REVIEW OF PARTICLE PHYSICS*

Particle Data Group

Abstract

The *Review* summarizes much of particle physics and cosmology. Using data from previous editions, plus 2,143 new measurements from 709 papers, we list, evaluate, and average measured properties of gauge bosons and the recently discovered Higgs boson, leptons, quarks, mesons, and baryons. We summarize searches for hypothetical particles such as supersymmetric particles, heavy bosons, axions, dark photons, etc. Particle properties and search limits are listed in Summary Tables. We give numerous tables, figures, formulae, and reviews of topics such as Higgs Boson Physics, Supersymmetry, Grand Unified Theories, Neutrino Mixing, Dark Energy, Dark Matter, Cosmology, Particle Detectors, Colliders, Probability and Statistics. Among the 120 reviews are many that are new or heavily revised, including a new review on Machine Learning, and one on Spectroscopy of Light Meson Resonances.

The *Review* is divided into two volumes. Volume 1 includes the Summary Tables and 97 review articles. Volume 2 consists of the Particle Listings and contains also 23 reviews that address specific aspects of the data presented in the Listings.

The complete *Review* (both volumes) is published online on the website of the Particle Data Group (pdg.lbl.gov) and in a journal. Volume 1 is available in print as the *PDG Book*. A *Particle Physics Booklet* with the Summary Tables and essential tables, figures, and equations from selected review articles is available in print, as a web version optimized for use on phones, and as an Android app.

The 2022 edition of the *Review of Particle Physics* should be cited as:
R.L. Workman *et al.* (Particle Data Group), Prog. Theor. Exp. Phys. **2022**, 083C01 (2022)

DOI: 10.1093/ptep/ptac097

For the online version see pdg.lbl.gov:

© 2022

Except where otherwise noted, content of this work (the *Review of Particle Physics*) is licensed under a Creative Commons Attribution-NonCommercial 4.0 International (CC BY-NC 4.0) license.

*The publication of the *Review of Particle Physics* is supported by the Director, Office of Science, Office of High Energy Physics of the U.S. Department of Energy under Contract No. DE–AC02–05CH11231; by an implementing arrangement between the governments of Japan (MEXT: Ministry of Education, Culture, Sports, Science and Technology) and the United States (DOE) on cooperative research and development; by the Italian National Institute of Nuclear Physics (INFN); by the Physical Society of Japan (JPS); and by the European Laboratory for Particle Physics (CERN). Individual collaborators receive support for their PDG activities from their respective institutes or funding agencies.

Downloaded from https://academic.oup.com/ptep/article/2022/8/083C01/6651666 by KIT Library user on 27 September 2022

Particle Data Group

R.L. Workman,[1] V.D. Burkert,[2] V. Crede,[3] E. Klempt,[4] U. Thoma,[4] L. Tiator,[5] K. Agashe,[6] G. Aielli,[7] B.C. Allanach,[8] C. Amsler,[9] M. Antonelli,[10] E.C. Aschenauer,[11] D.M. Asner,[11] H. Baer,[12] Sw. Banerjee,[13] R.M. Barnett,[14] L. Baudis,[15] C.W. Bauer,[14] J.J. Beatty,[16] V.I. Belousov,[17] J. Beringer,[14] A. Bettini*,[18] O. Biebel,[19] K.M. Black,[20] E. Blucher,[21] R. Bonventre,[14] V.V. Bryzgalov,[17] O. Buchmuller,[22] M.A. Bychkov,[23] R.N. Cahn,[14] M. Carena,[24,21,25] A. Ceccucci,[26] A. Cerri,[27] R. Sekhar Chivukula,[28] G. Cowan,[29] K. Cranmer,[30] O. Cremonesi,[31] G. D'Ambrosio,[32] T. Damour,[33] D. de Florian,[34] A. de Gouvêa,[35] T. DeGrand,[36] P. de Jong,[37] S. Demers,[38] B.A. Dobrescu,[24] M. D'Onofrio,[39] M. Doser,[26] H.K. Dreiner,[40] P. Eerola,[41] U. Egede,[42] S. Eidelman†,[43,44] A.X. El-Khadra,[45] J. Ellis,[46,26] S. C. Eno,[6] J. Erler,[5] V.V. Ezhela,[17] W. Fetscher,[47] B.D. Fields,[48,45] A. Freitas,[49] H. Gallagher,[50] Y. Gershtein,[51] T. Gherghetta,[52] M.C. Gonzalez-Garcia,[53,54,55] M. Goodman,[56] C. Grab,[47] A.V. Gritsan,[57] C. Grojean,[58,59] D.E. Groom,[14] M. Grünewald,[60] A. Gurtu,[26,61] T. Gutsche,[62] H.E. Haber,[63] Matthieu Hamel,[64] C. Hanhart,[65] S. Hashimoto,[66] Y. Hayato,[67,68] A. Hebecker,[69] S. Heinemeyer,[70] J. J. Hernández-Rey‡,[71] K. Hikasa,[72,73,74] J. Hisano,[75] A. Höcker,[26] J. Holder,[76,77] L. Hsu,[24] J. Huston,[78] T. Hyodo,[79] Al. Ianni,[80] M. Kado,[81,82,83] M. Karliner,[84] U.F. Katz,[85] M. Kenzie,[86] V.A. Khoze,[87] S.R. Klein,[88,89] F. Krauss,[87] M. Kreps,[86] P. Križan,[90,91] B. Krusche†,[92] Y. Kwon,[93] O. Lahav,[94] J. Laiho,[95] L.P. Lellouch,[96] J. Lesgourgues,[97] A.R. Liddle,[98] Z. Ligeti,[14] C.-J. Lin,[14] C. Lippmann,[99] T.M. Liss,[100] L. Littenberg,[11] C. Lourenço,[26] K.S. Lugovsky,[14,17] S.B. Lugovsky,[17] A. Lusiani,[101,102] Y. Makida,[66] F. Maltoni,[103,104] T. Mannel,[105] A.V. Manohar,[28] W.J. Marciano,[11] A. Masoni,[106] J. Matthews,[107] U.-G. Meißner,[4,65] I.-A. Melzer-Pellmann,[58] M. Mikhasenko,[19] D.J. Miller,[108] D. Milstead,[109] R.E. Mitchell,[110] K. Mönig,[111] P. Molaro,[112,113] F. Moortgat,[26,114] M. Moskovic,[26] K. Nakamura,[66,68] M. Narain,[115] P. Nason,[31,116] S. Navas‡,[117] A. Nelles,[111,85] M. Neubert,[118] P. Nevski§,[11] Y. Nir,[119] K.A. Olive,[52] C. Patrignani,[120] J.A. Peacock,[121] V.A. Petrov,[17] E. Pianori,[14] A. Pich,[71] A. Piepke,[122] F. Pietropaolo,[26,123] A. Pomarol,[124,125] S. Pordes,[24] S. Profumo,[63] A. Quadt,[126] K. Rabbertz,[127] J. Rademacker,[128] G. Raffelt,[129] M. Ramsey-Musolf,[130,131,132] B.N. Ratcliff,[133] P. Richardson,[87] A. Ringwald,[58] D.J. Robinson,[14] S. Roesler,[26] S. Rolli,[134] A. Romaniouk,[135,136] L. J Rosenberg,[137] J.L. Rosner,[21] G. Rybka,[137] M.G. Ryskin,[138] R.A. Ryutin,[17] Y. Sakai,[66] S. Sarkar,[139] F. Sauli§,[26] O. Schneider,[140] S. Schönert,[141] K. Scholberg,[142] A.J. Schwartz,[143] J. Schwiening,[99] D. Scott,[144] F. Sefkow,[58] U. Seljak,[89,14] V. Sharma,[28] S.R. Sharpe,[137] V. Shiltsev¶,[24] G. Signorelli,[102] M. Silari,[26] F. Simon,[129] T. Sjöstrand,[145] P. Skands,[42] T. Skwarnicki,[95] G.F. Smoot,[146,89,14,147,148] A. Soffer,[84] M.S. Sozzi,[149] S. Spanier,[150] C. Spiering,[111] A. Stahl,[151] S.L. Stone†,[95] Y. Sumino,[74] M.J. Syphers,[152,24] F. Takahashi,[74] M. Tanabashi,[153,75] J. Tanaka,[154] M. Taševský,[155] K. Terao,[133,156] K. Terashi,[154] J. Terning,[157] R.S. Thorne,[94] M. Titov,[158] N.P. Tkachenko,[17] D.R. Tovey,[159] K. Trabelsi,[83] P. Urquijo,[160] G. Valencia,[42] R. Van de Water,[24] N. Varelas,[161] G. Venanzoni,[102] L. Verde,[55,54] I. Vivarelli,[27] P. Vogel,[162] W. Vogelsang,[62] V. Vorobyev,[43,44] S.P. Wakely,[21,25] W. Walkowiak,[105] C.W. Walter,[142] D. Wands,[163] D.H. Weinberg,[164] E.J. Weinberg,[165] N. Wermes,[40] M. White,[89,14] L.R. Wiencke,[166] S. Willocq,[132] C.G. Wohl,[14] C.L. Woody,[11] W.-M. Yao,[14] M. Yokoyama,[167,68] R. Yoshida,[56] G. Zanderighi,[168] G.P. Zeller,[24] O.V. Zenin,[17,169] R.-Y. Zhu,[170] Shi-Lin Zhu,[171] F. Zimmermann,[26] P.A. Zyla[14]

Technical Associates: J. Anderson,[14] T. Basaglia,[26] P. Schaffner,[14] W. Zheng,[172]

1. *George Washington University, Department of Physics, Washington, D.C., USA*
2. *Jefferson Lab, Newport News, VA, USA*
3. *Florida State University, Department of Physics, Tallahassee, FL, USA*
4. *Universität Bonn, Helmholtz-Institut für Strahlen- und Kernphysik, Bonn, Germany*
5. *Institut für Kernphysik, Johannes Gutenberg University, Mainz, Germany*
6. *University of Maryland, Department of Physics, College Park, MD, USA*
7. *Università degli Studi di Roma "Tor Vergata", Rome, Italy*
8. *Department of Applied Mathematics and Theoretical Physics, University of Cambridge, Cambridge, UK*
9. *Stefan Meyer Institute for Subatomic Physics, Austrian Academy of Sciences, Vienna, Austria*
10. *Lab. Nazionali di Frascati dell'INFN, Frascati, Italy*
11. *Brookhaven National Laboratory, Nuclear and Particle Physics Directorate, Upton, NY, USA*
12. *University of Oklahoma, Department of Physics and Astronomy, Norman, OK, USA*
13. *University of Louisville, Louisville, KY, USA*
14. *Physics Division, Lawrence Berkeley National Laboratory, Berkeley, CA, USA*
15. *Universität Zürich, Physik-Institut, Zürich, Switzerland*
16. *Ohio State University, Department of Physics, Columbus, OH, USA*

*Coordination activities supported directly by INFN.
†Deceased.
‡Support from Programa Estatal de Generación de Conocimiento MCIU, Spain and ERDF of the European Union (PGC2018-096663-B-C41 and C44).
§Retired.
¶Supported by Fermi Research Alliance, LLC under Contract No. DE-AC02-07CH11359 with DOE.

Downloaded from https://academic.oup.com/ptep/article/2022/8/083C01/6651666 by KIT Library user on 27 September 2022

17. *Institute for High Energy Physics of the National Research Centre Kurchatov Institute, COMPAS Group, Protvino, Russia*
18. *INFN and Dipartimento di Fisica e Astronomia, Università di Padova, Padova, Italy*
19. *Ludwig-Maximilians-Universität, Fakultät für Physik, München, Germany*
20. *University of Wisconsin, Department of Physics, Madison, WI, USA*
21. *University of Chicago, Enrico Fermi Institute and Department of Physics, Chicago, IL, USA*
22. *Imperial College, High Energy Physics Group, Blackett Laboratory, London, UK*
23. *University of Virginia, Department of Physics, Charlottesville, VA, USA*
24. *Fermi National Accelerator Laboratory, Batavia, IL, USA*
25. *University of Chicago, Kavli Institute for Cosmological Physics, Chicago, IL, USA*
26. *CERN, European Organization for Nuclear Research, Genève, Switzerland*
27. *Department of Physics and Astronomy, University of Sussex, Brighton, UK*
28. *Department of Physics, University of California at San Diego, La Jolla, CA, USA*
29. *Department of Physics, Royal Holloway, University of London, London, UK*
30. *State University of New York, Institute for Theoretical Physics, Stony Brook, NY, USA*
31. *INFN Sezione di Milano-Bicocca, Piazza della Scienza, Milano, Italy*
32. *INFN Sezione di Napoli, Napoli, Italy*
33. *Institut des Hautes Etudes Scientifiques, Bures-sur-Yvette, France*
34. *UNSAM - Universidad Nacional de San Martin, International Center for Advanced Studies (ICAS) and Instituto de Ciencias Físicas (ICIFI), Buenos Aires, Argentina*
35. *Northwestern University, Department of Physics and Astronomy, Evanston, IL, USA*
36. *University of Colorado at Boulder, Department of Physics, Boulder, CO, USA*
37. *Nikhef and University of Amsterdam, Amsterdam, The Netherlands*
38. *Yale University, New Haven, CT, USA*
39. *University of Liverpool, Department of Physics, Liverpool, UK*
40. *Universität Bonn, Physikalisches Institut, Bonn, Germany*
41. *University of Helsinki, Department of Physics, Helsinki, Finland*
42. *Monash University, School of Physics and Astronomy, Melbourne, Australia*
43. *Budker Institute of Nuclear Physics SB RAS, Novosibirsk, Russia*
44. *Novosibirsk State University, Novosibirsk, Russia*
45. *University of Illinois, Department of Physics, Urbana, IL, USA*
46. *King's College London, Department of Physics, London, UK*
47. *ETH Zurich, Institute for Particle Physics and Astrophysics, Zurich, Switzerland*
48. *University of Illinois, Department of Astronomy, Urbana, IL, USA*
49. *University of Pittsburgh, Department of Physics and Astronomy, Pittsburgh, PA, USA*
50. *Tufts University, Department of Physics and Astronomy, Medford, MA, USA*
51. *Department of Physics and Astronomy, Rutgers University, NJ, USA*
52. *University of Minnesota, School of Physics and Astronomy, Minneapolis, MN, USA*
53. *CN Yang Institute for Theoretical Physics, Stony Brook University, Stony Brook, NY, USA*
54. *Institució Catalana de Recerca i Estudis Avancats, Barcelona, Spain*
55. *Instituto de ciencias del Cosmos (ICC), University of Barcelona, Barcelona, Spain*
56. *Argonne National Laboratory, Argonne, IL, USA*
57. *Johns Hopkins University, Baltimore, MD, USA*
58. *Deutsches Elektronen-Synchrotron DESY, Hamburg, Germany*
59. *Institut für Physik, Humboldt-Universität zu Berlin, Berlin, Germany*
60. *University College Dublin, School of Physics, Dublin, Ireland*
61. *TIFR, Mumbai, India*
62. *Universität Tübingen, Institut für Theoretische Physik, Tübingen, Germany*
63. *Santa Cruz Institute for Particle Physics, University of California, Santa Cruz, CA, USA*
64. *Université Paris-Saclay, CEA, LIST, F-91120 Palaiseau, France*
65. *Institut für Kernphysik and Institute for Advanced Simulation, Forschungszentrum Jülich, Jülich, Germany*
66. *KEK, High Energy Accelerator Research Organization, Tsukuba, Japan*
67. *Kamioka Observatory, ICRR, The University of Tokyo, Tokyo, Japan*
68. *The University of Tokyo, Kavli IPMU (WPI), The University of Tokyo Institutes for Advanced Study, Kashiwa, Japan*
69. *Heidelberg University, Institute for Theoretical Physics, Heidelberg, Germany*

Downloaded from https://academic.oup.com/ptep/article/2022/8/083C01/6651666 by KIT Library user on 27 September 2022

70. *Instituto de Física Teórica (UAM/CSIC), Universidad Autónoma de Madrid, Madrid, Spain*
71. *IFIC — Instituto de Física Corpuscular, Universitat de València — C.S.I.C., Valencia, Spain*
72. *Division for Interdisciplinary Advanced Research and Education, Tohoku University, Sendai, Japan*
73. *Institute of Liberal Arts and Sciences, Tohoku University, Sendai, Japan*
74. *Tohoku University, Department of Physics, Sendai, Japan*
75. *Nagoya University, Kobayashi-Maskawa Institute, Nagoya, Japan*
76. *University of Delaware, Department of Physics and Astronomy, Newark, DE, USA*
77. *University of Delaware, Bartol Research Institute, Newark, DE, USA*
78. *Michigan State University, Dept. of Physics and Astronomy, East Lansing, MI, USA*
79. *Department of Physics, Tokyo Metropolitan University, Tokyo, Japan*
80. *INFN - Laboratori Nazionali del Gran Sasso, Assergi, Italy*
81. *Dipartimento di Fisica, Sapienza Università di Roma, Rome, Italy*
82. *INFN Sezione di Roma, Rome, Italy*
83. *IJCLab, CNRS/IN2P3, Université Paris-Saclay, Orsay, France*
84. *Department of Particle Physics, Tel-Aviv University, Tel Aviv, Israel*
85. *Friedrich-Alexander-Universität Erlangen-Nürnberg, Erlangen Centre for Astroparticle Physics, Erlangen, Germany*
86. *University of Warwick, Department of Physics, Coventry, UK*
87. *University of Durham, Institute for Particle Physics Phenomenology, Department of Physics, Durham, UK*
88. *Nuclear Science Division, Lawrence Berkeley National Laboratory, Berkeley, CA, USA*
89. *University of California, Department of Physics, Berkeley, CA, USA*
90. *Faculty of Mathematics and Physics, University of Ljubljana, Jadranska, Slovenia*
91. *Jozef Stefan Institute, Ljubljana, Slovenia*
92. *University of Basel, Institute of Physics, Basel, Switzerland*
93. *Yonsei University, Department of Physics, Seoul, Republic of Korea*
94. *University College London, Department of Physics and Astronomy, London, UK*
95. *Syracuse University, Department of Physics, Syracuse, NY, USA*
96. *Aix-Marseille Univ, Université de Toulon, CNRS, CPT, Marseille, France*
97. *Institute of Theoretical Particle Physics and Cosmology (TTK), RWTH, Aachen, Germany*
98. *Instituto de Astrofísica e Ciências do Espaço, Universidade de Lisboa, Lisbon, Portugal*
99. *GSI, Helmholtzzentrum für Schwerionenforschung, Darmstadt, Germany*
100. *The City College of New York, New York, NY, USA*
101. *Scuola Normale Superiore, Pisa, Italy*
102. *INFN Sezione di Pisa, Pisa, Italy*
103. *Universitè catholique de Louvain, Centre for Cosmology, Particle Physics and Phenomenology (CP3), Louvain-la-Neuve, Belgium*
104. *Università di Bologna and INFN, Dipartimento di Fisica e Astronomia, Bologna, Italy*
105. *Universität Siegen, Department für Physik, Siegen, Germany*
106. *INFN Sezione di Cagliari, Monserrato, Italy*
107. *Louisiana State University, Department of Physics and Astronomy, Baton Rouge, LA, USA*
108. *University of Glasgow, School of Physics and Astronomy, Glasgow, UK*
109. *Stockholms Universitet, AlbaNova University Centre, Fysikum, Stockholm, Sweden*
110. *Indiana University, Department of Physics, Bloomington, IN, USA*
111. *Deutsches Elektronen-Synchrotron DESY, Zeuthen, Germany*
112. *INAF-OATS, Trieste, Italy*
113. *Institute for Fundamental Physics of the Universe, Trieste, Italy*
114. *University of Ghent, Dept. of Physics and Astronomy, Ghent, Belgium*
115. *Brown University, Department of Physics, Providence, RI, USA*
116. *Dip. di Fisica "G. Occhialini", Università di Milano-Bicocca, Milano, Italy*
117. *Universidad de Granada, Dpto. de Física Teórica y del Cosmos & C.A.F.P.E., Granada, Spain*
118. *Johannes Gutenberg University, PRISMA Cluster of Excellence and Mainz Institute for Theoretical Physics, Mainz, Germany*
119. *Department of Particle Physics and Astrophysics, Weizmann Institute of Science, Rehovot, Israel*
120. *Università di Bologna and INFN, Dip. Scienze per la Qualità della Vita, Rimini, Italy*
121. *University of Edinburgh, Royal Observatory, Institute for Astronomy, Edinburgh, UK*
122. *University of Alabama, Department of Physics and Astronomy, Tuscaloosa, AL, USA*

Downloaded from https://academic.oup.com/ptep/article/2022/8/083C01/6651666 by KIT Library user on 27 September 2022

123. INFN Sezione di Padova, Padua, Italy
124. Universitat Autònoma de Barcelona, Departament de Física, Barcelona, Spain
125. IFAE, Universitat Autònoma de Barcelona, Barcelona, Spain
126. Georg-August-Universität Göttingen, II. Physikalisches Institut, Göttingen, Germany
127. Karlsruhe Institute of Technology, Karlsruhe, Germany
128. University of Bristol, HH Wills Physics Laboratory, Bristol, UK
129. Max-Planck-Institut für Physik (Werner-Heisenberg-Institut), München, Germany
130. Tsung-Dao Lee Institute, Shanghai Jiao Tong University, Shanghai, China
131. Shanghai Jiao Tong University, Shanghai, China
132. University of Massachusetts, Department of Physics, Amherst, MA, USA
133. SLAC National Accelerator Laboratory, Menlo Park, CA, USA
134. DOE, Washington, DC, USA
135. Institut für Astro- und Teilchenphysik, Leopold-Franzens-Universität, Innsbruck, Austria
136. National Research Nuclear University "MEPhI", Moscow, Russia
137. University of Washington, Department of Physics, Seattle, WA, USA
138. Petersburg Nuclear Physics Institute, Petersburg, Russia
139. University of Oxford, Rudolf Peierls Centre for Theoretical Physics, Oxford, UK
140. Institute of Physics, Ecole Polytechnique Fédérale de Lausanne (EPFL), Lausanne, Switzerland
141. Department of Physics, Technical University Munich, Munich, Germany
142. Duke University, Physics Department, Durham, NC, USA
143. University of Cincinnati, Department of Physics, Cincinnati, OH, USA
144. University of British Columbia, Department of Physics and Astronomy, Vancouver, BC, Canada
145. Lund University, Department of Astronomy and Theoretical Physics, Lund, Sweden
146. The Hong Kong University of Science and Technology, Kowloon, Hong Kong
147. Donostia International Physics Center (DIPC), Donostia-San Sebastián, Spain
148. Paris Centre for Cosmological Physics, APC (CNRS), Université de Paris, Paris, France
149. Pisa University, Pisa, Italy
150. University of Tennessee, Department of Physics and Astronomy, Knoxville, TN, USA
151. III. Physikalisches Institut, Physikzentrum, RWTH Aachen University, Aachen, Germany
152. Department of Physics, Northern Illinois University, DeKalb, IL, USA
153. Department of Physics, Nagoya University, Nagoya, Japan
154. International Center for Elementary Particle Physics (ICEPP), The University of Tokyo, Tokyo, Japan
155. Institute of Physics, Czech Academy of Sciences, Prague, Czech Republic
156. Stanford University, Stanford, CA, USA
157. Department of Physics, University of California, Davis, CA, USA
158. IRFU, CEA, Université Paris-Saclay, F-91191 Gif-sur-Yvette, France
159. University of Sheffield, Department of Physics and Astronomy, Sheffield, UK
160. University of Melbourne, School of Physics, Victoria, Australia
161. University of Illinois at Chicago, Chicago, IL, USA
162. California Institute of Technology, Kellogg Radiation Laboratory, Pasadena, CA, USA
163. University of Portsmouth, Institute of Cosmology and Gravitation, Portsmouth, UK
164. Ohio State University, Department of Astronomy and CCAPP, Columbus, OH, USA
165. Columbia University, Department of Physics, New York, NY, USA
166. Dept. of Physics, Colorado School of Mines, Golden, CO, USA
167. The University of Tokyo, Department of Physics, Tokyo, Japan
168. Max-Planck-Institute of Physics, Munich, Germany
169. Moscow Institute of Physics and Technology, Dolgoprudny, Russia
170. California Institute of Technology, High Energy Physics, Pasadena, CA, USA
171. School of Physics, Peking University, Beijing, China
172. Institute of High Energy Physics, Beijing, China

Downloaded from https://academic.oup.com/ptep/article/2022/8/083C01/6651666 by KIT Library user on 27 September 2022

HIGHLIGHTS OF THE 2022 EDITION OF THE REVIEW OF PARTICLE PHYSICS

All PDG data and review articles are available online at **pdg.lbl.gov**.

709 new papers with 2,143 new measurements

120 reviews (most are revised)

- 267 new papers from *LHC* experiments (ATLAS, CMS and LHCb).
- Extensive up-to-date *Higgs boson* coverage from 58 new papers with 88 measurements, including latest results on mass, couplings, decay width and branching ratios, plus searches for other neutral and charged Higgs bosons.
- *Supersymmetry*: 62 new papers with major exclusions.
- *Top quark*: 24 new papers provide latest results on mass, coupling, and the first direct evidence of four top quark production at LHC.
- Latest from *b-hadron physics*: 83 papers and 326 measurements provide the world-best data on CKM angles, mixing, CP violation, and constraints on new physics from b-flavored hadrons.
- Substantial reorganization of several *meson resonances* sections. Also, recently observed states such as tetraquark candidates are included, several mesons now considered established are added to Summary Tables, and complex pole positions are listed when available.
- Revised naming and status of the Lambda and Sigma resonances.
- New most precise measurement of neutron lifetime.
- Naming scheme for hadrons extended to accommodate states with quantum numbers not allowed for $q\bar{q}$ and qqq states.
- New reviews on:
  - *Machine Learning*.
  - *Spectroscopy of Light Meson Resonances*.
- Significant update/revision to reviews on:
  - Major revision of review on *Accelerator Physics of Colliders*.
  - New section *LAr Time Projection Chamber* added to *Particle Detectors at Accelerators* review; extensive revision of sections on *Organic scintillators*, *Gaseous detectors*, *Semiconductor detectors*, *Low-noise detector readout*, and *Hadronic calorimeters*.
  - Major updates of sections on *Sub-Kelvin detectors*, *Low-radioactivity background techniques*, and *Radio emission from (ultra-)high energy particle showers* in *Particle Detectors for Non-Accelerator Physics* review.
  - Updated EWK fit in *Electroweak Model and Constraints on New Physics* review.
  - *Quark Model* review includes new discussion on magnetic moments and charmed and bottom baryons.
  - *Top Quark* review summarizes latest LHC results and constraints on new physics from top quark.
  - Review on *Semileptonic B Hadron Decays, Determination of V_{cb} and V_{ub}* summarizes latest results and discusses long-standing issues with inclusive and exclusive measurements.
  - Curated *Online Particle Physics Information* review now paired with more extensive online version on github open to community contributions.

Downloaded from https://academic.oup.com/ptep/article/2022/8/083C01/6651666 by KIT Library user on 27 September 2022

VOLUME 1: SUMMARY TABLES AND REVIEWS

Highlights 6
Introduction 11
History plots 19
Online particle physics information (rev.) 20

SUMMARY TABLES

Gauge and Higgs bosons 25
Leptons 28
Quarks 32
Mesons 33
Meson quick reference table 88
Baryon quick reference table 89
Baryons 90
Searches not in Other Sections 108
Tests of conservation laws 110

REVIEWS, TABLES, AND PLOTS

Constants, Units, Atomic and Nuclear Properties

1. Physical constants (rev.) 133
2. Astrophysical constants and parameters (rev.) 134
3. International system of units (SI) (rev.) 136
4. Periodic table of the elements (rev.) 137
5. Electronic structure of the elements 138
6. Atomic and nuclear properties of materials (rev.) 140
7. Electromagnetic relations 142
8. Naming scheme for hadrons (rev.) 144

Standard Model and Related Topics

9. Quantum chromodynamics (rev.) 149
10. Electroweak model and constraints on new physics (rev.) 177
11. Higgs boson physics, status of (rev.) 201
12. CKM quark-mixing matrix (rev.) 261
13. CP violation in the quark sector (rev.) 271
14. Neutrino masses, mixing, and oscillations (rev.) 285
15. Quark model (rev.) 312
16. Heavy-quark & soft-collinear effective theory 329
17. Lattice quantum chromodynamics (rev.) 337
18. Structure functions (rev.) 353
19. Fragmentation functions in e^+e^-, ep and pp collisions (rev.) 375
20. High Energy Soft QCD and Diffraction 392

Astrophysics and Cosmology

21. Experimental tests of gravitational theory (rev.) 417
22. Big-Bang cosmology (rev.) 430
23. Inflation (rev.) 443
24. Big-Bang nucleosynthesis (rev.) 459
25. Cosmological parameters (rev.) 467
26. Neutrinos in cosmology (rev.) 476
27. Dark matter (rev.) 483
28. Dark energy (rev.) 499
29. Cosmic microwave background (rev.) 509
30. Cosmic rays (rev.) 520

Experimental Methods and Colliders

31. Accelerator physics of colliders (rev.) 533
32. High-energy collider parameters (rev.) 543
33. Neutrino beam lines at high-energy proton synchrotrons (rev.) 548
34. Passage of particles through matter (rev.) 549
35. Particle detectors at accelerators (rev.) 565
36. Particle detectors for non-accelerator phys. (rev.) 618
37. Radioactivity and radiation protection (rev.) 646
38. Commonly used radioactive sources (rev.) 652

Mathematical Tools

39. Probability (rev.) 655
40. Statistics (rev.) 660
41. Machine Learning (new) 676
42. Monte Carlo techniques (rev.) 713
43. Monte Carlo event generators (rev.) 717
44. Monte Carlo neutrino event generators (rev.) 729
45. Monte Carlo particle numbering scheme (rev.) 733
46. Clebsch-Gordan coefficients, spherical harmonics, and d functions 737
47. SU(3) isoscalar factors and representation matrices 738
48. SU(n) multiplets and Young diagrams 739

Kinematics, Cross-Section Formulae, and Plots

49. Kinematics (rev.) 743
50. Resonances (rev.) 747
51. Cross-section formulae for specific processes (rev.) 756
52. Neutrino cross section measurements (rev.) 765
53. Plots of cross sections and related quantities (rev.) 770

Particle Properties

Gauge Bosons

54. Mass and width of the W boson (rev.) 789
55. Z boson 791

Charged Leptons

56. Muon anomalous magnetic moment (rev.) 796
57. Muon decay parameters (rev.) 800
58. τ branching fractions (rev.) 803
59. τ-lepton decay parameters (rev.) 806

Quarks

60. Quark masses (rev.) 808
61. Top quark (rev.) 817

(Continued on next page.)

Downloaded from https://academic.oup.com/ptep/article/2022/8/083C01/6651666 by KIT Library user on 27 September 2022

Mesons
62. Form factors for semileptonic kaon ($K_{\ell 3}$), radiative pion ($\pi_{\ell 2\gamma}$) & kaon ($K_{\ell 2\gamma}$) decays (rev.) 842
63. Spectroscopy of light meson resonances (new) 845
64. Scalar mesons below 1 GeV (rev.) 858
65. Rare kaon decays (rev.) 865
66. CPT invariance tests in neutral kaon decay (rev.) 871
67. V_{ud}, V_{us}, Cabibbo angle, and CKM unitarity (rev.) 873
68. CP-violation in K_L decays (rev.) 877
69. Review of multibody charm analyses (rev.) 880
70. D^0–$\overline{D}^0$ mixing (rev.) 885
71. D_s^+ branching fractions (rev.) 895
72. Leptonic decays of charged pseudoscalar mesons (rev.) 897
73. Production and decay of b-flavored hadrons (rev.) 908
74. Polarization in B decays (rev.) 919
75. B^0–$\overline{B}^0$ mixing (rev.) 923
76. Semileptonic B-hadron decays, V_{cb} and V_{ub} (rev.) 930
77. CKM angles from B hadrons, determination of (rev.) 946
78. Spectroscopy of mesons containing two heavy quarks (rev.) 951
79. Heavy non-$q\overline{q}$ mesons (rev.) 959

Baryons
80. Baryon decay parameters 964
81. N and Δ resonances 965
82. Λ and Σ resonances (rev.) 970
83. Pole structure of the $\Lambda(1405)$ region (rev.) 973
84. Pentaquarks (rev.) 975

Hypothetical Particles and Concepts
85. Extra dimensions (rev.) 983
86. W'-boson searches (rev.) 991
87. Z'-boson searches (rev.) 995
88. Supersymmetry: theory (rev.) 1000
89. Supersymmetry: experiment (rev.) 1019
90. Axions and other similar particles (rev.) 1038
91. Quark and lepton compositeness, searches for (rev.) 1055
92. Dynamical electroweak symmetry breaking: implications of the H^0 (rev.) 1061
93. Grand unified theories 1076
94. Leptoquarks (rev.) 1090
95. Magnetic monopoles (rev.) 1093

INDEX (Volumes 1 and 2 combined) 1101

VOLUME 2: PARTICLE LISTINGS (available online only)

Illustrative key and abbreviations
Illustrative key 1127
Abbreviations 1128

Gauge and Higgs bosons
(γ, gluon, graviton, W, Z, Higgs, Axions) 1141

Leptons
(e, μ, τ, Heavy-charged lepton searches, Neutrino properties, Number of neutrino types Double-β decay, Neutrino mixing, Heavy-neutral lepton searches) 1239

Quarks
(u, d, s, c, b, t, b', t' (4th gen.), Free quarks) 1311

Mesons
Light unflavored (π, ρ, a, b) (η, ω, f, ϕ, h) 1349
Strange (K, K^*) 1473
Charmed (D, D^*) 1527
Charmed, strange (D_s, D_s^*, D_{sJ}) 1588
Bottom (B, V_{cb}/V_{ub}, B^*, B_J^*) 1609
Bottom, strange (B_s, B_s^*, B_{sJ}^*) 1786
Bottom, charmed (B_c) 1813
$c\overline{c}$ (η_c, $J/\psi(1S)$, χ_c, h_c, ψ) 1818
$b\overline{b}$ (η_b, Υ, χ_b, h_b) 1940
Other mesons 1980

Baryons
N 1987
Δ 2042
Λ 2065
Σ 2090
Ξ 2121
Ω 2133
Charmed (Λ_c, Σ_c, Ξ_c, Ω_c) 2136
Doubly charmed (Ξ_{cc}) 2160
Bottom (Λ_b, Σ_b, Ξ_b, Ω_b, b-baryon admixture) 2161
Exotic baryons (P_c pentaquarks) 2181

Searches not in Other Sections
Magnetic monopole searches 2185
Supersymmetric particle searches 2187
Technicolor 2238
Searches for quark and lepton compositeness 2239
Extra dimensions 2243
WIMP and dark matter searches 2249
Other particle searches 2263

Downloaded from https://academic.oup.com/ptep/article/2022/8/083C01/6651666 by KIT Library user on 27 September 2022

INTRODUCTION

1. Overview . . . 11
2. Particle Listings responsibilities . . . 11
3. Consultants . . . 12
4. Naming scheme for hadrons . . . 15
5. Procedures . . . 15
   5.1 Selection and treatment of data . . . 15
   5.2 Averages and fits . . . 15
      5.2.1 Treatment of errors . . . 15
      5.2.2 Unconstrained averaging . . . 16
      5.2.3 Constrained fits . . . 16
   5.3 Rounding . . . 17
   5.4 Discussion . . . 17
History plots . . . 19

ONLINE PARTICLE PHYSICS INFORMATION

1. Introduction . . . 20
2. Particle Data Group (PDG) resources . . . 20
3. Particle physics information platform . . . 20
4. Literature databases . . . 20
5. Journals . . . 21
6. Conference and seminars databases . . . 21
7. Research institutions . . . 21
8. People . . . 21
9. Experiments . . . 21
10. Jobs . . . 21
11. Software packages and repositories . . . 21
12. Data repositories and preservation . . . 21
13. Particle physics education and outreach . . . 21

Downloaded from https://academic.oup.com/ptep/article/2022/8/083C01/6651666 by KIT Library user on 27 September 2022

Downloaded from https://academic.oup.com/ptep/article/2022/8/083C01/6651666 by KIT Library user on 27 September 2022

Introduction

1 Overview

The *Review of Particle Physics* is a comprehensive review of the field of Particle Physics and of related areas in Cosmology. It is divided into two volumes. Volume 1 includes the "Summary Tables" and "Reviews, Tables, and Plots". Volume 2 consists of the "Particle Listings".

The *Review* is updated each year and made available on the PDG website (pdg.lbl.gov). In even-numbered years, the *Review* is also published in a journal and printed as the *PDG Book* together with an abridged *Particle Physics Booklet* containing Summary Tables and essential tables, figures, and equations from selected review articles. This edition is an updating through January 2022.

The Summary Tables give our best values and limits for particle properties such as masses, widths or lifetimes, and branching fractions, as well as an extensive summary of searches for hypothetical particles and a summary of experimental tests of conservation laws.

The 95 review articles in Reviews, Tables and Plots cover a wide variety of theoretical and experimental topics. Together with the Summary Tables they provide a quick reference for the practicing particle physicist. Two more review articles, Online Particle Physics Information and Tests of Conservation Laws, can be found in the introduction and Summary Tables, respectively.

The Particle Listings are a compilation/evaluation of data on particle properties. They contain all the data used to get the values given in the Summary Tables. They also give information on unconfirmed particles and particle searches. In this edition, the Particle Listings include 2,143 new measurements from 709 papers, in addition to the 44,695 measurements from 12,200 papers that first appeared in previous editions [1]. 23 review articles are part of the Particle Listings and address specific aspects of the data presented in the Listings. Because of the large quantity of data, the Particle Listings are not an archive of all published data on particle properties. We refer interested readers to earlier editions for data now considered to be obsolete.

We organize the particles into six categories:

- Gauge and Higgs bosons
- Leptons
- Quarks
- Mesons
- Baryons
- Searches not in other sections

The last category only includes searches for particles that do not belong to the previous groups. For example, it includes searches for supersymmetric particles, compositeness and extra dimensions, while searches for heavy charged leptons are with the leptons.

In Sec. 2 of this Introduction, we list the main areas of responsibility of the authors of the Particle Listings. Our many consultants, without whom we would not have been able to produce this *Review*, are acknowledged in Sec. 3. In Sec. 4, we mention briefly the naming scheme for hadrons, and in Sec. 5, we discuss our procedures for choosing among measurements of particle properties and for obtaining best values of the properties from the measurements.

The accuracy and usefulness of this *Review* depend in large part on interaction between its users and the authors. We appreciate comments, criticisms, and suggestions for improvements of any kind. Please send them to the appropriate author, according to the list of responsibilities in Sec. 2 below, or to pdg@lbl.gov.

In addition to the online publication at pdg.lbl.gov, the Review is available in different formats:

- The printed *PDG Book* includes volume 1 only, *i.e.* it contains the Summary Tables and most review articles. Since the 2016 edition [2] the detailed tables from the Particle Listings are no longer printed.
- The *Particle Physics Booklet* includes the Summary Tables plus essential tables, figures, and equations from selected review articles. Starting with the Booklets of the 2018 edition, we have excluded most text and explanations in order to revert back to a more pocket-sized format. The Booklet is available in print, as a web version optimized for use on phones, and as an Android app (see pdg.lbl.gov/booklet).
- *pdgLive* (pdgLive.lbl.gov) is a web application giving more interactive access to PDG data than the static web pages and PDF files that are also available.
- Files that can be downloaded from the PDG website include a table of masses, widths, and PDG Monte Carlo particle ID numbers; PDF files of volume 1 (PDG Book), volume 2 (Particle Listings) and Booklet; individual review articles; all figures; and an archive file containing the complete PDG website (except for pdgLive).

Copies of the *PDG Book* or the *Particle Physics Booklet* can be ordered from our website or directly at pdg.lbl.gov/order. For special requests only, please email pdg@lbl.gov in North and South America, Australia, and the Far East, and pdg-products@cern.ch in all other areas.

This *Review* is considered to be a single comprehensive review of particle physics and related areas. Therefore we prefer that it be cited as a whole, rather than citing *e.g.* an individual review article that is part of this *Review*. For the 2022 edition, the proper citation is:

R.L. Workman *et al.* (Particle Data Group), Prog. Theor. Exp. Phys. **2022**, 083C01 (2022).

If you wish to refer to a specific part of the *Review*, for example to the Higgs boson review article, the following form should be used:

Status of Higgs Boson Physics in R.L. Workman *et al.* (Particle Data Group), Prog. Theor. Exp. Phys. **2022**, 083C01 (2022).

2 Particle Listings responsibilities

* Asterisk indicates the people to contact with questions or comments about Particle Listings sections.

- Gauge and Higgs bosons

γ	A. Bettini, D.E. Groom*
Gluons	R.M. Barnett,* A.V. Manohar
Graviton	A. Bettini,* D.E. Groom
W, Z	M. Grünewald,* A. Gurtu*
Higgs bosons	S. Heinemeyer,* K. Hikasa, J. Tanaka
Heavy bosons	R. Bonventre,* K.A. Olive, M. Tanabashi
Axions	K.A. Olive, G. Raffelt,* F. Takahashi

- Leptons

Neutrinos	M. Goodman, C.-J. Lin,* K. Nakamura, K.A. Olive, A. Piepke
Double-β decay	A. Piepke, A. Bettini*
e, μ	A. Bettini,* C. Grab
τ	A. Lusiani, K. Mönig*

- Quarks

Quarks	R.M. Barnett,* A.V. Manohar
Top quark	W.-M. Yao,* Y. Sumino
b', t'	W.-M. Yao,* Y. Sumino
Free quark	A. Bettini,* C.-J. Lin

- Mesons

π, η	A. Bettini,* C. Grab
Unstable mesons	C. Amsler,* T. Gutsche, C. Hanhart, J.J. Hernández-Rey, C. Lourenco, A. Masoni, M. Mikhasenko, R.E. Mitchell, S. Navas, C. Patrignani, S. Spanier, G. Venanzoni, V. Vorobyev
K (stable)	G. D'Ambrosio, C.-J. Lin*
D (stable, no mix.)	D.M. Asner, R. Bonventre, J. Rademacker, D. Robinson*
D^0 mixing	D.M. Asner, R. Bonventre, J. Rademacker, D. Robinson*
B (stable)	A. Cerri,* P. Eerola, M. Kreps, Y. Kwon, W.-M. Yao*

Downloaded from https://academic.oup.com/ptep/article/2022/8/083C01/6651666 by KIT Library user on 27 September 2022

- Baryons

Stable baryons	C. Grab, D. Robinson*
Unstable baryons	V. Burkert, V. Crede, U. Thoma, L. Tiator, R.L. Workman*
Charmed baryons	R. Bonventre, J. Rademacker, D. Robinson*
Bottom baryons	A. Cerri,* P. Eerola, M. Kreps, Y. Kwon, W.-M. Yao*

- Miscellanoues searches

Monopole	A. Bettini,* D. Milstead
Supersymmetry	H.K. Dreiner,* I.-A. Melzer-Pellmann, A. de Gouvêa, K.A. Olive, I. Vivarelli
Technicolor	K. Agashe,* K.A. Olive, M. Tanabashi
Compositeness	M. Tanabashi, J. Terning*
Extra Dimensions	T. Gherghetta, K.A. Olive, D. Robinson*
WIMP, DM, Other	H. Baer, A. Bettini,* W.-M. Yao*

3 Consultants

The Particle Data Group benefits greatly from the assistance of hundreds of physicists who are asked to referee review articles and verify every piece of data entered into this *Review*. Of special value is the advice of the PDG Advisory Committee, which meets biennially and thoroughly reviews all aspects of our operation. The members of the 2022 committee are:

S. Demers (Yale)
D. d'Enterria (CERN)
J. Frieman (FNAL)
T. Nakada (EPFL)
M. Yokoyama (Tokyo)
Q. Zhao (IHEP Beijing)

We have especially relied on the expertise of the following people for advice on particular topics:

- K.N. Abazajian (UC Irvine)
- I. Abt (MPI Munich)
- R. Acciarri (FNAL)
- M. Achasov (Budker Inst., Novosibirsk)
- E.G. Adelberger (FNAL)
- J. Aebischer (Munich Tech. U.)
- F. Afzal (Bonn U.)
- M. Aleksa (CERN)
- P. Alvarez (CERN)
- L. Alvarez-Ruso (IFIC, Valencia)
- L. An (CERN)
- A. Antognini (ETH Zurich)
- F. Anulli (INFN, Rome)
- E. Aprile (Columbia U.)
- F. Archilli (CERN)
- G. Arduini (CERN)
- C. Armand (LAPTH)
- E. Armengaud (CEA Saclay, DSM/IRFU/SPP)
- M. Artuso (Syracuse U.)
- P. Athron (Nanjing U.)
- Avnish (Physics U. Bhubaneswar)
- G. Azuelos (U. de Montreal)
- P. Azzurri (INFN, Pisa)
- C. Balazs (Monash U.)
- A. Baldini (INFN, Pisa)
- A. Ball (CERN)
- D. Barney (CERN)
- R. Beck (Bonn U.)
- O. Behnke (DESY, Hamburg)
- V. Belyaev (ITEP)
- G. Bertone (Amsterdam U.)
- M. Bettler (CERN)
- T. Biekötter (DESY, Hamburg)
- T. Blum (UConn)
- S. Bolognesi (CERN)
- A. Bolz (Heidelberg U.)
- M. Bona (QMUL)
- A. Bondar (Budker Inst., Novosibirsk)
- M. Borsato (CERN)
- M. Boulay (Carleton U.)
- A. Boyarsky (Leiden U.)
- P. Brady (Wisconsin U.)
- E. Bratkovskaya (GSI Darmstadt; Frankfurt U.)
- J.E. Brau (Oregon U.)
- R.A. Briere (Carnegie Mellon U.)
- J. Brod (U. of Cincinnati)
- J. Brodzicka (IFJ PAN)
- G. Brooijmans (Columbia U.)
- R. Bruce (CERN)
- O. Bruning (CERN)
- D.A. Bryman (TRIUMF)
- A. Buckley (Glasgow U.)
- A. Buras (Munich Tech. U.)
- A. Cabrera (APC, Paris)
- L. Calibbi (NKU)
- J. Camalich (IAC)
- I. Campos Plasencia (CSIC)
- P. Carenza (Stockholm U.)
- T. Carli (CERN)
- N. Cartiglia (INFN, Torino)
- G. Casarosa (Pisa U.; INFN, Pisa)
- V. Cavaliere (BNL)
- G. Cavallero (CERN)
- G. Cavoto (Rome U.; INFN, Rome)
- S. Cebrian Guajardo (U. de Zaragoza)
- M. Cepeda (CIEMAT)
- F. Cerutti (LBNL)
- M. Charles (CNRS)
- A.E. Chavarria (U. Washington)
- K. Chen (Taiwan National U. Physics Dep.)
- Y. Chen (MIT)
- D. Chiesa (Milano-Bicocca U.; INFN, Milano-Bicocca)
- V. Chobanova (CERN)
- J. Chou (Rutgers U.)
- M. Cirelli (LPTHE, Paris)
- C. Clement (Stockholm U.)
- G. Colangelo (Bern U.)
- J.I. Collar (Chicago U.)
- P. Coloma (UAM/CSIC, U. Autónoma de Madrid)
- N. Crisosto (U. Washington)
- P. Crivelli (ETH Zurich)
- A. Cukierman (Stanford U.; SLAC)
- J.P. Cumalat (Colorado U.)
- A. Dainese (INFN, Padua)
- S. Dalla Torre (SISSA/INFN, Trieste)
- J. Dalseno (Santiago de Compostela U.)
- J. Darling (Colorado U.)
- C. Da Via (Manchester U.)
- C. Davies (Glasgow U.)
- A. De Angelis (INFN, Padova)
- C. De La Taille (OMEGA-CNRS-Ecole Polytechnique)

Downloaded from https://academic.oup.com/ptep/article/2022/8/083C01/6651666 by KIT Library user on 27 September 2022

- M. Delmastro (CERN; LAPP)
- Z. Demiragli (Boston U.)
- P.B. Denton (BNL)
- F. Deppisch (UCL)
- A. Derbin (NRC Kurchatov Inst. PNPI)
- A. Di Domenico (INFN, Rome)
- L. Dong (IHEP)
- A. Dragone (SLAC)
- J.J. Dudek (IReS)
- K. Dundas (Columbia U.)
- M. Dunford (CERN)
- B. Dutta (TAMU)
- V. Dutta (UC Santa Barbara)
- D.A. Dwyer (LBNL)
- S.R. Elliott (LANL)
- K. Ellis (Durham U.)
- C. Englert (Glasgow U.)
- D. Epifanov (Budker Inst., Novosibirsk)
- J. Erdmann (TU)
- S. Esen (CERN)
- R. Essig (YITP, Stony Brook)
- I. Esteban (Ohio State U.)
- J. Estrada (FNAL)
- P. Everaerts (MIT)
- S. Fang (IHEP Beijing)
- M. Fedderke (Stanford U.)
- T. Ferber (KIT)
- A. Ferrari (CERN)
- A. Ferrari (Uppsala U.)
- C. Finley (Stokholm U.)
- W. Fischer (BNL)
- P. Fonte (LIP)
- J. Formaggio (MIT)
- S. Forte (INFN, Milano-Bicocca)
- M. Frank (Concordia U.)
- S. Friedrich (LLNL)
- T. Fujii (Kyoto U.)
- K. Fujikura (UTokyo)
- E. Gabriel (CERN)
- P. Gambino (INFN, Torino)
- J. Gao (IHEP Beijing)
- Y. Gao (IHEP Beijing)
- O. Gaponenko (INR, Moscow)
- R. Garisto (APS)
- M. Garny (Munich Tech. U.)
- A. Gasparian (Jefferson Lab)
- C. Gatti (INFN, LNF)
- P. Gauzzi (INFN, Rome; Rome U. Sapienza)
- M. Gazdzicki (CERN)
- S. Ghosh (Yale U.)
- M. Giovannozzi (CERN)
- T.A. Girard (Lisbon U.)
- C. Giunti (INFN, Torino)
- L. Gladilin (SINP)
- S. Gleyzer (Alabama U.)
- V. Gligorov (CNRS)
- S.N. Gninenko (Russian Academy of Sciences)
- J. Gomez Cadenas (DIPC)
- G. Gomez-Ceballos (CERN)
- J. Goodman (U. Maryland)
- M. Goodsell (LPTHE, Paris)
- S.A. Gottlieb (Indiana U.)
- P. Govoni (INFN, Milano-Bicocca)
- P. Grabmayr (Tübingen U.)
- G. Gratta (Stanford U.)
- E. Graziani (INFN, Rome)
- P. Guzowski (Manchester U.)
- C. Gwenlan (Phys. Dep. Oxford U.)
- F. Halzen (Wisconsin U.)
- S. Hannestad (Aarhus U.)
- F.A. Harris (Hawaii U.)
- F. Hartmann (KIT)
- J. He (CERN)
- B. Heacock (NIST)
- A. Heijboen (NIKHEF)
- W. Heil (JGU, Mainz)
- B. Heinemann (DESY, Hamburg; Freiburg U.)
- F. Heisse (MPIK)
- J. Heitger (WWU)
- K.H. Hicks (Ohio State U.)
- A. Hinzmann (Hamburg U.)
- F. Hiskens (School of Phys. U. of Melbourne)
- A. Hoang (HEPHY, Vienna)
- M. Hoferichter (Bern U.)
- N. Houston (BJUT)
- T. Huege (KIT)
- T. Ikeda (Kyoto U.)
- N. Ilic (Toronto U.)
- S. Ito (Osaka U.)
- L. Jacob (LPSC, IN2P3)
- N. Jafari (DESY, Zeuthen)
- C. James (CIRA)
- B. Jayatilaka (FNAL)
- L. Jeanty (CERN)
- I. John (Stokholm U.)
- D. Johnson (CERN)
- B. Jose (Adelaide U.)
- A. Jung (Purdue U.)
- N. Jurik (CERN)
- A. Juste (IFAE; ICREA, Barcelona)
- M. Kagan (SLAC)
- A. Kahn (MPIK)
- D. Karlen (Victoria U.)
- S. Karshenboim (Pulkovo Obs., St.Petersburg)
- K. Kawagoe (Kyushu U.)
- O. Kepka (CERN)
- S. Kim (Seoul National U.)
- Y. Kim (IBS, Daejeon)
- K. Kirch (ETH Zurich)
- R. Klanner (DESY, Hamburg)
- M. Knecht (CPT, Marseille)
- B. Ko (IBS, Daejeon)
- Y. Kolomensky (LBNL)
- B. Kopf (Ruhr U. Bochum)
- A. Kopylov (INR, Moscow)
- U. Kose (ETH Zurich)
- T. Koseki (KEK)
- S. Kraml (LPSC, Grenoble)
- N. Krasnikov (INR, Moscow; JINR, Dubna)
- G. Kribs (Oregon U.)
- A. Krieger (LBNL)
- P. Krokovny (Budker Inst., Novosibirsk)

Downloaded from https://academic.oup.com/ptep/article/2022/8/083C01/6651666 by KIT Library user on 27 September 2022

- A. Kronfeld (FNAL)
- C. Lange (CERN)
- F. Lanusse (CEA Saclay)
- C. Lazzeroni (Birmingham U.)
- K. Leney (Southern Methodist U.)
- A. Lenz (Siegen U.)
- O. Leroy (CPPM Marseille)
- H. Li (IHEP Beijing)
- P. Li (Heidelberg U.)
- J. Libby (Indian Inst. Tech., Madras)
- E. Lisi (INFN, Bari)
- L. Lista (INFN, Napoli U.)
- J. Liu (School of Physics, Peking U.)
- J. Liu (SJTU)
- S. Lloyd (Phys. Dep. Durham U.)
- L. Longke (DESY, Hamburg)
- S. Lowette (ULB, Brussels)
- G. Lucente (INFN, Bari)
- M. Lucio (Santiago de Compostela U.)
- X. Luo (UC Santa Barbara)
- H. Ma (IHEP Beijing)
- F. Mahmoudi (IP2I, Lyon)
- P. Maksimovic (Johns Hopkins U.)
- B. Malaescu (LPNHE Paris)
- R. Manzoni (ETH Zurich)
- A. Marchionni (FNAL)
- M. Margoni (INFN, Padova)
- F. Marianna (LPNHE Paris)
- D. Marsh (King's Coll. London)
- C. Marshall (Rochester U.)
- M. Martinez-Perez (IFAE)
- T. Masubuchi (UTokyo)
- A. Mathad (ETH Zurich)
- M. Mazziotta (INFN, Bari)
- M. Mihovilovic (Jozef Stefan Inst.)
- C. Milardi (INFN, LNF)
- E. Minucci (CERN)
- R. Mizuk (MIPT Moscow)
- S. Moch (Hamburg U.)
- R.N. Mohapatra (U. Maryland)
- P. Mohr (NIST)
- D. Moore (Yale U.)
- M. Morello (SNS, Pisa)
- S. Moriyama (ICRR)
- V.M. Mostepanenko (Pulkovo Obs., St.Petersburg)
- M. Mulder (CERN)
- E. Myers (Florida State U.)
- B. Nachman (LBNL)
- P. Nadav (Stanford U.)
- P. Naik (Bristol U.)
- S. Narison (Montpellier U.)
- K. Ng (MIT)
- J. Nico (NIST)
- V. Obraztsov (IHEP, Protvino)
- A. Ochi (Kobe U.)
- H.B. O'Connell (FNAL)
- S. OGURI (JAXA)
- C. O'Hare (Sydney U.)
- K. Oide (KEK)
- F. Olness (Southern Methodist U.)
- P.E. Onyisi (Texas U. Austin)
- W. Ootani (ICEPP, UTokyo)
- G. Orebi Gann (LBNL)
- J.L. Ouellet (MIT)
- L. Pagnanini (GSSI)
- A. Palano (INFN, Bari)
- N. Palanque-Delabrouille (Paris U.)
- L. PDG-BMesons-verifiers (CERN)
- P. Pedroni (INFN, Pavia)
- H. Peiris (UCL; Stockholm U.)
- J.R. Pelaez (UCM, Madrid)
- M. Peruzzi (CERN)
- F. Petricca (MPI Munich)
- M. Pierini (CERN)
- L. Piilonen (Virginia Tech)
- P. Piminov (Budker Inst., Novosibirsk)
- T. Plehn (Heidelberg U.)
- S. Polikarpov (MEPhI Moscow)
- I. Polyakov (Syracuse U.)
- A. Pompili (INFN, Bari)
- A. Popov (IHEP, Protvino)
- W. Porod (Würzburg U.)
- J. Pradler (HEPHY, Vienna)
- G. Pugliese (INFN, Bari)
- A. Read (Oslo U.)
- A. Rebhan (TU Vienna)
- M. REGIS (INFN, Torino; Torino U.)
- F. Resnati (ETH Zurich)
- J. Richard (IP2I, Lyon)
- C.D. Roberts (Nanjing U.)
- A. Rodas (UCM, Madrid)
- M. Rotondo (INFN, Frascati)
- T. Roussy (Colorado U.)
- G. Ruggiero (Lancaster U.)
- T. Saab (Florida State U.)
- B. Safdi (UC Berkeley)
- R. Salerno (CNRS)
- D. Salvat (Indiana U.)
- N. Saoulidou (Athens U.)
- A.V. Sarantsev (Bonn U.)
- M. Sarsa (U. de Zaragoza)
- K. Schmidt-Hoberg (DESY, Hamburg)
- M. Schott (JGU, Mainz)
- S. Schramm (Geneva U.)
- K. Schutz (MIT; McGill U.)
- C. Schwanda (HEPHY, Vienna)
- B. Schwingenheur (MPIK)
- S. Scorza (Adelaide U.)
- Y.K. Semertzidis (IBS, Daejeon; KAIST)
- S. Seo (IBS, Daejeon)
- A.P. Serebrov (Petersburg Nuclear Phys. Inst.)
- L. Sestini (INFN, Padua)
- L. Shao (Beijng U. Kavli Inst. for Astronomy and Astrophysics)
- D. Shwartz (Budker Inst., Novosibirsk)
- C.V. Sierra (CERN)
- R. Simoniello (CERN)
- S. Simula (INFN, Rome)
- J. Smiga (JGU, Mainz; GSI Darmstadt)
- E. Smith (CERN)
- J. Sobczyk (Wrocław U.)
- F. Spano (RHUL)

Downloaded from https://academic.oup.com/ptep/article/2022/8/083C01/6651666 by KIT Library user on 27 September 2022

- J. Steggemann (ETH Zurich)
- L. Sun (ANU)
- A. Sushkov (Boston U.)
- A. Suzuki (LBNL)
- E.S. Swanson (Pittsburgh U.)
- R. Tesarek (FNAL)
- J. Thaler (MIT)
- D. Tonelli (Trieste U.)
- D. Tovey (Sheffield U.)
- N. Tran (FNAL)
- R. Trotta (Imperial Coll. Physics Dep.)
- Y. Tsai (UC Irvine)
- J. Tyson (UC Davis)
- S. Ulmer (RIKEN)
- Y. Unno (KEK)
- P.L. Vahle (William and Mary Coll.)
- R.G. Van De Water (LANL)
- D. Vanegas (UdeMedellín)
- C. van Eldik (Erlangen U.)
- R. Van Kooten (Indiana U.)
- D. Veberic (KIT)
- J. Vlimant (CALTECH)
- B. von Krosigk (Hamburg U.; KIT)
- M. Vos (IFIC, Valencia)
- D. Wang (School of Physics, Peking U.)
- N. Wardle (Imperial Coll. Physics Dep.)
- A. Watson (Leeds U.)
- G. Watt (Durham U.)
- M. Weber (Bern U.)
- R. Wendell (Kyoto U.)
- A.P. White (Texas U.)
- M. Wilkinson (U. of Cincinnati)
- C. Will (Florida State U.)
- M. Williams (Manchester U.)
- J. Wilson (Johns Hopkins U.)
- M. Wilson (Toronto U.)
- Z. Xu (CERN)
- A. Yamamoto (KEK)
- T. Yamanaka (Osaka U.)
- N. Yamasaki (JAXA)
- S. Yang (Sun Yat-sen U.)
- P. Yin (IHEP Beijing)
- K. Yokoya (KEK)
- C. Yuan (IHEP Beijing)
- Q. Yue (Tsinghua U.)
- D. Zerwas (LAL Orsay)
- C. Zhang (IHEP Beijing)
- J. Zhang (IHEP)
- B. Zheng (South China U.)
- K. Zhu (IHEP Beijing)
- K. Zioutas (U. Patras)
- B. Zou (Academia Sinica, Inst. of Physics)

4 Naming scheme for hadrons

We introduced in the 1986 edition [3] a new naming scheme for the hadrons. Changes from older terminology affected mainly the heavier mesons made of u, d, and s quarks. Otherwise, the only important change to known hadrons was that the $F^{\pm}$ became the $D_s^{\pm}$. None of the lightest pseudoscalar or vector mesons changed names, nor did the $c\overline{c}$ or $b\overline{b}$ mesons (we do, however, now use χ_c for the $c\overline{c}$ χ states), nor did any of the established baryons. The Summary Tables give both the new and old names whenever a change has occurred.

In the 2018 edition [4], the naming scheme was extended to address the naming of charmonium and bottomonium states that are commonly referred to as X, Y or Z states in the literature. The current scheme is described in "Naming Scheme for Hadrons" (p. 1) of this *Review*. A table details the correspondence between the names newly adopted by the PDG and those that have appeared in the literature. For this edition the naming scheme was further extended to accommodate states with quantum numbers not allowed for $q\bar{q}$ and qqq states.

We give here our conventions on type-setting style. Particle symbols are italic (or slanted) characters: e^-, p, Λ, π^0, K_L, D_s^+, b. Charge is indicated by a superscript: B^-, Δ^{++}. Charge is not normally indicated for p, n, or the quarks, and is optional for neutral isosinglets: η or η^0. Antiparticles and particles are distinguished by charge for charged leptons and mesons: τ^+, K^-. Otherwise, distinct antiparticles are indicated by a bar (overline): $\overline{\nu}_\mu$, $\bar{t}$, $\overline{p}$, $\overline{K}^0$, and $\overline{\Sigma}^+$ (the antiparticle of the Σ^-).

5 Procedures

5.1 *Selection and treatment of data*

The Particle Listings contain all relevant data known to us that are published in journals. With very few exceptions, we do not include results from preprints or conference reports. Nor do we include data that are of historical importance only (the Listings are not an archival record). We search every volume of 30 journals through our cutoff date for relevant data. We also include later published papers that are sent to us by the authors (or others).

In the Particle Listings, we clearly separate measurements that are used to calculate or estimate values given in the Summary Tables from measurements that are not used. We give explanatory comments in many such cases. Among the reasons a measurement might be excluded are the following:

- It is superseded by or included in later results.
- No error is given.
- It involves assumptions we question.
- It has a poor signal-to-noise ratio, low statistical significance, or is otherwise of poorer quality than other data available.
- It is clearly inconsistent with other results that appear to be more reliable. Usually we then state the criterion, which sometimes is quite subjective, for selecting "more reliable" data for averaging. See Sec. 5.4.
- It is not independent of other results.
- It is not the best limit (see below).
- It is quoted from a preprint or a conference report.

In some cases, *none* of the measurements is entirely reliable and no average is calculated. For example, the masses of many of the baryon resonances, obtained from partial-wave analyses, are quoted as estimated ranges thought to probably include the true values, rather than as averages with errors. This is discussed in the Baryon Particle Listings.

For upper limits, we normally quote in the Summary Tables the strongest limit. We do not average or combine upper limits except in a very few cases where they may be re-expressed as measured numbers with Gaussian errors.

As is customary, we assume that particle and antiparticle share the same spin, mass, and mean life. The Tests of Conservation Laws table, following the Summary Tables, lists tests of CPT as well as other conservation laws.

We use the following indicators in the Particle Listings to tell how we get values from the tabulated measurements:

- OUR AVERAGE —From a weighted average of selected data.
- OUR FIT —From a constrained or overdetermined multiparameter fit of selected data.
- OUR EVALUATION —Not from a direct measurement, but evaluated from measurements of related quantities.
- OUR ESTIMATE —Based on the observed range of the data. Not from a formal statistical procedure.

Downloaded from https://academic.oup.com/ptep/article/2022/8/083C01/6651666 by KIT Library user on 27 September 2022

- OUR LIMIT —For special cases where the limit is evaluated by us from measured ratios or other data. Not from a direct measurement.

An experimentalist who sees indications of new a particle will of course want to know what has been seen in that region in the past. Hence, we include in the Particle Listings all reported states that, in our opinion, have sufficient statistical merit and that have not been disproved by more reliable data. However, we promote to the Summary Tables only those states that we feel are well-established. This judgment is, of course, somewhat subjective and no precise criteria can be given. For more detailed discussions, see the reviews section on Particle Properties.

5.2 *Averages and fits*

We divide this discussion on obtaining averages and errors into three sections: (1) treatment of errors; (2) unconstrained averaging; (3) constrained fits.

5.2.1 *Treatment of errors*

In what follows, the "error" δx means that the range $x \pm \delta x$ is intended to be a 68.3% confidence interval about the central value x. We treat this error as if it were Gaussian. Thus, when the error *is* Gaussian, δx is the usual one standard deviation (1σ). Many experimenters now give statistical and systematic errors separately, in which case we usually quote both errors, with the statistical error first. For averages and fits, we then add the two errors in quadrature and use this combined error for δx.

When experimenters quote asymmetric errors $(\delta x)^+$ and $(\delta x)^-$ for a measurement x, the error that we use for that measurement in making an average or a fit with other measurements is a continuous function of these three quantities. When the resultant average or fit $\overline{x}$ is less than $x - (\delta x)^-$, we use $(\delta x)^-$; when it is greater than $x + (\delta x)^+$, we use $(\delta x)^+$. In between, the error we use is a linear function of x. Since the errors we use are functions of the result, we iterate to get the final result. Asymmetric output errors are determined from the input errors assuming a linear relation between the input and output quantities.

In fitting or averaging, we usually do not include correlations between different measurements, but we try to select data in such a way as to reduce correlations. Correlated errors are, however, treated explicitly when there are a number of results of the form $A_i \pm \sigma_i \pm \Delta$ that have identical systematic errors Δ. In this case, one can first average the $A_i \pm \sigma_i$ and then combine the resulting statistical error with Δ. One obtains, however, the same result by averaging $A_i \pm (\sigma_i^2 + \Delta_i^2)^{1/2}$, where $\Delta_i = \sigma_i \Delta [\sum (1/\sigma_j^2)]^{1/2}$. This procedure has the advantage that, with the modified systematic errors Δ_i, each measurement may be treated as independent and averaged in the usual way with other data. Therefore, when appropriate, we adopt this procedure. We tabulate Δ and invoke an automated procedure that computes Δ_i before averaging, and we include a note saying that there are common systematic errors.

Another common case of correlated errors occurs when experimenters measure two quantities and then quote the two and their difference, *e.g.*, m_1, m_2, and $\Delta = m_2 - m_1$. We cannot enter all of m_1, m_2 and Δ into a constrained fit because they are not independent. In some cases, it is a good approximation to ignore the quantity with the largest error and put the other two into the fit. However, in some cases correlations are such that the errors on m_1, m_2 and Δ are comparable and none of the three values can be ignored. In this case, we put all three values into the fit and invoke an automated procedure to increase the errors prior to fitting such that the three quantities can be treated as independent measurements in the constrained fit. We include a note saying that this has been done.

5.2.2 *Unconstrained averaging*

To average data, we use a standard weighted least-squares procedure and in some cases, discussed below, increase the errors with a "scale factor." We begin by assuming that measurements of a given quantity are uncorrelated, and calculate a weighted average and error as

$$\overline{x} \pm \delta\overline{x} = \frac{\sum_i w_i\, x_i}{\sum_i w_i} \pm \left(\sum_i w_i\right)^{-1/2} , \qquad (1)$$

where

$$w_i = 1/(\delta x_i)^2 .$$

Here x_i and δx_i are the value and error reported by the ith experiment, and the sums run over the N experiments. We then calculate $\chi^2 = \sum w_i(\overline{x} - x_i)^2$ and compare it with $N-1$, which is the expectation value of χ^2 if the measurements are from a Gaussian distribution.

If $\chi^2/(N-1)$ is less than or equal to 1, and there are no known problems with the data, we accept the results.

If $\chi^2/(N-1)$ is very large, we may choose not to use the average at all. Alternatively, we may quote the calculated average, but then make an educated guess of the error, a conservative estimate designed to take into account known problems with the data.

Finally, if $\chi^2/(N-1)$ is greater than 1, but not greatly so, we still average the data, but then also do the following:

(a) We increase our quoted error, $\delta\overline{x}$ in Eq. (1), by a scale factor S defined as

$$S = \left[\chi^2/(N-1)\right]^{1/2} . \qquad (2)$$

Our reasoning is as follows. The large value of the χ^2 is likely to be due to underestimation of errors in at least one of the experiments. Not knowing which of the errors are underestimated, we assume they are all underestimated by the same factor S. If we scale up all the input errors by this factor, the χ^2 becomes $N-1$, and of course the output error $\delta\overline{x}$ scales up by the same factor. See Ref. [5].

When combining data with widely varying errors, we modify this procedure slightly. We evaluate S using only the experiments with smaller errors. Our cutoff or ceiling on δx_i is arbitrarily chosen to be

$$\delta_0 = 3N^{1/2}\, \delta\overline{x} ,$$

where $\delta\overline{x}$ is the unscaled error of the mean of all the experiments. Our reasoning is that although the low-precision experiments have little influence on the values $\overline{x}$ and $\delta\overline{x}$, they can make significant contributions to the χ^2, and the contribution of the high-precision experiments thus tends to be obscured. Note that if each experiment has the same error δx_i, then $\delta\overline{x}$ is $\delta x_i/N^{1/2}$, so each δx_i is well below the cutoff. (More often, however, we simply exclude measurements with relatively large errors from averages and fits: new, precise data chase out old, imprecise data.)

Our scaling procedure has the property that if there are two values with comparable errors separated by much more than their stated errors (with or without a number of other values of lower accuracy), the scaled-up error $\delta\,\overline{x}$ is approximately half the interval between the two discrepant values.

We emphasize that our scaling procedure for *errors* in no way affects central values. And if you wish to recover the unscaled error $\delta\overline{x}$, simply divide the quoted error by S.

(b) If the number M of experiments with an error smaller than δ_0 is at least three, and if $\chi^2/(M-1)$ is greater than 1.25, we show in the Particle Listings an ideogram of the data. Figure 1 is an example. Sometimes one or two data points lie apart from the main body; other times the data split into two or more groups. We extract no numbers from these ideograms; they are simply visual aids, which the reader may use as he or she sees fit.

Each measurement in an ideogram is represented by a Gaussian with a central value x_i, error δx_i, and area proportional to $1/\delta x_i$. The choice of $1/\delta x_i$ for the area is somewhat arbitrary. With this choice, the center of gravity of the ideogram corresponds to an average that uses weights $1/\delta x_i$ rather than the $(1/\delta x_i)^2$ actually used in the averages. This may be appropriate when some of the experiments have seriously underestimated systematic errors. However, since for this choice of area the height of the Gaussian for each measurement is proportional to $(1/\delta\, x_i)^2$, the peak position of the ideogram will often favor the high-precision measurements at least as much as does the least-squares average. See our 1986 edition [3] for a detailed discussion of the use of ideograms.

5.2.3 *Constrained fits*

In some cases, such as branching ratios or masses and mass differences, a constrained fit may be needed to obtain the best values of a set of parameters. For example, most branching ratios

Downloaded from https://academic.oup.com/ptep/article/2022/8/083C01/6651666 by KIT Library user on 27 September 2022

and rate measurements are analyzed by making a simultaneous least-squares fit to all the data and extracting the partial decay fractions P_i, the partial widths Γ_i, the full width Γ (or mean life), and the associated error matrix.

Assume, for example, that a state has m partial decay fractions P_i, where $\sum P_i = 1$. These have been measured in N_r different ratios R_r, where, e.g., $R_1 = P_1/P_2$, $R_2 = P_1/P_3$, *etc.* [We can handle any ratio R of the form $\sum \alpha_i P_i / \sum \beta_i P_i$, where α_i and β_i are constants, usually 1 or 0. The forms $R = P_i P_j$ and $R = (P_i P_j)^{1/2}$ are also allowed.] Further, assume that *each* ratio R has been measured by N_k experiments (we designate each experiment with a subscript k, e.g., R_{1k}). We then find the best values of the fractions P_i by minimizing the χ^2 as a function of the $m-1$ independent parameters:

$$\chi^2 = \sum_{r=1}^{N_r} \sum_{k=1}^{N_k} \left(\frac{R_{rk} - R_r}{\delta R_{rk}} \right)^2 , \tag{3}$$

where the R_{rk} are the measured values and R_r are the fitted values of the branching ratios.

In addition to the fitted values $\overline{P}_i$, we calculate an error matrix $\langle \delta\overline{P}_i \ \delta\overline{P}_j \rangle$. We tabulate the diagonal elements of $\delta\,\overline{P}_i = \langle \delta\,\overline{P}_i \ \delta\,\overline{P}_i \rangle^{1/2}$ (except that some errors are scaled as discussed below). In the Particle Listings, we give the complete correlation matrix; we also calculate the fitted value of each ratio, for comparison with the input data, and list it above the relevant input, along with a simple unconstrained average of the same input.

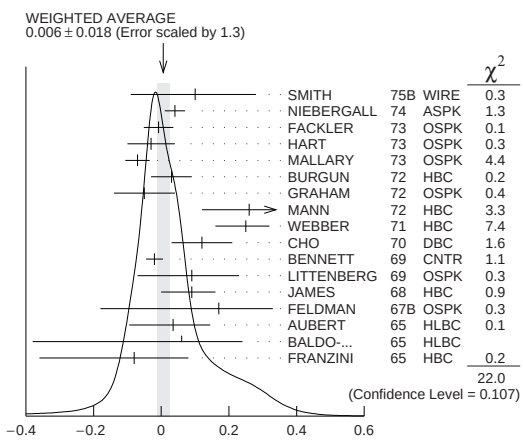

Figure 1: A typical ideogram. The arrow at the top shows the position of the weighted average, while the width of the shaded pattern shows the error in the average after scaling by the factor S. The column on the right gives the χ^2 contribution of each of the experiments. Note that the next-to-last experiment, denoted by the incomplete error flag ($\perp$), is not used in the calculation of S (see the text).

Three comments on the example above:

(1) There was no connection assumed between measurements of the full width and the branching ratios. But often we also have information on partial widths Γ_i as well as the total width Γ. In this case we must introduce Γ as a parameter in the fit, along with the P_i, and we give correlation matrices for the widths in the Particle Listings.

(2) We try to pick those ratios and widths that are as independent and as close to the original data as possible. When one experiment measures all the branching fractions and constrains their sum to be one, we leave one of them (usually the least well-determined one) out of the fit to make the set of input data more nearly independent. We now do allow for correlations between input data.

(3) We calculate scale factors for both the R_r and P_i when the measurements for any R give a larger-than-expected contribution to the χ^2. According to Eq. (3), the double sum for χ^2 is first summed over experiments $k = 1$ to N_k, leaving a single sum over ratios $\chi^2 = \sum \chi_r^2$. One is tempted to define a scale factor for the ratio r as $S_r^2 = \chi_r^2 / \langle \chi_r^2 \rangle$. However, since $\langle \chi_r^2 \rangle$ is not a fixed quantity (it is somewhere between N_k and N_{k-1}), we do not know how to evaluate this expression. Instead, we define

$$S_r^2 = \frac{1}{N_k} \sum_{k=1}^{N_k} \frac{\left(R_{rk} - \overline{R}_r\right)^2}{\langle (R_{rk} - \overline{R}_r)^2 \rangle}. \tag{4}$$

With this definition the expected value of S_r^2 is one. We can show that

$$\langle (R_{rk} - \overline{R}_r)^2 \rangle = \langle (\delta R_{rk})^2 \rangle - (\delta \overline{R}_r)^2, \tag{5}$$

where $\delta\overline{R}_r$ is the fitted error for ratio r.

The fit is redone using errors for the branching ratios that are scaled by the larger of S_r and unity, from which new and often larger errors $\delta\overline{P}_i'$ are obtained. The scale factors we finally list in such cases are defined by $S_i = \delta\overline{P}_i'/\delta\overline{P}_i$. However, in line with our policy of not letting S affect the central values, we give the values of $\overline{P}_i$ obtained from the original (unscaled) fit.

There is one special case in which the errors that are obtained by the preceding procedure may be changed. When a fitted branching ratio (or rate) $\overline{P}_i$ turns out to be less than three standard deviations ($\delta\overline{P}_i'$) from zero, a new smaller error $(\delta\overline{P}_i'')^-$ is calculated on the low side by requiring the area under the Gaussian between $\overline{P}_i - (\delta\,\overline{P}_i'')^-$ and $\overline{P}_i$ to be 68.3% of the area between zero and $\overline{P}_i$. A similar correction is made for branching fractions that are within three standard deviations of one. This keeps the quoted errors from overlapping the boundary of the physical region.

5.3 *Rounding*

While the results shown in the Particle Listings are usually exactly those published by the experiments, the numbers that appear in the Summary Tables (means, averages and limits) are subject to a set of rounding rules.

The basic rule states that if the three highest order digits of the error lie between 100 and 354, we round to two significant digits. If they lie between 355 and 949, we round to one significant digit. Finally, if they lie between 950 and 999, we round up to 1000 and keep two significant digits. In all cases, the central value is given with a precision that matches that of the error. So, for example, the result (coming from an average) 0.827 ± 0.119 would appear as 0.83 ± 0.12, while 0.827 ± 0.367 would turn into 0.8 ± 0.4.

In cases where there are asymmetric errors, if these errors differ by less than 10 percent of the average of the two errors, the average is instead used as a symmetric error in the displayed result and the rounding is determined by this average. Otherwise, the narrower of the two asymmetric errors is used to determine the rounding on both.

Rounding of this form is also performed on the value of limits that come from calculations (but not on limits that are directly taken from a single source).

Finally, we should point out that in several instances, when a group of results come from a single fit to a set of data, we have chosen to keep two significant digits for all the results. This happens, for instance, for several properties of the W and Z bosons and the τ lepton.

5.4 *Discussion*

The problem of averaging data containing discrepant values is nicely discussed by Taylor in Ref. [6]. He considers a number of algorithms that attempt to incorporate inconsistent data into a meaningful average. However, it is difficult to develop a procedure that handles simultaneously in a reasonable way two basic types of situations: (a) data that lie apart from the main body of the data are incorrect (contain unreported errors); and (b) the opposite—it is the main body of data that is incorrect. Unfortunately, as Taylor shows, case (b) is not infrequent. He concludes that the choice of procedure is less significant than the initial choice of data to include or exclude.

We place much emphasis on this choice of data. Often we solicit the help of outside experts (consultants). Sometimes, however, it

Downloaded from https://academic.oup.com/ptep/article/2022/8/083C01/6651666 by KIT Library user on 27 September 2022

is simply impossible to determine which of a set of discrepant measurements are correct. Our scale-factor technique is an attempt to address this ignorance by increasing the error. In effect, we are saying that present experiments do not allow a precise determination of this quantity because of unresolvable discrepancies, and one must await further measurements. The reader is warned of this situation by the size of the scale factor, and if he or she desires can go back to the literature (via the Particle Listings) and redo the average with a different choice of data.

Our situation is less severe than most of the cases Taylor considers, such as estimates of the fundamental constants like $\hbar$, *etc.* Most of the errors in his case are dominated by systematic effects. For our data, statistical errors are often at least as large as systematic errors, and statistical errors are usually easier to estimate. A notable exception occurs in partial-wave analyses, where different techniques applied to the same data yield different results. In this case, as stated earlier, we often do not make an average but just quote a range of values.

A brief history of early Particle Data Group averages is given in Ref. [5]. Our History Plots show the time evolution of some of our values of a few particle properties. Sometimes large changes occur. These usually reflect the introduction of significant new data or the discarding of older data. Older data are discarded in favor of newer data when it is felt that the newer data have smaller systematic errors, or have more checks on systematic errors, or have made corrections unknown at the time of the older experiments, or simply have much smaller errors. Sometimes, the scale factor becomes large near the time at which a large jump takes place, reflecting the uncertainty introduced by the new and inconsistent data. By and large, however, a full scan of our history plots shows a dull progression toward greater precision at central values quite consistent with the first data points shown.

We conclude that the reliability of the combination of experimental data and our averaging procedures is usually good, but it is important to be aware that fluctuations outside of the quoted errors can and do occur.

ACKNOWLEDGMENTS

The publication of the *Review of Particle Physics* is supported by the Director, Office of Science, Office of High Energy Physics of the U.S. Department of Energy under Contract No. DE–AC02–05CH11231; by an implementing arrangement between the governments of Japan (MEXT: Ministry of Education, Culture, Sports, Science and Technology) and the United States (DOE) on cooperative research and development; by the Italian National Institute of Nuclear Physics (INFN); by the Physical Society of Japan (JPS); and by the European Laboratory for Particle Physics (CERN). Individual collaborators receive support for their PDG activities from their respective institutes or funding agencies.

We thank all those who have assisted in the many phases of preparing this *Review*. We particularly thank the many who have responded to our requests for verification of data entered in the Listings, and those who have made suggestions or pointed out errors.

We are grateful to the staff at CERN, IHEP Beijing, KEK, and LBNL who take care of the mailing and distribution of our products.

This work used resources of the National Energy Research Scientific Computing Center, a DOE Office of Science User Facility supported by the Office of Science of the U.S. Department of Energy under Contract No. DE-AC02-05CH11231.

References

[1] The previous edition was: P.A. Zyla *et al.* (Particle Data Group), Prog. Theor. Exp. Phys. **2020**, 083C01 (2020).

[2] C. Patrignani *et al.* (Particle Data Group), Chin. Phys. **C40**, 10, 100001 (2016).

[3] M. Aguilar-Benitez *et al.* (Particle Data Group), Phys. Lett. **170B**, 1 (1986).

[4] M. Tanabashi *et al.* (Particle Data Group), Phys. Rev. D **98**, 3, 030001 (2018).

[5] A. H. Rosenfeld, Ann. Rev. Nucl. Part. Sci. **25**, 555 (1975).

[6] B.N. Taylor, "Numerical Comparisons of Several Algorithms for Treating Inconsistent Data in a Least-Squares Adjustment of the Fundamental Constants," U.S. National Bureau of Standards NBSIR 81-2426 (1982).

Downloaded from https://academic.oup.com/ptep/article/2022/8/083C01/6651666 by KIT Library user on 27 September 2022

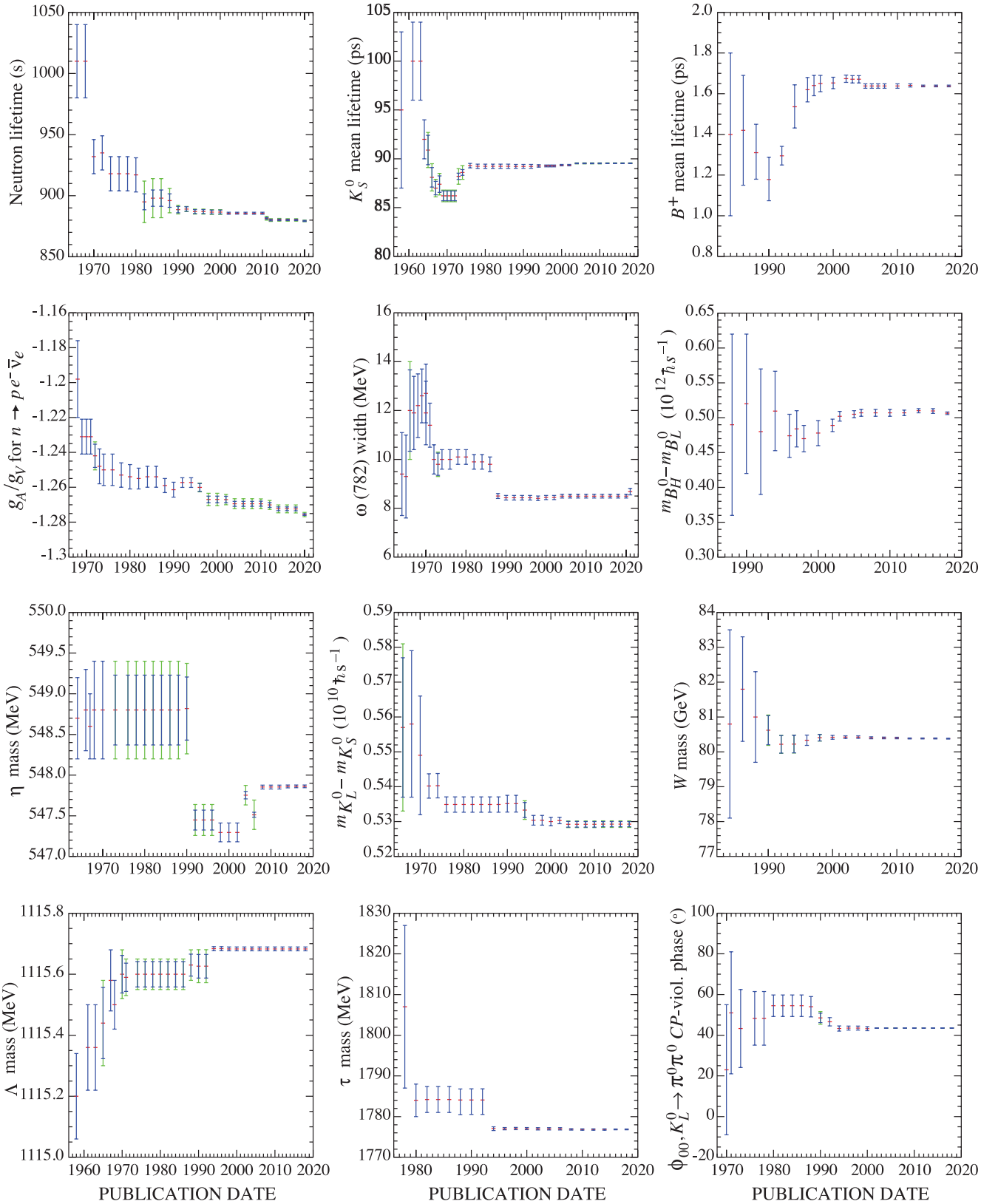

Figure 1: A historical perspective of values of a few particle properties tabulated in this *Review* as a function of date of publication of the *Review*. A full error bar indicates the quoted error; a thick-lined portion indicates the same but without the "scale factor."

Downloaded from https://academic.oup.com/ptep/article/2022/8/083C01/6651666 by KIT Library user on 27 September 2022

Online Particle Physics Information

Revised August 2021 by S. Demers (Yale U.) and M. Moskovic (CERN).

1	Introduction	20
2	Particle Data Group (PDG) resources	20
3	Particle physics information platform	20
4	Literature databases	20
5	Journals	21
6	Conference and seminars databases	21
7	Research institutions	21
8	People	21
9	Experiments	21
10	Jobs	21
11	Software packages and repositories	21
12	Data repositories and preservation	21
13	Particle physics education and outreach	21

1 Introduction

Online resources are used in a diverse and expanding set of ways in particle physics. Many of these resources have become central to our collective work. We provide a brief curated selection of the major resources here. An expanded and regularly updated online repository is referred to below and can be found at

`https://github.com/particledatagroup/hep-resources`

By contrast, it is meant to be inclusive and catalog all useful resources related to particle physics. The community is warmly invited to contribute in order to ensure a broad and up to date coverage of relevant resources. Practical details are available online.

2 Particle Data Group (PDG) resources

- **Review of Particle Physics (RPP):** A comprehensive report on the fields of particle physics and related areas of cosmology and astrophysics, including both review articles and a compilation/evaluation of data on particle properties. The review section includes articles, tables and plots on a wide variety of theoretical and experimental topics of interest to particle physicists and astrophysicists. The particle properties section provides tables of published measurements as well as the Particle Data Group's best values and limits for particle properties such as masses, widths, lifetimes, and branching fractions, as well as an extensive summary of searches for hypothetical particles. RPP is published as a large book every two years, with partial updates made available once each year on the web.
  All the contents of the book version of RPP are available online:
  `https://pdg.lbl.gov`
  The printed book can be ordered:
  `https://pdg.lbl.gov/current/receive_our_products.html`
  Of historical interest is the complete RPP collection which can be found online:
  `https://pdg.lbl.gov/rpp-archive/`
  `https://scientific-info.cern/search-and-read/online-resources/review-particle-physics`
- **Particle Physics booklet:** An abridged version of the Review of Particle Physics, available as a pocket-sized 250-page booklet. It is one of the most useful summaries of physics data. The booklet contains an abbreviated set of reviews and the summary tables from the most recent edition of the Review of Particle Physics.
  The PDF file of the booklet can be downloaded:
  `https://pdg.lbl.gov/current/booklet.pdf`
  The printed booklet can be ordered:
  `https://pdg.lbl.gov/current/receive_our_products.html`
- **PDGLive:** A web application for browsing the contents of the PDG database that contains the information published in the Review of Particle Physics. It allows one to navigate to a particle of interest, see a summary of the information available, and then proceed to the detailed information published in the Review of Particle Physics. Data entries are directly linked to the corresponding bibliographic information in INSPIRE.
  `https://pdglive.lbl.gov`
- **Computer-readable files:** Data files that can be downloaded from the PDG include tables of particle masses and widths, PDG Monte Carlo particle numbers, and cross-section data. The files are updated with each new edition of the Review of Particle Physics.
  `https://pdg.lbl.gov/current/html/computer_read.html`

3 Particle physics information platform

INSPIRE: INSPIRE serves as a one-stop information platform for the particle physics community, comprising interlinked databases on literature, authors, jobs, seminars, conferences, institutions and experiments (each described in more detail below). Run in collaboration by CERN, DESY, Fermilab, IHEP, IN2P3, and SLAC, it has been serving the scientific community for almost 50 years. Previously known as SPIRES, it was the first website outside Europe and the first database on the web. Close interaction with the user community and with arXiv, ADS, HEPData, ORCID, PDG and publishers is the backbone of INSPIRE's evolution. Since 2020, it is running on a modernized platform that is continuously being improved.

`https://inspirehep.net/`

4 Literature databases

Most research articles in the field of high-energy physics are first made available on the arXiv eprint server, where researchers can learn about the latest developments by browsing through the new announcements five days a week. They are indexed, together with all other publications in high-energy physics and related fields, in the INSPIRE literature collection. For neighboring fields such as astrophysics or mathematics, other databases are more exhaustive.

- **arXiv.org:** A repository of full-text articles in physics, astronomy, mathematics, computer science, statistics, nonlinear sciences, quantitative finance, quantitative biology, electrical engineering and systems science, and economics. Papers are submitted by registered authors to arXiv, often as preprints in advance of submission to a journal for publication; includes postprints, working papers, and other relevant material. Established in 1991, the repository is interlinked with ADS and INSPIRE, among others. Readers can browse subject categories or search by author, title, abstract, date, and other fields. Receive daily update alerts for subfields by email or RSS.
  `https://arXiv.org`
- **INSPIRE Literature:** The literature collection, the flagship of the INSPIRE suite, serves more than 1.4 million bibliographic records with a growing number of full-text articles attached and metadata including author affiliations, abstracts, references, experiments, keywords as well as links to arXiv, ADS, PDG, HEPData, publisher platforms and other servers. It provides fast metadata searches that can be easily refined using facets, plots extracted from full text, author disambiguation, author profile pages and citation analysis.
  `https://inspirehep.net/literature`
- **ADS:** The SAO/NASA Astrophysics Data System is a Digital Library portal offering access to 15 million bibliographic records in Astronomy and Physics. The ADS search engine also indexes the full-text for many publications in this collection and tracks citations. The system also provides access and links to a wealth of external resources, including electronic articles hosted by publishers and arXiv, data catalogs and a variety of data products hosted by the astronomy archives worldwide. The ADS can be accessed at:
  `http://ads.harvard.edu/`
- **MathSciNet:** This database of almost 4 million items provides reviews, abstracts and bibliographic information for

Downloaded from https://academic.oup.com/ptep/article/2022/8/083C01/6651666 by KIT Library user on 27 September 2022

much of the mathematical sciences literature. Over 100,000 new items, most of them classified according to the Mathematics Subject Classification, and more than 80,000 reviews of the current published literature are added each year. Author identification allows users to search for publications by author and citation data allows users to track the history and influence of research publications.

`https://www.ams.org/mathscinet`

5 Journals

SCOAP^3 Journals: A list of journals currently financed by the SCOAP^3 consortium. All HEP publications in those journals are made freely available under Open Access conditions at no cost for the authors.

`https://www.scoap3.org/phase3-journals/`

6 Conference and seminars databases

- **INSPIRE Conferences:** The database of more than 24,000 past, present, and future conferences, schools, and meetings relevant to high-energy physics and related fields is searchable by title, acronym, series, date and location. Included are information about published proceedings, links to conference contributions in the INSPIRE HEP database, and links to the conference website when available. New conferences can be submitted from the entry page.

  `https://inspirehep.net/conferences`

- **INSPIRE Seminars:** Created to support the surge of online seminars during the COVID19 pandemic, this database already contains more than 1,500 seminars in high-energy physics and related fields. Seminars can be filtered by date, series and subject and exported to a calendar. Direct links to join the online seminar and external resources are included. All seminars are community-maintained and can be submitted from the entry page.

  `https://inspirehep.net/seminars`

7 Research institutions

INSPIRE Institutions: INSPIRE Institutions contains over 11,500 institutes, laboratories, and universities, where research on particle physics and astrophysics is led. Every record includes, whenever possible, as detailed information, such as address, web links, experiments, and links to INSPIRE papers authored by people affiliated to that institution. One can search for a particular institution by name, acronym, and location.

`https://inspirehep.net/institutions`

8 People

- **INSPIRE Authors:** Searchable worldwide database of more than a hundred thousand active, departed, retired, and deceased people associated with particle physics and related fields. The affiliation history of these researchers, their e-mail addresses, ORCIDs, web pages, experiments they participated in, PhD advisor, information on their graduate students and links to their papers and seminars are provided, as well as a user interface to update this information.

  `https://inspirehep.net/authors`

- **ORCID**: Registry providing persistent digital identifiers allowing to unambiguously identify researchers. Through integration in key research workflows such as manuscript and grant submission, it supports automated linkages between scientists and their professional activities ensuring that their work is recognized.

  `https://orcid.org`

9 Experiments

INSPIRE Experiments: Contains more than 3,700 past, present, and future experiments in particle physics. It lists and classifies both accelerator and non-accelerator experiments as well as theory collaborations. Includes official experiment name and number, location, and collaboration lists. Simple searches by participant, title, experiment number, institution, date approved, accelerator, or detector, return a description of the experiment, including a complete list of authors, title, overview of the experiment's goals and methods, and a link to the experiment's web page if available. Recently, it has expanded its scope to include particle accelerators besides experiments and to link them together.

`https://inspirehep.net/experiments`

10 Jobs

INSPIRE Jobs: Lists academic and research jobs in high energy physics, nuclear physics, accelerator physics and astrophysics with the option to post a job or to receive email notices of new job listings. Several hundreds of jobs are listed all year round, with more activity during the application season.

`https://inspirehep.net/jobs`

11 Software packages and repositories

A vast number of software tools are used for various aspects of high-energy physics research. Due to their number, their often specialized purpose and the quickly-changing nature of software, no attempt has been made to present them in this chapter. The accompanying online version contains an extensive categorized list of software.

12 Data repositories and preservation

Initiatives to preserve and disseminate data produced during different stages of research, from Monte Carlo events to machine-readable versions of tables in papers, have grown in recent years. Unfortunately, there currently exists no central resource aggregating all these data as is the case for the more established means of scholarly communication. Instead, there are a number of repositories targeting different types of data and research subjects. They are listed in the online version.

13 Particle physics education and outreach

Particle physics public engagement efforts are widespread, with laboratories, experiments, universities and individual researchers engaged in a range of efforts. The online version of this chapter provides links to resources for particle physicists wanting to become engaged in public education as well as resources that physicists can provide directly to students or lay people. There are classroom activities, interactive websites, films, and direct links to education offices at institutions and experiments. Additionally, news sites relevant for experts and for the general public are provided.

Downloaded from https://academic.oup.com/ptep/article/2022/8/083C01/6651666 by KIT Library user on 27 September 2022

Downloaded from https://academic.oup.com/ptep/article/2022/8/083C01/6651666 by KIT Library user on 27 September 2022

SUMMARY TABLES OF PARTICLE PHYSICS

Gauge and Higgs bosons 25
Leptons 28
Quarks 32
Mesons 33
Baryons 90
Searches not in Other Sections* 108
Tests of conservation laws 110

Meson Quick Reference Table 88
Baryon Quick Reference Table 89

* There are also search limits in the Summary Tables for the Gauge and Higgs Bosons, the Leptons, the Quarks, and the Mesons.

Downloaded from https://academic.oup.com/ptep/article/2022/8/083C01/6651666 by KIT Library user on 27 September 2022

Downloaded from https://academic.oup.com/ptep/article/2022/8/083C01/6651666 by KIT Library user on 27 September 2022

SUMMARY TABLES OF PARTICLE PROPERTIES

Extracted from the Particle Listings of the
Review of Particle Physics
R.L. Workman *et al.* (Particle Data Group),
Prog. Theor. Exp. Phys. **2022**, 083C01 (2022)
Available at `https://pdg.lbl.gov`

Particle Data Group

R.L. Workman, V.D. Burkert, V. Crede, E. Klempt, U. Thoma, L. Tiator, K. Agashe, G. Aielli, B.C. Allanach, C. Amsler, M. Antonelli, E.C. Aschenauer, D.M. Asner, H. Baer, Sw. Banerjee, R.M. Barnett, L. Baudis, C.W. Bauer, J.J. Beatty, V.I. Belousov, J. Beringer, A. Bettini, O. Biebel, K.M. Black, E. Blucher, R. Bonventre, V.V. Bryzgalov, O. Buchmuller, M.A. Bychkov, R.N. Cahn, M. Carena, A. Ceccucci, A. Cerri, R. Sekhar Chivukula, G. Cowan, K. Cranmer, O. Cremonesi, G. D'Ambrosio, T. Damour, D. de Florian, A. de Gouvêa, T. DeGrand, P. de Jong, S. Demers, B.A. Dobrescu, M. D'Onofrio, M. Doser, H.K. Dreiner, P. Eerola, U. Egede, S. Eidelman, A.X. El-Khadra, J. Ellis, S. C. Eno, J. Erler, V.V. Ezhela, W. Fetscher, B.D. Fields, A. Freitas, H. Gallagher, Y. Gershtein, T. Gherghetta, M.C. Gonzalez-Garcia, M. Goodman, C. Grab, A.V. Gritsan, C. Grojean, D.E. Groom, M. Grünewald, A. Gurtu, T. Gutsche, H.E. Haber, Matthieu Hamel, C. Hanhart, S. Hashimoto, Y. Hayato, A. Hebecker, S. Heinemeyer, J. J. Hernández-Rey, K. Hikasa, J. Hisano, A. Höcker, J. Holder, L. Hsu, J. Huston, T. Hyodo, Al. Ianni, M. Kado, M. Karliner, U.F. Katz, M. Kenzie, V.A. Khoze, S.R. Klein, F. Krauss, M. Kreps, P. Križan, B. Krusche, Y. Kwon, O. Lahav, J. Laiho, L.P. Lellouch, J. Lesgourgues, A.R. Liddle, Z. Ligeti, C.-J. Lin, C. Lippmann, T.M. Liss, L. Littenberg, C. Lourenço, K.S. Lugovsky, S.B. Lugovsky, A. Lusiani, Y. Makida, F. Maltoni, T. Mannel, A.V. Manohar, W.J. Marciano, A. Masoni, J. Matthews, U.-G. Meißner, I.-A. Melzer-Pellmann, M. Mikhasenko, D.J. Miller, D. Milstead, R.E. Mitchell, K. Mönig, P. Molaro, F. Moortgat, M. Moskovic, K. Nakamura, M. Narain, P. Nason, S. Navas, A. Nelles, M. Neubert, P. Nevski, Y. Nir, K.A. Olive, C. Patrignani, J.A. Peacock, V.A. Petrov, E. Pianori, A. Pich, A. Piepke, F. Pietropaolo, A. Pomarol, S. Pordes, S. Profumo, A. Quadt, K. Rabbertz, J. Rademacker, G. Raffelt, M. Ramsey-Musolf, B.N. Ratcliff, P. Richardson, A. Ringwald, D.J. Robinson, S. Roesler, S. Rolli, A. Romaniouk, L. J Rosenberg, J.L. Rosner, G. Rybka, M.G. Ryskin, R.A. Ryutin, Y. Sakai, S. Sarkar, F. Sauli, O. Schneider, S. Schnert, K. Schölberg, A.J. Schwartz, J. Schwiening, D. Scott, F. Sefkow, U. Seljak, V. Sharma, S.R. Sharpe, V. Shiltsev, G. Signorelli, M. Silari, F. Simon, T. Sjöstrand, P. Skands, T. Skwarnicki, G.F. Smoot, A. Soffer, M.S. Sozzi, S. Spanier, C. Spiering, A. Stahl, S.L. Stone, Y. Sumino, M.J. Syphers, F. Takahashi, M. Tanabashi, J. Tanaka, M. Taševský, K. Terao, K. Terashi, J. Terning, R.S. Thorne, M. Titov, N.P. Tkachenko, D.R. Tovey, K. Trabelsi, P. Urquijo, G. Valencia, R. Van de Water, N. Varelas, G. Venanzoni, L. Verde, I. Vivarelli, P. Vogel, W. Vogelsang, V. Vorobyev, S.P. Wakely, W. Walkowiak, C.W. Walter, D. Wands, D.H. Weinberg, E.J. Weinberg, N. Wermes, M. White, L.R. Wiencke, S. Willocq, C.G. Wohl, C.L. Woody, W.-M. Yao, M. Yokoyama, R. Yoshida, G. Zanderighi, G.P. Zeller, O.V. Zenin, R.-Y. Zhu, Shi-Lin Zhu, F. Zimmermann, P.A. Zyla

Technical Associates:

J. Anderson, T. Basaglia, P. Schaffner, W. Zheng

©2022
(Approximate closing date for data: January 15, 2022)

GAUGE AND HIGGS BOSONS

γ (photon)

$I(J^{PC}) = 0,1(1^{--})$

Mass $m < 1 \times 10^{-18}$ eV
Charge $q < 1 \times 10^{-46}\ e$ (mixed charge)
Charge $q < 1 \times 10^{-35}\ e$ (single charge)
Mean life τ = Stable

g or gluon

$I(J^P) = 0(1^-)$

Mass $m = 0$ [a]
SU(3) color octet

graviton

$J = 2$

W

$J = 1$

Charge = $\pm 1\ e$
Mass $m = 80.377 \pm 0.012$ GeV
W/Z mass ratio = 0.88145 ± 0.00013
$m_Z - m_W = 10.811 \pm 0.012$ GeV
$m_{W^+} - m_{W^-} = -0.029 \pm 0.028$ GeV
Full width $\Gamma = 2.085 \pm 0.042$ GeV
$\langle N_{\pi^\pm} \rangle = 15.70 \pm 0.35$
$\langle N_{K^\pm} \rangle = 2.20 \pm 0.19$
$\langle N_p \rangle = 0.92 \pm 0.14$
$\langle N_{\rm charged} \rangle = 19.39 \pm 0.08$

W^- modes are charge conjugates of the modes below.

W^+ DECAY MODES		Fraction (Γ_i/Γ)	Confidence level	p (MeV/c)
$\ell^+\nu$	[b]	(10.86 ± 0.09) %		–
$e^+\nu$		(10.71 ± 0.16) %		40189
$\mu^+\nu$		(10.63 ± 0.15) %		40189
$\tau^+\nu$		(11.38 ± 0.21) %		40170
hadrons		(67.41 ± 0.27) %		–
$\pi^+\gamma$		$< 7 \times 10^{-6}$	95%	40189
$D_s^+\gamma$		$< 1.3 \times 10^{-3}$	95%	40165
cX		(33.3 ± 2.6) %		–
$c\overline{s}$		$(31\ ^{+13}_{-11})$ %		–
invisible	[c]	(1.4 ± 2.9) %		–
$\pi^+\pi^+\pi^-$		$< 1.01 \times 10^{-6}$	95%	40189

Z

$J = 1$

Charge = 0
Mass $m = 91.1876 \pm 0.0021$ GeV [d]
Full width $\Gamma = 2.4952 \pm 0.0023$ GeV
$\Gamma(\ell^+\ell^-) = 83.984 \pm 0.086$ MeV [b]
$\Gamma(\text{invisible}) = 499.0 \pm 1.5$ MeV [e]
$\Gamma(\text{hadrons}) = 1744.4 \pm 2.0$ MeV
$\Gamma(\mu^+\mu^-)/\Gamma(e^+e^-) = 1.0001 \pm 0.0024$
$\Gamma(\tau^+\tau^-)/\Gamma(e^+e^-) = 1.0020 \pm 0.0032$ [f]

Average charged multiplicity

$\langle N_{charged} \rangle = 20.76 \pm 0.16$ (S = 2.1)

Couplings to quarks and leptons

$g_V^\ell = -0.03783 \pm 0.00041$
$g_V^u = 0.266 \pm 0.034$
$g_V^d = -0.38^{+0.04}_{-0.05}$
$g_A^\ell = -0.50123 \pm 0.00026$
$g_A^u = 0.519^{+0.028}_{-0.033}$
$g_A^d = -0.527^{+0.040}_{-0.028}$
$g^{\nu_\ell} = 0.5008 \pm 0.0008$
$g^{\nu_e} = 0.53 \pm 0.09$
$g^{\nu_\mu} = 0.502 \pm 0.017$

Downloaded from https://academic.oup.com/ptep/article/2022/8/083C01/6651666 by KIT Library user on 27 September 2022

Asymmetry parameters [g]

$A_e = 0.1515 \pm 0.0019$
$A_\mu = 0.142 \pm 0.015$
$A_\tau = 0.143 \pm 0.004$
$A_s = 0.90 \pm 0.09$
$A_c = 0.670 \pm 0.027$
$A_b = 0.923 \pm 0.020$

Charge asymmetry (%) at Z pole

$A_{FB}^{(0\ell)} = 1.71 \pm 0.10$
$A_{FB}^{(0u)} = 4 \pm 7$
$A_{FB}^{(0s)} = 9.8 \pm 1.1$
$A_{FB}^{(0c)} = 7.07 \pm 0.35$
$A_{FB}^{(0b)} = 9.92 \pm 0.16$

Z DECAY MODES		Fraction (Γ_i/Γ)	Scale factor/ Confidence level	p (MeV/c)
e^+e^-	[h]	(3.3632 ± 0.0042) %		45594
$\mu^+\mu^-$	[h]	(3.3662 ± 0.0066) %		45594
$\tau^+\tau^-$	[h]	(3.3696 ± 0.0083) %		45559
$\ell^+\ell^-$	[b,h]	(3.3658 ± 0.0023) %		–
$\ell^+\ell^-\ell^+\ell^-$	[i]	$(4.55 \pm 0.17) \times 10^{-6}$		45594
invisible	[h]	(20.000 ± 0.055) %		–
hadrons	[h]	(69.911 ± 0.056) %		–
$(u\overline{u}+c\overline{c})/2$		(11.6 ± 0.6) %		–
$(d\overline{d}+s\overline{s}+b\overline{b})/3$		(15.6 ± 0.4) %		–
$c\overline{c}$		(12.03 ± 0.21) %		–
$b\overline{b}$		(15.12 ± 0.05) %		–
$b\overline{b}b\overline{b}$		$(3.6 \pm 1.3) \times 10^{-4}$		–
ggg		< 1.1 %	CL=95%	–
$\pi^0\gamma$		$< 2.01 \times 10^{-5}$	CL=95%	45594
$\eta\gamma$		$< 5.1 \times 10^{-5}$	CL=95%	45592
$\rho^0\gamma$		$< 2.5 \times 10^{-5}$	CL=95%	45591
$\omega\gamma$		$< 6.5 \times 10^{-4}$	CL=95%	45590
$\eta'(958)\gamma$		$< 4.2 \times 10^{-5}$	CL=95%	45589
$\phi\gamma$		$< 9 \times 10^{-7}$	CL=95%	45588
$\gamma\gamma$		$< 1.46 \times 10^{-5}$	CL=95%	45594
$\pi^0\pi^0$		$< 1.52 \times 10^{-5}$	CL=95%	45594
$\gamma\gamma\gamma$		$< 2.2 \times 10^{-6}$	CL=95%	45594
$\pi^\pm W^\mp$	[j]	$< 7 \times 10^{-5}$	CL=95%	10167
$\rho^\pm W^\mp$	[j]	$< 8.3 \times 10^{-5}$	CL=95%	10142
$J/\psi(1S)X$		$(3.51 {}^{+0.23}_{-0.25}) \times 10^{-3}$	S=1.1	–
$J/\psi(1S)\gamma$		$< 1.4 \times 10^{-6}$	CL=95%	45541
$\psi(2S)X$		$(1.60 \pm 0.29) \times 10^{-3}$		–
$\psi(2S)\gamma$		$< 4.5 \times 10^{-6}$	CL=95%	45519
$J/\psi(1S)J/\psi(1S)$		$< 2.2 \times 10^{-6}$	CL=95%	45489
$\chi_{c1}(1P)X$		$(2.9 \pm 0.7) \times 10^{-3}$		–
$\chi_{c2}(1P)X$		$< 3.2 \times 10^{-3}$	CL=90%	–
$\Upsilon(1S)X + \Upsilon(2S)X + \Upsilon(3S)X$		$(1.0 \pm 0.5) \times 10^{-4}$		–
$\Upsilon(1S)X$		$< 4.4 \times 10^{-5}$	CL=95%	–
$\Upsilon(1S)\gamma$		$< 2.8 \times 10^{-6}$	CL=95%	45103
$\Upsilon(2S)X$		$< 1.39 \times 10^{-4}$	CL=95%	–
$\Upsilon(2S)\gamma$		$< 1.7 \times 10^{-6}$	CL=95%	45043
$\Upsilon(3S)X$		$< 9.4 \times 10^{-5}$	CL=95%	–
$\Upsilon(3S)\gamma$		$< 4.8 \times 10^{-6}$	CL=95%	45006
$\Upsilon(1,2,3S)\Upsilon(1,2,3S)$		$< 1.5 \times 10^{-6}$	CL=95%	–
$(D^0/\overline{D}^0)X$		(20.7 ± 2.0) %		–
$D^\pm X$		(12.2 ± 1.7) %		–
$D^*(2010)^\pm X$	[j]	(11.4 ± 1.3) %		–
$D_{s1}(2536)^\pm X$		$(3.6 \pm 0.8) \times 10^{-3}$		–
$D_{sJ}(2573)^\pm X$		$(5.8 \pm 2.2) \times 10^{-3}$		–
$D^{*\prime}(2629)^\pm X$		searched for		–
B^+X	[k]	(6.08 ± 0.13) %		–
B_s^0X	[k]	(1.59 ± 0.13) %		–
B_c^+X		searched for		–
Λ_c^+X		(1.54 ± 0.33) %		–
Ξ_c^0X		seen		–
Ξ_bX		seen		–
b-baryon X	[k]	(1.38 ± 0.22) %		–
anomalous $\gamma+$ hadrons	[l]	$< 3.2 \times 10^{-3}$	CL=95%	–
$e^+e^-\gamma$	[l]	$< 5.2 \times 10^{-4}$	CL=95%	45594
$\mu^+\mu^-\gamma$	[l]	$< 5.6 \times 10^{-4}$	CL=95%	45594
$\tau^+\tau^-\gamma$	[l]	$< 7.3 \times 10^{-4}$	CL=95%	45559
$\ell^+\ell^-\gamma\gamma$	[n]	$< 6.8 \times 10^{-6}$	CL=95%	–
$q\overline{q}\gamma\gamma$	[n]	$< 5.5 \times 10^{-6}$	CL=95%	–
$\nu\overline{\nu}\gamma\gamma$	[n]	$< 3.1 \times 10^{-6}$	CL=95%	45594
$e^\pm\mu^\mp$	LF [j]	$< 7.5 \times 10^{-7}$	CL=95%	45594
$e^\pm\tau^\mp$	LF [j]	$< 5.0 \times 10^{-6}$	CL=95%	45576
$\mu^\pm\tau^\mp$	LF [j]	$< 6.5 \times 10^{-6}$	CL=95%	45576
pe	L,B	$< 1.8 \times 10^{-6}$	CL=95%	45589
$p\mu$	L,B	$< 1.8 \times 10^{-6}$	CL=95%	45589

H^0

$J = 0$

Mass $m = 125.25 \pm 0.17$ GeV (S = 1.5)
Full width $\Gamma = 3.2^{+2.8}_{-2.2}$ MeV (assumes equal on-shell and off-shell effective couplings)

H^0 Signal Strengths in Different Channels

Combined Final States $= 1.13 \pm 0.06$
$WW^* = 1.19 \pm 0.12$
$ZZ^* = 1.01 \pm 0.07$
$\gamma\gamma = 1.10 \pm 0.07$
$c\overline{c}$ Final State $= 37 \pm 20$
$b\overline{b} = 0.98 \pm 0.12$
$\mu^+\mu^- = 1.19 \pm 0.34$
$\tau^+\tau^- = 1.15^{+0.16}_{-0.15}$
$Z\gamma < 3.6$, CL = 95%
$\gamma^*\gamma$ Final State $= 1.5 \pm 0.5$
$t\overline{t}H^0$ Production $= 1.10 \pm 0.18$
tH^0 production $= 6 \pm 4$
H^0 Production Cross Section in pp Collisions at $\sqrt{s} = 13$ TeV $= 56 \pm 4$ pb

H^0 DECAY MODES		Fraction (Γ_i/Γ)	Confidence level	p (MeV/c)
e^+e^-		$< 3.6 \times 10^{-4}$	95%	62625
$Z\rho(770)$		< 1.21 %	95%	29423
$Z\phi(1020)$		$< 3.6 \times 10^{-3}$	95%	29417
$J/\psi\gamma$		$< 3.5 \times 10^{-4}$	95%	62587
$J/\psi J/\psi$		$< 1.8 \times 10^{-3}$	95%	62548
$\psi(2S)\gamma$		$< 2.0 \times 10^{-3}$	95%	62571
$\Upsilon(1S)\gamma$		$< 4.9 \times 10^{-4}$	95%	62268
$\Upsilon(2S)\gamma$		$< 5.9 \times 10^{-4}$	95%	62224
$\Upsilon(3S)\gamma$		$< 5.7 \times 10^{-4}$	95%	62197
$\Upsilon(nS)\Upsilon(mS)$		$< 1.4 \times 10^{-3}$	95%	–
$\rho(770)\gamma$		$< 8.8 \times 10^{-4}$	95%	62623
$\phi(1020)\gamma$		$< 4.8 \times 10^{-4}$	95%	62621
$e\mu$	LF	$< 6.1 \times 10^{-5}$	95%	62625
$e\tau$	LF	$< 2.2 \times 10^{-3}$	95%	62612
$\mu\tau$	LF	$< 1.5 \times 10^{-3}$	95%	62612
invisible		<19 %	95%	–

Neutral Higgs Bosons, Searches for

Mass limits for heavy neutral Higgs bosons (H_2^0, A^0) in the MSSM

m > 389 GeV, CL = 95% ($\tan\beta = 10$)
m > 863 GeV, CL = 95% ($\tan\beta = 20$)
m > 1157 GeV, CL = 95% ($\tan\beta = 30$)
m > 1341 GeV, CL = 95% ($\tan\beta = 40$)
m > 1496 GeV, CL = 95% ($\tan\beta = 50$)
m > 1613 GeV, CL = 95% ($\tan\beta = 60$)

Charged Higgs Bosons ($H^\pm$ and $H^{\pm\pm}$), Searches for

Mass limits for $m_{H^+} < m(top)$

m > 155 GeV, CL = 95%

Mass limits for $m_{H^+} > m(top)$

m > 181 GeV, CL = 95% ($\tan\beta = 10$)
m > 249 GeV, CL = 95% ($\tan\beta = 20$)
m > 390 GeV, CL = 95% ($\tan\beta = 30$)
m > 894 GeV, CL = 95% ($\tan\beta = 40$)
m > 1017 GeV, CL = 95% ($\tan\beta = 50$)
m > 1103 GeV, CL = 95% ($\tan\beta = 60$)

Downloaded from https://academic.oup.com/ptep/article/2022/8/083C01/6651666 by KIT Library user on 27 September 2022

New Heavy Bosons (W', Z', leptoquarks, etc.), Searches for

Additional W Bosons

W' with standard couplings
Mass $m >$ 6000 GeV, CL = 95% (pp direct search)
W_R (Right-handed W Boson)
Mass $m >$ 715 GeV, CL = 90% (electroweak fit)

Additional Z Bosons

Z'_{SM} with standard couplings
Mass $m >$ 5150 GeV, CL = 95% (pp direct search)
Z_{LR} of $SU(2)_L \times SU(2)_R \times U(1)$ (with $g_L = g_R$)
Mass $m >$ 630 GeV, CL = 95% ($p\overline{p}$ direct search)
Mass $m >$ 1162 GeV, CL = 95% (electroweak fit)
Z_χ of $SO(10) \rightarrow SU(5) \times U(1)_\chi$ (with $g_\chi = e/\cos\theta_W$)
Mass $m >$ 4800 GeV, CL = 95% (pp direct search)
Z_ψ of $E_6 \rightarrow SO(10) \times U(1)_\psi$ (with $g_\psi = e/\cos\theta_W$)
Mass $m >$ 4560 GeV, CL = 95% (pp direct search)
Z_η of $E_6 \rightarrow SU(3) \times SU(2) \times U(1) \times U(1)_\eta$ (with $g_\eta = e/\cos\theta_W$)
Mass $m >$ 3.900×10^3 GeV, CL = 95% (pp direct search)

Scalar Leptoquarks

$m >$ 1800 GeV, CL = 95% (1st gen., pair prod., B(eq)=1)
$m >$ 1755 GeV, CL = 95% (1st gen., single prod., B(eq)=1)
$m >$ 1700 GeV, CL = 95% (2nd gen., pair prod., B(μq)=1)
$m >$ 660 GeV, CL = 95% (2nd gen., single prod., B(μq)=1)
$m >$ 1430 GeV, CL = 95% (3rd gen., pair prod., B(τt)=1)
$m >$ 740 GeV, CL = 95% (3rd gen., single prod., B(τb)=1)
(See the Particle Listings for assumptions on leptoquark quantum numbers and branching fractions.)

Diquarks

Mass $m >$ 7200 GeV, CL = 95% (E_6 diquark)

Axigluon

Mass $m >$ 6600 GeV, CL = 95%

Axions (A^0) and Other Very Light Bosons, Searches for

See the review on "Axions and other similar particles."

The best limit for the half-life of neutrinoless double beta decay with Majoron emission is $> 7.2 \times 10^{24}$ years (CL = 90%).

NOTES

In this Summary Table:

When a quantity has "(S = ...)" to its right, the error on the quantity has been enlarged by the "scale factor" S, defined as $S = \sqrt{\chi^2/(N-1)}$, where N is the number of measurements used in calculating the quantity. We do this when $S > 1$, which often indicates that the measurements are inconsistent. When $S > 1.25$, we also show in the Particle Listings an ideogram of the measurements. For more about S, see the Introduction.

A decay momentum p is given for each decay mode. For a 2-body decay, p is the momentum of each decay product in the rest frame of the decaying particle. For a 3-or-more-body decay, p is the largest momentum any of the products can have in this frame.

[a] Theoretical value. A mass as large as a few MeV may not be precluded.
[b] ℓ indicates each type of lepton (e, μ, and τ), not sum over them.
[c] This represents the width for the decay of the W boson into a charged particle with momentum below detectability, p< 200 MeV.
[d] The Z-boson mass listed here corresponds to a Breit-Wigner resonance parameter. It lies approximately 34 MeV above the real part of the position of the pole (in the energy-squared plane) in the Z-boson propagator.
[e] This partial width takes into account Z decays into $\nu\overline{\nu}$ and any other possible undetected modes.
[f] This ratio has not been corrected for the τ mass.
[g] Here $A \equiv 2g_V g_A/(g_V^2+g_A^2)$.
[h] This parameter is not directly used in the overall fit but is derived using the fit results; see the note "The Z boson" and ref. LEP-SLC 06 (Physics Reports (Physics Letters C) **427** 257 (2006)).
[i] Here ℓ indicates e or μ.
[j] The value is for the sum of the charge states or particle/antiparticle states indicated.
[k] This value is updated using the product of (i) the $Z \rightarrow b\overline{b}$ fraction from this listing and (ii) the b-hadron fraction in an unbiased sample of weakly decaying b-hadrons produced in Z-decays provided by the Heavy Flavor Averaging Group (HFLAV, http://www.slac.stanford.edu/xorg/hflav/osc/PDG_2009/#FRACZ).
[l] See the Z Particle Listings for the γ energy range used in this measurement.
[n] For $m_{\gamma\gamma} = (60 \pm 5)$ GeV.

Downloaded from https://academic.oup.com/ptep/article/2022/8/083C01/6651666 by KIT Library user on 27 September 2022

LEPTONS

e

$J = \frac{1}{2}$

Mass $m = (548.579909065 \pm 0.000000016) \times 10^{-6}$ u
Mass $m = 0.51099895000 \pm 0.00000000015$ MeV
$|m_{e^+} - m_{e^-}|/m < 8 \times 10^{-9}$, CL = 90%
$|q_{e^+} + q_{e^-}|/e < 4 \times 10^{-8}$
Magnetic moment anomaly
$(g-2)/2 = (1159.65218076 \pm 0.00000028) \times 10^{-6}$
$(g_{e^+} - g_{e^-}) / g_{\rm average} = (-0.5 \pm 2.1) \times 10^{-12}$
Electric dipole moment $d < 0.11 \times 10^{-28}$ $e$cm, CL = 90%
Mean life $\tau > 6.6 \times 10^{28}$ yr, CL = 90% [a]

μ

$J = \frac{1}{2}$

Mass $m = 0.1134289259 \pm 0.0000000025$ u
Mass $m = 105.6583755 \pm 0.0000023$ MeV
Mean life $\tau = (2.1969811 \pm 0.0000022) \times 10^{-6}$ s
$\tau_{\mu^+}/\tau_{\mu^-} = 1.00002 \pm 0.00008$
$c\tau = 658.6384$ m
Magnetic moment anomaly $(g-2)/2 = (11659206 \pm 4) \times 10^{-10}$
$(g_{\mu^+} - g_{\mu^-}) / g_{\rm average} = (-0.11 \pm 0.12) \times 10^{-8}$
Electric dipole moment $|d| < 1.8 \times 10^{-19}$ $e$cm, CL = 95%

Decay parameters [b]

$\rho = 0.74979 \pm 0.00026$
$\eta = 0.057 \pm 0.034$
$\delta = 0.75047 \pm 0.00034$
$\xi P_\mu = 1.0009^{+0.0016}_{-0.0007}$ [c]
$\xi P_\mu \delta/\rho = 1.0018^{+0.0016}_{-0.0007}$ [c]
$\xi' = 1.00 \pm 0.04$
$\xi'' = 0.98 \pm 0.04$
$\alpha/A = (0 \pm 4) \times 10^{-3}$
$\alpha'/A = (-10 \pm 20) \times 10^{-3}$
$\beta/A = (4 \pm 6) \times 10^{-3}$
$\beta'/A = (2 \pm 7) \times 10^{-3}$
$\overline{\eta} = 0.02 \pm 0.08$

μ^+ modes are charge conjugates of the modes below.

μ^- DECAY MODES		Fraction (Γ_i/Γ)	Confidence level	p (MeV/c)
$e^- \overline{\nu}_e \nu_\mu$		$\approx 100\%$		53
$e^- \overline{\nu}_e \nu_\mu \gamma$	[d]	$(6.0 \pm 0.5) \times 10^{-8}$		53
$e^- \overline{\nu}_e \nu_\mu e^+ e^-$	[e]	$(3.4 \pm 0.4) \times 10^{-5}$		53
Lepton Family number (LF) violating modes				
$e^- \nu_e \overline{\nu}_\mu$	LF	[f] < 1.2 %	90%	53
$e^- \gamma$	LF	$< 4.2 \times 10^{-13}$	90%	53
$e^- e^+ e^-$	LF	$< 1.0 \times 10^{-12}$	90%	53
$e^- 2\gamma$	LF	$< 7.2 \times 10^{-11}$	90%	53

τ

$J = \frac{1}{2}$

Mass $m = 1776.86 \pm 0.12$ MeV
$(m_{\tau^+} - m_{\tau^-})/m_{\rm average} < 2.8 \times 10^{-4}$, CL = 90%
Mean life $\tau = (290.3 \pm 0.5) \times 10^{-15}$ s
$c\tau = 87.03$ μm
Magnetic moment anomaly > -0.052 and < 0.013, CL = 95%
$\mathrm{Re}(d_\tau) = -0.220$ to 0.45×10^{-16} $e$cm, CL = 95%
$\mathrm{Im}(d_\tau) = -0.250$ to 0.0080×10^{-16} $e$cm, CL = 95%

Weak dipole moment

$\mathrm{Re}(d^w_\tau) < 0.50 \times 10^{-17}$ $e$cm, CL = 95%
$\mathrm{Im}(d^w_\tau) < 1.1 \times 10^{-17}$ $e$cm, CL = 95%

Weak anomalous magnetic dipole moment

$\mathrm{Re}(\alpha^w_\tau) < 1.1 \times 10^{-3}$, CL = 95%
$\mathrm{Im}(\alpha^w_\tau) < 2.7 \times 10^{-3}$, CL = 95%
$\tau^\pm \to \pi^\pm K^0_S \nu_\tau$ (RATE DIFFERENCE) / (RATE SUM) = (-0.36 ± 0.25)%

Decay parameters

See the τ Particle Listings for a note concerning τ-decay parameters.

$\rho(e \text{ or } \mu) = 0.745 \pm 0.008$
$\rho(e) = 0.747 \pm 0.010$
$\rho(\mu) = 0.763 \pm 0.020$
$\xi(e \text{ or } \mu) = 0.985 \pm 0.030$
$\xi(e) = 0.994 \pm 0.040$
$\xi(\mu) = 1.030 \pm 0.059$
$\eta(e \text{ or } \mu) = 0.013 \pm 0.020$
$\eta(\mu) = 0.094 \pm 0.073$
$(\delta\xi)(e \text{ or } \mu) = 0.746 \pm 0.021$
$(\delta\xi)(e) = 0.734 \pm 0.028$
$(\delta\xi)(\mu) = 0.778 \pm 0.037$
$\xi(\pi) = 0.993 \pm 0.022$
$\xi(\rho) = 0.994 \pm 0.008$
$\xi(a_1) = 1.001 \pm 0.027$
$\xi(\text{all hadronic modes}) = 0.995 \pm 0.007$
$\overline{\eta}(\mu) = -1.3 \pm 1.7$
$(\xi\kappa)(e \text{ or } \mu)$ PARAMETER $= 0.5 \pm 0.4$
$(\xi\kappa)(e) = -0.4 \pm 1.2$
$(\xi\kappa)(\mu) = 0.8 \pm 0.6$

τ^+ modes are charge conjugates of the modes below. "$h^\pm$" stands for $\pi^\pm$ or $K^\pm$. "ℓ" stands for e or μ. "Neutrals" stands for γ's and/or π^0's.

τ^- DECAY MODES		Fraction (Γ_i/Γ)	Scale factor/ Confidence level	p (MeV/c)
Modes with one charged particle				
particle$^- \geq 0$ neutrals $\geq 0K^0 \nu_\tau$ ("1-prong")		(85.24 ± 0.06) %		–
particle$^- \geq 0$ neutrals $\geq 0K^0_L \nu_\tau$		(84.58 ± 0.06) %		–
$\mu^- \overline{\nu}_\mu \nu_\tau$	[g]	(17.39 ± 0.04) %		885
$\mu^- \overline{\nu}_\mu \nu_\tau \gamma$	[e]	$(3.67 \pm 0.08) \times 10^{-3}$		885
$e^- \overline{\nu}_e \nu_\tau$	[g]	(17.82 ± 0.04) %		888
$e^- \overline{\nu}_e \nu_\tau \gamma$	[e]	(1.83 ± 0.05) %		888
$h^- \geq 0K^0_L \nu_\tau$		(12.03 ± 0.05) %		883
$h^- \nu_\tau$		(11.51 ± 0.05) %		883
$\pi^- \nu_\tau$	[g]	(10.82 ± 0.05) %		883
$K^- \nu_\tau$	[g]	$(6.96 \pm 0.10) \times 10^{-3}$		820
$h^- \geq 1$ neutrals ν_τ		(37.01 ± 0.09) %		–
$h^- \geq 1\pi^0 \nu_\tau$ (ex.K^0)		(36.51 ± 0.09) %		–
$h^- \pi^0 \nu_\tau$		(25.93 ± 0.09) %		878
$\pi^- \pi^0 \nu_\tau$	[g]	(25.49 ± 0.09) %		878
$\pi^- \pi^0$ non-$\rho(770)$ ν_τ		$(3.0 \pm 3.2) \times 10^{-3}$		878
$K^- \pi^0 \nu_\tau$	[g]	$(4.33 \pm 0.15) \times 10^{-3}$		814
$h^- \geq 2\pi^0 \nu_\tau$		(10.81 ± 0.09) %		–
$h^- 2\pi^0 \nu_\tau$		(9.48 ± 0.10) %		862
$h^- 2\pi^0 \nu_\tau$ (ex.K^0)		(9.32 ± 0.10) %		862
$\pi^- 2\pi^0 \nu_\tau$ (ex.K^0)	[g]	(9.26 ± 0.10) %		862
$\pi^- 2\pi^0 \nu_\tau$ (ex.K^0), scalar		< 9	$\times 10^{-3}$ CL=95%	862
$\pi^- 2\pi^0 \nu_\tau$ (ex.K^0), vector		< 7	$\times 10^{-3}$ CL=95%	862
$K^- 2\pi^0 \nu_\tau$ (ex.K^0)	[g]	$(6.5 \pm 2.2) \times 10^{-4}$		796
$h^- \geq 3\pi^0 \nu_\tau$		(1.34 ± 0.07) %		–
$h^- \geq 3\pi^0 \nu_\tau$ (ex. K^0)		(1.25 ± 0.07) %		–
$h^- 3\pi^0 \nu_\tau$		(1.18 ± 0.07) %		836
$\pi^- 3\pi^0 \nu_\tau$ (ex.K^0)	[g]	(1.04 ± 0.07) %		836
$K^- 3\pi^0 \nu_\tau$ (ex.K^0, η)	[g]	$(4.8 \pm 2.1) \times 10^{-4}$		765
$h^- 4\pi^0 \nu_\tau$ (ex.K^0)		$(1.6 \pm 0.4) \times 10^{-3}$		800
$h^- 4\pi^0 \nu_\tau$ (ex.K^0,η)	[g]	$(1.1 \pm 0.4) \times 10^{-3}$		800
$a_1(1260) \nu_\tau \to \pi^- \gamma \nu_\tau$		$(3.8 \pm 1.5) \times 10^{-4}$		–
$K^- \geq 0\pi^0 \geq 0K^0 \geq 0\gamma \nu_\tau$		(1.552 ± 0.029) %		820
$K^- \geq 1$ (π^0 or K^0 or γ) ν_τ		$(8.59 \pm 0.28) \times 10^{-3}$		–
Modes with K^0's				
K^0_S(particles)$^- \nu_\tau$		$(9.43 \pm 0.28) \times 10^{-3}$		–
$h^- \overline{K}^0 \nu_\tau$		$(9.87 \pm 0.14) \times 10^{-3}$		812
$\pi^- \overline{K}^0 \nu_\tau$	[g]	$(8.38 \pm 0.14) \times 10^{-3}$		812
$\pi^- \overline{K}^0$ (non-$K^*(892)^-$) ν_τ		$(5.4 \pm 2.1) \times 10^{-4}$		812
$K^- K^0 \nu_\tau$	[g]	$(1.486 \pm 0.034) \times 10^{-3}$		737
$K^- K^0 \geq 0\pi^0 \nu_\tau$		$(2.99 \pm 0.07) \times 10^{-3}$		737
$h^- \overline{K}^0 \pi^0 \nu_\tau$		$(5.32 \pm 0.13) \times 10^{-3}$		794
$\pi^- \overline{K}^0 \pi^0 \nu_\tau$	[g]	$(3.82 \pm 0.13) \times 10^{-3}$		794

Downloaded from https://academic.oup.com/ptep/article/2022/8/083C01/6651666 by KIT Library user on 27 September 2022

$\overline{K}^0 \rho^- \nu_\tau$		$(2.2 \pm 0.5) \times 10^{-3}$		612
$K^- K^0 \pi^0 \nu_\tau$	[g]	$(1.50 \pm 0.07) \times 10^{-3}$		685
$\pi^- \overline{K}^0 \geq 1\pi^0 \nu_\tau$		$(4.08 \pm 0.25) \times 10^{-3}$		–
$\pi^- \overline{K}^0 \pi^0 \pi^0 \nu_\tau$ (ex.K^0)	[g]	$(2.6 \pm 2.3) \times 10^{-4}$		763
$K^- K^0 \pi^0 \pi^0 \nu_\tau$		$< 1.6 \times 10^{-4}$	CL=95%	619
$\pi^- K^0 \overline{K}^0 \nu_\tau$		$(1.55 \pm 0.24) \times 10^{-3}$		682
$\pi^- K^0_S K^0_S \nu_\tau$	[g]	$(2.35 \pm 0.06) \times 10^{-4}$		682
$\pi^- K^0_S K^0_L \nu_\tau$	[g]	$(1.08 \pm 0.24) \times 10^{-3}$		682
$\pi^- K^0_L K^0_L \nu_\tau$		$(2.35 \pm 0.06) \times 10^{-4}$		682
$\pi^- K^0 \overline{K}^0 \pi^0 \nu_\tau$		$(3.6 \pm 1.2) \times 10^{-4}$		614
$\pi^- K^0_S K^0_S \pi^0 \nu_\tau$	[g]	$(1.82 \pm 0.21) \times 10^{-5}$		614
$K^{*-} K^0 \pi^0 \nu_\tau \to \pi^- K^0_S K^0_S \pi^0 \nu_\tau$		$(1.08 \pm 0.21) \times 10^{-5}$		–
$f_1(1285) \pi^- \nu_\tau \to \pi^- K^0_S K^0_S \pi^0 \nu_\tau$		$(6.8 \pm 1.5) \times 10^{-6}$		–
$f_1(1420) \pi^- \nu_\tau \to \pi^- K^0_S K^0_S \pi^0 \nu_\tau$		$(2.4 \pm 0.8) \times 10^{-6}$		–
$\pi^- K^0_S K^0_L \pi^0 \nu_\tau$	[g]	$(3.2 \pm 1.2) \times 10^{-4}$		614
$\pi^- K^0_L K^0_L \pi^0 \nu_\tau$		$(1.82 \pm 0.21) \times 10^{-5}$		614
$K^- K^0_S K^0_S \nu_\tau$		$< 6.3 \times 10^{-7}$	CL=90%	466
$K^- K^0_S K^0_S \pi^0 \nu_\tau$		$< 4.0 \times 10^{-7}$	CL=90%	337
$K^0 h^+ h^- h^- \geq 0$ neutrals ν_τ		$< 1.7 \times 10^{-3}$	CL=95%	760
$K^0 h^+ h^- h^- \nu_\tau$	[g]	$(2.5 \pm 2.0) \times 10^{-4}$		760

Modes with three charged particles

$h^- h^- h^+ \geq 0$ neutrals $\geq 0 K^0_L \nu_\tau$		(15.20 ± 0.06) %		861
$h^- h^- h^+ \geq 0$ neutrals ν_τ (ex. $K^0_S \to \pi^+ \pi^-$) ("3-prong")		(14.55 ± 0.06) %		861
$h^- h^- h^+ \nu_\tau$		(9.80 ± 0.05) %		861
$h^- h^- h^+ \nu_\tau$ (ex.K^0)		(9.46 ± 0.05) %		861
$h^- h^- h^+ \nu_\tau$ (ex.K^0,ω)		(9.43 ± 0.05) %		861
$\pi^- \pi^+ \pi^- \nu_\tau$		(9.31 ± 0.05) %		861
$\pi^- \pi^+ \pi^- \nu_\tau$ (ex.K^0)		(9.02 ± 0.05) %		861
$\pi^- \pi^+ \pi^- \nu_\tau$ (ex.K^0), non-axial vector		< 2.4 %	CL=95%	861
$\pi^- \pi^+ \pi^- \nu_\tau$ (ex.K^0,ω)	[g]	(8.99 ± 0.05) %		861
$h^- h^- h^+ \geq 1$ neutrals ν_τ		(5.29 ± 0.05) %		–
$h^- h^- h^+ \geq 1\pi^0 \nu_\tau$ (ex. K^0)		(5.09 ± 0.05) %		–
$h^- h^- h^+ \pi^0 \nu_\tau$		(4.76 ± 0.05) %		834
$h^- h^- h^+ \pi^0 \nu_\tau$ (ex.K^0)		(4.57 ± 0.05) %		834
$h^- h^- h^+ \pi^0 \nu_\tau$ (ex. K^0, ω)		(2.79 ± 0.07) %		834
$\pi^- \pi^+ \pi^- \pi^0 \nu_\tau$		(4.62 ± 0.05) %		834
$\pi^- \pi^+ \pi^- \pi^0 \nu_\tau$ (ex.K^0)		(4.49 ± 0.05) %		834
$\pi^- \pi^+ \pi^- \pi^0 \nu_\tau$ (ex.K^0,ω)	[g]	(2.74 ± 0.07) %		834
$h^- h^- h^+ \geq 2\pi^0 \nu_\tau$ (ex. K^0)		$(5.17 \pm 0.31) \times 10^{-3}$		–
$h^- h^- h^+ 2\pi^0 \nu_\tau$		$(5.05 \pm 0.31) \times 10^{-3}$		797
$h^- h^- h^+ 2\pi^0 \nu_\tau$ (ex.K^0)		$(4.95 \pm 0.31) \times 10^{-3}$		797
$h^- h^- h^+ 2\pi^0 \nu_\tau$ (ex.K^0,ω,η)	[g]	$(10 \pm 4) \times 10^{-4}$		797
$h^- h^- h^+ 3\pi^0 \nu_\tau$		$(2.13 \pm 0.30) \times 10^{-4}$		749
$2\pi^- \pi^+ 3\pi^0 \nu_\tau$ (ex.K^0)		$(1.95 \pm 0.30) \times 10^{-4}$		749
$2\pi^- \pi^+ 3\pi^0 \nu_\tau$ (ex.K^0, η, $f_1(1285)$)		$(1.7 \pm 0.4) \times 10^{-4}$		–
$2\pi^- \pi^+ 3\pi^0 \nu_\tau$ (ex.K^0, η, ω, $f_1(1285)$)	[g]	$(1.4 \pm 2.7) \times 10^{-5}$		–
$K^- h^+ h^- \geq 0$ neutrals ν_τ		$(6.29 \pm 0.14) \times 10^{-3}$		794
$K^- h^+ \pi^- \nu_\tau$ (ex.K^0)		$(4.37 \pm 0.07) \times 10^{-3}$		794
$K^- h^+ \pi^- \pi^0 \nu_\tau$ (ex.K^0)		$(8.6 \pm 1.2) \times 10^{-4}$		763
$K^- \pi^+ \pi^- \geq 0$ neutrals ν_τ		$(4.77 \pm 0.14) \times 10^{-3}$		794
$K^- \pi^+ \pi^- \geq 0\pi^0 \nu_\tau$ (ex.K^0)		$(3.73 \pm 0.13) \times 10^{-3}$		794
$K^- \pi^+ \pi^- \nu_\tau$		$(3.45 \pm 0.07) \times 10^{-3}$		794
$K^- \pi^+ \pi^- \nu_\tau$ (ex.K^0)		$(2.93 \pm 0.07) \times 10^{-3}$		794
$K^- \pi^+ \pi^- \nu_\tau$ (ex.K^0,ω)	[g]	$(2.93 \pm 0.07) \times 10^{-3}$		794
$K^- \rho^0 \nu_\tau \to K^- \pi^+ \pi^- \nu_\tau$		$(1.4 \pm 0.5) \times 10^{-3}$		–
$K^- \pi^+ \pi^- \pi^0 \nu_\tau$		$(1.31 \pm 0.12) \times 10^{-3}$		763
$K^- \pi^+ \pi^- \pi^0 \nu_\tau$ (ex.K^0)		$(7.9 \pm 1.2) \times 10^{-4}$		763
$K^- \pi^+ \pi^- \pi^0 \nu_\tau$ (ex.K^0,η)		$(7.6 \pm 1.2) \times 10^{-4}$		763
$K^- \pi^+ \pi^- \pi^0 \nu_\tau$ (ex.K^0,ω)		$(3.7 \pm 0.9) \times 10^{-4}$		763
$K^- \pi^+ \pi^- \pi^0 \nu_\tau$ (ex.K^0,ω,η)	[g]	$(3.9 \pm 1.4) \times 10^{-4}$		763
$K^- \pi^+ K^- \geq 0$ neut. ν_τ		$< 9 \times 10^{-4}$	CL=95%	685
$K^- K^+ \pi^- \geq 0$ neut. ν_τ		$(1.496 \pm 0.033) \times 10^{-3}$		685
$K^- K^+ \pi^- \nu_\tau$	[g]	$(1.435 \pm 0.027) \times 10^{-3}$		685
$K^- K^+ \pi^- \pi^0 \nu_\tau$	[g]	$(6.1 \pm 1.8) \times 10^{-5}$		618
$K^- K^+ K^- \nu_\tau$		$(2.2 \pm 0.8) \times 10^{-5}$	S=5.4	472
$K^- K^+ K^- \nu_\tau$ (ex. ϕ)		$< 2.5 \times 10^{-6}$	CL=90%	–
$K^- K^+ K^- \pi^0 \nu_\tau$		$< 4.8 \times 10^{-6}$	CL=90%	345
$\pi^- K^+ \pi^- \geq 0$ neut. ν_τ		$< 2.5 \times 10^{-3}$	CL=95%	794
$e^- e^- e^+ \overline{\nu}_e \nu_\tau$		$(2.8 \pm 1.5) \times 10^{-5}$		888
$\mu^- e^- e^+ \overline{\nu}_\mu \nu_\tau$		$< 3.2 \times 10^{-5}$	CL=90%	885
$\pi^- e^- e^+ \nu_\tau$		seen		883
$\pi^- \mu^- \mu^+ \nu_\tau$		$< 1.14 \times 10^{-5}$	CL=90%	870

Modes with five charged particles

$3h^- 2h^+ \geq 0$ neutrals ν_τ (ex. $K^0_S \to \pi^- \pi^+$) ("5-prong")		$(9.9 \pm 0.4) \times 10^{-4}$		794
$3h^- 2h^+ \nu_\tau$ (ex.K^0)		$(8.29 \pm 0.31) \times 10^{-4}$		794
$3\pi^- 2\pi^+ \nu_\tau$ (ex.K^0, ω)		$(8.27 \pm 0.31) \times 10^{-4}$		794
$3\pi^- 2\pi^+ \nu_\tau$ (ex.K^0, ω, $f_1(1285)$)	[g]	$(7.75 \pm 0.30) \times 10^{-4}$		–
$K^- 2\pi^- 2\pi^+ \nu_\tau$ (ex.K^0)	[g]	$(6 \pm 12) \times 10^{-7}$		716
$K^+ 3\pi^- \pi^+ \nu_\tau$		$< 5.0 \times 10^{-6}$	CL=90%	716
$K^+ K^- 2\pi^- \pi^+ \nu_\tau$		$< 4.5 \times 10^{-7}$	CL=90%	528
$3h^- 2h^+ \pi^0 \nu_\tau$ (ex.K^0)		$(1.65 \pm 0.11) \times 10^{-4}$		746
$3\pi^- 2\pi^+ \pi^0 \nu_\tau$ (ex.K^0)		$(1.63 \pm 0.11) \times 10^{-4}$		746
$3\pi^- 2\pi^+ \pi^0 \nu_\tau$ (ex.K^0, η, $f_1(1285)$)		$(1.11 \pm 0.10) \times 10^{-4}$		–
$3\pi^- 2\pi^+ \pi^0 \nu_\tau$ (ex.K^0, η, ω, $f_1(1285)$)	[g]	$(3.8 \pm 0.9) \times 10^{-5}$		–
$K^- 2\pi^- 2\pi^+ \pi^0 \nu_\tau$ (ex.K^0)	[g]	$(1.1 \pm 0.6) \times 10^{-6}$		657
$K^+ 3\pi^- \pi^+ \pi^0 \nu_\tau$		$< 8 \times 10^{-7}$	CL=90%	657
$3h^- 2h^+ 2\pi^0 \nu_\tau$		$< 3.4 \times 10^{-6}$	CL=90%	687

Miscellaneous other allowed modes

$(5\pi)^- \nu_\tau$		$(7.8 \pm 0.5) \times 10^{-3}$		800
$4h^- 3h^+ \geq 0$ neutrals ν_τ ("7-prong")		$< 3.0 \times 10^{-7}$	CL=90%	682
$4h^- 3h^+ \nu_\tau$		$< 4.3 \times 10^{-7}$	CL=90%	682
$4h^- 3h^+ \pi^0 \nu_\tau$		$< 2.5 \times 10^{-7}$	CL=90%	612
$X^-(S=-1) \nu_\tau$		(2.92 ± 0.04) %		–
$K^*(892)^- \geq 0$ neutrals $\geq 0 K^0_L \nu_\tau$		(1.42 ± 0.18) %	S=1.4	665
$K^*(892)^- \nu_\tau$		(1.20 ± 0.07) %	S=1.8	665
$K^*(892)^- \nu_\tau \to \pi^- \overline{K}^0 \nu_\tau$		$(7.82 \pm 0.26) \times 10^{-3}$		–
$K^*(892)^0 K^- \geq 0$ neutrals ν_τ		$(3.2 \pm 1.4) \times 10^{-3}$		542
$K^*(892)^0 K^- \nu_\tau$		$(2.1 \pm 0.4) \times 10^{-3}$		542
$\overline{K}^*(892)^0 \pi^- \geq 0$ neutrals ν_τ		$(3.8 \pm 1.7) \times 10^{-3}$		655
$\overline{K}^*(892)^0 \pi^- \nu_\tau$		$(2.2 \pm 0.5) \times 10^{-3}$		655
$(\overline{K}^*(892)\pi)^- \nu_\tau \to \pi^- \overline{K}^0 \pi^0 \nu_\tau$		$(1.0 \pm 0.4) \times 10^{-3}$		–
$K_1(1270)^- \nu_\tau$		$(4.7 \pm 1.1) \times 10^{-3}$		447
$K_1(1400)^- \nu_\tau$		$(1.7 \pm 2.6) \times 10^{-3}$	S=1.7	335
$K^*(1410)^- \nu_\tau$		$(1.5 {}^{+1.4}_{-1.0}) \times 10^{-3}$		326
$K^*_0(1430)^- \nu_\tau$		$< 5 \times 10^{-4}$	CL=95%	317
$K^*_2(1430)^- \nu_\tau$		$< 3 \times 10^{-3}$	CL=95%	315
$\eta \pi^- \nu_\tau$		$< 9.9 \times 10^{-5}$	CL=95%	797
$\eta \pi^- \pi^0 \nu_\tau$	[g]	$(1.39 \pm 0.07) \times 10^{-3}$		778
$\eta \pi^- \pi^0 \pi^0 \nu_\tau$	[g]	$(2.0 \pm 0.4) \times 10^{-4}$		746
$\eta K^- \nu_\tau$	[g]	$(1.55 \pm 0.08) \times 10^{-4}$		719
$\eta K^*(892)^- \nu_\tau$		$(1.38 \pm 0.15) \times 10^{-4}$		511
$\eta K^- \pi^0 \nu_\tau$	[g]	$(4.8 \pm 1.2) \times 10^{-5}$		665
$\eta K^- \pi^0$ (non-$K^*(892)$) ν_τ		$< 3.5 \times 10^{-5}$	CL=90%	–
$\eta \overline{K}^0 \pi^- \nu_\tau$	[g]	$(9.4 \pm 1.5) \times 10^{-5}$		661
$\eta \overline{K}^0 \pi^- \pi^0 \nu_\tau$		$< 5.0 \times 10^{-5}$	CL=90%	590
$\eta K^- K^0 \nu_\tau$		$< 9.0 \times 10^{-6}$	CL=90%	430
$\eta \pi^+ \pi^- \pi^- \geq 0$ neutrals ν_τ		$< 3 \times 10^{-3}$	CL=90%	744
$\eta \pi^- \pi^+ \pi^- \nu_\tau$ (ex.K^0)	[g]	$(2.20 \pm 0.13) \times 10^{-4}$		744
$\eta \pi^- \pi^+ \pi^- \nu_\tau$ (ex.K^0,$f_1(1285)$)		$(9.9 \pm 1.6) \times 10^{-5}$		–
$\eta a_1(1260)^- \nu_\tau \to \eta \pi^- \rho^0 \nu_\tau$		$< 3.9 \times 10^{-4}$	CL=90%	–
$\eta \eta \pi^- \nu_\tau$		$< 7.4 \times 10^{-6}$	CL=90%	637
$\eta \eta \pi^- \pi^0 \nu_\tau$		$< 2.0 \times 10^{-4}$	CL=95%	559
$\eta \eta K^- \nu_\tau$		$< 3.0 \times 10^{-6}$	CL=90%	382
$\eta'(958) \pi^- \nu_\tau$		$< 4.0 \times 10^{-6}$	CL=90%	620
$\eta'(958) \pi^- \pi^0 \nu_\tau$		$< 1.2 \times 10^{-5}$	CL=90%	591
$\eta'(958) K^- \nu_\tau$		$< 2.4 \times 10^{-6}$	CL=90%	495
$\phi \pi^- \nu_\tau$		$(3.4 \pm 0.6) \times 10^{-5}$		585
$\phi K^- \nu_\tau$	[g]	$(4.4 \pm 1.6) \times 10^{-5}$		445
$f_1(1285) \pi^- \nu_\tau$		$(3.9 \pm 0.5) \times 10^{-4}$	S=1.9	408
$f_1(1285) \pi^- \nu_\tau \to \eta \pi^- \pi^+ \pi^- \nu_\tau$		$(1.18 \pm 0.07) \times 10^{-4}$	S=1.3	–
$f_1(1285) \pi^- \nu_\tau \to 3\pi^- 2\pi^+ \nu_\tau$	[g]	$(5.2 \pm 0.4) \times 10^{-5}$		–

Downloaded from https://academic.oup.com/ptep/article/2022/8/083C01/6651666 by KIT Library user on 27 September 2022

$\pi(1300)^- \nu_\tau \to (\rho\pi)^- \nu_\tau \to (3\pi)^- \nu_\tau$		< 1.0	$\times 10^{-4}$ CL=90%	–
$\pi(1300)^- \nu_\tau \to ((\pi\pi)_{S-\text{wave}}\, \pi)^- \nu_\tau \to (3\pi)^- \nu_\tau$		< 1.9	$\times 10^{-4}$ CL=90%	–
$h^- \omega \geq 0$ neutrals ν_τ		(2.40 ± 0.08) %		708
$h^- \omega \nu_\tau$		(1.99 ± 0.06) %		708
$\pi^- \omega \nu_\tau$	[g]	(1.95 ± 0.06) %		708
$K^- \omega \nu_\tau$	[g]	$(4.1 \pm 0.9) \times 10^{-4}$		610
$h^- \omega \pi^0 \nu_\tau$	[g]	$(4.1 \pm 0.4) \times 10^{-3}$		684
$h^- \omega 2\pi^0 \nu_\tau$		$(1.4 \pm 0.5) \times 10^{-4}$		644
$\pi^- \omega 2\pi^0 \nu_\tau$	[g]	$(7.2 \pm 1.6) \times 10^{-5}$		644
$h^- 2\omega \nu_\tau$		< 5.4	$\times 10^{-7}$ CL=90%	250
$2h^- h^+ \omega \nu_\tau$		$(1.20 \pm 0.22) \times 10^{-4}$		641
$2\pi^- \pi^+ \omega \nu_\tau$ (ex.K^0)	[g]	$(8.4 \pm 0.6) \times 10^{-5}$		641

Lepton Family number (*LF*), Lepton number (*L*), or Baryon number (*B*) violating modes

L means lepton number violation (*e.g.* $\tau^- \to e^+\pi^-\pi^-$). Following common usage, *LF* means lepton family violation *and not* lepton number violation (*e.g.* $\tau^- \to e^-\pi^+\pi^-$). *B* means baryon number violation.

$e^-\gamma$	*LF*	< 3.3	$\times 10^{-8}$ CL=90%	888
$e^-\gamma\gamma$		< 2.5	$\times 10^{-4}$ CL=90%	888
$\mu^-\gamma$	*LF*	< 4.2	$\times 10^{-8}$ CL=90%	885
$\mu^-\gamma\gamma$		< 5.8	$\times 10^{-4}$ CL=90%	885
$e^-\pi^0$	*LF*	< 8.0	$\times 10^{-8}$ CL=90%	883
$\mu^-\pi^0$	*LF*	< 1.1	$\times 10^{-7}$ CL=90%	880
$e^- K^0_S$	*LF*	< 2.6	$\times 10^{-8}$ CL=90%	819
$\mu^- K^0_S$	*LF*	< 2.3	$\times 10^{-8}$ CL=90%	815
$e^-\eta$	*LF*	< 9.2	$\times 10^{-8}$ CL=90%	804
$\mu^-\eta$	*LF*	< 6.5	$\times 10^{-8}$ CL=90%	800
$e^-\rho^0$	*LF*	< 1.8	$\times 10^{-8}$ CL=90%	719
$\mu^-\rho^0$	*LF*	< 1.2	$\times 10^{-8}$ CL=90%	715
$e^-\omega$	*LF*	< 4.8	$\times 10^{-8}$ CL=90%	716
$\mu^-\omega$	*LF*	< 4.7	$\times 10^{-8}$ CL=90%	711
$e^- K^*(892)^0$	*LF*	< 3.2	$\times 10^{-8}$ CL=90%	665
$\mu^- K^*(892)^0$	*LF*	< 5.9	$\times 10^{-8}$ CL=90%	659
$e^- \overline{K}^*(892)^0$	*LF*	< 3.4	$\times 10^{-8}$ CL=90%	665
$\mu^- \overline{K}^*(892)^0$	*LF*	< 7.0	$\times 10^{-8}$ CL=90%	659
$e^-\eta'(958)$	*LF*	< 1.6	$\times 10^{-7}$ CL=90%	630
$\mu^-\eta'(958)$	*LF*	< 1.3	$\times 10^{-7}$ CL=90%	625
$e^- f_0(980) \to e^-\pi^+\pi^-$	*LF*	< 3.2	$\times 10^{-8}$ CL=90%	–
$\mu^- f_0(980) \to \mu^-\pi^+\pi^-$	*LF*	< 3.4	$\times 10^{-8}$ CL=90%	–
$e^-\phi$	*LF*	< 3.1	$\times 10^{-8}$ CL=90%	596
$\mu^-\phi$	*LF*	< 8.4	$\times 10^{-8}$ CL=90%	590
$e^- e^+ e^-$	*LF*	< 2.7	$\times 10^{-8}$ CL=90%	888
$e^-\mu^+\mu^-$	*LF*	< 2.7	$\times 10^{-8}$ CL=90%	882
$e^+\mu^-\mu^-$	*LF*	< 1.7	$\times 10^{-8}$ CL=90%	882
$\mu^- e^+ e^-$	*LF*	< 1.8	$\times 10^{-8}$ CL=90%	885
$\mu^+ e^- e^-$	*LF*	< 1.5	$\times 10^{-8}$ CL=90%	885
$\mu^-\mu^+\mu^-$	*LF*	< 2.1	$\times 10^{-8}$ CL=90%	873
$e^-\pi^+\pi^-$	*LF*	< 2.3	$\times 10^{-8}$ CL=90%	877
$e^+\pi^-\pi^-$	*L*	< 2.0	$\times 10^{-8}$ CL=90%	877
$\mu^-\pi^+\pi^-$	*LF*	< 2.1	$\times 10^{-8}$ CL=90%	866
$\mu^+\pi^-\pi^-$	*L*	< 3.9	$\times 10^{-8}$ CL=90%	866
$e^-\pi^+ K^-$	*LF*	< 3.7	$\times 10^{-8}$ CL=90%	813
$e^-\pi^- K^+$	*LF*	< 3.1	$\times 10^{-8}$ CL=90%	813
$e^+\pi^- K^-$	*L*	< 3.2	$\times 10^{-8}$ CL=90%	813
$e^- K^0_S K^0_S$	*LF*	< 7.1	$\times 10^{-8}$ CL=90%	736
$e^- K^+ K^-$	*LF*	< 3.4	$\times 10^{-8}$ CL=90%	738
$e^+ K^- K^-$	*L*	< 3.3	$\times 10^{-8}$ CL=90%	738
$\mu^-\pi^+ K^-$	*LF*	< 8.6	$\times 10^{-8}$ CL=90%	800
$\mu^-\pi^- K^+$	*LF*	< 4.5	$\times 10^{-8}$ CL=90%	800
$\mu^+\pi^- K^-$	*L*	< 4.8	$\times 10^{-8}$ CL=90%	800
$\mu^- K^0_S K^0_S$	*LF*	< 8.0	$\times 10^{-8}$ CL=90%	696
$\mu^- K^+ K^-$	*LF*	< 4.4	$\times 10^{-8}$ CL=90%	699
$\mu^+ K^- K^-$	*L*	< 4.7	$\times 10^{-8}$ CL=90%	699
$e^-\pi^0\pi^0$	*LF*	< 6.5	$\times 10^{-6}$ CL=90%	878
$\mu^-\pi^0\pi^0$	*LF*	< 1.4	$\times 10^{-5}$ CL=90%	867
$e^-\eta\eta$	*LF*	< 3.5	$\times 10^{-5}$ CL=90%	699
$\mu^-\eta\eta$	*LF*	< 6.0	$\times 10^{-5}$ CL=90%	653
$e^-\pi^0\eta$	*LF*	< 2.4	$\times 10^{-5}$ CL=90%	798
$\mu^-\pi^0\eta$	*LF*	< 2.2	$\times 10^{-5}$ CL=90%	784
$p e^- e^-$	*L,B*	< 3.0	$\times 10^{-8}$ CL=90%	641
$\overline{p} e^+ e^-$	*L,B*	< 3.0	$\times 10^{-8}$ CL=90%	641
$\overline{p} e^+ \mu^-$	*L,B*	< 2.0	$\times 10^{-8}$ CL=90%	635
$\overline{p} e^- \mu^+$	*L,B*	< 1.8	$\times 10^{-8}$ CL=90%	635
$p\mu^-\mu^-$	*L,B*	< 4.0	$\times 10^{-8}$ CL=90%	618
$\overline{p}\mu^+\mu^-$	*L,B*	< 1.8	$\times 10^{-8}$ CL=90%	618
$\overline{p}\gamma$	*L,B*	< 3.5	$\times 10^{-6}$ CL=90%	641
$\overline{p}\pi^0$	*L,B*	< 1.5	$\times 10^{-5}$ CL=90%	632
$\overline{p}2\pi^0$	*L,B*	< 3.3	$\times 10^{-5}$ CL=90%	604
$\overline{p}\eta$	*L,B*	< 8.9	$\times 10^{-6}$ CL=90%	475
$\overline{p}\pi^0\eta$	*L,B*	< 2.7	$\times 10^{-5}$ CL=90%	360
$\Lambda\pi^-$	*L,B*	< 7.2	$\times 10^{-8}$ CL=90%	525
$\overline{\Lambda}\pi^-$	*L,B*	< 1.4	$\times 10^{-7}$ CL=90%	525
e^-light boson	*LF*	< 2.7	$\times 10^{-3}$ CL=95%	–
μ^-light boson	*LF*	< 5	$\times 10^{-3}$ CL=95%	–

Heavy Charged Lepton Searches

$L^\pm$ – charged lepton

Mass $m >$ 100.8 GeV, CL = 95% [h] Decay to νW.

$L^\pm$ – stable charged heavy lepton

Mass $m >$ 102.6 GeV, CL = 95%

Neutrino Properties

See the note on "Neutrino properties listings" in the Particle Listings.

Mass $m <$ 1.1 eV, CL = 90% (tritium decay)
Mean life/mass, $\tau/m >$ 300 s/eV, CL = 90% (reactor)
Mean life/mass, $\tau/m > 7 \times 10^9$ s/eV (solar)
Mean life/mass, $\tau/m >$ 15.4 s/eV, CL = 90% (accelerator)
Magnetic moment $\mu < 0.28 \times 10^{-10}\ \mu_B$, CL = 90% (solar + radiochemical)

Number of Neutrino Types

Number $N = 2.996 \pm 0.007$ (Standard Model fits to LEP-SLC data)
Number $N = 2.92 \pm 0.05$ (S = 1.2) (Direct measurement of invisible Z width)

Neutrino Mixing

The following values are obtained through data analyses based on the 3-neutrino mixing scheme described in the review "Neutrino Masses, Mixing, and Oscillations."

$\sin^2(\theta_{12}) = 0.307 \pm 0.013$
$\Delta m^2_{21} = (7.53 \pm 0.18) \times 10^{-5}$ eV^2
$\sin^2(\theta_{23}) = 0.539 \pm 0.022$ (S = 1.1) (Inverted order)
$\sin^2(\theta_{23}) = 0.546 \pm 0.021$ (Normal order)
$\Delta m^2_{32} = (-2.536 \pm 0.034) \times 10^{-3}$ eV^2 (Inverted order)
$\Delta m^2_{32} = (2.453 \pm 0.033) \times 10^{-3}$ eV^2 (Normal order)
$\sin^2(\theta_{13}) = (2.20 \pm 0.07) \times 10^{-2}$
δ, *CP* violating phase $= 1.36^{+0.20}_{-0.16}\ \pi$ rad
$\langle \Delta m^2_{21} - \Delta \overline{m}^2_{21} \rangle < 1.1 \times 10^{-4}$ eV^2, CL = 99.7%
$\langle \Delta m^2_{32} - \Delta \overline{m}^2_{32} \rangle = (-0.12 \pm 0.25) \times 10^{-3}$ eV^2

NOTES

In this Summary Table:

When a quantity has "(S = ...)" to its right, the error on the quantity has been enlarged by the "scale factor" S, defined as $S = \sqrt{\chi^2/(N-1)}$, where N is the number of measurements used in calculating the quantity. We do this when $S > 1$, which often indicates that the measurements are inconsistent. When $S > 1.25$, we also show in the Particle Listings an ideogram of the measurements. For more about S, see the Introduction.

A decay momentum p is given for each decay mode. For a 2-body decay, p is the momentum of each decay product in the rest frame of the decaying particle. For a 3-or-more-body decay, p is the largest momentum any of the products can have in this frame.

[a] This is the best limit for the mode $e^- \to \nu\gamma$. The best limit for Nuclear de-excitation experiments is 6.4×10^{24} yr.

[b] See the review on "Muon Decay Parameters" for definitions and details.

[c] P_μ is the longitudinal polarization of the muon from pion decay. For $V-A$ coupling, $P_\mu = 1$ and $\rho = \delta = 3/4$.

Downloaded from https://academic.oup.com/ptep/article/2022/8/083C01/6651666 by KIT Library user on 27 September 2022

[d] This only includes events with energy of $e > 45$ MeV and energy of $\gamma > 40$ MeV. Since the $e^- \overline{\nu}_e \nu_\mu$ and $e^- \overline{\nu}_e \nu_\mu \gamma$ modes cannot be clearly separated, we regard the latter mode as a subset of the former.

[e] See the relevant Particle Listings for the energy limits used in this measurement.

[f] A test of additive vs. multiplicative lepton family number conservation.

[g] Basis mode for the τ.

[h] $L^\pm$ mass limit depends on decay assumptions; see the Full Listings.

Downloaded from https://academic.oup.com/ptep/article/2022/8/083C01/6651666 by KIT Library user on 27 September 2022

QUARKS

The u-, d-, and s-quark masses are the $\overline{\text{MS}}$ masses at the scale μ = 2 GeV. The c- and b-quark masses are the $\overline{\text{MS}}$ masses renormalized at the $\overline{\text{MS}}$ mass, i.e. $\overline{m} = \overline{m}(\mu = \overline{m})$. The t-quark mass is extracted from event kinematics (see the review "The Top Quark").

u

$I(J^P) = \frac{1}{2}(\frac{1}{2}^+)$

$m_u = 2.16^{+0.49}_{-0.26}$ MeV Charge $= \frac{2}{3}\ e$ $I_z = +\frac{1}{2}$
$m_u/m_d = 0.474^{+0.056}_{-0.074}$

d

$I(J^P) = \frac{1}{2}(\frac{1}{2}^+)$

$m_d = 4.67^{+0.48}_{-0.17}$ MeV Charge $= -\frac{1}{3}\ e$ $I_z = -\frac{1}{2}$
$m_s/m_d = 17$–22
$\overline{m} = (m_u+m_d)/2 = 3.45^{+0.35}_{-0.15}$ MeV

s

$I(J^P) = 0(\frac{1}{2}^+)$

$m_s = 93.4^{+8.6}_{-3.4}$ MeV Charge $= -\frac{1}{3}\ e$ Strangeness $= -1$
$m_s\ /\ ((m_u + m_d)/2) = 27.33^{+0.67}_{-0.77}$

c

$I(J^P) = 0(\frac{1}{2}^+)$

$m_c = 1.27 \pm 0.02$ GeV Charge $= \frac{2}{3}\ e$ Charm $= +1$
$m_c/m_s = 11.76^{+0.05}_{-0.10}$
$m_b/m_c = 4.58 \pm 0.01$
$m_b - m_c = 3.45 \pm 0.05$ GeV

b

$I(J^P) = 0(\frac{1}{2}^+)$

$m_b = 4.18^{+0.03}_{-0.02}$ GeV Charge $= -\frac{1}{3}\ e$ Bottom $= -1$

t

$I(J^P) = 0(\frac{1}{2}^+)$

Charge $= \frac{2}{3}\ e$ Top $= +1$

Mass (direct measurements) $m = 172.69 \pm 0.30$ GeV [a,b] (S = 1.3)
Mass (from cross-section measurements) $m = 162.5^{+2.1}_{-1.5}$ GeV [a]
Mass (Pole from cross-section measurements) $m = 172.5 \pm 0.7$ GeV
$m_t - m_{\overline{t}} = -0.15 \pm 0.20$ GeV (S = 1.1)
Full width $\Gamma = 1.42^{+0.19}_{-0.15}$ GeV (S = 1.4)
$\Gamma(Wb)/\Gamma(Wq(q = b, s, d)) = 0.957 \pm 0.034$ (S = 1.5)

t-quark EW Couplings

$F_0 = 0.693 \pm 0.013$
$F_- = 0.315 \pm 0.010$
$F_+ = -0.005 \pm 0.007$
$F_{V+A} < 0.29$, CL = 95%

t DECAY MODES		Fraction (Γ_i/Γ)	Confidence level	p (MeV/c)
$Wq(q = b, s, d)$				–
Wb				–
$e\nu_e b$		(11.10 ± 0.30) %		–
$\mu\nu_\mu b$		(11.40 ± 0.20) %		–
$\tau\nu_\tau b$		(10.7 ± 0.5) %		–
$q\overline{q}b$		(66.5 ± 1.4) %		–
$\gamma q(q=u,c)$	[c]	$< 1.8 \times 10^{-4}$	95%	–
$\Delta T = 1$ weak neutral current ($T1$) modes				
$Zq(q=u,c)$	$T1$	[d] $< 5 \times 10^{-4}$	95%	–
Hu	$T1$	$< 1.2 \times 10^{-3}$	95%	–
Hc	$T1$	$< 1.1 \times 10^{-3}$	95%	–
$\ell^+\overline{q}q'(q=d,s,b;\ q'=u,c)$	$T1$	$< 1.6 \times 10^{-3}$	95%	–

b′ (4th Generation) Quark, Searches for

Mass $m >$ 190 GeV, CL = 95% ($p\overline{p}$, quasi-stable b')
Mass $m >$ 1390 GeV, CL = 95% (B($b' \to Zb$) = 1)
Mass $m >$ 1350 GeV, CL = 95% (B($b' \to Wt$) = 1)
Mass $m >$ 1570 GeV, CL = 95% (B($b' \to Hb$) = 1)
Mass $m >$ 46.0 GeV, CL = 95% (e^+e^-, all decays)

t′ (4th Generation) Quark, Searches for

$m(t'(2/3)) >$ 1280 GeV, CL = 95% (B($t' \to Zt$) = 1)
$m(t'(2/3)) >$ 1295 GeV, CL = 95% (B($t' \to Wb$) = 1)
$m(t'(2/3)) >$ 1310 GeV, CL = 95% (singlet t')
$m(t'(2/3)) >$ 1350 GeV, CL = 95% (t' in a weak isospin doublet (t',b'))
$m(t'(5/3)) > 1.350\times10^3$ GeV, CL = 95% ($t'(5/3) \to tW^+$)

Free Quark Searches

All searches since 1977 have had negative results.

NOTES

[a] A discussion of the definition of the top quark mass in these measurements can be found in the review "The Top Quark."

[b] Based on published top mass measurements using data from Tevatron Run-I and Run-II and LHC at $\sqrt{s} = 7$ TeV. Including the most recent unpublished results from Tevatron Run-II, the Tevatron Electroweak Working Group reports a top mass of 173.2 ± 0.9 GeV. See the note "The Top Quark' in the Quark Particle Listings of this *Review*.

[c] This limit is for $\Gamma(t \to \gamma q)/\Gamma(t \to Wb)$.

[d] This limit is for $\Gamma(t \to Zq)/\Gamma(t \to Wb)$.

Downloaded from https://academic.oup.com/ptep/article/2022/8/083C01/6651666 by KIT Library user on 27 September 2022

LIGHT UNFLAVORED MESONS ($S = C = B = 0$)

For $I = 1$ (π, b, ρ, a): $u\overline{d}$, $(u\overline{u}-d\overline{d})/\sqrt{2}$, $d\overline{u}$;
for $I = 0$ (η, η', h, h', ω, ϕ, f, f'): $c_1(u\overline{u} + d\overline{d}) + c_2(s\overline{s})$

$\pi^\pm$

$I^G(J^P) = 1^-(0^-)$

Mass $m = 139.57039 \pm 0.00018$ MeV (S = 1.8)
Mean life $\tau = (2.6033 \pm 0.0005) \times 10^{-8}$ s (S = 1.2)
$c\tau = 7.8045$ m

$\pi^\pm \to \ell^\pm \nu\gamma$ form factors [a]

$F_V = 0.0254 \pm 0.0017$
$F_A = 0.0119 \pm 0.0001$
F_V slope parameter $a = 0.10 \pm 0.06$
$R = 0.059^{+0.009}_{-0.008}$

π^- modes are charge conjugates of the modes below.

For decay limits to particles which are not established, see the section on Searches for Axions and Other Very Light Bosons.

π^+ DECAY MODES		Fraction (Γ_i/Γ)	Confidence level	p (MeV/c)
$\mu^+\nu_\mu$	[b]	(99.98770 ± 0.00004) %		30
$\mu^+\nu_\mu\gamma$	[c]	$(2.00 \pm 0.25) \times 10^{-4}$		30
$e^+\nu_e$	[b]	$(1.230 \pm 0.004) \times 10^{-4}$		70
$e^+\nu_e\gamma$	[c]	$(7.39 \pm 0.05) \times 10^{-7}$		70
$e^+\nu_e\pi^0$		$(1.036 \pm 0.006) \times 10^{-8}$		4
$e^+\nu_e e^+e^-$		$(3.2 \pm 0.5) \times 10^{-9}$		70
$\mu^+\nu_\mu\nu\overline{\nu}$		$< 9 \times 10^{-6}$	90%	30
$e^+\nu_e\nu\overline{\nu}$		$< 1.6 \times 10^{-7}$	90%	70
Lepton Family number (*LF*) or Lepton number (*L*) violating modes				
$\mu^+\overline{\nu}_e$	*L* [d]	$< 1.5 \times 10^{-3}$	90%	30
$\mu^+\nu_e$	*LF* [d]	$< 8.0 \times 10^{-3}$	90%	30
$\mu^-e^+e^+\nu$	*LF*	$< 1.6 \times 10^{-6}$	90%	30

π^0

$I^G(J^{PC}) = 1^-(0^{-+})$

Mass $m = 134.9768 \pm 0.0005$ MeV (S = 1.1)
$m_{\pi^\pm} - m_{\pi^0} = 4.5936 \pm 0.0005$ MeV
Mean life $\tau = (8.43 \pm 0.13) \times 10^{-17}$ s (S = 1.2)
$c\tau = 25.3$ nm

For decay limits to particles which are not established, see the appropriate Search sections (A^0 (axion) and Other Light Boson (X^0) Searches, etc.).

π^0 DECAY MODES		Fraction (Γ_i/Γ)	Scale factor/ Confidence level	p (MeV/c)
2γ		(98.823 ± 0.034) %	S=1.5	67
$e^+e^-\gamma$		(1.174 ± 0.035) %	S=1.5	67
γpositronium		$(1.82 \pm 0.29) \times 10^{-9}$		67
$e^+e^+e^-e^-$		$(3.34 \pm 0.16) \times 10^{-5}$		67
e^+e^-		$(6.46 \pm 0.33) \times 10^{-8}$		67
4γ		$< 2 \times 10^{-8}$	CL=90%	67
$\nu\overline{\nu}$	[e]	$< 4.4 \times 10^{-9}$	CL=90%	67
$\nu_e\overline{\nu}_e$		$< 1.7 \times 10^{-6}$	CL=90%	67
$\nu_\mu\overline{\nu}_\mu$		$< 1.6 \times 10^{-6}$	CL=90%	67
$\nu_\tau\overline{\nu}_\tau$		$< 2.1 \times 10^{-6}$	CL=90%	67
$\gamma\nu\overline{\nu}$		$< 1.9 \times 10^{-7}$	CL=90%	67
Charge conjugation (*C*) or Lepton Family number (*LF*) violating modes				
3γ	*C*	$< 3.1 \times 10^{-8}$	CL=90%	67
μ^+e^-	*LF*	$< 3.8 \times 10^{-10}$	CL=90%	26
μ^-e^+	*LF*	$< 3.2 \times 10^{-10}$	CL=90%	26
$\mu^+e^- + \mu^-e^+$	*LF*	$< 3.6 \times 10^{-10}$	CL=90%	26

η

$I^G(J^{PC}) = 0^+(0^{-+})$

Mass $m = 547.862 \pm 0.017$ MeV
Full width $\Gamma = 1.31 \pm 0.05$ keV

C-nonconserving decay parameters

$\pi^+\pi^-\pi^0$ left-right asymmetry $= (0.09^{+0.11}_{-0.12}) \times 10^{-2}$
$\pi^+\pi^-\pi^0$ sextant asymmetry $= (0.12^{+0.10}_{-0.11}) \times 10^{-2}$
$\pi^+\pi^-\pi^0$ quadrant asymmetry $= (-0.09 \pm 0.09) \times 10^{-2}$
$\pi^+\pi^-\gamma$ left-right asymmetry $= (0.9 \pm 0.4) \times 10^{-2}$
$\pi^+\pi^-\gamma$ β (D-wave) $= -0.02 \pm 0.07$ (S = 1.3)

CP-nonconserving decay parameters

$\pi^+\pi^-e^+e^-$ decay-plane asymmetry $A_\phi = (-0.6 \pm 3.1) \times 10^{-2}$

Other decay parameters

$\pi^0\pi^0\pi^0$ Dalitz plot $\alpha = -0.0288 \pm 0.0012$ (S = 1.1)
Parameter Λ in $\eta \to \ell^+\ell^-\gamma$ decay $= 0.716 \pm 0.011$ GeV/c^2

η DECAY MODES		Fraction (Γ_i/Γ)	Scale factor/ Confidence level	p (MeV/c)
Neutral modes				
neutral modes		(71.96 ± 0.30) %	S=1.3	–
2γ		(39.36 ± 0.18) %	S=1.1	274
$3\pi^0$		(32.57 ± 0.21) %	S=1.2	179
$\pi^0 2\gamma$		$(2.55 \pm 0.22) \times 10^{-4}$		257
$2\pi^0 2\gamma$		$< 1.2 \times 10^{-3}$	CL=90%	238
4γ		$< 2.8 \times 10^{-4}$	CL=90%	274
invisible		$< 1.0 \times 10^{-4}$	CL=90%	–
Charged modes				
charged modes		(28.04 ± 0.30) %	S=1.3	–
$\pi^+\pi^-\pi^0$		(23.02 ± 0.25) %	S=1.2	174
$\pi^+\pi^-\gamma$		(4.28 ± 0.07) %	S=1.1	236
$e^+e^-\gamma$		$(6.9 \pm 0.4) \times 10^{-3}$	S=1.2	274
$\mu^+\mu^-\gamma$		$(3.1 \pm 0.4) \times 10^{-4}$		253
e^+e^-		$< 7 \times 10^{-7}$	CL=90%	274
$\mu^+\mu^-$		$(5.8 \pm 0.8) \times 10^{-6}$		253
$2e^+2e^-$		$(2.40 \pm 0.22) \times 10^{-5}$		274
$\pi^+\pi^-e^+e^-(\gamma)$		$(2.68 \pm 0.11) \times 10^{-4}$		235
$e^+e^-\mu^+\mu^-$		$< 1.6 \times 10^{-4}$	CL=90%	253
$2\mu^+2\mu^-$		$< 3.6 \times 10^{-4}$	CL=90%	161
$\mu^+\mu^-\pi^+\pi^-$		$< 3.6 \times 10^{-4}$	CL=90%	113
$\pi^+e^-\overline{\nu}_e +$ c.c.		$< 1.7 \times 10^{-4}$	CL=90%	256
$\pi^+\pi^-2\gamma$		$< 2.1 \times 10^{-3}$		236
$\pi^+\pi^-\pi^0\gamma$		$< 6 \times 10^{-4}$	CL=90%	174
$\pi^0\mu^+\mu^-\gamma$		$< 3 \times 10^{-6}$	CL=90%	210
Charge conjugation (*C*), Parity (*P*), Charge conjugation × Parity (*CP*), or Lepton Family number (*LF*) violating modes				
$\pi^0\gamma$	*C*	[f] $< 9 \times 10^{-5}$	CL=90%	257
$\pi^+\pi^-$	*P,CP*	$< 4.4 \times 10^{-6}$	CL=90%	236
$2\pi^0$	*P,CP*	$< 3.5 \times 10^{-4}$	CL=90%	238
$2\pi^0\gamma$	*C*	$< 5 \times 10^{-4}$	CL=90%	238
$3\pi^0\gamma$	*C*	$< 6 \times 10^{-5}$	CL=90%	179
3γ	*C*	$< 1.6 \times 10^{-5}$	CL=90%	274
$4\pi^0$	*P,CP*	$< 6.9 \times 10^{-7}$	CL=90%	40
$\pi^0e^+e^-$	*C*	[g] $< 8 \times 10^{-6}$	CL=90%	257
$\pi^0\mu^+\mu^-$	*C*	[g] $< 5 \times 10^{-6}$	CL=90%	210
$\mu^+e^- + \mu^-e^+$	*LF*	$< 6 \times 10^{-6}$	CL=90%	264

$f_0(500)$

$I^G(J^{PC}) = 0^+(0^{++})$

also known as σ; was $f_0(600)$

See the review on "Scalar Mesons below 1 GeV."
Mass (T-Matrix Pole $\sqrt{s}$) = (400–550)$-i$(200–350) MeV
Mass (Breit-Wigner) = 400 to 800 MeV
Full width (Breit-Wigner) = 100 to 800 MeV

$f_0(500)$ DECAY MODES	Fraction (Γ_i/Γ)	p (MeV/c)
$\pi\pi$	seen	–
$\gamma\gamma$	seen	–

$\rho(770)$

$I^G(J^{PC}) = 1^+(1^{--})$

See the review on "Spectroscopy of Light Meson Resonances."
Mass $m = 775.26 \pm 0.23$ MeV
Full width $\Gamma = 149.1 \pm 0.8$ MeV

Downloaded from https://academic.oup.com/ptep/article/2022/8/083C01/6651666 by KIT Library user on 27 September 2022

$\rho(770)$ DECAY MODES	Fraction (Γ_i/Γ)	Scale factor/ Confidence level	p (MeV/c)
$\pi\pi$	~ 100 %		363
$\rho(770)^\pm$ decays			
$\pi^\pm\gamma$	$(4.5 \pm 0.5) \times 10^{-4}$	S=2.2	375
$\pi^\pm\eta$	$< 6 \times 10^{-3}$	CL=84%	152
$\pi^\pm\pi^+\pi^-\pi^0$	$< 2.0 \times 10^{-3}$	CL=84%	254
$\rho(770)^0$ decays			
$\pi^+\pi^-\gamma$	$(9.9 \pm 1.6) \times 10^{-3}$		362
$\pi^0\gamma$	$(4.7 \pm 0.8) \times 10^{-4}$	S=1.7	376
$\eta\gamma$	$(3.00 \pm 0.21) \times 10^{-4}$		194
$\pi^0\pi^0\gamma$	$(4.5 \pm 0.8) \times 10^{-5}$		363
$\mu^+\mu^-$ [h]	$(4.55 \pm 0.28) \times 10^{-5}$		373
e^+e^- [h]	$(4.72 \pm 0.05) \times 10^{-5}$		388
$\pi^+\pi^-\pi^0$	$(1.01^{+0.54}_{-0.36} \pm 0.34) \times 10^{-4}$		323
$\pi^+\pi^-\pi^+\pi^-$	$(1.8 \pm 0.9) \times 10^{-5}$		251
$\pi^+\pi^-\pi^0\pi^0$	$(1.6 \pm 0.8) \times 10^{-5}$		257
$\pi^0 e^+e^-$	$< 1.2 \times 10^{-5}$	CL=90%	376

$\omega(782)$

$I^G(J^{PC}) = 0^-(1^{--})$

Mass $m = 782.66 \pm 0.13$ MeV (S = 2.0)
Full width $\Gamma = 8.68 \pm 0.13$ MeV

$\omega(782)$ DECAY MODES	Fraction (Γ_i/Γ)	Scale factor/ Confidence level	p (MeV/c)
$\pi^+\pi^-\pi^0$	(89.2 ± 0.7) %		327
$\pi^0\gamma$	(8.35 ± 0.27) %	S=2.2	380
$\pi^+\pi^-$	$(1.53^{+0.11}_{-0.13})$ %	S=1.2	366
neutrals (excluding $\pi^0\gamma$)	$(7^{+8}_{-4}) \times 10^{-3}$	S=1.1	–
$\eta\gamma$	$(4.5 \pm 0.4) \times 10^{-4}$	S=1.1	200
$\pi^0 e^+e^-$	$(7.7 \pm 0.6) \times 10^{-4}$		380
$\pi^0\mu^+\mu^-$	$(1.34 \pm 0.18) \times 10^{-4}$	S=1.5	349
e^+e^-	$(7.38 \pm 0.22) \times 10^{-5}$	S=1.9	391
$\pi^+\pi^-\pi^0\pi^0$	$< 2 \times 10^{-4}$	CL=90%	262
$\pi^+\pi^-\gamma$	$< 3.6 \times 10^{-3}$	CL=95%	366
$\pi^+\pi^-\pi^+\pi^-$	$< 1 \times 10^{-3}$	CL=90%	256
$\pi^0\pi^0\gamma$	$(6.7 \pm 1.1) \times 10^{-5}$		367
$\eta\pi^0\gamma$	$< 3.3 \times 10^{-5}$	CL=90%	162
$\mu^+\mu^-$	$(7.4 \pm 1.8) \times 10^{-5}$		377
3γ	$< 1.9 \times 10^{-4}$	CL=95%	391
Charge conjugation (C) violating modes			
$\eta\pi^0$ C	$< 2.1 \times 10^{-4}$	CL=90%	162
$2\pi^0$ C	$< 2.2 \times 10^{-4}$	CL=90%	367
$3\pi^0$ C	$< 2.3 \times 10^{-4}$	CL=90%	330
invisible	$< 7 \times 10^{-5}$	CL=90%	–

$\eta'(958)$

$I^G(J^{PC}) = 0^+(0^{-+})$

Mass $m = 957.78 \pm 0.06$ MeV
Full width $\Gamma = 0.188 \pm 0.006$ MeV

$\eta'(958)$ DECAY MODES	Fraction (Γ_i/Γ)	Confidence level	p (MeV/c)
$\pi^+\pi^-\eta$	(42.5 ± 0.5) %		232
$\rho^0\gamma$ (including non-resonant $\pi^+\pi^-\gamma$)	(29.5 ± 0.4) %		165
$\pi^0\pi^0\eta$	(22.4 ± 0.5) %		239
$\omega\gamma$	(2.52 ± 0.07) %		159
ωe^+e^-	$(2.0 \pm 0.4) \times 10^{-4}$		159
$\gamma\gamma$	(2.307 ± 0.033) %		479
$3\pi^0$	$(2.50 \pm 0.17) \times 10^{-3}$		430
$\mu^+\mu^-\gamma$	$(1.13 \pm 0.28) \times 10^{-4}$		467
$\pi^+\pi^-\mu^+\mu^-$	$(2.0 \pm 0.4) \times 10^{-5}$		401
$\pi^+\pi^-\pi^0$	$(3.61 \pm 0.17) \times 10^{-3}$		428
$(\pi^+\pi^-\pi^0)$ S-wave	$(3.8 \pm 0.5) \times 10^{-3}$		428
$\pi^\mp\rho^\pm$	$(7.4 \pm 2.3) \times 10^{-4}$		106
$\pi^0\rho^0$	< 4 %	90%	111
$2(\pi^+\pi^-)$	$(8.4 \pm 0.9) \times 10^{-5}$		372
$\pi^+\pi^-2\pi^0$	$(1.8 \pm 0.4) \times 10^{-4}$		376
$2(\pi^+\pi^-)$ neutrals	< 1 %	95%	–
$2(\pi^+\pi^-)\pi^0$	$< 1.8 \times 10^{-3}$	90%	298
$2(\pi^+\pi^-)2\pi^0$	< 1 %	95%	197
$3(\pi^+\pi^-)$	$< 3.1 \times 10^{-5}$	90%	189
$K^\pm\pi^\mp$	$< 4 \times 10^{-5}$	90%	334
$\pi^+\pi^-e^+e^-$	$(2.42 \pm 0.10) \times 10^{-3}$		458
$\pi^+e^-\nu_e$ + c.c.	$< 2.1 \times 10^{-4}$	90%	469
γe^+e^-	$(4.91 \pm 0.27) \times 10^{-4}$		479
$\pi^0\gamma\gamma$	$(3.20 \pm 0.24) \times 10^{-3}$		469
$\pi^0\gamma\gamma$ (non resonant)	$(6.2 \pm 0.9) \times 10^{-4}$		–
$\eta\gamma\gamma$	$< 1.33 \times 10^{-4}$	90%	322
$4\pi^0$	$< 4.94 \times 10^{-5}$	90%	380
e^+e^-	$< 5.6 \times 10^{-9}$	90%	479
invisible	$< 6 \times 10^{-4}$	90%	–
Charge conjugation (C), Parity (P), Lepton family number (LF) violating modes			
$\pi^+\pi^-$ P,CP	$< 1.8 \times 10^{-5}$	90%	458
$\pi^0\pi^0$ P,CP	$< 4 \times 10^{-4}$	90%	459
$\pi^0 e^+e^-$ C	[g] $< 1.4 \times 10^{-3}$	90%	469
ηe^+e^- C	[g] $< 2.4 \times 10^{-3}$	90%	322
3γ C	$< 1.0 \times 10^{-4}$	90%	479
$\mu^+\mu^-\pi^0$ C	[g] $< 6.0 \times 10^{-5}$	90%	445
$\mu^+\mu^-\eta$ C	[g] $< 1.5 \times 10^{-5}$	90%	273
$e\mu$ LF	$< 4.7 \times 10^{-4}$	90%	473

$f_0(980)$

$I^G(J^{PC}) = 0^+(0^{++})$

See the review on "Scalar Mesons below 1 GeV."
T-matrix pole $\sqrt{s} = (980\text{–}1010) - i\,(20\text{–}35)$ MeV [i]
Mass $m = 990 \pm 20$ MeV [i]
Full width $\Gamma = 10$ to 100 MeV [i]

$f_0(980)$ DECAY MODES	Fraction (Γ_i/Γ)	p (MeV/c)
$\pi\pi$	seen	476
$K\overline{K}$	seen	36
$\gamma\gamma$	seen	495

$a_0(980)$

$I^G(J^{PC}) = 1^-(0^{++})$

See the review on "Scalar Mesons below 1 GeV."
T-matrix pole $\sqrt{s} = (960\text{–}1030) - i\,(20\text{–}70)$ MeV [i]
Mass $m = 980 \pm 20$ MeV [i]
Full width $\Gamma = 50$ to 100 MeV [i]

$a_0(980)$ DECAY MODES	Fraction (Γ_i/Γ)	p (MeV/c)
$\eta\pi$	seen	319
$K\overline{K}$	seen	†
$\eta'\pi$	seen	†
$\rho\pi$	not seen	137
$\gamma\gamma$	seen	490

$\phi(1020)$

$I^G(J^{PC}) = 0^-(1^{--})$

Mass $m = 1019.461 \pm 0.016$ MeV
Full width $\Gamma = 4.249 \pm 0.013$ MeV (S = 1.1)

$\phi(1020)$ DECAY MODES	Fraction (Γ_i/Γ)	Scale factor/ Confidence level	p (MeV/c)
K^+K^-	(49.1 ± 0.5) %	S=1.3	127
$K^0_L K^0_S$	(33.9 ± 0.4) %	S=1.2	110
$\rho\pi + \pi^+\pi^-\pi^0$	(15.4 ± 0.4) %	S=1.2	–
$\eta\gamma$	(1.301 ± 0.025) %	S=1.2	363
$\pi^0\gamma$	$(1.32 \pm 0.05) \times 10^{-3}$		501
$\ell^+\ell^-$	—		510
e^+e^-	$(2.979 \pm 0.033) \times 10^{-4}$	S=1.3	510
$\mu^+\mu^-$	$(2.85 \pm 0.19) \times 10^{-4}$		499
ηe^+e^-	$(1.08 \pm 0.04) \times 10^{-4}$		363
$\pi^+\pi^-$	$(7.3 \pm 1.3) \times 10^{-5}$		490
$\omega\pi^0$	$(4.7 \pm 0.5) \times 10^{-5}$		171
$\omega\gamma$	< 5 %	CL=84%	209
$\rho\gamma$	$< 1.2 \times 10^{-5}$	CL=90%	215
$\pi^+\pi^-\gamma$	$(4.1 \pm 1.3) \times 10^{-5}$		490
$f_0(980)\gamma$	$(3.22 \pm 0.19) \times 10^{-4}$	S=1.1	29

Downloaded from https://academic.oup.com/ptep/article/2022/8/083C01/6651666 by KIT Library user on 27 September 2022

$\pi^0\pi^0\gamma$	$(1.12 \pm 0.06) \times 10^{-4}$			492
$\pi^+\pi^-\pi^+\pi^-$	$(3.9 {}^{+2.8}_{-2.2}) \times 10^{-6}$			410
$\pi^+\pi^+\pi^-\pi^-\pi^0$	$< 4.6 \times 10^{-6}$	CL=90%		342
$\pi^0 e^+ e^-$	$(1.33 {}^{+0.07}_{-0.10}) \times 10^{-5}$			501
$\pi^0\eta\gamma$	$(7.27 \pm 0.30) \times 10^{-5}$	S=1.5		346
$a_0(980)\gamma$	$(7.6 \pm 0.6) \times 10^{-5}$			39
$K^0\overline{K}^0\gamma$	$< 1.9 \times 10^{-8}$	CL=90%		110
$\eta'(958)\gamma$	$(6.21 \pm 0.21) \times 10^{-5}$			60
$\eta\pi^0\pi^0\gamma$	$< 2 \times 10^{-5}$	CL=90%		293
$\mu^+\mu^-\gamma$	$(1.4 \pm 0.5) \times 10^{-5}$			499
$\rho\gamma\gamma$	$< 1.2 \times 10^{-4}$	CL=90%		215
$\eta\pi^+\pi^-$	$< 1.8 \times 10^{-5}$	CL=90%		288
$\eta\mu^+\mu^-$	$< 9.4 \times 10^{-6}$	CL=90%		321
$\eta U \to \eta e^+ e^-$	$< 1 \times 10^{-6}$	CL=90%		–
invisible	$< 1.7 \times 10^{-4}$	CL=90%		–
Lepton Family number (LF) violating modes				
$e^\pm\mu^\mp$ *LF*	$< 2 \times 10^{-6}$	CL=90%		504

$h_1(1170)$

$I^G(J^{PC}) = 0^-(1^{+-})$

Mass $m = 1166 \pm 6$ MeV
Full width $\Gamma = 375 \pm 35$ MeV

$h_1(1170)$ DECAY MODES	Fraction (Γ_i/Γ)	p (MeV/c)
$\rho\pi$	seen	305

$b_1(1235)$

$I^G(J^{PC}) = 1^+(1^{+-})$

Mass $m = 1229.5 \pm 3.2$ MeV (S = 1.6)
Full width $\Gamma = 142 \pm 9$ MeV (S = 1.2)

$b_1(1235)$ DECAY MODES	Fraction (Γ_i/Γ)	Confidence level	p (MeV/c)
$\omega\pi$	seen		348
[D/S amplitude ratio $= 0.277 \pm 0.027$]			
$\pi^\pm\gamma$	$(1.6 \pm 0.4) \times 10^{-3}$		607
$\eta\rho$	seen		†
$\pi^+\pi^+\pi^-\pi^0$	< 50 %	84%	535
$K^*(892)^\pm K^\mp$	seen		†
$(K\overline{K})^\pm\pi^0$	< 8 %	90%	248
$K^0_S K^0_L \pi^\pm$	< 6 %	90%	235
$K^0_S K^0_S \pi^\pm$	< 2 %	90%	235
$\phi\pi$	< 1.5 %	84%	147

$a_1(1260)$ [j]

$I^G(J^{PC}) = 1^-(1^{++})$

Mass $m = 1230 \pm 40$ MeV [i]
Full width $\Gamma = 250$ to 600 MeV [i]

$a_1(1260)$ DECAY MODES	Fraction (Γ_i/Γ)	p (MeV/c)
3π	seen	577
$(\rho\pi)_{S-\text{wave}}$, $\rho \to \pi\pi$	seen	353
$(\rho\pi)_{D-\text{wave}}$, $\rho \to \pi\pi$	seen	353
$(\rho(1450)\pi)_{S-\text{wave}}$, $\rho \to \pi\pi$	seen	†
$(\rho(1450)\pi)_{D-\text{wave}}$, $\rho \to \pi\pi$	seen	†
$f_0(500)\pi$, $f_0 \to \pi\pi$	seen	–
$f_0(980)\pi$, $f_0 \to \pi\pi$	not seen	179
$f_0(1370)\pi$, $f_0 \to \pi\pi$	seen	†
$f_2(1270)\pi$, $f_2 \to \pi\pi$	seen	†
$\pi^+\pi^-\pi^0$	seen	576
$\pi^0\pi^0\pi^0$	not seen	577
$KK\pi$	seen	250
$K^*(892)K$	seen	†
$\pi\gamma$	seen	608

$f_2(1270)$

$I^G(J^{PC}) = 0^+(2^{++})$

Mass $m = 1275.5 \pm 0.8$ MeV
Full width $\Gamma = 186.7^{+2.2}_{-2.5}$ MeV (S = 1.4)

$f_2(1270)$ DECAY MODES	Fraction (Γ_i/Γ)	Scale factor/ Confidence level	p (MeV/c)
$\pi\pi$	$(84.2 {}^{+2.9}_{-0.9})$ %	S=1.1	623
$\pi^+\pi^-2\pi^0$	$(7.7 {}^{+1.1}_{-3.2})$ %	S=1.2	563
$K\overline{K}$	$(4.6 {}^{+0.5}_{-0.4})$ %	S=2.7	404
$2\pi^+2\pi^-$	(2.8 ± 0.4) %	S=1.2	560
$\eta\eta$	$(4.0 \pm 0.8) \times 10^{-3}$	S=2.1	326
$4\pi^0$	$(3.0 \pm 1.0) \times 10^{-3}$		565
$\gamma\gamma$	$(1.42 \pm 0.24) \times 10^{-5}$	S=1.4	638
$\eta\pi\pi$	$< 8 \times 10^{-3}$	CL=95%	478
$K^0K^-\pi^+$ + c.c.	$< 3.4 \times 10^{-3}$	CL=95%	293
e^+e^-	$< 6 \times 10^{-10}$	CL=90%	638

$f_1(1285)$

$I^G(J^{PC}) = 0^+(1^{++})$

Mass $m = 1281.9 \pm 0.5$ MeV (S = 1.8)
Full width $\Gamma = 22.7 \pm 1.1$ MeV (S = 1.5)

$f_1(1285)$ DECAY MODES	Fraction (Γ_i/Γ)	Scale factor/ Confidence level	p (MeV/c)
4π	(32.7 ± 1.9) %	S=1.2	568
$\pi^0\pi^0\pi^+\pi^-$	(21.8 ± 1.3) %	S=1.2	566
$2\pi^+2\pi^-$	(10.9 ± 0.6) %	S=1.2	563
$\rho^0\pi^+\pi^-$	(10.9 ± 0.6) %	S=1.2	336
$\rho^0\rho^0$	seen		†
$4\pi^0$	$< 7 \times 10^{-4}$	CL=90%	568
$\eta\pi^+\pi^-$	(35 ± 15) %		479
$\eta\pi\pi$	(52.2 ± 2.0) %	S=1.2	482
$a_0(980)\pi$ [ignoring $a_0(980) \to K\overline{K}$]	(38 ± 4) %		238
$\eta\pi\pi$ [excluding $a_0(980)\pi$]	(14 ± 4) %		482
$K\overline{K}\pi$	(9.0 ± 0.4) %	S=1.1	308
$K\overline{K}^*(892)$	not seen		†
$\pi^+\pi^-\pi^0$	$(3.0 \pm 0.9) \times 10^{-3}$		603
$\rho^\pm\pi^\mp$	$< 3.1 \times 10^{-3}$	CL=95%	390
$\gamma\rho^0$	(6.1 ± 1.0) %	S=1.7	406
$\phi\gamma$	$(7.4 \pm 2.6) \times 10^{-4}$		236
e^+e^-	$< 9.4 \times 10^{-9}$	CL=90%	641

$\eta(1295)$

$I^G(J^{PC}) = 0^+(0^{-+})$

See the review on "Spectroscopy of Light Meson Resonances."
Mass $m = 1294 \pm 4$ MeV (S = 1.6)
Full width $\Gamma = 55 \pm 5$ MeV

$\eta(1295)$ DECAY MODES	Fraction (Γ_i/Γ)	p (MeV/c)
$\eta\pi^+\pi^-$	seen	487
$a_0(980)\pi$	seen	248
$\eta\pi^0\pi^0$	seen	490
$\eta(\pi\pi)_{S\text{-wave}}$	seen	–

$\pi(1300)$

$I^G(J^{PC}) = 1^-(0^{-+})$

Mass $m = 1300 \pm 100$ MeV [i]
Full width $\Gamma = 200$ to 600 MeV [i]

$\pi(1300)$ DECAY MODES	Fraction (Γ_i/Γ)	p (MeV/c)
$\rho\pi$	seen	404
$\pi(\pi\pi)_{S\text{-wave}}$	seen	–

$a_2(1320)$

$I^G(J^{PC}) = 1^-(2^{++})$

Mass $m = 1318.2 \pm 0.6$ MeV (S = 1.2)
Full width $\Gamma = 107 \pm 5$ MeV [i]

$a_2(1320)$ DECAY MODES	Fraction (Γ_i/Γ)	Scale factor/ Confidence level	p (MeV/c)
3π	(70.1 ± 2.7) %	S=1.2	624
$\eta\pi$	(14.5 ± 1.2) %		535
$\omega\pi\pi$	(10.6 ± 3.2) %	S=1.3	366
$K\overline{K}$	(4.9 ± 0.8) %		437
$\eta'(958)\pi$	$(5.5 \pm 0.9) \times 10^{-3}$		288

Downloaded from https://academic.oup.com/ptep/article/2022/8/083C01/6651666 by KIT Library user on 27 September 2022

$\pi^\pm\gamma$	$(2.91\pm0.27)\times10^{-3}$		652
$\gamma\gamma$	$(9.4\pm0.7)\times10^{-6}$		659
e^+e^-	$<5\times10^{-9}$	CL=90%	659

$f_0(1370)$

$I^G(J^{PC}) = 0^+(0^{++})$

See the review on "Spectroscopy of Light Meson Resonances."
Mass $m = 1200$ to 1500 MeV
Full width $\Gamma = 200$ to 500 MeV

$f_0(1370)$ DECAY MODES	Fraction (Γ_i/Γ)	p (MeV/c)
$\pi\pi$	seen	672
4π	seen	617
$4\pi^0$	seen	617
$2\pi^+2\pi^-$	seen	612
$\pi^+\pi^-2\pi^0$	seen	615
$\rho\rho$	seen	†
$2(\pi\pi)_{S\text{-wave}}$	seen	–
$\pi(1300)\pi$	seen	†
$a_1(1260)\pi$	seen	35
$\eta\eta$	seen	411
$K\overline{K}$	seen	475
$K\overline{K}n\pi$	not seen	†
6π	not seen	508
$\omega\omega$	not seen	†
$\gamma\gamma$	seen	685
e^+e^-	not seen	685

$\pi_1(1400)$

$I^G(J^{PC}) = 1^-(1^{-+})$

Coupled channel analyses favor the existence of only one broad 1^{-+} isovector state consistent with $\pi_1(1600)$ in the 1400–1600 MeV region. See the review on "Spectroscopy of Light Meson Resonances." See also $\pi_1(1600)$.
Mass $m = 1354 \pm 25$ MeV (S = 1.8)
Full width $\Gamma = 330 \pm 35$ MeV

$\pi_1(1400)$ DECAY MODES	Fraction (Γ_i/Γ)	p (MeV/c)
$\eta\pi^0$	seen	557
$\eta\pi^-$	seen	556
$\rho(770)\pi$	not seen	442

$\eta(1405)$

$I^G(J^{PC}) = 0^+(0^{-+})$

See the review on "Spectroscopy of Light Meson Resonances." See also $\eta(1475)$.
Mass $m = 1408.8 \pm 2.0$ MeV (S = 2.2)
Full width $\Gamma = 50.1 \pm 2.6$ MeV (S = 1.7)

$\eta(1405)$ DECAY MODES	Fraction (Γ_i/Γ)	Confidence level	p (MeV/c)
$K\overline{K}\pi$	seen		424
$\eta\pi\pi$	seen		562
$a_0(980)\pi$	seen		345
$\eta(\pi\pi)_{S\text{-wave}}$	seen		–
$f_0(980)\pi^0 \to \pi^+\pi^-\pi^0$	not seen		–
$f_0(980)\eta$	seen		†
4π	seen		639
$\rho\rho$	<58 %	99.85%	†
$\rho^0\gamma$	seen		491
$K^*(892)K$	seen		123

$h_1(1415)$

$I^G(J^{PC}) = 0^-(1^{+-})$

was $h_1(1380)$
Mass $m = 1416 \pm 8$ MeV (S = 1.5)
Full width $\Gamma = 90 \pm 15$ MeV

$f_1(1420)$

$I^G(J^{PC}) = 0^+(1^{++})$

See the review on "Spectroscopy of Light Meson Resonances."
Mass $m = 1426.3 \pm 0.9$ MeV (S = 1.1)
Full width $\Gamma = 54.5 \pm 2.6$ MeV

$f_1(1420)$ DECAY MODES	Fraction (Γ_i/Γ)	p (MeV/c)
$K\overline{K}\pi$	seen	438
$K\overline{K}^*(892)+$ c.c.	seen	163
$\eta\pi\pi$	possibly seen	573
$\phi\gamma$	seen	349

$\omega(1420)$ [k]

$I^G(J^{PC}) = 0^-(1^{--})$

Mass $m = 1410 \pm 60$ MeV [i]
Full width $\Gamma = 290 \pm 190$ MeV [i]

$\omega(1420)$ DECAY MODES	Fraction (Γ_i/Γ)	p (MeV/c)
$\rho\pi$	seen	480
$\omega\pi\pi$	seen	437
$b_1(1235)\pi$	seen	112
e^+e^-	seen	705

$a_0(1450)$

$I^G(J^{PC}) = 1^-(0^{++})$

See the review on "Spectroscopy of Light Meson Resonances."
Mass $m = 1474 \pm 19$ MeV
Full width $\Gamma = 265 \pm 13$ MeV

Branching fractions are given relative to the one **DEFINED AS 1**.

$a_0(1450)$ DECAY MODES	Fraction (Γ_i/Γ)	p (MeV/c)
$\pi\eta$	0.093 ± 0.020	627
$\pi\eta'(958)$	0.033 ± 0.017	410
$K\overline{K}$	0.082 ± 0.028	547
$\omega\pi\pi$	**DEFINED AS 1**	484
$a_0(980)\pi\pi$	seen	342
$\gamma\gamma$	seen	737

$\rho(1450)$

$I^G(J^{PC}) = 1^+(1^{--})$

See the review on "Spectroscopy of Light Meson Resonances."
Mass $m = 1465 \pm 25$ MeV [i]
Full width $\Gamma = 400 \pm 60$ MeV [i]

$\rho(1450)$ DECAY MODES	Fraction (Γ_i/Γ)	p (MeV/c)
$\pi\pi$	seen	720
$\pi^+\pi^-$	seen	719
4π	seen	669
e^+e^-	seen	732
$\eta\rho$	seen	311
$a_2(1320)\pi$	not seen	55
$K\overline{K}$	seen	541
K^+K^-	seen	541
$K\overline{K}^*(892)+$ c.c.	possibly seen	229
$\eta\gamma$	seen	630
$f_0(500)\gamma$	not seen	–
$f_0(980)\gamma$	not seen	398
$f_0(1370)\gamma$	not seen	92
$f_2(1270)\gamma$	not seen	177

$\eta(1475)$

$I^G(J^{PC}) = 0^+(0^{-+})$

See the review on "Spectroscopy of Light Meson Resonances." See also $\eta(1405)$.
Mass $m = 1475 \pm 4$ MeV (S = 1.4)
Full width $\Gamma = 90 \pm 9$ MeV (S = 1.6)

$\eta(1475)$ DECAY MODES	Fraction (Γ_i/Γ)	p (MeV/c)
$K\overline{K}\pi$	seen	477
$K\overline{K}^*(892)+$ c.c.	seen	244
$a_0(980)\pi$	seen	396
$\gamma\gamma$	seen	738
$K^0_SK^0_S\eta$	possibly seen	†
$\gamma\phi(1020)$	possibly seen	385

Downloaded from https://academic.oup.com/ptep/article/2022/8/083C01/6651666 by KIT Library user on 27 September 2022

$f_0(1500)$

$I^G(J^{PC}) = 0^+(0^{++})$

See the review on "Spectroscopy of Light Meson Resonances."
Mass $m = 1506 \pm 6$ MeV (S = 1.4)
Full width $\Gamma = 112 \pm 9$ MeV

$f_0(1500)$ DECAY MODES	Fraction (Γ_i/Γ)	Scale factor	p (MeV/c)
$\pi\pi$	(34.5±2.2) %	1.2	741
$\pi^+\pi^-$	seen		740
$2\pi^0$	seen		741
4π	(48.9±3.3) %	1.2	692
$4\pi^0$	seen		692
$2\pi^+2\pi^-$	seen		687
$2(\pi\pi)_{S\text{-wave}}$	seen		–
$\rho\rho$	seen		†
$\pi(1300)\pi$	seen		145
$a_1(1260)\pi$	seen		219
$\eta\eta$	(6.0±0.9) %	1.1	517
$\eta\eta'(958)$	(2.2±0.8) %	1.4	20
$K\overline{K}$	(8.5±1.0) %	1.1	569
$\gamma\gamma$	not seen		753

$f_2'(1525)$

$I^G(J^{PC}) = 0^+(2^{++})$

Mass $m = 1517.4 \pm 2.5$ MeV (S = 2.8)
Full width $\Gamma = 86 \pm 5$ MeV (S = 2.2)

$f_2'(1525)$ DECAY MODES	Fraction (Γ_i/Γ)	Scale factor	p (MeV/c)
$K\overline{K}$	(87.6±2.2) %	1.1	576
$\eta\eta$	(11.6±2.2) %	1.1	525
$\pi\pi$	(8.3±1.6) $\times 10^{-3}$		747
$\gamma\gamma$	(9.5±1.1) $\times 10^{-7}$	1.1	759

$\pi_1(1600)$

$I^G(J^{PC}) = 1^-(1^{-+})$

See the review on "Spectroscopy of Light Meson Resonances" and a note in PDG 06, Journal of Physics **G33** 1 (2006). See also $\pi_1(1400)$.
Mass $m = 1661^{+15}_{-11}$ MeV (S = 1.2)
Full width $\Gamma = 240 \pm 50$ MeV (S = 1.7)

$\pi_1(1600)$ DECAY MODES	Fraction (Γ_i/Γ)	p (MeV/c)
$\pi\pi\pi$	seen	803
$\rho^0\pi^-$	seen	641
$f_2(1270)\pi^-$	not seen	318
$b_1(1235)\pi$	seen	357
$\eta'(958)\pi^-$	seen	543
$f_1(1285)\pi$	seen	314

$a_1(1640)$

$I^G(J^{PC}) = 1^-(1^{++})$

Mass $m = 1655 \pm 16$ MeV (S = 1.2)
Full width $\Gamma = 254 \pm 40$ MeV (S = 1.8)

$a_1(1640)$ DECAY MODES	Fraction (Γ_i/Γ)	p (MeV/c)
$\pi\pi\pi$	seen	800
$f_2(1270)\pi$	seen	314
$\sigma\pi$	seen	–
$\rho\pi\ S-wave$	seen	638
$\rho\pi\ D-wave$	seen	638
$\omega\pi\pi$	seen	607
$f_1(1285)\pi$	seen	309
$a_1(1260)\eta$	not seen	†

$\eta_2(1645)$

$I^G(J^{PC}) = 0^+(2^{-+})$

Mass $m = 1617 \pm 5$ MeV
Full width $\Gamma = 181 \pm 11$ MeV

$\eta_2(1645)$ DECAY MODES	Fraction (Γ_i/Γ)	p (MeV/c)
$a_2(1320)\pi$	seen	242
$K\overline{K}\pi$	seen	580
$K^*\overline{K}$	seen	404
$\eta\pi^+\pi^-$	seen	685
$a_0(980)\pi$	seen	499
$f_2(1270)\eta$	not seen	†

$\omega(1650)$ [l]

$I^G(J^{PC}) = 0^-(1^{--})$

Mass $m = 1670 \pm 30$ MeV [i]
Full width $\Gamma = 315 \pm 35$ MeV [i]

$\omega(1650)$ DECAY MODES	Fraction (Γ_i/Γ)	p (MeV/c)
$\rho\pi$	seen	647
$\rho(1450)\pi$	seen	145
$\omega\pi\pi$	seen	617
$\omega\eta$	seen	500
e^+e^-	seen	835
$\pi^0\gamma$	not seen	830

$\omega_3(1670)$

$I^G(J^{PC}) = 0^-(3^{--})$

Mass $m = 1667 \pm 4$ MeV
Full width $\Gamma = 168 \pm 10$ MeV

$\omega_3(1670)$ DECAY MODES	Fraction (Γ_i/Γ)	p (MeV/c)
$\rho\pi$	seen	645
$\omega\pi\pi$	seen	615
$b_1(1235)\pi$	possibly seen	361

$\pi_2(1670)$

$I^G(J^{PC}) = 1^-(2^{-+})$

Mass $m = 1670.6^{+2.9}_{-1.2}$ MeV (S = 1.3)
Full width $\Gamma = 258^{+8}_{-9}$ MeV (S = 1.2)

$\pi_2(1670)$ DECAY MODES	Fraction (Γ_i/Γ)	Confidence level	p (MeV/c)
3π	(95.8±1.4) %		808
$f_2(1270)\pi$	(56.3±3.2) %		327
$\rho\pi$	(31 ±4) %		647
$\sigma\pi$	(10 ±4) %		–
$\pi(\pi\pi)_{S\text{-wave}}$	(8.7±3.4) %		–
$\pi^\pm\pi^+\pi^-$	(53 ±4) %		806
$K\overline{K}^*(892)+$ c.c.	(4.2±1.4) %		453
$\omega\rho$	(2.7±1.1) %		302
$\pi^\pm\gamma$	(7.0±1.2) $\times 10^{-4}$		829
$\gamma\gamma$	< 2.8 $\times 10^{-7}$	90%	835
$\eta\pi$	< 5 %		739
$\pi^\pm 2\pi^+2\pi^-$	< 5 %		735
$\rho(1450)\pi$	< 3.6 $\times 10^{-3}$	97.7%	145
$b_1(1235)\pi$	< 1.9 $\times 10^{-3}$	97.7%	364
$f_1(1285)\pi$	possibly seen		322
$a_2(1320)\pi$	not seen		291

$\phi(1680)$

$I^G(J^{PC}) = 0^-(1^{--})$

Mass $m = 1680 \pm 20$ MeV [i]
Full width $\Gamma = 150 \pm 50$ MeV [i]

$\phi(1680)$ DECAY MODES	Fraction (Γ_i/Γ)	p (MeV/c)
$K\overline{K}^*(892)+$ c.c.	seen	462
$K^0_S K\pi$	seen	621
$K\overline{K}$	seen	680
e^+e^-	seen	840
$\omega\pi\pi$	not seen	623
$K^+K^-\pi^+\pi^-$	seen	544
$\eta\phi$	seen	290
$\eta\gamma$	seen	751

Downloaded from https://academic.oup.com/ptep/article/2022/8/083C01/6651666 by KIT Library user on 27 September 2022

$\rho_3(1690)$

$I^G(J^{PC}) = 1^+(3^{--})$

Mass $m = 1688.8 \pm 2.1$ MeV
Full width $\Gamma = 161 \pm 10$ MeV (S = 1.5)

$\rho_3(1690)$ DECAY MODES	Fraction (Γ_i/Γ)	Scale factor	p (MeV/c)
4π	(71.1 ± 1.9) %		790
$\pi^\pm\pi^+\pi^-\pi^0$	(67 ±22) %		787
$\omega\pi$	(16 ± 6) %		655
$\pi\pi$	(23.6 ± 1.3) %		834
$K\overline{K}\pi$	(3.8 ± 1.2) %		629
$K\overline{K}$	(1.58± 0.26) %	1.2	685
$\eta\pi^+\pi^-$	seen		727
$\rho(770)\eta$	seen		520
$\pi\pi\rho$	seen		633
$a_2(1320)\pi$	seen		307
$\rho\rho$	seen		335

$\rho(1700)$

$I^G(J^{PC}) = 1^+(1^{--})$

See the review on "Spectroscopy of Light Meson Resonances."
Mass $m = 1720 \pm 20$ MeV [i] ($\eta\rho^0$ and $\pi^+\pi^-$ modes)
Full width $\Gamma = 250 \pm 100$ MeV [i] ($\eta\rho^0$ and $\pi^+\pi^-$ modes)

$\rho(1700)$ DECAY MODES	Fraction (Γ_i/Γ)	p (MeV/c)
$2(\pi^+\pi^-)$	seen	803
$\rho\pi\pi$	seen	653
$\rho^0\pi^+\pi^-$	seen	651
$\rho^\pm\pi^\mp\pi^0$	seen	652
$a_1(1260)\pi$	seen	404
$h_1(1170)\pi$	seen	450
$\pi(1300)\pi$	seen	349
$\rho\rho$	seen	372
$\pi^+\pi^-$	seen	849
$\pi\pi$	seen	849
$K\overline{K}^*(892)+$ c.c.	seen	496
$\eta\rho$	seen	545
$a_2(1320)\pi$	not seen	334
$K\overline{K}$	seen	704
e^+e^-	seen	860
$\pi^0\omega$	seen	674
$\pi^0\gamma$	not seen	855

$a_2(1700)$

$I^G(J^{PC}) = 1^-(2^{++})$

Mass $m = 1698 \pm 40$ MeV
Full width $\Gamma = 265 \pm 60$ MeV

$a_2(1700)$ DECAY MODES	Fraction (Γ_i/Γ)	p (MeV/c)
$\eta\pi$	(3.6 ±1.1) %	754
$\gamma\gamma$	$(1.13\pm0.30)\times10^{-6}$	849
$\rho\pi$	seen	664
$f_2(1270)\pi$	seen	350
$K\overline{K}$	(1.9 ±1.2) %	691
$\omega\pi^-\pi^0$	seen	634
$\omega\rho$	seen	338

$f_0(1710)$

$I^G(J^{PC}) = 0^+(0^{++})$

See the review on "Spectroscopy of Light Meson Resonances."
Mass $m = 1704 \pm 12$ MeV
Full width $\Gamma = 123 \pm 18$ MeV

$f_0(1710)$ DECAY MODES	Fraction (Γ_i/Γ)	p (MeV/c)
$K\overline{K}$	seen	694
$\eta\eta$	seen	652
$\pi\pi$	seen	841
$\gamma\gamma$	seen	852
$\omega\omega$	seen	337

$\pi(1800)$

$I^G(J^{PC}) = 1^-(0^{-+})$

Mass $m = 1810^{+9}_{-11}$ MeV (S = 2.2)
Full width $\Gamma = 215^{+7}_{-8}$ MeV

$\pi(1800)$ DECAY MODES	Fraction (Γ_i/Γ)	p (MeV/c)
$\pi^+\pi^-\pi^-$	seen	878
$f_0(500)\pi^-$	seen	–
$f_0(980)\pi^-$	seen	624
$f_0(1370)\pi^-$	seen	366
$f_0(1500)\pi^-$	not seen	247
$\rho\pi^-$	not seen	731
$\eta\eta\pi^-$	seen	660
$a_0(980)\eta$	seen	471
$a_2(1320)\eta$	not seen	†
$f_2(1270)\pi$	not seen	441
$f_0(1370)\pi^-$	not seen	366
$f_0(1500)\pi^-$	seen	247
$\eta\eta'(958)\pi^-$	seen	373
$K_0^*(1430)K^-$	seen	†
$K^*(892)K^-$	not seen	568

$\phi_3(1850)$

$I^G(J^{PC}) = 0^-(3^{--})$

Mass $m = 1854 \pm 7$ MeV
Full width $\Gamma = 87^{+28}_{-23}$ MeV (S = 1.2)

$\phi_3(1850)$ DECAY MODES	Fraction (Γ_i/Γ)	p (MeV/c)
$K\overline{K}$	seen	785
$K\overline{K}^*(892)+$ c.c.	seen	602

$\eta_2(1870)$

$I^G(J^{PC}) = 0^+(2^{-+})$

Mass $m = 1842 \pm 8$ MeV
Full width $\Gamma = 225 \pm 14$ MeV

$\eta_2(1870)$ DECAY MODES	Fraction (Γ_i/Γ)	p (MeV/c)
$\eta\pi\pi$	seen	816
$a_2(1320)\pi$	seen	434
$f_2(1270)\eta$	seen	119
$a_0(980)\pi$	seen	651
$\gamma\gamma$	seen	921

$\pi_2(1880)$

$I^G(J^{PC}) = 1^-(2^{-+})$

Mass $m = 1874^{+26}_{-5}$ MeV (S = 1.6)
Full width $\Gamma = 237^{+33}_{-30}$ MeV (S = 1.2)

$\pi_2(1880)$ DECAY MODES	Fraction (Γ_i/Γ)	p (MeV/c)
$\eta\eta\pi^-$	seen	702
$a_0(980)\eta$	seen	528
$a_2(1320)\eta$	seen	76
$f_0(1500)\pi$	seen	308
$f_1(1285)\pi$	seen	485
$\omega\pi^-\pi^0$	seen	744

$f_2(1950)$

$I^G(J^{PC}) = 0^+(2^{++})$

Mass $m = 1936 \pm 12$ MeV (S = 1.3)
Full width $\Gamma = 464 \pm 24$ MeV

$f_2(1950)$ DECAY MODES	Fraction (Γ_i/Γ)	p (MeV/c)
$K^*(892)\overline{K}^*(892)$	seen	377
$\pi^+\pi^-$	seen	958
$\pi^0\pi^0$	seen	959
4π	seen	921
$\eta\eta$	seen	798
$K\overline{K}$	seen	833
$\gamma\gamma$	seen	968
$p\overline{p}$	seen	238

Downloaded from https://academic.oup.com/ptep/article/2022/8/083C01/6651666 by KIT Library user on 27 September 2022

$a_4(1970)$

$I^G(J^{PC}) = 1^-(4^{++})$

was $a_4(2040)$

Mass $m = 1967 \pm 16$ MeV (S = 2.1)
Full width $\Gamma = 324^{+15}_{-18}$ MeV

$a_4(1970)$ DECAY MODES	Fraction (Γ_i/Γ)	p (MeV/c)
$K\overline{K}$	seen	851
$\pi^+\pi^-\pi^0$	seen	959
$\rho\pi$	seen	825
$f_2(1270)\pi$	seen	559
$\omega\pi^-\pi^0$	seen	801
$\omega\rho$	seen	601
$\eta\pi$	seen	902
$\eta'(958)\pi$	seen	743

$f_2(2010)$

$I^G(J^{PC}) = 0^+(2^{++})$

Mass $m = 2011^{+60}_{-80}$ MeV
Full width $\Gamma = 202 \pm 60$ MeV

$f_2(2010)$ DECAY MODES	Fraction (Γ_i/Γ)	p (MeV/c)
$\phi\phi$	seen	†
$K\overline{K}$	seen	876

$f_4(2050)$

$I^G(J^{PC}) = 0^+(4^{++})$

Mass $m = 2018 \pm 11$ MeV (S = 2.1)
Full width $\Gamma = 237 \pm 18$ MeV (S = 1.9)

$f_4(2050)$ DECAY MODES	Fraction (Γ_i/Γ)	p (MeV/c)
$\omega\omega$	seen	637
$\pi\pi$	(17.0 ± 1.5) %	1000
$K\overline{K}$	$(6.8^{+3.4}_{-1.8}) \times 10^{-3}$	880
$\eta\eta$	$(2.1 \pm 0.8) \times 10^{-3}$	848
$4\pi^0$	< 1.2 %	964
$\gamma\gamma$	seen	1009
$a_2(1320)\pi$	seen	567

$\phi(2170)$

$I^G(J^{PC}) = 0^-(1^{--})$

Mass $m = 2162 \pm 7$ MeV [i] (S = 1.1)
Full width $\Gamma = 100^{+31}_{-23}$ MeV [i] (S = 2.5)

$\phi(2170)$ DECAY MODES	Fraction (Γ_i/Γ)	p (MeV/c)
e^+e^-	seen	1081
$\phi f_0(980)$	seen	399
$K^+K^- f_0(980) \to K^+K^-\pi^+\pi^-$	seen	–
$K^+K^- f_0(980) \to K^+K^-\pi^0\pi^0$	seen	–
$K^{*0}K^\pm\pi^\mp$	not seen	761
$K^*(892)^0\overline{K}^*(892)^0$	not seen	612

$f_2(2300)$

$I^G(J^{PC}) = 0^+(2^{++})$

Mass $m = 2297 \pm 28$ MeV
Full width $\Gamma = 149 \pm 40$ MeV

$f_2(2300)$ DECAY MODES	Fraction (Γ_i/Γ)	p (MeV/c)
$\phi\phi$	seen	529
$K\overline{K}$	seen	1037
$\gamma\gamma$	seen	1149
$\Lambda\overline{\Lambda}$	seen	273

$f_2(2340)$

$I^G(J^{PC}) = 0^+(2^{++})$

Mass $m = 2345^{+50}_{-40}$ MeV
Full width $\Gamma = 322^{+70}_{-60}$ MeV

$f_2(2340)$ DECAY MODES	Fraction (Γ_i/Γ)	p (MeV/c)
$\phi\phi$	seen	580
$\eta\eta$	seen	1037

STRANGE MESONS
($S = \pm1$, $C = B = 0$)

$K^+ = u\overline{s}$, $K^0 = d\overline{s}$, $\overline{K}^0 = \overline{d}s$, $K^- = \overline{u}s$, similarly for K^*'s

$K^\pm$

$I(J^P) = \frac{1}{2}(0^-)$

Mass $m = 493.677 \pm 0.016$ MeV [n] (S = 2.8)
Mean life $\tau = (1.2380 \pm 0.0020) \times 10^{-8}$ s (S = 1.8)
$c\tau = 3.711$ m

CPT violation parameters (Δ = rate difference/sum)

$\Delta(K^\pm \to \mu^\pm\nu_\mu) = (-0.27 \pm 0.21)\%$
$\Delta(K^\pm \to \pi^\pm\pi^0) = (0.4 \pm 0.6)\%$ [o]

CP violation parameters (Δ = rate difference/sum)

$\Delta(K^\pm \to \pi^\pm e^+e^-) = (-2.2 \pm 1.6) \times 10^{-2}$
$\Delta(K^\pm \to \pi^\pm\mu^+\mu^-) = 0.010 \pm 0.023$
$\Delta(K^\pm \to \pi^\pm\pi^0\gamma) = (0.0 \pm 1.2) \times 10^{-3}$
$\Delta(K^\pm \to \pi^\pm\pi^+\pi^-) = (0.04 \pm 0.06)\%$
$\Delta(K^\pm \to \pi^\pm\pi^0\pi^0) = (-0.02 \pm 0.28)\%$

T violation parameters

$K^+ \to \pi^0\mu^+\nu_\mu$ $P_T = (-1.7 \pm 2.5) \times 10^{-3}$
$K^+ \to \mu^+\nu_\mu\gamma$ $P_T = (-0.6 \pm 1.9) \times 10^{-2}$
$K^+ \to \pi^0\mu^+\nu_\mu$ $\mathrm{Im}(\xi) = -0.006 \pm 0.008$

Slope parameter g [p]

(See Particle Listings for quadratic coefficients and alternative parametrization related to $\pi\pi$ scattering)

$K^\pm \to \pi^\pm\pi^+\pi^-$ $g = -0.21134 \pm 0.00017$
$(g_+ - g_-) / (g_+ + g_-) = (-1.5 \pm 2.2) \times 10^{-4}$
$K^\pm \to \pi^\pm\pi^0\pi^0$ $g = 0.626 \pm 0.007$
$(g_+ - g_-) / (g_+ + g_-) = (1.8 \pm 1.8) \times 10^{-4}$

$K^\pm$ decay form factors [a,q]

Assuming μ-e universality
$\lambda_+(K^+_{\mu3}) = \lambda_+(K^+_{e3}) = (2.959 \pm 0.025) \times 10^{-2}$
$\lambda_0(K^+_{\mu3}) = (1.76 \pm 0.25) \times 10^{-2}$ (S = 2.7)

Not assuming μ-e universality
$\lambda_+(K^+_{e3}) = (2.956 \pm 0.025) \times 10^{-2}$
$\lambda_+(K^+_{\mu3}) = (3.09 \pm 0.25) \times 10^{-2}$ (S = 1.5)
$\lambda_0(K^+_{\mu3}) = (1.73 \pm 0.27) \times 10^{-2}$ (S = 2.6)

K_{e3} form factor quadratic fit
λ'_+ ($K^\pm_{e3}$) linear coeff. $= (2.59 \pm 0.04) \times 10^{-2}$
λ''_+($K^\pm_{e3}$) quadratic coeff. $= (0.186 \pm 0.021) \times 10^{-2}$

λ'_+ (LINEAR $K^\pm_{\mu3}$ FORM FACTOR FROM QUADRATIC FIT) $= (24 \pm 4) \times 10^{-3}$
λ''_+ (QUADRATIC $K^\pm_{\mu3}$ FORM FACTOR) $= (1.8 \pm 1.5) \times 10^{-3}$
M_V (VECTOR POLE MASS FOR $K^\pm_{e3}$ DECAY) $= 890.3 \pm 2.8$ MeV
M_V (VECTOR POLE MASS FOR $K^\pm_{\mu3}$ DECAY) $= 878 \pm 12$ MeV
M_S (SCALAR POLE MASS FOR $K^\pm_{\mu3}$ DECAY) $= 1215 \pm 50$ MeV
Λ_+ (DISPERSIVE VECTOR FORM FACTOR IN $K^\pm_{e3}$ DECAY) $= (2.460 \pm 0.017) \times 10^{-2}$
Λ_+ (DISPERSIVE VECTOR FORM FACTOR IN $K^\pm_{\mu3}$ DECAY) $= (25.4 \pm 0.9) \times 10^{-3}$
$\ln(C)$ (DISPERSIVE SCALAR FORM FACTOR in $K^\pm_{\mu3}$ decays) $= (182 \pm 16) \times 10^{-3}$
K^+_{e3} $|f_S/f_+| = (-0.08^{+0.34}_{-0.40}) \times 10^{-2}$
K^+_{e3} $|f_T/f_+| = (-1.2^{+1.3}_{-1.1}) \times 10^{-2}$
$K^+_{\mu3}$ $|f_S/f_+| = (0.2 \pm 0.6) \times 10^{-2}$
$K^+_{\mu3}$ $|f_T/f_+| = (-0.1 \pm 0.7) \times 10^{-2}$
$K^+ \to e^+\nu_e\gamma$ $|F_A + F_V| = 0.133 \pm 0.008$ (S = 1.3)
$K^+ \to \mu^+\nu_\mu\gamma$ $|F_A + F_V| = 0.165 \pm 0.013$
$K^+ \to e^+\nu_e\gamma$ $|F_A - F_V| < 0.49$, CL = 90%
$K^+ \to \mu^+\nu_\mu\gamma$ $|F_A - F_V| = -0.153 \pm 0.033$ (S = 1.1)

Downloaded from https://academic.oup.com/ptep/article/2022/8/083C01/6651666 by KIT Library user on 27 September 2022

Charge radius

$\langle r \rangle = 0.560 \pm 0.031$ fm

Forward-backward asymmetry

$A_{FB}(K^{\pm}_{\pi\mu\mu}) = \frac{\Gamma(cos(\theta_{K\mu})>0)-\Gamma(cos(\theta_{K\mu})<0)}{\Gamma(cos(\theta_{K\mu})>0)+\Gamma(cos(\theta_{K\mu})<0)} < 2.3 \times 10^{-2}$, CL = 90%

K^- modes are charge conjugates of the modes below.

K^+ DECAY MODES		Fraction (Γ_i/Γ)	Scale factor/ Confidence level	p (MeV/c)
Leptonic and semileptonic modes				
$e^+ \nu_e$		$(1.582 \pm 0.007) \times 10^{-5}$		247
$\mu^+ \nu_\mu$		(63.56 ± 0.11) %	S=1.2	236
$\pi^0 e^+ \nu_e$ Called K^+_{e3}.		(5.07 ± 0.04) %	S=2.1	228
$\pi^0 \mu^+ \nu_\mu$ Called $K^+_{\mu3}$.		(3.352 ± 0.033) %	S=1.9	215
$\pi^0 \pi^0 e^+ \nu_e$		$(2.55 \pm 0.04) \times 10^{-5}$	S=1.1	206
$\pi^+ \pi^- e^+ \nu_e$		$(4.247 \pm 0.024) \times 10^{-5}$		203
$\pi^+ \pi^- \mu^+ \nu_\mu$		$(1.4 \pm 0.9) \times 10^{-5}$		151
$\pi^0 \pi^0 \pi^0 e^+ \nu_e$		$< 3.5 \times 10^{-6}$	CL=90%	135
Hadronic modes				
$\pi^+ \pi^0$		(20.67 ± 0.08) %	S=1.2	205
$\pi^+ \pi^0 \pi^0$		(1.760 ± 0.023) %	S=1.1	133
$\pi^+ \pi^+ \pi^-$		(5.583 ± 0.024) %		125
Leptonic and semileptonic modes with photons				
$\mu^+ \nu_\mu \gamma$	[r,s]	$(6.2 \pm 0.8) \times 10^{-3}$		236
$\mu^+ \nu_\mu \gamma (SD^+)$	[a,t]	$(1.33 \pm 0.22) \times 10^{-5}$		–
$\mu^+ \nu_\mu \gamma (SD^+ INT)$	[a,t]	$< 2.7 \times 10^{-5}$	CL=90%	–
$\mu^+ \nu_\mu \gamma (SD^- + SD^- INT)$	[a,t]	$< 2.6 \times 10^{-4}$	CL=90%	–
$e^+ \nu_e \gamma$		$(9.4 \pm 0.4) \times 10^{-6}$		247
$\pi^0 e^+ \nu_e \gamma$	[r,s]	$(2.66 \pm 0.09) \times 10^{-4}$		228
$\pi^0 e^+ \nu_e \gamma (SD)$	[a,t]	$< 5.3 \times 10^{-5}$	CL=90%	228
$\pi^0 \mu^+ \nu_\mu \gamma$	[r,s]	$(1.25 \pm 0.25) \times 10^{-5}$		215
$\pi^0 \pi^0 e^+ \nu_e \gamma$		$< 5 \times 10^{-6}$	CL=90%	206
Hadronic modes with photons or $\ell\overline{\ell}$ pairs				
$\pi^+ \pi^0 \gamma (INT)$		$(-4.2 \pm 0.9) \times 10^{-6}$		–
$\pi^+ \pi^0 \gamma (DE)$	[r,u]	$(6.0 \pm 0.4) \times 10^{-6}$		205
$\pi^+ \pi^0 e^+ e^-$		$(4.24 \pm 0.14) \times 10^{-6}$		205
$\pi^+ \pi^0 \pi^0 \gamma$	[r,s]	$(7.6 {}^{+6.0}_{-3.0}) \times 10^{-6}$		133
$\pi^+ \pi^+ \pi^- \gamma$	[r,s]	$(7.1 \pm 0.5) \times 10^{-6}$		125
$\pi^+ \gamma \gamma$	[r]	$(1.01 \pm 0.06) \times 10^{-6}$		227
$\pi^+ 3\gamma$	[r]	$< 1.0 \times 10^{-4}$	CL=90%	227
$\pi^+ e^+ e^- \gamma$		$(1.19 \pm 0.13) \times 10^{-8}$		227
Leptonic modes with $\ell\overline{\ell}$ pairs				
$e^+ \nu_e \nu\overline{\nu}$		$< 6 \times 10^{-5}$	CL=90%	247
$\mu^+ \nu_\mu \nu\overline{\nu}$		$< 1.0 \times 10^{-6}$	CL=90%	236
$e^+ \nu_e e^+ e^-$		$(2.48 \pm 0.20) \times 10^{-8}$		247
$\mu^+ \nu_\mu e^+ e^-$		$(7.06 \pm 0.31) \times 10^{-8}$		236
$e^+ \nu_e \mu^+ \mu^-$		$(1.7 \pm 0.5) \times 10^{-8}$		223
$\mu^+ \nu_\mu \mu^+ \mu^-$		$< 4.1 \times 10^{-7}$	CL=90%	185
Lepton family number (LF), Lepton number (L), $\Delta S = \Delta Q$ (SQ) violating modes, or $\Delta S = 1$ weak neutral current ($S1$) modes				
$\pi^+ \pi^+ e^- \overline{\nu}_e$	SQ	$< 1.3 \times 10^{-8}$	CL=90%	203
$\pi^+ \pi^+ \mu^- \overline{\nu}_\mu$	SQ	$< 3.0 \times 10^{-6}$	CL=95%	151
$\pi^+ e^+ e^-$	$S1$	$(3.00 \pm 0.09) \times 10^{-7}$		227
$\pi^+ \mu^+ \mu^-$	$S1$	$(9.4 \pm 0.6) \times 10^{-8}$	S=2.6	172
$\pi^+ \nu\overline{\nu}$	$S1$	$(1.14 {}^{+0.40}_{-0.33}) \times 10^{-10}$		227
$\pi^+ \pi^0 \nu\overline{\nu}$	$S1$	$< 4.3 \times 10^{-5}$	CL=90%	205
$\mu^- \nu e^+ e^+$	LF	$< 2.1 \times 10^{-8}$	CL=90%	236
$\mu^+ \nu_e$	LF	[d] $< 4 \times 10^{-3}$	CL=90%	236
$\pi^+ \mu^+ e^-$	LF	$< 1.3 \times 10^{-11}$	CL=90%	214
$\pi^+ \mu^- e^+$	LF	$< 6.6 \times 10^{-11}$	CL=90%	214
$\pi^- \mu^+ e^+$	L	$< 4.2 \times 10^{-11}$	CL=90%	214
$\pi^- e^+ e^+$	L	$< 2.2 \times 10^{-10}$	CL=90%	227
$\pi^- \mu^+ \mu^+$	L	$< 4.2 \times 10^{-11}$	CL=90%	172
$\mu^+ \overline{\nu}_e$	L	[d] $< 3.3 \times 10^{-3}$	CL=90%	236
$\pi^0 e^+ \overline{\nu}_e$	L	$< 3 \times 10^{-3}$	CL=90%	228
$\pi^+ \gamma$		[v] $< 2.3 \times 10^{-9}$	CL=90%	227

K^0

$I(J^P) = \frac{1}{2}(0^-)$

50% K_S, 50% K_L

Mass $m = 497.611 \pm 0.013$ MeV (S = 1.2)

$m_{K^0} - m_{K^\pm} = 3.934 \pm 0.020$ MeV (S = 1.6)

Mean square charge radius

$\langle r^2 \rangle = -0.077 \pm 0.010$ fm^2

***T*-violation parameters in K^0-$\overline{K}^0$ mixing** [q]

Asymmetry A_T in K^0-$\overline{K}^0$ mixing $= (6.6 \pm 1.6) \times 10^{-3}$

***CP*-violation parameters**

$\mathrm{Re}(\epsilon) = (1.596 \pm 0.013) \times 10^{-3}$

***CPT*-violation parameters** [q]

$\mathrm{Re}\,\delta = (2.5 \pm 2.3) \times 10^{-4}$

$\mathrm{Im}\,\delta = (-1.5 \pm 1.6) \times 10^{-5}$

Re(y), K_{e3} parameter $= (0.4 \pm 2.5) \times 10^{-3}$

Re(x$_-$), K_{e3} parameter $= (-2.9 \pm 2.0) \times 10^{-3}$

$|m_{K^0} - m_{\overline{K}^0}| / m_{\mathrm{average}} < 6 \times 10^{-19}$, CL = 90% [x]

$(\Gamma_{K^0} - \Gamma_{\overline{K}^0})/m_{\mathrm{average}} = (8 \pm 8) \times 10^{-18}$

Tests of $\Delta S = \Delta Q$

Re(x$_+$), K_{e3} parameter $= (-0.9 \pm 3.0) \times 10^{-3}$

K^0_S

$I(J^P) = \frac{1}{2}(0^-)$

Mean life $\tau = (0.8954 \pm 0.0004) \times 10^{-10}$ s (S = 1.1) Assuming *CPT*

Mean life $\tau = (0.89564 \pm 0.00033) \times 10^{-10}$ s Not assuming *CPT*

$c\tau = 2.6844$ cm Assuming *CPT*

***CP*-violation parameters** [y]

$\mathrm{Im}(\eta_{+-0}) = -0.002 \pm 0.009$

$\mathrm{Im}(\eta_{000}) = -0.001 \pm 0.016$

$|\eta_{000}| = |A(K^0_S \to 3\pi^0)/A(K^0_L \to 3\pi^0)| < 0.0088$, CL = 90%

CP asymmetry A in $\pi^+ \pi^- e^+ e^- = (-0.4 \pm 0.8)$%

K^0_S DECAY MODES		Fraction (Γ_i/Γ)	Scale factor/ Confidence level	p (MeV/c)
Hadronic modes				
$\pi^0 \pi^0$		(30.69 ± 0.05) %		209
$\pi^+ \pi^-$		(69.20 ± 0.05) %		206
$\pi^+ \pi^- \pi^0$		$(3.5 {}^{+1.1}_{-0.9}) \times 10^{-7}$		133
Modes with photons or $\ell\overline{\ell}$ pairs				
$\pi^+ \pi^- \gamma$	[s,z]	$(1.79 \pm 0.05) \times 10^{-3}$		206
$\pi^+ \pi^- e^+ e^-$		$(4.79 \pm 0.15) \times 10^{-5}$		206
$\pi^0 \gamma \gamma$	[z]	$(4.9 \pm 1.8) \times 10^{-8}$		230
$\gamma \gamma$		$(2.63 \pm 0.17) \times 10^{-6}$	S=3.1	249
Semileptonic modes				
$\pi^\pm e^\mp \nu_e$	[aa]	$(7.04 \pm 0.08) \times 10^{-4}$		229
***CP* violating (*CP*) and $\Delta S = 1$ weak neutral current (*S1*) modes**				
$3\pi^0$	CP	$< 2.6 \times 10^{-8}$	CL=90%	139
$\mu^+ \mu^-$	$S1$	$< 2.1 \times 10^{-10}$	CL=90%	225
$e^+ e^-$	$S1$	$< 9 \times 10^{-9}$	CL=90%	249
$\pi^0 e^+ e^-$	$S1$	[z] $(3.0 {}^{+1.5}_{-1.2}) \times 10^{-9}$		230
$\pi^0 \mu^+ \mu^-$	$S1$	$(2.9 {}^{+1.5}_{-1.2}) \times 10^{-9}$		177

K^0_L

$I(J^P) = \frac{1}{2}(0^-)$

$m_{K_L} - m_{K_S}$

$= (0.5293 \pm 0.0009) \times 10^{10}\ \hbar\ \mathrm{s}^{-1}$ (S = 1.3) Assuming *CPT*

$= (3.484 \pm 0.006) \times 10^{-12}$ MeV Assuming *CPT*

$= (0.5289 \pm 0.0010) \times 10^{10}\ \hbar\ \mathrm{s}^{-1}$ Not assuming *CPT*

Mean life $\tau = (5.116 \pm 0.021) \times 10^{-8}$ s (S = 1.1)

$c\tau = 15.34$ m

Downloaded from https://academic.oup.com/ptep/article/2022/8/083C01/6651666 by KIT Library user on 27 September 2022

Slope parameters [p]

(See Particle Listings for other linear and quadratic coefficients)

$K^0_L \to \pi^+\pi^-\pi^0$: $g = 0.678 \pm 0.008$ (S = 1.5)
$K^0_L \to \pi^+\pi^-\pi^0$: $h = 0.076 \pm 0.006$
$K^0_L \to \pi^+\pi^-\pi^0$: $k = 0.0099 \pm 0.0015$
$K^0_L \to \pi^0\pi^0\pi^0$: $h = (0.6 \pm 1.2) \times 10^{-3}$

K_L decay form factors [q]

Linear parametrization assuming μ-e universality
$\lambda_+(K^0_{\mu3}) = \lambda_+(K^0_{e3}) = (2.82 \pm 0.04) \times 10^{-2}$ (S = 1.1)
$\lambda_0(K^0_{\mu3}) = (1.38 \pm 0.18) \times 10^{-2}$ (S = 2.2)

Quadratic parametrization assuming μ-e universality
$\lambda'_+(K^0_{\mu3}) = \lambda'_+(K^0_{e3}) = (2.40 \pm 0.12) \times 10^{-2}$ (S = 1.2)
$\lambda''_+(K^0_{\mu3}) = \lambda''_+(K^0_{e3}) = (0.20 \pm 0.05) \times 10^{-2}$ (S = 1.2)
$\lambda_0(K^0_{\mu3}) = (1.16 \pm 0.09) \times 10^{-2}$ (S = 1.2)

Pole parametrization assuming μ-e universality
$M^\mu_V\ (K^0_{\mu3}) = M^e_V\ (K^0_{e3}) = 878 \pm 6$ MeV (S = 1.1)
$M^\mu_S\ (K^0_{\mu3}) = 1252 \pm 90$ MeV (S = 2.6)

Dispersive parametrization assuming μ-e universality
$\Lambda_+ = (2.51 \pm 0.06) \times 10^{-2}$ (S = 1.5)
$\ln(C) = (1.75 \pm 0.18) \times 10^{-1}$ (S = 2.0)

K^0_{e3} $|f_S/f_+| = (1.5^{+1.4}_{-1.6}) \times 10^{-2}$
K^0_{e3} $|f_T/f_+| = (5^{+4}_{-5}) \times 10^{-2}$
$K^0_{\mu3}$ $|f_T/f_+| = (12 \pm 12) \times 10^{-2}$
$K_L \to \ell^+\ell^-\gamma$, $K_L \to \ell^+\ell^-\ell'^+\ell'^-$: $\alpha_{K^*} = -0.205 \pm 0.022$ (S = 1.8)
$K^0_L \to \ell^+\ell^-\gamma$, $K^0_L \to \ell^+\ell^-\ell'^+\ell'^-$: $\alpha_{DIP} = -1.69 \pm 0.08$ (S = 1.7)
$K_L \to \pi^+\pi^-e^+e^-$: $a_1/a_2 = -0.737 \pm 0.014$ GeV^2
$K_L \to \pi^0 2\gamma$: $a_V = -0.43 \pm 0.06$ (S = 1.5)

***CP*-violation parameters** [y]

$A_L = (0.332 \pm 0.006)\%$
$|\eta_{00}| = (2.220 \pm 0.011) \times 10^{-3}$ (S = 1.8)
$|\eta_{+-}| = (2.232 \pm 0.011) \times 10^{-3}$ (S = 1.8)
$|\epsilon| = (2.228 \pm 0.011) \times 10^{-3}$ (S = 1.8)
$|\eta_{00}/\eta_{+-}| = 0.9950 \pm 0.0007$ [bb] (S = 1.6)
$\mathrm{Re}(\epsilon'/\epsilon) = (1.66 \pm 0.23) \times 10^{-3}$ [bb] (S = 1.6)

Assuming *CPT*
$\phi_{+-} = (43.51 \pm 0.05)^\circ$ (S = 1.2)
$\phi_{00} = (43.52 \pm 0.05)^\circ$ (S = 1.3)
$\phi_\epsilon = \phi_{SW} = (43.52 \pm 0.05)^\circ$ (S = 1.2)
$\mathrm{Im}(\epsilon'/\epsilon) = -(\phi_{00} - \phi_{+-})/3 = (-0.002 \pm 0.005)^\circ$ (S = 1.7)

Not assuming *CPT*
$\phi_{+-} = (43.4 \pm 0.5)^\circ$ (S = 1.2)
$\phi_{00} = (43.7 \pm 0.6)^\circ$ (S = 1.2)
$\phi_\epsilon = (43.5 \pm 0.5)^\circ$ (S = 1.3)

CP asymmetry *A* in $K^0_L \to \pi^+\pi^-e^+e^- = (13.7 \pm 1.5)\%$
β_{CP} from $K^0_L \to e^+e^-e^+e^- = -0.19 \pm 0.07$
γ_{CP} from $K^0_L \to e^+e^-e^+e^- = 0.01 \pm 0.11$ (S = 1.6)
j for $K^0_L \to \pi^+\pi^-\pi^0 = 0.0012 \pm 0.0008$
f for $K^0_L \to \pi^+\pi^-\pi^0 = 0.004 \pm 0.006$
$|\eta_{+-\gamma}| = (2.35 \pm 0.07) \times 10^{-3}$
$\phi_{+-\gamma} = (44 \pm 4)^\circ$
$|\epsilon'_{+-\gamma}|/\epsilon < 0.3$, CL = 90%
$|g_{E1}|$ for $K^0_L \to \pi^+\pi^-\gamma < 0.21$, CL = 90%

***T*-violation parameters**

$\mathrm{Im}(\xi)$ in $K^0_{\mu3} = -0.007 \pm 0.026$

***CPT* invariance tests**

$\phi_{00} - \phi_{+-} = (0.34 \pm 0.32)^\circ$
$\mathrm{Re}(\frac{2}{3}\eta_{+-} + \frac{1}{3}\eta_{00}) - \frac{A_L}{2} = (-3 \pm 35) \times 10^{-6}$

$\Delta S = -\Delta Q$ in $K^0_{\ell3}$ decay

Re $x = -0.002 \pm 0.006$
Im $x = 0.0012 \pm 0.0021$

K^0_L DECAY MODES		Fraction (Γ_i/Γ)	Scale factor/ Confidence level	p (MeV/c)
Semileptonic modes				
$\pi^\pm e^\mp \nu_e$ Called K^0_{e3}.	[aa]	(40.55 ± 0.11) %	S=1.7	229
$\pi^\pm \mu^\mp \nu_\mu$ Called $K^0_{\mu3}$.	[aa]	(27.04 ± 0.07) %	S=1.1	216
$(\pi\mu\text{atom})\nu$		$(1.05 \pm 0.11) \times 10^{-7}$		188
$\pi^0\pi^\pm e^\mp \nu$	[aa]	$(5.20 \pm 0.11) \times 10^{-5}$		207
$\pi^\pm e^\mp \nu e^+ e^-$	[aa]	$(1.26 \pm 0.04) \times 10^{-5}$		229
Hadronic modes, including Charge conjugation×Parity Violating (*CPV*) modes				
$3\pi^0$		(19.52 ± 0.12) %	S=1.6	139
$\pi^+\pi^-\pi^0$		(12.54 ± 0.05) %		133
$\pi^+\pi^-$	*CPV* [cc]	$(1.967 \pm 0.010) \times 10^{-3}$	S=1.5	206
$\pi^0\pi^0$	*CPV*	$(8.64 \pm 0.06) \times 10^{-4}$	S=1.8	209
Semileptonic modes with photons				
$\pi^\pm e^\mp \nu_e \gamma$	[s,aa,dd]	$(3.79 \pm 0.06) \times 10^{-3}$		229
$\pi^\pm \mu^\mp \nu_\mu \gamma$		$(5.65 \pm 0.23) \times 10^{-4}$		216
Hadronic modes with photons or $\ell\bar{\ell}$ pairs				
$\pi^0\pi^0\gamma$		$< 2.43 \times 10^{-7}$	CL=90%	209
$\pi^+\pi^-\gamma$	[s,dd]	$(4.15 \pm 0.15) \times 10^{-5}$	S=2.8	206
$\pi^+\pi^-\gamma$(DE)		$(2.84 \pm 0.11) \times 10^{-5}$	S=2.0	206
$\pi^0 2\gamma$	[dd]	$(1.273 \pm 0.033) \times 10^{-6}$		230
$\pi^0\gamma e^+e^-$		$(1.62 \pm 0.17) \times 10^{-8}$		230
Other modes with photons or $\ell\bar{\ell}$ pairs				
2γ		$(5.47 \pm 0.04) \times 10^{-4}$	S=1.1	249
3γ		$< 7.4 \times 10^{-8}$	CL=90%	249
$e^+e^-\gamma$		$(9.4 \pm 0.4) \times 10^{-6}$	S=2.0	249
$\mu^+\mu^-\gamma$		$(3.59 \pm 0.11) \times 10^{-7}$	S=1.3	225
$e^+e^-\gamma\gamma$	[dd]	$(5.95 \pm 0.33) \times 10^{-7}$		249
$\mu^+\mu^-\gamma\gamma$	[dd]	$(1.0 {}^{+0.8}_{-0.6}) \times 10^{-8}$		225
Charge conjugation × Parity (*CP*) or Lepton Family number (*LF*) violating modes, or $\Delta S = 1$ weak neutral current (*S1*) modes				
$\mu^+\mu^-$	*S1*	$(6.84 \pm 0.11) \times 10^{-9}$		225
e^+e^-	*S1*	$(9 {}^{+6}_{-4}) \times 10^{-12}$		249
$\pi^+\pi^-e^+e^-$	*S1* [dd]	$(3.11 \pm 0.19) \times 10^{-7}$		206
$\pi^0\pi^0e^+e^-$	*S1*	$< 6.6 \times 10^{-9}$	CL=90%	209
$\pi^0\pi^0\mu^+\mu^-$	*S1*	$< 9.2 \times 10^{-11}$	CL=90%	57
$\mu^+\mu^-e^+e^-$	*S1*	$(2.69 \pm 0.27) \times 10^{-9}$		225
$e^+e^-e^+e^-$	*S1*	$(3.56 \pm 0.21) \times 10^{-8}$		249
$\pi^0\mu^+\mu^-$	*CP,S1* [ee]	$< 3.8 \times 10^{-10}$	CL=90%	177
$\pi^0e^+e^-$	*CP,S1* [ee]	$< 2.8 \times 10^{-10}$	CL=90%	230
$\pi^0\nu\bar{\nu}$	*CP,S1* [ff]	$< 3.0 \times 10^{-9}$	CL=90%	230
$\pi^0\pi^0\nu\bar{\nu}$	*S1*	$< 8.1 \times 10^{-7}$	CL=90%	209
$e^\pm\mu^\mp$	*LF* [aa]	$< 4.7 \times 10^{-12}$	CL=90%	238
$e^\pm e^\pm\mu^\mp\mu^\mp$	*LF* [aa]	$< 4.12 \times 10^{-11}$	CL=90%	225
$\pi^0\mu^\pm e^\mp$	*LF* [aa]	$< 7.6 \times 10^{-11}$	CL=90%	217
$\pi^0\pi^0\mu^\pm e^\mp$	*LF*	$< 1.7 \times 10^{-10}$	CL=90%	159
Lorentz invariance violating modes				
$\pi^0\gamma$		$< 1.7 \times 10^{-7}$	CL=90%	230

$K^*_0(700)$

$I(J^P) = \frac{1}{2}(0^+)$

also known as κ; was $K^*_0(800)$

See the review on "Scalar Mesons below 1 GeV."

Mass (T-Matrix Pole $\sqrt{s}$) = (630–730) $- i$ (260–340) MeV
Mass (Breit-Wigner) = 845 ± 17 MeV
Full width (Breit-Wigner) = 468 ± 30 MeV

$K^*_0(700)$ DECAY MODES	Fraction (Γ_i/Γ)	p (MeV/c)
$K\pi$	100 %	256

Downloaded from https://academic.oup.com/ptep/article/2022/8/083C01/6651666 by KIT Library user on 27 September 2022

$K^*(892)$

$I(J^P) = \frac{1}{2}(1^-)$

Mass (T-Matrix Pole $\sqrt{s}$) = $(890 \pm 14) - i\,(26 \pm 6)$ MeV
$K^*(892)^\pm$ hadroproduced mass $m = 891.67 \pm 0.26$ MeV
$K^*(892)^\pm$ in τ decays mass $m = 895.5 \pm 0.8$ MeV
$K^*(892)^0$ mass $m = 895.55 \pm 0.20$ MeV (S = 1.7)
$K^*(892)^\pm$ hadroproduced full width $\Gamma = 51.4 \pm 0.8$ MeV
$K^*(892)^\pm$ in τ decays full width $\Gamma = 46.2 \pm 1.3$ MeV
$K^*(892)^0$ full width $\Gamma = 47.3 \pm 0.5$ MeV (S = 1.9)

$K^*(892)$ DECAY MODES	Fraction (Γ_i/Γ)	Confidence level	p (MeV/c)
$K\pi$	~ 100 %		289
$K^0\gamma$	$(2.46\pm0.21)\times10^{-3}$		307
$K^\pm\gamma$	$(9.8\pm0.9)\times10^{-4}$		309
$K\pi\pi$	$< 7\times10^{-4}$	95%	223

$K_1(1270)$

$I(J^P) = \frac{1}{2}(1^+)$

Mass $m = 1253 \pm 7$ MeV (S = 2.2)
Full width $\Gamma = 90 \pm 20$ MeV [i]

$K_1(1270)$ DECAY MODES	Fraction (Γ_i/Γ)	Scale factor	p (MeV/c)
$K\rho$	(38 ± 13) %	2.2	†
$K_0^*(1430)\pi$	(28 ± 4) %		†
$K^*(892)\pi$	(21 ± 10) %	2.2	286
$K\omega$	(11.0 ± 2.0) %		†
$Kf_0(1370)$	(3.0 ± 2.0) %		†
γK^0	seen		528

$K_1(1400)$

$I(J^P) = \frac{1}{2}(1^+)$

Mass $m = 1403 \pm 7$ MeV
Full width $\Gamma = 174 \pm 13$ MeV (S = 1.6)

$K_1(1400)$ DECAY MODES	Fraction (Γ_i/Γ)	p (MeV/c)
$K^*(892)\pi$	(94 ± 6) %	402
$K\rho$	(3.0 ± 3.0) %	293
$Kf_0(1370)$	(2.0 ± 2.0) %	†
$K\omega$	(1.0 ± 1.0) %	284
$K_0^*(1430)\pi$	not seen	†
γK^0	seen	613
$K\phi$	seen	†

$K^*(1410)$

$I(J^P) = \frac{1}{2}(1^-)$

Mass $m = 1414 \pm 15$ MeV (S = 1.3)
Full width $\Gamma = 232 \pm 21$ MeV (S = 1.1)

$K^*(1410)$ DECAY MODES	Fraction (Γ_i/Γ)	Confidence level	p (MeV/c)
$K^*(892)\pi$	> 40 %	95%	410
$K\pi$	(6.6 ± 1.3) %		612
$K\rho$	< 7 %	95%	305
γK^0	$< 2.3\times10^{-4}$	90%	619
$K\phi$	seen		†

$K_0^*(1430)$

$I(J^P) = \frac{1}{2}(0^+)$

Mass $m = 1425 \pm 50$ MeV [i]
Full width $\Gamma = 270 \pm 80$ MeV [i]

$K_0^*(1430)$ DECAY MODES	Fraction (Γ_i/Γ)	p (MeV/c)
$K\pi$	(93 ± 10) %	619
$K\eta$	$(8.6^{+2.7}_{-3.4})$ %	486
$K\eta'(958)$	seen	†

$K_2^*(1430)$

$I(J^P) = \frac{1}{2}(2^+)$

$K_2^*(1430)^\pm$ mass $m = 1427.3 \pm 1.5$ MeV (S = 1.3)
$K_2^*(1430)^0$ mass $m = 1432.4 \pm 1.3$ MeV
$K_2^*(1430)^\pm$ full width $\Gamma = 100.0 \pm 2.1$ MeV
$K_2^*(1430)^0$ full width $\Gamma = 109 \pm 5$ MeV (S = 1.9)

$K_2^*(1430)$ DECAY MODES	Fraction (Γ_i/Γ)	Scale factor / Confidence level	p (MeV/c)
$K\pi$	(49.9 ± 1.2) %		620
$K^*(892)\pi$	(24.7 ± 1.5) %		420
$K^*(892)\pi\pi$	(13.4 ± 2.2) %		373
$K\rho$	(8.7 ± 0.8) %	S=1.2	320
$K\omega$	(2.9 ± 0.8) %		313
$K^+\gamma$	$(2.4\pm0.5)\times10^{-3}$	S=1.1	628
$K\eta$	$(1.5^{+3.4}_{-1.0})\times10^{-3}$	S=1.3	488
$K\omega\pi$	$< 7.2\times10^{-4}$	CL=95%	106
$K^0\gamma$	$< 9\times10^{-4}$	CL=90%	627

$K(1460)$

$I(J^P) = \frac{1}{2}(0^-)$

$K(1460)$ DECAY MODES	Fraction (Γ_i/Γ)	p (MeV/c)
$K^*(892)\pi$	seen	–
$K\rho$	seen	–
$K_0^*(1430)\pi$	seen	–
$K\phi$	seen	–

$K_1(1650)$

$I(J^P) = \frac{1}{2}(1^+)$

Mass $m = 1650 \pm 50$ MeV
Full width $\Gamma = 150 \pm 50$ MeV

$K^*(1680)$

$I(J^P) = \frac{1}{2}(1^-)$

Mass $m = 1718 \pm 18$ MeV
Full width $\Gamma = 322 \pm 110$ MeV (S = 4.2)

$K^*(1680)$ DECAY MODES	Fraction (Γ_i/Γ)	p (MeV/c)
$K\pi$	(38.7 ± 2.5) %	782
$K\rho$	$(31.4^{+5.0}_{-2.1})$ %	571
$K^*(892)\pi$	$(29.9^{+2.2}_{-5.0})$ %	618
$K\phi$	seen	387
$K\eta$	$(1.4^{+1.0}_{-0.8})$ %	683

$K_2(1770)$ [gg]

$I(J^P) = \frac{1}{2}(2^-)$

Mass $m = 1773 \pm 8$ MeV
Full width $\Gamma = 186 \pm 14$ MeV

$K_2(1770)$ DECAY MODES	Fraction (Γ_i/Γ)	p (MeV/c)
$K\pi\pi$		794
$K_2^*(1430)\pi$	seen	287
$K^*(892)\pi$	seen	654
$Kf_2(1270)$	seen	53
$K\phi$	seen	441
$K\omega$	seen	607

$K_3^*(1780)$

$I(J^P) = \frac{1}{2}(3^-)$

Mass $m = 1779 \pm 8$ MeV (S = 1.2)
Full width $\Gamma = 161 \pm 17$ MeV (S = 1.1)

$K_3^*(1780)$ DECAY MODES	Fraction (Γ_i/Γ)	Confidence level	p (MeV/c)
$K\rho$	(31 ± 9) %		616
$K^*(892)\pi$	(20 ± 5) %		657
$K\pi$	(18.8 ± 1.0) %		815
$K\eta$	(30 ± 13) %		721
$K_2^*(1430)\pi$	< 16 %	95%	292

Downloaded from https://academic.oup.com/ptep/article/2022/8/083C01/6651666 by KIT Library user on 27 September 2022

$K_2(1820)$ [gg]

$I(J^P) = \frac{1}{2}(2^-)$

Mass $m = 1819 \pm 12$ MeV
Full width $\Gamma = 264 \pm 34$ MeV

$K_2(1820)$ DECAY MODES	Fraction (Γ_i/Γ)	p (MeV/c)
$K\pi\pi$	seen	819
$K_2^*(1430)\pi$	seen	328
$K^*(892)\pi$	seen	683
$Kf_2(1270)$	seen	191
$K\omega$	seen	640
$K\phi$	seen	483

$K_2^*(1980)$

$I(J^P) = \frac{1}{2}(2^+)$

Mass $m = 1994^{+60}_{-50}$ MeV (S = 2.8)
Full width $\Gamma = 348^{+50}_{-30}$ MeV (S = 1.3)

$K_2^*(1980)$ DECAY MODES	Fraction (Γ_i/Γ)	p (MeV/c)
$K^*(892)\pi$	possibly seen	791
$K\rho$	possibly seen	762
$Kf_2(1270)$	possibly seen	424
$K\phi$	seen	627
$K\eta$	seen	850

$K_4^*(2045)$

$I(J^P) = \frac{1}{2}(4^+)$

Mass $m = 2048^{+8}_{-9}$ MeV (S = 1.1)
Full width $\Gamma = 199^{+27}_{-19}$ MeV

$K_4^*(2045)$ DECAY MODES	Fraction (Γ_i/Γ)	p (MeV/c)
$K\pi$	(9.9 ± 1.2) %	960
$K^*(892)\pi\pi$	(9 ± 5) %	804
$K^*(892)\pi\pi\pi$	(7 ± 5) %	770
$\rho K\pi$	(5.7 ± 3.2) %	744
$\omega K\pi$	(5.0 ± 3.0) %	740
$\phi K\pi$	(2.8 ± 1.4) %	597
$\phi K^*(892)$	(1.4 ± 0.7) %	368

CHARMED MESONS ($C = \pm1$)

$D^+ = c\overline{d}$, $D^0 = c\overline{u}$, $\overline{D}^0 = \overline{c}u$, $D^- = \overline{c}d$, similarly for D^*'s

$D^\pm$

$I(J^P) = \frac{1}{2}(0^-)$

Mass $m = 1869.66 \pm 0.05$ MeV
Mean life $\tau = (1033 \pm 5) \times 10^{-15}$ s
$c\tau = 309.8\ \mu$m

c-quark decays

$\Gamma(c \to \ell^+ \text{anything})/\Gamma(c \to \text{anything}) = 0.096 \pm 0.004$ [hh]
$\Gamma(c \to D^*(2010)^+ \text{anything})/\Gamma(c \to \text{anything}) = 0.255 \pm 0.017$

CP-violation decay-rate asymmetries

$A_{CP}(\mu^\pm\nu) = (8 \pm 8)\%$
$A_{CP}(K_L^0 e^\pm\nu) = (-0.6 \pm 1.6)\%$
$A_{CP}(K_S^0\pi^\pm) = (-0.41 \pm 0.09)\%$
$A_{CP}(K_L^0 K^\pm)$ in $D^\pm \to K_L^0 K^\pm = (-4.2 \pm 3.4) \times 10^{-2}$
$A_{CP}(K^\mp 2\pi^\pm) = (-0.18 \pm 0.16)\%$
$A_{CP}(K^\mp\pi^\pm\pi^\pm\pi^0) = (-0.3 \pm 0.7)\%$
$A_{CP}(K_S^0\pi^\pm\pi^0) = (-0.1 \pm 0.7)\%$
$A_{CP}(K_S^0\pi^\pm\eta)$ in $D^\pm \to K_S^0\pi^\pm\eta = (-0.9 \pm 3.1) \times 10^{-2}$
$A_{CP}(K_S^0\pi^\pm\pi^+\pi^-) = (0.0 \pm 1.2)\%$
$A_{CP}(K^\pm\pi^+\pi^-\pi^0)$ in $D^\pm \to K^\pm\pi^+\pi^-\pi^0 = -0.04 \pm 0.06$
$A_{CP}(\pi^\pm\pi^0) = (0.4 \pm 1.3)\%$ (S = 1.7)
$A_{CP}(\pi^\pm\eta) = (0.3 \pm 0.8)\%$ (S = 1.2)
$A_{CP}(\pi^\pm\pi^0\eta)$ in $D^\pm \to \pi^\pm\pi^0\eta = (-6 \pm 7) \times 10^{-2}$
$A_{CP}(\pi^\pm\eta\eta)$ in $D^\pm \to \pi^\pm\eta\eta = (8 \pm 9) \times 10^{-2}$
$A_{CP}(\pi^\pm\eta'(958)) = (-0.6 \pm 0.7)\%$
$A_{CP}(\overline{K}^0/K^0K^\pm) = (0.11 \pm 0.17)\%$
$A_{CP}(K_S^0K^\pm) = (-0.01 \pm 0.07)\%$
$A_{CP}(K_S^0K^\pm\pi^0)$ in $D^\pm \to K_S^0K^\pm\pi^0 = (1 \pm 4) \times 10^{-2}$
$A_{CP}(K_L^0K^\pm\pi^0)$ in $D^\pm \to K_L^0K^\pm\pi^0 = (-1 \pm 4) \times 10^{-2}$
$A_{CP}(K^+K^-\pi^\pm) = (0.37 \pm 0.29)\%$
$A_{CP}(K^\pm K^{*0}) = (-0.3 \pm 0.4)\%$
$A_{CP}(\phi\pi^\pm) = (0.01 \pm 0.09)\%$ (S = 1.8)
$A_{CP}(K^\pm K_0^*(1430)^0) = (8^{+7}_{-6})\%$
$A_{CP}(K^\pm K_2^*(1430)^0) = (43^{+20}_{-26})\%$
$A_{CP}(K^\pm K_0^*(700)) = (-12^{+18}_{-13})\%$
$A_{CP}(a_0(1450)^0\pi^\pm) = (-19^{+14}_{-16})\%$
$A_{CP}(\phi(1680)\pi^\pm) = (-9 \pm 26)\%$
$A_{CP}(\pi^+\pi^-\pi^\pm) = (-2 \pm 4)\%$
$A_{CP}(\pi^+\pi^-\pi^\pm\eta)$ in $D^\pm \to \pi^+\pi^-\pi^\pm\eta = (3 \pm 5) \times 10^{-2}$
$A_{CP}(K_S^0K^\pm\pi^+\pi^-) = (-4 \pm 7)\%$
$A_{CP}(K^\pm\pi^0) = (-3 \pm 5)\%$
$A_{CP}(K^\pm\eta)$ in $D^\pm \to K^\pm\eta = (-6 \pm 11) \times 10^{-2}$

χ^2 tests of CP-violation (CPV)

Local CPV in $D^\pm \to \pi^+\pi^-\pi^\pm = 78.1\%$
Local CPV in $D^\pm \to K^+K^-\pi^\pm = 31\%$

CP violating asymmetries of P-odd (T-odd) moments

$A_T(K_S^0K^\pm\pi^+\pi^-) = (-12 \pm 11) \times 10^{-3}$ [ii]

D^+ form factors

$f_+(0)|V_{cs}|$ in $\overline{K}^0\ell^+\nu_\ell = 0.719 \pm 0.011$ (S = 1.6)
$r_1 \equiv a_1/a_0$ in $\overline{K}^0\ell^+\nu_\ell = -2.13 \pm 0.14$
$r_2 \equiv a_2/a_0$ in $\overline{K}^0\ell^+\nu_\ell = -3 \pm 12$ (S = 1.5)
$f_+(0)|V_{cd}|$ in $\pi^0\ell^+\nu_\ell = 0.1407 \pm 0.0025$
$r_1 \equiv a_1/a_0$ in $\pi^0\ell^+\nu_\ell = -2.00 \pm 0.13$
$r_2 \equiv a_2/a_0$ in $\pi^0\ell^+\nu_\ell = -4 \pm 5$
$f_+(0)|V_{cd}|$ in $D^+ \to \eta\ell^+\nu_\ell$ ($\ell = e$ or ν) $= (8.4 \pm 0.4) \times 10^{-2}$
$r_1 \equiv a_1/a_0$ in $D^+ \to \eta e^+\nu_e = -5.3 \pm 2.7$ (S = 1.9)
$r_v \equiv V(0)/A_1(0)$ in $D^+ \to \omega e^+\nu_e = 1.24 \pm 0.11$
$r_2 \equiv A_2(0)/A_1(0)$ in $D^+ \to \omega e^+\nu_e = 1.06 \pm 0.16$
$r_v \equiv V(0)/A_1(0)$ in $D^+, D^0 \to \rho e^+\nu_e = 1.64 \pm 0.10$ (S = 1.2)
$r_2 \equiv A_2(0)/A_1(0)$ in $D^+, D^0 \to \rho e^+\nu_e = 0.84 \pm 0.06$
$r_v \equiv V(0)/A_1(0)$ in $\overline{K}^*(892)^0\ell^+\nu_\ell = 1.49 \pm 0.05$ (S = 2.1)
$r_2 \equiv A_2(0)/A_1(0)$ in $\overline{K}^*(892)^0\ell^+\nu_\ell = 0.802 \pm 0.021$
$r_3 \equiv A_3(0)/A_1(0)$ in $\overline{K}^*(892)^0\ell^+\nu_\ell = 0.0 \pm 0.4$
Γ_L/Γ_T in $\overline{K}^*(892)^0\ell^+\nu_\ell = 1.13 \pm 0.08$
Γ_+/Γ_- in $\overline{K}^*(892)^0\ell^+\nu_\ell = 0.22 \pm 0.06$ (S = 1.6)

Most decay modes (other than the semileptonic modes) that involve a neutral K meson are now given as K_S^0 modes, not as $\overline{K}^0$ modes. Nearly always it is a K_S^0 that is measured, and interference between Cabibbo-allowed and doubly Cabibbo-suppressed modes can invalidate the assumption that $2\Gamma(K_S^0) = \Gamma(\overline{K}^0)$.

D^+ DECAY MODES	Fraction (Γ_i/Γ)	Scale factor/ Confidence level	p (MeV/c)
Inclusive modes			
e^+ semileptonic	(16.07 ± 0.30) %		–
μ^+ anything	(17.6 ± 3.2) %		–
K^- anything	(25.7 ± 1.4) %		–
$\overline{K}^0$ anything + K^0 anything	(61 ± 5) %		–
K^+ anything	(5.9 ± 0.8) %		–
$K^*(892)^-$ anything	(6 ± 5) %		–
$\overline{K}^*(892)^0$ anything	(23 ± 5) %		–
$K^*(892)^0$ anything	< 6.6 %	CL=90%	–
η anything	(6.3 ± 0.7) %		–
η' anything	(1.04 ± 0.18) %		–
ϕ anything	(1.12 ± 0.04) %		–
Leptonic and semileptonic modes			
$e^+\nu_e$	$< 8.8 \times 10^{-6}$	CL=90%	935
$\gamma e^+\nu_e$	$< 3.0 \times 10^{-5}$	CL=90%	935
$\mu^+\nu_\mu$	$(3.74 \pm 0.17) \times 10^{-4}$		932
$\tau^+\nu_\tau$	$(1.20 \pm 0.27) \times 10^{-3}$		90
$\overline{K}^0 e^+\nu_e$	(8.72 ± 0.09) %		869
$\overline{K}^0\mu^+\nu_\mu$	(8.76 ± 0.19) %		865
$K^-\pi^+e^+\nu_e$	(4.02 ± 0.18) %	S=3.2	864
$\overline{K}^*(892)^0 e^+\nu_e$, $\overline{K}^*(892)^0 \to K^-\pi^+$	(3.77 ± 0.17) %		722
$(K^-\pi^+)_{[0.8-1.0]\text{GeV}} e^+\nu_e$	(3.39 ± 0.09) %		864
$(K^-\pi^+)_{S-wave} e^+\nu_e$	$(2.28 \pm 0.11) \times 10^{-3}$		–

Downloaded from https://academic.oup.com/ptep/article/2022/8/083C01/6651666 by KIT Library user on 27 September 2022

$\overline{K}^*(1410)^0 e^+ \nu_e$, $\overline{K}^*(1410)^0 \to K^- \pi^+$		$< 6 \times 10^{-3}$	CL=90%	–
$\overline{K}_2^*(1430)^0 e^+ \nu_e$, $\overline{K}_2^*(1430)^0 \to K^- \pi^+$		$< 5 \times 10^{-4}$	CL=90%	–
$K^- \pi^+ e^+ \nu_e$ nonresonant		$< 7 \times 10^{-3}$	CL=90%	864
$\overline{K}^*(892)^0 e^+ \nu_e$		(5.40 ± 0.10) %	S=1.1	722
$K^- \pi^+ \mu^+ \nu_\mu$		(3.65 ± 0.34) %		851
$\overline{K}^*(892)^0 \mu^+ \nu_\mu$, $\overline{K}^*(892)^0 \to K^- \pi^+$		(3.52 ± 0.10) %		717
$K^- \pi^+ \mu^+ \nu_\mu$ nonresonant		$(1.9 \pm 0.5) \times 10^{-3}$		851
$\overline{K}^*(892)^0 \mu^+ \nu_\mu$		(5.27 ± 0.15) %		717
$K^- \pi^+ \pi^0 \mu^+ \nu_\mu$		$< 1.5 \times 10^{-3}$	CL=90%	825
$\overline{K}_1(1270)^0 e^+ \nu_e$, $\overline{K}_1^0 \to K^- \pi^+ \pi^0$		$(1.06 \pm 0.15) \times 10^{-3}$		–
$\overline{K}_0^*(1430)^0 \mu^+ \nu_\mu$		$< 2.3 \times 10^{-4}$	CL=90%	380
$\overline{K}^*(1680)^0 \mu^+ \nu_\mu$		$< 1.5 \times 10^{-3}$	CL=90%	105
$\pi^0 e^+ \nu_e$		$(3.72 \pm 0.17) \times 10^{-3}$	S=2.0	930
$\pi^0 \mu^+ \nu_\mu$		$(3.50 \pm 0.15) \times 10^{-3}$		927
$\eta e^+ \nu_e$		$(1.11 \pm 0.07) \times 10^{-3}$		855
$\eta \mu^+ \nu_\mu$		$(1.04 \pm 0.11) \times 10^{-3}$		851
$\pi^- \pi^+ e^+ \nu_e$		$(2.45 \pm 0.10) \times 10^{-3}$		924
$f_0(500)^0 e^+ \nu_e$, $f_0(500)^0 \to \pi^+ \pi^-$		$(6.3 \pm 0.5) \times 10^{-4}$		–
$\rho^0 e^+ \nu_e$		$(2.18 {}^{+0.17}_{-0.25}) \times 10^{-3}$		774
$\rho^0 \mu^+ \nu_\mu$		$(2.4 \pm 0.4) \times 10^{-3}$		770
$\omega e^+ \nu_e$		$(1.69 \pm 0.11) \times 10^{-3}$		771
$\omega \mu^+ \nu_\mu$		$(1.77 \pm 0.21) \times 10^{-3}$		767
$\eta'(958) e^+ \nu_e$		$(2.0 \pm 0.4) \times 10^{-4}$		690
$a(980)^0 e^+ \nu_e$, $a(980)^0 \to \eta \pi^0$		$(1.7 {}^{+0.8}_{-0.7}) \times 10^{-4}$		–
$b_1(1235)^0 e^+ \nu_e$, $b_1^0 \to \omega \pi^0$		$< 1.75 \times 10^{-4}$	CL=90%	–
$\phi e^+ \nu_e$		$< 1.3 \times 10^{-5}$	CL=90%	657
$D^0 e^+ \nu_e$		$< 1.0 \times 10^{-4}$	CL=90%	5

Hadronic modes with a $\overline{K}$ or $\overline{K}K\overline{K}$

$K_S^0 \pi^+$		(1.562 ± 0.031) %	S=1.7	863
$K_L^0 \pi^+$		(1.46 ± 0.05) %		863
$K^- 2\pi^+$	[jj]	(9.38 ± 0.16) %	S=1.6	846
$(K^- \pi^+)_{S-\text{wave}} \pi^+$		(7.52 ± 0.17) %		846
$\overline{K}_0^*(1430)^0 \pi^+$, $\overline{K}_0^*(1430)^0 \to K^- \pi^+$	[kk]	(1.25 ± 0.06) %		382
$\overline{K}^*(892)^0 \pi^+$, $\overline{K}^*(892)^0 \to K^- \pi^+$		(1.04 ± 0.12) %		714
$\overline{K}^*(1410)^0 \pi^+$, $\overline{K}^{*0} \to K^- \pi^+$		not seen		381
$\overline{K}_2^*(1430)^0 \pi^+$, $\overline{K}_2^*(1430)^0 \to K^- \pi^+$	[kk]	$(2.3 \pm 0.7) \times 10^{-4}$		371
$\overline{K}^*(1680)^0 \pi^+$, $\overline{K}^*(1680)^0 \to K^- \pi^+$	[kk]	$(2.2 \pm 1.1) \times 10^{-4}$		58
$K^- (2\pi^+)_{I=2}$		(1.45 ± 0.26) %		–
$K_S^0 \pi^+ \pi^0$	[jj]	(7.36 ± 0.21) %		845
$K_S^0 \rho^+$		$(6.14 {}^{+0.60}_{-0.35})$ %		677
$K_S^0 \rho(1450)^+$, $\rho^+ \to \pi^+ \pi^0$		$(1.5 {}^{+1.2}_{-1.4}) \times 10^{-3}$		–
$\overline{K}^*(892)^0 \pi^+$, $\overline{K}^*(892)^0 \to K_S^0 \pi^0$		$(2.64 \pm 0.32) \times 10^{-3}$		714
$\overline{K}_0^*(1430)^0 \pi^+$, $\overline{K}_0^{*0} \to K_S^0 \pi^0$		$(2.7 \pm 0.9) \times 10^{-3}$		–
$\overline{K}_0^*(1680)^0 \pi^+$, $\overline{K}_0^{*0} \to K_S^0 \pi^0$		$(10 {}^{+7}_{-10}) \times 10^{-4}$		–
$\overline{\kappa}^0 \pi^+$, $\overline{\kappa}^0 \to K_S^0 \pi^0$		$(6 {}^{+5}_{-4}) \times 10^{-3}$		–
$K_S^0 \pi^+ \pi^0$ nonresonant		$(3 \pm 4) \times 10^{-3}$		845
$K_S^0 \pi^+ \pi^0$ nonresonant and $\overline{\kappa}^0 \pi^+$		$(1.37 {}^{+0.21}_{-0.40})$ %		–
$(K_S^0 \pi^0)_{S-\text{wave}} \pi^+$		$(1.27 {}^{+0.27}_{-0.33})$ %		845
$K_S^0 \pi^+ \eta$		(1.31 ± 0.05) %		722
$K_S^0 \pi^+ \eta'(958)$		$(1.90 \pm 0.21) \times 10^{-3}$		481
$K^- 2\pi^+ \pi^0$	[ll]	(6.25 ± 0.18) %		817
$K_S^0 2\pi^+ \pi^-$	[ll]	(3.10 ± 0.09) %		814
$K^- 2\pi^+ \eta$		$(1.35 \pm 0.12) \times 10^{-3}$		657
$K_S^0 \pi^+ \pi^0 \eta$		$(1.22 \pm 0.25) \times 10^{-3}$		657
$K^- 3\pi^+ \pi^-$	[jj]	$(5.7 \pm 0.5) \times 10^{-3}$	S=1.1	772
$\overline{K}^*(892)^0 2\pi^+ \pi^-$, $\overline{K}^*(892)^0 \to K^- \pi^+$		$(1.2 \pm 0.4) \times 10^{-3}$		645
$\overline{K}^*(892)^0 \rho^0 \pi^+$, $\overline{K}^*(892)^0 \to K^- \pi^+$		$(2.3 \pm 0.4) \times 10^{-3}$		239
$\overline{K}^*(892)^0 a_1(1260)^+$	[nn]	$(9.3 \pm 1.9) \times 10^{-3}$		†
$K^- \rho^0 2\pi^+$		$(1.72 \pm 0.28) \times 10^{-3}$		524
$K^- 3\pi^+ \pi^-$ nonresonant		$(4.0 \pm 2.9) \times 10^{-4}$		772
$K^+ 2K_S^0$		$(2.54 \pm 0.13) \times 10^{-3}$		545
$K^+ K^- K_S^0 \pi^+$		$(2.4 \pm 0.5) \times 10^{-4}$		436

Pionic modes

$\pi^+ \pi^0$		$(1.247 \pm 0.033) \times 10^{-3}$		925
$2\pi^+ \pi^-$		$(3.27 \pm 0.18) \times 10^{-3}$		909
$\rho^0 \pi^+$		$(8.3 \pm 1.5) \times 10^{-4}$		767
$\pi^+ (\pi^+ \pi^-)_{S-\text{wave}}$		$(1.83 \pm 0.16) \times 10^{-3}$		909
$\sigma \pi^+$, $\sigma \to \pi^+ \pi^-$		$(1.38 \pm 0.12) \times 10^{-3}$		–
$f_0(980) \pi^+$, $f_0(980) \to \pi^+ \pi^-$		$(1.56 \pm 0.33) \times 10^{-4}$		669
$f_0(1370) \pi^+$, $f_0(1370) \to \pi^+ \pi^-$		$(8 \pm 4) \times 10^{-5}$		–
$f_2(1270) \pi^+$, $f_2(1270) \to \pi^+ \pi^-$		$(5.0 \pm 0.9) \times 10^{-4}$		485
$\rho(1450)^0 \pi^+$, $\rho(1450)^0 \to \pi^+ \pi^-$		$< 8 \times 10^{-5}$	CL=95%	338
$f_0(1500) \pi^+$, $f_0(1500) \to \pi^+ \pi^-$		$(1.1 \pm 0.4) \times 10^{-4}$		–
$f_0(1710) \pi^+$, $f_0(1710) \to \pi^+ \pi^-$		$< 5 \times 10^{-5}$	CL=95%	–
$f_0(1790) \pi^+$, $f_0(1790) \to \pi^+ \pi^-$		$< 7 \times 10^{-5}$	CL=95%	–
$(\pi^+ \pi^+)_{S-\text{wave}} \pi^-$		$< 1.2 \times 10^{-4}$	CL=95%	909
$2\pi^+ \pi^-$ nonresonant		$< 1.1 \times 10^{-4}$	CL=95%	909
$\pi^+ 2\pi^0$		$(4.7 \pm 0.4) \times 10^{-3}$		910
$2\pi^+ \pi^- \pi^0$		(1.16 ± 0.08) %		883
$3\pi^+ 2\pi^-$		$(1.66 \pm 0.16) \times 10^{-3}$	S=1.1	845
$\eta \pi^+$		$(3.77 \pm 0.09) \times 10^{-3}$		848
$\eta \pi^+ \pi^0$		$(2.05 \pm 0.35) \times 10^{-3}$	S=2.2	831
$\eta 2\pi^+ \pi^-$		$(3.41 \pm 0.20) \times 10^{-3}$		798
$\eta \pi^+ 2\pi^0$		$(3.20 \pm 0.33) \times 10^{-3}$		801
$\eta \eta \pi^+$		$(2.96 \pm 0.26) \times 10^{-3}$		700
$\omega \pi^+$		$(2.8 \pm 0.6) \times 10^{-4}$		764
$\omega \pi^+ \pi^0$		$(3.9 \pm 0.9) \times 10^{-3}$		742
$\eta'(958) \pi^+$		$(4.97 \pm 0.19) \times 10^{-3}$		681
$\eta'(958) \pi^+ \pi^0$		$(1.6 \pm 0.5) \times 10^{-3}$		654

Hadronic modes with a $K\overline{K}$ pair

$K_S^0 K^+$		$(3.04 \pm 0.09) \times 10^{-3}$	S=2.2	793
$K_L^0 K^+$		$(3.21 \pm 0.16) \times 10^{-3}$		793
$K_S^0 K^+ \pi^0$		$(5.07 \pm 0.30) \times 10^{-3}$		744
$K^*(892)^+ K_S^0$		$(2.89 \pm 0.30) \times 10^{-3}$		612
$\overline{K}^*(892)^0 K^+$		$(5.2 \pm 1.4) \times 10^{-4}$		613
$K_L^0 K^+ \pi^0$		$(5.24 \pm 0.31) \times 10^{-3}$		744
$K^+ K^- \pi^+$	[jj]	$(9.68 \pm 0.18) \times 10^{-3}$		744
$K^+ \overline{K}^*(892)^0$, $\overline{K}^*(892)^0 \to K^- \pi^+$		$(2.49 {}^{+0.08}_{-0.13}) \times 10^{-3}$		613
$K^+ \overline{K}_0^*(1430)^0$, $\overline{K}_0^*(1430)^0 \to K^- \pi^+$		$(1.82 \pm 0.35) \times 10^{-3}$		–
$K^+ \overline{K}_2^*(1430)^0$, $\overline{K}_2^* \to K^- \pi^+$		$(1.6 {}^{+1.2}_{-0.8}) \times 10^{-4}$		–
$K^+ \overline{K}_0^*(700)$, $\overline{K}_0^* \to K^- \pi^+$		$(6.8 {}^{+3.5}_{-2.1}) \times 10^{-4}$		–
$a_0(1450)^0 \pi^+$, $a_0^0 \to K^+ K^-$		$(4.5 {}^{+7.0}_{-1.8}) \times 10^{-4}$		–
$\phi(1680) \pi^+$, $\phi \to K^+ K^-$		$(4.9 {}^{+4.0}_{-1.9}) \times 10^{-5}$		–
$\phi \pi^+$, $\phi \to K^+ K^-$		$(2.69 {}^{+0.07}_{-0.08}) \times 10^{-3}$		647
$\phi \pi^+$		$(5.70 \pm 0.14) \times 10^{-3}$		647
$K^+ K^- \pi^+ \pi^0$		$(6.62 \pm 0.32) \times 10^{-3}$		682
$K_S^0 K_S^0 \pi^+$		$(2.70 \pm 0.13) \times 10^{-3}$		741
$K_S^0 K_S^0 \pi^+ \pi^0$		$(1.34 \pm 0.21) \times 10^{-3}$		679
$K_S^0 K^+ \eta$		$(1.8 \pm 0.5) \times 10^{-4}$		516
$K^+ K_S^0 \pi^+ \pi^-$		$(1.89 \pm 0.13) \times 10^{-3}$		678
$K_S^0 K^+ \pi^0 \pi^0$		$(5.8 \pm 1.3) \times 10^{-4}$		683
$K_S^0 K^- 2\pi^+$		$(2.27 \pm 0.13) \times 10^{-3}$		678
$K^+ K^- 2\pi^+ \pi^-$		$(2.3 \pm 1.2) \times 10^{-4}$		601

Downloaded from https://academic.oup.com/ptep/article/2022/8/083C01/6651666 by KIT Library user on 27 September 2022

A few poorly measured branching fractions:

$\phi\pi^+\pi^0$	(2.3 ± 1.0) %			619
$\phi\rho^+$	< 1.5 %		CL=90%	260
$K^+K^-\pi^+\pi^0$ non-ϕ	$(1.5^{+0.7}_{-0.6})$ %			682

Doubly Cabibbo-suppressed modes

$K^+\pi^0$	$(2.08 \pm 0.21) \times 10^{-4}$	S=1.4		864
$K^+\eta$	$(1.25 \pm 0.16) \times 10^{-4}$	S=1.1		776
$K^+\eta'(958)$	$(1.85 \pm 0.20) \times 10^{-4}$			571
$K^+\pi^+\pi^-$	$(4.91 \pm 0.09) \times 10^{-4}$			846
$K^+\rho^0$	$(1.9 \pm 0.5) \times 10^{-4}$			679
$K^*(892)^0\pi^+$, $K^*(892)^0 \to K^+\pi^-$	$(2.3 \pm 0.4) \times 10^{-4}$			714
$K^+f_0(980)$, $f_0(980) \to \pi^+\pi^-$	$(4.4 \pm 2.6) \times 10^{-5}$			–
$K_2^*(1430)^0\pi^+$, $K_2^*(1430)^0 \to K^+\pi^-$	$(3.9 \pm 2.7) \times 10^{-5}$			–
$K^+\pi^+\pi^-$ nonresonant	not seen			846
$K^+\pi^+\pi^-\pi^0$	$(1.21 \pm 0.09) \times 10^{-3}$			817
$K^+\pi^+\pi^-\pi^0$ nonresonant	$(1.10 \pm 0.07) \times 10^{-3}$			817
$K^+\omega$	$(5.7^{+2.5}_{-2.1}) \times 10^{-5}$			675
$2K^+K^-$	$(6.14 \pm 0.11) \times 10^{-5}$			550
$\phi(1020)^0K^+$	$< 2.1 \times 10^{-5}$		CL=90%	–
$K^+\phi(1020)$, $\phi \to K^+K^-$	$(4.4 \pm 0.6) \times 10^{-6}$			–
$K^+(K^+K^-)_{S-wave}$	$(5.77 \pm 0.12) \times 10^{-5}$			550

$\Delta C = 1$ weak neutral current ($C1$) modes, or Lepton Family number (LF), or Lepton number (L), or Baryon number (B) violating modes

$\pi^+e^+e^-$	$C1$	$< 1.1 \times 10^{-6}$	CL=90%		930
$\pi^+\pi^0e^+e^-$		$< 1.4 \times 10^{-5}$	CL=90%		925
$\pi^+\phi$, $\phi \to e^+e^-$		$[oo]$ $(1.7^{+1.4}_{-0.9}) \times 10^{-6}$			–
$\pi^+\mu^+\mu^-$	$C1$	$< 6.7 \times 10^{-8}$	CL=90%		918
$\pi^+\phi$, $\phi \to \mu^+\mu^-$		$[oo]$ $(1.8 \pm 0.8) \times 10^{-6}$			–
$\rho^+\mu^+\mu^-$	$C1$	$< 5.6 \times 10^{-4}$	CL=90%		757
$K^+e^+e^-$		$[pp]$ $< 8.5 \times 10^{-7}$	CL=90%		870
$K^+\pi^0e^+e^-$		$< 1.5 \times 10^{-5}$	CL=90%		864
$K^0_S\pi^+e^+e^-$		$< 2.6 \times 10^{-5}$	CL=90%		–
$K^0_SK^+e^+e^-$		$< 1.1 \times 10^{-5}$	CL=90%		792
$K^+\mu^+\mu^-$		$[pp]$ $< 5.4 \times 10^{-8}$	CL=90%		856
$\pi^+e^+\mu^-$	LF	$< 2.1 \times 10^{-7}$	CL=90%		927
$\pi^+e^-\mu^+$	LF	$< 2.2 \times 10^{-7}$	CL=90%		927
$K^+e^+\mu^-$	LF	$< 7.5 \times 10^{-8}$	CL=90%		866
$K^+e^-\mu^+$	LF	$< 1.0 \times 10^{-7}$	CL=90%		866
π^-2e^+	L	$< 5.3 \times 10^{-7}$	CL=90%		930
$\pi^-2\mu^+$	L	$< 1.4 \times 10^{-8}$	CL=90%		918
$\pi^-e^+\mu^+$	L	$< 1.3 \times 10^{-7}$	CL=90%		927
$\rho^-2\mu^+$	L	$< 5.6 \times 10^{-4}$	CL=90%		757
K^-2e^+	L	$< 9 \times 10^{-7}$	CL=90%		870
$K^0_S\pi^-2e^+$		$< 3.3 \times 10^{-6}$	CL=90%		863
$K^-\pi^02e^+$		$< 8.5 \times 10^{-6}$	CL=90%		864
$K^-2\mu^+$	L	$< 1.0 \times 10^{-5}$	CL=90%		856
$K^-e^+\mu^+$	L	$< 1.9 \times 10^{-6}$	CL=90%		866
$K^*(892)^-2\mu^+$	L	$< 8.5 \times 10^{-4}$	CL=90%		703
Λe^+	L,B	$< 1.1 \times 10^{-6}$	CL=90%		602
$\overline{\Lambda}e^+$	L,B	$< 6.5 \times 10^{-7}$	CL=90%		602
Σ^0e^+	L,B	$< 1.7 \times 10^{-6}$	CL=90%		554
$\overline{\Sigma}^0e^+$	L,B	$< 1.3 \times 10^{-6}$	CL=90%		554

D^0

$I(J^P) = \frac{1}{2}(0^-)$

Mass $m = 1864.84 \pm 0.05$ MeV
$m_{D^\pm} - m_{D^0} = 4.822 \pm 0.015$ MeV
Mean life $\tau = (410.3 \pm 1.0) \times 10^{-15}$ s
$c\tau = 123.01\ \mu$m

Mixing and related parameters

$|m_{D^0_1} - m_{D^0_2}| = (0.997 \pm 0.116) \times 10^{10}\ \hbar\ \mathrm{s}^{-1}$
$(\Gamma_{D^0_1} - \Gamma_{D^0_2})/\Gamma = 2y = (1.23 \pm 0.11) \times 10^{-2}$
$|q/p| = 0.995 \pm 0.016$
$A_\Gamma = (0.089 \pm 0.113) \times 10^{-3}$
$\phi^{K^0_S\pi\pi} = 0.02^{+0.04}_{-0.05}$
$K^+\pi^-$ relative strong phase: $\cos\delta = 0.97 \pm 0.11$
$K^-\pi^+\pi^0$ coherence factor $R_{K\pi\pi^0} = 0.792 \pm 0.033$
$K^-\pi^+\pi^0$ average relative strong phase $\delta^{K\pi\pi^0} = (198 \pm 10)^\circ$
$K^-\pi^-2\pi^+$ coherence factor $R_{K3\pi} = 0.52^{+0.10}_{-0.09}$
$K^-\pi^-2\pi^+$ average relative strong phase $\delta^{K3\pi} = (149^{+26}_{-16})^\circ$ (S = 1.4)
$D^0 \to K^-\pi^-2\pi^+$, $R_{K3\pi}$ (y $\cos\delta^{K3\pi}$ − x $\sin\delta^{K3\pi}$) $= (-3.0 \pm 0.7) \times 10^{-3}$ TeV^{-1}
$K^0_SK^+\pi^-$ coherence factor $R_{K^0_SK\pi} = 0.70 \pm 0.08$
$K^0_SK^+\pi^-$ average relative strong phase $\delta^{K^0_SK\pi} = (0 \pm 16)^\circ$
K^*K coherence factor $R_{K^*K} = 0.94 \pm 0.12$
K^*K average relative strong phase $\delta^{K^*K} = (-17 \pm 18)^\circ$

***CP*-violation decay-rate asymmetries (labeled by the D^0 decay)**

$A_{CP}(K^+K^-) = (-0.07 \pm 0.11)\%$
$A_{CP}(2K^0_S) = (-1.9 \pm 1.1)\%$ (S = 1.1)
$A_{CP}(\pi^+\pi^-) = (0.13 \pm 0.14)\%$
$A_{CP}(\pi^0\pi^0) = (0.0 \pm 0.6)\%$
$A_{CP}(\rho\gamma) = (6 \pm 15) \times 10^{-2}$
$A_{CP}(\phi\gamma) = (-9 \pm 7) \times 10^{-2}$
$A_{CP}(\overline{K}^*(892)^0\gamma) = (-0.3 \pm 2.0) \times 10^{-2}$
$A_{CP}(\pi^+\pi^-\pi^0) = (0.3 \pm 0.4)\%$
$A_{CP}(\eta\pi^+\pi^-)$ in $D^0, \overline{D}^0 \to \eta\pi^+\pi^- = (0.9 \pm 1.3) \times 10^{-2}$
$A_{CP}(\rho(770)^+\pi^- \to \pi^+\pi^-\pi^0) = (1.2 \pm 0.9)\%$ [qq]
$A_{CP}(\rho(770)^0\pi^0 \to \pi^+\pi^-\pi^0) = (-3.1 \pm 3.0)\%$ [qq]
$A_{CP}(\rho(770)^-\pi^+ \to \pi^+\pi^-\pi^0) = (-1.0 \pm 1.7)\%$ [qq]
$A_{CP}(\rho(1450)^+\pi^- \to \pi^+\pi^-\pi^0) = (0 \pm 70)\%$ [qq]
$A_{CP}(\rho(1450)^0\pi^0 \to \pi^+\pi^-\pi^0) = (-20 \pm 40)\%$ [qq]
$A_{CP}(\rho(1450)^-\pi^+ \to \pi^+\pi^-\pi^0) = (6 \pm 9)\%$ [qq]
$A_{CP}(\rho(1700)^+\pi^- \to \pi^+\pi^-\pi^0) = (-5 \pm 14)\%$ [qq]
$A_{CP}(\rho(1700)^0\pi^0 \to \pi^+\pi^-\pi^0) = (13 \pm 9)\%$ [qq]
$A_{CP}(\rho(1700)^-\pi^+ \to \pi^+\pi^-\pi^0) = (8 \pm 11)\%$ [qq]
$A_{CP}(f_0(980)\pi^0 \to \pi^+\pi^-\pi^0) = (0 \pm 35)\%$ [qq]
$A_{CP}(f_0(1370)\pi^0 \to \pi^+\pi^-\pi^0) = (25 \pm 18)\%$ [qq]
$A_{CP}(f_0(1500)\pi^0 \to \pi^+\pi^-\pi^0) = (0 \pm 18)\%$ [qq]
$A_{CP}(f_0(1710)\pi^0 \to \pi^+\pi^-\pi^0) = (0 \pm 24)\%$ [qq]
$A_{CP}(f_2(1270)\pi^0 \to \pi^+\pi^-\pi^0) = (-4 \pm 6)\%$ [qq]
$A_{CP}(\sigma(400)\pi^0 \to \pi^+\pi^-\pi^0) = (6 \pm 8)\%$ [qq]
$A_{CP}(\text{nonresonant } \pi^+\pi^-\pi^0) = (-13 \pm 23)\%$ [qq]
$A_{CP}(a_1(1260)^+\pi^- \to 2\pi^+2\pi^-) = (5 \pm 6)\%$
$A_{CP}(a_1(1260)^-\pi^+ \to 2\pi^+2\pi^-) = (14 \pm 18)\%$
$A_{CP}(\pi(1300)^+\pi^- \to 2\pi^+2\pi^-) = (-2 \pm 15)\%$
$A_{CP}(\pi(1300)^-\pi^+ \to 2\pi^+2\pi^-) = (-6 \pm 30)\%$
$A_{CP}(a_1(1640)^+\pi^- \to 2\pi^+2\pi^-) = (9 \pm 26)\%$
$A_{CP}(\pi_2(1670)^+\pi^- \to 2\pi^+2\pi^-) = (7 \pm 18)\%$
$A_{CP}(\sigma f_0(1370) \to 2\pi^+2\pi^-) = (-15 \pm 19)\%$
$A_{CP}(\sigma\rho(770)^0 \to 2\pi^+2\pi^-) = (3 \pm 27)\%$
$A_{CP}(2\rho(770)^0 \to 2\pi^+2\pi^-) = (-6 \pm 6)\%$
$A_{CP}(2f_2(1270) \to 2\pi^+2\pi^-) = (-28 \pm 24)\%$
$A_{CP}(\pi^+\pi^-\pi^0\eta)$ in $D^0, \overline{D}^0 \to \pi^+\pi^-\pi^0\eta = (-6 \pm 6) \times 10^{-2}$
$A_{CP}(K^+K^-\pi^0) = (-1.0 \pm 1.7)\%$
$A_{CP}(K^*(892)^+K^- \to K^+K^-\pi^0) = (-0.9 \pm 1.3)\%$ [qq]
$A_{CP}(K^*(1410)^+K^- \to K^+K^-\pi^0) = (-21 \pm 24)\%$ [qq]
$A_{CP}((K^+\pi^0)_{S-wave}K^- \to K^+K^-\pi^0) = (7 \pm 15)\%$ [qq]
$A_{CP}(\phi(1020)\pi^0 \to K^+K^-\pi^0) = (1.1 \pm 2.2)\%$ [qq]
$A_{CP}(f_0(980)\pi^0 \to K^+K^-\pi^0) = (-3 \pm 19)\%$ [qq]
$A_{CP}(a_0(980)^0\pi^0 \to K^+K^-\pi^0) = (-5 \pm 16)\%$ [qq]
$A_{CP}(f'_2(1525)\pi^0 \to K^+K^-\pi^0) = (0 \pm 160)\%$ [qq]
$A_{CP}(K^*(892)^-K^+ \to K^+K^-\pi^0) = (-5 \pm 4)\%$ [qq]
$A_{CP}(K^*(1410)^-K^+ \to K^+K^-\pi^0) = (-17 \pm 29)\%$ [qq]
$A_{CP}((K^-\pi^0)_{S-wave}K^+ \to K^+K^-\pi^0) = (-10 \pm 40)\%$ [qq]
$A_{CP}(K^+K^-\eta)$ in $D^0, \overline{D}^0 \to K^+K^-\eta = (-1.4 \pm 3.5) \times 10^{-2}$
$A_{CP}(\phi(1020)\eta \to K^+K^-\eta)$ in $D^0, \overline{D}^0 \to \phi(1020)\eta = (-2 \pm 4) \times 10^{-2}$
$A_{CP}(K^0_S\pi^0) = (-0.20 \pm 0.17)\%$
$A_{CP}(K^0_S\eta) = (0.5 \pm 0.5)\%$
$A_{CP}(K^0_S\eta') = (1.0 \pm 0.7)\%$
$A_{CP}(K^0_S\phi) = (-3 \pm 9)\%$
$A_{CP}(K^-\pi^+) = (0.2 \pm 0.5)\%$
$A_{CP}(K^+\pi^-) = (-0.9 \pm 1.4)\%$
$A_{CP}(D_{CP(\pm1)} \to K^\mp\pi^\pm) = (12.7 \pm 1.5)\%$
$A_{CP}(K^-\pi^+\pi^0) = (0.1 \pm 0.5)\%$
$A_{CP}(K^+\pi^-\pi^0) = (0 \pm 5)\%$
$A_{CP}(K^0_S\pi^+\pi^-) = (-0.1 \pm 0.8)\%$
$A_{CP}(K^\mp\pi^\pm\eta)$ in $D^0, \overline{D}^0 \to K^\mp\pi^\pm\eta = (-1.9 \pm 1.6) \times 10^{-2}$
$A_{CP}(K^0_S\pi^0\eta)$ in $D^0, \overline{D}^0 \to K^0_S\pi^0\eta = (-3.9 \pm 3.3) \times 10^{-2}$

Downloaded from https://academic.oup.com/ptep/article/2022/8/083C01/6651666 by KIT Library user on 27 September 2022

$A_{CP}(K^{\mp}\pi^{\pm}\pi^0\eta)$ in $D^0, \overline{D}^0 \to K^{\mp}\pi^{\pm}\pi^0\eta = (-8 \pm 5) \times 10^{-2}$
$A_{CP}(K^*(892)^-\pi^+ \to K^0_S\pi^+\pi^-) = (0.4 \pm 0.5)\%$
$A_{CP}(K^*(892)^+\pi^- \to K^0_S\pi^+\pi^-) = (1 \pm 6)\%$
$A_{CP}(\overline{K}^0\rho^0 \to K^0_S\pi^+\pi^-) = (-0.1 \pm 0.5)\%$
$A_{CP}(\overline{K}^0\omega \to K^0_S\pi^+\pi^-) = (-13 \pm 7)\%$
$A_{CP}(\overline{K}^0 f_0(980) \to K^0_S\pi^+\pi^-) = (-0.4 \pm 2.7)\%$
$A_{CP}(\overline{K}^0 f_2(1270) \to K^0_S\pi^+\pi^-) = (-4 \pm 5)\%$
$A_{CP}(\overline{K}^0 f_0(1370) \to K^0_S\pi^+\pi^-) = (-1 \pm 9)\%$
$A_{CP}(\overline{K}^0\rho^0(1450) \to K^0_S\pi^+\pi^-) = (-4 \pm 10)\%$
$A_{CP}(\overline{K}^0 f_0(600) \to K^0_S\pi^+\pi^-) = (-3 \pm 5)\%$
$A_{CP}(K^*(1410)^-\pi^+ \to K^0_S\pi^+\pi^-) = (-2 \pm 9)\%$
$A_{CP}(K^*_0(1430)^-\pi^+ \to K^0_S\pi^+\pi^-) = (4 \pm 4)\%$
$A_{CP}(K^*_0(1430)^+\pi^- \to K^0_S\pi^+\pi^-) = (12 \pm 15)\%$
$A_{CP}(K^*_2(1430)^-\pi^+ \to K^0_S\pi^+\pi^-) = (3 \pm 6)\%$
$A_{CP}(K^*_2(1430)^+\pi^- \to K^0_S\pi^+\pi^-) = (-10 \pm 32)\%$
$A_{CP}(K^-\pi^+\pi^+\pi^-) = (0.2 \pm 0.5)\%$
$A_{CP}(K^+\pi^-\pi^+\pi^-) = (-2 \pm 4)\%$
$A_{CP}(K^+K^-\pi^+\pi^-) = (1.3 \pm 1.7)\%$
$A_{CP}(K^*_1(1270)^+K^- \to K^+K^-\pi^+\pi^-) = (-2.3 \pm 1.7)\%$
$A_{CP}(K^*_1(1270)^+K^- \to K^{*0}\pi^+K^-) = (-1 \pm 10)\%$
$A_{CP}(K^*_1(1270)^-K^+ \to \overline{K}^{*0}\pi^-K^+) = (-10 \pm 32)\%$
$A_{CP}(K^*_1(1270)^-K^+ \to K^+K^-\pi^+\pi^-) = (1.7 \pm 3.5)\%$
$A_{CP}(K^*_1(1270)^+K^- \to \rho^0K^+K^-) = (-7 \pm 17)\%$
$A_{CP}(K^*_1(1270)^-K^+ \to \rho^0K^-K^+) = (10 \pm 13)\%$
$A_{CP}(K_1(1400)^+K^- \to K^+K^-\pi^+\pi^-) = (-4.4 \pm 2.1)\%$
$A_{CP}(K^*(1410)^+K^- \to K^{*0}\pi^+K^-) = (-20 \pm 17)\%$
$A_{CP}(K^*(1410)^-K^+ \to \overline{K}^{*0}\pi^-K^+) = (-1 \pm 14)\%$
$A_{CP}(K^*(1680)^+K^- \to K^+K^-\pi^+\pi^-) = (-17 \pm 29)\%$
$A_{CP}(K^{*0}\overline{K}^{*0})$ in $D^0, \overline{D}^0 \to K^{*0}\overline{K}^{*0} = (-5 \pm 14)\%$
$A_{CP}(K^{*0}\overline{K}^{*0}$ S-wave$) = (-3.9 \pm 2.2)\%$
$A_{CP}(\phi\rho^0)$ in $D^0, \overline{D}^0 \to \phi\rho^0 = (1 \pm 9)\%$
$A_{CP}(\phi\rho^0$ S-wave$) = (-3 \pm 5)\%$
$A_{CP}(\phi\rho^0$ D-wave$) = (-37 \pm 19)\%$
$A_{CP}(\phi(\pi^+\pi^-)_{S-wave}) = (6 \pm 6)\%$
$A_{CP}(K^*(892)^0(K^-\pi^+)_{S-wave}) = (-10 \pm 40)\%$
$A_{CP}(K^+K^-\pi^+\pi^-$ non-resonant$) = (8 \pm 20)\%$
$A_{CP}((K^-\pi^+)_{P-wave}(K^+\pi^-)_{S-wave}) = (3 \pm 11)\%$
$A_{CP}(K^+K^-\mu^+\mu^-)$ in $D^0, \overline{D}^0 \to K^+K^-\mu^+\mu^- = (0 \pm 11)\%$
$A_{CP}(\pi^+\pi^-\mu^+\mu^-)$ in $D^0, \overline{D}^0 \to \pi^+\pi^-\mu^+\mu^- = (5 \pm 4)\%$

CP-even fractions (labeled by the D^0 decay)

CP-even fraction in $D^0 \to \pi^+\pi^-\pi^0$ decays $= (97.3 \pm 1.7)\%$
CP-even fraction in $D^0 \to K^+K^-\pi^0$ decays $= (73 \pm 6)\%$
CP-even fraction in $D^0 \to \pi^+\pi^-\pi^+\pi^-$ decays $= (76.9 \pm 2.3)\%$
CP-even fraction in $D^0 \to K^0_S\pi^+\pi^-\pi^0$ decays $= (23.8 \pm 1.7)\%$
CP-even fraction in $D^0 \to K^+K^-\pi^+\pi^-$ decays $= (75 \pm 4)\%$

CP-violation asymmetry difference

$\Delta A_{CP} = A_{CP}(K^+K^-) - A_{CP}(\pi^+\pi^-) = (-0.154 \pm 0.029)\%$

χ^2 tests of CP-violation (CPV) p-values

Local CPV in $D^0, \overline{D}^0 \to \pi^+\pi^-\pi^0 = 4.9\%$
Local CPV in $D^0, \overline{D}^0 \to \pi^+\pi^-\pi^+\pi^- = (0.6 \pm 0.2)\%$
Local CPV in $D^0, \overline{D}^0 \to K^0_S\pi^+\pi^- = 96\%$
Local CPV in $D^0, \overline{D}^0 \to K^+K^-\pi^0 = 16.6\%$
Local CPV in $D^0, \overline{D}^0 \to K^+K^-\pi^+\pi^- = 9.1\%$

T-violation decay-rate asymmetry

$A_T(K^+K^-\pi^+\pi^-) = (2.9 \pm 2.2) \times 10^{-3}$ [ii]
$A_{T\text{viol}}(K_S\pi^+\pi^-\pi^0)$ in $D^0, \overline{D}^0 \to K_S\pi^+\pi^-\pi^0 = (-0.3^{+1.4}_{-1.6}) \times 10^{-3}$

CPT-violation decay-rate asymmetry

$A_{CPT}(K^{\mp}\pi^{\pm}) = 0.008 \pm 0.008$

Form factors

$r_V \equiv V(0)/A_1(0)$ in $D^0 \to K^*(892)^-\ell^+\nu_\ell = 1.46 \pm 0.07$
$r_2 \equiv A_2(0)/A_1(0)$ in $D^0 \to K^*(892)^-\ell^+\nu_\ell = 0.68 \pm 0.06$
$f_+(0)$ in $D^0 \to K^-\ell^+\nu_\ell = 0.736 \pm 0.004$
$f_+(0)|V_{cs}|$ in $D^0 \to K^-\ell^+\nu_\ell = 0.7166 \pm 0.0030$
$r_1 \equiv a_1/a_0$ in $D^0 \to K^-\ell^+\nu_\ell = -2.40 \pm 0.16$
$r_2 \equiv a_2/a_0$ in $D^0 \to K^-\ell^+\nu_\ell = 5 \pm 4$
$f_+(0)$ in $D^0 \to \pi^-\ell^+\nu_\ell = 0.637 \pm 0.009$
$f_+(0)|V_{cd}|$ in $D^0 \to \pi^-\ell^+\nu_\ell = 0.1436 \pm 0.0026$ (S = 1.5)
$r_1 \equiv a_1/a_0$ in $D^0 \to \pi^-\ell^+\nu_\ell = -1.97 \pm 0.28$ (S = 1.4)
$r_2 \equiv a_1/a_0$ in $D^0 \to \pi^-\ell^+\nu_\ell = -0.2 \pm 2.2$ (S = 1.7)

Most decay modes (other than the semileptonic modes) that involve a neutral K meson are now given as K^0_S modes, not as $\overline{K}^0$ modes. Nearly always it is a K^0_S that is measured, and interference between Cabibbo-allowed and doubly Cabibbo-suppressed modes can invalidate the assumption that $2\Gamma(K^0_S) = \Gamma(\overline{K}^0)$.

D^0 DECAY MODES		Fraction (Γ_i/Γ)	Scale factor/ Confidence level	p (MeV/c)
Topological modes				
0-prongs	[rr]	(15 ± 6) %		–
2-prongs		(71 ± 6) %		–
4-prongs	[ss]	(14.6 ± 0.5) %		–
6-prongs	[tt]	$(6.5 \pm 1.3) \times 10^{-4}$		–
Inclusive modes				
e^+ anything	[uu]	(6.49 ± 0.11) %		–
μ^+ anything		(6.8 ± 0.6) %		–
K^- anything		(54.7 ± 2.8) %	S=1.3	–
$\overline{K}^0$ anything + K^0 anything		(47 ± 4) %		–
K^+ anything		(3.4 ± 0.4) %		–
$K^*(892)^-$ anything		(15 ± 9) %		–
$\overline{K}^*(892)^0$ anything		(9 ± 4) %		–
$K^*(892)^+$ anything		< 3.6 %	CL=90%	–
$K^*(892)^0$ anything		(2.8 ± 1.3) %		–
η anything		(9.5 ± 0.9) %		–
η' anything		(2.48 ± 0.27) %		–
ϕ anything		(1.08 ± 0.04) %		–
invisibles		$< 9.4 \times 10^{-5}$	CL=90%	–
Semileptonic modes				
$K^-e^+\nu_e$		(3.549 ± 0.026) %	S=1.2	867
$K^-\mu^+\nu_\mu$		(3.41 ± 0.04) %		864
$K^*(892)^-e^+\nu_e$		(2.15 ± 0.16) %		719
$K^*(892)^-\mu^+\nu_\mu$		(1.89 ± 0.24) %		714
$K^-\pi^0e^+\nu_e$		$(1.6 {}^{+1.3}_{-0.5})$ %		861
$\overline{K}^0\pi^-e^+\nu_e$		(1.44 ± 0.04) %		860
$(\overline{K}^0\pi^-)_{S-wave}e^+\nu_e$		$(7.9 \pm 1.7) \times 10^{-4}$		860
$K^-\pi^+\pi^-e^+\nu_e$		$(2.8 {}^{+1.4}_{-1.1}) \times 10^{-4}$		843
$K_1(1270)^-e^+\nu_e$		$(1.01 \pm 0.18) \times 10^{-3}$		511
$K^-\pi^+\pi^-\mu^+\nu_\mu$		$< 1.3 \times 10^{-3}$	CL=90%	821
$(\overline{K}^*(892)\pi)^-\mu^+\nu_\mu$		$< 1.5 \times 10^{-3}$	CL=90%	692
$\pi^-e^+\nu_e$		$(2.91 \pm 0.04) \times 10^{-3}$		927
$\pi^-\mu^+\nu_\mu$		$(2.67 \pm 0.12) \times 10^{-3}$	S=1.3	924
$\pi^-\pi^0e^+\nu_e$		$(1.45 \pm 0.07) \times 10^{-3}$		922
$\rho^-e^+\nu_e$		$(1.50 \pm 0.12) \times 10^{-3}$	S=1.9	771
$\rho^-\mu^+\nu_\mu$		$(1.35 \pm 0.13) \times 10^{-3}$		767
$a(980)^-e^+\nu_e$, $a^- \to \eta\pi^-$		$(1.33 {}^{+0.34}_{-0.30}) \times 10^{-4}$		–
$b_1(1235)^-e^+\nu_e$, $b_1^- \to \omega\pi^-$		$< 1.12 \times 10^{-4}$	CL=90%	–
Hadronic modes with one $\overline{K}$				
$K^-\pi^+$		(3.947 ± 0.030) %	S=1.2	861
$K^0_S\pi^0$		(1.240 ± 0.022) %		860
$K^0_L\pi^0$		$(10.0 \pm 0.7) \times 10^{-3}$		860
$K^0_S\pi^+\pi^-$	[jj]	(2.80 ± 0.18) %	S=1.1	842
$K^0_S\rho^0$		$(6.3 {}^{+0.6}_{-0.8}) \times 10^{-3}$		674
$K^0_S\omega$, $\omega \to \pi^+\pi^-$		$(2.0 \pm 0.6) \times 10^{-4}$		670
$K^0_S(\pi^+\pi^-)_{S-wave}$		$(3.3 \pm 0.8) \times 10^{-3}$		842
$K^0_S f_0(980)$, $f_0 \to \pi^+\pi^-$		$(1.20 {}^{+0.40}_{-0.23}) \times 10^{-3}$		549
$K^0_S f_0(1370)$, $f_0 \to \pi^+\pi^-$		$(2.8 {}^{+0.9}_{-1.3}) \times 10^{-3}$		†
$K^0_S f_2(1270)$, $f_2 \to \pi^+\pi^-$		$(9 {}^{+10}_{-6}) \times 10^{-5}$		262
$K^*(892)^-\pi^+$, $K^{*-} \to K^0_S\pi^-$		$(1.64 {}^{+0.14}_{-0.17})$ %		711
$K^*_0(1430)^-\pi^+$, $K^{*-}_0 \to K^0_S\pi^-$		$(2.67 {}^{+0.40}_{-0.33}) \times 10^{-3}$		378
$K^*_2(1430)^-\pi^+$, $K^{*-}_2 \to K^0_S\pi^-$		$(3.4 {}^{+1.9}_{-1.0}) \times 10^{-4}$		367
$K^*(1680)^-\pi^+$, $K^{*-} \to K^0_S\pi^-$		$(4.4 \pm 3.5) \times 10^{-4}$		46
$K^*(892)^+\pi^-$, $K^{*+} \to K^0_S\pi^+$	[vv]	$(1.13 {}^{+0.60}_{-0.34}) \times 10^{-4}$		711
$K^*_0(1430)^+\pi^-$, $K^{*+}_0 \to K^0_S\pi^+$	[vv]	$< 1.4 \times 10^{-5}$	CL=95%	–

Downloaded from https://academic.oup.com/ptep/article/2022/8/083C01/6651666 by KIT Library user on 27 September 2022

$K_2^*(1430)^+\pi^-$, $K_2^{*+} \to K_S^0\pi^+$	[vv]	$< 3.4 \times 10^{-5}$	CL=95%	–
$K_S^0\pi^+\pi^-$ nonresonant		$(2.5 {}^{+6.0}_{-1.6}) \times 10^{-4}$		842
$K^-\pi^+\pi^0$	[jj]	(14.4 ± 0.5) %	S=2.0	844
$K^-\rho^+$		(11.2 ± 0.7) %		675
$K^-\rho(1700)^+$, $\rho^+ \to \pi^+\pi^0$		$(8.2 \pm 1.8) \times 10^{-3}$		†
$K^*(892)^-\pi^+$, $K^*(892)^- \to K^-\pi^0$		$(2.31 {}^{+0.40}_{-0.20})$ %		711
$\overline{K}^*(892)^0\pi^0$, $\overline{K}^*(892)^0 \to K^-\pi^+$		(1.95 ± 0.24) %		711
$K_0^*(1430)^-\pi^+$, $K_0^{*-} \to K^-\pi^0$		$(4.8 \pm 2.2) \times 10^{-3}$		378
$\overline{K}_0^*(1430)^0\pi^0$, $\overline{K}_0^{*0} \to K^-\pi^+$		$(5.9 {}^{+5.0}_{-1.6}) \times 10^{-3}$		379
$K^*(1680)^-\pi^+$, $K^{*-} \to K^-\pi^0$		$(1.9 \pm 0.7) \times 10^{-3}$		46
$K^-\pi^+\pi^0$ nonresonant		$(1.15 {}^{+0.60}_{-0.20})$ %		844
$K_S^0 2\pi^0$		$(9.1 \pm 1.1) \times 10^{-3}$	S=2.2	843
$K_S^0(2\pi^0)_{S-wave}$		$(2.6 \pm 0.7) \times 10^{-3}$		–
$\overline{K}^*(892)^0\pi^0$, $\overline{K}^{*0} \to K_S^0\pi^0$		$(8.1 \pm 0.7) \times 10^{-3}$		711
$\overline{K}^*(1430)^0\pi^0$, $\overline{K}^{*0} \to K_S^0\pi^0$		$(4 \pm 23) \times 10^{-5}$		–
$\overline{K}^*(1680)^0\pi^0$, $\overline{K}^{*0} \to K_S^0\pi^0$		$(1.0 \pm 0.4) \times 10^{-3}$		–
$K_S^0 f_2(1270)$, $f_2 \to 2\pi^0$		$(2.3 \pm 1.1) \times 10^{-4}$		–
$2K_S^0$, one $K_S^0 \to 2\pi^0$		$(3.2 \pm 1.1) \times 10^{-4}$		–
$K^-2\pi^+\pi^-$	[jj]	(8.22 ± 0.14) %	S=1.1	813
$K^-\pi^+\rho^0$ total		(6.87 ± 0.31) %		609
$K^-\pi^+\rho^0$ 3-body		$(6.1 \pm 1.6) \times 10^{-3}$		609
$\overline{K}^*(892)^0\rho^0$, $\overline{K}^{*0} \to K^-\pi^+$		(1.01 ± 0.05) %		416
$\overline{K}^*(892)^0\rho^0$ transverse, $\overline{K}^{*0} \to K^-\pi^+$		(1.2 ± 0.4) %		417
$K^-a_1(1260)^+$, $a_1^+ \to \rho^0\pi^+$		(4.32 ± 0.32) %		327
$K_1(1270)^-\pi^+$, $K_1^- \to K^-\pi^+\pi^-$ total		$(3.9 \pm 0.4) \times 10^{-3}$		–
$K_1(1270)^-\pi^+$, $K_1^- \to \overline{K}^*(892)^0\pi^-$, $\overline{K}^{*0} \to K^-\pi^+$		$(6.6 \pm 2.3) \times 10^{-4}$		484
$K^-2\pi^+\pi^-$ nonresonant		(1.81 ± 0.07) %		813
$K_S^0\pi^+\pi^-\pi^0$	[xx]	(5.2 ± 0.6) %		813
$K_S^0\eta$, $\eta \to \pi^+\pi^-\pi^0$		$(1.17 \pm 0.03) \times 10^{-3}$		772
$K_S^0\omega$, $\omega \to \pi^+\pi^-\pi^0$		$(9.9 \pm 0.6) \times 10^{-3}$		670
$K^-\pi^+2\pi^0$		(8.86 ± 0.23) %		815
$K^-2\pi^+\pi^-\pi^0$		(4.3 ± 0.4) %		771
$\overline{K}^*(892)^0\pi^+\pi^-\pi^0$, $\overline{K}^{*0} \to K^-\pi^+$		(1.3 ± 0.6) %		643
$K^-\pi^+\omega$, $\omega \to \pi^+\pi^-\pi^0$		(2.8 ± 0.5) %		605
$\overline{K}^*(892)^0\omega$, $\overline{K}^{*0} \to K^-\pi^+$, $\omega \to \pi^+\pi^-\pi^0$		$(6.5 \pm 3.0) \times 10^{-3}$		410
$K_S^0\eta\pi^0$		(1.01 ± 0.05) %		721
$K_S^0 a_0(980)$, $a_0 \to \eta\pi^0$		(1.20 ± 0.28) %		–
$\overline{K}^*(892)^0\eta$, $\overline{K}^{*0} \to K_S^0\pi^0$		$(2.9 \pm 0.7) \times 10^{-3}$		–
$K^-\pi^+\eta$		(1.88 ± 0.05) %	S=1.4	721
$K^*(892)^0\eta$, $K^{*0} \to K^-\pi^+$		$(8.9 {}^{+0.8}_{-0.6}) \times 10^{-3}$		–
$a_0(980)^+K^-$, $a_0^+ \to \eta\pi^+$		$(7.4 {}^{+0.9}_{-0.7}) \times 10^{-3}$		–
$K_2^*(1980)^-\pi^+$, $K_2^{*-} \to K^-\eta$		$(2.2 {}^{+1.7}_{-1.9}) \times 10^{-4}$		–
$K^-\pi^+\pi^0\eta$		$(4.49 \pm 0.27) \times 10^{-3}$		656
$K_S^0\pi^+\pi^-\eta$		$(2.80 \pm 0.21) \times 10^{-3}$		651
$K_S^0 2\pi^0\eta$		$(1.76 \pm 0.26) \times 10^{-3}$		656
$K_S^0 2\pi^+2\pi^-$		$(2.66 \pm 0.30) \times 10^{-3}$		768
$K_S^0\rho^0\pi^+\pi^-$, no $K^*(892)^-$		$(1.1 \pm 0.7) \times 10^{-3}$		–
$K^*(892)^-2\pi^+\pi^-$, $K^*(892)^- \to K_S^0\pi^-$, no ρ^0		$(5 \pm 7) \times 10^{-4}$		642
$K^*(892)^-\rho^0\pi^+$, $K^*(892)^- \to K_S^0\pi^-$		$(1.6 \pm 0.6) \times 10^{-3}$		230
$K_S^0 2\pi^+2\pi^-$ nonresonant		$< 1.2 \times 10^{-3}$	CL=90%	768
$K^-3\pi^+2\pi^-$		$(2.2 \pm 0.6) \times 10^{-4}$		713

Fractions of some of the following modes with resonances have already appeared above as submodes of particular charged-particle modes. These nine modes below are all corrected for unseen decays of the resonances.

$K_S^0\eta$	$(5.09 \pm 0.13) \times 10^{-3}$		772
$K_S^0\omega$	(1.11 ± 0.06) %		670
$K_S^0\eta'(958)$	$(9.49 \pm 0.32) \times 10^{-3}$		565
$\overline{K}^*(892)^0\pi^+\pi^-\pi^0$	(1.9 ± 0.9) %		643
$\overline{K}^*(892)^0\eta$	(1.41 ± 0.12) %		583
$K^-\pi^+\omega$	(3.1 ± 0.6) %		605
$\overline{K}^*(892)^0\omega$	(1.1 ± 0.5) %		410
$K^-\pi^+\eta'(958)$	$(6.43 \pm 0.34) \times 10^{-3}$		479
$K_S^0\eta'(958)\pi^0$	$(2.52 \pm 0.27) \times 10^{-3}$		479
$\overline{K}^*(892)^0\eta'(958)$	$< 1.0 \times 10^{-3}$	CL=90%	119

Hadronic modes with three K's

$K_S^0K^+K^-$	$(4.42 \pm 0.32) \times 10^{-3}$		544
$K_S^0 a_0(980)^0$, $a_0^0 \to K^+K^-$	$(2.9 \pm 0.4) \times 10^{-3}$		–
$K^-a_0(980)^+$, $a_0^+ \to K^+K_S^0$	$(5.9 \pm 1.8) \times 10^{-4}$		–
$K^+a_0(980)^-$, $a_0^- \to K^-K_S^0$	$< 1.1 \times 10^{-4}$	CL=95%	–
$K_S^0 f_0(980)$, $f_0 \to K^+K^-$	$< 9 \times 10^{-5}$	CL=95%	–
$K_S^0\phi$, $\phi \to K^+K^-$	$(2.03 \pm 0.15) \times 10^{-3}$		520
$K_S^0 f_0(1370)$, $f_0 \to K^+K^-$	$(1.7 \pm 1.1) \times 10^{-4}$		–
$3K_S^0$	$(7.5 \pm 0.7) \times 10^{-4}$	S=1.4	539
$K^+2K^-\pi^+$	$(2.25 \pm 0.32) \times 10^{-4}$		434
$K^+K^-\overline{K}^*(892)^0$, $\overline{K}^{*0} \to K^-\pi^+$	$(4.5 \pm 1.8) \times 10^{-5}$		†
$K^-\pi^+\phi$, $\phi \to K^+K^-$	$(4.0 \pm 1.7) \times 10^{-5}$		422
$\phi\overline{K}^*(892)^0$, $\phi \to K^+K^-$, $\overline{K}^{*0} \to K^-\pi^+$	$(1.08 \pm 0.21) \times 10^{-4}$		†
$K^+2K^-\pi^+$ nonresonant	$(3.4 \pm 1.5) \times 10^{-5}$		434
$2K_S^0K^\pm\pi^\mp$	$(5.9 \pm 1.3) \times 10^{-4}$		427

Pionic modes

$\pi^+\pi^-$	$(1.454 \pm 0.024) \times 10^{-3}$	S=1.4	922
$2\pi^0$	$(8.26 \pm 0.25) \times 10^{-4}$		923
$\pi^+\pi^-\pi^0$	(1.49 ± 0.06) %	S=2.1	907
$\rho^+\pi^-$	(1.01 ± 0.04) %		764
$\rho^0\pi^0$	$(3.86 \pm 0.23) \times 10^{-3}$		764
$\rho^-\pi^+$	$(5.15 \pm 0.25) \times 10^{-3}$		764
$\rho(1450)^+\pi^-$, $\rho^+ \to \pi^+\pi^0$	$(1.6 \pm 2.1) \times 10^{-5}$		–
$\rho(1450)^0\pi^0$, $\rho^0 \to \pi^+\pi^-$	$(4.5 \pm 2.0) \times 10^{-5}$		–
$\rho(1450)^-\pi^+$, $\rho^- \to \pi^-\pi^0$	$(2.7 \pm 0.4) \times 10^{-4}$		–
$\rho(1700)^+\pi^-$, $\rho^+ \to \pi^+\pi^0$	$(6.1 \pm 1.5) \times 10^{-4}$		–
$\rho(1700)^0\pi^0$, $\rho^0 \to \pi^+\pi^-$	$(7.4 \pm 1.8) \times 10^{-4}$		–
$\rho(1700)^-\pi^+$, $\rho^- \to \pi^-\pi^0$	$(4.8 \pm 1.1) \times 10^{-4}$		–
$f_0(980)\pi^0$, $f_0 \to \pi^+\pi^-$	$(3.7 \pm 0.9) \times 10^{-5}$		–
$f_0(500)\pi^0$, $f_0 \to \pi^+\pi^-$	$(1.22 \pm 0.22) \times 10^{-4}$		–
$f_0(1370)\pi^0$, $f_0 \to \pi^+\pi^-$	$(5.5 \pm 2.1) \times 10^{-5}$		–
$f_0(1500)\pi^0$, $f_0 \to \pi^+\pi^-$	$(5.8 \pm 1.6) \times 10^{-5}$		–
$f_0(1710)\pi^0$, $f_0 \to \pi^+\pi^-$	$(4.6 \pm 1.6) \times 10^{-5}$		–
$f_2(1270)\pi^0$, $f_2 \to \pi^+\pi^-$	$(1.97 \pm 0.21) \times 10^{-4}$		–
$\pi^+\pi^-\pi^0$ nonresonant	$(1.3 \pm 0.4) \times 10^{-4}$		907
$3\pi^0$	$(2.0 \pm 0.5) \times 10^{-4}$		908
$2\pi^+2\pi^-$	$(7.56 \pm 0.20) \times 10^{-3}$		880
$a_1(1260)^+\pi^-$, $a_1^+ \to 2\pi^+\pi^-$ total	$(4.53 \pm 0.31) \times 10^{-3}$		–
$a_1(1260)^+\pi^-$, $a_1^+ \to \rho^0\pi^+$ S-wave	$(3.13 \pm 0.21) \times 10^{-3}$		–
$a_1(1260)^+\pi^-$, $a_1^+ \to \rho^0\pi^+$ D-wave	$(1.9 \pm 0.5) \times 10^{-4}$		–
$a_1(1260)^+\pi^-$, $a_1^+ \to \sigma\pi^+$	$(6.4 \pm 0.7) \times 10^{-4}$		–
$a_1(1260)^-\pi^+$, $a_1^- \to \rho^0\pi^-$ S-wave	$(2.3 \pm 0.9) \times 10^{-4}$		–
$a_1(1260)^-\pi^+$, $a_1^- \to \sigma\pi^-$	$(6.0 \pm 3.4) \times 10^{-5}$		–
$\pi(1300)^+\pi^-$, $\pi(1300)^+ \to \sigma\pi^+$	$(5.1 \pm 2.7) \times 10^{-4}$		–
$\pi(1300)^-\pi^+$, $\pi(1300)^- \to \sigma\pi^-$	$(2.3 \pm 2.2) \times 10^{-4}$		–
$a_1(1640)^+\pi^-$, $a_1^+ \to \rho^0\pi^+$ D-wave	$(3.2 \pm 1.6) \times 10^{-4}$		–
$a_1(1640)^+\pi^-$, $a_1^+ \to \sigma\pi^+$	$(1.8 \pm 1.4) \times 10^{-4}$		–
$\pi_2(1670)^+\pi^-$, $\pi_2^+ \to f_2(1270)^0\pi^+$, $f_2^0 \to \pi^+\pi^-$	$(2.0 \pm 0.9) \times 10^{-4}$		–

Downloaded from https://academic.oup.com/ptep/article/2022/8/083C01/6651666 by KIT Library user on 27 September 2022

$\pi_2(1670)^+\pi^-$, $\pi_2^+ \to \sigma\pi^+$		$(2.6 \pm 1.0) \times 10^{-4}$		–
$2\rho^0$ total		$(1.85 \pm 0.13) \times 10^{-3}$		518
$2\rho^0$, parallel helicities		$(8.3 \pm 3.2) \times 10^{-5}$		–
$2\rho^0$, perpendicular helicities		$(4.8 \pm 0.6) \times 10^{-4}$		–
$2\rho^0$, longitudinal helicities		$(1.27 \pm 0.10) \times 10^{-3}$		–
$2\rho(770)^0$, S-wave		$(1.8 \pm 1.3) \times 10^{-4}$		–
$2\rho(770)^0$, P-wave		$(5.3 \pm 1.3) \times 10^{-4}$		–
$2\rho(770)^0$, D-wave		$(6.2 \pm 3.0) \times 10^{-4}$		–
Resonant $(\pi^+\pi^-)\pi^+\pi^-$ 3-body total		$(1.51 \pm 0.12) \times 10^{-3}$		–
$\sigma\pi^+\pi^-$		$(6.2 \pm 0.9) \times 10^{-4}$		–
$\sigma\rho(770)^0$		$(5.0 \pm 2.5) \times 10^{-4}$		–
$f_0(980)\pi^+\pi^-$, $f_0 \to \pi^+\pi^-$		$(1.8 \pm 0.5) \times 10^{-4}$		–
$f_2(1270)\pi^+\pi^-$, $f_2 \to \pi^+\pi^-$		$(3.7 \pm 0.6) \times 10^{-4}$		–
$2f_2(1270)$, $f_2 \to \pi^+\pi^-$		$(1.6 \pm 1.8) \times 10^{-4}$		–
$f_0(1370)\sigma$, $f_0 \to \pi^+\pi^-$		$(1.6 \pm 0.5) \times 10^{-3}$		–
$\pi^+\pi^-2\pi^0$		(1.02 ± 0.09) %		882
$\eta\pi^0$	[yy]	$(6.3 \pm 0.6) \times 10^{-4}$	S=1.1	846
$\omega\pi^0$	[yy]	$(1.17 \pm 0.35) \times 10^{-4}$		761
$\omega\eta$		$(1.98 \pm 0.18) \times 10^{-3}$	S=1.1	648
$2\pi^+2\pi^-\pi^0$		$(4.2 \pm 0.5) \times 10^{-3}$		844
$\eta\pi^+\pi^-$	[yy]	$(1.16 \pm 0.07) \times 10^{-3}$		827
$\omega\pi^+\pi^-$	[yy]	$(1.33 \pm 0.20) \times 10^{-3}$		738
$\omega\pi^0\pi^0$		$< 1.10 \times 10^{-3}$	CL=90%	740
$\eta 2\pi^0$		$(3.8 \pm 1.3) \times 10^{-4}$		829
$\pi^+\pi^-\pi^0\eta$		$(3.23 \pm 0.22) \times 10^{-3}$		797
$3\pi^+3\pi^-$		$(4.3 \pm 1.2) \times 10^{-4}$		795
$\eta'(958)\pi^0$		$(9.2 \pm 1.0) \times 10^{-4}$		678
$\eta'(958)\pi^+\pi^-$		$(4.5 \pm 1.7) \times 10^{-4}$		650
2η		$(2.11 \pm 0.19) \times 10^{-3}$	S=2.2	754
$2\eta\pi^0$		$(7.3 \pm 2.2) \times 10^{-4}$		699
3η		$< 1.3 \times 10^{-4}$	CL=90%	421
$\eta\eta'(958)$		$(1.01 \pm 0.19) \times 10^{-3}$		537

Hadronic modes with a $K\overline{K}$ pair

K^+K^-		$(4.08 \pm 0.06) \times 10^{-3}$	S=1.6	791
$2K^0_S$		$(1.41 \pm 0.05) \times 10^{-4}$	S=1.1	789
$K^0_S K^-\pi^+$		$(3.3 \pm 0.5) \times 10^{-3}$	S=1.1	739
$\overline{K}^*(892)^0 K^0_S$, $\overline{K}^{*0} \to K^-\pi^+$		$(8.2 \pm 1.6) \times 10^{-5}$		608
$K^*(892)^+K^-$, $K^{*+} \to K^0_S\pi^+$		$(1.89 \pm 0.30) \times 10^{-3}$		–
$\overline{K}^*(1410)^0 K^0_S$, $\overline{K}^{*0} \to K^-\pi^+$		$(1.3 \pm 1.9) \times 10^{-4}$		–
$K^*(1410)^+K^-$, $K^{*+} \to K^0_S\pi^+$		$(3.2 \pm 1.9) \times 10^{-4}$		–
$(K^-\pi^+)_{S-wave}K^0_S$		$(6.0 \pm 2.9) \times 10^{-4}$		739
$(K^0_S\pi^+)_{S-wave}K^-$		$(3.9 \pm 1.0) \times 10^{-4}$		739
$a_0(980)^-\pi^+$, $a_0^- \to K^0_S K^-$		$(1.3 \pm 1.4) \times 10^{-4}$		–
$a_0(1450)^-\pi^+$, $a_0^- \to K^0_S K^-$		$(2.5 \pm 2.0) \times 10^{-5}$		–
$a_2(1320)^-\pi^+$, $a_2^- \to K^0_S K^-$		$(5 \pm 5) \times 10^{-6}$		–
$\rho(1450)^-\pi^+$, $\rho^- \to K^0_S K^-$		$(4.6 \pm 2.5) \times 10^{-5}$		–
$K^0_S K^+\pi^-$		$(2.17 \pm 0.34) \times 10^{-3}$	S=1.1	739
$K^*(892)^0 K^0_S$, $K^{*0} \to K^+\pi^-$		$(1.12 \pm 0.21) \times 10^{-4}$		608
$K^*(892)^-K^+$, $K^{*-} \to K^0_S\pi^-$		$(6.2 \pm 1.0) \times 10^{-4}$		–
$K^*(1410)^0 K^0_S$, $K^{*0} \to K^+\pi^+$		$(5 \pm 8) \times 10^{-5}$		–
$K^*(1410)^-K^+$, $K^{*-} \to K^0_S\pi^-$		$(2.6 \pm 2.0) \times 10^{-4}$		–
$(K^+\pi^-)_{S-wave}K^0_S$		$(3.7 \pm 1.9) \times 10^{-4}$		739
$(K^0_S\pi^-)_{S-wave}K^+$		$(1.4 \pm 0.6) \times 10^{-4}$		739
$a_0(980)^+\pi^-$, $a_0^+ \to K^0_S K^+$		$(6 \pm 4) \times 10^{-4}$		–
$a_0(1450)^+\pi^-$, $a_0^+ \to K^0_S K^+$		$(3.2 \pm 2.5) \times 10^{-5}$		–
$\rho(1700)^+\pi^-$, $\rho^+ \to K^0_S K^+$		$(1.1 \pm 0.6) \times 10^{-5}$		–
$K^+K^-\pi^0$		$(3.42 \pm 0.14) \times 10^{-3}$		743
$K^*(892)^+K^-$, $K^*(892)^+ \to K^+\pi^0$		$(1.52 \pm 0.07) \times 10^{-3}$		–
$K^*(892)^-K^+$, $K^*(892)^- \to K^-\pi^0$		$(5.4 \pm 0.4) \times 10^{-4}$		–
$(K^+\pi^0)_{S-wave}K^-$		$(2.43 \pm 0.18) \times 10^{-3}$		743
$(K^-\pi^0)_{S-wave}K^+$		$(1.3 \pm 0.5) \times 10^{-4}$		743
$f_0(980)\pi^0$, $f_0 \to K^+K^-$		$(3.6 \pm 0.6) \times 10^{-4}$		–
$\phi\pi^0$, $\phi \to K^+K^-$		$(6.6 \pm 0.4) \times 10^{-4}$		–
$2K^0_S\pi^0$		$< 5.9 \times 10^{-4}$		740
$K^+K^-\eta$		$(5.9 \pm 1.9) \times 10^{-5}$		514
$\phi(1020)\eta$		$(1.84 \pm 0.12) \times 10^{-4}$		489
$K^+K^-\eta$ nonresonant		$(9.9 \,{}^{+0.9}_{-0.8}) \times 10^{-5}$		514
$2K^0_S\eta$		$(1.3 \pm 0.6) \times 10^{-4}$		508
$K^+K^-\pi^0\pi^0$		$(6.9 \pm 0.8) \times 10^{-4}$		681
$K^+K^-\pi^+\pi^-$		$(2.47 \pm 0.11) \times 10^{-3}$		677
$\phi(\pi^+\pi^-)_{S-wave}$, $\phi \to K^+K^-$		$(10 \pm 5) \times 10^{-5}$		614
$(\phi\rho^0)_{S-wave}$, $\phi \to K^+K^-$		$(6.9 \pm 0.6) \times 10^{-4}$		250
$(\phi\rho^0)_{P-wave}$, $\phi \to K^+K^-$		$(4.0 \pm 1.9) \times 10^{-5}$		–
$(\phi\rho^0)_{D-wave}$, $\phi \to K^+K^-$		$(4.2 \pm 1.4) \times 10^{-5}$		–
$(K^*(892)^0\overline{K}^*(892)^0)_{S-wave}$, $K^{*0} \to K^\pm\pi^\mp$		$(2.24 \pm 0.13) \times 10^{-4}$		–
$(K^*(892)^0\overline{K}^*(892)^0)_{P-wave}$, $K^* \to K^\pm\pi^\mp$		$(1.20 \pm 0.08) \times 10^{-4}$		–
$(K^*(892)^0\overline{K}^*(892)^0)_{D-wave}$, $K^* \to K^\pm\pi^\mp$		$(4.7 \pm 0.4) \times 10^{-5}$		–
$K^*(892)^0(K^-\pi^+)_{S-wave}$ 3-body, $K^{*0} \to K^+\pi^-$		$(1.4 \pm 0.6) \times 10^{-4}$		–
$K_1(1270)^+K^-$, $K_1^+ \to K^{*0}\pi^+$		$(1.4 \pm 0.9) \times 10^{-4}$		–
$K_1(1270)^+K^-$, $K_1^+ \to K^*(1430)^0\pi^+$, $K^{*0} \to K^+\pi^-$		$(1.5 \pm 0.5) \times 10^{-4}$		–
$K_1(1270)^+K^-$, $K_1^+ \to \rho^0K^+$		$(2.2 \pm 0.6) \times 10^{-4}$		–
$K_1(1270)^+K^-$, $K_1^+ \to \omega(782)K^+$, $\omega \to \pi^+\pi^-$		$(1.5 \pm 1.2) \times 10^{-5}$		–
$K_1(1270)^-K^+$, $K_1^- \to \rho^0K^-$		$(1.3 \pm 0.4) \times 10^{-4}$		–
$K_1(1400)^+K^-$, $K_1^+ \to K^*(892)^0\pi^+$, $K^{*0} \to K^+\pi^-$		$(4.6 \pm 0.4) \times 10^{-4}$		–
$K^*(1410)^-K^+$, $K^{*-} \to \overline{K}^{*0}\pi^-$		$(7.0 \pm 1.1) \times 10^{-5}$		–
$K_1(1680)^+K^-$, $K_1^+ \to K^{*0}\pi^+$, $K^{*0} \to K^+\pi^-$		$(8.9 \pm 3.2) \times 10^{-5}$		–
$K^+K^-\pi^+\pi^-$ non-resonant		$(2.7 \pm 0.6) \times 10^{-4}$		–
$2K^0_S\pi^+\pi^-$		$(5.3 \pm 0.9) \times 10^{-4}$		673
$K^0_S K^-\pi^+\pi^0$		$(1.32 \pm 0.16) \times 10^{-3}$		677
$K^0_S K^+\pi^-\pi^0$		$(6.5 \pm 0.7) \times 10^{-4}$		677
$K^0_S K^-2\pi^+\pi^-$		$< 1.4 \times 10^{-4}$	CL=90%	595
$K^+K^-\pi^+\pi^-\pi^0$		$(3.1 \pm 2.0) \times 10^{-3}$		600

Other $K\overline{K}X$ modes. They include all decay modes of the ϕ, η, and ω.

$\phi\pi^0$		$(1.17 \pm 0.04) \times 10^{-3}$		645
$\phi\eta$		$(1.8 \pm 0.5) \times 10^{-4}$		489
$\phi\omega$		$(6.5 \pm 1.0) \times 10^{-4}$		238

Radiative modes

$\rho^0\gamma$		$(1.82 \pm 0.32) \times 10^{-5}$		771
$\omega\gamma$		$< 2.4 \times 10^{-4}$	CL=90%	768
$\phi\gamma$		$(2.81 \pm 0.19) \times 10^{-5}$		654
$\overline{K}^*(892)^0\gamma$		$(4.1 \pm 0.7) \times 10^{-4}$		719

Doubly Cabibbo suppressed (DC) modes or $\Delta C = 2$ forbidden via mixing ($C2M$) modes

$K^+\ell^-\overline{\nu}_\ell$ via $\overline{D}^0$		$< 2.2 \times 10^{-5}$	CL=90%	–
K^+ or $K^*(892)^+e^-\overline{\nu}_e$ via $\overline{D}^0$		$< 6 \times 10^{-5}$	CL=90%	–
$K^+\pi^-$	DC	$(1.50 \pm 0.07) \times 10^{-4}$	S=3.0	861
$K^+\pi^-$ via DCS		$(1.363 \pm 0.025) \times 10^{-4}$		–
$K^+\pi^-$ via $\overline{D}^0$		$< 1.6 \times 10^{-5}$	CL=95%	861
$K^0_S\pi^+\pi^-$ in $D^0 \to \overline{D}^0$		$< 1.8 \times 10^{-4}$	CL=95%	–
$K^*(892)^+\pi^-$, $K^{*+} \to K^0_S\pi^+$	DC	$(1.13 \,{}^{+0.60}_{-0.34}) \times 10^{-4}$		711
$K_0^*(1430)^+\pi^-$, $K_0^{*+} \to K^0_S\pi^+$	DC	$< 1.4 \times 10^{-5}$		–
$K_2^*(1430)^+\pi^-$, $K_2^{*+} \to K^0_S\pi^+$	DC	$< 3.4 \times 10^{-5}$		–

Downloaded from https://academic.oup.com/ptep/article/2022/8/083C01/6651666 by KIT Library user on 27 September 2022

$K^+\pi^-\pi^0$	DC	$(3.05 \pm 0.15) \times 10^{-4}$			844
$K^+\pi^-\pi^0$ via $\overline{D}^0$		$(7.6 {}^{+0.5}_{-0.6}) \times 10^{-4}$			–
$K^+\pi^+2\pi^-$ via DCS		$(2.49 \pm 0.07) \times 10^{-4}$			–
$K^+\pi^+2\pi^-$	DC	$(2.65 \pm 0.06) \times 10^{-4}$			813
$K^+\pi^+2\pi^-$ via $\overline{D}^0$		$(7.9 \pm 3.0) \times 10^{-6}$			812
μ^- anything via $\overline{D}^0$		$< 4 \times 10^{-4}$		CL=90%	–

$\Delta C = 1$ weak neutral current ($C1$) modes, Lepton Family number (LF) violating modes, Lepton (L) or Baryon (B) number violating modes

$\gamma\gamma$	C1	$< 8.5 \times 10^{-7}$		CL=90%	932
e^+e^-	C1	$< 7.9 \times 10^{-8}$		CL=90%	932
$\mu^+\mu^-$	C1	$< 6.2 \times 10^{-9}$		CL=90%	926
$\pi^0e^+e^-$	C1	$< 4 \times 10^{-6}$		CL=90%	928
$\pi^0\mu^+\mu^-$	C1	$< 1.8 \times 10^{-4}$		CL=90%	915
ηe^+e^-	C1	$< 3 \times 10^{-6}$		CL=90%	852
$\eta\mu^+\mu^-$	C1	$< 5.3 \times 10^{-4}$		CL=90%	838
$\pi^+\pi^-e^+e^-$	C1	$< 7 \times 10^{-6}$		CL=90%	922
$\rho^0e^+e^-$	C1	$< 1.0 \times 10^{-4}$		CL=90%	771
$\pi^+\pi^-\mu^+\mu^-$	C1	$(9.6 \pm 1.2) \times 10^{-7}$			894
$\pi^+\pi^-\mu^+\mu^-$ (non-res)		$< 5.5 \times 10^{-7}$		CL=90%	–
$\rho^0\mu^+\mu^-$	C1	$< 2.2 \times 10^{-5}$		CL=90%	754
ωe^+e^-	C1	$< 6 \times 10^{-6}$		CL=90%	768
$\omega\mu^+\mu^-$	C1	$< 8.3 \times 10^{-4}$		CL=90%	751
$K^-K^+e^+e^-$	C1	$< 1.1 \times 10^{-5}$		CL=90%	791
ϕe^+e^-	C1	$< 5.2 \times 10^{-5}$		CL=90%	654
$K^-K^+\mu^+\mu^-$	C1	$(1.54 \pm 0.32) \times 10^{-7}$			710
$K^-K^+\mu^+\mu^-$ (non-res)		$< 3.3 \times 10^{-5}$		CL=90%	–
$\phi\mu^+\mu^-$	C1	$< 3.1 \times 10^{-5}$		CL=90%	631
$\overline{K}^0e^+e^-$		[pp] $< 2.4 \times 10^{-5}$		CL=90%	866
$\overline{K}^0\mu^+\mu^-$		[pp] $< 2.6 \times 10^{-4}$		CL=90%	852
$K^-\pi^+e^+e^-$, $675 < m_{ee} < 875$ MeV		$(4.0 \pm 0.5) \times 10^{-6}$			–
$K^-\pi^+e^+e^-$, $1.005 < m_{ee} < 1.035$ GeV		$< 5 \times 10^{-7}$		CL=90%	–
$\overline{K}^*(892)^0e^+e^-$		[pp] $< 4.7 \times 10^{-5}$		CL=90%	719
$K^-\pi^+\mu^+\mu^-$	C1	$< 3.59 \times 10^{-4}$		CL=90%	829
$K^-\pi^+\mu^+\mu^-$, $675 < m_{\mu\mu} < 875$ MeV		$(4.2 \pm 0.4) \times 10^{-6}$			–
$\overline{K}^*(892)^0\mu^+\mu^-$		[pp] $< 2.4 \times 10^{-5}$		CL=90%	700
$\pi^+\pi^-\pi^0\mu^+\mu^-$	C1	$< 8.1 \times 10^{-4}$		CL=90%	863
$\mu^\pm e^\mp$	LF	[aa] $< 1.3 \times 10^{-8}$		CL=90%	929
$\pi^0e^\pm\mu^\mp$	LF	[aa] $< 8.0 \times 10^{-7}$		CL=90%	924
$\eta e^\pm\mu^\mp$	LF	[aa] $< 2.25 \times 10^{-6}$		CL=90%	848
$\pi^+\pi^-e^\pm\mu^\mp$	LF	[aa] $< 1.71 \times 10^{-6}$		CL=90%	911
$\rho^0e^\pm\mu^\mp$	LF	[aa] $< 5.0 \times 10^{-7}$		CL=90%	767
$\omega e^\pm\mu^\mp$	LF	[aa] $< 1.71 \times 10^{-6}$		CL=90%	764
$K^-K^+e^\pm\mu^\mp$	LF	[aa] $< 1.00 \times 10^{-6}$		CL=90%	754
$\phi e^\pm\mu^\mp$	LF	[aa] $< 5.1 \times 10^{-7}$		CL=90%	648
$\overline{K}^0e^\pm\mu^\mp$	LF	[aa] $< 1.74 \times 10^{-6}$		CL=90%	863
$K^-\pi^+e^\pm\mu^\mp$	LF	[aa] $< 1.90 \times 10^{-6}$		CL=90%	848
$\overline{K}^*(892)^0e^\pm\mu^\mp$	LF	[aa] $< 1.25 \times 10^{-6}$		CL=90%	714
$2\pi^-2e^+$	L	$< 9.1 \times 10^{-7}$		CL=90%	922
$2\pi^-2\mu^+$	L	$< 1.52 \times 10^{-6}$		CL=90%	894
$K^-\pi^-2e^+$	L	$< 5.0 \times 10^{-7}$		CL=90%	861
$K^-\pi^-2\mu^+$	L	$< 5.3 \times 10^{-7}$		CL=90%	829
$2K^-2e^+$	L	$< 3.4 \times 10^{-7}$		CL=90%	791
$2K^-2\mu^+$	L	$< 1.0 \times 10^{-7}$		CL=90%	710
$\pi^-\pi^-e^+\mu^+$	L	$< 3.06 \times 10^{-6}$		CL=90%	911
$K^-\pi^-e^+\mu^+$	L	$< 2.10 \times 10^{-6}$		CL=90%	848
$2K^-e^+\mu^+$	L	$< 5.8 \times 10^{-7}$		CL=90%	754
pe^-	L,B	[zz] $< 1.0 \times 10^{-5}$		CL=90%	696
$\overline{p}e^+$	L,B	[aaa] $< 1.1 \times 10^{-5}$		CL=90%	696

$D^*(2007)^0$

$I(J^P) = \frac{1}{2}(1^-)$
I, J, P need confirmation.

Mass $m = 2006.85 \pm 0.05$ MeV (S = 1.1)
$m_{D^{*0}} - m_{D^0} = 142.014 \pm 0.030$ MeV (S = 1.5)
Full width $\Gamma < 2.1$ MeV, CL = 90%

$\overline{D}^*(2007)^0$ modes are charge conjugates of modes below.

$D^*(2007)^0$ DECAY MODES	Fraction (Γ_i/Γ)	p (MeV/c)
$D^0\pi^0$	(64.7 ± 0.9) %	43
$D^0\gamma$	(35.3 ± 0.9) %	137
$D^0e^+e^-$	$(3.91 \pm 0.33) \times 10^{-3}$	137

$D^*(2010)^\pm$

$I(J^P) = \frac{1}{2}(1^-)$
I, J, P need confirmation.

Mass $m = 2010.26 \pm 0.05$ MeV
$m_{D^*(2010)^+} - m_{D^+} = 140.603 \pm 0.015$ MeV
$m_{D^*(2010)^+} - m_{D^0} = 145.4258 \pm 0.0017$ MeV
Full width $\Gamma = 83.4 \pm 1.8$ keV

$D^*(2010)^-$ modes are charge conjugates of the modes below.

$D^*(2010)^\pm$ DECAY MODES	Fraction (Γ_i/Γ)	p (MeV/c)
$D^0\pi^+$	(67.7 ± 0.5) %	39
$D^+\pi^0$	(30.7 ± 0.5) %	38
$D^+\gamma$	(1.6 ± 0.4) %	136

$D_0^*(2300)$

$I(J^P) = \frac{1}{2}(0^+)$

was $D_0^*(2400)$

Mass $m = 2343 \pm 10$ MeV (S = 1.5)
Full width $\Gamma = 229 \pm 16$ MeV

$D_0^*(2300)$ DECAY MODES	Fraction (Γ_i/Γ)	p (MeV/c)
$D\pi^\pm$	seen	411

$D_1(2420)$

$I(J^P) = \frac{1}{2}(1^+)$

Mass $m = 2422.1 \pm 0.6$ MeV (S = 1.7)
$m_{D_1(2420)^0} - m_{D^{*+}} = 411.8 \pm 0.6$ MeV (S = 1.7)
$m_{D_1(2420)^\pm} - m_{D_1(2420)^0} = 4 \pm 4$ MeV
Full width $\Gamma = 31.3 \pm 1.9$ MeV (S = 2.8)

$\overline{D}_1(2420)$ modes are charge conjugates of modes below.

$D_1(2420)$ DECAY MODES	Fraction (Γ_i/Γ)	p (MeV/c)
$D^*(2007)^0\pi$	seen	359

$D_1(2430)^0$

$I(J^P) = \frac{1}{2}(1^+)$

Mass $m = 2412 \pm 9$ MeV
Full width $\Gamma = 314 \pm 29$ MeV

$D_1(2430)^0$ DECAY MODES	Fraction (Γ_i/Γ)	p (MeV/c)
$D^*(2010)^+\pi^-$	seen	345

$D_2^*(2460)$

$I(J^P) = \frac{1}{2}(2^+)$

Mass $m = 2461.1 {}^{+0.7}_{-0.8}$ MeV (S = 6.2)
$m_{D_2^*(2460)^0} - m_{D^+} = 591.5 {}^{+0.7}_{-0.8}$ MeV (S = 5.9)
$m_{D_2^*(2460)^0} - m_{D^{*+}} = 450.9 {}^{+0.7}_{-0.8}$ MeV (S = 5.9)
$m_{D_2^*(2460)^\pm} - m_{D_2^*(2460)^0} = 2.4 \pm 1.7$ MeV
Full width $\Gamma = 47.3 \pm 0.8$ MeV (S = 1.5)

$\overline{D}_2^*(2460)$ modes are charge conjugates of modes below.

$D_2^*(2460)$ DECAY MODES	Fraction (Γ_i/Γ)	p (MeV/c)
$D\pi^-$	seen	509
$D^*(2010)\pi^-$	seen	389

$D_3^*(2750)$

$I(J^P) = \frac{1}{2}(3^-)$

Mass $m = 2763.1 \pm 3.2$ MeV (S = 2.1)
Full width $\Gamma = 66 \pm 5$ MeV

$D_3^*(2750)$ DECAY MODES	Fraction (Γ_i/Γ)	p (MeV/c)
$D\pi$	seen	743
$D^+\pi^-$	seen	739
$D^0\pi^\pm$	seen	743
$D^*\pi$	seen	639
$D^{*+}\pi^-$	seen	639

Downloaded from https://academic.oup.com/ptep/article/2022/8/083C01/6651666 by KIT Library user on 27 September 2022

CHARMED, STRANGE MESONS ($C = \pm 1, S = \pm 1$) (including possibly non-$q\overline{q}$ states)

$D_s^+ = c\overline{s}$, $D_s^- = \overline{c}s$, similarly for D_s^*'s

$D_s^\pm$

$I(J^P) = 0(0^-)$

Mass $m = 1968.35 \pm 0.07$ MeV
$m_{D_s^\pm} - m_{D^\pm} = 98.69 \pm 0.05$ MeV
Mean life $\tau = (504 \pm 4) \times 10^{-15}$ s (S = 1.2)
$c\tau = 151.2\ \mu$m

CP-violating decay-rate asymmetries

$A_{CP}(\mu^\pm\nu) = (-0.2 \pm 2.5)\%$
$A_{CP}(\tau^\pm\nu)$ in $D_s^+ \to \tau^+\nu_\tau$, $D_s^- \to \tau^-\overline{\nu}_\tau = (3 \pm 5)\%$
$A_{CP}(K^\pm K_S^0) = (0.09 \pm 0.26)\%$
$A_{CP}(K^\pm K_L^0)$ in $D_s^\pm \to K^\pm K_L^0 = (-1.1 \pm 2.7) \times 10^{-2}$
$A_{CP}(K^+K^-\pi^\pm) = (-0.5 \pm 0.9)\%$
$A_{CP}(\phi\pi^\pm) = (-0.38 \pm 0.27)\%$
$A_{CP}(K^\pm K_S^0\pi^0) = (-2 \pm 6)\%$
$A_{CP}(2K_S^0\pi^\pm) = (3 \pm 5)\%$
$A_{CP}(K^+K^-\pi^\pm\pi^0) = (0.0 \pm 3.0)\%$
$A_{CP}(K^\pm K_S^0\pi^+\pi^-) = (-6 \pm 5)\%$
$A_{CP}(K_S^0K^\mp 2\pi^\pm) = (4.1 \pm 2.8)\%$
$A_{CP}(\pi^+\pi^-\pi^\pm) = (-0.7 \pm 3.1)\%$
$A_{CP}(\pi^\pm\eta) = (0.3 \pm 0.4)\%$
$A_{CP}(\pi^\pm\eta') = (-0.9 \pm 0.5)\%$
$A_{CP}(\eta\pi^\pm\pi^0) = (-1 \pm 4)\%$
$A_{CP}(\eta'\pi^\pm\pi^0) = (0 \pm 8)\%$
$A_{CP}(K^\pm\pi^0) = (2 \pm 4)\%$ (S = 1.2)
$A_{CP}(\overline{K}^0/K^0\pi^\pm) = (0.4 \pm 0.5)\%$
$A_{CP}(K_S^0\pi^\pm) = (0.20 \pm 0.18)\%$
$A_{CP}(K^\pm\pi^+\pi^-) = (4 \pm 5)\%$
$A_{CP}(K_S^0\pi^+\pi^0)$ in $D_s^\pm \to K_S^0\pi^+\pi^0 = (3 \pm 6)\%$
$A_{CP}(K^\pm\eta) = (1.8 \pm 1.9)\%$
$A_{CP}(K^\pm\eta'(958)) = (6 \pm 19)\%$

CP violating asymmetries of P-odd (T-odd) moments

$A_T(K_S^0K^\pm\pi^+\pi^-) = (-14 \pm 8) \times 10^{-3}$ [ii]

$D_s^+ \to \phi\ell^+\nu_\ell$ form factors

$r_2 = 0.84 \pm 0.11$ (S = 2.4)
$r_V = 1.80 \pm 0.08$
$\Gamma_L/\Gamma_T = 0.72 \pm 0.18$
$f_+(0)\,|V_{cs}|$ in $D_s^+ \to \eta e^+\nu_e = 0.446 \pm 0.007$
$f_+(0)\,|V_{cs}|$ in $D_s^+ \to \eta' e^+\nu_e = 0.48 \pm 0.05$
$f_+(0)|V_{cd}|$ in $D_s^+ \to K^0 e^+\nu_e = 0.162 \pm 0.019$
$r_V \equiv V(0)/A_1(0)$ in $D_s^+ \to K^*(892)^0 e^+\nu_e = 1.7 \pm 0.4$
$r_2 \equiv A_2(0)/A_1(0)$ in $D_s^+ \to K^*(892)^0 e^+\nu_e = 0.77 \pm 0.29$
$f_{D_s^+}\,|V_{cs}|$ in $D_s^+ \to \mu^+\nu_\mu = 243 \pm 5$ MeV
$f_{D_s^+}\,|V_{cs}|$ in $D_s^+ \to \tau^+\nu_\tau = 245.3 \pm 3.0$ MeV

Unless otherwise noted, the branching fractions for modes with a resonance in the final state include all the decay modes of the resonance. D_s^- modes are charge conjugates of the modes below.

D_s^+ DECAY MODES		Fraction (Γ_i/Γ)	Scale factor/ Confidence level	p (MeV/c)
Inclusive modes				
e^+ semileptonic	[bbb]	(6.33 ± 0.15) %		–
π^+ anything		(119.3 ± 1.4) %		–
π^- anything		(43.2 ± 0.9) %		–
π^0 anything		(123 ± 7) %		–
K^- anything		(18.7 ± 0.5) %		–
K^+ anything		(28.9 ± 0.7) %		–
K_S^0 anything		(19.0 ± 1.1) %		–
η anything	[ccc]	(29.9 ± 2.8) %		–
ω anything		(6.1 ± 1.4) %		–
η' anything	[ddd]	(10.3 ± 1.4) %	S=1.1	–
$f_0(980)$ anything, $f_0 \to \pi^+\pi^-$		< 1.3 %	CL=90%	–
ϕ anything		(15.7 ± 1.0) %		–
K^+K^- anything		(15.8 ± 0.7) %		–
$K_S^0K^+$ anything		(5.8 ± 0.5) %		–
$K_S^0K^-$ anything		(1.9 ± 0.4) %		–
$2K_S^0$ anything		(1.70 ± 0.32) %		–
$2K^+$ anything		< 2.6 $\times 10^{-3}$	CL=90%	–
$2K^-$ anything		< 6 $\times 10^{-4}$	CL=90%	–
Leptonic and semileptonic modes				
$e^+\nu_e$		< 8.3 $\times 10^{-5}$	CL=90%	984
$\mu^+\nu_\mu$		(5.43 ± 0.15) $\times 10^{-3}$		981
$\tau^+\nu_\tau$		(5.32 ± 0.11) %		182
$\gamma e^+\nu_e$		< 1.3 $\times 10^{-4}$	CL=90%	984
$K^+K^-e^+\nu_e$		—		851
$\phi e^+\nu_e$	[eee]	(2.39 ± 0.16) %	S=1.3	720
$\phi\mu^+\nu_\mu$		(1.9 ± 0.5) %		715
$\eta e^+\nu_e + \eta'(958) e^+\nu_e$	[eee]	(3.03 ± 0.24) %		–
$\eta e^+\nu_e$	[eee]	(2.32 ± 0.08) %		908
$\eta'(958) e^+\nu_e$	[eee]	(8.0 ± 0.7) $\times 10^{-3}$		751
$\eta\mu^+\nu_\mu$		(2.4 ± 0.5) %		905
$\eta'(958)\mu^+\nu_\mu$		(1.1 ± 0.5) %		747
$\omega e^+\nu_e$	[fff]	< 2.0 $\times 10^{-3}$	CL=90%	829
$K^0 e^+\nu_e$		(3.4 ± 0.4) $\times 10^{-3}$		921
$K^*(892)^0 e^+\nu_e$	[eee]	(2.15 ± 0.28) $\times 10^{-3}$	S=1.1	782
$a_0(980)^0 e^+\nu_e$, $a_0(980)^0 \to \pi^0\eta$		< 1.2 $\times 10^{-4}$	CL=90%	–
Hadronic modes with a $K\overline{K}$ pair				
$K^+K_S^0$		(1.453 ± 0.035) %		850
$K^+K_L^0$		(1.49 ± 0.06) %		850
$K^+\overline{K}^0$		(2.95 ± 0.14) %		850
$K^+K^-\pi^+$	[jj]	(5.38 ± 0.10) %	S=1.1	805
$\phi\pi^+$	[eee,ggg]	(4.5 ± 0.4) %		712
$\phi\pi^+$, $\phi \to K^+K^-$	[ggg]	(2.22 ± 0.06) %		712
$K^+\overline{K}^*(892)^0$, $\overline{K}^{*0} \to K^-\pi^+$		(2.58 ± 0.06) %		416
$f_0(980)\pi^+$, $f_0 \to K^+K^-$		(1.11 ± 0.19) %		732
$f_0(1370)\pi^+$, $f_0 \to K^+K^-$		(7.1 ± 2.9) $\times 10^{-4}$		–
$f_0(1710)\pi^+$, $f_0 \to K^+K^-$		(6.7 ± 2.8) $\times 10^{-4}$		198
$K^+\overline{K}_0^*(1430)^0$, $\overline{K}_0^* \to K^-\pi^+$		(1.76 ± 0.25) $\times 10^{-3}$		218
$K^+K_S^0\pi^0$		(1.52 ± 0.22) %		805
$2K_S^0\pi^+$		(7.7 ± 0.6) $\times 10^{-3}$		802
$K^0\overline{K}^0\pi^+$		—		802
$K^*(892)^+\overline{K}^0$	[eee]	(5.4 ± 1.2) %		683
$K^+K^-\pi^+\pi^0$		(5.50 ± 0.24) %	S=1.3	748
$\phi\rho^+$	[eee]	(5.59 ± 0.34) %		401
$\overline{K}_1(1270)^0K^+$, $\overline{K}_1(1270)^0 \to K^-\rho^+$		(5.7 ± 0.6) $\times 10^{-3}$		–
$\overline{K}_1(1270)^0K^+$, $\overline{K}_1(1270)^0 \to K^*(892)\pi$		(1.31 ± 0.25) %		–
$\overline{K}_1(1400)^0K^+$, $\overline{K}_1(1400)^0 \to K^*(892)\pi$		(2.0 ± 0.4) %		–
$a_0(980)^0\rho^+$, $a_0(980)^0 \to K^+K^-$		(1.9 ± 0.4) $\times 10^{-3}$		–
$f_1(1420)^0\pi^+$, $f_1(1420)^0 \to K^*(892)^\mp K^\pm$		(3.9 ± 0.7) $\times 10^{-3}$		–
$f_1(1420)^0\pi^+$, $f_1(1420)^0 \to a_0(980)^0\pi^0$, $a_0(980)^0 \to K^+K^-$		(4.0 ± 1.4) $\times 10^{-4}$		–
$\eta(1475)\pi^+$, $\eta(1475) \to a_0(980)^0\pi^0$, $a_0(980)^0 \to K^+K^-$		(7.0 ± 2.8) $\times 10^{-4}$		–
$K_S^0K^-2\pi^+$		(1.53 ± 0.08) %	S=1.5	744
$K^*(892)^+\overline{K}^*(892)^0$	[eee]	(5.64 ± 0.35) %		417
$\eta(1475)K_S^0$, $\eta \to K^*(892)^0\pi^+$, $K^{*0} \to K^-\pi^+$		(3.4 ± 1.0) $\times 10^{-4}$		–
$\eta(1475)\pi^+$, $\eta \to \overline{K}^*(892)^+K^-$, $\overline{K}^{*+} \to K_S^0\pi^+$		(3.4 ± 1.0) $\times 10^{-4}$		–
$\eta(1475)\pi^+$, $\eta \to a_0(980)^-\pi^+$, $a_0^- \to K_S^0K^-$		(1.7 ± 0.9) $\times 10^{-3}$		–

Downloaded from https://academic.oup.com/ptep/article/2022/8/083C01/6651666 by KIT Library user on 27 September 2022

$f_1(1285)\pi^+$, $f_1 \to a_0(980)^-\pi^+$, $a_0^- \to K^0_S K^-$		$(3.4 \pm 0.8) \times 10^{-4}$		–
$K^+ K^0_S \pi^+\pi^-$		$(9.5 \pm 0.8) \times 10^{-3}$	S=1.1	744
$K^+ K^- 2\pi^+\pi^-$		$(8.6 \pm 1.5) \times 10^{-3}$		673
$\phi 2\pi^+\pi^-$	[eee]	(1.21 ± 0.16) %		640
$\phi\rho^0\pi^+$, $\phi \to K^+K^-$		$(6.4 \pm 1.3) \times 10^{-3}$		181
$\phi a_1(1260)^+$, $\phi \to K^+K^-$, $a_1^+ \to \rho^0\pi^+$		$(7.4 \pm 1.2) \times 10^{-3}$		†
$\phi 2\pi^+\pi^-$ non-ρ, $\phi \to K^+K^-$		$(1.8 \pm 0.7) \times 10^{-3}$		–
$K^+K^-\rho^0\pi^+$ non-ϕ		$< 2.6 \times 10^{-4}$	CL=90%	249
$K^+K^-2\pi^+\pi^-$ nonresonant		$(9 \pm 7) \times 10^{-4}$		673
$2K^0_S 2\pi^+\pi^-$		$(7.8 \pm 3.3) \times 10^{-4}$		669

Hadronic modes without K's

$\pi^+\pi^0$		$< 1.2 \times 10^{-4}$	CL=90%	975
$2\pi^+\pi^-$		(1.08 ± 0.04) %		959
$\rho^0\pi^+$		$(1.9 \pm 1.2) \times 10^{-4}$		825
$\pi^+(\pi^+\pi^-)_{S-\text{wave}}$	[hhh]	$(9.0 \pm 0.4) \times 10^{-3}$		959
$f_2(1270)\pi^+$, $f_2 \to \pi^+\pi^-$		$(1.09 \pm 0.19) \times 10^{-3}$		559
$\rho(1450)^0\pi^+$, $\rho^0 \to \pi^+\pi^-$		$(2.9 \pm 1.9) \times 10^{-4}$		421
$\pi^+ 2\pi^0$		$(6.5 \pm 1.3) \times 10^{-3}$		961
$2\pi^+\pi^-\pi^0$		—		935
$\eta\pi^+$	[eee]	(1.68 ± 0.09) %	S=1.1	902
$\omega\pi^+$	[eee]	$(1.92 \pm 0.30) \times 10^{-3}$		822
$3\pi^+ 2\pi^-$		$(7.9 \pm 0.8) \times 10^{-3}$		899
$2\pi^+\pi^-2\pi^0$		—		902
$\eta\rho^+$	[eee]	(8.9 ± 0.8) %		724
$\eta\pi^+\pi^0$		(9.5 ± 0.5) %		885
$\eta(\pi^+\pi^0)_{P-wave}$		$(5.1 \pm 3.1) \times 10^{-3}$		885
$2\pi^+\pi^-\eta$		(3.12 ± 0.16) %		855
$a_1(1260)^+\eta$, $a_1^+ \to \rho(770)^0\pi^+$, $\rho^0 \to \pi^+\pi^-$		(1.73 ± 0.16) %		–
$a_1(1260)^+\eta$, $a_1^+ \to f_0(500)\pi^+$, $f_0 \to \pi^+\pi^-$		$(2.5 \pm 0.9) \times 10^{-3}$		–
$a_0(980)^{+0}\pi^{0+}$, $a_0(980)^{+0} \to \eta\pi^{+0}$		(2.2 ± 0.4) %		–
$a_0(980)^+\rho(770)^0$, $a_0^+ \to \eta\pi^+$		$(2.1 \pm 0.9) \times 10^{-3}$		–
$\eta(1405)\pi^+$, $\eta(1405) \to a_0(980)^-\pi^+$, $a_0^- \to \eta\pi^-$		$(2.2 \pm 0.7) \times 10^{-4}$		–
$\eta(1405)\pi^+$, $\eta(1405) \to a_0(980)^+\pi^-$, $a_0^+ \to \eta\pi^+$		$(2.2 \pm 0.7) \times 10^{-4}$		–
$f_1(1420)\pi^+$, $f_1 \to a_0(980)^-\pi^+$, $a_0^- \to \eta\pi^-$		$(5.9 \pm 1.8) \times 10^{-4}$		–
$f_1(1420)\pi^+$, $f_1 \to a_0(980)^+\pi^-$, $a_0^+ \to \eta\pi^+$		$(5.3 \pm 1.8) \times 10^{-4}$		–
$\omega\pi^+\pi^0$	[eee]	(2.8 ± 0.7) %		802
$3\pi^+ 2\pi^-\pi^0$		(4.9 ± 3.2) %		856
$\omega 2\pi^+\pi^-$	[eee]	(1.6 ± 0.5) %		766
$\eta'(958)\pi^+$	[ddd,eee]	(3.94 ± 0.25) %		743
$3\pi^+ 2\pi^-2\pi^0$		—		803
$\omega\eta\pi^+$	[eee]	< 2.13 %	CL=90%	654
$\eta'(958)\rho^+$	[ddd,eee]	(5.8 ± 1.5) %		465
$\eta'(958)\pi^+\pi^0$		(5.6 ± 0.8) %		720
$\eta'(958)\pi^+\pi^0$ nonresonant		< 5.1 %	CL=90%	720

Modes with one or three K's

$K^+\pi^0$		$(7.4 \pm 0.5) \times 10^{-4}$		917
$K^0_S\pi^+$		$(1.10 \pm 0.05) \times 10^{-3}$		916
$K^+\eta$	[eee]	$(1.73 \pm 0.08) \times 10^{-3}$		835
$K^+\omega$	[eee]	$(8.7 \pm 2.5) \times 10^{-4}$		741
$K^+\eta'(958)$	[eee]	$(2.64 \pm 0.24) \times 10^{-3}$		646
$K^+\pi^+\pi^-$		$(6.5 \pm 0.4) \times 10^{-3}$		900
$K^+\rho^0$		$(2.5 \pm 0.4) \times 10^{-3}$		745
$K^+\rho(1450)^0$, $\rho^0 \to \pi^+\pi^-$		$(6.9 \pm 2.4) \times 10^{-4}$		–
$K^*(892)^0\pi^+$, $K^{*0} \to K^+\pi^-$		$(1.40 \pm 0.24) \times 10^{-3}$		775
$K^*(1410)^0\pi^+$, $K^{*0} \to K^+\pi^-$		$(1.22 \pm 0.28) \times 10^{-3}$		–
$K^*(1430)^0\pi^+$, $K^{*0} \to K^+\pi^-$		$(5.0 \pm 3.4) \times 10^{-4}$		–
$K^+\pi^+\pi^-$ nonresonant		$(1.03 \pm 0.34) \times 10^{-3}$		900
$K^0\pi^+\pi^0$		(1.08 ± 0.06) %		899
$K^0_S 2\pi^+\pi^-$		$(2.8 \pm 1.0) \times 10^{-3}$		870
$K^+\omega\pi^0$	[eee]	$< 8.2 \times 10^{-3}$	CL=90%	684
$K^+\omega\pi^+\pi^-$	[eee]	$< 5.4 \times 10^{-3}$	CL=90%	603
$K^+\omega\eta$	[eee]	$< 7.9 \times 10^{-3}$	CL=90%	366
$2K^+K^-$		$(2.15 \pm 0.20) \times 10^{-4}$		628
ϕK^+, $\phi \to K^+K^-$		$(8.8 \pm 2.0) \times 10^{-5}$		–

Doubly Cabibbo-suppressed modes

$2K^+\pi^-$		$(1.276 \pm 0.031) \times 10^{-4}$		805
$K^+K^*(892)^0$, $K^{*0} \to K^+\pi^-$		$(6.0 \pm 3.4) \times 10^{-5}$		–

Baryon-antibaryon mode

$p\overline{n}$		$(1.22 \pm 0.11) \times 10^{-3}$		295
$p\overline{p}e^+\nu_e$		$< 2.0 \times 10^{-4}$	CL=90%	296

$\Delta C = 1$ weak neutral current ($C1$) modes, Lepton family number (LF), or Lepton number (L) violating modes

$\pi^+e^+e^-$	[pp]	$< 5.5 \times 10^{-6}$	CL=90%	979
$\pi^+\phi$, $\phi \to e^+e^-$	[oo]	$(6 {}^{+8}_{-4}) \times 10^{-6}$		–
$\pi^+\mu^+\mu^-$	[pp]	$< 1.8 \times 10^{-7}$	CL=90%	968
$K^+e^+e^-$	$C1$	$< 3.7 \times 10^{-6}$	CL=90%	922
$K^+\mu^+\mu^-$	$C1$	$< 1.4 \times 10^{-7}$	CL=90%	909
$K^*(892)^+\mu^+\mu^-$	$C1$	$< 1.4 \times 10^{-3}$	CL=90%	765
$\pi^+e^+\mu^-$	LF	$< 1.1 \times 10^{-6}$	CL=90%	976
$\pi^+e^-\mu^+$	LF	$< 9.4 \times 10^{-7}$	CL=90%	976
$K^+e^+\mu^-$	LF	$< 7.9 \times 10^{-7}$	CL=90%	919
$K^+e^-\mu^+$	LF	$< 5.6 \times 10^{-7}$	CL=90%	919
π^-2e^+	L	$< 1.4 \times 10^{-6}$	CL=90%	979
$\pi^-2\mu^+$	L	$< 8.6 \times 10^{-8}$	CL=90%	968
$\pi^-e^+\mu^+$	L	$< 6.3 \times 10^{-7}$	CL=90%	976
K^-2e^+	L	$< 7.7 \times 10^{-7}$	CL=90%	922
$K^-2\mu^+$	L	$< 2.6 \times 10^{-8}$	CL=90%	909
$K^-e^+\mu^+$	L	$< 2.6 \times 10^{-7}$	CL=90%	919
$K^*(892)^-2\mu^+$	L	$< 1.4 \times 10^{-3}$	CL=90%	765

$D_s^{*\pm}$

$I(J^P) = 0(?^?)$

J^P is natural, width and decay modes consistent with 1^-.

Mass $m = 2112.2 \pm 0.4$ MeV
$m_{D_s^{*\pm}} - m_{D_s^\pm} = 143.8 \pm 0.4$ MeV
Full width $\Gamma < 1.9$ MeV, CL = 90%

D_s^{*-} modes are charge conjugates of the modes below.

D_s^{*+} DECAY MODES	Fraction (Γ_i/Γ)	p (MeV/c)
$D_s^+\gamma$	(93.5 ± 0.7) %	139
$D_s^+\pi^0$	(5.8 ± 0.7) %	48
$D_s^+e^+e^-$	$(6.7 \pm 1.6) \times 10^{-3}$	139

$D_{s0}^*(2317)^\pm$

$I(J^P) = 0(0^+)$
J, P need confirmation.

J^P is natural, low mass consistent with 0^+.

See the review on "Heavy Non-$q\overline{q}$ Mesons."

Mass $m = 2317.8 \pm 0.5$ MeV
$m_{D_{s0}^*(2317)^\pm} - m_{D_s^\pm} = 349.4 \pm 0.5$ MeV
Full width $\Gamma < 3.8$ MeV, CL = 95%

$D_{s0}^*(2317)^-$ modes are charge conjugates of modes below.

$D_{s0}^*(2317)^\pm$ DECAY MODES	Fraction (Γ_i/Γ)	Confidence level	p (MeV/c)
$D_s^+\pi^0$	$(100 {}^{+0}_{-20})$ %		298
$D_s^+\gamma$	< 5 %	90%	323
$D_s^*(2112)^+\gamma$	< 6 %	90%	–
$D_s^+\gamma\gamma$	< 18 %	95%	323
$D_s^*(2112)^+\pi^0$	< 11 %	90%	–

Downloaded from https://academic.oup.com/ptep/article/2022/8/083C01/6651666 by KIT Library user on 27 September 2022

$D_s^+ \pi^+ \pi^-$	$< 4 \times 10^{-3}$	90%	194
$D_s^+ \pi^0 \pi^0$	not seen		205

$D_{s1}(2460)^\pm$

$I(J^P) = 0(1^+)$

See the review on "Heavy Non-$q\overline{q}$ Mesons."

Mass $m = 2459.5 \pm 0.6$ MeV (S = 1.1)
$m_{D_{s1}(2460)^\pm} - m_{D_s^{*\pm}} = 347.3 \pm 0.7$ MeV (S = 1.2)
$m_{D_{s1}(2460)^\pm} - m_{D_s^\pm} = 491.1 \pm 0.6$ MeV (S = 1.1)
Full width $\Gamma < 3.5$ MeV, CL = 95%

$D_{s1}(2460)^-$ modes are charge conjugates of the modes below.

$D_{s1}(2460)^+$ DECAY MODES	Fraction (Γ_i/Γ)	Scale factor/ Confidence level	p (MeV/c)
$D_s^{*+} \pi^0$	(48 ± 11) %		297
$D_s^+ \gamma$	(18 ± 4) %		442
$D_s^+ \pi^+ \pi^-$	(4.3 ± 1.3) %	S=1.1	363
$D_s^{*+} \gamma$	< 8 %	CL=90%	323
$D_{s0}^*(2317)^+ \gamma$	$(3.7^{+5.0}_{-2.4})$ %		138

$D_{s1}(2536)^\pm$

$I(J^P) = 0(1^+)$
J, P need confirmation.

Mass $m = 2535.11 \pm 0.06$ MeV
$m_{D_{s1}(2536)^\pm} - m_{D_s^*(2111)} = 422.9 \pm 0.4$ MeV
$m_{D_{s1}(2536)^\pm} - m_{D^*(2010)^\pm} = 524.85 \pm 0.04$ MeV
$m_{D_{s1}(2536)^\pm} - m_{D^*(2007)^0} = 528.26 \pm 0.05$ MeV (S = 1.2)
Full width $\Gamma = 0.92 \pm 0.05$ MeV

Branching fractions are given relative to the one **DEFINED AS 1**.
$D_{s1}(2536)^-$ modes are charge conjugates of the modes below.

$D_{s1}(2536)^+$ DECAY MODES	Fraction (Γ_i/Γ)	Confidence level	p (MeV/c)
$D^*(2010)^+ K^0$	0.85 ± 0.12		149
$(D^*(2010)^+ K^0)_{S-wave}$	0.61 ± 0.09		149
$D^+ \pi^- K^+$	0.028 ± 0.005		176
$D^*(2007)^0 K^+$	**DEFINED AS 1**		167
$D^+ K^0$	<0.34	90%	381
$D^0 K^+$	<0.12	90%	391
$D_s^{*+} \gamma$	possibly seen		388
$D_s^+ \pi^+ \pi^-$	seen		437

$D_{s2}^*(2573)$

$I(J^P) = 0(2^+)$

Mass $m = 2569.1 \pm 0.8$ MeV (S = 2.4)
$m_{D_{s2}^*(2573)} - m_{D^0} = 704 \pm 3.2$ MeV
Full width $\Gamma = 16.9 \pm 0.7$ MeV

$D_{s2}^*(2573)^-$ modes are charge conjugates of the modes below.

$D_{s2}^*(2573)^+$ DECAY MODES	Fraction (Γ_i/Γ)	p (MeV/c)
$D^0 K^+$	seen	431
$D^*(2007)^0 K^+$	not seen	238
$D^+ K_S^0$	seen	422
$D^{*+} K_S^0$	seen	225

$D_{s1}^*(2700)^\pm$

$I(J^P) = 0(1^-)$

Mass $m = 2714 \pm 5$ MeV (S = 1.5)
Full width $\Gamma = 122 \pm 10$ MeV

$D_{s1}^*(2700)^\pm$ DECAY MODES	Fraction (Γ_i/Γ)	p (MeV/c)
$D^0 K^+$	seen	579
$D^+ K_S^0$	seen	573
$D^{*0} K^+$	seen	438
$D^{*+} K_S^0$	seen	431

$D_{s3}^*(2860)^\pm$

$I(J^P) = 0(3^-)$

Mass $m = 2860 \pm 7$ MeV
Full width $\Gamma = 53 \pm 10$ MeV

$D_{s3}^*(2860)^\pm$ DECAY MODES	Fraction (Γ_i/Γ)	p (MeV/c)
$D^0 K^+$	seen	710
$D^+ K_S^0$	seen	704
$D^{*0} K^+$	seen	589
$D^{*+} K_S^0$	seen	584

BOTTOM MESONS ($B = \pm 1$)

$B^+ = u\overline{b}$, $B^0 = d\overline{b}$, $\overline{B}^0 = \overline{d}b$, $B^- = \overline{u}b$, similarly for B^*'s

B-particle organization

Many measurements of B decays involve admixtures of B hadrons. Previously we arbitrarily included such admixtures in the $B^\pm$ section, but because of their importance we have created two new sections: "$B^\pm/B^0$ Admixture" for $\Upsilon(4S)$ results and "$B^\pm/B^0/B_s^0/b$-baryon Admixture" for results at higher energies. Most inclusive decay branching fractions and χ_b at high energy are found in the Admixture sections. B^0-$\overline{B}^0$ mixing data are found in the B^0 section, while B_s^0-$\overline{B}_s^0$ mixing data and B-$\overline{B}$ mixing data for a B^0/B_s^0 admixture are found in the B_s^0 section. CP-violation data are found in the $B^\pm$, B^0, and $B^\pm$ B^0 Admixture sections. b-baryons are found near the end of the Baryon section.

The organization of the B sections is now as follows, where bullets indicate particle sections and brackets indicate reviews.

- $B^\pm$
  mass, mean life, CP violation, branching fractions
- B^0
  mass, mean life, B^0-$\overline{B}^0$ mixing, CP violation, branching fractions
- $B^\pm/B^0$ Admixtures
  CP violation, branching fractions
- $B^\pm/B^0/B_s^0/b$-baryon Admixtures
  mean life, production fractions, branching fractions
- B^*
  mass
- $B_1(5721)^+$
  mass
- $B_1(5721)^0$
  mass
- $B_2^*(5747)^+$
  mass
- $B_2^*(5747)^0$
  mass
- $B_J^*(5970)^+$
  mass
- $B_J^*(5970)^0$
  mass
- B_s^0
  mass, mean life, B_s^0-$\overline{B}_s^0$ mixing, CP violation, branching fractions
- B_s^*
  mass
- $B_{s1}(5830)^0$
  mass
- $B_{s2}^*(5840)^0$
  mass
- $B_c^\pm$

Downloaded from https://academic.oup.com/ptep/article/2022/8/083C01/6651666 by KIT Library user on 27 September 2022

mass, mean life, branching fractions

At the end of Baryon Listings:

- Λ_b
  mass, mean life, branching fractions
- $\Lambda_b(5912)^0$
  mass, mean life
- $\Lambda_b(5920)^0$
  mass, mean life
- Σ_b
  mass
- Σ_b^*
  mass
- Ξ_b^0, Ξ_b^-
  mass, mean life, branching fractions
- $\Xi_b'(5935)^-$
  mass
- $\Xi_b(5945)^0$
  mass
- $\Xi_b^*(5955)^-$
  mass
- Ω_b^-
  mass, branching fractions
- b-baryon Admixture
  mean life, branching fractions

$B^\pm$ $\quad I(J^P) = \frac{1}{2}(0^-)$

I, J, P need confirmation. Quantum numbers shown are quark-model predictions.

Mass $m_{B^\pm} = 5279.34 \pm 0.12$ MeV
Mean life $\tau_{B^\pm} = (1.638 \pm 0.004) \times 10^{-12}$ s
$c\tau = 491.1\ \mu$m

CP violation

$A_{CP}(B^+ \to J/\psi(1S)K^+) = (1.8 \pm 3.0) \times 10^{-3}$ (S = 1.5)
$A_{CP}(B^+ \to J/\psi(1S)\pi^+) = (1.8 \pm 1.2) \times 10^{-2}$ (S = 1.3)
$A_{CP}(B^+ \to J/\psi\rho^+) = -0.05 \pm 0.05$
$A_{CP}(B^+ \to J/\psi K^*(892)^+) = -0.048 \pm 0.033$
$A_{CP}(B^+ \to \eta_c K^+) = 0.01 \pm 0.07$ (S = 2.2)
$A_{CP}(B^+ \to \psi(2S)\pi^+) = 0.03 \pm 0.06$
$A_{CP}(B^+ \to \psi(2S)K^+) = 0.012 \pm 0.020$ (S = 1.5)
$A_{CP}(B^+ \to \psi(2S)K^*(892)^+) = 0.08 \pm 0.21$
$A_{CP}(B^+ \to \chi_{c1}(1P)\pi^+) = 0.07 \pm 0.18$
$A_{CP}(B^+ \to \chi_{c0}K^+) = -0.20 \pm 0.18$ (S = 1.5)
$A_{CP}(B^+ \to \chi_{c1}K^+) = -0.009 \pm 0.033$
$A_{CP}(B^+ \to \chi_{c1}K^*(892)^+) = 0.5 \pm 0.5$
$A_{CP}(B^+ \to D^0\ell^+\nu_\ell) = (-0.14 \pm 0.20) \times 10^{-2}$
$A_{CP}(B^+ \to \overline{D}^0\pi^+) = -0.007 \pm 0.007$
$A_{CP}(B^+ \to D_{CP(+1)}\pi^+) = -0.0080 \pm 0.0024$
$A_{CP}(B^+ \to D_{CP(-1)}\pi^+) = 0.017 \pm 0.026$
$A_{CP}([K^\mp\pi^\pm\pi^+\pi^-]_D\pi^+) = 0.02 \pm 0.05$
$A_{CP}(B^+ \to [\pi^+\pi^+\pi^-\pi^-]_D K^+) = 0.10 \pm 0.04$
$A_{CP}(B^+ \to [\pi^+\pi^-\pi^+\pi^-]_D K^*(892)^+) = 0.02 \pm 0.11$
$A_{CP}(B^+ \to \overline{D}^0 K^+) = -0.017 \pm 0.005$
$A_{CP}([K^\mp\pi^\pm\pi^+\pi^-]_D K^+) = -0.31 \pm 0.11$
$A_{CP}(B^+ \to [\pi^+\pi^+\pi^-\pi^-]_D\pi^+) = (-4 \pm 8) \times 10^{-3}$
$A_{CP}(B^+ \to [K^-\pi^+]_D K^+) = -0.58 \pm 0.21$
$A_{CP}(B^+ \to [K^-\pi^+\pi^0]_D K^+) = 0.07 \pm 0.30$ (S = 1.5)
$A_{CP}(B^+ \to [K^+K^-\pi^0]_D K^+) = 0.30 \pm 0.20$
$A_{CP}(B^+ \to [\pi^+\pi^-\pi^0]_D K^+) = 0.05 \pm 0.09$
$A_{CP}(B^+ \to \overline{D}^0 K^*(892)^+) = -0.007 \pm 0.019$
$A_{CP}(B^+ \to [K^-\pi^+]_{\overline{D}} K^*(892)^+) = -0.75 \pm 0.16$
$A_{CP}(B^+ \to [K^-\pi^+\pi^-\pi^+]_{\overline{D}} K^*(892)^+) = -0.45 \pm 0.25$
$A_{CP}(B^+ \to [K^-\pi^+]_D\pi^+) = 0.00 \pm 0.09$
$A_{CP}(B^+ \to [K^-\pi^+\pi^0]_D\pi^+) = 0.35 \pm 0.16$
$A_{CP}(B^+ \to [K^+K^-\pi^0]_D\pi^+) = -0.03 \pm 0.04$
$A_{CP}(B^+ \to [\pi^+\pi^-\pi^0]_D\pi^+) = -0.016 \pm 0.020$
$A_{CP}(B^+ \to [K^-\pi^+]_{(D\pi)}\pi^+) = -0.09 \pm 0.27$
$A_{CP}(B^+ \to [K^-\pi^+]_{(D\gamma)}\pi^+) = -0.7 \pm 0.6$
$A_{CP}(B^+ \to [K^-\pi^+]_{(D\pi)}K^+) = 0.8 \pm 0.4$
$A_{CP}(B^+ \to [K^-\pi^+]_{(D\gamma)}K^+) = 0.4 \pm 1.0$
$A_{CP}(B^+ \to [\pi^+\pi^-\pi^0]_D K^+) = -0.02 \pm 0.15$
$A_{CP}(B^+ \to [K^0_S K^+\pi^-]_D K^+) = 0.10 \pm 0.09$
$A_{CP}(B^+ \to [K^0_S K^-\pi^+]_D K^+) = -0.04 \pm 0.08$
$A_{CP}(B^+ \to [K^0_S K^-\pi^+]_D\pi^+) = 0.003 \pm 0.015$
$A_{CP}(B^+ \to [K^0_S K^+\pi^-]_D\pi^+) = -0.034 \pm 0.020$
$A_{CP}(B^+ \to [K^*(892)^- K^+]_D K^+) = 0.08 \pm 0.05$
$A_{CP}(B^+ \to [K^*(892)^+ K^-]_D K^+) = 0.02 \pm 0.10$
$A_{CP}(B^+ \to [K^*(892)^+ K^-]_D\pi^+) = 0.007 \pm 0.017$
$A_{CP}(B^+ \to [K^*(892)^- K^+]_D\pi^+) = -0.020 \pm 0.011$
$\boldsymbol{A_{CP}(B^+ \to D_{CP(+1)}K^+)} = 0.132 \pm 0.015$ (S = 1.8)
$A_{ADS}(B^+ \to DK^+) = -0.451 \pm 0.026$
$A_{ADS}(B^+ \to D\pi^+) = 0.129 \pm 0.014$
$A_{ADS}(B^+ \to D^*(D\gamma)K^+) = -0.6 \pm 1.3$
$A_{ADS}(B^+ \to D^*(D\pi^0)K^+) = 0.72 \pm 0.29$
$A_{ADS}(B^+ \to D^*(D\gamma)\pi^+) = 0.08 \pm 0.13$
$A_{ADS}(B^+ \to D^*(D\pi^0)\pi^+) = -0.14 \pm 0.06$
$A_{ADS}(B^+ \to [K^-\pi^+]_D K^+\pi^-\pi^+) = -0.33 \pm 0.35$
$A_{ADS}(B^+ \to [K^-\pi^+]_D\pi^+\pi^-\pi^+) = -0.01 \pm 0.09$
$A_{CP}(B^+ \to D_{CP(-1)}K^+) = -0.10 \pm 0.07$
$A_{CP}(B^+ \to [K^+K^-]_D K^+\pi^-\pi^+) = -0.04 \pm 0.06$
$A_{CP}(B^+ \to [\pi^+\pi^-]_D K^+\pi^-\pi^+) = -0.05 \pm 0.10$
$A_{CP}(B^+ \to [K^-\pi^+]_D K^+\pi^-\pi^+) = 0.013 \pm 0.023$
$A_{CP}(B^+ \to [K^+K^-]_D\pi^+\pi^-\pi^+) = -0.019 \pm 0.015$
$A_{CP}(B^+ \to [\pi^+\pi^-]_D\pi^+\pi^-\pi^+) = -0.013 \pm 0.019$
$A_{CP}(B^+ \to [K^-\pi^+]_D\pi^+\pi^-\pi^+) = -0.002 \pm 0.011$
$A_{CP}(B^+ \to \overline{D}^{*0}\pi^+) = -0.0004 \pm 0.0021$ (S = 1.1)
$A_{CP}(B^+ \to (D^*_{CP(+1)})^0\pi^+) = 0.010 \pm 0.007$
$A_{CP}(B^+ \to (D^*_{CP(-1)})^0\pi^+) = -0.09 \pm 0.05$
$A_{CP}(B^+ \to D^{*0}K^+) = 0.012 \pm 0.010$ (S = 1.5)
$A_{CP}(B^+ \to D^0_{CP(+1)}K^+) = -0.09 \pm 0.05$ (S = 2.6)
$A_{CP}(B^+ \to D^*_{CP(-1)}K^+) = 0.07 \pm 0.10$
$A_{CP}(B^+ \to D_{CP(+1)}K^*(892)^+) = 0.08 \pm 0.06$
$A_{CP}(B^+ \to D_{CP(-1)}K^*(892)^+) = -0.23 \pm 0.22$
$A_{CP}(B^+ \to D_s^+\phi) = 0.0 \pm 0.4$
$A_{CP}(B^+ \to D_s^+\overline{D}^0) = (-0.4 \pm 0.7)\%$
$A_{CP}(B^+ \to D^{*+}\overline{D}^{*0}) = -0.15 \pm 0.11$
$A_{CP}(B^+ \to D^{*+}\overline{D}^0) = -0.06 \pm 0.13$
$A_{CP}(B^+ \to D^+\overline{D}^{*0}) = 0.13 \pm 0.18$
$A_{CP}(B^+ \to D^+\overline{D}^0) = 0.016 \pm 0.025$
$A_{CP}(B^+ \to K^0_S\pi^+) = -0.017 \pm 0.016$
$A_{CP}(B^+ \to K^+\pi^0) = 0.030 \pm 0.013$
$A_{CP}(B^+ \to \eta' K^+) = 0.004 \pm 0.011$
$A_{CP}(B^+ \to \eta' K^*(892)^+) = -0.26 \pm 0.27$
$A_{CP}(B^+ \to \eta' K^*_0(1430)^+) = 0.06 \pm 0.20$
$A_{CP}(B^+ \to \eta' K^*_2(1430)^+) = 0.15 \pm 0.13$
$\boldsymbol{A_{CP}(B^+ \to \eta K^+)} = -0.37 \pm 0.08$
$A_{CP}(B^+ \to \eta K^*(892)^+) = 0.02 \pm 0.06$
$A_{CP}(B^+ \to \eta K^*_0(1430)^+) = 0.05 \pm 0.13$
$A_{CP}(B^+ \to \eta K^*_2(1430)^+) = -0.45 \pm 0.30$
$A_{CP}(B^+ \to \omega K^+) = -0.02 \pm 0.04$
$A_{CP}(B^+ \to \omega K^{*+}) = 0.29 \pm 0.35$
$A_{CP}(B^+ \to \omega(K\pi)^{*+}_0) = -0.10 \pm 0.09$
$A_{CP}(B^+ \to \omega K^*_2(1430)^+) = 0.14 \pm 0.15$
$A_{CP}(B^+ \to K^{*0}\pi^+) = -0.04 \pm 0.09$ (S = 2.1)
$A_{CP}(B^+ \to K^*(892)^+\pi^0) = -0.39 \pm 0.21$ (S = 1.6)
$\boldsymbol{A_{CP}(B^+ \to K^+\pi^-\pi^+)} = 0.027 \pm 0.008$
$A_{CP}(B^+ \to K^+K^-K^+$ nonresonant$) = 0.06 \pm 0.05$
$A_{CP}(B^+ \to f(980)^0 K^+) = -0.08 \pm 0.09$
$\boldsymbol{A_{CP}(B^+ \to f_2(1270)K^+)} = -0.68^{+0.19}_{-0.17}$
$A_{CP}(B^+ \to f_0(1500)K^+) = 0.28 \pm 0.30$
$A_{CP}(B^+ \to f'_2(1525)^0 K^+) = -0.08^{+0.05}_{-0.04}$
$\boldsymbol{A_{CP}(B^+ \to \rho^0 K^+)} = 0.37 \pm 0.10$
$A_{CP}(B^+ \to K^0\pi^+\pi^0) = 0.07 \pm 0.06$
$A_{CP}(B^+ \to K^*_0(1430)^0\pi^+) = 0.061 \pm 0.032$
$A_{CP}(B^+ \to K^*_0(1430)^+\pi^0) = 0.26^{+0.18}_{-0.14}$
$A_{CP}(B^+ \to K^*_2(1430)^0\pi^+) = 0.05^{+0.29}_{-0.24}$

Downloaded from https://academic.oup.com/ptep/article/2022/8/083C01/6651666 by KIT Library user on 27 September 2022

$A_{CP}(B^+ \to K^+\pi^0\pi^0) = -0.06 \pm 0.07$
$A_{CP}(B^+ \to K^0\rho^+) = -0.03 \pm 0.15$
$A_{CP}(B^+ \to K^{*+}\pi^+\pi^-) = 0.07 \pm 0.08$
$A_{CP}(B^+ \to \rho^0 K^*(892)^+) = 0.31 \pm 0.13$
$A_{CP}(B^+ \to K^*(892)^+ f_0(980)) = -0.15 \pm 0.12$
$A_{CP}(B^+ \to a_1^+ K^0) = 0.12 \pm 0.11$
$A_{CP}(B^+ \to b_1^+ K^0) = -0.03 \pm 0.15$
$A_{CP}(B^+ \to K^*(892)^0\rho^+) = -0.01 \pm 0.16$
$A_{CP}(B^+ \to b_1^0 K^+) = -0.46 \pm 0.20$
$A_{CP}(B^+ \to K^0 K^+) = 0.04 \pm 0.14$
$A_{CP}(B^+ \to K_S^0 K^+) = -0.21 \pm 0.14$
$A_{CP}(B^+ \to K^+ K_S^0 K_S^0) = 0.025 \pm 0.031$
$\boldsymbol{A_{CP}(B^+ \to K^+K^-\pi^+)} = -0.122 \pm 0.021$
$A_{CP}(B^+ \to K^+K^-\pi^+ \text{ nonresonant}) = -0.11 \pm 0.06$
$A_{CP}(B^+ \to K^+\overline{K}^*(892)^0) = 0.12 \pm 0.10$
$A_{CP}(B^+ \to K^+\overline{K}_0^*(1430)^0) = 0.10 \pm 0.17$
$A_{CP}(B^+ \to \phi\pi^+) = 0.1 \pm 0.5$
$A_{CP}(B^+ \to \pi^+(K^+K^-)_{S-wave}) = -0.66 \pm 0.04$
$\boldsymbol{A_{CP}(B^+ \to K^+K^-K^+)} = -0.033 \pm 0.008$
$A_{CP}(B^+ \to \phi K^+) = 0.024 \pm 0.028$ (S = 2.3)
$A_{CP}(B^+ \to X_0(1550)K^+) = -0.04 \pm 0.07$
$A_{CP}(B^+ \to K^{*+}K^+K^-) = 0.11 \pm 0.09$
$A_{CP}(B^+ \to \phi K^*(892)^+) = -0.01 \pm 0.08$
$A_{CP}(B^+ \to \phi(K\pi)_0^{*+}) = 0.04 \pm 0.16$
$A_{CP}(B^+ \to \phi K_1(1270)^+) = 0.15 \pm 0.20$
$A_{CP}(B^+ \to \phi K_2^*(1430)^+) = -0.23 \pm 0.20$
$A_{CP}(B^+ \to K^+\phi\phi) = -0.08 \pm 0.07$
$A_{CP}(B^+ \to K^+[\phi\phi]_{\eta_c}) = 0.10 \pm 0.08$
$A_{CP}(B^+ \to K^*(892)^+\gamma) = 0.014 \pm 0.018$
$A_{CP}(B^+ \to X_s\gamma) = 0.028 \pm 0.019$
$A_{CP}(B^+ \to \eta K^+\gamma) = -0.12 \pm 0.07$
$A_{CP}(B^+ \to \phi K^+\gamma) = -0.13 \pm 0.11$ (S = 1.1)
$A_{CP}(B^+ \to \rho^+\gamma) = -0.11 \pm 0.33$
$A_{CP}(B^+ \to \pi^+\pi^0) = 0.03 \pm 0.04$
$\boldsymbol{A_{CP}(B^+ \to \pi^+\pi^-\pi^+)} = 0.057 \pm 0.013$
$A_{CP}(B^+ \to \rho^0\pi^+) = 0.009 \pm 0.019$
$A_{CP}(B^+ \to f_2(1270)\pi^+) = 0.40 \pm 0.06$
$A_{CP}(B^+ \to \rho^0(1450)\pi^+) = -0.11 \pm 0.05$
$A_{CP}(B^+ \to \rho_3(1690)\pi^+) = -0.80 \pm 0.28$
$\boldsymbol{A_{CP}(B^+ \to f_0(1370)\pi^+)} = 0.72 \pm 0.22$
$A_{CP}(B^+ \to \pi^+\pi^-\pi^+ \text{ nonresonant}) = -0.14^{+0.23}_{-0.16}$
$A_{CP}(B^+ \to \rho^+\pi^0) = 0.02 \pm 0.11$
$A_{CP}(B^+ \to \rho^+\rho^0) = -0.05 \pm 0.05$
$A_{CP}(B^+ \to \omega\pi^+) = -0.04 \pm 0.05$
$A_{CP}(B^+ \to \omega\rho^+) = -0.20 \pm 0.09$
$A_{CP}(B^+ \to \eta\pi^+) = -0.14 \pm 0.07$ (S = 1.4)
$A_{CP}(B^+ \to \eta\rho^+) = 0.11 \pm 0.11$
$A_{CP}(B^+ \to \eta'\pi^+) = 0.06 \pm 0.16$
$A_{CP}(B^+ \to \eta'\rho^+) = 0.26 \pm 0.17$
$A_{CP}(B^+ \to b_1^0\pi^+) = 0.05 \pm 0.16$
$A_{CP}(B^+ \to p\overline{p}\pi^+) = 0.00 \pm 0.04$
$A_{CP}(B^+ \to p\overline{p}K^+) = 0.00 \pm 0.04$ (S = 2.2)
$A_{CP}(B^+ \to p\overline{p}K^*(892)^+) = 0.21 \pm 0.16$ (S = 1.4)
$A_{CP}(B^+ \to p\overline{\Lambda}\gamma) = 0.17 \pm 0.17$
$A_{CP}(B^+ \to p\overline{\Lambda}\pi^0) = 0.01 \pm 0.17$
$A_{CP}(B^+ \to K^+\ell^+\ell^-) = -0.02 \pm 0.08$
$A_{CP}(B^+ \to K^+e^+e^-) = 0.14 \pm 0.14$
$A_{CP}(B^+ \to K^+\mu^+\mu^-) = 0.011 \pm 0.017$
$A_{CP}(B^+ \to \pi^+\mu^+\mu^-) = -0.11 \pm 0.12$
$A_{CP}(B^+ \to K^{*+}\ell^+\ell^-) = -0.09 \pm 0.14$
$A_{CP}(B^+ \to K^*e^+e^-) = -0.14 \pm 0.23$
$A_{CP}(B^+ \to K^*\mu^+\mu^-) = -0.12 \pm 0.24$
$\boldsymbol{\gamma} = (65.9^{+3.3}_{-3.5})^\circ$
$\boldsymbol{r_B(B^+ \to D^0K^+)} = 0.0994 \pm 0.0026$
$\boldsymbol{\delta_B(B^+ \to D^0K^+)} = (127.7^{+3.6}_{-3.9})^\circ$
$\boldsymbol{r_B(B^+ \to D^0K^{*+})} = 0.101^{+0.016}_{-0.034}$
$\boldsymbol{\delta_B(B^+ \to D^0K^{*+})} = (48^{+59}_{-16})^\circ$
$\boldsymbol{r_B(B^+ \to D^{*0}K^+)} = 0.104^{+0.013}_{-0.014}$
$\boldsymbol{\delta_B(B^+ \to D^{*0}K^+)} = (314.8^{+7.9}_{-9.9})^\circ$

B^- modes are charge conjugates of the modes below. Modes which do not identify the charge state of the B are listed in the $B^\pm/B^0$ ADMIXTURE section.

The branching fractions listed below assume 50% $B^0\overline{B}^0$ and 50% B^+B^- production at the $\Upsilon(4S)$. We have attempted to bring older measurements up to date by rescaling their assumed $\Upsilon(4S)$ production ratio to 50:50 and their assumed D, D_s, D^*, and ψ branching ratios to current values whenever this would affect our averages and best limits significantly.

Indentation is used to indicate a subchannel of a previous reaction. All resonant subchannels have been corrected for resonance branching fractions to the final state so the sum of the subchannel branching fractions can exceed that of the final state.

For inclusive branching fractions, *e.g.*, $B \to D^\pm X$, the values usually are multiplicities, not branching fractions. They can be greater than one.

B^+ DECAY MODES		Fraction (Γ_i/Γ)	Scale factor/ Confidence level	p (MeV/c)
Semileptonic and leptonic modes				
$\ell^+\nu_\ell X$	[iii]	(10.99 ± 0.28) %		–
$e^+\nu_e X_c$		(10.8 ± 0.4) %		–
$\ell^+\nu_\ell X_u$		$(1.65 \pm 0.21) \times 10^{-3}$		–
$D\ell^+\nu_\ell X$		(9.6 ± 0.7) %		–
$\overline{D}^0\ell^+\nu_\ell$	[iii]	(2.30 ± 0.09) %		2310
$\overline{D}^0\tau^+\nu_\tau$		$(7.7 \pm 2.5) \times 10^{-3}$		1911
$\overline{D}^*(2007)^0\ell^+\nu_\ell$	[iii]	(5.58 ± 0.22) %		2258
$\overline{D}^*(2007)^0\tau^+\nu_\tau$		(1.88 ± 0.20) %		1839
$D^-\pi^+\ell^+\nu_\ell$		$(4.4 \pm 0.4) \times 10^{-3}$		2306
$\overline{D}_0^*(2420)^0\ell^+\nu_\ell$, $\overline{D}_0^{*0} \to D^-\pi^+$		$(2.5 \pm 0.5) \times 10^{-3}$		–
$\overline{D}_2^*(2460)^0\ell^+\nu_\ell$, $\overline{D}_2^{*0} \to D^-\pi^+$		$(1.53 \pm 0.16) \times 10^{-3}$		2065
$D^{(*)}n\pi\ell^+\nu_\ell(n \geq 1)$		(1.85 ± 0.25) %		–
$D^{*-}\pi^+\ell^+\nu_\ell$		$(6.0 \pm 0.4) \times 10^{-3}$		2254
$\overline{D}_1(2420)^0\ell^+\nu_\ell$, $\overline{D}_1^0 \to D^{*-}\pi^+$		$(3.03 \pm 0.20) \times 10^{-3}$		2084
$\overline{D}_1'(2430)^0\ell^+\nu_\ell$, $\overline{D}_1'^0 \to D^{*-}\pi^+$		$(2.7 \pm 0.6) \times 10^{-3}$		–
$\overline{D}_2^*(2460)^0\ell^+\nu_\ell$, $\overline{D}_2^{*0} \to D^{*-}\pi^+$		$(1.01 \pm 0.24) \times 10^{-3}$	S=2.0	2065
$\overline{D}^0\pi^+\pi^-\ell^+\nu_\ell$		$(1.6 \pm 0.4) \times 10^{-3}$		2301
$\overline{D}^{*0}\pi^+\pi^-\ell^+\nu_\ell$		$(8 \pm 5) \times 10^{-4}$		2248
$D_s^{(*)-}K^+\ell^+\nu_\ell$		$(6.1 \pm 1.0) \times 10^{-4}$		–
$D_s^-K^+\ell^+\nu_\ell$		$(3.0 {}^{+1.4}_{-1.2}) \times 10^{-4}$		2242
$D_s^{*-}K^+\ell^+\nu_\ell$		$(2.9 \pm 1.9) \times 10^{-4}$		2185
$\pi^0\ell^+\nu_\ell$		$(7.80 \pm 0.27) \times 10^{-5}$		2638
$\eta\ell^+\nu_\ell$		$(3.9 \pm 0.5) \times 10^{-5}$		2611
$\eta'\ell^+\nu_\ell$		$(2.3 \pm 0.8) \times 10^{-5}$		2553
$\omega\ell^+\nu_\ell$	[iii]	$(1.19 \pm 0.09) \times 10^{-4}$		2582
$\rho^0\ell^+\nu_\ell$	[iii]	$(1.58 \pm 0.11) \times 10^{-4}$		2583
$\pi^+\pi^-\ell^+\nu_\ell$		$(2.3 \pm 0.4) \times 10^{-4}$		2636
$p\overline{p}\ell^+\nu_\ell$		$(5.8 {}^{+2.6}_{-2.3}) \times 10^{-6}$		2467
$p\overline{p}\mu^+\nu_\mu$		$(5.32 \pm 0.34) \times 10^{-6}$		2446
$p\overline{p}e^+\nu_e$		$(8.2 {}^{+4.0}_{-3.3}) \times 10^{-6}$		2467
$e^+\nu_e$		$< 9.8 \times 10^{-7}$	CL=90%	2640
$\mu^+\nu_\mu$		$< 8.6 \times 10^{-7}$	CL=90%	2639
$\tau^+\nu_\tau$		$(1.09 \pm 0.24) \times 10^{-4}$	S=1.2	2341
$\ell^+\nu_\ell\gamma$		$< 3.0 \times 10^{-6}$	CL=90%	2640
$e^+\nu_e\gamma$		$< 4.3 \times 10^{-6}$	CL=90%	2640
$\mu^+\nu_\mu\gamma$		$< 3.4 \times 10^{-6}$	CL=90%	2639
$\mu^+\mu^-\mu^+\nu_\mu$		$< 1.6 \times 10^{-8}$	CL=95%	2634
Inclusive modes				
D^0X		(8.6 ± 0.7) %		–
$\overline{D}^0X$		(79 ± 4) %		–
D^+X		(2.5 ± 0.5) %		–
D^-X		(9.9 ± 1.2) %		–
D_s^+X		$(7.9 {}^{+1.4}_{-1.3})$ %		–
D_s^-X		$(1.10 {}^{+0.40}_{-0.32})$ %		–
Λ_c^+X		$(2.1 {}^{+0.9}_{-0.6})$ %		–
$\overline{\Lambda}_c^-X$		$(2.8 {}^{+1.1}_{-0.9})$ %		–
$\overline{c}X$		(97 ± 4) %		–
cX		$(23.4 {}^{+2.2}_{-1.8})$ %		–
$c/\overline{c}X$		(120 ± 6) %		–

Downloaded from https://academic.oup.com/ptep/article/2022/8/083C01/6651666 by KIT Library user on 27 September 2022

D, D^*, or D_s modes

$\overline{D}^0 \pi^+$		$(4.68 \pm 0.13) \times 10^{-3}$		2308
$D_{CP(+1)} \pi^+$	[jjj]	$(2.05 \pm 0.20) \times 10^{-3}$		–
$D_{CP(-1)} \pi^+$	[jjj]	$(2.1 \pm 0.4) \times 10^{-3}$		–
$\overline{D}^0 \rho^+$		(1.34 ± 0.18) %		2237
$\overline{D}^0 K^+$		$(3.69 \pm 0.16) \times 10^{-4}$		2281
$D_{CP(+1)} K^+$	[jjj]	$(1.83 \pm 0.08) \times 10^{-4}$		–
$D_{CP(-1)} K^+$	[jjj]	$(1.99 \pm 0.19) \times 10^{-4}$		–
$D^0 K^+$		$(3.64 \pm 0.25) \times 10^{-6}$		2281
$[K^- \pi^+]_D K^+$	[kkk]	$< 2.8 \times 10^{-7}$	CL=90%	–
$[K^+ \pi^-]_D K^+$	[kkk]	$< 2.0 \times 10^{-5}$	CL=90%	–
$[K^- \pi^+ \pi^0]_D K^+$		seen		–
$[K^+ \pi^- \pi^0]_D K^+$		seen		–
$[K^- \pi^+ \pi^+ \pi^-]_D K^+$		seen		–
$[K^+ \pi^- \pi^+ \pi^-]_D K^+$		seen		–
$[K^- \pi^+]_D \pi^+$	[kkk]	$(6.3 \pm 1.1) \times 10^{-7}$		–
$[K^+ \pi^-]_D \pi^+$		$(1.7 \pm 0.4) \times 10^{-4}$		–
$[K^- \pi^+ \pi^0]_D \pi^+$		seen		–
$[K^+ \pi^- \pi^0]_D \pi^+$		seen		–
$[K^- \pi^+ \pi^+ \pi^-]_D \pi^+$		seen		–
$[K^+ \pi^- \pi^+ \pi^-]_D \pi^+$		seen		–
$[\pi^+ \pi^- \pi^0]_D K^-$		$(4.6 \pm 0.9) \times 10^{-6}$		–
$[K^0_S K^+ \pi^-]_D K^+$		seen		–
$[K^0_S K^- \pi^+]_D K^+$		seen		–
$[K^*(892)^+ K^-]_D K^+$		seen		–
$[K^0_S K^- \pi^+]_D \pi^+$		seen		–
$[K^*(892)^+ K^-]_D \pi^+$		seen		–
$[K^0_S K^+ \pi^-]_D \pi^+$		seen		–
$[K^*(892)^- K^+]_D \pi^+$		seen		–
$\overline{D}^0 K^*(892)^+$		$(5.3 \pm 0.4) \times 10^{-4}$		2213
$D_{CP(-1)} K^*(892)^+$	[jjj]	$(2.7 \pm 0.8) \times 10^{-4}$		–
$D_{CP(+1)} K^*(892)^+$	[jjj]	$(6.2 \pm 0.7) \times 10^{-4}$		–
$D^0 K^*(892)^+$		$(5.4 {}^{+1.8}_{-4.0}) \times 10^{-6}$		2213
$\overline{D}^0 K^+ \pi^+ \pi^-$		$(5.2 \pm 2.1) \times 10^{-4}$		2237
$\overline{D}^0 K^+ \overline{K}^0$		$(5.5 \pm 1.6) \times 10^{-4}$		2189
$\overline{D}^0 K^+ \overline{K}^*(892)^0$		$(7.5 \pm 1.7) \times 10^{-4}$		2072
$\overline{D}^0 \pi^+ \pi^+ \pi^-$		$(5.6 \pm 2.1) \times 10^{-3}$	S=3.6	2289
$\overline{D}^0 \pi^+ \pi^+ \pi^-$ nonresonant		$(5 \pm 4) \times 10^{-3}$		2289
$\overline{D}^0 \pi^+ \rho^0$		$(4.2 \pm 3.0) \times 10^{-3}$		2208
$\overline{D}^0 a_1(1260)^+$		$(4 \pm 4) \times 10^{-3}$		2123
$\overline{D}^0 \omega \pi^+$		$(4.1 \pm 0.9) \times 10^{-3}$		2206
$D^*(2010)^- \pi^+ \pi^+$		$(1.35 \pm 0.22) \times 10^{-3}$		2247
$D^*(2010)^- K^+ \pi^+$		$(8.2 \pm 1.4) \times 10^{-5}$		2206
$\overline{D}_1(2420)^0 \pi^+$, $\overline{D}^0_1 \to D^*(2010)^- \pi^+$		$(8.4 \pm 1.5) \times 10^{-4}$		2081
$D^- \pi^+ \pi^+$		$(1.07 \pm 0.05) \times 10^{-3}$		2299
$D^- K^+ \pi^+$		$(7.7 \pm 0.5) \times 10^{-5}$		2260
$D^*_0(2300)^0 K^+$, $D^{*0}_0 \to D^- \pi^+$		$(6.1 \pm 2.4) \times 10^{-6}$		–
$D^*_2(2460)^0 K^+$, $D^{*0}_2 \to D^- \pi^+$		$(2.32 \pm 0.23) \times 10^{-5}$		–
$D^*_1(2760)^0 K^+$, $D^{*0}_1 \to D^- \pi^+$		$(3.6 \pm 1.2) \times 10^{-6}$		–
$D^+ K^0$		$< 2.9 \times 10^{-6}$	CL=90%	2278
$D^+ K^+ \pi^-$		$(5.6 \pm 1.1) \times 10^{-6}$		2260
$D^*_2(2460)^0 K^+$, $D^{*0}_2 \to D^+ \pi^-$		$< 6.3 \times 10^{-7}$	CL=90%	–
$D^+ K^{*0}$		$< 4.9 \times 10^{-7}$	CL=90%	2211
$D^+ \overline{K}^{*0}$		$< 1.4 \times 10^{-6}$	CL=90%	2211
$\overline{D}^*(2007)^0 \pi^+$		$(5.18 \pm 0.15) \times 10^{-3}$		2256
$\overline{D}^{*0}_{CP(+1)} \pi^+$	[lll]	$(2.9 \pm 0.6) \times 10^{-3}$		–
$\overline{D}^{*0}_{CP(-1)} \pi^+$	[lll]	$(2.6 \pm 1.0) \times 10^{-3}$		–
$\overline{D}^*(2007)^0 \omega \pi^+$		$(4.5 \pm 1.2) \times 10^{-3}$		2149
$\overline{D}^*(2007)^0 \rho^+$		$(9.8 \pm 1.7) \times 10^{-3}$		2181
$\overline{D}^*(2007)^0 K^+$		$(4.20 {}^{+0.31}_{-0.28}) \times 10^{-4}$		2227
$\overline{D}^{*0}_{CP(+1)} K^+$	[lll]	$(2.75 \pm 0.35) \times 10^{-4}$		–
$\overline{D}^{*0}_{CP(-1)} K^+$	[lll]	$(2.31 \pm 0.31) \times 10^{-4}$		–
$D^*(2007)^0 K^+$		$(4.5 \pm 1.2) \times 10^{-6}$		2227
$\overline{D}^*(2007)^0 K^*(892)^+$		$(8.1 \pm 1.4) \times 10^{-4}$		2156
$\overline{D}^*(2007)^0 K^+ \overline{K}^0$		$< 1.06 \times 10^{-3}$	CL=90%	2132
$\overline{D}^*(2007)^0 K^+ \overline{K}^*(892)^0$		$(1.5 \pm 0.4) \times 10^{-3}$		2009
$\overline{D}^*(2007)^0 \pi^+ \pi^+ \pi^-$		(1.03 ± 0.12) %		2236
$\overline{D}^*(2007)^0 a_1(1260)^+$		(1.9 ± 0.5) %		2063
$\overline{D}^*(2007)^0 \pi^- \pi^+ \pi^+ \pi^0$		(1.8 ± 0.4) %		2219
$\overline{D}^{*0} 3\pi^+ 2\pi^-$		$(5.7 \pm 1.2) \times 10^{-3}$		2196
$D^*(2010)^+ \pi^0$		$< 3.6 \times 10^{-6}$		2255
$D^*(2010)^+ K^0$		$< 9.0 \times 10^{-6}$	CL=90%	2225
$D^*(2010)^- \pi^+ \pi^+ \pi^0$		(1.5 ± 0.7) %		2235
$D^*(2010)^- \pi^+ \pi^+ \pi^+ \pi^-$		$(2.6 \pm 0.4) \times 10^{-3}$		2217
$\overline{D}^{**0} \pi^+$	[nnn]	$(5.7 \pm 1.2) \times 10^{-3}$		–
$\overline{D}^*_1(2420)^0 \pi^+$		$(1.5 \pm 0.6) \times 10^{-3}$	S=1.3	2081
$\overline{D}_1(2420)^0 \pi^+ \times B(\overline{D}^0_1 \to \overline{D}^0 \pi^+ \pi^-)$		$(2.5 {}^{+1.6}_{-1.4}) \times 10^{-4}$	S=3.9	2081
$\overline{D}_1(2420)^0 \pi^+ \times B(\overline{D}^0_1 \to \overline{D}^0 \pi^+ \pi^-$ (nonresonant))		$(2.2 \pm 1.0) \times 10^{-4}$		2081
$\overline{D}_1(2430)^0 \pi^+$, $\overline{D}^0_1 \to D^*(2010)^- \pi^+$		$(3.5 \pm 0.6) \times 10^{-4}$		2079
$\overline{D}(2550)^0 \pi^+$, $\overline{D}^0 \to D^*(2010)^- \pi^+$		$(7.2 \pm 1.4) \times 10^{-5}$		–
$\overline{D}^*_J(2600)^0 \pi^+$, $\overline{D}^{*0}_J \to D^*(2010)^- \pi^+$		$(6.8 \pm 1.3) \times 10^{-5}$		–
$\overline{D}^*_2(2462)^0 \pi^+$, $\overline{D}^{*0}_2 \to D^- \pi^+$		$(3.56 \pm 0.24) \times 10^{-4}$		–
$\overline{D}^*_2(2462)^0 \pi^+$, $\overline{D}^{*0}_2 \to \overline{D}^0 \pi^- \pi^+$		$(2.2 \pm 1.0) \times 10^{-4}$		–
$\overline{D}^*_2(2462)^0 \pi^+$, $\overline{D}^{*0}_2 \to \overline{D}^0 \pi^- \pi^+$ (nonresonant)		$< 1.7 \times 10^{-4}$	CL=90%	–
$\overline{D}^*_2(2462)^0 \pi^+$, $\overline{D}^{*0}_2 \to D^*(2010)^- \pi^+$		$(2.2 \pm 1.1) \times 10^{-4}$		–
$\overline{D}^*_0(2400)^0 \pi^+ \times B(\overline{D}^*_0(2400)^0 \to D^- \pi^+)$		$(6.4 \pm 1.4) \times 10^{-4}$		2136
$\overline{D}_1(2421)^0 \pi^+$, $\overline{D}^0_1 \to D^{*-} \pi^+$		$(7.4 \pm 1.0) \times 10^{-4}$		–
$\overline{D}^*_2(2462)^0 \pi^+$, $\overline{D}^{*0}_2 \to D^{*-} \pi^+$		$(1.98 \pm 0.30) \times 10^{-4}$		–
$\overline{D}'_1(2427)^0 \pi^+$, $\overline{D}'^0_1 \to D^{*-} \pi^+$		$(3.5 \pm 0.9) \times 10^{-4}$	S=1.5	–
$\overline{D}_1(2420)^0 \pi^+ \times B(\overline{D}^0_1 \to \overline{D}^{*0} \pi^+ \pi^-)$		$< 6 \times 10^{-6}$	CL=90%	2081
$\overline{D}^*_1(2420)^0 \rho^+$		$< 1.4 \times 10^{-3}$	CL=90%	1996
$\overline{D}^*_2(2460)^0 \pi^+$		$< 1.3 \times 10^{-3}$	CL=90%	2063
$\overline{D}^*_2(2460)^0 \pi^+ \times B(\overline{D}^{*0}_2 \to \overline{D}^{*0} \pi^+ \pi^-)$		$< 2.2 \times 10^{-5}$	CL=90%	2063
$\overline{D}^*_1(2680)^0 \pi^+$, $\overline{D}^*_1(2680)^0 \to D^- \pi^+$		$(8.4 \pm 2.1) \times 10^{-5}$		–
$\overline{D}(2740)^0 \pi^+$, $\overline{D}^0 \to D^*(2010)^- \pi^+$		$(3.3 \pm 1.5) \times 10^{-5}$		–
$\overline{D}^*_3(2750)^0 \pi^+$, $\overline{D}^{*0}_3 \to D^*(2010)^- \pi^+$		$(1.10 \pm 0.32) \times 10^{-5}$		1913
$\overline{D}^*_3(2760)^0 \pi^+$, $\overline{D}^*_3(2760)^0 \pi^+ \to D^- \pi^+$		$(1.00 \pm 0.22) \times 10^{-5}$		–
$\overline{D}^*_2(3000)^0 \pi^+$, $\overline{D}^*_2(3000)^0 \pi^+ \to D^- \pi^+$		$(2.0 \pm 1.4) \times 10^{-6}$		–
$\overline{D}^*_2(2460)^0 \rho^+$		$< 4.7 \times 10^{-3}$	CL=90%	1977
$\overline{D}^0 D^+_s$		$(9.0 \pm 0.9) \times 10^{-3}$		1815
$D^*_{s0}(2317)^+ \overline{D}^0$, $D^{*+}_{s0} \to D^+_s \pi^0$		$(8.0 {}^{+1.6}_{-1.3}) \times 10^{-4}$		1605
$D_{s0}(2317)^+ \overline{D}^0 \times B(D_{s0}(2317)^+ \to D^{*+}_s \gamma)$		$< 7.6 \times 10^{-4}$	CL=90%	1605
$D_{s0}(2317)^+ \overline{D}^*(2007)^0 \times B(D_{s0}(2317)^+ \to D^+_s \pi^0)$		$(9 \pm 7) \times 10^{-4}$		1511
$D_{sJ}(2457)^+ \overline{D}^0$		$(3.1 {}^{+1.0}_{-0.9}) \times 10^{-3}$		–
$D_{sJ}(2457)^+ \overline{D}^0 \times B(D_{sJ}(2457)^+ \to D^+_s \gamma)$		$(4.6 {}^{+1.3}_{-1.1}) \times 10^{-4}$		–
$D_{sJ}(2457)^+ \overline{D}^0 \times B(D_{sJ}(2457)^+ \to D^+_s \pi^+ \pi^-)$		$< 2.2 \times 10^{-4}$	CL=90%	–
$D_{sJ}(2457)^+ \overline{D}^0 \times B(D_{sJ}(2457)^+ \to D^+_s \pi^0)$		$< 2.7 \times 10^{-4}$	CL=90%	–
$D_{sJ}(2457)^+ \overline{D}^0 \times B(D_{sJ}(2457)^+ \to D^{*+}_s \gamma)$		$< 9.8 \times 10^{-4}$	CL=90%	–
$D_{sJ}(2457)^+ \overline{D}^*(2007)^0$		(1.20 ± 0.30) %		–
$D_{sJ}(2457)^+ \overline{D}^*(2007)^0 \times B(D_{sJ}(2457)^+ \to D^+_s \gamma)$		$(1.4 {}^{+0.7}_{-0.6}) \times 10^{-3}$		–
$\overline{D}^0 D_{s1}(2536)^+ \times B(D_{s1}(2536)^+ \to D^*(2007)^0 K^+ + D^*(2010)^+ K^0)$		$(4.0 \pm 1.0) \times 10^{-4}$		1447

Downloaded from https://academic.oup.com/ptep/article/2022/8/083C01/6651666 by KIT Library user on 27 September 2022

$\overline{D}^0 D_{s1}(2536)^+ \times B(D_{s1}(2536)^+ \to D^*(2007)^0 K^+)$	$(2.2 \pm 0.7) \times 10^{-4}$			1447
$\overline{D}^*(2007)^0 D_{s1}(2536)^+ \times B(D_{s1}(2536)^+ \to D^*(2007)^0 K^+)$	$(5.5 \pm 1.6) \times 10^{-4}$			1339
$\overline{D}^0 D_{s1}(2536)^+ \times B(D_{s1}(2536)^+ \to D^{*+} K^0)$	$(2.3 \pm 1.1) \times 10^{-4}$			1447
$\overline{D}^0 D_{sJ}(2700)^+ \times B(D_{sJ}(2700)^+ \to D^0 K^+)$	$(5.6 \pm 1.8) \times 10^{-4}$	S=1.7		–
$\overline{D}^{*0} D_{s1}(2536)^+$, $D_{s1}^+ \to D^{*+} K^0$	$(3.9 \pm 2.6) \times 10^{-4}$			1339
$\overline{D}^0 D_{sJ}(2573)^+$, $D_{sJ}^+ \to D^0 K^+$	$(8 \pm 15) \times 10^{-6}$			–
$\overline{D}^{*0} D_{sJ}(2573)$, $D_{sJ}^+ \to D^0 K^+$	$< 2 \times 10^{-4}$	CL=90%		1306
$\overline{D}^*(2007)^0 D_{sJ}(2573)$, $D_{sJ}^+ \to D^0 K^+$	$< 5 \times 10^{-4}$	CL=90%		1306
$\overline{D}^0 D_s^{*+}$	$(7.6 \pm 1.6) \times 10^{-3}$			1734
$\overline{D}^*(2007)^0 D_s^+$	$(8.2 \pm 1.7) \times 10^{-3}$			1737
$\overline{D}^*(2007)^0 D_s^{*+}$	(1.71 ± 0.24) %			1651
$D_s^{(*)+} \overline{D}^{**0}$	(2.7 ± 1.2) %			–
$\overline{D}^*(2007)^0 D^*(2010)^+$	$(8.1 \pm 1.7) \times 10^{-4}$			1713
$\overline{D}^0 D^*(2010)^+ + \overline{D}^*(2007)^0 D^+$	< 1.30 %	CL=90%		1792
$\overline{D}^0 D^*(2010)^+$	$(3.9 \pm 0.5) \times 10^{-4}$			1792
$\overline{D}^0 D^+$	$(3.8 \pm 0.4) \times 10^{-4}$			1866
$\overline{D}^0 D^+ K^0$	$(1.55 \pm 0.21) \times 10^{-3}$			1571
$D^+ \overline{D}^*(2007)^0$	$(6.3 \pm 1.7) \times 10^{-4}$			1791
$\overline{D}^*(2007)^0 D^+ K^0$	$(2.1 \pm 0.5) \times 10^{-3}$			1475
$\overline{D}^0 D^*(2010)^+ K^0$	$(3.8 \pm 0.4) \times 10^{-3}$			1476
$\overline{D}^*(2007)^0 D^*(2010)^+ K^0$	$(9.2 \pm 1.2) \times 10^{-3}$			1362
$\overline{D}^0 D^0 K^+$	$(1.45 \pm 0.33) \times 10^{-3}$	S=2.6		1577
$\overline{D}^*(2007)^0 D^0 K^+$	$(2.26 \pm 0.23) \times 10^{-3}$			1481
$\overline{D}^0 D^*(2007)^0 K^+$	$(6.3 \pm 0.5) \times 10^{-3}$			1481
$\overline{D}^*(2007)^0 D^*(2007)^0 K^+$	(1.12 ± 0.13) %			1368
$D^- D^+ K^+$	$(2.2 \pm 0.7) \times 10^{-4}$			1571
$X_0(2900) D^+$, $X_0 \to D^- K^+$	$(1.2 \pm 0.5) \times 10^{-5}$			–
$X_1(2900) D^+$, $X_1 \to D^- K^+$	$(6.7 \pm 2.3) \times 10^{-5}$			–
$D^- D^+ K^+$ nonresonant	$(5.3 \pm 1.8) \times 10^{-5}$			1571
$D^- D^*(2010)^+ K^+$	$(6.3 \pm 1.1) \times 10^{-4}$			1475
$D^*(2010)^- D^+ K^+$	$(6.0 \pm 1.3) \times 10^{-4}$			1475
$D^*(2010)^- D^*(2010)^+ K^+$	$(1.32 \pm 0.18) \times 10^{-3}$			1363
$(\overline{D} + \overline{D}^*)(D + D^*) K$	(4.05 ± 0.30) %			–
$D_s^+ \pi^0$	$(1.6 \pm 0.5) \times 10^{-5}$			2270
$D_s^{*+} \pi^0$	$< 2.6 \times 10^{-4}$	CL=90%		2215
$D_s^+ \eta$	$< 4 \times 10^{-4}$	CL=90%		2235
$D_s^{*+} \eta$	$< 6 \times 10^{-4}$	CL=90%		2178
$D_s^+ \rho^0$	$< 3.0 \times 10^{-4}$	CL=90%		2197
$D_s^{*+} \rho^0$	$< 4 \times 10^{-4}$	CL=90%		2138
$D_s^+ \omega$	$< 4 \times 10^{-4}$	CL=90%		2195
$D_s^{*+} \omega$	$< 6 \times 10^{-4}$	CL=90%		2136
$D_s^+ a_1(1260)^0$	$< 1.8 \times 10^{-3}$	CL=90%		2079
$D_s^{*+} a_1(1260)^0$	$< 1.3 \times 10^{-3}$	CL=90%		2015
$D_s^+ K^+ K^-$	$(7.2 \pm 1.1) \times 10^{-6}$			2149
$D_s^+ \phi$	$< 4.2 \times 10^{-7}$	CL=90%		2141
$D_s^{*+} \phi$	$< 1.2 \times 10^{-5}$	CL=90%		2079
$D_s^+ \overline{K}^0$	$< 8 \times 10^{-4}$	CL=90%		2242
$D_s^{*+} \overline{K}^0$	$< 9 \times 10^{-4}$	CL=90%		2185
$D_s^+ \overline{K}^*(892)^0$	$< 4.4 \times 10^{-6}$	CL=90%		2172
$D_s^+ K^{*0}$	$< 3.5 \times 10^{-6}$	CL=90%		2172
$D_s^{*+} \overline{K}^*(892)^0$	$< 3.5 \times 10^{-4}$	CL=90%		2112
$D_s^- \pi^+ K^+$	$(1.80 \pm 0.22) \times 10^{-4}$			2222
$D_s^{*-} \pi^+ K^+$	$(1.45 \pm 0.24) \times 10^{-4}$			2164
$D_s^- \pi^+ K^*(892)^+$	$< 5 \times 10^{-3}$	CL=90%		2138
$D_s^{*-} \pi^+ K^*(892)^+$	$< 7 \times 10^{-3}$	CL=90%		2076
$D_s^- K^+ K^+$	$(9.7 \pm 2.1) \times 10^{-6}$			2149
$D_s^{*-} K^+ K^+$	$< 1.5 \times 10^{-5}$	CL=90%		2088

Charmonium modes

$\eta_c K^+$	$(1.09 \pm 0.08) \times 10^{-3}$			1751
$\eta_c K^+$, $\eta_c \to K_S^0 K^\mp \pi^\pm$	$(2.7 \pm 0.6) \times 10^{-5}$			–
$\eta_c K^*(892)^+$	$(1.1 {}^{+0.5}_{-0.4}) \times 10^{-3}$			1646
$\eta_c K^+ \pi^+ \pi^-$	$< 3.9 \times 10^{-4}$	CL=90%		1684
$\eta_c K^+ \omega(782)$	$< 5.3 \times 10^{-4}$	CL=90%		1475
$\eta_c K^+ \eta$	$< 2.2 \times 10^{-4}$	CL=90%		1588
$\eta_c K^+ \pi^0$	$< 6.2 \times 10^{-5}$	CL=90%		1723
$\eta_c(2S) K^+$	$(4.4 \pm 1.0) \times 10^{-4}$			1320
$\eta_c(2S) K^+$, $\eta_c \to p\overline{p}$	$(3.5 \pm 0.8) \times 10^{-8}$			–
$\eta_c(2S) K^+$, $\eta_c \to K_S^0 K^\mp \pi^\pm$	$(3.4 {}^{+2.3}_{-1.6}) \times 10^{-6}$			–
$\eta_c(2S) K^+$, $\eta_c \to p\overline{p}\pi^+\pi^-$	$(1.12 \pm 0.18) \times 10^{-6}$			–
$h_c(1P) K^+$, $h_c \to J/\psi \pi^+ \pi^-$	$< 3.4 \times 10^{-6}$	CL=90%		1401
$X(3730)^0 K^+$, $X^0 \to \eta_c \eta$	$< 4.6 \times 10^{-5}$	CL=90%		–
$X(3730)^0 K^+$, $X^0 \to \eta_c \pi^0$	$< 5.7 \times 10^{-6}$	CL=90%		–
$\eta_{c2}(1D) K^+$, $\eta_{c2} \to h_c \gamma$	$< 3.7 \times 10^{-5}$	CL=90%		–
$\eta_{c2}(1D) \pi^+ K_S^0$, $\eta_{c2} \to h_c \gamma$	$< 1.1 \times 10^{-4}$	CL=90%		–
$\psi_2(3823) K^+$, $\psi_2 \to J/\psi \pi^+ \pi^-$	$(2.8 \pm 0.6) \times 10^{-7}$			–
$\chi_{c1}(3872) K^+$	$(2.1 \pm 0.7) \times 10^{-4}$			1141
$\chi_{c0}(3915) K^+$	$< 2.8 \times 10^{-4}$	CL=90%		1101
$\chi_{c0}(3915) K^+$, $\chi_{c0} \to D^+ D^-$	$(8.1 \pm 3.3) \times 10^{-6}$			–
$\chi_{c0}(3915) K^+$, $\chi_{c0} \to \eta_c \eta$	$< 4.7 \times 10^{-5}$	CL=90%		–
$(Xchi)_{c0}(3915) K^+$, $\chi_{c0} \to \eta_c \pi^0$	$< 1.7 \times 10^{-5}$	CL=90%		–
$X(4014)^0 K^+$, $X^0 \to \eta_c \eta$	$< 3.9 \times 10^{-5}$	CL=90%		–
$X(4014)^0 K^+$, $X^0 \to \eta_c \pi^0$	$< 1.2 \times 10^{-5}$	CL=90%		–
$Z_c(3900)^0 K^+$, $Z_c^0 \to \eta_c \pi^+ \pi^-$	$< 4.7 \times 10^{-5}$	CL=90%		–
$X(4020)^0 K^+$, $X^0 \to \eta_c \pi^+ \pi^-$	$< 1.6 \times 10^{-5}$	CL=90%		–
$\chi_{c1}(3872) K^*(892)^+$	$< 6 \times 10^{-4}$	CL=90%		940
$\chi_{c1}(3872)^+ K^0$, $\chi_{c1}^+ \to J/\psi(1S) \pi^+ \pi^0$ [ooo]	$< 6.1 \times 10^{-6}$	CL=90%		–
$\chi_{c1}(3872) K^0 \pi^+$	$(2.8 \pm 1.2) \times 10^{-4}$			1085
$Z_c(4430)^+ K^0$, $Z_c^+ \to J/\psi \pi^+$	$< 1.5 \times 10^{-5}$	CL=95%		–
$Z_c(4430)^+ K^0$, $Z_c^+ \to \psi(2S) \pi^+$	$< 4.7 \times 10^{-5}$	CL=95%		–
$\psi(4230)^0 K^+$, $\psi^0 \to J/\psi \pi^+ \pi^-$	$< 1.56 \times 10^{-5}$	CL=95%		–
$\chi_{c0}(3915) K^+$, $\chi_{c0} \to J/\psi \gamma$	$< 1.4 \times 10^{-5}$	CL=90%		–
$\chi_{c0}(3915) K^+$, $\chi_{c0} \to \chi_{c1}(1P) \pi^0$	$< 3.8 \times 10^{-5}$	CL=90%		–
$X(3930)^0 K^+$, $X^0 \to J/\psi \gamma$	$< 2.5 \times 10^{-6}$	CL=90%		–
$J/\psi(1S) K^+$	$(1.020 \pm 0.019) \times 10^{-3}$			1684
$J/\psi(1S) K^0 \pi^+$	$(1.14 \pm 0.11) \times 10^{-3}$			1651
$J/\psi(1S) K^+ \pi^+ \pi^-$	$(8.1 \pm 1.3) \times 10^{-4}$	S=2.5		1612
$J/\psi(1S) K^+ K^- K^+$	$(3.37 \pm 0.29) \times 10^{-5}$			1252
$\chi_{c0}(3915) K^+$, $\chi_{c0} \to p\overline{p}$	$< 7.1 \times 10^{-8}$	CL=95%		–
$J/\psi(1S) K^*(892)^+$	$(1.43 \pm 0.08) \times 10^{-3}$			1571
$J/\psi(1S) K(1270)^+$	$(1.8 \pm 0.5) \times 10^{-3}$			1402
$J/\psi(1S) K(1400)^+$	$< 5 \times 10^{-4}$	CL=90%		1308
$J/\psi(1S) \eta K^+$	$(1.24 \pm 0.14) \times 10^{-4}$			1510
$\chi_{c1-odd}(3872) K^+$, $\chi_{c1-odd} \to J/\psi \eta$	$< 3.8 \times 10^{-6}$	CL=90%		–
$\psi(4160) K^+$, $\psi \to J/\psi \eta$	$< 7.4 \times 10^{-6}$	CL=90%		–
$J/\psi(1S) \eta' K^+$	$< 8.8 \times 10^{-5}$	CL=90%		1273
$J/\psi(1S) \phi K^+$	$(5.0 \pm 0.4) \times 10^{-5}$			1227
$J/\psi(1S) K_1(1650)$, $K_1 \to \phi K^+$	$(6 {}^{+10}_{-6}) \times 10^{-6}$			–
$J/\psi(1S) K^*(1680)^+$, $K^* \to \phi K^+$	$(3.4 {}^{+1.9}_{-2.2}) \times 10^{-6}$			–
$J/\psi(1S) K_2^*(1980)$, $K_2^* \to \phi K^+$	$(1.5 {}^{+0.9}_{-0.5}) \times 10^{-6}$			–
$J/\psi(1S) K(1830)^+$, $K(1830)^+ \to \phi K^+$	$(1.3 {}^{+1.3}_{-1.1}) \times 10^{-6}$			–
$\chi_{c1}(4140) K^+$, $\chi_{c1} \to J/\psi(1S) \phi$	$(10 \pm 4) \times 10^{-6}$			–
$\chi_{c1}(4274) K^+$, $\chi_{c1} \to J/\psi(1S) \phi$	$(3.6 {}^{+2.2}_{-1.8}) \times 10^{-6}$			–
$\chi_{c0}(4500) K^+$, $\chi_c^0 \to J/\psi(1S) \phi$	$(3.3 {}^{+2.1}_{-1.7}) \times 10^{-6}$			–
$\chi_{c0}(4700) K^+$, $\chi_{c0} \to J/\psi(1S) \phi$	$(6 {}^{+5}_{-4}) \times 10^{-6}$			–
$J/\psi(1S) \omega K^+$	$(3.20 {}^{+0.60}_{-0.32}) \times 10^{-4}$			1388
$\chi_{c0}(3915) K^+$, $\chi_{c0} \to J/\psi \omega$	$(3.0 {}^{+0.9}_{-0.7}) \times 10^{-5}$			1103

Downloaded from https://academic.oup.com/ptep/article/2022/8/083C01/6651666 by KIT Library user on 27 September 2022

$J/\psi(1S)\pi^+$	$(3.92 \pm 0.08)\times10^{-5}$		1728
$J/\psi(1S)\pi^+\pi^+\pi^+\pi^-\pi^-$	$(1.17 \pm 0.13)\times10^{-5}$		1635
$\psi(2S)\pi^+\pi^+\pi^-$	$(1.9 \pm 0.4)\times10^{-5}$		1304
$J/\psi(1S)\rho^+$	$(4.1 \pm 0.5)\times10^{-5}$	S=1.4	1611
$J/\psi(1S)\pi^+\pi^0$ nonresonant	$< 7.3 \times10^{-6}$	CL=90%	1717
$J/\psi(1S)a_1(1260)^+$	$< 1.2 \times10^{-3}$	CL=90%	1415
$J/\psi(1S)p\overline{p}\pi^+$	$< 5.0 \times10^{-7}$	CL=90%	643
$J/\psi(1S)p\overline{\Lambda}$	$(1.46 \pm 0.12)\times10^{-5}$		567
$J/\psi(1S)\overline{\Sigma}^0 p$	$< 1.1 \times10^{-5}$	CL=90%	–
$J/\psi(1S)D^+$	$< 1.2 \times10^{-4}$	CL=90%	871
$J/\psi(1S)\overline{D}^0\pi^+$	$< 2.5 \times10^{-5}$	CL=90%	665
$\psi(2S)\pi^+$	$(2.44 \pm 0.30)\times10^{-5}$		1347
$\psi(2S)K^+$	$(6.24 \pm 0.20)\times10^{-4}$		1284
$\psi(2S)K^*(892)^+$	$(6.7 \pm 1.4)\times10^{-4}$	S=1.3	1116
$\psi(2S)K^+\pi^+\pi^-$	$(4.3 \pm 0.5)\times10^{-4}$		1179
$\psi(2S)\phi(1020)K^+$	$(4.0 \pm 0.7)\times10^{-6}$		418
$\psi(3770)K^+$	$(4.3 \pm 1.1)\times10^{-4}$		1218
$\psi(3770)K+, \psi \to D^0\overline{D}^0$	$(1.5 \pm 0.5)\times10^{-4}$	S=1.4	1218
$\psi(3770)K+, \psi \to D^+D^-$	$(9.4 \pm 3.5)\times10^{-5}$		1218
$\psi(3770)K^+,\ \psi \to p\overline{p}$	$< 2 \times10^{-7}$	CL=95%	–
$\psi(4040)K^+$	$< 1.3 \times10^{-4}$	CL=90%	1003
$\psi(4040)K^+,\ \psi \to D^+D^-$	$(1.1 \pm 0.5)\times10^{-5}$		–
$\psi(4160)K^+$	$(5.1 \pm 2.7)\times10^{-4}$		868
$\psi(4160)K^+,\ \psi \to \overline{D}^0D^0$	$(8 \pm 5)\times10^{-5}$		–
$\psi(4160)K^+,\ \psi \to D^+D^-$	$(1.5 \pm 0.6)\times10^{-5}$		–
$\psi(4415)K^+,\ \psi \to D^+D^-$	$(2.0 \pm 0.8)\times10^{-5}$		–
$\chi_{c0}\pi^+,\ \chi_{c0} \to \pi^+\pi^-$	$< 1 \times10^{-7}$	CL=90%	1531
$\chi_{c0}K^+$	$(1.51 {}^{+0.15}_{-0.13})\times10^{-4}$		1478
$\chi_{c0}K^*(892)^+$	$< 2.1 \times10^{-4}$	CL=90%	1341
$\chi_{c1}(1P)\pi^+$	$(2.2 \pm 0.5)\times10^{-5}$		1468
$\chi_{c1}(1P)K^+$	$(4.74 \pm 0.22)\times10^{-4}$		1412
$\chi_{c1}(1P)K^*(892)^+$	$(3.0 \pm 0.6)\times10^{-4}$	S=1.1	1265
$\chi_{c1}(1P)K^0\pi^+$	$(5.8 \pm 0.4)\times10^{-4}$		1370
$\chi_{c1}(1P)K^+\pi^0$	$(3.29 \pm 0.35)\times10^{-4}$		1373
$\chi_{c1}(1P)K^+\pi^+\pi^-$	$(3.74 \pm 0.30)\times10^{-4}$		1319
$\chi_{c1}(2P)K^+,\ \chi_{c1}(2P) \to \pi^+\pi^-\chi_{c1}(1P)$	$< 1.1 \times10^{-5}$	CL=90%	–
$\chi_{c2}K^+$	$(1.1 \pm 0.4)\times10^{-5}$		1379
$\chi_{c2}K^+,\ \chi_{c2} \to p\overline{p}\pi^+\pi^-$	$< 1.9 \times10^{-7}$		–
$\chi_{c2}K^*(892)^+$	$< 1.2 \times10^{-4}$	CL=90%	1228
$\chi_{c2}K^0\pi^+$	$(1.16 \pm 0.25)\times10^{-4}$		1336
$\chi_{c2}K^+\pi^0$	$< 6.2 \times10^{-5}$	CL=90%	1339
$\chi_{c2}K^+\pi^+\pi^-$	$(1.34 \pm 0.19)\times10^{-4}$		1284
$\chi_{c2}(3930)K^+,\ \chi_{c2} \to D^+D^-$	$(1.6 \pm 0.6)\times10^{-5}$		–
$\chi_{c2}(3930)\pi^+,\ \chi_{c2} \to \pi^+\pi^-$	$< 1 \times10^{-7}$	CL=90%	1437
$h_c(1P)K^+$	$(3.7 \pm 1.2)\times10^{-5}$		1401
$h_c(1P)K^+,\ h_c \to p\overline{p}$	$< 6.4 \times10^{-8}$	CL=95%	–

K or *K** modes

$K^0\pi^+$	$(2.37 \pm 0.08)\times10^{-5}$		2614
$K^+\pi^0$	$(1.29 \pm 0.05)\times10^{-5}$		2615
$\eta' K^+$	$(7.04 \pm 0.25)\times10^{-5}$		2528
$\eta' K^*(892)^+$	$(4.8 {}^{+1.8}_{-1.6})\times10^{-6}$		2472
$\eta' K_0^*(1430)^+$	$(5.2 \pm 2.1)\times10^{-6}$		–
$\eta' K_2^*(1430)^+$	$(2.8 \pm 0.5)\times10^{-5}$		2346
ηK^+	$(2.4 \pm 0.4)\times10^{-6}$	S=1.7	2588
$\eta K^*(892)^+$	$(1.93 \pm 0.16)\times10^{-5}$		2534
$\eta K_0^*(1430)^+$	$(1.8 \pm 0.4)\times10^{-5}$		–
$\eta K_2^*(1430)^+$	$(9.1 \pm 3.0)\times10^{-6}$		2414
$\eta(1295)K^+ \times B(\eta(1295) \to \eta\pi\pi)$	$(2.9 {}^{+0.8}_{-0.7})\times10^{-6}$		2455
$\eta(1405)K^+ \times B(\eta(1405) \to \eta\pi\pi)$	$< 1.3 \times10^{-6}$	CL=90%	2425
$\eta(1405)K^+ \times B(\eta(1405) \to K^*K)$	$< 1.2 \times10^{-6}$	CL=90%	2425
$\eta(1475)K^+ \times B(\eta(1475) \to K^*K)$	$(1.38 {}^{+0.21}_{-0.18})\times10^{-5}$		2407
$f_1(1285)K^+$	$< 2.0 \times10^{-6}$	CL=90%	2458
$f_1(1420)K^+ \times B(f_1(1420) \to \eta\pi\pi)$	$< 2.9 \times10^{-6}$	CL=90%	2420
$f_1(1420)K^+ \times B(f_1(1420) \to K^*K)$	$< 4.1 \times10^{-6}$	CL=90%	2420
$\phi(1680)K^+ \times B(\phi(1680) \to K^*K)$	$< 3.4 \times10^{-6}$	CL=90%	2344
$f_0(1500)K^+$	$(3.7 \pm 2.2)\times10^{-6}$		2398
ωK^+	$(6.5 \pm 0.4)\times10^{-6}$		2558
$\omega K^*(892)^+$	$< 7.4 \times10^{-6}$	CL=90%	2503
$\omega(K\pi)_0^{*+}$	$(2.8 \pm 0.4)\times10^{-5}$		–
$\omega K_0^*(1430)^+$	$(2.4 \pm 0.5)\times10^{-5}$		–
$\omega K_2^*(1430)^+$	$(2.1 \pm 0.4)\times10^{-5}$		2379
$a_0(980)^+K^0 \times B(a_0(980)^+ \to \eta\pi^+)$	$< 3.9 \times10^{-6}$	CL=90%	–
$a_0(980)^0K^+ \times B(a_0(980)^0 \to \eta\pi^0)$	$< 2.5 \times10^{-6}$	CL=90%	–
$K^*(892)^0\pi^+$	$(1.01 \pm 0.08)\times10^{-5}$		2562
$K^*(892)^+\pi^0$	$(6.8 \pm 0.9)\times10^{-6}$		2563
$K^+\pi^-\pi^+$	$(5.10 \pm 0.29)\times10^{-5}$		2609
$K^+\pi^-\pi^+$ nonresonant	$(1.63 {}^{+0.21}_{-0.15})\times10^{-5}$		2609
$\omega(782)K^+$	$(6 \pm 9)\times10^{-6}$		2558
$K^+f_0(980) \times B(f_0(980) \to \pi^+\pi^-)$	$(9.4 {}^{+1.0}_{-1.2})\times10^{-6}$		2522
$f_2(1270)^0K^+$	$(1.07 \pm 0.27)\times10^{-6}$		–
$f_0(1370)^0K^+ \times B(f_0(1370)^0 \to \pi^+\pi^-)$	$< 1.07 \times10^{-5}$	CL=90%	–
$\rho^0(1450)K^+ \times B(\rho^0(1450) \to \pi^+\pi^-)$	$< 1.17 \times10^{-5}$	CL=90%	–
$f_2'(1525)K^+ \times B(f_2'(1525) \to \pi^+\pi^-)$	$< 3.4 \times10^{-6}$	CL=90%	2394
$K^+\rho^0$	$(3.7 \pm 0.5)\times10^{-6}$		2559
$K_0^*(1430)^0\pi^+$	$(3.9 {}^{+0.6}_{-0.5})\times10^{-5}$	S=1.4	2445
$K_2^*(1430)^0\pi^+$	$(5.6 {}^{+2.2}_{-1.5})\times10^{-6}$		2445
$K^*(1410)^0\pi^+$	$< 4.5 \times10^{-5}$	CL=90%	2448
$K^*(1680)^0\pi^+$	$< 1.2 \times10^{-5}$	CL=90%	2358
$K^+\pi^0\pi^0$	$(1.62 \pm 0.19)\times10^{-5}$		2610
$f_0(980)K^+ \times B(f_0 \to \pi^0\pi^0)$	$(2.8 \pm 0.8)\times10^{-6}$		2522
$K^-\pi^+\pi^+$	$< 4.6 \times10^{-8}$	CL=90%	2609
$K^-\pi^+\pi^+$ nonresonant	$< 5.6 \times10^{-5}$	CL=90%	2609
$K_1(1270)^0\pi^+$	$< 4.0 \times10^{-5}$	CL=90%	2489
$K_1(1400)^0\pi^+$	$< 3.9 \times10^{-5}$	CL=90%	2451
$K^0\pi^+\pi^0$	$< 6.6 \times10^{-5}$	CL=90%	2609
$K_0^*(1430)^+\pi^0$	$(1.19 {}^{+0.20}_{-0.23})\times10^{-5}$		–
$K^0\rho^+$	$(7.3 {}^{+1.0}_{-1.2})\times10^{-6}$		2558
$K^*(892)^+\pi^+\pi^-$	$(7.5 \pm 1.0)\times10^{-5}$		2557
$K^*(892)^+\rho^0$	$(4.6 \pm 1.1)\times10^{-6}$		2504
$K^*(892)^+f_0(980)$	$(4.2 \pm 0.7)\times10^{-6}$		2466
$a_1^+K^0$	$(3.5 \pm 0.7)\times10^{-5}$		–
$b_1^+K^0 \times B(b_1^+ \to \omega\pi^+)$	$(9.6 \pm 1.9)\times10^{-6}$		–
$K^*(892)^0\rho^+$	$(9.2 \pm 1.5)\times10^{-6}$		2504
$K_1(1400)^+\rho^0$	$< 7.8 \times10^{-4}$	CL=90%	2388
$K_2^*(1430)^+\rho^0$	$< 1.5 \times10^{-3}$	CL=90%	2381
$b_1^0K^+ \times B(b_1^0 \to \omega\pi^0)$	$(9.1 \pm 2.0)\times10^{-6}$		–
$b_1^+K^{*0} \times B(b_1^+ \to \omega\pi^+)$	$< 5.9 \times10^{-6}$	CL=90%	–
$b_1^0K^{*+} \times B(b_1^0 \to \omega\pi^0)$	$< 6.7 \times10^{-6}$	CL=90%	–
$K^+\overline{K}^0$	$(1.31 \pm 0.17)\times10^{-6}$	S=1.2	2593
$\overline{K}^0K^+\pi^0$	$< 2.4 \times10^{-5}$	CL=90%	2578
$K^+K_S^0K_S^0$	$(1.05 \pm 0.04)\times10^{-5}$		2521
$f_0(980)K^+,\ f_0 \to K_S^0K_S^0$	$(1.47 \pm 0.33)\times10^{-5}$		–
$f_0(1710)K^+,\ f_0 \to K_S^0K_S^0$	$(4.8 {}^{+4.0}_{-2.6})\times10^{-7}$		–
$K^+K_S^0K_S^0$ nonresonant	$(2.0 \pm 0.4)\times10^{-5}$		2521
$K_S^0K_S^0\pi^+$	$< 5.1 \times10^{-7}$	CL=90%	2577
$K^+K^-\pi^+$	$(5.2 \pm 0.4)\times10^{-6}$		2578
$K^+K^-\pi^+$ nonresonant	$(1.68 \pm 0.26)\times10^{-6}$		2578
$K^+\overline{K}^*(892)^0$	$(5.9 \pm 0.8)\times10^{-7}$		2540
$K^+\overline{K}_0^*(1430)^0$	$(3.8 \pm 1.3)\times10^{-7}$		2421
$\pi^+(K^+K^-)_{S-wave}$	$(8.5 \pm 0.9)\times10^{-7}$		2578
$K^+K^+\pi^-$	$< 1.1 \times10^{-8}$	CL=90%	2578
$K^+K^+\pi^-$ nonresonant	$< 8.79 \times10^{-5}$	CL=90%	2578
$f_2'(1525)K^+$	$(1.8 \pm 0.5)\times10^{-6}$	S=1.1	2394
$K^{*+}\pi^+K^-$	$< 1.18 \times10^{-5}$	CL=90%	2524
$K^*(892)^+K^*(892)^0$	$(9.1 \pm 2.9)\times10^{-7}$		2485
$K^{*+}K^+\pi^-$	$< 6.1 \times10^{-6}$	CL=90%	2524
$K^+K^-K^+$	$(3.40 \pm 0.14)\times10^{-5}$	S=1.4	2523
$K^+\phi$	$(8.8 {}^{+0.7}_{-0.6})\times10^{-6}$	S=1.1	2516
$f_0(980)K^+ \times B(f_0(980) \to K^+K^-)$	$(9.4 \pm 3.2)\times10^{-6}$		2522
$a_2(1320)K^+ \times B(a_2(1320) \to K^+K^-)$	$< 1.1 \times10^{-6}$	CL=90%	2449

Downloaded from https://academic.oup.com/ptep/article/2022/8/083C01/6651666 by KIT Library user on 27 September 2022

$X_0(1550)K^+ \times B(X_0(1550) \to K^+K^-)$	$(4.3 \pm 0.7) \times 10^{-6}$			–
$\phi(1680)K^+ \times B(\phi(1680) \to K^+K^-)$	$< 8 \times 10^{-7}$	CL=90%		2344
$f_0(1710)K^+ \times B(f_0(1710) \to K^+K^-)$	$(1.1 \pm 0.6) \times 10^{-6}$			2336
$K^+K^-K^+$ nonresonant	$(2.38 {}^{+0.28}_{-0.50}) \times 10^{-5}$			2523
$K^*(892)^+K^+K^-$	$(3.6 \pm 0.5) \times 10^{-5}$			2466
$K^*(892)^+\phi$	$(10.0 \pm 2.0) \times 10^{-6}$	S=1.7		2460
$\phi(K\pi)_0^{*+}$	$(8.3 \pm 1.6) \times 10^{-6}$			–
$\phi K_1(1270)^+$	$(6.1 \pm 1.9) \times 10^{-6}$			2380
$\phi K_1(1400)^+$	$< 3.2 \times 10^{-6}$	CL=90%		2339
$\phi K^*(1410)^+$	$< 4.3 \times 10^{-6}$	CL=90%		–
$\phi K_0^*(1430)^+$	$(7.0 \pm 1.6) \times 10^{-6}$			–
$\phi K_2^*(1430)^+$	$(8.4 \pm 2.1) \times 10^{-6}$			2332
$\phi K_2^*(1770)^+$	$< 1.50 \times 10^{-5}$	CL=90%		–
$\phi K_2^*(1820)^+$	$< 1.63 \times 10^{-5}$	CL=90%		–
$a_1^+K^{*0}$	$< 3.6 \times 10^{-6}$	CL=90%		–
$K^+\phi\phi$	$(4.2 \pm 0.8) \times 10^{-6}$	S=2.2		2306
$\eta'\eta'K^+$	$< 2.5 \times 10^{-5}$	CL=90%		2338
$\omega\phi K^+$	$< 1.9 \times 10^{-6}$	CL=90%		2374
$X(1812)K^+ \times B(X \to \omega\phi)$	$< 3.2 \times 10^{-7}$	CL=90%		–
$K^*(892)^+\gamma$	$(3.92 \pm 0.22) \times 10^{-5}$	S=1.7		2564
$K_1(1270)^+\gamma$	$(4.4 {}^{+0.7}_{-0.6}) \times 10^{-5}$			2491
$\eta K^+\gamma$	$(7.9 \pm 0.9) \times 10^{-6}$			2588
$\eta' K^+\gamma$	$(2.9 {}^{+1.0}_{-0.9}) \times 10^{-6}$			2528
$\phi K^+\gamma$	$(2.7 \pm 0.4) \times 10^{-6}$	S=1.2		2516
$K^+\pi^-\pi^+\gamma$	$(2.58 \pm 0.15) \times 10^{-5}$	S=1.3		2609
$K^*(892)^0\pi^+\gamma$	$(2.33 \pm 0.12) \times 10^{-5}$			2562
$K^+\rho^0\gamma$	$(8.2 \pm 0.9) \times 10^{-6}$			2559
$(K^+\pi^-)_{NR}\pi^+\gamma$	$(9.9 {}^{+1.7}_{-2.0}) \times 10^{-6}$			2609
$K^0\pi^+\pi^0\gamma$	$(4.6 \pm 0.5) \times 10^{-5}$			2609
$K_1(1400)^+\gamma$	$(10 {}^{+5}_{-4}) \times 10^{-6}$			2453
$K^*(1410)^+\gamma$	$(2.7 {}^{+0.8}_{-0.6}) \times 10^{-5}$			–
$K_0^*(1430)^0\pi^+\gamma$	$(1.32 {}^{+0.26}_{-0.32}) \times 10^{-6}$			2445
$K_2^*(1430)^+\gamma$	$(1.4 \pm 0.4) \times 10^{-5}$			2447
$K^*(1680)^+\gamma$	$(6.7 {}^{+1.7}_{-1.4}) \times 10^{-5}$			2360
$K_3^*(1780)^+\gamma$	$< 3.9 \times 10^{-5}$	CL=90%		2340
$K_4^*(2045)^+\gamma$	$< 9.9 \times 10^{-3}$	CL=90%		2242

Light unflavored meson modes

$\rho^+\gamma$	$(9.8 \pm 2.5) \times 10^{-7}$			2583
$\pi^+\pi^0$	$(5.5 \pm 0.4) \times 10^{-6}$	S=1.2		2636
$\pi^+\pi^+\pi^-$	$(1.52 \pm 0.14) \times 10^{-5}$			2630
$\rho^0\pi^+$	$(8.3 \pm 1.2) \times 10^{-6}$			2581
$\pi^+ f_0(980),\ f_0 \to \pi^+\pi^-$	$< 1.5 \times 10^{-6}$	CL=90%		2545
$\pi^+ f_2(1270)$	$(2.2 {}^{+0.7}_{-0.4}) \times 10^{-6}$			2484
$\rho(1450)^0\pi^+,\ \rho^0 \to \pi^+\pi^-$	$(1.4 {}^{+0.6}_{-0.9}) \times 10^{-6}$			2434
$\rho(1450)^0\pi^+,\ \rho^0 \to K^+K^-$	$(1.60 \pm 0.14) \times 10^{-6}$			–
$f_0(1370)\pi^+,\ f_0 \to \pi^+\pi^-$	$< 4.0 \times 10^{-6}$	CL=90%		2460
$f_0(500)\pi^+,\ f_0 \to \pi^+\pi^-$	$< 4.1 \times 10^{-6}$	CL=90%		–
$\pi^+\pi^-\pi^+$ nonresonant	$(5.3 {}^{+1.5}_{-1.1}) \times 10^{-6}$			2630
$\pi^+\pi^0\pi^0$	$< 8.9 \times 10^{-4}$	CL=90%		2631
$\rho^+\pi^0$	$(1.09 \pm 0.14) \times 10^{-5}$			2581
$\pi^+\pi^-\pi^+\pi^0$	$< 4.0 \times 10^{-3}$	CL=90%		2622
$\rho^+\rho^0$	$(2.40 \pm 0.19) \times 10^{-5}$			2523
$\rho^+ f_0(980),\ f_0 \to \pi^+\pi^-$	$< 2.0 \times 10^{-6}$	CL=90%		2486
$a_1(1260)^+\pi^0$	$(2.6 \pm 0.7) \times 10^{-5}$			2494
$a_1(1260)^0\pi^+$	$(2.0 \pm 0.6) \times 10^{-5}$			2494
$\omega\pi^+$	$(6.9 \pm 0.5) \times 10^{-6}$			2580
$\omega\rho^+$	$(1.59 \pm 0.21) \times 10^{-5}$			2522
$\eta\pi^+$	$(4.02 \pm 0.27) \times 10^{-6}$			2609
$\eta\rho^+$	$(7.0 \pm 2.9) \times 10^{-6}$	S=2.8		2553
$\eta'\pi^+$	$(2.7 \pm 0.9) \times 10^{-6}$	S=1.9		2551
$\eta'\rho^+$	$(9.7 \pm 2.2) \times 10^{-6}$			2492
$\phi\pi^+$	$(3.2 \pm 1.5) \times 10^{-8}$			2539
$\phi\rho^+$	$< 3.0 \times 10^{-6}$	CL=90%		2480
$a_0(980)^0\pi^+,\ a_0^0 \to \eta\pi^0$	$< 5.8 \times 10^{-6}$	CL=90%		–
$a_0(980)^+\pi^0,\ a_0^+ \to \eta\pi^+$	$< 1.4 \times 10^{-6}$	CL=90%		–
$\pi^+\pi^+\pi^+\pi^-\pi^-$	$< 8.6 \times 10^{-4}$	CL=90%		2608
$\rho^0 a_1(1260)^+$	$< 6.2 \times 10^{-4}$	CL=90%		2433
$\rho^0 a_2(1320)^+$	$< 7.2 \times 10^{-4}$	CL=90%		2410
$b_1^0\pi^+,\ b_1^0 \to \omega\pi^0$	$(6.7 \pm 2.0) \times 10^{-6}$			–
$b_1^+\pi^0,\ b_1^+ \to \omega\pi^+$	$< 3.3 \times 10^{-6}$	CL=90%		–
$\pi^+\pi^+\pi^+\pi^-\pi^-\pi^0$	$< 6.3 \times 10^{-3}$	CL=90%		2592
$b_1^+\rho^0,\ b_1^+ \to \omega\pi^+$	$< 5.2 \times 10^{-6}$	CL=90%		–
$a_1(1260)^+a_1(1260)^0$	< 1.3 %	CL=90%		2336
$b_1^0\rho^+,\ b_1^0 \to \omega\pi^0$	$< 3.3 \times 10^{-6}$	CL=90%		–

Charged particle ($h^\pm$) modes

$h^\pm = K^\pm$ or $\pi^\pm$

$h^+\pi^0$	$(1.6 {}^{+0.7}_{-0.6}) \times 10^{-5}$			2636
ωh^+	$(1.38 {}^{+0.27}_{-0.24}) \times 10^{-5}$			2580
h^+X^0 (Familon)	$< 4.9 \times 10^{-5}$	CL=90%		–
$K^+X^0,\ X^0 \to \mu^+\mu^-$	$< 1 \times 10^{-7}$	CL=95%		–

Baryon modes

$p\overline{p}\pi^+$	$(1.62 \pm 0.20) \times 10^{-6}$			2439
$p\overline{p}\pi^+$ nonresonant	$< 5.3 \times 10^{-5}$	CL=90%		2439
$p\overline{p}\pi^+\pi^0$	$(4.6 \pm 1.3) \times 10^{-6}$			2407
$p\overline{p}K^+$	$(5.9 \pm 0.5) \times 10^{-6}$	S=1.5		2348
$\Theta(1710)^{++}\overline{p},\ \Theta^{++} \to pK^+$	[ppp] $< 9.1 \times 10^{-8}$	CL=90%		–
$f_J(2220)K^+,\ f_J \to p\overline{p}$	[ppp] $< 4.1 \times 10^{-7}$	CL=90%		2135
$p\overline{\Lambda}(1520)$	$(3.1 \pm 0.6) \times 10^{-7}$			2322
$p\overline{p}K^+$ nonresonant	$< 8.9 \times 10^{-5}$	CL=90%		2348
$p\overline{p}K^*(892)^+$	$(3.6 {}^{+0.8}_{-0.7}) \times 10^{-6}$			2215
$f_J(2220)K^{*+},\ f_J \to p\overline{p}$	$< 7.7 \times 10^{-7}$	CL=90%		2059
$p\overline{\Lambda}$	$(2.4 {}^{+1.0}_{-0.9}) \times 10^{-7}$			2430
$p\overline{\Lambda}\gamma$	$(2.4 {}^{+0.5}_{-0.4}) \times 10^{-6}$			2430
$p\overline{\Lambda}\pi^0$	$(3.0 {}^{+0.7}_{-0.6}) \times 10^{-6}$			2402
$p\overline{\Sigma}(1385)^0$	$< 4.7 \times 10^{-7}$	CL=90%		2362
$\Delta^+\overline{\Lambda}$	$< 8.2 \times 10^{-7}$	CL=90%		–
$p\overline{\Sigma}\gamma$	$< 4.6 \times 10^{-6}$	CL=90%		2413
$p\overline{\Lambda}\pi^+\pi^-$	$(1.13 \pm 0.13) \times 10^{-5}$			2367
$p\overline{\Lambda}\pi^+\pi^-$ nonresonant	$(5.9 \pm 1.1) \times 10^{-6}$			2367
$p\overline{\Lambda}\rho^0,\ \rho^0 \to \pi^+\pi^-$	$(4.8 \pm 0.9) \times 10^{-6}$			2214
$p\overline{\Lambda}f_2(1270),\ f_2 \to \pi^+\pi^-$	$(2.0 \pm 0.8) \times 10^{-6}$			2026
$p\overline{\Lambda}K^+K^-$	$(4.1 \pm 0.7) \times 10^{-6}$			2132
$p\overline{\Lambda}\phi$	$(8.0 \pm 2.2) \times 10^{-7}$			2119
$\overline{p}\Lambda K^+K^-$	$(3.7 \pm 0.6) \times 10^{-6}$			2132
$\Lambda\overline{\Lambda}\pi^+$	$< 9.4 \times 10^{-7}$	CL=90%		2358
$\Lambda\overline{\Lambda}K^+$	$(3.4 \pm 0.6) \times 10^{-6}$			2251
$\Lambda\overline{\Lambda}K^{*+}$	$(2.2 {}^{+1.2}_{-0.9}) \times 10^{-6}$			2098
$\Lambda(1520)\overline{\Lambda}K^+$	$(2.2 \pm 0.7) \times 10^{-6}$			2126
$\Lambda\overline{\Lambda}(1520)K^+$	$< 2.08 \times 10^{-6}$			2126
$\overline{\Delta}^0 p$	$< 1.38 \times 10^{-6}$	CL=90%		2403
$\Delta^{++}\overline{p}$	$< 1.4 \times 10^{-7}$	CL=90%		2403
$D^+p\overline{p}$	$< 1.5 \times 10^{-5}$	CL=90%		1860
$D^*(2010)^+p\overline{p}$	$< 1.5 \times 10^{-5}$	CL=90%		1786
$\overline{D}^0p\overline{p}\pi^+$	$(3.72 \pm 0.27) \times 10^{-4}$			1789
$\overline{D}^{*0}p\overline{p}\pi^+$	$(3.73 \pm 0.32) \times 10^{-4}$			1709
$D^-p\overline{p}\pi^+\pi^-$	$(1.66 \pm 0.30) \times 10^{-4}$			1705
$D^{*-}p\overline{p}\pi^+\pi^-$	$(1.86 \pm 0.25) \times 10^{-4}$			1621
$p\overline{\Lambda}^0\overline{D}^0$	$(1.43 \pm 0.32) \times 10^{-5}$			–
$p\overline{\Lambda}^0\overline{D}^*(2007)^0$	$< 5 \times 10^{-5}$	CL=90%		–
$\overline{\Lambda}_c^-p\pi^+$	$(2.3 \pm 0.4) \times 10^{-4}$	S=2.2		1980
$\overline{\Lambda}_c^-\Delta(1232)^{++}$	$< 1.9 \times 10^{-5}$	CL=90%		1928
$\overline{\Lambda}_c^-\Delta_X(1600)^{++}$	$(4.7 \pm 1.0) \times 10^{-5}$			–
$\overline{\Lambda}_c^-\Delta_X(2420)^{++}$	$(3.7 \pm 0.8) \times 10^{-5}$			–
$(\overline{\Lambda}_c^-p)_s\pi^+$	[qqq] $(3.1 \pm 0.7) \times 10^{-5}$			–
$\overline{\Sigma}_c(2520)^0p$	$< 3 \times 10^{-6}$	CL=90%		1904
$\overline{\Sigma}_c(2800)^0p$	$(2.6 \pm 0.9) \times 10^{-5}$			–
$\overline{\Lambda}_c^-p\pi^+\pi^0$	$(1.8 \pm 0.6) \times 10^{-3}$			1935
$\overline{\Lambda}_c^-p\pi^+\pi^+\pi^-$	$(2.2 \pm 0.7) \times 10^{-3}$			1880
$\overline{\Lambda}_c^-p\pi^+\pi^+\pi^-\pi^0$	< 1.34 %	CL=90%		1823
$\Lambda_c^+\Lambda_c^-K^+$	$(4.9 \pm 0.7) \times 10^{-4}$			739
$\Xi_c(2930)\Lambda_c^+,\ \Xi_c \to K^+\Lambda_c^-$	$(1.7 \pm 0.5) \times 10^{-4}$			–
$\overline{\Sigma}_c(2455)^0p$	$(2.9 \pm 0.7) \times 10^{-5}$			1938
$\overline{\Sigma}_c(2455)^0p\pi^0$	$(3.5 \pm 1.1) \times 10^{-4}$			1896
$\overline{\Sigma}_c(2455)^0p\pi^-\pi^+$	$(3.5 \pm 1.1) \times 10^{-4}$			1845
$\overline{\Sigma}_c(2455)^{--}p\pi^+\pi^+$	$(2.37 \pm 0.20) \times 10^{-4}$			1845

Downloaded from https://academic.oup.com/ptep/article/2022/8/083C01/6651666 by KIT Library user on 27 September 2022

$\overline{\Lambda}_c(2593)^- / \overline{\Lambda}_c(2625)^- p\pi^+$		< 1.9 $\times 10^{-4}$	CL=90%	–
$\overline{\Xi}_c^0 \Lambda_c^+$		(9.5 ± 2.3) $\times 10^{-4}$		1144
$\overline{\Xi}_c^0 \Lambda_c^+$, $\overline{\Xi}_c^0 \to \overline{\Xi}^+ \pi^-$		(1.76 ± 0.29) $\times 10^{-5}$		1144
$\overline{\Xi}_c^0 \Lambda_c^+$, $\overline{\Xi}_c^0 \to \Lambda K^+ \pi^-$		(1.14 ± 0.26) $\times 10^{-5}$		1144
$\overline{\Xi}_c^0 \Lambda_c^+$, $\overline{\Xi}_c^0 \to p K^- K^- \pi^+$		(5.5 ± 1.9) $\times 10^{-6}$		–
$\Lambda_c^+ \overline{\Xi}_c^0$		< 6.5 $\times 10^{-4}$	CL=90%	1023
$\Lambda_c^+ \overline{\Xi}_c(2645)^0$		< 7.9 $\times 10^{-4}$	CL=90%	–
$\Lambda_c^+ \overline{\Xi}_c(2790)^0$		(1.1 ± 0.4) $\times 10^{-3}$		–

Lepton Family number (*LF*) or Lepton number (*L*) or Baryon number (*B*) violating modes, or/and $\Delta B = 1$ weak neutral current (*B1*) modes

$\pi^+ \ell^+ \ell^-$	*B1*	< 4.9 $\times 10^{-8}$	CL=90%	2638
$\pi^+ e^+ e^-$	*B1*	< 8.0 $\times 10^{-8}$	CL=90%	2638
$\pi^+ \mu^+ \mu^-$	*B1*	(1.78 ± 0.23) $\times 10^{-8}$		2634
$\pi^+ \nu\overline{\nu}$	*B1*	< 1.4 $\times 10^{-5}$	CL=90%	2638
$K^+ \ell^+ \ell^-$	*B1*	[*iii*] (4.7 ± 0.5) $\times 10^{-7}$	S=2.3	2617
$K^+ e^+ e^-$	*B1*	(5.6 ± 0.6) $\times 10^{-7}$		2617
$K^+ \mu^+ \mu^-$	*B1*	(4.53 ± 0.35) $\times 10^{-7}$	S=1.8	2612
$K^+ \mu^+ \mu^-$ nonresonant	*B1*	(4.37 ± 0.27) $\times 10^{-7}$		2612
$K^+ \tau^+ \tau^-$	*B1*	< 2.25 $\times 10^{-3}$	CL=90%	1687
$K^+ \overline{\nu}\nu$	*B1*	< 1.6 $\times 10^{-5}$	CL=90%	2617
$\rho^+ \nu\overline{\nu}$	*B1*	< 3.0 $\times 10^{-5}$	CL=90%	2583
$K^*(892)^+ \ell^+ \ell^-$	*B1*	[*iii*] (1.01 ± 0.11) $\times 10^{-6}$	S=1.1	2564
$K^*(892)^+ e^+ e^-$	*B1*	($1.55 {}^{+0.40}_{-0.31}$) $\times 10^{-6}$		2564
$K^*(892)^+ \mu^+ \mu^-$	*B1*	(9.6 ± 1.0) $\times 10^{-7}$		2560
$K^*(892)^+ \nu\overline{\nu}$	*B1*	< 4.0 $\times 10^{-5}$	CL=90%	2564
$K^+ \pi^+ \pi^- \mu^+ \mu^-$	*B1*	(4.3 ± 0.4) $\times 10^{-7}$		2593
$\phi K^+ \mu^+ \mu^-$	*B1*	($7.9 {}^{+2.1}_{-1.7}$) $\times 10^{-8}$		2490
$\overline{\Lambda} p \nu\overline{\nu}$		< 3.0 $\times 10^{-5}$	CL=90%	2430
$\pi^+ e^+ \mu^-$	*LF*	< 6.4 $\times 10^{-3}$	CL=90%	2637
$\pi^+ e^- \mu^+$	*LF*	< 6.4 $\times 10^{-3}$	CL=90%	2637
$\pi^+ e^\pm \mu^\mp$	*LF*	< 1.7 $\times 10^{-7}$	CL=90%	2637
$\pi^+ e^+ \tau^-$	*LF*	< 7.4 $\times 10^{-5}$	CL=90%	2338
$\pi^+ e^- \tau^+$	*LF*	< 2.0 $\times 10^{-5}$	CL=90%	2338
$\pi^+ e^\pm \tau^\mp$	*LF*	< 7.5 $\times 10^{-5}$	CL=90%	2338
$\pi^+ \mu^+ \tau^-$	*LF*	< 6.2 $\times 10^{-5}$	CL=90%	2334
$\pi^+ \mu^- \tau^+$	*LF*	< 4.5 $\times 10^{-5}$	CL=90%	2334
$\pi^+ \mu^\pm \tau^\mp$	*LF*	< 7.2 $\times 10^{-5}$	CL=90%	2334
$K^+ e^+ \mu^-$	*LF*	< 7.0 $\times 10^{-9}$	CL=90%	2616
$K^+ e^- \mu^+$	*LF*	< 6.4 $\times 10^{-9}$	CL=90%	2616
$K^+ e^\pm \mu^\mp$	*LF*	< 9.1 $\times 10^{-8}$	CL=90%	2616
$K^+ e^+ \tau^-$	*LF*	< 4.3 $\times 10^{-5}$	CL=90%	2312
$K^+ e^- \tau^+$	*LF*	< 1.5 $\times 10^{-5}$	CL=90%	2312
$K^+ e^\pm \tau^\mp$	*LF*	< 3.0 $\times 10^{-5}$	CL=90%	2312
$K^+ \mu^+ \tau^-$	*LF*	< 4.5 $\times 10^{-5}$	CL=90%	2298
$K^+ \mu^- \tau^+$	*LF*	< 2.8 $\times 10^{-5}$	CL=90%	2298
$K^+ \mu^\pm \tau^\mp$	*LF*	< 4.8 $\times 10^{-5}$	CL=90%	2298
$K^*(892)^+ e^+ \mu^-$	*LF*	< 1.3 $\times 10^{-6}$	CL=90%	2563
$K^*(892)^+ e^- \mu^+$	*LF*	< 9.9 $\times 10^{-7}$	CL=90%	2563
$K^*(892)^+ e^\pm \mu^\mp$	*LF*	< 1.4 $\times 10^{-6}$	CL=90%	2563
$\pi^- e^+ e^+$	*L*	< 2.3 $\times 10^{-8}$	CL=90%	2638
$\pi^- \mu^+ \mu^+$	*L*	< 4.0 $\times 10^{-9}$	CL=95%	2634
$\pi^- e^+ \mu^+$	*L*	< 1.5 $\times 10^{-7}$	CL=90%	2637
$\rho^- e^+ e^+$	*L*	< 1.7 $\times 10^{-7}$	CL=90%	2583
$\rho^- \mu^+ \mu^+$	*L*	< 4.2 $\times 10^{-7}$	CL=90%	2578
$\rho^- e^+ \mu^+$	*L*	< 4.7 $\times 10^{-7}$	CL=90%	2582
$K^- e^+ e^+$	*L*	< 3.0 $\times 10^{-8}$	CL=90%	2617
$K^- \mu^+ \mu^+$	*L*	< 4.1 $\times 10^{-8}$	CL=90%	2612
$K^- e^+ \mu^+$	*L*	< 1.6 $\times 10^{-7}$	CL=90%	2616
$K^*(892)^- e^+ e^+$	*L*	< 4.0 $\times 10^{-7}$	CL=90%	2564
$K^*(892)^- \mu^+ \mu^+$	*L*	< 5.9 $\times 10^{-7}$	CL=90%	2560
$K^*(892)^- e^+ \mu^+$	*L*	< 3.0 $\times 10^{-7}$	CL=90%	2563
$D^- e^+ e^+$	*L*	< 2.6 $\times 10^{-6}$	CL=90%	2309
$D^- e^+ \mu^+$	*L*	< 1.8 $\times 10^{-6}$	CL=90%	2307
$D^- \mu^+ \mu^+$	*L*	< 6.9 $\times 10^{-7}$	CL=95%	2303
$D^{*-} \mu^+ \mu^+$	*L*	< 2.4 $\times 10^{-6}$	CL=95%	2251
$D_s^- \mu^+ \mu^+$	*L*	< 5.8 $\times 10^{-7}$	CL=95%	2267
$\overline{D}^0 \pi^- \mu^+ \mu^+$	*L*	< 1.5 $\times 10^{-6}$	CL=95%	2295
$\Lambda^0 \mu^+$	*L,B*	< 6 $\times 10^{-8}$	CL=90%	–
$\Lambda^0 e^+$	*L,B*	< 3.2 $\times 10^{-8}$	CL=90%	–
$\overline{\Lambda}^0 \mu^+$	*L,B*	< 6 $\times 10^{-8}$	CL=90%	–
$\overline{\Lambda}^0 e^+$	*L,B*	< 8 $\times 10^{-8}$	CL=90%	–

B^0

$I(J^P) = \frac{1}{2}(0^-)$

I, *J*, *P* need confirmation. Quantum numbers shown are quark-model predictions.

Mass $m_{B^0} = 5279.66 \pm 0.12$ MeV
$m_{B^0} - m_{B^\pm} = 0.32 \pm 0.05$ MeV
Mean life $\tau_{B^0} = (1.519 \pm 0.004) \times 10^{-12}$ s
$c\tau = 455.4\ \mu$m
$\tau_{B^+}/\tau_{B^0} = 1.076 \pm 0.004$ (direct measurements)

B^0-$\overline{B}^0$ mixing parameters

χ_d (B^0-$\overline{B}^0$ mixing probability) $= 0.1858 \pm 0.0011$
$\Delta m_{B^0} = m_{B^0_H} - m_{B^0_L} = (0.5065 \pm 0.0019) \times 10^{12}\ \hbar\ \mathrm{s}^{-1}$
$= (3.334 \pm 0.013) \times 10^{-10}$ MeV
$x_d = \Delta m_{B^0}/\Gamma_{B^0} = 0.769 \pm 0.004$
$\mathrm{Re}(\lambda_{CP}\ /\ |\lambda_{CP}|)\ \mathrm{Re(z)} = 0.047 \pm 0.022$
$\Delta\Gamma\ \mathrm{Re(z)} = -0.007 \pm 0.004\ \mathrm{ps}^{-1}$
$\mathrm{Re(z)} = (-4 \pm 4) \times 10^{-2}$ (S = 1.4)
$\mathrm{Im(z)} = (-0.8 \pm 0.4) \times 10^{-2}$

CP violation parameters

$\mathrm{Re}(\epsilon_{B^0})/(1+|\epsilon_{B^0}|^2) = (-0.5 \pm 0.4) \times 10^{-3}$
$A_{T/CP}(B^0 \leftrightarrow \overline{B}^0) = 0.005 \pm 0.018$
$A_{CP}(B^0 \to D^*(2010)^+ D^-) = 0.013 \pm 0.014$
$A_{CP}(B^0 \to [K^+ K^-]_D K^*(892)^0) = -0.05 \pm 0.10$
$A_{CP}(B^0 \to [K^+ \pi^-]_D K^*(892)^0) = 0.047 \pm 0.029$
$A_{CP}(B^0 \to [K^+ \pi^- \pi^+ \pi^-]_D K^*(892)^0) = 0.037 \pm 0.034$
$A_{CP}(B^0 \to [K^- \pi^+]_D K^*(892)^0) = 0.19 \pm 0.19$
$A_{CP}(B^0 \to [K^- \pi^+ \pi^+ \pi^-]_D K^*(892)^0) = -0.01 \pm 0.24$
$R_d^+ = \Gamma(B^0 \to [\pi^+ K^-]_D K^{*0})\ /\ \Gamma(B^0 \to [\pi^- K^+]_D K^{*0}) = 0.064 \pm 0.021$
$R_d^- = \Gamma(\overline{B}^0 \to [\pi^- K^+]_D K^{*0})\ /\ \Gamma(\overline{B}^0 \to [\pi^+ K^-]_D K^{*0}) = 0.095 \pm 0.021$
$A_{CP}(B^0 \to [\pi^+ \pi^-]_D K^*(892)^0) = -0.18 \pm 0.14$
$A_{CP}(B^0 \to [\pi^+ \pi^- \pi^+ \pi^-]_D K^*(892)^0) = -0.03 \pm 0.15$
$R_d^+ = \Gamma(B^0 \to [\pi^+ K^- \pi^+ \pi^-]_D K^{*0})\ /\ \Gamma(B^0 \to [\pi^- K^+ \pi^+ \pi^-]_D K^{*0}) = 0.074 \pm 0.026$
$R_d^- = \Gamma(\overline{B}^0 \to [\pi^- K^+ \pi^+ \pi^-]_D K^{*0})\ /\ \Gamma(\overline{B}^0 \to [\pi^+ K^- \pi^+ \pi^-]_D K^{*0}) = 0.072 \pm 0.025$
$\boldsymbol{A_{CP}\ (B^0 \to K^+ \pi^-)} = -0.0834 \pm 0.0032$
$A_{CP}(B^0 \to \eta' K^*(892)^0) = -0.07 \pm 0.18$
$A_{CP}(B^0 \to \eta' K_0^*(1430)^0) = -0.19 \pm 0.17$
$A_{CP}(B^0 \to \eta' K_2^*(1430)^0) = 0.14 \pm 0.18$
$\boldsymbol{A_{CP}(B^0 \to \eta K^*(892)^0)} = 0.19 \pm 0.05$
$A_{CP}(B^0 \to \eta K_0^*(1430)^0) = 0.06 \pm 0.13$
$A_{CP}(B^0 \to \eta K_2^*(1430)^0) = -0.07 \pm 0.19$
$A_{CP}(B^0 \to b_1 K^+) = -0.07 \pm 0.12$
$A_{CP}(B^0 \to \omega K^{*0}) = 0.45 \pm 0.25$
$A_{CP}(B^0 \to \omega (K\pi)_0^{*0}) = -0.07 \pm 0.09$
$A_{CP}(B^0 \to \omega K_2^*(1430)^0) = -0.37 \pm 0.17$
$A_{CP}(B^0 \to K^+ \pi^- \pi^0) = (0 \pm 6) \times 10^{-2}$
$A_{CP}(B^0 \to \rho^- K^+) = 0.20 \pm 0.11$
$A_{CP}(B^0 \to \rho(1450)^- K^+) = -0.10 \pm 0.33$
$A_{CP}(B^0 \to \rho(1700)^- K^+) = -0.4 \pm 0.6$
$A_{CP}(B^0 \to K^+ \pi^- \pi^0 \text{nonresonant}) = 0.10 \pm 0.18$
$A_{CP}(B^0 \to K^0 \pi^+ \pi^-) = -0.01 \pm 0.05$
$\boldsymbol{A_{CP}(B^0 \to K^*(892)^+ \pi^-)} = -0.27 \pm 0.04$
$A_{CP}(B^0 \to (K\pi)_0^{*+} \pi^-) = 0.02 \pm 0.04$
$A_{CP}(B^0 \to K_2^*(1430)^+ \pi^-) = -0.29 \pm 0.24$
$A_{CP}(B^0 \to K^*(1680)^+ \pi^-) = -0.07 \pm 0.14$
$A_{CP}(B^0 \to f_0(980) K_S^0) = 0.28 \pm 0.31$
$A_{CP}(B^0 \to (K\pi)_0^{*0} \pi^0) = -0.15 \pm 0.11$
$A_{CP}(B^0 \to K^{*0} \pi^0) = -0.15 \pm 0.13$
$A_{CP}(B^0 \to K^*(892)^0 \pi^+ \pi^-) = 0.07 \pm 0.05$
$A_{CP}(B^0 \to K^*(892)^0 \rho^0) = -0.06 \pm 0.09$
$A_{CP}(B^0 \to K^{*0} f_0(980)) = 0.07 \pm 0.10$
$A_{CP}(B^0 \to K^{*+} \rho^-) = 0.21 \pm 0.15$
$A_{CP}(B^0 \to K^*(892)^0 K^+ K^-) = 0.01 \pm 0.05$
$A_{CP}(B^0 \to a_1^- K^+) = -0.16 \pm 0.12$
$A_{CP}(B^0 \to K^0 K^0) = -0.6 \pm 0.7$
$A_{CP}(B^0 \to K^*(892)^0 \phi) = 0.00 \pm 0.04$
$A_{CP}(B^0 \to K^*(892)^0 K^- \pi^+) = 0.2 \pm 0.4$
$A_{CP}(B^0 \to \phi (K\pi)_0^{*0}) = 0.12 \pm 0.08$

Downloaded from https://academic.oup.com/ptep/article/2022/8/083C01/6651666 by KIT Library user on 27 September 2022

$A_{CP}(B^0 \to \phi K_2^*(1430)^0) = -0.11 \pm 0.10$
$A_{CP}(B^0 \to K^*(892)^0\gamma) = -0.006 \pm 0.011$
$A_{CP}(B^0 \to K_2^*(1430)^0\gamma) = -0.08 \pm 0.15$
$A_{CP}(B^0 \to X_s\gamma) = -0.009 \pm 0.018$
$A_{CP}(B^0 \to \rho^+\pi^-) = 0.13 \pm 0.06$ (S = 1.1)
$A_{CP}(B^0 \to \rho^-\pi^+) = -0.08 \pm 0.08$
$A_{CP}(B^0 \to a_1(1260)^\pm\pi^\mp) = -0.07 \pm 0.06$
$A_{CP}(B^0 \to b_1^-\pi^+) = -0.05 \pm 0.10$
$A_{CP}(B^0 \to p\overline{p}K^*(892)^0) = 0.05 \pm 0.12$
$A_{CP}(B^0 \to p\overline{\Lambda}\pi^-) = 0.04 \pm 0.07$
$A_{CP}(B^0 \to K^{*0}\ell^+\ell^-) = -0.05 \pm 0.10$
$A_{CP}(B^0 \to K^{*0}e^+e^-) = -0.21 \pm 0.19$
$A_{CP}(B^0 \to K^{*0}\mu^+\mu^-) = -0.034 \pm 0.024$
$C_{D^{*-}D^+}(B^0 \to D^*(2010)^-D^+) = -0.02 \pm 0.08$
$S_{D^{*-}D^+}(B^0 \to D^*(2010)^-D^+) = -0.83 \pm 0.09$
$C_{D^{*+}D^-}(B^0 \to D^*(2010)^+D^-) = -0.03 \pm 0.09$ (S = 1.1)
$S_{D^{*+}D^-}(B^0 \to D^*(2010)^+D^-) = -0.80 \pm 0.09$
$C_{D^{*+}D^{*-}}(B^0 \to D^{*+}D^{*-}) = 0.01 \pm 0.09$ (S = 1.6)
$S_{D^{*+}D^{*-}}(B^0 \to D^{*+}D^{*-}) = -0.59 \pm 0.14$ (S = 1.8)
$C_+(B^0 \to D^{*+}D^{*-}) = 0.00 \pm 0.10$ (S = 1.6)
$S_+(B^0 \to D^{*+}D^{*-}) = -0.73 \pm 0.09$
$C_-(B^0 \to D^{*+}D^{*-}) = 0.19 \pm 0.31$
$S_-(B^0 \to D^{*+}D^{*-}) = 0.1 \pm 1.6$ (S = 3.5)
$C(B^0 \to D^*(2010)^+D^*(2010)^-K_S^0) = 0.01 \pm 0.29$
$S(B^0 \to D^*(2010)^+D^*(2010)^-K_S^0) = 0.1 \pm 0.4$
$C_{D^+D^-}(B^0 \to D^+D^-) = -0.22 \pm 0.24$ (S = 2.5)
$S_{D^+D^-}(B^0 \to D^+D^-) = -0.76^{+0.15}_{-0.13}$ (S = 1.2)
$C_{J/\psi(1S)\pi^0}(B^0 \to J/\psi(1S)\pi^0) = 0.03 \pm 0.17$ (S = 1.5)
$S_{J/\psi(1S)\pi^0}(B^0 \to J/\psi(1S)\pi^0) = -0.88 \pm 0.32$ (S = 2.2)
$C(B^0 \to J/\psi(1S)\rho^0) = -0.06 \pm 0.06$
$S(B^0 \to J/\psi(1S)\rho^0) = -0.66^{+0.16}_{-0.12}$
$C_{D^{(*)}_{CP}h^0}(B^0 \to D^{(*)}_{CP}h^0) = -0.02 \pm 0.08$
$S_{D^{(*)}_{CP}h^0}(B^0 \to D^{(*)}_{CP}h^0) = -0.66 \pm 0.12$
$C_{K^0\pi^0}(B^0 \to K^0\pi^0) = 0.00 \pm 0.13$ (S = 1.4)
$S_{K^0\pi^0}(B^0 \to K^0\pi^0) = 0.58 \pm 0.17$
$C_{\eta'(958)K_S^0}(B^0 \to \eta'(958)K_S^0) = -0.04 \pm 0.20$ (S = 2.5)
$S_{\eta'(958)K_S^0}(B^0 \to \eta'(958)K_S^0) = 0.43 \pm 0.17$ (S = 1.5)
$C_{\eta'K^0}(B^0 \to \eta'K^0) = -0.06 \pm 0.04$
$S_{\eta'K^0}(B^0 \to \eta'K^0) = 0.63 \pm 0.06$
$C_{\omega K_S^0}(B^0 \to \omega K_S^0) = 0.0 \pm 0.4$ (S = 3.0)
$S_{\omega K_S^0}(B^0 \to \omega K_S^0) = 0.70 \pm 0.21$
$C(B^0 \to K_S^0\pi^0\pi^0) = -0.21 \pm 0.20$
$S(B^0 \to K_S^0\pi^0\pi^0) = 0.89^{+0.27}_{-0.30}$
$C_{\rho^0K_S^0}(B^0 \to \rho^0K_S^0) = -0.04 \pm 0.20$
$S_{\rho^0K_S^0}(B^0 \to \rho^0K_S^0) = 0.50^{+0.17}_{-0.21}$
$C_{f_0K_S^0}(B^0 \to f_0(980)K_S^0) = 0.29 \pm 0.20$
$S_{f_0K_S^0}(B^0 \to f_0(980)K_S^0) = -0.50 \pm 0.16$
$S_{f_2K_S^0}(B^0 \to f_2(1270)K_S^0) = -0.5 \pm 0.5$
$C_{f_2K_S^0}(B^0 \to f_2(1270)K_S^0) = 0.3 \pm 0.4$
$S_{f_xK_S^0}(B^0 \to f_x(1300)K_S^0) = -0.2 \pm 0.5$
$C_{f_xK_S^0}(B^0 \to f_x(1300)K_S^0) = 0.13 \pm 0.35$
$S_{K^0\pi^+\pi^-}(B^0 \to K^0\pi^+\pi^-\text{nonresonant}) = -0.01 \pm 0.33$
$C_{K^0\pi^+\pi^-}(B^0 \to K^0\pi^+\pi^-\text{nonresonant}) = 0.01 \pm 0.26$
$C_{K_S^0K_S^0}(B^0 \to K_S^0K_S^0) = 0.0 \pm 0.4$ (S = 1.4)
$S_{K_S^0K_S^0}(B^0 \to K_S^0K_S^0) = -0.8 \pm 0.5$
$C_{K^+K^-K_S^0}(B^0 \to K^+K^-K_S^0\text{ nonresonant}) = 0.06 \pm 0.08$
$S_{K^+K^-K_S^0}(B^0 \to K^+K^-K_S^0\text{ nonresonant}) = -0.66 \pm 0.11$
$C_{K^+K^-K_S^0}(B^0 \to K^+K^-K_S^0\text{ inclusive}) = 0.01 \pm 0.09$
$S_{K^+K^-K_S^0}(B^0 \to K^+K^-K_S^0\text{ inclusive}) = -0.65 \pm 0.12$
$C_{\phi K_S^0}(B^0 \to \phi K_S^0) = 0.01 \pm 0.14$
$S_{\phi K_S^0}(B^0 \to \phi K_S^0) = 0.59 \pm 0.14$
$C_{K_SK_SK_S}(B^0 \to K_SK_SK_S) = -0.14 \pm 0.12$
$S_{K_SK_SK_S}(B^0 \to K_SK_SK_S) = -0.82 \pm 0.17$
$C_{K_S^0\pi^0\gamma}(B^0 \to K_S^0\pi^0\gamma) = 0.36 \pm 0.33$
$S_{K_S^0\pi^0\gamma}(B^0 \to K_S^0\pi^0\gamma) = -0.8 \pm 0.6$
$C_{K_S^0\pi^+\pi^-\gamma}(B^0 \to K_S^0\pi^+\pi^-\gamma) = -0.39 \pm 0.20$
$S_{K_S^0\pi^+\pi^-\gamma}(B^0 \to K_S^0\pi^+\pi^-\gamma) = 0.14 \pm 0.25$
$C_{K^{*0}\gamma}(B^0 \to K^*(892)^0\gamma) = -0.04 \pm 0.16$ (S = 1.2)
$S_{K^{*0}\gamma}(B^0 \to K^*(892)^0\gamma) = -0.15 \pm 0.22$
$C_{\eta K^0\gamma}(B^0 \to \eta K^0\gamma) = 0.1 \pm 0.4$ (S = 1.4)
$S_{\eta K^0\gamma}(B^0 \to \eta K^0\gamma) = -0.5 \pm 0.5$ (S = 1.2)
$C_{K^0\phi\gamma}(B^0 \to K^0\phi\gamma) = -0.3 \pm 0.6$
$S_{K^0\phi\gamma}(B^0 \to K^0\phi\gamma) = 0.7^{+0.7}_{-1.1}$
$C(B^0 \to K_S^0\rho^0\gamma) = -0.05 \pm 0.19$
$S(B^0 \to K_S^0\rho^0\gamma) = -0.04 \pm 0.23$
$C(B^0 \to \rho^0\gamma) = 0.4 \pm 0.5$
$S(B^0 \to \rho^0\gamma) = -0.8 \pm 0.7$
$C_{\pi\pi}(B^0 \to \pi^+\pi^-) = -0.314 \pm 0.030$
$S_{\pi\pi}(B^0 \to \pi^+\pi^-) = -0.670 \pm 0.030$
$C_{\pi^0\pi^0}(B^0 \to \pi^0\pi^0) = -0.33 \pm 0.22$
$C_{\rho\pi}(B^0 \to \rho^+\pi^-) = -0.03 \pm 0.07$ (S = 1.2)
$S_{\rho\pi}(B^0 \to \rho^+\pi^-) = 0.05 \pm 0.07$
$\Delta C_{\rho\pi}(B^0 \to \rho^+\pi^-) = 0.27 \pm 0.06$
$\Delta S_{\rho\pi}(B^0 \to \rho^+\pi^-) = 0.01 \pm 0.08$
$C_{\rho^0\pi^0}(B^0 \to \rho^0\pi^0) = 0.27 \pm 0.24$
$S_{\rho^0\pi^0}(B^0 \to \rho^0\pi^0) = -0.23 \pm 0.34$
$C_{a_1\pi}(B^0 \to a_1(1260)^+\pi^-) = -0.05 \pm 0.11$
$S_{a_1\pi}(B^0 \to a_1(1260)^+\pi^-) = -0.2 \pm 0.4$ (S = 3.2)
$\Delta C_{a_1\pi}(B^0 \to a_1(1260)^+\pi^-) = 0.43 \pm 0.14$ (S = 1.3)
$\Delta S_{a_1\pi}(B^0 \to a_1(1260)^+\pi^-) = -0.11 \pm 0.12$
$C(B^0 \to b_1^-K^+) = -0.22 \pm 0.24$
$\Delta C(B^0 \to b_1^-\pi^+) = -1.04 \pm 0.24$
$C_{\rho^0\rho^0}(B^0 \to \rho^0\rho^0) = 0.2 \pm 0.9$
$S_{\rho^0\rho^0}(B^0 \to \rho^0\rho^0) = 0.3 \pm 0.7$
$C_{\rho\rho}(B^0 \to \rho^+\rho^-) = 0.00 \pm 0.09$
$S_{\rho\rho}(B^0 \to \rho^+\rho^-) = -0.14 \pm 0.13$
$|\lambda|(B^0 \to J/\psi K^*(892)^0) < 0.25$, CL = 95%
$\cos 2\beta(B^0 \to J/\psi K^*(892)^0) = 1.7^{+0.7}_{-0.9}$ (S = 1.6)
$\cos 2\beta(B^0 \to [K_S^0\pi^+\pi^-]_{D^{(*)}}h^0) = 0.91 \pm 0.25$
$(S_+ + S_-)/2(B^0 \to D^{*-}\pi^+) = -0.039 \pm 0.011$
$(S_- - S_+)/2(B^0 \to D^{*-}\pi^+) = -0.009 \pm 0.015$
$(S_+ + S_-)/2(B^0 \to D^-\pi^+) = -0.046 \pm 0.023$
$(S_- - S_+)/2(B^0 \to D^-\pi^+) = -0.022 \pm 0.021$
$S_+(B^0 \to D^-\pi^+) = 0.058 \pm 0.023$
$S_-(B^0 \to D^+\pi^-) = 0.038 \pm 0.021$
$(S_+ + S_-)/2(B^0 \to D^-\rho^+) = -0.024 \pm 0.032$
$(S_- - S_+)/2(B^0 \to D^-\rho^+) = -0.10 \pm 0.06$
$C_{\eta_cK_S^0}(B^0 \to \eta_cK_S^0) = 0.08 \pm 0.13$
$S_{\eta_cK_S^0}(B^0 \to \eta_cK_S^0) = 0.93 \pm 0.17$
$C_{c\overline{c}K^{(*)0}}(B^0 \to c\overline{c}K^{(*)0}) = (-0.5 \pm 1.5) \times 10^{-2}$
$\sin(2\beta) = 0.699 \pm 0.017$
$C_{J/\psi(nS)K^0}(B^0 \to J/\psi(nS)K^0) = (-0.8 \pm 1.7) \times 10^{-2}$
$S_{J/\psi(nS)K^0}(B^0 \to J/\psi(nS)K^0) = 0.701 \pm 0.017$
$C_{J/\psi K^{*0}}(B^0 \to J/\psi K^{*0}) = 0.03 \pm 0.10$
$S_{J/\psi K^{*0}}(B^0 \to J/\psi K^{*0}) = 0.60 \pm 0.25$
$C_{\chi_{c0}K_S^0}(B^0 \to \chi_{c0}K_S^0) = -0.3^{+0.5}_{-0.4}$
$S_{\chi_{c0}K_S^0}(B^0 \to \chi_{c0}K_S^0) = -0.7 \pm 0.5$
$C_{\chi_{c1}K_S^0}(B^0 \to \chi_{c1}K_S^0) = 0.06 \pm 0.07$
$S_{\chi_{c1}K_S^0}(B^0 \to \chi_{c1}K_S^0) = 0.63 \pm 0.10$
$\sin(2\beta_{\rm eff})(B^0 \to \phi K^0) = 0.22 \pm 0.30$
$\sin(2\beta_{\rm eff})(B^0 \to \phi K_0^*(1430)^0) = 0.97^{+0.03}_{-0.52}$
$\sin(2\beta_{\rm eff})(B^0 \to K^+K^-K_S^0) = 0.77^{+0.13}_{-0.12}$
$\sin(2\beta_{\rm eff})(B^0 \to [K_S^0\pi^+\pi^-]_{D^{(*)}}h^0) = 0.80 \pm 0.16$
$\beta_{\rm eff}(B^0 \to [K_S^0\pi^+\pi^-]_{D^{(*)}}h^0) = (22 \pm 5)^\circ$
$2\beta_{\rm eff}(B^0 \to J/\psi\rho^0) = (42^{+10}_{-11})^\circ$
$|\lambda|(B^0 \to [K_S^0\pi^+\pi^-]_{D^{(*)}}h^0) = 1.01 \pm 0.08$
$|\sin(2\beta+\gamma)| > 0.40$, CL = 90%

Downloaded from https://academic.oup.com/ptep/article/2022/8/083C01/6651666 by KIT Library user on 27 September 2022

$2\beta + \gamma = (83 \pm 60)^\circ$
$\boldsymbol{\alpha} = (85.2^{+4.8}_{-4.3})^\circ$
$x_+(B^0 \to D K^{*0}) = 0.04 \pm 0.17$
$x_-(B^0 \to D K^{*0}) = -0.16 \pm 0.14$
$y_+(B^0 \to D K^{*0}) = -0.68 \pm 0.22$
$y_-(B^0 \to D K^{*0}) = 0.20 \pm 0.25$ (S = 1.2)
$\boldsymbol{r_{B^0}(B^0 \to D K^{*0})} = 0.257^{+0.021}_{-0.023}$
$\boldsymbol{\delta_{B^0}(B^0 \to D K^{*0})} = (194.1^{+9.6}_{-8.8})^\circ$

$\overline{B}^0$ modes are charge conjugates of the modes below. Reactions indicate the weak decay vertex and do not include mixing. Modes which do not identify the charge state of the B are listed in the $B^\pm/B^0$ ADMIXTURE section.

The branching fractions listed below assume 50% $B^0\overline{B}^0$ and 50% B^+B^- production at the $\Upsilon(4S)$. We have attempted to bring older measurements up to date by rescaling their assumed $\Upsilon(4S)$ production ratio to 50:50 and their assumed D, D_s, D^*, and ψ branching ratios to current values whenever this would affect our averages and best limits significantly.

Indentation is used to indicate a subchannel of a previous reaction. All resonant subchannels have been corrected for resonance branching fractions to the final state so the sum of the subchannel branching fractions can exceed that of the final state.

For inclusive branching fractions, *e.g.*, $B \to D^\pm X$, the values usually are multiplicities, not branching fractions. They can be greater than one.

B^0 DECAY MODES		Fraction (Γ_i/Γ)	Scale factor/ Confidence level	p (MeV/c)
$\ell^+ \nu_\ell X$	[iii]	(10.33 ± 0.28) %		–
$e^+ \nu_e X_c$		(10.1 ± 0.4) %		–
$\ell^+ \nu_\ell X_u$		$(1.51 \pm 0.19) \times 10^{-3}$		–
$D \ell^+ \nu_\ell X$		(9.3 ± 0.8) %		–
$D^- \ell^+ \nu_\ell$	[iii]	(2.24 ± 0.09) %		2309
$D^- \tau^+ \nu_\tau$		(1.05 ± 0.23) %		1909
$D^*(2010)^- \ell^+ \nu_\ell$	[iii]	(4.97 ± 0.12) %		2257
$D^*(2010)^- \tau^+ \nu_\tau$		(1.58 ± 0.09) %	S=1.1	1838
$\overline{D}^0 \pi^- \ell^+ \nu_\ell$		$(4.1 \pm 0.5) \times 10^{-3}$		2308
$D_0^*(2300)^- \ell^+ \nu_\ell$, $D_0^{*-} \to \overline{D}^0 \pi^-$		$(3.0 \pm 1.2) \times 10^{-3}$	S=1.8	–
$D_2^*(2460)^- \ell^+ \nu_\ell$, $D_2^{*-} \to \overline{D}^0 \pi^-$		$(1.21 \pm 0.33) \times 10^{-3}$	S=1.8	2065
$\overline{D}^{(*)} n\pi \ell^+ \nu_\ell (n \geq 1)$		(2.3 ± 0.5) %		–
$\overline{D}^{*0} \pi^- \ell^+ \nu_\ell$		$(5.8 \pm 0.8) \times 10^{-3}$	S=1.4	2256
$D_1(2420)^- \ell^+ \nu_\ell$, $D_1^- \to \overline{D}^{*0} \pi^-$		$(2.80 \pm 0.28) \times 10^{-3}$		–
$D_1'(2430)^- \ell^+ \nu_\ell$, $D_1'^- \to \overline{D}^{*0} \pi^-$		$(3.1 \pm 0.9) \times 10^{-3}$		–
$D_2^*(2460)^- \ell^+ \nu_\ell$, $D_2^{*-} \to \overline{D}^{*0} \pi^-$		$(6.8 \pm 1.2) \times 10^{-4}$		2065
$D^- \pi^+ \pi^- \ell^+ \nu_\ell$		$(1.3 \pm 0.5) \times 10^{-3}$		2299
$D^{*-} \pi^+ \pi^- \ell^+ \nu_\ell$		$(1.4 \pm 0.5) \times 10^{-3}$		2247
$\rho^- \ell^+ \nu_\ell$	[iii]	$(2.94 \pm 0.21) \times 10^{-4}$		2583
$\pi^- \ell^+ \nu_\ell$	[iii]	$(1.50 \pm 0.06) \times 10^{-4}$		2638
$\pi^- \tau^+ \nu_\tau$		$< 2.5 \times 10^{-4}$	CL=90%	2339
Inclusive modes				
$K^\pm X$		(78 ± 8) %		–
$D^0 X$		(8.1 ± 1.5) %		–
$\overline{D}^0 X$		(47.4 ± 2.8) %		–
$D^+ X$		< 3.9 %	CL=90%	–
$D^- X$		(36.9 ± 3.3) %		–
$D_s^+ X$		$(10.3 {}^{+2.1}_{-1.8})$ %		–
$D_s^- X$		< 2.6 %	CL=90%	–
$\Lambda_c^+ X$		< 3.1 %	CL=90%	–
$\overline{\Lambda}_c^- X$		$(5.0 {}^{+2.1}_{-1.5})$ %		–
$\overline{c} X$		(95 ± 5) %		–
$c X$		(24.6 ± 3.1) %		–
$\overline{c}/c X$		(119 ± 6) %		–
D, D^*, or D_s modes				
$D^- \pi^+$		$(2.51 \pm 0.08) \times 10^{-3}$		2306
$D^- \rho^+$		$(7.6 \pm 1.2) \times 10^{-3}$		2235
$D^- K^0 \pi^+$		$(4.9 \pm 0.9) \times 10^{-4}$		2259
$D^- K^*(892)^+$		$(4.5 \pm 0.7) \times 10^{-4}$		2211
$D^- \omega \pi^+$		$(2.8 \pm 0.6) \times 10^{-3}$		2204
$D^- K^+$		$(2.05 \pm 0.08) \times 10^{-4}$		2279
$D^- K^+ \pi^+ \pi^-$		$(3.5 \pm 0.8) \times 10^{-4}$		2236
$D^- K^+ \overline{K}^0$		$< 3.1 \times 10^{-4}$	CL=90%	2188
$D^- K^+ \overline{K}^*(892)^0$		$(8.8 \pm 1.9) \times 10^{-4}$		2070
$\overline{D}^0 \pi^+ \pi^-$		$(8.8 \pm 0.5) \times 10^{-4}$		2301
$D^*(2010)^- \pi^+$		$(2.74 \pm 0.13) \times 10^{-3}$		2255
$\overline{D}^0 K^+ K^-$		$(6.1 \pm 0.5) \times 10^{-5}$		2191
$D^- \pi^+ \pi^+ \pi^-$		$(6.0 \pm 0.6) \times 10^{-3}$		2287
$(D^- \pi^+ \pi^+ \pi^-)$ nonresonant		$(3.9 \pm 1.9) \times 10^{-3}$		2287
$D^- \pi^+ \rho^0$		$(1.1 \pm 1.0) \times 10^{-3}$		2206
$D^- a_1(1260)^+$		$(6.0 \pm 3.3) \times 10^{-3}$		2121
$D^*(2010)^- \pi^+ \pi^0$		(1.5 ± 0.5) %		2248
$D^*(2010)^- \rho^+$		$(6.8 \pm 0.9) \times 10^{-3}$		2180
$D^*(2010)^- K^+$		$(2.12 \pm 0.15) \times 10^{-4}$		2226
$D^*(2010)^- K^0 \pi^+$		$(3.0 \pm 0.8) \times 10^{-4}$		2205
$D^*(2010)^- K^*(892)^+$		$(3.3 \pm 0.6) \times 10^{-4}$		2155
$D^*(2010)^- K^+ \overline{K}^0$		$< 4.7 \times 10^{-4}$	CL=90%	2131
$D^*(2010)^- K^+ \overline{K}^*(892)^0$		$(1.29 \pm 0.33) \times 10^{-3}$		2007
$D^*(2010)^- \pi^+ \pi^+ \pi^-$		$(7.21 \pm 0.29) \times 10^{-3}$		2235
$(D^*(2010)^- \pi^+ \pi^+ \pi^-)$ nonresonant		$(0.0 \pm 2.5) \times 10^{-3}$		2235
$D^*(2010)^- \pi^+ \rho^0$		$(5.7 \pm 3.2) \times 10^{-3}$		2150
$D^*(2010)^- a_1(1260)^+$		(1.30 ± 0.27) %		2061
$\overline{D}_1(2420)^0 \pi^- \pi^+$, $\overline{D}_1^0 \to D^{*-} \pi^+$		$(1.47 \pm 0.35) \times 10^{-4}$		–
$D^*(2010)^- K^+ \pi^- \pi^+$		$(4.7 \pm 0.4) \times 10^{-4}$		2181
$D^*(2010)^- \pi^+ \pi^+ \pi^- \pi^0$		(1.76 ± 0.27) %		2218
$D^{*-} 3\pi^+ 2\pi^-$		$(4.7 \pm 0.9) \times 10^{-3}$		2195
$D^*(2010)^- \omega \pi^+$		$(2.46 \pm 0.18) \times 10^{-3}$	S=1.2	2148
$\overline{D}_1(2430)^0 \omega$, $\overline{D}_1^0 \to D^{*-} \pi^+$		$(2.7 {}^{+0.8}_{-0.4}) \times 10^{-4}$		1992
$D^{*-} \rho(1450)^+$, $\rho^+ \to \omega \pi^+$		$(1.07 {}^{+0.40}_{-0.34}) \times 10^{-3}$		–
$\overline{D}_1(2420)^0 \omega$, $\overline{D}_1^0 \to D^{*-} \pi^+$		$(7.0 \pm 2.2) \times 10^{-5}$		1995
$\overline{D}_2^*(2460)^0 \omega$, $\overline{D}_2^0 \to D^{*-} \pi^+$		$(4.0 \pm 1.4) \times 10^{-5}$		1975
$D^{*-} b_1(1235)^+$, $b_1^+ \to \omega \pi^+$		$< 7 \times 10^{-5}$	CL=90%	–
$\overline{D}^{**-} \pi^+$	[nnn]	$(1.9 \pm 0.9) \times 10^{-3}$		–
$D_1(2420)^- \pi^+$, $D_1^- \to D^- \pi^+ \pi^-$		$(9.9 {}^{+2.0}_{-2.5}) \times 10^{-5}$		–
$D_1(2420)^- \pi^+$, $D_1^- \to D^{*-} \pi^+ \pi^-$		$< 3.3 \times 10^{-5}$	CL=90%	–
$\overline{D}_2^*(2460)^- \pi^+$, $(D_2^*)^- \to D^0 \pi^-$		$(2.38 \pm 0.16) \times 10^{-4}$		2062
$\overline{D}_0^*(2400)^- \pi^+$, $(D_0^*)^- \to D^0 \pi^-$		$(7.6 \pm 0.8) \times 10^{-5}$		2090
$D_2^*(2460)^- \pi^+$, $(D_2^*)^- \to D^{*-} \pi^+ \pi^-$		$< 2.4 \times 10^{-5}$	CL=90%	–
$\overline{D}_2^*(2460)^- \rho^+$		$< 4.9 \times 10^{-3}$	CL=90%	1974
$D^0 \overline{D}^0$		$(1.4 \pm 0.7) \times 10^{-5}$		1868
$D^{*0} \overline{D}^0$		$< 2.9 \times 10^{-4}$	CL=90%	1794
$D^- D^+$		$(2.11 \pm 0.18) \times 10^{-4}$		1864
$D^\pm D^{*\mp}$ (CP-averaged)		$(6.1 \pm 0.6) \times 10^{-4}$		–
$D^- D_s^+$		$(7.2 \pm 0.8) \times 10^{-3}$		1812
$D^*(2010)^- D_s^+$		$(8.0 \pm 1.1) \times 10^{-3}$		1735
$D^- D_s^{*+}$		$(7.4 \pm 1.6) \times 10^{-3}$		1732
$D^*(2010)^- D_s^{*+}$		(1.77 ± 0.14) %		1649
$D_{s0}(2317)^- K^+$, $D_{s0}^- \to D_s^- \pi^0$		$(4.2 \pm 1.4) \times 10^{-5}$		2097
$D_{s0}(2317)^- \pi^+$, $D_{s0}^- \to D_s^- \pi^0$		$< 2.5 \times 10^{-5}$	CL=90%	2128
$D_{sJ}(2457)^- K^+$, $D_{sJ}^- \to D_s^- \pi^0$		$< 9.4 \times 10^{-6}$	CL=90%	–
$D_{sJ}(2457)^- \pi^+$, $D_{sJ}^- \to D_s^- \pi^0$		$< 4.0 \times 10^{-6}$	CL=90%	–
$D_s^- D_s^+$		$< 3.6 \times 10^{-5}$	CL=90%	1759
$D_s^{*-} D_s^+$		$< 1.3 \times 10^{-4}$	CL=90%	1674
$D_s^- D_s^{*+}$		$< 2.4 \times 10^{-4}$	CL=90%	1583
$D_{s0}^*(2317)^+ D^-$, $D_{s0}^{*+} \to D_s^+ \pi^0$		$(1.06 \pm 0.16) \times 10^{-3}$	S=1.1	1602
$D_{s0}(2317)^+ D^-$, $D_{s0}^+ \to D_s^{*+} \gamma$		$< 9.5 \times 10^{-4}$	CL=90%	–
$D_{s0}(2317)^+ D^*(2010)^-$, $D_{s0}^+ \to D_s^+ \pi^0$		$(1.5 \pm 0.6) \times 10^{-3}$		1509
$D_{sJ}(2457)^+ D^-$		$(3.5 \pm 1.1) \times 10^{-3}$		–

Downloaded from https://academic.oup.com/ptep/article/2022/8/083C01/6651666 by KIT Library user on 27 September 2022

$D_{sJ}(2457)^+ D^-$, $D_{sJ}^+ \to D_s^+ \gamma$	$(6.5 {}^{+1.7}_{-1.4}) \times 10^{-4}$			–
$D_{sJ}(2457)^+ D^-$, $D_{sJ}^+ \to D_s^{*+} \gamma$	$< 6.0 \times 10^{-4}$	CL=90%		–
$D_{sJ}(2457)^+ D^-$, $D_{sJ}^+ \to D_s^+ \pi^+ \pi^-$	$< 2.0 \times 10^{-4}$	CL=90%		–
$D_{sJ}(2457)^+ D^-$, $D_{sJ}^+ \to D_s^+ \pi^0$	$< 3.6 \times 10^{-4}$	CL=90%		–
$D^*(2010)^- D_{sJ}(2457)^+$	$(9.3 \pm 2.2) \times 10^{-3}$			–
$D_{sJ}(2457)^+ D^*(2010)$, $D_{sJ}^+ \to D_s^+ \gamma$	$(2.3 {}^{+0.9}_{-0.7}) \times 10^{-3}$			–
$D^- D_{s1}(2536)^+$, $D_{s1}^+ \to D^{*0} K^+ + D^{*+} K^0$	$(2.8 \pm 0.7) \times 10^{-4}$			1444
$D^- D_{s1}(2536)^+$, $D_{s1}^+ \to D^{*0} K^+$	$(1.7 \pm 0.6) \times 10^{-4}$			1444
$D^- D_{s1}(2536)^+$, $D_{s1}^+ \to D^{*+} K^0$	$(2.6 \pm 1.1) \times 10^{-4}$			1444
$D^*(2010)^- D_{s1}(2536)^+$, $D_{s1}^+ \to D^{*0} K^+ + D^{*+} K^0$	$(5.0 \pm 1.4) \times 10^{-4}$			1336
$D^*(2010)^- D_{s1}(2536)^+$, $D_{s1}^+ \to D^{*0} K^+$	$(3.3 \pm 1.1) \times 10^{-4}$			1336
$D^{*-} D_{s1}(2536)^+$, $D_{s1}^+ \to D^{*+} K^0$	$(5.0 \pm 1.7) \times 10^{-4}$			1336
$D^- D_{sJ}(2573)^+$, $D_{sJ}^+ \to D^0 K^+$	$(3.4 \pm 1.8) \times 10^{-5}$			1414
$D^*(2010)^- D_{sJ}(2573)^+$, $D_{sJ}^+ \to D^0 K^+$	$< 2 \times 10^{-4}$	CL=90%		1304
$D^- D_{sJ}(2700)^+$, $D_{sJ}^+ \to D^0 K^+$	$(7.1 \pm 1.2) \times 10^{-4}$			–
$D^+ \pi^-$	$(7.3 \pm 1.2) \times 10^{-7}$			2306
$D_s^+ \pi^-$	$(2.03 \pm 0.18) \times 10^{-5}$			2270
$D_s^{*+} \pi^-$	$(2.1 \pm 0.4) \times 10^{-5}$		S=1.4	2215
$D_s^+ \rho^-$	$< 2.4 \times 10^{-5}$	CL=90%		2197
$D_s^{*+} \rho^-$	$(4.1 \pm 1.3) \times 10^{-5}$			2138
$D_s^+ a_0^-$	$< 1.9 \times 10^{-5}$	CL=90%		–
$D_s^{*+} a_0^-$	$< 3.6 \times 10^{-5}$	CL=90%		–
$D_s^+ a_1(1260)^-$	$< 2.1 \times 10^{-3}$	CL=90%		2080
$D_s^{*+} a_1(1260)^-$	$< 1.7 \times 10^{-3}$	CL=90%		2015
$D_s^+ a_2^-$	$< 1.9 \times 10^{-4}$	CL=90%		–
$D_s^{*+} a_2^-$	$< 2.0 \times 10^{-4}$	CL=90%		–
$D_s^- K^+$	$(2.7 \pm 0.5) \times 10^{-5}$		S=2.7	2242
$D_s^{*-} K^+$	$(2.19 \pm 0.30) \times 10^{-5}$			2185
$D_s^- K^*(892)^+$	$(3.5 \pm 1.0) \times 10^{-5}$			2172
$D_s^{*-} K^*(892)^+$	$(3.2 {}^{+1.5}_{-1.3}) \times 10^{-5}$			2112
$D_s^- \pi^+ K^0$	$(9.7 \pm 1.4) \times 10^{-5}$			2222
$D_s^{*-} \pi^+ K^0$	$< 1.10 \times 10^{-4}$	CL=90%		2164
$D_s^- K^+ \pi^+ \pi^-$	$(1.7 \pm 0.5) \times 10^{-4}$			2198
$D_s^- \pi^+ K^*(892)^0$	$< 3.0 \times 10^{-3}$	CL=90%		2138
$D_s^{*-} \pi^+ K^*(892)^0$	$< 1.6 \times 10^{-3}$	CL=90%		2076
$\overline{D}^0 K^0$	$(5.2 \pm 0.7) \times 10^{-5}$			2280
$\overline{D}^0 K^+ \pi^-$	$(8.8 \pm 1.7) \times 10^{-5}$			2261
$\overline{D}^0 K^*(892)^0$	$(4.5 \pm 0.6) \times 10^{-5}$			2213
$\overline{D}^0 K^*(1410)^0$	$< 6.7 \times 10^{-5}$	CL=90%		2062
$\overline{D}^0 K_0^*(1430)^0$	$(7 \pm 7) \times 10^{-6}$			2058
$\overline{D}^0 K_2^*(1430)^0$	$(2.1 \pm 0.9) \times 10^{-5}$			2057
$D_0^*(2300)^- K^+$, $D_0^{*-} \to \overline{D}^0 \pi^-$	$(1.9 \pm 0.9) \times 10^{-5}$			–
$D_2^*(2460)^- K^+$, $D_2^{*-} \to \overline{D}^0 \pi^-$	$(2.03 \pm 0.35) \times 10^{-5}$			2029
$D_3^*(2760)^- K^+$, $D_3^{*-} \to \overline{D}^0 \pi^-$	$< 1.0 \times 10^{-6}$	CL=90%		–
$\overline{D}^0 K^+ \pi^-$ nonresonant	$< 3.7 \times 10^{-5}$	CL=90%		2261
$[K^+ K^-]_D K^*(892)^0$	$(4.2 \pm 0.7) \times 10^{-5}$			–
$[\pi^+ \pi^-]_D K^*(892)^0$	$(6.0 \pm 1.1) \times 10^{-5}$			–
$[\pi^+ \pi^- \pi^+ \pi^-]_D K^{*0}$	$(4.6 \pm 0.9) \times 10^{-5}$			–
$\overline{D}^0 \pi^0$	$(2.63 \pm 0.14) \times 10^{-4}$			2308
$\overline{D}^0 \rho^0$	$(3.21 \pm 0.21) \times 10^{-4}$			2237
$\overline{D}^0 f_2$	$(1.56 \pm 0.21) \times 10^{-4}$			–
$\overline{D}^0 \eta$	$(2.36 \pm 0.32) \times 10^{-4}$		S=2.5	2274
$\overline{D}^0 \eta'$	$(1.38 \pm 0.16) \times 10^{-4}$		S=1.3	2198
$\overline{D}^0 \omega$	$(2.54 \pm 0.16) \times 10^{-4}$			2235
$D^0 \phi$	$< 2.3 \times 10^{-6}$	CL=95%		2183
$D^0 K^+ \pi^-$	$(5.3 \pm 3.2) \times 10^{-6}$			2261
$D^0 K^*(892)^0$	$(3.0 \pm 0.6) \times 10^{-6}$			2213
$\overline{D}^{*0} \gamma$	$< 2.5 \times 10^{-5}$	CL=90%		2258
$\overline{D}^*(2007)^0 \pi^0$	$(2.2 \pm 0.6) \times 10^{-4}$		S=2.6	2256
$\overline{D}^*(2007)^0 \rho^0$	$< 5.1 \times 10^{-4}$	CL=90%		2182
$\overline{D}^*(2007)^0 \eta$	$(2.3 \pm 0.6) \times 10^{-4}$		S=2.8	2220
$\overline{D}^*(2007)^0 \eta'$	$(1.40 \pm 0.22) \times 10^{-4}$			2141
$\overline{D}^*(2007)^0 \pi^+ \pi^-$	$(6.2 \pm 2.2) \times 10^{-4}$			2249
$\overline{D}^*(2007)^0 K^0$	$(3.6 \pm 1.2) \times 10^{-5}$			2227
$\overline{D}^*(2007)^0 K^*(892)^0$	$< 6.9 \times 10^{-5}$	CL=90%		2157
$D^*(2007)^0 K^*(892)^0$	$< 4.0 \times 10^{-5}$	CL=90%		2157
$D^*(2007)^0 \pi^+ \pi^+ \pi^- \pi^-$	$(2.7 \pm 0.5) \times 10^{-3}$			2219
$D^*(2010)^+ D^*(2010)^-$	$(8.0 \pm 0.6) \times 10^{-4}$			1711
$\overline{D}^*(2007)^0 \omega$	$(3.6 \pm 1.1) \times 10^{-4}$		S=3.1	2180
$D^*(2010)^+ D^-$	$(6.1 \pm 1.5) \times 10^{-4}$		S=1.6	1790
$D^*(2007)^0 \overline{D}^*(2007)^0$	$< 9 \times 10^{-5}$	CL=90%		1715
$D^- D^0 K^+$	$(1.07 \pm 0.11) \times 10^{-3}$			1574
$D^- D^*(2007)^0 K^+$	$(3.5 \pm 0.4) \times 10^{-3}$			1478
$D^*(2010)^- D^0 K^+$	$(2.47 \pm 0.21) \times 10^{-3}$			1479
$D^*(2010)^- D^*(2007)^0 K^+$	(1.06 ± 0.09) %			1366
$D^- D^+ K^0$	$(7.5 \pm 1.7) \times 10^{-4}$			1568
$D^*(2010)^- D^+ K^0 + D^- D^*(2010)^+ K^0$	$(6.4 \pm 0.5) \times 10^{-3}$			1473
$D^*(2010)^- D^*(2010)^+ K^0$	$(8.1 \pm 0.7) \times 10^{-3}$			1360
$D^{*-} D_{s1}(2536)^+$, $D_{s1}^+ \to D^{*+} K^0$	$(8.0 \pm 2.4) \times 10^{-4}$			1336
$\overline{D}^0 D^0 K^0$	$(2.7 \pm 1.1) \times 10^{-4}$			1574
$\overline{D}^0 \overline{D}^0 K^+ \pi^-$	$(3.5 \pm 0.5) \times 10^{-4}$			1476
$\overline{D}^0 D^*(2007)^0 K^0 + \overline{D}^*(2007)^0 D^0 K^0$	$(1.1 \pm 0.5) \times 10^{-3}$			1478
$\overline{D}^*(2007)^0 D^*(2007)^0 K^0$	$(2.4 \pm 0.9) \times 10^{-3}$			1365
$(\overline{D} + \overline{D}^*)(D + D^*) K$	(3.68 ± 0.26) %			–

Charmonium modes

$\eta_c K^0$	$(8.0 \pm 1.1) \times 10^{-4}$			1751
$\eta_c(1S) K^+ \pi^-$	$(6.0 \pm 0.7) \times 10^{-4}$			1722
$\eta_c(1S) K^+ \pi^-$ (NR)	$(6.2 \pm 1.3) \times 10^{-5}$			–
$X(4100)^- K^+$, $X^- \to \eta_c \pi^-$	$(2.0 \pm 1.0) \times 10^{-5}$			–
$\eta_c(1S) K^*(1410)^0$	$(1.9 \pm 1.5) \times 10^{-4}$			1395
$\eta_c(1S) K_0^*(1430)^0$	$(1.6 \pm 0.4) \times 10^{-4}$			1388
$\eta_c(1S) K_2^*(1430)^0$	$(5.0 {}^{+2.3}_{-2.7}) \times 10^{-5}$			1386
$\eta_c(1S) K^*(1680)^0$	$(3 \pm 4) \times 10^{-5}$			1166
$\eta_c(1S) K_0^*(1950)^0$	$(4.4 {}^{+3.0}_{-4.0}) \times 10^{-5}$			–
$\eta_c K^*(892)^0$	$(5.2 {}^{+0.8}_{-0.9}) \times 10^{-4}$		S=1.6	1646
$\eta_c(2S) K_S^0$, $\eta_c \to p\overline{p}\pi^+\pi^-$	$(4.2 {}^{+1.4}_{-1.2}) \times 10^{-7}$			–
$\eta_c(2S) K^{*0}$	$< 3.9 \times 10^{-4}$	CL=90%		1159
$h_c(1P) K_S^0$	$< 1.4 \times 10^{-5}$			1401
$h_c(1P) K^{*0}$	$< 4 \times 10^{-4}$	CL=90%		1253
$J/\psi(1S) K^0$	$(8.91 \pm 0.21) \times 10^{-4}$			1683
$J/\psi(1S) K^+ \pi^-$	$(1.15 \pm 0.05) \times 10^{-3}$			1652
$J/\psi(1S) K^*(892)^0$	$(1.27 \pm 0.05) \times 10^{-3}$			1572
$J/\psi(1S) \eta K_S^0$	$(5.4 \pm 0.9) \times 10^{-5}$			1508
$J/\psi(1S) \eta' K_S^0$	$< 2.5 \times 10^{-5}$	CL=90%		1271
$J/\psi(1S) \phi K^0$	$(4.9 \pm 1.0) \times 10^{-5}$		S=1.3	1224
$J/\psi(1S) \omega K^0$	$(2.3 \pm 0.4) \times 10^{-4}$			1386
$\chi_{c0}(3915)$, $\chi_{c0} \to J/\psi\omega$	$(2.1 \pm 0.9) \times 10^{-5}$			1102
$J/\psi(1S) K(1270)^0$	$(1.3 \pm 0.5) \times 10^{-3}$			1402
$J/\psi(1S) \pi^0$	$(1.66 \pm 0.10) \times 10^{-5}$			1728
$J/\psi(1S) \eta$	$(1.08 \pm 0.23) \times 10^{-5}$		S=1.5	1673
$J/\psi(1S) \pi^+ \pi^-$	$(4.00 \pm 0.15) \times 10^{-5}$			1716
$J/\psi(1S) \pi^+ \pi^-$ nonresonant	$< 1.2 \times 10^{-5}$	CL=90%		1716
$J/\psi(1S) f_0(500)$, $f_0 \to \pi\pi$	$(8.8 {}^{+1.2}_{-1.6}) \times 10^{-6}$			–
$J/\psi(1S) f_2$	$(3.3 {}^{+0.5}_{-0.6}) \times 10^{-6}$		S=1.5	–
$J/\psi(1S) \rho^0$	$(2.55 {}^{+0.18}_{-0.16}) \times 10^{-5}$			1612
$J/\psi(1S) f_0(980)$, $f_0 \to \pi^+\pi^-$	$< 1.1 \times 10^{-6}$	CL=90%		–
$J/\psi(1S) \rho(1450)^0$, $\rho^0 \to \pi\pi$	$(2.9 {}^{+1.6}_{-0.7}) \times 10^{-6}$			–
$J/\psi \rho(1700)^0$, $\rho^0 \to \pi^+\pi^-$	$(2.0 \pm 1.3) \times 10^{-6}$			–
$J/\psi(1S) \omega$	$(1.8 {}^{+0.7}_{-0.5}) \times 10^{-5}$			1609
$J/\psi(1S) K^+ K^-$	$(2.54 \pm 0.35) \times 10^{-6}$			1534

Downloaded from https://academic.oup.com/ptep/article/2022/8/083C01/6651666 by KIT Library user on 27 September 2022

$J/\psi(1S)\,a_0(980),\ a_0 \to K^+K^-$		$(4.7 \pm 3.4) \times 10^{-7}$		–
$J/\psi(1S)\,\phi$		$< 1.1 \times 10^{-7}$	CL=90%	1520
$J/\psi(1S)\,\eta'(958)$		$(7.6 \pm 2.4) \times 10^{-6}$		1546
$J/\psi(1S)\,K^0\pi^+\pi^-$		$(4.5 \pm 0.4) \times 10^{-4}$		1611
$J/\psi(1S)\,K^0K^-\pi^+ +$ c.c.		$< 2.1 \times 10^{-5}$	CL=90%	1467
$J/\psi(1S)\,K^0K^+K^-$		$(2.5 \pm 0.7) \times 10^{-5}$	S=1.8	1249
$J/\psi(1S)\,K^0\rho^0$		$(5.4 \pm 3.0) \times 10^{-4}$		1390
$J/\psi(1S)\,K^*(892)^+\pi^-$		$(8 \pm 4) \times 10^{-4}$		1515
$J/\psi(1S)\,\pi^+\pi^-\pi^+\pi^-$		$(1.44 \pm 0.12) \times 10^{-5}$		1670
$J/\psi(1S)\,f_1(1285)$		$(8.4 \pm 2.1) \times 10^{-6}$		1385
$J/\psi(1S)\,K^*(892)^0\pi^+\pi^-$		$(6.6 \pm 2.2) \times 10^{-4}$		1447
$\eta_{c2}(1D)\,K^0_S,\ \eta_{c2} \to h_c\gamma$		$< 3.5 \times 10^{-5}$	CL=90%	–
$\eta_{c2}(1D)\,\pi^-K^+,\ \eta_{c2} \to h_c\gamma$		$< 1.0 \times 10^{-4}$	CL=90%	–
$\chi_{c1}(3872)^-K^+$		$< 5 \times 10^{-4}$	CL=90%	–
$\chi_{c1}(3872)^-K^+,\ \chi_{c1}(3872)^- \to J/\psi(1S)\pi^-\pi^0$	[ooo]	$< 4.2 \times 10^{-6}$	CL=90%	–
$\chi_{c1}(3872)\,K^0$		$(1.1 \pm 0.4) \times 10^{-4}$		1140
$\chi_{c1}(3872)\,K^*(892)^0$		$(1.0 \pm 0.5) \times 10^{-4}$		940
$\chi_{c1}(3872)\,K^+\pi^-$		$(2.1 \pm 0.8) \times 10^{-4}$		1087
$\chi_{c1}(3872)\gamma$		$< 1.3 \times 10^{-5}$	CL=90%	1220
$Z_c(4430)^\pm K^\mp,\ Z_c^\pm \to \psi(2S)\pi^\pm$		$(6.0 {}^{+3.0}_{-2.4}) \times 10^{-5}$		583
$Z_c(4430)^\pm K^\mp,\ Z_c^\pm \to J/\psi\pi^\pm$		$(5.4 {}^{+4.0}_{-1.2}) \times 10^{-6}$		583
$Z_c(3900)^\pm K^\mp,\ Z_c^\pm \to J/\psi\pi^\pm$		$< 9 \times 10^{-7}$		–
$Z_c(4200)^\pm K^\mp,\ X^\pm \to J/\psi\pi^\pm$		$(2.2 {}^{+1.3}_{-0.8}) \times 10^{-5}$		–
$J/\psi(1S)\,p\overline{p}$		$(4.5 \pm 0.6) \times 10^{-7}$		862
$J/\psi(1S)\gamma$		$< 1.5 \times 10^{-6}$	CL=90%	1732
$J/\psi(1S)\,\overline{D}^0$		$< 1.3 \times 10^{-5}$	CL=90%	877
$\psi(2S)\,\pi^0$		$(1.17 \pm 0.19) \times 10^{-5}$		1348
$\psi(2S)\,K^0$		$(5.8 \pm 0.5) \times 10^{-4}$		1283
$\psi(3770)\,K^0,\ \psi \to \overline{D}^0D^0$		$< 1.23 \times 10^{-4}$	CL=90%	1217
$\psi(3770)\,K^0,\ \psi \to D^-D^+$		$< 1.88 \times 10^{-4}$	CL=90%	1217
$\psi(2S)\,\pi^+\pi^-$		$(2.24 \pm 0.35) \times 10^{-5}$		1332
$\psi(2S)\,K^+\pi^-$		$(5.8 \pm 0.4) \times 10^{-4}$		1239
$\psi(2S)\,K^*(892)^0$		$(5.9 \pm 0.4) \times 10^{-4}$		1116
$\chi_{c0}\,K^0$		$(1.9 \pm 0.4) \times 10^{-4}$		1477
$\chi_{c0}\,K^*(892)^0$		$(1.7 \pm 0.4) \times 10^{-4}$		1342
$\chi_{c1}\,\pi^0$		$(1.12 \pm 0.28) \times 10^{-5}$		1468
$\chi_{c1}\,K^0$		$(3.95 \pm 0.27) \times 10^{-4}$		1411
$\chi_{c1}\,\pi^-K^+$		$(4.97 \pm 0.30) \times 10^{-4}$		1371
$\chi_{c1}\,K^*(892)^0$		$(2.38 \pm 0.19) \times 10^{-4}$	S=1.2	1265
$X(4051)^-K^+,\ X^- \to \chi_{c1}\pi^-$		$(3.0 {}^{+4.0}_{-1.8}) \times 10^{-5}$		–
$X(4248)^-K^+,\ X^- \to \chi_{c1}\pi^-$		$(4.0 {}^{+20.0}_{-1.0}) \times 10^{-5}$		–
$\chi_{c1}\,\pi^+\pi^-K^0$		$(3.2 \pm 0.5) \times 10^{-4}$		1318
$\chi_{c1}\,\pi^-\pi^0K^+$		$(3.5 \pm 0.6) \times 10^{-4}$		1321
$\chi_{c2}\,K^0$		$< 1.5 \times 10^{-5}$	CL=90%	1379
$\chi_{c2}\,K^*(892)^0$		$(4.9 \pm 1.2) \times 10^{-5}$	S=1.1	1228
$\chi_{c2}\,\pi^-K^+$		$(7.2 \pm 1.0) \times 10^{-5}$		1338
$\chi_{c2}\,\pi^+\pi^-K^0$		$< 1.70 \times 10^{-4}$	CL=90%	1282
$\chi_{c2}\,\pi^-\pi^0K^+$		$< 7.4 \times 10^{-5}$	CL=90%	1286
$\psi(4660)\,K^0,\ \psi \to \Lambda_c^+\Lambda_c^-$		$< 2.3 \times 10^{-4}$	CL=90%	–
$\psi(4230)^0K^0,\ \psi^0 \to J/\psi\pi^+\pi^-$		$< 1.7 \times 10^{-5}$	CL=90%	–

K or *K** modes

$K^+\pi^-$		$(1.96 \pm 0.05) \times 10^{-5}$		2615
$K^0\pi^0$		$(9.9 \pm 0.5) \times 10^{-6}$		2615
$\eta'K^0$		$(6.6 \pm 0.4) \times 10^{-5}$	S=1.4	2528
$\eta'K^*(892)^0$		$(2.8 \pm 0.6) \times 10^{-6}$		2472
$\eta'K^*_0(1430)^0$		$(6.3 \pm 1.6) \times 10^{-6}$		2346
$\eta'K^*_2(1430)^0$		$(1.37 \pm 0.32) \times 10^{-5}$		2346
ηK^0		$(1.23 {}^{+0.27}_{-0.24}) \times 10^{-6}$		2587
$\eta K^*(892)^0$		$(1.59 \pm 0.10) \times 10^{-5}$		2534
$\eta K^*_0(1430)^0$		$(1.10 \pm 0.22) \times 10^{-5}$		2415
$\eta K^*_2(1430)^0$		$(9.6 \pm 2.1) \times 10^{-6}$		2414
ωK^0		$(4.8 \pm 0.4) \times 10^{-6}$		2557
$a_0(980)^0K^0,\ a_0^0 \to \eta\pi^0$		$< 7.8 \times 10^{-6}$	CL=90%	–
$b_1^0K^0,\ b_1^0 \to \omega\pi^0$		$< 7.8 \times 10^{-6}$	CL=90%	–
$a_0(980)^\pm K^\mp,\ a_0^\pm \to \eta\pi^\pm$		$< 1.9 \times 10^{-6}$	CL=90%	–
$b_1^-K^+,\ b_1^- \to \omega\pi^-$		$(7.4 \pm 1.4) \times 10^{-6}$		–
$b_1^0K^{*0},\ b_1^0 \to \omega\pi^0$		$< 8.0 \times 10^{-6}$	CL=90%	–
$b_1^-K^{*+},\ b_1^- \to \omega\pi^-$		$< 5.0 \times 10^{-6}$	CL=90%	–
$a_0(1450)^\pm K^\mp,\ a_0^\pm \to \eta\pi^\pm$		$< 3.1 \times 10^{-6}$	CL=90%	–
$K^0_SX^0$ (Familon)		$< 5.3 \times 10^{-5}$	CL=90%	–
$\omega K^*(892)^0$		$(2.0 \pm 0.5) \times 10^{-6}$		2503
$\omega(K\pi)^*_0{}^0$		$(1.84 \pm 0.25) \times 10^{-5}$		–
$\omega K^*_0(1430)^0$		$(1.60 \pm 0.34) \times 10^{-5}$		2380
$\omega K^*_2(1430)^0$		$(1.01 \pm 0.23) \times 10^{-5}$		2380
$\omega K^+\pi^-$ nonresonant		$(5.1 \pm 1.0) \times 10^{-6}$		2542
$K^+\pi^-\pi^0$		$(3.78 \pm 0.32) \times 10^{-5}$		2609
$K^+\rho^-$		$(7.0 \pm 0.9) \times 10^{-6}$		2559
$K^+\rho(1450)^-$		$(2.4 \pm 1.2) \times 10^{-6}$		–
$K^+\rho(1700)^-$		$(6 \pm 7) \times 10^{-7}$		–
$(K^+\pi^-\pi^0)$ nonresonant		$(2.8 \pm 0.6) \times 10^{-6}$		2609
$(K\pi)^{*+}_0\pi^-,\ (K\pi)^{*+}_0 \to K^+\pi^0$		$(3.4 \pm 0.5) \times 10^{-5}$		–
$(K\pi)^{*0}_0\pi^0,\ (K\pi)^{*0}_0 \to K^+\pi^-$		$(8.6 \pm 1.7) \times 10^{-6}$		–
$K^*_2(1430)^0\pi^0$		$< 4.0 \times 10^{-6}$	CL=90%	2445
$K^*(1680)^0\pi^0$		$< 7.5 \times 10^{-6}$	CL=90%	2358
$K^{*0}_x\pi^0$	[rrr]	$(6.1 \pm 1.6) \times 10^{-6}$		–
$K^0\pi^+\pi^-$		$(4.97 \pm 0.18) \times 10^{-5}$		2609
$K^0\pi^+\pi^-$ nonresonant		$(1.39 {}^{+0.26}_{-0.18}) \times 10^{-5}$	S=1.6	2609
$K^0\rho^0$		$(3.4 \pm 1.1) \times 10^{-6}$	S=2.3	2558
$K^*(892)^+\pi^-$		$(7.5 \pm 0.4) \times 10^{-6}$		2563
$K^*_0(1430)^+\pi^-$		$(3.3 \pm 0.7) \times 10^{-5}$	S=2.0	–
$K^{*+}_x\pi^-$	[rrr]	$(5.1 \pm 1.6) \times 10^{-6}$		–
$K^*(1410)^+\pi^-,\ K^{*+} \to K^0\pi^+$		$< 3.8 \times 10^{-6}$	CL=90%	–
$(K\pi)^{*+}_0\pi^-,\ (K\pi)^{*+}_0 \to K^0\pi^+$		$(1.62 \pm 0.13) \times 10^{-5}$		–
$f_0(980)\,K^0,\ f_0 \to \pi^+\pi^-$		$(8.1 \pm 0.8) \times 10^{-6}$	S=1.3	2522
$K^0f_0(500)$		$(1.6 {}^{+2.5}_{-1.6}) \times 10^{-7}$		–
$K^0f_0(1500)$		$(1.3 \pm 0.8) \times 10^{-6}$		2397
$f_2(1270)\,K^0$		$(2.7 {}^{+1.3}_{-1.2}) \times 10^{-6}$		2459
$f_x(1300)\,K0, f_x \to \pi^+\pi^-$		$(1.8 \pm 0.7) \times 10^{-6}$		–
$K^*(892)^0\pi^0$		$(3.3 \pm 0.6) \times 10^{-6}$		2563
$K^*_2(1430)^+\pi^-$		$(3.65 \pm 0.34) \times 10^{-6}$		2445
$K^*(1680)^+\pi^-$		$(1.41 \pm 0.10) \times 10^{-5}$		2358
$K^+\pi^-\pi^+\pi^-$	[sss]	$< 2.3 \times 10^{-4}$	CL=90%	2600
$\rho^0K^+\pi^-$		$(2.8 \pm 0.7) \times 10^{-6}$		2543
$f_0(980)\,K^+\pi^-,\ f_0 \to \pi\pi$		$(1.4 {}^{+0.5}_{-0.6}) \times 10^{-6}$		2506
$K^+\pi^-\pi^+\pi^-$ nonresonant		$< 2.1 \times 10^{-6}$	CL=90%	2600
$K^*(892)^0\pi^+\pi^-$		$(5.5 \pm 0.5) \times 10^{-5}$		2557
$K^*(892)^0\rho^0$		$(3.9 \pm 1.3) \times 10^{-6}$	S=1.9	2504
$K^*(892)^0f_0(980),\ f_0 \to \pi\pi$		$(3.9 {}^{+2.1}_{-1.8}) \times 10^{-6}$	S=3.9	2466
$K_1(1270)^+\pi^-$		$< 3.0 \times 10^{-5}$	CL=90%	2489
$K_1(1400)^+\pi^-$		$< 2.7 \times 10^{-5}$	CL=90%	2451
$a_1(1260)^-K^+$	[sss]	$(1.6 \pm 0.4) \times 10^{-5}$		2471
$K^*(892)^+\rho^-$		$(1.03 \pm 0.26) \times 10^{-5}$		2504
$K^*_0(1430)^+\rho^-$		$(2.8 \pm 1.2) \times 10^{-5}$		–
$K_1(1400)^0\rho^0$		$< 3.0 \times 10^{-3}$	CL=90%	2388
$K^*_0(1430)^0\rho^0$		$(2.7 \pm 0.6) \times 10^{-5}$		2381
$K^*_0(1430)^0f_0(980),\ f_0 \to \pi\pi$		$(2.7 \pm 0.9) \times 10^{-6}$		–
$K^*_2(1430)^0f_0(980),\ f_0 \to \pi\pi$		$(8.6 \pm 2.0) \times 10^{-6}$		–
K^+K^-		$(7.8 \pm 1.5) \times 10^{-8}$		2593
$K^0\overline{K}^0$		$(1.21 \pm 0.16) \times 10^{-6}$		2593
$K^0K^-\pi^+$		$(6.7 \pm 0.5) \times 10^{-6}$		2578
$K^*(892)^\pm K^\mp$		$< 4 \times 10^{-7}$	CL=90%	2540
$\overline{K}^{*0}K^0 + K^{*0}\overline{K}^0$		$< 9.6 \times 10^{-7}$	CL=90%	–
$K^+K^-\pi^0$		$(2.2 \pm 0.6) \times 10^{-6}$		2579
$K^0_SK^0_S\pi^0$		$< 9 \times 10^{-7}$	CL=90%	2578
$K^0_SK^0_S\eta$		$< 1.0 \times 10^{-6}$	CL=90%	2515
$K^0_SK^0_S\eta'$		$< 2.0 \times 10^{-6}$	CL=90%	2453
$K^0K^+K^-$		$(2.68 \pm 0.11) \times 10^{-5}$		2522
$K^0\phi$		$(7.3 \pm 0.7) \times 10^{-6}$		2516
$f_0(980)\,K^0,\ f_0 \to K^+K^-$		$(7.0 {}^{+3.5}_{-3.0}) \times 10^{-6}$		–
$f_0(1500)\,K^0$		$(1.3 {}^{+0.7}_{-0.5}) \times 10^{-5}$		2397
$f'_2(1525)^0K^0$		$(3 {}^{+5}_{-4}) \times 10^{-7}$		–

Downloaded from https://academic.oup.com/ptep/article/2022/8/083C01/6651666 by KIT Library user on 27 September 2022

$f_0(1710)K^0,\ f_0 \to K^+K^-$		$(4.4 \pm 0.9) \times 10^{-6}$			–
$K^0K^+K^-$ nonresonant		$(3.3 \pm 1.0) \times 10^{-5}$			2522
$K^0_S K^0_S K^0_S$		$(6.0 \pm 0.5) \times 10^{-6}$		S=1.1	2521
$f_0(980)K^0,\ f_0 \to K^0_S K^0_S$		$(2.7 \pm 1.8) \times 10^{-6}$			–
$f_0(1710)K^0,\ f_0 \to K^0_S K^0_S$		$(5.0 {}^{+5.0}_{-2.6}) \times 10^{-7}$			–
$f_2(2010)K^0,\ f_2 \to K^0_S K^0_S$		$(5 \pm 6) \times 10^{-7}$			–
$K^0_S K^0_S K^0_S$ nonresonant		$(1.33 \pm 0.31) \times 10^{-5}$			2521
$K^0_S K^0_S K^0_L$		$< 1.6 \times 10^{-5}$	CL=90%		2521
$K^*(892)^0K^+K^-$		$(2.75 \pm 0.26) \times 10^{-5}$			2467
$K^*(892)^0\phi$		$(1.00 \pm 0.05) \times 10^{-5}$			2460
$K^+K^-\pi^+\pi^-$ nonresonant		$< 7.17 \times 10^{-5}$	CL=90%		2559
$K^*(892)^0K^-\pi^+$		$(4.5 \pm 1.3) \times 10^{-6}$			2524
$K^*(892)^0\overline{K}^*(892)^0$		$(8.3 \pm 2.4) \times 10^{-7}$		S=1.5	2485
$K^+K^+\pi^-\pi^-$ nonresonant		$< 6.0 \times 10^{-6}$	CL=90%		2559
$K^*(892)^0K^+\pi^-$		$< 2.2 \times 10^{-6}$	CL=90%		2524
$K^*(892)^0K^*(892)^0$		$< 2 \times 10^{-7}$	CL=90%		2485
$K^*(892)^+K^*(892)^-$		$< 2.0 \times 10^{-6}$	CL=90%		2485
$K_1(1400)^0\phi$		$< 5.0 \times 10^{-3}$	CL=90%		2339
$\phi(K\pi)^{*0}_0$		$(4.3 \pm 0.4) \times 10^{-6}$			–
$\phi(K\pi)^{*0}_0$ $(1.60<m_{K\pi}<2.15)$	[ttt]	$< 1.7 \times 10^{-6}$	CL=90%		–
$K^*_0(1430)^0K^-\pi^+$		$< 3.18 \times 10^{-5}$	CL=90%		2403
$K^*_0(1430)^0\overline{K}^*(892)^0$		$< 3.3 \times 10^{-6}$	CL=90%		2360
$K^*_0(1430)^0\overline{K}^*_0(1430)^0$		$< 8.4 \times 10^{-6}$	CL=90%		2222
$K^*_0(1430)^0\phi$		$(3.9 \pm 0.8) \times 10^{-6}$			2333
$K^*_0(1430)^0K^*(892)^0$		$< 1.7 \times 10^{-6}$	CL=90%		2360
$K^*_0(1430)^0K^*_0(1430)^0$		$< 4.7 \times 10^{-6}$	CL=90%		2222
$K^*(1680)^0\phi$		$< 3.5 \times 10^{-6}$	CL=90%		2238
$K^*(1780)^0\phi$		$< 2.7 \times 10^{-6}$	CL=90%		–
$K^*(2045)^0\phi$		$< 1.53 \times 10^{-5}$	CL=90%		–
$K^*_2(1430)^0\rho^0$		$< 1.1 \times 10^{-3}$	CL=90%		2381
$K^*_2(1430)^0\phi$		$(6.8 \pm 0.9) \times 10^{-6}$		S=1.2	2332
$K^0\phi\phi$		$(3.7 \pm 0.7) \times 10^{-6}$		S=1.3	2305
$\eta'\eta'K^0$		$< 3.1 \times 10^{-5}$	CL=90%		2337
$\eta K^0\gamma$		$(7.6 \pm 1.8) \times 10^{-6}$			2587
$\eta' K^0\gamma$		$< 6.4 \times 10^{-6}$	CL=90%		2528
$K^0\phi\gamma$		$(2.7 \pm 0.7) \times 10^{-6}$			2516
$K^+\pi^-\gamma$		$(4.6 \pm 1.4) \times 10^{-6}$			2615
$K^*(892)^0\gamma$		$(4.18 \pm 0.25) \times 10^{-5}$		S=2.1	2565
$K^*(1410)\gamma$		$< 1.3 \times 10^{-4}$	CL=90%		2451
$K^+\pi^-\gamma$ nonresonant		$< 2.6 \times 10^{-6}$	CL=90%		2615
$K^*(892)^0X(214),\ X \to \mu^+\mu^-$	[uuu]	$< 2.26 \times 10^{-8}$	CL=90%		–
$K^0\pi^+\pi^-\gamma$		$(1.99 \pm 0.18) \times 10^{-5}$			2609
$K^+\pi^-\pi^0\gamma$		$(4.1 \pm 0.4) \times 10^{-5}$			2609
$K_1(1270)^0\gamma$		$< 5.8 \times 10^{-5}$	CL=90%		2491
$K_1(1400)^0\gamma$		$< 1.2 \times 10^{-5}$	CL=90%		2454
$K^*_2(1430)^0\gamma$		$(1.24 \pm 0.24) \times 10^{-5}$			2447
$K^*(1680)^0\gamma$		$< 2.0 \times 10^{-3}$	CL=90%		2360
$K^*_3(1780)^0\gamma$		$< 8.3 \times 10^{-5}$	CL=90%		2340
$K^*_4(2045)^0\gamma$		$< 4.3 \times 10^{-3}$	CL=90%		2243

Light unflavored meson modes

$\rho^0\gamma$		$(8.6 \pm 1.5) \times 10^{-7}$			2583
$\rho^0X(214),\ X \to \mu^+\mu^-$	[uuu]	$< 1.73 \times 10^{-8}$	CL=90%		–
$\omega\gamma$		$(4.4 {}^{+1.8}_{-1.6}) \times 10^{-7}$			2582
$\phi\gamma$		$< 1.0 \times 10^{-7}$	CL=90%		2541
$\pi^+\pi^-$		$(5.12 \pm 0.19) \times 10^{-6}$			2636
$\pi^0\pi^0$		$(1.59 \pm 0.26) \times 10^{-6}$		S=1.4	2636
$\eta\pi^0$		$(4.1 \pm 1.7) \times 10^{-7}$			2610
$\eta\eta$		$< 1.0 \times 10^{-6}$	CL=90%		2582
$\eta'\pi^0$		$(1.2 \pm 0.6) \times 10^{-6}$		S=1.7	2551
$\eta'\eta'$		$< 1.7 \times 10^{-6}$	CL=90%		2460
$\eta'\eta$		$< 1.2 \times 10^{-6}$	CL=90%		2523
$\eta'\rho^0$		$< 1.3 \times 10^{-6}$	CL=90%		2492
$\eta' f_0(980),\ f_0 \to \pi^+\pi^-$		$< 9 \times 10^{-7}$	CL=90%		2454
$\eta\rho^0$		$< 1.5 \times 10^{-6}$	CL=90%		2553
$\eta f_0(980),\ f_0 \to \pi^+\pi^-$		$< 4 \times 10^{-7}$	CL=90%		2516
$\omega\eta$		$(9.4 {}^{+4.0}_{-3.1}) \times 10^{-7}$			2552
$\omega\eta'$		$(1.0 {}^{+0.5}_{-0.4}) \times 10^{-6}$			2491
$\omega\rho^0$		$< 1.6 \times 10^{-6}$	CL=90%		2522
$\omega f_0(980),\ f_0 \to \pi^+\pi^-$		$< 1.5 \times 10^{-6}$	CL=90%		2485
$\omega\omega$		$(1.2 \pm 0.4) \times 10^{-6}$			2521
$\phi\pi^0$		$< 1.5 \times 10^{-7}$	CL=90%		2540
$\phi\eta$		$< 5 \times 10^{-7}$	CL=90%		2511
$\phi\eta'$		$< 5 \times 10^{-7}$	CL=90%		2448
$\phi\pi^+\pi^-$		$(1.8 \pm 0.5) \times 10^{-7}$			2533
$\phi\rho^0$		$< 3.3 \times 10^{-7}$	CL=90%		2480
$\phi f_0(980),\ f_0 \to \pi^+\pi^-$		$< 3.8 \times 10^{-7}$	CL=90%		2441
$\phi\omega$		$< 7 \times 10^{-7}$	CL=90%		2479
$\phi\phi$		$< 2.7 \times 10^{-8}$	CL=90%		2435
$a_0(980)^\pm\pi^\mp,\ a_0^\pm \to \eta\pi^\pm$		$< 3.1 \times 10^{-6}$	CL=90%		–
$a_0(1450)^\pm\pi^\mp,\ a_0^\pm \to \eta\pi^\pm$		$< 2.3 \times 10^{-6}$	CL=90%		–
$\pi^+\pi^-\pi^0$		$< 7.2 \times 10^{-4}$	CL=90%		2631
$\rho^0\pi^0$		$(2.0 \pm 0.5) \times 10^{-6}$			2581
$\rho^\mp\pi^\pm$	[aa]	$(2.30 \pm 0.23) \times 10^{-5}$			2581
$\pi^+\pi^-\pi^+\pi^-$		$< 1.12 \times 10^{-5}$	CL=90%		2621
$\rho^0\pi^+\pi^-$		$< 8.8 \times 10^{-6}$	CL=90%		2575
$\rho^0\rho^0$		$(9.6 \pm 1.5) \times 10^{-7}$			2523
$f_0(980)\pi^+\pi^-,\ f_0 \to \pi^+\pi^-$		$< 3.0 \times 10^{-6}$	CL=90%		–
$\rho^0 f_0(980),\ f_0 \to \pi^+\pi^-$		$(7.8 \pm 2.5) \times 10^{-7}$			2486
$f_0(980)f_0(980),\ f_0 \to \pi^+\pi^-,\ f_0 \to \pi^+\pi^-$		$< 1.9 \times 10^{-7}$	CL=90%		2447
$f_0(980)f_0(980),\ f_0 \to \pi^+\pi^-,\ f_0 \to K^+K^-$		$< 2.3 \times 10^{-7}$	CL=90%		2447
$a_1(1260)^\mp\pi^\pm$	[aa]	$(2.6 \pm 0.5) \times 10^{-5}$		S=1.9	2494
$a_2(1320)^\mp\pi^\pm$	[aa]	$< 6.3 \times 10^{-6}$	CL=90%		2473
$\pi^+\pi^-\pi^0\pi^0$		$< 3.1 \times 10^{-3}$	CL=90%		2622
$\rho^+\rho^-$		$(2.77 \pm 0.19) \times 10^{-5}$			2523
$a_1(1260)^0\pi^0$		$< 1.1 \times 10^{-3}$	CL=90%		2495
$\omega\pi^0$		$< 5 \times 10^{-7}$	CL=90%		2580
$\pi^+\pi^+\pi^-\pi^-\pi^0$		$< 9.0 \times 10^{-3}$	CL=90%		2609
$a_1(1260)^+\rho^-$		$< 6.1 \times 10^{-5}$	CL=90%		2433
$a_1(1260)^0\rho^0$		$< 2.4 \times 10^{-3}$	CL=90%		2433
$b_1^\mp\pi^\pm,\ b_1^\mp \to \omega\pi^\mp$		$(1.09 \pm 0.15) \times 10^{-5}$			–
$b_1^0\pi^0,\ b_1^0 \to \omega\pi^0$		$< 1.9 \times 10^{-6}$	CL=90%		–
$b_1^-\rho^+,\ b_1^- \to \omega\pi^-$		$< 1.4 \times 10^{-6}$	CL=90%		–
$b_1^0\rho^0,\ b_1^0 \to \omega\pi^0$		$< 3.4 \times 10^{-6}$	CL=90%		–
$\pi^+\pi^+\pi^+\pi^-\pi^-\pi^-$		$< 3.0 \times 10^{-3}$	CL=90%		2592
$a_1(1260)^+a_1(1260)^-,\ a_1^+ \to 2\pi^+\pi^-,\ a_1^- \to 2\pi^-\pi^+$		$(1.18 \pm 0.31) \times 10^{-5}$			2336
$\pi^+\pi^+\pi^+\pi^-\pi^-\pi^-\pi^0$		< 1.1 %	CL=90%		2572

Baryon modes

$p\overline{p}$		$(1.25 \pm 0.32) \times 10^{-8}$			2467
$p\overline{p}\pi^+\pi^-$		$(2.87 \pm 0.19) \times 10^{-6}$			2406
$p\overline{p}K^+\pi^-$		$(6.3 \pm 0.5) \times 10^{-6}$			2306
$p\overline{p}K^0$		$(2.66 \pm 0.32) \times 10^{-6}$			2347
$\Theta(1540)^+\overline{p},\ \Theta^+ \to pK^0_S$	[vvv]	$< 5 \times 10^{-8}$	CL=90%		2318
$f_J(2220)K^0,\ f_J \to p\overline{p}$		$< 4.5 \times 10^{-7}$	CL=90%		2135
$p\overline{p}K^*(892)^0$		$(1.24 {}^{+0.28}_{-0.25}) \times 10^{-6}$			2216
$f_J(2220)K^*_0,\ f_J \to p\overline{p}$		$< 1.5 \times 10^{-7}$	CL=90%		–
$p\overline{p}K^+K^-$		$(1.21 \pm 0.32) \times 10^{-7}$			2179
$p\overline{p}\pi^0$		$(5.0 \pm 1.9) \times 10^{-7}$			2440
$p\overline{p}p\overline{p}$		$< 2.0 \times 10^{-7}$	CL=90%		1735
$p\overline{\Lambda}\pi^-$		$(3.14 \pm 0.29) \times 10^{-6}$			2401
$p\overline{\Lambda}\pi^-\gamma$		$< 6.5 \times 10^{-7}$	CL=90%		2401
$p\overline{\Sigma}(1385)^-$		$< 2.6 \times 10^{-7}$	CL=90%		2363
$\Delta(1232)^+\overline{p} + \Delta(1232)^-p$		$< 1.6 \times 10^{-6}$			–
$\Delta^0\overline{\Lambda}$		$< 9.3 \times 10^{-7}$	CL=90%		2364
$p\overline{\Lambda}K^-$		$< 8.2 \times 10^{-7}$	CL=90%		2308
$p\overline{\Lambda}D^-$		$(2.5 \pm 0.4) \times 10^{-5}$			1765
$p\overline{\Lambda}D^{*-}$		$(3.4 \pm 0.8) \times 10^{-5}$			1685
$p\overline{\Sigma}^0\pi^-$		$< 3.8 \times 10^{-6}$	CL=90%		2383
$\overline{\Lambda}\Lambda$		$< 3.2 \times 10^{-7}$	CL=90%		2392
$\overline{\Lambda}\Lambda K^0$		$(4.8 {}^{+1.0}_{-0.9}) \times 10^{-6}$			2250
$\overline{\Lambda}\Lambda K^{*0}$		$(2.5 {}^{+0.9}_{-0.8}) \times 10^{-6}$			2098
$\overline{\Lambda}\Lambda D^0$		$(1.00 {}^{+0.30}_{-0.26}) \times 10^{-5}$			1662
$D^0\Sigma^0\overline{\Lambda}$ + c.c.		$< 3.1 \times 10^{-5}$	CL=90%		1611
$\Delta^0\overline{\Delta}^0$		$< 1.5 \times 10^{-3}$	CL=90%		2335
$\Delta^{++}\overline{\Delta}^{--}$		$< 1.1 \times 10^{-4}$	CL=90%		2335
$\overline{D}^0p\overline{p}$		$(1.04 \pm 0.07) \times 10^{-4}$			1863
$D^-_s\overline{\Lambda}p$		$(2.8 \pm 0.9) \times 10^{-5}$			1710
$\overline{D}^*(2007)^0p\overline{p}$		$(9.9 \pm 1.1) \times 10^{-5}$			1788
$D^*(2010)^-p\overline{n}$		$(1.4 \pm 0.4) \times 10^{-3}$			1785
$D^-p\overline{p}\pi^+$		$(3.32 \pm 0.31) \times 10^{-4}$			1786
$D^*(2010)^-p\overline{p}\pi^+$		$(4.7 \pm 0.5) \times 10^{-4}$		S=1.2	1708
$\overline{D}^0p\overline{p}\pi^+\pi^-$		$(3.0 \pm 0.5) \times 10^{-4}$			1708
$\overline{D}^{*0}p\overline{p}\pi^+\pi^-$		$(1.9 \pm 0.5) \times 10^{-4}$			1623

Downloaded from https://academic.oup.com/ptep/article/2022/8/083C01/6651666 by KIT Library user on 27 September 2022

$\Theta_c \overline{p} \pi^+$, $\Theta_c \to D^- p$		< 9	$\times 10^{-6}$	CL=90%	–
$\Theta_c \overline{p} \pi^+$, $\Theta_c \to D^{*-} p$		< 1.4	$\times 10^{-5}$	CL=90%	–
$\overline{\Sigma}_c^{--} \Delta^{++}$		< 8	$\times 10^{-4}$	CL=90%	1839
$\overline{\Lambda}_c^- p \pi^+ \pi^-$		(1.02 ± 0.14)	$\times 10^{-3}$	S=1.3	1934
$\overline{\Lambda}_c^- p$		(1.54 ± 0.18)	$\times 10^{-5}$		2021
$\overline{\Lambda}_c^- p \pi^0$		(1.55 ± 0.19)	$\times 10^{-4}$		1982
$\overline{\Sigma}_c(2455)^- p$		< 2.4	$\times 10^{-5}$		–
$\overline{\Lambda}_c^- p \pi^+ \pi^- \pi^0$		< 5.07	$\times 10^{-3}$	CL=90%	1883
$\overline{\Lambda}_c^- p \pi^+ \pi^- \pi^+ \pi^-$		< 2.74	$\times 10^{-3}$	CL=90%	1821
$\overline{\Lambda}_c^- p \pi^+ \pi^-$ (nonresonant)		(5.5 ± 1.0)	$\times 10^{-4}$	S=1.3	1934
$\overline{\Sigma}_c(2520)^{--} p \pi^+$		(1.02 ± 0.18)	$\times 10^{-4}$		1860
$\overline{\Sigma}_c(2520)^0 p \pi^-$		< 3.1	$\times 10^{-5}$	CL=90%	1860
$\overline{\Sigma}_c(2455)^0 p \pi^-$		(1.08 ± 0.16)	$\times 10^{-4}$		1895
$\overline{\Sigma}_c(2455)^0 N^0$, $N^0 \to p \pi^-$		(6.4 ± 1.7)	$\times 10^{-5}$		–
$\overline{\Sigma}_c(2455)^{--} p \pi^+$		(1.83 ± 0.24)	$\times 10^{-4}$		1895
$\Lambda_c^- p K^+ \pi^-$		(3.4 ± 0.7)	$\times 10^{-5}$		1786
$\overline{\Sigma}_c(2455)^{--} p K^+$, $\overline{\Sigma}_c^{--} \to \overline{\Lambda}_c^- \pi^-$		(8.8 ± 2.5)	$\times 10^{-6}$		1754
$\Lambda_c^- p K^*(892)^0$		< 2.42	$\times 10^{-5}$	CL=90%	1647
$\Lambda_c^- p K^+ K^-$		(2.0 ± 0.4)	$\times 10^{-5}$		1588
$\Lambda_c^- p \phi$		< 1.0	$\times 10^{-5}$	CL=90%	1567
$\Lambda_c^- p \overline{p} p$		< 2.8	$\times 10^{-6}$		677
$\overline{\Lambda}_c^- \Lambda K^+$		(4.8 ± 1.1)	$\times 10^{-5}$		1767
$\overline{\Lambda}_c^- \Lambda_c^+$		< 1.6	$\times 10^{-5}$	CL=95%	1319
$\overline{\Lambda}_c(2593)^- / \overline{\Lambda}_c(2625)^- p$		< 1.1	$\times 10^{-4}$	CL=90%	–
$\overline{\Xi}_c^- \Lambda_c^+$		(1.2 ± 0.8)	$\times 10^{-3}$		1147
$\overline{\Xi}_c^- \Lambda_c^+$, $\overline{\Xi}_c^- \to \overline{\Xi}^+ \pi^- \pi^-$		(2.4 ± 1.1)	$\times 10^{-5}$	S=1.8	1147
$\overline{\Xi}_c^- \Lambda_c^+$, $\overline{\Xi}_c^- \to \overline{p} K^+ \pi^-$		(5.3 ± 1.7)	$\times 10^{-6}$		–
$\Lambda_c^+ \Lambda_c^- K^0$		(4.0 ± 0.9)	$\times 10^{-4}$		732
$\overline{\Xi}_c(2930)^- \Lambda_c^+$, $\overline{\Xi}_c^- \to \Lambda_c^- K^0$		(2.4 ± 0.6)	$\times 10^{-4}$		–

Lepton Family number (*LF*) or Lepton number (*L*) or Baryon number (*B*) violating modes, or/and $\Delta B = 1$ weak neutral current (*B1*) modes

$\gamma\gamma$	*B1*	< 3.2	$\times 10^{-7}$	CL=90%	2640
$e^+ e^-$	*B1*	< 2.5	$\times 10^{-9}$	CL=90%	2640
$e^+ e^- \gamma$	*B1*	< 1.2	$\times 10^{-7}$	CL=90%	2640
$\mu^+ \mu^-$	*B1*	(7^{+13}_{-11})	$\times 10^{-11}$	S=1.8	2638
$\mu^+ \mu^- \gamma$	*B1*	< 2.0	$\times 10^{-9}$	CL=95%	2638
$\mu^+ \mu^- \mu^+ \mu^-$	*B1*	< 6.9	$\times 10^{-10}$	CL=95%	2629
SP, $S \to \mu^+ \mu^-$, $P \to \mu^+ \mu^-$	*B1*	[*xxx*] < 6.0	$\times 10^{-10}$	CL=95%	–
$\tau^+ \tau^-$	*B1*	< 2.1	$\times 10^{-3}$	CL=95%	1952
$\pi^0 \ell^+ \ell^-$	*B1*	< 5.3	$\times 10^{-8}$	CL=90%	2638
$\pi^0 e^+ e^-$	*B1*	< 8.4	$\times 10^{-8}$	CL=90%	2638
$\pi^0 \mu^+ \mu^-$	*B1*	< 6.9	$\times 10^{-8}$	CL=90%	2634
$\eta \ell^+ \ell^-$	*B1*	< 6.4	$\times 10^{-8}$	CL=90%	2611
$\eta e^+ e^-$	*B1*	< 1.08	$\times 10^{-7}$	CL=90%	2611
$\eta \mu^+ \mu^-$	*B1*	< 1.12	$\times 10^{-7}$	CL=90%	2607
$\pi^0 \nu \overline{\nu}$	*B1*	< 9	$\times 10^{-6}$	CL=90%	2638
$K^0 \ell^+ \ell^-$	*B1*	[*iii*] (3.3 ± 0.6)	$\times 10^{-7}$		2616
$K^0 e^+ e^-$	*B1*	($2.5^{+1.1}_{-0.9}$)	$\times 10^{-7}$	S=1.3	2616
$K^0 \mu^+ \mu^-$	*B1*	(3.39 ± 0.35)	$\times 10^{-7}$	S=1.1	2612
$K^0 \nu \overline{\nu}$	*B1*	< 2.6	$\times 10^{-5}$	CL=90%	2616
$\rho^0 \nu \overline{\nu}$	*B1*	< 4.0	$\times 10^{-5}$	CL=90%	2583
$K^*(892)^0 \ell^+ \ell^-$	*B1*	[*iii*] ($9.9^{+1.2}_{-1.1}$)	$\times 10^{-7}$		2565
$K^*(892)^0 e^+ e^-$	*B1*	($1.03^{+0.19}_{-0.17}$)	$\times 10^{-6}$		2565
$K^*(892)^0 \mu^+ \mu^-$	*B1*	(9.4 ± 0.5)	$\times 10^{-7}$		2560
$\pi^+ \pi^- \mu^+ \mu^-$	*B1*	(2.1 ± 0.5)	$\times 10^{-8}$		2626
$K^*(892)^0 \nu \overline{\nu}$	*B1*	< 1.8	$\times 10^{-5}$	CL=90%	2565
invisible	*B1*	< 2.4	$\times 10^{-5}$	CL=90%	–
$\nu \overline{\nu} \gamma$	*B1*	< 1.6	$\times 10^{-5}$	CL=90%	2640
$\phi \nu \overline{\nu}$	*B1*	< 1.27	$\times 10^{-4}$	CL=90%	2541
$e^\pm \mu^\mp$	*LF*	[*aa*] < 1.0	$\times 10^{-9}$	CL=90%	2639
$\pi^0 e^\pm \mu^\mp$	*LF*	< 1.4	$\times 10^{-7}$	CL=90%	2637
$K^0 e^\pm \mu^\mp$	*LF*	< 3.8	$\times 10^{-8}$	CL=90%	2615
$K^*(892)^0 e^+ \mu^-$	*LF*	< 1.6	$\times 10^{-7}$	CL=90%	2563
$K^*(892)^0 e^- \mu^+$	*LF*	< 1.2	$\times 10^{-7}$	CL=90%	2563
$K^*(892)^0 e^\pm \mu^\mp$	*LF*	< 1.8	$\times 10^{-7}$	CL=90%	2563
$e^\pm \tau^\mp$	*LF*	[*aa*] < 1.6	$\times 10^{-5}$	CL=90%	2341
$\mu^\pm \tau^\mp$	*LF*	[*aa*] < 1.4	$\times 10^{-5}$	CL=95%	2340
$\Lambda_c^+ \mu^-$	*L,B*	< 1.4	$\times 10^{-6}$	CL=90%	2143
$\Lambda_c^+ e^-$	*L,B*	< 4	$\times 10^{-6}$	CL=90%	2145

$B^\pm/B^0$ ADMIXTURE

CP violation

$A_{CP}(B \to K^*(892)\gamma) = -0.003 \pm 0.011$
$A_{CP}(B \to s\gamma) = 0.015 \pm 0.011$
$A_{CP}(B \to (s+d)\gamma) = 0.010 \pm 0.031$
$A_{CP}(B \to X_s \ell^+ \ell^-) = 0.04 \pm 0.11$
$A_{CP}(B \to X_s \ell^+ \ell^-)$ $(1.0 < q^2 < 6.0\ \mathrm{GeV}^2/c^4) = -0.06 \pm 0.22$
$A_{CP}(B \to X_s \ell^+ \ell^-)$ $(10.1 < q^2 < 12.9$ or $q^2 > 14.2\ \mathrm{GeV}^2/c^4)$ $= 0.19 \pm 0.18$
$A_{CP}(B \to K^* e^+ e^-) = -0.18 \pm 0.15$
$A_{CP}(B \to K^* \mu^+ \mu^-) = -0.03 \pm 0.13$
$A_{CP}(B \to K^* \ell^+ \ell^-) = -0.04 \pm 0.07$
$A_{CP}(B \to \eta \mathrm{anything}) = -0.13^{+0.04}_{-0.05}$
$\Delta A_{CP}(X_s\gamma) = A_{CP}(B^\pm \to X_s\gamma) - A_{CP}(B^0 \to X_s\gamma) = 0.041 \pm 0.023$
$\overline{A}_{CP}(B \to X_s\gamma) = (A_{CP}(B^+ \to X_s\gamma) + A_{CP}(B^0 \to X_s\gamma))/2 = 0.009 \pm 0.012$
$\Delta A_{CP}(B \to K^*\gamma) = A_{CP}(B^+ \to K^{*+}\gamma) - A_{CP}(B^0 \to K^{*0}\gamma) = 0.024 \pm 0.028$
$\overline{A}_{CP}(B \to K^*\gamma) = (A_{CP}(B^+ \to K^{*+}\gamma) + A_{CP}(B^0 \to K^{*0}\gamma))/2 = -0.001 \pm 0.014$

The branching fraction measurements are for an admixture of B mesons at the $\Upsilon(4S)$. The values quoted assume that $B(\Upsilon(4S) \to B\overline{B}) = 100\%$.

For inclusive branching fractions, *e.g.*, $B \to D^\pm$ *anything*, the treatment of multiple D's in the final state must be defined. One possibility would be to count the number of events with one-or-more D's and divide by the total number of B's. Another possibility would be to count the total number of D's and divide by the total number of B's, which is the definition of average multiplicity. The two definitions are identical if only one D is allowed in the final state. Even though the "one-or-more" definition seems sensible, for practical reasons inclusive branching fractions are almost always measured using the multiplicity definition. For heavy final state particles, authors call their results inclusive branching fractions while for light particles some authors call their results multiplicities. In the B sections, we list all results as inclusive branching fractions, adopting a multiplicity definition. This means that inclusive branching fractions can exceed 100% and that inclusive partial widths can exceed total widths, just as inclusive cross sections can exceed total cross section.

$\overline{B}$ modes are charge conjugates of the modes below. Reactions indicate the weak decay vertex and do not include mixing.

***B* DECAY MODES**		Fraction (Γ_i/Γ)	Scale factor/ Confidence level	p (MeV/c)
Semileptonic and leptonic modes				
$\ell^+ \nu_\ell$ anything	[*iii,yyy*]	(10.84 ± 0.16) %		–
$D^- \ell^+ \nu_\ell$ anything	[*iii*]	(2.6 ± 0.5) %		–
$\overline{D}^0 \ell^+ \nu_\ell$ anything	[*iii*]	(7.3 ± 1.5) %		–
$\overline{D} \ell^+ \nu_\ell$		(2.42 ± 0.12) %		2310
$D^{*-} \ell^+ \nu_\ell$ anything	[*zzz*]	(6.7 ± 1.3) $\times 10^{-3}$		–
$\overline{D}^* \ell^+ \nu_\ell$	[*aaaa*]	(4.95 ± 0.11) %		2257
$\overline{D}^{**} \ell^+ \nu_\ell$	[*iii,bbaa*]	(2.7 ± 0.7) %		–
$\overline{D}_1(2420) \ell^+ \nu_\ell$ anything		(3.8 ± 1.3) $\times 10^{-3}$	S=2.4	–
$\overline{D} \pi \ell^+ \nu_\ell$ anything + $\overline{D}^* \pi \ell^+ \nu_\ell$ anything		(2.6 ± 0.5) %	S=1.5	–
$\overline{D} \pi \ell^+ \nu_\ell$ anything		(1.5 ± 0.6) %		–
$\overline{D}^* \pi \ell^+ \nu_\ell$ anything		(1.9 ± 0.4) %		–
$\overline{D}^*_2(2460) \ell^+ \nu_\ell$ anything		(4.4 ± 1.6) $\times 10^{-3}$		–
$D^{*-} \pi^+ \ell^+ \nu_\ell$ anything		(1.00 ± 0.34) %		–
$\overline{D} \pi^+ \pi^- \ell^+ \nu_\ell$		(1.62 ± 0.32) $\times 10^{-3}$		2301
$\overline{D}^* \pi^+ \pi^- \ell^+ \nu_\ell$		(9.4 ± 3.2) $\times 10^{-4}$		2247
$D_s^- \ell^+ \nu_\ell$ anything	[*iii*]	< 7 $\times 10^{-3}$	CL=90%	–
$D_s^- \ell^+ \nu_\ell K^+$ anything	[*iii*]	< 5 $\times 10^{-3}$	CL=90%	–
$D_s^- \ell^+ \nu_\ell K^0$ anything	[*iii*]	< 7 $\times 10^{-3}$	CL=90%	–
$X_c \ell^+ \nu_\ell$		(10.65 ± 0.16) %		–
$X_u \ell^+ \nu_\ell$		(1.91 ± 0.27) $\times 10^{-3}$		–
$X_u e^+ \nu_e$		(1.57 ± 0.19) $\times 10^{-3}$		–
$X_u \mu^+ \nu_\mu$		(1.62 ± 0.21) $\times 10^{-3}$		–
$K^+ \ell^+ \nu_\ell$ anything	[*iii*]	(6.3 ± 0.6) %		–
$K^- \ell^+ \nu_\ell$ anything	[*iii*]	(10 ± 4) $\times 10^{-3}$		–
$K^0/\overline{K}^0 \ell^+ \nu_\ell$ anything	[*iii*]	(4.6 ± 0.5) %		–
$\overline{D} \tau^+ \nu_\tau$		(8.2 ± 0.8) $\times 10^{-3}$		1911
$\overline{D}^* \tau^+ \nu_\tau$		(1.46 ± 0.08) %		1838

Downloaded from https://academic.oup.com/ptep/article/2022/8/083C01/6651666 by KIT Library user on 27 September 2022

D, D^*, or D_s modes

$D^\pm$ anything		(23.1 ± 1.2) %		S=1.3	–
$D^0/\overline{D}^0$ anything		(61.6 ± 2.9) %			–
$D^*(2010)^\pm$ anything		(22.5 ± 1.5) %			–
$\overline{D}^*(2007)^0$ anything		(26.0 ± 2.7) %			–
$D_s^\pm$ anything	[aa]	(8.3 ± 0.8) %			–
$D_s^{*\pm}$ anything		(6.3 ± 1.0) %			–
$D_s^{*\pm}\overline{D}^{(*)}$		(3.4 ± 0.6) %			–
$\overline{D}D_{s0}(2317)$		seen			1605
$\overline{D}D_{s,J}(2457)$		seen			–
$D^{(*)}\overline{D}^{(*)}K^0 + D^{(*)}\overline{D}^{(*)}K^\pm$	[aa,ccaa]	$(7.1 {}^{+2.7}_{-1.7})$ %			–
$b \to c\overline{c}s$		(22 ± 4) %			–
$D_s^{(*)}\overline{D}^{(*)}$	[aa,ccaa]	(3.9 ± 0.4) %			–
$D^*D^*(2010)^\pm$	[aa]	< 5.9	$\times 10^{-3}$	CL=90%	1711
$DD^*(2010)^\pm + D^*D^\pm$	[aa]	< 5.5	$\times 10^{-3}$	CL=90%	–
$DD^\pm$	[aa]	< 3.1	$\times 10^{-3}$	CL=90%	1866
$D_s^{(*)\pm}\overline{D}^{(*)}X\,(n\pi^\pm)$	[aa,ccaa]	$(9 {}^{+5}_{-4})$ %			–
$\overline{D}^*(2010)\gamma$		< 1.1	$\times 10^{-3}$	CL=90%	2257
$D_s^+\pi^-$, $D_s^{*+}\pi^-$, $D_s^+\rho^-$, $D_s^{*+}\rho^-$, $D_s^+\pi^0$, $D_s^{*+}\pi^0$, $D_s^+\eta$, $D_s^{*+}\eta$, $D_s^+\rho^0$, $D_s^{*+}\rho^0$, $D_s^+\omega$, $D_s^{*+}\omega$	[aa]	< 4	$\times 10^{-4}$	CL=90%	–
$D_{s1}(2536)^+$ anything		< 9.5	$\times 10^{-3}$	CL=90%	–

Charmonium modes

$J/\psi(1S)$ anything		(1.094 ± 0.032) %		S=1.1	–
$J/\psi(1S)$ (direct) anything		(7.8 ± 0.4)	$\times 10^{-3}$	S=1.1	–
$\psi(2S)$ anything		(3.07 ± 0.21)	$\times 10^{-3}$		–
$\chi_{c1}(1P)$ anything		(3.55 ± 0.27)	$\times 10^{-3}$	S=1.3	–
$\chi_{c1}(1P)$ (direct) anything		(3.08 ± 0.19)	$\times 10^{-3}$		–
$\chi_{c2}(1P)$ anything		(10.0 ± 1.7)	$\times 10^{-4}$	S=1.6	–
$\chi_{c2}(1P)$ (direct) anything		(7.5 ± 1.1)	$\times 10^{-4}$		–
$\eta_c(1S)$ anything		< 9	$\times 10^{-3}$	CL=90%	–
$K\chi_{c1}(3872)$		(2.3 ± 0.7)	$\times 10^{-4}$		1141
$KX(3940)$, $X \to D^{*0}D^0$		< 6.7	$\times 10^{-5}$	CL=90%	1084
$K\chi_{c0}(3915)$, $\chi_{c0} \to \omega J/\psi$	[ddaa]	(7.1 ± 3.4)	$\times 10^{-5}$		1103

K or K^* modes

$K^\pm$ anything	[aa]	(78.9 ± 2.5) %			–
K^+ anything		(66 ± 5) %			–
K^- anything		(13 ± 4) %			–
$K^0/\overline{K}^0$ anything	[aa]	(64 ± 4) %			–
$K^*(892)^\pm$ anything		(18 ± 6) %			–
$K^*(892)^0/\overline{K}^*(892)^0$ anything	[aa]	(14.6 ± 2.6) %			–
$K^*(892)\gamma$		(4.2 ± 0.6)	$\times 10^{-5}$		2565
$\eta K\gamma$		$(8.5 {}^{+1.8}_{-1.6})$	$\times 10^{-6}$		2588
$K_1(1400)\gamma$		< 1.27	$\times 10^{-4}$	CL=90%	2454
$K_2^*(1430)\gamma$		$(1.7 {}^{+0.6}_{-0.5})$	$\times 10^{-5}$		2447
$K_2(1770)\gamma$		< 1.2	$\times 10^{-3}$	CL=90%	2342
$K_3^*(1780)\gamma$		< 3.7	$\times 10^{-5}$	CL=90%	2340
$K_4^*(2045)\gamma$		< 1.0	$\times 10^{-3}$	CL=90%	2243
$K\eta'(958)$		(8.3 ± 1.1)	$\times 10^{-5}$		2528
$K^*(892)\eta'(958)$		(4.1 ± 1.1)	$\times 10^{-6}$		2472
$K\eta$		< 5.2	$\times 10^{-6}$	CL=90%	2588
$K^*(892)\eta$		(1.8 ± 0.5)	$\times 10^{-5}$		2534
$K\phi\phi$		(2.3 ± 0.9)	$\times 10^{-6}$		2306
$\overline{b} \to \overline{s}\gamma$		(3.49 ± 0.19)	$\times 10^{-4}$		–
$\overline{b} \to \overline{d}\gamma$		(9.2 ± 3.0)	$\times 10^{-6}$		–
$\overline{b} \to \overline{s}$gluon		< 6.8	%	CL=90%	–
η anything		$(2.6 {}^{+0.5}_{-0.8})$	$\times 10^{-4}$		–
η' anything		(4.2 ± 0.9)	$\times 10^{-4}$		–
K^+gluon (charmless)		< 1.87	$\times 10^{-4}$	CL=90%	–
K^0gluon (charmless)		(1.9 ± 0.7)	$\times 10^{-4}$		–

Light unflavored meson modes

$\rho\gamma$		(1.39 ± 0.25)	$\times 10^{-6}$	S=1.2	2583
$\rho/\omega\gamma$		(1.30 ± 0.23)	$\times 10^{-6}$	S=1.2	–
$\pi^\pm$ anything	[aa,eeaa]	(358 ± 7) %			–
π^0 anything		(235 ± 11) %			–
η anything		(17.6 ± 1.6) %			–
ρ^0 anything		(21 ± 5) %			–
ω anything		< 81 %		CL=90%	–
ϕ anything		(3.43 ± 0.12) %			–
$\phi K^*(892)$		< 2.2	$\times 10^{-5}$	CL=90%	2460
π^+ gluon (charmless)		(3.7 ± 0.8)	$\times 10^{-4}$		–

Baryon modes

$\Lambda_c^+ / \overline{\Lambda}_c^-$ anything		(3.6 ± 0.4) %			–
Λ_c^+ anything		< 1.3 %		CL=90%	–
$\overline{\Lambda}_c^-$ anything		< 7 %		CL=90%	–
$\overline{\Lambda}_c^-\ell^+$ anything		< 9	$\times 10^{-4}$	CL=90%	–
$\overline{\Lambda}_c^- e^+$ anything		< 1.8	$\times 10^{-3}$	CL=90%	–
$\overline{\Lambda}_c^- \mu^+$ anything		< 1.4	$\times 10^{-3}$	CL=90%	–
$\overline{\Lambda}_c^- p$ anything		(2.04 ± 0.33) %			–
$\overline{\Lambda}_c^- p e^+ \nu_e$		< 8	$\times 10^{-4}$	CL=90%	2021
$\overline{\Sigma}_c^{--}$ anything		(3.3 ± 1.7)	$\times 10^{-3}$		–
$\overline{\Sigma}_c^-$ anything		< 8	$\times 10^{-3}$	CL=90%	–
$\overline{\Sigma}_c^0$ anything		(3.7 ± 1.7)	$\times 10^{-3}$		–
$\overline{\Sigma}_c^0 N\,(N = p$ or $n)$		< 1.2	$\times 10^{-3}$	CL=90%	1938
Ξ_c^0 anything, $\Xi_c^0 \to \Xi^-\pi^+$		(1.93 ± 0.30)	$\times 10^{-4}$	S=1.1	–
Ξ_c^+, $\Xi_c^+ \to \Xi^-\pi^+\pi^+$		$(4.5 {}^{+1.3}_{-1.2})$	$\times 10^{-4}$		–
$p/\overline{p}$ anything	[aa]	(8.0 ± 0.4) %			–
$p/\overline{p}$ (direct) anything	[aa]	(5.5 ± 0.5) %			–
$\overline{p}e^+\nu_e$ anything		< 5.9	$\times 10^{-4}$	CL=90%	–
$\Lambda/\overline{\Lambda}$ anything	[aa]	(4.0 ± 0.5) %			–
Λ anything		seen			–
$\overline{\Lambda}$ anything		seen			–
$\Xi^-/\overline{\Xi}^+$ anything	[aa]	(2.7 ± 0.6)	$\times 10^{-3}$		–
baryons anything		(6.8 ± 0.6) %			–
$p\overline{p}$ anything		(2.47 ± 0.23) %			–
$\Lambda\overline{p}/\overline{\Lambda}p$ anything	[aa]	(2.5 ± 0.4) %			–
$\Lambda\overline{\Lambda}$ anything		< 5	$\times 10^{-3}$	CL=90%	–

Lepton Family number (LF) violating modes or $\Delta B = 1$ weak neutral current ($B1$) modes

$s e^+ e^-$	$B1$		(6.7 ± 1.7)	$\times 10^{-6}$	S=2.0	–
$s\mu^+\mu^-$	$B1$		(4.3 ± 1.0)	$\times 10^{-6}$		–
$s\ell^+\ell^-$	$B1$	[iii]	(5.8 ± 1.3)	$\times 10^{-6}$	S=1.8	–
$\pi\ell^+\ell^-$	$B1$		< 5.9	$\times 10^{-8}$	CL=90%	2638
$\pi e^+ e^-$	$B1$		< 1.10	$\times 10^{-7}$	CL=90%	2638
$\pi\mu^+\mu^-$	$B1$		< 5.0	$\times 10^{-8}$	CL=90%	2634
$K e^+ e^-$	$B1$		(4.4 ± 0.6)	$\times 10^{-7}$		2617
$K^*(892) e^+ e^-$	$B1$		(1.19 ± 0.20)	$\times 10^{-6}$	S=1.2	2565
$K\mu^+\mu^-$	$B1$		(4.4 ± 0.4)	$\times 10^{-7}$		2612
$K^*(892)\mu^+\mu^-$	$B1$		(1.06 ± 0.09)	$\times 10^{-6}$		2560
$K\ell^+\ell^-$	$B1$		(4.8 ± 0.4)	$\times 10^{-7}$		2617
$K^*(892)\ell^+\ell^-$	$B1$		(1.05 ± 0.10)	$\times 10^{-6}$		2565
$K\nu\overline{\nu}$	$B1$		< 1.6	$\times 10^{-5}$	CL=90%	2617
$K^*\nu\overline{\nu}$	$B1$		< 2.7	$\times 10^{-5}$	CL=90%	–
$\pi\nu\overline{\nu}$	$B1$		< 8	$\times 10^{-6}$	CL=90%	2638
$\rho\nu\overline{\nu}$	$B1$		< 2.8	$\times 10^{-5}$	CL=90%	2583
$s e^\pm\mu^\mp$	LF	[aa]	< 2.2	$\times 10^{-5}$	CL=90%	–
$\pi e^\pm\mu^\mp$	LF		< 9.2	$\times 10^{-8}$	CL=90%	2637
$\rho e^\pm\mu^\mp$	LF		< 3.2	$\times 10^{-6}$	CL=90%	2582
$K e^\pm\mu^\mp$	LF		< 3.8	$\times 10^{-8}$	CL=90%	2616
$K^*(892) e^\pm\mu^\mp$	LF		< 5.1	$\times 10^{-7}$	CL=90%	2563

$B^\pm/B^0/B_s^0/b$-baryon ADMIXTURE

These measurements are for an admixture of bottom particles at high energy (LHC, LEP, Tevatron, $Sp\overline{p}S$).

Mean life $\tau = (1.5672 \pm 0.0029) \times 10^{-12}$ s

Mean life $\tau = (1.72 \pm 0.10) \times 10^{-12}$ s Charged b-hadron admixture

Mean life $\tau = (1.58 \pm 0.14) \times 10^{-12}$ s Neutral b-hadron admixture

$\tau_{\text{charged } b\text{-hadron}}/\tau_{\text{neutral } b\text{-hadron}} = 1.09 \pm 0.13$

$|\Delta\tau_b|/\tau_{b,\overline{b}} = -0.001 \pm 0.014$

The branching fraction measurements are for an admixture of B mesons and baryons at energies above the $\Upsilon(4S)$. Only the highest energy results (LHC, LEP, Tevatron, $Sp\overline{p}S$) are used in the branching fraction averages. In the following, we assume that the production fractions are the same at the LHC, LEP, and at the Tevatron.

For inclusive branching fractions, *e.g.*, $B \to D^\pm$ anything, the values usually are multiplicities, not branching fractions. They can be greater than one.

Downloaded from https://academic.oup.com/ptep/article/2022/8/083C01/6651666 by KIT Library user on 27 September 2022

The modes below are listed for a $\overline{b}$ initial state. b modes are their charge conjugates. Reactions indicate the weak decay vertex and do not include mixing.

$\overline{b}$ DECAY MODES		Fraction (Γ_i/Γ)	Scale factor/ Confidence level	p (MeV/c)

PRODUCTION FRACTIONS

The production fractions for weakly decaying b-hadrons at high energy have been calculated from the best values of mean lives, mixing parameters, and branching fractions in this edition by the Heavy Flavor Averaging Group (HFLAV) as described in the note "B^0-$\overline{B}^0$ Mixing" in the B^0 Particle Listings. We no longer provide world averages of the b-hadron production fractions, where results from LEP, Tevatron and LHC are averaged together; indeed the available data (from CDF and LHCb) shows that the fractions depend on the kinematics (in particular the p_T) of the produced b hadron. Hence we would like to list the fractions in Z decays instead, which are well-defined physics observables. The production fractions in $p\overline{p}$ collisions at the Tevatron are also listed at the end of the section. Values assume

$$B(\overline{b} \to B^+) = B(\overline{b} \to B^0)$$
$$B(\overline{b} \to B^+) + B(\overline{b} \to B^0) + B(\overline{b} \to B^0_s) + B(b \to b\text{-baryon}) = 100\%.$$

The correlation coefficients between production fractions are also reported:

$$cor(B^0_s, b\text{-baryon}) = 0.064$$
$$cor(B^0_s, B^\pm{=}B^0) = -0.633$$
$$cor(b\text{-baryon}, B^\pm{=}B^0) = -0.813.$$

The notation for production fractions varies in the literature (f_d, d_{B^0}, $f(b \to \overline{B}^0)$, $Br(b \to \overline{B}^0)$). We use our own branching fraction notation here, $B(\overline{b} \to B^0)$.

Note these production fractions are b-hadronization fractions, not the conventional branching fractions of b-quark to a B-hadron, which may have considerable dependence on the initial and final state kinematic and production environment.

B^+		(40.8 ± 0.7) %		–
B^0		(40.8 ± 0.7) %		–
B^0_s		(10.0 ± 0.8) %		–
b-baryon		(8.4 ± 1.1) %		–

DECAY MODES

Semileptonic and leptonic modes

ν anything		(23.1 ± 1.5) %		–
$\ell^+ \nu_\ell$ anything	[iii]	(10.69± 0.22) %		–
$e^+ \nu_e$ anything		(10.86± 0.35) %		–
$\mu^+ \nu_\mu$ anything		(10.95 $^{+0.29}_{-0.25}$) %		–
$D^- \ell^+ \nu_\ell$ anything	[iii]	(2.2 ± 0.4) %	S=1.9	–
$D^- \pi^+ \ell^+ \nu_\ell$ anything		(4.9 ± 1.9) $\times 10^{-3}$		–
$D^- \pi^- \ell^+ \nu_\ell$ anything		(2.6 ± 1.6) $\times 10^{-3}$		–
$\overline{D}^0 \ell^+ \nu_\ell$ anything	[iii]	(6.79± 0.34) %		–
$\overline{D}^0 \pi^- \ell^+ \nu_\ell$ anything		(1.07± 0.27) %		–
$\overline{D}^0 \pi^+ \ell^+ \nu_\ell$ anything		(2.3 ± 1.6) $\times 10^{-3}$		–
$D^{*-} \ell^+ \nu_\ell$ anything	[iii]	(2.75± 0.19) %		–
$D^{*-} \pi^- \ell^+ \nu_\ell$ anything		(6 ± 7) $\times 10^{-4}$		–
$D^{*-} \pi^+ \ell^+ \nu_\ell$ anything		(4.8 ± 1.0) $\times 10^{-3}$		–
$\overline{D}^0_j \ell^+ \nu_\ell$ anything $\times$ $B(\overline{D}^0_j \to D^{*+} \pi^-)$	[iii,ffaa]	(2.6 ± 0.9) $\times 10^{-3}$		–
$D^-_j \ell^+ \nu_\ell$ anything $\times$ $B(D^-_j \to D^0 \pi^-)$	[iii,ffaa]	(7.0 ± 2.3) $\times 10^{-3}$		–
$\overline{D}^*_2(2460)^0 \ell^+ \nu_\ell$ anything $\times$ $B(\overline{D}^*_2(2460)^0 \to D^{*-} \pi^+)$		< 1.4 $\times 10^{-3}$	CL=90%	–
$D^*_2(2460)^- \ell^+ \nu_\ell$ anything $\times$ $B(D^*_2(2460)^- \to D^0 \pi^-)$		(4.2 $^{+1.5}_{-1.8}$) $\times 10^{-3}$		–
$\overline{D}^*_2(2460)^0 \ell^+ \nu_\ell$ anything $\times$ $B(\overline{D}^*_2(2460)^0 \to D^- \pi^+)$		(1.6 ± 0.8) $\times 10^{-3}$		–
charmless $\ell \overline{\nu}_\ell$	[iii]	(1.7 ± 0.5) $\times 10^{-3}$		–
$\tau^+ \nu_\tau$ anything		(2.41± 0.23) %		–
$D^{*-} \tau \nu_\tau$ anything		(9 ± 4) $\times 10^{-3}$		–
$\overline{c} \to \ell^- \overline{\nu}_\ell$ anything	[iii]	(8.02± 0.19) %		–
$c \to \ell^+ \nu$ anything		(1.6 $^{+0.4}_{-0.5}$) %		–

Charmed meson and baryon modes

$\overline{D}^0$ anything		(58.7 ± 2.8) %		–
$D^0 D^\pm_s$ anything	[aa]	(9.1 $^{+4.0}_{-2.8}$) %		–
$D^\mp D^\pm_s$ anything	[aa]	(4.0 $^{+2.3}_{-1.8}$) %		–
$\overline{D}^0 D^0$ anything	[aa]	(5.1 $^{+2.0}_{-1.8}$) %		–
$D^0 D^\pm$ anything	[aa]	(2.7 $^{+1.8}_{-1.6}$) %		–
$D^\pm D^\mp$ anything	[aa]	< 9 $\times 10^{-3}$	CL=90%	–
D^- anything		(22.7 ± 1.6) %		–
$D^*(2010)^+$ anything		(17.3 ± 2.0) %		–
$D_1(2420)^0$ anything		(5.0 ± 1.5) %		–
$D^*(2010)^\mp D^\pm_s$ anything	[aa]	(3.3 $^{+1.6}_{-1.3}$) %		–
$D^0 D^*(2010)^\pm$ anything	[aa]	(3.0 $^{+1.1}_{-0.9}$) %		–
$D^*(2010)^\pm D^\mp$ anything	[aa]	(2.5 $^{+1.2}_{-1.0}$) %		–
$D^*(2010)^\pm D^*(2010)^\mp$ anything	[aa]	(1.2 ± 0.4) %		–
$\overline{D} D$ anything		(10 $^{+11}_{-10}$) %		–
$D^*_2(2460)^0$ anything		(4.7 ± 2.7) %		–
D^-_s anything		(14.7 ± 2.1) %		–
D^+_s anything		(10.1 ± 3.1) %		–
Λ^+_c anything		(7.7 ± 1.1) %		–
$\overline{c}/c$ anything	[eeaa]	(116.2 ± 3.2) %		–

Charmonium modes

$J/\psi(1S)$ anything		(1.16± 0.10) %		–
$\psi(2S)$ anything		(3.06± 0.30) $\times 10^{-3}$		–
$\chi_{c0}(1P)$ anything		(1.5 ± 0.6) %		–
$\chi_{c1}(1P)$ anything		(1.4 ± 0.4) %		–
$\chi_{c2}(1P)$ anything		(6.2 ± 2.9) $\times 10^{-3}$		–
$\chi_c(2P)$ anything, $\chi_c \to \phi\phi$		< 2.8 $\times 10^{-7}$	CL=95%	–
$\eta_c(1S)$ anything		(5.6 ± 0.9) $\times 10^{-3}$		–
$\eta_c(2S)$ anything, $\eta_c \to \phi\phi$		(3.9 ± 1.4) $\times 10^{-7}$		–
$\chi_{c1}(3872)$ anything, $\chi_{c1} \to \phi\phi$		< 4.5 $\times 10^{-7}$	CL=95%	–
$\chi_{c0}(3915)$ anything, $\chi_{c0} \to \phi\phi$		< 3.1 $\times 10^{-7}$	CL=95%	–

K or K^* modes

$\overline{s}\gamma$		(3.1 ± 1.1) $\times 10^{-4}$		–
$\overline{s}\overline{\nu}\nu$	B1	< 6.4 $\times 10^{-4}$	CL=90%	–
$K^\pm$ anything		(74 ± 6) %		–
K^0_S anything		(29.0 ± 2.9) %		–

Pion modes

$\pi^\pm$ anything		(397 ±21) %		–
π^0 anything	[eeaa]	(278 ±60) %		–
ϕ anything		(2.82± 0.23) %		–

Baryon modes

$p/\overline{p}$ anything		(13.1 ± 1.1) %		–
$\Lambda/\overline{\Lambda}$ anything		(5.9 ± 0.6) %		–
b-baryon anything		(10.2 ± 2.8) %		–

Other modes

charged anything	[eeaa]	(497 ± 7) %		–
hadron$^+$ hadron$^-$		(1.7 $^{+1.0}_{-0.7}$) $\times 10^{-5}$		–
charmless		(7 ±21) $\times 10^{-3}$		–

$\Delta B = 1$ weak neutral current ($B1$) modes

$\mu^+ \mu^-$ anything	B1	< 3.2 $\times 10^{-4}$	CL=90%	–

B^*

$I(J^P) = \frac{1}{2}(1^-)$
I, J, P need confirmation.

Quantum numbers shown are quark-model predictions.

Mass $m_{B^*} = 5324.71 \pm 0.21$ MeV
$m_{B^*} - m_B = 45.21 \pm 0.21$ MeV
$m_{B^{*+}} - m_{B^+} = 45.37 \pm 0.21$ MeV

B^* DECAY MODES	Fraction (Γ_i/Γ)	p (MeV/c)
$B\gamma$	seen	45

Downloaded from https://academic.oup.com/ptep/article/2022/8/083C01/6651666 by KIT Library user on 27 September 2022

$B_1(5721)$

$I(J^P) = \frac{1}{2}(1^+)$
I, J, P need confirmation.

$B_1(5721)^+$ mass $= 5725.9^{+2.5}_{-2.7}$ MeV
$m_{B_1^+} - m_{B^{*0}} = 401.2^{+2.4}_{-2.7}$ MeV
$B_1(5721)^0$ mass $= 5726.1 \pm 1.3$ MeV (S = 1.2)
$m_{B_1^0} - m_{B^+} = 446.7 \pm 1.3$ MeV (S = 1.2)
$m_{B_1^0} - m_{B^{*+}} = 401.4 \pm 1.2$ MeV (S = 1.2)
Full width $\Gamma(B_1(5721)^+) = 31 \pm 6$ MeV (S = 1.1)
Full width $\Gamma(B_1(5721)^0) = 27.5 \pm 3.4$ MeV (S = 1.1)

$B_1(5721)$ DECAY MODES	Fraction (Γ_i/Γ)	p (MeV/c)
$B^*\pi$	seen	365

$B_2^*(5747)$

$I(J^P) = \frac{1}{2}(2^+)$
I, J, P need confirmation.

$B_2^*(5747)^+$ mass $= 5737.2 \pm 0.7$ MeV
$m_{B_2^{*+}} - m_{B^0} = 457.5 \pm 0.7$ MeV
$B_2^*(5747)^0$ mass $= 5739.5 \pm 0.7$ MeV (S = 1.4)
$m_{B_2^{*0}} - m_{B_1^0} = 13.4 \pm 1.4$ MeV (S = 1.3)
$m_{B_2^{*0}} - m_{B^+} = 460.2 \pm 0.6$ MeV (S = 1.4)
Full width $\Gamma(B_2^*(5747)^+) = 20 \pm 5$ MeV (S = 2.2)
Full width $\Gamma(B_2^*(5747)^0) = 24.2 \pm 1.7$ MeV

$B_2^*(5747)$ DECAY MODES	Fraction (Γ_i/Γ)	p (MeV/c)
$B\pi$	seen	420
$B^*\pi$	seen	376

$B_J(5970)$

$I(J^P) = \frac{1}{2}(?^?)$
I, J, P need confirmation.

$B_J(5970)^+$ mass $m = 5964 \pm 5$ MeV
$m_{B_J(5970)^+} - m_{B^0} = 685 \pm 5$ MeV
$B_J(5970)^0$ mass $m = 5971 \pm 5$ MeV
$m_{B_J(5970)^0} - m_{B^+} = 691 \pm 5$ MeV
$B_J(5970)^+$ full width $\Gamma = 62 \pm 20$ MeV
$B_J(5970)^0$ full width $\Gamma = 81 \pm 12$ MeV

$B_J(5970)$ DECAY MODES	Fraction (Γ_i/Γ)	p (MeV/c)
$B\pi$	possibly seen	633
$B^*\pi$	seen	592

BOTTOM, STRANGE MESONS ($B = \pm 1$, $S = \mp 1$)

$B_s^0 = s\overline{b}$, $\overline{B}_s^0 = \overline{s}b$, similarly for B_s^*'s

B_s^0

$I(J^P) = 0(0^-)$

I, J, P need confirmation. Quantum numbers shown are quark-model predictions.

Mass $m_{B_s^0} = 5366.92 \pm 0.10$ MeV
$m_{B_s^0} - m_B = 87.42 \pm 0.14$ MeV
Mean life $\tau = (1.520 \pm 0.005) \times 10^{-12}$ s
$c\tau = 455.7\ \mu$m
$\Delta\Gamma_{B_s^0} = \Gamma_{B_{sL}^0} - \Gamma_{B_{sH}^0} = (0.084 \pm 0.005) \times 10^{12}\ \mathrm{s}^{-1}$ (S = 1.7)

B_s^0-$\overline{B}_s^0$ mixing parameters

$\Delta m_{B_s^0} = m_{B_{sH}^0} - m_{B_{sL}^0} = (17.765 \pm 0.006) \times 10^{12}\ \hbar\ \mathrm{s}^{-1}$
$= (1.1693 \pm 0.0004) \times 10^{-8}$ MeV
$x_s = \Delta m_{B_s^0}/\Gamma_{B_s^0} = 27.01 \pm 0.10$
χ_s (B_s^0-$\overline{B}_s^0$ mixing parameter) $= 0.499318 \pm 0.000005$

CP violation parameters in B_s^0

$\mathrm{Re}(\epsilon_{B_s^0}) / (1 + |\epsilon_{B_s^0}|^2) = (-0.15 \pm 0.70) \times 10^{-3}$
$C_{KK}(B_s^0 \to K^+K^-) = 0.162 \pm 0.035$
$S_{KK}(B_s^0 \to K^+K^-) = 0.14 \pm 0.05$ (S = 1.3)
$r_B(B_s^0 \to D_s^\mp K^\pm) = 0.37^{+0.10}_{-0.09}$
$r_B(B_s^0 \to D_s^\mp K^\pm\pi^\pm\pi^\mp) = 0.47 \pm 0.08$
$\delta_B(B_s^0 \to D_s^\pm K^\mp) = (358 \pm 14)^\circ$
$\delta_B(B_s^0 \to D_s^\pm K^\mp\pi^\pm\pi^\mp) = (-6^{+10}_{-13})^\circ$
CP Violation phase $\beta_s = (2.5 \pm 1.0) \times 10^{-2}$ rad
$|\lambda|$ ($B_s^0 \to J/\psi(1S)\phi$) $= 1.001 \pm 0.018$ (S = 1.2)
$|\lambda| = 0.999 \pm 0.017$
A, CP violation parameter $= -0.79 \pm 0.08$
C, CP violation parameter $= 0.19 \pm 0.06$
S, CP violation parameter $= 0.17 \pm 0.06$
$A_{CP}^L(B_s \to J/\psi\overline{K}^*(892)^0) = -0.05 \pm 0.06$
$A_{CP}^\parallel(B_s \to J/\psi\overline{K}^*(892)^0) = 0.17 \pm 0.15$
$A_{CP}^\perp(B_s \to J/\psi\overline{K}^*(892)^0) = -0.05 \pm 0.10$
$\boldsymbol{A_{CP}(B_s \to \pi^+K^-)} = 0.224 \pm 0.012$
$A_{CP}(B_s^0 \to [K^+K^-]_D\overline{K}^*(892)^0) = -0.04 \pm 0.07$
$A_{CP}(B_s^0 \to [\pi^+K^-]_D K^*(892)^0) = -0.01 \pm 0.04$
$A_{CP}(B_s^0 \to [\pi^+\pi^-]_D K^*(892)^0) = 0.06 \pm 0.13$
$S(B_s^0 \to \phi\gamma) = 0.43 \pm 0.32$
$C(B_s^0 \to \phi\gamma) = 0.11 \pm 0.31$
$A^\Delta(B_s^0 \to \phi\gamma) = -0.7 \pm 0.4$
$\Delta a_\perp < 1.2 \times 10^{-12}$ GeV, CL = 95%
$\Delta a_\parallel = (-0.9 \pm 1.5) \times 10^{-14}$ GeV
$\Delta a_X = (1.0 \pm 2.2) \times 10^{-14}$ GeV
$\Delta a_Y = (-3.8 \pm 2.2) \times 10^{-14}$ GeV
$\mathrm{Re}(\xi) = -0.022 \pm 0.033$
$\mathrm{Im}(\xi) = 0.004 \pm 0.011$

These branching fractions all scale with $B(\overline{b} \to B_s^0)$.

The branching fraction $B(B_s^0 \to D_s^-\ell^+\nu_\ell \text{anything})$ is not a pure measurement since the measured product branching fraction $B(\overline{b} \to B_s^0) \times B(B_s^0 \to D_s^-\ell^+\nu_\ell \text{anything})$ was used to determine $B(\overline{b} \to B_s^0)$, as described in the note on "B^0-$\overline{B}^0$ Mixing"

For inclusive branching fractions, *e.g.*, $B \to D^\pm$ anything, the values usually are multiplicities, not branching fractions. They can be greater than one.

B_s^0 DECAY MODES		Fraction (Γ_i/Γ)	Scale factor/ Confidence level	p (MeV/c)
D_s^- anything		(62 ± 6) %		–
$\ell\nu_\ell X$		(9.6 ± 0.8) %		–
$e^+\nu X^-$		(9.1 ± 0.8) %		–
$\mu^+\nu X^-$		(10.2 ± 1.0) %		–
$D_s^-\ell^+\nu_\ell$ anything	[ggaa]	(8.1 ± 1.3) %		–
$D_s^{*-}\ell^+\nu_\ell$ anything		(5.4 ± 1.1) %		–
$D_s^-\mu^+\nu_\mu$		(2.44± 0.23) %		2321
$D_s^{*-}\mu^+\nu_\mu$		(5.3 ± 0.5) %		2266
$D_{s1}(2536)^-\mu^+\nu_\mu$, $D_{s1}^- \to D^{*-}K_S^0$		(2.7 ± 0.7) $\times 10^{-3}$		–
$D_{s1}(2536)^- X\mu^+\nu$, $D_{s1}^- \to \overline{D}^0K^+$		(4.4 ± 1.3) $\times 10^{-3}$		–
$D_{s2}(2573)^- X\mu^+\nu$, $D_{s2}^- \to \overline{D}^0K^+$		(2.7 ± 1.0) $\times 10^{-3}$		–
$K^-\mu^+\nu_\mu$		(1.06± 0.09) $\times 10^{-4}$		2660
$D_s^-\pi^+$		(2.98± 0.14) $\times 10^{-3}$		2320
$D_s^-\rho^+$		(6.8 ± 1.4) $\times 10^{-3}$		2249
$D_s^-\pi^+\pi^+\pi^-$		(6.1 ± 1.0) $\times 10^{-3}$		2301
$D_{s1}(2536)^-\pi^+$, $D_{s1}^- \to D_s^-\pi^+\pi^-$		(2.4 ± 0.8) $\times 10^{-5}$		–
$D_s^\mp K^\pm$		(2.25± 0.12) $\times 10^{-4}$		2293
$D_s^-K^+\pi^+\pi^-$		(3.2 ± 0.6) $\times 10^{-4}$		2249
$D_s^+D_s^-$		(4.4 ± 0.5) $\times 10^{-3}$		1824
$D_s^-D^+$		(2.8 ± 0.5) $\times 10^{-4}$		1875
D^+D^-		(2.2 ± 0.6) $\times 10^{-4}$		1925
$D^0\overline{D}^0$		(1.9 ± 0.5) $\times 10^{-4}$		1930
$D_s^{*-}\pi^+$		(1.9 $^{+0.5}_{-0.4}$) $\times 10^{-3}$		2265

Downloaded from https://academic.oup.com/ptep/article/2022/8/083C01/6651666 by KIT Library user on 27 September 2022

$D_s^{*\mp} K^\pm$	$(1.32^{+0.40}_{-0.32}) \times 10^{-4}$		–
$D_s^{*-} \rho^+$	$(9.5 \pm 2.0) \times 10^{-3}$		2191
$D_s^{*+} D_s^- + D_s^{*-} D_s^+$	(1.39 ± 0.17) %		1742
$D_s^{*+} D_s^{*-}$	(1.44 ± 0.21) %	S=1.1	1655
$D_s^{(*)+} D_s^{(*)-}$	(4.5 ± 1.4) %		–
$D^{*-} D_s^+$	$(3.9 \pm 0.8) \times 10^{-4}$		1801
$\overline{D}^{*0} \overline{K}^0$	$(2.8 \pm 1.1) \times 10^{-4}$		2278
$\overline{D}^0 \overline{K}^0$	$(4.3 \pm 0.9) \times 10^{-4}$		2330
$\overline{D}^0 K^- \pi^+$	$(1.04 \pm 0.13) \times 10^{-3}$		2312
$\overline{D}^0 \overline{K}^*(892)^0$	$(4.4 \pm 0.6) \times 10^{-4}$		2264
$\overline{D}^0 \overline{K}^*(1410)$	$(3.9 \pm 3.5) \times 10^{-4}$		2117
$\overline{D}^0 \overline{K}_0^*(1430)$	$(3.0 \pm 0.7) \times 10^{-4}$		2113
$\overline{D}^0 \overline{K}_2^*(1430)$	$(1.1 \pm 0.4) \times 10^{-4}$		2112
$\overline{D}^0 \overline{K}^*(1680)$	$< 7.8 \times 10^{-5}$	CL=90%	1997
$\overline{D}^0 \overline{K}_0^*(1950)$	$< 1.1 \times 10^{-4}$	CL=90%	1890
$\overline{D}^0 \overline{K}_3^*(1780)$	$< 2.6 \times 10^{-5}$	CL=90%	1970
$\overline{D}^0 \overline{K}_4^*(2045)$	$< 3.1 \times 10^{-5}$	CL=90%	1835
$\overline{D}^0 K^- \pi^+$ (non-resonant)	$(2.1 \pm 0.8) \times 10^{-4}$		2312
$D_{s2}^*(2573)^- \pi^+$, $D_{s2}^* \to \overline{D}^0 K^-$	$(2.6 \pm 0.4) \times 10^{-4}$		–
$D_{s1}^*(2700)^- \pi^+$, $D_{s1}^* \to \overline{D}^0 K^-$	$(1.6 \pm 0.8) \times 10^{-5}$		–
$D_{s1}^*(2860)^- \pi^+$, $D_{s1}^* \to \overline{D}^0 K^-$	$(5 \pm 4) \times 10^{-5}$		–
$D_{s3}^*(2860)^- \pi^+$, $D_{s3}^* \to \overline{D}^0 K^-$	$(2.2 \pm 0.6) \times 10^{-5}$		–
$\overline{D}^0 K^+ K^-$	$(5.6 \pm 0.9) \times 10^{-5}$		2243
$\overline{D}^0 f_0(980)$	$< 3.1 \times 10^{-6}$	CL=90%	2242
$\overline{D}^0 \phi$	$(3.0 \pm 0.5) \times 10^{-5}$		2235
$\overline{D}^{*0} \phi$	$(3.7 \pm 0.6) \times 10^{-5}$		2178
$D^{*\mp} \pi^\pm$	$< 6.1 \times 10^{-6}$	CL=90%	–
$\eta_c \phi$	$(5.0 \pm 0.9) \times 10^{-4}$		1663
$\eta_c \pi^+ \pi^-$	$(1.8 \pm 0.7) \times 10^{-4}$		1840
$J/\psi(1S) \phi$	$(1.04 \pm 0.04) \times 10^{-3}$		1588
$J/\psi(1S) \phi\phi$	$(1.20^{+0.14}_{-0.16}) \times 10^{-5}$		764
$J/\psi(1S) \pi^0$	$< 1.2 \times 10^{-3}$	CL=90%	1787
$J/\psi(1S) \eta$	$(4.0 \pm 0.7) \times 10^{-4}$	S=1.4	1733
$J/\psi(1S) K_S^0$	$(1.92 \pm 0.14) \times 10^{-5}$		1743
$J/\psi(1S) \overline{K}^*(892)^0$	$(4.1 \pm 0.4) \times 10^{-5}$		1637
$J/\psi(1S) \eta'$	$(3.3 \pm 0.4) \times 10^{-4}$		1612
$J/\psi(1S) \pi^+ \pi^-$	$(2.02 \pm 0.17) \times 10^{-4}$	S=1.7	1775
$J/\psi(1S) f_0(500)$, $f_0 \to \pi^+ \pi^-$	$< 4 \times 10^{-6}$	CL=90%	–
$J/\psi(1S) \rho$, $\rho \to \pi^+ \pi^-$	$< 3.4 \times 10^{-6}$	CL=90%	–
$J/\psi(1S) f_0(980)$, $f_0 \to \pi^+ \pi^-$	$(1.24 \pm 0.15) \times 10^{-4}$	S=2.1	–
$J/\psi(1S) f_2(1270)$, $f_2 \to \pi^+ \pi^-$	$(1.0 \pm 0.4) \times 10^{-6}$		–
$J/\psi(1S) f_2(1270)_0$, $f_2 \to \pi^+ \pi^-$	$(7.3 \pm 1.7) \times 10^{-7}$		–
$J/\psi(1S) f_2(1270)_\parallel$, $f_2 \to \pi^+ \pi^-$	$(1.05 \pm 0.33) \times 10^{-6}$		–
$J/\psi(1S) f_2(1270)_\perp$, $f_2 \to \pi^+ \pi^-$	$(1.3 \pm 0.7) \times 10^{-6}$		–
$J/\psi(1S) f_0(1370)$, $f_0 \to \pi^+ \pi^-$	$(4.4^{+0.6}_{-4.0}) \times 10^{-5}$		–
$J/\psi(1S) f_0(1500)$, $f_0 \to \pi^+ \pi^-$	$(2.04^{+0.32}_{-0.24}) \times 10^{-5}$		–
$J/\psi(1S) f_2'(1525)_0$, $f_2' \to \pi^+ \pi^-$	$(1.03 \pm 0.22) \times 10^{-6}$		–
$J/\psi(1S) f_2'(1525)_\parallel$, $f_2' \to \pi^+ \pi^-$	$(1.2^{+2.6}_{-0.8}) \times 10^{-7}$		–
$J/\psi(1S) f_2'(1525)_\perp$, $f_2' \to \pi^+ \pi^-$	$(5 \pm 4) \times 10^{-7}$		–
$J/\psi(1S) f_0(1790)$, $f_0 \to \pi^+ \pi^-$	$(4.9^{+10.0}_{-1.0}) \times 10^{-6}$		–
$J/\psi(1S) \pi^+ \pi^-$ (nonresonant)	$(1.74^{+1.10}_{-0.34}) \times 10^{-5}$		1775
$J/\psi(1S) \overline{K}^0 \pi^+ \pi^-$	$< 4.4 \times 10^{-5}$	CL=90%	1675
$J/\psi(1S) K^+ K^-$	$(7.9 \pm 0.7) \times 10^{-4}$		1601
$J/\psi(1S) K^0 K^- \pi^+ +$ c.c.	$(9.5 \pm 1.3) \times 10^{-4}$		1538
$J/\psi(1S) \overline{K}^0 K^+ K^-$	$< 1.2 \times 10^{-5}$	CL=90%	1333
$J/\psi K^*(892)^0 \overline{K}^*(892)^0$	$(1.10 \pm 0.09) \times 10^{-4}$		1083
$J/\psi(1S) f_2'(1525)$	$(2.6 \pm 0.6) \times 10^{-4}$		1310
$J/\psi(1S) p\overline{p}$	$(3.6 \pm 0.4) \times 10^{-6}$		982
$J/\psi(1S) \gamma$	$< 7.3 \times 10^{-6}$	CL=90%	1790
$J/\psi(1S) \pi^+ \pi^- \pi^+ \pi^-$	$(7.5 \pm 0.8) \times 10^{-5}$		1731
$J/\psi(1S) f_1(1285)$	$(7.2 \pm 1.4) \times 10^{-5}$		1460
$\psi(2S) \eta$	$(3.3 \pm 0.9) \times 10^{-4}$		1338
$\psi(2S) \eta'$	$(1.29 \pm 0.35) \times 10^{-4}$		1158
$\psi(2S) \pi^+ \pi^-$	$(6.9 \pm 1.2) \times 10^{-5}$		1397
$\psi(2S) \phi$	$(5.2 \pm 0.4) \times 10^{-4}$		1120
$\psi(2S) K^- \pi^+$	$(3.1 \pm 0.4) \times 10^{-5}$		1310
$\psi(2S) \overline{K}^*(892)^0$	$(3.3 \pm 0.5) \times 10^{-5}$		1196
$\chi_{c1} \phi$	$(1.97 \pm 0.25) \times 10^{-4}$		1274
$\chi_{c1}(3872) \phi$	$(1.1 \pm 0.4) \times 10^{-4}$		936
$\chi_{c1}(3872) (K^+ K^-)_{non-\phi}$	$(8.6 \pm 3.5) \times 10^{-5}$		961
$\pi^+ \pi^-$	$(7.0 \pm 1.0) \times 10^{-7}$		2680
$\pi^0 \pi^0$	$< 2.1 \times 10^{-4}$	CL=90%	2680
$\eta \pi^0$	$< 1.0 \times 10^{-3}$	CL=90%	2654
$\eta\eta$	$< 1.43 \times 10^{-4}$	CL=90%	2627
$\rho^0 \rho^0$	$< 3.20 \times 10^{-4}$	CL=90%	2569
$\eta' \eta$	$< 6.5 \times 10^{-5}$	CL=90%	2568
$\eta' \eta'$	$(3.3 \pm 0.7) \times 10^{-5}$		2507
$\eta' \phi$	$< 8.2 \times 10^{-7}$	CL=90%	2495
$\phi f_0(980)$, $f_0(980) \to \pi^+ \pi^-$	$(1.12 \pm 0.21) \times 10^{-6}$		–
$\phi f_2(1270)$, $f_2(1270) \to \pi^+ \pi^-$	$(6.1^{+1.8}_{-1.5}) \times 10^{-7}$		–
$\phi \rho^0$	$(2.7 \pm 0.8) \times 10^{-7}$		2526
$\phi \pi^+ \pi^-$	$(3.5 \pm 0.5) \times 10^{-6}$		2579
$\phi\phi$	$(1.85 \pm 0.14) \times 10^{-5}$		2482
$\phi\phi\phi$	$(2.2 \pm 0.6) \times 10^{-6}$		2165
$\pi^+ K^-$	$(5.8 \pm 0.7) \times 10^{-6}$		2659
$K^+ K^-$	$(2.66 \pm 0.22) \times 10^{-5}$		2638
$K^0 \overline{K}^0$	$(1.76 \pm 0.31) \times 10^{-5}$		2637
$K^0 \pi^+ \pi^-$	$(9.5 \pm 2.1) \times 10^{-6}$		2653
$K^0 K^\pm \pi^\mp$	$(8.4 \pm 0.9) \times 10^{-5}$		2622
$K^*(892)^- \pi^+$	$(2.9 \pm 1.1) \times 10^{-6}$		2607
$K^*(892)^\pm K^\mp$	$(1.9 \pm 0.5) \times 10^{-5}$		2585
$K_0^*(1430)^\pm K^\mp$	$(3.1 \pm 2.5) \times 10^{-5}$		–
$K_2^*(1430)^\pm K^\mp$	$(1.0 \pm 1.7) \times 10^{-5}$		–
$K^*(892)^0 \overline{K}^0 +$ c.c.	$(2.0 \pm 0.6) \times 10^{-5}$		2585
$K_0^*(1430) \overline{K}^0 +$ c.c.	$(3.3 \pm 1.0) \times 10^{-5}$		2468
$K_2^*(1430)^0 \overline{K}^0 +$ c.c.	$(1.7 \pm 2.2) \times 10^{-5}$		2467
$K_S^0 \overline{K}^*(892)^0 +$ c.c.	$(1.6 \pm 0.4) \times 10^{-5}$		2585
$K^0 K^+ K^-$	$(1.3 \pm 0.6) \times 10^{-6}$		2568
$\overline{K}^*(892)^0 \rho^0$	$< 7.67 \times 10^{-4}$	CL=90%	2550
$\overline{K}^*(892)^0 K^*(892)^0$	$(1.11 \pm 0.27) \times 10^{-5}$		2531
$\phi K^*(892)^0$	$(1.14 \pm 0.30) \times 10^{-6}$		2507
$p\overline{p}$	$< 1.5 \times 10^{-8}$	CL=90%	2514
$p\overline{p} K^+ K^-$	$(4.5 \pm 0.5) \times 10^{-6}$		2231
$p\overline{p} K^+ \pi^-$	$(1.39 \pm 0.26) \times 10^{-6}$		2355
$p\overline{p} \pi^+ \pi^-$	$(4.3 \pm 2.0) \times 10^{-7}$		2454
$p\overline{\Lambda} K^- +$ c.c.	$(5.5 \pm 1.0) \times 10^{-6}$		2358
$\Lambda_c^- \Lambda \pi^+$	$(3.6 \pm 1.6) \times 10^{-4}$		1979
$\Lambda_c^- \Lambda_c^+$	$< 8.0 \times 10^{-5}$	CL=95%	1405

Lepton Family number (*LF*) violating modes or $\Delta B = 1$ weak neutral current (*B1*) modes

$\gamma\gamma$	*B1*	$< 3.1 \times 10^{-6}$	CL=90%	2683
$\phi\gamma$	*B1*	$(3.4 \pm 0.4) \times 10^{-5}$		2587
$\mu^+ \mu^-$	*B1*	$(3.01 \pm 0.35) \times 10^{-9}$		2681
$e^+ e^-$	*B1*	$< 9.4 \times 10^{-9}$	CL=90%	2683
$\tau^+ \tau^-$	*B1*	$< 6.8 \times 10^{-3}$	CL=95%	2011
$\mu^+ \mu^- \mu^+ \mu^-$	*B1*	$< 2.5 \times 10^{-9}$	CL=95%	2673
SP, $S \to \mu^+ \mu^-$, $P \to \mu^+ \mu^-$	*B1* [xxx]	$< 2.2 \times 10^{-9}$	CL=95%	–
$\phi(1020) \mu^+ \mu^-$	*B1*	$(8.4 \pm 0.4) \times 10^{-7}$		2582
$f_2'(1525) \mu^+ \mu^-$		$(1.62 \pm 0.22) \times 10^{-7}$		2464
$\overline{K}^*(892)^0 \mu^+ \mu^-$	*B1*	$(2.9 \pm 1.1) \times 10^{-8}$		2605
$\pi^+ \pi^- \mu^+ \mu^-$	*B1*	$(8.4 \pm 1.7) \times 10^{-8}$		2670
$\phi \nu \overline{\nu}$	*B1*	$< 5.4 \times 10^{-3}$	CL=90%	2587
$e^\pm \mu^\mp$	*LF* [aa]	$< 5.4 \times 10^{-9}$	CL=90%	2682
$\mu^\pm \tau^\mp$	*LF*	$< 4.2 \times 10^{-5}$	CL=95%	2388

B_s^*

$I(J^P) = 0(1^-)$

I, *J*, *P* need confirmation. Quantum numbers shown are quark-model predictions.

Mass $m = 5415.4^{+1.8}_{-1.5}$ MeV (S = 2.9)

$m_{B_s^*} - m_{B_s} = 48.5^{+1.8}_{-1.5}$ MeV (S = 2.9)

Downloaded from https://academic.oup.com/ptep/article/2022/8/083C01/6651666 by KIT Library user on 27 September 2022

B_s^* DECAY MODES	Fraction (Γ_i/Γ)	p (MeV/c)
$B_s\gamma$	seen	48

$B_{s1}(5830)^0$

$I(J^P) = 0(1^+)$
I, J, P need confirmation.

Mass $m = 5828.70 \pm 0.20$ MeV
$m_{B_{s1}^0} - m_{B^{*+}} = 503.99 \pm 0.17$ MeV
Full width $\Gamma = 0.5 \pm 0.4$ MeV

$B_{s1}(5830)^0$ DECAY MODES	Fraction (Γ_i/Γ)	p (MeV/c)
$B^{*+}K^-$	seen	97

$B_{s2}^*(5840)^0$

$I(J^P) = 0(2^+)$
I, J, P need confirmation.

Mass $m = 5839.86 \pm 0.12$ MeV
$m_{B_{s2}^{*0}} - m_{B^+} = 560.52 \pm 0.14$ MeV
Full width $\Gamma = 1.49 \pm 0.27$ MeV

Branching fractions are given relative to the one **DEFINED AS 1**.

$B_{s2}^*(5840)^0$ DECAY MODES	Fraction (Γ_i/Γ)	p (MeV/c)
B^+K^-	**DEFINED AS 1**	252
$B^{*+}K^-$	0.093 ± 0.018	141
$B^0K_S^0$	0.43 ± 0.11	245
$B^{*0}K_S^0$	0.04 ± 0.04	–

BOTTOM, CHARMED MESONS ($B = C = \pm 1$)

$B_c^+ = c\overline{b}$, $B_c^- = \overline{c}b$, similarly for B_c^*'s

B_c^+

$I(J^P) = 0(0^-)$
I, J, P need confirmation.

Quantum numbers shown are quark-model predictions.

Mass $m = 6274.47 \pm 0.32$ MeV
$m_{B_c^+} - m_{B_s^0} = 907.8 \pm 0.5$ MeV
Mean life $\tau = (0.510 \pm 0.009) \times 10^{-12}$ s

B_c^- modes are charge conjugates of the modes below.

B_c^+ DECAY MODES × B($\overline{b} \to B_c$)	Fraction (Γ_i/Γ)	Confidence level	p (MeV/c)
$J/\psi(1S)\ell^+\nu_\ell$ anything	seen		–
$J/\psi(1S)\mu^+\nu_\mu$	seen		2372
$J/\psi(1S)\tau^+\nu_\tau$	seen		1932
$J/\psi(1S)\pi^+$	seen		2370
$J/\psi(1S)K^+$	seen		2341
$J/\psi(1S)\pi^+\pi^+\pi^-$	seen		2350
$J/\psi(1S)a_1(1260)$	not seen		2169
$J/\psi(1S)K^+K^-\pi^+$	seen		2203
$J/\psi(1S)\pi^+\pi^+\pi^+\pi^-\pi^-$	seen		2309
$\psi(2S)\pi^+$	seen		2051
$J/\psi(1S)D^0K^+$	seen		1539
$J/\psi(1S)D^*(2007)^0K^+$	seen		1411
$J/\psi(1S)D^*(2010)^+K^{*0}$	seen		919
$J/\psi(1S)D^+K^{*0}$	seen		1122
$J/\psi(1S)D_s^+$	seen		1821
$J/\psi(1S)D_s^{*+}$	seen		1727
$J/\psi(1S)p\overline{p}\pi^+$	seen		1791
$\chi_c^0\pi^+$	$(2.4^{+0.9}_{-0.8}) \times 10^{-5}$		2205
$p\overline{p}\pi^+$	not seen		2970
D^0K^+	seen		2837
$D^0\pi^+$	not seen		2858
$D^{*0}\pi^+$	not seen		2814
$D^{*0}K^+$	not seen		2792
$D_s^+\overline{D}^0$	$< 7.2 \times 10^{-4}$	90%	2483
$D_s^+D^0$	$< 3.0 \times 10^{-4}$	90%	2483
$D^+\overline{D}^0$	$< 1.9 \times 10^{-4}$	90%	2521
D^+D^0	$< 1.4 \times 10^{-4}$	90%	2521
$D_s^{*+}\overline{D}^0$	$< 5.3 \times 10^{-4}$	90%	2425
$D_s^+\overline{D}^*(2007)^0$	$< 4.6 \times 10^{-4}$	90%	2427
$D_s^{*+}D^0$	$< 9 \times 10^{-4}$	90%	2425
$D_s^+D^*(2007)^0$	$< 6.6 \times 10^{-4}$	90%	2427
$D^*(2010)^+\overline{D}^0$	$< 3.8 \times 10^{-4}$	90%	2467
$D^*(2010)^+\overline{D}^0$, $D^{*+} \to D^+\pi^0/\gamma$	not seen		–
$D^+\overline{D}^*(2007)^0$	$< 6.5 \times 10^{-4}$	90%	2466
$D^*(2007)^+D^0$	$< 2.0 \times 10^{-4}$	90%	–
$D^*(2010)^+D^0$, $D^{*+} \to D^+\pi^0/\gamma$	not seen		2467
$D^+D^*(2007)^0$	$< 3.7 \times 10^{-4}$	90%	2466
$D_s^{*+}\overline{D}^*(2007)^0$	$< 1.3 \times 10^{-3}$	90%	2366
$D_s^{*+}D^*(2007)^0$	$< 1.3 \times 10^{-3}$	90%	2366
$D^*(2010)^+\overline{D}^*(2007)^0$	$< 1.0 \times 10^{-3}$	90%	2410
$D^*(2010)^+D^*(2007)^0$	$< 7.7 \times 10^{-4}$	90%	2410
D^+K^{*0}	not seen		2783
$D^+\overline{K}^{*0}$	not seen		2783
$D_s^+K^{*0}$	not seen		2751
$D_s^+\overline{K}^{*0}$	not seen		2751
$D_s^+\phi$	not seen		2727
K^+K^0	not seen		3098
$B_s^0\pi^+$ / B($\overline{b} \to B_s$)	seen		–

$B_c(2S)^\pm$

$I(J^P) = 0(0^-)$

Mass $m = 6871.2 \pm 1.0$ MeV

$B_c(2S)^\pm$ DECAY MODES	Fraction (Γ_i/Γ)	p (MeV/c)
$B_c^+\pi^+\pi^-$	seen	504

$c\overline{c}$ MESONS (including possibly non-$q\overline{q}$ states)

$\eta_c(1S)$

$I^G(J^{PC}) = 0^+(0^{-+})$

Mass $m = 2983.9 \pm 0.4$ MeV (S = 1.2)
Full width $\Gamma = 32.0 \pm 0.7$ MeV

$\eta_c(1S)$ DECAY MODES	Fraction (Γ_i/Γ)	Confidence level	p (MeV/c)
Decays involving hadronic resonances			
$\eta'(958)\pi\pi$	(4.1 ± 1.7) %		1323
$\eta'(958)K\overline{K}$	(3.5 ± 1.5) %		1131
$\rho\rho$	(1.8 ± 0.5) %		1275
$K^*(892)^0K^-\pi^+$ + c.c.	(2.0 ± 0.7) %		1278
$K^*(892)\overline{K}^*(892)$	$(6.9 \pm 1.3) \times 10^{-3}$		1196
$K^*(892)^0\overline{K}^*(892)^0\pi^+\pi^-$	(1.1 ± 0.5) %		1073
ϕK^+K^-	$(2.9 \pm 1.4) \times 10^{-3}$		1104
$\phi\phi$	$(1.74 \pm 0.19) \times 10^{-3}$		1089
$\phi 2(\pi^+\pi^-)$	$< 4 \times 10^{-3}$	90%	1251
$a_0(980)\pi$	seen		1327
$a_2(1320)\pi$	< 2 %	90%	1196
$K^*(892)\overline{K}$ + c.c.	< 1.28 %	90%	1310
$f_2(1270)\eta$	< 1.1 %	90%	1145
$f_2(1270)\eta'$	seen		984
$\omega\omega$	$(2.9 \pm 0.8) \times 10^{-3}$		1270
$\omega\phi$	$< 2.5 \times 10^{-4}$	90%	1185
$f_2(1270)f_2(1270)$	$(9.8 \pm 2.5) \times 10^{-3}$		774
$f_2(1270)f_2'(1525)$	$(9.5 \pm 3.2) \times 10^{-3}$		524
$f_0(500)\eta$	seen		–
$f_0(500)\eta'$	seen		–
$f_0(980)\eta$	seen		1264
$f_0(980)\eta'$	seen		1130
$f_0(1500)\eta$	seen		1025
$f_0(1710)\eta'$	seen		653
$f_0(2100)\eta'$	seen		†

Downloaded from https://academic.oup.com/ptep/article/2022/8/083C01/6651666 by KIT Library user on 27 September 2022

$f_0(2200)\eta$	seen			498
$a_0(1320)\pi$	seen			–
$a_0(1450)\pi$	seen			1123
$a_0(1700)\pi$	seen			–
$a_0(1950)\pi$	seen			860
$K_0^*(1430)\overline{K}$	seen			–
$K_2^*(1430)\overline{K}$	seen			–
$K_0^*(1950)\overline{K}$	seen			–
Decays into stable hadrons				
$K\overline{K}\pi$	(7.3 ± 0.4) %			1381
$K\overline{K}\eta$	(1.36 ± 0.15) %			1265
$\eta\pi^+\pi^-$	(1.7 ± 0.6) %			1428
$\eta 2(\pi^+\pi^-)$	(4.4 ± 1.6) %			1386
$K^+K^-\pi^+\pi^-$	$(6.6 \pm 1.1) \times 10^{-3}$			1345
$K^+K^-\pi^+\pi^-\pi^0$	(3.5 ± 0.6) %			1304
$K^0K^-\pi^+\pi^-\pi^+$ +c.c.	(5.6 ± 1.9) %			–
$K^+K^-2(\pi^+\pi^-)$	$(7.5 \pm 2.4) \times 10^{-3}$			1254
$2(K^+K^-)$	$(1.43 \pm 0.30) \times 10^{-3}$			1056
$\pi^+\pi^-\pi^0$	$< 5 \times 10^{-4}$		90%	1476
$\pi^+\pi^-\pi^0\pi^0$	(4.7 ± 1.4) %			1460
$2(\pi^+\pi^-)$	$(9.1 \pm 1.2) \times 10^{-3}$			1459
$2(\pi^+\pi^-\pi^0)$	(15.8 ± 2.3) %			1409
$3(\pi^+\pi^-)$	(1.7 ± 0.4) %			1407
$p\overline{p}$	$(1.44 \pm 0.14) \times 10^{-3}$			1160
$p\overline{p}\pi^0$	$(3.6 \pm 1.5) \times 10^{-3}$			1101
$\Lambda\overline{\Lambda}$	$(1.06 \pm 0.23) \times 10^{-3}$			991
$K^+\overline{p}\Lambda$ + c.c.	$(2.5 \pm 0.4) \times 10^{-3}$			772
$\overline{\Lambda}(1520)\Lambda$ + c.c.	$(3.1 \pm 1.3) \times 10^{-3}$			694
$\Sigma^+\overline{\Sigma}^-$	$(2.1 \pm 0.6) \times 10^{-3}$			901
$\Xi^-\overline{\Xi}^+$	$(9.0 \pm 2.6) \times 10^{-4}$			692
$\pi^+\pi^-p\overline{p}$	$(5.3 \pm 2.1) \times 10^{-3}$			1027
Radiative decays				
$\gamma\gamma$	$(1.61 \pm 0.12) \times 10^{-4}$			1492
Charge conjugation (C), Parity (P), Lepton family number (LF) violating modes				
$\pi^+\pi^-$	P, CP	$< 1.1 \times 10^{-4}$	90%	1485
$\pi^0\pi^0$	P, CP	$< 4 \times 10^{-5}$	90%	1486
K^+K^-	P, CP	$< 6 \times 10^{-4}$	90%	1408
$K_S^0K_S^0$	P, CP	$< 3.1 \times 10^{-4}$	90%	1407

$J/\psi(1S)$

$I^G(J^{PC}) = 0^-(1^{--})$

Mass $m = 3096.900 \pm 0.006$ MeV
Full width $\Gamma = 92.6 \pm 1.7$ keV (S = 1.1)

$J/\psi(1S)$ DECAY MODES		Fraction (Γ_i/Γ)	Scale factor/ Confidence level	p (MeV/c)
hadrons		(87.7 ± 0.5) %		–
virtual $\gamma \to$ hadrons		(13.50 ± 0.30) %		–
ggg		(64.1 ± 1.0) %		–
γgg		(8.8 ± 1.1) %		–
e^+e^-		(5.971 ± 0.032) %		1548
$e^+e^-\gamma$	[hhaa]	$(8.8 \pm 1.4) \times 10^{-3}$		1548
$\mu^+\mu^-$		(5.961 ± 0.033) %		1545
Decays involving hadronic resonances				
$\rho\pi$		(1.69 ± 0.15) %	S=2.4	1448
$\rho^0\pi^0$		$(5.6 \pm 0.7) \times 10^{-3}$		1448
$a_2(1320)\rho$		(1.09 ± 0.22) %		1123
$\eta\pi^+\pi^-$		$(3.8 \pm 0.7) \times 10^{-4}$		1487
$\eta\pi^+\pi^-\pi^0$		(1.17 ± 0.20) %		1470
$\eta\pi^+\pi^-3\pi^0$		$(4.9 \pm 1.0) \times 10^{-3}$		1419
$\eta\rho$		$(1.93 \pm 0.23) \times 10^{-4}$		1396
$\eta\phi(2170) \to \eta\phi f_0(980) \to \eta\phi\pi^+\pi^-$		$(1.2 \pm 0.4) \times 10^{-4}$		628
$\eta\phi(2170) \to \eta K^*(892)^0\overline{K}^*(892)^0$		$< 2.52 \times 10^{-4}$	CL=90%	–
$\eta K^\pm K_S^0\pi^\mp$	[aa]	$(2.2 \pm 0.4) \times 10^{-3}$		1278
$\eta K^*(892)^0\overline{K}^*(892)^0$		$(1.15 \pm 0.26) \times 10^{-3}$		1003
$\rho\eta'(958)$		$(8.1 \pm 0.8) \times 10^{-5}$	S=1.6	1281
$\rho^\pm\pi^\mp\pi^+\pi^-2\pi^0$		(2.8 ± 0.8) %		1364
$\rho^+\rho^-\pi^+\pi^-\pi^0$		$(6 \pm 4) \times 10^{-3}$		1186
$\rho^\mp K^\pm K_S^0$		$(1.9 \pm 0.4) \times 10^{-3}$		1269
$\rho(1450)\pi \to \pi^+\pi^-\pi^0$		$(2.3 \pm 0.7) \times 10^{-3}$		–
$\rho(1450)^\pm\pi^\mp \to K_S^0K^\pm\pi^\mp$		$(3.5 \pm 0.6) \times 10^{-4}$		–
$\rho(1450)^0\pi^0 \to K^+K^-\pi^0$		$(2.7 \pm 0.6) \times 10^{-4}$		–
$\rho(1450)\eta'(958) \to \pi^+\pi^-\eta'(958)$		$(3.3 \pm 0.7) \times 10^{-6}$		–
$\rho(1700)\pi \to \pi^+\pi^-\pi^0$		$(1.7 \pm 1.1) \times 10^{-4}$		–
$\rho(2150)\pi \to \pi^+\pi^-\pi^0$		$(8 \pm 40) \times 10^{-6}$		–
$\omega\pi^0$		$(4.5 \pm 0.5) \times 10^{-4}$	S=1.4	1446
$\omega\pi^0 \to \pi^+\pi^-\pi^0$		$(1.7 \pm 0.8) \times 10^{-5}$		–
$\omega\pi^+\pi^-$		$(7.2 \pm 1.0) \times 10^{-3}$		1435
$\omega\pi^0\pi^0$		$(3.4 \pm 0.8) \times 10^{-3}$		1436
$\omega 3\pi^0$		$(1.9 \pm 0.6) \times 10^{-3}$		1419
$\omega f_2(1270)$		$(4.3 \pm 0.6) \times 10^{-3}$		1142
$\omega\eta$		$(1.74 \pm 0.20) \times 10^{-3}$	S=1.6	1394
$\omega\pi^+\pi^-\pi^0$		$(4.0 \pm 0.7) \times 10^{-3}$		1418
$\omega\pi^0\eta$		$(3.4 \pm 1.7) \times 10^{-4}$		1363
$\omega\pi^+\pi^+\pi^-\pi^-$		$(8.5 \pm 3.4) \times 10^{-3}$		1392
$\omega\pi^+\pi^-2\pi^0$		(3.3 ± 0.5) %		1394
$\omega\eta'\pi^+\pi^-$		$(1.12 \pm 0.13) \times 10^{-3}$		1173
$\omega\eta'(958)$		$(1.89 \pm 0.18) \times 10^{-4}$		1279
$\omega f_0(980)$		$(1.4 \pm 0.5) \times 10^{-4}$		1267
$\omega f_0(1710) \to \omega K\overline{K}$		$(4.8 \pm 1.1) \times 10^{-4}$		878
$\omega f_1(1420)$		$(6.8 \pm 2.4) \times 10^{-4}$		1062
$\omega f_2'(1525)$		$< 2.2 \times 10^{-4}$	CL=90%	1007
$\omega X(1835) \to \omega p\overline{p}$		$< 3.9 \times 10^{-6}$	CL=95%	–
$\omega X(1835),\ X \to \eta'\pi^+\pi^-$		$< 6.2 \times 10^{-5}$		–
$\omega K^\pm K_S^0\pi^\mp$	[aa]	$(3.4 \pm 0.5) \times 10^{-3}$		1210
$\omega K\overline{K}$		$(1.9 \pm 0.4) \times 10^{-3}$		1268
$\omega K^*(892)\overline{K}$ + c.c.		$(6.1 \pm 0.9) \times 10^{-3}$		1097
$\eta' K^{*\pm}K^\mp$		$(1.48 \pm 0.13) \times 10^{-3}$		–
$\eta' K^{*0}\overline{K}^0$ + c.c.		$(1.66 \pm 0.21) \times 10^{-3}$		1000
$\eta' h_1(1415) \to \eta' K^*\overline{K}$ + c.c.		$(2.16 \pm 0.31) \times 10^{-4}$		–
$\eta' h_1(1415) \to \eta' K^{*\pm}K^\mp$		$(1.51 \pm 0.23) \times 10^{-4}$		–
$\overline{K}K^*(892)$ +c.c. $\to K_S^0K^\pm\pi^\mp$		$(5.0 \pm 0.5) \times 10^{-3}$		–
$K^+K^*(892)^-$ + c.c.		$(6.0 {}^{+0.8}_{-1.0}) \times 10^{-3}$	S=2.9	1373
$K^+K^*(892)^-$ + c.c. $\to K^+K^-\pi^0$		$(2.69 {}^{+0.13}_{-0.20}) \times 10^{-3}$		–
$K^+K^*(892)^-$ + c.c. $\to K^0K^\pm\pi^\mp$ + c.c.		$(3.0 \pm 0.4) \times 10^{-3}$		–
$K^0\overline{K}^*(892)^0$ + c.c.		$(4.2 \pm 0.4) \times 10^{-3}$		1373
$K^0\overline{K}^*(892)^0$ + c.c. $\to K^0K^\pm\pi^\mp$ + c.c.		$(3.2 \pm 0.4) \times 10^{-3}$		–
$\overline{K}^*(892)^0K^+\pi^-$ + c.c.		$(7.7 \pm 1.6) \times 10^{-3}$		1343
$K^*(892)^\pm K^\mp\pi^0$		$(4.1 \pm 1.3) \times 10^{-3}$		1344
$K^*(892)^+K_S^0\pi^-$ + c.c.		$(2.0 \pm 0.5) \times 10^{-3}$		1342
$K^*(892)^+K_S^0\pi^-$ + c.c. $\to K_S^0K_S^0\pi^+\pi^-$		$(6.7 \pm 2.2) \times 10^{-4}$		–
$K^*(892)^0K_S^0 \to \gamma K_S^0K_S^0$		$(6.3 {}^{+0.6}_{-0.5}) \times 10^{-6}$		–
$K^*(892)^0K_S^0\pi^0$		$(7 \pm 4) \times 10^{-4}$		1343
$K^*(892)^\pm K^*(700)^\mp$		$(1.1 {}^{+1.0}_{-0.6}) \times 10^{-3}$		–
$K^*(892)^0\overline{K}^*(892)^0$		$(2.3 \pm 0.6) \times 10^{-4}$		1266
$K^*(892)^\pm K^*(892)^\mp$		$(1.00 {}^{+0.22}_{-0.40}) \times 10^{-3}$		1266
$K_1(1400)^\pm K^\mp$		$(3.8 \pm 1.4) \times 10^{-3}$		1170
$K^*(1410)\overline{K}$ +c.c $\to K^\pm K^\mp\pi^0$		$(7 \pm 4) \times 10^{-5}$		–
$K^*(1410)\overline{K}$ + c.c. $\to K_S^0K^\pm\pi^\mp$		$(8 \pm 6) \times 10^{-5}$		–
$K_2^*(1430)\overline{K}$ +c.c. $\to K^\pm K^\mp\pi^0$		$(1.0 \pm 0.5) \times 10^{-4}$		–
$K_2^*(1430)\overline{K}$ + c.c. $\to K_S^0K^\pm\pi^\mp$		$(4.0 \pm 1.0) \times 10^{-4}$		–
$\overline{K}_2^*(1430)K$ + c.c.		$< 4.0 \times 10^{-3}$	CL=90%	1158
$K_2^*(1430)^+K^-$ + c.c. $\to K^+K^-\pi^0$		$(2.69 {}^{+0.25}_{-0.19}) \times 10^{-4}$		–
$K_2^*(1430)^+K_S^0\pi^-$ + c.c.		$(3.6 \pm 1.8) \times 10^{-3}$		1116
$\overline{K}_2^*(1430)^0K^*(892)^0$ + c.c.		$(4.67 \pm 0.29) \times 10^{-3}$		1011
$K_2^*(1430)^-K^*(892)^+$ + c.c.		$(3.4 \pm 2.9) \times 10^{-3}$		1011
$K_2^*(1430)^-K^*(892)^+$ + c.c. $\to K^*(892)^+K_S^0\pi^-$ + c.c.		$(4 \pm 4) \times 10^{-4}$		–
$\overline{K}_2^*(1430)^0\overline{K}_2^*(1430)^0$		$< 2.9 \times 10^{-3}$	CL=90%	601
$\overline{K}_2(1770)^0K^*(892)^0$ + c.c. $\to K^*(892)^0K^-\pi^+$ + c.c.		$(6.9 \pm 0.9) \times 10^{-4}$		–
$K_2^*(1980)^+K^-$ + c.c. $\to K^+K^-\pi^0$		$(1.10 {}^{+0.60}_{-0.14}) \times 10^{-5}$		–

Downloaded from https://academic.oup.com/ptep/article/2022/8/083C01/6651666 by KIT Library user on 27 September 2022

$K_4^*(2045)^+ K^- +$ c.c. $\to K^+ K^- \pi^0$		$(6.2 \; {}^{+2.9}_{-1.6}) \times 10^{-6}$		–
$K_1(1270)^\pm K^\mp$		$< 3.0 \times 10^{-3}$	CL=90%	1240
$K_1(1270) K_S^0 \to \gamma K_S^0 K_S^0$		$(8.5 \pm 2.5) \times 10^{-7}$		–
$a_2(1320)^\pm \pi^\mp$	[aa]	$< 4.3 \times 10^{-3}$	CL=90%	1263
$\phi\pi^0$		3×10^{-6} or 1×10^{-7}		1377
$\phi\pi^+\pi^-$		$(9.4 \pm 1.5) \times 10^{-4}$	S=1.7	1365
$\phi\pi^0\pi^0$		$(5.0 \pm 1.0) \times 10^{-4}$		1366
$\phi 2(\pi^+\pi^-)$		$(1.60 \pm 0.32) \times 10^{-3}$		1318
$\phi\eta$		$(7.4 \pm 0.8) \times 10^{-4}$	S=1.5	1320
$\phi\eta'(958)$		$(4.6 \pm 0.5) \times 10^{-4}$	S=2.2	1192
$\phi\eta\eta'$		$(2.32 \pm 0.17) \times 10^{-4}$		885
$\phi f_0(980)$		$(3.2 \pm 0.9) \times 10^{-4}$	S=1.9	1178
$\phi f_0(980) \to \phi\pi^+\pi^-$		$(2.60 \pm 0.34) \times 10^{-4}$		–
$\phi f_0(980) \to \phi\pi^0\pi^0$		$(1.8 \pm 0.5) \times 10^{-4}$		–
$\phi\pi^0 f_0(980) \to \phi\pi^0\pi^+\pi^-$		$(4.5 \pm 1.0) \times 10^{-6}$		–
$\phi\pi^0 f_0(980) \to \phi\pi^0 p^0\pi^0$		$(1.7 \pm 0.6) \times 10^{-6}$		1045
$\phi f_0(980)\eta \to \eta\phi\pi^+\pi^-$		$(3.2 \pm 1.0) \times 10^{-4}$		–
$\phi a_0(980)^0 \to \phi\eta\pi^0$		$(4.4 \pm 1.4) \times 10^{-6}$		–
$\phi f_2(1270)$		$(3.2 \pm 0.6) \times 10^{-4}$		1036
$\phi f_1(1285)$		$(2.6 \pm 0.5) \times 10^{-4}$		1032
$\phi f_1(1285) \to \phi\pi^0 f_0(980) \to \phi\pi^0\pi^+\pi^-$		$(9.4 \pm 2.8) \times 10^{-7}$		952
$\phi f_1(1285) \to \phi\pi^0 f_0(980) \to \phi 3\pi^0$		$(2.1 \pm 2.2) \times 10^{-7}$		955
$\phi\eta(1405) \to \phi\eta\pi^+\pi^-$		$(2.0 \pm 1.0) \times 10^{-5}$		946
$\phi f_2'(1525)$		$(8 \pm 4) \times 10^{-4}$	S=2.7	877
$\phi X(1835) \to \phi p\overline{p}$		$< 2.1 \times 10^{-7}$	CL=90%	–
$\phi X(1835) \to \phi\eta\pi^+\pi^-$		$< 2.8 \times 10^{-4}$	CL=90%	578
$\phi X(1870) \to \phi\eta\pi^+\pi^-$		$< 6.13 \times 10^{-5}$	CL=90%	–
$\phi K\overline{K}$		$(1.77 \pm 0.16) \times 10^{-3}$	S=1.3	1179
$\phi f_0(1710) \to \phi K\overline{K}$		$(3.6 \pm 0.6) \times 10^{-4}$		875
ϕK^+K^-		$(8.3 \pm 1.1) \times 10^{-4}$		1179
$\phi K_S^0 K_S^0$		$(5.9 \pm 1.5) \times 10^{-4}$		1176
$\phi K^\pm K_S^0 \pi^\mp$	[aa]	$(7.2 \pm 0.8) \times 10^{-4}$		1114
$\phi K^*(892)\overline{K} +$ c.c.		$(2.18 \pm 0.23) \times 10^{-3}$		969
$b_1(1235)^\pm \pi^\mp$	[aa]	$(3.0 \pm 0.5) \times 10^{-3}$		1300
$b_1(1235)^0 \pi^0$		$(2.3 \pm 0.6) \times 10^{-3}$		1300
$f_2'(1525) K^+K^-$		$(1.06 \pm 0.35) \times 10^{-3}$		897
$\Delta(1232)^+\overline{p}$		$< 1 \times 10^{-4}$	CL=90%	1100
$\Delta(1232)^{++}\overline{p}\pi^-$		$(1.6 \pm 0.5) \times 10^{-3}$		1030
$\Delta(1232)^{++}\overline{\Delta}(1232)^{--}$		$(1.10 \pm 0.29) \times 10^{-3}$		938
$\overline{\Sigma}(1385)^0 p K^-$		$(5.1 \pm 3.2) \times 10^{-4}$		646
$\Sigma(1385)^0\overline{\Lambda} +$ c.c.		$< 8.2 \times 10^{-6}$	CL=90%	911
$\Sigma(1385)^-\overline{\Sigma}^+$ (or c.c.)	[aa]	$(3.1 \pm 0.5) \times 10^{-4}$		855
$\Sigma(1385)^-\overline{\Sigma}(1385)^+$ (or c.c.)	[aa]	$(1.16 \pm 0.05) \times 10^{-3}$		697
$\Sigma(1385)^0\overline{\Sigma}(1385)^0$		$(1.07 \pm 0.08) \times 10^{-3}$		697
$\Lambda(1520)\overline{\Lambda} +$ c.c. $\to \gamma\Lambda\overline{\Lambda}$		$< 4.1 \times 10^{-6}$	CL=90%	–
$\overline{\Lambda}(1520)\Lambda +$ c.c.		$< 1.80 \times 10^{-3}$	CL=90%	807
$\Xi^0\overline{\Xi}^0$		$(1.17 \pm 0.04) \times 10^{-3}$		818
$\Xi(1530)^-\overline{\Xi}^+ +$ c.c.		$(3.18 \pm 0.08) \times 10^{-4}$		600
$\Xi(1530)^0\overline{\Xi}^0$		$(3.2 \pm 1.4) \times 10^{-4}$		608
$\Theta(1540)\overline{\Theta}(1540) \to K_S^0 p K^-\overline{n} +$ c.c.	[iiaa]	$< 1.1 \times 10^{-5}$	CL=90%	–
$\Theta(1540) K^-\overline{n} \to K_S^0 p K^-\overline{n}$	[iiaa]	$< 2.1 \times 10^{-5}$	CL=90%	–
$\Theta(1540) K_S^0\overline{p} \to K_S^0\overline{p}K^+ n$	[iiaa]	$< 1.6 \times 10^{-5}$	CL=90%	–
$\overline{\Theta}(1540) K^+ n \to K_S^0\overline{p}K^+ n$	[iiaa]	$< 5.6 \times 10^{-5}$	CL=90%	–
$\overline{\Theta}(1540) K_S^0 p \to K_S^0 p K^-\overline{n}$	[iiaa]	$< 1.1 \times 10^{-5}$	CL=90%	–

Decays into stable hadrons

$2(\pi^+\pi^-)\pi^0$		(3.71 ± 0.28) %	S=1.3	1496
$3(\pi^+\pi^-)\pi^0$		(2.9 ± 0.6) %		1433
$\pi^+\pi^- 3\pi^0$		(1.9 ± 0.9) %		1497
$\pi^+\pi^- 4\pi^0$		$(6.5 \pm 1.3) \times 10^{-3}$		1470
$\rho^\pm\pi^\mp\pi^0\pi^0$		(1.41 ± 0.22) %		1421
$\rho^+\rho^-\pi^0$		$(6.0 \pm 1.1) \times 10^{-3}$		1298
$\pi^+\pi^-\pi^0$		(2.10 ± 0.08) %	S=1.6	1533
$2(\pi^+\pi^-\pi^0)$		(1.61 ± 0.20) %		1468
$\pi^+\pi^-\pi^0 K^+K^-$		(1.20 ± 0.30) %		1368
$\pi^+\pi^-$		$(1.47 \pm 0.14) \times 10^{-4}$		1542
$2(\pi^+\pi^-)$		$(3.57 \pm 0.30) \times 10^{-3}$		1517
$3(\pi^+\pi^-)$		$(4.3 \pm 0.4) \times 10^{-3}$		1466
$2(\pi^+\pi^-)3\pi^0$		(6.2 ± 0.9) %		1435
$4(\pi^+\pi^-)\pi^0$		$(9.0 \pm 3.0) \times 10^{-3}$		1345
$2(\pi^+\pi^-)\eta$		$(2.29 \pm 0.28) \times 10^{-3}$		1446
$3(\pi^+\pi^-)\eta$		$(7.2 \pm 1.5) \times 10^{-4}$		1379
$2(\pi^+\pi^-\pi^0)\eta$		$(1.6 \pm 0.5) \times 10^{-3}$		1381
$\pi^+\pi^-\pi^0\pi^0\eta$		$(2.4 \pm 0.5) \times 10^{-3}$		1448
$\rho^\pm\pi^\mp\pi^0\eta$		$(1.9 \pm 0.8) \times 10^{-3}$		1326
K^+K^-		$(2.86 \pm 0.21) \times 10^{-4}$		1468
$K_S^0 K_L^0$		$(1.95 \pm 0.11) \times 10^{-4}$	S=2.4	1466
$K_S^0 K_S^0$		$< 1.4 \times 10^{-8}$	CL=95%	1466
$K\overline{K}\pi$		$(6.1 \pm 1.0) \times 10^{-3}$		1442
$K^+K^-\pi^0$		$(2.88 \pm 0.12) \times 10^{-3}$		1442
$K_S^0 K^\pm\pi^\mp$		$(5.6 \pm 0.5) \times 10^{-3}$		1440
$K_S^0 K_L^0\pi^0$		$(2.06 \pm 0.26) \times 10^{-3}$		1440
$K^*(892)^0\overline{K}^0 +$ c.c. $\to K_S^0 K_L^0\pi^0$		$(1.21 \pm 0.18) \times 10^{-3}$		–
$K_2^*(1430)^0\overline{K}^0 +$ c.c. $\to K_S^0 K_L^0\pi^0$		$(4.3 \pm 1.3) \times 10^{-4}$		–
$K^+K^-\pi^+\pi^-$		$(6.86 \pm 0.28) \times 10^{-3}$		1407
$K^+K^-\pi^0\pi^0$		$(2.13 \pm 0.22) \times 10^{-3}$		1410
$K_S^0 K_L^0\pi^+\pi^-$		$(3.8 \pm 0.6) \times 10^{-3}$		1406
$K_S^0 K_L^0\pi^0\pi^0$		$(1.9 \pm 0.4) \times 10^{-3}$		1408
$K_S^0 K_L^0\eta$		$(1.45 \pm 0.33) \times 10^{-3}$		1328
$K_S^0 K_S^0\pi^+\pi^-$		$(1.68 \pm 0.19) \times 10^{-3}$		1406
$K^\mp K_S^0\pi^\pm\pi^0$		$(5.7 \pm 0.5) \times 10^{-3}$		1408
$K^+K^- 2(\pi^+\pi^-)$		$(3.1 \pm 1.3) \times 10^{-3}$		1320
$K^+K^-\pi^+\pi^-\eta$		$(4.7 \pm 0.7) \times 10^{-3}$		1221
$2(K^+K^-)$		$(7.2 \pm 0.8) \times 10^{-4}$		1131
$K^+K^- K_S^0 K_S^0$		$(4.2 \pm 0.7) \times 10^{-4}$		1127
$p\overline{p}$		$(2.120 \pm 0.029) \times 10^{-3}$		1232
$p\overline{p}\pi^0$		$(1.19 \pm 0.08) \times 10^{-3}$	S=1.1	1176
$p\overline{p}\pi^+\pi^-$		$(6.0 \pm 0.5) \times 10^{-3}$	S=1.3	1107
$p\overline{p}\pi^+\pi^-\pi^0$	[jjaa]	$(2.3 \pm 0.9) \times 10^{-3}$	S=1.9	1033
$p\overline{p}\eta$		$(2.00 \pm 0.12) \times 10^{-3}$		948
$p\overline{p}\rho$		$< 3.1 \times 10^{-4}$	CL=90%	774
$p\overline{p}\omega$		$(9.8 \pm 1.0) \times 10^{-4}$	S=1.3	768
$p\overline{p}\eta'(958)$		$(1.29 \pm 0.14) \times 10^{-4}$	S=2.0	596
$p\overline{p}a_0(980) \to p\overline{p}\pi^0\eta$		$(6.8 \pm 1.8) \times 10^{-5}$		–
$p\overline{p}\phi$		$(5.19 \pm 0.33) \times 10^{-5}$		527
$p\overline{n}\pi^-$		$(2.12 \pm 0.09) \times 10^{-3}$		1174
$n\overline{n}$		$(2.09 \pm 0.16) \times 10^{-3}$		1231
$n\overline{n}\pi^+\pi^-$		$(4 \pm 4) \times 10^{-3}$		1106
$nN(1440)$		seen		978
$nN(1520)$		seen		928
$nN(1535)$		seen		917
$\Lambda\overline{\Lambda}$		$(1.89 \pm 0.09) \times 10^{-3}$	S=2.8	1074
$\Lambda\overline{\Lambda}\pi^0$		$(3.8 \pm 0.4) \times 10^{-5}$		998
$\Lambda\overline{\Lambda}\pi^+\pi^-$		$(4.3 \pm 1.0) \times 10^{-3}$		903
$\Lambda\overline{\Lambda}\eta$		$(1.62 \pm 0.17) \times 10^{-4}$		672
$\Lambda\overline{\Sigma}^-\pi^+$ (or c.c.)	[aa]	$(8.3 \pm 0.7) \times 10^{-4}$	S=1.2	950
$pK^-\overline{\Lambda} +$c.c.		$(8.6 \pm 1.1) \times 10^{-4}$		876
$pK^-\overline{\Sigma}^0$		$(2.9 \pm 0.8) \times 10^{-4}$		819
$\overline{\Lambda}nK_S^0 +$ c.c.		$(6.5 \pm 1.1) \times 10^{-4}$		872
$\Lambda\overline{\Sigma} +$ c.c.		$(2.83 \pm 0.23) \times 10^{-5}$		1034
$\Sigma^+\overline{\Sigma}^-$		$(1.07 \pm 0.04) \times 10^{-3}$		992
$\Sigma^0\overline{\Sigma}^0$		$(1.172 \pm 0.032) \times 10^{-3}$	S=1.4	988
$\Xi^-\overline{\Xi}^+$		$(9.7 \pm 0.8) \times 10^{-4}$	S=1.4	807

Radiative decays

$\gamma\eta_c(1S)$		(1.7 ± 0.4) %	S=1.5	111
$\gamma\eta_c(1S) \to 3\gamma$		$(3.8 \; {}^{+1.3}_{-1.0}) \times 10^{-6}$	S=1.1	–
$\gamma\eta_c(1S) \to \gamma\eta\eta\eta'$		$(4.9 \pm 0.8) \times 10^{-5}$		–
3γ		$(1.16 \pm 0.22) \times 10^{-5}$		1548
4γ		$< 9 \times 10^{-6}$	CL=90%	1548
5γ		$< 1.5 \times 10^{-5}$	CL=90%	1548
$\gamma\pi^0$		$(3.56 \pm 0.17) \times 10^{-5}$		1546
$\gamma\pi^0\pi^0$		$(1.15 \pm 0.05) \times 10^{-3}$		1543
$\gamma 2\pi^+ 2\pi^-$		$(2.8 \pm 0.5) \times 10^{-3}$	S=1.9	1517
$\gamma f_2(1270) f_2(1270)$		$(9.5 \pm 1.7) \times 10^{-4}$		878
$\gamma f_2(1270) f_2(1270)$ (non resonant)		$(8.2 \pm 1.9) \times 10^{-4}$		–
$\gamma\pi^+\pi^- 2\pi^0$		$(8.3 \pm 3.1) \times 10^{-3}$		1518
$\gamma K_S^0 K_S^0$		$(8.1 \pm 0.4) \times 10^{-4}$		1466
$\gamma(K\overline{K}\pi)$ [$J^{PC} = 0^{-+}$]		$(7 \pm 4) \times 10^{-4}$	S=2.1	1442
$\gamma K^+K^-\pi^+\pi^-$		$(2.1 \pm 0.6) \times 10^{-3}$		1407
$\gamma K^*(892)\overline{K}^*(892)$		$(4.0 \pm 1.3) \times 10^{-3}$		1266
$\gamma\eta$		$(1.085 \pm 0.018) \times 10^{-3}$		1500
$\gamma\eta\pi^0$		$(2.14 \pm 0.31) \times 10^{-5}$		1497
$\gamma a_0(980)^0 \to \gamma\eta\pi^0$		$< 2.5 \times 10^{-6}$	CL=95%	–
$\gamma a_2(1320)^0 \to \gamma\eta\pi^0$		$< 6.6 \times 10^{-6}$	CL=95%	–

Downloaded from https://academic.oup.com/ptep/article/2022/8/083C01/6651666 by KIT Library user on 27 September 2022

$\gamma\eta\pi\pi$	$(6.1 \pm 1.0) \times 10^{-3}$			1487
$\gamma\eta_2(1870) \to \gamma\eta\pi^+\pi^-$	$(6.2 \pm 2.4) \times 10^{-4}$			–
$\gamma\eta'(958)$	$(5.25 \pm 0.07) \times 10^{-3}$	S=1.3		1400
$\gamma\rho\rho$	$(4.5 \pm 0.8) \times 10^{-3}$			1340
$\gamma\rho\omega$	$< 5.4 \times 10^{-4}$	CL=90%		1338
$\gamma\rho\phi$	$< 8.8 \times 10^{-5}$	CL=90%		1258
$\gamma\omega\omega$	$(1.61 \pm 0.33) \times 10^{-3}$			1336
$\gamma\phi\phi$	$(4.0 \pm 1.2) \times 10^{-4}$	S=2.1		1166
$\gamma\eta(1405/1475) \to \gamma K\overline{K}\pi$	$(2.8 \pm 0.6) \times 10^{-3}$	S=1.6		1223
$\gamma\eta(1405/1475) \to \gamma\gamma\rho^0$	$(7.8 \pm 2.0) \times 10^{-5}$	S=1.8		1223
$\gamma\eta(1405/1475) \to \gamma\eta\pi^+\pi^-$	$(3.0 \pm 0.5) \times 10^{-4}$			–
$\gamma\eta(1405/1475) \to \gamma\rho^0\rho^0$	$(1.7 \pm 0.4) \times 10^{-3}$	S=1.3		1223
$\gamma\eta(1405/1475) \to \gamma\gamma\phi$	$< 8.2 \times 10^{-5}$	CL=95%		–
$\gamma\eta(1405) \to \gamma\gamma\gamma$	$< 2.63 \times 10^{-6}$	CL=90%		–
$\gamma\eta(1475) \to \gamma\gamma\gamma$	$< 1.86 \times 10^{-6}$	CL=90%		–
$\gamma\eta(1760) \to \gamma\rho^0\rho^0$	$(1.3 \pm 0.9) \times 10^{-4}$			1048
$\gamma\eta(1760) \to \gamma\omega\omega$	$(1.98 \pm 0.33) \times 10^{-3}$			–
$\gamma\eta(1760) \to \gamma\gamma\gamma$	$< 4.80 \times 10^{-6}$	CL=90%		–
$\gamma\eta(2225)$	$(3.14 {}^{+0.50}_{-0.19}) \times 10^{-4}$			752
$\gamma f_2(1270)$	$(1.64 \pm 0.12) \times 10^{-3}$	S=1.3		1286
$\gamma f_2(1270) \to \gamma K^0_S K^0_S$	$(2.58 {}^{+0.60}_{-0.22}) \times 10^{-5}$			–
$\gamma f_1(1285)$	$(6.1 \pm 0.8) \times 10^{-4}$			1283
$\gamma f_0(1370) \to \gamma K\overline{K}$	$(4.2 \pm 1.5) \times 10^{-4}$			–
$\gamma f_0(1370) \to \gamma K^0_S K^0_S$	$(1.1 \pm 0.4) \times 10^{-5}$			–
$\gamma f_1(1420) \to \gamma K\overline{K}\pi$	$(7.9 \pm 1.3) \times 10^{-4}$			1220
$\gamma f_0(1500) \to \gamma\pi\pi$	$(1.09 \pm 0.24) \times 10^{-4}$			1183
$\gamma f_0(1500) \to \gamma\eta\eta$	$(1.7 {}^{+0.6}_{-1.4}) \times 10^{-5}$			–
$\gamma f_0(1500) \to \gamma K^0_S K^0_S$	$(1.59 {}^{+0.24}_{-0.60}) \times 10^{-5}$			–
$\gamma f_1(1510) \to \gamma\eta\pi^+\pi^-$	$(4.5 \pm 1.2) \times 10^{-4}$			–
$\gamma f'_2(1525)$	$(5.7 {}^{+0.8}_{-0.5}) \times 10^{-4}$	S=1.5		1177
$\gamma f'_2(1525) \to \gamma K^0_S K^0_S$	$(8.0 {}^{+0.7}_{-0.5}) \times 10^{-5}$			–
$\gamma f'_2(1525) \to \gamma\eta\eta$	$(3.4 \pm 1.4) \times 10^{-5}$			–
$\gamma f_2(1640) \to \gamma\omega\omega$	$(2.8 \pm 1.8) \times 10^{-4}$			–
$\gamma f_0(1710) \to \gamma\pi\pi$	$(3.8 \pm 0.5) \times 10^{-4}$			–
$\gamma f_0(1710) \to \gamma K\overline{K}$	$(9.5 {}^{+1.0}_{-0.5}) \times 10^{-4}$	S=1.5		1075
$\gamma f_0(1710) \to \gamma\omega\omega$	$(3.1 \pm 1.0) \times 10^{-4}$			–
$\gamma f_0(1710) \to \gamma\eta\eta$	$(2.4 {}^{+1.2}_{-0.7}) \times 10^{-4}$			–
$\gamma f_0(1710) \to \gamma\omega\phi$	$(2.5 \pm 0.6) \times 10^{-4}$			–
$\gamma f_0(1750) \to \gamma K^0_S K^0_S$	$(1.11 {}^{+0.20}_{-0.33}) \times 10^{-5}$			–
$\gamma f_2(1810) \to \gamma\eta\eta$	$(5.4 {}^{+3.5}_{-2.4}) \times 10^{-5}$			–
$\gamma f_2(1910) \to \gamma\omega\omega$	$(2.0 \pm 1.4) \times 10^{-4}$			–
$\gamma f_2(1950) \to \gamma K^*(892)\overline{K}^*(892)$	$(7.0 \pm 2.2) \times 10^{-4}$			–
$\gamma f_4(2050)$	$(2.7 \pm 0.7) \times 10^{-3}$			891
$\gamma f_0(2100) \to \gamma\eta\eta$	$(1.13 {}^{+0.60}_{-0.30}) \times 10^{-4}$			–
$\gamma f_0(2100) \to \gamma\pi\pi$	$(6.2 \pm 1.0) \times 10^{-4}$			–
$\gamma f_0(2200) \to \gamma K\overline{K}$	$(5.9 \pm 1.3) \times 10^{-4}$			–
$\gamma f_0(2200) \to \gamma K^0_S K^0_S$	$(2.72 {}^{+0.19}_{-0.50}) \times 10^{-4}$			–
$\gamma f_J(2220) \to \gamma\pi\pi$	$< 3.9 \times 10^{-5}$	CL=90%		–
$\gamma f_J(2220) \to \gamma K\overline{K}$	$< 4.1 \times 10^{-5}$	CL=90%		–
$\gamma f_J(2220) \to \gamma p\overline{p}$	$(1.5 \pm 0.8) \times 10^{-5}$			–
$\gamma f_0(2330) \to \gamma K^0_S K^0_S$	$(4.9 \pm 0.7) \times 10^{-5}$			–
$\gamma f_2(2340) \to \gamma\eta\eta$	$(5.6 {}^{+2.4}_{-2.2}) \times 10^{-5}$			–
$\gamma f_2(2340) \to \gamma K^0_S K^0_S$	$(5.5 {}^{+4.0}_{-1.5}) \times 10^{-5}$			–
$\gamma X(1835) \to \gamma\pi^+\pi^-\eta'$	$(2.7 {}^{+0.6}_{-0.8}) \times 10^{-4}$	S=1.6		1006
$\gamma X(1835) \to \gamma p\overline{p}$	$(7.7 {}^{+1.5}_{-0.9}) \times 10^{-5}$			–
$\gamma X(1835) \to \gamma K^0_S K^0_S \eta$	$(3.3 {}^{+2.0}_{-1.3}) \times 10^{-5}$			–
$\gamma X(1835) \to \gamma\gamma\gamma$	$< 3.56 \times 10^{-6}$	CL=90%		–
$\gamma X(1835) \to \gamma 3(\pi^+\pi^-)$	$(2.4 {}^{+0.7}_{-0.8}) \times 10^{-5}$			–
$\gamma X(2370) \to \gamma K^+K^-\eta'$	$(1.8 \pm 0.7) \times 10^{-5}$			–
$\gamma X(2370) \to \gamma K^0_S K^0_S \eta'$	$(1.2 \pm 0.5) \times 10^{-5}$			–
$\gamma X(2370) \to \gamma\eta\eta\eta'$	$< 9.2 \times 10^{-6}$	CL=90%		–
$\gamma p\overline{p}$	$(3.8 \pm 1.0) \times 10^{-4}$			1232
$\gamma p\overline{p}\pi^+\pi^-$	$< 7.9 \times 10^{-4}$	CL=90%		1107
$\gamma\Lambda\overline{\Lambda}$	$< 1.3 \times 10^{-4}$	CL=90%		1074
$\gamma A \to \gamma$ invisible	[kkaa] $< 1.7 \times 10^{-6}$	CL=90%		–
$\gamma A^0 \to \gamma\mu^+\mu^-$	[llaa] $< 5 \times 10^{-6}$	CL=90%		–
Dalitz decays				
$\pi^0 e^+ e^-$	$(7.6 \pm 1.4) \times 10^{-7}$			1546
$\eta e^+ e^-$	$(1.42 \pm 0.08) \times 10^{-5}$			1500
$\eta'(958) e^+ e^-$	$(6.59 \pm 0.18) \times 10^{-5}$			1400
$\eta U \to \eta e^+ e^-$	[nnaa] $< 9.11 \times 10^{-7}$	CL=90%		–
$\eta'(958) U \to \eta'(958) e^+ e^-$	[nnaa] $< 2.0 \times 10^{-7}$	CL=90%		–
$\phi e^+ e^-$	$< 1.2 \times 10^{-7}$	CL=90%		1381
Weak decays				
$D^- e^+ \nu_e +$ c.c.	$< 7.1 \times 10^{-8}$	CL=90%		984
$\overline{D}^0 e^+ e^- +$ c.c.	$< 8.5 \times 10^{-8}$	CL=90%		987
$D^-_s e^+ \nu_e +$ c.c.	$< 1.3 \times 10^{-6}$	CL=90%		923
$D^{*-}_s e^+ \nu_e +$ c.c.	$< 1.8 \times 10^{-6}$	CL=90%		828
$D^- \pi^+ +$ c.c.	$< 7.5 \times 10^{-5}$	CL=90%		977
$\overline{D}^0 K^0 +$ c.c.	$< 1.7 \times 10^{-4}$	CL=90%		898
$\overline{D}^0 K^{*0} +$ c.c.	$< 2.5 \times 10^{-6}$	CL=90%		670
$D^-_s \pi^+ +$ c.c.	$< 1.3 \times 10^{-4}$	CL=90%		915
$D^-_s \rho^+ +$ c.c.	$< 1.3 \times 10^{-5}$	CL=90%		663
Charge conjugation (C), Parity (P), Lepton Family number (LF) violating modes				
$\gamma\gamma$	C $< 2.7 \times 10^{-7}$	CL=90%		1548
$\gamma\phi$	C $< 1.4 \times 10^{-6}$	CL=90%		1381
$e^\pm\mu^\mp$	LF $< 1.6 \times 10^{-7}$	CL=90%		1547
$e^\pm\tau^\mp$	LF $< 7.5 \times 10^{-8}$	CL=90%		1039
$\mu^\pm\tau^\mp$	LF $< 2.0 \times 10^{-6}$	CL=90%		1035
$\Lambda^+_c e^-$ +c.c.	$< 6.9 \times 10^{-8}$	CL=90%		–
Other decays				
invisible	$< 7 \times 10^{-4}$	CL=90%		–

$\chi_{c0}(1P)$

$I^G(J^{PC}) = 0^+(0^{++})$

Mass $m = 3414.71 \pm 0.30$ MeV
Full width $\Gamma = 10.8 \pm 0.6$ MeV

$\chi_{c0}(1P)$ DECAY MODES	Fraction (Γ_i/Γ)	Scale factor/ Confidence level	p (MeV/c)
Hadronic decays			
$2(\pi^+\pi^-)$	(2.34 ± 0.18) %		1679
$\rho^0\pi^+\pi^-$	$(9.1 \pm 2.9) \times 10^{-3}$		1607
$f_0(980) f_0(980)$	$(6.6 \pm 2.1) \times 10^{-4}$		1391
$\pi^+\pi^-\pi^0\pi^0$	(3.3 ± 0.4) %		1680
$\rho^+\pi^-\pi^0 +$ c.c.	(2.9 ± 0.4) %		1607
$4\pi^0$	$(3.3 \pm 0.4) \times 10^{-3}$		1681
$\pi^+\pi^-K^+K^-$	(1.81 ± 0.14) %		1580
$K^*_0(1430)^0\overline{K}^*_0(1430)^0 \to \pi^+\pi^-K^+K^-$	$(9.8 {}^{+4.0}_{-2.8}) \times 10^{-4}$		–
$K^*_0(1430)^0\overline{K}^*_2(1430)^0 +$ c.c. $\to \pi^+\pi^-K^+K^-$	$(8.0 {}^{+2.0}_{-2.4}) \times 10^{-4}$		–
$K_1(1270)^+K^- +$ c.c. $\to \pi^+\pi^-K^+K^-$	$(6.3 \pm 1.9) \times 10^{-3}$		–
$K_1(1400)^+K^- +$ c.c. $\to \pi^+\pi^-K^+K^-$	$< 2.7 \times 10^{-3}$	CL=90%	–
$f_0(980) f_0(980)$	$(1.6 {}^{+1.0}_{-0.9}) \times 10^{-4}$		1391
$f_0(980) f_0(2200)$	$(7.9 {}^{+2.0}_{-2.5}) \times 10^{-4}$		586
$f_0(1370) f_0(1370)$	$< 2.7 \times 10^{-4}$	CL=90%	1019
$f_0(1370) f_0(1500)$	$< 1.7 \times 10^{-4}$	CL=90%	920
$f_0(1370) f_0(1710)$	$(6.7 {}^{+3.5}_{-2.3}) \times 10^{-4}$		740
$f_0(1500) f_0(1370)$	$< 1.3 \times 10^{-4}$	CL=90%	920
$f_0(1500) f_0(1500)$	$< 5 \times 10^{-5}$	CL=90%	804
$f_0(1500) f_0(1710)$	$< 7 \times 10^{-5}$	CL=90%	581
$K^+K^-\pi^+\pi^-\pi^0$	$(8.6 \pm 0.9) \times 10^{-3}$		1545
$K^0_S K^\pm\pi^\mp\pi^+\pi^-$	$(4.2 \pm 0.4) \times 10^{-3}$		1543
$K^+K^-\pi^0\pi^0$	$(5.6 \pm 0.9) \times 10^{-3}$		1582
$K^+\pi^-\overline{K}^0\pi^0 +$ c.c.	(2.49 ± 0.33) %		1581
$\rho^+K^-K^0 +$ c.c.	(1.21 ± 0.21) %		1458
$K^*(892)^-K^+\pi^0 \to K^+\pi^-\overline{K}^0\pi^0 +$ c.c.	$(4.6 \pm 1.2) \times 10^{-3}$		–
$K^0_S K^0_S \pi^+\pi^-$	$(5.7 \pm 1.1) \times 10^{-3}$		1579
$K^+K^-\eta\pi^0$	$(3.0 \pm 0.7) \times 10^{-3}$		1468
$3(\pi^+\pi^-)$	(1.20 ± 0.18) %		1633

Downloaded from https://academic.oup.com/ptep/article/2022/8/083C01/6651666 by KIT Library user on 27 September 2022

$K^+\overline{K}^*(892)^0\pi^-$ + c.c.	$(7.5 \pm 1.6) \times 10^{-3}$		1523
$K^*(892)^0\overline{K}^*(892)^0$	$(1.7 \pm 0.6) \times 10^{-3}$		1456
$\pi\pi$	$(8.51 \pm 0.33) \times 10^{-3}$		1702
$\pi^0\eta$	$< 1.8 \times 10^{-4}$		1661
$\pi^0\eta'$	$< 1.1 \times 10^{-3}$		1570
$\pi^0\eta_c$	$< 1.6 \times 10^{-3}$	CL=90%	383
$\eta\eta$	$(3.01 \pm 0.19) \times 10^{-3}$		1617
$\eta\eta'$	$(9.1 \pm 1.1) \times 10^{-5}$		1521
$\eta'\eta'$	$(2.17 \pm 0.12) \times 10^{-3}$		1413
$\omega\omega$	$(9.7 \pm 1.1) \times 10^{-4}$		1517
$\omega\phi$	$(1.41 \pm 0.13) \times 10^{-4}$		1447
ωK^+K^-	$(1.94 \pm 0.21) \times 10^{-3}$		1457
K^+K^-	$(6.05 \pm 0.31) \times 10^{-3}$		1634
$K^0_S K^0_S$	$(3.16 \pm 0.17) \times 10^{-3}$		1633
$\pi^+\pi^-\eta$	$< 2.0 \times 10^{-4}$	CL=90%	1651
$\pi^+\pi^-\eta'$	$< 4 \times 10^{-4}$	CL=90%	1560
$\overline{K}^0 K^+\pi^-$ + c.c.	$< 9 \times 10^{-5}$	CL=90%	1610
$K^+K^-\pi^0$	$< 6 \times 10^{-5}$	CL=90%	1611
$K^+K^-\eta$	$< 2.3 \times 10^{-4}$	CL=90%	1512
$K^+K^-K^0_S K^0_S$	$(1.4 \pm 0.5) \times 10^{-3}$		1331
$K^0_S K^0_S K^0_S K^0_S$	$(5.8 \pm 0.5) \times 10^{-4}$		1327
$K^+K^-K^+K^-$	$(2.82 \pm 0.29) \times 10^{-3}$		1333
$K^+K^-\phi$	$(9.7 \pm 2.5) \times 10^{-4}$		1381
$\overline{K}^0 K^+\pi^-\phi$ + c.c.	$(3.7 \pm 0.6) \times 10^{-3}$		1326
$K^+K^-\pi^0\phi$	$(1.90 \pm 0.35) \times 10^{-3}$		1329
$\phi\pi^+\pi^-\pi^0$	$(1.18 \pm 0.15) \times 10^{-3}$		1525
$\phi\phi$	$(8.0 \pm 0.7) \times 10^{-4}$		1370
$\phi\phi\eta$	$(8.4 \pm 1.0) \times 10^{-4}$		1100
$p\overline{p}$	$(2.21 \pm 0.08) \times 10^{-4}$		1426
$p\overline{p}\pi^0$	$(7.0 \pm 0.7) \times 10^{-4}$	S=1.3	1379
$p\overline{p}\eta$	$(3.5 \pm 0.4) \times 10^{-4}$		1187
$p\overline{p}\omega$	$(5.2 \pm 0.6) \times 10^{-4}$		1043
$p\overline{p}\phi$	$(6.0 \pm 1.4) \times 10^{-5}$		876
$p\overline{p}\pi^+\pi^-$	$(2.1 \pm 0.7) \times 10^{-3}$	S=1.4	1320
$p\overline{p}\pi^0\pi^0$	$(1.04 \pm 0.28) \times 10^{-3}$		1324
$p\overline{p}K^+K^-$ (non-resonant)	$(1.22 \pm 0.26) \times 10^{-4}$		890
$p\overline{p}K^0_S K^0_S$	$< 8.8 \times 10^{-4}$	CL=90%	884
$p\overline{n}\pi^-$	$(1.27 \pm 0.11) \times 10^{-3}$		1376
$\overline{p}n\pi^+$	$(1.37 \pm 0.12) \times 10^{-3}$		1376
$p\overline{n}\pi^-\pi^0$	$(2.34 \pm 0.21) \times 10^{-3}$		1321
$\overline{p}n\pi^+\pi^0$	$(2.21 \pm 0.18) \times 10^{-3}$		1321
$\Lambda\overline{\Lambda}$	$(3.59 \pm 0.15) \times 10^{-4}$		1292
$\Lambda\overline{\Lambda}\pi^+\pi^-$	$(1.18 \pm 0.13) \times 10^{-3}$		1153
$\Lambda\overline{\Lambda}\pi^+\pi^-$ (non-resonant)	$< 5 \times 10^{-4}$	CL=90%	1153
$\Sigma(1385)^+\overline{\Lambda}\pi^-$ + c.c.	$< 5 \times 10^{-4}$	CL=90%	1083
$\Sigma(1385)^-\overline{\Lambda}\pi^+$ + c.c.	$< 5 \times 10^{-4}$	CL=90%	1083
$K^+\overline{p}\Lambda$ + c.c.	$(1.25 \pm 0.12) \times 10^{-3}$	S=1.3	1132
$nK^0_S\overline{\Lambda}$ + c.c.	$(6.6 \pm 0.5) \times 10^{-4}$		1129
$K^*(892)^+\overline{p}\Lambda$ + c.c.	$(4.8 \pm 0.9) \times 10^{-4}$		845
$K^+\overline{p}\Lambda(1520)$ + c.c.	$(2.9 \pm 0.7) \times 10^{-4}$		859
$\Lambda(1520)\overline{\Lambda}(1520)$	$(3.1 \pm 1.2) \times 10^{-4}$		780
$\Sigma^0\overline{\Sigma}^0$	$(4.68 \pm 0.32) \times 10^{-4}$		1222
$\Sigma^+\overline{p}K^0_S$ + c.c.	$(3.52 \pm 0.27) \times 10^{-4}$		1089
$\Sigma^0\overline{p}K^+$ + c.c.	$(3.03 \pm 0.20) \times 10^{-4}$		1090
$\Sigma^+\overline{\Sigma}^-$	$(4.6 \pm 0.8) \times 10^{-4}$	S=2.6	1225
$\Sigma^-\overline{\Sigma}^+$	$(5.1 \pm 0.5) \times 10^{-4}$		1217
$\Sigma(1385)^+\overline{\Sigma}(1385)^-$	$(1.6 \pm 0.6) \times 10^{-4}$		1001
$\Sigma(1385)^-\overline{\Sigma}(1385)^+$	$(2.3 \pm 0.7) \times 10^{-4}$		1001
$K^-\Lambda\overline{\Xi}^+$ + c.c.	$(1.94 \pm 0.35) \times 10^{-4}$		873
$\Xi^0\overline{\Xi}^0$	$(3.1 \pm 0.8) \times 10^{-4}$		1089
$\Xi^-\overline{\Xi}^+$	$(4.8 \pm 0.7) \times 10^{-4}$		1081
$\eta_c\pi^+\pi^-$	$< 7 \times 10^{-4}$	CL=90%	307
Radiative decays			
$\gamma J/\psi(1S)$	(1.40 ± 0.05) %		303
$\gamma\rho^0$	$< 9 \times 10^{-6}$	CL=90%	1619
$\gamma\omega$	$< 8 \times 10^{-6}$	CL=90%	1618
$\gamma\phi$	$< 6 \times 10^{-6}$	CL=90%	1555
$\gamma\gamma$	$(2.04 \pm 0.09) \times 10^{-4}$		1707
$e^+e^-J/\psi(1S)$	$(1.33 \pm 0.29) \times 10^{-4}$		303
$\mu^+\mu^-J/\psi(1S)$	$< 1.9 \times 10^{-5}$	CL=90%	226

$\chi_{c1}(1P)$

$I^G(J^{PC}) = 0^+(1^{++})$

Mass $m = 3510.67 \pm 0.05$ MeV (S = 1.2)
Full width $\Gamma = 0.84 \pm 0.04$ MeV

$\chi_{c1}(1P)$ DECAY MODES	Fraction (Γ_i/Γ)	Scale factor/ Confidence level	p (MeV/c)
Hadronic decays			
$3(\pi^+\pi^-)$	$(5.8 \pm 1.4) \times 10^{-3}$	S=1.2	1683
$2(\pi^+\pi^-)$	$(7.6 \pm 2.6) \times 10^{-3}$		1728
$\pi^+\pi^-\pi^0\pi^0$	(1.19 ± 0.15) %		1729
$\rho^+\pi^-\pi^0$ + c.c.	(1.45 ± 0.24) %		1658
$\rho^0\pi^+\pi^-$	$(3.9 \pm 3.5) \times 10^{-3}$		1657
$4\pi^0$	$(5.4 \pm 0.8) \times 10^{-4}$		1729
$\pi^+\pi^-K^+K^-$	$(4.5 \pm 1.0) \times 10^{-3}$		1632
$K^+K^-\pi^0\pi^0$	$(1.12 \pm 0.27) \times 10^{-3}$		1634
$K^+K^-\pi^+\pi^-\pi^0$	(1.15 ± 0.13) %		1598
$K^0_S K^\pm\pi^\mp\pi^+\pi^-$	$(7.5 \pm 0.8) \times 10^{-3}$		1596
$K^+\pi^-\overline{K}^0\pi^0$ + c.c.	$(8.6 \pm 1.4) \times 10^{-3}$		1632
$\rho^-K^+\overline{K}^0$ + c.c.	$(5.0 \pm 1.2) \times 10^{-3}$		1514
$K^*(892)^0\overline{K}^0\pi^0 \to K^+\pi^-\overline{K}^0\pi^0$ + c.c.	$(2.3 \pm 0.6) \times 10^{-3}$		–
$K^+K^-\eta\pi^0$	$(1.12 \pm 0.34) \times 10^{-3}$		1523
$\pi^+\pi^-K^0_S K^0_S$	$(6.9 \pm 2.9) \times 10^{-4}$		1630
$K^+K^-\eta$	$(3.2 \pm 1.0) \times 10^{-4}$		1566
$\overline{K}^0 K^+\pi^-$ + c.c.	$(7.0 \pm 0.6) \times 10^{-3}$		1661
$K^*(892)^0\overline{K}^0$ + c.c.	$(10 \pm 4) \times 10^{-4}$		1602
$K^*(892)^+K^-$ + c.c.	$(1.4 \pm 0.6) \times 10^{-3}$		1602
$K^*_J(1430)^0\overline{K}^0$ + c.c. $\to K^0_S K^+\pi^-$ + c.c.	$< 8 \times 10^{-4}$	CL=90%	–
$K^*_J(1430)^+K^-$ + c.c. $\to K^0_S K^+\pi^-$ + c.c.	$< 2.1 \times 10^{-3}$	CL=90%	–
$K^+K^-\pi^0$	$(1.81 \pm 0.24) \times 10^{-3}$		1662
$\eta\pi^+\pi^-$	$(4.62 \pm 0.23) \times 10^{-3}$		1701
$a_0(980)^+\pi^-$ + c.c. $\to \eta\pi^+\pi^-$	$(3.2 \pm 0.4) \times 10^{-3}$	S=2.2	–
$a_2(1320)^+\pi^-$ + c.c. $\to \eta\pi^+\pi^-$	$(1.76 \pm 0.24) \times 10^{-4}$		–
$a_2(1700)^+\pi^-$ + c.c. $\to \eta\pi^+\pi^-$	$(4.6 \pm 0.7) \times 10^{-5}$		–
$f_2(1270)\eta \to \eta\pi^+\pi^-$	$(3.5 \pm 0.6) \times 10^{-4}$		–
$f_4(2050)\eta \to \eta\pi^+\pi^-$	$(2.5 \pm 0.9) \times 10^{-5}$		–
$\pi_1(1400)^+\pi^-$ + c.c. $\to \eta\pi^+\pi^-$	$< 5 \times 10^{-5}$	CL=90%	–
$\pi_1(1600)^+\pi^-$ + c.c. $\to \eta\pi^+\pi^-$	$< 1.5 \times 10^{-5}$	CL=90%	–
$\pi_1(2015)^+\pi^-$ + c.c. $\to \eta\pi^+\pi^-$	$< 8 \times 10^{-6}$	CL=90%	–
$f_2(1270)\eta$	$(6.7 \pm 1.1) \times 10^{-4}$		1467
$\pi^+\pi^-\eta'$	$(2.2 \pm 0.4) \times 10^{-3}$		1612
$K^+K^-\eta'(958)$	$(8.8 \pm 0.9) \times 10^{-4}$		1461
$K^*_0(1430)^+K^-$ + c.c.	$(6.4 {}^{+2.2}_{-2.8}) \times 10^{-4}$		–
$f_0(980)\eta'(958)$	$(1.6 {}^{+1.4}_{-0.7}) \times 10^{-4}$		1460
$f_0(1710)\eta'(958)$	$(7 {}^{+7}_{-5}) \times 10^{-5}$		1118
$f'_2(1525)\eta'(958)$	$(9 \pm 6) \times 10^{-5}$		1229
$\pi^0 f_0(980) \to \pi^0\pi^+\pi^-$	$(3.5 \pm 0.9) \times 10^{-7}$		–
$K^+\overline{K}^*(892)^0\pi^-$ + c.c.	$(3.2 \pm 2.1) \times 10^{-3}$		1577
$K^*(892)^0\overline{K}^*(892)^0$	$(1.4 \pm 0.4) \times 10^{-3}$		1512
$K^+K^-K^0_S K^0_S$	$< 4 \times 10^{-4}$	CL=90%	1390
$K^0_S K^0_S K^0_S K^0_S$	$(3.5 \pm 1.0) \times 10^{-5}$		1387
$K^+K^-K^+K^-$	$(5.4 \pm 1.1) \times 10^{-4}$		1393
$K^+K^-\phi$	$(4.1 \pm 1.5) \times 10^{-4}$		1440
$\overline{K}^0 K^+\pi^-\phi$ + c.c.	$(3.3 \pm 0.5) \times 10^{-3}$		1387
$K^+K^-\pi^0\phi$	$(1.62 \pm 0.30) \times 10^{-3}$		1390
$\phi\pi^+\pi^-\pi^0$	$(7.5 \pm 1.0) \times 10^{-4}$		1578
$\omega\omega$	$(5.7 \pm 0.7) \times 10^{-4}$		1571
ωK^+K^-	$(7.8 \pm 0.9) \times 10^{-4}$		1513
$\omega\phi$	$(2.7 \pm 0.4) \times 10^{-5}$		1503
$\phi\phi$	$(4.2 \pm 0.5) \times 10^{-4}$		1429
$\phi\phi\eta$	$(3.0 \pm 0.5) \times 10^{-4}$		1172
$p\overline{p}$	$(7.60 \pm 0.34) \times 10^{-5}$		1484
$p\overline{p}\pi^0$	$(1.55 \pm 0.18) \times 10^{-4}$		1438
$p\overline{p}\eta$	$(1.45 \pm 0.25) \times 10^{-4}$		1254
$p\overline{p}\omega$	$(2.12 \pm 0.31) \times 10^{-4}$		1117
$p\overline{p}\phi$	$< 1.7 \times 10^{-5}$	CL=90%	962
$p\overline{p}\pi^+\pi^-$	$(5.0 \pm 1.9) \times 10^{-4}$		1381
$p\overline{p}\pi^0\pi^0$	$< 5 \times 10^{-4}$	CL=90%	1385
$p\overline{p}K^+K^-$ (non-resonant)	$(1.27 \pm 0.22) \times 10^{-4}$		974
$p\overline{p}K^0_S K^0_S$	$< 4.5 \times 10^{-4}$	CL=90%	968
$p\overline{n}\pi^-$	$(3.8 \pm 0.5) \times 10^{-4}$		1435
$\overline{p}n\pi^+$	$(3.9 \pm 0.5) \times 10^{-4}$		1435
$p\overline{n}\pi^-\pi^0$	$(1.03 \pm 0.12) \times 10^{-3}$		1383

Downloaded from https://academic.oup.com/ptep/article/2022/8/083C01/6651666 by KIT Library user on 27 September 2022

$\overline{p}n\pi^+\pi^0$	$(1.01\pm0.12)\times10^{-3}$		1383
$\Lambda\overline{\Lambda}$	$(1.27\pm0.08)\times10^{-4}$		1355
$\Lambda\overline{\Lambda}\pi^+\pi^-$	$(2.9\pm0.5)\times10^{-4}$		1223
$\Lambda\overline{\Lambda}\pi^+\pi^-$ (non-resonant)	$(2.5\pm0.6)\times10^{-4}$		1223
$\Sigma(1385)^+\overline{\Lambda}\pi^-$ + c.c.	$<1.3\times10^{-4}$	CL=90%	1157
$\Sigma(1385)^-\overline{\Lambda}\pi^+$ + c.c.	$<1.3\times10^{-4}$	CL=90%	1157
$K^+\overline{p}\Lambda$+c.c.	$(4.2\pm0.4)\times10^{-4}$	S=1.2	1203
$nK^0_S\overline{\Lambda}$ + c.c.	$(1.66\pm0.17)\times10^{-4}$		1200
$K^*(892)^+\overline{p}\Lambda$+ c.c.	$(4.9\pm0.7)\times10^{-4}$		935
$K^+\overline{p}\Lambda(1520)$+ c.c.	$(1.7\pm0.4)\times10^{-4}$		951
$\Lambda(1520)\overline{\Lambda}(1520)$	$<9\times10^{-5}$	CL=90%	880
$\Sigma^0\overline{\Sigma}^0$	$(4.2\pm0.6)\times10^{-5}$		1288
$\Sigma^+\overline{p}K^0_S$+ c.c.	$(1.53\pm0.12)\times10^{-4}$		1163
$\Sigma^0\overline{p}K^+$+ c.c.	$(1.46\pm0.10)\times10^{-4}$		1163
$\Sigma^+\overline{\Sigma}^-$	$(3.6\pm0.7)\times10^{-5}$		1291
$\Sigma^-\overline{\Sigma}^+$	$(5.7\pm1.5)\times10^{-5}$		1283
$\Sigma(1385)^+\overline{\Sigma}(1385)^-$	$<9\times10^{-5}$	CL=90%	1081
$\Sigma(1385)^-\overline{\Sigma}(1385)^+$	$<5\times10^{-5}$	CL=90%	1081
$K^-\Lambda\overline{\Xi}^+$+ c.c.	$(1.35\pm0.24)\times10^{-4}$		963
$\Xi^0\overline{\Xi}^0$	$<6\times10^{-5}$	CL=90%	1163
$\Xi^-\overline{\Xi}^+$	$(8.0\pm2.1)\times10^{-5}$		1155
$\pi^+\pi^-+K^+K^-$	$<2.1\times10^{-3}$		–
$K^0_SK^0_S$	$<6\times10^{-5}$	CL=90%	1683
$\eta_c\pi^+\pi^-$	$<3.2\times10^{-3}$	CL=90%	413
Radiative decays			
$\gamma J/\psi(1S)$	(34.3 ± 1.0) %		389
$\gamma\rho^0$	$(2.16\pm0.17)\times10^{-4}$		1670
$\gamma\omega$	$(6.8\pm0.8)\times10^{-5}$		1668
$\gamma\phi$	$(2.4\pm0.5)\times10^{-5}$		1607
$\gamma\gamma$	$<6.3\times10^{-6}$	CL=90%	1755
$e^+e^-J/\psi(1S)$	$(3.46\pm0.22)\times10^{-3}$		389
$\mu^+\mu^-J/\psi(1S)$	$(2.33\pm0.29)\times10^{-4}$		335

$h_c(1P)$

$I^G(J^{PC})=0^-(1^{+-})$

Mass $m=3525.38\pm0.11$ MeV
Full width $\Gamma=0.7\pm0.4$ MeV

$h_c(1P)$ DECAY MODES	Fraction (Γ_i/Γ)	Confidence level	p (MeV/c)
$J/\psi(1S)\pi\pi$	not seen		312
$J/\psi(1S)\pi^+\pi^-$	$<2.3\times10^{-3}$	90%	305
$p\overline{p}$	$<1.5\times10^{-4}$	90%	1492
$p\overline{p}\pi^+\pi^-$	$(2.9\pm0.6)\times10^{-3}$		1390
$p\overline{p}\pi^0\pi^0$	$<5\times10^{-4}$	90%	1394
$\pi^+\pi^-\pi^0$	$(1.6\pm0.5)\times10^{-3}$		1749
$\pi^+\pi^-\pi^0\eta$	$(7.2\pm2.3)\times10^{-3}$		1695
$2\pi^+2\pi^-\pi^0$	$(8.1\pm1.8)\times10^{-3}$		1716
$3\pi^+3\pi^-\pi^0$	$<9\times10^{-3}$	90%	1661
$K^+K^-\pi^+\pi^-$	$<6\times10^{-4}$	90%	1640
$K^+K^-\pi^+\pi^-\pi^0$	$(3.2\pm0.8)\times10^{-3}$		1606
$K^+K^-\pi^+\pi^-\eta$	$<2.3\times10^{-3}$	90%	1480
$K^+K^-\pi^0$	$<6\times10^{-4}$	90%	1670
$K^+K^-\pi^0\eta$	$<2.1\times10^{-3}$	90%	1532
$K^+K^-\eta$	$<9\times10^{-4}$	90%	1574
$2K^+2K^-\pi^0$	$<2.4\times10^{-4}$	90%	1339
$K^0_SK^\pm\pi^\mp$	$<6\times10^{-4}$	90%	1668
$K^0_SK^\pm\pi^\mp\pi^+\pi^-$	$(2.8\pm1.0)\times10^{-3}$		1604
Radiative decays			
$\gamma\eta$	$(4.7\pm2.1)\times10^{-4}$		1720
$\gamma\eta'(958)$	$(1.5\pm0.4)\times10^{-3}$		1633
$\gamma\eta_c(1S)$	(50 ± 9) %		500

$\chi_{c2}(1P)$

$I^G(J^{PC})=0^+(2^{++})$

Mass $m=3556.17\pm0.07$ MeV
Full width $\Gamma=1.97\pm0.09$ MeV

$\chi_{c2}(1P)$ DECAY MODES	Fraction (Γ_i/Γ)	Confidence level	p (MeV/c)
Hadronic decays			
$2(\pi^+\pi^-)$	(1.02 ± 0.09) %		1751
$\pi^+\pi^-\pi^0\pi^0$	(1.83 ± 0.23) %		1752
$\rho^+\pi^-\pi^0$+ c.c.	(2.19 ± 0.34) %		1682
$4\pi^0$	$(1.11\pm0.15)\times10^{-3}$		1752
$K^+K^-\pi^0\pi^0$	$(2.1\pm0.4)\times10^{-3}$		1658
$K^+\pi^-\overline{K}^0\pi^0$+ c.c.	(1.38 ± 0.20) %		1657
$\rho^-K^+\overline{K}^0$+ c.c.	$(4.1\pm1.2)\times10^{-3}$		1540
$K^*(892)^0K^-\pi^+\to K^-\pi^+K^0\pi^0$+ c.c.	$(2.9\pm0.8)\times10^{-3}$		–
$K^*(892)^0\overline{K}^0\pi^0\to K^+\pi^-\overline{K}^0\pi^0$+ c.c.	$(3.8\pm0.9)\times10^{-3}$		–
$K^*(892)^-K^+\pi^0\to K^+\pi^-\overline{K}^0\pi^0$+ c.c.	$(3.7\pm0.8)\times10^{-3}$		–
$K^*(892)^+\overline{K}^0\pi^-\to K^+\pi^-\overline{K}^0\pi^0$+ c.c.	$(2.9\pm0.8)\times10^{-3}$		–
$K^+K^-\eta\pi^0$	$(1.3\pm0.4)\times10^{-3}$		1549
$K^+K^-\pi^+\pi^-$	$(8.4\pm0.9)\times10^{-3}$		1656
$K^+K^-\pi^+\pi^-\pi^0$	(1.17 ± 0.13) %		1623
$K^0_SK^\pm\pi^\mp\pi^+\pi^-$	$(7.3\pm0.8)\times10^{-3}$		1621
$K^+\overline{K}^*(892)^0\pi^-$+ c.c.	$(2.1\pm1.1)\times10^{-3}$		1602
$K^*(892)^0\overline{K}^*(892)^0$	$(2.3\pm0.4)\times10^{-3}$		1538
$3(\pi^+\pi^-)$	$(8.6\pm1.8)\times10^{-3}$		1707
$\phi\phi$	$(1.06\pm0.09)\times10^{-3}$		1457
$\phi\phi\eta$	$(5.3\pm0.6)\times10^{-4}$		1206
$\omega\omega$	$(8.4\pm1.0)\times10^{-4}$		1597
ωK^+K^-	$(7.3\pm0.9)\times10^{-4}$		1540
$\omega\phi$	$(9.6\pm2.7)\times10^{-6}$		1529
$\pi\pi$	$(2.23\pm0.09)\times10^{-3}$		1773
$\rho^0\pi^+\pi^-$	$(3.7\pm1.6)\times10^{-3}$		1682
$\pi^+\pi^-\pi^0$ (non-resonant)	$(2.0\pm0.4)\times10^{-5}$		1765
$\rho(770)^\pm\pi^\mp$	$(6\pm4)\times10^{-6}$		–
$\pi^+\pi^-\eta$	$(4.8\pm1.3)\times10^{-4}$		1724
$\pi^+\pi^-\eta'$	$(5.0\pm1.8)\times10^{-4}$		1636
$\eta\eta$	$(5.4\pm0.4)\times10^{-4}$		1692
K^+K^-	$(1.01\pm0.06)\times10^{-3}$		1708
$K^0_SK^0_S$	$(5.2\pm0.4)\times10^{-4}$		1707
$K^*(892)^\pm K^\mp$	$(1.44\pm0.21)\times10^{-4}$		1627
$K^*(892)^0\overline{K}^0$+ c.c.	$(1.24\pm0.27)\times10^{-4}$		1627
$K^*_2(1430)^\pm K^\mp$	$(1.48\pm0.12)\times10^{-3}$		–
$K^*_2(1430)^0\overline{K}^0$+ c.c.	$(1.24\pm0.17)\times10^{-3}$		1443
$K^*_3(1780)^\pm K^\mp$	$(5.2\pm0.8)\times10^{-4}$		–
$K^*_3(1780)^0\overline{K}^0$+ c.c.	$(5.6\pm2.1)\times10^{-4}$		1274
$a_2(1320)^0\pi^0$	$(1.29\pm0.34)\times10^{-3}$		–
$a_2(1320)^\pm\pi^\mp$	$(1.8\pm0.6)\times10^{-3}$		1530
$\overline{K}^0K^+\pi^-$+ c.c.	$(1.28\pm0.18)\times10^{-3}$		1685
$K^+K^-\pi^0$	$(3.0\pm0.8)\times10^{-4}$		1686
$K^+K^-\eta$	$<3.2\times10^{-4}$	90%	1592
$K^+K^-\eta'(958)$	$(1.94\pm0.34)\times10^{-4}$		1488
$\eta\eta'$	$(2.2\pm0.5)\times10^{-5}$		1600
$\eta'\eta'$	$(4.6\pm0.6)\times10^{-5}$		1498
$\pi^+\pi^-K^0_SK^0_S$	$(2.2\pm0.5)\times10^{-3}$		1655
$K^+K^-K^0_SK^0_S$	$<4\times10^{-4}$	90%	1418
$K^0_SK^0_SK^0_SK^0_S$	$(1.13\pm0.18)\times10^{-4}$		1415
$K^+K^-K^+K^-$	$(1.65\pm0.20)\times10^{-3}$		1421
$K^+K^-\phi$	$(1.42\pm0.29)\times10^{-3}$		1468
$\overline{K}^0K^+\pi^-\phi$+ c.c.	$(4.8\pm0.7)\times10^{-3}$		1416
$K^+K^-\pi^0\phi$	$(2.7\pm0.5)\times10^{-3}$		1419
$\phi\pi^+\pi^-\pi^0$	$(9.3\pm1.2)\times10^{-4}$		1603
$p\overline{p}$	$(7.33\pm0.33)\times10^{-5}$		1510
$p\overline{p}\pi^0$	$(4.7\pm0.4)\times10^{-4}$		1465
$p\overline{p}\eta$	$(1.74\pm0.25)\times10^{-4}$		1285
$p\overline{p}\omega$	$(3.6\pm0.4)\times10^{-4}$		1152
$p\overline{p}\phi$	$(2.8\pm0.9)\times10^{-5}$		1002
$p\overline{p}\pi^+\pi^-$	$(1.32\pm0.34)\times10^{-3}$		1410
$p\overline{p}\pi^0\pi^0$	$(7.8\pm2.3)\times10^{-4}$		1414
$p\overline{p}K^+K^-$ (non-resonant)	$(1.91\pm0.32)\times10^{-4}$		1013
$p\overline{p}K^0_SK^0_S$	$<7.9\times10^{-4}$	90%	1007
$p\overline{n}\pi^-$	$(8.5\pm0.9)\times10^{-4}$		1463
$\overline{p}n\pi^+$	$(8.9\pm0.8)\times10^{-4}$		1463
$p\overline{n}\pi^-\pi^0$	$(2.17\pm0.18)\times10^{-3}$		1411
$\overline{p}n\pi^+\pi^0$	$(2.11\pm0.18)\times10^{-3}$		1411
$\Lambda\overline{\Lambda}$	$(1.83\pm0.16)\times10^{-4}$		1384
$\Lambda\overline{\Lambda}\pi^+\pi^-$	$(1.25\pm0.15)\times10^{-3}$		1255
$\Lambda\overline{\Lambda}\pi^+\pi^-$ (non-resonant)	$(6.6\pm1.5)\times10^{-4}$		1255
$\Sigma(1385)^+\overline{\Lambda}\pi^-$+ c.c.	$<4\times10^{-4}$	90%	1192
$\Sigma(1385)^-\overline{\Lambda}\pi^+$+ c.c.	$<6\times10^{-4}$	90%	1192
$K^+\overline{p}\Lambda$ + c.c.	$(7.8\pm0.5)\times10^{-4}$		1236
$nK^0_S\overline{\Lambda}$ + c.c.	$(3.58\pm0.28)\times10^{-4}$		1233
$K^*(892)^+\overline{p}\Lambda$+ c.c.	$(8.2\pm1.1)\times10^{-4}$		976
$K^+\overline{p}\Lambda(1520)$+ c.c.	$(2.8\pm0.7)\times10^{-4}$		992
$\Lambda(1520)\overline{\Lambda}(1520)$	$(4.6\pm1.5)\times10^{-4}$		924

Downloaded from https://academic.oup.com/ptep/article/2022/8/083C01/6651666 by KIT Library user on 27 September 2022

$\Sigma^0 \overline{\Sigma}^0$	$(3.7 \pm 0.6) \times 10^{-5}$		1319
$\Sigma^+ \overline{p} K^0_S +$ c.c.	$(8.2 \pm 0.9) \times 10^{-5}$		1197
$\Sigma^0 \overline{p} K^+ +$ c.c.	$(9.1 \pm 0.8) \times 10^{-5}$		1197
$\Sigma^+ \overline{\Sigma}^-$	$(3.4 \pm 0.7) \times 10^{-5}$		1322
$\Sigma^- \overline{\Sigma}^+$	$(4.4 \pm 1.8) \times 10^{-5}$		1314
$\Sigma(1385)^+ \overline{\Sigma}(1385)^-$	$< 1.6 \times 10^{-4}$	90%	1118
$\Sigma(1385)^- \overline{\Sigma}(1385)^+$	$< 8 \times 10^{-5}$	90%	1118
$K^- \Lambda \overline{\Xi}^+ +$ c.c.	$(1.76 \pm 0.32) \times 10^{-4}$		1004
$\Xi^0 \overline{\Xi}^0$	$< 1.0 \times 10^{-4}$	90%	1197
$\Xi^- \overline{\Xi}^+$	$(1.42 \pm 0.32) \times 10^{-4}$		1189
$J/\psi(1S) \pi^+ \pi^- \pi^0$	< 1.5 %	90%	185
$\pi^0 \eta_c$	$< 3.2 \times 10^{-3}$	90%	511
$\eta_c(1S) \pi^+ \pi^-$	$< 5.4 \times 10^{-3}$	90%	459

Radiative decays

$\gamma J/\psi(1S)$	(19.0 ± 0.5) %		430
$\gamma \rho^0$	$< 1.9 \times 10^{-5}$	90%	1694
$\gamma \omega$	$< 6 \times 10^{-6}$	90%	1692
$\gamma \phi$	$< 7 \times 10^{-6}$	90%	1632
$\gamma \gamma$	$(2.85 \pm 0.10) \times 10^{-4}$		1778
$e^+ e^- J/\psi(1S)$	$(2.15 \pm 0.14) \times 10^{-3}$		430
$\mu^+ \mu^- J/\psi(1S)$	$(2.02 \pm 0.33) \times 10^{-4}$		381

$\eta_c(2S)$

$I^G(J^{PC}) = 0^+(0^{-+})$

Quantum numbers are quark model predictions.

Mass $m = 3637.5 \pm 1.1$ MeV (S = 1.2)
Full width $\Gamma = 11.3^{+3.2}_{-2.9}$ MeV

$\eta_c(2S)$ DECAY MODES	Fraction (Γ_i/Γ)	Confidence level	p (MeV/c)
hadrons	not seen		–
$K\overline{K}\pi$	(1.9 ± 1.2) %		1729
$K\overline{K}\eta$	$(5 \pm 4) \times 10^{-3}$		1637
$2\pi^+ 2\pi^-$	not seen		1792
$\rho^0 \rho^0$	not seen		1645
$3\pi^+ 3\pi^-$	not seen		1749
$K^+ K^- \pi^+ \pi^-$	not seen		1700
$K^{*0} \overline{K}^{*0}$	not seen		1585
$K^+ K^- \pi^+ \pi^- \pi^0$	(1.4 ± 1.0) %		1667
$K^+ K^- 2\pi^+ 2\pi^-$	not seen		1627
$K^0_S K^- 2\pi^+ \pi^- +$ c.c.	seen		1666
$2K^+ 2K^-$	not seen		1470
$\phi\phi$	not seen		1506
$p\overline{p}$	seen		1558
$p\overline{p}\pi^+ \pi^-$	seen		1461
$\gamma\gamma$	$(1.9 \pm 1.3) \times 10^{-4}$		1819
$\gamma J/\psi(1S)$	< 1.4 %	90%	500
$\pi^+ \pi^- \eta$	not seen		1766
$\pi^+ \pi^- \eta'$	not seen		1680
$\pi^+ \pi^- \eta_c(1S)$	< 25 %	90%	537

$\psi(2S)$

$I^G(J^{PC}) = 0^-(1^{--})$

Mass $m = 3686.10 \pm 0.06$ MeV (S = 5.9)
Full width $\Gamma = 294 \pm 8$ keV

$\psi(2S)$ DECAY MODES	Fraction (Γ_i/Γ)	Scale factor/ Confidence level	p (MeV/c)
hadrons	(97.85 ± 0.13) %		–
virtual $\gamma \to$ hadrons	(1.73 ± 0.14) %	S=1.5	–
ggg	(10.6 ± 1.6) %		–
γgg	(1.03 ± 0.29) %		–
light hadrons	(15.4 ± 1.5) %		–
K^0_S anything	(16.0 ± 1.1) %		–
$e^+ e^-$	$(7.93 \pm 0.17) \times 10^{-3}$		1843
$\mu^+ \mu^-$	$(8.0 \pm 0.6) \times 10^{-3}$		1840
$\tau^+ \tau^-$	$(3.1 \pm 0.4) \times 10^{-3}$		489

Decays into $J/\psi(1S)$ and anything

$J/\psi(1S)$ anything	(61.4 ± 0.6) %		–
$J/\psi(1S)$ neutrals	(25.38 ± 0.32) %		–
$J/\psi(1S) \pi^+ \pi^-$	(34.68 ± 0.30) %		477
$J/\psi(1S) \pi^0 \pi^0$	(18.24 ± 0.31) %		481
$J/\psi(1S) \eta$	(3.37 ± 0.05) %		199
$J/\psi(1S) \pi^0$	$(1.268 \pm 0.032) \times 10^{-3}$		528

Hadronic decays

$\pi^+ \pi^-$	$(7.8 \pm 2.6) \times 10^{-6}$		1838
$\pi^+ \pi^- \pi^0$	$(2.01 \pm 0.17) \times 10^{-4}$	S=1.7	1830
$\rho(770) \pi \to \pi^+ \pi^- \pi^0$	$(3.2 \pm 1.2) \times 10^{-5}$	S=1.8	–
$\rho(2150) \pi \to \pi^+ \pi^- \pi^0$	$(1.9 {}^{+1.2}_{-0.4}) \times 10^{-4}$		–
$2(\pi^+ \pi^-)$	$(2.4 \pm 0.6) \times 10^{-4}$	S=2.2	1817
$\rho^0 \pi^+ \pi^-$	$(2.2 \pm 0.6) \times 10^{-4}$	S=1.4	1750
$2(\pi^+ \pi^-) \pi^0$	$(2.9 \pm 1.0) \times 10^{-3}$	S=4.7	1799
$\rho a_2(1320)$	$(2.6 \pm 0.9) \times 10^{-4}$		1500
$\pi^+ \pi^- \pi^0 \pi^0 \pi^0$	$(5.3 \pm 0.9) \times 10^{-3}$		1800
$\pi^+ \pi^- 4\pi^0$	$(1.4 \pm 1.0) \times 10^{-3}$		1778
$\rho^\pm \pi^\mp \pi^0 \pi^0$	$< 2.7 \times 10^{-3}$	CL=90%	1737
$3(\pi^+ \pi^-)$	$(3.5 \pm 2.0) \times 10^{-4}$	S=2.8	1774
$2(\pi^+ \pi^- \pi^0)$	$(4.8 \pm 1.5) \times 10^{-3}$		1776
$3(\pi^+ \pi^-) \pi^0$	$(3.5 \pm 1.6) \times 10^{-3}$		1746
$2(\pi^+ \pi^-) 3\pi^0$	(1.42 ± 0.31) %		1748
$\eta \pi^+ \pi^-$	$< 1.6 \times 10^{-4}$	CL=90%	1791
$\eta \pi^+ \pi^- \pi^0$	$(9.5 \pm 1.7) \times 10^{-4}$		1778
$\eta 2(\pi^+ \pi^-)$	$(1.2 \pm 0.6) \times 10^{-3}$		1758
$\eta \pi^+ \pi^- \pi^0 \pi^0$	$< 4 \times 10^{-4}$	CL=90%	1760
$\eta \pi^+ \pi^- 3\pi^0$	$< 2.1 \times 10^{-3}$	CL=90%	1736
$\eta 2(\pi^+ \pi^- \pi^0)$	$< 2.1 \times 10^{-3}$	CL=90%	1705
$\rho\eta$	$(2.2 \pm 0.6) \times 10^{-5}$	S=1.1	1717
$\eta' \pi^+ \pi^- \pi^0$	$(4.5 \pm 2.1) \times 10^{-4}$		1692
$\eta' \rho$	$(1.9 {}^{+1.7}_{-1.2}) \times 10^{-5}$		1625
$\omega \pi^0$	$(2.1 \pm 0.6) \times 10^{-5}$		1757
$\omega \pi^+ \pi^-$	$(7.3 \pm 1.2) \times 10^{-4}$	S=2.1	1748
$\omega \pi^+ \pi^- 2\pi^0$	$(8.7 \pm 2.4) \times 10^{-3}$		1715
$b_1^\pm \pi^\mp$	$(4.0 \pm 0.6) \times 10^{-4}$	S=1.1	1635
$\omega f_2(1270)$	$(2.2 \pm 0.4) \times 10^{-4}$		1515
$\omega \pi^0 \pi^0$	$(1.11 \pm 0.35) \times 10^{-3}$		1749
$\omega 3\pi^0$	$< 8 \times 10^{-4}$	CL=90%	1736
$b_1^0 \pi^0$	$(2.4 \pm 0.6) \times 10^{-4}$		–
$\omega\eta$	$< 1.1 \times 10^{-5}$	CL=90%	1715
$\omega\eta'$	$(3.2 {}^{+2.5}_{-2.1}) \times 10^{-5}$		1623
$\phi \pi^0$	$< 4 \times 10^{-7}$	CL=90%	1699
$\phi \pi^+ \pi^-$	$(1.18 \pm 0.26) \times 10^{-4}$	S=1.5	1690
$\phi f_0(980) \to \pi^+ \pi^-$	$(7.5 \pm 3.3) \times 10^{-5}$	S=1.6	–
$\phi\eta$	$(3.10 \pm 0.31) \times 10^{-5}$		1654
$\eta\phi(2170)$, $\phi(2170) \to \phi f_0(980)$, $f_0 \to \pi^+ \pi^-$	$< 2.2 \times 10^{-6}$	CL=90%	–
$\phi\eta'$	$(1.54 \pm 0.20) \times 10^{-5}$		1555
$\phi f_1(1285)$	$(3.0 \pm 1.3) \times 10^{-5}$		1436
$\phi\eta(1405) \to \phi \pi^+ \pi^- \eta$	$(8.5 \pm 1.7) \times 10^{-6}$		–
$\phi f_2'(1525)$	$(4.4 \pm 1.6) \times 10^{-5}$		1325
$K^+ K^-$	$(7.5 \pm 0.5) \times 10^{-5}$		1776
$K^+ K^- \pi^+$	$(7.3 \pm 0.5) \times 10^{-4}$		1754
$K^+ K^- \pi^0$	$(4.07 \pm 0.31) \times 10^{-5}$		1754
$K^0_S K^0_S$	$< 4.6 \times 10^{-6}$		1775
$K^0_S K^0_L$	$(5.34 \pm 0.33) \times 10^{-5}$		1775
$K^0_S K^0_L \pi^0$	$< 3.0 \times 10^{-4}$	CL=90%	1753
$K^+ K^- \pi^0 \pi^0$	$(2.6 \pm 1.3) \times 10^{-4}$		1728
$K^+ K^- \pi^+ \pi^- \pi^0$	$(1.26 \pm 0.09) \times 10^{-3}$		1694
$\omega f_0(1710) \to \omega K^+ K^-$	$(5.9 \pm 2.2) \times 10^{-5}$		–
$K^*(892)^0 K^- \pi^+ \pi^0 +$ c.c.	$(8.6 \pm 2.2) \times 10^{-4}$		–
$K^*(892)^+ K^- \pi^+ \pi^- +$ c.c.	$(9.6 \pm 2.8) \times 10^{-4}$		–
$K^*(892)^+ K^- \rho^0 +$ c.c.	$(7.3 \pm 2.6) \times 10^{-4}$		–
$K^*(892)^0 K^- \rho^+ +$ c.c.	$(6.1 \pm 1.8) \times 10^{-4}$		–
$K^0_S K^0_S \pi^+ \pi^-$	$(2.2 \pm 0.4) \times 10^{-4}$		1724
$K^0_S K^0_L \pi^0 \pi^0$	$(1.3 \pm 0.6) \times 10^{-3}$		1726
$K^0_S K^0_L \eta$	$(1.3 \pm 0.5) \times 10^{-3}$		1661
$K^+ K^- \rho^0$	$(2.2 \pm 0.4) \times 10^{-4}$		1616
$K^*(892)^0 \overline{K}^*_2(1430)^0$	$(1.9 \pm 0.5) \times 10^{-4}$		1417
$K^+ K^- \pi^+ \pi^- \eta$	$(1.3 \pm 0.7) \times 10^{-3}$		1574
$K^+ K^- 2(\pi^+ \pi^-)$	$(1.9 \pm 0.9) \times 10^{-3}$		1654
$K^+ K^- 2(\pi^+ \pi^-) \pi^0$	$(1.00 \pm 0.31) \times 10^{-3}$		1611
$K^+ K^*(892)^- +$ c.c.	$(2.9 \pm 0.4) \times 10^{-5}$	S=1.2	1698
$2(K^+ K^-)$	$(6.3 \pm 1.3) \times 10^{-5}$		1499
$2(K^+ K^-) \pi^0$	$(1.10 \pm 0.28) \times 10^{-4}$		1440
$K^+ K^- \phi$	$(7.0 \pm 1.6) \times 10^{-5}$		1546
$K_1(1270)^\pm K^\mp$	$(1.00 \pm 0.28) \times 10^{-3}$		1588
$K^+ \overline{K}^*(892)^0 \pi^-$ + c.c.	$(6.7 \pm 2.5) \times 10^{-4}$		1674
$\eta K^+ K^-$, no $\eta\phi$	$(3.49 \pm 0.17) \times 10^{-5}$		1664
$X(1750) \eta \to K^+ K^- \eta$	$(4.8 \pm 2.8) \times 10^{-6}$		–
$K_1(1400)^\pm K^\mp$	$< 3.1 \times 10^{-4}$	CL=90%	1532

Downloaded from https://academic.oup.com/ptep/article/2022/8/083C01/6651666 by KIT Library user on 27 September 2022

$K_2^*(1430)^\pm K^\mp$	$(7.1\ ^{+1.3}_{-0.9}) \times 10^{-5}$			–
$K^*(892)^0 \overline{K}^0 +$ c.c.	$(1.09 \pm 0.20) \times 10^{-4}$			1697
$\omega K^+ K^-$	$(1.62 \pm 0.11) \times 10^{-4}$	S=1.1		1614
$\omega K_S^0 K_S^0$	$(7.0 \pm 0.5) \times 10^{-5}$			1612
$\omega K^*(892)^+ K^- +$ c.c.	$(2.07 \pm 0.26) \times 10^{-4}$			1482
$\omega K_2^*(1430)^+ K^-$ + c.c.	$(6.1 \pm 1.2) \times 10^{-5}$			1252
$\omega \overline{K}^*(892)^0 K^0$	$(1.68 \pm 0.30) \times 10^{-4}$			1481
$\omega \overline{K}_2^*(1430)^0 K^0$	$(5.8 \pm 2.2) \times 10^{-5}$			1250
$\omega X(1440) \to \omega K_S^0 K^- \pi^+ +$ c.c.	$(1.6 \pm 0.4) \times 10^{-5}$			–
$\omega X(1440) \to \omega K^+ K^- \pi^0$	$(1.09 \pm 0.26) \times 10^{-5}$			–
$\omega f_1(1285) \to \omega K_S^0 K^- \pi^+ +$ c.c.	$(3.0 \pm 1.0) \times 10^{-6}$			–
$\omega f_1(1285) \to \omega K^+ K^- \pi^0$	$(1.2 \pm 0.7) \times 10^{-6}$			–
$p\overline{p}$	$(2.94 \pm 0.08) \times 10^{-4}$			1586
$n\overline{n}$	$(3.06 \pm 0.15) \times 10^{-4}$			1586
$p\overline{p}\pi^0$	$(1.53 \pm 0.07) \times 10^{-4}$			1543
$N(940)\overline{p}+$ c.c. $\to p\overline{p}\pi^0$	$(6.4\ ^{+1.8}_{-1.3}) \times 10^{-5}$			–
$N(1440)\overline{p}+$ c.c. $\to p\overline{p}\pi^0$	$(7.3\ ^{+1.7}_{-1.5}) \times 10^{-5}$	S=2.5		–
$N(1520)\overline{p}+$ c.c. $\to p\overline{p}\pi^0$	$(6.4\ ^{+2.3}_{-1.8}) \times 10^{-6}$			–
$N(1535)\overline{p}+$ c.c. $\to p\overline{p}\pi^0$	$(2.5 \pm 1.0) \times 10^{-5}$			–
$N(1650)\overline{p}+$ c.c. $\to p\overline{p}\pi^0$	$(3.8\ ^{+1.4}_{-1.7}) \times 10^{-5}$			–
$N(1720)\overline{p}+$ c.c. $\to p\overline{p}\pi^0$	$(1.79\ ^{+0.26}_{-0.70}) \times 10^{-5}$			–
$N(2300)\overline{p}+$ c.c. $\to p\overline{p}\pi^0$	$(2.6\ ^{+1.2}_{-0.7}) \times 10^{-5}$			–
$N(2570)\overline{p}+$ c.c. $\to p\overline{p}\pi^0$	$(2.13\ ^{+0.40}_{-0.31}) \times 10^{-5}$			–
$p\overline{p}\pi^+\pi^-$	$(6.0 \pm 0.4) \times 10^{-4}$			1491
$p\overline{p}K^+K^-$	$(2.7 \pm 0.7) \times 10^{-5}$			1118
$p\overline{p}\eta$	$(6.0 \pm 0.4) \times 10^{-5}$			1373
$N(1535)\overline{p}+$ c.c. $\to p\overline{p}\eta$	$(4.5\ ^{+0.7}_{-0.6}) \times 10^{-5}$			–
$p\overline{p}\pi^+\pi^-\pi^0$	$(7.3 \pm 0.7) \times 10^{-4}$			1435
$p\overline{p}\rho^0$	$(5.0 \pm 2.2) \times 10^{-5}$			1252
$p\overline{p}\omega$	$(6.9 \pm 2.1) \times 10^{-5}$			1247
$p\overline{p}\eta'$	$(1.10 \pm 0.13) \times 10^{-5}$			1141
$p\overline{p}\phi$	$(6.1 \pm 0.6) \times 10^{-6}$			1109
$\phi X(1835) \to p\overline{p}\phi$	$< 1.82 \times 10^{-7}$	CL=90%		–
$p\overline{n}\pi^-$ or c.c.	$(2.48 \pm 0.17) \times 10^{-4}$			–
$p\overline{n}\pi^-\pi^0$	$(3.2 \pm 0.7) \times 10^{-4}$			1492
$\Lambda\overline{\Lambda}$	$(3.81 \pm 0.13) \times 10^{-4}$	S=1.4		1467
$\Lambda\overline{\Lambda}\pi^0$	$< 2.9 \times 10^{-6}$	CL=90%		1412
$\Lambda\overline{\Lambda}\eta$	$(2.5 \pm 0.4) \times 10^{-5}$			1197
$\Lambda\overline{\Lambda}\pi^+\pi^-$	$(2.8 \pm 0.6) \times 10^{-4}$			1346
$\Lambda\overline{p}K^+$	$(1.00 \pm 0.14) \times 10^{-4}$			1327
$\Lambda\overline{p}K^*(892)^+$ + c.c.	$(6.3 \pm 0.7) \times 10^{-5}$			1087
$\Lambda\overline{p}K^+\pi^+\pi^-$	$(1.8 \pm 0.4) \times 10^{-4}$			1167
$\overline{\Lambda}nK_S^0$ + c.c.	$(8.1 \pm 1.8) \times 10^{-5}$			1324
$\Delta^{++}\overline{\Delta}^{--}$	$(1.28 \pm 0.35) \times 10^{-4}$			1371
$\Lambda\overline{\Sigma}^+\pi^-$ + c.c.	$(1.40 \pm 0.13) \times 10^{-4}$			1376
$\Lambda\overline{\Sigma}^-\pi^+$ + c.c.	$(1.54 \pm 0.14) \times 10^{-4}$			1379
$\Lambda\overline{\Sigma}^0$ + c.c.	$(1.6 \pm 0.7) \times 10^{-6}$			1437
$\Sigma^0\overline{p}K^+$ + c.c.	$(1.67 \pm 0.18) \times 10^{-5}$			1291
$\Sigma^+\overline{\Sigma}^-$	$(2.43 \pm 0.10) \times 10^{-4}$	S=1.4		1408
$\Sigma^0\overline{\Sigma}^0$	$(2.35 \pm 0.09) \times 10^{-4}$	S=1.1		1405
$\Sigma(1385)^+\overline{\Sigma}(1385)^-$	$(8.5 \pm 0.7) \times 10^{-5}$			1218
$\Sigma(1385)^-\overline{\Sigma}(1385)^+$	$(8.5 \pm 0.8) \times 10^{-5}$			1218
$\Sigma(1385)^0\overline{\Sigma}(1385)^0$	$(6.9 \pm 0.7) \times 10^{-5}$			1218
$\Xi^-\overline{\Xi}^+$	$(2.87 \pm 0.11) \times 10^{-4}$	S=1.1		1284
$\Xi^0\overline{\Xi}^0$	$(2.3 \pm 0.4) \times 10^{-4}$	S=4.2		1291
$\Xi(1530)^0\overline{\Xi}(1530)^0$	$(6.8 \pm 0.4) \times 10^{-5}$			1025
$\Lambda\overline{\Xi}^+K^-$ + c.c.	$(3.9 \pm 0.4) \times 10^{-5}$			1114
$\Xi(1530)^-\overline{\Xi}(1530)^+$	$(1.15 \pm 0.07) \times 10^{-4}$			1025
$\Xi(1530)^-\overline{\Xi}^+$	$(7.0 \pm 1.2) \times 10^{-6}$			1165
$\Xi(1530)^0\overline{\Xi}^0$	$(5.3 \pm 0.5) \times 10^{-6}$			1169
$\Xi(1690)^-\overline{\Xi}^+ \to K^-\Lambda\overline{\Xi}^+ +$ c.c.	$(5.2 \pm 1.6) \times 10^{-6}$			–
$\Xi(1820)^-\overline{\Xi}^+ \to K^-\Lambda\overline{\Xi}^+ +$ c.c.	$(1.20 \pm 0.32) \times 10^{-5}$			–
$\Sigma^0\overline{\Xi}^+K^-$ + c.c.	$(3.7 \pm 0.4) \times 10^{-5}$			1060
$\Omega^-\overline{\Omega}^+$	$(5.66 \pm 0.30) \times 10^{-5}$	S=1.3		774
$\eta_c\pi^+\pi^-\pi^0$	$< 1.0 \times 10^{-3}$	CL=90%		512
$h_c(1P)\pi^0$	$(8.6 \pm 1.3) \times 10^{-4}$			85
$\Lambda_c^+\overline{p}e^+e^-$ + c.c.	$< 1.7 \times 10^{-6}$	CL=90%		830
$\Theta(1540)\overline{\Theta}(1540) \to K_S^0 p K^- \overline{n}$ + c.c.	[iiaa] $< 8.8 \times 10^{-6}$	CL=90%		–
$\Theta(1540)K^-\overline{n} \to K_S^0 p K^- \overline{n}$	[iiaa] $< 1.0 \times 10^{-5}$	CL=90%		–
$\Theta(1540)K_S^0\overline{p} \to K_S^0\overline{p}K^+n$	[iiaa] $< 7.0 \times 10^{-6}$	CL=90%		–
$\overline{\Theta}(1540)K^+n \to K_S^0\overline{p}K^+n$	[iiaa] $< 2.6 \times 10^{-5}$	CL=90%		–
$\overline{\Theta}(1540)K_S^0 p \to K_S^0 p K^- \overline{n}$	[iiaa] $< 6.0 \times 10^{-6}$	CL=90%		–
Radiative decays				
$\gamma\chi_{c0}(1P)$	(9.79 ± 0.20) %			261
$\gamma\chi_{c1}(1P)$	(9.75 ± 0.24) %			171
$\gamma\chi_{c2}(1P)$	(9.52 ± 0.20) %			128
$\gamma\eta_c(1S)$	$(3.4 \pm 0.5) \times 10^{-3}$	S=1.3		635
$\gamma\eta_c(2S)$	$(7 \pm 5) \times 10^{-4}$			48
$\gamma\pi^0$	$(1.04 \pm 0.22) \times 10^{-6}$	S=1.4		1841
$\gamma 2(\pi^+\pi^-)$	$(4.0 \pm 0.6) \times 10^{-4}$			1817
$\gamma 3(\pi^+\pi^-)$	$< 1.7 \times 10^{-4}$	CL=90%		1774
$\gamma\eta'(958)$	$(1.24 \pm 0.04) \times 10^{-4}$			1719
$\gamma f_2(1270)$	$(2.73\ ^{+0.29}_{-0.25}) \times 10^{-4}$	S=1.8		1622
$\gamma f_0(1370) \to \gamma K\overline{K}$	$(3.1 \pm 1.7) \times 10^{-5}$			1588
$\gamma f_0(1500)$	$(9.3 \pm 1.9) \times 10^{-5}$			1535
$\gamma f_2'(1525)$	$(3.3 \pm 0.8) \times 10^{-5}$			1531
$\gamma f_0(1710) \to \gamma\pi\pi$	$(3.5 \pm 0.6) \times 10^{-5}$			–
$\gamma f_0(1710) \to \gamma K\overline{K}$	$(6.6 \pm 0.7) \times 10^{-5}$			–
$\gamma f_0(2100) \to \gamma\pi\pi$	$(4.8 \pm 1.0) \times 10^{-6}$			1244
$\gamma f_0(2200) \to \gamma K\overline{K}$	$(3.2 \pm 1.0) \times 10^{-6}$			1193
$\gamma f_J(2220) \to \gamma\pi\pi$	$< 5.8 \times 10^{-6}$	CL=90%		1168
$\gamma f_J(2220) \to \gamma K\overline{K}$	$< 9.5 \times 10^{-6}$	CL=90%		1168
$\gamma\eta$	$(9.2 \pm 1.8) \times 10^{-7}$			1802
$\gamma\eta\pi^+\pi^-$	$(8.7 \pm 2.1) \times 10^{-4}$			1791
$\gamma\eta(1405) \to \gamma K\overline{K}\pi$	$< 9 \times 10^{-5}$	CL=90%		1569
$\gamma\eta(1405) \to \gamma\eta\pi^+\pi^-$	$(3.6 \pm 2.5) \times 10^{-5}$			–
$\gamma\eta(1405) \to \gamma f_0(980)\pi^0 \to \gamma\pi^+\pi^-\pi^0$	$< 5.0 \times 10^{-7}$	CL=90%		–
$\gamma\eta(1475) \to \gamma K\overline{K}\pi$	$< 1.4 \times 10^{-4}$	CL=90%		–
$\gamma\eta(1475) \to \gamma\eta\pi^+\pi^-$	$< 8.8 \times 10^{-5}$	CL=90%		–
$\gamma K^{*0}K^+\pi^-$ + c.c.	$(3.7 \pm 0.9) \times 10^{-4}$			1674
$\gamma K^{*0}\overline{K}^{*0}$	$(2.4 \pm 0.7) \times 10^{-4}$			1613
$\gamma K_S^0 K^+\pi^-$ + c.c.	$(2.6 \pm 0.5) \times 10^{-4}$			1753
$\gamma K^+K^-\pi^+\pi^-$	$(1.9 \pm 0.5) \times 10^{-4}$			1726
$\gamma K^+K^-2(\pi^+\pi^-)$	$< 2.2 \times 10^{-4}$	CL=90%		1654
$\gamma 2(K^+K^-)$	$< 4 \times 10^{-5}$	CL=90%		1499
$\gamma p\overline{p}$	$(3.9 \pm 0.5) \times 10^{-5}$	S=2.0		1586
$\gamma f_2(1950) \to \gamma p\overline{p}$	$(1.20 \pm 0.22) \times 10^{-5}$			–
$\gamma f_2(2150) \to \gamma p\overline{p}$	$(7.2 \pm 1.8) \times 10^{-6}$			–
$\gamma X(1835) \to \gamma p\overline{p}$	$(4.6\ ^{+1.8}_{-4.0}) \times 10^{-6}$			–
$\gamma X \to \gamma p\overline{p}$	[ooaa] $< 2 \times 10^{-6}$	CL=90%		–
$\gamma p\overline{p}\pi^+\pi^-$	$(2.8 \pm 1.4) \times 10^{-5}$			1491
$\gamma\gamma$	$< 1.5 \times 10^{-4}$	CL=90%		1843
$\gamma\gamma J/\psi$	$(3.1\ ^{+1.0}_{-1.2}) \times 10^{-4}$			542
$e^+e^-\eta'$	$(1.90 \pm 0.26) \times 10^{-6}$			1719
$e^+e^-\chi_{c0}(1P)$	$(1.06 \pm 0.24) \times 10^{-3}$			261
$e^+e^-\chi_{c1}(1P)$	$(8.5 \pm 0.6) \times 10^{-4}$			171
$e^+e^-\chi_{c2}(1P)$	$(7.0 \pm 0.8) \times 10^{-4}$			128
Weak decays				
$D^0e^+e^-$ + c.c.	$< 1.4 \times 10^{-7}$	CL=90%		1371
Other decays				
invisible	< 1.6 %	CL=90%		–

$\psi(3770)$

$I^G(J^{PC}) = 0^-(1^{--})$

Mass $m = 3773.7 \pm 0.4$ MeV (S = 1.4)
Full width $\Gamma = 27.2 \pm 1.0$ MeV

$\psi(3770)$ DECAY MODES	Fraction (Γ_i/Γ)	Scale factor/ Confidence level	p (MeV/c)
$D\overline{D}$	$(93\ ^{+8}_{-9})$ %	S=2.0	287
$D^0\overline{D}^0$	$(52\ ^{+4}_{-5})$ %	S=2.0	287
D^+D^-	(41 ± 4) %	S=2.0	254
$J/\psi X$	$(5.0 \pm 2.2) \times 10^{-3}$		–
$J/\psi\pi^+\pi^-$	$(1.93 \pm 0.28) \times 10^{-3}$		561
$J/\psi\pi^0\pi^0$	$(8.0 \pm 3.0) \times 10^{-4}$		565
$J/\psi\eta$	$(9 \pm 4) \times 10^{-4}$		361
$J/\psi\pi^0$	$< 2.8 \times 10^{-4}$	CL=90%	604
e^+e^-	$(9.6 \pm 0.7) \times 10^{-6}$	S=1.3	1887

Downloaded from https://academic.oup.com/ptep/article/2022/8/083C01/6651666 by KIT Library user on 27 September 2022

Decays to light hadrons

$b_1(1235)\pi$	< 1.4	$\times 10^{-5}$	CL=90%	1684
$\phi\eta'$	< 7	$\times 10^{-4}$	CL=90%	1607
$\omega\eta'$	< 4	$\times 10^{-4}$	CL=90%	1672
$\rho^0\eta'$	< 6	$\times 10^{-4}$	CL=90%	1674
$\phi\eta$	(3.1 ± 0.7)	$\times 10^{-4}$		1703
$\omega\eta$	< 1.4	$\times 10^{-5}$	CL=90%	1762
$\rho^0\eta$	< 5	$\times 10^{-4}$	CL=90%	1764
$\phi\pi^0$	< 3	$\times 10^{-5}$	CL=90%	1746
$\omega\pi^0$	< 6	$\times 10^{-4}$	CL=90%	1803
$\pi^+\pi^-\pi^0$	< 5	$\times 10^{-6}$	CL=90%	1874
$\rho\pi$	< 5	$\times 10^{-6}$	CL=90%	1805
$K^*(892)^+K^- +$ c.c.	< 1.4	$\times 10^{-5}$	CL=90%	1745
$K^*(892)^0\overline{K}^0 +$ c.c.	< 1.2	$\times 10^{-3}$	CL=90%	1745
$K^0_S K^0_L$	< 1.2	$\times 10^{-5}$	CL=90%	1820
$2(\pi^+\pi^-)$	< 1.12	$\times 10^{-3}$	CL=90%	1861
$2(\pi^+\pi^-)\pi^0$	< 1.06	$\times 10^{-3}$	CL=90%	1844
$2(\pi^+\pi^-\pi^0)$	< 5.85	%	CL=90%	1821
$\omega\pi^+\pi^-$	< 6.0	$\times 10^{-4}$	CL=90%	1794
$3(\pi^+\pi^-)$	< 9.1	$\times 10^{-3}$	CL=90%	1820
$3(\pi^+\pi^-)\pi^0$	< 1.37	%	CL=90%	1792
$3(\pi^+\pi^-)2\pi^0$	< 11.74	%	CL=90%	1760
$\eta\pi^+\pi^-$	< 1.24	$\times 10^{-3}$	CL=90%	1836
$\pi^+\pi^-2\pi^0$	< 8.9	$\times 10^{-3}$	CL=90%	1862
$\rho^0\pi^+\pi^-$	< 6.9	$\times 10^{-3}$	CL=90%	1796
$\eta 3\pi$	< 1.34	$\times 10^{-3}$	CL=90%	1824
$\eta 2(\pi^+\pi^-)$	< 2.43	%	CL=90%	1804
$\eta\rho^0\pi^+\pi^-$	< 1.45	%	CL=90%	1708
$\eta' 3\pi$	< 2.44	$\times 10^{-3}$	CL=90%	1741
$K^+K^-\pi^+\pi^-$	< 9.0	$\times 10^{-4}$	CL=90%	1773
$\phi\pi^+\pi^-$	< 4.1	$\times 10^{-4}$	CL=90%	1737
$K^+K^-2\pi^0$	< 4.2	$\times 10^{-3}$	CL=90%	1774
$4(\pi^+\pi^-)$	< 1.67	%	CL=90%	1757
$4(\pi^+\pi^-)\pi^0$	< 3.06	%	CL=90%	1720
$\phi f_0(980)$	< 4.5	$\times 10^{-4}$	CL=90%	1597
$K^+K^-\pi^+\pi^-\pi^0$	< 2.36	$\times 10^{-3}$	CL=90%	1741
$K^+K^-\rho^0\pi^0$	< 8	$\times 10^{-4}$	CL=90%	1624
$K^+K^-\rho^+\pi^-$	< 1.46	%	CL=90%	1623
ωK^+K^-	< 3.4	$\times 10^{-4}$	CL=90%	1664
$\phi\pi^+\pi^-\pi^0$	< 3.8	$\times 10^{-3}$	CL=90%	1723
$K^{*0}K^-\pi^+\pi^0 +$ c.c.	< 1.62	%	CL=90%	1694
$K^{*+}K^-\pi^+\pi^- +$ c.c.	< 3.23	%	CL=90%	1693
$K^+K^-\pi^+\pi^-2\pi^0$	< 2.67	%	CL=90%	1705
$K^+K^-2(\pi^+\pi^-)$	< 1.03	%	CL=90%	1702
$K^+K^-2(\pi^+\pi^-)\pi^0$	< 3.60	%	CL=90%	1661
ηK^+K^-	< 4.1	$\times 10^{-4}$	CL=90%	1712
$\eta K^+K^-\pi^+\pi^-$	< 1.24	%	CL=90%	1624
$\rho^0K^+K^-$	< 5.0	$\times 10^{-3}$	CL=90%	1666
$2(K^+K^-)$	< 6.0	$\times 10^{-4}$	CL=90%	1552
ϕK^+K^-	< 7.5	$\times 10^{-4}$	CL=90%	1598
$2(K^+K^-)\pi^0$	< 2.9	$\times 10^{-4}$	CL=90%	1494
$2(K^+K^-)\pi^+\pi^-$	< 3.2	$\times 10^{-3}$	CL=90%	1426
$K^0_S K^-\pi^+$	< 3.2	$\times 10^{-3}$	CL=90%	1799
$K^0_S K^-\pi^+\pi^0$	< 1.33	%	CL=90%	1773
$K^0_S K^-\rho^+$	< 6.6	$\times 10^{-3}$	CL=90%	1665
$K^0_S K^-2\pi^+\pi^-$	< 8.7	$\times 10^{-3}$	CL=90%	1740
$K^0_S K^-\pi^+\rho^0$	< 1.6	%	CL=90%	1621
$K^0_S K^-\pi^+\eta$	< 1.3	%	CL=90%	1670
$K^0_S K^-2\pi^+\pi^-\pi^0$	< 4.18	%	CL=90%	1703
$K^0_S K^-2\pi^+\pi^-\eta$	< 4.8	%	CL=90%	1570
$K^0_S K^-\pi^+2(\pi^+\pi^-)$	< 1.22	%	CL=90%	1658
$K^0_S K^-\pi^+2\pi^0$	< 2.65	%	CL=90%	1742
$K^0_S K^-K^+K^-\pi^+$	< 4.9	$\times 10^{-3}$	CL=90%	1491
$K^0_S K^-K^+K^-\pi^+\pi^0$	< 3.0	%	CL=90%	1427
$K^0_S K^-K^+K^-\pi^+\eta$	< 2.2	%	CL=90%	1214
$K^{*0}K^-\pi^+ +$ c.c.	< 9.7	$\times 10^{-3}$	CL=90%	1722
$p\overline{p}\pi^0$	< 4	$\times 10^{-5}$	CL=90%	1595
$p\overline{p}\pi^+\pi^-$	< 5.8	$\times 10^{-4}$	CL=90%	1544
$\Lambda\overline{\Lambda}$	< 1.2	$\times 10^{-4}$	CL=90%	1522
$p\overline{p}\pi^+\pi^-\pi^0$	< 1.85	$\times 10^{-3}$	CL=90%	1490
$\omega p\overline{p}$	< 2.9	$\times 10^{-4}$	CL=90%	1310
$\Lambda\overline{\Lambda}\pi^0$	< 7	$\times 10^{-5}$	CL=90%	1469
$p\overline{p}2(\pi^+\pi^-)$	< 2.6	$\times 10^{-3}$	CL=90%	1426
$\eta p\overline{p}$	< 5.4	$\times 10^{-4}$	CL=90%	1431
$\eta p\overline{p}\pi^+\pi^-$	< 3.3	$\times 10^{-3}$	CL=90%	1284
$\rho^0 p\overline{p}$	< 1.7	$\times 10^{-3}$	CL=90%	1314
$p\overline{p}K^+K^-$	< 3.2	$\times 10^{-4}$	CL=90%	1186
$\eta p\overline{p}K^+K^-$	< 6.9	$\times 10^{-3}$	CL=90%	737
$\pi^0 p\overline{p}K^+K^-$	< 1.2	$\times 10^{-3}$	CL=90%	1094
$\phi p\overline{p}$	< 1.3	$\times 10^{-4}$	CL=90%	1178
$\Lambda\overline{\Lambda}\pi^+\pi^-$	< 2.5	$\times 10^{-4}$	CL=90%	1405
$\Lambda\overline{p}K^+$	< 2.8	$\times 10^{-4}$	CL=90%	1387
$\Lambda\overline{p}K^+\pi^+\pi^-$	< 6.3	$\times 10^{-4}$	CL=90%	1234
$\Lambda\overline{\Lambda}\eta$	< 1.9	$\times 10^{-4}$	CL=90%	1263
$\Sigma^+\overline{\Sigma}^-$	< 1.0	$\times 10^{-4}$	CL=90%	1465
$\Sigma^0\overline{\Sigma}^0$	< 4	$\times 10^{-5}$	CL=90%	1462
$\Xi^+\overline{\Xi}^-$	< 1.5	$\times 10^{-4}$	CL=90%	1347
$\Xi^0\overline{\Xi}^0$	< 1.4	$\times 10^{-4}$	CL=90%	1353

Radiative decays

$\gamma\chi_{c2}$	< 6.4	$\times 10^{-4}$	CL=90%	211
$\gamma\chi_{c1}$	(2.49 ± 0.23)	$\times 10^{-3}$		254
$\gamma\chi_{c0}$	(6.9 ± 0.6)	$\times 10^{-3}$		342
$\gamma\eta_c$	< 7	$\times 10^{-4}$	CL=90%	707
$\gamma\eta_c(2S)$	< 9	$\times 10^{-4}$	CL=90%	134
$\gamma\eta'$	< 1.8	$\times 10^{-4}$	CL=90%	1765
$\gamma\eta$	< 1.5	$\times 10^{-4}$	CL=90%	1847
$\gamma\pi^0$	< 2	$\times 10^{-4}$	CL=90%	1884

$\psi_2(3823)$

$I^G(J^{PC}) = 0^-(2^{--})$
I, J, P need confirmation.

was $\psi(3823)$, $X(3823)$

Mass $m = 3823.7 \pm 0.5$ MeV (S = 1.1)
Full width $\Gamma < 5.2$ MeV, CL = 90%

Branching fractions are given relative to the one **DEFINED AS 1**.

$\psi_2(3823)$ DECAY MODES	Fraction (Γ_i/Γ)	Confidence level	p (MeV/c)
$J/\psi(1S)\pi^+\pi^-$	<0.06	90%	607
$J/\psi(1S)\pi^0\pi^0$	<0.11	90%	610
$J/\psi(1S)\pi^0$	<0.030	90%	646
$J/\psi(1S)\eta$	<0.14	90%	431
$\chi_{c0}\gamma$	<0.24	90%	387
$\chi_{c1}\gamma$	**DEFINED AS 1**		300
$\chi_{c2}\gamma$	$0.28\ ^{+0.14}_{-0.11}$		258

$\psi_3(3842)$

$I^G(J^{PC}) = 0^-(3^{--})$
J, P need confirmation.

Seen by a single experiment only.
Mass $m = 3842.71 \pm 0.20$ MeV
Full width $\Gamma = 2.8 \pm 0.6$ MeV

$\psi_3(3842)$ DECAY MODES	Fraction (Γ_i/Γ)	p (MeV/c)
D^+D^-	seen	443
$D^0\overline{D}^0$	seen	463

$\chi_{c1}(3872)$

$I^G(J^{PC}) = 0^+(1^{++})$

also known as $X(3872)$

Mass $m = 3871.65 \pm 0.06$ MeV
$m_{\chi_{c1}(3872)} - m_{J/\psi} = 775 \pm 4$ MeV
Full width $\Gamma = 1.19 \pm 0.21$ MeV (S = 1.1)

$\chi_{c1}(3872)$ DECAY MODES	Fraction (Γ_i/Γ)	Confidence level	p (MeV/c)
e^+e^-	$< 2.8 \times 10^{-6}$	90%	1936
$\pi^+\pi^-J/\psi(1S)$	(3.8 ± 1.2) %		650
$\pi^+\pi^-\pi^0J/\psi(1S)$	not seen		588
$\omega\eta_c(1S)$	< 33 %	90%	368
$\omega J/\psi(1S)$	(4.3 ± 2.1) %		†
$\phi\phi$	not seen		1646
$D^0\overline{D}^0\pi^0$	$(49\ ^{+18}_{-20})$ %		116
$\overline{D}^{*0}D^0$	(37 ± 9) %		†
$\gamma\gamma$	< 11 %	90%	1936
$D^0\overline{D}^0$	< 29 %	90%	519
D^+D^-	< 19 %	90%	502
$\pi^0\chi_{c2}$	< 4 %	90%	273
$\pi^0\chi_{c1}$	(3.4 ± 1.6) %		319
$\pi^0\chi_{c0}$	< 70 %	90%	–

Downloaded from https://academic.oup.com/ptep/article/2022/8/083C01/6651666 by KIT Library user on 27 September 2022

$\pi^+\pi^-\eta_c(1S)$	< 14	%	90%	745
$\pi^+\pi^-\chi_{c1}$	< 7	$\times 10^{-3}$	90%	218
$p\overline{p}$	< 2.4	$\times 10^{-5}$	95%	1693
Radiative decays				
γD^+D^-	< 4	%	90%	502
$\gamma \overline{D}^0 D^0$	< 6	%	90%	519
$\gamma J/\psi$	$(8 \pm 4) \times 10^{-3}$			697
$\gamma\chi_{c1}$	< 9	$\times 10^{-3}$	90%	344
$\gamma\chi_{c2}$	< 3.2	%	90%	303
$\gamma\psi(2S)$	(4.5 ± 2.0)	%		181
***C*-violating decays**				
$\eta J/\psi$	< 1.8	%	90%	491

$Z_c(3900)$

$I^G(J^{PC}) = 1^+(1^{+-})$

was $X(3900)$

Mass $m = 3887.1 \pm 2.6$ MeV (S = 1.7)
Full width $\Gamma = 28.4 \pm 2.6$ MeV

$Z_c(3900)$ DECAY MODES	Fraction (Γ_i/Γ)	p (MeV/c)
$J/\psi\pi$	seen	699
$h_c\pi^\pm$	not seen	318
$\eta_c\pi^+\pi^-$	not seen	759
$(D\overline{D}^*)^\pm$	seen	–
D^0D^{*-} + c.c.	seen	152
D^-D^{*0} + c.c.	seen	143
$\omega\pi^\pm$	not seen	1862
$J/\psi\eta$	not seen	510
D^+D^{*-} + c.c	seen	–
$D^0\overline{D}^{*0}$ + c.c	seen	–

$\chi_{c0}(3915)$

$I^G(J^{PC}) = 0^+(0^{++})$

was $X(3915)$

Mass $m = 3921.7 \pm 1.8$ MeV (S = 1.5)
Full width $\Gamma = 18.8 \pm 3.5$ MeV

$\chi_{c0}(3915)$ DECAY MODES	Fraction (Γ_i/Γ)	p (MeV/c)
$\omega J/\psi$	seen	231
$\overline{D}^{*0}D^0$	not seen	312
D^+D^-	seen	591
$\pi^+\pi^-\eta_c(1S)$	not seen	788
$\eta_c\eta$	not seen	668
$\eta_c\pi^0$	not seen	817
$K\overline{K}$	not seen	1898
$\gamma\gamma$	seen	1961
$\pi^0\chi_{c1}$	not seen	368

$\chi_{c2}(3930)$

$I^G(J^{PC}) = 0^+(2^{++})$

Mass $m = 3922.5 \pm 1.0$ MeV (S = 1.7)
Full width $\Gamma = 35.2 \pm 2.2$ MeV (S = 1.2)

$\chi_{c2}(3930)$ DECAY MODES	Fraction (Γ_i/Γ)	p (MeV/c)
$\gamma\gamma$	seen	1961
$D\overline{D}$	seen	607
D^+D^-	seen	592
$D^0\overline{D}^0$	seen	607
$\pi^+\pi^-\eta_c(1S)$	not seen	788
$K\overline{K}$	not seen	1898

$X(4020)^\pm$

$I^G(J^{PC}) = 1^+(?^{?-})$

Mass $m = 4024.1 \pm 1.9$ MeV
Full width $\Gamma = 13 \pm 5$ MeV (S = 1.7)

$X(4020)^\pm$ DECAY MODES	Fraction (Γ_i/Γ)	p (MeV/c)
$h_c(1P)\pi$	seen	450
$D^*\overline{D}^*$	seen	85
$D\overline{D}^*$ + c.c.	not seen	542
$\eta_c\pi^+\pi^-$	not seen	872
$J/\psi(1S)\pi^\pm$	not seen	811

$\psi(4040)$ [ppaa]

$I^G(J^{PC}) = 0^-(1^{--})$

Mass $m = 4039 \pm 1$ MeV
Full width $\Gamma = 80 \pm 10$ MeV

Due to the complexity of the $c\overline{c}$ threshold region, in this listing, "seen" ("not seen") means that a cross section for the mode in question has been measured at effective $\sqrt{s}$ near this particle's central mass value, more (less) than 2σ above zero, without regard to any peaking behavior in $\sqrt{s}$ or absence thereof. See mode listing(s) for details and references.

$\psi(4040)$ DECAY MODES	Fraction (Γ_i/Γ)	Confidence level	p (MeV/c)
e^+e^-	$(1.07 \pm 0.16) \times 10^{-5}$		2019
$D\overline{D}$	seen		775
$D^0\overline{D}^0$	seen		775
D^+D^-	seen		763
$D^*\overline{D}$ + c.c.	seen		569
$D^*(2007)^0\overline{D}^0$ + c.c.	seen		575
$D^*(2010)^+D^-$ + c.c.	seen		561
$D^*\overline{D}^*$	seen		193
$D^*(2007)^0\overline{D}^*(2007)^0$	seen		226
$D^*(2010)^+D^*(2010)^-$	seen		193
$D^0D^-\pi^+$ +c.c. (excl. $D^*(2007)^0\overline{D}^0$ +c.c., $D^*(2010)^+D^-$ +c.c.)	not seen		–
$D\overline{D}^*\pi$ (excl. $D^*\overline{D}^*$)	not seen		–
$D^0\overline{D}^{*-}\pi^+$ +c.c. (excl. $D^*(2010)^+D^*(2010)^-$)	seen		–
$D_s^+D_s^-$	seen		452
$J/\psi\pi^+\pi^-$	< 4	$\times 10^{-3}$ 90%	794
$J/\psi\pi^0\pi^0$	< 2	$\times 10^{-3}$ 90%	797
$J/\psi\eta$	$(5.2 \pm 0.7) \times 10^{-3}$		675
$J/\psi\pi^0$	< 2.8	$\times 10^{-4}$ 90%	823
$J/\psi\pi^+\pi^-\pi^0$	< 2	$\times 10^{-3}$ 90%	746
$\chi_{c1}\gamma$	< 3.4	$\times 10^{-3}$ 90%	494
$\chi_{c2}\gamma$	< 5	$\times 10^{-3}$ 90%	454
$\chi_{c1}\pi^+\pi^-\pi^0$	< 1.1	% 90%	306
$\chi_{c2}\pi^+\pi^-\pi^0$	< 3.2	% 90%	233
$h_c(1P)\pi^+\pi^-$	< 3	$\times 10^{-3}$ 90%	403
$\phi\pi^+\pi^-$	< 3	$\times 10^{-3}$ 90%	1880
$\Lambda\overline{\Lambda}\pi^+\pi^-$	< 2.9	$\times 10^{-4}$ 90%	1578
$\Lambda\overline{\Lambda}\pi^0$	< 9	$\times 10^{-5}$ 90%	1636
$\Lambda\overline{\Lambda}\eta$	< 3.0	$\times 10^{-4}$ 90%	1452
$\Lambda\overline{\Lambda}$	< 6	$\times 10^{-6}$ 90%	1683
$\Sigma^+\overline{\Sigma}^-$	< 1.3	$\times 10^{-4}$ 90%	1632
$\Sigma^0\overline{\Sigma}^0$	< 7	$\times 10^{-5}$ 90%	1630
$\Xi^+\overline{\Xi}^-$	< 1.6	$\times 10^{-4}$ 90%	1527
$\Xi^0\overline{\Xi}^0$	< 1.8	$\times 10^{-4}$ 90%	1533
$\mu^+\mu^-$	$(9 \pm 6) \times 10^{-6}$		2017

$\chi_{c1}(4140)$

$I^G(J^{PC}) = 0^+(1^{++})$

was $X(4140)$

Mass $m = 4146.5 \pm 3.0$ MeV (S = 1.3)
Full width $\Gamma = 19^{+7}_{-5}$ MeV

$\chi_{c1}(4140)$ DECAY MODES	Fraction (Γ_i/Γ)	p (MeV/c)
$J/\psi\phi$	seen	216
$\gamma\gamma$	not seen	2073

$\psi(4160)$ [ppaa]

$I^G(J^{PC}) = 0^-(1^{--})$

Mass $m = 4191 \pm 5$ MeV
Full width $\Gamma = 70 \pm 10$ MeV

Due to the complexity of the $c\overline{c}$ threshold region, in this listing, "seen" ("not seen") means that a cross section for the mode in question has been measured at effective $\sqrt{s}$ near this particle's central mass value, more (less) than 2σ above zero, without regard to any peaking behavior in $\sqrt{s}$ or absence thereof. See mode listing(s) for details and references.

Downloaded from https://academic.oup.com/ptep/article/2022/8/083C01/6651666 by KIT Library user on 27 September 2022

$\psi(4160)$ DECAY MODES	Fraction (Γ_i/Γ)	Confidence level	p (MeV/c)
e^+e^-	$(6.9 \pm 3.3) \times 10^{-6}$		2096
$\mu^+\mu^-$	seen		2093
$D\overline{D}$	seen		956
$D^0\overline{D}^0$	seen		956
D^+D^-	seen		947
$D^*\overline{D}+$ c.c.	seen		798
$D^*(2007)^0\overline{D}^0+$ c.c.	seen		802
$D^*(2010)^+D^-+$ c.c.	seen		792
$D^*\overline{D}^*$	seen		592
$D^*(2007)^0\overline{D}^*(2007)^0$	seen		604
$D^*(2010)^+D^*(2010)^-$	seen		592
$D^0D^-\pi^+$+c.c. (excl. $D^*(2007)^0\overline{D}^0$ +c.c., $D^*(2010)^+D^-$ +c.c.)	not seen		–
$D\overline{D}^*\pi$+c.c. (excl. $D^*\overline{D}^*$)	seen		–
$D^0D^{*-}\pi^+$+c.c. (excl. $D^*(2010)^+D^*(2010)^-$)	not seen		–
$D_s^+D_s^-$	not seen		719
$D_s^{*+}D_s^-$+c.c.	seen		385
$J/\psi\pi^+\pi^-$	$< 3 \times 10^{-3}$	90%	919
$J/\psi\pi^0\pi^0$	$< 3 \times 10^{-3}$	90%	922
$J/\psi K^+K^-$	$< 2 \times 10^{-3}$	90%	407
$J/\psi\eta$	$< 8 \times 10^{-3}$	90%	822
$J/\psi\pi^0$	$< 1 \times 10^{-3}$	90%	944
$J/\psi\eta'$	$< 5 \times 10^{-3}$	90%	457
$J/\psi\pi^+\pi^-\pi^0$	$< 1 \times 10^{-3}$	90%	879
$\psi(2S)\pi^+\pi^-$	$< 4 \times 10^{-3}$	90%	396
$\chi_{c1}\gamma$	$< 5 \times 10^{-3}$	90%	625
$\chi_{c2}\gamma$	< 1.3 %	90%	587
$\chi_{c1}\pi^+\pi^-\pi^0$	$< 2 \times 10^{-3}$	90%	496
$\chi_{c2}\pi^+\pi^-\pi^0$	$< 8 \times 10^{-3}$	90%	445
$h_c(1P)\pi^+\pi^-$	$< 5 \times 10^{-3}$	90%	556
$h_c(1P)\pi^0\pi^0$	$< 2 \times 10^{-3}$	90%	560
$h_c(1P)\eta$	$< 2 \times 10^{-3}$	90%	348
$h_c(1P)\pi^0$	$< 4 \times 10^{-4}$	90%	600
$\phi\pi^+\pi^-$	$< 2 \times 10^{-3}$	90%	1961
$\gamma\chi_{c1}(3872)$	$< 1.8 \times 10^{-3}$	90%	308
$\gamma\chi_{c0}(3915) \to \gamma J/\psi\pi^+\pi^-$	$< 1.36 \times 10^{-4}$	90%	–
$\gamma X(3930) \to \gamma J/\psi\pi^+\pi^-$	$< 1.18 \times 10^{-4}$	90%	–
$\gamma X(3940) \to \gamma J/\psi\pi^+\pi^-$	$< 1.47 \times 10^{-4}$	90%	–
$\gamma\chi_{c0}(3915) \to \gamma\gamma J/\psi$	$< 1.26 \times 10^{-4}$	90%	–
$\gamma X(3930) \to \gamma\gamma J/\psi$	$< 8.8 \times 10^{-5}$	90%	–
$\gamma X(3940) \to \gamma\gamma J/\psi$	$< 1.79 \times 10^{-4}$	90%	–
$p\overline{p}p\overline{p}$	not seen		834
$\Lambda\overline{\Lambda}$	$< 1.5 \times 10^{-6}$	90%	1774

$\psi(4230)$

$I^G(J^{PC}) = 0^-(1^{--})$

also known as $Y(4230)$; was $\psi(4260)$

Mass $m = 4222.7 \pm 2.6$ MeV (S = 1.7)
Full width $\Gamma = 49 \pm 8$ MeV (S = 3.5)

$\psi(4230)$ DECAY MODES	Fraction (Γ_i/Γ)	p (MeV/c)
$\mu^+\mu^-$	$(3.1 \pm 2.8) \times 10^{-5}$	2107
$\eta_c(1S)\pi^+\pi^-$	not seen	1027
$\eta_c(1S)\pi^+\pi^-\pi^0$	seen	992
$J/\psi\pi^+\pi^-$	seen	942
$J/\psi f_0(980)$, $f_0(980) \to \pi^+\pi^-$	seen	–
$Z_c(3900)^\pm\pi^\mp$, $Z_c^\pm \to J/\psi\pi^\pm$	seen	–
$J/\psi\pi^0\pi^0$	seen	944
$J/\psi K^+K^-$	seen	460
$J/\psi K_S^0K_S^0$	not seen	447
$J/\psi\eta$	seen	848
$J/\psi\pi^0$	not seen	966
$J/\psi\eta'$	seen	504
$J/\psi\pi^+\pi^-\pi^0$	not seen	904
$J/\psi\eta\pi^0$	not seen	770
$J/\psi\eta\eta$	not seen	211
$\psi(2S)\pi^+\pi^-$	seen	426
$\psi(2S)\eta$	not seen	†
$\chi_{c0}\omega$	seen	171
$\chi_{c1}\pi^+\pi^-\pi^0$	not seen	527
$\chi_{c2}\pi^+\pi^-\pi^0$	not seen	477
$h_c(1P)\pi^+\pi^-$	seen	583
$\phi\pi^+\pi^-$	not seen	1976
$\phi f_0(980) \to \phi\pi^+\pi^-$	not seen	–
$D\overline{D}$	not seen	987
$D^0\overline{D}^0$	not seen	987
D^+D^-	not seen	978
$D^*\overline{D}$+c.c.	not seen	887
$D^*(2007)^0\overline{D}^0$+c.c.	not seen	–
$D^*(2010)^+D^-$+c.c.	not seen	–
$D^*(2007)^0\overline{D}^*(2007)^0$	not seen	652
$D^*(2010)^+D^*(2010)^-$	not seen	641
$D^0D^-\pi^+$+c.c. (excl. $D^*(2007)^0\overline{D}^{*0}$ +c.c., $D^*(2010)^+D^-$ +c.c.)	not seen	–
$D\overline{D}^*\pi$+c.c. (excl. $D^*\overline{D}^*$)	not seen	723
$D^0D^{*-}\pi^+$+c.c. (excl. $D^*(2010)^+D^*(2010)^-$)	not seen	–
$D^0D^*(2010)^-\pi^+$+c.c.	seen	716
$D_1(2420)\overline{D}+$ c.c.	not seen	†
$D^*\overline{D}^*\pi$	not seen	367
$D_s^+D_s^-$	not seen	760
$D_s^{*+}D_s^-$+c.c.	not seen	615
$D_s^{*+}D_s^{*-}$	not seen	†
$p\overline{p}$	not seen	1890
$p\overline{p}\pi^0$	not seen	1854
$p\overline{p}\eta$	not seen	1712
$p\overline{p}\omega$	not seen	1610
$\Xi^-\overline{\Xi}^+$	not seen	1645
$\pi^+\pi^+\pi^-\pi^-$	not seen	2087
$\pi^+\pi^+\pi^-\pi^-\pi^0$	not seen	2071
$K_S^0K^\pm\pi^\mp$	not seen	2032
$K_S^0K^\pm\pi^\mp\pi^0$	not seen	2009
$K_S^0K^\pm\pi^\mp\eta$	not seen	1917
$K^+K^-\pi^0$	not seen	2033
$K^+K^-\pi^+\pi^-$	not seen	2008
$K^+K^-\pi^+\pi^-\pi^0$	not seen	1981
$K^+K^+K^-K^-$	not seen	1813
$K^+K^+K^-K^-\pi^0$	not seen	1762
$p\overline{p}\pi^+\pi^-$	not seen	1810
$p\overline{p}\pi^+\pi^-\pi^0$	not seen	1764
$p\overline{p}p\overline{p}$	not seen	864
$\Lambda\overline{\Lambda}$	not seen	1791
Radiative decays		
$\eta_c(1S)\gamma$	possibly seen	1055
$\eta_c(1S)\pi^0\gamma$	not seen	1049
$\chi_{c1}\gamma$	not seen	650
$\chi_{c2}\gamma$	not seen	612
$\chi_{c1}(3872)\gamma$	seen	334

$\chi_{c1}(4274)$

$I^G(J^{PC}) = 0^+(1^{++})$

was $X(4274)$

Mass $m = 4286^{+8}_{-9}$ MeV (S = 1.7)
Full width $\Gamma = 51 \pm 7$ MeV

$\chi_{c1}(4274)$ DECAY MODES	Fraction (Γ_i/Γ)	p (MeV/c)
$J/\psi\phi$	seen	522

$\psi(4360)$

$I^G(J^{PC}) = 0^-(1^{--})$

also known as $Y(4360)$; was $X(4360)$

$\psi(4360)$ MASS $= 4372 \pm 9$ MeV (S = 2.9)
$\psi(4360)$ WIDTH $= 115 \pm 13$ MeV (S = 2.2)

$\psi(4360)$ DECAY MODES	Fraction (Γ_i/Γ)	p (MeV/c)
$h_c\pi^+\pi^-$	seen	721
$\psi(2S)\pi^+\pi^-$	seen	577
$\psi(3770)\pi^+\pi^-$	possibly seen	493
$\psi_2(3823)\pi^+\pi^-$	possibly seen	442
$J/\psi\eta$	seen	981
$D_1(2420)\overline{D}+$ c.c.	possibly seen	426
$p\overline{p}\eta$	not seen	1805
$p\overline{p}\omega$	not seen	1707

Downloaded from https://academic.oup.com/ptep/article/2022/8/083C01/6651666 by KIT Library user on 27 September 2022

$\psi(4415)$ [ppaa]

$I^G(J^{PC}) = 0^-(1^{--})$

Mass $m = 4421 \pm 4$ MeV
Full width $\Gamma = 62 \pm 20$ MeV

Due to the complexity of the $c\overline{c}$ threshold region, in this listing, "seen" ("not seen") means that a cross section for the mode in question has been measured at effective $\sqrt{s}$ near this particle's central mass value, more (less) than 2σ above zero, without regard to any peaking behavior in $\sqrt{s}$ or absence thereof. See mode listing(s) for details and references.

$\psi(4415)$ DECAY MODES	Fraction (Γ_i/Γ)	Confidence level	p (MeV/c)
$D\overline{D}$	seen		1187
$D^0\overline{D}^0$	seen		1187
D^+D^-	seen		1179
$D^*\overline{D}+$ c.c.	seen		1063
$D^*(2007)^0\overline{D}^0+$ c.c.	seen		1067
$D^*(2010)^+D^-+$ c.c.	seen		1059
$D^*\overline{D}^*$	seen		919
$D^*(2007)^0\overline{D}^*(2007)^0+$ c.c.	seen		927
$D^*(2010)^+D^*(2010)^-+$ c.c.	seen		919
$D^0D^-\pi^+$ (excl. $D^*(2007)^0\overline{D}^0$ +c.c., $D^*(2010)^+D^-$ +c.c.	< 2.3 %	90%	–
$D\overline{D}_2^*(2460) \to D^0D^-\pi^+$+c.c.	(10 ± 4) %		–
$D^0D^{*-}\pi^+$+c.c.	< 11 %	90%	926
$D_1(2420)\overline{D}+$ c.c.	possibly seen		537
$D_s^+D_s^-$	not seen		1006
$\omega\chi_{c2}$	possibly seen		330
$D_s^{*+}D_s^-$+c.c.	seen		–
$D_s^{*+}D_s^{*-}$	not seen		652
$\psi_2(3823)\pi^+\pi^-$	possibly seen		492
$\psi(3770)\pi^+\pi^-$	possibly seen		541
$J/\psi\eta$	$< 6 \times 10^{-3}$	90%	1022
$\chi_{c1}\gamma$	$< 8 \times 10^{-4}$	90%	817
$\chi_{c2}\gamma$	$< 4 \times 10^{-3}$	90%	780
$\Lambda\overline{\Lambda}$	$< 3.1 \times 10^{-6}$	90%	1908
e^+e^-	$(9.4 \pm 3.2) \times 10^{-6}$		2210
$\mu^+\mu^-$	$(2.0 \pm 1.0) \times 10^{-5}$		2208

$Z_c(4430)$

$I^G(J^{PC}) = 1^+(1^{+-})$
G, C need confirmation.

was $X(4430)^\pm$

Quantum numbers not established.

Mass $m = 4478^{+15}_{-18}$ MeV
Full width $\Gamma = 181 \pm 31$ MeV

$Z_c(4430)$ DECAY MODES	Fraction (Γ_i/Γ)	p (MeV/c)
$\pi^+\psi(2S)$	seen	711
π^+J/ψ	seen	1162

$\psi(4660)$

$I^G(J^{PC}) = 0^-(1^{--})$

also known as $Y(4660)$; was $X(4660)$

$\psi(4660)$ MASS $= 4630 \pm 6$ MeV (S = 1.4)
$\psi(4660)$ WIDTH $= 72^{+14}_{-12}$ MeV (S = 1.7)

$\psi(4660)$ DECAY MODES	Fraction (Γ_i/Γ)	p (MeV/c)
e^+e^-	not seen	2315
$\psi(2S)\pi^+\pi^-$	seen	809
$J/\psi\eta$	not seen	1192
$D^0D^{*-}\pi^+$	not seen	1153
$\chi_{c1}\gamma$	not seen	984
$\chi_{c2}\gamma$	not seen	949
$\Lambda_c^+\Lambda_c^-$	seen	363
$D_s^+D_{s1}(2536)^-$	seen	534

$b\overline{b}$ MESONS (including possibly non-$q\overline{q}$ states)

$\eta_b(1S)$

$I^G(J^{PC}) = 0^+(0^{-+})$

Mass $m = 9398.7 \pm 2.0$ MeV (S = 1.5)
Full width $\Gamma = 10^{+5}_{-4}$ MeV

$\eta_b(1S)$ DECAY MODES	Fraction (Γ_i/Γ)	Confidence level	p (MeV/c)
hadrons	seen		–
$3h^+3h^-$	not seen		4672
$2h^+2h^-$	not seen		4689
$4h^+4h^-$	not seen		4648
$\gamma\gamma$	not seen		4699
$\mu^+\mu^-$	$< 9 \times 10^{-3}$	90%	4698
$\tau^+\tau^-$	< 8 %	90%	4350

$\Upsilon(1S)$

$I^G(J^{PC}) = 0^-(1^{--})$

Mass $m = 9460.30 \pm 0.26$ MeV (S = 3.3)
Full width $\Gamma = 54.02 \pm 1.25$ keV

$\Upsilon(1S)$ DECAY MODES	Fraction (Γ_i/Γ)	Scale factor/ Confidence level	p (MeV/c)
$\tau^+\tau^-$	(2.60 ± 0.10) %		4384
e^+e^-	(2.38 ± 0.11) %		4730
$\mu^+\mu^-$	(2.48 ± 0.05) %		4729
Hadronic decays			
ggg	(81.7 ± 0.7) %		–
γgg	(2.2 ± 0.6) %		–
$\eta'(958)$ anything	(2.94 ± 0.24) %		–
$J/\psi(1S)$ anything	$(5.4 \pm 0.4) \times 10^{-4}$	S=1.4	4223
$J/\psi(1S)\eta_c$	$< 2.2 \times 10^{-6}$	CL=90%	3623
$J/\psi(1S)\chi_{c0}$	$< 3.4 \times 10^{-6}$	CL=90%	3429
$J/\psi(1S)\chi_{c1}$	$(3.9 \pm 1.2) \times 10^{-6}$		3382
$J/\psi(1S)\chi_{c2}$	$< 1.4 \times 10^{-6}$	CL=90%	3359
$J/\psi(1S)\eta_c(2S)$	$< 2.2 \times 10^{-6}$	CL=90%	3317
$J/\psi(1S)X(3940)$	$< 5.4 \times 10^{-6}$	CL=90%	3148
$J/\psi(1S)X(4160)$	$< 5.4 \times 10^{-6}$	CL=90%	3020
$X(4350)$ anything, $X \to J/\psi(1S)\phi$	$< 8.1 \times 10^{-6}$	CL=90%	–
$Z_c(3900)^\pm$ anything, $Z_c \to J/\psi(1S)\pi^\pm$	$< 1.3 \times 10^{-5}$	CL=90%	–
$Z_c(4200)^\pm$ anything, $Z_c \to J/\psi(1S)\pi^\pm$	$< 6.0 \times 10^{-5}$	CL=90%	–
$Z_c(4430)^\pm$ anything, $Z_c \to J/\psi(1S)\pi^\pm$	$< 4.9 \times 10^{-5}$	CL=90%	–
$X_{cs}^\pm$ anything, $X \to J/\psi K^\pm$	$< 5.7 \times 10^{-6}$	CL=90%	–
$\psi(4230)$ anything, $\psi \to J/\psi(1S)\pi^+\pi^-$	$< 3.8 \times 10^{-5}$	CL=90%	–
$\psi(4230)$ anything, $\psi \to J/\psi(1S)K^+K^-$	$< 7.5 \times 10^{-6}$	CL=90%	–
$\chi_{c1}(4140)$ anything, $\chi_{c1} \to J/\psi(1S)\phi$	$< 5.2 \times 10^{-6}$	CL=90%	–
χ_{c0} anything	$< 4 \times 10^{-3}$	CL=90%	–
χ_{c1} anything	$(1.90 \pm 0.35) \times 10^{-4}$		–
$\chi_{c1}(1P)X_{tetra}$	$< 3.78 \times 10^{-5}$	CL=90%	–
χ_{c2} anything	$(2.8 \pm 0.8) \times 10^{-4}$		–
$\psi(2S)$ anything	$(1.23 \pm 0.20) \times 10^{-4}$		–
$\psi(2S)\eta_c$	$< 3.6 \times 10^{-6}$	CL=90%	3345
$\psi(2S)\chi_{c0}$	$< 6.5 \times 10^{-6}$	CL=90%	3124
$\psi(2S)\chi_{c1}$	$< 4.5 \times 10^{-6}$	CL=90%	3070
$\psi(2S)\chi_{c2}$	$< 2.1 \times 10^{-6}$	CL=90%	3043
$\psi(2S)\eta_c(2S)$	$< 3.2 \times 10^{-6}$	CL=90%	2994
$\psi(2S)X(3940)$	$< 2.9 \times 10^{-6}$	CL=90%	2797
$\psi(2S)X(4160)$	$< 2.9 \times 10^{-6}$	CL=90%	2645
$\psi(4230)$ anything, $\psi \to \psi(2S)\pi^+\pi^-$	$< 7.9 \times 10^{-5}$	CL=90%	–
$\psi(4360)$ anything, $\psi \to \psi(2S)\pi^+\pi^-$	$< 5.2 \times 10^{-5}$	CL=90%	–
$\psi(4660)$ anything, $\psi \to \psi(2S)\pi^+\pi^-$	$< 2.2 \times 10^{-5}$	CL=90%	–

Downloaded from https://academic.oup.com/ptep/article/2022/8/083C01/6651666 by KIT Library user on 27 September 2022

$X(4050)^\pm$ anything, $X \to \psi(2S)\pi^\pm$		< 8.8	$\times 10^{-5}$	CL=90%	–
$Z_c(4430)^\pm$ anything, $Z_c \to \psi(2S)\pi^\pm$		< 6.7	$\times 10^{-5}$	CL=90%	–
$\chi_{c1}(3872)$ anything		< 2.5	$\times 10^{-4}$	CL=90%	–
$Z_c(4200)^+ Z_c(4200)^-$		< 2.23	$\times 10^{-5}$	CL=90%	–
$Z_c(3900)^\pm Z_c(4200)^\mp$		< 8.1	$\times 10^{-6}$	CL=90%	–
$Z_c(3900)^+ Z_c(3900)^-$		< 1.8	$\times 10^{-6}$	CL=90%	–
$X(4050)^+ X(4050)^-$		< 1.58	$\times 10^{-5}$	CL=90%	–
$X(4250)^+ X(4250)^-$		< 2.66	$\times 10^{-5}$	CL=90%	–
$X(4050)^\pm X(4250)^\mp$		< 4.42	$\times 10^{-5}$	CL=90%	–
$Z_c(4430)^+ Z_c(4430)^-$		< 2.03	$\times 10^{-5}$	CL=90%	–
$X(4055)^\pm X(4055)^\mp$		< 2.33	$\times 10^{-5}$	CL=90%	–
$X(4055)^\pm Z_c(4430)^\mp$		< 4.55	$\times 10^{-5}$	CL=90%	–
$\rho\pi$		< 3.68	$\times 10^{-6}$	CL=90%	4697
$\omega\pi^0$		< 3.90	$\times 10^{-6}$	CL=90%	4697
$\pi^+\pi^-$		< 5	$\times 10^{-4}$	CL=90%	4728
K^+K^-		< 5	$\times 10^{-4}$	CL=90%	4704
$p\overline{p}$		< 5	$\times 10^{-4}$	CL=90%	4636
$\pi^+\pi^-\pi^0$		$(2.1 \pm 0.8) \times 10^{-6}$			4725
ϕK^+K^-		$(2.4 \pm 0.5) \times 10^{-6}$			4622
$\omega\pi^+\pi^-$		$(4.5 \pm 1.0) \times 10^{-6}$			4694
$K^*(892)^0 K^-\pi^+ +$ c.c.		$(4.4 \pm 0.8) \times 10^{-6}$			4667
$\phi f_2'(1525)$		< 1.63	$\times 10^{-6}$	CL=90%	4551
$\omega f_2(1270)$		< 1.79	$\times 10^{-6}$	CL=90%	4611
$\rho(770) a_2(1320)$		< 2.24	$\times 10^{-6}$	CL=90%	4605
$K^*(892)^0 \overline{K}_2^*(1430)^0 +$ c.c.		$(3.0 \pm 0.8) \times 10^{-6}$			4578
$K_1(1270)^\pm K^\mp$		< 2.41	$\times 10^{-6}$	CL=90%	4634
$K_1(1400)^\pm K^\mp$		$(1.0 \pm 0.4) \times 10^{-6}$			4613
$b_1(1235)^\pm \pi^\mp$		< 1.25	$\times 10^{-6}$	CL=90%	4649
$\pi^+\pi^-\pi^0\pi^0$		$(1.28 \pm 0.30) \times 10^{-5}$			4720
$K_S^0 K^+\pi^- +$ c.c.		$(1.6 \pm 0.4) \times 10^{-6}$			4696
$K^*(892)^0 \overline{K}^0 +$ c.c.		$(2.9 \pm 0.9) \times 10^{-6}$			4675
$K^*(892)^- K^+ +$ c.c.		< 1.11	$\times 10^{-6}$	CL=90%	4675
$f_1(1285)$ anything		$(4.6 \pm 3.1) \times 10^{-3}$			–
$D^*(2010)^\pm$ anything		(2.52 ± 0.20) %			–
$f_1(1285) X_{tetra}$		< 6.24	$\times 10^{-5}$	CL=90%	–
^2H anything		$(2.85 \pm 0.25) \times 10^{-5}$			–
Sum of 100 exclusive modes		(1.200 ± 0.017) %			–
Radiative decays					
$\gamma\pi^+\pi^-$		$(6.3 \pm 1.8) \times 10^{-5}$			4728
$\gamma\pi^0\pi^0$		$(1.7 \pm 0.7) \times 10^{-5}$			4728
$\gamma\pi\pi$(S-wave)		$(4.6 \pm 0.7) \times 10^{-5}$			4728
$\gamma\pi^0\eta$		< 2.4	$\times 10^{-6}$	CL=90%	4713
γK^+K^-	[qqaa]	$(1.14 \pm 0.13) \times 10^{-5}$			4704
$\gamma p\overline{p}$	[rraa]	< 6	$\times 10^{-6}$	CL=90%	4636
$\gamma 2h^+ 2h^-$		$(7.0 \pm 1.5) \times 10^{-4}$			4720
$\gamma 3h^+ 3h^-$		$(5.4 \pm 2.0) \times 10^{-4}$			4703
$\gamma 4h^+ 4h^-$		$(7.4 \pm 3.5) \times 10^{-4}$			4679
$\gamma\pi^+\pi^- K^+K^-$		$(2.9 \pm 0.9) \times 10^{-4}$			4686
$\gamma 2\pi^+ 2\pi^-$		$(2.5 \pm 0.9) \times 10^{-4}$			4720
$\gamma 3\pi^+ 3\pi^-$		$(2.5 \pm 1.2) \times 10^{-4}$			4703
$\gamma 2\pi^+ 2\pi^- K^+K^-$		$(2.4 \pm 1.2) \times 10^{-4}$			4658
$\gamma\pi^+\pi^- p\overline{p}$		$(1.5 \pm 0.6) \times 10^{-4}$			4604
$\gamma 2\pi^+ 2\pi^- p\overline{p}$		$(4 \pm 6) \times 10^{-5}$			4563
$\gamma 2K^+ 2K^-$		$(2.0 \pm 2.0) \times 10^{-5}$			4601
$\gamma\eta'(958)$		< 1.9	$\times 10^{-6}$	CL=90%	4682
$\gamma\eta$		< 1.0	$\times 10^{-6}$	CL=90%	4714
$\gamma f_0(980)$		< 3	$\times 10^{-5}$	CL=90%	4678
$\gamma f_2'(1525)$		$(2.9 \pm 0.6) \times 10^{-5}$			4608
$\gamma f_2(1270)$		$(1.01 \pm 0.06) \times 10^{-4}$			4644
$\gamma\eta(1405)$		< 8.2	$\times 10^{-5}$	CL=90%	4625
$\gamma f_0(1500)$		< 1.5	$\times 10^{-5}$	CL=90%	4610
$\gamma f_0(1500) \to \gamma K^+K^-$		$(1.0 \pm 0.4) \times 10^{-5}$			–
$\gamma f_0(1710)$		< 2.6	$\times 10^{-4}$	CL=90%	4577
$\gamma f_0(1710) \to \gamma K^+K^-$		$(1.01 \pm 0.32) \times 10^{-5}$			–
$\gamma f_0(1710) \to \gamma\pi^+\pi^-$		$(5.3 \pm 2.0) \times 10^{-6}$			–
$\gamma f_0(1710) \to \gamma\pi^0\pi^0$		< 1.4	$\times 10^{-6}$	CL=90%	–
$\gamma f_0(1710) \to \gamma\eta\eta$		< 1.8	$\times 10^{-6}$	CL=90%	–
$\gamma f_4(2050)$		< 5.3	$\times 10^{-5}$	CL=90%	4515
$\gamma f_0(2200) \to \gamma K^+K^-$		< 2	$\times 10^{-4}$	CL=90%	4475
$\gamma f_J(2220) \to \gamma K^+K^-$		< 8	$\times 10^{-7}$	CL=90%	4469
$\gamma f_J(2220) \to \gamma\pi^+\pi^-$		< 6	$\times 10^{-7}$	CL=90%	–
$\gamma f_J(2220) \to \gamma p\overline{p}$		< 1.1	$\times 10^{-6}$	CL=90%	–
$\gamma\eta(2225) \to \gamma\phi\phi$		< 3	$\times 10^{-3}$	CL=90%	4469
$\gamma\eta_c(1S)$		< 2.9	$\times 10^{-5}$	CL=90%	4260
$\gamma\eta_c(2S)$		< 4	$\times 10^{-4}$	CL=90%	4031
$\gamma\chi_{c0}$		< 6.6	$\times 10^{-5}$	CL=90%	4114
$\gamma\chi_{c1}$		$(4.7 \pm^{2.4}_{1.9}) \times 10^{-5}$			4079
$\gamma\chi_{c2}$		< 7.6	$\times 10^{-6}$	CL=90%	4062
$\gamma\chi_{c1}(3872)$		< 4	$\times 10^{-5}$	CL=90%	3938
$\gamma\chi_{c1}(3872), \chi_{c1} \to \pi^+\pi^-\pi^0 J/\psi$		< 2.8	$\times 10^{-6}$	CL=90%	–
$\gamma\chi_{c0}(3915) \to \omega J/\psi$		< 3.0	$\times 10^{-6}$	CL=90%	–
$\gamma\chi_{c1}(4140) \to \phi J/\psi$		< 2.2	$\times 10^{-6}$	CL=90%	–
γX	[ssaa]	< 4.5	$\times 10^{-6}$	CL=90%	–
$\gamma X\overline{X}(m_X < 3.1$ GeV)	[ttaa]	< 1	$\times 10^{-3}$	CL=90%	–
$\gamma X\overline{X}(m_X < 4.5$ GeV)	[uuaa]	< 2.4	$\times 10^{-4}$	CL=90%	–
$\gamma X \to \gamma + \geq 4$ prongs	[vvaa]	< 1.78	$\times 10^{-4}$	CL=95%	–
$\gamma a_1^0 \to \gamma\mu^+\mu^-$	[xxaa]	< 9	$\times 10^{-6}$	CL=90%	–
$\gamma a_1^0 \to \gamma\tau^+\tau^-$	[qqaa]	< 1.30	$\times 10^{-4}$	CL=90%	–
$\gamma a_1^0 \to \gamma gg$	[yyaa]	< 1	%	CL=90%	–
$\gamma a_1^0 \to \gamma s\overline{s}$	[yyaa]	< 1	$\times 10^{-3}$	CL=90%	–
Lepton Family number (*LF*) violating modes					
$\mu^\pm\tau^\mp$	*LF*	< 6.0	$\times 10^{-6}$	CL=95%	4563
Other decays					
invisible		< 3.0	$\times 10^{-4}$	CL=90%	–
hadrons		(97 ± 5) %			–

$\chi_{b0}(1P)$ [zzaa]

$I^G(J^{PC}) = 0^+(0^{++})$
J needs confirmation.

Mass $m = 9859.44 \pm 0.42 \pm 0.31$ MeV

$\chi_{b0}(1P)$ DECAY MODES	Fraction (Γ_i/Γ)	Confidence level	p (MeV/c)
$\gamma\Upsilon(1S)$	(1.94 ± 0.27) %		391
$D^0 X$	< 10.4 %	90%	–
$\pi^+\pi^- K^+K^-\pi^0$	$< 1.6 \times 10^{-4}$	90%	4875
$2\pi^+\pi^- K^- K_S^0$	$< 5 \times 10^{-5}$	90%	4875
$2\pi^+\pi^- K^- K_S^0 2\pi^0$	$< 5 \times 10^{-4}$	90%	4846
$2\pi^+ 2\pi^- 2\pi^0$	$< 2.1 \times 10^{-4}$	90%	4905
$2\pi^+ 2\pi^- K^+K^-$	$(1.1 \pm 0.6) \times 10^{-4}$		4861
$2\pi^+ 2\pi^- K^+K^-\pi^0$	$< 2.7 \times 10^{-4}$	90%	4846
$2\pi^+ 2\pi^- K^+K^- 2\pi^0$	$< 5 \times 10^{-4}$	90%	4828
$3\pi^+ 2\pi^- K^- K_S^0\pi^0$	$< 1.6 \times 10^{-4}$	90%	4827
$3\pi^+ 3\pi^-$	$< 8 \times 10^{-5}$	90%	4904
$3\pi^+ 3\pi^- 2\pi^0$	$< 6 \times 10^{-4}$	90%	4881
$3\pi^+ 3\pi^- K^+K^-$	$(2.4 \pm 1.2) \times 10^{-4}$		4827
$3\pi^+ 3\pi^- K^+K^-\pi^0$	$< 1.0 \times 10^{-3}$	90%	4808
$4\pi^+ 4\pi^-$	$< 8 \times 10^{-5}$	90%	4880
$4\pi^+ 4\pi^- 2\pi^0$	$< 2.1 \times 10^{-3}$	90%	4850
$J/\psi J/\psi$	$< 7 \times 10^{-5}$	90%	3836
$J/\psi\psi(2S)$	$< 1.2 \times 10^{-4}$	90%	3571
$\psi(2S)\psi(2S)$	$< 3.1 \times 10^{-5}$	90%	3273
$J/\psi(1S)$ anything	$< 2.3 \times 10^{-3}$	90%	–

$\chi_{b1}(1P)$ [zzaa]

$I^G(J^{PC}) = 0^+(1^{++})$
J needs confirmation.

Mass $m = 9892.78 \pm 0.26 \pm 0.31$ MeV

$\chi_{b1}(1P)$ DECAY MODES	Fraction (Γ_i/Γ)	Confidence level	p (MeV/c)
$\gamma\Upsilon(1S)$	(35.2 ± 2.0) %		423
$D^0 X$	(12.6 ± 2.2) %		–
$\pi^+\pi^- K^+K^-\pi^0$	$(2.0 \pm 0.6) \times 10^{-4}$		4892
$2\pi^+\pi^- K^- K_S^0$	$(1.3 \pm 0.5) \times 10^{-4}$		4892
$2\pi^+\pi^- K^- K_S^0 2\pi^0$	$< 6 \times 10^{-4}$	90%	4863
$2\pi^+ 2\pi^- 2\pi^0$	$(8.0 \pm 2.5) \times 10^{-4}$		4921
$2\pi^+ 2\pi^- K^+K^-$	$(1.5 \pm 0.5) \times 10^{-4}$		4878
$2\pi^+ 2\pi^- K^+K^-\pi^0$	$(3.5 \pm 1.2) \times 10^{-4}$		4863
$2\pi^+ 2\pi^- K^+K^- 2\pi^0$	$(8.6 \pm 3.2) \times 10^{-4}$		4845
$3\pi^+ 2\pi^- K^- K_S^0\pi^0$	$(9.3 \pm 3.3) \times 10^{-4}$		4844
$3\pi^+ 3\pi^-$	$(1.9 \pm 0.6) \times 10^{-4}$		4921
$3\pi^+ 3\pi^- 2\pi^0$	$(1.7 \pm 0.5) \times 10^{-3}$		4898
$3\pi^+ 3\pi^- K^+K^-$	$(2.6 \pm 0.8) \times 10^{-4}$		4844
$3\pi^+ 3\pi^- K^+K^-\pi^0$	$(7.5 \pm 2.6) \times 10^{-4}$		4825
$4\pi^+ 4\pi^-$	$(2.6 \pm 0.9) \times 10^{-4}$		4897
$4\pi^+ 4\pi^- 2\pi^0$	$(1.4 \pm 0.6) \times 10^{-3}$		4867
ω anything	(4.9 ± 1.4) %		–
ωX_{tetra}	$< 4.44 \times 10^{-4}$	90%	–

Downloaded from https://academic.oup.com/ptep/article/2022/8/083C01/6651666 by KIT Library user on 27 September 2022

$J/\psi J/\psi$	$< 2.7 \times 10^{-5}$	90%	3857
$J/\psi\psi(2S)$	$< 1.7 \times 10^{-5}$	90%	3594
$\psi(2S)\psi(2S)$	$< 6 \times 10^{-5}$	90%	3298
$J/\psi(1S)$ anything	$< 1.1 \times 10^{-3}$	90%	–
$J/\psi(1S) X_{tetra}$	$< 2.27 \times 10^{-4}$	90%	–

$h_b(1P)$

$I^G(J^{PC}) = 0^-(1^{+-})$

Mass $m = 9899.3 \pm 0.8$ MeV

$h_b(1P)$ DECAY MODES	Fraction (Γ_i/Γ)	p (MeV/c)
$\eta_b(1S)\gamma$	(52^{+6}_{-5}) %	488

$\chi_{b2}(1P)$ [zzaa]

$I^G(J^{PC}) = 0^+(2^{++})$
J needs confirmation.

Mass $m = 9912.21 \pm 0.26 \pm 0.31$ MeV

$\chi_{b2}(1P)$ DECAY MODES	Fraction (Γ_i/Γ)	Confidence level	p (MeV/c)
$\gamma\Upsilon(1S)$	(18.0 ± 1.0) %		442
$D^0 X$	< 7.9 %	90%	–
$\pi^+\pi^- K^+K^-\pi^0$	$(8 \pm 5) \times 10^{-5}$		4902
$2\pi^+\pi^- K^- K^0_S$	$< 1.0 \times 10^{-4}$	90%	4901
$2\pi^+\pi^- K^- K^0_S 2\pi^0$	$(5.3\pm2.4) \times 10^{-4}$		4873
$2\pi^+2\pi^-2\pi^0$	$(3.5\pm1.4) \times 10^{-4}$		4931
$2\pi^+2\pi^- K^+K^-$	$(1.1\pm0.4) \times 10^{-4}$		4888
$2\pi^+2\pi^- K^+K^-\pi^0$	$(2.1\pm0.9) \times 10^{-4}$		4872
$2\pi^+2\pi^- K^+K^- 2\pi^0$	$(3.9\pm1.8) \times 10^{-4}$		4855
$3\pi^+2\pi^- K^- K^0_S\pi^0$	$< 5 \times 10^{-4}$	90%	4854
$3\pi^+3\pi^-$	$(7.0\pm3.1) \times 10^{-5}$		4931
$3\pi^+3\pi^-2\pi^0$	$(1.0\pm0.4) \times 10^{-3}$		4908
$3\pi^+3\pi^- K^+K^-$	$< 8 \times 10^{-5}$	90%	4854
$3\pi^+3\pi^- K^+K^-\pi^0$	$(3.6\pm1.5) \times 10^{-4}$		4835
$4\pi^+4\pi^-$	$(8 \pm 4) \times 10^{-5}$		4907
$4\pi^+4\pi^-2\pi^0$	$(1.8\pm0.7) \times 10^{-3}$		4877
$J/\psi J/\psi$	$< 4 \times 10^{-5}$	90%	3869
$J/\psi\psi(2S)$	$< 5 \times 10^{-5}$	90%	3608
$\psi(2S)\psi(2S)$	$< 1.6 \times 10^{-5}$	90%	3313
$J/\psi(1S)$ anything	$(1.5\pm0.4) \times 10^{-3}$		–

$\Upsilon(2S)$

$I^G(J^{PC}) = 0^-(1^{--})$

Mass $m = 10023.26 \pm 0.31$ MeV
$m_{\Upsilon(3S)} - m_{\Upsilon(2S)} = 331.50 \pm 0.13$ MeV
Full width $\Gamma = 31.98 \pm 0.63$ keV

$\Upsilon(2S)$ DECAY MODES	Fraction (Γ_i/Γ)	Scale factor/ Confidence level	p (MeV/c)
$\Upsilon(1S)\pi^+\pi^-$	(17.85 ± 0.26) %		475
$\Upsilon(1S)\pi^0\pi^0$	(8.6 ± 0.4) %		480
$\tau^+\tau^-$	(2.00 ± 0.21) %		4686
$\mu^+\mu^-$	(1.93 ± 0.17) %	S=2.2	5011
e^+e^-	(1.91 ± 0.16) %		5012
$\Upsilon(1S)\pi^0$	$< 4 \times 10^{-5}$	CL=90%	531
$\Upsilon(1S)\eta$	$(2.9 \pm 0.4) \times 10^{-4}$	S=2.0	126
$J/\psi(1S)$ anything	$< 6 \times 10^{-3}$	CL=90%	4533
$J/\psi(1S)\eta_c$	$< 5.4 \times 10^{-6}$	CL=90%	3984
$J/\psi(1S)\chi_{c0}$	$< 3.4 \times 10^{-6}$	CL=90%	3808
$J/\psi(1S)\chi_{c1}$	$< 1.2 \times 10^{-6}$	CL=90%	3765
$J/\psi(1S)\chi_{c2}$	$< 2.0 \times 10^{-6}$	CL=90%	3744
$J/\psi(1S)\eta_c(2S)$	$< 2.5 \times 10^{-6}$	CL=90%	3707
$J/\psi(1S)X(3940)$	$< 2.0 \times 10^{-6}$	CL=90%	3555
$J/\psi(1S)X(4160)$	$< 2.0 \times 10^{-6}$	CL=90%	3442
χ_{c1} anything	$(2.2 \pm 0.5) \times 10^{-4}$		–
$\chi_{c1}(1P)^0 X_{tetra}$	$< 3.67 \times 10^{-5}$	CL=90%	–
χ_{c2} anything	$(2.3 \pm 0.8) \times 10^{-4}$		–
$\psi(2S)\eta_c$	$< 5.1 \times 10^{-6}$	CL=90%	3732
$\psi(2S)\chi_{c0}$	$< 4.7 \times 10^{-6}$	CL=90%	3536
$\psi(2S)\chi_{c1}$	$< 2.5 \times 10^{-6}$	CL=90%	3488
$\psi(2S)\chi_{c2}$	$< 1.9 \times 10^{-6}$	CL=90%	3464
$\psi(2S)\eta_c(2S)$	$< 3.3 \times 10^{-6}$	CL=90%	3422
$\psi(2S)X(3940)$	$< 3.9 \times 10^{-6}$	CL=90%	3250
$\psi(2S)X(4160)$	$< 3.9 \times 10^{-6}$	CL=90%	3120
$Z_c(3900)^+ Z_c(3900)^-$	$< 1.0 \times 10^{-6}$	CL=90%	–
$Z_c(4200)^+ Z_c(4200)^-$	$< 1.67 \times 10^{-5}$	CL=90%	–
$Z_c(3900)^\pm Z_c(4200)^\mp$	$< 7.3 \times 10^{-6}$	CL=90%	–
$X(4050)^+ X(4050)^-$	$< 1.35 \times 10^{-5}$	CL=90%	–
$X(4250)^+ X(4250)^-$	$< 2.67 \times 10^{-5}$	CL=90%	–
$X(4050)^\pm X(4250)^\mp$	$< 2.72 \times 10^{-5}$	CL=90%	–
$Z_c(4430)^+ Z_c(4430)^-$	$< 2.03 \times 10^{-5}$	CL=90%	–
$X(4055)^\pm X(4055)^\mp$	$< 1.11 \times 10^{-5}$	CL=90%	–
$X(4055)^\pm Z_c(4430)^\mp$	$< 2.11 \times 10^{-5}$	CL=90%	–
$\overline{{}^2H}$ anything	$(2.78^{+0.30}_{-0.26}) \times 10^{-5}$	S=1.2	–
hadrons	(94 ± 11) %		–
ggg	(58.8 ± 1.2) %		–
γgg	(1.87 ± 0.28) %		–
ϕK^+K^-	$(1.6 \pm 0.4) \times 10^{-6}$		4910
$\omega\pi^+\pi^-$	$< 2.58 \times 10^{-6}$	CL=90%	4977
$K^*(892)^0 K^-\pi^+$ + c.c.	$(2.3 \pm 0.7) \times 10^{-6}$		4952
$\phi f'_2(1525)$	$< 1.33 \times 10^{-6}$	CL=90%	4842
$\omega f_2(1270)$	$< 5.7 \times 10^{-7}$	CL=90%	4899
$\rho(770) a_2(1320)$	$< 8.8 \times 10^{-7}$	CL=90%	4894
$K^*(892)^0 \overline{K}^*_2(1430)^0$ + c.c.	$(1.5 \pm 0.6) \times 10^{-6}$		4869
$K_1(1270)^\pm K^\mp$	$< 3.22 \times 10^{-6}$	CL=90%	4921
$K_1(1400)^\pm K^\mp$	$< 8.3 \times 10^{-7}$	CL=90%	4901
$b_1(1235)^\pm\pi^\mp$	$< 4.0 \times 10^{-7}$	CL=90%	4935
$\rho\pi$	$< 1.16 \times 10^{-6}$	CL=90%	4981
$\pi^+\pi^-\pi^0$	$< 8.0 \times 10^{-7}$	CL=90%	5007
$\omega\pi^0$	$< 1.63 \times 10^{-6}$	CL=90%	4980
$\pi^+\pi^-\pi^0\pi^0$	$(1.30\pm 0.28) \times 10^{-5}$		5002
$K^0_S K^+\pi^-$ + c.c.	$(1.14\pm 0.33) \times 10^{-6}$		4979
$K^*(892)^0 \overline{K}^0$ + c.c.	$< 4.22 \times 10^{-6}$	CL=90%	4959
$K^*(892)^- K^+$ + c.c.	$< 1.45 \times 10^{-6}$	CL=90%	4960
$f_1(1285)$ anything	$(2.2 \pm 1.6) \times 10^{-3}$		–
$f_1(1285) X_{tetra}$	$< 6.47 \times 10^{-5}$	CL=90%	–
Sum of 100 exclusive modes	$(2.90\pm 0.30) \times 10^{-3}$		–
Radiative decays			
$\gamma\chi_{b1}(1P)$	(6.9 ± 0.4) %		130
$\gamma\chi_{b2}(1P)$	(7.15 ± 0.35) %		110
$\gamma\chi_{b0}(1P)$	(3.8 ± 0.4) %		162
$\gamma f_0(1710)$	$< 5.9 \times 10^{-4}$	CL=90%	4867
$\gamma f'_2(1525)$	$< 5.3 \times 10^{-4}$	CL=90%	4897
$\gamma f_2(1270)$	$< 2.41 \times 10^{-4}$	CL=90%	4930
$\gamma\eta_c(1S)$	$< 2.7 \times 10^{-5}$	CL=90%	4567
$\gamma\chi_{c0}$	$< 1.0 \times 10^{-4}$	CL=90%	4430
$\gamma\chi_{c1}$	$< 3.6 \times 10^{-6}$	CL=90%	4397
$\gamma\chi_{c2}$	$< 1.5 \times 10^{-5}$	CL=90%	4381
$\gamma\chi_{c1}(3872)$	$< 2.1 \times 10^{-5}$	CL=90%	4264
$\gamma\chi_{c1}(3872)$, $\chi_{c1} \to \pi^+\pi^-\pi^0 J/\psi$	$< 2.4 \times 10^{-6}$	CL=90%	–
$\gamma\chi_{c0}(3915) \to \omega J/\psi$	$< 2.8 \times 10^{-6}$	CL=90%	–
$\gamma\chi_{c1}(4140) \to \phi J/\psi$	$< 1.2 \times 10^{-6}$	CL=90%	–
$\gamma X(4350) \to \phi J/\psi$	$< 1.3 \times 10^{-6}$	CL=90%	–
$\gamma\eta_b(1S)$	$(5.5 \pm^{1.1}_{0.9}) \times 10^{-4}$	S=1.2	605
$\gamma\eta_b(1S) \to \gamma$Sum of 26 exclusive modes	$< 3.7 \times 10^{-6}$	CL=90%	–
$\gamma X_{b\overline{b}} \to \gamma$Sum of 26 exclusive modes	$< 4.9 \times 10^{-6}$	CL=90%	–
$\gamma X \to \gamma + \geq 4$ prongs [aabb]	$< 1.95 \times 10^{-4}$	CL=95%	–
$\gamma A^0 \to \gamma$hadrons	$< 8 \times 10^{-5}$	CL=90%	–
$\gamma a^0_1 \to \gamma\mu^+\mu^-$	$< 8.3 \times 10^{-6}$	CL=90%	–
Lepton Family number (*LF*) violating modes			
$e^\pm\tau^\mp$ *LF*	$< 3.2 \times 10^{-6}$	CL=90%	4854
$\mu^\pm\tau^\mp$ *LF*	$< 3.3 \times 10^{-6}$	CL=90%	4854

$\Upsilon_2(1D)$

$I^G(J^{PC}) = 0^-(2^{--})$

was $\Upsilon(1D)$

Mass $m = 10163.7 \pm 1.4$ MeV (S = 1.7)

$\Upsilon_2(1D)$ DECAY MODES	Fraction (Γ_i/Γ)	p (MeV/c)
$\gamma\gamma\Upsilon(1S)$	seen	679
$\gamma\chi_{bJ}(1P)$	seen	300
$\eta\Upsilon(1S)$	not seen	426
$\pi^+\pi^-\Upsilon(1S)$	$(6.6\pm1.6) \times 10^{-3}$	623

Downloaded from https://academic.oup.com/ptep/article/2022/8/083C01/6651666 by KIT Library user on 27 September 2022

$\chi_{b0}(2P)$ [zzaa]

$I^G(J^{PC}) = 0^+(0^{++})$
J needs confirmation.

Mass $m = 10232.5 \pm 0.4 \pm 0.5$ MeV

$\chi_{b0}(2P)$ DECAY MODES	Fraction (Γ_i/Γ)	Confidence level	p (MeV/c)
$\gamma\,\Upsilon(2S)$	(1.38 ± 0.30) %		207
$\gamma\,\Upsilon(1S)$	$(3.8 \pm 1.7) \times 10^{-3}$		743
$D^0 X$	< 8.2 %	90%	–
$\pi^+\pi^- K^+ K^- \pi^0$	$< 3.4 \times 10^{-5}$	90%	5064
$2\pi^+\pi^- K^- K^0_S$	$< 5 \times 10^{-5}$	90%	5063
$2\pi^+\pi^- K^- K^0_S 2\pi^0$	$< 2.2 \times 10^{-4}$	90%	5036
$2\pi^+ 2\pi^- 2\pi^0$	$< 2.4 \times 10^{-4}$	90%	5092
$2\pi^+ 2\pi^- K^+ K^-$	$< 1.5 \times 10^{-4}$	90%	5050
$2\pi^+ 2\pi^- K^+ K^- \pi^0$	$< 2.2 \times 10^{-4}$	90%	5035
$2\pi^+ 2\pi^- K^+ K^- 2\pi^0$	$< 1.1 \times 10^{-3}$	90%	5019
$3\pi^+ 2\pi^- K^- K^0_S \pi^0$	$< 7 \times 10^{-4}$	90%	5018
$3\pi^+ 3\pi^-$	$< 7 \times 10^{-5}$	90%	5091
$3\pi^+ 3\pi^- 2\pi^0$	$< 1.2 \times 10^{-3}$	90%	5070
$3\pi^+ 3\pi^- K^+ K^-$	$< 1.5 \times 10^{-4}$	90%	5017
$3\pi^+ 3\pi^- K^+ K^- \pi^0$	$< 7 \times 10^{-4}$	90%	4999
$4\pi^+ 4\pi^-$	$< 1.7 \times 10^{-4}$	90%	5069
$4\pi^+ 4\pi^- 2\pi^0$	$< 6 \times 10^{-4}$	90%	5039

$\chi_{b1}(2P)$ [zzaa]

$I^G(J^{PC}) = 0^+(1^{++})$
J needs confirmation.

Mass $m = 10255.46 \pm 0.22 \pm 0.50$ MeV
$m_{\chi_{b1}(2P)} - m_{\chi_{b0}(2P)} = 23.5 \pm 1.0$ MeV

$\chi_{b1}(2P)$ DECAY MODES	Fraction (Γ_i/Γ)	p (MeV/c)
$\omega\,\Upsilon(1S)$	$(1.63^{+0.40}_{-0.34})$ %	135
$\gamma\,\Upsilon(2S)$	(18.1 ± 1.9) %	230
$\gamma\,\Upsilon(1S)$	(9.9 ± 1.0) %	764
$\pi\pi\,\chi_{b1}(1P)$	$(9.1 \pm 1.3) \times 10^{-3}$	238
$D^0 X$	(8.8 ± 1.7) %	–
$\pi^+\pi^- K^+ K^- \pi^0$	$(3.1 \pm 1.0) \times 10^{-4}$	5075
$2\pi^+\pi^- K^- K^0_S$	$(1.1 \pm 0.5) \times 10^{-4}$	5075
$2\pi^+\pi^- K^- K^0_S 2\pi^0$	$(7.7 \pm 3.2) \times 10^{-4}$	5047
$2\pi^+ 2\pi^- 2\pi^0$	$(5.9 \pm 2.0) \times 10^{-4}$	5104
$2\pi^+ 2\pi^- K^+ K^-$	$(10 \pm 4) \times 10^{-5}$	5062
$2\pi^+ 2\pi^- K^+ K^- \pi^0$	$(5.5 \pm 1.8) \times 10^{-4}$	5047
$2\pi^+ 2\pi^- K^+ K^- 2\pi^0$	$(10 \pm 4) \times 10^{-4}$	5030
$3\pi^+ 2\pi^- K^- K^0_S \pi^0$	$(6.7 \pm 2.6) \times 10^{-4}$	5029
$3\pi^+ 3\pi^-$	$(1.2 \pm 0.4) \times 10^{-4}$	5103
$3\pi^+ 3\pi^- 2\pi^0$	$(1.2 \pm 0.4) \times 10^{-3}$	5081
$3\pi^+ 3\pi^- K^+ K^-$	$(2.0 \pm 0.8) \times 10^{-4}$	5029
$3\pi^+ 3\pi^- K^+ K^- \pi^0$	$(6.1 \pm 2.2) \times 10^{-4}$	5011
$4\pi^+ 4\pi^-$	$(1.7 \pm 0.6) \times 10^{-4}$	5080
$4\pi^+ 4\pi^- 2\pi^0$	$(1.9 \pm 0.7) \times 10^{-3}$	5051

$h_b(2P)$

$I^G(J^{PC}) = 0^-(1^{+-})$

Mass $m = 10259.8 \pm 1.2$ MeV

$h_b(2P)$ DECAY MODES	Fraction (Γ_i/Γ)	p (MeV/c)
hadrons	not seen	–
$\eta_b(1S)\gamma$	(22 ± 5) %	825
$\eta_b(2S)\gamma$	(48 ± 13) %	257

$\chi_{b2}(2P)$ [zzaa]

$I^G(J^{PC}) = 0^+(2^{++})$
J needs confirmation.

Mass $m = 10268.65 \pm 0.22 \pm 0.50$ MeV
$m_{\chi_{b2}(2P)} - m_{\chi_{b1}(2P)} = 13.10 \pm 0.24$ MeV

$\chi_{b2}(2P)$ DECAY MODES	Fraction (Γ_i/Γ)	Confidence level	p (MeV/c)
$\omega\,\Upsilon(1S)$	$(1.10^{+0.34}_{-0.30})$ %		194
$\gamma\,\Upsilon(2S)$	(8.9 ± 1.2) %		242
$\gamma\,\Upsilon(1S)$	(6.6 ± 0.8) %		777
$\pi\pi\,\chi_{b2}(1P)$	$(5.1 \pm 0.9) \times 10^{-3}$		229
$D^0 X$	< 2.4 %	90%	–
$\pi^+\pi^- K^+ K^- \pi^0$	$< 1.1 \times 10^{-4}$	90%	5082
$2\pi^+\pi^- K^- K^0_S$	$< 9 \times 10^{-5}$	90%	5082
$2\pi^+\pi^- K^- K^0_S 2\pi^0$	$< 7 \times 10^{-4}$	90%	5054
$2\pi^+ 2\pi^- 2\pi^0$	$(3.9 \pm 1.6) \times 10^{-4}$		5110
$2\pi^+ 2\pi^- K^+ K^-$	$(9 \pm 4) \times 10^{-5}$		5068
$2\pi^+ 2\pi^- K^+ K^- \pi^0$	$(2.4 \pm 1.1) \times 10^{-4}$		5054
$2\pi^+ 2\pi^- K^+ K^- 2\pi^0$	$(4.7 \pm 2.3) \times 10^{-4}$		5037
$3\pi^+ 2\pi^- K^- K^0_S \pi^0$	$< 4 \times 10^{-4}$	90%	5036
$3\pi^+ 3\pi^-$	$(9 \pm 4) \times 10^{-5}$		5110
$3\pi^+ 3\pi^- 2\pi^0$	$(1.2 \pm 0.4) \times 10^{-3}$		5088
$3\pi^+ 3\pi^- K^+ K^-$	$(1.4 \pm 0.7) \times 10^{-4}$		5036
$3\pi^+ 3\pi^- K^+ K^- \pi^0$	$(4.2 \pm 1.7) \times 10^{-4}$		5017
$4\pi^+ 4\pi^-$	$(9 \pm 5) \times 10^{-5}$		5087
$4\pi^+ 4\pi^- 2\pi^0$	$(1.3 \pm 0.5) \times 10^{-3}$		5058

$\Upsilon(3S)$

$I^G(J^{PC}) = 0^-(1^{--})$

Mass $m = 10355.2 \pm 0.5$ MeV
$m_{\Upsilon(3S)} - m_{\Upsilon(2S)} = 331.50 \pm 0.13$ MeV
Full width $\Gamma = 20.32 \pm 1.85$ keV

$\Upsilon(3S)$ DECAY MODES	Fraction (Γ_i/Γ)	Scale factor/ Confidence level	p (MeV/c)
$\Upsilon(2S)$ anything	(10.6 ± 0.8) %		296
$\Upsilon(2S)\pi^+\pi^-$	(2.82 ± 0.18) %	S=1.6	177
$\Upsilon(2S)\pi^0\pi^0$	(1.85 ± 0.14) %		190
$\Upsilon(2S)\gamma\gamma$	(5.0 ± 0.7) %		327
$\Upsilon(2S)\pi^0$	$< 5.1 \times 10^{-4}$	CL=90%	298
$\Upsilon(1S)\pi^+\pi^-$	(4.37 ± 0.08) %		813
$\Upsilon(1S)\pi^0\pi^0$	(2.20 ± 0.13) %		816
$\Upsilon(1S)\eta$	$< 1 \times 10^{-4}$	CL=90%	677
$\Upsilon(1S)\pi^0$	$< 7 \times 10^{-5}$	CL=90%	846
$h_b(1P)\pi^0$	$< 1.2 \times 10^{-3}$	CL=90%	426
$h_b(1P)\pi^0 \to \gamma\eta_b(1S)\pi^0$	$(4.3 \pm 1.4) \times 10^{-4}$		–
$h_b(1P)\pi^+\pi^-$	$< 1.2 \times 10^{-4}$	CL=90%	353
$\tau^+\tau^-$	(2.29 ± 0.30) %		4863
$\mu^+\mu^-$	(2.18 ± 0.21) %	S=2.1	5177
e^+e^-	(2.18 ± 0.20) %		5178
hadrons	(93 ± 12) %		–
ggg	(35.7 ± 2.6) %		–
γgg	$(9.7 \pm 1.8) \times 10^{-3}$		–
^2H anything	$(2.33 \pm 0.33) \times 10^{-5}$		–
Radiative decays			
$\gamma\chi_{b2}(2P)$	(13.1 ± 1.6) %	S=3.4	86
$\gamma\chi_{b1}(2P)$	(12.6 ± 1.2) %	S=2.4	99
$\gamma\chi_{b0}(2P)$	(5.9 ± 0.6) %	S=1.4	122
$\gamma\chi_{b2}(1P)$	$(10.0 \pm 1.0) \times 10^{-3}$	S=1.7	434
$\gamma\chi_{b1}(1P)$	$(9 \pm 5) \times 10^{-4}$	S=1.8	452
$\gamma\chi_{b0}(1P)$	$(2.7 \pm 0.4) \times 10^{-3}$		484
$\gamma\eta_b(2S)$	$< 6.2 \times 10^{-4}$	CL=90%	350
$\gamma\eta_b(1S)$	$(5.1 \pm 0.7) \times 10^{-4}$		912
$\gamma A^0 \to \gamma$ hadrons	$< 8 \times 10^{-5}$	CL=90%	–
$\gamma X \to \gamma + \geq 4$ prongs	[bbbb] $< 2.2 \times 10^{-4}$	CL=95%	–
$\gamma a_1^0 \to \gamma\mu^+\mu^-$	$< 5.5 \times 10^{-6}$	CL=90%	–
$\gamma a_1^0 \to \gamma\tau^+\tau^-$	[ccbb] $< 1.6 \times 10^{-4}$	CL=90%	–
Lepton Family number (*LF*) violating modes			
$e^\pm\tau^\mp$ *LF*	$< 4.2 \times 10^{-6}$	CL=90%	5025
$\mu^\pm\tau^\mp$ *LF*	$< 3.1 \times 10^{-6}$	CL=90%	5025

$\chi_{b1}(3P)$ [zzaa]

$I^G(J^{PC}) = 0^+(1^{++})$

J needs confirmation.
Mass $m = 10513.4 \pm 0.7$ MeV

$\chi_{b1}(3P)$ DECAY MODES	Fraction (Γ_i/Γ)	p (MeV/c)
$\Upsilon(1S)\gamma$	seen	1000
$\Upsilon(2S)\gamma$	seen	479
$\Upsilon(3S)\gamma$	seen	157

Downloaded from https://academic.oup.com/ptep/article/2022/8/083C01/6651666 by KIT Library user on 27 September 2022

$\chi_{b2}(3P)$ [zzaa]

$I^G(J^{PC}) = 0^+(2^{++})$

J needs confirmation.

Mass $m = 10524.0 \pm 0.8$ MeV

$\chi_{b2}(3P)$ DECAY MODES	Fraction (Γ_i/Γ)	p (MeV/c)
$\Upsilon(3S)\gamma$	seen	167

$\Upsilon(4S)$

$I^G(J^{PC}) = 0^-(1^{--})$

also known as $\Upsilon(10580)$

Mass $m = 10579.4 \pm 1.2$ MeV

Full width $\Gamma = 20.5 \pm 2.5$ MeV

$\Upsilon(4S)$ DECAY MODES	Fraction (Γ_i/Γ)	Confidence level	p (MeV/c)
$B\overline{B}$	> 96 %	95%	326
B^+B^-	(51.4 ± 0.6) %		331
D_s^+ anything + c.c.	(17.8 ± 2.6) %		–
$B^0\overline{B}^0$	(48.6 ± 0.6) %		326
$J/\psi K_S^0 + (J/\psi, \eta_c) K_S^0$	$< 4 \times 10^{-7}$	90%	–
non-$B\overline{B}$	< 4 %	95%	–
e^+e^-	$(1.57 \pm 0.08) \times 10^{-5}$		5290
$\rho^+\rho^-$	$< 5.7 \times 10^{-6}$	90%	5233
$K^*(892)^0\overline{K}^0$	$< 2.0 \times 10^{-6}$	90%	5240
$J/\psi(1S)$ anything	$< 1.9 \times 10^{-4}$	95%	–
D^{*+} anything + c.c.	< 7.4 %	90%	5099
ϕ anything	(7.1 ± 0.6) %		5240
$\phi\eta$	$< 1.8 \times 10^{-6}$	90%	5226
$\phi\eta'$	$< 4.3 \times 10^{-6}$	90%	5196
$\rho\eta$	$< 1.3 \times 10^{-6}$	90%	5247
$\rho\eta'$	$< 2.5 \times 10^{-6}$	90%	5217
$\Upsilon(1S)$ anything	$< 4 \times 10^{-3}$	90%	1053
$\Upsilon(1S)\pi^+\pi^-$	$(8.2 \pm 0.4) \times 10^{-5}$		1026
$\Upsilon(1S)\eta$	$(1.81 \pm 0.18) \times 10^{-4}$		924
$\Upsilon(1S)\eta'$	$(3.4 \pm 0.9) \times 10^{-5}$		–
$\Upsilon(2S)\pi^+\pi^-$	$(8.2 \pm 0.8) \times 10^{-5}$		468
$h_b(1P)\pi^+\pi^-$	not seen		600
$h_b(1P)\eta$	$(2.18 \pm 0.21) \times 10^{-3}$		390
$\eta_b(1S)\omega$	$< 1.8 \times 10^{-4}$	90%	–
^2H anything	$< 1.3 \times 10^{-5}$	90%	–
Double Radiative Decays			
$\gamma\gamma\,\Upsilon(D) \to \gamma\gamma\eta\,\Upsilon(1S)$	$< 2.3 \times 10^{-5}$	90%	–

$Z_b(10610)$

$I^G(J^{PC}) = 1^+(1^{+-})$

was $X(10610)$

Mass $m = 10607.2 \pm 2.0$ MeV

Full width $\Gamma = 18.4 \pm 2.4$ MeV

$Z_b(10610)$ DECAY MODES	Fraction (Γ_i/Γ)	p (MeV/c)
$\Upsilon(1S)\pi^+$	$(5.4^{+1.9}_{-1.5}) \times 10^{-3}$	1077
$\Upsilon(1S)\pi^0$	not seen	1077
$\Upsilon(2S)\pi^+$	$(3.6^{+1.1}_{-0.8})$ %	551
$\Upsilon(2S)\pi^0$	seen	552
$\Upsilon(3S)\pi^+$	$(2.1^{+0.8}_{-0.6})$ %	207
$\Upsilon(3S)\pi^0$	seen	210
$h_b(1P)\pi^+$	$(3.5^{+1.2}_{-0.9})$ %	671
$h_b(2P)\pi^+$	$(4.7^{+1.7}_{-1.3})$ %	313
$B^+\overline{B}^0$	not seen	505
$B^+\overline{B}^{*0} + B^{*+}\overline{B}^0$	$(85.6^{+2.1}_{-2.9})$ %	–

$Z_b(10650)$

$I^G(J^{PC}) = 1^+(1^{+-})$

I, G, C need confirmation.

was $X(10650)^\pm$

Mass $m = 10652.2 \pm 1.5$ MeV

Full width $\Gamma = 11.5 \pm 2.2$ MeV

$Z_b(10650)^-$ decay modes are charge conjugates of the modes below.

$Z_b(10650)^+$ DECAY MODES	Fraction (Γ_i/Γ)	p (MeV/c)
$\Upsilon(1S)\pi^+$	$(1.7^{+0.8}_{-0.6}) \times 10^{-3}$	1117
$\Upsilon(2S)\pi^+$	$(1.4^{+0.6}_{-0.4})$ %	595
$\Upsilon(3S)\pi^+$	$(1.6^{+0.7}_{-0.5})$ %	259
$h_b(1P)\pi^+$	$(8.4^{+2.9}_{-2.4})$ %	714
$h_b(2P)\pi^+$	(15 ± 4) %	360
$B^+\overline{B}^0$	not seen	703
$B^+\overline{B}^{*0} + B^{*+}\overline{B}^0$	not seen	–
$B^{*+}\overline{B}^{*0}$	(74^{+4}_{-6}) %	122

$\Upsilon(10860)$

$I^G(J^{PC}) = 0^-(1^{--})$

Mass $m = 10885.2^{+2.6}_{-1.6}$ MeV

Full width $\Gamma = 37 \pm 4$ MeV

$\Upsilon(10860)$ DECAY MODES	Fraction (Γ_i/Γ)	Confidence level	p (MeV/c)
$B\overline{B}X$	$(76.2^{+2.7}_{-4.0})$ %		–
$B\overline{B}$	(5.5 ± 1.0) %		1322
$B\overline{B}^* +$ c.c.	(13.7 ± 1.6) %		–
$B^*\overline{B}^*$	(38.1 ± 3.4) %		1127
$B\overline{B}^{(*)}\pi$	< 19.7 %	90%	1015
$B\overline{B}\pi$	(0.0 ± 1.2) %		1015
$B^*\overline{B}\pi + B\overline{B}^*\pi$	(7.3 ± 2.3) %		–
$B^*\overline{B}^*\pi$	(1.0 ± 1.4) %		739
$B\overline{B}\pi\pi$	< 8.9 %	90%	551
$B_s^{(*)}\overline{B}_s^{(*)}$	(20.1 ± 3.1) %		905
$B_s\overline{B}_s$	$(5 \pm 5) \times 10^{-3}$		905
$B_s\overline{B}_s^* +$ c.c.	(1.35 ± 0.32) %		–
$B_s^*\overline{B}_s^*$	(17.6 ± 2.7) %		543
no open-bottom	$(3.8^{+5.0}_{-0.5})$ %		–
e^+e^-	$(8.3 \pm 2.1) \times 10^{-6}$		5443
$K^*(892)^0\overline{K}^0$	$< 1.0 \times 10^{-5}$	90%	5395
$\Upsilon(1S)\pi^+\pi^-$	$(5.3 \pm 0.6) \times 10^{-3}$		1306
$\Upsilon(1S)\eta$	$(8.5 \pm 1.7) \times 10^{-4}$		1229
$\Upsilon(1S)\eta'$	$< 6.9 \times 10^{-5}$	90%	985
$\Upsilon(2S)\pi^+\pi^-$	$(7.8 \pm 1.3) \times 10^{-3}$		783
$\Upsilon(2S)\eta$	$(4.1 \pm 0.6) \times 10^{-3}$		639
$\Upsilon(3S)\pi^+\pi^-$	$(4.8^{+1.9}_{-1.7}) \times 10^{-3}$		440
$\Upsilon(1S)K^+K^-$	$(6.1 \pm 1.8) \times 10^{-4}$		959
$\eta\Upsilon_J(1D)$	$(4.8 \pm 1.1) \times 10^{-3}$		–
$h_b(1P)\pi^+\pi^-$	$(3.5^{+1.0}_{-1.3}) \times 10^{-3}$		903
$h_b(2P)\pi^+\pi^-$	$(5.7^{+1.7}_{-2.1}) \times 10^{-3}$		544
$\chi_{bJ}(1P)\pi^+\pi^-\pi^0$	$(2.5 \pm 2.3) \times 10^{-3}$		894
$\chi_{b0}(1P)\pi^+\pi^-\pi^0$	$< 6.3 \times 10^{-3}$	90%	894
$\chi_{b0}(1P)\omega$	$< 3.9 \times 10^{-3}$	90%	631
$\chi_{b0}(1P)(\pi^+\pi^-\pi^0)_{non-\omega}$	$< 4.8 \times 10^{-3}$	90%	–
$\chi_{b1}(1P)\pi^+\pi^-\pi^0$	$(1.85 \pm 0.33) \times 10^{-3}$		861
$\chi_{b1}(1P)\omega$	$(1.57 \pm 0.30) \times 10^{-3}$		582
$\chi_{b1}(1P)(\pi^+\pi^-\pi^0)_{non-\omega}$	$(5.2 \pm 1.9) \times 10^{-4}$		–
$\chi_{b2}(1P)\pi^+\pi^-\pi^0$	$(1.17 \pm 0.30) \times 10^{-3}$		841
$\chi_{b2}(1P)\omega$	$(6.0 \pm 2.7) \times 10^{-4}$		552
$\chi_{b2}(1P)(\pi^+\pi^-\pi^0)_{non-\omega}$	$(6 \pm 4) \times 10^{-4}$		–
$\gamma X_b \to \gamma\Upsilon(1S)\omega$	$< 3.8 \times 10^{-5}$	90%	–
$\eta_b(1S)\omega$	$< 1.3 \times 10^{-3}$	90%	1177
$\eta_b(2S)\omega$	$< 5.6 \times 10^{-3}$	90%	399
Inclusive Decays.			
These decay modes are submodes of one or more of the decay modes above.			
ϕ anything	$(13.8^{+2.4}_{-1.7})$ %		–
D^0 anything + c.c.	(108 ± 8) %		–
D_s anything + c.c.	(46 ± 6) %		–
J/ψ anything	(2.06 ± 0.21) %		–
B^0 anything + c.c.	(77 ± 8) %		–
B^+ anything + c.c.	(72 ± 6) %		–

Downloaded from https://academic.oup.com/ptep/article/2022/8/083C01/6651666 by KIT Library user on 27 September 2022

$\Upsilon(11020)$

$I^G(J^{PC}) = 0^-(1^{--})$

Mass $m = 11000 \pm 4$ MeV
Full width $\Gamma = 24^{+8}_{-6}$ MeV

$\Upsilon(11020)$ DECAY MODES	Fraction (Γ_i/Γ)	p (MeV/c)
e^+e^-	$(5.4^{+1.9}_{-2.1}) \times 10^{-6}$	5500
$\chi_{bJ}(1P)\pi^+\pi^-\pi^0$	$(9^{+9}_{-8}) \times 10^{-3}$	1007
$\chi_{b1}(1P)\pi^+\pi^-\pi^0$	seen	975
$\chi_{b2}(1P)\pi^+\pi^-\pi^0$	seen	956

NOTES

In this Summary Table:

When a quantity has "(S = ...)" to its right, the error on the quantity has been enlarged by the "scale factor" S, defined as $S = \sqrt{\chi^2/(N-1)}$, where N is the number of measurements used in calculating the quantity. We do this when $S > 1$, which often indicates that the measurements are inconsistent. When $S > 1.25$, we also show in the Particle Listings an ideogram of the measurements. For more about S, see the Introduction.

A decay momentum p is given for each decay mode. For a 2-body decay, p is the momentum of each decay product in the rest frame of the decaying particle. For a 3-or-more-body decay, p is the largest momentum any of the products can have in this frame.

[a] See the review on "Form Factors for Radiative Pion and Kaon Decays" for definitions and details.

[b] Measurements of $\Gamma(e^+\nu_e)/\Gamma(\mu^+\nu_\mu)$ always include decays with γ's, and measurements of $\Gamma(e^+\nu_e\gamma)$ and $\Gamma(\mu^+\nu_\mu\gamma)$ never include low-energy γ's. Therefore, since no clean separation is possible, we consider the modes with γ's to be subreactions of the modes without them, and let $[\Gamma(e^+\nu_e) + \Gamma(\mu^+\nu_\mu)]/\Gamma_{\rm total} = 100\%$.

[c] See the $\pi^\pm$ Particle Listings for the energy limits used in this measurement; low-energy γ's are not included.

[d] Derived from an analysis of neutrino-oscillation experiments.

[e] Astrophysical and cosmological arguments give limits of order 10^{-13}, but they are model dependent and for the summary value we use the best laboratory limit, which includes any final state of invisible particles.

[f] Forbidden by angular momentum conservation.

[g] C parity forbids this to occur as a single-photon process.

[h] The $\omega\rho$ interference is then due to $\omega\rho$ mixing only, and is expected to be small. If $e\mu$ universality holds, $\Gamma(\rho^0 \to \mu^+\mu^-) = \Gamma(\rho^0 \to e^+e^-) \times 0.99785$.

[i] Our estimate. See the Particle Listings for details.

[j] See the "Note on $a_1(1260)$" in the $a_1(1260)$ Particle Listings in PDG 06, Journal of Physics **G33** 1 (2006).

[k] See also the $\omega(1650)$.

[l] See also the $\omega(1420)$.

[n] See the note in the $K^\pm$ Particle Listings.

[o] Neglecting photon channels. See, *e.g.*, A. Pais and S.B. Treiman, Phys. Rev. **D12**, 2744 (1975).

[p] The definition of the slope parameters of the $K \to 3\pi$ Dalitz plot is as follows (see also "Note on Dalitz Plot Parameters for $K \to 3\pi$ Decays" in the $K^\pm$ Particle Listings):

$$|M|^2 = 1 + g(s_3 - s_0)/m^2_{\pi^+} + \cdots .$$

[q] For more details and definitions of parameters see the Particle Listings.

[r] See the $K^\pm$ Particle Listings for the energy limits used in this measurement.

[s] Most of this radiative mode, the low-momentum γ part, is also included in the parent mode listed without γ's.

[t] Structure-dependent part.

[u] Direct-emission branching fraction.

[v] Violates angular-momentum conservation.

[x] Derived from measured values of ϕ_{+-}, ϕ_{00}, $|\eta|$, $|m_{K^0_L} - m_{K^0_S}|$, and $\tau_{K^0_S}$, as described in the introduction to "Tests of Conservation Laws."

[y] The CP-violation parameters are defined as follows (see also "Note on CP Violation in $K_S \to 3\pi$" and "Note on CP Violation in K^0_L Decay" in the Particle Listings):

$$\eta_{+-} = |\eta_{+-}|e^{i\phi_{+-}} = \frac{A(K^0_L \to \pi^+\pi^-)}{A(K^0_S \to \pi^+\pi^-)} = \epsilon + \epsilon'$$

$$\eta_{00} = |\eta_{00}|e^{i\phi_{00}} = \frac{A(K^0_L \to \pi^0\pi^0)}{A(K^0_S \to \pi^0\pi^0)} = \epsilon - 2\epsilon'$$

$$\delta = \frac{\Gamma(K^0_L \to \pi^-\ell^+\nu) - \Gamma(K^0_L \to \pi^+\ell^-\nu)}{\Gamma(K^0_L \to \pi^-\ell^+\nu) + \Gamma(K^0_L \to \pi^+\ell^-\nu)} ,$$

$$\mathrm{Im}(\eta_{+-0})^2 = \frac{\Gamma(K^0_S \to \pi^+\pi^-\pi^0)^{CP\ \mathrm{viol.}}}{\Gamma(K^0_L \to \pi^+\pi^-\pi^0)} ,$$

$$\mathrm{Im}(\eta_{000})^2 = \frac{\Gamma(K^0_S \to \pi^0\pi^0\pi^0)}{\Gamma(K^0_L \to \pi^0\pi^0\pi^0)} .$$

where for the last two relations CPT is assumed valid, *i.e.*, $\mathrm{Re}(\eta_{+-0}) \simeq 0$ and $\mathrm{Re}(\eta_{000}) \simeq 0$.

[z] See the K^0_S Particle Listings for the energy limits used in this measurement.

[aa] The value is for the sum of the charge states or particle/antiparticle states indicated.

[bb] $\mathrm{Re}(\epsilon'/\epsilon) = \epsilon'/\epsilon$ to a very good approximation provided the phases satisfy CPT invariance.

[cc] This mode includes gammas from inner bremsstrahlung but not the direct emission mode $K^0_L \to \pi^+\pi^-\gamma(\mathrm{DE})$.

[dd] See the K^0_L Particle Listings for the energy limits used in this measurement.

[ee] Allowed by higher-order electroweak interactions.

[ff] Violates CP in leading order. Test of direct CP violation since the indirect CP-violating and CP-conserving contributions are expected to be suppressed.

[gg] See our minireview under the $K_2(1770)$ in the 2004 edition of this *Review*.

[hh] This result applies to $Z^0 \to c\overline{c}$ decays only. Here ℓ^+ is an average (not a sum) of e^+ and μ^+ decays.

[ii] See the Particle Listings for the (complicated) definition of this quantity.

[jj] The branching fraction for this mode may differ from the sum of the submodes that contribute to it, due to interference effects. See the relevant papers in the Particle Listings.

[kk] These subfractions of the $K^-2\pi^+$ mode are uncertain: see the Particle Listings.

[ll] Submodes of the $D^+ \to K^-2\pi^+\pi^0$ and $K^0_S 2\pi^+\pi^-$ modes were studied by ANJOS 92C and COFFMAN 92B, but with at most 142 events for the first mode and 229 for the second – not enough for precise results. With nothing new for 18 years, we refer to our 2008 edition, Physics Letters **B667** 1 (2008), for those results.

[nn] The unseen decay modes of the resonances are included.

[oo] This is *not* a test for the ΔC=1 weak neutral current, but leads to the $\pi^+\ell^+\ell^-$ final state.

[pp] This mode is not a useful test for a ΔC=1 weak neutral current because both quarks must change flavor in this decay.

[qq] In the 2010 *Review*, the values for these quantities were given using a measure of the asymmetry that was inconsistent with the usual definition.

[rr] This value is obtained by subtracting the branching fractions for 2-, 4- and 6-prongs from unity.

[ss] This is the sum of our $K^-2\pi^+\pi^-$, $K^-2\pi^+\pi^-\pi^0$, $\overline{K}^0 2\pi^+2\pi^-$, $K^+2K^-\pi^+$, $2\pi^+2\pi^-$, $2\pi^+2\pi^-\pi^0$, $K^+K^-\pi^+\pi^-$, and $K^+K^-\pi^+\pi^-\pi^0$, branching fractions.

[tt] This is the sum of our $K^-3\pi^+2\pi^-$ and $3\pi^+3\pi^-$ branching fractions.

[uu] The branching fractions for the $K^-e^+\nu_e$, $K^*(892)^-e^+\nu_e$, $\pi^-e^+\nu_e$, and $\rho^-e^+\nu_e$ modes add up to 6.17 ± 0.17 %.

[vv] This is a doubly Cabibbo-suppressed mode.

[xx] Submodes of the $D^0 \to K^0_S\pi^+\pi^-\pi^0$ mode with a K^* and/or ρ were studied by COFFMAN 92B, but with only 140 events. With nothing new for 18 years, we refer to our 2008 edition, Physics Letters **B667** 1 (2008), for those results.

[yy] This branching fraction includes all the decay modes of the resonance in the final state.

[zz] This limit is for either D^0 or $\overline{D}^0$ to pe^-.

Downloaded from https://academic.oup.com/ptep/article/2022/8/083C01/6651666 by KIT Library user on 27 September 2022

[*aaa*] This limit is for either D^0 or $\overline{D}^0$ to $\overline{p}e^+$.

[*bbb*] This is the purely e^+ semileptonic branching fraction: the e^+ fraction from τ^+ decays has been subtracted off. The sum of our (non-τ) e^+ exclusive fractions — an $e^+\nu_e$ with an η, η', ϕ, K^0, or K^{*0} — is 5.99 ± 0.31 %.

[*ccc*] This fraction includes η from η' decays.

[*ddd*] The sum of our exclusive η' fractions — $\eta' e^+\nu_e$, $\eta'\mu^+\nu_\mu$, $\eta'\pi^+$, $\eta'\rho^+$, and $\eta' K^+$ — is 11.8 ± 1.6%.

[*eee*] This branching fraction includes all the decay modes of the final-state resonance.

[*fff*] A test for $u\overline{u}$ or $d\overline{d}$ content in the D_s^+. Neither Cabibbo-favored nor Cabibbo-suppressed decays can contribute, and $\omega - \phi$ mixing is an unlikely explanation for any fraction above about 2×10^{-4}.

[*ggg*] We decouple the $D_s^+ \to \phi\pi^+$ branching fraction obtained from mass projections (and used to get some of the other branching fractions) from the $D_s^+ \to \phi\pi^+$, $\phi \to K^+K^-$ branching fraction obtained from the Dalitz-plot analysis of $D_s^+ \to K^+K^-\pi^+$. That is, the ratio of these two branching fractions is not exactly the $\phi \to K^+K^-$ branching fraction 0.491.

[*hhh*] This is the average of a model-independent and a K-matrix parametrization of the $\pi^+\pi^-$ S-wave and is a sum over several f_0 mesons.

[*iii*] An ℓ indicates an e or a μ mode, not a sum over these modes.

[*jjj*] An $CP(\pm 1)$ indicates the CP=+1 and CP=−1 eigenstates of the D^0-$\overline{D}^0$ system.

[*kkk*] D denotes D^0 or $\overline{D}^0$.

[*lll*] D^{*0}_{CP+} decays into $D^0\pi^0$ with the D^0 reconstructed in CP-even eigenstates K^+K^- and $\pi^+\pi^-$.

[*nnn*] $\overline{D}^{**}$ represents an excited state with mass $2.2 < \mathrm{M} < 2.8$ GeV/c^2.

[*ooo*] $\chi_{c1}(3872)^+$ is a hypothetical charged partner of the $\chi_{c1}(3872)$.

[*ppp*] $\Theta(1710)^{++}$ is a possible narrow pentaquark state and $G(2220)$ is a possible glueball resonance.

[*qqq*] $(\overline{\Lambda}_c^- p)_s$ denotes a low-mass enhancement near 3.35 GeV/c^2.

[*rrr*] Stands for the possible candidates of $K^*(1410)$, $K_0^*(1430)$ and $K_2^*(1430)$.

[*sss*] B^0 and B_s^0 contributions not separated. Limit is on weighted average of the two decay rates.

[*ttt*] This decay refers to the coherent sum of resonant and nonresonant $J^P = 0^+$ $K\pi$ components with $1.60 < m_{K\pi} < 2.15$ GeV/c^2.

[*uuu*] $X(214)$ is a hypothetical particle of mass 214 MeV/c^2 reported by the HyperCP experiment, Physical Review Letters **94** 021801 (2005)

[*vvv*] $\Theta(1540)^+$ denotes a possible narrow pentaquark state.

[*xxx*] Here S and P are the hypothetical scalar and pseudoscalar particles with masses of 2.5 GeV/c^2 and 214.3 MeV/c^2, respectively.

[*yyy*] These values are model dependent.

[*zzz*] Here "anything" means at least one particle observed.

[*aaaa*] This is a $\mathrm{B}(B^0 \to D^{*-}\ell^+\nu_\ell)$ value.

[*bbaa*] D^{**} stands for the sum of the $D(1\,^1P_1)$, $D(1\,^3P_0)$, $D(1\,^3P_1)$, $D(1\,^3P_2)$, $D(2\,^1S_0)$, and $D(2\,^1S_1)$ resonances.

[*ccaa*] $D^{(*)}\overline{D}^{(*)}$ stands for the sum of $D^*\overline{D}^*$, $D^*\overline{D}$, $D\overline{D}^*$, and $D\overline{D}$.

[*ddaa*] $X(3915)$ denotes a near-threshold enhancement in the $\omega J/\psi$ mass spectrum.

[*eeaa*] Inclusive branching fractions have a multiplicity definition and can be greater than 100%.

[*ffaa*] D_j represents an unresolved mixture of pseudoscalar and tensor D^{**} (P-wave) states.

[*ggaa*] Not a pure measurement. See note at head of B_s^0 Decay Modes.

[*hhaa*] For $E_\gamma > 100$ MeV.

[*iiaa*] $\Theta(1540)$ is a hypothetical pentaquark state of 1.54 GeV/c^2 mass and a width of less than 25 MeV/c^2.

[*jjaa*] Includes $p\overline{p}\pi^+\pi^-\gamma$ and excludes $p\overline{p}\eta$, $p\overline{p}\omega$, $p\overline{p}\eta'$.

[*kkaa*] For a narrow state A with mass less than 960 MeV.

[*llaa*] For a narrow scalar or pseudoscalar A^0 with mass 0.21–3.0 GeV.

[*nnaa*] For a dark photon U with mass between 100 and 2100 MeV.

[*ooaa*] For a narrow resonance in the range $2.2 < M(X) < 2.8$ GeV.

[*ppaa*] J^{PC} known by production in e^+e^- via single photon annihilation. I^G is not known; interpretation of this state as a single resonance is unclear because of the expectation of substantial threshold effects in this energy region.

[*qqaa*] $2m_\tau < \mathrm{M}(\tau^+\tau^-) < 9.2$ GeV

[*rraa*] 2 GeV $< m_{K^+K^-} <$ 3 GeV

[*ssaa*] X = scalar with $m < 8.0$ GeV

[*ttaa*] $X\overline{X}$ = vectors with $m < 3.1$ GeV

[*uuaa*] X and $\overline{X}$ = zero spin with $m < 4.5$ GeV

[*vvaa*] 1.5 GeV $< m_X <$ 5.0 GeV

[*xxaa*] 201 MeV $< \mathrm{M}(\mu^+\mu^-) <$ 3565 MeV

[*yyaa*] 0.5 GeV $< m_X <$ 9.0 GeV, where m_X is the invariant mass of the hadronic final state.

[*zzaa*] Spectroscopic labeling for these states is theoretical, pending experimental information.

[*aabb*] 1.5 GeV $< m_X <$ 5.0 GeV

[*bbbb*] 1.5 GeV $< m_X <$ 5.0 GeV

[*ccbb*] For $m_{\tau^+\tau^-}$ in the ranges 4.03–9.52 and 9.61–10.10 GeV.

Downloaded from https://academic.oup.com/ptep/article/2022/8/083C01/6651666 by KIT Library user on 27 September 2022

Meson Summary Table

See also the table of suggested $q\overline{q}$ quark-model assignments in the Quark Model section.
• Indicates particles that appear in the preceding Meson Summary Table. We do not regard the other entries as being established.

LIGHT UNFLAVORED
($S = C = B = 0$)

	$I^G(J^{PC})$
• $\pi^{\pm}$	$1^-(0^-)$
• π^0	$1^-(0^{-+})$
• η	$0^+(0^{-+})$
• $f_0(500)$	$0^+(0^{++})$
• $\rho(770)$	$1^+(1^{--})$
• $\omega(782)$	$0^-(1^{--})$
• $\eta'(958)$	$0^+(0^{-+})$
• $f_0(980)$	$0^+(0^{++})$
• $a_0(980)$	$1^-(0^{++})$
• $\phi(1020)$	$0^-(1^{--})$
• $h_1(1170)$	$0^-(1^{+-})$
• $b_1(1235)$	$1^+(1^{+-})$
• $a_1(1260)$	$1^-(1^{++})$
• $f_2(1270)$	$0^+(2^{++})$
• $f_1(1285)$	$0^+(1^{++})$
• $\eta(1295)$	$0^+(0^{-+})$
• $\pi(1300)$	$1^-(0^{-+})$
• $a_2(1320)$	$1^-(2^{++})$
• $f_0(1370)$	$0^+(0^{++})$
• $\pi_1(1400)$	$1^-(1^{-+})$
• $\eta(1405)$	$0^+(0^{-+})$
• $h_1(1415)$	$0^-(1^{+-})$
• $f_1(1420)$	$0^+(1^{++})$
• $\omega(1420)$	$0^-(1^{--})$
$f_2(1430)$	$0^+(2^{++})$
• $a_0(1450)$	$1^-(0^{++})$
• $\rho(1450)$	$1^+(1^{--})$
• $\eta(1475)$	$0^+(0^{-+})$
• $f_0(1500)$	$0^+(0^{++})$
$f_1(1510)$	$0^+(1^{++})$
• $f_2'(1525)$	$0^+(2^{++})$
$f_2(1565)$	$0^+(2^{++})$
$\rho(1570)$	$1^+(1^{--})$
$h_1(1595)$	$0^-(1^{+-})$
• $\pi_1(1600)$	$1^-(1^{-+})$
• $a_1(1640)$	$1^-(1^{++})$
$f_2(1640)$	$0^+(2^{++})$
• $\eta_2(1645)$	$0^+(2^{-+})$
• $\omega(1650)$	$0^-(1^{--})$
• $\omega_3(1670)$	$0^-(3^{--})$

	$I^G(J^{PC})$
• $\pi_2(1670)$	$1^-(2^{-+})$
• $\phi(1680)$	$0^-(1^{--})$
• $\rho_3(1690)$	$1^+(3^{--})$
• $\rho(1700)$	$1^+(1^{--})$
• $a_2(1700)$	$1^-(2^{++})$
• $f_0(1710)$	$0^+(0^{++})$
$X(1750)$	$?^-(1^{--})$
$\eta(1760)$	$0^+(0^{-+})$
• $\pi(1800)$	$1^-(0^{-+})$
$f_2(1810)$	$0^+(2^{++})$
$X(1835)$	$?^?(0^{-+})$
• $\phi_3(1850)$	$0^-(3^{--})$
• $\eta_2(1870)$	$0^+(2^{-+})$
• $\pi_2(1880)$	$1^-(2^{-+})$
$\rho(1900)$	$1^+(1^{--})$
$f_2(1910)$	$0^+(2^{++})$
$a_0(1950)$	$1^-(0^{++})$
• $f_2(1950)$	$0^+(2^{++})$
• $a_4(1970)$	$1^-(4^{++})$
$\rho_3(1990)$	$1^+(3^{--})$
$\pi_2(2005)$	$1^-(2^{-+})$
• $f_2(2010)$	$0^+(2^{++})$
$f_0(2020)$	$0^+(0^{++})$
• $f_4(2050)$	$0^+(4^{++})$
$\pi_2(2100)$	$1^-(2^{-+})$
$f_0(2100)$	$0^+(0^{++})$
$f_2(2150)$	$0^+(2^{++})$
$\rho(2150)$	$1^+(1^{--})$
• $\phi(2170)$	$0^-(1^{--})$
$f_0(2200)$	$0^+(0^{++})$
$f_J(2220)$	$0^+(2^{++}$ or $4^{++})$
$\eta(2225)$	$0^+(0^{-+})$
$\rho_3(2250)$	$1^+(3^{--})$
• $f_2(2300)$	$0^+(2^{++})$
$f_4(2300)$	$0^+(4^{++})$
$f_0(2330)$	$0^+(0^{++})$
• $f_2(2340)$	$0^+(2^{++})$
$\rho_5(2350)$	$1^+(5^{--})$
$X(2370)$	$?^?(?^{??})$
$f_6(2510)$	$0^+(6^{++})$

STRANGE
($S = \pm1$, $C = B = 0$)

	$I(J^P)$
• $K^{\pm}$	$1/2(0^-)$
• K^0	$1/2(0^-)$
• K^0_S	$1/2(0^-)$
• K^0_L	$1/2(0^-)$
• $K^*_0(700)$	$1/2(0^+)$
• $K^*(892)$	$1/2(1^-)$
• $K_1(1270)$	$1/2(1^+)$
• $K_1(1400)$	$1/2(1^+)$
• $K^*(1410)$	$1/2(1^-)$
• $K^*_0(1430)$	$1/2(0^+)$
• $K^*_2(1430)$	$1/2(2^+)$
• $K(1460)$	$1/2(0^-)$
$K_2(1580)$	$1/2(2^-)$
$K(1630)$	$1/2(?^?)$
• $K_1(1650)$	$1/2(1^+)$
• $K^*(1680)$	$1/2(1^-)$
• $K_2(1770)$	$1/2(2^-)$
• $K^*_3(1780)$	$1/2(3^-)$
• $K_2(1820)$	$1/2(2^-)$
$K(1830)$	$1/2(0^-)$
$K^*_0(1950)$	$1/2(0^+)$
• $K^*_2(1980)$	$1/2(2^+)$
• $K^*_4(2045)$	$1/2(4^+)$
$K_2(2250)$	$1/2(2^-)$
$K_3(2320)$	$1/2(3^+)$
$K^*_5(2380)$	$1/2(5^-)$
$K_4(2500)$	$1/2(4^-)$
$K(3100)$	$?^?(?^{??})$

CHARMED
($C = \pm1$)

• $D^{\pm}$	$1/2(0^-)$
• D^0	$1/2(0^-)$
• $D^*(2007)^0$	$1/2(1^-)$
• $D^*(2010)^{\pm}$	$1/2(1^-)$
• $D^*_0(2300)$	$1/2(0^+)$
• $D_1(2420)$	$1/2(1^+)$
• $D_1(2430)^0$	$1/2(1^+)$
• $D^*_2(2460)$	$1/2(2^+)$
$D_0(2550)^0$	$1/2(0^-)$
$D^*_1(2600)^0$	$1/2(1^-)$
$D^*(2640)^{\pm}$	$1/2(?^?)$
$D_2(2740)^0$	$1/2(2^-)$
• $D^*_3(2750)$	$1/2(3^-)$
$D^*_1(2760)^0$	$1/2(1^-)$
$D(3000)^0$	$1/2(?^?)$

CHARMED, STRANGE
($C = \pm1$, $S = \pm1$)
(+ possibly non-$q\overline{q}$ states)

	$I(J^P)$
• $D^{\pm}_s$	$0(0^-)$
• $D^{*\pm}_s$	$0(?^?)$
• $D^*_{s0}(2317)^{\pm}$	$0(0^+)$
• $D_{s1}(2460)^{\pm}$	$0(1^+)$
• $D_{s1}(2536)^{\pm}$	$0(1^+)$
• $D^*_{s2}(2573)$	$0(2^+)$
$D_{s0}(2590)^+$	$0(0^-)$
• $D^*_{s1}(2700)^{\pm}$	$0(1^-)$
$D^*_{s1}(2860)^{\pm}$	$0(1^-)$
• $D^*_{s3}(2860)^{\pm}$	$0(3^-)$
$X_0(2900)$	$?(0^+)$
$X_1(2900)$	$?(1^-)$
$D_{sJ}(3040)^{\pm}$	$0(?^?)$

BOTTOM
($B = \pm1$)

• $B^{\pm}$	$1/2(0^-)$
• B^0	$1/2(0^-)$
• $B^{\pm}/B^0$ ADMIXTURE	
• $B^{\pm}/B^0/B^0_s/b$-baryon ADMIXTURE	
V_{cb} and V_{ub} CKM Matrix Elements	
• B^*	$1/2(1^-)$
• $B_1(5721)$	$1/2(1^+)$
$B^*_J(5732)$	$?(?^?)$
• $B^*_2(5747)$	$1/2(2^+)$
$B_J(5840)$	$1/2(?^?)$
• $B_J(5970)$	$1/2(?^?)$

BOTTOM, STRANGE
($B = \pm1$, $S = \mp1$)

• B^0_s	$0(0^-)$
• B^*_s	$0(1^-)$
$X(5568)^{\pm}$	$?(?^?)$
• $B_{s1}(5830)^0$	$0(1^+)$
• $B^*_{s2}(5840)^0$	$0(2^+)$
$B^*_{sJ}(5850)$	$?(?^?)$
$B_{sJ}(6063)^0$	$0(?^?)$
$B_{sJ}(6114)^0$	$0(?^?)$

BOTTOM, CHARMED
($B = C = \pm1$)

• B^+_c	$0(0^-)$
• $B_c(2S)^{\pm}$	$0(0^-)$

$c\overline{c}$
(+ possibly non-$q\overline{q}$ states)

• $\eta_c(1S)$	$0^+(0^{-+})$
• $J/\psi(1S)$	$0^-(1^{--})$
• $\chi_{c0}(1P)$	$0^+(0^{++})$
• $\chi_{c1}(1P)$	$0^+(1^{++})$
• $h_c(1P)$	$0^-(1^{+-})$
• $\chi_{c2}(1P)$	$0^+(2^{++})$
• $\eta_c(2S)$	$0^+(0^{-+})$
• $\psi(2S)$	$0^-(1^{--})$
• $\psi(3770)$	$0^-(1^{--})$

$c\overline{c}$ continued

	$I^G(J^{PC})$
• $\psi_2(3823)$	$0^-(2^{--})$
• $\psi_3(3842)$	$0^-(3^{--})$
$\chi_{c0}(3860)$	$0^+(0^{++})$
• $\chi_{c1}(3872)$	$0^+(1^{++})$
• $Z_c(3900)$	$1^+(1^{+-})$
• $\chi_{c0}(3915)$	$0^+(0^{++})$
• $\chi_{c2}(3930)$	$0^+(2^{++})$
$X(3940)$	$?^?(?^{??})$
• $X(4020)^{\pm}$	$1^+(?^{?-})$
• $\psi(4040)$	$0^-(1^{--})$
$X(4050)^{\pm}$	$1^-(?^{?+})$
$X(4055)^{\pm}$	$1^+(?^{?-})$
$X(4100)^{\pm}$	$1^-(?^{??})$
• $\chi_{c1}(4140)$	$0^+(1^{++})$
• $\psi(4160)$	$0^-(1^{--})$
$X(4160)$	$?^?(?^{??})$
$Z_c(4200)$	$1^+(1^{+-})$
• $\psi(4230)$	$0^-(1^{--})$
$R_{c0}(4240)$	$1^+(0^{--})$
$X(4250)^{\pm}$	$1^-(?^{?+})$
• $\chi_{c1}(4274)$	$0^+(1^{++})$
$X(4350)$	$0^+(?^{?+})$
• $\psi(4360)$	$0^-(1^{--})$
• $\psi(4415)$	$0^-(1^{--})$
• $Z_c(4430)$	$1^+(1^{+-})$
$\chi_{c0}(4500)$	$0^+(0^{++})$
$X(4630)$	$0^+(?^{?+})$
• $\psi(4660)$	$0^-(1^{--})$
$\chi_{c1}(4685)$	$0^+(1^{++})$
$\chi_{c0}(4700)$	$0^+(0^{++})$

$b\overline{b}$
(+ possibly non-$q\overline{q}$ states)

• $\eta_b(1S)$	$0^+(0^{-+})$
• $\Upsilon(1S)$	$0^-(1^{--})$
• $\chi_{b0}(1P)$	$0^+(0^{++})$
• $\chi_{b1}(1P)$	$0^+(1^{++})$
• $h_b(1P)$	$0^-(1^{+-})$
• $\chi_{b2}(1P)$	$0^+(2^{++})$
$\eta_b(2S)$	$0^+(0^{-+})$
• $\Upsilon(2S)$	$0^-(1^{--})$
• $\Upsilon_2(1D)$	$0^-(2^{--})$
• $\chi_{b0}(2P)$	$0^+(0^{++})$
• $\chi_{b1}(2P)$	$0^+(1^{++})$
• $h_b(2P)$	$0^-(1^{+-})$
• $\chi_{b2}(2P)$	$0^+(2^{++})$
• $\Upsilon(3S)$	$0^-(1^{--})$
• $\chi_{b1}(3P)$	$0^+(1^{++})$
• $\chi_{b2}(3P)$	$0^+(2^{++})$
• $\Upsilon(4S)$	$0^-(1^{--})$
• $Z_b(10610)$	$1^+(1^{+-})$
• $Z_b(10650)$	$1^+(1^{+-})$
$\Upsilon(10753)$	$?^?(1^{--})$
• $\Upsilon(10860)$	$0^-(1^{--})$
• $\Upsilon(11020)$	$0^-(1^{--})$

OTHER

Further States

Downloaded from https://academic.oup.com/ptep/article/2022/8/083C01/6651666 by KIT Library user on 27 September 2022

Baryon Summary Table

This short table gives the name, the quantum numbers (where known), and the status of baryons in the Review. Only the baryons with 3- or 4-star status are included in the Baryon Summary Table. Due to insufficient data or uncertain interpretation, the other entries in the table are not established baryons. The names with masses are of baryons that decay strongly. The spin-parity J^P (when known) is given with each particle. For the strongly decaying particles, the J^P values are considered to be part of the names.

p	$1/2^+$	****	$\Delta(1232)$	$3/2^+$	****	Σ^+	$1/2^+$	****	Λ_c^+	$1/2^+$	****	Λ_b^0	$1/2^+$	***
n	$1/2^+$	****	$\Delta(1600)$	$3/2^+$	****	Σ^0	$1/2^+$	****	$\Lambda_c(2595)^+$	$1/2^-$	***	$\Lambda_b(5912)^0$	$1/2^-$	***
$N(1440)$	$1/2^+$	****	$\Delta(1620)$	$1/2^-$	****	Σ^-	$1/2^+$	****	$\Lambda_c(2625)^+$	$3/2^-$	***	$\Lambda_b(5920)^0$	$3/2^-$	***
$N(1520)$	$3/2^-$	****	$\Delta(1700)$	$3/2^-$	****	$\Sigma(1385)$	$3/2^+$	****	$\Lambda_c(2765)^+$		*	$\Lambda_b(6070)^0$	$1/2^+$	***
$N(1535)$	$1/2^-$	****	$\Delta(1750)$	$1/2^+$	*	$\Sigma(1580)$	$3/2^-$	*	$\Lambda_c(2860)^+$	$3/2^+$	***	$\Lambda_b(6146)^0$	$3/2^+$	***
$N(1650)$	$1/2^-$	****	$\Delta(1900)$	$1/2^-$	***	$\Sigma(1620)$	$1/2^-$	*	$\Lambda_c(2880)^+$	$5/2^+$	***	$\Lambda_b(6152)^0$	$5/2^+$	***
$N(1675)$	$5/2^-$	****	$\Delta(1905)$	$5/2^+$	****	$\Sigma(1660)$	$1/2^+$	***	$\Lambda_c(2940)^+$	$3/2^-$	***	Σ_b	$1/2^+$	***
$N(1680)$	$5/2^+$	****	$\Delta(1910)$	$1/2^+$	****	$\Sigma(1670)$	$3/2^-$	****	$\Sigma_c(2455)$	$1/2^+$	****	Σ_b^*	$3/2^+$	***
$N(1700)$	$3/2^-$	***	$\Delta(1920)$	$3/2^+$	***	$\Sigma(1750)$	$1/2^-$	***	$\Sigma_c(2520)$	$3/2^+$	***	$\Sigma_b(6097)^+$		***
$N(1710)$	$1/2^+$	****	$\Delta(1930)$	$5/2^-$	***	$\Sigma(1775)$	$5/2^-$	****	$\Sigma_c(2800)$		***	$\Sigma_b(6097)^-$		***
$N(1720)$	$3/2^+$	****	$\Delta(1940)$	$3/2^-$	**	$\Sigma(1780)$	$3/2^+$	*	Ξ_c^+	$1/2^+$	***	Ξ_b^-	$1/2^+$	***
$N(1860)$	$5/2^+$	**	$\Delta(1950)$	$7/2^+$	****	$\Sigma(1880)$	$1/2^+$	**	Ξ_c^0	$1/2^+$	****	Ξ_b^0	$1/2^+$	***
$N(1875)$	$3/2^-$	***	$\Delta(2000)$	$5/2^+$	**	$\Sigma(1900)$	$1/2^-$	**	$\Xi_c^{\prime +}$	$1/2^+$	***	$\Xi_b^{\prime}(5935)^-$	$1/2^+$	***
$N(1880)$	$1/2^+$	***	$\Delta(2150)$	$1/2^-$	*	$\Sigma(1910)$	$3/2^-$	***	$\Xi_c^{\prime 0}$	$1/2^+$	***	$\Xi_b(5945)^0$	$3/2^+$	***
$N(1895)$	$1/2^-$	****	$\Delta(2200)$	$7/2^-$	***	$\Sigma(1915)$	$5/2^+$	****	$\Xi_c(2645)$	$3/2^+$	***	$\Xi_b(5955)^-$	$3/2^+$	***
$N(1900)$	$3/2^+$	****	$\Delta(2300)$	$9/2^+$	**	$\Sigma(1940)$	$3/2^+$	*	$\Xi_c(2790)$	$1/2^-$	***	$\Xi_b(6100)^-$	$3/2^-$	***
$N(1990)$	$7/2^+$	**	$\Delta(2350)$	$5/2^-$	*	$\Sigma(2010)$	$3/2^-$	*	$\Xi_c(2815)$	$3/2^-$	***	$\Xi_b(6227)^-$		***
$N(2000)$	$5/2^+$	**	$\Delta(2390)$	$7/2^+$	*	$\Sigma(2030)$	$7/2^+$	****	$\Xi_c(2923)$		**	$\Xi_b(6227)^0$		***
$N(2040)$	$3/2^+$	*	$\Delta(2400)$	$9/2^-$	**	$\Sigma(2070)$	$5/2^+$	*	$\Xi_c(2930)$		**	Ω_b^-	$1/2^+$	***
$N(2060)$	$5/2^-$	***	$\Delta(2420)$	$11/2^+$	****	$\Sigma(2080)$	$3/2^+$	*	$\Xi_c(2970)$	$1/2^+$	***	$\Omega_b(6316)^-$		*
$N(2100)$	$1/2^+$	***	$\Delta(2750)$	$13/2^-$	**	$\Sigma(2100)$	$7/2^-$	*	$\Xi_c(3055)$		***	$\Omega_b(6330)^-$		*
$N(2120)$	$3/2^-$	***	$\Delta(2950)$	$15/2^+$	**	$\Sigma(2110)$	$1/2^-$	*	$\Xi_c(3080)$		***	$\Omega_b(6340)^-$		*
$N(2190)$	$7/2^-$	****				$\Sigma(2230)$	$3/2^+$	*	$\Xi_c(3123)$		*	$\Omega_b(6350)^-$		*
$N(2220)$	$9/2^+$	****	Λ	$1/2^+$	****	$\Sigma(2250)$		**	Ω_c^0	$1/2^+$	***			
$N(2250)$	$9/2^-$	****	$\Lambda(1380)$	$1/2^-$	**	$\Sigma(2455)$		*	$\Omega_c(2770)^0$	$3/2^+$	***	$P_c(4312)^+$		*
$N(2300)$	$1/2^+$	**	$\Lambda(1405)$	$1/2^-$	****	$\Sigma(2620)$		*	$\Omega_c(3000)^0$		***	$P_c(4380)^+$		*
$N(2570)$	$5/2^-$	**	$\Lambda(1520)$	$3/2^-$	****	$\Sigma(3000)$		*	$\Omega_c(3050)^0$		***	$P_c(4440)^+$		*
$N(2600)$	$11/2^-$	***	$\Lambda(1600)$	$1/2^+$	****	$\Sigma(3170)$		*	$\Omega_c(3065)^0$		***	$P_c(4457)^+$		*
$N(2700)$	$13/2^+$	**	$\Lambda(1670)$	$1/2^-$	****				$\Omega_c(3090)^0$		***			
			$\Lambda(1690)$	$3/2^-$	****	Ξ^0	$1/2^+$	****	$\Omega_c(3120)^0$		***			
			$\Lambda(1710)$	$1/2^+$	*	Ξ^-	$1/2^+$	****						
			$\Lambda(1800)$	$1/2^-$	***	$\Xi(1530)$	$3/2^+$	****	Ξ_{cc}^+		*			
			$\Lambda(1810)$	$1/2^+$	***	$\Xi(1620)$		*	Ξ_{cc}^{++}		***			
			$\Lambda(1820)$	$5/2^+$	****	$\Xi(1690)$		***						
			$\Lambda(1830)$	$5/2^-$	****	$\Xi(1820)$	$3/2^-$	***						
			$\Lambda(1890)$	$3/2^+$	****	$\Xi(1950)$		***						
			$\Lambda(2000)$	$1/2^-$	*	$\Xi(2030)$	$\geq \frac{5}{2}$?	***						
			$\Lambda(2050)$	$3/2^-$	*	$\Xi(2120)$		*						
			$\Lambda(2070)$	$3/2^+$	*	$\Xi(2250)$		**						
			$\Lambda(2080)$	$5/2^-$	*	$\Xi(2370)$		**						
			$\Lambda(2085)$	$7/2^+$	**	$\Xi(2500)$		*						
			$\Lambda(2100)$	$7/2^-$	****									
			$\Lambda(2110)$	$5/2^+$	***	Ω^-	$3/2^+$	****						
			$\Lambda(2325)$	$3/2^-$	*	$\Omega(2012)^-$	$?^-$	***						
			$\Lambda(2350)$	$9/2^+$	***	$\Omega(2250)^-$		***						
			$\Lambda(2585)$		*	$\Omega(2380)^-$		**						
						$\Omega(2470)^-$		**						

**** Existence is certain, and properties are at least fairly well explored.

*** Existence ranges from very likely to certain, but further confirmation is desirable and/or quantum numbers, branching fractions, etc. are not well determined.

** Evidence of existence is only fair.

* Evidence of existence is poor.

Downloaded from https://academic.oup.com/ptep/article/2022/8/083C01/6651666 by KIT Library user on 27 September 2022

N BARYONS ($S = 0$, $I = 1/2$)

p, $N^+ = uud$; n, $N^0 = udd$

p

$I(J^P) = \frac{1}{2}(\frac{1}{2}^+)$

Mass $m = 1.007276466621 \pm 0.000000000053$ u
Mass $m = 938.27208816 \pm 0.00000029$ MeV [a]
$|m_p - m_{\overline{p}}|/m_p < 7 \times 10^{-10}$, CL = 90% [b]
$|\frac{q_{\overline{p}}}{m_{\overline{p}}}|/(\frac{q_p}{m_p}) = 1.000000000003 \pm 0.000000000016$
$|q_p + q_{\overline{p}}|/e < 7 \times 10^{-10}$, CL = 90% [b]
$|q_p + q_e|/e < 1 \times 10^{-21}$ [c]
Magnetic moment $\mu = 2.7928473446 \pm 0.0000000008\ \mu_N$
$(\mu_p + \mu_{\overline{p}}) / \mu_p = (0.002 \pm 0.004) \times 10^{-6}$
Electric dipole moment $d < 0.021 \times 10^{-23}$ e cm
Electric polarizability $\alpha = (11.2 \pm 0.4) \times 10^{-4}$ fm^3
Magnetic polarizability $\beta = (2.5 \pm 0.4) \times 10^{-4}$ fm^3 (S = 1.2)
Charge radius, μp Lamb shift = 0.84087 ± 0.00039 fm [d]
Charge radius = 0.8409 ± 0.0004 fm [d]
Magnetic radius = 0.851 ± 0.026 fm [e]
Mean life $\tau > 3.6 \times 10^{29}$ years, CL = 90% [f] ($p \to$ invisible mode)
Mean life $\tau > 10^{31}$ to 10^{33} years [f] (mode dependent)

See the "Note on Nucleon Decay" in our 1994 edition (Phys. Rev. **D50**, 1173) for a short review.

The "partial mean life" limits tabulated here are the limits on τ/B_i, where τ is the total mean life and B_i is the branching fraction for the mode in question. For N decays, p and n indicate proton and neutron partial lifetimes.

p DECAY MODES	Partial mean life (10^{30} years)	Confidence level	p (MeV/c)
Antilepton + meson			
$N \to e^+ \pi$	> 5300 (n), > 16000 (p)	90%	459
$N \to \mu^+ \pi$	> 3500 (n), > 7700 (p)	90%	453
$N \to \nu \pi$	> 1100 (n), > 390 (p)	90%	459
$p \to e^+ \eta$	> 10000	90%	309
$p \to \mu^+ \eta$	> 4700	90%	297
$n \to \nu \eta$	> 158	90%	310
$N \to e^+ \rho$	> 217 (n), > 720 (p)	90%	149
$N \to \mu^+ \rho$	> 228 (n), > 570 (p)	90%	113
$N \to \nu \rho$	> 19 (n), > 162 (p)	90%	149
$p \to e^+ \omega$	> 1600	90%	143
$p \to \mu^+ \omega$	> 2800	90%	105
$n \to \nu \omega$	> 108	90%	144
$N \to e^+ K$	> 17 (n), > 1000 (p)	90%	339
$N \to \mu^+ K$	> 26 (n), > 1600 (p)	90%	329
$N \to \nu K$	> 86 (n), > 5900 (p)	90%	339
$n \to \nu K^0_S$	> 260	90%	338
$p \to e^+ K^*(892)^0$	> 84	90%	45
$N \to \nu K^*(892)$	> 78 (n), > 51 (p)	90%	45
Antilepton + mesons			
$p \to e^+ \pi^+ \pi^-$	> 82	90%	448
$p \to e^+ \pi^0 \pi^0$	> 147	90%	449
$n \to e^+ \pi^- \pi^0$	> 52	90%	449
$p \to \mu^+ \pi^+ \pi^-$	> 133	90%	425
$p \to \mu^+ \pi^0 \pi^0$	> 101	90%	427
$n \to \mu^+ \pi^- \pi^0$	> 74	90%	427
$n \to e^+ K^0 \pi^-$	> 18	90%	319
Lepton + meson			
$n \to e^- \pi^+$	> 65	90%	459
$n \to \mu^- \pi^+$	> 49	90%	453
$n \to e^- \rho^+$	> 62	90%	150
$n \to \mu^- \rho^+$	> 7	90%	115
$n \to e^- K^+$	> 32	90%	340
$n \to \mu^- K^+$	> 57	90%	330
Lepton + mesons			
$p \to e^- \pi^+ \pi^+$	> 30	90%	448
$n \to e^- \pi^+ \pi^0$	> 29	90%	449
$p \to \mu^- \pi^+ \pi^+$	> 17	90%	425
$n \to \mu^- \pi^+ \pi^0$	> 34	90%	427
$p \to e^- \pi^+ K^+$	> 75	90%	320
$p \to \mu^- \pi^+ K^+$	> 245	90%	279
Antilepton + photon(s)			
$p \to e^+ \gamma$	> 670	90%	469
$p \to \mu^+ \gamma$	> 478	90%	463
$n \to \nu \gamma$	> 550	90%	470
$p \to e^+ \gamma\gamma$	> 100	90%	469
$n \to \nu \gamma\gamma$	> 219	90%	470
Antilepton + single massless			
$p \to e^+ X$	> 790	90%	–
$p \to \mu^+ X$	> 410	90%	–
Three (or more) leptons			
$p \to e^+ e^+ e^-$	> 793	90%	469
$p \to e^+ \mu^+ \mu^-$	> 359	90%	457
$p \to e^+ \nu \nu$	> 170	90%	469
$n \to e^+ e^- \nu$	> 257	90%	470
$n \to \mu^+ e^- \nu$	> 83	90%	464
$n \to \mu^+ \mu^- \nu$	> 79	90%	458
$p \to \mu^+ e^+ e^-$	> 529	90%	463
$p \to \mu^- e^+ e^+$	$> 1.90 \times 10^{34}$		463
$p \to \mu^+ \mu^+ \mu^-$	> 675	90%	439
$p \to \mu^+ \nu \nu$	> 220	90%	463
$p \to e^- \mu^+ \mu^+$	> 6	90%	457
$n \to 3\nu$	$> 5 \times 10^{-4}$	90%	470
Inclusive modes			
$N \to e^+$ anything	> 0.6 (n, p)	90%	–
$N \to \mu^+$ anything	> 12 (n, p)	90%	–
$N \to e^+ \pi^0$ anything	> 0.6 (n, p)	90%	–
$\Delta B = 2$ dinucleon modes			
The following are lifetime limits per iron nucleus.			
$pp \to \pi^+ \pi^+$	> 72.2	90%	–
$pn \to \pi^+ \pi^0$	> 170	90%	–
$nn \to \pi^+ \pi^-$	> 0.7	90%	–
$nn \to \pi^0 \pi^0$	> 404	90%	–
$pp \to K^+ K^+$	> 170	90%	–
$pp \to e^+ e^+$	> 5.8	90%	–
$pp \to e^+ \mu^+$	> 3.6	90%	–
$pp \to \mu^+ \mu^+$	> 1.7	90%	–
$pn \to e^+ \overline{\nu}$	> 260	90%	–
$pn \to \mu^+ \overline{\nu}$	> 200	90%	–
$pn \to \tau^+ \overline{\nu}_\tau$	> 29	90%	–
$nn \to \nu_e \overline{\nu}_e$	> 1.4	90%	–
$nn \to \nu_\mu \overline{\nu}_\mu$	> 1.4	90%	–
$pn \to$ invisible	$> 2.1 \times 10^{-5}$	90%	–
$pp \to$ invisible	$> 5 \times 10^{-5}$	90%	–

$\overline{p}$ DECAY MODES

$\overline{p}$ DECAY MODES	Partial mean life (years)	Confidence level	p (MeV/c)
$\overline{p} \to e^- \gamma$	$> 7 \times 10^5$	90%	469
$\overline{p} \to \mu^- \gamma$	$> 5 \times 10^4$	90%	463
$\overline{p} \to e^- \pi^0$	$> 4 \times 10^5$	90%	459
$\overline{p} \to \mu^- \pi^0$	$> 5 \times 10^4$	90%	453
$\overline{p} \to e^- \eta$	$> 2 \times 10^4$	90%	309
$\overline{p} \to \mu^- \eta$	$> 8 \times 10^3$	90%	297
$\overline{p} \to e^- K^0_S$	> 900	90%	337
$\overline{p} \to \mu^- K^0_S$	$> 4 \times 10^3$	90%	326
$\overline{p} \to e^- K^0_L$	$> 9 \times 10^3$	90%	337
$\overline{p} \to \mu^- K^0_L$	$> 7 \times 10^3$	90%	326
$\overline{p} \to e^- \gamma\gamma$	$> 2 \times 10^4$	90%	469
$\overline{p} \to \mu^- \gamma\gamma$	$> 2 \times 10^4$	90%	463
$\overline{p} \to e^- \omega$	> 200	90%	143

n

$I(J^P) = \frac{1}{2}(\frac{1}{2}^+)$

Mass $m = 1.0086649160 \pm 0.0000000005$ u
Mass $m = 939.5654205 \pm 0.0000005$ MeV [a]
$(m_n - m_{\overline{n}})/ m_n = (9 \pm 6) \times 10^{-5}$
$m_n - m_p = 1.2933324 \pm 0.0000005$ MeV
$= 0.00138844919(45)$ u
Mean life $\tau = 878.4 \pm 0.5$ s (S = 1.8)
$c\tau = 2.6335 \times 10^8$ km
Magnetic moment $\mu = -1.9130427 \pm 0.0000005\ \mu_N$
Electric dipole moment $d < 0.18 \times 10^{-25}$ e cm, CL = 90%
Mean-square charge radius $\langle r_n^2 \rangle = -0.1155 \pm 0.0017$ fm^2

Downloaded from https://academic.oup.com/ptep/article/2022/8/083C01/6651666 by KIT Library user on 27 September 2022

Magnetic radius $\sqrt{\langle r_M^2 \rangle} = 0.864^{+0.009}_{-0.008}$ fm
Electric polarizability $\alpha = (11.8 \pm 1.1) \times 10^{-4}$ fm^3
Magnetic polarizability $\beta = (3.7 \pm 1.2) \times 10^{-4}$ fm^3
Charge $q = (-0.2 \pm 0.8) \times 10^{-21}$ e
Mean $n\overline{n}$-oscillation time $> 8.6 \times 10^7$ s, CL = 90% (free n)
Mean $n\overline{n}$-oscillation time $> 4.7 \times 10^8$ s, CL = 90% [g] (bound n)
Mean $n n'$-oscillation time > 448 s, CL = 90% [h]

$p e^- \nu_e$ decay parameters [i]

$\lambda \equiv g_A / g_V = -1.2754 \pm 0.0013$ (S = 2.7)
$A = -0.11958 \pm 0.00021$ (S = 1.2)
$B = 0.9807 \pm 0.0030$
$C = -0.2377 \pm 0.0026$
$a = -0.1049 \pm 0.0013$ (S = 1.8)
$\phi_{AV} = (180.017 \pm 0.026)^\circ$ [j]
$D = (-1.2 \pm 2.0) \times 10^{-4}$ [k]
$R = 0.004 \pm 0.013$ [k]
FIERZ INTERFERENCE TERM $b = 0.017 \pm 0.020$

n DECAY MODES		Fraction (Γ_i/Γ)	Confidence level	p (MeV/c)
$p e^- \overline{\nu}_e$		100 %		1
$p e^- \overline{\nu}_e \gamma$	[l]	$(9.2 \pm 0.7) \times 10^{-3}$		1
hydrogen-atom $\overline{\nu}_e$		$< 2.7 \times 10^{-3}$	95%	1.19
Charge conservation (Q) violating mode				
$p \nu_e \overline{\nu}_e$	Q	$< 8 \times 10^{-27}$	68%	1

$N(1440)\ 1/2^+$

$I(J^P) = \frac{1}{2}(\frac{1}{2}^+)$

Re(pole position) = 1360 to 1380 ($\approx$ 1370) MeV
-2Im(pole position) = 160 to 190 ($\approx$ 175) MeV
Breit-Wigner mass = 1410 to 1470 ($\approx$ 1440) MeV
Breit-Wigner full width = 250 to 450 ($\approx$ 350) MeV

$N(1440)$ DECAY MODES	Fraction (Γ_i/Γ)	p (MeV/c)
$N\pi$	55–75 %	398
$N\eta$	<1 %	†
$N\pi\pi$	17–50 %	347
$\Delta(1232)\pi$, P-wave	6–27 %	147
$N\sigma$	11–23 %	–
$p\gamma$, helicity=1/2	0.035–0.048 %	414
$n\gamma$, helicity=1/2	0.02–0.04 %	413

$N(1520)\ 3/2^-$

$I(J^P) = \frac{1}{2}(\frac{3}{2}^-)$

Re(pole position) = 1505 to 1515 ($\approx$ 1510) MeV
-2Im(pole position) = 105 to 120 ($\approx$ 110) MeV
Breit-Wigner mass = 1510 to 1520 ($\approx$ 1515) MeV
Breit-Wigner full width = 100 to 120 ($\approx$ 110) MeV

$N(1520)$ DECAY MODES	Fraction (Γ_i/Γ)	p (MeV/c)
$N\pi$	55–65 %	453
$N\eta$	0.07–0.09 %	142
$N\pi\pi$	25–35 %	410
$\Delta(1232)\pi$	22–34 %	225
$\Delta(1232)\pi$, S-wave	15–23 %	225
$\Delta(1232)\pi$, D-wave	7–11 %	225
$N\rho$	10–16 %	†
$N\rho$, S=3/2 , S-wave	10–16 %	†
$N\rho$, S=1/2 , D-wave	0.2–0.4 %	†
$N\sigma$	<10 %	–
$p\gamma$	0.31–0.52 %	467
$p\gamma$, helicity=1/2	0.01–0.02 %	467
$p\gamma$, helicity=3/2	0.30–0.50 %	467
$n\gamma$	0.30–0.53 %	466
$n\gamma$, helicity=1/2	0.04–0.10 %	466
$n\gamma$, helicity=3/2	0.25–0.45 %	466

$N(1535)\ 1/2^-$

$I(J^P) = \frac{1}{2}(\frac{1}{2}^-)$

Re(pole position) = 1500 to 1520 ($\approx$ 1510) MeV
-2Im(pole position) = 110 to 150 ($\approx$ 130) MeV
Breit-Wigner mass = 1515 to 1545 ($\approx$ 1530) MeV
Breit-Wigner full width = 125 to 175 ($\approx$ 150) MeV

$N(1535)$ DECAY MODES	Fraction (Γ_i/Γ)	p (MeV/c)
$N\pi$	32–52 %	464
$N\eta$	30–55 %	176
$N\pi\pi$	4–31 %	422
$\Delta(1232)\pi$, D-wave	1–4 %	240
$N\rho$	2–17 %	†
$N\rho$, S=1/2 , S-wave	2–16 %	†
$N\rho$, S=3/2 , D-wave	<1 %	†
$N\sigma$	2–10 %	–
$N(1440)\pi$	5–12 %	†
$p\gamma$, helicity=1/2	0.15–0.30 %	477
$n\gamma$, helicity=1/2	0.01–0.25 %	477

$N(1650)\ 1/2^-$

$I(J^P) = \frac{1}{2}(\frac{1}{2}^-)$

Re(pole position) = 1640 to 1670 ($\approx$ 1655) MeV
-2Im(pole position) = 100 to 170 ($\approx$ 135) MeV
Breit-Wigner mass = 1635 to 1665 ($\approx$ 1650) MeV
Breit-Wigner full width = 100 to 150 ($\approx$ 125) MeV

$N(1650)$ DECAY MODES	Fraction (Γ_i/Γ)	p (MeV/c)
$N\pi$	50–70 %	547
$N\eta$	15–35 %	348
ΛK	5–15 %	169
$N\pi\pi$	20–58 %	514
$\Delta(1232)\pi$, D-wave	6–18 %	345
$N\rho$	12–22 %	†
$N\rho$, S=1/2, S-wave	<4 %	†
$N\rho$, S=3/2, D-wave	12–18 %	†
$N\sigma$	2–18 %	–
$N(1440)\pi$	6–26 %	150
$p\gamma$, helicity=1/2	0.04–0.20 %	558
$n\gamma$, helicity=1/2	0.003–0.17 %	557

$N(1675)\ 5/2^-$

$I(J^P) = \frac{1}{2}(\frac{5}{2}^-)$

Re(pole position) = 1655 to 1665 ($\approx$ 1660) MeV
-2Im(pole position) = 125 to 150 ($\approx$ 135) MeV
Breit-Wigner mass = 1665 to 1680 ($\approx$ 1675) MeV
Breit-Wigner full width = 130 to 160 ($\approx$ 145) MeV

$N(1675)$ DECAY MODES	Fraction (Γ_i/Γ)	p (MeV/c)
$N\pi$	38–42 %	564
$N\eta$	< 1 %	376
ΛK	<0.04 %	216
$N\pi\pi$	25–45 %	532
$\Delta(1232)\pi$, D-wave	23–37 %	366
$N\rho$	0.1–0.9 %	†
$N\rho$, S=1/2	<0.2 %	†
$N\rho$, S=3/2 , D-wave	0.1–0.7 %	†
$N\sigma$	3–7 %	–
$p\gamma$	0–0.02 %	575
$p\gamma$, helicity=1/2	0–0.01 %	575
$p\gamma$, helicity=3/2	0–0.01 %	575
$n\gamma$	0–0.15 %	574
$n\gamma$, helicity=1/2	0–0.05 %	574
$n\gamma$, helicity=3/2	0–0.10 %	574

$N(1680)\ 5/2^+$

$I(J^P) = \frac{1}{2}(\frac{5}{2}^+)$

Re(pole position) = 1665 to 1680 ($\approx$ 1675) MeV
-2Im(pole position) = 110 to 135 ($\approx$ 120) MeV
Breit-Wigner mass = 1680 to 1690 ($\approx$ 1685) MeV
Breit-Wigner full width = 115 to 130 ($\approx$ 120) MeV

$N(1680)$ DECAY MODES	Fraction (Γ_i/Γ)	p (MeV/c)
$N\pi$	60–70 %	571
$N\eta$	<1 %	386
$N\pi\pi$	28–53 %	539
$\Delta(1232)\pi$	11–23 %	374
$\Delta(1232)\pi$, P-wave	4–10 %	374
$\Delta(1232)\pi$, F-wave	1–13 %	374
$N\rho$	8–11 %	†

Downloaded from https://academic.oup.com/ptep/article/2022/8/083C01/6651666 by KIT Library user on 27 September 2022

$N\rho$, S=3/2 , P-wave	6–8 %	†
$N\rho$, S=3/2 , F-wave	2–3 %	†
$N\sigma$	9–19 %	–
$p\gamma$	0.21–0.32 %	581
$p\gamma$, helicity=1/2	0.001–0.011 %	581
$p\gamma$, helicity=3/2	0.20–0.32 %	581
$n\gamma$	0.021–0.046 %	581
$n\gamma$, helicity=1/2	0.004–0.029 %	581
$n\gamma$, helicity=3/2	0.01–0.024 %	581

$N(1700)\ 3/2^-$

$I(J^P) = \frac{1}{2}(\frac{3}{2}^-)$

Re(pole position) = 1650 to 1750 (≈ 1700) MeV
−2Im(pole position) = 100 to 300 (≈ 200) MeV
Breit-Wigner mass = 1650 to 1800 (≈ 1720) MeV
Breit-Wigner full width = 100 to 300 (≈ 200) MeV

$N(1700)$ DECAY MODES	Fraction (Γ_i/Γ)	p (MeV/c)
$N\pi$	7–17 %	594
$N\eta$	1–2 %	422
$N\omega$	10–34 %	†
ΛK	1–2 %	283
$N\pi\pi$	>89 %	564
$\Delta(1232)\pi$	55–85 %	402
$\Delta(1232)\pi$, S-wave	50–80 %	402
$\Delta(1232)\pi$, D-wave	4–14 %	402
$N\rho$, S=3/2, S-wave	32–44 %	74
$N\sigma$	2–14 %	–
$N(1440)\pi$	3–11 %	225
$N(1520)\pi$	<4 %	145
$p\gamma$	0.01–0.05 %	604
$p\gamma$, helicity=1/2	0.0–0.024 %	604
$p\gamma$, helicity=3/2	0.002–0.026 %	604
$n\gamma$	0.01–0.13 %	603
$n\gamma$, helicity=1/2	0.0–0.09 %	603
$n\gamma$, helicity=3/2	0.01–0.05 %	603

$N(1710)\ 1/2^+$

$I(J^P) = \frac{1}{2}(\frac{1}{2}^+)$

Re(pole position) = 1680 to 1720 (≈ 1700) MeV
−2Im(pole position) = 80 to 160 (≈ 120) MeV
Breit-Wigner mass = 1680 to 1740 (≈ 1710) MeV
Breit-Wigner full width = 80 to 200 (≈ 140) MeV

$N(1710)$ DECAY MODES	Fraction (Γ_i/Γ)	p (MeV/c)
$N\pi$	5–20 %	588
$N\eta$	10–50 %	412
$N\omega$	1–5 %	†
ΛK	5–25 %	269
ΣK	seen	138
$N\pi\pi$	14–48 %	557
$\Delta(1232)\pi$, P-wave	3–9 %	394
$N\rho$, S=1/2, P-wave	11–23 %	†
$N\sigma$	<16 %	–
$N(1535)\pi$	9–21 %	113
$p\gamma$, helicity=1/2	0.002–0.08 %	598
$n\gamma$, helicity=1/2	0.0–0.02%	597

$N(1720)\ 3/2^+$

$I(J^P) = \frac{1}{2}(\frac{3}{2}^+)$

Re(pole position) = 1660 to 1690 (≈ 1675) MeV
−2Im(pole position) = 150 to 400 (≈ 250) MeV
Breit-Wigner mass = 1680 to 1750 (≈ 1720) MeV
Breit-Wigner full width = 150 to 400 (≈ 250) MeV

$N(1720)$ DECAY MODES	Fraction (Γ_i/Γ)	p (MeV/c)
$N\pi$	8–14 %	594
$N\eta$	1–5 %	422
$N\omega$	12–40 %	†
ΛK	4–19 %	283
$N\pi\pi$	>50 %	564
$\Delta(1232)\pi$	47–89 %	402
$\Delta(1232)\pi$, P-wave	47–77 %	402
$\Delta(1232)\pi$, F-wave	<12 %	402
$N\rho$, S=1/2, P-wave	1–2 %	74
$N\sigma$	2–14 %	–
$N(1440)\pi$	<2 %	225
$N(1520)\pi$, S-wave	1–5 %	145
$p\gamma$	0.05–0.25 %	604
$p\gamma$, helicity=1/2	0.05–0.15 %	604
$p\gamma$, helicity=3/2	0.002–0.16 %	604
$n\gamma$	0.0–0.016 %	603
$n\gamma$, helicity=1/2	0.0–0.01 %	603
$n\gamma$, helicity=3/2	0.0–0.015 %	603

$N(1875)\ 3/2^-$

$I(J^P) = \frac{1}{2}(\frac{3}{2}^-)$

Re(pole position) = 1850 to 1950 (≈ 1900) MeV
−2Im(pole position) = 100 to 220 (≈ 160) MeV
Breit-Wigner mass = 1850 to 1920 (≈ 1875) MeV
Breit-Wigner full width = 120 to 250 (≈ 200) MeV

$N(1875)$ DECAY MODES	Fraction (Γ_i/Γ)	p (MeV/c)
$N\pi$	3–11 %	695
$N\eta$	3–16 %	559
$N\omega$	15–25 %	371
ΛK	1–2 %	454
ΣK	0.3–1.1 %	384
$N\pi\pi$	>56 %	670
$\Delta(1232)\pi$	4–44 %	520
$\Delta(1232)\pi$, S-wave	2–21 %	520
$\Delta(1232)\pi$, D-wave	2–23 %	520
$N\rho$, S=3/2, S-wave	36–56 %	379
$N\sigma$	16–60 %	–
$N(1440)\pi$	2–8 %	365
$N(1520)\pi$	<2 %	301
$\Lambda K^*(892)$	<0.2 %	†
$p\gamma$	0.001–0.025 %	703
$p\gamma$, helicity=1/2	0.001–0.021 %	703
$p\gamma$, helicity=3/2	<0.003 %	703
$n\gamma$	<0.040 %	702
$n\gamma$, helicity=1/2	<0.007 %	702
$n\gamma$, helicity=3/2	<0.033 %	702

$N(1880)\ 1/2^+$

$I(J^P) = \frac{1}{2}(\frac{1}{2}^+)$

Re(pole position) = 1820 to 1900 (≈ 1860) MeV
−2Im(pole position) = 180 to 280 (≈ 230) MeV
Breit-Wigner mass = 1830 to 1930 (≈ 1880) MeV
Breit-Wigner full width = 200 to 400 (≈ 300) MeV

$N(1880)$ DECAY MODES	Fraction (Γ_i/Γ)	p (MeV/c)
$N\pi$	3–31 %	698
$N\eta$	1–55 %	563
$N\omega$	12–28 %	377
ΛK	1–3 %	459
ΣK	10–24 %	389
$N\pi\pi$	>32 %	673
$\Delta(1232)\pi$	5–42 %	524
$N\rho$, S=1/2, P-wave	19–45 %	385
$N\sigma$	8–40 %	539
$N(1535)\pi$	4–12 %	293
$Na_0(980)$	1–5 %	†
$\Lambda K^*(892)$	0.5–1.1 %	†
$p\gamma$, helicity=1/2	seen	706
$n\gamma$, helicity=1/2	0.002–0.63 %	705

$N(1895)\ 1/2^-$

$I(J^P) = \frac{1}{2}(\frac{1}{2}^-)$

Re(pole position) = 1890 to 1930 (≈ 1910) MeV
−2Im(pole position) = 80 to 140 (≈ 110) MeV
Breit-Wigner mass = 1870 to 1920 (≈ 1895) MeV
Breit-Wigner full width = 80 to 200 (≈ 120) MeV

$N(1895)$ DECAY MODES	Fraction (Γ_i/Γ)	p (MeV/c)
$N\pi$	2–18 %	707
$N\eta$	15–45 %	575

Downloaded from https://academic.oup.com/ptep/article/2022/8/083C01/6651666 by KIT Library user on 27 September 2022

$N\eta'$	10–40 %	†
$N\omega$	16–40 %	395
ΛK	3–23 %	473
ΣK	6–20 %	405
$N\pi\pi$	17–74 %	683
$\Delta(1232)\pi$, D-wave	3–11 %	535
$N\rho$	14–50 %	403
$N\rho$, S=1/2, S-wave	<18 %	403
$N\rho$, S=3/2, D-wave	14–32 %	403
$N\sigma$	<13 %	–
$N(1440)\pi$	2–12 %	382
$\Lambda K^*(892)$	4–9 %	†
$p\gamma$, helicity=1/2	0.01–0.06 %	715
$n\gamma$, helicity=1/2	0.003–0.05 %	715

$N(1900)\ 3/2^+$

$I(J^P) = \frac{1}{2}(\frac{3}{2}^+)$

Re(pole position) = 1900 to 1940 (≈ 1920) MeV
−2Im(pole position) = 100 to 200 (≈ 150) MeV
Breit-Wigner mass = 1890 to 1950 (≈ 1920) MeV
Breit-Wigner full width = 100 to 320 (≈ 200) MeV

$N(1900)$ DECAY MODES	Fraction (Γ_i/Γ)	p (MeV/c)
$N\pi$	1–20 %	723
$N\eta$	2–14 %	595
$N\eta'$	4–8 %	151
$N\omega$	7–13 %	424
ΛK	2–20 %	495
ΣK	3–7 %	431
$N\pi\pi$	>56 %	699
$\Delta(1232)\pi$	30–70 %	553
$\Delta(1232)\pi$, P-wave	9–25 %	553
$\Delta(1232)\pi$, F-wave	21–45 %	553
$N\rho$, S=1/2	25–40 %	432
$N\sigma$	1–7 %	–
$N(1520)\pi$	7–23 %	341
$N(1535)\pi$	4–10 %	328
$\Lambda K^*(892)$	< 0.2 %	†
$p\gamma$	0.001–0.025 %	731
$p\gamma$, helicity=1/2	0.001–0.021 %	731
$p\gamma$, helicity=3/2	<0.003 %	731
$n\gamma$	<0.040 %	730
$n\gamma$, helicity=1/2	<0.007 %	730
$n\gamma$, helicity=3/2	<0.033 %	730

$N(2060)\ 5/2^-$

$I(J^P) = \frac{1}{2}(\frac{5}{2}^-)$

Re(pole position) = 2020 to 2130 (≈ 2070) MeV
−2Im(pole position) = 350 to 430 (≈ 400) MeV
Breit-Wigner mass = 2030 to 2200 (≈ 2100) MeV
Breit-Wigner full width = 300 to 450 (≈ 400) MeV

$N(2060)$ DECAY MODES	Fraction (Γ_i/Γ)	p (MeV/c)
$N\pi$	7–12 %	834
$N\eta$	2–38 %	729
$N\omega$	1–7 %	600
ΛK	10–20 %	644
ΣK	1–5 %	593
$N\pi\pi$	12–52 %	814
$\Delta(1232)\pi$, D-wave	4–10 %	680
$N\rho$	5–33 %	605
$N\rho$, S=1/2, P-wave	<10 %	605
$N\rho$, S=3/2 , D-wave	5–23 %	605
$N\sigma$	3–9 %	–
$N(1440)\pi$	4–14 %	544
$N(1520)\pi$, P-wave	9–21 %	490
$N(1680)\pi$, S-wave	8–22 %	353
$\Lambda K^*(892)$	0.3–1.3 %	307
$p\gamma$	0.03–0.19 %	840
$p\gamma$, helicity=1/2	0.02–0.08 %	840
$p\gamma$, helicity=3/2	0.01–0.10 %	840
$n\gamma$	0.003–0.07 %	840
$n\gamma$, helicity=1/2	0.001–0.02 %	840
$n\gamma$, helicity=3/2	0.002–0.05 %	840

$N(2100)\ 1/2^+$

$I(J^P) = \frac{1}{2}(\frac{1}{2}^+)$

Re(pole position) = 2050 to 2150 (≈ 2100) MeV
−2Im(pole position) = 240 to 340 (≈ 300) MeV
Breit-Wigner mass = 2050 to 2150 (≈ 2100) MeV
Breit-Wigner full width = 200 to 320 (≈ 260) MeV

$N(2100)$ DECAY MODES	Fraction (Γ_i/Γ)	p (MeV/c)
$N\pi$	8–32 %	834
$N\eta$	5–45 %	729
$N\eta'$	5–11 %	451
$N\omega$	10–25 %	600
ΛK	<1.0 %	644
$N\pi\pi$	>55 %	814
$\Delta(1232)\pi$, P-wave	6–14 %	680
$N\rho$, S=1/2, P-wave	35–70	605
$N\sigma$	14–35 %	–
$N(1535)\pi$	26–34 %	478
$\Lambda K^*(892)$	3–11 %	307
$p\gamma$, helicity=1/2	0.001–0.13 %	840
$n\gamma$, helicity=1/2	0.004–0.09 %	840

$N(2120)\ 3/2^-$

$I(J^P) = \frac{1}{2}(\frac{3}{2}^-)$

Re(pole position) = 2050 to 2150 (≈ 2100) MeV
−2Im(pole position) = 200 to 360 (≈ 280) MeV
Breit-Wigner mass = 2060 to 2160 (≈ 2120) MeV
Breit-Wigner full width = 260 to 360 (≈ 300) MeV

$N(2120)$ DECAY MODES	Fraction (Γ_i/Γ)	p (MeV/c)
$N\pi$	5–15 %	846
$N\eta$	1–5 %	743
$N\eta'$	2–6 %	474
$N\omega$	4–20 %	617
ΛK	6–11 %	660
$N\pi\pi$	>27 %	827
$\Delta(1232)\pi$	>23 %	693
$\Delta(1232)\pi$, S-wave	15–70 %	693
$\Delta(1232)\pi$, D-wave	8–45 %	693
$N\rho$, S=3/2 , S-wave	< 3 %	622
$N\sigma$	4–15 %	–
$N(1535)\pi$	7–23 %	494
$\Lambda K^*(892)$	< 0.2 %	339
$p\gamma$	0.16–2.1 %	852
$p\gamma$, helicity=1/2	0.07–0.80 %	852
$p\gamma$, helicity=3/2	0.09–1.3 %	852
$n\gamma$	0.04–0.72 %	852
$n\gamma$, helicity=1/2	0.04–0.60 %	852
$n\gamma$, helicity=3/2	0.001–0.12 %	852

$N(2190)\ 7/2^-$

$I(J^P) = \frac{1}{2}(\frac{7}{2}^-)$

Re(pole position) = 2050 to 2150 (≈ 2100) MeV
−2Im(pole position) = 300 to 500 (≈ 400) MeV
Breit-Wigner mass = 2140 to 2220 (≈ 2180) MeV
Breit-Wigner full width = 300 to 500 (≈ 400) MeV

$N(2190)$ DECAY MODES	Fraction (Γ_i/Γ)	p (MeV/c)
$N\pi$	10–20 %	882
$N\eta$	1–5 %	785
$N\omega$	8–20 %	667
ΛK	0.2–0.8 %	705
$N\pi\pi$	22–51 %	864
$\Delta(1232)\pi$, D-wave	19–31 %	734
$N\rho$, S=3/2, D-wave	<11 %	672
$N\sigma$	3–9 %	–
$\Lambda K^*(892)$	0.2–0.8 %	423
$p\gamma$	<0.08 %	888
$p\gamma$, helicity=1/2	<0.06 %	888
$p\gamma$, helicity=3/2	<0.02 %	888
$n\gamma$	<0.04 %	888
$n\gamma$, helicity=1/2	<0.01 %	888
$n\gamma$, helicity=3/2	<0.03 %	888

Downloaded from https://academic.oup.com/ptep/article/2022/8/083C01/6651666 by KIT Library user on 27 September 2022

$N(2220)\ 9/2^+$

$I(J^P) = \frac{1}{2}(\frac{9}{2}^+)$

Re(pole position) = 2130 to 2200 (≈ 2170) MeV
−2Im(pole position) = 360 to 480 (≈ 400) MeV
Breit-Wigner mass = 2200 to 2300 (≈ 2250) MeV
Breit-Wigner full width = 350 to 500 (≈ 400) MeV

$N(2220)$ DECAY MODES	Fraction (Γ_i/Γ)	p (MeV/c)
$N\pi$	15–30 %	924

$N(2250)\ 9/2^-$

$I(J^P) = \frac{1}{2}(\frac{9}{2}^-)$

Re(pole position) = 2150 to 2250 (≈ 2200) MeV
−2Im(pole position) = 350 to 500 (≈ 420) MeV
Breit-Wigner mass = 2250 to 2320 (≈ 2280) MeV
Breit-Wigner full width = 300 to 600 (≈ 500) MeV

$N(2250)$ DECAY MODES	Fraction (Γ_i/Γ)	p (MeV/c)
$N\pi$	5–15 %	941
$N\eta$	<5 %	852
ΛK	1–3 %	777

$N(2600)\ 11/2^-$

$I(J^P) = \frac{1}{2}(\frac{11}{2}^-)$

Breit-Wigner mass = 2550 to 2750 (≈ 2600) MeV
Breit-Wigner full width = 500 to 800 (≈ 650) MeV

$N(2600)$ DECAY MODES	Fraction (Γ_i/Γ)	p (MeV/c)
$N\pi$	3–8 %	1126

Δ BARYONS ($S=0, I=3/2$)

$\Delta^{++} = uuu,\quad \Delta^{+} = uud,\quad \Delta^{0} = udd,\quad \Delta^{-} = ddd$

$\Delta(1232)\ 3/2^+$

$I(J^P) = \frac{3}{2}(\frac{3}{2}^+)$

Re(pole position) = 1209 to 1211 (≈ 1210) MeV
−2Im(pole position) = 98 to 102 (≈ 100) MeV
Breit-Wigner mass (mixed charges) = 1230 to 1234 (≈ 1232) MeV
Breit-Wigner full width (mixed charges) = 114 to 120 (≈ 117) MeV

$\Delta(1232)$ DECAY MODES	Fraction (Γ_i/Γ)	p (MeV/c)
$N\pi$	99.4 %	229
$N\gamma$	0.55–0.65 %	259
$N\gamma$, helicity=1/2	0.11–0.13 %	259
$N\gamma$, helicity=3/2	0.44–0.52 %	259
pe^+e^-	$(4.2\pm0.7)\times10^{-5}$	259

$\Delta(1600)\ 3/2^+$

$I(J^P) = \frac{3}{2}(\frac{3}{2}^+)$

Re(pole position) = 1460 to 1560 (≈ 1510) MeV
−2Im(pole position) = 200 to 340 (≈ 270) MeV
Breit-Wigner mass = 1500 to 1640 (≈ 1570) MeV
Breit-Wigner full width = 200 to 300 (≈ 250) MeV

$\Delta(1600)$ DECAY MODES	Fraction (Γ_i/Γ)	p (MeV/c)
$N\pi$	8–24%	492
$N\pi\pi$	58–84 %	454
$\Delta(1232)\pi$	58–82 %	276
$\Delta(1232)\pi$, P-wave	72–82%	276
$\Delta(1232)\pi$, F-wave	<2%	276
$N(1440)\pi$	17–27%	†
$N\gamma$	0.001–0.035 %	505
$N\gamma$, helicity=1/2	0.0–0.02 %	505
$N\gamma$, helicity=3/2	0.001–0.015 %	505

$\Delta(1620)\ 1/2^-$

$I(J^P) = \frac{3}{2}(\frac{1}{2}^-)$

Re(pole position) = 1590 to 1610 (≈ 1600) MeV
−2Im(pole position) = 100 to 140 (≈ 120) MeV
Breit-Wigner mass = 1590 to 1630 (≈ 1610) MeV
Breit-Wigner full width = 110 to 150 (≈ 130) MeV

$\Delta(1620)$ DECAY MODES	Fraction (Γ_i/Γ)	p (MeV/c)
$N\pi$	25–35 %	520
$N\pi\pi$	>67 %	484
$\Delta(1232)\pi$, D-wave	44–72 %	311
$N\rho$	23–32%	†
$N\rho$, S=1/2, S-wave	23–32%	†
$N\rho$, S=3/2, D-wave	<0.04%	†
$N(1440)\pi$	<9 %	98
$N\gamma$, helicity=1/2	0.03–0.10 %	532

$\Delta(1700)\ 3/2^-$

$I(J^P) = \frac{3}{2}(\frac{3}{2}^-)$

Re(pole position) = 1640 to 1690 (≈ 1665) MeV
−2Im(pole position) = 200 to 300 (≈ 250) MeV
Breit-Wigner mass = 1690 to 1730 (≈ 1710) MeV
Breit-Wigner full width = 220 to 380 (≈ 300) MeV

$\Delta(1700)$ DECAY MODES	Fraction (Γ_i/Γ)	p (MeV/c)
$N\pi$	10–20 %	588
$N\pi\pi$	>31 %	557
$\Delta(1232)\pi$	9–70 %	394
$\Delta(1232)\pi$, S-wave	5–54 %	394
$\Delta(1232)\pi$, D-wave	4–16 %	394
$N\rho$, S=3/2, S-wave	22–32%	†
$N(1520)\pi$, P-wave	1–5 %	133
$N(1535)\pi$	0.5–1.5 %	113
$\Delta(1232)\eta$	3–7 %	†
$N\gamma$	0.22–0.60 %	598
$N\gamma$, helicity=1/2	0.12–0.30 %	598
$N\gamma$, helicity=3/2	0.10–0.30 %	598

$\Delta(1900)\ 1/2^-$

$I(J^P) = \frac{3}{2}(\frac{1}{2}^-)$

Re(pole position) = 1830 to 1900 (≈ 1865) MeV
−2Im(pole position) = 180 to 300 (≈ 240) MeV
Breit-Wigner mass = 1840 to 1920 (≈ 1860) MeV
Breit-Wigner full width = 180 to 320 (≈ 250) MeV

$\Delta(1900)$ DECAY MODES	Fraction (Γ_i/Γ)	p (MeV/c)
$N\pi$	4–12%	685
ΣK	seen	367
$N\pi\pi$	> 52%	660
$\Delta(1232)\pi$, D-wave	30–70%	509
$N\rho$	22–60 %	360
$N\rho$, S=1/2, S-wave	11–35%	360
$N\rho$, S=3/2, D-wave	11–25%	360
$N(1440)\pi$	3–32%	353
$N(1520)\pi$	2–10%	288
$\Delta(1232)\eta$	< 2%	251
$N\gamma$, helicity=1/2	0.06–0.43 %	693

$\Delta(1905)\ 5/2^+$

$I(J^P) = \frac{3}{2}(\frac{5}{2}^+)$

Re(pole position) = 1770 to 1830 (≈ 1800) MeV
−2Im(pole position) = 260 to 340 (≈ 300) MeV
Breit-Wigner mass = 1855 to 1910 (≈ 1880) MeV
Breit-Wigner full width = 270 to 400 (≈ 330) MeV

$\Delta(1905)$ DECAY MODES	Fraction (Γ_i/Γ)	p (MeV/c)
$N\pi$	9–15%	698
$N\pi\pi$	>65%	673
$\Delta(1232)\pi$	>48%	524
$\Delta(1232)\pi$, P-wave	8–43%	524
$\Delta(1232)\pi$, F-wave	40–58%	524

Downloaded from https://academic.oup.com/ptep/article/2022/8/083C01/6651666 by KIT Library user on 27 September 2022

$N\rho$, S=3/2, P-wave	17–35%	385
$N(1535)\pi$	< 1 %	293
$N(1680)\pi$, P-wave	5–15%	133
$\Delta(1232)\eta$	2–6%	282
$N\gamma$	0.012–0.036 %	706
$N\gamma$, helicity=1/2	0.002–0.006 %	706
$N\gamma$, helicity=3/2	0.01–0.03 %	706

$\Delta(1910)\ 1/2^+$

$I(J^P) = \frac{3}{2}(\frac{1}{2}^+)$

Re(pole position) = 1830 to 1890 (≈ 1860) MeV
−2Im(pole position) = 200 to 400 (≈ 300) MeV
Breit-Wigner mass = 1850 to 1950 (≈ 1900) MeV
Breit-Wigner full width = 200 to 400 (≈ 300) MeV

$\Delta(1910)$ DECAY MODES	Fraction (Γ_i/Γ)	p (MeV/c)
$N\pi$	10–30%	710
ΣK	4–14%	410
$\Delta(1232)\pi$	34–66%	539
$N(1440)\pi$	3–45%	386
$\Delta(1232)\eta$	5–13%	310
$N\gamma$, helicity=1/2	0.0–0.02 %	718

$\Delta(1920)\ 3/2^+$

$I(J^P) = \frac{3}{2}(\frac{3}{2}^+)$

Re(pole position) = 1850 to 1950 (≈ 1900) MeV
−2Im(pole position) = 200 to 400 (≈ 300) MeV
Breit-Wigner mass = 1870 to 1970 (≈ 1920) MeV
Breit-Wigner full width = 240 to 360 (≈ 300) MeV

$\Delta(1920)$ DECAY MODES	Fraction (Γ_i/Γ)	p (MeV/c)
$N\pi$	5–20 %	723
ΣK	2–6 %	431
$N\pi\pi$	>46 %	699
$\Delta(1232)\pi$	>46 %	553
$\Delta(1232)\pi$, P-wave	2–28 %	553
$\Delta(1232)\pi$, F-wave	44–72 %	553
$N(1440)\pi$, P-wave	4–86 %	403
$N(1520)\pi$, S-wave	<5 %	341
$N(1535)\pi$	<2 %	328
$Na_0(980)$	seen	41
$\Delta(1232)\eta$	5–17 %	336
$N\gamma$	0.01–0.84 %	731
$N\gamma$, helicity=1/2	0.0–0.42 %	731
$N\gamma$, helicity=3/2	0.01–0.42 %	731

$\Delta(1930)\ 5/2^-$

$I(J^P) = \frac{3}{2}(\frac{5}{2}^-)$

Re(pole position) = 1840 to 1920 (≈ 1880) MeV
−2Im(pole position) = 230 to 330 (≈ 280) MeV
Breit-Wigner mass = 1900 to 2000 (≈ 1950) MeV
Breit-Wigner full width = 200 to 400 (≈ 300) MeV

$\Delta(1930)$ DECAY MODES	Fraction (Γ_i/Γ)	p (MeV/c)
$N\pi$	5–15 %	742
$N\gamma$	0.0–0.01 %	749
$N\gamma$, helicity=1/2	0.0–0.005 %	749
$N\gamma$, helicity=3/2	0.0–0.004 %	749

$\Delta(1950)\ 7/2^+$

$I(J^P) = \frac{3}{2}(\frac{7}{2}^+)$

Re(pole position) = 1870 to 1890 (≈ 1880) MeV
−2Im(pole position) = 220 to 260 (≈ 240) MeV
Breit-Wigner mass = 1915 to 1950 (≈ 1930) MeV
Breit-Wigner full width = 235 to 335 (≈ 285) MeV

$\Delta(1950)$ DECAY MODES	Fraction (Γ_i/Γ)	p (MeV/c)
$N\pi$	35–45 %	729
ΣK	0.3–0.5 %	441
$N\pi\pi$	37–77 %	706
$\Delta(1232)\pi$, F-wave	1–9 %	560
$N(1680)\pi$, P-wave	3–9 %	191
$\Delta(1232)\eta$	< 0.6 %	349
$N\gamma$	0.06–0.14 %	737
$N\gamma$, helicity=1/2	0.03–0.05 %	737
$N\gamma$, helicity=3/2	0.04–0.09 %	737

$\Delta(2200)\ 7/2^-$

$I(J^P) = \frac{3}{2}(\frac{7}{2}^-)$

Re(pole position) = 2050 to 2150 (≈ 2100) MeV
−2Im(pole position) = 260 to 420 (≈ 340) MeV
Breit-Wigner mass = 2150 to 2250 (≈ 2200) MeV
Breit-Wigner full width = 200 to 500 (≈ 350) MeV

$\Delta(2200)$ DECAY MODES	Fraction (Γ_i/Γ)	p (MeV/c)
$N\pi$	2–8 %	894
ΣK	1–7 %	672
$N\pi\pi$	>45 %	876
$\Delta\pi$	>45 %	747
$\Delta\pi$, D-wave	>40 %	747
$\Delta\pi$, G-wave	5–25 %	747
$\Delta\eta$, D-wave	seen	614

$\Delta(2420)\ 11/2^+$

$I(J^P) = \frac{3}{2}(\frac{11}{2}^+)$

Re(pole position) = 2300 to 2500 (≈ 2400) MeV
−2Im(pole position) = 350 to 550 (≈ 450) MeV
Breit-Wigner mass = 2300 to 2600 (≈ 2450) MeV
Breit-Wigner full width = 300 to 700 (≈ 500) MeV

$\Delta(2420)$ DECAY MODES	Fraction (Γ_i/Γ)	p (MeV/c)
$N\pi$	5–10 %	1040

Λ BARYONS
($S = -1$, $I = 0$)

$\Lambda^0 = uds$

Λ

$I(J^P) = 0(\frac{1}{2}^+)$

Mass $m = 1115.683 \pm 0.006$ MeV
$(m_\Lambda - m_{\overline{\Lambda}}) / m_\Lambda = (-0.1 \pm 1.1) \times 10^{-5}$ (S = 1.6)
Mean life $\tau = (2.632 \pm 0.020) \times 10^{-10}$ s (S = 1.6)
$(\tau_\Lambda - \tau_{\overline{\Lambda}}) / \tau_\Lambda = -0.001 \pm 0.009$
$c\tau = 7.89$ cm
Magnetic moment $\mu = -0.613 \pm 0.004\ \mu_N$
Electric dipole moment $d < 1.5 \times 10^{-16}$ e cm, CL = 95%

Decay parameters

$p\pi^-$ $\alpha_- = 0.732 \pm 0.014$ (S = 2.3)
$\overline{p}\pi^+$ $\alpha_+ = -0.758 \pm 0.012$
$\overline{\alpha}_0$ FOR $\overline{\Lambda} \to \overline{n}\pi^0 = -0.692 \pm 0.017$
$p\pi^-$ $\phi_- = (-6.5 \pm 3.5)^\circ$
" $\gamma_- = 0.76$ [n]
" $\Delta_- = (8 \pm 4)^\circ$ [n]
$\overline{\alpha}_0 / \alpha_+$ in $\overline{\Lambda} \to \overline{n}\pi^0, \overline{\Lambda} \to \overline{p}\pi^+ = 0.913 \pm 0.030$
$R = |G_E/G_M|$ in $\Lambda \to p\pi^-, \overline{\Lambda} \to \overline{p}\pi^+ = 0.96 \pm 0.14$
$\Delta\Phi = \Phi_E - \Phi_M$ in $\Lambda \to p\pi^-, \overline{\Lambda} \to \overline{p}\pi^+ = 37 \pm 13$ degrees
$n\pi^0$ $\alpha_0 = 0.74 \pm 0.05$
$pe^-\overline{\nu}_e$ $g_A/g_V = -0.718 \pm 0.015$ [i]

Λ DECAY MODES		Fraction (Γ_i/Γ)	Confidence level	p (MeV/c)
$p\pi^-$		(63.9 ±0.5) %		101
$n\pi^0$		(35.8 ±0.5) %		104
$n\gamma$		(1.75±0.15) × 10^{-3}		162
$p\pi^-\gamma$	[o]	(8.4 ±1.4) × 10^{-4}		101
$pe^-\overline{\nu}_e$		(8.32±0.14) × 10^{-4}		163
$p\mu^-\overline{\nu}_\mu$		(1.57±0.35) × 10^{-4}		131

Downloaded from https://academic.oup.com/ptep/article/2022/8/083C01/6651666 by KIT Library user on 27 September 2022

Lepton (L) and/or Baryon (B) number violating decay modes

$\pi^+ e^-$	L,B	< 6	$\times 10^{-7}$	90%	549
$\pi^+ \mu^-$	L,B	< 6	$\times 10^{-7}$	90%	544
$\pi^- e^+$	L,B	< 4	$\times 10^{-7}$	90%	549
$\pi^- \mu^+$	L,B	< 6	$\times 10^{-7}$	90%	544
$K^+ e^-$	L,B	< 2	$\times 10^{-6}$	90%	449
$K^+ \mu^-$	L,B	< 3	$\times 10^{-6}$	90%	441
$K^- e^+$	L,B	< 2	$\times 10^{-6}$	90%	449
$K^- \mu^+$	L,B	< 3	$\times 10^{-6}$	90%	441
$K^0_S \nu$	L,B	< 2	$\times 10^{-5}$	90%	447
$\overline{p}\pi^+$	B	< 9	$\times 10^{-7}$	90%	101

$\Lambda(1405)\ 1/2^-$

$I(J^P) = 0(\frac{1}{2}^-)$

Mass $m = 1405.1^{+1.3}_{-1.0}$ MeV
Full width $\Gamma = 50.5 \pm 2.0$ MeV
Below $\overline{K}N$ threshold

$\Lambda(1405)$ DECAY MODES	Fraction (Γ_i/Γ)	p (MeV/c)
$\Sigma\pi$	100 %	155

$\Lambda(1520)\ 3/2^-$

$I(J^P) = 0(\frac{3}{2}^-)$

Mass $m = 1518$ to 1520 (≈ 1519) MeV [p]
Full width $\Gamma = 15$ to 17 (≈ 16) MeV [p]

$\Lambda(1520)$ DECAY MODES	Fraction (Γ_i/Γ)	p (MeV/c)
$N\overline{K}$	(45 ±1) %	242
$\Sigma\pi$	(42 ±1) %	268
$\Lambda\pi\pi$	(10 ±1) %	259
$\Sigma\pi\pi$	(0.9 ±0.1) %	168
$\Lambda\gamma$	(0.85±0.15) %	350

$\Lambda(1600)\ 1/2^+$

$I(J^P) = 0(\frac{1}{2}^+)$

Mass $m = 1570$ to 1630 (≈ 1600) MeV
Full width $\Gamma = 150$ to 250 (≈ 200) MeV

$\Lambda(1600)$ DECAY MODES	Fraction (Γ_i/Γ)	p (MeV/c)
$N\overline{K}$	15–30 %	343
$\Sigma\pi$	10–60 %	338
$\Lambda\sigma$	(19±4) %	–
$\Sigma(1385)\pi$	(9±4) %	158

$\Lambda(1670)\ 1/2^-$

$I(J^P) = 0(\frac{1}{2}^-)$

Mass $m = 1670$ to 1678 (≈ 1674) MeV
Full width $\Gamma = 25$ to 35 (≈ 30) MeV

$\Lambda(1670)$ DECAY MODES	Fraction (Γ_i/Γ)	p (MeV/c)
$N\overline{K}$	20–30 %	418
$\Sigma\pi$	25–55 %	398
$\Lambda\eta$	10–25 %	88
$\Sigma(1385)\pi$, D-wave	(6.0±2.0) %	235
$N\overline{K}^*(892)$, S=3/2, D-wave	(5 ±4) %	†
$\Lambda\sigma$	(20 ±8) %	–

$\Lambda(1690)\ 3/2^-$

$I(J^P) = 0(\frac{3}{2}^-)$

Mass $m = 1685$ to 1695 (≈ 1690) MeV
Full width $\Gamma = 60$ to 80 (≈ 70) MeV

$\Lambda(1690)$ DECAY MODES	Fraction (Γ_i/Γ)	p (MeV/c)
$N\overline{K}$	20–30 %	433
$\Sigma\pi$	20–40 %	410
$\Lambda\sigma$	(5.0±2.0) %	–
$\Lambda\pi\pi$	$\sim$ 25 %	419
$\Sigma\pi\pi$	$\sim$ 20 %	358
$\Sigma(1385)\pi$, S-wave	(9 ±5) %	251
$\Sigma(1385)\pi$, D-wave	(3.0±2.0) %	251

$\Lambda(1800)\ 1/2^-$

$I(J^P) = 0(\frac{1}{2}^-)$

Mass $m = 1750$ to 1850 (≈ 1800) MeV
Full width $\Gamma = 150$ to 250 (≈ 200) MeV

$\Lambda(1800)$ DECAY MODES	Fraction (Γ_i/Γ)	p (MeV/c)
$N\overline{K}$	25–40 %	528
$\Sigma\pi$	seen	494
$\Lambda\sigma$	(15 ±4) %	–
$\Sigma(1385)\pi$	seen	349
$\Lambda\eta$	0.01 to 0.10	326
$N\overline{K}^*(892)$	seen	†

$\Lambda(1810)\ 1/2^+$

$I(J^P) = 0(\frac{1}{2}^+)$

Mass $m = 1740$ to 1840 (≈ 1790) MeV
Full width $\Gamma = 50$ to 170 (≈ 110) MeV

$\Lambda(1810)$ DECAY MODES	Fraction (Γ_i/Γ)	p (MeV/c)
$N\overline{K}$	0.05 to 0.35	520
$\Sigma\pi$	(16 ± 5) %	487
$\Sigma(1385)\pi$	(40 ±15) %	340
$N\overline{K}^*(892)$	30–60 %	†

$\Lambda(1820)\ 5/2^+$

$I(J^P) = 0(\frac{5}{2}^+)$

Mass $m = 1815$ to 1825 (≈ 1820) MeV
Full width $\Gamma = 70$ to 90 (≈ 80) MeV

$\Lambda(1820)$ DECAY MODES	Fraction (Γ_i/Γ)	p (MeV/c)
$N\overline{K}$	55–65 %	545
$\Sigma\pi$	8–14 %	509
$\Sigma(1385)\pi$	5–10 %	366
$N\overline{K}^*(892)$, S=3/2, P-wave	(3.0±1.0) %	†

$\Lambda(1830)\ 5/2^-$

$I(J^P) = 0(\frac{5}{2}^-)$

Mass $m = 1820$ to 1830 (≈ 1825) MeV
Full width $\Gamma = 60$ to 120 (≈ 90) MeV

$\Lambda(1830)$ DECAY MODES	Fraction (Γ_i/Γ)	Scale factor	p (MeV/c)
$N\overline{K}$	0.04 to 0.08		549
$\Sigma\pi$	35–75 %		512
$\Sigma(1385)\pi$	>15 %		370
$\Sigma(1385)\pi$, D-wave	(40 ±15) %	3.2	370

$\Lambda(1890)\ 3/2^+$

$I(J^P) = 0(\frac{3}{2}^+)$

Mass $m = 1870$ to 1910 (≈ 1890) MeV
Full width $\Gamma = 80$ to 160 (≈ 120) MeV

$\Lambda(1890)$ DECAY MODES	Fraction (Γ_i/Γ)	p (MeV/c)
$N\overline{K}$	0.24 to 0.36	599
$\Sigma\pi$	3–10 %	560
$\Sigma(1385)\pi$	seen	423
$\Sigma(1385)\pi$, P-wave	(6.0 ±3.0) %	423
$\Sigma(1385)\pi$, F-wave	(4.0 ±2.0) %	423
$N\overline{K}^*(892)$	seen	236

$\Lambda(2100)\ 7/2^-$

$I(J^P) = 0(\frac{7}{2}^-)$

Mass $m = 2090$ to 2110 (≈ 2100) MeV
Full width $\Gamma = 100$ to 250 (≈ 200) MeV

$\Lambda(2100)$ DECAY MODES	Fraction (Γ_i/Γ)	p (MeV/c)
$N\overline{K}$	25–35 %	751
$\Sigma\pi$	$\sim$ 5 %	705
$\Lambda\eta$	<3 %	617

Downloaded from https://academic.oup.com/ptep/article/2022/8/083C01/6651666 by KIT Library user on 27 September 2022

ΞK	<3 %	491
$\Lambda\omega$	<8 %	443
$\Sigma(1385)\pi$, G-wave	(1.0±1.0) %	584
$N\overline{K}^*(892)$	10–20 %	515
$N\overline{K}^*(892)$, S=3/2, D-wave	(4.0±2.0) %	515

$\Lambda(2110)\ 5/2^+$

$I(J^P) = 0(\frac{5}{2}^+)$

Mass m = 2050 to 2130 (≈ 2090) MeV
Full width Γ = 200 to 300 (≈ 250) MeV

$\Lambda(2110)$ DECAY MODES	Fraction (Γ_i/Γ)	p (MeV/c)
$N\overline{K}$	5–25 %	744
$\Sigma\pi$	10–40 %	698
$\Lambda\omega$	seen	432
$\Lambda\omega$, S=3/2, P-wave	(5.0±2.0) %	432
$\Sigma(1385)\pi$	seen	576
$N\overline{K}^*(892)$	10–60 %	505

$\Lambda(2350)\ 9/2^+$

$I(J^P) = 0(\frac{9}{2}^+)$

Mass m = 2340 to 2370 (≈ 2350) MeV
Full width Γ = 100 to 250 (≈ 150) MeV

$\Lambda(2350)$ DECAY MODES	Fraction (Γ_i/Γ)	p (MeV/c)
$N\overline{K}$	∼ 12 %	915
$\Sigma\pi$	∼ 10 %	867

Σ BARYONS ($S = -1, I = 1$)

$\Sigma^+ = uus$, $\Sigma^0 = uds$, $\Sigma^- = dds$

Σ^+

$I(J^P) = 1(\frac{1}{2}^+)$

Mass m = 1189.37 ± 0.07 MeV (S = 2.2)
Mean life $\tau = (0.8018 \pm 0.0026) \times 10^{-10}$ s
$c\tau$ = 2.404 cm
$(\tau_{\Sigma^+} - \tau_{\overline{\Sigma}^-}) / \tau_{\Sigma^+} = -0.0006 \pm 0.0012$
Magnetic moment $\mu = 2.458 \pm 0.010\ \mu_N$ (S = 2.1)
$(\mu_{\Sigma^+} + \mu_{\overline{\Sigma}^-}) / \mu_{\Sigma^+} = 0.014 \pm 0.015$
$\Gamma(\Sigma^+ \to n\ell^+\nu)/\Gamma(\Sigma^- \to n\ell^-\overline{\nu}_\ell) < 0.043$

Decay parameters

$p\pi^0$	$\alpha_0 = -0.982 \pm 0.014$
$\overline{\alpha}_0$ FOR $\overline{\Sigma}^- \to \overline{p}\pi^0$	$= 0.99 \pm 0.04$
$(\alpha_0 + \overline{\alpha}_0) / (\alpha_0 - \overline{\alpha}_0)$	$= 0.00 \pm 0.04$
"	$\phi_0 = (36 \pm 34)^\circ$
"	$\gamma_0 = 0.16$ [n]
"	$\Delta_0 = (187 \pm 6)^\circ$ [n]
$n\pi^+$	$\alpha_+ = 0.068 \pm 0.013$
"	$\phi_+ = (167 \pm 20)^\circ$ (S = 1.1)
"	$\gamma_+ = -0.97$ [n]
"	$\Delta_+ = (-73^{+133}_{-10})^\circ$ [n]
$p\gamma$	$\alpha_\gamma = -0.76 \pm 0.08$

Σ^+ DECAY MODES		Fraction (Γ_i/Γ)	Confidence level	p (MeV/c)
$p\pi^0$		(51.57±0.30) %		189
$n\pi^+$		(48.31±0.30) %		185
$p\gamma$		$(1.23 \pm 0.05) \times 10^{-3}$		225
$n\pi^+\gamma$	[o]	$(4.5 \pm 0.5) \times 10^{-4}$		185
$\Lambda e^+\nu_e$		$(2.0 \pm 0.5) \times 10^{-5}$		71
$\Delta S = \Delta Q$ (SQ) violating modes or $\Delta S = 1$ weak neutral current ($S1$) modes				
$ne^+\nu_e$	SQ	$< 5 \times 10^{-6}$	90%	224
$n\mu^+\nu_\mu$	SQ	$< 3.0 \times 10^{-5}$	90%	202
pe^+e^-	$S1$	$< 7 \times 10^{-6}$		225
$p\mu^+\mu^-$	$S1$	$(2.4^{+1.7}_{-1.3}) \times 10^{-8}$		121

Σ^0

$I(J^P) = 1(\frac{1}{2}^+)$

Mass m = 1192.642 ± 0.024 MeV
$m_{\Sigma^-} - m_{\Sigma^0} = 4.807 \pm 0.035$ MeV (S = 1.1)
$m_{\Sigma^0} - m_\Lambda = 76.959 \pm 0.023$ MeV
Mean life $\tau = (7.4 \pm 0.7) \times 10^{-20}$ s
$c\tau = 2.22 \times 10^{-11}$ m
Transition magnetic moment $|\mu_{\Sigma\Lambda}| = 1.61 \pm 0.08\ \mu_N$

Σ^0 DECAY MODES		Fraction (Γ_i/Γ)	Confidence level	p (MeV/c)
$\Lambda\gamma$		100 %		74
$\Lambda\gamma\gamma$		< 3 %	90%	74
Λe^+e^-	[q]	5×10^{-3}		74

Σ^-

$I(J^P) = 1(\frac{1}{2}^+)$

Mass m = 1197.449 ± 0.030 MeV (S = 1.2)
$m_{\Sigma^-} - m_{\Sigma^+} = 8.08 \pm 0.08$ MeV (S = 1.9)
$m_{\Sigma^-} - m_\Lambda = 81.766 \pm 0.030$ MeV (S = 1.2)
Mean life $\tau = (1.479 \pm 0.011) \times 10^{-10}$ s (S = 1.3)
$c\tau$ = 4.434 cm
Magnetic moment $\mu = -1.160 \pm 0.025\ \mu_N$ (S = 1.7)
Σ^- charge radius = 0.78 ± 0.10 fm

Decay parameters

$n\pi^-$	$\alpha_- = -0.068 \pm 0.008$
"	$\phi_- = (10 \pm 15)^\circ$
"	$\gamma_- = 0.98$ [n]
"	$\Delta_- = (249^{+12}_{-120})^\circ$ [n]
$ne^-\overline{\nu}_e$	$g_A/g_V = 0.340 \pm 0.017$ [i]
"	$f_2(0)/f_1(0) = 0.97 \pm 0.14$
"	$D = 0.11 \pm 0.10$
$\Lambda e^-\overline{\nu}_e$	$g_V/g_A = 0.01 \pm 0.10$ [i] (S = 1.5)
"	$g_{WM}/g_A = 2.4 \pm 1.7$ [i]

Σ^- DECAY MODES		Fraction (Γ_i/Γ)	Confidence level	p (MeV/c)
$n\pi^-$		(99.848±0.005) %		193
$n\pi^-\gamma$	[o]	$(4.6 \pm 0.6) \times 10^{-4}$		193
$ne^-\overline{\nu}_e$		$(1.017 \pm 0.034) \times 10^{-3}$		230
$n\mu^-\overline{\nu}_\mu$		$(4.5 \pm 0.4) \times 10^{-4}$		210
$\Lambda e^-\overline{\nu}_e$		$(5.73 \pm 0.27) \times 10^{-5}$		79
Σ^+X		$< 1.2 \times 10^{-4}$	90%	–
Lepton number (L) violating modes				
pe^-e^-	L	$< 6.7 \times 10^{-5}$	90%	231

$\Sigma(1385)\ 3/2^+$

$I(J^P) = 1(\frac{3}{2}^+)$

$\Sigma(1385)^+$ mass m = 1382.83 ± 0.34 MeV (S = 1.9)
$\Sigma(1385)^0$ mass m = 1383.7 ± 1.0 MeV (S = 1.4)
$\Sigma(1385)^-$ mass m = 1387.2 ± 0.5 MeV (S = 2.2)
$\Sigma(1385)^+$ full width Γ = 36.2 ± 0.7 MeV
$\Sigma(1385)^0$ full width Γ = 36 ± 5 MeV
$\Sigma(1385)^-$ full width Γ = 39.4 ± 2.1 MeV (S = 1.7)
Below $\overline{K}N$ threshold

$\Sigma(1385)$ DECAY MODES	Fraction (Γ_i/Γ)	Confidence level	p (MeV/c)
$\Lambda\pi$	(87.0 ±1.5) %		208
$\Sigma\pi$	(11.7 ±1.5) %		129
$\Lambda\gamma$	$(1.25^{+0.13}_{-0.12})$ %		241
$\Sigma^+\gamma$	$(7.0 \pm 1.7) \times 10^{-3}$		180
$\Sigma^-\gamma$	$< 2.4 \times 10^{-4}$	90%	173

$\Sigma(1660)\ 1/2^+$

$I(J^P) = 1(\frac{1}{2}^+)$

Re(pole position) = 1585 ± 20 MeV
−2Im(pole position) = 290^{+140}_{-40} MeV
Mass m = 1640 to 1680 (≈ 1660) MeV
Full width Γ = 100 to 300 (≈ 200) MeV

Downloaded from https://academic.oup.com/ptep/article/2022/8/083C01/6651666 by KIT Library user on 27 September 2022

$\Sigma(1660)$ DECAY MODES	Fraction (Γ_i/Γ)	p (MeV/c)
$N\overline{K}$	0.05 to 0.15 ($\approx$ 010)	405
$\Lambda\pi$	(35 ±12) %	440
$\Sigma\pi$	(37 ±10) %	387
$\Sigma\sigma$	(20 ± 8) %	–
$\Lambda(1405)\pi$	(4.0 ± 2.0) %	199

$\Sigma(1670)\ 3/2^-$

$I(J^P) = 1(\frac{3}{2}^-)$

Mass m = 1665 to 1685 ($\approx$ 1675) MeV
Full width Γ = 40 to 100 ($\approx$ 70) MeV

$\Sigma(1670)$ DECAY MODES	Fraction (Γ_i/Γ)	p (MeV/c)
$N\overline{K}$	0.06 to 0.12	419
$\Lambda\pi$	5–15 %	452
$\Sigma\pi$	30–60 %	398
$\Sigma\sigma$	(7.0 ±3.0) %	–

$\Sigma(1750)\ 1/2^-$

$I(J^P) = 1(\frac{1}{2}^-)$

Mass m = 1700 to 1800 ($\approx$ 1750) MeV
Full width Γ = 100 to 200 ($\approx$ 150) MeV

$\Sigma(1750)$ DECAY MODES	Fraction (Γ_i/Γ)	p (MeV/c)
$N\overline{K}$	0.06 to 0.12	486
$\Lambda\pi$	(14 ±5) %	507
$\Sigma\pi$	(16 ±4) %	456
$\Sigma\eta$	15–55 %	98
$\Sigma(1385)\pi$, D-wave	< 1 %	305
$\Lambda(1520)\pi$	(2.0 ±1.0) %	175
$N\overline{K}^*(892)$, S=1/2	(8 ±4) %	†

$\Sigma(1775)\ 5/2^-$

$I(J^P) = 1(\frac{5}{2}^-)$

Mass m = 1770 to 1780 ($\approx$ 1775) MeV
Full width Γ = 105 to 135 ($\approx$ 120) MeV

$\Sigma(1775)$ DECAY MODES	Fraction (Γ_i/Γ)	p (MeV/c)
$N\overline{K}$	37–43%	508
$\Lambda\pi$	14–20%	525
$\Sigma\pi$	2–5%	475
$\Sigma(1385)\pi$	8–12%	327
$\Lambda(1520)\pi$, P-wave	17–23%	202

$\Sigma(1910)\ 3/2^-$

$I(J^P) = 1(\frac{3}{2}^-)$

was $\Sigma(1940)$

Mass m = 1870 to 1950 ($\approx$ 1910) MeV
Full width Γ = 150 to 300 ($\approx$ 220) MeV

$\Sigma(1910)$ DECAY MODES	Fraction (Γ_i/Γ)	p (MeV/c)
$N\overline{K}$	0.01 to 0.05 ($\approx$ 0.02)	615
$\Lambda\pi$	(6 ± 4) %	619
$\Sigma\pi$	(86 ±21) %	574
$\Sigma(1385)\pi$	seen	439
$\Lambda(1520)\pi$	seen	329
$\Delta(1232)\overline{K}$	(3.0 ± 1.0) %	377
$N\overline{K}^*(892)$	seen	274
$N\overline{K}^*(892)$, S=1/2 , D-wave	(1.0 ± 1.0) %	274

$\Sigma(1915)\ 5/2^+$

$I(J^P) = 1(\frac{5}{2}^+)$

Mass m = 1900 to 1935 ($\approx$ 1915) MeV
Full width Γ = 80 to 160 ($\approx$ 120) MeV

$\Sigma(1915)$ DECAY MODES	Fraction (Γ_i/Γ)	p (MeV/c)
$N\overline{K}$	0.05 to 0.15	618
$\Lambda\pi$	(6.0 ±2.0) %	623
$\Sigma\pi$	(10.0 ±2.0) %	577
$\Sigma(1385)\pi$, P-wave	(2.0 ±2.0) %	443
$\Sigma(1385)\pi$, F-wave	(4.0 ±2.0) %	443
$\Lambda(1520)\pi$, D-wave	(8.0 ±2.0) %	334
$N\overline{K}^*(892)$, S=1/2, F-wave	(5.0 ±3.0) %	282
$N\overline{K}^*(892)$, S=3/2, F-wave	(5.0 ±2.0) %	282
$\Delta\overline{K}$, P-wave	(16 ±5) %	383
$\Delta\overline{K}$, F-wave	(5.0 ±3.0) %	383

$\Sigma(2030)\ 7/2^+$

$I(J^P) = 1(\frac{7}{2}^+)$

Mass m = 2025 to 2040 ($\approx$ 2030) MeV
Full width Γ = 150 to 200 ($\approx$ 180) MeV

$\Sigma(2030)$ DECAY MODES	Fraction (Γ_i/Γ)	p (MeV/c)
$N\overline{K}$	17–23 %	702
$\Lambda\pi$	17–23 %	700
$\Sigma\pi$	5–10 %	657
ΞK	<2 %	422
$\Sigma(1385)\pi$	5–15 %	532
$\Sigma(1385)\pi$, F-wave	(1.0±1.0) %	532
$\Lambda(1520)\pi$	10–20 %	431
$\Delta(1232)\overline{K}$	10–20 %	498
$\Delta(1232)\overline{K}$, F-wave	(15 ±5) %	498
$\Delta(1232)\overline{K}$, H-wave	(1.0±1.0) %	498
$N\overline{K}^*(892)$, S=3/2, F-wave	(14 ±8) %	439

Ξ BARYONS ($S = -2, I = 1/2$)

$\Xi^0 = uss, \quad \Xi^- = dss$

Ξ^0

$I(J^P) = \frac{1}{2}(\frac{1}{2}^+)$

P is not yet measured; + is the quark model prediction.

Mass m = 1314.86 ± 0.20 MeV
$m_{\Xi^-} - m_{\Xi^0}$ = 6.85 ± 0.21 MeV
Mean life $\tau = (2.90 \pm 0.09) \times 10^{-10}$ s
$c\tau$ = 8.71 cm
Magnetic moment $\mu = -1.250 \pm 0.014\ \mu_N$

Decay parameters

$\Lambda\pi^0$	$\alpha = -0.356 \pm 0.011$
"	$\phi = (21 \pm 12)^\circ$
"	$\gamma = 0.85$ [n]
"	$\Delta = (218^{+12}_{-19})^\circ$ [n]
$\Lambda\gamma$	$\alpha = -0.70 \pm 0.07$
$\Lambda e^+ e^-$	$\alpha = -0.8 \pm 0.2$
$\Sigma^0\gamma$	$\alpha = -0.69 \pm 0.06$
$\Sigma^+ e^- \overline{\nu}_e$	$g_1(0)/f_1(0) = 1.22 \pm 0.05$
$\Sigma^+ e^- \overline{\nu}_e$	$f_2(0)/f_1(0) = 2.0 \pm 0.9$

Ξ^0 DECAY MODES	Fraction (Γ_i/Γ)	Confidence level	p (MeV/c)
$\Lambda\pi^0$	(99.524±0.012) %		135
$\Lambda\gamma$	(1.17 ±0.07) $\times 10^{-3}$		184
$\Lambda e^+ e^-$	(7.6 ±0.6) $\times 10^{-6}$		184
$\Sigma^0\gamma$	(3.33 ±0.10) $\times 10^{-3}$		117
$\Sigma^+ e^- \overline{\nu}_e$	(2.52 ±0.08) $\times 10^{-4}$		120
$\Sigma^+ \mu^- \overline{\nu}_\mu$	(2.33 ±0.35) $\times 10^{-6}$		64
$\Delta S = \Delta Q$ (SQ) violating modes or $\Delta S = 2$ forbidden ($S2$) modes			
$\Sigma^- e^+ \nu_e$	SQ < 9 $\times 10^{-4}$	90%	112
$\Sigma^- \mu^+ \nu_\mu$	SQ < 9 $\times 10^{-4}$	90%	49
$p\pi^-$	$S2$ < 8 $\times 10^{-6}$	90%	299
$p e^- \overline{\nu}_e$	$S2$ < 1.3 $\times 10^{-3}$		323
$p\mu^- \overline{\nu}_\mu$	$S2$ < 1.3 $\times 10^{-3}$		309

Downloaded from https://academic.oup.com/ptep/article/2022/8/083C01/6651666 by KIT Library user on 27 September 2022

Ξ^-

$I(J^P) = \frac{1}{2}(\frac{1}{2}^+)$

P is not yet measured; + is the quark model prediction.

Mass $m = 1321.71 \pm 0.07$ MeV
$(m_{\Xi^-} - m_{\overline{\Xi}^+}) / m_{\Xi^-} = (-3 \pm 9) \times 10^{-5}$
Mean life $\tau = (1.639 \pm 0.015) \times 10^{-10}$ s
$c\tau = 4.91$ cm
$(\tau_{\Xi^-} - \tau_{\overline{\Xi}^+}) / \tau_{\Xi^-} = -0.01 \pm 0.07$
Magnetic moment $\mu = -0.6507 \pm 0.0025\ \mu_N$
$(\mu_{\Xi^-} + \mu_{\overline{\Xi}^+}) / |\mu_{\Xi^-}| = +0.01 \pm 0.05$

Decay parameters

$\Lambda\pi^-$ $\alpha = -0.401 \pm 0.010$
$[\alpha(\Xi^-)\alpha_-(\Lambda) - \alpha(\overline{\Xi}^+)\alpha_+(\overline{\Lambda})] / [\text{sum}] = (0 \pm 7) \times 10^{-4}$
" $\phi = (-2.1 \pm 0.8)^\circ$
" $\gamma = 0.89$ [n]
" $\Delta = (175.9 \pm 1.5)^\circ$ [n]
$\Lambda e^-\overline{\nu}_e$ $g_A/g_V = -0.25 \pm 0.05$ [l]

Ξ^- DECAY MODES		Fraction (Γ_i/Γ)	Confidence level	p (MeV/c)
$\Lambda\pi^-$		(99.887 ± 0.035) %		140
$\Sigma^-\gamma$		$(1.27 \pm 0.23) \times 10^{-4}$		118
$\Lambda e^-\overline{\nu}_e$		$(5.63 \pm 0.31) \times 10^{-4}$		190
$\Lambda\mu^-\overline{\nu}_\mu$		$(3.5\ ^{+3.5}_{-2.2}) \times 10^{-4}$		163
$\Sigma^0 e^-\overline{\nu}_e$		$(8.7 \pm 1.7) \times 10^{-5}$		123
$\Sigma^0\mu^-\overline{\nu}_\mu$		$< 8 \times 10^{-4}$	90%	70
$\Xi^0 e^-\overline{\nu}_e$		$< 2.59 \times 10^{-4}$	90%	7
$\Delta S = 2$ forbidden ($S2$) modes				
$n\pi^-$	$S2$	$< 1.9 \times 10^{-5}$	90%	304
$ne^-\overline{\nu}_e$	$S2$	$< 3.2 \times 10^{-3}$	90%	327
$n\mu^-\overline{\nu}_\mu$	$S2$	< 1.5 %	90%	314
$p\pi^-\pi^-$	$S2$	$< 4 \times 10^{-4}$	90%	223
$p\pi^-e^-\overline{\nu}_e$	$S2$	$< 4 \times 10^{-4}$	90%	305
$p\pi^-\mu^-\overline{\nu}_\mu$	$S2$	$< 4 \times 10^{-4}$	90%	251
$p\mu^-\mu^-$	L	$< 4 \times 10^{-8}$	90%	272

$\Xi(1530)\ 3/2^+$

$I(J^P) = \frac{1}{2}(\frac{3}{2}^+)$

$\Xi(1530)^0$ mass $m = 1531.80 \pm 0.32$ MeV (S = 1.3)
$\Xi(1530)^-$ mass $m = 1535.0 \pm 0.6$ MeV
$\Xi(1530)^0$ full width $\Gamma = 9.1 \pm 0.5$ MeV
$\Xi(1530)^-$ full width $\Gamma = 9.9^{+1.7}_{-1.9}$ MeV

$\Xi(1530)$ DECAY MODES	Fraction (Γ_i/Γ)	Confidence level	p (MeV/c)
$\Xi\pi$	100 %		158
$\Xi\gamma$	<3.7 %	90%	202

$\Xi(1690)$

$I(J^P) = \frac{1}{2}(?^?)$

Mass $m = 1690 \pm 10$ MeV [p]
Full width $\Gamma = 20 \pm 15$ MeV

$\Xi(1690)$ DECAY MODES	Fraction (Γ_i/Γ)	p (MeV/c)
$\Lambda\overline{K}$	seen	240
$\Sigma\overline{K}$	seen	70
$\Xi\pi$	seen	311
$\Xi^-\pi^+\pi^-$	possibly seen	213

$\Xi(1820)\ 3/2^-$

$I(J^P) = \frac{1}{2}(\frac{3}{2}^-)$

Mass $m = 1823 \pm 5$ MeV [p]
Full width $\Gamma = 24^{+15}_{-10}$ MeV [p]

$\Xi(1820)$ DECAY MODES	Fraction (Γ_i/Γ)	p (MeV/c)
$\Lambda\overline{K}$	large	402
$\Sigma\overline{K}$	small	324
$\Xi\pi$	small	421
$\Xi(1530)\pi$	small	237

$\Xi(1950)$

$I(J^P) = \frac{1}{2}(?^?)$

Mass $m = 1950 \pm 15$ MeV [p]
Full width $\Gamma = 60 \pm 20$ MeV [p]

$\Xi(1950)$ DECAY MODES	Fraction (Γ_i/Γ)	p (MeV/c)
$\Lambda\overline{K}$	seen	522
$\Sigma\overline{K}$	possibly seen	460
$\Xi\pi$	seen	519

$\Xi(2030)$

$I(J^P) = \frac{1}{2}(\geq \frac{5}{2}^?)$

Mass $m = 2025 \pm 5$ MeV [p]
Full width $\Gamma = 20^{+15}_{-5}$ MeV [p]

$\Xi(2030)$ DECAY MODES	Fraction (Γ_i/Γ)	p (MeV/c)
$\Lambda\overline{K}$	~ 20 %	585
$\Sigma\overline{K}$	~ 80 %	529
$\Xi\pi$	small	574
$\Xi(1530)\pi$	small	416
$\Lambda\overline{K}\pi$	small	499
$\Sigma\overline{K}\pi$	small	428

Ω BARYONS ($S = -3, I = 0$)

$\Omega^- = sss$

Ω^-

$I(J^P) = 0(\frac{3}{2}^+)$

$J^P = \frac{3}{2}^+$ is the quark-model prediction; and $J = 3/2$ is fairly well established.

Mass $m = 1672.45 \pm 0.29$ MeV
$(m_{\Omega^-} - m_{\overline{\Omega}^+}) / m_{\Omega^-} = (-1 \pm 8) \times 10^{-5}$
Mean life $\tau = (0.821 \pm 0.011) \times 10^{-10}$ s
$c\tau = 2.461$ cm
$(\tau_{\Omega^-} - \tau_{\overline{\Omega}^+}) / \tau_{\Omega^-} = 0.00 \pm 0.05$
Magnetic moment $\mu = -2.02 \pm 0.05\ \mu_N$

Decay parameters

$\alpha(\Omega^-)\ \alpha_-(\Lambda)$ FOR $\Omega^- \to \Lambda K^- = 0.0115 \pm 0.0015$
ΛK^- $\alpha = 0.0157 \pm 0.0021$
$\Lambda K^-, \overline{\Lambda} K^+$ $(\alpha + \overline{\alpha})/(\alpha - \overline{\alpha}) = -0.02 \pm 0.13$
$\Xi^0\pi^-$ $\alpha = 0.09 \pm 0.14$
$\Xi^-\pi^0$ $\alpha = 0.05 \pm 0.21$

Ω^- DECAY MODES		Fraction (Γ_i/Γ)	Confidence level	p (MeV/c)
ΛK^-		(67.8 ± 0.7) %		211
$\Xi^0\pi^-$		(23.6 ± 0.7) %		294
$\Xi^-\pi^0$		(8.6 ± 0.4) %		289
$\Xi^-\pi^+\pi^-$		$(3.7^{+0.7}_{-0.6}) \times 10^{-4}$		189
$\Xi(1530)^0\pi^-$		$< 7 \times 10^{-5}$	90%	17
$\Xi^0 e^-\overline{\nu}_e$		$(5.6 \pm 2.8) \times 10^{-3}$		319
$\Xi^-\gamma$		$< 4.6 \times 10^{-4}$	90%	314
$\Delta S = 2$ forbidden ($S2$) modes				
$\Lambda\pi^-$	$S2$	$< 2.9 \times 10^{-6}$	90%	449

$\Omega(2012)^-$

$I(J^P) = 0(?^-)$

Mass $m = 2012.4 \pm 0.9$ MeV
Full width $\Gamma = 6.4^{+3.0}_{-2.6}$ MeV

Branching fractions are given relative to the one **DEFINED AS 1**.

$\Omega(2012)^-$ DECAY MODES	Fraction (Γ_i/Γ)	Confidence level	p (MeV/c)
$\Xi^0 K^-$	**DEFINED AS 1**		403
$\Xi^-\overline{K}^0$	0.83 ± 0.21		392
$\Xi^0\pi^0 K^-$	<0.30	90%	245

Downloaded from https://academic.oup.com/ptep/article/2022/8/083C01/6651666 by KIT Library user on 27 September 2022

$\Xi^0\pi^-\overline{K}^0$	<0.21	90%	230
$\Xi^-\pi^0\overline{K}^0$	<0.7	90%	226
$\Xi^-\pi^+K^-$	<0.08	90%	224

$\Omega(2250)^-$

$I(J^P) = 0(?^?)$

Mass $m = 2252 \pm 9$ MeV
Full width $\Gamma = 55 \pm 18$ MeV

$\Omega(2250)^-$ DECAY MODES	Fraction (Γ_i/Γ)	p (MeV/c)
$\Xi^-\pi^+K^-$	seen	532
$\Xi(1530)^0K^-$	seen	437

CHARMED BARYONS ($C=+1$)

$\Lambda_c^+ = udc$, $\Sigma_c^{++} = uuc$, $\Sigma_c^+ = udc$, $\Sigma_c^0 = ddc$,
$\Xi_c^+ = usc$, $\Xi_c^0 = dsc$, $\Omega_c^0 = ssc$

Λ_c^+

$I(J^P) = 0(\frac{1}{2}^+)$

Mass $m = 2286.46 \pm 0.14$ MeV
Mean life $\tau = (201.5 \pm 2.7) \times 10^{-15}$ s (S = 1.6)
$c\tau = 60.4$ μm

Decay asymmetry parameters

$\Lambda\pi^+$ $\alpha = -0.84 \pm 0.09$
$\Sigma^+\pi^0$ $\alpha = -0.55 \pm 0.11$
α FOR $\Lambda_c^+ \to \Sigma^0\pi^+ = -0.73 \pm 0.18$
$\Lambda\ell^+\nu_\ell$ $\alpha = -0.86 \pm 0.04$
α FOR $\Lambda_c^+ \to pK_S^0 = 0.2 \pm 0.5$
$(\alpha+\overline{\alpha})/(\alpha-\overline{\alpha})$ in $\Lambda_c^+ \to \Lambda\pi^+$, $\overline{\Lambda}_c^- \to \overline{\Lambda}\pi^- = -0.07 \pm 0.31$
$(\alpha+\overline{\alpha})/(\alpha-\overline{\alpha})$ in $\Lambda_c^+ \to \Lambda e^+\nu_e$, $\overline{\Lambda}_c^- \to \overline{\Lambda}e^-\overline{\nu}_e = 0.00 \pm 0.04$
$A_{CP}(\Lambda X)$ in $\Lambda_c \to \Lambda X$, $\overline{\Lambda}_c \to \overline{\Lambda}X = (2 \pm 7)\%$
$\Delta A_{CP} = A_{CP}(\Lambda_c^+ \to pK^+K^-) - A_{CP}(\Lambda_c^+ \to p\pi^+\pi^-) = (0.3 \pm 1.1)\%$

Branching fractions marked with a footnote, e.g. [a], have been corrected for decay modes not observed in the experiments. For example, the submode fraction $\Lambda_c^+ \to p\overline{K}^*(892)^0$ seen in $\Lambda_c^+ \to pK^-\pi^+$ has been multiplied up to include $\overline{K}^*(892)^0 \to \overline{K}^0\pi^0$ decays.

Λ_c^+ DECAY MODES		Fraction (Γ_i/Γ)	Scale factor/ Confidence level	p (MeV/c)
Hadronic modes with a p or n: $S = -1$ final states				
pK_S^0		(1.59 ± 0.08) %	S=1.1	873
$pK^-\pi^+$		(6.28 ± 0.32) %	S=1.4	823
$p\overline{K}^*(892)^0$	[r]	(1.96 ± 0.27) %		685
$\Delta(1232)^{++}K^-$		(1.08 ± 0.25) %		710
$\Lambda(1520)\pi^+$	[r]	(2.2 ± 0.5) %		628
$pK^-\pi^+$ nonresonant		(3.5 ± 0.4) %		823
$pK_S^0\pi^0$		(1.97 ± 0.13) %	S=1.1	823
$nK_S^0\pi^+$		(1.82 ± 0.25) %		821
$p\overline{K}^0\eta$		$(8.3 \pm 1.8) \times 10^{-3}$		568
$pK_S^0\pi^+\pi^-$		(1.60 ± 0.12) %	S=1.1	754
$pK^-\pi^+\pi^0$		(4.46 ± 0.30) %	S=1.5	759
$pK^*(892)^-\pi^+$	[r]	(1.4 ± 0.5) %		580
$p(K^-\pi^+)_{\text{nonresonant}}\pi^0$		(4.6 ± 0.8) %		759
$\Delta(1232)\overline{K}^*(892)$		seen		419
$pK^-2\pi^+\pi^-$		$(1.4 \pm 0.9) \times 10^{-3}$		671
$pK^-\pi^+2\pi^0$		(1.0 ± 0.5) %		678
Hadronic modes with a p: $S = 0$ final states				
$p\pi^0$		$< 8 \times 10^{-5}$	CL=90%	945
$p\eta$		$(1.42 \pm 0.12) \times 10^{-3}$		856
$p\omega(782)^0$		$(8.3 \pm 1.1) \times 10^{-4}$		751
$p\pi^+\pi^-$		$(4.61 \pm 0.28) \times 10^{-3}$		927
$pf_0(980)$	[r]	$(3.5 \pm 2.3) \times 10^{-3}$		614
$p2\pi^+2\pi^-$		$(2.3 \pm 1.4) \times 10^{-3}$		852
pK^+K^-		$(1.06 \pm 0.06) \times 10^{-3}$		616
$p\phi$	[r]	$(1.06 \pm 0.14) \times 10^{-3}$		590
pK^+K^- non-ϕ		$(5.3 \pm 1.2) \times 10^{-4}$		616
$p\phi\pi^0$		$(10 \pm 4) \times 10^{-5}$		460
$pK^+K^-\pi^0$ nonresonant		$< 6.3 \times 10^{-5}$	CL=90%	494
Hadronic modes with a hyperon: $S = -1$ final states				
$\Lambda\pi^+$		(1.30 ± 0.07) %	S=1.1	864
$\Lambda(1670)\pi^+$, $\Lambda(1670) \to \eta\Lambda$		$(3.5 \pm 0.5) \times 10^{-3}$		–
$\Lambda\pi^+\pi^0$		(7.1 ± 0.4) %	S=1.1	844
$\Lambda\rho^+$		< 6 %	CL=95%	636
$\Lambda\pi^-2\pi^+$		(3.64 ± 0.29) %	S=1.4	807
$\Sigma(1385)^+\pi^+\pi^-$, $\Sigma^{*+} \to \Lambda\pi^+$		(1.0 ± 0.5) %		688
$\Sigma(1385)^-2\pi^+$, $\Sigma^{*-} \to \Lambda\pi^-$		$(7.6 \pm 1.4) \times 10^{-3}$		688
$\Lambda\pi^+\rho^0$		(1.5 ± 0.6) %		524
$\Sigma(1385)^+\rho^0$, $\Sigma^{*+} \to \Lambda\pi^+$		$(5 \pm 4) \times 10^{-3}$		363
$\Lambda\pi^-2\pi^+$ nonresonant		< 1.1 %	CL=90%	807
$\Lambda\pi^-\pi^02\pi^+$ total		(2.3 ± 0.8) %		757
$\Lambda\pi^+\eta$	[r]	(1.84 ± 0.26) %		691
$\Sigma(1385)^+\eta$	[r]	$(9.1 \pm 2.0) \times 10^{-3}$		570
$\Lambda\pi^+\omega$	[r]	(1.5 ± 0.5) %		517
$\Lambda\pi^-\pi^02\pi^+$, no η or ω		$< 8 \times 10^{-3}$	CL=90%	757
$\Lambda K^+\overline{K}^0$		$(5.7 \pm 1.1) \times 10^{-3}$	S=1.9	443
$\Xi(1690)^0K^+$, $\Xi^{*0} \to \Lambda\overline{K}^0$		$(1.6 \pm 0.5) \times 10^{-3}$		286
$\Sigma^0\pi^+$		(1.29 ± 0.07) %	S=1.1	825
$\Sigma^0\pi^+\eta$		$(7.5 \pm 0.8) \times 10^{-3}$		635
$\Sigma^+\pi^0$		(1.25 ± 0.10) %		827
$\Sigma^+\eta$		$(4.4 \pm 2.0) \times 10^{-3}$		713
$\Sigma^+\eta'$		(1.5 ± 0.6) %		391
$\Sigma^+\pi^+\pi^-$		(4.50 ± 0.25) %	S=1.3	804
$\Sigma^+\rho^0$		< 1.7 %	CL=95%	575
$\Sigma^-2\pi^+$		(1.87 ± 0.18) %		799
$\Sigma^0\pi^+\pi^0$		(3.5 ± 0.4) %		803
$\Sigma^+\pi^0\pi^0$		(1.55 ± 0.15) %		806
$\Sigma^0\pi^-2\pi^+$		(1.11 ± 0.30) %		763
$\Sigma^+\pi^+\pi^-\pi^0$		—		767
$\Sigma^+\omega$	[r]	(1.70 ± 0.21) %		569
$\Sigma^-\pi^02\pi^+$		(2.1 ± 0.4) %		762
$\Sigma^+K^+K^-$		$(3.5 \pm 0.4) \times 10^{-3}$	S=1.1	349
$\Sigma^+\phi$	[r]	$(3.9 \pm 0.6) \times 10^{-3}$	S=1.1	295
$\Xi(1690)^0K^+$, $\Xi^{*0} \to \Sigma^+K^-$		$(1.02 \pm 0.25) \times 10^{-3}$		286
$\Sigma^+K^+K^-$ nonresonant		$< 8 \times 10^{-4}$	CL=90%	349
Ξ^0K^+		$(5.5 \pm 0.7) \times 10^{-3}$		653
$\Xi^-K^+\pi^+$		$(6.2 \pm 0.6) \times 10^{-3}$	S=1.1	565
$\Xi(1530)^0K^+$		$(4.3 \pm 0.9) \times 10^{-3}$	S=1.1	473
Hadronic modes with a hyperon: $S = 0$ final states				
ΛK^+		$(6.1 \pm 1.2) \times 10^{-4}$		781
$\Lambda K^+\pi^+\pi^-$		$< 5 \times 10^{-4}$	CL=90%	637
Σ^0K^+		$(5.2 \pm 0.8) \times 10^{-4}$		735
$\Sigma^0K^+\pi^+\pi^-$		$< 2.6 \times 10^{-4}$	CL=90%	574
$\Sigma^+K^+\pi^-$		$(2.1 \pm 0.6) \times 10^{-3}$		670
$\Sigma^+K^*(892)^0$	[r]	$(3.5 \pm 1.0) \times 10^{-3}$		470
$\Sigma^-K^+\pi^+$		$< 1.2 \times 10^{-3}$	CL=90%	664
Doubly Cabibbo-suppressed modes				
$pK^+\pi^-$		$(1.11 \pm 0.18) \times 10^{-4}$		823
Semileptonic modes				
$\Lambda e^+\nu_e$		(3.6 ± 0.4) %		871
$\Lambda\mu^+\nu_\mu$		(3.5 ± 0.5) %		867
Inclusive modes				
e^+ anything		(3.95 ± 0.35) %		–
p anything		(50 ± 16) %		–
n anything		(50 ± 16) %		–
Λ anything		$(38.2 {}^{+2.9}_{-2.4})$ %		–
K_S^0 anything		(9.9 ± 0.7) %		–
3prongs		(24 ± 8) %		–
$\Delta C = 1$ weak neutral current ($C1$) modes, or Lepton Family number (LF), or Lepton number (L), or Baryon number (B) violating modes				
pe^+e^-	$C1$	$< 5.5 \times 10^{-6}$	CL=90%	951
$p\mu^+\mu^-$ non-resonant	$C1$	$< 7.7 \times 10^{-8}$	CL=90%	937
$pe^+\mu^-$	LF	$< 9.9 \times 10^{-6}$	CL=90%	947
$pe^-\mu^+$	LF	$< 1.9 \times 10^{-5}$	CL=90%	947
$\overline{p}2e^+$	L,B	$< 2.7 \times 10^{-6}$	CL=90%	951
$\overline{p}2\mu^+$	L,B	$< 9.4 \times 10^{-6}$	CL=90%	937
$\overline{p}e^+\mu^+$	L,B	$< 1.6 \times 10^{-5}$	CL=90%	947
$\overline{\Sigma}^-\mu^+\mu^+$	L	$< 7.0 \times 10^{-4}$	CL=90%	812

Downloaded from https://academic.oup.com/ptep/article/2022/8/083C01/6651666 by KIT Library user on 27 September 2022

$\Lambda_c(2595)^+$ $I(J^P) = 0(\frac{1}{2}^-)$

The spin-parity follows from the fact that $\Sigma_c(2455)\pi$ decays, with little available phase space, are dominant. This assumes that $J^P = 1/2^+$ for the $\Sigma_c(2455)$.

Mass $m = 2592.25 \pm 0.28$ MeV
$m - m_{\Lambda_c^+} = 305.79 \pm 0.24$ MeV
Full width $\Gamma = 2.6 \pm 0.6$ MeV

$\Lambda_c^+\pi\pi$ and its submode $\Sigma_c(2455)\pi$ — the latter just barely — are the only strong decays allowed to an excited Λ_c^+ having this mass; and the submode seems to dominate.

$\Lambda_c(2595)^+$ DECAY MODES	Fraction (Γ_i/Γ)	p (MeV/c)
$\Lambda_c^+\pi^+\pi^-$	[s] —	117
$\Sigma_c(2455)^{++}\pi^-$	24 ± 7 %	3
$\Sigma_c(2455)^0\pi^+$	24 ± 7 %	3
$\Lambda_c^+\pi^+\pi^-$ 3-body	18 ± 10 %	117
$\Lambda_c^+\pi^0$	[t] not seen	258
$\Lambda_c^+\gamma$	not seen	288

$\Lambda_c(2625)^+$ $I(J^P) = 0(\frac{3}{2}^-)$

J^P has not been measured; $\frac{3}{2}^-$ is the quark-model prediction.

Mass $m = 2628.11 \pm 0.19$ MeV (S = 1.1)
$m - m_{\Lambda_c^+} = 341.65 \pm 0.13$ MeV (S = 1.1)
Full width $\Gamma < 0.97$ MeV, CL = 90%

$\Lambda_c^+\pi\pi$ and its submode $\Sigma(2455)\pi$ are the only strong decays allowed to an excited Λ_c^+ having this mass.

$\Lambda_c(2625)^+$ DECAY MODES	Fraction (Γ_i/Γ)	Confidence level	p (MeV/c)
$\Lambda_c^+\pi^+\pi^-$	≈ 67%		184
$\Sigma_c(2455)^{++}\pi^-$	<5	90%	103
$\Sigma_c(2455)^0\pi^+$	<5	90%	103
$\Lambda_c^+\pi^+\pi^-$ 3-body	large		184
$\Lambda_c^+\pi^0$	[t] not seen		293
$\Lambda_c^+\gamma$	not seen		319

$\Lambda_c(2860)^+$ $I(J^P) = 0(\frac{3}{2}^+)$

Mass $m = 2856.1^{+2.3}_{-6.0}$ MeV
Full width $\Gamma = 68^{+12}_{-22}$ MeV

$\Lambda_c(2860)^+$ DECAY MODES	Fraction (Γ_i/Γ)	p (MeV/c)
$D^0 p$	seen	259

$\Lambda_c(2880)^+$ $I(J^P) = 0(\frac{5}{2}^+)$

Mass $m = 2881.63 \pm 0.24$ MeV
$m - m_{\Lambda_c^+} = 595.17 \pm 0.28$ MeV
Full width $\Gamma = 5.6^{+0.8}_{-0.6}$ MeV

$\Lambda_c(2880)^+$ DECAY MODES	Fraction (Γ_i/Γ)	p (MeV/c)
$\Lambda_c^+\pi^+\pi^-$	seen	471
$\Sigma_c(2455)^{0,++}\pi^\pm$	seen	376
$\Sigma_c(2520)^{0,++}\pi^\pm$	seen	317
pD^0	seen	316

$\Lambda_c(2940)^+$ $I(J^P) = 0(\frac{3}{2}^-)$

$J^P = 3/2^-$ is favored, but is not certain

Mass $m = 2939.6^{+1.3}_{-1.5}$ MeV
Full width $\Gamma = 20^{+6}_{-5}$ MeV

$\Lambda_c(2940)^+$ DECAY MODES	Fraction (Γ_i/Γ)	p (MeV/c)
pD^0	seen	420
$\Sigma_c(2455)^{0,++}\pi^\pm$	seen	–

$\Sigma_c(2455)$ $I(J^P) = 1(\frac{1}{2}^+)$

$\Sigma_c(2455)^{++}$ mass $m = 2453.97 \pm 0.14$ MeV
$\Sigma_c(2455)^+$ mass $m = 2452.65^{+0.22}_{-0.16}$ MeV
$\Sigma_c(2455)^0$ mass $m = 2453.75 \pm 0.14$ MeV
$m_{\Sigma_c(2455)^{++}} - m_{\Lambda_c^+} = 167.510 \pm 0.017$ MeV
$m_{\Sigma_c(2455)^+} - m_{\Lambda_c^+} = 166.19^{+0.16}_{-0.08}$ MeV
$m_{\Sigma^0_{c2455}} - m_{\Lambda_c^+} = 167.290 \pm 0.017$ MeV
$m_{\Sigma_c(2455)^{++}} - m_{\Sigma_c(2455)^0} = 0.220 \pm 0.013$ MeV
$m_{\Sigma_c(2455)^+} - m_{\Sigma_c(2455)^0} = -1.10^{+0.16}_{-0.08}$ MeV
$\Sigma_c(2455)^{++}$ full width $\Gamma = 1.89^{+0.09}_{-0.18}$ MeV (S = 1.1)
$\Sigma_c(2455)^+$ full width $\Gamma = 2.3 \pm 0.4$ MeV
$\Sigma_c(2455)^0$ full width $\Gamma = 1.83^{+0.11}_{-0.19}$ MeV (S = 1.2)

$\Lambda_c^+\pi$ is the only strong decay allowed to a Σ_c having this mass.

$\Sigma_c(2455)$ DECAY MODES	Fraction (Γ_i/Γ)	p (MeV/c)
$\Lambda_c^+\pi$	≈ 100 %	94

$\Sigma_c(2520)$ $I(J^P) = 1(\frac{3}{2}^+)$

J^P has not been measured; $\frac{3}{2}^+$ is the quark-model prediction.

$\Sigma_c(2520)^{++}$ mass $m = 2518.41^{+0.22}_{-0.18}$ MeV (S = 1.1)
$\Sigma_c(2520)^+$ mass $m = 2517.4^{+0.7}_{-0.5}$ MeV
$\Sigma_c(2520)^0$ mass $m = 2518.48 \pm 0.20$ MeV (S = 1.1)
$m_{\Sigma_c(2520)^{++}} - m_{\Lambda_c^+} = 231.95^{+0.18}_{-0.12}$ MeV (S = 1.3)
$m_{\Sigma_c(2520)^+} - m_{\Lambda_c^+} = 230.9^{+0.7}_{-0.5}$ MeV
$m_{\Sigma_c(2520)^0} - m_{\Lambda_c^+} = 232.02^{+0.16}_{-0.14}$ MeV (S = 1.3)
$m_{\Sigma_c(2520)^{++}} - m_{\Sigma_c(2520)^0} = 0.01 \pm 0.15$ MeV
$\Sigma_c(2520)^{++}$ full width $\Gamma = 14.78^{+0.30}_{-0.40}$ MeV
$\Sigma_c(2520)^+$ full width $\Gamma = 17.2^{+4.0}_{-2.2}$ MeV
$\Sigma_c(2520)^0$ full width $\Gamma = 15.3^{+0.4}_{-0.5}$ MeV

$\Lambda_c^+\pi$ is the only strong decay allowed to a Σ_c having this mass.

$\Sigma_c(2520)$ DECAY MODES	Fraction (Γ_i/Γ)	p (MeV/c)
$\Lambda_c^+\pi$	≈ 100 %	179

$\Sigma_c(2800)$ $I(J^P) = 1(?^?)$

$\Sigma_c(2800)^{++}$ mass $m = 2801^{+4}_{-6}$ MeV
$\Sigma_c(2800)^+$ mass $m = 2792^{+14}_{-5}$ MeV
$\Sigma_c(2800)^0$ mass $m = 2806^{+5}_{-7}$ MeV (S = 1.3)
$m_{\Sigma_c(2800)^{++}} - m_{\Lambda_c^+} = 514^{+4}_{-6}$ MeV
$m_{\Sigma_c(2800)^+} - m_{\Lambda_c^+} = 505^{+14}_{-5}$ MeV
$m_{\Sigma_c(2800)^0} - m_{\Lambda_c^+} = 519^{+5}_{-7}$ MeV (S = 1.3)
$\Sigma_c(2800)^{++}$ full width $\Gamma = 75^{+22}_{-17}$ MeV
$\Sigma_c(2800)^+$ full width $\Gamma = 62^{+60}_{-40}$ MeV
$\Sigma_c(2800)^0$ full width $\Gamma = 72^{+22}_{-15}$ MeV

$\Sigma_c(2800)$ DECAY MODES	Fraction (Γ_i/Γ)	p (MeV/c)
$\Lambda_c^+\pi$	seen	443

Ξ_c^+ $I(J^P) = \frac{1}{2}(\frac{1}{2}^+)$

J^P has not been measured; $\frac{1}{2}^+$ is the quark-model prediction.

Mass $m = 2467.71 \pm 0.23$ MeV (S = 1.3)
Mean life $\tau = (453 \pm 5) \times 10^{-15}$ s
$c\tau = 135.8\ \mu$m

Downloaded from https://academic.oup.com/ptep/article/2022/8/083C01/6651666 by KIT Library user on 27 September 2022

Branching fractions marked with a footnote, e.g. [a], have been corrected for decay modes not observed in the experiments. For example, the submode fraction $\Xi_c^+ \to \Sigma^+ \overline{K}^*(892)^0$ seen in $\Xi_c^+ \to \Sigma^+ K^- \pi^+$ has been multiplied up to include $\overline{K}^*(892)^0 \to \overline{K}^0 \pi^0$ decays.

Ξ_c^+ DECAY MODES		Fraction (Γ_i/Γ)	Scale factor / Confidence level	p (MeV/c)
Cabibbo-favored ($S = -2$) decays				
$p 2K_S^0$		$(2.5 \pm 1.3) \times 10^{-3}$		766
$\Lambda \overline{K}^0 \pi^+$		—		852
$\Sigma(1385)^+ \overline{K}^0$	[r]	(2.9 ± 2.0) %		746
$\Lambda K^- 2\pi^+$		$(9 \pm 4) \times 10^{-3}$		787
$\Lambda \overline{K}^*(892)^0 \pi^+$	[r]	$< 5 \times 10^{-3}$	CL=90%	608
$\Sigma(1385)^+ K^- \pi^+$	[r]	$< 6 \times 10^{-3}$	CL=90%	678
$\Sigma^+ K^- \pi^+$		(2.7 ± 1.2) %		810
$\Sigma^+ \overline{K}^*(892)^0$	[r]	(2.3 ± 1.1) %		658
$\Sigma^0 K^- 2\pi^+$		$(8 \pm 5) \times 10^{-3}$		735
$\Xi^0 \pi^+$		(1.6 ± 0.8) %		876
$\Xi^- 2\pi^+$		(2.9 ± 1.3) %		851
$\Xi(1530)^0 \pi^+$	[r]	$< 2.9 \times 10^{-3}$	CL=90%	749
$\Xi(1620)^0 \pi^+$		seen		–
$\Xi(1690)^0 \pi^+$		seen		644
$\Xi^0 \pi^+ \pi^0$		(6.7 ± 3.5) %		856
$\Xi^0 \pi^- 2\pi^+$		(5.0 ± 2.6) %		818
$\Xi^0 e^+ \nu_e$		(7 ± 4) %		884
$\Omega^- K^+ \pi^+$		$(2.0 \pm 1.5) \times 10^{-3}$		399
Cabibbo-suppressed decays				
$p K^- \pi^+$		$(6.2 \pm 3.0) \times 10^{-3}$	S=1.5	944
$p \overline{K}^*(892)^0$	[r]	$(3.3 \pm 1.7) \times 10^{-3}$		828
$\Sigma^+ \pi^+ \pi^-$		(1.4 ± 0.8) %		922
$\Sigma^- 2\pi^+$		$(5.1 \pm 3.4) \times 10^{-3}$		918
$\Sigma^+ K^+ K^-$		$(4.3 \pm 2.5) \times 10^{-3}$		579
$\Sigma^+ \phi$	[r]	$< 3.2 \times 10^{-3}$	CL=90%	549
$\Xi(1690)^0 K^+$, $\Xi^0 \to \Sigma^+ K^-$		$< 1.3 \times 10^{-3}$	CL=90%	501
$p \phi(1020)$		$(1.2 \pm 0.6) \times 10^{-4}$		751

Ξ_c^0

$I(J^P) = \frac{1}{2}(\frac{1}{2}^+)$

J^P has not been measured; $\frac{1}{2}^+$ is the quark-model prediction.

Mass $m = 2470.44 \pm 0.28$ MeV (S = 1.2)
$m_{\Xi_c^0} - m_{\Xi_c^+} = 2.72 \pm 0.23$ MeV (S = 1.1)
Mean life $\tau = (151.9 \pm 2.4) \times 10^{-15}$ s
$c\tau = 45.5\ \mu$m

Decay asymmetry parameters

$\Xi^- \pi^+$ $\alpha = -0.64 \pm 0.05$
α FOR $\overline{\Xi}_c^0 \to \overline{\Xi}^+ \pi^- = 0.61 \pm 0.05$
α FOR $\Xi_c^0 \to \Lambda \overline{K}^*(892)^0 = 0.15 \pm 0.22$
α FOR $\Xi_c^0 \to \Sigma^+ K^*(892)^- = -0.52 \pm 0.30$

Ξ_c^0 DECAY MODES	Fraction (Γ_i/Γ)	Scale factor	p (MeV/c)
Cabibbo-favored decays			
$p K^- K^- \pi^+$	$(4.8 \pm 1.2) \times 10^{-3}$	1.1	676
$p K^- \overline{K}^*(892)^0$, $\overline{K}^{*0} \to K^- \pi^+$	$(2.0 \pm 0.6) \times 10^{-3}$		413
$p K^- K^- \pi^+$ (no $\overline{K}^{*0}$)	$(3.0 \pm 0.9) \times 10^{-3}$		676
ΛK_S^0	$(3.2 \pm 0.7) \times 10^{-3}$		906
$\Lambda K^- \pi^+$	(1.45 ± 0.33) %	1.1	856
$\Lambda \overline{K}^*(892)^0$	$(2.6 \pm 0.7) \times 10^{-3}$		717
$\Lambda \overline{K}^0 \pi^+ \pi^-$	seen		786
$\Lambda K^- \pi^+ \pi^+ \pi^-$	seen		703
$\Sigma^0 K_S^0$	$(5.4 \pm 1.6) \times 10^{-4}$		864
$\Sigma^+ K^-$	$(1.8 \pm 0.4) \times 10^{-3}$		868
$\Sigma^0 \overline{K}^*(892)^0$	$(9.8 \pm 2.3) \times 10^{-3}$		658
$\Sigma^+ K^*(892)^-$	$(4.9 \pm 1.4) \times 10^{-3}$		661
$\Xi^- \pi^+$	(1.43 ± 0.32) %	1.1	875
$\Xi^- \pi^+ \pi^+ \pi^-$	(4.8 ± 2.3) %		816
$\Xi^0 \phi$, $\phi \to K^+ K^-$	$(5.1 \pm 1.3) \times 10^{-4}$		–
$\Xi^0 K^+ K^-$ nonresonant	$(5.6 \pm 1.4) \times 10^{-4}$		444
$\Omega^- K^+$	$(4.2 \pm 1.0) \times 10^{-3}$		522
$\Xi^- e^+ \nu_e$	(1.04 ± 0.24) %		882
$\Xi^- \mu^+ \nu_\mu$	(1.01 ± 0.25) %		878
Cabibbo-suppressed decays			
$\Lambda_c^+ \pi^-$	$(5.5 \pm 1.8) \times 10^{-3}$		115
$\Xi^- K^+$	$(3.9 \pm 1.2) \times 10^{-4}$		789
$\Lambda K^+ K^-$ (no ϕ)	$(4.1 \pm 1.4) \times 10^{-4}$		648
$\Lambda \phi$	$(4.9 \pm 1.5) \times 10^{-4}$		621

$\Xi_c'^+$

$I(J^P) = \frac{1}{2}(\frac{1}{2}^+)$

J^P has not been measured; $\frac{1}{2}^+$ is the quark-model prediction.

Mass $m = 2578.2 \pm 0.5$ MeV (S = 1.1)
$m_{\Xi_c'^+} - m_{\Xi_c^+} = 110.5 \pm 0.4$ MeV
$m_{\Xi_c'^+} - m_{\Xi_c'^0} = -0.5 \pm 0.6$ MeV

The $\Xi_c'^+$-Ξ_c^+ mass difference is too small for any strong decay to occur.

$\Xi_c'^+$ DECAY MODES	Fraction (Γ_i/Γ)	p (MeV/c)
$\Xi_c^+ \gamma$	seen	108

$\Xi_c'^0$

$I(J^P) = \frac{1}{2}(\frac{1}{2}^+)$

J^P has not been measured; $\frac{1}{2}^+$ is the quark-model prediction.

Mass $m = 2578.7 \pm 0.5$ MeV
$m_{\Xi_c'^0} - m_{\Xi_c^0} = 108.3 \pm 0.4$ MeV

The $\Xi_c'^0 - \Xi_c^0$ mass difference is too small for any strong decay to occur.

$\Xi_c'^0$ DECAY MODES	Fraction (Γ_i/Γ)	p (MeV/c)
$\Xi_c^0 \gamma$	seen	106

$\Xi_c(2645)$

$I(J^P) = \frac{1}{2}(\frac{3}{2}^+)$

J^P has not been measured; $\frac{3}{2}^+$ is the quark-model prediction.

$\Xi_c(2645)^+$ mass $m = 2645.10 \pm 0.30$ MeV (S = 1.2)
$\Xi_c(2645)^0$ mass $m = 2646.16 \pm 0.25$ MeV (S = 1.3)
$m_{\Xi_c(2645)^0} - m_{\Xi_c^0} = 174.67 \pm 0.09$ MeV
$m_{\Xi_c(2645)^0} - m_{\Xi_c^+} = 178.45 \pm 0.10$ MeV
$m_{\Xi_c(2645)^+} - m_{\Xi_c(2645)^0} = -1.06 \pm 0.27$ MeV (S = 1.1)
$\Xi_c(2645)^+$ full width $\Gamma = 2.14 \pm 0.19$ MeV (S = 1.1)
$\Xi_c(2645)^0$ full width $\Gamma = 2.35 \pm 0.22$ MeV

$\Xi_c \pi$ is the only strong decay allowed to a Ξ_c resonance having this mass.

$\Xi_c(2645)$ DECAY MODES	Fraction (Γ_i/Γ)	p (MeV/c)
$\Xi_c^0 \pi^+$	seen	102
$\Xi_c^+ \pi^-$	seen	106

$\Xi_c(2790)$

$I(J^P) = \frac{1}{2}(\frac{1}{2}^-)$

J^P has not been measured; $\frac{1}{2}^-$ is the quark-model prediction.

$\Xi_c(2790)^+$ mass = 2791.9 ± 0.5 MeV
$\Xi_c(2790)^0$ mass = 2793.9 ± 0.5 MeV
$m_{\Xi_c(2790)^+} - m_{\Xi_c'^0} = 213.20 \pm 0.22$ MeV
$m_{\Xi_c(2790)^0} - m_{\Xi_c'^+} = 215.70 \pm 0.22$ MeV
$m_{\Xi_c(2790)^+} - m_{\Xi_c(2790)^0} = -2.0 \pm 0.7$ MeV
$\Xi_c(2790)^+$ width = 8.9 ± 1.0 MeV
$\Xi_c(2790)^0$ width = 10.0 ± 1.1 MeV

$\Xi_c(2790)$ DECAY MODES	Fraction (Γ_i/Γ)	p (MeV/c)
$\Xi_c' \pi$	seen	159

Downloaded from https://academic.oup.com/ptep/article/2022/8/083C01/6651666 by KIT Library user on 27 September 2022

$\Xi_c(2815)$ $I(J^P) = \frac{1}{2}(\frac{3}{2}^-)$

J^P has not been measured; $\frac{3}{2}^-$ is the quark-model prediction.

$\Xi_c(2815)^+$ mass $m = 2816.51 \pm 0.25$ MeV (S = 1.2)
$\Xi_c(2815)^0$ mass $m = 2819.79 \pm 0.30$ MeV (S = 1.1)
$m_{\Xi_c(2815)^+} - m_{\Xi_c^+} = 348.80 \pm 0.10$ MeV
$m_{\Xi_c(2815)^0} - m_{\Xi_c^0} = 349.35 \pm 0.11$ MeV
$m_{\Xi_c(2815)^+} - m_{\Xi_c(2815)^0} = -3.27 \pm 0.27$ MeV
$\Xi_c(2815)^+$ full width $\Gamma = 2.43 \pm 0.26$ MeV
$\Xi_c(2815)^0$ full width $\Gamma = 2.54 \pm 0.25$ MeV

The $\Xi_c \pi\pi$ modes are consistent with being entirely via $\Xi_c(2645)\pi$.

$\Xi_c(2815)$ DECAY MODES	Fraction (Γ_i/Γ)	p (MeV/c)
$\Xi'_c \pi$	seen	188
$\Xi_c(2645)\pi$	seen	102
$\Xi_c^0 \gamma$	seen	325

$\Xi_c(2970)$ $I(J^P) = \frac{1}{2}(\frac{1}{2}^+)$

was $\Xi_c(2980)$

$\Xi_c(2970)^+$ $m = 2964.3 \pm 1.5$ MeV (S = 3.9)
$\Xi_c(2970)^0$ $m = 2967.1 \pm 1.7$ MeV (S = 6.7)
$m_{\Xi_c(2970)^+} - m_{\Xi_c^+} = 496.6 \pm 1.5$ MeV (S = 3.7)
$m_{\Xi_c(2970)^0} - m_{\Xi_c^0} = 496.7 \pm 1.8$ MeV (S = 5.3)
$m_{\Xi_c(2970)^+} - m_{\Xi_c(2970)^0} = -2.8 \pm 1.9$ MeV (S = 4.8)
$\Xi_c(2970)^+$ width $\Gamma = 20.9^{+2.4}_{-3.5}$ MeV (S = 1.2)

$\Xi_c(2970)$ DECAY MODES	Fraction (Γ_i/Γ)	p (MeV/c)
$\Lambda_c^+ \overline{K}\pi$	seen	223
$\Sigma_c(2455)\overline{K}$	seen	122
$\Lambda_c^+ \overline{K}$	not seen	410
$\Lambda_c^+ K^-$	seen	410
$\Xi_c 2\pi$	seen	381
$\Xi'_c \pi$	seen	–
$\Xi_c(2645)\pi$	seen	274

$\Xi_c(3055)$ $I(J^P) = ?(?^?)$

Mass $m = 3055.9 \pm 0.4$ MeV
Full width $\Gamma = 7.8 \pm 1.9$ MeV

$\Xi_c(3055)$ DECAY MODES	Fraction (Γ_i/Γ)	p (MeV/c)
$\Sigma^{++} K^-$	seen	–
ΛD^+	seen	316

$\Xi_c(3080)$ $I(J^P) = \frac{1}{2}(?^?)$

$\Xi_c(3080)^+$ $m = 3077.2 \pm 0.4$ MeV
$\Xi_c(3080)^0$ $m = 3079.9 \pm 1.4$ MeV (S = 1.3)
$\Xi_c(3080)^+$ width $\Gamma = 3.6 \pm 1.1$ MeV (S = 1.5)
$\Xi_c(3080)^0$ width $\Gamma = 5.6 \pm 2.2$ MeV

$\Xi_c(3080)$ DECAY MODES	Fraction (Γ_i/Γ)	p (MeV/c)
$\Lambda_c^+ \overline{K}\pi$	seen	415
$\Sigma_c(2455)\overline{K}$	seen	342
$\Sigma_c(2455)^{++} K^-$	seen	342
$\Sigma_c(2520)^{++} K^-$	seen	239
$\Sigma_c(2455)\overline{K} + \Sigma_c(2520)\overline{K}$	seen	–
$\Lambda_c^+ \overline{K}$	not seen	536
$\Lambda_c^+ \overline{K}\pi^+\pi^-$	not seen	144
ΛD^+	seen	362

Ω_c^0 $I(J^P) = 0(\frac{1}{2}^+)$

J^P has not been measured; $\frac{1}{2}^+$ is the quark-model prediction.

Mass $m = 2695.2 \pm 1.7$ MeV (S = 1.3)
Mean life $\tau = (268 \pm 26) \times 10^{-15}$ s
$c\tau = 80\ \mu$m

No absolute branching fractions have been measured. The following are branching *ratios* relative to $\Omega^-\pi^+$.

Ω_c^0 DECAY MODES	Fraction (Γ_i/Γ)	Confidence level	p (MeV/c)
Cabibbo-favored ($S = -3$) decays — relative to $\Omega^-\pi^+$			
$\Omega^-\pi^+$	**DEFINED AS 1**		821
$\Omega^-\pi^+\pi^0$	1.80 ± 0.33		797
$\Omega^-\rho^+$	>1.3	90%	532
$\Omega^-\pi^-2\pi^+$	0.31 ± 0.05		753
$\Omega^- e^+ \nu_e$	2.4 ± 1.2		829
$\Xi^0 \overline{K}^0$	1.64 ± 0.29		950
$\Xi^0 K^-\pi^+$	1.20 ± 0.18		901
$\Xi^0 \overline{K}^{*0}$, $\overline{K}^{*0} \to K^-\pi^+$	0.68 ± 0.16		764
$\Omega(2012)^-\pi^+$, $\Omega(2012)^- \to \Xi^0 K^-$	0.12 ± 0.05		–
$\Xi^- \overline{K}^0 \pi^+$	2.12 ± 0.28		895
$\Omega(2012)^-\pi^+$, $\Omega(2012)^- \to \Xi^- \overline{K}^0$	0.12 ± 0.06		–
$\Xi^- K^- 2\pi^+$	0.63 ± 0.09		830
$\Xi(1530)^0 K^-\pi^+$, $\Xi^{*0} \to \Xi^-\pi^+$	0.21 ± 0.06		757
$\Xi^- \overline{K}^{*0}\pi^+$	0.34 ± 0.11		653
$p K^- K^-\pi^+$	seen		864
$\Sigma^+ K^- K^-\pi^+$	<0.32	90%	689
$\Lambda \overline{K}^0 \overline{K}^0$	1.72 ± 0.35		837

$\Omega_c(2770)^0$ $I(J^P) = 0(\frac{3}{2}^+)$

J^P has not been measured; $\frac{3}{2}^+$ is the quark-model prediction.

Mass $m = 2765.9 \pm 2.0$ MeV (S = 1.2)
$m_{\Omega_c(2770)^0} - m_{\Omega_c^0} = 70.7^{+0.8}_{-0.9}$ MeV

The $\Omega_c(2770)^0$–Ω_c^0 mass difference is too small for any strong decay to occur.

$\Omega_c(2770)^0$ DECAY MODES	Fraction (Γ_i/Γ)	p (MeV/c)
$\Omega_c^0 \gamma$	presumably 100%	70

$\Omega_c(3000)^0$ $I(J^P) = ?(?^?)$

Mass $m = 3000.41 \pm 0.22$ MeV
Full width $\Gamma = 4.5 \pm 0.7$ MeV

$\Omega_c(3000)^0$ DECAY MODES	Fraction (Γ_i/Γ)	p (MeV/c)
$\Xi_c^+ K^-$	seen	182

$\Omega_c(3050)^0$ $I(J^P) = ?(?^?)$

Mass $m = 3050.19 \pm 0.13$ MeV
Full width $\Gamma < 1.2$ MeV, CL = 95%

$\Omega_c(3050)^0$ DECAY MODES	Fraction (Γ_i/Γ)	p (MeV/c)
$\Xi_c^+ K^-$	seen	278

$\Omega_c(3065)^0$ $I(J^P) = ?(?^?)$

Mass $m = 3065.54 \pm 0.26$ MeV
Full width $\Gamma = 3.3 \pm 0.6$ MeV (S = 1.5)

$\Omega_c(3065)^0$ DECAY MODES	Fraction (Γ_i/Γ)	p (MeV/c)
$\Xi_c^+ K^-$	seen	303

$\Omega_c(3090)^0$ $I(J^P) = ?(?^?)$

Mass $m = 3090.1 \pm 0.5$ MeV
Full width $\Gamma = 8.7 \pm 1.3$ MeV

$\Omega_c(3090)^0$ DECAY MODES	Fraction (Γ_i/Γ)	p (MeV/c)
$\Xi_c^+ K^-$	seen	340

Downloaded from https://academic.oup.com/ptep/article/2022/8/083C01/6651666 by KIT Library user on 27 September 2022

$\Omega_c(3120)^0$

$I(J^P) = ?(?^?)$

Mass $m = 3119.1 \pm 1.0$ MeV
Full width $\Gamma < 2.6$ MeV, CL = 95%

$\Omega_c(3120)^0$ DECAY MODES	Fraction (Γ_i/Γ)	p (MeV/c)
$\Xi_c^+ K^-$	seen	379

DOUBLY CHARMED BARYONS ($C=+2$)

$\Xi_{cc}^{++} = ucc$, $\Xi_{cc}^{+} = dcc$, $\Omega_{cc}^{+} = scc$

Ξ_{cc}^{++}

$I(J^P) = ?(?^?)$

Mass $m = 3621.6 \pm 0.4$ MeV
Mean life $\tau = (256 \pm 27) \times 10^{-15}$ s

Ξ_{cc}^{++} DECAY MODES	Fraction (Γ_i/Γ)	p (MeV/c)
$\Lambda_c^+ K^- \pi^+ \pi^+$	seen	880
$\Xi_c^+ \pi^+$, $\Xi_c^+ \to p K^- \pi^+$	seen	–

BOTTOM BARYONS ($B=-1$)

$\Lambda_b^0 = udb$, $\Xi_b^0 = usb$, $\Xi_b^- = dsb$, $\Omega_b^- = ssb$

Λ_b^0

$I(J^P) = 0(\frac{1}{2}^+)$

$I(J^P)$ not yet measured; $0(\frac{1}{2}^+)$ is the quark model prediction.
Mass $m = 5619.60 \pm 0.17$ MeV
$m_{\Lambda_b^0} - m_{B^0} = 339.2 \pm 1.4$ MeV
$m_{\Lambda_b^0} - m_{B^+} = 339.72 \pm 0.28$ MeV
Mean life $\tau = (1.471 \pm 0.009) \times 10^{-12}$ s
$c\tau = 441.0\ \mu$m
$A_{CP}(\Lambda_b \to p\pi^-) = -0.025 \pm 0.029$ (S = 1.2)
$A_{CP}(\Lambda_b \to pK^-) = -0.025 \pm 0.022$
$A_{CP}(\Lambda_b \to Dp K^-) = 0.12 \pm 0.09$
$\Delta A_{CP}(pK^-/\pi^-) = 0.014 \pm 0.024$
$A_{CP}(\Lambda_b \to p\overline{K}^0\pi^-) = 0.22 \pm 0.13$
$\Delta A_{CP}(J/\psi p\pi^-/K^-) = (5.7 \pm 2.7) \times 10^{-2}$
$A_{CP}(\Lambda_b \to \Lambda K^+\pi^-) = -0.53 \pm 0.25$
$A_{CP}(\Lambda_b \to \Lambda K^+K^-) = -0.28 \pm 0.12$
$\Delta A_{CP}(\Lambda_b^0 \to pK^-\mu^+\mu^-) = (-4 \pm 5) \times 10^{-2}$
$\Delta A_{CP}(\Lambda_b^0 \to p\pi^-\pi^+\pi^-) = (1.1 \pm 2.6) \times 10^{-2}$
$\Delta A_{CP}(\Lambda_b^0 \to (p\pi^-\pi^+\pi^-)_{LBM}) = (4 \pm 4) \times 10^{-2}$
$\Delta A_{CP}(\Lambda_b^0 \to pa_1(1260)^-) = (-1 \pm 4) \times 10^{-2}$
$\Delta A_{CP}(\Lambda_b^0 \to N(1520)^0\rho(770)^0) = (2 \pm 5) \times 10^{-2}$
$\Delta A_{CP}(\Lambda_b^0 \to \Delta(1232)^{++}\pi^-\pi^-) = (0.1 \pm 3.3) \times 10^{-2}$
$\Delta A_{CP}(\Lambda_b^0 \to pK^-\pi^+\pi^-) = (3.2 \pm 1.3) \times 10^{-2}$
$\Delta A_{CP}(\Lambda_b^0 \to (pK^-\pi^+\pi^-)_{LBM}) = (3.5 \pm 1.6) \times 10^{-2}$
$\Delta A_{CP}(\Lambda_b^0 \to N(1520)^0 K^*(892)^0) = (5.5 \pm 2.5) \times 10^{-2}$
$\Delta A_{CP}(\Lambda_b^0 \to \Lambda(1520)\rho(770)^0) = (1 \pm 6) \times 10^{-2}$
$\Delta A_{CP}(\Lambda_b^0 \to \Delta(1232)^{++}K^-\pi^-) = (4.4 \pm 2.7) \times 10^{-2}$
$\Delta A_{CP}(\Lambda_b^0 \to pK_1(1410)^-) = (5 \pm 4) \times 10^{-2}$
$\Delta A_{CP}(\Lambda_b^0 \to pK^-K^+\pi^-) = (-7 \pm 5) \times 10^{-2}$
$\Delta A_{CP}(\Lambda_b^0 \to pK^-K^+K^-) = (0.2 \pm 1.9) \times 10^{-2}$
$\Delta A_{CP}(\Lambda_b^0 \to \Lambda(1520)\phi(1020)) = (4 \pm 6) \times 10^{-2}$
$\Delta A_{CP}(\Lambda_b^0 \to (pK^-)_{highmass}\ \phi(1020)) = (-0.7 \pm 3.4) \times 10^{-2}$
$\Delta A_{CP}(\Lambda_b^0 \to (pK^-K^+K^-)_{LBM}) = (2.7 \pm 2.4) \times 10^{-2}$
$A_{FB}^{\ell}(\mu\mu)$ in $\Lambda_b \to \Lambda\mu^+\mu^- = -0.39 \pm 0.04$
$\Delta(A_{FB}^{\ell}(\mu\mu))$ in $\Lambda_b \to \Lambda\mu^+\mu^- = -0.05 \pm 0.09$
$A_{FB}^{h}(p\pi)$ in $\Lambda_b \to \Lambda(p\pi)\mu^+\mu^- = -0.30 \pm 0.05$
$A_{FB}^{\ell h}$ in $\Lambda_b \to \Lambda\mu^+\mu^- = 0.25 \pm 0.04$

The branching fractions B(b-baryon $\to \Lambda\ell^-\overline{\nu}_\ell$ anything) and B($\Lambda_b^0 \to \Lambda_c^+\ell^-\overline{\nu}_\ell$ anything) are not pure measurements because the underlying measured products of these with B($b \to b$-baryon) were used to determine B($b \to b$-baryon), as described in the note "Production and Decay of b-Flavored Hadrons."

For inclusive branching fractions, *e.g.*, $\Lambda_b \to \overline{\Lambda}_c$ anything, the values usually are multiplicities, not branching fractions. They can be greater than one.

Λ_b^0 DECAY MODES		Fraction (Γ_i/Γ)	Scale factor/ Confidence level	p (MeV/c)
$J/\psi(1S)\Lambda \times$ B($b \to \Lambda_b^0$)		$(5.8 \pm 0.8) \times 10^{-5}$		1740
$pD^0\pi^-$		$(6.3 \pm 0.6) \times 10^{-4}$		2370
pD^0K^-		$(4.6 \pm 0.8) \times 10^{-5}$		2269
$pJ/\psi\pi^-$		$(2.6\ ^{+0.5}_{-0.4}) \times 10^{-5}$		1755
$p\pi^- J/\psi$, $J/\psi \to \mu^+\mu^-$		$(1.6 \pm 0.8) \times 10^{-6}$		–
$pJ/\psi K^-$		$(3.2\ ^{+0.6}_{-0.5}) \times 10^{-4}$		1589
$p\eta_c(1S)K^-$		$(1.06 \pm 0.26) \times 10^{-4}$		1670
$P_c(4312)^+K^-$, $P_c(4312)^+ \to p\eta_c(1S)$		$< 2.5 \times 10^{-5}$	CL=95%	–
$P_c(4380)^+K^-$, $P_c \to pJ/\psi$	[u]	$(2.7 \pm 1.4) \times 10^{-5}$		–
$P_c(4450)^+K^-$, $P_c \to pJ/\psi$	[u]	$(1.3 \pm 0.4) \times 10^{-5}$		–
$\chi_{c1}(1P)pK^-$		$(7.6\ ^{+1.5}_{-1.3}) \times 10^{-5}$		1242
$\chi_{c1}(1P)p\pi^-$		$(5.0\ ^{+1.3}_{-1.1}) \times 10^{-6}$		1462
$\chi_{c2}(1P)pK^-$		$(7.9\ ^{+1.6}_{-1.4}) \times 10^{-5}$		1198
$\chi_{c2}(1P)p\pi^-$		$(4.8 \pm 1.9) \times 10^{-6}$		1427
$pJ/\psi(1S)\pi^+\pi^-K^-$		$(6.6\ ^{+1.3}_{-1.1}) \times 10^{-5}$		1410
$p\psi(2S)K^-$		$(6.6\ ^{+1.2}_{-1.0}) \times 10^{-5}$		1063
$\chi_{c1}(3872)pK^-$		$(3.2 \pm 1.4) \times 10^{-5}$		837
$\chi_{c1}(3872)\Lambda(1520)$		$(1.9 \pm 0.9) \times 10^{-5}$		721
$\psi(2S)p\pi^-$		$(7.5\ ^{+1.6}_{-1.4}) \times 10^{-6}$		1320
$p\overline{K}^0\pi^-$		$(1.3 \pm 0.4) \times 10^{-5}$		2693
pK^0K^-		$< 3.5 \times 10^{-6}$	CL=90%	2639
$\Lambda_c^+\pi^-$		$(4.9 \pm 0.4) \times 10^{-3}$	S=1.2	2342
$\Lambda_c^+K^-$		$(3.56 \pm 0.28) \times 10^{-4}$	S=1.2	2314
$\Lambda_c^+a_1(1260)^-$		seen		2153
$\Lambda_c^+D^-$		$(4.6 \pm 0.6) \times 10^{-4}$		1886
$\Lambda_c^+D_s^-$		(1.10 ± 0.10) %		1833
$\Lambda_c^+\pi^+\pi^-\pi^-$		$(7.6 \pm 1.1) \times 10^{-3}$	S=1.1	2323
$\Lambda_c(2595)^+\pi^-$, $\Lambda_c(2595)^+ \to \Lambda_c^+\pi^+\pi^-$		$(3.4 \pm 1.4) \times 10^{-4}$		2210
$\Lambda_c(2625)^+\pi^-$, $\Lambda_c(2625)^+ \to \Lambda_c^+\pi^+\pi^-$		$(3.3 \pm 1.3) \times 10^{-4}$		2193
$\Sigma_c(2455)^0\pi^+\pi^-$, $\Sigma_c^0 \to \Lambda_c^+\pi^-$		$(5.7 \pm 2.2) \times 10^{-4}$		2265
$\Sigma_c(2455)^{++}\pi^-\pi^-$, $\Sigma_c^{++} \to \Lambda_c^+\pi^+$		$(3.2 \pm 1.5) \times 10^{-4}$		2265
$\Lambda_c^+K^+K^-\pi^-$		$(1.02 \pm 0.11) \times 10^{-3}$		2184
$\Lambda_c^+p\overline{p}\pi^-$		$(2.63 \pm 0.27) \times 10^{-4}$		1805
$\Sigma_c(2455)^0p\overline{p}$, $\Sigma_c^0 \to \Lambda_c^+\pi^-$		$(2.3 \pm 0.5) \times 10^{-5}$		–
$\Sigma_c(2520)^0p\overline{p}$, $\Sigma_c(2520)^0 \to \Lambda_c^+\pi^-$		$(3.1 \pm 0.7) \times 10^{-5}$		–
$\Lambda_c^+\ell^-\overline{\nu}_\ell$ anything	[v]	(10.9 ± 2.2) %		–
$\Lambda_c^+\ell^-\overline{\nu}_\ell$		$(6.2\ ^{+1.4}_{-1.3})$ %		2345
$\Lambda_c^+\pi^+\pi^-\ell^-\overline{\nu}_\ell$		(5.6 ± 3.1) %		2335
$\Lambda_c(2595)^+\ell^-\overline{\nu}_\ell$		$(7.9\ ^{+4.0}_{-3.5}) \times 10^{-3}$		2212
$\Lambda_c(2625)^+\ell^-\overline{\nu}_\ell$		$(1.3\ ^{+0.6}_{-0.5})$ %		2195
ph^-	[x]	$< 2.3 \times 10^{-5}$	CL=90%	2730
$p\pi^-$		$(4.5 \pm 0.8) \times 10^{-6}$		2730
pK^-		$(5.4 \pm 1.0) \times 10^{-6}$		2709
pD_s^-		$< 4.8 \times 10^{-4}$	CL=90%	2364
$p\mu^-\overline{\nu}_\mu$		$(4.1 \pm 1.0) \times 10^{-4}$		2730
$\Lambda\mu^+\mu^-$		$(1.08 \pm 0.28) \times 10^{-6}$		2695
$p\pi^-\mu^+\mu^-$		$(6.9 \pm 2.5) \times 10^{-8}$		2720
$pK^-e^+e^-$		$(3.1 \pm 0.6) \times 10^{-7}$		2708

Downloaded from https://academic.oup.com/ptep/article/2022/8/083C01/6651666 by KIT Library user on 27 September 2022

$pK^-\mu^+\mu^-$	$(2.6\ ^{+0.5}_{-0.4}) \times 10^{-7}$		2685
$\Lambda\gamma$	$(7.1 \pm 1.7) \times 10^{-6}$		2699
$\Lambda\eta$	$(9\ ^{+7}_{-5}) \times 10^{-6}$		2670
$\Lambda\eta'(958)$	$< 3.1 \times 10^{-6}$	CL=90%	2611
$\Lambda\pi^+\pi^-$	$(4.6 \pm 1.9) \times 10^{-6}$		2692
$\Lambda K^+\pi^-$	$(5.6 \pm 1.2) \times 10^{-6}$		2660
ΛK^+K^-	$(1.60 \pm 0.22) \times 10^{-5}$		2605
$\Lambda\phi$	$(9.8 \pm 2.6) \times 10^{-6}$		2599
$p\pi^-\pi^+\pi^-$	$(2.10 \pm 0.22) \times 10^{-5}$		2715
$pK^-K^+\pi^-$	$(4.0 \pm 0.6) \times 10^{-6}$		2612
$pK^-\pi^+\pi^-$	$(5.0 \pm 0.5) \times 10^{-5}$		2675
$pK^-K^+K^-$	$(1.26 \pm 0.13) \times 10^{-5}$		2524

$\Lambda_b(5912)^0$

$J^P = \frac{1}{2}^-$

Mass $m = 5912.19 \pm 0.17$ MeV
Full width $\Gamma < 0.25$ MeV, CL = 90%

$\Lambda_b(5912)^0$ DECAY MODES	Fraction (Γ_i/Γ)	p (MeV/c)
$\Lambda_b^0\pi^+\pi^-$	seen	86

$\Lambda_b(5920)^0$

$J^P = \frac{3}{2}^-$

Mass $m = 5920.09 \pm 0.17$ MeV
Full width $\Gamma < 0.19$ MeV, CL = 90%

$\Lambda_b(5920)^0$ DECAY MODES	Fraction (Γ_i/Γ)	p (MeV/c)
$\Lambda_b^0\pi^+\pi^-$	seen	108

$\Lambda_b(6070)^0$

$J^P = \frac{1}{2}^+$

Quantum numbers based on quark model expectations.

Mass $m = 6072.3 \pm 2.9$ MeV
Full width $\Gamma = 72 \pm 11$ MeV

$\Lambda_b(6070)^0$ DECAY MODES	Fraction (Γ_i/Γ)	p (MeV/c)
$\Lambda_b^0\pi^+\pi^-$	seen	343

$\Lambda_b(6146)^0$

$J^P = \frac{3}{2}^+$

Mass $m = 6146.2 \pm 0.4$ MeV
$m_{\Lambda_b(6146)^0} - m_{\Lambda_b^0} = 526.55 \pm 0.34$ MeV
Full width $\Gamma = 2.9 \pm 1.3$ MeV

$\Lambda_b(6146)^0$ DECAY MODES	Fraction (Γ_i/Γ)	p (MeV/c)
$\Lambda_b^0\pi^+\pi^-$	seen	427

$\Lambda_b(6152)^0$

$J^P = \frac{5}{2}^+$

Mass $m = 6152.5 \pm 0.4$ MeV
$m_{\Lambda_b(6152)^0} - m_{\Lambda_b^0} = 532.89 \pm 0.28$ MeV
$m_{\Lambda_b(6152)^0} - m_{\Lambda_b(6146)^0} = 6.34 \pm 0.32$ MeV
Full width $\Gamma = 2.1 \pm 0.9$ MeV

$\Lambda_b(6152)^0$ DECAY MODES	Fraction (Γ_i/Γ)	p (MeV/c)
$\Lambda_b^0\pi^+\pi^-$	seen	434

Σ_b

$I(J^P) = 1(\frac{1}{2}^+)$
I, J, P need confirmation.

Mass $m(\Sigma_b^+) = 5810.56 \pm 0.25$ MeV
Mass $m(\Sigma_b^-) = 5815.64 \pm 0.27$ MeV
$m_{\Sigma_b^+} - m_{\Sigma_b^-} = -5.06 \pm 0.18$ MeV
$\Gamma(\Sigma_b^+) = 5.0 \pm 0.5$ MeV
$\Gamma(\Sigma_b^-) = 5.3 \pm 0.5$ MeV

Σ_b DECAY MODES	Fraction (Γ_i/Γ)	p (MeV/c)
$\Lambda_b^0\pi$	dominant	133

Σ_b^*

$I(J^P) = 1(\frac{3}{2}^+)$
I, J, P need confirmation.

Mass $m(\Sigma_b^{*+}) = 5830.32 \pm 0.27$ MeV
Mass $m(\Sigma_b^{*-}) = 5834.74 \pm 0.30$ MeV
$m_{\Sigma_b^{*+}} - m_{\Sigma_b^{*-}} = -4.37 \pm 0.33$ MeV (S = 1.6)
$m_{\Sigma_b^{*+}} - m_{\Sigma_b^+} = 19.73 \pm 0.18$
$m_{\Sigma_b^{*-}} - m_{\Sigma_b^-} = 19.09 \pm 0.22$
$\Gamma(\Sigma_b^{*+}) = 9.4 \pm 0.5$ MeV
$\Gamma(\Sigma_b^{*-}) = 10.4 \pm 0.8$ MeV (S = 1.3)
$m_{\Sigma_b^*} - m_{\Sigma_b} = 21.2 \pm 2.0$ MeV

Σ_b^* DECAY MODES	Fraction (Γ_i/Γ)	p (MeV/c)
$\Lambda_b^0\pi$	dominant	159

$\Sigma_b(6097)^+$

$J^P = ?^?$

Mass $m = 6095.8 \pm 1.7$ MeV
Full width $\Gamma = 31 \pm 6$ MeV

$\Sigma_b(6097)^+$ DECAY MODES	Fraction (Γ_i/Γ)	p (MeV/c)
$\Lambda_b\pi^+ \times B(b \to \Sigma_b(6097)^+)$	seen	–

$\Sigma_b(6097)^-$

$J^P = ?^?$

Mass $m = 6098.0 \pm 1.8$ MeV
Full width $\Gamma = 29 \pm 4$ MeV

$\Sigma_b(6097)^-$ DECAY MODES	Fraction (Γ_i/Γ)	p (MeV/c)
$\Lambda_b\pi^- \times B(b \to \Sigma_b(6097)^-)$	seen	–

Ξ_b^-

$I(J^P) = \frac{1}{2}(\frac{1}{2}^+)$
I, J, P need confirmation.

$m(\Xi_b^-) = 5797.0 \pm 0.6$ MeV (S = 1.7)
$m_{\Xi_b^-} - m_{\Lambda_b^0} = 177.46 \pm 0.31$ MeV (S = 1.3)
$m_{\Xi_b^-} - m_{\Xi_b^0} = 5.9 \pm 0.6$ MeV
Mean life $\tau_{\Xi_b^-} = (1.572 \pm 0.040) \times 10^{-12}$ s

Ξ_b^- DECAY MODES	Fraction (Γ_i/Γ)	p (MeV/c)
$J/\psi\,\Xi^- \times B(b \to \Xi_b^-)$	$(1.02\ ^{+0.26}_{-0.21}) \times 10^{-5}$	1782
$J/\psi\,\Lambda K^- \times B(b \to \Xi_b^-)$	$(2.5 \pm 0.4) \times 10^{-6}$	1631
$pK^-K^- \times B(b \to \Xi_b^-)$	$(3.7 \pm 0.8) \times 10^{-8}$	2731
pK^-K^-	seen	2731
$pK^-\pi^-$	seen	2783
$\Lambda_b^0\pi^- \times B(b \to \Xi_b^-)/B(b \to \Lambda_b^0)$	$(5.7 \pm 2.0) \times 10^{-4}$	99
$\Xi_c^0\pi^-$	seen	2367
$\Sigma(1385)K^-$	$(2.6 \pm 2.3) \times 10^{-7}$	2707
$\Lambda(1405)K^-$	$(1.9 \pm 1.2) \times 10^{-7}$	2702
$\Lambda(1520)K^-$	$(7.6 \pm 3.2) \times 10^{-7}$	2673
$\Lambda(1670)K^-$	$(4.5 \pm 2.3) \times 10^{-7}$	2629
$\Sigma(1775)K^-$	$(2.2 \pm 1.5) \times 10^{-7}$	2599
$\Sigma(1915)K^-$	$(2.6 \pm 2.5) \times 10^{-7}$	2553

Ξ_b^0

$I(J^P) = \frac{1}{2}(\frac{1}{2}^+)$
I, J, P need confirmation.

$m(\Xi_b^0) = 5791.9 \pm 0.5$ MeV
$m_{\Xi_b^0} - m_{\Lambda_b^0} = 172.5 \pm 0.4$ MeV
Mean life $\tau_{\Xi_b^0} = (1.480 \pm 0.030) \times 10^{-12}$ s

Ξ_b^0 DECAY MODES	Fraction (Γ_i/Γ)	Confidence level	p (MeV/c)
$pD^0K^- \times B(b \to \Xi_b^0)$	$(1.7 \pm 0.5) \times 10^{-6}$		2374
$p\overline{K}^0\pi^- \times B(b \to \Xi_b^0)/B(\overline{b} \to B^0)$	$< 1.6 \times 10^{-6}$	90%	2783
$pK^0K^- \times B(b \to \Xi_b^0)/B(\overline{b} \to B^0)$	$< 1.1 \times 10^{-6}$	90%	2730
$\Lambda\pi^+\pi^- \times B(b \to \Xi_b^0)/B(b \to \Lambda_b^0)$	$< 1.7 \times 10^{-6}$	90%	2781

Downloaded from https://academic.oup.com/ptep/article/2022/8/083C01/6651666 by KIT Library user on 27 September 2022

$\Lambda K^- \pi^+ \times$ B($b \to \Xi_b^0$)/B($b \to \Lambda_b^0$)	< 8	$\times 10^{-7}$	90%	2751
$\Lambda K^+ K^- \times$ B($b \to \Xi_b^0$)/B($b \to \Lambda_b^0$)	< 3	$\times 10^{-7}$	90%	2698
$J/\psi \Lambda$	seen			1868
$J/\psi \Xi^0$	seen			1785
$\Lambda_c^+ K^- \times$ B($b \to \Xi_b^0$)	$(6 \pm 4) \times 10^{-7}$			2416
$p K^- \pi^+ \pi^- \times$ B($b \to \Xi_b^0$)/B($b \to \Lambda_b^0$)	$(1.9 \pm 0.4) \times 10^{-6}$			2766
$p K^- K^- \pi^+ \times$ B($b \to \Xi_b^0$)/B($b \to \Lambda_b^0$)	$(1.71 \pm 0.31) \times 10^{-6}$			2704
$p K^- K^+ K^- \times$ B($b \to \Xi_b^0$)/B($b \to \Lambda_b^0$)	$(1.7 \pm 1.0) \times 10^{-7}$			2620

$\Xi_b'(5935)^-$

$J^P = \frac{1}{2}^+$

Mass $m = 5935.02 \pm 0.05$ MeV
$m_{\Xi_b'(5935)^-} - m_{\Xi_b^0} - m_{\pi^-} = 3.653 \pm 0.019$ MeV
Full width $\Gamma < 0.08$ MeV, CL = 95%

$\Xi_b'(5935)^-$ DECAY MODES	Fraction (Γ_i/Γ)	p (MeV/c)
$\Xi_b^0 \pi^- \times$ B($\overline{b} \to \Xi_b'(5935)^-$)/B($\overline{b} \to \Xi_b^0$)	(11.8 ± 1.8) %	31

$\Xi_b(5945)^0$

$J^P = \frac{3}{2}^+$

Mass $m = 5952.3 \pm 0.6$ MeV
Full width $\Gamma = 0.90 \pm 0.18$ MeV

$\Xi_b(5945)^0$ DECAY MODES	Fraction (Γ_i/Γ)	p (MeV/c)
$\Xi_b^- \pi^+$	seen	78

$\Xi_b(5955)^-$

$J^P = \frac{3}{2}^+$

Mass $m = 5955.33 \pm 0.13$ MeV
$m_{\Xi_b(5955)^-} - m_{\Xi_b^0} - m_{\pi^-} = 23.96 \pm 0.13$ MeV
Full width $\Gamma = 1.65 \pm 0.33$ MeV

$\Xi_b(5955)^-$ DECAY MODES	Fraction (Γ_i/Γ)	p (MeV/c)
$\Xi_b^0 \pi^- \times$ B($\overline{b} \to \Xi_b^*(5955)^-$)/B($\overline{b} \to \Xi_b^0$)	(20.7 ± 3.5) %	84

$\Xi_b(6100)^-$

$J^P = \frac{3}{2}^-$
J, P need confirmation.

Mass $m = 6100.3 \pm 0.6$ MeV
$m_{\Xi_b(6100)^-} - m_{\Xi_b^-} - 2\, m_{\pi^\pm} = 24.14 \pm 0.24$ MeV
Full width $\Gamma < 1.9$ MeV, CL = 95%

$\Xi_b(6100)^-$ DECAY MODES	Fraction (Γ_i/Γ)	p (MeV/c)
$\Xi_b^- \pi^+ \pi^-$	seen	128

$\Xi_b(6227)^-$

$J^P = ?^?$

Mass $m = 6227.9 \pm 0.9$ MeV
Full width $\Gamma = 19.9 \pm 2.6$ MeV

$\Xi_b(6227)^-$ DECAY MODES	Fraction (Γ_i/Γ)	Scale factor	p (MeV/c)
$\Lambda_b^0 K^- \times$ B($b \to \Xi_b(6227)$)/B($b \to \Lambda_b^0$)	$(3.20 \pm 0.35) \times 10^{-3}$		336
$\Xi_b^0 \pi^- \times$ B($b \to \Xi_b(6227)$)/B($b \to \Xi_b^0$)	(2.8 ± 1.1) %	1.8	398

$\Xi_b(6227)^0$

$J^P = ?^?$

Mass $m = 6226.8 \pm 1.6$ MeV
Full width $\Gamma = 19^{+5}_{-4}$ MeV

$\Xi_b(6227)^0$ DECAY MODES	Fraction (Γ_i/Γ)	p (MeV/c)
$\Xi_b^- \pi^+ \times$ B($b \to \Xi_b(6227)^0$)/B($b \to \Xi_b^-$)	(4.5 ± 0.9) %	398

Ω_b^-

$I(J^P) = 0(\frac{1}{2}^+)$
I, J, P need confirmation.

Mass $m = 6045.2 \pm 1.2$ MeV
$m_{\Omega_b^-} - m_{\Lambda_b^0} = 426.4 \pm 2.2$ MeV
$m_{\Omega_b^-} - m_{\Xi_b^-} = 247.3 \pm 3.2$ MeV
Mean life $\tau = (1.64^{+0.18}_{-0.17}) \times 10^{-12}$ s
$\tau(\Omega_b^-)/\tau(\Xi_b^-)$ mean life ratio $= 1.11 \pm 0.16$

Ω_b^- DECAY MODES	Fraction (Γ_i/Γ)	Confidence level	p (MeV/c)
$J/\psi\, \Omega^- \times$B($b \to \Omega_b$)	$(2.9^{+1.1}_{-0.8}) \times 10^{-6}$		1805
$p K^- K^- \times$B($\overline{b} \to \Omega_b$)	$< 2.3 \times 10^{-9}$	90%	2865
$p \pi^- \pi^- \times$B($\overline{b} \to \Omega_b$)	$< 1.5 \times 10^{-8}$	90%	2943
$p K^- \pi^- \times$B($\overline{b} \to \Omega_b$)	$< 7 \times 10^{-9}$	90%	2915
$\Omega_c^0 \pi^-$	seen		2419
$\Omega_c^0 \pi^-$, $\Omega_c^0 \to p K^- K^- \pi^+$	seen		–
$\Xi_c^+ K^- \pi^-$	seen		2472

b-baryon ADMIXTURE (Λ_b, Ξ_b, Ω_b)

These branching fractions are actually an average over weakly decaying b-baryons weighted by their production rates at the LHC, LEP, and Tevatron, branching ratios, and detection efficiencies. They scale with the b-baryon production fraction B($b \to b$-baryon).

The branching fractions B(b-baryon $\to \Lambda \ell^- \overline{\nu}_\ell$ anything) and B($\Lambda_b^0 \to \Lambda_c^+ \ell^- \overline{\nu}_\ell$ anything) are not pure measurements because the underlying measured products of these with B($b \to b$-baryon) were used to determine B($b \to b$-baryon), as described in the note "Production and Decay of b-Flavored Hadrons."

For inclusive branching fractions, *e.g.*, $B \to D^\pm$ anything, the values usually are multiplicities, not branching fractions. They can be greater than one.

b-baryon ADMIXTURE DECAY MODES (Λ_b,Ξ_b,Ω_b)	Fraction (Γ_i/Γ)	Scale factor	p (MeV/c)
$p \mu^- \overline{\nu}$ anything	$(5.8^{+2.3}_{-2.0})$ %		–
$p \ell \overline{\nu}_\ell$ anything	(5.6 ± 1.2) %		–
p anything	(70 ± 22) %		–
$\Lambda \ell^- \overline{\nu}_\ell$ anything	(3.8 ± 0.6) %		–
$\Lambda \ell^+ \nu_\ell$ anything	(3.2 ± 0.8) %		–
Λ anything	(39 ± 7) %		–
$\Xi^- \ell^- \overline{\nu}_\ell$ anything	$(4.6 \pm 1.4) \times 10^{-3}$	1.2	–

EXOTIC BARYONS

$P_c(4312)^+$

Mass $m = 4311.9^{+7.0}_{-0.9}$ MeV
Full width $\Gamma = 10 \pm 5$ MeV

$P_c(4312)^+$ DECAY MODES	Fraction (Γ_i/Γ)	p (MeV/c)
$J/\psi\, p$	seen	658

$P_c(4380)^+$

Mass $m = 4380 \pm 30$ MeV
Full width $\Gamma = 205 \pm 90$ MeV

$P_c(4380)^+$ DECAY MODES	Fraction (Γ_i/Γ)	p (MeV/c)
$J/\psi\, p$	seen	741

Downloaded from https://academic.oup.com/ptep/article/2022/8/083C01/6651666 by KIT Library user on 27 September 2022

$P_c(4440)^+$

Mass $m = 4440^{+4}_{-5}$ MeV
Full width $\Gamma = 21^{+10}_{-11}$ MeV

$P_c(4440)^+$ DECAY MODES	Fraction (Γ_i/Γ)	p (MeV/c)
$J/\psi p$	seen	810

$P_c(4457)^+$

was $P_c(4450)$

Mass $m = 4457.3^{+4.0}_{-1.8}$ MeV
Full width $\Gamma = 6.4^{+6.0}_{-2.8}$ MeV

$P_c(4457)^+$ DECAY MODES	Fraction (Γ_i/Γ)	p (MeV/c)
$J/\psi p$	seen	828

NOTES

This Summary Table only includes established baryons. The Particle Listings include evidence for other baryons. The masses, widths, and branching fractions for the resonances in this Table are Breit-Wigner parameters, but pole positions are also given for most of the N and Δ resonances.

For most of the resonances, the parameters come from various partial-wave analyses of more or less the same sets of data, and it is not appropriate to treat the results of the analyses as independent or to average them together. Furthermore, the systematic errors on the results are not well understood. Thus, we usually only give ranges for the parameters. We then also give a best guess for the mass (as part of the name of the resonance) and for the width. The *Note on N and Δ Resonances* and the *Note on Λ and Σ Resonances* in the Particle Listings review the partial-wave analyses.

When a quantity has "(S = ...)" to its right, the error on the quantity has been enlarged by the "scale factor" S, defined as $S = \sqrt{\chi^2/(N-1)}$, where N is the number of measurements used in calculating the quantity. We do this when $S > 1$, which often indicates that the measurements are inconsistent. When $S > 1.25$, we also show in the Particle Listings an ideogram of the measurements. For more about S, see the Introduction.

A decay momentum p is given for each decay mode. For a 2-body decay, p is the momentum of each decay product in the rest frame of the decaying particle. For a 3-or-more-body decay, p is the largest momentum any of the products can have in this frame. For any resonance, the *nominal* mass is used in calculating p. A dagger ("†") in this column indicates that the mode is forbidden when the nominal masses of resonances are used, but is in fact allowed due to the nonzero widths of the resonances.

[a] The masses of the p and n are most precisely known in u (unified atomic mass units). The conversion factor to MeV, 1 u = 931.494061(21) MeV, is less well known than are the masses in u.

[b] The $|m_p - m_{\overline{p}}|/m_p$ and $|q_p + q_{\overline{p}}|/e$ are not independent, and both use the more precise measurement of $|q_{\overline{p}}/m_{\overline{p}}|/(q_p/m_p)$.

[c] The limit is from neutrality-of-matter experiments; it assumes $q_n = q_p + q_e$. See also the charge of the neutron.

[d] The μp and ep values for the charge radius are much too different to average them. The disagreement is not yet understood.

[e] There is a lot of disagreement about the value of the proton magnetic charge radius. See the Listings.

[f] The first limit is for $p \to$ anything or "disappearance" modes of a bound proton. The second entry, a rough range of limits, assumes the dominant decay modes are among those investigated. For antiprotons the best limit, inferred from the observation of cosmic ray $\overline{p}$'s is $\tau_{\overline{p}} > 10^7$ yr, the cosmic-ray storage time, but this limit depends on a number of assumptions. The best direct observation of stored antiprotons gives $\tau_{\overline{p}}/B(\overline{p} \to e^-\gamma) > 7 \times 10^5$ yr.

[g] There is some controversy about whether nuclear physics and model dependence complicate the analysis for bound neutrons (from which the best limit comes). The first limit here is from reactor experiments with free neutrons.

[h] Lee and Yang in 1956 proposed the existence of a mirror world in an attempt to restore global parity symmetry—thus a search for oscillations between the two worlds. Oscillations between the worlds would be maximal when the magnetic fields B and B' were equal. The limit for any B' in the range 0 to 12.5 μT is >12 s (95% CL).

[i] The parameters g_A, g_V, and g_{WM} for semileptonic modes are defined by $\overline{B}_f[\gamma_\lambda(g_V + g_A\gamma_5) + i(g_{WM}/m_{B_i})\,\sigma_{\lambda\nu}\,q^\nu]B_i$, and ϕ_{AV} is defined by $g_A/g_V = |g_A/g_V|e^{i\phi_{AV}}$. See the "Note on Baryon Decay Parameters" in the neutron Particle Listings.

[j] Time-reversal invariance requires this to be 0° or 180°.

[k] This coefficient is zero if time invariance is not violated.

[l] This limit is for γ energies between 0.4 and 782 keV.

[n] The decay parameters γ and Δ are calculated from α and ϕ using

$$\gamma = \sqrt{1-\alpha^2}\,\cos\phi\,, \qquad \tan\Delta = -\frac{1}{\alpha}\sqrt{1-\alpha^2}\,\sin\phi\,.$$

See the "Note on Baryon Decay Parameters" in the neutron Particle Listings.

[o] See the Listings for the pion momentum range used in this measurement.

[p] Our estimate. See the Particle Listings for details.

[q] A theoretical value using QED.

[r] This branching fraction includes all the decay modes of the final-state resonance.

[s] See AALTONEN 11H, Fig. 8, for the calculated ratio of $\Lambda_c^+\pi^0\pi^0$ and $\Lambda_c^+\pi^+\pi^-$ partial widths as a function of the $\Lambda_c(2595)^+ - \Lambda_c^+$ mass difference. At our value of the mass difference, the ratio is about 4.

[t] A test that the isospin is indeed 0, so that the particle is indeed a Λ_c^+.

[u] P_c^+ is a pentaquark-charmonium state.

[v] Not a pure measurement. See note at head of Λ_b^0 Decay Modes.

[x] Here h^- means π^- or K^-.

Downloaded from https://academic.oup.com/ptep/article/2022/8/083C01/6651666 by KIT Library user on 27 September 2022

SEARCHES not in other sections

Magnetic Monopole Searches

The most sensitive experiments obtain negative results.

Best cosmic-ray supermassive monopole flux limit:

$< 1.4 \times 10^{-16}$ cm^{-2}sr^{-1}s^{-1} for $1.1 \times 10^{-4} < \beta < 1$

Supersymmetric Particle Searches

All supersymmetric mass bounds here are model dependent.

The limits assume:

1) $\widetilde{\chi}^0_1$ is the lightest supersymmetric particle; 2) R-parity is conserved, unless stated otherwise;

See the Particle Listings for a Note giving details of supersymmetry.

$\widetilde{\chi}^0_i$ — neutralinos (mixtures of $\widetilde{\gamma}$, $\widetilde{Z}^0$, and $\widetilde{H}^0_i$)

Mass $m_{\widetilde{\chi}^0_1} > 0$ GeV, CL = 95%
[general MSSM, non-universal gaugino masses]

Mass $m_{\widetilde{\chi}^0_1} > 46$ GeV, CL = 95%
[all tanβ, all m_0, all $m_{\widetilde{\chi}^0_2} - m_{\widetilde{\chi}^0_1}$]

Mass $m_{\widetilde{\chi}^0_2} > 62.4$ GeV, CL = 95%
[1<tanβ <40, all m_0, all $m_{\widetilde{\chi}^0_2} - m_{\widetilde{\chi}^0_1}$]

Mass $m_{\widetilde{\chi}^0_3} > 99.9$ GeV, CL = 95%
[1<tanβ <40, all m_0, all $m_{\widetilde{\chi}^0_2} - m_{\widetilde{\chi}^0_1}$]

Mass $m_{\widetilde{\chi}^0_4} > 116$ GeV, CL = 95%
[1<tanβ <40, all m_0, all $m_{\widetilde{\chi}^0_2} - m_{\widetilde{\chi}^0_1}$]

$\widetilde{\chi}^\pm_i$ — charginos (mixtures of $\widetilde{W}^\pm$ and $\widetilde{H}^\pm_i$)

Mass $m_{\widetilde{\chi}^\pm_1} > 94$ GeV, CL = 95%
[tan$\beta < 40$, $m_{\widetilde{\chi}^\pm_1} - m_{\widetilde{\chi}^0_1} > 3$ GeV, all m_0]

Mass $m_{\widetilde{\chi}^\pm_1} > 1000$ GeV, CL = 95%
[$2\ell + \not{E}_T$, Tchi1chi1C, $m_{\widetilde{\chi}^0_1}$=0 GeV]

$\widetilde{\chi}^\pm$ — long-lived chargino

Mass $m_{\widetilde{\chi}^\pm} > 620$ GeV, CL = 95% [stable $\widetilde{\chi}^\pm$]

$\widetilde{\nu}$ — sneutrino

Mass $m > 41$ GeV, CL = 95% [model independent]

Mass $m > 94$ GeV, CL = 95%
[CMSSM, $1 \le \tan\beta \le 40$, $m_{\widetilde{e}_R} - m_{\widetilde{\chi}^0_1} > 10$ GeV]

Mass $m > 3400$ GeV, CL = 95% [R-Parity Violating]
[$\widetilde{\nu}_\tau \to e\mu$, $\lambda_{312} = \lambda_{321} = 0.07$, $\lambda'_{311} = 0.11$]

$\widetilde{e}$ — scalar electron (selectron)

Mass $m > 107$ GeV, CL = 95% [all $m_{\widetilde{e}_L} - m_{\widetilde{\chi}^0_1}$]

Mass $m > 700$ GeV, CL = 95%
[$2\ell + \not{E}_T$, $m_{\widetilde{\ell}_R} = m_{\widetilde{\ell}_L}$ and $\widetilde{\ell} = \widetilde{e}, \widetilde{\mu}$, $m_{\widetilde{\chi}^0_1}$=0 GeV]

Mass $m > 250$ GeV, CL = 95%
[$\ell^\pm \ell^\mp + \not{E}_T$, $\widetilde{e}_R$, $m_{\widetilde{\chi}^0_1} = 0$ GeV]

Mass $m > 410$ GeV, CL = 95% [R-Parity Violating]
[$\ge 4\ell^\pm$, $\widetilde{\ell} \to l\widetilde{\chi}^0_1$, $\widetilde{\chi}^0_1 \to \ell^\pm \ell^\mp \nu$]

$\widetilde{\mu}$ — scalar muon (smuon)

Mass $m > 700$ GeV, CL = 95%
[$2\ell + \not{E}_T$, $m_{\widetilde{\ell}_R} = m_{\widetilde{\ell}_L}$ and $\widetilde{\ell} = \widetilde{e}, \widetilde{\mu}$, $m_{\widetilde{\chi}^0_1}$=0 GeV]

Mass $m > 210$, CL = 95%
[$\ell^\pm \ell^\mp + \not{E}_T$, $\widetilde{\mu}_R$, $m_{\widetilde{\chi}^0_1} = 0$ GeV]

Mass $m > 94$ GeV, CL = 95%
[CMSSM, $1 \le \tan\beta \le 40$, $m_{\widetilde{\mu}_R} - m_{\widetilde{\chi}^0_1} > 10$ GeV]

Mass $m > 410$ GeV, CL = 95% [R-Parity Violating]
[$\ge 4\ell^\pm$, $\widetilde{\ell} \to l\widetilde{\chi}^0_1$, $\widetilde{\chi}^0_1 \to \ell^\pm \ell^\mp \nu$]

$\widetilde{\tau}$ — scalar tau (stau)

Mass $m > 81.9$ GeV, CL = 95%
[$m_{\widetilde{\tau}_R} - m_{\widetilde{\chi}^0_1} > 15$ GeV, all θ_τ, B($\widetilde{\tau} \to \tau\widetilde{\chi}^0_1$) = 100%]

Mass $m > 90$ GeV, CL = 95%
[RPV, $\widetilde{\tau}_R$, indirect, $\Delta m > 5$ GeV]

Mass $m > 286$ GeV, CL = 95% [long-lived $\widetilde{\tau}$]

$\widetilde{q}$ – squarks of the first two quark generations

Mass $m > 1.220 \times 10^3$ GeV, CL = 95%
[jets + $\not{E}_T$, Tsqk1, 1 non-degenerate $\widetilde{q}$, $m_{\widetilde{\chi}^0_1} = 0$ GeV]

Mass $m > 1.600 \times 10^3$ GeV, CL = 95% [R-Parity Violating]
[$\widetilde{q} \to q\widetilde{\chi}^0_1$, $\widetilde{\chi}^0_1 \to \ell\ell\nu$, $\lambda_{121}, \lambda_{122} \ne 0$, $m_{\widetilde{g}}$=2400GeV]

$\widetilde{q}$ — long-lived squark

Mass $m > 1340$, CL = 95% [$\widetilde{t}$ R-hadrons]

Mass $m > 1250$, CL = 95% [$\widetilde{b}$ R-hadrons]

$\widetilde{b}$ — scalar bottom (sbottom)

Mass $m > 1.270 \times 10^3$ GeV, CL = 95%
[b-jets + $\not{E}_T$, Tsbot1, $m_{\widetilde{\chi}^0_1}$=0 GeV]

Mass $m > 307$ GeV, CL = 95% [R-Parity Violating]
[$\widetilde{b} \to t\,d$ or $t\,s$, λ''_{332} or λ''_{331} coupling]

$\widetilde{t}$ — scalar top (stop)

Mass $m > 1.310 \times 10^3$ GeV, CL = 95%
[jets + $\not{E}_T$, Tstop1, $m_{\widetilde{\chi}^0_1} < 300$ GeV]

Mass $m > 1100$ GeV, CL = 95% [R-Parity Violating]
[$\widetilde{t} \to b\,e$, Tstop2RPV, prompt]

$\widetilde{g}$ — gluino

Mass $m > 2.300 \times 10^3$ GeV, CL = 95%
[jets + $\not{E}_T$, Tglu1A, $m_{\widetilde{\chi}^0_1} < 200$ GeV]

Mass $m > 2.260 \times 10^3$ GeV, CL = 95% [R-Parity Violating]
[$\ge 4\ell$, $\lambda_{12k} \ne 0$, $m_{\widetilde{\chi}^0_1} > 1000$ GeV]

Technicolor

The limits for technicolor (and top-color) particles are quite varied depending on assumptions. See the Technicolor section of the full *Review* (the data listings).

Quark and Lepton Compositeness, Searches for

Scale Limits Λ for Contact Interactions (the lowest dimensional interactions with four fermions)

If the Lagrangian has the form

$$\pm \frac{g^2}{2\Lambda^2}\, \overline{\psi}_L \gamma_\mu \psi_L \overline{\psi}_L \gamma^\mu \psi_L$$

(with $g^2/4\pi$ set equal to 1), then we define $\Lambda \equiv \Lambda^\pm_{LL}$. For the full definitions and for other forms, see the Note in the Listings on Searches for Quark and Lepton Compositeness in the full *Review* and the original literature.

$\Lambda^+_{LL}(eeee) > 8.3$ TeV, CL = 95%

$\Lambda^-_{LL}(eeee) > 10.3$ TeV, CL = 95%

$\Lambda^+_{LL}(ee\mu\mu) > 8.5$ TeV, CL = 95%

$\Lambda^-_{LL}(ee\mu\mu) > 9.5$ TeV, CL = 95%

$\Lambda^+_{LL}(ee\tau\tau) > 7.9$ TeV, CL = 95%

$\Lambda^-_{LL}(ee\tau\tau) > 7.2$ TeV, CL = 95%

$\Lambda^+_{LL}(\ell\ell\ell\ell) > 9.1$ TeV, CL = 95%

$\Lambda^-_{LL}(\ell\ell\ell\ell) > 10.3$ TeV, CL = 95%

$\Lambda^+_{LL}(eeqq) > 24$ TeV, CL = 95%

$\Lambda^-_{LL}(eeqq) > 37$ TeV, CL = 95%

$\Lambda^+_{LL}(eeuu) > 23.3$ TeV, CL = 95%

$\Lambda^-_{LL}(eeuu) > 12.5$ TeV, CL = 95%

$\Lambda^+_{LL}(eedd) > 11.1$ TeV, CL = 95%

Downloaded from https://academic.oup.com/ptep/article/2022/8/083C01/6651666 by KIT Library user on 27 September 2022

$\Lambda^-_{LL}(eedd)$ > 26.4 TeV, CL = 95%
$\Lambda^+_{LL}(eecc)$ > 9.4 TeV, CL = 95%
$\Lambda^-_{LL}(eecc)$ > 5.6 TeV, CL = 95%
$\Lambda^+_{LL}(eebb)$ > 9.4 TeV, CL = 95%
$\Lambda^-_{LL}(eebb)$ > 10.2 TeV, CL = 95%
$\Lambda^+_{LL}(\mu\mu qq)$ > 22.3 TeV, CL = 95%
$\Lambda^-_{LL}(\mu\mu qq)$ > 40.0 TeV, CL = 95%
$\Lambda(\ell\nu\ell\nu)$ > 3.10 TeV, CL = 90%
$\Lambda(e\nu qq)$ > 2.81 TeV, CL = 95%
$\Lambda^+_{LL}(qqqq)$ > 13.1 none 17.4–29.5 TeV, CL = 95%
$\Lambda^-_{LL}(qqqq)$ > 21.8 TeV, CL = 95%
$\Lambda^+_{LL}(\nu\nu qq)$ > 5.0 TeV, CL = 95%
$\Lambda^-_{LL}(\nu\nu qq)$ > 5.4 TeV, CL = 95%

Excited Leptons

The limits from $\ell^{*+}\ell^{*-}$ do not depend on λ (where λ is the $\ell\ell^*$ transition coupling). The λ-dependent limits assume chiral coupling.

$e^{*\pm}$ — excited electron
Mass $m >$ 103.2 GeV, CL = 95% (from e^*e^*)
Mass $m >$ 5.600×10^3 GeV, CL = 95% (from ee^*)
Mass $m >$ 356 GeV, CL = 95% (if $\lambda_\gamma = 1$)

$\mu^{*\pm}$ — excited muon
Mass $m >$ 103.2 GeV, CL = 95% (from $\mu^*\mu^*$)
Mass $m >$ 5.700×10^3 GeV, CL = 95% (from $\mu\mu^*$)

$\tau^{*\pm}$ — excited tau
Mass $m >$ 103.2 GeV, CL = 95% (from $\tau^*\tau^*$)
Mass $m >$ 2.500×10^3 GeV, CL = 95% (from $\tau\tau^*$)

ν^* — excited neutrino
Mass $m >$ 1.600×10^3 GeV, CL = 95% (from $\nu^*\nu^*$)
Mass $m >$ 213 GeV, CL = 95% (from ν^*X)

q^* — excited quark
Mass $m >$ 338 GeV, CL = 95% (from q^*q^*)
Mass $m >$ 6700 GeV, CL = 95% (from q^*X)

Color Sextet and Octet Particles

Color Sextet Quarks (q_6)
Mass $m >$ 84 GeV, CL = 95% (Stable q_6)

Color Octet Charged Leptons (ℓ_8)
Mass $m >$ 86 GeV, CL = 95% (Stable ℓ_8)

Color Octet Neutrinos (ν_8)
Mass $m >$ 110 GeV, CL = 90% ($\nu_8 \to \nu g$)

Extra Dimensions

Please refer to the Extra Dimensions section of the full *Review* for a discussion of the model-dependence of these bounds, and further constraints.

Constraints on the radius of the extra dimensions, for the case of two-flat dimensions of equal radii

(direct tests of Newton's law)
$R <$ 3.8 μm, CL = 95% ($pp \to jG$)
$R <$ 0.16–916 nm (astrophysics; limits depend on technique and assumptions)

Constraints on the fundamental gravity scale

M_{TT} > 9.02 TeV, CL = 95% ($pp \to$ dijet, angular distribution)
M_c > 4.16 TeV, CL = 95% ($pp \to \ell\overline{\ell}$)

Constraints on the Kaluza-Klein graviton in warped extra dimensions

M_G > 4.78 TeV, CL = 95% ($pp \to e^+e^-,\ \mu^+\mu^-$)

Constraints on the Kaluza-Klein gluon in warped extra dimensions

$M_{g_{KK}}$ > 3.8 TeV, CL = 95% ($g_{KK} \to t\overline{t}$)

WIMP and Dark Matter Searches

No confirmed evidence found for galactic WIMPs from the GeV to the TeV mass scales and down to 1×10^{-10} pb spin independent cross section at M = 100 GeV.

Downloaded from https://academic.oup.com/ptep/article/2022/8/083C01/6651666 by KIT Library user on 27 September 2022

Tests of Conservation Laws

Revised May 2022 by A. Pich (IFIC, Valencia) and M. Ramsey-Musolf (Tsung-Dao Lee Inst.; SJTU; U. Massachusetts).

In keeping with the current interest in tests of conservation laws, we collect together a Table of experimental limits on all weak and electromagnetic decays, mass differences, and moments, and on a few reactions, whose observation would violate conservation laws. The Table is given only in the full Review of Particle Physics (RPP), not in the Particle Physics Booklet, and organizes the data in two main sections: "Discrete Space-Time Symmetries", *i.e.*, C, P, T, CP and CPT; and "Number Conservation Laws", *i.e.*, lepton, baryon, flavor and charge conservation. The references for these data can be found in the Particle Listings. The following text discusses the best limits among those included in the Table and gives a brief overview of the current status. For some topics, a more extensive discussion of the framework for theoretical interpretation is provided, particularly where the analogous discussion does not appear elsewhere in the RPP. References to more extensive review articles are also included where appropriate. Unless otherwise specified, all limits quoted in this review are given at a C.L. of 90%.

DISCRETE SPACE-TIME SYMMETRIES

Charge conjugation (C), parity (P) and time reversal (T) are empirically exact symmetries of the electromagnetic (QED) and strong (QCD) interactions, but they are violated by the weak forces. Owing to the left-handed nature of the $SU(2)_L \otimes U(1)_Y$ electroweak theory, C and P are maximally violated in the fermionic couplings of the $W^\pm$ and (up to $\sin^2\theta_W$ corrections) the Z. However, their product CP is still an exact symmetry when only one or two fermion families are considered. With three generations of fermions, CP is violated through the single complex phase present in the Cabibbo-Kobayashi-Maskawa (CKM) quark mixing matrix. An analogous CP-violating (CPV) phase appears in the lepton sector when non-vanishing neutrino masses are taken into account (plus two additional phases if neutrinos are Majorana particles). The product of the three discrete symmetries, CPT, is an exact symmetry of any local and Lorentz-invariant quantum field theory with a positive-definite hermitian Hamiltonian that preserves micro-causality [1, 2]. Therefore, the breaking of CP implies a corresponding violation of T.

Violations of charge-conjugation symmetry have never been observed in electromagnetic and strong phenomena. The most stringent limits are extracted from C-violating transitions of neutral (self-conjugate) particles such as $\mathrm{Br}(\pi^0 \to 3\gamma) < 3.1 \times 10^{-8}$ [3] and $\mathrm{Br}(J/\psi \to 2\gamma) < 2.7 \times 10^{-7}$ [4]. P (and CP) conservation has been also precisely tested through forbidden decays such as $\mathrm{Br}(\eta \to 4\pi^0) < 6.9 \times 10^{-7}$ [5], but the best limits on P and T are set by the non-observation of electric dipole moments (see section 2). Obviously, the interplay of the weak interaction puts a lower bound in sensitivity for this type of tests, beyond which violations of the corresponding conservation laws should be detected.

1 Violations of CP and T

The first evidence of CP non-invariance in particle physics was the observation in 1964 of $K^0_L \to \pi^+\pi^-$ decays [6]. For many years afterwards, the non-zero ratio

$$\begin{aligned} |\eta_{+-}| &\equiv |\mathcal{M}(K^0_L \to \pi^+\pi^-)/\mathcal{M}(K^0_S \to \pi^+\pi^-)| \\ &= (2.232 \pm 0.011) \times 10^{-3} \end{aligned} \tag{1}$$

could be explained as a K^0–$\overline{K}^0$ mixing effect, $\eta_{+-} = \epsilon$ (superweak CP violation), which would imply an identical ratio $\eta_{00} \equiv \mathcal{M}(K^0_L \to \pi^0\pi^0)/\mathcal{M}(K^0_S \to \pi^0\pi^0)$ in the neutral decay mode and successfully predicts the observed CPV semileptonic asymmetry ($A_L(e) \approx 2\,\mathrm{Re}\,\epsilon$)

$$\begin{aligned} A_L(e) &\equiv \frac{\Gamma(K^0_L \to \pi^- e^+\nu_e) - \Gamma(K^0_L \to \pi^+ e^-\bar{\nu}_e)}{\Gamma(K^0_L \to \pi^- e^+\nu_e) + \Gamma(K^0_L \to \pi^+ e^-\bar{\nu}_e)} \\ &= (3.34 \pm 0.07) \times 10^{-3}\,. \end{aligned} \tag{2}$$

A tiny difference between η_{+-} and η_{00} was reported for the first time in 1988 by the CERN NA31 collaboration [7], and later established at the 7.2σ level with the full data samples from the NA31 [8], E731 [9], NA48 [10] and KTeV [11] experiments:

$$\mathrm{Re}(\epsilon'/\epsilon) = \frac{1}{3}\,(1 - |\eta_{00}/\eta_{+-}|) = (1.66 \pm 0.23) \times 10^{-3}\,. \tag{3}$$

This important measurement confirmed that CP violation is associated with a $\Delta S = 1$ transition, as predicted by the CKM mechanism. The Standard Model (SM) prediction, $\mathrm{Re}(\epsilon'/\epsilon) = (1.4 \pm 0.5) \times 10^{-3}$ [12–14], is in good agreement with the measured ratio, although the theoretical uncertainty is unfortunately large.

Much larger CP asymmetries have been later measured in B meson decays, many of them involving the interference between B^0–$\overline{B}^0$ mixing and the decay amplitude. They provide many successful tests of the CKM unitarity structure, validating the SM mechanism of CP violation (see the review on CP violation in the quark sector). Prominent signals of direct CP violation have been also clearly established in several $B^\pm$, B^0_d and B^0_s decays, and, very recently, in charm decays [15]:

$$\begin{aligned} \Delta a^{\mathrm{dir}}_{CP} &\equiv a^{\mathrm{dir}}_{CP}(D^0 \to K^+K^-) - a^{\mathrm{dir}}_{CP}(D^0 \to \pi^+\pi^-) \\ &= (-15.7 \pm 2.9) \times 10^{-4}\,. \end{aligned} \tag{4}$$

These direct CP asymmetries necessarily involve the presence of a strong phase-shift difference between (at least) two interfering amplitudes, which makes very challenging to perform reliable SM predictions for heavy-flavored mesons.

Global fits to neutrino oscillation data provide some hints of a non-zero mixing phase [16, 17]. Although the statistical significance is not yet compelling, they suggest that CP-violation effects in neutrino oscillations could be large (see the review on neutrino masses, mixings and oscillations). The future DUNE and Hyper-Kamiokande experiments are expected to confirm the presence of CP violation in the lepton sector or constrain the phase in the leptonic mixing matrix to be smaller than $O(10^\circ)$.

While CP violation implies a breaking of time-reversal symmetry, direct tests of T violation are much more difficult. The CPLEAR experiment observed longtime ago a non-zero difference between the oscillation probabilities of $K^0 \to \overline{K}^0$ and $\overline{K}^0 \to K^0$ [18]. Initial neutral kaons with defined strangeness were produced from proton-antiproton annihilations at rest, $p\bar{p} \to K^-\pi^+K^0, K^+\pi^-\overline{K}^0$, and tagged by the accompanying charged kaon, while the strangeness of the final neutral kaon was identified through its semileptonic decay: $K^0 \to e^+\pi^-\nu_e$, $\overline{K}^0 \to e^-\pi^+\bar{\nu}_e$. The average asymmetry over the time interval from 1 to 20 K^0_S lifetimes was found to be different from zero at 4σ [18]:

$$\begin{aligned} &\frac{R[\overline{K}^0\,(t=0) \to e^+\pi^-\nu_e\,(t)] - R[K^0\,(t=0) \to e^-\pi^+\bar{\nu}_e\,(t)]}{R[\overline{K}^0\,(t=0) \to e^+\pi^-\nu_e\,(t)] + R[K^0\,(t=0) \to e^-\pi^+\bar{\nu}_e\,(t)]} = \\ &= (6.6 \pm 1.3 \pm 1.0) \times 10^{-3}\,. \end{aligned} \tag{5}$$

Since this asymmetry violates also CP, its interpretation as direct evidence of T violation requires a detailed analysis of the underlying K^0–$\overline{K}^0$ mixing process [19–21].

More recently, the exchange of initial and final states has been made possible in B decays, taking advantage of the entanglement of the two daughter mesons produced in the decay $\Upsilon(4S) \to B\bar{B}$ which allows for both flavor ($B^0 \to \ell^+X$, $\overline{B}^0 \to \ell^-X$) and CP ($B_+ \to J/\psi K^0_L$, $B_- \to J/\psi K^0_S$) tagging. Selecting events where one B candidate is reconstructed in a CP eigenstate and the flavor of the other B is identified, one can compare the rates of the $\overline{B}^0 \to B_\pm$ and $B^0 \to B_\pm$ transitions with their T-reversed $B_\pm \to \overline{B}^0$ and $B_\pm \to B^0$ processes, as a function of the time difference Δt between the two B decays [22–24]. Neglecting the small width difference between the two B^0_d mass eigenstates, each of these eight transitions has a time-dependent decay rate of the form $\mathrm{e}^{-\Gamma_d\Delta t}\,\{1 + S^\pm_{\alpha,\beta}\,\sin(\Delta m_d\Delta t) + C^\pm_{\alpha,\beta}\,\cos(\Delta m_d\Delta t)\}$, where Γ_d is the average decay width, Δm_d the B^0_d mass difference, the subindices $\alpha = \ell^+, \ell^-$ and $\beta = K^0_S, K^0_L$ stand for the reconstructed final states of the two B mesons and the superindex +

Downloaded from https://academic.oup.com/ptep/article/2022/8/083C01/6651666 by KIT Library user on 27 September 2022

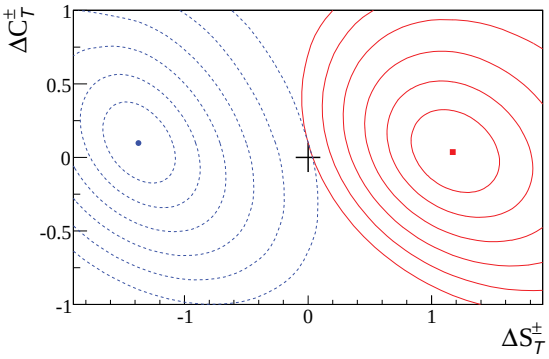

Figure 1: Measured values of ΔS_T^+, ΔC_T^+ (blue point, dashed lines) and ΔS_T^-, ΔC_T^- (red square, solid lines) [25]. The two-dimensional contours correspond to $1 - \mathrm{CL} = 0.317$, 4.55×10^{-2}, 2.70×10^{-3}, 6.33×10^{-5}, 5.73×10^{-7}, and 1.97×10^{-9}. The + sign indicates the T-invariant point.

or − indicates whether the decay to the flavor final state α occurs before or after the decay to the CP final state β. Figure 1 shows confidence-level contours for the T-asymmetry parameters $\Delta S_T^{\pm} \equiv S^{\mp}_{\ell^-,K_L^0} - S^{\pm}_{\ell^+,K_S^0}$ and $\Delta C_T^{\pm} \equiv C^{\mp}_{\ell^-,K_L^0} - C^{\pm}_{\ell^+,K_S^0}$, reported by the BABAR experiment [25], which clearly demonstrate a violation of T in $\Delta S_T^{\pm}$, with a significance of 14σ.

2 Electric dipole moments

Among the most powerful tests of CP invariance is the search for a permanent electric dipole moment (EDM) of an elementary fermion or non-degenerate quantum system. The EDM of an elementary spin-1/2 fermion f is defined by the effective, non-renormalizable interaction

$$\mathcal{L}_{\mathrm{EDM}} = -\frac{i}{2} d_f \, \bar{f} \sigma_{\mu\nu} \gamma_5 f \, F^{\mu\nu} \tag{6}$$

where $F^{\mu\nu}$ is the QED field strength tensor. The values for d_f are conventionally expressed in units of $e\,$cm. The interaction (6) is separately odd under T and P. In the non-relativistic limit, Eq. (6) reduces to

$$\mathcal{L}_{\mathrm{EDM}} \to d_f \, \chi_f^{\dagger} \vec{\sigma} \chi_f \cdot \vec{E} \tag{7}$$

where χ is a two-component Pauli spinor and $\vec{E}$ is the electric field. Note the interaction (7) is manifestly T-odd and carries no direct information on CP. The observation of a non-zero EDM of a non-relativistic (and non-degenerate) quantum system, such as the mercury atom (see below) would imply CP violation under the assumption of CPT invariance.

To date, no experimental observation of an EDM of an elementary particle or non-degenerate bound quantum system has been observed. The most stringent limits have been obtained for the EDMs of the electron, mercury atom, and neutron. A selection of the representative, most stringent limits is given in Table 1. The limits on the electron EDM are inferred from experiments involving polar molecules, paramagnetic systems with an unpaired electron spin. In contrast, the neutron and ^{199}Hg atom are diamagnetic. A variety of experimental efforts aimed at improved sensitivities are underway. For reviews of the experimental and theoretical situation, see, *e.g.* [26–29].

EDMs in the Standard Model

The SM provides two sources of d_f: the CPV phase in the CKM matrix and the P- and T-odd 'θ term' in the QCD Lagrangian. The former is characterized by the Jarlskog invariant [36]

$$\mathcal{J} = \mathrm{Im}(V_{us} V_{cs}^* V_{cb} V_{ub}^*) \sim A^2 \lambda^6 \eta < 10^{-4} \,, \tag{8}$$

while the latter is given by

$$\mathcal{L}_{\bar{\theta}} = -\frac{g_3^2}{16\pi^2} \, \bar{\theta} \, \mathrm{Tr} \left(G^{\mu\nu} \tilde{G}_{\mu\nu} \right) , \tag{9}$$

Table 1: Most stringent limits on electric dipole moments.

EDM	Limit ($e\,$cm)		Source
Electron	1.1×10^{-29}	(90% C.L.)	ThO [30]
	1.3×10^{-28}	(90% C.L.)	HfF^+ [31]
Muon	1.8×10^{-19}	(95% C.L.)	[32]
Neutron	1.8×10^{-26}	(90% C.L.)	[33]
^{199}Hg Atom	7.4×10^{-30}	(95% C.L.)	[34]
^{129}Xe Atom	1.5×10^{-27}	(95% C.L.)	[35]

where $G_{\mu\nu}$ ($\tilde{G}_{\mu\nu} = \epsilon_{\mu\nu\alpha\beta} \, G^{\alpha\beta}/2$) is the QCD field strength tensor (dual).

The CKM-induced EDMs of quarks and charged leptons arise at three- and four-loop orders, respectively [37–40]. The resulting numerical impact for the experimental observables (see below) falls well below present and prospective experimental sensitivities. The most important impact of $\mathcal{J}$ for the EDMs of the neutron and diamagnetic atoms arise via induced hadronic interactions. The resulting theoretical expectations for the electron, neutron and ^{199}Hg EDMs are

$$|d_e|_{\mathrm{CKM}} \approx 10^{-44} \; e\,\mathrm{cm} \quad [40], \tag{10a}$$

$$|d_n|_{\mathrm{CKM}} \approx (1-6) \times 10^{-32} \; e\,\mathrm{cm} \quad [41], \tag{10b}$$

$$|d_A(^{199}\mathrm{Hg})|_{\mathrm{CKM}} \lesssim 4 \times 10^{-34} \; e\,\mathrm{cm} \quad [26]. \tag{10c}$$

For d_n and $d_A(^{199}\mathrm{Hg})$, the dominant CKM contributions arise from four-quark operators (generated after integrating out the electroweak gauge bosons) rather than from the EDMs of the individual quarks. The corresponding sensitivities to the QCD $\bar{\theta}$ parameter are given by

$$|d_n|_{\bar{\theta}} \approx (0.9 - 1.2) \times 10^{-16} \; \bar{\theta} \; e\,\mathrm{cm} \quad [41], \tag{11a}$$

$$|d_A(^{199}\mathrm{Hg})|_{\bar{\theta}} \approx (0.07 - 8) \times 10^{-20} \; \bar{\theta} \; e\,\mathrm{cm} \quad [26,27], \tag{11b}$$

where the ranges quoted include the impacts of hadronic, nuclear, and atomic theory uncertainties. The neutron EDM puts then a stringent limit on 'strong' CP violation: $\bar{\theta} \lesssim 2 \times 10^{-10}$. The corresponding limit from $d_A(^{199}\mathrm{Hg})$ is weaker due to the large theoretical uncertainty.

EDMs Beyond the Standard Model

It is possible that the next generation of EDM searches will yield a non-zero result, arising from the $\bar{\theta}$-term interaction and/or physics beyond the SM (BSM). Most of the considered BSM scenarios involve new particles with masses well above the electroweak scale. At energies much lower than the BSM mass scale Λ, the dynamics can be described through an effective field theory (SMEFT) involving an infinite set of non-renormalizable operators $\mathcal{O}_k^{(d)}$, with dimensions $d > 4$, that are invariant under the SM gauge group:

$$\mathcal{L}_{\mathrm{SMEFT}} = \mathcal{L}_{\mathrm{SM}} + \sum_{k,d} \alpha_k^{(d)} \left(\frac{1}{\Lambda} \right)^{d-4} \mathcal{O}_k^{(d)} \,. \tag{12}$$

The operators contain only SM fields, while all short-distance information on the BSM physics is encoded in their Wilson coefficients $\alpha_k^{(d)}$. The $d = 4$ term corresponds to the SM Lagrangian.

For the systems of Table 1 and for many BSM scenarios of recent interest, it suffices to consider the leading contributions from $d = 6$ operators. Considering only the first-generation SM fermions, there exist 12 independent CPV pertinent operators. For a complete listing, see *e.g.*, Refs. [27, 42]. For a given elementary fermion f, two of these operators reduce to the EDM interaction in Eq. (6). Of the remaining, the most relevant include the chromo-electric dipole moments (cEDMs) of the quarks; a CP-odd three gluon operator; three semileptonic, four-fermion operators; two four-quark operators; and a CPV interaction involving two Higgs fields and a right-handed quark current. For the dipole operators, it is useful to define a rescaled Wilson coefficient $\alpha_{fV_j}^{(6)} \equiv g_j \, C_{fV_j}$, where V_j ($j = 1, 2, 3$) denote the gauge bosons for

Downloaded from https://academic.oup.com/ptep/article/2022/8/083C01/6651666 by KIT Library user on 27 September 2022

Table 2: Pertinent dimension-six EDM and cEDM sources (first generation fermions only).

System	$d=6$ Source	Wilson Coefficient
Paramagnetic	Electron EDM	Im $C_{e\gamma}$
	Electron-quark	$C_{eq}^{(\pm)}$
Diamagnetic	Quark EDM	Im $C_{q\gamma}$
	Quark cEDM	Im C_{qG}
	Three gluon	$C_{\tilde{G}}$
	Four quark	Im $C_{quqd}^{(1,8)}$
	Quark-Higgs	Im $C_{\varphi ud}$
	Electron-quark tensor*	Im $C_{\ell equ}^{(3)}$

*Applicable only to atoms.

the three SM gauge groups with corresponding couplings g_j; for all other $d=6$ operators we correspondingly identify $\alpha_k^{(6)} \equiv C_k$. In this case, one has for the EDM (d_f) and cEDM ($\tilde{d}_q$)

$$d_f = -(1.13\times 10^{-16}\ e\ \text{cm})\left(\frac{v}{\Lambda}\right)^2 \text{Im}\ C_{f\gamma}\,, \tag{13a}$$

$$\tilde{d}_q = -(1.13\times 10^{-16}\ \text{cm})\left(\frac{v}{\Lambda}\right)^2 \text{Im}\ C_{qG}\,, \tag{13b}$$

with $\text{Im}\ C_{f\gamma} = \text{Im}\ C_{fB} + 3I_3^f\ \text{Im}\ C_{fW}$. As the expressions (13a,13b) illustrate, the magnitude of the BSM contributions scales with two inverse powers of the scale Λ. A similar conclusion holds for the contributions from the other $d=6$ operators to the EDMs of Table 1.

It is important to emphasize that if the BSM mediators are light, with masses below the weak scale, the effective field theory description of Eq. (12) does not apply. For recent studies along these lines, see, *e.g.* [43, 44].

EDM Interpretation: From Short Distances to the Atomic Scale

The EDM limits in Table 1 are obtained using composite quantum systems, wherein the relevant dynamics involve physics at the hadronic, nuclear, atomic and molecular scales. The manifestation of a given CPV source (CKM, $\bar{\theta}$ term, BSM) involves an interplay of these dynamics. In all cases, one must first evolve the Wilson coefficients from the weak scale to the hadronic scale, then match onto the relevant low-energy degrees of freedom (electrons, nucleons, pions, *etc.*). At this level, the most straightforward interpretation involves the paramagnetic systems, for which two sources dominate: the electron EDM and the electron spin-dependent semileptonic interaction $\bar{e}\gamma_5 e\,\bar{q}q$. The latter gives rise to an spin-independent Hamiltonian, for an atom with Z electrons/protons and N neutrons,

$$\hat{H}_S = \frac{iG_F}{\sqrt{2}}\,\delta(\vec{r})\left[(Z+N)\,C_S^{(0)} + (Z-N)\,C_S^{(1)}\right]\gamma_0\gamma_5\,, \tag{14}$$

where $C_S^{(0)}$ ($C_S^{(1)}$) is proportional to $C_{eq}^{(+)}$ ($C_{eq}^{(-)}$). The computation of $C_S^{(0,1)}$ is relatively free from theoretical uncertainty since the operator $\bar{q}q$ essentially counts the number of quarks of flavor q in the nucleus. Experimental results for paramagnetic systems, thus, often quote bounds on

$$C_S \equiv C_S^{(0)} + \left(\frac{Z-N}{Z+N}\right) C_S^{(1)} \tag{15}$$

as well as on d_e, assuming only one of these two sources is non-vanishing. Combining results from ThO and HfF^+ (see Figure 2) allows one to obtain the global, 90% C.L. bounds

$$|d_e| < 1.8\times 10^{-28}\ e\ \text{cm}\,, \qquad |C_S| < 9.8\times 10^{-9}\,. \tag{16}$$

Note that the limits on d_e given in Table 1 have been obtained assuming $C_S = 0$.

For the diamagnetic systems, the situation is considerably more involved. For the neutron, a variety of approaches – including

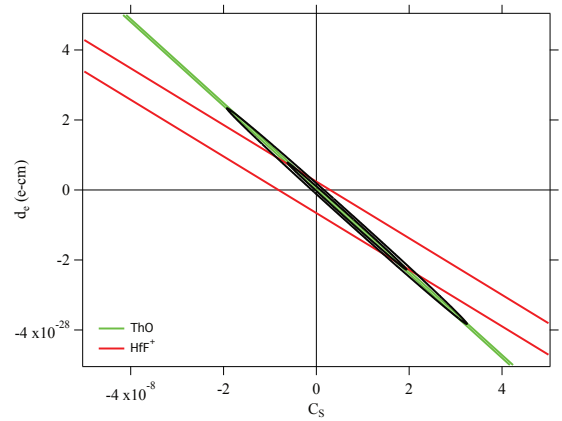

Figure 2: Constraints on d_e and C_S from EDM searches using polar molecules (updated by [45] from Ref. [26]).

lattice QCD, chiral perturbation theory, QCD sum rules, and the quark model – have been employed to compute the relevant hadronic matrix elements of the CPV sources (see, *e.g.*, [27,28,46,47]). For diamagnetic atoms, the non-leptonic sources of Table 2 give rise to the EDM of the nucleus as well as other P- and T-odd nuclear moments, as allowed by the nuclear spin. However, according to a theorem by Schiff [48], the nuclear EDM generates no contribution to the neutral-atom EDM due to screening by atomic electrons. The leading contribution from these sources, instead, arises via the nuclear Schiff moment, $\vec{S}$, an r^3-weighted moment of the T- and P-odd component of the nuclear charge density. The resulting effective atomic Hamiltonian is

$$\hat{H}_{\text{Schiff}} = -4\pi\,\vec{\nabla}\rho_e(0)\cdot\vec{S}\,, \tag{17}$$

where $\vec{\nabla}\rho_e(0)$ is the gradient of the electron density at the nucleus. To date, computations of the nuclear Schiff moment have assumed that the leading contribution arises from a pion-exchange induced nuclear force, with the P- and T-odd πN interaction given by

$$\mathcal{L}_{\pi N}^{T,P} = \bar{N}\left[\bar{g}_\pi^{(0)}\vec{\tau}\cdot\vec{\pi} + \bar{g}_\pi^{(1)}\pi^0 + \bar{g}_\pi^{(2)}(3\tau_3\pi^0 - \vec{\tau}\cdot\vec{\pi})\right]N\,. \tag{18}$$

Chiral effective field theory power counting implies that in general the magnitude of $\bar{g}_\pi^{(2)}$ is suppressed with respect to the isoscalar and isovector couplings. The CPV sources then generate a diamagnetic atom EDM d_A via the sequence

$$\text{CPV source} \longrightarrow \bar{g}_\pi^{(i)} \longrightarrow \vec{S} \longrightarrow d_A\,. \tag{19}$$

The steps in this sequence involve dynamics at the hadronic, nuclear, and atomic scales, respectively. In addition, d_A may receive contributions from the nuclear spin-dependent interaction generated by the semileptonic tensor interaction listed in Table 2, with the corresponding atomic Hamiltonian

$$\hat{H}_T = \frac{2iG_F}{\sqrt{2}}\,\delta(\vec{r})\sum_N\left[C_T^{(0)} + C_T^{(1)}\tau_3\right]\vec{\sigma}_N\cdot\vec{\gamma}\,, \tag{20}$$

where σ_N is the nucleon spin Pauli matrix and $C_T^{(0,1)} \propto \text{Im}\ C_{\ell equ}^{(3)}$.

Given the large number of CPV sources and existing diagmagnetic EDM limits, it is not possible to obtain a set of global constraints on the former. One may, however, do so for the low-energy effective parameters $\bar{g}_\pi^{(0,1)}$, $C_T^{(0,1)}$ and $\bar{d}_n^{\text{sr}}$, where the latter denotes a 'short-range' contribution to the neutron EDM [26, 49]. In this context, the dominant source of theoretical uncertainty involves computations of the nuclear Schiff moment. From the bounds on the low-energy parameters, one may then derive constraints on the CPV sources by utilizing computations of the hadronic matrix elements. Reducing the degree of theoretical hadronic and nuclear physics uncertainty is an area of active effort.

Downloaded from https://academic.oup.com/ptep/article/2022/8/083C01/6651666 by KIT Library user on 27 September 2022

3 Tests of CPT

CPT symmetry implies the equality of the masses and widths of a particle and its antiparticle. The most constraining limits are extracted from the neutral kaons [50, 51]:

$$\begin{aligned} 2\,\frac{|m_{K^0} - m_{\overline{K}^0}|}{(m_{K^0} + m_{\overline{K}^0})} &< 6\times 10^{-19}\,, \\ 2\,\frac{|\Gamma_{K^0} - \Gamma_{\overline{K}^0}|}{(\Gamma_{K^0} + \Gamma_{\overline{K}^0})} &= (8\pm 8)\times 10^{-18}\,. \end{aligned} \tag{21}$$

The limit on the K^0–$\overline{K}^0$ mass difference assumes that there is no other source of CPT violation. An upper bound on CPT breaking in $K^0_L \to 2\pi$ has been also set through the measured phase difference of the CPV ratios η_{00} and η_{+-}, $\phi_{00} - \phi_{+-} = (0.34\pm 0.32)^\circ$, thanks to the small value of $(1 - |\eta_{00}/\eta_{+-}|)$ (see the review on CP violation in K^0_L decays).

The measured masses and electric charges of the electron, the proton and their antiparticles provide also strong limits on CPT violation [52–54]:

$$\begin{aligned} &2\,\frac{|m_{e^+} - m_{e^-}|}{m_{e^+} + m_{e^-}} < 8\times 10^{-9}\,, \qquad \frac{|q_{e^+} + q_{e^-}|}{e} < 4\times 10^{-8}\,, \\ &\left|\frac{q_{\bar{p}}/m_{\bar{p}}}{q_p/m_p}\right| - 1 = (0.1\pm 6.9)\times 10^{-11}\,. \end{aligned} \tag{22}$$

Worth mentioning are also the tight constraints derived from the lepton and antilepton magnetic moments [55, 56],

$$\begin{aligned} 2\,\frac{g_{e^+} - g_{e^-}}{g_{e^+} + g_{e^-}} &= (-0.5\pm 2.1)\times 10^{-12}\,, \\ 2\,\frac{g_{\mu^+} - g_{\mu^-}}{g_{\mu^+} + g_{\mu^-}} &= (-0.11\pm 0.12)\times 10^{-8}\,, \end{aligned} \tag{23}$$

those of the proton and antiproton [57],

$$(\mu_p + \mu_{\bar{p}})/\mu_p = (2\pm 4)\times 10^{-9}\,, \tag{24}$$

and the recent measurement of the 1S-2S atomic transition in antihydrogen which agrees with the corresponding frequency spectral line in hydrogen at a relative precision of 2×10^{-12} [58].

A violation of CPT in an interacting local quantum field theory would imply that Lorentz symmetry is also violated [59]. Signatures of Lorentz-invariance violation have been searched for with atomic clocks, penning traps, matter and antimatter spectroscopy, colliders and astroparticle experiments, with so far negative results [60]. A compilation of experimental bounds is given in Ref. [61], parametrized through the coefficients of the so-called Standard Model Extension (SME) Lagrangian which contains all possible Lorentz- and CPT-violating operators preserving gauge invariance, renormalizability, locality and observer causality [62].

QUANTUM-NUMBER CONSERVATION LAWS

Conservation laws of several quantum numbers have been empirically established with a very high degree of confidence. They are usually associated with some global phase symmetry. However, while some of them are deeply rooted in basic principles such as gauge invariance (charge conservation; local symmetry implies global symmetry) or Lorentz symmetry (fermion number conservation), others appear to be accidental symmetries of the SM Lagrangian and could be broken by new physics interactions.

In fact, if one only assumes the SM gauge symmetries and particle content, the most general dynamics at energies below the BSM mass scale is described by the SMEFT Lagrangian in Eq. (12). All $d = 4$ operators (*i.e.*, the SM) happen to preserve the B and L quantum numbers, but this is no-longer true for the gauge-invariant structures of higher dimensionality. There is only one operator with $d = 5$ (up to hermitian conjugation and flavor assignments), and it violates lepton number by two units [63], giving rise to Majorana neutrino masses after the electroweak spontaneous symmetry breaking. With $d = 6$, there are five operators that violate B and L [64, 65]. Thus, violations of these quantum numbers can be generically expected, unless there is an explicit symmetry protecting them.

4 Electric charge

The conservation of electric charges is associated with the QED gauge symmetry. The most precise tests are the non-observation of the decays $e \to \nu_e\gamma$ (lifetime larger than 6.6×10^{28} yr [66]) and $n \to p\nu_e\bar{\nu}_e$ (Br $< 8\times 10^{-27}$, 68% C.L. [67]). The neutrality of matter can be also interpreted as a test of electric charge conservation. Worth mentioning are the experimental limits on the electric charge of the neutron, $q_n/e = (-0.2\pm 0.8)\times 10^{-21}$, and on the sum of the proton and electron charges, $|q_p + q_e|/e < 1\times 10^{-21}$ [68].

The isotropy of the cosmic microwave background has been used to set stringent limits on a possible charge asymmetry of the Universe [69]. Assuming that charge asymmetries produced by different particles are not anticorrelated, this implies upper bounds on the photon ($|q_\gamma|/e < 1\times 10^{-35}$) and neutrino ($|q_\nu|/e < 4\times 10^{-35}$) electric charges. A much stronger upper bound on the photon charge ($|q_\gamma|/e < 1\times 10^{-46}$) has been derived from the non-observation of Aharonov-Bohm phase differences in interferometric experiments with photons that have traversed cosmological distances, under the assumption that both positive and negative charged photons exist [70].

5 Lepton family numbers

In the SM with massless left-handed neutrinos there is a separate conservation number for each lepton family. However, neutrino oscillations show that neutrinos have tiny masses and there are sizable mixings among the different lepton flavors. Compelling evidence from solar, atmospheric, accelerator and reactor neutrino experiments has established a quite solid pattern of neutrino mass differences and mixing angles [16, 17]. (see the review on neutrino masses, mixings and oscillations). Nevertheless, flavor mixing among the different charged leptons has never been observed.

If neutrino masses and mixings among the three active neutrinos were the only sources of lepton-flavor violation (LFV), neutrinoless transitions from one charged lepton flavor to another would be heavily suppressed by powers of m_{ν_i} (GIM mechanism), leading to un-observably small rates; for instance [73–78],

$$\mathrm{Br}(\mu \to e\gamma) = \frac{3\alpha}{32\pi}\left|\sum_i U^*_{\mu i}U_{ei}\,\frac{m^2_{\nu_i} - m^2_{\nu_1}}{M^2_W}\right|^2 < 10^{-54}\,, \tag{25}$$

where U_{ia} are the relevant elements of the PMNS mixing matrix. This contribution is clearly too small to be observed in any realistic experiment, so any experimentally accessible effect would arise from BSM physics with sources of LFV not related to m_{ν_i}. The search for charged LFV (CLFV) remains an area of active interest, which has the potential to probe physics at scales much higher than the TeV.

Among the most sensitive probes are searches for the CLFV decays of the muon, $\mu \to e\gamma$ and $\mu \to 3e$, as well as the conversion process $\mu^- + A(N,Z) \to e^- + A(N,Z)$, where $A(N,Z)$ denotes a nucleus with N neutrons and Z protons. Searches for rare τ decays such as $\tau \to \ell\gamma$ ($\ell = e,\mu$) also provide interesting probes of CLFV. A variety of BSM scenarios predict that rates for these CLFV processes could be sufficiently large to be observed in the present or planned searches. To date, no observation has been reported, and the resulting null results place strong constraints on BSM scenarios. For extensive reviews of the experimental and theoretical status and prospects, see Refs. [72, 79, 80].

A detailed set of upper bounds on CLFV branching rations is given in the listings for the muon and tau leptons. Here we emphasize those with the strongest limits:

$$\begin{aligned} &\mathrm{Br}(\mu \to e\gamma) < 4.2\times 10^{-13} \quad [81], \\ &\mathrm{Br}(\mu \to 3e) < 1.0\times 10^{-12} \quad [82] \end{aligned} \tag{26}$$

and

$$B_{\mu\to e} \equiv \frac{\Gamma(\mu^- + A(N,Z) \to e^- + A(N,Z)}{\Gamma(\mu^- + A(N,Z) \to \nu + A(N+1,Z-1)} \tag{27}$$

Downloaded from https://academic.oup.com/ptep/article/2022/8/083C01/6651666 by KIT Library user on 27 September 2022

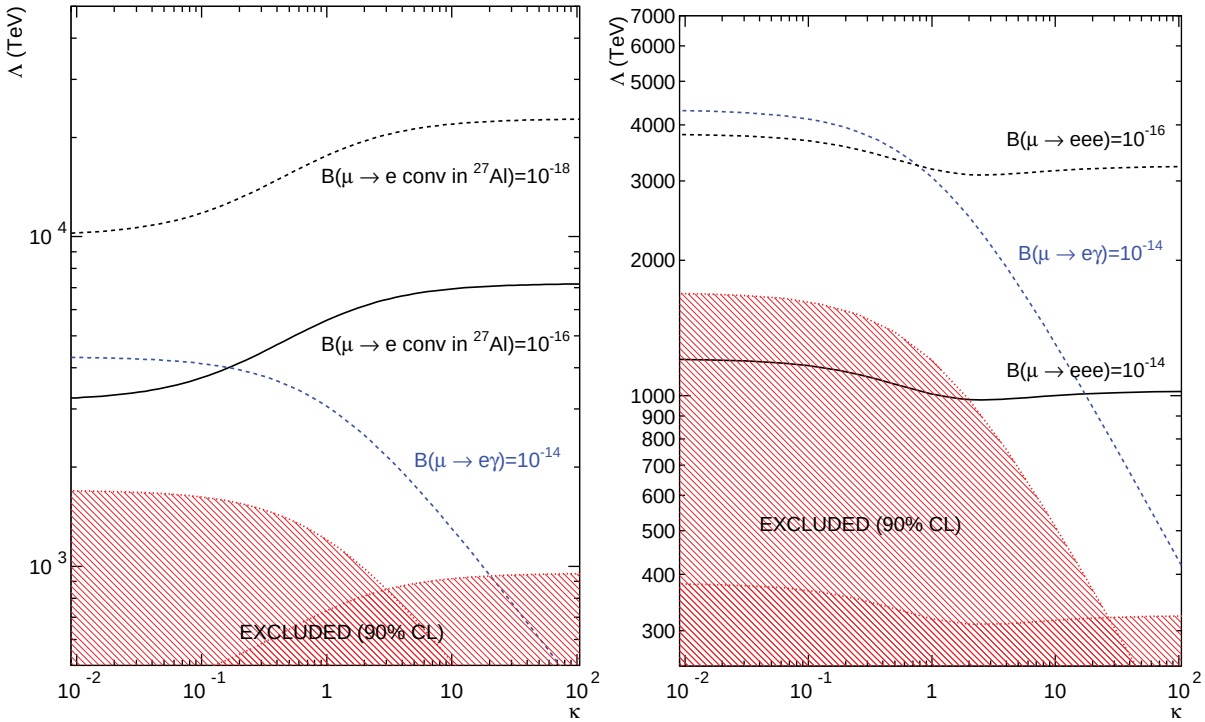

Figure 3: Model-independent CLFV sensitivities based on Eq (31). Left panel shows the comparison of present constraints with prospective future sensitivities for $\mu \to e\gamma$ and $\mu \to e$ conversion. Right panel gives analogous comparison for $\mu \to e\gamma$ and $\mu \to 3e$. Updated by [71] from Ref. [72].

with the best limit so far, $B_{\mu\to e} < 7 \times 10^{-13}$ [83], obtained with gold. Several proposed experiments aim to improve these limits by several orders of magnitude with different atoms.

One may interpret both $\mu \to e\gamma$ and $\mu \to e$ conversion in terms of the amplitudes to emit a real or virtual photon:

$$\mathcal{M}_{\mu\to e\gamma^{(*)}} = eG_\mu \varepsilon^{\alpha *} \bar{e}(p-q)\Big[\left(q^2\gamma_\alpha - \not{q}q_\alpha\right)\left(\tilde{A}_1^R P_R + \tilde{A}_1^L P_L\right) + im_\mu \sigma_{\alpha\beta} q^\beta \left(\tilde{A}_2^R P_R + \tilde{A}_2^L P_L\right)\Big]\mu(p)\,, \tag{28}$$

where it is conventional to normalize the amplitude to the Fermi constant. One then has

$$\mathrm{Br}(\mu \to e\gamma) = 48\pi^3\alpha\left(|\tilde{A}_2^R|^2 + |\tilde{A}_2^L|^2\right)\,. \tag{29}$$

For the conversion process, the virtual photon is absorbed by the quarks in the nucleus, yielding an effective four-fermion operator. In general, the exchange of other particles could lead to similar or alternate Lorentz structures, and it is not possible to distinguish between the exchange of a virtual photon or other particle. It is conventional to write the most general four-fermion amplitude, valid for energies below the electroweak scale as (adapted from Ref. [88])

$$\mathcal{M}_{\mu\to e} = G_\mu \sum_{n,a,q} a_{a,q}^{(n)}\, \bar{e}\Gamma^n P_a \mu\, \bar{q}\Gamma_n q\,, \tag{30}$$

where P_a $(a = L, R)$ denote the left and right-handed projectors and Γ^n denotes 1, γ_5, γ^μ, $\gamma^\mu\gamma_5$, and $\sigma_{\mu\nu}$. If any of the coefficients $a_{a,q}^{(n)}$ are generated by physics at a scale $\Lambda > v$, then their effects would be encoded in the SMEFT Lagrangian (12). For scenarios in which the leading CLFV operators occur at $d = 6$, the $a_{a,q}^{(n)}$ will scale as $(v/\Lambda)^2$. The corresponding decay and conversion rates will then scale as $(v/\Lambda)^4$. Note that the scalar and time component of the vector interactions are coherent over the nucleus, essentially counting the number of quarks. Consequently, these interactions typically yield the greatest sensitivities to high BSM mass scales.

It is sometimes convenient to compare the relative sensitivities of the decay and conversion processes using the following simplified effective Lagrangian [72]:

$$\mathcal{L}_{\mathrm{eff}}^{\mathrm{CLFV}} = \frac{m_\mu}{(\kappa+1)\Lambda^2}\,\bar{\mu}_R \sigma_{\mu\nu} e_L\, F^{\mu\nu} + \frac{\kappa}{(\kappa+1)\Lambda^2}\,\bar{\mu}\gamma_\mu e \sum_q \bar{q}\gamma^\mu q + \mathrm{h.c.}\,. \tag{31}$$

Note that one may replace the second term in Eq. (31) by any one of the other four-fermion interactions given in Eq. (30). An analogous expression applies to the process $\mu \to 3e$ when replacing the sum over quarks by the corresponding electron bilinear. A comparison of the present and prospective sensitivities for various muon CLFV searches in this framework is shown in Figure 3.

Stringent limits have been also set on the LFV decay modes of the τ lepton [89]. As shown in Figure 4, the large τ data samples collected at the B factories have made possible to reach a 10^{-8} sensitivity for many of its leptonic ($\tau \to \ell\gamma$, $\tau \to \ell'\ell^+\ell^-$) and semileptonic ($\tau \to \ell P^0$, $\tau \to \ell V^0$, $\tau \to \ell P^0 P^0$, $\tau \to \ell P^+ P'^-$) neutrinoless LFV decays, and BELLE-II is expected to push these limits beyond the 10^{-9} level [85]. Being a third generation lepton, the τ could be more sensitive to heavier new-physics scales, which makes his LFV decays particularly interesting. Compared to the muon, the τ decay amplitudes could be enhanced by a chirality ratio $(m_\tau/m_\mu)^2 \sim 280$ and/or by lepton-mixing factors such as $|U_{\tau 3}/U_{e3}|^2 \sim 20$, but the exact relation is model dependent. In any case, the τ LFV decays provide a rich data set that is very complementary to the μ bounds. If LFV is finally observed, the correlations between μ and τ data, and among different LFV τ decays will allow to probe the underlying mechanism of lepton flavor breaking.

Interesting limits on LFV are also obtained in meson decays. The best bounds come from kaon experiments, e.g., $\mathrm{Br}(K_L^0 \to e^\pm\mu^\mp) < 4.7 \times 10^{-12}$ [90], $\mathrm{Br}(K^+ \to \pi^+\mu^+e^-) < 1.3 \times 10^{-11}$ [91]. Quite strong limits have also been set in decays of B and D mesons, the best upper bounds being $\mathrm{Br}(B^0 \to e^\pm\mu^\mp) < 1.0 \times$

Downloaded from https://academic.oup.com/ptep/article/2022/8/083C01/6651666 by KIT Library user on 27 September 2022

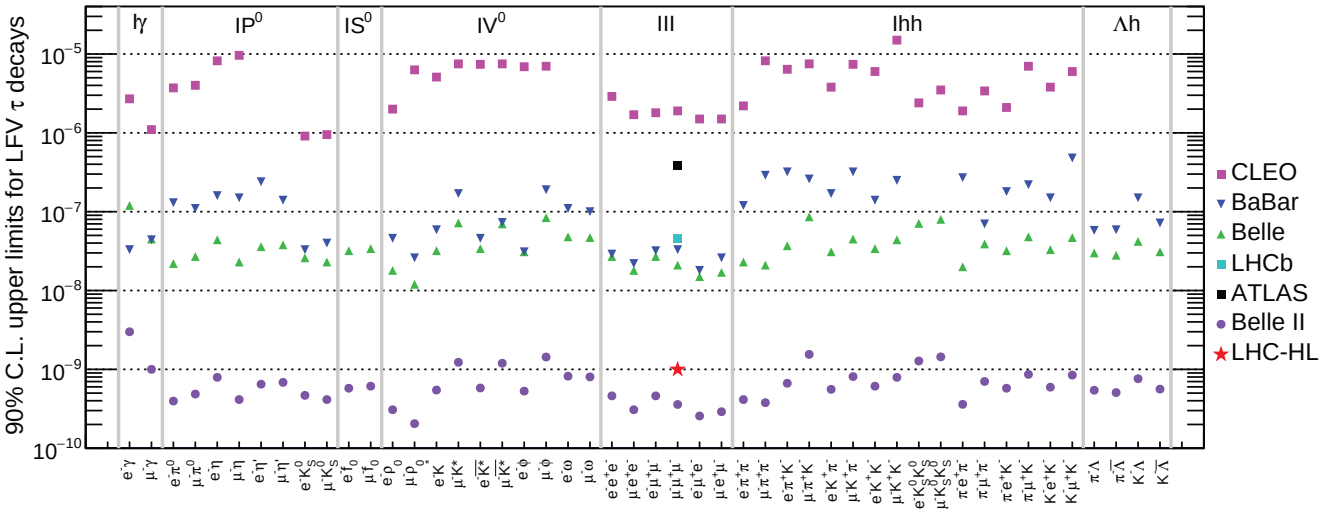

Figure 4: Current experimental limits on neutrinoless LFV τ decays [84]. Also shown are the future projections at Belle-II [85] and at the HL-LHC [86].

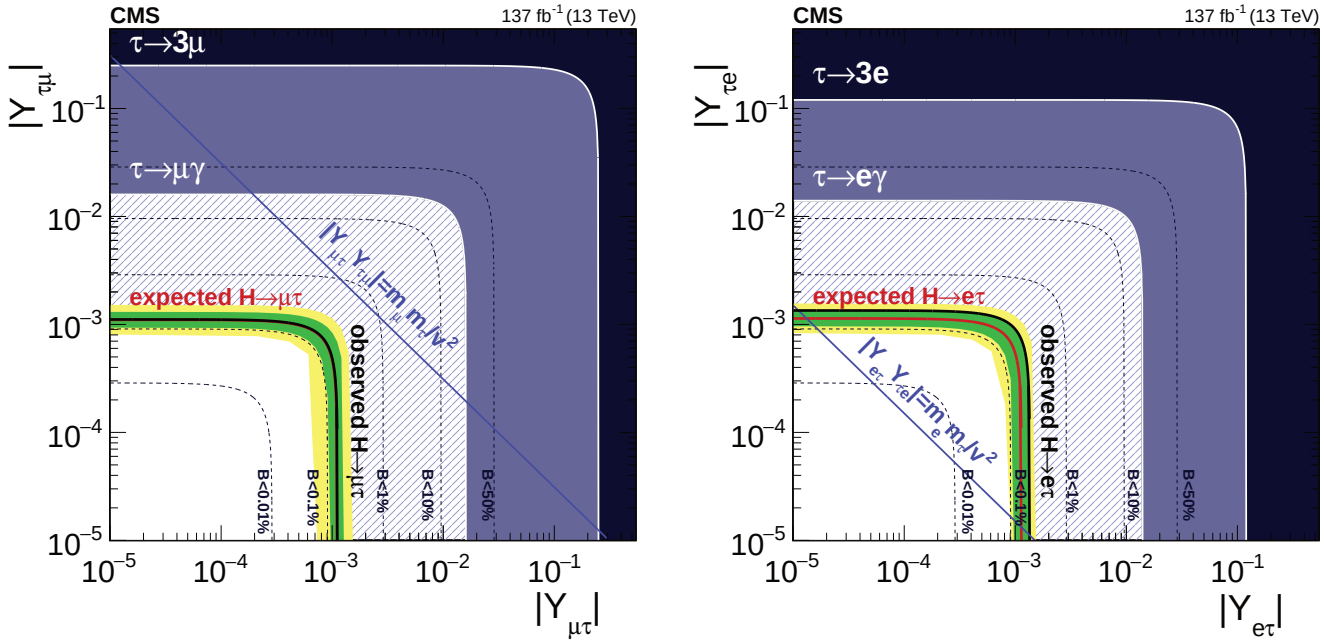

Figure 5: Current limits on the Higgs LFV τ Yukawas from direct $H^0 \to \ell^\pm\tau^\mp$ decays ($\ell = e, \mu$), and indirect constraints from τ decays [87].

10^{-9} [92] and $\mathrm{Br}(D^0 \to e^\pm\mu^\mp) < 1.3 \times 10^{-8}$ [93].

The LFV decays of the Z boson were probed at LEP at the 10^{-5} to 10^{-6} level. Stronger (95% C.L.) limits have been set recently by the LHC ATLAS collaboration [94, 95]:

$$\mathrm{Br}(Z \to e^\pm\mu^\mp) < 7.5 \times 10^{-7}\,, \qquad \mathrm{Br}(Z \to e^\pm\tau^\mp) < 5.0 \times 10^{-6}\,, \qquad \mathrm{Br}(Z \to \mu^\pm\tau^\mp) < 6.5 \times 10^{-6}\,. \tag{32}$$

LHC is now starting to test LFV in Higgs decays, within the available statistics. From the current (95% C.L.) experimental upper bounds [87, 96–98],

$$\mathrm{Br}(H^0 \to e^\pm\mu^\mp) < 6.1 \times 10^{-5}\,, \qquad \mathrm{Br}(H^0 \to e^\pm\tau^\mp) < 0.22\%\,, \qquad \mathrm{Br}(H^0 \to \mu^\pm\tau^\mp) < 0.15\%\,, \tag{33}$$

one can derive direct limits on the LFV Yukawa couplings of the Higgs boson,

$$\mathcal{L}_Y = -H^0 \sum_{i \neq j} \left(Y_{\ell_i \ell_j}\, \bar{\ell}^i_L \ell^j_R + \mathrm{h.c.} \right)\,. \tag{34}$$

From $H^0 \to e^\pm\mu^\mp$, one obtains $\sqrt{Y^2_{\mu e} + Y^2_{e\mu}} < 2.2 \times 10^{-4}$, which is not yet competitive with the indirect limit set by $\mu \to e\gamma$ through a (one-loop) virtual Higgs exchange:

$$\sqrt{Y^2_{\mu e} + Y^2_{e\mu}} < 3.6 \times 10^{-6}\,. \tag{35}$$

However, the LHC data provide at present the strongest bounds on the LFV τ Yukawas [87]:

$$\sqrt{Y^2_{e\tau} + Y^2_{\tau e}} < 1.35 \times 10^{-3}\,, \qquad \sqrt{Y^2_{\mu\tau} + Y^2_{\tau\mu}} < 1.11 \times 10^{-3}\,. \tag{36}$$

Figure 5 compares the Higgs exclusion limits on the τ Yukawas with the current indirect constraints from LFV τ decays.

Downloaded from https://academic.oup.com/ptep/article/2022/8/083C01/6651666 by KIT Library user on 27 September 2022

6 Baryon and Lepton Number

The transitions discussed in the previous section preserve the total lepton number $L = L_e + L_\mu + L_\tau$. In the SM, conservation of $B - L$ is an accidental symmetry of the Lagrangian. At the classical level, $B + L$ is also conserved, though it is violated at the loop level by the anomaly. The latter is a topological effect that is highly suppressed at zero temperature and, moreover, does not contribute to the processes discussed in the review. Going beyond renormalizable interactions, there exists a tower of operators in the SMEFT Lagrangian (12), containing only SM fields, that break one or both of these symmetries. We briefly review these possibilities in turn.

Lepton Number

The lowest-dimension operator containing only SM fields that breaks baryon or lepton number is the $d = 5$, lepton-number-violating (LNV) 'Weinberg' neutrino-mass operator [63]:

$$\mathcal{L}^{\rm LNV} = \frac{y}{\Lambda}\,\bar{L}^C H H^T L\,. \tag{37}$$

When the neutral component of the Higgs field obtains its vacuum expectation value, this $\Delta L = 2$ interaction yields a Majorana mass for the light, active neutrinos. The most comprehensive approach for probing this effect is the search for neutrinoless double-beta decay ($0\nu\beta\beta$) of atomic nuclei, $(Z, A) \to (Z + 2, A) + e^- + e^-$ [99, 100] (see the review on neutrinoless double-β decay). The detection of a non-zero $0\nu\beta\beta$ signal could represent a spectacular evidence of Majorana neutrinos. The current best limit, $\tau_{1/2} > 1.07 \times 10^{26}$ yr, was obtained by the KamLAND-Zen experiment with ^{136}Xe [101].

Theoretically, the interaction (37) can arise from BSM interactions in the well-known see-saw mechanism for neutrino mass (for a review, see [102]). In this context, the conventional choice for the scale Λ is of order the GUT scale, yielding light neutrino masses of order eV and below when the couplings y are of order the charged elementary fermion Yukawa couplings. BSM theories may also give rise to LNV observables in other contexts. In these scenarios, if the LNV scale is of order 1 TeV, one may observe signatures of LNV not only in $0\nu\beta\beta$ but also in collider searches for final states containing same sign dileptons. Searches for same sign dileptons plus a di-jet pair at the LHC have placed constraints on TeV-scale LNV [103, 104] that in some cases complement those obtained from $0\nu\beta\beta$.

Stringent constraints on violations of L have been also set in $\mu^- \to e^+$ conversion in muonic atoms, the best limit being $\sigma(\mu^-{\rm Ti} \to e^+{\rm Ca})/\sigma(\mu^-{\rm Ti} \to {\rm all}) < 3.6 \times 10^{-11}$ [105], and at the flavor factories through L-violating decays of the τ lepton and K, D and B mesons. Some representative examples are ${\rm Br}(\tau^- \to e^+\pi^-\pi^-) < 2.0 \times 10^{-8}$ [106], ${\rm Br}(K^+ \to \pi^-\mu^+\mu^+) < 4.2 \times 10^{-11}$ [107], ${\rm Br}(D^+ \to \pi^-\mu^+\mu^+) < 1.4 \times 10^{-8}$ [108] and ${\rm Br}(B^- \to \pi^+\mu^-\mu^-) < 4.0 \times 10^{-9}$ (95% CL) [109]. All these $|\Delta L| = 2$ processes could be mediated by a massive Majorana neutrino. They provide useful bounds on the effective Majorana neutrino mass matrix $m_{\ell\ell'} \sim \sum_i U_{\ell i} U_{\ell' i} m_{\nu_i}$ [110], although not as strong as the $0\nu\beta\beta$ constraint on m_{ee}.

Baryon Number

Grand Unified Theories (GUTs) combine leptons and quarks in the same symmetry multiplets and, therefore, predict the violation of the baryon and lepton quantum numbers. Many experiments have searched for B-violating transitions, but no positive signal has been identified so far. Proton decay would be the most relevant violation of B, as it would imply the unstability of matter. The current lower bound on the proton lifetime is 3.6×10^{29} yr [111]. Stronger limits have been set for particular decay modes, such as $\tau(p \to e^+\pi^0) > 1.6 \times 10^{34}$ yr [112]. For a discussion of proton decay in the context of GUTs, see the review on Grand Unified Theories.

Another spectacular signal would be neutron-antineutron oscillations. Searches have been performed for quasi-free n–$\bar{n}$ oscillations and for $n\bar{n}$ annihilation products in a nucleus. The latter would arise when the $\bar{n}$ produced through oscillations annihilates with another neutron in the nuclear medium. The corresponding best limits, expressed in terms of the free and bound oscillation times, $\tau_{n\bar{n}}$ and τ_m, respectively, are:

$$\tau_{n\bar{n}} > 0.86 \times 10^8 \text{ s} \quad [113], \tag{38a}$$

$$\tau_m > 1.9 \times 10^{32} \text{ yr} \quad [114]. \tag{38b}$$

From the latter, one may infer a bound $\tau_{n\bar{n}} > 2.7 \times 10^8$ s, as discussed below. See Ref. [115] for a recent review.

The theoretical interpretation of these bounds starts with an assumed, effective Hamiltonian for the free (anti-)neutron, $\mathcal{H}_{\rm eff}$ that contains a B-violating part, yielding matrix elements

$$\langle n|\mathcal{H}_{\rm eff}|n\rangle = \langle \bar{n}|\mathcal{H}_{\rm eff}|\bar{n}\rangle = m - i\frac{\lambda}{2}\,, \tag{39a}$$

$$\langle n|\mathcal{H}_{\rm eff}|\bar{n}\rangle = \langle \bar{n}|\mathcal{H}_{\rm eff}|n\rangle \equiv \delta m\,, \tag{39b}$$

where CPT is assumed to be conserved, the neutron lifetime $\tau_n = 1/\lambda$ and $\tau_{n\bar{n}} = 1/|\delta m|$. The rate for a neutron to oscillate into an antineutron after a time t is given by

$$\mathcal{P}_{n\bar{n}}(t) = \sin^2\left(\frac{t}{\tau_{n\bar{n}}}\right) e^{-\lambda t}\,. \tag{40}$$

For $t << \tau_n << \tau_{n\bar{n}}$, one has

$$\mathcal{P}_{n\bar{n}}(t) \to (t/\tau_{n\bar{n}})^2\,. \tag{41}$$

In realistic experiments, there exist effects, such as background magnetic fields, that split the energies of the neutron and antineutron. One must ensure that the observation time is sufficiently short so that these effects do not overwhelm the small B-violating term δm and that Eq. (40) applies.

In nuclei, the interactions of neutrons and antineutrons with the surrounding medium are sufficiently distinct that one must take the corresponding matter potentials into account. In particular, the matrix elements in Eq. (39a) become

$$\langle n|\mathcal{H}_{\rm eff}|n\rangle = m + V_n\,, \qquad \langle \bar{n}|\mathcal{H}_{\rm eff}|\bar{n}\rangle = m + V_{\bar{n}}\,, \tag{42}$$

with V_n being essentially real ($V_n \equiv V_{nR}$) and $V_{\bar{n}} = V_{\bar{n}R} - iV_{\bar{n}I}$. The imaginary part $V_{\bar{n}I}$ characterizes the annihilation of the antineutron with bound nucleons into secondary hadrons. The rate for a bound neutron to disappear is given by

$$\Gamma_m = \frac{2(\delta m)^2|V_{\bar{n}I}|}{(V_{nR} - V_{\bar{n}R})^2 + V_{\bar{n}I}^2} \equiv \left(R\,\tau_{n\bar{n}}^2\right)^{-1}\,. \tag{43}$$

For the nuclei of experimental interest, nuclear theory computations yield $R \sim 10^{23} s^{-1}$. Null results of bound n-$\bar{n}$ oscillation searches thus allow one to infer a bound on $\tau_{n\bar{n}}$ via Eq. (43).

From an elementary particle standpoint, n-$\bar{n}$ oscillations involve the conversion of three quarks into three antiquarks (and vice-versa). The lowest-dimension operators mediating such process arise at dimension nine in the SMEFT:

$$\mathcal{L}_{n\text{-}\bar{n}} = \frac{1}{\Lambda^5}\sum_j \alpha_j^{(9)}\,\mathcal{O}_j^{\rm BNV}\,. \tag{44}$$

Consequently, one expects

$$\delta m \sim \alpha_j^{(9)}\,\frac{\Lambda_{\rm HAD}^6}{\Lambda^5}\,, \tag{45}$$

where $\Lambda_{\rm HAD}$ is a hadronic scale set by the n-$\bar{n}$ matrix elements in Eq. (39b). Taking $\Lambda_{\rm HAD}$ to be of order the QCD scale and using the present bounds on $\tau_{n\bar{n}}$ yields a lower bound on the B-violating mass scale of ~ 100 TeV.

The search for B-violating decays of short-lived particles such as Z bosons, τ leptons and B mesons provides also relevant constraints. The best limits are ${\rm Br}(Z \to pe, p\mu) < 1.8 \times 10^{-6}$ (95% C.L.) [116], ${\rm Br}(\tau^- \to \bar{p}\mu^-\mu^+) < 1.8 \times 10^{-8}$ [117] and ${\rm Br}(B^+ \to \Lambda e^+) < 3.2 \times 10^{-8}$ [118].

Downloaded from https://academic.oup.com/ptep/article/2022/8/083C01/6651666 by KIT Library user on 27 September 2022

7 Quark flavors

While strong and electromagnetic forces preserve the quark flavor, the charged-current weak interactions generate transitions among the different quark species (see the review on the CKM quark-mixing matrix). Since the SM flavor-changing mechanism is associated with the $W^{\pm}$ fermionic vertices, the tree-level transitions satisfy a $\Delta F = \Delta Q$ rule where ΔQ denotes the change in charge of the relevant hadrons. Remember that the flavor quantum number F is defined to be $+1$ for positively charged quarks ($F = U, C, T$) and -1 for quarks with negative charges ($F = D, S, B$). The strongest tests on this conservation law have been obtained in kaon decays such as $\mathrm{Br}(K^+ \to \pi^+\pi^+e^-\bar{\nu}_e) < 1.3 \times 10^{-8}$ [119], and $(\mathrm{Re}\,x, \mathrm{Im}\,x) = (-0.002 \pm 0.006, 0.0012 \pm 0.0021)$ [120, 121] where $x \equiv \mathcal{M}(\overline{K}^0 \to \pi^-\ell^+\nu)/\mathcal{M}(K^0 \to \pi^-\ell^+\nu)$.

The $\Delta F = \Delta Q$ rule can be violated through quantum loop contributions giving rise to flavor-changing neutral-current transitions (FCNCs). Owing to the GIM mechanism, processes of this type are very suppressed in the SM, which makes them a superb tool in the search for new physics associated with the flavor dynamics. Within the SM itself, these transitions are also sensitive to the heavy-quark mass scales and have played a crucial role identifying the size of the charm (K^0–$\overline{K}^0$ mixing) and top (B^0–$\overline{B}^0$ mixing) masses before the discovery of those quarks. In addition to the well-established $\Delta F = 2$ mixings in neutral K and B mesons, $\Delta M_{K^0} \equiv M_{K^0_L} - M_{K^0_S} = (0.5293 \pm 0.0009) \times 10^{10}\ \mathrm{s}^{-1}$, $\Delta M_{B^0} \equiv M_{B^0_H} - M_{B^0_L} = (0.5065 \pm 0.0019) \times 10^{12}\ \mathrm{s}^{-1}$ and $\Delta M_{B^0_s} \equiv M_{B^0_{sH}} - M_{B^0_{sL}} = (17.765 \pm 0.006) \times 10^{12}\ \mathrm{s}^{-1}$, the mixing of the D^0 meson and its antiparticle has been recently observed with a significance of more than seven standard deviations [122], showing that there is a nonzero mass difference between the two neutral charm-meson eigenstates, of the expected size:

$$M_{D^0_H} - M_{D^0_L} = (0.997 \pm 0.116) \times 10^{10}\ \mathrm{s}^{-1}. \tag{46}$$

The SM prediction of the D^0_H–D^0_L mass difference is dominated by long-distance physics, because it involves virtual loops with down-type light quarks, and has unfortunately quite large uncertainties [123].

The FCNC kaon decays into lepton-antilepton pairs put stringent constraints on new flavor-changing interactions. The measured $K^0_L \to \mu^+\mu^-$ rate, $\mathrm{Br}(K^0_L \to \mu^+\mu^-) = (6.84 \pm 0.11) \times 10^{-9}$, is completely dominated by the known 2γ absorptive contribution, leaving very little room for new-physics, and $\mathrm{Br}(K^0_L \to e^+e^-) = (9^{+6}_{-4}) \times 10^{-12}$ [124] (the tiniest branching ratio ever measured) also agrees with the SM expectation [125]. The experimental K^0_S upper bounds on the electron, $\mathrm{Br}(K^0_S \to e^+e^-) < 9 \times 10^{-9}$ [126], and muon, $\mathrm{Br}(K^0_S \to \mu^+\mu^-) < 2.1 \times 10^{-10}$ [127], modes are still five and two orders of magnitude, respectively, larger than their SM predictions [125]. Another very clean test of FCNCs is provided by the decay $K^+ \to \pi^+\nu\bar{\nu}$. The CERN NA62 experiment has already observed 20 signal candidates, providing the first evidence of this decay [128]. This leads to $\mathrm{Br}(K^+ \to \pi^+\nu\bar{\nu}) = (1.14^{+0.40}_{-0.33}) \times 10^{-10}$, in agreement with the predicted SM branching fraction of $(7.73 \pm 0.61) \times 10^{-11}$ [129, 130]. Even more interesting is the CP-violating neutral mode $K^0_L \to \pi^0\nu\bar{\nu}$, expected at a rate of $(2.59 \pm 0.29) \times 10^{-11}$ [129, 130] that is still far away from the current upper bound of 3.0×10^{-9} [131]. The KOTO experiment at KEK is expected to substantially increase the sensitivity to this mode.

The strongest bound on FCNC transitions in charm decays is $\mathrm{Br}(D^0 \to \mu^+\mu^-) < 6.2 \times 10^{-9}$ [132], while in B decays the LHC experiments have recently reached the SM sensitivity: $\mathrm{Br}(B^0_d \to \mu^+\mu^-) = (0.07^{+0.13}_{-0.11}) \times 10^{-9}$ and $\mathrm{Br}(B^0_s \to \mu^+\mu^-) = (3.01 \pm 0.35) \times 10^{-9}$. At present, there is a lot of interest on the decays $B \to K^{(*)}\ell^+\ell^-$ where sizable discrepancies between the measured data and the SM predictions have been reported [133]. In particular, the LHCb experiment has found the ratios of produced muons versus electrons to be below the SM predictions (for dilepton invariant-masses squared in the range $q^2 \leq 6\ \mathrm{GeV}^2$), with a significance of 3.1σ in $B^+ \to K^+\ell^+\ell^-$ [134, 135] and 2.4σ in $B \to K^*\ell^+\ell^-$ [136], suggesting a significant violation of lepton universality. The current Belle-II measurements of these ratios [137, 138] are consistent with the SM, but they are also compatible with the LHCb results. Future analyses from LHCb and Belle-II are expected to clarify the situation.

References

[1] G. Luders, Kong. Dan. Vid. Sel. Mat. Fys. Med. **28N5**, 5, 1 (1954).

[2] W. Pauli, in L. Rosenfelf and V. Weisskopf, editors, "Niels Bohr and the Development of Physics," 30–51, McGraw-Hill, New York (1955).

[3] J. McDonough *et al.*, Phys. Rev. **D38**, 2121 (1988).

[4] M. Ablikim *et al.* (BESIII), Phys. Rev. **D90**, 9, 092002 (2014), [arXiv:1409.4040].

[5] S. Prakhov *et al.* (Crystal Ball), Phys. Rev. Lett. **84**, 4802 (2000).

[6] J. H. Christenson *et al.*, Phys. Rev. Lett. **13**, 138 (1964).

[7] H. Burkhardt *et al.* (NA31), Phys. Lett. **B206**, 169 (1988).

[8] G. D. Barr *et al.* (NA31), Phys. Lett. **B317**, 233 (1993).

[9] L. K. Gibbons *et al.*, Phys. Rev. Lett. **70**, 1203 (1993).

[10] J. R. Batley *et al.* (NA48), Phys. Lett. **B544**, 97 (2002), [hep-ex/0208009].

[11] E. Abouzaid *et al.* (KTeV), Phys. Rev. **D83**, 092001 (2011), [arXiv:1011.0127].

[12] H. Gisbert and A. Pich, Rept. Prog. Phys. **81**, 7, 076201 (2018), [arXiv:1712.06147].

[13] V. Cirigliano *et al.*, JHEP **02**, 032 (2020), [arXiv:1911.01359].

[14] R. Abbott *et al.* (RBC, UKQCD), Phys. Rev. D **102**, 5, 054509 (2020), [arXiv:2004.09440].

[15] R. Aaij *et al.* (LHCb), Phys. Rev. Lett. **122**, 21, 211803 (2019), [arXiv:1903.08726].

[16] P. F. de Salas *et al.*, JHEP **02**, 071 (2021), [arXiv:2006.11237].

[17] M. C. Gonzalez-Garcia, M. Maltoni and T. Schwetz, Universe **7**, 12, 459 (2021), [arXiv:2111.03086].

[18] A. Angelopoulos *et al.* (CPLEAR), Phys. Lett. **B444**, 43 (1998).

[19] L. Wolfenstein, Phys. Rev. Lett. **83**, 911 (1999).

[20] L. Alvarez-Gaume *et al.*, Phys. Lett. **B458**, 347 (1999), [hep-ph/9812326].

[21] H. J. Gerber, Eur. Phys. J. **C35**, 195 (2004).

[22] M. C. Bañuls and J. Bernabeu, Phys. Lett. **B464**, 117 (1999), [hep-ph/9908353].

[23] M. C. Bañuls and J. Bernabeu, Nucl. Phys. **B590**, 19 (2000), [hep-ph/0005323].

[24] J. Bernabeu, F. Martinez-Vidal and P. Villanueva-Perez, JHEP **08**, 064 (2012), [arXiv:1203.0171].

[25] J. P. Lees *et al.* (BaBar), Phys. Rev. Lett. **109**, 211801 (2012), [arXiv:1207.5832].

[26] T. Chupp *et al.*, Rev. Mod. Phys. **91**, 1, 015001 (2019), [arXiv:1710.02504].

[27] J. Engel, M. J. Ramsey-Musolf and U. van Kolck, Prog. Part. Nucl. Phys. **71**, 21 (2013), [arXiv:1303.2371].

[28] M. Pospelov and A. Ritz, Annals Phys. **318**, 119 (2005), [hep-ph/0504231].

[29] J. S. M. Ginges and V. V. Flambaum, Phys. Rept. **397**, 63 (2004), [arXiv:physics/0309054].

[30] V. Andreev *et al.* (ACME), Nature **562**, 7727, 355 (2018).

[31] W. B. Cairncross *et al.*, Phys. Rev. Lett. **119**, 15, 153001 (2017), [arXiv:1704.07928].

[32] G. W. Bennett *et al.* (Muon (g-2)), Phys. Rev. **D80**, 052008 (2009), [arXiv:0811.1207].

[33] C. Abel *et al.* (nEDM), Phys. Rev. Lett. **124**, 8, 081803 (2020), [arXiv:2001.11966].

Downloaded from https://academic.oup.com/ptep/article/2022/8/083C01/6651666 by KIT Library user on 27 September 2022

[34] B. Graner *et al.*, Phys. Rev. Lett. **116**, 16, 161601 (2016), [Erratum: Phys. Rev. Lett.119,no.11,119901(2017)], [arXiv:1601.04339].

[35] F. Allmendinger *et al.*, Phys. Rev. **A100**, 2, 022505 (2019), [arXiv:1904.12295].

[36] C. Jarlskog, Phys. Rev. Lett. **55**, 1039 (1985); C. Jarlskog, Z. Phys. **C29**, 491 (1985).

[37] E. P. Shabalin, Sov. J. Nucl. Phys. **28**, 75 (1978), [Yad. Fiz.28,151(1978)].

[38] E. P. Shabalin, Sov. Phys. Usp. **26**, 297 (1983), [Usp. Fiz. Nauk139,561(1983)].

[39] W. Bernreuther and M. Suzuki, Rev. Mod. Phys. **63**, 313 (1991), [Erratum: Rev. Mod. Phys.64,633(1992)].

[40] M. Pospelov and A. Ritz, Phys. Rev. **D89**, 5, 056006 (2014), [arXiv:1311.5537].

[41] C.-Y. Seng, Phys. Rev. **C91**, 2, 025502 (2015), [arXiv:1411.1476].

[42] B. Grzadkowski *et al.*, JHEP **10**, 085 (2010), [arXiv:1008.4884].

[43] S. Mantry, M. Pitschmann and M. J. Ramsey-Musolf, Phys. Rev. **D90**, 5, 054016 (2014), [arXiv:1401.7339].

[44] B. K. Sahoo, Phys. Rev. **D95**, 1, 013002 (2017), [arXiv:1612.09371].

[45] T. Chupp, Private Communication (2019).

[46] J. Bsaisou *et al.*, Annals Phys. **359**, 317 (2015), [arXiv:1412.5471].

[47] J. de Vries *et al.*, Annals Phys. **338**, 50 (2013), [arXiv:1212.0990].

[48] L. I. Schiff, Phys. Rev. **132**, 2194 (1963).

[49] T. Chupp and M. Ramsey-Musolf, Phys. Rev. **C91**, 3, 035502 (2015), [arXiv:1407.1064].

[50] J. Beringer *et al.* (Particle Data Group), Phys. Rev. **D86**, 010001 (2012).

[51] A. Angelopoulos *et al.* (CPLEAR), Phys. Lett. **B471**, 332 (1999).

[52] M. S. Fee *et al.*, Phys. Rev. **A48**, 192 (1993).

[53] R. J. Hughes and B. I. Deutch, Phys. Rev. Lett. **69**, 578 (1992).

[54] S. Ulmer *et al.* (BASE), Nature **524**, 7564, 196 (2015).

[55] R. S. Van Dyck, P. B. Schwinberg and H. G. Dehmelt, Phys. Rev. Lett. **59**, 26 (1987).

[56] G. W. Bennett *et al.* (Muon g-2), Phys. Rev. Lett. **92**, 161802 (2004), [hep-ex/0401008].

[57] C. Smorra *et al.* (BASE), Nature **550**, 7676, 371 (2017).

[58] M. Ahmadi *et al.*, Nature **557**, 7703, 71 (2018).

[59] O. W. Greenberg, Phys. Rev. Lett. **89**, 231602 (2002), [hep-ph/0201258].

[60] S. Liberati, Class. Quant. Grav. **30**, 133001 (2013), [arXiv:1304.5795].

[61] V. A. Kostelecky and N. Russell, Rev. Mod. Phys. **83**, 11 (2011), [arXiv:0801.0287].

[62] D. Colladay and V. A. Kostelecky, Phys. Rev. **D58**, 116002 (1998), [hep-ph/9809521].

[63] S. Weinberg, Phys. Rev. Lett. **43**, 1566 (1979).

[64] F. Wilczek and A. Zee, Phys. Rev. Lett. **43**, 1571 (1979).

[65] L. F. Abbott and M. B. Wise, Phys. Rev. **D22**, 2208 (1980).

[66] M. Agostini *et al.* (Borexino), Phys. Rev. Lett. **115**, 231802 (2015), [arXiv:1509.01223].

[67] E. B. Norman, J. N. Bahcall and M. Goldhaber, Phys. Rev. **D53**, 4086 (1996).

[68] G. Bressi *et al.*, Phys. Rev. **A83**, 5, 052101 (2011), [arXiv:1102.2766].

[69] C. Caprini, S. Biller and P. G. Ferreira, JCAP **0502**, 006 (2005), [hep-ph/0310066].

[70] B. Altschul, Phys. Rev. Lett. **98**, 261801 (2007), [hep-ph/0703126].

[71] A. de Gouvea, Private Communication (2019).

[72] A. de Gouvea and P. Vogel, Prog. Part. Nucl. Phys. **71**, 75 (2013), [arXiv:1303.4097].

[73] S. T. Petcov, Sov. J. Nucl. Phys. **25**, 340 (1977), [Erratum: Yad. Fiz.25,1336(1977)].

[74] W. J. Marciano and A. I. Sanda, Phys. Lett. **67B**, 303 (1977).

[75] S. M. Bilenky, S. T. Petcov and B. Pontecorvo, Phys. Lett. **67B**, 309 (1977).

[76] T.-P. Cheng and L.-F. Li, Phys. Rev. **D16**, 1425 (1977).

[77] B. W. Lee and R. E. Shrock, Phys. Rev. **D16**, 1444 (1977).

[78] B. W. Lee *et al.*, Phys. Rev. Lett. **38**, 937 (1977), [Erratum: Phys. Rev. Lett.38,1230(1977)].

[79] R. H. Bernstein and P. S. Cooper, Phys. Rept. **532**, 27 (2013), [arXiv:1307.5787].

[80] L. Calibbi and G. Signorelli, Riv. Nuovo Cim. **41**, 2, 71 (2018), [arXiv:1709.00294].

[81] A. M. Baldini *et al.* (MEG), Eur. Phys. J. **C76**, 8, 434 (2016), [arXiv:1605.05081].

[82] U. Bellgardt *et al.* (SINDRUM), Nucl. Phys. **B299**, 1 (1988).

[83] W. H. Bertl *et al.* (SINDRUM II), Eur. Phys. J. **C47**, 337 (2006).

[84] Y. S. Amhis *et al.* (HFLAV), Eur. Phys. J. C **81**, 3, 226 (2021), [arXiv:1909.12524].

[85] W. Altmannshofer *et al.* (Belle-II), PTEP **2019**, 12, 123C01 (2019), [arXiv:1808.10567].

[86] A. Cerri *et al.*, CERN Yellow Rep. Monogr. **7**, 867 (2019), [arXiv:1812.07638].

[87] A. M. Sirunyan *et al.* (CMS), Phys. Rev. D **104**, 3, 032013 (2021), [arXiv:2105.03007].

[88] R. Kitano, M. Koike and Y. Okada, Phys. Rev. **D66**, 096002 (2002), [Erratum: Phys. Rev.D76,059902(2007)], [hep-ph/0203110].

[89] A. Pich, Prog. Part. Nucl. Phys. **75**, 41 (2014), [arXiv:1310.7922].

[90] D. Ambrose *et al.* (BNL), Phys. Rev. Lett. **81**, 5734 (1998), [hep-ex/9811038].

[91] A. Sher *et al.*, Phys. Rev. **D72**, 012005 (2005), [hep-ex/0502020].

[92] R. Aaij *et al.* (LHCb), JHEP **03**, 078 (2018), [arXiv:1710.04111].

[93] R. Aaij *et al.* (LHCb), Phys. Lett. **B754**, 167 (2016), [arXiv:1512.00322].

[94] G. Aad *et al.* (ATLAS), Phys. Rev. **D90**, 7, 072010 (2014), [arXiv:1408.5774].

[95] G. Aad *et al.* (ATLAS), Nature Phys. **17**, 7, 819 (2021), [arXiv:2105.12491].

[96] G. Aad *et al.* (ATLAS), Phys. Lett. **B801**, 135148 (2020), [arXiv:1909.10235].

[97] G. Aad *et al.* (ATLAS), Phys. Lett. **B800**, 135069 (2020), [arXiv:1907.06131].

[98] A. M. Sirunyan *et al.* (CMS), JHEP **06**, 001 (2018), [arXiv:1712.07173].

[99] S. Dell'Oro *et al.*, Adv. High Energy Phys. **2016**, 2162659 (2016), [arXiv:1601.07512].

[100] J. Engel and J. Menéndez, Rept. Prog. Phys. **80**, 4, 046301 (2017), [arXiv:1610.06548].

Downloaded from https://academic.oup.com/ptep/article/2022/8/083C01/6651666 by KIT Library user on 27 September 2022

[101] A. Gando *et al.* (KamLAND-Zen), Phys. Rev. Lett. **117**, 8, 082503 (2016), [Addendum: Phys. Rev. Lett.117,no.10,109903(2016)], [arXiv:1605.02889].

[102] P. Fileviez Perez, Phys. Rept. **597**, 1 (2015), [arXiv:1501.01886].

[103] M. Aaboud *et al.* (ATLAS), JHEP **01**, 016 (2019), [arXiv:1809.11105].

[104] A. M. Sirunyan *et al.* (CMS), JHEP **05**, 05, 148 (2018), [arXiv:1803.11116].

[105] J. Kaulard *et al.* (SINDRUM II), Phys. Lett. **B422**, 334 (1998).

[106] Y. Miyazaki *et al.* (Belle), Phys. Lett. **B719**, 346 (2013), [arXiv:1206.5595].

[107] E. Cortina Gil *et al.* (NA62), Phys. Lett. **B797**, 134794 (2019), [arXiv:1905.07770].

[108] R. Aaij *et al.* (LHCb), JHEP **06**, 044 (2021), [arXiv:2011.00217].

[109] R. Aaij *et al.* (LHCb), Phys. Rev. Lett. **112**, 13, 131802 (2014), [arXiv:1401.5361].

[110] A. Abada *et al.*, JHEP **02**, 169 (2018), [arXiv:1712.03984].

[111] M. Anderson *et al.* (SNO+), Phys. Rev. D **99**, 3, 032008 (2019), [arXiv:1812.05552].

[112] K. Abe *et al.* (Super-Kamiokande), Phys. Rev. **D95**, 1, 012004 (2017), [arXiv:1610.03597].

[113] M. Baldo-Ceolin *et al.*, Z. Phys. **C63**, 409 (1994).

[114] K. Abe *et al.* (Super-Kamiokande), Phys. Rev. **D91**, 072006 (2015), [arXiv:1109.4227].

[115] D. G. Phillips, II *et al.*, Phys. Rept. **612**, 1 (2016), [arXiv:1410.1100].

[116] G. Abbiendi *et al.* (OPAL), Phys. Lett. **B447**, 157 (1999), [hep-ex/9901011].

[117] D. Sahoo *et al.* (Belle), Phys. Rev. D **102**, 111101 (2020), [arXiv:2010.15361].

[118] P. del Amo Sanchez *et al.* (BaBar), Phys. Rev. **D83**, 091101 (2011), [arXiv:1101.3830].

[119] P. Bloch *et al.* (Geneva-Saclay), Phys. Lett. **60B**, 393 (1976).

[120] A. Angelopoulos *et al.* (CPLEAR), Phys. Lett. **B444**, 38 (1998).

[121] A. Angelopoulos *et al.* (CPLEAR), Eur. Phys. J. **C22**, 55 (2001).

[122] R. Aaij *et al.* (LHCb), Phys. Rev. Lett. **127**, 11, 111801 (2021), [arXiv:2106.03744].

[123] A. A. Petrov, Int. J. Mod. Phys. **A21**, 5686 (2006), [hep-ph/0611361].

[124] D. Ambrose *et al.* (BNL E871), Phys. Rev. Lett. **81**, 4309 (1998), [hep-ex/9810007].

[125] V. Cirigliano *et al.*, Rev. Mod. Phys. **84**, 399 (2012), [arXiv:1107.6001].

[126] F. Ambrosino *et al.* (KLOE), Phys. Lett. **B672**, 203 (2009), [arXiv:0811.1007].

[127] R. Aaij *et al.* (LHCb), Phys. Rev. Lett. **125**, 23, 231801 (2020), [arXiv:2001.10354].

[128] E. Cortina Gil *et al.* (NA62), JHEP **06**, 093 (2021), [arXiv:2103.15389].

[129] J. Brod, M. Gorbahn and E. Stamou, Phys. Rev. **D83**, 034030 (2011), [arXiv:1009.0947].

[130] J. Brod, M. Gorbahn and E. Stamou, in "19th International Conference on B-Physics at Frontier Machines," (2021), [arXiv:2105.02868].

[131] J. K. Ahn *et al.* (KOTO), Phys. Rev. Lett. **122**, 2, 021802 (2019), [arXiv:1810.09655].

[132] R. Aaij *et al.* (LHCb), Phys. Lett. **B725**, 15 (2013), [arXiv:1305.5059].

[133] S. Bifani *et al.*, J. Phys. **G46**, 2, 023001 (2019), [arXiv:1809.06229].

[134] R. Aaij *et al.* (LHCb), Phys. Rev. Lett. **122**, 19, 191801 (2019), [arXiv:1903.09252].

[135] R. Aaij *et al.* (LHCb), Nature Phys. **18**, 3, 277 (2022), [arXiv:2103.11769].

[136] R. Aaij *et al.* (LHCb), JHEP **08**, 055 (2017), [arXiv:1705.05802].

[137] A. Abdesselam *et al.* (Belle), Phys. Rev. Lett. **126**, 16, 161801 (2021), [arXiv:1904.02440].

[138] S. Choudhury *et al.* (BELLE), JHEP **03**, 105 (2021), [arXiv:1908.01848].

Downloaded from https://academic.oup.com/ptep/article/2022/8/083C01/6651666 by KIT Library user on 27 September 2022

TESTS OF DISCRETE SPACE-TIME SYMMETRIES

CHARGE CONJUGATION (C) INVARIANCE

$\Gamma(\pi^0 \to 3\gamma)/\Gamma_{total}$		$<3.1 \times 10^{-8}$, CL = 90%
η C-nonconserving decay parameters		
$\pi^+\pi^-\pi^0$ left-right asymmetry		$(0.09^{+0.11}_{-0.12}) \times 10^{-2}$
$\pi^+\pi^-\pi^0$ sextant asymmetry		$(0.12^{+0.10}_{-0.11}) \times 10^{-2}$
$\pi^+\pi^-\pi^0$ quadrant asymmetry		$(-0.09 \pm 0.09) \times 10^{-2}$
$\pi^+\pi^-\gamma$ left-right asymmetry		$(0.9 \pm 0.4) \times 10^{-2}$
$\pi^+\pi^-\gamma$ parameter β (D-wave)		-0.02 ± 0.07 (S = 1.3)
$\Gamma(\eta \to \pi^0\gamma)/\Gamma_{total}$	[a]	$<9 \times 10^{-5}$, CL = 90%
$\Gamma(\eta \to 2\pi^0\gamma)/\Gamma_{total}$		$<5 \times 10^{-4}$, CL = 90%
$\Gamma(\eta \to 3\pi^0\gamma)/\Gamma_{total}$		$<6 \times 10^{-5}$, CL = 90%
$\Gamma(\eta \to 3\gamma)/\Gamma_{total}$		$<1.6 \times 10^{-5}$, CL = 90%
$\Gamma(\eta \to \pi^0 e^+ e^-)/\Gamma_{total}$	[b]	$<8 \times 10^{-6}$, CL = 90%
$\Gamma(\eta \to \pi^0 \mu^+ \mu^-)/\Gamma_{total}$	[b]	$<5 \times 10^{-6}$, CL = 90%
$\Gamma(\omega(782) \to \eta\pi^0)/\Gamma_{total}$		$<2.1 \times 10^{-4}$, CL = 90%
$\Gamma(\omega(782) \to 2\pi^0)/\Gamma_{total}$		$<2.2 \times 10^{-4}$, CL = 90%
$\Gamma(\omega(782) \to 3\pi^0)/\Gamma_{total}$		$<2.3 \times 10^{-4}$, CL = 90%
$\eta'(958) \to \pi^+\pi^-\gamma$ decay asymmetry parameter		-0.03 ± 0.04
$\Gamma(\eta'(958) \to \pi^0 e^+ e^-)/\Gamma_{total}$	[b]	$<1.4 \times 10^{-3}$, CL = 90%
$\Gamma(\eta'(958) \to \eta e^+ e^-)/\Gamma_{total}$	[b]	$<2.4 \times 10^{-3}$, CL = 90%
$\Gamma(\eta'(958) \to 3\gamma)/\Gamma_{total}$		$<1.0 \times 10^{-4}$, CL = 90%
$\Gamma(\eta'(958) \to \mu^+\mu^-\pi^0)/\Gamma_{total}$	[b]	$<6.0 \times 10^{-5}$, CL = 90%
$\Gamma(\eta'(958) \to \mu^+\mu^-\eta)/\Gamma_{total}$	[b]	$<1.5 \times 10^{-5}$, CL = 90%
$\Gamma(J/\psi(1S) \to \gamma\gamma)/\Gamma_{total}$		$<2.7 \times 10^{-7}$, CL = 90%
$\Gamma(J/\psi(1S) \to \gamma\phi)/\Gamma_{total}$		$<1.4 \times 10^{-6}$, CL = 90%

PARITY (P) INVARIANCE

e electric dipole moment		$<0.11 \times 10^{-28}$ $e$cm, CL = 90%
μ electric dipole moment $\lvert d \rvert$		$<1.8 \times 10^{-19}$ $e$cm, CL = 95%
Re($d_\tau = \tau$ electric dipole moment)		-0.220 to 0.45×10^{-16} $e$cm, CL = 95%
$\Gamma(\eta \to \pi^+\pi^-)/\Gamma_{total}$		$<4.4 \times 10^{-6}$, CL = 90%
$\Gamma(\eta \to 2\pi^0)/\Gamma_{total}$		$<3.5 \times 10^{-4}$, CL = 90%
$\Gamma(\eta \to 4\pi^0)/\Gamma_{total}$		$<6.9 \times 10^{-7}$, CL = 90%
$\Gamma(\eta'(958) \to \pi^+\pi^-)/\Gamma_{total}$		$<1.8 \times 10^{-5}$, CL = 90%
$\Gamma(\eta'(958) \to \pi^0\pi^0)/\Gamma_{total}$		$<4 \times 10^{-4}$, CL = 90%
$\Gamma(\eta_c(1S) \to \pi^+\pi^-)/\Gamma_{total}$		$<1.1 \times 10^{-4}$, CL = 90%
$\Gamma(\eta_c(1S) \to \pi^0\pi^0)/\Gamma_{total}$		$<4 \times 10^{-5}$, CL = 90%
$\Gamma(\eta_c(1S) \to K^+K^-)/\Gamma_{total}$		$<6 \times 10^{-4}$, CL = 90%
$\Gamma(\eta_c(1S) \to K^0_S K^0_S)/\Gamma_{total}$		$<3.1 \times 10^{-4}$, CL = 90%
p electric dipole moment		$<0.021 \times 10^{-23}$ $e$cm
n electric dipole moment		$<0.18 \times 10^{-25}$ $e$cm, CL = 90%
Λ electric dipole moment		$<1.5 \times 10^{-16}$ $e$cm, CL = 95%
$a_P(\Lambda^0_b \to p\pi^-\pi^+\pi^-)$		(-4.0 ± 0.7)%
$a_P(\Lambda^0_b \to pK^-\pi^+\pi^-)$		(-0.6 ± 0.9)%
$a_P(\Lambda^0_b \to pK^-K^+\pi^-)$		(4 ± 5)%
$a_P(\Lambda^0_b \to pK^-K^+K^-)$		(-1.6 ± 1.5)%
$a_P(\Lambda^0_b \to pK^-\mu^+\mu^-)$		(-5 ± 5)%

TIME REVERSAL (T) INVARIANCE

e electric dipole moment		$<0.11 \times 10^{-28}$ $e$cm, CL = 90%
μ electric dipole moment $\lvert d \rvert$		$<1.8 \times 10^{-19}$ $e$cm, CL = 95%
μ decay parameters		
transverse e^+ polarization normal to plane of μ spin, e^+ momentum		$(-2 \pm 8) \times 10^{-3}$
α'/A		$(-10 \pm 20) \times 10^{-3}$
β'/A		$(2 \pm 7) \times 10^{-3}$
Re($d_\tau = \tau$ electric dipole moment)		-0.220 to 0.45×10^{-16} $e$cm, CL = 95%
P_T in $K^+ \to \pi^0\mu^+\nu_\mu$		$(-1.7 \pm 2.5) \times 10^{-3}$
P_T in $K^+ \to \mu^+\nu_\mu\gamma$		$(-0.6 \pm 1.9) \times 10^{-2}$
Im(ξ) in $K^+ \to \pi^0\mu^+\nu_\mu$ decay (from transverse μ pol.)		-0.006 ± 0.008
asymmetry A_T in K^0-$\overline{K}^0$ mixing		$(6.6 \pm 1.6) \times 10^{-3}$
Im(ξ) in $K^0_{\mu3}$ decay (from transverse μ pol.)		-0.007 ± 0.026
$A_T(D^\pm \to K^0_S K^\pm\pi^+\pi^-)$	[c]	$(-12 \pm 11) \times 10^{-3}$
$A_T(D^0 \to K^+K^-\pi^+\pi^-)$	[c]	$(2.9 \pm 2.2) \times 10^{-3}$
$A_T(D^\pm_s \to K^0_S K^\pm\pi^+\pi^-)$	[c]	$(-14 \pm 8) \times 10^{-3}$
ΔS^+_T ($S^-_{\ell^-,K^0_S} - S^+_{\ell^+,K^0_S}$)		-1.37 ± 0.15
ΔS^-_T ($S^+_{\ell^-,K^0_S} - S^-_{\ell^+,K^0_S}$)		1.17 ± 0.21
ΔC^+_T ($C^-_{\ell^-,K^0_S} - C^+_{\ell^+,K^0_S}$)		0.10 ± 0.16
ΔC^-_T ($C^+_{\ell^-,K^0_S} - C^-_{\ell^+,K^0_S}$)		0.04 ± 0.16
p electric dipole moment		$<0.021 \times 10^{-23}$ $e$cm
n electric dipole moment		$<0.18 \times 10^{-25}$ $e$cm, CL = 90%
$n \to pe^-\overline{\nu}_e$ decay parameters		
ϕ_{AV}, phase of g_A relative to g_V	[d]	$(180.017 \pm 0.026)^\circ$
triple correlation coefficient D	[e]	$(-1.2 \pm 2.0) \times 10^{-4}$
triple correlation coefficient R	[e]	0.004 ± 0.013
Λ electric dipole moment		$<1.5 \times 10^{-16}$ $e$cm, CL = 95%
triple correlation coefficient D for $\Sigma^- \to ne^-\overline{\nu}_e$		0.11 ± 0.10

CP INVARIANCE

Re(d^W_τ)		$<0.50 \times 10^{-17}$ $e$cm, CL = 95%
Im(d^W_τ)		$<1.1 \times 10^{-17}$ $e$cm, CL = 95%
δ (CP violating phase in neutrino mixing)		$1.36^{+0.20}_{-0.16}$ π rad
$\eta \to \pi^+\pi^-e^+e^-$ decay-plane asymmetry		$(-0.6 \pm 3.1) \times 10^{-2}$
$\Gamma(\eta \to \pi^+\pi^-)/\Gamma_{total}$		$<4.4 \times 10^{-6}$, CL = 90%
$\Gamma(\eta \to 2\pi^0)/\Gamma_{total}$		$<3.5 \times 10^{-4}$, CL = 90%
$\Gamma(\eta \to 4\pi^0)/\Gamma_{total}$		$<6.9 \times 10^{-7}$, CL = 90%
$\Gamma(\eta'(958) \to \pi^+\pi^-)/\Gamma_{total}$		$<1.8 \times 10^{-5}$, CL = 90%
$\Gamma(\eta'(958) \to \pi^0\pi^0)/\Gamma_{total}$		$<4 \times 10^{-4}$, CL = 90%
$K^\pm \to \pi^\pm e^+e^-$ rate difference/sum		$(-2.2 \pm 1.6) \times 10^{-2}$
$K^\pm \to \pi^\pm\mu^+\mu^-$ rate difference/sum		0.010 ± 0.023
$K^\pm \to \pi^\pm\pi^0\gamma$ rate difference/sum		$(0.0 \pm 1.2) \times 10^{-3}$
$K^\pm \to \pi^\pm\pi^+\pi^-$ rate difference/sum		(0.04 ± 0.06)%
$K^\pm \to \pi^\pm\pi^0\pi^0$ rate difference/sum		(-0.02 ± 0.28)%
$K^\pm \to \pi^\pm\pi^+\pi^-$ $(g_+ - g_-)$ / $(g_+ + g_-)$		$(-1.5 \pm 2.2) \times 10^{-4}$
$K^\pm \to \pi^\pm\pi^0\pi^0$ $(g_+ - g_-)$ / $(g_+ + g_-)$		$(1.8 \pm 1.8) \times 10^{-4}$
$A_S = [\,\Gamma(K^0_S \to \pi^-e^+\nu_e) - \Gamma(K^0_S \to \pi^+e^-\overline{\nu}_e)\,]$ / SUM		$(-4 \pm 6) \times 10^{-3}$
Im(η_{+-0}) = Im(A($K^0_S \to \pi^+\pi^-\pi^0$, CP-violating) / A($K^0_L \to \pi^+\pi^-\pi^0$))		-0.002 ± 0.009
Im(η_{000}) = Im($A(K^0_S \to \pi^0\pi^0\pi^0)/A(K^0_L \to \pi^0\pi^0\pi^0)$)		-0.001 ± 0.016
$\lvert\eta_{000}\rvert = \lvert A(K^0_S \to 3\pi^0)/A(K^0_L \to 3\pi^0)\rvert$		<0.0088, CL = 90%
CP asymmetry A in $K^0_S \to \pi^+\pi^-e^+e^-$		(-0.4 ± 0.8)%
$\Gamma(K^0_S \to 3\pi^0)/\Gamma_{total}$		$<2.6 \times 10^{-8}$, CL = 90%
linear coefficient j for $K^0_L \to \pi^+\pi^-\pi^0$		0.0012 ± 0.0008
quadratic coefficient f for $K^0_L \to \pi^+\pi^-\pi^0$		0.004 ± 0.006
$\lvert\epsilon'_{+-\gamma}\rvert/\epsilon$ for $K^0_L \to \pi^+\pi^-\gamma$		<0.3, CL = 90%
$\lvert g_{E1}\rvert$ for $K^0_L \to \pi^+\pi^-\gamma$		<0.21, CL = 90%
$\Gamma(K^0_L \to \pi^0\mu^+\mu^-)/\Gamma_{total}$	[f]	$<3.8 \times 10^{-10}$, CL = 90%
$\Gamma(K^0_L \to \pi^0e^+e^-)/\Gamma_{total}$	[f]	$<2.8 \times 10^{-10}$, CL = 90%
$\Gamma(K^0_L \to \pi^0\nu\overline{\nu})/\Gamma_{total}$	[g]	$<3.0 \times 10^{-9}$, CL = 90%
$A_{CP}(D^\pm \to \mu^\pm\nu)$		(8 ± 8)%
$A_{CP}(D^\pm \to K^0_L e^\pm\nu)$		(-0.6 ± 1.6)%
$A_{CP}(D^\pm \to K^0_S\pi^\pm)$		(-0.41 ± 0.09)%
$A_{CP}(D^\pm \to K^\mp 2\pi^\pm)$		(-0.18 ± 0.16)%
$A_{CP}(D^\pm \to K^\mp\pi^\pm\pi^\pm\pi^0)$		(-0.3 ± 0.7)%
$A_{CP}(D^\pm \to K^0_S\pi^\pm\pi^0)$		(-0.1 ± 0.7)%
$A_{CP}(D^\pm \to K^0_S\pi^\pm\pi^+\pi^-)$		(0.0 ± 1.2)%
$A_{CP}(D^\pm \to \pi^\pm\pi^0)$		(0.4 ± 1.3)% (S = 1.7)
$A_{CP}(D^\pm \to \pi^\pm\eta)$		(0.3 ± 0.8)% (S = 1.2)
$A_{CP}(D^\pm \to \pi^\pm\eta'(958))$		(-0.6 ± 0.7)%
$A_{CP}(D^\pm \to \overline{K}^0/K^0K^\pm)$		(0.11 ± 0.17)%
$A_{CP}(D^\pm \to K^0_S K^\pm)$		(-0.01 ± 0.07)%
$A_{CP}(D^\pm \to K^+K^-\pi^\pm)$		(0.37 ± 0.29)%
$A_{CP}(D^\pm \to K^\pm K^{*0})$		(-0.3 ± 0.4)%
$A_{CP}(D^\pm \to \phi\pi^\pm)$		(0.01 ± 0.09)% (S = 1.8)
$A_{CP}(D^\pm \to K^\pm K^*_0(1430)^0)$		(8^{+7}_{-6})%
$A_{CP}(D^\pm \to K^\pm K^*_2(1430)^0)$		(43^{+20}_{-26})%

Downloaded from https://academic.oup.com/ptep/article/2022/8/083C01/6651666 by KIT Library user on 27 September 2022

$A_{CP}(D^{\pm} \to K^{\pm} K_0^*(700))$		$(-12^{+18}_{-13})\%$
$A_{CP}(D^{\pm} \to a_0(1450)^0 \pi^{\pm})$		$(-19^{+14}_{-16})\%$
$A_{CP}(D^{\pm} \to \phi(1680) \pi^{\pm})$		$(-9 \pm 26)\%$
$A_{CP}(D^{\pm} \to \pi^+ \pi^- \pi^{\pm})$		$(-2 \pm 4)\%$
$A_{CP}(D^{\pm} \to K_S^0 K^{\pm} \pi^+ \pi^-)$		$(-4 \pm 7)\%$
$A_{CP}(D^{\pm} \to K^{\pm} \pi^0)$		$(-3 \pm 5)\%$
Local CPV in $D^{\pm} \to \pi^+ \pi^- \pi^{\pm}$		78.1%
Local CPV in $D^{\pm} \to K^+ K^- \pi^{\pm}$		31%
$\lvert q/p \rvert$ of D^0–$\overline{D}^0$ mixing		0.995 ± 0.016
A_{Γ} of D^0–$\overline{D}^0$ mixing		$(0.089 \pm 0.113) \times 10^{-3}$
Where there is ambiguity, the CP test is labelled by the D^0 decay mode.		
$A_{CP}(D^0 \to K^+ K^-)$		$(-0.07 \pm 0.11)\%$
$A_{CP}(D^0 \to K_S^0 K_S^0)$		$(-1.9 \pm 1.1)\%$ (S = 1.1)
$A_{CP}(D^0 \to \pi^+ \pi^-)$		$(0.13 \pm 0.14)\%$
$A_{CP}(D^0 \to \pi^0 \pi^0)$		$(0.0 \pm 0.6)\%$
$A_{CP}(D^0 \to \rho\gamma)$		$(6 \pm 15) \times 10^{-2}$
$A_{CP}(D^0 \to \phi\gamma)$		$(-9 \pm 7) \times 10^{-2}$
$A_{CP}(D^0 \to \overline{K}^*(892)^0 \gamma)$		$(-0.3 \pm 2.0) \times 10^{-2}$
$A_{CP}(D^0 \to \pi^+ \pi^- \pi^0)$		$(0.3 \pm 0.4)\%$
$A_{CP}(D^0 \to \rho(770)^+ \pi^- \to \pi^+ \pi^- \pi^0)$	[h]	$(1.2 \pm 0.9)\%$
$A_{CP}(D^0 \to \rho(770)^0 \pi^0 \to \pi^+ \pi^- \pi^0)$	[h]	$(-3.1 \pm 3.0)\%$
$A_{CP}(D^0 \to \rho(770)^- \pi^+ \to \pi^+ \pi^- \pi^0)$	[h]	$(-1.0 \pm 1.7)\%$
$A_{CP}(D^0 \to \rho(1450)^+ \pi^- \to \pi^+ \pi^- \pi^0)$	[h]	$(0 \pm 70)\%$
$A_{CP}(D^0 \to \rho(1450)^0 \pi^0 \to \pi^+ \pi^- \pi^0)$	[h]	$(-20 \pm 40)\%$
$A_{CP}(D^0 \to \rho(1450)^- \pi^+ \to \pi^+ \pi^- \pi^0)$	[h]	$(6 \pm 9)\%$
$A_{CP}(D^0 \to \rho(1700)^+ \pi^- \to \pi^+ \pi^- \pi^0)$	[h]	$(-5 \pm 14)\%$
$A_{CP}(D^0 \to \rho(1700)^0 \pi^0 \to \pi^+ \pi^- \pi^0)$	[h]	$(13 \pm 9)\%$
$A_{CP}(D^0 \to \rho(1700)^- \pi^+ \to \pi^+ \pi^- \pi^0)$	[h]	$(8 \pm 11)\%$
$A_{CP}(D^0 \to f_0(980) \pi^0 \to \pi^+ \pi^- \pi^0)$	[h]	$(0 \pm 35)\%$
$A_{CP}(D^0 \to f_0(1370) \pi^0 \to \pi^+ \pi^- \pi^0)$	[h]	$(25 \pm 18)\%$
$A_{CP}(D^0 \to f_0(1500) \pi^0 \to \pi^+ \pi^- \pi^0)$	[h]	$(0 \pm 18)\%$
$A_{CP}(D^0 \to f_0(1710) \pi^0 \to \pi^+ \pi^- \pi^0)$	[h]	$(0 \pm 24)\%$
$A_{CP}(D^0 \to f_2(1270) \pi^0 \to \pi^+ \pi^- \pi^0)$	[h]	$(-4 \pm 6)\%$
$A_{CP}(D^0 \to \sigma(400) \pi^0 \to \pi^+ \pi^- \pi^0)$	[h]	$(6 \pm 8)\%$
$A_{CP}(\text{nonresonant } D^0 \to \pi^+ \pi^- \pi^0)$	[h]	$(-13 \pm 23)\%$
$A_{CP}(D^0, \overline{D}^0 \to 2\pi^+ 2\pi^-)$		$(0.5 \pm 1.2)\%$
$A_{CP}(D^0 \to a_1(1260)^+ \pi^- \to 2\pi^+ 2\pi^-)$		$(5 \pm 6)\%$
$A_{CP}(D^0 \to a_1(1260)^- \pi^+ \to 2\pi^+ 2\pi^-)$		$(14 \pm 18)\%$
$A_{CP}(D^0 \to \pi(1300)^+ \pi^- \to 2\pi^+ 2\pi^-)$		$(-2 \pm 15)\%$
$A_{CP}(D^0 \to \pi(1300)^- \pi^+ \to 2\pi^+ 2\pi^-)$		$(-6 \pm 30)\%$
$A_{CP}(D^0 \to a_1(1640)^+ \pi^- \to 2\pi^+ 2\pi^-)$		$(9 \pm 26)\%$
$A_{CP}(D^0 \to \pi_2(1670)^+ \pi^- \to 2\pi^+ 2\pi^-)$		$(7 \pm 18)\%$
$A_{CP}(D^0 \to \sigma f_0(1370) \to 2\pi^+ 2\pi^-)$		$(-15 \pm 19)\%$
$A_{CP}(D^0 \to \sigma\rho(770)^0 \to 2\pi^+ 2\pi^-)$		$(3 \pm 27)\%$
$A_{CP}(D^0 \to 2\rho(770)^0 \to 2\pi^+ 2\pi^-)$		$(-6 \pm 6)\%$
$A_{CP}(D^0 \to 2f_2(1270) \to 2\pi^+ 2\pi^-)$		$(-28 \pm 24)\%$
$A_{CP}(D^0 \to K^+ K^- \pi^0)$		$(-1.0 \pm 1.7)\%$
$A_{CP}(D^0 \to K^*(892)^+ K^- \to K^+ K^- \pi^0)$	[h]	$(-0.9 \pm 1.3)\%$
$A_{CP}(D^0 \to K^*(1410)^+ K^- \to K^+ K^- \pi^0)$	[h]	$(-21 \pm 24)\%$
$A_{CP}(D^0 \to (K^+ \pi^0)_S K^- \to K^+ K^- \pi^0)$	[h]	$(7 \pm 15)\%$
$A_{CP}(D^0 \to \phi(1020) \pi^0 \to K^+ K^- \pi^0)$	[h]	$(1.1 \pm 2.2)\%$
$A_{CP}(D^0 \to f_0(980) \pi^0 \to K^+ K^- \pi^0)$	[h]	$(-3 \pm 19)\%$
$A_{CP}(D^0 \to a_0(980)^0 \pi^0 \to K^+ K^- \pi^0)$	[h]	$(-5 \pm 16)\%$
$A_{CP}(D^0 \to f_2'(1525) \pi^0 \to K^+ K^- \pi^0)$	[h]	$(0 \pm 160)\%$
$A_{CP}(D^0 \to K^*(892)^- K^+ \to K^+ K^- \pi^0)$	[h]	$(-5 \pm 4)\%$
$A_{CP}(D^0 \to K^*(1410)^- K^+ \to K^+ K^- \pi^0)$	[h]	$(-17 \pm 29)\%$
$A_{CP}(D^0 \to (K^- \pi^0)_{S-wave} K^+ \to K^+ K^- \pi^0)$	[h]	$(-10 \pm 40)\%$
$A_{CP}(D^0 \to K_S^0 \pi^0)$		$(-0.20 \pm 0.17)\%$
$A_{CP}(D^0 \to K_S^0 \eta)$		$(0.5 \pm 0.5)\%$
$A_{CP}(D^0 \to K_S^0 \eta')$		$(1.0 \pm 0.7)\%$
$A_{CP}(D^0 \to K_S^0 \phi)$		$(-3 \pm 9)\%$
$A_{CP}(D^0 \to K^- \pi^+)$		$(0.2 \pm 0.5)\%$
$A_{CP}(D^0 \to K^+ \pi^-)$		$(-0.9 \pm 1.4)\%$
$A_{CP}(D_{CP(\pm 1)} \to K^{\mp} \pi^{\pm})$		$(12.7 \pm 1.5)\%$
$A_{CP}(D^0 \to K^- \pi^+ \pi^0)$		$(0.1 \pm 0.5)\%$
$A_{CP}(D^0 \to K^+ \pi^- \pi^0)$		$(0 \pm 5)\%$
$A_{CP}(D^0 \to K_S^0 \pi^+ \pi^-)$		$(-0.1 \pm 0.8)\%$
$A_{CP}(D^0 \to K^*(892)^- \pi^+ \to K_S^0 \pi^+ \pi^-)$		$(0.4 \pm 0.5)\%$
$A_{CP}(D^0 \to K^*(892)^+ \pi^- \to K_S^0 \pi^+ \pi^-)$		$(1 \pm 6)\%$
$A_{CP}(D^0 \to K_S^0 \rho^0 \to K_S^0 \pi^+ \pi^-)$		$(-0.1 \pm 0.5)\%$
$A_{CP}(D^0 \to K_S^0 \omega \to K_S^0 \pi^+ \pi^-)$		$(-13 \pm 7)\%$
$A_{CP}(D^0 \to K_S^0 f_0(980) \to K_S^0 \pi^+ \pi^-)$		$(-0.4 \pm 2.7)\%$
$A_{CP}(D^0 \to K_S^0 f_2(1270) \to K_S^0 \pi^+ \pi^-)$		$(-4 \pm 5)\%$
$A_{CP}(D^0 \to K_S^0 f_0(1370) \to K_S^0 \pi^+ \pi^-)$		$(-1 \pm 9)\%$
$A_{CP}(D^0 \to \overline{K}^0 \rho^0(1450) \to K_S^0 \pi^+ \pi^-)$		$(-4 \pm 10)\%$
$A_{CP}(D^0 \to \overline{K}^0 f_0(600) \to K_S^0 \pi^+ \pi^-)$		$(-3 \pm 5)\%$
$A_{CP}(D^0 \to K^*(1410)^- \pi^+ \to K_S^0 \pi^+ \pi^-)$		$(-2 \pm 9)\%$
$A_{CP}(D^0 \to K_0^*(1430)^- \pi^+ \to K_S^0 \pi^+ \pi^-)$		$(4 \pm 4)\%$
$A_{CP}(D^0 \to K_0^*(1430)^- \pi^+ \to K_S^0 \pi^+ \pi^-)$		$(12 \pm 15)\%$
$A_{CP}(D^0 \to K_2^*(1430)^- \pi^+ \to K_S^0 \pi^+ \pi^-)$		$(3 \pm 6)\%$
$A_{CP}(D^0 \to K_2^*(1430)^+ \pi^- \to K_S^0 \pi^+ \pi^-)$		$(-10 \pm 32)\%$
$A_{CP}(D^0 \to K^- \pi^+ \pi^+ \pi^-)$		$(0.2 \pm 0.5)\%$
$A_{CP}(D^0 \to K^+ \pi^- \pi^+ \pi^-)$		$(-2 \pm 4)\%$
$A_{CP}(D^0 \to K^+ K^- \pi^+ \pi^-)$		$(1.3 \pm 1.7)\%$
$A_{CP}(D^0 \to K_1^*(1270)^+ K^- \to K^+ K^- \pi^+ \pi^-)$		$(-2.3 \pm 1.7)\%$
$A_{CP}(D^0 \to K_1^*(1270)^+ K^- \to K^{*0} \pi^+ K^-)$		$(-1 \pm 10)\%$
$A_{CP}(D^0 \to K_1^*(1270)^- K^+ \to \overline{K}^{*0} \pi^- K^+)$		$(-10 \pm 32)\%$
$A_{CP}(D^0 \to K_1^*(1270)^- K^+ \to K^+ K^- \pi^+ \pi^-)$		$(1.7 \pm 3.5)\%$
$A_{CP}(D^0 \to K_1^*(1270)^+ K^- \to \rho^0 K^+ K^-)$		$(-7 \pm 17)\%$
$A_{CP}(D^0 \to K_1^*(1270)^- K^+ \to \rho^0 K^- K^+)$		$(10 \pm 13)\%$
$A_{CP}(D^0 \to K_1(1400)^+ K^- \to K^+ K^- \pi^+ \pi^-)$		$(-4.4 \pm 2.1)\%$
$A_{CP}(D^0 \to K^*(1410)^+ K^- \to K^{*0} \pi^+ K^-)$		$(-20 \pm 17)\%$
$A_{CP}(D^0 \to K^*(1410)^- K^+ \to \overline{K}^{*0} \pi^- K^+)$		$(-1 \pm 14)\%$
$A_{CP}(D^0 \to K^*(1680)^+ K^- \to K^+ K^- \pi^+ \pi^-)$		$(-17 \pm 29)\%$
$A_{CP}(K^{*0} \overline{K}^{*0})$ in $D^0, \overline{D}^0 \to K^{*0} \overline{K}^{*0}$		$(-5 \pm 14)\%$
$A_{CP}(D^0 \to K^{*0} \overline{K}^{*0}$ S-wave)		$(-3.9 \pm 2.2)\%$
$A_{CP}(\phi\rho^0)$ in $D^0, \overline{D}^0 \to \phi\rho^0$		$(1 \pm 9)\%$
$A_{CP}(D^0 \to \phi\rho^0$ S-wave)		$(-3 \pm 5)\%$
$A_{CP}(D^0 \to \phi\rho^0$ D-wave)		$(-37 \pm 19)\%$
$A_{CP}(D^0 \to \phi(\pi^+ \pi^-)_{S-wave})$		$(6 \pm 6)\%$
$A_{CP}(D^0 \to K^*(892)^0 (K^- \pi^+)_{S-wave})$		$(-10 \pm 40)\%$
$A_{CP}(D^0 \to K^+ K^- \pi^+ \pi^-$ non-resonant)		$(8 \pm 20)\%$
$A_{CP}((K^- \pi^+)_{P-wave} (K^+ \pi^-)_{S-wave})$		$(3 \pm 11)\%$
CP-even fraction in $D^0 \to \pi^+ \pi^- \pi^0$ decays		$(97.3 \pm 1.7)\%$
CP-even fraction in $D^0 \to K^+ K^- \pi^0$ decays		$(73 \pm 6)\%$
CP-even fraction in $D^0 \to \pi^+ \pi^- \pi^+ \pi^-$ decays		$(76.9 \pm 2.3)\%$
Local CPV p-value in $D^0, \overline{D}^0 \to \pi^+ \pi^- \pi^0$		4.9%
Local CPV p-value in $D^0, \overline{D}^0 \to \pi^+ \pi^- \pi^+ \pi^-$		$(0.6 \pm 0.2)\%$
Local CPV p-value in $D^0, \overline{D}^0 \to K_S^0 \pi^+ \pi^-$		96%
Local CPV p-value in $D^0, \overline{D}^0 \to K^+ K^- \pi^0$		16.6%
Local CPV p-value in $D^0, \overline{D}^0 \to K^+ K^- \pi^+ \pi^-$		9.1%
$A_{CP}(D_s^{\pm} \to \mu^{\pm} \nu)$		$(-0.2 \pm 2.5)\%$
$A_{CP}(D_s^{\pm} \to K^{\pm} K_S^0)$		$(0.09 \pm 0.26)\%$
$A_{CP}(D_s^{\pm} \to K^+ K^- \pi^{\pm})$		$(-0.5 \pm 0.9)\%$
$A_{CP}(D_s^{\pm} \to \phi\pi^{\pm})$		$(-0.38 \pm 0.27)\%$

Unless otherwise stated, limits are given at the 90% confidence level, while errors are given as ± 1 standard deviation.

Downloaded from https://academic.oup.com/ptep/article/2022/8/083C01/6651666 by KIT Library user on 27 September 2022

$A_{CP}(D_s^\pm \to K^\pm K_S^0 \pi^0)$	$(-2 \pm 6)\%$
$A_{CP}(D_s^\pm \to 2K_S^0 \pi^\pm)$	$(3 \pm 5)\%$
$A_{CP}(D_s^\pm \to K^+ K^- \pi^\pm \pi^0)$	$(0.0 \pm 3.0)\%$
$A_{CP}(D_s^\pm \to K^\pm K_S^0 \pi^+ \pi^-)$	$(-6 \pm 5)\%$
$A_{CP}(D_s^\pm \to K_S^0 K^\mp 2\pi^\pm)$	$(4.1 \pm 2.8)\%$
$A_{CP}(D_s^\pm \to \pi^+ \pi^- \pi^\pm)$	$(-0.7 \pm 3.1)\%$
$A_{CP}(D_s^\pm \to \pi^\pm \eta)$	$(0.3 \pm 0.4)\%$
$A_{CP}(D_s^\pm \to \pi^\pm \eta')$	$(-0.9 \pm 0.5)\%$
$A_{CP}(D_s^\pm \to \eta \pi^\pm \pi^0)$	$(-1 \pm 4)\%$
$A_{CP}(D_s^\pm \to \eta' \pi^\pm \pi^0)$	$(0 \pm 8)\%$
$A_{CP}(D_s^\pm \to K^\pm \pi^0)$	$(2 \pm 4)\%$ (S = 1.2)
$A_{CP}(D_s^\pm \to \overline{K}^0 / K^0 \pi^\pm)$	$(0.4 \pm 0.5)\%$
$A_{CP}(D_s^\pm \to K_S^0 \pi^\pm)$	$(0.20 \pm 0.18)\%$
$A_{CP}(D_s^\pm \to K^\pm \pi^+ \pi^-)$	$(4 \pm 5)\%$
$A_{CP}(D_s^\pm \to K^\pm \eta)$	$(1.8 \pm 1.9)\%$
$A_{CP}(D_s^\pm \to K^\pm \eta'(958))$	$(6 \pm 19)\%$
$A_{CP}(B^+ \to J/\psi(1S) K^+)$	$(1.8 \pm 3.0) \times 10^{-3}$ (S = 1.5)
$A_{CP}(B^+ \to J/\psi(1S) \pi^+)$	$(1.8 \pm 1.2) \times 10^{-2}$ (S = 1.3)
$A_{CP}(B^+ \to J/\psi \rho^+)$	-0.05 ± 0.05
$A_{CP}(B^+ \to J/\psi K^*(892)^+)$	-0.048 ± 0.033
$A_{CP}(B^+ \to \eta_c K^+)$	0.01 ± 0.07 (S = 2.2)
$A_{CP}(B^+ \to \psi(2S) \pi^+)$	0.03 ± 0.06
$A_{CP}(B^+ \to \psi(2S) K^+)$	0.012 ± 0.020 (S = 1.5)
$A_{CP}(B^+ \to \psi(2S) K^*(892)^+)$	0.08 ± 0.21
$A_{CP}(B^+ \to \chi_{c1}(1P) \pi^+)$	0.07 ± 0.18
$A_{CP}(B^+ \to \chi_{c0} K^+)$	-0.20 ± 0.18 (S = 1.5)
$A_{CP}(B^+ \to \chi_{c1} K^+)$	-0.009 ± 0.033
$A_{CP}(B^+ \to \chi_{c1} K^*(892)^+)$	0.5 ± 0.5
$A_{CP}(B^+ \to \overline{D}^0 \pi^+)$	-0.007 ± 0.007
$A_{CP}(B^+ \to D_{CP(+1)} \pi^+)$	-0.0080 ± 0.0024
$A_{CP}(B^+ \to D_{CP(-1)} \pi^+)$	0.017 ± 0.026
$A_{CP}([K^\mp \pi^\pm \pi^+ \pi^-]_D \pi^+)$	0.02 ± 0.05
$A_{CP}(B^+ \to [\pi^+ \pi^+ \pi^- \pi^-]_D K^+)$	0.10 ± 0.04
$A_{CP}(B^+ \to [\pi^+ \pi^- \pi^+ \pi^-]_D K^*(892)^+)$	0.02 ± 0.11
$A_{CP}(B^+ \to \overline{D}^0 K^+)$	-0.017 ± 0.005
$A_{CP}([K^\mp \pi^\pm \pi^+ \pi^-]_D K^+)$	-0.31 ± 0.11
$A_{CP}(B^+ \to [\pi^+ \pi^+ \pi^- \pi^-]_D \pi^+)$	$(-4 \pm 8) \times 10^{-3}$
$A_{CP}(B^+ \to [K^- \pi^+]_D K^+)$	-0.58 ± 0.21
$A_{CP}(B^+ \to [K^- \pi^+ \pi^0]_D K^+)$	0.07 ± 0.30 (S = 1.5)
$A_{CP}(B^+ \to [K^+ K^- \pi^0]_D K^+)$	0.30 ± 0.20
$A_{CP}(B^+ \to [\pi^+ \pi^- \pi^0]_D K^+)$	0.05 ± 0.09
$A_{CP}(B^+ \to \overline{D}^0 K^*(892)^+)$	-0.007 ± 0.019
$A_{CP}(B^+ \to [K^- \pi^+ \pi^- \pi^+]_{\overline{D}} K^*(892)^+)$	-0.45 ± 0.25
$A_{CP}(B^+ \to [K^- \pi^+]_D \pi^+)$	0.00 ± 0.09
$A_{CP}(B^+ \to [K^- \pi^+ \pi^0]_D \pi^+)$	0.35 ± 0.16
$A_{CP}(B^+ \to [K^+ K^- \pi^0]_D \pi^+)$	-0.03 ± 0.04
$A_{CP}(B^+ \to [\pi^+ \pi^- \pi^0]_D \pi^+)$	-0.016 ± 0.020
$A_{CP}(B^+ \to [K^- \pi^+]_{(D\pi)} \pi^+)$	-0.09 ± 0.27
$A_{CP}(B^+ \to [K^- \pi^+]_{(D\gamma)} \pi^+)$	-0.7 ± 0.6
$A_{CP}(B^+ \to [K^- \pi^+]_{(D\pi)} K^+)$	0.8 ± 0.4
$A_{CP}(B^+ \to [K^- \pi^+]_{(D\gamma)} K^+)$	0.4 ± 1.0
$A_{CP}(B^+ \to [\pi^+ \pi^- \pi^0]_D K^+)$	-0.02 ± 0.15
$A_{CP}(B^+ \to [K_S^0 K^+ \pi^-]_D K^+)$	0.10 ± 0.09
$A_{CP}(B^+ \to [K_S^0 K^- \pi^+]_D K^+)$	-0.04 ± 0.08
$A_{CP}(B^+ \to [K_S^0 K^- \pi^+]_D \pi^+)$	0.003 ± 0.015
$A_{CP}(B^+ \to [K_S^0 K^+ \pi^-]_D \pi^+)$	-0.034 ± 0.020
$A_{CP}(B^+ \to [K^*(892)^- K^+]_D K^+)$	0.08 ± 0.05
$A_{CP}(B^+ \to [K^*(892)^+ K^-]_D K^+)$	0.02 ± 0.10
$A_{CP}(B^+ \to [K^*(892)^+ K^-]_D \pi^+)$	0.007 ± 0.017
$A_{CP}(B^+ \to [K^*(892)^- K^+]_D \pi^+)$	-0.020 ± 0.011
$A_{ADS}(B^+ \to D \pi^+)$	0.129 ± 0.014
$A_{ADS}(B^+ \to D^*(D\gamma) K^+)$	-0.6 ± 1.3
$A_{ADS}(B^+ \to D^*(D\pi^0) K^+)$	0.72 ± 0.29
$A_{ADS}(B^+ \to D^*(D\gamma) \pi^+)$	0.08 ± 0.13
$A_{ADS}(B^+ \to D^*(D\pi^0) \pi^+)$	-0.14 ± 0.06
$A_{ADS}(B^+ \to [K^- \pi^+]_D K^+ \pi^- \pi^+)$	-0.33 ± 0.35
$A_{ADS}(B^+ \to [K^- \pi^+]_D \pi^+ \pi^- \pi^+)$	-0.01 ± 0.09
$A_{CP}(B^+ \to D_{CP(-1)} K^+)$	-0.10 ± 0.07
$A_{CP}(B^+ \to [K^+ K^-]_D K^+ \pi^- \pi^+)$	-0.04 ± 0.06
$A_{CP}(B^+ \to [\pi^+ \pi^-]_D K^+ \pi^- \pi^+)$	-0.05 ± 0.10
$A_{CP}(B^+ \to [K^- \pi^+]_D K^+ \pi^- \pi^+)$	0.013 ± 0.023
$A_{CP}(B^+ \to [K^+ K^-]_D \pi^+ \pi^- \pi^+)$	-0.019 ± 0.015
$A_{CP}(B^+ \to [\pi^+ \pi^-]_D \pi^+ \pi^- \pi^+)$	-0.013 ± 0.019
$A_{CP}(B^+ \to [K^- \pi^+]_D \pi^+ \pi^- \pi^+)$	-0.002 ± 0.011
$A_{CP}(B^+ \to \overline{D}^{*0} \pi^+)$	-0.0004 ± 0.0021 (S = 1.1)
$A_{CP}(B^+ \to (D^*_{CP(+1)})^0 \pi^+)$	0.010 ± 0.007
$A_{CP}(B^+ \to (D^*_{CP(-1)})^0 \pi^+)$	-0.09 ± 0.05
$A_{CP}(B^+ \to D^{*0} K^+)$	0.012 ± 0.010 (S = 1.5)
$A_{CP}(B^+ \to D^{*0}_{CP(+1)} K^+)$	-0.09 ± 0.05 (S = 2.6)
$A_{CP}(B^+ \to D^*_{CP(-1)} K^+)$	0.07 ± 0.10
$A_{CP}(B^+ \to D_{CP(+1)} K^*(892)^+)$	0.08 ± 0.06
$A_{CP}(B^+ \to D_{CP(-1)} K^*(892)^+)$	-0.23 ± 0.22
$A_{CP}(B^+ \to D_s^+ \phi)$	0.0 ± 0.4
$A_{CP}(B^+ \to D_s^+ \overline{D}^0)$	$(-0.4 \pm 0.7)\%$
$A_{CP}(B^+ \to D^{*+} \overline{D}^{*0})$	-0.15 ± 0.11
$A_{CP}(B^+ \to D^{*+} \overline{D}^0)$	-0.06 ± 0.13
$A_{CP}(B^+ \to D^+ \overline{D}^{*0})$	0.13 ± 0.18
$A_{CP}(B^+ \to D^+ \overline{D}^0)$	0.016 ± 0.025
$A_{CP}(B^+ \to K_S^0 \pi^+)$	-0.017 ± 0.016
$A_{CP}(B^+ \to K^+ \pi^0)$	0.030 ± 0.013
$A_{CP}(B^+ \to \eta' K^+)$	0.004 ± 0.011
$A_{CP}(B^+ \to \eta' K^*(892)^+)$	-0.26 ± 0.27
$A_{CP}(B^+ \to \eta' K_0^*(1430)^+)$	0.06 ± 0.20
$A_{CP}(B^+ \to \eta' K_2^*(1430)^+)$	0.15 ± 0.13
$A_{CP}(B^+ \to \eta K^*(892)^+)$	0.02 ± 0.06
$A_{CP}(B^+ \to \eta K_0^*(1430)^+)$	0.05 ± 0.13
$A_{CP}(B^+ \to \eta K_2^*(1430)^+)$	-0.45 ± 0.30
$A_{CP}(B^+ \to \omega K^+)$	-0.02 ± 0.04
$A_{CP}(B^+ \to \omega K^{*+})$	0.29 ± 0.35
$A_{CP}(B^+ \to \omega (K\pi)_0^{*+})$	-0.10 ± 0.09
$A_{CP}(B^+ \to \omega K_2^*(1430)^+)$	0.14 ± 0.15
$A_{CP}(B^+ \to K^{*0} \pi^+)$	-0.04 ± 0.09 (S = 2.1)
$A_{CP}(B^+ \to K^*(892)^+ \pi^0)$	-0.39 ± 0.21 (S = 1.6)
$A_{CP}(B^+ \to K^+ \pi^- \pi^+)$	0.027 ± 0.008
$A_{CP}(B^+ \to K^+ K^- K^+ \text{nonresonant})$	0.06 ± 0.05
$A_{CP}(B^+ \to f(980)^0 K^+)$	-0.08 ± 0.09
$A_{CP}(B^+ \to f_0(1500) K^+)$	0.28 ± 0.30
$A_{CP}(B^+ \to f_2'(1525)^0 K^+)$	$-0.08^{+0.05}_{-0.04}$
$A_{CP}(B^+ \to K_0^*(1430)^0 \pi^+)$	0.061 ± 0.032
$A_{CP}(B^+ \to K_0^*(1430)^+ \pi^0)$	$0.26^{+0.18}_{-0.14}$
$A_{CP}(B^+ \to K_2^*(1430)^0 \pi^+)$	$0.05^{+0.29}_{-0.24}$
$A_{CP}(B^+ \to K^+ \pi^0 \pi^0)$	-0.06 ± 0.07
$A_{CP}(B^+ \to K^0 \rho^+)$	-0.03 ± 0.15
$A_{CP}(B^+ \to K^{*+} \pi^+ \pi^-)$	0.07 ± 0.08
$A_{CP}(B^+ \to \rho^0 K^*(892)^+)$	0.31 ± 0.13
$A_{CP}(B^+ \to K^*(892)^+ f_0(980))$	-0.15 ± 0.12
$A_{CP}(B^+ \to a_1^+ K^0)$	0.12 ± 0.11
$A_{CP}(B^+ \to b_1^+ K^0)$	-0.03 ± 0.15
$A_{CP}(B^+ \to K^*(892)^0 \rho^+)$	-0.01 ± 0.16
$A_{CP}(B^+ \to b_1^0 K^+)$	-0.46 ± 0.20
$A_{CP}(B^+ \to K^0 K^+)$	0.04 ± 0.14
$A_{CP}(B^+ \to K^+ K_S^0 K_S^0)$	0.025 ± 0.031
$A_{CP}(B^+ \to \phi K^+)$	0.024 ± 0.028 (S = 2.3)
$A_{CP}(B^+ \to X_0(1550) K^+)$	-0.04 ± 0.07
$A_{CP}(B^+ \to K^{*+} K^+ K^-)$	0.11 ± 0.09
$A_{CP}(B^+ \to \phi K^*(892)^+)$	-0.01 ± 0.08
$A_{CP}(B^+ \to \phi (K\pi)_0^{*+})$	0.04 ± 0.16
$A_{CP}(B^+ \to \phi K_1(1270)^+)$	0.15 ± 0.20
$A_{CP}(B^+ \to \phi K_2^*(1430)^+)$	-0.23 ± 0.20
$A_{CP}(B^+ \to K^+ \phi\phi)$	-0.08 ± 0.07
$A_{CP}(B^+ \to K^+ [\phi\phi]_{\eta_c})$	0.10 ± 0.08
$A_{CP}(B^+ \to K^*(892)^+ \gamma)$	0.014 ± 0.018
$A_{CP}(B^+ \to X_s \gamma)$	0.028 ± 0.019
$A_{CP}(B^+ \to \eta K^+ \gamma)$	-0.12 ± 0.07
$A_{CP}(B^+ \to \phi K^+ \gamma)$	-0.13 ± 0.11 (S = 1.1)

Unless otherwise stated, limits are given at the 90% confidence level, while errors are given as ±1 standard deviation.

Downloaded from https://academic.oup.com/ptep/article/2022/8/083C01/6651666 by KIT Library user on 27 September 2022

$A_{CP}(B^+ \to \rho^+\gamma)$	-0.11 ± 0.33
$A_{CP}(B^+ \to \pi^+\pi^0)$	0.03 ± 0.04
$A_{CP}(B^+ \to \rho^0\pi^+)$	0.009 ± 0.019
$A_{CP}(B^+ \to \rho^0(1450)\pi^+)$	-0.11 ± 0.05
$A_{CP}(B^+ \to \pi^+\pi^-\pi^+$ nonresonant)	$-0.14^{+0.23}_{-0.16}$
$A_{CP}(B^+ \to \rho^+\pi^0)$	0.02 ± 0.11
$A_{CP}(B^+ \to \rho^+\rho^0)$	-0.05 ± 0.05
$A_{CP}(B^+ \to \omega\pi^+)$	-0.04 ± 0.05
$A_{CP}(B^+ \to \omega\rho^+)$	-0.20 ± 0.09
$A_{CP}(B^+ \to \eta\pi^+)$	-0.14 ± 0.07 (S = 1.4)
$A_{CP}(B^+ \to \eta\rho^+)$	0.11 ± 0.11
$A_{CP}(B^+ \to \eta'\pi^+)$	0.06 ± 0.16
$A_{CP}(B^+ \to \eta'\rho^+)$	0.26 ± 0.17
$A_{CP}(B^+ \to b_1^0\pi^+)$	0.05 ± 0.16
$A_{CP}(B^+ \to p\overline{p}\pi^+)$	0.00 ± 0.04
$A_{CP}(B^+ \to p\overline{p}K^+)$	0.00 ± 0.04 (S = 2.2)
$A_{CP}(B^+ \to p\overline{p}K^*(892)^+)$	0.21 ± 0.16 (S = 1.4)
$A_{CP}(B^+ \to p\overline{\Lambda}\gamma)$	0.17 ± 0.17
$A_{CP}(B^+ \to p\overline{\Lambda}\pi^0)$	0.01 ± 0.17
$A_{CP}(B^+ \to K^+\ell^+\ell^-)$	-0.02 ± 0.08
$A_{CP}(B^+ \to K^+e^+e^-)$	0.14 ± 0.14
$A_{CP}(B^+ \to K^+\mu^+\mu^-)$	0.011 ± 0.017
$A_{CP}(B^+ \to K^{*+}\ell^+\ell^-)$	-0.09 ± 0.14
$A_{CP}(B^+ \to K^*e^+e^-)$	-0.14 ± 0.23
$A_{CP}(B^+ \to K^*\mu^+\mu^-)$	-0.12 ± 0.24
$\mathrm{Re}(\epsilon_{B^0})/(1+\lvert\epsilon_{B^0}\rvert^2)$	$(-0.5 \pm 0.4) \times 10^{-3}$
$A_{T/CP}(B^0 \leftrightarrow \overline{B}^0)$	0.005 ± 0.018
$A_{CP}(B^0 \to D^*(2010)^+D^-)$	0.013 ± 0.014
$A_{CP}(B^0 \to [K^+K^-]_D K^*(892)^0)$	-0.05 ± 0.10
$A_{CP}(B^0 \to [K^+\pi^-]_D K^*(892)^0)$	0.047 ± 0.029
$A_{CP}(B^0 \to [\pi^+\pi^-]_D K^*(892)^0)$	-0.18 ± 0.14
$A_{CP}(B^0 \to \eta' K^*(892)^0)$	-0.07 ± 0.18
$A_{CP}(B^0 \to \eta' K_0^*(1430)^0)$	-0.19 ± 0.17
$A_{CP}(B^0 \to \eta' K_2^*(1430)^0)$	0.14 ± 0.18
$A_{CP}(B^0 \to \eta K_0^*(1430)^0)$	0.06 ± 0.13
$A_{CP}(B^0 \to \eta K_2^*(1430)^0)$	-0.07 ± 0.19
$A_{CP}(B^0 \to b_1 K^+)$	-0.07 ± 0.12
$A_{CP}(B^0 \to \omega K^{*0})$	0.45 ± 0.25
$A_{CP}(B^0 \to \omega(K\pi)_0^{*0})$	-0.07 ± 0.09
$A_{CP}(B^0 \to \omega K_2^*(1430)^0)$	-0.37 ± 0.17
$A_{CP}(B^0 \to K^+\pi^-\pi^0)$	$(0 \pm 6) \times 10^{-2}$
$A_{CP}(B^0 \to \rho^- K^+)$	0.20 ± 0.11
$A_{CP}(B^0 \to \rho(1450)^- K^+)$	-0.10 ± 0.33
$A_{CP}(B^0 \to \rho(1700)^- K^+)$	-0.4 ± 0.6
$A_{CP}(B^0 \to K^+\pi^-\pi^0$ nonresonant)	0.10 ± 0.18
$A_{CP}(B^0 \to K^0\pi^+\pi^-)$	-0.01 ± 0.05
$A_{CP}(B^0 \to (K\pi)_0^{*+}\pi^-)$	0.02 ± 0.04
$A_{CP}(B^0 \to K_2^*(1430)^+\pi^-)$	-0.29 ± 0.24
$A_{CP}(B^0 \to K^*(1680)^+\pi^-)$	-0.07 ± 0.14
$A_{CP}(B^0 \to f_0(980)K_S^0)$	0.28 ± 0.31
$A_{CP}(B^0 \to (K\pi)_0^{*0}\pi^0)$	-0.15 ± 0.11
$A_{CP}(B^0 \to K^{*0}\pi^0)$	-0.15 ± 0.13
$A_{CP}(B^0 \to K^*(892)^0\pi^+\pi^-)$	0.07 ± 0.05
$A_{CP}(B^0 \to K^*(892)^0\rho^0)$	-0.06 ± 0.09
$A_{CP}(B^0 \to K^{*0}f_0(980))$	0.07 ± 0.10
$A_{CP}(B^0 \to K^{*+}\rho^-)$	0.21 ± 0.15
$A_{CP}(B^0 \to K^*(892)^0K^+K^-)$	0.01 ± 0.05
$A_{CP}(B^0 \to a_1^- K^+)$	-0.16 ± 0.12
$A_{CP}(B^0 \to K^0K^0)$	-0.6 ± 0.7
$A_{CP}(B^0 \to K^*(892)^0\phi)$	0.00 ± 0.04
$A_{CP}(B^0 \to K^*(892)^0K^-\pi^+)$	0.2 ± 0.4
$A_{CP}(B^0 \to \phi(K\pi)_0^{*0})$	0.12 ± 0.08
$A_{CP}(B^0 \to \phi K_2^*(1430)^0)$	-0.11 ± 0.10
$A_{CP}(B^0 \to K^*(892)^0\gamma)$	-0.006 ± 0.011
$A_{CP}(B^0 \to K_2^*(1430)^0\gamma)$	-0.08 ± 0.15
$A_{CP}(B^0 \to X_s\gamma)$	-0.009 ± 0.018
$A_{CP}(B^0 \to \rho^+\pi^-)$	0.13 ± 0.06 (S = 1.1)
$A_{CP}(B^0 \to \rho^-\pi^+)$	-0.08 ± 0.08
$A_{CP}(B^0 \to a_1(1260)^\pm\pi^\mp)$	-0.07 ± 0.06
$A_{CP}(B^0 \to b_1^-\pi^+)$	-0.05 ± 0.10
$A_{CP}(B^0 \to p\overline{p}K^*(892)^0)$	0.05 ± 0.12
$A_{CP}(B^0 \to p\overline{\Lambda}\pi^-)$	0.04 ± 0.07
$A_{CP}(B^0 \to K^{*0}\ell^+\ell^-)$	-0.05 ± 0.10
$A_{CP}(B^0 \to K^{*0}e^+e^-)$	-0.21 ± 0.19
$A_{CP}(B^0 \to K^{*0}\mu^+\mu^-)$	-0.034 ± 0.024
$C_{D^*(2010)^-D^+}(B^0 \to D^*(2010)^-D^+)$	-0.02 ± 0.08
$C_{D^*(2010)^+D^-}(B^0 \to D^*(2010)^+D^-)$	-0.03 ± 0.09 (S = 1.1)
$C_{D^{*+}D^{*-}}(B^0 \to D^{*+}D^{*-})$	0.01 ± 0.09 (S = 1.6)
$C_+(B^0 \to D^{*+}D^{*-})$	0.00 ± 0.10 (S = 1.6)
$C_-(B^0 \to D^{*+}D^{*-})$	0.19 ± 0.31
$S_-(B^0 \to D^{*+}D^{*-})$	0.1 ± 1.6 (S = 3.5)
$C(B^0 \to D^*(2010)^+D^*(2010)^-K_S^0)$	0.01 ± 0.29
$S(B^0 \to D^*(2010)^+D^*(2010)^-K_S^0)$	0.1 ± 0.4
$C_{D^+D^-}(B^0 \to D^+D^-)$	-0.22 ± 0.24 (S = 2.5)
$C_{J/\psi(1S)\pi^0}(B^0 \to J/\psi(1S)\pi^0)$	0.03 ± 0.17 (S = 1.5)
$C(B^0 \to J/\psi(1S)\rho^0)$	-0.06 ± 0.06
$C_{D_{CP}^{(*)}h^0}(B^0 \to D_{CP}^{(*)}h^0)$	-0.02 ± 0.08
$S_{D_{CP}^{(*)}h^0}(B^0 \to D_{CP}^{(*)}h^0)$	-0.66 ± 0.12
$C_{K^0\pi^0}(B^0 \to K^0\pi^0)$	0.00 ± 0.13 (S = 1.4)
$C_{\eta'(958)K_S^0}(B^0 \to \eta'(958)K_S^0)$	-0.04 ± 0.20 (S = 2.5)
$S_{\eta'(958)K_S^0}(B^0 \to \eta'(958)K_S^0)$	0.43 ± 0.17 (S = 1.5)
$C_{\eta'K^0}(B^0 \to \eta'K^0)$	-0.06 ± 0.04
$C_{\omega K_S^0}(B^0 \to \omega K_S^0)$	0.0 ± 0.4 (S = 3.0)
$S_{\omega K_S^0}(B^0 \to \omega K_S^0)$	0.70 ± 0.21
$C(B^0 \to K_S^0\pi^0\pi^0)$	-0.21 ± 0.20
$S(B^0 \to K_S^0\pi^0\pi^0)$	$0.89^{+0.27}_{-0.30}$
$C_{\rho^0K_S^0}(B^0 \to \rho^0K_S^0)$	-0.04 ± 0.20
$S_{\rho^0K_S^0}(B^0 \to \rho^0K_S^0)$	$0.50^{+0.17}_{-0.21}$
$C_{f_0(980)K_S^0}(B^0 \to f_0(980)K_S^0)$	0.29 ± 0.20
$S_{f_0(980)K_S^0}(B^0 \to f_0(980)K_S^0)$	-0.50 ± 0.16
$S_{f_2(1270)K_S^0}(B^0 \to f_2(1270)K_S^0)$	-0.5 ± 0.5
$C_{f_2(1270)K_S^0}(B^0 \to f_2(1270)K_S^0)$	0.3 ± 0.4
$S_{f_x(1300)K_S^0}(B^0 \to f_x(1300)K_S^0)$	-0.2 ± 0.5
$C_{f_x(1300)K_S^0}(B^0 \to f_x(1300)K_S^0)$	0.13 ± 0.35
$S_{K^0\pi^+\pi^-}(B^0 \to K^0\pi^+\pi^-$ nonresonant)	-0.01 ± 0.33
$C_{K^0\pi^+\pi^-}(B^0 \to K^0\pi^+\pi^-$ nonresonant)	0.01 ± 0.26
$C_{K_S^0K_S^0}(B^0 \to K_S^0K_S^0)$	0.0 ± 0.4 (S = 1.4)
$S_{K_S^0K_S^0}(B^0 \to K_S^0K_S^0)$	-0.8 ± 0.5
$C_{K^+K^-K_S^0}(B^0 \to K^+K^-K_S^0$ nonresonant)	0.06 ± 0.08
$C_{K^+K^-K_S^0}(B^0 \to K^+K^-K_S^0$ inclusive)	0.01 ± 0.09
$C_{\phi K_S^0}(B^0 \to \phi K_S^0)$	0.01 ± 0.14
$S_{\phi K_S^0}(B^0 \to \phi K_S^0)$	0.59 ± 0.14
$C_{K_SK_SK_S}(B^0 \to K_SK_SK_S)$	-0.14 ± 0.12
$S_{K_SK_SK_S}(B^0 \to K_SK_SK_S)$	-0.82 ± 0.17
$C_{K_S^0\pi^0\gamma}(B^0 \to K_S^0\pi^0\gamma)$	0.36 ± 0.33
$S_{K_S^0\pi^0\gamma}(B^0 \to K_S^0\pi^0\gamma)$	-0.8 ± 0.6
$C_{K^*(892)^0\gamma}(B^0 \to K^*(892)^0\gamma)$	-0.04 ± 0.16 (S = 1.2)
$S_{K^*(892)^0\gamma}(B^0 \to K^*(892)^0\gamma)$	-0.15 ± 0.22
$C_{\eta K^0\gamma}(B^0 \to \eta K^0\gamma)$	0.1 ± 0.4 (S = 1.4)
$S_{\eta K^0\gamma}(B^0 \to \eta K^0\gamma)$	-0.5 ± 0.5 (S = 1.2)
$C_{K^0\phi\gamma}(B^0 \to K^0\phi\gamma)$	-0.3 ± 0.6
$S_{K^0\phi\gamma}(B^0 \to K^0\phi\gamma)$	$0.7^{+0.7}_{-1.1}$
$C(B^0 \to K_S^0\rho^0\gamma)$	-0.05 ± 0.19
$S(B^0 \to K_S^0\rho^0\gamma)$	-0.04 ± 0.23
$C(B^0 \to \rho^0\gamma)$	0.4 ± 0.5

Unless otherwise stated, limits are given at the 90% confidence level, while errors are given as ±1 standard deviation.

Downloaded from https://academic.oup.com/ptep/article/2022/8/083C01/6651666 by KIT Library user on 27 September 2022

$S\,(B^0 \to \rho^0\gamma)$	-0.8 ± 0.7
$C_{\pi^0\pi^0}(B^0 \to \pi^0\pi^0)$	-0.33 ± 0.22
$C_{\rho\pi}\,(B^0 \to \rho^+\pi^-)$	-0.03 ± 0.07 (S = 1.2)
$S_{\rho\pi}\,(B^0 \to \rho^+\pi^-)$	0.05 ± 0.07
$\Delta S_{\rho\pi}\,(B^0 \to \rho^+\pi^-)$	0.01 ± 0.08
$C_{\rho^0\pi^0}\,(B^0 \to \rho^0\pi^0)$	0.27 ± 0.24
$S_{\rho^0\pi^0}\,(B^0 \to \rho^0\pi^0)$	-0.23 ± 0.34
$C_{a_1\pi}\,(B^0 \to a_1(1260)^+\pi^-)$	-0.05 ± 0.11
$S_{a_1\pi}\,(B^0 \to a_1(1260)^+\pi^-)$	-0.2 ± 0.4 (S = 3.2)
$\Delta C_{a_1\pi}\,(B^0 \to a_1(1260)^+\pi^-)$	0.43 ± 0.14 (S = 1.3)
$\Delta S_{a_1\pi}\,(B^0 \to a_1(1260)^+\pi^-)$	-0.11 ± 0.12
$C\,(B^0 \to b_1^- K^+)$	-0.22 ± 0.24
$\Delta C\,(B^0 \to b_1^-\pi^+)$	-1.04 ± 0.24
$C_{\rho^0\rho^0}\,(B^0 \to \rho^0\rho^0)$	0.2 ± 0.9
$S_{\rho^0\rho^0}\,(B^0 \to \rho^0\rho^0)$	0.3 ± 0.7
$C_{\rho\rho}\,(B^0 \to \rho^+\rho^-)$	0.00 ± 0.09
$S_{\rho\rho}\,(B^0 \to \rho^+\rho^-)$	-0.14 ± 0.13
$\lvert\lambda\rvert\,(B^0 \to J/\psi K^*(892)^0)$	<0.25, CL = 95%
$\cos 2\beta\,(B^0 \to J/\psi K^*(892)^0)$	$1.7^{+0.7}_{-0.9}$ (S = 1.6)
$\cos 2\beta\,(B^0 \to [K^0_S\pi^+\pi^-]_{D^{(*)}}\,h^0)$	0.91 ± 0.25
$(S_+ + S_-)/2\,(B^0 \to D^{*-}\pi^+)$	-0.039 ± 0.011
$(S_- - S_+)/2\,(B^0 \to D^{*-}\pi^+)$	-0.009 ± 0.015
$(S_+ + S_-)/2\,(B^0 \to D^-\pi^+)$	-0.046 ± 0.023
$(S_- - S_+)/2\,(B^0 \to D^-\pi^+)$	-0.022 ± 0.021
$S_+\,(B^0 \to D^-\pi^+)$	0.058 ± 0.023
$S_-\,(B^0 \to D^+\pi^-)$	0.038 ± 0.021
$(S_+ + S_-)/2\,(B^0 \to D^-\rho^+)$	-0.024 ± 0.032
$(S_- - S_+)/2\,(B^0 \to D^-\rho^+)$	-0.10 ± 0.06
$C_{\eta_c K^0_S}\,(B^0 \to \eta_c K^0_S)$	0.08 ± 0.13
$C_{c\overline{c}K^{(*)0}}\,(B^0 \to c\overline{c}K^{(*)0})$	$(-0.5 \pm 1.5) \times 10^{-2}$
$C_{J/\psi(nS)K^0}\,(B^0 \to J/\psi(nS)K^0)$	$(-0.8 \pm 1.7) \times 10^{-2}$
$C_{J/\psi K^{*0}}\,(B^0 \to J/\psi K^{*0})$	0.03 ± 0.10
$S_{J/\psi K^{*0}}\,(B^0 \to J/\psi K^{*0})$	0.60 ± 0.25
$C_{\chi_{c0}K^0_S}\,(B^0 \to \chi_{c0}K^0_S)$	$-0.3^{+0.5}_{-0.4}$
$S_{\chi_{c0}K^0_S}\,(B^0 \to \chi_{c0}K^0_S)$	-0.7 ± 0.5
$C_{\chi_{c1}K^0_S}\,(B^0 \to \chi_{c1}K^0_S)$	0.06 ± 0.07
$\sin(2\beta_{\rm eff})(B^0 \to \phi K^0)$	0.22 ± 0.30
$\sin(2\beta_{\rm eff})(B^0 \to \phi K^*_0(1430)^0)$	$0.97^{+0.03}_{-0.52}$
$\sin(2\beta_{\rm eff})(B^0 \to [K^0_S\pi^+\pi^-]_{D^{(*)}}\,h^0)$	0.80 ± 0.16
$\lvert\lambda\rvert\,(B^0 \to [K^0_S\pi^+\pi^-]_{D^{(*)}}\,h^0)$	1.01 ± 0.08
$\lvert\sin(2\beta+\gamma)\rvert$	>0.40, CL = 90%
$2\beta+\gamma$	$(83 \pm 60)^\circ$
$x_+(B^0 \to DK^{*0})$	0.04 ± 0.17
$x_-(B^0 \to DK^{*0})$	-0.16 ± 0.14
$y_-(B^0 \to DK^{*0})$	0.20 ± 0.25 (S = 1.2)
$A_{CP}(B \to K^*(892)\gamma)$	-0.003 ± 0.011
$A_{CP}(B \to s\gamma)$	0.015 ± 0.011
$A_{CP}(B \to (s+d)\gamma)$	0.010 ± 0.031
$A_{CP}(B \to X_s\ell^+\ell^-)$	0.04 ± 0.11
$A_{CP}(B \to K^*e^+e^-)$	-0.18 ± 0.15
$A_{CP}(B \to K^*\mu^+\mu^-)$	-0.03 ± 0.13
$A_{CP}(B \to K^*\ell^+\ell^-)$	-0.04 ± 0.07
$A_{CP}(B \to \eta\,\text{anything})$	$-0.13^{+0.04}_{-0.05}$
$\Delta A_{CP}(X_s\gamma) = A_{CP}(B^\pm \to X_s\gamma) - A_{CP}(B^0 \to X_s\gamma)$	0.041 ± 0.023
$\overline{A}_{CP}(B \to X_s\gamma) = (A_{CP}(B^+ \to X_s\gamma) + A_{CP}(B^0 \to X_s\gamma))/2$	0.009 ± 0.012
$\overline{A}_{CP}(B \to K^*\gamma) = (A_{CP}(B^+ \to K^{*+}\gamma) + A_{CP}(B^0 \to K^{*0}\gamma))/2$	-0.001 ± 0.014
$\mathrm{Re}(\epsilon_{B^0_s})\,/\,(1+\lvert\epsilon_{B^0_s}\rvert^2)$	$(-0.15 \pm 0.70) \times 10^{-3}$
$S_{KK}(B^0_s \to K^+K^-)$	0.14 ± 0.05 (S = 1.3)
$\delta_B(B^0_s \to D^\pm_s K^\mp\pi^\pm\pi^\mp)$	$(-6^{+10}_{-13})^\circ$
CP Violation phase β_s	$(2.5 \pm 1.0) \times 10^{-2}$ rad
$A^L_{CP}(B_s \to J/\psi\overline{K}^*(892)^0)$	-0.05 ± 0.06
$A^{\parallel}_{CP}(B_s \to J/\psi\overline{K}^*(892)^0)$	0.17 ± 0.15
$A^{\perp}_{CP}(B_s \to J/\psi\overline{K}^*(892)^0)$	-0.05 ± 0.10
$A_{CP}(B^0_s \to [K^+K^-]_D\overline{K}^*(892)^0)$	-0.04 ± 0.07
$A_{CP}(B^0_s \to [\pi^+K^-]_D K^*(892)^0)$	-0.01 ± 0.04
$A_{CP}(B^0_s \to [\pi^+\pi^-]_D K^*(892)^0)$	0.06 ± 0.13
$\Gamma(\eta_c(1S) \to \pi^+\pi^-)/\Gamma_{\rm total}$	$<1.1 \times 10^{-4}$, CL = 90%
$\Gamma(\eta_c(1S) \to \pi^0\pi^0)/\Gamma_{\rm total}$	$<4 \times 10^{-5}$, CL = 90%
$\Gamma(\eta_c(1S) \to K^+K^-)/\Gamma_{\rm total}$	$<6 \times 10^{-4}$, CL = 90%
$\Gamma(\eta_c(1S) \to K^0_S K^0_S)/\Gamma_{\rm total}$	$<3.1 \times 10^{-4}$, CL = 90%
n electric dipole moment	$<0.18 \times 10^{-25}$ e cm, CL = 90%
$(\alpha+\overline{\alpha})/(\alpha-\overline{\alpha})$ in $\Lambda \to p\pi^-$, $\overline{\Lambda} \to \overline{p}\pi^+$	-0.002 ± 0.012
$\frac{[\alpha(\Xi^-)\alpha_-(\Lambda)-\alpha(\overline{\Xi}^+)\alpha_+(\overline{\Lambda})]}{[\alpha(\Xi^-)\alpha_-(\Lambda)+\alpha(\overline{\Xi}^+)\alpha_+(\overline{\Lambda})]}$	$(0 \pm 7) \times 10^{-4}$
$(\alpha+\overline{\alpha})/(\alpha-\overline{\alpha})$ in $\Omega^- \to \Lambda K^-$, $\overline{\Omega}^+ \to \overline{\Lambda}K^+$	-0.02 ± 0.13
$(\alpha+\overline{\alpha})/(\alpha-\overline{\alpha})$ in $\Lambda_c^+ \to \Lambda\pi^+$, $\overline{\Lambda}_c^- \to \overline{\Lambda}\pi^-$	-0.07 ± 0.31
$(\alpha+\overline{\alpha})/(\alpha-\overline{\alpha})$ in $\Lambda_c^+ \to \Lambda e^+\nu_e$, $\overline{\Lambda}_c^- \to \overline{\Lambda}e^-\overline{\nu}_e$	0.00 ± 0.04
$A_{CP}(\Lambda_b \to p\pi^-)$	-0.025 ± 0.029 (S = 1.2)
$A_{CP}(\Lambda_b \to pK^-)$	-0.025 ± 0.022
$A_{CP}(\Lambda_b \to DpK^-)$	0.12 ± 0.09
$\Delta A_{CP}(pK^-/\pi^-)$	0.014 ± 0.024
$A_{CP}(\Lambda_b \to p\overline{K}^0\pi^-)$	0.22 ± 0.13
$\Delta A_{CP}(J/\psi p\pi^-/K^-)$	$(5.7 \pm 2.7) \times 10^{-2}$
$A_{CP}(\Lambda_b \to \Lambda K^+\pi^-)$	-0.53 ± 0.25
$A_{CP}(\Lambda_b \to \Lambda K^+K^-)$	-0.28 ± 0.12
$\Delta A_{CP}(\Lambda^0_b \to pK^-\mu^+\mu^-)$	$(-4 \pm 5) \times 10^{-2}$
$\Delta A_{CP}(\Lambda^0_b \to p\pi^-\pi^+\pi^-)$	$(1.1 \pm 2.6) \times 10^{-2}$
$\Delta A_{CP}(\Lambda^0_b \to (p\pi^-\pi^+\pi^-)_{LBM})$	$(4 \pm 4) \times 10^{-2}$
$\Delta A_{CP}(\Lambda^0_b \to pa_1(1260)^-)$	$(-1 \pm 4) \times 10^{-2}$
$\Delta A_{CP}(\Lambda^0_b \to N(1520)^0\rho(770)^0)$	$(2 \pm 5) \times 10^{-2}$
$\Delta A_{CP}(\Lambda^0_b \to \Delta(1232)^{++}\pi^-\pi^-)$	$(0.1 \pm 3.3) \times 10^{-2}$
$\Delta A_{CP}(\Lambda^0_b \to pK^-\pi^+\pi^-)$	$(3.2 \pm 1.3) \times 10^{-2}$
$\Delta A_{CP}(\Lambda^0_b \to (pK^-\pi^+\pi^-)_{LBM})$	$(3.5 \pm 1.6) \times 10^{-2}$
$\Delta A_{CP}(\Lambda^0_b \to N(1520)^0K^*(892)^0)$	$(5.5 \pm 2.5) \times 10^{-2}$
$\Delta A_{CP}(\Lambda^0_b \to \Lambda(1520)\rho(770)^0)$	$(1 \pm 6) \times 10^{-2}$
$\Delta A_{CP}(\Lambda^0_b \to \Delta(1232)^{++}K^-\pi^-)$	$(4.4 \pm 2.7) \times 10^{-2}$
$\Delta A_{CP}(\Lambda^0_b \to pK_1(1410)^-)$	$(5 \pm 4) \times 10^{-2}$
$\Delta A_{CP}(\Lambda^0_b \to pK^-K^+\pi^-)$	$(-7 \pm 5) \times 10^{-2}$
$\Delta A_{CP}(\Lambda^0_b \to pK^-K^+K^-)$	$(0.2 \pm 1.9) \times 10^{-2}$
$\Delta A_{CP}(\Lambda^0_b \to \Lambda(1520)\phi(1020))$	$(4 \pm 6) \times 10^{-2}$
$\Delta A_{CP}(\Lambda^0_b \to (pK^-)_{highmass}\,\phi(1020))$	$(-0.7 \pm 3.4) \times 10^{-2}$
$\Delta A_{CP}(\Lambda^0_b \to (pK^-K^+K^-)_{LBM})$	$(2.7 \pm 2.4) \times 10^{-2}$
$A_c(\Lambda)$	-0.22 ± 0.13
$A_s(\Lambda)$	0.13 ± 0.13
$A_c(\phi)$	-0.01 ± 0.12
$A_s(\phi)$	-0.07 ± 0.12
$a_{CP}(\Lambda^0_b \to p\pi^-\pi^+\pi^-)$	(-0.7 ± 0.7)%
$a_{CP}(\Lambda^0_b \to pK^-\pi^+\pi^-)$	(-0.8 ± 0.9)%
$a_{CP}(\Lambda^0_b \to pK^-K^+\pi^-)$	(-1 ± 5)%
$a_{CP}(\Lambda^0_b \to pK^-K^+K^-)$	(1.1 ± 1.5)%
$a_{CP}(\Lambda^0_b \to pK^-\mu^+\mu^-)$	(1 ± 5)%

CP VIOLATION OBSERVED

$\mathrm{Re}(\epsilon)$	$(1.596 \pm 0.013) \times 10^{-3}$
charge asymmetry in $K^0_{\ell 3}$ decays	
A_L = weighted average of $A_L(\mu)$ and $A_L(e)$	(0.332 ± 0.006)%
$A_L(\mu) = [\Gamma(\pi^-\mu^+\nu_\mu) - \Gamma(\pi^+\mu^-\overline{\nu}_\mu)]/\text{sum}$	(0.304 ± 0.025)%
$A_L(e) = [\Gamma(\pi^-e^+\nu_e) - \Gamma(\pi^+e^-\overline{\nu}_e)]/\text{sum}$	(0.334 ± 0.007)%
parameters for $K^0_L \to 2\pi$ decay	
$\lvert\eta_{00}\rvert = \lvert A(K^0_L \to 2\pi^0)\,/\,A(K^0_S \to 2\pi^0)\rvert$	$(2.220 \pm 0.011) \times 10^{-3}$ (S = 1.8)
$\lvert\eta_{+-}\rvert = \lvert A(K^0_L \to \pi^+\pi^-)\,/\,A(K^0_S \to \pi^+\pi^-)\rvert$	$(2.232 \pm 0.011) \times 10^{-3}$ (S = 1.8)

Unless otherwise stated, limits are given at the 90% confidence level, while errors are given as ±1 standard deviation.

Downloaded from https://academic.oup.com/ptep/article/2022/8/083C01/6651666 by KIT Library user on 27 September 2022

$\lvert\epsilon\rvert = (2\lvert\eta_{+-}\rvert + \lvert\eta_{00}\rvert)/3$		$(2.228 \pm 0.011) \times 10^{-3}$ (S = 1.8)
$\lvert\eta_{00}/\eta_{+-}\rvert$	[i]	0.9950 ± 0.0007 (S = 1.6)
$\mathrm{Re}(\epsilon'/\epsilon) = (1-\lvert\eta_{00}/\eta_{+-}\rvert)/3$	[i]	$(1.66 \pm 0.23) \times 10^{-3}$ (S = 1.6)
Assuming CPT		
ϕ_{+-}, phase of η_{+-}		$(43.51 \pm 0.05)^\circ$ (S = 1.2)
ϕ_{00}, phase of η_{00}		$(43.52 \pm 0.05)^\circ$ (S = 1.3)
$\phi_\epsilon = (2\phi_{+-} + \phi_{00})/3$		$(43.52 \pm 0.05)^\circ$ (S = 1.2)
Not assuming CPT		
ϕ_{+-}, phase of η_{+-}		$(43.4 \pm 0.5)^\circ$ (S = 1.2)
ϕ_{00}, phase of η_{00}		$(43.7 \pm 0.6)^\circ$ (S = 1.2)
$\phi_\epsilon = (2\phi_{+-} + \phi_{00})/3$		$(43.5 \pm 0.5)^\circ$ (S = 1.3)
CP asymmetry A in $K^0_L \to \pi^+\pi^-e^+e^-$		$(13.7 \pm 1.5)\%$
β_{CP} from $K^0_L \to e^+e^-e^+e^-$		-0.19 ± 0.07
γ_{CP} from $K^0_L \to e^+e^-e^+e^-$		0.01 ± 0.11 (S = 1.6)
parameters for $K^0_L \to \pi^+\pi^-\gamma$ decay		
$\lvert\eta_{+-\gamma}\rvert = \lvert A(K^0_L \to \pi^+\pi^-\gamma,\ CP$ violating$)/A(K^0_S \to \pi^+\pi^-\gamma)\rvert$		$(2.35 \pm 0.07) \times 10^{-3}$
$\phi_{+-\gamma}$ = phase of $\eta_{+-\gamma}$		$(44 \pm 4)^\circ$
$\Gamma(K^0_L \to \pi^+\pi^-)/\Gamma_{\rm total}$	[j]	$(1.967 \pm 0.010) \times 10^{-3}$ (S = 1.5)
$\Gamma(K^0_L \to \pi^0\pi^0)/\Gamma_{\rm total}$		$(8.64 \pm 0.06) \times 10^{-4}$ (S = 1.8)
$\Delta A_{CP}^{D^0} = A_{CP}(K^+K^-) - A_{CP}(\pi^+\pi^-)$		$(-0.154 \pm 0.029)\%$
$A_{CP}(B^+ \to [K^-\pi^+]_{\overline{D}} K^*(892)^+)$		-0.75 ± 0.16
$A_{CP}(B^+ \to D_{CP(+1)} K^+)$		0.132 ± 0.015 (S = 1.8)
$A_{ADS}(B^+ \to D K^+)$		-0.451 ± 0.026
$A_{CP}(B^+ \to \eta K^+)$		-0.37 ± 0.08
$A_{CP}(B^+ \to f_2(1270) K^+)$		$-0.68^{+0.19}_{-0.17}$
$A_{CP}(B^+ \to \rho^0 K^+)$		0.37 ± 0.10
$A_{CP}(B^+ \to K^+K^-\pi^+)$		-0.122 ± 0.021
$A_{CP}(B^+ \to K^+K^-K^+)$		-0.033 ± 0.008
$A_{CP}(B^+ \to \pi^+\pi^-\pi^+)$		0.057 ± 0.013
$A_{CP}(B^+ \to f_2(1270)\pi^+)$		0.40 ± 0.06
$A_{CP}(B^+ \to f_0(1370)\pi^+)$		0.72 ± 0.22
γ		$(65.9^{+3.3}_{-3.5})^\circ$
$r_B(B^+ \to D^0 K^+)$		0.0994 ± 0.0026
$\delta_B(B^+ \to D^0 K^+)$		$(127.7^{+3.6}_{-3.9})^\circ$
$r_B(B^+ \to D^0 K^{*+})$		$0.101^{+0.016}_{-0.034}$
$\delta_B(B^+ \to D^0 K^{*+})$		$(48^{+59}_{-16})^\circ$
$r_B(B^+ \to D^{*0} K^+)$		$0.104^{+0.013}_{-0.014}$
$\delta_B(B^+ \to D^{*0} K^+)$		$(314.8^{+7.9}_{-9.9})^\circ$
$A_{CP}(B^0 \to K^+\pi^-)$		-0.0834 ± 0.0032
$A_{CP}(B^0 \to \eta K^*(892)^0)$		0.19 ± 0.05
$A_{CP}(B^0 \to K^*(892)^+\pi^-)$		-0.27 ± 0.04
$S_{D^*(2010)^-D^+}(B^0 \to D^*(2010)^-D^+)$		-0.83 ± 0.09
$S_{D^*(2010)^+D^-}(B^0 \to D^*(2010)^+D^-)$		-0.80 ± 0.09
$S_{D^{*+}D^{*-}}(B^0 \to D^{*+}D^{*-})$		-0.59 ± 0.14 (S = 1.8)
$S_+(B^0 \to D^{*+}D^{*-})$		-0.73 ± 0.09
$S_{D^+D^-}(B^0 \to D^+D^-)$		$-0.76^{+0.15}_{-0.13}$ (S = 1.2)
$S_{J/\psi(1S)\pi^0}(B^0 \to J/\psi(1S)\pi^0)$		-0.88 ± 0.32 (S = 2.2)
$S(B^0 \to J/\psi(1S)\rho^0)$		$-0.66^{+0.16}_{-0.12}$
$S_{K^0\pi^0}(B^0 \to K^0\pi^0)$		0.58 ± 0.17
$S_{\eta' K^0}(B^0 \to \eta' K^0)$		0.63 ± 0.06
$S_{K^+K^-K^0_S}(B^0 \to K^+K^-K^0_S$ nonresonant)		-0.66 ± 0.11
$S_{K^+K^-K^0_S}(B^0 \to K^+K^-K^0_S$ inclusive)		-0.65 ± 0.12
$C_{\pi\pi}(B^0 \to \pi^+\pi^-)$		-0.314 ± 0.030
$S_{\pi\pi}(B^0 \to \pi^+\pi^-)$		-0.670 ± 0.030
$\Delta C_{\rho\pi}(B^0 \to \rho^+\pi^-)$		0.27 ± 0.06
$S_{\eta_c K^0_S}(B^0 \to \eta_c K^0_S)$		0.93 ± 0.17
$\sin(2\beta)(B^0 \to J/\psi K^0_S)$		0.699 ± 0.017
$S_{J/\psi(nS)K^0}(B^0 \to J/\psi(nS)K^0)$		0.701 ± 0.017
$S_{\chi_{c1}K^0_S}(B^0 \to \chi_{c1}K^0_S)$		0.63 ± 0.10
$\sin(2\beta_{\rm eff})(B^0 \to K^+K^-K^0_S)$		$0.77^{+0.13}_{-0.12}$
α		$(85.2^{+4.8}_{-4.3})^\circ$
$r_{B^0}(B^0 \to D K^{*0})$		$0.257^{+0.021}_{-0.023}$
$\delta_{B^0}(B^0 \to D K^{*0})$		$(194.1^{+9.6}_{-8.8})^\circ$

Unless otherwise stated, limits are given at the 90% confidence level, while errors are given as ±1 standard deviation.

$C_{KK}(B^0_s \to K^+K^-)$		0.162 ± 0.035
$r_B(B^0_s \to D^\mp_s K^\pm)$		$0.37^{+0.10}_{-0.09}$
$r_B(B^0_s \to D^\mp_s K^\pm\pi^\pm\pi^\mp)$		0.47 ± 0.08
$\delta_B(B^0_s \to D^\pm_s K^\mp)$		$(358 \pm 14)^\circ$
$A_{CP}(B_s \to \pi^+K^-)$		0.224 ± 0.012

CPT INVARIANCE

$(m_{W^+} - m_{W^-}) / m_{\rm average}$		$(-3.7 \pm 3.5) \times 10^{-4}$
$(m_{e^+} - m_{e^-}) / m_{\rm average}$		$<8 \times 10^{-9}$, CL = 90%
$\lvert q_{e^+} + q_{e^-}\rvert/e$		$<4 \times 10^{-8}$
$(g_{e^+} - g_{e^-}) / g_{\rm average}$		$(-0.5 \pm 2.1) \times 10^{-12}$
$(\tau_{\mu^+} - \tau_{\mu^-}) / \tau_{\rm average}$		$(2 \pm 8) \times 10^{-5}$
$(g_{\mu^+} - g_{\mu^-}) / g_{\rm average}$		$(-0.11 \pm 0.12) \times 10^{-8}$
$(m_{\tau^+} - m_{\tau^-})/m_{\rm average}$		$<2.8 \times 10^{-4}$, CL = 90%
$\langle\Delta m^2_{21} - \Delta\overline{m}^2_{21}\rangle$ in neutrino mixing		$<1.1 \times 10^{-4}$ eV^2, CL = 99.7%
$\langle\Delta m^2_{32} - \Delta\overline{m}^2_{32}\rangle$ in neutrino mixing		$(-0.12 \pm 0.25) \times 10^{-3}$ eV^2
$m_t - m_{\overline{t}}$		-0.15 ± 0.20 GeV (S = 1.1)
$(m_{\pi^+} - m_{\pi^-}) / m_{\rm average}$		$(2 \pm 5) \times 10^{-4}$
$(\tau_{\pi^+} - \tau_{\pi^-}) / \tau_{\rm average}$		$(6 \pm 7) \times 10^{-4}$
$(m_{K^+} - m_{K^-}) / m_{\rm average}$		$(-0.6 \pm 1.8) \times 10^{-4}$
$(\tau_{K^+} - \tau_{K^-}) / \tau_{\rm average}$		$(0.10 \pm 0.09)\%$ (S = 1.2)
$K^\pm \to \mu^\pm\nu_\mu$ rate difference/sum		$(-0.27 \pm 0.21)\%$
$K^\pm \to \pi^\pm\pi^0$ rate difference/sum	[k]	$(0.4 \pm 0.6)\%$
δ in $K^0 - \overline{K}^0$ mixing		
real part of δ		$(2.5 \pm 2.3) \times 10^{-4}$
imaginary part of δ		$(-1.5 \pm 1.6) \times 10^{-5}$
Re(y), K_{e3} parameter		$(0.4 \pm 2.5) \times 10^{-3}$
Re(x$_-$), K_{e3} parameter		$(-2.9 \pm 2.0) \times 10^{-3}$
$\lvert m_{K^0} - m_{\overline{K}^0}\rvert / m_{\rm average}$	[l]	$<6 \times 10^{-19}$, CL = 90%
$(\Gamma_{K^0} - \Gamma_{\overline{K}^0})/m_{\rm average}$		$(8 \pm 8) \times 10^{-18}$
phase difference $\phi_{00} - \phi_{+-}$		$(0.34 \pm 0.32)^\circ$
$\mathrm{Re}(\frac{2}{3}\eta_{+-} + \frac{1}{3}\eta_{00}) - \frac{A_L}{2}$		$(-3 \pm 35) \times 10^{-6}$
$A_{CPT}(D^0 \to K^-\pi^+)$		0.008 ± 0.008
$\Delta S^+_{CPT}\ (S^-_{\ell^+,K^0_S} - S^+_{\ell^+,K^0_S})$		0.16 ± 0.23
$\Delta S^-_{CPT}\ (S^+_{\ell^+,K^0_S} - S^-_{\ell^+,K^0_S})$		-0.03 ± 0.14
$\Delta C^+_{CPT}\ (C^-_{\ell^+,K^0_S} - C^+_{\ell^+,K^0_S})$		0.14 ± 0.17
$\Delta C^-_{CPT}\ (C^+_{\ell^+,K^0_S} - C^-_{\ell^+,K^0_S})$		0.03 ± 0.14
$\lvert m_p - m_{\overline{p}}\rvert/m_p$	[n]	$<7 \times 10^{-10}$, CL = 90%
$(\lvert\frac{q_{\overline{p}}}{m_{\overline{p}}}\rvert - \frac{q_p}{m_p})/\frac{q_p}{m_p}$		$(0.1 \pm 6.9) \times 10^{-11}$
$\lvert q_p + q_{\overline{p}}\rvert/e$	[n]	$<7 \times 10^{-10}$, CL = 90%
$(\mu_p + \mu_{\overline{p}}) / \mu_p$		$(0.002 \pm 0.004) \times 10^{-6}$
$(m_n - m_{\overline{n}})/ m_n$		$(9 \pm 6) \times 10^{-5}$
$(m_\Lambda - m_{\overline{\Lambda}}) / m_\Lambda$		$(-0.1 \pm 1.1) \times 10^{-5}$ (S = 1.6)
$(\tau_\Lambda - \tau_{\overline{\Lambda}}) / \tau_\Lambda$		-0.001 ± 0.009
$(\tau_{\Sigma^+} - \tau_{\overline{\Sigma}^-}) / \tau_{\Sigma^+}$		-0.0006 ± 0.0012
$(\mu_{\Sigma^+} + \mu_{\overline{\Sigma}^-}) / \mu_{\Sigma^+}$		0.014 ± 0.015
$(m_{\Xi^-} - m_{\overline{\Xi}^+}) / m_{\Xi^-}$		$(-3 \pm 9) \times 10^{-5}$
$(\tau_{\Xi^-} - \tau_{\overline{\Xi}^+}) / \tau_{\Xi^-}$		-0.01 ± 0.07
$(\mu_{\Xi^-} + \mu_{\overline{\Xi}^+}) / \lvert\mu_{\Xi^-}\rvert$		$+0.01 \pm 0.05$
$(m_{\Omega^-} - m_{\overline{\Omega}^+}) / m_{\Omega^-}$		$(-1 \pm 8) \times 10^{-5}$
$(\tau_{\Omega^-} - \tau_{\overline{\Omega}^+}) / \tau_{\Omega^-}$		0.00 ± 0.05

TESTS OF NUMBER CONSERVATION LAWS

LEPTON FAMILY NUMBER

Lepton family number conservation means separate conservation of each of L_e, L_μ, L_τ.

$\Gamma(Z \to e^\pm\mu^\mp)/\Gamma_{\rm total}$	[o]	$<7.5 \times 10^{-7}$, CL = 95%
$\Gamma(Z \to e^\pm\tau^\mp)/\Gamma_{\rm total}$	[o]	$<5.0 \times 10^{-6}$, CL = 95%
$\Gamma(Z \to \mu^\pm\tau^\mp)/\Gamma_{\rm total}$	[o]	$<6.5 \times 10^{-6}$, CL = 95%

Downloaded from https://academic.oup.com/ptep/article/2022/8/083C01/6651666 by KIT Library user on 27 September 2022

$\Gamma(H^0 \to e\mu)/\Gamma_{total}$		$<6.1 \times 10^{-5}$, CL = 95%
$\Gamma(H^0 \to e\tau)/\Gamma_{total}$		$<2.2 \times 10^{-3}$, CL = 95%
$\Gamma(H^0 \to \mu\tau)/\Gamma_{total}$		$<1.5 \times 10^{-3}$, CL = 95%
$\sigma(e^+e^- \to e^\pm\tau^\mp)$ / $\sigma(e^+e^- \to \mu^+\mu^-)$		$<8.9 \times 10^{-6}$, CL = 95%
$\sigma(e^+e^- \to \mu^\pm\tau^\mp)$ / $\sigma(e^+e^- \to \mu^+\mu^-)$		$<4.0 \times 10^{-6}$, CL = 95%
limit on $\mu^- \to e^-$ conversion		
$\sigma(\mu^- {}^{32}S \to e^- {}^{32}S)$ / $\sigma(\mu^- {}^{32}S \to \nu_\mu {}^{32}P^*)$		$<7 \times 10^{-11}$, CL = 90%
$\sigma(\mu^- Ti \to e^- Ti)$ / $\sigma(\mu^- Ti \to$ capture)		$<4.3 \times 10^{-12}$, CL = 90%
$\sigma(\mu^- Pb \to e^- Pb)$ / $\sigma(\mu^- Pb \to$ capture)		$<4.6 \times 10^{-11}$, CL = 90%
$\sigma(\mu^- Au \to e^- Au)$ / $\sigma(\mu^- Au \to$ capture)		$<7 \times 10^{-13}$, CL = 90%
limit on muonium $\to$ antimuonium conversion $R_g = G_C$ / G_F		<0.0030, CL = 90%
$\Gamma(\mu^- \to e^-\nu_e\overline{\nu}_\mu)/\Gamma_{total}$	[p]	$<1.2 \times 10^{-2}$, CL = 90%
$\Gamma(\mu^- \to e^-\gamma)/\Gamma_{total}$		$<4.2 \times 10^{-13}$, CL = 90%
$\Gamma(\mu^- \to e^-e^+e^-)/\Gamma_{total}$		$<1.0 \times 10^{-12}$, CL = 90%
$\Gamma(\mu^- \to e^-2\gamma)/\Gamma_{total}$		$<7.2 \times 10^{-11}$, CL = 90%
$\Gamma(\tau^- \to e^-\gamma)/\Gamma_{total}$		$<3.3 \times 10^{-8}$, CL = 90%
$\Gamma(\tau^- \to \mu^-\gamma)/\Gamma_{total}$		$<4.2 \times 10^{-8}$, CL = 90%
$\Gamma(\tau^- \to e^-\pi^0)/\Gamma_{total}$		$<8.0 \times 10^{-8}$, CL = 90%
$\Gamma(\tau^- \to \mu^-\pi^0)/\Gamma_{total}$		$<1.1 \times 10^{-7}$, CL = 90%
$\Gamma(\tau^- \to e^-K^0_S)/\Gamma_{total}$		$<2.6 \times 10^{-8}$, CL = 90%
$\Gamma(\tau^- \to \mu^-K^0_S)/\Gamma_{total}$		$<2.3 \times 10^{-8}$, CL = 90%
$\Gamma(\tau^- \to e^-\eta)/\Gamma_{total}$		$<9.2 \times 10^{-8}$, CL = 90%
$\Gamma(\tau^- \to \mu^-\eta)/\Gamma_{total}$		$<6.5 \times 10^{-8}$, CL = 90%
$\Gamma(\tau^- \to e^-\rho^0)/\Gamma_{total}$		$<1.8 \times 10^{-8}$, CL = 90%
$\Gamma(\tau^- \to \mu^-\rho^0)/\Gamma_{total}$		$<1.2 \times 10^{-8}$, CL = 90%
$\Gamma(\tau^- \to e^-\omega)/\Gamma_{total}$		$<4.8 \times 10^{-8}$, CL = 90%
$\Gamma(\tau^- \to \mu^-\omega)/\Gamma_{total}$		$<4.7 \times 10^{-8}$, CL = 90%
$\Gamma(\tau^- \to e^-K^*(892)^0)/\Gamma_{total}$		$<3.2 \times 10^{-8}$, CL = 90%
$\Gamma(\tau^- \to \mu^-K^*(892)^0)/\Gamma_{total}$		$<5.9 \times 10^{-8}$, CL = 90%
$\Gamma(\tau^- \to e^-\overline{K}^*(892)^0)/\Gamma_{total}$		$<3.4 \times 10^{-8}$, CL = 90%
$\Gamma(\tau^- \to \mu^-\overline{K}^*(892)^0)/\Gamma_{total}$		$<7.0 \times 10^{-8}$, CL = 90%
$\Gamma(\tau^- \to e^-\eta'(958))/\Gamma_{total}$		$<1.6 \times 10^{-7}$, CL = 90%
$\Gamma(\tau^- \to \mu^-\eta'(958))/\Gamma_{total}$		$<1.3 \times 10^{-7}$, CL = 90%
$\Gamma(\tau^- \to e^-f_0(980) \to e^-\pi^+\pi^-)/\Gamma_{total}$		$<3.2 \times 10^{-8}$, CL = 90%
$\Gamma(\tau^- \to \mu^-f_0(980) \to \mu^-\pi^+\pi^-)/\Gamma_{total}$		$<3.4 \times 10^{-8}$, CL = 90%
$\Gamma(\tau^- \to e^-\phi)/\Gamma_{total}$		$<3.1 \times 10^{-8}$, CL = 90%
$\Gamma(\tau^- \to \mu^-\phi)/\Gamma_{total}$		$<8.4 \times 10^{-8}$, CL = 90%
$\Gamma(\tau^- \to e^-e^+e^-)/\Gamma_{total}$		$<2.7 \times 10^{-8}$, CL = 90%
$\Gamma(\tau^- \to e^-\mu^+\mu^-)/\Gamma_{total}$		$<2.7 \times 10^{-8}$, CL = 90%
$\Gamma(\tau^- \to e^+\mu^-\mu^-)/\Gamma_{total}$		$<1.7 \times 10^{-8}$, CL = 90%
$\Gamma(\tau^- \to \mu^-e^+e^-)/\Gamma_{total}$		$<1.8 \times 10^{-8}$, CL = 90%
$\Gamma(\tau^- \to \mu^+e^-e^-)/\Gamma_{total}$		$<1.5 \times 10^{-8}$, CL = 90%
$\Gamma(\tau^- \to \mu^-\mu^+\mu^-)/\Gamma_{total}$		$<2.1 \times 10^{-8}$, CL = 90%
$\Gamma(\tau^- \to e^-\pi^+\pi^-)/\Gamma_{total}$		$<2.3 \times 10^{-8}$, CL = 90%
$\Gamma(\tau^- \to \mu^-\pi^+\pi^-)/\Gamma_{total}$		$<2.1 \times 10^{-8}$, CL = 90%
$\Gamma(\tau^- \to e^-\pi^+K^-)/\Gamma_{total}$		$<3.7 \times 10^{-8}$, CL = 90%
$\Gamma(\tau^- \to e^-\pi^-K^+)/\Gamma_{total}$		$<3.1 \times 10^{-8}$, CL = 90%
$\Gamma(\tau^- \to e^-K^0_SK^0_S)/\Gamma_{total}$		$<7.1 \times 10^{-8}$, CL = 90%
$\Gamma(\tau^- \to e^-K^+K^-)/\Gamma_{total}$		$<3.4 \times 10^{-8}$, CL = 90%
$\Gamma(\tau^- \to \mu^-\pi^+K^-)/\Gamma_{total}$		$<8.6 \times 10^{-8}$, CL = 90%
$\Gamma(\tau^- \to \mu^-\pi^-K^+)/\Gamma_{total}$		$<4.5 \times 10^{-8}$, CL = 90%
$\Gamma(\tau^- \to \mu^-K^0_SK^0_S)/\Gamma_{total}$		$<8.0 \times 10^{-8}$, CL = 90%
$\Gamma(\tau^- \to \mu^-K^+K^-)/\Gamma_{total}$		$<4.4 \times 10^{-8}$, CL = 90%
$\Gamma(\tau^- \to e^-\pi^0\pi^0)/\Gamma_{total}$		$<6.5 \times 10^{-6}$, CL = 90%
$\Gamma(\tau^- \to \mu^-\pi^0\pi^0)/\Gamma_{total}$		$<1.4 \times 10^{-5}$, CL = 90%
$\Gamma(\tau^- \to e^-\eta\eta)/\Gamma_{total}$		$<3.5 \times 10^{-5}$, CL = 90%
$\Gamma(\tau^- \to \mu^-\eta\eta)/\Gamma_{total}$		$<6.0 \times 10^{-5}$, CL = 90%
$\Gamma(\tau^- \to e^-\pi^0\eta)/\Gamma_{total}$		$<2.4 \times 10^{-5}$, CL = 90%
$\Gamma(\tau^- \to \mu^-\pi^0\eta)/\Gamma_{total}$		$<2.2 \times 10^{-5}$, CL = 90%
$\Gamma(\tau^- \to e^-$light boson$)/\Gamma_{total}$		$<2.7 \times 10^{-3}$, CL = 95%
$\Gamma(\tau^- \to \mu^-$light boson$)/\Gamma_{total}$		$<5 \times 10^{-3}$, CL = 95%
LEPTON FAMILY NUMBER VIOLATION IN NEUTRINOS		
$\sin^2(\theta_{12})$		0.307 ± 0.013
Δm^2_{21}		$(7.53 \pm 0.18) \times 10^{-5}$ eV^2
$\sin^2(\theta_{23})$ (Normal order)		0.546 ± 0.021
Δm^2_{32} (Inverted order)		$(-2.536 \pm 0.034) \times 10^{-3}$ eV^2
Δm^2_{32} (Normal order)		$(2.453 \pm 0.033) \times 10^{-3}$ eV^2
$\sin^2(\theta_{13})$		$(2.20 \pm 0.07) \times 10^{-2}$
$\Gamma(\pi^+ \to \mu^+\nu_e)/\Gamma_{total}$	[q]	$<8.0 \times 10^{-3}$, CL = 90%
$\Gamma(\pi^+ \to \mu^-e^+e^+\nu)/\Gamma_{total}$		$<1.6 \times 10^{-6}$, CL = 90%
$\Gamma(\pi^0 \to \mu^+e^-)/\Gamma_{total}$		$<3.8 \times 10^{-10}$, CL = 90%
$\Gamma(\pi^0 \to \mu^-e^+)/\Gamma_{total}$		$<3.2 \times 10^{-10}$, CL = 90%
$\Gamma(\pi^0 \to \mu^+e^- + \mu^-e^+)/\Gamma_{total}$		$<3.6 \times 10^{-10}$, CL = 90%
$\Gamma(\eta \to \mu^+e^- + \mu^-e^+)/\Gamma_{total}$		$<6 \times 10^{-6}$, CL = 90%
$\Gamma(\eta'(958) \to e\mu)/\Gamma_{total}$		$<4.7 \times 10^{-4}$, CL = 90%
$\Gamma(\phi(1020) \to e^\pm\mu^\mp)/\Gamma_{total}$		$<2 \times 10^{-6}$, CL = 90%
$\Gamma(K^+ \to \mu^-\nu e^+e^+)/\Gamma_{total}$		$<2.1 \times 10^{-8}$, CL = 90%
$\Gamma(K^+ \to \mu^+\nu_e)/\Gamma_{total}$	[q]	$<4 \times 10^{-3}$, CL = 90%
$\Gamma(K^+ \to \pi^+\mu^+e^-)/\Gamma_{total}$		$<1.3 \times 10^{-11}$, CL = 90%
$\Gamma(K^+ \to \pi^+\mu^-e^+)/\Gamma_{total}$		$<6.6 \times 10^{-11}$, CL = 90%
$\Gamma(K^0_L \to e^\pm\mu^\mp)/\Gamma_{total}$	[o]	$<4.7 \times 10^{-12}$, CL = 90%
$\Gamma(K^0_L \to e^\pm e^\pm\mu^\mp\mu^\mp)/\Gamma_{total}$	[o]	$<4.12 \times 10^{-11}$, CL = 90%
$\Gamma(K^0_L \to \pi^0\mu^\pm e^\mp)/\Gamma_{total}$	[o]	$<7.6 \times 10^{-11}$, CL = 90%
$\Gamma(K^0_L \to \pi^0\pi^0\mu^\pm e^\mp)/\Gamma_{total}$		$<1.7 \times 10^{-10}$, CL = 90%
$\Gamma(D^+ \to \pi^+e^+\mu^-)/\Gamma_{total}$		$<2.1 \times 10^{-7}$, CL = 90%
$\Gamma(D^+ \to \pi^+e^-\mu^+)/\Gamma_{total}$		$<2.2 \times 10^{-7}$, CL = 90%
$\Gamma(D^+ \to K^+e^+\mu^-)/\Gamma_{total}$		$<7.5 \times 10^{-8}$, CL = 90%
$\Gamma(D^+ \to K^+e^-\mu^+)/\Gamma_{total}$		$<1.0 \times 10^{-7}$, CL = 90%
$\Gamma(D^0 \to \mu^\pm e^\mp)/\Gamma_{total}$	[o]	$<1.3 \times 10^{-8}$, CL = 90%
$\Gamma(D^0 \to \pi^0e^\pm\mu^\mp)/\Gamma_{total}$	[o]	$<8.0 \times 10^{-7}$, CL = 90%
$\Gamma(D^0 \to \eta e^\pm\mu^\mp)/\Gamma_{total}$	[o]	$<2.25 \times 10^{-6}$, CL = 90%
$\Gamma(D^0 \to \pi^+\pi^-e^\pm\mu^\mp)/\Gamma_{total}$	[o]	$<1.71 \times 10^{-6}$, CL = 90%
$\Gamma(D^0 \to \rho^0e^\pm\mu^\mp)/\Gamma_{total}$	[o]	$<5.0 \times 10^{-7}$, CL = 90%
$\Gamma(D^0 \to \omega e^\pm\mu^\mp)/\Gamma_{total}$	[o]	$<1.71 \times 10^{-6}$, CL = 90%
$\Gamma(D^0 \to K^-K^+e^\pm\mu^\mp)/\Gamma_{total}$	[o]	$<1.00 \times 10^{-6}$, CL = 90%
$\Gamma(D^0 \to \phi e^\pm\mu^\mp)/\Gamma_{total}$	[o]	$<5.1 \times 10^{-7}$, CL = 90%
$\Gamma(D^0 \to \overline{K}^0e^\pm\mu^\mp)/\Gamma_{total}$	[o]	$<1.74 \times 10^{-6}$, CL = 90%
$\Gamma(D^0 \to K^-\pi^+e^\pm\mu^\mp)/\Gamma_{total}$	[o]	$<1.90 \times 10^{-6}$, CL = 90%
$\Gamma(D^0 \to \overline{K}^*(892)^0e^\pm\mu^\mp)/\Gamma_{total}$	[o]	$<1.25 \times 10^{-6}$, CL = 90%
$\Gamma(D^+_s \to \pi^+e^+\mu^-)/\Gamma_{total}$		$<1.1 \times 10^{-6}$, CL = 90%
$\Gamma(D^+_s \to \pi^+e^-\mu^+)/\Gamma_{total}$		$<9.4 \times 10^{-7}$, CL = 90%
$\Gamma(D^+_s \to K^+e^+\mu^-)/\Gamma_{total}$		$<7.9 \times 10^{-7}$, CL = 90%
$\Gamma(D^+_s \to K^+e^-\mu^+)/\Gamma_{total}$		$<5.6 \times 10^{-7}$, CL = 90%
$\Gamma(B^+ \to \pi^+e^+\mu^-)/\Gamma_{total}$		$<6.4 \times 10^{-3}$, CL = 90%
$\Gamma(B^+ \to \pi^+e^-\mu^+)/\Gamma_{total}$		$<6.4 \times 10^{-3}$, CL = 90%
$\Gamma(B^+ \to \pi^+e^\pm\mu^\mp)/\Gamma_{total}$		$<1.7 \times 10^{-7}$, CL = 90%
$\Gamma(B^+ \to \pi^+e^+\tau^-)/\Gamma_{total}$		$<7.4 \times 10^{-5}$, CL = 90%
$\Gamma(B^+ \to \pi^+e^-\tau^+)/\Gamma_{total}$		$<2.0 \times 10^{-5}$, CL = 90%
$\Gamma(B^+ \to \pi^+e^\pm\tau^\mp)/\Gamma_{total}$		$<7.5 \times 10^{-5}$, CL = 90%
$\Gamma(B^+ \to \pi^+\mu^+\tau^-)/\Gamma_{total}$		$<6.2 \times 10^{-5}$, CL = 90%
$\Gamma(B^+ \to \pi^+\mu^-\tau^+)/\Gamma_{total}$		$<4.5 \times 10^{-5}$, CL = 90%
$\Gamma(B^+ \to \pi^+\mu^\pm\tau^\mp)/\Gamma_{total}$		$<7.2 \times 10^{-5}$, CL = 90%
$\Gamma(B^+ \to K^+e^+\mu^-)/\Gamma_{total}$		$<7.0 \times 10^{-9}$, CL = 90%
$\Gamma(B^+ \to K^+e^-\mu^+)/\Gamma_{total}$		$<6.4 \times 10^{-9}$, CL = 90%
$\Gamma(B^+ \to K^+e^\pm\mu^\mp)/\Gamma_{total}$		$<9.1 \times 10^{-8}$, CL = 90%
$\Gamma(B^+ \to K^+e^+\tau^-)/\Gamma_{total}$		$<4.3 \times 10^{-5}$, CL = 90%
$\Gamma(B^+ \to K^+e^-\tau^+)/\Gamma_{total}$		$<1.5 \times 10^{-5}$, CL = 90%
$\Gamma(B^+ \to K^+e^\pm\tau^\mp)/\Gamma_{total}$		$<3.0 \times 10^{-5}$, CL = 90%
$\Gamma(B^+ \to K^+\mu^+\tau^-)/\Gamma_{total}$		$<4.5 \times 10^{-5}$, CL = 90%
$\Gamma(B^+ \to K^+\mu^-\tau^+)/\Gamma_{total}$		$<2.8 \times 10^{-5}$, CL = 90%
$\Gamma(B^+ \to K^+\mu^\pm\tau^\mp)/\Gamma_{total}$		$<4.8 \times 10^{-5}$, CL = 90%
$\Gamma(B^+ \to K^*(892)^+e^+\mu^-)/\Gamma_{total}$		$<1.3 \times 10^{-6}$, CL = 90%
$\Gamma(B^+ \to K^*(892)^+e^-\mu^+)/\Gamma_{total}$		$<9.9 \times 10^{-7}$, CL = 90%
$\Gamma(B^+ \to K^*(892)^+e^\pm\mu^\mp)/\Gamma_{total}$		$<1.4 \times 10^{-6}$, CL = 90%
$\Gamma(B^0 \to e^\pm\mu^\mp)/\Gamma_{total}$	[o]	$<1.0 \times 10^{-9}$, CL = 90%
$\Gamma(B^0 \to \pi^0e^\pm\mu^\mp)/\Gamma_{total}$		$<1.4 \times 10^{-7}$, CL = 90%
$\Gamma(B^0 \to K^0e^\pm\mu^\mp)/\Gamma_{total}$		$<3.8 \times 10^{-8}$, CL = 90%
$\Gamma(B^0 \to K^*(892)^0e^+\mu^-)/\Gamma_{total}$		$<1.6 \times 10^{-7}$, CL = 90%
$\Gamma(B^0 \to K^*(892)^0e^-\mu^+)/\Gamma_{total}$		$<1.2 \times 10^{-7}$, CL = 90%
$\Gamma(B^0 \to K^*(892)^0e^\pm\mu^\mp)/\Gamma_{total}$		$<1.8 \times 10^{-7}$, CL = 90%
$\Gamma(B^0 \to e^\pm\tau^\mp)/\Gamma_{total}$	[o]	$<1.6 \times 10^{-5}$, CL = 90%
$\Gamma(B^0 \to \mu^\pm\tau^\mp)/\Gamma_{total}$	[o]	$<1.4 \times 10^{-5}$, CL = 95%
$\Gamma(B \to se^\pm\mu^\mp)/\Gamma_{total}$	[o]	$<2.2 \times 10^{-5}$, CL = 90%
$\Gamma(B \to \pi e^\pm\mu^\mp)/\Gamma_{total}$		$<9.2 \times 10^{-8}$, CL = 90%
$\Gamma(B \to \rho e^\pm\mu^\mp)/\Gamma_{total}$		$<3.2 \times 10^{-6}$, CL = 90%

Unless otherwise stated, limits are given at the 90% confidence level, while errors are given as ± 1 standard deviation.

Downloaded from https://academic.oup.com/ptep/article/2022/8/083C01/6651666 by KIT Library user on 27 September 2022

$\Gamma(B \to K e^{\pm}\mu^{\mp})/\Gamma_{total}$		$<3.8 \times 10^{-8}$, CL = 90%
$\Gamma(B \to K^*(892) e^{\pm}\mu^{\mp})/\Gamma_{total}$		$<5.1 \times 10^{-7}$, CL = 90%
$\Gamma(B^0_s \to e^{\pm}\mu^{\mp})/\Gamma_{total}$	[o]	$<5.4 \times 10^{-9}$, CL = 90%
$\Gamma(B^0_s \to \mu^{\pm}\tau^{\mp})/\Gamma_{total}$		$<4.2 \times 10^{-5}$, CL = 95%
$\Gamma(J/\psi(1S) \to e^{\pm}\mu^{\mp})/\Gamma_{total}$		$<1.6 \times 10^{-7}$, CL = 90%
$\Gamma(J/\psi(1S) \to e^{\pm}\tau^{\mp})/\Gamma_{total}$		$<7.5 \times 10^{-8}$, CL = 90%
$\Gamma(J/\psi(1S) \to \mu^{\pm}\tau^{\mp})/\Gamma_{total}$		$<2.0 \times 10^{-6}$, CL = 90%
$\Gamma(\Upsilon(1S) \to \mu^{\pm}\tau^{\mp})/\Gamma_{total}$		$<6.0 \times 10^{-6}$, CL = 95%
$\Gamma(\Upsilon(2S) \to e^{\pm}\tau^{\mp})/\Gamma_{total}$		$<3.2 \times 10^{-6}$, CL = 90%
$\Gamma(\Upsilon(2S) \to \mu^{\pm}\tau^{\mp})/\Gamma_{total}$		$<3.3 \times 10^{-6}$, CL = 90%
$\Gamma(\Upsilon(3S) \to e^{\pm}\tau^{\mp})/\Gamma_{total}$		$<4.2 \times 10^{-6}$, CL = 90%
$\Gamma(\Upsilon(3S) \to \mu^{\pm}\tau^{\mp})/\Gamma_{total}$		$<3.1 \times 10^{-6}$, CL = 90%
$\Gamma(\Lambda_c^+ \to p e^+\mu^-)/\Gamma_{total}$		$<9.9 \times 10^{-6}$, CL = 90%
$\Gamma(\Lambda_c^+ \to p e^-\mu^+)/\Gamma_{total}$		$<1.9 \times 10^{-5}$, CL = 90%

TOTAL LEPTON NUMBER

Violation of total lepton number conservation also implies violation of lepton family number conservation.

$\Gamma(Z \to p e)/\Gamma_{total}$		$<1.8 \times 10^{-6}$, CL = 95%
$\Gamma(Z \to p \mu)/\Gamma_{total}$		$<1.8 \times 10^{-6}$, CL = 95%
limit on $\mu^- \to e^+$ conversion		
$\sigma(\mu^- {}^{32}\mathrm{S} \to e^+ {}^{32}\mathrm{Si}^*)$ / $\sigma(\mu^- {}^{32}\mathrm{S} \to \nu_\mu {}^{32}\mathrm{P}^*)$		$<9 \times 10^{-10}$, CL = 90%
$\sigma(\mu^- {}^{127}\mathrm{I} \to e^+ {}^{127}\mathrm{Sb}^*)$ / $\sigma(\mu^- {}^{127}\mathrm{I} \to \text{anything})$		$<3 \times 10^{-10}$, CL = 90%
$\sigma(\mu^- \mathrm{Ti} \to e^+ \mathrm{Ca})$ / $\sigma(\mu^- \mathrm{Ti} \to \text{capture})$		$<3.6 \times 10^{-11}$, CL = 90%
$\Gamma(\tau^- \to e^+\pi^-\pi^-)/\Gamma_{total}$		$<2.0 \times 10^{-8}$, CL = 90%
$\Gamma(\tau^- \to \mu^+\pi^-\pi^-)/\Gamma_{total}$		$<3.9 \times 10^{-8}$, CL = 90%
$\Gamma(\tau^- \to e^+\pi^-K^-)/\Gamma_{total}$		$<3.2 \times 10^{-8}$, CL = 90%
$\Gamma(\tau^- \to e^+K^-K^-)/\Gamma_{total}$		$<3.3 \times 10^{-8}$, CL = 90%
$\Gamma(\tau^- \to \mu^+\pi^-K^-)/\Gamma_{total}$		$<4.8 \times 10^{-8}$, CL = 90%
$\Gamma(\tau^- \to \mu^+K^-K^-)/\Gamma_{total}$		$<4.7 \times 10^{-8}$, CL = 90%
$\Gamma(\tau^- \to p e^-e^-)/\Gamma_{total}$		$<3.0 \times 10^{-8}$, CL = 90%
$\Gamma(\tau^- \to \overline{p} e^+e^-)/\Gamma_{total}$		$<3.0 \times 10^{-8}$, CL = 90%
$\Gamma(\tau^- \to \overline{p} e^+\mu^-)/\Gamma_{total}$		$<2.0 \times 10^{-8}$, CL = 90%
$\Gamma(\tau^- \to \overline{p} e^-\mu^+)/\Gamma_{total}$		$<1.8 \times 10^{-8}$, CL = 90%
$\Gamma(\tau^- \to p \mu^-\mu^-)/\Gamma_{total}$		$<4.0 \times 10^{-8}$, CL = 90%
$\Gamma(\tau^- \to \overline{p} \mu^+\mu^-)/\Gamma_{total}$		$<1.8 \times 10^{-8}$, CL = 90%
$\Gamma(\tau^- \to \overline{p}\gamma)/\Gamma_{total}$		$<3.5 \times 10^{-6}$, CL = 90%
$\Gamma(\tau^- \to \overline{p}\pi^0)/\Gamma_{total}$		$<1.5 \times 10^{-5}$, CL = 90%
$\Gamma(\tau^- \to \overline{p}2\pi^0)/\Gamma_{total}$		$<3.3 \times 10^{-5}$, CL = 90%
$\Gamma(\tau^- \to \overline{p}\eta)/\Gamma_{total}$		$<8.9 \times 10^{-6}$, CL = 90%
$\Gamma(\tau^- \to \overline{p}\pi^0\eta)/\Gamma_{total}$		$<2.7 \times 10^{-5}$, CL = 90%
$\Gamma(\tau^- \to \Lambda\pi^-)/\Gamma_{total}$		$<7.2 \times 10^{-8}$, CL = 90%
$\Gamma(\tau^- \to \overline{\Lambda}\pi^-)/\Gamma_{total}$		$<1.4 \times 10^{-7}$, CL = 90%
$t_{1/2}({}^{76}\mathrm{Ge} \to {}^{76}\mathrm{Se} + 2e^-)$		$>9.0 \times 10^{25}$ yr, CL = 90%
$t_{1/2}({}^{136}\mathrm{Xe} \to {}^{136}\mathrm{Ba} + 2e^-)$		$>10.7 \times 10^{25}$ yr, CL = 90%
$t_{1/2}({}^{130}\mathrm{Te} \to {}^{130}\mathrm{Xe} + 2e^-)$		$>1.5 \times 10^{25}$ yr, CL = 90%
$\Gamma(\pi^+ \to \mu^+\overline{\nu}_e)/\Gamma_{total}$	[q]	$<1.5 \times 10^{-3}$, CL = 90%
$\Gamma(K^+ \to \pi^-\mu^+e^+)/\Gamma_{total}$		$<4.2 \times 10^{-11}$, CL = 90%
$\Gamma(K^+ \to \pi^-e^+e^+)/\Gamma_{total}$		$<2.2 \times 10^{-10}$, CL = 90%
$\Gamma(K^+ \to \pi^-\mu^+\mu^+)/\Gamma_{total}$		$<4.2 \times 10^{-11}$, CL = 90%
$\Gamma(K^+ \to \mu^+\overline{\nu}_e)/\Gamma_{total}$	[q]	$<3.3 \times 10^{-3}$, CL = 90%
$\Gamma(K^+ \to \pi^0e^+\overline{\nu}_e)/\Gamma_{total}$		$<3 \times 10^{-3}$, CL = 90%
$\Gamma(D^+ \to \pi^-2e^+)/\Gamma_{total}$		$<5.3 \times 10^{-7}$, CL = 90%
$\Gamma(D^+ \to \pi^-2\mu^+)/\Gamma_{total}$		$<1.4 \times 10^{-8}$, CL = 90%
$\Gamma(D^+ \to \pi^-e^+\mu^+)/\Gamma_{total}$		$<1.3 \times 10^{-7}$, CL = 90%
$\Gamma(D^+ \to \rho^-2\mu^+)/\Gamma_{total}$		$<5.6 \times 10^{-4}$, CL = 90%
$\Gamma(D^+ \to K^-2e^+)/\Gamma_{total}$		$<9 \times 10^{-7}$, CL = 90%
$\Gamma(D^+ \to K^-2\mu^+)/\Gamma_{total}$		$<1.0 \times 10^{-5}$, CL = 90%
$\Gamma(D^+ \to K^-e^+\mu^+)/\Gamma_{total}$		$<1.9 \times 10^{-6}$, CL = 90%
$\Gamma(D^+ \to K^*(892)^-2\mu^+)/\Gamma_{total}$		$<8.5 \times 10^{-4}$, CL = 90%
$\Gamma(D^+ \to \Lambda e^+)/\Gamma_{total}$		$<1.1 \times 10^{-6}$, CL = 90%
$\Gamma(D^+ \to \overline{\Lambda}e^+)/\Gamma_{total}$		$<6.5 \times 10^{-7}$, CL = 90%
$\Gamma(D^+ \to \Sigma^0e^+)/\Gamma_{total}$		$<1.7 \times 10^{-6}$, CL = 90%
$\Gamma(D^+ \to \overline{\Sigma}^0e^+)/\Gamma_{total}$		$<1.3 \times 10^{-6}$, CL = 90%
$\Gamma(D^0 \to 2\pi^-2e^+)/\Gamma_{total}$		$<9.1 \times 10^{-7}$, CL = 90%
$\Gamma(D^0 \to 2\pi^-2\mu^+)/\Gamma_{total}$		$<1.52 \times 10^{-6}$, CL = 90%
$\Gamma(D^0 \to K^-\pi^-2e^+)/\Gamma_{total}$		$<5.0 \times 10^{-7}$, CL = 90%
$\Gamma(D^0 \to K^-\pi^-2\mu^+)/\Gamma_{total}$		$<5.3 \times 10^{-7}$, CL = 90%
$\Gamma(D^0 \to 2K^-2e^+)/\Gamma_{total}$		$<3.4 \times 10^{-7}$, CL = 90%
$\Gamma(D^0 \to 2K^-2\mu^+)/\Gamma_{total}$		$<1.0 \times 10^{-7}$, CL = 90%
$\Gamma(D^0 \to \pi^-\pi^-e^+\mu^+)/\Gamma_{total}$		$<3.06 \times 10^{-6}$, CL = 90%
$\Gamma(D^0 \to K^-\pi^-e^+\mu^+)/\Gamma_{total}$		$<2.10 \times 10^{-6}$, CL = 90%
$\Gamma(D^0 \to 2K^-e^+\mu^+)/\Gamma_{total}$		$<5.8 \times 10^{-7}$, CL = 90%
$\Gamma(D^0 \to p e^-)/\Gamma_{total}$	[r]	$<1.0 \times 10^{-5}$, CL = 90%
$\Gamma(D^0 \to \overline{p} e^+)/\Gamma_{total}$	[s]	$<1.1 \times 10^{-5}$, CL = 90%
$\Gamma(D^+_s \to \pi^-2e^+)/\Gamma_{total}$		$<1.4 \times 10^{-6}$, CL = 90%
$\Gamma(D^+_s \to \pi^-2\mu^+)/\Gamma_{total}$		$<8.6 \times 10^{-8}$, CL = 90%
$\Gamma(D^+_s \to \pi^-e^+\mu^+)/\Gamma_{total}$		$<6.3 \times 10^{-7}$, CL = 90%
$\Gamma(D^+_s \to K^-2e^+)/\Gamma_{total}$		$<7.7 \times 10^{-7}$, CL = 90%
$\Gamma(D^+_s \to K^-2\mu^+)/\Gamma_{total}$		$<2.6 \times 10^{-8}$, CL = 90%
$\Gamma(D^+_s \to K^-e^+\mu^+)/\Gamma_{total}$		$<2.6 \times 10^{-7}$, CL = 90%
$\Gamma(D^+_s \to K^*(892)^-2\mu^+)/\Gamma_{total}$		$<1.4 \times 10^{-3}$, CL = 90%
$\Gamma(B^+ \to \pi^-e^+e^+)/\Gamma_{total}$		$<2.3 \times 10^{-8}$, CL = 90%
$\Gamma(B^+ \to \pi^-\mu^+\mu^+)/\Gamma_{total}$		$<4.0 \times 10^{-9}$, CL = 95%
$\Gamma(B^+ \to \pi^-e^+\mu^+)/\Gamma_{total}$		$<1.5 \times 10^{-7}$, CL = 90%
$\Gamma(B^+ \to \rho^-e^+e^+)/\Gamma_{total}$		$<1.7 \times 10^{-7}$, CL = 90%
$\Gamma(B^+ \to \rho^-\mu^+\mu^+)/\Gamma_{total}$		$<4.2 \times 10^{-7}$, CL = 90%
$\Gamma(B^+ \to \rho^-e^+\mu^+)/\Gamma_{total}$		$<4.7 \times 10^{-7}$, CL = 90%
$\Gamma(B^+ \to K^-e^+e^+)/\Gamma_{total}$		$<3.0 \times 10^{-8}$, CL = 90%
$\Gamma(B^+ \to K^-\mu^+\mu^+)/\Gamma_{total}$		$<4.1 \times 10^{-8}$, CL = 90%
$\Gamma(B^+ \to K^-e^+\mu^+)/\Gamma_{total}$		$<1.6 \times 10^{-7}$, CL = 90%
$\Gamma(B^+ \to K^*(892)^-e^+e^+)/\Gamma_{total}$		$<4.0 \times 10^{-7}$, CL = 90%
$\Gamma(B^+ \to K^*(892)^-\mu^+\mu^+)/\Gamma_{total}$		$<5.9 \times 10^{-7}$, CL = 90%
$\Gamma(B^+ \to K^*(892)^-e^+\mu^+)/\Gamma_{total}$		$<3.0 \times 10^{-7}$, CL = 90%
$\Gamma(B^+ \to D^-e^+e^+)/\Gamma_{total}$		$<2.6 \times 10^{-6}$, CL = 90%
$\Gamma(B^+ \to D^-e^+\mu^+)/\Gamma_{total}$		$<1.8 \times 10^{-6}$, CL = 90%
$\Gamma(B^+ \to D^-\mu^+\mu^+)/\Gamma_{total}$		$<6.9 \times 10^{-7}$, CL = 95%
$\Gamma(B^+ \to D^{*-}\mu^+\mu^+)/\Gamma_{total}$		$<2.4 \times 10^{-6}$, CL = 95%
$\Gamma(B^+ \to D_s^-\mu^+\mu^+)/\Gamma_{total}$		$<5.8 \times 10^{-7}$, CL = 95%
$\Gamma(B^+ \to \overline{D}^0\pi^-\mu^+\mu^+)/\Gamma_{total}$		$<1.5 \times 10^{-6}$, CL = 95%
$\Gamma(B^+ \to \Lambda^0\mu^+)/\Gamma_{total}$		$<6 \times 10^{-8}$, CL = 90%
$\Gamma(B^+ \to \Lambda^0e^+)/\Gamma_{total}$		$<3.2 \times 10^{-8}$, CL = 90%
$\Gamma(B^+ \to \overline{\Lambda}^0\mu^+)/\Gamma_{total}$		$<6 \times 10^{-8}$, CL = 90%
$\Gamma(B^+ \to \overline{\Lambda}^0e^+)/\Gamma_{total}$		$<8 \times 10^{-8}$, CL = 90%
$\Gamma(B^0 \to \Lambda_c^+\mu^-)/\Gamma_{total}$		$<1.4 \times 10^{-6}$, CL = 90%
$\Gamma(B^0 \to \Lambda_c^+e^-)/\Gamma_{total}$		$<4 \times 10^{-6}$, CL = 90%
$\Gamma(\Lambda \to \pi^+e^-)/\Gamma_{total}$		$<6 \times 10^{-7}$, CL = 90%
$\Gamma(\Lambda \to \pi^+\mu^-)/\Gamma_{total}$		$<6 \times 10^{-7}$, CL = 90%
$\Gamma(\Lambda \to \pi^-e^+)/\Gamma_{total}$		$<4 \times 10^{-7}$, CL = 90%
$\Gamma(\Lambda \to \pi^-\mu^+)/\Gamma_{total}$		$<6 \times 10^{-7}$, CL = 90%
$\Gamma(\Lambda \to K^+e^-)/\Gamma_{total}$		$<2 \times 10^{-6}$, CL = 90%
$\Gamma(\Lambda \to K^+\mu^-)/\Gamma_{total}$		$<3 \times 10^{-6}$, CL = 90%
$\Gamma(\Lambda \to K^-e^+)/\Gamma_{total}$		$<2 \times 10^{-6}$, CL = 90%
$\Gamma(\Lambda \to K^-\mu^+)/\Gamma_{total}$		$<3 \times 10^{-6}$, CL = 90%
$\Gamma(\Lambda \to K^0_S\nu)/\Gamma_{total}$		$<2 \times 10^{-5}$, CL = 90%
$\Gamma(\Sigma^- \to p e^-e^-)/\Gamma_{total}$		$<6.7 \times 10^{-5}$, CL = 90%
$\Gamma(\Xi^- \to p \mu^-\mu^-)/\Gamma_{total}$		$<4 \times 10^{-8}$, CL = 90%
$\Gamma(\Lambda_c^+ \to \overline{p}2e^+)/\Gamma_{total}$		$<2.7 \times 10^{-6}$, CL = 90%
$\Gamma(\Lambda_c^+ \to \overline{p}2\mu^+)/\Gamma_{total}$		$<9.4 \times 10^{-6}$, CL = 90%
$\Gamma(\Lambda_c^+ \to \overline{p}e^+\mu^+)/\Gamma_{total}$		$<1.6 \times 10^{-5}$, CL = 90%
$\Gamma(\Lambda_c^+ \to \Sigma^-\mu^+\mu^+)/\Gamma_{total}$		$<7.0 \times 10^{-4}$, CL = 90%

BARYON NUMBER

$\Gamma(Z \to p e)/\Gamma_{total}$		$<1.8 \times 10^{-6}$, CL = 95%
$\Gamma(Z \to p \mu)/\Gamma_{total}$		$<1.8 \times 10^{-6}$, CL = 95%
$\Gamma(\tau^- \to p e^-e^-)/\Gamma_{total}$		$<3.0 \times 10^{-8}$, CL = 90%
$\Gamma(\tau^- \to \overline{p} e^+e^-)/\Gamma_{total}$		$<3.0 \times 10^{-8}$, CL = 90%
$\Gamma(\tau^- \to \overline{p} e^+\mu^-)/\Gamma_{total}$		$<2.0 \times 10^{-8}$, CL = 90%
$\Gamma(\tau^- \to \overline{p} e^-\mu^+)/\Gamma_{total}$		$<1.8 \times 10^{-8}$, CL = 90%
$\Gamma(\tau^- \to p \mu^-\mu^-)/\Gamma_{total}$		$<4.0 \times 10^{-8}$, CL = 90%
$\Gamma(\tau^- \to \overline{p} \mu^+\mu^-)/\Gamma_{total}$		$<1.8 \times 10^{-8}$, CL = 90%
$\Gamma(\tau^- \to \overline{p}\gamma)/\Gamma_{total}$		$<3.5 \times 10^{-6}$, CL = 90%
$\Gamma(\tau^- \to \overline{p}\pi^0)/\Gamma_{total}$		$<1.5 \times 10^{-5}$, CL = 90%

Unless otherwise stated, limits are given at the 90% confidence level, while errors are given as ±1 standard deviation.

Downloaded from https://academic.oup.com/ptep/article/2022/8/083C01/6651666 by KIT Library user on 27 September 2022

$\Gamma(\tau^- \to \overline{p}2\pi^0)/\Gamma_{total}$		$<3.3 \times 10^{-5}$, CL = 90%
$\Gamma(\tau^- \to \overline{p}\eta)/\Gamma_{total}$		$<8.9 \times 10^{-6}$, CL = 90%
$\Gamma(\tau^- \to \overline{p}\pi^0\eta)/\Gamma_{total}$		$<2.7 \times 10^{-5}$, CL = 90%
$\Gamma(\tau^- \to \Lambda\pi^-)/\Gamma_{total}$		$<7.2 \times 10^{-8}$, CL = 90%
$\Gamma(\tau^- \to \overline{\Lambda}\pi^-)/\Gamma_{total}$		$<1.4 \times 10^{-7}$, CL = 90%
$\Gamma(D^+ \to \Lambda e^+)/\Gamma_{total}$		$<1.1 \times 10^{-6}$, CL = 90%
$\Gamma(D^+ \to \overline{\Lambda} e^+)/\Gamma_{total}$		$<6.5 \times 10^{-7}$, CL = 90%
$\Gamma(D^+ \to \Sigma^0 e^+)/\Gamma_{total}$		$<1.7 \times 10^{-6}$, CL = 90%
$\Gamma(D^+ \to \overline{\Sigma}^0 e^+)/\Gamma_{total}$		$<1.3 \times 10^{-6}$, CL = 90%
$\Gamma(D^0 \to p e^-)/\Gamma_{total}$	[r]	$<1.0 \times 10^{-5}$, CL = 90%
$\Gamma(D^0 \to \overline{p} e^+)/\Gamma_{total}$	[s]	$<1.1 \times 10^{-5}$, CL = 90%
$\Gamma(B^+ \to \Lambda^0 \mu^+)/\Gamma_{total}$		$<6 \times 10^{-8}$, CL = 90%
$\Gamma(B^+ \to \Lambda^0 e^+)/\Gamma_{total}$		$<3.2 \times 10^{-8}$, CL = 90%
$\Gamma(B^+ \to \overline{\Lambda}^0 \mu^+)/\Gamma_{total}$		$<6 \times 10^{-8}$, CL = 90%
$\Gamma(B^+ \to \overline{\Lambda}^0 e^+)/\Gamma_{total}$		$<8 \times 10^{-8}$, CL = 90%
$\Gamma(B^0 \to \Lambda_c^+ \mu^-)/\Gamma_{total}$		$<1.4 \times 10^{-6}$, CL = 90%
$\Gamma(B^0 \to \Lambda_c^+ e^-)/\Gamma_{total}$		$<4 \times 10^{-6}$, CL = 90%
p mean life	[t]	$>3.6 \times 10^{29}$ years, CL = 90%

A few examples of proton or bound neutron decay follow. For limits on many other nucleon decay channels, see the Baryon Summary Table.

$\tau(N \to e^+\pi)$		$> 5300\ (n)$, $> 16000\ (p) \times 10^{30}$ years, CL = 90%
$\tau(N \to \mu^+\pi)$		$> 3500\ (n)$, $> 7700\ (p) \times 10^{30}$ years, CL = 90%
$\tau(N \to e^+ K)$		$> 17\ (n)$, $> 1000\ (p) \times 10^{30}$ years, CL = 90%
$\tau(N \to \mu^+ K)$		$> 26\ (n)$, $> 1600\ (p) \times 10^{30}$ years, CL = 90%
limit on $n\overline{n}$ oscillations (free n)		$>0.86 \times 10^8$ s, CL = 90%
limit on $n\overline{n}$ oscillations (bound n)	[u]	$>2.7 \times 10^8$ s, CL = 90%
$\Gamma(\Lambda \to \pi^+ e^-)/\Gamma_{total}$		$<6 \times 10^{-7}$, CL = 90%
$\Gamma(\Lambda \to \pi^+ \mu^-)/\Gamma_{total}$		$<6 \times 10^{-7}$, CL = 90%
$\Gamma(\Lambda \to \pi^- e^+)/\Gamma_{total}$		$<4 \times 10^{-7}$, CL = 90%
$\Gamma(\Lambda \to \pi^- \mu^+)/\Gamma_{total}$		$<6 \times 10^{-7}$, CL = 90%
$\Gamma(\Lambda \to K^+ e^-)/\Gamma_{total}$		$<2 \times 10^{-6}$, CL = 90%
$\Gamma(\Lambda \to K^+ \mu^-)/\Gamma_{total}$		$<3 \times 10^{-6}$, CL = 90%
$\Gamma(\Lambda \to K^- e^+)/\Gamma_{total}$		$<2 \times 10^{-6}$, CL = 90%
$\Gamma(\Lambda \to K^- \mu^+)/\Gamma_{total}$		$<3 \times 10^{-6}$, CL = 90%
$\Gamma(\Lambda \to K_S^0 \nu)/\Gamma_{total}$		$<2 \times 10^{-5}$, CL = 90%
$\Gamma(\Lambda \to \overline{p}\pi^+)/\Gamma_{total}$		$<9 \times 10^{-7}$, CL = 90%
$\Gamma(\Lambda_c^+ \to \overline{p}2e^+)/\Gamma_{total}$		$<2.7 \times 10^{-6}$, CL = 90%
$\Gamma(\Lambda_c^+ \to \overline{p}2\mu^+)/\Gamma_{total}$		$<9.4 \times 10^{-6}$, CL = 90%
$\Gamma(\Lambda_c^+ \to \overline{p}e^+\mu^+)/\Gamma_{total}$		$<1.6 \times 10^{-5}$, CL = 90%

ELECTRIC CHARGE (Q)

γ charge (mixed)		$<1 \times 10^{-46}\ e$
γ charge (single)		$<1 \times 10^{-35}\ e$
$e \to \nu_e\gamma$ and astrophysical limits	[v]	$>6.6 \times 10^{28}$ yr, CL = 90%
ν charge		$<4 \times 10^{-35}\ e$, CL = 95%
$\lvert q_p + q_e \rvert / e$	[x]	$<1 \times 10^{-21}$
n charge		$(-0.2 \pm 0.8) \times 10^{-21}\ e$
$\Gamma(n \to p\nu_e\overline{\nu}_e)/\Gamma_{total}$		$<8 \times 10^{-27}$, CL = 68%

$\Delta S = \Delta Q$ RULE

Violations allowed in second-order weak interactions.

$\Gamma(K^+ \to \pi^+\pi^+ e^-\overline{\nu}_e)/\Gamma_{total}$		$<1.3 \times 10^{-8}$, CL = 90%
$\Gamma(K^+ \to \pi^+\pi^+ \mu^-\overline{\nu}_\mu)/\Gamma_{total}$		$<3.0 \times 10^{-6}$, CL = 95%
Re(x_+), K_{e3} parameter		$(-0.9 \pm 3.0) \times 10^{-3}$
$x = A(\overline{K}^0 \to \pi^-\ell^+\nu)/A(K^0 \to \pi^-\ell^+\nu) = A(\Delta S{=}-\Delta Q)/A(\Delta S{=}\Delta Q)$		
real part of x		-0.002 ± 0.006
imaginary part of x		0.0012 ± 0.0021
$\Gamma(\Sigma^+ \to n\ell^+\nu)/\Gamma(\Sigma^- \to n\ell^-\overline{\nu}_\ell)$		<0.043
$\Gamma(\Sigma^+ \to ne^+\nu_e)/\Gamma_{total}$		$<5 \times 10^{-6}$, CL = 90%
$\Gamma(\Sigma^+ \to n\mu^+\nu_\mu)/\Gamma_{total}$		$<3.0 \times 10^{-5}$, CL = 90%
$\Gamma(\Xi^0 \to \Sigma^- e^+\nu_e)/\Gamma_{total}$		$<9 \times 10^{-4}$, CL = 90%
$\Gamma(\Xi^0 \to \Sigma^- \mu^+\nu_\mu)/\Gamma_{total}$		$<9 \times 10^{-4}$, CL = 90%

$\Delta S = 2$ FORBIDDEN

Allowed in second-order weak interactions.

$\Gamma(\Xi^0 \to p\pi^-)/\Gamma_{total}$		$<8 \times 10^{-6}$, CL = 90%
$\Gamma(\Xi^0 \to pe^-\overline{\nu}_e)/\Gamma_{total}$		$<1.3 \times 10^{-3}$
$\Gamma(\Xi^0 \to p\mu^-\overline{\nu}_\mu)/\Gamma_{total}$		$<1.3 \times 10^{-3}$
$\Gamma(\Xi^- \to n\pi^-)/\Gamma_{total}$		$<1.9 \times 10^{-5}$, CL = 90%
$\Gamma(\Xi^- \to ne^-\overline{\nu}_e)/\Gamma_{total}$		$<3.2 \times 10^{-3}$, CL = 90%
$\Gamma(\Xi^- \to n\mu^-\overline{\nu}_\mu)/\Gamma_{total}$		$<1.5 \times 10^{-2}$, CL = 90%
$\Gamma(\Xi^- \to p\pi^-\pi^-)/\Gamma_{total}$		$<4 \times 10^{-4}$, CL = 90%
$\Gamma(\Xi^- \to p\pi^- e^-\overline{\nu}_e)/\Gamma_{total}$		$<4 \times 10^{-4}$, CL = 90%
$\Gamma(\Xi^- \to p\pi^- \mu^-\overline{\nu}_\mu)/\Gamma_{total}$		$<4 \times 10^{-4}$, CL = 90%
$\Gamma(\Omega^- \to \Lambda\pi^-)/\Gamma_{total}$		$<2.9 \times 10^{-6}$, CL = 90%

$\Delta S = 2$ VIA MIXING

Allowed in second-order weak interactions, e.g. mixing.

$m_{K_L^0} - m_{K_S^0}$	$(0.5293 \pm 0.0009) \times 10^{10}\ \hbar\ \mathrm{s}^{-1}$ (S = 1.3)
$m_{K_L^0} - m_{K_S^0}$	$(3.484 \pm 0.006) \times 10^{-12}$ MeV

$\Delta C = 2$ VIA MIXING

Allowed in second-order weak interactions, e.g. mixing.

$\lvert m_{D_1^0} - m_{D_2^0} \rvert = x\Gamma$	$(0.997 \pm 0.116) \times 10^{10}\ \hbar\ \mathrm{s}^{-1}$
$(\Gamma_{D_1^0} - \Gamma_{D_2^0})/\Gamma = 2y$	$(1.23 \pm 0.11) \times 10^{-2}$

$\Delta B = 2$ VIA MIXING

Allowed in second-order weak interactions, e.g. mixing.

χ_d (B^0-$\overline{B}^0$ mixing probability)	0.1858 ± 0.0011
$\Delta m_{B^0} = m_{B_H^0} - m_{B_L^0}$	$(0.5065 \pm 0.0019) \times 10^{12}\ \hbar\ \mathrm{s}^{-1}$
$x_d = \Delta m_{B^0}/\Gamma_{B^0}$	0.769 ± 0.004
$\Delta m_{B_s^0} = m_{B_{sH}^0} - m_{B_{sL}^0}$	$(17.765 \pm 0.006) \times 10^{12}\ \hbar\ \mathrm{s}^{-1}$
$x_s = \Delta m_{B_s^0}/\Gamma_{B_s^0}$	27.01 ± 0.10
χ_s (B_s^0-$\overline{B}_s^0$ mixing parameter)	0.499318 ± 0.000005

$\Delta S = 1$ WEAK NEUTRAL CURRENT FORBIDDEN

Allowed by higher-order electroweak interactions.

$\Gamma(K^+ \to \pi^+ e^+ e^-)/\Gamma_{total}$		$(3.00 \pm 0.09) \times 10^{-7}$
$\Gamma(K^+ \to \pi^+ \mu^+ \mu^-)/\Gamma_{total}$		$(9.4 \pm 0.6) \times 10^{-8}$ (S = 2.6)
$\Gamma(K^+ \to \pi^+ \nu\overline{\nu})/\Gamma_{total}$		$(1.14^{+0.40}_{-0.33}) \times 10^{-10}$
$\Gamma(K^+ \to \pi^+\pi^0 \nu\overline{\nu})/\Gamma_{total}$		$<4.3 \times 10^{-5}$, CL = 90%
$\Gamma(K_S^0 \to \mu^+\mu^-)/\Gamma_{total}$		$<2.1 \times 10^{-10}$, CL = 90%
$\Gamma(K_S^0 \to e^+e^-)/\Gamma_{total}$		$<9 \times 10^{-9}$, CL = 90%
$\Gamma(K_S^0 \to \pi^0 e^+ e^-)/\Gamma_{total}$	[y]	$(3.0^{+1.5}_{-1.2}) \times 10^{-9}$
$\Gamma(K_S^0 \to \pi^0 \mu^+ \mu^-)/\Gamma_{total}$		$(2.9^{+1.5}_{-1.2}) \times 10^{-9}$
$\Gamma(K_L^0 \to \mu^+\mu^-)/\Gamma_{total}$		$(6.84 \pm 0.11) \times 10^{-9}$
$\Gamma(K_L^0 \to e^+e^-)/\Gamma_{total}$		$(9^{+6}_{-4}) \times 10^{-12}$
$\Gamma(K_L^0 \to \pi^+\pi^- e^+ e^-)/\Gamma_{total}$	[z]	$(3.11 \pm 0.19) \times 10^{-7}$
$\Gamma(K_L^0 \to \pi^0\pi^0 e^+ e^-)/\Gamma_{total}$		$<6.6 \times 10^{-9}$, CL = 90%
$\Gamma(K_L^0 \to \pi^0\pi^0 \mu^+ \mu^-)/\Gamma_{total}$		$<9.2 \times 10^{-11}$, CL = 90%
$\Gamma(K_L^0 \to \mu^+\mu^- e^+ e^-)/\Gamma_{total}$		$(2.69 \pm 0.27) \times 10^{-9}$
$\Gamma(K_L^0 \to e^+e^- e^+ e^-)/\Gamma_{total}$		$(3.56 \pm 0.21) \times 10^{-8}$
$\Gamma(K_L^0 \to \pi^0 \mu^+ \mu^-)/\Gamma_{total}$		$<3.8 \times 10^{-10}$, CL = 90%
$\Gamma(K_L^0 \to \pi^0 e^+ e^-)/\Gamma_{total}$		$<2.8 \times 10^{-10}$, CL = 90%
$\Gamma(K_L^0 \to \pi^0 \nu\overline{\nu})/\Gamma_{total}$		$<3.0 \times 10^{-9}$, CL = 90%
$\Gamma(K_L^0 \to \pi^0\pi^0 \nu\overline{\nu})/\Gamma_{total}$		$<8.1 \times 10^{-7}$, CL = 90%
$\Gamma(\Sigma^+ \to pe^+e^-)/\Gamma_{total}$		$<7 \times 10^{-6}$
$\Gamma(\Sigma^+ \to p\mu^+\mu^-)/\Gamma_{total}$		$(2.4^{+1.7}_{-1.3}) \times 10^{-8}$

Unless otherwise stated, limits are given at the 90% confidence level, while errors are given as ±1 standard deviation.

Downloaded from https://academic.oup.com/ptep/article/2022/8/083C01/6651666 by KIT Library user on 27 September 2022

$\Delta C = 1$ WEAK NEUTRAL CURRENT FORBIDDEN

Allowed by higher-order electroweak interactions.

$\Gamma(D^+ \to \pi^+ e^+ e^-)/\Gamma_{total}$		$<1.1 \times 10^{-6}$, CL = 90%
$\Gamma(D^+ \to \pi^+ \mu^+ \mu^-)/\Gamma_{total}$		$<6.7 \times 10^{-8}$, CL = 90%
$\Gamma(D^+ \to \rho^+ \mu^+ \mu^-)/\Gamma_{total}$		$<5.6 \times 10^{-4}$, CL = 90%
$\Gamma(D^0 \to \gamma\gamma)/\Gamma_{total}$		$<8.5 \times 10^{-7}$, CL = 90%
$\Gamma(D^0 \to e^+ e^-)/\Gamma_{total}$		$<7.9 \times 10^{-8}$, CL = 90%
$\Gamma(D^0 \to \mu^+ \mu^-)/\Gamma_{total}$		$<6.2 \times 10^{-9}$, CL = 90%
$\Gamma(D^0 \to \pi^0 e^+ e^-)/\Gamma_{total}$		$<4 \times 10^{-6}$, CL = 90%
$\Gamma(D^0 \to \pi^0 \mu^+ \mu^-)/\Gamma_{total}$		$<1.8 \times 10^{-4}$, CL = 90%
$\Gamma(D^0 \to \eta e^+ e^-)/\Gamma_{total}$		$<3 \times 10^{-6}$, CL = 90%
$\Gamma(D^0 \to \eta \mu^+ \mu^-)/\Gamma_{total}$		$<5.3 \times 10^{-4}$, CL = 90%
$\Gamma(D^0 \to \pi^+ \pi^- e^+ e^-)/\Gamma_{total}$		$<7 \times 10^{-6}$, CL = 90%
$\Gamma(D^0 \to \rho^0 e^+ e^-)/\Gamma_{total}$		$<1.0 \times 10^{-4}$, CL = 90%
$\Gamma(D^0 \to \pi^+ \pi^- \mu^+ \mu^-)/\Gamma_{total}$		$(9.6 \pm 1.2) \times 10^{-7}$
$\Gamma(D^0 \to \rho^0 \mu^+ \mu^-)/\Gamma_{total}$		$<2.2 \times 10^{-5}$, CL = 90%
$\Gamma(D^0 \to \omega e^+ e^-)/\Gamma_{total}$		$<6 \times 10^{-6}$, CL = 90%
$\Gamma(D^0 \to \omega \mu^+ \mu^-)/\Gamma_{total}$		$<8.3 \times 10^{-4}$, CL = 90%
$\Gamma(D^0 \to K^- K^+ e^+ e^-)/\Gamma_{total}$		$<1.1 \times 10^{-5}$, CL = 90%
$\Gamma(D^0 \to \phi e^+ e^-)/\Gamma_{total}$		$<5.2 \times 10^{-5}$, CL = 90%
$\Gamma(D^0 \to K^- K^+ \mu^+ \mu^-)/\Gamma_{total}$		$(1.54 \pm 0.32) \times 10^{-7}$
$\Gamma(D^0 \to \phi \mu^+ \mu^-)/\Gamma_{total}$		$<3.1 \times 10^{-5}$, CL = 90%
$\Gamma(D^0 \to K^- \pi^+ \mu^+ \mu^-)/\Gamma_{total}$		$<3.59 \times 10^{-4}$, CL = 90%
$\Gamma(D^0 \to \pi^+ \pi^- \pi^0 \mu^+ \mu^-)/\Gamma_{total}$		$<8.1 \times 10^{-4}$, CL = 90%
$\Gamma(D_s^+ \to K^+ e^+ e^-)/\Gamma_{total}$		$<3.7 \times 10^{-6}$, CL = 90%
$\Gamma(D_s^+ \to K^+ \mu^+ \mu^-)/\Gamma_{total}$		$<1.4 \times 10^{-7}$, CL = 90%
$\Gamma(D_s^+ \to K^*(892)^+ \mu^+ \mu^-)/\Gamma_{total}$		$<1.4 \times 10^{-3}$, CL = 90%
$\Gamma(\Lambda_c^+ \to p e^+ e^-)/\Gamma_{total}$		$<5.5 \times 10^{-6}$, CL = 90%
$\Gamma(\Lambda_c^+ \to p \mu^+ \mu^-$ non-resonant$)/\Gamma_{total}$		$<7.7 \times 10^{-8}$, CL = 90%

$\Delta B = 1$ WEAK NEUTRAL CURRENT FORBIDDEN

Allowed by higher-order electroweak interactions.

$\Gamma(B^+ \to \pi^+ \ell^+ \ell^-)/\Gamma_{total}$		$<4.9 \times 10^{-8}$, CL = 90%
$\Gamma(B^+ \to \pi^+ e^+ e^-)/\Gamma_{total}$		$<8.0 \times 10^{-8}$, CL = 90%
$\Gamma(B^+ \to \pi^+ \mu^+ \mu^-)/\Gamma_{total}$		$(1.78 \pm 0.23) \times 10^{-8}$
$\Gamma(B^+ \to \pi^+ \nu\overline{\nu})/\Gamma_{total}$		$<1.4 \times 10^{-5}$, CL = 90%
$\Gamma(B^+ \to K^+ \ell^+ \ell^-)/\Gamma_{total}$	[aa]	$(4.7 \pm 0.5) \times 10^{-7}$ (S = 2.3)
$\Gamma(B^+ \to K^+ e^+ e^-)/\Gamma_{total}$		$(5.6 \pm 0.6) \times 10^{-7}$
$\Gamma(B^+ \to K^+ \mu^+ \mu^-)/\Gamma_{total}$		$(4.53 \pm 0.35) \times 10^{-7}$ (S = 1.8)
$\Gamma(B^+ \to K^+ \mu^+ \mu^-$ nonresonant$)/\Gamma_{total}$		$(4.37 \pm 0.27) \times 10^{-7}$
$\Gamma(B^+ \to K^+ \tau^+ \tau^-)/\Gamma_{total}$		$<2.25 \times 10^{-3}$, CL = 90%
$\Gamma(B^+ \to K^+ \overline{\nu}\nu)/\Gamma_{total}$		$<1.6 \times 10^{-5}$, CL = 90%
$\Gamma(B^+ \to \rho^+ \nu\overline{\nu})/\Gamma_{total}$		$<3.0 \times 10^{-5}$, CL = 90%
$\Gamma(B^+ \to K^*(892)^+ \ell^+ \ell^-)/\Gamma_{total}$	[aa]	$(1.01 \pm 0.11) \times 10^{-6}$ (S = 1.1)
$\Gamma(B^+ \to K^*(892)^+ e^+ e^-)/\Gamma_{total}$		$(1.55^{+0.40}_{-0.31}) \times 10^{-6}$
$\Gamma(B^+ \to K^*(892)^+ \mu^+ \mu^-)/\Gamma_{total}$		$(9.6 \pm 1.0) \times 10^{-7}$
$\Gamma(B^+ \to K^*(892)^+ \nu\overline{\nu})/\Gamma_{total}$		$<4.0 \times 10^{-5}$, CL = 90%
$\Gamma(B^+ \to K^+ \pi^+ \pi^- \mu^+ \mu^-)/\Gamma_{total}$		$(4.3 \pm 0.4) \times 10^{-7}$
$\Gamma(B^+ \to \phi K^+ \mu^+ \mu^-)/\Gamma_{total}$		$(7.9^{+2.1}_{-1.7}) \times 10^{-8}$
$\Gamma(B^0 \to \gamma\gamma)/\Gamma_{total}$		$<3.2 \times 10^{-7}$, CL = 90%
$\Gamma(B^0 \to e^+ e^-)/\Gamma_{total}$		$<2.5 \times 10^{-9}$, CL = 90%
$\Gamma(B^0 \to e^+ e^- \gamma)/\Gamma_{total}$		$<1.2 \times 10^{-7}$, CL = 90%
$\Gamma(B^0 \to \mu^+ \mu^-)/\Gamma_{total}$		$(7^{+13}_{-11}) \times 10^{-11}$ (S = 1.8)
$\Gamma(B^0 \to \mu^+ \mu^- \gamma)/\Gamma_{total}$		$<2.0 \times 10^{-9}$, CL = 95%
$\Gamma(B^0 \to \mu^+ \mu^- \mu^+ \mu^-)/\Gamma_{total}$		$<6.9 \times 10^{-10}$, CL = 95%
$\Gamma(B^0 \to SP,\ S \to \mu^+ \mu^-,\ P \to \mu^+ \mu^-)/\Gamma_{total}$	[bb]	$<6.0 \times 10^{-10}$, CL = 95%
$\Gamma(B^0 \to \tau^+ \tau^-)/\Gamma_{total}$		$<2.1 \times 10^{-3}$, CL = 95%
$\Gamma(B^0 \to \pi^0 \ell^+ \ell^-)/\Gamma_{total}$		$<5.3 \times 10^{-8}$, CL = 90%
$\Gamma(B^0 \to \pi^0 e^+ e^-)/\Gamma_{total}$		$<8.4 \times 10^{-8}$, CL = 90%
$\Gamma(B^0 \to \pi^0 \mu^+ \mu^-)/\Gamma_{total}$		$<6.9 \times 10^{-8}$, CL = 90%
$\Gamma(B^0 \to \eta \ell^+ \ell^-)/\Gamma_{total}$		$<6.4 \times 10^{-8}$, CL = 90%
$\Gamma(B^0 \to \eta e^+ e^-)/\Gamma_{total}$		$<1.08 \times 10^{-7}$, CL = 90%
$\Gamma(B^0 \to \eta \mu^+ \mu^-)/\Gamma_{total}$		$<1.12 \times 10^{-7}$, CL = 90%
$\Gamma(B^0 \to \pi^0 \nu\overline{\nu})/\Gamma_{total}$		$<9 \times 10^{-6}$, CL = 90%
$\Gamma(B^0 \to K^0 \ell^+ \ell^-)/\Gamma_{total}$	[aa]	$(3.3 \pm 0.6) \times 10^{-7}$
$\Gamma(B^0 \to K^0 e^+ e^-)/\Gamma_{total}$		$(2.5^{+1.1}_{-0.9}) \times 10^{-7}$ (S = 1.3)
$\Gamma(B^0 \to K^0 \mu^+ \mu^-)/\Gamma_{total}$		$(3.39 \pm 0.35) \times 10^{-7}$ (S = 1.1)
$\Gamma(B^0 \to K^0 \nu\overline{\nu})/\Gamma_{total}$		$<2.6 \times 10^{-5}$, CL = 90%
$\Gamma(B^0 \to \rho^0 \nu\overline{\nu})/\Gamma_{total}$		$<4.0 \times 10^{-5}$, CL = 90%
$\Gamma(B^0 \to K^*(892)^0 \ell^+ \ell^-)/\Gamma_{total}$	[aa]	$(9.9^{+1.2}_{-1.1}) \times 10^{-7}$
$\Gamma(B^0 \to K^*(892)^0 e^+ e^-)/\Gamma_{total}$		$(1.03^{+0.19}_{-0.17}) \times 10^{-6}$
$\Gamma(B^0 \to K^*(892)^0 \mu^+ \mu^-)/\Gamma_{total}$		$(9.4 \pm 0.5) \times 10^{-7}$
$\Gamma(B^0 \to \pi^+ \pi^- \mu^+ \mu^-)/\Gamma_{total}$		$(2.1 \pm 0.5) \times 10^{-8}$
$\Gamma(B^0 \to K^*(892)^0 \nu\overline{\nu})/\Gamma_{total}$		$<1.8 \times 10^{-5}$, CL = 90%
$\Gamma(B^0 \to$ invisible$)/\Gamma_{total}$		$<2.4 \times 10^{-5}$, CL = 90%
$\Gamma(B^0 \to \nu\overline{\nu}\gamma)/\Gamma_{total}$		$<1.6 \times 10^{-5}$, CL = 90%
$\Gamma(B^0 \to \phi\nu\overline{\nu})/\Gamma_{total}$		$<1.27 \times 10^{-4}$, CL = 90%
$\Gamma(B \to s e^+ e^-)/\Gamma_{total}$		$(6.7 \pm 1.7) \times 10^{-6}$ (S = 2.0)
$\Gamma(B \to s \mu^+ \mu^-)/\Gamma_{total}$		$(4.3 \pm 1.0) \times 10^{-6}$
$\Gamma(B \to s \ell^+ \ell^-)/\Gamma_{total}$	[aa]	$(5.8 \pm 1.3) \times 10^{-6}$ (S = 1.8)
$\Gamma(B \to \pi \ell^+ \ell^-)/\Gamma_{total}$		$<5.9 \times 10^{-8}$, CL = 90%
$\Gamma(B \to \pi e^+ e^-)/\Gamma_{total}$		$<1.10 \times 10^{-7}$, CL = 90%
$\Gamma(B \to \pi \mu^+ \mu^-)/\Gamma_{total}$		$<5.0 \times 10^{-8}$, CL = 90%
$\Gamma(B \to K e^+ e^-)/\Gamma_{total}$		$(4.4 \pm 0.6) \times 10^{-7}$
$\Gamma(B \to K^*(892) e^+ e^-)/\Gamma_{total}$		$(1.19 \pm 0.20) \times 10^{-6}$ (S = 1.2)
$\Gamma(B \to K \mu^+ \mu^-)/\Gamma_{total}$		$(4.4 \pm 0.4) \times 10^{-7}$
$\Gamma(B \to K^*(892) \mu^+ \mu^-)/\Gamma_{total}$		$(1.06 \pm 0.09) \times 10^{-6}$
$\Gamma(B \to K \ell^+ \ell^-)/\Gamma_{total}$		$(4.8 \pm 0.4) \times 10^{-7}$
$\Gamma(B \to K^*(892) \ell^+ \ell^-)/\Gamma_{total}$		$(1.05 \pm 0.10) \times 10^{-6}$
$\Gamma(B \to K \nu\overline{\nu})/\Gamma_{total}$		$<1.6 \times 10^{-5}$, CL = 90%
$\Gamma(B \to K^* \nu\overline{\nu})/\Gamma_{total}$		$<2.7 \times 10^{-5}$, CL = 90%
$\Gamma(B \to \pi \nu\overline{\nu})/\Gamma_{total}$		$<8 \times 10^{-6}$, CL = 90%
$\Gamma(B \to \rho \nu\overline{\nu})/\Gamma_{total}$		$<2.8 \times 10^{-5}$, CL = 90%
$\Gamma(\overline{b} \to \overline{s}\overline{\nu}\nu)/\Gamma_{total}$		$<6.4 \times 10^{-4}$, CL = 90%
$\Gamma(\overline{b} \to \mu^+ \mu^-$ anything$)/\Gamma_{total}$		$<3.2 \times 10^{-4}$, CL = 90%
$\Gamma(B_s^0 \to \gamma\gamma)/\Gamma_{total}$		$<3.1 \times 10^{-6}$, CL = 90%
$\Gamma(B_s^0 \to \phi\gamma)/\Gamma_{total}$		$(3.4 \pm 0.4) \times 10^{-5}$
$\Gamma(B_s^0 \to \mu^+ \mu^-)/\Gamma_{total}$		$(3.01 \pm 0.35) \times 10^{-9}$
$\Gamma(B_s^0 \to e^+ e^-)/\Gamma_{total}$		$<9.4 \times 10^{-9}$, CL = 90%
$\Gamma(B_s^0 \to \tau^+ \tau^-)/\Gamma_{total}$		$<6.8 \times 10^{-3}$, CL = 95%
$\Gamma(B_s^0 \to \mu^+ \mu^- \mu^+ \mu^-)/\Gamma_{total}$		$<2.5 \times 10^{-9}$, CL = 95%
$\Gamma(B_s^0 \to SP,\ S \to \mu^+ \mu^-,\ P \to \mu^+ \mu^-)/\Gamma_{total}$	[bb]	$<2.2 \times 10^{-9}$, CL = 95%
$\Gamma(B_s^0 \to \phi(1020) \mu^+ \mu^-)/\Gamma_{total}$		$(8.4 \pm 0.4) \times 10^{-7}$
$\Gamma(B_s^0 \to \overline{K}^*(892)^0 \mu^+ \mu^-)/\Gamma_{total}$		$(2.9 \pm 1.1) \times 10^{-8}$
$\Gamma(B_s^0 \to \pi^+ \pi^- \mu^+ \mu^-)/\Gamma_{total}$		$(8.4 \pm 1.7) \times 10^{-8}$
$\Gamma(B_s^0 \to \phi\nu\overline{\nu})/\Gamma_{total}$		$<5.4 \times 10^{-3}$, CL = 90%

$\Delta T = 1$ WEAK NEUTRAL CURRENT FORBIDDEN

Allowed by higher-order electroweak interactions.

$\Gamma(t \to Zq(q{=}u,c))/\Gamma_{total}$	[cc]	$<5 \times 10^{-4}$, CL = 95%
$\Gamma(t \to Hu)/\Gamma_{total}$		$<1.2 \times 10^{-3}$, CL = 95%
$\Gamma(t \to Hc)/\Gamma_{total}$		$<1.1 \times 10^{-3}$, CL = 95%
$\Gamma(t \to \ell^+ \overline{q}q'(q{=}d,s,b;\ q'{=}u,c))/\Gamma_{total}$		$<1.6 \times 10^{-3}$, CL = 95%

NOTES

In this Summary Table:

When a quantity has "(S = ...)" to its right, the error on the quantity has been enlarged by the "scale factor" S, defined as $S = \sqrt{\chi^2/(N-1)}$, where N is the number of measurements used in calculating the quantity. We do this when S > 1, which often indicates that the measurements are inconsistent. When S > 1.25, we also show in the Particle Listings an ideogram of the measurements. For more about S, see the Introduction.

[a] Forbidden by angular momentum conservation.
[b] C parity forbids this to occur as a single-photon process.
[c] See the Particle Listings for the (complicated) definition of this quantity.
[d] Time-reversal invariance requires this to be 0° or 180°.
[e] This coefficient is zero if time invariance is not violated.
[f] Allowed by higher-order electroweak interactions.

Unless otherwise stated, limits are given at the 90% confidence level, while errors are given as ±1 standard deviation.

Downloaded from https://academic.oup.com/ptep/article/2022/8/083C01/6651666 by KIT Library user on 27 September 2022

[g] Violates *CP* in leading order. Test of direct *CP* violation since the indirect *CP*-violating and *CP*-conserving contributions are expected to be suppressed.

[h] In the 2010 *Review*, the values for these quantities were given using a measure of the asymmetry that was inconsistent with the usual definition.

[i] $\mathrm{Re}(\epsilon'/\epsilon) = \epsilon'/\epsilon$ to a very good approximation provided the phases satisfy *CPT* invariance.

[j] This mode includes gammas from inner bremsstrahlung but not the direct emission mode $K^0_L \to \pi^+\pi^-\gamma(\mathrm{DE})$.

[k] Neglecting photon channels. See, *e.g.*, A. Pais and S.B. Treiman, Phys. Rev. **D12**, 2744 (1975).

[l] Derived from measured values of ϕ_{+-}, ϕ_{00}, $|\eta|$, $|m_{K^0_L} - m_{K^0_S}|$, and $\tau_{K^0_S}$, as described in the introduction to "Tests of Conservation Laws."

[n] The $|m_p - m_{\overline{p}}|/m_p$ and $|q_p + q_{\overline{p}}|/e$ are not independent, and both use the more precise measurement of $|q_{\overline{p}}/m_{\overline{p}}|/(q_p/m_p)$.

[o] The value is for the sum of the charge states or particle/antiparticle states indicated.

[p] A test of additive vs. multiplicative lepton family number conservation.

[q] Derived from an analysis of neutrino-oscillation experiments.

[r] This limit is for either D^0 or $\overline{D}^0$ to $p e^-$.

[s] This limit is for either D^0 or $\overline{D}^0$ to $\overline{p} e^+$.

[t] The first limit is for $p \to$ anything or "disappearance" modes of a bound proton. The second entry, a rough range of limits, assumes the dominant decay modes are among those investigated. For antiprotons the best limit, inferred from the observation of cosmic ray $\overline{p}$'s is $\tau_{\overline{p}} > 10^7$ yr, the cosmic-ray storage time, but this limit depends on a number of assumptions. The best direct observation of stored antiprotons gives $\tau_{\overline{p}}/\mathrm{B}(\overline{p} \to e^-\gamma) > 7 \times 10^5$ yr.

[u] There is some controversy about whether nuclear physics and model dependence complicate the analysis for bound neutrons (from which the best limit comes). The first limit here is from reactor experiments with free neutrons.

[v] This is the best limit for the mode $e^- \to \nu\gamma$. The best limit for Nuclear de-excitation experiments is 6.4×10^{24} yr.

[x] The limit is from neutrality-of-matter experiments; it assumes $q_n = q_p + q_e$. See also the charge of the neutron.

[y] See the K^0_S Particle Listings for the energy limits used in this measurement.

[z] See the K^0_L Particle Listings for the energy limits used in this measurement.

[aa] An ℓ indicates an e or a μ mode, not a sum over these modes.

[bb] Here S and P are the hypothetical scalar and pseudoscalar particles with masses of 2.5 GeV/c^2 and 214.3 MeV/c^2, respectively.

[cc] This limit is for $\Gamma(t \to Zq)/\Gamma(t \to Wb)$.

Unless otherwise stated, limits are given at the 90% confidence level, while errors are given as ± 1 standard deviation.

Downloaded from https://academic.oup.com/ptep/article/2022/8/083C01/6651666 by KIT Library user on 27 September 2022

REVIEWS, TABLES, AND PLOTS

Constants, Units, Atomic and Nuclear Properties

1. Physical constants (rev.) 133
2. Astrophysical constants and parameters (rev.) 134
3. International system of units (SI) (rev.) 136
4. Periodic table of the elements (rev.) 137
5. Electronic structure of the elements 138
6. Atomic and nuclear properties of materials (rev.) 140
7. Electromagnetic relations 142
8. Naming scheme for hadrons (rev.) 144

Downloaded from https://academic.oup.com/ptep/article/2022/8/083C01/6651666 by KIT Library user on 27 September 2022

Downloaded from https://academic.oup.com/ptep/article/2022/8/083C01/6651666 by KIT Library user on 27 September 2022

1. Physical Constants

Table 1.1: Revised 2021 by D. Robinson (LBNL). Reviewed by P. Mohr (NIST). Mainly from "CODATA Recommended Values of the Fundamental Physical Constants: 2018," E. Tiesinga, D.B. Newell, P.J. Mohr, and B.N. Taylor, NIST SP961 (May 2019) [1]. The electron charge magnitude e, and the Planck, Boltzmann, and Avogadro constants h, k, and N_A, now join c as having defined values; the free-space permittivity and permeability constants ϵ_0 and μ_0 are no longer exact. These changes affect practically everything else in the Table. Figures in parentheses after the values are the 1-standard-deviation uncertainties in the last digits; the fractional uncertainties in parts per 10^9 (ppb) are in the last column. The full 2018 CODATA Committee on Data for Science and Technology set of constants are found at `https://physics.nist.gov/constants`. The last set of constants (beginning with the Fermi coupling constant) comes from the Particle Data Group. See also "The International System of Units (SI)," 9th ed. (2019) of the International Bureau of Weights and Measures (BIPM), `https://www.bipm.org/utils/common/pdf/si-brochure/SI-Brochure-9-EN.pdf`.

Quantity	Symbol, equation	Value	Uncertainty (ppb)
speed of light in vacuum	c	299 792 458 m s^{-1}	exact
Planck constant	h	6.626 070 15$\times10^{-34}$ J s (or J/Hz) §	exact
Planck constant, reduced	$\hbar \equiv h/2\pi$	1.054 571 817... $\times 10^{-34}$ J s	exact*
		= 6.582 119 569... $\times 10^{-22}$ MeV s	exact*
electron charge magnitude	e	1.602 176 634$\times10^{-19}$ C	exact
conversion constant	$\hbar c$	197.326 980 4... MeV fm	exact*
conversion constant	$(\hbar c)^2$	0.389 379 372 1... GeV^2 mbarn	exact*
electron mass	m_e	0.510 998 950 00(15) MeV/c^2 = 9.109 383 7015(28)$\times10^{-31}$ kg	0.30
proton mass	m_p	938.272 088 16(29) MeV/c^2 = 1.672 621 923 69(51)$\times10^{-27}$ kg	0.31
		= 1.007 276 466 621(53) u = 1836.152 673 43(11) m_e	0.053, 0.060
neutron mass	m_n	939.565 420 52(54) MeV/c^2 = 1.008 664 915 95(49) u	0.57, 0.48
deuteron mass	m_d	1875.612 942 57(57) MeV/c^2	0.30
unified atomic mass unit**	u = (mass ^{12}C atom)/12	931.494 102 42(28) MeV/c^2 = 1.660 539 066 60(50)$\times10^{-27}$ kg	0.30
permittivity of free space	$\epsilon_0 = 1/\mu_0 c^2$	8.854 187 8128(13) $\times10^{-12}$ F m^{-1}	0.15
permeability of free space	$\mu_0/(4\pi\times10^{-7})$	1.000 000 000 55(15) N A^{-2}	0.15
fine-structure constant	$\alpha = e^2/4\pi\epsilon_0\hbar c$	7.297 352 5693(11)$\times10^{-3}$ = 1/137.035 999 084(21)† ‡‡	0.15
classical electron radius	$r_e = e^2/4\pi\epsilon_0 m_e c^2$	2.817 940 3262(13)$\times10^{-15}$ m	0.45
(e^- Compton wavelength)/2π	$\lambdabar_e = \hbar/m_e c = r_e\alpha^{-1}$	3.861 592 6796(12)$\times10^{-13}$ m	0.30
Bohr radius ($m_{\rm nucleus}=\infty$)	$a_\infty = 4\pi\epsilon_0\hbar^2/m_e e^2 = r_e\alpha^{-2}$	0.529 177 210 903(80)$\times10^{-10}$ m	0.15
wavelength of 1 eV/c particle	$hc/(1\ {\rm eV})$	1.239 841 984... $\times 10^{-6}$ m	exact*
Rydberg energy	$hcR_\infty = m_e e^4/2(4\pi\epsilon_0)^2\hbar^2 = m_e c^2\alpha^2/2$	13.605 693 122 994(26) eV	1.9$\times10^{-3}$
Thomson cross section	$\sigma_T = 8\pi r_e^2/3$	0.665 245 873 21(60) barn	0.91
Bohr magneton	$\mu_B = e\hbar/2m_e$	5.788 381 8060(17)$\times10^{-11}$ MeV T^{-1}	0.30
nuclear magneton	$\mu_N = e\hbar/2m_p$	3.152 451 258 44(96)$\times10^{-14}$ MeV T^{-1}	0.31
electron cyclotron freq./field	$\omega^e_{\rm cycl}/B = e/m_e$	1.758 820 010 76(53)$\times10^{11}$ rad s^{-1} T^{-1}	0.30
proton cyclotron freq./field	$\omega^p_{\rm cycl}/B = e/m_p$	9.578 833 1560(29)$\times10^{7}$ rad s^{-1} T^{-1}	0.31
gravitational constant‡	G_N	6.674 30(15)$\times10^{-11}$ m^3 kg^{-1} s^{-2}	2.2×10^4
		= 6.708 83(15)$\times10^{-39}$ $\hbar c$ (GeV/c^2)$^{-2}$	2.2×10^4
standard gravitational accel.	g_N	9.806 65 m s^{-2}	exact
Avogadro constant	N_A	6.022 140 76$\times10^{23}$ mol^{-1}	exact
Boltzmann constant	k	1.380 649$\times10^{-23}$ J K^{-1}	exact
		= 8.617 333 262... $\times 10^{-5}$ eV K^{-1}	exact*
molar volume, ideal gas at STP	$N_A k$ (273.15 K)/(101 325 Pa)	22.413 969 54... $\times 10^{-3}$ m^3 mol^{-1}	exact*
Wien displacement law constant	$b = \lambda_{\rm max}T$	2.897 771 955... $\times 10^{-3}$ m K	exact*
Stefan-Boltzmann constant	$\sigma = \pi^2k^4/60\hbar^3c^2$	5.670 374 419... $\times 10^{-8}$ W m^{-2} K^{-4}	exact*
Fermi coupling constant‡‡	$G_F/(\hbar c)^3$	1.166 378 8(6)$\times10^{-5}$ GeV^{-2}	510
weak-mixing angle	$\sin^2\widehat{\theta}(M_Z)\ (\overline{\rm MS})$	0.231 21(4)††	1.7×10^5
$W^\pm$ boson mass	m_W	80.377(12) GeV/c^2¶	1.5×10^5
Z^0 boson mass	m_Z	91.1876(21) GeV/c^2	2.3×10^4
strong coupling constant	$\alpha_s(m_Z)$	0.1179(9)	7.6×10^6

π = 3.141 592 653 589 793 238 ...		e = 2.718 281 828 459 045 235...	γ = 0.577 215 664 901 532 860...
1 in ≡ 0.0254 m	1 G ≡ 10^{-4} T	1 eV = 1.602 176 634 × 10^{-19} J (exact)	kT at 300 K = [38.681 727 0718...]$^{-1}$eV (exact*)
1 Å ≡ 0.1 nm	1 dyne ≡ 10^{-5} N	(1 kg)c^2 = 5.609 588 603... × 10^{35}eV(exact*)	0 °C ≡ 273.15K
1 barn ≡ 10^{-28} m^2	1 erg ≡ 10^{-7} J	1 C = 2.997 924 58 × 10^9 esu	1 atmosphere ≡ 760 Torr ≡ 101 325Pa

§CODATA recommends that the unit be J/Hz to stress that in $h = E/\nu$ the frequency ν is in cycles/sec (Hz), not radians/sec.
*These are calculated from exact values and are exact to the number of places given (*i.e.* no rounding).
**The molar mass of ^{12}C is 11.999 999 9958(36) g.
†At $Q^2 = 0$. At $Q^2 \approx m_W^2$ the value is $\sim 1/128$.
‡Absolute laboratory measurements of G_N have been made only on scales of about 1 cm to 1 m.
‡‡See the discussion in Ch. 10, "Electroweak model and constraints on new physics."
††The corresponding $\sin^2\theta$ for the effective angle is 0.23153(4).
¶See the "Mass and width of the W boson" review.

References

[1] E. Tiesinga *et al.*, Rev. Mod. Phys. **93**, 025010 (2021).

Downloaded from https://academic.oup.com/ptep/article/2022/8/083C01/6651666 by KIT Library user on 27 September 2022

2. Astrophysical Constants and Parameters

Table 2.1: Revised August 2021 by D.E. Groom (LBNL) and D. Scott (U. of British Columbia). The figures in parentheses after some values give the 1-σ uncertainties in the last digit(s). Physical constants are from Ref. [1]. While every effort has been made to obtain the most accurate current values of the listed quantities, this table does not represent a critical review or adjustment of the constants, and is not intended as a primary reference. The values and uncertainties for the cosmological parameters depend on the exact data sets, priors, and basis parameters used in the fit. Many of the derived parameters reported in this table have non-Gaussian likelihoods and parameters may be highly correlated, so care must be taken in propagating errors. Unless otherwise specified, cosmological parameters are derived from a 6-parameter ΛCDM cosmology fit to *Planck* cosmic microwave background 2018 temperature (TT) + polarization (TE,EE+lowE) + lensing data [2]. For more information see Ref. [3] and the original papers.

Quantity	Symbol, equation	Value	Reference, footnote
Newtonian constant of gravitation	G_N	$6.674\,30(15) \times 10^{-11}\,\mathrm{m^3\,kg^{-1}\,s^{-2}}$	[1]
Planck mass	$M_P = \sqrt{\hbar c/G_N}$	$1.220\,890(14) \times 10^{19}\ \mathrm{GeV}/c^2 = 2.176\,434(24) \times 10^{-8}\ \mathrm{kg}$	[1]
Planck length	$l_P = \sqrt{\hbar G_N/c^3}$	$1.616\,255(18) \times 10^{-35}\ \mathrm{m}$	[1]
tropical year (equinox to equinox, 2020)	yr	$31\,556\,925.1\ \mathrm{s} = 365.242\,189$ days	[4]
sidereal year (period of Earth around Sun relative to stars)		$31\,558\,149.8\ \mathrm{s} \approx \pi \times 10^7\ \mathrm{s}$	[4]
mean sidereal day (Earth rotation period relative to stars)		$23^{\mathrm{h}}\,56^{\mathrm{m}}\,04\overset{\mathrm{s}}{.}090\,53$	[4]
astronomical unit	au	$149\,597\,870\,700\ \mathrm{m}$	exact [5]
parsec (1 au/1 arc sec)	pc	$3.085\,677\,581\,49\ldots \times 10^{16}\ \mathrm{m} = 3.261\,56\ldots\mathrm{ly}$	exact [6]
light year (deprecated unit)	ly	$0.306\,601\ldots\ \mathrm{pc} = 0.946\,073\ldots \times 10^{16}\ \mathrm{m}$	[7]
solid angle	deg^2	$(\pi/180)^2\ \mathrm{sr} = 3.046\,17\ldots \times 10^{-4}\ \mathrm{sr}$	[8]
Schwarzschild radius of the Sun	$2G_N M_\odot/c^2$	$2.953\,250\,1\ \mathrm{km}$	[9]
Solar mass	$M_\odot$	$1.988\,41(4) \times 10^{30}\ \mathrm{kg}$	[10]
nominal Solar equatorial radius	$\mathcal{R}_\odot$	$6.957 \times 10^8\ \mathrm{m}$	exact [11]
nominal Solar constant	$\mathcal{S}_\odot$	$1361\ \mathrm{W\,m^{-2}}$	exact [11,12]
nominal Solar photosphere temperature	$\mathcal{T}_\odot$	$5772\ \mathrm{K}$	exact [11]
nominal Solar luminosity	$\mathcal{L}_\odot$	$3.828 \times 10^{26}\ \mathrm{W}$	exact [11,13]
Schwarzschild radius of the Earth	$2G_N M_\oplus/c^2$	$8.870\,056\ \mathrm{mm}$	[9]
Earth mass	$M_\oplus$	$5.972\,17(13) \times 10^{24}\ \mathrm{kg}$	[10]
nominal Earth equatorial radius	$\mathcal{R}_\oplus$	$6.3781 \times 10^6\ \mathrm{m}$	exact [11]
Chandrasekhar mass	M_{Ch}	$3.097\,972\,\mu^{-2}\,M_P^3/m_H^2 = 1.433\,77(6)\,(\mu/2)^{-2}\,M_\odot$	[14,15]
Eddington luminosity	L_{Ed}	$1.257\,065\,179\,8(12) \times 10^{31}\,(M/M_\odot)\ \mathrm{W}$	[16,17]
		$= 3.283\,869\,330\,8(31) \times 10^4\,(M/M_\odot)\ \mathcal{L}_\odot$	
jansky (flux density)	Jy	$10^{-26}\ \mathrm{W\,m^{-2}\,Hz^{-1}}$	definition
luminosity conversion	f_0	$3.0128 \times 10^{28} \times 10^{-0.4\ M_{\mathrm{Bol}}}\ \mathrm{W}$	exact [18]
		(M_{Bol} = absolute bolometric magnitude = bolometric magnitude at 10 pc)	
flux conversion	$\mathcal{F}$	$2.518\,021\,002 \times 10^{-8} \times 10^{-0.4\ m_{\mathrm{Bol}}}\ \mathrm{W\,m^{-2}}$	exact [18]
		(m_{Bol} = apparent bolometric magnitude)	
ABsolute monochromatic magnitude	AB	$-2.5\ \log_{10} f_\nu - 56.10$ (for f_ν in $\mathrm{W\,m^{-2}\,Hz^{-1}}$)	[19]
		$= -2.5\ \log_{10} f_\nu + 8.90$ (for f_ν in Jy)	
Solar angular velocity around Galactic center	Θ_0/R_0	$27.1(5)\ \mathrm{km\,s^{-1}\,kpc^{-1}}$	[20]
Solar distance from Galactic center	R_0	$8.178 \pm 0.013(\mathrm{stat.}) \pm 0.022(\mathrm{sys.})\ \mathrm{kpc}$	[21,22]
circular velocity at R_0	v_0 or Θ_0	$240(8)\ \mathrm{km\,s^{-1}}$	[22,23]
escape velocity from the Galaxy	v_{esc}	$492\,\mathrm{km\,s^{-1}} < v_{\mathrm{esc}} < 587\,\mathrm{km\,s^{-1}}$ (90%)	[24]
local disk density	ρ_{disk}	$6.6(9)\ \times 10^{-24}\ \mathrm{g\,cm^{-3}} = 3.7(5)\ \mathrm{GeV}/c^2\ \mathrm{cm^{-3}}$	[25]
local dark matter density	ρ_χ	canonical value $0.3\ \mathrm{GeV}/c^2\ \mathrm{cm^{-3}}$ within factor 2–3	[26]
present-day CMB temperature	T_0	$2.7255(6)\ \mathrm{K}$	[27,28]
present-day CMB dipole amplitude	d	$3.3621(10)\ \mathrm{mK}$	[27,29]
Solar velocity with respect to CMB	$v_\odot$	$369.82(11)\ \mathrm{km\,s^{-1}}$ towards (l,b)=(264.021(11)°, 48.253(5)°)	[29]
Local Group velocity with respect to CMB	v_{LG}	$620(15)\ \mathrm{km\,s^{-1}}$ towards $(l,b) = (271.9(20)°, 29.6(14)°)$	[29]
number density of CMB photons	n_γ	$410.73(27)\,(T/2.7255\,\mathrm{K})^3\ \mathrm{cm^{-3}}$	[30]
density of CMB photons	ρ_γ	$4.645(4)\,(T/2.7255\,\mathrm{K})^4 \times 10^{-34}\,\mathrm{g\,cm^{-3}} \approx 0.260\ \mathrm{eV\ cm^{-3}}$	[30]
entropy density/Boltzmann constant	s/k	$2\,891.2\,(T/2.7255\,\mathrm{K})^3\ \mathrm{cm^{-3}}$	[30]
present-day Hubble expansion rate	H_0	$100\,h\ \mathrm{km\,s^{-1}\,Mpc^{-1}} = h \times (9.777\,752\ \mathrm{Gyr})^{-1}$	[31]
scaling factor for Hubble expansion rate	h	$0.674(5)$	[2,32]
Hubble length	c/H_0	$0.925\,0629 \times 10^{26}\,h^{-1}\ \mathrm{m} = 1.372(10) \times 10^{26}\ \mathrm{m}$	
scaling for cosmological constant	$c^2/3H_0^2$	$2.85247 \times 10^{51}\,h^{-2}\ \mathrm{m^2} = 6.28(9) \times 10^{51}\ \mathrm{m^2}$	
critical density of the Universe	$\rho_{\mathrm{crit}} = 3H_0^2/8\pi G_N$	$1.878\,34(4) \times 10^{-29}\,h^2\ \mathrm{g\ cm^{-3}}$	
		$= 1.053\,672(24) \times 10^{-5}\,h^2\ (\mathrm{GeV}/c^2)\ \mathrm{cm^{-3}}$	
		$= 2.77536627 \times 10^{11}\,h^2\ M_\odot\mathrm{Mpc^{-3}}$	
baryon-to-photon ratio (from BBN)	$\eta = n_{\mathrm{b}}/n_\gamma$	$6.14(19) \times 10^{-10}$	[33,34]
number density of baryons	n_{b}	$2.515(17) \times 10^{-7}\ \mathrm{cm^{-3}}$ (from CMB)	[2,35]
		$2.52(8) \times 10^{-7}\ \mathrm{cm^{-3}}$ (from BBN, $\eta \times n_\gamma$)	[3,33]
CMB radiation density of the Universe	$\Omega_\gamma = \rho_\gamma/\rho_{\mathrm{crit}}$	$2.473 \times 10^{-5}(T/2.7255\,\mathrm{K})^4\,h^{-2} = 5.38(15) \times 10^{-5}$	[30]
- - - *Planck* 2018 6-parameter fit to flat ΛCDM cosmology - - -			
baryon density of the Universe	$\Omega_{\mathrm{b}} = \rho_{\mathrm{b}}/\rho_{\mathrm{crit}}$	$^\ddagger\,0.02237(15)\,h^{-2} = {}^\dagger\,0.0493(6)$	[2,3,27]
cold dark matter density of the Universe	$\Omega_{\mathrm{c}} = \rho_{\mathrm{c}}/\rho_{\mathrm{crit}}$	$^\ddagger\,0.1200(12)\,h^{-2} = {}^\dagger\,0.265(7)$	[2,3,27]
$100 \times$ approximation to r_*/D_{A}	$100 \times \theta_{\mathrm{MC}}$	$^\ddagger\,1.04092(31)$	[2,3,27]
reionization optical depth	τ	$^\ddagger\,0.054(7)$	[2,3,27]
ln(power prim. curv. pert.) ($k_0 = 0.05\,\mathrm{Mpc^{-1}}$)	$\ln(10^{10}\Delta^2_{\mathcal{R}})$	$^\ddagger\,3.044(14)$	[2,3,27]
scalar spectral index	n_{s}	$^\ddagger\,0.965(4)$	[2,3,27]
pressureless matter parameter	$\Omega_{\mathrm{m}} = \Omega_{\mathrm{c}} + \Omega_{\mathrm{b}}$	$^\dagger\,0.315(7)$	[2,3]
dark energy density parameter	Ω_Λ	$^\dagger\,0.685(7)$	[2,3]
energy density of dark energy	ρ_Λ	$^\dagger\,5.83(16) \times 10^{-30}\,\mathrm{g\,cm^{-3}}$	[2]
cosmological constant	Λ	$^\dagger\,1.088(30) \times 10^{-56}\,\mathrm{cm^{-2}}$	[2]
fluctuation amplitude at $8\,h^{-1}$ Mpc scale	σ_8	$^\dagger\,0.811(6)$	[2,3]

Downloaded from https://academic.oup.com/ptep/article/2022/8/083C01/6651666 by KIT Library user on 27 September 2022

Quantity	Symbol, equation.	Value	Reference,footnote
redshift of matter-radiation equality	$z_{\rm eq}$	† 3402(26)	[2, 36]
age at matter-radiation equality	$t_{\rm eq}$	† 51.1(8) kyr	[2, 37]
redshift at which optical depth equals unity	z_*	† 1089.92(25)	[2]
comoving size of sound horizon at z_*	r_*	† 144.43(26) Mpc	[2, 38]
age when optical depth equals unity	t_*	† 372.9(10) kyr	[2, 37]
redshift at half reionization	$z_{\rm i}$	† 7.7(7)	[2, 39]
age at half reionization	$t_{\rm i}$	† 690(90) Myr	[2]
redshift when acceleration was zero	z_q	† 0.636(18)	[2, 37]
age when acceleration was zero	t_q	† 7.70(10) Gyr	[2]
age of the Universe today	t_0	† 13.797(23) Gyr	[2]
effective number of neutrinos	$N_{\rm eff}$	♯ 2.99(17)	[2, 40, 41]
sum of neutrino masses	Σm_ν	♯ < 0.12 eV (95%, CMB + BAO); ≥ 0.06 eV (mixing)	[2, 41–43]
neutrino density of the Universe	$\Omega_\nu = h^{-2}\Sigma m_\nu/93.14\,{\rm eV}$	♯ < 0.003 (95%, CMB + BAO); ≥ 0.0012 (mixing)	[2, 42, 43]
curvature	Ω_K	♯ 0.0007(19)	[2]
running spectral index, $k_0 = 0.05\,{\rm Mpc}^{-1}$	$dn_{\rm s}/d\ln k$	♯ $-0.004(7)$	[2]
tensor-to-scalar perturbation ratio	$r_{0.05} = T/S$	< 0.036 (95% CL, $k_0 = 0.05\,{\rm Mpc}^{-1}$)	[2, 44–47]
dark energy equation of state parameter	w	♯ $-1.028(31)$	[2, 48]
primordial helium fraction	$Y_{\rm p}$	0.2453(34)	[49]

‡ Parameter in 6-parameter ΛCDM fit; † derived parameter in 6-parameter ΛCDM fit; ♯ extended model parameter, *Planck* + BAO data [2].

References

[1] CODATA recommended 2018 values of the fundamental physical constants: `physics.nist.gov/cuu/Constants/index.html`.

[2] Planck Collab. 2018 Results VI, Astron. Astrophys. **641**, A6 (2020), [arXiv:1807.06209].

[3] O. Lahav and A. R. Liddle, "The Cosmological Parameters," Sec. 25.1 in this *Review*.

[4] *The Astronomical Almanac for the year 2020*.

[5] The astronomical unit of length (au) in meters is re-defined (IAU XXVIII General Assembly 2012, Resolution B2) to be a conventional unit of length in agreement with the value adopted in IAU XXVII 2009 Resolution B2. It is to be used with all time scales.

[6] The distance at which 1 au subtends 1 arc sec: 1 au divided by $\pi/648\,000$.

[7] IAU XVI GA 1976, Recommendations.

[8] The number of square degrees on a sphere is $360^2/\pi = 41\,259.9\ldots$.

[9] Observationally determined mass parameter $G_N M \times 2/c^2$ [1] for either the Sun or the Earth, using the nominal values $\mathcal{GM}_\odot = 1.327\,124\,4 \times 10^{20}\,{\rm m}^3\,{\rm s}^{-2}$ and $\mathcal{GM}_\oplus = 3.986\,004 \times 10^{14}\,{\rm m}^3\,{\rm s}^{-2}$ [50]. The combination $G_N M$ is known much more precisely than either G_N or M individually. The digits are truncated here at the point where one would need to distinguish between Barycentic Coordinate Time (TCB) and Barycentric Dynamical Time (TDB).

[10] $G_N M \div G_N$ [1].

[11] IAU XXIX GA, 2015, Resolution B3, "on recommended nominal conversion constants ..." The calligraphic symbol indicates the recommended nominal value.

[12] See also G. Kopp and J. L. Lean, Geophys. Res. Lett. **38**, L01706 (2011), who give $(1360.8 \pm 0.6)\ {\rm W\,m}^{-2}$; see paper for caveats and other measurements.

[13] $4\pi\,(1\ {\rm au})^2 \times \mathcal{S}_\odot$, assuming isotropic irradiance.

[14] S. Chandrasekhar, Astrophys. J. **74**, 81 (1931).

[15] This value assumes an ideal Fermi gas, using a numerical constant from the Lane-Emden equation [51], and with μ the average molecular weight per electron, defined relative to the mass of the single-proton hydrogen atom.

[16] A. S. Eddington, Mon. Not. Roy. Astron. Soc. **77**, 16 (1916).

[17] The maximum luminosity assuming pure electron scattering for the outward force arising from radiation pressure: $4\pi G_N M m_p c/\sigma_T$.

[18] IAU XXIX GA, 2015, Resolution B2, "on recommended zero points for the absolute and apparent bolometric magnitude scales".

[19] J. B. Oke and J. E. Gunn, Astrophys. J. **266**, 713 (1983).

[20] J. Bovy, Mon. Not. Roy. Astron. Soc. **468**, 1, L63 (2017), [arXiv:1610.07610].

[21] R. Abuter *et al.*, Astron., Astrophys. **625**, L10 (2019), [arXiv:1904.05721].

[22] IAU XIX GA (1985) suggested that "in cases where standardization on a common set of galactic parameters is desirable" that the values $R_0 = (8.5 \pm 1.0)$ kpc and $\theta_0 = (220 \pm 20)\,{\rm km\,s}^{-1}$ should be used.

[23] M. J. Reid *et al.*, Astrophys. J. **783**, 130 (2014), [arXiv:1401.5377].

[24] T. Piffl *et al.*, Astron. Astrophys. **562**, A91 (2014), [arXiv:1309.4293].

[25] C. F. McKee, A. Parravano and D. J. Hollenbach, Astrophys. J. **814**, 1, 13 (2015), [arXiv:1509.05334]; this is representative of other published estimates.

[26] J. I. Read, J. Phys. **G41**, 063101 (2014), [arXiv:1404.1938]; A. M. Green, J. Phys. **G44**, 8, 084001 (2017), [arXiv:1703.10102]; the conclusion is $\rho_{\rm DM}^{\rm local} = 0.39 \pm 0.03\,{\rm GeV\,cm}^{-3}$.

[27] D. Scott and G. F. Smoot, "Cosmic Microwave Background," Sec. 29 in this *Review*.

[28] D. J. Fixsen, Astrophys. J. **707**, 916 (2009), [arXiv:0911.1955].

[29] Planck Collab. 2018 Results I, Astron. Astrophys. **641**, A1 (2020), [arXiv:1807.06205].

[30] $n_\gamma = \frac{2\zeta(3)}{\pi^2}\left(\frac{kT}{\hbar c}\right)^3$; $\rho_\gamma = \frac{\pi^2 kT}{15\,c^2}\left(\frac{kT}{\hbar c}\right)^3$; $s/k = \frac{2\cdot 43\cdot\pi^2}{11\cdot 45}\left(\frac{kT}{\hbar c}\right)^3$; $kT/\hbar c = 11.90\,235(T/2.7255)/{\rm cm}$.

[31] Conversion using length of sidereal year.

[32] Distance-ladder estimates of H_0 tend to give higher values than derived from the CMB, *e.g.* Riess *et al.*, Astrophys. J. **908**, L6 (2021) give $h = 0.732 \pm 0.013$; for discussion see O. Lahav and A. R. Liddle, "The Cosmological Parameters," Sec. 25.1 in this *Review*.

[33] B. D. Fields *et al.*, JCAP **03**, 010 (2020), [Erratum: JCAP 11, E02 (2020)], [arXiv:1912.01132].

[34] B. D. Fields, P. Molaro and S. Sarkar, "Big-Bang Nucleosynthesis," Sec. 24 in this *Review*.

[35] $n_{\rm b}$ depends only upon the measured $\Omega_{\rm b}h^2$, the average baryon mass at the present epoch (G. Steigman, J. Cosmol. Astropart. Phys., **0610**, 016 (2006), [astro-ph/0606206]), and G_N: $n_{\rm b} = (\Omega_{\rm b}h^2)(h^{-2}\rho_{\rm crit})/(0.93711\,{\rm GeV}/c^2$ per baryon).

[36] Here "radiation" includes three species of light neutrinos as well as photons.

[37] D. Scott, A. Narimani and D. N. Page, Phys. Canada **70**, 258 (2014), [arXiv:1309.2381].

[38] D. H. Weinberg and M. White, "Dark Energy," Sec. 28 in this *Review*.

[39] Planck Collab. Interm. Results XLVI, Astron. Astrophys., **596**, A108 (2016) extend the range by $\Delta z \approx 1$, depending on the reionization model.

[40] Summary Tables in this *Review* list $N_\nu = 2.984(8)$ (Standard Model fits to LEP-SLC data). Because neutrinos are not completely decoupled at $e^\pm$ annihilation, the effective number of massless neutrino species is 3.044, rather than 3.

[41] J. Lesgourgues and L. Verde, "Neutrinos in Cosmology," Sec. 26 in this *Review*.

[42] The sum is over all neutrino mass eigenstates, the lower limit following from neutrino mixing results reported in this *Review* combined with the assumptions that there are three light neutrinos and that the lightest neutrino is substantially less massive than the others.

[43] Astrophysical determinations of Σm_ν, reported in the Full Listings of this *Review* under "Sum of the neutrino masses," range from < 0.17 eV to < 2.3 eV in papers published since 2003.

[44] P. A. R. Ade *et al.* (BICEP2, Keck Array), Phys. Rev. Lett. **121**, 221301 (2018), [arXiv:1810.05216].

[45] M. Tristram *et al.*, Astron. Astrophys. **647**, A128 (2021), [arXiv:2010.01139].

[46] BICEP/Keck Collaboration, Phys. Rev. Lett. **127**, 151301 (2021), [arXiv:2110.00483].

[47] *Planck* data alone give $r < 0.056$, using all power spectra; the currently tightest constraint comes from BICEP/Keck data, using *WMAP* and *Planck* to remove foregrounds.

[48] This constraint uses BAO and SNe data, as described in Ref. [2]; see discussion in D. H. Weinberg and M. White, "Dark Energy," Sec. 28 in this *Review*.

[49] E. Aver *et al.*, JCAP **03**, 027 (2021), [arXiv:2010.04180].

[50] IAU XXIX GA 2015, Resolution B2.

[51] G. P. Horedt, Astrophys. Space Sci. **126**, 2, 357 (1986).

Downloaded from https://academic.oup.com/ptep/article/2022/8/083C01/6651666 by KIT Library user on 27 September 2022

3. International System of Units (SI)

See D.B. Newell and E. Tiesinga, ed. (2019), "The International System of Units (SI)" (National Institute of Standards and Technology, Gaithersburg, MD), NIST Special Publication **330**, 2019 edition, https://doi.org/10.6028/NIST.SP.330-2019; and A. Thompson and B.N. Taylor (2008), "Guide for the Use of the International System of Units (SI)" (National Institute of Standards and Technology, Gaithersburg, MD), NIST Special Publication **811**, 2008 edition, https://doi.org/10.6028/NIST.SP.811e2008.

SI prefixes

10^{24}	yotta	(Y)
10^{21}	zetta	(Z)
10^{18}	exa	(E)
10^{15}	peta	(P)
10^{12}	tera	(T)
10^{9}	giga	(G)
10^{6}	mega	(M)
10^{3}	kilo	(k)
10^{2}	hecto	(h)
10	deca	(da)
10^{-1}	deci	(d)
10^{-2}	centi	(c)
10^{-3}	milli	(m)
10^{-6}	micro	(μ)
10^{-9}	nano	(n)
10^{-12}	pico	(p)
10^{-15}	femto	(f)
10^{-18}	atto	(a)
10^{-21}	zepto	(z)
10^{-24}	yocto	(y)

Physical quantity	Name of unit	Symbol
Base units		
length	meter	m
mass	kilogram	kg
time	second	s
electric current	ampere	A
thermodynamic temperature	kelvin	K
amount of substance	mole	mol
luminous intensity	candela	cd
Derived units with special names		
plane angle	radian	rad
solid angle	steradian	sr
frequency	hertz	Hz
energy	joule	J
force	newton	N
pressure	pascal	Pa
power	watt	W
electric charge	coulomb	C
electric potential	volt	V
electric resistance	ohm	Ω
electric conductance	siemens	S
electric capacitance	farad	F
magnetic flux	weber	Wb
inductance	henry	H
magnetic flux density	tesla	T
luminous flux	lumen	lm
illuminance	lux	lx
celsius temperature	degree celsius	°C
activity (of a radioactive source)*	becquerel	Bq
absorbed dose (of ionizing radiation)*	gray	Gy
dose equivalent*	sievert	Sv

*See our section 37, on "Radioactivity and radiation protection."

Downloaded from https://academic.oup.com/ptep/article/2022/8/083C01/6651666 by KIT Library user on 27 September 2022

Downloaded from https://academic.oup.com/ptep/article/2022/8/083C01/6651666 by KIT Library user on 27 September 2022

Table 4.1. Revised June 2021 by D.E. Groom (LBNL). The atomic number (top left) is the number of protons in the nucleus. The atomic masses (bottom) of stable elements are weighted by isotopic abundances in the Earth's surface. Atomic masses are relative to the mass of ^{12}C, defined to be exactly 12 unified atomic mass units (u). The exceptions are Th, Pa, and U, which have no stable isotopes but do have characteristic terrestrial compositions. Relative isotopic abundances often vary considerably, both in natural and commercial samples; this is reflected in the number of significant figures given for the mass. Masses may be found at `https://physics.nist.gov/cgi-bin/Compositions/stand_alone.pl`. If there is no stable isotope, the atomic mass of the most stable isotope known as of June 2019 is given in parentheses.

IUPAC announced verification of the discoveries of elements 113, 115, 117, and 118 in December 2015. The names were approved November 2016. The 7th period of the periodic table is now complete. Attempts to synthesize elements with $Z > 118$ are under way, but as of July 2021 no discoveries have been announced.

PERIODIC TABLE OF THE ELEMENTS

1 IA																	18 VIIIA
1 H hydrogen 1.008	2 IIA											13 IIIA	14 IVA	15 VA	16 VIA	17 VIIA	2 He helium 4.002602
3 Li lithium 6.94	4 Be beryllium 9.012182											5 B boron 10.81	6 C carbon 12.0107	7 N nitrogen 14.007	8 O oxygen 15.999	9 F fluorine 18.998403163	10 Ne neon 20.1797
11 Na sodium 22.98976928	12 Mg magnesium 24.305	3 IIIB	4 IVB	5 VB	6 VIB	7 VIIB	8	9 VIII	10	11 IB	12 IIB	13 Al aluminum 26.9815385	14 Si silicon 28.085	15 P phosphorus 30.973761998	16 S sulfur 32.06	17 Cl chlorine 35.45	18 Ar argon 39.948
19 K potassium 39.0983	20 Ca calcium 40.078	21 Sc scandium 44.955908	22 Ti titanium 47.867	23 V vanadium 50.9415	24 Cr chromium 51.9961	25 Mn manganese 54.938044	26 Fe iron 55.845	27 Co cobalt 58.933195	28 Ni nickel 58.6934	29 Cu copper 63.546	30 Zn zinc 65.38	31 Ga gallium 69.723	32 Ge germanium 72.630	33 As arsenic 74.921595	34 Se selenium 78.971	35 Br bromine 79.904	36 Kr krypton 83.798
37 Rb rubidium 85.4678	38 Sr strontium 87.62	39 Y yttrium 88.90584	40 Zr zirconium 91.224	41 Nb niobium 92.90637	42 Mo molybdenum 95.95	43 Tc technetium (97.907212)	44 Ru ruthenium 101.07	45 Rh rhodium 102.90550	46 Pd palladium 106.42	47 Ag silver 107.8682	48 Cd cadmium 112.414	49 In indium 114.818	50 Sn tin 118.710	51 Sb antimony 121.760	52 Te tellurium 127.60	53 I iodine 126.90447	54 Xe xenon 131.293
55 Cs caesium 132.90545196	56 Ba barium 137.327	57–71 LANTHA-NIDES	72 Hf hafnium 178.49	73 Ta tantalum 180.94788	74 W tungsten 183.84	75 Re rhenium 186.207	76 Os osmium 190.23	77 Ir iridium 192.217	78 Pt platinum 195.084	79 Au gold 196.966569	80 Hg mercury 200.592	81 Tl thallium 204.38	82 Pb lead 207.2	83 Bi bismuth 208.98040	84 Po polonium (208.98243)	85 At astatine (209.98715)	86 Rn radon (222.01758)
87 Fr francium (223.01974)	88 Ra radium (226.02541)	89–103 ACTINIDES	104 Rf rutherford. (267.12169)	105 Db dubnium (268.12567)	106 Sg seaborgium (269.12863)	107 Bh bohrium (270.13336)	108 Hs hassium (269.13375)	109 Mt meitnerium (278.15631)	110 Ds darmstadt. (281.16451)	111 Rg roentgen. (282.16912)	112 Cn copernicium (285.17712)	113 Nh nihonium (286.18221)	114 Fl flerovium (289.19042)	115 Mc moscovium (290.19598)	116 Lv livermorium (293.20449	117 Ts tennessine (294.21046)	118 Og oganesson (294.21392)

Lanthanide series	57 La lanthanum 138.90547	58 Ce cerium 140.116	59 Pr praseodym. 140.90766	60 Nd neodymium 144.242	61 Pm promethium (144.91276)	62 Sm samarium 150.36	63 Eu europium 151.964	64 Gd gadolinum 157.25	65 Tb terbium 158.92535	66 Dy dysprosium 162.500	67 Ho holmium 164.93033	68 Er erbium 167.259	69 Tm thulium 168.93422	70 Yb ytterbium 173.054	71 Lu lutetium 174.9668
Actinide series	89 Ac actinium (227.02775)	90 Th thorium 232.0377	91 Pa protactinium 231.03588	92 U uranium 238.02891	93 Np neptunium (237.04817)	94 Pu plutonium (244.06420)	95 Am americium (243.06138)	96 Cm curium (247.07035)	97 Bk berkelium (247.07031)	98 Cf californium (251.07959)	99 Es einsteinium (252.08298)	100 Fm fermium (257.09511)	101 Md mendelevium (258.09844)	102 No nobelium (259.10103)	103 Lr lawrencium (262.10961)

5. Electronic Structure of the Elements

Table 5.1: Reviewed 2011 by J.E. Sansonetti (NIST). The electronic configurations and the ionization energies are from the NIST database, "Ground Levels and Ionization Energies for the Neutral Atoms," W.C. Martin, A. Musgrove, S. Kotochigova, and J.E. Sansonetti, `https://www.nist.gov/pml/data/ion_energy.cfm`. The electron configuration for, say, iron indicates an argon electronic core (see argon) plus six $3d$ electrons and two $4s$ electrons.

	Element		Electron configuration ($3d^5$ = five $3d$ electrons, *etc.*)					Ground state $^{2S+1}L_J$	Ionization energy (eV)
1	H	Hydrogen	$1s$					$^2S_{1/2}$	13.5984
2	He	Helium	$1s^2$					$^1S_0$	24.5874
3	Li	Lithium	(He)	2s				$^2S_{1/2}$	5.3917
4	Be	Beryllium	(He)	$2s^2$				$^1S_0$	9.3227
5	B	Boron	(He)	$2s^2$	$2p$			$^2P_{1/2}$	8.2980
6	C	Carbon	(He)	$2s^2$	$2p^2$			$^3P_0$	11.2603
7	N	Nitrogen	(He)	$2s^2$	$2p^3$			$^4S_{3/2}$	14.5341
8	O	Oxygen	(He)	$2s^2$	$2p^4$			$^3P_2$	13.6181
9	F	Fluorine	(He)	$2s^2$	$2p^5$			$^2P_{3/2}$	17.4228
10	Ne	Neon	(He)	$2s^2$	$2p^6$			$^1S_0$	21.5645
11	Na	Sodium	(Ne)	3s				$^2S_{1/2}$	5.1391
12	Mg	Magnesium	(Ne)	$3s^2$				$^1S_0$	7.6462
13	Al	Aluminum	(Ne)	$3s^2$	$3p$			$^2P_{1/2}$	5.9858
14	Si	Silicon	(Ne)	$3s^2$	$3p^2$			$^3P_0$	8.1517
15	P	Phosphorus	(Ne)	$3s^2$	$3p^3$			$^4S_{3/2}$	10.4867
16	S	Sulfur	(Ne)	$3s^2$	$3p^4$			$^3P_2$	10.3600
17	Cl	Chlorine	(Ne)	$3s^2$	$3p^5$			$^2P_{3/2}$	12.9676
18	Ar	Argon	(Ne)	$3s^2$	$3p^6$			$^1S_0$	15.7596
19	K	Potassium	(Ar)		$4s$			$^2S_{1/2}$	4.3407
20	Ca	Calcium	(Ar)		$4s^2$			$^1S_0$	6.1132
21	Sc	Scandium	(Ar)	$3d$	$4s^2$		T	$^2D_{3/2}$	6.5615
22	Ti	Titanium	(Ar)	$3d^2$	$4s^2$		r e	$^3F_2$	6.8281
23	V	Vanadium	(Ar)	$3d^3$	$4s^2$		a l	$^4F_{3/2}$	6.7462
24	Cr	Chromium	(Ar)	$3d^5$	$4s$		n e	$^7S_3$	6.7665
25	Mn	Manganese	(Ar)	$3d^5$	$4s^2$		s m	$^6S_{5/2}$	7.4340
26	Fe	Iron	(Ar)	$3d^6$	$4s^2$		i e	$^5D_4$	7.9024
27	Co	Cobalt	(Ar)	$3d^7$	$4s^2$		t n	$^4F_{9/2}$	7.8810
28	Ni	Nickel	(Ar)	$3d^8$	$4s^2$		i t	$^3F_4$	7.6399
29	Cu	Copper	(Ar)	$3d^{10}$	$4s$		o s	$^2S_{1/2}$	7.7264
30	Zn	Zinc	(Ar)	$3d^{10}$	$4s^2$		n	$^1S_0$	9.3942
31	Ga	Gallium	(Ar)	$3d^{10}$	$4s^2$	$4p$		$^2P_{1/2}$	5.9993
32	Ge	Germanium	(Ar)	$3d^{10}$	$4s^2$	$4p^2$		$^3P_0$	7.8994
33	As	Arsenic	(Ar)	$3d^{10}$	$4s^2$	$4p^3$		$^4S_{3/2}$	9.7886
34	Se	Selenium	(Ar)	$3d^{10}$	$4s^2$	$4p^4$		$^3P_2$	9.7524
35	Br	Bromine	(Ar)	$3d^{10}$	$4s^2$	$4p^5$		$^2P_{3/2}$	11.8138
36	Kr	Krypton	(Ar)	$3d^{10}$	$4s^2$	$4p^6$		$^1S_0$	13.9996
37	Rb	Rubidium	(Kr)		$5s$			$^2S_{1/2}$	4.1771
38	Sr	Strontium	(Kr)		$5s^2$			$^1S_0$	5.6949
39	Y	Yttrium	(Kr)	$4d$	$5s^2$		T	$^2D_{3/2}$	6.2173
40	Zr	Zirconium	(Kr)	$4d^2$	$5s^2$		r e	$^3F_2$	6.6339
41	Nb	Niobium	(Kr)	$4d^4$	$5s$		a l	$^6D_{1/2}$	6.7589
42	Mo	Molybdenum	(Kr)	$4d^5$	$5s$		n e	$^7S_3$	7.0924
43	Tc	Technetium	(Kr)	$4d^5$	$5s^2$		s m	$^6S_{5/2}$	7.28
44	Ru	Ruthenium	(Kr)	$4d^7$	$5s$		i e	$^5F_5$	7.3605
45	Rh	Rhodium	(Kr)	$4d^8$	$5s$		t n	$^4F_{9/2}$	7.4589
46	Pd	Palladium	(Kr)	$4d^{10}$			i t	$^1S_0$	8.3369
47	Ag	Silver	(Kr)	$4d^{10}$	$5s$		o s	$^2S_{1/2}$	7.5762
48	Cd	Cadmium	(Kr)	$4d^{10}$	$5s^2$		n	$^1S_0$	8.9938

Downloaded from https://academic.oup.com/ptep/article/2022/8/083C01/6651666 by KIT Library user on 27 September 2022

		Element	Electron configuration ($3d^5$ = five $3d$ electrons, *etc.*)						Ground state $^{2S+1}L_J$	Ionization energy (eV)
49	In	Indium	(Kr)	$4d^{10}$	$5s^2$	$5p$			$^2P_{1/2}$	5.7864
50	Sn	Tin	(Kr)	$4d^{10}$	$5s^2$	$5p^2$			$^3P_0$	7.3439
51	Sb	Antimony	(Kr)	$4d^{10}$	$5s^2$	$5p^3$			$^4S_{3/2}$	8.6084
52	Te	Tellurium	(Kr)	$4d^{10}$	$5s^2$	$5p^4$			$^3P_2$	9.0096
53	I	Iodine	(Kr)	$4d^{10}$	$5s^2$	$5p^5$			$^2P_{3/2}$	10.4513
54	Xe	Xenon	(Kr)	$4d^{10}$	$5s^2$	$5p^6$			$^1S_0$	12.1298
55	Cs	Cesium	(Xe)			$6s$			$^2S_{1/2}$	3.8939
56	Ba	Barium	(Xe)			$6s^2$			$^1S_0$	5.2117
57	La	Lanthanum	(Xe)		$5d$	$6s^2$			$^2D_{3/2}$	5.5769
58	Ce	Cerium	(Xe)	$4f$	$5d$	$6s^2$			$^1G_4$	5.5387
59	Pr	Praseodymium	(Xe)	$4f^3$		$6s^2$		L	$^4I_{9/2}$	5.473
60	Nd	Neodymium	(Xe)	$4f^4$		$6s^2$		a	$^5I_4$	5.5250
61	Pm	Promethium	(Xe)	$4f^5$		$6s^2$		n	$^6H_{5/2}$	5.582
62	Sm	Samarium	(Xe)	$4f^6$		$6s^2$		t	$^7F_0$	5.6437
63	Eu	Europium	(Xe)	$4f^7$		$6s^2$		a	$^8S_{7/2}$	5.6704
64	Gd	Gadolinium	(Xe)	$4f^7$	$5d$	$6s^2$		n	$^9D_2$	6.1498
65	Tb	Terbium	(Xe)	$4f^9$		$6s^2$		i	$^6H_{15/2}$	5.8638
66	Dy	Dysprosium	(Xe)	$4f^{10}$		$6s^2$		d	$^5I_8$	5.9389
67	Ho	Holmium	(Xe)	$4f^{11}$		$6s^2$		e	$^4I_{15/2}$	6.0215
68	Er	Erbium	(Xe)	$4f^{12}$		$6s^2$		s	$^3H_6$	6.1077
69	Tm	Thulium	(Xe)	$4f^{13}$		$6s^2$			$^2F_{7/2}$	6.1843
70	Yb	Ytterbium	(Xe)	$4f^{14}$		$6s^2$			$^1S_0$	6.2542
71	Lu	Lutetium	(Xe)	$4f^{14}$	$5d$	$6s^2$			$^2D_{3/2}$	5.4259
72	Hf	Hafnium	(Xe)	$4f^{14}$	$5d^2$	$6s^2$		T	$^3F_2$	6.8251
73	Ta	Tantalum	(Xe)	$4f^{14}$	$5d^3$	$6s^2$		r e	$^4F_{3/2}$	7.5496
74	W	Tungsten	(Xe)	$4f^{14}$	$5d^4$	$6s^2$		a l	$^5D_0$	7.8640
75	Re	Rhenium	(Xe)	$4f^{14}$	$5d^5$	$6s^2$		n e	$^6S_{5/2}$	7.8335
76	Os	Osmium	(Xe)	$4f^{14}$	$5d^6$	$6s^2$		s m	$^5D_4$	8.4382
77	Ir	Iridium	(Xe)	$4f^{14}$	$5d^7$	$6s^2$		i e	$^4F_{9/2}$	8.9670
78	Pt	Platinum	(Xe)	$4f^{14}$	$5d^9$	$6s$		t n	$^3D_3$	8.9588
79	Au	Gold	(Xe)	$4f^{14}$	$5d^{10}$	$6s$		i t	$^2S_{1/2}$	9.2255
80	Hg	Mercury	(Xe)	$4f^{14}$	$5d^{10}$	$6s^2$		o s	$^1S_0$	10.4375
								n		
81	Tl	Thallium	(Xe)	$4f^{14}$	$5d^{10}$	$6s^2$	$6p$		$^2P_{1/2}$	6.1082
82	Pb	Lead	(Xe)	$4f^{14}$	$5d^{10}$	$6s^2$	$6p^2$		$^3P_0$	7.4167
83	Bi	Bismuth	(Xe)	$4f^{14}$	$5d^{10}$	$6s^2$	$6p^3$		$^4S_{3/2}$	7.2855
84	Po	Polonium	(Xe)	$4f^{14}$	$5d^{10}$	$6s^2$	$6p^4$		$^3P_2$	8.414
85	At	Astatine	(Xe)	$4f^{14}$	$5d^{10}$	$6s^2$	$6p^5$		$^2P_{3/2}$	
86	Rn	Radon	(Xe)	$4f^{14}$	$5d^{10}$	$6s^2$	$6p^6$		$^1S_0$	10.7485
87	Fr	Francium	(Rn)			$7s$			$^2S_{1/2}$	4.0727
88	Ra	Radium	(Rn)			$7s^2$			$^1S_0$	5.2784
89	Ac	Actinium	(Rn)		$6d$	$7s^2$			$^2D_{3/2}$	5.3807
90	Th	Thorium	(Rn)		$6d^2$	$7s^2$			$^3F_2$	6.3067
91	Pa	Protactinium	(Rn)	$5f^2$	$6d$	$7s^2$		A	$^4K_{11/2}$*	5.89
92	U	Uranium	(Rn)	$5f^3$	$6d$	$7s^2$		c	$^5L_6$*	6.1939
93	Np	Neptunium	(Rn)	$5f^4$	$6d$	$7s^2$		t	$^6L_{11/2}$*	6.2657
94	Pu	Plutonium	(Rn)	$5f^6$		$7s^2$		i	$^7F_0$	6.0260
95	Am	Americium	(Rn)	$5f^7$		$7s^2$		n	$^8S_{7/2}$	5.9738
96	Cm	Curium	(Rn)	$5f^7$	$6d$	$7s^2$		i	$^9D_2$	5.9914
97	Bk	Berkelium	(Rn)	$5f^9$		$7s^2$		d	$^6H_{15/2}$	6.1979
98	Cf	Californium	(Rn)	$5f^{10}$		$7s^2$		e	$^5I_8$	6.2817
99	Es	Einsteinium	(Rn)	$5f^{11}$		$7s^2$		s	$^4I_{15/2}$	6.3676
100	Fm	Fermium	(Rn)	$5f^{12}$		$7s^2$			$^3H_6$	6.50
101	Md	Mendelevium	(Rn)	$5f^{13}$		$7s^2$			$^2F_{7/2}$	6.58
102	No	Nobelium	(Rn)	$5f^{14}$		$7s^2$			$^1S_0$	6.65
103	Lr	Lawrencium	(Rn)	$5f^{14}$		$7s^2$	$7p$?		$^2P_{1/2}$?	4.9?
104	Rf	Rutherfordium	(Rn)	$5f^{14}$	$6d^2$	$7s^2$?			$^3F_2$?	6.0?

* The usual LS coupling scheme does not apply for these three elements.
See the introductory note to the NIST table from which this table is taken.

Downloaded from https://academic.oup.com/ptep/article/2022/8/083C01/6651666 by KIT Library user on 27 September 2022

6. Atomic and Nuclear Properties of Materials

Table 6.1: Abridged from `https://pdg.lbl.gov/current/AtomicNuclearProperties` by D.E. Groom (2021). See web pages for more detail about entries in this table and for several hundred others. Parentheses in the dE/dx and density columns indicate gases at 20° C and 1 atm. Boiling points are at 1 atm. Refractive indices n are evaluated at the sodium D line blend (589.2 nm); values $\gg$1 in brackets indicate $(n-1)\times 10^6$ for gases at 0° C and 1 atm.

Material	Z	A	$\langle Z/A \rangle$	Nucl.coll. length λ_T {g cm^{-2}}	Nucl.inter. length λ_I {g cm^{-2}}	Rad.len. X_0 {g cm^{-2}}	$dE/dx\|_{\rm min}$ {MeV g^{-1}cm^2}	Density {g cm^{-3}} ({g ℓ^{-1}})	Melting point (K)	Boiling point (K)	Refract. index @ Na D
H_2	1	1.008(7)	0.99212	42.8	52.0	63.05	(4.103)	0.071(0.084)	13.81	20.28	1.11[132.]
D_2	1	2.014101764(8)	0.49650	51.3	71.8	125.97	(2.053)	0.169(0.168)	18.7	23.65	1.11[138.]
He	2	4.002602(2)	0.49967	51.8	71.0	94.32	(1.937)	0.125(0.166)		4.220	1.02[35.0]
Li	3	6.94(2)	0.43221	52.2	71.3	82.78	1.639	0.534	453.6	1615.	
Be	4	9.0121831(5)	0.44384	55.3	77.8	65.19	1.595	1.848	1560.	2744.	
C diamond	6	12.0107(8)	0.49955	59.2	85.8	42.70	1.725	3.520			2.419
C graphite	6	12.0107(8)	0.49955	59.2	85.8	42.70	1.742	2.210	Sublimes at 4098. K		
N_2	7	14.007(2)	0.49976	61.1	89.7	37.99	(1.825)	0.807(1.165)	63.15	77.29	1.20[298.]
O_2	8	15.999(3)	0.50002	61.3	90.2	34.24	(1.801)	1.141(1.332)	54.36	90.20	1.22[271.]
F_2	9	18.998403163(6)	0.47372	65.0	97.4	32.93	(1.676)	1.507(1.580)	53.53	85.03	[195.]
Ne	10	20.1797(6)	0.49555	65.7	99.0	28.93	(1.724)	1.204(0.839)	24.56	27.07	1.09[67.1]
Al	13	26.9815385(7)	0.48181	69.7	107.2	24.01	1.615	2.699	933.5	2792.	
Si	14	28.0855(3)	0.49848	70.2	108.4	21.82	1.664	2.329	1687.	3538.	3.95
Cl_2	17	35.453(2)	0.47951	73.8	115.7	19.28	(1.630)	1.574(2.980)	171.6	239.1	[773.]
Ar	18	39.948(1)	0.45059	75.7	119.7	19.55	(1.519)	1.396(1.662)	83.81	87.26	1.23[281.]
Ti	22	47.867(1)	0.45961	78.8	126.2	16.16	1.477	4.540	1941.	3560.	
Fe	26	55.845(2)	0.46557	81.7	132.1	13.84	1.451	7.874	1811.	3134.	
Cu	29	63.546(3)	0.45636	84.2	137.3	12.86	1.403	8.960	1358.	2835.	
Ge	32	72.630(1)	0.44053	86.9	143.0	12.25	1.370	5.323	1211.	3106.	
Sn	50	118.710(7)	0.42119	98.2	166.7	8.82	1.263	7.310	505.1	2875.	
Xe	54	131.293(6)	0.41129	100.8	172.1	8.48	(1.255)	2.953(5.483)	161.4	165.1	1.39[701.]
W	74	183.84(1)	0.40252	110.4	191.9	6.76	1.145	19.300	3695.	5828.	
Pt	78	195.084(9)	0.39983	112.2	195.7	6.54	1.128	21.450	2042.	4098.	
Au	79	196.966569(5)	0.40108	112.5	196.3	6.46	1.134	19.320	1337.	3129.	
Pb	82	207.2(1)	0.39575	114.1	199.6	6.37	1.122	11.350	600.6	2022.	
U	92	[238.02891(3)]	0.38651	118.6	209.0	6.00	1.081	18.950	1408.	4404.	
Air (dry, 1 atm)			0.49919	61.3	90.1	36.62	(1.815)	(1.205)		78.80	[289]
Shielding concrete			0.50274	65.1	97.5	26.57	1.711	2.300			
Borosilicate glass (Pyrex)			0.49707	64.6	96.5	28.17	1.696	2.230			
Lead glass			0.42101	95.9	158.0	7.87	1.255	6.220			
Standard rock			0.50000	66.8	101.3	26.54	1.688	2.650			
Methane (CH_4)			0.62334	54.0	73.8	46.47	(2.417)	(0.667)	90.68	111.7	[444.]
Ethane (C_2H_6)			0.59861	55.0	75.9	45.66	(2.304)	(1.263)	90.36	184.5	
Propane (C_3H_8)			0.58962	55.3	76.7	45.37	(2.262)	0.493(1.868)	85.52	231.0	
Butane (C_4H_{10})			0.59497	55.5	77.1	45.23	(2.278)	(2.489)	134.9	272.6	
Octane (C_8H_{18})			0.57778	55.8	77.8	45.00	2.123	0.703	214.4	398.8	
Paraffin ($CH_3(CH_2)_{n\approx 23}CH_3$)			0.57275	56.0	78.3	44.85	2.088	0.930			
Nylon (type 6, 6/6)			0.54790	57.5	81.6	41.92	1.973	1.18			
Polycarbonate (Lexan)			0.52697	58.3	83.6	41.50	1.886	1.20			
Polyethylene ($[CH_2CH_2]_n$)			0.57034	56.1	78.5	44.77	2.079	0.89			
Polyethylene terephthalate (Mylar)			0.52037	58.9	84.9	39.95	1.848	1.40			
Polyimide film (Kapton)			0.51264	59.2	85.5	40.58	1.820	1.42			
Polymethylmethacrylate (acrylic)			0.53937	58.1	82.8	40.55	1.929	1.19			1.49
Polypropylene			0.55998	56.1	78.5	44.77	2.041	0.90			
Polystyrene ($[C_6H_5CHCH_2]_n$)			0.53768	57.5	81.7	43.79	1.936	1.06			1.59
Polytetrafluoroethylene (Teflon)			0.47992	63.5	94.4	34.84	1.671	2.20			
Polyvinyltoluene			0.54141	57.3	81.3	43.90	1.956	1.03			1.58
Aluminum oxide (sapphire)			0.49038	65.5	98.4	27.94	1.647	3.970	2327.	3273.	1.77
Barium flouride (BaF_2)			0.42207	90.8	149.0	9.91	1.303	4.893	1641.	2533.	1.47
Bismuth germanate (BGO)			0.42065	96.2	159.1	7.97	1.251	7.130	1317.		2.15
Carbon dioxide gas (CO_2)			0.49989	60.7	88.9	36.20	1.819	(1.842)			[449.]
Solid carbon dioxide (dry ice)			0.49989	60.7	88.9	36.20	1.787	1.563	Sublimes at 194.7 K		
Cesium iodide (CsI)			0.41569	100.6	171.5	8.39	1.243	4.510	894.2	1553.	1.79
Lithium fluoride (LiF)			0.46262	61.0	88.7	39.26	1.614	2.635	1121.	1946.	1.39
Lithium hydride (LiH)			0.50321	50.8	68.1	79.62	1.897	0.820	965.		
Lead tungstate ($PbWO_4$)			0.41315	100.6	168.3	7.39	1.229	8.300	1403.		2.20
Silicon dioxide (SiO_2, fused quartz)			0.49930	65.2	97.8	27.05	1.699	2.200	1986.	3223.	1.46
Sodium chloride (NaCl)			0.47910	71.2	110.1	21.91	1.847	2.170	1075.	1738.	1.54
Sodium iodide (NaI)			0.42697	93.1	154.6	9.49	1.305	3.667	933.2	1577.	1.77
Water (H_2O)			0.55509	58.5	83.3	36.08	1.992	1.000	273.1	373.1	1.33
Silica aerogel			0.50093	65.0	97.3	27.25	1.740	0.200	(0.03 H_2O, 0.97 SiO_2)		
Epoxy (Epotek-301-1)			0.53409	58.1	83.0	41.22	1.925	1.190			

Downloaded from https://academic.oup.com/ptep/article/2022/8/083C01/6651666 by KIT Library user on 27 September 2022

Material	Dielectric constant ($\kappa = \epsilon/\epsilon_0$) () is ($\kappa$–1)×$10^6$ for gas	Young's modulus [10^6 psi]	Coeff. of thermal expansion [10^{-6}cm/cm-°C]	Specific heat [cal/g-°C]	Electrical resistivity [$\mu\Omega$cm(@°C)]	Thermal conductivity [cal/cm-°C-sec]
H_2	(253.9)	—	—	—	—	—
He	(64)	—	—	—	—	—
Li	—	—	56	0.86	8.55(0°)	0.17
Be	—	37	12.4	0.436	5.885(0°)	0.38
C	—	0.7	0.6–4.3	0.165	1375(0°)	0.057
N_2	(548.5)	—	—	—	—	—
O_2	(495)	—	—	—	—	—
Ne	(127)	—	—	—	—	—
Al	—	10	23.9	0.215	2.65(20°)	0.53
Si	11.9	16	2.8–7.3	0.162	—	0.20
Ar	(517)	—	—	—	—	—
Ti	—	16.8	8.5	0.126	50(0°)	—
Fe	—	28.5	11.7	0.11	9.71(20°)	0.18
Cu	—	16	16.5	0.092	1.67(20°)	0.94
Ge	16.0	—	5.75	0.073	—	0.14
Sn	—	6	20	0.052	11.5(20°)	0.16
Xe	—	—	—	—	—	—
W	—	50	4.4	0.032	5.5(20°)	0.48
Pt	—	21	8.9	0.032	9.83(0°)	0.17
Pb	—	2.6	29.3	0.038	20.65(20°)	0.083
U	—	—	36.1	0.028	29(20°)	0.064

Downloaded from https://academic.oup.com/ptep/article/2022/8/083C01/6651666 by KIT Library user on 27 September 2022

7. Electromagnetic Relations

Revised September 2005 by H.G. Spieler (LBNL).

Quantity	Gaussian CGS	SI
Conversion factors:		
Charge:	$2.997\,924\,58 \times 10^9$ esu	$= 1$ C $= 1$ A s
Potential:	(1/299.792 458) statvolt (ergs/esu)	$= 1$ V $= 1$ J C^{-1}
Magnetic field:	10^4 gauss $= 10^4$ dyne/esu	$= 1$ T $= 1$ N A^{-1}m^{-1}
	$\mathbf{F} = q\left(\mathbf{E} + \frac{\mathbf{v}}{c} \times \mathbf{B}\right)$	$\mathbf{F} = q\left(\mathbf{E} + \mathbf{v} \times \mathbf{B}\right)$
	$\nabla \bullet \mathbf{D} = 4\pi\rho$ $\nabla \times \mathbf{H} - \frac{1}{c}\frac{\partial \mathbf{D}}{\partial t} = \frac{4\pi}{c}\mathbf{J}$ $\nabla \bullet \mathbf{B} = 0$ $\nabla \times \mathbf{E} + \frac{1}{c}\frac{\partial \mathbf{B}}{\partial t} = 0$	$\nabla \bullet \mathbf{D} = \rho$ $\nabla \times \mathbf{H} - \frac{\partial \mathbf{D}}{\partial t} = \mathbf{J}$ $\nabla \bullet \mathbf{B} = 0$ $\nabla \times \mathbf{E} + \frac{\partial \mathbf{B}}{\partial t} = 0$
Constitutive relations:	$\mathbf{D} = \mathbf{E} + 4\pi\mathbf{P}, \quad \mathbf{H} = \mathbf{B} - 4\pi\mathbf{M}$	$\mathbf{D} = \epsilon_0\mathbf{E} + \mathbf{P}, \quad \mathbf{H} = \mathbf{B}/\mu_0 - \mathbf{M}$
Linear media:	$\mathbf{D} = \epsilon\mathbf{E}, \quad \mathbf{H} = \mathbf{B}/\mu$ 1 1	$\mathbf{D} = \epsilon\mathbf{E}, \quad \mathbf{H} = \mathbf{B}/\mu$ $\epsilon_0 = 8.854\,187\ldots \times 10^{-12}$ F m^{-1} $\mu_0 = 4\pi \times 10^{-7}$ N A^{-2}
	$\mathbf{E} = -\nabla V - \frac{1}{c}\frac{\partial \mathbf{A}}{\partial t}$ $\mathbf{B} = \nabla \times \mathbf{A}$	$\mathbf{E} = -\nabla V - \frac{\partial \mathbf{A}}{\partial t}$ $\mathbf{B} = \nabla \times \mathbf{A}$
	$V = \sum_{\text{charges}} \frac{q_i}{r_i} = \int \frac{\rho(\mathbf{r}')}{\lvert\mathbf{r}-\mathbf{r}'\rvert}\, d^3x'$ $\mathbf{A} = \frac{1}{c}\oint \frac{I\,d\boldsymbol{\ell}}{\lvert\mathbf{r}-\mathbf{r}'\rvert} = \frac{1}{c}\int \frac{\mathbf{J}(\mathbf{r}')}{\lvert\mathbf{r}-\mathbf{r}'\rvert}\, d^3x'$	$V = \frac{1}{4\pi\epsilon_0}\sum_{\text{charges}} \frac{q_i}{r_i} = \frac{1}{4\pi\epsilon_0}\int \frac{\rho(\mathbf{r}')}{\lvert\mathbf{r}-\mathbf{r}'\rvert}\, d^3x'$ $\mathbf{A} = \frac{\mu_0}{4\pi}\oint \frac{I\,d\boldsymbol{\ell}}{\lvert\mathbf{r}-\mathbf{r}'\rvert} = \frac{\mu_0}{4\pi}\int \frac{\mathbf{J}(\mathbf{r}')}{\lvert\mathbf{r}-\mathbf{r}'\rvert}\, d^3x'$
	$\mathbf{E}'_\parallel = \mathbf{E}_\parallel$ $\mathbf{E}'_\perp = \gamma(\mathbf{E}_\perp + \frac{1}{c}\mathbf{v} \times \mathbf{B})$ $\mathbf{B}'_\parallel = \mathbf{B}_\parallel$ $\mathbf{B}'_\perp = \gamma(\mathbf{B}_\perp - \frac{1}{c}\mathbf{v} \times \mathbf{E})$	$\mathbf{E}'_\parallel = \mathbf{E}_\parallel$ $\mathbf{E}'_\perp = \gamma(\mathbf{E}_\perp + \mathbf{v} \times \mathbf{B})$ $\mathbf{B}'_\parallel = \mathbf{B}_\parallel$ $\mathbf{B}'_\perp = \gamma(\mathbf{B}_\perp - \frac{1}{c^2}\mathbf{v} \times \mathbf{E})$
$\frac{1}{4\pi\epsilon_0} = c^2 \times 10^{-7}$ N A^{-2} $= 8.987\,55\ldots \times 10^9$ m F^{-1} ; $\frac{\mu_0}{4\pi} = 10^{-7}$ N A^{-2} ; $c = \frac{1}{\sqrt{\mu_0\epsilon_0}} = 2.997\,924\,58 \times 10^8$ m s^{-1}		

7.1 Impedances (SI units)

ρ = resistivity at room temperature in $10^{-8}\,\Omega$ m:

~ 1.7 for Cu ~ 5.5 for W
~ 2.4 for Au ~ 73 for SS 304
~ 2.8 for Al ~ 100 for Nichrome
(Al alloys may have double the Al value.)

For alternating currents, instantaneous current I, voltage V, angular frequency ω:

$$V = V_0\, e^{j\omega t} = ZI\ . \tag{7.1}$$

Impedance of self-inductance L: $Z = j\omega L$.

Impedance of capacitance C: $Z = 1/j\omega C$.

Impedance of free space: $Z = \sqrt{\mu_0/\epsilon_0} = 376.7\ \Omega$.

High-frequency surface impedance of a good conductor:

$$Z = \frac{(1+j)\,\rho}{\delta}\ , \quad \text{where } \delta = \text{skin depth}\ ; \tag{7.2}$$

$$\delta = \sqrt{\frac{\rho}{\pi\nu\mu}} \approx \frac{6.6\text{ cm}}{\sqrt{\nu\,(\text{Hz})}} \quad \text{for Cu}\ . \tag{7.3}$$

7.2 Capacitors, inductors, and transmission Lines

The capacitance between two parallel plates of area A spaced by the distance d and enclosing a medium with the dielectric constant ε is

$$C = K\varepsilon A/d\,, \tag{7.4}$$

where the correction factor K depends on the extent of the fringing field. If the dielectric fills the capacitor volume without extending beyond the electrodes. The correction factor $K \approx 0.8$ for capacitors of typical geometry.

The inductance at high frequencies of a straight wire whose length ℓ is much greater than the wire diameter d is

$$L \approx 2.0\left[\frac{\text{nH}}{\text{cm}}\right]\cdot \ell\left(\ln\left(\frac{4\ell}{d}\right) - 1\right)\ . \tag{7.5}$$

For very short wires, representative of vias in a printed circuit board, the inductance is

$$L(\text{in nH}) \approx \ell/d\,. \tag{7.6}$$

A transmission line is a pair of conductors with inductance L and capacitance C. The characteristic impedance $Z = \sqrt{L/C}$ and the phase velocity $v_p = 1/\sqrt{LC} = 1/\sqrt{\mu\varepsilon}$, which decreases with the inverse square root of the dielectric constant of the medium. Typical coaxial and ribbon cables have a propagation delay of about 5 ns/cm.

Downloaded from https://academic.oup.com/ptep/article/2022/8/083C01/6651666 by KIT Library user on 27 September 2022

The impedance of a coaxial cable with outer diameter D and inner diameter d is

$$Z = 60\,\Omega \cdot \frac{1}{\sqrt{\varepsilon_r}} \ln \frac{D}{d}\,, \tag{7.7}$$

where the relative dielectric constant $\varepsilon_r = \varepsilon/\varepsilon_0$. A pair of parallel wires of diameter d and spacing $a > 2.5\,d$ has the impedance

$$Z = 120\,\Omega \cdot \frac{1}{\sqrt{\varepsilon_r}} \ln \frac{2a}{d}\,. \tag{7.8}$$

This yields the impedance of a wire at a spacing h above a ground plane,

$$Z = 60\,\Omega \cdot \frac{1}{\sqrt{\varepsilon_r}} \ln \frac{4h}{d}\,. \tag{7.9}$$

A common configuration utilizes a thin rectangular conductor above a ground plane with an intermediate dielectric (microstrip). Detailed calculations for this and other transmission line configurations are given by Gunston [1].

7.3 Synchrotron radiation (CGS units)

For a particle of charge e, velocity $v = \beta c$, and energy $E = \gamma mc^2$, traveling in a circular orbit of radius R, the classical energy loss per revolution δE is

$$\delta E = \frac{4\pi}{3}\,\frac{e^2}{R}\,\beta^3\,\gamma^4\,. \tag{7.10}$$

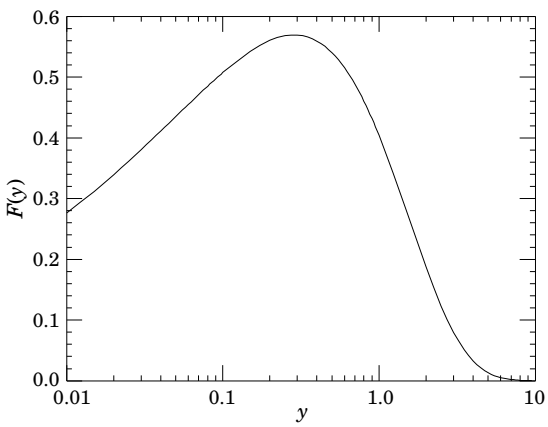

Figure 7.1: The normalized synchrotron radiation spectrum $F(y)$.

For high-energy electrons or positrons ($\beta \approx 1$), this becomes

$$\delta E \text{ (in MeV)} \approx 0.0885\,[E(\text{in GeV})]^4/R(\text{in m})\,. \tag{7.11}$$

For $\gamma \gg 1$, the energy radiated per revolution into the photon energy interval $d(\hbar\omega)$ is

$$dI = \frac{8\pi}{9}\alpha\,\gamma\,F(\omega/\omega_c)\,d(\hbar\omega)\,, \tag{7.12}$$

where $\alpha = e^2/\hbar c$ is the fine-structure constant and

$$\omega_c = \frac{3\gamma^3 c}{2R} \tag{7.13}$$

is the critical frequency. The normalized function $F(y)$ is

$$F(y) = \frac{9}{8\pi}\sqrt{3}\,y\int_y^\infty K_{5/3}(x)\;dx\,, \tag{7.14}$$

where $K_{5/3}(x)$ is a modified Bessel function of the third kind. For electrons or positrons,

$$\hbar\omega_c \text{ (in keV)} \approx 2.22\,[E(\text{in GeV})]^3/R(\text{in m})\,. \tag{7.15}$$

For $\gamma \gg 1$ and $\omega \ll \omega_c$,

$$\frac{dI}{d(\hbar\omega)} \approx 3.3\alpha\,(\omega R/c)^{1/3}\,, \tag{7.16}$$

whereas for

$$\gamma \gg 1 \text{ and } \omega \gtrsim 3\omega_c\,,$$

$$\frac{dI}{d(\hbar\omega)} \approx \sqrt{\frac{3\pi}{2}}\,\alpha\,\gamma\left(\frac{\omega}{\omega_c}\right)^{1/2} e^{-\omega/\omega_c}\left[1 + \frac{55}{72}\frac{\omega_c}{\omega} + \ldots\right]\,. \tag{7.17}$$

The radiation is confined to angles $\lesssim 1/\gamma$ relative to the instantaneous direction of motion. For $\gamma \gg 1$, where Eq. (7.12) applies, the mean number of photons emitted per revolution is

$$N_\gamma = \frac{5\pi}{\sqrt{3}}\alpha\gamma\,, \tag{7.18}$$

and the mean energy per photon is

$$\langle\hbar\omega\rangle = \frac{8}{15\sqrt{3}}\hbar\omega_c\,. \tag{7.19}$$

When $\langle\hbar\omega\rangle \gtrsim \mathrm{O}(E)$, quantum corrections are important [2].[1]

References

[1] M.A.R. Gunston. Microwave Transmission Line Data, Noble Publishing Corp., Atlanta (1997) ISBN 1-884932-57-6, TK6565.T73G85.

[2] J.D. Jackson, *Classical Electrodynamics*, 3rd edition (John Wiley & Sons, New York, 1998) for more formulae and details.

[1] Note that earlier editions of Ref. [2] had ω_c twice as large as Eq. (7.13).

Downloaded from https://academic.oup.com/ptep/article/2022/8/083C01/6651666 by KIT Library user on 27 September 2022

8. Naming Scheme for Hadrons

Revised August 2021 by V.D. Burkert (Jefferson Lab), C. Hanhart (Jülich), R.E. Mitchell (Indiana U.), C. Patrignani (Bologna U.), U. Thoma (Bonn U.), L. Tiator (KPH, JGU Mainz) and R.L. Workman (George Washington U.).

In the 1986 edition [1], the Particle Data Group extended and systematized the naming scheme for mesons and baryons. The extensions were necessary in order to name the new particles containing c or b quarks that were rapidly being discovered. With the discoveries of particles that are candidates for states with more complicated structures than just $q\overline{q}$ or qqq, it is necessary to extend the naming scheme again.

8.1 "Neutral-flavor" mesons

The naming of mesons is based on their quantum numbers. Although wherever possible we use names established within the naive quark model, the name does *not* necessarily designate a (predominantly) $q\overline{q}$ state. In other words, the name provides information on the quantum numbers of a given state and not about its dominant component, which might well be $q\overline{q}$ (if allowed) or tetraquark, molecule, etc. In many cases, exotic states will be difficult to distinguish from $q\overline{q}$ states and will likely mix with them, and we make no attempt to, e.g., distinguish those that are "mostly gluonium" from those that are "mostly $q\overline{q}$."

Table 8.1: Symbols for mesons with strangeness and heavy-flavor quantum numbers equal to zero. States that do not (yet?) appear in the RPP are listed in parentheses.

$J^{PC} = \left\{ \begin{array}{c} \\ \\ \\ \end{array} \right.$	0^{-+}	1^{+-}	1^{--}	0^{++}
	2^{-+}	3^{+-}	2^{--}	1^{++}
	$\vdots$	$\vdots$	$\vdots$	$\vdots$
Minimal quark content				
$u\bar{d}, u\bar{u}-d\bar{d}, d\bar{u}$ $(I=1)$	π	b	ρ	a
$d\bar{d}+u\bar{u}$ and/or $s\bar{s}$ $(I=0)$	η,η'	h,h'	ω,ϕ	f,f'
$c\bar{c}$	η_c	h_c	ψ^*	χ_c
$b\bar{b}$	η_b	h_b	Υ	χ_b
$I=1$ with $c\bar{c}$	(Π_c)	Z_c	R_c	(W_c)
$I=1/2$ with $sc\bar{c}$	(Π_{cs})	Z_{cs}	(R_{cs})	(W_{cs})
$I=1$ with $b\bar{b}$	(Π_b)	Z_b	(R_b)	(W_b)
$I=1/2$ with $sb\bar{b}$	(Π_{bs})	(Z_{bs})	(R_{bs})	(W_{bs})

*The J/ψ remains the J/ψ.

Table 8.1 shows the names for mesons having strangeness and all heavy-flavor quantum numbers equal to zero. The rows of Table 8.1 give the minimal $q\overline{q}$ content. The columns give the possible parity/charge-conjugation states,

$$PC = -+,\ +-,\ --,\ \text{and}\ ++\ .$$

Within the naive quark model, these combinations correspond one-to-one to the angular-momentum state $^{2S+1}L_J$ of the $q\overline{q}$ system being

$$^1(L\ \text{even})_J,\ ^1(L\ \text{odd})_J,\ ^3(L\ \text{even})_J,\ \text{or}\ ^3(L\ \text{odd})_J\ ,$$

respectively. Here S, L, and J are the spin, orbital, and total angular momenta of the $q\overline{q}$ system. Within the naive quark model, the quantum numbers are related by $P = (-1)^{L+1}$, $C = (-1)^{L+S}$, and G parity $= (-1)^{L+S+I}$, where the quantum number C is only relevant to neutral mesons with neutral-flavor quantum numbers and G extends to isovector mesons; see the review on the quark model. These expressions impose restrictions on the quantum numbers that are allowed for $q\overline{q}$ states. However, they do not apply to more complicated structures such as tetraquarks.

The spin J is added as a subscript in the name except for pseudoscalar, vector, and axial vector mesons when there is no risk of ambiguity. Moreover, the mass is added in parentheses for mesons that decay strongly. However, for some of the familiar mesons (e.g. η', ϕ, ω), we omit the mass.

Measurements of the mass, quark content (where relevant), and quantum numbers I, J, P, and C (or G) of a meson thus determine its symbol. Conversely, these properties may be inferred unambiguously from the symbol. The name X is used for states with still unknown quantum numbers.

The mass label used in particle names is chosen using the best information available when a name is assigned. A more accurate value of a particle mass may become available at a later time. PDG will decide on a case-by-case basis whether to revise the mass label, taking into account the updated information.

With u, d, and s quarks, there are two isospin-0 mesons. A prime is used to distinguish one from the other (e.g. η and η'). Vector mesons decoupling to $u\overline{u}+d\overline{d}$ and $s\overline{s}$ (ideal mixing) are labeled ω and ϕ, respectively. As usual, we assign the spectroscopic name (e.g. $\Upsilon(1S)$) as the primary name to most of those ψ, Υ, and χ states whose spectroscopic identity is known. We use the form $\Upsilon(9460)$ as an alternative, and as the primary name when the spectroscopic identity is not known.

Since the top quark is so heavy that it decays too rapidly to form bound states, no name is assigned to structures like $t\overline{t}$.

Mesons with quantum numbers $J^{PC} = 0^{--}, 0^{+-}, 1^{-+}, 2^{+-}, 3^{-+}$, etc. cannot be $q\overline{q}$. For such a "manifestly exotic" meson, we use the same symbol as for a $q\overline{q}$ meson; the exotic nature of the meson can be inferred from the values of the P and C quantum numbers (given by the symbol), and the spin J (given by the subscript). For example, an isospin-0 1^{-+} meson containing only u, d, and s quarks and antiquarks would be denoted η_1 and an isospin-1 0^{--} meson containing only u, d, and s quarks and antiquarks would be denoted ρ_0.

The last two lines of Table 8.1 list isospin-1 states that also contain hidden heavy flavor, i.e. whose minimal quark content includes $c\overline{c}$ or $b\overline{b}$. We have assigned new names to these states, in keeping with the practice in the light-quark sector, where the $I = 0$ and $I = 1$ states have distinct names. The currently established $I = 1$ states in the heavy-quark sector have quantum numbers $J^{PC} = 1^{+-}$ and the proposed scheme keeps their original names Z.

Recently two experiments claimed evidence for states with 1^{+-} decaying into final states containing $sc\overline{c}$ and a light quark calling them Z_{cs}. We therefore extended Tab. 8.1 by allowing also for multiquarks containing strangeness.

8.2 Remarks on "neutral-flavor" mesons with hidden charm or bottom not classified as $q\overline{q}$

In the heavy-quark sector, there are several states with properties – such as masses, decay patterns, and widths – that are in disagreement with predictions from the naive quark model. For example, the vector state at 4230 MeV does not decay into $D\overline{D}$, although within the naive quark model its quantum numbers would call for this decay channel to be dominant. In recent literature, these states have been called X, Y, or Z, with their masses added in parentheses. This nomenclature conflicts with the rules outlined in the previous section, since the meson names are not related to their quantum numbers. However, these states have properties in conflict with the naive quark model and therefore deserve some special labeling.

Therefore in the Review of Particle Physics we will keep two names, one that carries the quantum number information and the other the original name. However, the former name will be given priority. In particular, it will be used when the particle appears as a decay product. Thus, in the Listings as well as Summary Tables from the 2018 edition onwards (listed are only some examples of the particles that appear in the Summary Tables),

- $X(3872)$ will appear as '$\chi_{c1}(3872)$ also known as $X(3872)$';
- $X(3900)^{\pm}$ will appear as '$Z_c(3900)^{\pm}$';
- $X(4260)$ will appear as '$\psi(4230)$ also known as $Y(4230)$'[1];

In addition, states with quantum numbers allowed by the naive quark model but showing some peculiarities, such as an unusual decay pattern, will have the following information in the header:

[1] This is one example where the mass label needed to be shifted given improved experimental information

Downloaded from https://academic.oup.com/ptep/article/2022/8/083C01/6651666 by KIT Library user on 27 September 2022

> This state shows properties different from a conventional $q\bar{q}$ state. A candidate for an exotic structure. See the review on ⟨name of the proper review⟩.

The states that cannot be classified as $q\bar{q}$ states (such as charged states with strong decays to heavy quarkonia) will have in the header:

> Properties incompatible with a $q\bar{q}$ structure (exotic state). See the review on ⟨name of the proper review⟩.

The names Z_c and Z_b used in the literature for isovector states in the $c\bar{c}$ and $b\bar{b}$ sector, respectively, will now also be the official PDG names. No heavy isovector $PC = -+, --$, or $++$ states have yet been confirmed, but provisional names for such states – Π, R, and W, respectively – are listed in Table 8.1. Note that the heavy isovector $PC = ++$ states were predicted to exist as spin partners of the Z states in [2], where the name W was also introduced.

By analogy to the light-quark sector, states with quantum numbers that are in conflict with the naive quark model are labeled according to their I, P, C, and spin J. The exotic nature can be inferred from the quantum numbers.

Table 8.2 maps the names now used in the PDG to former commonly used names.

Table 8.2: A comparison of current PDG names to former names commonly used in the literature.

Mesons with complete $I^G J^{PC}$ assignment	
PDG Name	Former Common Name(s)
$\psi_2(3823)^*$	$X(3823)$
$\chi_{c1}(3872)$	$X(3872)$
$Z_c(3900)$	$Z_c(3900)$
$\chi_{c2}(3930)^\dagger$	$\chi_{c2}(2P)$, $Z(3930)$
$\chi_{c1}(4140)$	$Y(4140)$
$Z_c(4200)$	$Z_c(4200)$
$\psi(4230)$	$Y(4230)$, $Y(4260)$
$R_{c0}(4240)$	$Z_c(4240)$
$\chi_{c1}(4274)$	$Y(4274)$
$\psi(4360)$	$Y(4360)$
$Z_c(4430)$	$Z_c(4430)$
$\chi_{c0}(4500)$	$X(4500)$
$\psi(4660)$	$X(4630)$, $Y(4660)$
$\chi_{c0}(4700)$	$X(4700)$
$Z_b(10610)$	$Z_b(10610)$
$Z_b(10650)$	$Z_b^{(\prime)}(10650)$
Mesons with incomplete $I^G J^{PC}$ assignment	
PDG Name	Former Common Name(s)
$X(3915)^\ddagger$	$\chi_{c0}(3915)$, $X(3915)$, $Y(3940)$
$X(3940)$	$X(3940)$
$X(4020)$	$Z_c^{(\prime)}(4020)$
$X(4050)^\pm$	$Z_1(4050)$
$X(4055)^\pm$	$Z_c(4055)$
$X(4160)$	$X(4160)$
$X(4250)^\pm$	$Z_2(4250)$
$X(4350)$	$X(4350)$

*The 2016 edition used $\psi(3823)$.

†The 2016 edition used $\chi_{c2}(2P)$. The mass is now used in the name following the current prescription.

‡The 2016 edition used $\chi_{c0}(3915)$. The J^{PC} have since been questioned.

8.3 Mesons with nonzero S, C and/or B

Mesons with nonzero strangeness S or heavy flavor C and/or B are not eigenstates of charge conjugation, and in each of them one of the quarks is heavier than the other (as above, states containing top quarks are not considered). The rules have been and remain:

1. The main symbol is an upper-case italic letter indicating the heavier quark as follows:

$$s \to \overline{K} \qquad c \to D \qquad b \to \overline{B},$$

   We use the convention that *the flavor quantum number and the charge of a quark have the same sign.* Thus the strangeness of the s quark is negative, the charm of the c quark is positive, and the bottomness of the b quark is negative. The effect of this convention is as follows: *any flavor carried by a charged meson has the same sign as its charge.* Thus the K^+, D^+, and B^+ have positive strangeness, charm, and bottomness, respectively, and all have positive I_3. The D_s^+ has positive charm *and* strangeness. Furthermore, the Δ(flavor) = ΔQ rule, best known for the strange kaons, applies to every flavor.
2. If the lighter quark is not a u or a d quark, its identity is given by a subscript. The D_s^+ is an example.
3. When the spin-parity is in the natural series, $J^P = 0^+, 1^-, 2^+, \cdots$, a superscript "*" is added.
4. The spin is added as a subscript except for pseudoscalar or vector mesons.

8.4 Baryons with ordinary quantum numbers

All baryons having quantum numbers consistent with a minimal quark content of three quarks are denoted by the symbols N, Δ, Λ, Σ, Ξ, and Ω introduced more than 50 years ago. These symbols are followed by J^P signifying their spin J and parity P. For those where the minimal content involves one or more heavier quarks than the light (u, d, and s) quarks, subscripts are added to their symbols, (c and b) as appropriate. The rules are:

1. Baryons with miminal content of *three* u and/or d quarks are N's (isospin 1/2) or Δ's (isospin 3/2).
2. Baryons with *two* u and/or d quarks are Λ's (isospin 0) or Σ's (isospin 1). If the third quark is a c or b quark, its identity is given by a subscript.
3. Baryons with *one* u or d quark are Ξ's (isospin 1/2). One or two subscripts are used if one or both of the remaining quarks are heavy: thus Ξ_c, Ξ_{cc}, Ξ_b, etc.*
4. Baryons with *no* u or d quarks are Ω's (isospin 0), and subscripts indicate any heavy-quark content.
5. A baryon that decays strongly has its mass in parentheses. Examples are the $\Delta(1232)$ $3/2^+$, $\Sigma(1385)$ $3/2^+$, $N(1440)$ $1/2^+$, $\Xi_c(2645)$ $3/2^+$.
6. If individual states of isospin multiplets are addressed, the electric charge is specified as a superscript. The electric charge is not necessary for isospin-0 states (Λ and Ω), as there is no ambiguity, but may still be included.
7. Antibaryons are labeled by an overline (bar) (e.g. $\bar{p}$ for the antiproton). Alternatively, particle and antiparticle can be distinguished by including a charge-label superscript. For example using Λ_c and $\bar{\Lambda}_c$ is equivalent to Λ_c^+ and Λ_c^-.

In short, the minimal number of u plus d quarks together with the isospin determine the main symbol, and subscripts indicate any content of heavy quarks. A Σ always has isospin 1, an Ω always has isospin 0, etc.

8.5 Exotic baryons

In 2003, several experiments reported finding a strangeness $S = +1$, charge $Q = +1$ baryon, and one experiment reported finding an $S = -2$, $Q = -2$ baryon. Baryons with such quantum numbers cannot be made from three quarks, and thus they are exotic with respect to the naive quark model. However, these "discoveries" were then ruled out by many experiments with far larger statistics: See our 2008 *Review* [3].

More recently, the LHCb collaboration found a series of candidates for pentaquark states in the $J/\psi p$ system extracted from data on $\Lambda_b^0 \to J/\psi K^- p$ [4,5].** These have the quantum numbers of excited nucleons, but have a minimal quark content of $c\bar{c}uud$. Following the name established by the LHCb collaboration, we label these $P_c^+(\text{mass})J^P$, with the mass given in parentheses.

Footnotes:

* See the "Note on Charmed Baryons" in the Charmed Baryon Listings.

** See our review "Pentaquarks" in the 2016 Edition.

Downloaded from https://academic.oup.com/ptep/article/2022/8/083C01/6651666 by KIT Library user on 27 September 2022

References

[1] M. Aguilar-Benitez *et al.* (Particle Data Group), Phys. Lett. **170B**, 1 (1986).

[2] M. B. Voloshin, Phys. Rev. **D84**, 031502 (2011), [arXiv:1105.5829].

[3] C. Amsler *et al.* (Particle Data Group), Phys. Lett. **B667**, 1 (2008).

[4] R. Aaij *et al.* (LHCb), Phys. Rev. Lett. **115**, 072001 (2015), [arXiv:1507.03414].

[5] R. Aaij *et al.* (LHCb), Phys. Rev. Lett. **122**, 22, 222001 (2019), [arXiv:1904.03947].

Downloaded from https://academic.oup.com/ptep/article/2022/8/083C01/6651666 by KIT Library user on 27 September 2022

Standard Model and Related Topics

9. Quantum chromodynamics (rev.) 149
10. Electroweak model and constraints on new physics (rev.) . . . 177
11. Higgs boson physics, status of (rev.) 201
12. CKM quark-mixing matrix (rev.) 261
13. CP violation in the quark sector (rev.) 271
14. Neutrino masses, mixing, and oscillations (rev.) 285
15. Quark model (rev.) 312
16. Heavy-quark & soft-collinear effective theory 329
17. Lattice quantum chromodynamics (rev.) 337
18. Structure functions (rev.) 353
19. Fragmentation functions in e^+e^-, ep and pp collisions (rev.) . 375
20. High Energy Soft QCD and Diffraction 392

Downloaded from https://academic.oup.com/ptep/article/2022/8/083C01/6651666 by KIT Library user on 27 September 2022

Downloaded from https://academic.oup.com/ptep/article/2022/8/083C01/6651666 by KIT Library user on 27 September 2022

9. Quantum Chromodynamics

Revised August 2021 by J. Huston (Michigan State U.), K. Rabbertz (KIT) and G. Zanderighi (MPI Munich).

9.1 Basics . . . 149
9.1.1 Running coupling . . . 149
9.1.2 Quark masses . . . 150
9.2 Structure of QCD predictions . . . 150
9.2.1 Fully inclusive cross sections . . . 150
9.2.2 Processes with initial-state hadrons . . . 151
9.2.3 Cross sections with phase-space restrictions 153
9.2.4 Accuracy of predictions . . . 156
9.3 Experimental studies of QCD . . . 157
9.3.1 Hadronic final-state observables . . . 157
9.3.2 QCD measurements at colliders . . . 159
9.4 Determinations of the strong coupling constant . 162
9.4.1 Hadronic τ decays and low Q^2 continuum: 163
9.4.2 Heavy quarkonia decays: . . . 164
9.4.3 PDF fits: . . . 164
9.4.4 Hadronic final states of e^+e^- annihilations: 164
9.4.5 Observables from hadron-induced collisions: 165
9.4.6 Electroweak precision fit: . . . 165
9.4.7 Lattice QCD: . . . 166
9.4.8 Determination of the world average value of $\alpha_s(M_Z^2)$: . . . 166

9.1 Basics

Quantum Chromodynamics (QCD), the gauge field theory that describes the strong interactions of colored quarks and gluons, is the SU(3) component of the SU(3)×SU(2)×U(1) Standard Model of Particle Physics. The Lagrangian of QCD is given by

$$\mathcal{L} = \sum_q \bar{\psi}_{q,a}(i\gamma^\mu\partial_\mu\delta_{ab} - g_s\gamma^\mu t^C_{ab}\mathcal{A}^C_\mu - m_q\delta_{ab})\psi_{q,b} - \frac{1}{4}F^A_{\mu\nu}F^{A\,\mu\nu}\,, \tag{9.1}$$

where repeated indices are summed over. The γ^μ are the Dirac γ-matrices. The $\psi_{q,a}$ are quark-field spinors for a quark of flavor q and mass m_q, with a color-index a that runs from $a = 1$ to $N_c = 3$, *i.e.* quarks come in three "colors." Quarks are said to be in the fundamental representation of the SU(3) color group.

The $\mathcal{A}^C_\mu$ correspond to the gluon fields, with C running from 1 to $N_c^2-1 = 8$, *i.e.* there are eight kinds of gluon. Gluons transform under the adjoint representation of the SU(3) color group. The t^C_{ab} correspond to eight 3×3 matrices and are the generators of the SU(3) group (*cf.* the section on "SU(3) isoscalar factors and representation matrices" in this *Review*, with $t^C_{ab} \equiv \lambda^C_{ab}/2$). They encode the fact that a gluon's interaction with a quark rotates the quark's color in SU(3) space. The quantity g_s (or $\alpha_s = \frac{g_s^2}{4\pi}$) is the QCD coupling constant. Besides quark masses, which have electroweak origin, it is the only fundamental parameter of QCD. Finally, the field tensor $F^A_{\mu\nu}$ is given by

$$F^A_{\mu\nu} = \partial_\mu\mathcal{A}^A_\nu - \partial_\nu\mathcal{A}^A_\mu - g_s\, f_{ABC}\mathcal{A}^B_\mu\mathcal{A}^C_\nu\,,$$
$$[t^A, t^B] = i f_{ABC} t^C\,, \tag{9.2}$$

where the f_{ABC} are the structure constants of the SU(3) group.

Neither quarks nor gluons are observed as free particles. Hadrons are color-singlet (*i.e.* color-neutral) combinations of quarks, anti-quarks, and gluons.

Ab-initio predictive methods for QCD include lattice gauge theory and perturbative expansions in the coupling. The Feynman rules of QCD involve a quark-antiquark-gluon ($q\bar{q}g$) vertex, a 3-gluon vertex (both proportional to g_s), and a 4-gluon vertex (proportional to g_s^2). A full set of Feynman rules is to be found for example in Refs. [1, 2].

Adopting a standard notation where repeated indices are summed over, useful color-algebra relations include: $t^A_{ab}t^A_{bc} = C_F\delta_{ac}$, where $C_F \equiv (N_c^2-1)/(2N_c) = 4/3$ is the color factor ("Casimir") associated with gluon emission from a quark; $f_{ACD}f_{BCD} = C_A\delta_{AB}$, where $C_A \equiv N_c = 3$ is the color factor associated with gluon emission from a gluon; $t^A_{ab}t^B_{ab} = T_R\delta_{AB}$, where $T_R = 1/2$ is the color factor for a gluon to split to a $q\bar{q}$ pair.

There is freedom for an additional CP-violating term to be present in the QCD Lagrangian, $\theta\frac{\alpha_s}{8\pi}F^A_{\mu\nu}\tilde{F}^{A\,\mu\nu}$, where θ is an additional free parameter, and $\tilde{F}^{A\,\mu\nu}$ is the dual of the gluon field tensor, $\frac{1}{2}\epsilon_{\mu\nu\sigma\rho}F^{A\,\sigma\rho}$, with $\epsilon_{\mu\nu\sigma\rho}$ being the fully antisymmetric Levi-Civita symbol. Experimental limits on ultracold neutrons [3, 4] and atomic mercury [5] constrain the QCD vacuum angle to satisfy $|\theta| \lesssim 10^{-10}$. Further discussion is to be found in Ref. [6] and in the Axions section in the Listings of this *Review*.

This section will concentrate mainly on perturbative aspects of QCD as they relate to collider physics. Related textbooks and lecture notes include Refs. [1, 2, 7–9]. Aspects specific to Monte Carlo event generators are reviewed in the dedicated section 43. Lattice QCD is also reviewed in a section of its own, Sec. 17, with further discussion of perturbative and non-perturbative aspects to be found in the sections on "Quark Masses", "The CKM quark-mixing matrix", "Structure Functions", "Fragmentation Functions", "Passage of Particles Through Matter" and "Heavy-Quark and Soft-Collinear Effective Theory" in this *Review*.

9.1.1 *Running coupling*

In the framework of perturbative QCD (pQCD), predictions for observables are expressed in terms of the renormalized coupling $\alpha_s(\mu_R^2)$, a function of an (unphysical) renormalization scale μ_R. When one takes μ_R close to the scale of the momentum transfer Q in a given process, then $\alpha_s(\mu_R^2 \simeq Q^2)$ is indicative of the effective strength of the strong interaction in that process.

The coupling satisfies the following renormalization group equation (RGE):

$$\mu_R^2\frac{d\alpha_s}{d\mu_R^2} = \beta(\alpha_s) = -(b_0\alpha_s^2 + b_1\alpha_s^3 + b_2\alpha_s^4 + \cdots)\,, \tag{9.3}$$

where $b_0 = (11C_A - 4n_fT_R)/(12\pi) = (33-2n_f)/(12\pi)$ is referred to as the 1-loop β-function coefficient, the 2-loop coefficient is $b_1 = (17C_A^2 - n_fT_R(10C_A+6C_F))/(24\pi^2) = (153-19n_f)/(24\pi^2)$, and the 3-loop coefficient is $b_2 = (2857 - \frac{5033}{9}n_f + \frac{325}{27}n_f^2)/(128\pi^3)$ for the SU(3) values of C_A and C_F. Here n_f is the number of quark flavours. The 4-loop coefficient, b_3, is to be found in Refs. [10, 11], while the 5-loop coefficient, b_4, is in Refs. [12–16]. The coefficients b_2 and b_3 (and beyond) are renormalization-scheme-dependent and given here in the modified minimal subtraction scheme ($\overline{\text{MS}}$) [17], by far the most widely used scheme in QCD and the one adopted in the following.

The minus sign in Eq. (9.3) is the origin of "asymptotic freedom" [18, 19], *i.e.* the fact that the strong coupling becomes weak for processes involving large momentum transfers ("hard processes"). For momentum transfers in the 0.1–1 TeV range, $\alpha_s \sim 0.1$, while the theory is strongly interacting for scales around and below 1 GeV.

The β-function coefficients, the b_i, are given for the coupling of an *effective theory* in which n_f of the quark flavors are considered light ($m_q \ll \mu_R$), and in which the remaining heavier quark flavors decouple from the theory. One may relate the coupling for the theory with n_f+1 light flavors to that with n_f flavors through an equation of the form

$$\alpha_s^{(n_f+1)}(\mu_R^2) = \alpha_s^{(n_f)}(\mu_R^2)\times \times\left(1 + \sum_{n=1}^{\infty}\sum_{\ell=0}^{n} c_{n\ell}\,[\alpha_s^{(n_f)}(\mu_R^2)]^n \ln^\ell\frac{\mu_R^2}{m_h^2}\right)\,, \tag{9.4}$$

where m_h is the mass of the $(n_f+1)^{\text{th}}$ flavor, and the first few $c_{n\ell}$ coefficients are $c_{11} = \frac{1}{6\pi}$, $c_{10} = 0$, $c_{22} = c_{11}^2$, $c_{21} = \frac{11}{24\pi^2}$, and $c_{20} = -\frac{11}{72\pi^2}$ when m_h is the $\overline{\text{MS}}$ mass at scale m_h, while $c_{20} = \frac{7}{24\pi^2}$ when m_h is the pole mass (mass definitions are discussed below in Sec. (9.1.2) and in the review on "Quark Masses"). Terms up to $c_{4\ell}$ with $0 \le \ell \le 4$ are to be found in Refs. [20, 21].

Downloaded from https://academic.oup.com/ptep/article/2022/8/083C01/6651666 by KIT Library user on 27 September 2022

Numerically, when one chooses $\mu_R = m_h$, the matching is a modest effect, owing to the zero value for the c_{10} coefficient. Relations between n_f and (n_f+2) flavors where the two heavy flavors are close in mass are given to three loops in Ref. [22].

Working in an energy range where the number of flavors is taken constant, a simple exact analytic solution exists for Eq. (9.3) only if one neglects all but the b_0 term, giving $\alpha_s(\mu_R^2) = (b_0 \ln(\mu_R^2/\Lambda^2))^{-1}$. Here Λ is a constant of integration, which corresponds to the scale where the perturbatively-defined coupling would diverge. Its value is indicative of the energy range where non-perturbative dynamics dominates. A convenient approximate analytic solution to the RGE that includes terms up to b_4 is given by solving iteratively Eq. (9.3)

$$\alpha_s(\mu_R^2) \simeq \frac{1}{b_0 t}\left(1 - \frac{b_1}{b_0^2}\frac{\ell}{t} + \frac{b_1^2(\ell^2-\ell-1)+b_0 b_2}{b_0^4 t^2} + \right.$$
$$+ \frac{b_1^3\left(-2\ell^3+5\ell^2+4\ell-1\right) - 6b_0 b_2 b_1 \ell + b_0^2 b_3}{2b_0^6 t^3} +$$
$$+ \frac{18 b_0 b_2 b_1^2\left(2\ell^2-\ell-1\right) + b_1^4\left(6\ell^4-26\ell^3-9\ell^2+24\ell+7\right)}{6b_0^8 t^4}$$
$$\left. + \frac{-b_0^2 b_3 b_1(12\ell+1) + 2b_0^2\left(5b_2^2+b_0 b_4\right)}{6b_0^8 t^4}\right), \tag{9.5}$$

with $t \equiv \ln\frac{\mu_R^2}{\Lambda^2}$ and $\ell = \ln t$, again parametrized in terms of a constant Λ. Note that Eq. (9.5) is one of several possible approximate 4-loop solutions for $\alpha_s(\mu_R^2)$, and that a value for Λ only defines $\alpha_s(\mu_R^2)$ once one knows which particular approximation is being used. An alternative to the use of formulas such as Eq. (9.5) is to solve the RGE exactly, numerically (including the discontinuities, Eq. (9.4), at flavor thresholds). In such cases the quantity Λ does not directly arise (though it can be defined, *cf.* Eqs. (1–3) of Ref. [23]). For these reasons, in determinations of the coupling, it has become standard practice to quote the value of α_s at a given scale (typically the mass of the Z boson, M_Z) rather than to quote a value for Λ.

A discussion of determinations of the coupling and a graph illustrating its scale dependence ("running") are to be found in Section 9.4.

9.1.2 *Quark masses*

Free quarks have never been observed, which is understood as a result of a long-distance, confining property of the strong QCD force: up, down, strange, charm, and bottom quarks all *hadronize*, *i.e.* become part of a meson or baryon, on a timescale $\sim 1/\Lambda$; the top quark instead decays before it has time to hadronize. This means that the question of what one means by the quark mass is a complex one, which requires one to adopt a specific prescription. A perturbatively defined prescription is the pole mass, m_q, which corresponds to the position of the divergence of the propagator. This is close to one's physical picture of mass. However, when relating it to observable quantities, it suffers from a badly behaved perturbative series which makes it ambiguous to an amount related to Λ (see *e.g.* Ref. [24–26]). An alternative is the $\overline{\rm MS}$ mass, $\overline{m}_q(\mu_R^2)$, which depends on the renormalization scale μ_R.

Results for the masses of heavier quarks are often quoted either as the pole mass or as the $\overline{\rm MS}$ mass evaluated at a scale equal to the mass, $\overline{m}_q(\overline{m}_q^2)$; light quark masses are often quoted in the $\overline{\rm MS}$ scheme at a scale $\mu_R \sim 2\,\text{GeV}$. The pole and $\overline{\rm MS}$ masses are related by a series that starts as $m_q = \overline{m}_q(\overline{m}_q^2)(1 + \frac{4\alpha_s(\overline{m}_q^2)}{3\pi} + \mathcal{O}(\alpha_s^2))$, while the scale-dependence of $\overline{\rm MS}$ masses is given at lowest order by

$$\mu_R^2 \frac{d\overline{m}_q(\mu_R^2)}{d\mu_R^2} = \left[-\frac{\alpha_s(\mu_R^2)}{\pi} + \mathcal{O}(\alpha_s^2)\right]\overline{m}_q(\mu_R^2)\,. \tag{9.6}$$

A more detailed discussion is to be found in a dedicated section of the *Review*, "Quark Masses", with detailed formulas also in Ref. [27] and references therein.

In perturbative QCD calculations of scattering processes, it is common to work in an approximation in which one neglects (*i.e.* sets to zero) the masses of all quarks, whose mass is significantly smaller than the momentum transfer in the process.

9.2 Structure of QCD predictions

9.2.1 *Fully inclusive cross sections*

The simplest observables in perturbative QCD are those that do not involve initial-state hadrons and that are fully inclusive with respect to details of the final state. One example is the total cross section for $e^+e^- \to$ hadrons at center-of-mass energy Q, for which one can write

$$\frac{\sigma(e^+e^- \to \text{hadrons}, Q)}{\sigma(e^+e^- \to \mu^+\mu^-, Q)} \equiv R(Q) = R_{\rm EW}(Q)(1+\delta_{\rm QCD}(Q))\,, \tag{9.7}$$

where $R_{\rm EW}(Q)$ is the purely electroweak prediction for the ratio and $\delta_{\rm QCD}(Q)$ is the correction due to QCD effects. To keep the discussion simple, we can restrict our attention to energies $Q \ll M_Z$, where the process is dominated by photon exchange (neglecting electroweak and finite-quark-mass corrections $R_{\rm EW} = N_c \sum_q e_q^2$, where the e_q are the electric charges of the quarks) and

$$\delta_{\rm QCD}(Q) = \sum_{n=1}^{\infty} c_n \cdot \left(\frac{\alpha_s(Q^2)}{\pi}\right)^n + \mathcal{O}\left(\frac{\Lambda^4}{Q^4}\right)\,. \tag{9.8}$$

The first four terms in the α_s series expansion are then to be found in Ref. [28],

$$c_1 = 1\,, \qquad c_2 = 1.9857 - 0.1152 n_f\,, \tag{9.9a}$$
$$c_3 = -6.63694 - 1.20013 n_f - 0.00518 n_f^2 - 1.240\eta\,, \tag{9.9b}$$
$$c_4 = -156.61 + 18.775 n_f - 0.7974 n_f^2 + 0.0215 n_f^3 - (17.828 - 0.575 n_f)\eta\,, \tag{9.9c}$$

with $\eta = (\sum e_q)^2/(N_c \sum e_q^2)$ and $N_c = 3$. For corresponding expressions including also Z exchange and finite-quark-mass effects, see Refs. [29–31].

A related series holds also for the QCD corrections to the hadronic decay width of the τ lepton, which essentially involves an integral of $R(Q)$ over the allowed range of invariant masses of the hadronic part of the τ decay (see *e.g.* Ref. [32]). The series expansions for QCD corrections to Higgs-boson hadronic (partial) decay widths in the limit of heavy top quark and massless light flavours at N^{4}LO are given in Ref. [33].

One characteristic feature of Eqs. (9.8) and (9.9) is that the coefficients of α_s^n increase order by order: calculations in perturbative QCD tend to converge more slowly than would be expected based just on the size of α_s. The situation is significantly worse near thresholds or in the presence of tight kinematic cuts. Another feature is the existence of an extra "power-correction" term $\mathcal{O}(\Lambda^4/Q^4)$ in Eq. (9.8), which accounts for contributions that are fundamentally non-perturbative. All high-energy QCD predictions involve power corrections $(\Lambda/Q)^p$, although typically the suppression of these corrections with Q is smaller than given in Eq. (9.8), where $p = 4$. The exact power p depends on the observable and, for many processes and observables, it is possible to introduce an operator product expansion and associate power-suppressed terms with specific higher-dimension (non-perturbative) operators [34].

Scale dependence. In Eq. (9.8) the renormalization scale for α_s has been chosen equal to Q. The result can also be expressed in terms of the coupling at an arbitrary renormalization scale μ_R,

$$\delta_{\rm QCD}(Q) = \sum_{n=1}^{\infty} \bar{c}_n\left(\frac{\mu_R^2}{Q^2}\right) \cdot \left(\frac{\alpha_s(\mu_R^2)}{\pi}\right)^n + \mathcal{O}\left(\frac{\Lambda^4}{Q^4}\right)\,, \tag{9.10}$$

where $\bar{c}_1(\mu_R^2/Q^2) \equiv c_1$, $\bar{c}_2(\mu_R^2/Q^2) = c_2 + \pi b_0 c_1 \ln(\mu_R^2/Q^2)$, $\bar{c}_3(\mu_R^2/Q^2) = c_3 + (2b_0 c_2 \pi + b_1 c_1 \pi^2) \times \ln(\mu_R^2/Q^2) +$

Downloaded from https://academic.oup.com/ptep/article/2022/8/083C01/6651666 by KIT Library user on 27 September 2022

$b_0^2 c_1 \pi^2 \ln^2(\mu_R^2/Q^2)$, *etc.* Given an infinite number of terms in the α_s expansion, the μ_R dependence of the $\overline{c}_n(\mu_R^2/Q^2)$ coefficients will exactly cancel that of $\alpha_s(\mu_R^2)$, and the final result will be independent of the choice of μ_R: physical observables do not depend on unphysical scales.[1]

With just terms up to some finite $n = N$, a residual μ_R dependence will remain, which implies an uncertainty on the prediction of $R(Q)$ due to the arbitrariness of the scale choice. This uncertainty will be $\mathcal{O}(\alpha_s^{N+1})$, *i.e.* of the same order as the neglected higher-order terms. For this reason it is customary to use the scale dependence of QCD predictions as an estimate of the uncertainties due to neglected terms. One usually takes a central value for $\mu_R \sim Q$, in order to avoid the poor convergence of the perturbative series that results from the large $\ln^{n-1}(\mu_R^2/Q^2)$ terms in the $\overline{c}_n$ coefficients when $\mu_R \ll Q$ or $\mu_R \gg Q$. Uncertainties are then commonly determined by varying μ_R by a factor of two up and down around the central scale choice. This is not a rigorous prescription for determining the uncertainty, but is motivated by the requirement that there should not be large logarithms introduced into a calculation by large ratios of scales. A more detailed discussion on the accuracy of theoretical predictions and on ways to estimate the theoretical uncertainties can be found in Section 9.2.4.

9.2.2 *Processes with initial-state hadrons*

Deep-Inelastic Scattering. To illustrate the key features of QCD cross sections in processes with initial-state hadrons, let us consider deep-inelastic scattering (DIS), $e + p \to e + X$, where an electron e with four-momentum k emits a highly off-shell photon (momentum q) that interacts with the proton (momentum p). For photon virtualities $Q^2 \equiv -q^2$ far above the squared proton mass (but far below the squared Z mass), the differential cross section in terms of the kinematic variables Q^2, $x = Q^2/(2p \cdot q)$ and $y = (q \cdot p)/(k \cdot p)$ is

$$\frac{d^2\sigma}{dx dQ^2} = \frac{4\pi\alpha^2}{2xQ^4}\left[(1 + (1-y)^2)F_2(x,Q^2) - y^2 F_L(x,Q^2)\right], \tag{9.11}$$

where α is the electromagnetic coupling and $F_2(x,Q^2)$ and $F_L(x,Q^2)$ are proton structure functions, which encode the interaction between the photon (in given polarization states) and the proton. In the presence of parity-violating interactions (*e.g.* νp scattering) an additional F_3 structure function is present. For an extended review, including equations for the full electroweak and polarized cases, see Sec. 18 of this *Review*.

Structure functions are not calculable in perturbative QCD, nor is any other cross section that involves QCD interactions and initial-state hadrons. To zeroth order in α_s, the structure functions are given directly in terms of non-perturbative parton (quark or gluon) distribution functions (PDFs),

$$F_2(x,Q^2) = x\sum_q e_q^2 f_{q/p}(x), \qquad F_L(x,Q^2) = 0, \tag{9.12}$$

where $f_{q/p}(x)$ is the non-perturbative PDF for quarks of type q inside the proton, *i.e.* the number density of quarks of type q inside a fast-moving proton that carry a fraction x of its longitudinal momentum (the quark flavor index q, here, is not to be confused with the photon momentum q in the lines preceding Eq. (9.11)). Recently, some first determinations using lattice started to appear [35–44] but there is also some debate about the underlying methods [45]. Accordingly, for all practical uses, PDFs are currently determined from data (*cf.* Sec. 18 of this *Review* and also Refs. [46,47]) [2].

The above result, with PDFs $f_{q/p}(x)$ that are independent of the scale Q, corresponds to the "quark-parton model" picture, in which the photon interacts with point-like free quarks, or equivalently, one has incoherent elastic scattering between the electron and individual constituents of the proton. As a consequence, in this picture also F_2 and F_L are independent of Q [51]. When including higher orders in pQCD, one has

$$F_2(x,Q^2) = x\sum_{n=0}^{\infty}\frac{\alpha_s^n(\mu_R^2)}{(2\pi)^n}\times$$
$$\times\sum_{i=q,g}\int_x^1\frac{dz}{z}C_{2,i}^{(n)}(z,Q^2,\mu_R^2,\mu_F^2)f_{i/p}\left(\frac{x}{z},\mu_F^2\right) + \mathcal{O}\left(\frac{\Lambda^2}{Q^2}\right). \tag{9.13}$$

Just as in Eq. (9.10), we have a series in powers of $\alpha_s(\mu_R^2)$, each term involving a coefficient $C_{2,i}^{(n)}$ that can be calculated using Feynman graphs. At variance with the parton model, the PDFs in pQCD depend on an additional scale, the factorization scale μ_F, whose significance will be discussed in the following. Another important difference is the additional integral over z. The parton that comes from the proton can undergo a splitting before it interacts with the photon. As a result, the $C_{2,i}^{(n)}$ coefficients are functions that depend on the ratio, z, of the parton's momentum before and after radiation, and one must integrate over that ratio. For the electromagnetic component of DIS with light quarks and gluons, the zeroth order coefficient functions are $C_{2,q}^{(0)} = e_q^2\delta(1-z)$ and $C_{2,g}^{(0)} = 0$. Corrections are known up to $\mathcal{O}(\alpha_s^3)$ (next-to-next-to-next-to-leading order, N^{3}LO) for both electromagnetic [52] and weak currents [53,54]. For heavy-quark production they are known to $\mathcal{O}(\alpha_s^2)$ [55,56] (next-to-leading order, NLO, insofar as the series starts at $\mathcal{O}(\alpha_s)$). For precise comparisons of LHC cross sections with theoretical predictions, the photon PDF of the proton is also needed. It has been computed precisely in Ref. [57] and has now been implemented in most global PDF fits. More recently, the PDF for leptons has also been computed [58].

The majority of the emissions that modify a parton's momentum are collinear (parallel) to that parton, and do not depend on the fact that the parton is destined to interact with a photon. It is natural to view these emissions as modifying the proton's structure rather than being part of the coefficient function for the parton's interaction with the photon. Technically, one uses a procedure known as *collinear factorization* to give a well-defined meaning to this distinction, most commonly through the $\overline{\text{MS}}$ factorization scheme, defined in the context of dimensional regularization. The $\overline{\text{MS}}$ factorization scheme involves an arbitrary choice of *factorization scale*, μ_F, whose meaning can be understood roughly as follows: emissions with transverse momenta above μ_F are included in the $C_{2,q}^{(n)}(z,Q^2,\mu_R^2,\mu_F^2)$; emissions with transverse momenta below μ_F are accounted for within the PDFs, $f_{i/p}(x,\mu_F^2)$. While collinear factorization is generally believed to be valid for suitable (sufficiently inclusive) observables in processes with hard scales, Ref. [59], which reviews the factorization proofs in detail, is cautious in the statements it makes about their exhaustivity, notably for the hadron-collider processes which we shall discuss below. The transverse degrees of freedom have been integrated over for collinear PDFs. It is also possible to produce transverse-momentum dependent (or unintegrated) PDFs where

[1] With respect to pQCD there is an important caveat to this statement: at sufficiently high orders, perturbative series generally suffer from "renormalon" divergences $\alpha_s^n n!$ (reviewed in Ref. [24]). This phenomenon is not usually visible with the limited number of perturbative terms available today. However, it is closely connected with non-perturbative contributions and sets a limit on the possible precision of perturbative predictions. The cancellation of scale dependence will also ultimately be affected by this renormalon-induced breakdown of perturbation theory.

[2] PDFs can be determined from data in a global fit at LO, NLO and NNLO, depending on the order of the matrix elements used to describe the data. In modern global PDF fits, data are included from DIS, Drell-Yan (DY), jets and $t\bar{t}$ processes, and more LHC collider data, with the global PDF fits using 3000-4000 data points. There is a large change in the PDFs from LO to NLO, with a much smaller change from NLO to NNLO. LO PDFs can be unreliable for collider predictions, especially at low and high x. The uncertainties for the resulting PDFs are determined primarily from the experimental uncertainties of the data that serves as input to the global PDF fits. There is also a component due to the limitations of the parametrizations used, although this may be reduced with the use of more flexible forms. The PDF uncertainties can either be determined through a Hessian approach or through the use of Monte Carlo replicas. It is now relatively straightforward to convert results from one approach to the other. Recently, theoretical uncertainties related to missing higher orders have been included in global PDF determinations but so far only at NLO [48–50].

Downloaded from https://academic.oup.com/ptep/article/2022/8/083C01/6651666 by KIT Library user on 27 September 2022

these degrees of freedom remain. Further discussion is to be found in Refs. [60,61].

The PDFs' resulting dependence on μ_F is described by the Dokshitzer-Gribov-Lipatov-Altarelli-Parisi (DGLAP) equations [62], which to leading order (LO) read[3]

$$\mu_F^2 \frac{\partial f_{i/p}(x,\mu_F^2)}{\partial \mu_F^2} = \sum_j \frac{\alpha_s(\mu_F^2)}{2\pi} \int_x^1 \frac{dz}{z} P^{(1)}_{i\leftarrow j}(z) f_{j/p}\left(\frac{x}{z},\mu_F^2\right), \tag{9.14}$$

with, for example, $P^{(1)}_{q\leftarrow g}(z) = T_R(z^2+(1-z)^2)$. The other LO splitting functions are listed in Sec. 18 of this *Review*, while results up to NLO, α_s^2, and NNLO, α_s^3, are given in Refs. [63] and [64] respectively. At N^{3}LO accuracy, only partial results are currently available in Refs. [65–67]. Splitting functions for PDFs in the helicity dependent case are given in Ref. [68].

Beyond LO, the coefficient functions are also μ_F dependent, for example $C^{(1)}_{2,i}(x,Q^2,\mu_R^2,\mu_F^2) = C^{(1)}_{2,i}(x,Q^2,\mu_R^2,Q^2) - \ln\left(\frac{\mu_F^2}{Q^2}\right)\sum_j \int_x^1 \frac{dz}{z} \times C^{(0)}_{2,j}(\frac{x}{z}) P^{(1)}_{j\leftarrow i}(z)$. In certain contexts, higher-order QED and mixed QED-QCD corrections to the splitting functions are also needed [69].

As with the renormalization scale, the choice of factorization scale is arbitrary, but if one has an infinite number of terms in the perturbative series, the μ_F-dependencies of the coefficient functions and PDFs will compensate each other fully. Given only N terms of the series, a residual $\mathcal{O}(\alpha_s^{N+1})$ uncertainty is associated with the ambiguity in the choice of μ_F. As with μ_R, varying μ_F provides an input in estimating uncertainties on predictions. In inclusive DIS predictions, the default choice for the scales is usually $\mu_R = \mu_F = Q$.

As is the case for the running coupling, in DGLAP evolution one can introduce flavor thresholds near the heavy quark masses: below a given heavy quark's mass, that quark is not considered to be part of the proton's structure, while above it is considered to be part of the proton's structure and evolves with massless DGLAP splitting kernels. With appropriate parton distribution matching terms at threshold, such a variable flavor number scheme (VFNS), when used with massless coefficient functions, gives the full heavy-quark contributions at high Q^2 scales. For scales near the threshold, it is instead necessary to appropriately adapt the standard massive coefficient functions to account for the heavy-quark contribution already included in the PDFs [70–72].

At sufficiently small x and Q^2 in inclusive DIS, resummation of small x logarithms may be necessary [73,74]. This may in fact have been observed in Refs. [75] based on HERA data [76], in a kinematic region where useful information for PDFs for collider predictions is present. A better description of the data in this region can be gained by small x resummation matched to NNLO [75,77], or by the inclusion of power-suppressed contributions [78] or by using an x-dependent factorization scale in the NNLO DIS predictions [79].

In situations in which the total center-of-mass energy $\sqrt{s}$ is much larger than all other momentum-transfer scales in the problem (*e.g.* Q in DIS, m_b for $b\bar{b}$ production in pp collisions, *etc.*), each power of α_s beyond LO can be accompanied by a power of $\ln(s/Q^2)$ (or $\ln(s/m_b^2)$, *etc.*). This is variously referred to as the high-energy, small-x or Balitsky-Fadin-Kuraev-Lipatov (BFKL) limit [74,80,81]. Currently it is possible to account for the dominant and first sub-dominant [82,83] power of such logarithms at each order of α_s, and also to estimate further sub-dominant contributions that are numerically large (see Refs. [84–87] and references therein). Progress towards NNLO is discussed in Ref. [88].

Physically, the summation of all orders in α_s can be understood as leading to a growth with s of the gluon density in the proton. At sufficiently high energies this implies non-linear effects (commonly referred to as parton saturation), whose treatment has been the subject of intense study (see for example Refs. [89–91] and references thereto).

Hadron-hadron collisions.

The extension to processes with two initial-state hadrons can be illustrated with the example of the total (inclusive) cross section for W boson production in collisions of hadrons h_1 and h_2, which can be written as

$$\sigma(h_1h_2 \to W+X) = \sum_{n=0}^{\infty} \alpha_s^n(\mu_R^2) \times \sum_{i,j} \int dx_1 dx_2\, f_{i/h_1}\left(x_1,\mu_F^2\right) f_{j/h_2}\left(x_2,\mu_F^2\right) \times \hat{\sigma}^{(n)}_{ij\to W+X}\left(x_1x_2s,\mu_R^2,\mu_F^2\right) + \mathcal{O}\left(\frac{\Lambda^2}{M_W^4}\right), \tag{9.15}$$

where s is the squared center-of-mass energy of the collision. At LO, $n=0$, the hard (partonic) cross section $\hat{\sigma}^{(0)}_{ij\to W+X}(x_1x_2s,\mu_R^2,\mu_F^2)$ is simply proportional to $\delta(x_1x_2s - M_W^2)$, in the narrow W-boson width approximation (see Sec. 51 of this *Review* for detailed expressions for this and other hard scattering cross sections). It is non-zero only for choices of i,j that can directly give a W, such as $i=u$, $j=\bar{d}$. At higher orders, $n\geq 1$, new partonic channels contribute, such as gq, and $x_1x_2s \geq M_W^2$ in the narrow W-boson width approximation.

Equation (9.15) involves a collinear factorization between the hard cross section and the PDFs, just like Eq. (9.13). As long as the same factorization scheme is used in DIS and pp or $p\bar{p}$ (usually the $\overline{\text{MS}}$ scheme), then PDFs extracted in DIS can be directly used in pp and $p\bar{p}$ predictions [59,92] (with the anti-quark distributions in an anti-proton being the same as the quark distributions in a proton).

A number of fully inclusive cross-sections have been computed up to N^{3}LO, *i.e.* including corrections up to relative order α_s^3, in recent years. These include inclusive Higgs production through gluon fusion in the large m_t limit, calculated at N^{3}LO in Refs. [93,94]. Higgs boson pair production via gluon fusion in the same approximation was computed at N^{3}LO in Ref. [95]. Calculations at this order, differential in the Higgs rapidity [96,97] and fully differential [98] have been presented recently. Vector-boson fusion single- [99] and double-pair [100] production is also known to N^{3}LO [99] in the factorized approximation. Neutral [101,102] and charged [103] Drell-Yan processes have also been computed at N^{3}LO. Differential rapidity distributions are available, but not yet with fiducial cuts. The uncertainty band derived from scale variation is not contained in the uncertainty band of the previous order, as might be expected from a well-behaved process. This has been ascribed to cancellations between channels at NNLO that lead to underestimates of the uncertainty at that order. This effect does not seem to be present in other processes, such as Higgs boson production through gluon-gluon fusion. Note that there is currently a mis-match in N^{3}LO calculations in that PDFs at the same order are not yet available. The fully inclusive hard cross sections for several other processes are known to NNLO[4]. For instance, Higgs-boson production in association with a vector boson [104], Higgs-pair production in the large m_t approximation [105], and with full m_t dependence [106], top-antitop production [107,108] and vector-boson pair production [109–111]. For a comprehensive overview on other recent NNLO calculations see Ref. [112].

Photoproduction. γp (and $\gamma\gamma$) collisions are similar to pp collisions, with the subtlety that the photon can behave in two ways: there is "direct" photoproduction, in which the photon behaves as a point-like particle and takes part directly in the hard collision, with hard subprocesses such as $\gamma g \to q\bar{q}$; there is also resolved photoproduction, in which the photon behaves like a hadron, with non-perturbative partonic substructure and a corresponding PDF for its quark and gluon content, $f_{i/\gamma}(x,Q^2)$. While useful to understand the general structure of γp collisions, the distinction between direct and resolved photoproduction is not well defined beyond leading order, as discussed for example in Ref. [113].

[3] LO is generally taken to mean the lowest order at which a quantity is non-zero.

[4] Processes with jets or photons in the final state have divergent cross sections unless one places a cut on the jet or photon momentum. Accordingly, they are discussed below in Section 9.2.3.2.

Downloaded from https://academic.oup.com/ptep/article/2022/8/083C01/6651666 by KIT Library user on 27 September 2022

9.2.3 *Cross sections with phase-space restrictions*

QCD final states always consist of hadrons, while perturbative QCD calculations deal with partons. Physically, an energetic parton fragments ("showers") into many further partons, which then, on later timescales, undergo a transition to hadrons ("hadronization"). Fixed-order perturbation theory captures only a small part of these dynamics. This does not matter for the fully inclusive cross sections discussed above: the showering and hadronization stages are approximately unitary, *i.e.* they do not substantially change the overall probability of hard scattering, because they occur long after it has taken place (they introduce at most a correction proportional to a power of the ratio of timescales involved, *i.e.* a power of Λ/Q, where Q is the hard scattering scale).

Less inclusive measurements, in contrast, may be affected by the extra dynamics. For those sensitive just to the main directions of energy flow (jet rates, event shapes, *cf.* Sec. 9.3.1) fixed-order perturbation theory is often still adequate, because showering and hadronization do not substantially change the overall energy flow. This means that one can make a prediction using just a small number of partons, which should correspond well to a measurement of the same observable carried out on hadrons. For observables that instead depend on distributions of individual hadrons (which, *e.g.*, are the inputs to detector simulations), it is mandatory to account for showering and hadronization. The range of predictive techniques available for QCD final states reflects this diversity of needs of different measurements.

While illustrating the different methods, we shall for simplicity mainly use expressions that hold for e^+e^- scattering. The extension to cases with initial-state partons will be mostly straightforward (space constraints unfortunately prevent us from addressing diffraction and exclusive hadron-production processes; extensive discussion is to be found in Sec. 20 of this *Review* and in Refs. [114, 115]).

9.2.3.1 *Soft and collinear limits*

Before examining specific predictive methods, it is useful to be aware of a general property of QCD matrix elements in the soft and collinear limits. Consider a squared tree-level matrix element $|M_n^2(p_1,\ldots,p_n)|$ for the process $e^+e^- \to n$ partons with momenta $p_1,\ldots,p_n$, and a corresponding phase-space integration measure $d\Phi_n$. If particle n is a gluon, which becomes collinear (parallel) to another particle i and additionally its momentum tends to zero (is "soft"), the matrix element simplifies as follows,

$$\lim_{\theta_{in}\to 0,\, E_n\to 0} d\Phi_n |M_n^2(p_1,\ldots,p_n)| = d\Phi_{n-1}|M_{n-1}^2(p_1,\ldots,p_{n-1})| \frac{\alpha_s C_i}{\pi}\frac{d\theta_{in}^2}{\theta_{in}^2}\frac{dE_n}{E_n}\,, \qquad (9.16)$$

where $C_i = C_F$ (C_A) if i is a quark (gluon). This formula has non-integrable divergences both for the inter-parton angle $\theta_{in} \to 0$ and for the gluon energy $E_n \to 0$, which are mirrored also in the structure of divergences in loop diagrams. These divergences are important for at least two reasons: firstly, they govern the typical structure of events (inducing many emissions either with low energy or at small angle with respect to hard partons); secondly, they will determine which observables can be calculated within perturbative QCD.

9.2.3.2 *Fixed-order predictions*

Let us consider an observable $\mathcal{O}$ that is a function $\mathcal{O}_n(p_1,\ldots,p_n)$ of the four-momenta of the n final-state particles in an event (either partons or hadrons). In what follows, we shall consider the cross section for events weighted with the value of the observable, $\sigma_{\mathcal{O}}$. As examples, if $\mathcal{O}_n \equiv 1$ for all n, then $\sigma_{\mathcal{O}}$ is just the total cross section; if $\mathcal{O}_n \equiv \hat{\tau}(p_1,\ldots,p_n)$ where $\hat{\tau}$ is the value of the Thrust for that event (see Eq. (9.22) in Sec. 9.3.1.2), then the average value of the Thrust is $\langle\tau\rangle = \sigma_{\mathcal{O}}/\sigma_{\rm tot}$; if $\mathcal{O}_n \equiv \delta(\tau - \hat{\tau}(p_1,\ldots,p_n))$ then one gets the differential cross section as a function of the Thrust, $\sigma_{\mathcal{O}} \equiv d\sigma/d\tau$.

In the expressions below, we shall omit to write the non-perturbative power correction term, which for most common observables is proportional to a single power of Λ/Q.

Leading Order. If the observable $\mathcal{O}$ is non-zero only for events with at least n final-state particles, then the LO QCD prediction for the weighted cross section in e^+e^- annihilation is

$$\sigma_{\mathcal{O}}^{\rm LO} = \alpha_s^{n-2}(\mu_R^2)\int d\Phi_n |M_n^2(p_1,\ldots,p_n)|\,\mathcal{O}_n(p_1,\ldots,p_n)\,, \qquad (9.17)$$

where the squared tree-level matrix element, $|M_n^2(p_1,\ldots,p_n)|$, including relevant symmetry factors, has been summed over all subprocesses (*e.g.* $e^+e^- \to q\bar{q}q\bar{q}$, $e^+e^- \to q\bar{q}gg$) and has had all factors of α_s extracted in front. In processes other than e^+e^- collisions, the center-of-mass energy of the LO process is generally not fixed, and so the powers of the coupling are often brought inside the integrals, with the scale μ_R chosen event by event, as a function of the event kinematics.

Other than in the simplest cases (see the review on Cross Sections in this *Review*), the matrix elements in Eq. (9.17) are usually calculated automatically with programs such as CompHEP [116], MadGraph [117], Alpgen [118], Comix/Sherpa [119], and Helac/Phegas [120]. Some of these (CompHEP, MadGraph) use formulas obtained from direct evaluations of Feynman diagrams. Others (Alpgen, Helac/Phegas and Comix/Sherpa) use methods designed to be particularly efficient at high multiplicities, such as Berends-Giele recursion [121], which builds up amplitudes for complex processes from simpler ones (see also Refs. [122–124] for other tree-level calculational methods).

The phase-space integration is usually carried out by Monte Carlo sampling, because of the high dimensionality of the integration and in order to deal with the possibly involved kinematic cuts that are used in the corresponding experimental measurements. Perturbatively calculable observables should be insensitive to the emission of soft and collinear radiation. Because of the divergences in the matrix element, Eq. (9.16), at lowest order the integral converges only if the observable vanishes for kinematic configurations in which one of the n particles is arbitrarily soft or it is collinear to another particle. As an example, the cross section for producing any configuration of n partons will lead to an infinite integral, whereas a finite result will be obtained for the cross section for producing n deposits of energy (or jets, see Sec. 9.3.1.1), each above some energy threshold and well separated from each other in angle.

At a practical level, LO calculations can be carried out for $2 \to n$ processes with $n \lesssim 6-10$. The exact upper limit depends on the process, the method used to evaluate the matrix elements (recursive methods are more efficient), and the extent to which the phase-space integration can be optimized to work around the large variations in the values of the matrix elements.

NLO. Given an observable that is non-zero starting from n final-state particles, its prediction at NLO involves supplementing the LO result, Eq. (9.17), with the $2 \to (n+1)$-particle squared tree-level matrix element ($|M_{n+1}^2|$), and the interference of a $2 \to n$ tree-level and $2 \to n$ 1-loop amplitude ($2{\rm Re}(M_n M_{n,1-{\rm loop}}^*)$),

$$\begin{aligned}\sigma_{\mathcal{O}}^{\rm NLO} = \sigma_{\mathcal{O}}^{\rm LO} + \alpha_s^{n-1}(\mu_R^2)\int d\Phi_{n+1}|M_{n+1}^2(p_1,\ldots,p_{n+1})| \\ \times\, \mathcal{O}_{n+1}(p_1,\ldots,p_{n+1}) \;+\; \alpha_s^{n-1}(\mu_R^2) \\ \times \int d\Phi_n\, 2{\rm Re}\,[\, M_n(p_1,\ldots,p_n)\, M_{n,1-{\rm loop}}^*(p_1,\ldots,p_n)\,] \\ \times\, \mathcal{O}_n(p_1,\ldots,p_n)\,.\end{aligned} \qquad (9.18)$$

Relative to LO calculations, two important issues appear in the NLO calculations. Firstly, the extra complexity of loop-calculations relative to tree-level calculations means that automated calculations started to appear only about fifteen years ago (see below). Secondly, loop amplitudes are infinite in four dimensions, while tree-level amplitudes are finite, but their *integrals over the phase space* are infinite, due to the divergences of Eq. (9.16). These two sources of infinities have the same soft and collinear origins and cancel after the integration only if the observable $\mathcal{O}$ satisfies the property of infrared and collinear safety, which means that the observable is non-sensitive to soft emissions

Downloaded from https://academic.oup.com/ptep/article/2022/8/083C01/6651666 by KIT Library user on 27 September 2022

or to collinear splittings, *i.e.*

$$\begin{aligned}\mathcal{O}_{n+1}(p_1,\ldots,p_s,\ldots,p_n) &\to \mathcal{O}_n(p_1,\ldots,p_{s-1},p_{s+1},\ldots,p_n)\\ &\quad \text{if } p_s \to 0\\ \mathcal{O}_{n+1}(p_1,\ldots,p_a,p_b,\ldots,p_n) &\to \mathcal{O}_n(p_1,\ldots,p_a+p_b,\ldots,p_n)\\ &\quad \text{if } p_a \,||\, p_b\,.\end{aligned} \tag{9.19}$$

Examples of infrared-safe quantities include event-shape distributions and jet cross sections (with appropriate jet algorithms, see below). Unsafe quantities include the distribution of the momentum of the hardest QCD particle (which is not conserved under collinear splitting), observables that require the complete absence of radiation in some region of phase space (*e.g.* rapidity gaps or 100% isolation cuts, which are affected by soft emissions), or the particle multiplicity (affected by both soft and collinear emissions). The non-cancellation of divergences at NLO due to infrared or collinear unsafety compromises the usefulness not only of the NLO calculation, but also that of a LO calculation, since LO is only an acceptable approximation if one can prove that higher-order terms are smaller. Infrared and collinear unsafety usually also implies large non-perturbative effects.

As with LO calculations, the phase-space integrals in Eq. (9.18) are usually carried out by Monte Carlo integration, so as to facilitate the study of arbitrary observables. Various methods exist to obtain numerically efficient cancellation among the different infinities. These include notably dipole [125], FKS [126] and antenna [127] subtraction.

Thanks to new ideas like the OPP method [128], generalised [129] and D-dimensional [130] unitarity, onshell methods [131], and on-the-fly reduction algorithms [132], recent years have seen a breakthrough in the calculation of one-loop matrix elements (for reviews on unitarity based method see Ref. [133, 134]). Thanks to these innovative methods, automated tools for NLO calculations have been developed and a number of programs are available publicly: MadGraph5_aMC@NLO [117] and Helac-NLO [135] provide full frameworks for NLO calculations; GoSam [136], Njet [137], OpenLoops [138] and Recola [139] calculate just the 1-loop part and are typically interfaced with an external tool such as Sherpa [140] for a combination with the appropriate tree-level amplitudes. Other tools such as NLOJet++ [141], MCFM [142], VBFNLO [143], the Phox family [144] or BlackHat [145] implement analytic calculations for a selected class of processes.

Recently, a lot of attention has also been paid to the calculation of NLO electroweak corrections. Electroweak corrections are especially important for transverse momenta significantly above the W and Z masses, because they are enhanced by two powers of $\ln p_t/M_W$ for each power of the electroweak coupling, and close to Sudakov peaks, where most of the data lie and the best experimental precision can be achieved. In some cases the above programs (or development versions of them) can be used to calculate also NLO electroweak or beyond-standard-model corrections [146–152].

Given the progress in QCD and EW fixed-order computations, the largest unknown from fixed-order corrections is often given by the mixed QCD-electroweak corrections of $\mathcal{O}(\alpha_s\alpha)$. These mixed two-loop corrections are often available in an approximate form [153–162]. The first complete computation of the mixed QCD–EW corrections to the neutral-current Drell–Yan process appeared recently [163]. For a review on EW corrections to collider processes see Ref. [164].

NNLO. NNLO is considerably more complicated than NLO as it involves a further order in α_s, consisting of: the squared $(n+2)$-parton tree-level amplitude, the interference of the $(n+1)$-parton tree-level and 1-loop amplitudes, the interference of the n-parton tree-level and 2-loop amplitudes, and the squared n-parton 1-loop amplitude.

Each of these elements involves large numbers of soft and collinear divergences, satisfying relations analogous to Eq. (9.16) which now involve multiple collinear or soft particles and higher loop orders (see *e.g.* Refs. [165–167]). Arranging for the cancellation of the divergences after numerical Monte Carlo integration has been one of the significant challenges of NNLO calculations, as has been the determination of the relevant 2-loop amplitudes. For the cancellations of divergences a wide range of methods has been developed. Some of them [168–174] retain the approach, inherent in NLO methods, of directly combining the separate loop and tree-level amplitudes. Others combine a suitably chosen, partially inclusive $2 \to n$ NNLO calculation with a fully differential $2 \to n+1$ NLO calculation [175–180]. The q_T-subtraction method was extended to deal with mixed QCD–QED corrections at NNLO [181]. For an overview of NNLO subtraction methods see Ref [182].

Quite a number of processes have been calculated differentially at NNLO so far. The state of the art for e^+e^- collisions is $e^+e^- \to 3$ jets [183–185]. For DIS, dijet production is known at NNLO [186] and the description jet production has been recently pushed even to N^{3}LO using the Projection-to-Born method [187, 188]. For hadron colliders, all $2 \to 1$ processes are known, specifically vector boson [189, 190] and Higgs boson production in the large m_t limit [175, 191]. Recently, the finite top-mass corrections at this order have also been computed [192]. This calculation eliminates one important source of theoretical uncertainty to inclusive Higgs production at the LHC. For most of the above calculations there exist public codes (EERAD3 for e^+e^-, DYNNLO, FEWZ and MATRIX for W and Z production, Fehipro and HNNLO for Higgs production), links to which are to be found among the above references. Substantial progress has been made in the years for hadron-collider $2 \to 2$ processes, with calculations having been performed for nearly all relevant processes: ZZ [110] WW [109] and WZ [193], $\gamma\gamma$ [194, 195], $Z\gamma$ [196] and $W\gamma$ [197] (many of these colour singlet processes are available also in MCFM [198] or MATRIX [111]), inclusive photon [199, 200], $\gamma+$jet [200, 201], $W+$jet [177, 202], $Z+$jet [201, 203, 204] $H+$jet [205–208], WH [209] and ZH [210], t-channel single-top [211, 212], $t\bar{t}$ production [213], dijet production [214], W production in association with a c-jet [215] and HH [105] (in large-top-mass approximation, see also the exact (two-loop) NLO result [106]). Recently, also the NNLO corrections to identified B-hadron hadroproduction have been computed [216]. The frontier of NNLO calculation has now reached the complexity of $2 \to 3$ processes. The first $2 \to 3$ process known at NNLO has been Higgs production through vector-boson fusion, using an approximation in which the two underlying DIS-like $q \to qV$ scatterings are factorised, the so-called structure function approximation [180, 217]. Corrections beyond the structure function approximation are expected to be small, on the order of a percent or less [218]. More recently, first genuine $2 \to 3$ LHC processes have been described at NNLO accuracy, including three photon [219, 220], two photons and one jet [221], and three-jets [222]. The last calculation will be relevant for future extractions of $\alpha_s(M_Z^2)$ from three-jet observables at the LHC.

Cross sections at the LHC are most often measured with fiducial cuts, for example on the transverse momenta and rapidities of the measured objects, restricting the measurement to regions where the objects have a good efficiency to be detected and are well-reconstructed. Ideally, the theoretical predictions should also be constructed at the same fiducial level; the other possibility is to extrapolate the experimental fiducial results to the full phase space. Such an extrapolation, however, requires the extrapolation (typically using a parton shower Monte Carlo) to be accurate over the full phase space.

Comparisons of fixed order predictions to fiducial measurements can sometimes result in the presence of large logarithms which degrade the accuracy of the prediction. Such is the case, for example, in the calculation of the Higgs rapidity distribution, in the diphoton final state. The imposition of transverse momenta and rapidity cuts on the two photons leads to an uncertainty notably greater at N^{3}LO then at NNLO, due to the presence of these logs. One possible solution is to change the form of the kinematic cut on the photons, to a product of the two photon transverse momenta [223], reducing the impact of the logs; another solution is to perform a resummation of the logs, restoring the expected precision [224].

The Les Houches precision wishlist compiles predictions needed to fully exploit the data that will be taken at the High Luminosity LHC [225]. Most of the needed calculations require accuracy of at

Downloaded from https://academic.oup.com/ptep/article/2022/8/083C01/6651666 by KIT Library user on 27 September 2022

least NNLO QCD and NLO EW, and many require the prediction of $2 \to 3$ processes, such as $W/Z+ \geq 2$ jets, $H+ \geq 2$ jets, and ttH to NNLO.

As discussed in this section, calculations at NLO can now be relatively easily generated by non-experts using the programs described. However, many NNLO calculations can be too complex and CPU-intensive to allow such an approach. In these cases, the relevant matrix element information for a specific observable can be stored by means of interpolation grids developed originally for cross sections at NLO [226–228] and recently extended to include electroweak corrections [229]. The application to NNLO has been demonstrated for $t\bar{t}$ and for DIS jet cross sections in Refs. [230, 231]. Each such interpolation grid corresponds to one fixed observable with specific selection criteria and binning, but is flexible with respect to the renormalization or factorization scale, the PDF, or the α_s evolution chosen for the cross-section computation.

An even more flexible method, at the cost of requiring large amounts of storage space, saves huge numbers of partonic events in the form of ROOT ntuples, which allow predictions to be generated on-the-fly for many observables of a particular process [232, 233]. Recent developments of both techniques for pp collisions at NNLO are described in Ref. [225].

9.2.3.3 *Resummation*

Many experimental measurements place tight constraints on emissions in the final state. For example, in e^+e^- events, that (one minus) the Thrust should be less than some value $\tau \ll 1$, or, in $pp \to Z$, events that the Z-boson transverse momentum or the transverse momentum of the accompanying jet should be much smaller than the Z-boson mass. A further example is the production of heavy particles or jets near threshold (so that little energy is left over for real emissions) in DIS and pp collisions.

In such cases, the constraint vetoes a significant part of the integral over the soft and collinear divergence of Eq. (9.16). As a result, there is only a partial cancellation between real emission terms (subject to the constraint) and loop (virtual) contributions (not subject to the constraint), causing each order of α_s to be accompanied by a large coefficient $\sim L^2$, where *e.g.* $L = \ln\tau$ or $L = \ln(M_Z/p_t^Z)$. One ends up with a perturbative series, whose terms go as $\sim (\alpha_s L^2)^n$. It is not uncommon that $\alpha_s L^2 \gg 1$, so that the perturbative series converges very poorly if at all.[5] In such cases one may carry out a "resummation", which accounts for the dominant logarithmically enhanced terms to all orders in α_s, by making use of known properties of matrix elements for multiple soft and collinear emissions, and of the all-orders properties of the divergent parts of virtual corrections, following original works such as Refs. [234–243] and also through soft-collinear effective theory [244, 245] (*cf.* also the section on "Heavy-Quark and Soft-Collinear Effective Theory" in this *Review*, as well as Ref. [246]).

For cases with double logarithmic enhancements (two powers of logarithm per power of α_s), there are two classification schemes for resummation accuracy. Writing the cross section including the constraint as $\sigma(L)$ and the unconstrained (total) cross section as $\sigma_{\rm tot}$, the series expansion takes the form

$$\sigma(L) \simeq \sigma_{\rm tot} \sum_{n=0}^{\infty} \sum_{k=0}^{2n} R_{nk} \alpha_s^n(\mu_R^2) L^k, \qquad L \gg 1\,, \tag{9.20}$$

and leading log (LL) resummation means that one accounts for all terms with $k = 2n$, next-to-leading-log (NLL) includes additionally all terms with $k = 2n-1$, *etc.* Often $\sigma(L)$ (or its Fourier or Mellin transform) *exponentiates* [6],

$$\sigma(L) \simeq \sigma_{\rm tot} \exp\left[\sum_{n=1}^{\infty} \sum_{k=0}^{n+1} G_{nk} \alpha_s^n(\mu_R^2) L^k\right], \qquad L \gg 1\,, \tag{9.21}$$

where one notes the different upper limit on k ($\leq n+1$) compared to Eq. (9.20). This is a more powerful form of resummation: the G_{12} term alone reproduces the full LL series in Eq. (9.20). With the form Eq. (9.21) one still uses the nomenclature LL, but this now means that all terms with $k = n+1$ are included, and NLL implies all terms with $k = n$, *etc.*

For a large number of observables, NLL resummations are available in the sense of Eq. (9.21) (see Refs. [250–252] and references therein). NNLL has been achieved for the DY and Higgs-boson p_t distributions [253–256] (also available in the CuTe [257], HRes [258] and ResBos [259] families of programs and also differentially in vector-boson decay products [260]) and related variables [261], for the p_t of vector-boson pairs [262], for the back-to-back energy-energy correlation in e^+e^- [263], the jet broadening in e^+e^- collisions [264], the jet-veto survival probability in Higgs and Z boson production in pp collisions [265, 266] [7], an event-shape type observable known as the beam Thrust [267], hadron-collider jet masses in specific limits [268] (see also Ref. [269]), the production of top anti-top pairs near threshold [270–272] (and references therein), and high-p_t W and Z production [273]. Automation of NNLL jet-veto resummations for different processes has been achieved in Ref. [274] (*cf.* also the NLL automation in Ref. [275]), while automation for a certain class of e^+e^- observables has been achieved in Ref. [276]. N^{3}LL resummations are available for the Thrust variable, C-parameter and heavy-jet mass in e^+e^- annihilations [277–279] (confirmed for Thrust at NNLL in Ref. [280]), for p_t distribution of the Higgs boson [281] and weak gauge bosons [282] and for Higgs- and vector-boson production near threshold [283]. In order to make better contact with experimental measurements, recent years have seen an increasing interest in resummations in exclusive phase-space regions and joint resummations [284–291]. Finally, there has also been considerable progress in resummed calculations for jet substructure, whose observables involve more complicated definitions than is the case for standard resummations [292–299], see also Refs. [300–302].

9.2.3.4 *Fragmentation functions*

Since the parton-hadron transition is non-perturbative, it is not possible to perturbatively calculate quantities such as the energy-spectra of specific hadrons in high-energy collisions. However, one can factorize perturbative and non-perturbative contributions via the concept of fragmentation functions. These are the final-state analogue of the parton distribution functions which are used for initial-state hadrons. Like parton distribution functions, they depend on a (fragmentation) factorization scale and satisfy a DGLAP evolution equation.

It should be added that if one ignores the non-perturbative difficulties and just calculates the energy and angular spectrum of partons in perturbative QCD with some low cutoff scale $\sim \Lambda$ (using resummation to sum large logarithms of $\sqrt{s}/\Lambda$), then this reproduces many features of the corresponding hadron spectra [303]. This is often taken to suggest that hadronization is "local", in this sense it mainly involves partons that are close both in position and in momentum.

Section 19 of this *Review* provides further information (and references) on these topics, including also the question of heavy-quark fragmentation.

[5] To be precise one should be aware of two causes of the divergence of perturbative series. That which interests us here is associated with the presence of a new large parameter (*e.g.* ratio of scales). It is distinct from the "renormalon" induced factorial divergences of perturbation theory which were discussed above.

[6] Whether or not this happens depends on the quantity being resummed. A classic example involves two-jet rate in e^+e^- collisions as a function of a jet-resolution parameter $y_{\rm cut}$. The logarithms of $1/y_{\rm cut}$ exponentiate for the k_t (Durham) jet algorithm [247], but not [248] for the JADE algorithm [249] (both are discussed below in Sec. 9.3.1.1).

[7] A veto on the jet phase space can be severe, for example by requiring exactly zero jets above a given transverse momentum cut accompanying a Higgs boson, or relatively mild, for example by placing a transverse momentum cut of 30 GeV on the measurement of the production of a Higgs boson with one or more jets. In general, inclusive cross sections are preferable, as uncertainties on both the theoretical and experimental sides are smaller.

Downloaded from https://academic.oup.com/ptep/article/2022/8/083C01/6651666 by KIT Library user on 27 September 2022

9.2.3.5 *Parton-shower Monte Carlo event generators*

Parton-shower Monte Carlo (MC) event generators like PYTHIA [304–306], HERWIG [307–309], and SHERPA [140][8] provide fully exclusive simulations of QCD events at the level of measurable particles, the so-called "particle level" or "hadron level". Here, "measurable" refers to colour-neutral particles with mean lifetimes τ long enough to be associated with tracks or decay vertices in particle detectors. Usually, this requires mean decay lengths $c\tau$ of around 10 mm. As such the MC event generators are a crucial tool for all applications that involve simulating the response of detectors to QCD events. Here we give only a brief outline of how they work and refer the reader to Sec. 43 and Ref. [311] for a full overview.

The MC generation of an event involves several stages. It starts with the random generation of the kinematics and partonic channels of whatever *hard scattering process* the user has requested at some high scale Q_0 (for complex processes, this may be carried out by an external program). This is followed by a *parton shower*, usually based on the successive random generation of gluon emissions (or $g \to q\bar{q}$ splittings). Leading contributions to the shower have emissions that are ordered according to some ordering variable. Common choices of scale for the ordering of emissions are virtuality, transverse momentum or angle. Each emission is generated at a scale lower than the previous emission, following a (soft and collinear resummed) perturbative QCD distribution, which depends on the momenta of all previous emissions. Parton showering stops at a scale of order 1 GeV, at which point a *hadronization model* is used to convert the resulting partons into hadrons. One widely-used model involves stretching a color "string" across quarks and gluons, and breaking it up into hadrons [312, 313]. Another breaks each gluon into a $q\bar{q}$ pair and then groups quarks and anti-quarks into colorless "clusters", which then give the hadrons [307]. As both models are tuned primarily to LEP data, the cluster and string models provide similar results for most observables [314]. For pp and γp processes, modeling is also needed to treat the collision between the two hadron remnants, which generates an *underlying event* (UE), usually implemented via additional $2 \to 2$ scatterings ("multiple parton interactions", MPI) at a scale of a few GeV, following Ref. [315]. The parameter values for the MPI models must be determined from fits to underlying-event observables of LHC collision data. As the different MC event generators are adapted to essentially the same measurements, ideally the respective MPI implementations should lead to similar predictions for each program. One complication, however, is the non-universality of the underlying event for different physics processes.

A deficiency of the soft and collinear approximations that underlie parton showers is that they may fail to reproduce the full pattern of hard wide-angle emissions, important, for example, in many new physics searches. It is therefore common to use LO multi-parton matrix elements to generate hard high-multiplicity partonic configurations as additional starting points for the showering, supplemented with some prescription (CKKW [316], MLM [317]) for consistently merging samples with different initial multiplicities. Monte Carlo generators, as described above, compute cross sections for the requested hard process that are correct at LO.

A wide variety of processes are available in MC implementations that are correct also to NLO, using the MC@NLO [318] or POWHEG [319] prescriptions, notably through the MADGRAPH5_aMC@NLO [117], POWHEG-BOX [320] and SHERPA [119] programs. Techniques have also been developed to combine NLO plus shower accuracy for different multiplicities of final-state jets [321]. Building in part on some of that work, several groups have also obtained NNLO plus shower accuracy for Drell-Yan and Higgs production [322, 323], as well as for a handful of $2 \to 2$ processes [324–332].

It is important to understand/verify the accuracy of the parton shower predictions in the Monte Carlo programs. In the limit of large center-of-mass energy, parton showers and analytic resummation must yield the same prediction for physical observables. The expected agreement has been established at next-to-leading logarithmic order for a certain class of algorithms, and for both global [333–336] and non-global observables [337]. A general framework for assessing the logarithmic accuracy of parton-shower algorithms has been formulated, based on their ability to reproduce the singularity structure of multi-parton matrix elements, and their ability to reproduce logarithmic resummation results [338]. The dominant contributions relevant for the extension of parton showers to higher logarithmic accuracy have been computed [339–343] and included in some algorithms, although a parton shower at full next-to-next-to-leading logarithmic accuracy is still missing. There exist ways to improve on current parton-shower algorithms [336,337] and to demonstrate the shower accuracy through a comparison to analytic next-to-leading logarithmic calculations for a range of observables [337].

Parton showers are typically based on the leading color approximation, but sub-leading color effects arising from real emissions can be included on average [344, 345]. There are limitations of some routinely used parton shower algorithms, both in terms of leading (double) logarithms at subleading N_c and next-to-leading (single) logarithms at leading N_c [338].

In general, we expect parton-shower matched predictions to differ from the underlying fixed-order results in regions where (1) there is a large sensitivity to jet shapes (for instance small R jets), (2) there is a restriction in phase space such that soft gluon resummation effects become important, (3) the observable contains multiple disparate scales, (4) there are perturbative instabilities at fixed order, *e.g.* related to kinematical cuts, and (5) the observable is sensitive to higher multiplicity states than those described by the fixed-order calculation [314].

9.2.4 *Accuracy of predictions*

Estimating the accuracy of perturbative QCD predictions is not an exact science. It is often said that LO calculations are accurate to within a factor of two. This is based on experience with NLO corrections in the cases where these are available. In processes involving new partonic scattering channels at NLO and/or large ratios of scales (such as jet observables in processes with vector bosons, or the production of high-p_t jets containing B-hadrons), the ratio of the NLO to LO predictions, commonly called the "K factor", can be substantially larger than two. NLO corrections tend to be large for processes for which there is a great deal of color annihilation in the interaction. In addition, NLO corrections tend to decrease as more final state legs are added.

For calculations beyond LO, one approach to estimate the perturbative uncertainty is to base it on the last known perturbative correction; this may lead to misleading results if new sub-processes are present at the next-higher order. A more widely used method is to estimate it from the change in the prediction when varying the renormalization and factorization scales around a central value Q that is taken close to the physical scale of the process. A conventional range of variation is $Q/2 < \mu_R, \mu_F < 2Q$, varying the two scales independently with the restriction $\frac{1}{2}\mu_R < \mu_F < 2\mu_R$ [346]. This constraint limits the risk of misleadingly small uncertainties due to fortuitous cancellations between the μ_F and μ_R dependence when both are varied together, while avoiding the appearance of large logarithms of μ_R^2/μ_F^2 when both are varied completely independently. Where possible, it can be instructive to examine the two-dimensional scale distributions (μ_R *vs.* μ_F) to obtain a better understanding of the interplay between μ_R and μ_F. This procedure should not be assumed to always estimate the full uncertainty from missing higher orders, but it does indicate the size of one important known source of higher-order ambiguity.[9]

Calculations that involve resummations usually have an additional source of uncertainty associated with the choice of argument of the logarithms being resummed, *e.g.* $\ln(2\frac{p_t^Z}{M_Z})$ as opposed to

[8] The program ARIADNE [310] has also been widely used for simulating e^+e^- and DIS collisions.

[9] A number of prescriptions also exist for setting the scale automatically, *e.g.* Refs. [347–351], eliminating uncertainties from scale variation, though not from the truncation of the perturbative series itself. Various studies have been carried out on how to estimate uncertainties from missing higher orders that go beyond scale variations [352–355].

Downloaded from https://academic.oup.com/ptep/article/2022/8/083C01/6651666 by KIT Library user on 27 September 2022

$\ln(\frac{1}{2}\frac{p_t^Z}{M_Z})$. In addition to varying renormalization and factorization scales, it is therefore also advisable to vary the argument of the logarithm by a suitable factor in either direction with respect to the "natural" argument.

The accuracy of QCD predictions is limited also by non-perturbative (or hadronization) corrections, which typically scale as a power of Λ/Q.[10] For measurements that are directly sensitive to the structure of the hadronic final state, the corrections are usually linear in Λ/Q. The non-perturbative corrections are further enhanced in processes with a significant underlying event (*i.e.* in pp and $p\bar{p}$ collisions) and in cases where the perturbative cross sections fall steeply as a function of p_t or some other kinematic variable, for example in inclusive jet p_t or dijet mass spectra. In general, the underlying event for a hard scattering process, such as dijet production, is of a similar order, but somewhat harder, than the average energy density in a minimum-bias event [356]. Under high-luminosity running conditions, such as 13 TeV at the LHC, there can be on the order of 50 minimum-bias interactions occurring at each beam-beam crossing. This additional energy needs to be subtracted, and is typically removed by means of a rapidity-dependent transverse energy density determined on an event-by-event basis [357]. This subtraction, of necessity, also removes the underlying event, which must be added back in by means of MC event generator modelling to restore the measured event to the particle level.

Non-perturbative corrections are commonly estimated from the difference between Monte Carlo events at the "parton level" and at particle level. Parton level refers to the stage of the parton shower, where the evolution is stopped at an energy scale of typical hadron masses of a few GeV. An issue to be aware of is that "parton level" is not a uniquely defined concept. For example, in a MC event generator such a procedure depends on an arbitrary and tunable internal cutoff scale that separates the parton showering from the hadronization. In contrast, no such cutoff scale exists in an NLO or NNLO partonic calculation. The uncertainties in these corrections are often estimated by comparing different tunes of the various MC event generators. It should be noted that such estimates are not guaranteed to fully cover the true uncertainties.

Alternative methods exist for estimating hadronization corrections, that attempt to analytically deduce non-perturbative effects in one observable based on measurements of other observables (see the reviews [24,358]). While they directly address the problem of different possible definitions of parton level, it should also be said that they are far less flexible than Monte Carlo programs and not always able to provide equally good descriptions of the data.

One of the main issues is whether the fixed-order partonic final state of a NLO or NNLO prediction can match the parton shower in its ability to describe the experimental jet shape (minus any underlying event). Calculations at NNLO provide a better match to the parton shower predictions than do NLO ones, as might be expected from the additional gluon available to describe the jet shape. The hadronization predictions appear to work for both orders, but at an unknown accuracy. The impact of hadronization should fall as a power correction [1].

9.3 Experimental studies of QCD

Since we are not able to directly measure partons (quarks or gluons), but only hadrons and their decay products, a central issue for every experimental study of perturbative QCD is establishing a correspondence between observables obtained at the parton and the hadron level. The only theoretically sound correspondence is achieved by means of *infrared and collinear safe* quantities, which allow one to obtain finite predictions at any order of perturbative QCD.

As stated above, the simplest case of infrared- and collinear-safe observables are total cross sections. More generally, when measuring fully inclusive observables, the final state is not analyzed at all regarding its (topological, kinematical) structure or its composition. Basically the relevant information consists in the rate of a process ending up in a partonic or hadronic final state. In e^+e^- annihilation, widely used examples are the ratios of partial widths or branching ratios for the electroweak decay of particles into hadrons or leptons, such as Z or τ decays, (*cf.* Sec. 9.2.1). Such ratios are often favored over absolute cross sections or partial widths because of large cancellations of experimental and theoretical systematic uncertainties. The strong suppression of non-perturbative effects, $\mathcal{O}(\Lambda^4/Q^4)$, is one of the attractive features of such observables, however, at the same time, the sensitivity to radiative QCD corrections is small, which for example affects the statistical uncertainty when using them for the determination of the strong coupling constant. In the case of τ decays not only the hadronic branching ratio is of interest, but also moments of the spectral functions of hadronic tau decays, which sample different parts of the decay spectrum and thus provide additional information. Other examples of fully inclusive observables are structure functions (and related sum rules) in DIS. These are extensively discussed in Sec. 18 of this *Review*.

On the other hand, often the structure or composition of the final state are analyzed and cross sections differential in one or more variables characterizing this structure are of interest. Examples are jet rates, jet substructure, event shapes or transverse momentum distributions of jets or vector bosons in hadron collisions. The case of fragmentation functions, *i.e.* the measurement of hadron production as a function of the hadron momentum relative to some hard scattering scale, is discussed in Sec. 19 of this *Review*.

It is worth mentioning that, besides the correspondence between the parton and hadron level, also a correspondence between the hadron level and the actually measured quantities in the detector has to be established. The simplest examples are corrections for finite experimental acceptance and efficiencies. Whereas acceptance corrections essentially are of theoretical nature, since they involve extrapolations from the measurable (partial) to the full phase space, other corrections such as for efficiency, resolution and response are of experimental nature. For example, measurements of differential cross sections such as jet rates require corrections in order to relate, *e.g.*, the energy deposits in a calorimeter to the jets at the hadron level. Typically detector simulations and/or data-driven methods are used in order to obtain these corrections. Care should be taken here in order to have a clear separation between the parton-to-hadron level and hadron-to-detector level corrections. Finally, for the sake of an easy comparison to the results of other experiments and/or theoretical calculations, it is suggested to provide, whenever possible, measurements corrected for detector effects and/or all necessary information related to the detector response (*e.g.*, the detector response matrix). Any fiducial phase space for measurements should be defined as close as possible to the detector-level selection in order to minimize model-dependent extrapolations.

9.3.1 *Hadronic final-state observables*

9.3.1.1 *Jets*

In hard interactions, final-state partons and hadrons appear predominantly in collimated bunches, which are generically called *jets*. To a first approximation, a jet can be thought of as a hard parton that has undergone soft and collinear showering and then hadronization. Jets are used both for testing our understanding and predictions of high-energy QCD processes, and also for identifying the hard partonic structure of decays of massive particles such as top quarks and W, Z and Higgs bosons.

In order to map observed hadrons onto a set of jets, one uses a *jet definition*. The mapping involves explicit choices: for example when a gluon is radiated from a quark, for what range of kinematics should the gluon be part of the quark jet, or instead form a separate jet? Good jet definitions are infrared and collinear safe, simple to use in theoretical and experimental contexts, applicable to any type of inputs (parton or hadron momenta, charged particle tracks, and/or energy deposits in the detectors) and lead to jets that are not too sensitive to non-perturbative effects.

An extensive treatment of the topic of jet definitions is given in Ref. [359] (for e^+e^- collisions) and Refs. [360–362]. Here we briefly review the two main classes: cone algorithms, extensively used at older hadron colliders, and sequential recombination al-

[10] In some circumstances, the scale in the denominator could be a smaller kinematic or physical scale that depends on the observable.

Downloaded from https://academic.oup.com/ptep/article/2022/8/083C01/6651666 by KIT Library user on 27 September 2022

gorithms, more widespread in e^+e^- and ep colliders and at the LHC.

Very generically, most (iterative) cone algorithms start with some seed particle i, sum the momenta of all particles j within a cone of opening-angle R, typically defined in terms of rapidity and azimuthal angle. They then take the direction of this sum as a new seed and repeat until the direction of the cone is stable, and call the contents of the resulting stable cone a jet if its transverse momentum is above some threshold $p_{t,\min}$. The parameters R and $p_{t,\min}$ should be chosen according to the needs of a given analysis.

There are many variants of the cone algorithm, and they differ in the set of seeds they use and the manner in which they ensure a one-to-one mapping of particles to jets, given that two stable cones may share particles ("overlap"). The use of seed particles is a problem w.r.t. infrared and collinear safety. Seeded algorithms are generally not compatible with higher-order (or sometimes even leading-order) QCD calculations, especially in multi-jet contexts, as well as potentially subject to large non-perturbative corrections and instabilities. Seeded algorithms (JetCLU, MidPoint, and various other experiment-specific iterative cone algorithms) are therefore to be deprecated. Such algorithms are not used at the LHC, but were at the Fermilab Tevatron, where data still provide useful information, for example for global PDF fits. A modern alternative is to use a seedless variant, SISCone [363].

Sequential recombination algorithms at hadron colliders (and in DIS) are characterized by a distance $d_{ij} = \min(k_{t,i}^{2p}, k_{t,j}^{2p})\Delta_{ij}^2/R^2$ between all pairs of particles i, j, where Δ_{ij} is their separation in the rapidity-azimuthal plane, $k_{t,i}$ is the transverse momentum w.r.t. the incoming beams, and R is a free parameter. At the LHC, R is typically in the range from 0.4 to 0.8, although analyses can also use jet sizes up to 1.0-1.2. They also involve a "beam" distance $d_{iB} = k_{t,i}^{2p}$. One identifies the smallest of all the d_{ij} and d_{iB}, and if it is a d_{ij}, then i and j are merged into a new pseudo-particle (with some prescription, a recombination scheme, for the definition of the merged four-momentum). If the smallest distance is a d_{iB}, then i is removed from the list of particles and called a jet. As with cone algorithms, one usually considers only jets above some transverse-momentum threshold $p_{t,\min}$. The parameter p determines the kind of algorithm: $p = 1$ corresponds to the (*inclusive-*)k_t algorithm [247, 364, 365], $p = 0$ defines the *Cambridge-Aachen* algorithm [366, 367], while for the *anti-*k_t algorithm $p = -1$ [368]. All these variants are infrared and collinear safe. Whereas the former two lead to irregularly shaped jet boundaries, the latter results in cone-like boundaries, except in situations where there are nearby jets. The *anti-*k_t algorithm has become the de-facto standard for the LHC experiments.

In e^+e^- annihilation the k_t algorithm [247] uses $y_{ij} = 2\min(E_i^2, E_j^2)(1-\cos\theta_{ij})/Q^2$ as distance measure between two particles/partons i and j and repeatedly merges the pair with smallest y_{ij}, until all y_{ij} distances are above some threshold $y_{\rm cut}$, the jet resolution parameter. Q is a measure of the overall hardness of the event. The (pseudo)-particles that remain at this point are called the jets. Here it is $y_{\rm cut}$ (rather than R and $p_{t,\min}$) that should be chosen according to the needs of the analysis. The two-jet rate in the k_t algorithm has the property that logarithms $\ln(1/y_{\rm cut})$ exponentiate. This is one reason why it is preferred over the earlier JADE algorithm [249], which uses the distance measure $y_{ij} = 2\,E_i\,E_j\,(1-\cos\theta_{ij})/Q^2$. Note that other variants of sequential recombination algorithms for e^+e^- annihilations, using different definitions of the resolution measure y_{ij}, exhibit much larger sensitivities to fragmentation and hadronization effects than the k_t and JADE algorithms [369]. Efficient implementations of the above algorithms are available through the *FastJet* package [370].

9.3.1.2 *Event Shapes*

Event-shape variables are functions of the four momenta of the particles in the final state and characterize the topology of an event's energy flow. They are sensitive to QCD radiation (and correspondingly to the strong coupling) insofar as gluon emission changes the shape of the energy flow.

The classic example of an event shape is the *Thrust* [371, 372] in e^+e^- annihilations, defined as

$$\hat{\tau} = \max_{\vec{n}_\tau} \frac{\sum_i |\vec{p}_i \cdot \vec{n}_\tau|}{\sum_i |\vec{p}_i|}\,, \tag{9.22}$$

where $\vec{p}_i$ are the momenta of the particles or the jets in the final-state and the maximum is obtained for the Thrust axis $\vec{n}_\tau$. In the Born limit of the production of a perfect back-to-back $q\bar{q}$ pair, the limit $\hat{\tau} \to 1$ is obtained, whereas a perfectly spherical many-particle configuration leads to $\hat{\tau} \to 1/2$. Further event shapes of similar nature have been extensively measured at LEP and at HERA, and for their definitions and reviews we refer to Refs. [1, 7, 358, 373, 374]. The energy-energy correlation function [375], namely the energy-weighted angular distribution of produced hadron pairs, and its associated asymmetry are further shape variables which have been studied in detail at e^+e^- colliders. For hadron colliders the appropriate modification consists in only taking the transverse momentum component [376]. More recently, the event shape *N-jettiness* has been proposed [377], that measures the degree to which the hadrons in the final state are aligned along N jet axes or the beam direction. It vanishes in the limit of exactly N infinitely narrow jets.

Phenomenological discussions of event shapes at hadron colliders can be found in Refs. [377–381]. Measurements of hadronic event-shape distributions have been published by CDF [382], ATLAS [383–388] and CMS [389–392].

Event shapes are used for many purposes. These include measuring the strong coupling, tuning the parameters of Monte Carlo programs, investigating analytical models of hadronization and distinguishing QCD events from events that might involve decays of new particles (giving event-shape values closer to the spherical limit).

9.3.1.3 *Jet substructure, quark vs. gluon jets*

Jet substructure, which can be resolved by finding subjets or by measuring jet shapes, is sensitive to the details of QCD radiation in the shower development inside a jet and has been extensively used to study differences in the properties of quark and gluon induced jets, strongly related to their different color charges. In general, there is clear experimental evidence that gluon jets have a softer particle spectrum and are "broader" than (light-) quark jets (as expected from perturbative QCD) when looking at observables such as the jet shape $\Psi(r/R)$ [393]. This is the fraction of transverse momentum contained within a sub-cone of cone-size r for jets of cone-size R. It is sensitive to the relative fractions of quark and gluon jets in an inclusive jet sample and receives contributions from soft-gluon initial-state radiation and the underlying event. Therefore, it has been widely employed for validation and tuning of Monte Carlo parton-shower models. Furthermore, this quantity turns out to be sensitive to the modification of the gluon radiation pattern in heavy ion collisions (see *e.g.* Ref. [394]).

The most recent jet shape measurements using proton-proton collision data have been presented for inclusive jet samples [395–397] and for top-quark production [398]. Further discussions, references and summaries can be found in Refs. [374, 399, 400] and Sec. 4 of Ref. [401].

The use of jet substructure has also been investigated in order to distinguish QCD jets from jets that originate from hadronic decays of boosted massive particles (high-p_t electroweak bosons, top quarks and hypothesized new particles). A considerable number of experimental studies have been carried out with Tevatron and LHC data, in order to investigate the performance of the proposed algorithms for resolving jet substructure and to apply them to searches for new physics, as well as to the reconstruction of boosted top quarks, vector bosons and the Higgs boson. For reviews of this rapidly growing field, see sec. 5.3 of Ref. [360], Ref. [402] and Refs. [401, 403–406].

Neural network techniques and deep learning methods have also been applied to jet physics and jet substructure, see *e.g.* Refs. [407, 408]. Perhaps no other sub-field has benefited as much from machine learning techniques as the study of jet substructure. As a jet can have O(100) constituents each with kinematic and other information, jet substructure analysis is naturally a highly multivariate problem. Deep learning techniques can use all of the

Downloaded from https://academic.oup.com/ptep/article/2022/8/083C01/6651666 by KIT Library user on 27 September 2022

available information to study jets in their natural high dimensionality. Such techniques have not only improved discrimination between different final states/types of jets, but have also improved our understanding of perturbative QCD. See for example the review in Ref. [300].

9.3.2 *QCD measurements at colliders*

There exists a wealth of data on QCD-related measurements in e^+e^-, ep, pp, and $p\bar{p}$ collisions, to which a short overview like this would not be able to do any justice. Extensive reviews of the subject have been published in Refs. [373, 374] for e^+e^- colliders and in Ref. [409] for ep scattering, whereas for hadron colliders comprehensive overviews are given in, *e.g.*, Refs. [361, 400] and Refs. [2, 410–412].

Below we concentrate our discussion on measurements that are most sensitive to hard QCD processes with focus on jet production.

9.3.2.1 e^+e^- *colliders*

Analyses of jet production in e^+e^- collisions are mostly based on data from the JADE experiment at center-of-mass energies between 14 and 44 GeV, as well as on LEP collider data at the Z resonance and up to 209 GeV. The analyses cover the measurements of (differential or exclusive) jet rates (with multiplicities typically up to 4, 5 or 6 jets), the study of 3-jet events and particle production between the jets, as well as 4-jet production and angular correlations in 4-jet events.

Event-shape distributions from e^+e^- data have been an important input to the tuning of parton shower MC models, typically matched to matrix elements for 3-jet production. In general these models provide good descriptions of the available, highly precise data. Especially for the large LEP data sample at the Z peak, the statistical uncertainties are mostly negligible and the experimental systematic uncertainties are at the percent level or even below. These are usually dominated by the uncertainties related to the MC model dependence of the efficiency and acceptance corrections (often referred to as "detector corrections").

Observables measured in e^+e^- collisions have been used for determinations of the strong coupling constant (*cf.* Section 9.4 below) and for putting constraints on the QCD color factors (*cf.* Sec. 9.1 for their definitions), thus probing the non-Abelian nature of QCD. Angular correlations in 4-jet events give sensitivity at leading order. Some sensitivity to these color factors, although only at NLO, is also obtained from event-shape distributions. Scaling violations of fragmentation functions and the different subjet structure in quark and gluon induced jets also give access to these color factors. A compilation of results [374] quotes world average values of $C_A = 2.89 \pm 0.03(\text{stat}) \pm 0.21(\text{syst})$ and $C_F = 1.30 \pm 0.01(\text{stat}) \pm 0.09(\text{syst})$, with a correlation coefficient of 82%. These results are in perfect agreement with the expectations from SU(3) of $C_A = 3$ and $C_F = 4/3$.

9.3.2.2 *DIS and photoproduction*

Jet measurements in ep collisions, both in the DIS and photoproduction regimes, allow for tests of QCD factorization (as they involve only one initial state proton and thus one PDF function), and provide sensitivity to both the gluon PDF and to the strong coupling constant. Calculations are available at NNLO in both regimes [413, 414]. Experimental uncertainties of the order of 5–10% have been achieved, mostly dominated by the jet energy scale uncertainty, whereas statistical uncertainties are negligible to a large extent. For comparison to theoretical predictions, at large jet p_t the PDF uncertainty dominates the theoretical uncertainty (typically of order 5–10%, in some regions of phase space up to 20%), therefore jet observables become useful inputs for PDF fits.

In general, the data are well described by the NLO and NNLO matrix-element calculations, combined with DGLAP evolution equations, in particular at large Q^2 and central values of jet pseudo-rapidity. At low values of Q^2 and x, in particular for large jet pseudo-rapidities, certain features of the data have been interpreted as requiring BFKL-type evolution, though the predictions for such schemes are still limited. It is worth noting that there is no indication that the BKFL approximation is needed in the currently probed x, Q^2 values, and an alternative approach [415], which implements the merging of LO matrix-element based event generation with a parton shower (using the SHERPA framework), successfully describes the data in all kinematical regions, including the low Q^2, low x domain. At moderately small x values, it should perhaps not be surprising that the BFKL approach and fixed-order matrix-element merging with parton showers may both provide adequate descriptions of the data, because some part of the multi-parton phase space that they model is common to both approaches.

In the case of photoproduction, a wealth of measurements with low p_t jets were performed in order to constrain the photon content of the proton. The uncertainties related to such photon PDFs play a minor role at high jet p_t, which has allowed for precise tests of pQCD calculations.

A few examples of recent measurements can be found in Refs. [416–420] for photoproduction and in Refs. [421–430] for DIS.

9.3.2.3 *Hadron-hadron colliders*

The spectrum of observables and the number of measurements performed at hadron colliders is enormous, probing many regions of phase space and covering a huge range of cross sections, as illustrated in Fig. 9.1 for the case of the ATLAS and CMS experiments at the LHC. In general, the theory agreement with data is excellent for a wide variety of processes, indicating the success of perturbative QCD with the PDF and strong coupling inputs. For the sake of brevity, in the following only certain classes of those measurements will be discussed, which permit various aspects of the QCD studies to be addressed. Most of our discussion will focus on LHC results, which are available for center-of-mass energies of 2.76, 5, 7, 8 and 13 TeV with integrated luminosities of up to 140 fb^{-1}. Generally speaking, besides representing precision tests of the standard model and QCD in particular, these measurements serve several purposes, such as: (i) probing pQCD and its various approximations and implementations in MC models, in order to quantify the order of magnitude of not yet calculated contributions, and to gauge their precision when used as background predictions, or (ii) extracting/constraining model parameters such as the strong coupling constant or PDFs. Indeed, data from the LHC are becoming increasingly important for the determination of both PDFs and the strong coupling constant.

The final states measured at the LHC include single, double and triple gauge boson production, top production (single top, top pair and four top production), Higgs boson production, alone and in conjunction with a W or Z boson, and with a top quark pair. Many/most of these events are accompanied by additional jets. So far only relatively loose limits have been placed on double Higgs production. The volume of LHC results prohibits a comprehensive description in this *Review*; hence, only a few highlights will be presented.

Among the most important cross sections measured, and the one with the largest dynamic range, is the inclusive jet spectrum as a function of the jet transverse momentum (p_t), for several rapidity regions and for p_t up to 700 GeV at the Tevatron and ~ 3.5 TeV at the LHC. It is worth noting that this upper limit in p_t corresponds to a distance scale of $\sim 10^{-19}$ m: no other experiment so far is able to directly probe smaller distance scales of nature than this measurement. The Tevatron inclusive jet measurements in Run 2 (Refs. [433–436]) were carried out with the MidPoint jet clustering algorithm (or its equivalent) and with the k_t jet clustering algorithm. Most of the LHC measurements use the *anti-k_t* algorithm, with a variety of jet radii. The use of multiple jet radii in the same analysis allows a better understanding of the underlying QCD dynamics. Measurements by ALICE, ATLAS and CMS have been published in Refs. [437–446].

In general, we observe a good description of the data by the NLO and NNLO QCD predictions over about 11 orders of magnitude in cross section, as long as care is taken for the form of the central scale choice [447]. The experimental systematic uncertainties are dominated by the jet energy scale uncertainty, quoted to be in the range of a few percent (see for instance the review in Ref. [448]), leading to uncertainties of $\sim 5 - 30\%$ on the cross section, increasing with p_t and rapidity. The PDF uncertainties dominate the theoretical uncertainty at large p_t and rapidity. In fact, inclusive jet data are one of the most important inputs to

Downloaded from https://academic.oup.com/ptep/article/2022/8/083C01/6651666 by KIT Library user on 27 September 2022

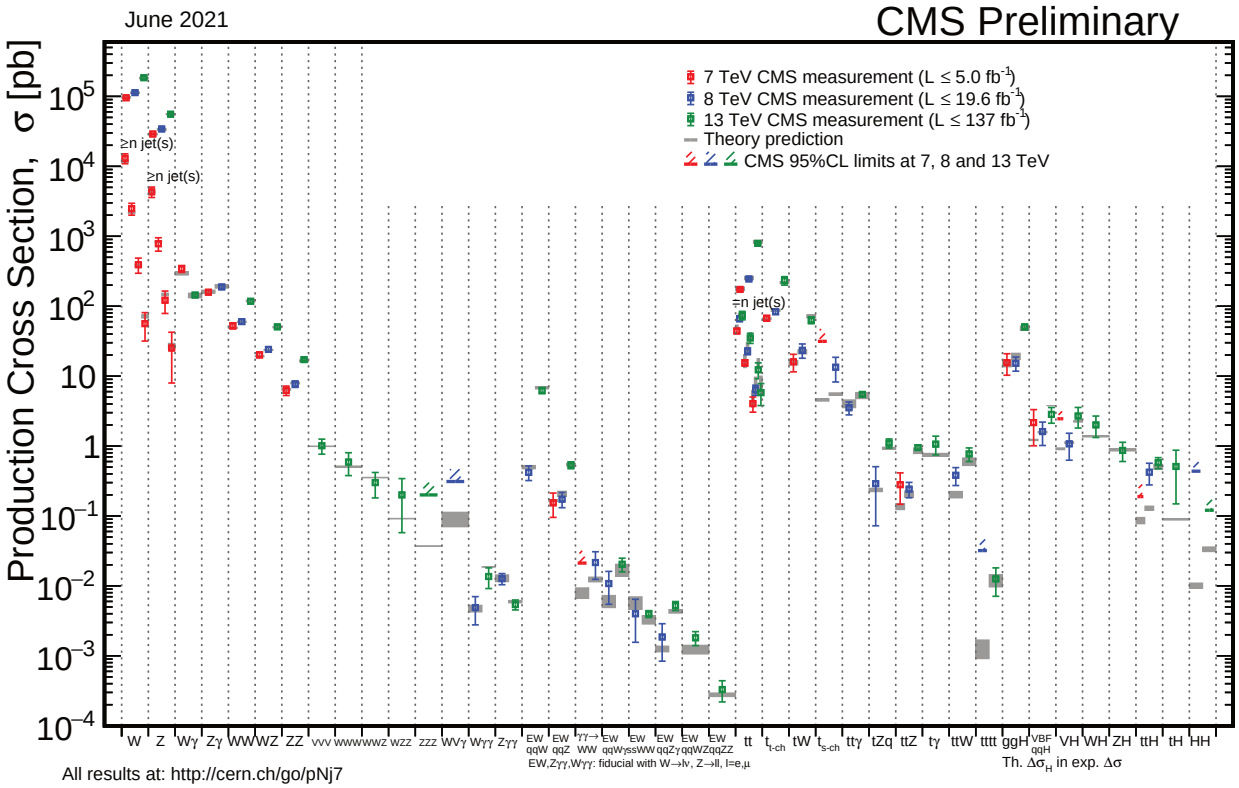

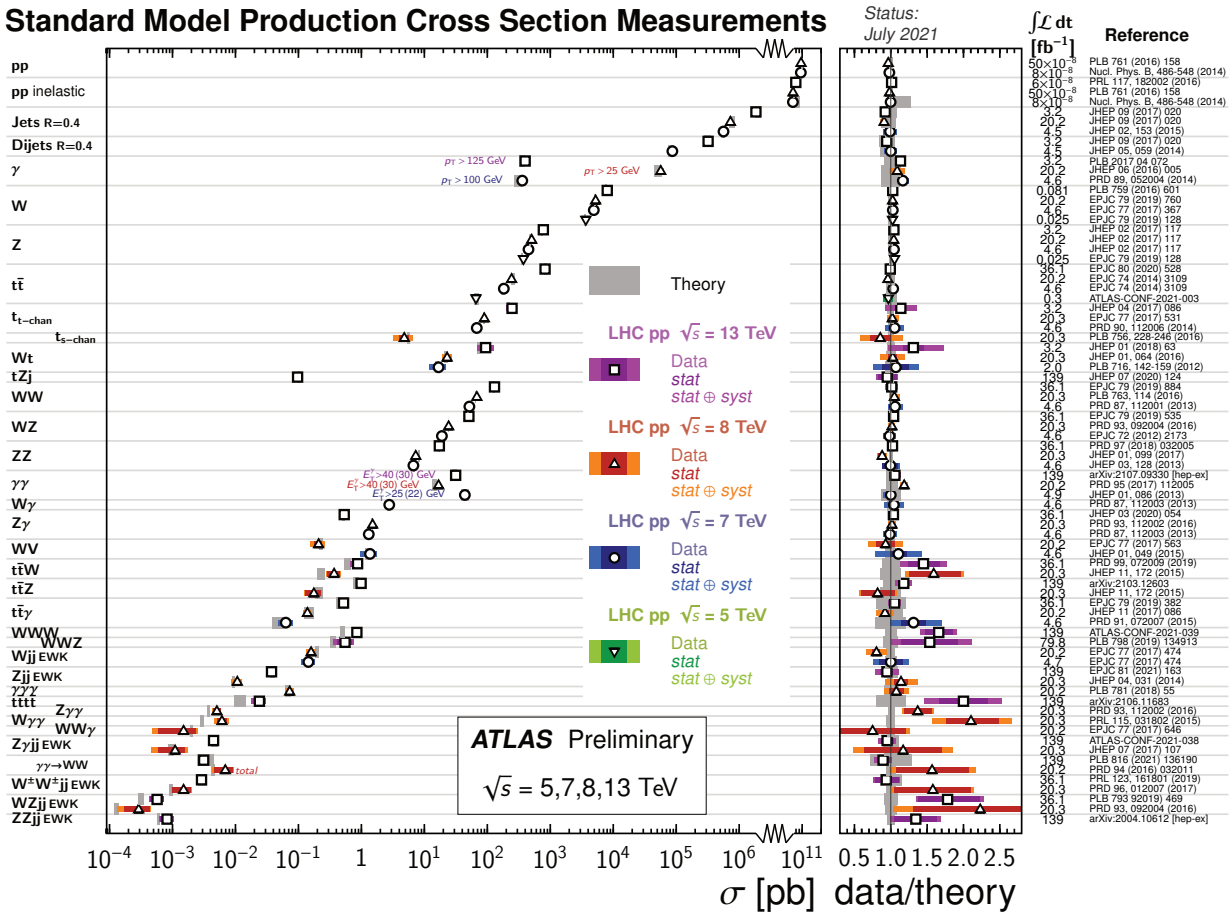

Figure 9.1: Overview of cross section measurements for a wide class of processes and observables, as obtained by the CMS [431] and ATLAS [432] experiments at the LHC, for centre-of-mass energies of 5, 7, 8 and 13 TeV. Also shown are the theoretical predictions and their uncertainties.

Downloaded from https://academic.oup.com/ptep/article/2022/8/083C01/6651666 by KIT Library user on 27 September 2022

global PDF fits, in particular for constraining the high-x gluon PDF [79, 449]. Constraints on the PDFs can also be obtained from ratios of inclusive cross sections at different center-of-mass energies [438, 443]. In general, ratios of jet cross sections are a means to (at least partially) cancel the jet energy scale uncertainties and thus provide jet observables with significantly improved precision.

Dijet events are typically analyzed in terms of their invariant mass or average dijet p_t and angular distributions, which allows for tests of NLO and NNLO QCD predictions (see *e.g.* Refs. [442, 450, 451] for recent LHC results), and for setting stringent limits on deviations from the Standard Model, such as quark compositeness or contact interactions (some examples can be found in Refs. [445, 452–458]). Furthermore, dijet azimuthal correlations between the two leading jets, normalized to the total dijet cross section, are an extremely valuable tool for studying the spectrum of gluon radiation in the event. The azimuthal separation of the two leading jets is sensitive to multi-jet production, avoiding at the same time large systematic uncertainties from the jet energy calibration. For example, results from the Tevatron [459, 460] and the LHC [388, 461–465] show that the LO (non-trivial) prediction for this observable, with at most three partons in the final state, is not able to describe the data for an azimuthal separation below $2\pi/3$, where NLO contributions (with 4 partons) restore the agreement with data. In addition, this observable can be employed to tune Monte Carlo predictions of soft gluon radiation. Further examples of dijet observables that probe special corners of phase space are those that involve forward (large rapidity) jets and where a large rapidity separation, possibly also a rapidity gap, is required between the two jets. Reviews of such measurements can be found in Ref. [400], showing that no single prediction is capable of describing the data in all phase-space regions. In particular, no conclusive evidence for BFKL effects in these observables has been established so far.

Beyond dijet final states, measurements of the production of three or more jets, including cross section ratios, have been performed (see Refs. [400, 466] for recent reviews), as a means of testing perturbative QCD predictions, determining the strong coupling constant (at NLO precision so far), and probing/tuning MC models, in particular those combining multi-parton matrix elements with parton showers. The calculation of 3-jet production to NNLO [222] will allow more precise predictions of the 3-jet to 2-jet ratio, and thus the extraction of $\alpha_s(M_Z^2)$ from this observable.

W and Z production serve as benchmark cross sections at the LHC. The large boson mass provides a stability for the perturbative predictions which results in better theoretical precision. In terms of experimental precision, measurements of inclusive vector boson (W, Z) production provide the most precisely determined observables at hadron colliders so far. This is because the experimental signatures are based on leptons which are measured much more accurately than jets or photons. At the LHC [467–474], the dominant uncertainty stems from the luminosity determination ($\leq$2–4%), while other uncertainties (*e.g.* statistical or from lepton efficiencies) are controlled at the $\sim$0.5–3% level. The uncertainty from the acceptance correction of about $\sim$1–2% can be reduced by measuring so-called fiducial cross sections, i.e. by applying kinematic cuts also to the particle level of the theoretical predictions. A further reduction or even complete elimination of particular uncertainties (*e.g.* luminosity) is achieved by measuring cross section ratios (W/Z or W^+/W^-) or differential distributions that are normalised to the inclusive cross section. On the theory side, as discussed earlier in this *Review*, the production of these color-singlet states has been calculated to N^3LO [101–103]. Since the dominant theoretical uncertainty is related to the choice of PDFs, these high-precision data provide useful handles for PDF determinations.

Further insights are obtained from measurements of differential vector boson production, as a function of the invariant dilepton mass, the boson's rapidity or its transverse momentum. For example, the dilepton invariant mass distribution has been measured [475–480] for masses between 15 and 3000 GeV, covering more than 8 orders of magnitude in cross section. NNLO QCD predictions, together with modern PDF sets and including higher-order electroweak and QED final-state radiation corrections, describe the data to within 5–10% over this large range, whereas NLO predictions show larger deviations, unless matched to a parton shower.

Similar conclusions can be drawn from the observed rapidity distribution of the dilepton system (see *e.g.* Refs. [467, 476, 481]) or, in the case of W production, from the observed charged lepton rapidity distribution and its charge asymmetry. The latter is particularly sensitive to differences among PDF sets [467, 482–484], also thanks to the high precision achieved by the ATLAS and CMS experiments for central rapidity ranges. These measurements are extended to the very forward region, up to 4.5 in lepton rapidity, by the LHCb experiment [473, 474, 485].

An overview of these kinds of measurement can be found in Ref. [400]. There one can also find a discussion of and references to LHC results from studies of the vector boson's transverse momentum distribution, p_t^V (see also Refs. [486–488]). This observable covers a wide kinematic range and probes different aspects of higher-order QCD effects. It is sensitive to jet production in association with the vector boson, without suffering from the large jet energy scale uncertainties. In the p_t^V region of several tens of GeV to over 1 TeV, the NNLO predictions for V+jet can be used to predict the high-p_t boson production cross section.[11] The NNLO predictions agree with the data to within about 10%, and agree somewhat better at high transverse momentum than do the NLO predictions [489]. At transverse momenta below $\sim$20 GeV, the fixed-order predictions fail and soft-gluon resummation is needed to restore the agreement with data. The soft gluon resummation can either be performed analytically, or effectively using parton showering implemented in Monte Carlo programs. While analytic approaches reach a higher perturbative precision, they typically refer to inclusive measurements without fiducial cuts. The addition of further jets to the final state extends the kinematic range as well as increasing the complexity of the calculation/measurements. The number of results obtained both at the Tevatron and at the LHC is extensive, summaries can be found in Refs. [400, 490], and more recent results can be found in Refs. [489, 491–494]. The measurements cover a very large phase space, *e.g.* with jet transverse momenta between 30 GeV and $\sim$ 1.5 TeV and jet rapidities up to $|y| < 4.4$ [489]. Jet multiplicities as high as seven jets accompanying the vector boson have already been probed at the LHC, together with a substantial number of other kinematical observables, such as angular correlations among the various jets or among the jets and the vector boson, or the sum of jet transverse momenta, H_T. Whereas the jet p_t and H_T distributions are dominated by jet energy scale uncertainties at levels similar to those discussed above for inclusive jet production, angular correlations and jet multiplicity ratios have been measured with a precision of $\sim$ 10%, see *e.g.* Refs. [390, 495].

NLO calculations for up to five jets [496] in addition to the vector boson are in good agreement with the data over that phase space, where the calculations are applicable. Predictions for V+jet at NNLO improve the description of the data for distributions involving the vector boson or the leading jet. MC models that implement parton shower matching to matrix elements (either at LO or NLO) have mixed results.

The challenges get even more severe in the case of vector boson plus heavy quark (b, c) production: on the theory side because an additional scale is introduced by the heavy quark mass, and different schemes exist for the handling of heavy quarks and their mass effects in the initial and/or final state; and on the experimental side because additional uncertainties related to the heavy-flavour tagging must be considered. A review of heavy quark production at the LHC is presented in Ref. [497], where the di-b-jet p_t and mass spectra are found to be well modeled within uncertainties by most generators for b-jet production with or without associated W and Z bosons. However, sizable differences between data and predictions are seen in the modeling of events with single b jets, particularly at large b-jet p_t, where gluon splitting processes

[11] For these calculations, there is a requirement of the presence of a jet, but the p_t cut is typically small (30 GeV) compared to the high p_t region being discussed here.

Downloaded from https://academic.oup.com/ptep/article/2022/8/083C01/6651666 by KIT Library user on 27 September 2022

become dominant, as also confirmed by studies of b-hadron and b-jet angular correlations.

The precision reached in photon measurements is in between that for lepton and jet measurements. The photon energy and angles can be measured at about the same precision as the lepton energy and angles in Drell-Yan production, but there are greater challenges encountered in photon reconstruction (for example isolation) and in purity determination. Note, though, that the photon purity approaches unity as the photon p_t increases. At high p_t, it becomes increasingly difficult for a jet to fragment into an isolated neutral electromagnetic cluster which mimics the photon signature. The inclusive photon cross section can be measured [450, 498–501], as well as the production of a photon accompanied by one or more jets [501–503, 503–506]. The kinematic range for photon production is less than that for jet production because of the presence of the electromagnetic coupling, but still reaches about 2 TeV. Better agreement is obtained with NNLO predictions for photon production than for NLO predictions, except when the latter are matched to matrix element plus parton shower predictions. Photon production in association with a heavy-flavor jet is a useful input for the determination of the b and c quark PDFs [507].

Electroweak corrections are expected to become more and more relevant now that the TeV energy range starts to be explored. For example, such corrections were found [508] to be sizable (tens of percent) when studying the ratio $(d\sigma^{\gamma}/dp_t)/(d\sigma^{Z}/dp_t)$ in $\gamma\,(Z)$+jet production, p_t being the boson's transverse momentum, and might account for (some of) the differences observed in a CMS measurement [509] of this quantity.

A number of interesting developments, in terms of probing higher-order QCD effects, have occurred in the sector of diboson production, in particular for the WW and $\gamma\gamma$ cases. Regarding the former, an early disagreement of about 10% between the LHC measurements and the NLO predictions had led to a number of speculations of possible new physics effects in this channel. However, more recent ATLAS and CMS measurements [510–513] are in agreement with the NNLO prediction [109]. The statistical reach of the LHC has resulted in evidence for triple massive gauge boson production [514].

In the case of diphoton production, ATLAS [515, 516] and CMS [517] have provided accurate measurements, in particular for phase-space regions that are sensitive to radiative QCD corrections (multi-jet production), such as small azimuthal photon separation. While there are large deviations between data and NLO predictions in this region, a calculation [194] at NNLO accuracy manages to mostly fill this gap. This is an interesting example where scale variations can not provide a reliable estimate of missing contributions beyond NLO, since at NNLO new channels appear in the initial state (gluon fusion in this case). These missing channels can be included in a matrix element plus parton shower calculation in which two additional jets are included at NLO. The result exhibits a similar level of agreement as that obtained at NNLO. Three-photon production has also been measured [518] and is in good agreement with NNLO theory predictions [219, 220].

In terms of heaviest particle involved, top-quark production at the LHC has become an important tool for probing higher-order QCD calculations, thanks to very impressive achievements both on the experimental and theoretical side, as extensively summarized in Ref. [519]. Regarding $t\bar{t}$ production, the most precise inclusive cross section measurements are achieved using the dilepton $(e\,\mu)$ final state, with a total uncertainty of 4% [520–523]. This is of about the same size as the uncertainty on the most advanced theoretical predictions [107, 108, 524, 525], obtained at NNLO with additional soft-gluon resummation at NNLL accuracy [526]. There is excellent agreement between data and the QCD predictions.

The $t\bar{t}$ final state allows multiple observables to be measured. A large number of differential cross section measurements have been performed at 7, 8 and 13 TeV centre-of-mass energy, studying distributions such as the top-quark p_t and rapidity, the transverse momentum and invariant mass of the $t\bar{t}$ system (probing the TeV range), or the number of additional jets. These measurements have been compared to a wide range of predictions, at fixed order up to NNLO as well as using LO or NLO matrix elements matched to parton showers. Each of the observables provides information on the high x gluon. However, there are tensions among the multiple observables that can lead to difficulties in PDF fits.

Thanks to both the precise measurements of, and predictions for, the inclusive top-pair cross section, which is sensitive to the strong coupling constant and the top-quark mass, this observable has been used to measure the strong coupling constant at NNLO accuracy from hadron collider data [527, 528] (*cf.* Section 9.4 below), as well as to obtain a measurement of the top-quark's pole mass without employing direct reconstruction methods [527, 529, 530].

The Higgs boson provides a tool for QCD studies, especially as the dominant production mechanism is gg fusion, which is subject to very large QCD corrections. Higgs boson production has been measured in the ZZ, $\gamma\gamma$, $b\bar{b}$, WW and $\tau\tau$ decay channels. The experimental cross section is now known with a precision approaching 10% [531, 532], similar to the size of the theoretical uncertainty [533], of which the PDF+α_s uncertainty is the largest component. The experimental precision has allowed detailed fiducial and differential cross section measurements. For example, with the diphoton final state, the transverse momentum of the Higgs boson can be measured out to the order of 650 GeV [534, 535], where top quark mass effects become important. The production of a Higgs boson with up to 4 jets has been measured [534, 536]. The experimental cross sections have been compared to NNLO predictions (for $H+\geq 1$ jet), NLO for 2 and 3 jets, and NNLO+NNLL for the transverse momentum distribution. In addition, finite top quark mass effects have been taken into account at NLO. The use of the boosted $H \to b\bar{b}$ topology allows probes of Higgs boson transverse momenta on the order of 600 GeV and greater [536]. So far the agreement with the perturbative QCD corrections is good.

9.4 Determinations of the strong coupling constant

Beside the quark masses, the only free parameter in the QCD Lagrangian is the strong coupling constant α_s. The coupling constant in itself is not a physical observable, but rather a quantity defined in the context of perturbation theory, which enters predictions for experimentally measurable observables, such as R in Eq. (9.7). The value of the strong coupling constant must be inferred from such measurements and is subject to experimental and theoretical uncertainties. The incomplete knowledge of α_s propagates into uncertainties in numerous precision tests of the Standard Model. Here, we present an update of the 2020 PDG average value of $\alpha_s(M_Z^2)$ and its uncertainty [537].

Many experimental observables are used to determine α_s. A number of recent determinations are collected in Ref. [538]. Further discussions and considerations on determinations of α_s can also be found in Refs. [539–541]. Such considerations include:

- The observable's sensitivity to α_s as compared to the experimental precision. For example, for the e^+e^- cross section to hadrons (*cf.* R in Sec. 9.2.1), QCD effects are only a small correction, since the perturbative series starts at order α_s^0; 3-jet production or event shapes in e^+e^- annihilations are directly sensitive to α_s since they start at order α_s; the hadronic decay width of heavy quarkonia, $\Gamma(\Upsilon \to \text{hadrons})$, is very sensitive to α_s since its leading order term is $\propto \alpha_s^3$.
- The accuracy of the perturbative prediction, or equivalently of the relation between α_s and the value of the observable. The minimal requirement is generally considered to be an NLO prediction. Several observables have been known to NNLO for quite some time. These include, for instance, inclusive observables, as well as 3-jet rates and event shapes in e^+e^- collisions, inclusive jet and dijet production in DIS, and inclusive jet, dijet, $t\bar{t}$, W/Z+jet and three-jet production cross sections in pp or $p\bar{p}$ collisions. The e^+e^- hadronic cross section and τ branching fraction to hadrons are even known to N^{3}LO, if one denotes the LO as the first non-trivial term. In certain cases, fixed-order predictions are supplemented with resummation. The precise magnitude of the associated theory uncertainties

Downloaded from https://academic.oup.com/ptep/article/2022/8/083C01/6651666 by KIT Library user on 27 September 2022

usually is estimated as discussed in Sec. 9.2.4.

- The size of non-perturbative effects. Sufficiently inclusive quantities, like the e^+e^- cross section to hadrons, have small non-perturbative contributions $\sim \Lambda^4/Q^4$. Others, such as event-shape distributions, have typically contributions $\sim \Lambda/Q$.
- The scale at which the measurement is performed. An uncertainty δ on a measurement of $\alpha_s(Q^2)$, at a scale Q, translates to an uncertainty $\delta' = (\alpha_s^2(M_Z^2)/\alpha_s^2(Q^2)) \cdot \delta$ on $\alpha_s(M_Z^2)$. For example, this enhances the already important impact of precise low-Q measurements, such as from τ decays, in combinations performed at the M_Z scale.

The selection of results from which to determine the world average value of $\alpha_s(M_Z^2)$ is restricted to those that are

- published in a peer-reviewed journal at the time of writing this report,
- based on the most complete perturbative QCD predictions of at least NNLO accuracy,
- accompanied by reliable estimates of all experimental and theoretical uncertainties.

Numerous measurements from jet production in DIS and at hadron colliders are still excluded from the average presented here, because the determination of $\alpha_s(M_Z^2)$ from those data sets has not yet been upgraded to NNLO. We expect that this will change in the near future. Still, the NLO analyses will be discussed in this *Review*, as they are important ingredients for the experimental evidence of the energy dependence of α_s, *i.e.* for asymptotic freedom, one of the key features of QCD.

In order to calculate the world average value of $\alpha_s(M_Z^2)$, we apply, as in earlier editions, an intermediate step of pre-averaging results within the sub-fields now labeled "Hadronic τ decays and low Q^2 continuum" (τ decays and low Q^2), "Heavy quarkonia decays" ($Q\bar{Q}$ bound states), "PDF fits" (PDF fits), "Hadronic final states of e^+e^- annihilations" (e^+e^- jets & shapes), "Observables from hadron-induced collisions" (hadron colliders), and "Electroweak precision fit" (electroweak) as explained in the following sections. For each sub-field, the *unweighted average* of all selected results is taken as the pre-average value of $\alpha_s(M_Z^2)$, and the unweighted average of the quoted uncertainties is assigned to be the respective overall error of this pre-average. For the "Lattice QCD" (lattice) sub-field we do not perform a pre-averaging; instead, we adopt for this sub-field the average value and uncertainty derived by the Flavour Lattice Averaging Group (FLAG) in Ref. [542].

Assuming that the six sub-fields (excluding lattice) are largely independent of each other, we determine a non-lattice world average value using a 'χ^2 *averaging*' method. In a last step we perform an unweighted average of the values and uncertainties of $\alpha_s(M_Z^2)$ from our non-lattice result and the lattice result presented in the FLAG2019 report [542].

9.4.1 *Hadronic τ decays and low Q^2 continuum:*

Based on complete N^{3}LO predictions [32], analyses of the τ hadronic decay width and spectral functions have been performed, *e.g.* in Refs. [32,543–548], and lead to precise determinations of α_s at the energy scale of M_τ^2. They are based on different approaches to treat perturbative and non-perturbative contributions, the impacts of which have been a matter of intense discussions for a long time, see *e.g.* Refs. [547–550]. In particular, in τ decays there is a significant difference between results obtained using fixed-order (FOPT) or contour-improved perturbation theory (CIPT),

such that analyses based on CIPT generally arrive at larger values of $\alpha_s(M_\tau^2)$ than those based on FOPT. In addition, some results show differences in $\alpha_s(M_\tau^2)$ between different groups using the same data sets and perturbative calculations, most likely due to different treatments of the non-perturbative contributions, *cf.* Ref. [548] with Refs. [547, 551]. References [552, 553] question the validity of using a truncated OPE at $Q^2 = m_\tau^2$ based on the disagreement found between experimental values of the spectral moments and the theory representations based on the truncated OPE fits at $Q^2 > m_\tau^2$.

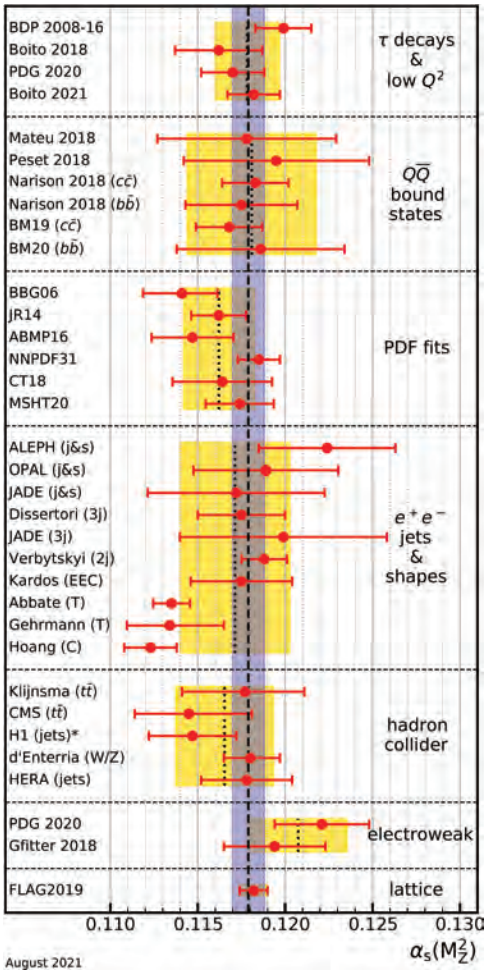

Figure 9.2: Summary of determinations of $\alpha_s(M_Z^2)$ from the seven sub-fields discussed in the text. The yellow (light shaded) bands and dotted lines indicate the pre-average values of each sub-field. The dashed line and blue (dark shaded) band represent the final world average value of $\alpha_s(M_Z^2)$. The "*" symbol within the "hadron colliders" sub-field indicates a determination including a simultaneous fit of PDFs.

We determine the pre-average value of $\alpha_s(M_Z^2)$ for this sub-field from studies that employ both FOPT and CIPT expansions, and that account for the difference among these in the quoted overall uncertainty. If necessary, we perform ourselves the averaging of FOPT and CIPT numbers and the quadratic addition of half their difference to the uncertainty. As the results from Refs. [32, 550, 551] are not totally independent, we pre-average as a first step the three results $\alpha_s(M_Z^2) = 0.1202 \pm 0.0019$ [32], $\alpha_s(M_Z^2) = 0.1199 \pm 0.0015$ [551], and $\alpha_s(M_Z^2) = 0.1197 \pm 0.0015$ [550] to $\alpha_s(M_Z^2) = 0.1199 \pm 0.0016$ (summarized as BDP2008-16 in Fig. 9.2). Subsequently, this is combined with $\alpha_s(M_Z^2) = 0.1162 \pm 0.0025$ [554], and $\alpha_s(M_Z^2) = 0.1182 \pm 0.0015$ [555], which replaces the previous result from Ref. [548]. We also include the result from τ decay and lifetime measurements, obtained in Sec. *Electroweak Model and constraints on New Physics* of the 2020 edition of this *Review* [537], $\alpha_s(M_Z^2) = 0.1170^{+0.0019}_{-0.0017}$. The latter result, being a global fit of τ data, involves some correlations with the other extractions of this category. However, since we perform an unweighted average of the central value and uncertainty, the effects of the potential correlations are reduced.

All these results are summarized in Fig. 9.2. Determining the unweighted average of the central values and their overall uncertainties, we arrive at $\alpha_s(M_Z^2) = 0.1178 \pm 0.0019$, which we will use as the first input for determining the world average value of

Downloaded from https://academic.oup.com/ptep/article/2022/8/083C01/6651666 by KIT Library user on 27 September 2022

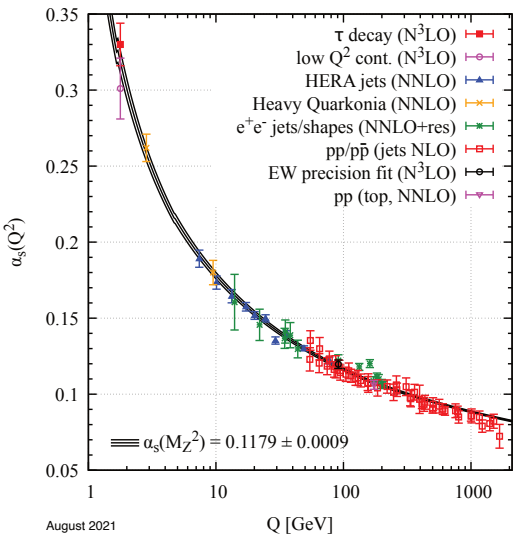

Figure 9.3: Summary of measurements of α_s as a function of the energy scale Q. The respective degree of QCD perturbation theory used in the extraction of α_s is indicated in brackets (NLO: next-to-leading order; NNLO: next-to-next-to-leading order; NNLO+res.: NNLO matched to a resummed calculation; N^{3}LO: next-to-NNLO).

$\alpha_s(M_Z^2)$. This corresponds to $\alpha_s(M_\tau^2) = 0.312 \pm 0.015$.

9.4.2 *Heavy quarkonia decays:*

Recently, two determinations have been performed [556, 557] that are based on N^{3}LO accurate predictions. Reference [556] performs a simultaneous fit of the strong coupling and the bottom mass $\overline{m_b}$, including states with principal quantum number up to $n \leq 2$ in order to break the degeneracy between α_s and $\overline{m_b}$, finding $\alpha_s(M_Z^2) = 0.1178 \pm 0.0051$. Reference [557] instead uses as input of the fit the renormalon-free combination of masses of the meson B_c, the bottomonium η_b and the charmonium η_c, $M_{B_c} - M_{\eta_b}/2 - M_{\eta_c}/2$, which is weakly dependent on the heavy quark masses, but shows a good dependence on α_s. Using this observable, they obtain $\alpha_s(M_Z^2) = 0.1195 \pm 0.0053$. Two further values are derived at NNLO in Ref. [558, 559] from mass splittings and sum rules giving $\alpha_s(M_Z^2) = 0.1183 \pm 0.0019$ and $\alpha_s(M_Z^2) = 0.1175 \pm 0.0032$ when evolved from the relevant charmonium respectively bottomonium mass scales to M_Z^2. Finally, by means of quarkonium sum rules, Refs. [560, 561] quote $\alpha_s(M_Z^2) = 0.1168 \pm 0.0019$ and $\alpha_s(M_Z^2) = 0.1186 \pm 0.0048$ for charmonium and bottomonium respectively. These six determinations satisfy our criteria to be included in the heavy-quarkonia category of the world average. Their unweighted combination leads to the pre-average for this category of $\alpha_s(M_Z^2) = 0.1181 \pm 0.0037$.

9.4.3 *PDF fits:*

Another class of studies, analyzing structure functions at NNLO QCD (and partly beyond), provide results that serve as relevant inputs for the world average of α_s. Most of these studies do *not*, however, explicitly include estimates of theoretical uncertainties when quoting fit results of α_s. In such cases we add, in quadrature, half of the difference between the results obtained in NNLO and NLO to the quoted errors.

A combined analysis of non-singlet structure functions from DIS [562], based on QCD predictions up to N^{3}LO in some of its parts, results in $\alpha_s(M_Z^2) = 0.1141 \pm 0.0022$ (BBG). Studies of singlet and non-singlet structure functions, based on NNLO predictions, result in $\alpha_s(M_Z^2) = 0.1162 \pm 0.0017$ [563] (JR14). The AMBP group [564, 565] determined a set of parton distribution functions using data from HERA, NOMAD, CHORUS, from the Tevatron and the LHC using the Drell-Yan process and the hadro-production of single-top and top-quark pairs, and determined $\alpha_s(M_Z^2) = 0.1147 \pm 0.0024$ [564].

The MSHT group [566], also including hadron collider data, determined a new set of parton density functions (MSHT20) together with $\alpha_s(M_Z^2) = 0.1174 \pm 0.0013$. Similarly, the CT group [567] determined the CT18 parton density set together with $\alpha_s(M_Z^2) = 0.1164 \pm 0.0026$. The NNPDF group [568] presented NNPDF3.1 parton distribution functions together with $\alpha_s(M_Z^2) = 0.1185 \pm 0.0012$.

We note that criticism has been expressed on some of the above extractions. Among the issues raised, we mention the neglect of singlet contributions at $x \geq 0.3$ in pure non-singlet fits [569], the impact and detailed treatment of particular classes of data in the fits [569, 570], possible biases due to insufficiently flexible parametrizations of the PDFs [571] and the use of a fixed-flavor number scheme [572, 573].

Summarizing the results from world data on structure functions, taking the *unweighted average* of the central values and errors of all selected results, leads to a pre-average value of $\alpha_s(M_Z^2) = 0.1162 \pm 0.0020$, see Fig. 9.2.

9.4.4 *Hadronic final states of e^+e^- annihilations:*

Re-analyses of jets and event shapes in e^+e^- annihilation (j&s), measured around the Z peak and at LEP2 center-of-mass energies up to 209 GeV, using NNLO predictions matched to NLL resummation and Monte Carlo models to correct for hadronization effects, resulted in $\alpha_s(M_Z^2) = 0.1224 \pm 0.0039$ (ALEPH) [574], and in $\alpha_s(M_Z^2) = 0.1189 \pm 0.0043$ (OPAL) [575]. Similarly, an analysis of JADE data [576] at center-of-mass energies between 14 and 46 GeV gives $\alpha_s(M_Z^2) = 0.1172 \pm 0.0051$, with contributions from the hadronization model and from perturbative QCD uncertainties of 0.0035 and 0.0030, respectively. Precise determinations of α_s from 3-jet production alone (3j), at NNLO, resulted in $\alpha_s(M_Z^2) = 0.1175 \pm 0.0025$ [577] from ALEPH data and in $\alpha_s(M_Z^2) = 0.1199 \pm 0.0059$ [578] from JADE. A recent determination is based on an NNLO+NNLL accurate calculation that allows to fit the region of lower 3-jet rate (2j) using data collected at LEP and PETRA at different energies. This fit gives $\alpha_s(M_Z^2) = 0.1188 \pm 0.0013$ [579], where the dominant uncertainty is the hadronization uncertainty, which is estimated from Monte Carlo simulations. A fit of energy-energy-correlation (EEC) also based on an NNLO+NNLL calculation together with a Monte Carlo based modeling of hadronization corrections gives $\alpha_s(M_Z^2) = 0.1175 \pm 0.0029$ [580]. These results are summarized in the upper seven rows of the e^+e^- sector of Fig. 9.2.

Another class of α_s determinations is based on analytic modeling of non-perturbative and hadronization effects, rather than on Monte Carlo models [581–584], using methods like power corrections, factorization of soft-collinear effective field theory, dispersive models and low scale QCD effective couplings. In these studies, the world data on Thrust distributions (T), or - most recently - C-parameter distributions (C), are analysed and fitted to perturbative QCD predictions at NNLO matched with resummation of leading logs up to N^{3}LL accuracy, see Sec. 9.2.3.3. The results are $\alpha_s(M_Z^2) = 0.1135 \pm 0.0011$ [582] and $\alpha_s(M_Z^2) = 0.1134^{+0.0031}_{-0.0025}$ [583] from Thrust, and $\alpha_s(M_Z^2) = 0.1123 \pm 0.0015$ [584] from C-parameter. They are displayed in the lower three rows of the e^+e^- sector of Fig. 9.2. A recent calculation has determined the leading non-perturbative contribution to the C-parameter in the three-jet limit, and has found that it differs by a factor of two from the two-jet limit [585]. Taking this result into account in analyses of the C-parameter would increase the value of the extracted α_s parameter, leaving it more in keeping with the world average.

The determination of Ref. [581], $\alpha_s(M_Z^2) = 0.1164^{+0.0028}_{-0.0024}$, is no longer included in the average as it is superseded by other determinations that use the same Thrust data but rely on more accurate theoretical predictions. Not included in the computation of the world average but worth mentioning are a computation of the NLO corrections to 5-jet production and comparison to the measured 5-jet rates at LEP [586], giving $\alpha_s(M_Z^2) = 0.1156^{+0.0041}_{-0.0034}$, and a computation of non-perturbative and perturbative QCD contributions to the scale evolution of quark and gluon jet multiplicities, including resummation, resulting in $\alpha_s(M_Z^2) = 0.1199 \pm 0.0026$ [587].

We note that there is criticism on both classes of α_s extractions

Downloaded from https://academic.oup.com/ptep/article/2022/8/083C01/6651666 by KIT Library user on 27 September 2022

described above: those based on corrections of non-perturbative hadronization effects using QCD-inspired Monte Carlo generators (since the parton level of a Monte Carlo simulation is not defined in a manner equivalent to that of a fixed-order calculation), as well as studies based on non-perturbative analytic modeling, as their systematics have not yet been fully verified. For the latter case, Refs. [582, 584] quote surprisingly small overall experimental, hadronization, and theoretical uncertainties of only 2, 5, and 9 per-mille, respectively, which calls for an independent confirmation.

A recent comparison of the non-perturbative corrections, using both Monte Carlo and analytic techniques, for both Thrust and the C-parameter, can be found in Ref. [588].

In view of these open questions, the determination of the *unweighted average* and uncertainties is intended to provide the most appropriate and unbiased estimate of the average value of $\alpha_s(M_Z^2)$ for this sub-field, which results in $\alpha_s(M_Z^2) = 0.1171 \pm 0.0031$.

9.4.5 ***Observables from hadron-induced collisions:***
Until recently, determinations of α_s using hadron collider data, mostly from jet or $t\bar{t}$ production processes, could be performed at NLO only. NNLO calculations have now become available for $t\bar{t}$ [107, 524, 525] and for inclusive jet and dijet production [214,589,590]. For $t\bar{t}$ production, in addition, logarithms to NNLL have been resummed [526]. Both should be supplemented by electroweak corrections [591–593], which become important for high-p_{T} collisions at the LHC. Z+jet production, studied with respect to an α_s determination at NLO from multi-jet events in Ref. [594], is also known at NNLO for the 1-jet case [204, 595]. Determinations of α_s from production cross sections at hadron colliders also require a knowledge of the relevant PDFs for those α_s values. Two strategies are pursued for the extraction of α_s, one using pre-determined PDFs as input and a second strategy fitting the proton PDFs together with the strong coupling constant. Each global PDF group produces PDF sets not only for the world average value of 0.118, but also for a wide range above and below that value, in increments of 0.001, that can be used in such determinations. The latter technique of simultaneously fitting α_s and the PDFs is technically more accurate, given that the new data used in the determination of α_s may modify the PDFs in a manner not taken into account by the α_s-variation PDFs provided by the fitting collaborations. The former technique may result in a bias of unknown magnitude [596]. As the LHC experiments have the ability to combine a PDF fit with the α_s determination, for example with tools like described in Ref. [597], we expect more experimental joint determinations of PDFs and of α_s for future iterations of this review.

The first determination of α_s at NNLO accuracy in QCD has been reported by CMS from the $t\bar{t}$ production cross section at $\sqrt{s} = 7$ TeV [527]. In recent *Reviews* this opened up a new subfield on its own. In the meantime, multiple datasets on $t\bar{t}$ production from Tevatron at $\sqrt{s} = 1.96$ TeV and from LHC at $\sqrt{s} = 7$, 8, and 13 TeV have been analyzed simultaneously to determine α_s [528] to

$$\alpha_s(M_Z^2) = 0.1177^{+0.0034}_{-0.0036},$$

where the largest uncertainties are associated with missing higher orders and with PDFs, and where an additional complication arises from the top-mass dependence. Since this combined analysis contains among other things an updated measurement as compared to the dataset used by CMS, the latter is replaced in the averaging by the new combined result. A second entry into this subfield is given by an analysis of $t\bar{t}$ production data at $\sqrt{s} = 13$ TeV from the CMS Collaboration [522]. From the four values derived for different PDF sets, the unweighted average is taken:

$$\alpha_s(M_Z^2) = 0.1145^{+0.0036}_{-0.0031}.$$

A second analysis by CMS using differential distributions of $t\bar{t}$ production [598] has been performed at NLO only and is not further considered.

From jet production, the α_s determination at NNLO using DIS data of the H1 Collaboration [430] has been corrected for an issue with the theory prediction reported in Ref. [413]. We choose the result

$$\alpha_s(M_Z^2) = 0.1147 \pm 0.0025$$

that is derived from a simultaneous fit of the strong coupling constant together with proton PDFs. We note that results of this section derived from such a simultaneous fit will be marked with a "*" in the corresponding figures.

Two new determinations without simultaneous PDF fit are considered for the unweighted pre-average of this sub-field. Reference [599] extracts the strong coupling constant from a fit at NNLO to measurements of inclusive Z and W boson production by experiments at the LHC and Tevatron colliders. From the four values quoted for different PDF sets we include the unweighted average for the CT14 and MMHT14 PDFs

$$\alpha_s(M_Z^2) = 0.1180^{+0.0017}_{-0.0015}.$$

The other two results suffer from either a bad fit quality or $\alpha_s(M_Z^2)$ values outside the range of validity for the PDF set.
The second determination [231] combines multiple datasets on inclusive jet production of the H1 and ZEUS collaborations at the HERA collider into one fit using interpolation grids at NNLO. The result of

$$\alpha_s(M_Z^2) = 0.1178 \pm 0.0026$$

has been updated for the same issue reported above [413].

As unweighted pre-average for this sub-field we obtain: $\alpha_s(M_Z^2) = 0.1165 \pm 0.0028$. If the stricter requirement of simultaneous fits with PDFs is imposed, then only the H1 result is left in this sub-field. In sect. 9.4.8 below, we will also report the outcome for this choice.

Many further α_s determinations from jet measurements either could not be advanced to NNLO accuracy yet, or the NNLO predictions are not yet available as is the case for observables requiring more than three jets in the final state. A selection of results from inclusive jet [429, 443, 600–605], dijet [451], and multi-jet measurements [385,387,388,429,606–610] is presented in Fig. 9.4, where the uncertainty in most cases is dominated by the impact of missing higher orders estimated through scale variations. From the CMS Collaboration we quote for the inclusive jet production at $\sqrt{s} = 7$ and 8 TeV, and for dijet production at TeV the values that have been derived in a simultaneous fit with the PDFs and marked with "*" in the figure. The last point of the inclusive jet sub-field from Ref. [605] is derived from a simultaneous fit to six datasets from different experiments and partially includes data used already for the other data points, *e.g.* the CMS result at 7 TeV.

The multi-jet α_s determinations are based on 3-jet cross sections (m3j), 3- to 2-jet cross-section ratios (R32), dijet angular decorrelations (RdR, RdPhi), and transverse energy-energy-correlations and their asymmetry (TEEC, ATEEC). The H1 result is extracted from a fit to inclusive 1-, 2-, and 3-jet cross sections (nj) simultaneously.

All NLO results are within their large uncertainties in agreement with the world average and the associated analyses provide valuable new values for the scale dependence of α_s at energy scales now extending up to almost 2.0 TeV as shown in Fig. 9.3.

9.4.6 ***Electroweak precision fit:***
For this category, we take the global electroweak fit of Ref. [611], which includes kinematic top quark and W boson mass measurements from the LHC, recent determinations of the effective leptonic electroweak mixing angles from the Tevatron, a Higgs mass measurement from ATLAS and CMS, and a new evaluation of the hadronic contribution to the running of the electromagnetic coupling at the Z-boson mass. In addition, we use the newer results of the electroweak fit at the Z mass pole from LEP and SLC data presented in Sec. *Electroweak Model and constraints on New Physics* of the 2020 edition of this *Review*. Both very similar results, $\alpha_s(M_Z^2) = 0.1221 \pm 0.0027$ [537], $\alpha_s(M_Z^2) = 0.1194 \pm 0.0029$ [611], are also in perfect agreement with the original result obtained from LEP and SLD data [612]. Our pre-averaging gives $\alpha_s(M_Z^2) = 0.1208 \pm 0.0028$.

We note, however, that results from electroweak precision data strongly depend on the strict validity of Standard Model predictions and the existence of the minimal Higgs mechanism to

Downloaded from https://academic.oup.com/ptep/article/2022/8/083C01/6651666 by KIT Library user on 27 September 2022

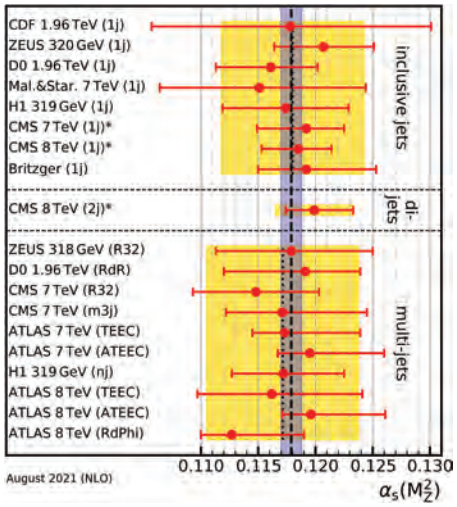

Figure 9.4: Summary of determinations of $\alpha_s(M_Z^2)$ at NLO from inclusive jet, dijet, and multi-jet measurements at hadron colliders. The uncertainty is dominated by estimates of the impact of missing higher orders. The yellow (light shaded) bands and dotted lines indicate average values for the two sub-fields. The dashed line and blue (dark shaded) band represent the final world average value of $\alpha_s(M_Z^2)$. The "*" symbol indicates determinations including a simultaneous fit of PDFs.

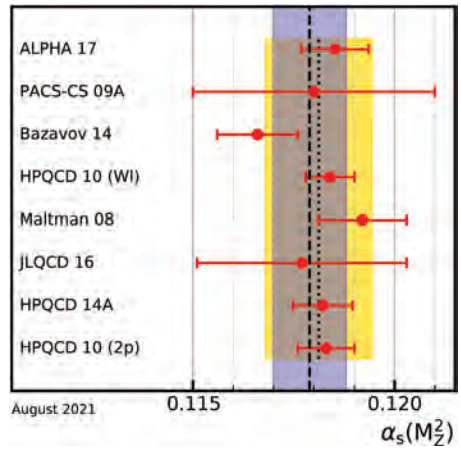

Figure 9.5: Lattice determinations that enter the FLAG2019 average. The yellow (light shaded) band and dotted line indicates the average value for this sub-field. The dashed line and blue (dark shaded) band represent the final world average value of $\alpha_s(M_Z^2)$. [a]

[a] In the previous edition, the JLQCD result was incorrectly labelled as "JLQCD17" and had a wrong (too small) uncertainty.

implement electroweak symmetry breaking. Any - even small - deviation of nature from this model could strongly influence this extraction of α_s.

9.4.7 *Lattice QCD:*

Several methods exist to extract the strong coupling constant from lattice QCD, as reviewed also in Sec. *Lattice QCD* of this *Review*. The Flavour Lattice Averaging Group has considered the most up-to-date determinations and combined them to produce an update of their average α_s [542]. Their final result is obtained by considering a multitude of possible input calculations [613–630] and by retaining in their final average only those eight [614–616, 622–624, 626] that fulfill their predefined quality criteria. These determinations, together with their uncertainties, are displayed in Fig. 9.5. The yellow (light shaded) band and dotted line indicate the FLAG2019 average, while the dashed line and blue (dark shaded) band represent the world average (see later). The level of agreement of individual results to the world average, or to the non-lattice world average is very similar. The criteria applied are detailed in the Sec. 9.2.1 of Ref. [542]. We note that, as in our case, the calculation must be published in a peer-reviewed journal for it to be eligible to be included in the FLAG average. We also note that the criteria applied now are considered relatively loose by the FLAG Collaboration and they have already formulated more stringent criteria. It is likely that in future FLAG averages only results satisfying these stricter criteria will be included in their averaging.

Similarly to what is done here, the FLAG Collaboration built pre-averages of results that belong to different classes. The four categories that contribute to the average are: step-scaling methods ($\alpha_s(M_Z^2) = 0.11848^{+0.00081}_{-0.00081}$), the potential at short distances ($\alpha_s(M_Z^2) = 0.11660^{+0.00160}_{-0.00160}$), Wilson loops ($\alpha_s(M_Z^2) = 0.11871^{+0.00128}_{-0.00128}$), and heavy-quark current two-point functions ($\alpha_s(M_Z^2) = 0.11818^{+0.00156}_{-0.00156}$). Other categories like the vacuum polarization at short distances, the calculation of QCD vertices, or of the eigenvalue spectrum of the Dirac operator have not yet published results that fulfill all requirements to be included in the average. Reference [631] has been completed after the publication of Ref. [542], hence these results have not been considered in the last FLAG average.

The final value is obtained by performing a weighted average of the pre-averages. The final uncertainty however is not the combined uncertainty of the pre-averages. Instead the smallest uncertainty of the pre-averages is taken, which is the one of the step-scaling category and which is dominated by the ALPHA 17 result [626]. The final FLAG average (rounded to four digits) is

$$\alpha_s(M_Z^2) = 0.1182 \pm 0.0008\,, \qquad \text{(lattice)}. \tag{9.23}$$

We believe that this result expresses to a large extent the consensus of the lattice community and that the imposed criteria and the rigorous assessment of systematic uncertainties qualify for a direct inclusion of this FLAG average here. As in the previous review, we therefore adopt the FLAG average with its uncertainty as our value of α_s for the lattice category. Moreover, this lattice result will not be directly combined with any other sub-field average, but with our non-lattice average to give our final world average value for α_s.

9.4.8 *Determination of the world average value of $\alpha_s(M_Z^2)$:*

Obtaining a world average value for $\alpha_s(M_Z^2)$ is a non-trivial exercise. A certain arbitrariness and subjective component is inevitable because of the choice of measurements to be included in the average, the treatment of (non-Gaussian) systematic uncertainties of mostly theoretical nature, as well as the treatment of correlations among the various inputs, of theoretical as well as experimental origin.

We have chosen to determine pre-averages for sub-fields of measurements that are considered to exhibit a maximum degree of independence among each other, considering experimental as well as theoretical issues. The seven pre-averages are summarized in Fig. 9.2. We recall that these are exclusively obtained from extractions that are based on (at least) full NNLO QCD predictions, and are published in peer-reviewed journals at the time of completing this *Review*. To obtain our final world average, we first combine six pre-averages, excluding the lattice result, using a χ^2 *averaging method*. This gives

$$0.1176 \pm 0.0010\,, \qquad \text{(without lattice)}\,. \tag{9.24}$$

This result is fully compatible with the lattice pre-average Eq. (9.23) and has a comparable error. To avoid a possible over-reduction, we combine these two numbers using an unweighted average and take as an uncertainty the average between these two uncertainties. This gives our final world average value

$$\alpha_s(M_Z^2) = 0.1179 \pm 0.0009\,. \tag{9.25}$$

Downloaded from https://academic.oup.com/ptep/article/2022/8/083C01/6651666 by KIT Library user on 27 September 2022

If for the sub-field of hadron colliders we are more restrictive instead and only accept results from a simultaneous fit of PDFs, we arrive at 0.1173 ± 0.0010 (without lattice) and $\alpha_s(M_Z^2) = 0.1177 \pm 0.0009$ for the final average.

Both the new world average value and the restricted result are in very good agreement with the last version of this *Review*, which was $\alpha_s(M_Z^2) = 0.1179 \pm 0.0010$, with a slightly larger overall uncertainty. Performing a weighted average of all seven categories gives $\alpha_s(M_Z^2) = 0.1180 \pm 0.0006$. Our uncertainty instead is 50% larger.

Notwithstanding the many open issues still present within each of the sub-fields summarized in this *Review*, the wealth of available results provides a rather precise and reasonably stable world average value of $\alpha_s(M_Z^2)$, as well as a clear signature and proof of the energy dependence of α_s, in full agreement with the QCD prediction of asymptotic freedom. This is demonstrated in Fig. 9.3, where results of $\alpha_s(Q^2)$ obtained at discrete energy scales Q, now also including those based just on NLO QCD, are summarized. Thanks to the results from the Tevatron and from the LHC, the energy scales, at which α_s is determined, now extend up to almost 2 TeV.[12]

In this combination, as in past combinations, we have considered lattice QCD calculations of α_s independently of experimental/phenomenological determinations. In the future, when the lattice continuum extrapolations are under better control, it may be useful to group lattice QCD determinations of α_s with experimental determinations of α_s that have systematics of similar origin, in a similar manner as we currently group, for example, hadron collider results together [632].

References

[1] R. K. Ellis, W. J. Stirling and B. R. Webber, Camb. Monogr. Part. Phys. Nucl. Phys. Cosmol. **8**, 1 (1996).

[2] J. Campbell, J. Huston, F. Krauss *"The Black Book of Quantum Chromodynamics, a Primer for the QCD Era,"*Oxford University Press, UK (2017).

[3] C. A. Baker *et al.*, Phys. Rev. Lett. **97**, 131801 (2006), [hep-ex/0602020].

[4] J. M. Pendlebury *et al.*, Phys. Rev. **D92**, 9, 092003 (2015), [arXiv:1509.04411].

[5] B. Graner *et al.*, Phys. Rev. Lett. **116**, 16, 161601 (2016), [Erratum: Phys. Rev. Lett.119,no.11,119901(2017)], [arXiv:1601.04339].

[6] J. E. Kim and G. Carosi, Rev. Mod. Phys. **82**, 557 (2010), [arXiv:0807.3125].

[7] G. Dissertori, I. G. Knowles and M. Schmelling, *High energy experiments and theory,* Oxford, UK: Clarendon (2003).

[8] R. Brock *et al.* (CTEQ), Rev. Mod. Phys. **67**, 157 (1995); See also `https://www.phys.psu.edu/~cteq/handbook/v1.1/handbook.pdf/`.

[9] K. Melnikov, CERN Yellow Rep. School Proc. **3**, 37 (2018).

[10] T. van Ritbergen, J. A. M. Vermaseren and S. A. Larin, Phys. Lett. **B400**, 379 (1997), [hep-ph/9701390].

[11] M. Czakon, Nucl. Phys. **B710**, 485 (2005), [hep-ph/0411261].

[12] P. A. Baikov, K. G. Chetyrkin and J. H. Kühn, Phys. Rev. Lett. **118**, 8, 082002 (2017), [arXiv:1606.08659].

[13] T. Luthe *et al.*, JHEP **07**, 127 (2016), [arXiv:1606.08662].

[14] F. Herzog *et al.*, JHEP **02**, 090 (2017), [arXiv:1701.01404].

[15] T. Luthe *et al.*, JHEP **10**, 166 (2017), [arXiv:1709.07718].

[16] K. G. Chetyrkin *et al.*, JHEP **10**, 179 (2017), [Addendum: JHEP12,006(2017)], [arXiv:1709.08541].

[17] W. A. Bardeen *et al.*, Phys. Rev. **D18**, 3998 (1978).

[18] D. J. Gross and F. Wilczek, Phys. Rev. Lett. **30**, 1343 (1973), [,271(1973)].

[19] H. D. Politzer, Phys. Rev. Lett. **30**, 1346 (1973), [,274(1973)].

[20] Y. Schroder and M. Steinhauser, JHEP **01**, 051 (2006), [hep-ph/0512058].

[21] K. G. Chetyrkin, J. H. Kuhn and C. Sturm, Nucl. Phys. **B744**, 121 (2006), [hep-ph/0512060].

[22] A. G. Grozin *et al.*, JHEP **09**, 066 (2011), [arXiv:1107.5970].

[23] M. Dalla Brida *et al.* (ALPHA), Phys. Rev. Lett. **117**, 18, 182001 (2016), [arXiv:1604.06193].

[24] M. Beneke, Phys. Rept. **317**, 1 (1999), [hep-ph/9807443].

[25] M. Beneke *et al.*, Phys. Lett. **B775**, 63 (2017), [arXiv:1605.03609].

[26] A. H. Hoang, C. Lepenik and M. Preisser, JHEP **09**, 099 (2017), [arXiv:1706.08526].

[27] P. Marquard *et al.*, Phys. Rev. Lett. **114**, 14, 142002 (2015), [arXiv:1502.01030].

[28] P. A. Baikov *et al.*, Phys. Lett. **B714**, 62 (2012), [arXiv:1206.1288].

[29] K. G. Chetyrkin, J. H. Kuhn and A. Kwiatkowski (1996), [Phys. Rept.277,189(1996)], [hep-ph/9503396].

[30] Y. Kiyo *et al.*, Nucl. Phys. **B823**, 269 (2009), [arXiv:0907.2120].

[31] P. A. Baikov *et al.*, Phys. Rev. Lett. **108**, 222003 (2012), [arXiv:1201.5804].

[32] P. A. Baikov, K. G. Chetyrkin and J. H. Kuhn, Phys. Rev. Lett. **101**, 012002 (2008), [arXiv:0801.1821].

[33] F. Herzog *et al.*, JHEP **08**, 113 (2017), [arXiv:1707.01044].

[34] V. A. Novikov *et al.*, Nucl. Phys. **B174**, 378 (1980).

[35] H.-W. Lin *et al.*, Phys. Rev. **D91**, 054510 (2015), [arXiv:1402.1462]; C. Alexandrou *et al.*, Phys. Rev. **D92**, 014502 (2015), [arXiv:1504.07455].

[36] H.-W. Lin *et al.*, Prog. Part. Nucl. Phys. **100**, 107 (2018), [arXiv:1711.07916].

[37] C. Alexandrou *et al.*, Phys. Rev. Lett. **121**, 11, 112001 (2018), [arXiv:1803.02685].

[38] J.-W. Chen *et al.* (2018), [arXiv:1803.04393].

[39] K. Cichy, L. Del Debbio and T. Giani (2019), [arXiv:1907.06037].

[40] K. Cichy and M. Constantinou, Adv. High Energy Phys. **2019**, 3036904 (2019), [arXiv:1811.07248].

[41] M. A. Ebert, I. W. Stewart and Y. Zhao, JHEP **09**, 037 (2019), [arXiv:1901.03685].

[42] L. Del Debbio, T. Giani and C. J. Monahan, JHEP **09**, 021 (2020), [arXiv:2007.02131].

[43] M. Constantinou, Eur. Phys. J. A **57**, 2, 77 (2021), [arXiv:2010.02445].

[44] M. Constantinou *et al.* (2020), [arXiv:2006.08636].

[45] G. C. Rossi and M. Testa, Phys. Rev. **D96**, 1, 014507 (2017), [arXiv:1706.04428].

[46] J. Gao, L. Harland-Lang and J. Rojo, Phys. Rept. **742**, 1 (2018), [arXiv:1709.04922].

[47] K. Kovařík, P. M. Nadolsky and D. E. Soper, Rev. Mod. Phys. **92**, 4, 045003 (2020), [arXiv:1905.06957].

[48] R. Abdul Khalek *et al.* (NNPDF), Eur. Phys. J. **C**, 79:838 (2019), [arXiv:1905.04311].

[49] R. Abdul Khalek *et al.* (NNPDF), Eur. Phys. J. C **79**, 11, 931 (2019), [arXiv:1906.10698].

[50] R. D. Ball and R. L. Pearson (2021), [arXiv:2105.05114].

[51] J. D. Bjorken and E. A. Paschos, Phys. Rev. **185**, 1975 (1969).

[12] We note, however, that in many such studies, like those based on exclusive states of jet multiplicities, the relevant energy scale of the measurement is not uniquely defined. For instance, in studies of the ratio of 3- to 2-jet cross sections at the LHC, the relevant scale was taken to be the average of the transverse momenta of the two leading jets [607], but could alternatively have been chosen to be the transverse momentum of the 3rd jet.

Downloaded from https://academic.oup.com/ptep/article/2022/8/083C01/6651666 by KIT Library user on 27 September 2022

[52] J. A. M. Vermaseren, A. Vogt and S. Moch, Nucl. Phys. **B724**, 3 (2005), [hep-ph/0504242].

[53] S. Moch, J. A. M. Vermaseren and A. Vogt, Nucl. Phys. **B813**, 220 (2009), [arXiv:0812.4168].

[54] J. Davies *et al.*, PoS **DIS2016**, 059 (2016), [arXiv:1606.08907].

[55] E. Laenen *et al.*, Nucl. Phys. **B392**, 162 (1993); S. Riemersma, J. Smith and W. L. van Neerven, Phys. Lett. **B347**, 143 (1995), [hep-ph/9411431].

[56] J. Blümlein *et al.* (2019), [arXiv:1903.06155].

[57] A. Manohar *et al.*, Phys. Rev. Lett. **117**, 24, 242002 (2016), [arXiv:1607.04266].

[58] L. Buonocore *et al.*, JHEP **08**, 08, 019 (2020), [arXiv:2005.06477].

[59] J. C. Collins, D. E. Soper and G. F. Sterman, Adv. Ser. Direct. High Energy Phys. **5**, 1 (1989), [hep-ph/0409313].

[60] J.C. Collins, *Foundations of Perturbative QCD*, Cambridge University Press, 2011.

[61] G. C. Nayak, J.-W. Qiu and G. F. Sterman, Phys. Rev. **D72**, 114012 (2005), [hep-ph/0509021].

[62] V. N. Gribov and L. N. Lipatov, Sov. J. Nucl. Phys. **15**, 438 (1972), [Yad. Fiz.15,781(1972)]; L. N. Lipatov, Sov. J. Nucl. Phys. **20**, 94 (1975), [Yad. Fiz.20,181(1974)]; G. Altarelli and G. Parisi, Nucl. Phys. **B126**, 298 (1977); Y. L. Dokshitzer, Sov. Phys. JETP **46**, 641 (1977), [Zh. Eksp. Teor. Fiz.73,1216(1977)].

[63] G. Curci, W. Furmanski and R. Petronzio, Nucl. Phys. **B175**, 27 (1980); W. Furmanski and R. Petronzio, Phys. Lett. **97B**, 437 (1980).

[64] A. Vogt, S. Moch and J. A. M. Vermaseren, Nucl. Phys. **B691**, 129 (2004), [hep-ph/0404111]; S. Moch, J. A. M. Vermaseren and A. Vogt, Nucl. Phys. **B688**, 101 (2004), [hep-ph/0403192].

[65] S. Moch *et al.*, JHEP **10**, 041 (2017), [arXiv:1707.08315].

[66] A. Vogt *et al.*, PoS **RADCOR2017**, 046 (2018), [arXiv:1801.06085].

[67] A. Vogt *et al.*, PoS **LL2018**, 050 (2018), [arXiv:1808.08981].

[68] S. Moch, J. A. M. Vermaseren and A. Vogt, Nucl. Phys. **B889**, 351 (2014), [arXiv:1409.5131].

[69] D. de Florian, G. F. R. Sborlini and G. Rodrigo, Eur. Phys. J. **C76**, 5, 282 (2016), [arXiv:1512.00612]; D. de Florian, G. F. R. Sborlini and G. Rodrigo, JHEP **10**, 056 (2016), [arXiv:1606.02887].

[70] R. S. Thorne, Phys. Rev. **D73**, 054019 (2006), [hep-ph/0601245].

[71] S. Forte *et al.*, Nucl. Phys. **B834**, 116 (2010), [arXiv:1001.2312].

[72] M. Guzzi *et al.*, Phys. Rev. **D86**, 053005 (2012), [arXiv:1108.5112].

[73] V. S. Fadin, E. A. Kuraev and L. N. Lipatov, Phys. Lett. **60B**, 50 (1975).

[74] I. I. Balitsky and L. N. Lipatov, Sov. J. Nucl. Phys. **28**, 822 (1978), [Yad. Fiz.28,1597(1978)].

[75] R. D. Ball *et al.*, Eur. Phys. J. **C78**, 4, 321 (2018), [arXiv:1710.05935].

[76] H. Abramowicz *et al.* (H1, ZEUS), Eur. Phys. J. **C75**, 12, 580 (2015), [arXiv:1506.06042].

[77] H. Abdolmaleki *et al.* (xFitter Developers' Team), Eur. Phys. J. **C78**, 8, 621 (2018), [arXiv:1802.00064].

[78] L. A. Harland-Lang *et al.*, Eur. Phys. J. **C76**, 4, 186 (2016), [arXiv:1601.03413].

[79] T.-J. Hou *et al.* (2019), [arXiv:1908.11238].

[80] L. N. Lipatov, Sov. J. Nucl. Phys. **23**, 338 (1976), [Yad. Fiz.23,642(1976)].

[81] E. A. Kuraev, L. N. Lipatov and V. S. Fadin, Sov. Phys. JETP **45**, 199 (1977), [Zh. Eksp. Teor. Fiz.72,377(1977)].

[82] V. S. Fadin and L. N. Lipatov, Phys. Lett. **B429**, 127 (1998), [hep-ph/9802290].

[83] M. Ciafaloni and G. Camici, Phys. Lett. **B430**, 349 (1998), [hep-ph/9803389].

[84] G. Altarelli, R. D. Ball and S. Forte, Nucl. Phys. **B799**, 199 (2008), [arXiv:0802.0032].

[85] M. Ciafaloni *et al.*, JHEP **08**, 046 (2007), [arXiv:0707.1453].

[86] C. D. White and R. S. Thorne, Phys. Rev. **D75**, 034005 (2007), [hep-ph/0611204].

[87] E. Iancu *et al.*, Phys. Lett. **B744**, 293 (2015), [arXiv:1502.05642].

[88] N. Gromov, F. Levkovich-Maslyuk and G. Sizov, Phys. Rev. Lett. **115**, 25, 251601 (2015), [arXiv:1507.04010]; V. N. Velizhanin (2015), [arXiv:1508.02857]; S. Caron-Huot and M. Herranen, JHEP **02**, 058 (2018), [arXiv:1604.07417].

[89] I. Balitsky, Nucl. Phys. **B463**, 99 (1996), [hep-ph/9509348].

[90] Y. V. Kovchegov, Phys. Rev. **D60**, 034008 (1999), [hep-ph/9901281].

[91] M. Davier *et al.*, Eur. Phys. J. C **56**, 305 (2008), [arXiv:0803.0979].

[92] J. C. Collins, D. E. Soper and G. F. Sterman, Nucl. Phys. **B261**, 104 (1985).

[93] C. Anastasiou *et al.*, Phys. Rev. Lett. **114**, 212001 (2015), [arXiv:1503.06056]; C. Anastasiou *et al.*, JHEP **05**, 058 (2016), [arXiv:1602.00695].

[94] B. Mistlberger, JHEP **05**, 028 (2018), [arXiv:1802.00833].

[95] L.-B. Chen *et al.*, Phys. Lett. B **803**, 135292 (2020), [arXiv:1909.06808].

[96] F. Dulat, B. Mistlberger and A. Pelloni, Phys. Rev. **D99**, 3, 034004 (2019), [arXiv:1810.09462].

[97] L. Cieri *et al.*, JHEP **02**, 096 (2019), [arXiv:1807.11501].

[98] X. Chen *et al.* (2021), [arXiv:2102.07607].

[99] F. A. Dreyer and A. Karlberg, Phys. Rev. Lett. **117**, 7, 072001 (2016), [arXiv:1606.00840].

[100] F. A. Dreyer and A. Karlberg, Phys. Rev. D **98**, 11, 114016 (2018), [arXiv:1811.07906].

[101] C. Duhr, F. Dulat and B. Mistlberger, Phys. Rev. Lett. **125**, 17, 172001 (2020), [arXiv:2001.07717].

[102] X. Chen *et al.* (2021), [arXiv:2107.09085].

[103] C. Duhr, F. Dulat and B. Mistlberger, JHEP **11**, 143 (2020), [arXiv:2007.13313].

[104] O. Brein, A. Djouadi and R. Harlander, Phys. Lett. **B579**, 149 (2004), [hep-ph/0307206].

[105] D. de Florian and J. Mazzitelli, Phys. Rev. Lett. **111**, 201801 (2013), [arXiv:1309.6594].

[106] S. Borowka *et al.*, Phys. Rev. Lett. **117**, 1, 012001 (2016), [Erratum: Phys. Rev. Lett.117,no.7,079901(2016)], [arXiv:1604.06447].

[107] M. Czakon, P. Fiedler and A. Mitov, Phys. Rev. Lett. **110**, 252004 (2013), [arXiv:1303.6254].

[108] S. Catani *et al.*, Phys. Rev. **D99**, 5, 051501 (2019), [arXiv:1901.04005].

[109] T. Gehrmann *et al.*, Phys. Rev. Lett. **113**, 21, 212001 (2014), [arXiv:1408.5243].

[110] F. Cascioli *et al.*, Phys. Lett. **B735**, 311 (2014), [arXiv:1405.2219].

[111] M. Grazzini, S. Kallweit and M. Wiesemann, Eur. Phys. J. **C78**, 7, 537 (2018), [arXiv:1711.06631].

[112] G. Heinrich, Phys. Rept. **922**, 1 (2021), [arXiv:2009.00516].

[113] M. Greco and A. Vicini, Nucl. Phys. **B415**, 386 (1994).

[114] A. Hebecker, Phys. Rept. **331**, 1 (2000), [hep-ph/9905226].

Downloaded from https://academic.oup.com/ptep/article/2022/8/083C01/6651666 by KIT Library user on 27 September 2022

[115] A. V. Belitsky and A. V. Radyushkin, Phys. Rept. **418**, 1 (2005), [hep-ph/0504030].

[116] E. Boos *et al.* (CompHEP), Nucl. Instrum. Meth. **A534**, 250 (2004), [hep-ph/0403113]; `http://compep.sinp.su.ru/`.

[117] J. Alwall *et al.*, JHEP **07**, 079 (2014), [arXiv:1405.0301]; `https://launchpad.net/mg5amcnlo`.

[118] M. L. Mangano *et al.*, JHEP **07**, 001 (2003), [hep-ph/0206293]; `http://cern.ch/mlm/alpgen/`.

[119] T. Gleisberg and S. Hoeche, JHEP **12**, 039 (2008), [arXiv:0808.3674]; `https://sherpa.hepforge.prg/trac/wiki`.

[120] A. Cafarella, C. G. Papadopoulos and M. Worek, Comput. Phys. Commun. **180**, 1941 (2009), [arXiv:0710.2427]; `http://cern.ch/helac-phegas/`.

[121] F. A. Berends and W. T. Giele, Nucl. Phys. **B306**, 759 (1988).

[122] L. J. Dixon, in "QCD and beyond. Proceedings, Theoretical Advanced Study Institute in Elementary Particle Physics, TASI-95, Boulder, USA, June 4-30, 1995," 539–584 (1996), [hep-ph/9601359], URL `http://www-public.slac.stanford.edu/sciDoc/docMeta.aspx?slacPubNumber=SLAC-PUB-7106`.

[123] R. Britto, F. Cachazo and B. Feng, Nucl. Phys. **B715**, 499 (2005), [hep-th/0412308].

[124] F. Cachazo, P. Svrcek and E. Witten, JHEP **09**, 006 (2004), [hep-th/0403047].

[125] S. Catani and M. H. Seymour, Nucl. Phys. **B485**, 291 (1997), [Erratum: Nucl. Phys.B510,503(1998)], [hep-ph/9605323].

[126] S. Frixione, Z. Kunszt and A. Signer, Nucl. Phys. **B467**, 399 (1996), [hep-ph/9512328].

[127] D. A. Kosower, Phys. Rev. **D57**, 5410 (1998), [hep-ph/9710213]; J. M. Campbell, M. A. Cullen and E. W. N. Glover, Eur. Phys. J. **C9**, 245 (1999), [hep-ph/9809429]; D. A. Kosower, Phys. Rev. **D71**, 045016 (2005), [hep-ph/0311272].

[128] G. Ossola, C. G. Papadopoulos and R. Pittau, Nucl. Phys. **B763**, 147 (2007), [hep-ph/0609007].

[129] R. Britto, F. Cachazo and B. Feng, Nucl. Phys. **B725**, 275 (2005), [hep-th/0412103].

[130] R. K. Ellis *et al.*, Nucl. Phys. **B822**, 270 (2009), [arXiv:0806.3467].

[131] C. F. Berger and D. Forde, Ann. Rev. Nucl. Part. Sci. **60**, 181 (2010), [arXiv:0912.3534].

[132] F. Cascioli, P. Maierhofer and S. Pozzorini, Phys. Rev. Lett. **108**, 111601 (2012), [arXiv:1111.5206].

[133] Z. Bern, L. J. Dixon and D. A. Kosower, Annals Phys. **322**, 1587 (2007), [arXiv:0704.2798].

[134] R. K. Ellis *et al.*, Phys. Rept. **518**, 141 (2012), [arXiv:1105.4319].

[135] G. Bevilacqua *et al.*, Comput. Phys. Commun. **184**, 986 (2013), [arXiv:1110.1499]; `http://cern.ch/helax-phegas/`.

[136] G. Cullen *et al.*, Eur. Phys. J. **C74**, 8, 3001 (2014), [arXiv:1404.7096]; `http://gosam.hepforge.org/`.

[137] S. Badger *et al.*, Comput. Phys. Commun. **184**, 1981 (2013), [arXiv:1209.0100]; `https://bitbucket.org/njet/wiki/Home/`.

[138] F. Buccioni, S. Pozzorini and M. Zoller, Eur. Phys. J. **C78**, 1, 70 (2018), [arXiv:1710.11452]; `https://openloops.hepforge.org/`.

[139] S. Actis *et al.*, Comput. Phys. Commun. **214**, 140 (2017), [arXiv:1605.01090].

[140] T. Gleisberg *et al.*, JHEP **02**, 007 (2009), [arXiv:0811.4622]; `http://projects.hepforge.org/sherpa`.

[141] Z. Nagy, Phys. Rev. **D68**, 094002 (2003), [hep-ph/0307268]; `http://www.desy.de.~znagy/Site/NLOJet++.html`.

[142] J. M. Campbell and R. K. Ellis, Phys. Rev. **D62**, 114012 (2000), [hep-ph/0006304].

[143] J. Baglio *et al.* (2011), [arXiv:1107.4038]; http://www-itp.particle.uni-karlsruhe.de/~vbfnloweb.

[144] T. Binoth *et al.*, Eur. Phys. J. **C16**, 311 (2000), [hep-ph/9911340]; `http://lapth.in2p3.fr/PHOX_FAMILY/`.

[145] Z. Bern *et al.*, PoS **LL2012**, 018 (2012), [arXiv:1210.6684].

[146] G. Cullen, N. Greiner and G. Heinrich, Eur. Phys. J. **C73**, 4, 2388 (2013), [arXiv:1212.5154].

[147] S. Kallweit *et al.*, JHEP **04**, 012 (2015), [arXiv:1412.5157].

[148] A. Denner *et al.*, JHEP **04**, 018 (2015), [arXiv:1412.7421].

[149] M. Chiesa, N. Greiner and F. Tramontano, J. Phys. **G43**, 1, 013002 (2016), [arXiv:1507.08579].

[150] S. Frixione *et al.*, JHEP **06**, 184 (2015), [arXiv:1504.03446].

[151] B. Biedermann *et al.*, Eur. Phys. J. **C77**, 492 (2017), [arXiv:1704.05783].

[152] R. Frederix *et al.*, JHEP **07**, 185 (2018), [arXiv:1804.10017].

[153] C. Anastasiou, R. Boughezal and F. Petriello, JHEP **04**, 003 (2009), [arXiv:0811.3458].

[154] S. Dittmaier, A. Huss and C. Schwinn, Nucl. Phys. **B885**, 318 (2014), [arXiv:1403.3216].

[155] S. Dittmaier, A. Huss and C. Schwinn, Nucl. Phys. **B904**, 216 (2016), [arXiv:1511.08016].

[156] D. de Florian, M. Der and I. Fabre, Phys. Rev. **D98**, 9, 094008 (2018), [arXiv:1805.12214].

[157] M. Bonetti, K. Melnikov and L. Tancredi, Phys. Rev. **D97**, 3, 034004 (2018), [arXiv:1711.11113].

[158] M. Bonetti, K. Melnikov and L. Tancredi, Phys. Rev. **D97**, 5, 056017 (2018), [Erratum: Phys. Rev.D97,no.9,099906(2018)], [arXiv:1801.10403].

[159] C. Anastasiou *et al.*, JHEP **03**, 162 (2019), [arXiv:1811.11211].

[160] V. Hirschi, S. Lionetti and A. Schweitzer, JHEP **05**, 002 (2019), [arXiv:1902.10167].

[161] M. Becchetti *et al.*, Phys. Rev. D **103**, 5, 054037 (2021), [arXiv:2010.09451].

[162] M. Bonetti *et al.*, JHEP **11**, 045 (2020), [arXiv:2007.09813].

[163] R. Bonciani *et al.* (2021), [arXiv:2106.11953].

[164] A. Denner and S. Dittmaier, Phys. Rept. **864**, 1 (2020), [arXiv:1912.06823].

[165] Z. Bern *et al.*, Nucl. Phys. **B425**, 217 (1994), [hep-ph/9403226].

[166] J. M. Campbell and E. W. N. Glover, Nucl. Phys. **B527**, 264 (1998), [hep-ph/9710255].

[167] S. Catani and M. Grazzini, Phys. Lett. **B446**, 143 (1999), [hep-ph/9810389].

[168] T. Binoth and G. Heinrich, Nucl. Phys. **B585**, 741 (2000), [hep-ph/0004013].

[169] C. Anastasiou, K. Melnikov and F. Petriello, Phys. Rev. **D69**, 076010 (2004), [hep-ph/0311311].

[170] A. Gehrmann-De Ridder, T. Gehrmann and E. W. N. Glover, JHEP **09**, 056 (2005), [hep-ph/0505111].

[171] G. Somogyi, Z. Trocsanyi and V. Del Duca, JHEP **01**, 070 (2007), [hep-ph/0609042].

[172] M. Czakon, Phys. Lett. **B693**, 259 (2010), [arXiv:1005.0274].

[173] F. Caola, K. Melnikov and R. Röntsch, Eur. Phys. J. C **77**, 4, 248 (2017), [arXiv:1702.01352].

[174] L. Magnea *et al.*, JHEP **12**, 107 (2018), [Erratum: JHEP 06, 013 (2019)], [arXiv:1806.09570].

[175] S. Catani and M. Grazzini, Phys. Rev. Lett. **98**, 222002 (2007), [hep-ph/0703012]; `http://theory.fi.infn.it/grazzini/codes.html`.

Downloaded from https://academic.oup.com/ptep/article/2022/8/083C01/6651666 by KIT Library user on 27 September 2022

[176] R. Bonciani *et al.*, Eur. Phys. J. C **75**, 12, 581 (2015), [arXiv:1508.03585].

[177] R. Boughezal *et al.*, Phys. Rev. Lett. **115**, 6, 062002 (2015), [arXiv:1504.02131].

[178] R. Boughezal, X. Liu and F. Petriello, Phys. Rev. D **91**, 9, 094035 (2015), [arXiv:1504.02540].

[179] J. Gaunt *et al.*, JHEP **09**, 058 (2015), [arXiv:1505.04794].

[180] M. Cacciari *et al.*, Phys. Rev. Lett. **115**, 8, 082002 (2015), [Erratum: Phys. Rev. Lett.120,no.13,139901(2018)], [arXiv:1506.02660].

[181] L. Cieri *et al.*, JHEP **09**, 155 (2020), [arXiv:2005.01315].

[182] W. J. Torres Bobadilla *et al.*, Eur. Phys. J. C **81**, 3, 250 (2021), [arXiv:2012.02567].

[183] A. Gehrmann-De Ridder *et al.*, Phys. Rev. Lett. **99**, 132002 (2007), [arXiv:0707.1285]; A. Gehrmann-De Ridder *et al.*, JHEP **12**, 094 (2007), [arXiv:0711.4711]; A. Gehrmann-De Ridder *et al.*, Phys. Rev. Lett. **100**, 172001 (2008), [arXiv:0802.0813].

[184] A. Gehrmann-De Ridder *et al.*, Comput. Phys. Commun. **185**, 3331 (2014), [arXiv:1402.4140]; `https://eerad3.epforge.org/`.

[185] S. Weinzierl, Phys. Rev. Lett. **101**, 162001 (2008), [arXiv:0807.3241]; S. Weinzierl, JHEP **06**, 041 (2009), [arXiv:0904.1077].

[186] J. Currie, T. Gehrmann and J. Niehues, Phys. Rev. Lett. **117**, 4, 042001 (2016), [arXiv:1606.03991].

[187] J. Currie *et al.*, JHEP **05**, 209 (2018), [arXiv:1803.09973].

[188] T. Gehrmann *et al.*, Phys. Lett. **B792**, 182 (2019), [arXiv:1812.06104].

[189] K. Melnikov and F. Petriello, Phys. Rev. **D74**, 114017 (2006), [hep-ph/0609070]; `http://gate.hep.anl.gov/fpetriello/FEWZ.html`.

[190] S. Catani *et al.*, Phys. Rev. Lett. **103**, 082001 (2009), [arXiv:0903.2120]; `http://theory.fi.infn.it/gazzani/dy.html`.

[191] C. Anastasiou, K. Melnikov and F. Petriello, Nucl. Phys. **B724**, 197 (2005), [hep-ph/0501130]; `http://www.phys.ethz.ch/∼pheno/fehipro/`.

[192] M. Czakon *et al.* (2021), [arXiv:2105.04436].

[193] M. Grazzini *et al.*, JHEP **05**, 139 (2017), [arXiv:1703.09065].

[194] S. Catani *et al.*, Phys. Rev. Lett. **108**, 072001 (2012), [Erratum: Phys. Rev. Lett.117,no.8,089901(2016)], [arXiv:1110.2375].

[195] J. M. Campbell *et al.*, JHEP **07**, 148 (2016), [arXiv:1603.02663].

[196] M. Grazzini *et al.*, Phys. Lett. **B731**, 204 (2014), [arXiv:1309.7000].

[197] M. Grazzini, S. Kallweit and D. Rathlev, JHEP **07**, 085 (2015), [arXiv:1504.01330].

[198] R. Boughezal *et al.*, Eur. Phys. J. **C77**, 1, 7 (2017), [arXiv:1605.08011].

[199] J. M. Campbell, R. K. Ellis and C. Williams, Phys. Rev. Lett. **118**, 22, 222001 (2017), [arXiv:1612.04333].

[200] X. Chen *et al.*, Submitted to: J. High Energy Phys. (2019), [arXiv:1904.01044].

[201] J. M. Campbell, R. K. Ellis and C. Williams, Phys. Rev. **D96**, 1, 014037 (2017), [arXiv:1703.10109].

[202] A. Gehrmann-De Ridder *et al.*, Phys. Rev. Lett. **120**, 12, 122001 (2018), [arXiv:1712.07543].

[203] A. Gehrmann-De Ridder *et al.*, Phys. Rev. Lett. **117**, 2, 022001 (2016), [arXiv:1507.02850].

[204] R. Boughezal *et al.*, Phys. Rev. Lett. **116**, 15, 152001 (2016), [arXiv:1512.01291].

[205] R. Boughezal *et al.*, Phys. Rev. Lett. **115**, 8, 082003 (2015), [arXiv:1504.07922].

[206] R. Boughezal *et al.*, Phys. Lett. **B748**, 5 (2015), [arXiv:1505.03893].

[207] F. Caola, K. Melnikov and M. Schulze, Phys. Rev. **D92**, 7, 074032 (2015), [arXiv:1508.02684].

[208] X. Chen *et al.*, JHEP **10**, 066 (2016), [arXiv:1607.08817].

[209] G. Ferrera, M. Grazzini and F. Tramontano, Phys. Rev. Lett. **107**, 152003 (2011), [arXiv:1107.1164].

[210] G. Ferrera, M. Grazzini and F. Tramontano, Phys. Lett. **B740**, 51 (2015), [arXiv:1407.4747].

[211] M. Brucherseifer, F. Caola and K. Melnikov, Phys. Lett. **B736**, 58 (2014), [arXiv:1404.7116].

[212] E. L. Berger *et al.*, Phys. Rev. **D94**, 7, 071501 (2016), [arXiv:1606.08463].

[213] M. Czakon, P. Fiedler and A. Mitov, Phys. Rev. Lett. **115**, 5, 052001 (2015), [arXiv:1411.3007].

[214] J. Currie, E. W. N. Glover and J. Pires, Phys. Rev. Lett. **118**, 7, 072002 (2017), [arXiv:1611.01460].

[215] M. Czakon *et al.* (2020), [arXiv:2011.01011].

[216] M. L. Czakon *et al.* (2021), [arXiv:2102.08267].

[217] J. Cruz-Martinez *et al.*, Phys. Lett. **B781**, 672 (2018), [arXiv:1802.02445].

[218] T. Liu, K. Melnikov and A. A. Penin (2019), [arXiv:1906.10899].

[219] H. A. Chawdhry *et al.*, JHEP **02**, 057 (2020), [arXiv:1911.00479].

[220] S. Kallweit, V. Sotnikov and M. Wiesemann, Phys. Lett. B **812**, 136013 (2021), [arXiv:2010.04681].

[221] H. A. Chawdhry *et al.* (2021), [arXiv:2105.06940].

[222] M. Czakon, A. Mitov and R. Poncelet (2021), [arXiv:2106.05331].

[223] G. P. Salam and E. Slade (2021), [arXiv:2106.08329].

[224] M. A. Ebert *et al.*, JHEP **04**, 102 (2021), [arXiv:2006.11382].

[225] S. Amoroso *et al.*, in "11th Les Houches Workshop on Physics at TeV Colliders: PhysTeV Les Houches," (2020), [arXiv:2003.01700].

[226] T. Carli *et al.*, Eur. Phys. J. C **66**, 503 (2010), [arXiv:0911.2985].

[227] T. Kluge, K. Rabbertz and M. Wobisch, in "14th International Workshop on Deep Inelastic Scattering (DIS 2006)," 483, Tsukuba, Japan, April 20-24 (2006), [hep-ph/0609285].

[228] D. Britzger *et al.*, in "Proceedings, XX. International Workshop on Deep-Inelastic Scattering and Related Subjects (DIS 2012)," 217, Bonn, Germany, March 26-30 (2012), [arXiv:1208.3641].

[229] S. Carrazza *et al.*, JHEP **12**, 108 (2020), [arXiv:2008.12789].

[230] M. Czakon, D. Heymes and A. Mitov (2017), [arXiv:1704.08551].

[231] D. Britzger *et al.*, Eur. Phys. J. C **79**, 10, 845 (2019), [Erratum: arXiv:1906.05303v3], [arXiv:1906.05303].

[232] D. Maître, J. Phys. Conf. Ser. **1525**, 1, 012014 (2020).

[233] D. Maître, G. Heinrich and M. Johnson, PoS **LL2016**, 016 (2016), [arXiv:1607.06259].

[234] Y. L. Dokshitzer, D. Diakonov and S. I. Troian, Phys. Rept. **58**, 269 (1980).

[235] G. Parisi and R. Petronzio, Nucl. Phys. **B154**, 427 (1979).

[236] G. Curci, M. Greco and Y. Srivastava, Nucl. Phys. **B159**, 451 (1979).

[237] A. Bassetto, M. Ciafaloni and G. Marchesini, Nucl. Phys. **B163**, 477 (1980).

[238] J. C. Collins and D. E. Soper, Nucl. Phys. **B193**, 381 (1981), [Erratum: Nucl. Phys.B213,545(1983)].

Downloaded from https://academic.oup.com/ptep/article/2022/8/083C01/6651666 by KIT Library user on 27 September 2022

[239] J. C. Collins and D. E. Soper, Nucl. Phys. **B197**, 446 (1982).

[240] J. Kodaira and L. Trentadue, Phys. Lett. **112B**, 66 (1982).

[241] J. Kodaira and L. Trentadue, Phys. Lett. **123B**, 335 (1983).

[242] J. C. Collins, D. E. Soper and G. F. Sterman, Nucl. Phys. **B250**, 199 (1985).

[243] S. Catani *et al.*, Nucl. Phys. **B407**, 3 (1993).

[244] C. W. Bauer *et al.*, Phys. Rev. **D63**, 114020 (2001), [hep-ph/0011336].

[245] C. W. Bauer, D. Pirjol and I. W. Stewart, Phys. Rev. **D65**, 054022 (2002), [hep-ph/0109045].

[246] T. Becher, A. Broggio and A. Ferroglia, Lect. Notes Phys. **896**, pp.1 (2015), [arXiv:1410.1892].

[247] S. Catani *et al.*, Phys. Lett. **B269**, 432 (1991).

[248] N. Brown and W. J. Stirling, Phys. Lett. **B252**, 657 (1990).

[249] W. Bartel *et al.* (JADE), Z. Phys. **C33**, 23 (1986), [,53(1986)].

[250] N. Kidonakis, G. Oderda and G. F. Sterman, Nucl. Phys. **B531**, 365 (1998), [hep-ph/9803241].

[251] R. Bonciani *et al.*, Phys. Lett. **B575**, 268 (2003), [hep-ph/0307035].

[252] A. Banfi, G. P. Salam and G. Zanderighi, JHEP **03**, 073 (2005), [hep-ph/0407286].

[253] D. de Florian and M. Grazzini, Phys. Rev. Lett. **85**, 4678 (2000), [hep-ph/0008152].

[254] G. Bozzi *et al.*, Nucl. Phys. **B737**, 73 (2006), [hep-ph/0508068]; `http://theory.fi.infn.it/grazzini/codes.html`.

[255] G. Bozzi *et al.*, Phys. Lett. **B696**, 207 (2011), [arXiv:1007.2351].

[256] T. Becher and M. Neubert, Eur. Phys. J. **C71**, 1665 (2011), [arXiv:1007.4005].

[257] T. Becher, M. Neubert, and D. Wilhelm, `http://cute.hepforge.org/`.

[258] D. de Florian *et al.*, JHEP **06**, 132 (2012), [arXiv:1203.6321]; `http://theory.fi.infn.it/grazzini/codes.html`.

[259] C. Balazs and C. P. Yuan, Phys. Rev. **D56**, 5558 (1997), [hep-ph/9704258].

[260] S. Catani *et al.*, JHEP **12**, 047 (2015), [arXiv:1507.06937].

[261] A. Banfi *et al.*, Phys. Lett. **B715**, 152 (2012), [arXiv:1205.4760].

[262] M. Grazzini *et al.*, JHEP **08**, 154 (2015), [arXiv:1507.02565].

[263] D. de Florian and M. Grazzini, Nucl. Phys. **B704**, 387 (2005), [hep-ph/0407241].

[264] T. Becher and G. Bell, JHEP **11**, 126 (2012), [arXiv:1210.0580].

[265] A. Banfi *et al.*, Phys. Rev. Lett. **109**, 202001 (2012), [arXiv:1206.4998]; T. Becher, M. Neubert and L. Rothen, JHEP **10**, 125 (2013), [arXiv:1307.0025].

[266] I. W. Stewart *et al.*, Phys. Rev. **D89**, 5, 054001 (2014), [arXiv:1307.1808].

[267] I. W. Stewart, F. J. Tackmann and W. J. Waalewijn, Phys. Rev. Lett. **106**, 032001 (2011), [arXiv:1005.4060].

[268] Y.-T. Chien *et al.*, Phys. Rev. **D87**, 1, 014010 (2013), [arXiv:1208.0010]; T. T. Jouttenus *et al.*, Phys. Rev. **D88**, 5, 054031 (2013), [arXiv:1302.0846].

[269] M. Dasgupta *et al.*, JHEP **10**, 126 (2012), [arXiv:1207.1640].

[270] V. Ahrens *et al.*, JHEP **09**, 097 (2010), [arXiv:1003.5827].

[271] M. Aliev *et al.*, Comput. Phys. Commun. **182**, 1034 (2011), [arXiv:1007.1327].

[272] N. Kidonakis, Phys. Rev. **D82**, 114030 (2010), [arXiv:1009.4935].

[273] T. Becher, C. Lorentzen and M. D. Schwartz, Phys. Rev. Lett. **108**, 012001 (2012), [arXiv:1106.4310].

[274] T. Becher *et al.*, Eur. Phys. J. **C75**, 4, 154 (2015), [arXiv:1412.8408].

[275] E. Gerwick *et al.*, JHEP **02**, 106 (2015), [arXiv:1411.7325].

[276] A. Banfi *et al.*, JHEP **05**, 102 (2015), [arXiv:1412.2126].

[277] T. Becher and M. D. Schwartz, JHEP **07**, 034 (2008), [arXiv:0803.0342].

[278] A. H. Hoang *et al.*, Phys. Rev. **D91**, 9, 094017 (2015), [arXiv:1411.6633].

[279] Y.-T. Chien and M. D. Schwartz, JHEP **08**, 058 (2010), [arXiv:1005.1644].

[280] P. F. Monni, T. Gehrmann and G. Luisoni, JHEP **08**, 010 (2011), [arXiv:1105.4560].

[281] W. Bizon *et al.*, JHEP **02**, 108 (2018), [arXiv:1705.09127].

[282] W. Bizon *et al.*, Eur. Phys. J. C **79**, 10, 868 (2019), [arXiv:1905.05171].

[283] S. Catani *et al.*, Nucl. Phys. **B888**, 75 (2014), [arXiv:1405.4827].

[284] A. Banfi *et al.*, JHEP **04**, 049 (2016), [arXiv:1511.02886].

[285] A. J. Larkoski and I. Moult, Phys. Rev. **D93**, 014017 (2016), [arXiv:1510.08459].

[286] G. Lustermans, W. J. Waalewijn and L. Zeune, Phys. Lett. **B762**, 447 (2016), [arXiv:1605.02740].

[287] C. Muselli, S. Forte and G. Ridolfi, JHEP **03**, 106 (2017), [arXiv:1701.01464].

[288] M. Bonvini and S. Marzani, Phys. Rev. Lett. **120**, 20, 202003 (2018), [arXiv:1802.07758].

[289] M. Procura, W. J. Waalewijn and L. Zeune, JHEP **10**, 098 (2018), [arXiv:1806.10622].

[290] G. Lustermans *et al.*, JHEP **03**, 124 (2019), [arXiv:1901.03331].

[291] P. F. Monni, L. Rottoli and P. Torrielli, Phys. Rev. Lett. **124**, 25, 252001 (2020), [arXiv:1909.04704].

[292] I. Feige *et al.*, Phys. Rev. Lett. **109**, 092001 (2012), [arXiv:1204.3898].

[293] M. Dasgupta *et al.*, JHEP **09**, 029 (2013), [arXiv:1307.0007].

[294] A. J. Larkoski *et al.*, JHEP **05**, 146 (2014), [arXiv:1402.2657].

[295] M. Dasgupta, A. Powling and A. Siodmok, JHEP **08**, 079 (2015), [arXiv:1503.01088].

[296] A. J. Larkoski, I. Moult and D. Neill, JHEP **05**, 117 (2016), [arXiv:1507.03018].

[297] C. Frye *et al.*, JHEP **07**, 064 (2016), [arXiv:1603.09338].

[298] A. J. Larkoski, I. Moult and D. Neill, JHEP **02**, 144 (2018), [arXiv:1710.00014].

[299] F. A. Dreyer *et al.*, JHEP **06**, 093 (2018), [arXiv:1804.03657].

[300] A. J. Larkoski, I. Moult and B. Nachman, Phys. Rept. **841**, 1 (2020), [arXiv:1709.04464].

[301] S. Marzani, G. Soyez and M. Spannowsky (2019), [Lect. Notes Phys.958,pp.(2019)], [arXiv:1901.10342].

[302] R. Kogler *et al.*, Rev. Mod. Phys. **91**, 4, 045003 (2019), [arXiv:1803.06991].

[303] Yu.L. Dokshitzer *et al.*, *"Basics of perturbative QCD,"* Gif-sur-Yvette, France: Éditions frontières (1991), see also `http://www.lpthe.jussieu.fr/~yuri/` BPQCD/-cover.html.

[304] T. Sjostrand *et al.*, Comput. Phys. Commun. **135**, 238 (2001), [hep-ph/0010017].

[305] T. Sjostrand, S. Mrenna and P. Z. Skands, JHEP **05**, 026 (2006), [hep-ph/0603175]; `http://projects.hepforge.org/pythia6/`.

Downloaded from https://academic.oup.com/ptep/article/2022/8/083C01/6651666 by KIT Library user on 27 September 2022

[306] T. Sjostrand *et al.*, Comput. Phys. Commun. **191**, 159 (2015), [arXiv:1410.3012]; http://home.thep.lu.se/∼torbjorn/Pythia.html.

[307] B. R. Webber, Nucl. Phys. **B238**, 492 (1984).

[308] G. Corcella *et al.*, JHEP **01**, 010 (2001), [hep-ph/0011363]; http://www.hep.phy.cam.ac.uk/theory/webber/Herwig/.

[309] M. Bahr *et al.*, Eur. Phys. J. **C58**, 639 (2008), [arXiv:0803.0883]; http://projects.hepforge.org/herwig/.

[310] L. Lonnblad, Comput. Phys. Commun. **71**, 15 (1992).

[311] A. Buckley *et al.*, Phys. Rept. **504**, 145 (2011), [arXiv:1101.2599].

[312] B. Andersson *et al.*, Phys. Rept. **97**, 31 (1983).

[313] T. Sjostrand, Nucl. Phys. **B248**, 469 (1984).

[314] J. Bellm *et al.*, Eur. Phys. J. C **80**, 2, 93 (2020), [arXiv:1903.12563].

[315] T. Sjostrand and M. van Zijl, Phys. Rev. **D36**, 2019 (1987).

[316] S. Catani *et al.*, JHEP **11**, 063 (2001), [hep-ph/0109231].

[317] J. Alwall *et al.*, Eur. Phys. J. **C53**, 473 (2008), [arXiv:0706.2569].

[318] S. Frixione and B. R. Webber, JHEP **06**, 029 (2002), [hep-ph/0204244].

[319] P. Nason, JHEP **11**, 040 (2004), [hep-ph/0409146].

[320] S. Alioli *et al.*, JHEP **06**, 043 (2010), [arXiv:1002.2581]; http://powhegbox.mib.infn.it/.

[321] S. Plätzer, JHEP **08**, 114 (2013), [arXiv:1211.5467]; R. Frederix and S. Frixione, JHEP **12**, 061 (2012), [arXiv:1209.6215]; K. Hamilton *et al.*, JHEP **05**, 082 (2013), [arXiv:1212.4504].

[322] K. Hamilton *et al.*, JHEP **10**, 222 (2013), [arXiv:1309.0017]; A. Karlberg, E. Re and G. Zanderighi, JHEP **09**, 134 (2014), [arXiv:1407.2940]; S. Höche, Y. Li and S. Prestel, Phys. Rev. **D91**, 7, 074015 (2015), [arXiv:1405.3607]; S. Höche, Y. Li and S. Prestel, Phys. Rev. **D90**, 5, 054011 (2014), [arXiv:1407.3773]; S. Alioli *et al.*, Phys. Rev. **D92**, 9, 094020 (2015), [arXiv:1508.01475]; P. F. Monni *et al.*, JHEP **05**, 143 (2020), [arXiv:1908.06987].

[323] S. Alioli *et al.* (2021), [arXiv:2102.08390].

[324] W. Astill *et al.*, JHEP **06**, 154 (2016), [arXiv:1603.01620].

[325] W. Astill *et al.*, JHEP **11**, 157 (2018), [arXiv:1804.08141].

[326] E. Re, M. Wiesemann and G. Zanderighi, JHEP **12**, 121 (2018), [arXiv:1805.09857].

[327] S. Alioli *et al.*, Phys. Rev. D **100**, 9, 096016 (2019), [arXiv:1909.02026].

[328] J. Mazzitelli *et al.* (2020), [arXiv:2012.14267].

[329] D. Lombardi, M. Wiesemann and G. Zanderighi (2020), [arXiv:2010.10478].

[330] S. Alioli *et al.*, JHEP **04**, 041 (2021), [arXiv:2010.10498].

[331] D. Lombardi, M. Wiesemann and G. Zanderighi (2021), [arXiv:2103.12077].

[332] S. Alioli *et al.*, Phys. Lett. B **818**, 136380 (2021), [arXiv:2103.01214].

[333] G. Marchesini and B. R. Webber, Nucl. Phys. B **238**, 1 (1984).

[334] G. Marchesini and B. R. Webber, Nucl. Phys. B **310**, 461 (1988).

[335] S. Catani, B. R. Webber and G. Marchesini, Nucl. Phys. B **349**, 635 (1991).

[336] G. Bewick *et al.*, JHEP **04**, 019 (2020), [arXiv:1904.11866].

[337] M. Dasgupta *et al.*, Phys. Rev. Lett. **125**, 5, 052002 (2020), [arXiv:2002.11114].

[338] M. Dasgupta *et al.*, JHEP **09**, 033 (2018), [Erratum: JHEP 03, 083 (2020)], [arXiv:1805.09327].

[339] L. Hartgring, E. Laenen and P. Skands, JHEP **10**, 127 (2013), [arXiv:1303.4974].

[340] H. T. Li and P. Skands, Phys. Lett. B **771**, 59 (2017), [arXiv:1611.00013].

[341] S. Höche and S. Prestel, Phys. Rev. D **96**, 7, 074017 (2017), [arXiv:1705.00742].

[342] F. Dulat, S. Höche and S. Prestel, Phys. Rev. D **98**, 7, 074013 (2018), [arXiv:1805.03757].

[343] A. Banfi, B. K. El-Menoufi and P. F. Monni, JHEP **01**, 083 (2019), [arXiv:1807.11487].

[344] G. Gustafson, Nucl. Phys. B **392**, 251 (1993).

[345] K. Hamilton *et al.* (2020), [arXiv:2011.10054].

[346] M. Cacciari *et al.*, JHEP **04**, 068 (2004), [hep-ph/0303085].

[347] P. M. Stevenson, Phys. Lett. **100B**, 61 (1981).

[348] P. M. Stevenson, Phys. Rev. **D23**, 2916 (1981).

[349] G. Grunberg, Phys. Rev. **D29**, 2315 (1984).

[350] S. J. Brodsky, G. P. Lepage and P. B. Mackenzie, Phys. Rev. **D28**, 228 (1983).

[351] S.-Q. Wang *et al.* (2019), [arXiv:1908.00060].

[352] M. Cacciari and N. Houdeau, JHEP **09**, 039 (2011), [arXiv:1105.5152].

[353] A. David and G. Passarino, Phys. Lett. **B726**, 266 (2013), [arXiv:1307.1843].

[354] E. Bagnaschi *et al.*, JHEP **02**, 133 (2015), [arXiv:1409.5036].

[355] C. Duhr *et al.* (2021), [arXiv:2106.04585].

[356] D. Acosta *et al.* (CDF), Phys. Rev. D **70**, 072002 (2004), [hep-ex/0404004].

[357] G. Soyez *et al.*, Phys. Rev. Lett. **110**, 16, 162001 (2013), [arXiv:1211.2811].

[358] M. Dasgupta and G. P. Salam, J. Phys. **G30**, R143 (2004), [hep-ph/0312283].

[359] S. Moretti, L. Lonnblad and T. Sjostrand, JHEP **08**, 001 (1998), [hep-ph/9804296].

[360] G. P. Salam, Eur. Phys. J. **C67**, 637 (2010), [arXiv:0906.1833].

[361] S. D. Ellis *et al.*, Prog. Part. Nucl. Phys. **60**, 484 (2008), [arXiv:0712.2447].

[362] M. Cacciari, Int. J. Mod. Phys. **A30**, 31, 1546001 (2015), [arXiv:1509.02272].

[363] G. P. Salam and G. Soyez, JHEP **05**, 086 (2007), [arXiv:0704.0292].

[364] S. Catani *et al.*, Nucl. Phys. **B406**, 187 (1993).

[365] S. D. Ellis and D. E. Soper, Phys. Rev. **D48**, 3160 (1993), [hep-ph/9305266].

[366] Y. L. Dokshitzer *et al.*, JHEP **08**, 001 (1997), [hep-ph/9707323].

[367] M. Wobisch and T. Wengler, in "Monte Carlo generators for HERA physics. Proceedings, Workshop, Hamburg, Germany, 1998-1999," 270–279 (1998), [hep-ph/9907280].

[368] M. Cacciari, G. P. Salam and G. Soyez, JHEP **04**, 063 (2008), [arXiv:0802.1189].

[369] S. Bethke *et al.*, Nucl. Phys. **B370**, 310 (1992), [Erratum: Nucl. Phys.B523,681(1998)].

[370] M. Cacciari and G. P. Salam, Phys. Lett. **B641**, 57 (2006), [hep-ph/0512210]; M. Cacciari, G. P. Salam and G. Soyez, Eur. Phys. J. **C72**, 1896 (2012), [arXiv:1111.6097].

[371] S. Brandt *et al.*, Phys. Lett. **12**, 57 (1964).

[372] E. Farhi, Phys. Rev. Lett. **39**, 1587 (1977).

[373] O. Biebel, Phys. Rept. **340**, 165 (2001).

[374] S. Kluth, Rept. Prog. Phys. **69**, 1771 (2006), [hep-ex/0603011].

[375] C. L. Basham *et al.*, Phys. Rev. Lett. **41**, 1585 (1978).

Downloaded from https://academic.oup.com/ptep/article/2022/8/083C01/6651666 by KIT Library user on 27 September 2022

[376] A. Ali, E. Pietarinen and W. J. Stirling, Phys. Lett. **141B**, 447 (1984).

[377] I. W. Stewart, F. J. Tackmann and W. J. Waalewijn, Phys. Rev. Lett. **105**, 092002 (2010), [arXiv:1004.2489].

[378] A. Banfi, G. P. Salam and G. Zanderighi, JHEP **08**, 062 (2004), [hep-ph/0407287].

[379] A. Banfi, G. P. Salam and G. Zanderighi, JHEP **06**, 038 (2010), [arXiv:1001.4082].

[380] T. Becher, X. Garcia i Tormo and J. Piclum, Phys. Rev. **D93**, 5, 054038 (2016), [Erratum: Phys. Rev.D93,no.7,079905(2016)], [arXiv:1512.00022].

[381] A. Gao *et al.*, Phys. Rev. Lett. **123**, 6, 062001 (2019), [arXiv:1901.04497].

[382] T. Aaltonen *et al.* (CDF), Phys. Rev. **D83**, 112007 (2011), [arXiv:1103.5143].

[383] G. Aad *et al.* (ATLAS), Eur. Phys. J. **C72**, 2211 (2012), [arXiv:1206.2135].

[384] G. Aad *et al.* (ATLAS), Phys. Rev. **D88**, 3, 032004 (2013), [arXiv:1207.6915].

[385] G. Aad *et al.* (ATLAS), Phys. Lett. **B750**, 427 (2015), [arXiv:1508.01579].

[386] G. Aad *et al.* (ATLAS), Eur. Phys. J. **C76**, 7, 375 (2016), [arXiv:1602.08980].

[387] M. Aaboud *et al.* (ATLAS), Eur. Phys. J. **C77**, 12, 872 (2017), [arXiv:1707.02562].

[388] M. Aaboud *et al.* (ATLAS), Phys. Rev. **D98**, 9, 092004 (2018), [arXiv:1805.04691].

[389] V. Khachatryan *et al.* (CMS), Phys. Lett. **B699**, 48 (2011), [arXiv:1102.0068].

[390] S. Chatrchyan *et al.* (CMS), Phys. Lett. **B722**, 238 (2013), [arXiv:1301.1646].

[391] V. Khachatryan *et al.* (CMS), JHEP **10**, 87 (2014), [arXiv:1407.2856].

[392] A. M. Sirunyan *et al.* (CMS), JHEP **12**, 117 (2018), [arXiv:1811.00588].

[393] A. Ali and G. Kramer, Eur. Phys. J. H **36**, 245 (2011), [arXiv:1012.2288].

[394] S. Chatrchyan *et al.* (CMS), Phys. Lett. **B730**, 243 (2014), [arXiv:1310.0878].

[395] G. Aad *et al.* (ATLAS), Phys. Rev. **D83**, 052003 (2011), [arXiv:1101.0070].

[396] S. Chatrchyan *et al.* (CMS), JHEP **06**, 160 (2012), [arXiv:1204.3170].

[397] B. B. Abelev *et al.* (ALICE), Phys. Rev. **D91**, 11, 112012 (2015), [arXiv:1411.4969].

[398] G. Aad *et al.* (ATLAS), Eur. Phys. J. **C73**, 12, 2676 (2013), [arXiv:1307.5749].

[399] C. Glasman (H1, ZEUS), Nucl. Phys. Proc. Suppl. **191**, 121 (2009), [arXiv:0812.0757].

[400] T. Carli, K. Rabbertz and S. Schumann, in T. Schörner-Sadenius, editor, "The Large Hadron Collider: Harvest of Run 1," 139–194 (2015), [arXiv:1506.03239].

[401] A. Abdesselam *et al.*, Eur. Phys. J. **C71**, 1661 (2011), [arXiv:1012.5412].

[402] D. Krohn, J. Thaler and L.-T. Wang, JHEP **02**, 084 (2010), [arXiv:0912.1342].

[403] A. Altheimer *et al.*, J. Phys. **G39**, 063001 (2012), [arXiv:1201.0008].

[404] A. Altheimer *et al.*, Eur. Phys. J. **C74**, 3, 2792 (2014), [arXiv:1311.2708].

[405] P. C. Stichel and W. J. Zakrzewski, Eur. Phys. J. **C75**, 1, 9 (2015), [arXiv:1409.1363].

[406] D. Adams *et al.*, Eur. Phys. J. **C75**, 9, 409 (2015), [arXiv:1504.00679].

[407] G. Louppe *et al.*, JHEP **01**, 057 (2019), [arXiv:1702.00748].

[408] D. Guest, K. Cranmer and D. Whiteson, Ann. Rev. Nucl. Part. Sci. **68**, 161 (2018), [arXiv:1806.11484].

[409] T. Schorner-Sadenius, Eur. Phys. J. **C72**, 2060 (2012), [Erratum: Eur. Phys. J.C72,2133(2012)].

[410] J. M. Campbell, J. W. Huston and W. J. Stirling, Rept. Prog. Phys. **70**, 89 (2007), [hep-ph/0611148].

[411] M. L. Mangano, Phys. Usp. **53**, 109 (2010), [Usp. Fiz. Nauk180,113(2010)].

[412] J. M. Butterworth, G. Dissertori and G. P. Salam, Ann. Rev. Nucl. Part. Sci. **62**, 387 (2012), [arXiv:1202.0583].

[413] J. Currie *et al.*, JHEP **07**, 018 (2017), [Erratum: JHEP 12, 042 (2020)], [arXiv:1703.05977].

[414] M. Klasen, G. Kramer and M. Michael, Phys. Rev. **D89**, 7, 074032 (2014), [arXiv:1310.1724].

[415] T. Carli, T. Gehrmann and S. Hoeche, Eur. Phys. J. **C67**, 73 (2010), [arXiv:0912.3715].

[416] S. Chekanov *et al.* (ZEUS), Nucl. Phys. **B792**, 1 (2008), [arXiv:0707.3749].

[417] S. Chekanov *et al.* (ZEUS), Phys. Rev. **D76**, 072011 (2007), [arXiv:0706.3809].

[418] A. Aktas *et al.* (H1), Phys. Lett. **B639**, 21 (2006), [hep-ex/0603014].

[419] H. Abramowicz *et al.* (ZEUS), Eur. Phys. J. **C71**, 1659 (2011), [arXiv:1104.5444].

[420] H. Abramowicz *et al.* (ZEUS), Nucl. Phys. **B864**, 1 (2012), [arXiv:1205.6153].

[421] F. D. Aaron *et al.* (H1), Eur. Phys. J. **C65**, 363 (2010), [arXiv:0904.3870].

[422] F. D. Aaron *et al.* (H1), Eur. Phys. J. **C54**, 389 (2008), [arXiv:0711.2606].

[423] S. Chekanov *et al.* (ZEUS), Eur. Phys. J. **C52**, 515 (2007), [arXiv:0707.3093].

[424] S. Chekanov *et al.* (ZEUS), Phys. Rev. **D78**, 032004 (2008), [arXiv:0802.3955].

[425] H. Abramowicz *et al.* (ZEUS), Eur. Phys. J. **C70**, 965 (2010), [arXiv:1010.6167].

[426] H. Abramowicz *et al.* (ZEUS), Phys. Lett. **B691**, 127 (2010), [arXiv:1003.2923].

[427] S. Chekanov *et al.* (ZEUS), Phys. Rev. **D85**, 052008 (2012), [arXiv:0808.3783].

[428] F. D. Aaron *et al.* (H1), Eur. Phys. J. **C67**, 1 (2010), [arXiv:0911.5678].

[429] V. Andreev *et al.* (H1), Eur. Phys. J. **C75**, 2, 65 (2015), [arXiv:1406.4709].

[430] V. Andreev *et al.* (H1), Eur. Phys. J. **C77**, 11, 791 (2017), [Erratum: Eur. Phys. J. **C81**, 8, 738 (2021)], [arXiv:1709.07251].

[431] `http://twiki.cern.ch/twiki/bin/view/CMSPublic/PhysicsResultsCombined`.

[432] `http://atlas.web.cern.ch/Atlas/GROUPS/PHYSICS/CombinedSummaryPlots/SM`.

[433] A. Abulencia *et al.* (CDF), Phys. Rev. **D75**, 092006 (2007), [Erratum: Phys. Rev.D75,119901(2007)], [hep-ex/0701051].

[434] T. Aaltonen *et al.* (CDF), Phys. Rev. **D78**, 052006 (2008), [Erratum: Phys. Rev.D79,119902(2009)], [arXiv:0807.2204].

[435] V. M. Abazov *et al.* (D0), Phys. Rev. Lett. **101**, 062001 (2008), [arXiv:0802.2400].

[436] V. M. Abazov *et al.* (D0), Phys. Rev. **D85**, 052006 (2012), [arXiv:1110.3771].

[437] B. Abelev *et al.* (ALICE), Phys. Lett. **B722**, 262 (2013), [arXiv:1301.3475].

[438] G. Aad *et al.* (ATLAS), Eur. Phys. J. **C73**, 8, 2509 (2013), [arXiv:1304.4739].

Downloaded from https://academic.oup.com/ptep/article/2022/8/083C01/6651666 by KIT Library user on 27 September 2022

[439] G. Aad *et al.* (ATLAS), JHEP **02**, 153 (2015), [Erratum: JHEP09,141(2015)], [arXiv:1410.8857].

[440] M. Aaboud *et al.* (ATLAS), JHEP **09**, 020 (2017), [arXiv:1706.03192].

[441] V. Khachatryan *et al.* (CMS), Eur. Phys. J. **C76**, 5, 265 (2016), [arXiv:1512.06212].

[442] S. Chatrchyan *et al.* (CMS), Phys. Rev. **D87**, 11, 112002 (2013), [Erratum: Phys. Rev.D87,no.11,119902(2013)], [arXiv:1212.6660].

[443] V. Khachatryan *et al.* (CMS), JHEP **03**, 156 (2017), [arXiv:1609.05331].

[444] V. Khachatryan *et al.* (CMS), Eur. Phys. J. **C76**, 8, 451 (2016), [arXiv:1605.04436].

[445] M. Aaboud *et al.* (ATLAS), JHEP **05**, 195 (2018), [arXiv:1711.02692].

[446] A. M. Sirunyan *et al.* (CMS), JHEP **12**, 082 (2020), [arXiv:2005.05159].

[447] J. Currie *et al.*, JHEP **10**, 155 (2018), [arXiv:1807.03692].

[448] A. Schwartzman, Int. J. Mod. Phys. **A30**, 31, 1546002 (2015), [arXiv:1509.05459].

[449] J. Rojo, Int. J. Mod. Phys. **A30**, 1546005 (2015), [arXiv:1410.7728].

[450] G. Aad *et al.* (ATLAS), JHEP **05**, 059 (2014), [arXiv:1312.3524].

[451] A. M. Sirunyan *et al.* (CMS), Eur. Phys. J. **C77**, 11, 746 (2017), [arXiv:1705.02628].

[452] T. Aaltonen *et al.* (CDF), Phys. Rev. **D79**, 112002 (2009), [arXiv:0812.4036].

[453] V. M. Abazov *et al.* (D0), Phys. Rev. Lett. **103**, 191803 (2009), [arXiv:0906.4819].

[454] S. Chatrchyan *et al.* (CMS), JHEP **05**, 055 (2012), [arXiv:1202.5535].

[455] V. Khachatryan *et al.* (CMS), Phys. Lett. **B746**, 79 (2015), [arXiv:1411.2646].

[456] A. M. Sirunyan *et al.* (CMS), JHEP **07**, 013 (2017), [arXiv:1703.09986].

[457] G. Aad *et al.* (ATLAS), JHEP **01**, 029 (2013), [arXiv:1210.1718].

[458] M. Aaboud *et al.* (ATLAS), Phys. Rev. **D96**, 5, 052004 (2017), [arXiv:1703.09127].

[459] V. M. Abazov *et al.* (D0), Phys. Rev. Lett. **94**, 221801 (2005), [hep-ex/0409040].

[460] V. M. Abazov *et al.* (D0), Phys. Lett. **B721**, 212 (2013), [arXiv:1212.1842].

[461] G. Aad *et al.* (ATLAS), Phys. Rev. Lett. **106**, 172002 (2011), [arXiv:1102.2696].

[462] V. Khachatryan *et al.* (CMS), Phys. Rev. Lett. **106**, 122003 (2011), [arXiv:1101.5029].

[463] V. Khachatryan *et al.* (CMS), Eur. Phys. J. **C76**, 10, 536 (2016), [arXiv:1602.04384].

[464] A. M. Sirunyan *et al.* (CMS), Eur. Phys. J. **C78**, 7, 566 (2018), [arXiv:1712.05471].

[465] A. M. Sirunyan *et al.* (CMS) (2019), [arXiv:1902.04374].

[466] P. Kokkas, Int. J. Mod. Phys. **A30**, 31, 1546004 (2015), [arXiv:1509.02144].

[467] M. Aaboud *et al.* (ATLAS), Eur. Phys. J. **C77**, 6, 367 (2017), [arXiv:1612.03016].

[468] G. Aad *et al.* (ATLAS), Phys. Lett. **B759**, 601 (2016), [arXiv:1603.09222].

[469] R. Aaij *et al.* (LHCb), JHEP **08**, 039 (2015), [arXiv:1505.07024].

[470] S. Chatrchyan *et al.* (CMS), JHEP **10**, 132 (2011), [arXiv:1107.4789].

[471] S. Chatrchyan *et al.* (CMS), Phys. Rev. Lett. **112**, 191802 (2014), [arXiv:1402.0923].

[472] R. Aaij *et al.* (LHCb), JHEP **06**, 058 (2012), [arXiv:1204.1620].

[473] R. Aaij *et al.* (LHCb), JHEP **01**, 155 (2016), [arXiv:1511.08039].

[474] R. Aaij *et al.* (LHCb), JHEP **09**, 136 (2016), [arXiv:1607.06495].

[475] S. Chatrchyan *et al.* (CMS), JHEP **10**, 007 (2011), [arXiv:1108.0566].

[476] V. Khachatryan *et al.* (CMS), Eur. Phys. J. **C75**, 4, 147 (2015), [arXiv:1412.1115].

[477] G. Aad *et al.* (ATLAS), Phys. Lett. **B725**, 223 (2013), [arXiv:1305.4192].

[478] G. Aad *et al.* (ATLAS), JHEP **06**, 112 (2014), [arXiv:1404.1212].

[479] G. Aad *et al.* (ATLAS), JHEP **08**, 009 (2016), [arXiv:1606.01736].

[480] A. M. Sirunyan *et al.* (CMS), Submitted to: JHEP (2018), [arXiv:1812.10529].

[481] M. Aaboud *et al.* (ATLAS), JHEP **12**, 059 (2017), [arXiv:1710.05167].

[482] S. Chatrchyan *et al.* (CMS), Phys. Rev. **D90**, 3, 032004 (2014), [arXiv:1312.6283].

[483] V. Khachatryan *et al.* (CMS), Eur. Phys. J. **C76**, 8, 469 (2016), [arXiv:1603.01803].

[484] G. Aad *et al.* (ATLAS), Submitted to: Eur. Phys. J. (2019), [arXiv:1904.05631].

[485] R. Aaij *et al.* (LHCb), JHEP **10**, 030 (2016), [arXiv:1608.01484].

[486] G. Aad *et al.* (ATLAS), Eur. Phys. J. **C76**, 5, 291 (2016), [arXiv:1512.02192].

[487] V. Khachatryan *et al.* (CMS), JHEP **02**, 096 (2017), [arXiv:1606.05864].

[488] A. M. Sirunyan *et al.* (CMS), JHEP **03**, 172 (2018), [arXiv:1710.07955].

[489] M. Aaboud *et al.* (ATLAS), JHEP **05**, 077 (2018), [arXiv:1711.03296].

[490] U. Blumenschein, Int. J. Mod. Phys. **A30**, 31, 1546007 (2015), [arXiv:1509.04885].

[491] G. Aad *et al.* (ATLAS) (2019), [arXiv:1907.06728].

[492] V. Khachatryan *et al.* (CMS), Phys. Rev. **D95**, 052002 (2017), [arXiv:1610.04222].

[493] A. M. Sirunyan *et al.* (CMS), Phys. Rev. **D96**, 7, 072005 (2017), [arXiv:1707.05979].

[494] A. M. Sirunyan *et al.* (CMS), Eur. Phys. J. **C78**, 11, 965 (2018), [arXiv:1804.05252].

[495] G. Aad *et al.* (ATLAS), JHEP **07**, 032 (2013), [arXiv:1304.7098].

[496] Z. Bern *et al.*, Phys. Rev. **D88**, 1, 014025 (2013), [arXiv:1304.1253].

[497] M. Voutilainen, Int. J. Mod. Phys. **A30**, 31, 1546008 (2015), [arXiv:1509.05026].

[498] G. Aad *et al.* (ATLAS), JHEP **08**, 005 (2016), [arXiv:1605.03495].

[499] G. Aad *et al.* (ATLAS) (2019), [arXiv:1908.02746].

[500] S. Chatrchyan *et al.* (CMS), Phys. Rev. **D84**, 052011 (2011), [arXiv:1108.2044].

[501] S. Chatrchyan *et al.* (CMS), JHEP **06**, 009 (2014), [arXiv:1311.6141].

[502] G. Aad *et al.* (ATLAS), Phys. Rev. **D89**, 5, 052004 (2014), [arXiv:1311.1440].

[503] M. Aaboud *et al.* (ATLAS), Phys. Lett. **B780**, 578 (2018), [arXiv:1801.00112].

Downloaded from https://academic.oup.com/ptep/article/2022/8/083C01/6651666 by KIT Library user on 27 September 2022

[504] M. Aaboud *et al.* (ATLAS), Nucl. Phys. **B918**, 257 (2017), [arXiv:1611.06586].

[505] A. M. Sirunyan *et al.* (CMS), Eur. Phys. J. **C79**, 1, 20 (2019), [arXiv:1807.00782].

[506] A. M. Sirunyan *et al.* (CMS) (2019), [arXiv:1907.08155].

[507] M. Aaboud *et al.* (ATLAS), Phys. Lett. **B776**, 295 (2018), [arXiv:1710.09560].

[508] J. H. Kuhn *et al.*, JHEP **03**, 059 (2006), [hep-ph/0508253].

[509] V. Khachatryan *et al.* (CMS), JHEP **10**, 128 (2015), [Erratum: JHEP04,010(2016)], [arXiv:1505.06520].

[510] G. Aad *et al.* (ATLAS), JHEP **09**, 029 (2016), [arXiv:1603.01702].

[511] M. Aaboud *et al.* (ATLAS), Phys. Lett. **B773**, 354 (2017), [arXiv:1702.04519].

[512] M. Aaboud *et al.* (ATLAS) (2019), [arXiv:1905.04242].

[513] V. Khachatryan *et al.* (CMS), Eur. Phys. J. **C76**, 7, 401 (2016), [arXiv:1507.03268].

[514] G. Aad *et al.* (ATLAS), Phys. Lett. B **798**, 134913 (2019), [arXiv:1903.10415].

[515] G. Aad *et al.* (ATLAS), JHEP **01**, 086 (2013), [arXiv:1211.1913].

[516] M. Aaboud *et al.* (ATLAS), Phys. Rev. **D95**, 11, 112005 (2017), [arXiv:1704.03839].

[517] S. Chatrchyan *et al.* (CMS), Eur. Phys. J. **C74**, 11, 3129 (2014), [arXiv:1405.7225].

[518] M. Aaboud *et al.* (ATLAS), Phys. Lett. **B781**, 55 (2018), [arXiv:1712.07291].

[519] K. Kröninger, A. B. Meyer and P. Uwer, in T. Schörner-Sadenius, editor, "The Large Hadron Collider: Harvest of Run 1," 259–300 (2015), [arXiv:1506.02800].

[520] M. Aaboud *et al.* (ATLAS), Phys. Rev. **D94**, 9, 092003 (2016), [arXiv:1607.07281].

[521] M. Aaboud *et al.* (ATLAS), Eur. Phys. J. **C77**, 5, 292 (2017), [arXiv:1612.05220].

[522] A. M. Sirunyan *et al.* (CMS), Eur. Phys. J. **C79**, 5, 368 (2019), [arXiv:1812.10505].

[523] A. M. Sirunyan *et al.* (CMS), Submitted to: Eur. Phys. J. (2019), [arXiv:1904.05237].

[524] M. Czakon, D. Heymes and A. Mitov, Phys. Rev. Lett. **116**, 8, 082003 (2016), [arXiv:1511.00549].

[525] S. Catani *et al.*, JHEP **07**, 100 (2019), [arXiv:1906.06535].

[526] M. Czakon *et al.*, JHEP **05**, 149 (2018), [arXiv:1803.07623].

[527] S. Chatrchyan *et al.* (CMS), Phys. Lett. **B728**, 496 (2014), [Erratum: Phys. Lett.B738,526(2014)], [arXiv:1307.1907].

[528] T. Klijnsma *et al.*, Eur. Phys. J. **C77**, 11, 778 (2017), [arXiv:1708.07495].

[529] G. Aad *et al.* (ATLAS), Eur. Phys. J. **C74**, 10, 3109 (2014), [Addendum: Eur. Phys. J.C76,no.11,642(2016)], [arXiv:1406.5375].

[530] A. M. Sirunyan *et al.* (CMS), JHEP **09**, 051 (2017), [arXiv:1701.06228].

[531] M. Aaboud *et al.* (ATLAS), Phys. Lett. **B786**, 114 (2018), [arXiv:1805.10197].

[532] A. M. Sirunyan *et al.* (CMS), Phys. Lett. **B792**, 369 (2019), [arXiv:1812.06504].

[533] D. de Florian *et al.* (LHC Higgs Cross Section Working Group) (2016), [arXiv:1610.07922].

[534] M. Aaboud *et al.* (ATLAS), Phys. Rev. **D98**, 052005 (2018), [arXiv:1802.04146].

[535] A. M. Sirunyan *et al.* (CMS), JHEP **01**, 183 (2019), [arXiv:1807.03825].

[536] A. M. Sirunyan *et al.* (CMS Collaboration), Phys. Lett. B **792**, arXiv:1812.06504. CMS-HIG-17-028-003, 369. 28 p (2018), submitted to Phys.Lett., URL `http://cds.cern.ch/record/2651932`.

[537] P. A. Zyla *et al.* (Particle Data Group), PTEP **2020**, 8, 083C01 (2020).

[538] D. d'Enterria *et al.*, in "Workshop on precision measurements of the QCD coupling constant (alphas-2019) Trento, Trentino, Italy, February 11-15, 2019," (2019), [arXiv:1907.01435].

[539] G. P. Salam, in A. Levy, S. Forte and G. Ridolfi, editors, "From My Vast Repertoire ...: Guido Altarelli's Legacy," 101–121 (2019), [arXiv:1712.05165].

[540] A. Pich *et al.*, in "13th Conference on Quark Confinement and the Hadron Spectrum (Confinement XIII) Maynooth, Ireland, July 31-August 6, 2018," (2018), [arXiv:1811.11801].

[541] A. Pich, Prog. Part. Nucl. Phys. **117**, 103846 (2021), [arXiv:2012.04716].

[542] S. Aoki *et al.* (Flavour Lattice Averaging Group), Eur. Phys. J. C **80**, 2, 113 (2020), [arXiv:1902.08191].

[543] M. Beneke and M. Jamin, JHEP **09**, 044 (2008), [arXiv:0806.3156].

[544] K. Maltman and T. Yavin, Phys. Rev. **D78**, 094020 (2008), [arXiv:0807.0650].

[545] S. Narison, Phys. Lett. **B673**, 30 (2009), [arXiv:0901.3823].

[546] I. Caprini and J. Fischer, Eur. Phys. J. **C64**, 35 (2009), [arXiv:0906.5211].

[547] A. Pich, Prog. Part. Nucl. Phys. **75**, 41 (2014), [arXiv:1310.7922].

[548] D. Boito *et al.*, Phys. Rev. **D91**, 3, 034003 (2015), [arXiv:1410.3528].

[549] G. Altarelli, PoS **Corfu2012**, 002 (2013), [arXiv:1303.6065].

[550] A. Pich and A. Rodríguez-Sánchez, Phys. Rev. **D94**, 3, 034027 (2016), [arXiv:1605.06830].

[551] M. Davier *et al.*, Eur. Phys. J. **C74**, 3, 2803 (2014), [arXiv:1312.1501].

[552] D. Boito *et al.*, Phys. Rev. **D95**, 3, 034024 (2017), [arXiv:1611.03457].

[553] D. Boito *et al.*, Phys. Rev. **D100**, 7, 074009 (2019), [arXiv:1907.03360].

[554] D. Boito *et al.*, Phys. Rev. **D98**, 7, 074030 (2018), [arXiv:1805.08176].

[555] D. Boito *et al.*, Phys. Rev. D **103**, 3, 034028 (2021), [arXiv:2012.10440].

[556] V. Mateu and P. G. Ortega, JHEP **01**, 122 (2018), [arXiv:1711.05755].

[557] C. Peset, A. Pineda and J. Segovia, JHEP **09**, 167 (2018), [arXiv:1806.05197].

[558] S. Narison, Int. J. Mod. Phys. A **33**, 10, 1850045 (2018), [Addendum: Int. J. Mod. Phys. A 33, 1850045 (2018)], [arXiv:1801.00592].

[559] S. Narison, Int. J. Mod. Phys. A **33**, 33, 1892004 (2018), [arXiv:1812.09360].

[560] D. Boito and V. Mateu, Phys. Lett. B **806**, 135482 (2020), [arXiv:1912.06237].

[561] D. Boito and V. Mateu, JHEP **03**, 094 (2020), [arXiv:2001.11041].

[562] J. Blumlein, H. Bottcher and A. Guffanti, Nucl. Phys. **B774**, 182 (2007), [hep-ph/0607200].

[563] P. Jimenez-Delgado and E. Reya, Phys. Rev. **D89**, 7, 074049 (2014), [arXiv:1403.1852].

[564] S. Alekhin *et al.*, Phys. Rev. **D96**, 1, 014011 (2017), [arXiv:1701.05838].

[565] S. Alekhin, J. Blümlein and S. Moch, Eur. Phys. J. **C78**, 6, 477 (2018), [arXiv:1803.07537].

[566] T. Cridge *et al.* (2021), [arXiv:2106.10289].

Downloaded from https://academic.oup.com/ptep/article/2022/8/083C01/6651666 by KIT Library user on 27 September 2022

[567] T.-J. Hou *et al.*, Phys. Rev. D **103**, 1, 014013 (2021), [arXiv:1912.10053].

[568] R. D. Ball *et al.* (NNPDF), Eur. Phys. J. **C78**, 5, 408 (2018), [arXiv:1802.03398].

[569] R. S. Thorne and G. Watt, JHEP **08**, 100 (2011), [arXiv:1106.5789].

[570] S. Alekhin, J. Blumlein and S. Moch, Eur. Phys. J. **C71**, 1723 (2011), [arXiv:1101.5261].

[571] R. D. Ball *et al.* (NNPDF), Phys. Lett. **B704**, 36 (2011), [arXiv:1102.3182].

[572] R. D. Ball *et al.* (NNPDF), Phys. Lett. **B723**, 330 (2013), [arXiv:1303.1189].

[573] R. S. Thorne, PoS **DIS2013**, 042 (2013), [arXiv:1306.3907].

[574] G. Dissertori *et al.*, JHEP **08**, 036 (2009), [arXiv:0906.3436].

[575] G. Abbiendi *et al.* (OPAL), Eur. Phys. J. **C71**, 1733 (2011), [arXiv:1101.1470].

[576] S. Bethke *et al.* (JADE), Eur. Phys. J. **C64**, 351 (2009), [arXiv:0810.1389].

[577] G. Dissertori *et al.*, Phys. Rev. Lett. **104**, 072002 (2010), [arXiv:0910.4283].

[578] J. Schieck *et al.* (JADE), Eur. Phys. J. **C73**, 3, 2332 (2013), [arXiv:1205.3714].

[579] A. Verbytskyi *et al.*, JHEP **08**, 129 (2019), [arXiv:1902.08158].

[580] A. Kardos *et al.*, Eur. Phys. J. **C78**, 6, 498 (2018), [arXiv:1804.09146].

[581] R. A. Davison and B. R. Webber, Eur. Phys. J. **C59**, 13 (2009), [arXiv:0809.3326].

[582] R. Abbate *et al.*, Phys. Rev. **D83**, 074021 (2011), [arXiv:1006.3080].

[583] T. Gehrmann, G. Luisoni and P. F. Monni, Eur. Phys. J. **C73**, 1, 2265 (2013), [arXiv:1210.6945].

[584] A. H. Hoang *et al.*, Phys. Rev. **D91**, 9, 094018 (2015), [arXiv:1501.04111].

[585] G. Luisoni, P. F. Monni and G. P. Salam, Eur. Phys. J. C **81**, 2, 158 (2021), [arXiv:2012.00622].

[586] R. Frederix *et al.*, JHEP **11**, 050 (2010), [arXiv:1008.5313].

[587] P. Bolzoni, B. A. Kniehl and A. V. Kotikov, Nucl. Phys. **B875**, 18 (2013), [arXiv:1305.6017].

[588] A. Kardos, G. Somogyi and A. Verbytskyi, Eur. Phys. J. C **81**, 4, 292 (2021), [arXiv:2009.00281].

[589] J. Currie *et al.*, Phys. Rev. Lett. **119**, 15, 152001 (2017), [arXiv:1705.10271].

[590] M. Czakon *et al.* (2019), [arXiv:1907.12911].

[591] S. Dittmaier, A. Huss and C. Speckner, JHEP **11**, 095 (2012), [arXiv:1210.0438].

[592] R. Frederix *et al.*, JHEP **04**, 076 (2017), [arXiv:1612.06548].

[593] M. Czakon *et al.*, JHEP **10**, 186 (2017), [arXiv:1705.04105].

[594] M. Johnson and D. Maître, Phys. Rev. **D97**, 5, 054013 (2018), [arXiv:1711.01408].

[595] A. Gehrmann-De Ridder *et al.*, JHEP **07**, 133 (2016), [arXiv:1605.04295].

[596] S. Forte and Z. Kassabov, Eur. Phys. J. C **80**, 3, 182 (2020), [arXiv:2001.04986].

[597] S. Alekhin *et al.*, Eur. Phys. J. C **75**, 304 (2015), [arXiv:1410.4412].

[598] A. M. Sirunyan *et al.* (CMS), Eur. Phys. J. C **80**, 7, 658 (2020), [arXiv:1904.05237].

[599] D. d'Enterria and A. Poldaru, JHEP **06**, 016 (2020), [arXiv:1912.11733].

[600] T. Affolder *et al.* (CDF), Phys. Rev. Lett. **88**, 042001 (2002), [hep-ex/0108034].

[601] S. Chekanov *et al.* (ZEUS), Phys. Lett. B **649**, 12 (2007), [hep-ex/0701039].

[602] V. M. Abazov *et al.* (D0), Phys. Rev. **D80**, 111107 (2009), [arXiv:0911.2710].

[603] B. Malaescu and P. Starovoitov, Eur. Phys. J. **C72**, 2041 (2012), [arXiv:1203.5416].

[604] V. Khachatryan *et al.* (CMS), Eur. Phys. J. **C75**, 6, 288 (2015), [arXiv:1410.6765].

[605] D. Britzger *et al.*, Eur. Phys. J. **C79**, 1, 68 (2019), [arXiv:1712.00480].

[606] S. Chekanov *et al.* (ZEUS), Eur. Phys. J. **C44**, 183 (2005), [hep-ex/0502007].

[607] S. Chatrchyan *et al.* (CMS), Eur. Phys. J. **C73**, 10, 2604 (2013), [arXiv:1304.7498].

[608] V. M. Abazov *et al.* (D0), Phys. Lett. **B718**, 56 (2012), [arXiv:1207.4957].

[609] V. Khachatryan *et al.* (CMS), Eur. Phys. J. **C75**, 5, 186 (2015), [arXiv:1412.1633].

[610] V. Andreev *et al.* (H1), Eur. Phys. J. C **77**, 4, 215 (2017), [arXiv:1611.03421].

[611] J. Haller *et al.*, Eur. Phys. J. **C78**, 8, 675 (2018), [arXiv:1803.01853].

[612] S. Schael *et al.* (ALEPH, DELPHI, L3, OPAL, SLD, LEP Electroweak Working Group, SLD Electroweak Group, SLD Heavy Flavour Group), Phys. Rept. **427**, 257 (2006), [hep-ex/0509008].

[613] I. Allison *et al.* (HPQCD), Phys. Rev. **D78**, 054513 (2008), [arXiv:0805.2999].

[614] K. Maltman *et al.*, Phys. Rev. **D78**, 114504 (2008), [arXiv:0807.2020].

[615] S. Aoki *et al.* (PACS-CS), JHEP **10**, 053 (2009), [arXiv:0906.3906].

[616] C. McNeile *et al.*, Phys. Rev. **D82**, 034512 (2010), [arXiv:1004.4285].

[617] E. Shintani *et al.*, Phys. Rev. **D82**, 7, 074505 (2010), [Erratum: Phys. Rev.D89,no.9,099903(2014)], [arXiv:1002.0371].

[618] B. Blossier *et al.*, Phys. Rev. **D85**, 034503 (2012), [arXiv:1110.5829].

[619] A. Bazavov *et al.*, Phys. Rev. **D86**, 114031 (2012), [arXiv:1205.6155].

[620] B. Blossier *et al.*, Phys. Rev. Lett. **108**, 262002 (2012), [arXiv:1201.5770].

[621] B. Blossier *et al.* (ETM), Phys. Rev. **D89**, 1, 014507 (2014), [arXiv:1310.3763].

[622] B. Chakraborty *et al.*, Phys. Rev. **D91**, 5, 054508 (2015), [arXiv:1408.4169].

[623] A. Bazavov *et al.*, Phys. Rev. **D90**, 7, 074038 (2014), [arXiv:1407.8437].

[624] K. Nakayama, B. Fahy and S. Hashimoto, Phys. Rev. **D94**, 5, 054507 (2016), [arXiv:1606.01002].

[625] Y. Maezawa and P. Petreczky, Phys. Rev. **D94**, 3, 034507 (2016), [arXiv:1606.08798].

[626] M. Bruno *et al.* (ALPHA), Phys. Rev. Lett. **119**, 10, 102001 (2017), [arXiv:1706.03821].

[627] R. J. Hudspith *et al.* (2018), [arXiv:1804.10286].

[628] H. Takaura *et al.*, Phys. Lett. **B789**, 598 (2019), [arXiv:1808.01632].

[629] H. Takaura *et al.*, JHEP **04**, 155 (2019), [arXiv:1808.01643].

[630] K. Nakayama, H. Fukaya and S. Hashimoto, Phys. Rev. **D98**, 1, 014501 (2018), [arXiv:1804.06695].

[631] A. Bazavov *et al.* (TUMQCD), Phys. Rev. D **100**, 11, 114511 (2019), [arXiv:1907.11747].

[632] L. Del Debbio and A. Ramos, Physics Reports **920**, 1 (2021), ISSN 0370-1573, [arXiv:2101.04762].

Downloaded from https://academic.oup.com/ptep/article/2022/8/083C01/6651666 by KIT Library user on 27 September 2022

10. Electroweak Model and Constraints on New Physics

Revised March 2022 by J. Erler (KPH, JGU Mainz) and A. Freitas (Pittsburgh U.).

10.1 Introduction . . . 177
10.2 Renormalization and radiative corrections . . . 177
10.2.1 The Fermi constant . . . 178
10.2.2 The electromagnetic coupling . . . 178
10.2.3 Quark masses . . . 179
10.2.4 The weak mixing angle . . . 179
10.2.5 Radiative corrections . . . 180
10.3 Low energy electroweak observables . . . 181
10.3.1 Neutrino scattering . . . 181
10.3.2 Parity violating lepton scattering . . . 182
10.3.3 Atomic parity violation . . . 183
10.4 Precision flavor physics . . . 183
10.4.1 The τ lifetime . . . 184
10.4.2 The muon anomalous magnetic moment . . . 184
10.5 Physics of the massive electroweak bosons . . . 185
10.5.1 Electroweak physics off the Z pole . . . 185
10.5.2 Z pole physics . . . 186
10.5.3 W and Z decays . . . 187
10.6 Global fit results . . . 189
10.7 Constraints on new physics . . . 191

10.1 Introduction

The standard model of the electroweak interactions (SM) [1–4] is based on the gauge group SU(2) × U(1), with gauge bosons W^i_μ, $i = 1, 2, 3$, and B_μ for the SU(2) and U(1) factors, respectively, and the corresponding gauge coupling constants g and g'. The left-handed fermion fields of the $i^{\rm th}$ fermion family transform as doublets $\Psi_i = \begin{pmatrix} \nu_i \\ \ell_i^- \end{pmatrix}$ and $\begin{pmatrix} u_i \\ d'_i \end{pmatrix}$ under SU(2), where $d'_i \equiv \sum_j V_{ij}\, d_j$, and V is the Cabibbo-Kobayashi-Maskawa mixing [5,6] matrix. The right-handed fields are SU(2) singlets. From Higgs and electroweak precision data it is known that there are precisely three sequential fermion families. Constraints on V and tests of universality are discussed in Ref. [7] and in the Section on the "CKM Quark-Mixing Matrix" in this *Review*. The extension of the formalism to allow an analogous leptonic mixing matrix is discussed in the Section on "Neutrino Masses, Mixing, and Oscillations" in this *Review*.

A complex scalar Higgs doublet, ϕ, is added to the model for mass generation through spontaneous symmetry breaking with potential[1] given by,

$$V(\phi) = \mu^2 \phi^\dagger \phi + \frac{\lambda^2}{2} (\phi^\dagger \phi)^2 \ , \qquad \phi \equiv \begin{pmatrix} \phi^+ \\ \phi^0 \end{pmatrix} \ . \tag{10.1}$$

For μ^2 negative, ϕ develops a vacuum expectation value, $v/\sqrt{2} = |\mu|/\lambda$, where $v = 246.22$ GeV, breaking part of the electroweak (EW) gauge symmetry, after which only one neutral Higgs scalar, H, remains in the physical particle spectrum. In non-minimal models there are additional charged and neutral scalar Higgs particles. Higgs boson physics is reviewed in the Section on the "Status of Higgs Boson Physics" in this *Review*.

After symmetry breaking the Lagrangian for the fermion fields, ψ_i, is

$$\mathscr{L}_F = \sum_i \bar\psi_i \left(i \partial\!\!\!/ - m_i - \frac{m_i H}{v} \right) \psi_i \tag{10.2}$$

$$- \frac{g}{2\sqrt{2}} \sum_i \overline{\Psi}_i \, \gamma^\mu \, (1 - \gamma^5)(T^+ \, W^+_\mu + T^- \, W^-_\mu) \, \Psi_i$$

$$- e \sum_i Q_i \, \bar\psi_i \, \gamma^\mu \, \psi_i \, A_\mu \tag{10.3}$$

$$- \frac{g}{2\cos\theta_W} \sum_i \bar\psi_i \, \gamma^\mu (g^i_V - g^i_A \gamma^5) \, \psi_i \, Z_\mu \ . \tag{10.4}$$

Here $\theta_W \equiv \tan^{-1}(g'/g)$ is the weak mixing angle and $e = g \sin\theta_W$ is the positron electric charge. Furthermore,

$$A_\mu \equiv B_\mu \cos\theta_W + W^3_\mu \sin\theta_W \ , \tag{10.5a}$$

$$W^\pm_\mu \equiv \frac{W^1_\mu \mp i W^2_\mu}{\sqrt{2}} \ , \tag{10.5b}$$

$$Z_\mu \equiv -B_\mu \sin\theta_W + W^3_\mu \cos\theta_W \ , \tag{10.5c}$$

are the photon field (γ) and the charged ($W^\pm$) and neutral (Z) weak boson fields, respectively.

The Yukawa coupling of H to ψ_i in the first term in $\mathscr{L}_F$, which is flavor diagonal in the minimal model, is $g m_i / 2M_W$. The boson masses in the EW sector are given (at tree level, *i.e.*, to lowest order in perturbation theory) by,

$$M_H = \lambda \, v \ , \tag{10.6a}$$

$$M_W = \frac{gv}{2} = \frac{ev}{2\sin\theta_W} \ , \tag{10.6b}$$

$$M_Z = \sqrt{g^2 + g'^2} \ \frac{v}{2} = \frac{ev}{2\sin\theta_W \cos\theta_W} \ , \tag{10.6c}$$

$$M_\gamma = 0 \ . \tag{10.6d}$$

The second term in $\mathscr{L}_F$ represents the charged-current weak interaction [8–10], where T^+ and T^- are the weak isospin raising and lowering operators. For example, the coupling of a W to an electron and a neutrino is

$$- \frac{e}{2\sqrt{2}\sin\theta_W} \left[W^-_\mu \, \bar e \, \gamma^\mu (1 - \gamma^5) \nu + W^+_\mu \, \bar\nu \, \gamma^\mu \, (1 - \gamma^5) e \right] \ . \tag{10.7}$$

For momenta small compared to M_W, this term gives rise to the effective four-fermion interaction with the Fermi constant given by $G_F/\sqrt{2} = 1/2v^2 = g^2/8M_W^2$. CP violation is incorporated into the EW model by a single observable phase in V_{ij}.

The third term in $\mathscr{L}_F$ describes electromagnetic interactions (QED) [11, 12], and the last is the weak neutral-current interaction [9, 10, 13]. The vector and axial-vector couplings are

$$g^i_V \equiv t_{3L}(i) - 2Q_i \sin^2\theta_W \ , \tag{10.8a}$$

$$g^i_A \equiv t_{3L}(i) \ , \tag{10.8b}$$

where $t_{3L}(i)$ is the weak isospin of fermion i ($+1/2$ for u_i and ν_i; $-1/2$ for d_i and e_i) and Q_i is the charge of ψ_i in units of e.

The first term in Eq. (10.4) also gives rise to fermion masses, and in the presence of right-handed neutrinos to Dirac neutrino masses. The possibility of Majorana masses is discussed in the Section on "Neutrino Mass, Mixing, and Oscillations" in this *Review*.

10.2 Renormalization and radiative corrections

In addition to the Higgs boson mass, M_H, the fermion masses and mixings, and the strong coupling constant, α_s, the SM has three parameters. The set with the smallest experimental errors contains the Z mass[2], the Fermi constant, and the fine structure constant, to be discussed in turn (the numerical values quoted in Sections 10.2−10.4 correspond to the main fit result in Table 10.7).

The Z boson mass, $M_Z = 91.1876 \pm 0.0021$ GeV, has been determined from the Z lineshape scan at LEP 1 [14]. This value of M_Z corresponds to a definition based on a Breit-Wigner shape with an energy-dependent width[3] (see the Section on the "Z Boson" in this *Review*).

[1] There is no generally accepted convention to write the quartic term. Our numerical coefficient simplifies Eq. (10.6a) below and the squared coupling preserves the relation between the number of external legs and the power counting of couplings at a given loop order. This structure also naturally emerges from physics beyond the SM, such as Supersymmetry.

[2] We emphasize that in the fits described in Sec. 10.6 and Sec. 10.7 the values of the SM parameters are affected by all observables that depend on them. This is of no practical consequence for α and G_F, however, since they are very precisely known.

[3] The theoretically consistent and gauge-invariant definition of the Z-

Downloaded from https://academic.oup.com/ptep/article/2022/8/083C01/6651666 by KIT Library user on 27 September 2022

10.2.1 *The Fermi constant*

The Fermi constant,

$$G_F = 1.1663788(6) \times 10^{-5}\ \mathrm{GeV}^{-2}\ , \tag{10.9}$$

is derived from the μ lifetime formula[4],

$$\frac{\hbar}{\tau_\mu} = \frac{G_F^2 m_\mu^5}{192\pi^3} F(\rho)\Big[1 + H_1(\rho)\frac{\widehat{\alpha}(m_\mu)}{\pi} + H_2(\rho)\frac{\widehat{\alpha}^2(m_\mu)}{\pi^2} + H_3\frac{\widehat{\alpha}^3(m_\mu)}{\pi^3}\Big]\ , \tag{10.10}$$

where $\rho = m_e^2/m_\mu^2$, and where

$$F(\rho) = 1 - 8\rho + 8\rho^3 - \rho^4 - 12\rho^2 \ln\rho = 0.99981295\ , \tag{10.11a}$$

$$H_1(\rho) = \frac{25}{8} - \frac{\pi^2}{2} - \Big(9 + 4\pi^2 + 12\ln\rho\Big)\rho + 16\pi^2\rho^{3/2} + \mathcal{O}(\rho^2) = -1.80793\ , \tag{10.11b}$$

$$H_2(\rho) = \frac{156815}{5184} - \frac{518}{81}\pi^2 - \frac{895}{36}\zeta(3) + \frac{67}{720}\pi^4 + \frac{53}{6}\pi^2\ln 2 - (0.042 \pm 0.002)_{\mathrm{had}} - \frac{5}{4}\pi^2\sqrt{\rho} + \mathcal{O}(\rho) = 6.64\ , \tag{10.11c}$$

$$\widehat{\alpha}(m_\mu)^{-1} = \alpha^{-1} + \frac{1}{3\pi}\ln\rho + \mathcal{O}(\alpha) = 135.901\ . \tag{10.11d}$$

H_1 and H_2 capture the QED corrections within the Fermi model. The results for $\rho = 0$ have been obtained in Refs. [16] and [17, 18] for H_1 and H_2, respectively, where the term in parentheses is from the hadronic vacuum polarization [17]. The mass corrections to H_1 have been known for some time [19], while those to H_2 are more recent [20]. Notice the term linear in m_e whose appearance was unforeseen and can be traced to the use of the muon pole mass in the prefactor [20]. The coefficient $H_3 = -15.3 \pm 2.3$ has been estimated in Refs. [21, 22]. The remaining uncertainty in G_F is mostly experimental and has been reduced by an order of magnitude by the MuLan collaboration [15] at the PSI.

10.2.2 *The electromagnetic coupling*

The fine structure constant, α, can be extracted from the anomalous magnetic moment of the electron, $a_e = (1159652180.73 \pm 0.28) \times 10^{-12}$ [23], giving the value [24] $\alpha^{-1} = 137.035999150(33)$. Another approach combines measurements of the Rydberg constant and atomic masses with interferometry of atomic recoil kinematics. Applied to ^{87}Rb [25] and ^{133}Cs [26], this method implies the results $\alpha^{-1} = 137.035999206(11)$ and $\alpha^{-1} = 137.035999046(27)$, respectively, which differ by 5.5 σ from each other, and when combined would give $\alpha^{-1} = 137.035999183(10)$. Finally, combining the anomalous magnetic moment and atomic interferometry methods, which unlike in the past are now in agreement, leads to the world average of

$$\alpha^{-1} = 137.035999180(10)\ . \tag{10.12}$$

In most EW renormalization schemes, it is convenient to define a running α dependent on the energy scale of the process, with $\alpha^{-1} \approx 137.036$ appropriate at very low energy, *i.e.* close to the Thomson limit. The OPAL [27] and L3 [28] collaborations at LEP could also observe the running directly in small and large angle Bhabha scattering, respectively. For scales above a few hundred MeV the low energy hadronic contribution to vacuum polarization introduces a theoretical uncertainty in α. In the modified minimal subtraction ($\overline{\mathrm{MS}}$) scheme[5] [29] (used for this *Review*), and with $\alpha_s(M_Z) = 0.1185 \pm 0.0016$ we have $\widehat{\alpha}^{(4)}(m_\tau)^{-1} = 133.471 \pm 0.007$ and $\widehat{\alpha}^{(5)}(M_Z)^{-1} = 127.951 \pm 0.009$. The latter corresponds to a quark sector contribution (without the top) to the conventional (on-shell) QED coupling,

$$\alpha(M_Z) = \frac{\alpha}{1 - \Delta\alpha(M_Z)}\ , \tag{10.13}$$

of $\Delta\alpha_{\mathrm{had}}^{(5)}(M_Z) = 0.02768 \pm 0.00007$. These values are updated from Ref. [30] with $\Delta\alpha_{\mathrm{had}}^{(5)}(M_Z)$ moved downwards and its uncertainty reduced (partly due to a more precise charm quark mass). Its correlation with a_μ, as well as the non-linear α_s dependence of $\widehat{\alpha}(M_Z)$ and the resulting correlation with the input variable α_s, are fully taken into account in the fits. This is done by using as actual input (fit constraint) instead of $\Delta\alpha_{\mathrm{had}}^{(5)}(M_Z)$ the low energy contribution by the three light quarks, $\Delta\alpha_{\mathrm{had}}^{(3)}(2.0\ \mathrm{GeV}) = (58.84 \pm 0.51) \times 10^{-4}$ [31], and by calculating the perturbative and heavy quark contributions to $\widehat{\alpha}(M_Z)$ in each call of the fits according to [30]. Part of the error ($\pm 0.37 \times 10^{-4}$) is from e^+e^- annihilation data below $\sqrt{s} = 2$ GeV, as well as isospin rotated data from τ decays into two- and four-pion final states [32] (including uncertainties from isospin breaking effects [33]), but uncalculated higher order perturbative ($\pm 0.21 \times 10^{-4}$) and non-perturbative ($\pm 0.28 \times 10^{-4}$ [31]) QCD corrections and the $\overline{\mathrm{MS}}$ quark mass values (see below) also contribute. Various evaluations of $\Delta\alpha_{\mathrm{had}}^{(5)}(M_Z)$ are summarized in Table 10.1, where the relation[6] between the $\overline{\mathrm{MS}}$ and on-shell definitions (obtained using Refs. [37, 38]) is given by,

$$\begin{aligned}
&\Delta\widehat{\alpha}(M_Z) - \Delta\alpha(M_Z) \\
&= \frac{\alpha}{\pi}\Bigg[\frac{100}{27} - \frac{1}{6} - \frac{7}{4}\ln\frac{M_Z^2}{M_W^2} + \frac{\alpha_s(M_Z)}{\pi}\left(\frac{605}{108} - \frac{44}{9}\zeta(3)\right) \\
&+ \frac{\alpha_s^2}{\pi^2}\left(\frac{976481}{23328} - \frac{253}{36}\zeta(2) - \frac{781}{18}\zeta(3) + \frac{275}{27}\zeta(5)\right) \\
&+ \frac{\alpha_s^3}{\pi^3}\Bigg(\frac{1483517111}{3359232} - \frac{22781}{144}\zeta(2) - \frac{3972649}{7776}\zeta(3) - \frac{31}{81}\zeta(2)^2 \\
&+ \frac{521255}{7776}\zeta(5) - \frac{7315}{324}\zeta(7) + \frac{5819}{54}\zeta(2)\zeta(3) + \frac{14675}{162}\zeta(3)^2\Bigg)\Bigg] \\
&= 0.007122(2)(5)\ ,
\end{aligned} \tag{10.14}$$

and where the first entry of the lowest order term is from fermions and the other two are from $W^\pm$ loops, which are usually excluded from the on-shell definition. Fermion mass effects and corrections of $\mathcal{O}(\alpha^2)$ contributing to Eq. (10.14) are small, partly cancel each other and are not included here. The first error in Eq. (10.14) is parametric (from α_s) and the second is from the truncation of the perturbative expansion. The most recent results on $\Delta\alpha_{\mathrm{had}}^{(5)}(M_Z)$ [31, 39–41] typically assume the validity of perturbative QCD (PQCD) at scales of ~ 2 GeV or above and are in good agreement with each other. In regions where PQCD is not trusted, one can use $e^+e^- \to$ hadrons cross-section data and τ decay spectral functions [42], where the latter derive from OPAL [43], CLEO [44], ALEPH [45], and Belle [46]. Recently, new data for various $e^+e^- \to$ hadrons channels was obtained from BaBar, BES III, CLEO, the SND and CMD-3 experiments at VEPP-2000, and the KEDR experiments at VEPP-4M (for a list of references see, *e.g.*, Ref. [31]). While VEPP-2000 and VEPP-4M scanned center-of-mass (CM) energies up to 2 GeV and

boson mass through the complex pole of the propagator would instead lead to a Breit-Wigner shape with a constant width. The two definitions differ numerically, and this difference has to be accounted for in theoretical calculations.

[4] In the spirit of the Fermi theory, we incorporated the small propagator correction, $3/5\ m_\mu^2/M_W^2$, into Δr (see below). This is also the convention adopted by the MuLan collaboration [15]. While this breaks with historical consistency, the numerical difference was negligible in the past.

[5] In this Section we denote quantities defined in the $\overline{\mathrm{MS}}$ scheme by a caret; the exception is the strong coupling constant, α_s, which will always correspond to the $\overline{\mathrm{MS}}$ definition and where the caret will be dropped. Furthermore, $\alpha^{(n)}$ and $\alpha_s^{(n)}$ denote the running couplings with n quark flavors.

[6] In practice, $\alpha(M_Z)$ is directly evaluated in the $\overline{\mathrm{MS}}$ scheme using the FORTRAN package GAPP [34], including the QED contributions of both leptons and quarks. The leptonic three-loop [35] and four-loop [36] contributions in the on-shell scheme have also been obtained.

Downloaded from https://academic.oup.com/ptep/article/2022/8/083C01/6651666 by KIT Library user on 27 September 2022

between about 3 and 4 GeV, respectively, the BaBar collaboration studied multi-hadron events radiatively returned from the $\Upsilon(4S)$, reconstructing the radiated photon and normalizing to $\mu^{\pm}\gamma$ final states. The precision of these results generally exceeds those from τ decays. There are significant discrepancies between the older (CMD-2) and newer (CMD-3) measurements of $e^+e^- \to K^+K^-$, which could be due to difficulties in determining the detection efficiency of low-momentum kaons. The radiative return data from BaBar is expected to be more reliable for this channel owing to an additional boost of the final-state hadrons.

10.2.3 *Quark masses*

Further free parameters entering into Eq. (10.4) are the quark and lepton masses, where m_i is the mass of the $i^{\rm th}$ fermion ψ_i. For the light quarks, as described in the Section on "Quark Masses" in this *Review*, $\widehat{m}_u = 2.16^{+0.49}_{-0.26}$ MeV, $\widehat{m}_d = 4.67^{+0.48}_{-0.17}$ MeV, and $\widehat{m}_s = 93^{+11}_{-\ 5}$ MeV. These are running $\overline{\rm MS}$ masses evaluated at the scale $\mu = 2$ GeV. For the charm mass we use the constraint [55],

$$\widehat{m}_c(\widehat{m}_c) = 1274 \pm 8 + 2616\,[\alpha_s(M_Z) - 0.1182]\ \text{MeV}\ , \qquad (10.15)$$

which is based on QCD sum rules [56, 57], and recalculate $\widehat{m}_c$ in each call of our fits to account for its α_s dependence. Similarly, for the bottom quark mass we use [58],

$$\widehat{m}_b(\widehat{m}_b) = 4180 \pm 8 - 108\,[\alpha_s(M_Z) - 0.1182]\ \text{MeV}\ , \qquad (10.16)$$

with a theoretical correlation of about 60% arising from the PQCD truncation uncertainty which is similar for $\widehat{m}_c(\widehat{m}_c)$ and $\widehat{m}_b(\widehat{m}_b)$. To improve the precisions in $\widehat{m}_c(\widehat{m}_c)$ and $\widehat{m}_b(\widehat{m}_b)$ in the future it would help to remeasure the threshold regions of the heavy quarks, as well as the electronic decay widths of the narrow $c\bar{c}$ and $b\bar{b}$ resonances. It would also be important to obtain data on the R-ratio in e^+e^- annihilation for center-of-mass energies $\gtrsim 11.2$ GeV, as in this region QCD perturbation theory cannot be sufficiently relied upon for b quarks [58].

The top quark "pole" mass (the quotation marks are a reminder that the experiments do not strictly measure the pole mass and that quarks do not form asymptotic states), has been kinematically reconstructed by the Tevatron collaborations, CDF and DØ, in leptonic, hadronic, and mixed channels with the result $m_t = 174.30 \pm 0.35_{\,\rm stat.} \pm 0.54_{\,\rm syst.}$ GeV [59]. Likewise, using data from CM energies $\sqrt{s} = 7$ and 8 TeV (Run 1), ATLAS and CMS (including alternative technique measurements) at the LHC obtained $m_t = 172.69 \pm 0.25_{\,\rm stat.} \pm 0.41_{\,\rm syst.}$ GeV [60] and $m_t = 172.43 \pm 0.13_{\,\rm stat.} \pm 0.46_{\,\rm syst.}$ GeV [61], respectively. In addition, there are first results with $\sqrt{s} = 13$ TeV data (Run 2). CMS obtained $m_t = 172.26 \pm 0.07_{\,\rm mostly\,stat.} \pm 0.61_{\,\rm syst.}$ GeV [62] in the lepton + jets and all-jets channels, $m_t = 172.33 \pm 0.14_{\,\rm stat.} \pm 0.69_{\,\rm syst.}$ GeV [63] in the di-lepton channel, and $m_t = 172.13 \pm 0.32_{\,\rm stat.} \pm 0.70_{\,\rm syst.}$ GeV [64] in t-channel single top events (leptonic decays). Using a leptonic invariant mass and thus featuring reduced correlation with the more traditional analysis approaches, ATLAS quotes $m_t = 174.48 \pm 0.40_{\,\rm stat.} \pm 0.67_{\,\rm syst.}$ GeV [65] from the lepton + jets channel. While there seems to be generally good agreement between all these measurements, we observe a 2.8 σ discrepancy (or more in case of correlated systematics) between the two most precise determinations, 174.98 ± 0.76 GeV [66] (by the DØ collaboration) and 172.25 ± 0.63 GeV [67] (by the CMS collaboration), both from the lepton + jets channels. In addition, the latter is also 2.2 σ lower than the preliminary result of Ref. [65]. Assuming a systematic error component of 0.17 GeV (the QCD, PDF and Monte Carlo type errors at ATLAS at Run 1) is common to all six results, we arrive at the combination,

$$m_t = 172.83 \pm 0.28_{\,\rm exp.}\ \text{GeV} + \Delta m_{\rm MC}\ , \qquad (10.17)$$

where $\Delta m_{\rm MC}$ is defined to account for any difference between the top pole mass, m_t, and the mass parameter implemented in the Monte Carlo event generators employed by the experimental groups. $\Delta m_{\rm MC}$ is expected to be of order $\alpha_s(Q_0)Q_0$ with a low scale $Q_0 \sim \mathcal{O}(1\ \text{GeV})$ [68], but its value is unknown in hadron collider environments so that we will treat it as an uncertainty instead[7], and choose for definiteness $Q_0 = \Gamma_t = 1.42$ GeV to arrive at $\Delta m_{\rm MC} = 0 \pm 0.52$ GeV. We further assume that an uncertainty [70] of ± 0.32 GeV in the relation [71] between m_t and the $\overline{\rm MS}$ definition, $\widehat{m}_t(\widehat{m}_t)$, entering electroweak radiative correction libraries, including the renormalon ambiguity [72], is already included in $\Delta m_{\rm MC}$, as m_t merely serves as an intermediate bookkeeping device in Ref. [68]. A promising future direction to arrive at a competitive independent constraint on m_t is to analyze differential top quark pair production cross-sections at next-to-next-to-leading order (NNLO) [73, 74] as m_t extraction based on them are easier to interpret, and experimentally they have become much more precise recently [75–77]. The combination in Eq. (10.17) differs slightly from the average, $m_t = 172.76 \pm 0.30_{\,\rm exp.}$ GeV, which appears in the Top Quark Listings in this *Review*, and which is based exclusively on published results. For more details and references, see the Section on the "Top Quark" and the Quarks Listings in this *Review*.

10.2.4 *The weak mixing angle*

The observables $\sin^2\theta_W$ and M_W can be calculated from M_Z, $\widehat{\alpha}(M_Z)$, and G_F, when values for m_t and M_H are given, or conversely, M_H can be constrained by $\sin^2\theta_W$ and M_W. The value of $\sin^2\theta_W$ is extracted from neutral-current processes (see Sec. 10.3) and Z pole observables (see Sec. 10.5.3) and depends on the renormalization prescription. There are a number of popular schemes [9] leading to values which differ by small factors depending on m_t and M_H. The notation for these schemes is shown in Table 10.2.

(i) The on-shell scheme [79] promotes the tree-level formula $\sin^2\theta_W = 1 - M_W^2/M_Z^2$ to a definition of the renormalized $\sin^2\theta_W$ to all orders in perturbation theory, *i.e.*,

$$\sin^2\theta_W \to s_W^2 \equiv 1 - \frac{M_W^2}{M_Z^2}\ , \qquad (10.18a)$$

$$M_W = \frac{A_0}{s_W(1-\Delta r)^{1/2}}\ , \qquad M_Z = \frac{M_W}{c_W}\ , \qquad (10.18b)$$

where $c_W \equiv \cos\theta_W$, $A_0 = (\pi\alpha/\sqrt{2}G_F)^{1/2} = 37.28038(1)$ GeV, and Δr includes the radiative corrections relating α, $\alpha(M_Z)$, G_F, M_W, and M_Z. One finds $\Delta r \sim \Delta r_0 - \rho_t \tan^{-2}\theta_W$, where $\Delta r_0 = 1 - \alpha/\widehat{\alpha}(M_Z) = 0.06630(7)$ is due to the running of α, and

$$\rho_t = \frac{3G_F m_t^2}{8\sqrt{2}\pi^2} = 0.00936 \times \frac{m_t^2}{(172.83\ \text{GeV})^2}\ , \qquad (10.19)$$

represents the dominant (quadratic) m_t dependence. There are additional contributions to Δr from bosonic loops, including those which depend logarithmically on M_H and higher-order corrections[8]. One has $\Delta r = 0.03657 \mp 0.00021 \pm 0.00007$, where the first uncertainty is from m_t and the second is from $\alpha(M_Z)$. Thus the value of s_W^2 extracted from M_Z includes an uncertainty (∓ 0.00007) from the currently allowed range of m_t. This scheme is simple conceptually. However, the relatively large ($\sim 3\%$) correction from ρ_t causes large spurious contributions in higher orders. s_W^2 depends not only on the gauge couplings but also on the spontaneous-symmetry breaking, and it is awkward in the presence of any extension of the SM which perturbs the value of M_Z (or M_W). Other definitions are motivated by the tree-level coupling constant definition $\theta_W = \tan^{-1}(g'/g)$:

(ii) In particular, the $\overline{\rm MS}$ scheme introduces the quantity,

$$\sin^2\widehat{\theta}_W(\mu) \equiv \frac{\widehat{g}'^2(\mu)}{\widehat{g}^2(\mu) + \widehat{g}'^2(\mu)}\ , \qquad (10.20)$$

[7] However, see Ref. [69] for a proposed procedure to calibrate the Monte-Carlo mass parameter at hadron colliders.

[8] All explicit numbers quoted here and below include the two- and three-loop corrections described near the end of Sec. 10.2.

Downloaded from https://academic.oup.com/ptep/article/2022/8/083C01/6651666 by KIT Library user on 27 September 2022

Table 10.1: Evaluations of the on-shell $\Delta\alpha^{(5)}_{\rm had}(M_Z)$ by different groups (for a more complete list of evaluations see the 2012 edition of this *Review*). For better comparison we adjusted central values and errors to correspond to a common and fixed value of $\alpha_s(M_Z) = 0.120$. References quoting results without the top quark decoupled are converted to the five flavor definition. Ref. [47] uses $\Lambda_{\rm QCD} = 380 \pm 60$ MeV; for the conversion we assumed $\alpha_s(M_Z) = 0.118 \pm 0.003$.

Reference	Result	Comment
Geshkenbein, Morgunov [48]	0.02780 ± 0.00006	$\mathcal{O}(\alpha_s)$ resonance model
Swartz [49]	0.02754 ± 0.00046	use of fitting function
Krasnikov, Rodenberg [50]	0.02737 ± 0.00039	PQCD for $\sqrt{s} > 2.3$ GeV
Kühn & Steinhauser [51]	0.02778 ± 0.00016	full $\mathcal{O}(\alpha_s^2)$ for $\sqrt{s} > 1.8$ GeV
Groote *et al.* [47]	0.02787 ± 0.00032	use of QCD sum rules
Martin *et al.* [52]	0.02741 ± 0.00019	incl. new BES data
de Troconiz, Yndurain [53]	0.02754 ± 0.00010	PQCD for $s > 2$ GeV^2
Burkhardt, Pietrzyk [54]	0.02750 ± 0.00033	PQCD for $\sqrt{s} > 12$ GeV
Erler, Ferro-Hernández [39]	0.02761 ± 0.00010	conv. from $\overline{\rm MS}$ scheme
Jegerlehner [40]	0.02755 ± 0.00013	Euclidean split technique
Davier *et al.* [31]	0.02760 ± 0.00010	PQCD for $\sqrt{s} = 1.8$–3.7 & > 5 GeV
Keshavarzi *et al.* [41]	0.02761 ± 0.00011	PQCD for $\sqrt{s} > 11.2$ GeV

Table 10.2: Notations used to indicate the various schemes discussed in the text. Each definition of $\sin^2\theta_W$ leads to values that differ by small factors depending on m_t and M_H. Numerical values and the uncertainties induced by the imperfectly known SM parameters and unknown higher orders [78] are also given for illustration.

Scheme	Notation	Value	Uncertainty
On-shell	s^2_W	0.22339	± 0.00010
$\overline{\rm MS}$	$\widehat{s}^2_Z$	0.23122	± 0.00004
$\overline{\rm MS}$ (ND)	$\widehat{s}^2_{\rm ND}$	0.23141	± 0.00004
$\overline{\rm MS}$	$\widehat{s}^2_0$	0.23863	± 0.00005
Effective angle	$\bar{s}^2_\ell$	0.23155	± 0.00004

where the couplings $\widehat{g}$ and $\widehat{g}'$ are defined by modified minimal subtraction and the scale μ is conveniently chosen to be M_Z for many EW processes. The value of $\widehat{s}^2_Z \equiv \sin^2\widehat{\theta}_W(M_Z)$ extracted from M_Z is less sensitive than s^2_W to m_t (by a factor of $\tan^2\theta_W$), and is less sensitive to most types of new physics. It is also very useful for comparing with the predictions of grand unification. There are actually several variant definitions of $\sin^2\widehat{\theta}_W(M_Z)$, differing according to whether or how finite $\alpha\ln(m_t/M_Z)$ terms are decoupled (subtracted from the couplings). One cannot entirely decouple the $\alpha\ln(m_t/M_Z)$ terms from all EW quantities because $m_t \gg m_b$ breaks SU(2) symmetry. The scheme that will be adopted here decouples the $\alpha\ln(m_t/M_Z)$ terms from the γ–Z mixing [29, 80], essentially eliminating any $\ln(m_t/M_Z)$ dependence in the formulae for asymmetries at the Z pole when written in terms of $\widehat{s}^2_Z$. (A similar definition is used for $\widehat{\alpha}$.) The on-shell and $\overline{\rm MS}$ definitions are related by

$$\widehat{s}^2_Z = c\,(m_t, M_H) s^2_W = (1.0351 \pm 0.0003) s^2_W \ . \qquad (10.21)$$

The quadratic m_t dependence is given by $c \sim 1 + \rho_t/\tan^2\theta_W$. The expressions for M_W and M_Z in the $\overline{\rm MS}$ scheme are

$$M_W = \frac{A_0}{\widehat{s}_Z(1-\Delta\widehat{r}_W)^{1/2}} \ , \qquad M_Z = \frac{M_W}{\widehat{\rho}^{\,1/2}\,\widehat{c}_Z} \ , \qquad (10.22)$$

and one predicts $\Delta\widehat{r}_W = 0.06922 \pm 0.00007$. $\Delta\widehat{r}_W$ has no quadratic m_t dependence, because shifts in M_W are absorbed into the observed G_F, so that the error in $\Delta\widehat{r}_W$ is almost entirely due to $\Delta r_0 = 1 - \alpha/\widehat{\alpha}(M_Z)$. The quadratic m_t dependence has been shifted into $\widehat{\rho} \sim 1 + \rho_t$, where including bosonic loops, $\widehat{\rho} = 1.01019 \pm 0.00009$.

(iii) A variant $\overline{\rm MS}$ quantity $\widehat{s}^2_{\rm ND}$ (used in the 1992 edition of this *Review*) does not decouple the $\alpha\ln(m_t/M_Z)$ terms [81]. It is related to $\widehat{s}^2_Z$ by

$$\widehat{s}^2_Z = \frac{\widehat{s}^2_{\rm ND}}{1+\frac{\alpha}{\pi}\widehat{d}} \ ,$$
$$d = \frac{1}{3}\left(\frac{1}{\widehat{s}^2} - \frac{8}{3}\right)\left[\left(1+\frac{\alpha_s}{\pi}\right)\ln\frac{m_t}{M_Z} - \frac{15\alpha_s}{8\pi}\right] \ . \qquad (10.23)$$

Thus, $\widehat{s}^2_Z - \widehat{s}^2_{\rm ND} = -0.0002$.

(iv) Some of the low-energy experiments discussed in the next section are sensitive to the weak mixing angle at almost vanishing momentum transfer [39, 82–84]. Thus, Table 10.2 also includes $\widehat{s}^2_0 \equiv \sin^2\widehat{\theta}_W(0)$.

(v) Yet another definition, the effective angle [85, 86], $\bar{s}^2_f \equiv \sin\theta^f_{\rm eff}$, for the Z vector coupling to fermion f, is based on Z pole observables and described in Sec. 10.5.

10.2.5 *Radiative corrections*

Experiments are at such level of precision [78] that complete one-loop, dominant two-loop, and partial three and four-loop radiative corrections must be applied. For neutral-current and Z pole processes, these corrections are conveniently divided into two classes:

1. QED diagrams involving the emission of real photons or the exchange of virtual photons in loops, but not including vacuum polarization diagrams. These graphs often yield finite and gauge-invariant contributions to observable processes. However, they are dependent on energies, experimental cuts, *etc.*, and must be calculated individually for each experiment.
2. EW corrections, including $\gamma\gamma$, γZ, ZZ, and WW vacuum polarization diagrams, as well as vertex corrections, box graphs, *etc.*, involving virtual W and Z bosons. One-loop corrections [87] are included for all processes, and many two-loop corrections are also important. In particular, two-loop corrections involving the top quark modify ρ_t in $\widehat{\rho}$, Δr, and elsewhere by

$$\rho_t \to \rho_t\left[1 + R(M_H, m_t)\,\frac{\rho_t}{3}\right] \ . \qquad (10.24)$$

$R(M_H, m_t)$ can be described as an expansion in M^2_Z/m^2_t, for which the leading m^4_t/M^4_Z [88, 89] and next-to-leading m^2_t/M^2_Z [90, 91] terms are known. The complete two-loop calculation of Δr (without further approximation) has been performed in Refs. [92–96]. More recently, Ref. [97] obtained the $\overline{\rm MS}$ quantities $\Delta\widehat{r}_W$ and $\widehat{\rho}$ to two-loop accuracy, confirming the prediction of M_W in the on-shell scheme from

Downloaded from https://academic.oup.com/ptep/article/2022/8/083C01/6651666 by KIT Library user on 27 September 2022

Refs. [94, 98] within about 4 MeV. Similarly, the EW two-loop corrections for the relation between $\bar{s}^2_{\ell,b}$ and s^2_W are known [99–104], as well as for the partial decay and total decay widths and the effective couplings of the Z boson [105–108]. For $\bar{s}_{s,c}$ only two-loop corrections from diagrams with closed fermion loops are available [109], but given the experimental precision this is more than adequate.

The mixed QCD-EW contributions to gauge boson self-energies of order $\alpha\alpha_s m_t^2$ [110, 111], $\alpha\alpha_s^2 m_t^2$ [112, 113], and $\alpha\alpha_s^3 m_t^2$ [114–116] increase the predicted value of m_t by 6%. This is, however, almost entirely an artifact of using the pole mass definition for m_t. The equivalent corrections when using the $\overline{\rm MS}$ definition $\widehat{m}_t(\widehat{m}_t)$ increase m_t by less than 0.5%. The sub-leading $\alpha\alpha_s$ corrections [117–120] are also included. Further three-loop corrections of order $\alpha\alpha_s^2$ [121,122], $\alpha^3 m_t^6$, and $\alpha^2\alpha_s m_t^4$ [123, 124], are rather small. The same is true for $\alpha^3 M_H^4$ [125] corrections unless M_H approaches 1 TeV. The theoretical uncertainty from unknown higher-order corrections [78] is estimated to amount to 4 MeV for the prediction of M_W [98] and 4.5×10^{-5} for $\bar{s}^2_\ell$ [109].

Throughout this *Review* we utilize EW radiative corrections from the program GAPP [34], which works entirely in the $\overline{\rm MS}$ scheme, and which is independent of the package ZFITTER [126].

10.3 Low energy electroweak observables

In the following we discuss EW precision observables obtained at low momentum transfers [127], *i.e.*, $Q^2 \ll M_Z^2$. It is convenient to write the four-fermion interactions relevant to ν-hadron, ν-e, as well as parity violating e-hadron and e-e neutral-current processes, in a form that is valid in an arbitrary gauge theory (assuming massless left-handed neutrinos). One has[9],

$$-\mathscr{L}^{\nu e} = \frac{G_F}{\sqrt{2}}\,\bar{\nu}\gamma_\mu(1-\gamma^5)\nu\;\bar{e}\,\gamma^\mu(g^{\nu e}_{LV} - g^{\nu e}_{LA}\,\gamma^5)e\;, \tag{10.25a}$$

$$-\mathscr{L}^{\nu h} = \frac{G_F}{\sqrt{2}}\,\bar{\nu}\,\gamma_\mu(1-\gamma^5)\nu\sum_q\Big[g^{\nu q}_{LL}\,\bar{q}\,\gamma^\mu(1-\gamma^5)q + g^{\nu q}_{LR}\,\bar{q}\,\gamma^\mu(1+\gamma^5)q\Big]\;, \tag{10.25b}$$

$$-\mathscr{L}^{ee} = -\frac{G_F}{\sqrt{2}}\,g^{ee}_{AV}\,\bar{e}\,\gamma_\mu\gamma^5 e\,\bar{e}\,\gamma^\mu e\;, \tag{10.25c}$$

$$-\mathscr{L}^{eh} = -\frac{G_F}{\sqrt{2}}\sum_q\Big[g^{eq}_{AV}\,\bar{e}\,\gamma_\mu\gamma^5 e\,\bar{q}\,\gamma^\mu q + g^{eq}_{VA}\,\bar{e}\,\gamma_\mu e\,\bar{q}\,\gamma^\mu\gamma^5 q\Big]\;, \tag{10.25d}$$

where one must include the charged-current contribution for ν_e-e and $\bar{\nu}_e$-e and the parity conserving QED contribution for electron scattering. The SM tree level expressions for the four-Fermi couplings are given in Table 10.3. Note that they differ from the respective products of the gauge couplings in (10.8) in the radiative corrections and in the presence of possible physics beyond the SM.

10.3.1 *Neutrino scattering*

The cross-section in the laboratory system for $\nu_\mu e \to \nu_\mu e$ or $\bar{\nu}_\mu e \to \bar{\nu}_\mu e$ elastic scattering [9,128] is (in this subsection we drop the redundant index L in the effective neutrino couplings),

$$\frac{d\sigma_{\nu,\bar{\nu}}}{dy} = \frac{G_F^2 m_e E_\nu}{2\pi}\Big[(g^{\nu e}_V \pm g^{\nu e}_A)^2 + (g^{\nu e}_V \mp g^{\nu e}_A)^2(1-y)^2 - (g^{\nu e2}_V - g^{\nu e2}_A)\frac{y\,m_e}{E_\nu}\Big]\;, \tag{10.26}$$

where the upper (lower) sign refers to $\nu_\mu(\bar{\nu}_\mu)$, and $y \equiv T_e/E_\nu$ (which runs from 0 to $(1+m_e/2E_\nu)^{-1}$) is the ratio of the kinetic energy of the recoil electron to the incident ν or $\bar{\nu}$ energy. For $E_\nu \gg m_e$ this yields a total cross-section

$$\sigma = \frac{G_F^2 m_e E_\nu}{2\pi}\Big[(g^{\nu e}_V \pm g^{\nu e}_A)^2 + \frac{1}{3}(g^{\nu e}_V \mp g^{\nu e}_A)^2\Big]\;. \tag{10.27}$$

[9] We use here slightly different definitions (and to avoid confusion also a different notation) for the coefficients of these four-Fermi operators than we did in previous editions of this *Review*. The new couplings [13] are defined in the static limit, $Q^2 \to 0$, with specific radiative corrections included, while others (more experiment specific ones) are assumed to be removed by the experimentalist. They are convenient in that their determinations from very different types of processes can be straightforwardly combined.

Table 10.3: SM tree level expressions for the neutral-current parameters for ν-hadron, ν-e, and e^- scattering processes. To obtain the SM values in the last column, the tree level expressions have to be multiplied by the low-energy neutral-current ρ parameter, $\rho_{\rm NC} = 1.00063$, and further vertex and box corrections need to be added as detailed in Ref. [13]. The dominant m_t dependence is again given by $\rho_{\rm NC} \sim 1 + \rho_t$.

Quantity	SM tree level	SM value
$g^{\nu_\mu e}_{LV}$	$-\frac{1}{2} + 2\,\widehat{s}^2_0$	-0.0397
$g^{\nu_\mu e}_{LA}$	$-\frac{1}{2}$	-0.5064
$g^{\nu_\mu u}_{LL}$	$\frac{1}{2} - \frac{2}{3}\,\widehat{s}^2_0$	0.3457
$g^{\nu_\mu d}_{LL}$	$-\frac{1}{2} + \frac{1}{3}\,\widehat{s}^2_0$	-0.4288
$g^{\nu_\mu u}_{LR}$	$-\frac{2}{3}\,\widehat{s}^2_0$	-0.1553
$g^{\nu_\mu d}_{LR}$	$\frac{1}{3}\,\widehat{s}^2_0$	0.0777
g^{ee}_{AV}	$\frac{1}{2} - 2\,\widehat{s}^2_0$	0.0226
g^{eu}_{AV}	$-\frac{1}{2} + \frac{4}{3}\,\widehat{s}^2_0$	-0.1887
g^{ed}_{AV}	$\frac{1}{2} - \frac{2}{3}\,\widehat{s}^2_0$	0.3419
g^{eu}_{VA}	$-\frac{1}{2} + 2\,\widehat{s}^2_0$	-0.0351
g^{ed}_{VA}	$\frac{1}{2} - 2\,\widehat{s}^2_0$	0.0248

The most accurate measurements of $\sin^2\theta_W$ from ν-lepton scattering (see Sec. 10.6) are from the ratio $R \equiv \sigma_{\nu_\mu e}/\sigma_{\bar{\nu}_\mu e}$, in which many of the systematic uncertainties cancel. The results are $\sin^2\theta_W = 0.211 \pm 0.037$ [129], $\sin^2\theta_W = 0.195 \pm 0.022$ [130], and $\sin^2\theta_W = 0.2324 \pm 0.0083$ [131], where radiative corrections (other than m_t effects) are small compared to the precision of present experiments and have negligible effect. As shown in Fig. 10.1, one can determine $g^{\nu e}_{V,A}$ from the experimental data as well. The cross-sections for ν_e-e and $\bar{\nu}_e$-e may be obtained from Eq. (10.26) by replacing $g^{\nu e}_{V,A}$ by $g^{\nu e}_{V,A} + 1$, where the 1 is due to the charged-current contribution.

A precise determination of the on-shell s^2_W, which depends only very weakly on m_t and M_H, is obtained from deep inelastic scattering (DIS) of neutrinos [128,135] from (approximately) isoscalar targets. The ratio $R_\nu \equiv \sigma^{NC}_{\nu N}/\sigma^{CC}_{\nu N}$ of neutral-to-charged-current cross-sections has been measured to 1% accuracy by CDHS [136] and CHARM [137] at CERN. CCFR [138] at Fermilab has obtained an even more precise result, so it is important to obtain theoretical expressions for R_ν and $R_{\bar{\nu}} \equiv \sigma^{NC}_{\bar{\nu}N}/\sigma^{CC}_{\bar{\nu}N}$ to comparable accuracy. Fortunately, many of the uncertainties from the strong interactions and neutrino spectra cancel in the ratio. A large theoretical uncertainty is associated with the c-threshold, which mainly affects σ^{CC}. Using the slow rescaling prescription [139, 140] the central value of $\sin^2\theta_W$ from CCFR varies as $0.0111(m_c/\text{GeV}-1.31)$, where m_c is the effective mass which is numerically close to the $\overline{\rm MS}$ mass $\widehat{m}_c(\widehat{m}_c)$, but their exact relation is unknown at higher orders. For $m_c = 1.31 \pm 0.24$ GeV, which was determined from ν-induced di-muon production [141], this contributes ±0.003 to the total uncertainty of $\Delta\sin^2\theta_W = \pm0.004$, where the experimental uncertainty was also ±0.003. This uncertainty largely cancels, however, in the Paschos-Wolfenstein ratio [142],

$$R^- = \frac{\sigma^{NC}_{\nu N} - \sigma^{NC}_{\bar{\nu}N}}{\sigma^{CC}_{\nu N} - \sigma^{CC}_{\bar{\nu}N}}\;. \tag{10.28}$$

It was measured by Fermilab's NuTeV collaboration [143] for the first time, and required a high-intensity and high-energy anti-neutrino beam.

Downloaded from https://academic.oup.com/ptep/article/2022/8/083C01/6651666 by KIT Library user on 27 September 2022

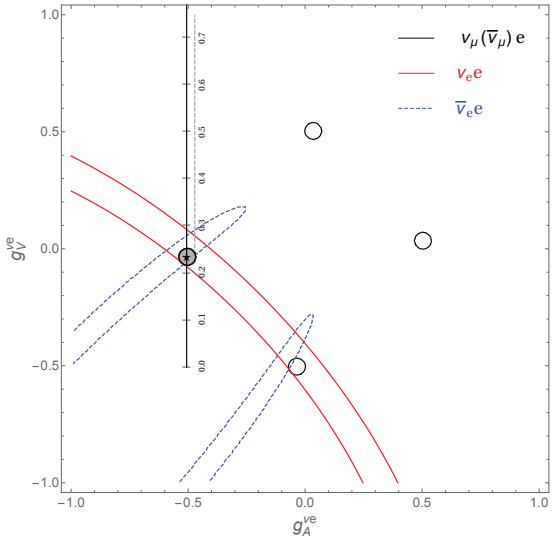

Figure 10.1: Allowed contours in $g_A^{\nu e}$ *vs.* $g_V^{\nu e}$ from neutrino-electron scattering and the SM prediction as a function of $\widehat{s}_Z^2$. (The SM best fit value, $\widehat{s}_Z^2 = 0.23122$, is also indicated.) The ν_e-e [132, 133] and $\bar{\nu}_e$-e [134] constraints are at 1 σ, while each of the four equivalent $\nu_\mu(\bar{\nu}_\mu)$-e [129–131] solutions ($g_{V,A} \to -g_{V,A}$ and $g_{V,A} \to g_{A,V}$) are at the 90% CL. The global best fit region (shaded) almost exactly coincides with the corresponding $\nu_\mu(\bar{\nu}_\mu)$-e region. The solution near $g_A = 0$ and $g_V = -0.5$ is eliminated by $e^+e^- \to \ell^+\ell^-$ data under the weak additional assumption that the neutral current is dominated by the exchange of a single Z boson.

A simple zeroth-order approximation is,

$$R_\nu = g_L^2 + g_R^2 r \ , \qquad R_{\bar{\nu}} = g_L^2 + \frac{g_R^2}{r} \ , \tag{10.29a}$$

$$R^- = g_L^2 - g_R^2 \ , \qquad r \equiv \frac{\sigma_{\bar{\nu}N}^{CC}}{\sigma_{\nu N}^{CC}} \ , \tag{10.29b}$$

where r is the ratio of $\bar{\nu}$ to ν charged-current cross-sections which can be measured directly[10], and

$$g_L^2 \equiv (g_{LL}^{\nu_\mu u})^2 + (g_{LL}^{\nu_\mu d})^2 \approx \frac{1}{2} - \sin^2\theta_W + \frac{5}{9}\sin^4\theta_W \ , \tag{10.30a}$$

$$g_R^2 \equiv (g_{LR}^{\nu_\mu u})^2 + (g_{LR}^{\nu_\mu d})^2 \approx \frac{5}{9}\sin^4\theta_W \ . \tag{10.30b}$$

In practice, Eq. (10.29b) must be corrected for quark mixing, quark sea effects, c quark threshold effects, non-isoscalarity, W–Z propagator differences, the finite muon mass, QED and EW radiative corrections. Details of the neutrino spectra, experimental cuts, x and Q^2 dependence of structure functions, and longitudinal structure functions, enter only at the level of these corrections and therefore lead to very small uncertainties. CCFR quotes $s_W^2 = 0.2236 \pm 0.0041$ for the reference values $(m_t, M_H) = (175, 150)$ GeV with very little sensitivity to (m_t, M_H).

The NuTeV collaboration found $s_W^2 = 0.2277 \pm 0.0016$ (for the same reference values), which was 3.0 σ higher than the SM prediction [143]. However, since then several groups have raised concerns about the interpretation of the NuTeV result, which could affect the extracted $g_{L,R}^2$ (and thus s_W^2) including their uncertainties and correlation. These include the assumption of symmetric strange and anti-strange sea quark distributions, the electron neutrino contamination from K_{e3} decays, isospin symmetry violation in the parton distribution functions and from QED splitting effects, nuclear shadowing effects, and a more complete treatment of EW and QCD radiative corrections. A more detailed discussion and a list of references can be found in the 2016 edition of this *Review*. The precise impact of these effects would need to be evaluated carefully by the collaboration, but in the absence of such an effort we do not include the νDIS constraints in our default set of fits.

Recently, the COHERENT collaboration was the first to observe the coherent elastic neutrino nucleus scattering (CEνNS) process [144] on a target consisting mostly of ^{133}Cs and ^{127}I, and at the opposite end of the kinematic scale where the momentum transfer is significantly smaller than the inverse of the nuclear radius. Subsequently, COHERENT [145] observed CEνNS using a liquid ^{40}Ar detector, as well. The coherence enhances the process roughly proportional to the square of the number of neutrons in the nuclei, but the process is difficult to observe as the experimental signature is a mere keV scale nuclear recoil.

10.3.2 *Parity violating lepton scattering*

Reviews on weak polarized electron scattering may be found in Refs. [9, 146]. The SLAC polarized electron-deuteron DIS (eDIS) experiment [147] measured the parity violating right-left asymmetry,

$$A_{RL} \equiv \frac{\sigma_R - \sigma_L}{\sigma_R + \sigma_L} \ , \tag{10.31}$$

where $\sigma_{R,L}$ is the cross-section for the deep-inelastic scattering of a right- or left-handed electron, $e_{R,L}N \to e$X. In the quark parton model,

$$\frac{A_{RL}}{Q^2} = a_1 + a_2 \frac{1-(1-y)^2}{1+(1-y)^2} \ , \tag{10.32}$$

where $Q^2 > 0$ is the momentum transfer and y is the fractional energy transfer from the electron to the hadrons. For the deuteron or other isoscalar targets, one has, neglecting the s quark and anti-quarks,

$$a_1 = \frac{3G_F}{5\sqrt{2}\pi\alpha}\left(g_{AV}^{eu} - \frac{1}{2}g_{AV}^{ed}\right) \approx \frac{3G_F}{5\sqrt{2}\pi\alpha}\left(-\frac{3}{4} + \frac{5}{3}\widehat{s}_0^2\right) \ , \tag{10.33a}$$

$$a_2 = \frac{3G_F}{5\sqrt{2}\pi\alpha}\left(g_{VA}^{eu} - \frac{1}{2}g_{VA}^{ed}\right) \approx \frac{9G_F}{5\sqrt{2}\pi\alpha}\left(\widehat{s}_0^2 - \frac{1}{4}\right) \ . \tag{10.33b}$$

The Jefferson Lab Hall A collaboration [148, 149] improved on the SLAC result by measuring A_{RL} at $Q^2 = 1.085$ GeV^2 and 1.901 GeV^2, and determined the weak mixing angle to 2% precision, $\widehat{s}^2(161\text{ MeV}) = 0.2403 \pm 0.0043$. In another polarized electron scattering experiment on deuterons, but in the quasi-elastic kinematic regime, the SAMPLE experiment [150, 151] at MIT-Bates extracted the combination $g_{VA}^{eu} - g_{VA}^{ed}$ at Q^2 values of 0.038 GeV^2 and 0.091 GeV^2. What was actually determined were nucleon form factors from which the quoted results were obtained by the removal of a multi-quark radiative correction [152]. Other linear combinations of the effective couplings have been determined in polarized lepton scattering at CERN in μ-^{12}C DIS [153] (the observable was the double charge-helicity cross-section asymmetry), at Mainz in e-^{9}Be (quasi-elastic) [154], and at Bates in e-^{12}C (elastic) [155]. More recent polarized electron scattering experiments, *i.e.*, SAMPLE, the PVA4 experiment at Mainz, and the HAPPEX and GØ experiments at Jefferson Lab, have focussed on the strange quark content of the nucleon [156].

A_{RL} can also be measured in fixed target polarized Møller scattering, $e^-e^- \to e^-e^-$, and reads [157],

$$\frac{A_{RL}}{Q^2} = -2\, g_{AV}^{ee} \frac{G_F}{\sqrt{2}\pi\alpha} \frac{1-y}{1+y^4+(1-y)^4} \ . \tag{10.34}$$

It has been determined at low $Q^2 = 0.026$ GeV^2 in the SLAC E158 experiment [158], with the result, $A_{RL} = (-1.31 \pm 0.14_{\text{stat.}} \pm 0.10_{\text{syst.}}) \times 10^{-7}$. Expressed in terms of the weak mixing angle in the $\overline{\text{MS}}$ scheme this yields $\widehat{s}^2(161\text{ MeV}) = 0.2403 \pm 0.0013$, and as shown in Fig. 10.2 established the scale dependence of the weak mixing angle at the level of 6.4 σ. One also extracts the model-independent effective coupling, $g_{AV}^{ee} = 0.0190 \pm 0.0027$ [13].

[10] In the simple parton model, ignoring hadron energy cuts, $r \approx (1 + 3\epsilon)/(3 + \epsilon)$, where $\epsilon \sim 0.125$ is the ratio of the fraction of the nucleon's momentum carried by anti-quarks to that carried by quarks.

Downloaded from https://academic.oup.com/ptep/article/2022/8/083C01/6651666 by KIT Library user on 27 September 2022

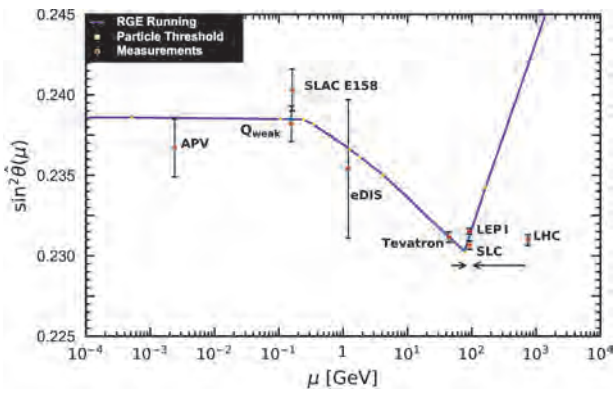

Figure 10.2: Scale dependence of the weak mixing angle defined in the $\overline{\text{MS}}$ scheme [39, 83] (for the scale dependence in a mass-dependent renormalization scheme, see Ref. [82]). The minimum of the curve corresponds to $\mu = M_W$, below which we switch to an effective theory with the $W^\pm$ bosons integrated out, and where the β-function for $\widehat{s}^2(\mu)$ changes sign. At M_W and each fermion mass there are also discontinuities arising from scheme dependent matching terms, which are necessary to ensure that the various effective field theories within a given loop order describe the same physics. However, in the $\overline{\text{MS}}$ scheme these are very small numerically and barely visible in the figure provided one decouples quarks at $\mu = \widehat{m}_q(\widehat{m}_q)$. The width of the curve exceeds the theory uncertainty from strong interaction effects which at low energies is at the level of $\pm 2 \times 10^{-5}$ [39]. The Tevatron and LHC measurements are strongly dominated by invariant masses of the final-state di-lepton pair of $\mathcal{O}(M_Z)$ and can thus be considered as additional Z pole data points. For clarity we displayed the Tevatron and LHC points horizontally to the left and right, respectively.

One-loop radiative corrections and implications are discussed in Ref. [82].

In a similar experiment and at about the same $Q^2 = 0.0248$ GeV^2, the Q_{weak} collaboration at Jefferson Lab obtained $A_{RL} = (-2.265 \pm 0.073_{\text{stat.}} \pm 0.058_{\text{syst.}}) \times 10^{-7}$ [159, 160] in elastic $e^-p \to e^-p$ scattering. To extract the physical quantity of interest, the weak charge of the proton [161], a large ($\approx 30\%$) correction had to be applied to A_{RL} arising from electromagnetic, strange, and axial form factors. This was achieved by performing a global fit [162] including a large number of A_{RL} data points at larger Q^2, dominated by the HAPPEX result at $Q^2 = 0.109$ GeV^2 [163]. Finally, the constraint, $2g_{AV}^{eu} + g_{AV}^{ed} = 0.0356 \pm 0.0023$, which translates into a weak mixing angle measurement of $\widehat{s}^2(157 \text{ MeV}) = 0.2382 \pm 0.0011$, could be deduced, after correcting for a relatively large and uncertain contribution from the γZ box diagram [164–167].

10.3.3 *Atomic parity violation*

There are precise measurements of atomic parity violation (APV) [9, 168, 169] in ^{133}Cs [170, 171] (at the 0.4% level [170]), ^{205}Tl [172, 173], ^{208}Pb [174], and ^{209}Bi [175]. The EW physics is contained in the nuclear weak charges $Q_W(Z, N)$, where Z and N are the numbers of protons and neutrons in the nucleus. In terms of the nucleon vector couplings,

$$g_{AV}^{ep} \equiv 2g_{AV}^{eu} + g_{AV}^{ed} \approx -\frac{1}{2} + 2\widehat{s}_0^2 \ , \tag{10.35a}$$

$$g_{AV}^{en} \equiv g_{AV}^{eu} + 2g_{AV}^{ed} \approx +\frac{1}{2} \ , \tag{10.35b}$$

one has,

$$Q_W(Z,N) \equiv -2\Big[Z(g_{AV}^{ep} + 0.00005) + N(g_{AV}^{en} + 0.00006)\Big]\left(1 - \frac{\alpha}{2\pi}\right) \ , \tag{10.36}$$

where the numerically small adjustments are discussed in Ref. [13] and include the result of the γZ-box correction from Ref. [176].

E.g., $Q_W(^{133}_{78}\text{Cs})$ is extracted by measuring experimentally the ratio of the parity violating amplitude, E_{PNC}, to the Stark vector transition polarizability, β, and by calculating theoretically E_{PNC} in terms of Q_W. One can then write,

$$Q_W(^{133}_{78}\text{Cs}) = N\left(\frac{\text{Im}\,E_{\text{PNC}}}{\beta}\right)_{\text{exp.}}\left(\frac{|e|\,a_B}{\text{Im}\,E_{\text{PNC}}}\frac{Q_W}{N}\right)_{\text{th.}} \times \left(\frac{\beta}{a_B^3}\right)_{\text{exp.+th.}}\left(\frac{a_B^2}{|e|}\right) \ , \tag{10.37}$$

where a_B is the Bohr radius. There are currently two semi-empirical approaches to β of similar precision. The ratio of the off-diagonal hyperfine amplitude to the vector polarizability was measured directly by the Boulder group [177]. Combined with the hyperfine amplitude, computed precisely in Ref. [178], one finds $\beta = (26.957 \pm 0.044_{\text{exp.}} \pm 0.027_{\text{th.}})\,a_B^3$. Alternatively, one can combine [179] the measurement of the ratio of scalar to vector transition polarizabilities [180] with the recent calculation of the scalar polarizability [181] to obtain $\beta = (27.139 \pm 0.030_{\text{exp.}} \pm 0.030_{\text{th.}})\,a_B^3$, in agreement with earlier results [182, 183] based on this approach. The two determinations average to $\beta = (27.064 \pm 0.025_{\text{exp.}} \pm 0.021_{\text{th.}})\,a_B^3$, while they differ by 2.7 σ.

The uncertainties associated with the atomic wave function calculations are relatively small for cesium [9, 184–186]. State-of-the-art many-body atomic structure computations of the parity non-conserving amplitude, $\text{Im}\,E_{\text{PNC}} = (0.8977 \pm 0.0040) \times 10^{-11}|e|\,a_B\,Q_W/N$ [187–192], together with the measurements [170, 171] which can be combined to give $\text{Im}\,E_{\text{PNC}}/\beta = -1.5924 \pm 0.0055$ mV/cm, imply,

$$Q_W(^{133}_{78}\text{Cs}) = -72.82 \pm 0.26_{\text{exp.}} \pm 0.33_{\text{th.}} \ , \tag{10.38}$$

or equivalently the constraint, $55g_{AV}^{ep} + 78g_{AV}^{en} = 36.46 \pm 0.21$. Within the SM this can also be translated into a determination of the weak mixing angle, $\widehat{s}^2(2.4 \text{ MeV}) = 0.2367 \pm 0.0018$, where the scale setting follows the estimate in Ref. [193] for the typical momentum transfer for parity violation experiments in Cs (the corresponding estimate for Tl amounts to 8 MeV). By comparing different hyperfine transitions, the Boulder experiment in cesium also observed the parity violating weak corrections to the nuclear electromagnetic vertex, called the nuclear anapole moment [194–196].

The theoretical atomic structure uncertainties are 3% for thallium [197] and even larger for the other atoms. However, they mostly cancel if one takes ratios of parity violation in different isotopes [198]. The first result of this type of experiment was announced very recently by the Mainz group [199], who studied APV in ^{100}Yb, ^{102}Yb, ^{104}Yb, and ^{106}Yb, at the 0.5% level. The resulting three ratios can be interpreted as a measurement of $\widehat{s}_0^2 = 0.258 \pm 0.052$, and represent a very complementary approach to search for BSM physics [200]. If the precision increases in the future, one would ultimately face uncertainties from differences in the neutron charge radii [201, 202]. These can be constrained experimentally [203], *e.g.*, by measuring A_{RL} in heavier nuclei as done by the CollaborationsPREX collaboration at Jefferson Lab on ^{208}Pb [204, 205].

10.4 Precision flavor physics

In addition to cross-sections, asymmetries, parity violation, W, Z, Higgs and other collider physics, there is a large number of experiments and observables testing the flavor structure of the SM. These are addressed elsewhere in this *Review*, and are generally not included in this Section. However, we identify three precision observables with sensitivity to similar types of new physics as the other processes discussed here. The branching fraction of the flavor changing transition $b \to s\gamma$ is of comparatively low precision, but since it is a loop-level process (in the SM) its sensitivity to new physics (and SM parameters, such as heavy quark masses) is enhanced. A discussion can be found in the 2010 edition of this *Review*.

The τ lepton lifetime and leptonic branching ratios are primarily sensitive to α_s and not affected significantly by many types

Downloaded from https://academic.oup.com/ptep/article/2022/8/083C01/6651666 by KIT Library user on 27 September 2022

of new physics. However, having an independent and reliable low energy measurement of α_s in a global analysis allows the comparison with the Z lineshape determination of α_s which shifts easily in the presence of new physics contributions. By far the most precise observable discussed here is the anomalous magnetic moment of the muon. Its combined experimental and theoretical uncertainty is smaller than typical electroweak scale contributions. The electron magnetic moment is measured to even greater precision, and as discussed in Sec. 10.2.2 can be used to determine α. Its new physics sensitivity, however, is suppressed by an additional factor of m_e^2/m_μ^2, unless there is a new light degree of freedom such as a dark Z [206] boson.

10.4.1 *The τ lifetime*

The extraction of α_s from the τ lifetime τ_τ [207,208] is standing out from other determinations because of a variety of independent reasons:

(i) The τ-scale is low, so that upon extrapolation to the Z scale (where it can be compared to the theoretically clean Z lineshape determinations) the α_s error shrinks by about an order of magnitude.

(ii) Yet, this scale is high enough that perturbation theory and the operator product expansion (OPE) can be applied.

(iii) These observables are fully inclusive and thus free of fragmentation and hadronization effects that would have to be modeled or measured.

(iv) Duality violation (DV) effects are most problematic near the branch cut but there they are suppressed by a double zero at $s = m_\tau^2$.

(v) There are data [43, 45, 209] to constrain non-perturbative effects both within and breaking the OPE.

(vi) A complete four-loop order QCD calculation is available [210–214] in the massless limit.

(vii) Large effects associated with the QCD β-function can be re-summed [215] in what has become known as contour improved perturbation theory (CIPT).

However, while CIPT certainly shows faster convergence in the lower (calculable) orders, doubts have been cast on the method by the observation that at least in a specific model [216], which includes the exactly known coefficients and theoretical constraints on the large-order behavior, ordinary fixed order perturbation theory (FOPT) may nevertheless give a better approximation to the full result. We therefore use the expressions [57, 214, 217],

$$\tau_\tau = \hbar \frac{1-\mathcal{B}_\tau^s}{\Gamma_\tau^e + \Gamma_\tau^\mu + \Gamma_\tau^{ud}} = 290.75 \pm 0.36 \text{ fs} , \tag{10.39}$$

and

$$\Gamma_\tau^{ud} = \frac{G_F^2 m_\tau^5 |V_{ud}|^2}{64\pi^3} S(m_\tau, M_Z) \left(1 + \frac{3}{5}\frac{m_\tau^2 - m_\mu^2}{M_W^2}\right) \times \left[1 + \frac{\alpha_s(m_\tau)}{\pi} + 5.202\,\frac{\alpha_s^2}{\pi^2} + 26.37\,\frac{\alpha_s^3}{\pi^3} + 127.1\,\frac{\alpha_s^4}{\pi^4} + \frac{\widehat{\alpha}}{\pi}\left(\frac{85}{24} - \frac{\pi^2}{2}\right) + \delta_{\rm NP}\right] , \tag{10.40}$$

where Γ_τ^e and Γ_τ^μ can be taken from Eq. (10.10) with obvious replacements. The relative fraction of strangeness changing ($\Delta S = -1$) decays, $\mathcal{B}_\tau^s = 0.0292 \pm 0.0004$, is based on experimental data since the value for the strange quark mass, $\widehat{m}_s(m_\tau)$, is not well known and the QCD expansion proportional to $\widehat{m}_s^2$ converges poorly and cannot be trusted. $S(m_\tau, M_Z) = 1.01907 \pm 0.0003$ is a logarithmically enhanced EW correction factor [218] with higher orders re-summed [219].

$\delta_{\rm NP}$ collects non-perturbative and quark-mass suppressed contributions, including the dimension four, six and eight terms in the OPE, as well as DV effects. We use the average $\delta_{\rm NP} = 0.0141 \pm 0.0072$ derived from the τ decay spectral functions provided by OPAL [43] and ALEPH [45, 209], which give $\delta_{\rm NP} = 0.000 \pm 0.012$ and $\delta_{\rm NP} = 0.022 \pm 0.009$, respectively. These numbers are based on the original analyses in Refs. [220, 221], but are modified to correspond to a strict FOPT analysis as is appropriate for our purpose[11] (for alternative analyses, see the Section on "Quantum Chromodynamics" in this Review).

The dominant uncertainty arises from the truncation of the FOPT series and is conservatively taken as the α_s^4 term (this is re-calculated in each call of the fits, leading to an α_s-dependent and thus asymmetric error) until a better understanding of the numerical differences between FOPT and CIPT has been gained. Our perturbative error covers almost the entire range from using CIPT to assuming that the nearly geometric series in Eq. (10.40) continues to higher orders. The experimental uncertainty in Eq. (10.39) is from the combination of the two leptonic branching ratios with the direct τ_τ. Included are also various smaller uncertainties (± 0.15 fs) from other sources. Based on the method of Refs. [57, 222], we obtain in total

$$\alpha_s^{(4)}(m_\tau) = 0.312^{+0.016}_{-0.013} , \quad \alpha_s^{(5)}(M_Z) = 0.1171^{+0.0018}_{-0.0017} , \tag{10.41}$$

which represents a 1.5% determination of $\alpha_s(M_Z)$. For more details, see Refs. [220,221] where the τ spectral functions themselves and an estimate of the unknown α_s^5 term were used as additional inputs.

10.4.2 *The muon anomalous magnetic moment*

The world average of the muon anomalous magnetic moment[12],

$$a_\mu^{\rm exp} = \frac{g_\mu - 2}{2} = (1165920.61 \pm 0.41) \times 10^{-9} , \tag{10.42}$$

is the combination of the final result of the BNL E821 collaboration [223] and the first result of the Muon $g-2$ collaboration at Fermilab [224]. The QED contribution has been calculated to five loops [225–227] (fully analytic to three loops [228–232] and semi-analytic to four loops [233]). The estimated SM EW contribution [234–239], $a_\mu^{\rm EW} = (1.54 \pm 0.01) \times 10^{-9}$, includes two-loop [240–244] and leading three-loop [245, 246] corrections and is at the level of two and a half times the current uncertainty.

The limiting factor in the interpretation of the result are the uncertainties from hadronic effects. The most recent evaluations of the leading-order (two-loop) hadronic vacuum polarization contribution obtained $a_\mu^{\rm had,VP}(\alpha^2) = (68.81 \pm 0.41) \times 10^{-9}$ [247], $a_\mu^{\rm had,VP}(\alpha^2) = (69.40 \pm 0.40) \times 10^{-9}$ [31], and $a_\mu^{\rm had,VP}(\alpha^2) = (69.28 \pm 0.24) \times 10^{-9}$ [41]. These are mainly based on data from $e^+e^- \to$ hadrons (see, *e.g.*, Ref. [31] for references). Our analysis combines the e^+e^- [31] and τ-decay data [32,33] for contributions up to $\sqrt{s} = 2$ GeV, $a_\mu^{\rm had,VP}(\alpha^2, 2\text{ GeV}) = (64.49 \pm 0.33) \times 10^{-9}$, with analytical PQCD expressions for energies beyond 2 GeV and for the c and b quark contributions [232, 248]. By now there are also precise results for the determination of $a_\mu^{\rm had,VP}(\alpha^2)$ from lattice QCD calculations, which were averaged in Ref. [249] with the result $a_\mu^{\rm had,VP}(\alpha^2) = (71.16 \pm 1.84) \times 10^{-9}$. The most recent lattice calculation has a 0.8% quoted uncertainty [250], $a_\mu^{\rm had,VP}(\alpha^2) = (70.75 \pm 0.55) \times 10^{-9}$, showing a roughly 2 σ conflict with the data-driven evaluations,. If confirmed, a more detailed understanding of the numerical differences between data-driven and lattice approaches will be needed.

The other hadronic uncertainty is induced by the three-loop light-by-light scattering amplitude, where a number of independent model calculations yield results which are in reasonable agreement with each other, $a_\mu^{\rm had,\gamma\times\gamma}(\alpha^3) = (1.36 \pm 0.25) \times 10^{-9}$ [251], $a_\mu^{\rm had,\gamma\times\gamma}(\alpha^3) = 1.37^{+0.15}_{-0.27} \times 10^{-9}$ [252],

[11] We are indebted to Diogo Boito, Maarten Golterman, Kim Maltman and Santiago Peris for privately communicating these results to us.

[12] In what follows, we summarize the most important aspects of a_μ and give some details on the evaluation in our fits. For more details and references, see the Section on the "Muon Anomalous Magnetic Moment" in this *Review*. There are some numerical differences, which are well understood and arise because internal consistency of the fits requires the calculation of all observables from analytical expressions and common inputs and fit parameters, so that an independent evaluation is necessary for this Section. Note, that in the spirit of a global analysis based on all available information we have chosen here to also include τ decay data [32], corrected for isospin breaking effects [33].

Downloaded from https://academic.oup.com/ptep/article/2022/8/083C01/6651666 by KIT Library user on 27 September 2022

$a_\mu^{\rm had,\gamma\times\gamma}(\alpha^3) = (1.05 \pm 0.26) \times 10^{-9}$ [253], and $a_\mu^{\rm had,\gamma\times\gamma}(\alpha^3) = (1.03\pm0.29)\times10^{-9}$ [247], but the sign of this effect is opposite [254] to the one quoted in the 2002 edition of this *Review*. There is also an upper bound given by $a_\mu^{\rm had,\gamma\times\gamma}(\alpha^3) < 1.59 \times 10^{-9}$ [252] but this requires an *ad hoc* assumption, too. Efforts to improve the evaluation by using experimental input where available yield the slightly lower values, $a_\mu^{\rm had,\gamma\times\gamma}(\alpha^3) = (0.87 \pm 0.13) \times 10^{-9}$ [255] and $a_\mu^{\rm had,\gamma\times\gamma}(\alpha^3) = (0.92 \pm 0.19) \times 10^{-9}$ [249]. The first two complete results from lattice simulations, both accounting for all systematic errors, $a_\mu^{\rm had,\gamma\times\gamma}(\alpha^3) = (0.79 \pm 0.35) \times 10^{-9}$ [256] and $a_\mu^{\rm had,\gamma\times\gamma}(\alpha^3) = (1.07 \pm 0.15) \times 10^{-9}$ [257], are consistent with the model and data-driven calculations. For our fits we take the result from Ref. [249], shifted by 1×10^{-11} to correspond to the charm quark treatment of Ref. [252] and with an increased error to also account for the precise constraint in Ref. [257], giving $a_\mu^{\rm had,\gamma\times\gamma}(\alpha^3) = (0.93 \pm 0.29) \times 10^{-9}$.

Sub-leading hadronic vacuum polarization effects at three-loop [258] and four-loop order [259] contribute $a_\mu^{\rm had,VP}(\alpha^3) = (-0.983\pm0.004)\times10^{-9}$ [41] and $a_\mu^{\rm had,VP}(\alpha^4) = (0.124\pm0.001)\times 10^{-9}$ [259], respectively. The correlations with the two-loop hadronic contribution and with $\Delta\alpha(M_Z)$ (see Sec. 10.2) were considered in Ref. [232]. The contributions with a hadronic light-by-light scattering subgraph have been estimated in Ref. [260] with the result, $a_\mu^{\rm had,\gamma\times\gamma}(\alpha^4) = (0.02 \pm 0.01) \times 10^{-9}$ [249].

Altogether, the SM prediction is

$$a_\mu^{\rm theory} = (1165918.34 \pm 0.44) \times 10^{-9} \ , \tag{10.43}$$

where the error is from the hadronic uncertainties excluding parametric ones such as from α_s and the heavy quark masses. We evaluate the correlation of the total (experimental plus theoretical) uncertainty in a_μ with $\Delta\alpha(M_Z)$ to amount to roughly 30%. The overall 3.8 σ discrepancy[13],

$$a_\mu^{\rm exp} - a_\mu^{\rm theory} = (2.27 \pm 0.60) \times 10^{-9} \ ,$$

could be due to fluctuations (the experimental results are statistics dominated) or underestimates of the theoretical uncertainties. On the other hand, the deviation could also arise from physics beyond the SM, such as supersymmetric models with large $\tan\beta$ and moderately light superparticle masses [261], or a dark Z boson [206].

10.5 Physics of the massive electroweak bosons

If the CM energy $\sqrt{s}$ is large compared to the fermion mass m_f, the unpolarized Born cross-section for $e^+e^- \to f\bar f$ [262] can be written as,

$$\frac{d\sigma}{d\cos\theta} = \frac{\pi\alpha^2(s)}{2s}\left[F_1(1+\cos^2\theta) + 2F_2\cos\theta\right] + B \ , \tag{10.44a}$$

$$F_1 = Q_e^2 Q_f^2 - 2\chi Q_e Q_f \bar g_V^e \bar g_V^f \cos\delta_R + \chi^2(\bar g_V^{e2} + \bar g_A^{e2})(\bar g_V^{f2} + \bar g_A^{f2}) \ , \tag{10.44b}$$

$$F_2 = -2\chi Q_e Q_f \bar g_A^e \bar g_A^f \cos\delta_R + 4\chi^2 \bar g_V^e \bar g_A^e \bar g_V^f \bar g_A^f \ , \tag{10.44c}$$

where

$$\tan\delta_R = \frac{\overline{M}_Z\overline{\Gamma}_Z}{\overline{M}_Z^2 - s} \ , \quad \chi = \frac{G_F}{2\sqrt{2}\pi\alpha(s)}\frac{s\overline{M}_Z^2}{\left[(\overline{M}_Z^2 - s)^2 + \overline{M}_Z^2\overline{\Gamma}_Z^2\right]^{1/2}} \ . \tag{10.45}$$

B accounts for box graphs involving virtual Z and W bosons, and the $\bar g_{V,A}^f$ are defined in Eq. (10.46) below. $\overline{M}_Z$ and $\overline{\Gamma}_Z$ correspond to mass and width definitions based on a Breit-Wigner shape with an energy-independent width (see the Section on the "Z Boson" in this *Review*). The differential cross-section receives important corrections from QED effects in the initial and final state, and interference between the two [263]. For $q\bar q$ production, there are additional final-state QCD corrections, which are relatively large. Note also that the equations above are written in the CM frame of the incident e^+e^- system, which may be boosted due to the initial-state QED radiation.

Some of the leading virtual EW corrections are captured by the running QED coupling $\alpha(s)$ and the Fermi constant G_F. The remaining corrections to the $Zf\bar f$ interactions are absorbed by replacing the tree-level couplings in Eq. (10.8) with the s-dependent *effective couplings* [14],

$$\bar g_V^f = \sqrt{\rho_f}\left(t_{3L}^f - 2Q_f\kappa_f\sin^2\theta_W\right) \ , \tag{10.46a}$$

$$\bar g_A^f = \sqrt{\rho_f}\, t_{3L}^f \ . \tag{10.46b}$$

In these equations, the effective couplings are to be taken at the scale $\sqrt{s}$, but for notational simplicity we do not show this explicitly. At tree-level, $\rho_f = \kappa_f = 1$, but inclusion of EW radiative corrections leads to $\rho_f \neq 1$ and $\kappa_f \neq 1$, which depend on the fermion f and on the renormalization scheme. In the on-shell scheme, the quadratic m_t dependence is given by,

$$\rho_f \sim 1 + \rho_t \ , \qquad \kappa_f \sim 1 + \frac{\rho_t}{\tan^2\theta_W} \ , \tag{10.47}$$

while in $\overline{\rm MS}$, $\widehat\rho_f \sim \widehat\kappa_f \sim 1$, for $f \neq b$, and

$$\widehat\rho_b \sim 1 - \frac{4}{3}\rho_t \ , \qquad \widehat\kappa_b \sim 1 + \frac{2}{3}\rho_t \ . \tag{10.48}$$

In the $\overline{\rm MS}$ scheme the normalization is changed according to $G_F M_Z^2/2\sqrt{2}\pi \to \widehat\alpha/4\widehat s_Z^2\widehat c_Z^2$ in the second Eq. (10.45).

As reviewed in Sec. 10.2.5, for the high precision Z pole observables discussed below, many additional bosonic and fermionic loop effects, vertex corrections, and higher order contributions, *etc.*, must be included. For example, in the $\overline{\rm MS}$ scheme one then has $\widehat\rho_\ell = 0.9977$, $\widehat\kappa_\ell = 1.0014$, $\widehat\rho_b = 0.9866$, and $\widehat\kappa_b = 1.0068$.

To connect to measured quantities, it is convenient to define an effective angle

$$\bar s_f^2 \equiv \sin^2\bar\theta_{Wf} \equiv \widehat\kappa_f \widehat s_Z^2 = \kappa_f s_W^2 \ , \tag{10.49}$$

in terms of which $\bar g_V^f$ and $\bar g_A^f$ are given by $\sqrt{\rho_f}$ times their tree-level formulae. One finds that the $\widehat\kappa_f$ ($f \neq b$) are almost independent of m_t and M_H, and thus one can write,

$$\bar s_\ell^2 = \widehat s_Z^2 + 0.00032 \ , \tag{10.50}$$

while the κ_f for the on-shell scheme are m_t dependent.

10.5.1 *Electroweak physics off the Z pole*

Experiments at PEP, PETRA and TRISTAN have measured the unpolarized forward-backward asymmetry, A_{FB}, and the total cross-section relative to pure QED, R, for $e^+e^- \to \ell^+\ell^-$, $\ell = \mu$ or τ at CM energies $\sqrt{s} < M_Z$. They are defined as

$$A_{FB} \equiv \frac{\sigma_F - \sigma_B}{\sigma_F + \sigma_B} \ , \qquad R = \frac{\sigma}{\mathcal{R}_{\rm ini}\otimes\sigma_{\rm QED}} \ , \tag{10.51}$$

where σ_F (σ_B) is the cross-section for ℓ^- to travel forward (backward) with respect to the e^- direction, $\sigma_{\rm QED}$ is the tree-level cross-section from s-channel photon exchange, and $\mathcal{R}_{\rm ini}\otimes$ denotes convolution with initial-state QED corrections. Neglecting box graph contributions, they are given by,

$$A_{FB} = \frac{3}{4}\frac{F_2}{F_1} \ , \qquad R = F_1 \ . \tag{10.52}$$

For the available data, it is sufficient to approximate the EW corrections through the leading running $\alpha(s)$ and quadratic m_t contributions [264], as described above. Reviews and formulae for $e^+e^- \to$ hadrons may be found in [9, 265, 266].

LEP 2 [267] ran at several energies above the Z pole up to $\sim$ 209 GeV. Measurements were made of a number of observables,

[13] Alternatively, if we employ the light-by-light scattering amplitude from Ref. [257] with the charm contribution [252] added, we find $a_\mu^{\rm exp} - a_\mu^{\rm theory} = (2.10 \pm 0.55) \times 10^{-9}$, likewise corresponding to a 3.8 σ discrepancy.

Downloaded from https://academic.oup.com/ptep/article/2022/8/083C01/6651666 by KIT Library user on 27 September 2022

including the total production cross-sections of $f\bar{f}$ pairs for $f = \mu, \tau$, and q (hadrons), of four-fermion final states, of $\gamma\gamma$, ZZ, WW, $WW\gamma$, and WWZ, as well as of single resonant W and Z bosons. The differential cross-sections for all three lepton flavors, and the leptonic and hadronic W branching ratios were also extracted.

Among the most important LEP 2 results were the measurements [267] of the W boson mass,

$$M_W = 80.376 \pm 0.025_{\,\text{stat.}} \pm 0.022_{\,\text{syst.}} \text{ GeV (LEP 2)} , \quad (10.53)$$

which were dominated by kinematic reconstruction, but included the complementary albeit statistics limited and thus much less precise determination from a WW threshold cross section measurement. The kinematic method was also employed at the Tevatron [268] and by ATLAS [270] and LHCb [271] at the LHC. They quote,

$$M_W = 80.387 \pm 0.016 \text{ GeV (Tevatron)} , \quad (10.54a)$$

$$M_W = 80.3695 \pm 0.0068_{\,\text{stat.}} \pm 0.0106_{\,\text{syst.}} \pm 0.0136_{\,\text{th.}} \text{ GeV (ATLAS)} , \quad (10.54b)$$

$$M_W = 80.354 \pm 0.023_{\,\text{stat.}} \pm 0.010_{\,\text{syst.}} \pm 0.017_{\,\text{th.}} \pm 0.009_{\,\text{PDF}} \text{ GeV (LHCb)} . \quad (10.54c)$$

To arrive at our LHC average, $M_W = 80.366 \pm 0.017$ GeV, we assume the PDF error from LHCb of 9 MeV to be common between the two LHC determinations. Furthermore, we assume an error component of 7 MeV to be common between the Tevatron and the LHC. This is smaller than the 10 MeV (9 MeV) PDF uncertainty quoted by CDF (LHCb), because the larger CM energy at the LHC enhances the sensitivity to second generation quark PDFs, in addition to the greater sea quark PDF dependence of the Drell-Yan process in the pp environment. There may also be some correlation due to other production modeling uncertainties. This implies for the average,

$$M_W = 80.377 \pm 0.012 \text{ GeV (world average)} . \quad (10.55)$$

For details and references, see the Section on the "Mass and Width of the W Boson" in this *Review*.

Strong constraints on anomalous triple and quartic gauge couplings have been obtained at LEP 2, the Tevatron, and the LHC. These are described in detail in the three Sections on the "Extraction of Triple Gauge Couplings (TGCs)", "Anomalous W/Z Quartic Couplings (QGCs)", and "Anomalous $ZZ\gamma$, $Z\gamma\gamma$, and ZZV Couplings" in this *Review*.

After their discovery of the Higgs boson [273, 274], the LHC experiments are now performing high precision measurements of its mass. We average the results, $M_H = 124.97 \pm 0.16_{\,\text{stat.}} \pm 0.18_{\,\text{syst.}}$ GeV from ATLAS [275], and $M_H = 125.38 \pm 0.11_{\,\text{stat.}} \pm 0.09_{\,\text{syst.}}$ GeV from CMS [276], by conservatively treating the smaller systematic error as common among the two determinations, and arrive at,

$$M_H = 125.30 \pm 0.09_{\,\text{stat.}} \pm 0.09_{\,\text{syst.}} \text{ GeV (LHC)} . \quad (10.56)$$

For further references and many more details on Higgs boson properties, see the Section on the "Status of Higgs Boson Physics" in this *Review*. The principal non-Z pole observables discussed here and in Sections 10.2–10.4 are summarized in Table 10.4. Included there is also the first measurement of the Higgs boson width (by CMS [277], assuming equal on- and off-shell effective couplings) and the SM prediction (without electroweak corrections as in Ref. [278]).

10.5.2 *Z pole physics*

High precision measurements of various Z pole ($\sqrt{s} \approx M_Z$) observables [9, 286, 287] have been performed at LEP 1 and SLC [14, 284, 285, 288, 289], as summarized in Table 10.5. These include the Z mass and total width, Γ_Z, and partial widths $\Gamma_{f\bar{f}}$ for $Z \to f\bar{f}$, where $f = e$, μ, τ, light hadrons, b, and c. It is convenient to use the variables M_Z, Γ_Z,

$$\sigma_{\text{had}} \equiv \frac{12\pi\Gamma_{e^+e^-}\Gamma_{\text{had}}}{M_Z^2\,\Gamma_Z^2} , \quad R_\ell \equiv \frac{\Gamma_{\text{had}}}{\Gamma_{\ell^+\ell^-}} , \quad R_q \equiv \frac{\Gamma_{q\bar{q}}}{\Gamma_{\text{had}}} , \quad (10.57)$$

for $\ell = e, \mu$ or τ, and $q = b$ or c, where Γ_{had} is the partial decay width into hadrons. Most of these are weakly correlated experimentally. The three values for R_ℓ are consistent with lepton universality (although R_τ is somewhat low compared to R_e and R_μ), but we use the general analysis in which the three observables are treated as independent. Similar remarks apply to $A_{FB}^{0,\ell}$ defined through Eq. (10.58) with $P_e = 0$, where $A_{FB}^{0,\tau}$ is somewhat high. Initial-state radiation reduces the peak cross section by more than 25%, where $\mathcal{O}(\alpha^3)$ QED effects induce a large anti-correlation (−30%) between Γ_Z and σ_{had}. The anti-correlation between R_b and R_c amounts to −18% [14]. The R_ℓ are insensitive to m_t except for the $Z \to b\bar{b}$ vertex, final-state corrections, and the implicit dependence through $\sin^2\theta_W$. Thus, they are especially useful for constraining α_s.

Very important constraints follow from measurements of various Z pole asymmetries. These include the forward-backward asymmetry, A_{FB}, and the polarization or left-right asymmetry, A_{LR}, defined analogously to Eq. (10.31). The latter was measured precisely by the SLD collaboration at the SLC [284], and has the advantages of being very sensitive to $\bar{s}_\ell^2$ and that systematic uncertainties largely cancel. After removing initial-state QED corrections and contributions from photon exchange, γ–Z interference, as well as the EW boxes in Eq. (10.44a), one can use the effective tree-level expressions,

$$A_{LR} = A_e P_e , \qquad A_{FB} = \frac{3}{4} A_f \, \frac{A_e + P_e}{1 + P_e A_e} , \quad (10.58)$$

where,

$$A_f \equiv \frac{2\bar{g}_V^f \bar{g}_A^f}{\bar{g}_V^{f2} + \bar{g}_A^{f2}} = \frac{1 - 4|Q_f|\bar{s}_f^2}{1 - 4|Q_f|\bar{s}_f^2 + 8(|Q_f|\bar{s}_f^2)^2} . \quad (10.59)$$

P_e is the initial e^- polarization, so that the second equality in Eq. (10.60) is reproduced for $P_e = 1$, and the Z pole forward-backward asymmetries at LEP 1 ($P_e = 0$) are given by $A_{FB}^{(0,f)} = \frac{3}{4} A_e A_f$ for $f = e$, μ, τ, b, c, s [14], and q, and where $A_{FB}^{(0,q)}$ refers to the hadronic charge asymmetry. Corrections for t-channel exchange and s/t-channel interference cause $A_{FB}^{(0,e)}$ to be strongly anti-correlated with R_e (−37%). Very recently, the m_b-dependence [290] of the $\mathcal{O}(\alpha_s^2)$ QCD correction [291], affecting the reference axis of the b quark asymmetry [292], increased the extracted[14] $A_{FB}^{(0,b)}$ by about 0.2 σ. The correlation between $A_{FB}^{(0,b)}$ and $A_{FB}^{(0,c)}$ amounts to 15%.

In addition, SLD extracted the final-state couplings A_b, A_c [14], A_s [288], A_τ, and A_μ [285], from left-right forward-backward asymmetries, using

$$A_{LR}^{FB}(f) = \frac{\sigma_{LF}^f - \sigma_{LB}^f - \sigma_{RF}^f + \sigma_{RB}^f}{\sigma_{LF}^f + \sigma_{LB}^f + \sigma_{RF}^f + \sigma_{RB}^f} = \frac{3}{4} A_f , \quad (10.60)$$

where, for example, σ_{LF}^f is the cross-section for a left-handed incident electron to produce a fermion f traveling in the forward hemisphere. Similarly, A_τ and A_e were measured at LEP 1 [14] through the τ polarization, $\mathcal{P}_\tau$, as a function of the scattering angle θ, which can be written as,

$$\mathcal{P}_\tau = -\frac{A_\tau(1 + \cos^2\theta) + 2A_e\cos\theta}{(1 + \cos^2\theta) + 2A_\tau A_e \cos\theta} . \quad (10.61)$$

The average polarization, $\langle\mathcal{P}_\tau\rangle$, obtained by integrating over $\cos\theta$ in the numerator and denominator of Eq. (10.61), yields

[14] We are grateful to Werner Bernreuther and Long Chen for the recalculation of their result employing the more appropriate $\overline{\text{MS}}$ mixing angle, $\widehat{s}_Z^2$, instead of the on-shell quantity, s_W^2.

Downloaded from https://academic.oup.com/ptep/article/2022/8/083C01/6651666 by KIT Library user on 27 September 2022

Table 10.4: Non-Z pole observables, compared with the SM best fit predictions. The first M_W and Γ_W values are from the Tevatron [268, 269], the second ones from LEP 2 [267], while the third M_W is from the LHC [270, 271]. The hadronic branching ratio for W decays combines LEP 2 [267] and CMS [272] and assumes lepton flavor universality. The world averages for $g_{V,A}^{\nu e}$ are dominated by the CHARM II [131] results, $g_V^{\nu e} = -0.035 \pm 0.017$ and $g_A^{\nu e} = -0.503 \pm 0.017$. The τ_τ value is the τ lifetime world average computed by combining the direct measurements with values derived from the leptonic branching ratios [57]; in this case, the theory error is included in the SM prediction. In all other SM predictions, the uncertainty is parametric from M_Z, M_H, m_t, m_b, m_c, $\widehat{\alpha}(M_Z)$, and α_s, and theoretical from unknown higher orders [78], where correlations due to both types have been accounted for. The column denoted by Pull gives the standard deviations.

Quantity	Value	Standard Model	Pull
m_t [GeV]	172.83 ± 0.59	173.13 ± 0.56	-0.5
M_H [GeV]	125.30 ± 0.13	125.30 ± 0.13	0.0
Γ_H [MeV]	$3.2^{+2.4}_{-1.7}$	4.12 ± 0.05	-0.4
M_W [GeV]	80.387 ± 0.016	80.360 ± 0.006	1.7
	80.376 ± 0.033		0.5
	80.366 ± 0.017		0.4
Γ_W [GeV]	2.046 ± 0.049	2.089 ± 0.001	-0.9
	2.195 ± 0.083		1.3
$\mathcal{B}(W \to \text{hadrons})$	0.6736 ± 0.0018	0.6751 ± 0.0001	-0.8
$g_V^{\nu e}$	-0.040 ± 0.015	-0.0397 ± 0.0001	0.0
$g_A^{\nu e}$	-0.507 ± 0.014	-0.5064	0.0
$Q_W(e)$	-0.0403 ± 0.0053	-0.0473 ± 0.0002	1.3
$Q_W(p)$	0.0719 ± 0.0045	0.0709 ± 0.0002	0.2
$Q_W(\text{Cs})$	-72.82 ± 0.42	-73.24 ± 0.01	1.0
$Q_W(\text{Tl})$	-116.4 ± 3.6	-116.90 ± 0.02	0.1
$\widehat{s}_Z^2(\text{eDIS})$	0.2299 ± 0.0043	0.23122 ± 0.00004	-0.3
τ_τ [fs]	290.75 ± 0.36	288.90 ± 2.24	0.8
$\frac{1}{2}(g_\mu - 2 - \frac{\alpha}{\pi})$	$(4510.88 \pm 0.60) \times 10^{-9}$	$(4508.61 \pm 0.03) \times 10^{-9}$	3.8

$\langle \mathcal{P}_\tau \rangle = -A_\tau$, and A_e can be extracted from the $\mathcal{P}_\tau$ angular distribution. The initial-state coupling, A_e, was also determined through the left-right charge asymmetry [289] and in polarized Bhabba scattering [285] at the SLC. Because $\bar{g}_V^\ell$ is very small, not only $A_{LR}^0 = A_e$, $A_{FB}^{(0,\ell)}$, and $\mathcal{P}_\tau$, but also $A_{FB}^{(0,q)}$ for $q = b$, c, and s, as well as the hadronic asymmetries are mainly sensitive to $\bar{s}_\ell^2$.

As an example of the precision of the Z pole observables, the values of $\bar{g}_A^f$ and $\bar{g}_V^f$ for $f = e, \mu, \tau$, and ℓ, extracted from the LEP and SLC lineshape and asymmetry data, are shown in Fig. 10.3. It may be compared with Fig. 10.1 as the two sets of parameters coincide at the SM at tree-level.

As for hadron colliders, the forward-backward asymmetry, A_{FB}, for e^+e^- and $\mu^+\mu^-$ final states (with invariant masses restricted to or dominated by values around M_Z) in $p\bar{p}$ collisions has been measured by the CDF [293] and DØ [294] collaborations, and the values $\bar{s}_\ell^2 = 0.23221 \pm 0.00046$ and $\bar{s}_\ell^2 = 0.23095 \pm 0.00040$ were extracted, respectively. The combination of these measurements (which differ by more than 2 σ) yields [279],

$$\bar{s}_\ell^2 = 0.23148 \pm 0.00033 \text{ (Tevatron)} . \tag{10.62}$$

By varying the invariant mass and the scattering angle (and assuming the electron couplings), information on the effective Z couplings to light quarks, $\bar{g}_{V,A}^{u,d}$, could also be obtained [295, 296], but with large uncertainties, mutual correlations, and not independently of $\bar{s}_\ell^2$ above. Similar analyses have also been reported by the H1 [297] and ZEUS [298] collaborations at HERA and by the LEP collaborations [14]. This kind of measurement is harder in the pp environment due to the difficulty to assign the initial quark and antiquark in the underlying Drell-Yan process to the protons, thus requiring excellent control of uncertainties from parton distribution functions. ATLAS obtained $\bar{s}_\ell^2 = 0.2308 \pm 0.0012$ using 7 TeV data [280] and $\bar{s}_\ell^2 = 0.23140 \pm 0.00036$ at 8 TeV [281], while CMS measured $\bar{s}_\ell^2 = 0.23101 \pm 0.00053$ (8 TeV) [282] and LHCb reported $\bar{s}_\ell^2 = 0.23142 \pm 0.00106$ (from both 7 and 8 TeV data, but only analyzing $\mu^+\mu^-$ final state) [283]. Assuming that the smallest theoretical and PDF uncertainty (± 0.00024 from ATLAS [281]) is fully correlated among the four determinations, they combine to

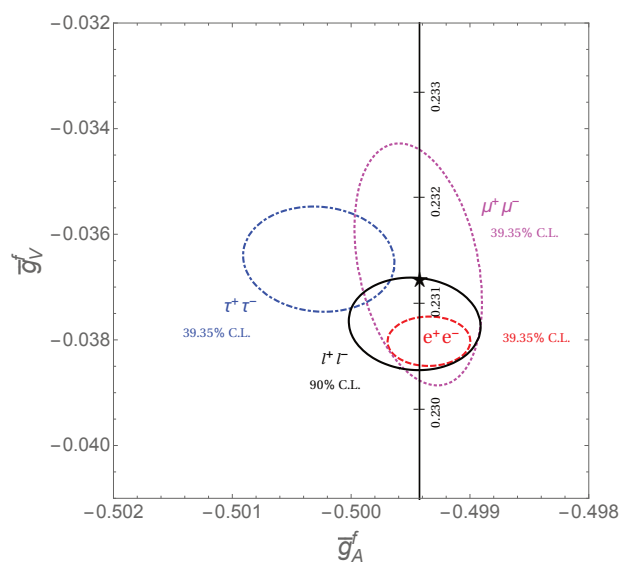

Figure 10.3: 1 σ (39.35% CL) contours of the effective couplings $\bar{g}_A^f$ and $\bar{g}_V^f$ for $f = e, \mu$ and τ from LEP and SLC, compared to the SM expectation as a function of $\widehat{s}_Z^2$. (The SM best fit value $\widehat{s}_Z^2 = 0.23122$ is also indicated.) Also shown is the 90% CL allowed region in $\bar{g}_{A,V}^\ell$ obtained assuming lepton universality.

$$\bar{s}_\ell^2 = 0.23129 \pm 0.00033 \text{ (LHC)} . \tag{10.63}$$

10.5.3 *W and Z decays*

The partial decay widths for gauge bosons to decay into massless fermions $f_1\bar{f}_2$ (the numerical values include the small EW

Downloaded from https://academic.oup.com/ptep/article/2022/8/083C01/6651666 by KIT Library user on 27 September 2022

Table 10.5: Principal Z pole observables and their SM predictions (*cf.* Table 10.4). The first $\bar{s}^2_\ell$ is the effective weak mixing angle extracted from the hadronic charge asymmetry at LEP 1 [14], the second is the combined value from the Tevatron [279], and the third is from the LHC [280–283]. The values of A_e are (i) from A_{LR} for hadronic final states [284]; (ii) from A_{LR} for leptonic final states and from polarized Bhabba scattering [285]; and (iii) from the angular distribution of the τ polarization at LEP 1 [14]. The A_τ values are from SLD [285] and the total τ polarization, respectively. Note that the SM errors in Γ_Z, the R_ℓ, and $\sigma_{\rm had}$ are largely dominated by the uncertainty in α_s.

Quantity	Value	Standard Model	Pull
M_Z [GeV]	91.1876 ± 0.0021	91.1882 ± 0.0020	-0.3
Γ_Z [GeV]	2.4955 ± 0.0023	2.4941 ± 0.0009	0.6
$\sigma_{\rm had}$ [nb]	41.481 ± 0.033	41.482 ± 0.008	0.0
R_e	20.804 ± 0.050	20.736 ± 0.010	1.4
R_μ	20.784 ± 0.034	20.736 ± 0.010	1.4
R_τ	20.764 ± 0.045	20.781 ± 0.010	-0.4
R_b	0.21629 ± 0.00066	0.21582 ± 0.00002	0.7
R_c	0.1721 ± 0.0030	0.17221 ± 0.00003	0.0
$A_{FB}^{(0,e)}$	0.0145 ± 0.0025	0.01617 ± 0.00007	-0.7
$A_{FB}^{(0,\mu)}$	0.0169 ± 0.0013		0.6
$A_{FB}^{(0,\tau)}$	0.0188 ± 0.0017		1.5
$A_{FB}^{(0,b)}$	0.0996 ± 0.0016	0.1029 ± 0.0002	-2.0
$A_{FB}^{(0,c)}$	0.0707 ± 0.0035	0.0735 ± 0.0002	-0.8
$A_{FB}^{(0,s)}$	0.0976 ± 0.0114	0.1030 ± 0.0002	-0.4
$\bar{s}^2_\ell$	0.2324 ± 0.0012	0.23155 ± 0.00004	0.7
	0.23148 ± 0.00033		-0.2
	0.23129 ± 0.00033		-0.8
A_e	0.15138 ± 0.00216	0.1468 ± 0.0003	2.1
	0.1544 ± 0.0060		1.3
	0.1498 ± 0.0049		0.6
A_μ	0.142 ± 0.015		-0.3
A_τ	0.136 ± 0.015		-0.7
	0.1439 ± 0.0043		-0.7
A_b	0.923 ± 0.020	0.9347	-0.6
A_c	0.670 ± 0.027	0.6677 ± 0.0001	0.1
A_s	0.895 ± 0.091	0.9356	-0.4

Table 10.6: Results derived from Table 10.5 and the corresponding covariance matrices [14, 299], and the SM predictions for the partial and total Z decay widths [in MeV]. In the (second) third column lepton universality is (not) assumed.

Quantity	Value	Value (universal)	Standard Model
$\Gamma_{e^+e^-}$	83.87 ± 0.12	83.942 ± 0.085	83.960 ± 0.009
$\Gamma_{\mu^+\mu^-}$	83.95 ± 0.18	83.941 ± 0.085	83.959 ± 0.009
$\Gamma_{\tau^+\tau^-}$	84.03 ± 0.21	83.759 ± 0.085	83.777 ± 0.009
$\Gamma_{\rm inv}$	498.9 ± 2.5	500.5 ± 1.5	501.445 ± 0.047
$\Gamma_{u\bar{u}}$	—	—	299.89 ± 0.20
$\Gamma_{c\bar{c}}$	300.3 ± 5.3	300.0 ± 5.2	299.81 ± 0.20
$\Gamma_{d\bar{d}}, \Gamma_{s\bar{s}}$	—	—	382.77 ± 0.14
$\Gamma_{b\bar{b}}$	377.4 ± 1.3	377.0 ± 1.2	375.73 ∓ 0.18
$\Gamma_{\rm had}$	1744.8 ± 2.6	1743.2 ± 1.9	1740.97 ± 0.85
Γ_Z	2495.5 ± 2.3	2495.5 ± 2.3	2494.11 ± 0.86

radiative corrections and final-state mass effects) are given by,

$$\Gamma(W^+ \to e^+\nu_e) = \frac{M_W^3}{12\pi v^2} = 226.33 \pm 0.05\,\text{MeV}\ , \tag{10.64a}$$

$$\Gamma(W^+ \to u_i\bar{d}_j) = \frac{M_W^3}{12\pi v^2}\,|V_{ij}|^2\mathcal{R}_V^q = (705.4 \pm 0.4\,\text{MeV})|V_{ij}|^2\ , \tag{10.64b}$$

$$\Gamma(Z \to f\bar{f}) = \frac{M_Z^3}{12\pi v^2}\left[\mathcal{R}_V^f\bar{g}_V^{f2} + \mathcal{R}_A^f\bar{g}_A^{f2}\right]\ , \tag{10.64c}$$

where the result for the latter are shown in Table 10.6. Final-state QED and QCD corrections [300] to the vector and axial-vector form factors are given by,

$$\mathcal{R}_{V,A}^f = N_C\left[1 + \frac{3}{4}\left(Q_f^2\frac{\alpha(s)}{\pi} + \frac{N_C^2-1}{2N_C}\frac{\alpha_s(s)}{\pi}\right) + \cdots\right]\ , \tag{10.65}$$

where $N_C = 3$ (1) is the color factor for quarks (leptons) and the dots indicate finite fermion mass effects proportional to m_f^2/s which are different for $\mathcal{R}_V^f$ and $\mathcal{R}_A^f$, as well as higher-order QCD corrections [301], which are known to $\mathcal{O}(\alpha_s^4)$ [214]. These include

Downloaded from https://academic.oup.com/ptep/article/2022/8/083C01/6651666 by KIT Library user on 27 September 2022

singlet contributions starting from two-loop order which are large, strongly top quark mass dependent, family universal, and flavor non-universal [302–306]. The $\mathcal{O}(\alpha^2)$ self-energy corrections from Ref. [307] are also taken into account.

For the W decay into quarks, Eq. (10.64b), only the universal massless part (non-singlet and $m_q = 0$) of the final-state QCD radiator function in $\mathcal{R}_V$ from Eq. (10.65) is used, and the QED corrections are modified. Expressing the widths in terms of $G_F M_{W,Z}^3$ incorporates the largest radiative corrections from the running QED coupling. EW corrections to the Z widths are then taken into account through the effective couplings $\bar{g}^{\,i\,2}_{V,A}$. Hence, in the on-shell scheme the Z widths are proportional to $\rho_i \sim 1 + \rho_t$. There is additional (negative) quadratic m_t dependence in the $Z \to b\bar{b}$ vertex corrections [308,309] which causes $\Gamma_{b\bar{b}}$ to decrease with m_t. The dominant effect is to multiply $\Gamma_{b\bar{b}}$ by the vertex correction $1 + \delta\rho_{b\bar{b}}$, where $\delta\rho_{b\bar{b}} \sim 10^{-2}(-\frac{1}{2}m_t^2/M_Z^2 + \frac{1}{5})$. In practice, the corrections are included in $\widehat{\rho}_b$ and $\widehat{\kappa}_b$, as discussed in Sec. 10.5.

Starting at $\mathcal{O}(\alpha\alpha_s)$, the factorized form indicated in Eq. (10.64) is violated and corrections need to be included [310–312]. They add coherently, resulting in a sizable effect, and shift $\alpha_s(M_Z)$ when extracted from Z lineshape observables by about $+0.0007$. Similar non-factorizable corrections are also known for mixed QED-EW corrections [106,107,109,313].

For three fermion families the total widths of the Z [314–318] and W [319,320] bosons are predicted to be,

$$\Gamma_Z = 2.4941 \pm 0.0009\,\text{GeV}\ , \quad \Gamma_W = 2.0895 \pm 0.0008\,\text{GeV}\ . \tag{10.66}$$

The uncertainties in these predictions are almost entirely induced by the parametric error in $\alpha_s(M_Z) = 0.1185 \pm 0.0016$ from the global fit. These predictions can be compared with the experimental results, $\Gamma_Z = 2.4955 \pm 0.0023$ GeV [14, 299] and $\Gamma_W = 2.085 \pm 0.042$ GeV [267,269] (see the Gauge & Higgs Bosons Particle Listings). The hadronic branching ratio of the W boson, $\mathcal{B}(W \to \text{hadrons})$ has been measured by both LEP 2 [267] and CMS [272] . The measurements of the total and partical widths are generally in good agreement with the SM. The exception is the branching ratio $W \to \tau + \nu_\tau$ from LEP 2, which is 2.6 σ larger than the electron-muon average [267][15].

The invisible decay width, $\Gamma_{\text{inv}} = \Gamma_Z - \Gamma_{e^+e^-} - \Gamma_{\mu^+\mu^-} - \Gamma_{\tau^+\tau^-} - \Gamma_{\text{had}}$, can be used to determine the number of neutrino flavors, N_ν, much lighter than $M_Z/2$. The hadronic peak cross section, and therefore the extracted Γ_{had}, depends strongly on the knowledge of the LEP 1 luminosity derived from small-angle Bhabha scattering. However, the prediction for the Bhabha cross-section was recently found to be overestimated, and consequently the luminosity underestimated [299]. The updated analysis involved an improved Z lineshape fit, significantly reducing σ_{had}, while slightly increasing Γ_Z, with the result, $N_\nu = 2.9963 \pm 0.0074$ [299]. In practice, we determine N_ν by allowing it as an additional fit parameter and obtain,

$$N_\nu = 3.0026 \pm 0.0061\ , \tag{10.67}$$

which is now in perfect agreement with the observed number of fermion generations and $N_\nu = 3$ (a 1.3 σ deviation was observed in the 2018 edition of this *Review* before including the correction in the luminosity determination).

10.6 Global fit results

In this section, we present the results of global fits, subject to the experimental data and theoretical constraints discussed in Section 10.2−10.5. For earlier analyses, see Refs. [14,78,322–325] and previous editions of this *Review*. The values for m_t, M_H [275,276], Γ_H [277], M_W [267,268,270,271], Γ_W [267,269], the weak charges of the electron [158], the proton [159], cesium [170,171] and thallium [172,173], the weak mixing angle extracted from eDIS [148], $\nu_\mu(\bar{\nu}_\mu)$-e scattering [129–131], the τ lifetime, and the μ anomalous magnetic moment [224] are listed in Table 10.4. Likewise, Table 10.5 summarizes the principal Z pole observables, where the LEP 1 averages of the ALEPH, DELPHI, L3, and OPAL results include common systematic uncertainties and correlations [14,299]. The heavy flavor results [14,290] of LEP 1 and SLD are based on common inputs, and are thus correlated, as well.

Also shown in both tables are the SM predictions for the values of M_Z, $\alpha_s(M_Z)$, $\Delta\alpha^{(3)}_{\text{had}}$ and the heavy quark masses shown in Table 10.7. The predictions result from a global least-square (χ^2) fit to all data using the minimization package MINUIT [326] and the EW library GAPP [34]. In most cases, we treat all input errors (the uncertainties of the values) as Gaussian. The reason is not that we assume that theoretical and systematic errors are intrinsically bell-shaped (which they are not) but because in most cases the input errors are either dominated by the statistical components or they are combinations of many different (including statistical) error sources, which should yield approximately Gaussian *combined* errors by the large number theorem. An exception is the theory dominated error on the τ lifetime, which we recalculate in each χ^2-function call since it depends itself on α_s. Sizes and shapes of the output errors (the uncertainties of the predictions and the SM fit parameters) are fully determined by the fit, and 1 σ errors are defined to correspond to $\Delta\chi^2 = \chi^2 - \chi^2_{\text{min}} = 1$, and do not necessarily correspond to the 68.3% probability range or the 39.3% probability contour (for 2 parameters).

The agreement is generally very good. Despite the few discrepancies addressed in the following, the global electroweak fit describes the data well, with a very good $\chi^2/\text{d.o.f.} = 46.7/43$. The probability of a larger χ^2 is 32%, and only $g_\mu - 2$ is currently showing a larger (3.8 σ) conflict. In addition, A^0_{LR} (SLD) from hadronic final states and $A^{(0,b)}_{FB}$ (LEP 1) deviate at the 2 σ level. g_L^2 from NuTeV is nominally in conflict with the SM, as well, but the precise status is unresolved (see Sec. 10.3.1). We also emphasize that there are a number of discrepancies among individual measurements of certain quantities, as discussed in previous sections, but that they are not reflected in the overall χ^2 of the fit as only the corresponding combinations are used as constraints.

A_b can be extracted from $A^{(0,b)}_{FB}$ when $A_e = 0.1501 \pm 0.0016$ is taken from a fit to leptonic asymmetries (using lepton universality). The result, $A_b = 0.885 \pm 0.017$, is 2.9 σ below the SM prediction[16] and also 1.4 σ below $A_b = 0.923 \pm 0.020$ obtained from $A^{FB}_{LR}(b)$ at SLD. Thus, it appears that at least some of the problem in A_b is due to a statistical fluctuation or other experimental effect in one of the asymmetries. Note, however, that the uncertainty in $A^{(0,b)}_{FB}$ is strongly statistics dominated. The combined value, $A_b = 0.901 \pm 0.013$ deviates by 2.6 σ.

The left-right asymmetry, $A^0_{LR} = 0.15138 \pm 0.00216$ [284], from hadronic decays at SLD, differs by 2.1 σ from the SM expectation of 0.1468 ± 0.0003. The combined value of $A_\ell = 0.1513 \pm 0.0021$ from SLD (using lepton-family universality and including correlations) is also 2.1 σ above the SM prediction; but there is experimental agreement between this SLD value and the LEP 1 value, $A_\ell = 0.1481 \pm 0.0027$, obtained from a fit to $A^{(0,\ell)}_{FB}$, $A_e(\mathcal{P}_\tau)$, and $A_\tau(\mathcal{P}_\tau)$, again assuming universality.

The observables in Table 10.4 and Table 10.5, as well as some other less precise observables, are used in the global fits described below. In all fits, the errors include full statistical, systematic, and theoretical uncertainties. The correlations from the LEP 1 lineshape and τ polarization measurements, the LEP/SLD heavy flavor observables, the SLD lepton asymmetries, and the ν-e scattering observables, are included. The theoretical correlations between $\Delta\alpha^{(5)}_{\text{had}}$, $\widehat{s}_0^2$, and $g_\mu - 2$, and between the M_W extractions from the LHC and the Tevatron, are also accounted for.

The electroweak data allow a simultaneous determination of M_Z, m_t, and $\alpha_s(M_Z)$. The direct measurements of M_H at the LHC [275,276] have reached a precision that the global fit result

[15] W-boson branching ratio measurements from CMS and ATLAS are in good agreement with lepton universality and slightly more precise than LEP-2 [272,321].

[16] Alternatively, one can use $A_\ell = 0.1481 \pm 0.0027$, which is from LEP 1 alone and in excellent agreement with the SM, and obtain $A_b = 0.897 \pm 0.022$ which is 1.7 σ low. This illustrates that some of the discrepancy is related to the one in A_{LR}.

Downloaded from https://academic.oup.com/ptep/article/2022/8/083C01/6651666 by KIT Library user on 27 September 2022

Table 10.7: Principal SM fit result including mutual correlations.

M_Z [GeV]	91.1882 ± 0.0020	1.00	−0.07	0.00	0.00	0.02	0.02
$\widehat{m}_t(\widehat{m}_t)$ [GeV]	163.45 ± 0.55	−0.07	1.00	0.00	−0.11	−0.22	0.04
$\widehat{m}_b(\widehat{m}_b)$ [GeV]	4.180 ± 0.008	0.00	0.00	1.00	0.20	−0.02	0.00
$\widehat{m}_c(\widehat{m}_c)$ [GeV]	1.274 ± 0.009	0.00	−0.11	0.20	1.00	0.47	0.00
$\alpha_s(M_Z)$	0.1185 ± 0.0016	0.02	−0.22	−0.02	0.47	1.00	−0.03
$\Delta\alpha^{(3)}_{\rm had}(2\ {\rm GeV})$	0.00593 ± 0.00005	0.02	0.04	0.00	0.00	−0.03	1.00

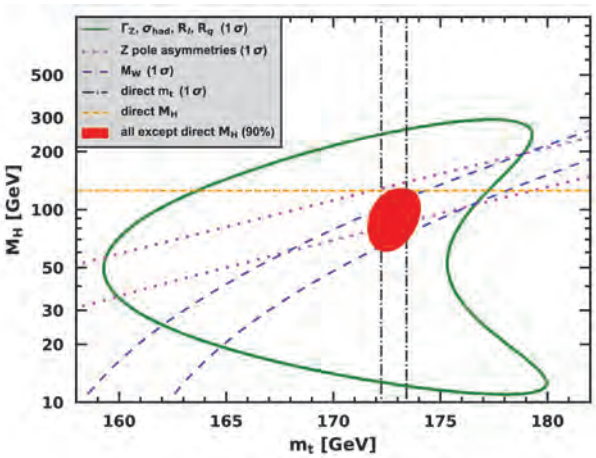

Figure 10.4: Fit result and one-standard-deviation (39.35% for the closed contours and 68% for the others) uncertainties in M_H as a function of m_t for various inputs, and the 90% CL region ($\Delta\chi^2 = 4.605$) allowed by all data. $\alpha_s(M_Z) = 0.1185$ is assumed except for the fits including the Z lineshape. The width of the horizontal dashed band is not visible on the scale of the plot.

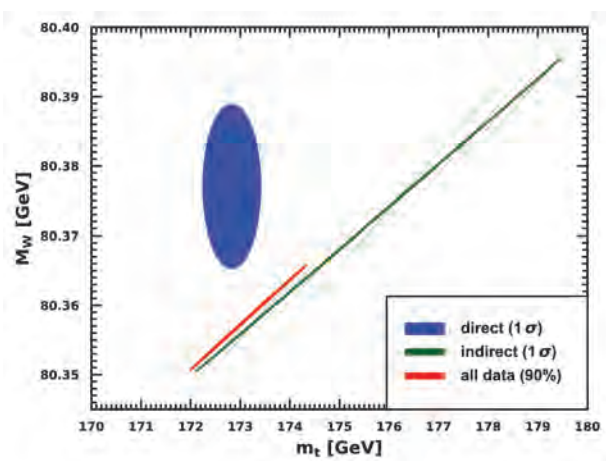

Figure 10.5: One-standard-deviation (39.35%) regions in M_W as a function of m_t for the direct and indirect data, and the 90% CL region ($\Delta\chi^2 = 4.605$) allowed by all data.

for M_H coincides with the constraint in Eq. (10.56) with negligible correlations with the other fit parameters. $\widehat{m}_c$, $\widehat{m}_b$, and $\Delta\alpha^{(3)}_{\rm had}$ are also allowed to float in the fits, subject to the theoretical constraints [30, 55] described in Sec. 10.2, and are correlated with α_s, which in turn is determined mainly through R_ℓ, Γ_Z, $\sigma_{\rm had}$, and τ_τ. The global fit to all data, including the hadron collider m_t average in Eq. (10.17), yields the results in Table 10.7, while those for the weak mixing angle in various schemes are summarized in Table 10.2.

Removing the kinematic constraint on M_H from LHC gives the loop-level determination from the precision data,

$$M_H = 91^{+18}_{-16}\ {\rm GeV}\ , \tag{10.68}$$

which is 1.7 σ below the value in Eq. (10.56). The latter is also slightly outside the 90% central confidence range,

$$65\ {\rm GeV} < M_H < 122\ {\rm GeV}\ . \tag{10.69}$$

This is mostly a reflection of the Tevatron determination of M_W, which is 1.7 σ higher than the SM best fit value in Table 10.4. This is shown in Fig. 10.4 where one sees that the precision data together with M_H from the LHC prefer m_t to be closer to the upper end of its 1 σ allowed range.

Conversely, one can remove the explicit M_W and Γ_W constraints from the global fit and use $M_H = 125.30 \pm 0.13$ GeV to obtain $M_W = 80.356 \pm 0.006$ GeV, which is 1.6 σ below the world average in Eq. (10.55). Finally, one can carry out a fit without including the direct constraint, $m_t = 172.83 \pm 0.59$ GeV, from the hadron colliders. One obtains $m_t = 176.2 \pm 1.9$ GeV, which is 1.7 σ higher than the collider average. (The indirect prediction is for the $\overline{\rm MS}$ mass definition, $\widehat{m}_t(\widehat{m}_t) = 166.4 \pm 1.8$ GeV, which is in the end converted to the pole mass.) The situation is summarized in Fig. 10.5 showing the 1 σ contours in the $M_W - m_t$ plane from the direct and indirect determinations, as well as the combined 90% CL region.

In view of these tensions it is instructive to study the effect of doubling the uncertainty in $\Delta\alpha^{(3)}_{\rm had}(2\ {\rm GeV}) = (58.84 \pm 0.51) \times 10^{-4}$ (see Sec. 10.2) on the loop-level determination of the Higgs boson mass. The result, $M_H = 88^{+19}_{-16}$ GeV, deviates even slightly *more* (1.8 σ) than Eq. (10.68), and demonstrates that the uncertainty in $\Delta\alpha_{\rm had}$ is currently of only secondary importance. Note also that an increase of 3×10^{-4} in $\Delta\alpha^{(3)}_{\rm had}(2\ {\rm GeV})$, as favored by the very recent lattice evaluation in Ref. [329], corresponds to a decrease of the indirectly extracted M_H by 13 GeV. The hadronic contribution to $\alpha(M_Z)$ is correlated with $g_\mu - 2$ (see Sec. 10.4). The measurement of the latter is higher than the SM prediction, and its inclusion in the fit favors a larger $\alpha(M_Z)$ and a lower M_H from the precision data (currently by 2.8 GeV).

The weak mixing angle can be determined from Z pole observables, M_W, and a variety of neutral-current processes spanning a very wide Q^2 range. The results (for older low energy neutral-current data see Refs. [322–325], as well as earlier editions of this *Review*) shown in Table 10.8 are in reasonable agreement with each other, indicating the quantitative success of the SM. One of the largest discrepancies is the value $\widehat{s}^2_Z = 0.23176 \pm 0.00027$ from $A^{(0,b)}_{FB}$ and $A^{(0,c)}_{FB}$, which is 2.0 σ above the value 0.23122 ± 0.00004 from the global fit to all data. Similarly, $\widehat{s}^2_Z = 0.23064 \pm 0.00028$ from the SLD asymmetries (in both cases when combined with M_Z, Γ_Z, and m_t) is 2.1 σ low.

The extracted Z pole value of $\alpha_s(M_Z)$ is based on a formula with negligible theoretical uncertainty if one assumes the exact validity of the SM. One should keep in mind, however, that this value, $\alpha_s(M_Z) = 0.1221 \pm 0.0027$, which increased after the updated analysis in Ref. [299], is very sensitive to certain types of new physics such as non-universal vertex corrections. In contrast, the value derived from τ decays, $\alpha_s(M_Z) = 0.1171^{+0.0018}_{-0.0017}$, is theory dominated but less sensitive to new physics. The agreement between the two values is only marginal, but the latter does agree well with the averages deduced from heavy quarkonia spectroscopy (0.1183 ± 0.0039), DIS and global PDF fits

Downloaded from https://academic.oup.com/ptep/article/2022/8/083C01/6651666 by KIT Library user on 27 September 2022

Table 10.8: Values of $\widehat{s}_Z^2$, s_W^2, α_s, m_t and M_H for various data sets. In the fit to the LHC data, the α_s constraint is from a combined NNLO analysis of inclusive electroweak boson production cross-sections at the LHC [327]. Likewise, for the Tevatron fit we use the α_s result from the inclusive jet cross-section at DØ [328].

data set	$\widehat{s}_Z^2$	s_W^2	$\alpha_s(M_Z)$	m_t [GeV]	M_H [GeV]
all data	0.23122(4)	0.22339(10)	0.1185(16)	173.1 ± 0.6	125
all data except M_H	0.23109(9)	0.22312(19)	0.1189(17)	172.8 ± 0.6	$91^{+\ 18}_{-\ 16}$
all data except M_Z	0.23113(6)	0.22335(10)	0.1185(16)	172.8 ± 0.6	125
all data except M_W	0.23125(4)	0.22346(11)	0.1189(17)	172.9 ± 0.6	125
all data except m_t	0.23115(6)	0.22307(21)	0.1190(17)	176.2 ± 1.9	125
$M_{H,Z} + \Gamma_{H,Z} + m_t$	0.23128(8)	0.22353(16)	0.1218(45)	172.8 ± 0.6	125
LHC	0.23116(10)	0.22340(12)	0.1187(16)	172.6 ± 0.6	125
Tevatron + M_Z	0.23103(14)	0.22294(30)	0.1160(45)	174.3 ± 0.8	$99^{+\ 31}_{-\ 27}$
LEP 1 + LEP 2	0.23137(18)	0.22352(46)	0.1234(29)	178 ± 11	195^{+267}_{-109}
LEP 1 + SLD	0.23116(17)	0.22345(58)	0.1221(27)	169 ± 10	$79^{+100}_{-\ 38}$
SLD + $M_Z + \Gamma_Z + m_t$	0.23064(28)	0.22226(54)	0.1191(48)	172.8 ± 0.6	$36^{+\ 29}_{-\ 21}$
$A_{FB}^{(b,c)} + M_Z + \Gamma_Z + m_t$	0.23176(27)	0.22465(66)	0.1267(45)	172.8 ± 0.6	$273^{+140}_{-\ 98}$
$M_{W,Z} + \Gamma_{W,Z} + m_t$	0.23106(12)	0.22306(25)	0.1201(42)	172.8 ± 0.6	$86^{+\ 23}_{-\ 20}$
low energy + $M_{H,Z}$	0.23174(94)	0.2253(35)	0.1172(18)	157 ± 29	125

Table 10.9: Values of model-independent neutral-current parameters, compared with the SM predictions, where the uncertainties in the latter are $\lesssim 0.0001$, throughout.

Quantity	Experimental Value	Standard Model	Correlation	
$g_{LV}^{\nu e}$	-0.040 ± 0.015	-0.0397		-0.05
$g_{LA}^{\nu e}$	-0.507 ± 0.014	-0.5064		
$g_{AV}^{eu} + 2\,g_{AV}^{ed}$	0.4927 ± 0.0031	0.4950	-0.88	0.20
$2\,g_{AV}^{eu} - \ g_{AV}^{ed}$	-0.7165 ± 0.0068	-0.7193		-0.22
$2\,g_{VA}^{eu} - \ g_{VA}^{ed}$	-0.13 ± 0.06	-0.0950		
g_{VA}^{ee}	0.0190 ± 0.0027	0.0226		

(0.1162 ± 0.0020), hadronic final states of e^+e^- annihilations (0.1171 ± 0.0031), hadron colliders (0.1165 ± 0.0028), as well as lattice QCD simulations (0.1182 ± 0.0008). For more details, other determinations, and references, see the Section on "Quantum Chromodynamics" in this *Review*. We also provide the values, computed with five-loop beta functions and four-loop matching,

$$\alpha_s^{(4)}(m_\tau) = 0.324 \pm 0.014, \tag{10.70}$$

$$\alpha_s^{(5)}(M_W) = 0.1208 \pm 0.0017, \tag{10.71}$$

$$\alpha_s^{(5)}(M_H) = 0.1131 \pm 0.0015, \tag{10.72}$$

$$\alpha_s^{(6)}(m_t) = 0.1089 \pm 0.0014, \tag{10.73}$$

to be used in precision calculations.

Using $\alpha(M_Z)$ and $\widehat{s}_Z^2$ as inputs, one can predict $\alpha_s(M_Z)$ assuming grand unification. One finds $\alpha_s(M_Z) = 0.13 \pm 0.01$ [330, 331] for the simplest theories based on the minimal supersymmetric extension of the SM, where the uncertainty is from the unknown particle thresholds. This is slightly larger, but consistent with $\alpha_s(M_Z) = 0.1185 \pm 0.0016$ from our fit and most other determinations, while minimal non-supersymmetric theories predict much lower and excluded values (see the Section on "Grand Unified Theories" in this *Review*).

Most of the parameters relevant to ν-hadron, ν-e, e-hadron, and e-e processes are determined uniquely and precisely from the data in "model-independent" fits, *i.e.*, fits allowing for an arbitrary EW gauge theory. The values for the parameters defined in Eq. (10.25) are given in Table 10.9 along with the predictions of the SM. The agreement is very good. (The ν-hadron results including NuTeV [143] and other ν-DIS data can be found in the 2006 edition of this *Review*, and fits with modified NuTeV constraints in the 2008 and 2010 editions.)

10.7 Constraints on new physics

The masses and decay properties of the electroweak bosons and low energy data can be used to search for and set limits on deviations from the SM. We will mainly discuss the effects of exotic particles (with heavy masses $M_{\rm new} \gg M_Z$ in an expansion in $M_Z/M_{\rm new}$) on the gauge boson self-energies. (Brief remarks are made on new physics which is not of this type.) Most of the effects on precision measurements can be described by three gauge self-energy parameters S, T, and U. We will define these, as well as the related parameters ρ_0, ϵ_i, and $\widehat{\epsilon}_i$, to arise from new physics only. In other words, they are equal to zero ($\rho_0 = 1$) exactly in the SM, and do not include any (loop induced) contributions that depend on m_t or M_H, which are treated separately. Our treatment differs from most of the original papers.

The dominant effect of many extensions of the SM can be described by the ρ_0 parameter,

$$\rho_0 \equiv \frac{M_W^2}{M_Z^2\,\widehat{c}_Z^2\,\widehat{\rho}}\,, \tag{10.74}$$

which describes new sources of SU(2) breaking that cannot be accounted for by the SM Higgs doublet or by m_t effects. $\widehat{\rho}$ is calculated as in Eq. (10.22) assuming the validity of the SM. In the presence of $\rho_0 \neq 1$, Eq. (10.74) generalizes the second Eq. (10.22) while the first remains unchanged. Provided that the new physics which yields $\rho_0 \neq 1$ is a small perturbation which does not significantly affect other radiative corrections, ρ_0 can be regarded as a phenomenological parameter which multiplies G_F in Eqs. (10.25) and (10.45), as well as Γ_Z in Eq. (10.64c). There are enough data to determine ρ_0, M_H, m_t, and α_s, simultaneously. From the

Downloaded from https://academic.oup.com/ptep/article/2022/8/083C01/6651666 by KIT Library user on 27 September 2022

global fit,

$$\rho_0 = 1.00038 \pm 0.00020 \ , \tag{10.75a}$$

$$\alpha_s(M_Z) = 0.1188 \ \ \pm 0.0017 \ , \tag{10.75b}$$

where as before the uncertainty is from the experimental inputs and includes an estimate of the error from unknown higher-order electroweak corrections. The result in Eq. (10.75a) is 2.0 σ above the SM expectation, $\rho_0 = 1$. It can be used to constrain higher-dimensional Higgs representations to have vacuum expectation values of less than a few percent of those of the doublets. Indeed, the relation between M_W and M_Z is modified if there are Higgs multiplets with weak isospin $> 1/2$ and significant vacuum expectation values. For a general (charge-conserving) Higgs structure,

$$\rho_0 = \frac{\sum_i [t_i(t_i+1) - t_{3i}^2]|v_i|^2}{2\sum_i t_{3i}^2 |v_i|^2} \ , \tag{10.76}$$

where v_i is the expectation value of the neutral component of a Higgs multiplet with weak isospin t_i and third component t_{3i}. In order to calculate to higher orders in such theories one must define a set of four fundamental renormalized parameters which one may conveniently choose to be α, G_F, M_Z, and M_W, since M_W and M_Z are directly measurable. Then $\widehat{s}_Z^2$ and ρ_0 can be considered dependent parameters.

Eq. (10.75a) can also be used to constrain other types of new physics. For example, non-degenerate multiplets of heavy fermions or scalars break the vector part of weak SU(2) and lead to a decrease in the value of M_Z/M_W. Each non-degenerate SU(2) doublet $\binom{f_1}{f_2}$ yields a positive contribution to ρ_0 [332–334] of

$$\frac{N_C\, G_F}{8\sqrt{2}\pi^2} \Delta m^2 \ , \tag{10.77}$$

where

$$\Delta m^2 \equiv m_1^2 + m_2^2 - \frac{4 m_1^2 m_2^2}{m_1^2 - m_2^2} \ln \frac{m_1}{m_2} \geq (m_1 - m_2)^2 \ , \tag{10.78}$$

and $N_C = 1$ (3) for color singlets (triplets). Eq. (10.75a) taken together with Eq. (10.77) implies the following constraint on the mass splitting at the 90% CL,

$$(14 \text{ GeV})^2 < \sum_i \frac{N_C^i}{3} \Delta m_i^2 < (48 \text{ GeV})^2 \ , \tag{10.79}$$

where the sum runs over all new-physics doublets, for example fourth-family quarks or leptons, $\binom{t'}{b'}$ or $\binom{\nu'}{\ell'-}$, vector-like fermion doublets (which contribute to the sum in Eq. (10.79) with an extra factor of 2), and scalar doublets such as $\binom{\tilde{t}}{\tilde{b}}$ in Supersymmetry (in the absence of L–R mixing).

Non-degenerate multiplets usually imply $\rho_0 > 1$. Similarly, heavy Z' bosons decrease the prediction for M_Z due to mixing and generally lead to $\rho_0 > 1$ [335]. On the other hand, extra Higgs doublets participating in spontaneous symmetry breaking [336–338] or heavy lepton doublets involving Majorana neutrinos [339], both of which have more complicated expressions, and the v_i of higher-dimensional Higgs representations can contribute to ρ_0 with either sign.

A number of authors [340–342] have considered the general effects on neutral-current, Z and W boson observables of various types of heavy (*i.e.*, $M_{\rm new} \gg M_Z$) physics which contribute to the W and Z self-energies but which do not have any direct coupling to the ordinary fermions (an alternative formulation is given by Ref. [343]). In addition to non-degenerate multiplets, which break the vector part of weak SU(2), these include heavy degenerate multiplets of chiral fermions which break the axial generators.

Such effects can be described by just three parameters, S, T, and U [344], at the (EW) one-loop level[17]. T is proportional to the difference between the W and Z self-energies at $Q^2 = 0$ (*i.e.*, vector SU(2)-breaking), while S ($S+U$) is associated with the difference between the Z (W) self-energy at $Q^2 = M_{Z,W}^2$ and $Q^2 = 0$ (axial SU(2)-breaking). Denoting the contributions of new physics to the various self-energies by $\Pi_{ij}^{\rm new}$, we have

$$\widehat{\alpha}(M_Z) T \equiv \frac{\Pi_{WW}^{\rm new}(0)}{M_W^2} - \frac{\Pi_{ZZ}^{\rm new}(0)}{M_Z^2} \ , \tag{10.80a}$$

$$\frac{\widehat{\alpha}(M_Z)}{4\widehat{s}_Z^2 \widehat{c}_Z^2} S \equiv \frac{\Pi_{ZZ}^{\rm new}(M_Z^2) - \Pi_{ZZ}^{\rm new}(0)}{M_Z^2} - \frac{\widehat{c}_Z^2 - \widehat{s}_Z^2}{\widehat{c}_Z \widehat{s}_Z} \frac{\Pi_{Z\gamma}^{\rm new}(M_Z^2)}{M_Z^2} - \frac{\Pi_{\gamma\gamma}^{\rm new}(M_Z^2)}{M_Z^2} \ , \tag{10.80b}$$

$$\frac{\widehat{\alpha}(M_Z)}{4\widehat{s}_Z^2} (S+U) \equiv \frac{\Pi_{WW}^{\rm new}(M_W^2) - \Pi_{WW}^{\rm new}(0)}{M_W^2} - \frac{\widehat{c}_Z}{\widehat{s}_Z} \frac{\Pi_{Z\gamma}^{\rm new}(M_Z^2)}{M_Z^2} - \frac{\Pi_{\gamma\gamma}^{\rm new}(M_Z^2)}{M_Z^2} \ . \tag{10.80c}$$

S, T, and U are defined with a factor proportional to $\widehat{\alpha}$ removed, so that they are expected to be of order unity in the presence of new physics. In the $\overline{\rm MS}$ scheme as defined in Ref. [80], the last two terms in Eqs. (10.80b) and (10.80c) can be omitted, as was done in some earlier editions of this *Review*. These parameters are related to other parameter sets, S_i [80], $\widehat{\epsilon}_i$ [348], and h_i [349], by

$$T = h_V = \frac{\widehat{\epsilon}_1}{\widehat{\alpha}(M_Z)} \ , \tag{10.81a}$$

$$S = h_{AZ} = S_Z = 4\widehat{s}_Z^2 \frac{\widehat{\epsilon}_3}{\widehat{\alpha}(M_Z)} \ , \tag{10.81b}$$

$$U = h_{AW} - h_{AZ} = S_W - S_Z = -4\widehat{s}_Z^2 \frac{\widehat{\epsilon}_2}{\widehat{\alpha}(M_Z)} \ . \tag{10.81c}$$

A heavy non-degenerate multiplet of fermions or scalars contributes positively to T as

$$\rho_0 - 1 = \frac{1}{1 - \widehat{\alpha}(M_Z) T} - 1 \approx \widehat{\alpha}(M_Z) T \ , \tag{10.82}$$

where $\rho_0 - 1$ is given in Eq. (10.77). The effects of non-standard Higgs representations cannot be separated from heavy non-degenerate multiplets unless the new physics has other consequences, such as vertex corrections. Most of the original papers defined T to include the effects of loops only. However, we will redefine T to include all new sources of SU(2) breaking, including non-standard Higgs, so that T and ρ_0 are equivalent by Eq. (10.82).

A multiplet of heavy degenerate chiral fermions yields

$$S = \frac{N_C}{3\pi} \sum_i \left(t_{3i}^L - t_{3i}^R \right)^2 \ , \tag{10.83}$$

where $t_{3i}^{L,R}$ is the 3rd component of weak isospin of the left-(right-)handed component of fermion i. For example, a heavy degenerate ordinary or mirror family would contribute $2/3\pi$ to S. In models with warped extra dimensions [350], sizeable corrections to the S parameter are generated through mixing between the SM gauge bosons and their Kaluza-Klein (KK) excitations, and one finds $S \approx 30\, v^2 M_{KK}^{-2}$ [351], where M_{KK} is the mass scale of the KK gauge bosons. Large positive values of S can also be generated in models with dynamical electroweak symmetry breaking, where the Higgs boson is composite. In simple composite Higgs models, the dominant contribution stems from heavy spin-1 resonances of the strong dynamics leading to $S \approx 4\pi v^2 (M_V^{-2} + M_A^{-2})$, where $M_{V,A}$ are the masses of the lightest vector and axial-vector resonances, respectively [352].

[17] Three additional parameters are needed if the new physics scale is comparable to M_Z [345]. Further generalizations, including effects relevant to LEP 2 and Drell-Yan production at the LHC, are described in Refs. [346] and [347], respectively.

Downloaded from https://academic.oup.com/ptep/article/2022/8/083C01/6651666 by KIT Library user on 27 September 2022

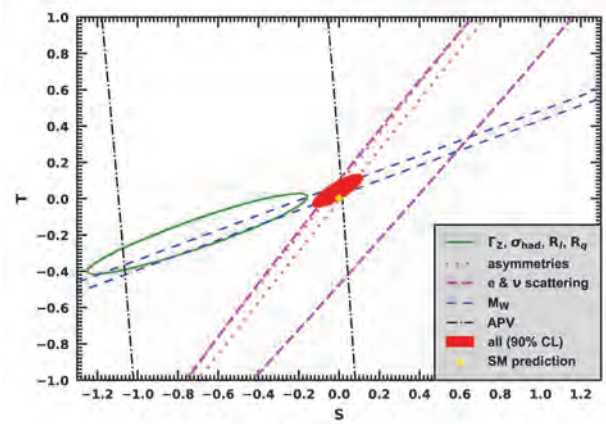

Figure 10.6: 1 σ constraints (39.35% for the closed contours and 68% for the others) on S and T (for $U = 0$) from various inputs combined with M_Z. S and T represent the contributions of new physics only. Data sets not involving M_W or Γ_W are insensitive to U. With the exception of the fit to all data, we fix $\alpha_s = 0.1185$. The yellow dot indicates the Standard Model values $S = T = 0$.

Negative values of S are possible, for example, in composite Higgs models [353], or from loops involving scalars or Majorana particles [354–356]. The simplest origin of $S < 0$ would probably be an additional heavy Z' boson [335]. Supersymmetric extensions of the SM [357, 358] generally give very small effects. For more details and references, see Refs. [359–368] and the Sections on "Supersymmetry" in this *Review*. Most simple types of new physics yield $U = 0$, although there are counter-examples, such as the effects of anomalous triple gauge vertices [348].

The SM expressions for observables are replaced by,

$$M_Z^2 = M_{Z0}^2 \frac{1 - \widehat{\alpha}(M_Z)T}{1 - G_F M_{Z0}^2 S/2\sqrt{2}\pi} , \tag{10.84a}$$

$$M_W^2 = M_{W0}^2 \frac{1}{1 - G_F M_{W0}^2 (S+U)/2\sqrt{2}\pi} , \tag{10.84b}$$

where M_{Z0} and M_{W0} are the SM expressions (as functions of m_t and M_H) in the $\overline{\text{MS}}$ scheme. Furthermore,

$$\Gamma_Z = \frac{M_Z^3 \beta_Z}{1 - \widehat{\alpha}(M_Z)T} , \tag{10.85a}$$

$$\Gamma_W = M_W^3 \beta_W , \tag{10.85b}$$

$$A_i = \frac{A_{i0}}{1 - \widehat{\alpha}(M_Z)T} , \tag{10.85c}$$

where $\beta_{Z,W}$ are the SM expressions for the reduced widths Γ_{Z0}/M_{Z0}^3 and Γ_{W0}/M_{W0}^3, M_Z and M_W are the physical masses, and A_i (A_{i0}) is a neutral-current amplitude (in the SM).

The data allows for a simultaneous determination of M_H and m_t (from the hadron colliders), S (from M_Z), T (mainly from Γ_Z), U (from M_W), $\widehat{s}_Z^2 = 0.23112 \pm 0.00013$ (from the Z pole asymmetries), and $\alpha_s(M_Z) = 0.1189 \pm 0.0018$ (from R_ℓ, σ_{had}, and τ_τ), giving,

$$S = -0.02 \pm 0.10 , \tag{10.86a}$$

$$T = 0.03 \pm 0.12 , \tag{10.86b}$$

$$U = 0.01 \pm 0.11 , \tag{10.86c}$$

with little correlation among the SM parameters, where the uncertainties are from unknown higher orders in the SM predictions and the inputs. The parameters in Eq. (10.86), which by definition are due to new physics only, are in excellent agreement with the SM values of zero. Fixing $U = 0$, which is motivated by the fact that U is suppressed by an additional factor M_{new}^2/M_Z^2 compared to S and T [369], greatly improves the precision on S and particularly T,

$$S = -0.01 \pm 0.07 , \tag{10.87a}$$

$$T = 0.04 \pm 0.06 . \tag{10.87b}$$

If only any one of the three parameters is allowed, then this parameter would deviate almost at the 2 σ level, reflecting the deviation in M_W. Using Eq. (10.82), the value of ρ_0 corresponding to T in Eqs. (10.86) is 1.0002 ± 0.0009, while the one corresponding to Eqs. (10.87) is 1.0003 ± 0.0005. Thus, the multi-parameter fits are consistent with $\rho_0 = 1$, in contrast to the fit with $S = U = 0$ in Eq. (10.75a). There is a strong correlation (92%) between the S and T parameters. The U parameter is -80% (-93%) anti-correlated with S (T). The allowed regions in S–T (for $U = 0$) are shown in Fig. 10.6. From Eq. (10.86) one obtains $S < 0.14$ and $T < 0.22$ at 95% CL, where the former puts the constraint $M_{KK} \gtrsim 3.6$ TeV on the masses of KK gauge bosons in warped extra dimensions. In minimal composite Higgs models, the bound on S requires $M_V \gtrsim 4$ TeV [370], but this constraint can be relaxed, *e.g.*, if the fermionic sector is also allowed to be partially composite [371, 372].

The S parameter can also be used to constrain the number of fermion families, *under the assumption* that there are no new contributions to T or U and therefore that any new families are degenerate; then an extra generation of SM fermions is excluded with almost 9 σ confidence, corresponding to $N_F = 2.74 \pm 0.15$. This can be compared to the fit to the number of light neutrinos given in Eq. (10.67), $N_\nu = 3.0026 \pm 0.0061$, but the S parameter fits are valid even for a very heavy fourth family neutrino. Allowing T to vary as well, the constraint on a fourth family is weaker [373]. However, a heavy fourth family would increase the Higgs production cross-section through gluon fusion by a factor of about 9 [374], which is in considerable tension with the observed Higgs signal at the LHC [375]. Combining the limits from electroweak precision data with the measured Higgs production rate and limits from direct searches for heavy quarks [376], a fourth family of chiral fermions is now excluded by more than five standard deviations [377, 378]. Similar remarks apply to a heavy mirror family [379] involving right-handed SU(2) doublets and left-handed singlets. In contrast, new doublets that receive most of their mass from a different source than the Higgs vacuum expectation value, such as vector-like fermion doublets or scalar doublets in Supersymmetry, give small or no contribution to S, T, U, and the Higgs production cross-section and are therefore still allowed. Partial or complete vector-like fermion families are predicted in many Grand Unified Theories [380] (see the Section on "Grand Unified Theories" in this *Review*), and many other models including supersymmetric and superstring inspired ones [381–384].

As discussed in Sec. 10.6, there is a 3.6% deviation in the asymmetry parameter A_b. Assuming that this is due to new physics affecting preferentially the third generation, we can perform a fit allowing additional $Z \to b\bar{b}$ vertex corrections ρ_b and κ_b as in Eq. (10.46) (here defined to be due to new physics only with the SM contributions removed), as well as S, T, U, and the SM parameters, with the result,

$$\rho_b = 0.058 \pm 0.020 , \tag{10.88a}$$

$$\kappa_b = 0.186 \pm 0.067 , \tag{10.88b}$$

with an almost perfect correlation of 99% (because R_b is much better determined than A_b). The central values of the oblique parameters are consistent with their SM values of zero, and there is little change in the SM parameters, except that the value of $\alpha_s(M_Z)$ is lower by 0.0008 compared to the SM fit. Given that an $\mathcal{O}(20\%)$ correction to κ_b would be necessary, it would be difficult to account for the deviation in A_b by new physics that enters only at the level of radiative corrections. Thus, if it is due to new physics, it is most likely of tree-level type affecting preferentially the third generation. Examples include the decay of a scalar neutrino resonance [385], mixing of the b quark with heavy exotics [386], and

Downloaded from https://academic.oup.com/ptep/article/2022/8/083C01/6651666 by KIT Library user on 27 September 2022

a heavy Z' with family non-universal couplings [387, 388]. It is difficult, however, to simultaneously account for R_b without tuning, which has been measured on the Z peak and off-peak [389] at LEP 1.

There is no simple parametrization to describe the effects of every type of new physics on every possible observable. The S, T, and U formalism describes many types of heavy physics which affect only the gauge self-energies, and it can be applied to all precision observables. However, new physics which couples directly to ordinary fermions cannot be fully parametrized in the S, T, and U framework. Examples include heavy Z' bosons [335], mixing with exotic fermions [9, 390, 391], leptoquark exchange [267, 392, 393], supersymmetric models, strong EW dynamics [371], Little Higgs models [394, 395], and TeV-scale extra spatial dimensions [396–399] (for more details and references, see the Section on "Extra Dimensions" in this *Review*). These types of new physics can be parametrized in a model-independent way by using an effective field theory description [400–403]. Here the SM is extended by a set of higher-dimensional operators, denoted $\mathcal{O}_i$,

$$\mathcal{L} = \mathcal{L}_{\rm SM} + \sum_{d>4} \sum_i \frac{C_i}{\Lambda^{d-4}} \mathcal{O}_i \ , \tag{10.89}$$

where Λ is the characteristic scale of the new physics sector, which is assumed to satisfy $\Lambda \gg v$. For EW precision observables, the leading new operators enter at dimension $d = 6$. Note that S and T can be identified with two of these operators (or linear combinations thereof, depending on the chosen operator basis), while U corresponds to a dimension-8 operator [369, 404]. With current data on M_W and Z pole observables, Λ is constrained to be larger than $\mathcal{O}$(TeV) if the Wilson coefficients C_i are of order unity [405–410].

Limits on new four-Fermi operators and on leptoquarks using LEP 2 and lower energy data are given in Refs. [267, 411–413], while constraints on various types of new physics are addressed in Refs. [9, 161, 287, 414, 415]. For a particularly well motivated and explored type of physics beyond the SM, see the Section on "Z'-Boson Searches" in this *Review*.

Acknowledgments
It is a pleasure to thank Rodolfo Ferro-Hernández for discussions, for performing some of the calculations and checks, and for updating the plots. J.E. is supported by the German–Mexican research collaboration grant SP 778/4–1 (DFG) and 278017 (CONACyT). A.F. is supported in part by the National Science Foundation under grant no. PHY–1820760.

References

[1] S. Glashow, Nucl. Phys. **22**, 579 (1961).
[2] S. Weinberg, Phys. Rev. Lett. **19**, 1264 (1967).
[3] A. Salam, Conf. Proc. C **680519**, 367 (1968).
[4] S. Glashow, J. Iliopoulos and L. Maiani, Phys. Rev. D **2**, 1285 (1970).
[5] N. Cabibbo, Phys. Rev. Lett. **10**, 531 (1963).
[6] M. Kobayashi and T. Maskawa, Prog. Theor. Phys. **49**, 652 (1973).
[7] S. Descotes-Genon and P. Koppenburg, Ann. Rev. Nucl. Part. Sci. **67**, 97 (2017), [arXiv:1702.08834].
[8] E. Commins and P. Bucksbaum, *Weak Interactions of Leptons and Quarks*, Cambridge Univ. Pr., Cambridge, USA (1983), ISBN 978-0-521-27370-1.
[9] P. Langacker, editor, *Precision tests of the standard electroweak model*, volume 14, WSP, Singapore (1996).
[10] P. Langacker, *The standard model and beyond*, CRC Pr., Boca Raton, USA (2010), ISBN 978-1-4200-7906-7.
[11] T. Kinoshita, editor, *Quantum electrodynamics*, volume 7, WSP, Singapore (1990).
[12] S. G. Karshenboim, Phys. Rept. **422**, 1 (2005), [hep-ph/0509010].
[13] J. Erler and S. Su, Prog. Part. Nucl. Phys. **71**, 119 (2013), [arXiv:1303.5522].
[14] S. Schael *et al.* (ALEPH, DELPHI, L3, OPAL, SLD, LEP Electroweak Working Group, SLD Electroweak Group, SLD Heavy Flavour Group), Phys. Rept. **427**, 257 (2006), [hep-ex/0509008].
[15] D. Webber *et al.* (MuLan), Phys. Rev. Lett. **106**, 041803 (2011), [arXiv:1010.0991].
[16] T. Kinoshita and A. Sirlin, Phys. Rev. **113**, 1652 (1959).
[17] T. van Ritbergen and R. G. Stuart, Nucl. Phys. B **564**, 343 (2000), [hep-ph/9904240].
[18] M. Steinhauser and T. Seidensticker, Phys. Lett. B **467**, 271 (1999), [hep-ph/9909436].
[19] Y. Nir, Phys. Lett. B **221**, 184 (1989).
[20] A. Pak and A. Czarnecki, Phys. Rev. Lett. **100**, 241807 (2008), [arXiv:0803.0960].
[21] A. Ferroglia, G. Ossola and A. Sirlin, Nucl. Phys. B **560**, 23 (1999), [hep-ph/9905442].
[22] B. Ananthanarayan, S. Friot and S. Ghosh, Phys. Rev. D **101**, 11, 116008 (2020), [arXiv:2003.12030].
[23] D. Hanneke, S. Fogwell and G. Gabrielse, Phys. Rev. Lett. **100**, 120801 (2008), [arXiv:0801.1134].
[24] T. Aoyama, T. Kinoshita and M. Nio, Atoms **7**, 1, 28 (2019).
[25] L. Morel *et al.*, Nature **588**, 7836, 61 (2020).
[26] R. H. Parker *et al.*, Science **360**, 191 (2018), [arXiv:1812.04130].
[27] G. Abbiendi *et al.* (OPAL), Eur. Phys. J. C **45**, 1 (2006), [hep-ex/0505072].
[28] P. Achard *et al.* (L3), Phys. Lett. B **623**, 26 (2005), [hep-ex/0507078].
[29] S. Fanchiotti, B. A. Kniehl and A. Sirlin, Phys. Rev. D **48**, 307 (1993), [hep-ph/9212285].
[30] J. Erler, Phys. Rev. D **59**, 054008 (1999), [hep-ph/9803453].
[31] M. Davier *et al.*, Eur. Phys. J. C **80**, 3, 241 (2020), [arXiv:1908.00921].
[32] F. Jegerlehner, EPJ Web Conf. **118**, 01016 (2016), [arXiv:1511.04473].
[33] F. Jegerlehner and R. Szafron, Eur. Phys. J. C **71**, 1632 (2011), [arXiv:1101.2872].
[34] J. Erler (1999), [hep-ph/0005084].
[35] M. Steinhauser, Phys. Lett. B **429**, 158 (1998), [hep-ph/9803313].
[36] C. Sturm, Nucl. Phys. B **874**, 698 (2013), [arXiv:1305.0581].
[37] K. Chetyrkin, J. H. Kuhn and M. Steinhauser, Nucl. Phys. B **482**, 213 (1996), [hep-ph/9606230].
[38] A. V. Nesterenko, *Strong interactions in spacelike and timelike domains: dispersive approach*, Elsevier (2016), ISBN 978-0-12-803448-4.
[39] J. Erler and R. Ferro-Hernández, JHEP **03**, 196 (2018), [arXiv:1712.09146].
[40] A. Blondel *et al.* (2019), [arXiv:1905.05078].
[41] A. Keshavarzi, D. Nomura and T. Teubner, Phys. Rev. D **101**, 1, 014029 (2020), [arXiv:1911.00367].
[42] M. Davier *et al.*, Eur. Phys. J. C **71**, 1515 (2011), [Erratum: Eur.Phys.J.C 72, 1874 (2012)], [arXiv:1010.4180].
[43] K. Ackerstaff *et al.* (OPAL), Eur. Phys. J. C **7**, 571 (1999), [hep-ex/9808019].
[44] S. Anderson *et al.* (CLEO), Phys. Rev. D **61**, 112002 (2000), [hep-ex/9910046].
[45] S. Schael *et al.* (ALEPH), Phys. Rept. **421**, 191 (2005), [hep-ex/0506072].
[46] M. Fujikawa *et al.* (Belle), Phys. Rev. D **78**, 072006 (2008), [arXiv:0805.3773].
[47] S. Groote *et al.*, Phys. Lett. B **440**, 375 (1998), [hep-ph/9802374].

Downloaded from https://academic.oup.com/ptep/article/2022/8/083C01/6651666 by KIT Library user on 27 September 2022

[48] B. Geshkenbein and V. Morgunov, Phys. Lett. B **352**, 456 (1995).

[49] M. L. Swartz, Phys. Rev. D **53**, 5268 (1996), [hep-ph/9509248].

[50] N. Krasnikov and R. Rodenberg, Nuovo Cim. A **111**, 217 (1998), [hep-ph/9711367].

[51] J. H. Kuhn and M. Steinhauser, Phys. Lett. B **437**, 425 (1998), [hep-ph/9802241].

[52] A. D. Martin, J. Outhwaite and M. Ryskin, Phys. Lett. B **492**, 69 (2000), [hep-ph/0008078].

[53] J. de Troconiz and F. Yndurain, Phys. Rev. D **65**, 093002 (2002), [hep-ph/0107318].

[54] H. Burkhardt and B. Pietrzyk, Phys. Rev. D **84**, 037502 (2011), [arXiv:1106.2991].

[55] J. Erler, P. Masjuan and H. Spiesberger, Eur. Phys. J. C **77**, 2, 99 (2017), [arXiv:1610.08531].

[56] V. Novikov *et al.*, Phys. Rept. **41**, 1 (1978).

[57] J. Erler and M. Luo, Phys. Lett. B **558**, 125 (2003), [hep-ph/0207114].

[58] J. Erler, P. Masjuan and H. Spiesberger (2022), [arXiv:2203.02348].

[59] T. Aaltonen *et al.* (CDF, DØ, Tevatron Electroweak Working Group) (2016), [arXiv:1608.01881].

[60] M. Aaboud *et al.* (ATLAS), Eur. Phys. J. C **79**, 4, 290 (2019), [arXiv:1810.01772].

[61] Technical Report CMS-PAS-TOP-15-012, CERN, Geneva (2016), URL `https://cds.cern.ch/record/2235162`.

[62] A. M. Sirunyan *et al.* (CMS), Eur. Phys. J. C **79**, 4, 313 (2019), [arXiv:1812.10534].

[63] A. M. Sirunyan *et al.* (CMS), Eur. Phys. J. C **79**, 5, 368 (2019), [arXiv:1812.10505].

[64] A. Tumasyan *et al.* (CMS), JHEP **12**, 161 (2021), [arXiv:2108.10407].

[65] Technical Report ATLAS-CONF-2019-046, CERN, Geneva (2019), URL `https://cds.cern.ch/record/2693954`.

[66] V. M. Abazov *et al.* (DØ), Phys. Rev. Lett. **113**, 032002 (2014), [arXiv:1405.1756].

[67] A. M. Sirunyan *et al.* (CMS), Eur. Phys. J. C **78**, 11, 891 (2018), [arXiv:1805.01428].

[68] A. H. Hoang, S. Plätzer and D. Samitz, JHEP **10**, 200 (2018), [arXiv:1807.06617].

[69] J. Kieseler, K. Lipka and S.-O. Moch, Phys. Rev. Lett. **116**, 16, 162001 (2016), [arXiv:1511.00841].

[70] M. Beneke *et al.*, Phys. Lett. B **775**, 63 (2017), [arXiv:1605.03609].

[71] P. Marquard *et al.*, Phys. Rev. Lett. **114**, 14, 142002 (2015), [arXiv:1502.01030].

[72] M. Beneke, Phys. Rept. **317**, 1 (1999), [hep-ph/9807443].

[73] S. Catani *et al.*, JHEP **07**, 100 (2019), [arXiv:1906.06535].

[74] S. Catani *et al.*, Eur. Phys. J. C **81**, 6, 491 (2021), [arXiv:2102.03256].

[75] A. M. Sirunyan *et al.* (CMS), Eur. Phys. J. C **80**, 7, 658 (2020), [arXiv:1904.05237].

[76] G. Aad *et al.* (ATLAS), JHEP **11**, 150 (2019), [arXiv:1905.02302].

[77] A. Tumasyan *et al.* (CMS), JHEP **02**, 142 (2022), [arXiv:2111.10431].

[78] J. Erler and M. Schott, Prog. Part. Nucl. Phys. **106**, 68 (2019), [arXiv:1902.05142].

[79] A. Sirlin, Phys. Rev. D **22**, 971 (1980).

[80] W. J. Marciano and J. L. Rosner, Phys. Rev. Lett. **65**, 2963 (1990), [Erratum: Phys.Rev.Lett. 68, 898 (1992)].

[81] G. Degrassi, S. Fanchiotti and A. Sirlin, Nucl. Phys. B **351**, 49 (1991).

[82] A. Czarnecki and W. J. Marciano, Int. J. Mod. Phys. A **15**, 2365 (2000), [hep-ph/0003049].

[83] J. Erler and M. J. Ramsey-Musolf, Phys. Rev. D **72**, 073003 (2005), [hep-ph/0409169].

[84] K. Kumar *et al.*, Ann. Rev. Nucl. Part. Sci. **63**, 237 (2013), [arXiv:1302.6263].

[85] G. Degrassi and A. Sirlin, Nucl. Phys. B **352**, 342 (1991).

[86] P. Gambino and A. Sirlin, Phys. Rev. D **49**, 1160 (1994), [hep-ph/9309326].

[87] W. Hollik, Fortsch. Phys. **38**, 165 (1990).

[88] R. Barbieri *et al.*, Nucl. Phys. B **409**, 105 (1993).

[89] J. Fleischer, O. Tarasov and F. Jegerlehner, Phys. Lett. B **319**, 249 (1993).

[90] G. Degrassi, P. Gambino and A. Vicini, Phys. Lett. B **383**, 219 (1996), [hep-ph/9603374].

[91] G. Degrassi, P. Gambino and A. Sirlin, Phys. Lett. B **394**, 188 (1997), [hep-ph/9611363].

[92] A. Freitas *et al.*, Phys. Lett. B **495**, 338 (2000), [Erratum: Phys.Lett.B 570, 265 (2003)], [hep-ph/0007091].

[93] M. Awramik and M. Czakon, Phys. Lett. B **568**, 48 (2003), [hep-ph/0305248].

[94] A. Freitas *et al.*, Nucl. Phys. B **632**, 189 (2002), [Erratum: Nucl.Phys.B 666, 305–307 (2003)], [hep-ph/0202131].

[95] M. Awramik and M. Czakon, Phys. Rev. Lett. **89**, 241801 (2002), [hep-ph/0208113].

[96] A. Onishchenko and O. Veretin, Phys. Lett. B **551**, 111 (2003), [hep-ph/0209010].

[97] G. Degrassi, P. Gambino and P. P. Giardino, JHEP **05**, 154 (2015), [arXiv:1411.7040].

[98] M. Awramik *et al.*, Phys. Rev. D **69**, 053006 (2004), [hep-ph/0311148].

[99] M. Awramik *et al.*, Phys. Rev. Lett. **93**, 201805 (2004), [hep-ph/0407317].

[100] W. Hollik, U. Meier and S. Uccirati, Nucl. Phys. B **731**, 213 (2005), [hep-ph/0507158].

[101] M. Awramik, M. Czakon and A. Freitas, Phys. Lett. B **642**, 563 (2006), [hep-ph/0605339].

[102] W. Hollik, U. Meier and S. Uccirati, Nucl. Phys. B **765**, 154 (2007), [hep-ph/0610312].

[103] M. Awramik *et al.*, Nucl. Phys. B **813**, 174 (2009), [arXiv:0811.1364].

[104] I. Dubovyk *et al.*, Phys. Lett. B **762**, 184 (2016), [arXiv:1607.08375].

[105] A. Freitas, Phys. Lett. B **730**, 50 (2014), [arXiv:1310.2256].

[106] A. Freitas, JHEP **04**, 070 (2014), [arXiv:1401.2447].

[107] I. Dubovyk *et al.*, Phys. Lett. B **783**, 86 (2018), [arXiv:1804.10236].

[108] I. Dubovyk *et al.*, JHEP **08**, 113 (2019), [arXiv:1906.08815].

[109] M. Awramik, M. Czakon and A. Freitas, JHEP **11**, 048 (2006), [hep-ph/0608099].

[110] A. Djouadi and C. Verzegnassi, Phys. Lett. B **195**, 265 (1987).

[111] A. Djouadi, Nuovo Cim. A **100**, 357 (1988).

[112] K. Chetyrkin, J. H. Kuhn and M. Steinhauser, Phys. Lett. B **351**, 331 (1995), [hep-ph/9502291].

[113] L. Avdeev *et al.*, Phys. Lett. B **336**, 560 (1994), [Erratum: Phys.Lett.B 349, 597–598 (1995)], [hep-ph/9406363].

[114] Y. Schroder and M. Steinhauser, Phys. Lett. B **622**, 124 (2005), [hep-ph/0504055].

[115] K. Chetyrkin *et al.*, Phys. Rev. Lett. **97**, 102003 (2006), [hep-ph/0605201].

[116] R. Boughezal and M. Czakon, Nucl. Phys. B **755**, 221 (2006), [hep-ph/0606232].

Downloaded from https://academic.oup.com/ptep/article/2022/8/083C01/6651666 by KIT Library user on 27 September 2022

[117] B. A. Kniehl, J. H. Kuhn and R. Stuart, Phys. Lett. B **214**, 621 (1988).

[118] B. A. Kniehl, Nucl. Phys. B **347**, 86 (1990).

[119] F. Halzen and B. A. Kniehl, Nucl. Phys. B **353**, 567 (1991).

[120] A. Djouadi and P. Gambino, Phys. Rev. D **49**, 3499 (1994), [Erratum: Phys.Rev.D 53, 4111 (1996)], [hep-ph/9309298].

[121] A. Anselm, N. Dombey and E. Leader, Phys. Lett. B **312**, 232 (1993).

[122] K. Chetyrkin, J. H. Kuhn and M. Steinhauser, Phys. Rev. Lett. **75**, 3394 (1995), [hep-ph/9504413].

[123] J. van der Bij *et al.*, Phys. Lett. B **498**, 156 (2001), [hep-ph/0011373].

[124] M. Faisst *et al.*, Nucl. Phys. B **665**, 649 (2003), [hep-ph/0302275].

[125] R. Boughezal, J. Tausk and J. van der Bij, Nucl. Phys. B **725**, 3 (2005), [hep-ph/0504092].

[126] A. Arbuzov *et al.*, Comput. Phys. Commun. **174**, 728 (2006), [hep-ph/0507146].

[127] J. Erler and M. J. Ramsey-Musolf, Prog. Part. Nucl. Phys. **54**, 351 (2005), [hep-ph/0404291].

[128] J. Formaggio and G. Zeller, Rev. Mod. Phys. **84**, 1307 (2012), [arXiv:1305.7513].

[129] J. Dorenbosch *et al.* (CHARM), Z. Phys. C **41**, 567 (1989), [Erratum: Z.Phys.C 51, 142 (1991)].

[130] L. Ahrens *et al.*, Phys. Rev. D **41**, 3297 (1990).

[131] P. Vilain *et al.* (CHARM-II), Phys. Lett. B **335**, 246 (1994).

[132] R. Allen *et al.*, Phys. Rev. D **47**, 11 (1993).

[133] L. Auerbach *et al.* (LSND), Phys. Rev. D **63**, 112001 (2001), [hep-ex/0101039].

[134] M. Deniz *et al.* (TEXONO), Phys. Rev. D **81**, 072001 (2010), [arXiv:0911.1597].

[135] J. M. Conrad, M. H. Shaevitz and T. Bolton, Rev. Mod. Phys. **70**, 1341 (1998), [hep-ex/9707015].

[136] A. Blondel *et al.*, Z. Phys. C **45**, 361 (1990).

[137] J. Allaby *et al.* (CHARM), Z. Phys. C **36**, 611 (1987).

[138] K. S. McFarland *et al.* (CCFR, E744, E770), Eur. Phys. J. C **1**, 509 (1998), [hep-ex/9701010].

[139] R. Barnett, Phys. Rev. D **14**, 70 (1976).

[140] H. Georgi and H. Politzer, Phys. Rev. D **14**, 1829 (1976).

[141] S. Rabinowitz *et al.*, Phys. Rev. Lett. **70**, 134 (1993).

[142] E. Paschos and L. Wolfenstein, Phys. Rev. D **7**, 91 (1973).

[143] G. Zeller *et al.* (NuTeV), Phys. Rev. Lett. **88**, 091802 (2002), [Erratum: Phys.Rev.Lett. 90, 239902 (2003)], [hep-ex/0110059].

[144] D. Akimov *et al.* (COHERENT), Science **357**, 6356, 1123 (2017), [arXiv:1708.01294].

[145] D. Akimov *et al.* (COHERENT), Phys. Rev. Lett. **126**, 1, 012002 (2021), [arXiv:2003.10630].

[146] J. Erler *et al.*, Ann. Rev. Nucl. Part. Sci. **64**, 269 (2014), [arXiv:1401.6199].

[147] C. Prescott *et al.*, Phys. Lett. B **84**, 524 (1979).

[148] D. Wang *et al.* (PVDIS), Nature **506**, 7486, 67 (2014).

[149] D. Wang *et al.*, Phys. Rev. C **91**, 4, 045506 (2015), [arXiv:1411.3200].

[150] R. Hasty *et al.* (SAMPLE), Science **290**, 2117 (2000), [arXiv:nucl-ex/0102001].

[151] E. Beise, M. Pitt and D. Spayde, Prog. Part. Nucl. Phys. **54**, 289 (2005), [arXiv:nucl-ex/0412054].

[152] S.-L. Zhu *et al.*, Phys. Rev. D **62**, 033008 (2000), [hep-ph/0002252].

[153] A. Argento *et al.*, Phys. Lett. B **120**, 245 (1983).

[154] W. Heil *et al.*, Nucl. Phys. B **327**, 1 (1989).

[155] P. Souder *et al.*, Phys. Rev. Lett. **65**, 694 (1990).

[156] D. Armstrong and R. McKeown, Ann. Rev. Nucl. Part. Sci. **62**, 337 (2012), [arXiv:1207.5238].

[157] E. Derman and W. J. Marciano, Annals Phys. **121**, 147 (1979).

[158] P. Anthony *et al.* (SLAC E158), Phys. Rev. Lett. **95**, 081601 (2005), [hep-ex/0504049].

[159] D. Androić *et al.* (Qweak), Nature **557**, 7704, 207 (2018), [arXiv:1905.08283].

[160] R. D. Carlini *et al.*, Ann. Rev. Nucl. Part. Sci. **69**, 191 (2019).

[161] J. Erler, A. Kurylov and M. J. Ramsey-Musolf, Phys. Rev. D **68**, 016006 (2003), [hep-ph/0302149].

[162] R. D. Young *et al.*, Phys. Rev. Lett. **99**, 122003 (2007), [arXiv:0704.2618].

[163] A. Acha *et al.* (HAPPEX), Phys. Rev. Lett. **98**, 032301 (2007), [arXiv:nucl-ex/0609002].

[164] M. Gorchtein and C. Horowitz, Phys. Rev. Lett. **102**, 091806 (2009), [arXiv:0811.0614].

[165] M. Gorchtein, C. Horowitz and M. J. Ramsey-Musolf, Phys. Rev. C **84**, 015502 (2011), [arXiv:1102.3910].

[166] N. Hall *et al.*, Phys. Lett. B **753**, 221 (2016), [arXiv:1504.03973].

[167] J. Erler *et al.*, Phys. Rev. D **100**, 5, 053007 (2019), [arXiv:1907.07928].

[168] M. Bouchiat and C. Bouchiat, Phys. Lett. B **48**, 111 (1974).

[169] M. Safronova *et al.*, Rev. Mod. Phys. **90**, 2, 025008 (2018), [arXiv:1710.01833].

[170] C. Wood *et al.*, Science **275**, 1759 (1997).

[171] J. Guena, M. Lintz and M. Bouchiat, Phys. Rev. A **71**, 042108 (2005), [arXiv:physics/0412017].

[172] N. Edwards *et al.*, Phys. Rev. Lett. **74**, 2654 (1995).

[173] P. Vetter *et al.*, Phys. Rev. Lett. **74**, 2658 (1995).

[174] D. Meekhof *et al.*, Phys. Rev. Lett. **71**, 3442 (1993).

[175] M. Macpherson *et al.*, Phys. Rev. Lett. **67**, 20, 2784 (1991).

[176] P. Blunden, W. Melnitchouk and A. Thomas, Phys. Rev. Lett. **109**, 262301 (2012), [arXiv:1208.4310].

[177] S. Bennett and C. E. Wieman, Phys. Rev. Lett. **82**, 2484 (1999), [Erratum: Phys.Rev.Lett. 82, 4153 (1999), Erratum: Phys.Rev.Lett. 83, 889 (1999)], [hep-ex/9903022].

[178] V. Dzuba and V. Flambaum., Phys. Rev. A **62**, 052101 (2000), [arXiv:physics/0005038].

[179] V. Dzuba, V. Flambaum and O. Sushkov, Phys. Rev. A **56**, 4357 (1997), [hep-ph/9709251].

[180] D. Cho *et al.*, Phys. Rev. A **55**, 1007 (1997).

[181] G. Toh *et al.*, Phys. Rev. Lett. **123**, 7, 073002 (2019), [arXiv:1905.02768].

[182] A. A. Vasilyev *et al.*, Phys. Rev. A **66**, 020101 (2002).

[183] V. Dzuba, V. Flambaum and J. Ginges, Phys. Rev. D **66**, 076013 (2002), [hep-ph/0204134].

[184] J. Ginges and V. Flambaum, Phys. Rept. **397**, 63 (2004), [arXiv:physics/0309054].

[185] A. Derevianko and S. G. Porsev, Eur. Phys. J. A **32**, 4, 517 (2007), [hep-ph/0608178].

[186] B. Roberts, V. Dzuba and V. Flambaum, Ann. Rev. Nucl. Part. Sci. **65**, 63 (2015), [arXiv:1412.6644].

[187] A. Derevianko, Phys. Rev. Lett. **85**, 1618 (2000), [hep-ph/0005274].

[188] W. Johnson, I. Bednyakov and G. Soff, Phys. Rev. Lett. **87**, 233001 (2001), [Erratum: Phys.Rev.Lett. 88, 079903 (2002)], [hep-ph/0110262].

[189] M. Kuchiev and V. Flambaum, Phys. Rev. Lett. **89**, 283002 (2002), [hep-ph/0206124].

Downloaded from https://academic.oup.com/ptep/article/2022/8/083C01/6651666 by KIT Library user on 27 September 2022

[190] A. Milstein, O. Sushkov and I. Terekhov, Phys. Rev. Lett. **89**, 283003 (2002), [hep-ph/0208227].

[191] S. Porsev, K. Beloy and A. Derevianko, Phys. Rev. Lett. **102**, 181601 (2009), [arXiv:0902.0335].

[192] V. Dzuba *et al.*, Phys. Rev. Lett. **109**, 203003 (2012), [arXiv:1207.5864].

[193] C. Bouchiat and C. Piketty, Phys. Lett. B **128**, 73 (1983).

[194] I. Zel'dovich, J. Exp. Theor. Phys. **6**, 1184 (1958).

[195] V. Flambaum and D. Murray, Phys. Rev. C **56**, 1641 (1997), [arXiv:nucl-th/9703050].

[196] W. Haxton and C. E. Wieman, Ann. Rev. Nucl. Part. Sci. **51**, 261 (2001), [arXiv:nucl-th/0104026].

[197] V. Dzuba *et al.*, J. Phys. B **20**, 3297 (1987).

[198] J. L. Rosner, Phys. Rev. D **53**, 2724 (1996), [hep-ph/9507375].

[199] D. Antypas *et al.*, Nature Phys. **15**, 2, 120 (2019), [arXiv:1804.05747].

[200] M. Ramsey-Musolf, Phys. Rev. C **60**, 015501 (1999), [hep-ph/9903264].

[201] S. Pollock, E. Fortson and L. Wilets, Phys. Rev. C **46**, 2587 (1992), [arXiv:nucl-th/9211004].

[202] B. Chen and P. Vogel, Phys. Rev. C **48**, 1392 (1993), [arXiv:nucl-th/9303003].

[203] C. Horowitz *et al.*, Phys. Rev. C **63**, 025501 (2001), [arXiv:nucl-th/9912038].

[204] S. Abrahamyan *et al.*, Phys. Rev. Lett. **108**, 112502 (2012), [arXiv:1201.2568].

[205] D. Adhikari *et al.* (PREX), Phys. Rev. Lett. **126**, 17, 172502 (2021), [arXiv:2102.10767].

[206] H. Davoudiasl, H.-S. Lee and W. J. Marciano, Phys. Rev. D **86**, 095009 (2012), [arXiv:1208.2973].

[207] E. Braaten, S. Narison and A. Pich, Nucl. Phys. B **373**, 581 (1992).

[208] A. Pich, Prog. Part. Nucl. Phys. **75**, 41 (2014), [arXiv:1310.7922].

[209] M. Davier *et al.*, Eur. Phys. J. C **74**, 3, 2803 (2014), [arXiv:1312.1501].

[210] K. Chetyrkin, A. Kataev and F. Tkachov, Phys. Lett. B **85**, 277 (1979).

[211] M. Dine and J. Sapirstein, Phys. Rev. Lett. **43**, 668 (1979).

[212] S. Gorishnii, A. Kataev and S. Larin, Phys. Lett. B **259**, 144 (1991).

[213] L. R. Surguladze and M. A. Samuel, Phys. Rev. Lett. **66**, 560 (1991), [Erratum: Phys.Rev.Lett. 66, 2416 (1991)].

[214] P. Baikov, K. Chetyrkin and J. H. Kuhn, Phys. Rev. Lett. **101**, 012002 (2008), [arXiv:0801.1821].

[215] F. Le Diberder and A. Pich, Phys. Lett. B **286**, 147 (1992).

[216] M. Beneke and M. Jamin, JHEP **09**, 044 (2008), [arXiv:0806.3156].

[217] E. Braaten and C.-S. Li, Phys. Rev. D **42**, 3888 (1990).

[218] W. Marciano and A. Sirlin, Phys. Rev. Lett. **61**, 1815 (1988).

[219] J. Erler, Rev. Mex. Fis. **50**, 200 (2004), [hep-ph/0211345].

[220] D. Boito *et al.*, Phys. Rev. D **85**, 093015 (2012), [arXiv:1203.3146].

[221] D. Boito *et al.*, Phys. Rev. D **91**, 3, 034003 (2015), [arXiv:1410.3528].

[222] J. Erler (2011), [arXiv:1102.5520].

[223] G. Bennett *et al.* (Muon g-2), Phys. Rev. Lett. **92**, 161802 (2004), [hep-ex/0401008].

[224] B. Abi *et al.* (Muon g-2), Phys. Rev. Lett. **126**, 14, 141801 (2021), [arXiv:2104.03281].

[225] T. Aoyama *et al.*, Phys. Rev. Lett. **109**, 111808 (2012), [arXiv:1205.5370].

[226] T. Aoyama *et al.*, PTEP **2012**, 01A107 (2012).

[227] P. Baikov, A. Maier and P. Marquard, Nucl. Phys. B **877**, 647 (2013), [arXiv:1307.6105].

[228] G. Li, R. Mendel and M. A. Samuel, Phys. Rev. D **47**, 1723 (1993).

[229] S. Laporta and E. Remiddi, Phys. Lett. B **301**, 440 (1993).

[230] S. Laporta and E. Remiddi, Phys. Lett. B **379**, 283 (1996), [hep-ph/9602417].

[231] A. Czarnecki and M. Skrzypek, Phys. Lett. B **449**, 354 (1999), [hep-ph/9812394].

[232] J. Erler and M. Luo, Phys. Rev. Lett. **87**, 071804 (2001), [hep-ph/0101010].

[233] S. Laporta, Phys. Lett. B **772**, 232 (2017), [arXiv:1704.06996].

[234] S. J. Brodsky and J. D. Sullivan, Phys. Rev. **156**, 1644 (1967).

[235] T. Burnett and M. Levine, Phys. Lett. B **24**, 467 (1967).

[236] R. Jackiw and S. Weinberg, Phys. Rev. D **5**, 2396 (1972).

[237] I. Bars and M. Yoshimura, Phys. Rev. D **6**, 374 (1972).

[238] K. Fujikawa, B. Lee and A. Sanda, Phys. Rev. D **6**, 2923 (1972).

[239] W. A. Bardeen, R. Gastmans and B. Lautrup, Nucl. Phys. B **46**, 319 (1972).

[240] T. Kukhto *et al.*, Nucl. Phys. B **371**, 567 (1992).

[241] S. Peris, M. Perrottet and E. de Rafael, Phys. Lett. B **355**, 523 (1995), [hep-ph/9505405].

[242] A. Czarnecki, B. Krause and W. J. Marciano, Phys. Rev. D **52**, 2619 (1995), [hep-ph/9506256].

[243] A. Czarnecki, B. Krause and W. J. Marciano, Phys. Rev. Lett. **76**, 3267 (1996), [hep-ph/9512369].

[244] C. Gnendiger, D. Stöckinger and H. Stöckinger-Kim, Phys. Rev. D **88**, 053005 (2013), [arXiv:1306.5546].

[245] G. Degrassi and G. Giudice, Phys. Rev. D **58**, 053007 (1998), [hep-ph/9803384].

[246] A. Czarnecki, W. J. Marciano and A. Vainshtein, Phys. Rev. D **67**, 073006 (2003), [Erratum: Phys.Rev.D 73, 119901 (2006)], [hep-ph/0212229].

[247] F. Jegerlehner, EPJ Web Conf. **166**, 00022 (2018), [arXiv:1705.00263].

[248] P. D. Kennedy, J. Erler and H. Spiesberger (2021), [arXiv:2111.13016].

[249] T. Aoyama *et al.*, Phys. Rept. **887**, 1 (2020), [arXiv:2006.04822].

[250] S. Borsanyi *et al.*, Nature **593**, 7857, 51 (2021), [arXiv:2002.12347].

[251] K. Melnikov and A. Vainshtein, Phys. Rev. D **70**, 113006 (2004), [hep-ph/0312226].

[252] J. Erler and G. Toledo Sanchez, Phys. Rev. Lett. **97**, 161801 (2006), [hep-ph/0605052].

[253] J. Prades, E. de Rafael and A. Vainshtein **20**, 303 (2009), [arXiv:0901.0306].

[254] M. Knecht and A. Nyffeler, Phys. Rev. D **65**, 073034 (2002), [hep-ph/0111058].

[255] I. Danilkin, C. F. Redmer and M. Vanderhaeghen, Prog. Part. Nucl. Phys. **107**, 20 (2019), [arXiv:1901.10346].

[256] T. Blum *et al.*, Phys. Rev. Lett. **124**, 13, 132002 (2020), [arXiv:1911.08123].

[257] E.-H. Chao *et al.*, Eur. Phys. J. C **81**, 7, 651 (2021), [arXiv:2104.02632].

[258] B. Krause, Phys. Lett. B **390**, 392 (1997), [hep-ph/9607259].

Downloaded from https://academic.oup.com/ptep/article/2022/8/083C01/6651666 by KIT Library user on 27 September 2022

[259] A. Kurz *et al.*, Phys. Lett. B **734**, 144 (2014), [arXiv:1403.6400].

[260] G. Colangelo *et al.*, Phys. Lett. B **735**, 90 (2014), [arXiv:1403.7512].

[261] J. L. Lopez, D. V. Nanopoulos and X. Wang, Phys. Rev. D **49**, 366 (1994), [hep-ph/9308336].

[262] G. Passarino and M. Veltman, Nucl. Phys. B **160**, 151 (1979).

[263] W. Hollik and G. Duckeck, Springer Tracts Mod. Phys. **162**, 1 (2000).

[264] B. Lynn and R. Stuart, Nucl. Phys. B **253**, 216 (1985).

[265] S. L. Wu, Phys. Rept. **107**, 59 (1984).

[266] R. Marshall, Z. Phys. C **43**, 607 (1989).

[267] S. Schael *et al.* (ALEPH, DELPHI, L3, OPAL, LEP Electroweak), Phys. Rept. **532**, 119 (2013), [arXiv:1302.3415].

[268] T. A. Aaltonen *et al.* (CDF, DØ), Phys. Rev. D **88**, 5, 052018 (2013), [arXiv:1307.7627].

[269] Technical Report TEVEWWG/WZ 2010/01, FERMILAB, Batavia (2010), [arXiv:1003.2826], URL `https://www-d0.fnal.gov/Run2Physics/WWW/results/prelim/EW/E34`.

[270] M. Aaboud *et al.* (ATLAS), Eur. Phys. J. C **78**, 2, 110 (2018), [Erratum: Eur.Phys.J.C 78, 898 (2018)], [arXiv:1701.07240].

[271] R. Aaij *et al.* (LHCb), JHEP **01**, 036 (2022), [arXiv:2109.01113].

[272] A. Tumasyan *et al.* (CMS) (2022), [arXiv:2201.07861].

[273] G. Aad *et al.* (ATLAS), Phys. Lett. B **716**, 1 (2012), [arXiv:1207.7214].

[274] S. Chatrchyan *et al.* (CMS), Phys. Lett. B **716**, 30 (2012), [arXiv:1207.7235].

[275] M. Aaboud *et al.* (ATLAS), Phys. Lett. B **784**, 345 (2018), [arXiv:1806.00242].

[276] A. M. Sirunyan *et al.* (CMS), Phys. Lett. B **805**, 135425 (2020), [arXiv:2002.06398].

[277] A. Tumasyan *et al.* (CMS) (2022), [arXiv:2202.06923].

[278] D. de Florian *et al.* (LHC Higgs Cross Section Working Group) (2016), [arXiv:1610.07922].

[279] T. A. Aaltonen *et al.* (CDF, DØ), Phys. Rev. D **97**, 11, 112007 (2018), [arXiv:1801.06283].

[280] G. Aad *et al.* (ATLAS), JHEP **09**, 049 (2015), [arXiv:1503.03709].

[281] Technical Report ATLAS-CONF-2018-037, CERN, Geneva (2018), URL `https://cds.cern.ch/record/2630340`.

[282] A. M. Sirunyan *et al.* (CMS), Eur. Phys. J. C **78**, 9, 701 (2018), [arXiv:1806.00863].

[283] R. Aaij *et al.* (LHCb), JHEP **11**, 190 (2015), [arXiv:1509.07645].

[284] K. Abe *et al.* (SLD), Phys. Rev. Lett. **84**, 5945 (2000), [hep-ex/0004026].

[285] K. Abe *et al.* (SLD), Phys. Rev. Lett. **86**, 1162 (2001), [hep-ex/0010015].

[286] D. Kennedy *et al.*, Nucl. Phys. B **321**, 83 (1989).

[287] S. Riemann, Rept. Prog. Phys. **73**, 126201 (2010).

[288] K. Abe *et al.* (SLD), Phys. Rev. Lett. **85**, 5059 (2000), [hep-ex/0006019].

[289] K. Abe *et al.* (SLD), Phys. Rev. Lett. **78**, 17 (1997), [hep-ex/9609019].

[290] W. Bernreuther *et al.*, JHEP **01**, 053 (2017), [arXiv:1611.07942].

[291] S. Catani and M. H. Seymour, JHEP **07**, 023 (1999), [hep-ph/9905424].

[292] A. Djouadi, J. H. Kuhn and P. Zerwas, Z. Phys. C **46**, 411 (1990).

[293] T. A. Aaltonen *et al.* (CDF), Phys. Rev. D **93**, 11, 112016 (2016), [Addendum: Phys.Rev.D 95, 119901 (2017)], [arXiv:1605.02719].

[294] V. M. Abazov *et al.* (DØ), Phys. Rev. Lett. **120**, 24, 241802 (2018), [arXiv:1710.03951].

[295] V. Abazov *et al.* (DØ), Phys. Rev. D **84**, 012007 (2011), [arXiv:1104.4590].

[296] D. Acosta *et al.* (CDF), Phys. Rev. D **71**, 052002 (2005), [hep-ex/0411059].

[297] V. Andreev *et al.* (H1), Eur. Phys. J. C **78**, 9, 777 (2018), [arXiv:1806.01176].

[298] H. Abramowicz *et al.* (ZEUS), Phys. Rev. D **93**, 9, 092002 (2016), [arXiv:1603.09628].

[299] P. Janot and S. Jadach, Phys. Lett. B **803**, 135319 (2020), [arXiv:1912.02067].

[300] D. Albert *et al.*, Nucl. Phys. B **166**, 460 (1980).

[301] K. Chetyrkin, J. H. Kuhn and A. Kwiatkowski, Phys. Rept. **277**, 189 (1996), [hep-ph/9503396].

[302] B. A. Kniehl and J. H. Kuhn, Nucl. Phys. B **329**, 547 (1990).

[303] K. Chetyrkin and A. Kwiatkowski, Phys. Lett. B **319**, 307 (1993), [hep-ph/9310229].

[304] S. Larin, T. van Ritbergen and J. Vermaseren, Phys. Lett. B **320**, 159 (1994), [hep-ph/9310378].

[305] K. Chetyrkin and O. Tarasov, Phys. Lett. B **327**, 114 (1994), [hep-ph/9312323].

[306] P. Baikov *et al.*, Phys. Rev. Lett. **108**, 222003 (2012), [arXiv:1201.5804].

[307] A. Kataev, Phys. Lett. B **287**, 209 (1992).

[308] B. W. Lynn and R. G. Stuart, Phys. Lett. B **252**, 676 (1990).

[309] J. Bernabeu, A. Pich and A. Santamaria, Nucl. Phys. B **363**, 326 (1991).

[310] A. Czarnecki and J. H. Kuhn, Phys. Rev. Lett. **77**, 3955 (1996), [hep-ph/9608366].

[311] R. Harlander, T. Seidensticker and M. Steinhauser, Phys. Lett. B **426**, 125 (1998), [hep-ph/9712228].

[312] J. Fleischer *et al.*, Phys. Lett. B **459**, 625 (1999), [hep-ph/9904256].

[313] P. A. Grassi, B. A. Kniehl and A. Sirlin, Phys. Rev. Lett. **86**, 389 (2001), [hep-th/0005149].

[314] A. Akhundov, D. Bardin and T. Riemann, Nucl. Phys. B **276**, 1 (1986).

[315] F. Jegerlehner, Z. Phys. C **32**, 425 (1986), [Erratum: Z.Phys.C 38, 519 (1988)].

[316] W. Beenakker and W. Hollik, Z. Phys. C **40**, 141 (1988).

[317] D. Bardin *et al.*, Z. Phys. C **44**, 493 (1989).

[318] A. Borrelli *et al.*, Nucl. Phys. B **333**, 357 (1990).

[319] A. Denner and T. Sack, Z. Phys. C **46**, 653 (1990).

[320] A. Denner, Fortsch. Phys. **41**, 307 (1993), [arXiv:0709.1075].

[321] G. Aad *et al.* (ATLAS), Nature Phys. **17**, 7, 813 (2021), [arXiv:2007.14040].

[322] U. Amaldi *et al.*, Phys. Rev. D **36**, 1385 (1987).

[323] G. Costa *et al.*, Nucl. Phys. B **297**, 244 (1988).

[324] P. Langacker and M. Luo, Phys. Rev. D **44**, 817 (1991).

[325] J. Erler and P. Langacker, Phys. Rev. D **52**, 441 (1995), [hep-ph/9411203].

[326] F. James and M. Roos, Comput. Phys. Commun. **10**, 343 (1975).

[327] D. d'Enterria and A. Poldaru, JHEP **06**, 016 (2020), [arXiv:1912.11733].

[328] V. Abazov *et al.* (DØ), Phys. Rev. D **80**, 111107 (2009), [arXiv:0911.2710].

[329] M. Cè *et al.* (2022), [arXiv:2203.08676].

Downloaded from https://academic.oup.com/ptep/article/2022/8/083C01/6651666 by KIT Library user on 27 September 2022

[330] J. Bagger, K. T. Matchev and D. Pierce, Phys. Lett. B **348**, 443 (1995), [hep-ph/9501277].

[331] P. Langacker and N. Polonsky, Phys. Rev. D **52**, 3081 (1995), [hep-ph/9503214].

[332] M. Veltman, Nucl. Phys. B **123**, 89 (1977).

[333] M. S. Chanowitz, M. Furman and I. Hinchliffe, Phys. Lett. B **78**, 285 (1978).

[334] J. van der Bij and F. Hoogeveen, Nucl. Phys. B **283**, 477 (1987).

[335] P. Langacker and M. Luo, Phys. Rev. D **45**, 278 (1992).

[336] A. Denner, R. Guth and J. H. Kuhn, Phys. Lett. B **240**, 438 (1990).

[337] W. Grimus *et al.*, J. Phys. G **35**, 075001 (2008), [arXiv:0711.4022].

[338] H. E. Haber and D. O'Neil, Phys. Rev. D **83**, 055017 (2011), [arXiv:1011.6188].

[339] S. Bertolini and A. Sirlin, Phys. Lett. B **257**, 179 (1991).

[340] M. Golden and L. Randall, Nucl. Phys. B **361**, 3 (1991).

[341] B. Holdom and J. Terning, Phys. Lett. B **247**, 88 (1990).

[342] M. E. Peskin and T. Takeuchi, Phys. Rev. Lett. **65**, 964 (1990).

[343] K. Hagiwara *et al.*, Z. Phys. C **64**, 559 (1994), [Erratum: Z.Phys.C 68, 352 (1995)], [hep-ph/9409380].

[344] M. E. Peskin and T. Takeuchi, Phys. Rev. D **46**, 381 (1992).

[345] I. Maksymyk, C. Burgess and D. London, Phys. Rev. D **50**, 529 (1994), [hep-ph/9306267].

[346] R. Barbieri *et al.*, Nucl. Phys. B **703**, 127 (2004), [hep-ph/0405040].

[347] M. Farina *et al.*, Phys. Lett. B **772**, 210 (2017), [arXiv:1609.08157].

[348] G. Altarelli and R. Barbieri, Phys. Lett. B **253**, 161 (1991).

[349] D. Kennedy and P. Langacker, Phys. Rev. D **44**, 1591 (1991).

[350] L. Randall and R. Sundrum, Phys. Rev. Lett. **83**, 3370 (1999), [hep-ph/9905221].

[351] M. Carena *et al.*, Nucl. Phys. B **759**, 202 (2006), [hep-ph/0607106].

[352] R. Contino (2011), [arXiv:1005.4269].

[353] D. D. Dietrich, F. Sannino and K. Tuominen, Phys. Rev. D **72**, 055001 (2005), [hep-ph/0505059].

[354] E. Gates and J. Terning, Phys. Rev. Lett. **67**, 1840 (1991).

[355] H. Georgi, Nucl. Phys. B **363**, 301 (1991).

[356] M. J. Dugan and L. Randall, Phys. Lett. B **264**, 154 (1991).

[357] H. E. Haber and G. L. Kane, Phys. Rept. **117**, 75 (1985).

[358] A. Djouadi, Phys. Rept. **459**, 1 (2008), [hep-ph/0503173].

[359] R. Barbieri *et al.*, Nucl. Phys. B **341**, 309 (1990).

[360] R. Barbieri, M. Frigeni and F. Caravaglios, Phys. Lett. B **279**, 169 (1992).

[361] J. Erler and D. M. Pierce, Nucl. Phys. B **526**, 53 (1998), [hep-ph/9801238].

[362] G.-C. Cho and K. Hagiwara, Nucl. Phys. B **574**, 623 (2000), [hep-ph/9912260].

[363] G. Altarelli *et al.*, JHEP **06**, 018 (2001), [hep-ph/0106029].

[364] S. Heinemeyer, W. Hollik and G. Weiglein, Phys. Rept. **425**, 265 (2006), [hep-ph/0412214].

[365] S. P. Martin, K. Tobe and J. D. Wells, Phys. Rev. D **71**, 073014 (2005), [hep-ph/0412424].

[366] M. Ramsey-Musolf and S. Su, Phys. Rept. **456**, 1 (2008), [hep-ph/0612057].

[367] S. Heinemeyer *et al.*, JHEP **04**, 039 (2008), [arXiv:0710.2972].

[368] O. Buchmueller *et al.*, Eur. Phys. J. C **72**, 2020 (2012), [arXiv:1112.3564].

[369] B. Grinstein and M. B. Wise, Phys. Lett. B **265**, 326 (1991).

[370] A. Pich, I. Rosell and J. Sanz-Cillero, JHEP **01**, 157 (2014), [arXiv:1310.3121].

[371] C. T. Hill and E. H. Simmons, Phys. Rept. **381**, 235 (2003), [Erratum: Phys.Rept. 390, 553–554 (2004)], [hep-ph/0203079].

[372] G. Panico and A. Wulzer **913** (2016), [arXiv:1506.01961].

[373] J. Erler and P. Langacker, Phys. Rev. Lett. **105**, 031801 (2010), [arXiv:1003.3211].

[374] J. Gunion, D. W. McKay and H. Pois, Phys. Rev. D **53**, 1616 (1996), [hep-ph/9507323].

[375] A. Lenz, Adv. High Energy Phys. **2013**, 910275 (2013).

[376] S. Chatrchyan *et al.* (CMS), Phys. Rev. D **86**, 112003 (2012), [arXiv:1209.1062].

[377] A. Djouadi and A. Lenz, Phys. Lett. B **715**, 310 (2012), [arXiv:1204.1252].

[378] O. Eberhardt *et al.*, Phys. Rev. Lett. **109**, 241802 (2012), [arXiv:1209.1101].

[379] J. Maalampi and M. Roos, Phys. Rept. **186**, 53 (1990).

[380] P. Langacker, Phys. Rept. **72**, 185 (1981).

[381] J. L. Hewett and T. G. Rizzo, Phys. Rept. **183**, 193 (1989).

[382] J. Kang, P. Langacker and B. D. Nelson, Phys. Rev. D **77**, 035003 (2008), [arXiv:0708.2701].

[383] S. P. Martin, Phys. Rev. D **81**, 035004 (2010), [arXiv:0910.2732].

[384] P. W. Graham *et al.*, Phys. Rev. D **81**, 055016 (2010), [arXiv:0910.3020].

[385] J. Erler, J. L. Feng and N. Polonsky, Phys. Rev. Lett. **78**, 3063 (1997), [hep-ph/9612397].

[386] D. Choudhury, T. M. Tait and C. Wagner, Phys. Rev. D **65**, 053002 (2002), [hep-ph/0109097].

[387] J. Erler and P. Langacker, Phys. Rev. Lett. **84**, 212 (2000), [hep-ph/9910315].

[388] P. Langacker and M. Plumacher, Phys. Rev. D **62**, 013006 (2000), [hep-ph/0001204].

[389] P. Abreu *et al.* (DELPHI), Eur. Phys. J. C **10**, 415 (1999).

[390] P. Langacker and D. London, Phys. Rev. D **38**, 886 (1988).

[391] F. del Aguila, J. de Blas and M. Perez-Victoria, Phys. Rev. D **78**, 013010 (2008), [arXiv:0803.4008].

[392] M. Chemtob, Prog. Part. Nucl. Phys. **54**, 71 (2005), [hep-ph/0406029].

[393] R. Barbier *et al.*, Phys. Rept. **420**, 1 (2005), [hep-ph/0406039].

[394] T. Han, H. E. Logan and L.-T. Wang, JHEP **01**, 099 (2006), [hep-ph/0506313].

[395] M. Perelstein, Prog. Part. Nucl. Phys. **58**, 247 (2007), [hep-ph/0512128].

[396] I. Antoniadis (2001), [hep-th/0102202].

[397] M. Carena *et al.*, Phys. Rev. D **68**, 035010 (2003), [hep-ph/0305188].

[398] K. Agashe *et al.*, JHEP **08**, 050 (2003), [hep-ph/0308036].

[399] I. Gogoladze and C. Macesanu, Phys. Rev. D **74**, 093012 (2006), [hep-ph/0605207].

[400] S. Weinberg, Phys. Rev. Lett. **43**, 1566 (1979).

[401] W. Buchmuller and D. Wyler, Nucl. Phys. B **268**, 621 (1986).

[402] B. Grzadkowski *et al.*, JHEP **10**, 085 (2010), [arXiv:1008.4884].

[403] R. Contino *et al.*, JHEP **07**, 035 (2013), [arXiv:1303.3876].

[404] K. Hagiwara *et al.*, Phys. Rev. D **48**, 2182 (1993).

Downloaded from https://academic.oup.com/ptep/article/2022/8/083C01/6651666 by KIT Library user on 27 September 2022

[405] A. Falkowski, F. Riva and A. Urbano, JHEP **11**, 111 (2013), [arXiv:1303.1812].

[406] A. Pomarol and F. Riva, JHEP **01**, 151 (2014), [arXiv:1308.2803].

[407] J. Ellis, V. Sanz and T. You, JHEP **03**, 157 (2015), [arXiv:1410.7703].

[408] A. Efrati, A. Falkowski and Y. Soreq, JHEP **07**, 018 (2015), [arXiv:1503.07872].

[409] J. de Blas *et al.*, PoS **EPS-HEP2017**, 467 (2017), [arXiv:1710.05402].

[410] S. Dawson and P. P. Giardino, Phys. Rev. D **101**, 1, 013001 (2020), [arXiv:1909.02000].

[411] G.-C. Cho, K. Hagiwara and S. Matsumoto, Eur. Phys. J. C **5**, 155 (1998), [hep-ph/9707334].

[412] K. Cheung, Phys. Lett. B **517**, 167 (2001), [hep-ph/0106251].

[413] Z. Han and W. Skiba, Phys. Rev. D **71**, 075009 (2005), [hep-ph/0412166].

[414] P. Langacker, M. Luo and A. K. Mann, Rev. Mod. Phys. **64**, 87 (1992).

[415] P. Langacker, Rev. Mod. Phys. **81**, 1199 (2009), [arXiv:0801.1345].

Downloaded from https://academic.oup.com/ptep/article/2022/8/083C01/6651666 by KIT Library user on 27 September 2022

11. Status of Higgs Boson Physics

Revised October 2021 by M. Carena (FNAL; Chicago U.; Chicago U., Kavli Inst.), C. Grojean (DESY, Hamburg; Physik, Humboldt U.), M. Kado (Rome U. Sapienza; INFN, Rome; U. Paris-Saclay, IJCLab) and V. Sharma (UC San Diego).

11.1 Introduction 201
11.2 The Standard Model and the mechanism of electroweak symmetry breaking 202
11.2.1 The SM Higgs boson mass, couplings and quantum numbers 203
11.2.2 The SM custodial symmetry 203
11.2.3 Stability of the Higgs potential 203
11.2.4 Higgs boson production and decay mechanisms 203
11.3 The experimental profile of the Higgs boson . . 208
11.3.1 The principal decay channels to vector bosons 208
11.3.2 Decays to third generation fermions ($b\bar{b}$ and $\tau^+\tau^-$) 210
11.3.3 Higgs boson production in association with top quarks or in top decays 212
11.3.4 Higgs boson pair production 214
11.3.5 Searches for rare decays of the Higgs boson 215
11.3.6 Searches for non-SM decay channels 217
11.4 Combining the main channels 219
11.4.1 Principles of the combination 219
11.4.2 Main decay modes 220
11.4.3 Main production modes 222
11.5 Main quantum numbers and width of the Higgs boson 222
11.5.1 Main quantum numbers J^{PC} 222
11.5.2 Off-shell couplings of the Higgs boson . . . 225
11.5.3 The Higgs boson width 226
11.6 Probing the coupling properties of the Higgs boson 227
11.6.1 Effective Lagrangian framework 228
11.6.2 Probing coupling properties 228
11.7 New physics models of EWSB in the light of the Higgs boson discovery 234
11.7.1 Higgs bosons in the minimal supersymmetric standard model (MSSM) 236
11.7.2 Supersymmetry with singlet extensions . . 238
11.7.3 Supersymmetry with extended gauge sectors 238
11.7.4 Effects of CP violation 239
11.7.5 Non-supersymmetric extensions of the Higgs sector 240
11.7.6 Composite Higgs models 242
11.7.7 Searches for signatures of extended Higgs sectors 245
11.8 Summary and outlook 250

11.1 Introduction

Understanding the mechanism that breaks the electroweak symmetry and generates the masses of the known elementary particles has been one of the fundamental endeavours in particle physics for several decades. The discovery in 2012 by the ATLAS [1] and the CMS [2] collaborations of a new resonance with a mass of approximately 125 GeV and the subsequent studies of its properties with the full data set from Run 1, from 2009 to 2012, with a centre-of-mass energy of 7 TeV and 8 TeV, conclusively provided a first portrait of the Electroweak Symmetry Breaking (EWSB) mechanism. The data collected during the LHC Run 2, from 2015 to 2018, with a higher centre-of-mass energy of 13 TeV and more conspicuous dataset, put in solid grounds the compatibility of the measured resonance with the Higgs boson of the Standard Model (SM) [3] and strongly challenge its contenders. LHC will start its Run 3 in 2022 and is expected to last until 2025. During this period the LHC is expected to deliver proton-proton collision data corresponding to an integrated luminosity of approximately 160 fb^{-1} per experiment.

In the SM, the electroweak interactions are described by a gauge field theory invariant under the $\mathrm{SU}(2)_L \times \mathrm{U}(1)_Y$ symmetry group. The mechanism of EWSB [4] provides a general framework to keep untouched the structure of these gauge interactions at high energies and still generate the observed masses of the W and Z gauge bosons. The EWSB mechanism posits a self-interacting complex EW doublet scalar field, whose CP-even neutral component acquires a vacuum expectation value (VEV) $v \approx 246$ GeV, which sets the scale of the symmetry breaking. Three massless Goldstone bosons are generated and are absorbed to give masses to the W and Z gauge bosons. The remaining component of the complex doublet becomes the Higgs boson – a new, and so far unique, fundamental scalar particle. The masses of all fermions are also a consequence of EWSB since the Higgs doublet is postulated to couple to the fermions through Yukawa interactions. Remarkably, these Yukawa interactions to the heaviest fermions have now been established.

The initial measurements during the LHC Run 1 were accessible mainly through production and decay channels related to the couplings of the Higgs boson to the vector gauge bosons (the mediators of the electroweak interactions, $W^\pm$, Z and γ, as well as the gluons, g, mediators of the strong interactions). The outstanding performance of the LHC Run 2, made it possible for the ATLAS and CMS experiments to independently and unambiguously establish the couplings of the Higgs boson to the charged fermions of the third generation (the top quark, the bottom quark, and the tau lepton). These observations of fundamental importance were made with partial Run 2 datasets. In all observed production and decay modes measured so far, the rates and differential measurements are found to be consistent, within experimental and theoretical uncertainties, with the SM predictions. In high resolution decay channels, such as the ones with four leptons (electrons or muons) or diphoton final states, the mass of the Higgs boson has been measured at the permill precision level. Nevertheless, several channels are still out of reach experimentally and the couplings of the Higgs boson to light fermions are very challenging and yet to be observed; however, the very recent results of the search for Higgs boson decays to muons by the ATLAS and CMS experiments provide evidence for the Yukawa coupling of the Higgs boson to muons. Moreover, within the current precision, a more complex sector with additional states, although significantly constrained, is not ruled out, nor has it been established whether the Higgs boson is an elementary particle or whether it has an internal structure like any other scalar particle observed before it.

Without the Higgs boson, the calculability of the SM would have been spoiled. In particular, perturbative unitarity [5] would be lost at high energies since the longitudinal W/Z boson scattering amplitude would grow with the centre-of-mass energy. In addition, the radiative corrections to the gauge boson self-energies would exhibit dangerous logarithmic divergences that would be difficult to reconcile with EW precision data. With the discovery of the Higgs boson, the SM is a spontaneously broken gauge theory and, as such, it could a priori be consistently extrapolated well above the masses of the W and Z bosons. Hence, formally there is no need for new physics at the EW scale. However, as the SM Higgs boson is a scalar particle, at the quantum level it has sensitivity to possible new physics scales. Quite generally, the Higgs boson mass is affected by the presence of heavy particles and it receives quantum corrections which destabilise the weak scale barring a large fine-tuning of unrelated parameters. This is known as the Higgs naturalness or hierarchy problem [6]. It has been the prime argument for expecting new physics right at the TeV scale. New theoretical paradigms have been imagined, such as a new fermion-boson symmetry called supersymmetry (SUSY) [7] (for recent reviews, see Refs. [8, 9]), or the existence of strong interactions at a scale of the order of a TeV from which the Higgs boson would emerge as a composite state [10] (see Refs. [11, 12] for recent reviews). Alternatively, new agents stabilising the weak scale could also be light but elusive, like in models of neutral naturalness [13, 14]. Other recent scenarios [15, 16], instead, rely on the cosmological evolution of the Universe to drive the Higgs boson mass to a value much smaller than the cutoff of the theory and aim at alleviating the hierarchy problem without the need for TeV scale new physics, even thought there might still be interesting and spectacular signatures [15, 17]. This new approach spurs a change in perspective invoking our Universe as part of a

Downloaded from https://academic.oup.com/ptep/article/2022/8/083C01/6651666 by KIT Library user on 27 September 2022

multiverse that should be treated as a quantum statistical system [18]. Beyond the naturalness problem, extensions of the SM Higgs sector without other low-energy particles have been proposed, for example, to provide explanations for the fermion mass hierarchies, see e.g. Ref. [19], to account for the Dark Matter abundance, see e.g. Ref. [20], or to modify the properties of the electroweak phase transition [21]. Such models with additional scalars provide grounds to explore new Higgs boson signals in concrete and complete scenarios, with different types of coupling structure to fermions and gauge bosons.

The Higgs boson is anyway special and, in the nine years since its discovery, it became a powerful tool to explore the manifestations of the SM and to probe the physics landscape beyond it. It might offer direct insights on what comes beyond the weak scale through possible sizeable effects on the Higgs boson properties. The Higgs boson couplings, however, are observed to be in good agreement with their SM predictions. This, together with the strong bounds from precision electroweak and flavour data, leaves open the possibility that the Higgs boson may well be elementary, weakly coupled and solitary up to the Planck scale, rendering the EW vacuum potentially metastable [22].

After completion of the first two runs, the LHC has only gathered approximately 5% of its projected full dataset. LHC is undergoing important upgrades in order to prepare for its high luminosity phase. The foreseen larger datasets to be collected during Run 3 and ultimately during the High Luminosity LHC (HL-LHC), will enable yet more fundamental and challenging measurements to explore new physics.

This review is organised as follows. Section 11.2 is a theoretical review of the SM Higgs boson, its properties, production mechanisms and decay rates. In Section 11.3, the experimental measurements are described. In Section 11.4, the combination of the main Higgs boson production and decay channels is presented. In Section 11.5, measurements of the main quantum numbers and CP properties of the Higgs boson are reported and the bounds on its total width are discussed. In Section 11.6, a general theoretical framework to describe the deviations of the Higgs boson couplings from the SM predictions is introduced and the experimental measurements of these Higgs couplings is reviewed. Measurements of differential cross sections are outlined. Section 11.7 presents, in detail, some interesting models proposed for extensions of the SM Higgs sector, addressing the hierarchy problem or not, and considers their experimental signatures. Section 11.8 provides a short summary and a brief outlook.

11.2 The Standard Model and the mechanism of electroweak symmetry breaking

In the SM [3], electroweak symmetry breaking [4] is responsible for generating mass for the W and Z gauge bosons rendering the weak interactions short ranged. The SM scalar potential reads:

$$V(\Phi) = m^2\Phi^\dagger\Phi + \lambda(\Phi^\dagger\Phi)^2 \tag{11.1}$$

with the Higgs field Φ being a self-interacting $\mathrm{SU}(2)_L$ complex doublet (four real degrees of freedom) with weak hypercharge $Y{=}1$ (the hypercharge is normalised such that $Q = T_{3L} + Y/2$, Q being the electric charge and T_{3L} the eigenvalue of the diagonal generator of $\mathrm{SU}(2)_L$):

$$\Phi = \frac{1}{\sqrt{2}}\begin{pmatrix}\sqrt{2}\phi^+\\ \phi^0 + ia^0\end{pmatrix}, \tag{11.2}$$

where ϕ^0 and a^0 are the CP-even and CP-odd neutral components, and ϕ^+ is the complex charged component of the Higgs doublet, respectively. $V(\Phi)$ is the most general renormalisable scalar potential. If the quadratic term is negative, the neutral component of the scalar doublet acquires a non-zero (real) vacuum expectation value (VEV)

$$\langle\Phi\rangle = \frac{1}{\sqrt{2}}\begin{pmatrix}0\\ v\end{pmatrix}, \tag{11.3}$$

with $\phi^0 = H + \langle\phi^0\rangle$ and $\langle\phi^0\rangle \equiv v$, inducing the spontaneous breaking of the SM gauge symmetry $\mathrm{SU}(3)_C \times \mathrm{SU}(2)_L \times \mathrm{U}(1)_Y$ into $\mathrm{SU}(3)_C \times \mathrm{U}(1)_{\mathrm{em}}$. The global minimum of the theory defines the ground state, and spontaneous symmetry breaking implies that there is a (global and/or local) symmetry of the system that is not respected by the ground state. From the four generators of the $\mathrm{SU}(2)_L \times \mathrm{U}(1)_Y$ SM gauge group, three are spontaneously broken, implying that they lead to non-trivial transformations of the ground state and indicate the existence of three massless Goldstone bosons identified with three of the four Higgs field degrees of freedom. The Higgs field couples to the W_μ and B_μ gauge fields associated with the $\mathrm{SU}(2)_L \times \mathrm{U}(1)_Y$ local symmetry through the covariant derivative appearing in the kinetic term of the Higgs Lagrangian,

$$\mathcal{L}_{\mathrm{Higgs}} = (D_\mu\Phi)^\dagger(D^\mu\Phi) - V(\Phi), \tag{11.4}$$

where $D_\mu\Phi = (\partial_\mu + ig\sigma^a W^a_\mu/2 + ig'YB_\mu/2)\Phi$, g and g' are the $\mathrm{SU}(2)_L$ and $\mathrm{U}(1)_Y$ gauge couplings, respectively, and $\sigma^a, a = 1,2,3$ are the usual Pauli matrices. As a result, the neutral and the two charged massless Goldstone degrees of freedom mix with the gauge fields corresponding to the broken generators of $\mathrm{SU}(2)_L \times \mathrm{U}(1)_Y$ and become, in the unitarity gauge, the longitudinal components of the Z and W physical gauge bosons, respectively. The Z and W gauge bosons acquire masses,

$$m_W^2 = \frac{g^2v^2}{4}, \quad m_Z^2 = \frac{(g'^2+g^2)v^2}{4}. \tag{11.5}$$

The fourth generator remains unbroken since it is the one associated to the conserved $\mathrm{U}(1)_{\mathrm{em}}$ gauge symmetry, and its corresponding gauge field, the photon, remains massless. Similarly, the eight color gauge bosons, the gluons, corresponding to the conserved $\mathrm{SU}(3)_C$ gauge symmetry with 8 unbroken generators, also remain massless (though confined inside hadrons and mesons as the result of the asymptotic freedom behaviour of Quantum ChromoDynamics (QCD)). Hence, from the initial four degrees of freedom of the Higgs field, two are absorbed by the $W^\pm$ gauge bosons, one by the Z gauge boson, and there is one remaining degree of freedom, H, that is the physical Higgs boson — a new scalar particle first imagined by P. Higgs [4]. The Higgs boson is neutral under the electromagnetic interactions and transforms as a singlet under $\mathrm{SU}(3)_C$ and hence does not couple at tree level to the massless photons and gluons.

The fermions of the SM acquire mass through renormalisable interactions between the Higgs field and the fermions: the Yukawa interactions,

$$\mathcal{L}_{\mathrm{Yukawa}} = -\hat{h}_{d_{ij}}\bar{q}_{L_i}\Phi\, d_{R_j} - \hat{h}_{u_{ij}}\bar{q}_{L_i}\tilde{\Phi}u_{R_j} - \hat{h}_{l_{ij}}\bar{l}_{L_i}\Phi\, e_{R_j} + h.c., \tag{11.6}$$

which respect the symmetries of the SM but generate fermion masses once EWSB occurs. In the Lagrangian above, $\tilde{\Phi} = i\sigma_2\Phi^*$ and q_L (l_L) and u_R, d_R (e_R) are the quark (lepton) $\mathrm{SU}(2)_L$ doublets and singlets, respectively, while in each term, $\hat{h}_{f_{ij}}$, $f = u, d, l$ is parametrized by a 3×3 matrix in family space. The mass term for neutrinos is omitted, but could be added in an analogous manner to the up-type quarks when right-handed neutrinos are supplementing the SM particle content (neutrinos can also acquire Majorana masses via non-renormalisable dimension-5 interactions with the Higgs field [23]). Once the Higgs field acquires a VEV, and after rotation to the fermion mass eigenstate basis that also diagonalises the Higgs-fermion interactions, $\hat{h}_{f_{ij}} \to h_{f_i}\delta_{ij}$ (the diagonal Yukawa coupling h_{f_i} is often denoted as y_{f_i}), all fermions acquire a mass given by $m_{f_i} = h_{f_i}v/\sqrt{2}$. The indices $i, j = 1,2,3$ refer to the three families in the up-quark, down-quark or charged lepton sectors. Remarkably, if the Yukawa interactions Eq. (11.6) are indeed fully responsible for the fermion masses, the Higgs interactions do not mediate flavour changing neutral currents at tree-level. It should be further noted that the EWSB mechanism provides no additional insight on possible underlying reasons for the large variety of mass values of the fermions, often referred to as the flavour hierarchy. The fermion masses, accounting for a large number of the free parameters of the SM, are simply translated into Yukawa couplings.

Downloaded from https://academic.oup.com/ptep/article/2022/8/083C01/6651666 by KIT Library user on 27 September 2022

11.2.1 *The SM Higgs boson mass, couplings and quantum numbers*

The SM Higgs boson is a CP-even scalar of spin 0. Its mass is given by $m_H = \sqrt{2\lambda}\, v$, where λ is the self coupling parameter in $V(\Phi)$. The expectation value of the Higgs field, $v = (\sqrt{2}G_F)^{-1/2} \approx 246\,\text{GeV}$, is fixed by the Fermi coupling G_F, which is determined with a precision of 0.6 ppm from muon decay measurements [24]. The quartic coupling λ is a free parameter in the SM, and hence, there is no a priori prediction for the Higgs mass. Moreover the sign of the mass parameter $m^2 = -\lambda v^2$ has to be negative for the EW symmetry breaking to take place, but there is no a priori understanding of what decides of this sign. The experimentally measured Higgs boson mass, $m_H = 125.25 \pm 0.17\,\text{GeV}$ [24], implies that $\lambda \simeq 0.13$ and $|m| \simeq 88.4\,\text{GeV}$.

The Higgs boson couplings to the fundamental particles are set by their masses. This is a new type of interaction; very weak for light particles, such as up and down quarks, and electrons, but strong for heavy particles such as the W and Z bosons and the top quark. More precisely, the SM Higgs couplings to fundamental fermions are linearly proportional to the fermion masses, whereas the couplings to bosons are proportional to the square of the boson masses. The SM Higgs boson couplings to gauge bosons and fermions, as well as the Higgs boson self coupling, are summarized in the following Lagrangian:

$$\begin{aligned}\mathcal{L} = -g_{Hf\bar{f}}\bar{f}fH + \frac{g_{HHH}}{6}H^3 + \frac{g_{HHHH}}{24}H^4 \\ + \delta_V V_\mu V^\mu \left(g_{HVV}H + \frac{g_{HHVV}}{2}H^2\right)\end{aligned} \tag{11.7}$$

with

$$\begin{aligned}&g_{Hf\bar{f}} \equiv y_f = \frac{m_f}{v},\ g_{HVV} = \frac{2m_V^2}{v},\ g_{HHVV} = \frac{2m_V^2}{v^2}, \\ &g_{HHH} = \frac{3m_H^2}{v},\ g_{HHHH} = \frac{3m_H^2}{v^2},\end{aligned} \tag{11.8}$$

where $V = W^\pm$ or Z and $\delta_W = 1, \delta_Z = 1/2$. As a result, the dominant mechanisms for Higgs boson production and decay involve the coupling of H to W, Z and/or the third generation quarks and leptons. The Higgs boson coupling to gluons [25,26] is induced at leading order by a one-loop process in which H couples to a virtual $t\bar{t}$ pair (with minor contributions from the other lighter quarks). Likewise, the Higgs boson coupling to photons is also generated via loops, although in this case the one-loop graph with a virtual W^+W^- pair provides the dominant contribution [27] and it is interfering destructively with the smaller contribution involving a virtual $t\bar{t}$ pair (as such, the Higgs coupling to photons is sensitive to the relative phase of the interactions between bosons and fermions).

11.2.2 *The SM custodial symmetry*

The SM Higgs Lagrangian, $\mathcal{L}_{\text{Higgs}} + \mathcal{L}_{\text{Yukawa}}$ of Eq. (11.4) and Eq. (11.6), is, by construction, $\text{SU}(2)_L \times \text{U}(1)_Y$ gauge invariant, but it also has an approximate global symmetry. In the limit $g' \to 0$ and $h_f \to 0$, a global $\text{SU}(2)_R$ symmetry emerges. This symmetry is preserved for non-vanishing Yukawa couplings, provided $h_u = h_d$. Once the Higgs acquires a VEV, both the $\text{SU}(2)_L$ and $\text{SU}(2)_R$ symmetry groups are broken but the diagonal subgroup $\text{SU}(2)_{L+R}$ remains unbroken and it is the subgroup that defines the custodial symmetry of the SM [28].

In the limit $g' \to 0$, the W and Z gauge bosons have equal mass and form a triplet of the $\text{SU}(2)_{L+R}$ unbroken global symmetry. Using the expressions for the W and Z gauge boson masses in term of the gauge couplings, one obtains at tree level

$$\frac{m_W^2}{m_Z^2} = \frac{g^2}{g'^2 + g^2} = \cos^2\theta_W \quad \text{or} \quad \rho \equiv \frac{m_W^2}{m_Z^2\cos^2\theta_W} = 1. \tag{11.9}$$

The custodial symmetry protects the above relation from large radiative corrections. All corrections to the ρ parameter are therefore proportional to terms that break the custodial symmetry. For instance, radiative corrections involving the Higgs boson are proportional to $\sin^2\theta_W$, $\delta\rho = -11G_F m_Z^2 \sin^2\theta_W \log(m_H^2/m_Z^2)/(24\sqrt{2}\pi^2)$, and vanish in the limit $g' \to 0$. Since $m_t \neq m_b$, there are also relevant radiative corrections generated by massive fermions. They are proportional to $m_t^2 + m_b^2 - 2(m_t^2 m_b^2)\log(m_t^2/m_b^2)/(m_t^2 - m_b^2)$ and would indeed vanish for $m_t = m_b$ [29].

11.2.3 *Stability of the Higgs potential*

The discovery of the Higgs boson with $m_H \approx 125\,\text{GeV}$ has far reaching consequences within the SM framework. In particular, the precise value of m_H determines the value of the quartic coupling λ at the electroweak scale and makes it possible to study its behavior up to high energy scales. A larger value of m_H would have implied that the self coupling λ would become non-perturbative at some scale Λ that could be well below the Planck scale [30].

However, for the value of Higgs boson mass experimentally measured, the EW vacuum of the Higgs potential is most likely metastable [22]. The high-energy evolution of λ shows that it becomes negative at energies $\Lambda = \mathcal{O}(10^{11})\,\text{GeV}$ (even though λ could remain positive till higher energy, maybe all the way to the Planck scale, if the top quark mass exceeds its current measured value by 3σ). When this occurs, the SM Higgs potential develops an instability and the long term existence of the EW vacuum is challenged. This behaviour may call for new physics at an intermediate scale before the instability develops, i.e., below M_{Planck}, even though new physics at M_{Planck} could influence the stability of the EW vacuum and possibly modify this conclusion [31]. The consequences of the instability of the EW vacuum on high-scale inflation have been discussed in Ref. [32]. It was also noticed that Higgs field fluctuations during inflation could seed the formation of primordial black holes, possibly making up the Dark Matter relic abundance [33] or they could produce a stochastic background of gravitational waves with characteristic structures [34], offering a probe of the EW vacuum near criticality.

The lifetime of the EW metastable vacuum is determined by the rate of quantum tunnelling from this vacuum into the true vacuum of the theory (for the most recent computation of the EW vacuum lifetime within the SM, see Ref. [35]). Within the SM, the running of the Higgs self coupling slows down at high energies with a cancellation of its β-function at energies just one to two orders of magnitude below the Planck scale [36]. This slow evolution of the quartic coupling is responsible for saving the EW vacuum from premature collapse. It might also help the Higgs boson to play the role of an inflaton [37] (see, however, Ref. [38] for potential issues with this Higgs-boson-as-an-inflaton idea).

11.2.4 *Higgs boson production and decay mechanisms*

Comprehensive reviews of the SM Higgs boson's properties and phenomenology, with an emphasis on the impact of loop corrections to the Higgs boson decay rates and cross sections, can be found in Refs. [39–46]. The main results are summarised here.

11.2.4.1 *Production mechanisms at hadron colliders*

The main production mechanisms at the Tevatron collider and the LHC are gluon fusion (ggF), weak-boson fusion (VBF), associated production with a gauge boson (VH), and associated production with a pair of $t\bar{t}$ quarks ($t\bar{t}H$) or with a single top quark (tHq). Figure 11.1 depicts representative diagrams for these dominant Higgs boson production processes.

The state-of-the-art of the theoretical calculations in the main different production channels is summarized in Table 11.1.

The cross sections for the production of a SM Higgs boson as a function of $\sqrt{s}$, the center of mass energy, for pp collisions, including bands indicating the theoretical uncertainties, are summarized in Fig. 11.2 (left) [47]. A detailed discussion, including uncertainties in the theoretical calculations due to missing higher-order effects and experimental uncertainties on the determination of SM parameters involved in the calculations, can be found in Refs. [43–46]. These references also contain state-of-the-art discussions on the impact of PDF uncertainties, QCD scale uncertainties and uncertainties due to different procedures for including higher-order corrections matched to parton shower simulations, as well as uncertainties due to hadronisation and parton-shower events.

Downloaded from https://academic.oup.com/ptep/article/2022/8/083C01/6651666 by KIT Library user on 27 September 2022

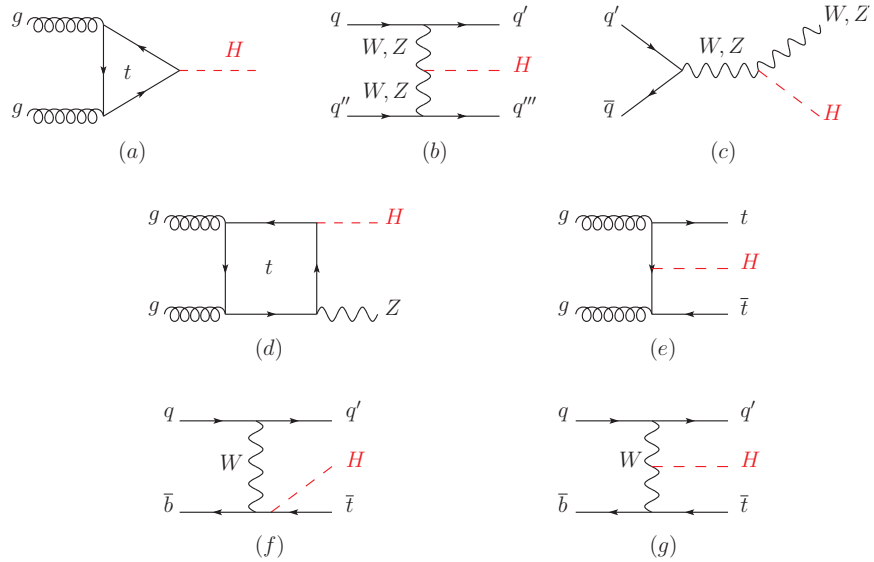

Figure 11.1: Main leading order Feynman diagrams contributing to the Higgs boson production in (a) gluon fusion, (b) Vector-boson fusion, (c) Higgs-strahlung (or associated production with a gauge boson at tree level from a quark-quark interaction), (d) associated production with a gauge boson (at loop level from a gluon-gluon interaction), (e) associated production with a pair of top quarks (there is a similar diagram for the associated production with a pair of bottom quarks), (f-g) production in association with a single top quark

Table 11.1: State-of-the-art of the theoretical calculations in the main Higgs boson production channels in the SM, and the major MC tools used in the simulations

ggF	VBF	VH	$t\bar{t}H$
Fixed order:	Fixed order:	Fixed order:	Fixed order:
N3LO QCD + NLO EW	NNLO/NLOPS QCD	NNLO QCD+EW	NNLO QCD
`(HIGLU, iHixs, FeHiPro, HNNLO)`	`(VBF@NNLO)`	`(V2HV and HAWK)`	`(Powheg)`
Resummed:	Fixed order:	Fixed order:	`(MG5_aMC@NLO)`
NNLO + NNLL QCD	NLO QCD + NLO EW	NNLO QCD	
`(HRes)`	`(HAWK)`	`(VH@NNLO)`	
Differential $p_T(H)$:			
N3LO			
`(HqT, HRes)`			
Fiducial:			
N3LO+N3LL'			

Table 11.2 summarizes the Higgs boson production cross sections and relative uncertainties for a Higgs boson mass of 125 GeV, for $\sqrt{s} = 7$, 8, 13 and 14 TeV.

i. *Gluon fusion production mechanism*

At high-energy hadron colliders, the Higgs boson production mechanism with the largest cross section is the gluon-fusion process, $gg \to H + X$, mediated by the exchange of a virtual, heavy top quark [49]. Contributions from lighter quarks propagating in the loop are suppressed proportionally to m_q^2. QCD radiative corrections to the gluon-fusion process are very important and have been studied in detail. Including the full dependence on the (top, bottom, charm) quark and Higgs boson masses, the cross section has been calculated at the next-to-leading order (NLO) in α_s [50, 51]. To a very good approximation, the leading top-quark contribution can be evaluated in the limit $m_t \to \infty$ by matching the SM to an effective theory. The gluon-fusion amplitude is then evaluated from an effective Lagrangian containing a local $HG^a_{\mu\nu}G^{a\,\mu\nu}$ operator [25, 26]. In this approximation, the cross section is known at next-to-next-to-next-to-leading order (N3LO) [52]. The validity of the effective theory with infinite m_t is greatly enhanced by rescaling the result by the exact LO result: $\sigma = (\sigma^{\rm LO}_{m_t}/\sigma^{\rm LO}_{m_t=\infty}) \times \sigma_{m_t=\infty}$ [46]. The large top-quark mass approximation, after this rescaling of the cross section, yields a NNLO result that has been established to be at the percent level accuracy [53]. Further progress is made to include full top mass dependence at NNLO [54].

The LO and NLO QCD corrections [55] amount to about 80% of the total N3LO cross section. The NNLO corrections [56] further enhance the cross section by approximately 30% of the LO plus NLO result (at $\mu_f = \mu_r = m_H/2$). Electroweak radiative corrections have been computed at NLO and increase the LO cross section by about 5% for $m_H \simeq 125$ GeV [57]. Mixed QCD-EW corrections are now being investigated with encouraging results on the computation of the exact 3-loop amplitude [58] complementing the results obtained in either limit of heavy [59] or massless [60] gauge bosons. The mixed QCD-EW corrections still have to be evaluated at large p_T.

At N3LO, the perturbation series is rather stable with a mere enhancement of 3% of the total cross section, with a central value quite insensitive to threshold resummation effects with the scale choice mentioned above ($\mu_f = \mu_r = m_H/2$) [46, 52, 61]. At the LHC with a center-of-mass energy of 13 TeV, the most up-to-date value for the production cross section of a 125.09 GeV Higgs boson amounts to [46]

$$\sigma^{\rm N3LO}_{\rm ggF} = 48.5 \pm 1.9(\pm 3.9\%)\,({\rm theory}) \pm 1.6\,(3.2\%)\,({\rm PDF} + \alpha_s)\,{\rm pb}. \tag{11.10}$$

Besides considering the inclusive Higgs boson production cross section at the LHC, it is important to study differential distributions in order to probe the properties of the Higgs boson in a detailed way. Fully-differential N3LO QCD predictions for Higgs production in gluon fusion have been obtained by combin-

Downloaded from https://academic.oup.com/ptep/article/2022/8/083C01/6651666 by KIT Library user on 27 September 2022

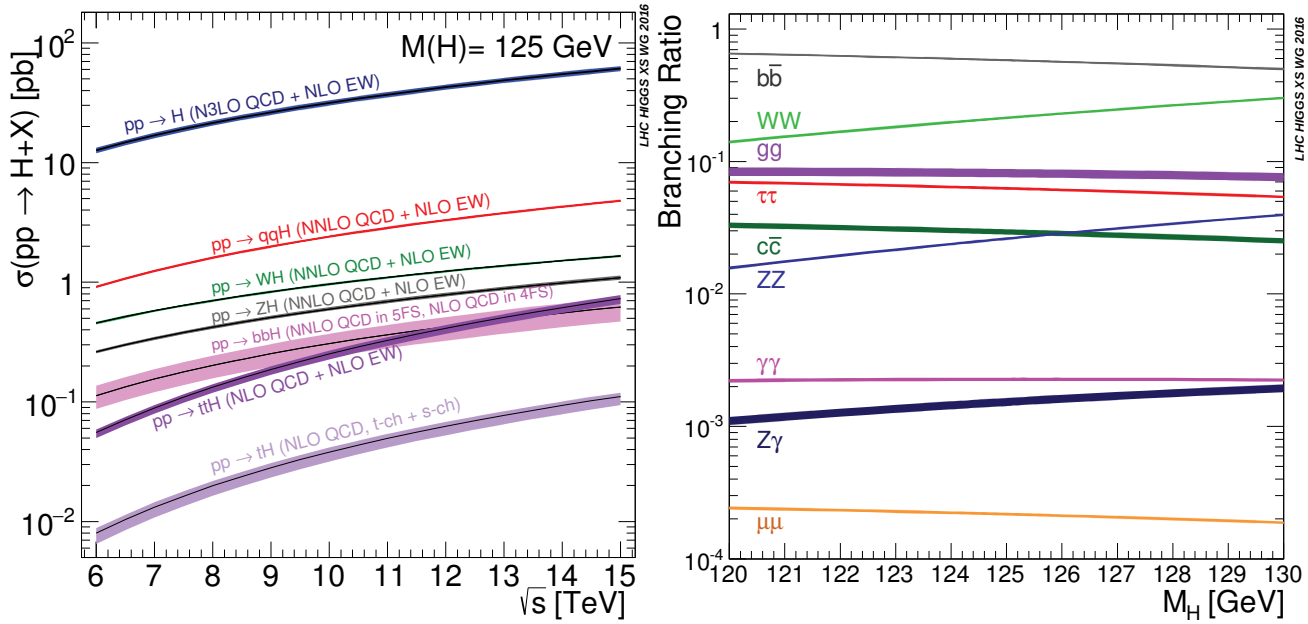

Figure 11.2: (Left) The SM Higgs boson production cross sections as a function of the center of mass energy, $\sqrt{s}$, for pp collisions [47]. The VBF process is indicated here as qqH. The theoretical uncertainties are indicated as bands. (Right) The branching ratios for the main decays of the SM Higgs boson near $m_H = 125\,\text{GeV}$ [45, 46]. The theoretical uncertainties are indicated as bands.

Table 11.2: The SM Higgs boson production cross sections for $m_H = 125\,\text{GeV}$ in pp collisions ($p\bar{p}$ collisions at $\sqrt{s} = 1.96\,\text{TeV}$ for the Tevatron), as a function of the center of mass energy, $\sqrt{s}$. The predictions for the LHC energies are taken from Refs. [43–46], the ones for the Tevatron energy are the ones used in Ref. [48]. The predictions for the ggF channel at the LHC include the latest N3LO results leading to reduced theoretical uncertainties by a factor around 2 compared to the NNLO+NLL results. The total uncertainties are estimated assuming no correlations between α_S and PDF uncertainties.

$\sqrt{s}$ (TeV)	Production cross section (in pb) for $m_H = 125\,\text{GeV}$					
	ggF	VBF	WH	ZH	$t\bar{t}H$	total
1.96	$0.95^{+17\%}_{-17\%}$	$0.065^{+8\%}_{-7\%}$	$0.13^{+8\%}_{-8\%}$	$0.079^{+8\%}_{-8\%}$	$0.004^{+10\%}_{-10\%}$	1.23
7	$16.9^{+5.5\%}_{-7.6\%}$	$1.24^{+2.2\%}_{-2.2\%}$	$0.58^{+2.2\%}_{-2.3\%}$	$0.34^{+3.1\%}_{-3.0\%}$	$0.09^{+5.6\%}_{-10.2\%}$	19.1
8	$21.4^{+5.4\%}_{-7.6\%}$	$1.60^{+2.1\%}_{-2.1\%}$	$0.70^{+2.1\%}_{-2.2\%}$	$0.42^{+3.4\%}_{-2.9\%}$	$0.13^{+5.9\%}_{-10.1\%}$	24.2
13	$48.6^{+5.6\%}_{-7.4\%}$	$3.78^{+2.1\%}_{-2.1\%}$	$1.37^{+2.0\%}_{-2.0\%}$	$0.88^{+4.1\%}_{-3.5\%}$	$0.50^{+6.8\%}_{-9.9\%}$	55.1
14	$54.7^{+5.6\%}_{-7.4\%}$	$4.28^{+2.1\%}_{-2.1\%}$	$1.51^{+1.8\%}_{-1.9\%}$	$0.99^{+4.1\%}_{-3.7\%}$	$0.61^{+6.9\%}_{-9.8\%}$	62.1

ing N3LO QCD predictions for Higgs rapidity distribution with NNLO predictions for H+jet [62]. A more exclusive account of Higgs boson production is also required because experimental analyses often impose cuts on the final states in order to improve the signal-to-background ratio. Using soft-collinear effective theory, large fiducial power corrections induced by fiducial cuts have been resummed at N3LO+N3LL' accuracy [63]. This is the most accurate result that can be directly compared with fiducial measurements. Different fiducial cuts are explored to suppress these fiducial effects. In addition, nice progress is made to improve the calculation of the Higgs boson production cross section with a jet veto (the "0-jet bin" or in the presence of a veto bounding the transverse momentum of the hardest accompanying jet) [64], reaching N2LL accuracy matched to N3LO. These accurate predictions for the jet-veto cross section are required, e.g., to suppress the $t\bar{t}$ background in the $H \to WW$ channel [65].

ii. *Vector boson fusion production mechanism*

The SM Higgs boson production mode with the second-largest cross section at the LHC is vector boson fusion. At the Tevatron collider, VBF also occurred, but for $m_H = 125\,\text{GeV}$ had a smaller cross section than Higgs boson production in association with a W or Z boson. Higgs boson production via VBF, $qq \to qqH$, proceeds by the scattering of two (anti-)quarks, mediated by t- or u-channel exchange of a W or Z boson, with the Higgs boson radiated off the weak-boson propagator. The scattered quarks give rise to two back-to-back hard jets in the forward and backward regions of the detector [66]. Because of the color-singlet nature of the weak-gauge boson exchange, gluon radiation from the central-rapidity regions is strongly suppressed. These characteristic features of VBF processes can be exploited to distinguish them from overwhelming QCD backgrounds, including gluon-fusion induced Higgs boson + 2 jet production, and from s-channel WH or ZH production with a hadronically decaying weak gauge boson. After the application of specific selection cuts, the VBF channel provides a clean environment, not only for the Higgs boson searches originally performed, but also for the subsequent determination of Higgs boson couplings at the LHC.

The cross-section is known at N3LO at the inclusive level and at N2LO enforcing the VBF cuts [67] with a residual uncertainty of the order of few permill. However, this result is obtained in the DIS/factorized approximation [68] where the fusing gauge bosons are emitted from the two quark legs independently. While, the exact NNLO VBF calculation will remain out-of-reach in the near future, the leading non-factorisable contributions with two forward jets have been estimated [69] and the impact of non-factorizable effects have been studied in Ref. [70]. They give some corrections, also of the order of few permill, to inclusive quantities, but they are an order of magnitude larger for differential observables. Overall, the residual uncertainty is of the order of a few percent but is quite sensitive to the tagging jet cuts and jet radius modelling [71]. Extensive studies on VBF at fixed order and with parton shower matched computations can be found in Ref. [72].

Downloaded from https://academic.oup.com/ptep/article/2022/8/083C01/6651666 by KIT Library user on 27 September 2022

iii. *WH and ZH associated production mechanism*

The next most relevant Higgs boson production mechanisms are associated production with W and Z gauge bosons. The cross sections for the associated production processes, $pp \to VH + X$, with $V = W^{\pm}, Z$ receive contributions at NLO given by NLO QCD corrections to the Drell–Yan cross section [73, 74] and from NLO EW corrections. The latter, unlike the QCD corrections, do not respect the factorisation into Drell–Yan production since there are irreducible box contributions already at one loop [75]. At NNLO, the Drell–Yan-like corrections to WH production also give the bulk of the corrections to ZH production [76]. For ZH production there are, however, gluon-gluon induced contributions that do not involve a virtual Z gauge boson but are such that the Z gauge boson and H boson couple to gluons via top-quark loops [77], see diagram (d) in Fig. 11.1. NLO virtual corrections to the partonic cross section for $gg \to ZH$, in the high-energy and large top mass limits are available in Refs. [78]. In addition, WH and ZH production receive non Drell–Yan-like corrections in the $q\bar{q}'$ and $q\bar{q}$ initiated channels, respectively, at the NNLO level, where the Higgs boson is radiated off top-quark loops [79]. The full QCD corrections up to NNLO order, the NLO EW corrections and the NLO corrections to the gluon-gluon channel are available in `VH@NNLO` [80]. NNLO QCD corrections to $pp \to WH$+jet are important for signal modelling. NLO corrections to cross section inclusive in the number of jets show excellent convergence while NNLO QCD corrections to exclusive single jet cross section are much more significant [81].

As neither the Higgs boson nor the weak gauge bosons are stable particles, their decays also have to be taken into account. Providing full kinematical information for the decay products can furthermore help in the suppression of large QCD backgrounds. Differential distributions for the processes $pp \to WH \to \bar{\nu}_\ell \ell H$ and $pp \to ZH \to \ell^+\ell^- H/\nu_\ell \bar{\nu}_\ell H$, including NLO QCD and EW corrections, have been presented in Ref. [82]. The NNLO QCD corrections to differential observables for WH production at the LHC, including the leptonic decays of the W boson and the decay of the Higgs boson into a $b\bar{b}$ pair, are presented in Ref. [83]. Calculations at the same level, including also the ZH process have been performed [84]. The WH production mode has also been matched to a parton shower at NNLO accuracy [85]. Full NNLO results for both the production and decay are available [86] and show a large impact of radiation from the final-state bottoms. The WH and ZH production modes, especially in the boosted regime, provide a relatively clean environment for studying the decay of the Higgs boson into bottom quarks [87]. Bottom mass effects have been computed at NNLO [88, 89] and tend to increase the rates by 6-7%.

iv. *Higgs boson production in association with $t\bar{t}$*

Higgs boson radiation off top quarks, $pp \to t\bar{t}H$, provides a direct probe of the top-Higgs Yukawa coupling. The LO cross section for this production process was computed in Ref. [90]. Later, the NLO(+NNLL) QCD [91] and NLO EW corrections [92] were evaluated yielding a moderate increase in the total cross section of at most 20%, but significantly reducing the scale dependence of the inclusive cross section. The EW corrections can be enhanced by large electroweak Sudakov logarithms in particular in the boosted regime often used in the phenomenological analyses [93]. The resummation of soft gluon contributions close to the partonic kinematical threshold are considered in Refs. [94]. Full off-shell calculations with decaying top quarks are computed at NLO QCD [95] and NLO QCD plus EW [96] order, respectively. Interfaces between NLO QCD calculations for $t\bar{t}H$ production with parton-shower Monte-Carlo programs have been provided in Refs. [97]. These programs provide the most flexible tools to date for the computation of differential distributions, including experimental selection cuts and vetoes on the final-state particles and their decay products. The fixed-order NLO QCD calculation has been interfaced with the standard Parton Shower Monte-Carlo generators, allowing an accurate description of the $t\bar{t}H$ signal, from the energy scale of the hard scattering to the hadronisation energy scale. The exploitation of this channel requires, however, a proper description of the background, in particular $t\bar{t}b\bar{b}$, which exhibits a huge k-factor[1] enhancement from shower effects, see Ref. [46] for a detailed discussion. The total theoretical uncertainties, estimated by combining the ones from factorisation and renormalisation scales, strong gauge coupling, and parton distributions, amount to 10–15% of the corresponding inclusive cross section. To match the experimental precision envisioned at the end of HL-LHC, NNLO QCD predictions are required. Using the q_T subtraction formalism for $t\bar{t}H$ production, Ref. [98] presented the first quantitative results at NLO and NNLO. The calculation is accurate at NLO in QCD and agrees with the results obtained using the conventional subtraction methods. The NNLO corrections are computed for the flavour off-diagonal partonic channels but their contribution turn out to be at the permill level. The results for the diagonal channels are still missing. Most recently, the fragmentation and splitting functions for the production of a Higgs boson have been computed at order $y_t^2\alpha_s$ and they can be used to compute differential cross sections with arbitrary top-quark and Higgs-boson masses directly from the results in the massless limit [99].

v. *Other single Higgs boson production mechanisms at the LHC*

The Higgs boson production in association with a single top quark, though subdominant, can bring valuable information, in particular regarding the sign of the top Yukawa coupling. This is due to an almost totally destructive interference between two large contributions, one where the Higgs boson couples to a space-like W boson and the other where it couples to the top quark. This process has been computed at NLO QCD in a five-flavour scheme [100] and amounts to about 90 fb at $\sqrt{s} = 14$ TeV (with the opposite sign of the top Yukawa coupling, the cross section increases by one order of magnitude while the cross section for associated production with a pair of top quarks is unaffected). Recently, the tHj (and tZj) process has been computed at NLO QCD+EW accuracy [101]. The NLO EW correction is found to be within the NLO QCD theory uncertainties if the 4 vs 5 flavor scheme uncertainty is taken into account. The EW corrections reduce the total cross section by 3-4%.

The Higgs boson production in association with a pair of bottom quarks ($b\bar{b}H$) is known at NNLO in the 5-flavour scheme [102–104]. The coupling of the Higgs boson to a b-quark is suppressed in the SM by the bottom-quark mass over the Higgs VEV, m_b/v, implying that associated production of a SM Higgs boson with b-quarks is small at the LHC. Yet, at high energy, large logarithms are present and need to be resummed, leading to an enhancement of the inclusive cross section. At $\sqrt{s} = 14$ TeV, the $b\bar{b}H$ cross section can be as large as 550 fb, still two orders of magnitude below the ggF production cross section. Furthermore, the overwhelming ZH and VBF backgrounds (at the inclusive but also differential levels) make it challenging to extract genuine bottom Yukawa signal in a traditional cut-based analysis [105] but innovative machine-learning techniques are a promising avenue to obtain information complementary to the ones extracted from $gg \to h \to b\bar{b}$, in particular for what concerns the phase of the bottom Yukawa coupling [106]. In a two Higgs doublet model or a SUSY model, which will be discussed in Section 11.7, this coupling is proportional to the ratio of neutral Higgs boson vacuum expectation values, $\tan\beta$, and can be significantly enhanced for large values of this ratio. Consequently, the $b\bar{b}H$ mode can even become the dominant production process for the Higgs boson, unlike in the SM.

The Higgs boson production in association with charm quarks is also known at NNLO and its cross section is approximately 85 fb at $\sqrt{s} = 13$ TeV [46].

vi. *Double Higgs boson production at the LHC*

The main interest in the double Higgs boson production is that it can provide invaluable information on the Higgs potential. In particular, it gives access to the Higgs trilinear self coupling. The

[1] the k-factor is defined as the ratio of a physical quantity with and without radiative corrections included.

Downloaded from https://academic.oup.com/ptep/article/2022/8/083C01/6651666 by KIT Library user on 27 September 2022

dominant production is via gluon fusion $gg \to HH$. It accounts for more than 90% of the total inclusive cross-section, the subleading production mechanisms are VBF $HHjj$ (around 1.7 fb at 13 TeV), HHW (0.50 fb), HHZ (0.36 fb) and $t\bar{t}HH$ (0.8 fb). The fixed order QCD corrections, computed in the infinite top mass limit, are large, typically doubling the cross section from LO to NLO [107], further enhancing it by 20% and reducing the scale uncertainty by a factor 2-3 from NLO to NNLO [108], with a milder increase of order 3% at N3LO [109] to finally reach at 13 TeV

$$\sigma(gg \to HH)^{\rm N3LO}_{\rm ggF} = 31.31\,{\rm fb}^{+0.66\%}_{-2.8\%}\,. \tag{11.11}$$

Recently, the complete NLO corrections with all top quark mass effects also became available numerically [110], intriguingly revealing a k-factor much less flat than predicted in the large top mass approximations. The non-trivial dependence of the results on the renormalisation scheme and scale for the top quark mass questions the assessment of the scale uncertainty and would warrant a proper NNLO computation that will however remain out of reach for quite some time. At the differential level, the destructive interference between the box and the triangle contributions complicates the predictions made in the infinite top mass limit for both the HH invariant mass and the leading Higgs boson p_T distributions. With an inclusive cross section of about 35 fb at $\sqrt{s} = 13$ TeV and a difficult signal vs background discrimination, the double Higgs boson production remains a challenging channel to probe and will greatly benefit from the high-luminosity run of the LHC and the combination of various decay modes [111]. The double Higgs channel is definitively a prime target on the Higgs physics agenda and the forthcoming analyses will greatly benefit from the solidification of the fixed order predictions and the detailed uncertainty budget estimate that is underway [112].

11.2.4.2 *Production mechanisms at e^+e^- colliders*

The dominant Higgs boson production cross sections at an e^+e^- collider are from the Higgs-strahlung process [25, 113], $e^+e^- \to ZH$, and the WW fusion process [114], $e^+e^- \to \bar{\nu}_e\nu_e W^*W^* \to \bar{\nu}_e\nu_e H$. The cross-section for the Higgs-strahlung process scales as s^{-1} and is predominant at low energies, while the cross-section for the WW fusion process scales as $\ln(s/m_H^2)$ and dominates at high energies [115]. The ZZ fusion mechanism, $e^+e^- \to e^+e^-Z^*Z^* \to e^+e^-H$, also contributes to the Higgs boson production, with a cross-section suppressed by an order of magnitude with respect to that of WW fusion. The process $e^+e^- \to t\bar{t}H$ [116] becomes important for $\sqrt{s} \geq 500$ GeV. For a more detailed discussion of Higgs boson production properties at lepton colliders, see for example Refs. [117]. Interesting progress has been made recently [118] to accurately account for beamstrahlung and initial state radiation using the factorisation approach primarily developed for hadron colliders and this method is being implemented in Monte Carlo event generators.

11.2.4.3 *SM Higgs boson branching ratios and total width*

For the understanding and interpretation of the experimental results, the computation of all relevant Higgs boson decay widths is essential, including an estimate of their uncertainties and, when appropriate, the effects of Higgs boson decays into off-shell particles with successive decays into lighter SM ones. A Higgs boson mass of about 125 GeV allows to explore the Higgs boson couplings to many SM particles. In particular the dominant decay modes are $H \to b\bar{b}$ and $H \to WW^*$, followed by $H \to gg$, $H \to \tau^+\tau^-$, $H \to c\bar{c}$ and $H \to ZZ^*$. With much smaller rates follow the Higgs boson decays into $H \to \gamma\gamma$, $H \to \gamma Z$ and $H \to \mu^+\mu^-$. Since the decays into gluons, diphotons and $Z\gamma$ are loop induced, they provide indirect information on the Higgs boson couplings to WW, ZZ and $t\bar{t}$ in different combinations. The uncertainties in the branching ratios include the missing higher-order corrections in the theoretical calculations as well as the errors in the SM input parameters, in particular fermion masses and the QCD gauge coupling, involved in the decay. In the following the state-of-the-art of the theoretical calculations compiled by the LHC Higgs Working Group [47] will be discussed and the reader is referred to Refs. [43–46, 119] for detail.

The evaluation of the radiative corrections to the fermionic decays of the SM Higgs boson are implemented in HDECAY [120] at different levels of accuracy. The computations of the $H \to b\bar{b}$ and $H \to c\bar{c}$ decays include the complete massless QCD corrections up to N4LO, with a corresponding scale dependence of about 0.1% [121]. Both the electroweak corrections to $H \to b\bar{b}$, $c\bar{c}$ as well as $H \to \tau^+\tau^-$ are known at NLO [122] providing predictions with an overall accuracy of about 1–2% for $m_H \simeq 125$ GeV.

The loop induced decays of the SM Higgs boson are known fully at NLO and partially beyond that approximation. For $H \to gg$, the QCD corrections are known up to N3LO in the limit of heavy top quarks [51,123] and the uncertainty from the scale dependence is about 3%. For the $H \to \gamma\gamma$, the full NLO QCD corrections are available [51, 124] and the three-loop QCD corrections have also been evaluated [125]. The NLO electroweak corrections to $H \to gg$ and $H \to \gamma\gamma$ have been computed in Ref. [126]. All these corrections are implemented in HDECAY [120]. For $m_H \simeq 125$ GeV, the overall impact of known QCD and EW radiative effects turns out to be well below 1%. In addition, the contribution of the $H \to \gamma e^+e^-$ decay via virtual photon conversion has been computed in Ref. [127]. The partial decay width $H \to Z\gamma$ is only implemented at LO in HDECAY, including the virtual W, top-, bottom-, and τ-loop contributions. The QCD corrections have been calculated and are at the percent level [128]. The theoretical uncertainty due to unknown electroweak corrections is estimated to be less than 5%, an accuracy that will be hard to achieve in the measurement of this process at the LHC.

Table 11.3: The branching ratios and the relative uncertainty for a SM Higgs boson with $m_H = 125$ GeV [45, 46].

Decay channel	Branching ratio	Rel. uncertainty
$H \to \gamma\gamma$	2.27×10^{-3}	2.1%
$H \to ZZ$	2.62×10^{-2}	±1.5%
$H \to W^+W^-$	2.14×10^{-1}	±1.5%
$H \to \tau^+\tau^-$	6.27×10^{-2}	±1.6%
$H \to b\bar{b}$	5.82×10^{-1}	$^{+1.2\%}_{-1.3\%}$
$H \to c\bar{c}$	2.89×10^{-2}	$^{+5.5\%}_{-2.0\%}$
$H \to Z\gamma$	1.53×10^{-3}	±5.8%
$H \to \mu^+\mu^-$	2.18×10^{-4}	±1.7%

The decays $H \to WW/ZZ \to 4f$ can be simulated with the `Prophecy4f` Monte-Carlo generator [129] that includes complete NLO QCD and EW corrections for Higgs decays into any possible four-fermion final state. All calculations are consistently performed with off-shell gauge bosons, without any on-shell approximation. For the SM Higgs boson, the missing higher-order corrections are estimated to be roughly 0.5%. Such uncertainties will have to be combined with the parametric uncertainties, in particular those associated to the bottom-quark mass and the strong gauge coupling, to arrive at the full theory uncertainty. A detailed treatment of the differential distributions for a Higgs boson decay into four charged leptons in the final state is discussed in Refs. [45, 130].

The total width of a 125 GeV SM Higgs boson is $\Gamma_H = 4.07 \times 10^{-3}$ GeV, with a relative uncertainty of $^{+4.0\%}_{-3.9\%}$. The branching ratios for the most relevant decay modes of the SM Higgs boson as a function of m_H, including the most recent theoretical uncertainties, are shown in Fig. 11.2 (right) and listed for $m_H = 125$ GeV in Table 11.3. Further details of these calculations can be found in the reviews [43–46] and references therein.

Downloaded from https://academic.oup.com/ptep/article/2022/8/083C01/6651666 by KIT Library user on 27 September 2022

11.3 The experimental profile of the Higgs boson

The observation [1,2] at the LHC of a narrow resonance with a mass of about 125 GeV was an important landmark in the decades-long direct search [48, 131] for the SM Higgs boson. This was followed by a detailed exploration of properties of the Higgs boson at the different runs of the LHC at $\sqrt{s}$ = 7, 8 and 13 TeV.

The dataset at $\sqrt{s}$ =13 TeV in the Run 2 phase of the LHC operation corresponds to an integrated luminosity of about 156 fb^{-1} to the ATLAS and CMS experiments, see Table 11.4. The datasets effectively useful for analysis need to take into account the data-taking efficiency with fully operational detectors and the data quality efficiency. The typical total inefficiency for both ATLAS and CMS is approximately 10%, where approximately half is due to the data taking inefficiency and half from data quality.

In this section, most of the references for the Run 1 measurements that have been updated at the Run 2 are given in the previous version of this review [132] and are not repeated herein.

Table 11.4: The LHC pp collision centre-of-mass energies and delivered data samples.

Year	$\sqrt{s}$ (TeV)	$\int$ L.dt (fb^{-1})	Period
2010	7	0.04	Run 1
2011	7	6.1	Run 1
2012	8	23.3	Run 1
2015	13	4.2	Run 2
2016	13	40.8	Run 2
2017	13	50.2	Run 2
2018	13	60.6	Run 2

11.3.1 *The principal decay channels to vector bosons*

For a given m_H, the sensitivity of a channel depends on the production cross section of the Higgs boson, its decay branching fraction, the reconstructed mass resolution, the selection efficiency and the level of background in the final state. For a low-mass Higgs boson (110 GeV $< m_H <$ 150 GeV) for which the SM width would be only a few MeV, five decay channels play an important role at the LHC. In the $H \to \gamma\gamma$ and $H \to ZZ^* \to 4\ell$ channels, all final state particles can be very precisely measured and the reconstructed m_H resolution is excellent (typically 1-2%). While the $H \to W^{\pm}W^{\mp(*)} \to \ell^+\nu_\ell\ell'^-\bar{\nu}_{\ell'}$ channel has relatively large branching fraction, however, due to the presence of neutrinos which are not reconstructed in the final state, the m_H resolution, obtained through observables sensitive to the Higgs boson mass such as the transverse mass, is poor (approximately 20%). The $H \to b\bar{b}$ and the $H \to \tau^+\tau^-$ (with the tau subsequently decaying to electrons or muons and two neutrinos $\tau \to \ell\nu\nu$ or to hadrons and one neutrino $\tau \to$ hadrons ν) channels suffer from large backgrounds and lead to an intermediate mass resolution of about 10% and 15% respectively.

With the increase in the size of datasets, measurements in the most sensitive channels are now carried out differentially or in exclusive modes depending on specific production characteristics. These measurements are discussed in Section 11.6.2.4.

The candidate events in each Higgs boson decay channel are split into several mutually exclusive categories (or event tags) based on the specific topological, kinematic or other features present in the event. The categorization of events increases the sensitivity of the overall analysis and allows a separation of different Higgs boson production processes. Most categories are dominated by signal from one Higgs boson decay mode but contain an admixture of various Higgs boson production processes. For example, a typical VBF selection requires Higgs boson candidates to be accompanied by two energetic jets ($\geq$ 30 GeV) with a large dijet mass ($\geq$ 400 GeV) and separated by a large pseudo-rapidity ($\Delta\eta_{jj} \geq 3.5$) [133]. While such a category is enriched in Higgs bosons produced via VBF, the contamination from the ggF production mechanism can be significant. Hence, a measurement of the signal rate in the VBF category does not imply a measurement of VBF production cross section since one cannot resolve the contamination from ggF. Simulations are used to determine the relative contributions of the various Higgs boson production modes in each specific categories.

An important difference between the Run 1 and Run 2 results, in particular when comparing signal strengths, and therefore in the measurement of the couplings of the Higgs boson as discussed in Section 11.4, is that values and errors of the predicted cross sections have been improved (mostly the scale and PDF uncertainties). The theoretical predictions are however compatible and therefore, the signal strengths can be compared on a sound basis.

11.3.1.1 $H \to \gamma\gamma$

In the diphoton channel, a search is performed for a narrow peak over a smoothly falling background in the invariant mass distribution of two high p_T photons. The background in this channel is conspicuous and stems from prompt $\gamma\gamma$ processes for the irreducible backgrounds, and the γ+jet and dijet processes for the reducible backgrounds where one jet fragments typically into a leading π^0. In order to optimise search sensitivity and also to separate the various Higgs boson production modes, ATLAS and CMS split events into several mutually exclusive categories. Diphoton events containing high p_T muons or electrons, or missing energy ($E_T^{\rm miss}$) consistent with the decay of a W or Z boson, are tagged in the VH production category. Diphoton events containing energetic dijets with a large mass and pseudo-rapidity difference are assigned to the VBF production category, and the remaining events are considered either in the VH category when the two jets are compatible with the hadronic decay of a W or a Z, or in the ggF production category. While the leptonic VH category is relatively pure, the VBF category has significant contamination from the gluon fusion process. Events which are not picked by any of the above selections are further categorised according to their expected $m_{\gamma\gamma}$ resolution and signal-to-background ratio. Categories with good m_H resolution and larger signal-to-background ratio contribute most to the sensitivity of the search.

Both ATLAS and CMS have studied in detail the calibration of the energy response of photons, in particular using $Z \to e^+e^-$, $Z \to \mu^+\mu^-\gamma$ and the response of muons in the calorimeter (for ATLAS) from $Z \to \mu^+\mu^-$ events. This information is used to correct the simulated signal mass line-shapes. In each category, parametric signal models are adjusted to these line-shapes to provide a functional form for the signal. Simple monotonic functional forms of the backgrounds are determined by a fit to the $m_{\gamma\gamma}$ distribution in each category (typically exponential, Bernstein polynomials, Laurent series or power laws). All categories are fitted simultaneously to determine the signal yield at the measured combined Run 1 mass of 125.09$\pm$ GeV [136] for ATLAS and m_H = 125.38 GeV for CMS as discussed in Section 11.3.1.3. The $m_{\gamma\gamma}$ distribution after combining all categories is shown in Fig. 11.3, using the full ATLAS Run 2 dataset.

The signal strength, $\mu = (\sigma \cdot {\rm BR})_{\rm obs}/(\sigma \cdot {\rm BR})_{\rm SM}$, which is the observed product of the Higgs boson production cross section (σ) and its branching ratio (BR) normalised to the corresponding SM values, is 1.17 $\pm$ 0.27 for ATLAS in Run 1 and 1.02 $\pm$ 0.14 in Run 2 [137] (where this signal strength measurement is estimated from the measured fiducial cross sections and thus neglects acceptance systematic uncertainties, which are not expected to be dominant in particular given that the measurement is inclusive). The signal strengths [2] measured in Run 1 and Run 2 by the CMS collaboration are $1.18^{+0.26}_{-0.23}$ and 1.12 ± 0.09 [138] respectively.

11.3.1.2 $H \to ZZ^* \to \ell^+\ell^-\ell'^+\ell'^-$

In the $H \to ZZ^* \to \ell^+\ell^-\ell'^+\ell'^-$ channel, a search is performed for a narrow mass peak over a small continuous background dominated by non-resonant ZZ^* production from $q\bar{q}$ annihilation and gg fusion processes. The contribution and the shape of this irreducible background is taken from simulation. The subdominant and reducible backgrounds stem from Z+$b\bar{b}$, $t\bar{t}$ and Z+jets events. Their contribution is suppressed by requirements on lepton isolation and lepton impact parameter and their yield is estimated from control samples in data.

To help to distinguish the Higgs boson signal from the dominant non-resonant ZZ^* background, both ATLAS and CMS [139]

[2] The Run 1 results for ATLAS and CMS are at fixed values of m_H = 125.4 GeV and 124.7 GeV, respectively.

Downloaded from https://academic.oup.com/ptep/article/2022/8/083C01/6651666 by KIT Library user on 27 September 2022

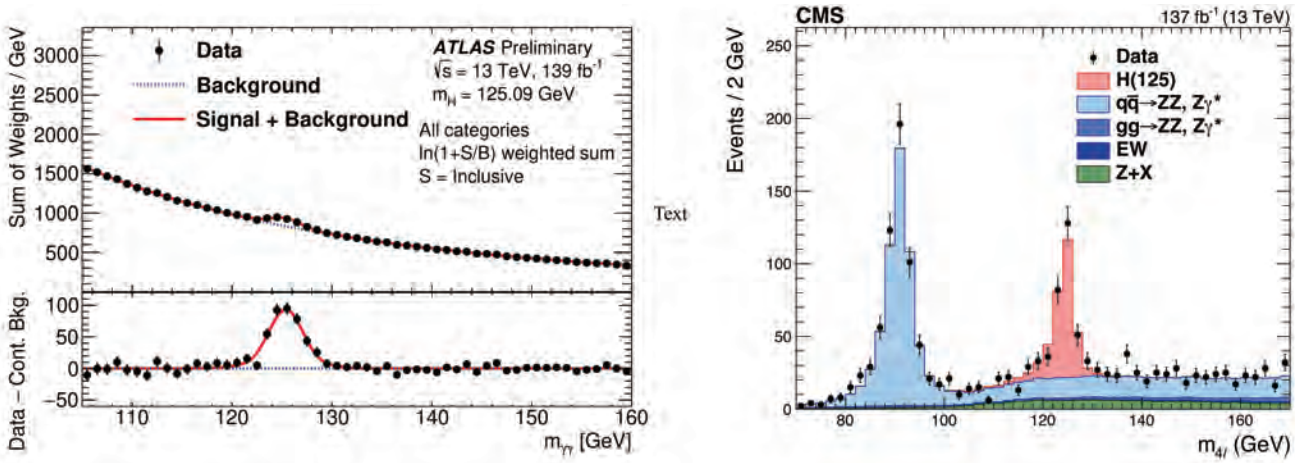

Figure 11.3: (Left) The invariant mass distribution of diphoton candidates, with each event weighted by the ratio of signal-to-background in each event category, observed by ATLAS [134] at Run 2. The residuals of the data with respect to the fitted background are displayed in the lower panel. (Right) The $m_{4\ell}$ distribution from CMS [135] Run 2 data.

use a matrix element likelihood approach to construct a kinematic discriminant built for each 4ℓ event based on the ratio of complete leading-order matrix elements $|\mathcal{M}_{\rm sig}{}^2/\mathcal{M}_{\rm bkg}{}^2|$ for the signal ($gg \to H \to 4\ell$) and background ($q\overline{q} \to ZZ \to 4\ell$) hypotheses. To further enhance the sensitivity, experiments also use multivariate techniques.

To improve the sensitivity to more exclusive production processes such as VBF, VH, and $t\bar{t}H$, the experiments divide 4ℓ events into mutually exclusive categories. Events are categorised in terms of the number of reconstructed jets, the number of additional leptons (from the decay of a vector boson in the associated production mode), number of jet tagged as containing a b-hadron, the transverse momentum of the Higgs boson (or e.g. its associated vector boson) and missing transverse momentum. The exclusive processes are also further separated in different kinematic regions in a framework referred to as Simplified Template Cross Sections (see Section 11.6.2.4). Dijets with a large mass and pseudo-rapidity difference populate the VBF category. ATLAS requires the presence of an additional lepton in the VH category. In events with less than two jets, CMS uses the $p_T^{4\ell}$ to distinguish between production via the gluon fusion and the VH/VBF processes.

Since the $m_{4\ell}$ resolutions and the reducible background levels are different in the 4μ, $4e$ and $2e2\mu$ sub-channels, they are analysed separately and the results are then combined. The distribution of the reconstructed invariant mass of the four leptons for CMS [135] is given in Fig. 11.3 (right), showing a clear excess at a mass of approximately $m_H = 125$ GeV. Both experiments also observe a clear peak at $m_{4\ell} = 91$ GeV from the production of a Z boson on-mass-shell and decaying to four leptons due typically to the emission of an off-shell photon from one of the primary leptons from the Z boson decay.

The signal strengths μ for the inclusive $H \to 4\ell$ production measured by ATLAS and CMS are $1.44^{+0.40}_{-0.33}$ at $m_H = 125.38$ GeV and $0.93^{+0.29}_{-0.25}$ at $m_H = 125.6$ GeV respectively, in Run 1. The signal strengths measured by ATLAS and CMS in Run 2 are 1.01 ± 0.11 [140] and $0.94^{+0.12}_{-0.11}$ [135] respectively (the ATLAS measurement is made at the combined Run 1 Higgs boson mass of $m_H = 125.09$ GeV and $m_H = 125.38$ GeV for the CMS measurement).

11.3.1.3 *Measurement of the Higgs boson mass*

To measure the mass of the Higgs boson, ATLAS and CMS collaborations rely on the two high mass-resolution and sensitive channels, $\gamma\gamma$ and $ZZ^*/4\ell$. The ATLAS and CMS approaches are very similar in these two analyses with small differences on the usage of categories, additional discriminating variables and per-event errors. In these two channels, the mass resolutions range from 1.4 GeV to 2 GeV for ATLAS and from 1.0 GeV to 2.8 GeV for CMS (see Ref. [136] and the reconstruction-performance references therein). An excellent mass resolution is obtained for both experiments in the diphoton channel for central diphoton pairs (typically for events where both photons are not converted). However, the best precision in this measurement at Run 2 is obtained using the four lepton channel and in particular in the sub-channel of four muons (followed by the two-electrons and two muons channel where the mass resolution is driven by the reconstruction of the lower mass di-lepton pair with typically lower transverse momentum leptons).

Both ATLAS and CMS have produced several Higgs boson mass measurements, including the individual and combined Run 1 measurements [136] and the Run 2 measurements by ATLAS [141,142] and CMS [139, 143] for both the 4ℓ and the diphoton channels. The current most precise result is obtained by CMS using a partial Run 2 dataset and a combination of Run 1 and Run 2 measurements yielding a measurement of 125.38 ± 0.11 (stat.) ± 0.08(syst.). The later measurement is used by CMS as reference Higgs boson mass.

The Run 1 combination including both ATLAS and CMS measurements of 125.09 ± 0.21 (stat.) ± 0.11(syst.) is currently used as a reference for Higgs measurement results by ATLAS. [136].

In the diphoton channel, as discussed in Section 11.5.3.2, a mass shift is expected to be induced by the deformation of the mass line-shape of the signal in presence of background, from the interference between the Higgs boson production and the continuum irreducible background. It is a small but non negligible effect of approximately 35 MeV [144] for a Higgs boson width close to that of the SM. This effect could be larger if the width of the Higgs boson were to be substantially larger. This effect estimated by ATLAS with a full simulation is still relatively small with respect to the total uncertainty on the mass and is therefore neglected.

11.3.1.4 $H \to W^+W^- \to \ell^+\nu\ell^-\overline{\nu}$

In this challenging channel, experiments search for an excess of events with two leptons (electrons or muons) of opposite charge accompanied by missing energy and/or jets. A typical event selection is described below in order to give an idea of the main intricacies. Specific selections vary between experiments and between Run 1 and Run 2 analyses. Events are divided into several categories depending on the lepton flavour combination (e^+e^-, $\mu^+\mu^-$and $e^\pm\mu^\mp$) and the number of accompanying jets ($N_{\rm jet} = 0, 1, \geq 2$). In the ATLAS analysis, the $N_{\rm jet} \geq 2$ category is optimised for the VBF production process by selecting two leading jets with a large pseudo-rapidity difference and with a large mass ($m_{jj} > 500$ GeV).

Backgrounds contributing to this channel are numerous and depend on the category of selected events. Reducing them and accurately estimating the remainder is a major challenge in this analysis. For events with opposite-flavour leptons and no ac-

Downloaded from https://academic.oup.com/ptep/article/2022/8/083C01/6651666 by KIT Library user on 27 September 2022

companying high p_T jets, the dominant background stems from non-resonant WW production. Events with same-flavour leptons suffer from large Drell–Yan contamination (note that also the opposite-flavour leptons analysis has Drell–Yan $\tau\bar{\tau}$ background in 0-jet category). The $t\bar{t}$, tW and $W+$jets (with the jet misidentified as a lepton) events contaminate all categories. Non-resonant WZ, ZZ and $W\gamma$ processes also contribute to the background at a sub-leading level.

A requirement of large missing transverse energy ($E_T^{\rm miss}$) is used to reduce the Drell–Yan and multijet backgrounds. In the e^+e^- and $\mu^+\mu^-$ categories, events with $m_{\ell\ell}$ consistent with the Z mass are vetoed. The $t\bar{t}$ background is suppressed by a veto against identified b-jets or low p_T muons assumed to be coming from semi-leptonic b-hadron decays within jets (this soft muon veto was not applied anymore in Run 2 analysis) and tight isolation requirements diminish the W+jets background. The scalar nature of the Higgs boson and the $V-A$ nature of the W boson decay implies that the two charged leptons in the final state are preferentially emitted at small angles with respect to each other. Therefore the dilepton invariant mass ($m_{\ell\ell}$) and the azimuthal angle difference between the leptons ($\Delta\phi_{\ell\ell}$) are used to discriminate between the signal and non-resonant WW events [145]. The transverse mass, constructed from the dilepton p_T ($p_T^{\ell\ell}$), $E_T^{\rm miss}$ and the azimuthal angle between $E_T^{\rm miss}$ and $p_T^{\ell\ell}$, is defined as $m_T = \sqrt{2p_T^{\ell\ell}E_T^{\rm miss}(1-\cos\Delta\phi_{E_T^{\rm miss}\ell\ell})}$ and serves as an effective discriminant against backgrounds. The transverse mass variable also tracks the Higgs boson mass but with a poor mass resolution. Background rates except for the small contributions typically from non-resonant WZ, ZZ and $W\gamma$ are evaluated from data control samples with floating normalisation.

At Run 1 ATLAS fitted the m_T distributions and observed an excess at $m_H = 125.38$ GeV with a local significance of 6.1σ similar to that expected from a 125 GeV SM Higgs boson. The measured inclusive signal strength is $\mu = 1.09^{+0.23}_{-0.21}$. In the VBF category, an excess with a significance of 3.2σ corresponding to a signal strength of $\mu = 1.27^{+0.53}_{-0.45}$ is observed. The CMS analysis of 0- and 1-jet categories, using all lepton flavour combinations, shows an excess with an observed significance of 4.3σ, lower than the expected sensitivity of 5.8σ for a 125.6 GeV SM Higgs boson. CMS observes no significant excess in the VBF production mode and sets a 95% CL limit on the signal strength of $\mu_{\rm VBF} < 1.7$ for $m_H = 125.6$ GeV.

ATLAS and CMS have also searched for the associated Higgs boson production in this channel. The signal consists of up to three (WH) or four (ZH) high p_T isolated leptons with missing transverse energy and low hadronic activity. The major backgrounds stem from triboson and diboson production where each boson decays leptonically. ATLAS observes [146] an excess at $m_H = 125.38$ GeV with a local significance of 2.5σ corresponding to a $\mu_{VH} = 3.0^{+1.6}_{-1.0}$. CMS instead sets a 95% CL limit of $\mu_{VH} < 4.7$.

Both ATLAS [147] and CMS [148] have performed this analysis with the full Run 2 dataset. The ATLAS analysis was done with the different flavour $WW \to e\nu\mu\nu$ decay mode in categories selected according to the numbers of jets with categories aiming specifically at the VBF production mode. The gluon fusion and VBF production cross sections are measured simultaneously. The measured signal strengths are:

$$\mu_{\rm ggF} = 1.20 \pm 0.05\ (\text{stat.})^{+0.09}_{-0.08}\ (\text{exp.sys.})^{+0.10}_{-0.08}\ (\text{sig.th.})^{+0.12}_{-0.11}\ (\text{bkg.th.})$$

$$\mu_{\rm VBF} = 0.99 \pm^{+0.13}_{-0.12}\ (\text{stat.})^{+0.07}_{-0.06}\ (\text{exp.sys.})^{+0.18}_{-0.12}\ (\text{sig.th.})^{+0.10}_{-0.08}\ (\text{bkg.th.}).$$

It is interesting to note that the largest uncertainty is from the theoretical prediction of the background in the gluon fusion process and that the statistical uncertainty is sub-dominant. While in the VBF mode the largest uncertainty is from the signal modelling.

With the entire Run 2 dataset CMS performed a fiducial measurement of the inclusive and differential production cross sections of the Higgs boson in the leptonic modes of its WW decay channel. The results are unfolded to correct for selection efficiency and purity as well as resolution effects. The measured cross section in the fiducial volume is 86.5 ± 9.5 fb, consistent with the Standard Model expectation of 82.5 ± 4.2 fb.

CMS has also performed with the full dataset an analysis of the WH and ZH production modes of the Higgs boson subsequently decaying to WW using both leptonic and hadronic decay modes of the W and Z boson. The selected channels are: (i) two same-sign leptons (electrons or muons) and jets targetting the WH production mode, (ii) 3 leptons targetting the WH production, (iii) 3 leptons to select events from the ZH production mode, and (iv) 4 lepton channels. In the (iii) and (iv) one pair of same flavour and opposite sign leptons are required to be compatible with the mass of the Z boson. The overall measured signal strenght is [149]:

$$\mu = 1.85 \pm 0.33\ (\text{stat.})^{+0.27}_{-0.25}\ (\text{exp.})^{+0.10}_{-0.07}\ (\text{th.})$$

11.3.2 *Decays to third generation fermions ($b\bar{b}$ and $\tau^+\tau^-$)*

In the SM, fermions acquire a mass through gauge invariant interactions with the Higgs field which is also responsible for the electroweak symmetry breaking and thus for generating the masses of gauge bosons (see Section 11.2 for more details). While this minimal solution is very elegant, there is no fundamental reason for it to be the case, and probing the couplings of the Higgs boson to fermions is therefore of fundamental importance, in particular since BSM physics can largely change the SM predictions.

The discovery of the Higgs boson was made essentially through bosonic final states. These decays probed mostly the couplings of the Higgs boson to vector bosons (the decay of the Higgs boson to photons occurring only through loops is also dominated in the SM by the coupling of the Higgs boson to W bosons). However, the predominant Higgs boson production mode is the gluon fusion, occurring only through loops dominated by the coupling of the Higgs boson to fermions. The observation of the Higgs boson in the two photons or two gluons decay modes is also an indirect evidence for the coupling of the Higgs boson to fermions (and in particular to the top quark). Nevertheless, the observation of either decays to fermions or production modes which unambiguously proceed through fermion couplings provide direct probes of the coupling of the Higgs boson to fermions and is thus of fundamental importance.

At hadron colliders, the most promising channel for probing the coupling of the Higgs field to the quarks and leptons are $H \to b\bar{b}$ and $H \to \tau^+\tau^-$, respectively. For a Higgs boson with $m_H \approx 125$ GeV, the branching fraction to $b\bar{b}$ is about 58% and to $\tau^+\tau^-$ is about 6%. Nevertheless, the presence of very large backgrounds makes the isolation of a Higgs boson signal in these channels quite challenging.

One of the most prominent goals of the LHC Run 2 for ATLAS and CMS was the direct observation of the Yukawa coupling of the Higgs boson to fermions of the third generation (bottom quarks, tau leptons and top quarks). This goal has been reached independently by both ATLAS and CMS and with only partial Run 2 datasets.

The Run 2 of the LHC has also delivered beyond expectations as it provided evidence for two new rare decay modes of the higgs boson in the $H \to \mu^+\mu^-$ and the $H \to \ell^+\ell^-\gamma$ channels (where ℓ denotes and electron or a muon).

11.3.2.1 $H \to \tau^+\tau^-$

In the $H \to \tau^+\tau^-$ search, τ leptons decaying to electrons (τ_e), muons (τ_μ) and hadrons (τ_{had}) are considered. The $\tau^+\tau^-$ invariant mass ($m_{\tau\tau}$) is reconstructed from a kinematic fit of the visible products from the two τ leptons and the missing energy observed in the event. Due to the presence of missing neutrinos, the $m_{\tau\tau}$ resolution is poor ($\approx 15\%$). As a result, a broad excess over the expected background in the $m_{\tau\tau}$ distribution is searched for. The major sources of background stem from Drell–Yan $Z \to \tau^+\tau^-$ and $Z \to e^+e^-$, W+jets, $t\bar{t}$ and multijet production. Events in all sub-channels are divided into categories based on the number and kinematic properties of additional energetic jets in the event and the transverse momentum of the reconstructed Higgs boson and the distance ΔR distance between the two τ's. The sensitivity

Downloaded from https://academic.oup.com/ptep/article/2022/8/083C01/6651666 by KIT Library user on 27 September 2022

of the search is generally higher for categories with one or more additional jets. The VBF category, consisting of a τ pair with two energetic jets separated by a large pseudo-rapidity, has the best signal-to-background ratio and search sensitivity, followed by the $\tau^+\tau^-$+1 jet category. The signal to background discrimination relies in part on the $m_{\tau\tau}$ resolution, which improves with the boost of the Higgs boson. The non-VBF categories are further subdivided according to the observed boost of the $\tau^+\tau^-$ system. CMS primarily uses the reconstructed $m_{\tau\tau}$ as the final discriminating variable while ATLAS combines various kinematic properties of each event categories with multivariate techniques to build the final discriminant [150].

Searches for $H \to \tau^+\tau^-$ decays in the VH production mode are also performed in final states where the W or Z boson decays into leptons or jets. The irreducible background in this search arises from non-resonant WZ and ZZ diboson production. The reducible backgrounds originate from W, Z, and $t\bar{t}$ events that contain at least one fake lepton in the final state due to a misidentified jet. The shape and yield of the major backgrounds in each category are estimated from control samples in data. Contributions from non-resonant WZ and ZZ diboson production are estimated from simulations but corrected for reconstruction efficiency using control samples formed from observed data.

For CMS, the significance of the observed excess at $m_H = 125\,\text{GeV}$ in Run 1 is 3.2σ, close to the expected 3.7σ sensitivity, and corresponds to a signal strength of $\mu = 0.86 \pm 0.29$. The observed (expected) deviation from the background-only hypothesis in ATLAS corresponds to a local significance of 4.5σ (3.4σ) and the best fit value of the signal strength is $\mu = 1.43^{+0.43}_{-0.37}$ [150].

When the ATLAS and CMS $H \to \tau\tau$ Run 1 measurements are combined [151], the significance of the observed excess corresponding to $m_H = 125.09\,\text{GeV}$ is 5.5σ and the combined signal strength is $\mu = 1.11^{+0.24}_{-0.22}$, consistent with the SM expectation.

The Run 1 evidence was strong only through the combination of the two experiments. The Run 2 larger dataset at a greater centre-of-mass energy is essential to further confirm this observation and perform first precision measurements in this important channel.

ATLAS [152] and CMS [153, 154] had analysed an early Run 2 dataset to provide independent observations, with significances of 4.4σ and 4.9σ respectively. These results in combination with the Run 1 results provide an unambiguous observation of this process. ATLAS quantified the combined result yielding a significance of 6.4σ [152].

CMS has also performed the search for Higgs boson decays to taus in the associated production with a vector boson [155] with a larger dataset corresponding to an integrated luminosity of almost $80\,\text{fb}^{-1}$ of data.

Both ATLAS [156] and CMS [157, 158] have then completed the analyses of the full Run 2 dataset. ATLAS performed simultaneously measurements not only of the VBF production mode, but also of the gluon fusion channel where the Higgs boson has a sizeable boost, the associated production with a vector boson as well as the associated production with a pair of top quarks. The measured total production cross-section is $2.90 \pm 0.21(\text{stat.})^{+0.37}_{-0.32}$ (sys.) corresponding to a signal strength of $\mu = 0.92 \pm 0.13$ in excellent agreement with the prediction from the Standard Model. The individual processes measured signal strenghts are: (i) for the VBF production mode $\mu_{VBF} = 0.89 \pm 0.18$, (ii) the gluon fusion mode $\mu_{ggF} = 0.95^{+0.34}_{-0.27}$ where the dominant uncertainty is systematic and mainly related to the signal acceptance in the high boost regime, (iii) the associated production with a vector boson where the vector boson decays hadronically $\mu_{VH} = 0.95^{+0.59}_{-0.57}$, and the associated production with a pair of top-quarks $\mu_{ttH} = 1.53^{+1.56}_{-1.32}$.

CMS has not yet combined its associated production channels, it has however performed a measurement in both the gluon fusion (boosted) and VBF production modes. The overall measured signal strength is $\mu = 0.85^{+0.12}_{-0.11}$. The gluon fusion signal and VBF signal strengths are $\mu_{ggF} = 0.98^{+0.20}_{-0.19}$ and $\mu_{VBF} = 0.67^{+0.23}_{-0.22}$ respectively. The precision of the former is limited by systematic uncertainties while for the latter the main uncertainty is from the data statistics [157]. The CMS collaboration also reported measurements of inclusive fiducial and differential cross sections, yielding a fiducial cross section of 426 ± 102 fb, in agreement with the Standard-Model expectation of 408 ± 27 fb [158].

11.3.2.2 $H \to b\bar{b}$

In the search for the decay of the Higgs boson to a pair of b-quarks, the most sensitive production modes are the associated WH and ZH processes allowing use of the leptonic W and Z decays for triggering, and to purify the signal and reject QCD backgrounds. The W bosons are reconstructed via their leptonic decay $W \to \ell\bar{\nu}_\ell$ where $\ell = e, \mu$ or τ. The Z bosons are reconstructed via their decay into $e^+e^-, \mu^+\mu^-$or $\nu\bar{\nu}$. The Higgs boson candidate mass is reconstructed from two b-tagged jets in the event. Backgrounds arise from production of W and Z bosons in association with gluon, light and heavy-flavoured jets (V+jets), $t\bar{t}$, diboson (ZZ and WZ with $Z \to b\bar{b}$) and QCD multi-jet processes. Due to the limited $m_{b\bar{b}}$ mass resolution, a SM Higgs boson signal is expected to appear as a broad enhancement in the reconstructed dijet mass distribution. The crucial elements in this search are b-jet tagging with high efficiency and low fake rate, accurate estimate of b-jet momentum and estimate of backgrounds from various signal depleted control samples constructed from data.

At the Tevatron, the $H \to b\bar{b}$ channel contributes the majority of the Higgs boson search sensitivity below $m_H = 130\,\text{GeV}$. To separate signal from background, CDF and D0 use multivariate analysis (MVA) techniques that combine several discriminating variables into a single final discriminant. Each channel is divided into exclusive sub-channels according to various lepton, jet multiplicity, and b-tagging characteristics in order to group events with similar signal-to-background ratio and thus optimise the overall search sensitivity. The combined CDF and D0 data show [48, 159] an excess of events with respect to the predicted background in the 115–140 GeV mass range in the most sensitive bins of the discriminant distributions suggesting the potential presence of a signal. At $m_H = 125\,\text{GeV}$, the observed signal strength is $\mu = 1.59^{+0.69}_{-0.72}$.

At the LHC, in order to reduce the dominant V+jets background, following Ref. [87], experiments select a region in the VH production phase space where the vector boson is significantly boosted and recoils from the $H \to b\bar{b}$ candidate with a large azimuthal angle $\Delta\phi_{VH}$. For each channel, events are categorised into different $p_T(V)$ regions with varying signal/background ratios. Events with higher $p_T(V)$ have smaller backgrounds and better $m_{b\bar{b}}$ resolution. CMS uses MVA classifiers based on kinematic, topological and quality of b-jet tagging and trained on different values of m_H to separate Higgs boson signal in each category from backgrounds. The MVA outputs for all categories are then fitted simultaneously.

The nominal results from ATLAS are also based on a combination of (i) a multivariate analysis of their 8 TeV data, incorporating various kinematic variables in addition to $m_{b\bar{b}}$ and b-tagging information and (ii) a statistical analysis of their 7 TeV data centered on $m_{b\bar{b}}$ as the main discriminant. In both cases, customised control samples devised from data are used to constrain the contributions of the dominant background processes.

The direct observation of the Higgs boson decaying to a pair of b-quarks, a major result of Run 2, was obtained by both ATLAS and CMS independently after the update of their search with similar analyses as those performed at Run 1 but with a larger dataset of approximately $80\,\text{fb}^{-1}$ of data collected in 2015, 2016 and 2017. The increase in signal cross sections of nearly a factor of 3 at the centre-of-mass energy of 13 TeV with respect to 7 TeV, has also been instrumental in bringing the two experiments to the required sensitivity to claim an evidence for this decay mode in the VH production mode (in the high transverse momentum of the vector boson fiducial region of interest for this channel). The expected significance for a SM Higgs boson is 4.3σ for ATLAS [160] and 4.9σ for CMS [161]. Both ATLAS and CMS observe significant excesses corresponding to 4.9σ and 4.8σ respectively with Run 2 data only. When combined with results obtained in Run 1, the observed (expected) significance of the excesses are 5.4σ (5.5σ) and 5.6σ (5.5σ) respectively. These results provide direct evidence for the $H \to b\bar{b}$ decay through the VH production mode.

Since these important observations, ATLAS has completed its

Downloaded from https://academic.oup.com/ptep/article/2022/8/083C01/6651666 by KIT Library user on 27 September 2022

Table 11.5: Summary of the results of measurements for a Higgs boson decaying to a pair of b-quarks by ATLAS and CMS. The results are given in terms of measured signal strength. When available, the statistical and systematic contributions to the total uncertainty are reported separately and in this order.

$H \to b\bar{b}$	Tevatron	ATLAS Run 1	CMS Run 1	ATLAS Run 2	CMS Run 2
VH	1.6 ± 0.7	$0.52 \pm 0.32 \pm 0.24$	1.0 ± 0.5	$1.02\,^{+0.12}_{-0.11}\,^{+0.14}_{-0.13}$	1.01 ± 0.22
VBF (γ)	—	-0.8 ± 2.3	$2.8 \pm 1.4 \pm 0.8$	$0.99\,^{+0.30}_{-0.30}\,^{+0.18}_{-0.16}$	1.3 ± 1.2
$t\bar{t}H$	—	$1.4 \pm 0.6 \pm 0.8$	0.7 ± 1.9	$0.79 \pm 0.29 \pm 0.53$	$1.49 \pm 0.21 \pm 0.39$
Inclusive	—	—	—	0.7 ± 3.3	3.7 ± 1.6

analysis of the full dataset using two reconstruction techniques. The first is based on the reconstruction of the Higgs boson with two jets is referred to as *resolved* [162]. The second is based on the reconstruction of the Higgs boson as a large radius jet and is referred to as *boosted* [163]. These measurements expand the range of measurements of the Higgs boson decays to b-quarks in association with a vector boson at higher transverse momentum, above 400 GeV. These results are summarized in Table 11.5. It should be noted that the sensitivity of these analyses are already limited by systematic uncertainties.

Also, the LHCb collaboration has performed a search for the VH production with subsequent decay of the Higgs boson to a pair of b-quarks [164] with $1.98\,\text{fb}^{-1}$ of data taken at a centre-of-mass energy of 8 TeV. The final state is required to have two reconstructed b quarks and one lepton in the LHCb acceptance of $2 < \eta < 5$. The sensitivity of this search is an expected 95% CL exclusion of 84 times the SM production rate. This analysis is also used to set a limit on the VH production with the subsequent decay of the Higgs boson in a pair of c quarks with a 95% CL limit at 6.4×10^3 times the SM production rate, while the expected sensitivity corresponds to an exclusion of 7.9×10^3 times the SM production rate.

ATLAS and CMS have also searched for $H \to b\bar{b}$ in the VBF production mode. The event topology consists of two VBF-tagging energetic light-quark jets in the forward and backward direction relative to the beam direction and two b-tagged jets in the central region of the detector. Due to the electroweak nature of the process, for the signal events, no additional energetic jet activity (excluding that from the Higgs boson) is expected in the rapidity gap between the two VBF-tagging jets. The dominant background in this search stems from QCD production of multi-jet events and the hadronic decays of vector bosons accompanied by additional jets. A contribution of Higgs boson events produced in the ggF process but with two or more associated jets is expected in the signal sample. The signal is expected as a broad enhancement in the $m_{b\bar{b}}$ distribution over the smoothly falling contribution from the SM background processes. Both ATLAS [165] and CMS [166] have produced results in this channel with Run 1 data, but with limited sensitivity. Both experiments performed a similar analysis with Run 2 data [167]. The results are summarized in Table 11.5.

Two of the main difficulties for the VBF production mode are the large QCD background and the difficulty in triggering fully hadronic events. Both difficulties are addressed, by the proposal made in Ref. [168], where the requirement of an additional photon in the final state reduces the background through an interference effect and enhances the possibilities for triggering. This analysis has been carried out by ATLAS at Run 2 [169] and its result combined with the standard VBF channel (see Table 11.5). The sensitivity in this channel is smaller than in the fully hadronic mode.

The sensitivity in the inclusive search for the Higgs boson in the ggF production mode with $H \to b\bar{b}$ is limited by the overwhelming background from the inclusive production of $pp \to b\bar{b} + X$ via the strong interaction. For this reason, no meaningful results exist with the Run 1 dataset for this production mode. With the increase in centre-of-mass energy to 13 TeV, and by taking advantage of the harder transverse momentum spectrum of the $gg \to H$ production mode with respect to the QCD background, a search for high p_T Higgs boson decaying to a pair of b quarks in association with an energetic Initial State Radiation (ISR) jet, has been performed by ATLAS [170] and CMS [171]. For this analysis with the Run 2 data, ATLAS and CMS require jets clustered with the anti-k_T algorithm [172] with a distance parameter of 1.0 and 0.8 respectively, with a transverse momentum in excess of 450 GeV. As in the case of VH production mode, this analysis is sensitive also to the $VZ, Z \to b\bar{b}$ production, which is an important step in the validation of the analysis chain. The $Z \to b\bar{b}$ decay is observed with a significance in excess of five standard deviations, in agreement with the expected rate from the Standard Model. CMS provides an expected sensitivity to the observation of a Higgs boson of 0.7σ. This estimate has a non negligible uncertainty from the precise estimate of the fiducial signal cross section in the specific acceptance of this analysis. CMS observes an excesses at $m_H = 125$ GeV of 2.5σ. ATLAS provides measurements in different regions of transverse momentum which are compatible with the Standard Model expectation for a signal, and which are also compatible with the absence of a signal within the current precision. These results are reported in Table 11.5.

Another important production mode sensitive to the decay of the Higgs boson to bottom quarks, is the associated production with a pair of top quarks. The results of the searches for this process have been combined with the channels described above, to provide an additional constraint on the Yukawa coupling of the Higgs boson to bottom quarks. The channels corresponding to this production mode are described in Section 11.3.3. The results are, however, also reported in Table 11.5.

11.3.3 *Higgs boson production in association with top quarks or in top decays*

11.3.3.1 *The associated production with top quark pairs*

As discussed in Section 11.2, the coupling of the Higgs boson to top quarks plays a special role in the electroweak symmetry breaking mechanism in the SM, as well as in its possible extensions. Substantial indirect evidence of this coupling is provided by the compatibility of observed rates of the Higgs boson in the principal discovery channels, given that the main production process – the gluon fusion – is dominated by a top quark loop. Direct evidence of this coupling at the LHC and the future e^+e^- colliders will be mainly available through the $t\bar{t}H$ final state and will permit a clean measurement of the top quark-Higgs boson Yukawa coupling. The $t\bar{t}H$ production cross section at the LHC is small in comparison with the ggF or even VH production modes. The production cross section for a 125 GeV Higgs boson in pp collisions at $\sqrt{s} = 8$ TeV of about 130 fb made it challenging to measure the $t\bar{t}H$ process with the LHC Run 1 dataset. However, in Run 2, the increase in cross section at $\sqrt{s} = 13$ TeV is substantial, reaching approximately 500 fb. For a sensitive search, at Run 1, it was important to target as many accessible experimental signatures as possible. The analysis channels for such complex final states can be separated in four classes according to the decays of the Higgs boson. In each of these classes, most of the decay final states of the top quarks are considered (fully hadronic, semi-leptonic and dilepton decay final states).

Downloaded from https://academic.oup.com/ptep/article/2022/8/083C01/6651666 by KIT Library user on 27 September 2022

The first analysis in this ensemble is the search for $t\bar{t}H$ production in the $H \to \gamma\gamma$ channel. This analysis relies on the search for a narrow mass peak in the $m_{\gamma\gamma}$ distribution. The background is estimated from the $m_{\gamma\gamma}$ sidebands. The sensitivity in this channel is mostly limited by the available statistics. The second analysis is the search for the Higgs boson decaying to ZZ^* and subsequently to four leptons (electrons and/or muons). This channel is currently limited by the low statistics due to the small branching fraction of the Z decays to leptons. The third analysis is the search in the $H \to b\bar{b}$ channel. This search is intricate due to the large backgrounds, both physical and combinatorial in resolving the $b\bar{b}$ system from the Higgs boson decay, in events with six jets and four b-tagged jets. Already with the Run 1 dataset, the sensitivity of this analysis was strongly impacted by the systematic uncertainties on the background predictions. The fourth analysis channel is a specific search for $\tau^+\tau^-$ where the two tau leptons decay to hadrons. Finally, the W^+W^- , $\tau^+\tau^-$ and ZZ^* final states can be searched for inclusively in multilepton event topologies (not including the resonant $H \to 4\ell$ channel that is covered in a more specific analysis). The corresponding $t\bar{t}H$ modes can be decomposed in terms of the decays of the Higgs boson and those of the top quarks as having two b-quarks and four W bosons (or two W and two taus, or two W and two Z) in the final state.

ATLAS and CMS have provided a complete set of results in these channels and their combination with the Run 1 data [173, 174].

With the large increase in production cross section for the $t\bar{t}H$ associated production process of a factor of 3.9 from 7 TeV to 13 TeV, an outstanding goal of the Run 2 physics program was the direct observation of the top Yukawa coupling through this production mode. As could be seen in the Run 1 results, the $H \to b\bar{b}$ channel sensitivity was already dominated by systematic uncertainties and the multilepton channel had already large systematic uncertainties, while channels such as the $H \to \gamma\gamma$ had very limited sensitivity due to the low statistics. With a conspicuous amount of data, the hierarchy of channels was therefore bound to change.

ATLAS and CMS have analysed Run 2 data in all the sensitive decay channels for this production mode, with datasets of variable size of up to the full Run 2 dataset in the case where it matters the most, i.e., the $t\bar{t}(H \to \gamma\gamma)$ channel. With this partial analysis of the Run 2 data, ATLAS and CMS were able to independently observe the production of the Higgs boson in association with a pair of top quarks, and therefore the Yukawa coupling of the Higgs boson to the top quark [175, 176]. This observation is particularly important in comparison to the indirect evidence through the gluon fusion production process dominated by the top quark loop.

The observation made independently by the two experiments was based on all the channels that were studied at the Run 1. ATLAS used up to 79.8 fb^{-1} of Run 2 data and CMS has used its 2016 dataset of 35.9 fb^{-1}. ATLAS reached an expected sensitivity of 4.9σ and an observed significance of 5.8σ with the Run 2 partial dataset alone, and 6.3σ (with 5.1σ expected) in combination with the Run 1 results. CMS reached a sensitivity of 4.2σ and observed an excess with respect to the background-only hypothesis of 5.2σ, combining the Run 1 and Run 2 results.

With the larger Run 2 dataset, the dominant mode is the $t\bar{t}(H \to \gamma\gamma)$ channel, where a narrow peak over a continuous background is searched for. At Run 2, this channel has reached a signal-to-background ratio in excess of 1 in the most signal-like categories. This is in contrast with the inclusive diphoton channel Higgs channels where the signal-to-background ratios are of the order of a few percents. ATLAS and CMS have analysed the entire Run 2 dataset reaching an observed (expected) sensitivity of 5.2σ (4.4σ) [177] and 6.6σ (4.7σ) [178], providing nearly unambiguous observations in this channel alone. These results are largely dominated by statistical uncertainty and are therefore expected to improve significantly with more data.

The search for the resonant Higgs boson decay to four leptons in the associated production with a pair of top quarks has also been updated in ATLAS [140] with the full Run 2 dataset and reported in Table 11.6, but it is also not included in the combination.

The ATLAS experiment performed a measurement of the Higgs boson decaying to b-quarks in the $t\bar{t}H$ production mode with the full Run 2 dataset [179]. This analysis was performed in the semi-leptonic and di-leptonic channels, including a resolved mode where the Higgs boson is reconstructed as two standard jets and a *boosted* mode where the Higgs boson is reconstructed as a single large radius jet. This analysis yields the following combined measurement:

$$\mu_{ttH} = 0.43\ ^{+0.20}_{-0.19}\,(\text{stat.})\ ^{+0.30}_{-0.27}\,(\text{syst.})$$

The precision of this result is already limited by systematic uncertainties. The dominant systematic unknown is the modelling of the top-quark pair poduction in association with heavy flavour jets [179].

An update of the $H \to b\bar{b}$ channel made by CMS with a partial Run 2 dataset of 41.5 fb^{-1} [180], using in particular the fully hadronic channel, is not in combination either. It is nevertheless reported in Table 11.5.

For the so-called "multi-lepton" channels which cover mostly the WW, ZZ and $\tau\tau$ decay modes, CMS has analysed the full Run 2 dataset [181] and ATLAS only part of it [182]. Using a dataset corresponding to an integrated luminosity of 36.1 fb^{-1}, the ATLAS experiment obtained an evidence in this channel [183]. In a preliminary release of this analysis using a larger, but not full Run 2 dataset corresponding to an integrated luminosity of approximately 80 fb^{-1}, the ATLAS experiment found that the normalisation of the $t\bar{t}W$ background was larger than expected from Standard Model calculations by factors ranging from 1.3 to 1.7 and modelling issues were observed in analysis regions where the $t\bar{t}W$ process is dominant [182]. It should be noted that a specific search for Higgs boson decays to tau leptons in association with a pair of top quarks was carried out by ATLAS with the full Run 2 dataset and discussed in 11.3.2.1 [156]. This search is orthogonal to the multi-lepton channel approach where the leptons (including taus) are searched for inclusively.

Using the full dataset in this channel CMS obtained an observation of the Higgs boson production in association with top quarks with an observed significance of 4.7 standard deviations (5.2σ expected). The rate of the $t\bar{t}W$ background in this analysis is also high by a factor of approximately 1.4. The combined result in this channel yields [181]:

$$\mu_{ttH} = 0.92 \pm 0.19\,(\text{stat.})\ ^{+0.17}_{-0.13}\,(\text{syst.})$$

All results, except the ATLAS update of the $t\bar{t}H(b\bar{b})$ channel reported above [179], are summarized in Table 11.6.

11.3.3.2 *The associated production with a single top quark*

An additional production mode of the Higgs boson in association with a top quark is the single top associated production mode. There is an interesting similarity between this production mode and the $H \to \gamma\gamma$ decay mode. Both processes proceed through either the top Yukawa coupling or the interaction of the Higgs boson with the W boson, with a negative interference between the two. Representative Feynman diagrams for this production process are shown in Fig. 11.1. Contrary to the diphoton decay channel, in this production mode the interference occurs at the tree level and is dominant. This process can therefore be used to further discriminate a negative relative sign between the couplings of the Higgs boson to fermions and its couplings to gauge bosons [186].

ATLAS and CMS have produced specific searches for the tH production mode with the Run 1 and Run 2 data exploiting a variety of Higgs boson decay modes resulting in final states with photons, bottom quarks, and multiple charged leptons, including tau leptons. In particular, with the Run 2 data, CMS has searched for multi-leptonic decay signatures from the $H \to WW^*$, $H \to \tau^+\tau^-$ and $H \to ZZ^*$ modes [187]. This analysis restricts values of κ_t, the top-Higgs coupling normalised to its SM value, to $[-1.25, 1.60]$ at 95% CL. CMS has also performed an analysis of the 2015 dataset to search for the $H \to b\bar{b}$ mode [188], yielding much less stringent constraints.

The diphoton channel has also been used to search specifically for this production mode by ATLAS using Run 1 data, yielding the restricted range of allowed values of κ_t at the 95% CL to $[-1.3, 8]$.

Downloaded from https://academic.oup.com/ptep/article/2022/8/083C01/6651666 by KIT Library user on 27 September 2022

Table 11.6: Summary of the results of searches for a Higgs boson in association with a top quark pair by ATLAS and CMS. The results are given in terms of a measured signal strength. When available, the statistical and systematic contributions to the total uncertainty are reported separately and in this order. The ATLAS [184] and CMS [185] diphoton and four-leptons results indicated by (∗) are not included in the overall combinations which include versions of the diphoton analyses with smaller Run 2 datasets. The combination includes the $t\bar{t}(H \to b\bar{b})$ channels reported in Table 11.5, but does not include the latest update of the multi-lepton channel [181].

$t\bar{t}H$	ATLAS Run 1	CMS Run 1	ATLAS Run 2	CMS Run 2
$H \to \gamma\gamma$	$1.3\,^{+2.6}_{-1.7}\,^{+2.5}_{-1.7}$	$1.2\,^{+2.5}_{-1.7}\,^{+2.6}_{-1.8}$	$1.38\,^{+0.33}_{-0.31}\,^{+0.26}_{-0.18}$ (∗)	$2.27^{+0.86}_{-0.74}$ (∗)
$H \to 4\ell$	—	—	$1.2\,^{+1.4}_{-0.8}$ (∗)	0.0 ± 1.2 (∗)
$WW/\tau\tau/ZZ$	$1.4 \pm 0.6 \pm 1.0$	3.3 ± 1.4	$1.56\,^{+0.30}_{-0.29}\,^{+0.30}_{-0.27}$	$0.92\,^{+0.26}_{-0.23}$
Combination	$1.7 \pm 0.5 \pm 0.8$	$2.6\,^{+1.0}_{-0.9}$	$1.32 \pm 0.18\,^{+0.21}_{-0.19}$	$1.49 \pm 0.16\,^{+0.27}_{-0.21}$

The strongest constraint on the negative (relative) sign of κ_t was obtained by CMS using the recent analysis of the full dataset [181] in the multilepton ($H \to WW$, $H \to ZZ$, $H \to \tau\tau$) discussed in 11.3.3.1, negative values of κ_t are disfavoured and the only non excluded negative values of κ_t at 95% CL. range between -0.9 and -0.7.

11.3.3.3 *Flavour changing neutral current decays of the top quark*

The discovery of the Higgs boson at a mass smaller than the top quark mass opened a new decay channel for the top quark. The decays of the top quark to a Higgs boson and a charm or an up quark proceed through a Flavour Changing Neutral Current (FCNC) which are forbidden at tree level and suppressed at higher orders through the Glashow–Iliopoulos–Maiani (GIM) mechanism [3]. The SM prediction for these branching fractions is $\mathrm{BR}(t \to Hc) = 10^{-15}$ and two orders of magnitude less for the Hu final state. These decay channels of the top quark are, therefore, very interesting to probe possible FCNC interactions in the Yukawa couplings to the quark sector, see Section 11.7.

ATLAS has searched for FCNC top decays specifically in channels involving a Higgs boson with subsequent decays to two photons and a pair of b-quarks [189]. It has also reinterpreted a search for the $t\bar{t}H$ production in the multilepton final state (discussed in Section 11.3.3.1) [174]. The latter channel covers Higgs boson decays to a pair of W bosons and a pair of taus. No significant excess was observed in any of the specific channels (as discussed in Section 11.3.3.1, a slight excess is observed in the $t\bar{t}H$ multilepton channel) and 95% CL upper limits are set on $\mathrm{BR}(t \to Hc) < 0.46\%$ with an expected sensitivity of 0.25% and $\mathrm{BR}(t \to Hu) < 0.45\%$ with an expected sensitivity of 0.29%. CMS has performed a search for these FCNC top decays in the diphoton and multi-lepton channels [190], placing a 95% CL upper limit on $\mathrm{BR}(t \to Hc) < 0.40\%$ with an expected sensitivity of 0.43%.

From these limits on branching fractions, constraints on non-flavour-diagonal Yukawa couplings of a FCNC Lagrangian of the form:

$$\mathcal{L}_{\mathrm{FCNC}} = \lambda_{tcH}\bar{t}Hc + \lambda_{tuH}\bar{t}Hu + h.c. \tag{11.12}$$

can be derived. The 95% CL observed (expected) upper limits from ATLAS on the $|\lambda_{tcH}|$ and $|\lambda_{tuH}|$ couplings are 0.13 (0.10) and 0.13 (0.10), respectively.

The results above are derived from the combination of several channels for searches performed with Run 1 data. Both ATLAS and CMS have produced updates of individual channels with Run 2 data. ATLAS has searched for FCNC top decays with subsequent decays of the Higgs boson to a pair of photons [191], yielding a 95% CL upper limit on $\mathrm{BR}(t \to Hc) < 0.22\%$ with an expected sensitivity of 0.16%. CMS has searched for FCNC top decays with subsequent decays of the Higgs boson to a pair of b-quarks [192], yiedling a 95% CL upper limit on $\mathrm{BR}(t \to Hc) < 0.47\%$ with an expected sensitivity of 0.44%.

11.3.4 *Higgs boson pair production*

Higgs boson pair production in the SM is a rare but very important mode to measure and search for. The measurement of Higgs boson pair production is essential to directly constrain the trilinear Higgs boson self coupling and the search for Higgs boson pair resonances is key in a variety of BSM models. The latter searches are discussed in Section 11.7.7.

In the SM, the main non-resonant production mode of two Higgs bosons proceeds through a loop, mainly of top quarks, see Fig. 11.4 (a). Another production mode is via the trilinear coupling of the Higgs boson, see Fig. 11.4 (b), whose amplitude is not negligible compared to the former. These diagrams interfere negatively, making the overall production rate smaller than what would be expected in the absence of a trilinear coupling.

Figure 11.4: Feynman diagrams contributing at leading order to Higgs boson pair production through (a) a top- and bottom-quark loop and (b) through the self coupling of the Higgs boson.

11.3.4.1 *Searches for Higgs boson pair production*

The searches for Higgs boson pair production both resonant and non-resonant are important probes for a variety of BSM theories, and they can be done in a large number of Higgs boson decay channels. At Run 1, ATLAS and CMS have searched for both resonant and non resonant Higgs boson pair production in the following channels: (i) $HH \to b\bar{b}\gamma\gamma$; (ii) $HH \to b\bar{b}\tau^+\tau^-$; (iii) $HH \to b\bar{b}b\bar{b}$; (iv) $HH \to b\bar{b}4\ell$; (v) $HH \to WW^*\gamma\gamma$; (vi) in final states containing multiple leptons (electrons or muons) covering the WW^*WW^*, WW^*ZZ^*, ZZ^*ZZ^*, $ZZ^*\tau^+\tau^-$, $WW^*\tau^+\tau^-$, $ZZ^*b\bar{b}$, $\tau^+\tau^-\tau^+\tau^-$ channels; and (vi) $\gamma\gamma\tau^+\tau^-$ channels.

At Run 2, similarly to the $t\bar{t}H$ production process, the di-Higgs production gains a substantial increase in production cross section of a factor in excess of 3 from 8 TeV to 13 TeV, and most of these channels have been updated both by ATLAS [193] and CMS [194]. The detailed description of the analyses can be found in the following references [193–200] and the references within the combination results published by the collaborations [193–195]. All the results and their combinations are summarised in Table 11.7. The channels (i)-(iii) are the most sensitive to the HH production. These three channels have been updated with the full Run 2 dataset except the $HH \to b\bar{b}\tau^+\tau^-$ channel by CMS and the $HH \to b\bar{b}b\bar{b}$ channel by ATLAS which have both been analysed using a partial Run 2 dataset.

In several of these analysis channels the VBF production mode is searched for separately providing sensitivity to the coupling involving two vector bosons and two Higgs bosons HHVV which is an expected coupling in the Standard Model.

The limits obtained on the HHVV coupling modifier denoted κ_{2V} are obtained from the analysis performed by CMS [199] in

Downloaded from https://academic.oup.com/ptep/article/2022/8/083C01/6651666 by KIT Library user on 27 September 2022

Table 11.7: Summary of the final states investigated in the search for Higgs boson pair production by ATLAS and CMS, the results reported in bold are based on the full Run 2 dataset. For ATLAS, the result indicated by (*) uses mostly the $b\bar{b}W^+W^-$ channel. Results are 95% CL upper limits on the observed (expected) SM signal strengths.

Channel	ATLAS	CMS
$b\bar{b}\gamma\gamma$	**4.1 (5.5)**	**7.7 (5.2)**
$b\bar{b}b\bar{b}$	12.9 (21)	**3.6 (7.3)**
$b\bar{b}\tau^+\tau^-$	**4.7 (3.9)**	31.4 (25.1)
$b\bar{b}4\ell$	-	**30 (37)**
$W^+W^-W^+W^-$	160 (120)	–
$W^+W^-\gamma\gamma$	230 (170)	–
$b\bar{b}VV$	305 (305)*	79 (89)
Combination	6.9 (10)	22.2 (12.8)

the $b\bar{b}\gamma\gamma$:

$$-1.3 < \kappa_{2V} < 3.5\,(\text{observed}), \quad -0.9 < \kappa_{2V} < 3.1\,(\text{expected})$$

11.3.4.2 *The Higgs boson self coupling*

The Higgs boson self coupling is an extremely important direct probe of the Higgs potential with implications on our understanding of the electroweak phase transition. Constraints on the trilinear self coupling from HH processes is an outstanding long term goal of the LHC and the reach in sensitivity has been reappraised in the light of the recent HH analyses from ATLAS and CMS, shedding a different light on the achievable sensitivity [111]. Constraints from the HHH final state on the quartic Higgs boson self coupling are out of reach at the LHC due mostly to the very small production rates and intricate final states.

In the SM, the Higgs boson pair production through the trilinear Higgs boson self coupling has an on-shell component and a large off-shell component. The on-shell $H \to H^*H^*$ is strongly disfavoured, requiring two off-shell Higgs bosons in the final state. The sensitivity region to the trilinear coupling production as in Fig. 11.4 (b), is mainly in the kinematic region where the two Higgs boson in the final state are on-shell and the Higgs boson acts as a propagator (off-shell). As discussed in the introduction to this section, this process interferes negatively with the background Higgs boson pair production (Fig. 11.4 (a)).

The measurement of the trilinear coupling requires separating the contributions of the diagram of Fig. 11.4 (b) from the box diagram of Fig. 11.4 (b), and therefore a precise knowledge of the top-Yukawa coupling is needed. Each diagram alone would produce rather distinct m_{HH} distribution. And, for values of the trilinear coupling close to the SM value, an additional discriminating feature of the signal with respect to one obtained with the box contribution alone is a deficit in the number of events. With large variations of the trilinear coupling, an excess of events over the SM prediction would be observed (for a value of the trilinear coupling about 6 times larger than its SM value, the number of events is equal to the SM expectation). Additional sensitivity to the trilinear coupling is also obtained from the kinematical distributions of the signal taking in particular into account the effect of the HH mass distribution which discriminates the main contributions of Fig. 11.4. This further discrimination is instrumental in resolving the degeneracy in the total cross section mentioned above. The bounds obtained by ATLAS [200] and CMS [199] for the $b\bar{b}\gamma\gamma$ channel alone for are the following:

$$\begin{aligned} \text{(ATLAS)}\ & -1.5 < \kappa_\lambda < 6.7\,(\text{observed}), \\ & -2.4 < \kappa_\lambda < 7.7\,(\text{expected}), \\ \text{(CMS)}\ & -3.3 < \kappa_\lambda < 8.5\,(\text{observed}), \\ & -2.5 < \kappa_\lambda < 8.2\,(\text{expected}), \end{aligned} \tag{11.13}$$

where κ_λ is the ratio between the trilinear coupling value left free in the fit and its expected value in the SM ($\kappa_\lambda = 1$ corresponds to the SM). These results are also illustrated in Fig. 11.5.

The analyses performed at Run 2 bring substantial improvements from those of Run 1, and they were used to reappraise the sensitivity of the LHC in the High Luminosity regime in the framework of the update of the European Strategy for Particle Physics [111]. The result in terms of bounds on the trilinear coupling are shown in Fig. 11.5, indicating that the significance of the observation of the HH process reaches 4σ. It is also apparent that the degeneracy of secondary minimum at intermediate values of κ_λ is resolved by the use of the kinematic discriminants. Indeed, this secondary minimum is expected to be excluded at 99.4% CL. This is very important to allow the measurement in the vicinity of the SM value at one standard deviation and to provide a meaningful confidence interval. At HL-LHC, the foreseen precision on κ_λ is approximately 50%.

Significantly higher precisions can be reached at pp colliders (and e^+e^- colliders) at higher centre-of-mass energies. The foreseen precision for a High-Energy (HE) LHC at a centre-of-mass energy of 27 TeV is expected to be within 10% to 20% [111]. At a very large hadron collider at a centre-of-mass energy of 100 TeV, a 5% sensitivity is expected to be reached, provided that the theoretical and parametric uncertainties are kept at the 1% level.

Indirect constraints on the Higgs boson trilinear coupling from single Higgs boson production processes will be discussed in Section 11.6.2.5.

11.3.5 *Searches for rare decays of the Higgs boson*

11.3.5.1 *$H \to Z\gamma$ and the first evidence for the Dalitz $H \to \ell^+\ell^-\gamma$ decay*

The search for $H \to Z\gamma$ is performed in the final states where the Z boson decays into opposite sign and same flavour leptons ($\ell^+\ell^-$), ℓ here refers to e or μ. While the branching fraction for $H \to Z\gamma$ is comparable to $H \to \gamma\gamma$ (about 10^{-3}) at $m_H = 125$ GeV, the observable signal yield is brought down by the small branching ratio of $Z \to (e^+e^- + \mu^+\mu^-) = 6.7 \times 10^{-2}$. In these channels, the $m_{\ell\ell\gamma}$ mass resolution is excellent (1–3%), therefore the analyses search for a narrow mass peak over a continuous background. The major backgrounds arise from the $Z+\gamma$ final state radiation in Drell–Yan decays and from the $Z+$ jets processes where a jet is misidentified as a photon. The ratio of signal over background in this channel is typically of the order of 0.5%. In a narrow window of a few GeV around 125 GeV, several hundreds of events are expected in a Run 2 dataset corresponding to approximately 36 fb^{-1}.

Events are divided into mutually exclusive categories on the basis either of the expected $m_{Z\gamma}$ resolution or exclusive production mode categories.

No excess of events is observed in either ATLAS or CMS in the Run 1 data. The CMS expected and observed 95% CL upper limits for $m_H = 125$ GeV on the signal strength μ are 10.0 and 9.5 respectively. The ATLAS expected and observed upper limits on the signal strength μ are 9.0 and 11.0 respectively, for $m_H = 125.5$ GeV.

With the full Run 2 dataset, ATLAS observes no significant excess and places a 95% CL observed (expected) upper limit on the signal strength of 3.6 (2.6) [201]. An excess with a significance of 2.2σ is observed. The expected significance of an excess with respect to the background hypothesis sensitivity is 1.2σ. With a partial dataset CMS reports a limit of 4.0 (11.4) times the SM cross section for $H \to Z\gamma$ [202] process.

Both ATLAS and CMS experiments have extended the search for the so-called Dalitz Higgs boson decays $H \to \gamma^*\gamma \to \ell^+\ell^-\gamma$ in the low mass γ^* range of approximately 20-30 GeV. This decay mode has a substantially larger branching fraction compared to

Downloaded from https://academic.oup.com/ptep/article/2022/8/083C01/6651666 by KIT Library user on 27 September 2022

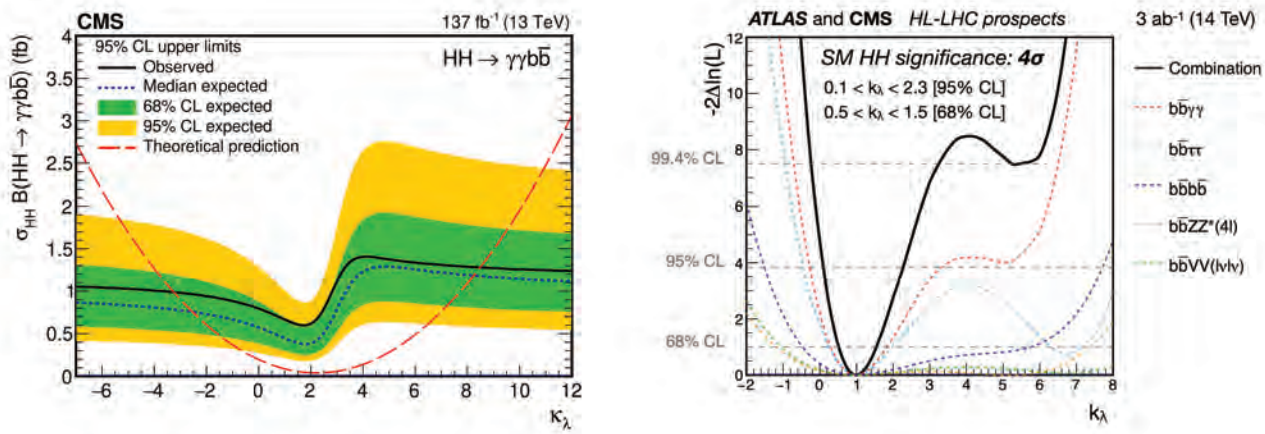

Figure 11.5: (Left) Upper limit obtained by CMS on the total $pp \to HH$ production cross section as a function of the trilinear coupling modifier κ_λ. The variation of the limit corresponds to variations in the signal acceptance. The expected total production cross section is also illustrated (red). (Right) Expected combined ATLAS and CMS likelihood for the searches for the $pp \to HH$ production at the High Luminosity LHC. The channels used in the combination are indicated in the figure.

the $Z\gamma$ decay, as $\Gamma(H \to \gamma^*\gamma \to e^+e^-\gamma) \sim 3.5\% \times \Gamma(H \to \gamma\gamma)$ and $\Gamma(H \to \gamma^*\gamma \to \mu^+\mu^-\gamma) \sim 1.7\% \times \Gamma(H \to \gamma\gamma)$, while $\Gamma(H \to Z\gamma) = 2.3\% \times \Gamma(H \to \gamma\gamma)$ (which does not account for the subsequent decay of the Z boson to electrons or muons). With the Run 1 dataset, CMS observes an upper limit of 6.7 times the SM branching ratio [203]. With a partial Run 2 dataset, in the $\gamma^*\gamma$ CMS obtained a much more stringent limits on cross section times the corresponding branching fractions of 1.4 (6.1) times the SM cross section [202]. CMS also performed a combination of the two this mode with $H \to Z\gamma$, obtaining a combined observed (expected) limit of 3.9 (2.0) times the SM branching fractions.

Using the full Run 2 dataset corresponding to $139\,\text{fb}^{-1}$, ATLAS obtained the first evidence for Higgs boson decays to a low-mass dilepton pair and a photon with a significance of 3.2 (2.1) standard deviations (expected) [204]. The invariance mass requirement on the di-lepton is $m_{\ell\ell} < 30\,\text{GeV}$. The corresponding signal strength is $\mu = 1.5 \pm 0.5$, compatible with the expectation from the Standard Model.

11.3.5.2 *First evidence of $H \to \mu^+\mu^-$*

The branching fraction in the $H \to \mu^+\mu^-$ channel for a 125 GeV SM Higgs boson is 2.2×10^{-4}, about ten times smaller than that for $H \to \gamma\gamma$. The dominant and irreducible background arises from the $Z/\gamma^* \to \mu^+\mu^-$ process which has a rate several orders of magnitude larger than that from the SM Higgs boson signal. Due to the precise muon momentum measurement achieved by ATLAS and CMS, the $m_{\mu^+\mu^-}$ mass resolution is very good ($\approx$ 2–3% for ATLAS and $\approx$ 1–3% for CMS depending on the selected categories; a better resolution is expected for CMS due its higher field in the inner detector). A search is performed for a narrow peak over a large but smoothly falling background. For optimal search sensitivity, events are divided into several categories. Either taking advantage of the superior muon momentum measurement in the central region, events can be subdivided by the pseudo-rapidity of the muons, or designing selections aiming at specific production processes such in particular as the vector boson fusion.

No excess in the $m_{\mu^+\mu^-}$ spectrum is observed near 125 GeV. From an analysis of the Run 1 data, ATLAS sets an observed (expected) 95% CL upper limit on the signal strength $\mu < 7.0$ (7.2). The CMS analysis of its 7 and 8 TeV data sets an observed (expected) limit of $\mu < 7.4$ (6.5).

ATLAS [205] and CMS [206] have performed a reoptimised analysis using the full Run 2 dataset. Both the ATLAS and CMS selections target all the main production modes including gluon fusion, the associated production with a vector boson (VH), the vector boson fusion and the associated production with a top-quark pair and in various cases further use multivariate and deep learning methods to discriminate signal from background in these categories. The signal in both experiments is extracted from a fit to the di-muon invariant mass spectrum and the background is modelled using an analytical function, except in the case of the most sensitive channel (VBF) in the CMS analysis where the discriminant Deep Neural Network output is used [206]. The reach in sensitivies of the analyses has been significantly improved. With the full dataset ATLAS and CMS have respectively an expected significance of 1.7σ and 2.5σ. Both ATLAS and CMS observe an excess of events respectively with signal strengths of $\mu = 1.2 \pm 0.6$ and $\mu = 1.19 \pm 0.40\,(\text{stat.}) \pm 0.15\,(\text{syst.})$. In both cases the measurement uncertainties are dominated by the data statistics. The observed significances are 2.0σ and 3.0σ respectively. These results show a first direct evidence for the decay of the Higgs boson to muons and thus of the Yukawa coupling of the Higgs boson to second generation fermions. The significant increase in sensitivity is very encouraging for these important measurements at the LHC Run 3.

11.3.5.3 $H \to e^+e^-$

A search similar to the $H \to \mu^+\mu^-$ is performed by CMS in the di-electron channel. In this search channel, the contribution from the peaking background from Higgs boson decays to diphotons mis-identified as di-electrons (when mostly converted photons are faking electrons) needs to be assessed. The sensitivity to the SM Higgs decays is negligible given the extremely small branching fraction to e^+e^-, approximately 40'000 times smaller than the branching fraction to dimuons. It is nevertheless interesting to probe this decay channel to search for potential large anomalous couplings. Assuming a SM Higgs boson production cross section, the observed limit on the branching fraction at the 95% CL is 0.0019, five orders of magnitude larger than the expected SM prediction. It is also important to note that processes not depending on the electron Yukawa coupling such as the $H \to e^+e^-\gamma$ (where the photon is soft), are sizeably larger than the direct Yukawa coupling process, but also much smaller than the current constraints, making any interpretation in terms of constraint on the electron Yukawa couplings far from straightforward.

At Run 2, ATLAS has also performed a search for the $H \to e^+e^-$ decay mode with the full dataset, improving the current limit by a factor of approximately 5, with a limit of 3.6×10^{-4} on the branching fraction [207].

11.3.5.4 *Lepton flavour violating (LFV) Higgs boson decays*

Given the Yukawa suppression of the couplings of the Higgs boson to quarks and leptons of the first two generations and the small total width of the Higgs boson, new physics contributions could easily have sizable branching fractions. One very interesting possibility is the Lepton Flavour Violating (LFV) decays of the Higgs boson, in particular in the $\tau\mu$ and τe modes. These

Downloaded from https://academic.oup.com/ptep/article/2022/8/083C01/6651666 by KIT Library user on 27 September 2022

decays are suppressed in the SM but they could easily be enhanced in theories such as two-Higgs-doublet models (discussed in Section 11.7).

There are already constraints on LFV Yukawa couplings $|Y_{\tau\mu}|$ from channels such as the $\tau \to 3\mu$ or $\tau \to \mu\gamma$, or a reinterpretation of the search for Higgs boson decays to $\tau^+\tau^-$. A direct search at the LHC, however, complements these indirect limits. The search for LFV decays in the $\tau\mu$ channel have been done with the Run 1 dataset in several channels according to the subsequent decay of the τ. The results from CMS [208] and from ATLAS for the hadronic [209], the leptonic [210] decays of the tau, and their combination [210] are reported in Table 11.8. It is interesting to note that the analysis strategies at Run 1 for the dilepton $\tau_{\rm lep}\mu$ channel are very different between ATLAS [210] and CMS [208]. The CMS results are obtained using the full Run 2 dataset.

As shown in Table 11.8, an excess was observed in this channel by CMS with a significance of 2.5σ, while in ATLAS analysis, the excess is smaller, about 1σ at Run 1. CMS has performed the search again with the full 2016 Run 2 dataset [211], relying on a multivariate analysis. The observed best fit branching fraction is $(0.00 \pm 0.12)\%$. These limits are reported in Table 11.8.

ATLAS and CMS have also performed a search for the LFV Higgs boson decays in the τe and μe channels [210–212]. No significant excess was observed and 95% CL limits are reported in Table 11.8, for the τe channel only. For the μe channel, the constraints from the $\mu \to e\gamma$ experiments [213] are much stronger than those from the direct LFV Higgs boson decay search. However these indirect constraints can be relaxed by the cancellation of LFV effects from new physics.

At Run 2, ATLAS has performed searches for LFV decays of the Higgs boson in the $e\tau$ and $\mu\tau$ channels [214] as well as in the $e\mu$ channel [207]. The searches for the $H \to e\tau$ and $H \to \mu\tau$ decays where done with the 2016 data only and yielded upper limits on the LFV decay branching fraction of 0.47% (0.34%) and 0.28% (0.37%), respectively.

CMS has also searched for LFV decays with the 2016 dataset at Run 2 and obtained observed (expected) limits on the LFV branching fraction of $\mathrm{BR}(H \to \mu\tau) < 0.25\%$ (0.25%) and $\mathrm{BR}(H \to e\tau) < 0.61\%$ (0.37%), at the 95% CL [215]. These limits were also interpreted in terms of constraints on the corresponding off-diagonal Yukawa couplings.

The results obtained by ATLAS and CMS at Run 2 do not confirm the excesses observed at Run 1.

11.3.5.5 *Probing charm- and light-quark-Yukawa couplings*

Probing the Yukawa couplings to quarks of the second or even the first generation is extremely challenging given the overwhelming backgrounds and very small signal rates.

The possibility of probing the Yukawa coupling to the charm has been discussed in Ref. [216] where indirect bounds are estimated from a combined fit to the Higgs data and the importance of using charm tagging is emphasised. Searches in the VH production mode have been carried out, in the channels very similarly to those aiming at the b-quark Yukawa coupling, by both ATLAS [217] and CMS [218] with Run 2 data. The upper limits obtained (expected) on the VH production cross section times the charm quark decay branching fraction of the Higgs boson are:

$$\text{(ATLAS)} \quad \frac{\sigma(VH) \times \mathrm{BR}(H \to c\bar{c})}{\sigma(VH)_{SM} \times \mathrm{BR}(H \to c\bar{c})_{SM}} < 26(31). \tag{11.14}$$

$$\text{(CMS)} \quad \frac{\sigma(VH) \times \mathrm{BR}(H \to c\bar{c})}{\sigma(VH)_{SM} \times \mathrm{BR}(H \to c\bar{c})_{SM}} < 70 \ \ (37^{+16}_{-10}). \tag{11.15}$$

The ATLAS search [217] was done with the full Run 2 dataset and the cross section times branching fraction upper limit is interpreted in terms of charm yukawa coupling modifier yielding an observed limit of $\kappa_c < 8.5$ (12.4 expected) at the 95% CL. It should be noted that these analyses are sensitive to the diboson VZ where Z$\to c\bar{c}$ and VW where W$\to c\bar{q}$. The ATLAS collaboration reported significances of 2.6σ and 3.8σ for these two standard signals respectively, in good agreement with the expectation from the Standard Model.

Another possibility to access the charm Yukawa coupling has been discussed in Ref. [219]. It relies on the decays of the Higgs boson to a final state with charmonium: $H \to J/\Psi\gamma$. Higgs boson decays in this final state have been searched for by ATLAS [220]. The sensitivity of this analysis is, however, several orders of magnitude above the branching fraction estimated in the SM: $\mathrm{BR}(H \to J/\Psi\gamma) = (2.8 \pm 0.2) \times 10^{-6}$. ATLAS [220] has also searched for Higgs boson decays to $\Upsilon(nS)\gamma$ where $(n = 1, 2, 3)$, a channel with much lower sensitivity than the $H \to b\bar{b}$ to the Yukawa coupling to b-quarks.

More recently, ATLAS [221] and CMS [222] haved searched, for quarkonia in the Higgs decay final state where the Higgs boson decays to $\phi\gamma$ or $\rho\gamma$ at the LHC Run 2 and a center-of-mass energy of 13 TeV. These channels require specific triggers and could probe deviations from the strange-quark or light-quarks Yukawa couplings respectively. Its sensitivity is several orders of magnitude above the SM expectation.

CMS has also performed a search of the decays of the Higgs boson in the $J/\Psi J/\Psi$ and $\Upsilon\Upsilon$ decay to cover the cases where the photon in the $J/\Psi\gamma$ decay is virtual and transforms into a J/Ψ meson, These decays provide an additional channel potentially sensitive to BSM phenomena [223].

11.3.5.6 *Rare decays outlook*

Rare decays such as those described in the above sections have clearly a limited sensitivity. However, they already deliver interesting messages. For example, if the coupling of the Higgs boson to muons was as strong as it is to top quarks, this mode should have been observed. Therefore, it can be concluded that the observed couplings of the Higgs boson are manifestly non-universal. Further, developing these rare decay modes is an important component of the High Luminosity program of the LHC in order to directly probe the couplings of the Higgs boson, and to potentially measure the Yukawa coupling to the fermions of the second generation, in particular to muons. It is also an integral part of the physics program of the discussed potential future Higgs boson factories.

11.3.6 *Searches for non-SM decay channels*

The main decay and production properties of the observed Higgs boson are consistent with the SM predictions. The Higgs boson may, however, have other decay channels beyond those anticipated in the SM. Among these, and of great interest, are the invisible decays into stable particles, such as DM particle candidates, that interact very weakly with the detector, and that remain undetected. Other non standard decay channels that have been investigated are the decays of the Higgs particle to hidden valley or dark particles.

11.3.6.1 *Invisible decays of the Higgs boson*

The discovery of the Higgs boson immediately raised the question of its couplings to DM and how it could be used to reveal at colliders the existence of a dark sector coupled to the SM via the Higgs boson portal, see Ref. [224] and references therein. If kinematically accessible and with a sufficiently large coupling to the Higgs boson, DM particles, such as, e.g., neutralinos in SUSY models, graviscalars in models with extra dimensions or heavy neutrinos in the context of four-generation fermion models, would manifest themselves as invisible decays of the Higgs boson, thus strongly motivating searches for the invisible decays of the Higgs boson.

To identify an invisibly decaying Higgs boson at the LHC, it must be produced in association with other particles. Searches for invisible decays of the Higgs particle at the LHC have been carried out in the three associated production modes of the Higgs boson with the highest SM cross sections and target events with large missing energy.

The ggF production mode has the largest SM cross section but it usually results in the Higgs boson being created alone and hence leaving no characteristic signature in the detector of its invisible decay. One way to search for invisible decays in ggF production mode is to look for events with the monojet topology arising from initial state gluon radiation and containing missing energy. The major irreducible background in such searches stems from Z + jets events where the Z boson decays into a pair of neutrinos [225].

Downloaded from https://academic.oup.com/ptep/article/2022/8/083C01/6651666 by KIT Library user on 27 September 2022

Table 11.8: Summary of the results of searches for lepton flavour violating decays of the Higgs boson in the $\tau\mu$ and τe channels from ATLAS and CMS. For the result with *, the expected sensitivity was not reported but appears consistent with the observed one. In its Run 2 analysis CMS reports no significant excess (NSE).

	ATLAS (Run 1)	CMS (Run 1)	CMS (Run 2)
$\mathrm{BR}(H \to \tau\mu)$	$(0.53 \pm 0.51)\%$	$(0.84^{+0.39}_{-0.37})\%$	NSE
95% CL Obs. (Exp.)	1.43% (1.01%)	1.51% (0.75%)	0.15% (0.15%)
$H \to \tau e$ 95% CL Obs. (Exp.)	1.02% (1.21%)	0.69%*	0.22% (0.16%)

The analysis with the best sensitivity targets the VBF production topology but it suffers from large backgrounds arising from events with two jets and large missing energy. The VH mode has much smaller cross section but the presence of a W or Z boson allows a variety of final states that can be tagged with relatively low background.

ATLAS and CMS have searched for such final states at Run 1 and have observed no significant excess over the predicted backgrounds (for references, see the previous edition of this review [132]). Table 11.9 summarizes the 95% CL limits on the invisible decays of the Higgs boson assuming a SM Higgs boson production cross section and the corresponding detector acceptances.

ATLAS has performed the search for invisible decays of the Higgs boson at Run 2 with the full dataset in the VBF production [226], the ZH associated production where the Z boson subsequently decays to a pair of leptons [227], and in the 2015 and 2016 datasets, corresponding to an integrated luminosity of approximately 36 fb^{-1} in the VH associated production where the vector boson (a W or a Z) subsequently decays hadonically [228]. The most stringent constraint is obtained through the VBF channel. All results and their combination [229] are reported in Table 11.9. Combined with the Run 1 results, the ATLAS limit on the invisible branching fraction reaches 11%, with an expected sensitivity of 11% [229].

CMS has updated the search for invisible decays of the Higgs boson in the vector boson fusion and the associated production with a vector boson channels (both with subsequent leptonic [230] and hadronic decays [231]) using Run 2 data collected in 2016 [232]. It has produced a combination with Run 1 channels, yielding a limit on the invisible branching fraction of 19%, with an expected sensitivity of 15% [232].

ATLAS and CMS have also reinterpreted a search for scalar top quarks in the all-hadronic, semi-leptonic and fully leptonic final state with the 2016 data of Run 2 to set limits on the invisible Higgs decays through the $pp \to t\bar{t}H$ production mode [229, 233]. The results of the search are reported in Table 11.9.

This constraint can then be further used to probe Higgs portal models to DM [224], where an additional weakly interacting particle χ with mass lower than $m_H/2$ is introduced as DM candidate and where the Higgs boson is considered as the only mediator between the SM particles and DM. In this model, it is interesting to express the limit on the invisible branching fraction in terms of strength of interaction of DM with standard matter, i.e., in terms of it interaction cross section with nucleons $\sigma_{\chi-N}$. In this model, the couplings of the Higgs boson to SM particles are assumed to be those of the SM and the interaction of the Higgs boson with the nucleon is parametrised in a Higgs-Nucleon form factor estimated using lattice QCD calculations [224]. The exclusion limits from the constraints on invisible Higgs boson decays, both direct and indirect from the measurement of the coupling properties of the Higgs boson can be compared to direct detection experiments. For comparison, the limit at 90% CL on the invisible branching fraction of $\mathrm{BR}_{\mathrm{inv}} < 19\%$ [232] is used and converted into limits on $\sigma_{\chi-N}$ under several hypotheses on the nature of DM particles depending mainly on their spin (scalar- or fermion-like). The vector DM hypothesis is not included since (renormalisable) models of vectorial DM require an extended dark sector that could imply modifications of the signal. The results are shown in Fig. 11.6.

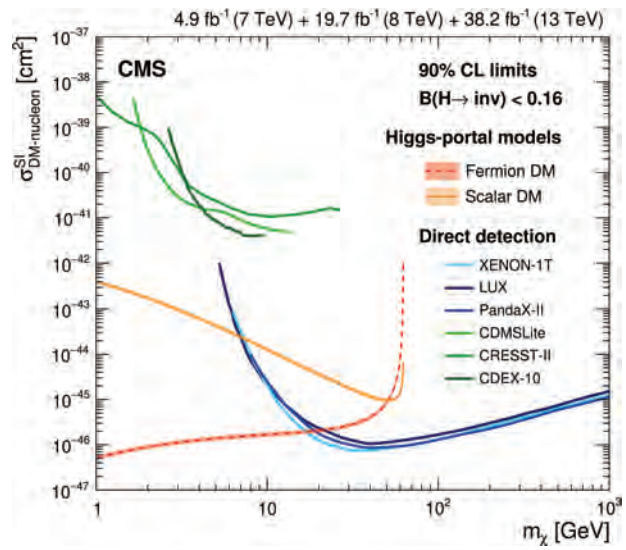

Figure 11.6: 90% CL upper limits on the WIMP-nucleon scattering cross section as a function of the DM particle mass in models where the Higgs boson is a portal between the SM matter and the Dark Sector. Spin-independent results excluded and favoured regions from direct detection experiments are also shown.

11.3.6.2 *Exotic Higgs boson decays*

The 125 GeV Higgs boson serves not only as a probe for potential DM candidates, but also to search for other exotic particles arising from fields associated with a low-mass hidden sector. Such hidden sectors are composed of fields that are singlet under the SM gauge group $\mathrm{SU}(3) \times \mathrm{SU}(2) \times U(1)$. These models are referred to as hidden valley models [234]. Since a light Higgs boson is a particle with a narrow width, even modest couplings to new states can give rise to a significant modification of the Higgs boson phenomenology through exotic decays. Simple hidden valley models exist in which the Higgs boson decays to an invisible fundamental particle, which has a long lifetime to decay back to SM particles through a small mixing with the SM Higgs boson, see Ref. [234] for a concrete example. The Higgs boson may also decay to a pair of hidden valley "v-quarks," which subsequently hadronise in the hidden sector, forming "v-mesons." These mesons often prefer to decay to the heaviest state kinematically available, so that a possible signature is $H \to 4b$. Some of the v-mesons may be stable, implying a mixed missing energy plus heavy flavour final state. In other cases, the v-mesons may decay to leptons, implying the presence of low mass lepton resonances in high-H_T events [235]. Other scenarios have been studied [236] in which the Higgs boson decays predominantly into light hidden sector particles, either directly, or through light SUSY states, and with subsequent cascades that increase the multiplicity of hidden sector particles. In such scenarios, the high-multiplicity hidden-sector particles, after decaying back into the SM, appear in the detector as clusters of collimated leptons known as "lepton jets".

A variety of models have been investigated searching for final states involving dark photons and hidden valley scalars. The resulting topologies typically have leptons or light hadrons which in some cases can be prompt (i.e., originating from the hard process interaction point) or not and are in some cases collimated and reconstructed as jets [237, 238], and long-lived weakly interacting particles. The latter occur not only in hidden valley scenarios, but

Downloaded from https://academic.oup.com/ptep/article/2022/8/083C01/6651666 by KIT Library user on 27 September 2022

Table 11.9: Summary of the channels searched for and the corresponding 95% CL limits from ATLAS and CMS on the branching fraction for the Higgs boson decay to invisible particles assuming a SM Higgs boson production cross section. The results in parentheses are the expected exclusions.

	ATLAS (Run 1)	ATLAS (Run 2)	CMS (Run 1)	CMS (Run 2)
ggF (monojet); $H \to$ inv.	–	–	67 (71) %	66 (59)%
VBF; $H \to$ inv.	28 (31) %	13 (13) %	57 (40) %	33 (25) %
ZH; $Z \to \ell^+\ell^-$; $H \to$ inv.	75 (62)%	18 (18) %	75 (91) %	40 (42)%
VH; $Z, W \to jj$; $H \to$ inv.	78 (86)%	83 (58) %	–	50 (48)%
ZH; $Z \to b\bar{b}$; $H \to$ inv.	–	–	182 (189)%	–
$t\bar{t}H$; $H \to$ inv.	–	40 (36)%	–	46 (48)%
Combination	25 (27)%	13 (12)%	–	26 (20) %
Run 1 & 2 Combination	11 (11)%		19 (15)%	

also in gauge-mediated extensions of the minimal SUSY standard model (MSSM), the MSSM with R-parity violation, and inelastic DM scenarios [239]. Finally, CMS has performed a search for pair production of light bosons [240]. Such a scenario can occur in SUSY models with additional hidden (or dark) valleys.

11.4 Combining the main channels

The analysis strategy used by the LHC experiments to perform the searches for the Higgs boson has been based on the Higgs boson decay modes. It is a natural choice given that it focusses on the decay products of the object searched for. However, for each channel, exclusive sub-channels have been defined to target different production modes and kinematic regimes, and these sub-channels have been combined. The natural extension of this approach in order to probe further the production and decay modes of the Higgs boson is to combine the analysis channels together. Such a combination is also used in Section 11.6 to further measure the coupling properties of the Higgs boson.

At the LHC, the total cross section cannot be measured in any of the production modes. As a consequence, neither the absolute branching fractions nor the total width of the Higgs boson can be directly measured, at least if the width is of the SM size. However, a combined measurement of the large variety of categories described in Section 11.3, with different sensitivities to various production and decay modes, permits a wide variety of measurements of the production, decay and coupling properties. These measurements require, in general, a limited but nevertheless restrictive number of assumptions.

In this section, three sets of results will be given. The first one is the ATLAS and CMS Run 1 combination [151]. The other two are the individual combinations of ATLAS and CMS independently with partial Run 2 dataset. It is important to note that, between the Run 1 and the Run 2 results, the signal theoretical systematic uncertainties have improved significantly.

The Run 1 full combination results were derived by the two collaborations, taking rigorously into account all correlations in the systematic uncertainties and in the large number of channels and their categories.

At Run 2, ATLAS [241] and CMS [242] have already produced combined measurements of the coupling properties and production cross section ratios of the Higgs boson.

In this section, only the results on the main Higgs boson production and decay modes will be discussed. Only a brief presentation of the combination framework is given here (a more detailed description is given in Ref. [243]). This framework will also be used in Section 11.6 to discuss the measurements of the coupling properties of the Higgs boson.

11.4.1 *Principles of the combination*

The combination of the Higgs boson analysis channels in each experiment and for the two experiments together was done using a fit of a signal and background model to the data. As described above, the data was made of a large number of categories, aiming at reconstructing exclusive production and decay modes. In the combination of ATLAS and CMS [151], there were approximately 600 categories. The combination was a simultaneous fit to all these categories, using a reduced number of parameters of interest and a Higgs boson mass fixed at its measured value (see Section 11.3.1.3). The much larger number of categories present in the ATLAS and CMS combination [151] is due to additional separation in terms of finer exclusive production regions, decay channels of the Z and the W bosons, and taus, control regions where little-to-no signal is present, and different center-of-mass energies. It should be noted that the individual combination performed by ATLAS [244] included two additional decay channels: the $\mu^+\mu^-$ and $Z\gamma$. For the sake of simplicity these channels were omitted in the ATLAS–CMS combination due to the very little sensitivity in these channels with this dataset.

In their Run 2 individual combinations, ATLAS and CMS have not considered the $Z\gamma$ channel. Both ATLAS and CMS experiment have included the $\mu\mu$ channel based on a partial Run 2 dataset corresponding to an integrated luminosity of 36 fb^{-1} only.

The key to understand how the combination of channels works relies on the combination master formula, which expresses for each category, indexed by c, of a given channel (typically a category covers mostly one decay mode, but possibly various production modes), the measured number of signal events n_s^c as a function of a limited number of parameters as follows:

$$n_s^c = \left(\sum_{i,f} \mu_i \, \sigma_i^{\rm SM} \times A_{if}^c \times \varepsilon_{if}^c \times \mu_f \, {\rm BR}_f^{\rm SM} \right) \times \mathcal{L}^c. \quad (11.16)$$

The production index is defined as $i \in \{\text{ggF}, \text{VBF}, VH, t\bar{t}H, tH, \ldots\}$ (including specific modes and regions of phase space) and the decay index is defined as $f \in \{\gamma\gamma, WW, ZZ, bb, \tau\tau\}$, while $\sigma_i^{\rm SM}$ and ${\rm BR}_f^{\rm SM}$ are the corresponding production cross sections and decay branching fractions, estimated as described in Section 11.2, assuming that the Higgs boson is that of the SM. A_{if}^c and ε_{if}^c are the signal acceptance and the reconstruction efficiency for the given production and decay modes in the category c. $\mathcal{L}^c$ is the integrated luminosity used for that specific category. For the purpose of this review, these parameters can be considered as fixed[3].

The parameters of interest in the master formula are the signal strength parameters μ_i and μ_f. It is important to note that the formula relies on the factorisation of the production cross section and decay branching fraction, which assumes the narrow width approximation. The width of the Higgs boson will be discussed in Section 11.5, however, for the precision needed here, the fact that the Higgs boson has been observed in decay channels with high mass resolution as a resonance is sufficient to validate this hypothesis. It is also manifest in the above equation that the ten parameters for the production modes (μ_i) and decay modes (μ_f) cannot be determined simultaneously. This illustrates that total cross sections or branching fractions cannot be measured without further assumptions in this fit.

The master formula also illustrates an important caveat to the measurement of signal strength parameters. In case these are interpreted as scale factors of the production cross sections or branching fractions, then all the other quantities such as the acceptances and efficiencies, A_{if}^c and ε_{if}^c, need to be assumed as

[3] In the combination performed by ATLAS and CMS, the systematic uncertainties on these parameters are taken into account by allowing these parameters to vary in the fit.

Downloaded from https://academic.oup.com/ptep/article/2022/8/083C01/6651666 by KIT Library user on 27 September 2022

Table 11.10: Summary, for the main production and decay processes at the LHC, of the observed (and expected) significances with respect to the background only hypothesis. When the observation has been established unambiguously, the measured signal strength is reported together with the total uncertainty or, when available, the statistical (first) and the systematic (last) uncertainties. The results for the gauge boson decays of the Higgs boson for the ATLAS experiment are not reported in the combination and are thus taken from the individual channels results (*) and when needed computed from the ratio of fiducial cross sections (**) discussed in this review. *The Run 2 VH significances reported in this table are obtained from the observation of the Higgs boson decays to b quarks, while the Run 1 combination corresponds to combination of all channels.

Decay modes				
	ATLAS (Run 1)	CMS (Run 1)	ATLAS (Run 2)	CMS (Run 2)
$\gamma\gamma$	4.6σ (5.3σ)	5.2σ (4.6σ)	1.02 ± 0.13**	$1.07\,^{+0.08}_{-0.08}\,^{+0.08}_{-0.07}$
ZZ	6.2σ (6.3σ)	8.1σ (6.5σ)	1.01 ± 0.11*	$0.93\,^{+0.07}_{-0.07}\,^{+0.07}_{-0.06}$
WW	5.9σ (5.4σ)	6.5σ (4.7σ)	1.05 ± 0.13**	$1.20\,^{+0.09}_{-0.09}\,^{+0.13}_{-0.12}$
$\tau^+\tau^-$	3.4σ (3.9σ)	4.5σ (3.8σ)	6.4σ (5.4σ)	$0.80\,^{+0.10}_{-0.10}\,^{+0.14}_{-0.13}$
	Comb. 5.0σ (5.5σ)			
$b\bar{b}$	2.6σ (2.5σ)	1.4σ (2.1σ)	5.4σ (5.5σ)	$1.11\,^{+0.13}_{-0.13}\,^{+0.16}_{-0.15}$
	Comb. 3.7σ (2.6σ)			
Production modes				
	ATLAS and CMS (Run 1)		ATLAS (Run 2)	CMS (Run 2)
$gg \to H$ (ggF)	NR		$1.00 \pm 0.05 \pm 0.05$	$1.04 \pm 0.05\,^{+0.08}_{-0.07}$
$qq \to qqH$ (VBF)	Comb. 5.4σ (4.6σ)		$1.15 \pm 0.13\,^{+0.12}_{-0.10}$	$0.75\,^{+0.16}_{-0.15}\,^{+0.10}_{-0.08}$
$pp \to WH$	Comb. 3.5σ (4.2σ)		$1.20\,^{+0.17}_{-0.16}\,^{+0.15}_{-0.14}$	$1.46\,^{+0.29}_{-0.28}\,^{+0.22}_{-0.21}$
$pp \to ZH$			$0.98 \pm 0.16\,^{+0.15}_{-0.13}$	$0.98\,^{+0.26}_{-0.25}\,^{+0.17}_{-0.16}$
$pp \to t\bar{t}H$	Comb. 4.4σ (2.2σ)		$1.10\,^{+0.16}_{-0.15}\,^{+0.14}_{-0.13}$	$1.14\,^{+0.13}_{-0.13}\,^{+0.17}_{-0.15}$

independent and fixed to their estimated values for the SM Higgs boson. An additional important caveat to note concerning these combined results is that only the normalisation is varied, while the discriminating variables for the signal are not modified and are still used in the fit. These caveats are of particular importance in the use of the combination to measure the coupling properties of the Higgs boson, as discussed in Section 11.6. For relatively small perturbations of the couplings of the Higgs boson from the SM values, this hypothesis is valid.

However, the products $\mu_i \times \mu_f$ can be considered as free parameters and in principle measurable (if there is sufficient sensitivity from specific categories). Measuring the products of signal strengths can be viewed as measuring the cross sections times the branching fraction, $\sigma \cdot \mathrm{BR}$. An illustration of the results for the Run 2 combinations of ATLAS is presented in Fig. 11.7 and for CMS in Fig. 11.8.

Other fits involving ratios of cross sections, which are less sensitive to theory uncertainties, are performed and reported in Ref. [243].

The most constrained fit in the combination allows for only one single parameter to vary, i.e., $\forall(i,f), \mu_i = \mu_f = \mu$. This global-signal-strength model provides the simplest probe of the compatibility of the signal with the SM Higgs boson. Indeed, it is sensitive to any deviation from the SM Higgs boson couplings provided that these deviations do not cancel overall. The full Run 1 combination determines the global signal strength to be

$$\begin{aligned}\mu = 1.09 \pm 0.11 =& 1.09 \pm 0.07\ (\text{stat.})\ \pm 0.04\ (\text{expt.}) \\ &\pm 0.03\ (\text{th. bkg.})\ \pm 0.07\ (\text{th. sig.}),\end{aligned} \tag{11.17}$$

where the statistical, experimental uncertainties as well as the theoretical uncertainties on the background and on the signal are reported separately. The ATLAS Run 2 combination of the global signal strength yields [241]:

$$\begin{aligned}\mu = 1.06 \pm 0.07 = 1.06\ &\pm 0.04\ (\text{stat.}) \pm 0.03\ (\text{exp.}) \\ &\pm 0.02\ (\text{th. bkg.})\ ^{+0.05}_{-0.04}\ (\text{th. sig.}),\end{aligned} \tag{11.18}$$

while the CMS Run 2 combination yields [242]:

$$\begin{aligned}\mu = 1.02\ ^{+0.07}_{-0.06} = 1.02\ &\pm 0.04\ (\text{stat.}) \pm 0.04\ (\text{th}) \\ &\pm 0.04\ (\text{exp.}).\end{aligned} \tag{11.19}$$

These overall signal strengths are fully compatible with the SM expectation, $\mu = 1$, with a precision of 7%. It is interesting to note that the main uncertainty in these measurements arises from the limited precision in the theoretical predictions for the signal production processes. The precision reached with the individual experiments combinations using partial Run 2 data sets have already exceeded the full Run 1 ATLAS and CMS combination precision.

11.4.2 *Main decay modes*

Despite the large number of decay channels, since the cross sections cannot be independently measured, from the measurements described in this section it is impossible to measure the decay branching fractions without a loss of generality. The simplest assumption that can be made is that the production cross sections are those of the SM, which is equivalent to assume that, for all i indices, $\mu_i = 1$. All branching fractions μ_f can then be measured in a simple 5 parameter fit. The results of these fits are reported in Table 11.10 in terms of significances to highlight their unambiguous observations: all the measured branching fractions are compatible with the SM values.

As illustrated in Table 11.10, for all channels directly sensitive to the third generation Yukawa couplings (*i.e.* the $H \to \tau\tau$ the $\mathrm{V}H(\to b\bar{b})$ the Run 2 data made a significant difference. The

Downloaded from https://academic.oup.com/ptep/article/2022/8/083C01/6651666 by KIT Library user on 27 September 2022

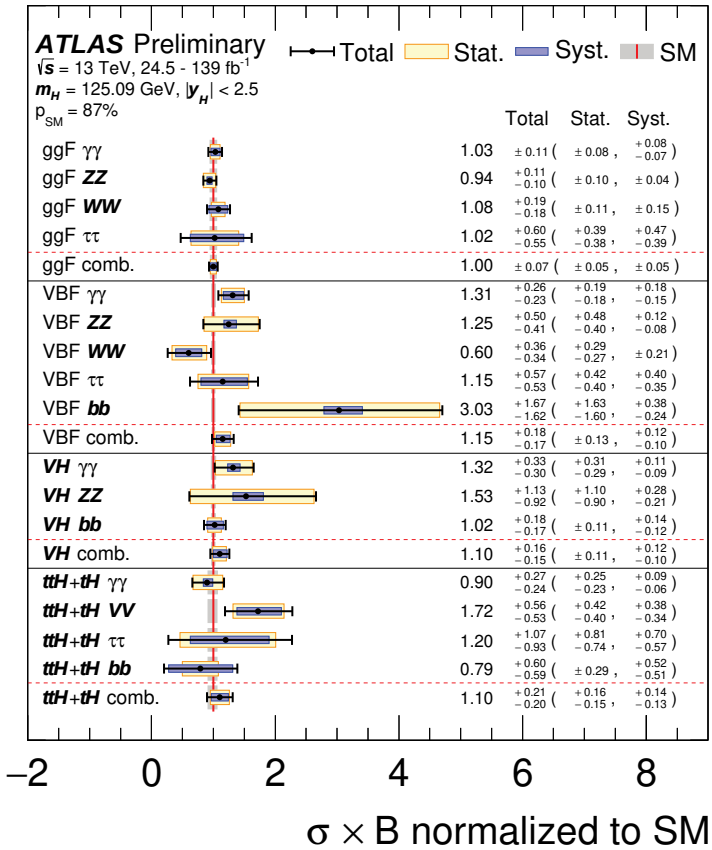

Figure 11.7: Combined measurements by ATLAS of the products $\sigma \cdot \mathrm{BR}$, normalised to the SM predictions, for the five main production and five main decay modes.

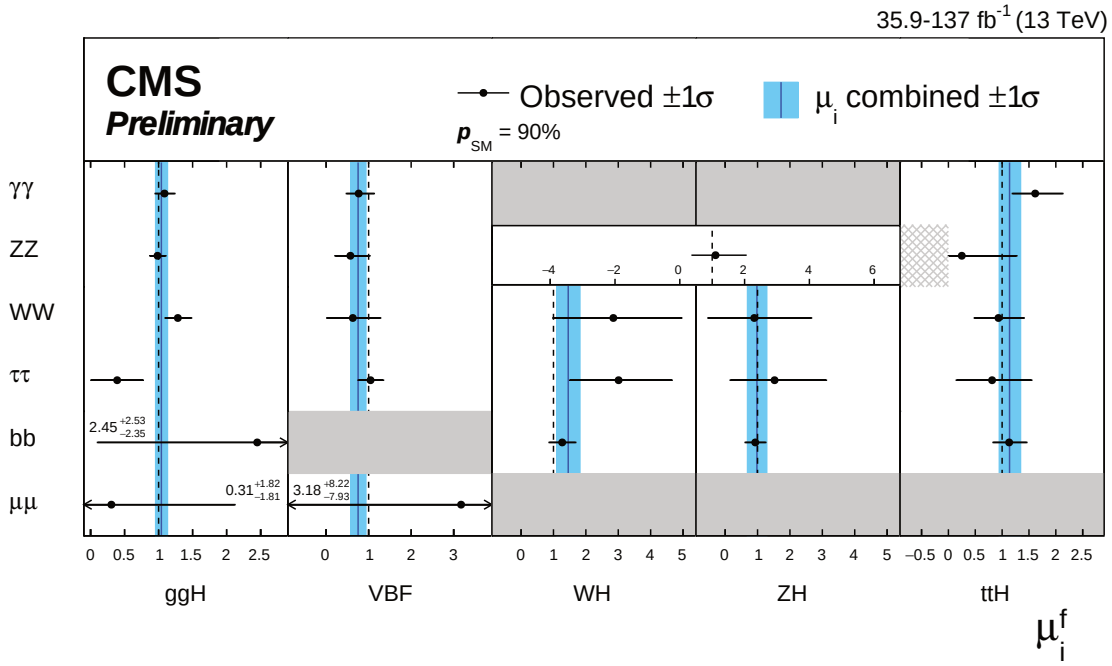

Figure 11.8: Combined measurements by CMS of signal strengths for the five main production and five main decay modes. The hatched combinations require more data for a meaningful confidence interval to be provided.

available sensitivity came mostly from the VH process. The combined significance of 3.7σ at Run 1 was sufficient to suggest ev-

Downloaded from https://academic.oup.com/ptep/article/2022/8/083C01/6651666 by KIT Library user on 27 September 2022

idence, however ATLAS and CMS observations were both low with respect to the rate expected in the SM. At Run 2, this channel benefited largely from the increased production cross sections at 13 TeV and the much larger dataset. In this case as well, it is with the addition of the Run 2 data that both experiments were able to establish a measurement in this channel (as discussed in Section 11.3.2).

These are major milestones of the LHC physics program.

11.4.3 *Main production modes*

Most analysis channels are divided into exclusive categories allowing for an increased overall sensitivity and permitting to access the various Higgs boson production modes. The cross sections of the main production modes can be measured assuming that the branching fractions are those of the SM, i.e., for all f indices $\mu_f = 1$. These assumptions lead to a 5 parameter combination. The results are reported in terms of significances of observation of the production modes in Table 11.10.

The gluon fusion production process is the dominant production mode. Although no numerical estimate of combined significance of observation for this process has been given by the experiments, it is considered as established due to the overwhelming evidence from the three main discovery channels. None of the other production modes have been firmly established by the experiments individually. However, the table shows that, for the VBF production mode, the combination had a large sensitivity and produced a combined observation of 5.4σ, therefore establishing this process with a rate compatible with that expected in the SM.

The VH production mode has only very recently been unambiguously observed by ATLAS and CMS independently (as discussed in Section 11.3.2) through the $V(H \to b\bar{b})$ channel. This is illustrated in the relative contributions of all channels to the VH process shown in Fig. 11.7 and Fig. 11.8.

With the Run 2 data, all production processes have been established, and in particular the $pp \to t\bar{t}H$ process, which provides direct evidence of the coupling of the Higgs boson to top quarks. This is another milestone in the LHC physics program.

11.5 Main quantum numbers and width of the Higgs boson

11.5.1 *Main quantum numbers* J^{PC}

Probing the Higgs boson quantum numbers is essential to further unveiling its coupling properties. The measurements of the signal event yields in all the channels discussed in Sections 11.3 and 11.4, and their compatibility with the SM Higgs boson predictions, give a qualitative but, nonetheless, compelling indication of its nature. This qualitative picture is further complemented by the implications of the observation of the particle in the diphoton channel. According to the Landau–Yang theorem [245], the observation made in the diphoton channel excludes the spin-1 hypothesis and restricts possibilities for the spin to 0 or 2.

The Landau–Yang theorem does not apply if the observed state is not decaying to a pair of photons but to a pair of scalars subsequently decaying to two very collimated pairs of photons (as for example in the case of $H \to a_1 a_1 \to 4\gamma$). This possibility has not been rigorously excluded but is not experimentally favoured since tight selection criteria are applied on the electromagnetic shower shapes of the reconstructed photons. A more systematic analysis of shower shapes and the fraction of conversions could be performed to further discriminate between the single prompt photon and the two overlapping photons hypotheses. There are also potential theoretical loopholes concerning the applicability of the Landau–Yang theorem, such as off-shell vector boson decays. However, for the observed particle not to be of spin 0 and +1 parity would require an improbable conspiracy of effects. It is nevertheless important to test this hypothesis independently, in particular since the measurements of coupling properties of the Higgs boson assume that it is a CP-even state.

11.5.1.1 *Charge conjugation*

The charge conjugation quantum number is multiplicative, therefore given that the Higgs-like particle is observed in the $H \to \gamma\gamma$ channel, and given that photons are C-odd eigenstates, assuming C conservation, the observed neutral particle should be C-even.

11.5.1.2 *Spin and parity*

To probe the spin and parity quantum numbers of the discovered particle, a systematic analysis of its production and decay processes is performed in several analyses. These analyses are designed to be independent of the measured event yields and they rely instead on the production and the decay angles, and on the threshold distributions as long as a significant signal is observed, i.e., in situations when an excess over the expected background can be used to further discriminate between signal hypotheses. These analyses are based on probing various alternative models of spin and parity [246]. These models can be expressed in terms of an effective Lagrangian [247] or in terms of helicity amplitudes [248]. The two approaches are equivalent. In the following, the effective Lagrangian formalism is chosen to describe the models considered and a restricted number of models are discussed [247]. In the analysis performed by CMS [248], a larger number of models have been investigated, however, the main channels studied by both experiments are essentially the same and the main conclusions are similar and fully consistent.

i. *Spin-0 model*

The interaction Lagrangian relevant for the analysis of spin-0 particle interaction with a pair of W or Z bosons with either fixed or mixed SM and BSM CP-even couplings or CP-odd couplings, is the following [249]:

$$\begin{aligned}\mathcal{L}_0^{W,Z} \supset \Big\{ &\cos(\alpha)\kappa_{\rm SM}\left[\frac{1}{2}g_{HZZ}Z_\mu Z^\mu + g_{HWW}W^+_\mu W^{-\mu}\right] \\ &- \frac{1}{4\Lambda}\left[\cos(\alpha)\kappa_{HZZ}Z_{\mu\nu}Z^{\mu\nu} + \sin(\alpha)\kappa_{AZZ}Z_{\mu\nu}\tilde{Z}^{\mu\nu}\right] \\ &- \frac{1}{2\Lambda}\left[\cos(\alpha)\kappa_{HWW}W^+_{\mu\nu}W^{-\mu\nu} + \sin(\alpha)\kappa_{AWW}W^+_{\mu\nu}\tilde{W}^{-\mu\nu}\right]\Big\} H,\end{aligned} \tag{11.20}$$

where $V^\mu = Z^\mu, W^{+\mu}$ are the vector boson fields, $V^{\pm\mu\nu}$ are the reduced field tensors and $\tilde{V}^{\pm\mu\nu} = 1/2\,\varepsilon^{\mu\nu\rho\sigma}V_{\rho\sigma}$ are the dual tensor fields. And Λ defines an effective theory energy scale. The factors $\kappa_{\rm SM}, \kappa_{HZZ}, \kappa_{HWW}, \kappa_{AZZ}, \kappa_{AWW}$ denote the coupling constants corresponding of the coupling of the SM and BSM CP-even and CP-odd components of the Higgs boson to the W and Z fields. The mixing angle α allows for the production of a CP-mixed state and the CP-symmetry is broken when $\alpha \neq 0, \pi$.

This formalism can be used to probe both CP-mixing for a spin-0 state, as discussed in Section 11.5.1.4 or specific alternative hypotheses, as discussed below in Section 11.5.1.3, such as a pure CP-odd state ($J^P = 0^-$) corresponding to $\alpha = \pi/2$, $\kappa_{\rm SM} = \kappa_{HVV} = 0$ and $\kappa_{AVV} = 1$. A BSM CP-even state $J^P = 0^+$ corresponds to $\alpha = 0$, $\kappa_{AVV} = 0$, $\kappa_{HVV} = 1$ and $\kappa_{\rm SM}$ arbitrary. These hypotheses are compared to the SM Higgs boson hypothesis corresponding to $\alpha = 0$ and $\kappa_{HVV} = \kappa_{AVV} = 0$ and $\kappa_{\rm SM} = 1$. This formalism has been adopted by the ATLAS experiment. The analysis of these benchmarks are illustrated in Fig. 11.9.

A different parametrisation of anomalous couplings of a spin-zero boson with two gauge bosons VV can also expressed in the general form of the scattering amplitude A:

$$\begin{aligned}A \sim &\left[a_1^{VV} - \frac{\kappa_1^{VV}q_1^2 + \kappa_2^{VV}q_2^2}{(\Lambda_1^{VV})^2} - \frac{\kappa_3^{VV}(q_1+q_2)^2}{(\Lambda_Q^{VV})^2}\right] m_{V_1}^2 \varepsilon^*_{V_1}\varepsilon^*_{V_2} \\ &+ a_2^{VV} f^{*(1)}_{\mu\nu} f^{*(2)\mu\nu} + a_3^{VV} f^{*(1)}_{\mu\nu}\tilde{f}^{*(2)\mu\nu}\end{aligned} \tag{11.21}$$

where ε_i is the polarization vector of the boson V_i, $f^{*(i)}_{\mu\nu} = \varepsilon^\mu_i q^\nu - \varepsilon^\nu_i q^\mu$ is a scalar tensor constructed from the vector boson V_i polarization and four momentum, $\tilde{f}^{*(i)}_{\mu\nu} = \frac{1}{2}\varepsilon_{\mu\nu\rho\sigma}f^{*(i)\rho\sigma}$ is the corresponding pseudo-scalar tensor. Λ_1 and Λ_Q are new physics scales, $a_{1,2,3}$ are coupling strength modifiers and $|\kappa^{VV}_{(1,2,3)}| = 0$ or 1. The custodial symmetry would require that $a^{WW} = a^{ZZ}$ and, at tree-level, the only non-zero contributions would come from the a_1

Downloaded from https://academic.oup.com/ptep/article/2022/8/083C01/6651666 by KIT Library user on 27 September 2022

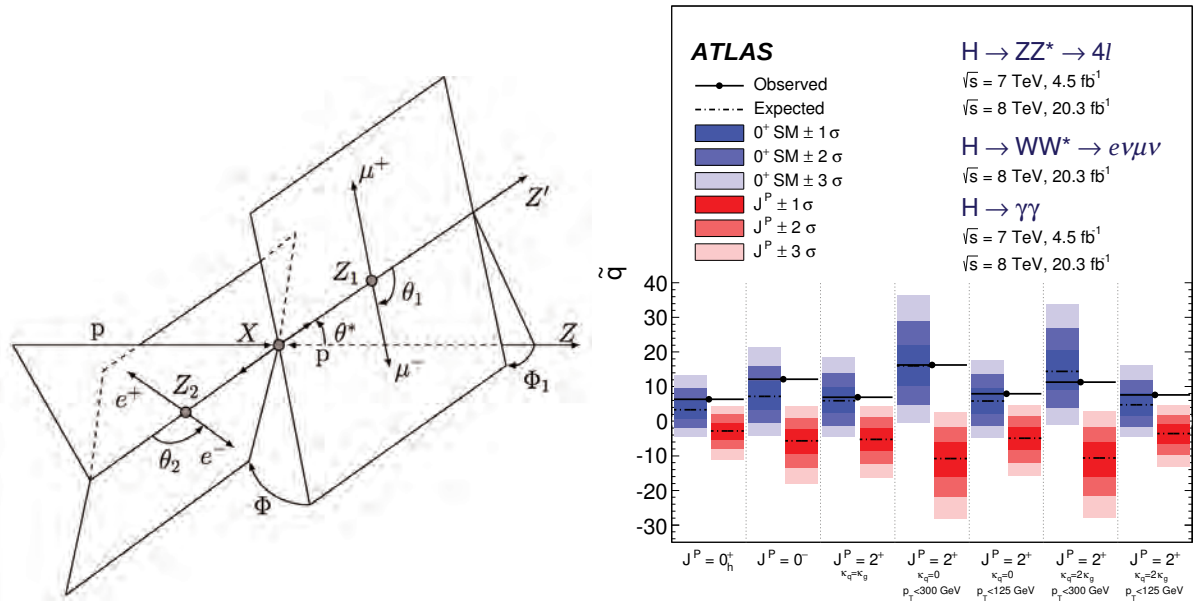

Figure 11.9: (Left) Definition of the production and decay angles defined for the $H \to ZZ^{(*)} \to 4\ell$ final state [248]. (Right) Expected distributions of the test statistic for the SM hypothesis (in blue) and several alternative spin and parity hypotheses (in red).

term. This parametrisation is used by CMS. It is fully equivalent to the interaction Lagrangian approach described above.

ii. *Spin-2 model*

The graviton-inspired interaction Lagrangian for a spin-2 boson $X^{\mu\nu}$ that does not carry any color, weak and electromagnetic charge and that uniquely interacts with the energy momentum tensor $\mathcal{T}^{V,f}$ of vector bosons V or fermions f, can be written as follows [249]:

$$\mathcal{L}_2 \supset \frac{1}{\Lambda}\left[\sum_V \xi_V \mathcal{T}^V_{\mu\nu} X^{\mu\nu} + \sum_f \xi_f \mathcal{T}^f_{\mu\nu} X^{\mu\nu}\right], \qquad (11.22)$$

where the strength of the interaction is determined by the couplings ξ_V and ξ_f. The simplest scenarios, referred to as universal couplings (UC), correspond to $\xi_V = \xi_f$. They predict a large branching ratio to photons (of approximately 5%) and negligible couplings to massive gauge bosons (W and Z). They are therefore disfavoured, and other models are investigated where the couplings of the W, Z and γ are assumed to be independent. Universality of the couplings refers to $\xi_g = \xi_q$. Two other scenarios are considered: $\xi_q = 0$ and $\xi_q = 2\xi_g$. In these scenarios, a large enhancement of the tail of the transverse momentum of the spin-2 state is expected and requires a further selection requirement in order to probe the models within the range of validity of the effective field theory. Two requirements are considered, $p_T^X < 300\,\text{GeV}$ and $p_T^X < 125\,\text{GeV}$ [247]. The analysss of these benchmarks are discussed below and results are illustrated in Fig. 11.9.

11.5.1.3 *Probing fixed J^P scenarios*

At the LHC, the determination of the spin and CP properties of the Higgs boson is done independently from the total rates measurement, it uses a global angular helicity analysis and, when applicable, the study of threshold effects. The channels used for this analysis, $H \to \gamma\gamma$, $H \to WW^{(*)} \to \ell\nu\ell\nu$ and $H \to ZZ^{(*)} \to 4\ell$, are those where the observation of a signal is unambiguous.

At the Tevatron, an analysis using the threshold distribution in the associated production mode VH with subsequent decay to a pair of b quarks was performed by the D0 collaboration.

i. *The VH production at D0*

The mass of the VH system is a powerful discriminant to distinguish a $J^P = 0^+$, with a threshold behaviour in $d\sigma/dM^2 \sim \beta, \beta^3, \beta^5$ from a 0^+, 0^- and 2^+ state, respectively [250]. The VH mass observable not only discriminates signal hypotheses, but also has an increased separation between the 0^- and 2^+ hypotheses with respect to the backgrounds, thus allowing, with a small and not yet significant signal yield, to exclude that the observed state is 0^- at 98% CL [251] and 2^+ at the 99.9% CL [252], assuming a signal produced with their best fit signal strength (which was $\mu = 1.23$).

ii. *The $\gamma\gamma$ channel at the LHC*

In the $H \to \gamma\gamma$ channel, the analysis is performed inclusively using the production angle $\cos\theta^*_{CS}$ and the transverse momentum of the diphoton pair [247]. The polar angle in the rest frame is defined with respect to the bisector axis of the momenta of the incoming protons and is referred to as the polar angle in the Collins–Soper frame [253]. The SM Higgs boson signal distribution is expected to be uniform with a cutoff due to the selection requirements on the photons transverse momentum. The $H \to \gamma\gamma$ channel is mostly sensitive to the gluon-initiated spin-2 production scenarios, which yield a $\cos\theta^*_{CS}$ distribution peaking at values close to 1. The ATLAS limits are derived from a fit of the signal in bins of $\cos\theta^*_{CS}$ and diphoton transverse momentum and are summarized in Fig. 11.9 (right) (only combined results are shown). The data shows a good compatibility with the SM 0^+ hypothesis and contributes strongly to the exclusion of several spin-2 scenarios. The conclusions are the same from CMS results [248].

iii. *The $H \to WW^{(*)} \to \ell\nu\ell\nu$ channel at the LHC*

In the $H \to WW^{(*)} \to \ell\nu\ell\nu$ channel, the production and decay angles cannot be easily reconstructed due to the presence of neutrinos in the final state, however, sensitivity arises from the $V-A$ structure of the decay of the W bosons. A scalar state thus yields a clear spin correlation pattern that implies that the charged leptons e or μ from the decays of the W bosons are produced close to one another in the transverse plane. This feature impacts observables such as the azimuthal angle between the two leptons $\Delta\Phi_{\ell\ell}$ or their invariant mass $m_{\ell\ell}$ in addition to the threshold behaviour of the decay. It can be used to discriminate between various spin and parity hypotheses. The approach adopted by ATLAS uses a multivariate discriminant, whereas CMS uses a 2D-fit of the dilepton mass and the transverse mass. Figure 11.9 (right) summarizes the ATLAS results of the $H \to WW^{(*)} \to \ell\nu\ell\nu$ analyses alone and in combination with other channels. Spin-1 hypotheses

Downloaded from https://academic.oup.com/ptep/article/2022/8/083C01/6651666 by KIT Library user on 27 September 2022

(1^+ and 1^-) have also been tested in this channel by ATLAS and CMS. ATLAS and CMS exclude the 1^+ and 1^- hypotheses at more than 95% CL.

iv. *The $H \to ZZ^{(*)} \to 4\ell$ channel at the LHC*

The $H \to ZZ^{(*)} \to 4\ell$ coupling analysis, as described in Section 11.3, also uses a discriminant based on the 0^+ nature of the Higgs boson to further separate signal and background. In this analysis, this feature is used to discriminate between signal hypotheses. The observables sensitive to the spin and parity are [254] the masses of the two Z bosons (due to the threshold dependence of the mass of the off-shell Z boson), two production angle θ^* and Φ_1, and three decay angles, Φ, θ_1 and θ_2. The production and decay angles are defined as:

– θ_1 and θ_2, the angles between the negative final state lepton and the direction of flight of Z_1 and Z_2 in the rest frame.

– Φ, the angle between the decay planes of the four final state leptons expressed in the four lepton rest frame.

– Φ_1, the angle defined between the decay plane of the leading lepton pair and a plane defined by the vector of the Z_1 in the four lepton rest frame and the positive direction of the proton axis.

– θ^*, the production angle of the Z_1 defined in the four lepton rest frame with respect to the proton axis.

These angles are illustrated in Fig. 11.9 (left). There are two approaches to this analysis. The first, used by CMS, is a matrix element likelihood approach where a kinematic discriminant is defined based on the ratio of the signal and background probabilities. These probabilities are defined using the leading-order matrix elements. A similar approach is also performed by ATLAS as a cross check of their main result. The main approach adopted by ATLAS is the combination of sensitive observables with a Boosted Decision Tree. These analyses are sensitive to various J^P hypotheses and in particular discriminate the 0^+ hypothesis from the 0^-. In all scenarios investigated, and for both ATLAS and CMS, the data is compatible with the 0^+ hypothesis. ATLAS and CMS exclude a pure pseudo-scalar nature of the observed boson at CL_S levels of 98% and 99.8% [248].

11.5.1.4 *Probing CP-mixing and anomalous HVV couplings*

The careful study of the kinematic properties of the events observed in the $H \to ZZ^{(*)} \to 4\ell$ and $H \to WW^{(*)} \to \ell\nu\ell\nu$ channel, and in particular the angular distributions described above, allows one to further probe the HVV coupling beyond testing fixed hypotheses. Assuming that the observed particle is a spin-0 state, and using several discriminating observables in the $H \to ZZ^{(*)} \to 4\ell$ and $H \to WW^{(*)} \to \ell\nu\ell\nu$ channels, the anomalous terms in the formalism of Eq. (11.20) can be probed. In the approach of helicity amplitudes used by CMS [248], all terms are essentially equivalent, except for one additional phase which is neglected in Eq. (11.20).

Results are derived in terms of the parameters $\tilde{\kappa}_{HVV} = v\,\kappa_{HVV}/\Lambda$ and $\tilde{\kappa}_{AVV} = v\,\kappa_{AVV}/\Lambda$, and, more precisely, as measurements of $\tilde{\kappa}_{HVV}/\kappa_{\mathrm{SM}}$ and $\tan\alpha \cdot \tilde{\kappa}_{AVV}/\kappa_{\mathrm{SM}}$, as shown in Fig. 11.10. These parameters can be interpreted as mixing parameters of a tensor anomalous CP-even coupling and a CP-odd component. The measurements are made in the $H \to ZZ^{(*)} \to 4\ell$ and $H \to WW^{(*)} \to \ell\nu\ell\nu$ channels independently and then combined assuming that the $\tilde{\kappa}_{HVV}/\kappa_{\mathrm{SM}}$ and $\tan\alpha \cdot \tilde{\kappa}_{AVV}/\kappa_{\mathrm{SM}}$ are the same for the W and Z vector bosons. Only the combination of the WW and ZZ channels is shown in Fig. 11.10. The asymmetric shape of the likelihood as a function of $\tilde{\kappa}_{HWW,\,HZZ}/\kappa_{\mathrm{SM}}$ is mainly due to the interference between the BSM and the SM contributions that gives a maximal deviation from the SM predictions for negative relative values of the BSM couplings. In Fig. 11.10, the expected likelihood profiles for a SM Higgs boson are also displayed. While no significant deviation from the SM expectation is observed, the precision of the measurements of the mixing parameters is fairly low. The results and conclusions from the CMS measurements [248] are very similar.

An individual ZZ^* channel measurement has also been carried out with a partial Run 2 dataset by ATLAS [255]. CMS has performed a CP-mixing analysis of a partial Run 2 dataset of $36\,\mathrm{pb}^{-1}$ combined with the full Run 1 data using the ZZ^* channel [256]. In this analysis the CMS experiment sets constraints on the following parameters defined in the scattering amplitude parametrisation (11.21):

$$f_{a_i} = \frac{|a_i|^2\sigma_i}{\sum_{j=1,2,3}|a_j|^2\sigma_j}, \quad \phi_{a_i} = \arg\left(\frac{a_i}{a_1}\right), \tag{11.23}$$

where σ_i is the cross section for process with $a_i = 1$ and $a_{j\neq i} = 0$. The constraints on these parameters are shown in Fig. 11.11.

CP invariance in the HVV coupling can also be probed with the VBF production process in the $H \to \tau^+\tau^-$ channel. CMS has performed an analysis in this channel and has combined its results with the aforementioned ZZ^* channel using the same dataset [257].

ATLAS has also performed an analysis using optimal observables [258], defined as the ratio of the interference between the CP-odd and the SM contributions normalised to the SM matrix element squared, using the Run 1 data. In this study, the CP-mixing contributions are described in the framework of an effective field theory governed by a single parameter $\tilde{d}$, found to be consistent with its SM value of $\tilde{d} = 0$ and constrained to the interval [-0.11,0.05] at the 68% CL.

11.5.1.5 *Probing $Hf\overline{f}$ coupling CP properties in $pp \to t\bar{t}H$ production*

The CP-properties of the Hggs boson coupling to fermions can be probed with the $p\overline{p} \to t\bar{t}H$ process. The increased sensitivity to the this process in particular in The channels where the higgs boson decays to a pair of photons provide a good sensitivity to the CP properties of the coupling through kinematics and angular distributions between the Higgs boson and the top quarks produced in the final state. The

$$\mathcal{L} \supset -\frac{m_t}{v}\overline{\psi_t}(\kappa_t + i\gamma_5\tilde{\kappa}_t)\psi_t$$

To probe the CP properties of the Higgs to fermion couplings, ATLAS [177] and CMS [178] use slightly different observables. ATLAS measures an overall coupling-strength factor denoted κ_t' and a CP-mixing angle α which are related to the above Lagrangian by:

$$\kappa_t' = \frac{\kappa_t}{\cos\alpha} \quad \text{and} \quad \alpha = \arctan\frac{\tilde{\kappa}_t}{\kappa_t}$$

With the full Run 2 dataset, ATLAS [177] excludes CP-mixing angle greater (less) than 43° (−43°) is excluded at 95% confidence level.

CMS provides a measurement of the fraction of CP-odd contribution to the scattering amplitude from the above Lagrangian estimated as:

$$f_{CP} = \frac{|\tilde{\kappa}_t|^2}{|\kappa_t|^2| + |\tilde{\kappa}_t|^2} \times \mathrm{sign}(\tilde{\kappa}_t/\kappa_t)$$

Also using the full Run 2 dataset, CMS [178] measures the CP-odd fraction $f_{CP} = 0.00 \pm 0.33$.

Both he ATLAS and CMS experiments used multivariate analyses in order to maximize the sensitivity to the measurement of the CP properties of the $Hf\overline{f}$ coupling. Both experiments used leptonic and hadronic decays of the top quarks.

11.5.1.6 *Probing $Hf\overline{f}$ coupling CP properties in $H \to \tau^+\tau^-$ decays*

Another interesting channel to investigate the CP properties of the $Hf\overline{f}$ coupling is the Higgs decay to taus through tau polarisation sensitive variables. Preliminary studies of the sensitivity to CP properties in this channel have been carried out by ATLAS [259]. At HL-LHC this analysis has investigated $H \to \tau^+\tau^-$ decaus where taus decay via the $\tau^\pm \to \rho^\pm\nu_\tau \to \pi^0\pi^\pm\nu_\tau$. This analysis is foreseen to constrain the CP-mixing angle to be measured with a precision between $\pm 18^o$ to $\pm 30^o$, depending on the precision of the reconstruction of the π^0.

Downloaded from https://academic.oup.com/ptep/article/2022/8/083C01/6651666 by KIT Library user on 27 September 2022

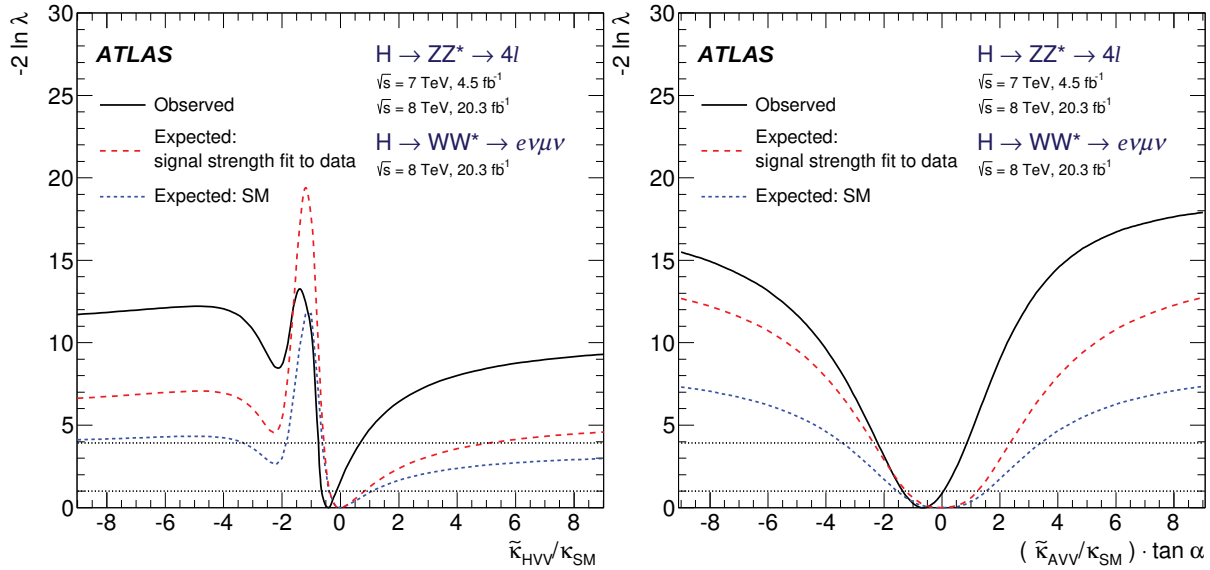

Figure 11.10: Likelihood profiles for the $\tilde{\kappa}_{HVV}$ and $\tilde{\kappa}_{AVV} \cdot \tan\alpha$ parameters, representing respectively CP-even and CP-odd anomalous couplings of the Higgs boson.

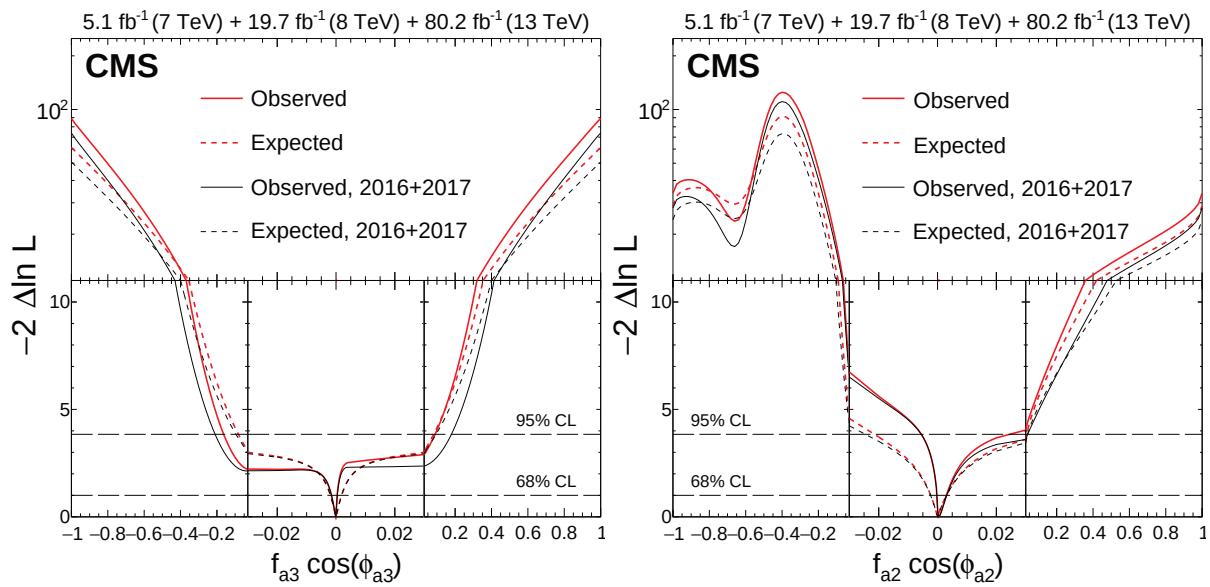

Figure 11.11: Observed (solid) and expected (dashed) likelihoods as a function of $f_{a_3}\cos(\phi_{a_3})$ (left), $f_{a_2}\cos(\phi_{a_2})$ (right) for the Run 1 and Run 2 datasets separately and combined.

11.5.2 *Off-shell couplings of the Higgs boson*

In the dominant ggF production mode with a subsequent decay of the Higgs boson into a pair of Z bosons, the production cross section of an off-shell Higgs boson is known to be sizeable. This follows as a consequence of the enhanced couplings of the Higgs boson to the longitudinal polarization of the massive vector bosons at high energy.

The off-shell to on-shell cross section ratio is approximately 8% in the SM [260]. Still, the Higgs contribution to VV production at large invariant mass remains small compared to the background. It is nevertheless interesting to probe Higgs production in this regime as it is sensitive to new physics beyond the SM.

The difficulty in the off-shell VV analysis, beyond the small signal-to-background ratio, is due to a large negative interference between the signal and the $gg \to VV$ background.

The resulting presence of a SM Higgs boson signal in the far off-shell domain results in a deficit of events with respect to the expectation from background only events. It is only when the off-shell couplings of the Higgs boson are larger than expected in the SM that the presence of a signal appears as an excess over the background expectation. One additional intricacy arises from the precision in the prediction of the rate for $gg \to VV$, a loop process at lowest order, and its interference with the signal. At the time of the publication of the original ATLAS and CMS results, a full NLO prediction had not been computed.

It is interesting to note that, in this regime, the Higgs boson is studied as a propagator and not as a particle. The measurement of its off-shell couplings is therefore absolute and does not rely on the knowledge of the total Higgs boson width. The off-shell coupling constraints can then be used to indirectly constrain the width of the Higgs boson, under specific assumptions detailed in Section 11.5.3.3.

This measurement has been carried out in the $H \to ZZ \to 4\ell$, $H \to ZZ \to \ell\ell\nu\nu$ and $H \to WW \to \ell\nu\ell\nu$ channels. To enhance the sensitivity of the analysis, the knowledge of the full kinematics of the events is important. In particular the signal and the background can be further distinguished by the invariant mass of the VV system, which is more accurately accessible in the

Downloaded from https://academic.oup.com/ptep/article/2022/8/083C01/6651666 by KIT Library user on 27 September 2022

$H \to ZZ \to 4\ell$ channel. Angular distributions also play an important role in this analysis. For these reasons, the $H \to ZZ^{(*)} \to 4\ell$ channel is significantly more sensitive than $H \to WW^{(*)} \to \ell\nu\ell\nu$. The CMS results in Refs. [261] include the VBF and VH processes through the selection of two additional jets in the final state. The ATLAS results do not have a specific selection for the VBF or VH production processes, but their contributions are taken into account.

Limits on the off-shell rates have been reported for the two channels by ATLAS [262] and CMS [261] with Run 1 data. The combined results, assuming that the off-shell rates in the ZZ and WW channels scale equally, are given for two different hypotheses on the VBF production rate: fixing it to its SM value or scaling it as the gluon fusion rate. The observed (expected) limits on the off-shell rate fraction with respect to its SM expectation is 6.7 (9.1) for ATLAS [262] with the VBF rate fixed to its SM value and 2.4 (6.2) for CMS [261] where no assumption is made on the relative production rates of gluon-fusion and VBF. In both cases, the custodial symmetry is assumed and the ratio of the rates in the ZZ and WW decays are fixed to those of the SM. Results without this assumption have also been reported in Ref. [261].

Both ATLAS [263] and CMS [256] have performed off-shell Higgs boson analyses to constrain the off-shell Higgs boson production rates with partial Run 2 datasets, corresponding respectively to luminosities of $36.1\,\mathrm{fb}^{-1}$ and $80.2\,\mathrm{fb}^{-1}$. With the increase in centre-of-mass energy and luminosities, significantly better sensitivities are achieved. The ATLAS analysis is based on two decay channels, $H \to 4\ell$ and $H \to 2\ell 2\nu$, and the two main ggF and VBF production modes, while the CMS analysis is based on the $H \to 4\ell$ channel exclusively, but uses the exclusive VH categories. The results obtained have already reached an impressive sensitivity, with 95% CL upper limits on the off shell signal strength $\mu_{\mathrm{off-shell}}$ (the CMS Run 2 results are combined with the measurements made with Run 1 data):

$$\begin{aligned} &(\mathrm{ATLAS})\ \ \mu_{\mathrm{off-shell}} < 3.8\ (\mathrm{obs})\ \ [3.4\ (\mathrm{exp})], \\ &(\mathrm{CMS})\ \ \mu_{\mathrm{off-shell}} = 0.78^{+0.72}_{-0.53}(\mathrm{obs})\ \ [1.00^{+1.20}_{-0.99}\ (\mathrm{exp})]. \end{aligned} \tag{11.24}$$

11.5.3 *The Higgs boson width*

In the SM, the Higgs boson width is very precisely predicted once the Higgs boson mass is known. For a mass of 125 GeV, the Higgs boson has a very narrow width of 4.1 MeV [46]. It is dominated by the fermionic decays partial width at approximately 75%, while the vector boson modes are suppressed and contribute 25% only.

At the LHC or the Tevatron, in all production modes, only the cross sections times branching fractions can be measured. As a consequence, the total width of the Higgs boson cannot be inferred from measurements of Higgs boson rates. Direct constraints on the Higgs boson width are much larger than the expected width of the SM Higgs boson.

11.5.3.1 *Direct constraints*

Analyses of the reconstructed mass line-shape in the two channels with a good mass resolution, the $H \to \gamma\gamma$ and $H \to ZZ^{(*)} \to 4\ell$ channels, allow for a direct measurement of the width of the SM Higgs boson. The intrinsic mass resolution in these channels is about 1–2 GeV, much larger than the expected width of the SM Higgs boson. As a result, only upper limits on the Higgs boson width have been set by ATLAS [264] and CMS [265]. The two main challenges of direct constraints on the width through the measurement of the line-shape are: (i) the modelling of resolution uncertainties and (ii) the modelling of the interference between the signal and the continuum background which can be sizeable for large widths, in particular in the range where direct constraints are set. Given that these interference effects are small with respect to the individual channels sensitivity, they are neglected in deriving constraints on the total width. The combined constraints, however, being more precise, could be affected by the interference. ATLAS [264] has therefore not combined the constraints on the width from the two channels. The results are reported in Table 11.11. These constraints are still three orders of magnitude larger than the expected SM width and are fully compatible with the SM hypothesis.

Another direct constraint on the Higgs boson width can be obtained, in the $H \to ZZ^{(*)} \to 4\ell$ channel, from the measurement of the average lifetime of the Higgs boson calculated from the displacement of the four-lepton vertex from the beam spot. This analysis has been carried out by CMS (see references in Ref. [132]), using the measured decay length. The measured $c\tau_H$ is 2^{+25}_{-2} μm, yielding an observed (and expected) limit at the 95% CL of $c\tau_H < 57(56)\,\mu$m. From this upper limit on the lifetime of the Higgs boson, the 95% CL lower limit on its width is $\Gamma_H > 3.5 \times 10^{-12}$ GeV.

11.5.3.2 *Indirect constraints from mass shift in the diphoton channel*

In the diphoton channel, it was noticed in Ref. [266], that the effect of the interference between the main signal $gg \to H \to \gamma\gamma$ and the continuum irreducible background $gg \to \gamma\gamma$, taking into account detector resolution effects, is responsible for a non negligible mass shift. The size of the mass shift depends on the total width of the Higgs boson and it was suggested that measuring this mass shift could provide a constraint on the width [266]. It was further noticed that the mass shift has a dependence also on the diphoton transverse momentum. The total width of the Higgs boson could therefore be constrained using the diphoton channel alone.

Further studies were performed by ATLAS to estimate the size of the expected mass shift [144]. The expected shift in mass in the diphoton channel is 35±9 MeV for the SM Higgs boson. Very preliminary studies of the sensitivity of this method to estimate the width of the Higgs boson in the High-Luminosity regime have been made by ATLAS [267] and yield an expected 95% CL upper limit on the total width of approximately 200 MeV from $3\,\mathrm{ab}^{-1}$ of 14 TeV data.

11.5.3.3 *Indirect constraints from on-shell rate in the diphoton channel*

In the diphoton channel, it was noticed in Ref. [268], that the interference between the main signal $gg \to H \to \gamma\gamma$ amplitude and the continuum irreducible background $gg \to \gamma\gamma$ amplitude generates non-negligible change in the on-shell cross sections, as a result of the existence of a relative phase between these amplitudes. The size of this on-shell interference effect depends on the total width of the Higgs boson and it was suggested that measuring this on-shell cross section precisely could provide a constraint on the Higgs total width. This interference effect yields around 2% reduction for the $gg \to H \to \gamma\gamma$ cross section measurement. The current evaluation of this interference effect is performed at NLO and has a $^{+50\%}_{-30\%}$ uncertainty, due to the fact that the large relative phase is driven by the two-loop $gg \to \gamma\gamma$ background amplitude [266, 268]. This on-shell interference effect has a dependence on the p_T of the diphoton system and the photon polar angle in the diphoton rest frame, which can be further exploited to improve the measurement to constrain the Higgs total width.

Taking the ratios of the on-shell cross section of Higgs boson to diphoton channel and the cross section of Higgs boson to four-leptons channel where the interference effect is negligible could put bound on the Higgs boson total width. This ratio is free from many dominant sources of systematic uncertainties for cross section measurements, i.e., PDF uncertainty and luminosity uncertainty, and can be further improved by the accumulation of the LHC data. From this cross section ratio measurement alone, a preliminary estimation of the current limit from this interference effect with current 30% precision puts an upper bound of 800 MeV on the Higgs boson total width and the limit improves to 60 MeV with $3\,\mathrm{ab}^{-1}$ of 14 TeV data [268, 269].

11.5.3.4 *Indirect constraints from off-shell couplings*

Using simultaneously on-shell and off-shell measurements in the VV channels, it was noticed [260, 270] that the total width of the Higgs boson could be constrained. This can be illustrated from the parametrisation of the signal strength measurements both on-shell ($\mu_{\mathrm{on-shell}}$) and off-shell ($\mu_{\mathrm{off-shell}}$) as a function of the couplings modifiers κ_g and κ_V parameterizing the main process $gg \to H \to VV$ (see Section 11.6.2 for the definition of these coupling modifiers). The on-shell and off-shell signal strengths can

Downloaded from https://academic.oup.com/ptep/article/2022/8/083C01/6651666 by KIT Library user on 27 September 2022

Table 11.11: Run 1 observed (expected) direct 95% CL constraints on the width of the 125 GeV resonance from fits to the $\gamma\gamma$ and ZZ mass spectra and to the 4ℓ vertex lifetime. *The CMS measurement from the 4ℓ mass line-shape was performed using Run 2 data.

Exp.	$M_{\gamma\gamma}$ mass spectrum	$M_{4\ell}$ spectrum	4ℓ vertex lifetime
ATLAS	$< 5.0\,(6.2)$ GeV	$< 2.6\,(6.2)$ GeV	—
CMS	$< 2.4\,(3.1)$ GeV	$< 1.1\,(1.6)$ GeV*	$> 3.5 \times 10^{-12}$ GeV

be written as:

$$\mu_{\text{on-shell}} = \frac{\kappa^2_{g,\,\text{on-shell}}\,\kappa^2_{V,\,\text{on-shell}}}{\Gamma_H/\Gamma_{\text{SM}}}, \qquad (11.25)$$
$$\mu_{\text{off-shell}} = \kappa^2_{g,\,\text{off-shell}}\,\kappa^2_{V,\,\text{off-shell}}.$$

A bound on the Higgs boson width can then be obtained from the measurements of the on-shell and off-shell signal strengths. This assumes that no new physics alters the Higgs boson couplings in the off-shell regime, i.e., that the running of its couplings is negligible in the off-shell regime [271,272]. Both ATLAS [262] and CMS [261] have used their off-shell production limits to constrain the width of the Higgs boson.

Both ATLAS and CMS analyses use the kinematic event characteristics to further gain in sensitivity to discriminate between the signal and background. The ATLAS analysis assumed that there are no anomalous couplings of the Higgs boson to vector bosons, and obtains 95% CL observed (expected) upper limit on the total width of $5.5\times\Gamma_{\text{SM}}$ ($8.0\times\Gamma_{\text{SM}}$) with the Run 1 dataset. In the CMS analysis, the observed (expected) limit on the total width is $6.2\times\Gamma_{\text{SM}}$ ($9.8\times\Gamma_{\text{SM}}$) for the ZZ channel only at Run 1.

In addition, in the CMS analysis, results are also derived allowing for anomalous couplings of the Higgs boson, therefore reducing the discriminating power of the kinematic variables used in the analysis but reducing the model dependence. The observed (expected) limit on the total width is $10.9\times\Gamma_{\text{SM}}$ ($17.4\times\Gamma_{\text{SM}}$).

CMS has also combined the ZZ and W^+W^- channels while keeping the gluon-fusion and VBF production processes separate. For the gluon fusion mode, the observed (expected) combined upper limit at the 95% CL on the total width of the Higgs boson is $2.4\times\Gamma_{\text{SM}}$ ($6.2\times\Gamma_{\text{SM}}$) [261], while for the VBF production mode the exclusion limits are $19.3\times\Gamma_{\text{SM}}$ ($34.4\times\Gamma_{\text{SM}}$) [261].

At Run 2, using the ATLAS [263] and CMS [256] analyses described in Section 11.5.2, the following bounds were obtained:

$$\text{(ATLAS)}\ \ \Gamma_H/\Gamma_H^{SM} < 3.5\ \ [3.7\ (\text{exp})], \qquad (11.26)$$
$$\text{(CMS)}\ \ \Gamma_H < 9.16\ \ [13.7\ (\text{exp})]\ \text{MeV}$$
$$\text{or}\ \ \Gamma_H = 3.2^{+2.8}_{-2.2}\ \ [4.1^{+5.0}_{-4.0}\ (\text{exp})]\ \text{MeV}. \qquad (11.27)$$

The CMS combination includes results obtained with run 1 data. CMS has also performed this analysis considering possible anomalous HZZ couplings as discussed in Section 11.5.1.4. Neither the results nor the sensitivities are significantly affected by allowing specific anomalous coupling parameters to float in the fits.

ATLAS and CMS have also performed a study of the prospects for measuring the Higgs boson width mainly in the four lepton channel. Projecting to a luminosity of $3\,\text{ab}^{-1}$, it was concluded that, within assumptions similar to the ones mentioned above and assuming the SM central value, the observed (expected) combined upper limit at the 95% CL on the total width of the Higgs boson would be $3.8\times\Gamma_{\text{SM}}$ ($3.4\times\Gamma_{\text{SM}}$), i.e., the width of the Higgs boson could be constrained with the following precision [111]:

$$\Gamma_H = 4.1^{+0.7}_{-0.8}\ \text{MeV}. \qquad (11.28)$$

11.6 Probing the coupling properties of the Higgs boson

As discussed in Section 11.2, within the SM, all the Higgs boson couplings are fixed unambiguously once all the particle masses are known. Any deviation in the measurement of the couplings of the Higgs boson could therefore signal BSM physics.

Measuring the Higgs boson couplings without relying on the SM assumption requires a general framework treating deviations from the SM coherently at the quantum level in order to provide theoretical predictions for relevant observables to be confronted with experimental data. An attempt in that direction has been formalised in the so-called κ-formalism [273], following earlier attempts [274] and initial phenomenological studies of the first hints of the existence of the Higgs boson [275]. In this LO-inspired approach, the SM Higgs boson couplings are rescaled by arbitrary factors, κ's, keeping the same Lorentz structure of the interactions. This formalism allows for simple interpretation of the signal strengths measured in the various Higgs channels. It has been utilised to test various physics scenarios, like the existence of additional new particles contributing to the radiative Higgs boson production and decays, or to probe various symmetries of the SM itself, as for example the custodial symmetry. It only compares the experimental measurements to their best SM predictions and does not require any new BSM computations per se. And, from a more theoretical perspective, its relevance arises from the fact that it actually fully captures the leading effects in single Higgs processes of well motivated scenarios. Still, the κ-formalism has obvious limitations and certainly does not capture the most general deformations of the SM, even under the assumptions of heavy and decoupling new physics. A particularly acute shortcoming at the time Higgs physics is entering a precision era is the lack of proficiency to assert the richness of kinematical distributions beyond simple signal strength measurements. Several extensions and alternative approaches are being developed as part of the activities of the LHC Higgs Cross Section Working Group [47].

The Higgs Pseudo-Observable (HPO) approach [276] allows one to report the data in terms of a finite set of on-shell form factors parametrising amplitudes of physical processes subject to constraints from Lorentz invariance and other general requirements like analyticity, unitarity, and crossing symmetry. These form factors are expanded in powers of kinematical invariants of the process around the known poles of SM particles, assuming that poles from BSM particles are absent in the relevant energy regime. A set of HPOs have been proposed to characterise both the Higgs boson decays and the EW Higgs boson production channels, thus exploring different kinematical regimes. Prospective studies concluded that these HPOs can be measured/bounded at the percent level at the HL-LHC and could therefore be used to constrain some explicit models of new physics.

Another systematic approach to characterise the possible Higgs boson coupling deviations induced by BSM physics is the use of Effective Field Theories (EFT) [277,278]. This approach assumes again that the new physics degrees of freedom are sufficiently heavy to be integrated out, and they give rise to effective interactions among the light SM particles. By construction, the effective Lagrangians cannot account for deviations in Higgs physics induced by light degrees of freedom, unless they are added themselves as extra fields in the effective Lagrangians. In Section 11.7, several examples of models with light degrees of freedom affecting Higgs boson production and decay rates will be presented. The main advantage of EFTs is their prowess to relate different observables in different sectors and at different energies to constrain a finite set of effective interactions among the SM degrees of freedom. In an EFT, the SM Lagrangian is extended by a set of higher-dimensional operators, and it reproduces the low-energy limit of a more fundamental UV description. It will be assumed that the Higgs boson is part of a CP-even EW doublet, Φ, and that the Lagrangian is an analytic function of the gauge invariant $\Phi^\dagger\Phi$. This scenario is commonly refereed as SMEFT. Even though it is not fully established experimentally, this set-up is motivated by the measurements of the Higgs couplings to the different SM particles that show an alignement with their masses, such an alignment naturally follows under this assumption of a linear realisation of the $\text{SU}(2)_L \times \text{U}(1)_Y$ symmetry of the SM but would require an ad hoc tuning otherwise. General Lagrangians bypass-

Downloaded from https://academic.oup.com/ptep/article/2022/8/083C01/6651666 by KIT Library user on 27 September 2022

ing this linear assumption have been explicitly written down, see for instance Ref. [279]. They rely on a chiral expansion with a specific power-counting, effectively resumming the expansion in powers of the Higgs field, usually referred as HEFT as opposed to SMEFT.

11.6.1 *Effective Lagrangian framework*

The SMEFT has the same field content and it respects the same linearly-realised $\mathrm{SU}(3)_C \times \mathrm{SU}(2)_L \times \mathrm{U}(1)_Y$ local symmetry as the SM. The difference is the presence of operators with canonical mass-dimension d larger than 4. These are organised in a systematic expansion in d, where each consecutive term is suppressed by a larger power of a high mass scale. Assuming baryon and lepton number conservation, the most general Lagrangian takes the form

$$\mathcal{L}_{\mathrm{eff}} = \mathcal{L}_{\mathrm{SM}} + \sum_i c_i^{(6)} \mathcal{O}_i^{(6)} + \sum_j c_j^{(8)} \mathcal{O}_j^{(8)} + \cdots . \tag{11.29}$$

The contribution of the higher order operators of dimension d to physical amplitudes is suppressed by $(E/\Lambda)^{d-4}$, where E is the relevant energy scale of the process and Λ is the energy scale suppressing the higher-dimensional operators. The Wilson coefficients $c_i^{(d)}$ encode the virtual effects of the heavy new physics in low-energy observables. Their precise forms in terms of masses and couplings of the new particles can be obtained via matching with the ultraviolet (UV) completion of the SM, see, e.g., Ref. [280], or inferred using specific power-counting rules [277, 281].

The list of dimension-6 operators was first classified in a systematic way in Ref. [282] after the works of Ref. [283]. Subsequent analyses pointed out the presence of redundant operators, and a minimal and complete list of operators was finally provided in Ref. [284][4]. For a single family of fermions, there are 76 real ways to deform the SM generated by 59 independent operators. With the 3 families of fermions of the SM, flavour indices can be added to these 59 operators, and furthermore, new operator structures, that have been dismissed by means of Fierz transformations in the single family case, have to be considered, for a total of 2499 real deformations [287]. When considering Higgs data, one can reasonably focus on a relatively small subset of the 2499 operators of dimension 6. In particular the vast subset of 4-fermion operators, whether flavour and CP preserving or not, can be more strongly constrained by other processes. Thus, it makes sense to neglect this whole class, with the exception of one particular four-fermion interaction that contributes to the muon decay and thus directly affects the Fermi constant. The dipole operators, instead do directly affect Higgs boson production, however, under very general and plausible assumptions on the flavour structure of new physics, the coefficients of these operators display the same structure and the same chiral suppression of the Yukawa couplings. The consequence is that, with the possible exception of processes involving the top quark, their effect in Higgs boson production is expected to be negligible. Furthermore, as far as Higgs boson decays are concerned, the dipole operators only contribute to three (or more)-body final states (for instance $H \to \bar{b}b\gamma$) and as such they can easily be neglected too. Eliminating these two classes, there remain three other classes: 1) purely bosonic operators, 2) generalised Yukawas, 3) Higgs-fermion current operators. Operators in class 2 and 3, per se, can still contain CP- or flavour-violating terms, on which experimental constraints are rather strong. Under the assumption of flavour universality (respectively diagonality), one is left with 12 (14) parameters affecting EW precision measurements, diboson processes and single- and double-Higgs data and 7 (17) other parameters modifying the EW gauge boson couplings to fermions, see Ref. [46] for further technical details. Working in the unitary gauge and performing suitable redefinition of fields and input parameters the effective Lagrangian can be conveniently expressed in the parameterisation of Ref. [288], the so-called *Higgs basis* that conveniently single out these special less constrained parameters. Such a classification reflects the current experimental situation and the hierarchy in the sensitivity of the experimental measurements in the various sectors of the SM. As the sensitivity of the measurements in the Higgs sector improves, another and more general parametrisation of the SM deformation will have to be retained, in particular a parametrisation more suited for a treatment at the quantum level. In other bases of operators, in particular the so-called Warsaw basis [284] used in some experimental EFT analyses [137, 289, 290], one finds strong correlations among the operators affecting the EW gauge couplings to fermions, leaving 12 (14) linear combinations of operators with weaker constraints.

Section 11.6.2 illustrates how the Higgs data accumulated at the LHC can (partially) constrain the SM deformations, i.e., the dimension-6 operators of the SEMFT Lagrangian. Automatic tools are being developed to analyse the experimental data within an EFT framework, see the report [291] and references therein.

11.6.2 *Probing coupling properties*

As described in Section 11.3, a framework was developed by ATLAS and CMS [151], individually and together, to combine the very large number of exclusive categories aimed at reconstructing the five main decay modes and the five main production modes of the Higgs boson. The general conclusion of this combination, illustrating the compatibility of the observation with the SM expectations, is given in Section 11.3. The same framework with its master formula, Eq. (11.16), can be used to further measure coupling properties of the Higgs boson under specific additional assumptions.

11.6.2.1 *Combined measurements of the Higgs boson coupling properties*

i. *From effective Lagrangians to Higgs observables*

The κ framework, described in detail in Ref. [45, 273], facilitates the characterisation of Higgs coupling properties in terms of a series of Higgs coupling strength modifier parameters κ_i, which are defined as the ratios of the couplings of the Higgs bosons to particles i to their corresponding SM values. The κ framework assumes a single narrow resonance so that the zero-width approximation can be used to decompose the cross section as a product of two factors characterising the production and the decay of the Higgs boson. The κ parameters are introduced by expressing each of the these factors as their SM expectation multiplied by the square of a coupling strength modifier for the corresponding process at leading order:

$$\begin{aligned}(\sigma \cdot \mathrm{BR})(i \to \mathrm{H} \to f) &= \frac{\sigma_i^{SM}\kappa_i^2 \cdot \Gamma_f^{SM}\kappa_f^2}{\Gamma_H^{SM}\kappa_H^2} \quad \to \\ \to \quad \mu_i^f &\equiv \frac{\sigma \cdot \mathrm{BR}}{\sigma_{\mathrm{SM}} \cdot \mathrm{BR}_{\mathrm{SM}}} = \frac{\kappa_i^2 \cdot \kappa_f^2}{\kappa_H^2},\end{aligned} \tag{11.30}$$

where μ_i^f is the rate relative to the SM expectation and κ_H^2 is an expression that adjusts the SM Higgs width to take into account the modifications induced by the deformed Higgs boson couplings. When all κ_i are set to 1, the SM is reproduced. For loop-induced processes, e.g. $H \to \gamma\gamma$, there is a choice of either resolving the coupling strength modification in its SM expectation, i.e., $\kappa_\gamma(\kappa_t, \kappa_W)$ or keeping κ_γ as an effective coupling strength parameter.

The κ-framework is the simplest parametrisation directly related to experimental measurements of the Higgs boson production and decay modes. For this reason, it has been widely used by the community. It can also be connected to the SMEFT formalism as follows. Restricting to the EFT directions not probed outside Higgs physics [292], the Higgs boson couplings are written

[4] Complete enumerations of d=8 operators have been obtained [285] and some preliminary constraints on peculiar subsets of these operators have been derived from experimental measurements [286]. Still, in this review, the EFT Lagrangians will be truncated at the level of dimension-6 operators.

Downloaded from https://academic.oup.com/ptep/article/2022/8/083C01/6651666 by KIT Library user on 27 September 2022

in the unitary gauge as:

$$\begin{aligned}\mathcal{L} &= \kappa_Z \frac{m_Z^2}{v} Z_\mu Z^\mu H + \kappa_W \frac{2m_W^2}{v} W_\mu^+ W^{-\mu} H \\ &+ \kappa_{VV} \frac{\alpha}{2\pi v} \left(\cos^2\theta_W Z_{\mu\nu} Z^{\mu\nu} + 2\, W_{\mu\nu}^+ W^{-\mu\nu}\right) H \\ &+ \kappa_g \frac{\alpha_s}{12\pi v} G_{\mu\nu}^a G^{a\mu\nu} H + \kappa_\gamma \frac{\alpha}{2\pi v} A_{\mu\nu} A^{\mu\nu} H + \kappa_{Z\gamma} \frac{\alpha}{\pi v} A_{\mu\nu} Z^{\mu\nu} H \\ &- \sum_f \kappa_f \frac{m_f}{v} f\bar{f} H + \kappa_3 \frac{m_H^2}{2v} H^3 + \ldots .\end{aligned} \tag{11.31}$$

The exact correspondence between the effective coefficients of the dimension-6 operators and the κ's can be found for instance in Ref. [46]. In the SM, the Higgs boson does not couple to massless gauge bosons at tree level, hence $\kappa_g = \kappa_\gamma = \kappa_{Z\gamma} = 0$. Nonetheless, the contact operators are generated radiatively by SM particles loops. In particular, the top quark gives a contribution to the 3 coefficients $\kappa_g, \kappa_\gamma, \kappa_{Z\gamma}$ that does not decouple in the infinite top mass limit. For instance, in that limit $\kappa_\gamma = \kappa_g = 1$ [25, 26, 293].

The coefficient for the contact interactions of the Higgs boson to the W and Z field strengths is not independent but obeys the relation

$$(1 - \cos^4\theta_W)\kappa_{VV} = \sin 2\theta_W \kappa_{Z\gamma} + \sin^2\theta_W \kappa_{\gamma\gamma}. \tag{11.32}$$

This relation is a general consequence of the custodial symmetry [294], which also imposes $\kappa_Z = \kappa_W$ at leading order ($\kappa_Z/\kappa_W - 1$ is a measure of custodial symmetry breaking and, as such, is already constrained by electroweak precision data and the bounds on anomalous gauge couplings). When the Higgs boson is part of a $\mathrm{SU}(2)_L$ doublet, the custodial symmetry in the bosonic sector could only be broken by the $\mathcal{O}_T = \frac{1}{2}\left(\Phi^\dagger \overleftrightarrow{D}^\mu \Phi\right)^2$ operator at the level of dimension-6 operators and it is accidentally realised among the interactions with four derivatives, like the contact interactions considered.

The coefficient κ_3 can be accessed directly only through double Higgs boson production processes, hence it will remain largely unconstrained at the LHC. Before the associated production of a Higgs boson with a pair of top quarks was observed, the Higgs boson coupling to the top quark was only probed indirectly via the one-loop gluon fusion production or the radiative decay into two photons. However, these two processes are only sensitive to the combinations of couplings $(\kappa_t + \kappa_g)$ and $(\kappa_t + \kappa_\gamma)$ and not to the individual couplings. Therefore a deviation in the Higgs boson coupling to the top quark can in principle always be masked by new contact interactions to photons and gluons (and this is precisely what is happening in minimal incarnations of composite Higgs models [295]). The current and still limited sensitivity, of the order of 20%, in the $t\bar{t}H$ channel leaves elongated ellipses in the direction $\kappa_g = \kappa_\gamma = 1 - \kappa_t$.

The operators already bounded by EW precision data and the limits on anomalous gauge couplings modify in general the Lorentz structure of the Higgs couplings and hence induce some modifications of the kinematical differential distributions [296]. A promising way to have a direct access to the effective coefficients of these operators in Higgs physics is to study the VH associated production with a W or a Z at large invariant mass of the VH system [297]. These differential distributions could also be a way to test the hypothesis that the Higgs boson belongs to a $\mathrm{SU}(2)_L$ doublet together with the longitudinal components of the massive electroweak gauge bosons.

ii. *Interpretations of the experimental data*

The measurements of the coupling properties of the Higgs boson are entirely based on the formalism of the effective Lagrangian described above. Measurements of coupling properties in this framework implies assessing the parameters of the model Eq. (11.31) or combinations of these parameters with different sets of assumptions.

These measurements are carried out with the combination framework described in Section 11.4, where the μ_i and μ_f signal strength parameters are further interpreted in terms of modifiers of the SM couplings κ_k where $k \in \{Z, W, f, g, \gamma, Z\gamma\}$ as in Eq. (11.31). The number of signal events per category for the various production modes are typically estimated at higher orders in the analyses but are scaled by these single LO-inspired factors, thus not taking into account possible intricacies and correlations of these parameters through the higher-order corrections. This approximation is valid within the level of precision of current results and their compatibility with the SM expectation.

In this formalism, further assumptions are explicitly made: (i) the signals observed in the different search channels originate from a single narrow resonance with a mass of 125 GeV; (ii) similarly to the combination described in Section 11.4, the narrow width approximation is assumed (to allow the decomposition of signal yields into products of production and decay signal strengths); (iii) the tensor structure of the couplings is assumed to be the same as that of a SM Higgs boson. This means in particular that the observed state is assumed to be a CP-even scalar as in the SM.

Loop-level couplings such as the $gg \to H$, $H \to \gamma\gamma$ and $H \to Z\gamma$ can either be treated effectively, with κ_g, κ_γ and $\kappa_{Z\gamma}$ as free parameters in the fit or these parameters can be expressed in terms of the know SM field content and as a function of the SM coupling modifiers, in the following way [298]:

$$\begin{aligned}\kappa_g^2(\kappa_t, \kappa_b, \kappa_c) &= 1.042\,\kappa_t^2 - 0.040\,\kappa_t\kappa_b + 0.002\,\kappa_b^2 \\ &\quad - 0.005\kappa_t\kappa_c + 0.0005\kappa_b\kappa_c + 0.00002\kappa_c^2, \\ \kappa_\gamma^2(\kappa_F, \kappa_V) &= 1.59\,\kappa_V^2 - 0.66\,\kappa_V\kappa_F + 0.07\,\kappa_F^2, \\ \kappa_{Z\gamma}^2(\kappa_F, \kappa_V) &= 1.12\,\kappa_V^2 - 0.15\,\kappa_V\kappa_F + 0.03\,\kappa_F^2.\end{aligned} \tag{11.33}$$

The $\kappa_{Z\gamma}$ parametrisation has been used only in the ATLAS Run 1 combined measurements of the coupling properties of the Higgs boson. The $\mu^+\mu^-$ channels is not included in the CMS and ATLAS-CMS Run 1 combinations, while it is included in the ATLAS [241] and the CMS [242] Run 2 combinations.

The parametrisations are given for a Higgs boson mass hypothesis of 125.09 GeV (and in the last two expressions, all the Higgs-fermion couplings are assumed to be rescaled by an universal multiplicative factor κ_F). It can be noted from the expression of κ_γ that the coupling of the Higgs boson to photons is dominated by the loop of W bosons, and it is affected by the top quark loop mostly through its interference with the W loop. The sensitivity of the current measurements to the relative sign of the fermion and vector boson couplings to the Higgs boson is due to this large negative interference term. The κ_g parameter is expressed in terms of the scaling of production cross sections and therefore also depends on the pp collisions centre-of-mass energy. The parametrisations of κ_γ and $\kappa_{Z\gamma}$ are obtained from the scaling of partial widths and are only dependent on the Higgs boson mass hypothesis. Experiments use a more complete parametrisation with the contributions from the b-quarks, τ-leptons in the loops [45, 273].

The global fit is then performed expressing the μ_i and μ_f parameters in terms of a limited number of κ_k parameters or their ratios, under various assumptions. The parametrisation for the main production modes are: (i) $\mu_{\mathrm{ggF}} = \kappa_g^2$ for the gluon fusion and an effective coupling of the Higgs boson to the gluons; (ii) $\mu_{\mathrm{VBF},VH} = \kappa_V^2$ for the VBF and VH processes when the W and Z couplings are assumed to scale equally, and $\mu_{\mathrm{VBF}}^2(\kappa_W, \kappa_Z) = (\kappa_W^2\sigma_{WWH} + \kappa_Z^2\sigma_{ZZH})/(\sigma_{WWH} + \sigma_{ZZH})$, when the couplings to the W and Z bosons are varied independently (σ_{WWH} and σ_{ZZH} denote the VBF cross sections via the fusion of a W and a Z boson respectively, the small interference term is neglected); (iii) $\mu_{t\bar{t}H} = \kappa_t^2$ for the $t\bar{t}H$ production mode. Numerically the production modes signal strengths as a function of the coupling modifiers to the SM fields are:

$$\begin{aligned}\mu_{\mathrm{ggF}} &= 1.06\kappa_t^2 + 0.01\kappa_b^2 - 0.07\kappa_t\kappa_b, \quad \text{and} \\ \mu_{\mathrm{VBF}} &= 0.74\kappa_W^2 + 0.26\kappa_Z^2.\end{aligned} \tag{11.34}$$

The decay mode signal strengths are parametrised as $\mu_k = \kappa_k^2/\kappa_H^2$ where $k \in \{Z, W, f, g, \gamma, Z\gamma\}$ denotes the decay mode and κ_H,

Downloaded from https://academic.oup.com/ptep/article/2022/8/083C01/6651666 by KIT Library user on 27 September 2022

the overall modifier of the total width that affects all the signal yields. κ_H is a priori an independent parameter. However, when it is assumed that the Higgs boson cannot decay to new particles beyond those of the SM, κ_H can also be treated as an effective parameter and expressed in terms of the coupling modifiers to the SM field content. Its general expression is:

$$\kappa_H^2 = 0.57\kappa_b^2 + 0.06\kappa_\tau^2 + 0.03\kappa_c^2 + 0.22\kappa_W^2 + 0.03\kappa_Z^2 + 0.09\kappa_g^2 + 0.0023\kappa_\gamma^2. \tag{11.35}$$

The general expression of the total width of the Higgs boson can be written as follows:

$$\Gamma_H = \frac{\kappa_H^2 \Gamma_H^{\rm SM}}{1 - {\rm BR}_{\rm BSM}} \tag{11.36}$$

where $\Gamma_H^{\rm SM}$ is the total width of the SM Higgs boson and ${\rm BR}_{\rm BSM}$ is the branching fraction of the Higgs boson to new particles beyond the SM.

It is worth reminding that the inability to determine ${\rm BR}_{BSM}$ and Γ_H at the LHC requires some hypotheses in order to extract the Higgs couplings from the measured Higgs signal strengths. In particular, one can assume either (i) no BSM particles in the decay, or (ii) all invisible decays are detectable, or (iii) $|\kappa_V| \leq 1$. These scenarios will be examined below.

Specific parametrisations will be made in order to address the following aspects of the coupling properties of the Higgs boson under different assumptions: (i) the relative couplings of the Higgs boson to fermions and bosons; (ii) the potential impact of the presence of new particles beyond the SM either in the loops or both in the loops and the decay of the H; and (iii) also, more general models either of coupling modifiers or their ratios, under different assumptions.

iii. *Couplings to bosons and fermions*

As it will be discussed in Section 11.7.6.3, it is interesting to probe a model where no additional field content is considered in the decay width of the Higgs boson and where the relative couplings of the Higgs boson to W- and Z-bosons is fixed to its SM value, i.e., $\kappa_W = \kappa_Z$, and where all Yukawa couplings scale with one coupling modifier. In this model, only the SM particles are assumed to contribute to the gluon fusion and the diphoton loops, and all fermion couplings modifiers are required to scale simultaneously with a unique factor κ_F while all vector boson couplings modifiers also scale with a common factor κ_V. It is a two-parameter fit with κ_V and κ_F as free variables of interest. The ATLAS-CMS combined results for each channel independently, the combinations of all channels for the two experiments separately and the results of the overall combination are all shown in Fig. 11.12.

The global fit is only sensitive to the relative sign of κ_V and κ_F. By convention, either κ_F or κ_V can be considered positive and negative values of κ_V or κ_F respectively can be considered. Such values are not excluded a priori, but would imply the existence of new physics at a light scale and would also raise questions about the validity of the perturbative treatment of the SM deformations and also about the stability of the vacuum [300]. Among the five main Higgs boson decay channels, only the $\gamma\gamma$ is sensitive to the sign of κ_F (or κ_V) through the interference of the W and t loops as shown in Eq. (11.33). The current global fit disfavours a negative value of κ_F at more than five standard deviations. A specific analysis for the Higgs boson production in association with a single top quark has been proposed in order to more directly probe the sign of κ_F (see references in Ref. [132]). All available experimental data show a fair agreement of the SM prediction of the couplings of the Higgs boson to fermions and gauge bosons. The results shown in Fig. 11.12 assume that $\kappa_F \geq 0$, however, in Ref. [151], a similar combination is done without this assumption. The observed exclusion is fully compatible with the SM expectation The ATLAS and CMS combined measurements with the Run 1 dataset lead to

$$\kappa_V = 1.03 \pm 0.03 \quad \text{and} \quad \kappa_F = 0.97 \pm 0.07, \tag{11.37}$$

and were already at an impressive 5% level of accuracy for the κ_V parameter. The ATLAS Run 2 combination yielded:

$$\kappa_V = 1.05 \pm 0.04 \quad \text{and} \quad \kappa_F = 1.05 \pm 0.09. \tag{11.38}$$

The ATLAS Run 2 results are also reported as likelihood contours shown in Fig. 11.12.

iv. *Probing new physics in the loops (and the decay)*

A more constrained model fully focussing on BSM scenarios with new heavy particles contributing to the loops and where all couplings to the SM particles are assumed to be the same as in the SM ($\kappa_W = \kappa_Z = \kappa_t = \kappa_b = \kappa_\tau = 1$) is also used to constrain the κ_g and κ_γ parameters only. In this model, it can be assumed that the new physics affecting the loops are either introducing new decay channels (i.e., ${\rm BR}_{\rm BSM}$ allowed to vary in the fit) or not (i.e., ${\rm BR}_{\rm BSM} = 0$). In the two cases, the results on the couplings through loops (to gluons and photons) do not change significantly. The constraints on ${\rm BR}_{\rm BSM}$ will be discussed in the next section, while here the focus will be on the effective couplings of the Higgs boson to gluons and photons. The contours of the combined likelihood in the $(\kappa_\gamma, \kappa_g)$ plane for the ATLAS and CMS experiments and their combination are shown in Fig. 11.13. The measured values of these parameters for the ATLAS and CMS Run 1 combination are:

$$\kappa_g = 0.78^{+0.13}_{-0.10} \quad \text{and} \quad \kappa_\gamma = 0.87^{+0.14}_{-0.09}. \tag{11.39}$$

At Run 2, the ATLAS combination yielded:

$$\kappa_g = 0.98 \pm 0.05 \quad \text{and} \quad \kappa_\gamma = 1.06 \pm 0.05. \tag{11.40}$$

In this model as well, all results are fully compatible with the SM expectations.

v. *Coupling measurements and probing BSM physics in loops and in the decay*

In the models described above, it was either assumed that no new BSM degree of freedom distorts neither the loop-induced Higgs boson couplings to gluons and photons nor the total Higgs boson width, or that all tree level couplings to SM particles are SM-like. These assumptions can be relaxed.

In order to probe simultaneously the Higgs boson couplings to massive and massless particles, only the assumption ${\rm BR}_{\rm BSM} = 0$ is kept. The couplings to photons and gluons are then parametrised by independent effective couplings, κ_g and κ_γ, and κ_Z, κ_W, κ_t, $|\kappa_\tau|$, and $|\kappa_b|$ are measured simultaneously. The absolute values of certain coupling modifiers only indicate the degeneracy of combined likelihood for the two signs. It can be noted that when the coupling to gluons is not considered effective, there is some sensitivity to the sign of κ_b through the interference between the top- and bottom-quark loops in the gluon fusion process. In this analysis, the constraint on the top quark Yukawa coupling comes from the $t\bar{t}H$ direct search channels only. The complete set of results from this model is given in Table 11.12 for the ATLAS-CMS combination using the full Run 1 dataset [299] and for the ATLAS [241] and CMS [301] individual combinations using partial Run 2 datasets. Figure 11.14 also displays the results of the individual ATLAS and CMS combinations. A negative relative sign is allowed for the κ_W and κ_Z parameters without loss of generality. This convention is used in the ATLAS and CMS Run 1 combination and in the CMS Run 2 combination. Neglecting the very small interference between the W and Z exchanges in the VBF production and when treating the photon and gluon couplings as effective, the sensitivity to the negative signs of the couplings of the Higgs boson to the W and the top quark and that of the Z to the gluon come respectively from the tH and the $ggHZ$ production processes. In the case of the ATLAS Run 2 combination, only a relative negative sign of the coupling of the Higgs boson to the top quark is allowed. The cases reported in Table 11.12 of negative values of the couplings correspond to *quasi*-degenerate cases and the choice of sign is therefore not significant. For instance, the negative value of κ_W obtained by CMS in its Run 2

Downloaded from https://academic.oup.com/ptep/article/2022/8/083C01/6651666 by KIT Library user on 27 September 2022

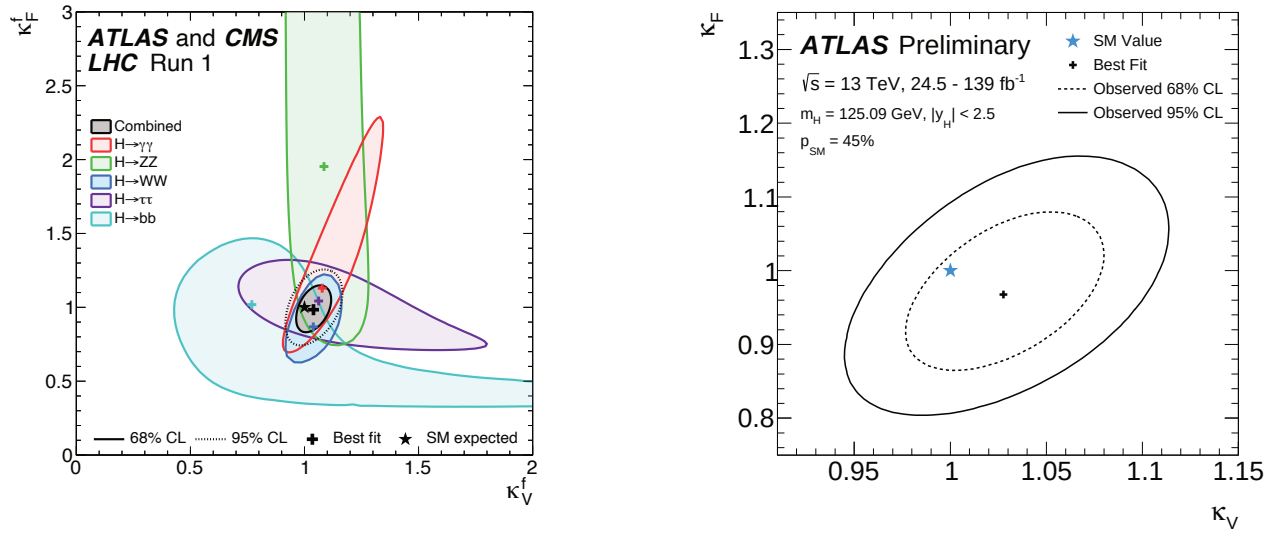

Figure 11.12: Likelihood contours in the (κ_F, κ_V) plane for the ATLAS-CMS Run 1 combination [299] (left) and ATLAS [241] (right) individual Run 2 combinations. These results correspond to a 2-parameter fit assuming a universal rescaling of the Higgs couplings to all fermions and also $\kappa_W = \kappa_Z$.

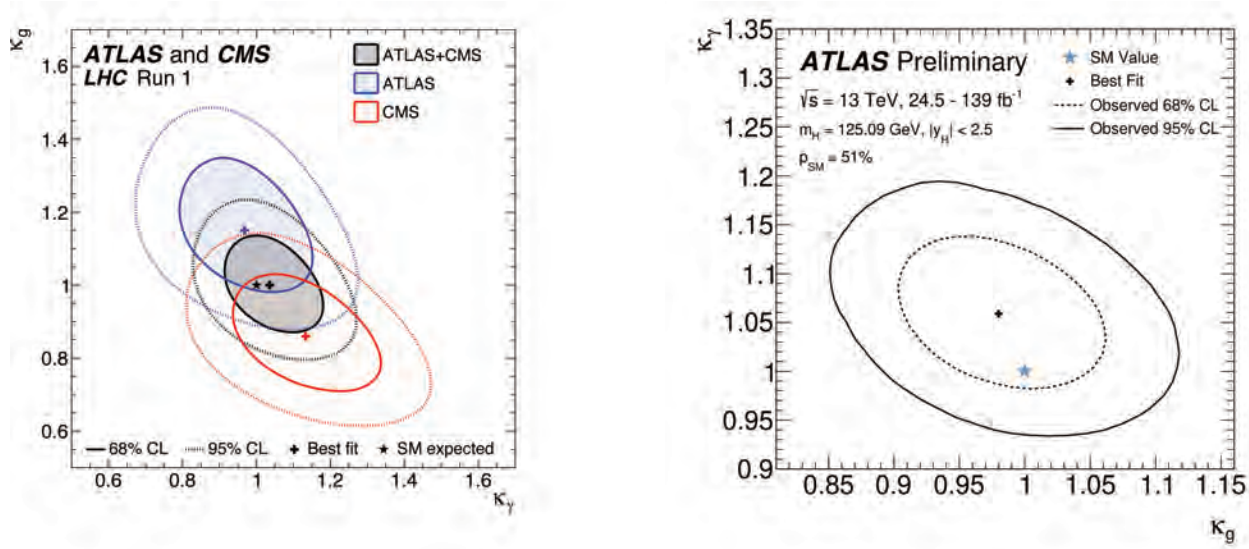

Figure 11.13: Likelihood contours in the $(\kappa_g, \kappa_\gamma)$ plane for the ATLAS-CMS [299] combination (left) and for the ATLAS [241] (right) under the assumption that undetected and invisible branching fractions vanish and that all the couplings to SM particles are those expected from the SM. This model probes new physics in the loops.

combination is due to tH contribution to the $t\bar{t}H$ channels as the specific tH analyses described in Section 11.3.3 are not included in the combination.

It is interesting to note that, with a partial Run 2 dataset, the sensitivity of individual experiments is already better than the one obtained at Run 1. This is in large part due to the improved systematic uncertainties related to the predictions of the Higgs boson production and decay that have been discussed in Section 11.2.

The results above are obtained under the assumption that the Higgs boson decays only to SM particles. This assumption is necessary since the signal rates cannot resolve separately κ_H and the absolute couplings of the Higgs boson to the SM particles. This degeneracy can, however, be resolved using an independent constraint on the Higgs boson width as the one derived from off-shell couplings measurements. This approach was used by the ATLAS experiment (see references in Ref. [132]), thus yielding a priori an absolute measurement of the couplings of the Higgs boson. The validity of the results obtained still relies on assumptions that have been discussed in Section 11.5.2. Another well-motivated assumption to resolve the aforementioned degeneracy preventing the determination of κ_H is inspired by unitarity conditions. Requiring that $\kappa_V \leq 1$ allows to free the $\mathrm{BR}_{\mathrm{BSM}}$ parameter and further probe new physics in the decay of the Higgs boson. An intuitive understanding of how this constraint works can be given by a simple example. In the VBF $H \to W^+W^-$ channel, the number of signal events compared to the SM prediction is rescaled by $(1 - \mathrm{BR}_{\mathrm{BSM}})\kappa_W^4/\kappa_H^2$, and, an observed signal close to the SM expectation cannot accommodate a large value of $\mathrm{BR}_{\mathrm{BSM}}$ since the depletion factor $(1 - \mathrm{BR}_{\mathrm{BSM}})$ cannot be compensated by an enhanced value $\kappa_W > 1$. Or, in other terms, if $\kappa_W \sim 1$ is preferred from other channels, a low signal in the VBF $H \to W^+W^-$ channel would be a sign of the presence of BSM physics in the Higgs boson decays. Within this framework, all the Higgs boson couplings to massive and massless SM particles can be measured in addition to $\mathrm{BR}_{\mathrm{BSM}}$. The results of this combination are shown in Fig. 11.14 (left). The results for all parameters do not change significantly with respect to the previous fit that assumed $\mathrm{BR}_{\mathrm{BSM}} = 0$. But a 95% CL bound on this parameter

Downloaded from https://academic.oup.com/ptep/article/2022/8/083C01/6651666 by KIT Library user on 27 September 2022

Table 11.12: Coupling modifier combined measurements assuming the absence of perceptible new physics in the decay of the Higgs boson. No assumption is made for the loop level couplings of the Higgs boson to gluons and photons which are considered as effective. The last column gives the expected precision at the HL-LHC [111].

	LHC Run 1	ATLAS Run 2	CMS Run 2	HL-LHC (expected)
κ_γ	$0.87^{+0.14}_{-0.09}$	$1.06^{+0.08}_{-0.07}$	$1.01^{+0.07}_{-0.07}{}^{+0.06}_{-0.12}$	1.8%
κ_W	$0.87^{+0.13}_{-0.09}$	1.06 ± 0.07	$-1.11^{+0.13}_{-0.07}{}^{+0.05}_{-0.06}$	1.7%
κ_Z	-0.98 ± 0.10	1.02 ± 0.06	$0.96^{+0.06}_{-0.06}{}^{+0.04}_{-0.05}$	1.5%
κ_g	$0.78^{+0.13}_{-0.10}$	$0.96^{+0.09}_{-0.08}$	$1.16^{+0.08}_{-0.08}{}^{+0.08}_{-0.08}$	2.5%
κ_t	$1.40^{+0.24}_{-0.21}$	1.00 ± 0.12	$1.01^{+0.06}_{-0.06}{}^{+0.09}_{-0.08}$	3.4%
κ_b	$0.49^{+0.27}_{-0.15}$	$0.98^{+0.14}_{-0.13}$	$1.18^{+0.14}_{-0.13}{}^{+0.13}_{-0.24}$	3.7%
κ_τ	$0.84^{+0.15}_{-0.11}$	$1.05^{+0.15}_{-0.14}$	$0.94^{+0.08}_{-0.11}{}^{+0.09}_{-0.06}$	1.9%

can now be obtained:

$$\mathrm{BR_{BSM}} < 34\% \ \text{(ATLAS)}, \quad \mathrm{BR_{BSM}} < 38\% \ \text{(CMS)}. \tag{11.41}$$

Both ATLAS and CMS in their Run 2 combinations have included the search for invisible decays of the Higgs boson [301,302], described in Section 11.3. This allows for a coherent interpretation of the constraints on invisible decays and the measurements in the visible channels as well as simultaneously constraining $\mathrm{BR_{inv}}$ and the overall branching fraction to potentially "visible" particles but to which none of the considered measurements are sensitive, as for example Higgs boson decays to light quarks or BSM particles decaying subsequently mainly to light quarks ($\mathrm{BR_{und}}$ referred to as branching fraction to undetected particles). The limits obtained on the invisible branching fractions are:

$$\mathrm{BR_{inv}} < 30\% \ \text{(ATLAS)}, \quad \mathrm{BR_{inv}} < 22\% \ \text{(CMS)}. \tag{11.42}$$

Models which are less sensitive to modelling systematic uncertainties and requiring no constraints on the natural width of the Higgs bosons have been considered, either through the ratio of cross section and branching ratios (see results in Ref. [132]) or through a more generic approach to avoid the degeneracy in the measurement of the coupling modifiers, probing the coupling properties of the Higgs boson through ratio of couplings. In the latter model, the cross section times branching fraction of the $gg \to H \to ZZ$ process is parametrised as a function of a single coupling modifier:

$$\kappa_{gZ} = \kappa_g \times \frac{\kappa_Z}{\kappa_H} \tag{11.43}$$

Then all combination signals can be parametrised with the following ratios of coupling modifiers: (i) the $\lambda_{Zg} = \kappa_Z/\kappa_g$ ratio which is mainly probed by the measurements of the VBF and ZH production; (ii) the $\lambda_{tg} = \kappa_t/\kappa_g$ ratio constrained by the $t\bar{t}H$ production process; (iii) the $\lambda_{WZ} = \kappa_W/\kappa_Z$ ratio mainly probed by the WW and ZZ decay modes; (iv) the $\lambda_{\tau Z} = \kappa_\tau/\kappa_Z$ ratio constrained by the $\tau^+\tau^-$ channel; (v) the $\lambda_{bZ} = \kappa_b/\kappa_Z$ ratio probed mainly by the $VH(b\bar{b})$ channels; and (vi) the $\lambda_{\gamma Z} = \kappa_\gamma/\kappa_Z$ ratio constrained by the diphoton channel. In this parametrisation, the ZZ channel plays an important normalisation role (the results are discussed in detail in the previous edition of this review [132]).

11.6.2.2 *Differential cross sections*

To further characterise the production and decay properties of the Higgs boson, with the increase in size of the LHC datasets, measurements of fiducial and differential cross sections are being carried out by ATLAS and CMS both at Run 1 (the references can be found in the previous edition of this review [132]) and Run 2 [289,303] and in several channels: (i) the diphoton, (ii) the four leptons, and (iii) the WW channels.

The definition of a fiducial volume as close as possible to the reconstruction level selection criteria is very important as it will minimise the model dependence from possible variations in the signal reconstruction efficiencies. Minimising model dependence of unfolded fiducial differential cross section measurements is also key to ensure their usefulness to further probe and tune more accurate models in the future.

As an example in the diphoton channel for the ATLAS Run 1 analysis (similar criteria are used at Run 2 and by CMS), the selection criteria defining the fiducial volume are the following: the two highest transverse momentum (E_T), isolated final state photons, within $|\eta| < 2.37$ and with $105\,\mathrm{GeV} < M_{\gamma\gamma} < 160\,\mathrm{GeV}$ are selected (the transition region between the barrel and end-cap calorimeters is not removed); after the pair is selected, the same cut on $E_T/M_{\gamma\gamma}$ as in the event selection, i.e., in excess of 0.35 (0.25) for the two photons is applied. The requirement of the isolation of the photon to define the fiducial volume is particularly important to avoid potentially large variations of the reconstruction efficiency within this volume for production processes as different as the gluon fusion and $t\bar{t}H$.

While strict fiducial requirements are key to minimise model dependence, these make combinations of decay channels impossible. To gain precision in the measurement of the production properties of the Higgs boson, the fiducial volume defined on the decay products of the Higgs boson can be removed and channels can be combined relying on the extrapolation from the reconstruction acceptance using Monte Carlo simulations. This has been used to combine differential cross section for instance in the transverse momentum of the Higgs boson. Such hybrid approaches are also discussed in Section 11.6.2.4.

A large number of observables have been studied aiming at probing the accuracy of the modelling of the Higgs boson production simulations. Some examples include (i) the transverse momentum and pseudo rapidity of the objects, such as jets or leptons, produced in association with the Higgs boson in several modes, the principal distributions of the Higgs boson decay products such for instance in the diphoton channel; (ii) the production angle in the Collins–Soper frame [253] in the diphoton channel; (iii) the overall distribution of the Higgs boson transverse momentum.

The measured differential cross section in the Higgs boson transverse momentum by ATLAS and CMS using the full Run 2 datasets are illustrated in Fig. 11.15.

11.6.2.3 *Constraints on non-SM Higgs boson interactions in an effective Lagrangian*

An example of the possible use of differential cross sections in constraining non-SM Higgs boson couplings in an EFT is given by ATLAS [305]. In this analysis, differential cross section measured in the diphoton channel are used to constrain an effective Lagrangian where the SM is supplemented by dimension six CP-even operators of the Strongly Interacting Light Higgs (SILH) formulation [277] and corresponding CP-odd operators. The diphoton differential cross sections are mainly sensitive to the operators that affect the Higgs boson interactions with gauge bosons. CMS has also recently analysed [289] the Higgs boson transverse momentum distribution to constrain the Higgs boson couplings to top, bottom, and charm quarks as well as the effective coupling

Downloaded from https://academic.oup.com/ptep/article/2022/8/083C01/6651666 by KIT Library user on 27 September 2022

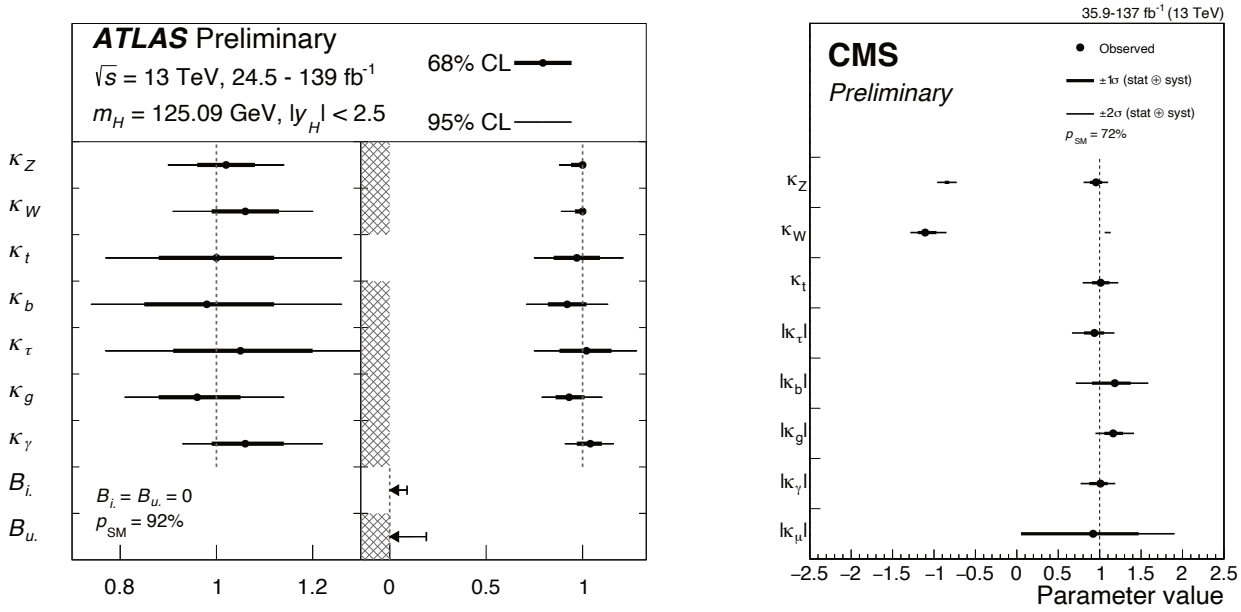

Figure 11.14: ATLAS [241] (left) and CMS [242] (right) combined measurements of coupling modifiers with various assumptions o the $\kappa_V < 1$ scenario, and in the case of the ATLAS measurements with the assumption $\mathrm{BR}_{\mathrm{BSM}} = 0$ and using the off-shell Higgs measurements.

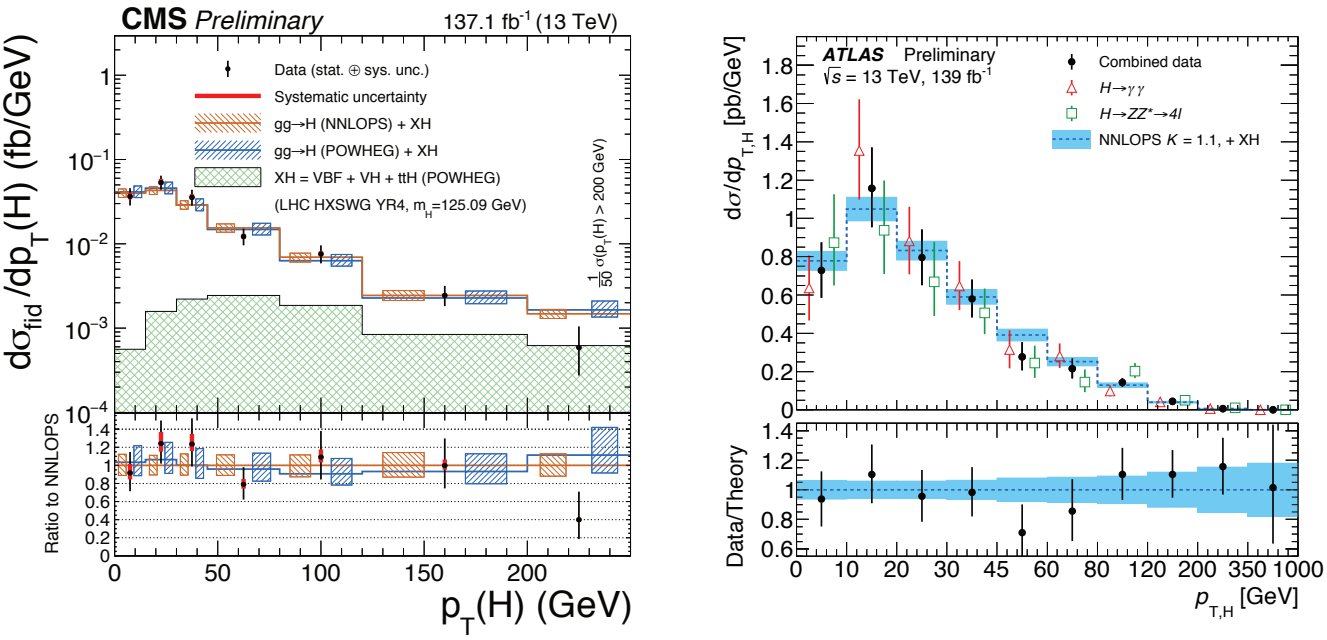

Figure 11.15: (Left) Fiducial differential, closely matching the reconstruction level selections, cross sections in Higgs boson transverse momentum in the $H \to 4\ell$ channel from the CMS experiment [304]. (Right) Partially fiducial combined cross sections using the $H \to \gamma\gamma$ and $H \to 4\ell$ channels from the ATLAS experiment [303].

to gluons. This analysis is, however, not performed in an EFT framework.

The differential distributions used in this combination are: (i) the transverse momentum of the Higgs boson, (ii) the number of reconstructed jets produced in association with the diphoton pair, (iii) the invariant mass of the diphoton system and (iv) the difference in azimuthal angle of the leading and sub-leading jets in events with two or more jets. This analysis shows how differential information significantly improves the sensitivity to dimension-6 operators.

11.6.2.4 *Simplified Template Cross Sections (STXS)*

An overarching subject of discussion between the theory and experimental communities in the field of Higgs physics has been how experimentalists could best communicate their results for them to be most efficiently used by others for further interpretation. In the field of precision SM measurements, the commonly used practise is that results are given at particle level within a well-defined fiducial volume of phase space. The fiducial volume is usually defined close enough to the experimental reconstruction to minimise the possible variations of the reconstruction efficiency within the particle level fiducial volume. In this way, results minimise their dependence on theoretical uncertainties.

Downloaded from https://academic.oup.com/ptep/article/2022/8/083C01/6651666 by KIT Library user on 27 September 2022

ATLAS and CMS have produced fiducial and unfolded cross sections based on all objects reconstructed in the events. These measurements could be used for further interpretation. However, performing a proper combination of channels taking into account all experimental systematic uncertainties is non trivial. A proposal [46, 306] was made by the LHC Higgs Working Group to produce results in each decay channel with a well defined fiducial phase space of the Higgs boson (and not its decay products) and for other associated objects pertaining to all channels, such as jets and missing transverse momentum (MET). The definition of the fiducial regions is motivated by maximising the experimental sensitivity, isolating possible BSM effects, and minimising the dependence on theoretical uncertainties. The number of regions is also minimised to avoid the loss of experimental sensitivity. The observables that are measured in this approach are still the standard production cross sections (the gluon fusion, the vector boson fusion, the VH and $t\bar{t}H$ associated production modes) within the defined fiducial volumes.

In summary, this approach is hybrid. It is fiducial on specific objects to reduce the theory dependence and inclusive in the Higgs kinematics in order to allow for a more straightforward combination. This approach also allows the use of multivariate techniques to enhance the sensitivity within given fiducial regions, at the expense of a greater extrapolation and therefore increased model dependence.

The currently used Simplified Template Cross Sections (STXS) scheme covers, with a limited number of bins, the ggF process in four categories in number of jets (0, 1, 2 and 2 VBF-like jets, where VBF-like means a selection of two high invariant mass jets with large pseudo rapidity difference) further subdivided in four transverse momentum categories covering the full spectrum with the last bin being inclusive for $p_T > 200\,\text{GeV}$. The VH process is subdivided two categories depending on the number of reconstructed charged leptons corresponding to the decays of either a W boson or a Z boson, and two bins in transverse momentum. VBF and hadronic VH categories are defined using jet cuts and two bins in transverse momentum.

Measurements in this framework have been made in various decay channels. The first measurements have been performed in the main Higgs boson discovery channels. ATLAS has produced measurements of the diphoton and the 4ℓ channels with Run 2 data [255, 265, 307–309]. And full Run 2 results are available for the $H \to 4\ell$ channel from ATLAS [310] and CMS [311].

CMS has carried out a measurement of the STXS in the $H \to \tau^+\tau^-$ decay channel targeting the high transverse momentum of the Higgs boson [154], in particular in the channel where the Higgs boson is produced with one jet of transverse energy in excess of 200 GeV.

ATLAS [312] has made a measurement of the STXS aiming at the VH production mode in the $H \to b\bar{b}$ decay mode at high transverse momentum of the vector boson above 250 GeV, where the discrimination of the background further increases.

A combination of STXS across decay channels has also been carried out by ATLAS with the full Run 2 dataset [241, 313].

11.6.2.5 *Indirect constraints on the Higgs boson couplings*

The direct measurements at the LHC provide direct probes of the Higgs boson couplings to the vector bosons (photons, W, Z and gluons) and to a limited number of Yukawa couplings to fermions. Currently these include essentially the third generation fermions – tau leptons, bottom and top quarks. For the High-Luminosity run, prospective studies [111] have shown that a good precision will be reached in the measurement of the coupling of the Higgs boson to muons and an evidence of the Higgs boson trilinear self-coupling with a precision of the order of 50% can be achieved. For the couplings of the Higgs boson to the other light SM fermions, direct evidences will be hard to reach at the LHC. However, from the measurements of the main observed Higgs final states, it is possible to constrain specific couplings through their radiative corrections to dominant processes. Two prime examples are: (i) the trilinear self-coupling can be constrained through loop corrections to the single Higgs boson production [314–316], see the interpretation carried out by ATLAS of the combination of the main decay channels [317]; (ii) the charm Yukawa coupling can

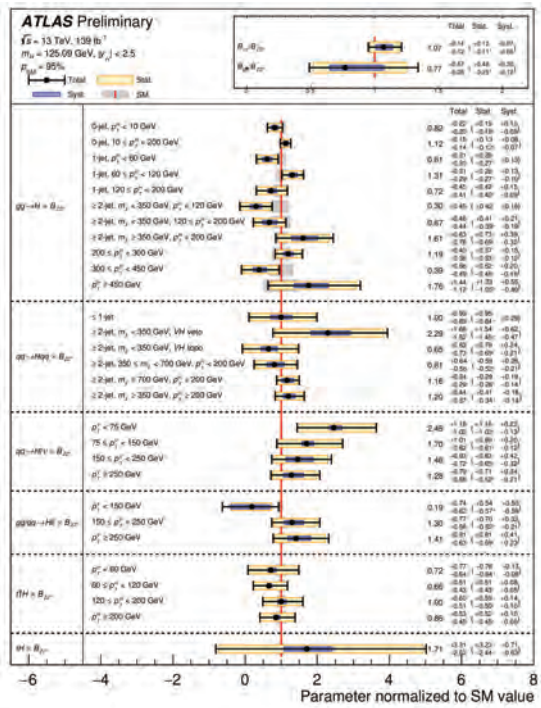

Figure 11.16: Simultaneous measurement of the simplified template cross sections times the branching fraction $\text{BR}(H \to ZZ)$ (normalised to their Standard Model expectations) and the ratios of branching fractions $\text{BR}(f)/\text{BR}(ZZ)$ [241].

be constrained from the differential cross section in Higgs boson transverse momentum [318], see the ATLAS [319] and CMS [289] analyses in the diphoton channel. These indirect constraints, however, require assumptions on the possible variations of all the other couplings.

ATLAS has also performed a preliminary combination of the single Higgs boson production measurements [320], using the approach and parametrisations of Ref. [315], which yield the following constraint:

$$-3.2 < \kappa_\lambda < 11.9. \tag{11.44}$$

When combined with results of the double Higgs boson production searches, the following combined constraint on the Higgs boson trilinear coupling yields:

$$-2.3 < \kappa_\lambda < 10.3\,(\text{obs}) \quad [-5.1 < \kappa_\lambda < 11.2.\,(\text{exp})]. \tag{11.45}$$

The *direct* and *indirect* constraints on the Higgs boson trilinear self-coupling are currently of similar strength. The double Higgs boson measurements are dominated by statistical uncertainties and are expected to improve much more rapidly than the precision on single Higgs boson measurements. Furthermore, it should be stressed that the constraints on the trilinear self-coupling obtained via the NLO fit of single Higgs boson data are less robust and more model-dependent since the NLO effects induced by a shift of the trilinear self-coupling compete with possible LO effects sourced by the deviations of the Higgs boson couplings to the other SM particles. The different effects can be disentangled by the measurements of various kinematical differential distributions in addition to the study of the inclusive rates [321], but the expected sensitivity in such global fits is not as promising as the one obtained when only the Higgs boson self-coupling is allowed to deviate from its SM value [112].

11.7 New physics models of EWSB in the light of the Higgs boson discovery

The discovery of a light scalar with couplings to gauge bosons and fermions that are consistent with SM predictions, together with the slow running of the Higgs boson self-coupling at high

Downloaded from https://academic.oup.com/ptep/article/2022/8/083C01/6651666 by KIT Library user on 27 September 2022

energies allow one to consider the SM as a valid perturbative description of nature all the way to the Planck scale. This picture is admittedly very attractive, but it posits that the Higgs boson is an elementary scalar field, whose mass has quantum sensitivity to possible new physics scales. This EW/Higgs naturalness problem [6] has become much more definite after the Higgs boson discovery.

There are two broad classes of models addressing the naturalness problem[5]. One is based on SUSY [7] (for recent reviews, see Refs. [8, 9]). This is a weakly coupled approach to EWSB, maintaining the perturbativity of the SM, and, the Higgs boson remains elementary and the corrections to its mass are screened at the scale at which SUSY is broken so the value of the weak scale remains insensitive to the details of the physics at higher scales. These theories predict at least three neutral Higgs particles and a pair of charged Higgs particles [27]. One of the neutral Higgs bosons, most often the lightest CP-even one, has properties that can resemble those of the SM Higgs boson (at least in some regions of the parameter space like the so-called decoupling limit). It is referred to as a SM-like Higgs boson, meaning that its couplings are close to the ones predicted in the SM, and one talk of the alignment limit. The other approach invokes the existence of strong interactions at a scale of the order of one TeV or above and these new interactions induce the breaking of the electroweak symmetry [323]. In the original incarnation, dubbed technicolor, the strong interactions themselves trigger EWSB without the need of a Higgs boson. Another possibility, more compatible with the ATLAS and CMS discovery, is that the strong interactions produce four light resonances identified with the Higgs doublet and EWSB proceeds through vacuum misalignment [10] (see Refs. [11, 12] for recent reviews). In that case, the Higgs boson itself has a finite size and thus never feels the UV degrees of freedom that would otherwise have dragged its mass to much higher scales. The Higgs boson could also correspond to the Goldstone boson associated with the spontaneous breaking of scale invariance, see Ref. [324] and references therein. However, this dilaton/radion scenario now requires a jumbled model-building to be consistent with the constraints from the coupling measurements. All these BSM scenarios can have important effects on the phenomenology of the Higgs boson. Also, in each case, the role of the Higgs boson in the unitarisation of scattering amplitudes is shared by other particles which remain targets of experimental searches.

The realisation of SUSY at low energies has many good qualities that render it attractive as a model of new physics. First of all since, for every SM degree of freedom, there is a superpartner of different spin but of equal mass and effective coupling to the SM-like Higgs boson, in the case of exact SUSY, an automatic cancellation of quantum corrections to the Higgs mass parameter holds. In practice, it is known that SUSY must be broken since no superpartners of the SM particles have been observed so far. The mass difference between the precise value of the mass of any particle and that of its corresponding superpartner is proportional to the correlated soft SUSY breaking parameter, generically called $M_{\rm SUSY}$. The quantum corrections to the Higgs boson mass parameter are proportional to $M^2_{\rm SUSY}$, and provided $M_{\rm SUSY}$ is of order of a few TeV, the low energy mass parameters of the Higgs sector become insensitive to physics at the GUT or Planck scale. Another interesting feature of SUSY theories is related to the dynamical generation of EWSB [325]. In the SM, a negative Higgs mass parameter, m^2, needs to be inserted by hand to induce EWSB, see Eq. (11.1). In SUSY, instead, even if the relevant Higgs mass parameter is positive in the ultraviolet, it may become negative and induce EWSB radiatively through the strong effect of the top quark-Higgs boson coupling in its renormalisation group evolution [325].

In the following, the Higgs sector will be explored in specific SUSY models. In all of them, it is often possible to find regions of the parameter space that accommodate one neutral Higgs boson with properties that resemble those of the SM Higgs boson, whereas additional neutral and charged Higgs bosons are also predicted and are intensively being sought for at the LHC (see Section 11.7.7). In the simplest SUSY model, accommodating a SM-like Higgs boson mass of about 125 GeV results in constraints on the stop sector, with at least one stop mass in the few TeV mass range. In non-minimal SUSY extensions of the SM (details and related references can be found in the previous edition of this review [132]), a SM-like Higgs boson with mass of 125 GeV can be accommodated with less restrictions on the stop sector. While naturalness dictates relatively light stops and - at the two loop level - also gluinos, the first and second generation of squarks and sleptons couple weakly to the Higgs sector and may be heavy. Moreover, small values of the μ parameter and therefore light Higgsinos, the fermionic superpartners of the Higgs bosons, would be a signature of a natural realization of electroweak symmetry breaking [326]. Such SUSY spectra, consisting of TeV range stop masses and light Higgsinos, continue to be under intense scrutiny by the experimental collaborations [327] in order to understand if such natural SUSY scenarios endure and can explain why the Higgs boson remains light.

In the context of weakly coupled models of EWSB, one can also consider multiple Higgs $\mathrm{SU}(2)_L$ doublets as well as additional Higgs singlets, triplets or even more complicated multiplet structures, with or without low energy SUSY. In general, for such models, one needs to take into account experimental constraints from precision measurements and flavour changing neutral currents. The LHC signatures of such extended Higgs sectors are largely shaped by the role of the exotic scalar fields in EWSB.

The idea that the Higgs boson itself could be a composite bound state emerging from a new strongly-coupled sector has been reconsidered thanks to the insights gained from the AdS/CFT duality. The composite Higgs boson idea is an incarnation of EWSB via strong dynamics that smoothly interpolates between the standard technicolor approach and the true SM limit. To avoid the usual conflict with EW data, it is sufficient, if not necessary, that a mass gap separates the Higgs resonance from the other resonances of the strong sector. Such a mass gap can naturally follow from dynamics if the strongly-interacting sector exhibits a global symmetry, G, broken dynamically to a subgroup H at the scale f, such that, in addition to the three Nambu–Goldstone bosons of SO(4)/SO(3) that describe the longitudinal components of the massive W and Z, the coset G/H contains a fourth Nambu–Goldstone boson that can be identified with the physical Higgs boson. Simple examples of such a coset are SU(3)/SU(2) or SO(5)/SO(4), the latter being favoured since it is invariant under the custodial symmetry. It is also possible to have non-minimal custodial cosets with extra Goldstone bosons leading to additional Higgs bosons in the spectrum, see for instance Ref. [328]. Modern incarnations of composite Higgs models have been recently investigated in the framework of 5D warped models where, according to the principles of the AdS/CFT correspondence, the holographic composite Higgs boson then originates from a component of a gauge field along the 5th dimension with appropriate boundary conditions.

A last crucial ingredient in the construction of viable composite Higgs boson models is the concept of partial compositeness [329], i.e., the idea that there are only linear mass mixings between elementary fields and composite states. After diagonalisation of the mass matrices, the SM particles, fermions and gauge bosons, are admixtures of elementary and composite states and thus they interact with the strong sector, and in particular with the Higgs boson, through their composite component. This setup has important consequences on the flavour properties, chiefly the suppression of large flavour changing neutral currents involving light fermions. It also plays an important role in dynamically generating a potential for the would-be Goldstone bosons. Partial compositeness also links the properties of the Higgs boson to the spectrum of the fermionic resonances, i.e., the partners of the top quark. As in the MSSM, these top partners are really the agents that trigger the EWSB and also generate the mass of the Higgs boson that otherwise would remain an exact Goldstone boson and hence massless. The bounds from the direct searches for the top partners, in addition to the usual constraints from EW precision data, force the minimal composite Higgs models into some unnatural corners of their parameter spaces [330].

[5] Another solution to the naturalness problem is to lower the fundamental scale of quantum gravity, like for instance in models with large extra-dimensions, see Ref. [322].

Downloaded from https://academic.oup.com/ptep/article/2022/8/083C01/6651666 by KIT Library user on 27 September 2022

11.7.1 *Higgs bosons in the minimal supersymmetric standard model (MSSM)*

The particle masses and interactions in a SUSY theory are uniquely defined as a function of the superpotential and the Kähler potential [9]. A fundamental theory of SUSY breaking, however, is unknown at this time. Nevertheless, one can parametrise the low-energy theory in terms of the most general set of soft SUSY-breaking operators [9]. The simplest realistic model of low-energy SUSY is the minimal SUSY extension of the SM (MSSM) [9, 331], that associates a SUSY partner to each gauge boson and chiral fermion of the SM, and provides a realistic model of physics at the weak scale. However, even in this minimal model with the most general set of soft SUSY-breaking terms, more than 100 new parameters are introduced. However, only a subset of these parameters impact the Higgs boson phenomenology either directly at tree-level or through quantum effects.

The MSSM contains the particle spectrum of a two-Higgs-doublet model (2HDM) extension of the SM and the corresponding SUSY partners. Two Higgs doublets, Φ_1 and Φ_2, with hypercharge $Y = -1$ and $Y = 1$, respectively, are required to ensure an anomaly-free SUSY extension of the SM and to generate mass for down-type quarks/charged leptons (Φ_1) and up-type quarks (Φ_2) [27]. The Higgs potential reads

$$\begin{aligned} V =& m_1^2 \Phi_1^\dagger \Phi_1 + m_2^2 \Phi_2^\dagger \Phi_2 - m_3^2 (\Phi_1^T i\sigma_2 \Phi_2 + \text{h.c.}) \\ &+ \frac{1}{2}\lambda_1 (\Phi_1^\dagger \Phi_1)^2 + \frac{1}{2}\lambda_2 (\Phi_2^\dagger \Phi_2)^2 + \lambda_3 (\Phi_1^\dagger \Phi_1)(\Phi_2^\dagger \Phi_2) \\ &+ \lambda_4 |\Phi_1^T i\sigma_2 \Phi_2|^2 + \frac{1}{2}\lambda_5 \left[(\Phi_1^T i\sigma_2 \Phi_2)^2 + \text{h.c.} \right] \\ &+ \left[[\lambda_6 (\Phi_1^\dagger \Phi_1) + \lambda_7 (\Phi_2^\dagger \Phi_2)] \Phi_1^T i\sigma_2 \Phi_2 + \text{h.c.} \right] , \end{aligned} \tag{11.46}$$

where $m_i^2 = \mu^2 + m_{H_i}^2$ $(i = 1, 2)$, with μ being the supersymmetric Higgsino mass parameter and m_{H_i} the soft supersymmetric breaking mass parameters of the two Higgs doublets; $m_3^2 \equiv B\mu$ is associated to the B-term soft SUSY breaking parameter; and λ_i, for $i = 1$ to 7, are all the Higgs quartic couplings.

After the spontaneous breaking of the electroweak symmetry, five physical Higgs particles are left in the MSSM spectrum: one charged Higgs pair, $H^\pm$, one CP-odd neutral scalar, A, and two CP-even neutral states, H and h, with h being the lightest.[6] The Higgs sector at tree level depends on the electroweak gauge coupling constants and the vacuum expectation value v – or equivalently the Z gauge boson mass – and is determined by only two free parameters: $\tan\beta$ - the ratio of the two Higgs doublets' vacuum expectation values v_2/v_1 - and one Higgs boson mass, conventionally chosen to be the CP-odd Higgs boson mass, m_A. The other tree-level Higgs boson masses are then given in terms of these parameters. The tree level value of m_h is maximised not only for $m_A \gg m_Z$ but also for $\tan\beta \gg 1$. For $m_A \gg m_Z$ it acquires a maximum value $m_h = m_Z \cos 2\beta$.

Radiative corrections have a significant impact on the values of Higgs boson masses and couplings in the MSSM. The dominant radiative effects to the SM-like Higgs boson mass arise from the incomplete cancellation between top and scalar-top (stop) loops and at large $\tan\beta$ also from sbottom and stau loops. The stop, sbottom and stau masses and mixing angles depend on the SUSY Higgsino mass parameter μ and on the soft-SUSY-breaking parameters [9, 331]: M_Q, M_U, M_D, M_L, M_E, and A_t, A_b A_τ. The first three of these are the left-chiral and the right-chiral top and bottom scalar quark mass parameters. The next two are the left-chiral stau/sneutrino and the right-chiral stau mass parameters, and the last three are the trilinear parameters that enter in the off-diagonal squark/slepton mixing elements: $X_t \equiv A_t - \mu \cot\beta$ and $X_{b,\tau} \equiv A_{b,\tau} - \mu \tan\beta$. At one-loop, the electroweak gauginos yield a small contribution to the Higgs boson mass, and at the two-loop level, the masses of the gluinos also enter in the calculations. Radiative corrections to the Higgs boson masses have been computed using a number of techniques, with a variety of approximations, see Ref. [332] for a recent review.

[6] Observe that in the SM sections of this review, H denotes the SM Higgs boson, whereas in the sections about SUSY, or extensions of the SM with two Higgs doublets, H is used for the heaviest CP-even Higgs boson, since this is the standard notation in the literature, and the 125 GeV SM-like light Higgs boson will be denoted by h. Generically, in the MSSM, the lightest CP-even Higgs boson is indeed SM-like and thus it is naturally identified with the 125 GeV Higgs boson discovered by ATLAS and CMS, while in 2HDM extensions, with or without SUSY, there could still be lighter scalar states below 125 GeV.

Figure 11.17: Values of the SUSY mass scale $M_{\rm SUSY} = M_S$ versus the stop mixing parameter normalised by the SUSY mass scale $X_t/M_{\rm SUSY}$, for fixed $\tan\beta = 20$, $\mu = 200$ GeV and $A_t = A_b = A_\tau$. The solid black line corresponds to $m_h = 125$ GeV while in the grey band m_h varies by ± 1 GeV. The red dotted lines are iso-values of the stop mass. This figure is based on Ref. [333].

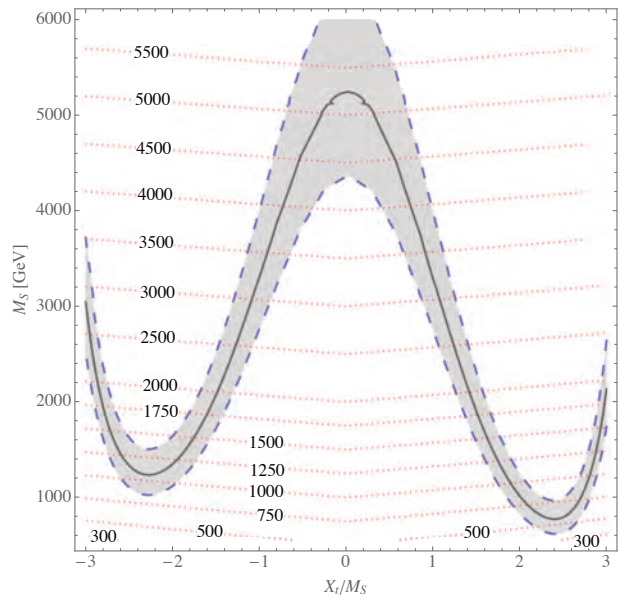

The discovered SM-like Higgs boson, if interpreted as the lightest MSSM Higgs boson with a mass of about 125 GeV, provides information on the possible MSSM parameter space, see Fig. 11.17.

The phenomenology of the Higgs sector depends on the couplings of the Higgs bosons to gauge bosons and fermions. At tree-level, the couplings of the two CP-even Higgs bosons to W and Z bosons are given in terms of the angles α, that diagonalises the CP-even Higgs boson squared-mass matrix, and β

$$g_{hVV} = g_V m_V \sin(\beta - \alpha), \quad g_{HVV} = g_V m_V \cos(\beta - \alpha), \tag{11.47}$$

where $g_V \equiv 2m_V/v$, for $V = W$ or Z ($g_V m_V$ is the SM hVV coupling). Observe that in the limit $\cos(\beta - \alpha) \to 0$, the lightest CP-even Higgs boson h behaves as the SM Higgs boson. This situation is called alignment and is achieved in specific regions of parameter space for $m_A \geq m_Z$ [334] or in the large $m_A \gg m_Z$ limit, in which alignment is achieved through decoupling [334, 335]. There are no tree-level couplings of A or $H^\pm$ to VV. The couplings of the Z boson to two neutral Higgs bosons are given by $g_{\phi AZ}(p_\phi - p_A)$, where $\phi = H$ or h, the momenta p_ϕ and p_A point into the vertex, and

$$g_{hAZ} = g_Z \cos(\beta - \alpha)/2, \quad g_{HAZ} = -g_Z \sin(\beta - \alpha)/2 . \tag{11.48}$$

The expressions of the couplings between a charged Higgs boson, a neutral Higgs boson and the W boson as well as the expressions of the four-point couplings of vector bosons and Higgs bosons can be found in Ref. [27].

The tree-level Higgs boson couplings to fermions obey the following property: the neutral components of one Higgs doublet, Φ_1, couple exclusively to down-type fermion pairs while the neutral components of the other doublet, Φ_2, couple exclusively to up-type fermion pairs [27]. This Higgs-fermion coupling structure defines the Type-II 2HDM. In the MSSM, fermion masses are generated when both neutral Higgs components acquire a vacuum expectation value, and the relations between Yukawa couplings

Downloaded from https://academic.oup.com/ptep/article/2022/8/083C01/6651666 by KIT Library user on 27 September 2022

and fermion masses are (in third-generation notation)

$$h_{b,\tau} = \sqrt{2}\, m_{b,\tau}/(v\cos\beta), \quad h_t = \sqrt{2}\, m_t/(v\sin\beta)\,. \tag{11.49}$$

The couplings of the neutral Higgs bosons to $f\bar{f}$, relative to their SM values, $g\, m_f/(2m_W)$, are therefore given by

$$\begin{aligned} &hb\bar{b}: \ -\sin\alpha/\cos\beta, && ht\bar{t}: \cos\alpha/\sin\beta\,, \\ &Hb\bar{b}: \ \cos\alpha/\cos\beta, && Ht\bar{t}: \sin\alpha/\sin\beta\,, \\ &Ab\bar{b}: \ \gamma_5\tan\beta, && At\bar{t}: \gamma_5\cot\beta\,. \end{aligned} \tag{11.50}$$

In each relation above, the factor listed for $b\bar{b}$ also pertains to $\tau^+\tau^-$. The charged Higgs boson couplings to fermion pairs, normalised to $g/(\sqrt{2}m_W)$, are given by

$$\begin{aligned} &g_{H^-t\bar{b}}: m_t\cot\beta\frac{1+\gamma_5}{2} + m_b\tan\beta\frac{1-\gamma_5}{2}, \\ &g_{H^-\tau^+\nu}: m_\tau\tan\beta\frac{1-\gamma_5}{2}\,. \end{aligned} \tag{11.51}$$

The non-standard neutral Higgs bosons have significantly enhanced couplings to down-type fermions at sizeable $\tan\beta$. Radiative corrections can modify significantly the values of the Higgs boson couplings to fermion pairs and to vector boson pairs, through a radiatively-corrected value for $\cos(\beta-\alpha)$ as well as from the one-loop vertex corrections to tree-level Higgs-fermion Yukawa couplings, see Ref. [9] and references therein, for a detailed discussion.

11.7.1.1 *MSSM Higgs boson phenomenology*

The MSSM parameters have to be arranged such that the mass, the CP properties, the decay and production properties of one of the neutral Higgs bosons agree with the LHC Higgs data. Given that present data allows only for moderate departures from the SM predictions, it implies that some degree of alignment is necessary.

The SM-like branching ratios of h can be modified if decays into SUSY particles are kinematically allowed, and, in particular, decays into a pair of the lightest SUSY particles – i.e., the lightest neutralinos, $\tilde{\chi}_1^0$ – can become dominant and would be invisible if R-parity is conserved [336]. Moreover, if light superpartners exist and couple to photons and/or gluons, the h loop-induced coupling to gg and $\gamma\gamma$ could deviate sizeably from the corresponding SM predictions (see for instance the review [337]), and would be in conflict with present data (see Section 11.3). For the heavier Higgs states, there are two possibilities to be considered[7]:

i) Alignment triggered by decoupling, hence $m_A \geq$ several hundred GeV: The HWW and HZZ couplings are very small. The dominant H, A decay branching ratios strongly depend on $\tan\beta$. The decay modes $H, A \to b\bar{b}, \tau^+\tau^-$ dominate when $\tan\beta$ is large (this holds even away from decoupling). For small $\tan\beta$, the $t\bar{t}$ decay mode dominates above its kinematic threshold. For the charged Higgs boson, $H^+ \to t\bar{b}$ dominates.

ii) Some degree of alignment without decoupling, hence $m_A \leq$ a few hundred GeV: The main difference with the previous case is that, in the low $\tan\beta$ regime ($\tan\beta \leq 5$), additional decay channels may be allowed which involve decays into the lightest SM-like Higgs boson; $A \to Zh$, $H \to hh$ as well as $H \to WW/ZZ$ decay modes are available (they are suppressed in the strict alignment limit). When kinematically open, the decays $A/H \to t\bar{t}$ become relevant or even dominant for sufficiently small $\tan\beta$. For the charged Higgs boson, $H^+ \to \tau^+\nu_\tau$ dominates below the $t\bar{b}$ threshold, and also $H^\pm \to W^\pm h$ may be searched for.

In both cases i) and ii), the heavier Higgs states, H, A and $H^\pm$, are roughly mass degenerate (with masses $\pm$ 20 GeV or less apart). If kinematically allowed, the heavy Higgs boson decays into charginos, neutralinos and third-generation squarks and sleptons can be important [340].

[7] In very special regions of the parameter space, there is still the possibility that the heavier CP-even Higgs state is identified with the 125 GeV Higgs boson discovered by ATLAS and CMS, see for instance the discussion in Ref. [338] and the benchmark M_H^{125} defined in Ref. [339].

At hadron colliders, the dominant neutral Higgs boson production mechanism at moderate values of $\tan\beta$ is gluon fusion, mediated by loops containing heavy top and bottom quarks and the corresponding SUSY partners. The effect of light stops that may contribute to the gluon fusion production can be partially cancelled by mixing effects. Higgs boson radiation off bottom quarks becomes important for large $\tan\beta$, where at least two of the three neutral Higgs bosons have enhanced couplings to bottom-type fermions [341, 342]. Detailed discussions of the impact of radiative corrections in these search modes are presented for instance in Ref. [343]. The vector boson fusion and Higgs-strahlung production of the CP-even Higgs bosons as well as the associated production of neutral Higgs bosons with top quark pairs have lower production cross sections by at least an order of magnitude with respect to the dominant ones, depending on the precise region of MSSM parameter space [43–46]. Higgs boson pair production of non-standard MSSM Higgs bosons has been studied in Ref. [344]. For a discussion of charged Higgs boson production at LHC, see Refs. [44, 45, 345].

Strong production of a heavy neutral Higgs boson followed by its decay into top-quark pairs is a challenging channel, only most recently being searched for by ATLAS and CMS. Interference effects between the signal and the SM $t\bar{t}$ background need to be carefully taken into account [346].

Summarising, the additional Higgs bosons are sought for mainly via the channels:

$$\begin{aligned} &pp \to A/H \to \tau^+\tau^- \ \text{(inclusive)}, \\ &b\bar{b}A/H, A/H \to \tau^+\tau^- \ \text{(with } b\text{-tag)}, \\ &b\bar{b}A/H, A/H \to b\bar{b} \ \text{(with } b\text{-tag)}, \\ &pp \to t\bar{t} \to H^\pm W^\mp b\bar{b}, \ H^\pm \to \tau\nu_\tau\ , \\ &gb \to H^-t \ \text{ or } \ g\bar{b} \to H^+\bar{t}, \ H^\pm \to \tau\nu_\tau\ . \end{aligned} \tag{11.52}$$

After the Higgs boson discovery, updated MSSM benchmarks scenarios have been defined to highlight interesting conditions for the MSSM Higgs boson searches [45, 339] and are scrutinised by the LHC Higgs Working Group [347]. The latest benchmark scenarios update [339], partly based in MSSM parameter space discussions in Ref. [348], considers six benchmarks to illustrate different aspects of Higgs phenomenology in the MSSM. They include one case with complex parameters, but they all assume R-parity conservation and no flavour mixing. Each scenario contains one CP-even scalar with mass around 125 GeV and SM-like couplings. These scenarios include a M_h^{125} scenario with relatively heavy superparticles, so the Higgs phenomenology at the LHC resembles that of a 2HDM with MSSM-inspired Higgs boson couplings. Other two scenarios are characterised by some of the superparticles – staus or electroweakinos – being relatively light, that in turn is of relevance for heavy neutral Higgs boson searches. In particular, the traditional $A/H \to \tau^+\tau^-$ search channel varies depending on the values of μ and M_2, that may enable the A/H decays into electroweakinos. Another two scenarios are characterised by the phenomenon of alignment without decoupling, in which one of the two neutral CP-even scalars has SM-like couplings independently of the mass spectrum of the remaining Higgs bosons, hence allowing for all the Higgs bosons to have relatively low mass values (about few hundred GeV). Finally, there is one scenario which incorporates CP violation in the Higgs sector and gives rise to a strong admixture of the two heavier neutral states. All the above scenarios assume all parameters in the mass range from 1 to a few TeV, hence they are not applicable for values of $\tan\beta$ of order a few, for which a Higgs boson mass value of 125 GeV is out of reach. An additional study [349], relying on an EFT approach in the MSSM, focusses on two scenarios specifically designed for the low $\tan\beta$ region and ensures a 125 GeV Higgs boson mass in almost the entire parameter space by employing a flexible supersymmetric mass scale, reaching values of up to 10^{16} GeV.

An alternative approach to reduce the large number of parameters relevant to the Higgs sector is to consider that, in the Higgs basis, the only important radiative corrections are those affecting the Higgs boson mass [350]. This approximation is called hMSSM and works well in large regions of parameter space but it breaks

Downloaded from https://academic.oup.com/ptep/article/2022/8/083C01/6651666 by KIT Library user on 27 September 2022

down for sizeable values of μ and A_t, and moderate values of $\tan\beta$, for which the radiative corrections to the mixing between the two CP even eigenstates become relevant. The effect of such radiative corrections is to allow for alignment for small to intermediate values of $\tan\beta$, independent of the specific value of m_A [351]. In addition, the hMSSM assumption that the right value of the Higgs boson mass may be obtained for all values of m_A and $\tan\beta$ is in conflict with the MSSM predictions for the Higgs boson mass for small values of m_A and $\tan\beta \simeq \mathcal{O}(1)$. The recent M_h^{125} [339] and EFTMSSM benchmarks [349], are designed to address the limitations of the hMSSM, in particular the low $\tan\beta$ region for the EFTMSSM.

The compatibility between the predicted and measured Higgs boson mass sets stringent constraints on the parameter space of BSM models. The predictions are illustrated in Fig. 11.18 for two concrete scenarios. Note that to use the predicted Higgs boson mass as a constraint (exclusion at nearly constant $\tan\beta$ at high M_A in the (M_A,$\tan\beta$) plane), it is important to account for the theoretical uncertainty on the prediction which is in excess of an order of magnitude larger than the experimental uncertainty on the measured mass of the Higgs boson. The theoretical uncertainty depends itself on the specific SUSY spectrum for a given MSSM parameter set and should be estimated accordingly, however, a more generic estimate of ± 3 GeV is made and found to be a conservative choice [332].

Reviews of the properties and phenomenology of the Higgs bosons of the MSSM can be found for example in Refs. [9,41,337]. Future precision measurements of the Higgs boson couplings to fermions and gauge bosons together with information on heavy Higgs boson searches will provide powerful information on the SUSY parameter space [353].

Improvements in our understanding of B-physics observables put indirect constraints on additional Higgs bosons in mass ranges that would be accessible in direct LHC searches. In particular, $\mathrm{BR}(B_s \to \mu^+\mu^-)$, $\mathrm{BR}(b \to s\gamma)$, and $\mathrm{BR}(B_u \to \tau\nu)$ play an important role within minimal flavour-violating (MFV) models [354], in which flavor effects proportional to the CKM matrix elements are induced as in the SM.

11.7.2 *Supersymmetry with singlet extensions*

The Higgs mass parameter μ is a SUSY parameter, and as such, it should naturally be of order M_{GUT} or M_{Planck}. The fact that phenomenologically it is required that μ be at the electroweak/TeV scale is known as the μ problem [355]. SUSY models with additional singlets can provide a solution to the μ problem, by promoting the μ parameter to a dynamical singlet superfield S that only interacts with the MSSM Higgs doublets through a coupling λ_S at the level of the superpotential. An effective μ is generated when the real scalar component of S acquires a vacuum expectation value v_S, yielding $\mu_{eff} = \lambda_S\, v_S$. After the minimization of the Higgs potential, the vacuum state relates the vacuum expectation values of the three CP-even neutral scalars, v_1, v_2 and v_S, to the scalar doublet and singlet soft SUSY breaking masses, hence, one expects that these VEVs should all be of order M_{SUSY} and therefore the μ problem is solved.

The addition of a singlet superfield to the MSSM may come along with additional symmetries imposed to the theory. Depending on such symmetries, different models with singlet extensions of the MSSM (xMSSM) have been proposed, see Ref. [356] for a general review. Among the most studied examples are the NMSSM with an additional discrete Z_3 symmetry (first introduced in Ref. [357]), the Nearly-Minimal SUSY SM (nMSSM), with additional discrete Z_5^R, and Z_7^R symmetries [358], and the $\mathrm{U}(1)'$-extended MSSM (UMSSM) [359]. A Secluded $\mathrm{U}(1)'$-extended MSSM (sMSSM) [360] contains three singlets in addition to the standard UMSSM Higgs boson singlet; this model is equivalent to the nMSSM in the limit that the additional singlet VEV's are large, and the trilinear singlet coupling, λ_S, is small [361]. The non-zero neutrino masses provide also a motivation for a particular extension of the MSSM, $\mu\nu$SSM [362], which also happens to address the address the $-mu$ problem. The computation of the Higgs boson spectrum in these various models has been reviewed in Ref. [332].

A singlet extended SUSY Higgs sector opens new avenues for discovery. Since the singlet pseudoscalar particle may be identified as the pseudo-Goldstone boson of a spontaneously broken Peccei–Quinn symmetry, it may become naturally light [363]. Generally, there is mixing of the singlet sector with the MSSM Higgs sector, and for a sufficiently light, singlet-dominated scalar or pseudoscalar, h_S or A_S, respectively, the SM-like Higgs boson h may decay to pairs of h_S or A_S. The light scalar and/or pseudoscalar may subsequently decay to $\tau\tau$ or $b\bar{b}$ pairs. Such cascade decays are more difficult to detect than in standard searches due to the potentially soft decay products. There is also a rich phenomenology for the decays of the heavy CP-even and CP-odd doublets, H and A into two lighter Higgs bosons such as $H \to hh_S$, hh, h_Sh_S or $A \to A_Sh_S$, A_Sh as well as into a light Higgs boson and a gauge boson: $H \to A_SZ$; $A \to h_SZ$, hZ. If kinematically allowed, the heavy Higgs bosons decay into $t\bar{t}$. If the singlet-dominated scalar or pseudoscalar are somewhat heavier, the decays $h_S \to WW$ or $A_S \to h_SZ$ will be allowed.

In addition, the light singlet scenario in the NMSSM or nMSSM is typically associated with a light singlino-dominated neutralino. The 125 GeV SM-like Higgs boson can then decay to pairs of this neutralino [364], opening an invisible decay mode that is not excluded by present data. All of the Higgs bosons can decay into electroweakinos depending on kinematics and on the singlino or Higgsino composition of the electroweakinos.

In models with extended singlets, at low $\tan\beta$, it is possible to trade the requirement of a large stop mixing by a sizeable trilinear Higgs-singlet Higgs coupling λ_S, rendering more freedom on the requirements for gluon fusion production. As in the MSSM, mixing in the Higgs sector – additionally triggered by the extra new parameter λ_S – can produce variations in the Higgs–$b\bar{b}$ and Higgs–$\tau^-\tau^+$ couplings that can alter the Higgs to ZZ/WW and to diphoton rates. Light charginos at low $\tan\beta$ can independently contribute to enhance the di-photon rate, without altering any other of the Higgs boson decay rates, see for instance Ref. [365].

There is much activity in exploring the NMSSM phenomenology in the light of the 125 GeV Higgs boson as well as in defining benchmark scenarios with new topologies including Higgs decay chains, see Refs. [46, 366] and references therein. An analytic understanding of the alignment condition in the NMSSM is presented in Ref. [367]. The NMSSM with a Higgs boson of mass 125 GeV can be compatible with stop masses of order of the electroweak/TeV scale, thereby reducing the degree of fine-tuning necessary to achieve electroweak symmetry breaking. Interestingly, the alignment conditions point toward a more natural region of parameter space for electroweak symmetry breaking, while allowing for perturbativity of the theory up to the Planck scale and yielding a rich and interesting Higgs boson phenomenology at the LHC.

11.7.3 *Supersymmetry with extended gauge sectors*

In the MSSM, the tree-level value of the lightest CP-even Higgs boson mass originates from the D-term dependence of the scalar potential that comes from the SUSY kinetic terms in the Kähler potential. The D-terms lead to tree-level quartic couplings which are governed by the squares of the gauge couplings of the weak interactions, under which the Higgs boson has non-trivial charges. Hence, the lightest Higgs mass is bounded to be smaller than M_Z. In the presence of new gauge interactions at the TeV scale, and if the Higgs fields had non-trivial charges under them, new D-term contributions would lead to an enhancement of the tree-level Higgs boson mass value. Since the low energy gauge interactions reduce to the known $\mathrm{SU}(3)_c \times \mathrm{SU}(2)_L \times \mathrm{U}(1)_Y$ ones, in order for this mechanism to work, the extended gauge and Higgs sectors should be integrated out in a non-SUSY way. This means that there must be SUSY breaking terms that are of the order of, or larger than, the new gauge boson masses. The tree-level quartic couplings would then be enhanced through their dependence on the square of the gauge couplings of the extended Higgs sector. This effect will be suppressed when the heavy gauge boson masses are larger than the SUSY breaking scale and will acquire its full potential only for large values of this scale.

One of the simplest possibilities is to extend the weak interactions to a $\mathrm{SU}(2)_1 \times \mathrm{SU}(2)_2$ sector, such that the known weak interactions are obtained after the spontaneous breaking of these

Downloaded from https://academic.oup.com/ptep/article/2022/8/083C01/6651666 by KIT Library user on 27 September 2022

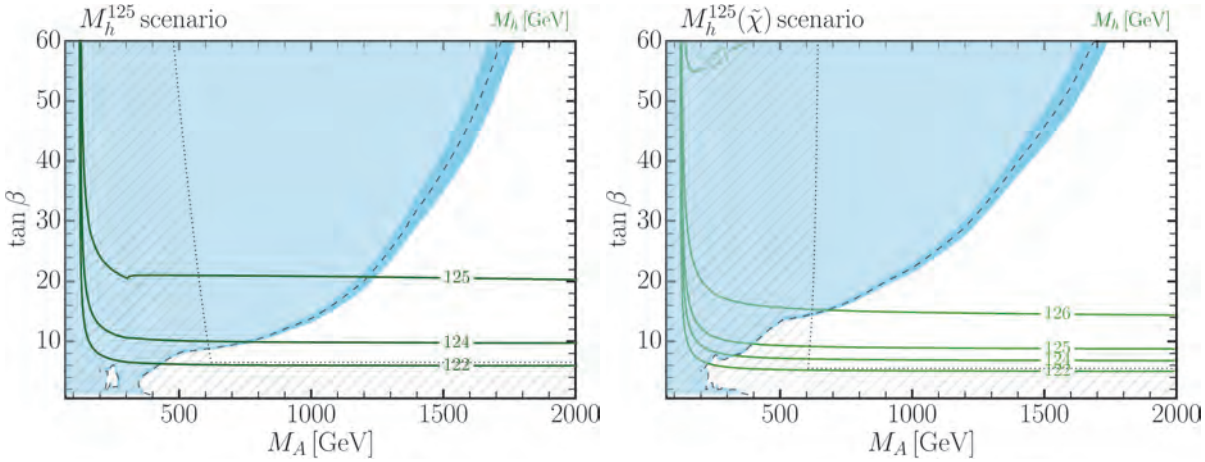

Figure 11.18: The 95% CL exclusion contours in the $(M_A, \tan\beta)$ parameter space for the M_h^{125} (right) and $M_h^{125}(\tilde{\chi})$(left) benchmark scenarios [352]. The M_h^{125} benchmark assumes that super partners are heavy, so that the phenomenology of the observed Higgs boson is not altered except in its couplings due to the existence of another doublet. The $M_h^{125}(\tilde{\chi})$ scenario on the other hand considers light electroweakinos and therefore the heavy Higgs bosons H and A can have sizeable decay rates to charginos and neutralinos, consequently suppressing the $\tau^+\tau^-$ decay rate. The nearly vertical dotted line illustrated the lower limit on the mass of the A boson and the close-to horizontal dotted line represents the limit on $\tan\beta$ from the compatibility of the measured mass of the observed Higgs boson and the prediction using radiative corrections (mostly from the stop sector).

groups to $\mathrm{SU}(2)_L$ [368]. This example is briefly summarized in the previous editions of this review [132]. Assuming SUSY breaking terms of the order of the new gauge boson masses, enhancements of order 50% of the MSSM D-term contribution to the Higgs boson mass may be obtained. Such enhancements are sufficient to obtain the measured Higgs mass value without the need for very heavy stops or large stop mixing parameters. This gauge extension leads to new, heavy gauge and Higgs bosons, as well as new neutralinos and charginos, that depending on the region of parameter space can induce novel phenomenology at the LHC. Gauge extensions including new Abelian gauge groups have also been considered.

Gauge extensions of the MSSM can also lead to an enhancement of the Higgs boson mass value by modifying the renormalisation group evolution of the Higgs quartic coupling to low energies. In the MSSM, the evolution of the quartic coupling is governed by the top-quark Yukawa interactions and depends on the fourth power of the top-quark Yukawa coupling. The neutralino and chargino contributions, which depend on the fourth power of the weak gauge couplings, are small due to the smallness of these couplings. Depending on the values of the soft SUSY breaking parameters in the gaugino and Higgsino sectors, the $\mathrm{SU}(2)_1$ gauginos may become light, with masses of the order of the weak scale. Since the $\mathrm{SU}(2)_1$ coupling may be significantly larger than the $\mathrm{SU}(2)_L$ one, for small values of the Higgsino mass parameter μ, the associated charginos and neutralinos may modify the evolution of the quartic coupling in a significant way [369]. This may lead to a significant increase of the lightest CP-even Higgs boson mass, even for small values of $\tan\beta \simeq 1$ for which the D-term contributions become small. Radiative corrections should be properly taken into account in this scenario as they might modify the tree-level result.

11.7.4 *Effects of CP violation*

SUSY scenarios with CP-violation (CPV) phases are theoretically appealing, since additional CPV beyond that observed in the K, D, and B meson systems is required to explain the observed cosmic matter-antimatter asymmetry. In the MSSM, CP-violation effects in the Higgs sector appear at the quantum level, while in singlet extensions of the MSSM CP-violation effects can already be effective at tree level. In general, CP-violation effects in the Higgs sector have significant constraints from electric dipole moments data [370].

In the MSSM, the gaugino mass parameters ($M_{1,2,3}$), the Higgsino mass parameter, μ, the bilinear Higgs squared-mass parameter, m_{12}^2, and the trilinear couplings of the squark and slepton fields to the Higgs fields, A_f, may carry non-trivial phases. The two parameter combinations $\arg[\mu A_f (m_{12}^2)^*]$ and $\arg[\mu M_i (m_{12}^2)^*]$ are invariant under phase redefinitions of the MSSM fields [371, 372]. Therefore, if one of these quantities is non-zero, there would be new sources of CP-violation affecting the Higgs sector through radiative corrections, see Ref. [373] and references therein. The mixing of the neutral CP-odd and CP-even Higgs boson states is no longer forbidden. Hence, m_A is no longer a physical parameter. However, the charged Higgs boson mass $m_{H^\pm}$ is still physical and can be used as an input for the computation of the neutral Higgs boson spectrum of the theory. For large values of $m_{H^\pm}$, corresponding to the decoupling limit, the properties of the lightest neutral Higgs boson state approach those of the SM Higgs boson. In particular, the upper bound on the lightest neutral Higgs boson mass takes the same value as in the CP-conserving case [372]. Nevertheless, there still can be significant mixing between the two heavier neutral mass eigenstates. For a detailed study of the Higgs boson mass spectrum and parametric dependence of the associated radiative corrections, see Ref. [373] and references therein.

Major variations to the Higgs boson phenomenology occur in the presence of explicit CPV phases. In the CPV case, vector boson pairs couple to all three neutral Higgs boson mass eigenstates, H_i $(i = 1, 2, 3)$, with couplings

$$\begin{aligned} g_{H_i VV} &= \cos\beta\, \mathcal{O}_{1i} + \sin\beta\, \mathcal{O}_{2i}\,, \\ g_{H_i H_j Z} &= \mathcal{O}_{3i}\, (\cos\beta\, \mathcal{O}_{2j} - \sin\beta\, \mathcal{O}_{1j}) \\ &\quad - \mathcal{O}_{3j}\, (\cos\beta\, \mathcal{O}_{2i} - \sin\beta\, \mathcal{O}_{1i})\,, \end{aligned} \tag{11.53}$$

where the $g_{H_i VV}$ couplings are normalised to the analogous SM coupling and the $g_{H_i H_j Z}$ have been normalised to $g_Z^{\mathrm{SM}}/2$. The orthogonal matrix $\mathcal{O}_{ij}$, only defined in the $p^2 \to 0$ limit, is relating the weak eigenstates to the mass eigenstates. It has non-zero off-diagonal entries mixing the CP-even and CP-odd components of the weak eigenstates. Moreover, CPV phases imply that all neutral Higgs bosons can couple to both scalar and pseudoscalar fermion bilinear densities. The couplings of the mass eigenstates H_i to fermions depend on the loop-corrected fermion Yukawa couplings (similarly to the CP conserving (CPC) case), on $\tan\beta$ and on $\mathcal{O}_{ji}$ [374].

The production processes of neutral MSSM Higgs bosons in the CPV scenario are similar to those in the CPC scenario. Regarding the decay properties, the lightest mass eigenstate, H_1, predominantly decays to $b\bar{b}$ if kinematically allowed, with a smaller fraction decaying to $\tau^+\tau^-$. If kinematically allowed, a SM-like neutral Higgs boson, H_2 or H_3 can decay predominantly to $H_1 H_1$

Downloaded from https://academic.oup.com/ptep/article/2022/8/083C01/6651666 by KIT Library user on 27 September 2022

leading to many new interesting signals both at lepton and hadron colliders; otherwise it will decay preferentially to $b\bar{b}$.

The discovery of a 125 GeV Higgs boson has put strong constraints on the realisation of the CPV scenario within the MSSM. This is partly due to the fact that the observed Higgs boson rates are close to the SM values, and a large CP-violating component would necessarily induce a large variation in the rate of the SM-like Higgs boson decays into the weak gauge bosons $W^{\pm}$ and Z. The measured Higgs mass imposes additional constraints on the realisation of this scenario. Once all effects are considered, the CP-odd Higgs boson A component of the lightest Higgs boson tends to be smaller than about 10% [375]. This restriction can be alleviated in the NMSSM or more general two Higgs doublet models. CP-violating effects can still be significant in the heavy Higgs sector. For instance, the Higgs bosons H_2 and H_3 may be admixtures of CP-even and CP-odd scalars, and therefore both may be able to decay into pairs of weak gauge bosons. The observation of such decays would be a clear signal of CP-violation. In the MSSM, the proximity of the masses of H_2 and H_3 makes the measurement of such effect quite challenging, but in generic two Higgs doublet models, the mass splitting between the two heavy mass eigenstates may become larger, facilitating the detection of CP-violating effects at collider experiments [376].

11.7.5 *Non-supersymmetric extensions of the Higgs sector*

There are many ways to extend the minimal Higgs sector of the SM. In the preceding sections the phenomenology of SUSY Higgs sectors is considered, which at tree level implies a constrained type-II 2HDM (with restrictions on the Higgs boson masses and couplings). In the following discussion, more generic 2HDM's are presented (for some comprehensive reviews, see the reviews [377]). These models are theoretically less compelling since they do not provide an explanation for the SM Higgs naturalness problem, but can lead to different patterns of Higgs-fermion couplings, hence, to different phenomenology. It is also possible to consider models with a SM Higgs boson and one or more additional scalar SU(2) doublets that acquire no VEV and hence play no role in the EWSB mechanism. Such models are dubbed Inert Higgs Doublet Models (IHD) [378]. Without a VEV associated to it, a Higgs boson from an inert doublet has no tree-level coupling to gauge bosons and hence cannot decay into a pair of them. Moreover, imposing a Z_2 symmetry that prevents them from coupling to the fermions, it follows that, if the lightest inert Higgs boson is neutral, it becomes a good DM candidate with interesting associated collider signals. Various studies of IHD models in the light of a 125 GeV Higgs boson have been performed, see for instance Ref. [379], showing an interesting interplay between collider and direct DM detection signals.

An interesting type of 2HDMs are those in which an Abelian flavour symmetry broken at the electroweak scales creates the fermion mass hierarchies and mixing angles [19]. This idea is based on the Froggatt–Nielsen model [380], where a flavon field couples differently to the SM fermions of different flavour charges. Such flavon acquires a vacuum expectation value, breaking the flavour symmetry but leaving both the flavour breaking and the new physics scales undetermined. In Refs. [381], it was proposed to relate the flavour breaking scale to the electroweak scale by identifying the flavon with the modulus square of the Higgs field. A 2HDM, however, provides a more compelling realisation of the electroweak scale flavour breaking idea. In the most ambitious constructions of two Higgs doublet flavour models (2HDFM), the textures of the Yukawa couplings are a result of an Abelian flavour symmetry that only allows renormalisable Yukawa couplings of the top quark to the Higgs bosons. All other Yukawa couplings are generated by higher dimensional operators that produce hierarchical entries of the Yukawa matrices, explaining the observed quark masses and mixing angles. Flavour observables, LHC Higgs signal strength measurements, electroweak precision measurements, unitarity and perturbativity bounds, as well as collider searches for new scalar resonances result in precise predictions for the parameters of these 2HDFMs. In particular, correlated departures from SM Higgs boson couplings, as well as additional Higgs bosons with masses < 700 GeV must be observed at the LHC. Other incarnations of 2HDFMs can aim at only partially explaining the fermion mass hierarchies but are therefore less restrictive.

Other extensions of the Higgs sector can include multiple copies of $\mathrm{SU}(2)_L$ doublets [382], additional Higgs singlets [383], triplets or more complicated combinations of Higgs multiplets. It is also possible to enlarge the gauge symmetry beyond $\mathrm{SU}(2)_L\times\mathrm{U}(1)_Y$ along with the necessary Higgs field structure to generate gauge boson and fermion masses. There are two main experimental constraints on these extensions: (i) precision measurements which constrain $\rho = m_W^2/(m_Z^2\cos^2\theta_W)$ to be very close to 1 and (ii) flavour changing neutral current (FCNC) effects. In electroweak models based on the SM gauge group, the tree-level value of ρ is determined by the Higgs multiplet structure. By suitable choices for the hypercharges, and in some cases the mass splitting between the charged and neutral Higgs sector or the vacuum expectation values of the Higgs fields, it is possible to obtain a richer combination of singlets, doublets, triplets and higher multiplets compatible with precision measurements. Concerning the constraints coming from FCNC effects, the Glashow–Weinberg (GW) criterion [384] states that, in the presence of multiple Higgs doublets, the tree-level FCNC's mediated by neutral Higgs bosons will be absent if all fermions of a given electric charge couple to no more than one Higgs doublet. An alternative way of suppressing FCNC in a two Higgs doublet model has been considered in Ref. [385], where it is shown that it is possible to have tree level FCNC completely fixed by the CKM matrix, as a result of an Abelian symmetry.

There is a lot of activity on the study of non-supersymmetric models with an extended Higgs sector with an intense collaboration between theorists and experimentalists, in particular inside the LHC Higgs Working Group [347].

11.7.5.1 *Two-Higgs-doublet models*

General two Higgs doublet models [377] can have a more diverse Higgs-fermion coupling structure than in SUSY, and can be viewed as a simple extension of the SM to realise the spontaneous breakdown of $\mathrm{SU}(2)_L \times \mathrm{U}(1)_Y$ to $\mathrm{U}(1)_{\mathrm{em}}$. Quite generally, if the two Higgs doublets contain opposite hypercharges, the scalar potential will contain mixing mass parameters of the kind $m_{12}^2\Phi_1^T i\sigma_2\Phi_2 + h.c.$. In the presence of such terms, both Higgs doublets will acquire vacuum expectation values, $v_1/\sqrt{2}$ and $v_2/\sqrt{2}$, respectively, and the gauge boson masses will keep their SM expressions with the Higgs VEV v replaced by $\sqrt{v_1^2+v_2^2}$. Apart from the mass terms, the most generic renormalisable and gauge invariant scalar potential for two Higgs doublets with opposite hypercharges contains seven quartic couplings, as presented in Eq. (11.46).

Just as in the MSSM case, after electroweak symmetry breaking and in the absence of CP-violation, the physical spectrum contains a pair of charged Higgs bosons $H^{\pm}$, a CP-odd Higgs boson A and two neutral CP-even Higgs bosons, h and H. The angles α and β diagonalise the CP-even, and the CP-odd and charged Higgs sectors, respectively. The complete 2HDM is defined only after considering the interactions of the Higgs fields to fermions. Yukawa couplings of the generic form

$$-h_{ij}^a\bar{\Psi}_L^i H_a \Psi_R^j + h.c. \tag{11.54}$$

may be added to the renormalisable Lagrangian of the theory. Contrary to the SM, the two Higgs doublet structure does not ensure the alignment of the fermion mass terms $m_{ij} = h_{ij}^a v_a/\sqrt{2}$ with the Yukawa couplings h_{ij}^a. This implies that quite generally the neutral Higgs boson will mediate flavour changing interactions between the different mass eigenstates of the fermion fields. Such flavour changing interactions should be suppressed in order to describe properly the Kaon, D and B meson phenomenology. Based on the Glashow–Weinberg criterion, it is clear that the simplest way of avoiding such transitions is to assume the existence of a symmetry that ensures the couplings of the fermions of each given quantum number (up-type and down-type quarks, charged and neutral leptons) to only one of the two Higgs doublets. Different models may be defined depending on which of these fermion fields couple to a given Higgs boson, see Table 11.13. Models of type-I are those in which all SM fermions couple to a single Higgs field. In type-II models, down-type quarks and charged leptons

Downloaded from https://academic.oup.com/ptep/article/2022/8/083C01/6651666 by KIT Library user on 27 September 2022

couple to a common Higgs field, while the up-type quarks and neutral leptons couple to the other. In models of type-III (lepton-specific), quarks couple to one of the Higgs bosons, while leptons couple to the other. Finally, in models of type-IV (flipped), up-type quarks and charged leptons couple to one of the Higgs fields while down-quarks and neutral leptons couple to the other.

Table 11.13: Higgs boson couplings to up, down and charged lepton-type $SU(2)_L$ singlet fermions in the four discrete types of 2HDM models that satisfy the Glashow–Weinberg criterion.

Model	2HDM I	2HDM II	2HDM III	2HDM IV
u	Φ_2	Φ_2	Φ_2	Φ_2
d	Φ_2	Φ_1	Φ_2	Φ_1
e	Φ_2	Φ_1	Φ_1	Φ_2

The two Higgs doublet model phenomenology depends strongly on the size of the mixing angle α and therefore on the quartic couplings. For large values of m_A, $\sin\alpha \to -\cos\beta$, $\cos\alpha \to \sin\beta$, $\cos(\beta-\alpha) \to 0$, and the lightest CP-even Higgs boson h behaves as the SM Higgs boson. The same behaviour is obtained if the quartic couplings are such that $\mathcal{M}_{12}^2 \sin\beta = -(\mathcal{M}_{11}^2 - m_h^2)\cos\beta$. The latter condition represents a situation in which the couplings of h to fermions and weak gauge bosons become the same as in the SM, without decoupling the rest of the non-standard scalars and it is of particular interest due to the fact that the discovered Higgs boson has SM-like properties. This situation will be referred to as alignment, as in the MSSM case.

In analogy to the effects of CP violation in the SUSY 2HDM, some parameters of the Higgs potential can be complex and one has a model that is explicitly CP violating. The three neutral mass eigenstates mixed with each other and the Higgs phenomenology is analogous to the one described for the SUSY case above, with the caveat that when considering the neutral Higgs boson couplings to the scalar and pseudoscalar fermion bilinear densities, the proper weight should be considered for the respective 2HDM's.

In type-II Higgs doublet models, at large values of $\tan\beta$ and moderate values of m_A, the non-standard Higgs bosons H, A and $H^\pm$ couple strongly to bottom quarks and τ leptons. Hence, the decay modes of the non-standard Higgs bosons tend to be dominated by the b-quark and τ-lepton modes, including top quarks or neutrinos in the case of the charged Higgs boson. However, for large and negative values of λ_4, the charged Higgs boson mass may be sufficiently heavy to allow on-shell decays $H^\pm \to W^\pm + (H, A)$, via a trilinear coupling

$$g_{H^\pm W^\mp H,A} \simeq \frac{M_W}{v}\sin(\beta-\alpha)(p_{H^+} - p_{H,A})\,, \quad (11.55)$$

where p_{H^+} and $p_{H,A}$ are the charged and neutral scalar Higgs boson momenta pointing into the vertex. On the other hand, for large and positive values of λ_5, the above charged Higgs boson decay into a $W^\pm$ and the CP-odd Higgs boson may be allowed, but the heavy Higgs boson H may be sufficiently heavy to decay into a CP-odd Higgs boson and an on-shell Z, $H \to Z + A$, via

$$g_{HZA} \simeq \frac{M_Z}{v}\sin(\beta-\alpha)(p_H - p_A). \quad (11.56)$$

The decay $H^\pm \to W^\pm + H$, on the other hand may be allowed only if $\lambda_4 < -\lambda_5$. The couplings controlling all the above decay modes are proportional to $\sin(\beta-\alpha)$ and therefore they are unsuppressed in the alignment limit. Moreover, these could still be the dominant decay modes at moderate values of $\tan\beta$, offering a way to evade the current bounds obtained assuming a dominant decay into b-quarks or τ-leptons.

The quartic couplings are restricted by the condition of stability of the effective potential as well as by the restriction of obtaining the proper value of the lightest CP-even Higgs boson mass. Close to the alignment limit, the lightest CP-even Higgs boson mass becomes

$$\begin{aligned} m_h^2 \simeq\ & v^2(\lambda_1\cos^4\beta + \lambda_2\sin^4\beta + 2\tilde{\lambda}_3 v^2\cos^2\beta\sin^2\beta \\ & + 4\lambda_6\cos^3\beta\sin\beta + 4\lambda_7\sin^3\beta\cos\beta)\,, \end{aligned} \quad (11.57)$$

where $\tilde{\lambda}_3 = \lambda_3 + \lambda_4 + \lambda_5$.

The stability conditions imply the positiveness of all masses, as well as the avoidance of run-away solutions to large negative values of the fields in the scalar potential. These conditions imply

$$\begin{aligned} & \lambda_1 \geq 0,\ \ \lambda_2 \geq 0,\ \ \lambda_3 + \lambda_4 - |\lambda_5| \geq -\sqrt{\lambda_1\lambda_2},\ \ \lambda_3 \geq -\sqrt{\lambda_1\lambda_2}, \\ & 2|\lambda_6 + \lambda_7| < \frac{\lambda_1 + \lambda_2}{2} + \tilde{\lambda}_3, \end{aligned} \quad (11.58)$$

where the first four conditions are necessary and sufficient conditions in the case of $\lambda_6 = \lambda_7 = 0$, while the last one is a necessary condition in the case all couplings are non-zero. Therefore, to obtain the conditions that allow the decays $H^\pm \to W^\pm H, A$ and $H \to ZA$, λ_3 should take large positive values in order to compensate for the effects of λ_4 and λ_5. For more detailed discussions about 2HDM phenomenology, see for example Refs. [46, 377].

11.7.5.2 *Higgs triplets*

Electroweak triplet scalars are the simplest non-doublet extension of the SM that can participate in the spontaneous breakdown of $\mathrm{SU}(2)_L \times \mathrm{U}(1)_Y$ to $\mathrm{U}(1)_{\mathrm{em}}$. Two types of model have been developed in enough detail to make a meaningful comparison to LHC data: the Higgs triplet model (HTM) [386] and the Georgi–Machacek model (GM) [387].

The Higgs triplet model extends the SM by the addition of a complex $\mathrm{SU}(2)_L$ triplet scalar field Δ with hypercharge $Y = 2$, and a general gauge-invariant renormalisable potential $V(\Phi, \Delta)$ for Δ and the SM Higgs doublet Φ. The components of the triplet field can be parameterised as

$$\Delta = \frac{1}{\sqrt{2}}\begin{pmatrix} \Delta^+ & \sqrt{2}\Delta^{++} \\ v_\Delta + \delta + i\xi & -\Delta^+ \end{pmatrix}. \quad (11.59)$$

where Δ^+ is a singly-charged field, Δ^{++} is a doubly-charged field, δ is a neutral CP-even scalar, ξ is a neutral CP-odd scalar, and v_Δ is the triplet VEV. The general scalar potential mixes the doublet and triplet components. After electroweak symmetry breaking there are seven physical mass eigenstates, denoted $H^{\pm\pm}$, $H^\pm$, A, H, and h.

A distinguishing feature of the HTM is that it violates the custodial symmetry of the SM; thus the ρ parameter deviates from 1 even at tree level. Letting x denote the ratio of triplet and doublet VEVs, the tree level expression is

$$\rho = \frac{1 + 2x^2}{1 + 4x^2}\,. \quad (11.60)$$

The measured value of the ρ parameter then limits the triplet VEV to be quite small, $x \lesssim 0.03$, or $v_\Delta < 8\,\mathrm{GeV}$. This constraint severely limits the role of the triplet scalar in the EWSB mechanism.

The small VEV of the Higgs triplet in the HTM is a virtue from the point of view of generating neutrino masses without the necessity for introducing right-handed neutrino fields. The gauge invariant dimension four interaction

$$h_{\nu_{ij}}\,\ell_i^T C^{-1} i\sigma_2\,\Delta\,\ell_j\,, \quad (11.61)$$

where ℓ_i are the lepton doublets, C is the charge conjugation matrix, and $h_{\nu_{ij}}$ is a complex symmetric coupling matrix, generates a Majorana mass matrix for the neutrinos:

$$m_{\nu_{ij}} = \sqrt{2}h_{\nu_{ij}}v_\Delta\,. \quad (11.62)$$

This can be combined with the usual neutrino seesaw to produce what is known as the type-II seesaw [388].

The HTM suggests the exciting possibility of measuring parameters of the neutrino mass matrix at the LHC. If the doubly-charged Higgs boson is light enough and/or its couplings to

Downloaded from https://academic.oup.com/ptep/article/2022/8/083C01/6651666 by KIT Library user on 27 September 2022

W^+W^+ are sufficiently suppressed, then its primary decay is into same-sign lepton pairs: $H^{++} \to \ell_i^+\ell_j^+$; from Eq. (11.61) and Eq. (11.62), it is apparent that these decays are in general lepton-flavor violating with branchings proportional to elements of the neutrino mass matrix [389].

Precision electroweak data constrain the mass spectrum as well as the triplet VEV of the HTM [390]. These constraints favour a spectrum where H^{++} is the lightest of the exotic bosons, and where the mass difference between H^+ and H^{++} is a few hundred GeV. The favoured triplet VEV is a few GeV, which also favours H^{++} decays into W^+W^+ over same-sign dileptons.

The GM model addresses the ρ parameter constraint directly by building in a custodial symmetry (it was however argued that large corrections to $\rho = 1$ are generated at one-loop [391], requiring some fine-tuning to preserves agreement with EW precision data). Writing the complex scalar doublet of the SM as a $(2,2)$ under $\mathrm{SU}(2)_L \times \mathrm{SU}(2)_R$, it is obvious that the next simplest construction respecting custodial symmetry is a scalar transforming like a $(3,3)$ [392]. These nine real degrees of freedom correspond to a complex electroweak triplet combined with a real triplet, with the scalar potential required to be invariant under $\mathrm{SU}(2)_R$. Under the custodial $\mathrm{SU}(2)_{L+R}$, they transform as $1 \oplus 3 \oplus 5$, with a CP-even neutral scalar as the custodial singlet (thus matching the SM Higgs boson), a CP-odd neutral scalar in the custodial triplet, and another CP-even neutral scalar in the custodial 5-plet.

The scalar components can be decomposed as

$$\Xi = \begin{pmatrix} \chi_3^* & \xi_1 & \chi_1 \\ -\chi_2^* & \xi_2 & \chi_2 \\ \chi_1^* & -\xi_1^* & \chi_3 \end{pmatrix}, \tag{11.63}$$

where ξ_2 is a real scalar and the others are complex scalars. Linear combinations of these scalars account for the neutral custodial singlet, a neutral and singly-charged field making up the custodial triplet, and neutral, singly-charged, and doubly-charged fields making up the custodial 5-plet.

When combined with the usual SM doublet field Φ, the electroweak scale v is now related to the doublet and triplet VEVs by

$$v^2 = v_\Phi^2 + 8v_\Xi^2 \ . \tag{11.64}$$

Note that the GM triplets by themselves are sufficient to explain electroweak symmetry breaking and the existence of a 125 GeV neutral boson along with a custodial triplet of Goldstone bosons; the complex doublet field in the GM model is required to generate fermion masses via the usual dimension four Yukawa couplings. This raises the question of whether one can rule out the possibility that the 125 GeV boson is the neutral member of a custodial 5-plet rather than a custodial singlet, without invoking decays to fermions. A conclusive answer is given by observing that the ratio of the branching fractions to W versus Z bosons is completely determined by the custodial symmetry properties of the boson. For a custodial 5-plet, the ratio of the signal strength to WW over that to ZZ is predicted to be 1/4 that of a SM Higgs boson [392], and thus already ruled out by the experimental results presented in Section 11.6.

Another interesting general feature of Higgs triplet models is that, after mixing, the SM-like neutral boson can have stronger couplings to WW and ZZ than predicted by the SM [393]; this is in contrast to mixing with additional doublets and singlet, which can only reduce the WW and ZZ couplings versus the SM. This emphasises that LHC Higgs data cannot extract model independent coupling strengths for the Higgs boson [273].

Because of the built-in custodial symmetry, the triplet VEV in the GM model can be large compared to the doublet VEV. The custodial singlet neutral boson from the triplets mixes with the neutral boson from the doublet. Two interesting special cases are (i) the triplet VEV is small and the 125 GeV boson is SM-like except for small deviations, and (ii) the 125 GeV boson is mostly the custodial singlet neutral boson from the electroweak triplets. The phenomenology of the doubly-charged and singly-charged bosons is similar to that of the HTM. The constraints on the GM model from precision electroweak data, LEP data, and current LHC data are summarised in Ref. [46].

11.7.6 *Composite Higgs models*

Within the SM, EWSB is posited but has no dynamical origin. Furthermore, the Higgs boson appears to be unnaturally light. A scenario that remedies these two catches is to consider the Higgs boson as a bound state of new dynamics becoming strong around the weak scale. The Higgs boson can be made significantly lighter than the other resonances of the strong sector if it appears as a pseudo-Nambu–Goldstone boson, see Refs. [11] for reviews.

11.7.6.1 *Little Higgs models*

The idea behind the Little Higgs boson models [394] is to identify the Higgs doublet as a (pseudo) Nambu–Goldstone boson while keeping some sizeable non-derivative interactions, in particular a largish Higgs quartic interaction. By analogy with QCD where the pions $\pi^{\pm,0}$ appear as Nambu–Goldstone bosons associated to the breaking of the chiral symmetry $\mathrm{SU}(2)_\mathrm{L} \times \mathrm{SU}(2)_\mathrm{R}/\mathrm{SU}(2)$, switching on some interactions that break explicitly the global symmetry will generate masses for the would-be massless Nambu–Goldstone bosons of the order of $g\Lambda_{G/H}/(4\pi)$, where g is the coupling of the symmetry breaking interaction and $\Lambda_{G/H} = 4\pi f_{G/H}$ is the dynamical scale of the global symmetry breaking G/H. In the case of the Higgs boson, the top Yukawa interaction or the gauge interactions themselves will certainly break explicitly (part of) the global symmetry since they act non-linearly on the Higgs boson. Therefore, obtaining a Higgs boson mass around 125 GeV would demand a dynamical scale $\Lambda_{G/H}$ of the order of 1 TeV, which is known to lead to too large oblique corrections. Raising the strong dynamical scale by at least one order of magnitude requires an additional selection rule to ensure that a Higgs boson mass is generated at the 2-loop level only

$$m_H^2 = \frac{g^2}{16\pi^2}\Lambda_{G/H}^2 \to m_H^2 = \frac{g_1^2 g_2^2}{(16\pi^2)^2}\Lambda_{G/H}^2. \tag{11.65}$$

The way to enforce this selection rule is through a "collective breaking" of the global symmetry:

$$\mathcal{L} = \mathcal{L}_{G/H} + g_1\mathcal{L}_1 + g_2\mathcal{L}_2. \tag{11.66}$$

Each interaction $\mathcal{L}_1$ or $\mathcal{L}_2$ individually preserves a subset of the global symmetry such that the Higgs boson remains an exact Nambu–Goldstone boson whenever either g_1 or g_2 is vanishing. A mass term for the Higgs boson can be generated only by diagrams involving simultaneously both interactions. At one-loop, such diagrams are not quadratically divergent, so the Higgs boson mass is not UV sensitive. Explicitly, the cancellation of the SM quadratic divergences is achieved by a set of new particles around the Fermi scale: gauge bosons, vector-like quarks, and extra massive scalars, which are related, by the original global symmetry, to the SM particles with the same spin. Contrary to SUSY, the cancellation of the quadratic divergences is achieved by same-spin particles. These new particles, with definite couplings to SM particles as dictated by the global symmetries of the theory, are perfect goals for the LHC.

The simplest incarnation of the collective breaking idea, the so-called littlest Higgs boson model, is based on a non-linear σ-model describing the spontaneous breaking SU(5) down to SO(5). A subgroup $\mathrm{SU}(2)_1 \times \mathrm{U}(1)_1 \times \mathrm{SU}(2)_2 \times \mathrm{U}(1)_2$ is weakly gauged. This model contains a weak doublet, that is identified with the Higgs doublet, and a complex weak triplet whose mass is not protected by collective breaking. Other popular little Higgs models are based on different coset spaces: minimal moose $(\mathrm{SU}(3)^2/\mathrm{SU}(3))$, the simplest little Higgs $(\mathrm{SU}(3)^2/\mathrm{SU}(2)^2)$, the bestest little Higgs $(\mathrm{SO}(6)^2/\mathrm{SO}(6))$. For comprehensive reviews, see Ref. [395].

Generically, oblique corrections in Little Higgs models are reduced either by increasing the coupling of one of the gauge groups (in the case of product group models) or by increasing the masses of the W and Z partners, leading ultimately to a fine-tuning of the order of a few percents (see for instance Ref. [396] and references therein). The compatibility of Little Higgs models with experimental data is significantly improved when the global symmetry involves a custodial symmetry as well as a T-parity [397] under which, in analogy with R-parity in SUSY models, the SM particles are even and their partners are odd. Such Little Higgs models would therefore appear in colliders as jet(s) with missing

Downloaded from https://academic.oup.com/ptep/article/2022/8/083C01/6651666 by KIT Library user on 27 September 2022

transverse energy [398] and the ATLAS and CMS searches for squarks and gluinos can be recast to obtain limits on the masses of the heavy vector-like quarks. The T-even top partner, with an expected mass below 1 TeV to cancel the top loop quadratic divergence without too much fine-tuning, would decay dominantly into a $t+Z$ pair or into a $b+W$ pair or even into $t+H$. The latest CMS and ATLAS direct searches [399] for vector-like top partners put a lower bound around 1.1–1.3 TeV (for various branching fraction combinations), excluding the most natural region of the parameter space of these models, i.e., imposing a fine-tuning below the percent level.

The motivation for Little Higgs models is to solve the little hierarchy problem, i.e., to push the need for new physics (responsible for the stability of the weak scale) up to around 10 TeV. Per se, Little Higgs models are effective theories valid up to their cut-off scale $\Lambda_{G/H}$. Their UV completions could either be weakly or strongly coupled.

11.7.6.2 *Models of partial compositeness*

Even in composite models, the Higgs boson cannot appear as a regular resonance of the strong sector without endangering the viability of the setup when confronted to data. The way out is that the Higgs boson appears as a pseudo Nambu–Goldstone boson: the new strongly coupled sector is supposed to be invariant under a global symmetry G spontaneously broken to a subgroup H at the scale f (the typical mass scale of the resonances of the strong sector is $m_\rho \sim g_\rho f$ with g_ρ the characteristic coupling of the strong sector). To avoid conflict with EW precision measurements, the strong interactions themselves should better not break the EW symmetry. Hence the SM gauge symmetry itself should be contained in H. See Table 11.14 for a few examples of coset spaces.

Table 11.14: Global symmetry breaking patterns and the corresponding Goldstone boson contents of the SM, the minimal composite Higgs model, the next to minimal composite Higgs model, and the minimal composite two Higgs doublet model. Note that the SU(3) model does not have a custodial invariance. a denotes a CP-odd scalar while h and H are CP-even scalars.

Model	Symmetry Pattern	Goldstones
SM	SO(4)/SO(3)	W_L, Z_L
–	SU(3)/SU(2)×U(1)	W_L, Z_L, H
MCHM	SO(5)/SO(4)	W_L, Z_L, H
NMCHM	SO(6)/SO(5)	W_L, Z_L, H, a
MC2HM	SO(6)/SO(4)×SO(2)	$W_L, Z_L, h, H, H^\pm, a$

The SM (light) fermions and gauge bosons cannot be part of the strong sector itself since LEP data have already put stringent bounds on the compositeness scale of these particles far above the TeV scale. The gauge bosons couple to the strong sector by a weak gauging of a SU(2)×U(1) subgroup of the global symmetry G. Inspiration for the construction of such models comes from the AdS/CFT correspondence: the components of a gauge field along an extra warped space dimension can be interpreted as the Goldstone bosons resulting from the breaking of global symmetry of the strong sector. The couplings of the SM fermions to the strong sector could a priori take two different forms:

(i) a bilinear coupling of two SM fermions to a composite scalar operator, $\mathcal{O}$, of the form $\mathcal{L} = y\,\bar{q}_L u_R \mathcal{O} + h.c.$, in simple analogy with the SM Yukawa interactions. This is the way fermion masses were introduced in technicolor theories and it generically comes with severe flavour problems and calls for extended model-building gymnastics [12] to circumvent them;

(ii) a linear mass mixing with fermionic vector-like operators: $\mathcal{L} = \lambda_L\,\bar{q}_L \mathcal{Q}_R + \lambda_R \bar{\mathcal{U}}_L u_R$. $\mathcal{Q}$ and $\mathcal{U}$ are two fermionic composite operators of mass M_Q and M_U.

Being part of the composite sector, the composite fermionic operators can have a direct coupling of generic order Y_* to the Higgs boson. In analogy with the photon-ρ mixing in QCD, once the linear mixings are diagonalised, the physical states are a linear combination of elementary and composite fields. Effective Yukawa couplings are generated and read for instance for the up-type quark

$$y = Y_* \sin\theta_L \sin\theta_R \tag{11.67}$$

where $\sin\theta_i = \lambda_i/\sqrt{M_{Q,U}^2 + \lambda_i^2}$, $i = L, R$, measure the amount of compositeness of the SM left- and right-handed up-type quark. If the strong sector is flavour-anarchic, i.e., if the couplings of the Higgs boson to the composite fermions does not exhibit any particular flavour structure, the relation Eq. (11.67) implies that the light fermions are mostly elementary states ($\sin\theta_i \ll 1$), while the third generation quarks need to have a sizable degree of compositeness. The partial compositeness paradigm offers an appealing dynamical explanation of the hierarchies in the fermion masses. In fact, assuming the strong sector to be almost conformal above the confinement scale, the low-energy values of the mass-mixing parameters $\lambda_{L,R}$ are determined by the (constant) anomalous dimension of the composite operator they mix with. If the UV scale at which the linear mixings are generated is large, then $\mathcal{O}(1)$ differences in the anomalous dimensions can generate naturally large hierarchies in the fermion masses via renormalisation group running [400]. While the introduction of partial compositeness greatly ameliorated the flavor problem of the original composite Higgs models, nevertheless, it did not solve the issue completely, at least in the case where the strong sector is assumed to be flavour-anarchic [401]. While the partial compositeness set-up naturally emerges in models built in space-times with extra dimensions, no fully realistic microscopic realisation of partial compositeness has been proposed in the literature.

Another nice aspect of the partial compositeness structure is the dynamical generation of the Higgs potential that is not arbitrary like in the SM. The Higgs boson being a pseudo-Nambu–Goldstone boson, its mass does not receive any contribution from the strong sector itself but it is generated at the one-loop level via the couplings of the SM particles to the strong sector since these interactions are breaking the global symmetries under which the Higgs doublet transforms non-linearly. Obtaining $v \ll f$, as required phenomenologically, requires some degree of tuning, which scales like $\xi \equiv v^2/f^2$. A mild tuning of the order of 10% ($\xi \approx 0.1$) is typically enough to comply with electroweak precision constraints. This is an important point: in partial compositeness models, the entire Higgs potential is generated at one loop, therefore the separation between v and f can only be obtained at a price of a tuning. This marks a difference with respect to the Little Higgs models which realise a parametric hierarchy between the quartic and mass terms through the collective symmetry breaking mechanism. In fact in Little Higgs models, the quartic coupling is a tree-level effect, leading to a potential

$$V(H) \approx \frac{g_{\rm SM}^2}{16\pi^2} m_\rho^2 H^2 + g_{\rm SM}^2 H^4, \tag{11.68}$$

where $g_{\rm SM}$ generically denotes the SM couplings. The minimisation condition reads $v^2/f^2 \sim g_\rho^2/(16\pi^2)$, therefore v is formally loop suppressed with respect to f. This is the major achievement of the Little Higgs constructions, which however comes at the price of the presence of sub-TeV vectors carrying EW quantum numbers and therefore giving rise generically to large oblique corrections to the propagators of the W and the Z gauge bosons.

After minimisation, the dynamically generated potential leads to an estimate of the Higgs boson mass as

$$m_H^2 \approx g_\rho^3\, y_t 2\pi^2 v^2. \tag{11.69}$$

It follows that the limit $f \to \infty$, i.e., $\xi \to 0$, is a true decoupling limit: all the resonances of the strong sector become heavy but the Higgs boson whose mass is protected by the symmetries of the coset G/H. When compared to the experimentally measured Higgs boson mass, this estimate puts an upper bound on the strength of the strong interactions: $g_\rho \lesssim 2$. In this limit of not so large coupling, the Higgs potential receives additional contributions. In particular, the fermionic resonances in the top

Downloaded from https://academic.oup.com/ptep/article/2022/8/083C01/6651666 by KIT Library user on 27 September 2022

sector which follow from the global symmetry structure of the new physics sector can help raising the Higgs boson mass. Using some dispersion relation techniques, the mass of the Higgs is connected to the resonance masses. In the minimal SO(5)/SO(4) model, it was shown [402] that a 125 GeV mass can be obtained if at least one of the fermionic resonances is lighter than $\sim 1.4\,f$. As in SUSY scenarios, the top sector is playing a crucial role in the dynamics of EWSB and can provide the first direct signs of new physics. The direct searches for these top partners, in particular the ones with exotic electric charges 5/3, are already exploring the natural parameter spaces of these models [403].

The main physics properties of a pseudo Nambu–Goldstone Higgs boson can be captured in a model-independent way by a small number of higher-dimensional operators. Indeed, the strong dynamics at the origin of the composite Higgs boson singles out a few operators among the complete list discussed earlier in Section 11.6: these are the operators that involve extra powers of the Higgs doublets, and they are therefore generically suppressed by a factor $1/f^2$ as opposed to the operators that involve extra derivatives or gauge bosons that are suppressed by a factor $1/(g_\rho^2 f^2)$. The relevant effective Lagrangian describing a strongly interacting light Higgs boson is:

$$\mathcal{L}_{\rm SILH} = \frac{c_H}{2f^2}\left(\partial_\mu\left(\Phi^\dagger\Phi\right)\right)^2 + \frac{c_T}{2f^2}\left(\Phi^\dagger \overleftrightarrow{D}^\mu \Phi\right)^2 - \frac{c_6\lambda}{f^2}\left(\Phi^\dagger\Phi\right)^3 + \left(\sum_f \frac{c_f\, y_f}{f^2}\Phi^\dagger\Phi \bar{f}_L \Phi f_R + \text{h.c.}\right). \tag{11.70}$$

Typically, these new interactions induce deviations in the Higgs boson couplings that scale like $\mathcal{O}(v^2/f^2)$. Hence, the measurements of the Higgs boson couplings can be translated into some constraints on the compositeness scale, $4\pi f$, of the Higgs boson. The peculiarity of these composite models is that, due to the Goldstone nature of the Higgs boson, the direct couplings to photons and gluons are further suppressed and generically the coupling modifiers scale like

$$\kappa_{W,Z,f} \sim 1 + \mathcal{O}\left(\frac{v^2}{f^2}\right), \quad \kappa_{Z\gamma} \sim \mathcal{O}\left(\frac{v^2}{f^2}\right), \quad \kappa_{\gamma,g} \sim \mathcal{O}\left(\frac{v^2}{f^2}\times\frac{y_t^2}{g_\rho^2}\right), \tag{11.71}$$

where g_ρ denotes the typical coupling strength among the states of the strongly coupled sector and y_t is the top Yukawa coupling, the largest interaction that breaks the Goldstone symmetry. The $\kappa_{Z\gamma,\gamma,g}$ coupling modifiers are not generated by the strong coupling operators of Eq. (11.70) but by some subleading form-factor operator generated by loops of heavy resonances of the strong sector. The coupling modifiers also receive additional contributions from the other resonances of the strong sector, in particular the fermionic resonances of the top sector that are required to be light to generate a 125 GeV Higgs boson mass. Some indirect information on the resonance spectrum could thus be inferred by a precise measurement of the Higgs boson coupling deviations. However, it was realised, see in particular Ref. [295], that the task is actually complicated by the fact that, in the minimal models, these top partners give a contribution to both κ_t (resulting from a modification of the top Yukawa coupling) and κ_γ and κ_g (resulting from new heavy particles running into the loops) and the structure of interactions is such that the net effect vanishes for inclusive quantities like $\sigma(gg \to H)$ or $\Gamma(H \to \gamma\gamma)$ as a consequence of the Higgs low energy theorem [25, 26, 293]. So, one would need to rely on differential distribution, like the Higgs boson p_T distribution discussed in Section 11.2.4.1, to *see* the top partner effects in Higgs data [404]. The off-shell channel $gg \to H^* \to 4\ell$ [272] and the double Higgs boson production $gg \to HH$ [405] can also help to resolve the gluon loop and separate the top and top-partner contributions.

11.7.6.3 *Minimal composite Higgs models*

The minimal composite Higgs models (MCHM) are concrete examples of the partial compositeness paradigm. The Higgs doublet is described by the coset space SO(5)/SO(4) where a subgroup $\mathrm{SU}(2)_L\times\ \mathrm{U}(1)_Y$ is weakly gauged and under which the four Goldstone bosons transform as a doublet of hypercharge 1. There is some freedom on how the global symmetry is acting on the SM fermions: in MCHM4 the quarks and leptons are embedded into spinorial representations of SO(5), while in MHCM5 they are part of fundamental representations (it might also be interesting phenomenologically to consider larger representations like MCHM14 [406] with the SM fermions inside a representation of dimension 14). It is also possible to consider that fermions of different chirality and flavour are in different representations of SO(5), leading to a more varied phenomenology [407]. The non-linearly realised symmetry acting on the Goldstone bosons leads to general predictions of the coupling of the Higgs boson to the EW gauge bosons. For instance, it can be shown that the quadratic terms in the W and Z bosons read

$$m_W^2(H)\left(W_\mu W^\mu + \frac{1}{2\cos^2\theta_W} Z_\mu Z^\mu\right), \tag{11.72}$$

with $m_W(H) = \frac{gf}{2}\sin\frac{H}{f}$. Expanding around the EW vacuum, the expression of the weak scale is $v = f\sin(\langle H\rangle/f)$. And the values of the modified Higgs boson couplings to the W and Z become:

$$g_{HVV} = \frac{2m_V^2}{v}\sqrt{1-v^2/f^2}, \quad g_{HHVV} = \frac{2m_V^2}{v^2}(1-2v^2/f^2). \tag{11.73}$$

Note that the Higgs boson couplings to gauge bosons is always suppressed compared to the SM prediction. This is a general result [408] that holds as long as the coset space is compact.

The Higgs boson couplings to the fermions depend on the representation which the SM fermions are embedded into. The most commonly used embeddings consider all fermion doublets and singlets in the same representations. While, in MCHM4 and MCHM5, the modifications of the couplings depend only on the Higgs boson compositeness scale, in MCHM14 the leading corrections depend also on the mass spectrum of the resonances [406]. This is due to the fact that more than one SO(5) invariant gives rise to SM fermion masses. The (κ_V, κ_f) experimental fit of the Higgs boson couplings can be used to derive a lower bound on the Higgs boson compositeness scale $4\pi f \gtrsim 9$ TeV, which is less stringent than the indirect bound obtained from EW precision data, $4\pi f \gtrsim 15$ TeV [409] but more robust and less subject on assumptions [410].

11.7.6.4 *Twin Higgs models*

In all composite models presented above, the particles responsible for canceling the quadratic divergences in the Higgs boson mass are charged under the SM gauge symmetries. In particular, the top partner carries color charge, implying a reasonably large minimal production cross section at the LHC. An alternative scenario, which is experimentally quite challenging and might explain the null result in various new physics searches, is the case nowadays referred to as "neutral naturalness" [13, 14], where the particles canceling the 1-loop quadratic divergences are neutral under the SM. The canonical example for such theories is the Twin Higgs model of Ref. [13]. This is an example of a pseudo-Goldstone boson model with an approximate global SU(4) symmetry broken to SU(3). The Twin Higgs model is obtained by gauging the $\mathrm{SU}(2)_A\times\ \mathrm{SU}(2)_B$ subgroup of SU(4), where $\mathrm{SU}(2)_A$ is identified with the SM $\mathrm{SU}(2)_L$, while $\mathrm{SU}(2)_B$ is the twin SU(2) group. Gauging this subgroup breaks the SU(4) symmetry explicitly, but quadratically divergent corrections do not involve the Higgs boson when the gauge couplings of the two SU(2) subgroups are equal, $g_A = g_B$. The SU(4)$\to$ SU(3) breaking will also result in the breaking of the twin $\mathrm{SU}(2)_B$ group and, as a result, three of the seven Goldstone bosons will be eaten, leaving 4 Goldstone bosons corresponding to the SM Higgs doublet. In fact, imposing the Z_2 symmetry on the full model will ensure the cancellation of all 1-loop quadratic divergences to the Higgs boson mass. Logarithmically divergent terms can, however, arise for example from

Downloaded from https://academic.oup.com/ptep/article/2022/8/083C01/6651666 by KIT Library user on 27 September 2022

gauge loops, leading to a Higgs boson mass of order $g^2 f/4\pi$, which is of the order of the physical Higgs boson mass for $f \sim 1$ TeV. The quadratic divergences from the top sector can be eliminated if the Z_2 protecting the Higgs boson mass remains unbroken by the couplings that result in the top Yukawa coupling. This can be achieved by introducing top partners charged under a twin $\mathrm{SU}(3)_C$. In this case, the quadratic divergences are cancelled by top partners that are neutral under the SM gauge symmetries.

Twin Higgs models are low-energy effective theories valid up to a cutoff scale of order $\Lambda \sim 4\pi f \sim$ 5–10 TeV, beyond which a UV completion has to be specified. The simplest such possibility is to also make the Higgs boson composite, and to UV complete the twin Higgs model via gauge and top partners at masses of the order of a few TeV. A concrete implementation is the holographic twin Higgs model [411], which also incorporates a custodial symmetry to protect the T-parameter from large corrections. It is based on a warped extra dimensional theory with a bulk SO(8) gauge group, which incorporates the SU(4) global symmetry discussed above enlarged to contain the $\mathrm{SU}(2)_L \times \mathrm{SU}(2)_R$ custodial symmetry. In addition, the bulk contains either a full SU(7) group or an $\mathrm{SU}(3) \times \mathrm{SU}(3) \times \mathrm{U}(1) \times \mathrm{U}(1) \times Z_2$ subgroup of it to incorporate the QCD, its twin, and the hypercharge local symmetries. The breaking on the UV brane is to the SM symmetries and their twin symmetries, while on the IR brane $\mathrm{SO}(8) \to \mathrm{SO}(7)$, giving rise to the 7 Goldstone bosons, three of which will be again eaten by the twin W, Z. The main difference compared to ordinary composite Higgs models is that, in composite twin Higgs models, the cancellation of the one-loop quadratic divergences is achieved by the twin partners. They have a mass of order 700 GeV–1 TeV and they are uncharged under the SM gauge group. This allows the IR scale of the warped extra dimension to be raised to the multi-TeV range without reintroducing the hierarchy problem. The role of the composite partners is to UV complete the theory, rather than to cancel the one-loop quadratic divergences. For more details about the composite twin Higgs models, see Refs. [412].

11.7.7 *Searches for signatures of extended Higgs sectors*

The measurements described in Sections 11.3 to 11.6 have established the existence of one state of the electroweak symmetry breaking sector, compatible with a SM Higgs boson, but not that it is the only one. As was discussed above, several classes of models beyond the SM require extended Higgs sectors. The searches are typically designed to be as model-independent as possible[8] and can be categorised in the classes summarised as follows:

- **(i)** the search for an additional CP-even state mostly in the high mass domain decaying to vector bosons, which would correspond either to the heavy CP-even state in a generic 2HDM where the light state would be the discovered Higgs boson at 125 GeV or to a generic additional singlet;
- **(ii)** the search for a state in the high mass domain decaying to pairs of fermions, which would correspond to the CP-odd A or the heavy CP-even state H in a generic 2HDM;
- **(iii)** the search for charged Higgs bosons, which also appear in generic 2HDMs;
- **(iv)** the search for a CP-odd state a in the low mass region which appears in the NMSSM in a variety of final states, e.g., with one or two a bosons decaying to pairs of photons, muons, taus, and b-quarks;
- **(v)** the search for doubly charged Higgs bosons which are expected in extensions of the Higgs sector with triplets.

Below is a concise description of the most recent searches performed at the LHC and elsewhere. A summary of these searches in terms of final states is given in Table 11.15 where the corresponding references are given for more details.

11.7.7.1 *Searches for an additional CP-even state*

(a) Exclusion limits from LEP

The searches for the SM Higgs boson at LEP provided an absolute lower limit of 114 GeV on its mass. These searches are also relevant for non-SM Higgs bosons. These searches were interpreted as 95% CL upper bounds on the ratio of the coupling g_{HZZ} to its SM prediction as a function of the Higgs boson mass [131, 485]. These results have an impact on MSSM benchmarks such as the low-m_H scenario where the heavy CP-even Higgs boson is the discovered 125 GeV boson [348], which is also nearly ruled out by current direct constraints and charged Higgs boson limits from LHC. These results also impact scenarios of light CP-even Higgs boson of the NMSSM which are constrained to project predominantly onto the EW singlet component. Additional interest for these scenarios is due to the slight excess observed at LEP [131] at a Higgs boson mass hypothesis of approximately 98 GeV, bolstered by a possible excess in the diphoton channel at 96 GeV in Run 2 data of CMS [416].

(b) Searches at the LHC

At the LHC, the searches for the SM Higgs boson before the 2012 discovery covered a wide range of mass hypotheses up to approximately 1 TeV. After the discovery, the SM Higgs boson searches have been reappraised to search for a heavy CP-even state, extending progressively the search mass range beyond 1 TeV. This state could be the heavy CP-even Higgs boson of a 2HDM, or a generic additional singlet. In both cases, the natural width of the additional H state can be very different from that of the SM Higgs boson. To preserve unitarity of the longitudinal vector boson scattering and the longitudinal vector boson scattering into fermion pairs, the couplings of the additional CP-even Higgs boson to gauge bosons and fermions should not be too large and should constrain the natural width to be smaller than that of a unique Higgs boson at high mass with couplings to fermions and gauge bosons as predicted by the SM (and provided that trilinear and quartic couplings are not too large and that no new state affects the heavy state total width). It is therefore reasonable to consider total widths for the high mass CP-even state smaller than the equivalent SM width. Two specific cases have been considered: (i) the SM width using the complex pole scheme (CPS), and (ii) the narrow width approximation. For the sake of generality, these searches are now done as a function of the Higgs boson mass and total width.

Searches for the Higgs boson in the channels $H \to \gamma\gamma$, $H \to Z\gamma$, $H \to WW^{(*)}$ leptonic and semi-leptonic, and in the $H \to ZZ^{(*)}$ searches in the 4ℓ, $\ell\ell q\bar{q}$ and $\ell\ell\nu\nu$ channels have also been done, but some of them are simple reinterpretations of the SM Higgs boson search in the CPS scheme. References for these searches are summarised in Table 11.15.

(c) Searches for an additional resonance decaying to a pair of Higgs bosons

In addition to the rare and expected Higgs boson pair production mode, high mass CP-even Higgs bosons can be searched for in the resonant double Higgs boson mode. Searches for such processes, where the Higgs boson is used as a tool for searches for BSM phenomena, have been carried out in a variety of distinct modes depending on the subsequent decays of each Higgs bosons. ATLAS and CMS have searched for the $H \to hh \to b\bar{b}\tau\tau$, $b\bar{b}\gamma\gamma$, $H \to hh \to 4b$, $H \to hh \to \gamma\gamma WW^*$, $H \to hh \to bbWW^*$, $H \to hh \to WW^*WW^*$ and $H \to hh \to bbZZ^*$ final states. For mass hypotheses of an additional Higgs boson below 500 GeV, the two dominant search channels are the $b\bar{b}\gamma\gamma$ and the $b\bar{b}\tau\tau$ channels. For masses above 500 GeV, the most powerful search is with the $4b$ final state. As illustrated in Figure 11.19, these searches provide useful limits in the low $\tan\beta$ and high mass domain. The list of references for these searches is given in Table 11.15.

(d) Searches for an additional state with the presence of the Higgs boson

In the post-discovery era, analyses searching for additional Higgs bosons need to take into account the presence of the 125 GeV Higgs boson. For searches with sufficiently high mass resolution to disentangle the additional states which are not degenerate in mass, the strength of the observed state and limits on the signal

[8] Still, most non-SUSY models are likely to include further states and dynamics above the weak scale to stabilise the scalar sector and this new and unknown physics may influence the searches described in this section in a way difficult to estimate.

Downloaded from https://academic.oup.com/ptep/article/2022/8/083C01/6651666 by KIT Library user on 27 September 2022

Table 11.15: Summary of references to the searches for additional states from extended Higgs sectors. (BBr) denotes the BaBar experiment and (TeV), the Tevatron experiments. V denotes either the W or the Z boson. Only Run 2 searches references are indicated except when searches have been carried out using Run 1 data only. References for Run 1 searches are available in Ref. [132].

	ATLAS	CMS	Other experiments
CP-even H			
$H \to \gamma\gamma$	[413]	[414]	—
$H \to \gamma\gamma$ (low mass)	[415]	[416]	—
$H \to Z\gamma$	[417]	[418]	—
$H \to ZZ \to 4\ell$	[419]	[420]	—
$H \to ZZ \to \ell\ell\nu\nu$	[419]	[421]	—
$H \to ZZ \to \ell\ell q\bar{q}$	[422]	[423, 424]	—
$H \to ZZ \to \nu\nu q\bar{q}$	[425]	—	—
$H \to WW \to \ell\nu\ell\nu$	[426]	[427]	—
$H \to WW \to \ell\nu q\overline{q'}$	[428]	[427]	—
$H \to VV \to q\overline{q'}q\overline{q'}(JJ)$	[429, 430]	—	—
$H \to VV$ combination	[431]	—	—
$H \to hh \to b\bar{b}\tau\tau, b\bar{b}\gamma\gamma, 4b,$ $\gamma\gamma WW^*, bbWW^*, WW^*WW^*, bbZZ^*$	[432, 433]	[424, 434, 435]	—
CP-odd A (and/or CP-even H)			
$H, A \to \tau^+\tau^-$	[436]	[437]	[438, 439] (TeV) [440] (LHCb)
$A \to \tau^+\tau^-$ (low mass)	—	[441]	—
$H, A \to \mu^+\mu^-$	[442]	[443]	—
$H \to \mu\tau, e\tau$ LFV		[444]	—
$bj\mu^+\mu^-$ (low $\mu^+\mu^-$ mass)	[445]	[446]	—
$H, A \to t\bar{t}$	[430, 447]	[448]	
$H, A \to b\bar{b}$	[449]	[450]	[451, 452] (TeV)
$A \to hV \to b\bar{b}q\overline{q'}, b\bar{b}\ell\nu, b\bar{b}\ell\ell, \ell\ell\tau\tau, \nu\bar{\nu}b\bar{b}$	[453, 454]	[455, 456]	
$H \to ZA \to b\bar{b}\ell^+\ell^-$	[457]	[458]	—
Charged $H^\pm$			
$H^\pm \to \tau^\pm\nu$	[459, 460]	[461]	—
$H^\pm \to cs$	[462]	[463]	—
$H^\pm \to tb$	[464]	[465]	—
$H^\pm \to W^\pm Z$	[466]	[467, 468]	—
$H^\pm \to W^\pm A$	—	[469]	—
$H^\pm \to cb$	—	[470]	—
CP-odd NMSSM a			
$a \to \mu^+\mu^-$	[471]	[472]	—
$h \to aa \to 4\mu, 4\tau, 2\mu 2\tau, 4\gamma,$	[473]	[474–477]	[478] (TeV)
$aa \to \mu^+\mu^-\mu^+\mu^-$	—	[479]	—
$bb\mu\mu, bb\tau\tau$			[480] (LEP)
$\Upsilon_{1s,3s} \to a\gamma$	—	—	[481, 482] (BBr)
Doubly charged $H^{\pm\pm}$	[483]	[468, 484]	—

strength of a potential additional state can be set independently, as discussed in the next section. However, in some cases where channels do not have a sufficiently fine mass resolution to resolve states nearly degenerate in mass, specific analyses need to be designed. There are two examples of such analyses: (i) the search for an additional state in the $H \to WW^{(*)} \to \ell\nu\ell\nu$ channel in ATLAS, and (ii) the search for nearly degenerate states in the $H \to \gamma\gamma$ channel with the CMS detector.

In the $H \to WW^{(*)} \to \ell\nu\ell\nu$ channel, the search for an additional state is done using a boosted decision tree combining several discriminating kinematic characteristics to separate both the signal from the background and a high mass signal H from the lower mass state h [486]. A simultaneous fit of the two states h and H is then made to test the presence of an additional state. In this case, the usual null hypothesis of background includes the SM signal.

The CMS search for nearly degenerate mass states decaying to a pair of photons [487] is more generic and could for instance apply to CP-odd Higgs bosons as well. It consists of a fit to the diphoton mass spectrum using two nearly degenerate mass templates.

(e) Type I 2HDM and fermiophobia

The measurements of coupling properties of the 125 GeV Higgs boson directly establish its couplings to fermions. However, the presence of an additional fermiophobic state, as predicted by Type I 2HDMs, is not excluded. Prior to the discovery, ATLAS and CMS have performed searches for a fermiophobic Higgs boson, i.e., produced through couplings with vector bosons only (VBF and VH) and decaying in two photons. CMS has further combined these results with searches in the W^+W^- and ZZ channels, assuming fermiophobic production and decay. This way, CMS excluded a fermiophobic Higgs boson in the range 110 GeV $< m_H <$ 188 GeV at the 95% CL. References for these Run 1 measurements can be found in Ref. [132]

11.7.7.2 *Searches for additional neutral states ($\phi \equiv h$, H, A) decaying to fermions*

(a) Exclusion limits from LEP

In e^+e^- collisions, around the centre-of-mass energies reached by LEP, the main production mechanisms of the neutral MSSM Higgs bosons were the Higgs-strahlung processes $e^+e^- \to hZ$, HZ and the pair production processes $e^+e^- \to hA$, HA, while the vector boson fusion processes played a marginal role. Higgs boson decays to $b\bar{b}$ and $\tau^+\tau^-$ were used in these searches.

The searches and limits from the four LEP experiments are described in Refs. [488]. The combined LEP data did not contain any excess of events which would imply the production of a Higgs boson. Combined limits were derived [485]. For $m_A \gg M_Z$, the limit on m_h is nearly that of the SM searches, as $\sin^2(\beta - \alpha) \approx 1$. For high values of $\tan\beta$ and low m_A ($m_A \leq m_h^{max}$), the $e^+e^- \to hA$ searches become the most important, and the lightest

Downloaded from https://academic.oup.com/ptep/article/2022/8/083C01/6651666 by KIT Library user on 27 September 2022

Higgs boson h is non SM-like. In this region, the 95% CL mass bounds are $m_h > 92.8\,\text{GeV}$ and $m_A > 93.4\,\text{GeV}$. In the m_h^{max} scenario [489], values of $\tan\beta$ from 0.7 to 2.0 are excluded taking $m_t = 174.3\,\text{GeV}$, while a much larger $\tan\beta$ region is excluded for other benchmark scenarios such as the no-mixing one.

A flavour-independent limit for Higgs bosons in the Higgs-strahlung process at LEP has also been set at 112 GeV [490].

Neutral Higgs bosons may also be produced by Yukawa processes $e^+e^- \to f\bar{f}\phi$, where the Higgs particle $\phi \equiv h,\ H,\ A$, is radiated off a massive fermion ($f \equiv b$ or $\tau^\pm$). These processes can be dominant at low masses, and whenever the $e^+e^- \to hZ$ and hA processes are suppressed. The corresponding ratios of the $f\bar{f}h$ and $f\bar{f}A$ couplings to the SM coupling are $-\sin\alpha/\cos\beta$ and $\tan\beta$, respectively. The LEP data have been used to search for $b\bar{b}\,b\bar{b}$, $b\bar{b}\tau^+\tau^-$, and $\tau^+\tau^-\,\tau^+\tau^-$ final states [491]. Regions of low mass and high enhancement factors are excluded by these searches.

The searches for the Higgs boson at LEP also included the case where it does not predominantly decay to a pair of b quarks. All four collaborations conducted dedicated searches for the Higgs boson with reduced model dependence, assuming it is produced via the Higgs-strahlung process, and not addressing its flavour of decay, a lower limit on the Higgs boson mass of 112.9 GeV is set by combining the data of all four experiments [490].

Using an effective Lagrangian approach and combining results sensitive to the $h\gamma\gamma$, $hZ\gamma$ and hZZ couplings, an interpretation of several searches for the Higgs boson was made and set a lower limit of 106.7 GeV on the mass of a Higgs boson that can couple anomalously to photons [490].

(b) Searches at the Tevatron and the LHC

The best sensitivity is in the regime with low to moderate m_A and with large $\tan\beta$ which enhances the couplings of the Higgs bosons to down-type fermions. The corresponding limits on the Higgs boson production cross section times the branching ratio of the Higgs boson into down-type fermions can be interpreted in MSSM benchmark scenarios [492]. The most promising channels at the Tevatron are the inclusive $p\bar{p} \to \phi \to \tau^+\tau^-$ process ($\phi = A, H, h$), with contributions from both $gg \to \phi$ and $b\bar{b}\phi$ production, and $b\bar{b}\phi, \phi \to \tau^+\tau^-$ or $\phi \to b\bar{b}$, with $b\tau\tau$ or three tagged b-jets in the final state, respectively. Although the Higgs boson production via gluon fusion has a higher cross section in general than via associated production, it cannot be used to study the $\phi \to b\bar{b}$ decay mode since the signal is overwhelmed by the QCD background.

CDF and D0 have searched for neutral Higgs bosons produced in association with bottom quarks and which decay into $b\bar{b}$ [451, 452], or into $\tau^+\tau^-$ [438,439]. The most recent searches in the $b\bar{b}\phi$ channel with $\phi \to b\bar{b}$ analyse approximately $2.6\,\text{fb}^{-1}$ (CDF) and $5.2\,\text{fb}^{-1}$ (D0) of data, seeking events with at least three b-tagged jets. The cross section is defined such that at least one b quark not from ϕ decay is required to have $p_T > 20\,\text{GeV}$ and $|\eta| < 5$. The invariant mass of the two leading jets as well as b-tagging variables are used to discriminate the signal from the backgrounds. The QCD background rates and shapes are inferred from data control samples, in particular, the sample with two b-tagged jets and a third, untagged jet. Separate-signal hypotheses are tested and limits are placed on $\sigma(p\bar{p} \to b\bar{b}\phi) \times \text{BR}(\phi \to b\bar{b})$. A local excess of approximately 2.5σ significance has been observed in the mass range of 130–160 GeV, but D0's search is more sensitive and sets stronger limits. The D0 result had a $\mathcal{O}(2\sigma)$ local upward fluctuation in the 110 to 125 GeV mass range. These results have been superseded by the LHC searches and the excess seen by D0 has not been confirmed elsewhere.

A substantially larger sensitivity in the search for the $\phi \to \tau^+\tau^-$ is obtained with the ATLAS and CMS analyses. The higher centre-of-mass energy reached at the Run 2 brings a substantial, though not excessively large, increase in sensitivity due to the intermediate masses probed. Both ATLAS and CMS have reported the result of their searches in this important channel with the full 2016 dataset. The searches are performed in categories of the decays of the two tau leptons: $e\tau_{\text{had}}$, $\mu\tau_{\text{had}}$, $e\mu$, and $\mu\mu$, where τ_{had} denotes a tau lepton which decays to one or more hadrons plus a tau neutrino, e denotes $\tau \to e\nu\nu$, and μ denotes $\tau \to \mu\nu\nu$. The dominant background comes from $Z \to \tau^+\tau^-$ decays, although $t\bar{t}$, W+jets and Z+jets events contribute as well. Separating events into categories based on the number of b-tagged jets improves the sensitivity in the MSSM. The $b\bar{b}$ annihilation process and radiation of a Higgs boson from a b quark gives rise to events in which the Higgs boson is accompanied by a $b\bar{b}$ pair in the final state. Requiring the presence of one or more b-jets reduces the background from Z+jets. Data control samples are used to constrain background rates. The rates for jets to be identified as a hadronically decaying tau lepton are measured in dijet samples, and W+jets samples provide a measurement of the rate of events that, with a fake hadronic tau, can pass the signal selection requirements. Lepton fake rates are measured using samples of isolated lepton candidates and same-sign lepton candidates. Constraints from the ATLAS searches are shown in Fig. 11.19 (left) in the hMSSM approximation defined in Ref. [350]. The neutral Higgs boson searches consider the contributions of both the CP-odd and CP-even neutral Higgs bosons with enhanced couplings to bottom quarks, similarly to was done for the Tevatron results. In Fig. 11.19, decays of the charged Higgs boson into $\tau\nu$ and decays of the heavy Higgs boson into a pair of SM-like Higgs bosons or gauge bosons, or decays of A into hZ are also being constrained. In addition, decays of the neutral Higgs bosons into muon pairs are also being explored. In the $m_h^{\text{mod}+}$ scenario, the region of $\tan\beta$ lower than 5 does not allow for a Higgs boson mass m_h close to 125 GeV. For the hMSSM scenario, instead, the SM-like Higgs boson mass is fixed as an input and hence the requirement that it is close to 125 GeV is always fulfilled, although this may imply other limitations as discussed in Section 11.7.1.1.

A search for $\phi \to \mu^+\mu^-$ has also been performed by ATLAS [442] and CMS [443] and no significant deviations from the SM expectation were observed, allowing to set model-independent limit on the product of the branching fraction for the decay into a muon pair and the cross section for the production of a scalar neutral boson, either via gluon fusion, or in association with b quarks, in the mass range from 130 to 1000 GeV.

Finally, searches for a resonance decaying to a top quark pair were done by ATLAS [447, 493] and CMS [448, 494]. These searches were interpreted as searches for scalar resonances by ATLAS [447], however, an important component of these searches is an accurate treatment of the interference effects between the signal and the continuum background. These effects can yield a dip and peak structure instead of a simple peak [346]. ATLAS has performed a search for a high mass state decaying to a pair of top quarks taking into account the deformation in mass shape of the signal in the presence of the continuum background [495].

The LHC has the potential to explore a broad range of SUSY parameter space through the search for non-SM-like Higgs bosons. As illustrated in Fig. 11.19, the parameter space corresponding to large $\tan\beta$ values and large masses of the A boson are covered mostly by the searches in the $A, H \to \tau^+\tau^-$ channel. A projection of the combined sensitivity of ATLAS and CMS at the HL-LHC has been performed in Ref. [111], showing that, compared to the current sensitivity, the full HL-LHC luminosity can expand the exclusion domain by nearly 1 TeV. In the low $\tan\beta$ limit, the parameter space spanning large A boson masses is best excluded indirectly from the observed Higgs boson measurements. This is illustrated in the M_h^{125} scenario by the nearly horizontal exclusion which is due to the compatibility of the Higgs boson mass measurement with its prediction from radiative corrections (mostly from the stop sector). Nevertheless, Fig. 11.19 (right) shows a broad region with intermediate $\tan\beta$ and large values of m_A that is not accessed by current searches, and in which the most promising channel is the very difficult search for $t\bar{t}$ decays with its aforementioned intricacies [353]. In this region of parameter space, it is possible that only the SM-like Higgs boson can be within the LHC's reach. If no other state of the EWSB sector than the 125 GeV state is discovered, it may be challenging to determine only from the Higgs sector whether there is a SUSY extension of the SM in nature.

Downloaded from https://academic.oup.com/ptep/article/2022/8/083C01/6651666 by KIT Library user on 27 September 2022

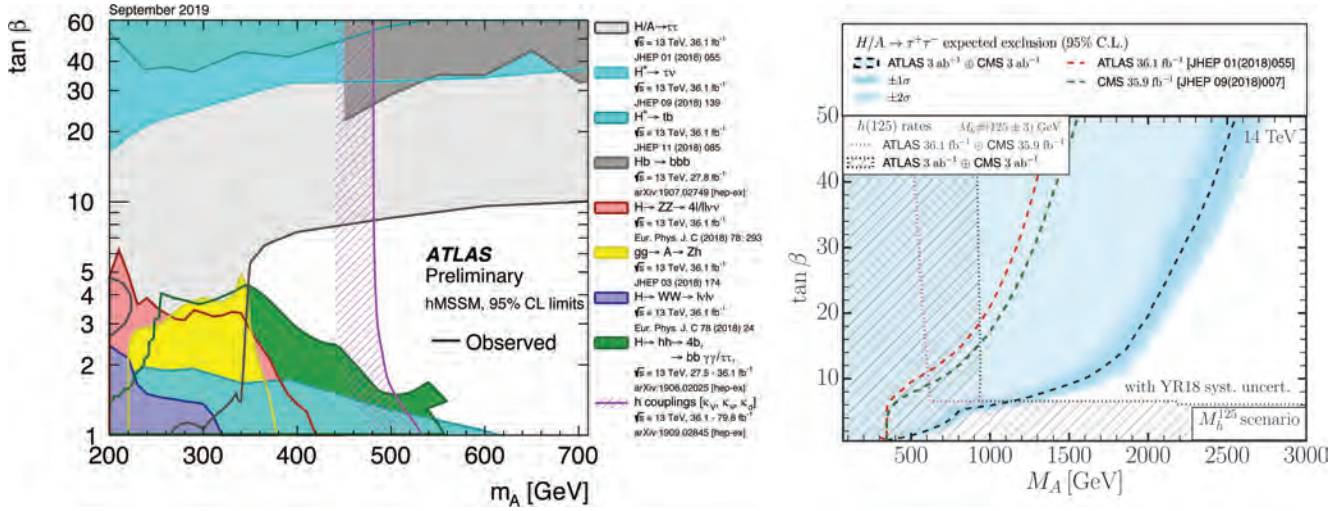

Figure 11.19: The 95% CL exclusion contours in the $(M_A, \tan\beta)$ parameter space for: (left) a summary of ATLAS Run 2 searches in the hMSSM and (right) the projected sensitivity for the combination of ATLAS and CMS searches in the $A, H \to \tau^+\tau^-$ channel at HL-LHC and the interpretation of the constraints from the measurements of the Higgs boson couplings in the M_h^{125} benchmark [353] (the projected ATLAS sensitivity in the $A, H \to \tau^+\tau^-$ channel used for this projection was not optimised for high masses, when re-optimised similar sensitivities are obtained between ATLAS and CMS).

11.7.7.3 *Searches for a CP-odd state decaying to hZ*

Similarly, to the search for a CP-even high mass Higgs boson decaying to a pair of Higgs bosons, the search for a CP-odd states decaying to hZ was carried out at the LHC by ATLAS and CMS in various channels:

(i) $(Z \to \ell\ell)(h \to b\bar{b})$,
(ii) $(Z \to \nu\nu)(h \to b\bar{b})$,
(iii) $(Z \to \ell\ell)(h \to \tau\tau)$,
(iv) and $(Z \to \ell\ell)(h \to \tau\tau)$.

The searches where the A boson decays to a pair of b quarks have been performed both in the regime where both b-jets are resolved and in the boosted regime where the two b-jets are merged in a single larger radius jet. These searches have been used to constrain the parameter space of 2HDMs. In the MSSM, these searches place limits on small values of $\tan\beta$ for masses of A between 220 GeV and 360 GeV.

11.7.7.4 *Searches for low mass states*

Searches for pseudo-scalar Higgs boson at intermediate to low masses, below the Z mass (in the 25 GeV to 80 GeV mass range) have been performed by CMS both in the $\tau^+\tau^-$ [496] and the $\mu^+\mu^-$ [497] decay channels. A light pseudo-scalar in this mass range is excluded by current direct constraints in the MSSM but not in general 2HDMs [498]. These searches are done in the decay channels where the pseudo-scalar Higgs boson is produced in association with a pair of b-quarks and decays into a pair of taus or muons.

CMS has also reported an anomaly observed in the search for $\mu^+\mu^-$ resonances produced with one jet tagged as containing a b-hadron and a forward jet in the Run 1 data. A mild excess appeared in the di-muon mass distribution at approximately 28 GeV. Another very mild excess was then also found in the 2016 Run 2 data [446]. ATLAS then performed a similar analysis with the full Run 2 dataset corresponding to an integrated luminosity of approximately 139 fb^{-1}, and no significant excess was found [445].

Searches for low mass Higgs bosons were also performed in the diphoton channel by both ATLAS and CMS [499, 500] at Run 1. CMS has updated the results of this search with Run 2 data [416]. A modest excess has been observed by CMS at a mass of 95.3 GeV with a local significance of 2.8σ (the corresponding global significance is 1.3σ). A slight excess was also seen by CMS in the 8 TeV data at a slightly higher mass of 97.6 GeV with a local significance of 2.0σ (1.47σ global). No significant excess has been observed in this region by ATLAS neither in the Run 1 nor Run 2 [413] data. It should, however, be noted that the ATLAS search does not reach the level of sensitivity to exclude at the 95% CL the excess seen in CMS. This mildly significant excess also coincides in mass with the excess observed at LEP and discussed in Section 11.7.7.1. It has therefore raised interest and speculations on its possible nature, see for instance Ref. [501] and references therein.

11.7.7.5 *Searches for charged Higgs bosons $H^\pm$*

At e^+e^- colliders, charged Higgs bosons can be pair produced in the s-channel via γ or Z boson exchange. This process is dominant in the LEP centre-of-mass energies range, i.e., up to 209 GeV. At higher centre-of-mass energies, other processes can play an important role such as the production in top quark decays via $t \to b + H^+$ if $m_{H^\pm} < m_t - m_b$ or via the one-loop process $e^+e^- \to W^\pm H^\mp$ [502, 503], which allows the production of a charged Higgs boson with $m_{H^\pm} > \sqrt{s}/2$, even when H^+H^- production is kinematically forbidden. Other single charged Higgs boson production mechanisms include $t\bar{b}H^-/\bar{t}bH^+$ production [116], $\tau^+\nu H^-/\tau^-\bar{\nu}H^+$ production [504], and a variety of processes in which $H^\pm$ is produced in association with a one or two other gauge and/or Higgs bosons [505].

At hadron colliders, charged Higgs bosons can be produced in several different modes depending on the value of its mass with respect to the top-quark mass. For light values of the charged Higgs boson mass, defined by Higgs boson masses smaller than the mass of the top quark (with experimental analyses typically considering masses up to $m_{H^\pm} \leq 160$ GeV), the top-quark decay $t \to Hb$ is allowed and the charged Higgs boson is light enough so that top-quark off-shell effects can be neglected. The cross section for the production of a light charged Higgs boson is simply given by the product of the top-pair production cross section and the branching ratio of a top quark into a charged Higgs boson. The top-pair production cross section is known up to NNLO in perturbative QCD [506], and relevant QCD and SUSY-QCD including NLO corrections to the branching ratio for $t \to H^+b$ have been computed in the literature, see Refs. [507–509] and references therein. At present, the theoretical accuracy for the production of a light charged Higgs boson is at the few percent level. For the intermediate mass range, values of $m_{H^\pm}$ near m_t, the finite top-width effects as well as the interplay between top-quark resonant and non-resonant diagrams cannot be neglected. Hence, the full process $pp \to H^\pm W^\mp b\bar{b}$ (with massive b-quarks) must be considered to perform a reliable perturbative calculation of the charged Higgs boson production cross section [509]. For heavy charged Higgs boson scenarios, with charged Higgs boson masses larger than the top-quark mass (typically above 180 GeV), the dominant charged

Downloaded from https://academic.oup.com/ptep/article/2022/8/083C01/6651666 by KIT Library user on 27 September 2022

Higgs boson production channel is the associated production with a top quark/antiquark and a (possibly low transverse momentum) bottom antiquark/quark. Theoretical calculation at NLO have been computed both at the inclusive and fully-differential level in the five-flavour scheme and in the four-flavour scheme, see Ref. [46] and references therein. Charged Higgs bosons can also be produced via associated production with $W^{\pm}$ bosons through $b\bar{b}$ annihilation and gg-fusion annihilation [510].

For charged Higgs boson production cross section predictions for the Tevatron and the LHC, see Refs. [44, 45, 345].

(a) Exclusion limits from LEP

Charged Higgs bosons have been searched for at LEP, where the combined data of the four experiments, ALEPH, DELPHI, L3, and OPAL, were sensitive to masses of up to about 90 GeV [485] in two decay channels, $\tau\nu$ and $c\bar{s}$. The combined LEP data exclude, at 95% CL, charged Higgs bosons with mass below 80 GeV (Type II scenario) or 72.5 GeV (Type I scenario) [511].

(b) Exclusion limits from Tevatron

Compared to the mass domain covered by LEP searches, the Tevatron covered a complementary range of charged Higgs boson masses. CDF and D0 have also searched for charged Higgs bosons in top quark decays with subsequent decays to $\tau\nu$ or to $c\bar{s}$ [512]. For the $H^+ \to c\bar{s}$ channel, the limits on $\mathrm{BR}(t \to H^+ b)$ from CDF and D0 are $\approx 20\%$ in the mass range $90\,\mathrm{GeV} < m_{H^+} < 160\,\mathrm{GeV}$ and assuming a branching fraction of 100% in this specific final state. $H^+ \to \tau^+\nu_\tau$ channel, D0's limits on $\mathrm{BR}(t \to H^+ b)$ are also $\approx 20\%$ in the same mass range and assuming a branching fraction of 100% in this final state. These limits are valid in general 2HDMs, and they have also been interpreted in terms of the MSSM [512].

(c) Exclusion limits from LHC

Similarly, to the Tevatron, at the LHC, light charged Higgs bosons can be searched for in the decays of top quarks. The main initial production mode for light charged Higgs bosons ($m_{H^\pm} < m_t - m_b$) is top pair production. The subsequent decay modes of the charged Higgs boson for these searches are $\tau\nu$ and $c\bar{s}$. More recently, ATLAS and CMS have also searched for higher mass charged Higgs bosons ($m_{H^\pm} > m_t + m_b$) in $H^+ \to t\bar{b}$. The main production modes are the associated production of a charged Higgs boson in association with a top and a bottom quark or in association with a top quark only.

The decay $H^+ \to \tau^+\nu_\tau$ is searched typically in three final state topologies:

(i) lepton+jets: with $t\bar{t} \to \bar{b}WH^+ \to b\bar{b}(q\bar{q}')(\tau_{\mathrm{lep}}\nu)$, i.e., the W boson decays hadronically and the tau decays into an electron or a muon, with two neutrinos;

(ii) τ +lepton: with $t\bar{t} \to \bar{b}WH^+ \to b\bar{b}(l\nu)(\tau_{\mathrm{had}}\nu)$, i.e., the W boson decays leptonically (with $\ell = e, \mu$) and the tau decays hadronically;

(iii) τ+jets: $t\bar{t} \to \bar{b}WH^+ \to b\bar{b}(q\bar{q}')(\tau_{\mathrm{had}}\nu)$, i.e., both the W boson and the τ decay hadronically.

CMS has also searched for the charged Higgs boson in the decay products of top quark pairs: $t\bar{t} \to H^\pm W^\mp b\bar{b}$ and $t\bar{t} \to H^+H^- b\bar{b}$ as well. Three types of final states with large missing transverse energy and jets originating from b-quark hadronisation have been analysed: the fully-hadronic channel with a hadronically decaying tau in association with jets, the dilepton channel with a hadronically decaying tau in association with an electron or muon and the dilepton channel with an electron-muon pair. The results of the searches at the LHC are illustrated in Figure 11.19.

Both ATLAS and CMS have also searched for high mass charged Higgs bosons decaying to a top and bottom quarks. The main production mode for this search is the associated production with one top quark (5-flavour scheme) or a top quark and and bottom quark (4-flavour scheme) in the final state. The s-channel production mode where the charged Higgs boson is produced alone in the final state at tree level is also considered. This search is particularly intricate and it is sensitive to the modelling of the top pair production background produced in association with additional partons and in particular b-quarks. No excess was found and the results are expressed in terms of exclusion limits of cross section times branching fractions.

ATLAS and CMS have also searched for charged Higgs bosons in top quark decays assuming $\mathrm{BR}(H^+ \to c\bar{s}) = 100\%$ [462, 513], and sets limits of $\approx 20\%$ on $\mathrm{BR}(t \to H^+ b)$ in the $90\,\mathrm{GeV} < m_{H^+} < 160\,\mathrm{GeV}$ mass range.

In 2HDMs, the decay of the charged Higgs boson to a W and a Z boson is allowed only at loop level and is therefore suppressed. However the $H^\pm \to W^\pm Z$ decay channel is allowed in Higgs triplet models. ATLAS [466] has searched for such decays, requiring that the charged Higgs boson is produced through the fusion of vector bosons. No excess with respect to the SM backgrounds has been observed in this channel, and the results are interpreted in the Georgi–Machacek model [387] discussed in Section 11.7.5.2.

At the LHC, various other channels still remain to be explored, in particular searches involving additional neutral scalars in particular in the WH, WA channels (A is the pseudo-scalar MSSM Higgs boson), and in the Wa channel (a is the light CP-odd scalars of the NMSSM).

11.7.7.6 *Interpretation of the measurements of the coupling properties of the Higgs boson*

The 125 GeV Higgs boson being part of any hypothetically extended EWSB sector, it can be used through the compatibility of its measured couplings and mass with those predicted in specific models to provide constraints on these specific models parameters.

As discussed in Section 11.7.1.1, the mass of the Higgs boson limits drastically the MSSM parameter space and can be used to set limits on specific MSSM benchmarks. This is the case for the Mh125 scenario as illustrated in Figure 11.18 and in Figure 11.19, corresponding approximately to a lower limit on $\tan\beta$ in this model [111].

The measurements of the Higgs boson couplings, discussed in Section 11.6, can be interpreted in the framework of a constrained model where the couplings of the Higgs boson to vector bosons, up-type quarks, down-type quarks and leptons, are varied. In 2HDMs, these couplings are functions of the mixing angle α between the observed Higgs boson and the heavy CP-even neutral scalar, and of the ratio of the vacuum expectation values of the two doublets, $\tan\beta$. In the case of the MSSM, the two parameters are the A boson mass and $\tan\beta$ (the sole two parameters needed to describe the MSSM Higgs sector at tree level). The coupling measurements have been interpreted both by ATLAS [514] and CMS [301] in specific MSSM benchmarks and in 2HDMs. The exclusion contour in the hMSSM for the ATLAS combination [514] is illustrated in Figure 11.19.

11.7.7.7 *Searches for a light CP-odd Higgs boson*

A light pseudo-scalar boson a is present in any two Higgs doublet model enhanced with an additional singlet field. A prominent example is the NMSSM. The theoretical motivations for singlet extensions of the MSSM are discussed in Section 11.7.2. There is also a variety of other models with light additional spin-0 bosons such as two Higgs doublet models with a scalar, Little Higgs models or light scalar mediator to a dark sector.

In the framework of the NMSSM, the searches now focus on the low a mass region for several reasons:

(i) in the NMSSM, the light pseudo-scalar a boson can, as a pseudo-Goldstone boson, be a natural candidate for an axion;

(ii) scenarios where $m_a > 2m_b$ and a CP-even state h decaying to a pair of a ($m_h > 2m_a$) are excluded by direct searches at LEP in the four b's channel [478, 485, 515];

(iii) in the pre-discovery era, LEP limits on a CP-even Higgs boson resulted in fine-tuning MSSM constraints [516] which could be evaded through non standard decays of the Higgs boson to aa;

(iv) in the NMSSM, a CP-odd a boson with a mass in the range 9.2–12 GeV can also account for the difference observed between the measured anomalous muon magnetic moment and its prediction [517].

Downloaded from https://academic.oup.com/ptep/article/2022/8/083C01/6651666 by KIT Library user on 27 September 2022

The benchmark scenarios have also changed in the light of the Higgs boson discovery. The 125 GeV state could be the lightest or the next-to-lightest of the three CP-even states of the NMSSM. Light pseudo-scalar scenarios are still very interesting in particular for the potential axion candidate. There are three main types of direct searches for the light a boson:

(i) for masses below the Υ resonance, the search is for radiative decays $\Upsilon \to a\gamma$ at B-factories;

(ii) the inclusive search in high energy pp collisions at the LHC;

(iii) the search for decays of the observed CP-even Higgs h boson into a pair of a bosons.

Radiative decays $\Upsilon \to a\gamma$ have been searched for in various colliders, the most recent results are searches for radiative decays of the $\Upsilon(1s)$ to $a\gamma$ with a subsequent decay of the a boson to a pair of taus at CLEO [518], and the radiative decays of the $\Upsilon(1s, 2s, 3s)$ to $a\gamma$ with subsequent decays to a pair of muons or taus by BaBar [481, 482].

Direct inclusive searches for the light pseudo scalar a boson were performed in the $a \to \mu\mu$ channel at the Tevatron by D0 [478] and by ATLAS [471], CMS [472], and LHCb [165] at the LHC.

Finally, searches for the decays of the Higgs boson to a pair of a bosons where performed with subsequent decays to four photons, in the four muons final state, in the two muons and two taus final state, and in the four taus final state.

No significant excess in the searches for a light CP-odd a boson was found and limits on the production times branching fractions of the a boson have been set.

References for all these searches are summarised in Table 11.15.

11.7.7.8 *Searches for doubly charged Higgs bosons $H^{\pm\pm}$*

As discussed in Section 11.7.5, the generation of small neutrino masses via the standard EWSB mechanism described in Section 11.2 requires unnaturally small Yukawa couplings, provided that neutrinos are Dirac-type fermions. A Majorana mass term with a see-saw mechanism for neutrinos, would allow for naturally small masses and would also yield a framework for the appealing scenario of leptogenesis. However, within the SM, Majorana mass terms correspond to (non-renomalizable) dimension-5 operators. Such effective interactions can be generated via renormalisable interactions with an electroweak triplet of complex scalar fields (corresponding to a type-II see-saw mechanism). Other models such as the Zee–Babu model, with the introduction of two $\mathrm{SU}(2)_L$ singlets, also generate Majorana mass terms. The signature of such models would be the presence of doubly charged Higgs bosons $H^{\pm\pm}$.

The main production mechanisms of $H^{\pm\pm}$ bosons at hadron colliders are the pair production in the s-channel through the exchange of a Z boson or a photon and the associated production with a charged Higgs boson through the exchange of a W boson. Various searches for doubly charged Higgs bosons have been performed by ATLAS and CMS at Run 1 [519] and Run 2 [483, 484]. Typically, these searches aim at low values of the Higgs triplet vacuum expectation for which the doubly charged Higgs boson will decay mostly to leptons (for high values, the decay to W bosons will become predominant). These searches assume that the coupling to W bosons is negligible and that the main production mode is through the Drell–Yan process.

11.7.7.9 *Searches for non-standard production processes of the Higgs boson*

The discovery of the Higgs boson has also allowed for searches of BSM processes involving standard decays of the Higgs boson. One example directly pertaining to the search for additional states of the EWSB sector is the search for Higgs bosons in the cascade decay of a heavy CP-even Higgs boson decaying to charged Higgs boson and a W boson, and the charged Higgs boson subsequently decaying to H and another W boson. This search has been performed by ATLAS in $b\bar{b}$ decays of the 125 GeV Higgs boson [520].

11.7.7.10 *Outlook on searches for additional states*

The LHC program of searches for additional states covers a large variety of decay and production channels. Since the Higgs boson discovery, many new channels have been explored at the LHC, e.g., the searches for additional states decaying into hh or Vh or ZA. The search for charged Higgs bosons has been extended to include the WZ, WA and the very difficult $t\bar{b}$ decay channel.

11.8 Summary and outlook

Summary– The discovery of the Higgs boson is a major milestone in the history of particle physics as well as an extraordinary achievement of the LHC machine and the ATLAS and CMS experiments. Nine years after the discovery, substantial progress in the field of Higgs boson physics has been accomplished and a significant number of measurements probing the nature of this unique particle have been made. They are revealing an increasingly precise profile of the Higgs boson.

The LHC has now concluded its Run 2, delivering a dataset of 13 TeV pp collisions corresponding to an integrated luminosity of approximately 140 fb^{-1} of data collected by ATLAS and CMS. With the substantial increase in production rates at the higher center-of-mass energy and the larger datasets, new landmark results in Higgs physics have been achieved.

Three new results of fundamental importance have been achieved with Run 2 datasets by ATLAS and CMS independently: (i) the clear and unambiguous observation of the Higgs boson decay to taus; (ii) the clear and unambiguous observation of the Higgs boson decay to a pair of b quarks; (iii) the clear and unambiguous observation of the production of the Higgs boson through the $t\bar{t}H$ process. These results provide direct evidence for the Yukawa coupling of the Higgs boson to fermions of the third generation: taus, bottom quarks and top quarks, at rates compatible with those expected in the SM. In addition, with the full Run 2 dataset, a first evidence for the decay of the Higgs boson to muons was achieved. These, and all other experimental measurements, are consistent with the EWSB mechanism of the SM.

New theoretical calculations and developments in Monte-Carlo simulation pertaining to Higgs physics are still occurring at a rapid pace. For example, the theoretical prediction for the dominant gluon fusion production mode now includes the latest N3LO result, which is twice as precise as previous N2LO calculations. With these improvements in the state-of-the-art theory predictions and the increase in luminosity and center-of-mass energy, Higgs physics has definitively entered a precision era. Its impact can already be seen on the latest Run 2 combined measurements of the Higgs boson couplings (see Section 11.6).

Since the discovery of the Higgs boson, new ideas have emerged to probe its rare decays and production modes, as well as to indirectly measure the Higgs boson width through the study of its off-shell couplings, or via on-shell interference effects. The Higgs boson has now become part of the standard toolkit in searches for new physics.

Many extensions of the SM at higher energies call for an enlargement of the EWSB sector. Hence, direct searches for additional scalar states can provide valuable insights on the dynamics of the EWSB mechanism. The ATLAS and CMS experiments have searched for additional Higgs bosons in the Run 2 data, and have imposed constraints in broad ranges of mass and couplings for various scenarios with an extended Higgs sector.

The landscape of Higgs physics has been extended extraordinarily since its discovery. The current precisions on the measurements of the couplings of the Higgs boson to gauge bosons and third generation fermions are typically of the order of 10–20%. The uncertainty on the Higgs boson coupling to the muon shrank below 50%, and the upper limits on the branching fraction to new invisible particles are approximately 10%. The sensitivity to the Higgs boson self-coupling has not reached the SM value yet and there is no information on how the Higgs field acquired its VEV in the early times of the Universe. This situation allows for new challenges to ultimately increase further the reach in precision and it also widens the possibilities of unveiling the true nature and the dynamics of the electroweak symmetry breaking.

Outlook– The unitarisation of the vector boson scattering (VBS) amplitudes, dominated at high energies by their longitudinal polarisation, has been the basis of the *no lose* theorem at the LHC, and was a determining consideration in the building of the accelerator and detectors. It motivated the existence of a Higgs

Downloaded from https://academic.oup.com/ptep/article/2022/8/083C01/6651666 by KIT Library user on 27 September 2022

boson or the observability of manifestations of strong dynamics at the TeV scale. Now that a Higgs boson has been found and its couplings to gauge bosons are consistent with the SM predictions, perturbative unitarity is preserved to a large extent with the sole exchange of the Higgs boson, and without the need for any additional states. VBS is, however, still an important channel to further investigate in order to better understand the nature of the Higgs sector and the possible completion of the SM at the TeV scale. In association with the double Higgs boson production channel by vector boson fusion, VBS could, for instance, confirm that the Higgs boson is part of a weak doublet and also establish whether it is an elementary object or a composite state that could emerge as a pseudo-Nambu–Goldstone boson from a new underlying broken symmetry.

The fermion-Higgs boson couplings are not governed by local gauge symmetry. Thus, in addition to a new particle, the LHC has also discovered a new force, different in nature from the other fundamental interactions since it is non-universal and distinguishes between the three families of quarks and leptons. The existence of the Higgs boson embodies the problem of an unnatural cancellation among the quantum corrections to its mass if new physics is present at scales significantly higher than the EW scale. The non-observation of additional states which could stabilise the Higgs boson mass is a challenge for natural scenarios like SUSY or models with a new strong interaction in which the Higgs boson is not a fundamental particle. This increasingly pressing paradox starts questioning the principle of naturalness or inspires new solutions tied to the cosmological evolution of the Universe.

The search for the Higgs boson has occupied the particle physics community for the last 50 years. Its discovery has shaped and sharpened the physics programs of the LHC and of prospective future accelerators [521]. With the HL-LHC, the precision will improve by a factor 5–10 on all observables with respect to current data. Table 11.12 displays the expected sensitivities in the characterization of the Higgs boson at HL-LHC: in this table, the parameters κ_i specify by how much the coupling of the Higgs boson to a given particle i deviates from the SM expectation. The only channels which are expected to be limited by data statistics are the rare decays to muons and $Z\gamma$. In all other cases, the experimental systematic uncertainties are similar to the statistical uncertainties, but the dominant source of uncertainty arises from theory, and this remains the case even after assuming that, by the end of the HL-LHC run, the theory uncertainties can be reduced by a factor two compared to the current uncertainties, a hypothesis that appears realistic but still requires dedicated and concerted work [111]. For both hadron and lepton colliders, some theoretical progress is crucial to fully exploit and capitalise on the experimental data. In particular, the expected HL-LHC data together with rapid ongoing progress in theoretical calculations are defining a new era of precision Higgs boson measurements.

Acknowledgements

We would like to thank many of our colleagues for proofreading this review, for useful criticism and for their input in general: W. Altmannshofer, J. de Blas, G. Branco, J. Campbell, F. Caola, F. Cerutti, C. Csáki, R. Contino, J. Conway, N. Craig, A. David, S. Dawson, J.B. De Vivie, J. D'Hondt, G. Durieux, C. Englert, J.R. Espinosa, A. Falkowski, L. Fayard, W. Fischer, S. Forte, M. Grazzini, J. Gu, H. Haber, B. Heinemann, S. Heinemeyer, J. Hubisz, A. Korytov, B. Jäger, H. Ji, T. Junk, P. Langacker, J. Lykken, F. Maltoni, M.L. Mangano, B. Mansoulié, M. McCullough, R. Mishra, M. Mühlleitner, B. Murray, M. Neubert, A. Nisati, Y. Paul, G. Perez, G. Petrucciani, A. Pomarol, E. Pontón, R. Rattazzi, D. Rebuzzi, F. Riva, R. Salerno, E. Salvioni, N. Shah, G. Shaughnessy, M. Spira, O. Stål, A. Strumia, K. Tackmann, R. Tanaka, J. Terning, A. Vartak, C. Wagner, A. Weiler, A. Wulzer, and G. Zanderighi. We are also most grateful to the ATLAS, CDF, CMS and D0 collaborations for their help with this review.

M.C. is supported by Fermilab, that is operated by Fermi Research Alliance, LLC under Contract No. DE–AC02–07CH11359 with the United States Department of Energy. C.G. is supported by the Helmholtz Association and by the Deutsche Forschungsgemeinschaft under Germany's Excellence Strategy – EXC 2121 "Quantum Universe" – 390833306. V.S. is supported by the grant DE–SC0009919 of the United States Department of Energy.

References

[1] G. Aad *et al.* (ATLAS), Phys. Lett. **B716**, 1 (2012), [arXiv:1207.7214].

[2] S. Chatrchyan *et al.* (CMS), Phys. Lett. **B716**, 30 (2012), [arXiv:1207.7235].

[3] S.L. Glashow, Nucl. Phys. **20**, 579 (1961); S. Weinberg, Phys. Rev. Lett. **19**, 1264 (1967); A. Salam, *Elementary Particle Theory*, eds.: Svartholm, Almquist and Wiksells, Stockholm, 1968; S. L. Glashow, J. Iliopoulos and L. Maiani, Phys. Rev. **D2**, 1285 (1970).

[4] F. Englert and R. Brout, Phys. Rev. Lett. **13**, 321 (1964), [,157(1964)]; P. W. Higgs, Phys. Rev. **145**, 1156 (1966); G. S. Guralnik, C. R. Hagen and T. W. B. Kibble, Phys. Rev. Lett. **13**, 585 (1964), [,162(1964)].

[5] J. M. Cornwall, D. N. Levin and G. Tiktopoulos, Phys. Rev. Lett. **30**, 1268 (1973), [Erratum: Phys. Rev. Lett. **31**, 572 (1973)]; J. M. Cornwall, D. N. Levin and G. Tiktopoulos, Phys. Rev. **D10**, 1145 (1974), [Erratum: Phys. Rev. **D11**, 972 (1975)]; C. H. Llewellyn Smith, Phys. Lett. **46B**, 233 (1973); B. W. Lee, C. Quigg and H. B. Thacker, Phys. Rev. **D16**, 1519 (1977).

[6] K. G. Wilson, Phys. Rev. **D3**, 1818 (1971); G. 't Hooft, in *Proc. of 1979 Cargèse Institute on Recent Developments in Gauge Theories,* p. 135 Press, New York 1980; For a modern discussion, see the GGI Tea Break's Seminar by G.F. Giudice and R. Rattazzi, https://is.gd/nUnjAr (2021).

[7] J. Wess and B. Zumino, Phys. Lett. **49B**, 52 (1974).

[8] S. P. Martin, Adv. Ser. Direct. High Energy Phys. 1–98 (1998), [hep-ph/9709356].

[9] B.C. Allanach and H.E. Haber, *Supersymmetry, Part I (Theory)*, in this volume.

[10] D. B. Kaplan and H. Georgi, Phys. Lett. **136B**, 183 (1984).

[11] B. Bellazzini, C. Csaki and J. Serra, Eur. Phys. J. **C74**, 5, 2766 (2014), [arXiv:1401.2457]; G. Panico and A. Wulzer, Lect. Notes Phys. **913**, pp.1 (2016), [arXiv:1506.01961]; C. Csaki, C. Grojean and J. Terning, Rev. Mod. Phys. **88**, 4, 045001 (2016), [arXiv:1512.00468].

[12] K.M. Black, R.S. Chivukula and M. Narain, *Dynamical Electroweak Symmetry Breaking: Implications of the H0*, in this volume.

[13] Z. Chacko, H.-S. Goh and R. Harnik, Phys. Rev. Lett. **96**, 231802 (2006), [hep-ph/0506256]; Z. Chacko, H.-S. Goh and R. Harnik, JHEP **01**, 108 (2006), [hep-ph/0512088].

[14] N. Craig *et al.*, JHEP **07**, 105 (2015), [arXiv:1501.05310]; N. Craig, S. Knapen and P. Longhi, Phys. Rev. Lett. **114**, 6, 061803 (2015), [arXiv:1410.6808].

[15] P. W. Graham, D. E. Kaplan and S. Rajendran, Phys. Rev. Lett. **115**, 22, 221801 (2015), [arXiv:1504.07551]; J. R. Espinosa *et al.*, Phys. Rev. Lett. **115**, 25, 251803 (2015), [arXiv:1506.09217]; G. Dvali (2019), [arXiv:1908.05984].

[16] C. Csaki *et al.*, Phys. Rev. Lett. **126**, 091801 (2021), [arXiv:2007.14396]; N. Arkani-Hamed, R. Tito D'agnolo and H. D. Kim (2020), [arXiv:2012.04652]; R. Tito D'Agnolo and D. Teresi (2021), [arXiv:2106.04591].

[17] T. Flacke *et al.*, JHEP **06**, 050 (2017), [arXiv:1610.02025].

[18] J. Khoury and O. Parrikar, JCAP **12**, 014 (2019), [arXiv:1907.07693]; G. F. Giudice, M. McCullough and T. You (2021), [arXiv:2105.08617].

[19] M. Bauer, M. Carena and K. Gemmler, JHEP **11**, 016 (2015), [arXiv:1506.01719]; M. Bauer, M. Carena and K. Gemmler, Phys. Rev. **D94**, 11, 115030 (2016), [arXiv:1512.03458].

[20] R. Barbieri, L. J. Hall and V. S. Rychkov, Phys. Rev. **D74**, 015007 (2006), [hep-ph/0603188].

Downloaded from https://academic.oup.com/ptep/article/2022/8/083C01/6651666 by KIT Library user on 27 September 2022

[21] D. E. Morrissey and M. J. Ramsey-Musolf, New J. Phys. **14**, 125003 (2012), [arXiv:1206.2942].

[22] G. Degrassi *et al.*, JHEP **08**, 098 (2012), [arXiv:1205.6497]; S. Alekhin, A. Djouadi and S. Moch, Phys. Lett. **B716**, 214 (2012), [arXiv:1207.0980]; D. Buttazzo *et al.*, JHEP **12**, 089 (2013), [arXiv:1307.3536].

[23] S. Weinberg, Phys. Rev. Lett. **43**, 1566 (1979).

[24] See the particle listing section at `http://pdg.lbl.gov`.

[25] J. R. Ellis, M. K. Gaillard and D. V. Nanopoulos, Nucl. Phys. **B106**, 292 (1976).

[26] M. A. Shifman *et al.*, Sov. J. Nucl. Phys. **30**, 711 (1979), [Yad. Fiz.30,1368(1979)].

[27] J. F. Gunion *et al.*, *The Higgs Hunter's Guide*, Addison-Wesley (1990).

[28] P. Sikivie *et al.*, Nucl. Phys. **B173**, 189 (1980); H. Georgi, Ann. Rev. Nucl. Part. Sci. **43**, 209 (1993).

[29] M. J. G. Veltman, Nucl. Phys. **B123**, 89 (1977).

[30] M. Luscher and P. Weisz, Nucl. Phys. **B290**, 25 (1987); M. Luscher and P. Weisz, Nucl. Phys. **B295**, 65 (1988).

[31] V. Branchina, E. Messina and M. Sher, Phys. Rev. **D91**, 013003 (2015), [arXiv:1408.5302].

[32] A. Hook *et al.*, JHEP **01**, 061 (2015), [arXiv:1404.5953]; J. Kearney, H. Yoo and K. M. Zurek, Phys. Rev. **D91**, 12, 123537 (2015), [arXiv:1503.05193].

[33] J. R. Espinosa, D. Racco and A. Riotto, Phys. Rev. Lett. **120**, 12, 121301 (2018), [arXiv:1710.11196].

[34] J. R. Espinosa, D. Racco and A. Riotto, JCAP **1809**, 09, 012 (2018), [arXiv:1804.07732].

[35] A. Andreassen, W. Frost and M. D. Schwartz, Phys. Rev. **D97**, 5, 056006 (2018), [arXiv:1707.08124]; S. Chigusa, T. Moroi and Y. Shoji, Phys. Rev. Lett. **119**, 21, 211801 (2017), [arXiv:1707.09301].

[36] M. Shaposhnikov and C. Wetterich, Phys. Lett. **B683**, 196 (2010), [arXiv:0912.0208]; M. Holthausen, K. S. Lim and M. Lindner, JHEP **02**, 037 (2012), [arXiv:1112.2415].

[37] F. L. Bezrukov and M. Shaposhnikov, Phys. Lett. **B659**, 703 (2008), [arXiv:0710.3755]; F. L. Bezrukov, A. Magnin and M. Shaposhnikov, Phys. Lett. **B675**, 88 (2009), [arXiv:0812.4950].

[38] C. P. Burgess, H. M. Lee and M. Trott, JHEP **09**, 103 (2009), [arXiv:0902.4465]; J. L. F. Barbon and J. R. Espinosa, Phys. Rev. **D79**, 081302 (2009), [arXiv:0903.0355]; M. P. Hertzberg, JHEP **11**, 023 (2010), [arXiv:1002.2995].

[39] B. A. Kniehl, Phys. Rept. **240**, 211 (1994).

[40] M. Spira, Fortsch. Phys. **46**, 203 (1998), [hep-ph/9705337].

[41] M. Carena and H. E. Haber, Prog. Part. Nucl. Phys. **50**, 63 (2003), [hep-ph/0208209].

[42] A. Djouadi, Phys. Rept. **457**, 1 (2008), [hep-ph/0503172].

[43] S. Dittmaier *et al.* (LHC Higgs Cross Section Working Group), CERN Report **2011-002** (2011), [arXiv:1101.0593].

[44] S. Dittmaier *et al.* (LHC Higgs Cross Section Working Group), CERN Report **2012-002** (2012), [arXiv:1201.3084].

[45] S. Heinemeyer *et al.* (LHC Higgs Cross Section Working Group), CERN Report **2013-004** (2013), [arXiv:1307.1347].

[46] D. de Florian *et al.* (LHC Higgs Cross Section Working Group), CERN Report **2017-002** (2016), [arXiv:1610.07922].

[47] LHC Higgs Working Group, `https://twiki.cern.ch/twiki/bin/view/LHCPhysics/LHCHWG`.

[48] T. Aaltonen *et al.* (CDF, D0), Phys. Rev. **D88**, 5, 052014 (2013), [arXiv:1303.6346].

[49] H. M. Georgi *et al.*, Phys. Rev. Lett. **40**, 692 (1978).

[50] D. Graudenz, M. Spira and P. M. Zerwas, Phys. Rev. Lett. **70**, 1372 (1993).

[51] M. Spira *et al.*, Nucl. Phys. **B453**, 17 (1995), [hep-ph/9504378].

[52] C. Anastasiou *et al.*, Phys. Rev. Lett. **114**, 212001 (2015), [arXiv:1503.06056]; C. Anastasiou *et al.*, JHEP **05**, 058 (2016), [arXiv:1602.00695].

[53] R. V. Harlander and K. J. Ozeren, JHEP **11**, 088 (2009), [arXiv:0909.3420]; A. Pak, M. Rogal and M. Steinhauser, JHEP **02**, 025 (2010), [arXiv:0911.4662].

[54] J. Davies *et al.*, Phys. Rev. **D100**, 3, 034017 (2019), [arXiv:1906.00982]; M. Czakon *et al.* (2021), [arXiv:2105.04436].

[55] S. Dawson, Nucl. Phys. **B359**, 283 (1991); A. Djouadi, M. Spira and P. M. Zerwas, Phys. Lett. **B264**, 440 (1991).

[56] R. V. Harlander and W. B. Kilgore, Phys. Rev. Lett. **88**, 201801 (2002), [hep-ph/0201206]; C. Anastasiou and K. Melnikov, Nucl. Phys. **B646**, 220 (2002), [hep-ph/0207004]; V. Ravindran, J. Smith and W. L. van Neerven, Nucl. Phys. **B665**, 325 (2003), [hep-ph/0302135].

[57] A. Djouadi and P. Gambino, Phys. Rev. Lett. **73**, 2528 (1994), [hep-ph/9406432]; S. Actis *et al.*, Phys. Lett. **B670**, 12 (2008), [arXiv:0809.1301]; U. Aglietti *et al.*, Phys. Lett. **B595**, 432 (2004), [hep-ph/0404071]; G. Degrassi and F. Maltoni, Phys. Lett. **B600**, 255 (2004), [hep-ph/0407249].

[58] M. Bonetti, K. Melnikov and L. Tancredi, Phys. Rev. **D97**, 5, 056017 (2018), [Erratum: Phys. Rev. **D97**, 9, 099906 (2018)], [arXiv:1801.10403]; M. Bonetti *et al.*, JHEP **11**, 045 (2020), [arXiv:2007.09813]; M. Becchetti *et al.*, Phys. Rev. D **103**, 5, 054037 (2021), [arXiv:2010.09451].

[59] C. Anastasiou, R. Boughezal and F. Petriello, JHEP **04**, 003 (2009), [arXiv:0811.3458].

[60] C. Anastasiou *et al.*, JHEP **03**, 162 (2019), [arXiv:1811.11211].

[61] M. Bonvini *et al.*, JHEP **08**, 105 (2016), [arXiv:1603.08000]; B. Mistlberger, JHEP **05**, 028 (2018), [arXiv:1802.00833].

[62] X. Chen *et al.*, Phys. Rev. Lett. **127**, 7, 072002 (2021), [arXiv:2102.07607].

[63] G. Billis *et al.*, Phys. Rev. Lett. **127**, 7, 072001 (2021), [arXiv:2102.08039].

[64] A. Banfi, G. P. Salam and G. Zanderighi, JHEP **06**, 159 (2012), [arXiv:1203.5773]; T. Becher, M. Neubert and D. Wilhelm, JHEP **05**, 110 (2013), [arXiv:1212.2621]; A. Banfi *et al.*, JHEP **04**, 049 (2016), [arXiv:1511.02886]; J. K. L. Michel, P. Pietrulewicz and F. J. Tackmann, JHEP **04**, 142 (2019), [arXiv:1810.12911]; P. F. Monni, L. Rottoli and P. Torrielli, Phys. Rev. Lett. **124**, 25, 252001 (2020), [arXiv:1909.04704].

[65] I. Moult and I. W. Stewart, JHEP **09**, 129 (2014), [arXiv:1405.5534].

[66] V. D. Barger *et al.*, Phys. Rev. **D44**, 1426 (1991).

[67] M. Cacciari *et al.*, Phys. Rev. Lett. **115**, 8, 082002 (2015), [Erratum: Phys. Rev. Lett. **120**, 13,139901 (2018)], [arXiv:1506.02660]; F. A. Dreyer and A. Karlberg, Phys. Rev. Lett. **117**, 7, 072001 (2016), [arXiv:1606.00840]; J. Cruz-Martinez *et al.*, Phys. Lett. **B781**, 672 (2018), [arXiv:1802.02445].

[68] T. Han, G. Valencia and S. Willenbrock, Phys. Rev. Lett. **69**, 3274 (1992), [hep-ph/9206246].

[69] T. Liu, K. Melnikov and A. A. Penin, Phys. Rev. Lett. **123**, 12, 122002 (2019), [arXiv:1906.10899].

[70] F. A. Dreyer, A. Karlberg and L. Tancredi, JHEP **10**, 131 (2020), [arXiv:2005.11334].

[71] M. Rauch and D. Zeppenfeld, Phys. Rev. **D95**, 11, 114015 (2017), [arXiv:1703.05676].

[72] A. Buckley *et al.* (2021), [arXiv:2105.11399].

Downloaded from https://academic.oup.com/ptep/article/2022/8/083C01/6651666 by KIT Library user on 27 September 2022

[73] S. L. Glashow, D. V. Nanopoulos and A. Yildiz, Phys. Rev. **D18**, 1724 (1978); T. Han and S. Willenbrock, Phys. Lett. **B273**, 167 (1991); T. Han, G. Valencia, and S. Willenbrock, Phys. Rev. Lett. **69**, 3274 (1992); H. Baer, B. Bailey and J. F. Owens, Phys. Rev. **D47**, 2730 (1993); J. Ohnemus and W. J. Stirling, Phys. Rev. **D47**, 2722 (1993).

[74] A. Stange, W. J. Marciano and S. Willenbrock, Phys. Rev. **D49**, 1354 (1994), [hep-ph/9309294]; A. Stange, W. J. Marciano and S. Willenbrock, Phys. Rev. **D50**, 4491 (1994), [hep-ph/9404247].

[75] M. L. Ciccolini, S. Dittmaier and M. Kramer, Phys. Rev. **D68**, 073003 (2003), [hep-ph/0306234]; A. Denner *et al.*, JHEP **03**, 075 (2012), [arXiv:1112.5142].

[76] R. Hamberg, W. L. van Neerven and T. Matsuura, Nucl. Phys. **B359**, 343 (1991), [Erratum: Nucl. Phys. **B644**, 403 (2002)].

[77] O. Brein, A. Djouadi and R. Harlander, Phys. Lett. **B579**, 149 (2004), [hep-ph/0307206]; L. Altenkamp *et al.*, JHEP **02**, 078 (2013), [arXiv:1211.5015].

[78] J. Davies, G. Mishima and M. Steinhauser, JHEP **03**, 034 (2021), [arXiv:2011.12314]; L. Chen *et al.*, JHEP **03**, 125 (2021), [arXiv:2011.12325].

[79] O. Brein *et al.*, Eur. Phys. J. **C72**, 1868 (2012), [arXiv:1111.0761].

[80] O. Brein, R. V. Harlander and T. J. E. Zirke, Comput. Phys. Commun. **184**, 998 (2013), [arXiv:1210.5347]; R. V. Harlander *et al.*, JHEP **05**, 089 (2018), [arXiv:1802.04817].

[81] R. Gauld *et al.*, Phys. Lett. B **817**, 136335 (2021), [arXiv:2009.14209].

[82] A. Denner *et al.*, JHEP **03**, 075 (2012), [arXiv:1112.5142].

[83] G. Ferrera, M. Grazzini, and F. Tramontano, Phys. Rev. Lett. **107**, 152003 (2011).

[84] G. Ferrera, M. Grazzini and F. Tramontano, Phys. Lett. **B740**, 51 (2015), [arXiv:1407.4747]; J. M. Campbell, R. K. Ellis and C. Williams, JHEP **06**, 179 (2016), [arXiv:1601.00658].

[85] W. Astill *et al.*, JHEP **06**, 154 (2016), [arXiv:1603.01620].

[86] F. Caola *et al.*, Phys. Rev. **D97**, 7, 074022 (2018), [arXiv:1712.06954]; R. Gauld *et al.*, JHEP **10**, 002 (2019), [arXiv:1907.05836].

[87] J. M. Butterworth *et al.*, Phys. Rev. Lett. **100**, 242001 (2008), [arXiv:0802.2470].

[88] A. Behring *et al.*, Phys. Rev. D **101**, 11, 114012 (2020), [arXiv:2003.08321].

[89] W. Bizon *et al.* (2021), [arXiv:2106.06328].

[90] R. Raitio and W. W. Wada, Phys. Rev. **D19**, 941 (1979); Z. Kunszt, Nucl. Phys. **B247**, 339 (1984); J. N. Ng and P. Zakarauskas, Phys. Rev. D **29**, 876 (1984); J. F. Gunion, Phys. Lett. **B261**, 510 (1991); W. J. Marciano and F. E. Paige, Phys. Rev. Lett. **66**, 2433 (1991).

[91] W. Beenakker *et al.*, Phys. Rev. Lett. **87**, 201805 (2001), [hep-ph/0107081]; L. Reina and S. Dawson, Phys. Rev. Lett. **87**, 201804 (2001), [hep-ph/0107101]; L. Reina, S. Dawson and D. Wackeroth, Phys. Rev. D **65**, 053017 (2002), [hep-ph/0109066]; S. Dawson *et al.*, Phys. Rev. **D67**, 071503 (2003), [hep-ph/0211438]; W. Beenakker *et al.*, Nucl. Phys. **B653**, 151 (2003), [hep-ph/0211352]; S. Dawson *et al.*, Phys. Rev. **D68**, 034022 (2003), [hep-ph/0305087].

[92] Y. Zhang *et al.*, Phys. Lett. **B738**, 1 (2014), [arXiv:1407.1110]; S. Frixione *et al.*, JHEP **09**, 065 (2014), [arXiv:1407.0823]; S. Frixione *et al.*, JHEP **06**, 184 (2015), [arXiv:1504.03446].

[93] T. Plehn, G. P. Salam and M. Spannowsky, Phys. Rev. Lett. **104**, 111801 (2010), [arXiv:0910.5472].

[94] A. Kulesza *et al.*, JHEP **03**, 065 (2016), [arXiv:1509.02780]; A. Broggio *et al.*, JHEP **03**, 124 (2016), [arXiv:1510.01914]; A. Broggio *et al.*, JHEP **02**, 126 (2017), [arXiv:1611.00049]; A. Kulesza *et al.*, Phys. Rev. D **97**, 11, 114007 (2018), [arXiv:1704.03363]; A. Broggio *et al.*, JHEP **08**, 039 (2019), [arXiv:1907.04343]; A. Kulesza *et al.*, Eur. Phys. J. C **80**, 5, 428 (2020), [arXiv:2001.03031].

[95] A. Denner and R. Feger, JHEP **11**, 209 (2015), [arXiv:1506.07448].

[96] A. Denner *et al.*, JHEP **02**, 053 (2017), [arXiv:1612.07138].

[97] R. Frederix *et al.*, Phys. Lett. **B701**, 427 (2011), [arXiv:1104.5613]; M. V. Garzelli *et al.*, EPL **96**, 1, 11001 (2011), [arXiv:1108.0387].

[98] S. Catani *et al.*, Eur. Phys. J. C **81**, 6, 491 (2021), [arXiv:2102.03256].

[99] C. Brancaccio *et al.*, JHEP **08**, 145 (2021), [arXiv:2106.06516].

[100] F. Demartin *et al.*, Eur. Phys. J. **C75**, 6, 267 (2015), [arXiv:1504.00611].

[101] D. Pagani, I. Tsinikos and E. Vryonidou, JHEP **08**, 082 (2020), [arXiv:2006.10086].

[102] K.A. Assamagan *et al.*, [Higgs Working Group, "Physics at TeV Colliders" workshop, Les Houches, 2003], `arXiv:hep-ph/0406152` (2004).

[103] R. V. Harlander and W. B. Kilgore, Phys. Rev. **D68**, 013001 (2003), [hep-ph/0304035]; J. M. Campbell *et al.*, Phys. Rev. **D67**, 095002 (2003), [hep-ph/0204093]; S. Dawson *et al.*, Phys. Rev. Lett. **94**, 031802 (2005), [hep-ph/0408077]; S. Dittmaier, M. Krämer and M. Spira, Phys. Rev. **D70**, 074010 (2004), [hep-ph/0309204]; S. Dawson *et al.*, Phys. Rev. **D69**, 074027 (2004), [hep-ph/0311067].

[104] W. J. Stirling and D. J. Summers, Phys. Lett. **B283**, 411 (1992); F. Maltoni *et al.*, Phys. Rev. **D64**, 094023 (2001), [hep-ph/0106293].

[105] D. Pagani, H.-S. Shao and M. Zaro, JHEP **11**, 036 (2020), [arXiv:2005.10277].

[106] C. Grojean, A. Paul and Z. Qian, JHEP **04**, 139 (2021), [arXiv:2011.13945].

[107] S. Dawson, S. Dittmaier and M. Spira, Phys. Rev. **D58**, 115012 (1998), [hep-ph/9805244].

[108] D. de Florian and J. Mazzitelli, Phys. Rev. Lett. **111**, 201801 (2013), [arXiv:1309.6594].

[109] L.-B. Chen *et al.*, Phys. Lett. B **803**, 135292 (2020), [arXiv:1909.06808].

[110] S. Borowka *et al.*, Phys. Rev. Lett. **117**, 1, 012001 (2016), [Erratum: Phys. Rev. Lett. **117**, 7, 079901 (2016)], [arXiv:1604.06447]; J. Baglio *et al.*, Eur. Phys. J. **C79**, 6, 459 (2019), [arXiv:1811.05692]; J. Davies *et al.*, JHEP **11**, 024 (2019), [arXiv:1907.06408].

[111] M. Cepeda *et al.* (HL/HE-LHC WG2 group) (2019), [arXiv:1902.00134].

[112] J. Alison *et al.*, Rev. Phys. **5**, 100045 (2020), [arXiv:1910.00012].

[113] B.L. Ioffe and V.A. Khoze, Sov. J. Nucl. Phys. **9**, 50 (1978).

[114] D. R. T. Jones and S. T. Petcov, Phys. Lett. **84B**, 440 (1979); R. N. Cahn and S. Dawson, Phys. Lett. **136B**, 196 (1984), [Erratum: Phys. Lett. **138B**, 464 (1984)]; G. L. Kane, W. W. Repko and W. B. Rolnick, Phys. Lett. **148B**, 367 (1984); G. Altarelli, B. Mele and F. Pitolli, Nucl. Phys. **B287**, 205 (1987); W. Kilian, M. Kramer and P. M. Zerwas, Phys. Lett. **B373**, 135 (1996), [hep-ph/9512355].

[115] B. A. Kniehl, Z. Phys. **C55**, 605 (1992); J. Fleischer and F. Jegerlehner, Nucl. Phys. **B216**, 469 (1983); A. Denner *et al.*, Z. Phys. **C56**, 261 (1992); B. A. Kniehl, Int. J. Mod. Phys. **A17**, 1457 (2002), [hep-ph/0112023].

[116] K. J. F. Gaemers and G. J. Gounaris, Phys. Lett. **77B**, 379 (1978); A. Djouadi, J. Kalinowski and P. M. Zerwas, Z. Phys. **C54**, 255 (1992); B. A. Kniehl, F. Madricardo and M. Steinhauser, Phys. Rev. **D66**, 054016 (2002), [hep-ph/0205312]; S. Dittmaier *et al.*, Phys. Lett. **B441**,

Downloaded from https://academic.oup.com/ptep/article/2022/8/083C01/6651666 by KIT Library user on 27 September 2022

383 (1998), [hep-ph/9808433]; S. Dittmaier *et al.*, Phys. Lett. **B478**, 247 (2000), [hep-ph/0002035]; S. Dawson and L. Reina, Phys. Rev. **D59**, 054012 (1999), [hep-ph/9808443].

[117] A. Arbey *et al.*, Eur. Phys. J. **C75**, 8, 371 (2015), [arXiv:1504.01726]; A. Freitas *et al.* (2019), [arXiv:1906.05379].

[118] S. Frixione *et al.* (2021), [arXiv:2108.10261].

[119] A. Denner *et al.*, Eur. Phys. J. **C71**, 1753 (2011), [arXiv:1107.5909].

[120] A. Djouadi, J. Kalinowski, and M. Spira, Comp. Phys. Comm. **108**, 56 (1998); A. Djouadi *et al.*, `arXiv:1003.1643 [hep-ph]` (2010).

[121] S. G. Gorishnii *et al.*, Mod. Phys. Lett. **A5**, 2703 (1990); S. G. Gorishnii *et al.*, Phys. Rev. **D43**, 1633 (1991); A. L. Kataev and V. T. Kim, Mod. Phys. Lett. **A9**, 1309 (1994); L. R. Surguladze, Phys. Lett. **B341**, 60 (1994), [hep-ph/9405325]; S. A. Larin, T. van Ritbergen and J. A. M. Vermaseren, Phys. Lett. **B362**, 134 (1995), [hep-ph/9506465]; K. G. Chetyrkin and A. Kwiatkowski, Nucl. Phys. **B461**, 3 (1996), [hep-ph/9505358]; K. G. Chetyrkin, Phys. Lett. **B390**, 309 (1997), [hep-ph/9608318]; P. A. Baikov, K. G. Chetyrkin and J. H. Kuhn, Phys. Rev. Lett. **96**, 012003 (2006), [hep-ph/0511063].

[122] J. Fleischer and F. Jegerlehner, Phys. Rev. **D23**, 2001 (1981); D. Yu. Bardin, B. M. Vilensky and P. K. Khristova, Sov. J. Nucl. Phys. **53**, 152 (1991), [Yad. Fiz.53,240(1991)]; A. Dabelstein and W. Hollik, Z. Phys. **C53**, 507 (1992); B. A. Kniehl, Nucl. Phys. **B376**, 3 (1992); A. Djouadi *et al.*, in "In *Munich/Annecy/Hamburg 1991, Proceedings, e+ e- collisions at 500-GeV, pt. A* 11-30," (1991).

[123] T. Inami, T. Kubota and Y. Okada, Z. Phys. **C18**, 69 (1983); K. G. Chetyrkin, B. A. Kniehl and M. Steinhauser, Phys. Rev. Lett. **79**, 353 (1997), [hep-ph/9705240]; P. A. Baikov and K. G. Chetyrkin, Phys. Rev. Lett. **97**, 061803 (2006), [hep-ph/0604194].

[124] H.-Q. Zheng and D.-D. Wu, Phys. Rev. **D42**, 3760 (1990); A. Djouadi *et al.*, Phys. Lett. **B257**, 187 (1991); S. Dawson and R. P. Kauffman, Phys. Rev. **D47**, 1264 (1993); A. Djouadi, M. Spira and P. M. Zerwas, Phys. Lett. **B311**, 255 (1993), [hep-ph/9305335]; K. Melnikov and O. I. Yakovlev, Phys. Lett. **B312**, 179 (1993), [hep-ph/9302281]; M. Inoue *et al.*, Mod. Phys. Lett. **A9**, 1189 (1994).

[125] P. Maierhöfer and P. Marquard, Phys. Lett. **B721**, 131 (2013), [arXiv:1212.6233].

[126] U. Aglietti *et al.*, Phys. Lett. **B595**, 432 (2004), [hep-ph/0404071]; G. Degrassi and F. Maltoni, Phys. Lett. **B600**, 255 (2004), [hep-ph/0407249]; S. Actis *et al.*, Phys. Lett. **B670**, 12 (2008), [arXiv:0809.1301]; U. Aglietti *et al.*, Phys. Lett. **B600**, 57 (2004), [hep-ph/0407162]; G. Degrassi and F. Maltoni, Nucl. Phys. **B724**, 183 (2005), [hep-ph/0504137]; U. Aglietti *et al.*, FERMILAB-CONF (2006), [hep-ph/0612172].

[127] A. Abbasabadi *et al.*, Phys. Rev. **D55**, 5647 (1997), [hep-ph/9611209]; A. Abbasabadi and W. W. Repko, Phys. Rev. **D71**, 017304 (2005), [hep-ph/0411152]; A. Abbasabadi and W. W. Repko, JHEP **08**, 048 (2006), [hep-ph/0602087]; D. A. Dicus and W. W. Repko, Phys. Rev. **D87**, 7, 077301 (2013), [arXiv:1302.2159]; L.-B. Chen, C.-F. Qiao and R.-L. Zhu, Phys. Lett. **B726**, 306 (2013), [arXiv:1211.6058]; Y. Sun, H.-R. Chang and D.-N. Gao, JHEP **05**, 061 (2013), [arXiv:1303.2230]; G. Passarino, Phys. Lett. **B727**, 424 (2013), [arXiv:1308.0422].

[128] M. Spira, A. Djouadi and P. M. Zerwas, Phys. Lett. **B276**, 350 (1992).

[129] A. Bredenstein *et al.*, Phys. Rev. **D74**, 013004 (2006), [hep-ph/0604011]; A. Bredenstein *et al.*, JHEP **02**, 080 (2007), [hep-ph/0611234]; A. Bredenstein *et al.*, `Prophecy4f`: A Monte Carlo generator for a proper description of the Higgs decay into 4 fermions, `http://omnibus.uni-freiburg.de/~sd565/programs/prophecy4f/prophecy4f.html`.

[130] A. Ghinculov, Phys. Lett. **B337**, 137 (1994), [Erratum: Phys. Lett. **B346**, 426 (1995)], [hep-ph/9405394]; L. Durand, B. A. Kniehl and K. Riesselmann, Phys. Rev. **D51**, 5007 (1995), [hep-ph/9412311]; L. Durand, K. Riesselmann and B. A. Kniehl, Phys. Rev. Lett. **72**, 2534 (1994), [Erratum: Phys. Rev. Lett. **74**, 1699 (1995)].

[131] R. Barate *et al.* (LEP Working Group for Higgs boson searches, ALEPH, DELPHI, L3, OPAL), Phys. Lett. **B565**, 61 (2003), [hep-ex/0306033].

[132] M. Tanabashi *et al.* (Particle Data Group), Phys. Rev. **D98**, 3, 030001 (2018).

[133] Y. L. Dokshitzer, S. I. Troian and V. A. Khoze, Sov. J. Nucl. Phys. **46**, 712 (1987), [Yad. Fiz.46,1220(1987)].

[134] ATLAS Collaboration, ATLAS-CONF-2020-026 (2020).

[135] A. M. Sirunyan *et al.* (CMS), Eur. Phys. J. C **81**, 6, 488 (2021), [arXiv:2103.04956].

[136] G. Aad *et al.* (ATLAS, CMS), Phys. Rev. Lett. **114**, 191803 (2015), [arXiv:1503.07589].

[137] ATLAS Collaboration, ATLAS-CONF-2019-029 (2019).

[138] A. M. Sirunyan *et al.* (CMS), JHEP **07**, 027 (2021), [arXiv:2103.06956].

[139] A. M. Sirunyan *et al.* (CMS), JHEP **11**, 047 (2017), [arXiv:1706.09936].

[140] G. Aad *et al.* (ATLAS), Eur. Phys. J. C **80**, 10, 957 (2020), [Erratum: Eur.Phys.J.C 81, 29 (2021), Erratum: Eur.Phys.J.C 81, 398 (2021)], [arXiv:2004.03447].

[141] M. Aaboud *et al.* (ATLAS), Phys. Lett. **B784**, 345 (2018), [arXiv:1806.00242].

[142] ATLAS Collaboration, ATLAS-CONF-2020-005 (2020).

[143] A. M. Sirunyan *et al.* (CMS), Phys. Lett. B **805**, 135425 (2020), [arXiv:2002.06398].

[144] ATLAS Collaboration, ATL-PHYS-PUB-2016-009 (2016).

[145] M. Dittmar and H. K. Dreiner, Phys. Rev. **D55**, 167 (1997), [hep-ph/9608317].

[146] G. Aad *et al.* (ATLAS), JHEP **08**, 137 (2015), [arXiv:1506.06641].

[147] ATLAS Collaboration, ATLAS-CONF-2021-014 (2021).

[148] A. M. Sirunyan *et al.* (CMS), JHEP **03**, 003 (2021), [arXiv:2007.01984].

[149] CMS Collaboration, CMS-PAS-HIG-19-017 (2021).

[150] G. Aad *et al.* (ATLAS), JHEP **04**, 117 (2015), [arXiv:1501.04943].

[151] ATLAS and CMS Collaborations, ATLAS-CONF-2015-044 and CMS-PAS-HIG-15-002 (2015).

[152] M. Aaboud *et al.* (ATLAS), Phys. Rev. **D99**, 072001 (2019), [arXiv:1811.08856].

[153] A. M. Sirunyan *et al.* (CMS), Phys. Lett. **B779**, 283 (2018), [arXiv:1708.00373].

[154] CMS Collaboration, CMS-PAS-HIG-18-032 (2019).

[155] A. M. Sirunyan *et al.* (CMS), JHEP **06**, 093 (2019), [arXiv:1809.03590].

[156] ATLAS Collaboration, ATLAS-CONF-2021-044 (2021).

[157] CMS Collaboration, CMS-PAS-HIG-19-010 (2020).

[158] A. Tumasyan *et al.* (CMS) (2021), [arXiv:2107.11486].

[159] T. Aaltonen *et al.* (CDF, D0), Phys. Rev. Lett. **109**, 071804 (2012), [arXiv:1207.6436].

[160] M. Aaboud *et al.* (ATLAS), Phys. Lett. **B786**, 59 (2018), [arXiv:1808.08238].

[161] A. M. Sirunyan *et al.* (CMS), Phys. Rev. Lett. **121**, 12, 121801 (2018), [arXiv:1808.08242].

[162] G. Aad *et al.* (ATLAS), Eur. Phys. J. C **81**, 2, 178 (2021), [arXiv:2007.02873].

Downloaded from https://academic.oup.com/ptep/article/2022/8/083C01/6651666 by KIT Library user on 27 September 2022

[163] G. Aad *et al.* (ATLAS), Phys. Lett. B **816**, 136204 (2021), [arXiv:2008.02508].

[164] LHCb-CONF-2016-006, CERN-LHCb-CONF-2016-006.

[165] M. Aaboud *et al.* (ATLAS), JHEP **11**, 112 (2016), [arXiv:1606.02181].

[166] V. Khachatryan *et al.* (CMS), Phys. Rev. **D92**, 3, 032008 (2015), [arXiv:1506.01010].

[167] G. Aad *et al.* (ATLAS), Eur. Phys. J. C **81**, 6, 537 (2021), [arXiv:2011.08280]; CMS Collaboration, CMS-PAS-HIG-16-003 (2019).

[168] E. Gabrielli *et al.*, Nucl. Phys. **B781**, 64 (2007), [hep-ph/0702119].

[169] G. Aad *et al.* (ATLAS), JHEP **03**, 268 (2021), [arXiv:2010.13651].

[170] ATLAS Collaboration, ATLAS-CONF-2021-010 (2021).

[171] A. M. Sirunyan *et al.* (CMS), JHEP **12**, 085 (2020), [arXiv:2006.13251].

[172] M. Cacciari, G. P. Salam and G. Soyez, JHEP **04**, 063 (2008), [arXiv:0802.1189].

[173] V. Khachatryan *et al.* (CMS), Eur. Phys. J. **C75**, 6, 251 (2015), [arXiv:1502.02485].

[174] G. Aad *et al.* (ATLAS), Phys. Lett. **B749**, 519 (2015), [arXiv:1506.05988].

[175] M. Aaboud *et al.* (ATLAS), Phys. Lett. **B784**, 173 (2018), [arXiv:1806.00425].

[176] A. M. Sirunyan *et al.* (CMS), Phys. Rev. Lett. **120**, 23, 231801 (2018), [arXiv:1804.02610].

[177] G. Aad *et al.* (ATLAS), Phys. Rev. Lett. **125**, 6, 061802 (2020), [arXiv:2004.04545].

[178] A. M. Sirunyan *et al.* (CMS), Phys. Rev. Lett. **125**, 6, 061801 (2020), [arXiv:2003.10866].

[179] ATLAS Collaboration, ATLAS-CONF-2020-058 (2020).

[180] CMS Collaboration, CMS-PAS-HIG-18-030 (2019).

[181] A. M. Sirunyan *et al.* (CMS), Eur. Phys. J. C **81**, 4, 378 (2021), [arXiv:2011.03652].

[182] ATLAS Collaboration, ATLAS-CONF-2019-045 (2019).

[183] ATLAS Collaboration, ATLAS-CONF-2017-077 (2017).

[184] ATLAS Collaboration, ATLAS-CONF-2019-004 (2019).

[185] CMS Collaboration, CMS-PAS-HIG-18-018 (2019).

[186] M. Farina *et al.*, JHEP **05**, 022 (2013), [arXiv:1211.3736].

[187] CMS Collaboration, CMS-PAS-HIG-17-005 (2017).

[188] CMS Collaboration, CMS-PAS-HIG-16-019 (2016).

[189] G. Aad *et al.* (ATLAS), JHEP **12**, 061 (2015), [arXiv:1509.06047].

[190] V. Khachatryan *et al.* (CMS), JHEP **02**, 079 (2017), [arXiv:1610.04857].

[191] ATLAS Collaboration, JHEP **129**, 010 (2017).

[192] CMS Collaboration, CMS-PAS-TOP-2017-003 (2017).

[193] G. Aad *et al.* (ATLAS) (2019), [arXiv:1906.02025].

[194] A. M. Sirunyan *et al.* (CMS), Phys. Rev. Lett. **122**, 12, 121803 (2019), [arXiv:1811.09689].

[195] ATLAS Collaboration, ATLAS-CONF-2021-030 (2021).

[196] CMS Collaboration, CMS-PAS-HIG-20-004 (2020).

[197] G. Aad *et al.* (ATLAS), JHEP **07**, 108 (2020), [Erratum: JHEP 01, 145 (2021), Erratum: JHEP 05, 207 (2021)], [arXiv:2001.05178].

[198] CMS Collaboration, CMS-PAS-HIG-20-005 (2021).

[199] A. M. Sirunyan *et al.* (CMS), JHEP **03**, 257 (2021), [arXiv:2011.12373].

[200] ATLAS Collaboration, ATLAS-CONF-2021-016 (2021).

[201] G. Aad *et al.* (ATLAS), Phys. Lett. B **809**, 135754 (2020), [arXiv:2005.05382].

[202] A. M. Sirunyan *et al.* (CMS), JHEP **11**, 152 (2018), [arXiv:1806.05996].

[203] V. Khachatryan *et al.* (CMS), Phys. Lett. **B753**, 341 (2016), [arXiv:1507.03031].

[204] G. Aad *et al.* (ATLAS), Phys. Lett. B **819**, 136412 (2021), [arXiv:2103.10322].

[205] G. Aad *et al.* (ATLAS), Phys. Lett. B **812**, 135980 (2021), [arXiv:2007.07830].

[206] A. M. Sirunyan *et al.* (CMS), JHEP **01**, 148 (2021), [arXiv:2009.04363].

[207] ATLAS Collaboration, ATLAS-CONF-2019-037 (2019).

[208] A. M. Sirunyan *et al.* (CMS), Phys. Rev. D **104**, 3, 032013 (2021), [arXiv:2105.03007].

[209] G. Aad *et al.* (ATLAS), JHEP **11**, 211 (2015), [arXiv:1508.03372].

[210] G. Aad *et al.* (ATLAS), Eur. Phys. J. **C77**, 2, 70 (2017), [arXiv:1604.07730].

[211] CMS Collaboration, CMS-PAS-HIG-17-001 (2017).

[212] V. Khachatryan *et al.* (CMS), Phys. Lett. **B763**, 472 (2016), [arXiv:1607.03561].

[213] R. Harnik, J. Kopp and J. Zupan, JHEP **03**, 026 (2013), [arXiv:1209.1397].

[214] G. Aad *et al.* (ATLAS) (2019), [arXiv:1907.06131].

[215] A. M. Sirunyan *et al.* (CMS), JHEP **06**, 001 (2018), [arXiv:1712.07173].

[216] C. Delaunay *et al.*, Phys. Rev. **D89**, 3, 033014 (2014), [arXiv:1310.7029].

[217] ATLAS Collaboration, ATLAS-CONF-2021-021 (2021).

[218] A. M. Sirunyan *et al.* (CMS), JHEP **03**, 131 (2020), [arXiv:1912.01662].

[219] G. Isidori, A. V. Manohar and M. Trott, Phys. Lett. **B728**, 131 (2014), [arXiv:1305.0663]; G. T. Bodwin *et al.*, Phys. Rev. **D88**, 5, 053003 (2013), [arXiv:1306.5770]; M. König and M. Neubert, JHEP **08**, 012 (2015), [arXiv:1505.03870].

[220] G. Aad *et al.* (ATLAS), Phys. Rev. Lett. **114**, 12, 121801 (2015), [arXiv:1501.03276].

[221] M. Aaboud *et al.* (ATLAS), Phys. Rev. Lett. **117**, 11, 111802 (2016), [arXiv:1607.03400].

[222] A. M. Sirunyan *et al.* (CMS), JHEP **11**, 039 (2020), [arXiv:2007.05122].

[223] A. M. Sirunyan *et al.* (CMS), Phys. Lett. **B797**, 134811 (2019), [arXiv:1905.10408].

[224] A. Djouadi *et al.*, Eur. Phys. J. **C73**, 6, 2455 (2013), [arXiv:1205.3169].

[225] O. J. P. Eboli and D. Zeppenfeld, Phys. Lett. **B495**, 147 (2000), [hep-ph/0009158].

[226] ATLAS Collaboration, ATLAS-CONF-2020-008 (2020).

[227] ATLAS Collaboration, ATLAS-CONF-2021-029 (2021).

[228] M. Aaboud *et al.* (ATLAS), JHEP **10**, 180 (2018), [arXiv:1807.11471].

[229] ATLAS Collaboration, ATLAS-CONF-2020-052 (2020).

[230] A. M. Sirunyan *et al.* (CMS), Eur. Phys. J. **C78**, 4, 291 (2018), [arXiv:1711.00431].

[231] A. M. Sirunyan *et al.* (CMS), Phys. Rev. **D97**, 9, 092005 (2018), [arXiv:1712.02345].

[232] A. M. Sirunyan *et al.* (CMS), Phys. Lett. **B793**, 520 (2019), [arXiv:1809.05937].

[233] CMS Collaboration, CMS-PAS-HIG-18-008 (2019).

[234] M. J. Strassler and K. M. Zurek, Phys. Lett. **B651**, 374 (2007), [hep-ph/0604261]; M. J. Strassler and K. M. Zurek, Phys. Lett. **B661**, 263 (2008), [hep-ph/0605193].

[235] T. Han *et al.*, JHEP **07**, 008 (2008), [arXiv:0712.2041].

Downloaded from https://academic.oup.com/ptep/article/2022/8/083C01/6651666 by KIT Library user on 27 September 2022

[236] A. Falkowski *et al.*, Phys. Rev. Lett. **105**, 241801 (2010), [arXiv:1007.3496].

[237] G. Aad *et al.* (ATLAS), Eur. Phys. J. C **80**, 5, 450 (2020), [arXiv:1909.01246].

[238] CMS Collaboration, CMS-PAS-EXO-19-007 (2019).

[239] D. Tucker-Smith and N. Weiner, Phys. Rev. **D64**, 043502 (2001), [hep-ph/0101138].

[240] S. Chatrchyan *et al.* (CMS), Phys. Lett. **B726**, 564 (2013), [arXiv:1210.7619].

[241] ATLAS Collaboration, ATLAS-CONF-2020-027 (2020).

[242] CMS Collaboration, CMS-PAS-HIG-19-005 (2020).

[243] C. Patrignani *et al.* (Particle Data Group), Chin. Phys. **C40**, 10, 100001 (2016).

[244] G. Aad *et al.* (ATLAS), Eur. Phys. J. **C76**, 1, 6 (2016), [arXiv:1507.04548].

[245] L. D. Landau, Dokl. Akad. Nauk Ser. Fiz. **60**, 2, 207 (1948); C.-N. Yang, Phys. Rev. **77**, 242 (1950).

[246] S. Bolognesi *et al.*, Phys. Rev. **D86**, 095031 (2012), [arXiv:1208.4018].

[247] G. Aad *et al.* (ATLAS), Eur. Phys. J. **C75**, 10, 476 (2015), [Erratum: Eur. Phys. J. **C76**, 3, 152 (2016)], [arXiv:1506.05669].

[248] V. Khachatryan *et al.* (CMS), Phys. Rev. **D92**, 1, 012004 (2015), [arXiv:1411.3441]; G. Aad *et al.* (ATLAS), Phys. Lett. **B726**, 120 (2013), [arXiv:1307.1432].

[249] P. Artoisenet *et al.*, JHEP **11**, 043 (2013), [arXiv:1306.6464].

[250] J. Ellis *et al.*, JHEP **11**, 134 (2012), [arXiv:1208.6002].

[251] D0 Collaboration, Note 6387-CONF (2013).

[252] D0 Collaboration, Note 6406-CONF (2013).

[253] J. C. Collins and D. E. Soper, Phys. Rev. **D16**, 2219 (1977).

[254] A. De Rujula *et al.*, Phys. Rev. **D82**, 013003 (2010), [arXiv:1001.5300].

[255] ATLAS Collaboration, ATLAS-CONF-2017-043 (2017).

[256] A. M. Sirunyan *et al.* (CMS), Phys. Rev. **D99**, 11, 112003 (2019), [arXiv:1901.00174].

[257] A. M. Sirunyan *et al.* (CMS), Submitted to: Phys. Rev. (2019), [arXiv:1903.06973].

[258] G. Aad *et al.* (ATLAS), Eur. Phys. J. **C76**, 12, 658 (2016), [arXiv:1602.04516].

[259] ATLAS Collaboration, ATL-PHYS-PUB-2019-008 (2019).

[260] N. Kauer and G. Passarino, JHEP **08**, 116 (2012), [arXiv:1206.4803].

[261] V. Khachatryan *et al.* (CMS), JHEP **09**, 051 (2016), [arXiv:1605.02329].

[262] G. Aad *et al.* (ATLAS), Eur. Phys. J. **C75**, 7, 335 (2015), [arXiv:1503.01060].

[263] M. Aaboud *et al.* (ATLAS), Phys. Lett. **B786**, 223 (2018), [arXiv:1808.01191].

[264] G. Aad *et al.* (ATLAS), Phys. Rev. **D90**, 5, 052004 (2014), [arXiv:1406.3827].

[265] CMS Collaboration, CMS-PAS-HIG-16-041 (2017).

[266] L. J. Dixon and M. S. Siu, Phys. Rev. Lett. **90**, 252001 (2003), [hep-ph/0302233]; S. P. Martin, Phys. Rev. **D86**, 073016 (2012), [arXiv:1208.1533]; L. J. Dixon and Y. Li, Phys. Rev. Lett. **111**, 111802 (2013), [arXiv:1305.3854].

[267] ATLAS Collaboration, ATL-PHYS-PUB-2013-014 (2013).

[268] J. Campbell *et al.*, Phys. Rev. Lett. **119**, 18, 181801 (2017), [Addendum: Phys. Rev. Lett.119,19,199901(2017)], [arXiv:1704.08259].

[269] ATLAS Collaboration, ATL-PHYS-PUB-2014-016 (2014).

[270] F. Caola and K. Melnikov, Phys. Rev. **D88**, 054024 (2013), [arXiv:1307.4935]; J. M. Campbell, R. K. Ellis and C. Williams, JHEP **04**, 060 (2014), [arXiv:1311.3589]; J. M. Campbell, R. K. Ellis and C. Williams, Phys. Rev. **D89**, 5, 053011 (2014), [arXiv:1312.1628].

[271] C. Englert and M. Spannowsky, Phys. Rev. **D90**, 053003 (2014), [arXiv:1405.0285].

[272] A. Azatov *et al.*, Zh. Eksp. Teor. Fiz. **147**, 410 (2015), [J. Exp. Theor. Phys.120,354(2015)], [arXiv:1406.6338]; A. Azatov *et al.*, JHEP **09**, 123 (2016), [arXiv:1608.00977].

[273] A. David *et al.* (LHC Higgs Cross Section Working Group), "LHC HXSWG interim recommendations to explore the coupling structure of a Higgs-like particle," (2012), [arXiv:1209.0040].

[274] M. Dührssen, "Prospects for the measurement of Higgs boson coupling parameters in the mass range from 110–190 GeV," (2003); M. Duhrssen *et al.*, Phys. Rev. **D70**, 113009 (2004), [hep-ph/0406323]; R. Lafaye *et al.*, JHEP **08**, 009 (2009), [arXiv:0904.3866].

[275] J. R. Espinosa *et al.*, JHEP **05**, 097 (2012), [arXiv:1202.3697]; A. Azatov, R. Contino and J. Galloway, JHEP **04**, 127 (2012), [Erratum: JHEP **04**, 140 (2013)], [arXiv:1202.3415]; D. Carmi *et al.*, JHEP **07**, 136 (2012), [arXiv:1202.3144]; J. R. Espinosa *et al.*, JHEP **12**, 045 (2012), [arXiv:1207.1717].

[276] M. Gonzalez-Alonso *et al.*, Eur. Phys. J. **C75**, 128 (2015), [arXiv:1412.6038]; A. Greljo *et al.*, Eur. Phys. J. **C76**, 3, 158 (2016), [arXiv:1512.06135].

[277] G. F. Giudice *et al.*, JHEP **06**, 045 (2007), [hep-ph/0703164].

[278] S. Willenbrock and C. Zhang, Ann. Rev. Nucl. Part. Sci. **64**, 83 (2014), [arXiv:1401.0470]; I. Brivio and M. Trott, Phys. Rept. **793**, 1 (2019), [arXiv:1706.08945]; S. Dawson, C. Englert and T. Plehn, Phys. Rept. **816**, 1 (2019), [arXiv:1808.01324]; T. Cohen, PoS **TASI2018**, 011 (2019), [arXiv:1903.03622].

[279] F. Feruglio, Int. J. Mod. Phys. **A8**, 4937 (1993), [hep-ph/9301281]; G. Buchalla, O. Catà and C. Krause, Nucl. Phys. **B880**, 552 (2014), [Erratum: Nucl. Phys. **B913**, 475 (2016)], [arXiv:1307.5017]; R. Alonso *et al.*, Phys. Lett. **B722**, 330 (2013), [Erratum: Phys. Lett. **B726**, 926 (2013)], [arXiv:1212.3305]; A. V. Manohar, in "Les Houches summer school: EFT in Particle Physics and Cosmology Les Houches, Chamonix Valley, France, July 3-28, 2017," (2018), [arXiv:1804.05863]; I. Brivio *et al.*, JHEP **03**, 024 (2014), [arXiv:1311.1823].

[280] J. de Blas *et al.*, JHEP **03**, 109 (2018), [arXiv:1711.10391].

[281] A. Manohar and H. Georgi, Nucl. Phys. **B234**, 189 (1984); M. A. Luty, Phys. Rev. **D57**, 1531 (1998), [hep-ph/9706235]; D. Liu *et al.*, JHEP **11**, 141 (2016), [arXiv:1603.03064].

[282] W. Buchmuller and D. Wyler, Nucl. Phys. **B268**, 621 (1986).

[283] C. J. C. Burges and H. J. Schnitzer, Nucl. Phys. **B228**, 464 (1983); C. N. Leung, S. T. Love and S. Rao, Z. Phys. **C31**, 433 (1986).

[284] B. Grzadkowski *et al.*, JHEP **10**, 085 (2010), [arXiv:1008.4884].

[285] L. Lehman and A. Martin, JHEP **02**, 081 (2016), [arXiv:1510.00372]; B. Henning *et al.*, JHEP **08**, 016 (2017), [arXiv:1512.03433].

[286] C. Hays *et al.*, JHEP **02**, 123 (2019), [arXiv:1808.00442].

[287] R. Alonso *et al.*, JHEP **04**, 159 (2014), [arXiv:1312.2014].

[288] A. Falkowski, LHCHXSWG-INT-2015-001 (2015); A. Falkowski, Pramana **87**, 3, 39 (2016), [arXiv:1505.00046].

[289] A. M. Sirunyan *et al.* (CMS), Phys. Lett. **B792**, 369 (2019), [arXiv:1812.06504].

Downloaded from https://academic.oup.com/ptep/article/2022/8/083C01/6651666 by KIT Library user on 27 September 2022

[290] M. Aaboud *et al.* (ATLAS), Phys. Rev. **D98**, 052005 (2018), [arXiv:1802.04146].

[291] F. Maltoni *et al.* (2019), [arXiv:1906.12310].

[292] R. S. Gupta, A. Pomarol and F. Riva, Phys. Rev. **D91**, 3, 035001 (2015), [arXiv:1405.0181].

[293] B. A. Kniehl and M. Spira, Z. Phys. **C69**, 77 (1995), [hep-ph/9505225].

[294] R. Contino *et al.*, JHEP **07**, 035 (2013), [arXiv:1303.3876].

[295] A. Azatov and J. Galloway, Phys. Rev. **D85**, 055013 (2012), [arXiv:1110.5646].

[296] G. Isidori and M. Trott, JHEP **02**, 082 (2014), [arXiv:1307.4051]; A. Pomarol and F. Riva, JHEP **01**, 151 (2014), [arXiv:1308.2803].

[297] J. Ellis, V. Sanz and T. You, JHEP **07**, 036 (2014), [arXiv:1404.3667]; A. Biekötter *et al.*, Phys. Rev. **D91**, 055029 (2015), [arXiv:1406.7320].

[298] LHC Higgs Cross Section Working Group, `https://twiki.cern.ch/twiki/bin/view/LHCPhysics/LHCHWG2KAPPA`.

[299] ATLAS and CMS Collaborations, CMS-PAS-HIG-15-002 (2015).

[300] M. Reece, New J. Phys. **15**, 043003 (2013), [arXiv:1208.1765].

[301] A. M. Sirunyan *et al.* (CMS), Eur. Phys. J. **C79**, 5, 421 (2019), [arXiv:1809.10733].

[302] G. Aad *et al.* (ATLAS) (2019), [arXiv:1909.02845].

[303] ATLAS Collaboration, ATLAS-CONF-2019-032 (2019).

[304] CMS Collaboration, CMS-PAS-HIG-19-001 (2019).

[305] G. Aad *et al.* (ATLAS), Phys. Lett. **B753**, 69 (2016), [arXiv:1508.02507].

[306] N. Berger *et al.* (2019), [arXiv:1906.02754].

[307] ATLAS Collaboration, ATLAS-CONF-2017-045 (2017).

[308] CMS Collaboration, CMS-PAS-HIG-16-040 (2017).

[309] ATLAS Collaboration, ATLAS-CONF-2018-028 (2018).

[310] ATLAS Collaboration, ATLAS-CONF-2019-025 (2019).

[311] ATLAS Collaboration, CMS-PAS-HIG-19-001 (2019).

[312] M. Aaboud *et al.* (ATLAS), JHEP **05**, 141 (2019), [arXiv:1903.04618].

[313] ATLAS Collaboration, ATLAS-CONF-2020-053 (2020).

[314] M. McCullough, Phys. Rev. **D90**, 1, 015001 (2014), [Erratum: Phys. Rev. **D92**, 3, 039903 (2015)], [arXiv:1312.3322].

[315] G. Degrassi *et al.*, JHEP **12**, 080 (2016), [arXiv:1607.04251].

[316] M. Gorbahn and U. Haisch, JHEP **10**, 094 (2016), [arXiv:1607.03773].

[317] ATLAS Collaboration, ATL-PHYS-PUB-2019-009 (2019).

[318] F. Bishara *et al.*, Phys. Rev. Lett. **118**, 12, 121801 (2017), [arXiv:1606.09253].

[319] ATLAS Collaboration, ATLAS-CONF-2019-029 (2019).

[320] ATLAS Collaboration, ATLAS-CONF-2019-049 (2019).

[321] S. Di Vita *et al.*, JHEP **09**, 069 (2017), [arXiv:1704.01953]; F. Maltoni *et al.*, Eur. Phys. J. **C77**, 12, 887 (2017), [arXiv:1709.08649].

[322] Y. Gershtein, and A. Pomarol, *Extra Dimenions*, in this volume.

[323] S. Weinberg, Phys. Rev. **D13**, 974 (1976), [Addendum: Phys. Rev.D19,1277(1979)]; L. Susskind, Phys. Rev. **D20**, 2619 (1979); For a review, see C. T. Hill and E. H. Simmons, Phys. Reports **381**, 235 (2003) [Erratum: 390, 553 (2004)], [arXiv:hep-ph/0203079].

[324] Z. Chacko, R. Franceschini and R. K. Mishra, JHEP **04**, 015 (2013), [arXiv:1209.3259].

[325] L. E. Ibanez and G. G. Ross, Phys. Lett. **110B**, 215 (1982); L. E. Ibanez, Phys. Lett. **118B**, 73 (1982); J. R. Ellis, D. V. Nanopoulos and K. Tamvakis, Phys. Lett. **121B**, 123 (1983); L. Alvarez-Gaume, J. Polchinski and M. B. Wise, Nucl. Phys. **B221**, 495 (1983).

[326] S. Dimopoulos and G. F. Giudice, Phys. Lett. **B357**, 573 (1995), [hep-ph/9507282]; M. Papucci, J. T. Ruderman and A. Weiler, JHEP **09**, 035 (2012), [arXiv:1110.6926].

[327] ATLAS Collaboration, `https://twiki.cern.ch/twiki/bin/view/AtlasPublic/Publications`; CMS Collaboration, `http://cms-results.web.cern.ch/cms-results/public-results/publications/SUS/STOP.html`.

[328] J. Mrazek *et al.*, Nucl. Phys. **B853**, 1 (2011), [arXiv:1105.5403].

[329] D. B. Kaplan, Nucl. Phys. **B365**, 259 (1991).

[330] G. Panico *et al.*, JHEP **03**, 051 (2013), [arXiv:1210.7114].

[331] H. E. Haber and G. L. Kane, Phys. Rept. **117**, 75 (1985).

[332] P. Slavich *et al.*, Eur. Phys. J. C **81**, 5, 450 (2021), [arXiv:2012.15629].

[333] P. Draper, G. Lee and C. E. M. Wagner, Phys. Rev. **D89**, 5, 055023 (2014), [arXiv:1312.5743].

[334] J. F. Gunion and H. E. Haber, Phys. Rev. **D67**, 075019 (2003), [hep-ph/0207010].

[335] H. E. Haber and Y. Nir, Nucl. Phys. **B335**, 363 (1990).

[336] E. L. Berger *et al.*, Phys. Rev. **D66**, 095001 (2002), [hep-ph/0205342].

[337] A. Djouadi, Phys. Rept. **459**, 1 (2008), [hep-ph/0503173].

[338] P. Bechtle *et al.*, Eur. Phys. J. **C77**, 2, 67 (2017), [arXiv:1608.00638].

[339] E. Bagnaschi *et al.*, Eur. Phys. J. **C79**, 7, 617 (2019), [arXiv:1808.07542].

[340] A. Djouadi, J. Kalinowski and P. M. Zerwas, Z. Phys. **C57**, 569 (1993).

[341] G. Lee and C. E. M. Wagner, Phys. Rev. **D92**, 7, 075032 (2015), [arXiv:1508.00576].

[342] D. Dicus *et al.*, Phys. Rev. **D59**, 094016 (1999), [hep-ph/9811492].

[343] M. Carena *et al.*, JHEP **07**, 091 (2012), [arXiv:1203.1041].

[344] A. A. Barrientos Bendezu and B. A. Kniehl, Phys. Rev. **D64**, 035006 (2001), [hep-ph/0103018].

[345] LHC Higgs Working Group, `https://twiki.cern.ch/twiki/bin/view/LHCPhysics/LHCHWGMSSMCharged`.

[346] A. Djouadi, J. Ellis and J. Quevillon, JHEP **07**, 105 (2016), [arXiv:1605.00542]; M. Carena and Z. Liu, JHEP **11**, 159 (2016), [arXiv:1608.07282].

[347] LHC Higgs Working Group for BSM Higgs, `https://twiki.cern.ch/twiki/bin/view/LHCPhysics/LHCHWG3`.

[348] M. Carena *et al.*, Eur. Phys. J. **C73**, 9, 2552 (2013), [arXiv:1302.7033].

[349] H. Bahl, S. Liebler and T. Stefaniak, Eur. Phys. J. **C79**, 3, 279 (2019), [arXiv:1901.05933].

[350] L. Maiani, A. D. Polosa and V. Riquer, Phys. Lett. **B718**, 465 (2012), [arXiv:1209.4816]; A. Djouadi and J. Quevillon, JHEP **10**, 028 (2013), [arXiv:1304.1787]; A. Djouadi *et al.*, Eur. Phys. J. **C73**, 2650 (2013), [arXiv:1307.5205].

[351] M. Carena *et al.*, Phys. Rev. **D91**, 3, 035003 (2015), [arXiv:1410.4969].

[352] E. Bagnaschi *et al.*, Eur. Phys. J. C **79**, 7, 617 (2019), [arXiv:1808.07542].

[353] H. Bahl *et al.*, Eur. Phys. J. C **80**, 10, 916 (2020), [arXiv:2005.14536].

[354] R. S. Chivukula and H. Georgi, Phys. Lett. **B188**, 99 (1987); L. J. Hall and L. Randall, Phys. Rev. Lett. **65**, 2939 (1990); A. J. Buras *et al.*, Phys. Lett. **B500**, 161 (2001), [hep-ph/0007085]; G. D'Ambrosio *et al.*, Nucl. Phys. **B645**, 155 (2002), [hep-ph/0207036].

Downloaded from https://academic.oup.com/ptep/article/2022/8/083C01/6651666 by KIT Library user on 27 September 2022

[355] L. J. Hall, J. D. Lykken and S. Weinberg, Phys. Rev. **D27**, 2359 (1983); J. E. Kim and H. P. Nilles, Phys. Lett. **138B**, 150 (1984); G. F. Giudice and A. Masiero, Phys. Lett. **B206**, 480 (1988).

[356] U. Ellwanger, C. Hugonie and A. M. Teixeira, Phys. Rept. **496**, 1 (2010), [arXiv:0910.1785].

[357] P. Fayet, Nucl. Phys. **B90**, 104 (1975).

[358] C. Panagiotakopoulos and K. Tamvakis, Phys. Lett. **B469**, 145 (1999), [hep-ph/9908351]; A. Dedes *et al.*, Phys. Rev. **D63**, 055009 (2001), [hep-ph/0009125]; A. Menon, D. E. Morrissey and C. E. M. Wagner, Phys. Rev. **D70**, 035005 (2004), [hep-ph/0404184].

[359] M. Cvetic *et al.*, Phys. Rev. **D56**, 2861 (1997), [Erratum: Phys. Rev. **D58**, 119905 (1998)], [hep-ph/9703317]; P. Langacker and J. Wang, Phys. Rev. **D58**, 115010 (1998), [hep-ph/9804428].

[360] J. Erler, P. Langacker and T.-j. Li, Phys. Rev. **D66**, 015002 (2002), [hep-ph/0205001]; T. Han, P. Langacker and B. McElrath, Phys. Rev. **D70**, 115006 (2004), [hep-ph/0405244]; V. Barger *et al.*, Phys. Rev. **D73**, 115010 (2006), [hep-ph/0603247].

[361] V. Barger, P. Langacker and G. Shaughnessy, Phys. Rev. **D75**, 055013 (2007), [hep-ph/0611239].

[362] D. E. Lopez-Fogliani and C. Munoz, Phys. Rev. Lett. **97**, 041801 (2006), [hep-ph/0508297].

[363] B. A. Dobrescu, G. L. Landsberg and K. T. Matchev, Phys. Rev. **D63**, 075003 (2001), [hep-ph/0005308]; R. Dermisek and J. F. Gunion, Phys. Rev. Lett. **95**, 041801 (2005), [hep-ph/0502105].

[364] O. J. P. Eboli and D. Zeppenfeld, Phys. Lett. **B495**, 147 (2000), [hep-ph/0009158]; H. Davoudiasl, T. Han and H. E. Logan, Phys. Rev. **D71**, 115007 (2005), [hep-ph/0412269].

[365] J.-J. Cao *et al.*, JHEP **03**, 086 (2012), [arXiv:1202.5821].

[366] LHC Higgs Working Group, Beyond the Standard Model Higgs – NMSSM, `https://twiki.cern.ch/twiki/bin/view/LHCPhysics/LHCHWGNMSSM`.

[367] M. Carena *et al.*, Phys. Rev. **D93**, 3, 035013 (2016), [arXiv:1510.09137].

[368] P. Batra *et al.*, JHEP **02**, 043 (2004), [hep-ph/0309149].

[369] R. Huo *et al.*, Phys. Rev. **D87**, 5, 055011 (2013), [arXiv:1212.0560].

[370] J. Engel, M. J. Ramsey-Musolf and U. van Kolck, Prog. Part. Nucl. Phys. **71**, 21 (2013), [arXiv:1303.2371].

[371] S. Dimopoulos and S. D. Thomas, Nucl. Phys. **B465**, 23 (1996), [hep-ph/9510220]; S. D. Thomas, Int. J. Mod. Phys. **A13**, 2307 (1998), [hep-ph/9803420].

[372] A. Pilaftsis and C. E. M. Wagner, Nucl. Phys. **B553**, 3 (1999), [hep-ph/9902371].

[373] M. Frank *et al.*, JHEP **02**, 047 (2007), [hep-ph/0611326].

[374] M. Carena *et al.*, Nucl. Phys. **B586**, 92 (2000), [hep-ph/0003180].

[375] B. Li and C. E. M. Wagner, Phys. Rev. **D91**, 095019 (2015), [arXiv:1502.02210].

[376] M. D. Goodsell and F. Staub, Eur. Phys. J. **C77**, 1, 46 (2017), [arXiv:1604.05335]; A. Chakraborty *et al.*, Phys. Rev. **D90**, 5, 055005 (2014), [arXiv:1301.2745]; M. Carena *et al.*, JHEP **02**, 123 (2016), [arXiv:1512.00437].

[377] J. F. Gunion and H. E. Haber, Phys. Rev. **D67**, 075019 (2003), [hep-ph/0207010]; G. C. Branco *et al.*, Phys. Rept. **516**, 1 (2012), [arXiv:1106.0034].

[378] N. G. Deshpande and E. Ma, Phys. Rev. **D18**, 2574 (1978).

[379] A. Goudelis, B. Herrmann and O. Stål, JHEP **09**, 106 (2013), [arXiv:1303.3010].

[380] C. D. Froggatt and H. B. Nielsen, Nucl. Phys. **B147**, 277 (1979).

[381] K. S. Babu and S. Nandi, Phys. Rev. **D62**, 033002 (2000), [hep-ph/9907213]; G. F. Giudice and O. Lebedev, Phys. Lett. **B665**, 79 (2008), [arXiv:0804.1753].

[382] E. Accomando *et al.*, CERN Report **2006-009** (2006), [hep-ph/0608079].

[383] T. Robens and T. Stefaniak, Eur. Phys. J. **C75**, 104 (2015), [arXiv:1501.02234].

[384] S. L. Glashow and S. Weinberg, Phys. Rev. **D15**, 1958 (1977); E. A. Paschos, Phys. Rev. **D15**, 1966 (1977).

[385] G. C. Branco, W. Grimus and L. Lavoura, Phys. Lett. **B380**, 119 (1996), [hep-ph/9601383]; F. J. Botella, G. C. Branco and M. N. Rebelo, Phys. Lett. **B687**, 194 (2010), [arXiv:0911.1753].

[386] J. Schechter and J. W. F. Valle, Phys. Rev. **D22**, 2227 (1980); T. P. Cheng and L.-F. Li, Phys. Rev. **D22**, 2860 (1980).

[387] H. Georgi and M. Machacek, Nucl. Phys. **B262**, 463 (1985); M. S. Chanowitz and M. Golden, Phys. Lett. **165B**, 105 (1985); J. F. Gunion, R. Vega and J. Wudka, Phys. Rev. **D42**, 1673 (1990).

[388] P. Nath *et al.*, Nucl. Phys. Proc. Suppl. **200-202**, 185 (2010), [arXiv:1001.2693].

[389] J. Garayoa and T. Schwetz, JHEP **03**, 009 (2008), [arXiv:0712.1453].

[390] H. E. Haber and H. E. Logan, Phys. Rev. **D62**, 015011 (2000), [hep-ph/9909335]; S. Kanemura and K. Yagyu, Phys. Rev. **D85**, 115009 (2012), [arXiv:1201.6287].

[391] J. F. Gunion, R. Vega and J. Wudka, Phys. Rev. **D43**, 2322 (1991).

[392] I. Low and J. Lykken, JHEP **10**, 053 (2010), [arXiv:1005.0872]; I. Low, J. Lykken and G. Shaughnessy, Phys. Rev. **D86**, 093012 (2012), [arXiv:1207.1093].

[393] H. E. Logan and M.-A. Roy, Phys. Rev. **D82**, 115011 (2010), [arXiv:1008.4869]; A. Falkowski, S. Rychkov and A. Urbano, JHEP **04**, 073 (2012), [arXiv:1202.1532].

[394] N. Arkani-Hamed *et al.*, JHEP **07**, 034 (2002), [hep-ph/0206021]; N. Arkani-Hamed, A. G. Cohen and H. Georgi, Phys. Lett. **B513**, 232 (2001), [hep-ph/0105239].

[395] M. Perelstein, Prog. Part. Nucl. Phys. **58**, 247 (2007), [hep-ph/0512128]; M. Schmaltz and D. Tucker-Smith, Ann. Rev. Nucl. Part. Sci. **55**, 229 (2005), [hep-ph/0502182].

[396] J. A. Casas, J. R. Espinosa and I. Hidalgo, JHEP **03**, 038 (2005), [hep-ph/0502066].

[397] H.-C. Cheng and I. Low, JHEP **09**, 051 (2003), [hep-ph/0308199].

[398] M. Carena *et al.*, Phys. Rev. **D75**, 091701 (2007), [hep-ph/0610156].

[399] M. Aaboud *et al.* (ATLAS), Phys. Rev. Lett. **121**, 21, 211801 (2018), [arXiv:1808.02343]; A. M. Sirunyan *et al.* (CMS), Eur. Phys. J. **C79**, 4, 364 (2019), [arXiv:1812.09768].

[400] H. Georgi, A. E. Nelson and A. Manohar, Phys. Lett. **126B**, 169 (1983); A. E. Nelson and M. J. Strassler, JHEP **09**, 030 (2000), [hep-ph/0006251]; S. Davidson, G. Isidori and S. Uhlig, Phys. Lett. **B663**, 73 (2008), [arXiv:0711.3376].

[401] C. Csaki, A. Falkowski and A. Weiler, JHEP **09**, 008 (2008), [arXiv:0804.1954]; B. Keren-Zur *et al.*, Nucl. Phys. **B867**, 394 (2013), [arXiv:1205.5803].

[402] O. Matsedonskyi, G. Panico and A. Wulzer, JHEP **01**, 164 (2013), [arXiv:1204.6333]; M. Redi and A. Tesi, JHEP **10**, 166 (2012), [arXiv:1205.0232]; D. Marzocca, M. Serone and J. Shu, JHEP **08**, 013 (2012), [arXiv:1205.0770]; A. Pomarol and F. Riva, JHEP **08**, 135 (2012), [arXiv:1205.6434].

[403] R. Contino and G. Servant, JHEP **06**, 026 (2008), [arXiv:0801.1679]; J. Mrazek and A. Wulzer, Phys. Rev. **D81**, 075006 (2010), [arXiv:0909.3977]; A. De Simone *et al.*, JHEP **04**, 004 (2013), [arXiv:1211.5663]; A. Azatov *et al.*, Phys. Rev. **D89**, 7, 075001 (2014), [arXiv:1308.6601].

Downloaded from https://academic.oup.com/ptep/article/2022/8/083C01/6651666 by KIT Library user on 27 September 2022

[404] A. Banfi, A. Martin and V. Sanz, JHEP **08**, 053 (2014), [arXiv:1308.4771]; A. Azatov and A. Paul, JHEP **01**, 014 (2014), [arXiv:1309.5273]; C. Grojean *et al.*, JHEP **05**, 022 (2014), [arXiv:1312.3317].

[405] A. Azatov *et al.*, Phys. Rev. **D92**, 3, 035001 (2015), [arXiv:1502.00539].

[406] K. Agashe, R. Contino and A. Pomarol, Nucl. Phys. **B719**, 165 (2005), [hep-ph/0412089]; R. Contino, L. Da Rold and A. Pomarol, Phys. Rev. **D75**, 055014 (2007), [hep-ph/0612048]; D. Pappadopulo, A. Thamm and R. Torre, JHEP **07**, 058 (2013), [arXiv:1303.3062]; M. Montull *et al.*, Phys. Rev. **D88**, 095006 (2013), [arXiv:1308.0559].

[407] M. Carena, L. Da Rold and E. Pontón, JHEP **06**, 159 (2014), [arXiv:1402.2987]; D. Liu, I. Low and C. E. M. Wagner, Phys. Rev. **D96**, 3, 035013 (2017), [arXiv:1703.07791].

[408] I. Low, R. Rattazzi and A. Vichi, JHEP **04**, 126 (2010), [arXiv:0907.5413].

[409] M. Ciuchini *et al.*, JHEP **08**, 106 (2013), [arXiv:1306.4644].

[410] C. Grojean, O. Matsedonskyi and G. Panico, JHEP **10**, 160 (2013), [arXiv:1306.4655].

[411] M. Geller and O. Telem, Phys. Rev. Lett. **114**, 191801 (2015), [arXiv:1411.2974].

[412] P. Batra and Z. Chacko, Phys. Rev. **D79**, 095012 (2009), [arXiv:0811.0394]; R. Barbieri *et al.*, JHEP **08**, 161 (2015), [arXiv:1501.07803]; M. Low, A. Tesi and L.-T. Wang, Phys. Rev. **D91**, 095012 (2015), [arXiv:1501.07890].

[413] G. Aad *et al.* (ATLAS), Phys. Lett. B **822**, 136651 (2021), [arXiv:2102.13405].

[414] CMS Collaboration, CMS-PAS-HIG-17-13 (2017); V. Khachatryan *et al.* (CMS), Phys. Lett. **B767**, 147 (2017), [arXiv:1609.02507].

[415] M. Aaboud *et al.* (ATLAS), Phys. Lett. **B775**, 105 (2017), [arXiv:1707.04147].

[416] A. M. Sirunyan *et al.* (CMS), Phys. Lett. B **793**, 320 (2019), [arXiv:1811.08459].

[417] M. Aaboud *et al.* (ATLAS), JHEP **10**, 112 (2017), [arXiv:1708.00212].

[418] CMS Collaboration, CMS-PAS-HIG-16-014 (2016).

[419] G. Aad *et al.* (ATLAS), Eur. Phys. J. C **81**, 4, 332 (2021), [arXiv:2009.14791].

[420] CMS Collaboration, CMS-PAS-HIG-16-033 (2016).

[421] CMS Collaboration, CMS-PAS-HIG-16-023 (2016).

[422] G. Aad *et al.* (ATLAS), Eur. Phys. J. C **80**, 12, 1165 (2020), [arXiv:2004.14636].

[423] CMS Collaboration, CMS-PAS-HIG-16-034 (2017).

[424] A. M. Sirunyan *et al.* (CMS), Phys. Rev. D **102**, 3, 032003 (2020), [arXiv:2006.06391].

[425] ATLAS Collaboration, ATLAS-CONF-2016-082 (2016).

[426] ATLAS Collaboration, ATLAS-CONF-2013-067 (2013).

[427] A. M. Sirunyan *et al.* (CMS), JHEP **03**, 034 (2020), [arXiv:1912.01594].

[428] ATLAS Collaboration, ATLAS-CONF-2012-018 (2012).

[429] M. Aaboud *et al.* (ATLAS), Phys. Lett. **B777**, 91 (2018), [arXiv:1708.04445].

[430] G. Aad *et al.* (ATLAS), JHEP **09**, 091 (2019), [arXiv:1906.08589].

[431] M. Aaboud *et al.* (ATLAS), Phys. Rev. **D98**, 5, 052008 (2018), [arXiv:1808.02380].

[432] ATLAS Collaboration, ATLAS-CONF-2016-004 (2016); M. Aaboud *et al.* (ATLAS), JHEP **05**, 124 (2019), [arXiv:1811.11028]; M. Aaboud *et al.* (ATLAS), Eur. Phys. J. **C78**, 12, 1007 (2018), [arXiv:1807.08567].

[433] ATLAS Collaboration, ATLAS-CONF-2019-030 (2019); M. Aaboud *et al.* (ATLAS), Phys. Rev. Lett. **121**, 19, 191801 (2018), [Erratum: Phys. Rev. Lett. **122**, 089901 (2019)], [arXiv:1808.00336]; G. Aad *et al.* (ATLAS) (2019), [arXiv:1908.06765].

[434] A. M. Sirunyan *et al.* (CMS), Phys. Lett. B **788**, 7 (2019), [arXiv:1806.00408].

[435] V. Khachatryan *et al.* (CMS), Phys. Lett. **B755**, 217 (2016), [arXiv:1510.01181].

[436] G. Aad *et al.* (ATLAS), Phys. Rev. Lett. **125**, 5, 051801 (2020), [arXiv:2002.12223].

[437] A. M. Sirunyan *et al.* (CMS), JHEP **09**, 007 (2018), [arXiv:1803.06553].

[438] V. M. Abazov *et al.* (D0), Phys. Rev. Lett. **104**, 151801 (2010), [arXiv:0912.0968].

[439] D0 Collaboration, D0Note 5974-CONF (2011).

[440] R. Aaij *et al.* (LHCb), JHEP **05**, 132 (2013), [arXiv:1304.2591].

[441] A. M. Sirunyan *et al.* (CMS), JHEP **05**, 210 (2019), [arXiv:1903.10228].

[442] M. Aaboud *et al.* (ATLAS), JHEP **07**, 117 (2019), [arXiv:1901.08144].

[443] A. M. Sirunyan *et al.* (CMS) (2019), [arXiv:1907.03152].

[444] A. M. Sirunyan *et al.* (CMS), JHEP **03**, 103 (2020), [arXiv:1911.10267].

[445] ATLAS Collaboration, ATLAS-CONF-2019-036 (2019).

[446] A. M. Sirunyan *et al.* (CMS), JHEP **11**, 161 (2018), [arXiv:1808.01890].

[447] G. Aad *et al.* (ATLAS), JHEP **08**, 148 (2015), [arXiv:1505.07018].

[448] A. M. Sirunyan *et al.* (CMS), JHEP **04**, 171 (2020), [arXiv:1908.01115].

[449] G. Aad *et al.* (ATLAS), Phys. Rev. D **102**, 3, 032004 (2020), [arXiv:1907.02749].

[450] S. Chatrchyan *et al.* (CMS), Phys. Lett. **B722**, 207 (2013), [arXiv:1302.2892]; CMS Collaboration, CMS-PAS-HIG-16-025 (2016); A. M. Sirunyan *et al.* (CMS), JHEP **08**, 113 (2018), [arXiv:1805.12191].

[451] V. M. Abazov *et al.* (D0), Phys. Lett. **B698**, 97 (2011), [arXiv:1011.1931].

[452] T. Aaltonen *et al.* (CDF), Phys. Rev. **D85**, 032005 (2012), [arXiv:1106.4782].

[453] ATLAS Collaboration, ATLAS-CONF-2017-055 (2017).

[454] G. Aad *et al.* (ATLAS), Phys. Rev. D **102**, 11, 112008 (2020), [arXiv:2007.05293]; G. Aad *et al.* (ATLAS), Phys. Lett. **B744**, 163 (2015), [arXiv:1502.04478].

[455] A. M. Sirunyan *et al.* (CMS), JHEP **03**, 065 (2020), [arXiv:1910.11634].

[456] A. M. Sirunyan *et al.* (CMS), Eur. Phys. J. **C79**, 7, 564 (2019), [arXiv:1903.00941].

[457] G. Aad *et al.* (ATLAS), Phys. Rev. Lett. **125**, 22, 221802 (2020), [arXiv:2004.01678].

[458] A. M. Sirunyan *et al.* (CMS), JHEP **03**, 055 (2020), [arXiv:1911.03781].

[459] M. Aaboud *et al.* (ATLAS), Phys. Lett. **B759**, 555 (2016), [arXiv:1603.09203].

[460] M. Aaboud *et al.* (ATLAS), JHEP **09**, 139 (2018), [arXiv:1807.07915].

[461] CMS Collaboration, CMS-PAS-HIG-16-031 (2016); A. M. Sirunyan *et al.* (CMS), JHEP **07**, 142 (2019), [arXiv:1903.04560].

[462] ATLAS Collaboration, ATLAS-CONF-2012-010 (2012).

[463] A. M. Sirunyan *et al.* (CMS), Phys. Rev. D **102**, 7, 072001 (2020), [arXiv:2005.08900].

Downloaded from https://academic.oup.com/ptep/article/2022/8/083C01/6651666 by KIT Library user on 27 September 2022

[464] G. Aad *et al.* (ATLAS), JHEP **06**, 145 (2021), [arXiv:2102.10076].

[465] A. M. Sirunyan *et al.* (CMS), JHEP **07**, 126 (2020), [arXiv:2001.07763]; V. Khachatryan *et al.* (CMS), JHEP **11**, 018 (2015), [arXiv:1508.07774]; A. M. Sirunyan *et al.* (CMS) (2019), [arXiv:1908.09206].

[466] G. Aad *et al.* (ATLAS), Phys. Rev. Lett. **114**, 23, 231801 (2015), [arXiv:1503.04233].

[467] A. M. Sirunyan *et al.* (CMS), Phys. Rev. Lett. **119**, 14, 141802 (2017), [arXiv:1705.02942].

[468] A. M. Sirunyan *et al.* (CMS), Eur. Phys. J. C **81**, 8, 723 (2021), [arXiv:2104.04762].

[469] A. M. Sirunyan *et al.* (CMS), Phys. Rev. Lett. **123**, 13, 131802 (2019), [arXiv:1905.07453].

[470] A. M. Sirunyan *et al.* (CMS), JHEP **11**, 115 (2018), [arXiv:1808.06575].

[471] ATLAS Collaboration, ATLAS-CONF-2011-020 (2011).

[472] A. M. Sirunyan *et al.* (CMS), JHEP **11**, 010 (2017), [arXiv:1707.07283].

[473] G. Aad *et al.* (ATLAS), Phys. Rev. **D92**, 5, 052002 (2015), [arXiv:1505.01609]; ATLAS Collaboration, ATLAS-CONF-2012-079 (2012).

[474] CMS Collaboration, CMS-PAS-HIG-21-003 (2021).

[475] A. Tumasyan *et al.* (CMS), JHEP **11**, 057 (2021), [arXiv:2106.10361].

[476] CMS Collaboration, CMS-PAS-HIG-16-055 (2016).

[477] A. M. Sirunyan *et al.* (CMS), JHEP **08**, 139 (2020), [arXiv:2005.08694]; V. Khachatryan *et al.* (CMS), JHEP **10**, 076 (2017), [arXiv:1701.02032]; A. M. Sirunyan *et al.* (CMS), Phys. Lett. **B795**, 398 (2019), [arXiv:1812.06359]; A. M. Sirunyan *et al.* (CMS) (2019), [arXiv:1907.07235]; A. M. Sirunyan *et al.* (CMS), Phys. Lett. **B785**, 462 (2018), [arXiv:1805.10191]; A. M. Sirunyan *et al.* (CMS), JHEP **11**, 018 (2018), [arXiv:1805.04865]; CMS Collaboration, CMS-PAS-HIG-18-015 (2019).

[478] V. M. Abazov *et al.* (D0), Phys. Rev. Lett. **103**, 061801 (2009), [arXiv:0905.3381].

[479] A. M. Sirunyan *et al.* (CMS), Phys. Lett. **B796**, 131 (2019), [arXiv:1812.00380].

[480] S. Schael *et al.* (ALEPH), JHEP **05**, 049 (2010), [arXiv:1003.0705].

[481] B. Aubert *et al.* (BaBar), Phys. Rev. Lett. **103**, 081803 (2009), [arXiv:0905.4539].

[482] B. Aubert *et al.* (BaBar), Phys. Rev. Lett. **103**, 181801 (2009), [arXiv:0906.2219].

[483] ATLAS Collaboration, ATLAS-CONF-2016-051 (2016); ATLAS Collaboration, ATLAS-CONF-2017-053 (2017); M. Aaboud *et al.* (ATLAS), Eur. Phys. J. **C79**, 1, 58 (2019), [arXiv:1808.01899].

[484] CMS Collaboration, CMS-PAS-HIG-16-036 (2017).

[485] S. Schael *et al.* (ALEPH, DELPHI, L3, OPAL, LEP Working Group for Higgs Boson Searches), Eur. Phys. J. **C47**, 547 (2006), [hep-ex/0602042].

[486] ATLAS Collaboration, ATLAS-CONF-2013-027 (2013).

[487] CMS Collaboration, CMS-PAS-HIG-13-016 (2013).

[488] A. Heister *et al.* (ALEPH), Phys. Lett. **B526**, 191 (2002), [hep-ex/0201014]; P. Achard *et al.* (L3), Phys. Lett. **B545**, 30 (2002), [hep-ex/0208042].

[489] M. Carena *et al.* (1999), [hep-ph/9912223].

[490] M. M. Kado and C. G. Tully, Ann. Rev. Nucl. Part. Sci. **52**, 65 (2002).

[491] G. Abbiendi *et al.* (OPAL), Eur. Phys. J. **C23**, 397 (2002), [hep-ex/0111010]; J. Abdallah *et al.* (DELPHI), Eur. Phys. J. **C38**, 1 (2004), [hep-ex/0410017].

[492] M. Carena *et al.*, Eur. Phys. J. **C45**, 797 (2006), [hep-ph/0511023].

[493] ATLAS Collaboration, ATLAS-CONF-2016-104 (2016).

[494] S. Chatrchyan *et al.* (CMS), JHEP **09**, 029 (2012), [Erratum: JHEP **03**, 132 (2014)], [arXiv:1204.2488].

[495] M. Aaboud *et al.* (ATLAS), Phys. Rev. Lett. **119**, 19, 191803 (2017), [arXiv:1707.06025].

[496] V. Khachatryan *et al.* (CMS), Phys. Lett. **B758**, 296 (2016), [arXiv:1511.03610].

[497] A. M. Sirunyan *et al.* (CMS), JHEP **11**, 010 (2017), [arXiv:1707.07283].

[498] J. Bernon *et al.*, Phys. Rev. **D91**, 7, 075019 (2015), [arXiv:1412.3385].

[499] G. Aad *et al.* (ATLAS), Phys. Rev. Lett. **113**, 17, 171801 (2014), [arXiv:1407.6583].

[500] CMS Collaboration, CMS-PAS-HIG-14-037 (2015).

[501] T. Biekötter, M. Chakraborti and S. Heinemeyer, Eur. Phys. J. C **80**, 1, 2 (2020), [arXiv:1903.11661].

[502] S. H. Zhu, arXiv preprint (1999), [hep-ph/9901221].

[503] H. E. Logan and S.-f. Su, Phys. Rev. **D66**, 035001 (2002), [hep-ph/0203270].

[504] A. Gutierrez-Rodriguez and O. A. Sampayo, Phys. Rev. **D62**, 055004 (2000).

[505] S. Kanemura, S. Moretti and K. Odagiri, JHEP **02**, 011 (2001), [hep-ph/0012030].

[506] M. Czakon, P. Fiedler and A. Mitov, Phys. Rev. Lett. **110**, 252004 (2013), [arXiv:1303.6254].

[507] M. Carena *et al.*, Nucl. Phys. **B577**, 88 (2000), [hep-ph/9912516].

[508] J. M. Campbell, R. K. Ellis and F. Tramontano, Phys. Rev. **D70**, 094012 (2004), [hep-ph/0408158].

[509] C. Degrande *et al.*, Phys. Lett. **B772**, 87 (2017), [arXiv:1607.05291].

[510] A. A. Barrientos Bendezu and B. A. Kniehl, Phys. Rev. **D63**, 015009 (2001), [hep-ph/0007336]; A. A. Barrientos Bendezu and B. A. Kniehl, Nucl. Phys. **B568**, 305 (2000), [hep-ph/9908385].

[511] G. Abbiendi *et al.* (ALEPH, DELPHI, L3, OPAL, LEP), Eur. Phys. J. **C73**, 2463 (2013), [arXiv:1301.6065].

[512] B. Abbott *et al.* (D0), Phys. Rev. Lett. **82**, 4975 (1999), [hep-ex/9902028]; A. Abulencia *et al.* (CDF), Phys. Rev. Lett. **96**, 042003 (2006), [hep-ex/0510065]; V. M. Abazov *et al.* (D0), Phys. Lett. **B682**, 278 (2009), [arXiv:0908.1811].

[513] V. Khachatryan *et al.* (CMS), JHEP **12**, 178 (2015), [arXiv:1510.04252].

[514] G. Aad *et al.* (ATLAS), Phys. Rev. D **101**, 1, 012002 (2020), [arXiv:1909.02845].

[515] J. Abdallah *et al.* (DELPHI), Eur. Phys. J. **C54**, 1 (2008), [Erratum: Eur. Phys. J. **C56**, 165 (2008)], [arXiv:0801.3586].

[516] R. Dermisek, Mod. Phys. Lett. **A24**, 1631 (2009), [arXiv:0907.0297].

[517] J. F. Gunion, JHEP **08**, 032 (2009), [arXiv:0808.2509].

[518] W. Love *et al.* (CLEO), Phys. Rev. Lett. **101**, 151802 (2008), [arXiv:0807.1427].

[519] G. Aad *et al.* (ATLAS), Eur. Phys. J. **C72**, 2244 (2012), [arXiv:1210.5070]; S. Chatrchyan *et al.* (CMS), Eur. Phys. J. **C72**, 2189 (2012), [arXiv:1207.2666].

[520] G. Aad *et al.* (ATLAS), Phys. Rev. **D89**, 3, 032002 (2014), [arXiv:1312.1956].

[521] J. de Blas *et al.*, JHEP **01**, 139 (2020), [arXiv:1905.03764].

Downloaded from https://academic.oup.com/ptep/article/2022/8/083C01/6651666 by KIT Library user on 27 September 2022

12. CKM Quark-Mixing Matrix

Revised March 2022 by A. Ceccucci (CERN), Z. Ligeti (LBNL) and Y. Sakai (KEK).

12.1 Introduction

The masses and mixings of quarks have a common origin in the Standard Model (SM). They arise from the Yukawa interactions with the Higgs condensate,

$$\mathcal{L}_Y = -Y^d_{ij}\,\overline{Q^I_{Li}}\,\phi\,d^I_{Rj} - Y^u_{ij}\,\overline{Q^I_{Li}}\,\epsilon\,\phi^*\,u^I_{Rj} + \text{h.c.}, \tag{12.1}$$

where $Y^{u,d}$ are 3×3 complex matrices, ϕ is the Higgs field, i,j are generation labels, and ϵ is the 2×2 antisymmetric tensor. Q^I_L are left-handed quark doublets, and d^I_R and u^I_R are right-handed down- and up-type quark singlets, respectively, in the weak-eigenstate basis. When ϕ acquires a vacuum expectation value, $\langle\phi\rangle = (0, v/\sqrt{2})$, Eq. (12.1) yields mass terms for the quarks. The physical states are obtained by diagonalizing $Y^{u,d}$ by four unitary matrices, $V^{u,d}_{L,R}$, as $M^f_{\rm diag} = V^f_L\,Y^f\,V^{f\dagger}_R(v/\sqrt{2})$, $f = u, d$. As a result, the charged-current $W^\pm$ interactions couple to the physical u_{Lj} and d_{Lk} quarks with couplings given by

$$\frac{-g}{\sqrt{2}}(\overline{u_L},\,\overline{c_L},\,\overline{t_L})\gamma^\mu\,W^+_\mu\,V_{\rm CKM}\begin{pmatrix} d_L\\ s_L\\ b_L\end{pmatrix} + \text{h.c.},$$
$$V_{\rm CKM} \equiv V^u_L V^{d\dagger}_L = \begin{pmatrix} V_{ud} & V_{us} & V_{ub}\\ V_{cd} & V_{cs} & V_{cb}\\ V_{td} & V_{ts} & V_{tb}\end{pmatrix}. \tag{12.2}$$

This Cabibbo-Kobayashi-Maskawa (CKM) matrix [1,2] is a 3×3 unitary matrix. It can be parameterized by three mixing angles and the CP-violating KM phase [2]. Of the many possible conventions, a standard choice has become [3]

$$\begin{aligned} V_{\rm CKM} &= \begin{pmatrix} 1 & 0 & 0\\ 0 & c_{23} & s_{23}\\ 0 & -s_{23} & c_{23}\end{pmatrix}\begin{pmatrix} c_{13} & 0 & s_{13}e^{-i\delta}\\ 0 & 1 & 0\\ -s_{13}e^{i\delta} & 0 & c_{13}\end{pmatrix}\begin{pmatrix} c_{12} & s_{12} & 0\\ -s_{12} & c_{12} & 0\\ 0 & 0 & 1\end{pmatrix}\\ &= \begin{pmatrix} c_{12}c_{13} & s_{12}c_{13} & s_{13}e^{-i\delta}\\ -s_{12}c_{23} - c_{12}s_{23}s_{13}e^{i\delta} & c_{12}c_{23} - s_{12}s_{23}s_{13}e^{i\delta} & s_{23}c_{13}\\ s_{12}s_{23} - c_{12}c_{23}s_{13}e^{i\delta} & -c_{12}s_{23} - s_{12}c_{23}s_{13}e^{i\delta} & c_{23}c_{13}\end{pmatrix}, \end{aligned} \tag{12.3}$$

where $s_{ij} = \sin\theta_{ij}$, $c_{ij} = \cos\theta_{ij}$, and δ is the phase responsible for all CP-violating phenomena in flavor-changing processes in the SM. The angles θ_{ij} can be chosen to lie in the first quadrant, so $s_{ij}, c_{ij} \geq 0$.

It is known experimentally that $s_{13} \ll s_{23} \ll s_{12} \ll 1$, and it is convenient to exhibit this hierarchy using the Wolfenstein parameterization. We define [4–6]

$$s_{12} = \lambda = \frac{|V_{us}|}{\sqrt{|V_{ud}|^2 + |V_{us}|^2}}\,, \qquad s_{23} = A\lambda^2 = \lambda\left|\frac{V_{cb}}{V_{us}}\right|,$$
$$s_{13}e^{i\delta} = V^*_{ub} = A\lambda^3(\rho + i\eta) = \frac{A\lambda^3(\bar\rho + i\bar\eta)\sqrt{1 - A^2\lambda^4}}{\sqrt{1-\lambda^2}\,[1 - A^2\lambda^4(\bar\rho + i\bar\eta)]}\,. \tag{12.4}$$

These relations ensure that $\bar\rho + i\bar\eta = -(V_{ud}V^*_{ub})/(V_{cd}V^*_{cb})$ is phase convention independent, and the CKM matrix written in terms of λ, A, $\bar\rho$, and $\bar\eta$ is unitary to all orders in λ. The definitions of $\bar\rho$, $\bar\eta$ reproduce all approximate results in the literature; *i.e.*, $\bar\rho = \rho(1 - \lambda^2/2 + \ldots)$ and $\bar\eta = \eta(1 - \lambda^2/2 + \ldots)$, and one can write $V_{\rm CKM}$ to $\mathcal{O}(\lambda^4)$ either in terms of $\bar\rho, \bar\eta$ or, traditionally,

$$V_{\rm CKM} = \begin{pmatrix} 1 - \lambda^2/2 & \lambda & A\lambda^3(\rho - i\eta)\\ -\lambda & 1 - \lambda^2/2 & A\lambda^2\\ A\lambda^3(1 - \rho - i\eta) & -A\lambda^2 & 1\end{pmatrix} + \mathcal{O}(\lambda^4)\,. \tag{12.5}$$

The CKM matrix elements are fundamental parameters of the SM, so their precise determination is important. The unitarity of the CKM matrix imposes $\sum_i V_{ij}V^*_{ik} = \delta_{jk}$ and $\sum_j V_{ij}V^*_{kj} = \delta_{ik}$. The six vanishing combinations can be represented as triangles in a complex plane, of which those obtained by taking scalar products of neighboring rows or columns are nearly degenerate. The areas of all triangles are the same, half of the Jarlskog invariant, J [7], which is a phase-convention-independent measure of CP violation, defined by $\text{Im}\left[V_{ij}V_{kl}V^*_{il}V^*_{kj}\right] = J\sum_{m,n}\varepsilon_{ikm}\varepsilon_{jln}$.

The most commonly used unitarity triangle arises from

$$V_{ud}\,V^*_{ub} + V_{cd}\,V^*_{cb} + V_{td}\,V^*_{tb} = 0\,, \tag{12.6}$$

by dividing each side by $V_{cd}V^*_{cb}$ (see Fig. 12.1). Its vertices are exactly $(0,0)$, $(1,0)$, and, due to the definition in Eq. (12.4), $(\bar\rho, \bar\eta)$. An important goal of flavor physics is to overconstrain the CKM elements, and many measurements can be conveniently displayed and compared in the $\bar\rho, \bar\eta$ plane. While the Lagrangian in Eq. (12.1) is renormalized, and the CKM matrix has a well-known scale dependence above the weak scale [8], below $\mu = m_W$ the CKM elements can be treated as constants, with all μ-dependence contained in the running of quark masses and higher-dimension operators.

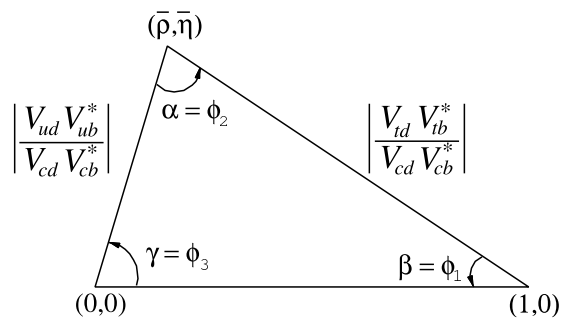

Figure 12.1: Sketch of the unitarity triangle.

Unless explicitly stated otherwise, we describe all measurements assuming the SM, to extract magnitudes and phases of CKM elements in Sec. 12.2 and 12.3. Processes dominated by loop-level contributions in the SM are particularly sensitive to new physics beyond the SM (BSM). We give the global fit results for the CKM elements in Sec. 12.4, and discuss some implications for beyond standard model physics in Sec. 12.5.

12.2 Magnitudes of CKM elements

12.2.1 $|V_{ud}|$

The most precise determination of $|V_{ud}|$ comes from the study of superallowed $0^+ \to 0^+$ nuclear beta decays, which are pure vector transitions. Taking the average of the fifteen most precise determinations [9] yields [10]

$$|V_{ud}| = 0.97373 \pm 0.00031\,. \tag{12.7}$$

This uncertainty is slightly more than twice larger than that in the previous edition, due to a more conservative estimate of the nuclear structure uncertainties. A less precise determination of $|V_{ud}|$ can be obtained from the measurement of the neutron lifetime. The theoretical uncertainties are very small, but the determination is limited by the knowledge of the ratio of the axial-vector and vector couplings, $g_A = G_A/G_V$ [10]. The PIBETA experiment [11] has improved the measurement of the $\pi^+ \to \pi^0 e^+\nu$ branching ratio to 0.6%, and quotes $|V_{ud}| = 0.9739 \pm 0.0029$, in

Downloaded from https://academic.oup.com/ptep/article/2022/8/083C01/6651666 by KIT Library user on 27 September 2022

agreement with the more precise result listed above. The interest in this measurement is that the determination of $|V_{ud}|$ is very clean theoretically, because it is a pure vector transition and is free from nuclear-structure uncertainties.

12.2.2 $|V_{us}|$

The product of $|V_{us}|$ and the form factor at $q^2 = 0$, $|V_{us}|\, f_+(0)$, has been extracted traditionally from $K_L^0 \to \pi e \nu$ decays in order to avoid isospin-breaking corrections ($\pi^0 - \eta$ mixing) that affect $K^\pm$ semileptonic decay, and the complications induced by a second (scalar) form factor present in the muonic decays. The last round of measurements has led to enough experimental constraints to justify the comparison between different decay modes. Systematic errors related to the experimental quantities, *e.g.*, the lifetime of neutral or charged kaons, and the form factor determinations for electron and muonic decays, differ among decay modes, and the consistency between different determinations enhances the confidence in the final result. For this reason, we follow the prescription [12] to average $K_L^0 \to \pi e \nu$, $K_L^0 \to \pi \mu \nu$, $K^\pm \to \pi^0 e^\pm \nu$, $K^\pm \to \pi^0 \mu^\pm \nu$ and $K_S^0 \to \pi e \nu$. The average of these five decay modes yields $|V_{us}|\, f_+(0) = 0.21635 \pm 0.00038$. Results obtained from each decay mode, and exhaustive references to the experimental data, are listed for instance in Ref. [10]. The form factor average $f_+(0) = 0.9698 \pm 0.0017$ [13] from $N_f = 2+1+1$ lattice QCD calculations gives $|V_{us}| = 0.2231 \pm 0.0006$ [10].[1] The broadly used classic calculation of $f_+(0)$ [15] is in good agreement with this value, while other calculations [17] differ by as much as 2%.

The calculation of the ratio of the kaon and pion decay constants enables one to extract $|V_{us}/V_{ud}|$ from $K \to \mu\nu(\gamma)$ and $\pi \to \mu\nu(\gamma)$, where (γ) indicates that radiative decays are included [18]. The value of $\Gamma(K \to \mu\nu(\gamma))$ [10] derived from the KLOE measurement of the corresponding branching ratio [19], combined with the lattice QCD result, $f_K/f_\pi = 1.1932 \pm 0.0021$ [13], leads to $|V_{us}| = 0.2252 \pm 0.0005$, where the accuracy is limited by the knowledge of the ratio of the decay constants. The average of these two determinations, with the error scaled according to the PDG prescription [20] by $\sqrt{\chi^2} = 2.0$, is quoted as [10]

$$|V_{us}| = 0.2243 \pm 0.0008\,. \tag{12.8}$$

It is important to include both QED and QCD isospin violations in the lattice QCD calculations.

The latest determination from hyperon decays can be found in Ref. [21]. The authors focus on the analysis of the vector form factor, protected from first order $SU(3)$ breaking effects by the Ademollo-Gatto theorem [22], and treat the ratio between the axial and vector form factors g_1/f_1 as experimental input, thus avoiding first order $SU(3)$ breaking effects in the axial-vector contribution. They find $|V_{us}| = 0.2250 \pm 0.0027$, although this does not include an estimate of the theoretical uncertainty due to second-order $SU(3)$ breaking, contrary to Eq. (12.8). Concerning hadronic τ decays to strange particles, averaging the inclusive decay and the exclusive $\tau \to h\nu$ ($h = \pi, K$) measurements yields $|V_{us}| = 0.2221 \pm 0.0013$ [23].

12.2.3 $|V_{cd}|$

The magnitude of V_{cd} can be extracted from semileptonic charm decays, using theoretical knowledge of the form factors. In semileptonic D decays, lattice QCD calculations have predicted the normalization of the $D \to \pi\ell\nu$ and $D \to K\ell\nu$ form factors [13]. The dependence on the invariant mass of the lepton pair, q^2, is determined from lattice QCD and theoretical constraints from analyticity [14]. Using $N_f = 2+1+1$ lattice QCD calculations for $D \to \pi\ell\nu$, $f_+^{D\pi}(0) = 0.612 \pm 0.035$ [13], and the average [23] of the measurements of $D \to \pi\ell\nu$ decays by *BaBar* [24], BESIII [25,26], CLEO-c [27], and Belle [28], one obtains $|V_{cd}| = 0.2330 \pm 0.0029 \pm 0.0133$, where the first uncertainty is experimental, and the second is from the theoretical uncertainty of the form factor.

[1] For lattice QCD inputs, we use the averages from Ref. [13], unless the minireviews [10,14] choose different values. We only use unquenched results, and if both $N_f = 2+1+1$ and $2+1$ calculations are available, we use the former.

The determination of $|V_{cd}|$ is also possible from the leptonic decay $D^+ \to \mu^+\nu$ and $\tau^+\nu$. The experimental uncertainties have not decreased significantly recently. Averaging the BESIII [29] and earlier CLEO [30] for $\mu^+\nu$ and BESIII [31] for $\tau^+\nu$ measurements, and using the $N_f = 2+1+1$ lattice QCD result, $f_D = 212.0 \pm 0.7$ MeV [13], yields $|V_{cd}| = 0.2181 \pm 0.0049 \pm 0.0007$ [23,32].[2]

Earlier determinations of $|V_{cd}|$ came from neutrino scattering data. The difference of the ratio of double-muon to single-muon production by neutrino and antineutrino beams is proportional to the charm cross section off valence d quarks, and therefore to $|V_{cd}|^2$ times the average semileptonic branching ratio of charm mesons, $\mathcal{B}_\mu$. The method was used first by CDHS [33] and then by CCFR [34,35] and CHARM II [36]. Averaging these results is complicated, because it requires assumptions about the scale of the QCD corrections, and because $\mathcal{B}_\mu$ is an effective quantity, which depends on the specific neutrino beam characteristics. With no recent experimental input available, we quote the average from a past review, $\mathcal{B}_\mu |V_{cd}|^2 = (0.463 \pm 0.034) \times 10^{-2}$ [37]. Analysis cuts make these experiments insensitive to neutrino energies smaller than 30 GeV. Thus, $\mathcal{B}_\mu$ should be computed using only neutrino interactions with visible energy larger than 30 GeV. An appraisal [38] based on charm-production fractions measured in neutrino interactions [39,40] gives $\mathcal{B}_\mu = 0.088 \pm 0.006$. Data from the CHORUS experiment [41] are sufficiently precise to extract $\mathcal{B}_\mu$ directly, by comparing the number of charm decays with a muon to the total number of charmed hadrons found in the nuclear emulsions. Requiring the visible energy to be larger than 30 GeV, CHORUS found $\mathcal{B}_\mu = 0.085 \pm 0.009 \pm 0.006$. We use the average of these two determinations, $\mathcal{B}_\mu = 0.087 \pm 0.005$, and obtain $|V_{cd}| = 0.230 \pm 0.011$. Averaging the three determinations above, we find

$$|V_{cd}| = 0.221 \pm 0.004\,. \tag{12.9}$$

12.2.4 $|V_{cs}|$

The direct determination of $|V_{cs}|$ is possible from semileptonic D or leptonic D_s decays, using lattice QCD calculations of the semileptonic D form factor or the D_s decay constant. For muonic decays, the average of Belle [42], CLEO-c [43], *BaBar* [44], and BESIII [45,46] is $\mathcal{B}(D_s^+ \to \mu^+\nu) = (5.43 \pm 0.16) \times 10^{-3}$ [23]. For decays to τ leptons, the average of CLEO-c [43,47,48], *BaBar* [44], Belle [42], and BESIII [45] gives $\mathcal{B}(D_s^+ \to \tau^+\nu) = (5.40 \pm 0.23) \times 10^{-2}$ [23]. From each of these values, determinations of $|V_{cs}|$ can be obtained using the PDG values for the mass and lifetime of the D_s, the masses of the leptons, and $f_{D_s} = (249.9 \pm 0.5)$ MeV [13]. The average of these determinations gives $|V_{cs}| = 0.984 \pm 0.012$, where the error is dominated by the experimental uncertainty. In semileptonic D decays, lattice QCD calculations of the $D \to K\ell\nu$ form factor are available [13]. Using $f_+^{DK}(0) = 0.7385 \pm 0.0044$ and the average [23] of CLEO-c [27], Belle [28], *BaBar* [49], and recent BESIII [25,50] measurements of $D \to K\ell\nu$ decays, one obtains $|V_{cs}| = 0.972 \pm 0.007$, where the dominant uncertainty is from the theoretical calculation of the form factor. Averaging the determinations from leptonic and semileptonic decays, we find

$$|V_{cs}| = 0.975 \pm 0.006\,. \tag{12.10}$$

Measurements of on-shell $W^\pm$ decays sensitive to $|V_{cs}|$ were made by LEP-2. The W branching ratios depend on the six CKM elements involving quarks lighter than m_W. The W branching ratio to each lepton flavor is $1/\mathcal{B}(W \to \ell\bar{\nu}_\ell) = 3\Big[1 + \sum_{u,c,d,s,b} |V_{ij}|^2\,(1 + \alpha_s(m_W)/\pi) + \ldots\Big]$. Assuming lepton universality, the measurement $\mathcal{B}(W \to \ell\bar{\nu}_\ell) = (10.83 \pm 0.07 \pm 0.07)\,\%$ [51] implies $\sum_{u,c,d,s,b} |V_{ij}|^2 = 2.002 \pm 0.027$. This is a precise test of unitarity; however, only flavor-tagged W-decays determine $|V_{cs}|$ directly, such as DELPHI's tagged $W^+ \to c\bar{s}$ analysis, yielding $|V_{cs}| = 0.94^{+0.32}_{-0.26} \pm 0.13$ [52].

[2] Hereafter the first error is statistical and the second is systematic, unless mentioned otherwise.

Downloaded from https://academic.oup.com/ptep/article/2022/8/083C01/6651666 by KIT Library user on 27 September 2022

12.2.5 $|V_{cb}|$

This matrix element can be determined from exclusive and inclusive semileptonic decays of B mesons to charm. The inclusive determinations use the semileptonic decay rate measurement, together with (certain moments of) the lepton energy and the hadronic invariant-mass spectra. The theoretical basis is the operator product expansion [53, 54], which allows calculation of the decay rate and various spectra as expansions in α_s and inverse powers of the heavy-quark mass. The dependence on m_b, m_c, and the parameters that occur at subleading order is different for different moments. The measurements of many moments overconstrain these parameters, and also test the consistency of their determination. The precise extraction of $|V_{cb}|$ requires using a "threshold" quark mass definition [55, 56]. Inclusive measurements have been performed using B mesons from Z^0 decays at LEP, and at e^+e^- colliders operated at the $\Upsilon(4S)$. At LEP, the large boost of B mesons from the Z^0 decay allows the determination of the moments throughout phase space, which is not possible otherwise, but the large statistics available at the B factories lead to more precise determinations. An average of the measurements and a compilation of the references are provided in Ref. [14]: $|V_{cb}| = (42.2 \pm 0.8) \times 10^{-3}$.

Complementary determinations are based on exclusive semileptonic B decays to D and D^*. In the $m_{b,c} \gg \Lambda_{\rm QCD}$ limit, all form factors are given by a single Isgur-Wise function [57], which depends on the product of the four-velocities of the B and $D^{(*)}$ mesons, $w = v \cdot v'$. Heavy-quark symmetry determines the rate at $w = 1$ (in the symmetry limit), the maximum momentum transfer to the $\ell\bar{\nu}$ pair, and $|V_{cb}|$ is obtained from extrapolating a fit to the spectrum to $w = 1$. The current update of the V_{cb} and V_{ub} minireview quotes from exclusive decays $|V_{cb}| = (39.4 \pm 0.8) \times 10^{-3}$ [14], based on the only unfolded measurement of $B \to D^*$ semileptonic decay distributions [58], and using a more general fit [59] than in earlier B factory measurements. With the uncertainty scaled by $\sqrt{\chi^2} = 2.4$, this yields the combination [14],

$$|V_{cb}| = (40.8 \pm 1.4) \times 10^{-3} \,. \tag{12.11}$$

Determinations of $|V_{cb}|$ that are currently less precise and not included in this average, can be obtained from the measurement of $B_s \to D_s^{(*)}\mu\bar{\nu}$ decays [60]. In addition, semileptonic decays to τ leptons measured in $B \to D^{(*)}\tau\bar{\nu}$ and related modes are also sensitive to $|V_{cb}|$. The most precise data involving τ leptons are the $|V_{cb}|$-independent ratios, $\mathcal{B}(B \to D^{(*)}\tau\bar{\nu})/\mathcal{B}(B \to D^{(*)}\ell\bar{\nu})$ measured by BaBar, Belle, and LHCb. If the current, approximately $3\,\sigma$ [23], hint of lepton non-universality prevails, the determination of $|V_{cb}|$ becomes more complicated.

12.2.6 $|V_{ub}|$

The determination of $|V_{ub}|$ from inclusive $B \to X_u\ell\bar{\nu}$ decay is complicated due to large $B \to X_c\ell\bar{\nu}$ backgrounds. In most regions of phase space where the charm background is kinematically forbidden, the hadronic physics enters via unknown nonperturbative functions, so-called shape functions. (In contrast, the nonperturbative physics for $|V_{cb}|$ is encoded in a few parameters.) At leading order in $\Lambda_{\rm QCD}/m_b$, there is only one shape function, which can be extracted from the photon energy spectrum in $B \to X_s\gamma$ [61, 62], and applied to several spectra in $B \to X_u\ell\bar{\nu}$. The subleading shape functions are modeled in the current determinations. Phase space cuts for which the rate has only subleading dependence on the shape function are also possible [63]. The measurements of both the hadronic and the leptonic systems are important for an optimal choice of phase space. A different approach is to make the measurements more inclusive by extending them deeper into the $B \to X_c\ell\bar{\nu}$ region, and thus reduce the theoretical uncertainties. Analyses of the electron-energy endpoint from CLEO [64], BABAR [65], and Belle [66] quote $B \to X_u e\bar{\nu}$ partial rates for $|\vec{p}_e| \geq 2.0\,$GeV and $1.9\,$GeV, which are well below the charm endpoint. The large and pure $B\overline{B}$ samples at the B factories permit the selection of $B \to X_u\ell\bar{\nu}$ decays in events where the other B is fully reconstructed [67]. With this full-reconstruction tag method, the four-momenta of both the leptonic and the hadronic final states can be measured. It also gives access to a wider kinematic region, because of improved signal purity. Ref. [14] quotes the inclusive average, $|V_{ub}| = (4.13 \pm 0.12\ ^{+0.13}_{-0.14} \pm 0.18) \times 10^{-3}$, where the first error is experimental, the second arises from the model dependence quoted by the individual measurements, and the third is an additional one estimated in Ref. [14].

To extract $|V_{ub}|$ from exclusive decays, the form factors have to be known. Experimentally, better signal-to-background ratios are offset by smaller yields. The $B \to \pi\ell\bar{\nu}$ branching ratio is now known to 5%. Lattice QCD calculations of the $B \to \pi\ell\bar{\nu}$ form factor are available [68] for the high q^2 region ($q^2 > 16$ or $18\,{\rm GeV}^2$). A fit to the experimental partial rates and lattice QCD results versus q^2 yields $|V_{ub}| = (3.70 \pm 0.10 \pm 0.12) \times 10^{-3}$ [23]. Light-cone QCD sum rules are supposed to be applicable for $q^2 < 12\,{\rm GeV}^2$ [69], yielding a combination, $|V_{ub}| = (3.67 \pm 0.09 \pm 0.12) \times 10^{-3}$ [14, 23].

The uncertainties in extracting $|V_{ub}|$ from inclusive and exclusive decays are different to a large extent. An average of these determinations, with the uncertainty scaled by $\sqrt{\chi^2} = 1.4$, is [14]

$$|V_{ub}| = (3.82 \pm 0.20) \times 10^{-3} \,. \tag{12.12}$$

A determination of $|V_{ub}|$ not included in this average can be obtained from $\mathcal{B}(B \to \tau\bar{\nu}) = (1.06 \pm 0.19) \times 10^{-4}$ [23]. Using $f_B = (190.0 \pm 1.3)\,$MeV [13] and $\tau_{B^\pm} = (1.638 \pm 0.004)\,$ps [70], we find the remarkably consistent result, $|V_{ub}| = (4.05 \pm 0.36) \times 10^{-3}$. This decay is sensitive, for example, to tree-level charged Higgs contributions, and the measured rate is consistent with the SM expectation. The LHCb measurement $|V_{ub}/V_{cb}| = 0.084 \pm 0.007$ [14] from the ratios of $\Lambda_b \to p^+\mu^-\bar{\nu}$ and $\Lambda_b \to \Lambda_c^+\mu^-\bar{\nu}$ [71] and $B_s^0 \to K^-\mu^+\nu$ and $B_s^0 \to D_s^-\mu^+\nu$ [72] in different regions of q^2, provides another complementary determination.

12.2.7 $|V_{td}|$ *and* $|V_{ts}|$

The CKM elements $|V_{td}|$ and $|V_{ts}|$ are not likely to be precisely measurable in tree-level processes involving top quarks, so one has to rely on determinations from B–$\overline{B}$ oscillations dominated by box diagrams with top quarks, or loop-mediated rare K and B decays. Theoretical uncertainties in hadronic effects limit the accuracy of the current determinations. These can be reduced by taking ratios of processes that are equal in the flavor $SU(3)$ limit to determine $|V_{td}/V_{ts}|$.

The mixing of the two B^0 mesons was discovered by ARGUS [73], and the mass difference is now precisely measured as $\Delta m_d = (0.5065 \pm 0.0019)\,{\rm ps}^{-1}$ [74]. In the B_s^0 system, Δm_s was first measured significantly by CDF [75] and the world average, dominated by an LHCb measurement [76], is $\Delta m_s = (17.765 \pm 0.006)\,{\rm ps}^{-1}$ [74]. Neglecting corrections suppressed by $|V_{tb}| - 1$, and using the lattice QCD results $f_{B_d}\sqrt{\widehat{B}_{B_d}} = (210.6 \pm 5.5)\,$MeV and $f_{B_s}\sqrt{\widehat{B}_{B_s}} = (256.1 \pm 5.7)\,$MeV [13],

$$|V_{td}| = (8.6 \pm 0.2) \times 10^{-3} \,, \qquad |V_{ts}| = (41.5 \pm 0.9) \times 10^{-3} \,. \tag{12.13}$$

The uncertainties are dominated by lattice QCD. Several uncertainties are reduced in the calculation of the ratio $\xi = \left(f_{B_s}\sqrt{\widehat{B}_{B_s}}\right)/\left(f_{B_d}\sqrt{\widehat{B}_{B_d}}\right) = 1.216 \pm 0.016$ [13] and therefore the constraint on $|V_{td}/V_{ts}|$ from $\Delta m_d/\Delta m_s$ is more reliable theoretically. These provide a theoretically clean and significantly improved determination,

$$\left|V_{td}/V_{ts}\right| = 0.207 \pm 0.001 \pm 0.003 \,. \tag{12.14}$$

The inclusive branching ratio $\mathcal{B}(B \to X_s\gamma) = (3.32 \pm 0.15) \times 10^{-4}$ extrapolated to $E_\gamma > E_0 = 1.6\,$GeV [23] is also sensitive to $|V_{tb}V_{ts}|$. In addition to t-quark penguins, a substantial part of the rate comes from charm contributions proportional to $V_{cb}V_{cs}^*$ via the application of 3×3 CKM unitarity (which is used here). With the NNLO calculation of $\mathcal{B}(B \to X_s\gamma)_{E_\gamma > E_0}/\mathcal{B}(B \to X_c e\bar{\nu})$ [77], we obtain $|V_{ts}/V_{cb}| = 0.98 \pm 0.04$. The $B_s \to \mu^+\mu^-$ rate is also proportional to $|V_{tb}V_{ts}|^2$ in the SM, and the world average, $\mathcal{B}(B_s \to \mu^+\mu^-) = (2.9 \pm 0.4) \times 10^{-9}$ [70], is consistent with the SM, with sizable uncertainties.

A complementary determination of $|V_{td}/V_{ts}|$ is possible from the ratio of $B \to \rho\gamma$ and $K^*\gamma$ rates. The ratio of the neutral modes

Downloaded from https://academic.oup.com/ptep/article/2022/8/083C01/6651666 by KIT Library user on 27 September 2022

is theoretically cleaner than that of the charged ones, because the poorly known spectator-interaction contribution is expected to be smaller (W-exchange vs. weak annihilation). For now, because of low statistics, we average the charged and neutral rates assuming the isospin symmetry and heavy-quark limit motivated relation, $|V_{td}/V_{ts}|^2/\xi_\gamma^2 = [\Gamma(B^+ \to \rho^+\gamma) + 2\Gamma(B^0 \to \rho^0\gamma)]/[\Gamma(B^+ \to K^{*+}\gamma) + \Gamma(B^0 \to K^{*0}\gamma)] = (3.37 \pm 0.49)\%$ [23]. Here ξ_γ contains the poorly known hadronic physics. Using $\xi_\gamma = 1.2 \pm 0.2$ [78] gives $|V_{td}/V_{ts}| = 0.220 \pm 0.016 \pm 0.037$, where the first uncertainty is experimental and the second is theoretical.

A theoretically clean determination of $|V_{td}V_{ts}^*|$ is possible from $K^+ \to \pi^+\nu\bar{\nu}$ decay [79]. Experimentally, more than 20 candidates have been observed [80, 81] and the rate is consistent with the SM within errors. Much more data are needed for a precision measurement.

12.2.8 $|V_{tb}|$

The determination of $|V_{tb}|$ from top decays uses the ratio of branching fractions $R = \mathcal{B}(t \to Wb)/\mathcal{B}(t \to Wq) = |V_{tb}|^2/(\sum_q |V_{tq}|^2) = |V_{tb}|^2$, where $q = b, s, d$. The CDF and DØ measurements performed on data collected during Run II of the Tevatron give $|V_{tb}| > 0.78$ [82] and $0.99 > |V_{tb}| > 0.90$ [83], respectively, at 95% CL. CMS measured the same quantity at 8 TeV and obtained $|V_{tb}| > 0.975$ [84] at 95% CL.

The direct determination of $|V_{tb}|$, without assuming unitarity, is possible from the single top quark production cross section. The $(3.30^{+0.52}_{-0.40})$ pb combined cross section [85] of DØ and CDF measurements implies $|V_{tb}| = 1.02^{+0.06}_{-0.05}$. The LHC experiments, ATLAS and CMS, have measured single top quark production cross sections (and extracted $|V_{tb}|$) in t-channel, Wt-channel, and s-channel at 7 TeV, 8 TeV, and 13 TeV [86]. The average of these $|V_{tb}|$ values is calculated to be $|V_{tb}| = 1.014 \pm 0.035$, where all systematic errors and theoretical errors are treated to be fully correlated. The average of Tevatron and LHC values gives

$$|V_{tb}| = 1.014 \pm 0.029\,. \tag{12.15}$$

The experimental systematic uncertainties dominate, and a dedicated combination would be welcome.

A weak constraint on $|V_{tb}|$ can be obtained from precision electroweak data, where top quarks enter in loops. The sensitivity is best in $\Gamma(Z \to b\bar{b})$ and yields $|V_{tb}| = 0.77^{+0.18}_{-0.24}$ [87].

12.3 Phases of CKM elements

As can be seen from Fig. 12.1, the angles of the unitarity triangle are

$$\beta = \phi_1 = \arg\left(-\frac{V_{cd}V_{cb}^*}{V_{td}V_{tb}^*}\right),$$
$$\alpha = \phi_2 = \arg\left(-\frac{V_{td}V_{tb}^*}{V_{ud}V_{ub}^*}\right),$$
$$\gamma = \phi_3 = \arg\left(-\frac{V_{ud}V_{ub}^*}{V_{cd}V_{cb}^*}\right). \tag{12.16}$$

Since CP violation involves phases of CKM elements, many measurements of CP-violating observables can be used to constrain these angles and the $\bar{\rho}, \bar{\eta}$ parameters.

12.3.1 ϵ *and* ϵ'

The measurement of CP violation in K^0–$\overline{K}^0$ mixing, $|\epsilon| = (2.228 \pm 0.011) \times 10^{-3}$ [88], provides important information about the CKM matrix. The phase of ϵ is determined by long-distance physics, $\epsilon = \frac{1}{2}\, e^{i\phi_\epsilon} \sin\phi_\epsilon \arg(-M_{12}/\Gamma_{12})$, where $\phi_\epsilon = \arctan|2\Delta m_K/\Delta\Gamma_K| \simeq 43.5°$. The SM prediction can be written as

$$\epsilon = \kappa_\epsilon\, e^{i\phi_\epsilon} \frac{G_F^2 m_W^2 m_K}{12\sqrt{2}\,\pi^2 \Delta m_K} f_K^2 \widehat{B}_K \Big\{ \eta_{tt} S(x_t)\, \mathrm{Im}[(V_{ts}V_{td}^*)^2] + 2\eta_{ct} S(x_c, x_t)\, \mathrm{Im}(V_{cs}V_{cd}^* V_{ts}V_{td}^*) + \eta_{cc}\, x_c\, \mathrm{Im}[(V_{cs}V_{cd}^*)^2] \Big\}, \tag{12.17}$$

where $\kappa_\epsilon \simeq 0.94 \pm 0.02$ [89] includes the effects of strangeness changing $\Delta s = 1$ operators and additional dependence on $\phi_\epsilon \neq \pi/4$ (see also Ref. [90]). The displayed terms are the short-distance $\Delta s = 2$ contribution to $\mathrm{Im}M_{12}$ in the usual phase convention, S is an Inami-Lim function [91], $x_q = m_q^2/m_W^2$, and η_{ij} are perturbative QCD corrections. The constraint from ϵ in the $\bar{\rho}, \bar{\eta}$ plane is bounded by approximate hyperbolas. Lattice QCD determined the bag parameter $\widehat{B}_K = 0.717 \pm 0.024$ [13] and the main uncertainties are from $(V_{ts}V_{td}^*)^2$ (approximately given by that of $|V_{cb}|^4$ or A^4), the η_{ij} coefficients, and estimates of κ_ϵ.

The measurement of $6\,\mathrm{Re}(\epsilon'/\epsilon) = 1 - |\eta_{00}/\eta_{+-}|^2$, where each $\eta_{ij} = \langle\pi^i\pi^j|\mathcal{H}|K_L\rangle/\langle\pi^i\pi^j|\mathcal{H}|K_S\rangle$ violates CP, provides a qualitative test of the CKM mechanism, and strong constraints on many BSM scenarios. Its nonzero value, $\mathrm{Re}(\epsilon'/\epsilon) = (1.67 \pm 0.23) \times 10^{-3}$ [88], demonstrated the existence of direct CP violation, a prediction of the KM ansatz. While $\mathrm{Re}(\epsilon'/\epsilon) \propto \mathrm{Im}(V_{td}V_{ts}^*)$, this quantity cannot easily be used to extract CKM parameters, because cancellations between the electromagnetic and gluonic penguin contributions for large m_t [92] enhance the hadronic uncertainties. Most SM estimates [93] agree with the observed value, indicating that $\bar{\eta}$ is positive. Progress in lattice QCD [94] may yield a precise SM prediction in the future, and trigger new work on assessing the consistency of the SM with the measured value [95, 96].

12.3.2 β / ϕ_1

12.3.2.1 *Charmonium modes*

CP-violation measurements in B-meson decays provide direct information on the angles of the unitarity triangle, shown in Fig. 12.1. These overconstraining measurements serve to improve the determination of the CKM elements, and to reveal possible effects beyond the SM.

The time-dependent CP asymmetry of neutral B decays to a final state f common to B^0 and $\overline{B}^0$ is given by [97–99]

$$\mathcal{A}_f = \frac{\Gamma(\overline{B}^0(t) \to f) - \Gamma(B^0(t) \to f)}{\Gamma(\overline{B}^0(t) \to f) + \Gamma(B^0(t) \to f)}\,, \quad = S_f \sin(\Delta m_d\, t) - C_f \cos(\Delta m_d\, t)\,, \tag{12.18}$$

where

$$S_f = \frac{2\,\mathrm{Im}\lambda_f}{1 + |\lambda_f|^2}\,, \qquad C_f = \frac{1 - |\lambda_f|^2}{1 + |\lambda_f|^2}\,, \qquad \lambda_f = \frac{q}{p}\frac{\bar{A}_f}{A_f}\,. \tag{12.19}$$

Here, q/p describes B^0–$\overline{B}^0$ mixing and, to a good approximation in the SM, $q/p = V_{tb}^* V_{td}/V_{tb}V_{td}^* = e^{-2i\beta + \mathcal{O}(\lambda^4)}$ in the usual phase convention. A_f ($\bar{A}_f$) is the amplitude of the $B^0 \to f$ ($\overline{B}^0 \to f$) decay. If f is a CP eigenstate, and amplitudes with one CKM phase dominate the decay, then $|A_f| = |\bar{A}_f|$, $C_f = 0$, and $S_f = \sin(\arg\lambda_f) = \eta_f \sin 2\phi$, where η_f is the CP eigenvalue of f and 2ϕ is the phase difference between the $B^0 \to f$ and $B^0 \to \overline{B}^0 \to f$ decay paths. A contribution of another amplitude to the decay with a different CKM phase makes the value of S_f sensitive to relative strong-interaction phases between the decay amplitudes (it also makes $C_f \neq 0$ possible).

The $b \to c\bar{c}s$ decays to CP eigenstates ($B^0 \to$ charmonium $K^0_{S,L}$) give currently the most precise measurements of $S_f = -\eta_f \sin 2\beta$. The $b \to s$ penguin amplitudes have dominantly the same weak phase as the $b \to c\bar{c}s$ tree amplitude. Since only λ^2-suppressed penguin amplitudes introduce a different CP-violating phase, amplitudes with a single weak phase dominate, and we expect $\left|\bar{A}_{\psi K}/A_{\psi K}| - 1\right| < 0.01$. The e^+e^- asymmetric-energy B-factory experiments, BABAR [100] and Belle [101], and LHCb [102] provided precise measurements. The world average, including some other measurements, is [23]

$$\sin 2\beta = 0.699 \pm 0.017\,. \tag{12.20}$$

This measurement has a four-fold ambiguity in β, which can be resolved by a global fit as mentioned in Sec. 12.4. Experimentally, the two-fold ambiguity $\beta \to \pi/2 - \beta$ (but not $\beta \to \pi + \beta$) can be resolved by a time-dependent angular analysis of $B^0 \to J/\psi K^{*0}$ [103, 104], or a time-dependent Dalitz plot analysis of $B^0 \to \overline{D}^0 h^0$. The time-dependent Dalitz plot analysis of $B^0 \to \overline{D}^0 h^0$ ($h^0 = \pi^0, \eta, \omega$) with $\overline{D}^0 \to K^0_S\pi^+\pi^-$, jointly performed by Belle and BABAR, excludes the $\pi/2 - \beta$ solution with

Downloaded from https://academic.oup.com/ptep/article/2022/8/083C01/6651666 by KIT Library user on 27 September 2022

7.3σ confidence level [105]. These results exclude the negative $\cos 2\beta$ solutions, in agreement with the global CKM fit, which is no longer shown in Fig. 12.2.

The $b \to c\bar{c}d$ mediated transitions, such as $B^0 \to J/\psi\pi^0$ and $B^0 \to D^{(*)+}D^{(*)-}$, also measure approximately $\sin 2\beta$. However, the dominant component of the $b \to d$ penguin amplitude has a different CKM phase ($V_{tb}^*V_{td}$) than the tree amplitude ($V_{cb}^*V_{cd}$), and their magnitudes are of the same order in λ. Therefore, the effect of penguins could be large, resulting in $S_f \neq -\eta_f \sin 2\beta$ and $C_f \neq 0$. Such decay modes have been measured by *BaBar*, Belle, and LHCb. The world averages [23], $S_{J/\psi\pi^0} = -0.86 \pm 0.14$, $S_{J/\psi\rho^0} = -0.66^{+0.16}_{-0.12}$, $S_{D^+D^-} = -0.84 \pm 0.12$, and $S_{D^{*+}D^{*-}} = -0.71 \pm 0.09$ (where $\eta_f = +1$ for the $J/\psi\pi^0$ and D^+D^- modes, while $J/\psi\rho^0$ and $D^{*+}D^{*-}$ are mixtures of CP even and odd states), are consistent with $\sin 2\beta$ obtained from $B^0 \to$ charmonium K^0 decays, and the C_f's are consistent with zero, although the uncertainties are sizable.

The $b \to c\bar{u}d$ decays $B^0 \to \overline{D}^{0(*)}h^0$, with $\overline{D}^0 \to CP$ eigenstates and $\overline{D}^0 \to K_S^0\pi^+\pi^-$ with Dalitz plot analysis, have no penguin contributions, and provide theoretically clean $\sin 2\beta$ measurements. The average of joint analyses of *BaBar* and Belle data [105, 106] give $\sin 2\beta = 0.71 \pm 0.09$ [23, 107].

12.3.2.2 *Penguin-dominated modes*

The $b \to s\bar{q}q$ penguin-dominated decays have the same CKM phase as the $b \to c\bar{c}s$ tree level decays, up to corrections suppressed by λ^2, since $V_{tb}^*V_{ts} = -V_{cb}^*V_{cs}[1 + \mathcal{O}(\lambda^2)]$. Therefore, decays such as $B^0 \to \phi K^0$ and $\eta' K^0$ provide $\sin 2\beta$ measurements in the SM. Any BSM contribution to the amplitude with a different weak phase would give rise to $S_f \neq -\eta_f \sin 2\beta$, and possibly $C_f \neq 0$. Therefore, the main interest in these modes is not simply to measure $\sin 2\beta$, but to search for new physics. Measurements of many other decay modes in this category, such as $B \to \pi^0 K_S^0$, $K_S^0 K_S^0 K_S^0$, *etc.*, have also been performed by *BaBar* and Belle. The results and their uncertainties are summarized in Fig. 13.3 and Table 13.1 of Ref. [98]. The comparison of CP violation measurements between tree-dominated and penguin-dominated modes in B_s^0 decays provides similar sensitivity to new physics.

12.3.3 α / ϕ_2

Since α is the phase between $V_{tb}^*V_{td}$ and $V_{ub}^*V_{ud}$, only time-dependent CP asymmetries in decay modes dominated by $b \to u\bar{u}d$ transitions can directly measure $\sin 2\alpha$, in contrast to $\sin 2\beta$, where several different quark-level transitions can be used. Since $b \to d$ penguin amplitudes have a different CKM phase than $b \to u\bar{u}d$ tree amplitudes, and their magnitudes are of the same order in λ, the penguin contribution can be sizable, which makes the determination of α complicated. To date, α has been measured in $B \to \pi\pi$, $\rho\pi$ and $\rho\rho$ decay modes.

12.3.3.1 $B \to \pi\pi$

It is well-established from the data that there is a sizable contribution of $b \to d$ penguin amplitudes in $B \to \pi\pi$ decays. Thus, $S_{\pi^+\pi^-}$ in the time-dependent $B^0 \to \pi^+\pi^-$ analysis does not measure $\sin 2\alpha$, but

$$S_{\pi^+\pi^-} = \sqrt{1 - C^2_{\pi^+\pi^-}}\,\sin(2\alpha + 2\Delta\alpha)\,, \tag{12.21}$$

where $2\Delta\alpha$ is the phase difference between $e^{2i\gamma}\bar{A}_{\pi^+\pi^-}$ and $A_{\pi^+\pi^-}$. The value of $\Delta\alpha$, and hence α, can be extracted using the isospin relation among the amplitudes of $B^0 \to \pi^+\pi^-$, $B^0 \to \pi^0\pi^0$, and $B^+ \to \pi^+\pi^0$ decays [108],

$$\frac{1}{\sqrt{2}}\,A_{\pi^+\pi^-} + A_{\pi^0\pi^0} - A_{\pi^+\pi^0} = 0\,, \tag{12.22}$$

and a similar expression for the $\bar{A}_{\pi\pi}$'s. This method utilizes the fact that a pair of pions from $B \to \pi\pi$ decay must be in a zero angular momentum state, and, because of Bose statistics, they must have even isospin. Consequently, $\pi^\pm\pi^0$ is in a pure isospin-2 state, while the penguin amplitudes only contribute to the isospin-0 final state. The latter does not hold for the electroweak penguin amplitudes, but their effect is expected to be small. The isospin analysis uses the world averages of *BaBar*, Belle, and LHCb measurements, $S_{\pi^+\pi^-} = -0.666 \pm 0.029$, $C_{\pi^+\pi^-} = -0.311 \pm 0.030$, the decay widths of all three modes, and the direct CP asymmetry $C_{\pi^0\pi^0} = -0.33 \pm 0.22$ [23]. This analysis leads to 16 mirror solutions for $0 \leq \alpha < 2\pi$. Because of this, and due to the experimental uncertainties, some of these solutions are not well separated [99].

12.3.3.2 $B \to \rho\rho$

The decay $B^0 \to \rho^+\rho^-$ contains two vector mesons in the final state, and so in general is a mixture of CP-even and CP-odd components. At the current level of precision, it simplifies the analysis that the longitudinal polarization fractions in $B^+ \to \rho^+\rho^0$ and $B^0 \to \rho^+\rho^-$ decays were measured to be close to unity [109], which implies that the final states are almost purely CP-even. Furthermore, $\mathcal{B}(B^0 \to \rho^0\rho^0) = (0.95 \pm 0.16) \times 10^{-6}$ is much smaller than $\mathcal{B}(B^0 \to \rho^+\rho^-) = (27.7 \pm 1.9) \times 10^{-6}$ and $\mathcal{B}(B^+ \to \rho^+\rho^0) = (24.0^{+1.9}_{-2.0}) \times 10^{-6}$ [23], which implies that the effect of the penguin contributions is small. The isospin analysis using the world averages, $S_{\rho^+\rho^-} = -0.14 \pm 0.13$ and $C_{\rho^+\rho^-} = 0.00 \pm 0.09$ [23], together with the time-dependent CP asymmetry, $S_{\rho^0\rho^0} = -0.3 \pm 0.7$ and $C_{\rho^0\rho^0} = -0.2 \pm 0.9$ [110], and the above mentioned branching fractions and longitudinal polarization fractions, gives two solutions (with mirror solutions at $3\pi/2 - \alpha$) [99]. A possible small violation of Eq. (12.22) due to the finite width of the ρ [111] is so far neglected.

12.3.3.3 $B \to \rho\pi$

The final state in $B^0 \to \rho^+\pi^-$ decay is not a CP eigenstate, but this decay proceeds via the same quark-level diagrams as $B^0 \to \pi^+\pi^-$, and both B^0 and $\overline{B}^0$ can decay to $\rho^+\pi^-$, while the final state in $B^0 \to \rho^0\pi^0$ is a CP eigenstate. Consequently, mixing-induced CP violation can occur in B^0 and $\overline{B}^0$ decays to $\rho^\pm\pi^\mp$ and $\rho^0\pi^0$. The time-dependent Dalitz plot analysis of $B^0 \to \pi^+\pi^-\pi^0$ decays permits the extraction of α with a single discrete ambiguity, $\alpha \to \alpha + \pi$, since one knows the variation of the strong phases in the interference regions of the $\rho^+\pi^-$, $\rho^-\pi^+$, and $\rho^0\pi^0$ amplitudes in the Dalitz plot [112]. The combination of Belle [113] and *BaBar* [114] measurements gives only moderate constraints [99].

Combining the $B \to \pi\pi$, $\rho\pi$, and $\rho\rho$ decay modes [23, 99], α is constrained as

$$\alpha = \left(85.2^{+4.8}_{-4.3}\right)^\circ\,. \tag{12.23}$$

Similar results can be found in Refs. [115, 116].

12.3.4 γ / ϕ_3

By virtue of Eq. (12.16), γ does not depend on CKM elements involving the top quark, so it can be measured in tree-level B decays. This is an important distinction from the measurements of α and β, and implies that measurements of γ are unlikely to be affected by physics beyond the SM.

12.3.4.1 $B_{(s)} \to D_{(s)}K^{(*)}$

The interference of $B^- \to D^0K^-$ ($b \to c\bar{u}s$) and $B^- \to \overline{D}^0K^-$ ($b \to u\bar{c}s$) transitions can be studied in final states accessible in both D^0 and $\overline{D}^0$ decays [97]. In principle, it is possible to extract the B and D decay amplitudes, the relative strong phases, and the weak phase γ from the data [99].

A practical complication is that the precision depends sensitively on the ratio of the interfering amplitudes

$$r_B = \left|A(B^- \to \overline{D}^0K^-)\big/A(B^- \to D^0K^-)\right|, \tag{12.24}$$

which is around 0.1. The original GLW method [117, 118] considers D decays to CP eigenstates, such as $B^\pm \to D^{(*)}_{CP}(\to \pi^+\pi^-)K^{(*)\pm}$. To alleviate the smallness of r_B and make the interfering amplitudes (which are products of the B and D decay amplitudes) comparable in magnitude, the ADS method [119] considers final states where Cabibbo-allowed $\overline{D}^0$ and doubly-Cabibbo-suppressed D^0 decays interfere. Measurements have been made by the B factories, CDF, and LHCb, using both methods [23]. The GLW method currently gives only a loose constraint on γ, $13.7^\circ < \gamma < 80.0^\circ$, $100.0^\circ < \gamma < 166.3^\circ$ at 68% CL with 4 solutions at $26^\circ, 72^\circ, 107^\circ$, and 154°; while the ADS method provides $\gamma = (70^{+15}_{-33})^\circ$ [99, 107].

Downloaded from https://academic.oup.com/ptep/article/2022/8/083C01/6651666 by KIT Library user on 27 September 2022

The BPGGSZ method [120, 121] utilizes the fact that both D^0 and $\overline{D}^0$ can have large branching fractions to CP self-conjugate three-body final states, such as $K^0_S\pi^+\pi^-$, and the analysis can be optimized by studying the Dalitz plot dependence of the interferences. The best present determination of γ comes from this method. Combining the Belle [122], *BaBar* [123], and now dominant LHCb [124] measurements, $\gamma = (69.3 \pm 4.5)^\circ$ is obtained [99, 107]. The uncertainty is sensitive to the central value of the amplitude ratio r_B (and r^*_B for the D^*K mode), for which Belle found somewhat larger central values than *BaBar* and LHCb. The same values of $r_B^{(*)}$ enter the ADS analyses, and the data can be combined to fit for $r_B^{(*)}$ and γ. The effect of D^0–$\overline{D}^0$ mixing on γ is either below the present experimental accuracy or can be taken into account in the analysis [125, 126] (even if D^0–$\overline{D}^0$ mixing is due to CP-violating new physics [127]).

The amplitude ratio is much larger in the analogous $B^0_s \to D^\pm_s K^\mp$ decays, which allows a model-independent extraction of $\gamma - 2\beta_s$ [128] (here $\beta_s = \arg(-V_{ts}V^*_{tb}/V_{cs}V^*_{cb})$ is related to the phase of B_s mixing). Measurements by LHCb with $B^0_s \to D^\pm_s K^\mp$ [129] and $B^0_s \to D^\pm_s K^\mp\pi^+\pi^-$ [130] give $\gamma = (79^{+19}_{-21})^\circ$ using a constraint on $2\beta_s$ (see Sec. 12.5).

Combining all the above measurements [99, 107], γ is constrained as

$$\gamma = \left(65.9^{+3.3}_{-3.5}\right)^\circ . \tag{12.25}$$

Similar results can be found in Refs. [115, 116].

12.3.4.2 $B^0 \to D^{(*)\pm}\pi^\mp$

The interference of $b \to u$ and $b \to c$ transitions can be studied in $\overline{B}^0 \to D^{(*)+}\pi^-$ ($b \to c\bar{u}d$) and $\overline{B}^0 \to B^0 \to D^{(*)+}\pi^-$ ($\bar{b} \to \bar{u}c\bar{d}$) decays and their CP conjugates, since both B^0 and $\overline{B}^0$ decay to $D^{(*)\pm}\pi^\mp$ (or $D^\pm\rho^\mp$, *etc.*). Since there are only tree and no penguin contributions to these decays, in principle, it is possible to extract from the four time-dependent rates the magnitudes of the two hadronic amplitudes, their relative strong phase, and the weak phase between the two decay paths, which is $2\beta + \gamma$.

A complication is that the ratio of the interfering amplitudes is very small, $r_{D\pi} = A(B^0 \to D^+\pi^-)/A(\overline{B}^0 \to D^+\pi^-) = \mathcal{O}(0.01)$ (and similarly for $r_{D^*\pi}$ and $r_{D\rho}$), and therefore it has not been possible to measure it. To obtain $2\beta + \gamma$, $SU(3)$ flavor symmetry and dynamical assumptions have been used to relate $A(\overline{B}^0 \to D^-\pi^+)$ to $A(\overline{B}^0 \to D^-_s\pi^+)$, so this measurement is not model independent at present. Combining the $D^\pm\pi^\mp$, $D^{*\pm}\pi^\mp$ and $D^\pm\rho^\mp$ measurements [131] gives $\sin(2\beta + \gamma) > 0.68$ at 68% CL [115], consistent with the previously discussed results for β and γ.

12.4 Global fit in the Standard Model

Using the independently measured CKM elements mentioned in the previous sections, the unitarity of the CKM matrix can be checked. We obtain $|V_{ud}|^2 + |V_{us}|^2 + |V_{ub}|^2 = 0.9985 \pm 0.0007$ (1st row), $|V_{cd}|^2 + |V_{cs}|^2 + |V_{cb}|^2 = 1.001 \pm 0.012$ (2nd row), $|V_{ud}|^2 + |V_{cd}|^2 + |V_{td}|^2 = 0.9972 \pm 0.0020$ (1st column), and $|V_{us}|^2 + |V_{cs}|^2 + |V_{ts}|^2 = 1.004 \pm 0.012$ (2nd column), respectively. Due to the recent reduction of the value of $|V_{ud}|$, there is a 2.2σ tension with unitarity in the 1st row, leading also to poor consistency of the SM fit below. The uncertainties in the second row and column are dominated by that of $|V_{cs}|$. For the second row, another check is obtained from the measurement of $\sum_{u,c,d,s,b} |V_{ij}|^2$ in Sec. 12.2.4, minus the sum in the first row above: $|V_{cd}|^2 + |V_{cs}|^2 + |V_{cb}|^2 = 1.002 \pm 0.027$. These provide strong tests of the unitarity of the CKM matrix. With the significantly improved direct determination of $|V_{tb}|$, the unitarity checks for the third row and column have also become fairly precise, leaving decreasing room for mixing with other states. The sum of the three angles of the unitarity triangle, $\alpha + \beta + \gamma = \left(173 \pm 6\right)^\circ$, is also consistent with the SM expectation.

The CKM matrix elements can be most precisely determined using a global fit to all available measurements and imposing the SM constraints (*i.e.*, three generation unitarity). The fit must also use theory predictions for hadronic matrix elements, which sometimes have significant uncertainties. There are several approaches to combining the experimental data. CKMfitter [6, 115] and Ref. [132] (which develops [133, 134] further) use frequentist statistics, while UTfit [116, 135] uses a Bayesian approach. These approaches provide similar results.

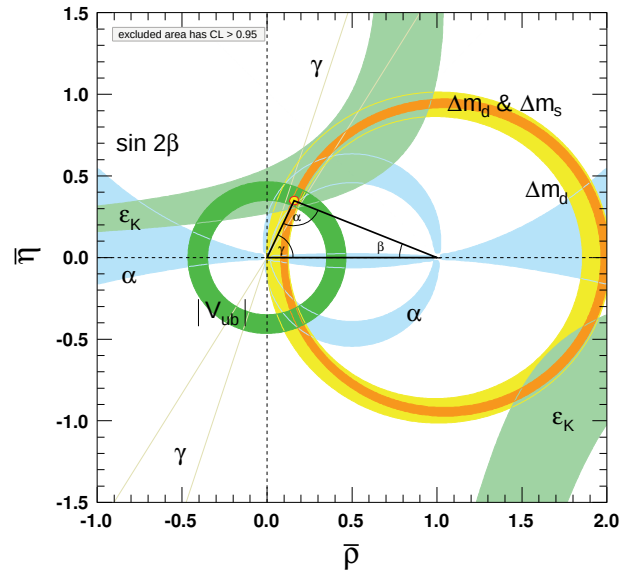

Figure 12.2: Constraints on the $\bar{\rho}, \bar{\eta}$ plane. The shaded areas have 95% CL.

The constraints implied by the unitarity of the three generation CKM matrix significantly reduce the allowed range of some of the CKM elements. The fit for the Wolfenstein parameters defined in Eq. (12.4) gives

$$\lambda = 0.22500 \pm 0.00067\,, \qquad A = 0.826^{+0.018}_{-0.015}\,,$$
$$\bar{\rho} = 0.159 \pm 0.010\,, \qquad \bar{\eta} = 0.348 \pm 0.010\,. \tag{12.26}$$

These values are obtained using the method of Refs. [6, 115]. The prescription of Refs. [116, 135] gives $\lambda = 0.22499 \pm 0.00067$, $A = 0.833 \pm 0.011$, $\bar{\rho} = 0.159 \pm 0.010$, and $\bar{\eta} = 0.348 \pm 0.009$ [136]; these results are now very close to one another. The fit results for the magnitudes of all nine CKM elements are

$$\left|V_{\rm CKM}\right| = \begin{pmatrix} 0.97435 \pm 0.00016 & 0.22500 \pm 0.00067 & 0.00369 \pm 0.00011 \\ 0.22486 \pm 0.00067 & 0.97349 \pm 0.00016 & 0.04182^{+0.00085}_{-0.00074} \\ 0.00857^{+0.00020}_{-0.00018} & 0.04110^{+0.00083}_{-0.00072} & 0.999118^{+0.000031}_{-0.000036} \end{pmatrix}, \tag{12.27}$$

and the Jarlskog invariant is $J = \left(3.08^{+0.15}_{-0.13}\right) \times 10^{-5}$. The parameters in Eq. (12.3) are

$$\sin\theta_{12} = 0.22500 \pm 0.00067\,, \qquad \sin\theta_{13} = 0.00369 \pm 0.00011\,,$$
$$\sin\theta_{23} = 0.04182^{+0.00085}_{-0.00074}\,, \qquad \delta = 1.144 \pm 0.027\,. \tag{12.28}$$

Fig. 12.2 illustrates the constraints on the $\bar{\rho}, \bar{\eta}$ plane from various measurements, and the global fit result. The shaded 95% CL regions all overlap consistently around the global fit region. This reverts a change in the 2020 edition, when the shown CL of each region was increased to 99%, because of poor consistency (primarily due to changes in $|V_{ud}|$), which is no longer the case.

If one uses only tree-level inputs (magnitudes of CKM elements not coupling to the top quark and the angle γ), the resulting fit is almost identical for λ in Eq. (12.26), while the other parameters' central values can change by about a sigma and their uncertainties double, yielding $\lambda = 0.22507 \pm 0.00068$, $A = 0.805 \pm 0.028$, $\bar{\rho} = 0.166^{+0.026}_{-0.024}$, and $\bar{\eta} = 0.370^{+0.029}_{-0.028}$. This illustrates how the constraints can be less tight in the presence of BSM physics.

Downloaded from https://academic.oup.com/ptep/article/2022/8/083C01/6651666 by KIT Library user on 27 September 2022

12.5 Implications beyond the SM

The effects in B, B_s, K, and D decays and mixings due to high-scale physics (W, Z, t, H in the SM, and unknown heavier particles) can be parameterized by operators composed of SM fields, obeying the $SU(3)\times SU(2)\times U(1)$ gauge symmetry. Flavor-changing neutral currents, suppressed in the SM, are especially sensitive to beyond SM contributions. Processes studied in great detail, both experimentally and theoretically, include neutral meson mixings, $B_{(s)} \to X\gamma$, $X\ell^+\ell^-$, $\ell^+\ell^-$, $K \to \pi\nu\bar{\nu}$, etc. The BSM contributions to these operators are suppressed by powers of the scale at which they are generated. Already at lowest order, there are many dimension-6 operators, and the observable effects of BSM interactions are encoded in their coefficients. In the SM, these coefficients are determined by just the four CKM parameters, and the W, Z, and quark masses. For example, Δm_d, $\Gamma(B \to \rho\gamma)$, $\Gamma(B \to \pi\ell^+\ell^-)$, and $\Gamma(B \to \ell^+\ell^-)$ are all proportional to $|V_{td}V_{tb}|^2$ in the SM, however, they may receive unrelated BSM contributions. These BSM contributions may or may not obey the SM relations. (For example, the flavor sector of the MSSM contains 69 CP-conserving parameters and 41 CP-violating phases, *i.e.*, 40 new ones [137]). Thus, similar to the measurements of $\sin 2\beta$ in tree- and loop-dominated decay modes, overconstraining measurements of the magnitudes and phases of flavor-changing neutral-current amplitudes gives good sensitivity to BSM.

To illustrate the level of suppression required for BSM contributions, consider a class of models in which the unitarity of the CKM matrix is maintained, and the dominant BSM effects modify the neutral meson mixing amplitudes [138] by $(z_{ij}/\Lambda^2)(\bar{q}_i\gamma^\mu P_L q_j)^2$, where z_{ij} is an unknown coefficient and Λ is the scale suppressing this BSM contribution (see, [139, 140]). It is only known since the first measurements of γ and α that the SM gives the leading contribution to $B^0-\overline{B}^0$ mixing [6,141]. Nevertheless, new physics with a generic weak phase may still contribute to neutral meson mixings at a significant fraction of the SM [135, 142, 143]. The existing data imply that $\Lambda/|z_{ij}|^{1/2}$ has to exceed about 10^4 TeV for $K^0-\overline{K}^0$ mixing, 10^3 TeV for $D^0-\overline{D}^0$ mixing, 500 TeV for $B^0-\overline{B}^0$ mixing, and 100 TeV for $B_s^0-\overline{B}_s^0$ mixing [135, 140]. (Some other operators are even better constrained [135].) The constraints are the strongest in the kaon sector, because the CKM suppression is the most severe. Thus, if there is new physics at the TeV scale, $|z_{ij}| \ll 1$ is required. Even if $|z_{ij}|$ are suppressed by a loop factor and $|V_{ti}^*V_{tj}|^2$ (in the down quark sector), similar to the SM, one expects percent-level effects, which may be observable in forthcoming flavor physics experiments. To constrain such extensions of the SM, many measurements irrelevant for the SM-CKM fit, such as the CP asymmetry in semileptonic $B_{d,s}^0$ decays, $A_{\rm SL}^{d,s}$, are important [144]. The current world averages [23] are consistent with the SM, with experimental uncertainties far greater than those of the theory predictions.

There are many key measurements sensitive to BSM physics, which do not constrain the unitarity triangle in Fig. 12.1. For example, a key quantity in the B_s system is $\beta_s = \arg(-V_{ts}V_{tb}^*/V_{cs}V_{cb}^*)$, which is the small, λ^2-suppressed, angle of a "squashed" unitarity triangle, obtained by taking the scalar product of the second and third columns of the CKM matrix. This angle can be measured via time-dependent CP violation in $B_s^0 \to J/\psi\,\phi$, similar to β in $B^0 \to J/\psi K^0$. Since the $J/\psi\,\phi$ final state is not a CP eigenstate, an angular analysis of the decay products is needed to separate the CP-even and CP-odd components, which give opposite asymmetries. In the SM, the asymmetry for the CP-even part is $2\beta_s$, when one neglects subdominant amplitudes with a weak phase V_{ub}. (Sometimes the notation $\phi_s = -2\beta_s$ plus a possible BSM contribution to the B_s mixing phase is used.) Testing if the data agree with the SM prediction, $2\beta_s = 0.0369^{+0.0011}_{-0.0010}$ [115], is another sensitive probe of the SM. The current world average, dominated by LHC measurements [145] including the $B_s \to J/\psi\,K^+K^-$ and $J/\psi\,\pi^+\pi^-$ decay modes, is $2\beta_s = 0.050 \pm 0.019$ [74]. Since the uncertainty is much larger than that in the SM, a lot will be learned from more precise future measurements. Searches for CP violation in the charm sector, in particular in $D^0-\overline{D}^0$ mixing, provide complementary sensitivity to BSM.

In the kaon sector, the CP-violating observables, ϵ and ϵ', are tiny, so models in which all sources of CP violation are small were viable before the B-factory measurements. Since the measurement of $\sin 2\beta$, we know that CP violation can be an $\mathcal{O}(1)$ effect, and only flavor mixing is suppressed between the three quark generations. Thus, many models with spontaneous CP violation were excluded. In the kaon sector, clean tests of the SM can come from measurements of $K^+ \to \pi^+\nu\bar{\nu}$ [81] and $K_L^0 \to \pi^0\nu\bar{\nu}$ [146]. These loop-induced rare decays are sensitive to BSM, and will allow precise tests [147] of the CKM paradigm, independent of B decays.

The CKM elements are fundamental parameters, so they should be measured as precisely as possible. The overconstraining measurements of CP asymmetries, mixing, semileptonic, and rare decays severely constrain the magnitudes and phases of possible BSM contributions to flavor-changing interactions. If new particles are observed at the LHC, it will be important to explore their flavor parameters as precisely as possible to understand the underlying physics.

References

[1] N. Cabibbo, Phys. Rev. Lett. **10**, 531 (1963).

[2] M. Kobayashi and T. Maskawa, Prog. Theor. Phys. **49**, 652 (1973).

[3] L.-L. Chau and W.-Y. Keung, Phys. Rev. Lett. **53**, 1802 (1984).

[4] L. Wolfenstein, Phys. Rev. Lett. **51**, 1945 (1983).

[5] A. J. Buras, M. E. Lautenbacher and G. Ostermaier, Phys. Rev. **D50**, 3433 (1994), [hep-ph/9403384].

[6] J. Charles *et al.* (CKMfitter Group), Eur. Phys. J. **C41**, 1, 1 (2005), [hep-ph/0406184].

[7] C. Jarlskog, Phys. Rev. Lett. **55**, 1039 (1985).

[8] W. J. Marciano and A. Sirlin, Nucl. Phys. **B93**, 303 (1975); K. S. Babu, Z. Phys. **C35**, 69 (1987).

[9] J. C. Hardy and I. S. Towner, Phys. Rev. C **102**, 4, 045501 (2020).

[10] E. Blucher and W.J. Marciano, "V_{ud}, V_{us}, the Cabibbo Angle and CKM Unitarity," in this *Review*.

[11] D. Pocanic *et al.*, Phys. Rev. Lett. **93**, 181803 (2004), [hep-ex/0312030].

[12] M. Antonelli *et al.* (FlaviaNet Working Group on Kaon Decays), Eur. Phys. J. **C69**, 399 (2010), [arXiv:1005.2323]; see also `http://www.lnf.infn.it/wg/vus`.

[13] S. Aoki *et al.* (Flavour Lattice Averaging Group) "FLAG Review 2021", `http://flag.unibe.ch/2021`; The original papers that led to the quoted averages are cited in this reference.

[14] T. Mannel and P. Urquijo, "Semileptonic b-Hadron Decays, Determination of V_{cb} and V_{ub}," in this *Review*.

[15] H. Leutwyler and M. Roos, Z. Phys. **C25**, 91 (1984); For earlier fits for $|V_{ud}|$ and $|V_{us}|$ in the 3-generation SM, see Ref. [16].

[16] R. E. Shrock and L.-L. Wang, Phys. Rev. Lett. **41**, 1692 (1978).

[17] J. Bijnens and P. Talavera, Nucl. Phys. **B669**, 341 (2003), [hep-ph/0303103]; M. Jamin, J. A. Oller and A. Pich, JHEP **02**, 047 (2004), [hep-ph/0401080]; V. Cirigliano *et al.*, JHEP **04**, 006 (2005), [hep-ph/0503108]; C. Dawson *et al.*, PoS **LAT2005**, 337 (2006), [hep-lat/0510018]; N. Tsutsui *et al.* (JLQCD), PoS **LAT2005**, 357 (2006), [hep-lat/0510068]; M. Okamoto (Fermilab Lattice, MILC, HPQCD), in "3rd Conference on Flavor Physics and CP Violation (FPCP 2004) Daegu, Korea, October 4-9, 2004," (2004), [hep-lat/0412044].

[18] W. J. Marciano, Phys. Rev. Lett. **93**, 231803 (2004), [hep-ph/0402299].

[19] F. Ambrosino *et al.* (KLOE), Phys. Lett. **B632**, 76 (2006), [hep-ex/0509045].

Downloaded from https://academic.oup.com/ptep/article/2022/8/083C01/6651666 by KIT Library user on 27 September 2022

[20] See Sec. 5.2, "Averages and fits," in the Introduction to this *Review*, http://pdg.lbl.gov/2019/reviews/rpp2019-rev-rpp-intro.pdf.

[21] N. Cabibbo, E. C. Swallow and R. Winston, Ann. Rev. Nucl. Part. Sci. **53**, 39 (2003), [hep-ph/0307298]; N. Cabibbo, E. C. Swallow and R. Winston, Phys. Rev. Lett. **92**, 251803 (2004), [hep-ph/0307214].

[22] M. Ademollo and R. Gatto, Phys. Rev. Lett. **13**, 264 (1964).

[23] Y. S. Amhis *et al.* (HFLAV), Eur. Phys. J. C **81**, 3, 226 (2021), [arXiv:1909.12524]; and updates at https://hflav.web.cern.ch/.

[24] J. P. Lees *et al.* (BaBar), Phys. Rev. **D91**, 5, 052022 (2015), [arXiv:1412.5502].

[25] M. Ablikim *et al.* (BESIII), Phys. Rev. **D92**, 7, 072012 (2015), [arXiv:1508.07560].

[26] M. Ablikim *et al.* (BESIII), Phys. Rev. **D96**, 1, 012002 (2017), [arXiv:1703.09084].

[27] D. Besson *et al.* (CLEO), Phys. Rev. **D80**, 032005 (2009), [arXiv:0906.2983].

[28] L. Widhalm *et al.* (Belle), Phys. Rev. Lett. **97**, 061804 (2006), [hep-ex/0604049].

[29] M. Ablikim *et al.* (BESIII), Phys. Rev. **D89**, 5, 051104 (2014), [arXiv:1312.0374].

[30] B. I. Eisenstein *et al.* (CLEO), Phys. Rev. **D78**, 052003 (2008), [arXiv:0806.2112].

[31] M. Ablikim *et al.* (BESIII), Phys. Rev. Lett. **123**, 21, 211802 (2019), [arXiv:1908.08877].

[32] Heavy Flavor Averaging Group [23], June 2021 update of Charm Leptonic Decays https://hflav-eos.web.cern.ch/hflav-eos/charm/Vcd/june21/Vcd~from~leptonic~D~decays.html.

[33] H. Abramowicz *et al.*, Z. Phys. **C15**, 19 (1982).

[34] S. A. Rabinowitz *et al.*, Phys. Rev. Lett. **70**, 134 (1993).

[35] A. O. Bazarko *et al.* (CCFR), Z. Phys. **C65**, 189 (1995), [hep-ex/9406007].

[36] P. Vilain *et al.* (CHARM II), Eur. Phys. J. **C11**, 19 (1999).

[37] F. J. Gilman, K. Kleinknecht and B. Renk (2004).

[38] G. De Lellis, P. Migliozzi and P. Santorelli, Phys. Rept. **399**, 227 (2004), [Erratum: Phys. Rept.411,323(2005)].

[39] N. Ushida *et al.* (Fermilab E531), Phys. Lett. **B206**, 380 (1988).

[40] T. Bolton (1997), [hep-ex/9708014].

[41] A. Kayis-Topaksu *et al.* (CHORUS), Phys. Lett. **B626**, 24 (2005).

[42] A. Zupanc *et al.* (Belle), JHEP **09**, 139 (2013), [arXiv:1307.6240].

[43] J. P. Alexander *et al.* (CLEO), Phys. Rev. **D79**, 052001 (2009), [arXiv:0901.1216].

[44] P. del Amo Sanchez *et al.* (BaBar), Phys. Rev. **D82**, 091103 (2010), [Erratum: Phys. Rev.D91,no.1,019901(2015)], [arXiv:1008.4080].

[45] M. Ablikim *et al.* (BESIII), Phys. Rev. **D94**, 7, 072004 (2016), [arXiv:1608.06732].

[46] M. Ablikim *et al.* (BESIII), Phys. Rev. D **104**, 5, 052009 (2021), [arXiv:2102.11734].

[47] P. U. E. Onyisi *et al.* (CLEO), Phys. Rev. **D79**, 052002 (2009), [arXiv:0901.1147].

[48] P. Naik *et al.* (CLEO), Phys. Rev. **D80**, 112004 (2009), [arXiv:0910.3602].

[49] B. Aubert *et al.* (BaBar), Phys. Rev. **D76**, 052005 (2007), [arXiv:0704.0020].

[50] M. Ablikim *et al.* (BESIII), Phys. Rev. Lett. **122**, 1, 011804 (2019), [arXiv:1810.03127].

[51] LEP W branching fraction results for this Review of Particle Physics, LEPEWWG/XSEC/2005-01, http://lepewwg.web.cern.ch/LEPEWWG/lepww/4f/Winter05.

[52] P. Abreu *et al.* (DELPHI), Phys. Lett. **B439**, 209 (1998).

[53] I. I. Y. Bigi *et al.*, Phys. Rev. Lett. **71**, 496 (1993), [hep-ph/9304225].

[54] A. V. Manohar and M. B. Wise, Phys. Rev. **D49**, 1310 (1994), [hep-ph/9308246].

[55] I. I. Y. Bigi *et al.*, Phys. Rev. **D56**, 4017 (1997), [hep-ph/9704245].

[56] A. H. Hoang, Z. Ligeti and A. V. Manohar, Phys. Rev. **D59**, 074017 (1999), [hep-ph/9811239]; A. H. Hoang, Z. Ligeti and A. V. Manohar, Phys. Rev. Lett. **82**, 277 (1999), [hep-ph/9809423]; A. H. Hoang and T. Teubner, Phys. Rev. **D60**, 114027 (1999), [hep-ph/9904468].

[57] N. Isgur and M. B. Wise, Phys. Lett. **B237**, 527 (1990); N. Isgur and M. B. Wise, Phys. Lett. **B232**, 113 (1989).

[58] A. Abdesselam *et al.* (Belle) (2017), [arXiv:1702.01521].

[59] C. G. Boyd, B. Grinstein and R. F. Lebed, Phys. Rev. **D56**, 6895 (1997), [hep-ph/9705252]; C. G. Boyd, B. Grinstein and R. F. Lebed, Nucl. Phys. **B461**, 493 (1996), [hep-ph/9508211].

[60] R. Aaij *et al.* (LHCb), Phys. Rev. D **101**, 7, 072004 (2020), [arXiv:2001.03225].

[61] M. Neubert, Phys. Rev. **D49**, 3392 (1994), [hep-ph/9311325]; M. Neubert, Phys. Rev. **D49**, 4623 (1994), [hep-ph/9312311].

[62] I. I. Y. Bigi *et al.*, Int. J. Mod. Phys. **A9**, 2467 (1994), [hep-ph/9312359].

[63] C. W. Bauer, Z. Ligeti and M. E. Luke, Phys. Lett. **B479**, 395 (2000), [hep-ph/0002161]; C. W. Bauer, Z. Ligeti and M. E. Luke, Phys. Rev. **D64**, 113004 (2001), [hep-ph/0107074].

[64] A. Bornheim *et al.* (CLEO), Phys. Rev. Lett. **88**, 231803 (2002), [hep-ex/0202019].

[65] B. Aubert *et al.* (BaBar), Phys. Rev. **D73**, 012006 (2006), [hep-ex/0509040].

[66] A. Limosani *et al.* (Belle), Phys. Lett. **B621**, 28 (2005), [hep-ex/0504046].

[67] P. Urquijo *et al.* (Belle), Phys. Rev. Lett. **104**, 021801 (2010), [arXiv:0907.0379]; J. P. Lees *et al.* (BaBar), Phys. Rev. **D86**, 032004 (2012), [arXiv:1112.0702].

[68] J. A. Bailey *et al.* (Fermilab Lattice, MILC), Phys. Rev. **D92**, 1, 014024 (2015), [arXiv:1503.07839]; J. M. Flynn *et al.*, Phys. Rev. **D91**, 7, 074510 (2015), [arXiv:1501.05373]; B. Colquhoun *et al.*, Phys. Rev. **D93**, 3, 034502 (2016), [arXiv:1510.07446].

[69] P. Ball and R. Zwicky, Phys. Rev. **D71**, 014015 (2005), [hep-ph/0406232]; A. Khodjamirian *et al.*, Phys. Rev. **D83**, 094031 (2011), [arXiv:1103.2655].

[70] Particle listing, in this *Review*.

[71] R. Aaij *et al.* (LHCb), Nature Phys. **11**, 743 (2015), [arXiv:1504.01568].

[72] R. Aaij *et al.* (LHCb), Phys. Rev. Lett. **126**, 8, 081804 (2021), [arXiv:2012.05143].

[73] H. Albrecht *et al.* (ARGUS), Phys. Lett. **B192**, 245 (1987).

[74] O. Schneider, "B^0–$\overline{B}^0$ mixing," in this *Review*.

[75] A. Abulencia *et al.* (CDF), Phys. Rev. Lett. **97**, 242003 (2006), [hep-ex/0609040].

[76] R. Aaij *et al.* (LHCb), Nature Phys. **18**, 1, 1 (2022), [arXiv:2104.04421].

[77] M. Misiak *et al.*, Phys. Rev. Lett. **114**, 22, 221801 (2015), [arXiv:1503.01789]; M. Czakon *et al.*, JHEP **04**, 168 (2015), [arXiv:1503.01791].

Downloaded from https://academic.oup.com/ptep/article/2022/8/083C01/6651666 by KIT Library user on 27 September 2022

[78] B. Grinstein and D. Pirjol, Phys. Rev. **D62**, 093002 (2000), [hep-ph/0002216]; A. Ali, E. Lunghi and A. Ya. Parkhomenko, Phys. Lett. **B595**, 323 (2004), [hep-ph/0405075]; M. Beneke, T. Feldmann and D. Seidel, Nucl. Phys. **B612**, 25 (2001), [hep-ph/0106067]; S. W. Bosch and G. Buchalla, Nucl. Phys. **B621**, 459 (2002), [hep-ph/0106081]; Z. Ligeti and M. B. Wise, Phys. Rev. **D60**, 117506 (1999), [hep-ph/9905277]; D. Becirevic *et al.*, JHEP **05**, 007 (2003), [hep-lat/0301020]; P. Ball, G. W. Jones and R. Zwicky, Phys. Rev. **D75**, 054004 (2007), [hep-ph/0612081]; W. Wang, R.-H. Li and C.-D. Lu (2007), [arXiv:0711.0432]; C.-D. Lu, W. Wang and Z.-T. Wei, Phys. Rev. **D76**, 014013 (2007), [hep-ph/0701265].

[79] A. J. Buras *et al.*, Phys. Rev. Lett. **95**, 261805 (2005), [hep-ph/0508165].

[80] A. V. Artamonov *et al.* (E949), Phys. Rev. Lett. **101**, 191802 (2008), [arXiv:0808.2459]; A. V. Artamonov *et al.* (BNL-E949), Phys. Rev. **D79**, 092004 (2009), [arXiv:0903.0030].

[81] E. Cortina Gil *et al.* (NA62), JHEP **06**, 093 (2021), [arXiv:2103.15389].

[82] D. Acosta *et al.* (CDF), Phys. Rev. Lett. **95**, 102002 (2005), [hep-ex/0505091].

[83] V. M. Abazov *et al.* (D0), Phys. Rev. Lett. **107**, 121802 (2011), [arXiv:1106.5436].

[84] V. Khachatryan *et al.* (CMS), Phys. Lett. **B736**, 33 (2014), [arXiv:1404.2292].

[85] T. A. Aaltonen *et al.* (CDF, D0), Phys. Rev. Lett. **115**, 15, 152003 (2015), [arXiv:1503.05027].

[86] LHC Top Working Group summary plots, single top quark production, Sep. 2021, `https://twiki.cern.ch/twiki/bin/view/LHCPhysics/LHCTopWGSummaryPlots`.

[87] J. Swain and L. Taylor, Phys. Rev. **D58**, 093006 (1998), [hep-ph/9712420].

[88] "K_L^0 meson" particle listing, in this *Review*.

[89] A. J. Buras, D. Guadagnoli and G. Isidori, Phys. Lett. **B688**, 309 (2010), [arXiv:1002.3612]; For earlier discussions, see Ref. [90].

[90] E. A. Andriyash, G. G. Ovanesyan and M. I. Vysotsky, Phys. Lett. **B599**, 253 (2004), [hep-ph/0310314]; K. Anikeev *et al.*, in "Workshop on B Physics at the Tevatron: Run II and Beyond Batavia, Illinois, September 23-25, 1999," (2001), [hep-ph/0201071]; A. J. Buras and D. Guadagnoli, Phys. Rev. **D78**, 033005 (2008), [arXiv:0805.3887].

[91] T. Inami and C. S. Lim, Prog. Theor. Phys. **65**, 297 (1981), [Erratum: Prog. Theor. Phys.65,1772(1981)].

[92] J. M. Flynn and L. Randall, Phys. Lett. **B224**, 221 (1989), [Erratum: Phys. Lett.B235,412(1990)]; G. Buchalla, A. J. Buras and M. K. Harlander, Nucl. Phys. **B337**, 313 (1990).

[93] M. Ciuchini *et al.*, Phys. Lett. **B301**, 263 (1993), [hep-ph/9212203]; A. J. Buras, M. Jamin and M. E. Lautenbacher, Nucl. Phys. **B408**, 209 (1993), [hep-ph/9303284]; T. Hambye *et al.*, Nucl. Phys. **B564**, 391 (2000), [hep-ph/9906434]; S. Bertolini, J. O. Eeg and M. Fabbrichesi, Phys. Rev. **D63**, 056009 (2001), [hep-ph/0002234]; V. Cirigliano *et al.*, Phys. Rev. Lett. **91**, 162001 (2003), [hep-ph/0307030].

[94] R. Abbott *et al.* (RBC, UKQCD), Phys. Rev. D **102**, 5, 054509 (2020), [arXiv:2004.09440].

[95] A. J. Buras *et al.*, JHEP **11**, 202 (2015), [arXiv:1507.06345].

[96] V. Cirigliano *et al.*, JHEP **02**, 032 (2020), [arXiv:1911.01359].

[97] A. B. Carter and A. I. Sanda, Phys. Rev. Lett. **45**, 952 (1980); A. B. Carter and A. I. Sanda, Phys. Rev. **D23**, 1567 (1981).

[98] A more detailed discussion and references can be found in: T. Gershon and Y. Nir, "CP violation in meson decays," in this *Review*.

[99] T. Gershon, M. Kenzie and K. Trabelsi, "Determination of CKM angles from B hadrons," in this *Review*.

[100] B. Aubert *et al.* (BaBar), Phys. Rev. **D79**, 072009 (2009), [arXiv:0902.1708].

[101] I. Adachi *et al.* (Belle), Phys. Rev. Lett. **108**, 171802 (2012), [arXiv:1201.4643].

[102] R. Aaij *et al.* (LHCb), Phys. Rev. Lett. **115**, 3, 031601 (2015), [arXiv:1503.07089].

[103] B. Aubert *et al.* (BaBar), Phys. Rev. **D71**, 032005 (2005), [hep-ex/0411016].

[104] R. Itoh *et al.* (Belle), Phys. Rev. Lett. **95**, 091601 (2005), [hep-ex/0504030].

[105] I. Adachi *et al.* (BaBar, Belle), Phys. Rev. Lett. **121**, 26, 261801 (2018), [arXiv:1804.06152]; I. Adachi *et al.* (BaBar, Belle), Phys. Rev. **D98**, 11, 112012 (2018), [arXiv:1804.06153].

[106] A. Abdesselam *et al.* (BaBar, Belle), Phys. Rev. Lett. **115**, 12, 121604 (2015), [arXiv:1505.04147].

[107] Heavy Flavor Averaging Group [23], Results on Time-Dependent CP Violation and Measurements Related to the Angles of the Unitarity Triangle: Winter conferences (Moriond, etc.) and PDG 2022: `https://hflav-eos.web.cern.ch/hflav-eos/triangle/pdg2022/`.

[108] M. Gronau and D. London, Phys. Rev. Lett. **65**, 3381 (1990).

[109] J. Zhang *et al.* (Belle), Phys. Rev. Lett. **91**, 221801 (2003), [hep-ex/0306007]; A. Somov *et al.* (Belle), Phys. Rev. Lett. **96**, 171801 (2006), [hep-ex/0601024]; B. Aubert *et al.* (BaBar), Phys. Rev. Lett. **97**, 261801 (2006), [hep-ex/0607092]; B. Aubert *et al.* (BaBar), Phys. Rev. **D76**, 052007 (2007), [arXiv:0705.2157].

[110] B. Aubert *et al.* (BaBar), Phys. Rev. **D78**, 071104 (2008), [arXiv:0807.4977].

[111] A. F. Falk *et al.*, Phys. Rev. **D69**, 011502 (2004), [hep-ph/0310242].

[112] A. E. Snyder and H. R. Quinn, Phys. Rev. **D48**, 2139 (1993).

[113] A. Kusaka *et al.* (Belle), Phys. Rev. Lett. **98**, 221602 (2007), [hep-ex/0701015].

[114] J. P. Lees *et al.* (BaBar), Phys. Rev. **D88**, 1, 012003 (2013), [arXiv:1304.3503].

[115] A. Hocker *et al.*, Eur. Phys. J. **C21**, 225 (2001), [hep-ph/0104062]; and updates at `http://ckmfitter.in2p3.fr/`.

[116] M. Bona *et al.* (UTfit), JHEP **07**, 028 (2005), [hep-ph/0501199]; and updates at `http://www.utfit.org`.

[117] M. Gronau and D. London, Phys. Lett. **B253**, 483 (1991).

[118] M. Gronau and D. Wyler, Phys. Lett. **B265**, 172 (1991).

[119] D. Atwood, I. Dunietz and A. Soni, Phys. Rev. Lett. **78**, 3257 (1997), [hep-ph/9612433]; D. Atwood, I. Dunietz and A. Soni, Phys. Rev. **D63**, 036005 (2001), [hep-ph/0008090].

[120] A. Bondar, talk at the Belle analysis workshop, Novosibirsk, September 2002; A. Poluektov *et al.* (Belle), Phys. Rev. **D70**, 072003 (2004), [hep-ex/0406067].

[121] A. Giri *et al.*, Phys. Rev. **D68**, 054018 (2003), [hep-ph/0303187].

[122] A. Poluektov *et al.* (Belle), Phys. Rev. **D81**, 112002 (2010), [arXiv:1003.3360].

[123] P. del Amo Sanchez *et al.* (BaBar), Phys. Rev. Lett. **105**, 121801 (2010), [arXiv:1005.1096].

[124] R. Aaij *et al.* (LHCb), JHEP **02**, 169 (2021), [arXiv:2010.08483].

[125] Y. Grossman, A. Soffer and J. Zupan, Phys. Rev. **D72**, 031501 (2005), [hep-ph/0505270].

[126] M. Rama, Phys. Rev. D **89**, 1, 014021 (2014), [arXiv:1307.4384].

Downloaded from https://academic.oup.com/ptep/article/2022/8/083C01/6651666 by KIT Library user on 27 September 2022

[127] A. Amorim, M. G. Santos and J. P. Silva, Phys. Rev. **D59**, 056001 (1999), [hep-ph/9807364].

[128] R. Aleksan, I. Dunietz and B. Kayser, Z. Phys. **C54**, 653 (1992).

[129] R. Aaij *et al.* (LHCb), JHEP **03**, 059 (2018), [arXiv:1712.07428].

[130] R. Aaij *et al.* (LHCb), JHEP **03**, 137 (2021), [arXiv:2011.12041].

[131] B. Aubert *et al.* (BaBar), Phys. Rev. **D71**, 112003 (2005), [hep-ex/0504035]; B. Aubert *et al.* (BaBar), Phys. Rev. **D73**, 111101 (2006), [hep-ex/0602049]; F. J. Ronga *et al.* (Belle), Phys. Rev. **D73**, 092003 (2006), [hep-ex/0604013]; S. Bahinipati *et al.* (Belle), Phys. Rev. **D84**, 021101 (2011), [arXiv:1102.0888]; R. Aaij *et al.* (LHCb), JHEP **06**, 084 (2018), [arXiv:1805.03448].

[132] G. P. Dubois-Felsmann *et al.*, *Sensitivity of CKM fits to theoretical uncertainties and their representation* (2003), [hep-ph/0308262]; G. Eigen *et al.*, Phys. Rev. **D89**, 3, 033004 (2014), [arXiv:1301.5867].

[133] D. Boutigny *et al.* (BaBar), in "Workshop on Physics at an Asymmetric B Factory (BaBar Collaboration Meeting) Pasadena, California, September 22-24, 1997," (1998), URL `http://www-public.slac.stanford.edu/sciDoc/docMeta.aspx?slacPubNumber=SLAC-R-504`.

[134] S. Plaszczynski and M.-H. Schune hf8/019 (1999), [PoShf8,019(1999)], [hep-ph/9911280].

[135] M. Bona *et al.* (UTfit), JHEP **03**, 049 (2008), [arXiv:0707.0636].

[136] We thank the CKMfitter and UTfit groups for performing fits and preparing plots using input values from this *Review*.

[137] H. E. Haber, Nucl. Phys. Proc. Suppl. **62**, 469 (1998), [hep-ph/9709450]; Y. Nir, *CP violation: A New era* (2001), [hep-ph/0109090].

[138] J. M. Soares and L. Wolfenstein, Phys. Rev. **D47**, 1021 (1993); T. Goto *et al.*, Phys. Rev. **D53**, 6662 (1996), [hep-ph/9506311]; J. P. Silva and L. Wolfenstein, Phys. Rev. **D55**, 5331 (1997), [hep-ph/9610208].

[139] Y. Grossman, Z. Ligeti and Y. Nir, Prog. Theor. Phys. **122**, 125 (2009), [arXiv:0904.4262].

[140] G. Isidori, Y. Nir and G. Perez, Ann. Rev. Nucl. Part. Sci. **60**, 355 (2010), [arXiv:1002.0900]; G. Isidori, in "Proceedings, 2012 European School of High-Energy Physics (ESHEP 2012): La Pommeraye, Anjou, France, June 06-19, 2012," 69–105 (2014), [arXiv:1302.0661].

[141] Z. Ligeti, Int. J. Mod. Phys. **A20**, 5105 (2005), [hep-ph/0408267].

[142] J. Charles *et al.*, Phys. Rev. **D89**, 3, 033016 (2014), [arXiv:1309.2293].

[143] K. Agashe *et al.* (2005), [hep-ph/0509117].

[144] S. Laplace *et al.*, Phys. Rev. **D65**, 094040 (2002), [hep-ph/0202010].

[145] R. Aaij *et al.* (LHCb), JHEP **08**, 037 (2017), [arXiv:1704.08217]; G. Aad *et al.* (ATLAS) (2020), [arXiv:2001.07115]; V. Khachatryan *et al.* (CMS), Phys. Lett. **B757**, 97 (2016), [arXiv:1507.07527].

[146] J. K. Ahn *et al.* (KOTO), Phys. Rev. Lett. **122**, 2, 021802 (2019), [arXiv:1810.09655].

[147] A. J. Buras *et al.*, JHEP **11**, 033 (2015), [arXiv:1503.02693].

Downloaded from https://academic.oup.com/ptep/article/2022/8/083C01/6651666 by KIT Library user on 27 September 2022

13. *CP* Violation in the Quark Sector

Revised August 2021 by T. Gershon (Warwick U.) and Y. Nir (Weizmann Inst.).

The *CP* transformation combines charge conjugation C with parity P. Under C, particles and antiparticles are interchanged, by conjugating all internal quantum numbers, *e.g.*, $Q \to -Q$ for electromagnetic charge. Under P, the handedness of space is reversed, $\vec{x} \to -\vec{x}$. Thus, for example, a left-handed electron e^-_L is transformed under *CP* into a right-handed positron, e^+_R.

If *CP* were an exact symmetry, the laws of nature would be the same for matter and for antimatter. We observe that most phenomena are C- and P-symmetric, and therefore, also *CP*-symmetric. In particular, these symmetries are respected by the electromagnetic and strong interactions. The weak interactions, on the other hand, violate C and P in the strongest possible way. For example, the W bosons couple to left-handed electrons, e^-_L, and to their *CP*-conjugate right-handed positrons, e^+_R, but to neither their C-conjugate left-handed positrons, e^+_L, nor their P-conjugate right-handed electrons, e^-_R. While weak interactions violate C and P separately, *CP* is still preserved in most weak interaction processes. The *CP* symmetry is, however, violated in certain processes involving interference effects, as discovered in neutral K decays in 1964 [1], and established later in B (2001) and D (2019) decays. For example, as discovered in 1967, a K_L meson decays more often to $\pi^- e^+ \nu_e$ than to $\pi^+ e^- \overline{\nu}_e$, thus allowing electrons and positrons to be unambiguously distinguished, but the decay-rate asymmetry is only at the 0.003 level. The *CP*-violating effects observed in the B system are larger: the parameter describing the *CP* asymmetry in the decay time distribution of $B^0/\overline{B}^0$ meson transitions to *CP* eigenstates like $J/\psi K_S$ is about 0.7 [2,3]. These effects are related to K^0–$\overline{K}^0$ and B^0–$\overline{B}^0$ mixing, but *CP* violation arising solely from decay amplitudes has also been observed, first in $K \to \pi\pi$ decays [4–6], subsequently in B^0 [7,8], B^+ [9–11], and B^0_s [12] decays, and most recently in charm decays [13]. All of these observed *CP* asymmetries are consistent with the Standard Model predictions. Similar effects could also occur in decays of baryons, but have not yet been observed. Given that neutrino masses and lepton mixing have been established, it is expected that *CP* is violated also in the lepton sector [14]. Discovering *CP* violation in the lepton sector is one of the main goals of current and near-future experiments. *CP* violation has not yet been observed in processes involving the top quark, nor in flavor-conserving processes such as electric dipole moments; for these, any significant observation would be a clear indication of physics beyond the Standard Model.

In addition to parity and to continuous Lorentz transformations, there is one other spacetime operation that could be a symmetry of the interactions: time reversal T, $t \to -t$. Violations of T symmetry have been observed in neutral K decays [15]. More recently, T violation has been observed between states that are not *CP*-conjugate [16], exploiting the fact that for neutral B mesons both flavor tagging and *CP* tagging can be used [17]. Moreover, T violation is expected as a corollary of *CP* violation if the combined *CPT* transformation is a fundamental symmetry of nature [18]. All observations indicate that *CPT* is indeed a symmetry of nature [15]. Furthermore, one cannot build a locally Lorentz-invariant quantum field theory with a Hermitian Hamiltonian that violates *CPT*. (At several points in our discussion, we avoid assumptions about *CPT*, in order to identify cases where evidence for *CP* violation relies on assumptions about *CPT*.)

Within the Standard Model, *CP* symmetry is broken by complex phases in the Yukawa couplings (that is, the couplings of the Higgs scalar to quarks). When all transformations to remove unphysical phases in this model are exhausted, a single *CP*-violating parameter remains [19]. In the basis of mass eigenstates, this single phase appears in the 3×3 unitary matrix that gives the W-boson couplings to an up-type antiquark and a down-type quark. (If the Standard Model is supplemented with Majorana mass terms for the neutrinos, the analogous mixing matrix for leptons has three *CP*-violating phases.) The beautifully consistent and economical Standard-Model description of *CP* violation in terms of Yukawa couplings, known as the Kobayashi-Maskawa (KM) mechanism [19], agrees with all measurements to date. Furthermore, one can fit the data allowing contributions from beyond the Standard Model (referred to subsequently as new physics) to loop processes to compete with, or even dominate over, the Standard Model amplitudes [20,21]. Such an analysis provides model-independent proof that the KM phase is different from zero, and that the matrix of three-generation quark mixing is the dominant source of *CP* violation in meson decays.

The current level of experimental accuracy and the theoretical uncertainties involved in the interpretation of the various observations leave room, however, for additional subdominant sources of *CP* violation from new physics. Indeed, almost all extensions of the Standard Model imply that there are such additional sources. Moreover, *CP* violation is a necessary condition for baryogenesis, the process of dynamically generating the matter-antimatter asymmetry of the Universe [22]. Despite the phenomenological success of the KM mechanism, it fails (by several orders of magnitude) to accommodate the observed asymmetry [23]. This discrepancy strongly suggests that nature provides additional sources of *CP* violation beyond the KM mechanism. The evidence for neutrino masses implies that *CP* can be violated also in the lepton sector. This situation makes leptogenesis [24,25], a scenario where *CP*-violating phases in the Yukawa couplings of the neutrinos play a crucial role in the generation of the baryon asymmetry, a very attractive possibility. The expectation of new sources motivates the large ongoing experimental effort to find deviations from the predictions of the KM mechanism.

CP violation can be experimentally searched for in a variety of processes, such as hadron decays, electric dipole moments of neutrons, electrons and nuclei, and neutrino oscillations. Hadron decays via the weak interaction probe flavor-changing *CP* violation. The search for electric dipole moments may find (or constrain) sources of *CP* violation that, unlike the KM phase, are not related to flavor-changing couplings. Following the discovery of the Higgs boson [26,27], searches for *CP* violation in the Higgs sector are becoming feasible. Future searches for *CP* violation in neutrino oscillations might provide further input on leptogenesis.

The present measurements of *CP* asymmetries provide some of the strongest constraints on the weak couplings of quarks. Future measurements of *CP* violation in K, D, B, and B^0_s meson decays will provide additional constraints on the flavor parameters of the Standard Model, and can probe new physics. In this review, we give the formalism and basic physics motivations that are relevant to present and near future measurements of *CP* violation in the quark sector.

13.1 Formalism

The phenomenology of *CP* violation for neutral flavored mesons is particularly interesting, since many of the observables can be cleanly interpreted. Although the phenomenology is superficially different for K^0, D^0, B^0, and B^0_s decays, this is primarily because each of these systems is governed by a different balance between decay rates, oscillations, and lifetime splitting. However, the general considerations presented in this section are identical for all flavored neutral pseudoscalar mesons. The phenomenology of *CP* violation for neutral mesons that do not carry flavor quantum numbers (such as the $\eta^{(\prime)}$ state) is quite different: such states are their own antiparticles and have definite *CP* eigenvalues, so the signature of *CP* violation is simply the decay to a final state with the opposite *CP*. Such decays are mediated by the electromagnetic or (OZI-suppressed [28–30]) strong interaction, where *CP* violation is not expected and has not yet been observed. In the remainder of this review, we restrict ourselves to considerations of weakly decaying hadrons.

In this section, we present a general formalism for, and classification of, *CP* violation in the decay of a weakly decaying hadron, denoted M. We pay particular attention to the case that M is a K^0, D^0, B^0, or B^0_s meson. Subsequent sections describe the *CP*-violating phenomenology, approximations, and alternative formalisms that are specific to each system.

13.1.1 *Charged- and neutral-hadron decays*

We define decay amplitudes of M (which could be charged or neutral) and its *CP* conjugate $\overline{M}$ to a multi-particle final state f

Downloaded from https://academic.oup.com/ptep/article/2022/8/083C01/6651666 by KIT Library user on 27 September 2022

and its CP conjugate $\overline{f}$ as

$$A_f = \langle f\,|\mathcal{H}|\,M\rangle\ , \quad \overline{A}_f = \langle f\,|\mathcal{H}|\,\overline{M}\rangle\ , \tag{13.1a}$$

$$A_{\overline{f}} = \langle \overline{f}\,|\mathcal{H}|\,M\rangle\ , \quad \overline{A}_{\overline{f}} = \langle \overline{f}\,|\mathcal{H}|\,\overline{M}\rangle\ , \tag{13.1b}$$

where $\mathcal{H}$ is the Hamiltonian governing weak interactions. The action of CP on these states introduces phases ξ_M and ξ_f that depend on their flavor content, according to

$$CP|M\rangle = e^{+i\xi_M}\,|\overline{M}\rangle\ , \quad CP|f\rangle = e^{+i\xi_f}\,|\overline{f}\rangle\ , \tag{13.2a}$$

$$CP|\overline{M}\rangle = e^{-i\xi_M}\,|M\rangle\ , \quad CP|\overline{f}\rangle = e^{-i\xi_f}\,|f\rangle\ , \tag{13.2b}$$

so that $(CP)^2 = 1$. The phases ξ_M and ξ_f are arbitrary and unobservable because of the flavor symmetry of the strong interaction. If CP is conserved by the dynamics, $[CP, \mathcal{H}] = 0$, then A_f and $\overline{A}_{\overline{f}}$ have the same magnitude and an arbitrary unphysical relative phase

$$\overline{A}_{\overline{f}} = e^{i(\xi_f - \xi_M)}\,A_f\ . \tag{13.3}$$

13.1.2 *Neutral-meson mixing*

A state that is initially a superposition of M^0 and $\overline{M}^0$, say

$$|\psi(0)\rangle = a(0)|M^0\rangle + b(0)|\overline{M}^0\rangle\ , \tag{13.4}$$

will evolve in time acquiring components that describe all possible decay final states $\{f_1, f_2, \ldots\}$, that is,

$$|\psi(t)\rangle = a(t)|M^0\rangle + b(t)|\overline{M}^0\rangle + c_1(t)|f_1\rangle + c_2(t)|f_2\rangle + \cdots\ . \tag{13.5}$$

If we are interested in computing only the values of $a(t)$ and $b(t)$ (and not the values of all $c_i(t)$), and if the times t under study are much larger than the typical strong interaction scale, then we can use a much simplified formalism [31]. The simplified time evolution is determined by a 2×2 effective Hamiltonian $\mathbf{H}$ that is not Hermitian, since otherwise the mesons would only oscillate and not decay. Any complex matrix, such as $\mathbf{H}$, can be written in terms of Hermitian matrices $\mathbf{M}$ and $\mathbf{\Gamma}$ as

$$\mathbf{H} = \mathbf{M} - \frac{i}{2}\,\mathbf{\Gamma}\ . \tag{13.6}$$

$\mathbf{M}$ and $\mathbf{\Gamma}$ are associated with $(M^0, \overline{M}^0) \leftrightarrow (M^0, \overline{M}^0)$ transitions via off-shell (dispersive), and on-shell (absorptive) intermediate states, respectively. Diagonal elements of $\mathbf{M}$ and $\mathbf{\Gamma}$ are associated with the flavor-conserving transitions $M^0 \to M^0$ and $\overline{M}^0 \to \overline{M}^0$, while off-diagonal elements are associated with flavor-changing transitions $M^0 \leftrightarrow \overline{M}^0$.

The eigenvectors of $\mathbf{H}$ have well-defined masses and decay widths. To specify the components of the strong interaction eigenstates, M^0 and $\overline{M}^0$, in the light (M_L) and heavy (M_H) mass eigenstates, we introduce three complex parameters: p, q, and, for the case that both CP and CPT are violated in mixing, z. Then

$$|M_L\rangle \propto p\sqrt{1-z}\,|M^0\rangle + q\sqrt{1+z}\,|\overline{M}^0\rangle\ , \tag{13.7a}$$

$$|M_H\rangle \propto p\sqrt{1+z}\,|M^0\rangle - q\sqrt{1-z}\,|\overline{M}^0\rangle\ , \tag{13.7b}$$

with the normalization $|q|^2 + |p|^2 = 1$ when $z = 0$. (Another possible choice of labeling, which is in standard usage for K mesons, defines the mass eigenstates according to their lifetimes: K_S for the short-lived and K_L for the long-lived state. The K_L is experimentally found to be the heavier state. Yet another choice is often used for the D mesons [32]: the eigenstates are labeled according to their dominant CP content.)

The real and imaginary parts of the eigenvalues $\omega_{L,H}$ corresponding to $|M_{L,H}\rangle$ represent their masses and decay widths, respectively. The mass and width splittings are

$$\Delta m \equiv m_H - m_L = \mathcal{R}e(\omega_H - \omega_L)\ , \tag{13.8a}$$

$$\Delta\Gamma \equiv \Gamma_H - \Gamma_L = -2\,\mathcal{I}m(\omega_H - \omega_L)\ . \tag{13.8b}$$

Note that here Δm is positive by definition, while the sign of $\Delta\Gamma$ must be experimentally determined. The sign of $\Delta\Gamma$ has not yet been established for B^0 mesons, while $\Delta\Gamma < 0$ is established for K and B^0_s mesons. The Standard Model predicts $\Gamma_L > \Gamma_H$ for $B^0_{(s)}$ mesons; for this reason, $\Delta\Gamma = \Gamma_L - \Gamma_H$, which is still a signed quantity, is often used in the $B^0_{(s)}$ literature and is the convention used in the PDG experimental summaries.

Solving the eigenvalue problem for $\mathbf{H}$ yields

$$\left(\frac{q}{p}\right)^2 = \frac{\mathbf{M}^*_{12} - (i/2)\mathbf{\Gamma}^*_{12}}{\mathbf{M}_{12} - (i/2)\mathbf{\Gamma}_{12}} \tag{13.9}$$

and

$$z \equiv \frac{\delta m - (i/2)\delta\Gamma}{\Delta m - (i/2)\Delta\Gamma}\ , \tag{13.10}$$

where

$$\delta m \equiv \mathbf{M}_{11} - \mathbf{M}_{22}\ , \quad \delta\Gamma \equiv \mathbf{\Gamma}_{11} - \mathbf{\Gamma}_{22} \tag{13.11}$$

are the differences in effective mass and decay-rate expectation values for the strong interaction states M^0 and $\overline{M}^0$.

If either CP or CPT is a symmetry of $\mathbf{H}$ (independently of whether T is conserved or violated), then the values of δm and $\delta\Gamma$ are both zero, and hence $z = 0$. We also find that

$$\omega_H - \omega_L = 2\sqrt{\left(\mathbf{M}_{12} - \frac{i}{2}\mathbf{\Gamma}_{12}\right)\left(\mathbf{M}^*_{12} - \frac{i}{2}\mathbf{\Gamma}^*_{12}\right)}\ . \tag{13.12}$$

If either CP or T is a symmetry of $\mathbf{H}$ (independently of whether CPT is conserved or violated), then $\mathbf{\Gamma}_{12}/\mathbf{M}_{12}$ is real, leading to

$$\left(\frac{q}{p}\right)^2 = e^{2i\xi_M} \quad \Rightarrow \quad \left|\frac{q}{p}\right| = 1\ , \tag{13.13}$$

where ξ_M is the arbitrary unphysical phase introduced in Eq. (13.2). If, and only if, CP is a symmetry of $\mathbf{H}$ (independently of CPT and T), then both of the above conditions hold, with the result that the mass eigenstates are orthogonal

$$\langle M_H|M_L\rangle = |p|^2 - |q|^2 = 0\ . \tag{13.14}$$

13.1.3 *CP-violating observables*

All CP-violating observables in M and $\overline{M}$ decays to final states f and $\overline{f}$ can be expressed in terms of phase-convention-independent combinations of A_f, $\overline{A}_f$, $A_{\overline{f}}$, and $\overline{A}_{\overline{f}}$, together with, for neutral meson decays only, q/p. CP violation in charged meson and all baryon decays depends only on the combination $|\overline{A}_{\overline{f}}/A_f|$, while CP violation in flavored neutral meson decays is enriched by $M^0 \leftrightarrow \overline{M}^0$ oscillations, and depends, additionally, on $|q/p|$ and on $\lambda_f \equiv (q/p)(\overline{A}_f/A_f)$.

The decay rates of the two neutral kaon mass eigenstates, K_S and K_L, are different enough ($\Gamma_S/\Gamma_L \sim 500$) that one can, in most cases, actually study their decays independently. For D^0, B^0, and B^0_s mesons, however, values of $\Delta\Gamma/\Gamma$ (where $\Gamma \equiv (\Gamma_H + \Gamma_L)/2$) are relatively small, and so both mass eigenstates must be considered in their evolution. We denote the state of an initially pure $|M^0\rangle$ or $|\overline{M}^0\rangle$ after an elapsed proper time t as $|M^0_{\rm phys}(t)\rangle$ or $|\overline{M}^0_{\rm phys}(t)\rangle$, respectively. Using the effective Hamiltonian approximation, but not assuming CPT to be a good symmetry, we obtain

$$|M^0_{\rm phys}(t)\rangle = (g_+(t) + z\,g_-(t))\,|M^0\rangle - \sqrt{1-z^2}\,\frac{q}{p}\,g_-(t)|\overline{M}^0\rangle\ , \tag{13.15a}$$

$$|\overline{M}^0_{\rm phys}(t)\rangle = (g_+(t) - z\,g_-(t))\,|\overline{M}^0\rangle - \sqrt{1-z^2}\,\frac{p}{q}\,g_-(t)|M^0\rangle\ , \tag{13.15b}$$

where

$$g_\pm(t) \equiv \frac{1}{2}\left[\exp\left(-im_H t - \frac{1}{2}\Gamma_H t\right) \pm \exp\left(-im_L t - \frac{1}{2}\Gamma_L t\right)\right] \tag{13.16}$$

and $z = 0$ if either CPT or CP is conserved.

Downloaded from https://academic.oup.com/ptep/article/2022/8/083C01/6651666 by KIT Library user on 27 September 2022

Defining $x \equiv \Delta m/\Gamma$ and $y \equiv \Delta\Gamma/(2\Gamma)$, and assuming $z = 0$, one obtains the following time-dependent decay rates:

$$\begin{aligned}\frac{d\Gamma\left[M^0_{\rm phys}(t)\to f\right]/dt}{e^{-\Gamma t}\mathcal{N}_f} &= \left(|A_f|^2 + |(q/p)\overline{A}_f|^2\right)\cosh(y\Gamma t)\\ &+ \left(|A_f|^2 - |(q/p)\overline{A}_f|^2\right)\cos(x\Gamma t)\\ &+ 2\,\mathcal{R}e((q/p)A_f^*\overline{A}_f)\sinh(y\Gamma t)\\ &- 2\,\mathcal{I}m((q/p)A_f^*\overline{A}_f)\sin(x\Gamma t)\ ,\end{aligned} \tag{13.17a}$$

$$\begin{aligned}\frac{d\Gamma\left[\overline{M}^0_{\rm phys}(t)\to f\right]/dt}{e^{-\Gamma t}\mathcal{N}_f} &= \left(|(p/q)A_f|^2 + |\overline{A}_f|^2\right)\cosh(y\Gamma t)\\ &- \left(|(p/q)A_f|^2 - |\overline{A}_f|^2\right)\cos(x\Gamma t)\\ &+ 2\,\mathcal{R}e((p/q)A_f\overline{A}_f^*)\sinh(y\Gamma t)\\ &- 2\,\mathcal{I}m((p/q)A_f\overline{A}_f^*)\sin(x\Gamma t)\ ,\end{aligned} \tag{13.17b}$$

where $\mathcal{N}_f$ is a common, time-independent, normalization factor that can be determined bearing in mind that the range of t is $0 < t < \infty$. Decay rates to the *CP*-conjugate final state $\overline{f}$ are obtained analogously, with $\mathcal{N}_f = \mathcal{N}_{\overline{f}}$ and the substitutions $A_f \to A_{\overline{f}}$ and $\overline{A}_f \to \overline{A}_{\overline{f}}$ in Eqs. (13.17a) and (13.17b). Terms proportional to $|A_f|^2$ or $|\overline{A}_f|^2$ are associated with decays that occur without any net $M^0 \leftrightarrow \overline{M}^0$ oscillation, while terms proportional to $|(q/p)\overline{A}_f|^2$ or $|(p/q)A_f|^2$ are associated with decays following a net oscillation. The $\sinh(y\Gamma t)$ and $\sin(x\Gamma t)$ terms of Eqs. (13.17a) and (13.17b) are associated with the interference between these two cases. Note that, in multi-body decays such as $D^0 \to K_S\pi^+\pi^-$ or $B^0 \to \pi^+\pi^-\pi^+\pi^-$, amplitudes are functions of variables that describe the phase-space of the final state. Interference may be present in some regions but not others, and is strongly influenced by resonant substructure.

When neutral pseudoscalar mesons are produced coherently in pairs from the decay of a vector resonance, $V \to M^0\overline{M}^0$ (for example, $\Upsilon(4S) \to B^0\overline{B}^0$, $\psi(3770) \to D^0\overline{D}^0$ or $\phi \to K^0\overline{K}^0$), the time-dependence of their subsequent decays to final states f_1 and f_2 has a similar form to Eqs. (13.17a) and (13.17b):

$$\begin{aligned}\frac{d\Gamma\left[V_{\rm phys}(t_1,t_2)\to f_1 f_2\right]/d(\Delta t)}{e^{-\Gamma|\Delta t|}\mathcal{N}_{f_1 f_2}} &= \left(|a_+|^2 + |a_-|^2\right)\cosh(y\Gamma\Delta t)\\ &+ \left(|a_+|^2 - |a_-|^2\right)\cos(x\Gamma\Delta t)\\ &- 2\,\mathcal{R}e(a_+^* a_-)\sinh(y\Gamma\Delta t)\\ &+ 2\,\mathcal{I}m(a_+^* a_-)\sin(x\Gamma\Delta t)\ ,\end{aligned} \tag{13.18}$$

where $\Delta t \equiv t_2 - t_1$ is the difference in the production times, t_1 and t_2, of f_1 and f_2, respectively, and the dependence on the average decay time and on decay angles has been integrated out. The normalization factor $\mathcal{N}_{f_1 f_2}$ can be evaluated, noting that the range of Δt is $-\infty < \Delta t < \infty$. The coefficients in Eq. (13.18) are determined by the amplitudes for no net oscillation from $t_1 \to t_2$, $\overline{A}_{f_1}A_{f_2}$, and $A_{f_1}\overline{A}_{f_2}$, and for a net oscillation, $(q/p)\overline{A}_{f_1}\overline{A}_{f_2}$ and $(p/q)A_{f_1}A_{f_2}$, via

$$a_+ \equiv \overline{A}_{f_1}A_{f_2} - A_{f_1}\overline{A}_{f_2}\ , \tag{13.19a}$$

$$\begin{aligned}a_- \equiv -\sqrt{1-z^2}\left(\frac{q}{p}\overline{A}_{f_1}\overline{A}_{f_2} - \frac{p}{q}A_{f_1}A_{f_2}\right)\\ + z\left(\overline{A}_{f_1}A_{f_2} + A_{f_1}\overline{A}_{f_2}\right)\ .\end{aligned} \tag{13.19b}$$

Assuming *CPT* conservation, $z = 0$, and identifying $\Delta t \to t$ and $f_2 \to f$, we find that Eqs. (13.18) and (13.19) reduce to Eq. (13.17a) with $A_{f_1} = 0$, $\overline{A}_{f_1} = 1$, or to Eq. (13.17b) with $\overline{A}_{f_1} = 0$, $A_{f_1} = 1$. Indeed, this plays an important role in experiments that exploit the coherence of $V \to M^0\overline{M}^0$ production. Final states f_1 with $A_{f_1} = 0$ or $\overline{A}_{f_1} = 0$ are called tagging states, because they identify the decaying pseudoscalar meson as, respectively, $\overline{M}^0$ or M^0. Before one of M^0 or $\overline{M}^0$ decays, they evolve in phase, so that there is always one M^0 and one $\overline{M}^0$ present. A tagging decay of one meson sets the clock for the time evolution of the other: it starts at t_1 as purely M^0 or $\overline{M}^0$, with time evolution that depends only on $t_2 - t_1$.

When f_1 is a state that both M^0 and $\overline{M}^0$ can decay into, then Eq. (13.18) contains interference terms proportional to $A_{f_1}\overline{A}_{f_1} \neq 0$ that are not present in Eqs. (13.17a) and (13.17b). Even when f_1 is dominantly produced by M^0 decays rather than $\overline{M}^0$ decays, or vice versa, $A_{f_1}\overline{A}_{f_1}$ can be non-zero owing to doubly-CKM-suppressed decays (with amplitudes suppressed by at least two powers of λ relative to the dominant amplitude, in the language of Section 13.3), and these terms should be considered for precision studies of *CP* violation in coherent $V \to M^0\overline{M}^0$ decays [33]. The correlations in $V \to M^0\overline{M}^0$ decays can also be exploited to determine strong phase differences between favored and suppressed decay amplitudes [34].

13.1.4 *Classification of CP-violating effects*

We distinguish three types of *CP*-violating effects that can occur in the quark sector:

I. *CP* violation in decay is defined by

$$|\overline{A}_{\overline{f}}/A_f| \neq 1\ . \tag{13.20}$$

In charged meson (and all baryon) decays, where mixing effects are absent, this is the only possible source of *CP* asymmetries:

$$\mathcal{A}_{f^\pm} \equiv \frac{\Gamma(M^-\to f^-) - \Gamma(M^+\to f^+)}{\Gamma(M^-\to f^-) + \Gamma(M^+\to f^+)} = \frac{|\overline{A}_{f^-}/A_{f^+}|^2 - 1}{|\overline{A}_{f^-}/A_{f^+}|^2 + 1}\ . \tag{13.21}$$

Note that the usual sign convention for *CP* asymmetries of hadrons is for the difference between the rate involving the particle that contains a heavy quark and that which contains an antiquark. Hence, Eq. (13.21) corresponds to the definition for $B^\pm$ mesons, but the opposite sign is used for $D^\pm_{(s)}$ decays.

II. *CP* (and *T*) violation in mixing is defined by

$$|q/p| \neq 1\ . \tag{13.22}$$

In charged-current semileptonic neutral meson decays $M, \overline{M} \to \ell^\pm X^\mp$ (taking $|A_{\ell^+X^-}| = |\overline{A}_{\ell^-X^+}|$ and $A_{\ell^-X^+} = \overline{A}_{\ell^+X^-} = 0$, as is the case in the Standard Model, to lowest order in G_F, and in most of its extensions), this is the only source of *CP* violation, and can be measured via the asymmetry of "wrong-sign" decays induced by oscillations:

$$\begin{aligned}&\mathcal{A}_{\rm SL}(t)\\ &\equiv \frac{d\Gamma/dt\left[\overline{M}^0_{\rm phys}(t)\to \ell^+X^-\right] - d\Gamma/dt\left[M^0_{\rm phys}(t)\to \ell^-X^+\right]}{d\Gamma/dt\left[\overline{M}^0_{\rm phys}(t)\to \ell^+X^-\right] + d\Gamma/dt\left[M^0_{\rm phys}(t)\to \ell^-X^+\right]}\ ,\end{aligned} \tag{13.23a}$$

$$= \frac{1-|q/p|^4}{1+|q/p|^4}\ . \tag{13.23b}$$

Note that this asymmetry of time-dependent decay rates is actually time-independent.

III. *CP* violation in interference between a decay without mixing, $M^0 \to f$, and a decay with mixing, $M^0 \to \overline{M}^0 \to f$ (such an effect occurs only in decays to final states that are common to M^0 and $\overline{M}^0$, including all *CP* eigenstates), is defined by

$$\arg(\lambda_f) + \arg(\lambda_{\overline{f}}) \neq 0\ , \qquad \text{with} \qquad \lambda_f \equiv \frac{q}{p}\frac{\overline{A}_f}{A_f}\ . \tag{13.24}$$

For final *CP* eigenstates, f_{CP}, the condition Eq. (13.24) simplifies to

$$\mathcal{I}m(\lambda_{f_{CP}}) \neq 0\ , \tag{13.25}$$

Downloaded from https://academic.oup.com/ptep/article/2022/8/083C01/6651666 by KIT Library user on 27 September 2022

This form of CP violation can be observed, for example, using the asymmetry of neutral meson decay rates into CP eigenstates

$$\mathcal{A}_{f_{CP}}(t) \equiv \equiv \frac{d\Gamma/dt\left[\overline{M}^0_{\rm phys}(t) \to f_{CP}\right] - d\Gamma/dt\left[M^0_{\rm phys}(t) \to f_{CP}\right]}{d\Gamma/dt\left[\overline{M}^0_{\rm phys}(t) \to f_{CP}\right] + d\Gamma/dt\left[M^0_{\rm phys}(t) \to f_{CP}\right]} . \tag{13.26}$$

If $\Delta\Gamma = 0$, as expected to a good approximation for B^0 mesons but not for K^0 and B^0_s mesons, and $|q/p| = 1$, then $\mathcal{A}_{f_{CP}}$ has a particularly simple form (see Eq. (13.75), below). If, in addition, the decay amplitudes fulfill $|\overline{A}_{f_{CP}}| = |A_{f_{CP}}|$, the interference between decays with and without mixing is the only source of asymmetry and $\mathcal{A}_{f_{CP}}(t) = \mathcal{I}m(\lambda_{f_{CP}})\sin(x\Gamma t)$.

Examples of these three types of CP violation will be given in Sections 13.4, 13.5, and 13.6.

13.2 Theoretical Interpretation: General Considerations

Consider the $M \to f$ decay amplitude A_f, and the CP conjugate process, $\overline{M} \to \overline{f}$, with decay amplitude $\overline{A}_{\overline{f}}$. There are two types of phases that may appear in these decay amplitudes. Complex parameters in any Lagrangian term that contributes to the amplitude will appear in complex conjugate form in the CP-conjugate amplitude. Thus, their phases appear in A_f and $\overline{A}_{\overline{f}}$ with opposite signs. In the Standard Model, these phases occur only in the couplings of the $W^\pm$ bosons, and hence, are often called "weak phases." The weak phase of any single term is convention-dependent. However, the difference between the weak phases in two different terms in A_f is convention-independent. A second type of phase can appear in scattering or decay amplitudes, even when the Lagrangian is real. This phase originates from the possible contribution from intermediate on-shell states in the decay process. Since such phases are generated by CP-invariant interactions, they are the same in A_f and $\overline{A}_{\overline{f}}$. Usually the dominant rescattering is due to strong interactions; hence the designation "strong phases" for the phase shifts so induced. Again, only the relative strong phases between different terms in the amplitude are physically meaningful.

The "weak" and "strong" phases discussed here appear in addition to the spurious CP-transformation phases of Eq. (13.3). Those spurious phases are due to an arbitrary choice of phase convention, and do not originate from any dynamics or induce any CP violation. For simplicity, we set them to zero from here on.

It is useful to write each contribution a_i to A_f in three parts: its magnitude $|a_i|$, its weak phase ϕ_i, and its strong phase δ_i. If, for example, there are two such contributions, $A_f = a_1 + a_2$, we have

$$A_f = |a_1|e^{i(\delta_1+\phi_1)} + |a_2|e^{i(\delta_2+\phi_2)} , \tag{13.27a}$$

$$\overline{A}_{\overline{f}} = |a_1|e^{i(\delta_1-\phi_1)} + |a_2|e^{i(\delta_2-\phi_2)} . \tag{13.27b}$$

Similarly, for neutral mesons, it is useful to write

$$\mathbf{M}_{12} = |\mathbf{M}_{12}|e^{i\phi_M} , \quad \mathbf{\Gamma}_{12} = |\mathbf{\Gamma}_{12}|e^{i\phi_\Gamma} . \tag{13.28}$$

Each of the phases appearing in Eqs. (13.27) and (13.28) is convention-dependent, but combinations such as $\delta_1 - \delta_2$, $\phi_1 - \phi_2$, $\phi_M - \phi_\Gamma$, and $\phi_M + \phi_1 - \overline{\phi}_1$ (where $\overline{\phi}_1$ is a weak phase contributing to $\overline{A}_f$) are physical.

It is now straightforward to evaluate the various asymmetries in terms of the theoretical parameters introduced here. We will do so with approximations that are often relevant to the most interesting measured asymmetries.

1. The CP asymmetry in charged meson and all baryon decays [Eq. (13.21)] is given by

$$\mathcal{A}_f = -\frac{2|a_1a_2|\sin(\delta_2-\delta_1)\sin(\phi_2-\phi_1)}{|a_1|^2+|a_2|^2+2|a_1a_2|\cos(\delta_2-\delta_1)\cos(\phi_2-\phi_1)} . \tag{13.29}$$

The quantity of most interest to theory is the weak phase difference $\phi_2 - \phi_1$. Its extraction from the asymmetry requires, however, that the amplitude ratio $|a_2/a_1|$ and the strong phase difference $\delta_2 - \delta_1$ are known. Both quantities depend on non-perturbative hadronic parameters that are difficult to calculate, but in some cases can be obtained from experiment.

2. In the approximation that $|\mathbf{\Gamma}_{12}/\mathbf{M}_{12}| \ll 1$ (valid for B^0 and B^0_s mesons), the CP asymmetry in semileptonic neutral-meson decays [Eq. (13.23)] is given by

$$\mathcal{A}_{\rm SL} = -\left|\frac{\mathbf{\Gamma}_{12}}{\mathbf{M}_{12}}\right|\sin(\phi_M - \phi_\Gamma) . \tag{13.30}$$

The quantity of most interest to theory is the weak phase $\phi_M - \phi_\Gamma$. Its extraction from the asymmetry requires, however, that $|\mathbf{\Gamma}_{12}/\mathbf{M}_{12}|$ is known. State of the art calculations of this quantity for the B^0 and B^0_s mesons have uncertainties of around 15–20% [35].

3. In the approximations that only a single weak phase contributes to decay, $A_f = |a_f|e^{i(\delta_f+\phi_f)}$, and that $|\mathbf{\Gamma}_{12}/\mathbf{M}_{12}| = 0$, we obtain $|\lambda_f| = 1$, and the CP asymmetries in decays to a final CP eigenstate f [Eq. (13.26)] with eigenvalue $\eta_f = \pm 1$ are given by

$$\mathcal{A}_{f_{CP}}(t) = \mathcal{I}m(\lambda_f)\ \sin(\Delta m t)\ \text{ with }\ \mathcal{I}m(\lambda_f) = \eta_f \sin(\phi_M + 2\phi_f) . \tag{13.31}$$

Note that the phase measured is purely a weak phase, and no hadronic parameters are involved in the extraction of its value from $\mathcal{I}m(\lambda_f)$.

The discussion above allows us to introduce another classification of CP-violating effects:

1. *Indirect CP violation* is consistent with taking $\phi_M \neq 0$ and setting all other CP violating phases to zero. CP violation in mixing (type II) belongs to this class.
2. *Direct CP violation* cannot be accounted for by just $\phi_M \neq 0$. CP violation in decay (type I) belongs to this class.

The historical significance of this classification is related to theory. In superweak models [36], CP violation appears only in diagrams that contribute to $\mathbf{M}_{12}$, hence predicting no direct CP violation. In most models and, in particular, in the Standard Model, CP violation is both direct and indirect. As concerns type III CP violation, a single observation of such an effect would be consistent with indirect CP violation, but observing $\eta_{f_1}\mathcal{I}m(\lambda_{f_1}) \neq \eta_{f_2}\mathcal{I}m(\lambda_{f_2})$ (for the same decaying meson and two different final CP eigenstates f_1 and f_2) would establish direct CP violation. The experimental observation of $\epsilon' \neq 0$, which was achieved by establishing that $\mathcal{I}m(\lambda_{\pi^+\pi^-}) \neq \mathcal{I}m(\lambda_{\pi^0\pi^0})$ (see Section 13.4), excluded the superweak scenario.

13.3 Theoretical Interpretation: The KM Mechanism

Of all the Standard Model quark parameters, only the Kobayashi-Maskawa (KM) phase is CP-violating. Having a single source of CP violation, the Standard Model is very predictive for CP asymmetries: some vanish, and those that do not are correlated.

To be precise, CP could be violated also by strong interactions. The experimental upper bound on the electric-dipole moment of the neutron [37] implies, however, that $\theta_{\rm QCD}$, the non-perturbative parameter that determines the strength of this type of CP violation, is tiny, if not zero [38]. The smallness of $\theta_{\rm QCD}$ constitutes a theoretical puzzle, known as "the strong CP problem." This, however, is irrelevant to our discussion of hadron decays.

The charged current interactions (that is, the $W^\pm$ interactions) for quarks are given by

$$-\mathcal{L}_{W^\pm} = \frac{g}{\sqrt{2}}\ \overline{u_{Li}}\ \gamma^\mu\ (V_{\rm CKM})_{ij}\ d_{Lj}\ W^+_\mu + \text{h.c.} \tag{13.32}$$

Downloaded from https://academic.oup.com/ptep/article/2022/8/083C01/6651666 by KIT Library user on 27 September 2022

Here $i, j = 1, 2, 3$ are generation numbers. The Cabibbo-Kobayashi-Maskawa (CKM) mixing matrix for quarks is a 3×3 unitary matrix [39]. Ordering the quarks by their masses, *i.e.*, $(u_1, u_2, u_3) \to (u, c, t)$ and $(d_1, d_2, d_3) \to (d, s, b)$, the elements of $V_{\rm CKM}$ are written as follows:

$$V_{\rm CKM} = \begin{pmatrix} V_{ud} & V_{us} & V_{ub} \\ V_{cd} & V_{cs} & V_{cb} \\ V_{td} & V_{ts} & V_{tb} \end{pmatrix} . \tag{13.33}$$

While a general 3×3 unitary matrix depends on three real angles and six phases, the freedom to redefine the phases of the quark mass eigenstates can be used to remove five of the phases, leaving a single physical phase, the Kobayashi-Maskawa phase, that is responsible for all *CP* violation in the Standard Model.

The fact that one can parameterize $V_{\rm CKM}$ by three real and only one imaginary physical parameters can be made manifest by choosing an explicit parametrization. The Wolfenstein parametrization [40, 41] is particularly useful:

$$V_{\rm CKM} = \begin{pmatrix} 1 - \frac{1}{2}\lambda^2 - \frac{1}{8}\lambda^4 & \lambda & A\lambda^3(\rho - i\eta) \\ -\lambda + \frac{1}{2}A^2\lambda^5[1 - 2(\rho + i\eta)] & 1 - \frac{1}{2}\lambda^2 - \frac{1}{8}\lambda^4(1 + 4A^2) & A\lambda^2 \\ A\lambda^3[1 - (1 - \frac{1}{2}\lambda^2)(\rho + i\eta)] & -A\lambda^2 + \frac{1}{2}A\lambda^4[1 - 2(\rho + i\eta)] & 1 - \frac{1}{2}A^2\lambda^4 \end{pmatrix} . \tag{13.34}$$

Here $\lambda \approx 0.23$ (not to be confused with λ_f), the sine of the Cabibbo angle, plays the role of an expansion parameter, and η represents the *CP*-violating phase. Terms of $\mathcal{O}(\lambda^6)$ have been neglected.

The unitarity of the CKM matrix, $(VV^\dagger)_{ij} = (V^\dagger V)_{ij} = \delta_{ij}$, leads to twelve distinct complex relations among the matrix elements. The six relations with $i \neq j$ can be represented geometrically as triangles in the complex plane. Two of these,

$$V_{ud}V_{ub}^* + V_{cd}V_{cb}^* + V_{td}V_{tb}^* = 0 , \tag{13.35a}$$
$$V_{td}V_{ud}^* + V_{ts}V_{us}^* + V_{tb}V_{ub}^* = 0 , \tag{13.35b}$$

have terms of equal order, $\mathcal{O}(A\lambda^3)$, and so have corresponding triangles whose interior angles are all $\mathcal{O}(1)$ physical quantities that can be independently measured. The angles of the first triangle (see Fig. 13.1) are given by

$$\alpha \equiv \varphi_2 \equiv \arg\left(-\frac{V_{td}V_{tb}^*}{V_{ud}V_{ub}^*}\right) \simeq \arg\left(-\frac{1 - \rho - i\eta}{\rho + i\eta}\right) , \tag{13.36a}$$
$$\beta \equiv \varphi_1 \equiv \arg\left(-\frac{V_{cd}V_{cb}^*}{V_{td}V_{tb}^*}\right) \simeq \arg\left(\frac{1}{1 - \rho - i\eta}\right) , \tag{13.36b}$$
$$\gamma \equiv \varphi_3 \equiv \arg\left(-\frac{V_{ud}V_{ub}^*}{V_{cd}V_{cb}^*}\right) \simeq \arg(\rho + i\eta) . \tag{13.36c}$$

The angles of the second triangle are equal to (α, β, γ) up to corrections of $\mathcal{O}(\lambda^2)$. The notations (α, β, γ) and $(\varphi_1, \varphi_2, \varphi_3)$ are both in common usage but, for convenience, we only use the first convention in the following.

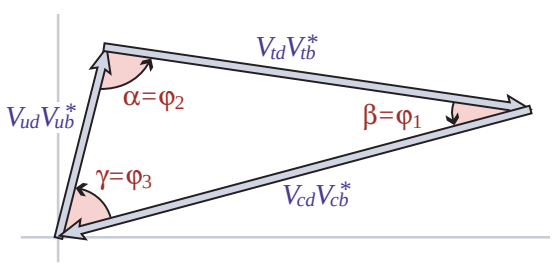

Figure 13.1: Graphical representation of the unitarity constraint $V_{ud}V_{ub}^* + V_{cd}V_{cb}^* + V_{td}V_{tb}^* = 0$ as a triangle in the complex plane.

Another relation that can be represented as a triangle,

$$V_{us}V_{ub}^* + V_{cs}V_{cb}^* + V_{ts}V_{tb}^* = 0 , \tag{13.37}$$

and, in particular, its small angle, of $\mathcal{O}(\lambda^2)$,

$$\beta_s \equiv \arg\left(-\frac{V_{ts}V_{tb}^*}{V_{cs}V_{cb}^*}\right) , \tag{13.38}$$

is convenient for analyzing *CP* violation in the B_s^0 sector.

All unitarity triangles have the same area, commonly denoted by $J/2$ [42]. If *CP* is violated, J is different from zero and can be taken as the single *CP*-violating parameter. In the Wolfenstein parametrization of Eq. (13.34), $J \simeq \lambda^6 A^2 \eta$.

13.4 Kaons

CP violation was discovered in $K \to \pi\pi$ decays in 1964 [1]. The same mode provided the first observation of direct *CP* violation [4–6].

The decay amplitudes actually measured in neutral K decays refer to the mass eigenstates K_L and K_S, rather than to the K and $\overline{K}$ states referred to in Eq. (13.1). The final $\pi^+\pi^-$ and $\pi^0\pi^0$ states are *CP*-even. In the *CP* conservation limit, K_S (K_L) would be *CP*-even (odd), and therefore would (would not) decay to two pions. We define *CP*-violating amplitude ratios for two-pion final states,

$$\eta_{00} \equiv \frac{\langle \pi^0\pi^0|\mathcal{H}|K_L\rangle}{\langle \pi^0\pi^0|\mathcal{H}|K_S\rangle} , \quad \eta_{+-} \equiv \frac{\langle \pi^+\pi^-|\mathcal{H}|K_L\rangle}{\langle \pi^+\pi^-|\mathcal{H}|K_S\rangle} . \tag{13.39}$$

Another important observable is the asymmetry of time-integrated semileptonic decay rates:

$$\delta_L \equiv \frac{\Gamma(K_L \to \ell^+\nu_\ell\pi^-) - \Gamma(K_L \to \ell^-\overline{\nu}_\ell\pi^+)}{\Gamma(K_L \to \ell^+\nu_\ell\pi^-) + \Gamma(K_L \to \ell^-\overline{\nu}_\ell\pi^+)} . \tag{13.40}$$

CP violation has been observed as an appearance of K_L decays to two-pion final states [43],

$$|\eta_{00}| = (2.220 \pm 0.011) \times 10^{-3} , \tag{13.41a}$$
$$|\eta_{+-}| = (2.232 \pm 0.011) \times 10^{-3} , \tag{13.41b}$$
$$|\eta_{00}/\eta_{+-}| = 0.9950 \pm 0.0007 , \tag{13.41c}$$

where the *CP*-conserving phases ϕ_{ij} of the amplitude ratios η_{ij} have been determined both assuming *CPT* invariance:

$$\phi_{00} = (43.52 \pm 0.05)^\circ , \qquad \phi_{+-} = (43.51 \pm 0.05)^\circ , \tag{13.42}$$

and without assuming *CPT* invariance:

$$\phi_{00} = (43.7 \pm 0.6)^\circ , \qquad \phi_{+-} = (43.4 \pm 0.5)^\circ . \tag{13.43}$$

CP violation has also been observed in semileptonic K_L decays [43]

$$\delta_L = (3.32 \pm 0.06) \times 10^{-3} , \tag{13.44}$$

where δ_L is a weighted average of muon and electron measurements, as well as in K_L decays to $\pi^+\pi^-\gamma$ and $\pi^+\pi^-e^+e^-$ [43]. *CP* violation in $K \to 3\pi$ decays has not yet been observed [43, 44].

Historically, *CP* violation in neutral K decays has been described in terms of the complex parameters ϵ and ϵ'. The observables η_{00}, η_{+-}, and δ_L are related to these parameters, and to

Downloaded from https://academic.oup.com/ptep/article/2022/8/083C01/6651666 by KIT Library user on 27 September 2022

those of Section 13.1, by

$$\eta_{00} = \frac{1-\lambda_{\pi^0\pi^0}}{1+\lambda_{\pi^0\pi^0}} = \epsilon - 2\epsilon' , \tag{13.45a}$$

$$\eta_{+-} = \frac{1-\lambda_{\pi^+\pi^-}}{1+\lambda_{\pi^+\pi^-}} = \epsilon + \epsilon' , \tag{13.45b}$$

$$\delta_L = \frac{1-|q/p|^2}{1+|q/p|^2} = \frac{2\mathcal{R}e(\epsilon)}{1+|\epsilon|^2} , \tag{13.45c}$$

where, in the last line, we have assumed that $\left|A_{\ell^+\nu_\ell\pi^-}\right| = \left|\overline{A}_{\ell^-\overline{\nu}_\ell\pi^+}\right|$ and $\left|A_{\ell^-\overline{\nu}_\ell\pi^+}\right| = \left|\overline{A}_{\ell^+\nu_\ell\pi^-}\right| = 0$. (The convention-dependent parameter $\tilde{\epsilon} \equiv (1-q/p)/(1+q/p)$, sometimes used in the literature, is, in general, different from ϵ but yields a similar expression, $\delta_L = 2\mathcal{R}e(\tilde{\epsilon})/(1+|\tilde{\epsilon}|^2)$.) A fit to the $K \to \pi\pi$ data yields [43]

$$|\epsilon| = (2.228 \pm 0.011) \times 10^{-3} , \tag{13.46a}$$

$$\mathcal{R}e(\epsilon'/\epsilon) = (1.66 \pm 0.23) \times 10^{-3} . \tag{13.46b}$$

In discussing two-pion final states, it is useful to express the amplitudes $A_{\pi^0\pi^0}$ and $A_{\pi^+\pi^-}$ in terms of their isospin components via

$$A_{\pi^0\pi^0} = \sqrt{\frac{1}{3}}\,|A_0|\,e^{i(\delta_0+\phi_0)} - \sqrt{\frac{2}{3}}\,|A_2|\,e^{i(\delta_2+\phi_2)} , \tag{13.47a}$$

$$A_{\pi^+\pi^-} = \sqrt{\frac{2}{3}}\,|A_0|\,e^{i(\delta_0+\phi_0)} + \sqrt{\frac{1}{3}}\,|A_2|\,e^{i(\delta_2+\phi_2)} , \tag{13.47b}$$

where we parameterize the amplitude $A_I(\overline{A}_I)$ for $K^0(\overline{K}^0)$ decay into two pions with total isospin $I = 0$ or 2 as

$$A_I \equiv \langle(\pi\pi)_I\,|\mathcal{H}|\,K^0\rangle = |A_I|\,e^{i(\delta_I+\phi_I)} , \tag{13.48a}$$

$$\overline{A}_I \equiv \langle(\pi\pi)_I\,|\mathcal{H}|\,\overline{K}^0\rangle = |A_I|\,e^{i(\delta_I-\phi_I)} . \tag{13.48b}$$

The smallness of $|\eta_{00}|$ and $|\eta_{+-}|$ allows us to approximate

$$\epsilon \simeq \frac{1}{2}(1-\lambda_{(\pi\pi)_{I=0}}) , \qquad \epsilon' \simeq \frac{1}{6}\left(\lambda_{\pi^0\pi^0} - \lambda_{\pi^+\pi^-}\right) . \tag{13.49}$$

The parameter ϵ represents indirect *CP* violation, while ϵ' parameterizes direct *CP* violation: $\mathcal{R}e(\epsilon')$ measures *CP* violation in decay (type I), $\mathcal{R}e(\epsilon)$ measures *CP* violation in mixing (type II), and $\mathcal{I}m(\epsilon)$ and $\mathcal{I}m(\epsilon')$ measure the interference between decays with and without mixing (type III).

The following expressions for ϵ and ϵ' are useful for theoretical evaluations:

$$\epsilon \simeq \frac{e^{i\pi/4}}{\sqrt{2}}\frac{\mathcal{I}m(\mathbf{M}_{12})}{\Delta m} , \qquad \epsilon' = \frac{i}{\sqrt{2}}\left|\frac{A_2}{A_0}\right| e^{i(\delta_2-\delta_0)}\sin(\phi_2-\phi_0) . \tag{13.50}$$

The expression for ϵ is only valid in a phase convention where $\phi_2 = 0$, corresponding to a real $V_{ud}V_{us}^*$, and in the approximation that also $\phi_0 = 0$. The phase of ϵ, $\arg(\epsilon) \approx \arctan(-2\Delta m/\Delta\Gamma)$, is determined by non-perturbative QCD dynamics and is experimentally determined to be about $\pi/4$. The calculation of ϵ benefits from the fact that $\mathcal{I}m(\mathbf{M}_{12})$ is dominated by short distance physics. Consequently, the main sources of uncertainty in theoretical interpretations of ϵ are the values of matrix elements, such as $\langle K^0\,|(\overline{s}d)_{V-A}(\overline{s}d)_{V-A}|\,\overline{K}^0\rangle$. The expression for ϵ' is valid to first order in $|A_2/A_0| \sim 1/20$. The phase of ϵ' is experimentally determined, $\pi/2+\delta_2-\delta_0 \approx \pi/4$, and is independent of the model of electroweak interactions. Note that, accidentally, ϵ'/ϵ is real to a good approximation. Determination of weak phase information from the measurement of $\mathcal{R}e(\epsilon'/\epsilon)$ given in Eq. (13.46) has until now been precluded by uncertainties in the hadronic parameters, but recent advances in lattice QCD calculations [45, 46] suggest that it may become possible [47].

A future measurement of much interest is that of *CP* violation in the rare $K \to \pi\nu\overline{\nu}$ decays. The signal for *CP* violation is simply observing the $K_L \to \pi^0\nu\overline{\nu}$ decay. The effect here is that of interference between decays with and without mixing (type III) [48]:

$$\frac{\Gamma(K_L \to \pi^0\nu\overline{\nu})}{\Gamma(K^+ \to \pi^+\nu\overline{\nu})} = \frac{1}{2}\left[1 + |\lambda_{\pi\nu\overline{\nu}}|^2 - 2\,\mathcal{R}e(\lambda_{\pi\nu\overline{\nu}})\right] \simeq 1 - \mathcal{R}e(\lambda_{\pi\nu\overline{\nu}}) , \tag{13.51}$$

where in the last equation we neglect *CP* violation in decay and in mixing (expected, model-independently, to be of order 10^{-5} and 10^{-3}, respectively). Such a measurement is experimentally very challenging but would be theoretically very rewarding [49]. Similar to the *CP* asymmetry in $B^0 \to J/\psi K_S$, the *CP* violation in $K \to \pi\nu\overline{\nu}$ decay is predicted to be large (that is, the ratio in Eq. (13.51) is neither CKM- nor loop-suppressed) and can be very cleanly interpreted. In particular, the independent determinations of the CKM parameters via *B*-meson and *K*-meson decays and mixing will over-constrain the unitarity triangle and provide a stringent text of the KM mechanism.

Within the Standard Model, the $K_L \to \pi^0\nu\overline{\nu}$ decay is dominated by an intermediate top quark contribution and, consequently, can be interpreted in terms of CKM parameters [50]. (For the charged mode, $K^+ \to \pi^+\nu\overline{\nu}$, the contribution from an intermediate charm quark is not negligible, and constitutes a source of hadronic uncertainty.) In particular, $\mathcal{B}(K_L \to \pi^0\nu\overline{\nu})$ provides a theoretically clean way to determine the Wolfenstein parameter η [51]:

$$\mathcal{B}(K_L \to \pi^0\nu\overline{\nu}) = \kappa_L[X(m_t^2/m_W^2)]^2 A^4\eta^2 , \tag{13.52}$$

where the hadronic parameter $\kappa_L \sim 2 \times 10^{-10}$ incorporates the value of the four-fermion matrix element which is deduced, using isospin relations, from $\mathcal{B}(K^+ \to \pi^0 e^+\nu_e)$, and $X(m_t^2/m_W^2)$ is a known function of the top mass. An explicit calculation gives $\mathcal{B}(K_L \to \pi^0\nu\overline{\nu}) = (3.00 \pm 0.30) \times 10^{-11}$ [52].

Currently the most stringent experimental limit is $\mathcal{B}(K_L \to \pi^0\nu\overline{\nu}) < 3.0 \times 10^{-9}$ [53, 54], which does not yet reach the bound that can be derived from Eq. (13.51), $\mathcal{B}(K_L \to \pi^0\nu\overline{\nu}) < 4.4 \times \mathcal{B}(K^+ \to \pi^+\nu\overline{\nu})$ [48], with the most precise result for the charged kaon decay being $\mathcal{B}(K^+ \to \pi^+\nu\overline{\nu}) = \left(10.6\,^{+4.0}_{-3.4} \pm 0.9\right) \times 10^{-11}$ [55]. Significant further progress is anticipated from experiments searching for $K \to \pi\nu\overline{\nu}$ decays in the next few years.

13.5 Charm

The existence of D^0–$\overline{D}^0$ mixing is well established [56–60], with the latest experimental constraints giving [61, 62] $x \equiv \Delta m/\Gamma = (0.41 \pm 0.05) \times 10^{-2}$ and $y \equiv \Delta\Gamma/(2\Gamma) = (0.62 \pm 0.06) \times 10^{-2}$. Long-distance contributions make it difficult to calculate Standard Model predictions for the D^0–$\overline{D}^0$ mixing parameters. Therefore, the goal of the search for D^0–$\overline{D}^0$ mixing is not to constrain the CKM parameters, but rather to probe new physics. Here *CP* violation plays an important role. Within the Standard Model, the *CP*-violating effects are predicted to be small, since the mixing and the relevant decays are described, to an excellent approximation, by the physics of the first two generations only. The expectation is that the Standard Model size of *CP* violation in *D* decays is $\mathcal{O}(10^{-3})$ or less. At present, the most sensitive searches involve the $D^0 \to K^+K^-$, $D^0 \to \pi^+\pi^-$ and $D^0 \to K^\pm\pi^\mp$ modes.

The neutral *D* mesons decay via a singly-Cabibbo-suppressed transition to the *CP* eigenstates K^+K^- and $\pi^+\pi^-$. These decays are dominated by Standard-Model tree diagrams. Thus, we can write, for $f = K^+K^-$ or $\pi^+\pi^-$,

$$A_f = A_f^T e^{+i\phi_f^T}\left[1 + r_f e^{i(\delta_f+\phi_f)}\right] , \tag{13.53a}$$

$$\bar{A}_f = A_f^T e^{-i\phi_f^T}\left[1 + r_f e^{i(\delta_f-\phi_f)}\right] , \tag{13.53b}$$

where $A_f^T e^{\pm i\phi_f^T}$ is the Standard Model tree-level contribution, ϕ_f^T and ϕ_f are weak, *CP* violating phases, δ_f is a strong phase difference, and r_f is the ratio between a subleading ($r_f \ll 1$) contribution with a weak phase different from ϕ_f^T and the Standard Model tree-level contribution. Neglecting r_f, λ_f is universal, and

Downloaded from https://academic.oup.com/ptep/article/2022/8/083C01/6651666 by KIT Library user on 27 September 2022

we can define an observable phase ϕ_D via

$$\lambda_f \equiv -|q/p|e^{i\phi_D} \,. \tag{13.54}$$

(In the limit of CP conservation, choosing $\phi_D = 0$ is equivalent to defining the mass eigenstates by their CP eigenvalue: $|D_\mp\rangle = p|D^0\rangle \pm q|\overline{D}^0\rangle$, with D_- (D_+) being the CP-odd (CP-even) state; that is, the state that does not (does) decay into K^+K^-.)

We define the time integrated CP asymmetry for a final CP eigenstate f as follows:

$$a_f \equiv \frac{\int_0^\infty \Gamma(D^0_{\rm phys}(t) \to f)dt - \int_0^\infty \Gamma(\overline{D}^0_{\rm phys}(t) \to f)dt}{\int_0^\infty \Gamma(D^0_{\rm phys}(t) \to f)dt + \int_0^\infty \Gamma(\overline{D}^0_{\rm phys}(t) \to f)dt} \,. \tag{13.55}$$

(This expression corresponds to the D meson being tagged at production, hence the integration goes from 0 to $+\infty$; measurements are also possible with $\psi(3770) \to D^0\overline{D}^0$, in which case the integration goes from $-\infty$ to $+\infty$ giving slightly different results; see the discussion in Section 13.1.3.) We take $x, y, r_f \ll 1$ and expand to leading order in these parameters. We can then separate the contribution to a_f into three parts [63],

$$a_f = a_f^d + a_f^m + a_f^i \,, \tag{13.56}$$

with the following underlying mechanisms:

1. a_f^d signals CP violation in decay (similar to Eq. (13.21)):

$$a_f^d = 2r_f \sin\phi_f \sin\delta_f \,. \tag{13.57}$$

2. a_f^m signals CP violation in mixing (similar to Eq. (13.30)). With our approximations, it is universal:

$$a^m = -\frac{y}{2}\left(\left|\frac{q}{p}\right| - \left|\frac{p}{q}\right|\right)\cos\phi_D \,. \tag{13.58}$$

3. a_f^i signals CP violation in the interference of mixing and decay (similar to Eq. (13.31)). With our approximations, it is universal:

$$a^i = \frac{x}{2}\left(\left|\frac{q}{p}\right| + \left|\frac{p}{q}\right|\right)\sin\phi_D \,. \tag{13.59}$$

In the SM, both a^m and a^i are $\mathcal{O}(10^{-5})$ or less, while a^d could be up to two orders of magnitude larger.

One can isolate the effects of direct CP violation by taking the difference between the CP asymmetries in the K^+K^- and $\pi^+\pi^-$ modes:

$$\Delta a_{CP} \equiv a_{K^+K^-} - a_{\pi^+\pi^-} = a^d_{K^+K^-} - a^d_{\pi^+\pi^-} \,, \tag{13.60}$$

where we neglected a residual, experiment-dependent, contribution from indirect CP violation due to the fact that there may be a decay time-dependent acceptance function that can be different for the K^+K^- and $\pi^+\pi^-$ channels. The current average gives [13, 61]:

$$a^d_{K^+K^-} - a^d_{\pi^+\pi^-} = (-0.164 \pm 0.028) \times 10^{-2} \,, \tag{13.61}$$

demonstrating CP violation in charm decay. While the asymmetry is somewhat larger than the theoretical predictions that preceded the measurement, it can in principle be explained by non-perturbative QCD effects.

One can also isolate the effects of indirect CP violation in the following way. Consider the time-dependent decay rates in Eq. (13.17a) and Eq. (13.17b). The mixing processes modify the time dependence from a pure exponential. However, given the small values of x and y, the time dependences can be recast, to a good approximation, into purely exponential form, but with modified decay-rate parameters [64,65] (given here for the K^+K^- final state):

$$\Gamma_{D^0\to K^+K^-} = \Gamma \times [1 + |q/p|\,(y\cos\phi_D - x\sin\phi_D)] \,, \tag{13.62a}$$

$$\Gamma_{\overline{D}^0\to K^+K^-} = \Gamma \times [1 + |p/q|\,(y\cos\phi_D + x\sin\phi_D)] \,. \tag{13.62b}$$

One can define CP-conserving and CP-violating combinations of these two observables (normalized to the true width Γ):

$$\begin{aligned} y_{CP} &\equiv \frac{\Gamma_{\overline{D}^0\to K^+K^-} + \Gamma_{D^0\to K^+K^-}}{2\Gamma} - 1 \\ &= (y/2)\,(|q/p| + |p/q|)\cos\phi_D - (x/2)\,(|q/p| - |p/q|)\sin\phi_D \,, \end{aligned} \tag{13.63a}$$

$$\begin{aligned} A_\Gamma &\equiv \frac{\Gamma_{D^0\to K^+K^-} - \Gamma_{\overline{D}^0\to K^+K^-}}{2\Gamma} \\ &= -(a^m + a^i) \,. \end{aligned} \tag{13.63b}$$

In the limit of CP conservation (and, in particular, within the Standard Model), $y_{CP} = (\Gamma_+ - \Gamma_-)/2\Gamma = y$ (where $\Gamma_+(\Gamma_-)$ is the decay width of the CP-even (-odd) mass eigenstate) and $A_\Gamma = 0$. Indeed, present measurements imply that CP violation is small [61],

$$y_{CP} = (+0.72 \pm 0.11) \times 10^{-2} \,, \tag{13.64a}$$

$$A_\Gamma = (0.009 \pm 0.011) \times 10^{-2} \,. \tag{13.64b}$$

The $K^\pm\pi^\mp$ states are not CP eigenstates, but they are still common final states for D^0 and $\overline{D}^0$ decays. Since $D^0(\overline{D}^0) \to K^-\pi^+$ is a Cabibbo-favored (doubly-Cabibbo-suppressed) process, these processes are particularly sensitive to x and/or $y = \mathcal{O}(\lambda^2)$. Taking into account that $|\lambda_{K^-\pi^+}|\,, \left|\lambda^{-1}_{K^+\pi^-}\right| \ll 1$ and $x, y \ll 1$, assuming that there is no direct CP violation (these are Standard Model tree-level decays dominated by a single weak phase, and there is no contribution from penguin-like and chromomagnetic operators), and expanding the time-dependent rates for $xt, yt \lesssim \Gamma^{-1}$, one obtains

$$\begin{aligned} &\Gamma[D^0_{\rm phys}(t) \to K^+\pi^-] = e^{-\Gamma t}|\overline{A}_{K^-\pi^+}|^2 \\ &\times \left[r_d^2 + r_d\left|\frac{q}{p}\right|(y'\cos\phi_D - x'\sin\phi_D)\Gamma t + \left|\frac{q}{p}\right|^2 \frac{y^2+x^2}{4}(\Gamma t)^2\right] \,, \end{aligned} \tag{13.65a}$$

$$\begin{aligned} &\Gamma[\overline{D}^0_{\rm phys}(t) \to K^-\pi^+] = e^{-\Gamma t}|\overline{A}_{K^-\pi^+}|^2 \\ &\times \left[r_d^2 + r_d\left|\frac{p}{q}\right|(y'\cos\phi_D + x'\sin\phi_D)\Gamma t + \left|\frac{p}{q}\right|^2 \frac{y^2+x^2}{4}(\Gamma t)^2\right] \,, \end{aligned} \tag{13.65b}$$

where

$$y' \equiv y\cos\delta - x\sin\delta \quad \text{and} \quad x' \equiv x\cos\delta + y\sin\delta \,. \tag{13.66}$$

The weak phase ϕ_D is the same as that of Eq. (13.54) (a consequence of neglecting direct CP violation) and $r_d = \mathcal{O}(\tan^2\theta_c)$ is the amplitude ratio, $r_d = \left|\overline{A}_{K^-\pi^+}/A_{K^-\pi^+}\right| = \left|A_{K^+\pi^-}/\overline{A}_{K^+\pi^-}\right|$, that is, $\lambda_{K^-\pi^+} = r_d|q/p|e^{-i(\delta-\phi_D)}$ and $\lambda^{-1}_{K^+\pi^-} = r_d|p/q|e^{-i(\delta+\phi_D)}$. The parameter δ is a strong-phase difference for these processes, that can be obtained from measurements of quantum correlated $\psi(3770) \to D^0\overline{D}^0$ decays [66,67]. By fitting to the six coefficients of the various time-dependences, one can determine r_d, $|q/p|$, (x^2+y^2), $y'\cos\phi_D$, and $x'\sin\phi_D$. In particular, finding CP violation ($|q/p| \neq 1$ and/or $\sin\phi_D \neq 0$) at a level much higher than 10^{-3} would constitute evidence for new physics. The most stringent constraints to date on CP violation in charm mixing have been obtained with this method [68] and from the A_Γ measurement [69].

A fit to all data [61], including also results from time-dependent analyses of $D^0 \to K_S\pi^+\pi^-$ decays, from which x, y, $|q/p|$ and ϕ_D can be determined directly, yields no evidence for indirect CP violation:

$$1 - |q/p| = +0.005 \pm 0.016 \,, \tag{13.67a}$$

$$\phi_D = (-2.5 \pm 1.2)^\circ \,. \tag{13.67b}$$

With the additional assumption of no direct CP violation in doubly-Cabibbo-suppressed D decays [70–72], more stringent con-

Downloaded from https://academic.oup.com/ptep/article/2022/8/083C01/6651666 by KIT Library user on 27 September 2022

straints are obtained:

$$1 - |q/p| = -0.005 \pm 0.007\,, \tag{13.68a}$$

$$\phi_D = (-0.2 \pm 0.3)^\circ\ . \tag{13.68b}$$

More details on various theoretical and experimental aspects of D^0–$\overline{D}^0$ mixing can be found in Ref. [32].

Searches for *CP* violation in charged $D_{(s)}$ decays have been performed in many modes. Searches in decays mediated by Cabibbo-suppressed amplitudes are particularly interesting, since in other channels effects are likely to be too small to be observable in current experiments. Examples of relevant two-body modes are $D^+ \to \pi^+\pi^0$, $K_S K^+$, $\phi\pi^+$ and $D_s^+ \to K^+\pi^0$, $K_S\pi^+$, ϕK^+. The most precise results are $\mathcal{A}_{D^+\to K_S K^+} = +0.0011 \pm 0.0017$ and $\mathcal{A}_{D_s^+\to K_S\pi^+} = +0.0038 \pm 0.0048$ [61]. The precision of experiments is now sufficient that the effect from *CP* violation in the neutral kaon system can be seen in $D^+ \to K_S\pi^+$ decays [73, 74].

Three- and four-body final states provide additional possibilities to search for *CP* violation, since effects may vary over the phase-space [75]. A number of methods have been proposed to exploit this feature and search for *CP* violation in ways that do not require modelling of the decay distribution [76–79]. Such methods are useful for analysis of charm decays since they are less sensitive to biases from production asymmetries, and are well suited to address the issue of whether or not *CP* violation effects are present. They can also be applied to tagged neutral D meson as well as to charged $D_{(s)}$ decays (flavor tagging is typically achieved from the charge of the pion produced in $D^{*+} \to D^0\pi^+$ decays). The results of all searches to date are consistent with the absence of *CP* violation, with the most significant hint at the level of 2.7σ [80].

13.6 Beauty

13.6.1 *CP violation in mixing of B^0 and B_s^0 mesons*

The upper bound on the *CP* asymmetry in semileptonic B decays [81] implies that *CP* violation in B^0–$\overline{B}^0$ mixing is a small effect (we use $\mathcal{A}_{\rm SL}/2 \approx 1 - |q/p|$, see Eq. (13.23)):

$$\mathcal{A}^d_{\rm SL} = (-2.1 \pm 1.7) \times 10^{-3} \quad\Longrightarrow\quad |q/p| = 1.0010 \pm 0.0008\ . \tag{13.69}$$

The Standard Model prediction is

$$\mathcal{A}^d_{\rm SL} = \mathcal{O}\left[(m_c^2/m_t^2)\sin\beta\right] \lesssim 0.001\ . \tag{13.70}$$

An explicit calculation gives $(-4.7 \pm 0.6) \times 10^{-4}$ [35].

The experimental constraint on *CP* violation in B_s^0–$\overline{B}_s^0$ mixing is somewhat weaker than that in the B^0–$\overline{B}^0$ system [81]

$$\mathcal{A}^s_{\rm SL} = (-0.6 \pm 2.8) \times 10^{-3} \quad\Longrightarrow\quad |q/p| = 1.0003 \pm 0.0014\ . \tag{13.71}$$

The Standard Model prediction is $\mathcal{A}^s_{\rm SL} = \mathcal{O}\left[(m_c^2/m_t^2)\sin\beta_s\right] \lesssim 10^{-4}$, with an explicit calculation giving $(2.22 \pm 0.27) \times 10^{-5}$ [35].

The fit to experimental data that results in the averages quoted above has a χ^2 probability of 4.5% indicating some tension between the different measurements [61]. This originates in part from a result from the D0 collaboration for the inclusive same-sign dimuon asymmetry that deviates from the Standard Model prediction by 3.6σ [82]. As yet, this has not been confirmed by independent studies.

In models where $\mathbf{\Gamma}_{12}/\mathbf{M}_{12}$ is approximately real, such as the Standard Model, an upper bound on $\Delta\Gamma/\Delta m \approx \mathcal{R}e(\mathbf{\Gamma}_{12}/\mathbf{M}_{12})$ provides yet another upper bound on the deviation of $|q/p|$ from one. This constraint does not hold if $\mathbf{\Gamma}_{12}/\mathbf{M}_{12}$ is approximately imaginary. (An alternative parameterization uses $q/p = (1 - \tilde{\epsilon}_B)/(1 + \tilde{\epsilon}_B)$, leading to $\mathcal{A}_{\rm SL} \simeq 4\mathcal{R}e(\tilde{\epsilon}_B)$.)

13.6.2 *CP violation in interference of B^0 decays with and without mixing*

The small deviation (less than one percent) of $|q/p|$ from 1 implies that, at the present level of experimental precision, *CP* violation in B^0 mixing is a negligible effect. Thus, for the purpose of analyzing *CP* asymmetries in hadronic B^0 decays, we can use

$$\lambda_f = e^{-i\phi_{M(B^0)}}(\overline{A}_f/A_f)\ , \tag{13.72}$$

where $\phi_{M(B^0)}$ refers to the phase of $\mathbf{M}_{12}$ appearing in Eq. (13.28) that is appropriate for B^0–$\overline{B}^0$ oscillations. Within the Standard Model, the corresponding phase factor is given by

$$e^{-i\phi_{M(B^0)}} = (V_{tb}^* V_{td})/(V_{tb} V_{td}^*)\ . \tag{13.73}$$

The class of *CP* violation effects in interference between mixing and decay is studied with final states that are common to B^0 and $\overline{B}^0$ decays [83–85]. It is convenient to rewrite Eq. (13.26) for B^0 decays as [86–88]

$$\mathcal{A}_f(t) = S_f \sin(\Delta m t) - C_f \cos(\Delta m t)\ , \tag{13.74}$$

$$S_f \equiv \frac{2\,\mathcal{I}m(\lambda_f)}{1 + \left|\lambda_f\right|^2}\ , \quad C_f \equiv \frac{1 - \left|\lambda_f\right|^2}{1 + \left|\lambda_f\right|^2}\ , \tag{13.75}$$

where we assume that $\Delta\Gamma = 0$ and $|q/p| = 1$. An alternative notation in use is $A_f \equiv -C_f$ – this A_f should not be confused with the A_f of Eq. (13.1), but in the limit that $|q/p| = 1$ is equivalent with the $\mathcal{A}_f$ of Eq. (13.21).

A large class of interesting processes proceed via quark transitions of the form $\overline{b} \to \overline{q}q\overline{q}'$ with $q' = s$ or d. For $q = c$ or u, there are contributions from both tree (t) and penguin (p^{q_u}, where $q_u = u, c, t$ is the quark in the loop) diagrams (see Fig. 13.2) which carry different weak phases:

$$A_f = \left(V_{qb}^* V_{qq'}\right) t_f + \sum_{q_u=u,c,t} \left(V_{q_u b}^* V_{q_u q'}\right) p_f^{q_u}\ . \tag{13.76}$$

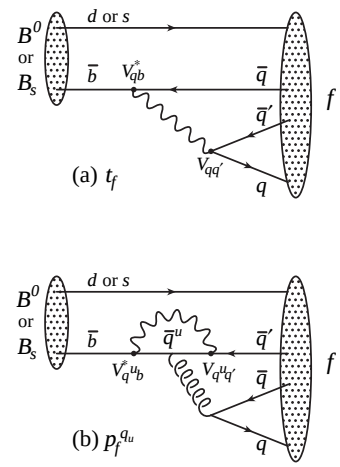

Figure 13.2: Feynman diagrams for (a) tree and (b) penguin amplitudes contributing to $B^0 \to f$ or $B_s^0 \to f$ via a $\overline{b} \to \overline{q}q\overline{q}'$ quark-level process.

(The distinction between tree and penguin contributions is a heuristic one; the separation by the operator that enters is more precise. A more detailed discussion of the operator product expansion approach, which also includes higher order QCD corrections, can be found in Ref. [89, 90] for example.) Using CKM unitarity, the various decay amplitudes can always be written in terms of just two CKM combinations. For example, for $f = \pi\pi$, which proceeds via a $\overline{b} \to \overline{u}u\overline{d}$ transition, we can write

$$A_{\pi\pi} = \left(V_{ub}^* V_{ud}\right) T_{\pi\pi} + \left(V_{tb}^* V_{td}\right) P_{\pi\pi}^t\ , \tag{13.77}$$

where $T_{\pi\pi} = t_{\pi\pi} + p_{\pi\pi}^u - p_{\pi\pi}^c$ and $P_{\pi\pi}^t = p_{\pi\pi}^t - p_{\pi\pi}^c$. *CP*-violating phases in Eq. (13.77) appear only in the CKM elements, so that

$$\frac{\overline{A}_{\pi\pi}}{A_{\pi\pi}} = \frac{\left(V_{ub} V_{ud}^*\right) T_{\pi\pi} + \left(V_{tb} V_{td}^*\right) P_{\pi\pi}^t}{\left(V_{ub}^* V_{ud}\right) T_{\pi\pi} + \left(V_{tb}^* V_{td}\right) P_{\pi\pi}^t}\ . \tag{13.78}$$

For $f = J/\psi K$, which proceeds via a $\overline{b} \to \overline{c}c\overline{s}$ transition, we can write

$$A_{\psi K} = \left(V_{cb}^* V_{cs}\right) T_{\psi K} + \left(V_{ub}^* V_{us}\right) P_{\psi K}^u\ , \tag{13.79}$$

Downloaded from https://academic.oup.com/ptep/article/2022/8/083C01/6651666 by KIT Library user on 27 September 2022

where $T_{\psi K} = t_{\psi K} + p^c_{\psi K} - p^t_{\psi K}$ and $P^u_{\psi K} = p^u_{\psi K} - p^t_{\psi K}$. A subtlety arises in this decay that is related to the fact that B^0 decays into a final $J/\psi K^0$ state while $\overline{B}^0$ decays into a final $J/\psi \overline{K}^0$ state. A common final state, *e.g.*, $J/\psi K_S$, is reached only via K^0–$\overline{K}^0$ mixing. Consequently, the phase factor (defined in Eq. (13.28)) corresponding to neutral K mixing, $e^{-i\phi_{M(K)}} = (V^*_{cd}V_{cs})/(V_{cd}V^*_{cs})$, plays a role:

$$\frac{\overline{A}_{\psi K_S}}{A_{\psi K_S}} = -\frac{\left(V_{cb}V^*_{cs}\right) T_{\psi K} + \left(V_{ub}V^*_{us}\right) P^u_{\psi K}}{\left(V^*_{cb}V_{cs}\right) T_{\psi K} + \left(V^*_{ub}V_{us}\right) P^u_{\psi K}} \times \frac{V^*_{cd}V_{cs}}{V_{cd}V^*_{cs}} \ . \quad (13.80)$$

For $q = s$ or d, there are only penguin contributions to A_f, that is, $t_f = 0$ in Eq. (13.76). (The tree $\overline{b} \to \overline{u}u\overline{q}'$ transition followed by $\overline{u}u \to \overline{q}q$ rescattering is included below in the P^u terms.) Again, CKM unitarity allows us to write A_f in terms of two CKM combinations. For example, for $f = \phi K_S$, which proceeds via a $\overline{b} \to \overline{s}s\overline{s}$ transition, we can write

$$\frac{\overline{A}_{\phi K_S}}{A_{\phi K_S}} = -\frac{\left(V_{cb}V^*_{cs}\right) P^c_{\phi K} + \left(V_{ub}V^*_{us}\right) P^u_{\phi K}}{\left(V^*_{cb}V_{cs}\right) P^c_{\phi K} + \left(V^*_{ub}V_{us}\right) P^u_{\phi K}} \times \frac{V^*_{cd}V_{cs}}{V_{cd}V^*_{cs}} \ , \quad (13.81)$$

where $P^c_{\phi K} = p^c_{\phi K} - p^t_{\phi K}$ and $P^u_{\phi K} = p^u_{\phi K} - p^t_{\phi K}$.

Since in general the amplitude A_f involves two different weak phases, the corresponding decays can exhibit both *CP* violation in the interference of decays with and without mixing, $S_f \neq 0$, and *CP* violation in decay, $C_f \neq 0$. (At the present level of experimental precision, the contribution to C_f from *CP* violation in mixing is negligible, see Eq. (13.69).) If the contribution from a second weak phase is suppressed, then the interpretation of S_f in terms of Lagrangian *CP*-violating parameters is clean, while C_f is small. If such a second contribution is not suppressed, S_f depends on hadronic parameters and, if the relevant strong phase difference is large, C_f is large.

A summary of $\overline{b} \to \overline{q}q\overline{q}'$ modes with $q' = s$ or d is given in Table 13.1. The $\overline{b} \to \overline{d}d\overline{q}$ transitions lead to final states that are similar to those from $\overline{b} \to \overline{u}u\overline{q}$ transitions and have similar phase dependence. Final states that consist of two vector mesons ($\psi\phi$ and $\phi\phi$) are not *CP* eigenstates, and angular analysis is needed to separate the *CP*-even from the *CP*-odd contributions.

The cleanliness of the theoretical interpretation of S_f can be assessed from the information in the last column of Table 13.1. In case of small uncertainties, the expression for S_f in terms of CKM phases can be deduced from the fourth column of Table 13.1 in combination with Eq. (13.73) (and, for $b \to q\overline{q}s$ decays, the example in Eq. (13.80)). Here we consider several interesting examples.

For $B^0 \to J/\psi K_S$ and other $\overline{b} \to \overline{c}c\overline{s}$ processes, we can neglect the P^u contribution to A_f, in the Standard Model, to an approximation that is better than one percent, giving

$$\lambda_{\psi K_S} = -e^{-2i\beta} \ \Rightarrow \ S_{\psi K_S} = \sin(2\beta) \ , \quad C_{\psi K_S} = 0 \ . \quad (13.82)$$

It is important to verify experimentally the level of suppression of the penguin contribution. Methods based on flavor symmetries [91–94] allow limits to be obtained. All are currently consistent with the P^u term being negligible. Explicit calculations [94–97] also support this conclusion.

In the presence of new physics, A_f is still likely to be dominated by the T term, but the mixing amplitude might be modified. Thus, model-independently, $C_f \approx 0$ while S_f cleanly determines the mixing phase $(\phi_M - 2\arg(V_{cb}V^*_{cd}))$. The experimental measurement [61], $S_{\psi K} = +0.699 \pm 0.017$, gave the first precision test of the Kobayashi-Maskawa mechanism, and its consistency with the predictions for $\sin 2\beta$ makes it very likely that this mechanism is indeed the dominant source of *CP* violation in the quark sector.

For $B^0 \to \phi K_S$ and other $\overline{b} \to \overline{s}s\overline{s}$ processes (as well as some $\overline{b} \to \overline{u}u\overline{s}$ processes), we can neglect the subdominant contributions, in the Standard Model, to an approximation that is good to the order of a few percent:

$$\lambda_{\phi K_S} = -e^{-2i\beta} \ \Rightarrow \ S_{\phi K_S} = \sin 2\beta \ , \quad C_{\phi K_S} = 0 \ . \quad (13.83)$$

A review of explicit calculations of the effects of subleading amplitudes can be found in Ref. [98]. In the presence of new physics, both A_f and $\mathbf{M}_{12}$ can have contributions that are comparable in size to those of the Standard Model and carry new weak phases. Such a situation gives several interesting consequences for penguin-dominated $\overline{b} \to \overline{q}q\overline{s}$ decays ($q = u, d, s$) to a final state f:

1. The value of $-\eta_f S_f$ may be different from $S_{\psi K_S}$ by more than a few percent, where η_f is the *CP* eigenvalue of the final state.
2. The values of $\eta_f S_f$ for different final states f may be different from each other by more than a few percent (for example, $S_{\phi K_S} \neq S_{\eta' K_S}$).
3. The value of C_f may be different from zero by more than a few percent.

While a clear interpretation of such signals in terms of Lagrangian parameters will be difficult because, under these circumstances, hadronic parameters play a role, any of the above three options will clearly signal new physics. In addition, flavor symmetry relations, such as those that relate observables in $B \to K\pi$ decays [99, 100] can be used to provide further tests of the Standard Model. Fig. 13.3 summarizes the present experimental results: none of the possible signatures listed above is unambiguously established, but there is definitely still room for new physics.

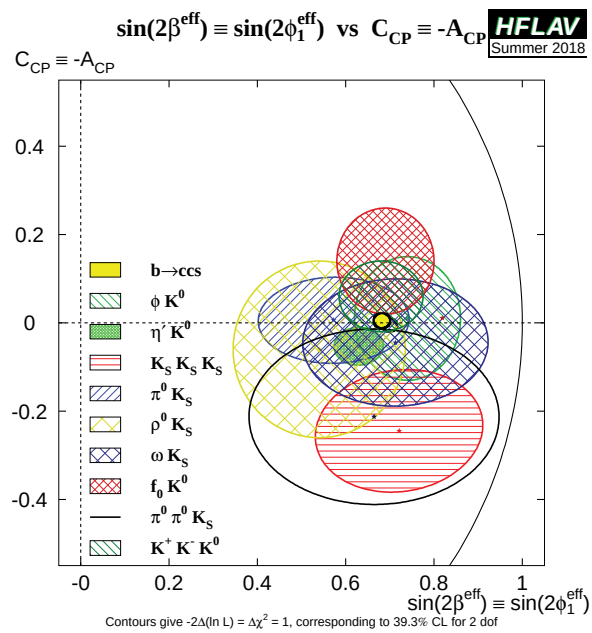

Figure 13.3: Summary of the results [61] of time-dependent analyses of $b \to q\overline{q}s$ decays, which are potentially sensitive to new physics.

For the $\overline{b} \to \overline{u}u\overline{d}$ process $B \to \pi\pi$ and other related channels, the penguin-to-tree ratio can be estimated using SU(3) relations and experimental data on related $B \to K\pi$ decays. The result (for $\pi\pi$) is that the suppression is at the level of $0.2 - 0.3$ and so cannot be neglected. The expressions for $S_{\pi\pi}$ and $C_{\pi\pi}$ to leading order in $R_{PT} \equiv (|V_{tb}V_{td}|\, P^t_{\pi\pi})/(|V_{ub}V_{ud}|\, T_{\pi\pi})$ are:

$$\lambda_{\pi\pi} = e^{2i\alpha}\left[(1 - R_{PT}e^{-i\alpha})/(1 - R_{PT}e^{+i\alpha})\right] \ \Rightarrow \quad (13.84)$$

$$S_{\pi\pi} \approx \sin 2\alpha + 2\,\mathcal{R}e(R_{PT})\cos 2\alpha \sin\alpha \ , \quad C_{\pi\pi} \approx 2\,\mathcal{I}m(R_{PT})\sin\alpha \ . \quad (13.85)$$

Note that R_{PT} is mode-dependent and, in particular, could be different for $\pi^+\pi^-$ and $\pi^0\pi^0$. If strong phases can be neglected, then R_{PT} is real, resulting in $C_{\pi\pi} = 0$. The size of $C_{\pi\pi}$ is an indicator of how large the strong phase is. The present experimental average is $C_{\pi^+\pi^-} = -0.31 \pm 0.03$ [61]. As concerns $S_{\pi\pi}$, it is clear from Eq. (13.85) that the relative size or strong phase of the penguin contribution must be known to extract α. The theoretical uncertainty stemming from $|R_{PT}| \not\ll 1$ is referred to in the literature as penguin pollution.

Downloaded from https://academic.oup.com/ptep/article/2022/8/083C01/6651666 by KIT Library user on 27 September 2022

Table 13.1: Summary of $\bar{b} \to \bar{q}q\bar{q}'$ modes with $q' = s$ or d. The second and third columns give examples of hadronic final states (usually those which are experimentally most convenient to study). The fourth column gives the CKM dependence of the amplitude A_f, using the notation of Eqs. ((13.77), (13.79), (13.81)), with the dominant term first and the subdominant second. The suppression factor of the second term compared to the first is given in the last column. "Loop" refers to a penguin versus tree-suppression factor (it is mode-dependent and roughly $\mathcal{O}(0.2-0.3)$) and $\lambda \simeq 0.23$ is the expansion parameter of Eq. (13.34).

$\bar{b} \to \bar{q}q\bar{q}'$	$B^0 \to f$	$B_s^0 \to f$	CKM dependence of A_f	Suppression
$\bar{b} \to \bar{c}c\bar{s}$	ψK_S	$\psi\phi$	$(V_{cb}^* V_{cs})T + (V_{ub}^* V_{us})P^u$	loop $\times \lambda^2$
$\bar{b} \to \bar{s}s\bar{s}$	ϕK_S	$\phi\phi$	$(V_{cb}^* V_{cs})P^c + (V_{ub}^* V_{us})P^u$	λ^2
$\bar{b} \to \bar{u}u\bar{s}$	$\pi^0 K_S$	K^+K^-	$(V_{cb}^* V_{cs})P^c + (V_{ub}^* V_{us})T$	λ^2/loop
$\bar{b} \to \bar{c}c\bar{d}$	D^+D^-	ψK_S	$(V_{cb}^* V_{cd})T + (V_{tb}^* V_{td})P^t$	loop
$\bar{b} \to \bar{s}s\bar{d}$	$K_S K_S$	ϕK_S	$(V_{tb}^* V_{td})P^t + (V_{cb}^* V_{cd})P^c$	$\lesssim 1$
$\bar{b} \to \bar{u}u\bar{d}$	$\pi^+\pi^-$	$\rho^0 K_S$	$(V_{ub}^* V_{ud})T + (V_{tb}^* V_{td})P^t$	loop
$\bar{b} \to \bar{c}u\bar{d}$	$D_{CP}\pi^0$	$D_{CP}K_S$	$(V_{cb}^* V_{ud})T + (V_{ub}^* V_{cd})T'$	λ^2
$\bar{b} \to \bar{c}u\bar{s}$	$D_{CP}K_S$	$D_{CP}\phi$	$(V_{cb}^* V_{us})T + (V_{ub}^* V_{cs})T'$	$\lesssim 1$

The cleanest solution involves isospin relations among the $B \to \pi\pi$ amplitudes [101]:

$$\frac{1}{\sqrt{2}} A_{\pi^+\pi^-} + A_{\pi^0\pi^0} = A_{\pi^+\pi^0} \ . \tag{13.86}$$

The method exploits the fact that the penguin contribution to $P^t_{\pi\pi}$ is pure $\Delta I = 1/2$ (this is not true for the electroweak penguins which, however, are expected to be small), while the tree contribution to $T_{\pi\pi}$ contains amplitudes that are both $\Delta I = 1/2$ and $\Delta I = 3/2$. A simple geometric construction then allows one to find R_{PT} and extract α cleanly from $S_{\pi^+\pi^-}$. The key experimental difficulty is that one must measure accurately the separate rates for B^0 and $\overline{B}^0 \to \pi^0\pi^0$.

CP asymmetries in $B \to \rho\pi$ and $B \to \rho\rho$ can also be used to determine α. In particular, the $B \to \rho\rho$ measurements are presently very significant in constraining α. The extraction proceeds via isospin analysis similar to that of $B \to \pi\pi$. There are, however, several important differences. First, due to the finite width of the ρ mesons, a final $(\rho\rho)_{I=1}$ state is possible [102]. The effect is, however, of the order of $(\Gamma_\rho/m_\rho)^2 \sim 0.04$. Second, due to the presence of three helicity states for the two vector mesons, angular analysis is needed to separate the *CP*-even and *CP*-odd components. The theoretical expectation is that the *CP*-odd component is small. This is supported by experiments which find that the $\rho^+\rho^-$ and $\rho^\pm\rho^0$ modes are dominantly longitudinally polarized. Third, an important advantage of the $\rho\rho$ modes is that the penguin contribution is expected to be small due to different hadronic dynamics. This expectation is confirmed by the smallness of $\mathcal{B}(B^0 \to \rho^0\rho^0) = (0.95 \pm 0.16) \times 10^{-6}$ compared to $\mathcal{B}(B^0 \to \rho^+\rho^-) = (24.2 \pm 3.1) \times 10^{-6}$ [61]. Thus, $S_{\rho^+\rho^-}$ is not far from $\sin 2\alpha$. Finally, both $S_{\rho^0\rho^0}$ and $C_{\rho^0\rho^0}$ are experimentally accessible, which may allow a precise determination of α. However, a full isospin analysis should allow that the fractions of longitudinal polarization in B and $\overline{B}$ decays may differ, which has not yet been done by the experiments.

Detailed discussion of the determination of α with these methods, and the latest world average, can be found in Refs. [103,104]. The consistency between the range of α determined by the $B \to \pi\pi$, $\rho\pi$ and $\rho\rho$ measurements and the range allowed by CKM fits (excluding these direct determinations) provides further support to the Kobayashi-Maskawa mechanism.

All modes discussed in this Section so far have possible contributions from penguin amplitudes. As shown in Table 13.1, *CP* violation can also be studied with final states, typically containing charmed mesons, where no such contribution is possible. The neutral charmed meson must be reconstructed in a final state, such as a *CP* eigenstate, common to D^0 and $\overline{D}^0$ so that the amplitudes for the B and $\overline{B}$ meson decays interfere. Although there is a second tree amplitude with a different weak phase, the contributions of the different diagrams can in many cases be separated experimentally (for example by exploiting different decays of the neutral D mesons) making these channels very clean theoretically. The first determination of $\sin(2\beta)$, with significance of *CP* violation over 5σ, with this method has recently been reported [105]. Moreover, the interference between the two tree diagrams gives sensitivity to γ, as will be discussed in Section 13.6.4.

13.6.3 *CP violation in interference of B_s^0 decays with and without mixing*

As discussed in Section 13.6.1, the world average for $|q/p|$ in the B_s^0 system currently deviates from the Standard Model expectation due to an anomalous value of the dimuon asymmetry. Attributing the dimuon asymmetry result to a fluctuation, we again neglect the deviation of $|q/p|$ from 1, and use

$$\lambda_f = e^{-i\phi_M(B_s^0)}(\overline{A}_f/A_f) \ . \tag{13.87}$$

Within the Standard Model,

$$e^{-i\phi_{M(B_s^0)}} = (V_{tb}^* V_{ts})/(V_{tb} V_{ts}^*) \ . \tag{13.88}$$

Note that $\Delta\Gamma/\Gamma = 0.132 \pm 0.008$ [61] and therefore y should not be put to zero in Eqs. (13.17a) and (13.17b). However, $|q/p| = 1$ is expected to hold to an even better approximation than for B^0 mesons. One therefore obtains

$$\mathcal{A}_f(t) = \frac{S_f \sin(\Delta m t) - C_f \cos(\Delta m t)}{\cosh(\Delta\Gamma t/2) - A_f^{\Delta\Gamma} \sinh(\Delta\Gamma t/2)} \ , \tag{13.89}$$

$$A_f^{\Delta\Gamma} \equiv \frac{-2\,\mathcal{R}e(\lambda_f)}{1 + \left|\lambda_f\right|^2} \ . \tag{13.90}$$

The presence of the $A_f^{\Delta\Gamma}$ term implies that information on λ_f can be obtained from analyses that do not use tagging of the initial flavor, through so-called effective lifetime measurements [106].

The $B_s^0 \to J/\psi\phi$ decay proceeds via the $\bar{b} \to \bar{c}c\bar{s}$ transition. The *CP* asymmetry in this mode thus determines (with angular analysis to disentangle the *CP*-even and *CP*-odd components of the final state) $\sin 2\beta_s$, where β_s is defined in Eq. (13.38) [107]. The $B_s^0 \to J/\psi\pi^+\pi^-$ decay, which has a large contribution from $J/\psi f_0(980)$ and is assumed to also proceed dominantly via the $\bar{b} \to \bar{c}c\bar{s}$ transition, has also been used to determine β_s. In this case no angular analysis is necessary, since the final state has been shown to be dominated by the *CP*-odd component [108]. The combination of measurements yields [61]

$$2\beta_s = 0.050 \pm 0.019 \, , \tag{13.91}$$

consistent with the Standard Model prediction, assuming negligible penguin contributions, $\beta_s = 0.0184 \pm 0.0004$ [20].

A time-dependent *CP* asymmetry was established in $B_s^0 \to K^+K^-$ decay, which proceeds via the $\bar{b} \to \bar{u}u\bar{s}$ transition [109]:

$$C_{KK} = +0.172 \pm 0.039, \ , \quad S_{KK} = +0.139 \pm 0.032 \ . \tag{13.92}$$

For both C_{KK} and S_{KK}, the hadronic ratio (T/P^c) plays an important role (see Table 13.1), making a clean theoretical interpretation challenging. First results on the $\bar{b} \to \bar{q}q\bar{s}$ decays $B_s^0 \to \phi\phi$ and $K^{*0}\overline{K}^{*0}$ have also been reported. Parameters of *CP* violation have also been determined from the decay-time distributions of $B_s^0 \to D_s^\mp K^\pm$ and $D_s^\mp K^\pm\pi^+\pi^-$ decays, involving interference between $\bar{b} \to \bar{c}u\bar{s}$ and $\bar{b} \to \bar{u}c\bar{s}$ amplitudes.

Downloaded from https://academic.oup.com/ptep/article/2022/8/083C01/6651666 by KIT Library user on 27 September 2022

13.6.4 *Direct CP violation in the B system*

An interesting class of decay modes is that of the tree-level decays $B^\pm \to D^{(*)}K^\pm$, which allow a theoretically pristine determination of the angle γ [110–115]. The method uses the decays $B^+ \to D^0K^+$, which proceeds via the quark transition $\overline{b} \to \overline{u}c\overline{s}$, and $B^+ \to \overline{D}^0K^+$, which proceeds via the quark transition $\overline{b} \to \overline{c}u\overline{s}$, with the D^0 and $\overline{D}^0$ decaying into a common final state. The decays into common final states, such $(\pi^0K_S)_DK^+$, involve interference effects between the two amplitudes, with sensitivity to the relative phase, $\delta+\gamma$ (δ is the relevant strong phase difference). The *CP*-conjugate processes are sensitive to $\delta-\gamma$. Measurements of branching ratios and *CP* asymmetries allow the determination of γ and δ from amplitude triangle relations. The method suffers from discrete ambiguities but, since all hadronic parameters can be determined from the data, has negligible theoretical uncertainty [116].

Unfortunately, the smallness of the CKM-suppressed $b \to u$ transitions makes it difficult to use the simplest methods alone [110–112] to determine γ. These difficulties are overcome (and the discrete ambiguities are removed) by performing a Dalitz plot analysis for multi-body D decays [113–115]. Detailed discussion of the determination of γ with these methods can be found in Ref. [104].

Constraints on γ from combinations of results on various $B \to D^{(*)}K^{(*)}$ processes have been obtained by experiments [117,118]. The latest world average is [61,104]

$$\gamma = \left(66.2\,^{+3.4}_{-3.6}\right)^\circ \,. \tag{13.93}$$

The consistency between the range of γ determined by the $B \to DK$ measurements and the range allowed by CKM fits (excluding these direct determinations) provides further support to the Kobayashi-Maskawa mechanism. As more data become available, determinations of γ from $B_s^0 \to D_s^\mp K^\pm$ [119, 120] and $B^0 \to DK^{*0}$ [121–124] are expected to also give competitive measurements.

Decays to the final state $K^\mp\pi^\pm$ provided the first observations of direct *CP* violation in both B^0 and B_s^0 systems. The asymmetry arises due to interference between tree and penguin diagrams [125], similar to the effect discussed in Section 13.6.2. In principle, measurements of $\mathcal{A}_{B^0\to K^+\pi^-}$ and $\mathcal{A}_{B_s^0\to K^-\pi^+}$ could be used to determine the weak phase difference γ, but lack of knowledge of the relative magnitude and strong phase of the contributing amplitudes limits the achievable precision. The uncertainties on these hadronic parameters can be reduced by exploiting flavor symmetries, which predict a number of relations between asymmetries in different modes. One such relation is that the partial rate differences for B^0 and B_s^0 decays to $K^\mp\pi^\pm$ are expected to be approximately equal and opposite [126], which is consistent with current data. It is also expected that the partial rate asymmetries for $B^0 \to K^+\pi^-$ and $B^+ \to K^+\pi^0$ should be approximately equal; however, the experimental results currently show a significant discrepancy [61]:

$$\mathcal{A}_{B^0\to K^+\pi^-} = -0.083\pm0.004\,, \quad \mathcal{A}_{B^+\to K^+\pi^0} = +0.029\pm0.013\,. \tag{13.94}$$

It is therefore of great interest to understand whether this originates from Standard Model QCD corrections, or whether it is a signature of new dynamics. Improved tests of a more precise relation between the partial rate differences of all four $K\pi$ final states [127–130], currently limited by knowledge of the *CP* asymmetry in $\overline{B}^0 \to K_S\pi^0$ decays, may help to resolve the situation.

It is also of interest to investigate whether similar patterns appear among the *CP* violating asymmetries in B meson decays to final states containing one pseudoscalar and one vector meson. Since the vector resonance decays to two particles, such channels can be studied through Dalitz plot analysis of the three-body final state. Model-independent analyses of $B^+ \to K^+K^-K^+$, $\pi^+\pi^-K^+$, $\pi^+\pi^-\pi^+$ and $K^+K^-\pi^+$ decays have revealed large *CP* violation effects in certain regions of phase space [131]. For the $B^+ \to K^+K^-\pi^+$ decay, an amplitude analysis has established a large *CP* violation effect associated with $\pi\pi \leftrightarrow KK$ S-wave rescattering [132]. In $B^+ \to \pi^+\pi^-\pi^+$ decays, amplitude analysis has established *CP* violation effects in the decay amplitude involving the $f_2(1270)$ resonance, in the $\pi^+\pi^-$ S-wave at low invariant mass, and in the interference between the $\pi^+\pi^-$ S-wave and the P-wave $B^+ \to \rho(770)^0\pi^+$ amplitude [133, 134]. For the other channels it remains to be seen whether the *CP* violation effects are associated to particular resonances or to interference effects, which will be necessary to understand the underlying dynamics.

13.7 Summary and Outlook

CP violation has been experimentally established in K, D and B meson decays. A full list of *CP* asymmetries that have been measured at a level higher than 5σ is given in the introduction to this review. In Section 13.1.4 we introduced three types of *CP*-violating effects. Examples of these three types include the following:

1. All three types of *CP* violation have been observed in $K \to \pi\pi$ decays:

$$\begin{aligned}
\mathcal{R}e(\epsilon') &= \frac{1}{6}\left(\left|\frac{\overline{A}_{\pi^0\pi^0}}{A_{\pi^0\pi^0}}\right| - \left|\frac{\overline{A}_{\pi^+\pi^-}}{A_{\pi^+\pi^-}}\right|\right) \\
&= (2.5\pm0.4)\times10^{-6}\,, \qquad \text{(I)} \qquad (13.95a)\\
\mathcal{R}e(\epsilon) &= \frac{1}{2}\left(1-\left|\frac{q}{p}\right|\right) \\
&= (1.66\pm0.02)\times10^{-3}\,, \qquad \text{(II)} \qquad (13.95b)\\
\mathcal{I}m(\epsilon) &= -\frac{1}{2}\mathcal{I}m(\lambda_{(\pi\pi)_{I=0}}) \\
&= (1.57\pm0.02)\times10^{-3}\,. \qquad \text{(III)} \qquad (13.95c)
\end{aligned}$$

2. For D mesons, *CP* violation in decay has been established in the difference of asymmetries for $D^0 \to K^+K^-$ and $D^0 \to \pi^+\pi^-$ decays.

$$\begin{aligned}
\Delta a_{CP} &= \frac{|\overline{A}_{K^+K^-}/A_{K^+K^-}|^2-1}{|\overline{A}_{K^+K^-}/A_{K^+K^-}|^2+1} - \frac{|\overline{A}_{\pi^+\pi^-}/A_{\pi^+\pi^-}|^2-1}{|\overline{A}_{\pi^+\pi^-}/A_{\pi^+\pi^-}|^2+1} \\
&= (-0.164\pm0.028)\times10^{-2}\,, \quad \text{(I)}
\end{aligned} \tag{13.96}$$

3. In the B meson system, *CP* violation in decay has been observed in, for example, $B^0 \to K^+\pi^-$ transitions, while *CP* violation in interference of decays with and without mixing has been observed in, for example, the $B^0 \to J/\psi K_S$ channel:

$$\begin{aligned}
\mathcal{A}_{K^+\pi^-} &= \frac{|\overline{A}_{K^-\pi^+}/A_{K^+\pi^-}|^2-1}{|\overline{A}_{K^-\pi^+}/A_{K^+\pi^-}|^2+1} \\
&= -0.083\pm0.004\,, \qquad \text{(I)} \qquad (13.97a)\\
S_{\psi K} &= \mathcal{I}m(\lambda_{\psi K}) \\
&= +0.699\pm0.017\,. \qquad \text{(III)} \qquad (13.97b)
\end{aligned}$$

Based on Standard Model predictions, further observations of *CP* violation in B^0, B^+ and B_s^0 decays seem likely in the near future, at both LHCb and its upgrades [135–137] as well as the Belle II experiment [138]. The first observation of *CP* violation in b baryons is also likely to be within reach of LHCb. Further improvements in the sensitivity to *CP* violation effects in the charm sector can also be anticipated, though uncertainty in the Standard Model predictions makes it difficult to forecast whether or not additional discoveries will be forthcoming. A number of upcoming experiments have potential to make significant progress on rare kaon decays. Observables that are subject to clean theoretical interpretation, such as β from $S_{\psi K_S}$, β_s from $B_s^0 \to J/\psi\phi$, $\mathcal{B}(K_L \to \pi^0\nu\overline{\nu})$ and γ from *CP* violation in $B \to DK$ decays, are of particular value for constraining the values of the CKM parameters and probing the flavor sector of extensions to the Standard Model. Progress in lattice QCD calculations is also needed to complement the anticipated experimental results. Other probes of *CP* violation now being pursued experimentally include the electric dipole moments of the neutron and electron, and the decays of tau leptons. Additional processes that are likely to play an

Downloaded from https://academic.oup.com/ptep/article/2022/8/083C01/6651666 by KIT Library user on 27 September 2022

important role in future *CP* studies include top-quark production and decay, Higgs boson decays and neutrino oscillations.

All measurements of *CP* violation to date are consistent with the predictions of the Kobayashi-Maskawa mechanism of the Standard Model. In fact, it is now established that the KM mechanism plays a dominant role in the *CP* violation measured in the quark sector. However, a dynamically-generated matter-antimatter asymmetry of the universe requires additional sources of *CP* violation, and such sources are naturally generated by extensions to the Standard Model. New sources might eventually reveal themselves as small deviations from the predictions of the KM mechanism, or else might not be observable in the quark sector at all, but observable with future probes such as neutrino oscillations or electric dipole moments. The fundamental nature of *CP* violation demands a vigorous search.

A number of excellent reviews of *CP* violation are available [139–146], where the interested reader may find a detailed discussion of the various topics that are briefly reviewed here.

We thank David Kirkby for significant contributions to earlier versions of this review.

13.8 Observed *CP* violation effects

We conclude by listing the observables where *CP* violation has been observed at a level above 5σ [43, 61, 81]:

- Indirect *CP* violation in $K \to \pi\pi$ and $K \to \pi\ell\nu$ decays, and in the $K_L \to \pi^+\pi^-e^+e^-$ decay, is given by

$$|\epsilon| = (2.228 \pm 0.011) \times 10^{-3}\,. \tag{13.98}$$

- Direct *CP* violation in $K \to \pi\pi$ decays is given by

$$\mathcal{R}e(\epsilon'/\epsilon) = (1.65 \pm 0.26) \times 10^{-3}\,. \tag{13.99}$$

- *CP* violation in the interference of mixing and decay in the tree-dominated $b \to c\bar{c}s$ transitions, such as $B^0 \to \psi K^0$, is given by (we use K^0 throughout to denote results that combine K_S and K_L modes, but use the sign appropriate to K_S):

$$S_{\psi K^0} = +0.699 \pm 0.017\,. \tag{13.100}$$

- *CP* violation in the interference of mixing and decay in modes governed by the tree-dominated $b \to c\bar{u}d$ transitions is given by

$$S_{D^{(*)}h^0} = +0.71 \pm 0.09\,, \tag{13.101}$$

- *CP* violation in the interference of mixing and decay in various modes related to $b \to c\bar{c}d$ transitions is given by

$$\begin{aligned} S_{\psi\pi^0} &= -0.86 \pm 0.14\,,\\ S_{D^+D^-} &= -0.84 \pm 0.12\,,\\ S_{D^{*\pm}D^{\mp}} &= -0.81 \pm 0.06\,,\\ S_{D^{*+}D^{*-}} &= -0.71 \pm 0.09\,. \end{aligned} \tag{13.102}$$

- *CP* violation in the interference of mixing and decay in various modes related to $b \to q\bar{q}s$ (penguin) transitions is given by

$$\begin{aligned} S_{\phi K^0} &= +0.74\,^{+0.11}_{-0.13}\,,\\ S_{\eta' K^0} &= +0.63 \pm 0.06\,,\\ S_{f_0 K^0} &= +0.69\,^{+0.10}_{-0.12}\,,\\ S_{K^+K^-K_S} &= +0.68\,^{+0.09}_{-0.10}\,. \end{aligned} \tag{13.103}$$

- *CP* violation in the interference of mixing and decay in the $B^0 \to \pi^+\pi^-$ mode is given by

$$S_{\pi^+\pi^-} = -0.67 \pm 0.03\,. \tag{13.104}$$

- Direct *CP* violation in the $B^0 \to \pi^+\pi^-$ mode is given by

$$C_{\pi^+\pi^-} = -0.31 \pm 0.03\,. \tag{13.105}$$

- Direct *CP* violation in the $B^0_s \to K^+K^-$ mode is given by

$$C_{K^+K^-} = 0.17 \pm 0.03\,. \tag{13.106}$$

- Direct *CP* violation in $B^+ \to D^{(*)}_+ K^+$ decays ($D^{(*)}_+$ is the *CP*-even neutral $D^{(*)}$ state) are given by

$$\begin{aligned} \mathcal{A}_{B^+\to D_+K^+} &= +0.139 \pm 0.009 \quad \text{and}\\ \mathcal{A}_{B^+\to D^*_+K^+} &= -0.109 \pm 0.019\,, \end{aligned} \tag{13.107}$$

  while the corresponding quantity in the case that the neutral D meson is reconstructed in the suppressed $K^-\pi^+$ final state is

$$\mathcal{A}_{B^+\to D_{K^-\pi^+}K^+} = -0.453 \pm 0.026\,, \tag{13.108}$$

- Direct *CP* violation has also been observed in $B^+ \to DK^+$ decays through differences between the Dalitz plot distributions of subsequent $D \to K_S\pi^+\pi^-$ decays.
- Direct *CP* violation in the $B^0 \to K^+\pi^-$ mode is given by

$$\mathcal{A}_{B^0\to K^+\pi^-} = -0.083 \pm 0.004\,. \tag{13.109}$$

- Direct *CP* violation in the $B^0_s \to K^-\pi^+$ mode is given by

$$\mathcal{A}_{B^0_s\to K^-\pi^+} = +0.225 \pm 0.012\,. \tag{13.110}$$

- Direct *CP* violation in $B^+ \to K^+K^-\pi^+$ decays is given by

$$\mathcal{A}_{B^+\to K^+K^-\pi^+} = -0.118 \pm 0.022\,. \tag{13.111}$$

- Large *CP* violation effects have been observed model-independently in certain regions of the phase space of $B^+ \to K^+K^-K^+$, $K^+K^-\pi^+$, $\pi^+\pi^-K^+$ and $\pi^+\pi^-\pi^+$ decays. An amplitude analysis has established a large *CP* violation effect associated with $\pi\pi \leftrightarrow KK$ S-wave rescattering in $B^+ \to K^+K^-\pi^+$ decays. In $B^+ \to \pi^+\pi^-\pi^+$ decays, amplitude analysis has established *CP* violation effects in the decay amplitude involving the $f_2(1270)$ resonance, in the $\pi^+\pi^-$ S-wave at low invariant mass, and in the interference between the $\pi^+\pi^-$ S-wave and the P-wave $B^+ \to \rho(770)^0\pi^+$ amplitude.
- Direct *CP* violation has been established in the difference of asymmetries for $D^0 \to K^+K^-$ and $D^0 \to \pi^+\pi^-$ decays

$$\Delta a_{CP} = (-0.164 \pm 0.028) \times 10^{-2}\,. \tag{13.112}$$

References

[1] J. H. Christenson *et al.*, Phys. Rev. Lett. **13**, 138 (1964).

[2] B. Aubert *et al.* (BaBar), Phys. Rev. Lett. **87**, 091801 (2001), [hep-ex/0107013].

[3] K. Abe *et al.* (Belle), Phys. Rev. Lett. **87**, 091802 (2001), [hep-ex/0107061].

[4] H. Burkhardt *et al.* (NA31), Phys. Lett. **B206**, 169 (1988).

[5] V. Fanti *et al.* (NA48), Phys. Lett. **B465**, 335 (1999), [hep-ex/9909022].

[6] A. Alavi-Harati *et al.* (KTeV), Phys. Rev. Lett. **83**, 22 (1999), [hep-ex/9905060].

[7] B. Aubert *et al.* (BaBar), Phys. Rev. Lett. **93**, 131801 (2004), [hep-ex/0407057].

[8] Y. Chao *et al.* (Belle), Phys. Rev. Lett. **93**, 191802 (2004), [hep-ex/0408100].

[9] A. Poluektov *et al.* (Belle), Phys. Rev. **D81**, 112002 (2010), [arXiv:1003.3360].

[10] P. del Amo Sanchez *et al.* (BaBar), Phys. Rev. **D82**, 072004 (2010), [arXiv:1007.0504].

[11] R. Aaij *et al.* (LHCb), Phys. Lett. **B712**, 203 (2012), [Erratum-ibid. **B713**, 351 (2012)], [arXiv:1203.3662].

[12] R. Aaij *et al.* (LHCb), Phys. Rev. Lett. **110**, 221601 (2013), [arXiv:1304.6173].

[13] R. Aaij *et al.* (LHCb), Phys. Rev. Lett. **122**, 211803 (2019), [arXiv:1903.08726].

[14] See the review on "Neutrino Masses, Mixing, and Oscillations," in this *Review*.

Downloaded from https://academic.oup.com/ptep/article/2022/8/083C01/6651666 by KIT Library user on 27 September 2022

[15] See the review on "Tests of Conservation Laws," in this *Review*.

[16] J. P. Lees *et al.* (BaBar), Phys. Rev. Lett. **109**, 211801 (2012), [arXiv:1207.5832].

[17] J. Bernabeu, F. Martinez-Vidal and P. Villanueva-Perez, JHEP **08**, 064 (2012), [arXiv:1203.0171].

[18] See, for example, R. F. Streater and A. S. Wightman, *CPT, Spin and Statistics, and All That,* reprinted by Addison-Wesley, New York (1989).

[19] M. Kobayashi and T. Maskawa, Prog. Theor. Phys. **49**, 652 (1973).

[20] J. Charles *et al.* (CKMfitter Group), Eur. Phys. J. **C41**, 1 (2005), updated results and plots available at: `http://ckmfitter.in2p3.fr`, [hep-ph/0406184].

[21] M. Bona *et al.* (UTfit), JHEP **10**, 081 (2006), updated results and plots available at: `http://www.utfit.org/UTfit`, [hep-ph/0606167].

[22] A. D. Sakharov, Pisma Zh. Eksp. Teor. Fiz. **5**, 32 (1967), [Usp. Fiz. Nauk161,no.5,61(1991)].

[23] A. Riotto, in "Proceedings, Summer School in High-energy physics and cosmology: Trieste, Italy, June 29-July 17, 1998," 326–436 (1998), [hep-ph/9807454].

[24] M. Fukugita and T. Yanagida, Phys. Lett. **B174**, 45 (1986).

[25] S. Davidson, E. Nardi and Y. Nir, Phys. Rept. **466**, 105 (2008), [arXiv:0802.2962].

[26] G. Aad *et al.* (ATLAS), Phys. Lett. **B716**, 1 (2012), [arXiv:1207.7214].

[27] S. Chatrchyan *et al.* (CMS), Phys. Lett. **B716**, 30 (2012), [arXiv:1207.7235].

[28] S. Okubo, Phys. Lett. **5**, 165 (1963).

[29] G. Zweig (1964), *An SU_3 model for strong interaction symmetry and its breaking; Version 2*, CERN-TH-412.

[30] J. Iizuka, Prog. Theor. Phys. Suppl. **37**, 21 (1966).

[31] V. Weisskopf and E. P. Wigner, Z. Phys. **63**, 54 (1930).

[32] See the review on "D^0–$\overline{D}^0$ Mixing" in this *Review*.

[33] O. Long *et al.*, Phys. Rev. **D68**, 034010 (2003), [hep-ex/0303030].

[34] M. Gronau, Y. Grossman and J. L. Rosner, Phys. Lett. **B508**, 37 (2001), [hep-ph/0103110].

[35] M. Artuso, G. Borissov and A. Lenz, Rev. Mod. Phys. **88**, 045002 (2016), [arXiv:1511.09466].

[36] L. Wolfenstein, Phys. Rev. Lett. **13**, 562 (1964).

[37] C. Abel *et al.* (nEDM), Phys. Rev. Lett. **124**, 081803 (2020), [arXiv:2001.11966].

[38] R. J. Crewther *et al.*, Phys. Lett. **B88**, 123 (1979), [Erratum-ibid. **B91**, 487 (1980)].

[39] See the review on "Cabibbo-Kobayashi-Maskawa Mixing Matrix," in this *Review*.

[40] L. Wolfenstein, Phys. Rev. Lett. **51**, 1945 (1983).

[41] A. J. Buras, M. E. Lautenbacher and G. Ostermaier, Phys. Rev. **D50**, 3433 (1994), [hep-ph/9403384].

[42] C. Jarlskog, Phys. Rev. Lett. **55**, 1039 (1985).

[43] See the K-meson Listings in this *Review*.

[44] See the review on "CP violation in $K_S \to 3\pi$," in this *Review*.

[45] T. Blum *et al.*, Phys. Rev. **D91**, 074502 (2015), [arXiv:1502.00263].

[46] Z. Bai *et al.* (RBC, UKQCD), Phys. Rev. Lett. **115**, 212001 (2015), [arXiv:1505.07863].

[47] A. J. Buras *et al.*, JHEP **11**, 202 (2015), [arXiv:1507.06345].

[48] Y. Grossman and Y. Nir, Phys. Lett. **B398**, 163 (1997), [hep-ph/9701313].

[49] L. S. Littenberg, Phys. Rev. **D39**, 3322 (1989).

[50] A. J. Buras, Phys. Lett. **B333**, 476 (1994), [hep-ph/9405368].

[51] G. Buchalla and A. J. Buras, Nucl. Phys. **B400**, 225 (1993).

[52] A. J. Buras *et al.*, JHEP **11**, 033 (2015), [arXiv:1503.02693].

[53] J. K. Ahn *et al.* (KOTO), Phys. Rev. Lett. **122**, 021802 (2019), [arXiv:1810.09655].

[54] J. K. Ahn *et al.* (KOTO), Phys. Rev. Lett. **126**, 121801 (2021), [arXiv:2012.07571].

[55] E. Cortina Gil *et al.* (NA62), JHEP **06**, 093 (2021), [arXiv:2103.15389].

[56] B. Aubert *et al.* (BaBar), Phys. Rev. Lett. **98**, 211802 (2007), [hep-ex/0703020].

[57] M. Staric *et al.* (Belle), Phys. Rev. Lett. **98**, 211803 (2007), [hep-ex/0703036].

[58] T. Aaltonen *et al.* (CDF), Phys. Rev. Lett. **100**, 121802 (2008), [arXiv:0712.1567].

[59] R. Aaij *et al.* (LHCb), Phys. Rev. Lett. **110**, 101802 (2013), [arXiv:1211.1230].

[60] R. Aaij *et al.* (LHCb) (2021), to appear in PRL, [arXiv:2106.03744].

[61] Y. S. Amhis *et al.* (HFLAV), Eur. Phys. J. **C81**, 226 (2021), updated results and plots available at `https://hflav.web.cern.ch/`, [arXiv:1909.12524].

[62] See the D-meson Listings in this *Review*.

[63] Y. Grossman, A. L. Kagan and Y. Nir, Phys. Rev. **D75**, 036008 (2007), [hep-ph/0609178].

[64] S. Bergmann *et al.*, Phys. Lett. **B486**, 418 (2000), [hep-ph/0005181].

[65] M. Gersabeck *et al.*, J. Phys. **G39**, 045005 (2012), [arXiv:1111.6515].

[66] D. M. Asner *et al.* (CLEO), Phys. Rev. **D78**, 012001 (2008), [arXiv:0802.2268].

[67] M. Ablikim *et al.* (BESIII), Phys. Lett. **B734**, 227 (2014), [arXiv:1404.4691].

[68] R. Aaij *et al.* (LHCb), Phys. Rev. Lett. **111**, 251801 (2013), [arXiv:1309.6534].

[69] R. Aaij *et al.* (LHCb), Phys. Rev. Lett. **118**, 261803 (2017), [arXiv:1702.06490].

[70] M. Ciuchini *et al.*, Phys. Lett. **B655**, 162 (2007), [hep-ph/0703204].

[71] Y. Grossman, Y. Nir and G. Perez, Phys. Rev. Lett. **103**, 071602 (2009), [arXiv:0904.0305].

[72] A. L. Kagan and M. D. Sokoloff, Phys. Rev. **D80**, 076008 (2009), [arXiv:0907.3917].

[73] Y. Grossman and Y. Nir, JHEP **04**, 002 (2012), [arXiv:1110.3790].

[74] B. R. Ko *et al.* (Belle), Phys. Rev. Lett. **109**, 021601 (2012), [Erratum-ibid. **109**, 119903 (2012)], [arXiv:1203.6409].

[75] See the "Review of Multibody Charm Analyses" in this *Review*.

[76] B. Aubert *et al.* (BaBar), Phys. Rev. **D78**, 051102 (2008), [arXiv:0802.4035].

[77] I. Bediaga *et al.*, Phys. Rev. **D80**, 096006 (2009), [arXiv:0905.4233].

[78] I. Bediaga *et al.*, Phys. Rev. **D86**, 036005 (2012), [arXiv:1205.3036].

[79] M. Williams, Phys. Rev. **D84**, 054015 (2011), [arXiv:1105.5338].

[80] R. Aaij *et al.* (LHCb), Phys. Lett. **B769**, 345 (2017), [arXiv:1612.03207].

[81] See the B-meson Listings in this *Review*.

[82] V. M. Abazov *et al.* (D0), Phys. Rev. **D82**, 032001 (2010), [arXiv:1005.2757].

Downloaded from https://academic.oup.com/ptep/article/2022/8/083C01/6651666 by KIT Library user on 27 September 2022

[83] A. B. Carter and A. I. Sanda, Phys. Rev. Lett. **45**, 952 (1980).

[84] A. B. Carter and A. I. Sanda, Phys. Rev. **D23**, 1567 (1981).

[85] I. I. Y. Bigi and A. I. Sanda, Nucl. Phys. **B193**, 85 (1981).

[86] I. Dunietz and J. L. Rosner, Phys. Rev. **D34**, 1404 (1986).

[87] Y. I. Azimov, N. G. Uraltsev and V. A. Khoze, Sov. J. Nucl. Phys. **45**, 878 (1987), [Yad. Fiz. **45**, 1412 (1987)].

[88] I. I. Y. Bigi and A. I. Sanda, Nucl. Phys. **B281**, 41 (1987).

[89] G. Buchalla, A. J. Buras and M. E. Lautenbacher, Rev. Mod. Phys. **68**, 1125 (1996), [hep-ph/9512380].

[90] A. J. Buras and L. Silvestrini, Nucl. Phys. **B569**, 3 (2000), [hep-ph/9812392].

[91] R. Fleischer, Eur. Phys. J. **C10**, 299 (1999), [hep-ph/9903455].

[92] M. Ciuchini, M. Pierini and L. Silvestrini, Phys. Rev. Lett. **95**, 221804 (2005), [hep-ph/0507290].

[93] S. Faller *et al.*, Phys. Rev. **D79**, 014030 (2009), [arXiv:0809.0842].

[94] M. Jung, Phys. Rev. **D86**, 053008 (2012), [arXiv:1206.2050].

[95] H.-n. Li and S. Mishima, JHEP **03**, 009 (2007), [hep-ph/0610120].

[96] K. De Bruyn and R. Fleischer, JHEP **03**, 145 (2015), [arXiv:1412.6834].

[97] P. Frings, U. Nierste and M. Wiebusch, Phys. Rev. Lett. **115**, 061802 (2015), [arXiv:1503.00859].

[98] L. Silvestrini, Ann. Rev. Nucl. Part. Sci. **57**, 405 (2007), [arXiv:0705.1624].

[99] R. Fleischer *et al.*, Phys. Rev. **D78**, 111501 (2008), [arXiv:0806.2900].

[100] R. Fleischer *et al.*, Eur. Phys. J. **C78**, 943 (2018), [arXiv:1806.08783].

[101] M. Gronau and D. London, Phys. Rev. Lett. **65**, 3381 (1990).

[102] A. F. Falk *et al.*, Phys. Rev. **D69**, 011502 (2004), [hep-ph/0310242].

[103] J. Charles *et al.*, Eur. Phys. J. **C77**, 574 (2017), [arXiv:1705.02981].

[104] See the review on "Determination of CKM Angles from B hadrons," in this *Review*.

[105] A. Abdesselam *et al.* (BaBar, Belle), Phys. Rev. Lett. **115**, 121604 (2015), [arXiv:1505.04147].

[106] R. Fleischer and R. Knegjens, Eur. Phys. J. **C71**, 1789 (2011), [arXiv:1109.5115].

[107] A. S. Dighe, I. Dunietz and R. Fleischer, Eur. Phys. J. **C6**, 647 (1999), [hep-ph/9804253].

[108] R. Aaij *et al.* (LHCb), Phys. Rev. **D89**, 092006 (2014), [arXiv:1402.6248].

[109] R. Aaij *et al.* (LHCb), JHEP **03**, 075 (2021), [arXiv:2012.05319].

[110] M. Gronau and D. London, Phys. Lett. **B253**, 483 (1991).

[111] M. Gronau and D. Wyler, Phys. Lett. **B265**, 172 (1991).

[112] D. Atwood, I. Dunietz and A. Soni, Phys. Rev. Lett. **78**, 3257 (1997), [hep-ph/9612433].

[113] D. Atwood, I. Dunietz and A. Soni, Phys. Rev. **D63**, 036005 (2001), [hep-ph/0008090].

[114] A. Giri *et al.*, Phys. Rev. **D68**, 054018 (2003), [hep-ph/0303187].

[115] A. Bondar, *Proceedings of BINP special analysis meeting on Dalitz analysis*, 24-26 Sep. 2002, unpublished.

[116] J. Brod and J. Zupan, JHEP **01**, 051 (2014), [arXiv:1308.5663].

[117] J. P. Lees *et al.* (BaBar), Phys. Rev. **D87**, 052015 (2013), [arXiv:1301.1029].

[118] R. Aaij *et al.* (LHCb), JHEP **12**, 087 (2016), [arXiv:1611.03076].

[119] R. Aleksan, I. Dunietz and B. Kayser, Z. Phys. **C54**, 653 (1992).

[120] R. Fleischer, Nucl. Phys. **B671**, 459 (2003), [hep-ph/0304027].

[121] I. Dunietz, Phys. Lett. **B270**, 75 (1991).

[122] M. Gronau, Phys. Lett. **B557**, 198 (2003), [hep-ph/0211282].

[123] T. Gershon, Phys. Rev. **D79**, 051301 (2009), [arXiv:0810.2706].

[124] T. Gershon and M. Williams, Phys. Rev. **D80**, 092002 (2009), [arXiv:0909.1495].

[125] M. Bander, D. Silverman and A. Soni, Phys. Rev. Lett. **43**, 242 (1979).

[126] X.-G. He, Eur. Phys. J. **C9**, 443 (1999), [hep-ph/9810397].

[127] D. Atwood and A. Soni, Phys. Rev. **D58**, 036005 (1998), [hep-ph/9712287].

[128] M. Gronau and J. L. Rosner, Phys. Rev. **D59**, 113002 (1999), [hep-ph/9809384].

[129] H. J. Lipkin, Phys. Lett. **B445**, 403 (1999), [hep-ph/9810351].

[130] M. Gronau, Phys. Lett. **B627**, 82 (2005), [hep-ph/0508047].

[131] R. Aaij *et al.* (LHCb), Phys. Rev. **D90**, 112004 (2014), [arXiv:1408.5373].

[132] R. Aaij *et al.* (LHCb) (2019), [arXiv:1905.09244].

[133] R. Aaij *et al.* (LHCb), Phys. Rev. Lett. **124**, 031801 (2020), [arXiv:1909.05211].

[134] R. Aaij *et al.* (LHCb), Phys. Rev. **D101**, 012006 (2020), [arXiv:1909.05212].

[135] A. A. Alves, Jr. *et al.* (LHCb), JINST **3**, S08005 (2008).

[136] I. Bediaga *et al.* (LHCb) (2012), CERN-LHCC-2012-007.

[137] R. Aaij *et al.* (LHCb) (2017), CERN-LHCC-2017-003.

[138] W. Altmannshofer *et al.* (Belle-II), PTEP **2019**, 123C01 (2019), [Erratum-ibid. **2020**, 029201 (2020)], [arXiv:1808.10567].

[139] G. C. Branco, L. Lavoura and J. P. Silva, Int. Ser. Monogr. Phys. **103**, 1 (1999).

[140] I. I. Bigi and A. I. Sanda (2000), [Camb. Monogr. Part. Phys. Nucl. Phys. Cosmol.9,1(2009)].

[141] A. J. Bevan *et al.* (BaBar, Belle), Eur. Phys. J. **C74**, 3026 (2014), [arXiv:1406.6311].

[142] H.R. Quinn and Y. Nir, *"The Mystery of the Missing Antimatter,"* Princeton University Press, Princeton (2008).

[143] T. E. Browder *et al.*, Rev. Mod. Phys. **81**, 1887 (2009), [arXiv:0802.3201].

[144] M. Ciuchini and A. Stocchi, Ann. Rev. Nucl. Part. Sci. **61**, 491 (2011), [arXiv:1110.3920].

[145] R. Aaij *et al.* (LHCb), Eur. Phys. J. **C73**, 2373 (2013), [arXiv:1208.3355].

[146] T. Gershon and V. V. Gligorov, Rept. Prog. Phys. **80**, 046201 (2017), [arXiv:1607.06746].

Downloaded from https://academic.oup.com/ptep/article/2022/8/083C01/6651666 by KIT Library user on 27 September 2022

14. Neutrino Masses, Mixing, and Oscillations

Revised October 2021 by M.C. Gonzalez-Garcia (YITP, Stony Brook; ICREA, Barcelona; ICC, U. of Barcelona) and M. Yokoyama (UTokyo; Kavli IPMU (WPI), UTokyo).

14.1 Neutrinos in the Standard Model: Massless Neutrinos . . . 285
14.2 Extending the Standard Model to Introduce Massive Neutrinos . . . 285
14.2.1 Dirac Neutrinos . . . 286
14.2.2 The See-saw Mechanism . . . 286
14.2.3 Light Sterile Neutrinos . . . 287
14.2.4 Neutrino Masses from Generic New Physics 287
14.3 Lepton Mixing . . . 287
14.4 Mass-Induced Flavour Oscillations in Vacuum . 288
14.5 Propagation of Massive Neutrinos in Matter . . 289
14.5.1 The Mikheyev-Smirnov-Wolfenstein Effect for Solar Neutrinos . . . 291
14.6 Experimental Study of Neutrino Oscillations . . 291
14.6.1 Solar Neutrinos . . . 292
14.6.2 Atmospheric Neutrinos . . . 293
14.6.3 Accelerator Neutrinos . . . 294
14.6.4 Reactor Antineutrinos . . . 298
14.7 Combined Analysis of Experimental Results: The 3ν Paradigm . . . 300
14.7.1 3ν Oscillation Probabilities . . . 301
14.7.2 3ν Oscillation Analysis . . . 302
14.7.3 Convention-independent Measures of Leptonic CP Violation in 3ν Mixing . . . 302
14.8 Beyond 3ν: Additional Neutrinos at the eV Scale 304
14.9 Laboratory Probes of ν Mass Scale and its Nature 305
14.9.1 Constraints from Kinematics of Weak Decays 305
14.9.2 Dirac vs. Majorana: Neutrinoless Double-beta Decay . . . 307
14.9.3 Experimental Search for Neutrinoless Double-beta Decay . . . 307

14.1 Neutrinos in the Standard Model: Massless Neutrinos

The gauge symmetry principle is one of the pillars of the great success of modern particle physics as it establishes an unambiguous connection between local (gauge) symmetries and forces mediated by spin-1 particles. In the Standard Model (SM) of particle physics the strong, weak, and electromagnetic interactions are connected to gauge symmetry under $SU(3)_{\rm C} \times SU(2)_L \times U(1)_Y$ where C stands for colour, L for left-handedness, and Y for hypercharge. The SM gauge symmetry is spontaneously broken to $SU(3)_{\rm C} \times U(1)_{\rm EM}$ where $U(1)_{\rm EM}$ couples to the electromagnetic charge $Q_{\rm EM} = T_{L3} + Y$ (T_{L3} is the weak isospin which is the third generator of $SU(2)_L$). The model explains all the interactions of the known fermions once they are assigned to a well defined representation of the gauge group. The construction and tests of the Standard Model as a gauge theory are covered in Chapter 9 "Quantum chromodynamics" and Chapter 10 "Electroweak model and constraints on new physics" of this *Review*. Here we emphasize that the gauge invariance principle requires that all terms in the Lagrangian, including the mass terms, respect the local symmetry. This has important implications for the neutrino and in particular for the question of the neutrino mass [1].

In the SM, neutrinos are fermions that do not have strong nor electromagnetic interactions. Consequently, they are singlets of the subgroup $SU(3)_C \times U(1)_{\rm EM}$. They are part of the lepton doublets $L_{L\ell} = \begin{pmatrix} \nu_\ell \\ \ell \end{pmatrix}_L$ where f_L is the left-handed component of the fermion f, $f_L = P_L f \equiv \frac{1-\gamma_5}{2} f$. In what follows we will refer as *active* neutrinos to neutrinos that are part of these lepton doublets. In the SM there is one active neutrino for each charged leptons, $\ell = e, \mu, \tau$. $SU(2)_L$ gauge invariance dictates the form of weak charged current (CC) interactions between the neutrinos and their corresponding charged leptons and neutral current (NC) among themselves to be:

$$-\mathcal{L}_{\rm CC} = \frac{g}{\sqrt{2}} \sum_\ell \bar{\nu}_{L\ell} \gamma^\mu \ell_L^- W_\mu^+ + \text{h.c.}\,, \tag{14.1}$$

$$-\mathcal{L}_{\rm NC} = \frac{g}{2\cos\theta_W} \sum_\ell \bar{\nu}_{L\ell} \gamma^\mu \nu_{L\ell} Z_\mu^0\,. \tag{14.2}$$

In the above equations, g is the coupling constant associated with $SU(2)$ and θ_W is the Weinberg angle. Equations(14.1) and (14.2) describe all the neutrino interactions in the SM. In particular, Eq.(14.2) determines the decay width of the Z boson into light ($m_\nu \leq m_Z/2$) left-handed neutrinos states. Thus from the measurement of the total decay width of the Z one can infer the number of such states. At present the measurement implies $N_\nu = 2.984 \pm 0.008$ (see Particle Listing). As a result any extension of the SM should contain three, and only three, light active neutrinos.

Sterile neutrinos are defined as having no SM gauge interactions, that is, they are singlets of the complete SM gauge group. Thus the SM, as the gauge theory able to describe all known particle interactions, contains no sterile neutrinos.

The SM with its gauge symmetry and the particle content required for the gauge interactions, that is, in the absence of SM singlets, respects an accidental global symmetry that is not imposed but appears as a consequence of the gauge symmetry and the representation of the matter fields:

$$G_{\rm SM}^{\rm global} = U(1)_B \times U(1)_{L_e} \times U(1)_{L_\mu} \times U(1)_{L_\tau}\,, \tag{14.3}$$

where $U(1)_B$ is the baryon number symmetry, and $U(1)_{L_e,L_\mu,L_\tau}$ are the three lepton flavour symmetries. The total lepton number, $L_e + L_\mu + L_\tau$, is then also an accidental symmetry since it is a subgroup of $G_{\rm SM}^{\rm global}$. This fact has consequences that are relevant to the question of the neutrino mass as we argue next.

In the SM, the masses of the fermions are generated via a Yukawa coupling of the scalar Higgs doublet ϕ with a fermion right-handed and left-handed component. The former is an $SU(2)_L$ singlet, the latter is part of a doublet. For leptons, we can build such a term coupling the left-handed lepton doublets L_L with the right-handed charged lepton fields E_R:

$$-\mathcal{L}_{\rm Yukawa,lep} = Y_{ij}^\ell \bar{L}_{Li} \phi E_{Rj} + \text{h.c.}\,. \tag{14.4}$$

After spontaneous symmetry breaking these terms lead to charged lepton masses

$$m_{ij}^\ell = Y_{ij}^\ell \frac{v}{\sqrt{2}}\,, \tag{14.5}$$

where v is the vacuum expectation value of the Higgs field. However, since the model does not contain right-handed neutrinos, no such Yukawa interaction can be built for the neutrinos, which are consequently massless at the Lagrangian level.

In principle, a neutrino mass term could be generated at loop level. With the particle content of the SM the only possible neutrino mass term that could be constructed is the bilinear $\bar{L}_L L_L^c$, where L_L^c is the charge conjugated field, $L_L^c = C\bar{L_L}^T$ and C is the charge conjugation matrix. However this term is forbidden in the SM because it violates the total lepton symmetry by two units and therefore it cannot be induced by loop corrections because it breaks the accidental symmetry of the model. Also, because $U(1)_{B-L}$ is a non-anomalous subgroup of $G_{\rm SM}^{\rm global}$, the bilinear $\bar{L}_L L_L^c$, cannot be induced by nonperturbative corrections either since it breaks $B - L$.

We conclude that within the SM neutrinos are precisely massless. Consequently one must go beyond the SM in order to add a mass to the neutrino.

14.2 Extending the Standard Model to Introduce Massive Neutrinos

From the above discussion, we conclude that it is not possible to construct a renormalizable mass term for the neutrinos with the

[1] The physics of massive neutrinos has been the subject of excellent books such as [1–5] and multiple review articles. The contents of the present review is built upon the structure and the contents of the review articles [6, 7].

Downloaded from https://academic.oup.com/ptep/article/2022/8/083C01/6651666 by KIT Library user on 27 September 2022

fermionic content and gauge symmetry of the SM. The obvious consequence is that in order to introduce a neutrino mass in the theory one must extend the particle content of the model, depart from gauge invariance and/or renormalizability, or do both.

As a matter of fact, neutrino mass terms can be constructed in different ways. In the following we shall assume to maintain the gauge symmetry and explore the different possibilities to introduce a neutrino mass term adding to the SM an arbitrary number of sterile neutrinos ν_{si} $(i = 1, \dots m)$.

In the SM extended with the addition of m number of sterile neutrinos one can construct two gauge invariant renormalizable operators leading to two types of mass terms

$$-\mathcal{L}_{M_\nu} = M_{D\,ij}\bar{\nu}_{si}\nu_{Lj} + \frac{1}{2}M_{N\,ij}\bar{\nu}_{si}\nu^c_{sj} + \text{h.c.}\,, \tag{14.6}$$

where ν^c is the neutrino charge conjugated field (defined in section 14.1). M_D is a complex matrix of dimension $m \times 3$ and M_N is a symmetric $m \times m$ matrix.

The first term is generated after spontaneous electroweak symmetry breaking from Yukawa interactions,

$$Y^\nu_{ij}\bar{\nu}_{si}\tilde{\phi}^\dagger L_{Lj} \Rightarrow M_{D\,ij} = Y^\nu_{ij}\frac{v}{\sqrt{2}}\,, \tag{14.7}$$

in similarity to Eqs.(14.4) and (14.5) for the charged fermion masses. It is correspondingly called a Dirac mass term. It conserves total lepton number but it can break the lepton flavour number symmetries.

The second term in Eq.(14.6) is a Majorana mass term and it differs from the Dirac mass terms in several relevant aspects. First, it is a singlet of the SM gauge group and, as such, it can appear as a bare mass term in the Lagrangian. Second, since it involves two neutrino fields (right-handed in this case), it breaks lepton number by two units. In general, such a term is not allowed if the neutrinos carry any additive conserved charge.

It is possible to rewrite Eq.(14.6) as:

$$-\mathcal{L}_{M_\nu} = \frac{1}{2}(\overline{\vec{\nu}^c_L}, \overline{\vec{\nu}_s})\begin{pmatrix} 0 & M_D^T \\ M_D & M_N \end{pmatrix}\begin{pmatrix} \vec{\nu}_L \\ \vec{\nu}^c_s \end{pmatrix} + \text{h.c.} \equiv \overline{\vec{\nu}^c}M_\nu\vec{\nu} + \text{h.c.}\,, \tag{14.8}$$

where $\vec{\nu} = (\vec{\nu}_L,\, \vec{\nu}^c_s)^T$ is a $(3+m)$-dimensional vector. The matrix M_ν is complex and symmetric [2]. Thus it can be diagonalized by a unitary matrix V^ν of dimension$(3+m)$, so

$$(V^\nu)^T M_\nu V^\nu = \text{diag}(m_1, m_2, \dots, m_{3+m})\,. \tag{14.9}$$

One can express the original weak eigenstates in terms of the resulting $3+m$ mass eigenstates

$$\vec{\nu}_{\text{mass}} = (V^\nu)^\dagger\vec{\nu}\,, \tag{14.10}$$

and in terms of the mass eigenstates, Eq.(14.8) takes the form:

$$\begin{aligned} -\mathcal{L}_{M_\nu} &= \frac{1}{2}\sum_{k=1}^{3+m} m_k\left(\bar{\nu}^c_{\text{mass},k}\nu_{\text{mass},k} + \bar{\nu}_{\text{mass},k}\nu^c_{\text{mass},k}\right) \\ &= \frac{1}{2}\sum_{k=1}^{3+m} m_k\bar{\nu}_{Mk}\nu_{Mk}\,, \end{aligned} \tag{14.11}$$

where

$$\nu_{Mk} = \nu_{\text{mass},k} + \nu^c_{\text{mass},k} = (V^{\nu\dagger}\vec{\nu})_k + (V^{\nu\dagger}\vec{\nu})^c_k\,. \tag{14.12}$$

So these states obey the Majorana condition

$$\nu_M = \nu^c_M\,, \tag{14.13}$$

and are referred to as Majorana neutrinos. The Majorana condition implies that only one field describes both neutrino and antineutrino states, unlike the case of a charge of which particles and antiparticles are described by two different fields. So a Majorana neutrino can be described by a two-component spinor unlike the charged fermions, which are Dirac particles, and are represented by four-component spinors.

[2] Notice that Eq.(14.8) corresponds to the tree-level neutrino mass matrix. Corrections are induced at the loop level, which in particular lead to non-vanishing $\bar{\nu}^c_L\nu_L$ entry [8].

Inverting Eq.(14.12) we can write the weak-doublet components of the neutrino fields as:

$$\nu_{Li} = P_L\sum_{j=1}^{3+m} V^\nu_{ij}\nu_{Mj} \quad i = 1, 2, 3\,, \tag{14.14}$$

where P_L is the left projector.

In the following, we will discuss some interesting particular cases of this general framework: light Dirac neutrinos in Sec.14.2.1, and light Majorana neutrinos and the see-saw mechanism in Sec.14.2.2. A special case of the second example is the possibility of light-sterile neutrinos discussed in Sec.14.2.3. In Sec.14.2.4 we shall discuss the effective generation of neutrino masses from non-renormalizable operators (of which the see-saw mechanism is a particular realization).

14.2.1 *Dirac Neutrinos*

Imposing $M_N = 0$ is equivalent to imposing lepton number symmetry on the model. In doing this only the first term in Eq.(14.6), the Dirac mass term, is allowed. If sterile neutrinos are three ($m = 3$), we can identify them with the right-handed component of a four-spinor neutrino field. In this case the Dirac mass term can be diagonalized with two 3×3 unitary matrices, V^ν and V^ν_R as:

$$V^{\nu\dagger}_R M_D V^\nu = \text{diag}(m_1, m_2, m_3)\,. \tag{14.15}$$

The neutrino mass term can be written as:

$$-\mathcal{L}_{M_\nu} = \sum_{k=1}^{3} m_k\bar{\nu}_{Dk}\nu_{Dk}\,, \tag{14.16}$$

where

$$\nu_{D\,k} = (V^{\nu\dagger}\vec{\nu}_L)_k + (V^{\nu\dagger}_R\vec{\nu}_s)_k\,, \tag{14.17}$$

so the weak-doublet components of the neutrino fields are

$$\nu_{Li} = P_L\sum_{j=1}^{3} V^\nu_{ij}\nu_{Dj}\,. \qquad i = 1, 2, 3\,. \tag{14.18}$$

Let us stress that in this case both the low-energy matter content and the assumed symmetries are different from those of the SM. Consequently, the SM is not even a good low-energy effective theory. Furthermore, this scenario does not explain the fact that neutrinos are much lighter than the corresponding charged fermions, because all acquire their mass via the same mechanism.

14.2.2 *The See-saw Mechanism*

If the mass eigenvalues of M_N are much higher than the scale of electroweak symmetry breaking v, the diagonalization of M_ν leads to three light neutrinos, ν_l, and m heavy neutrinos, N:

$$-\mathcal{L}_{M_\nu} = \frac{1}{2}\bar{\nu}_l M^l\nu_l + \frac{1}{2}\bar{N}M^h N\,, \tag{14.19}$$

with

$$M^l \simeq -V_l^T M_D^T M_N^{-1} M_D V_l, \qquad M^h \simeq V_h^T M_N V_h\,, \tag{14.20}$$

and

Downloaded from https://academic.oup.com/ptep/article/2022/8/083C01/6651666 by KIT Library user on 27 September 2022

$$V^\nu \simeq \begin{bmatrix} \left(1-\frac{1}{2}M_D^\dagger M_N^{*-1}M_N^{-1}M_D\right)\ V_l & M_D^\dagger M_N^{*-1}V_h \\ -M_N^{-1}M_D V_l & \left(1-\frac{1}{2}M_N{}^{-1}M_D M_D^\dagger M_N^{*-1}\right)V_h \end{bmatrix}, \tag{14.21}$$

where V_l and V_h are 3×3 and $m\times m$ unitary matrices respectively. From Eq.(14.20) we see that the masses of the heavier states are proportional to M_N while those of the lighter ones to M_N^{-1}, hence the name *see-saw mechanism* [9–13]. Also, as seen from Eq.(14.21), the heavy states are mostly right-handed while the light ones are mostly left-handed. Both the light and the heavy neutrinos are Majorana particles. Two well-known examples of extensions of the SM leading to a see-saw mechanism for neutrino masses are SO(10) Grand Unified Theories [10, 11] and left-right symmetry [13].

In this case, the SM is a good effective low energy theory. Indeed the see-saw mechanism is a particular example of a full theory whose low energy effective realization is the SM with three light Majorana neutrinos which we describe in Sec.14.2.4.

14.2.3 *Light Sterile Neutrinos*

If the scale of some $n_s \le m$ eigenvalues of M_N are not higher than the electroweak scale, the low energy spectrum contains n_s additional light states with a large admixture of sterile component. As in the case with Dirac Neutrinos, the SM is not a good low energy effective theory: there are more than three $(3+n_s)$ light neutrinos, and they are admixtures of doublet and singlet fields. As in the general case, both light and heavy neutrinos are Majorana particles.

14.2.4 *Neutrino Masses from Generic New Physics*

Under the generic hypothesis that new physics (NP) beyond the SM only manifests itself directly above some scale $\Lambda_{\rm NP}$, we can consider that the SM is an effective low energy theory which is valid to describe the physical world at energies well below $\Lambda_{\rm NP}$ with the same gauge group, fermionic spectrum, and the pattern of spontaneous symmetry breaking of the SM. However, this is an effective theory, holding only till energy below $\Lambda_{\rm NP}$, and consequently does not need to be renormalizable. In this case, the low energy Lagrangian can contain non-renormalizable higher dimensional terms whose effect will be suppressed by powers $1/\Lambda_{\rm NP}^{\rm dim-4}$.

In this approach, the least suppressed NP effects at low energy are expected to come from dim= 5 operators. With the SM fields and gauge symmetry one can only construct the following set of dimension-five terms

$$\mathcal{O}_5 = \frac{Z^\nu_{ij}}{\Lambda_{\rm NP}}\left(\bar L_{Li}\tilde\phi\right)\left(\tilde\phi^T L^C_{Lj}\right) + \text{h.c.}\,. \tag{14.22}$$

This set violates (14.3), which poses no problem since, in general, there is no reason for the NP to respect the accidental symmetries of the SM. In particular, it violates the total lepton number by two units, and after spontaneous symmetry breaking it generates a bilinear neutrino field term:

$$-\mathcal{L}_{M_\nu} = \frac{Z^\nu_{ij}}{2}\frac{v^2}{\Lambda_{\rm NP}}\bar\nu_{Li}\nu^c_{Lj} + \text{h.c.}\,. \tag{14.23}$$

This is a Majorana mass term (see Eq.(14.8)). It is built with the left-handed neutrino fields and with mass matrix:

$$(M_\nu)_{ij} = Z^\nu_{ij}\frac{v^2}{\Lambda_{\rm NP}}\,. \tag{14.24}$$

We conclude that Eq.(14.24) would arise in a generic extension of the SM and that neutrino masses are very likely to appear if there is NP. Comparing Eq.(14.24) and Eq.(14.5), we also find that the scale of neutrino masses is suppressed by $v/\Lambda_{\rm NP}$ when compared to the scale of charged fermion masses, which provides an explanation for their smallness. Furthermore, both total lepton number and the lepton flavour symmetry $U(1)_e\times U(1)_\mu\times U(1)_\tau$ are broken by Eq.(14.24), which means that, generically, in the absence of additional symmetries on the coefficients Z_{ij}, we can expect lepton flavour mixing and CP violation as we discuss in the next section.

Finally, we notice that, as mentioned in Sec.14.2.2, a theory where the NP is composed of m heavy sterile neutrinos, provides an specific example of a theory which at low energy theory contains three light mass eigenstates with an effective dim-5 interaction of the form (14.22) with $\Lambda_{\rm NP} = M_N$. In this case, the NP scale is the characteristic mass scale of the heavy sterile neutrinos.

14.3 Lepton Mixing

Let us start by considering $n = 3+m$ massive neutrino states and denote the neutrino mass eigenstates by $(\nu_1,\nu_2,\nu_3,\ldots,\nu_n)$. The neutrino interaction eigenstates are denoted by $\vec\nu = (\nu_{Le},\nu_{L\mu},\nu_{L\tau},\nu_{s1},\ldots,\nu_{sm})$. We label the corresponding mass and interaction eigenstates for the charged leptons as (e,μ,τ) and (e^I,μ^I,τ^I), respectively. The Lagrangian for the leptonic charged current interactions in the mass basis takes the form:

$$-\mathcal{L}_{\rm CC} = \frac{g}{\sqrt2}(\bar e_L,\,\bar\mu_L,\,\bar\tau_L)\gamma^\mu U\begin{pmatrix}\nu_1\\ \nu_2\\ \nu_3\\ \vdots\\ \nu_n\end{pmatrix}W^+_\mu + \text{h.c.}\,, \tag{14.25}$$

where U is a $3\times n$ matrix [14–16]. It satisfies the unitary condition

$$UU^\dagger = I_{3\times 3}\,. \tag{14.26}$$

However, in general $U^\dagger U \ne I_{n\times n}$.

In the interaction basis, the mass terms for the leptons are:

$$-\mathcal{L}_M = [(\bar e^I_L,\,\bar\mu^I_L,\,\bar\tau^I_L)M_\ell\begin{pmatrix}e^I_R\\ \mu^I_R\\ \tau^I_R\end{pmatrix} + \text{h.c.}] - \mathcal{L}_{M_\nu}\,, \tag{14.27}$$

with $\mathcal{L}_{M_\nu}$ given in Eq.(14.8). M_ℓ can be diagonalized with two 3×3 unitary matrices V^ℓ and V^ℓ_R which satisfy

$$V^{\ell\dagger}M_\ell V^\ell_R = \text{diag}(m_e, m_\mu, m_\tau)\,. \tag{14.28}$$

Then for the charged leptons we have

$$-\mathcal{L}_{M_\ell} = \sum_{k=1}^{3} m_{\ell_k}\bar\ell_k\ell_k\,, \tag{14.29}$$

with

$$\ell_k = (V^{\ell\dagger}\ell^I_L)_k + (V^{\ell\dagger}_R\ell^I_R)_k\,. \tag{14.30}$$

Inverting the equation above we find that the weak-doublet components of the charged lepton fields are

$$\ell^I_{Li} = P_L\sum_{j=1}^{3}V^\ell_{ij}\ell_j\,. \qquad i=1,2,3 \tag{14.31}$$

From Eqs.(14.14), (14.18) and (14.31) we find that the mixing matrix U can be expressed as:

$$U_{ij} = \mathcal{P}_{\ell,ii}\,V^{\ell\,\dagger}_{ik}\,V^\nu_{kj}\,(\mathcal{P}_{\nu,jj}). \tag{14.32}$$

The matrix $V^{\ell\dagger}V^\nu$ contains a number of phases that are not physical. Three of them are eliminated by the diagonal 3×3 phase matrix $\mathcal{P}_\ell$ that absorbs them in the charged lepton mass eigenstates. If neutrinos are Dirac states, further $n-1$ are similarly eliminated by absorbing them in the neutrino mass eigenstates with the diagonal $n\times n$ phase matrix $\mathcal{P}_\nu$. For Majorana neutrinos, $\mathcal{P}_\nu = I_{n\times n}$ because one cannot rotate by an arbitrary phase a Majorana field without physical effects. If one rotates a Majorana neutrino by a phase, this phase will appear in its mass term, which will no longer be real. Consequently, the number of phases that can be absorbed by redefining the mass eigenstates

Downloaded from https://academic.oup.com/ptep/article/2022/8/083C01/6651666 by KIT Library user on 27 September 2022

depends on whether the neutrinos are Dirac or Majorana particles. Altogether for $n \geq 3$ Majorana [Dirac] neutrinos, the U matrix contains a total of $6(n-2)$ $[5n-11]$ real parameters, of which $3(n-2)$ are angles, and $3(n-2)$ $[2n-5]$ can be interpreted as physical phases.

The possibility of arbitrary mixing between massive neutrino states was first discussed in the context of two neutrinos introduced in Ref. [17] (the possibility of two mixed massless flavour neutrino states had been previously considered in the literature [18], and the possibility of mixing between neutrino and antineutrino states even earlier, in the seminal paper of Pontecorvo [19]). For that case, in which only mixing between two generations is considered with $n = 2$ distinct neutrino masses, the U matrix is 2×2 and contains one mixing angle if the neutrinos are Dirac and an additional physical phase if they are Majorana.

If there are only $n = 3$ Majorana neutrinos, U is a 3×3 matrix analogous to the CKM matrix for the quarks [20, 21], but due to the Majorana nature of the neutrinos it depends on six independent parameters: three mixing angles and three phases. In this case the mixing matrix can be conveniently parameterized as:

$$U = \begin{pmatrix} 1 & 0 & 0 \\ 0 & c_{23} & s_{23} \\ 0 & -s_{23} & c_{23} \end{pmatrix} \cdot \begin{pmatrix} c_{13} & 0 & s_{13}e^{-i\delta_{\rm CP}} \\ 0 & 1 & 0 \\ -s_{13}e^{i\delta_{\rm CP}} & 0 & c_{13} \end{pmatrix} \cdot \begin{pmatrix} c_{12} & s_{12} & 0 \\ -s_{12} & c_{12} & 0 \\ 0 & 0 & 1 \end{pmatrix} \cdot \begin{pmatrix} e^{i\eta_1} & 0 & 0 \\ 0 & e^{i\eta_2} & 0 \\ 0 & 0 & 1 \end{pmatrix} , \tag{14.33}$$

where $c_{ij} \equiv \cos\theta_{ij}$ and $s_{ij} \equiv \sin\theta_{ij}$. The angles θ_{ij} can be taken without loss of generality to lie in the first quadrant, $\theta_{ij} \in [0, \pi/2]$ and the phases $\delta_{\rm CP}$, $\eta_i \in [0, 2\pi]$. This is to be compared to the case of three Dirac neutrinos. In this case, the Majorana phases, η_1 and η_2, can be absorbed in the neutrino states so the number of physical phases is one (similar to the CKM matrix). Thus we can write U as:

$$U = \begin{pmatrix} c_{12}\, c_{13} & s_{12}\, c_{13} & s_{13}\, e^{-i\delta_{\rm CP}} \\ -s_{12}\, c_{23} - c_{12}\, s_{13}\, s_{23}\, e^{i\delta_{\rm CP}} & c_{12}\, c_{23} - s_{12}\, s_{13}\, s_{23}\, e^{i\delta_{\rm CP}} & c_{13}\, s_{23} \\ s_{12}\, s_{23} - c_{12}\, s_{13}\, c_{23}\, e^{i\delta_{\rm CP}} & -c_{12}\, s_{23} - s_{12}\, s_{13}\, c_{23}\, e^{i\delta_{\rm CP}} & c_{13}\, c_{23} \end{pmatrix} . \tag{14.34}$$

This matrix is often called the Pontecorvo-Maki-Nakagawa-Sakata (PMNS) mixing matrix.

Notice that when the charged leptons have no other interactions than the SM ones, one can identify their interaction eigenstates with the corresponding mass eigenstates up to phase redefinition. This implies that, in this case, U is just a $3 \times n$ sub-matrix of the unitary neutrino mass diagonalizing matrix V^ν.

Finally, let us point out that for the case of 3 light Dirac neutrinos, the procedure above leads to a unitary U matrix for the light states. But for three light Majorana neutrinos, this is not the case when the full spectrum contains states which are heavy and are not in the low energy spectrum as seen, for example, in Eq.(14.21). This implies that, strictly speaking, the parametrization in Eq.(14.33) is not valid to describe the flavour mixing of the three light Majorana neutrinos in the see-saw mechanism. The violation of unitarity, however, is rather small, of the order $\mathcal{O}(M_D/M_N)$ as seen in Eq.(14.21). It is also severely constrained experimentally [22, 23]. For all these reasons, for all practical purposes, we will consider the U matrix for the 3ν mixing case to be unitary independently of whether neutrinos are Dirac or Majorana particles.

14.4 Mass-Induced Flavour Oscillations in Vacuum

If neutrinos have masses and lepton flavours are mixed in the weak CC interactions, lepton flavour is not conserved in neutrino propagation [19, 24]. This phenomenon is usually referred to as *neutrino oscillations*. In brief, a weak eigenstates, ν_α, which by default is the state produced in the weak CC interaction of a charged lepton ℓ_α, is the linear combination determined by the mixing matrix U

$$|\nu_\alpha\rangle = \sum_{i=1}^{n} U^*_{\alpha i} |\nu_i\rangle , \tag{14.35}$$

where ν_i are the mass eigenstates, and here n is the number of light neutrino species (implicit in our definition of the state $|\nu\rangle$ is its energy-momentum and space-time dependence). After traveling a distance L ($L \simeq ct$ for relativistic neutrinos), that state evolves as:

$$|\nu_\alpha(t)\rangle = \sum_{i=1}^{n} U^*_{\alpha i} |\nu_i(t)\rangle . \tag{14.36}$$

This neutrino can then undergo a charged-current (CC) interaction producing a charge lepton ℓ_β, $\nu_\alpha(t)N' \to \ell_\beta N$, with a probability

$$P_{\alpha\beta} = |\langle\nu_\beta|\nu_\alpha(t)\rangle|^2 = |\sum_{i=1}^{n}\sum_{j=1}^{n} U^*_{\alpha i} U_{\beta j} \langle\nu_j|\nu_i(t)\rangle|^2 . \tag{14.37}$$

Assuming that $|\nu\rangle$ is a plane wave, $|\nu_i(t)\rangle = e^{-i\,E_i t}|\nu_i(0)\rangle$, [3] with $E_i = \sqrt{p_i^2 + m_i^2}$ and m_i being, respectively, the energy and the mass of the neutrino mass eigenstate ν_i. In all practical cases neutrinos are very relativistic ,so $p_i \simeq p_j \equiv p \simeq E$. We can then write

$$E_i = \sqrt{p_i^2 + m_i^2} \simeq p + \frac{m_i^2}{2E} , \tag{14.38}$$

and use the orthogonality of the mass eigenstates, $\langle\nu_j|\nu_i\rangle = \delta_{ij}$, to arrive to the following form for $P_{\alpha\beta}$:

$$P_{\alpha\beta} = \delta_{\alpha\beta} - 4\sum_{i<j}^{n} {\rm Re}[U_{\alpha i} U^*_{\beta i} U^*_{\alpha j} U_{\beta j}] \sin^2 X_{ij} + 2\sum_{i<j}^{n} {\rm Im}[U_{\alpha i} U^*_{\beta i} U^*_{\alpha j} U_{\beta j}] \sin 2X_{ij} , \tag{14.39}$$

where

$$X_{ij} = \frac{(m_i^2 - m_j^2)L}{4E} = 1.267\, \frac{\Delta m^2_{ij}}{{\rm eV}^2}\, \frac{L/E}{{\rm m/MeV}} . \tag{14.40}$$

If we had made the same derivation for antineutrino states, we would have ended with a similar expression but with the exchange $U \to U^*$. Consequently, we conclude that the first term in the right-hand-side of Eq.(14.39) is CP conserving since it is the same for neutrinos and antineutrinos, while the last one is CP violating because it has opposite signs for neutrinos and antineutrinos.

Equation (14.39) is oscillatory in distance with oscillation lengths

$$L^{\rm osc}_{0,ij} = \frac{4\pi E}{|\Delta m^2_{ij}|} , \tag{14.41}$$

and with amplitudes proportional to products of elements in the mixing matrix. Thus, neutrinos must have different masses

[3] For a pedagogical discussion of the quantum mechanical description of flavour oscillations in the wave package approach see for example Ref. [3]. A recent review of the quantum mechanical aspects and subtleties on neutrino oscillations can be found in in Ref. [25].

Downloaded from https://academic.oup.com/ptep/article/2022/8/083C01/6651666 by KIT Library user on 27 September 2022

Table 14.1: Characteristic values of L and E for experiments performed using various neutrino sources and the corresponding ranges of $|\Delta m^2|$ to which they can be most sensitive to flavour oscillations in vacuum. SBL stands for Short Baseline, VSBL stands for Very Short Baseline , MBL stands for Medium Baseline, and LBL for Long Baseline.

Experiment		L (m)	E (MeV)	$\lvert\Delta m^2\rvert$ (eV^2)
Solar		10^{10}	1	10^{-10}
Atmospheric		$10^4 - 10^7$	10^2–10^5	$10^{-1} - 10^{-4}$
Reactor	VSBL–SBL–MBL	$10 - 10^3$	1	$1 - 10^{-3}$
	LBL	$10^4 - 10^5$		$10^{-4} - 10^{-5}$
Accelerator	SBL	10^2	10^3–10^4	> 0.1
	LBL	$10^5 - 10^6$	$10^3 - 10^4$	$10^{-2} - 10^{-3}$

($\Delta m^2_{ij} \neq 0$) and they must have not vanishing mixing ($U_{\alpha_i} U_{\beta i} \neq 0$) in order to undergo flavour oscillations. Also, from Eq.(14.39) we see that the Majorana phases cancel out in the oscillation probability. This is expected because flavour oscillation is a total lepton number conserving process.

Ideally, a neutrino oscillation experiment would like to measure an oscillation probability over a distance L between the source and the detector, for neutrinos of a definite energy E. In practice, neutrino beams, both from natural or artificial sources, are never monoenergetic but have an energy spectrum $\Phi(E)$. In addition, each detector has a finite energy resolution. Under these circumstances what is measured is an average probability

$$\begin{aligned}\langle P_{\alpha\beta}\rangle &= \frac{\int dE \frac{d\Phi}{dE}\sigma(E) P_{\alpha\beta}(E)\epsilon(E)}{\int dE \frac{d\Phi}{dE}\sigma_{CC}(E)\epsilon(E)} \\ &= \delta_{\alpha\beta} - 4\sum_{i<j}^{n} \mathrm{Re}[U_{\alpha i}U^*_{\beta i}U^*_{\alpha j}U_{\beta j}]\langle \sin^2 X_{ij}\rangle \\ &\quad + 2\sum_{i<j}^{n} \mathrm{Im}[U_{\alpha i}U^*_{\beta i}U^*_{\alpha j}U_{\beta j}]\langle \sin 2X_{ij}\rangle\,.\end{aligned} \tag{14.42}$$

σ is the cross-section for the process in which the neutrino flavour is detected, and $\epsilon(E)$ is the detection efficiency. The minimal range of the energy integral is determined by the energy resolution of the experiment.

It is clear from the above expression that if $(E/L) \gg |\Delta m^2_{ij}|$ ($L \ll L^{\rm osc}_{0,ij}$) so $\sin^2 X_{ij} \ll 1$, the oscillation phase does not give any appreciable effect. Conversely, if $L \gg L^{\rm osc}_{0,ij}$, many oscillation cycles occur between production and detection, so the oscillating term is averaged to $\langle \sin^2 X_{ij}\rangle = 1/2$.

We summarize in Table 14.1 the typical values of L/E for different types of neutrino sources and experiments and the corresponding ranges of Δm^2 to which they can be most sensitive.

Historically, the results of neutrino oscillation experiments were interpreted assuming two-neutrino states so there is only one oscillating phase; the mixing matrix depends on a single mixing angle θ, and no CP violation effect in oscillations is possible. At present, as we will discuss in Sec.14.7, we need at least the mixing among three-neutrino states to fully describe the bulk of experimental results. However, in many cases, the observed results can be understood in terms of oscillations dominantly driven by one Δm^2. In this limit $P_{\alpha\beta}$ of Eq.(14.39) takes the form [24]

$$P_{\alpha\beta} = \delta_{\alpha\beta} - (2\delta_{\alpha\beta} - 1)\sin^2 2\theta \sin^2 X\,. \tag{14.43}$$

In this effective $2-\nu$ limit, changing the sign of the mass difference, $\Delta m^2 \to -\Delta m^2$, and changing the octant of the mixing angle, $\theta \to \frac{\pi}{2} - \theta$, is just redefining the mass eigenstates, $\nu_1 \leftrightarrow \nu_2$: $P_{\alpha\beta}$ must be invariant under such transformation. So the physical parameter space can be covered with either $\Delta m^2 \geq 0$ with $0 \leq \theta \leq \frac{\pi}{2}$, or, alternatively, $0 \leq \theta \leq \frac{\pi}{4}$ with either sign for Δm^2.

However, from Eq.(14.43) we see that $P_{\alpha\beta}$ is actually invariant under the change of sign of the mass splitting *and* the change of octant of the mixing angle separately. This implies that there is a two-fold discrete ambiguity since the two different sets of physical parameters, $(\Delta m^2, \theta)$ and $(\Delta m^2, \frac{\pi}{2} - \theta)$, give the same transition probability in vacuum. In other words, one could not tell from a measurement of, say, $P_{e\mu}$ in vacuum whether the larger component of ν_e resides in the heavier or in the lighter neutrino mass eigenstate. This symmetry is broken when one considers mixing of three or more neutrinos in the flavour evolution and or when the neutrinos traverse regions of dense matter as we describe in Sec.14.7.1 and Sec.14.5, respectively.

14.5 Propagation of Massive Neutrinos in Matter

Neutrinos propagating in a dense medium can interact with the particles in the medium. The probability of an incoherent inelastic scattering is very small. For example the characteristic cross section for ν-proton scattering is of the order

$$\sigma \sim \frac{G_F^2 s}{\pi} \sim 10^{-43}\ \mathrm{cm}^2 \left(\frac{E}{\mathrm{MeV}}\right)^2, \tag{14.44}$$

where G_F is the Fermi constant and s is the square of the center of mass energy of the collision.

But when neutrinos propagate in dense matter, they can also interact coherently with the particles in the medium. By definition, in coherent interactions, the medium remains unchanged so it is possible to have interference of the forward scattered and the unscattered neutrino waves which enhances the effect of matter in the neutrino propagation. In this case, the effect of the medium is not on the intensity of the propagating neutrino beam, which remains unchanged, but on the phase velocity of the neutrino wave, and for this reason the effect is proportional to G_F, instead of the G_F^2 dependence of the incoherent scattering. Coherence also allows decoupling the evolution equation of the neutrinos from those of the medium. In this limit, the effect of the medium is introduced in the evolution equation for the neutrinos in the form of an effective potential which depends on the density and composition of the matter [26].

As an example, let us consider the evolution of ν_e in a medium with electrons, protons, and neutrons with corresponding n_e, n_p, and n_n number densities. The effective low-energy Hamiltonian describing the relevant neutrino interactions at point x is given by

$$H_W = \frac{G_F}{\sqrt{2}}\left[J^{(+)\alpha}(x)J^{(-)}_\alpha(x) + \frac{1}{4}J^{(N)\alpha}(x)J^{(N)}_\alpha(x)\right], \tag{14.45}$$

where the J_α's are the standard fermionic currents

$$J^{(+)}_\alpha(x) = \bar\nu_e(x)\gamma_\alpha(1-\gamma_5)e(x)\,, \tag{14.46}$$

$$J^{(-)}_\alpha(x) = \bar e(x)\gamma_\alpha(1-\gamma_5)\nu_e(x)\,, \tag{14.47}$$

$$\begin{aligned}J^{(N)}_\alpha(x) &= \bar\nu_e(x)\gamma_\alpha(1-\gamma_5)\nu_e(x) \\ &\quad - \bar e(x)[\gamma_\alpha(1-\gamma_5) - 4\sin^2\theta_W\gamma_\alpha]e(x) \\ &\quad + \bar p(x)[\gamma_\alpha(1-g^{(p)}_A\gamma_5) - 4\sin^2\theta_W\gamma_\alpha]p(x) \\ &\quad - \bar n(x)\gamma_\alpha(1-g^{(n)}_A\gamma_5)n(x)\,,\end{aligned} \tag{14.48}$$

and $g^{(n,p)}_A$ are the axial couplings for neutrons and protons, respectively.

Downloaded from https://academic.oup.com/ptep/article/2022/8/083C01/6651666 by KIT Library user on 27 September 2022

Let us focus first on the effect of the charged current interactions. The effective CC Hamiltonian due to electrons in the medium is

$$\begin{aligned} H_C^{(e)} &= \frac{G_F}{\sqrt{2}} \int d^3p_e f(E_e,T) \times \Big\langle \langle e(s,p_e) \,|\, \bar{e}(x)\gamma^\alpha(1-\gamma_5)\nu_e(x)\bar{\nu}_e(x)\gamma_\alpha(1-\gamma_5)e(x) \,|\, e(s,p_e)\rangle \Big\rangle \\ &= \frac{G_F}{\sqrt{2}} \bar{\nu}_e(x)\gamma_\alpha(1-\gamma_5)\nu_e(x) \int d^3p_e f(E_e,T) \Big\langle \langle e(s,p_e) \,|\, \bar{e}(x)\gamma_\alpha(1-\gamma_5)e(x) \,|\, e(s,p_e)\rangle \Big\rangle . \end{aligned} \tag{14.49}$$

In the above equation, we denote by s the electron spin, and by p_e its momentum, and $f(E_e,T)$ is the energy distribution function of the electrons in the medium which is assumed to be homogeneous and isotropic and is normalized as

$$\int d^3p_e f(E_e,T) = 1 . \tag{14.50}$$

We denote by $\Big\langle \ldots \Big\rangle$ the averaging over electron spinors and summing over all electrons in the medium. Coherence dictates that s, p_e are the same for initial and final electrons. The axial current reduces to the spin in the non-relativistic limit and therefore averages to zero for a background of non-relativistic electrons. The spatial components of the vector current cancel because of isotropy. Therefore, the only non-trivial average is

$$\int d^3p_e f(E_e,T) \Big\langle \langle e(s,p_e) \,|\, \bar{e}(x)\gamma_0 e(x) \,|\, e(s,p_e)\rangle \Big\rangle = n_e(x) , \tag{14.51}$$

which gives a contribution to the effective Hamiltonian

$$H_C^{(e)} = \sqrt{2}G_F n_e \bar{\nu}_{eL}(x)\gamma_0\nu_{eL}(x) . \tag{14.52}$$

This can be interpreted as a contribution to the ν_{eL} potential energy

$$V_C = \sqrt{2}G_F n_e . \tag{14.53}$$

Should we have considered antineutrino states, we would have ended up with $V_C = -\sqrt{2}G_F n_e$ For a more detailed derivation of the matter potentials see, for example, Ref. [3].

With an equivalent derivation, we find that for ν_μ and ν_τ, the potential due to its CC interactions is zero for most media since neither μ's nor $\tau's$ are present, while the effective potential for any active neutrino due to the neutral current interactions is found to be

$$V_{NC} = \frac{\sqrt{2}}{2} G_F \left[-n_e(1-4\sin^2\theta_w) + n_p(1-4\sin^2\theta_w) - n_n \right] . \tag{14.54}$$

In neutral matter, $n_e = n_p$ and the contribution from electrons and protons cancel each other. So we are left only with the neutron contribution

$$V_{NC} = -1/\sqrt{2}G_F n_n . \tag{14.55}$$

After including these effects, the evolution equation for n ultra-relativistic neutrinos propagating in matter written in the mass basis is (see for instance Ref. [27–29] for the derivation):

$$i\frac{d\vec{\nu}}{dx} = H\,\vec{\nu}, \qquad H = H_m + U^{\nu\,\dagger}\, V\, U^\nu . \tag{14.56}$$

Here $\vec{\nu} \equiv (\nu_1, \nu_2, \ldots, \nu_n)^T$, H_m is the the kinetic Hamiltonian,

$$H_m = \frac{1}{2E}\,\mathrm{diag}(m_1^2, m_2^2, \ldots, m_n^2), \tag{14.57}$$

and V is the effective neutrino potential in the interaction basis. U^ν is the $n\times n$ submatrix of the unitary V^ν matrix corresponding to the n ultrarelativistic neutrino states. For the three SM active neutrinos with purely SM interactions crossing a neutral medium with electrons, protons and neutrons, the evolution equation takes the form (14.56) with $U^\nu \equiv U$, and the effective potential:

$$V = \mathrm{diag}\left(\pm\sqrt{2}G_F n_e(x),\, 0,\, 0\right) \equiv \mathrm{diag}\,(V_e,\, 0,\, 0) . \tag{14.58}$$

The sign + (−) in Eq.(14.58) applies to neutrinos (antineutrinos), and $n_e(x)$ is the electron number density in the medium, which in general is not constant along the neutrino trajectory so the potential is not constant. The characteristic value of the potential at the Earth core is $V_e \sim 10^{-13}$ eV, while at the solar core $V_e \sim 10^{-12}$ eV. Since the neutral current potential Eq.(14.55) is flavour diagonal, it can be eliminated from the evolution equation as it only contributes to an overall unobservable phase.

The instantaneous mass eigenstates in matter, ν_i^m, are the eigenstates of the Hamiltonian H in (14.56) for a fixed value of x, and they are related to the interaction basis by

$$\vec{\nu} = \tilde{U}(x)\nu^{\vec{m}} . \tag{14.59}$$

The corresponding instantaneous eigenvalues of H are $\mu_i(x)^2/(2E)$ with $\mu_i(x)$ being the instantaneous effective neutrino masses.

Let us take for simplicity a neutrino state which is an admixture of only two neutrino species $|\nu_\alpha\rangle$ and $|\nu_\beta\rangle$, so the two instantaneous mass eigenstates in matter ν_1^m and ν_2^m have instantaneous effective neutrino masses

$$\begin{aligned} \mu_{1,2}^2(x) &= \frac{m_1^2+m_2^2}{2} + E[V_\alpha + V_\beta] \\ &\mp \frac{1}{2}\sqrt{[\Delta m^2\cos 2\theta - A]^2 + [\Delta m^2 \sin 2\theta]^2} , \end{aligned} \tag{14.60}$$

and $\tilde{U}(x)$ is a 2x2 rotation matrix with the instantaneous mixing angle in matter given by

$$\tan 2\theta_m = \frac{\Delta m^2 \sin 2\theta}{\Delta m^2 \cos 2\theta - A} . \tag{14.61}$$

In the Eqs.(14.60) and (14.61) A is

$$A \equiv 2E(V_\alpha - V_\beta) , \tag{14.62}$$

and its sign depends on the composition of the medium and on the flavour composition of the neutrino state considered. From the expressions above, we see that for a given sign of A the mixing angle in matter is larger(smaller) than in vacuum if this last one is in the first (second) octant. We see that the symmetry about $\theta = 45°$ which exists in vacuum oscillations between two neutrino states is broken by the matter potential in propagation in a medium. The expressions above show that signficant effects are present when A, is close to $\Delta m^2\cos 2\theta$. In particular, as seen in Eq.(14.61), the tangent of the mixing angle changes sign if, along its path, the neutrino passes by some matter density region satisfying, for its energy, the *resonance condition*

$$A_R = \Delta m^2 \cos 2\theta . \tag{14.63}$$

This implies that if the neutrino is created in a region where the relevant potential satisfies $A_0 > A_R$ (A_0 here is the value of the relevant potential at the production point), then the effective mixing angle in matter at the production point is such that $\mathrm{sgn}(\cos 2\theta_{m,0}) = -\mathrm{sgn}(\cos 2\theta)$. So the flavour component of the mass eigenstates is inverted as compared to their composition in vacuum. In particular, if at the production point we have $A_0 = 2A_R$, then $\theta_{m,0} = \frac{\pi}{2} - \theta$. Asymptotically, for $A_0 \gg A_R$, $\theta_{m,0} \to \frac{\pi}{2}$. In other words, if in vacuum the lightest (heaviest) mass eigenstate has a larger projection on the flavour α (β), inside a matter with density and composition such that $A > A_R$,

Downloaded from https://academic.oup.com/ptep/article/2022/8/083C01/6651666 by KIT Library user on 27 September 2022

the opposite holds. So if the neutrino system is traveling across a monotonically varying matter potential, the dominant flavour component of a given mass eigenstate changes when crossing the region with $A = A_R$. This phenomenon is known as *level crossing*.

Taking the derivative of Eq.(14.59) with respect to x and using Eq.(14.56), we find that in the instantaneous mass basis the evolution equation reads:

$$i\frac{d\vec{\nu}^m}{dx} = \\ = \left[\frac{1}{2E}\,\mathrm{diag}\left(\mu_1^2(x),\,\mu_2^2(x),\,\ldots,\,\mu_n^2(x)\right) - i\,\tilde{U}^\dagger(x)\,\frac{d\tilde{U}(x)}{dx}\right]\vec{\nu}^m\,. \tag{14.64}$$

The presence of the last term, Eq.(14.64) implies that this is a system of coupled equations. So, in general, the instantaneous mass eigenstates, ν_i^m are not energy eigenstates. For constant or slowly enough varying matter potential this last term can be neglected and the instantaneous mass eigenstates, ν_i^m, behave approximately as energy eigenstates, and they do not mix in the evolution. This is the *adiabatic* transition approximation. On the contrary, when the last term in Eq.(14.64) cannot be neglected, the instantaneous mass eigenstates mix along the neutrino path. This implies there can be *level-jumping* [30–33], and the evolution is *non-adiabatic*.

For adiabatic evolution in matter, the oscillation probability take a form very similar to the vacuum oscillation expression, Eq.(14.39). For example, neglecting CP violation:

$$P_{\alpha\beta} = \left|\sum_i \tilde{U}_{\alpha i}(0)\tilde{U}_{\beta i}(L)\exp\left(-\frac{i}{2E}\int_0^L \mu_i^2(x')dx'\right)\right|^2 . \tag{14.65}$$

To compute $P_{\alpha\beta}$ in a varying potential, one can always solve the evolution equation numerically. Also, several analytic approximations for specific profiles of the matter potential can be found in the literature [34].

14.5.1 *The Mikheyev-Smirnov-Wolfenstein Effect for Solar Neutrinos*

The matter effects discussed in the previous section are of special relevance for solar neutrinos. As the Sun produces ν_e's in its core, we consider the propagation of a $\nu_e - \nu_X$ neutrino system (X is some superposition of μ and τ, which is arbitrary because ν_μ and ν_τ have only and equal neutral current interactions) in the matter density of the Sun.

The density of solar matter is a monotonically decreasing function of the distance R from the center of the Sun, and it can be approximated by an exponential for $R < 0.9R_\odot$

$$n_e(R) = n_e(0)\exp\left(-R/r_0\right)\ , \tag{14.66}$$

with $r_0 = R_\odot/10.54 = 6.6\times10^7$ m $= 3.3\times10^{14}$ eV^{-1}.

As mentioned above, the nuclear reactions in the Sun produce electron neutrinos. After crossing the Sun, the composition of the neutrino state exiting the Sun will depend on the relative size of $\Delta m^2\cos2\theta$ versus $A_0 = 2\,E\,G_F\,n_{e,0}$ (where 0 refers to the neutrino production point, which is near but not exactly at the center of the Sun, $R = 0$).

If the relevant matter potential at production is well below the resonant value, $A_R = \Delta m^2\cos2\theta \gg A_0$, matter effects are negligible. With the characteristic matter density and energy of the solar neutrinos, this condition is fulfilled for values of Δm^2 such that $\Delta m^2/E \gg L_{\mathrm{Sun-Earth}}$. So the propagation occurs as in vacuum with the oscillating phase averaged to 1/2 and the survival probability at the exposed surface of the Earth is

$$P_{ee}(\Delta m^2\cos2\theta \gg A_0) = 1 - \frac{1}{2}\sin^2 2\theta > \frac{1}{2}\,. \tag{14.67}$$

If the relevant matter potential at production is only slightly below the resonant value, $A_R = \Delta m^2\cos2\theta \gtrsim A_0$, the neutrino does not cross a region with resonant density, but matter effects are sizable enough to modify the mixing. The oscillating phase is averaged in the propagation between the Sun and the Earth. This regime is well described by an adiabatic propagation, Eq.(14.65). Using that $\tilde{U}(0)$ is a 2x2 rotation of angle $\theta_{m,0}$ – the mixing angle in matter at the neutrino production point–, and $\tilde{U}(L)$ is the corresponding rotation with vacuum mixing angle θ, we get

$$P_{ee}(\Delta m^2\cos2\theta \geq A_0) = \cos^2\theta_{m,0}\cos^2\theta + \sin^2\theta_{m,0}\sin^2\theta \\ = \frac{1}{2}\left[1+\cos2\theta_{m,0}\cos2\theta\right]\,. \tag{14.68}$$

This expression reflects that an electron neutrino produced at A_0 is an admixture of ν_1 with fraction $P_{e1,0} = \cos^2\theta_{m,0}$ and ν_2 with fraction $P_{e2,0} = \sin^2\theta_{m,0}$. On exiting the Sun, ν_1 consists of ν_e with fraction $P_{1e} = \cos^2\theta$, and ν_2 consists of ν_e with fraction $P_{2e} = \sin^2\theta$ so $P_{ee} = P_{e1,0}P_{1e} + P_{e2,0}P_{2e} = \cos^2\theta_{m,0}\cos^2\theta + \sin^2\theta_{m,0}\sin^2\theta$ [35–37], exactly as given in Eq.(14.68). Since $A_0 < A_R$ the resonance is not crossed so $\cos2\theta_{m,0}$ has the same sign as $\cos2\theta$ and still $P_{ee} \geq 1/2$.

Finally, in the case that $A_R = \Delta m^2\cos2\theta < A_0$, the neutrino can cross the resonance on its way out. In the convention of $\Delta m^2 > 0$ this occurs if $\cos2\theta > 0$ ($\theta < \pi/4$). which means that in vacuum ν_e is a combination of ν_1 and ν_2 with a larger ν_1 component, while at the production point ν_e is a combination of ν_1^m and ν_2^m with larger ν_2^m component. In particular, if the density at the production point is much higher than the resonant density, $\Delta m^2\cos2\theta \ll A_0$,

$$\theta_{m,0} = \frac{\pi}{2} \quad\Rightarrow\quad \cos2\theta_{m,0} = -1\,, \tag{14.69}$$

and the produced ν_e is purely ν_2^m.

In this regime, the evolution of the neutrino ensemble can be adiabatic or non-adiabatic depending on the particular values of Δm^2 and the mixing angle. The oscillation parameters (see Secs.14.6.1 and 14.7) happen to be such that the transition is adiabatic in all ranges of solar neutrino energies. Thus the survival probability at the exposed surface of the Earth is given by Eq.(14.68) but now with mixing angle (14.69) so

$$P_{ee}(\Delta m^2\cos2\theta < A_0) = \frac{1}{2}\left[1+\cos2\theta_{m,0}\cos2\theta\right] = \sin^2\theta\,. \tag{14.70}$$

So, in this case, P_{ee} can be much smaller than 1/2 because $\cos2\theta_{m,0}$ and $\cos2\theta$ have opposite signs. This is referred to as the Mihheev-Smirnov-Wolfenstein (MSW) effect [26, 38], which plays a fundamental role in the interpretation of the solar neutrino data.

The resulting energy dependence of the survival probability of solar neutrinos is shown in Fig.14.3 (together with a compilation of data from solar experiments). The plotted curve corresponds to $\Delta m^2 \sim 7.5\times10^{-5}$ eV^2 and $\sin^2\theta \sim 0.3$ (the so-called large mixing angle, LMA, solution). The figure illustrates the regimes described above. For these values of the oscillation parameters, neutrinos with $E \ll 1$ MeV are in the regime with $\Delta m^2\cos2\theta \gg A_0$ so the curve represents the value of vacuum averaged survival probability, Eq.(14.67), and therefore $P_{ee} > 0.5$. For $E > 10$ MeV, on the contrary, $\Delta m^2\cos2\theta \ll A_0$ and the survival probability is given by Eq.(14.70), so $P_{ee} = \sin^2\theta \sim 0.3$. In between, the survival probability is given by Eq.(14.68) with θ_0 changing rapidly from its vacuum value to the asymptotic matter value (14.69), 90°.

14.6 Experimental Study of Neutrino Oscillations

Neutrino flavour transitions, or neutrino oscillations, have been experimentally studied using various neutrino sources and detection techniques. Intense sources and large detectors are mandatory because of a large distance necessary for observable oscillation effects in addition to the tiny cross-sections. Also, the relevant neutrino flux before oscillations should be known with sufficient precision for a definitive measurement. Here, the experimental status of neutrino oscillations with the different neutrino sources: the Sun, Earth's atmosphere, accelerators, and nuclear reactors are reviewed.

Downloaded from https://academic.oup.com/ptep/article/2022/8/083C01/6651666 by KIT Library user on 27 September 2022

14.6.1 *Solar Neutrinos*

14.6.1.1 *Solar neutrino flux*

In the Sun, electron neutrinos are produced in the thermonuclear reactions which generate solar energy. These reactions occur via two main chains, the *pp* chain and the CNO cycle. The *pp* chain includes reactions $p+p \to d+e^+ +\nu$ (*pp*), $p+e^- +p \to d+\nu$ (*pep*), $^3\mathrm{He}+p \to {}^4\mathrm{He}+e^+ +\nu$ (*hep*), $^7\mathrm{Be}+e^- \to {}^7\mathrm{Li}+\nu(+\gamma)$ (^{7}Be), and $^8\mathrm{B} \to {}^8\mathrm{Be}^* + e^+ + \nu$ (^{8}B). The CNO cycle involves $^{13}\mathrm{N} \to {}^{13}\mathrm{C}+e^+ +\nu$ (^{13}N), $^{15}\mathrm{O} \to {}^{15}\mathrm{N}+e^+ +\nu$ (^{15}O), and $^{17}\mathrm{F} \to {}^{17}\mathrm{O}+e^+ +\nu$ (^{17}F). Those reactions result in the overall fusion of protons into ^{4}He, $4p \to {}^4\mathrm{He}+2e^+ +2\nu_e$, where the energy released in the reaction, $Q = 4m_p - m_{4\mathrm{He}} - 2m_e \sim 26$ MeV, is mostly radiated through the photons and only a small fraction is carried by the neutrinos, $\langle E_{2\nu_e}\rangle = 0.59$ MeV. In addition, electron capture on ^{13}N, ^{15}O, and ^{17}F produces line spectra of neutrinos called ecCNO neutrinos. Dividing the solar luminosity by the energy released per neutrino production, the total neutrino flux can be estimated. At Earth, the *pp* solar neutrino flux is about 6×10^{10} cm^{-2}s^{-1}.

The solar neutrino flux has been calculated based on the Standard Solar Model (SSM). The SSM describes the structure and evolution of the Sun based on a variety of inputs such as the mass, luminosity, radius, surface temperature, age, and surface elemental abundances. In addition, the knowledge of the absolute nuclear reaction cross sections for relevant fusion reactions and radiative opacities are necessary. John Bahcall and his collaborators continuously updated the SSM calculations over several decades [39, 40]. Figure 14.1 shows the solar neutrino fluxes predicted by the SSM calculation in [41] and ecCNO neutrinos in [42].

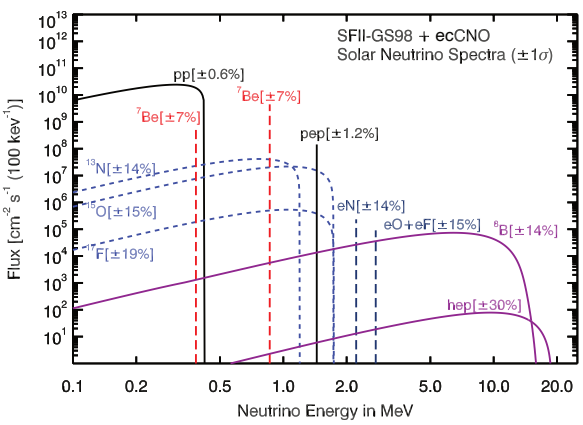

Figure 14.1: Spectrum of solar neutrino fluxes predicted by SSM calculation in [41]. In addition to standard fluxes, ecCNO neutrinos have been added based on [42]. Electron capture fluxes are given in cm^{-2}s^{-1}. Taken from [43].

14.6.1.2 *Detection of solar neutrinos and the solar neutrino problem*

Experiments that observed solar neutrinos are summarized in Table 14.2. A pioneering solar neutrino experiment was carried out by R. Davis, Jr. and collaborators at Homestake starting in the late 1960s [44]. The Davis' experiment utilizes the reaction $\nu_e + {}^{37}\mathrm{Cl} \to e^- + {}^{37}\mathrm{Ar}$. Because this process has an energy threshold of 814 keV, the most relevant fluxes are the ^{7}Be and ^{8}B neutrinos. The detector contained ~ 615 t of C_2Cl_4. The produced ^{37}Ar, which has a half-life of 34.8 d, was chemically extracted and introduced into a low-background proportional chamber every few months. The Auger electrons from electron capture of ^{37}Ar were counted to determine the reaction rate.

From the beginning, the observed number of neutrinos in the Homestake mine experiment was significantly smaller than the prediction by SSM — it was almost one-third. After thorough checks of both experimental and theoretical work, the discrepancy remained. This became to be known as the solar neutrino problem. The final result from the Homestake experiment is $2.56 \pm 0.16 \pm 0.16$ SNU [45], where SNU (solar neutrino unit) is a unit of event rate, 1 SNU $= 10^{-36}$ captures/(s atom). On the other hand, prediction based on SSM is $8.46^{+0.87}_{-0.88}$ SNU [46].

The detection of neutrinos from other production processes was recognized as an important input to investigate the origin of the solar neutrino problem. In particular, the *pp* neutrino is most abundant, and its flux prediction has the smallest uncertainty. Using the radiochemical technique with gallium, the reaction $\nu_e + {}^{71}\mathrm{Ga} \to e^- + {}^{71}\mathrm{Ge}$ has an energy threshold of 233 keV and can be used for the *pp* neutrino detection. According to the SSM, more than half of the events on ^{71}Ga are due to the *pp* neutrinos, with the second dominant contribution coming from the ^{7}Be neutrinos. ^{71}Ge decays via electron capture with a half-life of 11.4 d. The SAGE experiment in Baksan [47] used about 50 t of liquid metallic gallium as a target. The GALLEX experiment in LNGS [48] used 101 t of $GaCl_3$, containing 30.3 t of gallium. Both experiments used natural gallium, containing 39.9% of ^{71}Ga isotope. GALLEX was followed by its successor GNO experiment. The measured capture rate is $69.3 \pm 4.1 \pm 3.6$ SNU for GALLEX+GNO [49] and $65.4^{+3.1+2.6}_{-3.0-2.8}$ SNU for SAGE [50]. A SSM prediction is $127.9^{+8.1}_{-8.2}$ SNU [46].

The radiochemical detectors measure the reaction rate integrated between extractions. The real-time measurement of solar neutrinos was realized by the Kamiokande experiment [51]. The Kamiokande detector was a 3,000-t water-Cherenkov detector in the Kamioka mine. Super-Kamiokande, the successor of Kamiokande, started operation in April 1996. It is a large upright cylindrical water Cherenkov detector containing 50 kt of pure water [4]. An inner detector volume corresponding to 32 kt water mass is viewed by more than 11,000 inward-facing 50 cm diameter photomultiplier tubes (PMTs). Kamiokande and Super-Kamiokande can observe solar neutrinos using ν-e elastic scattering (ES), $\nu_x + e^- \to \nu_x + e^-$. The ES reaction occurs via both charged and neutral current interactions. Consequently, it is sensitive to all active neutrino flavours, although the cross-section for ν_e, which is the only flavour to interact via charged current, is about six times larger than that for ν_μ or ν_τ. Because the energy threshold is 6.5 MeV for Kamiokande and 3.5 MeV for the present Super-Kamiokande (for the kinetic energy of recoil electron), these experiments are sensitive to primarily to ^{8}B neutrinos.

The results from Kamiokande [52, 53] and Super-Kamiokande [54, 55] showed significantly smaller numbers of observed solar neutrinos compared to the prediction. The latest ^{8}B neutrino flux measured by Super-Kamiokande is $(2.345\pm0.014\pm0.036)\times10^6$ cm^{-2}s^{-1} [56], while a prediction based on the SSM is $(5.46 \pm 0.66) \times 10^6$ cm^{-2}s^{-1} [57]. In addition, no significant zenith angle variation nor spectrum distortion were observed in the initial phase of Super-Kamiokande, which placed strong constraints on the solution of the solar neutrino problem [58, 59].

14.6.1.3 *Solution of the solar neutrino problem*

The SNO experiment in Canada used 1,000 t of heavy water (D_2O) contained in a spherical acrylic vessel which was surrounded by an H_2O shield. An array of PMTs installed on a stainless steel structure detected Cherenkov radiation produced in both the D_2O and H_2O. The SNO detector observed ^{8}B neutrinos via three different reactions. In addition to the ES scattering with an electron, with D_2O target the CC $\nu_e + d \to e^- + p + p$ and the NC $\nu_x + d \to \nu_x + p + n$ interactions are possible. The CC reaction is sensitive to only ν_e, while NC reaction is sensitive to all active flavours of neutrinos with equal cross-sections. Therefore, by comparing the measurements of different reactions, SNO could provide a model-independent test of the neutrino flavour change.

In 2001, SNO reported the initial result of CC measurement [62]. Combined with the high statistics measurement of ν-e elastic scattering from Super-Kamiokande [58], it provided a direct evidence for the existence of non-ν_e component in solar neutrino flux. The result of the NC measurement in 2002 [63] established it with 5.3σ of statistical significance. Figure 14.2 shows the fluxes of electron neutrinos ($\phi(\nu_e)$) and muon and tau neutrinos ($\phi(\nu_{\mu,\tau})$) with the 68%, 95%, and 99% joint probability contours obtained with the SNO data. Finally, together with

[4] From 2020, gadolinium (0.01% by weight) is loaded in the water.

Downloaded from https://academic.oup.com/ptep/article/2022/8/083C01/6651666 by KIT Library user on 27 September 2022

Table 14.2: List of solar neutrino experiments

Name	Target material	Energy threshold (MeV)	Mass (ton)	Years
Homestake	C_2Cl_4	0.814	615	1970–1994
SAGE	Ga	0.233	50	1989–
GALLEX	$GaCl_3$	0.233	100 [30.3 for Ga]	1991–1997
GNO	$GaCl_3$	0.233	100 [30.3 for Ga]	1998–2003
Kamiokande	H_2O	6.5	3,000	1987–1995
Super-Kamiokande	H_2O	3.5	50,000	1996–
SNO	D_2O	3.5	1,000	1999–2006
KamLAND	Liquid scintillator	0.5/5.5	1,000	2001–
Borexino	Liquid scintillator	0.19	300	2007–

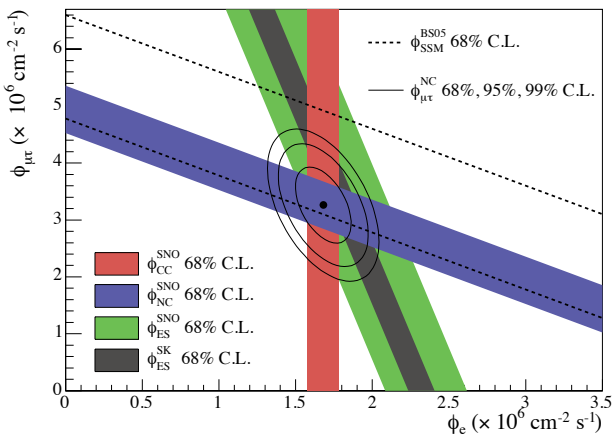

Figure 14.2: Fluxes of ^{8}B solar neutrinos, $\phi(\nu_e)$, and $\phi(\nu_{\mu,\tau})$, deduced from the SNO's CC, ES, and NC results [60]. The Super-Kamiokande ES flux is from [61]. The BS05(OP) standard solar model prediction [40] is also shown. The bands represent the 1σ error. The contours show the 68%, 95%, and 99% joint probability for $\phi(\nu_e)$ and $\phi(\nu_{\mu,\tau})$. The figure is from [60].

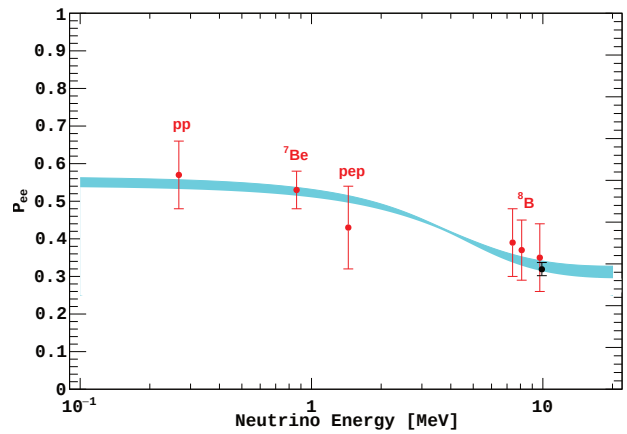

Figure 14.3: Electron neutrino survival probability as a function of neutrino energy. The points represent, from left to right, the Borexino pp, ^{7}Be, pep, and ^{8}B data (red points) and the SNO+SK ^{8}B data (black point). The three Borexino ^{8}B data points correspond, from left to right, to the low-energy (LE) range, LE+HE range, and the high-energy (HE) range. The electron neutrino survival probabilities from experimental points are determined using a high metallicity SSM from Ref. [57]. The error bars represent the $\pm 1\sigma$ experimental + theoretical uncertainties. The curve corresponds to the $\pm 1\sigma$ prediction of the MSW-LMA solution using the parameter values given in [65]. This figure is provided by A. Ianni.

the reactor neutrino experiment KamLAND (see Sec.14.6.4), the solution of solar neutrino problem was found to be the MSW adiabatic flavour transitions in the solar matter, the so-called large mixing angle (LMA) solution. From a combined result of three phases of SNO [64], the total flux of ^{8}B solar neutrino is found to be $(5.25 \pm 0.16^{+0.11}_{-0.13})$ cm^{-2}s^{-1}, consistent with the SSM prediction. This consistency is one of the major accomplishments of SSM.

In order to understand the SSM as well as to study the MSW effect for the solar neutrino, measurements of solar neutrinos other than ^{8}B are important. The Borexino experiment at Gran Sasso, Italy, detects solar neutrino via ν-e scattering in real-time with a low energy threshold. The Borexino detector consists of 300 t of ultra-pure liquid scintillator, which achieved 0.19 MeV of energy threshold and 5% energy resolution at 1 MeV. Borexino reported the first real-time detection of ^{7}Be solar neutrinos [66]. They also measured the fluxes of *pep* [67], *pp* [68], and CNO [69] neutrino for the first time. Together with ^{8}B [70] neutrino measurement, Borexino provides important data to study the MSW effect. The KamLAND experiment also measured ^{8}B [71] and ^{7}Be [72] solar neutrinos.

Figure 14.3 shows the survival probability of solar ν_e as a function of neutrino energy. The data points are from the Borexino results [73, 74] and the SNO+SK ^{8}B data. The theoretical curve shows the prediction of the MSW-LMA solution. All the data shown in this plot are consistent with the theoretically calculated curve. This indicates that these solar neutrino measurements are consistent with the MSW-LMA solution of the solar neutrino problem.

The matter effects can also be relevant to the propagation of solar neutrinos through the Earth. Because solar neutrinos go through the Earth before interaction in the detector during the nighttime, a comparison of measured event rate between daytime and nighttime provides a clean and direct test of matter effects on neutrino oscillations. Super-Kamiokande reported the indication of the day/night asymmetry in ^{8}B solar neutrinos [75, 76]. The measured asymmetry, defined as the difference of the average day rate and average night rate divided by the average of those two rates, is $(-3.3 \pm 1.0 \pm 0.5)\%$, corresponding to a statistical significance of 2.9σ.

14.6.2 *Atmospheric Neutrinos*

14.6.2.1 *Atmospheric neutrino flux*

Atmospheric neutrinos are produced by the decays of pions and kaons generated in the interaction of cosmic rays and nucleons in the Earth's atmosphere. They have a broad range of energy ($\sim$0.1 GeV to >TeV) and long travel distances before detection ($\sim$10 to $\sim 10^4$ km), and contain all the flavours of neutrinos and antineutrinos.

Considering their dominant production modes, some generic relations for flux ratios of different flavours of neutrinos can be derived without detailed calculations. From the decay chain of a charged pion $\pi^+ \to \mu^+\nu_\mu$ followed by $\mu^+ \to e^+\nu_e\bar{\nu}_\mu$ (and the charge conjugate for π^-), the ratio $(\nu_\mu+\bar{\nu}_\mu)/(\nu_e+\bar{\nu}_e)$ is expected to be around 2 at low energies ($\sim$ 1 GeV), where most muons decay in the atmosphere. For higher energies, some muons reach the Earth before they decay and the ratio increases. One can also expect that the zenith angle distributions of atmospheric neu-

Downloaded from https://academic.oup.com/ptep/article/2022/8/083C01/6651666 by KIT Library user on 27 September 2022

trinos are symmetric between upward-going and downward-going neutrinos. It is true for the energy above 1 GeV, but at lower energies, the Earth's geomagnetic field induces up-down asymmetries in the primary cosmic ray. The zenith angle corresponds to the flight length of atmospheric neutrinos. Vertically upward-going neutrinos come from the other side of the Earth with flight lengths of $\sim 10^4$ km, while downward-going neutrinos produced just above the experimental site travel $\sim$10 km before detection.

The atmospheric neutrino fluxes are calculated in detail based on the energy spectrum and composition of primary cosmic rays and their hadronic interactions in the atmosphere. The effects of solar activity and geomagnetic field are also taken into account. Results of calculations by several groups are available [77–80]. A typical uncertainty of the absolute flux is 10–20%, while the ratio of fluxes between different flavour has much smaller uncertainty ($< 5\%$).

14.6.2.2 *Observation of atmospheric neutrino oscillations*

The first detection of atmospheric neutrinos was reported in the 1960's by the underground experiments in the Kolar Gold Field experiment in India [81] and in South Africa [82]. In the 1980's, experiments searching for nucleon decays started operation. They used large underground detectors which could also observe atmospheric neutrinos that were studied as backgrounds to nucleon decays. Among the early experiments were Kamiokande [83] and IMB [84] using water Cherenkov detectors, and Frejus [85] and NUSEX [86] using iron tracking calorimeters.

The flavour of an atmospheric neutrino can be identified in charged current interaction with nuclei, which produces the corresponding charged lepton. Those detectors originally designed for nucleon decay search had the capability to distinguish muons and electrons. For example, a water Cherenkov detector can utilize the information from Cherenkov ring patterns for particle identification; e-like particles ($e^{\pm}$, γ) produce more diffuse ring than μ-like particles ($\mu^{\pm}$, $\pi^{\pm}$) because of electromagnetic cascades and multiple Coulomb scattering effects.

To reduce the uncertainty, in early results the flux ratio $\nu_\mu/\nu_e \equiv (\nu_\mu + \bar{\nu}_\mu)/(\nu_e + \bar{\nu}_e)$ was measured, and the double ratio between observation and expectation $(\nu_\mu/\nu_e)_{\rm obs}/(\nu_\mu/\nu_e)_{\rm exp}$ was reported. The Kamiokande experiment reported an indication of a deficit of $(\nu_\mu + \bar{\nu}_\mu)$ flux [83]. IMB also observed a similar deficit [84], but measurements by Frejus [85] and NUSEX [86] were consistent with the expectations. This was called the atmospheric neutrino anomaly. Kamiokande reported studies with an increased data set of the sub-GeV (< 1.33 GeV) [87] as well as the multi-GeV (> 1.33 GeV) [88] samples. In the latter, they reported an analysis of zenith angle distributions, which showed an indication that the muon disappearance probability is dependent on the zenith angle, hence the travel length of neutrinos. However, the statistical significance was not sufficient to provide a conclusive interpretation.

The solution to the atmospheric neutrino anomaly was brought by Super-Kamiokande, which reported compelling evidence for neutrino oscillations in atmospheric neutrinos in 1998 [89]. The zenith angle (θ_z, with $\theta_z = 0$ for vertically downward-going) distributions of μ-like events showed a clear deficit of upward-going events, while no significant asymmetry was observed for e-like events. The asymmetry is defined as $A = (U - D)/(U + D)$, where U is the number of upward-going ($-1 < \cos\theta_z < -0.2$) events and D is the number of downward-going ($0.2 < \cos\theta_z < 1.0$) events. With multi-GeV (visible energy > 1.33 GeV) μ-like events alone, the measured asymmetry was $A = -0.296 \pm 0.048 \pm 0.001$, deviating from zero by more than 6σ. The sub-GeV (< 1.33 GeV) μ-like, upward through going, and upward stopping μ samples which correspond to different energy ranges of neutrinos, showed the consistent behaviour which strengthens the credibility of the observation. Super-Kamiokande's results were confirmed by other atmospheric neutrino observations MACRO [90] and Soudan2 [91].

Although the energy and zenith-angle-dependent muon neutrino disappearance observed with atmospheric neutrinos could be consistently explained by the neutrino oscillations predominantly between ν_μ and ν_τ, other exotic explanations such as neutrino decay [92] or decoherence [93] were not initially ruled out. By using a selected sample from Super-Kamiokande's atmospheric data with good L/E resolution, the L/E dependence of the survival probability was measured [94]. The observed dip in the L/E distribution was consistent with the expectation from neutrino oscillation, while alternative models were strongly disfavored.

As an experimental proof of ν_μ-ν_τ oscillation, an appearance signal of ν_τ was searched for in the atmospheric neutrino data. Because of the high energy threshold (> 3.5 GeV) of ν_τ CC interaction and the short lifetime of τ lepton (0.3 ps), identifying the appearance of ν_τ experimentally is challenging. Super-Kamiokande reported evidence of tau neutrino appearance using atmospheric neutrino data with 4.6σ significance [95]. The definitive observation of ν_τ appearance was made by the long-baseline experiment, OPERA (See Sec.14.6.3.3), and recently IceCube also reported the ν_τ appearance analysis [96] using atmospheric neutrinos.

14.6.2.3 *Neutrino oscillation measurements using atmospheric neutrinos*

Figure 14.4 shows the zenith angle distributions of atmospheric neutrino data from Super-Kamiokande. For a wide range of neutrino energy and path length, the observed distributions are consistent with the expectation from neutrino oscillation. Atmospheric neutrinos in the energy region of a few to $\sim$10 GeV provide information for the determination of the neutrino mass ordering [97].

The neutrino telescopes primarily built for high-energy neutrino astronomy such as ANTARES and IceCube can also measure neutrino oscillations with atmospheric neutrinos. ANTARES consists of a sparse array of PMTs deployed under the Mediterranean Sea at a depth of about 2.5 km to instrument a 10^5 m^3 volume. IceCube is a detector deployed in ice in Antarctica at the South Pole, at a depth between 1.45 and 2.45 km. In the bottom center of IceCube there is a region of $\sim 10^7$ m^3 volume with denser PMT spacing called DeepCore to extend the observable energies to the lower energy region. By observing the charged current interaction of up-going ν_μ, they measure the ν_μ disappearance. ANTARES reported a measurement of ν_μ disappearance with 20 GeV threshold [98]. With analysis of events with 6–56 GeV energy range, the results on ν_μ disappearance measurements from IceCube DeepCore [99] provided a precision comparable to the measurements by Super-Kamiokande and long-baseline accelerator neutrino experiments.

There are several projects for atmospheric neutrino observations either proposed or under preparation. The atmospheric neutrino observation program is included in the plans for future neutrino telescopes such as ORCA in the KM3NeT project [100] in the Mediterranean Sea and the IceCube Upgrade [101]. In India, a 50 kt magnetized iron tracking calorimeter ICAL is planned at the INO [102]. Future large underground detectors, Hyper-Kamiokande in Japan [103] and DUNE in US [104] can also study the atmospheric neutrinos.

14.6.3 *Accelerator Neutrinos*

14.6.3.1 *Accelerator neutrino beams*

A comprehensive description of the accelerator neutrino beams is found in [105]. Conventional neutrino beams from accelerators are produced by colliding high-energy protons onto a target, producing π and K, which then decay into neutrinos. Undecayed mesons and muons are stopped in a beam dump and soil. Because pions are the most abundant product of the high energy collisions, a conventional neutrino beam contains a dominant amount of muon-type neutrinos (or antineutrinos).

Focusing devices called magnetic horns are used to concentrate the neutrino beam flux towards the desired direction [106]. A magnetic horn is a pulsed electromagnet with toroidal magnetic fields to focus charged particles that are parents of neutrinos. One can choose the dominant component of the beam to be either neutrinos or antineutrinos by selecting the direction of current in the magnetic horns. Even with the focusing with horns, *wrong sign* neutrinos contaminate in the beam. Also, there is a small amount of contamination of ν_e and $\bar{\nu}_e$ coming primarily from kaon and muon decays.

In order to maximize the sensitivity of the experiment, the ratio of baseline and neutrino energy (L/E) should be chosen to match the oscillation effects to be studied. In addition to maximizing the flux of neutrinos with relevant energy, neutrinos with irrele-

Downloaded from https://academic.oup.com/ptep/article/2022/8/083C01/6651666 by KIT Library user on 27 September 2022

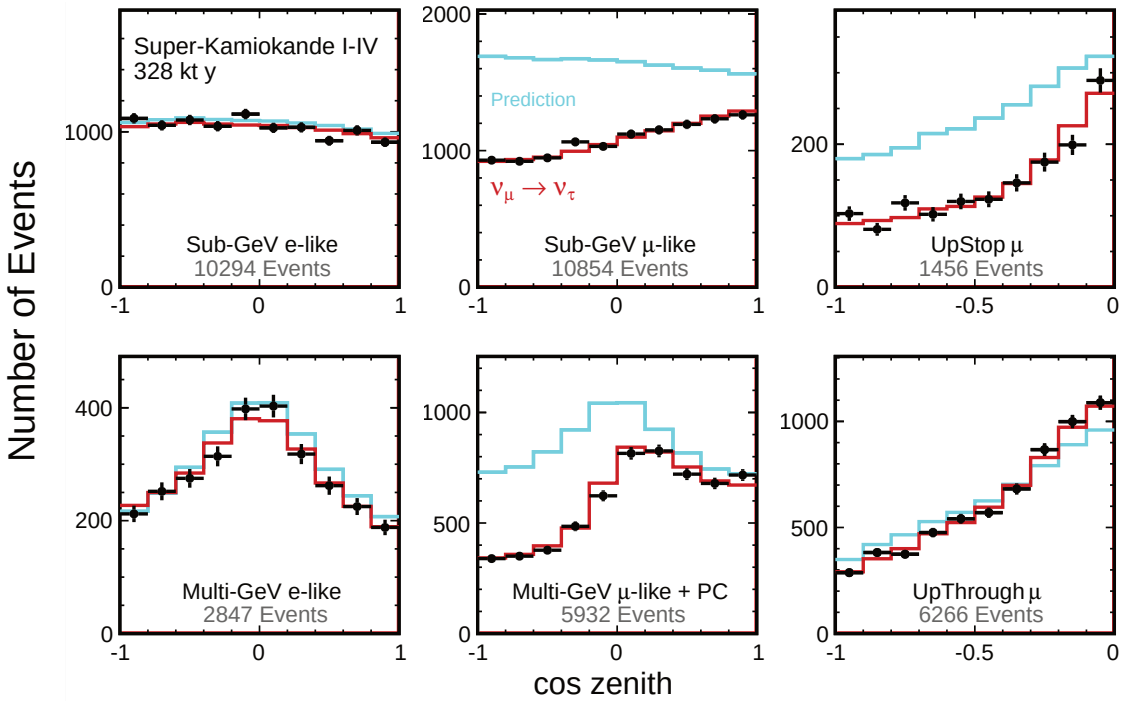

Figure 14.4: The zenith angle distributions of Super-Kamiokande atmospheric neutrino events. A data set corresponding to 328 kton-years of exposure is used. Fully contained 1-ring e-like and μ-like events with visible energy < 1.33 GeV (sub-GeV) and > 1.33 GeV (multi-GeV), as well as upward stopping and upward through going μ samples are shown. Partially contained (PC) events are combined with multi-GeV μ-like events. The blue histograms show the non-oscillated Monte Carlo events, and the red histograms show the best-fit expectations for neutrino oscillations. (This figure is provided by the Super-Kamiokande Collaboration)

vant energy that result in unwanted background process should be suppressed. The energy of a neutrino from a pion decay is

$$E_\nu = \frac{[1-(m_\mu/m_\pi)^2]E_\pi}{1+\gamma^2\theta^2}, \tag{14.71}$$

where E_ν and E_π are the energy of neutrino and pion, respectively, θ is the angle between the pion and neutrino direction, and $\gamma = E_\pi/m_\pi$. For $\theta = 0$, the energy of neutrino is linearly proportional to the energy of pion. In this case, a narrow band beam can be made by selecting the momentum of pions. On the other hand, for $\theta \neq 0$, the energy of neutrino is not strongly dependent on the parent energy for a wide range of pion energy, but dependent on the off-axis angle θ. Using this relation, a neutrino beam with narrow energy spectrum, around the energy determined by θ, can be produced. This off-axis beam method was first introduced for BNL E889 proposal [107] and adopted in T2K and NOvA experiments. For a list of neutrino beamlines, see also Chapter 33 of this *Review*, "Neutrino Beam Lines at High-Energy Proton Synchrotrons."

As indicated in Table 14.1, there are two different scales of baselines for accelerator-based experiments to study different ranges of Δm^2. The atmospheric mass splitting $\Delta m^2 \sim 2.5 \times 10^{-3}$ eV^2 gives rise to the first oscillation maximum at $L/E \sim 500$ GeV/km. In order to study this parameter region with a ~ 1 GeV accelerator neutrino beam, a long baseline of a few hundred to a thousand km is necessary. On the other hand, there have been reports of possible neutrino oscillations at the ~ 1 eV^2 scale, which can be studied at ~ 1 km baseline with neutrinos from accelerators. These experiments are called short-baseline oscillation experiments.

The flux of a neutrino beam is calculated using Monte Carlo simulation based on the configuration of the beamline. An important ingredient of the neutrino flux prediction is the hadron production cross-section. Data from dedicated hadron production experiments [108–110] are used to tune the beam simulation and constrain the uncertainty. The uncertainty of predicted neutrino flux for the most relevant energy region is ∼5–10% with the latest hadron production data [111–113].

14.6.3.2 *Near detectors and neutrino interaction cross sections*

Many long-baseline experiments use two detectors to reduce the systematic uncertainties arising from neutrino flux and neutrino-nucleus interactions. The near detectors either use the same technology as the far detector or consist of sub-detectors with complementary functions to obtain detailed information of the neutrino beam and interactions. The near detectors provide information for the neutrino flux, energy spectrum, and the interaction cross-sections, which is used as input to make predictions of observables at the far detector. However, even with the two-detector configuration, one should note that the neutrino flux is inevitably different between the near and the far detectors. In addition to the fact that the neutrino source looks like a line source for the near detector while it looks like a point source for the far detector, the neutrino oscillations alter the flavour composition of the neutrino beam quite significantly, as the design of a neutrino oscillation experiment requires.

For the precision measurements of neutrino oscillations with long-baseline experiments, the understanding of the neutrino-nucleus interaction becomes crucial. Because heavy nuclei are used as the interaction target, the nuclear effects complicate the understanding of the neutrino-nucleus interaction. For more information on the neutrino cross-sections, see also Chapter 52 of this *Review*, "Neutrino Cross Section Measurements."

14.6.3.3 *Long-baseline experiments*

Long-baseline neutrino oscillation experiments are summarized in Table 14.3. The first long-baseline experiment was the K2K experiment which used a neutrino beam from the KEK 12 GeV proton synchrotron directed towards Super-Kamiokande with a baseline of 250 km. The beam had an average energy of 1.3 GeV. The K2K near detectors, located 300 m downstream of the production target, consisted of a combination of a 1 kt water Cherenkov detector and a set of fine-grained detectors. K2K confirmed the muon neutrino disappearance originally reported by Super-Kamiokande atmospheric neutrino observation [114].

The MINOS experiment used a beam from Fermilab and a de-

Downloaded from https://academic.oup.com/ptep/article/2022/8/083C01/6651666 by KIT Library user on 27 September 2022

Table 14.3: List of long-baseline neutrino oscillation experiments

Name	Beamline	Far Detector	L (km)	E_ν (GeV)	Year
K2K	KEK-PS	Water Cherenkov	250	1.3	1999–2004
MINOS	NuMI	Iron-scintillator	735	3	2005–2013
MINOS+	NuMI	Iron-scintillator	735	7	2013–2016
OPERA	CNGS	Emulsion hybrid	730	17	2008–2012
ICARUS	CNGS	Liquid argon TPC	730	17	2010–2012
T2K	J-PARC	Water Cherenkov	295	0.6	2010–
NOvA	NuMI	Liquid scint. tracking calorimeter	810	2	2014–
DUNE	LBNF	Liquid argon TPC	1300	2–3	
Hyper-Kamiokande	J-PARC	Water Cherenkov	295	0.6	

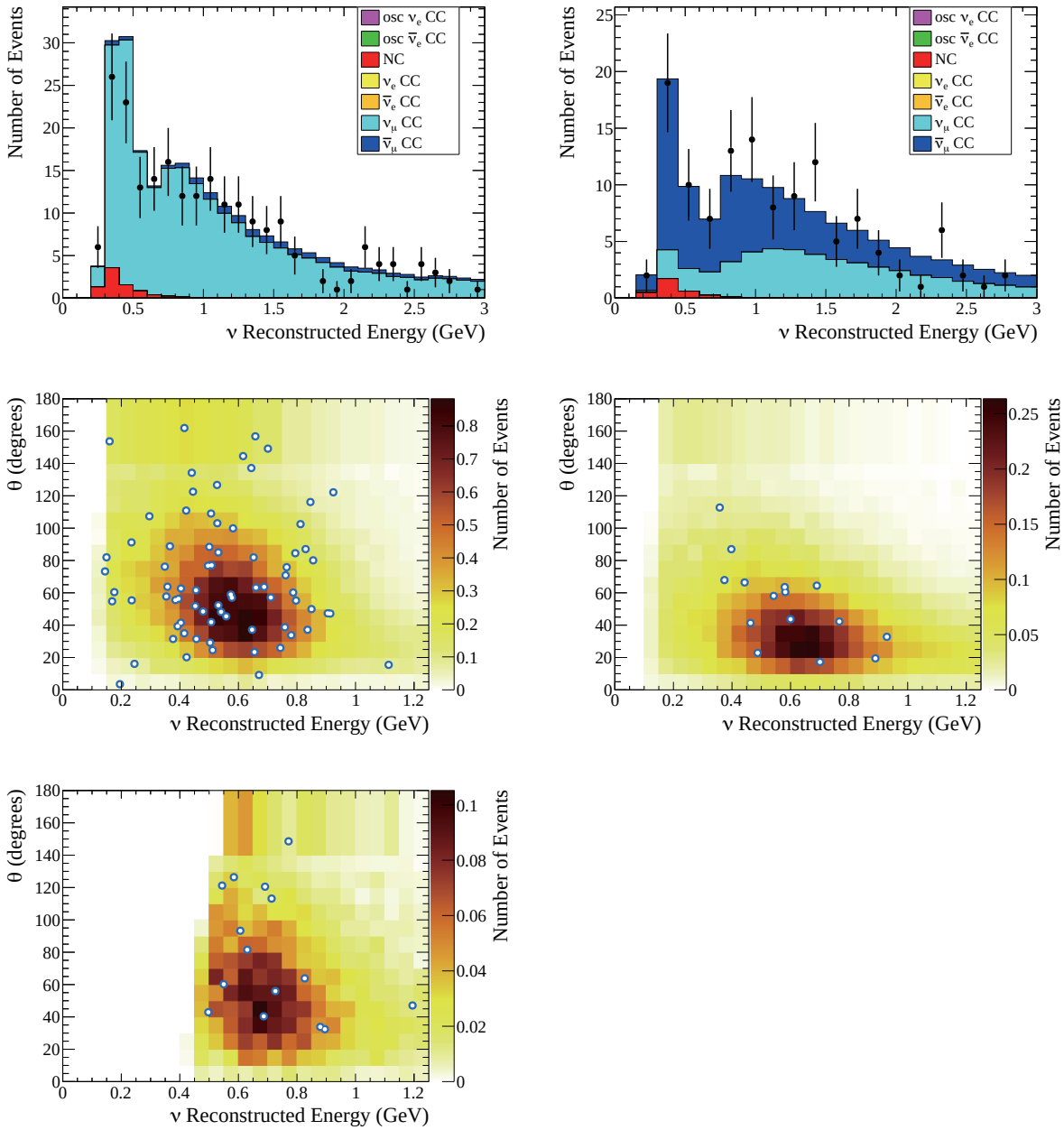

Figure 14.5: Observed kinematic distributions from T2K compared to the expectations assuming neutrino oscillations. Left and right panels correspond to data from neutrino and antineutrino beam mode, respectively. Top: Reconstructed energy distribution of single ring μ-like events. The error bars indicate the statistical uncertainty. Middle: Reconstructed energy vs. angle from beam direction of single ring e-like events with no associated decay electron. Bottom: Reconstructed energy vs. angle from beam direction of single ring e-like events with one associated decay electron for neutrino beam mode data.

Downloaded from https://academic.oup.com/ptep/article/2022/8/083C01/6651666 by KIT Library user on 27 September 2022

tector in the Soudan mine 735 km away. The neutrino beam is produced in the NuMI beamline with a 120 GeV proton beam from the Main Injector. The MINOS detectors are both iron-scintillator tracking calorimeters with toroidal magnetic fields. The far detector was 5.4 kt, while the near detector had a total mass of 0.98 kt and was located 1 km downstream of the production target. The energy spectrum of the NuMI beamline can be varied by changing the relative position of the target and horns. Most of MINOS data were taken with the "low energy" configuration with a peak energy of around 3 GeV. Since 2013, NuMI was operated with a "medium energy" configuration with the peak neutrino energy of around 7 GeV. The experiment for this period was called MINOS+. MINOS and MINOS+ combined accelerator and atmospheric neutrino data in both disappearance and appearance modes to measure oscillation parameters [115–117].

In Europe, the CNGS neutrino beamline provided a beam with mean energy of 17 GeV from CERN to LNGS for long-baseline experiments with about 730 km of baseline. The beam energy was chosen so that CC interaction of ν_τ can occur for direct confirmation of ν_τ appearance. There was no near detector in CNGS because it was not necessary for the ν_τ appearance search. The OPERA experiment used a detector consisting of an emulsion/lead target with about 1.25 kt total mass, complemented by electronic detectors. The excellent spatial resolution of the emulsion enabled the event-by-event identification of τ leptons. OPERA observed ten ν_τ CC candidate events with 2.0±0.4 expected background [118] and confirmed $\nu_\mu \to \nu_\tau$ oscillation in appearance mode with a statistical significance of 6.1σ. Another neutrino experiment, ICARUS [119], which used 600 t liquid argon time projection chambers (TPCs), was operated in Gran Sasso from 2010 to 2012.

The first generation of long-baseline experiments confirmed the existence of neutrino oscillation. The major initial goal of second-generation experiments was the observation of $\nu_\mu \to \nu_e$ oscillation. Using this appearance mode, and by comparison of neutrino and antineutrino oscillation probabilities, search for CP violation in the neutrino mixing and measurement of the mass ordering and the octant of θ_{23} become possible.

The T2K experiment started in 2010 using a newly constructed high-intensity proton synchrotron J-PARC and the Super-Kamiokande detector. It is the first long-baseline experiment to employ the off-axis neutrino beam. The off-axis angle of 2.5° was chosen to set the peak of the neutrino energy spectrum at 0.6 GeV, matching the first maximum of oscillation probability at the 295 km baseline for $\Delta m^2 \sim 2.5 \times 10^{-3}$ eV^2. T2K employs a set of near detectors at about 280 m from the production target. In 2011, T2K reported the first indication of $\nu_\mu \to \nu_e$ oscillation with a statistical significance of 2.5σ [120]. In the framework of 3ν mixing, it corresponds to detecting non-zero amplitude generated by the mixing angle θ_{13} (see Eq.14.33). Later $\nu_\mu \to \nu_e$ oscillation was established by T2K with more than 7σ in 2014 [121]. Figure 14.5 shows the observed kinematic distributions from T2K, for neutrino and antineutrino beam mode and also for muon and electron candidates. By a combined analysis of the neutrino and antineutrino data, T2K reported a hint of CP violation at the 2σ level [122, 123].

The NOvA experiment uses the upgraded NuMI beamline with an off-axis configuration. The 14 kt NOvA far detector is located near Ash River, Minnesota, 810 km away from the source. At 14.6 mrad off-axis from the central axis of the NuMI beam, the neutrino energy spectrum at the far detector has a peak of around 2 GeV. The near detector, located around 1 km from the source, has a functionally identical design to the far detector with a total mass of 290 t. Both detectors are tracking calorimeters consisting of planes of polyvinyl chloride cells alternating in vertical and horizontal orientation filled with liquid scintillator. The physics run of NOvA was started in 2014. After confirmation of ν_e appearance from ν_μ beam [124, 125], NOvA started data taking with antineutrino beam in 2016. Using the antineutrino beam data, NOvA has reported the observation of $\bar{\nu}_e$ appearance from $\bar{\nu}_\mu$ beam with 4.4σ significance [126]. Figure 14.6 shows the reconstructed neutrino energy distributions from NOvA. Some values of the CP-violating phase $\delta_{\rm CP}$ (see Eq.14.33) have been excluded for the inverted mass ordering ($m_3 < m_2 < m_1$, see Sec.14.7 for definitions), while no significant limit has been set for the case of normal mass ordering ($m_1 < m_2 < m_3$, see Sec.14.7 for definitions).

Two large-scale long-baseline experiments are under preparation. DUNE [127] will be a 1,300 km long-baseline experiment based in the US. The DUNE far detector will consist of four modules of at least 10 kt fiducial mass liquid argon time projection chambers, located 1.5 km underground at the Sanford Underground Research Facility in South Dakota. The beamline for DUNE, 1.2 MW at start and upgradable to 2.4 MW, as well as the facility for near detectors will be newly constructed at Fermilab. The Hyper-Kamiokande detector [128] in Japan will be the successor of the Super-Kamiokande detector. It will be a water Cherenkov detector with 260 kt total water mass. With upgrades to the existing accelerator and beamline, J-PARC will provide a 1.3 MW neutrino beam to Hyper-Kamiokande with a baseline of 295 km. Both DUNE and Hyper-Kamiokande will have a rich physics program besides the long-baseline experiment, such as searches for nucleon decays and study of supernova neutrinos.

14.6.3.4 *Short-baseline experiments*

The LSND experiment searched for neutrino oscillation using neutrinos from stopped pions at Los Alamos. A 800 MeV linac was used to produce pions that stopped in the target. Most of π^-s are absorbed by the nuclei inside the target, while π^+s and their daughter μ^+s decay and produce neutrinos. Therefore, the produced neutrinos are mostly ν_μ, $\bar{\nu}_\mu$, and ν_e with minimal contamination of $\bar{\nu}_e$. The detector was a tank filled with 167 t of diluted liquid scintillator, located about 30 m from the neutrino source. LSND searched for $\bar{\nu}_\mu \to \bar{\nu}_e$ appearance using the inverse beta decay process, $\bar{\nu}_e + p \to e^+ + n$, and found an excess of $87.9 \pm 22.4 \pm 6.0$ events over the expected background [129].

The KARMEN experiment was performed at the neutron spallation facility ISIS of the Rutherford Appleton Laboratory. The KARMEN 2 detector was a segmented liquid scintillation calorimeter with a total volume of 65 m^3 located at a mean distance of 17.7 m from the ISIS target. KARMEN found a number of events consistent with the total background expectation, showing no signal for $\bar{\nu}_\mu \to \bar{\nu}_e$ oscillations [130]. The resulting limits exclude large regions of the parameter area favored by LSND.

The MiniBooNE experiment at Fermilab used a conventional neutrino beam to search for ν_e and $\bar{\nu}_e$ appearance in the same parameter region as LSND. The booster neutrino beamline (BNB) with a single magnetic horn uses an 8 GeV proton beam from the Fermilab booster to produce a neutrino (antineutrino) beam with an energy spectrum peak of 600 (400) MeV. The MiniBooNE detector consists of a 12.2 m diameter sphere filled with 818 t of mineral and oil located 541 m from the target. MiniBooNE reported ν_e and $\bar{\nu}_e$ event excess in both neutrino and antineutrino running modes. In total, $638.0 \pm 52.1 \pm 122.2$ excess events are observed over the expected backgrounds, corresponding to 4.8σ significance [131].

Both LSND and MiniBooNE are single detector experiments. The reported excess will be further investigated with the multi-detector short-baseline neutrino (SBN) program at Fermilab BNB [132]. The SBN program comprises three liquid argon time projection chambers at different baselines in the same neutrino beamline. The 112 t Short-Baseline Near Detector will be located at 110 m from the target. The 85 t MicroBooNE detector has been operated at 470 m from the target. The ICARUS detector was transported from Europe after refurbishment at CERN and is located at a baseline of 600 m.

JSNS^2 experiment at J-PARC has started the search for neutrino oscillations with $\Delta m^2 \sim 1$ eV^2 [133]. 1MW proton beam from the 3 GeV Rapid Cycling Synchrotron of J-PARC produces neutrinos from muon decay at rest. With a detector filled with a gadolinium-loaded liquid scintillator of 17 t fiducial mass at 24 m from the target, JSNS^2 is aiming to provide a direct test of the LSND anomaly. The second phase with additional second detector at 48 m is under preparation.

Downloaded from https://academic.oup.com/ptep/article/2022/8/083C01/6651666 by KIT Library user on 27 September 2022

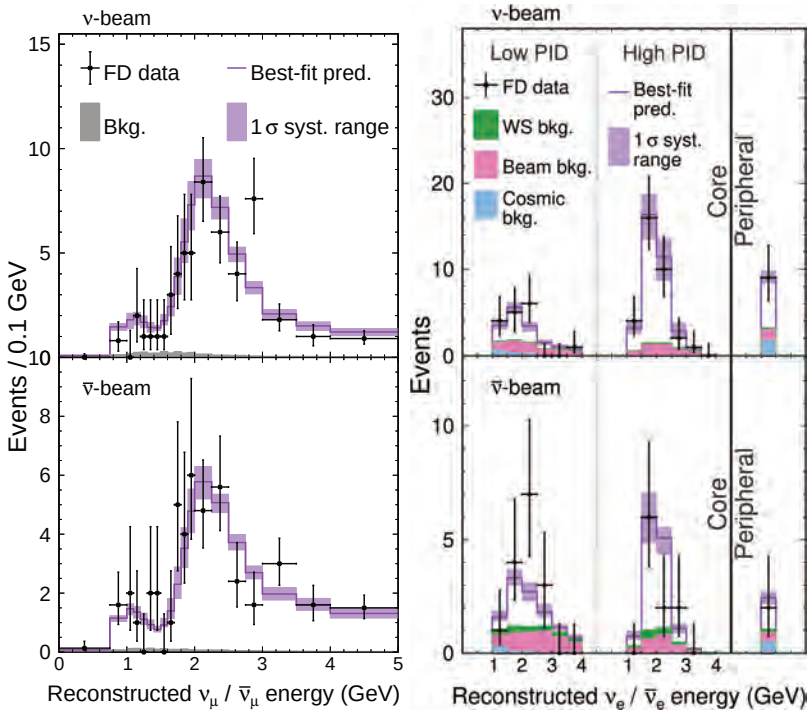

Figure 14.6: Reconstructed neutrino energy distributions from the NOvA far detector [126]. Top plots are for neutrino beam mode, and bottom plots are for antineutrino beam mode. Left: muon-type candidates. Right: electron-type candidates, split into a low and high purity sample as well as the event counts in the peripheral sample which occurred near the edge of the detector.

14.6.4 *Reactor Antineutrinos*

14.6.4.1 *Reactor antineutrino flux*

Nuclear reactors are very intense sources of $\bar{\nu}_e$'s in the MeV energy region, which are generated in nuclear fission of heavy isotopes (mainly ^{235}U, ^{238}U, ^{239}Pu, and ^{241}Pu). The $\bar{\nu}_e$ flux from a reactor can be estimated based on the thermal power output and fuel composition as a function of time. On average, about six $\bar{\nu}_e$'s are emitted, and about 200 MeV of energy is released per fission. Therefore, a 1 $\mathrm{GW_{th}}$ (thermal power) reactor produces about 2×10^{20} $\bar{\nu}_e$'s per second.

The detailed estimate of $\bar{\nu}_e$ flux and energy spectrum can be obtained by either summing up the spectra of beta decays involved using available nuclear data information of each fission fragment and its decays, or by using measurements of cumulative electron spectra associated with the beta decays of fission fragments. Because the fission of four main fuel isotopes involves thousands of beta-decay branches, a complete *ab initio* calculation is challenging. The cumulative electron spectra for ^{235}U, ^{239}Pu, and ^{241}Pu were measured at the Institut Laue-Langevin (ILL) reactor in Grenoble, France in the 1980s [134–136]. For the prediction of $\bar{\nu}_e$ flux from ^{238}U, a summation calculation in [137] was often used together with the ILL results.

A recent calculation of the reactor $\bar{\nu}_e$ flux [138] uses an improved *ab initio* approach for ^{238}U and combined information from nuclear databases and electron spectra measured at ILL for ^{235}U, ^{239}Pu, and ^{241}Pu. Another calculation [139] is provided for ^{235}U, ^{239}Pu, and ^{241}Pu based on the ILL measurement of electron spectra, taking into account higher-order corrections and minimizing the use of nuclear databases. Both calculations predict a few percent higher normalization for the energy-averaged antineutrino fluxes of ^{235}U, ^{239}Pu, and ^{241}Pu compared to the original analyses of ILL data. However, the reactor antineutrino flux measurement at Daya Bay [140] is consistent with the old flux predictions and the flux measurement results. Also, an excess of $\bar{\nu}_e$ flux around 5 MeV, compared to the prediction, has been observed by recent reactor experiments [141–144].

14.6.4.2 *Reactor antineutrino oscillation experiments*

Charged current interaction cannot happen if a reactor $\bar{\nu}_e$ changes its flavour to $\bar{\nu}_\mu$ or $\bar{\nu}_\tau$, because its energy is not sufficient to produce heavier charged leptons. Thus, $\bar{\nu}_e$ disappearance is the only channel to study neutrino flavour change with reactor experiments. The inverse beta decay $\bar{\nu}_e + p \to e^+ + n$ provides a way to detect $\bar{\nu}_e$ in the relevant energy region. The energy of prompt signal from e^+, E_p, is related to the energy of $\bar{\nu}_e$, $E_{\bar{\nu}} \sim E_p + 0.8$ MeV. The delayed coincidence with the signal from γ ray emitted by neutron capture on nucleus after thermalization very efficiently suppresses the backgrounds. A liquid scintillator is often used to realize large detectors containing hydrogen as the target of inverse beta decay. In order to increase the neutron detection efficiency, a liquid scintillator is sometimes loaded with gadolinium because of a large neutron capture cross-section and higher energy of emitted γ rays, the total energy of about 8 MeV, by gadolinium, in contrast to 2.2 MeV for the capture by hydrogen.

Early reactor experiments that searched for neutrino oscillations at short or intermediate baselines reported negative results. The CHOOZ [145] and Palo Verde [146] experiments in the 1990's searched for neutrino oscillations in the $\Delta m^2 \sim 10^{-2}$–10^{-3} eV^2 range and set a limit on the corresponding mixing angle $\sin^2 2\theta < 0.1$ at 90% CL.

Table 14.4 shows a list of reactor antineutrino experiments measuring neutrino oscillation. As was also shown in Table 14.1, experiments are designed with different baselines because of the different scale of mass splittings found by solar and atmospheric neutrino experiments. Experiments with O(100) km baseline are sensitive to Δm^2 of 10^{-4}–10^{-5} eV^2, while $\sim$ 1 km of baseline results in a sensitivity in the range of 10^{-2}–10^{-3} eV^2.

The KamLAND detector consists of 1,000 t of ultra-pure liquid scintillator contained in a 13-m diameter spherical balloon [147]. The detector is located in the original Kamiokande cavern, where the $\bar{\nu}_e$ flux was dominated by a few reactors at an average distance of $\sim$180 km until 2011. KamLAND reported the first results in 2002 showing that the ratio of the observed number of $\bar{\nu}_e$ events and expectation without disappearance is $0.611 \pm 0.085 \pm 0.041$, evidence for reactor $\bar{\nu}_e$ disappearance at the 99.95% confidence

Downloaded from https://academic.oup.com/ptep/article/2022/8/083C01/6651666 by KIT Library user on 27 September 2022

Table 14.4: List of reactor antineutrino oscillation experiments

Name	Reactor power (GW_{th})	Baseline (km)	Detector mass (t)	Year
KamLAND	various	180 (ave.)	1,000	2001–
Double Chooz	4.25×2	1.05	8.3	2011–2018
Daya Bay	2.9×6	1.65	20×4	2011–2020
RENO	2.8×6	1.38	16	2011–
JUNO	26.6 (total)	53	20,000	

Table 14.5: List of reactor antineutrino experiments for O(eV^2) oscillations

Name	Reactor power (MW_{th})	Baseline (m)	Detector mass (t)	Detector technology	σ_E/E @1 MeV(%)	S/B
NEOS	2,800	24	1	Gd-LS	5	22
DANSS	3,100	10–13	0.9	Gd-PS	34	∼30
STEREO	57	9–11	1.7	Gd-LS	10	0.9
PROSPECT	85	7–9	4	^{6}Li-LS	4.5	1.3
NEUTRINO-4	100	6–12	1.5	Gd-LS	16	0.5
SoLid	80	6–9	1.6	^{6}Li-PS	14	

level [147]. It confirmed a large value of the mixing angle corresponding to the LMA solution, which was reported by solar neutrino experiments. KamLAND also showed the evidence of $\bar{\nu}_e$ spectrum distortion consistent with the expectation from neutrino oscillations [148]. Figure 14.7 shows the ratio of observed $\bar{\nu}_e$ spectrum to the expectation for no-oscillation as a function of L_0/E ($L_0 = 180$ km) for the KamLAND data. A clear oscillatory signature can be seen.

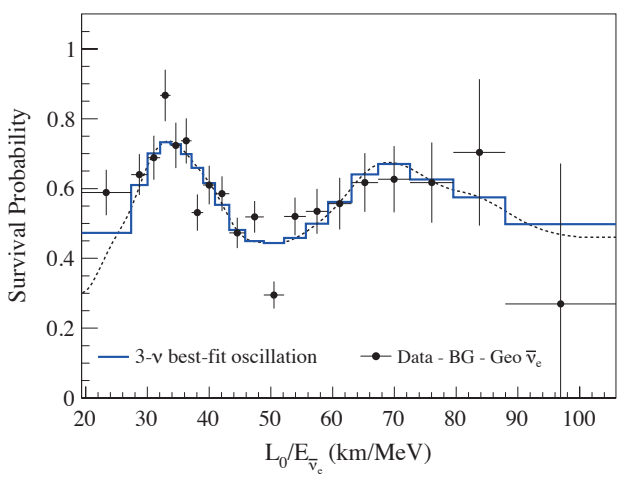

Figure 14.7: Ratio of the observed $\bar{\nu}_e$ spectrum to the expectation for no-oscillation versus L_0/E for the KamLAND data. $L_0 = 180$ km is the flux-weighted average reactor baseline. The 3-ν histogram is the best-fit survival probability curve from the three-flavour unbinned maximum-likelihood analysis using only the KamLAND data. This figure is taken from [149].

Following the establishment of neutrino oscillations with atmospheric, solar, accelerator, and reactor experiments, the measurement of the remaining mixing angle θ_{13} was recognized as the next major milestone. A reactor neutrino experiment with a baseline of ∼1 km can make an almost pure measurement of $\sin^2 2\theta_{13}$ from the disappearance of $\bar{\nu}_e$. To be sensitive to a small value below the limit set by CHOOZ and Palo Verde, experiments with two detectors were proposed. Among several proposals, three experiments have been realized: Double Chooz in France, Daya Bay in China, and RENO in Korea.

These three experiments employ a similar detector design optimized for the precise measurement of a reactor antineutrino. An antineutrino detector consists of a cylindrical stainless steel vessel that houses two nested acrylic cylindrical vessels. The innermost vessel is filled with gadolinium-doped liquid scintillator as the primary antineutrino target. It is surrounded by a liquid scintillator layer to contain γ rays from the target volume. A buffer layer of mineral oil is placed outside to shield inner volumes from radioactivity of PMTs and surrounding rock. The light from liquid scintillator is detected by an array of PMTs mounted on the stainless steel vessel. Optically separated by the stainless steel vessel, the outside region is instrumented as a veto detector with either liquid scintillator (Double Chooz) or water Cherenkov (Daya Bay and RENO) detector.

The Double Chooz detector has a gadolinium-doped liquid scintillator with a mass of 8.3 t. The far detector at a baseline of ∼1050 m from the two 4.25 GW_{th} reactors started physics data taking in 2011. The near detector, located at ∼400 m from the reactors, was completed in the end of 2014. Double Chooz finished data taking in early 2018. Daya Bay has two near (flux-weighted baseline 470 m and 576 m), and one far (1648 m) underground experimental halls near six reactors with 2.9 GW_{th} each. Daya Bay has eight antineutrino detectors in total; two detectors in each of the near detector halls, and four detectors in the far detector hall. Each detector contains 20 t of gadolinium-loaded liquid scintillator. RENO has two identical detectors located at 294 m and 1383 m from the center of an array of six 2.8 GW_{th} reactors. The mass of the gadolinium-loaded liquid scintillator is 16 t per detector. RENO started data taking with both near and far detectors from August 2011.

All three reactor neutrino experiments published their first results in 2012. First, Double Chooz reported an indication of reactor electron antineutrino disappearance with the ratio of observed to expected events of $R = 0.944 \pm 0.016 \pm 0.04$, ruling out the no-oscillation hypothesis at the 94.6% CL [150]. Daya Bay observed $R = 0.940 \pm 0.011 \pm 0.004$, corresponding to 5.2σ significance of non-zero value of θ_{13} [151]. RENO also reported $R = 0.920 \pm 0.009 \pm 0.014$, indicating a non-zero value of θ_{13} with a significance of 4.9σ [152]. These results established a non-zero value of θ_{13}.

Both Daya Bay [141] and RENO [142] report results constraining mass-squared difference as well as the mixing angle by using both relative $\bar{\nu}_e$ rate and energy spectra information. Double Chooz has reported the analysis based on both far and near detectors [143] for the mixing angle, using neutron capture on any elements (primarily gadolinium and hydrogen) to increase the effective target mass. Figure 14.8 shows the energy spectra of the prompt signals observed in the far detector of three experiments.

In all three experiments, as well as in the NEOS experiment [144], an excess of $\bar{\nu}_e$ events over the expected energy spectrum has been observed around 5 MeV, as mentioned earlier. This excess is observed in both near and far detectors and scales with

Downloaded from https://academic.oup.com/ptep/article/2022/8/083C01/6651666 by KIT Library user on 27 September 2022

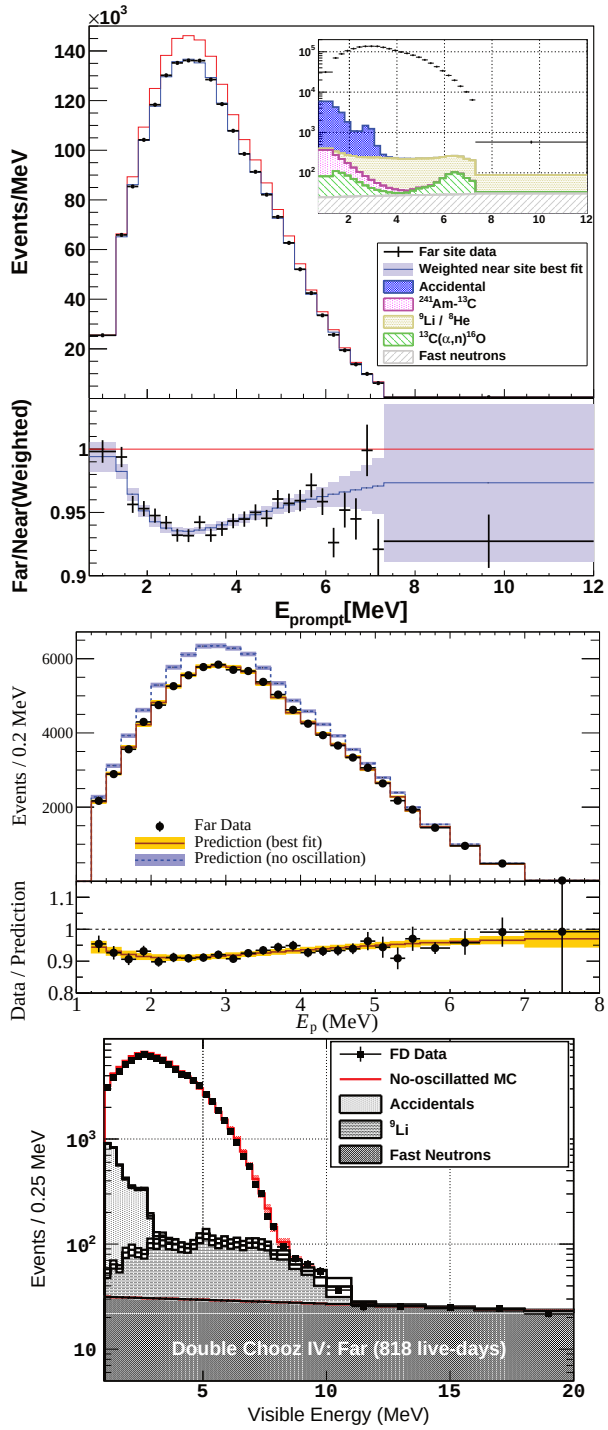

Figure 14.8: Energy spectra for prompt events at the far detectors for Daya Bay [141], RENO [142], and Double Chooz [143].

the reactor power. Thanks to the cancellation between the near and far detectors, the neutrino oscillation measurements are not affected in a multi-detector setup.

With a baseline of ∼50 km and an excellent energy measurement, reactor antineutrino experiments have significant sensitivity to the mass ordering. The JUNO detector, which is under construction, will consist of a 20 kt liquid scintillator and be located at 53 km from two nuclear power plants in China [153]. The JUNO experiment aims to determine the mass ordering with this technique as its primary goal. It can also provide precision measurements of neutrino mixing parameters as well as a broad non-oscillation science program.

14.6.4.3 *New reactor experiments sensitive to O(1) eV² oscillations*

Possible hints of neutrino oscillation at a scale of $\Delta m^2 \sim 1$ eV^2 (see Sec.14.8) have motivated reactor experiments at a distance of ∼10 m from the core. Recent experiments searching for ∼1 eV^2 oscillation at reactors are summarized in Table 14.5.

As the antineutrino source, some use commercial reactors, which can provide a large flux leading to high statistical precision. On the other hand, though the flux is orders of magnitude smaller, a research reactor could have favorable conditions such as relatively easier access to a short baseline, simpler fuel composition, and compact core size.

The detectors are based on organic scintillators, either liquid scintillator (LS) or solid plastic scintillator (PS), which contain hydrogen as the target for inverse beta decay ($\bar{\nu}_e + p \to e^+ + n$). To identify the signal, neutron capture on either gadolinium (Gd) or ^{6}Li is detected with delayed coincidence. When a neutron is captured by Gd, γ rays with a total energy of 8 MeV are emitted. After neutron capture, ^{6}Li decays into triton and α. The effect of neutrino oscillation appears as a distortion of energy spectrum. To be independent from the reactor neutrino spectrum uncertainties, some experiments compare the spectra at different baselines by using a segmented detector or moving the detector.

NEOS [144] uses about 1 t of gadolinium-loaded liquid scintillator in an unsegmented detector. It is located at 23.7 m from the center of a commercial reactor and covered by an overburden of about 20 meters of water equivalent.

DANSS [154] is another experiment using a commercial reactor. The detector is highly segmented, consisting of 2,500 plastic scintillator strips, each with the size of $1 \times 4 \times 100$ cm^3 and coated with a thin gadolinium-loaded reflective layer. The detector is placed on a movable platform below the reactor core, which varies the distance to the core from 10.7 to 12.7 m.

The STEREO detector [155] has six identical target cells of 37 cm length, ∼ 2m^3 of volume in total, filled with gadolinium-loaded liquid scintillator. They are placed from 9.4 to 11.1 m from the compact (80 cm high, 40 cm diameter) core of the ILL research reactor.

The PROSPECT detector [156] consists of a segmented 4 t ^{6}Li-doped liquid scintillator detector. It covers a baseline range of 7–9 m from the highly ^{235}U enriched reactor core of the High Flux Isotope Reactor (HFIR) at Oak Ridge National Laboratory. Thin reflecting panels divide the LS volume into an 11 × 14 two-dimensional array of 154 optically isolated rectangular segments ($14.5 \times 14.5 \times 117.6$ cm^3).

NEUTRINO-4 [157, 158] uses a gadolinium-loaded liquid scintillator detector segmented in 10×5 sections with a total volume of 1.8 m^3. The detector is installed on a movable platform and moved to various positions with baselines of 6–12 m from the SM-3 reactor core in Russia.

The SoLid detector [159] is a finely segmented detector made of $5 \times 5 \times 5$ cm^3 plastic scintillator cubes and ^{6}LiF:ZnS sheets. Using the difference of time constant of scintillation between ZnS and the plastic scintillator a n-γ separation capability is achieved. A detector with 1.6 t of active volume is installed at a distance of 6–9 m from the research reactor core in the BR2 reactor, Belgium.

14.7 Combined Analysis of Experimental Results: The 3ν Paradigm

From the experimental situation described in Sec.14.6 we conclude that

- Atmospheric ν_μ and $\bar{\nu}_\mu$ disappear most likely converting to ν_τ and $\bar{\nu}_\tau$. The results show an energy and distance dependence perfectly described by mass-induced oscillations.
- Accelerator ν_μ and $\bar{\nu}_\mu$ disappear over distances of ∼ 200 to 800 km. The energy spectrum of the results show a clear oscillatory behavior also in accordance with mass-induced oscillations with a wavelength in agreement with the effect observed in atmospheric neutrinos.
- Accelerator ν_μ and $\bar{\nu}_\mu$ appear as ν_e and $\bar{\nu}_e$ at distances ∼ 200 to 800 km.

Downloaded from https://academic.oup.com/ptep/article/2022/8/083C01/6651666 by KIT Library user on 27 September 2022

- Solar ν_e convert to ν_μ and/or ν_τ. The observed energy dependence of the effect is well described by massive neutrino conversion in the Sun matter according to the MSW effect
- Reactor $\bar{\nu}_e$ disappear over distances of ~ 200 km and ~ 1.5 km with different probabilities. The observed energy spectra show two different mass-induced oscillation wavelengths: at short distances in agreement with the one observed in accelerator ν_μ disappearance, and a long-distance compatible with the required parameters for MSW conversion in the Sun.

The minimum scenario to describe these results requires the mixing between the three flavour neutrinos of the standard model in three distinct mass eigenstates. In this case U in Eq. (14.32) is a 3×3 matrix analogous to the CKM matrix for the quarks [21], but due to the possible Majorana nature of the neutrinos it can depend on six independent parameters: three mixing angles and three phases. There are several possible conventions for the ranges of the angles and ordering of the states. The community finally agreed to a parametrization of the leptonic mixing matrix as in Eq. (14.33). The angles θ_{ij} can be taken without loss of generality to lie in the first quadrant, $\theta_{ij} \in [0, \pi/2]$, and the phase $\delta_{\rm CP} \in [0, 2\pi]$. Values of $\delta_{\rm CP}$ different from 0 and π imply CP violation in neutrino oscillations in vacuum [160–162]. The Majorana phases η_1 and η_2 play no role in neutrino oscillations [161, 163]. Hence for the study of neutrino oscillations in the 3ν mixing scenario one can use the parametrization in Eq. (14.34) irrespective of whether neutrinos are Dirac or Majorana particles. Indeed, Majorana phases are very hard to measure since they are only physical if neutrino mass is non-zero, and therefore, the amplitude of any process involving them is suppressed by a factor m_ν/E to some power where E is the energy involved in the process, which is typically much larger than the neutrino mass. The most sensitive experimental probe of Majorana phases is the rate of neutrinoless $\beta\beta$ decay discussed in Secs. 14.9.3 and 14.9.2.

In this convention there are two non-equivalent orderings for the spectrum of neutrino masses:

– Spectrum with Normal Ordering (NO) with $m_1 < m_2 < m_3$
– Spectrum Inverted ordering (IO) with $m_3 < m_1 < m_2$.

Furthermore, the data show a hierarchy between the mass splittings, $\Delta m^2_{21} \ll |\Delta m^2_{31}| \simeq |\Delta m^2_{32}|$ with $\Delta m^2_{ij} \equiv m_i^2 - m_j^2$.

In this section, we follow the convention used in the listing section of the PDG and discuss the results for both, NO and IO, using Δm^2_{21}, which is always the smallest mass splitting, and Δm^2_{32}, which up to a sign, is the largest mass splitting for IO, while for NO the largest mass splitting is $\Delta m^2_{31} = \Delta m^2_{32} + \Delta m^2_{21}$.

With what we know of the mass differences (see table 14.7) and the neutrino mass scale (see Sec. 14.9), depending on the value of the lightest neutrino mass, the neutrino mass spectrum can be further classified in:

– Normal Hierarchical Spectrum (NH): $m_1 \ll m_2 < m_3$, $\Rightarrow m_2 \simeq \sqrt{\Delta m^2_{21}} \sim 8.6\times10^{-3}$eV, $m_3 \simeq \sqrt{\Delta m^2_{32} + \Delta m^2_{21}} \sim 0.05$eV,

– Inverted Hierarchical Spectrum (IH): $m_3 \ll m_1 < m_2$, $\Rightarrow m_1 \simeq \sqrt{|\Delta m^2_{32} + \Delta m^2_{21}|} \sim 0.0492$eV, $m_2 \simeq \sqrt{|\Delta m^2_{32}|} \sim 0.05$eV,

– Quasidegenerate Spectrum (QD): $m_1 \simeq m_2 \simeq m_3 \gg \sqrt{|\Delta m^2_{32}|}$.

Sometimes in the literature the determination of the neutrino mass spectrum is referred to as determination of the neutrino hierarchy. However, as described above, with what we know so far of the neutrino mass scale, the neutrino spectrum may or may not be hierarchical. Therefore determination of neutrino mass ordering is a more precise expression, and it is the one used in this review.

In total, the 3-ν oscillation analysis of the existing data involves six parameters: 2 mass differences (one of which can be positive or negative), 3 mixing angles, and the CP phase. The different experiments described in Sec.14.6 provide information on different subsets of these parameters. The precise statistical analysis of the data requires the numerical evaluation of the corresponding oscillation probabilities by solving the evolution equation of the neutrino ensemble from their source to the experiment. Nevertheless, the dominant effects in the different experiments can be qualitatively understood in terms of approximate expressions for the oscillation probabilities which, for convenience, we briefly summarize here.

14.7.1 *3ν Oscillation Probabilities*

The relevant survival probabilities for solar and KamLAND experiments in the framework of three neutrino oscillations can be written as:

$$P^{3\nu}_{ee} = \sin^4\theta_{13} + \cos^4\theta_{13} P^{2\nu}_{ee}(\Delta m^2_{21}, \theta_{12}), \tag{14.72}$$

where we have used the fact that $L^{\rm osc}_{0,32} = 4\pi E_\nu/\Delta m^2_{32}$ is much shorter than the distance traveled by both solar and KamLAND neutrinos, so that the oscillations related to $L^{\rm osc}_{0,32}$ are averaged. In the presence of matter effects $P^{2\nu}_{ee}(\Delta m^2_{21}, \theta_{12})$ should be calculated, taking into account the evolution in an effective matter density $n_e^{\rm eff} = n_e \cos^2\theta_{13}$. For $10^{-5} \lesssim \Delta m^2/{\rm eV}^2 \lesssim 10^{-4}$, $P^{2\nu}_{ee}(\Delta m^2_{21}, \theta_{12})$ presents the following asymptotic behaviors [164]:

$$P^{2\nu,{\rm sun}}_{ee} \simeq 1 - \frac{1}{2}\sin^2(2\theta_{12}) \qquad \text{for } E_\nu \lesssim \text{few} \times 100 \text{ keV}, \tag{14.73}$$

$$P^{2\nu,{\rm sun}}_{ee} \simeq \sin^2(\theta_{12}) \qquad \text{for } E_\nu \gtrsim \text{few} \times 1 \text{ MeV}, \tag{14.74}$$

$$P^{2\nu,{\rm kam}}_{ee} = 1 - \sin^2(2\theta_{12})\sin^2\frac{\Delta m^2_{21} L}{4E_\nu}. \tag{14.75}$$

At present most of the precision of the solar analysis is provided by SNO and SK, for which the relevant MSW survival probability provides a direct measurement of $\sin^2\theta_{12}$, as seen in Eq. (14.74). In the MSW regime, the determination of Δm^2_{21} in solar experiments comes dominantly from the ratio between the solar potential and the Δm^2_{21} term required to simultaneously describe the CC/NC data at SNO and the undistorted spectra of ^{8}B neutrinos as measured in both SK and SNO. Conversely, KamLAND $\bar{\nu}_e$ survival probability proceeds dominantly as vacuum oscillations and provides a most precise determination of Δm^2_{21} via the strong effect of the oscillating phase in the distortion of the reactor energy spectrum. On the contrary, it yields a weaker constraint on θ_{12} as the vacuum oscillation probability depends on the double-valued and "flatter" function $\sin^2(2\theta_{12})$.

In what respects the interpretation of ν_μ disappearance data, at LBL experiments, the ν_μ survival probability can be expanded in the small parameters $\sin\theta_{13}$ and $\alpha \equiv \Delta m^2_{21}/\Delta m^2_{31}$ to good accuracy as [165, 166]

$$\begin{aligned} P_{\nu_\mu\to\nu_\mu} &\approx 1 - \sin^2 2\theta_{\mu\mu}\sin^2\frac{\Delta m^2_{\mu\mu} L}{4E_\nu} \\ &\approx 1 - \cos^2\theta_{13}\sin^2(2\theta_{23})\sin^2\frac{\Delta m^2_{32} L}{4E_\nu} + \mathcal{O}(\alpha, s^2_{13}), \end{aligned} \tag{14.76}$$

with

$$\begin{aligned} \sin^2\theta_{\mu\mu} &= \cos^2\theta_{13}\sin^2\theta_{23}, \\ \Delta m^2_{\mu\mu} &= \sin^2\theta_{12}\Delta m^2_{31} + \cos^2\theta_{12}\Delta m^2_{32} \\ &\quad + \cos\delta_{\rm CP}\sin\theta_{13}\sin 2\theta_{12}\tan\theta_{23}\Delta m^2_{21}. \end{aligned}$$

At present ν_μ disappearance results at LBL provide the best determination of $|\Delta m^2_{32}|$ and θ_{23}, but as seen above, the probability is symmetric with respect to the octant of $\theta_{\mu\mu}$, which implies symmetry around $s^2_{23} = 0.5/c^2_{13}$.

The relevant oscillation probability for ν_e appearance at LBL experiments can be expanded at the second order in the small

Downloaded from https://academic.oup.com/ptep/article/2022/8/083C01/6651666 by KIT Library user on 27 September 2022

parameters $\sin\theta_{13}$ and α, and assuming a constant matter density it takes the form [167–169]:

$$P_{\nu_\mu\to\nu_e,(\bar\nu_\mu\to\bar\nu_e)} \approx 4\,\sin^2\theta_{13}\,\sin^2\theta_{23}\frac{\sin^2\Delta}{(1-A)^2} + \alpha^2\sin^2 2\theta_{12}\,\cos^2\theta_{23}\frac{\sin^2 A\Delta}{A^2} + 8\,\alpha\,J_{\rm CP}^{\rm max}\cos(\Delta\pm\delta_{\rm CP})\,\frac{\sin\Delta A}{A}\,\frac{\sin\Delta(1-A)}{1-A}\,, \tag{14.77}$$

with

$$J_{\rm CP}^{\rm max} = \cos\theta_{12}\sin\theta_{12}\cos\theta_{23}\sin\theta_{23}\cos^2\theta_{13}\sin\theta_{13}\,, \tag{14.78}$$

and

$$\Delta \equiv \frac{\Delta m_{31}^2 L}{4E_\nu}\,,\quad A \equiv \frac{2E_\nu V}{\Delta m_{31}^2}\,, \tag{14.79}$$

where V is the effective matter potential in the Earth's crust. Results on ν_e appearance at LBL provide us with the dominant information on leptonic CP violation. Furthermore, α, Δ, and A are sensitive to the sign of Δm_{32}^2 (*i.e.*, the type of the neutrino mass ordering). The plus (minus) sign in Eq. (14.77) applies for neutrinos (antineutrinos), and for antineutrinos $V\to -V$, which implies $A\to -A$. Numerically one finds for a typical Earth crust matter density of 3 g/cm^3 that at T2K with $E\sim 0.7$ GeV, matter effects cause $\sim\pm 10\%$ differences in the rates, whereas in NOvA with $E\sim 2$ GeV, we can have $|A|\sim 0.2$. Also, $\alpha^2\approx 10^{-3}$, which implies that the second term in the first line of Eq. (14.77) gives a very small contribution compared to the other terms. Also, the first term in Eq. (14.77) (which dominates for large θ_{13}) depends on $\sin^2\theta_{23}$ and therefore is sensitive to the octant.

The ν_e survival probability relevant for reactor experiments with medium baseline (MBL), $L\sim 1$ km, can be approximated as [166, 170]:

$$P_{\nu_e\to\nu_e} = 1-\sin^2 2\theta_{13}\sin^2\frac{\Delta m_{ee}^2 L}{4E_\nu} + \mathcal{O}(\alpha^2)\,, \tag{14.80}$$

where

$$\Delta m_{ee}^2 = \cos^2\theta_{12}\Delta m_{31}^2 + \sin^2\theta_{12}\Delta m_{32}^2\,. \tag{14.81}$$

These MBL reactor experiments provide the most precise determination of θ_{13}. Furthermore there is an additional effect sensitive to the mass ordering when comparing the disappearance of ν_μ at LBL experiments – which is symmetric with respect to the sign of $\Delta m_{\mu\mu}^2$ given in Eq.(14.7.1) – with that of ν_e disappearance at MBL reactors which is symmetric with respect to the slightly different effective mass-squared difference Δm_{ee}^2 given in Eq. (14.81).

Finally, for atmospheric neutrinos, the fluxes contain ν_e, ν_μ, $\bar\nu_e$, and $\bar\nu_\mu$, and for a good fraction of the events, neutrinos travel through the Earth's matter. In the context of 3ν mixing, the dominant oscillation channel of atmospheric neutrinos is $\nu_\mu\to\nu_\tau$ driven by $|\Delta m_{32}^2|$ with an amplitude controlled by θ_{23} with subleading oscillation modes, triggered by Δm_{21}^2 and/or θ_{13}, which depend on the octant of θ_{23}, on the mass ordering, and on $\delta_{\rm CP}$. In that respect, an interesting observable is the deviation of e-like events relative to the no-oscillation prediction N_e^0, since in the two-flavour limit one expects $N_e = N_e^0$. Such deviation can be written in the following way (see, *e.g.*, [171]):

$$\frac{N_e}{N_e^0} - 1 \approx (r\sin^2\theta_{23}-1)P_{2\nu}(\Delta m_{32}^2,\theta_{13}) + (r\cos^2\theta_{23}-1)P_{2\nu}(\Delta m_{21}^2,\theta_{12}) - \sin\theta_{13}\sin 2\theta_{23}\,r\,\Re(A_{ee}^* A_{\mu e})\,. \tag{14.82}$$

Here $r\equiv\Phi_\mu/\Phi_e$ is the flux ratio with $r\approx 2$ in the sub-GeV range and $r\approx 2.6\to 4.5$ in the multi-GeV range. $P_{2\nu}(\Delta m^2,\theta)$ is an effective two-flavour oscillation probability, and $A_{ee}, A_{\mu e}$ are elements of a transition amplitude matrix. The three terms appearing in Eq. (14.82) have a well-defined physical interpretation. The first term is important in the multi-GeV range and is controlled by the mixing angle θ_{13} in $P_{2\nu}(\Delta m_{32}^2,\theta_{13})$. This probability can be strongly affected by resonant matter effects [172–177]. Depending on the mass ordering, the resonance will occur either for neutrinos or antineutrinos. The second term is important for sub-GeV events, and it takes into account the effect of oscillations due to Δm_{21}^2 and θ_{12} [178–181]. Via the pre-factor containing the flux ratio r both, the first and second terms in Eq. (14.82) depend on the octant of θ_{23}, though in opposite directions: the multi-GeV (sub-GeV) excess is suppressed (enhanced) for $\theta_{23}<45^\circ$. Finally, the last term in Eq. (14.82) is an interference term between θ_{13} and Δm_{21}^2 amplitudes and this term shows also dependence on the CP phase $\delta_{\rm CP}$ [171, 181].

Subdominant three neutrino effects can also affect μ-like events. For example, for multi-GeV muon events one can write the excess in μ-like events as [182, 183]

$$\frac{N_\mu}{N_\mu^0} - 1 \approx \sin^2\theta_{23}\left(\frac{1}{r}-\sin^2\theta_{23}\right)P_{2\nu}(\Delta m_{32}^2,\theta_{13}) - \frac{1}{2}\sin^2 2\theta_{23}\,[1-\Re(A_{33})]\,. \tag{14.83}$$

The first term is controlled by θ_{13} and is subject to resonant matter effects, similar to the first term in Eq. (14.82), though with a different dependence on θ_{23} and the flux ratio. In the second term, A_{33} is a probability amplitude satisfying $P_{2\nu}(\Delta m_{32}^2,\theta_{13}) = 1-|A_{33}|^2$. In the limit $\theta_{13}=0$ we have $\Re(A_{33})=\cos(\Delta m_{32}^2 L/2E)$, such that the second term in Eq. (14.83) just describes two-flavour $\nu_\mu\to\nu_\mu$ vacuum oscillations.

14.7.2 *3ν Oscillation Analysis*

We summarize in Table 14.6 the different experiments which dominantly contribute to the present determination of the different parameters in the chosen convention.

The table illustrates that the determination of the leptonic parameters requires global analyses of the data from the different experiments. Over the years, these analyses have been in the hands of a few phenomenological groups. We show in Table 14.7 the results from the latest analyses in Refs. [184–187]. For the sake of comparison, all results are presented in the convention of the listing section as described above.

The table illustrates the dependence of the present determination of the parameters on variations of the statistical analysis performed by the different groups and on the data samples included. In that last respect, the main difference resides in the results from Super-Kamiokande atmospheric data [97] which, at present, can only be included in this analysis by directly adding the χ^2 tabulated χ^2 map provided by the experiment.

Altogether the different analyses find consistent results, in particular on the better-known parameters, θ_{12}, θ_{13} and Δm_{21}^2 and $|\Delta m_{32}^2|$. The issues which still require clarification are the mass ordering discrimination, the determination of θ_{23} and the leptonic CP phase $\delta_{\rm CP}$:

- In all analyses the best fit is for the normal mass ordering. Inverted ordering is disfavoured with a $\Delta\chi^2$, which ranges from slightly above 2σ – driven by the interplay of long-baseline accelerator and short-baseline reactor data – to 3σ when adding the atmospheric χ^2 table from Ref. [97].
- All analyses find some preference for the second octant of θ_{23} but with statistical significance still well below 3σ.
- The best fit for the complex phase in NO is at $\delta_{\rm CP}\sim 120^\circ$, but CP conservation (for $\delta_{\rm CP}\sim 180^\circ$) is still allowed at a confidence level (CL) of 1-2σ. We notice that, at present, the significance of CP violation in the global analysis is reduced with respect to that reported by T2K [188] because NOvA data does not show a significant indication of CP violation.

14.7.3 *Convention-independent Measures of Leptonic CP Violation in 3ν Mixing*

In the framework of 3ν mixing leptonic CP violation can also be quantified in terms of the leptonic Jarlskog invariant [189],

Downloaded from https://academic.oup.com/ptep/article/2022/8/083C01/6651666 by KIT Library user on 27 September 2022

Table 14.6: Experiments contributing to the present determination of the oscillation parameters.

Experiment	Dominant	Important
Solar Experiments	θ_{12}	Δm^2_{21} , θ_{13}
Reactor LBL (KamLAND)	Δm^2_{21}	θ_{12} , θ_{13}
Reactor MBL (Daya-Bay, Reno, D-Chooz)	θ_{13}, $\lvert\Delta m^2_{31,32}\rvert$	
Atmospheric Experiments (SK, IC-DC)		θ_{23},$\lvert\Delta m^2_{31,32}\rvert$, θ_{13},$\delta_{\rm CP}$
Accel LBL ν_μ,$\bar\nu_\mu$, Disapp (K2K, MINOS, T2K, NOνA)	$\lvert\Delta m^2_{31,32}\rvert$, θ_{23}	
Accel LBL ν_e,$\bar\nu_e$ App (MINOS, T2K, NOνA)	$\delta_{\rm CP}$	θ_{13} , θ_{23}

Table 14.7: 3ν oscillation parameters obtained from different global analyses of neutrino data. In all cases, the numbers labeled as NO (IO) are obtained assuming NO (IO), *i.e.*, relative to the respective local minimum. SK-ATM makes reference to the tabulated χ^2 map from the Super-Kamiokande analysis of their data in Ref. [97].

	Ref. [185] w/o SK-ATM		Ref. [185] w SK-ATM		Ref. [186] w SK-ATM		Ref. [187] w SK-ATM	
NO	Best Fit Ordering		Best Fit Ordering		Best Fit Ordering		Best Fit Ordering	
Param	bfp $\pm1\sigma$	3σ range	bfp $\pm1\sigma$	3σ range	bfp $\pm1\sigma$	3σ range	bfp $\pm1\sigma$	3σ range
$\frac{\sin^2\theta_{12}}{10^{-1}}$	$3.10^{+0.13}_{-0.12}$	$2.75 \to 3.50$	$3.10^{+0.13}_{-0.12}$	$2.75 \to 3.50$	$3.04^{+0.14}_{-0.13}$	$2.65 \to 3.46$	$3.20^{+0.20}_{-0.16}$	$2.73 \to 3.79$
$\theta_{12}/^\circ$	$33.82^{+0.78}_{-0.76}$	$31.61 \to 36.27$	$33.82^{+0.78}_{-0.76}$	$31.61 \to 36.27$	$33.46^{+0.87}_{-0.88}$	$30.98 \to 36.03$	$34.5^{+1.2}_{-1.0}$	$31.5 \to 38.0$
$\frac{\sin^2\theta_{23}}{10^{-1}}$	$5.58^{+0.20}_{-0.33}$	$4.27 \to 6.09$	$5.63^{+0.18}_{-0.24}$	$4.33 \to 6.09$	$5.51^{+0.19}_{-0.80}$	$4.30 \to 6.02$	$5.47^{+0.20}_{-0.30}$	$4.45 \to 5.99$
$\theta_{23}/^\circ$	$48.3^{+1.2}_{-1.9}$	$40.8 \to 51.3$	$48.6^{+1.0}_{-1.4}$	$41.1 \to 51.3$	$47.9^{+1.1}_{-4.0}$	$41.0 \to 50.9$	$47.7^{+1.2}_{-1.7}$	$41.8 \to 50.7$
$\frac{\sin^2\theta_{13}}{10^{-2}}$	$2.241^{+0.066}_{-0.065}$	$2.046 \to 2.440$	$2.237^{+0.066}_{-0.065}$	$2.044 \to 2.435$	$2.14^{+0.09}_{-0.07}$	$1.90 \to 2.39$	$2.160^{+0.083}_{-0.069}$	$1.96 \to 2.41$
$\theta_{13}/^\circ$	$8.61^{+0.13}_{-0.13}$	$8.22 \to 8.99$	$8.60^{+0.13}_{-0.13}$	$8.22 \to 8.98$	$8.41^{+0.18}_{-0.14}$	$7.9 \to 8.9$	$8.45^{+0.16}_{-0.14}$	$8.0 \to 8.9$
$\delta_{\rm CP}/^\circ$	222^{+38}_{-28}	$141 \to 370$	221^{+39}_{-28}	$144 \to 357$	238^{+41}_{-33}	$149 \to 358$	218^{+38}_{-27}	$157 \to 349$
$\frac{\Delta m^2_{21}}{10^{-5}\ \mathrm{eV}^2}$	$7.39^{+0.21}_{-0.20}$	$6.79 \to 8.01$	$7.39^{+0.21}_{-0.20}$	$6.79 \to 8.01$	$7.34^{+0.17}_{-0.14}$	$6.92 \to 7.91$	$7.55^{+0.20}_{-0.16}$	$7.05 \to 8.24$
$\frac{\Delta m^2_{32}}{10^{-3}\ \mathrm{eV}^2}$	$2.449^{+0.032}_{-0.030}$	$2.358 \to 2.544$	$2.454^{+0.029}_{-0.031}$	$2.362 \to 2.544$	$2.419^{+0.035}_{-0.032}$	$2.319 \to 2.521$	2.424 ± 0.03	$2.334 \to 2.524$
IO	$\Delta\chi^2 = 6.2$		$\Delta\chi^2 = 10.4$		$\Delta\chi^2 = 9.5$		$\Delta\chi^2 = 11.7$	
$\frac{\sin^2\theta_{12}}{10^{-1}}$	$3.10^{+0.13}_{-0.12}$	$2.75 \to 3.50$	$3.10^{+0.13}_{-0.12}$	$2.75 \to 3.50$	$3.03^{+0.14}_{-0.13}$	$2.64 \to 3.45$	$3.20^{+0.20}_{-0.16}$	$2.73 \to 3.79$
$\theta_{12}/^\circ$	$33.82^{+0.78}_{-0.76}$	$31.61 \to 36.27$	$33.82^{+0.78}_{-0.75}$	$31.62 \to 36.27$	$33.40^{+0.87}_{-0.81}$	$30.92 \to 35.97$	$34.5^{+1.2}_{-1.0}$	$31.5 \to 38.0$
$\frac{\sin^2\theta_{23}}{10^{-1}}$	$5.63^{+0.19}_{-0.26}$	$4.30 \to 6.12$	$5.65^{+0.17}_{-0.22}$	$4.36 \to 6.10$	$5.57^{+0.17}_{-0.24}$	$4.44 \to 6.03$	$5.51^{+0.18}_{-0.30}$	$4.53 \to 5.98$
$\theta_{23}/^\circ$	$48.6^{+1.1}_{-1.5}$	$41.0 \to 51.5$	$48.8^{+1.0}_{-1.2}$	$41.4 \to 51.3$	$48.2^{+1.0}_{-1.4}$	$41.8 \to 50.9$	$47.9^{+1.0}_{-1.7}$	$42.3 \to 50.7$
$\frac{\sin^2\theta_{13}}{10^{-2}}$	$2.261^{+0.067}_{-0.064}$	$2.066 \to 2.461$	$2.259^{+0.065}_{-0.065}$	$2.064 \to 2.457$	$2.18^{+0.08}_{-0.07}$	$1.95 \to 2.43$	$2.220^{+0.074}_{-0.076}$	$1.99 \to 2.44$
$\theta_{13}/^\circ$	$8.65^{+0.13}_{-0.12}$	$8.26 \to 9.02$	$8.64^{+0.12}_{-0.13}$	$8.26 \to 9.02$	$8.49^{+0.15}_{-0.14}$	$8.0 \to 9.0$	$8.53^{+0.14}_{-0.15}$	$8.1 \to 9.0$
$\delta_{\rm CP}/^\circ$	285^{+24}_{-26}	$205 \to 354$	282^{+23}_{-25}	$205 \to 348$	247^{+26}_{-27}	$193 \to 346$	281^{+23}_{-27}	$202 \to 349$
$\frac{\Delta m^2_{21}}{10^{-5}\ \mathrm{eV}^2}$	$7.39^{+0.21}_{-0.20}$	$6.79 \to 8.01$	$7.39^{+0.21}_{-0.20}$	$6.79 \to 8.01$	$7.34^{+0.17}_{-0.14}$	$6.92 \to 7.91$	$7.55^{+0.20}_{-0.16}$	$7.05 \to 8.24$
$\frac{\Delta m^2_{32}}{10^{-3}\ \mathrm{eV}^2}$	$-2.509^{+0.032}_{-0.032}$	$-2.603 \to -2.416$	$-2.510^{+0.030}_{-0.031}$	$-2.601 \to -2.419$	$-2.478^{+0.035}_{-0.033}$	$-2.577 \to -2.375$	$-2.50\pm^{+0.04}_{-0.03}$	$-2.59 \to -2.39$

defined by:

$$\Im\Big[U_{\alpha i}U^*_{\alpha j}U^*_{\beta i}U_{\beta j}\Big] \equiv \sum_{\gamma=e,\mu,\tau}\sum_{k=1,2,3} J_{\rm CP}\,\epsilon_{\alpha\beta\gamma}\,\epsilon_{ijk} \equiv J^{\rm max}_{\rm CP}\,\sin\delta_{\rm CP}\,. \tag{14.84}$$

With the convention in Eq. (14.33) $J^{\rm max}_{\rm CP}$ is the combination of mixing angles in Eq. (14.78). For example, from the analysis in Ref. [184, 185]

$$J^{\rm max}_{\rm CP} = 0.03359 \pm 0.0006\,(\pm 0.0019)\,, \tag{14.85}$$

at 1σ (3σ) for both orderings, and the preference of the present data for non-zero $\delta_{\rm CP}$ implies a non-zero best fit value $J^{\rm best}_{\rm CP} = -0.019$.

The status of the determination of leptonic CP violation can also be graphically displayed by projecting the results of the global analysis in terms of leptonic unitarity triangles [190–192]. Since in the analysis U is unitary by construction, any given pair of rows or columns can be used to define a triangle in the complex plane. There are a total of six possible triangles corresponding to the unitary conditions

$$\sum_{i=1,2,3} U_{\alpha i}U^*_{\beta i} = 0 \text{ with } \alpha \neq \beta\,, \qquad \sum_{\alpha=e,\mu,\tau} U_{\alpha i}U^*_{\alpha j} = 0 \text{ with } i \neq j\,. \tag{14.86}$$

As an illustration we show in Fig. 14.9 the recasting of the allowed regions of the analysis in Ref. [184, 185] in terms of one leptonic unitarity triangle. We show the triangle corresponding to the unitarity conditions on the first and third columns (after the shown rescaling), which is the equivalent to the one usually shown for the quark sector. In this figure, the absence of CP violation would imply a flat triangle, *i.e.*, $\Im(z) = 0$. So the CL at which leptonic CP violation is being observed would be given by the CL at which the region crosses the horizontal axis. Notice however, that this representation is made *under the assumption of a unitary U matrix* and therefore does not provide any test of unitarity in the leptonic sector.

Downloaded from https://academic.oup.com/ptep/article/2022/8/083C01/6651666 by KIT Library user on 27 September 2022

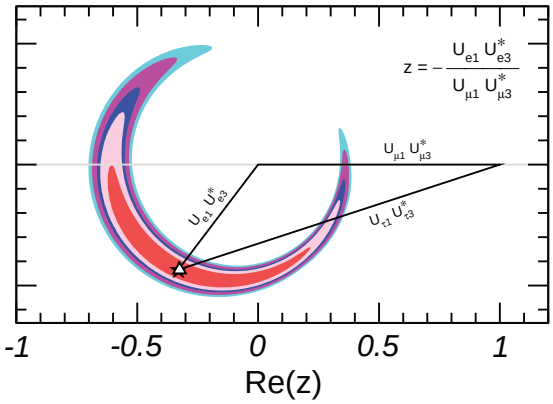

Figure 14.9: Leptonic unitarity triangle for the first and third columns of the mixing matrix. After scaling and rotating the triangle so that two of its vertices always coincide with $(0,0)$ and $(1,0)$ the figure shows the 1σ, 90%, 2σ, 99%, 3σ CL (2 dof) allowed regions of the third vertex for the NO from the analysis in Ref. [184, 185].

14.8 Beyond 3ν: Additional Neutrinos at the eV Scale

Besides the huge success of three-flavour oscillations described in Sec.14.7, as mentioned in Secs.14.6.3 and 14.6.4, there are some anomalies which cannot be explained within the 3ν framework and which might point towards the existence of additional neutrino states with masses at the eV scale. In brief:

- the LSND experiment [129] reports evidence for $\bar{\nu}_\mu \to \bar{\nu}_e$ transitions with $E/L \sim 1$ eV^2, where E and L are the neutrino energy and the distance between source and detector, respectively (see *Short Baseline Experiments* subsection of Sec.14.6.3).
- this effect has also been searched for by the MiniBooNE experiment [193], which reports a yet unexplained event excess in the low-energy region of the electron neutrino and antineutrino event spectra. No significant excess is found at higher neutrino energies. Interpreting the data in terms of oscillations, parameter values consistent with the ones from LSND are obtained, but the test is not definitive;
- radioactive source experiments at the Gallium solar neutrino experiments both in SAGE and GALLEX/GNO have obtained an event rate that is somewhat lower than expected. If not due to uncertainties in the interaction cross-section, this effect can be explained by the hypothesis of ν_e disappearance due to oscillations with $\Delta m^2 \gtrsim 1$ eV^2 ("Gallium anomaly") [194, 195];
- new calculations of the neutrino flux emitted by nuclear reactors [138, 139] predict a neutrino rate that is a few percent higher than observed in short-baseline ($L \lesssim 100$ m) reactor experiments [5]. If not due to systematic or theoretical uncertainties, a decrease rate at those distances can be explained by assuming $\bar{\nu}_e$ disappearance due to oscillations with $\Delta m^2 \sim 1$ eV^2 ("reactor anomaly") [198]. This reactor anomaly is under study both by the experimental community – with a set of follow-up measurements performed at SBL both at reactors and accelerators (see the corresponding subsections in Sec.14.6.4 and Sec.14.6.3)– , and by the theory community for improvements of the reactor flux calculations.

As mentioned in Sec.14.1, whatever the extension of the SM we want to consider, it must contain only three light active neutrinos. Therefore if we need more than three light massive neutrinos, we must add sterile neutrinos to the particle content of the model.

[5] However, as discussed in Sec.14.6.4, the reactor antineutrino flux measurement at Daya Bay [196, 197] is consistent with the old flux predictions and the flux measurement results in the previous short-baseline reactor neutrino oscillation experiments.

The most immediate question as these anomalies were reported was whether they could all be consistently described in combination with the rest of the neutrino data – in particular with the negative results on the disappearance of ν_μ at short distances – if one adds those additional sterile states. Quantitatively one can start by adding a fourth massive neutrino state to the spectrum and perform a global data analysis to answer this question. Although the answer is always the same, the physical reason behind it depends on ordering assumed for the states. In brief, there are six possible four-neutrino schemes that can, in principle, accommodate the results of solar+KamLAND and atmospheric+LBL neutrino experiments as well as the SBL result. They can be divided into two classes: (2+2) and (3+1). In the (3+1) schemes, there is a group of three close-by neutrino masses (as on the 3ν schemes described in the previous section) that is separated from the fourth one by a gap of the order of 1 eV, which is responsible for the SBL oscillations. In (2+2) schemes, there are two pairs of close masses (one pair responsible for solar results and the other for atmospheric [199]) separated by the $\mathcal{O}$(eV) gap. The main difference between these two classes is the following: if a (2+2)-spectrum is realized in nature, the transition into the sterile neutrino is a solution of either the solar or the atmospheric neutrino problem, or the sterile neutrino takes part in both. Consequently, a (2+2)-spectrum is easier to test because the required mixing of sterile neutrinos in either solar and/or atmospheric oscillations would modify their effective matter potential in the Sun and in the Earth, giving distinctive effects in the solar and/or atmospheric neutrino observables. Those distinctive effects were not observed so oscillations into sterile neutrinos did not describe well either solar or atmospheric data. Consequently, as soon as the early 2000's 2+2 spectra could be ruled out already beyond 3-4 σ as seen in the left panel in Fig.14.10 taken from Ref. [200].

On the contrary, for a (3+1)-spectrum (and more generally for a $3+N$-spectrum with an arbitrary N number of sterile states), the sterile neutrino(s) could be only slightly mixed with the active ones and mainly provide a description of the SBL results. In this case, the oscillation probabilities for experiments working at $E/L \sim 1$ eV^2 take a simple form:

$$P_{\alpha\alpha} = 1 - \sin^2 2\theta_{\alpha\alpha} \sin^2 \Delta\,, \qquad P_{\mu e} = \sin^2 2\theta_{\mu e} \sin^2 \Delta\,, \quad (14.87)$$

where $\Delta \equiv \Delta m^2_{41} L/4E$ and one can define effective mixing angles

$$\sin^2 2\theta_{\alpha\alpha} \equiv 4|U_{\alpha 4}|^2(1 - |U_{\alpha 4}|^2)\,, \qquad \sin^2 2\theta_{\mu e} \equiv 4|U_{\mu 4}|^2|U_{e4}|^2\,. \quad (14.88)$$

In here $\alpha = e, \mu$ and $U_{\alpha 4}$ are the elements of the lepton mixing matrix describing the mixing of the 4th neutrino mass state with the electron and muon flavour. In this scenario, there is no sensitivity to CP violation in the the Δ driven oscillations, so the relations above are valid for both neutrinos and antineutrinos. At linear order in the mixing elements one can derive a relation between the amplitudes of appearance and disappearance probabilities:

$$4 \sin^2 2\theta_{\mu e} \approx \sin^2 2\theta_{ee} \sin^2 2\theta_{\mu\mu}\,. \quad (14.89)$$

This relation implies a constraint between the possible results in disappearance and appearance experiments. Consequently, it is not trivial to find a consistent description to all the SBL anomalies. Over the years, different groups have performed a variety of such global analyses leading to different quantitative conclusions on the statistical quality of the global fit (see for example [201–206], see also Refs. [207, 208] for recent reviews on the subject). Generically, the results of the global analysis show that there is significant tension between groups of different data sets – in particular between appearance and disappearance results – and Eq.(14.89) makes it difficult to obtain a good global fit as illustrated in the right panel in Fig.14.10 taken from Ref. [201] which concluded that 3+1 scenario is excluded at 4.7σ level.

A straightforward question to ask is whether the situation improves if more neutrino states at the eV scale are introduced. The simplest extension is the introduction of 2 states with eV scale mass splittings, ν_4 and ν_5. The ordering of the states can be such that Δm^2_{41} and Δm^2_{51} are both positive ("3+2"), or one of them

Downloaded from https://academic.oup.com/ptep/article/2022/8/083C01/6651666 by KIT Library user on 27 September 2022

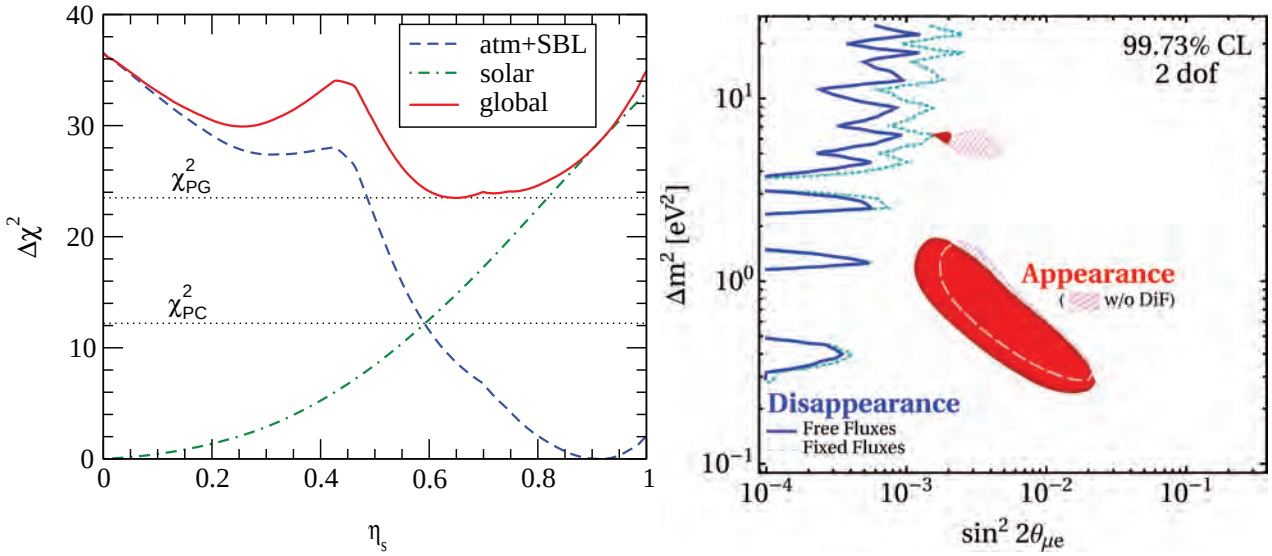

Figure 14.10: *Left*: Status of the 2+2 oscillation scenarios from Ref. [200] ($\eta_S = \sum_i |U_{is}|^2$ where i runs over the two massive states mostly relevant for solar neutrino oscillations). In the figure also shown are the values of $\chi^2_{\rm PC}$ and $\chi^2_{\rm PG}$ relevant for parameter consistency test and parameter goodness of fit, respectively. *Right*: Present status of 3+1 oscillation scenarios from Ref. [201].

is negative ("1+3+1"). From the point of view of the description of the data, the most important new qualitative feature is that now, non-zero CP violation at $E/L \sim$ eV^2 is possibly observable [204, 209–211]. This allows some additional freedom in fitting neutrino versus antineutrino data from LSND and MiniBooNE together. However, it still holds that a non-zero $\nu_\mu \to \nu_e$ appearance at SBL necessarily predicts SBL disappearance for both ν_e and ν_μ. So, generically, the tension between appearance and disappearance results remains, though differences in the methodology of statistical quantification of the degree of agreement/disagreement in these scenarios can lead to different conclusions on whether they can provide a successful description of all the data [201,207,208]. Cosmological observations can provide complementary information on the number of relativistic neutrino states in thermal equilibrium in the early Universe and on the sum of their masses, which sets further constraints on light sterile neutrino scenarios (see Chapter 26 of this *Review*, "Neutrinos in cosmology").

14.9 Laboratory Probes of ν Mass Scale and its Nature

As described in Secs.14.4 and 14.5, neutrino flavour oscillations in vacuum and flavour transitions in matter only depend on the differences between the neutrino masses-squared, Δm^2_{ij}, and on the mixing matrix elements, U_{ij}. However, they are insensitive to the absolute mass scale for the neutrinos, m_i. They also give us no information on whether they are Dirac or Majorana particles.

Clearly, the observation of flavour oscillations implies a lower bound on the mass of the heavier neutrino in Δm^2_{ij}, $|m_i| \geq \sqrt{\Delta m^2_{ij}}$ for $\Delta m^2_{ij} > 0$. However, there is no upper bound on m_i. In particular, oscillation results allow the neutrino spectrum to be approximately degenerate at a mass scale that is much higher than the $\sqrt{\Delta m^2_{ij}}$ that they determine. Information of the mass scale of the neutrino is provided by other types of experiments. Here we briefly summarize the most sensitive laboratory probes of the neutrino mass scale and on whether they are Dirac or Majorana particles. Cosmological observations provide, albeit indirectly, complementary information on the neutrino mass scale as it is reviewed in Chapter 26 of this *Review*, "Neutrinos in cosmology".

14.9.1 *Constraints from Kinematics of Weak Decays*

The only model-independent information on the neutrino masses, rather than mass differences, can be extracted from energy-momentum conservation relation in reactions in which a neutrino or an antineutrino is involved.

Historically these bounds were labeled as limits on the mass of the flavour neutrino states corresponding to the charged flavour involved in the decay. Fermi proposed in 1933 such a kinematic search for the ν_e neutrino mass (which we will label here as $m^{\rm eff}_{\nu_e}$) in the end part of the beta spectra in ^{3}H beta decay $^3{\rm H} \to {}^3{\rm He} + e^- + \bar{\nu}_e$.

Because ^{3}H beta decay is a superallowed transition, the nuclear matrix elements are energy independent, so the electron spectrum is determined exclusively by the phase space

$$\begin{aligned} \frac{dN}{dE} &= C\,p\,E\,(Q-T)\sqrt{(Q-T)^2-(m^{\rm eff}_{\nu_e})^2}\,F(E) \\ &\equiv R(E)\,\sqrt{(E_0-E)^2-(m^{\rm eff}_{\nu_e})^2}\,. \end{aligned} \tag{14.90}$$

E_0 is the mass difference between the inital and final nucleus, $E = T + m_e$ is the total electron energy, p its momentum, $Q \equiv E_0 - m_e$ is the maximum kinetic energy of the electron and Final state Coulomb interactions are contained in the Fermi function $F(E)$. $R(E)$ in the second equality contains all the m_ν-independent factors.

The Kurie function is defined as $K(T) \equiv \sqrt{\frac{dN}{dE}\,\frac{1}{pEF(E)}}$. From Eq.(14.90), we see that if $m^{\rm eff}_{\nu_e}$=0 $K(T)$ would depend linearly on T. A non-vanishing neutrino mass then provokes a distortion from the straight-line T-dependence at the endpoint, So for $m^{\rm eff}_{\nu_e} = 0$, $T_{\rm max} = Q$, while for $m^{\rm eff}_{\nu_e} \neq 0$, $T_{\rm max} = Q - m^{\rm eff}_{\nu_e}$. In ^{3}H beta decay $Q = 18.6$ KeV is very small and therefore, this decay is more sensitive to this $m^{\rm eff}_{\nu_e}$-induced distortion.

The most recent result on the kinematic search for neutrino mass in tritium decay is from KATRIN [212], an experiment which has found so far no indication of $m_{\nu_e} \neq 0$ and sets an upper limit

$$m^{\rm eff}_{\nu_e} < 1.1 \text{ eV}\,, \tag{14.91}$$

at 90% CL improving over the previous bound from the Mainz [213] and Troitsk [214] experiments which constrained $m^{\rm eff}_{\nu_e} < 2.2$ eV at 95% CL. KATRIN continues running with an estimated sensitivity limit of $m^{\rm eff}_{\nu_e} \sim 0.2$ eV. Project 8 is exploring a new technique for β-spectrometry based on cyclotron radiation [215].

An alternative isotope to Tritium is ^{163}Ho [216] which presents the advantage of a smaller $Q = 2.8$ KeV. It decays via electron capture to ^{163}Dy. Currently, there are three experiments

Downloaded from https://academic.oup.com/ptep/article/2022/8/083C01/6651666 by KIT Library user on 27 September 2022

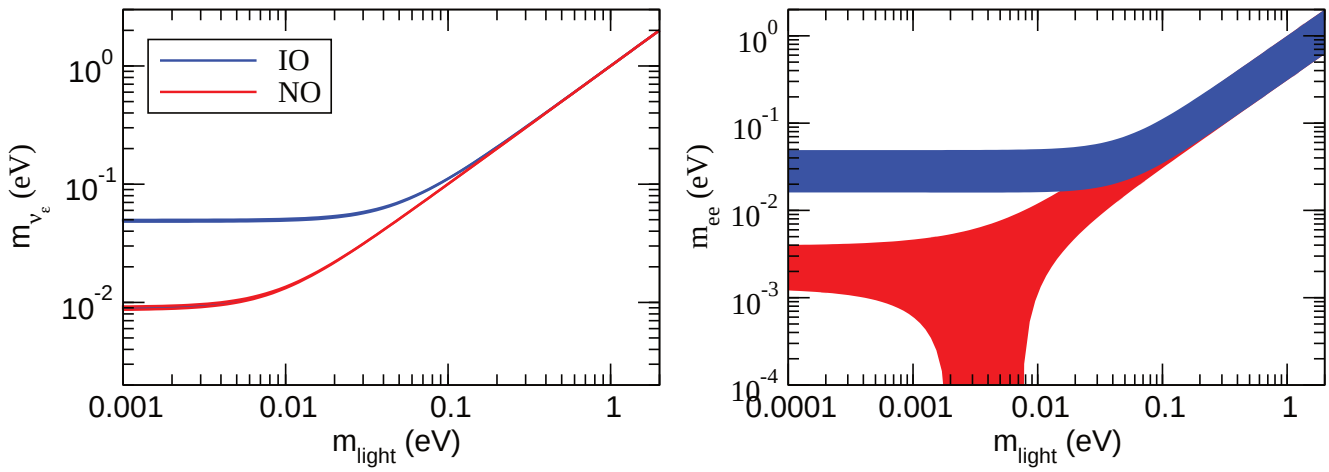

Figure 14.11: Allowed 95% CL ranges (1 dof) for the neutrino mass observable determined in ^{3}H beta decay (left panel) and in $0\nu\beta\beta$ (right panel) in the framework of 3ν mixing as a function of the lightest neutrino mass. The ranges are obtained by projecting the results of the global analysis of oscillation data (w/o SK-atm) in Ref. [184]. The region for each ordering is defined with respect to its local minimum.

exploring this decay to probe the neutrino mass: ECHo [217], HOLMES [218], and NuMECS [219]. These experiments are complementary to tritium-based searches from a technical point of view. Also, the decay of ^{163}Ho determines the effective electron neutrino mass as opposed to antineutrino in Tritium.

For the other flavours the present limits compiled in the listing section of the PDG read

$$m^{\rm eff}_{\nu_\mu} < 190 \text{ keV (90\% CL)} \qquad \text{from} \qquad \pi^- \to \mu^- + \bar\nu_\mu\,, \quad (14.92)$$

$$m^{\rm eff}_{\nu_\tau} < 18.2 \text{ MeV (95\% CL)} \qquad \text{from} \qquad \tau^- \to n\pi + \nu_\tau\,. \quad (14.93)$$

In the presence of mixing and for neutrinos with small mass differences, the distortion of the beta spectrum is given by the sum of the individual spectra generated incoherently by each neutrino massive state weighted with the relevant mixing matrix element squared [220]:

$$\frac{dN}{dE} = R(E)\sum_i |U_{ei}|^2 \sqrt{(E_0-E)^2 - m_i^2}\,\Theta(E_0-E-m_i)\,. \quad (14.94)$$

The step function $\Theta(E_0-E-m_i)$ arises because a neutrino with a given mass m_i can only be produced if the available energy is larger than its mass. Equation (14.94) shows the two main effects of the neutrino masses and mixings on the electron energy spectrum: First, kinks appear at the electron energies $E_e^{(i)} = E \sim E_0 - m_i$ with sizes that are determined by $|U_{ei}|^2$. Second, the endpoint shifts to $E_{\rm ep} = E_0 - m_0$, where m_0 is the lightest neutrino mass. Corrections are induced once the energy resolution of the experiment is considered. [221, 222]

In the 3-ν mixing scenario, the distortion of the spectrum can still be effectively described by a single parameter – which we will still denote as m_{ν_e} – if for all neutrino states $E_0 - E = Q - T \gg m_i$. In this case, one can expand Eq.(14.94) as:

$$\frac{dN}{dE} \simeq R(E)\sum_i |U_{ei}|^2 \sqrt{(E_0-E)^2 - (m^{\rm eff}_{\nu_e})^2}\,, \quad (14.95)$$

with

$$(m^{\rm eff}_{\nu_e})^2 = \frac{\sum_i m_i^2|U_{ei}|^2}{\sum_i |U_{ei}|^2} = \sum_i m_i^2|U_{ei}|^2\,, \quad (14.96)$$

where unitarity is assumed in the second equality. In this approximation, the distortion of the endpoint of the spectrum is described by a single parameter, and with the present results from KATRIN, it is bounded to be

$$1.1 \text{ eV} \geq m^{\rm eff}_{\nu_e} = \sqrt{\sum_i m_i^2|U_{ei}|^2} = \begin{cases} \sqrt{m_0^2 + \Delta m^2_{21}(1-c^2_{13}c^2_{12}) + \Delta m^2_{32}s^2_{13}} & \text{in NO}\,, \\ \sqrt{m_0^2 + \Delta m^2_{21}c^2_{13}c^2_{12} - \Delta m^2_{32}c^2_{13}} & \text{in IO}\,, \end{cases} \quad (14.97)$$

where $m_0 = m_1\,(m_3)$ is the lightest neutrino mass in the NO (IO) spectrum. Correspondingly the bounds in Eqs.(14.92) and (14.93) apply to the combinations $\sum_i m_i^2|U_{\alpha i}|^2$ for $\alpha = \mu$ and τ respectively. So with the values known of the mixing matrix elements, the strongest constraint on the absolute value of the neutrino mass comes from Tritium beta decay.

From Eq.(14.97) we see that, given the present knowledge of the neutrino mass differences and their mixing from oscillation experiments, it is possible to translate the experimental information of m_{ν_e} on a corresponding range for the lightest neutrino mass and that such relation depends on the ordering of the states. We plot in Fig.14.11 the recasting of the allowed regions of the analysis in Ref. [184] in terms of the allowed range m_{ν_e} as a function of $m_{\rm light} \equiv m_0$. In particular, one finds that the results of oscillation experiments imply a lower bound on $m_{\nu_e} > 0.048$ (0.0085) eV for IO (NO) at 95% CL.

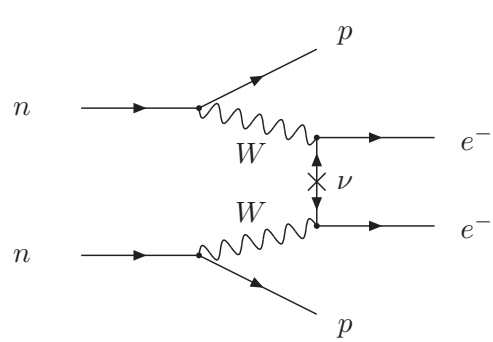

Figure 14.12: Feynman diagram for neutrinoless double-beta decay.

Downloaded from https://academic.oup.com/ptep/article/2022/8/083C01/6651666 by KIT Library user on 27 September 2022

14.9.2 *Dirac vs. Majorana: Neutrinoless Double-beta Decay*

The most sensitive probe to whether neutrinos are Dirac or Majorana states is the neutrinoless double beta decay ($0\nu\beta\beta$):

$$(A, Z) \to (A, Z+2) + e^- + e^-. \tag{14.98}$$

In the presence of neutrino masses and mixing, the process in Eq.(14.98) can be generated at lower order in perturbation theory by the term represented in Fig.14.12. The corresponding amplitude is proportional to the product of the two leptonic currents

$$\begin{aligned} M_{\alpha\beta} &\propto [\bar{e}\gamma_\alpha(1-\gamma_5)\nu_e]\left[\bar{e}\gamma_\beta(1-\gamma_5)\nu_e\right] \\ &\propto \sum_i (U_{ei})^2 [\bar{e}\gamma_\alpha(1-\gamma_5)\nu_i]\left[\bar{e}\gamma_\beta(1-\gamma_5)\nu_i\right] . \end{aligned} \tag{14.99}$$

The neutrino propagator in Fig.14.12 can only arise from the contraction $\langle 0 \,|\, \nu_i(x)\nu_i(y)^T \,|\, 0\rangle$. However, if the neutrino is a Dirac particle ν_i field annihilates a neutrino state and creates an antineutrino state, and neutrino and antineutrino states are different, so the contraction $\langle 0 \,|\, \nu_i(x)\nu_i(y)^T \,|\, 0\rangle = 0$ and $M_{\alpha\beta} = 0$. On the other hand, if ν_i is a Majorana particle, neutrino and antineutrino are described by the same field and $\langle 0 \,|\, \nu_i(x)\nu_i(y)^T \,|\, 0\rangle \neq 0$.

The conclusion is that in order to induce the $0\nu\beta\beta$ decay, neutrinos must be Majorana particles. This is consistent with the fact that the process (14.98) violates the total lepton number by two units. Conversely, if $0\nu\beta\beta$ decay is observed, massive neutrinos cannot be Dirac states [223].

It is important to stress that neutrinoless double-beta decay could be dominantly induced by other new physics effects beyond that of Majorana neutrino masses. Consequently, the connection between the observation or limitation of the neutrinoless double beta decay and the neutrino mass can only be made under some assumption about the source of total lepton number violation in the model.

The observable determined by the experiments is the half-life of the decay. Under the assumption that the Majorana neutrino mass is the only source of lepton number violation at low energies, the decay half-life is given by:

$$(T^{0\nu}_{1/2})^{-1} = G^{0\nu}\left|M^{0\nu}\right|^2 \left(\frac{m_{ee}}{m_e}\right)^2 , \tag{14.100}$$

where $G^{0\nu}$ is the phase space integral taking into account the final atomic state, $|M^{0\nu}\ |$ is the nuclear matrix element of the transition, and m_{ee} is the *effective Majorana mass of* ν_e,

$$\begin{aligned} m_{ee} &= \left|\sum_i m_i U_{ei}^2\right| \\ &= \begin{cases} \left|m_0 c_{12}^2 c_{13}^2 + \sqrt{\Delta m_{21}^2 + m_0^2}\, s_{12}^2 c_{13}^2 e^{2i(\eta_2-\eta_1)} + \sqrt{\Delta m_{32}^2 + \Delta m_{21}^2 + m_0^2}\, s_{13}^2 e^{-2i(\delta_{\rm CP}+\eta_1)}\right| & \text{in NO}\,, \\ \left|m_0 s_{13}^2 + \sqrt{m_0^2 - \Delta m_{32}^2}\, s_{12}^2 c_{13}^2 e^{2i(\eta_2+\delta_{\rm CP})} + \sqrt{m_0^2 - \Delta m_{32}^2 - \Delta m_{21}^2}\, c_{12}^2 c_{13}^2 e^{2i(\eta_1+\delta_{\rm CP})}\right| & \text{in IO}\,, \end{cases} \end{aligned}$$

which, in addition to the masses and mixing parameters that affect the tritium beta decay spectrum, also depends on the leptonic CP-violating phases. We plot in Fig.14.11 the recasting of the allowed regions of the analysis in Ref. [184] in terms of the allowed range m_{ee} as a function of $m_{\rm light} \equiv m_0$ for the two orderings. As a consequence of the dependence on the unknown Majorana phases, the allowed range of m_{ee} for a given value of $m_{\rm light}$ and ordering is substantially broader than that of m_{ν_e}. Nevertheless, the results of oscillation experiments imply a lower bound on the effective Majorana mass for the IO, which at 95%CL reads $m_{ee} > 0.016$ eV.

From Eq.(14.100) we see that nuclear structure details enter relation between the decay rate (or lifetime) and the effective Majorana mass. As a consequence, uncertainties in the nuclear structure calculations result in a spread of m_{ee} values for a given $T^{0\nu}_{1/2}$ by a factor of 2–3 [224].

We present in Sec.14.9.3 a brief description of the experimental searches for neutrinoless double-beta decay. At the time of writing of this review, the strongest bound on $0\nu\beta\beta$ decay lifetimes came for Xenon and Germanium from the KamLAND-Zen [225] and GERDA [226] experiments, respectively. They have set a bound on the corresponding half-lives of $T^{0\nu}_{1/2} > 1.07 \times 10^{26}$ yr, and $T^{0\nu}_{1/2} > 1.8 \times 10^{26}$ yr, at 90% CL. Using a variety of nuclear matrix element calculations, the corresponding upper bounds on the effective Majorana mass are

$$m_{ee} < 61 - 165 \text{ meV} \tag{14.101}$$

$$m_{ee} < 79 - 180 \text{ meV} . \tag{14.102}$$

14.9.3 *Experimental Search for Neutrinoless Double-beta Decay*

There are 35 candidate nuclei for double-beta decay. Currently, experiments using ^{136}Xe and ^{76}Ge have reported the most sensitive results of $0\nu\beta\beta$ search. Because of the uncertainties related to the nuclear matrix element, the complementarity of technologies, different backgrounds, and the investigation of the mechanism behind the $0\nu\beta\beta$ in case of a positive signal, it is important to pursue the searches with as many isotopes as possible.

The signature of $0\nu\beta\beta$ is that the sum of the energy of two electrons is equal to the Q-value of the nuclear transition. The energy from electrons is measured with either ionization, scintillation, or through phonons. In some experiments, a combination of two techniques is used to enhance the sensitivity. In the case of background-free measurement, the sensitivity to the half-life is proportional to the product of the detection efficiency of the signal ε, the source mass M, and the measurement time t. If background exists, it is proportional to $\varepsilon\sqrt{\frac{Mt}{b\Delta E}}$, where b is the background rate, and ΔE is the energy resolution.

Among the experiments using ionization detection, ultra-high-purity germanium detector provides the best sensitivity thanks to high energy resolution and low background. GERDA, in its final phase, used a total of 20.0 kg of broad energy germanium (BEGe), 14.6 kg of coaxial detectors, and 9.6 kg of inverted coaxial detectors. A background level of $(5.2^{+1.6}_{-1.3}) \times 10^{-4}$ counts/(keV·kg·year) was achieved [226], which enabled a background-free search. The final result from GERDA for the half-life limit for $0\nu\beta\beta$ decay of ^{76}Ge is $T_{1/2} > 1.8 \times 10^{26}$ years at 90% CL. The Majorana Demonstrator [227] consisted of 44.1 kg of Ge (29.7 kg enriched to 88% in ^{76}Ge) detectors split between two modules. It achieved energy resolution of 2.53 keV FWHM (full width at half maximum) at the Q-value (2.039 MeV). GERDA and Majorana collaborations have united and formed, together with new groups, the LEGEND collaboration. LEGEND has adopted a phased approach toward the deployment of a tonne of enriched Ge detectors [228]. The first phase of LEGEND, based on 200 kg of enriched Ge and using the GERDA infrastructure at LNGS, is expected to start in 2022. The second phase of LEGEND is planned as a one-ton experiment in a new cryostat, reaching a discovery sensitivity of half-life beyond 10^{28} years.

Liquid scintillator detectors have a simple structure and can utilize existing large detectors with low background environments. By adding an inner balloon to contain xenon-loaded liquid scintillator to the KamLAND detector, KamLAND-Zen used 380 kg of xenon with 90.1% enrichment in ^{136}Xe. Reducing the background

Downloaded from https://academic.oup.com/ptep/article/2022/8/083C01/6651666 by KIT Library user on 27 September 2022

level by purification of scintillator, KamLAND-Zen reported the half-life limit above 10^{26} years at 90% CL [225]. KamLAND-Zen has been accumulating more data with about 750 kg of enriched xenon. The SNO detector has also been upgraded to be filled with a liquid scintillator in the SNO+ experiment [229]. The SNO+ detector will be loaded with 0.5% natural tellurium, corresponding to approximately 1.3 t of ^{130}Te, to search for $0\nu\beta\beta$.

With a time projection chamber, one can utilize both ionization and scintillation. EXO-200 used a liquid xenon time projection chamber with enrichment to 80.6%, corresponding to 74.7 kg of ^{136}Xe in the fiducial mass [230]. An energy resolution of 1.15% (σ/E) is achieved at the Q-value of ^{136}Xe $0\nu\beta\beta$. Based on the technology validated by EXO-200, nEXO plans to use 5,000 kg of xenon enriched to 90% in ^{136}Xe to achieve beyond 10^{28} year half-life sensitivity [231, 232]. NEXT has been developing a high-pressure xenon gas time projection chamber with electroluminescent amplification and optical readouts. An energy resolution of 1% FWHM at the Q-value of ^{136}Xe $0\nu\beta\beta$ is demonstrated with NEXT-White detector [233]. NEXT proved background suppression by exploiting differences in the spatial ionization patterns of double beta decay and single-electron events [234]. A robust identification of signal is possible by tagging Ba^{2+} ions produced in ^{136}Xe decay. NEXT [235–238] and nEXO [239] have made significant progress in this technology. AXEL develops a cellular readout structure based on electroluminescence for the ^{136}Xe $0\nu\beta\beta$ search using a high-pressure xenon gas time projection chamber [240].

CUORE uses a cryogenic bolometer to measure the energy in a calorimetric way. The detector is located in Gran Sasso and composed of 988 TeO_2 bolometers for a total mass of 742 kg, corresponding to 206 kg of ^{130}Te. An effective energy resolution of (7.0±0.4) keV FWHM is achieved [241]. For further reduction of background towards future search based on the CUORE technology, CUPID proposes to simultaneously measure the calorimetric signal and the scintillation light with a tonne-scale bolometric detector [242]. Using the prototype CUPID-0, the technology is demonstrated, and $0\nu\beta\beta$ is also searched for with ^{82}Se [243] and ^{100}Mo [244].

AMoRE also uses the simultaneous detection of heat and scintillation. Six ^{100}Mo-enriched and ^{48}Ca-depleted $CaMoO_4$ crystals with a total mass of 1.9 kg (AMoRE-Pilot) are operated in Yangyang underground laboratory located in South Korea, searching for $0\nu\beta\beta$ of ^{100}Mo [245]. Currently, AMoRE-I experiment [246] using 13 enriched $CaMoO_4$ crystals and 5 enriched Li_2MoO_4 crystals (6 kg total mass) is under operation in Yemilab.

A tracker-calorimeter technique is employed in NEMO. Source isotopes are hosted in thin foils surrounded by a tracking detector, which in turn is surrounded by a calorimeter. Full topological event reconstruction with this configuration enables background rejection and gives additional information after discovery. The NEMO-3 experiment used 7 isotopes, with the largest mass comprised of ^{100}Mo (7 kg) [247]. NEMO-3 also reported the first search for neutrinoless quadruple-β decay of ^{150}Nd [248].

References

[1] J. N. Bahcall, *NEUTRINO ASTROPHYSICS* (1989), ISBN 9780521379755.

[2] R. N. Mohapatra and P. B. Pal, World Sci. Lect. Notes Phys. **60**, 1 (1998), [World Sci. Lect. Notes Phys.72,1(2004)].

[3] C. W. Kim and A. Pevsner, Contemp. Concepts Phys. **8**, 1 (1993).

[4] B. Kayser, F. Gibrat-Debu and F. Perrier, World Sci. Lect. Notes Phys. **25**, 1 (1989).

[5] C. Giunti and C. W. Kim, *Fundamentals of Neutrino Physics and Astrophysics* (2007), ISBN 9780198508717.

[6] M. C. Gonzalez-Garcia and Y. Nir, Rev. Mod. Phys. **75**, 345 (2003), [hep-ph/0202058].

[7] M. C. Gonzalez-Garcia and M. Maltoni, Phys. Rept. **460**, 1 (2008), [arXiv:0704.1800].

[8] A. Pilaftsis, Z. Phys. **C55**, 275 (1992), [hep-ph/9901206].

[9] P. Minkowski, Phys. Lett. **67B**, 421 (1977).

[10] P. Ramond, in "International Symposium on Fundamentals of Quantum Theory and Quantum Field Theory," (1979), [hep-ph/9809459].

[11] M. Gell-Mann, P. Ramond and R. Slansky, Conf. Proc. **C790927**, 315 (1979), [arXiv:1306.4669].

[12] T. Yanagida, Conf. Proc. C **7902131**, 95 (1979).

[13] R. N. Mohapatra and G. Senjanovic, Phys. Rev. Lett. **44**, 912 (1980).

[14] J. Schechter and J. W. F. Valle, Phys. Rev. **D21**, 309 (1980).

[15] J. Schechter and J. W. F. Valle, Phys. Rev. **D22**, 2227 (1980).

[16] J. Schechter and J. W. F. Valle, Phys. Rev. **D24**, 1883 (1981), [Erratum: Phys. Rev.D25,283(1982)].

[17] Z. Maki, M. Nakagawa and S. Sakata, Prog. Theor. Phys. **28**, 870 (1962).

[18] Y. Katayama *et al.*, Prog. Theor. Phys. **28**, 675 (1962).

[19] B. Pontecorvo, Zh. Eksp. Teor. Fiz. **53**, 1717 (1967).

[20] N. Cabibbo, Phys. Rev. Lett. **10**, 531 (1963).

[21] M. Kobayashi and T. Maskawa, Prog. Theor. Phys. **49**, 652 (1973).

[22] S. Antusch *et al.*, JHEP **10**, 084 (2006), [hep-ph/0607020].

[23] S. Antusch and O. Fischer, JHEP **10**, 094 (2014), [arXiv:1407.6607].

[24] V. N. Gribov and B. Pontecorvo, Phys. Lett. **28B**, 493 (1969).

[25] E. Akhmedov, in "International Conference on History of the Neutrino: 1930-2018 Paris, France, September 5-7, 2018," (2019), [arXiv:1901.05232].

[26] L. Wolfenstein, Phys. Rev. D **17**, 2369 (1978).

[27] A. Halprin, Phys. Rev. **D34**, 3462 (1986).

[28] A. J. Baltz and J. Weneser, Phys. Rev. **D37**, 3364 (1988).

[29] P. D. Mannheim, Phys. Rev. **D37**, 1935 (1988).

[30] L. Landau, Phys. Z. Sov. **2**, 46 (1932).

[31] C. Zener, Proc. Roy. Soc. Lond. **A137**, 696 (1932).

[32] E. Majorana, Nuovo Cim. **9**, 43 (1932).

[33] E. C. G. Stueckelberg, Helv. Phys. Acta **5**, 369 (1932).

[34] T.-K. Kuo and J. T. Pantaleone, Rev. Mod. Phys. **61**, 937 (1989).

[35] S. J. Parke, Phys. Rev. Lett. **57**, 1275 (1986).

[36] W. C. Haxton, Phys. Rev. Lett. **57**, 1271 (1986).

[37] S. T. Petcov, Phys. Lett. B **191**, 299 (1987).

[38] S. P. Mikheyev and A. Y. Smirnov, Sov. J. Nucl. Phys. **42**, 913 (1985).

[39] J. N. Bahcall *et al.*, Rev. Mod. Phys. **54**, 767 (1982).

[40] J. N. Bahcall, A. M. Serenelli and S. Basu, Astrophys. J. **621**, L85 (2005), [arXiv:astro-ph/0412440].

[41] A. M. Serenelli, W. C. Haxton and C. Pena-Garay, Astrophys. J. **743**, 24 (2011), [arXiv:1104.1639].

[42] F. L. Villante, Phys. Lett. **B742**, 279 (2015), [arXiv:1410.2796].

[43] A. Serenelli, Eur. Phys. J. **A52**, 4, 78 (2016), [arXiv:1601.07179].

[44] R. Davis, Jr., D. S. Harmer and K. C. Hoffman, Phys. Rev. Lett. **20**, 1205 (1968).

[45] B. T. Cleveland *et al.*, Astrophys. J. **496**, 505 (1998).

[46] C. Pena-Garay and A. Serenelli (2008), [arXiv:0811.2424].

[47] J. N. Abdurashitov *et al.* (SAGE), J. Exp. Theor. Phys. **95**, 181 (2002), [Zh. Eksp. Teor. Fiz.122,211(2002)], [arXiv:astro-ph/0204245].

[48] W. Hampel *et al.* (GALLEX), Phys. Lett. **B447**, 127 (1999).

[49] M. Altmann *et al.* (GNO), Phys. Lett. **B616**, 174 (2005), [hep-ex/0504037].

Downloaded from https://academic.oup.com/ptep/article/2022/8/083C01/6651666 by KIT Library user on 27 September 2022

[50] J. N. Abdurashitov *et al.* (SAGE), Phys. Rev. **C80**, 015807 (2009), [arXiv:0901.2200].

[51] K. S. Hirata *et al.* (Kamiokande-II), Phys. Rev. Lett. **63**, 16 (1989).

[52] K. S. Hirata *et al.* (Kamiokande-II), Phys. Rev. **D44**, 2241 (1991), [Erratum: Phys. Rev.D45, 2170 (1992)].

[53] Y. Fukuda *et al.* (Kamiokande), Phys. Rev. Lett. **77**, 1683 (1996).

[54] Y. Fukuda *et al.* (Super-Kamiokande), Phys. Rev. Lett. **81**, 1158 (1998), [Erratum: Phys. Rev. Lett. 81, 4279 (1998)], [hep-ex/9805021].

[55] Y. Fukuda *et al.* (Super-Kamiokande), Phys. Rev. Lett. **82**, 2430 (1999), [hep-ex/9812011].

[56] K. Abe *et al.* (Super-Kamiokande), Phys. Rev. **D94**, 5, 052010 (2016), [arXiv:1606.07538].

[57] N. Vinyoles *et al.*, Astrophys. J. **835**, 2, 202 (2017), [arXiv:1611.09867].

[58] S. Fukuda *et al.* (Super-Kamiokande), Phys. Rev. Lett. **86**, 5651 (2001), [hep-ex/0103032].

[59] S. Fukuda *et al.* (Super-Kamiokande), Phys. Rev. Lett. **86**, 5656 (2001), [hep-ex/0103033].

[60] B. Aharmim *et al.* (SNO), Phys. Rev. **C72**, 055502 (2005), [arXiv:nucl-ex/0502021].

[61] S. Fukuda *et al.* (Super-Kamiokande), Phys. Lett. **B539**, 179 (2002), [hep-ex/0205075].

[62] Q. R. Ahmad *et al.* (SNO), Phys. Rev. Lett. **87**, 071301 (2001), [arXiv:nucl-ex/0106015].

[63] Q. R. Ahmad *et al.* (SNO), Phys. Rev. Lett. **89**, 011301 (2002), [arXiv:nucl-ex/0204008].

[64] B. Aharmim *et al.* (SNO), Phys. Rev. **C88**, 025501 (2013), [arXiv:1109.0763].

[65] J. Bergstrom *et al.*, JHEP **03**, 132 (2016), [arXiv:1601.00972].

[66] C. Arpesella *et al.* (Borexino), Phys. Lett. B **658**, 101 (2008), [arXiv:0708.2251].

[67] G. Bellini *et al.* (Borexino), Phys. Rev. Lett. **108**, 051302 (2012), [arXiv:1110.3230].

[68] M. Agostini *et al.* (BOREXINO), Nature **562**, 7728, 505 (2018).

[69] M. Agostini *et al.* (BOREXINO), Nature **587**, 577 (2020), [arXiv:2006.15115].

[70] G. Bellini *et al.* (Borexino), Phys. Rev. D **82**, 033006 (2010), [arXiv:0808.2868].

[71] S. Abe *et al.* (KamLAND), Phys. Rev. **C84**, 035804 (2011), [arXiv:1106.0861].

[72] A. Gando *et al.* (KamLAND), Phys. Rev. **C92**, 5, 055808 (2015), [arXiv:1405.6190].

[73] M. Agostini *et al.* (Borexino), Phys. Rev. D **100**, 8, 082004 (2019), [arXiv:1707.09279].

[74] M. Agostini *et al.* (Borexino), Phys. Rev. D **101**, 6, 062001 (2020), [arXiv:1709.00756].

[75] A. Renshaw *et al.* (Super-Kamiokande), Phys. Rev. Lett. **112**, 9, 091805 (2014), [arXiv:1312.5176].

[76] K. Abe *et al.* (Super-Kamiokande), Phys. Rev. D **94**, 5, 052010 (2016), [arXiv:1606.07538].

[77] M. Honda *et al.*, Phys. Rev. **D92**, 2, 023004 (2015), [arXiv:1502.03916].

[78] G. D. Barr *et al.*, Phys. Rev. **D74**, 094009 (2006), [arXiv:astro-ph/0611266].

[79] G. Battistoni *et al.*, Astropart. Phys. **19**, 269 (2003), [Erratum: Astropart. Phys.19,291(2003)], [hep-ph/0207035].

[80] J. Evans *et al.*, Phys. Rev. **D95**, 2, 023012 (2017), [arXiv:1612.03219].

[81] C. V. Achar *et al.*, Phys. Lett. **18**, 196 (1965).

[82] F. Reines *et al.*, Phys. Rev. Lett. **15**, 429 (1965).

[83] K. S. Hirata *et al.* (Kamiokande-II), Phys. Lett. B **205**, 416 (1988).

[84] D. Casper *et al.*, Phys. Rev. Lett. **66**, 2561 (1991).

[85] K. Daum *et al.* (Frejus), Z. Phys. **C66**, 417 (1995).

[86] M. Aglietta *et al.* (NUSEX), Europhys. Lett. **8**, 611 (1989).

[87] K. S. Hirata *et al.* (Kamiokande-II), Phys. Lett. **B280**, 146 (1992).

[88] Y. Fukuda *et al.* (Kamiokande), Phys. Lett. **B335**, 237 (1994).

[89] Y. Fukuda *et al.* (Super-Kamiokande), Phys. Rev. Lett. **81**, 1562 (1998), [hep-ex/9807003].

[90] M. Ambrosio *et al.* (MACRO), Phys. Lett. **B517**, 59 (2001), [hep-ex/0106049].

[91] M. C. Sanchez *et al.* (Soudan 2), Phys. Rev. **D68**, 113004 (2003), [hep-ex/0307069].

[92] V. D. Barger *et al.*, Phys. Rev. Lett. **82**, 2640 (1999), [arXiv:astro-ph/9810121].

[93] E. Lisi, A. Marrone and D. Montanino, Phys. Rev. Lett. **85**, 1166 (2000), [hep-ph/0002053].

[94] Y. Ashie *et al.* (Super-Kamiokande), Phys. Rev. Lett. **93**, 101801 (2004), [hep-ex/0404034].

[95] Z. Li *et al.* (Super-Kamiokande), Phys. Rev. **D98**, 5, 052006 (2018), [arXiv:1711.09436].

[96] M. G. Aartsen *et al.* (IceCube), Phys. Rev. **D99**, 3, 032007 (2019), [arXiv:1901.05366].

[97] K. Abe *et al.* (Super-Kamiokande), Phys. Rev. **D97**, 7, 072001 (2018), [arXiv:1710.09126].

[98] A. Albert *et al.* (ANTARES), JHEP **06**, 113 (2019), [arXiv:1812.08650].

[99] M. G. Aartsen *et al.* (IceCube), Phys. Rev. Lett. **120**, 7, 071801 (2018), [arXiv:1707.07081].

[100] S. Adrian-Martinez *et al.* (KM3Net), J. Phys. **G43**, 8, 084001 (2016), [arXiv:1601.07459].

[101] M. G. Aartsen *et al.* (IceCube-Gen2), J. Phys. G **48**, 6, 060501 (2021), [arXiv:2008.04323].

[102] S. Ahmed *et al.* (ICAL), Pramana **88**, 5, 79 (2017), [arXiv:1505.07380].

[103] K. Abe *et al.* (Hyper-Kamiokande) (2018), [arXiv:1805.04163].

[104] B. Abi *et al.* (DUNE) (2018), [arXiv:1807.10334].

[105] S. E. Kopp, Phys. Rept. **439**, 101 (2007), [arXiv:physics/0609129].

[106] S. van der Meer (1961), CERN-61-07.

[107] D. Beavis *et al.* (E899) (1995), BNL-52459.

[108] M. G. Catanesi *et al.* (HARP), Nucl. Instrum. Meth. **A571**, 527 (2007).

[109] J. M. Paley *et al.* (MIPP), Phys. Rev. **D90**, 3, 032001 (2014), [arXiv:1404.5882].

[110] N. Abgrall *et al.* (NA61), JINST **9**, P06005 (2014), [arXiv:1401.4699].

[111] J. M. Paley *et al.* (MIPP), Phys. Rev. D **90**, 3, 032001 (2014), [arXiv:1404.5882].

[112] N. Abgrall *et al.* (NA61/SHINE), Phys. Rev. C **84**, 034604 (2011), [arXiv:1102.0983].

[113] N. Abgrall *et al.* (NA61/SHINE), Eur. Phys. J. C **76**, 11, 617 (2016), [arXiv:1603.06774].

[114] M. H. Ahn *et al.* (K2K), Phys. Rev. **D74**, 072003 (2006), [hep-ex/0606032].

[115] P. Adamson *et al.* (MINOS), Phys. Rev. Lett. **110**, 25, 251801 (2013), [arXiv:1304.6335].

[116] P. Adamson *et al.* (MINOS), Phys. Rev. Lett. **112**, 191801 (2014), [arXiv:1403.0867].

Downloaded from https://academic.oup.com/ptep/article/2022/8/083C01/6651666 by KIT Library user on 27 September 2022

[117] P. Adamson *et al.* (MINOS+), Phys. Rev. Lett. **125**, 13, 131802 (2020), [arXiv:2006.15208].

[118] N. Agafonova *et al.* (OPERA), Phys. Rev. Lett. **120**, 21, 211801 (2018), [Erratum: Phys. Rev. Lett.121,no.13,139901(2018)], [arXiv:1804.04912].

[119] C. Rubbia *et al.*, JINST **6**, P07011 (2011), [arXiv:1106.0975].

[120] K. Abe *et al.* (T2K), Phys. Rev. Lett. **107**, 041801 (2011), [arXiv:1106.2822].

[121] K. Abe *et al.* (T2K), Phys. Rev. Lett. **112**, 061802 (2014), [arXiv:1311.4750].

[122] K. Abe *et al.* (T2K), Nature **580**, 7803, 339 (2020), [Erratum: Nature 583, E16 (2020)], [arXiv:1910.03887].

[123] K. Abe *et al.* (T2K), Phys. Rev. D **103**, 11, 112008 (2021), [arXiv:2101.03779].

[124] P. Adamson *et al.* (NOvA), Phys. Rev. Lett. **116**, 15, 151806 (2016), [arXiv:1601.05022].

[125] P. Adamson *et al.* (NOvA), Phys. Rev. Lett. **118**, 23, 231801 (2017), [arXiv:1703.03328].

[126] M. A. Acero *et al.* (NOvA), Phys. Rev. Lett. **123**, 15, 151803 (2019), [arXiv:1906.04907].

[127] B. Abi *et al.* (DUNE), JINST **15**, 08, T08008 (2020), [arXiv:2002.02967].

[128] K. Abe *et al.* (Hyper-Kamiokande) (2018), [arXiv:1805.04163].

[129] A. Aguilar-Arevalo *et al.* (LSND), Phys. Rev. **D64**, 112007 (2001), [hep-ex/0104049].

[130] B. Armbruster *et al.* (KARMEN), Phys. Rev. **D65**, 112001 (2002), [hep-ex/0203021].

[131] A. A. Aguilar-Arevalo *et al.* (MiniBooNE), Phys. Rev. D **103**, 5, 052002 (2021), [arXiv:2006.16883].

[132] M. Antonello *et al.* (MicroBooNE, LAr1-ND, ICARUS-WA104) (2015), [arXiv:1503.01520].

[133] S. Ajimura *et al.* (JSNS2), Nucl. Instrum. Meth. A **1014**, 165742 (2021), [arXiv:2104.13169].

[134] F. Von Feilitzsch, A. A. Hahn and K. Schreckenbach, Phys. Lett. **118B**, 162 (1982).

[135] K. Schreckenbach *et al.*, Phys. Lett. **160B**, 325 (1985).

[136] A. A. Hahn *et al.*, Phys. Lett. **B218**, 365 (1989).

[137] P. Vogel *et al.*, Phys. Rev. **C24**, 1543 (1981).

[138] T. A. Mueller *et al.*, Phys. Rev. **C83**, 054615 (2011), [arXiv:1101.2663].

[139] P. Huber, Phys. Rev. **C84**, 024617 (2011), [Erratum: Phys. Rev.C85,029901(2012)], [arXiv:1106.0687].

[140] D. Adey *et al.* (Daya Bay), Phys. Rev. **D100**, 5, 052004 (2019), [arXiv:1808.10836].

[141] D. Adey *et al.* (Daya Bay), Phys. Rev. Lett. **121**, 24, 241805 (2018), [arXiv:1809.02261].

[142] G. Bak *et al.* (RENO), Phys. Rev. Lett. **121**, 20, 201801 (2018), [arXiv:1806.00248].

[143] H. de Kerret *et al.* (Double Chooz), Nature Phys. **16**, 5, 558 (2020), [arXiv:1901.09445].

[144] Y. J. Ko *et al.* (NEOS), Phys. Rev. Lett. **118**, 12, 121802 (2017), [arXiv:1610.05134].

[145] M. Apollonio *et al.* (CHOOZ), Eur.Phys.J. **C27**, 331 (2003), [hep-ex/0301017].

[146] F. Boehm *et al.*, Phys. Rev. **D64**, 112001 (2001), [hep-ex/0107009].

[147] K. Eguchi *et al.* (KamLAND), Phys. Rev. Lett. **90**, 021802 (2003), [hep-ex/0212021].

[148] T. Araki *et al.* (KamLAND), Phys. Rev. Lett. **94**, 081801 (2005), [hep-ex/0406035].

[149] A. Gando *et al.* (KamLAND), Phys. Rev. **D88**, 3, 033001 (2013), [arXiv:1303.4667].

[150] Y. Abe *et al.* (Double Chooz), Phys. Rev. Lett. **108**, 131801 (2012), [arXiv:1112.6353].

[151] F. P. An *et al.* (Daya Bay), Phys. Rev. Lett. **108**, 171803 (2012), [arXiv:1203.1669].

[152] J. K. Ahn *et al.* (RENO), Phys. Rev. Lett. **108**, 191802 (2012), [arXiv:1204.0626].

[153] F. An *et al.* (JUNO), J. Phys. **G43**, 3, 030401 (2016), [arXiv:1507.05613].

[154] I. Alekseev *et al.* (DANSS), Phys. Lett. **B787**, 56 (2018), [arXiv:1804.04046].

[155] H. Almazán *et al.* (STEREO), Phys. Rev. D **102**, 5, 052002 (2020), [arXiv:1912.06582].

[156] M. Andriamirado *et al.* (PROSPECT), Phys. Rev. D **103**, 3, 032001 (2021), [arXiv:2006.11210].

[157] A. P. Serebrov *et al.* (NEUTRINO-4), Pisma Zh. Eksp. Teor. Fiz. **109**, 4, 209 (2019), [JETP Lett.109,no.4,213(2019)], [arXiv:1809.10561].

[158] A. P. Serebrov *et al.*, Phys. Rev. D **104**, 3, 032003 (2021), [arXiv:2005.05301].

[159] Y. Abreu *et al.* (SoLid), JINST **16**, 02, P02025 (2021), [arXiv:2002.05914].

[160] N. Cabibbo, Phys. Lett. **72B**, 333 (1978).

[161] S. M. Bilenky, J. Hosek and S. T. Petcov, Phys. Lett. **94B**, 495 (1980).

[162] V. D. Barger, K. Whisnant and R. J. N. Phillips, Phys. Rev. Lett. **45**, 2084 (1980).

[163] P. Langacker *et al.*, Nucl. Phys. **B282**, 589 (1987).

[164] S. Goswami and A. Yu. Smirnov, Phys. Rev. **D72**, 053011 (2005), [hep-ph/0411359].

[165] N. Okamura, Prog. Theor. Phys. **114**, 1045 (2006), [hep-ph/0411388].

[166] H. Nunokawa, S. J. Parke and R. Zukanovich Funchal, Phys. Rev. **D72**, 013009 (2005), [hep-ph/0503283].

[167] A. Cervera *et al.*, Nucl. Phys. **B579**, 17 (2000), [Erratum: Nucl. Phys.B593,731(2001)], [hep-ph/0002108].

[168] M. Freund, Phys. Rev. **D64**, 053003 (2001), [hep-ph/0103300].

[169] E. K. Akhmedov *et al.*, JHEP **04**, 078 (2004), [hep-ph/0402175].

[170] H. Minakata *et al.*, Phys. Rev. **D74**, 053008 (2006), [hep-ph/0607284].

[171] O. L. G. Peres and A. Yu. Smirnov, Nucl. Phys. **B680**, 479 (2004), [hep-ph/0309312].

[172] S. Petcov, Phys.Lett. **B434**, 321 (1998), [hep-ph/9805262].

[173] E. K. Akhmedov *et al.*, Nucl.Phys. **B542**, 3 (1999), [hep-ph/9808270].

[174] E. K. Akhmedov, Nucl.Phys. **B538**, 25 (1999), [hep-ph/9805272].

[175] M. Chizhov, M. Maris and S. Petcov (1998), SISSA-53-98-EP, [hep-ph/9810501].

[176] M. Chizhov and S. Petcov, Phys.Rev.Lett. **83**, 1096 (1999), [hep-ph/9903399].

[177] E. K. Akhmedov, M. Maltoni and A. Y. Smirnov, JHEP **0705**, 077 (2007), [hep-ph/0612285].

[178] C. Kim and U. Lee, Phys.Lett. **B444**, 204 (1998), [hep-ph/9809491].

[179] O. Peres and A. Y. Smirnov, Phys.Lett. **B456**, 204 (1999), [hep-ph/9902312].

[180] M. Gonzalez-Garcia, M. Maltoni and A. Y. Smirnov, Phys.Rev. **D70**, 093005 (2004), [hep-ph/0408170].

[181] E. K. Akhmedov, M. Maltoni and A. Y. Smirnov, JHEP **0806**, 072 (2008), [arXiv:0804.1466].

[182] J. Bernabeu, S. Palomares Ruiz and S. Petcov, Nucl.Phys. **B669**, 255 (2003), [hep-ph/0305152].

Downloaded from https://academic.oup.com/ptep/article/2022/8/083C01/6651666 by KIT Library user on 27 September 2022

[183] S. Petcov and T. Schwetz, Nucl.Phys. **B740**, 1 (2006), [hep-ph/0511277].

[184] I. Esteban *et al.*, JHEP **01**, 106 (2019), [arXiv:1811.05487].

[185] I. Esteban *et al.*, "Nufit4.1 at nufit webpage," `http://www.nu-fit.org`.

[186] F. Capozzi *et al.*, Prog. Part. Nucl. Phys. **102**, 48 (2018), [arXiv:1804.09678].

[187] P. F. de Salas *et al.*, Phys. Lett. **B782**, 633 (2018), [arXiv:1708.01186].

[188] M. Friend, "Updated Results from the T2K Experiment with 3.13×10^{21} Protons on Target," (2019), KEK/J-PARC Physics seminar, January 10, 2019, URL `https://t2k.org/docs/talk/335/2019kekseminar`.

[189] C. Jarlskog, Phys. Rev. Lett. **55**, 1039 (1985).

[190] M. C. Gonzalez-Garcia, M. Maltoni and T. Schwetz, JHEP **11**, 052 (2014), [arXiv:1409.5439].

[191] Y. Farzan and A. Yu. Smirnov, Phys. Rev. **D65**, 113001 (2002), [hep-ph/0201105].

[192] A. Dueck, S. Petcov and W. Rodejohann, Phys. Rev. **D82**, 013005 (2010), [arXiv:1006.0227].

[193] A. Aguilar-Arevalo *et al.* (MiniBooNE) (2012), [arXiv:1207.4809].

[194] M. A. Acero, C. Giunti and M. Laveder, Phys. Rev. **D78**, 073009 (2008), [arXiv:0711.4222].

[195] C. Giunti and M. Laveder, Phys. Rev. **C83**, 065504 (2011), [arXiv:1006.3244].

[196] F. P. An *et al.* (Daya Bay), Phys. Rev. Lett. **116**, 6, 061801 (2016), [Erratum: Phys. Rev. Lett.118,no.9,099902(2017)], [arXiv:1508.04233].

[197] F. P. An *et al.* (Daya Bay), Phys. Rev. Lett. **118**, 25, 251801 (2017), [arXiv:1704.01082].

[198] G. Mention *et al.*, Phys. Rev. **D83**, 073006 (2011), [arXiv:1101.2755].

[199] J. J. Gomez-Cadenas and M. C. Gonzalez-Garcia, Z. Phys. **C71**, 443 (1996), [hep-ph/9504246].

[200] M. Maltoni *et al.*, Nucl. Phys. **B643**, 321 (2002), [hep-ph/0207157].

[201] M. Dentler *et al.*, JHEP **08**, 010 (2018), [arXiv:1803.10661].

[202] C. Giunti and M. Laveder, Phys. Rev. **D84**, 093006 (2011), [arXiv:1109.4033].

[203] J. M. Conrad *et al.*, Adv. High Energy Phys. **2013**, 163897 (2013), [arXiv:1207.4765].

[204] J. Kopp *et al.*, JHEP **05**, 050 (2013), [arXiv:1303.3011].

[205] G. H. Collin *et al.*, Phys. Rev. Lett. **117**, 22, 221801 (2016), [arXiv:1607.00011].

[206] S. Gariazzo *et al.*, JHEP **06**, 135 (2017), [arXiv:1703.00860].

[207] A. Diaz *et al.*, Phys. Rept. **884**, 1 (2020), [arXiv:1906.00045].

[208] S. Böser *et al.*, Prog. Part. Nucl. Phys. **111**, 103736 (2020), [arXiv:1906.01739].

[209] G. Karagiorgi *et al.*, Phys. Rev. **D75**, 013011 (2007), [Erratum: Phys. Rev.D80,099902(2009)], [hep-ph/0609177].

[210] M. Maltoni and T. Schwetz, Phys. Rev. **D76**, 093005 (2007), [arXiv:0705.0107].

[211] C. Giunti and M. Laveder, Phys. Rev. **D84**, 073008 (2011), [arXiv:1107.1452].

[212] M. Aker *et al.* (KATRIN) (2019), [arXiv:1909.06048].

[213] J. Bonn *et al.*, Nucl. Phys. B Proc. Suppl. **91**, 273 (2001).

[214] V. M. Lobashev *et al.*, Nucl. Phys. B Proc. Suppl. **91**, 280 (2001).

[215] B. Monreal and J. A. Formaggio, Phys. Rev. **D80**, 051301 (2009), [arXiv:0904.2860].

[216] A. De Rujula and M. Lusignoli, Phys. Lett. **118B**, 429 (1982).

[217] L. Gastaldo *et al.*, J. Low Temp. Phys. **176**, 5-6, 876 (2014), [arXiv:1309.5214].

[218] B. Alpert *et al.*, Eur. Phys. J. **C75**, 3, 112 (2015), [arXiv:1412.5060].

[219] M. P. Croce *et al.*, J. Low. Temp. Phys. **184**, 3-4, 958 (2016), [arXiv:1510.03874].

[220] R. E. Shrock, Phys. Lett. **96B**, 159 (1980).

[221] F. Vissani, Nucl. Phys. B Proc. Suppl. **100**, 273 (2001), [hep-ph/0012018].

[222] Y. Farzan, O. L. G. Peres and A. Yu. Smirnov, Nucl. Phys. **B612**, 59 (2001), [hep-ph/0105105].

[223] J. Schechter and J. W. F. Valle, Phys. Rev. D **25**, 2951 (1982).

[224] J. Engel and J. Menendez, Rept. Prog. Phys. **80**, 4, 046301 (2017), [arXiv:1610.06548].

[225] A. Gando *et al.* (KamLAND-Zen), Phys. Rev. Lett. **117**, 8, 082503 (2016), [Addendum: Phys.Rev.Lett. 117, 109903 (2016)], [arXiv:1605.02889].

[226] M. Agostini *et al.* (GERDA), Phys. Rev. Lett. **125**, 25, 252502 (2020), [arXiv:2009.06079].

[227] S. I. Alvis *et al.* (Majorana), Phys. Rev. C **100**, 2, 025501 (2019), [arXiv:1902.02299].

[228] N. Abgrall *et al.* (LEGEND) (2021), [arXiv:2107.11462].

[229] V. Albanese *et al.* (SNO+), JINST **16**, 08, P08059 (2021), [arXiv:2104.11687].

[230] G. Anton *et al.* (EXO-200), Phys. Rev. Lett. **123**, 16, 161802 (2019), [arXiv:1906.02723].

[231] S. A. Kharusi *et al.* (nEXO) (2018), [arXiv:1805.11142].

[232] G. Adhikari *et al.* (nEXO) (2021), [arXiv:2106.16243].

[233] J. Renner *et al.* (NEXT), JINST **13**, 10, P10020 (2018), [arXiv:1808.01804].

[234] A. Simón *et al.* (NEXT), JHEP **21**, 146 (2020), [arXiv:2102.11931].

[235] D. R. Nygren, J. Phys. Conf. Ser. **650**, 1, 012002 (2015).

[236] B. J. P. Jones, A. D. McDonald and D. R. Nygren, JINST **11**, 12, P12011 (2016), [arXiv:1609.04019].

[237] A. D. McDonald *et al.*, Phys. Rev. Lett. **120**, 13, 132504 (2018), [arXiv:1711.04782].

[238] I. Rivilla *et al.*, Nature **583**, 7814, 48 (2020).

[239] C. Chambers *et al.* (nEXO), Nature **569**, 7755, 203 (2019), [arXiv:1806.10694].

[240] S. Ban *et al.*, PTEP **2020**, 3, 033H01 (2020), [arXiv:2001.03281].

[241] D. Q. Adams *et al.* (CUORE), Phys. Rev. Lett. **124**, 12, 122501 (2020), [arXiv:1912.10966].

[242] W. R. Armstrong *et al.* (CUPID) (2019), [arXiv:1907.09376].

[243] O. Azzolini *et al.* (CUPID), Phys. Rev. Lett. **123**, 3, 032501 (2019), [arXiv:1906.05001].

[244] E. Armengaud *et al.* (CUPID), Phys. Rev. Lett. **126**, 18, 181802 (2021), [arXiv:2011.13243].

[245] V. Alenkov *et al.* (AMoRE), Eur. Phys. J. **C79**, 9, 791 (2019), [arXiv:1903.09483].

[246] M. H. Lee (AMoRE), JINST **15**, 08, C08010 (2020), [arXiv:2005.05567].

[247] R. Arnold *et al.* (NEMO-3), Phys. Rev. **D92**, 7, 072011 (2015), [arXiv:1506.05825].

[248] R. Arnold *et al.* (NEMO-3), Phys. Rev. Lett. **119**, 4, 041801 (2017), [arXiv:1705.08847].

Downloaded from https://academic.oup.com/ptep/article/2022/8/083C01/6651666 by KIT Library user on 27 September 2022

15. Quark Model

Revised August 2021 by C. Amsler (Stefan Meyer Inst.), T. DeGrand (Colorado U., Boulder) and B. Krusche (Basel U.).

15.1 Introduction 312
15.2 Quantum numbers of the quarks 312
15.3 Mesons 312
15.4 Exotic mesons 316
15.5 Baryons: qqq states 317
15.5.1 Light baryons 317
15.5.2 Charmed and bottom baryons 320
15.6 Magnetic moments 321
15.7 Dynamics 322
15.8 Lattice Calculations of Hadronic Spectroscopy . 323
15.8.1 Spectroscopy of low-lying states 323
15.8.2 Excited state spectroscopy 324
15.8.3 Electromagnetic effects 326

15.1 Introduction

Quantum chromodynamics (QCD) is the theory of strong interactions. QCD is a quantum field theory with an $SU(N_c)$ local "color" gauge symmetry with $N_c = 3$ colors and a collection of N_f "flavors" of colored fermions, the quarks. It involves a set of $N_c^2 - 1 = 8$ non-Abelian gauge fields, the gluons. QCD is believed to confine, that is, its physical states are color singlets with internal quark and gluon degrees of freedom. This review is concerned with the description of the properties (masses and matrix elements for couplings to electromagnetism and the weak intractions) of the low lying bound states of QCD. The shorthand expression for describing this physics is called the "quark model."

The spectrum of strongly interacting particles consists of a tower of many states, which can be either bosons (labelled as "mesons") or fermions (labelled as "baryons"). The spectrum of baryons and mesons exhibits a high degree of regularity. The organizational principle which best categorizes this regularity is encoded in the quark model. All descriptions of strongly interacting states use the language of the quark model. At the same time, the language is not precise. The quark model exists on many levels: at the simplest level, it is an almost dynamics-free picture of strongly interacting particles as bound states of quarks and antiquarks. As one refines the description, the quark model can become a a framework with more detailed descriptions of dynamics. At its most fundamental level, it might be a description of QCD.

At its heart, the quark model assumes that mesons are bound states of a quark - antiquark pair, and baryons are bound states of three quarks. These are the minimal particle content states which can be color singlets in an $SU(3)$ gauge theory. This approach cannot be justified directly from QCD; however, there is indirect evidence that this description has some fundamental validity from the version of QCD where the number of colors N_c is taken to infinity [1–3]. In that limit, mesons are dominantly narrow (width proportional to $1/N_c$) bound states of a quark - antiquark pair, and baryons have a mass which scales as N_c.

A better justification is that this approach works. Indeed, the quark model is much older (circa 1963-64) than QCD as a theory of the strong interactions (1973-1974). In fact, the principle issue in strong interaction physics before QCD was to justify the success of the quark model in systemizing the properties of mesons and baryons in terms of some more fundamental dynamics (QCD).

Today one knows that this is not the whole story. There are experimentally observed states which either cannot be described, or have an uncomfortable description, as minimal quark number states. Some of them have "exotic" (non- $\bar{q}q$ or qqq) quantum numbers. Given the successes of the quark model, these are classified as "tetraquarks, "pentaquarks" (or more) or "glueballs" (bound states of the gluonic degrees of freedom in QCD). Of course, such labels are imprecise: bound states with the same overall quantum numbers can mix, regardless of their internal degrees of freedom.

This review has several parts. We start by describing the properties of strongly interacting particles in terms of the properties of states made of a minimal number of quark fields which can be coupled into a color singlet – two fields (a quark and an antiquark) for the mesons, and three quarks, for a baryon. Quarks come in six flavors. We describe the properties of mesons as $\bar{q}q$ systems and baryons as qqq systems. Along the way we discuss hadronic bound states which do not fit into this classification.

Finally, at the end of this review, we present results from lattice simulations of QCD, a direct approach to the solution of QCD from its Lagrangian, without reference to models. Lattice simulations interact with the quark model in (at least) two ways: first, the interpolating fields which are used in lattice simulations are usually directly based on quark model constructions. That is the simplest way to create states with the desired quantum numbers, which can then be processed by the lattice calculation. The second way that lattice calculations interact with the quark model comes when one wishes to put the lattice calculations into some context: without the quark model, there are simply the results from the lattice calculations, and the results from experiment, and no way to understand why they are similar or different. The quark model is the framework which is almost universally used to generate that context. Of course, that statement is equally valid when one tries to systemize actual experimental data: the context is always some variation of a quark model.

15.2 Quantum numbers of the quarks

As gluons carry no intrinsic quantum numbers beyond color charge, and because color is believed to be permanently confined, the quantum numbers of strongly interacting particles are given by the quantum numbers of their constituent quarks and antiquarks.

Quarks are strongly interacting fermions with spin 1/2 and, by convention, positive parity. Antiquarks have negative parity. Quarks have the additive baryon number 1/3, antiquarks -1/3. Table 15.1 gives the other additive quantum numbers (flavors) for the three generations of quarks. They are related to the charge Q (in units of the elementary charge e) through the generalized Gell-Mann-Nishijima formula

$$\mathsf{Q} = \mathsf{I}_z + \frac{\mathcal{B} + \mathsf{S} + \mathsf{C} + \mathsf{B} + \mathsf{T}}{2} , \qquad (15.1)$$

where $\mathcal{B}$ is the baryon number. The convention is that the quark *flavor* (I_z, S, C, B, or T) has the same sign as its *charge* Q. With this convention, any flavor carried by a charged meson has

Table 15.1: Quark quantum numbers.

	d	u	s	c	b	t
Q – electric charge	$-\frac{1}{3}$	$+\frac{2}{3}$	$-\frac{1}{3}$	$+\frac{2}{3}$	$-\frac{1}{3}$	$+\frac{2}{3}$
I – isospin	$\frac{1}{2}$	$\frac{1}{2}$	0	0	0	0
I_z – isospin z-component	$-\frac{1}{2}$	$+\frac{1}{2}$	0	0	0	0
S – strangeness	0	0	-1	0	0	0
C – charm	0	0	0	$+1$	0	0
B – bottomness	0	0	0	0	-1	0
T – topness	0	0	0	0	0	$+1$

the same sign as its charge, *e.g.*, the strangeness of the K^+ is $+1$, the bottomness of the B^+ is $+1$, and the charm and strangeness of the D_s^- are each -1. Antiquarks have the opposite flavor signs. The hypercharge is defined as

$$\mathsf{Y} = \mathcal{B} + \mathsf{S} - \frac{\mathsf{C} - \mathsf{B} + \mathsf{T}}{3} .$$

Thus Y is equal to $\frac{1}{3}$ for the u and d quarks, $-\frac{2}{3}$ for the s quark, and 0 for all other quarks. More details and derivations on the quark structure of mesons and baryons can be found *e.g.* in Ref. [4].

15.3 Mesons

Mesons have baryon number $\mathcal{B} = 0$. In the quark model, they are $q\bar{q}'$ bound states of quarks q and antiquarks $\bar{q}'$ (the flavors of q and q' may be different). If the orbital angular momentum of the $q\bar{q}'$ state is ℓ, then the parity P is $(-1)^{\ell+1}$. The meson spin

Downloaded from https://academic.oup.com/ptep/article/2022/8/083C01/6651666 by KIT Library user on 27 September 2022

J is given by the usual relation $|\ell - s| \leq J \leq |\ell + s|$, where s is 0 (antiparallel quark spins) or 1 (parallel quark spins). The charge conjugation, or C-parity $C = (-1)^{\ell+s}$, is defined only for the $q\bar{q}$ states made of quarks and their own antiquarks. The C-parity can be generalized to the G-parity $G = (-1)^{I+\ell+s}$ for mesons made of quarks and their own antiquarks (isospin $\mathsf{I}_z = 0$), and for the charged $u\bar{d}$ and $d\bar{u}$ states (isospin $\mathsf{I} = 1$).

The mesons are classified in J^{PC} multiplets. The $\ell = 0$ states are the pseudoscalars (0^{-+}) and the vectors (1^{--}). The orbital excitations $\ell = 1$ are the scalars (0^{++}), the axial vectors (1^{++}) and (1^{+-}), and the tensors (2^{++}). Assignments for many of the known mesons are given in Tables 15.2, 15.3 and 15.4. Radial excitations are denoted by the principal quantum number n. The very short lifetime of the t quark makes it likely that bound-state hadrons containing t quarks and/or antiquarks do not exist.

States in the natural spin-parity series $P = (-1)^J$ must, according to the above, have $s = 1$ and hence, $CP = +1$. Thus, mesons with natural spin-parity and $CP = -1$ (0^{+-}, 1^{-+}, 2^{+-}, 3^{-+}, *etc.*) are forbidden in the $q\bar{q}'$ model. The $J^{PC} = 0^{--}$ state is forbidden as well. Mesons with such *exotic* quantum numbers may exist, but would lie outside the $q\bar{q}'$ model (see section 15.4 below on exotic mesons).

Following SU(3), the nine possible $q\bar{q}'$ combinations containing the light u, d, and s quarks are grouped into an octet and a singlet of light quark mesons:

$$\mathbf{3} \otimes \bar{\mathbf{3}} = \mathbf{8} \oplus \mathbf{1} \ . \tag{15.2}$$

A fourth quark such as charm c can be included by extending SU(3) to SU(4). However, SU(4) is badly broken owing to the much heavier c quark. Nevertheless, in an SU(4) classification, the sixteen mesons are grouped into a 15-plet and a singlet:

$$\mathbf{4} \otimes \bar{\mathbf{4}} = \mathbf{15} \oplus \mathbf{1} \ . \tag{15.3}$$

The *weight diagrams* for the ground-state pseudoscalar (0^{-+}) and vector (1^{--}) mesons are depicted in Fig. 15.1. The light quark mesons are members of nonets building the middle plane in Fig. 15.1(a) and (b).

Isoscalar states with the same J^{PC} mix, but mixing between the two light quark isoscalar mesons, and the much heavier charmonium and bottomonium states, are generally assumed to be negligible. In the following, we shall use the generic names a for the $\mathsf{I} = 1$, K for the $\mathsf{I} = 1/2$, and f and f' for the $\mathsf{I} = 0$ members of the light quark nonets. Thus, the physical isoscalars are mixtures of the SU(3) wave function ψ_8 and ψ_1:

$$f' = \psi_8 \cos\theta - \psi_1 \sin\theta \ , \tag{15.4}$$

$$f = \psi_8 \sin\theta + \psi_1 \cos\theta \ , \tag{15.5}$$

where θ is the nonet mixing angle and

$$\psi_8 = \frac{1}{\sqrt{6}}(u\bar{u} + d\bar{d} - 2s\bar{s}) \ , \tag{15.6}$$

$$\psi_1 = \frac{1}{\sqrt{3}}(u\bar{u} + d\bar{d} + s\bar{s}) \ . \tag{15.7}$$

The mixing relations are often rewritten to exhibit the $u\bar{u} + d\bar{d}$ and $s\bar{s}$ components which decouple for the "ideal" mixing angle θ_i, such that $\tan\theta_i = 1/\sqrt{2}$ (or $\theta_i = 35.3°$). Defining $\alpha = \theta + 54.7°$, one obtains the physical isoscalar state in the flavor basis

$$f' = \frac{1}{\sqrt{2}}(u\bar{u} + d\bar{d})\cos\alpha - s\bar{s} \ \sin\alpha \ , \tag{15.8}$$

and its orthogonal partner f (replace α by α –90°). Thus for ideal mixing ($\alpha_i = 90°$), the f' becomes pure $s\bar{s}$ and the f pure $u\bar{u} + d\bar{d}$. The mixing angle θ can be derived by diagonalizing the mass matrix

$$\begin{pmatrix} m_8 & m_{81} \\ m_{18} & m_1 \end{pmatrix} .$$

The mass eigenvalues are $m_{f'}$ and m_f. The mixing angle is given by

$$\tan\theta = \frac{m_8 - m_{f'}}{m_{81}} \ .$$

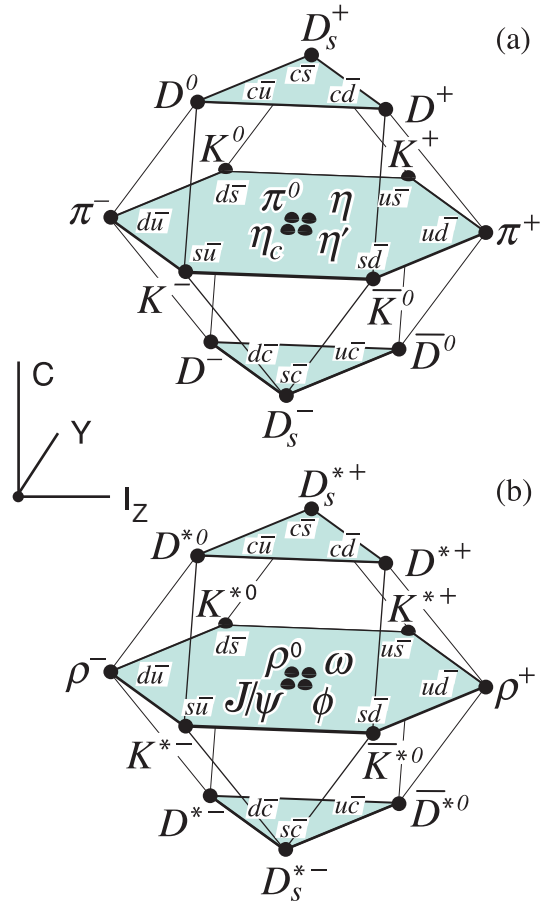

Figure 15.1: SU(4) weight diagram showing the 16-plets for the pseudoscalar (a) and vector mesons (b) made of the u, d, s, and c quarks as a function of isospin I_z, charm C, and hypercharge $\mathsf{Y} = \mathcal{B} + \mathsf{S} - \frac{\mathsf{C}}{3}$. The nonets of light mesons occupy the central planes to which the $c\bar{c}$ states have been added.

Calculating m_8 and m_{81} from the wave functions Eq. (15.6) and Eq. (15.7), and expressing the quark masses as a function of the $\mathsf{I} = 1/2$ and $\mathsf{I} = 1$ meson masses, one obtains

$$\tan\theta = \frac{4m_K - m_a - 3m_{f'}}{2\sqrt{2}(m_a - m_K)} \ , \tag{15.9}$$

which also determines the sign of θ. Alternatively, one can express the mixing angle as a function of all nonet masses. The octet mass is given by

$$m_8 = m_{f'} \cos^2\theta + m_f \sin^2\theta$$

whence

$$\tan^2\theta = \frac{4m_K - m_a - 3m_{f'}}{-4m_K + m_a + 3m_f} \ . \tag{15.10}$$

Eliminating θ from Eq. (15.9) and Eq. (15.10) leads to the sum rule [10]

$$(m_f + m_{f'})(4m_K - m_a) - 3m_f m_{f'} = 8m_K^2 - 8m_K m_a + 3m_a^2. \tag{15.11}$$

This relation is verified for the ground-state vector mesons. We identify the $\phi(1020)$ with the f' and the $\omega(783)$ with the f. Thus

$$\phi(1020) = \psi_8 \cos\theta_V - \psi_1 \sin\theta_V \ , \tag{15.12}$$

$$\omega(782) = \psi_8 \sin\theta_V + \psi_1 \cos\theta_V \ , \tag{15.13}$$

with the vector mixing angle $\theta_V = 36.5°$ from Eq. (15.10), very close to ideal mixing. Thus $\phi(1020)$ is nearly pure $s\bar{s}$. For ideal mixing, Eq. (15.9) and Eq. (15.10) lead to the relations

$$m_K = \frac{m_f + m_{f'}}{2} \ , \quad m_a = m_f \ , \tag{15.14}$$

Downloaded from https://academic.oup.com/ptep/article/2022/8/083C01/6651666 by KIT Library user on 27 September 2022

Table 15.2: Suggested $q\bar{q}$ quark-model assignments for the lightest mesons made of u, d and s quarks. Mesons in boldface are included in the Meson Summary Table. The wave functions f and f' are given in the text (Eq. (15.8)) and the singlet-octet mixing angles in Table 15.5 below for the well established nonets. The classification of the 0^{++} mesons is tentative: (i) the scalars $a_0(980)$, $K_0^*(700)$, $f_0(980)$ and $f_0(500)$, omitted from the table, are often considered to be four-quark states, see Eq. (15.21) below, but are also proposed for the ground state scalar nonet (see the chapter "Scalar Mesons below 1 GeV" in this *Review*); (ii) the isoscalar 0^{++} mesons $f_0(1370)$, $f_0(1500)$ (not shown) and $f_0(1710)$ are expected to mix. The isoscalar assignments in the 2^1S_0 (0^{-+}) nonet are also tentative. Details and alternative schemes can be found in "Spectroscopy of Light Meson Resonances" in this *Review*.
[a] The $1^{+\pm}$ and $2^{-\pm}$ isospin $\frac{1}{2}$ states mix. In particular, the K_{1A} and K_{1B} are nearly equal mixtures of the $K_1(1270)$ and $K_1(1400)$ [5].
[b] The physical vector mesons are mixtures of 1^3D_1 and 2^3S_1 [6].
[c] The $\eta(1475)$ and $\eta(1405)$ (not shown) may be manifestations of a single state [7].
[d] This state has also been proposed as a tetraquark state [8].

$n^{2s+1}\ell_J$	J^{PC}	I = 1 $u\bar{d}$, $\bar{u}d$, $\frac{1}{\sqrt{2}}(d\bar{d}-u\bar{u})$	I = $\frac{1}{2}$ $u\bar{s}$, $d\bar{s}$; $\bar{d}s$, $\bar{u}s$	I = 0 f'	I = 0 f
1^1S_0	0^{-+}	$\boldsymbol{\pi}$	$\boldsymbol{K}$	$\boldsymbol{\eta}$	$\boldsymbol{\eta'}(958)$
1^3S_1	1^{--}	$\boldsymbol{\rho(770)}$	$\boldsymbol{K^*(892)}$	$\boldsymbol{\phi(1020)}$	$\boldsymbol{\omega(782)}$
1^1P_1	1^{+-}	$\boldsymbol{b_1(1235)}$	$\boldsymbol{K_{1B}}$[a]	$\boldsymbol{h_1(1415)}$	$\boldsymbol{h_1(1170)}$
1^3P_0	0^{++}	$\boldsymbol{a_0(1450)}$	$\boldsymbol{K_0^*(1430)}$	$\boldsymbol{f_0(1710)}$	$\boldsymbol{f_0(1370)}$
1^3P_1	1^{++}	$\boldsymbol{a_1(1260)}$	$\boldsymbol{K_{1A}}$[a]	$\boldsymbol{f_1(1420)}$	$\boldsymbol{f_1(1285)}$
1^3P_2	2^{++}	$\boldsymbol{a_2(1320)}$	$\boldsymbol{K_2^*(1430)}$	$\boldsymbol{f_2'(1525)}$	$\boldsymbol{f_2(1270)}$
1^1D_2	2^{-+}	$\boldsymbol{\pi_2(1670)}$	$\boldsymbol{K_2(1770)}$[a]	$\boldsymbol{\eta_2(1870)}$	$\boldsymbol{\eta_2(1645)}$
1^3D_1	1^{--}	$\boldsymbol{\rho(1700)}$	$\boldsymbol{K^*(1680)}$[b]	$\phi(2170)$[d]	$\boldsymbol{\omega(1650)}$
1^3D_2	2^{--}		$\boldsymbol{K_2(1820)}$[a]		
1^3D_3	3^{--}	$\boldsymbol{\rho_3(1690)}$	$\boldsymbol{K_3^*(1780)}$	$\boldsymbol{\phi_3(1850)}$	$\boldsymbol{\omega_3(1670)}$
1^3F_4	4^{++}	$\boldsymbol{a_4(1970)}$	$\boldsymbol{K_4^*(2045)}$	$f_4(2300)$	$\boldsymbol{f_4(2050)}$
1^3G_5	5^{--}	$\rho_5(2350)$	$K_5^*(2380)$		
2^1S_0	0^{-+}	$\boldsymbol{\pi(1300)}$	$\boldsymbol{K(1460)}$	$\boldsymbol{\eta(1475)}$[c]	$\boldsymbol{\eta(1295)}$
2^3S_1	1^{--}	$\boldsymbol{\rho(1450)}$	$\boldsymbol{K^*(1410)}$[b]	$\boldsymbol{\phi(1680)}$	$\boldsymbol{\omega(1420)}$
2^3P_1	1^{++}	$\boldsymbol{a_1(1640)}$			
2^3P_2	2^{++}	$\boldsymbol{a_2(1700)}$	$\boldsymbol{K_2^*(1980)}$	$\boldsymbol{f_2(1950)}$	$f_2(1640)$

Table 15.3: $c\bar{c}$ quark-model assignments for the charmonium mesons with established J^{PC} and their corresponding open charm mesons. Mesons in bold face are included in the Meson Summary Table. The open flavor states in the 1^{+-} and 1^{++} rows are mixtures of the $1^{+\pm}$ states.
[a] This meson splits into two states. The ground state scalar meson lies around 2100 MeV [9].
[b] The masses are considerably smaller than most theoretical predictions. They have also been considered as tetraquark or $D^{(*)}K$ molecular states.
[c] Mixtures of the $1\,^3D_1$ and $2\,^3S_1$ states.

$n^{2s+1}\ell_J$	J^{PC}	I = 0 $c\bar{c}$	I = $\frac{1}{2}$ $c\bar{u}$, cd; $\bar{c}u$, $\bar{c}d$	I = 0 $c\bar{s}$; $\bar{c}s$
$1\,^1S_0$	0^{-+}	$\boldsymbol{\eta_c(1S)}$	$\boldsymbol{D}$	$\boldsymbol{D_s^\pm}$
$1\,^3S_1$	1^{--}	$\boldsymbol{J/\psi(1S)}$	$\boldsymbol{D^*}$	$\boldsymbol{D_s^{*\pm}}$
$1\,^3P_0$	0^{++}	$\boldsymbol{\chi_{c0}(1P)}$	$\boldsymbol{D_0^*(2300)}$[a]	$\boldsymbol{D_{s0}^*(2317)^\pm}$[b]
$1\,^3P_1$	1^{++}	$\boldsymbol{\chi_{c1}(1P)}$	$D_1(2430)$	$\boldsymbol{D_{s1}(2460)^\pm}$[b]
$1\,^1P_1$	1^{+-}	$\boldsymbol{h_c(1P)}$	$\boldsymbol{D_1(2420)}$	$\boldsymbol{D_{s1}(2536)^\pm}$
$1\,^3P_2$	2^{++}	$\boldsymbol{\chi_{c2}(1P)}$	$\boldsymbol{D_2^*(2460)}$	$\boldsymbol{D_{s2}^*(2573)^\pm}$
$2\,^1S_0$	0^{-+}	$\boldsymbol{\eta_c(2S)}$	$D_0(2500)^0$	$D_{s0}(2590)^+$
$2\,^3S_1$	1^{--}	$\boldsymbol{\psi(2S)}$	$D_1^*(2760)^0$	$\boldsymbol{D_{s1}^*(2700)^\pm}$[c]
$1\,^3D_1$	1^{--}	$\boldsymbol{\psi(3770)}$		$D_{s1}^*(2860)^\pm$[c]
$1\,^3D_2$	2^{--}	$\boldsymbol{\psi_2(3823)}$	$D_2(2740)^0$	
$2\,^3P_J$	$0^{++}, 1^{++}$	$\chi_{c0}(3860)$		
	2^{++}	$\boldsymbol{\chi_{c2}(3930)}$		
$3\,^3S_1$	1^{--}	$\boldsymbol{\psi(4040)}$		
$2\,^3D_1$	1^{--}	$\boldsymbol{\psi(4160)}$		
$4\,^3S_1$	1^{--}	$\boldsymbol{\psi(4415)}$		
$1\,^3D_3$	3^{--}	$\boldsymbol{\psi_3(3842)}$	$D_3^*(2750)$	$D_{s3}^*(2860)^\pm$

Downloaded from https://academic.oup.com/ptep/article/2022/8/083C01/6651666 by KIT Library user on 27 September 2022

Table 15.4: $b\bar{b}$ quark-model assignments for the bottomonium mesons with established J^{PC} and their corresponding open bottom mesons.

$n^{2s+1}\ell_J$	J^{PC}	I = 0 $b\bar{b}$	I = $\frac{1}{2}$ $b\bar{u}$, $b\bar{d}$; $\bar{b}u$, $\bar{b}d$	I = 0 $b\bar{s}$; $\bar{b}s$	I = 0 $b\bar{c}$; $\bar{b}c$
$1\,^1S_0$	0^{-+}	$\boldsymbol{\eta_b(1S)}$	$\boldsymbol{B}$	$\boldsymbol{B_s^0}$	$\boldsymbol{B_c^\pm}$
$1\,^3S_1$	1^{--}	$\boldsymbol{\Upsilon(1S)}$	$\boldsymbol{B^*}$	$\boldsymbol{B_s^*}$	
$1\,^3P_0$	0^{++}	$\boldsymbol{\chi_{b0}(1P)}$			
$1\,^3P_1$	1^{++}	$\boldsymbol{\chi_{b1}(1P)}$			
$1\,^1P_1$	1^{+-}	$\boldsymbol{h_b(1P)}$	$\boldsymbol{B_1(5721)}$	$\boldsymbol{B_{s1}(5830)^0}$	
$1\,^3P_2$	2^{++}	$\boldsymbol{\chi_{b2}(1P)}$	$\boldsymbol{B_2^*(5747)}$	$\boldsymbol{B_{s2}^*(5840)^0}$	
$2\,^1S_0$	0^{-+}	$\eta_b(2S)$			$\boldsymbol{B_c(2S)^\pm}$
$2\,^3S_1$	1^{--}	$\boldsymbol{\Upsilon(2S)}$			
$1\,^3D_2$	2^{--}	$\boldsymbol{\Upsilon_2(1D)}$			
$2\,^3P_J$	$0,1,2^{++}$	$\boldsymbol{\chi_{b0,1,2}(2P)}$			
$2\,^1P_1$	1^{+-}	$\boldsymbol{h_b(2P)}$			
$3\,^3S_1$	1^{--}	$\boldsymbol{\Upsilon(3S)}$			
$3\,^3P_J$	$0,1,2^{++}$	$\boldsymbol{\chi_{b1,2}(3P)}$			
$4\,^3S_1$	1^{--}	$\boldsymbol{\Upsilon(4S)}$			

which are satisfied for the vector mesons.

The situation for the pseudoscalar and scalar mesons is not so clear cut, either theoretically or experimentally. For the pseudoscalars, the mixing angle is small. This can be understood qualitatively via gluon-line counting of the mixing process. The size of the mixing process between the nonstrange and strange mass bases scales as α_s^2, not α_s^3, because of two rather than three gluon exchange as it does for the vector mesons. It may also be that the lightest isoscalar pseudoscalars mix more strongly with excited states or with states of substantial non-$\bar{q}q$ content, as will be discussed below.

In fact a large mixing from hadronic loops is expected for scalar mesons, no matter what model is assumed for $q\bar{q}$ pair production [11]. A variety of analysis methods lead to similar results: First, for these states, Eq. (15.11) is satisfied only approximately. Then Eq. (15.9) and Eq. (15.10) lead to somewhat different values for the mixing angle. Identifying the η with the f' one gets

$$\eta = \psi_8 \cos\theta_P - \psi_1 \sin\theta_P \ , \tag{15.15}$$

$$\eta' = \psi_8 \sin\theta_P + \psi_1 \cos\theta_P \ . \tag{15.16}$$

Following chiral perturbation theory, the meson masses in the mass formulae (Eq. (15.9) and Eq. (15.10)) might be replaced by their squares. Table 15.5 lists the mixing angle $\theta_{\rm lin}$ from Eq. (15.10) (using the neutral members of the nonets) and the corresponding $\theta_{\rm quad}$ obtained by replacing the meson masses by their squares throughout. The mixing angles in the 1^{--}, 2^{++} and 3^{--} nonets are not far from ideal, while larger $s\bar{s}$-$(u\bar{u}+d\bar{d})$ mixing is predicted from hadronic loops in the 0^{++}, 0^{-+} and $1^{+\pm}$ nonets [11].

Table 15.5: Singlet-octet mixing angles for the well established nonets from the linear mass formula Eq. (15.10) and its quadratic version in which the masses are squared. The 1^{++} and 1^{+-} nonet mixing angles depend on the mixing angle θ_{K_1} between K_{1A} and K_{1B}. The recommended values are $\sim$23° and $\sim$28° for 1^{++} and 1^{+-}, respectively, with $\theta_{K_1}\sim$35° [5].

$n^{2s+1}\ell_J$	J^{PC}	$\theta_{\rm quad}$ [°]	$\theta_{\rm lin}$ [°]
1^1S_0	0^{-+}	−11.3	−24.5
1^3S_1	1^{--}	39.2	36.5
1^3P_2	2^{++}	29.6	28.0
1^3D_3	3^{--}	31.8	30.8

The pseudoscalar mixing angle θ_P can also be measured by comparing the partial widths for radiative J/ψ decay into a vector and a pseudoscalar [12], radiative $\phi(1020)$ decay into η and η' [13], radiative decays between pseudoscalar and vector mesons [14], or $\bar{p}p$ annihilation at rest into a pair of vector and pseudoscalar or into two pseudoscalars [15, 16]. One obtains a mixing angle between –10° and –20°. More recently, a lattice QCD simulation, Ref. [17], has successfully reproduced the masses of the η and η', and as a byproduct find a mixing angle $\theta_{lin} = -14.1(2.8)°$. We return to this point in Sec. 15.8.

The nonet mixing angles can be measured in $\gamma\gamma$ collisions, *e.g.*, for the 0^{-+}, 0^{++}, and 2^{++} nonets. In the quark model, the amplitude for the coupling of neutral mesons to two photons is proportional to $\sum_i Q_i^2$, where Q_i is the charge of the i-th quark. The 2γ partial width of an isoscalar meson with mass m is then given in terms of the mixing angle α by

$$\Gamma_{2\gamma} = C(5\cos\alpha - \sqrt{2}\sin\alpha)^2 m^3 \ , \tag{15.17}$$

for f' and f ($\alpha \to \alpha - 90°$). The coupling C may depend on the meson mass. It is often assumed to be a constant in the nonet. For the isovector a, one finds $\Gamma_{2\gamma} = 9\ C\ m^3$. Thus the members of an ideally mixed nonet couple to 2γ with partial widths in the ratios $f : f' : a = 25 : 2 : 9$. For tensor mesons, one finds from the ratios of the measured 2γ partial widths for the $f_2(1270)$ and $f_2'(1525)$ mesons a mixing angle α_T of $(81\pm 1)°$, or $\theta_T = (27 \pm 1)°$, in accord with the linear mass formula. For the pseudoscalars, one finds from the ratios of partial widths $\Gamma(\eta' \to 2\gamma)/\Gamma(\eta \to 2\gamma)$ a mixing angle $\theta_P = (-18 \pm 2)°$, while the ratio $\Gamma(\eta' \to 2\gamma)/\Gamma(\pi^0 \to 2\gamma)$ leads to $\sim$ –24 °. SU(3) breaking effects for pseudoscalars are discussed in [18].

The partial width Γ for the decay of a scalar or a tensor meson into a pair of pseudoscalar mesons is model-dependent. Following Ref. [19],

$$\Gamma = C \times \gamma^2 \times |F(q)|^2 \times q \ , \tag{15.18}$$

where C is a nonet constant, q the momentum of the decay products, $F(q)$ a form factor, and γ^2 the SU(3) coupling. Details and explicit expressions for γ^2 and $F(q)$ are given in "Spectroscopy of Light Meson Resonances". The decay of a $q\bar{q}$ meson into a pair of mesons involves the creation of a $q\bar{q}$ pair, and SU(3) symmetry assumes that the matrix elements for the creation of $s\bar{s}$, $u\bar{u}$, and $d\bar{d}$ pairs are equal. An excellent fit to the tensor meson decay widths is obtained assuming SU(3) symmetry and a pseudoscalar mixing angle $\theta_P \simeq$ –17 ° [19].

The analysis of resonances is complicated by the presence of thresholds such as $K\bar{K}$ in $a_0(980) \to \eta\pi$ or $f_0(980) \to \pi\pi$, which affect the resonance masses and widths. A particularly nasty kinematic effect is the triangle singularity in which one of the primary decay daughters in turn decays and is emitted backwards, catching up and scattering with the second primary product. This mechanism generates fake peaks in the final state and has been proposed as alternative explanation for several meson (and baryon) signals. Prominent examples are the $\eta(1475) \to K^*(\to K\pi)\bar{K}$

Downloaded from https://academic.oup.com/ptep/article/2022/8/083C01/6651666 by KIT Library user on 27 September 2022

and $\eta(1410) \to a_0(980)(\to \eta\pi)\pi$ signals which could be due to one single state [7] (see also Table 15.2).

15.4 Exotic mesons

The existence of a light nonet composed of four quarks (tetraquarks) with masses below 1 GeV was suggested a long time ago [20,21]. Coupling two triplets of light quarks u, d, and s, one obtains nine states, of which the six symmetric (uu, dd, ss, $ud+du$, $us+su$, $ds+sd$) form the six dimensional representation $\mathbf{6}$, while the three antisymmetric ($ud-du$, $us-su$, $ds-sd$) form the three dimensional representation $\overline{\mathbf{3}}$ of SU(3):

$$\mathbf{3} \otimes \mathbf{3} = \mathbf{6} \oplus \overline{\mathbf{3}} \ . \tag{15.19}$$

Hence for tetraquarks one gets the reduction

$$\begin{aligned} &\mathbf{3} \otimes \mathbf{3} \otimes \overline{\mathbf{3}} \otimes \overline{\mathbf{3}} \\ &= \mathbf{6} \oplus \overline{\mathbf{3}} \otimes \overline{\mathbf{6}} \otimes \mathbf{3} \\ &= \overline{\mathbf{3}} \otimes \mathbf{3} \oplus \mathbf{6} \otimes \overline{\mathbf{6}} \oplus \mathbf{6} \otimes \mathbf{3} \oplus \overline{\mathbf{3}} \otimes \overline{\mathbf{6}} \\ &= \mathbf{9} \oplus \mathbf{36} \oplus \mathbf{18} \oplus \overline{\mathbf{18}}. \end{aligned} \tag{15.20}$$

Combining with spin and color and requiring antisymmetry for diquarks and antidiquarks, one finds for ground states (zero angular momenta) that the most deeply bound tetraquarks (and hence the lightest ones) lie in the nonet and are scalar mesons (see also [4]). The average mass is estimated to be around 900 MeV from the mass differences between the ρ and π masses. Letting the strange quark determine the mass splittings one obtains a mass inverted spectrum with a light isosinglet, a medium heavy isodoublet and a heavy isotriplet + isosinglet. It is then tempting to identify these mesons as the lightest scalars

$$\begin{aligned} f_0(500) &= \bar{u}\bar{d}ud, \\ K_0^*(700) &= (\bar{s}\bar{d}ud, \bar{s}\bar{u}ud) \quad \text{and} \quad (\bar{u}\bar{d}us, \bar{u}\bar{d}ds), \\ a_0(980) &= (us\bar{d}\bar{s}, \frac{1}{\sqrt{2}}[u\bar{u} - d\bar{d}]s\bar{s}, \bar{u}\bar{s}ds), \\ f_0(980) &= \frac{1}{\sqrt{2}}[u\bar{u} + d\bar{d}]s\bar{s}. \end{aligned} \tag{15.21}$$

In alternative schemes these states build the lightest $q\bar{q}$ scalar nonet (for details see "Scalar mesons below 1 GeV" in this *"Review"*).

A plethora of new states have been reported in the charmonium and bottomonium spectra. The most prominent one is the $\chi_{c1}(3872)$ (formerly $X(3872)$), first observed in 2003 in B-decays in the final state $J/\psi\,\pi^+\pi^-$ (see Fig. 15.2). Even more remarkable is the observation of isovector (charged) candidates decaying into $c\bar{c}$ plus a charged pion, such as the $Z^{\pm}(4430)$ decaying into $\psi(2S)\pi^{\pm}$, which a priori excludes an interpretation as true $c\bar{c}$ (charmonium) state. Similar states are also observed in the bottomonium spectrum. Some of these states may be tetraquarks (e.g. $cq\bar{c}\bar{q}$), molecular structures (e.g. $c\bar{q}\bar{c}q$) made of pairs of mesons such as D, D_s and D^*, D_s^* excitations, or their B and B^* counterparts. They could also be mimicked by kinematical effects such as triangle singularities. Details and references can be found in recent reviews [23], [24] and in the review "Heavy non-$q\bar{q}$ Mesons" .

QCD predicts the existence of extra isoscalar mesons which cannot be addressed by the quark model. In the pure gauge theory they contain only gluons, and are called glueballs. The ground state glueball is predicted by lattice gauge theories to be 0^{++}, the first excited state 2^{++}. Errors on the mass predictions are large. From Ref. [25] one obtains 1750 (50) (80) MeV for the mass of the lightest 0^{++} glueball from quenched QCD. As an example for the glueball mass spectrum, we show in Fig. 15.3 a calculation from Ref. [22]. A mass of 1710 MeV is predicted for the ground state, also with an error of about 100 MeV. Earlier work by other groups produced masses at 1650 MeV [26] and 1550 MeV [27] (see also [28]. The first excited state has a mass of about 2.4 GeV, and the lightest glueball with exotic quantum numbers (2^{+-}) has a mass of about 4 GeV.

These calculations are made in the so-called "quenched approximation" which neglects $q\bar{q}$ loops. However, both glue and $q\bar{q}$ states

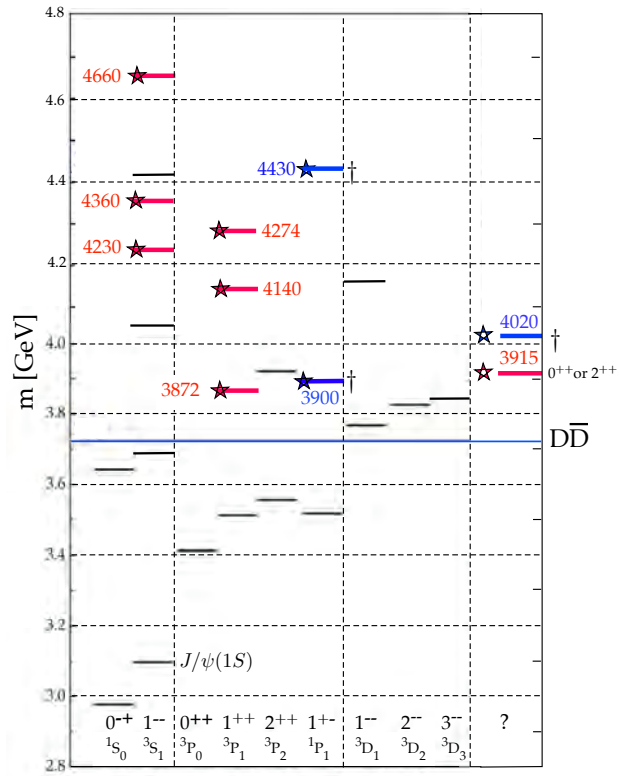

Figure 15.2: Established states populating the charmonium spectrum that are listed in the Summary Tables. The $c\bar{c}$ states are shown in black, the exotic ones are tagged by stars (red for the isoscalars, blue for the isovectors). The quantum numbers of the two states in the right column are not firmly established.

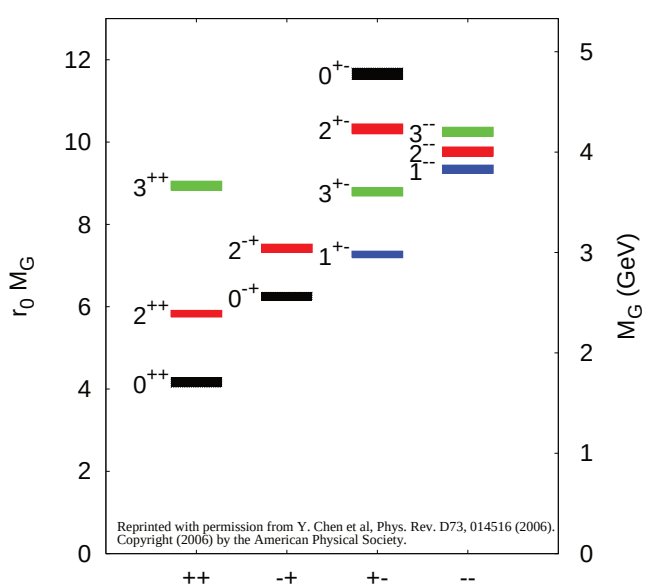

Figure 15.3: Predicted glueball mass spectrum from the lattice in quenched approximation (from [22]).

Downloaded from https://academic.oup.com/ptep/article/2022/8/083C01/6651666 by KIT Library user on 27 September 2022

couple to singlet scalar mesons. Therefore glueballs will mix with nearby $q\bar{q}$ states of the same quantum numbers. For example, the two isoscalar 0^{++} mesons around 1500 MeV will mix with the pure ground state glueball to generate the observed physical states $f_0(1370)$, $f_0(1500)$, and $f_0(1710)$ [19, 29]. The first results from lattice calculations, which include these effects, indicate that the mass shifts are small. We return to a discussion of this point in Sec. 15.8, see also Fig. 15.15.

The existence of three singlet scalar mesons around 1.5 GeV suggests additional degrees of freedom such as glue, since only two mesons are predicted in this mass range. The $f_0(1500)$ [19, 29] or, alternatively, the $f_0(1710)$ [26], have been proposed as candidates for the scalar glueball, both states having considerable mixing also with the $f_0(1370)$. Other mixing schemes, in particular with the $f_0(500)$ and the $f_0(980)$, have also been proposed [30]. According to a holographic model of low-energy QCD scalar glueballs decay strongly into kaons and η mesons, in good agreement with data on the $f_0(1710)$ [31]. Details can be found in the review "Spectroscopy of Light Meson Resonances" and in Ref. [32]. See also the review "Scalar Mesons below 1 GeV" in this *Review*.

Mesons made of $q\bar{q}$ pairs bound by excited gluons g, the hybrid states $q\bar{q}g$, are also predicted. They should lie in the 1.9 GeV mass region, according to gluon flux tube models [33]. Lattice QCD also predicts the lightest hybrid, an exotic 1^{-+}, at a mass of 1.8 to 1.9 GeV [34]. However, the bag model predicts four nonets, among them an exotic 1^{-+} around or above 1.4 GeV [35, 36]. There are so far two candidates for exotic states with quantum numbers 1^{-+}, the $\pi_1(1400)$ and $\pi_1(1600)$, which could be hybrids or four-quark states. However, a recent combined re-analysis of π_1 production in diffractive $\pi^- p$ interaction and low energy $\bar{p}p$ annihilation leads to a single pole at ∼1560 MeV with a width of ∼390 MeV, although a two-pole scenario cannot be excluded [37]. (See the review "Spectroscopy of Light Meson Resonances" in this *Review* and Ref. [32].)

15.5 Baryons: qqq states

Baryons are fermions with baryon number $\mathcal{B} = 1$, *i.e.*, in the most general case, they are composed of three quarks plus any number of quark - antiquark pairs. Until recently, all established baryons were 3-quark (qqq) configurations, which we mainly discuss in this section. However, in 2015 the LHCb collaboration published first evidence for charmed 'pentaquark' states of minimal quark content $c\bar{c}uud$ at invariant masses close to 4.4 GeV [38]. More refined LHCb experiments have revealed evidence for three such states called $P_c(4312)^+$, $P_c(4440)^+$, and $P_c(4457)^+$ [39]. These states are located close to the thresholds of the production of ordinary baryon-meson pairs like $\Sigma_c^+ \bar{D}^0$ and $\Sigma_c^+ \bar{D}^{\star 0}$ and are consistent with the predictions [40, 41] in terms of molecular-like states. A nice overview on the discussion of pentaquark and tetraquark states is given in Ref. [42].

The color part of baryon state functions is an SU(3) singlet, a completely antisymmetric state of the three colors. Since the quarks are fermions, the state function must be antisymmetric under interchange of any two equal-mass quarks (up and down quarks in the limit of isospin symmetry). Thus it can be written as

$$|\, qqq \,\rangle_A = |\, \text{color} \,\rangle_A \times |\, \text{space, spin, flavor} \,\rangle_S, \tag{15.22}$$

where the subscripts S and A indicate symmetry or antisymmetry under interchange of any two equal-mass quarks. Note the contrast with the state function for the three nucleons in ^{3}H or ^{3}He:

$$|\, NNN \,\rangle_A = |\, \text{space, spin, isospin} \,\rangle_A. \tag{15.23}$$

This difference has major implications for internal structure, magnetic moments, *etc.* (For a nice discussion, see Ref. [43].)

15.5.1 *Light baryons*

The "ordinary" baryons are made up of u, d, and s quarks. The three flavors imply an approximate flavor SU(3), which requires that baryons made of these quarks belong to the multiplets on the right side of

$$\mathbf{3} \otimes \mathbf{3} \otimes \mathbf{3} = \mathbf{10}_S \oplus \mathbf{8}_M \oplus \mathbf{8}_M \oplus \mathbf{1}_A \tag{15.24}$$

(see the section on "SU(n) Multiplets and Young Diagrams" in this *Review*). Here the subscripts indicate symmetric, mixed-symmetry, or antisymmetric states under interchange of any two quarks. The **1** is a uds state (Λ_1), and the octet contains a similar state (Λ_8). If these have the same spin and parity, they can mix. The mechanism is the same as for the mesons (see above). In the ground state multiplet, the SU(3) flavor singlet Λ_1 is forbidden by Fermi statistics. The section on "SU(3) Isoscalar Factors and Representation Matrices," shows how relative decay rates in, say, $\mathbf{10} \to \mathbf{8} \otimes \mathbf{8}$ decays may be calculated.

For the "ordinary" baryons (no c or b quark), flavor and spin may be combined in an approximate flavor-spin SU(6), in which the six basic states are $d\uparrow$, $d\downarrow$, $\cdots$, $s\downarrow$ ($\uparrow, \downarrow$ = spin up, down). Then the baryons belong to the multiplets on the right side of

$$\mathbf{6} \otimes \mathbf{6} \otimes \mathbf{6} = \mathbf{56}_S \oplus \mathbf{70}_M \oplus \mathbf{70}_M \oplus \mathbf{20}_A. \tag{15.25}$$

These SU(6) multiplets decompose into flavor SU(3) multiplets as follows:

$$\mathbf{56} = {}^4\mathbf{10} \oplus {}^2\mathbf{8} \tag{15.26a}$$

$$\mathbf{70} = {}^2\mathbf{10} \oplus {}^4\mathbf{8} \oplus {}^2\mathbf{8} \oplus {}^2\mathbf{1} \tag{15.26b}$$

$$\mathbf{20} = {}^2\mathbf{8} \oplus {}^4\mathbf{1}, \tag{15.26c}$$

where the superscript $(2S{+}1)$ gives the net spin S of the quarks for each particle in the SU(3) multiplet. The $J^P = 1/2^+$ octet containing the nucleon and the $J^P = 3/2^+$ decuplet containing the $\Delta(1232)$ together make up the "ground-state" 56-plet, in which the orbital angular momenta between the quark pairs are zero (so that the spatial part of the state function is trivially symmetric). The **70** and **20** require some excitation of the spatial part of the state function in order to make the overall state function symmetric. States with nonzero orbital angular momenta are classified in SU(6)⊗O(3) supermultiplets.

It is useful to classify the baryons into bands that have the same number N of quanta of excitation. Each band consists of a number of supermultiplets, specified by (D, L_N^P), where D is the dimensionality of the SU(6) representation, L is the total quark orbital angular momentum, and P is the total parity. Supermultiplets contained in bands up to N = 12 are given in Ref. [44]. The N = 0 band, which contains the nucleon and $\Delta(1232)$, consists only of the $(56,0_0^+)$ supermultiplet. The N = 1 band consists only of the $(70,1_1^-)$ multiplet and contains the negative-parity baryons with masses below about 1.9 GeV. The N = 2 band contains five supermultiplets: $(56,0_2^+)$, $(70,0_2^+)$, $(56,2_2^+)$, $(70,2_2^+)$, and $(20,1_2^+)$.

The wave functions of the non-strange baryons in the harmonic oscillator basis are often labeled by $|X^{2S+1}L_\pi J^P\rangle$, where S, L, J, P are as above, $X = N$ or Δ, and $\pi = S, M$ or A denotes the symmetry of the spatial wave function. The possible model states for the bands with N=0,1,2 are given in Table 15.7. The assignment of experimentally observed states is only complete and well established up to the N=1 band. Some more tentative assignments for higher multiplets are suggested in [45].

In Table 15.6, quark-model assignments are given for many of the established baryons whose SU(6)⊗O(3) compositions are relatively unmixed. One must, however, keep in mind that apart from the mixing of the Λ singlet and octet states, states with same J^P but different L, S combinations can also mix. In the quark model with one-gluon exchange motivated interactions, the size of the mixing is determined by the relative strength of the tensor term with respect to the contact term (see below). The mixing is more important for the decay patterns of the states than for their positions. An example are the lowest lying $(70, 1_1^-)$ states with J^P=1/2$^-$ and 3/2$^-$. The physical states are:

$$|\, N(1535)1/2^- \rangle = \cos(\Theta_S)|N^2 P_M 1/2^-\rangle - \sin(\Theta_S)|N^4 P_M 1/2^-\rangle \tag{15.27}$$

$$|\, N(1520)3/2^- \rangle = \cos(\Theta_D)|N^2 P_M 3/2^-\rangle - \sin(\Theta)_D|N^4 P_M 3/2^-\rangle \tag{15.28}$$

and the orthogonal combinations for $N(1650)1/2^-$ and $N(1700)3/2^-$. The mixing is large for the J^P=1/2$^-$ states ($\Theta_S \approx$ -32°), but small for the J^P=3/2$^-$ states ($\Theta_D \approx +6^o$) [47–49].

All baryons of the ground state multiplets are known. Many of their properties, in particular their masses, are in good agreement

Downloaded from https://academic.oup.com/ptep/article/2022/8/083C01/6651666 by KIT Library user on 27 September 2022

Table 15.6: Quark-model assignments for some of the known baryons in terms of a flavor-spin SU(6) basis. Only the dominant representation is listed. Assignments for several states, especially for the $\Lambda(1810)$, $\Lambda(2350)$, $\Xi(1820)$, and $\Xi(2030)$, are merely educated guesses.
† suggestions for assignments and re-assignments from Ref. [46].

J^P	(D, L_N^P)	S	Octet members				Singlets
$1/2^+$	$(56,0_0^+)$	1/2	$N(939)$	$\Lambda(1116)$	$\Sigma(1193)$	$\Xi(1318)$	
$1/2^+$	$(56,0_2^+)$	1/2	$N(1440)$	$\Lambda(1600)$	$\Sigma(1660)$	$\Xi(1690)^\dagger$	
$1/2^-$	$(70,1_1^-)$	1/2	$N(1535)$	$\Lambda(1670)$	$\Sigma(1620)$	$\Xi(?)$	$\Lambda(1405)$
					$\Sigma(1560)^\dagger$		
$3/2^-$	$(70,1_1^-)$	1/2	$N(1520)$	$\Lambda(1690)$	$\Sigma(1670)$	$\Xi(1820)$	$\Lambda(1520)$
$1/2^-$	$(70,1_1^-)$	3/2	$N(1650)$	$\Lambda(1800)$	$\Sigma(1750)$	$\Xi(?)$	
					$\Sigma(1620)^\dagger$		
$3/2^-$	$(70,1_1^-)$	3/2	$N(1700)$	$\Lambda(?)$	$\Sigma(1940)^\dagger$	$\Xi(?)$	
$5/2^-$	$(70,1_1^-)$	3/2	$N(1675)$	$\Lambda(1830)$	$\Sigma(1775)$	$\Xi(1950)^\dagger$	
$1/2^+$	$(70,0_2^+)$	1/2	$N(1710)$	$\Lambda(1810)$	$\Sigma(1880)$	$\Xi(?)$	$\Lambda(1810)^\dagger$
$3/2^+$	$(56,2_2^+)$	1/2	$N(1720)$	$\Lambda(1890)$	$\Sigma(?)$	$\Xi(?)$	
$5/2^+$	$(56,2_2^+)$	1/2	$N(1680)$	$\Lambda(1820)$	$\Sigma(1915)$	$\Xi(2030)$	
$7/2^-$	$(70,3_3^-)$	1/2	$N(2190)$	$\Lambda(?)$	$\Sigma(?)$	$\Xi(?)$	$\Lambda(2100)$
$9/2^-$	$(70,3_3^-)$	3/2	$N(2250)$	$\Lambda(?)$	$\Sigma(?)$	$\Xi(?)$	
$9/2^+$	$(56,4_4^+)$	1/2	$N(2220)$	$\Lambda(2350)$	$\Sigma(?)$	$\Xi(?)$	
			Decuplet members				
$3/2^+$	$(56,0_0^+)$	3/2	$\Delta(1232)$	$\Sigma(1385)$	$\Xi(1530)$	$\Omega(1672)$	
$3/2^+$	$(56,0_2^+)$	3/2	$\Delta(1600)$	$\Sigma(1690)^\dagger$	$\Xi(?)$	$\Omega(?)$	
$1/2^-$	$(70,1_1^-)$	1/2	$\Delta(1620)$	$\Sigma(1750)^\dagger$	$\Xi(?)$	$\Omega(?)$	
$3/2^-$	$(70,1_1^-)$	1/2	$\Delta(1700)$	$\Sigma(?)$	$\Xi(?)$	$\Omega(?)$	
$5/2^+$	$(56,2_2^+)$	3/2	$\Delta(1905)$	$\Sigma(?)$	$\Xi(?)$	$\Omega(?)$	
$7/2^+$	$(56,2_2^+)$	3/2	$\Delta(1950)$	$\Sigma(2030)$	$\Xi(?)$	$\Omega(?)$	
$11/2^+$	$(56,4_4^+)$	3/2	$\Delta(2420)$	$\Sigma(?)$	$\Xi(?)$	$\Omega(?)$	

Table 15.7: N and Δ states in the N=0,1,2 harmonic oscillator bands. L^P denotes angular momentum and parity, S the three-quark spin and 'sym'=A,S,M the symmetry of the spatial wave function. Listed are all possible spin/parity combinations and assignments of experimentally observed states. Only dominant components are indicated. Assignments in the N=2 band are partly tentative.

N	sym	L^P	S	$N(I=1/2)$			
2	A	1^+	1/2	$1/2^+$	$3/2^+$	-	-
2	M	2^+	3/2	$1/2^+$	$3/2^+$	$5/2^+$	$7/2^+$
2	M	2^+	1/2	-	$3/2^+$	$5/2^+$	-
2	M	0^+	3/2	-	$3/2^+$	-	-
2	M	0^+	1/2	$1/2^+$ $N(1710)$	-	-	-
2	S	2^+	3/2	-	-	-	-
2	S	2^+	1/2	-	$3/2^+$ $N(1720)$	$5/2^+$ $N(1680)$	-
2	S	0^+	3/2	-	-	-	-
2	S	0^+	1/2	$1/2^+$ $N(1440)$	-	-	-
1	M	1^-	3/2	$1/2^-$ $N(1650)$	$3/2^-$ $N(1700)$	$5/2^-$ $N(1675)$	-
1	M	1^-	1/2	$1/2^-$ $N(1535)$	$3/2^-$ $N(1520)$	-	-
0	S	0^+	3/2	-	-	-	-
0	S	0^+	1/2	$1/2^+$ $N(938)$	-	-	-
N	sym	L^P	S	$\Delta(I=3/2)$			
2	A	1^+	1/2	-	-	-	-
2	M	2^+	3/2	-	-	-	-
2	M	2^+	1/2	-	$3/2^+$	$5/2^+$	-
2	M	0^+	3/2	-	-	-	-
2	M	0^+	1/2	$1/2^+$ $\Delta(1750)$	-	-	-
2	S	2^+	3/2	$1/2^+$ $\Delta(1910)$	$3/2^+$ $\Delta(1920)$	$5/2^+$ $\Delta(1905)$	$7/2^+$ $\Delta(1950)$
2	S	2^+	1/2	-	-	-	-
2	S	0^+	3/2	-	$3/2^+$ $\Delta(1600)$	-	-
2	S	0^+	1/2	-	-	-	-
1	M	1^-	3/2	-	-	-	-
1	M	1^-	1/2	$1/2^-$ $\Delta(1620)$	$3/2^-$ $\Delta(1700)$	-	-
0	S	0^+	3/2	-	$3/2^+$ $\Delta(1232)$	-	
0	S	0^+	1/2	-	-	-	-

Downloaded from https://academic.oup.com/ptep/article/2022/8/083C01/6651666 by KIT Library user on 27 September 2022

even with the most basic versions of the quark model, including harmonic (or linear) confinement and a spin-spin interaction, which is responsible for the octet - decuplet mass shifts. A consistent description of the ground-state electroweak properties, however, requires refined relativistic constituent quark models.

The situation for the excited states is much less clear. The assignment of some experimentally observed states with strange quarks to model configurations is only tentative and in many cases candidates are completely missing. Melde, Plessas and Sengl [46] have calculated baryon properties in relativistic constituent quark models, using one-gluon exchange and Goldstone-boson exchange for the modeling of the hyperfine interactions (see Sec. 15.7 on Dynamics). Both types of models give qualitatively comparable results, and underestimate in general experimentally observed decay widths. Nevertheless, in particular on the basis of the observed decay patterns, the authors have assigned some additional states with strangeness to the SU(3) multiplets and suggest reassignments for a few others. Among the new assignments are states with weak experimental evidence (two or three star ratings) and partly without firm spin/parity assignments, so that further experimental efforts are necessary before final conclusions can be drawn. We have added their suggestions in Table 15.6.

In the non-strange sector there are two main problems which are illustrated in Fig. 15.4, where the experimentally observed excitation spectrum of the nucleon (N and Δ resonances) is compared to the results of a typical quark model calculation [50]. The lowest states from the N=2 band, the $N(1440)1/2^+$, and the $\Delta(1600)3/2^+$, appear lower than the negative parity states from the N=1 band (see Table 15.7) and much lower than predicted by most models. Also negative parity Δ states from the N=3 band ($\Delta(1900)1/2^-$, $\Delta(1940)3/2^-$, and $\Delta(1930)5/2-$) are too low in energy. The low lying states show a clustering in groups of levels around 1700 MeV and 1900 MeV for $N^\star$ states and around 1900 MeV for Δ states which is not reflected in models.

Furthermore, many more states are predicted than observed. This has been known for a long time as the 'missing resonance' problem [47]. Up to an excitation energy of 2.4 GeV, about 45 N states are predicted, but only 20 are established (four- or three-star; see Note on N and Δ Resonances for the rating of the status of resonances) and 5 are tentative (two- or one-star). Even for the N=2 band, up to now only half of the predicted states have been observed. However, there is some recent progress. The total number of states has not much changed but the number of states with four- or three-star rating has increased from 14 to 20 compared to the 2018 PDG particle listings. Most of this progress is due to the programs concentrating on the study of meson photoproduction reactions, while the most recent partial wave analysis of elastic pion scattering and charge exchange data by Arndt and collaborators [51] found no evidence for almost half of the states listed in this review (and included in Fig. 15.4). Such analyses are of course biased against resonances which couple only weakly to the $N\pi$ channel. Quark model predictions for the couplings to other hadronic channels and to photons are given in Ref. [50]. The large experimental effort ongoing at several electron accelerators to study the baryon resonance spectrum with real and virtual photon-induced meson production reactions includes the search for as-yet-unobserved states, as well as detailed studies of the properties of the low lying states (decay patterns, electromagnetic couplings, magnetic moments, *etc.*) (see Ref. [52] for reviews). There are two major new aspects of this program. The investigation of single and double polarization observables allows, via the study of interference terms, access to small partial waves that do not leave a footprint in unpolarized cross sections. An example for the impact of such data is given by a comparison of results from different multipole analyses of pion photoproduction [53]. It shows clearly that with the inclusion of polarization observables the reaction model results start to converge. This will in the near future much improve the data basis for excited baryons in the light quark sector.

The other aspect is the study of final states with meson pairs, in particular $\pi\pi$ and $\pi\eta$ pairs, which made large progress during the last few years. This is important for higher lying states, which in the quark model may have both possible oscillations excited. Such

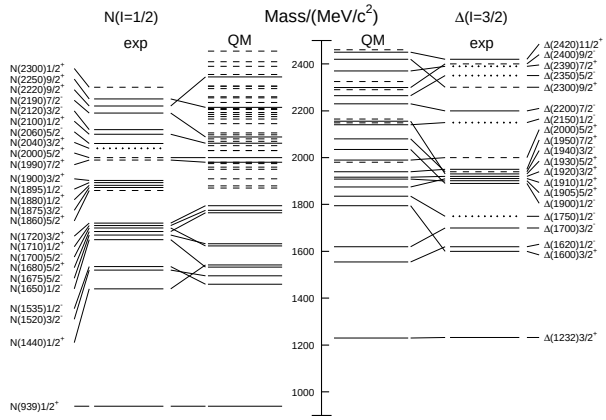

Figure 15.4: Excitation spectrum of the nucleon. Compared are the positions of the excited states identified in experiment, to those predicted by a relativized quark model calculation. Left hand side: isospin $I = 1/2$ N-states, right hand side: isospin $I = 3/2$ Δ-states. Experimental: (columns labeled 'exp'), three- and four-star states are indicated by full lines (two-star dashed lines, one-star dotted lines). At the very left and right of the figure, the spectroscopic notation of these states is given. Quark model [50, 54]: (columns labeled 'QM'), all states for the N=1,2 bands, low-lying states for the N=3,4,5 bands. Full lines: at least tentative assignment to observed states, dashed lines: so far no observed counterparts. Many of the assignments between predicted and observed states are highly tentative.

states can be expected to decay in sequential processes de-exciting the two oscillations step-by-step so that they couple strongly to multiple-meson final states but not to single-meson production. Detailed analyses of such data are for example given in [55, 56] and had already significant impact on partial wave analyses.

The excitation spectrum of hyperons containing s-quarks is even less well explored. Many experimental results date back to before 2000, although parameters listed in the review are in many cases updated by more modern partial wave analyses. A recent review on the quark model interpretation of the Λ and Σ states is given in Ref. [57], a new Ω^- state was reported with high significance from the Belle experiment [58]. In the near future significant progress is expected from the PANDA experiment at FAIR [59, 60].

In quark models, the number of excited states is determined by the effective degrees of freedom, while their ordering and decay properties are related to the residual quark - quark interaction. An overview of quark models for baryons is given in [61], recent discussions of baryon spectroscopy are given in [45, 62]. The effective degrees of freedom in the standard nonrelativistic quark model are three equivalent valence quarks with one-gluon exchange-motivated, flavor-independent color-magnetic interactions. The QCD aspect of gluon-gluon interactions is emphasized by the hypercentral quark model [63, 64], which includes in a natural way three-body forces between the quarks. A different class of models uses interactions which give rise to a quark - diquark clustering of the baryons: for a review see [65]. If there is a tightly bound diquark, only two degrees of freedom are available at low energies, and thus *fewer* states are predicted. Furthermore, selection rules in the decay pattern may arise from the quantum numbers of the diquark. *More* states are predicted by collective models of the baryon like the algebraic approach in [66]. In this approach, the quantum numbers of the valence quarks are distributed over a Y-shaped string-like configuration, and additional states arise *e.g.*, from vibrations of the strings. *More* states are also predicted in the framework of flux-tube models, see [67], which are motivated by lattice QCD. In addition to the quark degrees of freedom, flux-tubes responsible for the confinement of the quarks are considered as degrees of freedom. These models

Downloaded from https://academic.oup.com/ptep/article/2022/8/083C01/6651666 by KIT Library user on 27 September 2022

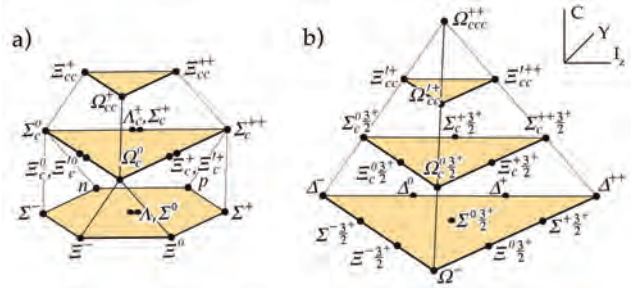

Figure 15.5: $SU(4)_f$ multiplets of ground state baryons made of u, d, s, and c quarks. (a) The spin $\frac{1}{2}$ 20-plet extends the charmless $SU(3)_f$ octet to $\mathsf{C} = 1,2$; (b) the spin $\frac{3}{2}$ 20-plet extends the $SU(3)_f$ decuplet to $\mathsf{C} = 1, 2, 3$.

include hybrid baryons containing explicit excitations of the gluon fields. However, since all half integral J^P quantum numbers are possible for ordinary baryons, such 'exotics' will be very hard to identify, and probably always mix with ordinary states. So far, the experimentally observed number of states is still far lower even than predicted by the quark–diquark models.

The influence of chiral symmetry on the excitation spectrum of the nucleon has been debated from a somewhat different perspective. Chiral symmetry, the fundamental symmetry of QCD, is strongly broken for the low lying states, resulting in large mass differences of parity partners like the J^P=1/2$^+$ $N(938)1/2^+$ ground state and the J^P=1/2$^-$ $N(1535)1/2^-$ excitation. However, at higher excitation energies there is some evidence for parity doublets and even some very tentative suggestions for full chiral multiplets of $N^\star$ and Δ resonances. An effective restoration of chiral symmetry at high excitation energies due to a decoupling from the quark condensate of the vacuum has been discussed (see Ref. [68] for recent reviews) as a possible cause. In this case, the mass generating mechanisms for low and high lying states would be essentially different. As a further consequence, the parity doublets would decouple from pions, so that experimental bias would be worse. However, parity doublets might also arise from the spin-orbital dynamics of the 3-quark system. Presently, the status of data does not allow final conclusions.

The most recent developments on the theory side are the first unquenched lattice calculations for the excitation spectrum discussed in Sec. 15.8. The results are basically consistent with the level counting of SU(6)⊗O(3) in the standard non-relativistic quark model and show no indication for quark-diquark structures or parity doubling. Consequently, there is as yet no indication from lattice that the mis-match between the excitation spectrum predicted by the standard quark model and experimental observations is due to inappropriate degrees of freedom in the quark model.

15.5.2 *Charmed and bottom baryons*

The naming scheme for baryons with c or b quarks follows that of the light baryons: the Λ is an isosinglet and the Σ an isotriplet with one heavy (s, c or b) quark. The Ξ is an isodoublet which contains two heavy quarks, and the Ω an isosinglet with three heavy quarks. The number of c or b quarks is indicated by the subscripts c or b. Hyperons are baryons with at least one s quark.

For charmed baryons the addition of the c quark to the light quarks extends the flavor symmetry to $SU(4)_f$. Due to the large mass of the c quark, this symmetry is much more strongly broken than the $SU(3)_f$ of the three light quarks. Nevertheless, the $SU(4)_f$ representation is still useful for bookkeeping purposes. With the additive charm quantum number C the baryons are classified in a 3-dimensional representation with the three coordinates (I_z, Y , C). Figure 15.5 shows the $SU(4)_f$ weight diagrams.

With four quarks the 64 possible configurations decompose into

$$\mathbf{4} \otimes \mathbf{4} \otimes \mathbf{4} = \bar{\mathbf{4}}_A \oplus \mathbf{20}_S \oplus \mathbf{20}_{MS} \oplus \mathbf{20}_{MA}, \tag{15.29}$$

(for a review on $SU(N)$ symmetries see *e.g.* [69]). The subscripts

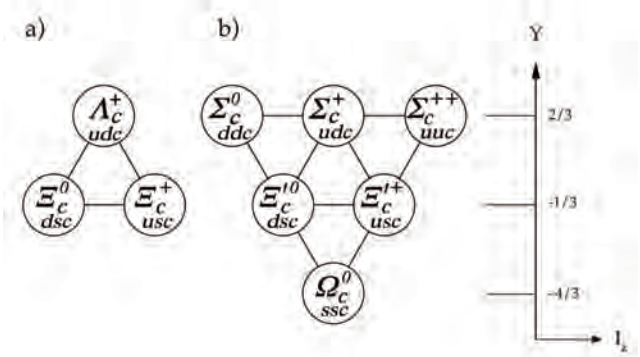

Figure 15.6: The $SU(3)_f$ $\bar{\mathbf{3}}$ (a) and $\mathbf{6}$ (b) ground state $J^P = 1/2^+$ representations. The structure of the $\mathbf{6}$ ground state with $J^P = 3/2^+$ is identical to the one in (b).

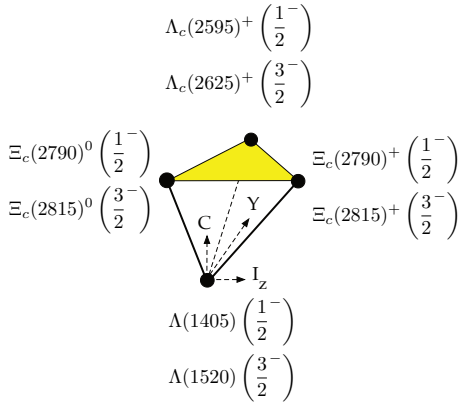

Figure 15.7: Weight diagram of the $\bar{\mathbf{4}}$ $SU(4)_f$ multiplet with the experimentally observed negative parity baryons.

S and A refer to the symmetry and antisymmetry properties of the flavor wave functions. The flavor symmetric 20_S multiplet, associated with spin-$\frac{3}{2}$ baryons, contains the charmless $SU(3)_f$ decuplet at the bottom level. The 20_{MS} and 20_{MA} multiplets correspond to the mixed symmetric and mixed antisymmetric flavour wave functions of the spin-$\frac{1}{2}$ baryons, with the charmless octet baryons at the bottom level. There are two dsc and two usc spin-$\frac{1}{2}$ states, labeled Ξ_c^0, $\Xi_c'^{\,0}$ and Ξ_c^+, $\Xi_c'^{\,+}$. This is because one of the qq pairs can have spin 1 (symmetric) or spin 0 (antisymmetric), giving both the total spin $j = \frac{1}{2}$ with the third quark (see also Fig. 15.6 below).

For $\mathsf{C} = 1$ baryons the flavor decomposition of the diquark, made of u, d, or s quarks, is

$$\mathbf{3} \otimes \mathbf{3} = \bar{\mathbf{3}}_A \oplus \mathbf{6}_S. \tag{15.30}$$

For ground-state baryons, the overall antisymmetry of baryon wave function (including color) requires the light diquark to be symmetric under the exchange of spin and flavor, hence both symmetric or both antisymmetric, that is spin 1 for the $\mathbf{6}_S$ and spin 0 for the $\bar{\mathbf{3}}_A$. The $\bar{\mathbf{3}}$ then combines with the c quark to form the $J^P = 1/2^+$ states, while the $\mathbf{6}$ combines to form $J^P = 1/2^+$ or $J^P = 3/2^+$. The weight diagrams of the $\bar{\mathbf{3}}$ and $\mathbf{6}$ ground-state representations are shown in Fig. 15.6. Within each multiplet the $\mathsf{C} = 1$ baryons obey isospin and $SU(3)_f$ mass relations at the expected orders.

The antisymmetric quadruplet in (15.29) does not exist in the ground state but is realized for the first orbital excitations ($L = 1$). Figure 15.7 shows the weight diagram with the experimentally observed states. In the quark model the quadruplet consists of four baryons with spins coupling to $\frac{1}{2}$, leading to four $L = 1$

Downloaded from https://academic.oup.com/ptep/article/2022/8/083C01/6651666 by KIT Library user on 27 September 2022

excitations with $J^P = \frac{1}{2}^-$ and four excitations with $\frac{3}{2}^-$. The charmed ones are the partners of the $\Lambda(1405)$ and $\Lambda(1520)$ singlets of $\mathrm{SU}(3)_f$.

For a detailed review on charmed baryons see Ref. [62]. Quark model predictions for baryons with two heavy quarks are given in Ref. [70] and lattice results for doubly and triply charmed states are discussed in Sec. 15.8 of this *Review*.

The $\mathsf{C} = 1$ ground state baryons have all been observed. Due to their relatively narrow widths the states are much easier to isolate than the light quark baryon resonances which require intricate partial wave analyses. The production cross sections are small, but the recent measurements at the e^+e^- B-factories, at the $p\bar{p}$ Tevatron collider, and at LHCb have boosted the field. The LHCb collaboration has published evidence for five new narrow Ω_c^0 states (css) [71] in proton-proton collisions. Four of these states have been confirmed by the Belle experiment in e^+e^- collisions [72]. Their quantum numbers are still unknown, but they could correspond to the $L = 1$ ssc orbital excitations. Constituent quark models, lattice QCD, quark-diquark models, molecular models, and pentaquark states, have been discussed to describe their structure (see e.g. [73] for references). In the meantime, also four Ω_b^- states of the bss type have been reported from LHCb [73]. They lie in a narrow range between 6316 - 6350 MeV, but since their intrinsic widths are on the order of just a few MeV they are well separated in the invariant mass spectra. Spectroscopy and theory in this field is rapidly evolving.

LHCb has also reported a doubly charmed Ξ_{cc}^{++} (ccu) baryon [74]. The quantum numbers of this state are undetermined, but its significance is already rated three stars in the current compilation. Doubly charmed baryons have a very different structure from light baryons, more resembling heavy 'double-star' systems with attached light 'planets', which opens a new window for QCD properties. The first candidate for a doubly charmed baryon Ξ_{cc}^+ (ccd) had been reported earlier by the SELEX experiment [75, 76]. A significance of 6.3σ was claimed for the $\Lambda_c^+ K^- \pi^+$ decay and 4.8σ for pD^+K- but searches by other experiments have not confimed it so far (see *e.g.* [77] and Refs. therein) and it is not included in the particle listings. The SELEX and LHCb masses lie in the predicted 3500 – 3700 MeV mass range (see *e.g.* [70]). The LHCb Ξ_{cc}^{++} state lies about 100 MeV above the SELEX one, with a mass splitting far too large for ucc and dcc isospin partners. However, it has also been discussed that due to the different production mechanisms this is not necessarily a contradiction [78].

Figure 15.8 shows the spectrum of the established singly-charmed baryons (3* and 4* baryons in the *Listings* with known quantum numbers). The parity of the Λ_c^+ is that of the c quark, defined as positive. Spin and parity have not been determined experimentally for most of the states. They follow the ordering and expectation from the quark model. Candidates for $L = 2$ orbital excitations of the Λ_c (with $J^P = \frac{3}{2}^+$ and $J^P = \frac{5}{2}^+$) have already been observed, as well as a $\frac{3}{2}^-$ state at 2940 MeV, possibly a radial $L = 1$ excitation [79].

The same $\mathrm{SU}(4)_f$ multiplets can be constructed for the bottom baryons by replacing the c quark by a b quark.The established 3* and 4* bottom baryons are shown in Fig.15.8. The quadruplet $\bar{\mathbf{4}}$ contains the two negative parity candidates $\Lambda_b(5912)^0$ and $\Lambda_b(5920)^0$. It appears that the confining potential is only weakly flavour dependent. For example, the mass difference between the Ξ_b and the Λ_b is roughly the same as that between the Ξ_c and the Λ_c, the mass splitting between the spin-$\frac{1}{2}$ Ω_b and the Λ_b close to that between the spin-$\frac{1}{2}$ Ω_c and the Λ_c. The spin-$\frac{3}{2}$ states are also heavier than the spin-$\frac{1}{2}$ ones, in agreement with expectations from the spin-spin force.

The bottom hadrons can also be embedded in a larger $\mathrm{SU}(5)_f$ group that accounts for all baryons constructed from the five quark flavors. (The existence of baryons with t-quarks is very unlikely due to the short lifetime of the t-quark.) One predicts the decomposition

$$\mathbf{5} \otimes \mathbf{5} \otimes \mathbf{5} = \overline{\mathbf{10}}_A \oplus \mathbf{40}_{MS} \oplus \mathbf{40}_{MA} \oplus \mathbf{35}_S. \tag{15.31}$$

The decuplet is not realized in the ground state. The two 40-plets have mixed symmetry ($\frac{1}{2}$-spin) and the 35-plet is symmetric

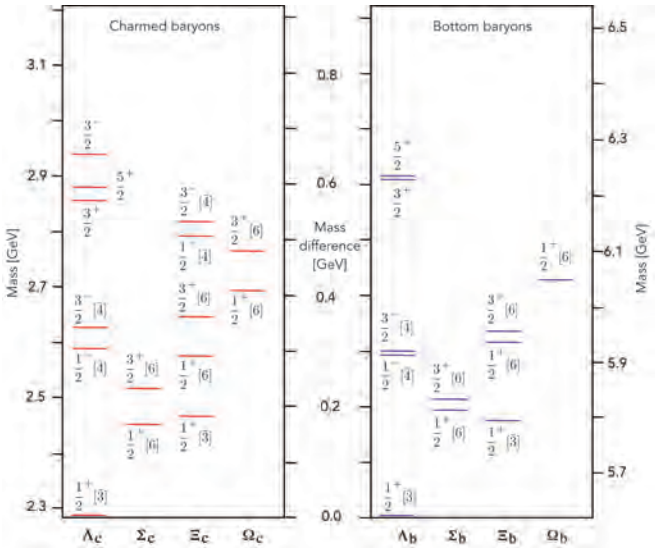

Figure 15.8: Mass spectrum of the established $\mathsf{C} = 1$ charmed and $\mathsf{B} = -1$ bottom baryons with known J^P. The flavor symmetry assignments are given by the square brackets. According to their isospins the $\Sigma_{c,b}$ ($\Xi_{c,b}$) consist of three (two) charged or neutral states that are nearly degenerate.

($\frac{3}{2}$-spin). The $\mathrm{SU}(4)_f$ spin-$\frac{1}{2}$ multiplet in Fig. 15.5 contains 20 spin-$\frac{1}{2}$ baryons and the corresponding one with bottom quarks an additional 12, giving together 32 states. Similarly there are 30 spin-$\frac{3}{2}$ baryons. One expects 75 ground state mesons from (15.31). Thus 13 ground state baryons containing both b and c quarks are predicted (8 spin-$\frac{1}{2}$ $[4\Omega + 4\Xi]$ and 5 spin-$\frac{3}{2}$ $[3\Omega + 2\Xi]$).

15.6 Magnetic moments

The magnetic dipole moment of a baryon is conventionally written relative to the mass of the proton:

$$\vec{\mu}_B = g_B \mu_N \vec{s}, \tag{15.32}$$

where $\mu_N = \frac{e}{2m_p}$ is the nuclear magneton (in natural units). The factor g_B is calculated by adding the quark contributions. The magnetic moment of quark i with charge $q_i e$ and constituent mass m_i is $\vec{\mu}_i = 2(\frac{q_i e}{2m_i})\vec{s}$, hence for the three light quarks,

$$\mu_u = \frac{2}{3}\kappa_u, \;\; \mu_d = -\frac{1}{3}\kappa_d, \;\; \mu_s = -\frac{1}{3}\kappa_s, \;\; \text{with} \;\; \kappa_i \equiv \frac{e}{2m_i}. \tag{15.33}$$

The magnetic dipole moment of a baryon is then given by

$$\mu_B = \sum_{i=1}^{3} \langle B \uparrow | \mu_i \sigma_{zi} | B \uparrow \rangle, \tag{15.34}$$

where $|B \uparrow\rangle$ is the wavefunction for a baryon with its spin along the z-axis and $\vec{\sigma} = 2\vec{s}$. Since the quark model uses the totally *symmetric* SU(6) wavefunctions (flavor SU(3) $\times$ spin SU(2)) one predicts for the proton:

$$\mu_p = \frac{4}{3}\mu_u - \frac{1}{3}\mu_d = \frac{e}{2m} \equiv \kappa, \tag{15.35}$$

assuming $m_u = m_d \simeq m$ (for the detailed derivation see *e.g.* Ref. [4]). For the magnetic moment of the neutron one obtains likewise

$$\mu_n = -\frac{1}{3}\mu_u + \frac{4}{3}\mu_d = -\frac{2}{3}\kappa, \tag{15.36}$$

which leads to the simple prediction $\mu_n/\mu_p = g_n/g_p = -2/3$.

The famous Frisch and Stern experiment showed for the first time that $g_p \sim 5.58 \gg 2$. Modern measurements are performed

Downloaded from https://academic.oup.com/ptep/article/2022/8/083C01/6651666 by KIT Library user on 27 September 2022

in electromagnetic traps, see the *Listings*, while the magnetic moment of the neutron is measured with cold neutron beams. The experimental ratio $\mu_n/\mu_p = -0.6849793 \pm 0.0000003$ is impressively close to the prediction of the quark model (note that using instead the *antisymmetric* SU(6) wavefunctions would lead to $\mu_n/\mu_p = -2$ [4]). The constituent mass m of the u and d quarks can be estimated from (15.32) and (15.35): $m = 2m_p/g_p \simeq 336$ MeV.

The magnetic moment of the Λ is easy to predict: the diquark ud has isospin $i = 0$, since $i(s) = 0$ and $i(\Lambda) = 0$, and is therefore an antisymmetric isospin state. The symmetric quark model then also requires the spin to be zero, so that the magnetic moment of the Λ stems from the s quark:

$$\mu_\Lambda = \mu_s = -\frac{1}{3}\kappa_s. \tag{15.37}$$

The magnetic moment of the Λ is obtained from the Larmor precession frequency of the polarization vector in an homogeneous magnetic field. The latter is derived from the asymmetric distribution of the proton in $\Lambda \to \pi^- p$ [80]. The experimental result is listed in Table 15.8. The constituent mass of the s quark is then $m_s = -m\mu_p/3\mu_\Lambda = 509$ MeV.

Table 15.8: Quark model predictions and measured magnetic dipole moments of the ground state baryons in units of μ_N; $\kappa \equiv \frac{e}{2m} = 2.793$ μ_N and $\kappa_s \equiv \frac{e}{2m_s} = -3\mu_\Lambda = 1.84\ \mu_N$. $^\dagger\Sigma^0 \to \Lambda$ transition magnetic moment.

Baryon	Quark model			Experimental value		
p	κ		input	2.793		
n	$-\frac{2}{3}\kappa$	=	–1.86	–1.913		
Λ	$-\frac{1}{3}\kappa_s$		input	–0.6138	±	0.0047
Σ^+	$\frac{8}{9}\kappa + \frac{1}{9}\kappa_s$	=	2.68	2.458	±	0.010
Σ^0	$\frac{2}{9}\kappa + \frac{1}{9}\kappa_s$	=	0.82			
$\Sigma^{0\dagger}$	$-\frac{1}{\sqrt{3}}\kappa$	=	–1.61	–1.61	±	0.08
Σ^-	$-\frac{4}{9}\kappa + \frac{1}{9}\kappa_s$	=	–1.04	–1.160	±	0.025
Ξ^0	$-\frac{2}{9}\kappa - \frac{4}{9}\kappa_s$	=	–1.44	–1.250	±	0.014
Ξ^-	$\frac{1}{9}\kappa - \frac{4}{9}\kappa_s$	=	–0.51	–0.6507	±	0.0025
Ω^-	$-\kappa_s$	=	–1.84	–2.024	±	0.056
Δ^{++}	2κ	=	5.58	4.52	±	0.67
Δ^+	κ	=	2.79	2.3	-	4.5

The magnetic moments of the other baryons (Table 15.8) are predicted from κ and κ_s. The magnetic moment of the Σ^+ is obtained by replacing the d quark in (15.35) by an s quark, and for the Σ^- the u quark by an s quark in (15.36). The magnetic moment of the Σ^+ has also been measured with the precession method using its decay into $p\pi^0$ [81], that of the $\Sigma^- \to n\pi^-$ likewise, or by detecting the X-rays emitted by cascading Σ^- captured in the Coulomb shells of target atoms. The magnetic moment is then derived from the fine-structure splitting [82].

The magnetic moments of the Ξ^0, Ξ^- and Ω^- are obtained from the polarization of the Λ in the decays $\Lambda\pi^0$, $\Lambda\pi^-$ and ΛK^-, respectively. The SU(6) wavefunction of the (spin 3/2) Ω^- is the product of the two symmetric SU(3) flavor and SU(2) spin wavefunctions. Summing over the three s quarks one gets

$$\mu_{\Omega^-} = \sum_{i=1}^{3} \langle \Omega^- \uparrow | \mu_i \sigma_{zi} | \Omega^- \uparrow \rangle = 3\mu_s = 3\mu_\Lambda. \tag{15.38}$$

The magnetic moment of the Ω^- is hard to measure, because the Ω^- is unpolarized at high energies, in contrast to the other hyperons. Polarized Ω^- hyperons have been obtained from polarized Λ and Ξ^0 impinging on a nuclear target [83].

In quark models with full isospin symmetry the magnetic moments of the Δ-resonances are simply related to the magnetic moment of the proton by $\mu_\Delta = Q_\Delta \cdot \mu_N$, ($Q_\Delta$ = charge) i.e. the moment of the Δ^+ should equal the proton moment and the moment of the Δ^{++} should be twice as large (sum of the three u-quarks). Magnetic moments of the decuplet baryons (with the exception of the Ω^-) are very difficult to measure because their lifetimes are so short that spin precession techniques cannot be used. For the Δ one can profit from an electromagnetic spin-reorientation transition inside the large width of the state. This leads to the emission of a magnetic dipole photon in reactions like $\pi^+ p \to \pi^+ p\gamma$ or $\gamma p \to \pi^0 p\gamma'$ which is related to the magnetic moment of the resonance. The first reaction has been used to study the magnetic moment of the Δ^{++} by measuring the left-right asymmetry with polarized protons [84]. The second one was used for the Δ^+ state [85, 86]. Taking all experimental and systematic uncertainties into account the result spans the range from (2.3 - 4.5)μ_N, covering the quark model prediction of $\approx 2.8\mu_N$, but is not very precise.

Table 15.8 lists the current experimental values for the magnetic moments of the ground state baryons, together with the predictions from the quark model. There are significant discrepancies, but given its crudeness, the quark model performs surprisingly well.

15.7 Dynamics

Quantum chromodynamics (QCD) is well-established as the theory for the strong interactions. As such, one of the goals of QCD is to predict the spectrum of strongly-interacting particles. To date, the only first-principles calculations of spectroscopy from QCD use lattice methods. These are the subject of Sec. 15.8. These calculations are difficult and unwieldy, and many interesting questions do not have a good lattice-based method of solution. Therefore, it is natural to build models, whose ingredients are abstracted from QCD, or from the low-energy limit of QCD (such as chiral Lagrangians) or from the data itself. The words "quark model" are a shorthand for such phenomenological models. Many specific quark models exist, but most contain a similar basic set of dynamical ingredients. These include:

1. A confining interaction, which is generally spin-independent (*e.g.*, harmonic oscillator or linear confinement);
2. Different types of spin-dependent interactions:

   a) commonly used is a color-magnetic flavor-independent interaction modeled after the effects of gluon exchange in QCD (see *e.g.*, Ref. [87]). For example, in the S-wave states, there is a spin-spin hyperfine interaction of the form

   $$H_{HF} = -\alpha_S M \sum_{i>j} (\vec{\sigma}\lambda_a)_i (\vec{\sigma}\lambda_a)_j, \tag{15.39}$$

   where M is a constant with units of energy, λ_a ($a = 1, \cdots, 8,$) is the set of SU(3) unitary spin matrices, defined in the review "SU(3) Isoscalar Factors and Representation Matrices," and the sum runs over constituent quarks or antiquarks. Spin-orbit interactions, although allowed, seem to be small in general, but a tensor term is responsible for the mixing of states with the same J^P but different L, S combinations.

   b) other approaches include flavor-dependent short-range quark forces from instanton effects (see *e.g.*, [88, 89]). This interaction acts only on scalar, isoscalar pairs of quarks in a relative S-wave state:

   $$\langle q^2; S, L, T | W | q^2; S, L, T \rangle = -4g\delta_{S,0}\delta_{L,0}\delta_{I,0}\mathcal{W} \tag{15.40}$$

   where $\mathcal{W}$ is the radial matrix element of the contact interaction.

   c) a rather different and somewhat controversial approach is based on flavor-dependent spin-spin forces arising from one-boson exchange. The interaction term is of the form:

   $$H_{HF} \propto \sum_{i<j} V(\vec{r}_{ij}) \lambda_i^F \cdot \lambda_j^F \vec{\sigma}_i \cdot \vec{\sigma}_j \tag{15.41}$$

   where the λ_i^F are in flavor space (see *e.g.*, Ref. [90]).

Downloaded from https://academic.oup.com/ptep/article/2022/8/083C01/6651666 by KIT Library user on 27 September 2022

3. A strange quark mass somewhat larger than the up and down quark masses, in order to split the SU(3) multiplets;
4. In the case of spin-spin interactions, a flavor-symmetric interaction for mixing $q\bar{q}$ configurations of different flavors (*e.g.*, $u\bar{u} \leftrightarrow d\bar{d} \leftrightarrow s\bar{s}$), in isoscalar channels, so as to reproduce *e.g.*, the η - η' and ω - ϕ mesons.

These ingredients provide the basic mechanisms that determine the hadron spectrum in the standard quark model.

15.8 Lattice Calculations of Hadronic Spectroscopy

Lattice calculations are a major source of information about QCD masses and matrix elements. The necessary theoretical background is given in Sec. 17 of this *Review*. Here we confine ourselves to some general comments and illustrations of lattice calculations for spectroscopy.

It might seem a bit out of place to have a section about lattice calculations in a review of the quark model, since to many readers, the quark model is just a model while QCD could be thought of as a construct which is something deeper than a model. But this review is, despite its title, actually an introduction to the spectroscopy and related quantities of the strong interactions. From that perspective, a presentation of lattice results is entirely appropriate.

Lattice calculations are from first principles – their input is a discretized version of the QCD Lagrangian, and the predictions of a lattice calculation are predictions of QCD, once the lattice spacing is taken to zero, the simulation volume is taken to infinity, and the quark masses are tuned to their physical values. Lattice calculations make extensive use of quark model ideas – for example, the operators used to create and annihilate hadrons are almost always based on the quark model. (This may not be clear in the lattice literature, since the final answer should not depend on the choice of operators used.)

There is only a sporadic literature connecting lattice results to the quark model (one recent example is [91]) but of course the qualitative understanding of lattice results depends as heavily on quark model ideas as does the qualitative understanding of experimental data.

In general, the cleanest lattice results come from computations of processes in which there is only one particle in the simulation volume. These quantities include masses of hadrons, simple decay constants, like pseudoscalar meson decay constants, and semileptonic form factors (such as the ones appropriate to $B \to Dl\nu$, $Kl\nu$, $\pi l\nu$). The cleanest predictions for masses are for states which have narrow decay widths and are far below any thresholds to open channels, since the effects of final state interactions are not yet under complete control on the lattice. As a simple corollary, the lightest state in a channel is easier to study than the heavier ones. "Difficult" states for the quark model (such as exotics) are also difficult for the lattice because of the lack of simple operators which couple well to them.

Good-quality modern lattice calculations will present multipart error budgets with their predictions. A small part of the uncertainty is statistical, from sample size. Typically, the quoted statistical uncertainty includes uncertainty from a fit: it is rare that a simulation computes one global quantity which is the desired observable. Simulations which include virtual quark-antiquark pairs (also known as "dynamical quarks" or "sea quarks") are often done at up and down quark mass values heavier than the experimental ones, and it is then necessary to extrapolate in these quark masses. Simulations can work at the physical values of the heavier quarks' masses. They are always done at nonzero lattice spacing, and so it is necessary to extrapolate to zero lattice spacing. Some theoretical input is needed to do this. Much of the uncertainty in these extrapolations is systematic, from the choice of fitting function. Other systematics include the effect of finite simulation volume, the number of flavors of dynamical quarks actually simulated, and technical issues with how these dynamical quarks are included. The particular choice of a fiducial mass (to normalize other predictions) is not standardized; there are many possible choices, each with its own set of strengths and weaknesses, and determining it usually requires a second lattice simulation from that used to calculate the quantity under consideration.

A systematic error of major historical interest is the "quenched approximation," in which dynamical quarks are simply left out of the simulation. This was done because the addition of these virtual pairs presented an expensive computational problem. No generally-accepted methodology has ever allowed one to correct for quenching effects, short of redoing all calculations with dynamical quarks. Recent advances in algorithms and computer hardware have rendered it obsolete.

With these brief remarks, we turn to examples. The field of lattice QCD simulations is vast, and so it is not possible to give a comprehensive review of them in a small space. The history of lattice QCD simulations is a story of thirty years of incremental improvements in physical understanding, algorithm development, and ever faster computers, which have combined to bring the field to a present state where it is possible to carry out very high quality calculations. We present a few representative illustrations, to show the current state of the art.

15.8.1 *Spectroscopy of low-lying states*

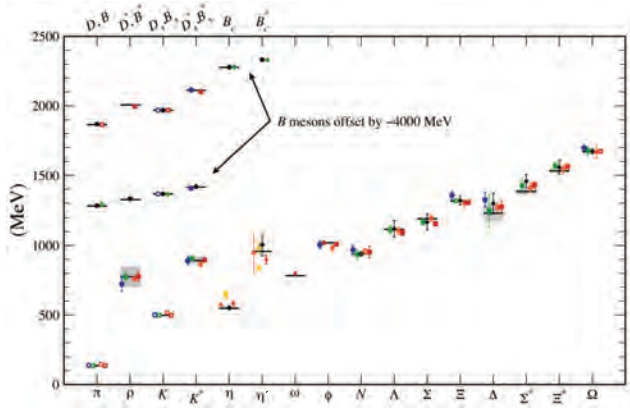

Figure 15.9: Hadron spectrum from lattice QCD. Comprehensive results for mesons and baryons are from MILC [92,93], PACS-CS [94], BMW [95], QCDSF [96], and ETM [97]. Results for η and η' are from RBC & UKQCD [17], Hadron Spectrum [98] (also the only ω mass), UKQCD [99], and Michael, Ottnad, and Urbach [100]. Results for heavy-light hadrons from Fermilab-MILC [101], HPQCD [102, 103], and Mohler and Woloshyn [104]. Circles, squares, diamonds, and triangles stand for staggered, Wilson, twisted-mass Wilson, and chiral sea quarks, respectively. Asterisks represent anisotropic lattices. Open symbols denote the masses used to fix parameters. Filled symbols (and asterisks) denote results. Red, orange, yellow, green, and blue stand for increasing numbers of ensembles (i.e., lattice spacing and sea quark mass) Black symbols stand for results with 2+1+1 flavors of sea quarks. Horizontal bars (gray boxes) denote experimentally measured masses (widths). *b*-flavored meson masses are offset by −4000 MeV.

By far, the major part of all lattice spectroscopy is concerned with that of the light hadrons, and so we illustrate results in Fig. 15.9, a comprehensive summary provided by A. Kronfeld (private communication; see also [105]).

Mesons with a valence structure of identical quark - antiquark pairs such as the eta or eta-prime, $|\eta\rangle \sim \alpha|\bar{u}u + \bar{d}d\rangle + \beta|\bar{s}s\rangle$, are at the frontier of lattice QCD calculations, because one must include the effects of "annihilation graphs" for the valence q and $\bar{q}$. Recently, several groups, Refs. [17, 99, 106], have reported calculations of the η and η' mesons. The numbers of [17] are typical, finding masses of 573(6) and 947(142) MeV for the η and η'. The singlet-octet mixing angle (in the conventions of Table 15.2) is $\theta_{lin} = -14.1(2.8)^\circ$.

The spectroscopy of mesons containing heavy quarks has become a truly high-precision endeavor. These simulations use Non-Relativistic QCD (NRQCD) or Heavy Quark Effective Theory

Downloaded from https://academic.oup.com/ptep/article/2022/8/083C01/6651666 by KIT Library user on 27 September 2022

(HQET), systematic expansions of the QCD Lagrangian in powers of the heavy quark velocity, or the heavy quark mass. Terms in the Lagrangian have obvious quark model analogs, but are derived directly from QCD. For example, the heavy quark potential is a derived quantity, extracted from simulations. Figs. 15.10 and 15.11 show the low lying mass spectrum for charmonium and bottomonium states from two different groups [103, 107]. Most of the results are for the lightest state with a given value of quantum numbers. We return to this point below.

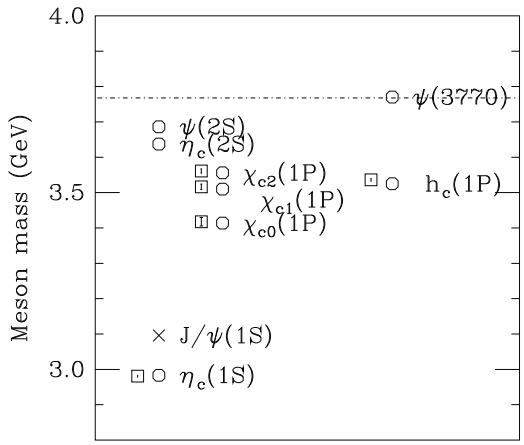

Figure 15.10: Spectroscopy of the $\bar{c}c$ spectrum, compared to lattice data from Ref. [107]. Particles whose masses are used to fix lattice parameters are shown with crosses; octagons label experimental values, and lattice results are shown as squares. The dotted line shows the threshold value for two charmed mesons.

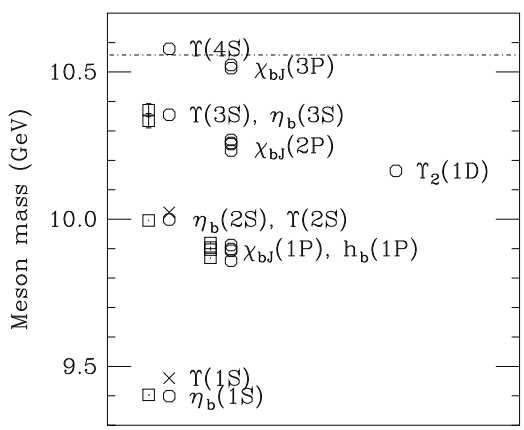

Figure 15.11: Spectroscopy of the $\bar{b}b$ system, adapted from Ref. [103]. Particles whose masses are used to fix lattice parameters are shown with crosses; octagons label experimental values, and lattice results are shown as squares. The dotted line shows the threshold value for two bottom mesons.

Fig. 15.12 shows a compilation of recent lattice results for doubly and triply charmed baryons, provided by S. Meinel [115]. The state recently announced by LHCb [74] is also shown. Note that the lattice calculations for the mass of this state were predictions, not postdictions.

15.8.2 *Excited state spectroscopy*

Lattice calculations of excited states are much more difficult than those for the lightest states. There are two issues:

1. The states are unstable resonances
2. There are many states with the same quantum numbers

While these two problems appear together in excited state spectroscopy, almost all lattice calculations we know of deal with them separately (i. e. there are studies of many stable states, or studies of a single state with a single decay channel).

The first point is an issue because lattice calculations do not see decays directly; instead, they give energies of single or multiple particle states in a box of finite size. The combined mass is shifted from being the sum of the individual masses because the finite box size forces the hadrons to interact with each other. The volume-dependent mass shift yields the phase shift for the continuum scattering amplitude, which in turn can be used to extract the resonance mass and width, with some degree of modeling. So far only two-body resonances, the rho meson and a few others, have been well studied. This is an active research area. A recent review, [117], summarizes the situation, and example of a calculation of the rho meson decay width is [118]. The mass and decay width of the $f_0(500)$ have recently been computed in [119] and [120]. Ref. [121] studies the decay width of the $\Delta(1238)$.

The second point is an issue for lattice calculations since the observables which give masses have a typical functional form

$$C(t) = \sum_n A_n \exp(-E_n t). \tag{15.42}$$

E_n is the energy of the nth state and t is a parameter (the spatial distance of separation of operators) which is accessible to the lattice simulator. The contribution of excited states is exponentially suppressed at large t. The size of a given state's contribution, A_n, is related to the choice of interpolating field use to create the state. (This is where the quark model comes in.) As we move away from hadrons which can be created by the simplest quark model operators (appropriate to the lightest meson and baryon multiplets) we encounter a host of new problems: either no good interpolating fields, or too many possible interpolating fields, and many states with the same quantum numbers. Techniques for dealing with these interrelated problems vary from collaboration to collaboration, but all share common features: typically, correlation functions from many different interpolating fields are used, and the signal is extracted in what amounts to a variational calculation using the chosen operator basis. In addition to mass spectra, wave function information can be garnered from the form of the best variational wave function. Of course, the same problems which are present in the spectroscopy of the lightest hadrons (the need to extrapolate to infinite volume, physical values of the light quark masses, and zero lattice spacing) are also present. We briefly touch on three different kinds of hadrons: excited states of mesons (including hybrids), excited states of baryons, and glueballs. The quality of the data is not as good as for the ground states, and so the results continue to evolve. Shifts in the masses which occur because the state can decay are not included in the calculations.

Modern calculations use a large basis of trial states, which allow them to probe many quantum number channels simultaneously. This is vital for studying "difficult sectors" of QCD, such as the isoscalar mesons. A recent example of meson spectroscopy where this is done, by [116], is shown in Fig. 15.13. The quark masses are still heavier than their physical values, so the pion is at 392 MeV. The authors can assign a relative composition of nonstrange and strange quark content to their states, observing, for example, a nonstrange ω and a strange ϕ. Some states also have a substantial component of gluonic excitation. Note especially the three exotic channels $J^{PC} = 1^{-+}$, 0^{+-}, and 2^{+-}, with states around 2 GeV. These calculations will become more realistic as the quark masses are carried lower and resonance effects are included.

The interesting physics questions of excited baryon spectroscopy to be addressed are precisely those enumerated in the last section. An example of a recent calculation, due to Ref. [122] is shown in Fig. 15.14. Notice that the pion is not yet at its physical value. The lightest positive parity state is the nucleon, and the Roper resonance has not yet appeared as a light state.

Studies which observe a large basis of states across many volumes can probe excited state spectroscopy as resonances. These calculations are just beginning and the ones we know about are performed at unphysically heavy quark masses. Examples include the decays of an exotic $J^{PC} = 1^{-+}$ resonance [123] and the spec-

Downloaded from https://academic.oup.com/ptep/article/2022/8/083C01/6651666 by KIT Library user on 27 September 2022

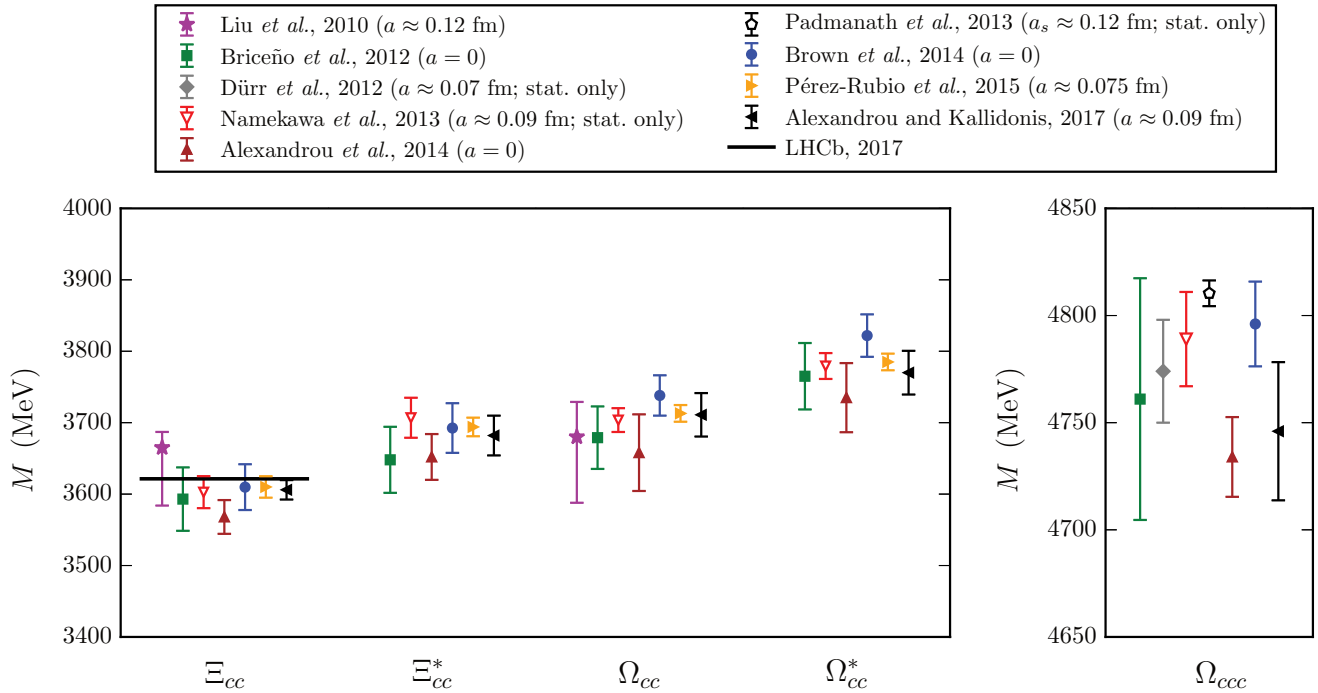

Figure 15.12: Comparison of lattice QCD results for the doubly and triply charmed baryon masses. Labels are Liu, *et al.*, [108]; Briceno, *et al.*, [109]; Namekawa, *et al.*, [110]; Padmanath, *et al.*, [111]; Alexandrou, *et al.*, [97]; Brown, *et al.*, [112]; Perez-Rubio *et al.*, [113]; Alexandrou and Kallidonis 2017, [114]. Only calculations with dynamical light quarks are included; for the doubly charmed baryons, only calculations were performed at or extrapolated to the physical pion mass are shown. Results without estimates of systematic uncertainties are labeled "stat. only". The lattice spacing values used in the calculations are also given; $a = 0$ indicates that the results have been extrapolated to the continuum limit. In the plot of the doubly charmed baryons, the recently announced experimental result for the Ξ_{cc}^{+} mass from LHCb [74] is shown with a horizontal line.

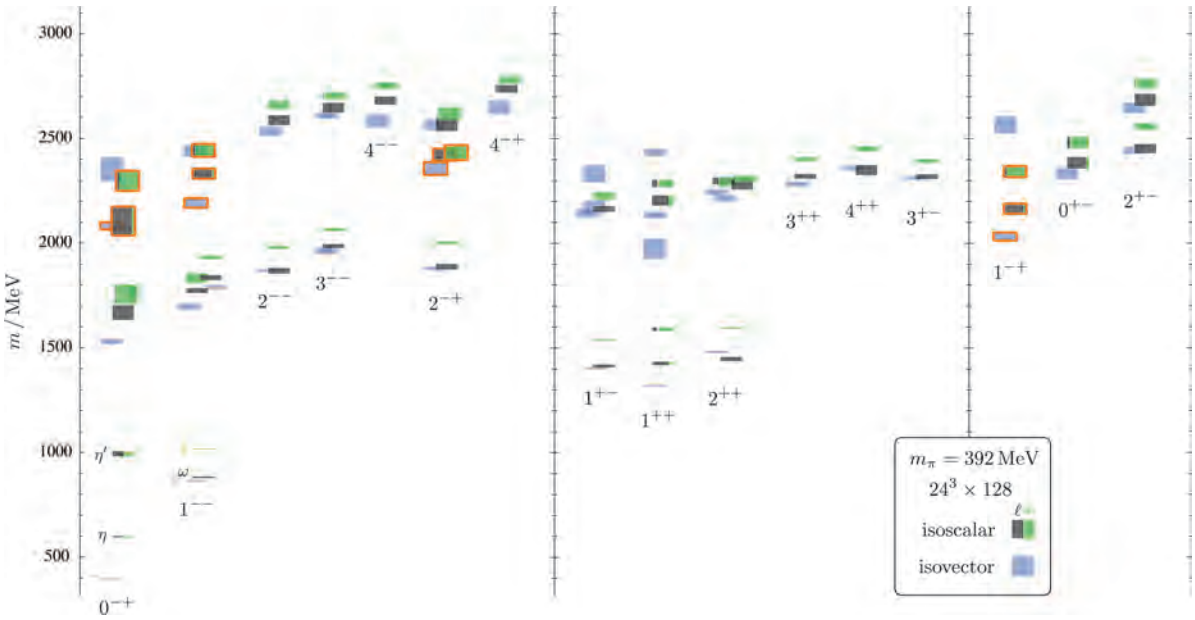

Figure 15.13: Isoscalar (green and black) and isovector (blue) spectrum from Ref. [116]. States are labeled J^{PC}. The quark mass is heavier than its physical value; $m_\pi = 392$ MeV. The vertical height of each box indicates the statistical uncertainty in the mass. Black and green indicate relative nonstrange and strange composition. Orange outlines show states with a large chromomagnetic component to their wave function, which the authors argue are hybrid states. Note the exotic states in the three rightmost columns.

Downloaded from https://academic.oup.com/ptep/article/2022/8/083C01/6651666 by KIT Library user on 27 September 2022

troscopy of J^{--} resonances [124]. We expect to see considerable progress in this area over the next few years.

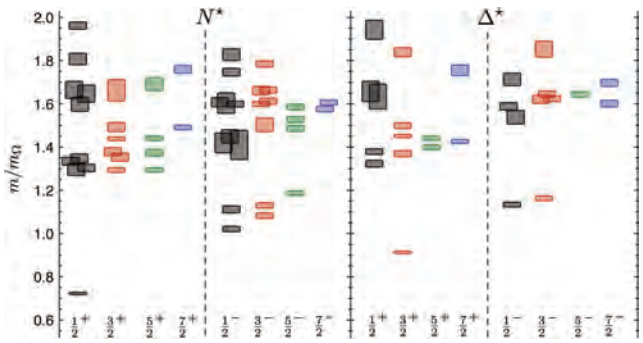

Figure 15.14: Spin-identified spectrum of nucleons and deltas, from lattices where $m_\pi = 396$ MeV, in units of the calculated Ω mass, from Ref. [122]. The colors just correspond to the different J assignments: grey for $J = 1/2$, red for $J = 3/2$, green for $5/2$, blue for $J = 7/2$.

Glueballs present similar issues. In Fig. 15.3 we showed a figure from [22] presenting a lattice prediction for the glueball mass spectrum in quenched approximation. A true QCD prediction of the glueball spectrum requires dynamical light quarks, some way to deal with the mixing of glue states and quark-antiquark (and beyond) states and (because glueball operators are intrinsically noisy) high statistics. Only recently have the first useful such calculations appeared, in [125, 126]. Fig. 15.15 shows results from [125], done with dynamical u, d and s quarks at two lattice spacings, 0.123 and 0.092 fm, along with comparisons to the quenched lattice calculation of [25] and to experimental isosinglet mesons. The dynamical simulation is, of course, not the last word on this subject, but it shows that the effects of quenching seem to be small.

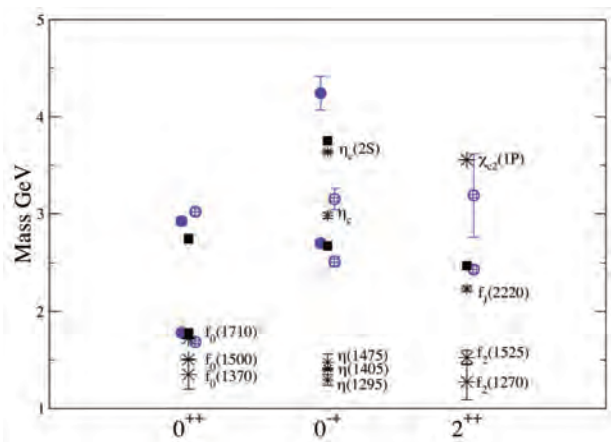

Figure 15.15: Lattice QCD predictions for glueball masses. The open and closed circles are the larger and smaller lattice spacing data of the full QCD calculation of glueball masses of Ref. [125]. Squares are the quenched data for glueball masses of Ref. [25]. The bursts labeled by particle names are experimental states with the appropriate quantum numbers.

Lattice calculations relevant to the extra states observed in the charmonium and bottomonium spectrum (Sec. 15.4) are difficult, because the states sit high in the spectrum of most channels, because of the number of nearby multiparticle states, and because it is necessary to have the technology to study heavy and light quarks together. There is a hybrid literature of studies which combines lattice calculations of the potential of static sources in a solution of a Schrödinger equation for the light quarks in a Born - Oppenheimer approximation (see [127] for context).

The system with the largest lattice literature is a bound state of two heavy quarks and two light antiquarks, for example $\bar{b}\bar{b}ud$. There are excellent reasons for expecting this state to be stable in the limit that the b mass goes to infinity [128] but finding the precise degree of stability at the physical b mass takes a phenomenological estimate or a lattice calculation. The $I(J^P) = 0(1^+)$ state is predicted to be stable by about 128(26) MeV [129] or 189(10) MeV [130]. (These authors put the $\bar{b}\bar{b}sd$ state at 98 MeV below threshold.) These numbers are in reasonable agreement with phenomenological estimates from Refs. [128, 131].

15.8.3 *Electromagnetic effects*

As a final part of spectroscopy we mention electromagnetic mass splittings (such as the neutron - proton mass difference). They are interesting but difficult. These calculations are important for determining the values of the quark masses (for a discussion see Sec. 60 in this Review). Knowing that the neutron is heavier than the proton tells us that these splittings have a complicated origin. One part of the shift is because the up and down quarks have slightly different masses. The second is that the quarks have (different) charges. Phenomenologists (compare Ref. [132]) combine Coulomb forces and spin-dependent electromagnetic hyperfine interactions to model their charge effects. In order to compute hadronic mass differences on the lattice, electromagnetic interactions must be included in the simulations. This creates a host of technical issues. An important one is that electromagnetic interactions are long range, but lattice simulations are done in finite volumes. The theoretical situation is summarized in the recent Flavour Lattice Averaging Group (FLAG) review [133]. A recent calculation, Ref. [134], has presented the first results for electromagnetic mass splittings in the baryon octet, with good agreement with observation. Refs. [135–137] have performed calculations for meson splittings.

There is a small lattice literature associated with magnetic moments of baryons. The calculations are done by including a static magnetic field in the simulation and computing the energy difference between baryons in different spin states. We are aware of no calculations at physical quark masses. A recent calculation [138] used 800 and 450 MeV pions. When expressed in units of the nucleon magneton at the simulation point $(e/(2M_N(m_\pi))$ the moments are in reasonable agreement with experiment and with quark model expectations.

References

[1] G. 't Hooft, Nucl. Phys. B **72**, 461 (1974).

[2] G. 't Hooft, Nucl. Phys. B **75**, 461 (1974).

[3] E. Witten, Nucl. Phys. B **160**, 57 (1979).

[4] C. Amsler in the Quark Structure of Hadrons, Lecture Notes in Physics **949** (2018), ed. Springer.

[5] H.-Y. Cheng, Physics Letters B **707**, 1, 116 (2012), ISSN 0370-2693, URL `https://www.sciencedirect.com/science/article/pii/S0370269311014705`.

[6] L. Burakovsky and J. T. Goldman, Nucl. Phys. **A625**, 220 (1997), [hep-ph/9703272].

[7] M.-C. Du and Q. Zhao, Phys. Rev. D **100**, 036005 (2019), URL `https://link.aps.org/doi/10.1103/PhysRevD.100.036005`.

[8] H.-W. Ke and X.-Q. Li, Phys. Rev. D **99**, 036014 (2019), URL `https://link.aps.org/doi/10.1103/PhysRevD.99.036014`.

[9] M.-L. Du *et al.*, Phys. Rev. Lett. **126**, 192001 (2021), URL `https://link.aps.org/doi/10.1103/PhysRevLett.126.192001`.

[10] J. Schwinger, Phys. Rev. **135**, B816 (1964).

[11] H. J. Lipkin and B.-s. Zou, Phys. Rev. D **53**, 6693 (1996).

[12] A. Bramon, R. Escribano and M. D. Scadron, Phys. Lett. **B403**, 339 (1997), [hep-ph/9703313].

[13] A. Aloisio *et al.* (KLOE), Phys. Lett. **B541**, 45 (2002), [hep-ex/0206010].

[14] F. Ambrosino *et al.*, JHEP **07**, 105 (2009), [arXiv:0906.3819].

Downloaded from https://academic.oup.com/ptep/article/2022/8/083C01/6651666 by KIT Library user on 27 September 2022

[15] C. Amsler *et al.* (Crystal Barrel), Phys. Lett. **B294**, 451 (1992).

[16] C. Amsler, Rev. Mod. Phys. **70**, 1293 (1998), [hep-ex/9708025].

[17] N. H. Christ *et al.*, Phys. Rev. Lett. **105**, 241601 (2010), [arXiv:1002.2999].

[18] T. Feldmann, Int. J. Mod. Phys. **A915**, 159 (2000).

[19] C. Amsler and F. E. Close, Phys. Rev. **D53**, 295 (1996), [hep-ph/9507326].

[20] R. L. Jaffe, Phys. Rev. **D15**, 267 (1977).

[21] R. L. Jaffe, Phys. Rev. **D15**, 281 (1977).

[22] Y. Chen *et al.*, Phys. Rev. **D73**, 014516 (2006), [hep-lat/0510074].

[23] S.L. Olsen, Front. Phys. **10**, 121 (2015).

[24] S. L. Olsen, T. Skwarnicki and D. Zieminska, Rev. Mod. Phys. **90**, 1, 015003 (2018), [arXiv:1708.04012].

[25] C. J. Morningstar and M. J. Peardon, Phys. Rev. **D60**, 034509 (1999), [hep-lat/9901004].

[26] W.-J. Lee and D. Weingarten, Phys. Rev. **D61**, 014015 (2000), [hep-lat/9910008].

[27] G. S. Bali *et al.* (UKQCD), Phys. Lett. **B309**, 378 (1993), [hep-lat/9304012].

[28] C. Michael, AIP Conf. Proc. **432**, 1, 657 (1998), [hep-ph/9710502].

[29] F. E. Close and A. Kirk, Eur. Phys. J. **C21**, 531 (2001), [hep-ph/0103173].

[30] W. Ochs, J. Phys. **G40**, 043001 (2013), [arXiv:1301.5183].

[31] F. Brünner and A. Rebhan, Phys. Rev. Lett. **115**, 13, 131601 (2015), [arXiv:1504.05815].

[32] C. Amsler and N. A. Tornqvist, Phys. Rept. **389**, 61 (2004).

[33] N. Isgur and J. E. Paton, Phys. Rev. **D31**, 2910 (1985).

[34] P. Lacock *et al.* (UKQCD), Phys. Lett. **B401**, 308 (1997), [hep-lat/9611011].

[35] M. S. Chanowitz and S. R. Sharpe, Nucl. Phys. **B222**, 211 (1983), [Erratum: Nucl. Phys.B228,588(1983)].

[36] T. Barnes *et al.*, Nucl. Phys. **B224**, 241 (1983).

[37] B. Kopf *et al.* (2020), [arXiv:2008.11566].

[38] R. Aaij *et al.* (LHCb), Phys. Rev. Lett. **115**, 072001 (2015), [arXiv:1507.03414].

[39] R. Aaij *et al.* (LHCb), Phys. Rev. Lett. **122**, 22, 222001 (2019), [arXiv:1904.03947].

[40] J.-J. Wu *et al.*, Phys. Rev. Lett. **105**, 232001 (2010), URL `https://link.aps.org/doi/10.1103/PhysRevLett.105.232001`.

[41] J.-J. Wu, T.-S. H. Lee and B. S. Zou, Phys. Rev. C **85**, 044002 (2012), URL `https://link.aps.org/doi/10.1103/PhysRevC.85.044002`.

[42] Y.-R. Liu *et al.*, Prog. Part. Nucl. Phys. **107**, 237 (2019), [arXiv:1903.11976].

[43] F.E. Close, in *Quarks and Nuclear Forces* (Springer-Verlag, 1982), p. 56.

[44] R.H. Dalitz and L.J. Reinders, in "Hadron Structure as Known from Electromagnetic and Strong Interactions," *Proceedings of the Hadron '77 Conference* (Veda, 1979), p. 11.

[45] E. Klempt and J.-M. Richard, Rev. Mod. Phys. **82**, 1095 (2010), [arXiv:0901.2055].

[46] T. Melde, W. Plessas and B. Sengl, Phys. Rev. **D77**, 114002 (2008), [arXiv:0806.1454].

[47] N. Isgur and G. Karl, Phys. Rev. **D18**, 4187 (1978).

[48] N. Isgur and G. Karl, Phys. Rev. **D19**, 2653 (1979), [Erratum: Phys. Rev.D23,817(1981)].

[49] S. Capstick and W. Roberts, Prog. Part. Nucl. Phys. **45**, S241 (2000), [arXiv:nucl-th/0008028].

[50] S. Capstick and W. Roberts, Phys. Rev. **D58**, 074011 (1998), [arXiv:nucl-th/9804070].

[51] R. A. Arndt *et al.*, Phys. Rev. **C74**, 045205 (2006), [arXiv:nucl-th/0605082].

[52] B. Krusche and S. Schadmand, Prog. Part. Nucl. Phys. **51**, 399 (2003), [arXiv:nucl-ex/0306023].

[53] A. V. Anisovich *et al.*, Eur. Phys. J. **A52**, 9, 284 (2016), [arXiv:1604.05704].

[54] S. Capstick, Phys. Rev. **D46**, 2864 (1992).

[55] E. Gutz *et al.* (CBELSA/TAPS), Eur. Phys. J. **A50**, 74 (2014), [arXiv:1402.4125].

[56] V. Sokhoyan *et al.* (CBELSA/TAPS), Eur. Phys. J. **A51**, 8, 95 (2015), [Erratum: Eur. Phys. J.A51,no.12,187(2015)], [arXiv:1507.02488].

[57] E. Klempt *et al.*, Eur. Phys. J. **A56**, 261 (2020).

[58] J. Yelton *et al.*, Phys. Rev. Lett. **121**, 052003 (2018).

[59] G. Barruca *et al.*, Eur. Phys. J. **A57**, 154 (2021).

[60] G. Barucca *et al.*, Eur. Phys. J **A57**, 4, 154 (2021).

[61] S. Capstick and W. Roberts, Prog. in Part. Nucl. Phys. **45**, 241 (2000).

[62] V. Crede and W. Roberts, Rept. on Prog. in Phys. **76**, 076301 (2013).

[63] M. Ferraris *et al.*, Phys. Lett. **B364**, 231 (1995).

[64] M. M. Giannini and E. Santopinto, Chin. J. Phys. **53**, 020301 (2015), [arXiv:1501.03722].

[65] M. Anselmino *et al.*, Rev. Mod. Phys. **65**, 1199 (1993).

[66] R. Bijker, F. Iachello and A. Leviatan, Annals Phys. **236**, 69 (1994), [arXiv:nucl-th/9402012].

[67] S. Capstick and P. R. Page, Phys. Rev. **C66**, 065204 (2002), [arXiv:nucl-th/0207027].

[68] R. L. Jaffe, D. Pirjol and A. Scardicchio, Phys. Rept. **435**, 157 (2006), [hep-ph/0602010].

[69] R. Slansky, Phys. Rept. **79**, 1 (1981).

[70] M. Karliner and J. L. Rosner, Phys. Rev. **D90**, 9, 094007 (2014), [arXiv:1408.5877].

[71] R. Aaij *et al.* (LHCb), Phys. Rev. Lett. **118**, 18, 182001 (2017), [arXiv:1703.04639].

[72] Y. Yelton *et al.*, Phys. Rev. **D97**, 051102(R) (2018).

[73] R. Aaij *et al.*, Phys. Rev. Lett **124**, 082002 (2020).

[74] R. Aaij *et al.* (LHCb), Phys. Rev. Lett. **119**, 11, 112001 (2017), [arXiv:1707.01621].

[75] M. Mattson *et al.* (SELEX), Phys. Rev. Lett. **89**, 112001 (2002), [hep-ex/0208014].

[76] A. Ocherashvili *et al.* (SELEX), Phys. Lett. **B628**, 18 (2005), [hep-ex/0406033].

[77] R. Aaij *et al.* (LHCb), Sci. China Phys. Mech. Astron. **63**, 2, 221062 (2020), [arXiv:1909.12273].

[78] S. G. S.J. Brodsky and S. Koshkarev, Eur. Phys. J. **C78**, 483 (2018).

[79] R. Aaij *et al.* (LHCb), JHEP **05**, 030 (2017), [arXiv:1701.07873].

[80] L. Schachinger *et al.*, Phys. Rev. Lett. **41**, 1348 (1978).

[81] A. Morelos Pineda *et al.* (E761), Phys. Rev. Lett. **71**, 3417 (1993).

[82] D. W. Hertzog *et al.*, Phys. Rev. D **37**, 1142 (1988).

[83] N. B. Wallace *et al.*, Phys. Rev. Lett. **74**, 3732 (1995).

[84] A. Bosshard *et al.*, Phys. Rev. D **44**, 1962 (1991).

[85] M. Kotulla *et al.*, Phys. Rev. Lett **27**, 272001 (2002).

[86] S. Schumann *et al.*, Eur. Phys. J. **A43**, 269 (2010).

Downloaded from https://academic.oup.com/ptep/article/2022/8/083C01/6651666 by KIT Library user on 27 September 2022

[87] A. De Rujula, H. Georgi and S. L. Glashow, Phys. Rev. **D12**, 147 (1975).

[88] W. H. Blask *et al.*, Z. Phys. **A337**, 327 (1990).

[89] U. Loring *et al.*, Eur. Phys. J. **A10**, 309 (2001), [hep-ph/0103287].

[90] L. Ya. Glozman and D. O. Riska, Phys. Rept. **268**, 263 (1996), [hep-ph/9505422].

[91] T. DeGrand and E. T. Neil, Phys. Rev. D **101**, 3, 034504 (2020), [arXiv:1910.08561].

[92] C. Aubin *et al.*, Phys. Rev. **D70**, 094505 (2004), [hep-lat/0402030].

[93] A. Bazavov *et al.* (MILC), Rev. Mod. Phys. **82**, 1349 (2010), [arXiv:0903.3598].

[94] S. Aoki *et al.* (PACS-CS), Phys. Rev. **D79**, 034503 (2009), [arXiv:0807.1661].

[95] S. Durr *et al.*, Science **322**, 1224 (2008), [arXiv:0906.3599].

[96] W. Bietenholz *et al.*, Phys. Rev. **D84**, 054509 (2011), [arXiv:1102.5300].

[97] C. Alexandrou *et al.*, Phys. Rev. **D90**, 7, 074501 (2014), [arXiv:1406.4310].

[98] J. J. Dudek *et al.*, Phys. Rev. **D83**, 111502 (2011), [arXiv:1102.4299].

[99] E. B. Gregory *et al.* (UKQCD), Phys. Rev. **D86**, 014504 (2012), [arXiv:1112.4384].

[100] C. Michael, K. Ottnad and C. Urbach (ETM), Phys. Rev. Lett. **111**, 18, 181602 (2013), [arXiv:1310.1207].

[101] C. Bernard *et al.* (Fermilab Lattice, MILC), Phys. Rev. **D83**, 034503 (2011), [arXiv:1003.1937].

[102] E. B. Gregory *et al.*, Phys. Rev. **D83**, 014506 (2011), [arXiv:1010.3848].

[103] R. J. Dowdall *et al.*, Phys. Rev. **D86**, 094510 (2012), [arXiv:1207.5149].

[104] D. Mohler and R. M. Woloshyn, Phys. Rev. **D84**, 054505 (2011), [arXiv:1103.5506].

[105] A. S. Kronfeld, Ann. Rev. Nucl. Part. Sci. **62**, 265 (2012), [arXiv:1203.1204].

[106] K. Ottnad, C. Urbach and F. Zimmermann (OTM), Nucl. Phys. **B896**, 470 (2015), [arXiv:1501.02645].

[107] C. DeTar *et al.* (Fermilab Lattice, MILC), Phys. Rev. D **99**, 3, 034509 (2019), [arXiv:1810.09983].

[108] L. Liu *et al.*, Phys. Rev. **D81**, 094505 (2010), [arXiv:0909.3294].

[109] R. A. Briceno, H.-W. Lin and D. R. Bolton, Phys. Rev. **D86**, 094504 (2012), [arXiv:1207.3536].

[110] Y. Namekawa *et al.* (PACS-CS), Phys. Rev. **D87**, 9, 094512 (2013), [arXiv:1301.4743].

[111] M. Padmanath *et al.*, Phys. Rev. **D90**, 7, 074504 (2014), [arXiv:1307.7022].

[112] Z. S. Brown *et al.*, Phys. Rev. **D90**, 9, 094507 (2014), [arXiv:1409.0497].

[113] P. Pérez-Rubio, S. Collins and G. S. Bali, Phys. Rev. **D92**, 3, 034504 (2015), [arXiv:1503.08440].

[114] C. Alexandrou and C. Kallidonis, Phys. Rev. **D96**, 3, 034511 (2017), [arXiv:1704.02647].

[115] S. Meinel, private comunication .

[116] J. J. Dudek *et al.* (Hadron Spectrum), Phys. Rev. **D88**, 9, 094505 (2013), [arXiv:1309.2608].

[117] R. A. Briceno, J. J. Dudek and R. D. Young, Rev. Mod. Phys. **90**, 2, 025001 (2018), [arXiv:1706.06223].

[118] J. Bulava *et al.*, Nucl. Phys. **B910**, 842 (2016), [arXiv:1604.05593].

[119] R. A. Briceno *et al.*, Phys. Rev. Lett. **118**, 2, 022002 (2017), [arXiv:1607.05900].

[120] D. Guo *et al.*, Phys. Rev. D **98**, 1, 014507 (2018), [arXiv:1803.02897].

[121] C. W. Andersen *et al.*, Phys. Rev. **D97**, 1, 014506 (2018), [arXiv:1710.01557].

[122] R. G. Edwards *et al.*, Phys. Rev. **D84**, 074508 (2011), [arXiv:1104.5152].

[123] A. J. Woss *et al.* (Hadron Spectrum), Phys. Rev. D **103**, 5, 054502 (2021), [arXiv:2009.10034].

[124] C. T. Johnson and J. J. Dudek (Hadron Spectrum), Phys. Rev. D **103**, 7, 074502 (2021), [arXiv:2012.00518].

[125] C. M. Richards *et al.* (UKQCD), Phys. Rev. **D82**, 034501 (2010), [arXiv:1005.2473].

[126] E. Gregory *et al.*, JHEP **10**, 170 (2012), [arXiv:1208.1858].

[127] R. F. Lebed, R. E. Mitchell and E. S. Swanson, Prog. Part. Nucl. Phys. **93**, 143 (2017), [arXiv:1610.04528].

[128] E. J. Eichten and C. Quigg, Phys. Rev. Lett. **119**, 20, 202002 (2017), [arXiv:1707.09575].

[129] L. Leskovec *et al.*, Phys. Rev. D **100**, 1, 014503 (2019), [arXiv:1904.04197].

[130] A. Francis *et al.*, Phys. Rev. Lett. **118**, 14, 142001 (2017), [arXiv:1607.05214].

[131] M. Karliner and J. L. Rosner, Phys. Rev. Lett. **119**, 20, 202001 (2017), [arXiv:1707.07666].

[132] M. Karliner and J. L. Rosner (2019), [arXiv:1906.07799].

[133] S. Aoki *et al.* (Flavour Lattice Averaging Group), Eur. Phys. J. C **80**, 2, 113 (2020), [arXiv:1902.08191].

[134] S. Borsanyi *et al.*, Science **347**, 1452 (2015), [arXiv:1406.4088].

[135] G. M. de Divitiis *et al.* (RM123), Phys. Rev. D **87**, 11, 114505 (2013), [arXiv:1303.4896].

[136] D. Giusti *et al.*, Phys. Rev. **D95**, 11, 114504 (2017), [arXiv:1704.06561].

[137] S. Basak *et al.* (MILC), Phys. Rev. D **99**, 3, 034503 (2019), [arXiv:1807.05556].

[138] A. Parreno *et al.*, Phys. Rev. D **95**, 11, 114513 (2017), [arXiv:1609.03985].

Downloaded from https://academic.oup.com/ptep/article/2022/8/083C01/6651666 by KIT Library user on 27 September 2022

16. Heavy-Quark and Soft-Collinear Effective Theory

Revised August 2019 by C.W. Bauer (LBNL) and M. Neubert (PRISMA, Mainz Inst. for Theor. Physics, JG U.).

16.1 Effective Field Theories

Quantum field theories provide the most precise computational tools for describing physics at the highest energies. One of their characteristic features is that they almost inevitably involve multiple length scales. When trying to determine the value of an observable, quantum field theory demands that all possible virtual states and hence all particles be included in the calculation. Since these particles have widely different masses, the final prediction is sensitive to many scales. This fact represents a formidable challenge from a practical point of view. No realistic quantum field theories can be solved exactly, so that one needs to resort to approximation schemes; these, however, are typically most straightforward when only a single scale is involved at a time.

Effective field theories (EFTs) provide a general theoretical framework to deal with the multi-scale problems of realistic quantum field theories. This framework aims at reducing such problems to a combination of separate and simpler single-scale problems; simultaneously, however, it provides an organization scheme whereby the other scales are not omitted but allowed to play their role in a separate step of the computation. The philosophy and basic principles of this approach are very generic, and correspondingly EFTs represent a widely used method in many different areas of high-energy physics, from the low-energy scales of atomic and nuclear physics to the high-energy scales of (partly yet unknown) elementary-particle physics, see [1–3] for some early references. EFTs can play a role both within analytic perturbative computations and in the context of non-perturbative numerical simulations; One of the simplest applications of EFTs to particle physics concerns the description of an underlying theory that is only probed at energy scales $E < \Lambda$. Any particle with mass $m > \Lambda$ cannot be produced as a real state and therefore only leads to short-distance virtual effects. Thus, one can construct an effective theory in which the quantum fluctuations of such heavy particles are "integrated out" from the generating functional for Green functions. This results in a simpler theory containing only those degrees of freedom that are relevant to the energy scales under consideration. In fact, the standard model of particle physics itself is widely viewed as an EFT of some yet unknown, more fundamental theory.

The development of any effective theory starts by identifying the degrees of freedom that are relevant to describe the physics at a given energy (or length) scale and constructing the Lagrangian describing the interactions among these fields. Short-distance quantum fluctuations associated with much smaller length scales are absorbed into the coefficients of the various operators in the effective theory. These coefficients are determined in a matching procedure, by requiring that the EFT reproduces the matrix elements of the full theory up to power corrections. In many cases the effective Lagrangian exhibits enhanced symmetries compared with the fundamental theory, allowing for simple and sometimes striking predictions relating different observables.

16.2 Heavy-Quark Effective Theory

Heavy-quark systems provide prime examples for applications of the EFT technology, because the hierarchy $m_Q \gg \Lambda_{\rm QCD}$ (with $Q = b, c$) provides a natural separation of scales. Physics at the scale m_Q is of a short-distance nature and can be treated perturbatively, while for heavy-quark systems there is always also some hadronic physics governed by the confinement scale $\Lambda_{\rm QCD}$ of the strong interaction. Being able to separate the short-distance and long-distance effects associated with these two scales is crucial for any quantitative description. For instance, if the long-distance hadronic matrix elements are obtained from lattice QCD, then it is necessary to analytically compute the effects of short-wavelength modes that do not fit on the lattice. In many other instances, the long-distance physics can be encoded in a small number of hadronic parameters.

16.2.1 *General idea and derivation of the effective Lagrangian*

The simplest effective theory for heavy-quark systems is the heavy-quark effective theory (HQET) [4–7] (see [8, 9] for detailed discussions). It provides a simplified description of the soft interactions of a single heavy quark with light partons. This includes the interactions that bind the heavy quark with other light partons inside heavy mesons and baryons.

A softly interacting heavy quark is nearly on-shell. Its momentum may be decomposed as $p_Q = m_Q v + k$, where v is the 4-velocity of the hadron containing the heavy quark. The "residual momentum" k results from the soft interactions of the heavy quark with its environment and satisfies $v \cdot k \sim \Lambda_{\rm QCD}$ and $k^2 \sim \Lambda_{\rm QCD}^2$, which in the rest frame of the heavy hadron reduces to $k^\mu \sim \Lambda_{\rm QCD}$. In the limit $m_Q \gg \Lambda_{\rm QCD}$, the soft interactions do not change the 4-velocity of the heavy quark, which is therefore a conserved quantum number that is often used as a label on the effective heavy-quark fields. A nearly on-shell Dirac spinor has two large and two small components. We define

$$Q(x) = e^{-im_Q v\cdot x}\,[h_v(x) + H_v(x)]\,, \tag{16.1}$$

where

$$h_v(x) = e^{im_Q v\cdot x}\,\frac{1+\not v}{2}\,Q(x)\,, \qquad H_v(x) = e^{im_Q v\cdot x}\,\frac{1-\not v}{2}\,Q(x) \tag{16.2}$$

are the large ("upper") and small ("lower") components of the spinor field, respectively. The extraction of the phase factor in (16.1) implies that the fields h_v and H_v carry the residual momentum k. The field H_v is $1/m_Q$ suppressed relative to h_v and describes quantum fluctuations far off the mass shell. Integrating it out using its equations of motion yields the HQET Lagrangian

$$\begin{aligned}\mathcal{L}_{\rm HQET} &= \bar h_v\, iv\cdot D_s\, h_v \\ &\quad + \frac{1}{2m_Q}\left[\bar h_v (iD_s)^2 h_v + C_{\rm mag}(\mu)\,\frac{g}{2}\,\bar h_v\,\sigma_{\mu\nu}\,G_s^{\mu\nu} h_v\right] + \dots\,.\end{aligned} \tag{16.3}$$

The covariant derivative $iD_s^\mu = i\partial^\mu + gA_s^\mu$ and the field strength $G_s^{\mu\nu}$ contain only the soft gluon field. Hard gluons have been integrated out, and their effects are contained in the Wilson coefficients of the operators in the effective Lagrangian. From the leading operator one derives the Feynman rules of HQET. The new operators entering at subleading order are referred to as the "kinetic energy" and "chromo-magnetic interaction". The kinetic-energy operator corresponds to the first correction term in the Taylor expansion of the relativistic energy $E = m_Q + \vec p^{\,2}/2m_Q + \dots$. Lorentz invariance, which is encoded as a reparametrization invariance of the effective Lagrangian [10], ensures that its Wilson coefficient is not renormalized ($C_{\rm kin} \equiv 1$). The coefficient $C_{\rm mag}$ of the chromo-magnetic operator receives corrections starting at one-loop order.

16.2.2 *Spin-flavor symmetry*

The leading term in the HQET Lagrangian exhibits a global spin-flavor symmetry. Its physical meaning is that, in the infinite mass limit, the properties of hadronic systems containing a single heavy quark are insensitive to the spin and flavor of the heavy quark [11, 12]. The spin symmetry results from the fact that there are no Dirac matrices in the leading term of the effective Lagrangian in (16.3), implying that the interactions of the heavy quark with soft gluons leave its spin unchanged. The flavor symmetry arises since the mass of the heavy quark does not appear at leading order. For n_Q heavy quarks moving at the same velocity, one can simply extend (16.3) by summing over n_Q identical terms for heavy-quark fields h_v^i. The result is invariant under rotations in flavor space. When combined with the spin symmetry, the symmetry group becomes promoted to $SU(2n_Q)$. These symmetries are broken by the operators at subleading power in the $1/m_Q$ expansion.

The spin-flavor symmetry leads to many interesting relations between the properties of hadrons containing a heavy quark. The most direct consequences concern the spectroscopy of such states

Downloaded from https://academic.oup.com/ptep/article/2022/8/083C01/6651666 by KIT Library user on 27 September 2022

[13]. In the heavy-quark limit, the spin of the heavy quark and the total angular momentum j of the light degrees of freedom are separately conserved by the strong interactions. Because of heavy-quark symmetry, the dynamics is independent of the spin and mass of the heavy quark. Hadronic states can thus be classified by the quantum numbers (flavor, spin, parity, etc.) of the light degrees of freedom. The spin symmetry predicts that, for fixed $j \neq 0$, there is a doublet of degenerate states with total spin $J = j \pm \frac{1}{2}$. The flavor symmetry relates the properties of states with different heavy-quark flavor.

16.2.3 *Weak decay form factors*

Of particular interest are the relations between the weak decay form factors of heavy mesons, which parametrize hadronic matrix elements of currents between two mesons containing a heavy quark. These relations have been derived by Isgur and Wise [12], generalizing ideas developed by Nussinov and Wetzel [14] and Voloshin and Shifman [15]. For the purpose of this discussion, it is convenient to work with a mass-independent normalization of meson states and use velocity rather than momentum variables.

Consider the elastic scattering of a pseudoscalar meson, $P(v) \to P(v')$, induced by an external vector current coupled to the heavy quark contained in P, which acts as a color source moving with the meson's velocity v. The action of the current is to replace instantaneously the color source by one moving at velocity v'. Soft gluons need to be exchanged in order to rearrange the light degrees of freedom and build up the final state meson moving at velocity v'. This rearrangement leads to a form-factor suppression. The important observation is that, in the $m_Q \to \infty$ limit, the form factor can only depend on the Lorentz boost $\gamma = v \cdot v'$ connecting the rest frames of the initial and final-state mesons (as long as $\gamma = \mathcal{O}(1)$). In the effective theory the hadronic matrix element describing the scattering process can therefore be written as

$$\langle P(v')|\, \bar{h}_{v'} \gamma^\mu h_v \,|P(v)\rangle = \xi(v \cdot v')(v + v')^\mu, \tag{16.4}$$

with a form factor $\xi(v \cdot v')$ that is real and independent of m_Q. By flavor symmetry, the form factor remains identical when one replaces the heavy quark Q in one of the meson states by a heavy quark Q' of a different flavor, thereby turning P into another pseudoscalar meson P'. At the same time, the current becomes a flavor-changing vector current. This universal form factor is called the Isgur-Wise function [12]. For equal velocities the vector current $J^\mu = \bar{h}_v \gamma^\mu h_v$ is conserved in the effective theory, irrespective of the flavor of the heavy quarks. The corresponding conserved charges are the generators of the flavor symmetry. It follows that the Isgur-Wise function is normalized at the point of equal velocities: $\xi(1) = 1$. Since the recoil energy of the daughter meson P' in the rest frame of the parent meson P is $E_{\rm recoil} = m_{P'}\,(v \cdot v' - 1)$, the point $v \cdot v' = 1$ is referred to as the zero-recoil limit. The heavy-quark spin symmetry leads to additional relations among weak decay form factors. It can be used to relate matrix elements involving vector mesons to those involving pseudoscalar mesons, which once again can be described completely in terms of the universal Isgur-Wise function.

The form factor relations imposed by heavy-quark symmetry describe the semileptonic decay processes $\bar{B} \to D\,\ell\,\bar{\nu}$ and $\bar{B} \to D^*\ell\,\bar{\nu}$ in the limit of infinite heavy-quark masses. They are model-independent consequences of QCD. The known normalization of the Isgur-Wise function at zero recoil can be used to obtain a model-independent measurement of the element $|V_{cb}|$ of the Cabibbo-Kobayashi-Maskawa (CKM) matrix. The semileptonic decay $\bar{B} \to D^*\ell\,\bar{\nu}$ is particularly well suited for this purpose [16]. Experimentally this is a very clean mode, since the reconstruction of the D^* meson mass provides a powerful rejection against background. From the theoretical point of view, it is ideal since the decay rate at zero recoil is protected by Luke's theorem against first-order power corrections in $1/m_Q$ [17]. This is described in more detail in Section 12. Corrections to the heavy-quark symmetry relations for the $\bar{B} \to D^{(*)}$ form factors near zero recoil can also be constrained using sum rules derived in the small-velocity limit [18, 19].

16.2.4 *Decoupling transformation*

At leading order in $1/m_Q$, the couplings of soft gluons to heavy quarks in the effective Lagrangian (16.3) can be removed by the field redefinition $h_v(x) = Y_v(x)\, h_v^{(0)}(x)$, where $Y_v(x)$ is a soft Wilson line along the direction of v, extending from minus infinity to the point x. In terms of the new fields the leading-order HQET Lagrangian becomes $\mathcal{L}_{\rm HQET} = \bar{h}_v^{(0)} iv \cdot \partial\, h_v^{(0)}$. It describes a free theory as far as the strong interactions of heavy quarks are concerned. However, the theory is nevertheless non-trivial in the presence of external sources. Consider, e.g., the case of a weak-interaction heavy-quark current

$$\bar{h}_{v'} \gamma^\mu (1 - \gamma_5) h_v = \bar{h}_{v'}^{(0)} \gamma^\mu (1 - \gamma_5)\, Y_{v'}^\dagger Y_v\, h_v^{(0)}, \tag{16.5}$$

where v and v' are the velocities of the heavy mesons containing the heavy quarks. Unless the two velocities are equal, corresponding to the zero-recoil limit discussed above, the object $Y_{v'}^\dagger Y_v$ is non-trivial, and hence the soft gluons do not decouple from the heavy quarks inside the current operator. One may interpret $Y_{v'}^\dagger Y_v$ as a Wilson loop with a cusp at the point x, where the two paths parallel to the different velocity vectors intersect. The presence of the cusp leads to non-trivial ultra-violet behavior (for $v \neq v'$), which is described by a cusp anomalous dimension $\Gamma_{\rm cusp}(v \cdot v')$ that was calculated at two-loop order in [20]. It coincides with the velocity-dependent anomalous dimension of heavy-quark currents, which was introduced in the context of HQET in [21]. The interpretation of heavy quarks as Wilson lines is a useful tool, which was put forward in one of the very first papers on the subject [4]. This technology will be useful in the study of the interactions of heavy quarks with collinear degrees of freedom discussed later in this review.

16.2.5 *Heavy-quark expansion for inclusive decays*

The theoretical description of inclusive decays of hadrons containing a heavy quark exploits two observations [22–26]: bound-state effects related to the initial state can be calculated using the heavy-quark expansion, and the fact that the final state consists of a sum over many hadronic channels eliminates the sensitivity to the properties of individual final-state hadrons. The second feature rests on the hypothesis of quark-hadron duality, i.e. the assumption that decay rates are calculable in QCD after a smearing procedure has been applied [27]. In semileptonic decays, the integration over the lepton spectrum provides a smearing over the invariant hadronic mass of the final state (global duality). For nonleptonic decays, where the total hadronic mass is fixed, the summation over many hadronic final states provides an averaging (local duality). Since global duality is a much weaker assumption, the theoretical control of inclusive semileptonic decays is on firmer footing.

Using the optical theorem, the inclusive decay width of a hadron H_b containing a b quark can be written in the form

$$\Gamma(H_b) = \frac{1}{M_{H_b}}\, {\rm Im}\, \langle H_b|\, i \int {\rm d}^4x\, T\, \{\mathcal{H}_{\rm eff}(x), \mathcal{H}_{\rm eff}(0)\}\, |H_b\rangle\,. \tag{16.6}$$

The effective weak Hamiltonian for b-quark decays consists of dimension-6 four-fermion operators and dipole operators [28]. Because of the large mass of the b quark, it follows that the separation of fields in the time-ordered product in (16.6) is small, of order $x \sim 1/m_b$. It is thus possible to construct an operator-product expansion (OPE) for the time-ordered product, in which it is represented as a series of local operators in HQET. The leading operator $\bar{h}_v h_v$ has a trivial matrix element. The next contributions arise at $\mathcal{O}(1/m_b^2)$ and give rise to two parameters $\mu_\pi^2(H_b)$ and $\mu_G^2(H_b)$, which are defined as the matrix elements of the heavy-quark kinetic energy and chromo-magnetic interaction inside the hadron H_b, respectively [29]. For the ground-state heavy mesons and baryons, one has $\mu_G^2(B) = 3(m_{B^*}^2 - m_B^2)/4 \simeq 0.36\,{\rm GeV}^2$ and $\mu_G^2(\Lambda_b) = 0$. Thus, the total inclusive decay rate of a hadron H_b

Downloaded from https://academic.oup.com/ptep/article/2022/8/083C01/6651666 by KIT Library user on 27 September 2022

can be written as [23, 24]

$$\Gamma(H_b) = \frac{G_F^2 m_b^5 |V_{cb}|^2}{192\pi^3} \left[c_1 + c_2 \frac{\mu_\pi^2(H_b)}{2m_b^2} + c_3 \frac{\mu_G^2(H_b)}{2m_b^2} + \mathcal{O}\left(\frac{1}{m_b^3}\right) + \dots \right], \tag{16.7}$$

where the prefactor arises from the loop integrations and is proportional to the fifth power of the b-quark mass. The coefficient functions c_i are calculable order by order in perturbation theory. While c_1 corresponds to the decay rate of a free heavy quark, the higher-order coefficients systematically account for bound-state effects. The coefficients of the subleading operators and of the leading operator at third order in $1/m_b$ have recently been calculated at NLO [30–34], and the heavy-quark expansion has been pushed to fifth order in $1/m_b$ [35].

From the fully inclusive width in (16.7) one can obtain the lifetime of a heavy hadron via $\tau(H_b) = 1/\Gamma(H_b)$. Due to the universality of the leading term in the heavy-quark expansion, lifetime ratios such as $\tau(B^-)/\tau(\bar{B}^0)$, $\tau(\bar{B}_s^0)/\tau(\bar{B}^0)$ and $\tau(\Lambda_b)/\tau(\bar{B}^0)$ are particularly sensitive to the hadronic parameters determining the power corrections in the expansion. In order to understand these ratios theoretically, it is necessary to include phase-space enhanced power corrections of order $(\Lambda_{\rm QCD}/m_b)^3$ [36, 37] as well as short-distance perturbative effects [38] in the calculation (see [39] for a recent discussion of the status of the corresponding calculations).

A formula analogous to (16.7) can be derived for differential distributions in specific inclusive decay processes, assuming that these distributions are integrated over a sufficiently large region of phase space to ensure quark-hadron duality. Important examples are the distributions in the lepton energy and the lepton invariant mass, as well as moments of the invariant hadronic mass distribution in the semileptonic processes $\bar{B} \to X_u\, \ell\, \bar{\nu}$ and $\bar{B} \to X_c\, \ell\, \bar{\nu}$. A global fit of semileptonic decay distributions can be used to determine the CKM matrix elements $|V_{ub}|$ and $|V_{cb}|$ along with heavy-quark parameters such as the masses m_b, m_c and the hadronic parameters $\mu_\pi^2(B)$, $\mu_G^2(B)$. These determinations provide some of the most accurate values for these parameters (see e.g. [40–42]).

16.2.6 *Shape functions and non-local power corrections*

In certain regions of phase space, in which the hadronic final state in an inclusive heavy-hadron decay is made up of light energetic partons, the local OPE for inclusive decays must be replaced by a more complicated expansion involving hadronic matrix elements of non-local light-ray operators [43, 44]. Prominent examples are the radiative decay $\bar{B} \to X_s\gamma$ for large photon energy E_γ near $m_B/2$, and the semileptonic decay $\bar{B} \to X_u\, \ell\, \bar{\nu}$ at large lepton energy or small hadronic invariant mass. In these cases, the differential decay rates at leading order in the heavy-quark expansion can be written in the factorized form $d\Gamma = H\, J \otimes S$ [45], where the hard function H and the jet function J are calculable in perturbation theory. The characteristic scales for these functions are set by m_b and $(m_b\Lambda_{\rm QCD})^{1/2}$, respectively. The soft function

$$S(\omega) = \int \frac{dt}{4\pi}\, e^{-i\omega t}\, \langle \bar{B}(v)|\, \bar{h}_v(tn) Y_n(tn) Y_n^\dagger(0) h_v(0) |\bar{B}(v)\rangle \tag{16.8}$$

is a non-perturbative object called the shape function [43, 44]. Here Y_n are soft Wilson lines along a light-like direction n aligned with the momentum of the hadronic final-state jet. The jet function and the shape function share a common variable $\omega \sim \Lambda_{\rm QCD}$, and the symbol $\otimes$ denotes a convolution in this variable.

While the hard functions are different for the decays $\bar{B} \to X_s\gamma$ and $\bar{B} \to X_u\, \ell\bar{\nu}$, the jet and soft functions are identical at leading order in $\Lambda_{\rm QCD}/m_Q$. This is particularly important for the shape function, which introduces non-perturbative physics into the theoretical predictions for the decay rates in the regions of experimental interest. The fact that both processes depend on the same non-perturbative function makes it possible to use the measured shape of the $\bar{B} \to X_s\gamma$ photon spectrum to reduce the theoretical uncertainties in the determination of the CKM element $|V_{ub}|$ from semileptonic decays. In higher orders of the heavy-quark expansion, an increasing number of subleading jet and soft functions are required to describe the decay distributions [46]. These have been analyzed in detail at order $1/m_b$ [47–49]. In the case of $\bar{B} \to X_s\gamma$ (and also in the related case of $\bar{B} \to X_s\ell\bar{\ell}$), some of these non-local effects survive in the total decay rate and give rise to irreducible hadronic uncertainties [50]. The technology for deriving the corresponding factorization theorems relies on the soft-collinear effective theory, to which we now turn.

16.3 Soft-Collinear Effective Theory

As discussed in the previous section, soft gluons that bind a heavy quark inside a heavy meson cannot change the virtuality of that heavy quark by a significant amount. The ratio $\Lambda_{\rm QCD}/m_Q$ provides the expansion parameter in HQET, which is a small parameter since $m_Q \gg \Lambda_{\rm QCD}$. This obviously does not work when considering light quarks. However, if the energy Q of the quarks is large, the ratio $\Lambda_{\rm QCD}/Q$ provides a small parameter, which can be used to construct an effective theory. One major difference to HQET is that light energetic quarks cannot only emit soft gluons, but they can also emit collinear gluons (an energetic gluon in the same direction as the original quark), without parametrically changing their virtuality. Thus, to fully reproduce the long-distance physics of energetic quarks requires that one includes their interactions with both soft and collinear particles. The resulting effective theory is therefore called soft-collinear effective theory (SCET) [51–53] (see [54] for a review).

A single energetic particle can always be boosted to a frame where all momentum components have similar size, in which case there is no small expansion parameter. Thus, the presence of energetic particles must refer to a reference frame defined by external kinematics. SCET has a wide range of applications; some examples are the production of energetic, light states in the decay of a heavy particle in its rest frame, the production of energetic jets in collider environments, and the scattering of energetic particles off a target at rest. In this brief review we will outline the main features of this effective theory and mention a few selected applications.

16.3.1 *General idea of the expansion*

Consider a quark with virtuality much less than its energy Q, moving along the direction $\vec{n}$. It is convenient to parameterize the momentum p_n of this particle in terms of its light-cone components, defined by $(p_n^-, p_n^+, p_n^\perp) = (\bar{n}\cdot p_n, n\cdot p_n, p_n^\perp)$, where $n^\mu = (1, \vec{n})$ and $\bar{n}^\mu = (1, -\vec{n})$ are light-like vectors, and $n\cdot p_n^\perp = \bar{n}\cdot p_n^\perp = 0$. The subscript n on the momentum indicates the direction of the collinear particle. In terms of these light-cone components, the virtuality satisfies $p_n^2 = p_n^+ p_n^- + p_n^{\perp 2}$. The individual components of the momentum obey

$$(p_n^-, p_n^+, p_n^\perp) \sim Q(1, \lambda^2, \lambda)\,, \tag{16.9}$$

where $\lambda^2 = p^2/Q^2$ is the expansion parameter of SCET. The virtuality of such an energetic particle remains parametrically unchanged if it interacts with energetic particles in the same direction n, or with soft particles with momentum scaling as

$$(p_s^-, p_s^+, p_s^\perp) \sim Q(\lambda^2, \lambda^2, \lambda^2)\,. \tag{16.10}$$

SCET is constructed in such a way as to reproduce the long-distance dynamics arising from the interactions of collinear and soft degrees of freedom.

In the above power counting the transverse momenta of soft degrees of freedom scale as $p_s^\perp \sim Q\lambda^2$, which is much smaller than the transverse momenta $p_c^\perp \sim Q\lambda$ of collinear fields. This theory is usually called $\mathrm{SCET_I}$. If the external kinematics require that the transverse momenta of both soft and collinear fields are of the same size, $p_c^\perp \sim p_s^\perp$, then the appropriate degrees of freedom have the scaling $p_c \sim Q(1, \lambda^2, \lambda)$ and $p_s \sim Q(\lambda, \lambda, \lambda)$. This theory is usually called $\mathrm{SCET_{II}}$ and is required, e.g., for exclusive hadronic decays such as $\bar{B} \to D\pi$, where the virtuality of both collinear and soft degrees of freedom are set by $\Lambda_{\rm QCD}$, or for the description of transverse-momentum distributions at colliders. $\mathrm{SCET_I}$ power counting is assumed in the following sections, while $\mathrm{SCET_{II}}$ is discussed in more detail in 16.3.6.

Downloaded from https://academic.oup.com/ptep/article/2022/8/083C01/6651666 by KIT Library user on 27 September 2022

16.3.2 *Leading-order Lagrangian*

The derivation of the SCET Lagrangian follows similar steps as described for HQET in Section 16.2.1. One begins by deriving the Lagrangian for a theory containing only a single collinear sector. Similar to HQET, one separates the full QCD field into two components, $q_n(x) = \psi_n(x) + \Xi_n(x)$, where (with $n \cdot \bar{n} = 2$)

$$\psi_n(x) = \frac{\not{n}\not{\bar{n}}}{4}\, q_n(x)\,, \qquad \Xi_n(x) = \frac{\not{\bar{n}}\not{n}}{4}\, q_n(x)\,. \tag{16.11}$$

The degrees of freedom described by the field Ξ_n are far off shell and can therefore be eliminated using its equation of motion. This gives

$$\mathcal{L}_n = \bar{\psi}_n(x) \left[in \cdot D + i\not{D}^\perp \frac{1}{i\bar{n}\cdot D}\, i\not{D}^\perp \right] \frac{\not{\bar{n}}}{2}\, \psi_n(x)\,. \tag{16.12}$$

As a next step, one separates the large and residual momentum components by decomposing the collinear momentum into a "label" and a residual momentum, $p^\mu = P^\mu + k^\mu$ with $n \cdot P = 0$. One then performs a phase redefinition on the collinear fields, such that $\psi_n(x) = e^{iP\cdot x}\, \xi_n(x)$. Derivatives acting on the fields $\xi_n(x)$ now only pick out the residual momentum. Since unlike in HQET the label momentum in SCET is not conserved, one defines a label operator $\mathcal{P}^\mu$ acting as $\mathcal{P}^\mu \xi_n(x) = P^\mu \xi_n(x)$ [52], as well as a corresponding covariant label operator $i\mathcal{D}_n^\mu = \mathcal{P}^\mu + gA_n^\mu(x)$. Note that at leading order in power counting $i\mathcal{D}_n^\mu$ does not contain the soft gluon field. This leads to the final SCET Lagrangian [52,53,55,56]

$$\mathcal{L}_n = \bar{\xi}_n(x) \left[in \cdot D_n + gn \cdot A_s + i\not{\mathcal{P}}_n^\perp \frac{1}{i\bar{n}\cdot \mathcal{D}_n}\, i\not{\mathcal{P}}_n^\perp \right] \frac{\not{\bar{n}}}{2}\, \xi_n(x) + \ldots\,, \tag{16.13}$$

where we have split $in \cdot D$ into a collinear piece $in \cdot D_n = in \cdot \partial + gn \cdot A_n$ and a soft piece $gn \cdot A_s$. This latter term gives rise to the only interaction between a collinear quark and soft gluons at leading power in λ. The ellipses represent higher-order interactions between soft and collinear particles.

The Lagrangian describing collinear fields in different light-like directions is simply given by the sum of the Lagrangians for each direction n, i.e. $\mathcal{L} = \sum_n \mathcal{L}_n$. The soft gluons are the same in each individual Lagrangian. An alternative way to understand the separation between large and small momentum components is to derive the Lagrangian of SCET in position space [56]. In this case no label operators are required, and the dependence on short-distance effects is contained in non-localities at short distances. An important difference between SCET and HQET is that the SCET Lagrangian is not corrected by short distance fluctuations. The physical reason is that in the construction described above no high-momentum modes have been integrated out [56]. Such hard modes arise when different collinear sectors are coupled via some external current (e.g. in jet production at e^+e^- or hadron colliders), or when collinear particles are produced in the rest frame of a decaying heavy object (such as in B decays). Short-distance effects are then incorporated in the Wilson coefficients of the external source operators.

16.3.3 *Collinear gauge invariance and Wilson lines*

An important aspect of SCET is the implementation of local gauge invariance. Because the effective field operators describe modes with certain momentum scalings, the effective Lagrangian respects only residual gauge symmetries. One of them satisfies the collinear scaling

$$(\bar{n}\cdot\partial, n\cdot\partial, \partial^\perp)\, U_n(x) \sim Q(1, \lambda^2, \lambda)\, U_n(x)\,, \tag{16.14}$$

and one the soft scaling

$$(\bar{n}\cdot\partial, n\cdot\partial, \partial^\perp)\, U_s(x) \sim Q(\lambda^2, \lambda^2, \lambda^2)\, U_s(x)\,. \tag{16.15}$$

While the soft gauge transformation is common for all fields, collinear fields in different directions each transform under their own collinear gauge transformation, which means that each collinear sector, containing particles with large momenta along a certain direction, has to be separately gauge invariant under its collinear gauge transformation. This requires the introduction of collinear Wilson lines [52]

$$W_n(x) = \mathrm{P}\exp\left[-ig \int_{-\infty}^0 ds\, \bar{n}\cdot A_n(s\bar{n} + x) \right], \tag{16.16}$$

which transform under collinear gauge transformations according to $W_n \to U_n W_n$. Thus, the combination $\chi_n \equiv W_n^\dagger\, \psi_n$ is gauge invariant. In a similar manner, one can define the gauge-invariant gluon field $B_n^\mu = g^{-1} W_n^\dagger\, iD_n^\mu\, W_n$ [57, 58]. Collinear operators in SCET are typically constructed from such collinearly gauge-invariant building blocks.

16.3.4 *Derivation of factorization theorems*

One of the important applications of SCET is to understand how to factorize cross sections involving energetic particles moving in different directions into simpler pieces that can either be calculated perturbatively or determined from data. Factorization theorems have been around for much longer than SCET (see [59] for a review). However, the effective theory allows for a conceptually simpler understanding of certain classes of factorization theorems [57], since most simplifications happen already at the level of the Lagrangian. The discussion in this section is valid to leading order in the power counting of the effective theory.

As discussed in the previous section, the Lagrangian of SCET does not involve any couplings between collinear particles moving in different directions. Soft gluons couple to collinear quarks only through the term $\bar{\xi}_n\, gn \cdot A_s\, (\not{\bar{n}}/2)\, \xi_n$ in the effective Lagrangian in (16.13). This coupling is similar to the coupling of soft gluons to heavy quarks in HQET, see Section 16.2.4. It can be removed by means of the field redefinition [53]

$$\psi_n(x) = Y_n(x)\, \psi_n^{(0)}(x)\,, \qquad A_n^a(x) = Y_n^{ab}(x)\, A_n^{b(0)}(x)\,, \tag{16.17}$$

where Y_n and Y_n^{ab} live in the fundamental and adjoint representations of $SU(3)$, respectively. This fact greatly facilitates proofs of factorization theorems in SCET. A QCD operator $O(x)$ describing the interactions of collinear partons moving in different directions can thus be written as (omitting color indices for simplicity)

$$\langle O(x) \rangle = C_O(\mu)\, \langle \left[\mathcal{C}_{n_a}^{(0)}\, \mathcal{C}_{n_b}^{(0)}\, \mathcal{C}_{n_1}^{(0)} \ldots \mathcal{C}_{n_N}^{(0)} \right](x) \left[\mathcal{Y}_{n_a}\, \mathcal{Y}_{n_b}\, \mathcal{Y}_{n_1} \ldots \mathcal{Y}_{n_N} \right](x) \rangle_\mu\,. \tag{16.18}$$

Here $\mathcal{C}_{n_i}^{(0)}(x)$ denotes a gauge-invariant combination of collinear fields (either quark or gluon fields) in the direction n_i. The hard matching coefficient C_O accounts for short-distance effects at the scale Q. The soft Wilson lines can either be in a color triplet or color octet representation, and are collectively denoted by $\mathcal{Y}_{n_i}$. Both the matrix elements and the coefficient C_O depend on the renormalization scale μ.

Having defined the operator mediating a given process, one can calculate the cross section by squaring the operator, taking the forward matrix element and integrating over the phase space of all final-state particles. The absence of interactions between collinear degrees of freedom moving along different directions or soft degrees of freedom implies that the forward matrix element can be factorized as

$$\begin{aligned} \left\langle \mathrm{in} \middle| O(x)\, O^\dagger(0) \middle| \mathrm{in} \right\rangle &= |C_O(\mu)|^2 \left\langle \mathrm{in}_a \middle| \mathcal{C}_{n_a}(x)\, \mathcal{C}_{n_a}^\dagger(0) \middle| \mathrm{in}_a \right\rangle_\mu \\ &\times \left\langle \mathrm{in}_b \middle| \mathcal{C}_{n_b}(x)\, \mathcal{C}_{n_b}^\dagger(0) \middle| \mathrm{in}_b \right\rangle_\mu \\ &\times \left\langle 0 \middle| \mathcal{C}_{n_1}(x)\, \mathcal{C}_{n_1}^\dagger(0) \middle| 0 \right\rangle_\mu \cdots \left\langle 0 \middle| \mathcal{C}_{n_N}(x)\, \mathcal{C}_{n_N}^\dagger(0) \middle| 0 \right\rangle_\mu \\ &\times \left\langle 0 \middle| \left[\mathcal{Y}_{n_a} \ldots \mathcal{Y}_{n_N} \right](x) \left[\mathcal{Y}_{n_a} \ldots \mathcal{Y}_{n_N} \right]^\dagger(0) \middle| 0 \right\rangle_\mu\,. \end{aligned} \tag{16.19}$$

Thus, the matrix element can be written as a product of simpler structures, each of which can be evaluated separately.

The vacuum matrix elements of the outgoing collinear fields are determined by jet functions $J_i(\mu)$. As long as the relevant scale (for example the jet mass) is sufficiently large, these functions can

Downloaded from https://academic.oup.com/ptep/article/2022/8/083C01/6651666 by KIT Library user on 27 September 2022

be calculated perturbatively. The matrix elements of the incoming collinear fields are non-perturbative objects $B_{p/N}(\mu)$ called beam functions for parton p in nucleon N [60]. For many applications they can be related perturbatively to the well-known parton distribution functions. Finally, the vacuum matrix element of the soft Wilson lines defines a so-called soft function $S_{ab\ldots N}(\mu)$. The shared dependence on x in the above equation implies that in momentum space the various components of the factorization theorem are convoluted with one another. Deriving this convolution requires a careful treatment of the phase-space integration and the factorization of the measurement defining the cross section of interest, in particular treating the large and residual components of each momentum appropriately.

Putting all information together, the differential cross section for a proton-proton collision with N jet-like objects can schematically be written as

$$d\sigma \sim \sum_{ab} H_{ab}(\mu) \left[B_{a/P}(\mu)\, B_{b/P}(\mu)\right] \otimes \left[J_1(\mu)\ldots J_N(\mu)\right] \otimes S_{ab\ldots N}(\mu)\,. \tag{16.20}$$

The hard function is equal to the square of the matching coefficient, $H_{ab}(\mu) = |C_O(\mu)|^2$, and the beam, jet, and soft functions and their convolution structure depend on the specific N-jet measurement. It should be mentioned that the most difficult part of traditional factorization proofs involves showing that so-called Glauber gluons do not spoil the above factorization theorem [61]. Significant progress toward the description of Glauber effects within SCET has been made in [62], where a closed form for the effective Lagrangian describing these interactions was derived. In this context, a proof of factorization requires demonstrating that this Lagrangian has no impact on a particular cross section, and such proofs have not yet been fully derived within SCET.

16.3.5 *Resummation of large logarithms*

SCET can be used to sum the large logarithms arising in perturbative calculations to all orders in the strong coupling constant α_s. In general, perturbation theory will generate a logarithmic dependence on any ratio of scales r in a problem. For processes that involve initial or final states with energy much in excess of their mass, there are two powers of logarithms for every power of α_s. These are referred to as Sudakov logarithms. For widely separated scales these large logarithms can spoil the convergence of fixed-order perturbation theory. One thus needs to reorganize the expansion in such a way that $\alpha_s L = \mathcal{O}(1)$ is kept fixed, with $L = \ln r$. More precisely, a proper resummation requires summing logarithms of the form $\alpha_s^n L^m$ with $m \leq (n+1)$ in the logarithm of a cross section, by writing $\ln\sigma \sim L\, g_0(\alpha_s L) + g_1(\alpha_s L) + \alpha_s\, g_2(\alpha_s L) + \ldots$, with functions $g_n(x)$ that need to be determined.

The important ingredient in achieving this resummation is the fact that SCET factorizes a given cross section into simpler pieces, each of which depends on a single physical scale. The only dependence on that scale can arise through logarithms of its ratio with the renormalization scale μ. Thus, for each of the components in the factorization theorem one can choose a renormalization scale μ for which the large logarithmic terms are absent. Of course, the factorization formula requires a common renormalization scale μ in all its components, and one therefore has to use the renormalization group (RG) to evolve the various component functions from their preferred scale to the common scale μ. A novel feature of RG equations in SCET, as opposed to other EFTs, is that the anomalous dimensions entering the evolution equations of the hard, beam, jet and soft functions in a factorization formula such as (16.20) contain a single power of the logarithm of the relevant energy scale. For example, the anomalous dimension γ_H of the hard function has the form

$$\gamma_H(\mu) = c_H\, \Gamma_{\rm cusp}(\alpha_s)\, \ln\frac{Q^2}{\mu^2} + \gamma(\alpha_s)\,, \tag{16.21}$$

where c_H is a process-dependent coefficient and $\Gamma_{\rm cusp}$ denotes the so-called cusp anomalous dimension [20, 63]. Collinear and soft functions have similar anomalous dimensions, which also involve a cusp and a non-cusp part. The non-cusp part γ of the anomalous dimensions is process (and observable) dependent. The presence of a logarithm in the anomalous dimension is characteristic of Sudakov problems and arises since the perturbative series contains double logarithms of scale ratios.

Solving the RG equations one can systematically resum all large logarithms of scale ratios in the factorized cross section and express the functions $g_n(\alpha_s L)$ introduced above in terms of ratios of running coupling constants. In order to compute the first two terms $L\, g_0(\alpha_s L) + g_1(\alpha_s L)$ in $\ln\sigma$, corresponding to the next-to-leading logarithmic (NLL) approximation, one needs two-loop expressions for the cusp anomalous dimension and β function, one-loop expressions for the non-cusp pieces in the anomalous dimensions, and tree-level matching conditions for all component functions at their characteristic scales. To calculate the next term $\alpha_s g_2(\alpha_s L)$ in the expansion, corresponding to NNLL order, one needs to go one order higher in the loop expansion, and so on.

16.3.6 *Factorization and resummation in* $\mathbf{SCET_{II}}$

The effective theory $\mathrm{SCET_{II}}$ contains collinear and soft particles with momenta scaling as $(p_n^-, p_n^+, p_n^\perp) \sim Q(1, \lambda^2, \lambda)$ and $(p_s^-, p_s^+, p_s^\perp) \sim Q(\lambda, \lambda, \lambda)$. They have the same small virtuality ($p_n^2 \sim p_s^2 \sim Q^2\lambda^2$) but differ in their rapidities. An important class of observables, for which this scaling is relevant, contains cross sections for processes in which the transverse momenta of particles are constrained by external kinematics. The prime example are the transverse-momentum distributions of electroweak gauge bosons or Higgs bosons produced at hadron colliders. The parton transverse momenta are constrained by the fact that their vector sum must be equal and opposite to the transverse momentum q_T of the boson. Standard RG evolution in the effective theory controls the logarithms arising from the fact that the virtualities of the collinear and soft modes are much smaller than the hard scale Q in the process (the boson mass). However, additional large logarithms arise since the rapidities of collinear and soft modes are parametrically different, such that $e^{|y_c - y_s|} \sim 1/\lambda$. These logarithms can be traced to a new source of divergences and an unusual failure of dimensional regularization. They need to be factorized in the cross section and resummed by other means.

Two equivalent approaches exist for how to deal with the additional rapidity logarithms in SCET. In the approach of [64], they are interpreted as a consequence of a "collinear anomaly" of the effective theory $\mathrm{SCET_{II}}$, resulting from the fact that a classical rescaling symmetry of the effective Lagrangian is broken by quantum effects. The extra large logarithms can be resummed by means of simple differential equations, which typically state that to all orders in perturbation theory (and in an appropriate space) the logarithm of the cross section contains only a single extra logarithm of $\lambda \sim q_T/Q$ not contained in the hard function. Another approach to resum the rapidity logarithms uses the "rapidity renormalization group" [65], in which the relevant differential equations are obtained by considering a new type of scale variation in a parameter ν, which separates the phase space for collinear and soft particles along a hyperbola in the (p_-, p_+) plane. In contrast to the standard RG, there is no running coupling involved in the ν evolution, since the different contributions live at the same virtuality.

$\mathrm{SCET_{II}}$ also plays an important role in the study of factorization for a variety of exclusive B meson decays, such as $\bar{B} \to \pi\ell\bar{\nu}$, $\bar{B} \to K^*\gamma$ and $\bar{B} \to \pi\pi$, for which the virtualities of energetic (collinear) final-state particles are of order $\Lambda_{\rm QCD}$, which is also the scale for the soft light degrees of freedom contained in the initial-state B meson.

16.3.7 *Applications*

Most of the applications of SCET are either in flavor physics, where the decay of a heavy B meson can give rise to energetic light partons, or in collider physics, where the presence of jets naturally leads to collimated sets of energetic particles. For some of these applications alternative approaches existed before the invention of SCET, but the effective theory has opened up alternative ways to understand the physics of these processes. For

Downloaded from https://academic.oup.com/ptep/article/2022/8/083C01/6651666 by KIT Library user on 27 September 2022

many examples, however, SCET has allowed new insights and new applications. The investigation of heavy-to-light form factors has been instrumental for understanding factorization in exclusive semileptonic B decays [66]. SCET has also provided a field-theoretic basis for the QCD factorization approach to exclusive, non-leptonic decays of B mesons [67]. Using SCET methods, proofs of factorization were derived for the color-allowed decay $\bar{B}^0 \to D^+\pi^-$ [68], the color-suppressed decay $\bar{B}^0 \to D^0\pi^0$ [69], and the radiative decay $\bar{B} \to K^*\gamma$ [70]. Further examples are factorization theorems and the resummation of endpoint logarithms for quarkonia production [71], the resummation of large logarithmic terms for the thrust [72] and jet broadening [73] distributions in e^+e^- annihilation beyond NLL order, the development of new factorizable observables to veto extra jets [60, 74], all-orders factorization theorems for processes containing electroweak Sudakov logarithms [75], and the resummation of threshold (soft gluon) logarithms in momentum space for several important processes at hadron colliders [76–78]. There has also been a lot of activity describing p_T-based resummation at hadron colliders. Prominent examples are the transverse-momentum distributions of electroweak bosons [64, 65, 79]. Finally, SCET has given new insights into the jet substructure methods (see [80] for a recent review). We now describe a few of these applications in more detail.

Event-shape distributions, in particular the thrust distribution, have been measured to high accuracy at LEP [81]. They can be used for a determination of the strong coupling constant α_s. SCET has increased the theoretical accuracy in the calculations of the thrust and C-parameter distributions significantly. First, it has allowed to increase the perturbative accuracy of the thrust spectrum. The resummation of logarithms of τ, which become important for $\tau \ll 1$, has been performed to N^{3}LL [72], two orders beyond what was previously available. Combining this resummation with the known two-loop spectrum [82, 83] gives precise perturbative predictions both at small and large values of τ. Second, the factorization of the cross section in SCET has made it possible to include non-perturbative physics through a shape function, in analogy with the B-physics case discussed in Section 16.2.6. Comparing the theoretical predictions to the measured thrust and C-parameter distributions yields a precise value of the strong coupling constant $\alpha_s(m_Z)$, which however is lower than the average value cited in Section 9 by several standard deviations [84, 85]. For more discussions on this, see Section 9.

The Higgs-boson production cross section in gluon fusion at the LHC, defined with a jet veto stating that no jet in the final state has transverse momentum above a threshold $p_T^{\rm veto}$, can be factorized in the form [86, 87] (see [88] for a corresponding calculation outside the SCET framework)

$$\sigma(p_T^{\rm veto}) = H(m_H,\mu)\left(\frac{\nu_B}{\nu_S}\right)^{-2F_{gg}(R,p_T^{\rm veto},\mu)} S_{gg}(R,p_T^{\rm veto},\mu,\frac{\nu_S}{p_T^{\rm veto}}) \times \int_\tau^1 \frac{dz}{z}\, B_{g/P}\left(z,R,p_T^{\rm veto},\mu,\frac{\nu_B}{m_H}\right) B_{g/P}\left(\frac{\tau}{z},R,p_T^{\rm veto},\mu,\frac{\nu_B}{m_H}\right), \tag{16.22}$$

where $\tau = m_H^2/s$, and $\mu \sim p_T^{\rm veto}$ is a common factorization scale. The beam functions $B_{g/P}$, the soft function S_{gg} and the exponent F_{gg} all depend on the jet radius R as well as the jet clustering algorithm. The scale dependence of the hard function H is controlled by standard RG evolution in SCET. The beam functions can be factorized further into calculable collinear kernels convoluted with parton distribution functions. In addition to the renormalization scale μ, the beam and soft functions depend on two rapidity scales $\nu_B \sim m_H$ and $\nu_S \sim p_T^{\rm veto}$, respectively. In [86] the default values $\nu_B = m_H$ and $\nu_S = p_T^{\rm veto}$ are used for these scales, and the soft function S_{gg} is absorbed into the beam functions. In [87] the exponent F_{gg} is called $-\gamma_\nu^g/2$. The second factor on the right-hand side of the factorization formula (16.22), which resums large rapidity logarithms, implies that the logarithm of the jet-veto cross section contains a single large logarithm $\ln\sigma = -2F_{gg}(R,p_T^{\rm veto},\mu)\,\ln(m_H/p_T^{\rm veto}) + \ldots$ not contained in the hard function. Its coefficient can be calculated in fixed-order perturbation theory.

Obtaining more precise fixed-order calculations has been an important goal for many years. A major difficulty in these calculations is the proper handling of the infrared singularities that arise in both virtual and real contributions. A method based on N-jettiness ($\mathcal{T}_N$) slicing [89,90] allows one to obtain the NNLO result from a much easier NLO calculation, combined with information about the singular dependence of the cross section on the $\mathcal{T}_N$ resolution variable [74]. This has been used to compute various processes with final states containing up to one hard, colored particle [91–95]. While the NLO calculations can be performed using well established techniques, the singular dependence on $\mathcal{T}_N$ can be calculated using SCET at NNLO. Calculations of the leading power corrections in $\mathcal{T}_0/Q$ [96, 97] have helped to improved the numerical stability for several processes. The N-jettiness ($\mathcal{T}_N$) slicing method has been used prior to the fixed-order application in the combination of higher order resummation with parton showers [98, 99].

More generally, there is currently a strong effort to push the applications of SCET toward factorization and resummation at subleading power in the expansion in λ. The subleading SCET Lagrangian [56, 100] and current operators arising in B-meson decays and their anomalous dimensions [55,56,101–103] have been studied a long time ago. More recently, the focus has shifted to subleading operators arising in important collider processes, such as Drell-Yan or Higgs production. The general set of operators for such processes have been identified [104–106], and several of their anomalous dimensions have been calculated [106, 107]. First resummed results at subleading power have been presented for event shapes [108] and the Drell-Yan process [109].

16.4 Open issues and perspectives

HQET has successfully passed many experimental tests, and there are not many open questions that still need to be addressed. One concept that has not been derived from first principles is the notion of quark-hadron duality, which underlies the application of HQET to the description of inclusive decays of B mesons. The validity of global duality (at energies even lower than those relevant in B decays) has been tested experimentally using high-precision data on semileptonic B decays and on hadronic τ decays. However, assigning a theoretical uncertainty due to possible duality violations remains a difficult task. Another known issue is that the measured values of the CKM element $|V_{ub}|$ extracted from exclusive or inclusive decays of B mesons differ from each other by several standard deviations (see Section 76). This measurement relies on the heavy-quark limit, and the uncertainty quoted includes a theoretical estimate of the effect of power corrections arising from the finite b-quark mass. It remains an open question whether the discrepancy is due to underestimated theoretical or experimental uncertainties, or whether it may hint to the existence of new physics.

SCET, on the other hand, is still an active field of research, and new results are being obtained regularly. An important example concerns the understanding of non-global logarithms arising in hadron-collider processes with jets [110, 111]. For a long time a fully factorized form of non-global jet cross sections has not been available, despite significant progress towards this goal [112, 113]. A consistent factorization formula for non-global jet observables was developed in [114, 115]. It requires the introduction of a collinear-soft mode in the SCET Lagrangian. The first application of this formalism was to the light jet mass distribution [116], and significant steps toward an extension to NLL accuracy have been taken in [117]. It is believed that the results obtained from the factorization theorem derived in [114, 115] are equivalent to those obtained using the approaches proposed in [112, 113]. The various methods differ in the way in which they organize the all-order expansion for the appearing complicated multi-Wilson-line structures.

Another active field concerns the study of Glauber gluons in SCET [118] and their relation to the BFKL equation familiar from small-x physics [119]. A systematic account of the effects of Glauber gluons in the context of the SCET Lagrangian has been developed in [62]. The formalism has been extended to Glauber quarks in [120]. These developments set the basis for

Downloaded from https://academic.oup.com/ptep/article/2022/8/083C01/6651666 by KIT Library user on 27 September 2022

a solid understanding of the impact of Glauber exchanges on factorization theorems. Glauber gluons also play an important role in SCET-based analysis of jet propagation in dense QCD media [121, 122], which gives rise to the jet-quenching phenomenon in heavy-ion collisions. An important open question facing some applications of SCET concerns factorized expressions containing endpoint-divergent convolution integrals.

We close this short review by mentioning a particularly nice application combining the methods of heavy-particle EFTs such as HQET and non-relativistic QCD with SCET in the context of describing the interactions of heavy dark matter (with mass $M \gg v$) with SM particles. In [123] it was realized that the interactions of heavy, weakly interacting massive particles (WIMPs) with nuclear targets can be described in a model-independent way using heavy-particle EFTs. The WIMPs are charged under $SU(2)_L$ and can interact with electroweak gauge bosons and the Higgs boson. The WIMP EFT was later extended by describing the produced, highly energetic electroweak gauge bosons in terms of soft or collinear fields in SCET [124–126]. This allows one to systematically separate all relevant mass scales, resum electroweak Sudakov logarithms and disentangle the so-called Sommerfeld enhancement from the short-distance hard annihilation process.

References

[1] E. Witten, Nucl. Phys. **B122**, 109 (1977).

[2] S. Weinberg, Phys. Lett. **91B**, 51 (1980).

[3] L. J. Hall, Nucl. Phys. **B178**, 75 (1981).

[4] E. Eichten and B. R. Hill, Phys. Lett. **B234**, 511 (1990).

[5] H. Georgi, Phys. Lett. **B240**, 447 (1990).

[6] B. Grinstein, Nucl. Phys. **B339**, 253 (1990).

[7] T. Mannel, W. Roberts and Z. Ryzak, Nucl. Phys. **B368**, 204 (1992).

[8] M. Neubert, Phys. Rept. **245**, 259 (1994), [hep-ph/9306320].

[9] A. V. Manohar and M. B. Wise, Camb. Monogr. Part. Phys. Nucl. Phys. Cosmol. **10**, 1 (2000).

[10] M. E. Luke and A. V. Manohar, Phys. Lett. **B286**, 348 (1992), [hep-ph/9205228].

[11] E. V. Shuryak, Phys. Lett. **93B**, 134 (1980).

[12] N. Isgur and M. B. Wise, Phys. Lett. **B232**, 113 (1989).

[13] N. Isgur and M. B. Wise, Phys. Rev. Lett. **66**, 1130 (1991).

[14] S. Nussinov and W. Wetzel, Phys. Rev. **D36**, 130 (1987).

[15] M. A. Shifman and M. B. Voloshin, Sov. J. Nucl. Phys. **45**, 292 (1987), [Yad. Fiz.45,463(1987)].

[16] M. Neubert, Phys. Lett. **B264**, 455 (1991).

[17] M. E. Luke, Phys. Lett. **B252**, 447 (1990).

[18] I. I. Y. Bigi *et al.*, Phys. Rev. **D52**, 196 (1995), [hep-ph/9405410].

[19] N. Uraltsev, Phys. Lett. **B501**, 86 (2001), [,195(2000)], [hep-ph/0011124].

[20] G. P. Korchemsky and A. V. Radyushkin, Nucl. Phys. **B283**, 342 (1987).

[21] A. F. Falk *et al.*, Nucl. Phys. **B343**, 1 (1990).

[22] J. Chay, H. Georgi and B. Grinstein, Phys. Lett. **B247**, 399 (1990).

[23] I. I. Y. Bigi, N. G. Uraltsev and A. I. Vainshtein, Phys. Lett. **B293**, 430 (1992), [Erratum: Phys. Lett.B297,477(1992)], [hep-ph/9207214].

[24] A. V. Manohar and M. B. Wise, Phys. Rev. **D49**, 1310 (1994), [hep-ph/9308246].

[25] T. Mannel, Nucl. Phys. **B413**, 396 (1994), [hep-ph/9308262].

[26] A. F. Falk, M. E. Luke and M. J. Savage, Phys. Rev. **D49**, 3367 (1994), [hep-ph/9308288].

[27] E. C. Poggio, H. R. Quinn and S. Weinberg, Phys. Rev. **D13**, 1958 (1976).

[28] G. Buchalla, A. J. Buras and M. E. Lautenbacher, Rev. Mod. Phys. **68**, 1125 (1996), [hep-ph/9512380].

[29] A. F. Falk and M. Neubert, Phys. Rev. **D47**, 2965 (1993), [hep-ph/9209268].

[30] T. Becher, H. Boos and E. Lunghi, JHEP **12**, 062 (2007), [arXiv:0708.0855].

[31] A. Alberti, P. Gambino and S. Nandi, JHEP **01**, 147 (2014), [arXiv:1311.7381].

[32] T. Mannel, A. A. Pivovarov and D. Rosenthal, Phys. Lett. **B741**, 290 (2015), [arXiv:1405.5072].

[33] T. Mannel, A. A. Pivovarov and D. Rosenthal, Phys. Rev. **D92**, 5, 054025 (2015), [arXiv:1506.08167].

[34] T. Mannel and A. A. Pivovarov, Phys. Rev. **D100**, 9, 093001 (2019), [arXiv:1907.09187].

[35] T. Mannel, S. Turczyk and N. Uraltsev, JHEP **11**, 109 (2010), [arXiv:1009.4622].

[36] M. Neubert and C. T. Sachrajda, Nucl. Phys. **B483**, 339 (1997), [hep-ph/9603202].

[37] M. Beneke, G. Buchalla and I. Dunietz, Phys. Rev. **D54**, 4419 (1996), [Erratum: Phys. Rev.D83,119902(2011)], [hep-ph/9605259].

[38] M. Beneke *et al.*, Phys. Lett. **B459**, 631 (1999), [hep-ph/9808385].

[39] M. Kirk, A. Lenz and T. Rauh, JHEP **12**, 068 (2017), [arXiv:1711.02100].

[40] P. Gambino and C. Schwanda, Phys. Rev. **D89**, 1, 014022 (2014), [arXiv:1307.4551].

[41] Y. Amhis *et al.* (HFLAV), Eur. Phys. J. **C77**, 12, 895 (2017), [arXiv:1612.07233].

[42] P. Gambino, M. Jung and S. Schacht, Phys. Lett. **B795**, 386 (2019), [arXiv:1905.08209].

[43] M. Neubert, Phys. Rev. **D49**, 3392 (1994), [hep-ph/9311325].

[44] I. I. Y. Bigi *et al.*, Int. J. Mod. Phys. **A9**, 2467 (1994), [hep-ph/9312359].

[45] G. P. Korchemsky and G. F. Sterman, Phys. Lett. **B340**, 96 (1994), [hep-ph/9407344].

[46] C. W. Bauer, M. E. Luke and T. Mannel, Phys. Rev. **D68**, 094001 (2003), [hep-ph/0102089].

[47] K. S. M. Lee and I. W. Stewart, Nucl. Phys. **B721**, 325 (2005), [hep-ph/0409045].

[48] S. W. Bosch, M. Neubert and G. Paz, JHEP **11**, 073 (2004), [hep-ph/0409115].

[49] M. Beneke *et al.*, JHEP **06**, 071 (2005), [hep-ph/0411395].

[50] M. Benzke *et al.*, JHEP **08**, 099 (2010), [arXiv:1003.5012].

[51] C. W. Bauer, S. Fleming and M. E. Luke, Phys. Rev. **D63**, 014006 (2000), [hep-ph/0005275].

[52] C. W. Bauer and I. W. Stewart, Phys. Lett. **B516**, 134 (2001), [hep-ph/0107001].

[53] C. W. Bauer, D. Pirjol and I. W. Stewart, Phys. Rev. **D65**, 054022 (2002), [hep-ph/0109045].

[54] T. Becher, A. Broggio and A. Ferroglia, Lect. Notes Phys. **896**, pp.1 (2015), [arXiv:1410.1892].

[55] J. Chay and C. Kim, Phys. Rev. **D65**, 114016 (2002), [hep-ph/0201197].

[56] M. Beneke *et al.*, Nucl. Phys. **B643**, 431 (2002), [hep-ph/0206152].

[57] C. W. Bauer *et al.*, Phys. Rev. **D66**, 014017 (2002), [hep-ph/0202088].

[58] R. J. Hill and M. Neubert, Nucl. Phys. **B657**, 229 (2003), [hep-ph/0211018].

[59] J. C. Collins, D. E. Soper and G. F. Sterman, Adv. Ser. Direct. High Energy Phys. **5**, 1 (1989), [hep-ph/0409313].

Downloaded from https://academic.oup.com/ptep/article/2022/8/083C01/6651666 by KIT Library user on 27 September 2022

[60] I. W. Stewart, F. J. Tackmann and W. J. Waalewijn, Phys. Rev. **D81**, 094035 (2010), [arXiv:0910.0467].

[61] J. C. Collins, D. E. Soper and G. F. Sterman, Nucl. Phys. **B261**, 104 (1985).

[62] I. Z. Rothstein and I. W. Stewart, JHEP **08**, 025 (2016), [arXiv:1601.04695].

[63] I. A. Korchemskaya and G. P. Korchemsky, Phys. Lett. **B287**, 169 (1992).

[64] T. Becher and M. Neubert, Eur. Phys. J. **C71**, 1665 (2011), [arXiv:1007.4005].

[65] J.-Y. Chiu *et al.*, JHEP **05**, 084 (2012), [arXiv:1202.0814].

[66] M. Beneke and T. Feldmann, Nucl. Phys. **B685**, 249 (2004), [hep-ph/0311335].

[67] M. Beneke *et al.*, Phys. Rev. Lett. **83**, 1914 (1999), [hep-ph/9905312].

[68] C. W. Bauer, D. Pirjol and I. W. Stewart, Phys. Rev. Lett. **87**, 201806 (2001), [hep-ph/0107002].

[69] S. Mantry, D. Pirjol and I. W. Stewart, Phys. Rev. **D68**, 114009 (2003), [hep-ph/0306254].

[70] T. Becher, R. J. Hill and M. Neubert, Phys. Rev. **D72**, 094017 (2005), [hep-ph/0503263].

[71] S. Fleming, A. K. Leibovich and T. Mehen, Phys. Rev. **D68**, 094011 (2003), [hep-ph/0306139].

[72] T. Becher and M. D. Schwartz, JHEP **07**, 034 (2008), [arXiv:0803.0342].

[73] T. Becher and G. Bell, JHEP **11**, 126 (2012), [arXiv:1210.0580].

[74] I. W. Stewart, F. J. Tackmann and W. J. Waalewijn, Phys. Rev. Lett. **105**, 092002 (2010), [arXiv:1004.2489].

[75] J.-y. Chiu, R. Kelley and A. V. Manohar, Phys. Rev. **D78**, 073006 (2008), [arXiv:0806.1240].

[76] T. Becher, M. Neubert and G. Xu, JHEP **07**, 030 (2008), [arXiv:0710.0680].

[77] V. Ahrens *et al.*, Eur. Phys. J. **C62**, 333 (2009), [arXiv:0809.4283].

[78] X. Liu, S. Mantry and F. Petriello, Phys. Rev. **D86**, 074004 (2012), [arXiv:1205.4465].

[79] M. G. Echevarria, A. Idilbi and I. Scimemi, JHEP **07**, 002 (2012), [arXiv:1111.4996].

[80] A. J. Larkoski, I. Moult and B. Nachman (2017), [arXiv:1709.04464].

[81] S. Kluth, Rept. Prog. Phys. **69**, 1771 (2006), [hep-ex/0603011].

[82] A. Gehrmann-De Ridder *et al.*, Phys. Rev. Lett. **99**, 132002 (2007), [arXiv:0707.1285].

[83] S. Weinzierl, Phys. Rev. Lett. **101**, 162001 (2008), [arXiv:0807.3241].

[84] R. Abbate *et al.*, Phys. Rev. **D83**, 074021 (2011), [arXiv:1006.3080].

[85] A. H. Hoang *et al.*, Phys. Rev. **D91**, 9, 094018 (2015), [arXiv:1501.04111].

[86] T. Becher and M. Neubert, JHEP **07**, 108 (2012), [arXiv:1205.3806].

[87] I. W. Stewart *et al.*, Phys. Rev. **D89**, 5, 054001 (2014), [arXiv:1307.1808].

[88] A. Banfi *et al.*, Phys. Rev. Lett. **109**, 202001 (2012), [arXiv:1206.4998].

[89] R. Boughezal, X. Liu and F. Petriello, Phys. Rev. **D91**, 9, 094035 (2015), [arXiv:1504.02540].

[90] J. Gaunt *et al.*, JHEP **09**, 058 (2015), [arXiv:1505.04794].

[91] R. Boughezal *et al.*, Phys. Lett. **B748**, 5 (2015), [arXiv:1505.03893].

[92] R. Boughezal *et al.*, Phys. Rev. Lett. **116**, 15, 152001 (2016), [arXiv:1512.01291].

[93] J. M. Campbell, R. K. Ellis and C. Williams, JHEP **06**, 179 (2016), [arXiv:1601.00658].

[94] J. M. Campbell *et al.*, JHEP **07**, 148 (2016), [arXiv:1603.02663].

[95] G. Heinrich *et al.*, JHEP **03**, 142 (2018), [arXiv:1710.06294].

[96] I. Moult *et al.*, Phys. Rev. **D95**, 7, 074023 (2017), [arXiv:1612.00450].

[97] R. Boughezal, X. Liu and F. Petriello, JHEP **03**, 160 (2017), [arXiv:1612.02911].

[98] S. Alioli *et al.*, JHEP **09**, 120 (2013), [arXiv:1211.7049].

[99] S. Alioli *et al.*, Phys. Rev. **D92**, 9, 094020 (2015), [arXiv:1508.01475].

[100] C. W. Bauer, D. Pirjol and I. W. Stewart, Phys. Rev. **D68**, 034021 (2003), [hep-ph/0303156].

[101] D. Pirjol and I. W. Stewart, Phys. Rev. **D67**, 094005 (2003), [Erratum: Phys. Rev.D69,019903(2004)], [hep-ph/0211251].

[102] R. J. Hill *et al.*, JHEP **07**, 081 (2004), [hep-ph/0404217].

[103] M. Beneke and D. Yang, Nucl. Phys. **B736**, 34 (2006), [hep-ph/0508250].

[104] I. Moult, I. W. Stewart and G. Vita, JHEP **07**, 067 (2017), [arXiv:1703.03408].

[105] I. Feige *et al.*, JHEP **11**, 142 (2017), [arXiv:1703.03411].

[106] M. Beneke *et al.*, JHEP **03**, 001 (2018), [arXiv:1712.04416].

[107] S. Alte, M. König and M. Neubert, JHEP **08**, 095 (2018), [arXiv:1806.01278].

[108] I. Moult *et al.*, JHEP **08**, 013 (2018), [arXiv:1804.04665].

[109] M. Beneke *et al.*, JHEP **03**, 043 (2019), [arXiv:1809.10631].

[110] M. Dasgupta and G. P. Salam, Phys. Lett. **B512**, 323 (2001), [hep-ph/0104277].

[111] R. B. Appleby and M. H. Seymour, JHEP **12**, 063 (2002), [hep-ph/0211426].

[112] S. Caron-Huot, JHEP **03**, 036 (2018), [arXiv:1501.03754].

[113] A. J. Larkoski, I. Moult and D. Neill, JHEP **09**, 143 (2015), [arXiv:1501.04596].

[114] T. Becher *et al.*, Phys. Rev. Lett. **116**, 19, 192001 (2016), [arXiv:1508.06645].

[115] T. Becher *et al.*, JHEP **11**, 019 (2016), [Erratum: JHEP05,154(2017)], [arXiv:1605.02737].

[116] T. Becher, B. D. Pecjak and D. Y. Shao, JHEP **12**, 018 (2016), [arXiv:1610.01608].

[117] M. Balsiger, T. Becher and D. Y. Shao, JHEP **04**, 020 (2019), [arXiv:1901.09038].

[118] C. W. Bauer, B. O. Lange and G. Ovanesyan, JHEP **07**, 077 (2011), [arXiv:1010.1027].

[119] S. Fleming, Phys. Lett. **B735**, 266 (2014), [arXiv:1404.5672].

[120] I. Moult *et al.*, JHEP **02**, 134 (2018), [arXiv:1709.09174].

[121] A. Idilbi and A. Majumder, Phys. Rev. **D80**, 054022 (2009), [arXiv:0808.1087].

[122] G. Ovanesyan and I. Vitev, JHEP **06**, 080 (2011), [arXiv:1103.1074].

[123] R. J. Hill and M. P. Solon, Phys. Lett. **B707**, 539 (2012), [arXiv:1111.0016].

[124] M. Bauer *et al.*, JHEP **01**, 099 (2015), [arXiv:1409.7392].

[125] M. Baumgart, I. Z. Rothstein and V. Vaidya, Phys. Rev. Lett. **114**, 211301 (2015), [arXiv:1409.4415].

[126] G. Ovanesyan, T. R. Slatyer and I. W. Stewart, Phys. Rev. Lett. **114**, 21, 211302 (2015), [arXiv:1409.8294].

Downloaded from https://academic.oup.com/ptep/article/2022/8/083C01/6651666 by KIT Library user on 27 September 2022

17. Lattice Quantum Chromodynamics

Revised August 2021 by S. Hashimoto (KEK) and S.R. Sharpe (U. Washington), written September 2011 with J. Laiho (Syracuse U.)

17.1 Lattice regularization of QCD . . . 337
17.1.1 Gauge invariance, gluon fields and the gluon action . . . 337
17.1.2 Lattice fermions . . . 338
17.1.3 Heavy quarks on the lattice . . . 339
17.1.4 QED on the lattice . . . 340
17.1.5 Basic inputs for lattice calculations . . . 340
17.1.6 Sources of systematic error . . . 341
17.2 Methods and status . . . 342
17.2.1 Monte-Carlo method . . . 342
17.2.2 Two-point functions . . . 342
17.2.3 Three-point functions . . . 343
17.2.4 Scattering amplitudes and resonances . . . 343
17.2.5 Recent advances . . . 344
17.2.6 Status of LQCD simulations . . . 344
17.3 Physics applications . . . 344
17.3.1 Spectrum . . . 344
17.3.2 Decay constants and bag parameters . . . 345
17.3.3 Form factors ($K \to \pi\ell\nu$, $D \to K\ell\nu$, $B \to \pi\ell\nu$, $B \to D^{(*)}\ell\nu$) . . . 345
17.3.4 Strong gauge coupling . . . 346
17.3.5 Quark masses . . . 346
17.3.6 Other applications . . . 346
17.4 Outlook . . . 347
17.5 Acknowledgments . . . 347

Many physical processes considered in the Review of Particle Properties (RPP) involve hadrons. The properties of hadrons—which are composed of quarks and gluons—are governed primarily by Quantum Chromodynamics (QCD) (with small corrections from Quantum Electrodynamics [QED]). Theoretical calculations of these properties require non-perturbative methods, and Lattice Quantum Chromodynamics (LQCD) is a tool to carry out such calculations. It has been successfully applied to many properties of hadrons. Most important for the RPP are the calculation of electroweak decay constants and form factors, which are needed to extract Cabbibo-Kobayashi-Maskawa (CKM) matrix elements when combined with the corresponding experimental measurements. LQCD has also been used to determine other fundamental parameters of the standard model, in particular the strong gauge coupling and quark masses, as well as to predict hadronic contributions to the anomalous magnetic moment of the muon, $g_\mu - 2$.

This review describes the theoretical foundations of LQCD and sketches the methods used to calculate the quantities relevant for the RPP. It also describes the various sources of error that must be controlled in a LQCD calculation. Results for hadronic quantities are given in the corresponding dedicated reviews.

17.1 Lattice regularization of QCD

Gauge theories form the building blocks of the Standard Model. While the SU(2) and U(1) parts have weak couplings and can be studied accurately with perturbative methods, the SU(3) component—QCD—is only amenable to a perturbative treatment at high energies. The growth of the gauge coupling in the infrared—the flip-side of asymptotic freedom—requires the use of non-perturbative methods to determine the low energy properties of QCD. Lattice gauge theory, proposed by K. Wilson in 1974 [1], provides such a method, for it gives a non-perturbative definition of vector-like gauge field theories such as QCD. In lattice regularized QCD—commonly called lattice QCD or LQCD—Euclidean space-time is discretized, usually on a hypercubic lattice with lattice spacing a, with quark fields placed on sites and gauge fields on the links between sites. The lattice spacing plays the role of the ultraviolet regulator, rendering the quantum field theory finite. The continuum theory is recovered by taking the limit of vanishing lattice spacing, which can be reached by tuning the bare gauge coupling to zero according to the renormalization group.

Unlike dimensional regularization, which is commonly used in continuum QCD calculations, the definition of LQCD does not rely on the perturbative expansion. Indeed, LQCD allows non-perturbative calculations by numerical evaluation of the path integral that defines the theory.

Practical LQCD calculations are limited by the availability of computational resources and the efficiency of algorithms. Because of this, LQCD results come with both statistical and systematic errors, the former arising from the use of Monte-Carlo integration, the latter, for example, from the use of non-zero values of a. There are also different ways in which the QCD action can be discretized, and all must give consistent results in the continuum limit, $a \to 0$. It is the purpose of this review to provide an outline of the methods of LQCD, with particular focus on applications to particle physics, and an overview of the various sources of error. This should allow the reader to better understand the LQCD results that are presented in other reviews, primarily those on "Quark Masses," "Quark Model," "Quantum Chromodynamics," "CKM quark-mixing matrix," "V_{ud}, V_{us}, Cabibbo angle and CKM Unitarity," "Leptonic Decays of Charged Pseudoscalar Mesons," "B^0-$\bar{B}^0$ Mixing," and "Semileptonic b-Hadron Decays, Determination of V_{cb} and V_{ub}." For more extensive explanations the reader should consult the available textbooks or lecture notes, the most up-to-date of which are Refs. [2–4].

17.1.1 *Gauge invariance, gluon fields and the gluon action*

A key feature of the lattice formulation of QCD is that it preserves gauge invariance. This is in contrast to perturbative calculations, where gauge fixing is an essential step. The preservation of gauge invariance leads to considerable simplifications, e.g., restricting the form of operators that can mix under renormalization.

The gauge transformations of lattice quark fields are just as in the continuum: $q(x) \longrightarrow V(x)q(x)$ and $\bar{q}(x) \longrightarrow \bar{q}(x)V^\dagger(x)$, with $V(x)$ an arbitrary element of SU(3). The only difference is that the Euclidean space-time positions x are restricted to lie on the sites of the lattice, i.e. $x = a(n_1, n_2, n_3, n_4)$ for a hypercubic lattice, with the n_j being integers. Quark bilinears involving different lattice points can be made gauge invariant by introducing the gluon field $U_\mu(x)$. For example, for adjacent points the bilinear is $\bar{q}(x)U_\mu(x)q(x+a\hat{\mu})$, with $\hat{\mu}$ the unit vector in the μ'th direction. (This form is used in the construction of the lattice covariant derivative.) This is illustrated in Fig. 17.1. The gluon field (or "gauge link") is an element of the group, SU(3), in contrast to the continuum field A_μ which takes values in the Lie algebra. The bilinear is invariant if U_μ transforms as $U_\mu(x) \to V(x)U_\mu(x)V^\dagger(x+a\hat{\mu})$. The lattice gluon field is naturally associated with the link joining x and $x+a\hat{\mu}$, and corresponds in the continuum to a Wilson line connecting these two points, $\mathrm{P}\exp(i\int_x^{x+a\hat{\mu}} dx_\mu A_\mu^{\mathrm{cont}}(x))$ (where P indicates a path-ordered integral, and the superscript on A_μ indicates that it is a continuum field). The trace of a product of the $U_\mu(x)$ around any closed loop is easily seen to be gauge invariant and is the lattice version of a Wilson loop.

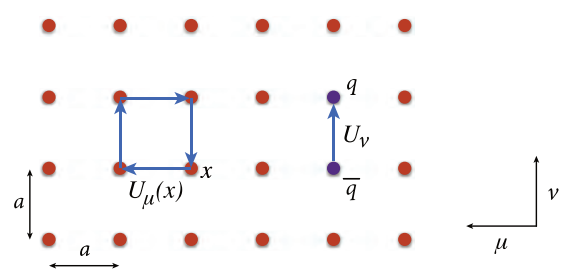

Figure 17.1: Sketch of a two-dimensional slice through the $\mu-\nu$ plane of a lattice, showing gluon fields lying on links and forming either the plaquette product appearing in the gauge action or a component of the covariant derivative connecting quark and antiquark fields.

The simplest possible gauge action, usually called the Wilson gauge action, is given by the product of gauge links around elementary plaquettes:

Downloaded from https://academic.oup.com/ptep/article/2022/8/083C01/6651666 by KIT Library user on 27 September 2022

$$S_g = \beta \sum_{x,\mu,\nu} [1 - \frac{1}{3}\mathrm{ReTr}[U_\mu(x)U_\nu(x+a\hat{\mu})U_\mu^\dagger(x+a\hat{\nu})U_\nu^\dagger(x)]] \,. \quad (17.1)$$

This is illustrated in Fig. 17.1. For small a, assuming that the fields are slowly varying, one can expand the action in powers of a using $U_\mu(x) = \exp(iaA_\mu(x))$. Keeping only the leading non-vanishing term, and replacing the sum with an integral, one finds the continuum form,

$$S_g \longrightarrow \int d^4x \frac{1}{4g_{\mathrm{lat}}^2} \mathrm{Tr}[F_{\mu\nu}^2(x)] \,, \quad (17.2)$$
$$(F_{\mu\nu} = \partial_\mu A_\nu - \partial_\nu A_\mu + i[A_\mu, A_\nu])$$

as long as one chooses $\beta = 6/g_{\mathrm{lat}}^2$ for the lattice coupling. In this expression, g_{lat} is the bare gauge coupling in the lattice scheme, which can be related (by combining continuum and lattice perturbation theory) to a more conventional gauge coupling such as that in the $\overline{\mathrm{MS}}$ scheme (see Sec. 17.3.4 below).

In practice, the lattice spacing a is non-zero, leading to discretization errors. In particular, the lattice breaks Euclidean rotational invariance (which is the Euclidean version of Lorentz invariance) down to a discrete hypercubic subgroup. One wants to reduce discretization errors as much as possible. A very useful tool for understanding and then reducing discretization errors is the Symanzik effective action: the interactions of quarks and gluons with momenta low compared to the lattice cutoff ($|p| \ll 1/a$) are described by a continuum action consisting of the standard continuum terms (e.g., the gauge action given in Eq. (17.2)) augmented by higher dimensional operators suppressed by powers of a [5]. For the Wilson lattice gauge action, the leading corrections come in at $\mathcal{O}(a^2)$. They take the form $\sum_j a^2 c_j O_6^{(j)}$, with the sum running over all dimension-six operators $O_6^{(j)}$ allowed by the *lattice* symmetries, and c_j unknown coefficients. Some of these operators violate Euclidean rotational invariance, and all of them lead to discretization errors of the form $a^2\Lambda^2$ (up to $\log(a)$ corrections that will be discussed below), where Λ is a typical momentum scale for the quantity being calculated. These errors can, however, be reduced by adding corresponding operators to the lattice action and tuning their coefficients to eliminate the dimension-six operators in the effective action to a given order in perturbation theory or even non-perturbatively. This is the idea of the Symanzik improvement program [5]. In the case of the gauge action, one adds Wilson loops involving six gauge links (as opposed to the four links needed for the original plaquette action, Eq. (17.1)) to define the $\mathcal{O}(a^2)$ improved (or "Symanzik") action [6]. In practical implementations, the improvement is either at tree-level (so that residual errors are proportional to $\alpha_s a^2$, where the coupling is evaluated at a scale $\sim 1/a$), or at one loop order (errors proportional to $\alpha_s^2 a^2$). Another popular choice is motivated by studies of renormalization group (RG) flow. It has the same terms as the $\mathcal{O}(a^2)$ improved action but with different coefficients, and is called the RG-improved or "Iwasaki" action [7].

17.1.2 *Lattice fermions*

Discretizing the fermion action turns out to involve subtle issues, and the range of actions being used is more extensive than for gauge fields. Recall that the continuum fermion action is $S_f = \int d^4x \bar{q}[iD_\mu\gamma_\mu + m_q]q$, where $D_\mu = \partial_\mu + iA_\mu$ is the gauge-covariant derivative. The simplest discretization replaces the derivative with a symmetric difference:

$$D_\mu q(x) \longrightarrow \frac{1}{2a}[U_\mu(x)q(x+a\hat{\mu}) - U_\mu(x-a\hat{\mu})^\dagger q(x-a\hat{\mu})] \,. \quad (17.3)$$

The factors of U_μ ensure that $D_\mu q(x)$ transforms under gauge transformations in the same way as $q(x)$, so that the discretized version of $\bar{q}(x)D_\mu\gamma_\mu q(x)$ is gauge invariant. The choice in Eq. (17.3) leads to the so-called naive fermion action. This, however, suffers from the fermion doubling problem—in d dimensions it describes 2^d equivalent fermion fields in the continuum limit. The appearance of the extra "doubler" fermions is related to the deeper theoretical problem of formulating chirally symmetric fermions on the lattice. This is encapsulated by the Nielsen-Ninomiya theorem [8]: one cannot define lattice fermions having exact, continuum-like chiral symmetry without producing doublers. Naive lattice fermions do have chiral symmetry but at the cost of introducing 15 unwanted doublers (for $d = 4$).

There are a number of different strategies for dealing with the doubling problem, each with their own theoretical and computational advantages and disadvantages. Wilson fermions [1] add a term proportional to $a\bar{q}\Delta q$ to the fermion action (the "Wilson term"—in which Δ is a covariant lattice Laplacian). This gives a mass of $\mathcal{O}(1/a)$ to the doublers, so that they decouple in the continuum limit. The Wilson term, however, violates chiral symmetry, and also introduces discretization errors linear in a. A commonly used variant that eliminates the $\mathcal{O}(a)$ discretization error is the $\mathcal{O}(a)$-improved Wilson (or "clover") action [9]. In this application of Symanzik improvement, methods have been developed to remove $\mathcal{O}(a)$ terms non-perturbatively using auxiliary simulations to tune parameters [10]. Such "non-perturbetive improvement" is of great practical importance as it brings the discretization error from the fermion action down to the same level as that from the gauge action.

The advantages of Wilson fermions are their theoretical simplicity and relatively low computational cost. Their main disadvantage is the lack of chiral symmetry, which makes them difficult to use in cases where mixing with wrong chirality operators can occur, particularly if this involves divergences proportional to powers of $1/a$. A related problem is the presence of potential numerical instabilities due to spurious near-zero modes of the lattice Dirac operator. There are, however, studies that successfully ameliorate these problems and increase the range of quantities for which Wilson fermions can be used (see, e.g., Refs. [11–14]).

Twisted-mass fermions [15] are a variant of Wilson fermions in which two flavors are treated together with an isospin-breaking mass term (the "twisted mass" term). The main advantage of this approach is that all errors linear in a are automatically removed (without the need for tuning of parameters) by a clever choice of twisted mass and operators [16]. A disadvantage is the presence of isospin breaking effects (such as a splitting between charged and neutral pion masses even when up and down quarks are degenerate), which, however, vanish as $a^2\Lambda^2$ in the continuum limit. Strange and charm quarks can be added as a second pair, with a term added to split their masses [17, 18].

Staggered fermions are a reduced version of naive fermions in which there is only a single fermion Dirac component on each lattice site, with the full Dirac structure built up from neighboring sites [19]. They have the advantages of being somewhat faster to simulate than Wilson-like fermions, of preserving some chiral symmetry, and of having discretization errors of $\mathcal{O}(a^2)$. Their disadvantage is that they retain some of the doublers (3 for $d = 4$). The action thus describes four degenerate fermions in the continuum limit. These are usually called "tastes", to distinguish them from physical flavors, and the corresponding SU(4) symmetry is referred to as the "taste symmetry". The preserved chiral symmetry in this formulation has non-singlet taste. Practical applications usually introduce one staggered fermion for each physical flavor, and remove contributions from the unwanted tastes by taking the fourth-root of the fermion determinant appearing in the path integral. The validity of this "rooting" procedure is not obvious because taste symmetry is violated for non-zero lattice spacing. Theoretical arguments, supported by numerical evidence, suggest that the procedure is valid as long as one takes the continuum limit before approaching the light quark mass region [20]. Additional issues arise for the valence quarks (those appearing in quark propagators, as described in Sec. 17.2 below), where rooting is not possible, and one must ignore the extra tastes, or account for them by including appropriate factors [21], which can be nontrivial in applications involving baryons [22].

Just as for Wilson fermions, the staggered action can be improved, so as to reduce discretization errors. The Asqtad (a-squared tadpole improved) action [23] was used until recently in many large scale simulations [24]. More recent calculations use the HISQ (highly improved staggered quark) action, introduced in

Downloaded from https://academic.oup.com/ptep/article/2022/8/083C01/6651666 by KIT Library user on 27 September 2022

Ref. [25]. At tree-level it removes both $\mathcal{O}(a^2)$ errors and, to lowest order in the quark speed v/c, $\mathcal{O}([am]^4)$ errors. It also substantially reduces effects caused by taste-symmetry breaking. This makes it attractive not only for light quarks, but means that it is also quite accurate for heavy quarks because it suppresses $(am)^n$ errors. It is being used to directly simulate charm quarks and to approach direct simulations of bottom quarks (see, e.g., [26–28]).

There is an important class of lattice fermions, "Ginsparg-Wilson fermions," that possess a continuum-like chiral symmetry without introducing unwanted doublers. The lattice Dirac operator D for these fermions satisfies the Ginsparg-Wilson relation $D\gamma_5 + \gamma_5 D = aD\gamma_5 D$ [29]. In the continuum, the right-hand-side vanishes, leading to chiral symmetry. On the lattice, it is non-vanishing, but with a particular form (with two factors of D) that restricts the violations of chiral symmetry in Ward-Takahashi identities to short-distance terms that do not contribute to physical matrix elements [30]. In fact, one can define a modified chiral transformation on the lattice (by including dependence on the gauge fields) such that Ginsparg-Wilson fermions have an exact chiral symmetry for on-shell quantities [31]. The net result is that such fermions essentially have the same properties under chiral transformations as do continuum fermions, including the index theorem [30]. Their leading discretization errors are of $\mathcal{O}(a^2)$.

Two types of Ginsparg-Wilson fermions are currently being used in large-scale numerical simulations. The first is Domain-wall fermions (DWF). These are defined on a five-dimensional space, in which the fifth dimension is fictitious [32]. The action is chosen so that the low-lying modes are chiral, with left- and right-handed modes localized on opposite four-dimensional surfaces. For an infinite fifth dimension, these fermions satisfy the Ginsparg-Wilson relation. In practice, the fifth dimension is kept finite, and there remains a small, controllable violation of chiral symmetry. The second type is Overlap fermions. These appeared from a completely different context and have an explicit form that exactly satisfies the Ginsparg-Wilson relation [33]. Their numerical implementation requires an approximation of the matrix sign function of a Wilson-like fermion operator, and various approaches are being used. In fact, it is possible to rewrite these approximations in terms of a five-dimensional formulation, showing that the DWF and Overlap approaches are essentially equivalent [34, 35]. Numerically, the five-dimensional approach appears to be more computationally efficient.

The various lattice fermion formulations are often combined with the technique of link smearing. Here one couples the fermions to a smoother gauge link, defined by averaging with adjacent links in a gauge invariant manner. Several closely related implementations are being used. All reduce the coupling of fermions to the short-distance fluctuations in the gauge field, leading to an improvement in the numerical stability and speed of algorithms. One cannot perform this smearing too aggressively, however, since the smearing may distort short distance physics and enhance discretization errors.

As noted above, each fermion formulation has its own advantages and disadvantages. For instance, domain-wall and overlap fermions are theoretically preferred as they have chiral symmetry without doublers, but their computational cost is greater than for other choices. If the physics application of interest and the target precision do not require near-exact chiral symmetry, there is no strong motivation to use these expensive formulations. On the other hand, there is a class of applications (including the calculation of the $\Delta I = 1/2$ amplitude for $K \to \pi\pi$ decays and the S-parameter [36]) where chiral symmetry plays an essential role and for which the use of Ginsparg-Wilson fermions is strongly favored.

17.1.3 *Heavy quarks on the lattice*

The fermion formulations described in the previous subsection can be used straightforwardly only for quarks whose masses are small compared to the lattice cutoff, $m_q \lessapprox 1/a$. This is because there are discretization errors proportional to powers of am_q, and if $am_q \gtrapprox 1$ these errors are large and uncontrolled. Present LQCD simulations typically have cutoffs in the range of $1/a = 2-4$ GeV (corresponding to $a \approx 0.1 - 0.05$ fm). Thus, while for the up, down and strange quarks one has $am_q \ll 1$, for bottom quarks (with $m_b \approx 4.5$ GeV) one must use alternative approaches. Charm quarks ($m_c \approx 1.5$ GeV) are an intermediate case, allowing simulations using both direct and alternative approaches.

For the charm quark, the straightforward approach is to simultaneously reduce the lattice spacing and to improve the fermion action so as to reduce the size of errors proportional to powers of am_c. This approach has been followed successfully using the HISQ, twisted-mass and domain-wall actions [25, 26, 28, 37, 38]. It is important to note, however, that reducing a increases the computational cost because an increased number of lattice points are needed for the same physical volume. One cannot reduce the spatial size below 2–3 fm without introducing finite volume errors. Present lattices have typical sizes of $\sim 64^3 \times 128$ (with the long direction being Euclidean time), and thus allow a lattice cutoff up to $1/a \sim 4$ GeV.

This approach can, to some extent, be extended to the bottom quark, by the use of simulations with small lattice spacings [27]. This has been pursued with the HISQ action [39], using lattices of size up to $144^3 \times 288$ and lattice spacings down to $a \approx 0.03$ fm ($1/a \approx 6.6$ GeV). Extrapolation in m_b is still needed [40], however, and this makes use of the mass dependence predicted by Heavy Quark Effective Theory (HQET).

Alternative approaches for discretizing heavy quarks are motivated by effective field theories. For a bottom quark in heavy-light hadrons, one can use HQET to expand about the infinite quark-mass limit. In this limit, the bottom quark is a static color source, and one can straightforwardly write the corresponding lattice action [41]. Corrections, proportional to powers of $1/m_b$, can be introduced as operator insertions, with coefficients that can be determined non-perturbatively using existing techniques [42]. This method allows the continuum limit to be taken controlling all $1/m_b$ corrections.

Another way of introducing the $1/m_b$ corrections is to include the relevant terms in the effective action. This leads to a non-relativistic QCD (NRQCD) action, in which the heavy quark is described by a two-component spinor [43]. This approach has the advantage over HQET that it can also be used for heavy-heavy systems, such as the Upsilon states. Moreover, the bottom quark can be treated without any extrapolation in m_b. A disadvantage is that some of the parameters in this effective theory are determined perturbatively (at tree-level or at one-loop [44]), which limits the precision of the final results. Although discretization effects can be controlled with good numerical precision for a range of lattice spacings, these artifacts cannot be extrapolated away by taking the lattice spacing to zero. This is because NRQCD is a nonrelativistic effective field theory and so ceases to work when the cutoff π/a becomes much larger than the heavy-quark mass. In practice these effects are accounted for in the error budget.

This problem can be avoided if one uses HQET power counting to analyze and reduce discretization effects for heavy quarks while using conventional fermion actions [45]. For instance, one can tune the parameters of an improved Wilson quark action so that the leading HQET corrections to the static quark limit are correctly accounted for. As the lattice spacing becomes finer, the action smoothly goes over to that of a light Wilson quark action, where the continuum limit can be taken as usual. In principle, one can improve the action in the heavy quark regime up to arbitrarily high orders using HQET, but so far large-scale simulations have typically used clover improved Wilson quarks, where tuning the parameters of the action corresponds to including all corrections through next-to-leading order in HQET. Three different methods for tuning the parameters of the clover action are being used: the Fermilab [45], Tsukuba [46] and Columbia [47] approaches. An advantage of this HQET approach is that the c and b quarks can be treated on the same footing. Parameter tuning has been done perturbatively, as in NRQCD, or using non-perturbative tuning of some of the parameters [48, 49]. One can improve the effective theory including the terms beyond the next-to-leading order. The Oktay-Kronfeld action that includes dimension-six and -seven operators has been constructed [50] and used in large-scale numerical calculations [51].

Another approach is the "ratio method" introduced in Ref. [52]. Here one uses quarks with masses lying at, or slightly above, the

Downloaded from https://academic.oup.com/ptep/article/2022/8/083C01/6651666 by KIT Library user on 27 September 2022

charm mass m_c, which can be simulated with a relativistic action, and extrapolates to m_b incorporating the behavior predicted by HQET. The particular implementation relies on the use of ratios. As an example, consider the B meson decay constant f_B. According to HQET, this scales as $1/\sqrt{m_B}$ for $m_B \gg \Lambda_{\rm QCD}$, up to a logarithmic dependence that is calculable in perturbative QCD (but will be suppressed in the following). Here m_B is the B meson mass, which differs from m_b by $\sim \Lambda_{\rm QCD}$. One considers the ratio $y(\lambda, m_{b'}) \equiv f_{B''}\sqrt{m_{B''}}/f_{B'}\sqrt{m_{B'}}$ for fictitious B mesons containing b quarks with unphysical masses $m_{b'}$ and $m_{b''} = \lambda m_{b'}$. HQET implies that $y(\lambda, m_{b'})$ approaches unity for large $m_{b'}$ and any fixed $\lambda > 1$. The ratios are evaluated on the lattice for the sequence of masses $m_{b'} = m_c$, λm_c, $\lambda^2 m_c$, all well below the physical m_b, and for each the continuum limit is taken. The form of the ratio for larger values of $m_{b'}$ is obtained by fitting, incorporating the constraints implied by HQET. The result for $f_B\sqrt{m_B}$ is then obtained as a product of y's with $f_D\sqrt{m_D}$.

17.1.4 *QED on the lattice*

Quarks in nature are electrically charged, and the resultant coupling to photons leads to shifts in the properties of hadrons that are generically of $\mathcal{O}(\alpha_{\rm EM})$. Thus, for example, the proton mass is increased by ~ 1 MeV relative to that of the neutron due to its overall charge although this effect is more than compensated for by the ~ 2.5 MeV relative decrease due to the up quark being lighter than the down quark [53]. This example shows that once pure QCD, isospin-symmetric lattice calculations reach percent level accuracy, further improvement requires the inclusion of effects due to both electromagnetism and the up-down mass difference. This level of accuracy has in fact been obtained for various quantities, e.g., light hadron masses and decay constants (see Ref. [54]), and simulations including QED in addition to QCD are becoming more common.

The extension of lattice methods to include QED is straightforward, although some new subtleties arise. The essential change is that the quark must now propagate through a background field containing both gluons and photons. The gauge field U_μ that appears in the covariant derivative of Eq. (17.3) is extended from an SU(3) matrix to one living in U(3): $U_\mu \to U_\mu e^{iaqeA_\mu^{\rm EM}}$. Here $A_\mu^{\rm EM}$ is the photon field, e the electromagnetic coupling, and q the charge of the quark, e.g., $q = 2/3$ for up and $-1/3$ for down and strange quarks. The lattice action for the photon that is typically used is a discretized version of the continuum action Eq. (17.2), rather than the form used for the gluons, Eq. (17.1). This "non-compact" action has the advantage that it is quadratic in $A_\mu^{\rm EM}$, which simplifies the QED part of the generation of configurations.

One subtlety that arises is that Gauss' law forbids a charged particle in a box with periodic boundary conditions. This finite volume effect can be overcome by including a uniform background charge, and this can be shown to be equivalent to removing the zero-momentum mode from the photon field. This is an example of the enhanced finite-volume effects that arise in the presence of the massless photon.

Simulations including QED have progressed over the last few years, and now a full inclusion of QED has been achieved for a range of quark masses approaching the physical values [53,55–57]. Alternative approaches have also been used: reweighting the QCD fields *a posteriori* [58, 59], and keeping only the linear term in an expansion in $\alpha_{\rm EM}$ about the QCD only case [60]. In addition, some calculations have included QED effects for the valence quarks but not the sea quarks (the "electroquenched approximation") [61–65].

The QED corrections to processes including leptons, such as the leptonic and semileptonic decays of hadrons, involve additional diagrams in which a photon propagator bridges between a hadron and a lepton. Such diagrams induce infrared divergences that cancel against soft photon radiation (Bloch-Nordsieck theorem [66]). Methods have been developed to implement this cancellation in lattice calculations, treating the soft photon analytically [67], with first results reported recently for leptonic pion and kaon decays [68, 69]. An application to semi-leptonic decays has also been discussed [70, 71].

17.1.5 *Basic inputs for lattice calculations*

Since LQCD is nothing but a regularization of QCD, the renormalizability of QCD implies that the number of input parameters in LQCD is the same as for continuum QCD—the strong gauge coupling $\alpha_s = g^2/(4\pi)$, the quark masses for each flavor, and the CP violating phase θ. The θ parameter is usually assumed to be zero, while the other parameters must be determined using experimental inputs.

17.1.5.1 *Lattice spacing*

In QCD, the gauge coupling is a function of scale. With lattice regularization, this scale is the inverse lattice spacing $1/a$, and choosing the bare gauge coupling is equivalent to fixing the lattice spacing.

In principle, a can be determined using any dimensionful quantity measured by experiments. For example, using the mass of hadron H one has $a = (am_H)^{\rm lat}/m_H^{\rm exp}$. One chooses quantities that can be calculated accurately on the lattice, and that are only weakly dependent on the light quark masses. The latter property minimizes errors from extrapolating or interpolating to the physical light quark masses or from mistuning of these masses.

Commonly used choices are the spin-averaged 1S-1P or 1S-2S splittings in the Upsilon system, the mass of the Ω^- baryon, and the pion decay constant f_π. Ultimately, all choices must give consistent results for a, and that this is the case provides a highly non-trivial check of both the calculational method and of QCD.

Many recent lattice calculations use intermediate length scales in place of a direct determination of the lattice spacing. These length scales, which we denote $\mathcal{R}$, have the advantage that they can be precisely, and relatively cheaply, computed numerically. Examples are r_0, derived from the heavy quark potential [72], and t_0 and w_0, determined from the gradient flow of the gauge field [73]. These scales are used in the following manner, explained here in the context of calculating a quantity Q with mass dimension d (e.g. a decay constant for which $d = 1$). In the first step, one calculates the dimensionless quantities a^dQ and $\mathcal{R}/a$ in a given lattice calculation, and forms the product $(a^dQ)\times(\mathcal{R}/a)^d = Q\mathcal{R}^d$. In a second step, one uses results available from previous dedicated lattice calculations that have determined $\mathcal{R}$ in physical units (i.e. fm) by relating them to physical quantities as discussed above. Then one obtains $Q = (Q\mathcal{R}^d)/\mathcal{R}^d$. The results of this second step are reviewed in the latest edition of the Flavor Lattice Averaging Group (FLAG) report [74].

17.1.5.2 *Light quark masses*

In LQCD simulations, the up, down and strange quarks are usually referred to as the light quarks, in the sense that $m_q < \Lambda_{\rm QCD}$. (The standard definition of $\Lambda_{\rm QCD}$ is given in the "Quantum Chromodynamics" review; in this review we are using it only to indicate the approximate non-perturbative scale of QCD.) This condition is stronger than that used above to distinguish quarks with small discretization errors, $m_q < 1/a$. Loop effects from light quarks must be included in the simulations to accurately represent QCD. At present, most simulations are done in the isospin symmetric limit $m_u = m_d \equiv m_\ell < m_s$, and are often referred to as "$N_f = 2 + 1$" simulations. Increasingly, simulations also include loops of charm quarks (denoted $N_f = 2 + 1 + 1$ simulations), although the effect of charmed sea quarks on low-energy physics is generically expected to be at the sub-percent level [75–79]. Precision is now reaching the point where isospin breaking effects must be included. To do so without approximation requires simulating with nondegenerate up and down quarks (leading to $N_f = 1+1+1$ or $1+1+1+1$ simulations) as well as including electromagnetism (as described above). This has been done in Ref. [53]. Alternatively, one can use the perturbative approach mentioned above, expanding about the isospin symmetric theory and working to linear order in $\alpha_{\rm EM}$ and $m_u - m_d$ [60, 80].

We now describe the tuning of m_ℓ, m_s and m_c to their physical values. (For brevity, we ignore isospin violation in the following discussion.) The most commonly used quantities for these tunings are, respectively, m_π, m_K and m_{η_c}. If the scale is being set by m_Ω, then one adjusts the lattice quark masses until the ratios m_π/m_Ω, m_K/m_Ω and m_{η_c}/m_Ω take their physical values. In the past, most calculations needed to extrapolate to the physical value

Downloaded from https://academic.oup.com/ptep/article/2022/8/083C01/6651666 by KIT Library user on 27 September 2022

of m_ℓ (typically using forms based on chiral perturbation theory [ChPT]), while simulating directly at or near to the physical values of m_s and m_c. Present calculations are increasingly done with physical or near physical values of m_ℓ, requiring at most only a short extrapolation or interpolation.

17.1.5.3 *Heavy quark masses*

The b quark is usually treated only as a valence quark, with no loop effects included. The errors introduced by this approximation can be estimated to be $\sim \alpha_s(m_b)\Lambda^2_{\rm QCD}/m_b^2$ and are likely to be very small. In the past, the same approximation has been made for the c quark, leading to errors $\sim \alpha_s(m_c)\Lambda^2_{\rm QCD}/m_c^2$. (See Ref. [75] for a quantitative estimate of the effects of including the charm quark on some low energy physical quantities, and Ref. [81] for similar estimates for B-meson matrix elements.) For high precision, however, dynamical charm quarks are necessary, and some of the most recent simulations now include them.

The b quark mass can be tuned by setting heavy-heavy (Υ) or heavy-light (B) meson masses to their experimental values. Consistency between these two determinations provides an important check that the determination of parameters in the heavy quark lattice formulations is being done correctly (see, e.g., Ref. [27,82,83])

17.1.6 *Sources of systematic error*

Lattice results have statistical and systematic errors that must be quantified for any calculation in order for the result to be a useful input to phenomenology. The statistical error is due to the use of Monte Carlo importance sampling to evaluate the path integral (a method discussed below). There are, in addition, a number of systematic errors that are always present to some degree in lattice calculations, although the size of any given error depends on the particular quantity under consideration and the parameters of the ensembles being used. The most common lattice errors are reviewed below.

Although not strictly a systematic error, it is important to note that the presence of long autocorrelations in the sequence of lattice configurations generated by the Monte Carlo method can lead to underestimates of statistical errors [84]. It is known that the global topological charge of the gauge fields decorrelates very slowly with certain algorithms [84, 85]. The effect of poorly sampling topological charge is expected to be most significant for the pion mass and related quantities [86–88]. This issue becomes more relevant as the precision of the final results increases.

17.1.6.1 *Continuum limit*

Physical results are obtained in the limit that the lattice spacing a goes to zero. The Symanzik effective theory (SET) determines the scaling of lattice artefacts with a. Most lattice calculations use improved actions with leading discretizations errors of $\mathcal{O}(\alpha_s a\Lambda)$, $\mathcal{O}(a^2\Lambda^2)$, or $\mathcal{O}(\alpha_s a^2\Lambda^2)$, where Λ is a typical momentum scale in the system. Knowledge of the scaling of the leading discretization errors allows controlled extrapolation to $a = 0$ when multiple lattice spacings are available, as in current state-of-the-art calculations. Residual errors arise from the exclusion of subleading a dependence from the fits, either that due to prefactors containing powers of $\log(a)$, or from higher powers of a. The former can, in principle, be understood using the SET, and first studies of this in pure gauge QCD have been undertaken [89].

For many quantities the typical momentum scale in the system is $\sim \Lambda_{\rm QCD} \approx 300$ MeV. Discretization errors are expected to be larger for quantities involving larger scales, for example form factors or decays involving particles with momenta larger than $\Lambda_{\rm QCD}$.

17.1.6.2 *Infinite volume limit*

LQCD calculations are necessarily carried out in finite space-time boxes, leading to departures of physical quantities (masses, decay constants, etc.) from their measured, infinite volume values. These finite-volume shifts are an important systematic that must be estimated and minimized.

Typical lattices are asymmetric, with N_s points in the three spatial directions and N_t in the (Euclidean) temporal direction. The spatial and temporal sizes in physical units are thus $L_s = aN_s$ and $L_t = aN_t$, respectively. (Anisotropic lattice spacings are also sometimes used, as discussed below in Sec. 17.2.2.) Typically, $L_t \geq 2L_s$, a longer temporal direction being used to allow excited-state contributions to correlators to decay. This means that the dominant impact of using finite volume is from the presence of a finite spatial box.

High-precision LQCD calculations are of quantities involving no more than a single strongly-interacting particle in initial and final states (with the exception of the $K \to \pi\pi$ decay amplitudes). For such quantities, once the volume exceeds about 2 fm (so that the particle is not "squeezed"), the dominant finite-volume effect comes from virtual pions wrapping around the lattice in the spatial directions. This effect is exponentially suppressed as the volume becomes large, roughly as $\sim \exp(-m_\pi L_s)$, and has been estimated using ChPT [90] or other methods [91]. The estimates suggest that finite volume shifts are sub-percent effects when $m_\pi L_s \gtrsim 4$, and most large-scale simulations use lattices satisfying this condition. This becomes challenging as one approaches the physical pion mass, for which $L_s \gtrsim 5$ fm is required.

Finite volume errors are usually determined by repeating the simulations on two or more different volumes (with other parameters fixed). If different volumes are not available, the ChPT estimate can be used, often inflated to account for the fact that the ChPT calculation is truncated at some order.

In the future, LQCD calculations involving more than a single hadron will become increasingly precise. Examples include the calculation of resonance parameters and the above-mentioned $K \to \pi\pi$ amplitudes. Finite volume effects are much larger in these cases, with power-law terms (e.g., $1/L_s^3$) in addition to exponential dependence. Indeed, as will be discussed in Sec. 17.2.4, one can use the volume dependence to indirectly extract infinite-volume quantities such as scattering lengths. Doing so, however, requires a set of lattice volumes satisfying $m_\pi L_s \gtrsim 4$ and is thus more challenging than for single-particle quantities.

17.1.6.3 *Chiral extrapolation*

Until recently, an important source of systematic error in LQCD calculations was the need to extrapolate in m_u and m_d (or, equivalently, in m_π). This extrapolation was usually done using functional forms based on ChPT, or with analytic functions, with the difference between different fits used as an estimate of the systematic error, which was often substantial. Increasingly, however, calculations work directly at, or very close to, the physical quark masses. This either removes entirely, or greatly reduces, the uncertainties in the extrapolation, such that this error is subdominant.

17.1.6.4 *Operator matching*

Many of the quantities that LQCD can precisely calculate involve hadronic matrix elements of operators from the electroweak Hamiltonian. Examples include the pion and kaon decay constants, semileptonic form factors and the kaon mixing parameter B_K (the latter defined in Eq. (17.13)). The operators in the lattice matrix elements are defined in the lattice regularization scheme. To be used in tests of the Standard Model, however, they must be matched to the continuum regularization scheme in which the corresponding Wilson coefficients have been calculated. The only case in which such matching is not needed is if the operator is a conserved or partially conserved current. Similar matching is also needed for the conversion of lattice bare quark masses to those in the continuum $\overline{\rm MS}$ scheme.

Several methods are used to calculate the matching factors: perturbation theory (usually to one- or two-loop order), non-perturbative renormalization (NPR) using Landau-gauge quark and gluon external states [92], NPR using gauge-invariant methods based on the Schrödinger functional [93], NPR using gauge-invariant short-distance hadron correlators [94], and NPR using gauge-invariant heavy-heavy correlators [28, 95]. The NPR methods replace truncation errors (which can only be approximately estimated) by statistical and systematic errors that can be determined reliably and systematically reduced.

An issue that arises in some of such calculations (e.g., for quark masses and B_K) is that, using NPR with Landau-gauge quark and gluon external states, one ends up with operators regularized in a MOM-like scheme (or a Schrödinger-functional scheme), rather than the $\overline{\rm MS}$ scheme mostly used for calculating the Wilson coef-

Downloaded from https://academic.oup.com/ptep/article/2022/8/083C01/6651666 by KIT Library user on 27 September 2022

ficients. To make contact with this scheme requires a purely continuum perturbative matching calculation supplemented by the operator product expansion (OPE). (The importance of power corrections is emphasized in [96].) The resultant truncation error of perturbative expansion and OPE can be minimized by pushing up the momentum scale at which the matching is done using step-scaling techniques as part of the NPR calculation [97].

It should also be noted that this final step in the conversion to the $\overline{\text{MS}}$ scheme could be avoided if continuum calculations used a MOM-like scheme or if one imposes a renormalization condition for quantities that are calculable both in the $\overline{\text{MS}}$ scheme and in LQCD, such as the hadron correlators at short distances (see, e.g., Ref. [98]).

17.2 Methods and status

Once the lattice action is chosen, it is straightforward to define the quantum theory using the path integral formulation. The Euclidean-space partition function is

$$Z = \int [dU] \prod_f [dq_f][d\bar{q}_f] e^{-S_g[U] - \sum_f \bar{q}_f (D[U]+m_f) q_f}, \quad (17.4)$$

where link variables are integrated over the SU(3) manifold, q_f and $\bar{q}_f$ are Grassmann (anticommuting) quark and antiquark fields of flavor f, and $D[U]$ is the chosen lattice Dirac operator with m_f the quark mass in lattice units. Integrating out the quark and antiquark fields, one arrives at a form suitable for simulation:

$$Z = \int [dU] e^{-S_g[U]} \prod_f \det(D[U] + m_f). \quad (17.5)$$

The building blocks for calculations are expectation values of multi-local gauge-invariant operators, also known as "correlation functions",

$$\langle \mathcal{O}(U, q, \bar{q}) \rangle = (1/Z) \int [dU] \prod_f [dq_f][d\bar{q}_f] \mathcal{O}(U, q, \bar{q}) e^{-S_g[U] - \sum_f \bar{q}_f (D[U]+m_f) q_f}. \quad (17.6)$$

If the operators depend on the (anti-)quark fields q_f and $\bar{q}_f$, then integrating these fields out leads not only to the fermion determinant but also, through Wick's theorem, to a series of quark "propagators", $(D[U] + m_f)^{-1}$, connecting the positions of the fields.

This set-up allows one to choose, by hand, the masses of the quarks in the determinant (the sea quarks) differently from those in the propagators (valence quarks). This is called "partial quenching", and is used by some calculations as a way of obtaining more data points from which to extrapolate both sea and valence quarks to their physical values.

17.2.1 *Monte-Carlo method*

Since the number of integration variables U is huge ($N_s^3 \times N_t \times 4 \times 9$), direct numerical integration is impractical and one has to use Monte-Carlo techniques. In this method, one generates a Markov chain of gauge configurations (a "configuration" being the set of U's on all links) distributed according to the probability measure $[dU] e^{-S_g[U]} \prod_f \det(D[U] + m_f)$. Once the configurations are generated, expectation values $\langle \mathcal{O}(U, q, \bar{q}) \rangle$ are calculated by averaging over those configurations. In this way the configurations can be used for many different calculations, and there are several large collections of ensembles of configurations (with a range of values of a, lattice sizes and quark masses) that are publicly available through the International Lattice Data Grid (ILDG). As the number of the configurations, N, is increased, the error decreases as $1/\sqrt{N}$.

The most challenging part of the generation of gauge configurations is the need to include the fermion determinant. Direct evaluation of the determinant is not feasible, as it requires $\mathcal{O}((N_s^3 \times N_t)^3)$ computations. Instead, one rewrites it in terms of "pseudofermion" fields ϕ (auxiliary fermion fields with bosonic statistics). For example, for two degenerate quarks one has

$$\det(D[U] + m_f)^2 = \int [d\phi] e^{-\phi^\dagger (D[U]+m_f)^{-2} \phi}. \quad (17.7)$$

By treating the pseudofermions as additional integration variables in the path integral, one obtains a totally bosonic representation. The price one pays is that the pseudofermion effective action is highly non-local since it includes the inverse Dirac operator $(D[U] + m_f)^{-1}$. Thus, the large sparse matrix $(D[U] + m)$ has to be inverted every time one needs an evaluation of the effective action.

Present simulations generate gauge configurations using the Hybrid Monte Carlo (HMC) algorithm [99], or variants thereof. This algorithm combines molecular dynamics (MD) evolution in a fictitious time (which is also discretized) with a Metropolis "accept-reject" step. It makes a global update of the configuration, and is made exact by the Metropolis step. In its original form it can be used only for two degenerate flavors, but extensions (particularly the rational HMC [100]) are available for single flavors. Considerable speed-up of the algorithms has been achieved over the last two decades using a variety of techniques.

All these algorithms spend the bulk of their computational time on the repeated inversion of $(D[U]+m)$ acting on a source (which is required at every step of the MD evolution). Inversions are done using a variety of iterative algorithms, e.g., the conjugate gradient algorithm. In this class of algorithms, computational cost is proportional to the condition number of the matrix, which is the ratio of maximum and minimum eigenvalues. For $(D[U]+m)$ the smallest eigenvalue is $\approx m$, so the condition number and cost are inversely proportional to the quark mass. This is a major reason why simulations at the physical quark mass are challenging.

Recent algorithmic improvements have significantly reduced this problem. The main idea is to separate different length scales. Since the low eigenvalues of $(D[U] + m)$ are associated with long wavelength quark modes, one may project the problem onto that of a coarse-grained lattice by averaging the field within a block of sublattices and carrying out the inversion on this coarse lattice. The result is then fed back to the original lattice as an efficient *preconditioner* for the iterative solver, and the whole procedure may be nested multiple times. Variants of such methods have been implemented, specifically domain-decomposition [11,12], deflation [101–104] and multigrid [105,106]. They are increasingly used in large-scale lattice simulations.

A practical concern is the inevitable presence of correlations between configurations in the Markov chain. These are characterized by an autocorrelation length in the fictitious MD time. One aims to use configurations separated in MD time by greater than this autocorrelation length. In practice, it is difficult to measure this length accurately, see, e.g., [107], and this leads to some uncertainty in the resulting statistical errors, as well as the possibility of insufficient equilibration.

The computational cost of gauge generation grows with the lattice volume, $V_{\text{lat}} = N_s^3 N_t$, as $V_{\text{lat}}^{1+\delta}$. Here $\delta = 1/4$ for the HMC algorithm [108] and can be reduced slightly using modern variants. Such growth with V_{lat} provides a (time-dependent) limit on the largest lattice volumes that can be simulated. At present, the largest lattices being used have $N_s = 144$ and $N_t = 288$. Typically, one aims to create an ensemble of $\sim 10^3$ statistically independent configurations at each choice of parameters (a, m_q and V_{lat}). For most physical quantities of interest, this is sufficient to make the resulting statistical errors smaller than or comparable to the systematic errors.

In the past, the cost of generating gauge configurations was larger than that of performing "measurements" on those configurations. However, as the number of quantities being calculated and their complexity has increased, the balance has shifted to the point that the total cost of measurements exceeds that of generation.

17.2.2 *Two-point functions*

One can extract properties of stable hadrons using two-point correlation functions, $\langle O_X(x) O_Y^\dagger(0) \rangle$. Here $O_{X,Y}(x)$ are opera-

Downloaded from https://academic.oup.com/ptep/article/2022/8/083C01/6651666 by KIT Library user on 27 September 2022

tors that have non-zero overlaps with the hadronic state of interest $|H\rangle$, *i.e.* $\langle 0|O_{X,Y}(x)|H\rangle \neq 0$. One usually Fourier transforms in the spatial directions and considers correlators as a function of Euclidean time:

$$C_{XY}(t;\boldsymbol{p}) = \sum_{\boldsymbol{x}} \langle O_X(t,\boldsymbol{x}) O_Y^\dagger(0)\rangle e^{-i\boldsymbol{p}\cdot\boldsymbol{x}}. \tag{17.8}$$

(Here and throughout this section all quantities are expressed in dimensionless lattice units, so that, for example, $\boldsymbol{p} = a\boldsymbol{p}_{\rm phys}$.) By inserting a complete set of states having spatial momentum $\boldsymbol{p}$, the two-point function can be written as

$$C_{XY}(t;\boldsymbol{p}) = \sum_{i=0}^{\infty} \frac{1}{2E_i(\boldsymbol{p})} \langle 0|O_X(0)|H_i(\boldsymbol{p})\rangle\langle H_i(\boldsymbol{p})|O_Y^\dagger(0)|0\rangle e^{-E_i(\boldsymbol{p})t}, \tag{17.9}$$

where the energy of the i-th state $E_i(\boldsymbol{p})$ appears as an eigenvalue of the time evolution operator e^{-Ht} in the Euclidean time direction. The factor of $1/[2E_i(\boldsymbol{p})]$ is due to the relativistic normalization used for the states. For large enough t, the dominant contribution is that of the lowest energy state $|H_0(\boldsymbol{p})\rangle$:

$$C_{XY}(t) \overset{t\to\infty}{\longrightarrow} \frac{1}{2E_0(\boldsymbol{p})} \langle 0|O_X(0)|H_0(\boldsymbol{p})\rangle\langle H_0(\boldsymbol{p})|O_Y^\dagger(0)|0\rangle e^{-E_0(\boldsymbol{p})t}. \tag{17.10}$$

One can thus obtain the energy $E_0(\boldsymbol{p})$, which equals the hadron mass m_H when $\vec{p} = 0$, and the product of matrix elements $\langle 0|O_X(0)|H_i(\boldsymbol{p})\rangle\langle H_i(\boldsymbol{p})|O_Y^\dagger(0)|0\rangle$.

This method can be used to determine the masses of all the stable mesons and baryons by making appropriate choices of operators. For example, if one uses the axial current, $O_X = O_Y = A_\mu = \bar{d}\gamma_\mu\gamma_5 u$, then one can determine m_{π^+} from the rate of exponential fall-off, and in addition the decay constant f_π from the coefficient of the exponential.

The expression given above for the correlator $C_{XY}(t;\boldsymbol{p})$ shows how, in principle, one can determine the energies of the excited hadron states having the same quantum numbers as the operators $O_{X,Y}$, by fitting the correlation function to a sum of exponentials, which is also important to precisely determine the ground-state exponential. In practice, in order to reliably identify the excited state, one often needs to use a large basis of operators and to adopt the variational approach such as that of Ref. [109]. One can also use an anisotropic lattice in which a_t, the lattice spacing in the time direction, is smaller than its spatial counterpart a_s. Using a combination of these and other technical improvements extensive excited-state spectra have been obtained [110–115].

A complication arises for states with high spins ($j \geq 4$ for bosons) because the spatial rotation group on the lattice is a discrete subgroup of the continuum group SO(3). This implies that lattice operators, even when chosen to lie in irreducible representations of the lattice rotation group, have overlap with states that have a number of values of j in the continuum limit [116]. For example $j = 0$ operators can also create mesons with $j = 4$. Methods to overcome this problem in practice are available [110, 117] and have been used successfully.

17.2.3 *Three-point functions*

Hadronic matrix elements needed to calculate semileptonic form factors and neutral meson mixing amplitudes can be computed from three-point correlation functions. We discuss here, as a representative example, the $D \to K$ amplitude. As in the case of two-point correlation functions one constructs operators O_D and O_K having overlap, respectively, with the D and K mesons. We are interested in calculating the matrix element $\langle K|V_\mu|D\rangle$, with $V_\mu = \bar{c}\gamma_\mu s$ the vector current calculations of this contribution.

To obtain this, we use the three-point correlator

$$C_{KV_\mu D}(t_x,t_y;\boldsymbol{p}) = \sum_{\boldsymbol{x},\boldsymbol{y}} \langle O_K(t_x,\boldsymbol{x}) V_\mu(0) O_D^\dagger(t_y,\boldsymbol{y})\rangle e^{-i\boldsymbol{p}\cdot\boldsymbol{x}}, \tag{17.11}$$

and focus on the limit $t_x \to \infty$, $t_y \to -\infty$. In this example we set the D-meson at rest while the kaon carries three-momentum $\boldsymbol{p}$. Momentum conservation then implies that the weak operator V_μ inserts three-momentum $-\boldsymbol{p}$. Inserting a pair of complete sets of states between each pair of operators, we find

$$C_{KV_\mu D}(t_x,t_y;\boldsymbol{p}) = \sum_{i,j} \frac{1}{2m_{D_i}2E_{K_j}(\boldsymbol{p})} e^{-m_{D_i}t_x - E_{K_j}(\boldsymbol{p})|t_y|} \times \langle 0|O_K(0)|K_i(\boldsymbol{p})\rangle\langle K_i(\boldsymbol{p})|V_\mu(0)|D_j(\boldsymbol{0})\rangle\langle D_j(\boldsymbol{0})|O_D^\dagger(0)|0\rangle. \tag{17.12}$$

The matrix element $\langle K_i(\boldsymbol{p})|V_\mu(0)|D_j(\boldsymbol{0})\rangle$ can then be extracted, since all other quantities in this expression can be obtained from two-point correlation functions. Typically, one is interested in the weak matrix elements of ground states, such as the lightest pseudoscalar mesons. In the limit of large separation between the three operators in Euclidean time, the three-point correlation function yields the weak matrix element of the transition between ground states.

17.2.4 *Scattering amplitudes and resonances*

The methods described thus far yield matrix elements involving single, stable particles (where by stable we mean here absolutely stable to strong interaction decays). Most of the particles listed in the Review of Particle Properties are, however, unstable—they are resonances decaying into final states consisting of multiple strongly interacting particles. LQCD simulations cannot directly calculate resonance properties, but methods have been developed to do so indirectly for resonances coupled to two-particle final states in the elastic regime, starting from the seminal work of Lüscher [118].

The difficulty faced by LQCD calculations is that, to obtain resonance properties, or, more generally, scattering phase-shifts, one must calculate multiparticle scattering amplitudes in momentum space and put the external particles on their mass-shells. This requires analytically continuing from Euclidean to Minkowski momenta. Although it is straightforward in LQCD to generalize the methods described above to calculate four- and higher-point correlation functions, one necessarily obtains them at a discrete and finite set of Euclidean momenta. Analytic continuation to $p_E^2 = -m^2$ is then an ill-posed and numerically unstable problem. The same problem arises for single-particle states, but can be largely overcome by picking out the exponential fall-off of the Euclidean correlator, as described above. With a multi-particle state there is no corresponding trick, except for two particles at threshold [119], although recent ideas using smeared correlators and advanced spectral-reconstruction methods offer hope for future progress [120–123].

What LQCD can calculate are the energies of the eigenstates of the QCD Hamiltonian in a finite box. The energies of states containing two stable particles, e.g., two pions, clearly depend on the interactions between the particles. It is possible to invert this dependence and, with plausible assumptions, determine the scattering phase-shifts at a discrete set of momenta from a calculation of the two-particle energy levels for a variety of spatial volumes [118]. This is a challenging calculation, but it has been carried through in several channels with quark masses approaching physical values. Channels studied include $\pi\pi$ (for $I = 2$, 1 and 0), $\bar{K}K$, $K\pi$, $\pi\omega$, $\pi\phi$, KD, DD^* and $B\pi$. For recent comprehensive reviews see [124]. Extensions to nucleon interactions are also being actively studied [125]. The formalism has been generalized to three spinless particles (both identical and nondegenerate) [126], and has been applied to three pions and kaons at maximal isospin [127]. For recent reviews, see [128].

It is also possible to extend the methodology to calculate electroweak decay amplitudes to two particles below the inelastic threshold, e.g., $A(K \to \pi\pi)$ [129]. Results for both the $\Delta I = 3/2$ and 1/2 amplitudes with physical quark masses have been obtained [130–132], the former now including a controlled continuum limit [133]. First results for the CP-violating quantity ϵ' have been obtained [131, 132].

Partial extensions of the formalism above the elastic threshold have been worked out, in particular for the case of multiple two-particle channels [134]. Another theoretical extension is to allow the calculation of form factors between a stable particle and a resonance [135] , and between two resonances [136]. The former

Downloaded from https://academic.oup.com/ptep/article/2022/8/083C01/6651666 by KIT Library user on 27 September 2022

has been used to calculate the $\gamma\pi \to \rho$ amplitude, albeit for unphysically large quark masses [137]. Finally, the formalism for using LQCD to calculate electroweak decays or transitions to three particles, e.g $\gamma^* \to 3\pi$ and $K \to 3\pi$, has recently been worked out [138, 139].

While a systematic extension to decays with many multiparticle channels, e.g., hadronic B decays, has, however, yet to be formulated, some interesting new ideas have been recently proposed [140, 141], including a method to compute inclusive decay rates or cross sections [142, 143].

17.2.5 *Recent advances*

In some physics applications, one is interested in the two-point correlation function $\langle O_X(x)O_Y^\dagger(0)\rangle$ for all values of the separation x, not just its asymptotic form for large separations (which is used to determine the hadron spectrum as sketched above). A topical example is the hadronic vacuum polarization function $\Pi_{\mu\nu}(x) = \langle V_\mu(x)V_\nu(0)\rangle$ and its Fourier transform $\Pi_{\mu\nu}(q^2)$. Since the lattice is in Euclidean space-time, only space-like momenta, $q^2 = -Q^2 < 0$, are accessible. Nevertheless, this quantity is of significant interest. It is related by a dispersion relation to the cross section for $e^+e^- \to$ hadrons, and is needed for a first-principles calculation of the "hadronic vacuum polarization" contribution to the muon anomalous magnetic moment a_μ. There are a number of lattice calculations of this contribution (see, e.g., Refs. [144–160] following the pioneering work Ref. [161]; see also Ref. [162] for the summary of the status as of March 2020). Since the relevant scale is set by the muon mass m_μ, this quantity is most sensitive to the low-energy region $Q^2 \simeq m_\mu^2$ of $\Pi_{\mu\nu}(-Q^2)$, where the long-range contribution of multibody states become relevant. The lattice calculation is challenging because of this and also because the necessary precision is high (below 1%). Many systematic effects must be carefully studied and controlled in order to achieve this precision, including finite volume errors [163, 164], isospin breaking [156,165,166], quark-line disconnected diagrams [150,156,166], and QED corrections [156, 166]. Very recently, a lattice calculation has achieved the required sub-percent precision [167], a level that is comparable to the determination from the e^+e^- data. The result is, however, in tension with the data-driven approach, disagreeing with intermediate quantities by as much as 3.7σ. More calculations are anticipated to appear in the near future.

Calculations of the light-by-light scattering contribution to a_μ are also underway. These involve the calculations of four-point correlation functions with various external momenta. Ingenious methods to evaluate the contribution to a_μ have been developed by two groups and the results are in good agreement [168–175].

A summary of the theoretical studies needed to provide the hadronic quantities related to a_μ has been given by the "Muon $g-2$ Theory Initiative" [162]. This work quotes a conservative average of all results for a_μ available before April 2019, and thus does not include the result from Ref. [167].

There are other processes for which lattice calculations can make a significant contribution to establishing a quantitative understanding. One example is the long-distance contribution to the neutral kaon mass splitting, ΔM_K. This also requires the evaluation of a four-point function, constructed from the two-point functions described above by the insertion of two electroweak Hamiltonians [176, 177]. Rare kaon decays $K \to \pi\ell^+\ell^-$ and $K \to \pi\nu\bar{\nu}$ are also important processes for which first lattice studies have appeared [178–183]. Radiative leptonic decays of pion and kaon, $\pi \to \ell\nu\gamma$ and $K \to \ell\nu\gamma$, also include two operator insertions, i.e. an electroweak Hamiltonian and an electromagnetic current, and similar techniques developed for the rare decays can be applied. First lattice results have appeared [184, 185].

17.2.6 *Status of LQCD simulations*

Until the 1990s, most large-scale lattice simulations were limited to the "quenched" approximation, wherein the fermion determinant is omitted from the path integral. While much of the basic methodology was developed in this era, the results obtained had uncontrolled systematic errors and were not suitable for use in placing precision constraints on the Standard Model. During the 1990s, more extensive simulations including the fermion determinant (also known as simulations with "dynamical" fermions) were begun, but with unphysically heavy quark masses ($m_\ell \sim 50 - 100$ MeV), such that the extrapolation to the physical light quark masses was a source of large systematic errors [186]. During the 2000s, advances in both algorithms and computers allowed simulations to reach much smaller quark masses ($m_\ell \sim 10 - 20$ MeV) such that LQCD calculations of selected quantities with all sources of error controlled and small became available. Their results played an important role in constraints on the CKM matrix and other phenomenological analyses. In the last decade, simulations directly at the physical isospin-symmetric light quark masses have become standard, removing the need for a chiral extrapolation and thus significantly reducing the overall error. The present frontier, as noted above, is the inclusion of isospin breaking. This will be needed to push the accuracy of calculations below the percent level.

On a more qualitative level, analytic and numerical results from LQCD have demonstrated that QCD confines color and spontaneously breaks chiral symmetry. Confinement can be seen as a linearly rising potential between heavy quark and anti-quark in the absence of quark loops. Analytically, this can be shown in the strong coupling limit $g_{\rm lat} \to \infty$ [1]. At weaker couplings there are precise numerical calculations of the potential that clearly show that this behavior persists in the continuum limit [187–189].

Chiral symmetry breaking was also demonstrated in the strong coupling limit on the lattice [19,190], and there have been a number of numerical studies showing that this holds also in the continuum limit. The accumulation of low-lying modes of the Dirac operator, which is the analog of Cooper pair condensation in superconductors, has been observed, yielding a determination of the chiral condensate [191–197]. Many relations among physical quantities that can be derived under the assumption of broken chiral symmetry have been confirmed by a number of lattice groups [198].

17.3 Physics applications

In this section we describe the main applications of LQCD that are both computationally mature and relevant for the determination of particle properties.

A general feature to keep in mind is that, since there are many different choices for lattice actions, all of which lead to the same continuum theory, a crucial test is that results for any given quantity are consistent. In many cases, different lattice calculations are completely independent and often have very different systematic errors. Thus, final agreement, if found, is a highly non-trivial check, just as it is for different experimental measurements.

The number, variety and precision of the calculations has progressed to the point that an international collaboration, FLAG, has been formed, which aims to collect all lattice results of relevance for a variety of phenomenologically interesting quantities and provide averages of those results that pass appropriate quality criteria. The averages attempt to account for possible correlations between results (which can arise, for example, if they use common gauge configurations). The quantities considered are those we discuss in this section, with the exception of the hadron spectrum, as well as the intermediate scale-setting quantities discussed earlier. The most recent FLAG review is from 2021 [74] (see also older editions, Refs. [54, 198]). The interested reader can consult this review for very extensive discussions of the details of the calculations and of the sources of systematic errors.

We stress that the results we quote below are those obtained using the physical complement of light quarks (i.e. $N_f = 2+1$ or $2+1+1$ simulations).

17.3.1 *Spectrum*

The most basic prediction of LQCD is of the hadron spectrum. Once the input parameters are fixed as described in Sec. 17.1.5, the masses or resonance parameters of all other states can be predicted. This includes hadrons composed of light (u, d and s) quarks, as well as heavy-light and heavy-heavy hadrons. It also includes quark-model exotics (e.g., $J^{PC} = 1^{-+}$ mesons) and glueballs. Thus, in principle, LQCD calculations should be able to reproduce many of the experimental results compiled in the Review of Particle Properties. Doing so would test both that the error budgets of LQCD calculations are accurate and that QCD

Downloaded from https://academic.oup.com/ptep/article/2022/8/083C01/6651666 by KIT Library user on 27 September 2022

indeed describes the strong interactions in the low-energy domain. The importance of the latter test can hardly be overstated.

What is the status of this fundamental test? As discussed in Sec. 1.2, LQCD calculations are most straightforward for stable, low-lying hadrons. Calculations of the properties of resonances that can decay into only two particles are more challenging, but are becoming standard in the meson sector, with the frontier being decays involving baryons. As noted above, the formalism for resonances decaying to three particles that are a mix of pions and kaons exists, but has yet to be applied to resonant channels. It is also more technically challenging to calculate masses of flavor singlet states (which can annihilate into purely gluonic intermediate states) than those of flavor non-singlets, although again algorithmic and computational advances have begun to make such calculations accessible, including first calculations that reach physical quark masses [199].

The present status for light hadrons is that fully controlled results are available for the masses of the octet light baryons, while results with less than complete control are available for the decuplet baryon resonances, the vector meson resonances and the η and η'. This is discussed in the "Quark Model" review—see, in particular, Fig. 15.9. In addition, it has been possible to calculate the isospin splitting in light mesons and baryons (due to the up-down mass difference and the incorporation of QED). There are also extensive results for heavy-light (D and B systems) and heavy-heavy (J/ψ and Υ systems). All present results, which are discussed in the "Quark Model" review, are consistent with experimental values, and several predictions have been made. We refer the reader to that review for references to the relevant work.

17.3.2 *Decay constants and bag parameters*

The pseudoscalar decay constants can be determined from two-point correlation functions involving the axial-vector current, as discussed in Sec. 17.2.2. The decay constant f_P of a meson P is extracted from the weak matrix element involving the axial-vector current using the definition $\langle 0|A_\mu(x)|P(\boldsymbol{p})\rangle = f_P p_\mu \exp(-ip\cdot x)$, where p_μ is the momentum of P and $A_\mu(x)$ is the axial-vector current. (In practice, results with the smallest errors are obtained using the pseudoscalar density $P(x)$ instead of $A_\mu(x)$.) Since they are among the simplest quantities to calculate, decay constants provide good benchmarks for lattice methods, in addition to being important inputs for flavor physics phenomenology in their own right. Results from several lattice groups for the pion and kaon decay constants now have subpercent errors. The decay constants in the charm and bottom sectors, f_D, f_{D_s}, f_B, and f_{B_s}, have also been calculated to high precision, with subpercent errors for charmed mesons, and percent-level errors for bottom mesons. Lattice results for all of these decay constants are discussed in detail in the review "Leptonic Decays of Charged Pseudoscalar Mesons."

Another important lattice quantity is the kaon bag parameter, B_K, which is needed to turn the precise measurement of CP-violation in kaon mixing into a constraint on the Standard Model. It is defined by

$$\frac{8}{3}m_K^2 f_K^2 B_K(\mu) = \langle \overline{K}^0|Q_{\Delta S=2}(\mu)|K^0\rangle, \tag{17.13}$$

where m_K is the kaon mass, f_K is the kaon decay constant, $Q_{\Delta S=2} = \bar{s}\gamma_\mu(1-\gamma_5)d\bar{s}\gamma_\mu(1-\gamma_5)d$ is the four-quark operator of the effective electroweak Hamiltonian and μ is the renormalization scale. The short distance contribution to the electroweak Hamiltonian can be calculated perturbatively, but the hadronic matrix element parameterized by B_K must be computed using non-perturbative methods. In order to be of use to phenomenology, the renormalization factor of the four-quark operator must be matched to a continuum renormalization scheme, e.g., to $\overline{\text{MS}}$, as described in Sec. 17.1.6.4. Determinations with percent-level precision using different fermion actions and $N_f = 2+1$ light sea quarks are now available using DWF [200] , staggered fermions [201], DWF valence on staggered sea quarks [202], and Wilson fermions [13]. The results are all consistent, and the present FLAG average is $\hat{B}_K = 0.7625(97)$ [74] (for original papers, see [13, 202–204]).

The bag parameters for B and B_s meson mixing are defined analogously to that for kaon mixing. The B and B_s mesons contain a valence b-quark so that calculations of these quantities must use one of the methods for heavy quarks described above. Calculations have been done using NRQCD [205, 206], the Fermilab formalism [81], and static heavy quarks [207]. All results are consistent. The FLAG averages for the quantities relevant for B_s and B mixing with $N_f = 2+1$, which are based on results from Refs. [81, 205, 207], are $f_{B_s}\sqrt{\hat{B}_{B_s}} = 274(8)$ MeV and $f_B\sqrt{\hat{B}_B} = 225(9)$ MeV, with their ratio (which is somewhat better determined) being $\xi = 1.206(17)$. FLAG also quotes an "average" for $N_f = 2+1+1$, which comes from a single calculation [206] and gives $f_{B_s}\sqrt{\hat{B}_{B_s}} = 256(6)$ MeV $f_B\sqrt{\hat{B}_B} = 211(6)$ MeV, and $\xi = 1.216(16)$. These are consistent with the $N_f = 2+1$ results at the 2σ level. Errors for quantities involving b quarks are typically larger than those for quantities involving only light quarks, although the difference has steadily decreased in recent years.

For the K, D and B systems, one can also consider the matrix elements of four-fermion operators that arise in beyond-the-standard-model (BSM) theories, which can have a different chiral structure. Knowledge of these matrix elements allows one to constrain the parameters of the BSM theories, and is complementary to direct searches at the LHC. Reliable results are now available from lattice calculations, and are reviewed by FLAG in the case of kaon mixing [74]. Complete results for D and B mixing are presented in Ref. [208, 209] and Ref. [81, 210], respectively.

The results for mixing matrix elements are used in the reviews "The CKM Quark-Mixing Matrix," and "$B^0 - \bar{B}^0$ Mixing."

17.3.3 *Form factors ($K \to \pi\ell\nu$, $D \to K\ell\nu$, $B \to \pi\ell\nu$, $B \to D^{(*)}\ell\nu$)*

Semileptonic decay rates can be used to extract CKM matrix elements once the semileptonic form factors are known from lattice calculations. For example, the matrix element of a pseudoscalar meson P undergoing semileptonic decay to another pseudoscalar meson D is mediated by the vector current, and can be written in terms of form factors as

$$\langle D(p_D)|V_\mu|P(p_P)\rangle = f_+(q^2)(p_D+p_P-\Delta)_\mu + f_0(q^2)\Delta_\mu\,, \tag{17.14}$$

where $q = p_D - p_P$, $\Delta_\mu = (m_D^2 - m_P^2)q_\mu/q^2$ and V_μ is the quark vector current. The shape of the form factor is typically well determined by experiment, and the value of $f_+(q^2)$ at some reference value of q^2 is needed from the lattice in order to extract CKM matrix elements. Typically, $f_+(q^2)$ dominates the decay rate, since the contribution from $f_0(q^2)$ is suppressed when the final state lepton is light.

The form factor $f_+(0)$ for $K \to \pi\ell\nu$ decays is highly constrained by the Ademollo-Gatto theorem [211] and chiral symmetry. Old estimates using chiral perturbation theory combined with quark models quote sub-percent precision [212], though they suffer from some model dependence. Utilizing the constraint from the vector current conservation that $f_+(0)$ is normalized to unity in the limit of degenerate up and strange quark masses, the lattice calculation can be made very precise and has now matched the precision of the phenomenological estimates [213–220]. The present FLAG average (from $N_f = 2+1+1$ simulations) is $f_+(0) = 0.9698(17)$, based on Refs. [220].

Charm meson semileptonic decays have been calculated by different groups using methods similar to those used for charm decay constants, and results are steadily improving in precision [221–225]. For semileptonic decays involving a bottom quark, one uses HQET or NRQCD to control the discretization errors of the bottom quark. The form factors for the semileptonic decay $B \to \pi\ell\nu$ have been calculated in unquenched lattice QCD by a number of groups [226–231]. These B semileptonic form factors are difficult to calculate at low q^2, *i.e.* when the mass of the B-meson must be balanced by a large pion momentum, in order to transfer a large momentum to the lepton pair. The low q^2 region has large discretization errors and very large statistical errors, while the high q^2 region is much more accessible to the lattice. For experiment, the opposite is true. To combine lattice and experimental results it has proved helpful to use the z-parameter

Downloaded from https://academic.oup.com/ptep/article/2022/8/083C01/6651666 by KIT Library user on 27 September 2022

expansion [232]. This provides a theoretically constrained parameterization of the entire q^2 range, and allows one to obtain $|V_{ub}|$ without model dependence [233, 234].

The semileptonic decays $B \to D\ell\nu$ and $B \to D^*\ell\nu$ (and the similar decays $B_s \to D_s\ell\nu$ and $B_s \to D_s^*\ell\nu$) can be used to extract $|V_{cb}|$ once the corresponding form factors are known. The lattice calculation is most precise at zero recoil since the bulk of the systematic error cancels for appropriate ratios between $B \to D^{(*)}$ and $B \to B$ or $D^{(*)} \to D^{(*)}$ [235, 236]. The unquenched calculation of the $B \to D^{(*)}\ell\nu$ form factor at zero recoil has been performed with various formulations for the heavy quark [237–241]. Calculations at non-zero recoil have also been performed to constrain the functional form of the form factor, which can be used to extrapolate the experimental data to the zero-recoil point or to determine $|V_{cb}|$ directly at the non-zero recoil points [242]. Semileptonic decays of the Λ_b baryon can also be used to constrain $|V_{cb}|$ and $|V_{ub}|$ using lattice calculations of the relevant form factors [243, 244].

The rare decays $B \to K^{(*)}\ell^+\ell^-$ involve matrix elements similar to those needed for semileptonic decays, Eq. (17.14), except that the vector current V_μ is replaced by the operators $\bar{s}\gamma^\mu(1-\gamma_5)b$ or $\bar{s}\sigma^{\mu\nu}(1+\gamma_5)b$. Lattice calculations of the corresponding form factors involve similar techniques to those for the semileptonic form factors. The values of q^2 for which lattice calculations can be done are limited as for B semileptonic decays, and, in addition, the region of $c\bar{c}$ resonances has to be avoided. Recent lattice calculations [230, 245–247] have been used to constrain the standard model and new physics contributions.

The results discussed in this section are used in the reviews "The CKM Quark-Mixing Matrix," "V_{ud}, V_{us}, the Cabibbo Angle and CKM Unitarity," and "Semileptonic b-hadron decays, determination of V_{cb}, V_{ub}."

17.3.4 *Strong gauge coupling*

As explained in Sec. 17.1.5.1, for a given lattice action, the choice of bare lattice gauge coupling, $g_{\rm lat}$, determines the lattice spacing a. If one then calculates a as described in Sec. 17.1.5.1, one knows the strong gauge coupling in the bare lattice scheme at the scale $1/a$, $\alpha_{\rm lat} = g_{\rm lat}^2/(4\pi)$. This is not, however, useful for comparing to results for α_s obtained from other inputs, such as deep inelastic scattering or jet shape variables. This is because the latter results give α_s in the $\overline{\rm MS}$ scheme, which is commonly used in such analyses, and the conversion factor between these two schemes is known to converge extremely poorly in perturbation theory. Instead, one must use a method which directly determines α_s on the lattice in a scheme closer to $\overline{\rm MS}$.

Several such methods have been used, all following a similar strategy. One calculates a short-distance quantity K both perturbatively ($K^{\rm PT}$) and non-perturbatively ($K^{\rm NP}$) on the lattice, and requires equality: $K^{\rm NP} = K^{\rm PT} = \sum_{i=0}^{n} c_i \alpha_s^i$. Solving this equation one obtains α_s at a scale related to the quantity being used. Often, α_s thus obtained is not defined in the conventional $\overline{\rm MS}$ scheme, and one has to convert among the different schemes using perturbation theory. Unlike for the bare lattice scheme, the required conversion factors are reasonably convergent. As a final step, one uses the renormalization group to run the resulting coupling to a canonical scale (such as M_Z).

In the work of the HPQCD collaboration [248, 249], the short-distance quantities are Wilson loops of several sizes and their ratios. These quantities are perturbatively calculated through $\mathcal{O}(\alpha_s^3)$ using the V-scheme defined through the heavy quark potential. The coefficients of even higher orders are estimated using the data at various values of a. In addition, this work obtains a result for α_s by matching with $\alpha_{\rm lat}$ in a tadpole-improved scheme that improves convergence.

Another choice of short-distance quantities is to use current-current correlators. Appropriate moments of these correlators are ultraviolet finite, and by matching lattice results to the *continuum* perturbative predictions, one can directly extract the $\overline{\rm MS}$ coupling [250]. The method can be applied for light meson correlators [251–254] as well as heavy meson correlators [38, 249, 255–258]. Yet another choice of short-distance quantity is the static-quark potential, where the lattice result for the potential is compared to perturbative calculations; this method was used to compute α_s within 2+1 flavor QCD [259–264]. There is also a determination of α_s from a comparison of lattice data for the ghost-gluon coupling with that of perturbation theory [265, 266].

With a definition of α_s given using the Schrödinger functional, one can non-perturbatively control the evolution of α_s to high-energy scales, such as 100 GeV, where the perturbative expansion converges very well. This method developed by the ALPHA collaboration [97] has been applied to 2+1-flavor QCD in [267–269].

The various lattice methods for calculating α_s have significantly different sources of systematic error. The FLAG review [74] reports an estimate $\alpha_{\overline{\rm MS}}^{(5)}(M_Z) = 0.1184(8)$, based on Refs. [249, 254, 256, 264, 267, 269–271]. A comparison to other phenomenological determinations can be found in the "Quantum Chromodynamics" review.

17.3.5 *Quark masses*

Once the quark mass parameters are tuned in the lattice action, the remaining task is to convert them to those of the conventional definition. Since the quarks do not appear as asymptotic states due to confinement, the pole mass of the quark propagator is not a physical quantity. Instead, one defines the quark mass after subtracting the ultra-violet divergences in some particular way. The conventional choice is again the $\overline{\rm MS}$ scheme at a canonical scale such as 2 or 3 GeV. Ratios such as m_c/m_s and m_b/m_c are also useful as they are free from multiplicative renormalization (in a mass-independent scheme).

As discussed in Sec. 17.1.6.4, one must convert the lattice bare quark mass to that in the $\overline{\rm MS}$ scheme. Older calculations did so directly using perturbation theory; most recent calculations use an intermediate NPR method (e.g., RI/MOM or RI/SMOM) which is then converted to the $\overline{\rm MS}$ scheme using perturbation theory (see, e.g., [63, 200, 272–276]).

Alternatively, one can use a definition based on the Schrödinger functional, which allows one to evolve the quark mass to a high scale non-perturbatively [277, 278]. In practice, one can reach scales as high as ∼100 GeV, at which matching to the $\overline{\rm MS}$ scheme can be reliably calculated in perturbation theory.

Other approaches available for heavy quarks are to match current-current correlators at short distances calculated on the lattice to those obtained in continuum perturbation theory in the $\overline{\rm MS}$ scheme [38, 65, 249, 255–257], or to use HQET mass relations [275, 279]. This has allowed an accurate determination of m_c and m_b [95, 249, 256].

The ratio method for heavy quarks (discussed earlier) can also be used to determine m_b [280].

Results are summarized in the review of "Quark Masses."

17.3.6 *Other applications*

In this review we have concentrated on applications of LQCD that are relevant to the quantities discussed in the Review of Particle Properties. We have not discussed at all several other applications that are being actively pursued by simulations. Here we list the major such applications. The reader can consult the aforementioned texts [2–4] for further details, as well as the proceedings of recent lattice conferences [281], and several recent white papers [282–288].

LQCD can be used, in principle, to simulate QCD at non-zero temperature and density, and in particular to study how confinement and chiral-symmetry breaking are lost as T and μ (the chemical potential) are increased. For example, as T is increased at $\mu = 0$, It is found that, for the physical values of the quark masses, the deconfinement and chiral-symmetry-restoration transitions are smooth crossovers, rather than phase transitions, and that they occur together. This is of relevance to heavy-ion collisions, the early Universe and neutron-star structure. In practice, finite temperature simulations are computationally tractable and relatively mature, while simulations at finite μ suffer from a "sign problem" and are at a rudimentary stage.

Another topic under active investigation is nucleon structure and inter-nucleon interactions. The simplest nucleon matrix elements are calculable with a precision that is now starting to rival that for some mesonic quantities. Of particular interest are those of the axial current (leading to g_A) and of the scalar density (with

Downloaded from https://academic.oup.com/ptep/article/2022/8/083C01/6651666 by KIT Library user on 27 September 2022

$\langle N|\bar{s}s|N\rangle$ needed for dark matter searches), both of which are reviewed by FLAG [54, 74]. Other such matrix elements provide information on the parton distribution functions (PDFs) including their low moments. More recently, methods to directly access PDFs are being developed (see, e.g., Ref. [282] for a recent summary).

Finally, we note that there is much recent interest in studying QCD-like theories with more fermions, possibly in other representations of the gauge group (see, e.g., [284]). The main interest is to find nearly conformal theories which might be candidates for "walking technicolor" models.

17.4 Outlook

While LQCD calculations have made major strides in the last decade, and are now playing an important role in constraining the Standard Model, there are many calculations that could be done in principle but are not yet mature due to limitations in computational resources. As we move to exascale resources (10^{18} floating point operations per second), the list of mature calculations will grow. Examples that we expect to mature in the next few years are results for B meson and Λ_b baryon form factors covering the full range of q^2; results for excited hadrons, including quark-model exotics, at close to physical light-quark masses; results for moments of structure functions; results for the simplest nucleon matrix elements; $K \to \pi\pi$ amplitudes (allowing a prediction of ϵ'/ϵ from the Standard Model); hadronic vacuum polarization contributions to $g_\mu - 2$, the running of $\alpha_{\rm EM}$ and α_s (the status of the first of which was discussed in Sec. 17.2.5); $\pi \to \gamma\gamma$ and related amplitudes; long-distance contributions to $\overline{K} \leftrightarrow K$ mixing; the light-by-light contribution to $g_\mu - 2$; and determinations of long distance contributions to rare kaon decays such as $K \to \pi\nu\bar{\nu}$. There will also be steady improvement in the precision attained for the mature quantities discussed above. As already noted, for several of these quantities, attaining the desired precision will ultimately require simulations with $m_u \neq m_d$ and the inclusion of electromagnetic effects.

17.5 Acknowledgments

We are grateful to Jack Laiho for his collaboration on previous editions of this review, and to Christine Davies, Aida El-Khadra, and Andreas Kronfeld for comments and suggestions.

References

[1] K. G. Wilson, Phys. Rev. **D10**, 2445 (1974).

[2] T. Degrand & C. DeTar, "Lattice Methods for Quantum Chromodynamics," World Scientific (2006).

[3] C. Gattringer & C.B. Lang, "Quantum Chromodynamics on the Lattice: An Introductory Presentation," Springer (2009).

[4] "Modern Pespectives in Lattice QCD: quantum field theory and high performance computing" (Lecture notes of the Les Houches Summer School, Vol. 93) eds. L. Lellouch *et al.*, Oxford Univ. Press. (Aug. 2011).

[5] W. Zimmermann, in "Lectures on Elementary Particles and Quantum Field Theory", ed. S. Deser et al., MIT Press, Cambridge, MA (1971); K. Symanzik, Nucl. Phys. **B226**, 187 (1983); K. Symanzik, Nucl. Phys. **B226**, 205 (1983).

[6] M. Lüscher and P. Weisz, Commun. Math. Phys. **97**, 59 (1985), [Erratum: Commun. Math. Phys. 98, 433(1985)].

[7] Y. Iwasaki (1983), UT-HEP-118, [arXiv:1111.7054].

[8] H. B. Nielsen and M. Ninomiya, Phys. Lett. **105B**, 219 (1981).

[9] B. Sheikholeslami and R. Wohlert, Nucl. Phys. **B259**, 572 (1985).

[10] K. Jansen *et al.*, Phys. Lett. **B372**, 275 (1996), [hep-lat/9512009].

[11] M. Lüscher, JHEP **05**, 052 (2003), [hep-lat/0304007].

[12] M. Lüscher, Comput. Phys. Commun. **156**, 209 (2004), [hep-lat/0310048]; M. Lüscher, Comput. Phys. Commun. **165**, 199 (2005), [hep-lat/0409106]; M. Hasenbusch, Phys. Lett. **B519**, 177 (2001), [hep-lat/0107019]; C. Urbach *et al.*, Comput. Phys. Commun. **174**, 87 (2006), [hep-lat/0506011].

[13] S. Dürr *et al.*, Phys. Lett. B **705**, 477 (2011), [arXiv:1106.3230].

[14] N. Ishizuka *et al.*, Phys. Rev. **D92**, 7, 074503 (2015), [arXiv:1505.05289].

[15] R. Frezzotti *et al.* (Alpha), JHEP **08**, 058 (2001), [hep-lat/0101001].

[16] R. Frezzotti and G. C. Rossi, JHEP **08**, 007 (2004), [hep-lat/0306014].

[17] R. Frezzotti and G. C. Rossi, Nucl. Phys. Proc. Suppl. **128**, 193 (2004), [hep-lat/0311008].

[18] R. Frezzotti and G. C. Rossi, JHEP **10**, 070 (2004), [hep-lat/0407002].

[19] L. Susskind, Phys. Rev. **D16**, 3031 (1977); N. Kawamoto and J. Smit, Nucl. Phys. B **192**, 100 (1981); H. S. Sharatchandra, H. J. Thun and P. Weisz, Nucl. Phys. B **192**, 205 (1981).

[20] M. Golterman, PoS **CONFINEMENT8**, 014 (2008), [arXiv:0812.3110].

[21] C. Bernard, Phys. Rev. **D73**, 114503 (2006), [hep-lat/0603011]; S. R. Sharpe, PoS **LAT2006**, 022 (2006), [hep-lat/0610094].

[22] J. A. Bailey, Phys. Rev. D **75**, 114505 (2007), [hep-lat/0611023]; Y. Lin *et al.*, Phys. Rev. D **103**, 5, 054510 (2021), [arXiv:2010.10455].

[23] G. P. Lepage, Phys. Rev. **D59**, 074502 (1999), [hep-lat/9809157].

[24] A. Bazavov *et al.* (MILC), Rev. Mod. Phys. **82**, 1349 (2010), [arXiv:0903.3598].

[25] E. Follana *et al.* (HPQCD, UKQCD), Phys. Rev. **D75**, 054502 (2007), [hep-lat/0610092].

[26] C. T. H. Davies *et al.*, Phys. Rev. **D82**, 114504 (2010), [arXiv:1008.4018].

[27] C. McNeile *et al.*, Phys. Rev. **D85**, 031503 (2012), [arXiv:1110.4510].

[28] G. C. Donald *et al.*, Phys. Rev. **D86**, 094501 (2012), [arXiv:1208.2855].

[29] P. H. Ginsparg and K. G. Wilson, Phys. Rev. **D25**, 2649 (1982).

[30] P. Hasenfratz, V. Laliena and F. Niedermayer, Phys. Lett. **B427**, 125 (1998), [hep-lat/9801021].

[31] M. Lüscher, Phys. Lett. **B428**, 342 (1998), [hep-lat/9802011].

[32] D. B. Kaplan, Phys. Lett. **B288**, 342 (1992), [hep-lat/9206013]; Y. Shamir, Nucl. Phys. **B406**, 90 (1993), [hep-lat/9303005]; Y. Shamir, Nucl. Phys. **B417**, 167 (1994), [hep-lat/9310006].

[33] H. Neuberger, Phys. Lett. **B417**, 141 (1998), [hep-lat/9707022]; H. Neuberger, Phys. Lett. **B427**, 353 (1998), [hep-lat/9801031].

[34] A. Borici, NATO Sci. Ser. C **553**, 41 (2000), [hep-lat/9912040].

[35] A. D. Kennedy (2006), [hep-lat/0607038].

[36] E. Shintani *et al.* (JLQCD), Phys. Rev. Lett. **101**, 242001 (2008), [arXiv:0806.4222].

[37] P. A. Boyle *et al.*, JHEP **12**, 008 (2017), [arXiv:1701.02644].

[38] K. Nakayama, B. Fahy and S. Hashimoto, Phys. Rev. **D94**, 5, 054507 (2016), [arXiv:1606.01002].

[39] A. Bazavov *et al.*, Phys. Rev. **D98**, 7, 074512 (2018), [arXiv:1712.09262].

[40] A. Bazavov *et al.* (Fermilab Lattice, MILC, TUMQCD), Phys. Rev. **D98**, 5, 054517 (2018), [arXiv:1802.04248].

[41] E. Eichten and B. R. Hill, Phys. Lett. **B234**, 511 (1990).

[42] J. Heitger and R. Sommer (ALPHA), JHEP **02**, 022 (2004), [hep-lat/0310035]; B. Blossier *et al.* (ALPHA), JHEP **12**, 039 (2010), [arXiv:1006.5816].

Downloaded from https://academic.oup.com/ptep/article/2022/8/083C01/6651666 by KIT Library user on 27 September 2022

[43] B. A. Thacker and G. P. Lepage, Phys. Rev. **D43**, 196 (1991); G. P. Lepage *et al.*, Phys. Rev. **D46**, 4052 (1992), [hep-lat/9205007].

[44] R. J. Dowdall *et al.* (HPQCD), Phys. Rev. **D85**, 054509 (2012), [arXiv:1110.6887].

[45] A. X. El-Khadra, A. S. Kronfeld and P. B. Mackenzie, Phys. Rev. **D55**, 3933 (1997), [hep-lat/9604004].

[46] S. Aoki, Y. Kuramashi and S.-i. Tominaga, Prog. Theor. Phys. **109**, 383 (2003), [hep-lat/0107009].

[47] N. H. Christ, M. Li and H.-W. Lin, Phys. Rev. **D76**, 074505 (2007), [hep-lat/0608006].

[48] Y. Aoki *et al.* (RBC, UKQCD), Phys. Rev. **D86**, 116003 (2012), [arXiv:1206.2554].

[49] N. H. Christ *et al.*, Phys. Rev. **D91**, 5, 054502 (2015), [arXiv:1404.4670].

[50] M. B. Oktay and A. S. Kronfeld, Phys. Rev. **D78**, 014504 (2008), [arXiv:0803.0523].

[51] J. A. Bailey *et al.*, Eur. Phys. J. **C77**, 11, 768 (2017), [arXiv:1701.00345].

[52] B. Blossier *et al.* (ETM), JHEP **04**, 049 (2010), [arXiv:0909.3187].

[53] S. Borsanyi *et al.*, Science **347**, 1452 (2015), [arXiv:1406.4088].

[54] S. Aoki *et al.* (Flavour Lattice Averaging Group) (2019), [arXiv:1902.08191].

[55] R. Horsley *et al.*, J. Phys. G **43**, 10, 10LT02 (2016), [arXiv:1508.06401].

[56] R. Horsley *et al.* (CSSM, QCDSF, UKQCD), J. Phys. G **46**, 115004 (2019), [arXiv:1904.02304].

[57] Z. R. Kordov *et al.* (CSSM/QCDSF/UKQCD), Phys. Rev. D **101**, 3, 034517 (2020), [arXiv:1911.02186].

[58] S. Aoki *et al.* (HAL QCD), PTEP **2012**, 01A105 (2012), [arXiv:1206.5088].

[59] T. Ishikawa *et al.*, Phys. Rev. Lett. **109**, 072002 (2012), [arXiv:1202.6018].

[60] G. M. de Divitiis *et al.* (RM123), Phys. Rev. **D87**, 11, 114505 (2013), [arXiv:1303.4896].

[61] P. Boyle *et al.*, JHEP **09**, 153 (2017), [arXiv:1706.05293].

[62] S. Basak *et al.* (MILC), Phys. Rev. D **99**, 3, 034503 (2019), [arXiv:1807.05556].

[63] D. Hatton *et al.* (HPQCD), Phys. Rev. D **102**, 5, 054511 (2020), [arXiv:2005.01845].

[64] D. Hatton, C. T. H. Davies and G. P. Lepage, Phys. Rev. D **102**, 9, 094514 (2020), [arXiv:2009.07667].

[65] D. Hatton *et al.*, Phys. Rev. D **103**, 11, 114508 (2021), [arXiv:2102.09609].

[66] F. Bloch and A. Nordsieck, Phys. Rev. **52**, 54 (1937).

[67] N. Carrasco *et al.*, Phys. Rev. **D91**, 7, 074506 (2015), [arXiv:1502.00257].

[68] D. Giusti *et al.*, Phys. Rev. Lett. **120**, 7, 072001 (2018), [arXiv:1711.06537].

[69] M. Di Carlo *et al.*, Phys. Rev. D **100**, 3, 034514 (2019), [arXiv:1904.08731].

[70] C. T. Sachrajda *et al.*, PoS **LATTICE2019**, 162 (2019), [arXiv:1910.07342].

[71] C.-Y. Seng *et al.*, JHEP **10**, 179 (2020), [arXiv:2009.00459].

[72] R. Sommer, Nucl. Phys. B **411**, 839 (1994), [hep-lat/9310022].

[73] M. Lüscher, JHEP **08**, 071 (2010), [Erratum: JHEP 03, 092 (2014)], [arXiv:1006.4518].

[74] Y. Aoki *et al.* (2021), [arXiv:2111.09849].

[75] M. Bruno *et al.* (ALPHA), Phys. Rev. Lett. **114**, 10, 102001 (2015), [arXiv:1410.8374].

[76] F. Knechtli *et al.* (ALPHA), Phys. Lett. **B774**, 649 (2017), [arXiv:1706.04982].

[77] A. Athenodorou *et al.* (ALPHA), Nucl. Phys. **B943**, 114612 (2019), [arXiv:1809.03383].

[78] S. Cali, F. Knechtli and T. Korzec, Eur. Phys. J. **C79**, 7, 607 (2019), [arXiv:1905.12971].

[79] S. Cali *et al.* (2021), [arXiv:2105.12278].

[80] D. Giusti *et al.*, Phys. Rev. **D95**, 11, 114504 (2017), [arXiv:1704.06561].

[81] A. Bazavov *et al.* (Fermilab Lattice, MILC), Phys. Rev. **D93**, 11, 113016 (2016), [arXiv:1602.03560].

[82] R. J. Dowdall *et al.*, Phys. Rev. **D86**, 094510 (2012), [arXiv:1207.5149].

[83] C. McNeile *et al.*, Phys. Rev. **D86**, 074503 (2012), [arXiv:1207.0994].

[84] S. Schaefer, R. Sommer and F. Virotta (ALPHA), Nucl. Phys. **B845**, 93 (2011), [arXiv:1009.5228].

[85] M. Lüscher, PoS **LATTICE2010**, 015 (2010), [arXiv:1009.5877].

[86] R. Brower *et al.*, Phys. Lett. **B560**, 64 (2003), [hep-lat/0302005].

[87] S. Aoki *et al.*, Phys. Rev. **D76**, 054508 (2007), [arXiv:0707.0396].

[88] C. Bernard and D. Toussaint (MILC), Phys. Rev. D **97**, 7, 074502 (2018), [arXiv:1707.05430].

[89] N. Husung, P. Marquard and R. Sommer, Eur. Phys. J. C **80**, 3, 200 (2020), [arXiv:1912.08498].

[90] G. Colangelo, S. Dürr and C. Haefeli, Nucl. Phys. **B721**, 136 (2005), [hep-lat/0503014].

[91] M. Lüscher, Commun. Math. Phys. **104**, 177 (1986).

[92] G. Martinelli *et al.*, Nucl. Phys. **B445**, 81 (1995), [hep-lat/9411010].

[93] M. Lüscher *et al.*, Nucl. Phys. **B384**, 168 (1992), [hep-lat/9207009].

[94] G. Martinelli *et al.*, Phys. Lett. **B411**, 141 (1997), [hep-lat/9705018].

[95] B. Colquhoun *et al.*, Phys. Rev. **D91**, 7, 074514 (2015), [arXiv:1408.5768].

[96] D. Hatton *et al.* (HPQCD), Phys. Rev. D **100**, 11, 114513 (2019), [arXiv:1909.00756].

[97] M. Lüscher *et al.*, Nucl. Phys. **B413**, 481 (1994), [hep-lat/9309005]; M. Della Morte *et al.* (ALPHA), Nucl. Phys. **B713**, 378 (2005), [hep-lat/0411025].

[98] M. Tomii *et al.* (JLQCD), Phys. Rev. **D94**, 5, 054504 (2016), [arXiv:1604.08702].

[99] S. Duane *et al.*, Phys. Lett. **B195**, 216 (1987).

[100] M. A. Clark and A. D. Kennedy, Phys. Rev. Lett. **98**, 051601 (2007), [hep-lat/0608015].

[101] M. Lüscher, JHEP **07**, 081 (2007), [arXiv:0706.2298].

[102] M. Lüscher, JHEP **12**, 011 (2007), [arXiv:0710.5417].

[103] A. Stathopoulos and K. Orginos, SIAM J. Sci. Comput. **32**, 439 (2010), [arXiv:0707.0131].

[104] P. A. Boyle (2014), [arXiv:1402.2585].

[105] R. Babich *et al.*, Phys. Rev. Lett. **105**, 201602 (2010), [arXiv:1005.3043].

[106] A. Frommer *et al.*, SIAM J. Sci. Comput. **36**, A1581 (2014), [arXiv:1303.1377].

[107] M. Bruno, S. Schaefer and R. Sommer (ALPHA), JHEP **08**, 150 (2014), [arXiv:1406.5363].

[108] M. Creutz, Phys. Rev. **D38**, 1228 (1988); R. Gupta, G. W. Kilcup and S. R. Sharpe, Phys. Rev. **D38**, 1278 (1988).

[109] M. Lüscher and U. Wolff, Nucl. Phys. **B339**, 222 (1990).

Downloaded from https://academic.oup.com/ptep/article/2022/8/083C01/6651666 by KIT Library user on 27 September 2022

[110] J. J. Dudek *et al.*, Phys. Rev. **D82**, 034508 (2010), [arXiv:1004.4930]; J. J. Dudek *et al.*, Phys. Rev. **D83**, 111502 (2011), [arXiv:1102.4299]; R. G. Edwards *et al.*, Phys. Rev. **D84**, 074508 (2011), [arXiv:1104.5152].

[111] G. P. Engel *et al.* (BGR [Bern-Graz-Regensburg]), Phys. Rev. **D82**, 034505 (2010), [arXiv:1005.1748]; D. Mohler *et al.*, Phys. Rev. Lett. **111**, 22, 222001 (2013), [arXiv:1308.3175].

[112] M. S. Mahbub *et al.*, Annals Phys. **342**, 270 (2014), [arXiv:1310.6803].

[113] J. Bulava *et al.*, Nucl. Phys. **B910**, 842 (2016), [arXiv:1604.05593].

[114] R. Brett *et al.*, Nucl. Phys. **B932**, 29 (2018), [arXiv:1802.03100].

[115] B. Hörz and A. Hanlon, Phys. Rev. Lett. **123**, 14, 142002 (2019), [arXiv:1905.04277].

[116] J. E. Mandula, G. Zweig and J. Govaerts, Nucl. Phys. **B228**, 91 (1983); J. E. Mandula and E. Shpiz, Nucl. Phys. **B232**, 180 (1984).

[117] H. B. Meyer and M. J. Teper, Nucl. Phys. **B658**, 113 (2003), [hep-lat/0212026].

[118] M. Lüscher, Commun. Math. Phys. **105**, 153 (1986); M. Lüscher, Nucl. Phys. **B364**, 237 (1991).

[119] L. Maiani and M. Testa, Phys. Lett. **B245**, 585 (1990).

[120] M. T. Hansen, H. B. Meyer and D. Robaina, Phys. Rev. **D96**, 9, 094513 (2017), [arXiv:1704.08993].

[121] M. Hansen, A. Lupo and N. Tantalo, Phys. Rev. **D99**, 9, 094508 (2019), [arXiv:1903.06476].

[122] J. Bulava and M. T. Hansen, Phys. Rev. D **100**, 3, 034521 (2019), [arXiv:1903.11735].

[123] M. Bruno and M. T. Hansen (2020), [arXiv:2012.11488].

[124] R. A. Briceno, J. J. Dudek and R. D. Young, Rev. Mod. Phys. **90**, 2, 025001 (2018), [arXiv:1706.06223]; N. Brambilla *et al.* (2019), [arXiv:1907.07583].

[125] M. J. Savage, Prog. Part. Nucl. Phys. **67**, 140 (2012), [arXiv:1110.5943]; T. Inoue *et al.* (HAL QCD), Phys. Rev. **C91**, 1, 011001 (2015), [arXiv:1408.4892]; B. Hörz *et al.*, Phys. Rev. C **103**, 1, 014003 (2021), [arXiv:2009.11825].

[126] K. Polejaeva and A. Rusetsky, Eur. Phys. J. **A48**, 67 (2012), [arXiv:1203.1241]; R. A. Briceno and Z. Davoudi, Phys. Rev. **D87**, 9, 094507 (2013), [arXiv:1212.3398]; M. T. Hansen and S. R. Sharpe, Phys. Rev. **D90**, 11, 116003 (2014), [arXiv:1408.5933]; M. T. Hansen and S. R. Sharpe, Phys. Rev. **D92**, 11, 114509 (2015), [arXiv:1504.04248]; R. Briceño, M. T. Hansen and S. R. Sharpe, Phys. Rev. **D95**, 7, 074510 (2017), [arXiv:1701.07465]; H. W. Hammer, J. Y. Pang and A. Rusetsky, JHEP **10**, 115 (2017), [arXiv:1707.02176]; R. A. Briceno, M. T. Hansen and S. R. Sharpe, Phys. Rev. **D99**, 1, 014516 (2019), [arXiv:1810.01429]; M. Mai and M. Döring, Eur. Phys. J. **A53**, 12, 240 (2017), [arXiv:1709.08222]; M. T. Hansen, F. Romero-López and S. R. Sharpe, JHEP **07**, 047 (2020), [Erratum: JHEP 02, 014 (2021)], [arXiv:2003.10974]; T. D. Blanton and S. R. Sharpe, Phys. Rev. D **103**, 5, 054503 (2021), [arXiv:2011.05520].

[127] T. D. Blanton, F. Romero-López and S. R. Sharpe, Phys. Rev. Lett. **124**, 3, 032001 (2020), [arXiv:1909.02973]; C. Culver *et al.*, Phys. Rev. D **101**, 11, 114507 (2020), [arXiv:1911.09047]; A. Alexandru *et al.*, Phys. Rev. D **102**, 11, 114523 (2020), [arXiv:2009.12358].

[128] M. T. Hansen and S. R. Sharpe (2019), [arXiv:1901.00483]; M. Mai, M. Döring and A. Rusetsky, Eur. Phys. J. ST **230**, 6, 1623 (2021), [arXiv:2103.00577].

[129] L. Lellouch and M. Lüscher, Commun. Math. Phys. **219**, 31 (2001), [hep-lat/0003023].

[130] T. Blum *et al.*, Phys. Rev. Lett. **108**, 141601 (2012), [arXiv:1111.1699]; T. Blum *et al.*, Phys. Rev. **D86**, 074513 (2012), [arXiv:1206.5142].

[131] Z. Bai *et al.* (RBC, UKQCD), Phys. Rev. Lett. **115**, 21, 212001 (2015), [arXiv:1505.07863].

[132] R. Abbott *et al.* (RBC, UKQCD), Phys. Rev. D **102**, 5, 054509 (2020), [arXiv:2004.09440].

[133] T. Blum *et al.*, Phys. Rev. **D91**, 7, 074502 (2015), [arXiv:1502.00263].

[134] V. Bernard *et al.*, JHEP **01**, 019 (2011), [arXiv:1010.6018]; M. Doring *et al.*, Eur. Phys. J. **A47**, 139 (2011), [arXiv:1107.3988]; M. T. Hansen and S. R. Sharpe, Phys. Rev. **D86**, 016007 (2012), [arXiv:1204.0826]; R. A. Briceño and Z. Davoudi, Phys. Rev. **D88**, 9, 094507 (2013), [arXiv:1204.1110].

[135] R. Briceño, M. T. Hansen and A. Walker-Loud, Phys. Rev. **D91**, 3, 034501 (2015), [arXiv:1406.5965].

[136] R. Briceño and M. T. Hansen, Phys. Rev. **D94**, 1, 013008 (2016), [arXiv:1509.08507].

[137] R. Briceño *et al.*, Phys. Rev. **D93**, 11, 114508 (2016), [arXiv:1604.03530].

[138] F. Müller and A. Rusetsky, JHEP **03**, 152 (2021), [arXiv:2012.13957].

[139] M. T. Hansen, F. Romero-López and S. R. Sharpe, JHEP **04**, 113 (2021), [arXiv:2101.10246].

[140] D. Agadjanov *et al.*, JHEP **06**, 043 (2016), [arXiv:1603.07205].

[141] S. Hashimoto, PTEP **2017**, 5, 053B03 (2017), [arXiv:1703.01881].

[142] P. Gambino and S. Hashimoto, Phys. Rev. Lett. **125**, 3, 032001 (2020), [arXiv:2005.13730].

[143] H. Fukaya *et al.*, Phys. Rev. D **102**, 11, 114516 (2020), [arXiv:2010.01253].

[144] X. Feng *et al.*, Phys. Rev. Lett. **107**, 081802 (2011), [arXiv:1103.4818].

[145] P. Boyle *et al.*, Phys. Rev. **D85**, 074504 (2012), [arXiv:1107.1497].

[146] M. Della Morte *et al.*, JHEP **03**, 055 (2012), [arXiv:1112.2894].

[147] F. Burger *et al.* (ETM), JHEP **02**, 099 (2014), [arXiv:1308.4327].

[148] B. Chakraborty *et al.* (HPQCD), Phys. Rev. **D89**, 11, 114501 (2014), [arXiv:1403.1778].

[149] F. Burger *et al.*, Eur. Phys. J. C **76**, 8, 464 (2016), [arXiv:1501.05110].

[150] B. Chakraborty *et al.*, Phys. Rev. **D93**, 7, 074509 (2016), [arXiv:1512.03270].

[151] B. Chakraborty *et al.*, Phys. Rev. **D96**, 3, 034516 (2017), [arXiv:1601.03071].

[152] T. Blum *et al.* (RBC/UKQCD), JHEP **04**, 063 (2016), [Erratum: JHEP05, 034(2017)], [arXiv:1602.01767].

[153] S. Borsanyi *et al.*, Phys. Rev. **D96**, 7, 074507 (2017), [arXiv:1612.02364].

[154] M. Della Morte *et al.*, JHEP **10**, 020 (2017), [arXiv:1705.01775].

[155] S. Borsanyi *et al.* (Budapest-Marseille-Wuppertal), Phys. Rev. Lett. **121**, 2, 022002 (2018), [arXiv:1711.04980].

[156] T. Blum *et al.* (RBC, UKQCD), Phys. Rev. Lett. **121**, 2, 022003 (2018), [arXiv:1801.07224].

[157] D. Giusti, F. Sanfilippo and S. Simula, Phys. Rev. **D98**, 11, 114504 (2018), [arXiv:1808.00887].

[158] C. T. H. Davies *et al.* (Fermilab Lattice, HPQCD, MILC), Phys. Rev. D **101**, 3, 034512 (2020), [arXiv:1902.04223].

[159] A. Gérardin *et al.*, Phys. Rev. D **100**, 1, 014510 (2019), [arXiv:1904.03120].

[160] C. Aubin *et al.*, Phys. Rev. D **101**, 1, 014503 (2020), [arXiv:1905.09307].

Downloaded from https://academic.oup.com/ptep/article/2022/8/083C01/6651666 by KIT Library user on 27 September 2022

[161] T. Blum, Phys. Rev. Lett. **91**, 052001 (2003), [hep-lat/0212018].

[162] T. Aoyama *et al.*, Phys. Rept. **887**, 1 (2020), [arXiv:2006.04822].

[163] T. Izubuchi *et al.* (PACS), Phys. Rev. D **98**, 5, 054505 (2018), [arXiv:1805.04250].

[164] E. Shintani and Y. Kuramashi (PACS), Phys. Rev. D **100**, 3, 034517 (2019), [arXiv:1902.00885].

[165] B. Chakraborty *et al.* (Fermilab Lattice, HPQCD, MILC), Phys. Rev. Lett. **120**, 15, 152001 (2018), [arXiv:1710.11212].

[166] D. Giusti *et al.*, Phys. Rev. D **99**, 11, 114502 (2019), [arXiv:1901.10462].

[167] S. Borsanyi *et al.*, Nature **593**, 7857, 51 (2021), [arXiv:2002.12347].

[168] T. Blum *et al.*, Phys. Rev. Lett. **114**, 1, 012001 (2015), [arXiv:1407.2923].

[169] T. Blum *et al.*, Phys. Rev. **D93**, 1, 014503 (2016), [arXiv:1510.07100].

[170] J. Green *et al.*, Phys. Rev. Lett. **115**, 22, 222003 (2015), [arXiv:1507.01577].

[171] T. Blum *et al.*, Phys. Rev. Lett. **118**, 2, 022005 (2017), [arXiv:1610.04603].

[172] T. Blum *et al.*, Phys. Rev. **D96**, 3, 034515 (2017), [arXiv:1705.01067].

[173] T. Blum *et al.*, "Hadronic Light-by-Light Scattering Contribution to the Muon Anomalous Magnetic Moment from Lattice QCD," (2020), [arXiv:1911.08123].

[174] E.-H. Chao *et al.*, Eur. Phys. J. C **80**, 9, 869 (2020), [arXiv:2006.16224].

[175] E.-H. Chao *et al.*, Eur. Phys. J. C **81**, 7, 651 (2021), [arXiv:2104.02632].

[176] Z. Bai *et al.*, Phys. Rev. Lett. **113**, 112003 (2014), [arXiv:1406.0916].

[177] N. H. Christ *et al.*, Phys. Rev. D **91**, 11, 114510 (2015), [arXiv:1504.01170].

[178] N. H. Christ *et al.* (RBC, UKQCD), Phys. Rev. **D92**, 9, 094512 (2015), [arXiv:1507.03094].

[179] N. H. Christ *et al.* (RBC, UKQCD), Phys. Rev. **D93**, 11, 114517 (2016), [arXiv:1605.04442].

[180] N. H. Christ *et al.*, Phys. Rev. **D94**, 11, 114516 (2016), [arXiv:1608.07585].

[181] Z. Bai *et al.*, Phys. Rev. Lett. **118**, 25, 252001 (2017), [arXiv:1701.02858].

[182] Z. Bai *et al.*, Phys. Rev. **D98**, 7, 074509 (2018), [arXiv:1806.11520].

[183] N. H. Christ *et al.* (RBC, UKQCD), Phys. Rev. D **100**, 11, 114506 (2019), [arXiv:1910.10644].

[184] C. Kane *et al.*, PoS **LATTICE2019**, 134 (2019), [arXiv:1907.00279].

[185] A. Desiderio *et al.*, Phys. Rev. D **103**, 1, 014502 (2021), [arXiv:2006.05358].

[186] C. Bernard *et al.*, Nucl. Phys. Proc. Suppl. **119**, 170 (2003), [hep-lat/0209086].

[187] S. Perantonis and C. Michael, Nucl. Phys. **B347**, 854 (1990).

[188] G. S. Bali and K. Schilling, Phys. Rev. **D46**, 2636 (1992).

[189] S. Necco and R. Sommer, Nucl. Phys. **B622**, 328 (2002), [hep-lat/0108008].

[190] J. M. Blairon *et al.*, Nucl. Phys. **B180**, 439 (1981).

[191] H. Fukaya *et al.* (JLQCD), Phys. Rev. Lett. **104**, 122002 (2010), [Erratum: Phys. Rev. Lett.105,159901(2010)], [arXiv:0911.5555].

[192] H. Fukaya *et al.* (JLQCD, TWQCD), Phys. Rev. **D83**, 074501 (2011), [arXiv:1012.4052].

[193] L. Giusti and M. Lüscher, JHEP **03**, 013 (2009), [arXiv:0812.3638].

[194] K. Cichy, E. Garcia-Ramos and K. Jansen, JHEP **10**, 175 (2013), [arXiv:1303.1954].

[195] G. P. Engel *et al.*, Phys. Rev. Lett. **114**, 11, 112001 (2015), [arXiv:1406.4987].

[196] G. P. Engel *et al.*, Phys. Rev. **D91**, 5, 054505 (2015), [arXiv:1411.6386].

[197] G. Cossu *et al.*, PTEP **2016**, 9, 093B06 (2016), [arXiv:1607.01099].

[198] S. Aoki *et al.*, Eur. Phys. J. **C77**, 2, 112 (2017), [arXiv:1607.00299].

[199] G. S. Bali *et al.* (2021), [arXiv:2106.05398].

[200] T. Blum *et al.* (RBC, UKQCD), Phys. Rev. **D93**, 7, 074505 (2016), [arXiv:1411.7017].

[201] B. J. Choi *et al.* (SWME), Phys. Rev. **D93**, 1, 014511 (2016), [arXiv:1509.00592].

[202] J. Laiho and R. S. Van de Water, PoS **LATTICE2011**, 293 (2011), [arXiv:1112.4861].

[203] T. Blum *et al.* (RBC, UKQCD), Phys. Rev. D **93**, 7, 074505 (2016), [arXiv:1411.7017].

[204] B. J. Choi *et al.* (SWME), Phys. Rev. D **93**, 1, 014511 (2016), [arXiv:1509.00592].

[205] E. Gamiz *et al.* (HPQCD), Phys. Rev. **D80**, 014503 (2009), [arXiv:0902.1815].

[206] R. J. Dowdall *et al.*, Phys. Rev. D **100**, 9, 094508 (2019), [arXiv:1907.01025].

[207] Y. Aoki *et al.*, Phys. Rev. **D91**, 11, 114505 (2015), [arXiv:1406.6192].

[208] N. Carrasco *et al.* (ETM), Phys. Rev. D **92**, 3, 034516 (2015), [arXiv:1505.06639].

[209] A. Bazavov *et al.*, Phys. Rev. **D97**, 3, 034513 (2018), [arXiv:1706.04622].

[210] C. T. H. Davies *et al.* (HPQCD), Phys. Rev. Lett. **124**, 8, 082001 (2020), [arXiv:1910.00970].

[211] M. Ademollo and R. Gatto, Phys. Rev. Lett. **13**, 264 (1964).

[212] H. Leutwyler and M. Roos, Z. Phys. **C25**, 91 (1984).

[213] P. A. Boyle *et al.*, Phys. Rev. Lett. **100**, 141601 (2008), [arXiv:0710.5136].

[214] V. Lubicz *et al.* (ETM), Phys. Rev. **D80**, 111502 (2009), [arXiv:0906.4728]; V. Lubicz *et al.* (ETM), PoS **LATTICE2010**, 316 (2010), [arXiv:1012.3573].

[215] P. A. Boyle *et al.* (RBC-UKQCD), Eur. Phys. J. **C69**, 159 (2010), [arXiv:1004.0886].

[216] A. Bazavov *et al.*, Phys. Rev. **D87**, 073012 (2013), [arXiv:1212.4993].

[217] T. Kaneko *et al.* (JLQCD), PoS **LATTICE2012**, 111 (2012), [arXiv:1211.6180].

[218] P. A. Boyle *et al.*, JHEP **08**, 132 (2013), [arXiv:1305.7217].

[219] P. A. Boyle *et al.* (RBC/UKQCD), JHEP **06**, 164 (2015), [arXiv:1504.01692].

[220] N. Carrasco *et al.*, Phys. Rev. **D93**, 11, 114512 (2016), [arXiv:1602.04113]; A. Bazavov *et al.* (Fermilab Lattice, MILC), Phys. Rev. D **99**, 11, 114509 (2019), [arXiv:1809.02827].

[221] H. Na *et al.*, Phys. Rev. **D82**, 114506 (2010), [arXiv:1008.4562].

[222] H. Na *et al.*, Phys. Rev. **D84**, 114505 (2011), [arXiv:1109.1501].

[223] V. Lubicz *et al.* (ETM), Phys. Rev. **D96**, 5, 054514 (2017), [Erratum: Phys. Rev. D99, 099902(2019)], [arXiv:1706.03017].

[224] T. Kaneko *et al.* (JLQCD), EPJ Web Conf. **175**, 13007 (2018), [arXiv:1711.11235].

Downloaded from https://academic.oup.com/ptep/article/2022/8/083C01/6651666 by KIT Library user on 27 September 2022

[225] B. Chakraborty *et al.* (2021), [arXiv:2104.09883].

[226] E. Dalgic *et al.*, Phys. Rev. **D73**, 074502 (2006), [Erratum: Phys. Rev. D75,119906(2007)], [hep-lat/0601021].

[227] J. M. Flynn *et al.*, Phys. Rev. **D91**, 7, 074510 (2015), [arXiv:1501.05373].

[228] J. A. Bailey *et al.* (Fermilab Lattice, MILC), Phys. Rev. **D92**, 1, 014024 (2015), [arXiv:1503.07839].

[229] B. Colquhoun *et al.*, Phys. Rev. **D93**, 3, 034502 (2016), [arXiv:1510.07446].

[230] Z. Gelzer *et al.*, EPJ Web Conf. **175**, 13024 (2018), [arXiv:1710.09442].

[231] B. Colquhoun, S. Hashimoto and T. Kaneko, PoS **LATTICE2018**, 274 (2018), [arXiv:1811.00227].

[232] C. Bourrely, B. Machet and E. de Rafael, Nucl. Phys. **B189**, 157 (1981); C. G. Boyd, B. Grinstein and R. F. Lebed, Phys. Rev. Lett. **74**, 4603 (1995), [hep-ph/9412324]; T. Becher and R. J. Hill, Phys. Lett. **B633**, 61 (2006), [hep-ph/0509090]; C. Bourrely, I. Caprini and L. Lellouch, Phys. Rev. **D79**, 013008 (2009), [Erratum: Phys. Rev. D82, 099902(2010)], [arXiv:0807.2722].

[233] M. C. Arnesen *et al.*, Phys. Rev. Lett. **95**, 071802 (2005), [hep-ph/0504209].

[234] J. A. Bailey *et al.*, Phys. Rev. **D79**, 054507 (2009), [arXiv:0811.3640].

[235] S. Hashimoto *et al.*, Phys. Rev. **D61**, 014502 (1999), [hep-ph/9906376].

[236] S. Hashimoto *et al.*, Phys. Rev. **D66**, 014503 (2002), [hep-ph/0110253].

[237] C. Bernard *et al.*, Phys. Rev. **D79**, 014506 (2009), [arXiv:0808.2519].

[238] J. A. Bailey *et al.* (Fermilab Lattice, MILC), Phys. Rev. **D89**, 11, 114504 (2014), [arXiv:1403.0635].

[239] J. Harrison, C. Davies and M. Wingate (HPQCD), Phys. Rev. **D97**, 5, 054502 (2018), [arXiv:1711.11013].

[240] E. McLean *et al.*, Phys. Rev. **D99**, 11, 114512 (2019), [arXiv:1904.02046].

[241] T. Bhattacharya *et al.* (LANL/SWME), PoS **LATTICE2018**, 283 (2018).

[242] J. A. Bailey *et al.* (MILC), Phys. Rev. **D92**, 3, 034506 (2015), [arXiv:1503.07237]; H. Na *et al.* (HPQCD), Phys. Rev. **D92**, 5, 054510 (2015), [Erratum: Phys. Rev. D93, 19906(2016)], [arXiv:1505.03925]; T. Kaneko *et al.* (JLQCD), PoS **LATTICE2018**, 311 (2018), [arXiv:1811.00794]; E. McLean *et al.*, Phys. Rev. D **101**, 7, 074513 (2020), [arXiv:1906.00701]; J. Harrison and C. T. H. Davies (HPQCD) (2021), [arXiv:2105.11433]; A. Bazavov *et al.* (Fermilab Lattice, MILC) (2021), [arXiv:2105.14019].

[243] W. Detmold, C. Lehner and S. Meinel, Phys. Rev. **D92**, 3, 034503 (2015), [arXiv:1503.01421].

[244] W. Detmold and S. Meinel, Phys. Rev. **D93**, 7, 074501 (2016), [arXiv:1602.01399].

[245] R. R. Horgan *et al.*, Phys. Rev. **D89**, 9, 094501 (2014), [arXiv:1310.3722].

[246] J. A. Bailey *et al.*, Phys. Rev. **D93**, 2, 025026 (2016), [arXiv:1509.06235].

[247] D. Du *et al.*, Phys. Rev. **D93**, 3, 034005 (2016), [arXiv:1510.02349].

[248] C. T. H. Davies *et al.* (HPQCD), Phys. Rev. **D78**, 114507 (2008), [arXiv:0807.1687].

[249] C. McNeile *et al.*, Phys. Rev. **D82**, 034512 (2010), [arXiv:1004.4285].

[250] A. Bochkarev and P. de Forcrand, Nucl. Phys. B **477**, 489 (1996), [hep-lat/9505025].

[251] E. Shintani *et al.*, Phys. Rev. **D82**, 7, 074505 (2010), [Erratum: Phys. Rev. D89, 099903(2014)], [arXiv:1002.0371].

[252] R. J. Hudspith *et al.*, Mod. Phys. Lett. **A31**, 32, 1630037 (2016).

[253] R. J. Hudspith *et al.* (2018), [arXiv:1804.10286].

[254] S. Cali *et al.*, Phys. Rev. Lett. **125**, 242002 (2020), [arXiv:2003.05781].

[255] I. Allison *et al.* (HPQCD), Phys. Rev. **D78**, 054513 (2008), [arXiv:0805.2999].

[256] B. Chakraborty *et al.*, Phys. Rev. **D91**, 5, 054508 (2015), [arXiv:1408.4169].

[257] Y. Maezawa and P. Petreczky, Phys. Rev. **D94**, 3, 034507 (2016), [arXiv:1606.08798].

[258] P. Petreczky and J. H. Weber, Phys. Rev. D **100**, 3, 034519 (2019), [arXiv:1901.06424].

[259] Q. Mason *et al.* (HPQCD, UKQCD), Phys. Rev. Lett. **95**, 052002 (2005), [hep-lat/0503005].

[260] A. Bazavov *et al.*, Phys. Rev. **D86**, 114031 (2012), [arXiv:1205.6155].

[261] A. Bazavov *et al.*, Phys. Rev. **D90**, 7, 074038 (2014), [arXiv:1407.8437].

[262] F. Karbstein, M. Wagner and M. Weber, Phys. Rev. **D98**, 11, 114506 (2018), [arXiv:1804.10909].

[263] H. Takaura *et al.*, JHEP **04**, 155 (2019), [arXiv:1808.01643].

[264] A. Bazavov *et al.* (TUMQCD), Phys. Rev. D **100**, 11, 114511 (2019), [arXiv:1907.11747].

[265] B. Blossier *et al.*, Phys. Rev. **D85**, 034503 (2012), [arXiv:1110.5829]; B. Blossier *et al.*, Phys. Rev. Lett. **108**, 262002 (2012), [arXiv:1201.5770].

[266] S. Zafeiropoulos *et al.*, Phys. Rev. Lett. **122**, 16, 162002 (2019), [arXiv:1902.08148].

[267] S. Aoki *et al.* (PACS-CS), JHEP **10**, 053 (2009), [arXiv:0906.3906].

[268] P. Fritzsch *et al.*, PoS **LATTICE2014**, 291 (2014), [arXiv:1411.7648].

[269] M. Bruno *et al.* (ALPHA), Phys. Rev. Lett. **119**, 10, 102001 (2017), [arXiv:1706.03821].

[270] C. Ayala, X. Lobregat and A. Pineda, JHEP **09**, 016 (2020), [arXiv:2005.12301].

[271] K. Maltman *et al.*, Phys. Rev. D **78**, 114504 (2008), [arXiv:0807.2020].

[272] S. Dürr *et al.*, Phys. Lett. **B701**, 265 (2011), [arXiv:1011.2403].

[273] S. Dürr *et al.*, JHEP **08**, 148 (2011), [arXiv:1011.2711].

[274] A. T. Lytle *et al.* (HPQCD), Phys. Rev. D **98**, 1, 014513 (2018), [arXiv:1805.06225].

[275] A. Bazavov *et al.* (Fermilab Lattice, MILC, TUMQCD), Phys. Rev. D **98**, 5, 054517 (2018), [arXiv:1802.04248].

[276] C. Alexandrou *et al.* (2021), [arXiv:2104.13408].

[277] S. Capitani *et al.*, Nucl. Phys. **B544**, 669 (1999), [Erratum: Nucl. Phys. B582, 762(2000)], [hep-lat/9810063].

[278] M. Bruno *et al.* (ALPHA), PoS **LATTICE2018**, 220 (2019), [arXiv:1903.04094].

[279] J. Komijani, JHEP **08**, 062 (2017), [arXiv:1701.00347]; N. Brambilla *et al.* (TUMQCD), Phys. Rev. D **97**, 3, 034503 (2018), [arXiv:1712.04983].

[280] A. Bussone *et al.* (ETM), Phys. Rev. **D93**, 11, 114505 (2016), [arXiv:1603.04306].

[281] *Proceedings, 36th International Symposium on Lattice Field Theory*, volume PoS **LATTICE2018** (2019), URL `https://pos.sissa.it/334/`.

[282] W. Detmold *et al.* (USQCD) (2019), [arXiv:1904.09512].

[283] A. S. Kronfeld *et al.* (USQCD) (2019), [arXiv:1904.09931].

[284] R. C. Brower *et al.* (USQCD) (2019), [arXiv:1904.09964].

[285] C. Lehner *et al.* (USQCD) (2019), [arXiv:1904.09479].

Downloaded from https://academic.oup.com/ptep/article/2022/8/083C01/6651666 by KIT Library user on 27 September 2022

[286] A. Bazavov *et al.* (USQCD) (2019), [arXiv:1904.09951].
[287] V. Cirigliano *et al.* (USQCD) (2019), [arXiv:1904.09704].
[288] B. Joó *et al.* (USQCD) (2019), [arXiv:1904.09725].

Downloaded from https://academic.oup.com/ptep/article/2022/8/083C01/6651666 by KIT Library user on 27 September 2022

18. Structure Functions

Revised August 2021 by E.C. Aschenauer (BNL), R.S. Thorne (UCL) and R. Yoshida (ANL).

18.1 Deep inelastic scattering

High-energy lepton-nucleon scattering plays a key role in determining the partonic structure of the proton. The process $\ell N \to \ell' X$ is illustrated in Fig. 18.1. The filled circle in this figure represents the internal structure of the proton which can be expressed in terms of structure functions.

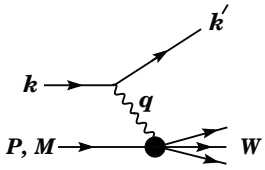

Figure 18.1: Kinematic quantities for the description of deep inelastic scattering. The quantities k and k' are the four-momenta of the incoming and outgoing leptons, P is the four-momentum of a nucleon with mass M, and W is the mass of the recoiling system X. The exchanged particle is a γ, $W^{\pm}$, or Z; it transfers four-momentum $q = k - k'$ to the nucleon.

Invariant quantities:

$\nu = \frac{q\cdot P}{M} = E - E'$ is the lepton's energy loss in the nucleon rest frame (in earlier literature sometimes $\nu = q \cdot P$). Here, E and E' are the initial and final lepton energies in the nucleon rest frame.

$Q^2 = -q^2 = 2(EE' - \vec{k} \cdot \vec{k}\,') - m_\ell^2 - m_{\ell'}^2$ where $m_\ell(m_{\ell'})$ is the initial (final) lepton mass. If $EE' \sin^2(\theta/2) \gg m_\ell^2,\, m_{\ell'}^2$, then

$\approx 4EE' \sin^2(\theta/2)$, where θ is the lepton's scattering angle with respect to the lepton beam direction.

$x = \frac{Q^2}{2M\nu}$ where, in the parton model, x is the fraction of the nucleon's momentum carried by the struck quark. Beyond leading order the equation remains the definition of x, but this is no longer identical to nucleon momentum fraction.

$y = \frac{q\cdot P}{k\cdot P} = \frac{\nu}{E}$ is the fraction of the lepton's energy lost in the nucleon rest frame.

$W^2 = (P+q)^2 = M^2 + 2M\nu - Q^2$ is the mass squared of the system X recoiling against the scattered lepton.

$s = (k+P)^2 = \frac{Q^2}{xy} + M^2 + m_\ell^2$ is the center-of-mass energy squared of the lepton-nucleon system.

The process in Fig. 18.1 is called deep ($Q^2 \gg M^2$) inelastic ($W^2 \gg M^2$) scattering (DIS). In what follows, the masses of the initial and scattered leptons, m_ℓ and $m_{\ell'}$, are neglected.

18.1.1 *DIS cross sections*

The double-differential cross section for deep inelastic scattering can be expressed in terms of kinematic variables in several ways.

$$\frac{d^2\sigma}{dx\,dy} = x\,(s - M^2)\,\frac{d^2\sigma}{dx\,dQ^2} = \frac{2\pi\,M\nu}{E'}\,\frac{d^2\sigma}{d\Omega_{\rm Nrest}\,dE'}\ . \qquad (18.1)$$

In lowest-order perturbation theory, the cross section for the scattering of polarized leptons on polarized nucleons can be expressed in terms of the products of leptonic and hadronic tensors associated with the coupling of the exchanged bosons at the upper and lower vertices in Fig. 18.1 (see Refs. [1–4])

$$\frac{d^2\sigma}{dxdy} \;=\; \frac{2\pi y\alpha^2}{Q^4}\,\sum_j \eta_j\, L_j^{\mu\nu}\, W_{\mu\nu}^j\ . \qquad (18.2)$$

For neutral-current processes, the summation is over $j = \gamma, Z$ and γZ representing photon and Z exchange and the interference between them, whereas for charged-current interactions there is only W exchange, $j = W$. (For transverse nucleon polarization, there is a dependence on the azimuthal angle of the scattered lepton.) The lepton tensor $L_{\mu\nu}$ is associated with the coupling of the exchange boson to the leptons. For incoming leptons of charge $e = \pm 1$ and helicity $\lambda = \pm 1$,

$$\begin{aligned}
L_{\mu\nu}^{\gamma} &= 2\left(k_\mu k'_\nu + k'_\mu k_\nu - (k\cdot k' - m_\ell^2) g_{\mu\nu} - i\lambda\varepsilon_{\mu\nu\alpha\beta} k^\alpha k'^\beta\right),\\
L_{\mu\nu}^{\gamma Z} &= (g_V^e + e\lambda g_A^e)\, L_{\mu\nu}^{\gamma}, \quad L_{\mu\nu}^{Z} = (g_V^e + e\lambda g_A^e)^2\, L_{\mu\nu}^{\gamma},\\
L_{\mu\nu}^{W} &= (1 + e\lambda)^2\, L_{\mu\nu}^{\gamma},
\end{aligned} \qquad (18.3)$$

where $g_V^e = -\frac{1}{2} + 2\sin^2\theta_W, \qquad g_A^e = -\frac{1}{2}$.

Although here the helicity basis is adopted, an alternative approach is to express the tensors in Eq. (18.3) in terms of the polarization of the lepton.

The factors η_j in Eq. (18.2) denote the ratios of the corresponding propagators and couplings to the photon propagator and coupling squared

$$\begin{aligned}
\eta_\gamma &= 1\ ;\ \eta_{\gamma Z} = \left(\frac{G_F M_Z^2}{2\sqrt{2}\pi\alpha}\right)\left(\frac{Q^2}{Q^2 + M_Z^2}\right);\\
\eta_Z &= \eta_{\gamma Z}^2\ ;\ \eta_W = \frac{1}{2}\left(\frac{G_F M_W^2}{4\pi\alpha}\,\frac{Q^2}{Q^2 + M_W^2}\right)^2.
\end{aligned} \qquad (18.4)$$

The hadronic tensor, which describes the interaction of the appropriate electroweak currents with the target nucleon, is given by

$$W_{\mu\nu} \;=\; \frac{1}{4\pi}\int d^4z\; e^{iq\cdot z}\;\left\langle P,S\,\middle|\left[J_\mu^\dagger(z), J_\nu(0)\right]\middle|\,P,S\right\rangle, \qquad (18.5)$$

where J_α is the hadronic contribution to the electromagnetic, or weak current and S denotes the nucleon-spin 4-vector, with $S^2 = -M^2$ and $S\cdot P = 0$.

18.2 Structure functions of the proton

The structure functions are defined in terms of the hadronic tensor (see Refs. [1–3])

$$\begin{aligned}
W_{\mu\nu} &= \left(-g_{\mu\nu} + \frac{q_\mu q_\nu}{q^2}\right) F_1(x,Q^2) + \frac{\hat{P}_\mu \hat{P}_\nu}{P\cdot q}\, F_2(x,Q^2)\\
&- i\varepsilon_{\mu\nu\alpha\beta}\,\frac{q^\alpha P^\beta}{2P\cdot q}\, F_3(x,Q^2)\\
&+ i\varepsilon_{\mu\nu\alpha\beta}\,\frac{q^\alpha}{P\cdot q}\left[S^\beta g_1(x,Q^2) + \left(S^\beta - \frac{S\cdot q}{P\cdot q}\,P^\beta\right) g_2(x,Q^2)\right]\\
&+ \frac{1}{P\cdot q}\left[\frac{1}{2}\left(\hat{P}_\mu \hat{S}_\nu + \hat{S}_\mu \hat{P}_\nu\right) - \frac{S\cdot q}{P\cdot q}\,\hat{P}_\mu \hat{P}_\nu\right] g_3(x,Q^2)\\
&+ \frac{S\cdot q}{P\cdot q}\left[\frac{\hat{P}_\mu \hat{P}_\nu}{P\cdot q}\, g_4(x,Q^2) + \left(-g_{\mu\nu} + \frac{q_\mu q_\nu}{q^2}\right) g_5(x,Q^2)\right]
\end{aligned} \qquad (18.6)$$

where

$$\hat{P}_\mu \;=\; P_\mu - \frac{P\cdot q}{q^2}\, q_\mu, \qquad \hat{S}_\mu \;=\; S_\mu - \frac{S\cdot q}{q^2}\, q_\mu\ . \qquad (18.7)$$

In [2],the definition of $W_{\mu\nu}$ with $\mu \leftrightarrow \nu$ is adopted, which changes the sign of the $\varepsilon_{\mu\nu\alpha\beta}$ terms in Eq. (18.6), although the formulae given below are unchanged. Ref. [1] tabulates the relation between the structure functions defined in Eq. (18.6) and other choices available in the literature.

The cross sections for neutral- and charged-current deep inelastic scattering on unpolarized nucleons can be written in terms of

Downloaded from https://academic.oup.com/ptep/article/2022/8/083C01/6651666 by KIT Library user on 27 September 2022

the structure functions in the generic form

$$\frac{d^2\sigma^i}{dxdy} = \frac{4\pi\alpha^2}{xyQ^2}\,\eta^i\left\{\left(1 - y - \frac{x^2y^2M^2}{Q^2}\right)F_2^i + y^2xF_1^i \mp \left(y - \frac{y^2}{2}\right)xF_3^i\right\}, \tag{18.8}$$

where $i = \mathrm{NC}, \mathrm{CC}$ corresponds to neutral-current ($eN \to eX$) or charged-current ($eN \to \nu X$ or $\nu N \to eX$) processes, respectively. For incoming neutrinos, $L^W_{\mu\nu}$ of Eq. (18.3) is still true, but with e, λ corresponding to the outgoing charged lepton. In the last term of Eq. (18.8), the $-$ sign is taken for an incoming e^+ or $\overline{\nu}$ and the $+$ sign for an incoming e^- or ν. The factor $\eta^{\mathrm{NC}} = 1$ for unpolarized $e^\pm$ beams, whereas

$$\eta^{\mathrm{CC}} = (1 \pm \lambda)^2\eta_W \tag{18.9}$$

with $\pm$ for $\ell^\pm$; and where λ is the helicity of the incoming lepton and η_W is defined in Eq. (18.4); for incoming neutrinos $\eta^{\mathrm{CC}} = 4\eta_W$. The CC structure functions, which derive exclusively from W exchange, are

$$F_1^{\mathrm{CC}} = F_1^W,\ F_2^{\mathrm{CC}} = F_2^W,\ xF_3^{\mathrm{CC}} = xF_3^W. \tag{18.10}$$

The NC structure functions $F_2^\gamma, F_2^{\gamma Z}, F_2^Z$ are, for $e^\pm N \to e^\pm X$, given by [5],

$$F_2^{\mathrm{NC}} = F_2^\gamma - (g_V^e \pm \lambda g_A^e)\eta_{\gamma Z}F_2^{\gamma Z} + ({g_V^e}^2 + {g_A^e}^2 \pm 2\lambda g_V^e g_A^e)\,\eta_Z F_2^Z \tag{18.11}$$

and similarly for F_1^{NC}, whereas

$$xF_3^{\mathrm{NC}} = -(g_A^e \pm \lambda g_V^e)\eta_{\gamma Z}xF_3^{\gamma Z} + [2g_V^e g_A^e \pm \lambda({g_V^e}^2 + {g_A^e}^2)]\eta_Z xF_3^Z. \tag{18.12}$$

The polarized cross-section difference

$$\Delta\sigma = \sigma(\lambda_n = -1, \lambda_\ell) - \sigma(\lambda_n = 1, \lambda_\ell), \tag{18.13}$$

where λ_ℓ, λ_n are the helicities (± 1) of the incoming lepton and nucleon, respectively, may be expressed in terms of the five structure functions $g_{1,\ldots 5}(x, Q^2)$ of Eq. (18.6). Explicitly,

$$\frac{d^2\Delta\sigma^i}{dxdy} = \frac{8\pi\alpha^2}{xyQ^2}\,\eta^i\left\{-\lambda_\ell y\left(2 - y - 2x^2y^2\frac{M^2}{Q^2}\right)xg_1^i + \lambda_\ell 4x^3y^2\,\frac{M^2}{Q^2}\,g_2^i + 2x^2y\frac{M^2}{Q^2}\left(1 - y - x^2y^2\frac{M^2}{Q^2}\right)g_3^i - \left(1 + 2x^2y\frac{M^2}{Q^2}\right)\left[\left(1 - y - x^2y^2\frac{M^2}{Q^2}\right)g_4^i + xy^2g_5^i\right]\right\} \tag{18.14}$$

with $i = \mathrm{NC}$ or CC as before. The Eq. (18.13) corresponds to the difference of antiparallel minus parallel spins of the incoming particles for e^- or ν initiated reactions, but the difference of parallel minus antiparallel for e^+ or $\overline{\nu}$ initiated processes. For longitudinal nucleon polarization, the contributions of g_2 and g_3 are suppressed by powers of M^2/Q^2. These structure functions give an unsuppressed contribution to the cross section for transverse polarization [1], but in this case the cross-section difference vanishes as $M/Q \to 0$.

Because the same tensor structure occurs in the spin-dependent and spin-independent parts of the hadronic tensor of Eq. (18.6) in the $M^2/Q^2 \to 0$ limit, the differential cross-section difference of Eq. (18.14) may be obtained from the differential cross section Eq. (18.8) by replacing

$$F_1 \to -g_5\,,\quad F_2 \to -g_4\,,\quad F_3 \to 2g_1\,, \tag{18.15}$$

and multiplying by two, since the total cross section is the average over the initial-state polarizations. In this limit, Eq. (18.8) and Eq. (18.14) may be written in the form

$$\frac{d^2\sigma^i}{dxdy} = \frac{2\pi\alpha^2}{xyQ^2}\,\eta^i\left[Y_+F_2^i \mp Y_-xF_3^i - y^2F_L^i\right],$$

$$\frac{d^2\Delta\sigma^i}{dxdy} = \frac{4\pi\alpha^2}{xyQ^2}\,\eta^i\left[-Y_+g_4^i \mp Y_-2xg_1^i + y^2g_L^i\right], \tag{18.16}$$

with $i = \mathrm{NC}$ or CC, where $Y_\pm = 1 \pm (1-y)^2$ and

$$F_L^i = F_2^i - 2xF_1^i\,,\qquad g_L^i = g_4^i - 2xg_5^i\,. \tag{18.17}$$

In the naive quark-parton model, the analogy with the Callan-Gross relations [6]$F_L^i = 0$, are the Dicus relations [7] $g_L^i = 0$. Therefore, there are only two independent polarized structure functions: g_1 (parity conserving) and g_5 (parity violating), in analogy with the unpolarized structure functions F_1 and F_3.

18.2.1 *Structure functions in the quark parton model*

In the naive quark-parton model [8, 9], contributions to the structure functions F^i and g^i can be expressed in terms of the quark distribution functions $q(x, Q^2)$ of the proton, where $q = u, \overline{u}, d, \overline{d}$ etc. The quantity $q(x, Q^2)dx$ is the number of quarks (or antiquarks) of designated flavor that carry a momentum fraction between x and $x + dx$ of the proton's momentum in a frame in which the proton momentum is large. One of the most striking predictions of the quark-parton model is that the structure functions F_i, g_i *scale*, i.e., $F_i(x, Q^2) \to F_i(x)$ in the Bjorken limit that Q^2 and $\nu \to \infty$ with x fixed [10]. This property is related to the assumption that the transverse momentum of the partons in the infinite-momentum frame of the proton is small.

For the neutral-current processes $ep \to eX$,

$$\left[F_2^\gamma,\ F_2^{\gamma Z},\ F_2^Z\right] = x\sum_q\left[e_q^2,\ 2e_qg_V^q,\ {g_V^q}^2 + {g_A^q}^2\right]\,(q + \overline{q})\,,$$

$$\left[F_3^\gamma,\ F_3^{\gamma Z},\ F_3^Z\right] = \sum_q\left[0,\ 2e_qg_A^q,\ 2g_V^qg_A^q\right]\,(q - \overline{q})\,,$$

$$\left[g_1^\gamma,\ g_1^{\gamma Z},\ g_1^Z\right] = \frac{1}{2}\sum_q\left[e_q^2,\ 2e_qg_V^q,\ {g_V^q}^2 + {g_A^q}^2\right]\,(\Delta q + \Delta\overline{q})\,,$$

$$\left[g_5^\gamma,\ g_5^{\gamma Z},\ g_5^Z\right] = \sum_q\left[0,\ e_qg_A^q,\ g_V^qg_A^q\right]\,(\Delta\overline{q} - \Delta q)\,, \tag{18.18}$$

where $g_V^q = \pm\frac{1}{2} - 2e_q\sin^2\theta_W$ and $g_A^q = \pm\frac{1}{2}$, with $\pm$ according to whether q is a $u-$ or $d-$type quark respectively. The quantity Δq is the difference $q\uparrow - q\downarrow$ of the distributions with the quark spin parallel and antiparallel to the proton spin.

For the charged-current processes $e^-p \to \nu X$ and $\overline{\nu}p \to e^+X$, the structure functions are:

$$\begin{aligned} F_2^{W^-} &= 2x(u + \overline{d} + \overline{s} + c\ldots)\,,\\ F_3^{W^-} &= 2(u - \overline{d} - \overline{s} + c\ldots)\,,\\ g_1^{W^-} &= (\Delta u + \Delta\overline{d} + \Delta\overline{s} + \Delta c\ldots)\,,\\ g_5^{W^-} &= (-\Delta u + \Delta\overline{d} + \Delta\overline{s} - \Delta c\ldots)\,, \end{aligned} \tag{18.19}$$

where only the active flavors have been kept and where CKM mixing has been neglected. For $e^+p \to \overline{\nu}X$ and $\nu p \to e^-X$, the structure functions F^{W^+}, g^{W^+} are obtained by the flavor interchanges $d \leftrightarrow u, s \leftrightarrow c$ in the expressions for F^{W^-}, g^{W^-}. The structure functions for scattering on a neutron are obtained from those of the proton by the interchange $u \leftrightarrow d$. For both the neutral- and charged-current processes, the quark-parton model predicts $2xF_1^i = F_2^i$ and $g_4^i = 2xg_5^i$.

Neglecting masses, the structure functions g_2 and g_3 contribute only to scattering from transversely polarized nucleons, and have no simple interpretation in terms of the quark-parton model. They arise from off-diagonal matrix elements

Downloaded from https://academic.oup.com/ptep/article/2022/8/083C01/6651666 by KIT Library user on 27 September 2022

$\langle P,\lambda'|[J^\dagger_\mu(z), J_\nu(0)]|P,\lambda\rangle$, where the proton helicities satisfy $\lambda' \neq \lambda$. In fact, the leading-twist contributions to both g_2 and g_3 are both twist-2 and twist-3, which contribute at the same order of Q^2. The Wandzura-Wilczek relation [11] expresses the twist-2 part of g_2 in terms of g_1 as

$$g_2^i(x) \;=\; -g_1^i(x) \;+\; \int_x^1 \frac{dy}{y}\, g_1^i(y)\;. \tag{18.20}$$

However, the twist-3 component of g_2 is unknown. Similarly, there is a relation expressing the twist-2 part of g_3 in terms of g_4. A complete set of relations, including M^2/Q^2 effects, can be found in [12].

18.2.2 *Structure functions and QCD*

In QCD, there are perturbative corrections to the partonic cross sections defining structure functions. Also, the radiation of hard gluons from the quarks violates the assumption that the transverse momentum of the partons is small, leading to logarithmic scaling violations, which are particularly large at small x, see Fig. 18.2. The radiation of gluons produces the evolution of the partons and structure functions. As Q^2 increases, more and more gluons are radiated, which in turn split into $q\bar{q}$ pairs. This process leads both to the softening of the initial quark momentum distributions and to the growth of the gluon density and the $q\bar{q}$ sea as x decreases.

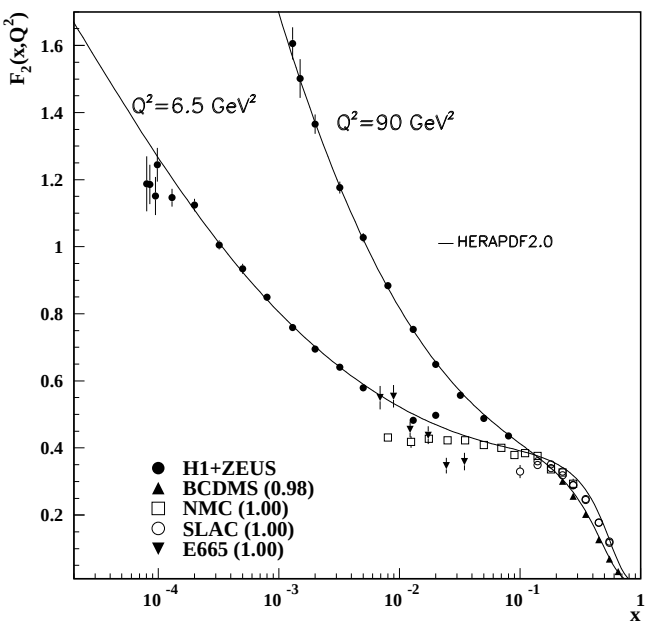

Figure 18.2: The proton structure function F_2^p given at two Q^2 values (6.5 GeV^2 and 90 GeV^2), which exhibit scaling at the 'pivot' point $x \sim 0.14$. See the captions in Fig. 18.10 and Fig. 18.12 for the references of the data. The various data sets have been renormalized by the factors shown in brackets in the key to the plot, which were globally determined in a previous HERAPDF analysis [13]. The curves were obtained using the PDFs from the HERAPDF analysis [14]. In practice, data for the reduced cross section, $F_2(x,Q^2) - (y^2/Y_+)F_L(x,Q^2)$, were fitted, rather than F_2 and F_L separately. The agreement between data and theory at low Q^2 and x can be improved by a positive higher-twist correction to $F_L(x,Q^2)$ [15, 16] (see Fig. 8 of Ref. [16]), or small-x resummation [17, 18].

For $Q^2 \gg M^2$, the structure functions satisfy the factorization theorem [19],

$$F_i = \sum_a C_i^a \otimes f_a + \mathcal{O}(M^2/Q^2), \tag{18.21}$$

where $\otimes$ denotes the convolution integral

$$C \;\otimes\; f \;=\; \int_x^1 \frac{dy}{y}\, C(y)\, f\left(\frac{x}{y}\right)\;, \tag{18.22}$$

and where the coefficient functions C_i^a, where $a = g$ or q, are given as a power series in α_s. The scale-dependent parton distribution $f_a(x,\mu^2)$ corresponds, at a given x, to the density of parton a in the proton integrated over transverse momentum k_t up to the factorization scale μ. Typically, μ is the scale of the probe Q. For parton distributions x always refers to the nucleon momentum fraction of the parton, whereas for structure functions it retains the definition in Sec. 18.1. The parton evolution in μ is described in QCD by a DGLAP equation (see Refs. [20–23]) which has the schematic form

$$\frac{\partial f_a}{\partial \ln \mu^2} \sim \frac{\alpha_s(\mu^2)}{2\pi} \sum_b (P_{ab} \otimes f_b)\;, \tag{18.23}$$

where the P_{ab}, which describe the parton splitting $b \to a$, are also given as a power series in α_s. Although perturbative QCD can predict, via Eq. (18.23), the evolution of the parton distribution functions from a particular scale, μ_0, these DGLAP equations cannot predict them *a priori* at any particular μ_0. Thus they must be measured at a starting point μ_0 before the predictions of QCD can be compared to the data at other scales, μ. In general, all observables involving a hard hadronic interaction (such as structure functions) can be expressed as a convolution of calculable, process-dependent coefficient functions and these universal parton distributions, e.g. Eq. (18.21).

Table 18.1: The main processes relevant to global PDF analyses, ordered in three groups: fixed-target experiments, HERA and the $p\bar{p}$ Tevatron / pp LHC. For each process we give an indication of their dominant partonic subprocesses, the primary partons which are probed and the approximate range of x constrained by the data. This list expands as more processes are measured and calculated with sufficient precision.

Process	Subprocess	Partons	x range
$\ell^\pm\,\{p,n\} \to \ell^\pm\,X$	$\gamma^* q \to q$	$q, \bar{q}, g$	$x \gtrsim 0.01$
$\ell^\pm\, n/p \to \ell^\pm\,X$	$\gamma^*\, d/u \to d/u$	d/u	$x \gtrsim 0.01$
$pp \to \mu^+\mu^-\,X$	$u\bar{u}, d\bar{d} \to \gamma^*$	$\bar{q}$	$0.015 \lesssim x \lesssim 0.35$
$pn/pp \to \mu^+\mu^-\,X$	$(u\bar{d})/(u\bar{u}) \to \gamma^*$	$\bar{d}/\bar{u}$	$0.015 \lesssim x \lesssim 0.35$
$\nu(\bar{\nu})\,N \to \mu^-(\mu^+)\,X$	$W^* q \to q'$	$q, \bar{q}$	$0.01 \lesssim x \lesssim 0.5$
$\nu\,N \to \mu^-\mu^+\,X$	$W^* s \to c$	s	$0.01 \lesssim x \lesssim 0.2$
$\bar{\nu}\,N \to \mu^+\mu^-\,X$	$W^* \bar{s} \to \bar{c}$	$\bar{s}$	$0.01 \lesssim x \lesssim 0.2$
$e^\pm\,p \to e^\pm\,X$	$\gamma^* q \to q$	$g, q, \bar{q}$	$10^{-4} \lesssim x \lesssim 0.1$
$e^+\,p \to \bar{\nu}\,X$	$W^+\,\{d,s\} \to \{u,c\}$	d, s	$x \gtrsim 0.01$
$e^\pm p \to e^\pm\,c\bar{c}X, e^\pm\,b\bar{b}X$	$\gamma^* c \to c,\ \gamma^* g \to c\bar{c}$	c, b, g	$10^{-4} \lesssim x \lesssim 0.01$
$e^\pm p \to$ jet$+X$	$\gamma^* g \to q\bar{q}$	g	$0.01 \lesssim x \lesssim 0.1$
$p\bar{p}, pp \to$ jet(dijet)$+X$	$gg, qg, qq \to 2j$	g, q	$0.00005 \lesssim x \lesssim 0.5$
$p\bar{p} \to (W^\pm \to \ell^\pm\nu)\,X$	$ud \to W^+, \bar{u}\bar{d} \to W^-$	$u, d, s, \bar{u}, \bar{d}, \bar{s}$	$x \gtrsim 0.05$
$pp \to (W^\pm \to \ell^\pm\nu)\,X$	$u\bar{d} \to W^+, d\bar{u} \to W^-$	$u, d, s, \bar{u}, \bar{d}, \bar{s}, g$	$x \gtrsim 0.001$
$p\bar{p}(pp) \to (Z \to \ell^+\ell^-)X$	$uu, dd, ..(u\bar{u}, ..) \to Z$	$u, d, s, ..(g)$	$x \gtrsim 0.001$
$pp \to W^-c,\ W^+\bar{c}$	$gs \to W^-c$	$s, \bar{s}$	$x \sim 0.01$
$pp \to (\gamma^* \to \ell^+\ell^-)X$	$u\bar{u}, d\bar{d}, .. \to \gamma^*$	$\bar{q}, g$	$x \gtrsim 10^{-5}$
$pp \to (\gamma^* \to \ell^+\ell^-)X$	$u\gamma, d\gamma, .. \to \gamma^*$	γ	$x \gtrsim 10^{-2}$
$pp \to b\bar{b}\,X,\ \ t\bar{t}X$	$gg \to b\bar{b},\ \ t\bar{t}$	g	$x \gtrsim 10^{-5}, 10^{-2}$
$pp \to t(\bar{t})\,X,$	$bu(\bar{b}d) \to td(\bar{t}u)$	$b, d/u$	$x \gtrsim 10^{-2}$
$pp \to$ exclusive $J/\psi,\,\Upsilon$	$\gamma^*(gg) \to J/\psi,\,\Upsilon$	g	$x \gtrsim 10^{-5}, 10^{-4}$
$pp \to \gamma\,X$	$gq \to \gamma q,\ g\bar{q} \to \gamma\bar{q}$	g	$x \gtrsim 0.005$

Downloaded from https://academic.oup.com/ptep/article/2022/8/083C01/6651666 by KIT Library user on 27 September 2022

It is often convenient to write the evolution equations in terms of the gluon, non-singlet (q^{NS}) and singlet (q^S) quark distributions, such that

$$q^{NS} = q_i - \overline{q}_i \quad (\text{or } q_i - q_j), \qquad q^S = \sum_i (q_i + \overline{q}_i) \ . \quad (18.24)$$

The non-singlet distributions have non-zero values of flavor quantum numbers, such as isospin and baryon number. The DGLAP evolution equations then take the form

$$\frac{\partial q^{NS}}{\partial \ln \mu^2} = \frac{\alpha_s(\mu^2)}{2\pi} \, P_{qq} \otimes q^{NS} \ ,$$

$$\frac{\partial}{\partial \ln \mu^2} \begin{pmatrix} q^S \\ g \end{pmatrix} = \frac{\alpha_s(\mu^2)}{2\pi} \begin{pmatrix} P_{qq} & 2n_f \, P_{qg} \\ P_{gq} & P_{gg} \end{pmatrix} \otimes \begin{pmatrix} q^S \\ g \end{pmatrix}, \quad (18.25)$$

where P are splitting functions that describe the probability of a given parton splitting into two others, and n_f is the number of (active) quark flavors. The leading-order Altarelli-Parisi [22] splitting functions are

$$P_{qq} = \frac{4}{3} \left[\frac{1+x^2}{(1-x)} \right]_+ = \frac{4}{3} \left[\frac{1+x^2}{(1-x)_+} \right] + 2\delta(1-x) \ , \quad (18.26)$$

$$P_{qg} = \frac{1}{2} \left[x^2 + (1-x)^2 \right] \ , \ P_{gq} = \frac{4}{3} \left[\frac{1+(1-x)^2}{x} \right] \ , \quad (18.27)$$

$$P_{gg} = 6 \left[\frac{1-x}{x} + x(1-x) + \frac{x}{(1-x)_+} \right] + \left[\frac{11}{2} - \frac{n_f}{3} \right] \delta(1-x), \quad (18.28)$$

where the notation $[F(x)]_+$ defines a distribution such that for any sufficiently regular test function, $f(x)$,

$$\int_0^1 dx f(x) [F(x)]_+ = \int_0^1 dx \, (f(x) - f(1)) F(x) \ . \quad (18.29)$$

In general, the splitting functions can be expressed as a power series in α_s. The series contains both terms proportional to $\ln \mu^2$ and to $\ln(1/x)$ and $\ln(1-x)$. The leading-order DGLAP evolution sums up the $(\alpha_s \ln \mu^2)^n$ contributions, while at next-to-leading order (NLO) the sum over the $\alpha_s(\alpha_s \ln \mu^2)^{n-1}$ terms is included [24, 25]. The NNLO contributions to the splitting functions and the DIS coefficient functions are also all known [26–28], as are the N^{3}LO corrections to the coefficient functions [29].

In the kinematic region of very small x, one may also sum leading terms in $\ln(1/x)$, independent of the value of $\ln \mu^2$. At leading order, LLx, this is done by the BFKL equation for the unintegrated distributions (see Refs. [32, 33].) The leading-order $(\alpha_s \ln(1/x))^n$ terms result in a power-like growth, $x^{-\omega}$ with $\omega = (12\alpha_s \ln 2)/\pi$, at asymptotic values of $\ln 1/x$. The next-to-leading $\ln 1/x$ (NLLx) contributions are also available [34, 35]. They are so large (and negative) that the results initially appeared to be perturbatively unstable. Methods, based on a combination of collinear and small-x resummations, have been developed which reorganize the perturbative series into a more stable hierarchy [36–39], and this has been used as the basis for a framework for including the corrections in phenomenological studies [40, 41]. There are some limited indications that small-x resummations become necessary for sufficient precision for $x \lesssim 10^{-3}$ at low scales [17, 18]. At sufficiently small x it is expected that evolution should also be affected by non-linear/saturation effects due to a high density of partons, i.e. the gluon density would be so high that gluon-gluon recombination effects would become significant,

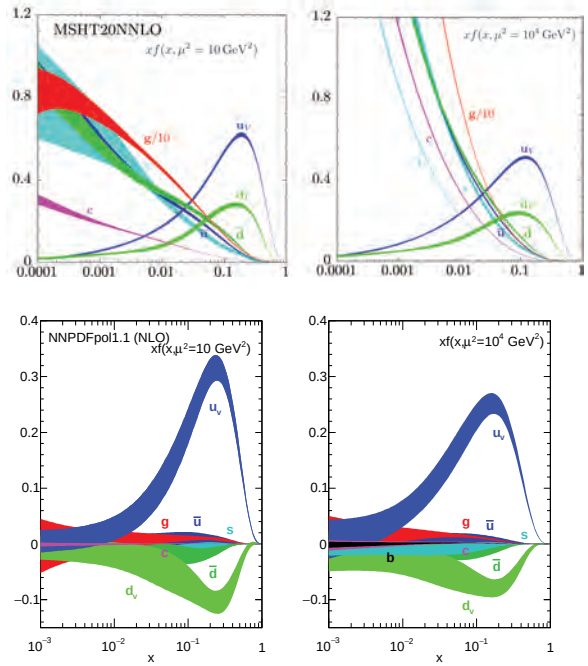

Figure 18.3: The bands are x times the unpolarized parton distributions $f(x)$ (where $f = u_v, d_v, \overline{u}, \overline{d}, s \simeq \overline{s}, c = \overline{c}, b = \overline{b}, g$) obtained in the NNLO MSHT20 global analysis [30] (top) at scales $\mu^2 = 10$ GeV^2 (left) and $\mu^2 = 10^4$ GeV^2 (right), with $\alpha_s(M_Z^2) = 0.118$. The polarized parton distributions $f(x)$ obtained in the NLO NNPDFpol1.1 fit [31] (bottom).

see [42–44] for reviews. However, there is not yet any very convincing indication for a non-linear regime for $Q^2 \gtrsim 2$ GeV^2 in hadron DIS. Better evidence for saturation may be found in more exclusive final states such as dihadron correlations in proton-nucleus collisions, e.g. [45, 46].

The precision of the experimental data demands that at least NLO, and preferably NNLO, DGLAP evolution be used in comparisons between QCD theory and experiment. Beyond the leading order, it is necessary to specify, and to use consistently, both a renormalization and a factorization scheme. The renormalization scheme used almost universally is the modified minimal subtraction ($\overline{\text{MS}}$) scheme [47, 48]. The most popular choices for the factorization scheme is also $\overline{\text{MS}}$ [49]. Historically, sometimes the DIS [50] scheme was adopted, in which there are no higher-order corrections to the F_2 structure function, and this was extended to a specific definition appropriate to small x [51]. The two schemes differ in how the non-divergent pieces are assimilated in the parton distribution functions.

The discussion above relates to the Q^2 behavior of leading-twist (twist-2) contributions to the structure functions. Higher-twist terms, which involve their own non-perturbative input, exist. These die off as powers of Q; specifically twist-n terms are damped by $1/Q^{n-2}$. Provided a cut, say $W^2 > 15$ GeV^2 is imposed, the higher-twist terms appear to be numerically unimportant for Q^2 above a few GeV^2, except possibly for very small x and more definitely for x close to 1 [52–54], though it is important to note that they are likely to be larger in $xF_3(x, Q^2)$ than in $F_2(x, Q^2)$ (see e.g. [55])due to a lack of a constraining sum rule for $xF_3(x, Q^2)$.

18.3 Determination of parton distributions

The parton distribution functions (PDFs) can be determined from an analysis of data for deep inelastic lepton-nucleon scattering and for related hard-scattering processes initiated by nucleons; see Refs. [56–62] for reviews. Table 18.1 highlights some of the processes and their primary sensitivity to PDFs. LHC data are playing an increasing role [63], and new processes are continually being added to the list. Fixed-target and collider experiments have complementary kinematic reach (as is shown in Fig. 18.4),

Downloaded from https://academic.oup.com/ptep/article/2022/8/083C01/6651666 by KIT Library user on 27 September 2022

which enables the determination of PDFs over a wide range in x and μ^2. As more precise LHC data for $W^{\pm}$, Z, γ, jet, $b\bar{b}$ and $t\bar{t}$ production become available, tighter constraints on the PDFs are expected in a wider kinematic range. At present about half the constraint on PDFs comes from LHC data [30], but much of the constraint still comes from structure functions.

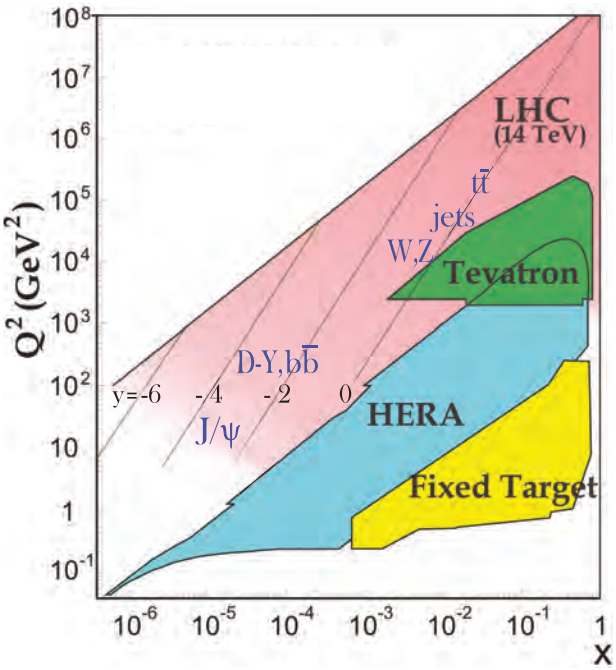

Figure 18.4: Kinematic domains in x and Q^2 probed by fixed-target and collider experiments, where here Q^2 can refer either the literal Q^2 for deep inelastic scattering, or the hard scale of the process in hadron-hadron collisions, e.g. invariant mass or transverse momentum p_T^2. Some of the final states accessible at the LHC are indicated in the appropriate regions, where y is the rapidity. The incoming partons have $x_{1,2} = (Q/14\ \text{TeV})e^{\pm y}$ where Q is the hard scale of the process shown in blue in the figure. For example, open charm production [64] and exclusive J/ψ and Υ production [65] at high $|y|$ at the LHC may probe the gluon PDF down to $x \sim 10^{-5}$.

Recent determinations and releases of the unpolarized PDFs up to NNLO have been made by five groups: MSHT [30], NNPDF [66], CT [67], HERAPDF [14] and ABMP [68]. The CJ group produce PDFs at NLO and concentrate on the high x, low Q^2 regime, including data with lower kinematic cuts [69]. All groups start evolution at $Q_0^2 = 1-4$ GeV^2. Most groups use input PDFs of the form $xf = x^a(...)(1-x)^b$ with 14-32 free parameters in total. In these cases the PDF uncertainties are made available using the "Hessian" formulation. The free parameters are expanded around their best fit values, and orthogonal eigenvector sets of PDFs depending on linear combinations of the parameter variations are obtained. The uncertainty is then the quadratic sum of the uncertainties arising from each eigenvector. The NNPDF group combines a Monte Carlo representation of the probability measure in the space of PDFs with the use of neural networks. Fits are performed to a very large number of "replica" data sets obtained by allowing individual data points to fluctuate randomly by amounts determined by the size of the data uncertainties. This results in a set of replicas of unbiased PDF sets. In this case the best prediction is the average obtained using all PDF replicas and the uncertainty is the standard deviation over all replicas. It is possible to convert the eigenvectors of Hessian-based PDFs to Monte Carlo replicas [70] and *vice versa* [71].

In these analyses, the u, d and s quarks are taken to be massless, but the treatment of the heavy c and b quark masses, m_Q, differs, and has a long history, which may be traced from Refs. [72–83]. The MSHT, CT, NNPDF and HERAPDF analyses use different variants of the General-Mass Variable-Flavour-Number Scheme (GM-VFNS). This combines fixed-order contributions to the coefficient functions (or partonic cross sections) calculated with the full m_Q dependence, with the all-order resummation of contributions via DGLAP evolution in which the heavy quarks are treated as massless after starting evolution at some transition point. Transition matrix elements are computed, following [75], which provide the boundary conditions between n_f and $n_f + 1$ PDFs. The ABMP analysis uses for structure function calculations a FFNS where only the three light (massless) quarks enter the evolution, while the heavy quarks enter the partonic cross sections with their full m_Q dependence. The GM-VFNS and FFNS approaches yield different results: in particular $\alpha_s(M_Z^2)$ and the large-x gluon PDF at large Q^2 are both significantly smaller in the FFNS. It has been argued [53, 54, 82] that the difference is due to the slow convergence of the $\ln^n(Q^2/m_Q^2)$ terms in certain regions in a FFNS. The final HERA combination of heavy flavour structure function data has been published [84], and the evolution of these measurements and their interpretation may be traced in [85].

The recent determinations of the groups fitting a variety of data and using a GM-VFNS (MSHT, NNPDF and CT) have converged, so that now a good agreement has been achieved between the resulting PDFs. Indeed, the previous round of global fit PDF sets, CT14 [86], MMHT2014 [87], and NNPDF3.0 [88], have been combined [89] using the Monte Carlo approach [70] mentioned above. The single combined set of PDFs is discussed in detail in Ref. [89]. An update for the most recent PDFs is in progress [90].

For illustration, we show in Fig. 18.3 the PDFs obtained in the NNLO MSHT analysis [30] at scales $\mu^2 = 10$ and 10^4 GeV^2 (and an equivalent plot for polarized PDFs from NNPDF [31]). The values of α_s found by MSHT [91] may be taken as representative of those resulting from the GM-VFNS analyses

$$\text{NLO} : \alpha_s(M_Z^2) = 0.1203 \pm 0.0015,$$

$$\text{NNLO} : \alpha_s(M_Z^2) = 0.1174 \pm 0.0013,$$

where the error (at 68% C.L.) corresponds to the uncertainties resulting from the data fitted (the uncertainty that might be expected from the neglect of higher orders is at least as large). A similar results is found by the NNPDF group [92], who find $\alpha_s(M_Z^2) = 0.1185 \pm 0.0012$ at NNLO and the CT group [67], who obtain $\alpha_s(M_Z^2) = 0.1164 \pm 0.0026$. The ABMP analysis [68],which uses a FFNS, finds $\alpha_s(M_Z^2) = 0.1147 \pm 0.0011$ at NNLO.

As a first step towards the inclusion of higher order electroweak corrections a recent development has been a vastly increased understanding of the photon content of the proton. Sets of PDFs with a photon contribution were considered in Refs. [93–95]. However, due to weak data constraints, the uncertainty was extremely large. Subsequently, there has been a much improved understanding of the separation into elastic and inelastic contributions [96–98]. This gives much more theoretical precision, since the elastic contribution, arising from coherent emission of a photon from the proton, can be directly related to the well-known proton electric and magnetic form factors; the model dependence of the inelastic (incoherent) contribution, related to the quark PDFs, is at the level of tens of percent. A final and decisive development directly relating the entire photon contribution to the proton structure function [99] resulted in a determination of the photon content of the proton as precise as that of the light quarks. The framework has been applied within global fits to PDFs via an iterative procedure in [100] and to provide the low-scale input photon PDF in [101, 102]. A further development is the calculation of photon-initiated collider processes directly from structure functions [103].

There are also some calculations of PDFs using lattice QCD, see [104,105] for a recent review. There has been significant recent progress in the development of efficient algorithms for generating ensembles of gauge field configurations and in tools for extracting the required information from correlation functions. However, there remain a number of sources of systematic uncertainty; discretization effects, pion mass dependence, finite volume effects, excited state contamination and renormalization, which need to

Downloaded from https://academic.oup.com/ptep/article/2022/8/083C01/6651666 by KIT Library user on 27 September 2022

be determined and ideally minimised. Moreover, PDFs cannot be determined directly in Euclidean lattice QCD because they depend on quantum fields at light-like separations. Traditionally the lattice has been used to determine matrix elements of twist two operators which can be related to integer moments of PDFs. Until recently these did not always agree well with determinations using global fit PDFs [104]. However, there have been recent improvements [106, 107], though uncertainties are still relatively large. An alternative approach [108] suggested the computation of the matrix elements of frame-dependent, equal-time correlators in the large momentum limit. This leads to so-called Quasi-PDFs, which in the infinite momentum frame can be related to light-cone PDFs via a matching procedure. Recent results using physical values of the light quark masses are in [109].

Comprehensive sets of PDFs are available from the LHAPDF library [110], which can be linked directly into a user's programme to provide access to recent PDFs in a standard format. This also includes many nuclear and polarized PDFs.

Nuclear PDFs: The study of the parton distributions for nucleons within nuclei, so-called nuclear parton distribution functions (nPDFs), is now reaching a level of maturity and sophistication similar to nucleon PDFs (and some nuclear target data is often included in determinations of nucleon PDFs), though they are still typically performed at NLO in perturbative QCD. The PDFs are also a function of the nucleon number of the nucleus, A. The nPDFs are obtained via fits to deep inelastic scattering data and dilepton (Drell-Yan) and pion production from proton-nucleus, and most recently also from jet and heavy flavour production data. There are a number of recent examples of NLO analyses, DSSZ [111], nCTEQ15 [112], EPPS16 [113], while NNLO analyses with a smaller selection of data types now also exist [114,115]. The NNPDF group has recently introduced its first nuclear PDFs, with nNNPDF1.0 [116] at NNLO and based only on neutral current DIS data and nNNPDF2.0 [117] at NLO, which additionally contains charged current DIS data and vector boson production data from the LHC. A comparison of the nuclear modification factors for nCTEQ15WZ+SIH [118], EPPS16 [113] and nNNPDF2.0 [117] is shown in Fig. 18.5 where, for example, for the up quark $R_u^{\rm Pb} = (Z_{Pb}u_{Pb} + (A_{Pb} - Z_{Pb})d_{Pb})/(Z_{Pb}u_p + (A_{Pb} - Z_{Pb})d_p)$ i.e. it involves "physical" nuclear PDFs and is normalised such that $R_u^{\rm Pb} = 1$ corresponds to no nuclear effects.

Much of the heavy-nucleus data included are in the form of ratios to proton or deuteron measurements. Initially most nuclear PDFs were related to a particular proton PDF via a nuclear modification factor, i.e.

$$f_i^{p/A}(x, Q^2) = R_i^A(x, Q^2) f_i^p(x, Q^2). \qquad (18.30)$$

The first exception was the PDFs in [112] which parameterise the nuclear PDFs directly but are equal to proton PDFs in the limit $A = 1$, and this approch has been repeated in [115–117]. There is some variation in whether charged current neutrino DIS data is used as well as neutral current DIS data since there is no clear compatibility in the modification factors obtained [119, 120]. Recently, LHC data from vector boson production [121–124] in proton-lead collisions has been studied [125] or used directly [113,117], and LHC jet data [126] has been included [113], giving extra constraint on the gluon within nuclei. Further information at smaller x values should soon be extracted from heavy meson production at LHCb [127], dijet production at CMS [128]. Single inclusive hadron production e.g. [129,130], is already sometimes used. There have been PDF reweighting studies at NLO including some of these data [131–133], indicating a substantial uncertainty reduction at small x, but no fully updated nuclear PDF sets so far include them. All the PDF extractions above are based on the Hessian formulation, except for the NNPDF studies which use Monte Carlo replicas. Agreement between the different nuclear PDFs is generally good, though uncertainty is still large compared to proton PDFs. As well as improved constraints from further LHC data, nPDFs would be very significantly improved by data from a potential high-energy Electron-Ion Collider [134–136].

Double Parton Distributions Double parton scattering (DPS) occurs when two pairs of partons initiate two distinct hard scattering processes in a single collision. It becomes more prevalent at higher collider energies as the parton flux increases. Hence, it is becoming relevant at the LHC, and even moreso for planning of higher energy colliders. It has a long theoretical history [137–141], and in recent years experimental studies have started. DPS is often supressed, but this is less the case in certain kinematic regions, e.g. when the total transverse momentum of the two hard-scattering processes is small [142–145], when they have a large rapidity separation [146, 147], or when single particle production is supressed by coupling constants, e.g. like-sign W production [148]. There have been results with some evidence for DPS found from both the Tevatron [149, 150] involving final states with multijets and photons, and at the LHC [151–153] in states with multiple vector bosons or mesons. Recent developments have been involved in putting the theoretical foundations of DPS on a much more rigorous footing and describing it in terms of well-defined double partons distributions (DPDs) which extend the concept of parton distribution functions (PDFs) to the case of two partons [142–145,154–156]. The current knowledge of DPDs is still limited, though there are a number of attempts to impose theoretical constrains as a limit on the forms [157–159]. The DPDs can be calculated quite accurately when the tranverse separtion of the two partons is small, since in this limit the observed partons are produced by a splitting from a single parton. This limit is complicated by potential double counting [145], and an approach to deal with this has been devised [156]. The full splitting functions for DPS have been calculated at LO [145].

Polarized PDFs: For spin-dependent structure functions, data exists for a more restricted range of Q^2 and has lower precision, so that the scaling violations are not seen so clearly. However, spin-dependent (or polarized) parton distributions have been extracted by comparison to data using NLO global analyses which include measurements of the g_1 structure function in inclusive polarized DIS, 'flavour-tagged' semi-inclusive DIS data, open–charm production in DIS and results from polarized pp scattering at RHIC. There are recent results on DIS from JLAB [160] (for g_1^n/F_1^n), COMPASS [161,162] and CLAS [163]. NLO analyses are given in Refs. [164–167] and more recent extractions [168,169]. Improved parton-to-hadron fragmentation functions, needed to describe the semi-inclusive DIS (SIDIS) data, can be found in Refs. [170–173]. Only the DSSV collaboration includes in their NLO analysis to extract polarized PDFs all the world data, inclusive and semi-inclusive DIS, double spin asymmetries in jet [174], dijet [175] and inclusive π^0-production [176], but not yet the single spin asymmetries in $W^\pm, Z^0$ production [177]. A determination [178], using the NNPDF methodology, concentrates just on the inclusive polarized DIS data, and finds the uncertainties on the polarized gluon PDF have been underestimated in the earlier analyses. An update to this [31], where jet and $W^\pm$ data from pp collisions and open–charm DIS data have been included via reweighting, reduces the uncertainty and suggests a positive polarized gluon PDF. The evidence for a positive gluon polarization is strengthened by the most recent jet [179,180] and inclusive π^0 [181] data. The DSSV group has recently implemented a Monte Carlo sampling strategy to extract helicity parton densities and their uncertainties from a reference set of longitudinally polarized scattering data [182]. Calculations of polarised PDFs on the lattice are frequently produced by the same studies as for unpolarised PDFs. These are usually in better agreement with the corresponding moments obtained from global fits, than the unpolarised PDFs, and also tend to have much more competitive uncertainties, see [104,105] for a review and e.g. [107,183] for more recent results.

A comparison of the polarized gluon PDFs obtained in the NLO analyses of NNPDF [31] and DSSV [182] is shown in Fig. 18.6 at scale $\mu^2 = 10$ GeV^2. The world data of the inclusive structure function g_1 for proton and deuterium included in these analysis are shown in Fig. 18.16 and Fig. 18.17.

Downloaded from https://academic.oup.com/ptep/article/2022/8/083C01/6651666 by KIT Library user on 27 September 2022

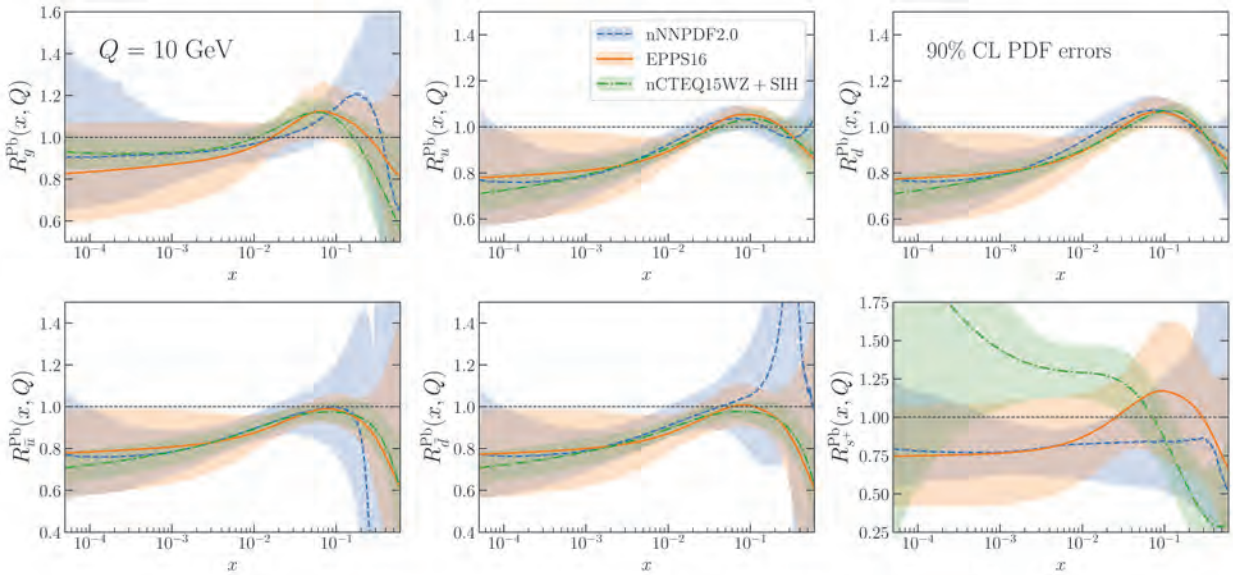

Figure 18.5: Comparison of the nNNPDF2.0, CTEQ15WZ+SIH and EPPS16 nuclear PDFs. The curves shown are ratios to the result in the limit of no nuclear corrections. Plot from NNPDF collaboration (Juan Rojo – private communication).

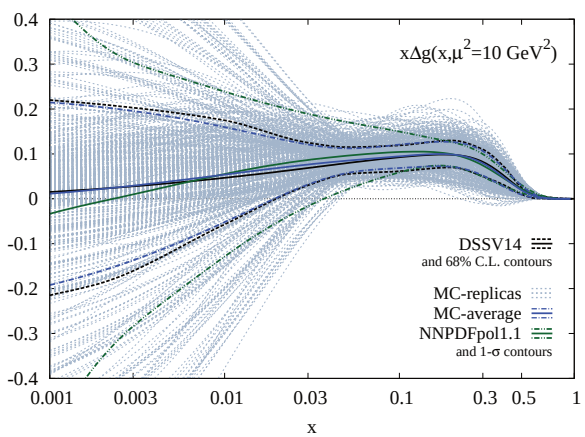

Figure 18.6: Ensemble of replicas (dotted blue lines) for the NLO gluon helicity density $\Delta g(x, Q^2)$ at $Q^2 = 10$ GeV^2 shown along with its statistical average (solid blue line) and variance (dot-dashed blue lines). The corresponding results from the DSSV14 fit (black lines) [168] and the NNPDFpol1.1 analysis (green lines) [31] are shown for comparison. Figure taken from Ref. [182].

18.4 The hadronic structure of the photon

Besides the *direct* interactions of the photon, it is possible for it to fluctuate into a hadronic state via the process $\gamma \to q\bar{q}$. While in this state, the partonic content of the photon may be *resolved*, for example, through the process $e^+e^- \to e^+e^-\gamma^\star\gamma \to e^+e^-X$, where the virtual photon emitted by the DIS lepton probes the hadronic structure of the quasi-real photon emitted by the other lepton. The perturbative LO QED contributions to this process with $\gamma \to q\bar{q}$ in conjunction with $\gamma^\star q(\bar{q}) \to q(\bar{q})$, are subject to QCD corrections due to the radiation of gluons from these quarks.

Often the equivalent-photon approximation is used to express the differential cross section for deep inelastic electron–photon scattering in terms of the structure functions of the transverse quasi-real photon times a flux factor N_γ^T (for these incoming quasi-real photons of transverse polarization)

$$\frac{d^2\sigma}{dxdQ^2} = N_\gamma^T \frac{2\pi\alpha^2}{xQ^4} \left[\left(1 + (1-y)^2\right) F_2^\gamma(x, Q^2) - y^2 F_L^\gamma(x, Q^2) \right], \tag{18.31}$$

where we have used $F_2^\gamma = 2xF_T^\gamma + F_L^\gamma$ (where F_T is the transverse structure function), not to be confused with F_2^γ of Sec. 18.2. Complete formulae are given, for example, in the comprehensive review of [184].

The hadronic photon structure function, F_2^γ, evolves with increasing Q^2 from the 'hadron-like' behavior, calculable via the vector-meson-dominance model, to the dominating 'point-like' behaviour, calculable in perturbative QCD. Due to the point-like coupling, the logarithmic evolution of F_2^γ with Q^2 has a *positive* slope for all values of x, see Fig. 18.18. The 'loss' of quarks at large x due to gluon radiation is over-compensated by the 'creation' of quarks via the point-like $\gamma \to q\bar{q}$ coupling. The logarithmic evolution was first predicted in the quark–parton model ($\gamma^\star\gamma \to q\bar{q}$) [185, 186], and then an improved expression was obtained using QCD corrections in the limit of large Q^2 [187]. The evolution is now known to NLO [188–190]. The NLO data analyses to determine the parton densities of the photon can be found in Refs. [191–193].

18.5 Diffractive DIS (DDIS)

Some 10% of DIS events are diffractive, $\gamma^* p \to X + p$, in which the slightly deflected proton and the cluster X of outgoing hadrons are well-separated in rapidity [194]. Besides x and Q^2, two extra variables are needed to describe a DDIS event: the fraction $x_{I\!P}$ of the proton's momentum transferred across the rapidity gap and t, the square of the 4-momentum transfer of the proton. The DDIS data [199, 200] are usually analysed using two levels of factorization. First, the diffractive structure function $F_2^{\rm D}$ satisfies *collinear factorization*, and can be expressed as the convolution [201]

$$F_2^{\rm D} = \sum_{a=q,g} C_2^a \otimes f_{a/p}^{\rm D}, \tag{18.32}$$

with the same coefficient functions as in DIS (see Eq. (18.21)), and where the diffractive parton distributions $f_{a/p}^{\rm D}$ $(a = q, g)$ satisfy DGLAP evolution. Second, *Regge factorization* is assumed [202],

$$f_{a/p}^{\rm D}(x_{I\!P}, t, z, \mu^2) = f_{I\!P/p}(x_{I\!P}, t)\, f_{a/I\!P}(z, \mu^2), \tag{18.33}$$

where $f_{a/I\!P}$ are the parton densities of the Pomeron, which itself is treated like a hadron, and $z \in [x/x_{I\!P}, 1]$ is the fraction of the Pomeron's momentum carried by the parton entering the hard subprocess. The Pomeron flux factor $f_{I\!P/p}(x_{I\!P}, t)$ is taken from Regge phenomenology. There are also secondary Reggeon contributions to Eq. (18.33). A sample of the t-integrated diffractive parton densities, obtained in this way, is shown in Fig. 18.7.

Downloaded from https://academic.oup.com/ptep/article/2022/8/083C01/6651666 by KIT Library user on 27 September 2022

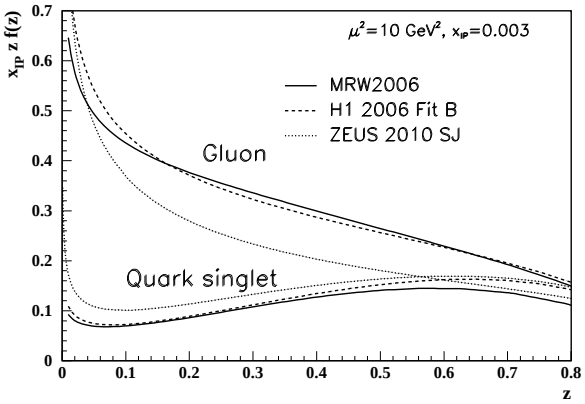

Figure 18.7: Diffractive parton distributions, $x_{I\!P}\, z f^{\rm D}_{a/p}$, obtained from fitting to the ZEUS data with $Q^2 > 5$ GeV^2 [195],H1 data with $Q^2 > 8.5$ GeV^2 assuming Regge factorization [196], and from MRW2006 [197] using a more perturbative QCD approach [197]. Only the Pomeron contributions are shown and not the secondary Reggeon contributions, which are negligible at the value of $x_{I\!P} = 0.003$ chosen here. The H1 2007 Jets distribution [198] is similar to H1 2006 Fit B.

A more recent extraction of the parton densities may be found in [203].

Although collinear factorization holds as $\mu^2 \to \infty$, there are non-negligible corrections for finite μ^2 and small $x_{I\!P}$. Besides the *resolved* interactions of the Pomeron, the perturbative QCD Pomeron may also interact *directly* with the hard subprocess, giving rise to an inhomogeneous evolution equation for the diffractive parton densities analogous to the photon case. The results of the MRW analysis [197],which includes these contributions, are also shown in Fig. 18.7.

Unlike the inclusive case, the diffractive parton densities cannot be directly used to calculate diffractive hadron-hadron cross sections, since account must first be taken of "soft" rescattering effects.

18.6 Three-dimensional structure of hadrons

Generalized parton distributions (GPDs) and their compliment, transverse momentum dependent distributions (TMDs) describe the three-dimensional structure of hadrons. While GPDs encode the transverse position of a parton in a nucleon, TMDs, encompassing both the parton distributions (TMD PDF) and fragmentation functions (TMD FF), encode their transverse momenta and lead to observable transverse momenta in the final state. Both TMDs and GPDs derive, via integration over the appropriate variable, from Wigner distributions [204–206] that depend on the average transverse momentum and position of partons.

18.6.1 *Generalized parton distributions*

The parton distributions of the proton of Sec. 18.3 are given by the diagonal matrix elements $\langle P,\lambda|\hat{O}|P,\lambda\rangle$, where P and λ are the 4-momentum and helicity of the proton, and $\hat{O}$ is a twist-2 quark or gluon operator. However, there is new information in the so-called generalised parton distributions (GPDs) defined in terms of the off-diagonal matrix elements $\langle P',\lambda'|\hat{O}|P,\lambda\rangle$; see Refs. [207–212] for reviews. Unlike the diagonal PDFs, the GPDs cannot be regarded as parton densities, but are to be interpreted as probability amplitudes.

The physical significance of GPDs is best seen using light-cone coordinates, $z^\pm = (z^0 \pm z^3)/\sqrt{2}$, and in the light-cone gauge, $A^+ = 0$. It is conventional to define the generalised quark distributions in terms of quark operators at light-like separation

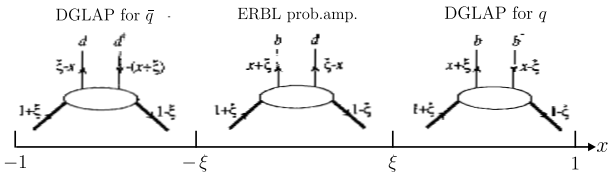

Figure 18.8: Schematic diagrams of the three distinct kinematic regions of the imaginary part of H_q. The proton and quark momentum fractions refer to $\bar{P}^+$, and x covers the interval (-1,1). In the ERBL domain the GPDs are generalisations of distribution amplitudes which occur in processes such as $p\bar{p} \to J/\psi$.

$$F_q(x,\xi,t) = \frac{1}{2}\int \frac{dz^-}{2\pi} e^{ix\bar{P}^+z^-} \langle P'|\bar{\psi}(-z/2)\gamma^+\psi(z/2)|P\rangle \Big|_{z^+=z^1=z^2=0} = \frac{1}{2\bar{P}^+} \times \left(H_q(x,\xi,t)\ \bar{u}(P')\gamma^+u(P) + E_q(x,\xi,t)\ \bar{u}(P')\frac{i\sigma^{+\alpha}\Delta_\alpha}{2m}u(P)\right) \tag{18.34}$$

with $\bar{P} = (P+P')/2$ and $\Delta = P' - P$, and where we have suppressed the helicity labels of the protons and spinors. We now have two extra kinematic variables:

$$t = \Delta^2, \qquad \xi = -\Delta^+/(P+P')^+. \tag{18.35}$$

We see that $-1 \le \xi \le 1$. Similarly, we may define GPDs $\tilde{H}_q$ and $\tilde{E}_q$ with an additional γ_5 between the quark operators in Eq. (18.34); and also an analogous set of gluon GPDs, H_g, E_g, $\tilde{H}_g$ and $\tilde{E}_g$. After a Fourier transform with respect to the transverse components of Δ, we are able to describe the spatial distribution of partons in the impact parameter plane in terms of GPDs [213, 214].

For $P' = P$, $\lambda' = \lambda$ the matrix elements reduce to the ordinary PDFs of Sec. 18.2.1

$$H_q(x,0,0) = q(x), \quad H_q(-x,0,0) = -\bar{q}(x), \quad H_g(x,0,0) = xg(x), \tag{18.36}$$

$$\tilde{H}_q(x,0,0) = \Delta q(x),\ \tilde{H}_q(-x,0,0) = \Delta\bar{q}(x),\ \tilde{H}_g(x,0,0) = x\Delta g(x), \tag{18.37}$$

where $\Delta q = q\uparrow - q\downarrow$ as in Eq. (18.18). No corresponding relations exist for E, $\tilde{E}$ as they decouple in the forward limit, $\Delta = 0$.

The functions H_g, E_g are even in x, and $\tilde{H}_g, \tilde{E}_g$ are odd functions of x. We can introduce valence and 'singlet' quark distributions which are even and odd functions of x respectively. For example

$$H_q^V(x,\xi,t) \equiv H_q(x,\xi,t) + H_q(-x,\xi,t) = H_q^V(-x,\xi,t), \tag{18.38}$$

$$H_q^S(x,\xi,t) \equiv H_q(x,\xi,t) - H_q(-x,\xi,t) = -H_q^S(-x,\xi,t). \tag{18.39}$$

All the GPDs satisfy relations of the form

$$H(x,-\xi,t) = H(x,\xi,t) \qquad \text{and} \qquad H(x,-\xi,t)^* = H(x,\xi,t), \tag{18.40}$$

and so are real-valued functions. Moreover, the moments of GPDs, that is the x integrals of $x^n H_q$ etc., are *polynomials* in ξ of order $n+1$. Another important property of GPDs are Ji's sum rule [207]

$$\frac{1}{2}\int_{-1}^{1} dx\ x\,(H_q(x,\xi,t) + E_q(x,\xi,t)) = J_q(t), \tag{18.41}$$

where $J_q(0)$ is the total angular momentum carried by quarks and antiquarks of flavour q, with a similar relation for gluons.

Downloaded from https://academic.oup.com/ptep/article/2022/8/083C01/6651666 by KIT Library user on 27 September 2022

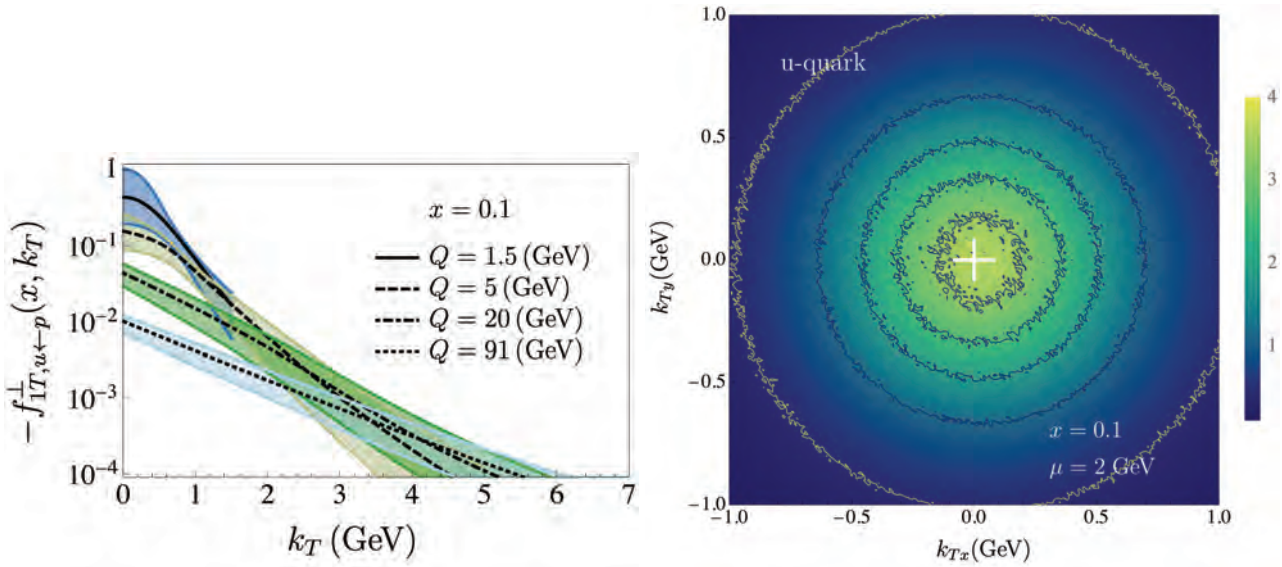

Figure 18.9: (Left) Sivers function in the momentum space for u quark [215] at $x = 0.1$ as a function of transverse momentum k_T for different values of Q. The bands are 68%CI. (Right) Momentum space density function as defined in [215] for the unpolarized u quark in a proton totally polarized in the y direction. The white cross indicates the origin with respect to which a shift of the distribution along the x-direction due to the Sivers function can be seen. The width of the patterns in the plot roughly indicates the uncertainty of the extraction.

To visualize the physical content of H_q, we Fourier expand ψ and $\bar{\psi}$ in terms of quark, antiquark creation (b, d) and annihilation $(b^\dagger, d^\dagger)$ operators, and sketch the result in Fig. 18.8. There are two types of domain: (i) the time-like or 'annihilation' domain, with $|x| < |\xi|$, where the GPDs describe the wave functions of a t-channel $q\bar{q}$ (or gluon) pair and evolve according to modified ERBL equations [216,217]; (ii) the space-like or 'scattering' domain, with $|x| > |\xi|$, where the GPDs generalise the familiar $\bar{q}$, q (and gluon) PDFs and describe processes such as 'deeply virtual Compton scattering' ($\gamma^* p \to \gamma p$), $\gamma p \to J/\psi p$, etc., and evolve according to modified DGLAP equations. The splitting functions for the evolution of GPDs are known to NLO [218–220].

GPDs describe new aspects of proton structure and must be determined from experiment. We can parametrise them in terms of 'double distributions' [221,222], which reduce to diagonal PDFs as $\xi \to 0$. Alternatively, flexible $SO(3)$-based parametrisations have been used to determine GPDs from DVCS data [223,224]; a more recent summary may be found in Ref. [225,226].

18.6.2 *Transverse momentum dependent distributions*

For a proton, there are eight independent transverse dependent distribution (TMD) PDFs, at leading twist, three of which correspond to the usual unpolarized, longitudinally polarized and transversely polarized quark parton distributions [227,228]. The novel TMD PDFs have physical interpretations. For example, the Sivers function [229] represents the distribution of unpolarized partons inside a transversely polarized hadron. For (pseudo)scalar particles, such as kaon and pions, there are two independent leading-twist TMD FFs, one being the ordinary unpolarized fragmentation function and the other the Collins FF [230] which is related to the probability of a polarized quark fragmenting into an unpolarized hadron.

Factorization of TMDs has been shown for semi-inclusive DIS, for the Drell-Yan process as well as for electron-position annihilation into dihadrons [231–236]. Recently first TMD global fits have become available [237–244], although problems with consistent descriptions still remain [245,246]. The results of a recent extraction of Sivers function from a global fit to polarized Semi-Inclusive DIS, polarized pion-induced Drell-Yan and W+-/Z boson production data is shown in Fig. 18.9 [215].

Because TMD PDFs encode nonperturbative information about transverse momentum and polarization degrees of freedom, they are important for descriptions of multi-scale, non-inclusive collider observables, for example, production of electroweak gauge bosons at LHC [247] and can have an effect on determination of the W boson mass [248]. The combination of TMD PDFs and FFs can give consistent global description of spin and azimuthal asymmetries and provide predictions. Some recent reviews of this rapidly developing field are given here [247, 249–252].

References

[1] J. Blumlein and N. Kochelev, Nucl. Phys. **B498**, 285 (1997), [hep-ph/9612318].

[2] S. Forte, M. L. Mangano and G. Ridolfi, Nucl. Phys. **B602**, 585 (2001), [hep-ph/0101192].

[3] M. Anselmino, P. Gambino and J. Kalinowski, Z. Phys. **C64**, 267 (1994), [hep-ph/9401264].

[4] M. Anselmino, A. Efremov and E. Leader, Phys. Rept. **261**, 1 (1995), [Erratum: Phys. Rept.281,399(1997)], [hep-ph/9501369].

[5] M. Klein and T. Riemann, Z. Phys. **C24**, 151 (1984).

[6] C. G. Callan, Jr. and D. J. Gross, Phys. Rev. Lett. **22**, 156 (1969).

[7] D. A. Dicus, Phys. Rev. **D5**, 1367 (1972).

[8] J. D. Bjorken and E. A. Paschos, Phys. Rev. **185**, 1975 (1969).

[9] R.P. Feynman, Photon Hadron Interactions (Benjamin, New York, 1972).

[10] J. D. Bjorken, Phys. Rev. **179**, 1547 (1969).

[11] S. Wandzura and F. Wilczek, Phys. Lett. **72B**, 195 (1977).

[12] J. Blumlein and A. Tkabladze, Nucl. Phys. **B553**, 427 (1999), [hep-ph/9812478].

[13] A.M. Cooper-Sarkar, private communication.

[14] H. Abramowicz *et al.* (H1, ZEUS), Eur. Phys. J. **C75**, 12, 580 (2015), [arXiv:1506.06042].

[15] L. A. Harland-Lang *et al.*, Eur. Phys. J. **C76**, 4, 186 (2016), [arXiv:1601.03413].

[16] I. Abt *et al.*, Phys. Rev. **D94**, 3, 034032 (2016), [arXiv:1604.02299].

[17] R. D. Ball *et al.*, Eur. Phys. J. **C78**, 4, 321 (2018), [arXiv:1710.05935].

[18] H. Abdolmaleki *et al.* (xFitter Developers' Team), Eur. Phys. J. **C78**, 8, 621 (2018), [arXiv:1802.00064].

Downloaded from https://academic.oup.com/ptep/article/2022/8/083C01/6651666 by KIT Library user on 27 September 2022

[19] J. C. Collins, D. E. Soper and G. F. Sterman, Adv. Ser. Direct. High Energy Phys. **5**, 1 (1989), [hep-ph/0409313].

[20] V. N. Gribov and L. N. Lipatov, Sov. J. Nucl. Phys. **15**, 438 (1972), [Yad. Fiz.15,781(1972)].

[21] L.N. Lipatov, Sov. J. Nucl. Phys. **20**, 95 (1975).

[22] G. Altarelli and G. Parisi, Nucl. Phys. **B126**, 298 (1977).

[23] Y. L. Dokshitzer, Sov. Phys. JETP **46**, 641 (1977), [Zh. Eksp. Teor. Fiz.73,1216(1977)].

[24] G. Curci, W. Furmanski and R. Petronzio, Nucl. Phys. **B175**, 27 (1980); W. Furmanski and R. Petronzio, Phys. Lett. **97B**, 437 (1980).

[25] R.K. Ellis *et al.*, QCD and Collider Physics (Cambridge UP, 1996).

[26] W. L. van Neerven and E. B. Zijlstra, Phys. Lett. **B272**, 127 (1991); E. B. Zijlstra and W. L. van Neerven, Phys. Lett. **B273**, 476 (1991); E. B. Zijlstra and W. L. van Neerven, Phys. Lett. **B297**, 377 (1992); E. B. Zijlstra and W. L. van Neerven, Nucl. Phys. **B383**, 525 (1992).

[27] S. Moch and J. A. M. Vermaseren, Nucl. Phys. **B573**, 853 (2000), [hep-ph/9912355].

[28] S. Moch, J. A. M. Vermaseren and A. Vogt, Nucl. Phys. **B688**, 101 (2004), [hep-ph/0403192]; A. Vogt, S. Moch and J. A. M. Vermaseren, Nucl. Phys. **B691**, 129 (2004), [hep-ph/0404111]; S. Moch, J. A. M. Vermaseren and A. Vogt, Phys. Lett. **B606**, 123 (2005), [hep-ph/0411112].

[29] J. A. M. Vermaseren, A. Vogt and S. Moch, Nucl. Phys. **B724**, 3 (2005), [hep-ph/0504242].

[30] S. Bailey *et al.*, Eur. Phys. J. C **81**, 4, 341 (2021), [arXiv:2012.04684].

[31] E. R. Nocera *et al.* (NNPDF), Nucl. Phys. **B887**, 276 (2014), [arXiv:1406.5539].

[32] V. S. Fadin, E. A. Kuraev and L. N. Lipatov, Phys. Lett. **60B**, 50 (1975); E. A. Kuraev, L. N. Lipatov and V. S. Fadin, Sov. Phys. JETP **44**, 443 (1976), [Zh. Eksp. Teor. Fiz.71,840(1976)]; E. A. Kuraev, L. N. Lipatov and V. S. Fadin, Sov. Phys. JETP **45**, 199 (1977), [Zh. Eksp. Teor. Fiz.72,377(1977)].

[33] I. I. Balitsky and L. N. Lipatov, Sov. J. Nucl. Phys. **28**, 822 (1978), [Yad. Fiz.28,1597(1978)].

[34] V. S. Fadin and L. N. Lipatov, Phys. Lett. **B429**, 127 (1998), [hep-ph/9802290].

[35] G. Camici and M. Ciafaloni, Phys. Lett. **B412**, 396 (1997), [Erratum: Phys. Lett.B417,390(1998)], [hep-ph/9707390]; M. Ciafaloni and G. Camici, Phys. Lett. **B430**, 349 (1998), [hep-ph/9803389].

[36] M. Ciafaloni, D. Colferai and G. P. Salam, Phys. Rev. **D60**, 114036 (1999), [hep-ph/9905566]; M. Ciafaloni, D. Colferai and G. P. Salam, JHEP **07**, 054 (2000), [hep-ph/0007240].

[37] M. Ciafaloni *et al.*, Phys. Lett. **B576**, 143 (2003), [hep-ph/0305254]; M. Ciafaloni *et al.*, Phys. Rev. **D68**, 114003 (2003), [hep-ph/0307188].

[38] G. Altarelli, R. D. Ball and S. Forte, Nucl. Phys. **B742**, 1 (2006), [hep-ph/0512237]; G. Altarelli, R. D. Ball and S. Forte, Nucl. Phys. **B799**, 199 (2008), [arXiv:0802.0032].

[39] C. D. White and R. S. Thorne, Phys. Rev. **D75**, 034005 (2007), [hep-ph/0611204].

[40] M. Bonvini, S. Marzani and T. Peraro, Eur. Phys. J. **C76**, 11, 597 (2016), [arXiv:1607.02153].

[41] M. Bonvini, S. Marzani and C. Muselli, JHEP **12**, 117 (2017), [arXiv:1708.07510].

[42] Y. V. Kovchegov and E. Levin, *Quantum chromodynamics at high energy*, volume 33, Cambridge University Press (2012), ISBN 978-0-521-11257-4, 978-1-139-55768-9.

[43] J. L. Albacete and C. Marquet, Prog. Part. Nucl. Phys. **76**, 1 (2014), [arXiv:1401.4866].

[44] A. Morreale and F. Salazar, Universe **7**, 8, 312 (2021), [arXiv:2108.08254].

[45] G. Giacalone and C. Marquet, Nucl. Phys. A **982**, 291 (2019), [arXiv:1807.06388].

[46] X. Chu (STAR), in "28th International Workshop on Deep Inelastic Scattering and Related Subjects," (2021), [arXiv:2110.03731].

[47] G. 't Hooft and M. J. G. Veltman, Nucl. Phys. **B44**, 189 (1972).

[48] G. 't Hooft, Nucl. Phys. **B61**, 455 (1973).

[49] W. A. Bardeen *et al.*, Phys. Rev. **D18**, 3998 (1978).

[50] G. Altarelli, R. K. Ellis and G. Martinelli, Nucl. Phys. **B143**, 521 (1978), [Erratum: Nucl. Phys.B146,544(1978)].

[51] S. Catani, Z. Phys. C **70**, 263 (1996), [hep-ph/9506357].

[52] A. D. Martin *et al.*, Eur. Phys. J. **C35**, 325 (2004), [hep-ph/0308087].

[53] R. D. Ball *et al.* (NNPDF), Phys. Lett. **B723**, 330 (2013), [arXiv:1303.1189].

[54] R. S. Thorne, Eur. Phys. J. **C74**, 7, 2958 (2014), [arXiv:1402.3536].

[55] M. Dasgupta and B. R. Webber, Phys. Lett. **B382**, 273 (1996), [hep-ph/9604388].

[56] A. De Roeck and R. S. Thorne, Prog. Part. Nucl. Phys. **66**, 727 (2011), [arXiv:1103.0555].

[57] S. Forte and G. Watt, Ann. Rev. Nucl. Part. Sci. **63**, 291 (2013), [arXiv:1301.6754].

[58] J. Blumlein, Prog. Part. Nucl. Phys. **69**, 28 (2013), [arXiv:1208.6087].

[59] E. Perez and E. Rizvi, Rept. Prog. Phys. **76**, 046201 (2013), [arXiv:1208.1178].

[60] R. D. Ball *et al.*, JHEP **04**, 125 (2013), [arXiv:1211.5142].

[61] J. Gao, L. Harland-Lang and J. Rojo, Phys. Rept. **742**, 1 (2018), [arXiv:1709.04922].

[62] J. J. Ethier and E. R. Nocera, Ann. Rev. Nucl. Part. Sci. **70**, 43 (2020), [arXiv:2001.07722].

[63] J. Rojo *et al.*, J. Phys. **G42**, 103103 (2015), [arXiv:1507.00556].

[64] V. Bertone, R. Gauld and J. Rojo, JHEP **01**, 217 (2019), [arXiv:1808.02034].

[65] R. Aaij *et al.* (LHCb), JHEP **10**, 167 (2018), [arXiv:1806.04079].

[66] R. D. Ball *et al.* (NNPDF), Eur. Phys. J. **C77**, 10, 663 (2017), [arXiv:1706.00428].

[67] T.-J. Hou *et al.*, Phys. Rev. D **103**, 1, 014013 (2021), [arXiv:1912.10053].

[68] S. Alekhin *et al.*, Phys. Rev. **D96**, 1, 014011 (2017), [arXiv:1701.05838].

[69] A. Accardi *et al.*, Phys. Rev. D **93**, 11, 114017 (2016), [arXiv:1602.03154].

[70] G. Watt and R. S. Thorne, JHEP **08**, 052 (2012), [arXiv:1205.4024].

[71] S. Carrazza *et al.*, Eur. Phys. J. **C75**, 8, 369 (2015), [arXiv:1505.06736].

[72] J. C. Collins, F. Wilczek and A. Zee, Phys. Rev. **D18**, 242 (1978).

[73] E. Laenen *et al.*, Nucl. Phys. **B392**, 162 (1993).

[74] M. A. G. Aivazis *et al.*, Phys. Rev. **D50**, 3102 (1994), [hep-ph/9312319].

[75] M. Buza *et al.*, Eur. Phys. J. **C1**, 301 (1998), [hep-ph/9612398].

[76] J. C. Collins, Phys. Rev. **D58**, 094002 (1998), [hep-ph/9806259].

[77] A. Chuvakin, J. Smith and W. L. van Neerven, Phys. Rev. **D61**, 096004 (2000), [hep-ph/9910250].

Downloaded from https://academic.oup.com/ptep/article/2022/8/083C01/6651666 by KIT Library user on 27 September 2022

[78] R. S. Thorne, Phys. Rev. **D73**, 054019 (2006), [hep-ph/0601245].

[79] R. S. Thorne and W. K. Tung, in "Proceedings, HERA and the LHC Workshop Series on the implications of HERA for LHC physics: 2006-2008," 332–351 (2008), [,2(2008)], [arXiv:0809.0714].

[80] S. Alekhin and S. Moch, Phys. Lett. **B699**, 345 (2011), [arXiv:1011.5790].

[81] S. Forte *et al.*, Nucl. Phys. **B834**, 116 (2010), [arXiv:1001.2312].

[82] R. S. Thorne, Phys. Rev. **D86**, 074017 (2012), [arXiv:1201.6180].

[83] E. G. de Oliveira *et al.*, Eur. Phys. J. **C73**, 10, 2616 (2013), [arXiv:1307.3508].

[84] H. Abramowicz *et al.* (H1, ZEUS), Eur. Phys. J. **C78**, 6, 473 (2018), [arXiv:1804.01019].

[85] O. Behnke, A. Geiser and M. Lisovyi, Prog. Part. Nucl. Phys. **84**, 1 (2015), [arXiv:1506.07519].

[86] S. Dulat *et al.*, Phys. Rev. D **93**, 3, 033006 (2016), [arXiv:1506.07443].

[87] L. A. Harland-Lang *et al.*, Eur. Phys. J. **C75**, 5, 204 (2015), [arXiv:1412.3989].

[88] R. D. Ball *et al.* (NNPDF), JHEP **04**, 040 (2015), [arXiv:1410.8849].

[89] J. Butterworth *et al.*, J. Phys. **G43**, 023001 (2016), [arXiv:1510.03865].

[90] T. Cridge (PDF4LHC21 combination group), in "28th International Workshop on Deep Inelastic Scattering and Related Subjects," (2021), [arXiv:2108.09099].

[91] T. Cridge *et al.*, Eur. Phys. J. C **81**, 744 (2021), [arXiv:2106.10289].

[92] R. D. Ball *et al.* (NNPDF), Eur. Phys. J. **C78**, 5, 408 (2018), [arXiv:1802.03398].

[93] A. D. Martin *et al.*, Eur. Phys. J. **C39**, 155 (2005), [hep-ph/0411040].

[94] R. D. Ball *et al.* (NNPDF), Nucl. Phys. **B877**, 290 (2013), [arXiv:1308.0598].

[95] C. Schmidt *et al.*, Phys. Rev. **D93**, 11, 114015 (2016), [arXiv:1509.02905].

[96] M. Gluck, C. Pisano and E. Reya, Phys. Lett. **B540**, 75 (2002), [hep-ph/0206126].

[97] A. D. Martin and M. G. Ryskin, Eur. Phys. J. **C74**, 3040 (2014), [arXiv:1406.2118].

[98] L. A. Harland-Lang, V. A. Khoze and M. G. Ryskin, Phys. Rev. **D94**, 7, 074008 (2016), [arXiv:1607.04635].

[99] A. Manohar *et al.*, Phys. Rev. Lett. **117**, 24, 242002 (2016), [arXiv:1607.04266].

[100] V. Bertone *et al.* (NNPDF), SciPost Phys. **5**, 1, 008 (2018), [arXiv:1712.07053].

[101] L. A. Harland-Lang *et al.*, Eur. Phys. J. **C79**, 10, 811 (2019), [arXiv:1907.02750].

[102] K. Xie *et al.* (CTEQ-TEA) (2021), [arXiv:2106.10299].

[103] L. A. Harland-Lang, JHEP **03**, 128 (2020), [arXiv:1910.10178].

[104] H.-W. Lin *et al.*, Prog. Part. Nucl. Phys. **100**, 107 (2018), [arXiv:1711.07916].

[105] M. Constantinou *et al.*, Prog. Part. Nucl. Phys. **121**, 103908 (2021), [arXiv:2006.08636].

[106] Y.-B. Yang *et al.*, Phys. Rev. Lett. **121**, 21, 212001 (2018), [arXiv:1808.08677].

[107] C. Alexandrou *et al.*, Phys. Rev. D **101**, 9, 094513 (2020), [arXiv:2003.08486].

[108] X. Ji, Phys. Rev. Lett. **110**, 262002 (2013), [arXiv:1305.1539].

[109] C. Alexandrou *et al.*, Phys. Rev. Lett. **121**, 11, 112001 (2018), [arXiv:1803.02685].

[110] A. Buckley *et al.*, Eur. Phys. J. **C75**, 132 (2015), [arXiv:1412.7420].

[111] D. de Florian *et al.*, Phys. Rev. **D85**, 074028 (2012), [arXiv:1112.6324].

[112] K. Kovarik *et al.*, Phys. Rev. **D93**, 8, 085037 (2016), [arXiv:1509.00792].

[113] K. J. Eskola *et al.*, Eur. Phys. J. **C77**, 3, 163 (2017), [arXiv:1612.05741].

[114] H. Khanpour and S. Atashbar Tehrani, Phys. Rev. **D93**, 1, 014026 (2016), [arXiv:1601.00939].

[115] M. Walt, I. Helenius and W. Vogelsang, Phys. Rev. D **100**, 9, 096015 (2019), [arXiv:1908.03355].

[116] R. Abdul Khalek, J. J. Ethier and J. Rojo (NNPDF), Eur. Phys. J. C **79**, 6, 471 (2019), [arXiv:1904.00018].

[117] R. Abdul Khalek *et al.*, JHEP **09**, 183 (2020), [arXiv:2006.14629].

[118] P. Duwentäster *et al.* (2021), [arXiv:2105.09873].

[119] K. Kovarik *et al.*, Phys. Rev. Lett. **106**, 122301 (2011), [arXiv:1012.0286].

[120] H. Paukkunen and C. A. Salgado, Phys. Rev. Lett. **110**, 21, 212301 (2013), [arXiv:1302.2001].

[121] G. Aad *et al.* (ATLAS), Phys. Rev. **C92**, 4, 044915 (2015), [arXiv:1507.06232].

[122] V. Khachatryan *et al.* (CMS), Phys. Lett. **B750**, 565 (2015), [arXiv:1503.05825].

[123] V. Khachatryan *et al.* (CMS), Phys. Lett. B **759**, 36 (2016), [arXiv:1512.06461].

[124] A. M. Sirunyan *et al.* (CMS), Phys. Lett. B **800**, 135048 (2020), [arXiv:1905.01486].

[125] A. Kusina *et al.*, Eur. Phys. J. **C77**, 7, 488 (2017), [arXiv:1610.02925].

[126] S. Chatrchyan *et al.* (CMS), Eur. Phys. J. **C74**, 7, 2951 (2014), [arXiv:1401.4433].

[127] R. Aaij *et al.* (LHCb), JHEP **10**, 090 (2017), [arXiv:1707.02750].

[128] A. M. Sirunyan *et al.* (CMS), Phys. Rev. Lett. **121**, 6, 062002 (2018), [arXiv:1805.04736].

[129] S. Acharya *et al.* (ALICE), Eur. Phys. J. **C78**, 8, 624 (2018), [arXiv:1801.07051].

[130] S. S. Adler *et al.* (PHENIX), Phys. Rev. Lett. **98**, 172302 (2007), [arXiv:nucl-ex/0610036].

[131] K. J. Eskola *et al.*, JHEP **05**, 037 (2020), [arXiv:1906.02512].

[132] K. J. Eskola, P. Paakkinen and H. Paukkunen, Eur. Phys. J. C **79**, 6, 511 (2019), [arXiv:1903.09832].

[133] A. Kusina *et al.*, Phys. Rev. D **104**, 1, 014010 (2021), [arXiv:2012.11462].

[134] E. C. Aschenauer *et al.*, Phys. Rev. **D96**, 11, 114005 (2017), [arXiv:1708.05654].

[135] R. Abdul Khalek *et al.* (2021), [arXiv:2103.05419].

[136] R. A. Khalek *et al.*, Phys. Rev. D **103**, 9, 096005 (2021), [arXiv:2102.00018].

[137] P. V. Landshoff and J. C. Polkinghorne, Phys. Rev. D **18**, 3344 (1978).

[138] R. Kirschner, Phys. Lett. B **84**, 266 (1979).

[139] N. Paver and D. Treleani, Nuovo Cim. A **70**, 215 (1982).

[140] V. P. Shelest, A. M. Snigirev and G. M. Zinovev, Phys. Lett. B **113**, 325 (1982).

[141] M. Mekhfi, Phys. Rev. D **32**, 2371 (1985).

[142] B. Blok *et al.*, Phys. Rev. D **83**, 071501 (2011), [arXiv:1009.2714].

Downloaded from https://academic.oup.com/ptep/article/2022/8/083C01/6651666 by KIT Library user on 27 September 2022

[143] M. Diehl and A. Schafer, Phys. Lett. B **698**, 389 (2011), [arXiv:1102.3081].

[144] B. Blok *et al.*, Eur. Phys. J. C **72**, 1963 (2012), [arXiv:1106.5533].

[145] M. Diehl, D. Ostermeier and A. Schafer, JHEP **03**, 089 (2012), [Erratum: JHEP 03, 001 (2016)], [arXiv:1111.0910].

[146] C. H. Kom, A. Kulesza and W. J. Stirling, Phys. Rev. Lett. **107**, 082002 (2011), [arXiv:1105.4186].

[147] C. H. Kom, A. Kulesza and W. J. Stirling, Eur. Phys. J. C **71**, 1802 (2011), [arXiv:1109.0309].

[148] J. R. Gaunt *et al.*, Eur. Phys. J. C **69**, 53 (2010), [arXiv:1003.3953].

[149] F. Abe *et al.* (CDF), Phys. Rev. D **56**, 3811 (1997).

[150] V. M. Abazov *et al.* (D0), Phys. Rev. D **93**, 5, 052008 (2016), [arXiv:1512.05291].

[151] R. Aaij *et al.* (LHCb), JHEP **06**, 047 (2017), [Erratum: JHEP 10, 068 (2017)], [arXiv:1612.07451].

[152] M. Aaboud *et al.* (ATLAS), Phys. Lett. B **790**, 595 (2019), [arXiv:1811.11094].

[153] A. M. Sirunyan *et al.* (CMS), Eur. Phys. J. C **80**, 1, 41 (2020), [arXiv:1909.06265].

[154] A. V. Manohar and W. J. Waalewijn, Phys. Rev. D **85**, 114009 (2012), [arXiv:1202.3794].

[155] B. Blok *et al.*, Eur. Phys. J. C **74**, 2926 (2014), [arXiv:1306.3763].

[156] M. Diehl, J. R. Gaunt and K. Schönwald, JHEP **06**, 083 (2017), [arXiv:1702.06486].

[157] J. R. Gaunt and W. J. Stirling, JHEP **03**, 005 (2010), [arXiv:0910.4347].

[158] K. Golec-Biernat *et al.*, Phys. Lett. B **750**, 559 (2015), [arXiv:1507.08583].

[159] M. Diehl *et al.*, Eur. Phys. J. C **80**, 5, 468 (2020), [arXiv:2001.10428].

[160] D. Flay *et al.* (Jefferson Lab Hall A), Phys. Rev. **D94**, 5, 052003 (2016), [arXiv:1603.03612].

[161] C. Adolph *et al.* (COMPASS), Phys. Lett. **B753**, 18 (2016), [arXiv:1503.08935].

[162] C. Adolph *et al.* (COMPASS), Phys. Lett. **B769**, 34 (2017), [arXiv:1612.00620].

[163] R. Fersch *et al.* (CLAS), Phys. Rev. **C96**, 6, 065208 (2017), [arXiv:1706.10289].

[164] M. Hirai and S. Kumano (Asymmetry Analysis), Nucl. Phys. **B813**, 106 (2009), [arXiv:0808.0413].

[165] D. de Florian *et al.*, Phys. Rev. Lett. **101**, 072001 (2008), [arXiv:0804.0422]; D. de Florian *et al.*, Phys. Rev. **D80**, 034030 (2009), [arXiv:0904.3821].

[166] E. Leader, A. V. Sidorov and D. B. Stamenov, Phys. Rev. **D82**, 114018 (2010), [arXiv:1010.0574].

[167] J. Blumlein and H. Bottcher, Nucl. Phys. **B841**, 205 (2010), [arXiv:1005.3113].

[168] D. de Florian *et al.*, Phys. Rev. Lett. **113**, 1, 012001 (2014), [arXiv:1404.4293].

[169] N. Sato *et al.* (Jefferson Lab Angular Momentum), Phys. Rev. **D93**, 7, 074005 (2016), [arXiv:1601.07782].

[170] D. de Florian *et al.*, Phys. Rev. **D91**, 1, 014035 (2015), [arXiv:1410.6027].

[171] D. de Florian *et al.*, Phys. Rev. **D95**, 9, 094019 (2017), [arXiv:1702.06353].

[172] V. Bertone *et al.* (NNPDF), Eur. Phys. J. **C77**, 8, 516 (2017), [arXiv:1706.07049].

[173] V. Bertone *et al.* (NNPDF), Eur. Phys. J. **C78**, 8, 651 (2018), [arXiv:1807.03310].

[174] L. Adamczyk *et al.* (STAR), Phys. Rev. Lett. **115**, 9, 092002 (2015), [arXiv:1405.5134].

[175] L. Adamczyk *et al.* (STAR), Phys. Rev. D **95**, 7, 071103 (2017), [arXiv:1610.06616].

[176] A. Adare *et al.* (PHENIX), Phys. Rev. D **90**, 1, 012007 (2014), [arXiv:1402.6296].

[177] J. Adam *et al.* (STAR), Phys. Rev. D **99**, 5, 051102 (2019), [arXiv:1812.04817].

[178] R. D. Ball *et al.* (NNPDF), Nucl. Phys. **B874**, 36 (2013), [arXiv:1303.7236].

[179] J. Adam *et al.* (STAR), Phys. Rev. D **100**, 5, 052005 (2019), [arXiv:1906.02740].

[180] M. Abdallah *et al.* (STAR), Phys. Rev. D **103**, 9, L091103 (2021), [arXiv:2103.05571].

[181] A. Adare *et al.* (PHENIX), Phys. Rev. D **93**, 1, 011501 (2016), [arXiv:1510.02317].

[182] D. De Florian *et al.*, Phys. Rev. D **100**, 11, 114027 (2019), [arXiv:1902.10548].

[183] J. Liang *et al.*, Phys. Rev. D **98**, 7, 074505 (2018), [arXiv:1806.08366].

[184] R. Nisius, Phys. Rept. **332**, 165 (2000), [hep-ex/9912049].

[185] T. F. Walsh and P. M. Zerwas, Phys. Lett. **44B**, 195 (1973).

[186] R. L. Kingsley, Nucl. Phys. **B60**, 45 (1973).

[187] E. Witten, Nucl. Phys. **B120**, 189 (1977).

[188] W. A. Bardeen and A. J. Buras, Phys. Rev. **D20**, 166 (1979), [Erratum: Phys. Rev.D21,2041(1980)].

[189] M. Fontannaz and E. Pilon, Phys. Rev. **D45**, 382 (1992).

[190] M. Gluck, E. Reya and A. Vogt, Phys. Rev. **D45**, 3986 (1992).

[191] F. Cornet, P. Jankowski and M. Krawczyk, Phys. Rev. **D70**, 093004 (2004), [hep-ph/0404063].

[192] P. Aurenche, M. Fontannaz and J. P. Guillet, Eur. Phys. J. **C44**, 395 (2005), [hep-ph/0503259].

[193] W. Slominski, H. Abramowicz and A. Levy, Eur. Phys. J. **C45**, 633 (2006), [hep-ph/0504003].

[194] H. Abramowicz and A. Caldwell, Rev. Mod. Phys. **71**, 1275 (1999), [hep-ex/9903037].

[195] S. Chekanov *et al.* (ZEUS), Nucl. Phys. **B831**, 1 (2010), [arXiv:0911.4119].

[196] A. Aktas *et al.* (H1), Eur. Phys. J. **C48**, 715 (2006), [hep-ex/0606004].

[197] A. D. Martin, M. G. Ryskin and G. Watt, Phys. Lett. **B644**, 131 (2007), [hep-ph/0609273].

[198] A. Aktas *et al.* (H1), JHEP **10**, 042 (2007), [arXiv:0708.3217].

[199] F. D. Aaron *et al.* (H1, ZEUS), Eur. Phys. J. **C72**, 2175 (2012), [arXiv:1207.4864].

[200] F. D. Aaron *et al.* (H1), Eur. Phys. J. **C72**, 2074 (2012), [arXiv:1203.4495].

[201] J. C. Collins, Phys. Rev. **D57**, 3051 (1998), [Erratum: Phys. Rev.D61,019902(2000)], [hep-ph/9709499].

[202] G. Ingelman and P. E. Schlein, Phys. Lett. **152B**, 256 (1985).

[203] M. Goharipour, H. Khanpour and V. Guzey, Eur. Phys. J. **C78**, 4, 309 (2018), [arXiv:1802.01363].

[204] X. Ji, Phys. Rev. Lett. **91**, 062001 (2003), [hep-ph/0304037].

[205] A. V. Belitsky, X. Ji and F. Yuan, Phys. Rev. **D69**, 074014 (2004), [hep-ph/0307383].

[206] C. Lorce, B. Pasquini and M. Vanderhaeghen, JHEP **05**, 041 (2011), [arXiv:1102.4704].

[207] X.-D. Ji, J. Phys. **G24**, 1181 (1998), [hep-ph/9807358].

[208] K. Goeke, M. V. Polyakov and M. Vanderhaeghen, Prog. Part. Nucl. Phys. **47**, 401 (2001), [hep-ph/0106012].

[209] M. Diehl, Phys. Rept. **388**, 41 (2003), [hep-ph/0307382].

Downloaded from https://academic.oup.com/ptep/article/2022/8/083C01/6651666 by KIT Library user on 27 September 2022

[210] A. V. Belitsky and A. V. Radyushkin, Phys. Rept. **418**, 1 (2005), [hep-ph/0504030].

[211] S. Boffi and B. Pasquini, Riv. Nuovo Cim. **30**, 387 (2007), [arXiv:0711.2625].

[212] K. Kumericki, S. Liuti and H. Moutarde, Eur. Phys. J. **A52**, 6, 157 (2016), [arXiv:1602.02763].

[213] M. Burkardt, Int. J. Mod. Phys. **A18**, 173 (2003), [hep-ph/0207047].

[214] M. Diehl, Eur. Phys. J. **C25**, 223 (2002), [Erratum: Eur. Phys. J.C31,277(2003)], [hep-ph/0205208].

[215] M. Bury, A. Prokudin and A. Vladimirov, JHEP **05**, 151 (2021), [arXiv:2103.03270].

[216] A. V. Efremov and A. V. Radyushkin, Phys. Lett. **94B**, 245 (1980).

[217] G. P. Lepage and S. J. Brodsky, Phys. Rev. **D22**, 2157 (1980).

[218] A. V. Belitsky, A. Freund and D. Mueller, Phys. Lett. **B493**, 341 (2000), [hep-ph/0008005].

[219] A. V. Belitsky, A. Freund and D. Mueller, Nucl. Phys. **B574**, 347 (2000), [hep-ph/9912379].

[220] V. M. Braun *et al.*, JHEP **06**, 037 (2017), [arXiv:1703.09532].

[221] A. V. Radyushkin, Phys. Rev. **D59**, 014030 (1999), [hep-ph/9805342].

[222] A. V. Radyushkin, Phys. Lett. **B449**, 81 (1999), [hep-ph/9810466].

[223] K. Kumerički and D. Mueller, Nucl. Phys. **B841**, 1 (2010), [arXiv:0904.0458].

[224] N. d'Hose, S. Niccolai and A. Rostomyan, Eur. Phys. J. **A52**, 6, 151 (2016).

[225] M. Guidal, H. Moutarde and M. Vanderhaeghen, Rept. Prog. Phys. **76**, 066202 (2013), [arXiv:1303.6600].

[226] M. Anselmino, M. Guidal and P. Rossi, The European Physical Journal A **52**, 6, 149 (2016), ISSN 1434-601X, URL `https://doi.org/10.1140/epja/i2016-16164-4`.

[227] P. J. Mulders and R. D. Tangerman, Nucl. Phys. **B461**, 197 (1996), [Erratum: Nucl. Phys.B484,538(1997)], [hep-ph/9510301].

[228] D. Boer and P. J. Mulders, Phys. Rev. **D57**, 5780 (1998), [hep-ph/9711485].

[229] D. W. Sivers, Phys. Rev. **D41**, 83 (1990).

[230] J. C. Collins, Nucl. Phys. **B396**, 161 (1993), [hep-ph/9208213].

[231] X. Ji, J. Ma and F. Yuan, Phys. Rev. **D71**, 034005 (2005), [hep-ph/0404183].

[232] J. Collins, Foundations of perturbative QCD Camb. Monogr. Part. Phys. Nucl. Phys. Cosmol. 32 (2011) 1-624 and references therein.

[233] S. M. Aybat and T. C. Rogers, Phys. Rev. **D83**, 114042 (2011), [arXiv:1101.5057].

[234] M. G. Echevarria, A. Idilbi and I. Scimemi, JHEP **07**, 002 (2012), [arXiv:1111.4996].

[235] M. G. A. Buffing, A. Mukherjee and P. J. Mulders, Phys. Rev. **D88**, 054027 (2013), [arXiv:1306.5897].

[236] T. C. Rogers and P. J. Mulders, Phys. Rev. **D81**, 094006 (2010), [arXiv:1001.2977].

[237] A. Signori *et al.*, JHEP **11**, 194 (2013), [arXiv:1309.3507].

[238] M. Anselmino *et al.*, JHEP **04**, 005 (2014), [arXiv:1312.6261].

[239] U. D'Alesio *et al.*, JHEP **11**, 098 (2014), [arXiv:1407.3311].

[240] M. G. Echevarria *et al.*, Phys. Rev. **D89**, 074013 (2014), [arXiv:1401.5078].

[241] P. Sun *et al.*, Int. J. Mod. Phys. **A33**, 11, 1841006 (2018), [arXiv:1406.3073].

[242] A. Bacchetta *et al.*, JHEP **06**, 081 (2017), [Erratum: JHEP06,051(2019)], [arXiv:1703.10157].

[243] I. Scimemi and A. Vladimirov, Eur. Phys. J. **C78**, 2, 89 (2018), [arXiv:1706.01473].

[244] V. Bertone, I. Scimemi and A. Vladimirov, JHEP **06**, 028 (2019), [arXiv:1902.08474].

[245] J. O. Gonzalez-Hernandez *et al.*, Phys. Rev. **D98**, 11, 114005 (2018), [arXiv:1808.04396].

[246] A. Bacchetta *et al.*, Phys. Rev. **D100**, 1, 014018 (2019), [arXiv:1901.06916].

[247] R. Angeles-Martinez *et al.*, Acta Phys. Polon. **B46**, 12, 2501 (2015), [arXiv:1507.05267].

[248] A. Bacchetta *et al.*, Phys. Lett. **B788**, 542 (2019), [arXiv:1807.02101].

[249] M. Diehl, Eur. Phys. J. **A52**, 6, 149 (2016), [arXiv:1512.01328].

[250] A. Bacchetta, Eur. Phys. J. **A52**, 6, 163 (2016).

[251] `http://hepdata.cedar.ac.uk/pdfs`.

[252] I. Scimemi, Adv. High Energy Phys. **2019**, 3142510 (2019), [arXiv:1901.08398].

Downloaded from https://academic.oup.com/ptep/article/2022/8/083C01/6651666 by KIT Library user on 27 September 2022

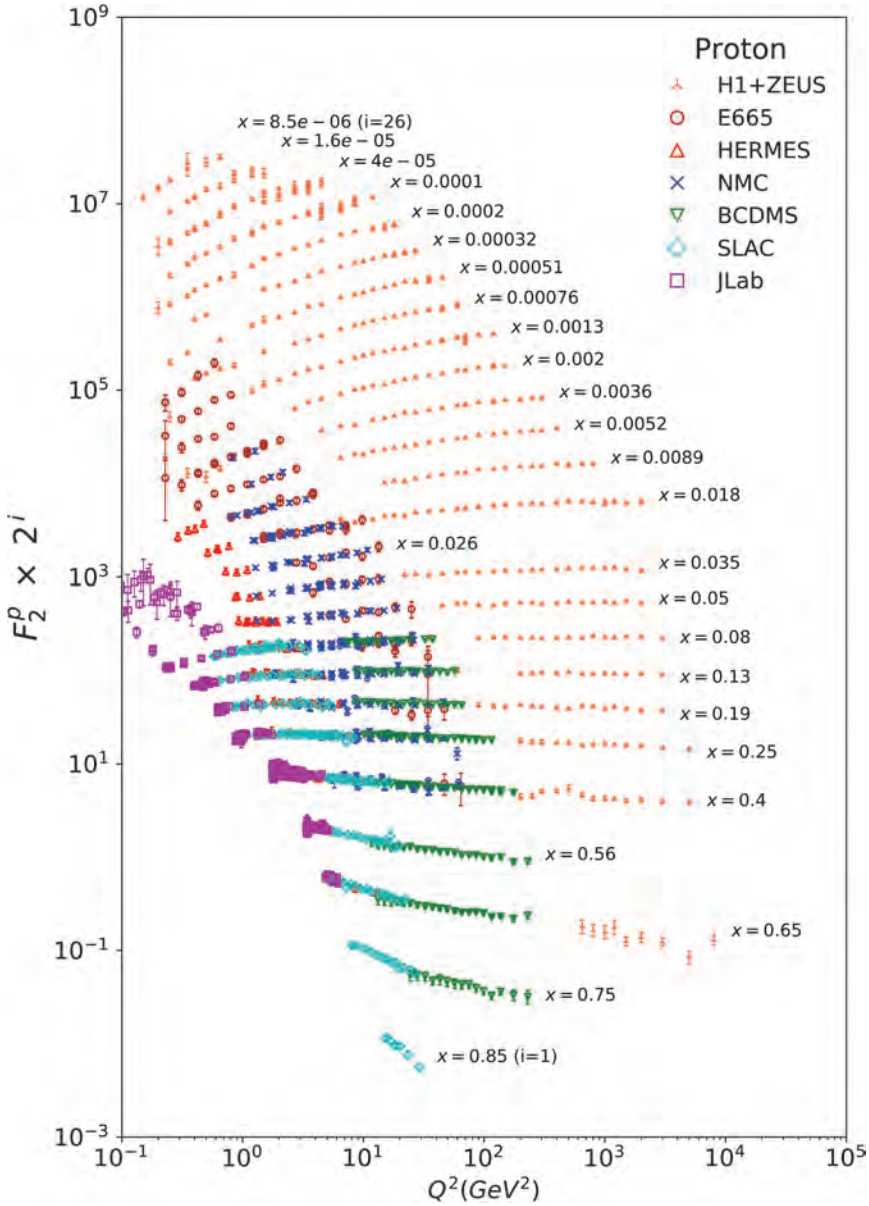

Figure 18.10: The proton structure function F_2^p measured in electromagnetic scattering of electrons and positrons on protons, and for electrons/positrons (SLAC,HERMES,JLAB) and muons (BCDMS, E665, NMC) on a fixed target. Statistical and systematic errors added in quadrature are shown. The H1+ZEUS combined values are obtained from the measured reduced cross section and converted to F_2^p with a HERAPDF NLO fit, for all measured points where the predicted ratio of F_2^p to reduced cross-section was within 10% of unity. The data are plotted as a function of Q^2 in bins of fixed x. Some points have been slightly offset in Q^2 for clarity. The H1+ZEUS combined binning in x is used in this plot; all other data are rebinned to the x values of these data. For the purpose of plotting, F_2^p has been multiplied by 2^{i_x}, where i_x is the number of the x bin, ranging from $i_x = 1$ ($x = 0.85$) to $i_x = 26$ ($x = 0.0000085$). Only data with $W^2 > 3.5$ GeV^2 is included. Plot from CJ collaboration (Shujie Li – private communication).
References: **H1 and ZEUS**—H. Abramowicz *et al.*, Eur. Phys. J. **C75**, 580 (2015) (for both data and HERAPDF parameterization); **BCDMS**—A.C. Benvenuti *et al.*, Phys. Lett. **B223**, 485 (1989) (as given in [251]) **E665**—M.R. Adams *et al.*, Phys. Rev. **D54**, 3006 (1996); **NMC**—M. Arneodo *et al.*, Nucl. Phys. **B483**, 3 (1997); **SLAC**—L.W. Whitlow *et al.*, Phys. Lett. **B282**, 475 (1992); **HERMES**—A. Airapetian *et al.*, JHEP **1105**, 126 (2011);**JLAB**—Y. Liang *et al.*, Jefferson Lab Hall C E94-110 collaboration, nucl-ex/0410027, M.E. Christy *et al.*, Jefferson Lab Hall C E94-110 Collaboration, Phys. Rev. **C70**, 015206 (2004), S. Malace *et al.*, Jefferson Lab Hall C E00-116 Collaboration, Phys. Rev. **C80**, 035207 (2009), V. Tvaskis *et al.*, Jefferson Lab Hall C E99-118 Collaboration, Phys. Rev. **C81**, 055207 (2010), M. Osipenko *et al.*, Jefferson Lab Hall B CLAS6 Collaboration, Phys. Rev. **D67**, 092001 (2003).

Downloaded from https://academic.oup.com/ptep/article/2022/8/083C01/6651666 by KIT Library user on 27 September 2022

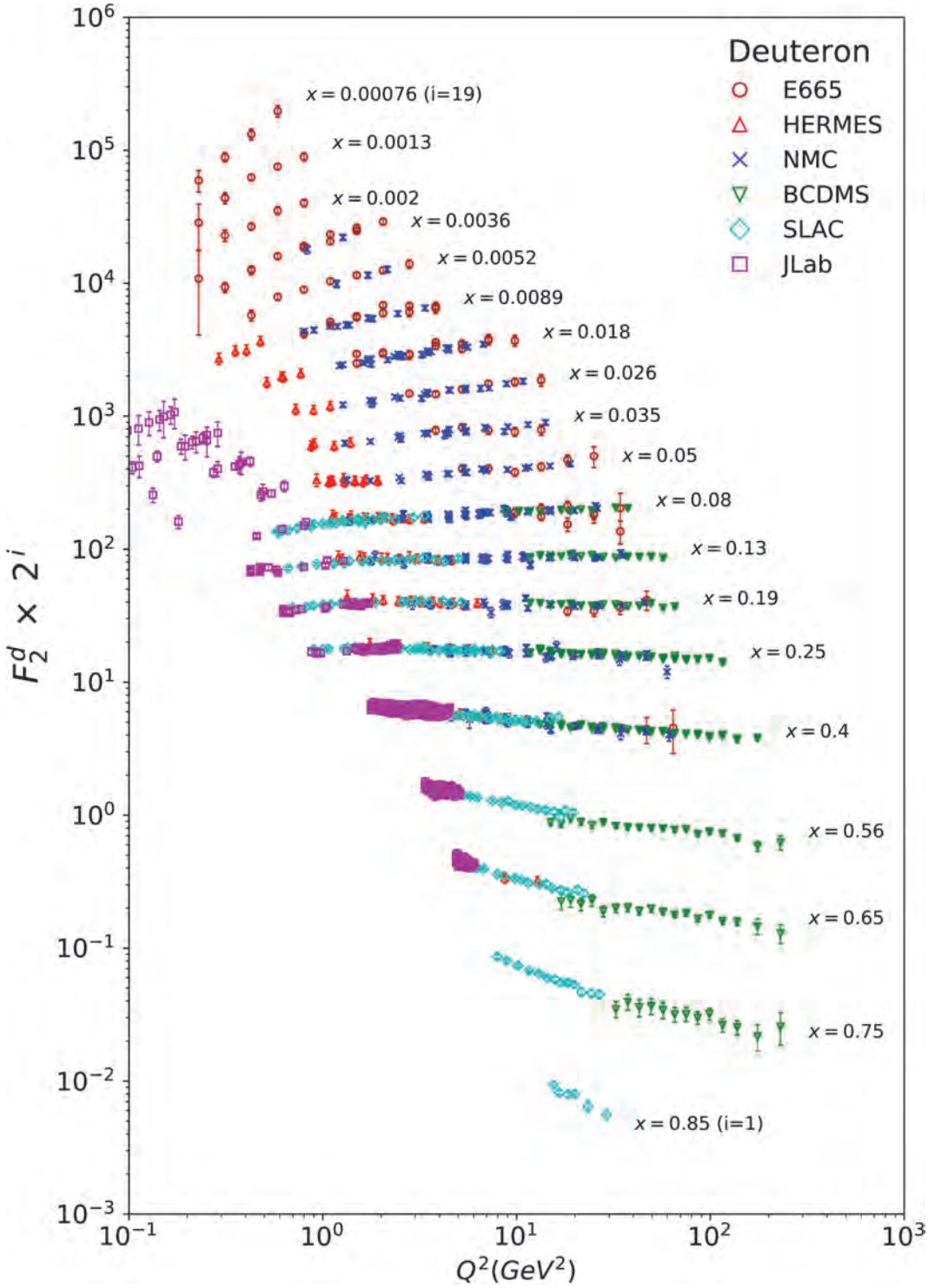

Figure 18.11: The deuteron structure function F_2^d measured in electromagnetic scattering of electrons/positrons (SLAC,HERMES,JLAB) and muons (BCDMS, E665, NMC) on a fixed target, shown as a function of Q^2 for bins of fixed x. Statistical and systematic errors added in quadrature are shown. For the purpose of plotting, F_2^d has been multiplied by 2^{i_x}, where i_x is the number of the x bin, ranging from 1 ($x = 0.85$) to 29 ($x = 0.00076$). Only data with $W^2 > 3.5$ GeV^2 is included. Plot from CJ collaboration (Shujie Li – private communication) References: **BCDMS**—A.C. Benvenuti *et al.*, Phys. Lett. **B237**, 592 (1990). **E665, NMC, SLAC,HERMES**—same references as Fig. 18.10; **JLAB**—S. Malace *et al.*, Jefferson Lab Hall C E00-116 Collaboration, Phys. Rev. **C80**, 035207 (2009), V. Tvaskis *et al.*, Jefferson Lab Hall C E99-118 Collaboration, Phys. Rev. **C81**, 055207 (2010), J. Seely (MIT, LNS) *et al.*, Jefferson Lab Hall C E03-103 Collaboration, Phys. Rev. Lett. **103**, 202301 (2009), M. Osipenko *et al.*, Jefferson Lab Hall B CLAS6 Collaboration, Phys. Rev. **C73**, 045205 (2006).

Downloaded from https://academic.oup.com/ptep/article/2022/8/083C01/6651666 by KIT Library user on 27 September 2022

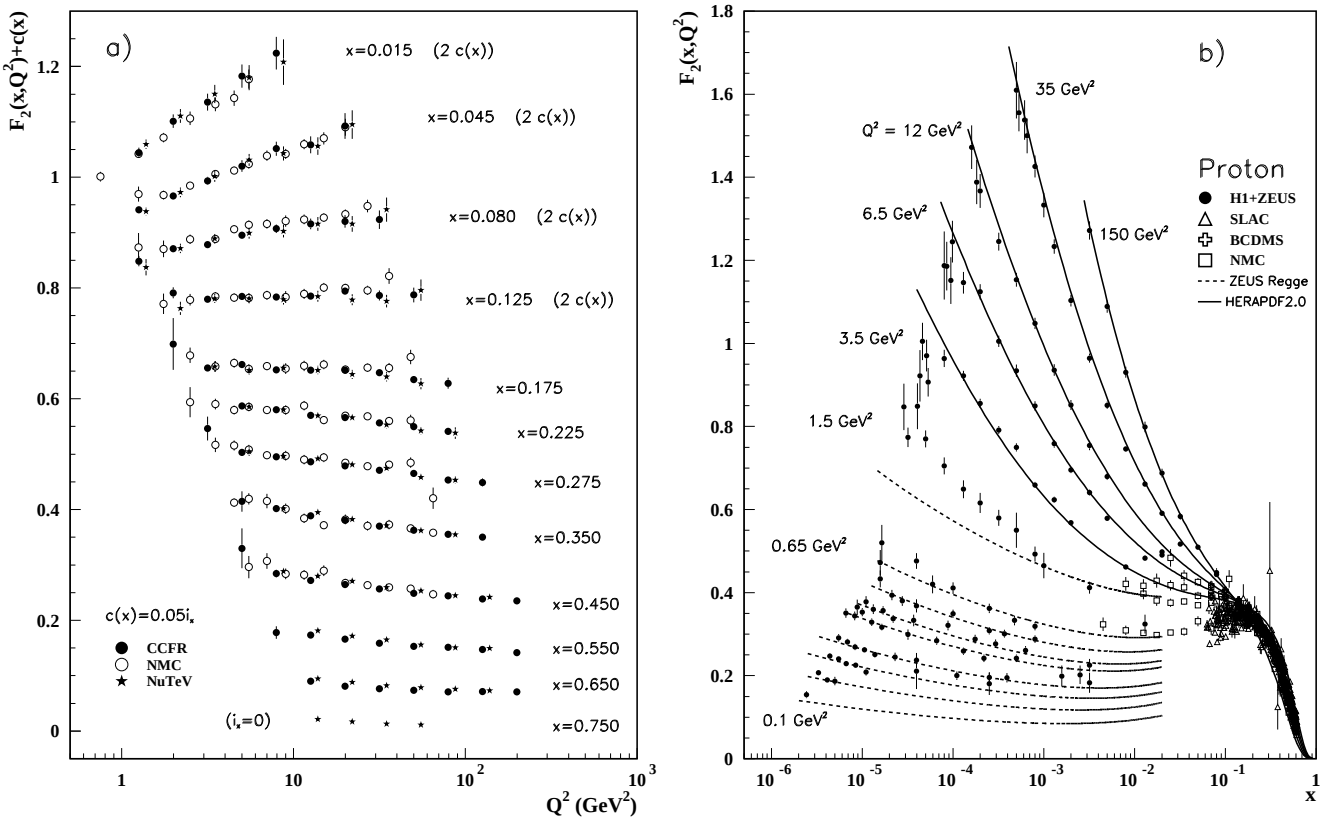

Figure 18.12: a) The deuteron structure function F_2 measured in deep inelastic scattering of muons on a fixed target (NMC) is compared to the structure function F_2 from neutrino-iron scattering (CCFR and NuTeV) using $F_2^{\mu} = (5/18)F_2^{\nu} - x(s+\overline{s})/6$, where heavy-target effects have been taken into account. The data are shown versus Q^2, for bins of fixed x. The NMC data have been rebinned to CCFR and NuTeV x values. For the purpose of plotting, a constant $c(x) = 0.05i_x$ is added to F_2, where i_x is the number of the x bin, ranging from 0 ($x = 0.75$) to 7 ($x = 0.175$). For $i_x = 8$ ($x = 0.125$) to 11 ($x = 0.015$), $2c(x)$ has been added. References: **NMC**—M. Arneodo *et al.*, Nucl. Phys. **B483**, 3 (1997); **CCFR/NuTeV**—U.K. Yang *et al.*, Phys. Rev. Lett. **86**, 2741 (2001); **NuTeV**—M. Tzanov *et al.*, Phys. Rev. **D74**, 012008 (2006).
b) The proton structure function F_2^p mostly at small x and Q^2, measured in electromagnetic scattering of electrons and positrons (H1, ZEUS), electrons (SLAC), and muons (BCDMS, NMC) on protons. Lines are ZEUS Regge and HERAPDF parameterizations for lower and higher Q^2, respectively. The width of the bins can be up to 10% of the stated Q^2. Some points have been slightly offset in x for clarity. The H1+ZEUS combined values for $Q^2 \geq 3.5$ GeV^2 are obtained from the measured reduced cross section and converted to F_2^p with a HERAPDF NLO fit, for all measured points where the predicted ratio of F_2^p to reduced cross-section was within 10% of unity. A turn-over is visible in the low-x points at medium Q^2 (3.5 GeV^2 and 6 GeV^2) for the H1+ZEUS combined values. In order to obtain F_2^p from the measured reduced cross-section, F_L must be estimated; for the points shown, this estimate is obtained from HERAPDF2.0. No F_L value consistent with the HERA data can eliminate the turn-over. This may indicate that at low x and Q^2 there are contributions to the structure functions that cannot be described in standard DGLAP evolution.
References: **H1 and ZEUS**—F.D. Aaron *et al.*, JHEP **1001**, 109 (2010) (data for $Q^2 < 3.5$ GeV^2), H. Abramowicz *et al.*, Eur. Phys. J. **C75**, 580 (2015) (data for $Q^2 \geq 3.5$ GeV^2 and HERAPDF parameterization); **ZEUS**—J. Breitweg *et al.*, Phys. Lett. **B487**, 53 (2000) (ZEUS Regge parameterization); **BCDMS, NMC, SLAC**—same references as Fig. 18.10.
Statistical and systematic errors added in quadrature are shown for both plots.

Downloaded from https://academic.oup.com/ptep/article/2022/8/083C01/6651666 by KIT Library user on 27 September 2022

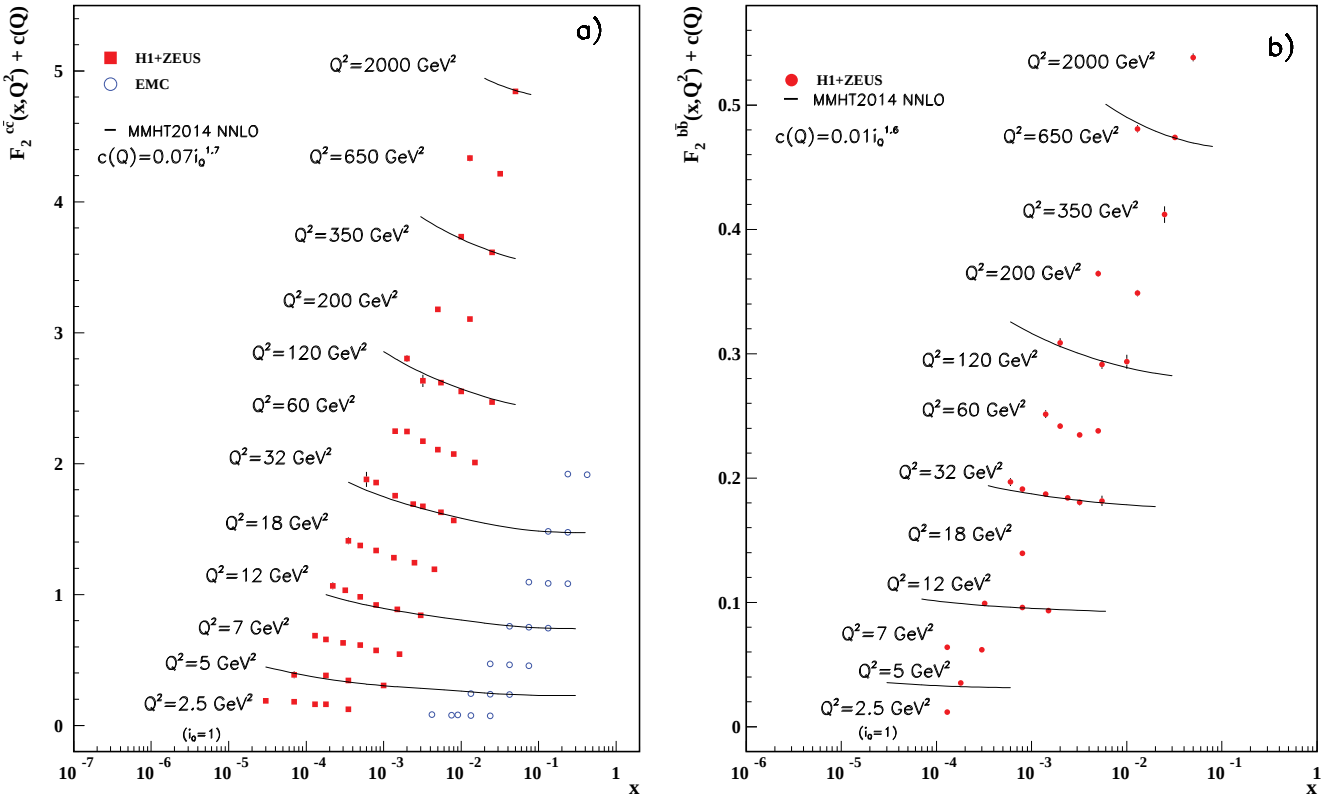

Figure 18.13: a) The charm-quark structure function $F_2^{c\bar{c}}(x)$, i.e. that part of the inclusive structure function F_2^p arising from the production of charm quarks, measured in electromagnetic scattering of positrons on protons (H1, ZEUS) (the values are obtained from the measured reduced cross section and converted to $F_2^{c\bar{c}}$ using the PDFs from the MMHT NNLO fit) and muons on iron (EMC). For the purpose of plotting, a constant $c(Q) = 0.07{i_Q}^{1.7}$ is added to $F_2^{c\bar{c}}$ where i_Q is the number of the Q^2 bin, ranging from 1 ($Q^2 = 2.5$ GeV^2) to 12 ($Q^2 = 2000$ GeV^2). References: **H1 and ZEUS run I +II combination**—H. Abramowicz *et al.*, Eur. Phys. J. **C78**, 473 (2018); **EMC**—J.J. Aubert *et al.*, Nucl. Phys. **B213**, 31 (1983).

b) The bottom-quark structure function $F_2^{b\bar{b}}(x)$. For the purpose of plotting, a constant $c(Q) = 0.01 i_Q^{1.6}$ is added to $F_2^{b\bar{b}}$ where i_Q is the number of the Q^2 bin, ranging from 1 ($Q^2 = 2.5$ GeV^2) to 12 ($Q^2 = 2000$ GeV^2). References: **H1 and ZEUS run I combination**—H. Abramowicz *et al.*, Eur. Phys. J. **C78**, 473 (2018).

For both plots, statistical and systematic errors added in quadrature are shown. The data are given as a function of x in bins of Q^2. Points may have been slightly offset in x for clarity. Some data have been rebinned to common Q^2 values. Also shown is the MMHT2014 parameterization given at several Q^2 values (L. A. Harland-Lang *et al.*, Eur. Phys. J. **C75**, 204 (2015)).

Downloaded from https://academic.oup.com/ptep/article/2022/8/083C01/6651666 by KIT Library user on 27 September 2022

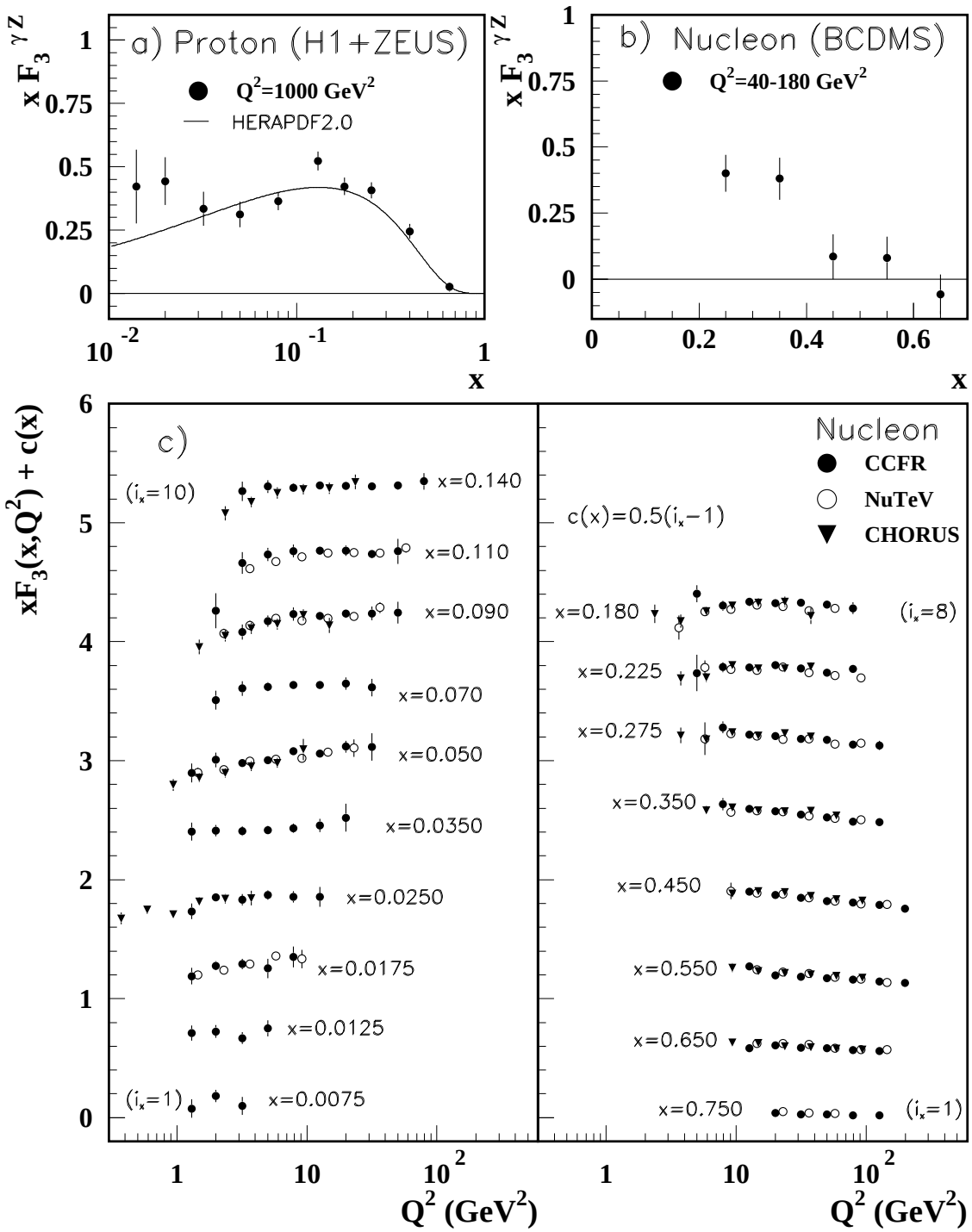

Figure 18.14: The structure function $xF_3^{\gamma Z}$ measured in electroweak scattering of **a)** electrons on protons (H1 and ZEUS) and **b)** muons on carbon (BCDMS). The line in **a)** is the HERAPDF parameterization. References: **H1 and ZEUS**—H. Abramowicz *et al.*, Eur. Phys. J. **C75**, 580 (2015) (for both data and HERAPDF parameterization); **BCDMS**—A. Argento *et al.*, Phys. Lett. **B140**, 142 (1984).
c) The structure function xF_3 of the nucleon measured in ν-Fe scattering. The data are plotted as a function of Q^2 in bins of fixed x. For the purpose of plotting, a constant $c(x) = 0.5(i_x - 1)$ is added to xF_3, where i_x is the number of the x bin as shown in the plot. The NuTeV and CHORUS points have been shifted to the nearest corresponding x bin as given in the plot and slightly offset in Q^2 for clarity. References: **CCFR**—W.G. Seligman *et al.*, Phys. Rev. Lett. **79**, 1213 (1997); **NuTeV**—M. Tzanov *et al.*, Phys. Rev. **D74**, 012008 (2006); **CHORUS**—G. Önengüt *et al.*, Phys. Lett. **B632**, 65 (2006).

Statistical and systematic errors added in quadrature are shown for all plots.

Downloaded from https://academic.oup.com/ptep/article/2022/8/083C01/6651666 by KIT Library user on 27 September 2022

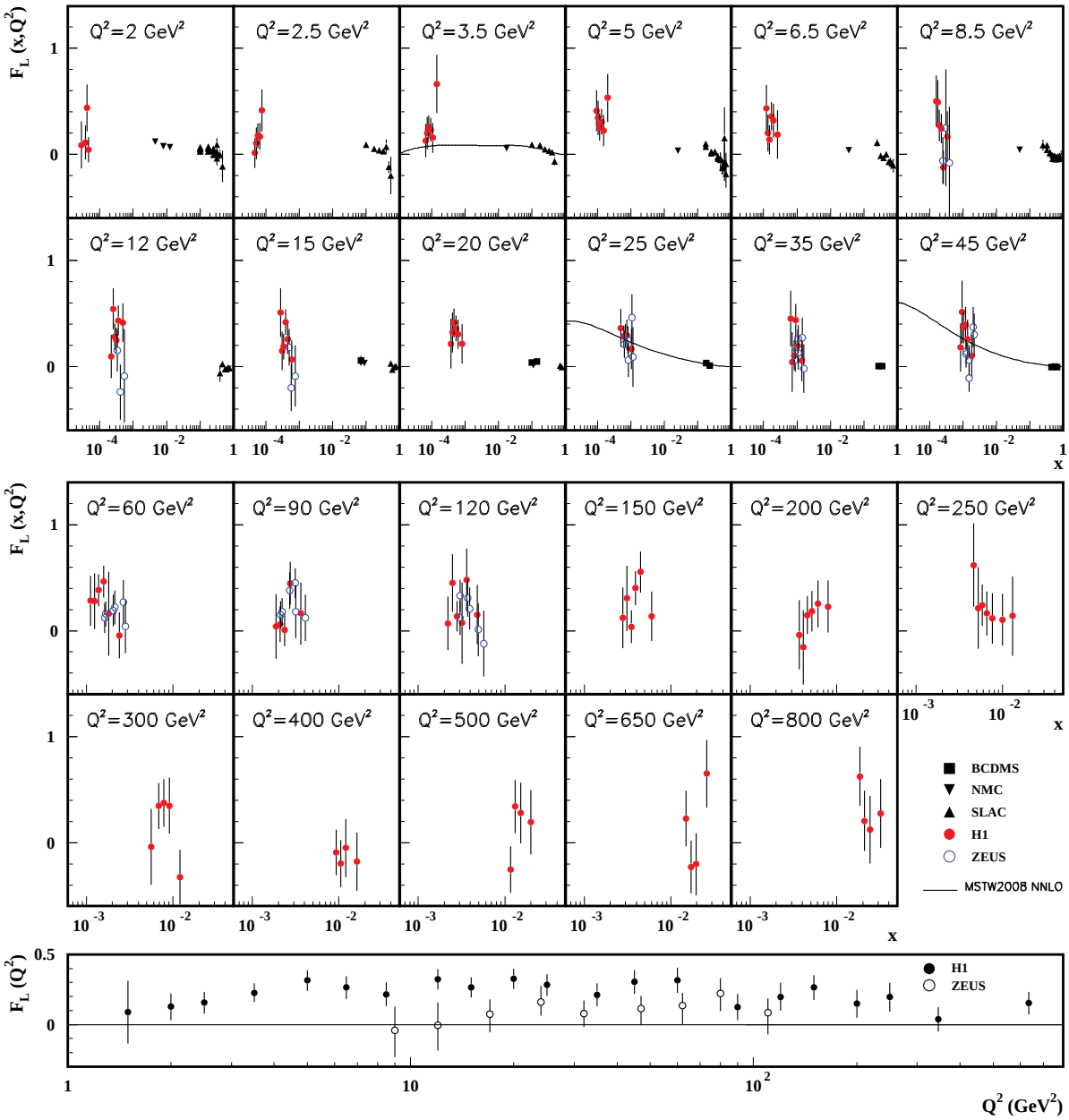

Figure 18.15: Top panels: The longitudinal structure function F_L as a function of x in bins of fixed Q^2 measured on the proton (except for the SLAC data which also contain deuterium data). BCDMS, NMC, and SLAC results are from measurements of R (the ratio of longitudinal to transverse photon absorption cross sections) which are converted to F_L by using the BDCMS parameterization of F_2 (A.C. Benvenuti *et al.*, Phys. Lett. **B223**, 485 (1989)). It is assumed that the Q^2 dependence of the fixed-target data is small within a given Q^2 bin. Some of the other data may have been rebinned to common Q^2 values. Some points have been slightly offset in x for clarity. Also shown is the MSTW2008 parameterization given at three Q^2 values (A.D. Martin *et al.*, Eur. Phys. J. **C63**, 189 (2009)). References: **H1**—V. Andreev *et al.*, Eur. Phys. J. **C74**, 2814 (2014); **ZEUS**—S. Chekanov *et al.*, Phys. Lett. **B682**, 8 (2009); H. Abramowicz et al., Phys. Rev. **D90**, 072002 (2014); **BCDMS**—A. Benvenuti *et al.*, Phys. Lett. **B223**, 485 (1989); **NMC**—M. Arneodo *et al.*, Nucl. Phys. **B483**, 3 (1997); **SLAC**—L.W. Whitlow *et al.*, Phys. Lett. **B250**, 193 (1990) and numerical values from the thesis of L.W. Whitlow (SLAC-357).
Bottom panel: The longitudinal structure function F_L as a function of Q^2. Some points have been slightly offset in Q^2 for clarity. References: **H1**—V. Andreev *et al.*, Eur. Phys. J. **C74**, 2814 (2014); **ZEUS**—H. Abramowicz et al., Phys. Rev. **D90**, 072002 (2014).
The results shown in the bottom plot require the assumption of the validity of the QCD form for the F_2 structure function in order to extract F_L. Statistical and systematic errors added in quadrature are shown for both plots.

Downloaded from https://academic.oup.com/ptep/article/2022/8/083C01/6651666 by KIT Library user on 27 September 2022

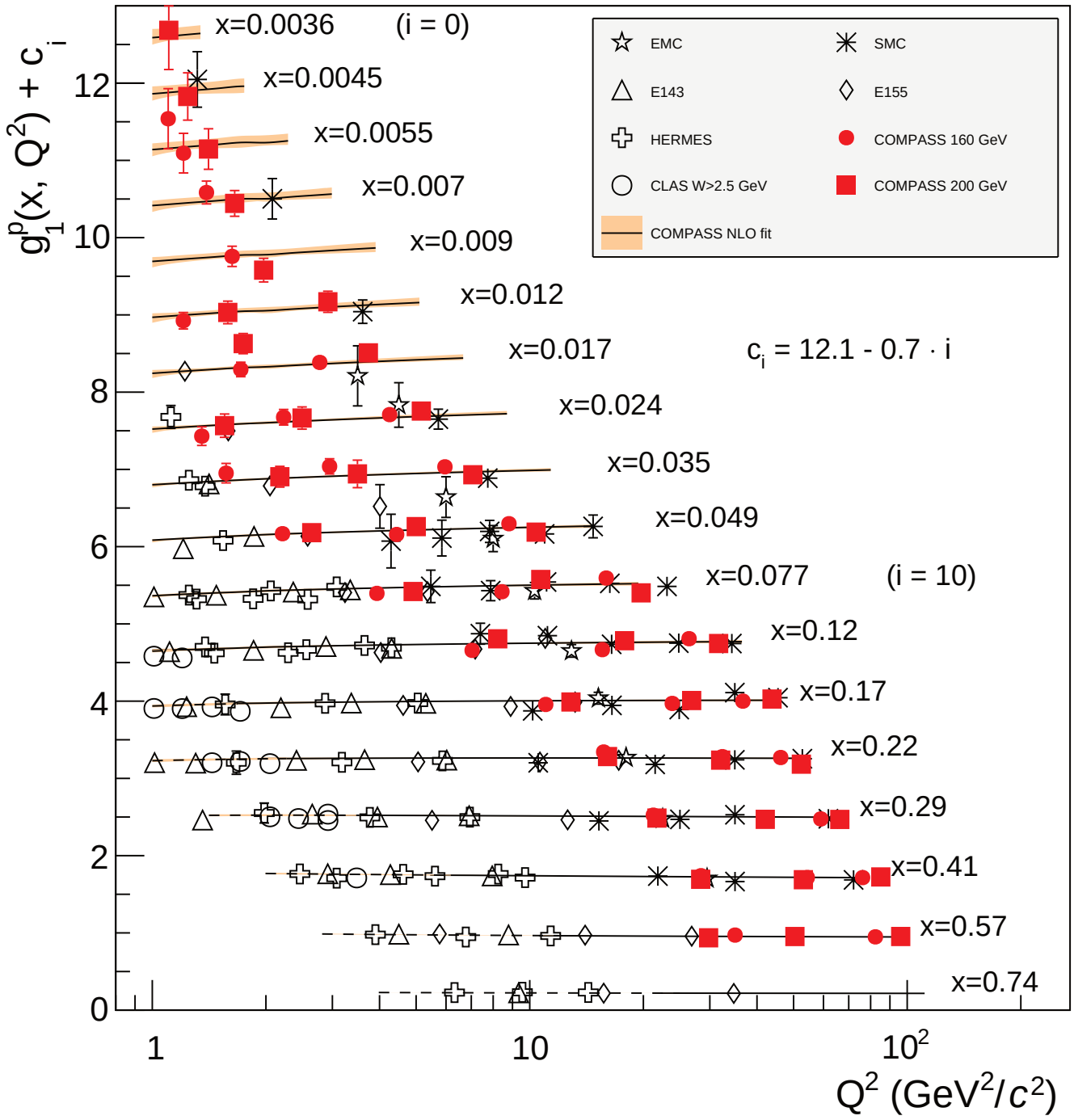

Figure 18.16: World data on the spin-dependent structure function g_1^p as a function of Q^2 for various values of x The lines represent the Q^2 dependence for each value of x, as determined from a NLO QCD fit. The dashed ranges represent the region with $W^2 < 10$ (GeV/c^2)^2. References: **EMC**—J. Ashman *et al.*, Phys. Lett. **B206**, 363 (1988); Nucl. Phys. **B328**, 1 (1989); **E143**—K. Abe *et al.*, Phys. Rev. **D58**, 112003 (1998); **SMC**—B. Adeva *et al.*, Phys. Rev. **D58**, 112001 (1998); **HERMES**—A. Airapetian *et al.*, Phys. Rev. **D75**, 012007 (2007); **E155**—P.L. Anthony *et al.*, Phys. Lett. **B493**, 19 (2000); **COMPASS**—M.G. Alekseev *et al.*, Phys. Lett. **B690**, 466 (2010), C. Adolph, *et al.*, Phys. Lett. **B753**, 18 (2016); **CLAS**—K.V. Dharmawardane *et al.*, Phys. Lett. **B641**, 11 (2006) (which also includes resonance region data not shown on this plot — there is also low W^2 CLAS data in Y. Prok *et al.*, Phys. Rev. **C90**, 025212 (2014) and N. Guler *et al.*, Phys. Rev. **C92**, 055201 (2015)).

Downloaded from https://academic.oup.com/ptep/article/2022/8/083C01/6651666 by KIT Library user on 27 September 2022

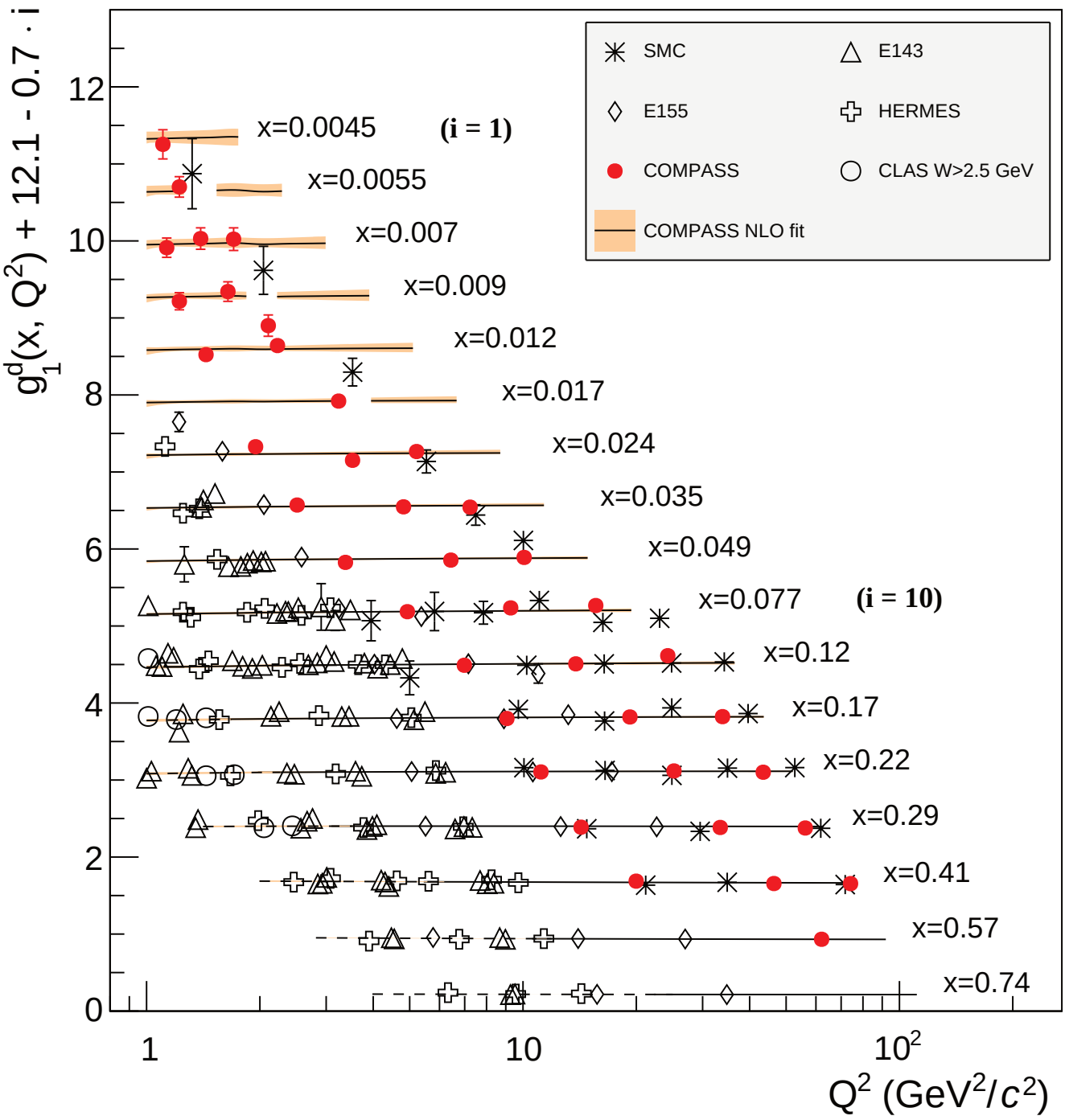

Figure 18.17: World data on the spin-dependent structure function g_1^d as a function of Q^2 for various values of x The lines represent the Q^2 dependence for each value of x, as determined from a NLO QCD fit. The dashed ranges represent the region with $W^2 < 10$ (GeV/c^2)^2. **CLAS**—K.V. Dharmawardane *et al.*, Phys. Lett. **B641**, 11 (2006) **HERMES**—A. Airapetian *et al.*, Phys. Rev. **D75**, 012007 (2007); **SMC**—B. Adeva *et al.*, Phys. Rev. **D58**, 112001 (1998); **E155**—P.L. Anthony *et al.*, Phys. Lett. **B463**, 339 (1999); **E143**—K. Abe *et al.*, Phys. Rev. **D58**, 112003 (1998); **COMPASS**—C. Adolph, *et al.*, Phys. Lett. **B769**, 34 (2017);

Downloaded from https://academic.oup.com/ptep/article/2022/8/083C01/6651666 by KIT Library user on 27 September 2022

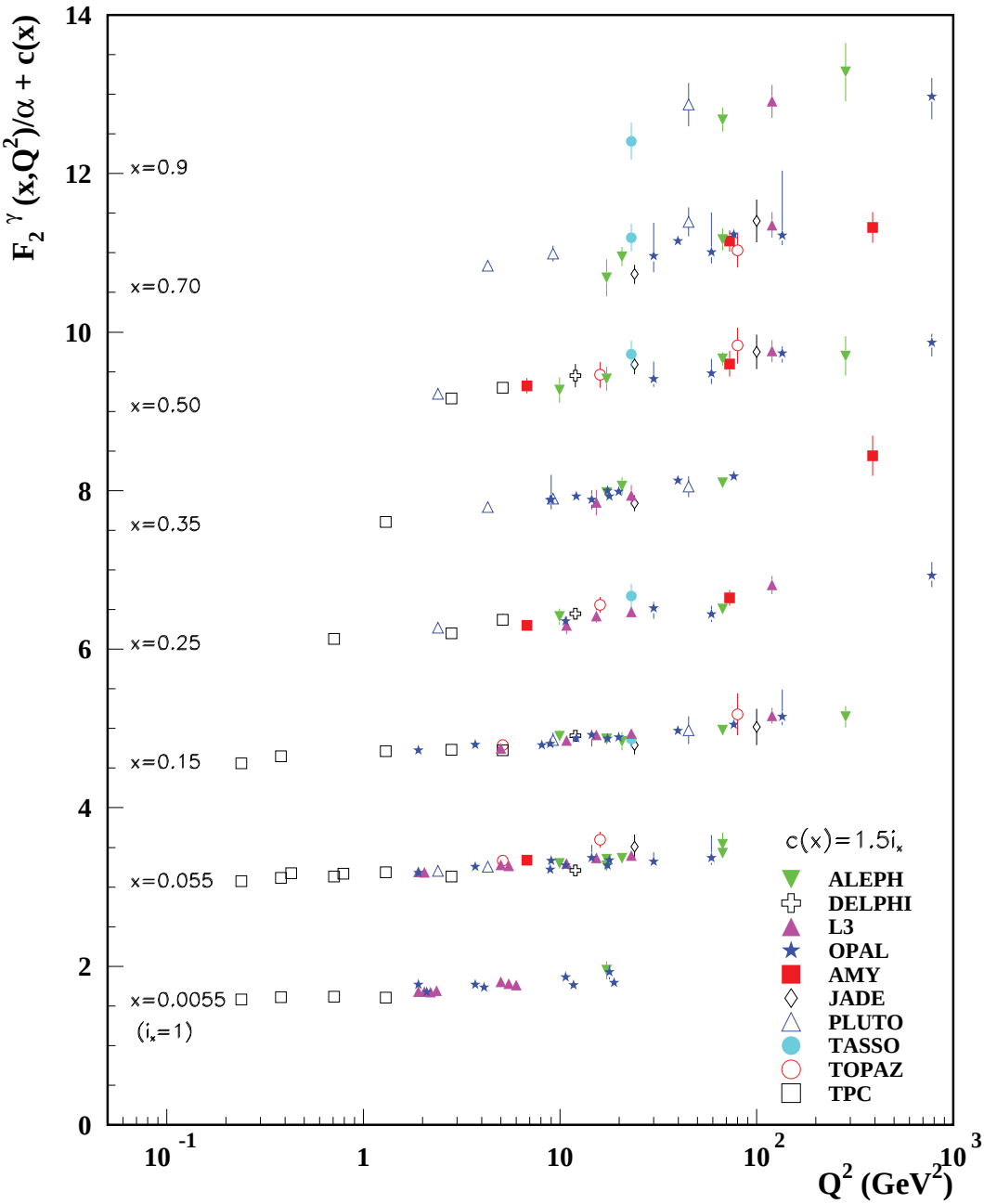

Figure 18.18: The hadronic structure function of the photon F_2^γ divided by the fine structure constant α measured in e^+e^- scattering, shown as a function of Q^2 for bins of x. Data points have been shifted to the nearest corresponding x bin as given in the plot. Some points have been offset in Q^2 for clarity. Statistical and systematic errors added in quadrature are shown. For the purpose of plotting, a constant $c(x) = 1.5i_x$ is added to F_2^γ/α where i_x is the number of the x bin, ranging from 1 ($x = 0.0055$) to 8 ($x = 0.9$). References: **ALEPH**–R. Barate *et al.*, Phys. Lett. **B458**, 152 (1999); A. Heister *et al.*, Eur. Phys. J. **C30**, 145 (2003);**DELPHI**–P. Abreu *et al.*, Z. Phys. **C69**, 223 (1995); **L3**–M. Acciarri *et al.*, Phys. Lett. **B436**, 403 (1998); M. Acciarri *et al.*, Phys. Lett. **B447**, 147 (1999); M. Acciarri *et al.*, Phys. Lett. **B483**, 373 (2000); **OPAL**–A. Ackerstaff *et al.*, Phys. Lett. **B411**, 387 (1997); A. Ackerstaff *et al.*, Z. Phys. **C74**, 33 (1997); G. Abbiendi *et al.*, Eur. Phys. J. **C18**, 15 (2000); G. Abbiendi *et al.*, Phys. Lett. **B533**, 207 (2002) (note that there is overlap of the data samples in these last two papers); **AMY**–S.K. Sahu *et al.*, Phys. Lett. **B346**, 208 (1995); T. Kojima *et al.*, Phys. Lett. **B400**, 395 (1997); **JADE**–W. Bartel *et al.*, Z. Phys. **C24**, 231 (1984); **PLUTO**–C. Berger *et al.*, Phys. Lett. **142B**, 111 (1984); C. Berger *et al.*, Nucl. Phys. **B281**, 365 (1987); **TASSO**–M. Althoff *et al.*, Z. Phys. **C31**, 527 (1986); **TOPAZ**–K. Muramatsu *et al.*, Phys. Lett. **B332**, 477 (1994); **TPC/Two Gamma**–H. Aihara *et al.*, Z. Phys. **C34**, 1 (1987).

Downloaded from https://academic.oup.com/ptep/article/2022/8/083C01/6651666 by KIT Library user on 27 September 2022

19. Fragmentation Functions in e^+e^-, ep, and pp Collisions

Revised August 2021 by O. Biebel (Ludwig-Maximilians U.), D. de Florian (ICAS and ICIFI, UNSAM), D. Milstead (Stockholm U.) and W. Vogelsang (Tübingen U.).

19.1 Introduction to fragmentation

Quarks and gluons produced in hard-scattering reactions will ultimately give rise to the colorless hadronic bound states that may be observed in the detector. The associated hadronization process is described by fragmentation functions $D_i^h(x,\mu^2)$ $(i = q, \bar{q}, g)$ which are universal functions representing, in the simplest picture, a measure of the probability density that an outgoing parton produces a hadron h. Here, x is the fraction of the parton's momentum transferred to the hadron, and μ is a 'resolution' scale known as factorization scale. The $D_i^h(x,\mu^2)$ may be viewed as the final-state analogs of the initial-state parton distribution functions (PDFs) addressed in Section 18 of this *Review*. They are also sometimes referred to as *timelike* distributions since they are primarily accessed in e^+e^- annihilation via a timelike intermediate boson. (See Refs. [1,2] for introductory reviews, and Refs. [3–5] for summaries of experimental and theoretical research in this field).

The cleanest laboratory for the study of fragmentation functions is provided by semi-inclusive electron-positron annihilation, $e^+e^- \to \gamma/Z \to h+X$. The cross section for this reaction may be expressed in terms of 'fragmentation structure functions' $F_{T,L,A}$ that are directly related to the fragmentation functions. At center-of-mass (CM) energy $\sqrt{s} = q^2$ we have

$$\frac{1}{\sigma_0}\frac{d^2\sigma^h}{dx\,d\cos\theta} = \frac{3}{8}(1+\cos^2\theta)F_T^h(x,q^2) + \frac{3}{4}\sin^2\theta\,F_L^h(x,q^2) + \frac{3}{4}\cos\theta\,F_A^h(x,q^2)\,. \tag{19.1}$$

Here, q is the four-momentum of the intermediate photon or Z-boson, with $q^2 > 0$, and $x = 2P_h \cdot q/q^2$ with the hadron's four-momentum P_h is the fragmentation counterpart of the familiar DIS Bjorken variable. (Note that $x = 2E_h/\sqrt{s} \le 1$ in terms of the energy E_h of the produced hadron in the CM frame of the electron positron pair.) Furthermore, in the same frame, θ is the hadron's angle relative to the electron beam direction. Eq. (19.1) is the most general form for unpolarized inclusive single-particle production via vector bosons [6]. The fragmentation structure functions F_T and F_L represent the contributions from γ/Z polarizations transverse or longitudinal with respect to the direction of motion of the hadron. The parity-violating term with the asymmetric fragmentation function F_A arises from the interference between vector and axial-vector contributions. Various normalization factors σ_0 are used in the literature, ranging from the total cross section $\sigma_{\rm tot}$ for $e^+e^- \to$ hadrons, including all weak and QCD contributions, to $\sigma_0 = 4\pi\alpha^2 N_c/3s$ with $N_c = 3$, the lowest-order QED cross section for $e^+e^- \to \mu^+\mu^-$ times the number of colors N_c. LEP1 measurements of the three fragmentation structure functions are shown in Fig. 19.1.

Integration of Eq. (19.1) over all θ yields the total fragmentation structure function $F^h = F_T^h + F_L^h$:

$$\frac{1}{\sigma_0}\frac{d\sigma^h}{dx} = F^h(x,q^2) = \sum_i \int_x^1 \frac{dz}{z}\,C_i\left(z,\alpha_{\rm s}(\mu),\frac{q^2}{\mu^2}\right) D_i^h\left(\frac{x}{z},\mu^2\right)\,. \tag{19.2}$$

On the right we have written the factorized expression for the structure function in terms of a sum over convolutions of the fragmentation functions D_i^h for partons $i = u, \bar{u}, d, \bar{d}, \ldots, g$ with perturbative coefficient functions C_i. Since photons and Z bosons do not distinguish between quarks and antiquarks, e^+e^- annihilation primarily constrains the combinations $D_q^h + D_{\bar{q}}^h$. Gluon fragmentation contributes only at higher order in perturbation theory or by scaling violations. Corrections to the factorized expression in Eq. (19.2) are suppressed by inverse powers of q^2. They arise from quark and hadron mass terms and from non-perturbative effects.

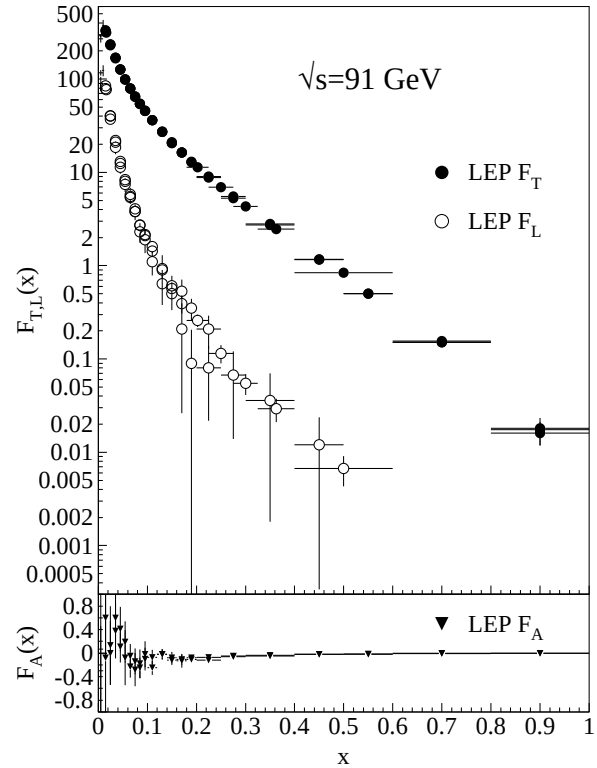

Figure 19.1: LEP1 measurements of total transverse (F_T), longitudinal (F_L), and asymmetric (F_A) fragmentation structure functions [7]. Data points with relative errors greater than 100% are omitted.

Analogous factorized expressions as in Eq. (19.2) may be written for each of the structure functions $F_{T,L,A}$ individually.

The fragmentation functions obey the momentum sum rule constraint

$$\sum_h \int_0^1 dx\,x\,D_i^h(x,\mu^2) = 1\,, \tag{19.3}$$

separately for each flavor i. Note that the sum rule involves a sum over all possible produced hadrons. The dependence of the functions D_i^h on the factorization scale μ^2 will be discussed in the next section.

Measurements of hadron production in deeply-inelastic lepton-proton scattering and hadron-hadron scattering are complementary to those in e^+e^- annihilation. The former process, $\ell p \to \ell' + h + X$, is known as *semi-inclusive deep-inelastic scattering (SIDIS)*. Here, in analogy with Eq. (19.2), the high virtuality of the photon in DIS also permits factorization of the cross section in terms of fragmentation functions, PDFs for the incoming proton, and perturbative hard-scattering cross sections. Likewise, factorization also occurs for $pp \to h + X$ at large transverse momentum of the produced hadron, and for $pp \to {\rm jet}(h) + X$, where the hadron is part of a fully reconstructed jet. The fragmentation functions contributing to $e^+e^- \to h + X$, $\ell p \to \ell' + h + X$, and $pp \to h + X$, $pp \to {\rm jet}(h) + X$ are universal in the sense that the same functions appear in the factorized expressions for the three reactions. Modern QCD analyses of fragmentation functions "globally" take into account experimental data sets for all three types of processes in order to obtain optimal sets of fragmentation functions.

Electron-positron annihilation has the advantage that there is no hadronic initial state and hence no beam remnant. This is in contrast to $\ell p \to \ell' + h + X$ or $pp \to h + X$, which are affected by hadron remnant contributions associated with the partons of the initial-state hadron(s) which are collaterally involved in the hard lepton-parton or parton-parton collision. On the other hand,

Downloaded from https://academic.oup.com/ptep/article/2022/8/083C01/6651666 by KIT Library user on 27 September 2022

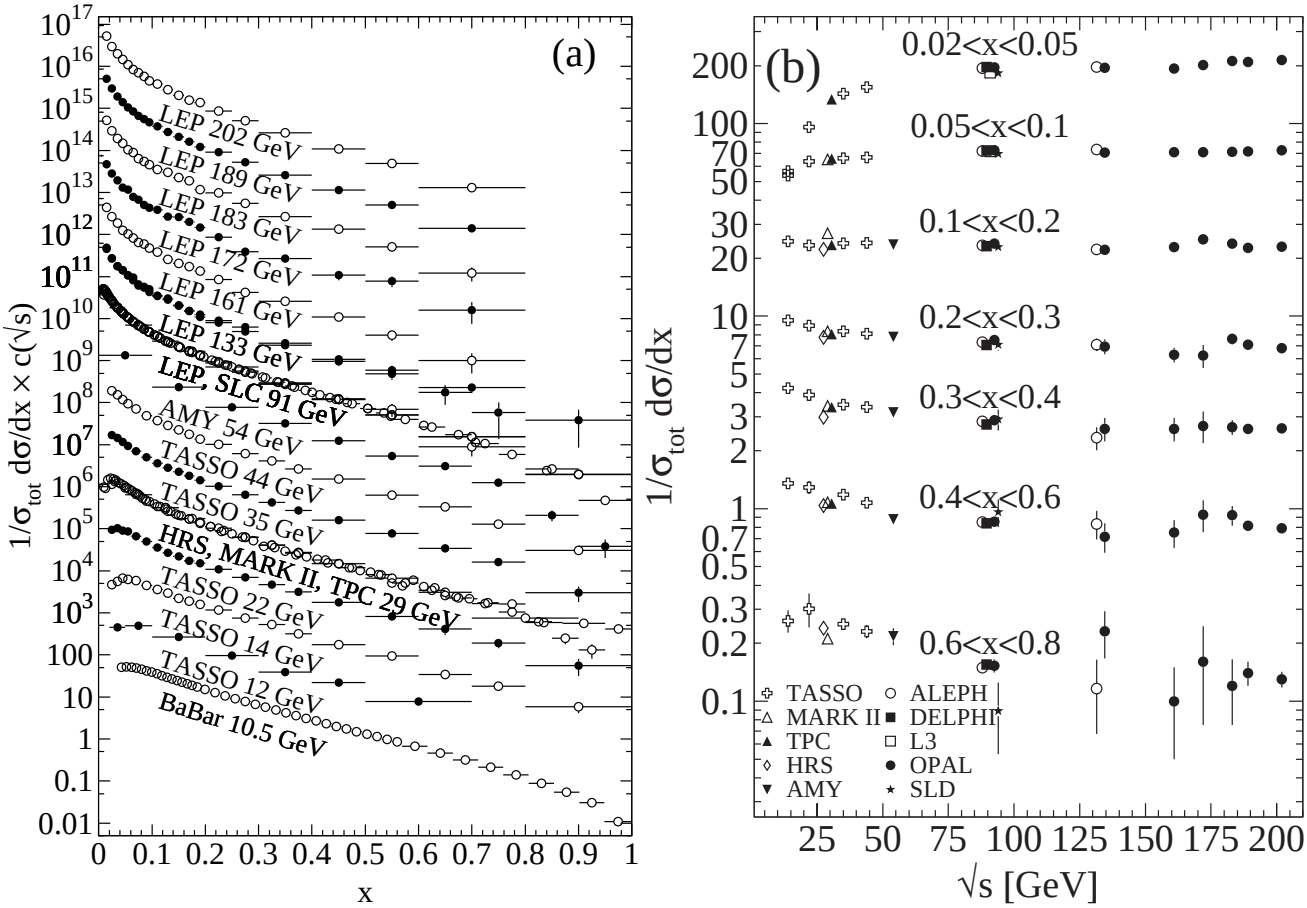

Figure 19.2: Cross section for $e^+e^- \to h + X$ for all charged hadrons [8–26], (a) for different CM energies $\sqrt{s}$ versus x, and (b) for various ranges of x versus $\sqrt{s}$. For (a) the distributions have been scaled by $c(\sqrt{s}) = 10^i$ with i ranging from $i = 0$ ($\sqrt{s} = 12$ GeV) to $i = 13$ ($\sqrt{s} = 202$ GeV).

$e^+e^- \to h + X$ has little sensitivity to D_g^h and is insensitive to the charge asymmetries $D_q^h - D_{\bar{q}}^h$. These quantities are best constrained in proton–(anti-)proton and electron-proton scattering, respectively. Especially the latter provides an environment that allows the study of the influence of initial-state QCD radiation on the fragmentation process, of the partonic and spin structure of the hadron target, and of the target remnant system. (See Ref. [27] for a comprehensive review of the measurements and models of fragmentation in lepton-hadron scattering).

Moreover, unlike e^+e^- annihilation where $q^2 = s$ is fixed by the collider energy, lepton-hadron scattering has two independent scales, $Q^2 = -q^2$ and the invariant mass squared, $W^2 \approx Q^2(1-x)/x$, of the hadronic final state, which both can vary by several orders of magnitudes for a given CM energy, thus allowing the study of fragmentation in different environments by a single experiment. For example, in photoproduction the exchanged photon is quasi-real ($Q^2 \approx 0$), leading to processes akin to hadron-hadron scattering. In DIS ($Q^2 \gg 1$ GeV^2), using factorization, the hadronic fragments of the struck quark can be directly compared with quark fragmentation in e^+e^- in a suitable frame. Results from lepton-hadron experiments quoted in this report primarily concern fragmentation in the DIS regime. Studies performed by lepton-hadron experiments of fragmentation with photoproduction data containing high transverse momentum jets or particles are also reported, when these are directly comparable to DIS and e^+e^- results.

Fragmentation studies in lepton-hadron collisions are usually performed in one of two frames in which the target hadron and the exchanged boson are collinear. The hadronic center-of-mass frame (HCMS) is defined as the rest system of the exchanged boson and incoming hadron, with the z^*-axis defined along the direction of the exchanged boson. The positive z^* direction defines the so-called current fragmentation region. Fragmentation measurements performed in the HCMS often use the Feynman-x variable $x_F = 2p_z^*/W$, where p_z^* is the longitudinal momentum of the particle in this frame. As W is the invariant mass of the hadronic final state, x_F ranges between -1 and 1.

The Breit system [28, 29] is related to the HCMS by a longitudinal boost such that the time component of q vanishes, i.e, $q = (0, 0, 0, -Q)$. In the parton model, the struck parton then has the longitudinal momentum $Q/2$ which becomes $-Q/2$ after the collision. As compared with the HCMS, the current fragmentation region of the Breit frame is more closely matched to the partonic scattering process, and is thus appropriate for direct comparisons of fragmentation functions in DIS with those from e^+e^- annihilation. The variable $x_p = 2p^*/Q$, where p^* is the particle's momentum in the current region of the Breit frame, is used at HERA for measurements in the Breit frame, enabling rather direct comparisons of DIS and e^+e^- results.

19.2 Scaling violations and QCD corrections

As mentioned, the coefficient functions for the fragmentation structure functions in $e^+e^- \to h + X$ are amenable to QCD perturbation theory. For each of the structure functions $F_{T,L,A}(x, q^2)$ in Eq. (19.1) (and hence for the total structure function F^h in Eq. (19.2)) the coefficient function has an expansion of the form

$$C_{a,i}\left(z, \alpha_s(\mu), \frac{q^2}{\mu^2}\right) = (1-\delta_{aL})\,\delta_{iq}\,\delta(1-z) + \frac{\alpha_s(\mu)}{2\pi}\,c_{a,i}^{(1)}\left(z, \frac{q^2}{\mu^2}\right) + \left(\frac{\alpha_s(\mu)}{2\pi}\right)^2 c_{a,i}^{(2)}\left(z, \frac{q^2}{\mu^2}\right) + . \quad (19,4)$$

Downloaded from https://academic.oup.com/ptep/article/2022/8/083C01/6651666 by KIT Library user on 27 September 2022

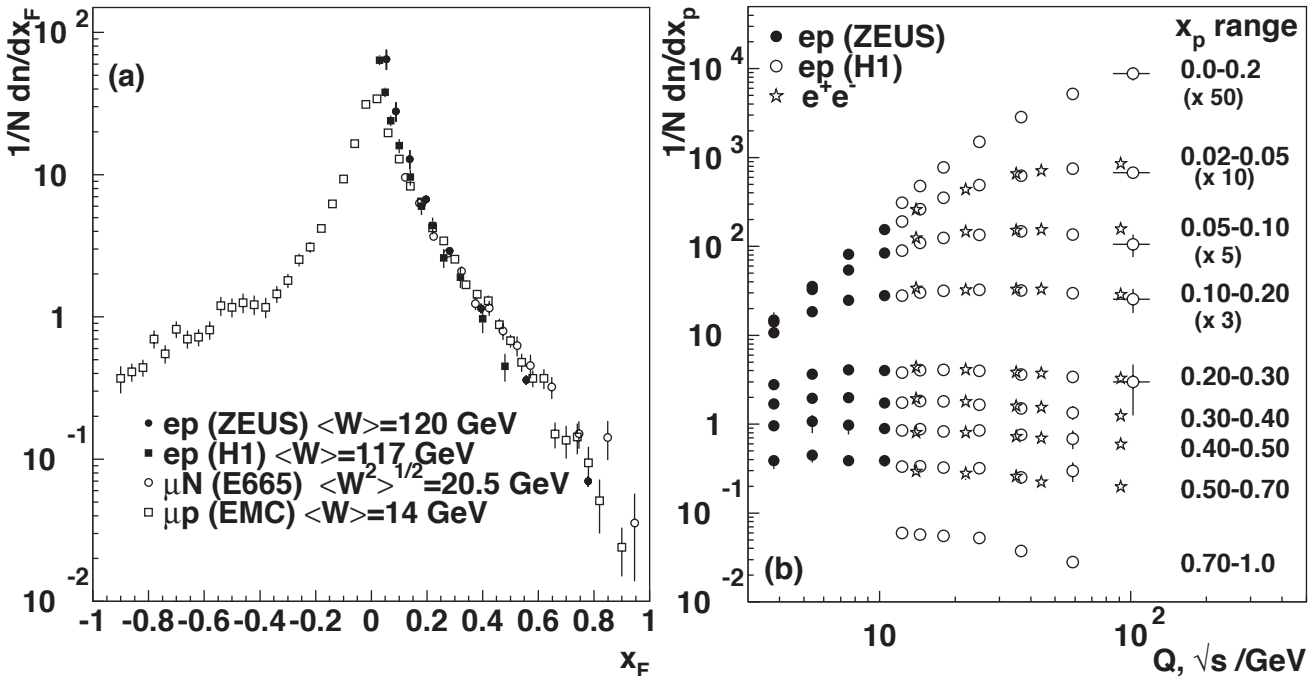

Figure 19.3: (a) The distribution $1/N \cdot dN/dx_F$ for all charged particles in DIS lepton-hadron experiments at different values of W, measured in the HCMS [30–33]. (b) Scaling violations of the fragmentation structure function for all charged particles in the current region of the Breit frame of DIS [34, 35] and in e^+e^- interactions [19, 36]. The data are shown as a function of $\sqrt{s}$ for e^+e^- results, and as a function of Q for the DIS results, each within the same indicated intervals of the scaled momentum x_p. The data for the four lowest intervals of x_p are multiplied by factors 50, 10, 5, and 3, respectively for better visibility.

where $a = T, L, A$. At the zeroth order in the strong coupling α_s the coefficient functions C_g for gluons vanish, while for (anti-) quarks $C_i = g_i(s)\,\delta(1-z)$ (except for F_L for which the leading contribution is of order α_s, as indicated in Eq. (19.4)). Here $g_i(s)$ is the appropriate electroweak coupling. In particular, $g_i(s)$ is proportional to the squared charge of the quark i at $s \ll M_Z^2$, when weak effects can be neglected. The full electroweak prefactors $g_i(s)$ can be found in Ref. [6]. The first-order QCD corrections to the coefficient functions have been calculated in Refs. [37,38], and the second-order terms in [39–41]. Thus, the coefficient functions are known to NNLO, except for F_L. We note that beyond the leading order the coefficient functions, and hence the fragmentation functions, start to depend on the choice of factorization scheme. The standard choice in the literature is the $\overline{\text{MS}}$ scheme.

The simplest parton-model approach would predict scale-independent ('scaling') x-distributions for both the structure function F^h and the parton fragmentation functions D_i^h. Perturbative QCD corrections lead to logarithmic scaling violations via the evolution equations [42]

$$\frac{\partial}{\partial \ln \mu^2} D_i^h(x,\mu^2) \;=\; \sum_j \int_x^1 \frac{dz}{z}\, P_{ji}\big(z, \alpha_s(\mu^2)\big) D_j^h\left(\frac{x}{z}, \mu^2\right) , \tag{19.5}$$

where the functions $P_{ij}(z, \alpha_s(\mu^2))$ describe the splitting process $i \to j + X$, where parton j carries the longitudinal momentum fraction z of parton i. Note that for fragmentation the relevant splitting functions are P_{ji} (rather than P_{ij} as for the PDFs) since D_j^h represents the fragmentation of the final parton. Usually the system of evolution equations is decomposed into a 2×2 flavor-singlet sector comprising the gluon and the sum of all quark and antiquark fragmentation functions, and scalar ('non-singlet') equations for quark-antiquark and flavor differences.

The splitting functions in Eq. (19.5) have the perturbative expansion

$$P_{ji}(z, \alpha_s) \;=\; \frac{\alpha_s}{2\pi} P_{ji}^{(0)}(z) + \left(\frac{\alpha_s}{2\pi}\right)^2 P_{ji}^{(1)}(z) + \left(\frac{\alpha_s}{2\pi}\right)^3 P_{ji}^{(2)}(z) + \ldots , \tag{19.6}$$

where the leading-order (LO) functions $P^{(0)}(z)$ [42, 43] are the same as those for the initial-state parton distributions. The next-to-leading order (NLO) corrections $P^{(1)}(z)$ have been calculated in Refs. [44–48] (there are well-known misprints in the journal version of Ref. [45]). Ref. [48] also includes the spin-dependent case. The timelike functions are different from, but related to, their spacelike counterparts, see also Ref. [49]. The connections between the two sets of functions has facilitated recent calculations of the next-to-next-to-leading order (NNLO) quantities $P_{qq}^{(2)}(z)$ and $P_{gg}^{(2)}(z)$ in Eq. (19.6) [40,50]. In the same way, the corresponding off-diagonal quantities $P_{qg}^{(2)}$ and $P_{gq}^{(2)}$ were recently obtained in Ref. [51] with the help of constraints from the momentum sum rule Eq. (19.3) [50] and of the limit of $C_A = C_F = n_f$ for which QCD becomes supersymmetric. An uncertainty still remains for the $P_{qg}^{(2)}$ kernel, which however does not affect the logarithmic behavior at small and large momentum fractions. With the exception of Ref. [47], all these higher-order results refer to the standard $\overline{\text{MS}}$ scheme with a fixed number n_f of light flavors. When the threshold for the production of a heavier quark flavor is crossed in the course of the scale evolution, fragmentation functions change. The NLO treatment of these flavor thresholds in the evolution has been addressed in Ref. [52].

The phenomenological effect of scale evolution is similar in the timelike and spacelike cases: As the scale increases, one observes a scaling violation in which the x-distribution is shifted towards lower values. This can be seen from Fig. 19.2 where a set of measurements of the total fragmentation structure function in e^+e^- annihilation are shown. In particular, the figure on the right exhibits the dependence on $\sqrt{q^2} = \sqrt{s}$ at fixed values of x. QCD analyses of these data are discussed in Section 19.5 below.

The NLO coefficient functions for SIDIS, $ep \to e + h + X$, have been presented in Refs. [37, 38] Corresponding results have also been obtained for the case that a non-vanishing hadron transverse momentum is required in the HCMS frame [53, 54].

Scaling violations in DIS are shown in Fig. 19.3 for both the HCMS and the Breit frames. In Fig. 1.3(a) the distribution in terms of $x_F = 2p_z^*/W$ shows a steeper slope in ep data than for the lower-energy μp data for $x_F > 0.15$, indicating the scaling

Downloaded from https://academic.oup.com/ptep/article/2022/8/083C01/6651666 by KIT Library user on 27 September 2022

violations. At smaller values of x_F in the current jet region, the multiplicity of particles substantially increases with W, owing to the increased phase space available for the fragmentation process. The EMC data access both the current region and the region of the fragmenting target remnant system. At higher values of $|x_F|$, due to the extended nature of the remnant, the multiplicity in the target region far exceeds that in the current region. For acceptance reasons the remnant hemisphere of the HCMS is only accessible by the lower-energy fixed-target experiments.

Using hadrons from the current hemisphere in the Breit frame, measurements of fragmentation functions and the production properties of particles in *ep* scattering have been reported in Refs. [34, 35, 55–58]. Fig. 19.3(b) compares results from *ep* scattering and e^+e^- experiments; the latter results have been divided by two as they cover both event hemispheres. The agreement between the DIS and e^+e^- results is fairly good. However, processes in DIS which are not present in e^+e^- annihilation, such as boson-gluon fusion and initial-state QCD radiation, can depopulate the current region. These effects become most prominent at low values of Q and x_p. Hence, when compared with e^+e^- annihilation data at $\sqrt{s} = 5.2$, 6.5 GeV [59] not shown here, the DIS particle rates tend to lie below those observed in e^+e^- annihilation. A ZEUS study [60] finds that the direct comparability of the *ep* data to e^+e^- results at low scales is improved if twice the energy in the current hemisphere of the Breit frame, $2E_B^{\rm cr}$, is used instead of $Q/2$ as the fragmentation scale. Choosing $2E_B^{\rm cr}$ for the fragmentation scale approximates QCD radiation effects relevant at low scales, as detailed in Ref. [29].

19.3 Fragmentation functions for small particle momenta

The higher-order timelike splitting functions in Eq. (19.6) are singular at small values of x. They show a double-logarithmic enhancement, with leading terms of the form $\alpha_{\rm s}^k\left(\ln^{2k-2}x\right)/x$ at the kth order of perturbation theory, corresponding to poles $\alpha_{\rm s}^k\,(N-1)^{1-2k}$ for the Mellin moments

$$P^{(k)}(N) \;=\; \int_0^1 dx\; x^{N-1}\; P^{(k)}(x)\;. \tag{19.7}$$

Despite large cancellations between leading and non-leading logarithms at non-asymptotic values of x, the resulting small-x rise in the timelike splitting functions dwarfs that of their spacelike counterparts for the evolution of the parton distributions in Section 18 of this *Review*, see Fig. 1 of Ref. [50]. Consequently, in fragmentation the fixed-order approximation to the evolution breaks down orders of magnitude earlier in x than in DIS.

The pattern of the known coefficients and other considerations suggest that the double-logarithmic terms sum to all-order expressions without any pole at $N = 1$, such as [61, 62]

$$P_{gg}^{\rm LL}(N) \;=\; -\frac{1}{4}\left(N-1-\sqrt{(N-1)^2\cdot 24\,\alpha_{\rm s}/\pi}\right) \tag{19.8}$$

for the gluon-to-gluon splitting function at leading logarithmic order. Keeping the first three terms in the resulting expansion of Eq. (19.5) around $N = 1$ and taking the Mellin inverse yields a Gaussian in the variable $\xi = \ln(1/x)$ for the small-x fragmentation functions,

$$xD(x, q^2 = s) \;\propto\; \exp\left[-\frac{1}{2\sigma^2}(\xi-\xi_p)^2\right]\;, \tag{19.9}$$

with the peak position and width varying with the energy as [63] (see also Ref. [2])

$$\xi_p \;\simeq\; \frac{1}{4}\ln\left(\frac{s}{\Lambda^2}\right)\;,\quad \sigma \;\propto\; \left[\ln\left(\frac{s}{\Lambda^2}\right)\right]^{3/4}\;. \tag{19.10}$$

Next-to-leading logarithmic corrections to the above predictions have been calculated [64]. In the method of Ref. [65], see also Refs. [66, 67], the corrections are included in an analytical form known as the 'modified leading logarithmic approximation' (MLLA). Alternatively they can be used to compute higher-moment corrections to the shape in Eq. (19.9) [68]. The small-x resummation of the coefficient functions for semi-inclusive e^+e^- annihilation and of the timelike spitting functions in the standard $\overline{\rm MS}$ scheme was extended in Refs. [69–73] and has reached full next-to-next-to-leading logarithmic accuracy. Applications of these results to gluon and quark jet multiplicities have been presented in Refs. [74].

Fig. 19.4 shows the ξ distribution for charged particles produced in the current region of the Breit frame in DIS and in e^+e^- annihilation. Consistently with Eq. (19.9) (the 'hump backed plateau') and Eq. (19.10) the distributions have a Gaussian shape, with the peak position and area increasing with CM energy (e^+e^-) and Q^2 (DIS).

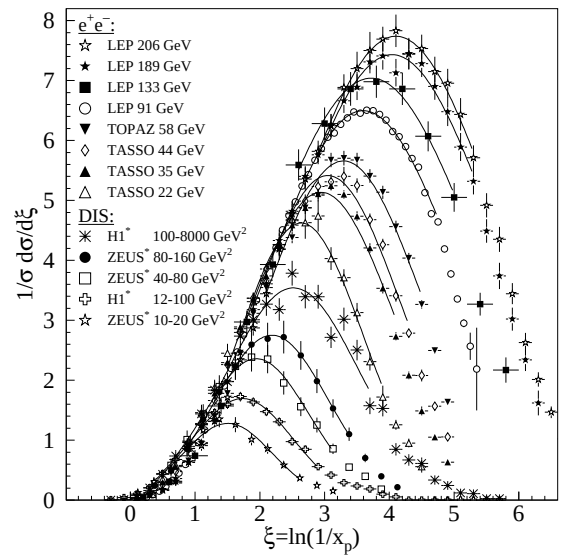

Figure 19.4: Distribution of the normalized fragmentation cross sections in $\xi = \ln(1/x_p)$ at several CM energies (e^+e^-) [10,11,16–19,57,58,75–78] and for intervals of Q^2 (DIS). At each energy only one representative measurement is displayed. For clarity some measurements at intermediate CM energies (e^+e^-) or Q^2 ranges (DIS) are not shown. The DIS measurements ($*$) have been scaled by a factor of 2 for direct comparability with the e^+e^- results. Fits of simple Gaussian functions are overlaid for illustration.

The predicted energy dependence of the peak in the ξ distribution (see Eq. (19.10)) is explained by soft gluon coherence (angular ordering), *i.e.*, the destructive interference of the color wavefunction of low energy gluon radiation, which correctly predicts the suppression of hadron production at small x. Of course, a decrease at very small x is expected on purely kinematical grounds, but this would occur at particle energies proportional to their masses, *i.e.*, at $x \propto m/\sqrt{s}$ and hence $\xi \sim \frac{1}{2}\ln s$. Thus, if the suppression were purely kinematic, the peak position ξ_p would vary twice as rapidly with the energy, which is ruled out by the data in Fig. 19.5. The e^+e^- and DIS data agree well with each other, demonstrating the universality of hadronization and the MLLA prediction. Measurements of the higher moments of the ξ distribution in e^+e^- [19,78–80] and DIS [58] have also been performed and show consistency with each other.

The average charged-particle multiplicity is another observable sensitive to fragmentation functions for small particle momenta. Perturbative predictions using both NLO [89] and MLLA [90, 91] have been obtained by solving Eq. (19.5) yielding

$$\left\langle n_G(Q^2)\right\rangle \propto \alpha_{\rm s}^b(Q^2)\cdot\exp\left[\frac{c}{4\pi b_0\sqrt{\alpha_{\rm s}(Q^2)}}\cdot\left(1+6a_2\frac{\alpha_{\rm s}(Q^2)}{\pi}\right)\right]\,, \tag{19.11}$$

where $b = \frac{1}{4} + \frac{10}{27}\frac{n_f}{4\pi b_0}$, $c = \sqrt{96\pi}$, with $b_0 = (33-2n_f)/(12\pi)$, cf. Section 9 of this *Review*, for n_f contributing quark flavors. Higher-order corrections to Eq. (19.11) are known up to next-to-next-to-next-to-leading order ($\rm N^3LO$), for details and references

Downloaded from https://academic.oup.com/ptep/article/2022/8/083C01/6651666 by KIT Library user on 27 September 2022

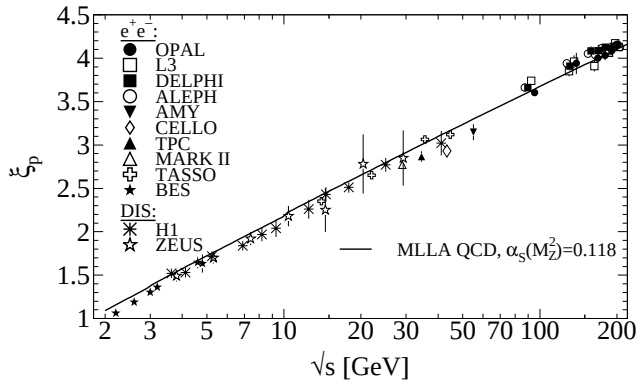

Figure 19.5: Evolution of the peak position, ξ_p, of the ξ distribution with the CM energy $\sqrt{s}$. The MLLA QCD prediction using $\alpha_s(s = M_Z^2) = 0.118$ is superimposed to the data of Refs. [10, 12, 15, 19, 56, 57, 76, 77, 80–88].

see [92]. The term proportional to $a_2 \approx -0.502 + 0.0421\, n_f - 0.00036\, n_f^2$ in Eq. (19.11) is the contribution due to NNLO corrections [93]. The quantity $\langle n_G(Q^2)\rangle$ refers to the average number of gluons, while for $\langle n_q(Q^2)\rangle$ for quarks a correction factor $1/r$ is required due to the different color factors in quark and gluon couplings, so that $\langle n_q(Q^2)\rangle = \langle n_G(Q^2)\rangle/r$. The correction factor depends only weakly on Q^2; higher-order corrections up to N^{3}LO on the asymptotic value $r = C_A/C_F = 9/4$ [94] are quoted in [92].

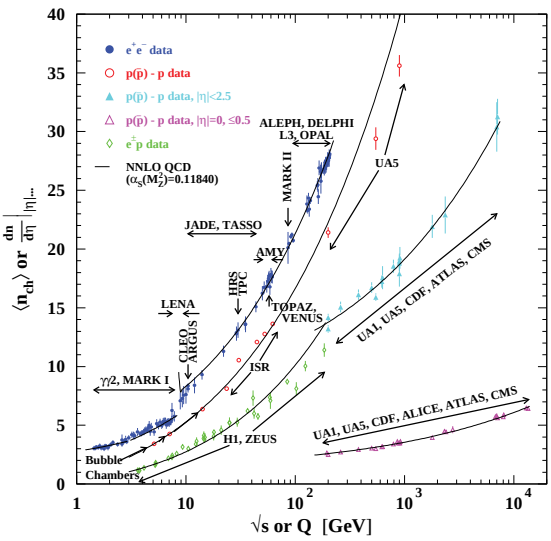

Figure 19.6: Average charged-particle multiplicity $\langle n_{\rm ch}\rangle$ as a function of $\sqrt{s}$ or Q for e^+e^- and $p\overline{p}$ annihilations, and pp and ep collisions. The indicated errors are statistical and systematic uncertainties added in quadrature, except when no systematic uncertainties are given. All NNLO QCD curves are from Eq. (19.11) with fitted normalization, $K_{\rm LHPD}$, and offset, n_0, using a fixed $\alpha_s(M_Z^2) = 0.1184$ [95] and for e^+e^- annihilation data $n_f = 3$, 4, or 5 depending on $\sqrt{s}$, else $n_f = 3$. $\mathbf{e^+e^-}$: Contributions from K_S^0 and Λ decays included. Data compiled from Refs. [8,10,16,16,22,77,83,96–106]; $\mathbf{e^\pm p}$: Multiplicities have been measured in the current fragmentation region of the Breit frame. Data compiled from Refs. [35, 57, 58, 60, 107]; $\mathbf{p^{(}\overline{p}^{)}}$: Measured values above 20 GeV refer to non-single diffractive (NSD) processes. Central pseudorapidity multiplicities $(\mathrm{d}n/\mathrm{d}\eta)|_{|\eta|\ldots}$ refer to either $|\eta| < 2.5$ (CMS: $|\eta| < 2.4$) or $|\eta| = 0$ (UA5, CMS, ALICE: $|\eta| < 0.5$). Data compiled from Refs. [108–123].

Employing the hypothesis of 'Local Parton-Hadron Duality' (LPHD) [90], *i.e.*, that the color charge of partons is balanced locally in phase space and, hence, their hadronization occurs locally such that (Mellin transformed) parton and hadron inclusive distributions directly correspond, Eq. (19.11) can be applied to describe average charged particle multiplicities obtained in e^+e^- annihilation. The equation can also be applied to $e^\pm p$ scattering if the current fragmentation region of the Breit frame is considered for measuring the average charged-particle multiplicity. Fig. 19.6 shows corresponding data and fits of Eq. (19.11) where apart from an LPHD normalization factor a constant offset has been allowed for, so that $\langle n_{\rm ch}(Q)\rangle = K_{\rm LHPD} \cdot \langle n_G(Q)\rangle/r + n_0$.

In hadron-hadron collisions beam remnants, e.g. from single-diffractive (SD) scattering where one colliding proton is negligibly deflected while hadrons related with the other colliding proton are well-separated in rapidity from the former proton, contribute to the measurement of the hadron multiplicity from a hard parton-parton scattering, making interpretation of the data more model dependent. Experimental results are usually given for inelastic processes or for non-single diffractive processes (NSD). Due to the large beam particle momenta at Tevatron and LHC, not all final state particles can be detected within the limited detector acceptance. Therefore, experiments at Tevatron and LHC quote particle multiplicities for limited ranges of pseudo-rapidity $\eta = -\ln\tan(\vartheta/2)$ or at central rapidity, i.e. $\eta = 0$, as shown in Fig. 19.6.

A universality of the average particle multiplicities in e^+e^- and $p^{(}\overline{p}^{)}$ processes has been reported in Ref. [124] when considering an effective collision energy $Q_{\rm eff} = \sqrt{s}/k$ in $p^{(}\overline{p}^{)}$ reduced by a factor of $k \approx 3$, plus a constant offset of $n_0 \approx 2$. A more detailed review is available in Ref. [125]. According to the investigations presented in Ref. [126] the universality of the energy dependence of average particle multiplicities also applies to hadron-hadron and nucleus-nucleus collisions for both full and central rapidity multiplicities. Evidence for this universality is given by the good agreement for the energy dependence of Eq. (19.11) when fit to the $p^{(}\overline{p}^{)}$ data as shown in Fig. 19.6.

19.4 Fragmentation models

Although the scaling violations can be calculated perturbatively, the actual form of the parton fragmentation functions is non-perturbative. Perturbative evolution gives rise to a shower of quarks and gluons (partons). Multi-parton final states from leading and higher order matrix element calculations are linked to these parton showers using factorization prescriptions, also called matching schemes, see Ref. [127] for an overview.

Phenomenological schemes are then used to model the carry-over of parton momenta and flavor to the hadrons. Implemented in Monte Carlo event generators (see Section 43 of this *Review*), these schemes have been tuned using e^+e^- data and provide good description of hadron collisions as well, thus providing evidence of the universality of fragmentation. However, e^+e^- mainly fix the quark jet fragmentation while it provides less constraints for modelling the gluon jet fragmentation.

19.5 Phenomenology of quark and gluon fragmentation functions

The fragmentation functions are solutions to the evolution equations Eq. (19.5), but need to be specified at some initial scale μ_0^2 (usually around 1 GeV^2 for light quarks and gluons, and at m_Q^2 for heavy quarks). A typical parameterization for a given light hadron is [128, 131–139]

$$D_i^h(x, \mu_0^2) = N_i\, x^{\alpha_i}(1-x)^{\beta_i}\left(1 + \gamma_i(1-x)^{\delta_i}\right) , \qquad (19.12)$$

where as indicated the normalization N_i, and the parameters α_i, β_i, γ_i and δ_i depend on the type i of the fragmenting parton. Heavy flavor fragmentation into heavy mesons is discussed in Sec. 19.8 below. The parameters of Eq. (19.12) are obtained by performing global fits to data on various hadron types for different combinations of partons and hadrons in e^+e^-, lepton-hadron and hadron-hadron collisions. We note that the choice of parameterization of the fragmentation functions at the initial scale necessarily introduces a bias since it imposes a certain form of the functions. This bias is largely avoided in neural network approaches which offer a wide flexibility of the initial functions and have recently been applied to fragmentation functions as well [130]. Sets of fragmentation functions are now available for

Downloaded from https://academic.oup.com/ptep/article/2022/8/083C01/6651666 by KIT Library user on 27 September 2022

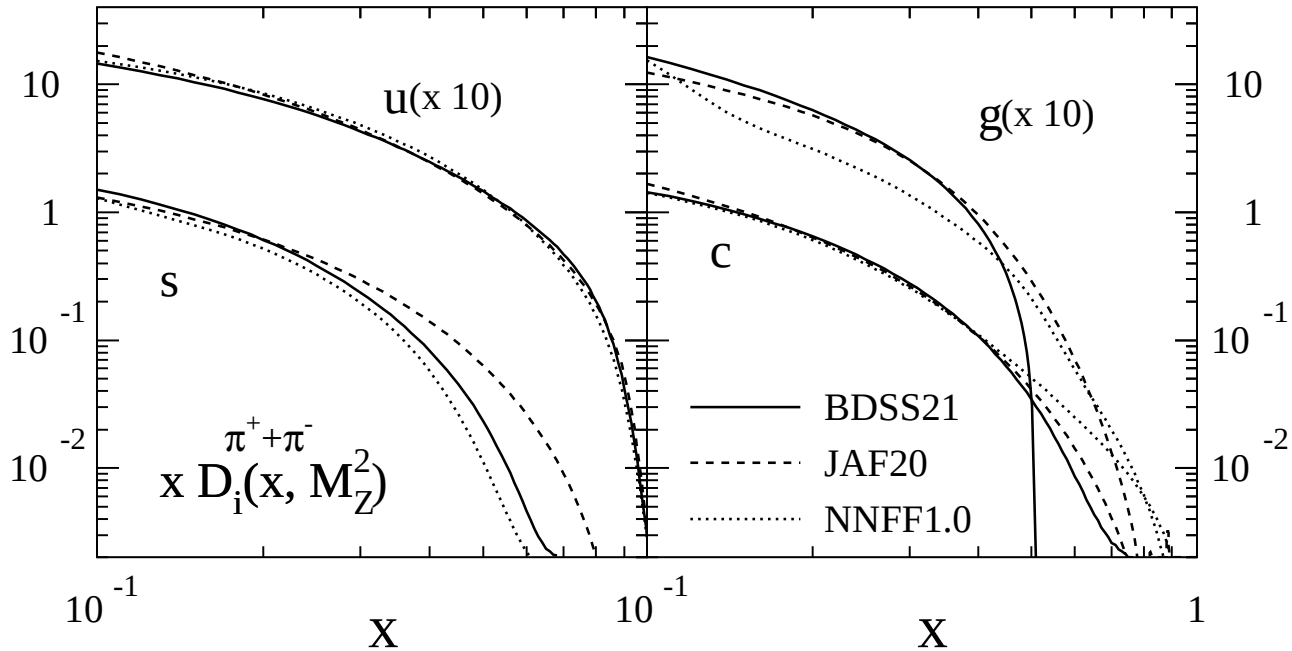

Figure 19.7: Comparison of up, strange, charm and gluon NLO fragmentation functions for $\pi^+ + \pi^-$ at the mass of the Z. The different lines correspond to the results of the analyses performed in Refs. [128–130].

pions, kaons, protons, neutrons, η mesons, Λ baryons, and charged hadrons [129, 130, 132–144]. They are all at NLO level, except for Refs. [130, 141, 144] which have been performed at NNLO level. The latter sets are restricted to the analysis of e^+e^- annihilation data. Recently, data from hadron-hadron collisions have been added in the framework of the neural network approach at NLO accuracy for charged hadrons [145]. It is noteworthy that the NNLO effects lead to an improvement in the theoretical description of the data in e^+e^- annihilation.

Data from e^+e^- annihilation present the cleanest experimental source for the measurement of fragmentation functions, but cannot be used to disentangle quark from antiquark fragmentation. Since the bulk of the e^+e^- annihilation data is obtained at the mass of the Z-boson, where the electroweak couplings are roughly the same for the different partons, it provides the most precise determination of the flavor-singlet combination of quark and antiquark fragmentation functions. Flavor-tagged results [146], distinguishing between the light quark, charm and bottom contributions are of particular value for flavor decomposition, even though those measurements cannot be unambiguously interpreted in perturbative QCD.

The most relevant source for quark-antiquark (and also flavor) separation is provided by SIDIS data. Semi-inclusive measurements are usually performed at much lower scales than for e^+e^- annihilation. The inclusion of SIDIS data in global fits allows for a wider coverage in the evolution of the fragmentation functions, resulting at the same time in a stringent test of the universality of the distributions. Charged-hadron production data in hadronic collisions also have sensitivity to (anti-)quark fragmentation functions. A recent analysis [129] performs a simultaneous extraction of parton distributions and fragmentation functions based on SIDIS data.

The gluon fragmentation function $D_g^h(x)$ can be extracted, in principle, from the longitudinal fragmentation structure function F_L in Eq. (19.2), as the coefficient functions $C_{L,i}$ for quarks and gluons are comparable at order α_s. However at NLO, *i.e.*, including the $\mathcal{O}(\alpha_s^2)$ coefficient functions $C_{L,i}^{(2)}$ [39], quark fragmentation is dominant in F_L over a large part of the kinematic range, reducing the sensitivity to D_g^h. This distribution could be determined

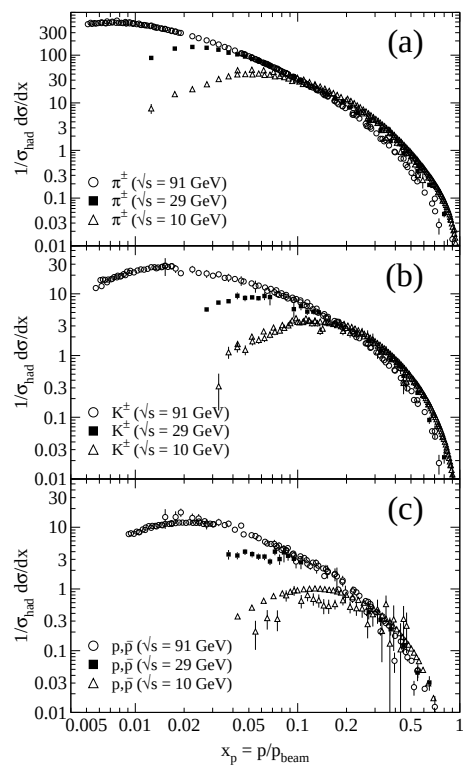

Figure 19.8: Scaled momentum spectra of (a) $\pi^\pm$, (b) $K^\pm$, and (c) $p, \overline{p}$ at $\sqrt{s} = 10$, 29, and 91 GeV [24, 26, 85, 147, 148].

also by analyzing the scale evolution of the fragmentation functions. This possibility is limited by the lack of sufficiently precise data at energy scales away from the Z-resonance and the dominance of the quark contributions at medium and large values of x. In e^+e^- annihilation, D_g^h can also be deduced from the study

Downloaded from https://academic.oup.com/ptep/article/2022/8/083C01/6651666 by KIT Library user on 27 September 2022

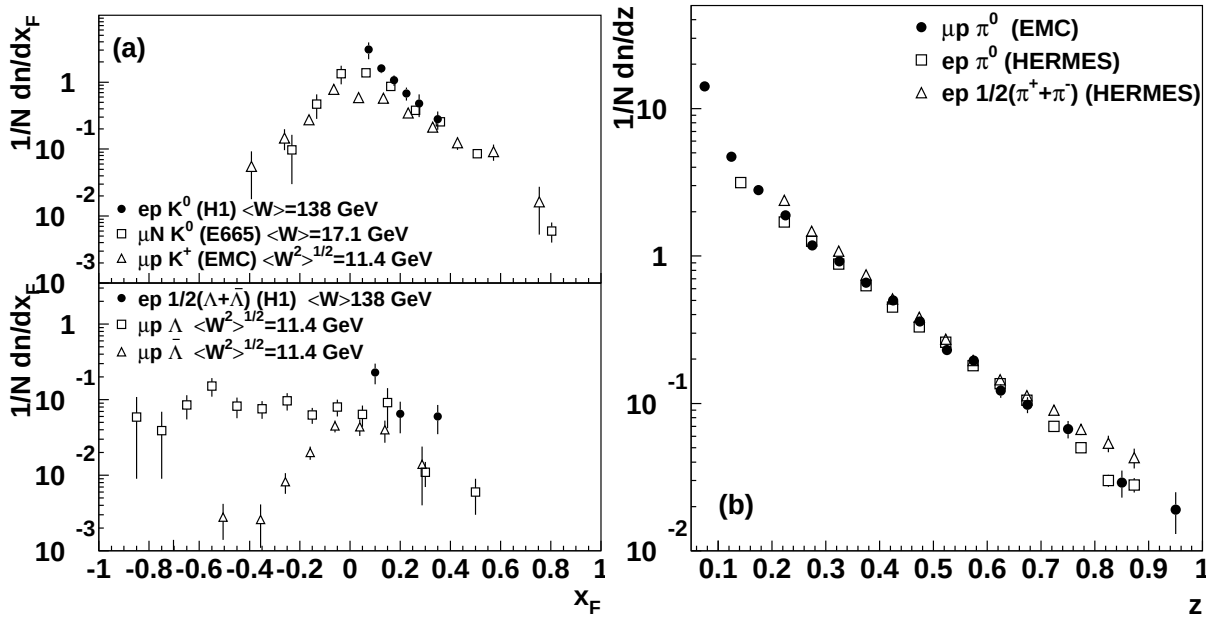

Figure 19.9: (a) $1/N \cdot dn/dx_F$ for identified strange particles in DIS at various values of W [149–151]. (b) $1/N \cdot dn/dz$ for measurements of pions in fixed-target DIS experiments [152–154].

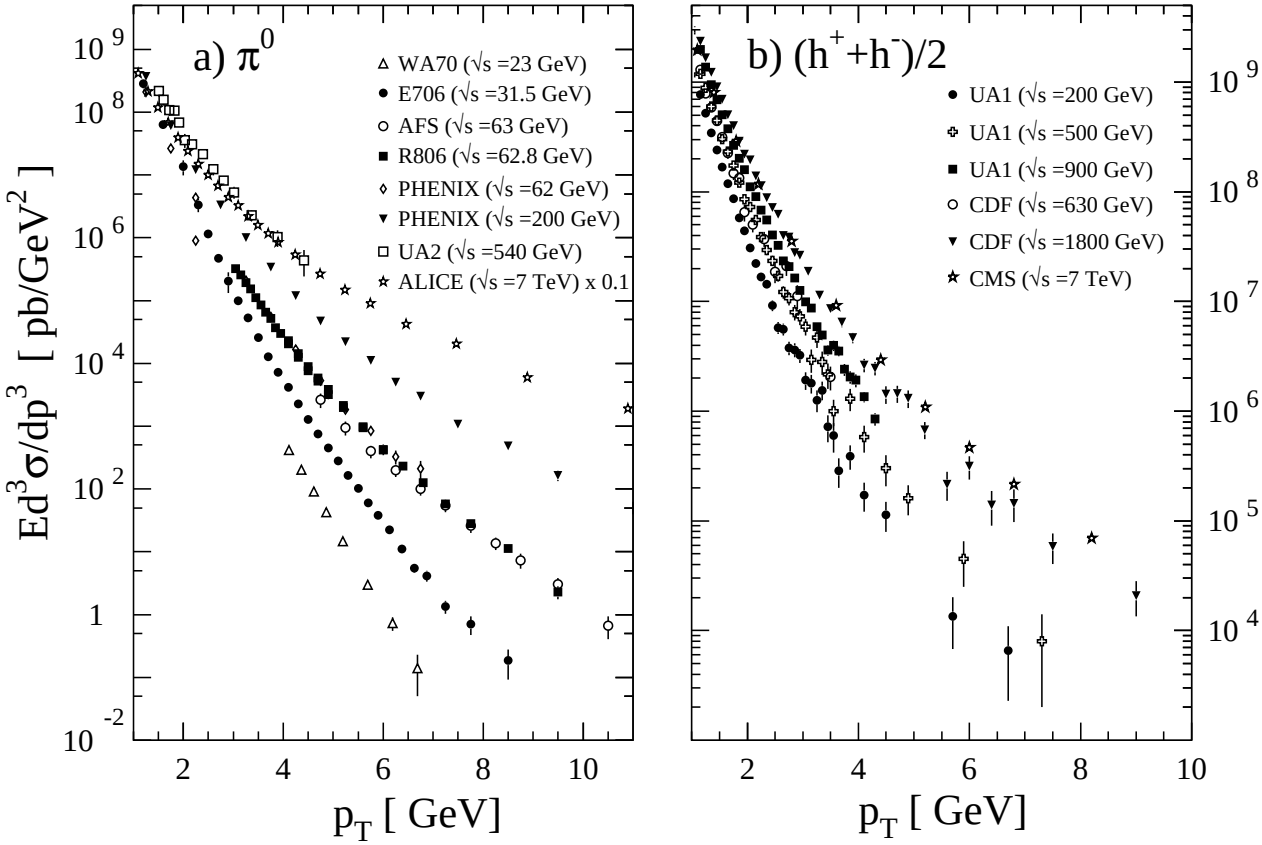

Figure 19.10: Selection of inclusive (a) π^0 and (b) charged-hadron production data from pp [118, 155–160] and $p\bar{p}$ [114, 161, 162] collisions.

of three-jet events in which the gluon jet is identified, for example, by tagging the other two jets with heavy quark decays. To leading order, the measured distributions of $x = E_{\rm had}/E_{\rm jet}$ for particles in gluon jets can be identified directly with the gluon fragmentation function $D_g^h(x)$.

Data for $p^{(}\overline{p}^{)} \to h + X$ provide much more direct constraint on D_g^h. At variance with e^+e^- annihilation and SIDIS, here gluon fragmentation contributes already at the lowest order in the coupling constant. At large $x \gtrsim 0.5$, where information from e^+e^- is sparse, data from hadronic colliders significantly improve extractions of D_g^h [131, 132, 138, 140]. Recent LHC data has been included in the NLO analyses [128,138,139] of pion-fragmentation functions; see Sec.(17.7) for more details. Note that these analyses are currently the only ones that 'globally' incorporate avail-

Downloaded from https://academic.oup.com/ptep/article/2022/8/083C01/6651666 by KIT Library user on 27 September 2022

Table 19.1: Classification of spin- and transverse-momentum dependent quark fragmentation functions. For simplicity we have left out the ubiquitous label for flavor i of the fragmenting quark and for hadron species h. Each of the functions carries the argument $(x, x^2k_T^2)$ (plus dependence on a factorization scale), where $xk_T = p_T^h$ is the hadron's transverse momentum. λ and Λ are the quark's and hadron's helicities, respectively, and $\vec{s}_T$ and $\vec{S}_T$ are their transverse spin vectors. We have defined $\left[\vec{a} \times \vec{b}\right] \equiv a^1b^2 - a^2b^1$. Finally, m_h is the mass of the produced hadron.

	quark polarization		
hadron pol.	unpolarized	long. polarized	transv. polarized
unpol.	D	–	$\frac{\left[\vec{k}_T \times \vec{s}_T\right]}{m_h} H^\perp$
long. pol.	–	$\lambda \Lambda G_L$	$\frac{\vec{k}_T \cdot \vec{s}_T}{m_h} \Lambda H_L^\perp$
transv. pol.	$\frac{\left[\vec{k}_T \times \vec{S}_T\right]}{m_h} D_T^\perp$	$\frac{\vec{k}_T \cdot \vec{S}_T}{m_h} \lambda G_T^\perp$	$(\vec{s}_T \cdot \vec{S}_T) H_T + \frac{\vec{k}_T \cdot \vec{S}_T}{m_h} \frac{\vec{k}_T \cdot \vec{s}_T}{m_h} H_T^\perp$

able data from all sources, $e^+e^- \to h + X$, $ep \to e'h + X$ and $pp \to h + X$.

We note that recently a 'hybrid' type of high-p_T jet/hadron observable has also been considered both theoretically [163–169] and experimentally [170–177]. It is defined by an identified specific hadron found inside a fully reconstructed jet. This gives rise to a *same-side* hadron-jet momentum correlation that may be addressed using perturbative methods. One of several relevant kinematical variables (see [168] for an overview) is $z_h \equiv (\vec{p}_T^{\,h} \cdot \vec{p}_T^{\,\rm jet})/(p_T^{\rm jet})^2$, where $\vec{p}_T^{\,h}$ and $\vec{p}_T^{\,\rm jet}$ are the transverse momenta of the hadron and the jet, respectively. The observable provides an alternative window on fragmentation functions in a more exclusive setting, enabling novel tests of the universality of fragmentation functions. Varying z_h and/or the hadron species, one can map out the fragmentation functions 'locally' as functions of x. This is in contrast to the single-inclusive observable $pp \to h + X$, which inevitably samples over a broad range of x. Although hadron-in-jet data are not yet routinely included in analyse of fragmentation functions, a 'proof-of-principle' analysis does exist [178] that shows the potential of the observable in providing constraint on fragmentation functions.

A comparison of recent NLO fits of fragmentation functions for $\pi^+ + \pi^-$ obtained by the updated version of BDSS21 [128], JAF20 [129] and NNPDF1.0 [130] is shown in Fig. 19.7. Differences among the functions for these sets are visible, especially for the gluon fragmentation function over the full range of x and for the quark functions at large momentum fractions. The differences are even larger for other species of hadrons like kaons and protons [131,132,136,140]. Recent analyses [128–130,136,138,139,179,180] estimate the uncertainties involved in the extraction of fragmentation functions.

Photonic fragmentation functions play a relevant role in the theoretical understanding of inclusive photon production in (leptonic and hadronic) high energy processes. In the sprit of the analogy between parton fragmentation functions and parton distribution functions, also photonic fragmentation functions are analogous to the photon structure function F_2^γ and to the proton's photonic parton distributions (see review on structure functions in Section 18 of this *Review*). Since photons have a pointlike coupling to quarks [181], the corresponding fragmentation functions obey inhomogeneous evolution equations and are generally decomposed into a perturbative and a non-perturbative component [135, 182, 183]. The hadronic part, sometimes approximated by the Vector Meson Dominance Model, can in principle be obtained by performing a global analysis to the available prompt photon production data [7,12,15,19–21,85,147,184,185], although in practice this has not been done. We note that also the cross section for photons produced in fully reconstructed jets has been proposed [186] as a new tool for obtaining access to photon fragmentation functions, in analogy to the hadron-in-jet cross section discussed above.

19.6 Identified particles in e^+e^- and semi-inclusive DIS

There is a great wealth of measurements of e^+e^- fragmentation into identified particles. A collection of references for data on fragmentation into identified particles is provided in Table 53.1 of this *Review*. As a representative example, Figure 19.8 shows differential charged-hadron spectra as functions of the scaled hadron momentum at several CM energies.

Quantitative results of studies of scaling violations in e^+e^- fragmentation have been reported in [7,21,187,188]. Scaling violations may be used to extract a value of $\alpha_{\rm s}$; the values obtained are consistent with the world average (see review on QCD in Section 9 of this *Review*).

Many studies have been made of production of identified particles in lepton-hadron scattering, although fewer particle species have been measured than in e^+e^- collisions. References [149, 150, 152–154, 189–191] and [151, 192–197] are representative of the data from fixed target and ep collider experiments, respectively. QCD calculations performed at NLO provide an overall good description of the HERA data [33, 34, 58, 197–199], both for SIDIS [200] and for the hadron transverse momentum distribution [53,201] in the kinematic regions in which the calculations are predictive. A first step towards an NNLO calculation for SIDIS has been presented in [202].

Fig. 19.9(a) compares lower-energy fixed-target and HERA data on strangeness production, showing that the HERA spectra have substantially increased multiplicities, albeit with statistical precision that is insufficient to study scaling violations. The fixed-target data show that the Λ rate substantially exceeds the $\overline{\Lambda}$ rate in the remnant region, owing to the conserved baryon number from the baryon target. Fig. 19.9(b) shows $1/N \cdot dn/dz$ for neutral and charged pion production, where z is defined as the ratio of the pion energy to that of the exchanged boson, both measured in the laboratory frame. Results are shown from the HERMES and the EMC experiments, where the HERMES data have been evolved to $\langle Q^2 \rangle = 25$ GeV^2 at NLO QCD, in order to be comparable with the EMC data. Each of the experiments uses various kinematic cuts to ensure that the measured particles lie in the region that is expected to be associated with the struck quark. In the DIS kinematic regime accessed at these experiments, and over the range in z shown in Fig. 19.9, the z and x_F variables have similar values [30]. The precision data on identified particles can be used in the study of the quark flavor content of the proton [179, 218, 219].

Data on identified particle production can aid the investigation of the universality of jet fragmentation in e^+e^- and DIS. The strangeness suppression factor γ_s, as derived principally from tuning the Lund string model [220] within JETSET [221], is typically found to be around 0.3 in e^+e^- experiments [75], although values closer to 0.2 [222] have also been obtained. A number of measurements of so-called V^0-particles (K^0, Λ^0) and the relative rates of V^0's and inclusively produced charged particles have been performed at HERA [151,192,223] and fixed target experiments [149].

Downloaded from https://academic.oup.com/ptep/article/2022/8/083C01/6651666 by KIT Library user on 27 September 2022

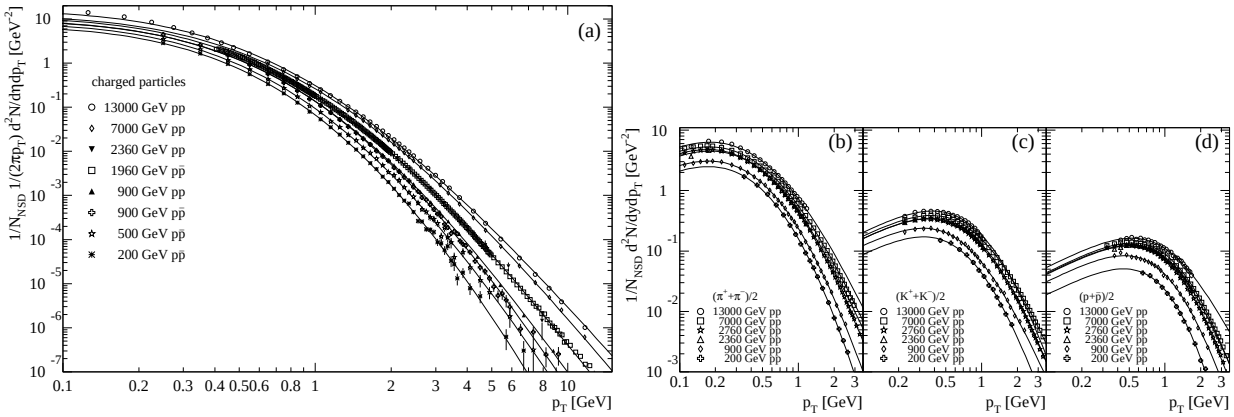

Figure 19.11: (a) Selection of inclusive charged-particle transverse momentum spectra [114, 117, 119, 121, 161, 203, 204], normalized to the non-single diffractive cross section (NSD). (b)-(d) Selection of identified charged-particle transverse momentum spectra [205–210] normalized to the NSD cross section. All spectra are scaled to the NSD cross-section using measurements of total, inelastic, elastic, single, or non-single diffractive cross sections from [211–215, 215–217]. The overall normalization uncertainty of about 3% is not shown. Superimposed are fits of the Tsallis distribution in Eq. (19.13).

These typically favour a stronger suppression ($\gamma_s \approx 0.2$) than usually obtained from e^+e^- data, although values close to 0.3 have also been obtained [224, 225].

However, when comparing the description of QCD-based models for lepton-hadron interactions and e^+e^- collisions, it is important to note that the overall description by event generators of inclusively produced hadronic final states is more accurate in e^+e^- collisions than in lepton-hadron interactions [226]. Predictions of particle rates in lepton-hadron scattering are affected by uncertainties in the modelling of the parton composition of the proton and photon, the extended target remnant, and initial and final-state QCD radiation. Furthermore, the tuning of event generators for e^+e^- collisions is typically based on a larger set of parameters and uses more observables [75] than are used when optimizing models for lepton-hadron data [227].

19.7 Fragmentation in hadron-hadron collisions

An extensive set on high-transverse momentum (p_T) single-inclusive hadron data has been collected in $h_1h_2 \to hX$ scattering processes, both at high energy colliders and fixed-target experiments [155–162, 185, 228–250]. Fig. 19.10 shows the invariant cross sections $E\mathrm{d}^3\sigma/\mathrm{d}p^3$ for a compilation of neutral-pion and charged-hadron production data for energies in the range $\sqrt{s} \approx 23$ - 7000 GeV.

The differential cross section for high-transverse momentum hadron production has been computed to NLO accuracy in perturbative QCD [251]. The NLO corrections are typically large and can even double the prediction for the cross section at fixed-target energies. Nevertheless, the NLO calculations significantly under-predict the cross-section for several fixed-target energy data sets [246, 252, 253]. Different strategies have been developed to ameliorate the theoretical description at fixed-target energies. A possible phenomenological approach involves the introduction of a non-perturbative intrinsic partonic transverse momentum [160, 246, 254, 255]. Furthermore, the resummation of the dominant higher order corrections at threshold produces an enhancement of the theoretical calculation that significantly improves the description of the data [256, 257].

Data collected at high energy colliders are either included in global fit analyses or used as a test for the universality of fragmentation functions. A certain tension has been observed between data sets from RHIC and the LHC [258]. The tension can be largely resolved [128] by taking properly into account the theoretical scale dependence in the global analysis, allowing factorization and renormalization scales to variate according to the kinematics of each experiment within a conventional range.

Transverse momentum distributions can usually be fit by power laws [259]. An approach to describe the low p_T particle spectra is the Tsallis distribution [260–262], which is based on a non-extensive generalization of the Boltzmann-Gibbs statistics. The functional form [263]

$$\frac{\mathrm{d}^2N}{\mathrm{d}p_T\mathrm{d}y} = p_T\frac{\mathrm{d}N}{\mathrm{d}y}\frac{(n-1)(n-2)}{nT(nT+m_0(n-2))}\left[1+\frac{m_T-m_0}{nT}\right]^{-n} \tag{19.13}$$

is frequently used to fit the transverse momentum spectra, where $\mathrm{d}N/\mathrm{d}y$ is the particle's multiplicity, T and n are fit parameters of the Tsallis distribution, m_0 is the either the mass of the most abundant particle, i.e. the pion for inclusive spectra, or the mass of an identified particle, and $m_T = \sqrt{p_T^2 + m_0^2}$. The parameter n is related to the non-extensive parameter $q = n/(n-1)$ of the original Tsallis formula [264], and T is connected to the temperature in the Boltzmann-Gibbs statistics. The Tsallis distribution has been very successfully fit to measured transverse momentum distributions of both inclusive charged particles and identified particle spectra for hadron-hadron collisions, see for example [265–267], for collisions of heavy nuclei, see for example [268], and also for e^+e^- collisions, see for example [269]. The energy dependence of the fitted Tsallis parameters has also been investigated in detail, see [263, 270]. Fig. 19.11 shows examples of hadron production data in pp and $p\bar{p}$ collisions compared to Tsallis distributions.

Hadron production provides a critical observable for probing the high energy-density matter produced in heavy-ion collisions. Measurements at colliders show a suppression of inclusive hadron yields at high transverse momentum for AA collisions compared to pp scattering, indicating the formation of a dense medium opaque to quark and gluons, see e.g. [271].

19.8 Heavy quark fragmentation

It was recognized very early [272] that a heavy flavored meson should retain a large fraction of the momentum of the primordial heavy quark, and therefore its fragmentation function should be much harder than that of a light hadron. In the limit of a very heavy quark, one expects the fragmentation function for a heavy quark to go into any heavy hadron to be peaked near $x = 1$.

When the heavy quark is produced at a momentum much larger than its mass, one expects important perturbative effects, enhanced by powers of the logarithm of the transverse momentum over the heavy quark mass, to intervene and modify the shape of the fragmentation function. In leading logarithmic order (*i.e.*, including all powers of $\alpha_s \log(m_Q/p_T)$), the total (*i.e.*, summed over all hadron types) perturbative fragmentation function is simply obtained by solving the leading evolution equation for fragmentation functions, Eq. (19.5), with the initial condition due to the finite mass of the heavy quark given by $D_Q(x,\mu^2)\big|_{\mu^2=m_Q^2} = \delta(1-x)$ and $D_i(x,\mu^2)\big|_{\mu^2=m_Q^2} = 0$ for $i \neq Q$ (here $D_i(x,\mu^2)$, stands for the probability to produce a heavy quark Q from parton i with a fraction x of the parton momentum).

Downloaded from https://academic.oup.com/ptep/article/2022/8/083C01/6651666 by KIT Library user on 27 September 2022

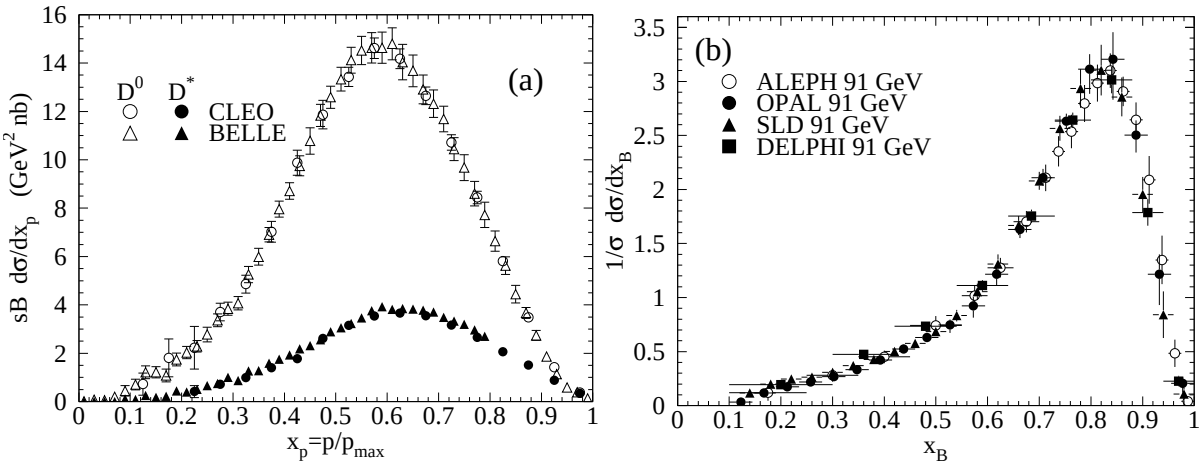

Figure 19.12: (a) Efficiency-corrected inclusive cross-section measurements for the production of D^0 and D^{*+} in e^+e^- measurements at $\sqrt{s} \approx 10.6$ GeV, excluding B decay products [273] [274]. (b) Measured e^+e^- fragmentation function of b quarks into B hadrons at $\sqrt{s} \approx 91$ GeV [275].

Several extensions of the leading logarithmic result have appeared in the literature. Next-to-leading-log (NLL) order results for the perturbative heavy quark fragmentation function have been obtained in [276]. The resummation of the dominant logarithmic contributions at large x was performed in [277] to next-to-leading-log accuracy. Fixed-order calculations of the fragmentation function at order α_s^2 in e^+e^- annihilation have appeared in [278] while the initial condition for the perturbative heavy quark fragmentation function has been extended to NNLO in [279].

Inclusion of non-perturbative effects in the calculation of the heavy-quark fragmentation function is done by convoluting the perturbative result with a phenomenological non-perturbative form. This form follows from the simple kinematical consideration that the formation of a hadron by attaching light quarks/antiquarks to the heavy quark will slightly decelerate the heavy quark. Thus, its shape will show a peak that becomes increasingly centered next to $x = 1$ the higher the quark mass. Among the most popular parameterizations we have the following:

$$\text{Peterson } et\ al.\ [280]: \quad D_{\rm np}(x) \propto \frac{1}{x}\left(1 - \frac{1}{x} - \frac{\epsilon}{1-x}\right)^{-2}, \tag{19.14}$$

$$\text{Kartvelishvili } et\ al.\ [281]: \quad D_{\rm np}(x) \propto x^{\alpha}(1-x), \tag{19.15}$$

$$\text{Collins \& Spiller } [282]: \quad D_{\rm np}(x) \propto \left(\frac{1-x}{x} + \frac{(2-x)\epsilon_C}{1-x}\right) \times (1+x^2) \times \left(1 - \frac{1}{x} - \frac{\epsilon_C}{1-x}\right)^{-2} \tag{19.16}$$

$$\text{Colangelo \& Nason } [283]: \quad D_{\rm np}(x) \propto (1-x)^{\alpha} x^{\beta} \tag{19.17}$$

$$\text{Bowler } [284]: \quad D_{\rm np}(x) \propto x^{-(1+bm_{h,\perp}^2)} \times (1-x)^a \exp\left(-\frac{bm_{h,\perp}^2}{x}\right) \tag{19.18}$$

$$\text{Braaten } et\ al.\ [285]: \quad \text{(see Eqs. (31), (32) in [285])} \tag{19.19}$$

where ϵ, ϵ_C, a, $bm_{h,\perp}^2$, α, and β are non-perturbative parameters that depend on the heavy hadron considered. The parameters entering the non-perturbative forms are fitted together with some model of hard radiation, which can be either a shower Monte Carlo, a leading-log or NLL calculation (which may or may not include Sudakov resummation), or a fixed order calculation. In [278], for example, the Peterson *et al.* [280] ϵ parameter for charm and bottom production is fitted from the measured distributions of Refs. [286, 287] for charm, and of [288] for bottom. If the leading-logarithmic approximation (LLA) is used for the perturbative part, one finds $\epsilon_c \approx 0.05$ and $\epsilon_b \approx 0.006$; if a second order calculation is used one finds $\epsilon_c \approx 0.035$ and $\epsilon_b \approx 0.0033$; if a NLL improved fixed order $\mathcal{O}(\alpha_s^2)$ calculation is used instead of NLO $\mathcal{O}(\alpha_s)$ one finds $\epsilon_c \approx 0.022$ and $\epsilon_b \approx 0.0023$. The larger values found in the LL approximation are consistent with what is obtained in the context of parton shower models [289], as expected. The ϵ parameter for charm and bottom scales roughly with the inverse square of the heavy flavor mass. This behavior can be justified by several arguments [272, 290, 291]. It can be used to relate the non-perturbative parts of the fragmentation functions of charm and bottom quarks [278, 283, 292].

A more conventional approach [293] involves the introduction of a unique set of heavy quark fragmentation functions of non-perturbative nature that obey the usual massless evolution equations in Eq. (19.5). Finite mass terms of the form $(m_Q/p_T)^n$ are kept in the corresponding short distance coefficient function for each scattering process. Within this approach, the initial condition for the perturbative fragmentation function provides the term needed to define the correct subtraction scheme to match the massless limit for the coefficient function (see e.g. [294]). Such an implementation is in line with the variable flavor number scheme introduced for parton distributions functions, as described in Section 18 of this *Review*.

High statistics data for charmed-meson production near the Υ resonance (excluding decay products of B mesons) have been published [273, 274]. They include results for D and D^*, D_s (see also [295, 296]) and Λ_c. Shown in Fig. 19.12(a) are the CLEO and BELLE inclusive cross-sections times branching ratio $\mathcal{B}$, $s\mathcal{B}d\sigma/dx_p$, for the production of D^0 and D^{*+}. The variable x_p approximates the light-cone momentum fraction x, but is not identical to it. The two measurements are consistent with each other.

The branching ratio $\mathcal{B}$ represents $D^0 \to K^-\pi^+$ for the D^0 results and for the D^{*+} the product of the branching fractions for $D^{*+} \to D^0\pi^+$ and $D^0 \to K^-\pi^+$. Given the high precision of CLEO's and BELLE's data, a superposition of different parametric forms for the non-perturbative contribution is needed to obtain a good fit [52]. Older studies are reported in Refs. [287, 297, 298]. Charmed meson spectra on the Z peak have been published by OPAL and ALEPH [299, 300].

Charm quark production has also been extensively studied at HERA by the H1 and ZEUS collaborations. Measurements have been made of $D^{*\pm}$, $D^{\pm}$, and $D_s^{\pm}$ mesons and the Λ_c baryon. See, for example, Refs. [301, 302].

Experimental studies of the fragmentation function for b quarks, shown in Fig. 19.12(b), have been performed at LEP and SLD [275, 288, 303]. Commonly used methods identify the B meson

Downloaded from https://academic.oup.com/ptep/article/2022/8/083C01/6651666 by KIT Library user on 27 September 2022

through its semileptonic decay or based upon tracks emerging from the B secondary vertex. Heavy flavor contributions from gluon splitting are usually explicitly removed before fitting for the fragmentation functions. The studies in [275] fit the B spectrum using a Monte Carlo shower model supplemented with non-perturbative fragmentation functions yielding consistent results.

The experiments measure primarily the spectrum of B mesons. This defines a fragmentation function that includes the effect of the decay of higher mass excitations, like the B^* and B^{**}. In the literature (cf. details in Ref. [304]), there is sometimes ambiguity in what is defined to be the bottom fragmentation function. Instead of using what is directly measured (*i.e.*, the B meson spectrum), in some cases corrections are applied to account for B^* or B^{**} production.

Heavy-flavor production in e^+e^- collisions is the primary source of information for the role of fragmentation effects in heavy-flavor production in hadron-hadron and lepton-hadron collisions. The QCD calculations tend to underestimate the data in certain regions of phase space. Some experimental results from LHC summarized in [305] show such deviations e.g. at high transverse jet momentum and also at low di-jet separation angles, see [306] for details, and were already theoretically investigated in [307].

Both bottomed- and charmed-meson spectra have been measured at the Tevatron with unprecedented accuracy [308]. The measured spectra are in good agreement with QCD calculations (including non-perturbative fragmentation effects inferred from e^+e^- data [309]).

The HERA collaborations have produced a number of measurements of beauty production; see, for example, Refs. [301,310–313]. As for the Tevatron data, the HERA results are described well by QCD-based calculations using fragmentation models optimized with e^+e^- data.

Besides degrading the fragmentation function by gluon radiation, QCD evolution can also generate soft heavy quarks, increasing in the small x region as $\sqrt{s}$ increases. Several theoretical studies are available on the issue of how often $b\bar{b}$ or $c\bar{c}$ pairs are produced indirectly via a gluon splitting mechanism [314–316]. Experimental results from studies on charm and bottom production via gluon splitting, given in [300, 317–321], yield weighted averages of $\overline{n}_{g\to c\bar{c}} = 3.05 \pm 0.45\%$ and $\overline{n}_{g\to b\bar{b}} = 0.277 \pm 0.072\%$, respectively. The production of bottom-antibottom quark pairs via gluon splitting has also been investigated at hadron colliders, see for example [322–324].

19.9 Spin-dependent and transverse-momentum dependent fragmentation functions

The fragmentation functions we have considered so far apply to the spin-averaged case in which the polarization of the produced hadron is not observed, or the hadron has spin-0. We have also only considered 'collinear' fragmentation functions $D_i^h(x,\mu^2)$ which carry only one kinematical variable, the momentum fraction x. New insights into fragmentation and hadronization become available when also the dependence of fragmentation functions on the spin of the produced hadron and/or its relative transverse momentum with respect to the fragmenting parton are considered. In the latter case, one refers to the fragmentation functions as 'transverse-momentum dependent (TMD)' fragmentation functions.

Staying first with collinear fragmentation functions, two types of spin-dependent fragmentation functions to spin-1/2 hadrons can be considered. The helicity-dependent fragmentation function measures the transfer of longitudinal spin from the fragmenting parton to the hadron [38, 325–328]. It is given by

$$\Delta D_i^h(x,\mu^2) \equiv D_{i+}^{h^+}(x,\mu^2) - D_{i+}^{h^-}(x,\mu^2)\,, \tag{19.20}$$

where the superscripts $\pm$ refer to the helicities of the parton and hadron. Λ hyperons are ideally suited for measurements of the ΔD_i^h, thanks to their self-analyzing weak decay $\Lambda \to \pi p$. Measurements of the longitudinal spin transfer to Lambda hyperons have been presented in e^+e^- (on the Z resonance), ℓp, and pp scattering in Refs. [329–335]. One may readily extend Eq. (19.20) to the case of transverse polarization of hadrons and quarks [336], where the corresponding fragmentation functions are known as 'transversity' fragmentation functions. There are also measurements constraining these fragmentation functions [330, 337, 338]. A recent phenomenological analysis was presented in [339].

If the transverse-momentum (k_T) dependence of fragmentation functions is considered, there are eight types of leading-twist functions, defined by the correlations among the hadronic and partonic spin vectors and transverse-momentum vectors they represent. (For review, see [5]). We note that the eight fragmentation functions given in the table below exist separately for each quark and antiquark flavor, and a similar set may be introduced for gluons. Upon integration over the transverse momentum k_T the collinear unpolarized, helicity, and transversity fragmentation functions are reproduced.

The various fragmentation functions may be obtained from spin asymmetries and angular distributions in hadron production processes. There is a large body of precision data by now on transverse-momentum distributions in e^+e^- annihilation [340] and SIDIS [190, 341] that provide constraints on the unpolarized TMD fragmentation functions D_i^h, which have been analyzed theoretically, partly also including TMD evolution effects and high orders of perturbation theory [342–349].

Besides the unpolarized functions D most of the attention in experiment and theory has been on the function $H^\perp$ which describes the production of unpolarized (or spin-0) hadrons by transversely polarized quarks. This function is known as the 'Collins function' [350]. Its importance also derives from the fact that it may be used to probe the quark transversity PDF of the nucleon [351] which gives the probability of finding a transversely polarized quark with its spin aligned or anti-aligned with the spin of a transversely polarized nucleon. The transversity function is chiral-odd, and therefore not accessible through measurements of inclusive lepton-hadron scattering. The Collins effect in semi-inclusive DIS, on the other hand, provides an avenue for accessing transversity. The Collins fragmentation function is chiral-odd and T-odd, leading to a characteristic single-spin asymmetry in the azimuthal angular distribution of the produced hadron in the hadron scattering plane. A number of SIDIS [352–363] and e^+e^- experiments [364–368] have performed measurements of the Collins effect, for charged pions and kaons. These have been analyzed theoretically [369, 370], leading to an extraction of the nucleon's transversity distributions [370]. The Collins effect has also been studied in pp scattering, where one considers azimuthal transverse single-spin asymmetries for distributions of hadrons inside jets [177, 371, 372].

In the context of extractions of transversity PDFs also fragmentation functions for same-side pairs of hadrons with small invariant mass, *dihadrons*, have been introduced and studied [373–381]. Compared to the Collins effect, dihadron fragmentation functions have the advantage that they may be defined purely in collinear factorization. The relevant spin-dependent dihadron fragmentation function exploits a correlation between the transverse polarization of the fragmenting quark and the relative momentum of the two hadrons. In SIDIS with a transversely polarized hadron beam, the dihadron cross section then contains a specific modulation in the azimuthal orientation of the plane containing the momenta of the two hadrons. The coefficient of this modulation is a product of the spin-dependent dihadron fragmentation function and the target's transversity PDF. The dihadron fragmentation functions may be separately extracted from measurements in e^+e^- annihilation, and the Belle experiment has presented data [382] that have been analyzed theoretically [383, 384]. In lepton scattering, HERMES [385] and COMPASS [386, 387] have reported data sensitive to the spin-dependent dihadron fragmentation functions, and recently the STAR experiment at RHIC has presented data in the azimuthal distribution of $\pi^+\pi^-$ pairs produced in pp scattering with one transversely polarized proton [388]. The results have been successfully used for the extraction of transversity PDFs [384, 389–391].

References

[1] G. Altarelli, Phys. Rept. **81**, 1 (1982).

[2] R.K. Ellis *et al.*, *QCD and Collider Physics*, Cambridge

Downloaded from https://academic.oup.com/ptep/article/2022/8/083C01/6651666 by KIT Library user on 27 September 2022

University Press (1996).

[3] S. Albino *et al.* (2008), [arXiv:0804.2021].

[4] F. Arleo, Eur. Phys. J. **C61**, 603 (2009), [arXiv:0810.1193].

[5] A. Metz and A. Vossen, Prog. Part. Nucl. Phys. **91**, 136 (2016), [arXiv:1607.02521].

[6] P. Nason and B. R. Webber, Nucl. Phys. **B421**, 473 (1994), [Erratum: Nucl. Phys.B480,755(1996)].

[7] D. Buskulic *et al.* (ALEPH), Phys. Lett. **B357**, 487 (1995), [Erratum: Phys. Lett.B364,247(1995)].

[8] P. Abreu *et al.* (DELPHI), Eur. Phys. J. **C6**, 19 (1999).

[9] R. Barate *et al.* (ALEPH), Phys. Rept. **294**, 1 (1998).

[10] D. Buskulic *et al.* (ALEPH), Z. Phys. **C73**, 409 (1997).

[11] B. Adeva *et al.* (L3), Phys. Lett. **B259**, 199 (1991).

[12] Y. K. Li *et al.* (AMY), Phys. Rev. **D41**, 2675 (1990).

[13] D. Bender *et al.*, Phys. Rev. **D31**, 1 (1985).

[14] G. S. Abrams *et al.*, Phys. Rev. Lett. **64**, 1334 (1990).

[15] A. Petersen *et al.*, Phys. Rev. **D37**, 1 (1988).

[16] G. Alexander *et al.* (OPAL), Z. Phys. **C72**, 191 (1996).

[17] K. Ackerstaff *et al.* (OPAL), Z. Phys. **C75**, 193 (1997).

[18] G. Abbiendi *et al.* (OPAL), Eur. Phys. J. **C16**, 185 (2000), [hep-ex/0002012].

[19] W. Braunschweig *et al.* (TASSO), Z. Phys. **C47**, 187 (1990).

[20] K. Ackerstaff *et al.* (OPAL), Eur. Phys. J. **C7**, 369 (1999), [hep-ex/9807004].

[21] P. Abreu *et al.* (DELPHI), Phys. Lett. **B398**, 194 (1997).

[22] G. Abbiendi *et al.* (OPAL), Eur. Phys. J. **C37**, 1, 25 (2004), [hep-ex/0404026].

[23] R. Brandelik *et al.* (TASSO), Phys. Lett. **114B**, 65 (1982).

[24] K. Abe *et al.* (SLD), Phys. Rev. **D69**, 072003 (2004), [hep-ex/0310017].

[25] H. Aihara *et al.* (TPC/Two Gamma), Phys. Rev. Lett. **61**, 1263 (1988).

[26] M. Leitgab *et al.* (Belle), Phys. Rev. Lett. **111**, 062002 (2013), [arXiv:1301.6183].

[27] W. Kittel and E.A. De Wolf, *Soft Multihadron Dynamics*, World Scientific (2005).

[28] H.F. Jones, Nuovo Cimento **40A**, 1018 (1965).

[29] K. H. Streng, T. F. Walsh and P. M. Zerwas, Z. Phys. **C2**, 237 (1979).

[30] M. R. Adams *et al.* (E-665), Phys. Lett. **B272**, 163 (1991).

[31] M. Arneodo *et al.* (European Muon), Z. Phys. **C35**, 417 (1987).

[32] I. Abt *et al.* (H1), Z. Phys. **C63**, 377 (1994).

[33] M. Derrick *et al.* (ZEUS), Z. Phys. **C70**, 1 (1996), [hep-ex/9511010].

[34] J. Breitweg *et al.* (ZEUS), Phys. Lett. **B414**, 428 (1997), [hep-ex/9710011].

[35] F. D. Aaron *et al.* (H1), Phys. Lett. **B654**, 148 (2007), [arXiv:0706.2456].

[36] P. Abreu *et al.* (DELPHI), Phys. Lett. **B311**, 408 (1993).

[37] G. Altarelli *et al.*, Nucl. Phys. **B160**, 301 (1979); R. Baier and K. Fey, Z. Phys. **C2**, 339 (1979).

[38] D. de Florian, M. Stratmann and W. Vogelsang, Phys. Rev. **D57**, 5811 (1998), [hep-ph/9711387].

[39] P. J. Rijken and W. L. van Neerven, Phys. Lett. **B386**, 422 (1996), [hep-ph/9604436]; P. J. Rijken and W. L. van Neerven, Phys. Lett. **B392**, 207 (1997), [hep-ph/9609379]; P. J. Rijken and W. L. van Neerven, Nucl. Phys. **B487**, 233 (1997), [hep-ph/9609377].

[40] A. Mitov, S. Moch and A. Vogt, Phys. Lett. **B638**, 61 (2006), [hep-ph/0604053].

[41] A. Mitov and S.-O. Moch, Nucl. Phys. **B751**, 18 (2006), [hep-ph/0604160].

[42] V. N. Gribov and L. N. Lipatov, Sov. J. Nucl. Phys. **15**, 438 (1972), [Yad. Fiz.15,781(1972)]; V. N. Gribov and L. N. Lipatov, Sov. J. Nucl. Phys. **15**, 675 (1972), [Yad. Fiz.15,1218(1972)]; L.N. Lipatov, Sov. J. Nucl. Phys. **20**, 95 (1975); Yu.L. Dokshitzer, Sov. Phys. JETP Lett. **46**, 641 (1977); G. Altarelli and G. Parisi, Nucl. Phys. **B126**, 298 (1977).

[43] H. Georgi and H. D. Politzer, Nucl. Phys. **B136**, 445 (1978); J. F. Owens, Phys. Lett. **76B**, 85 (1978); T. Uematsu, Phys. Lett. **79B**, 97 (1978).

[44] G. Curci, W. Furmanski and R. Petronzio, Nucl. Phys. **B175**, 27 (1980).

[45] W. Furmanski and R. Petronzio, Phys. Lett. **97B**, 437 (1980).

[46] E. G. Floratos, C. Kounnas and R. Lacaze, Nucl. Phys. **B192**, 417 (1981).

[47] J. Kalinowski, K. Konishi and T. R. Taylor, Nucl. Phys. **B181**, 221 (1981).

[48] M. Stratmann and W. Vogelsang, Nucl. Phys. **B496**, 41 (1997), [hep-ph/9612250].

[49] Yu. L. Dokshitzer, G. Marchesini and G. P. Salam, Phys. Lett. **B634**, 504 (2006), [hep-ph/0511302].

[50] S. Moch and A. Vogt, Phys. Lett. **B659**, 290 (2008), [arXiv:0709.3899].

[51] A. A. Almasy, S. Moch and A. Vogt, Nucl. Phys. **B854**, 133 (2012), [arXiv:1107.2263].

[52] M. Cacciari, P. Nason and C. Oleari, JHEP **04**, 006 (2006), [hep-ph/0510032]; M. Cacciari, P. Nason and C. Oleari, JHEP **10**, 034 (2005), [hep-ph/0504192].

[53] P. Aurenche *et al.*, Eur. Phys. J. **C34**, 277 (2004), [hep-ph/0312359]; A. Daleo, D. de Florian and R. Sassot, Phys. Rev. **D71**, 034013 (2005), [hep-ph/0411212]; B. A. Kniehl, G. Kramer and M. Maniatis, Nucl. Phys. **B711**, 345 (2005), [Erratum: Nucl. Phys.B720,231(2005)], [hep-ph/0411300].

[54] B. Wang *et al.*, Phys. Rev. **D99**, 9, 094029 (2019), [arXiv:1903.01529].

[55] S. Aid *et al.* (H1), Nucl. Phys. **B445**, 3 (1995), [hep-ex/9505003].

[56] M. Derrick *et al.* (ZEUS), Z. Phys. **C67**, 93 (1995), [hep-ex/9501012].

[57] C. Adloff *et al.* (H1), Nucl. Phys. **B504**, 3 (1997), [hep-ex/9707005].

[58] J. Breitweg *et al.* (ZEUS), Eur. Phys. J. **C11**, 251 (1999), [hep-ex/9903056].

[59] J. F. Patrick *et al.*, Phys. Rev. Lett. **49**, 1232 (1982).

[60] S. Chekanov *et al.* (ZEUS), JHEP **06**, 061 (2008), [arXiv:0803.3878].

[61] A. H. Mueller, Phys. Lett. **104B**, 161 (1981).

[62] A. Bassetto *et al.*, Nucl. Phys. **B207**, 189 (1982).

[63] Yu.L. Dokshitzer *et al.*, Z. Phys. **C15**, 324 (1982).

[64] A. H. Mueller, Nucl. Phys. **B213**, 85 (1983); A. H. Mueller, Nucl. Phys. **B241**, 141 (1984).

[65] Y. L. Dokshitzer, V. A. Khoze and S. I. Troian, Int. J. Mod. Phys. **A7**, 1875 (1992).

[66] Yu.L. Dokshitzer *et al.*, *Basics of Perturbative QCD*, Editions Frontières (1991).

[67] V. A. Khoze and W. Ochs, Int. J. Mod. Phys. **A12**, 2949 (1997), [hep-ph/9701421].

[68] C. P. Fong and B. R. Webber, Nucl. Phys. **B355**, 54 (1991).

[69] S. Albino *et al.*, Phys. Rev. Lett. **95**, 232002 (2005), [hep-ph/0503170].

[70] S. Albino *et al.*, Phys. Rev. **D73**, 054020 (2006), [hep-ph/0510319].

Downloaded from https://academic.oup.com/ptep/article/2022/8/083C01/6651666 by KIT Library user on 27 September 2022

[71] S. Albino *et al.*, Nucl. Phys. **B851**, 86 (2011), [arXiv:1104.3018]; S. Albino *et al.*, Nucl. Phys. **B855**, 801 (2012), [arXiv:1108.3948].

[72] A. Vogt, JHEP **10**, 025 (2011), [arXiv:1108.2993]; C. H. Kom, A. Vogt and K. Yeats, JHEP **10**, 033 (2012), [arXiv:1207.5631].

[73] D. P. Anderle *et al.*, Phys. Rev. **D95**, 5, 054003 (2017), [arXiv:1611.03371].

[74] P. Bolzoni, B. A. Kniehl and A. V. Kotikov, Phys. Rev. Lett. **109**, 242002 (2012), [arXiv:1209.5914]; P. Bolzoni, B. A. Kniehl and A. V. Kotikov, Nucl. Phys. **B875**, 18 (2013), [arXiv:1305.6017].

[75] P. Abreu *et al.* (DELPHI), Z. Phys. **C73**, 11 (1996).

[76] P. Abreu *et al.* (DELPHI), Z. Phys. **C73**, 229 (1997).

[77] P. Achard *et al.* (L3), Phys. Rept. **399**, 71 (2004), [hep-ex/0406049].

[78] R. Itoh *et al.* (TOPAZ), Phys. Lett. **B345**, 335 (1995), [hep-ex/9412015].

[79] M. Althoff *et al.* (TASSO), Z. Phys. **C22**, 307 (1984).

[80] M. Z. Akrawy *et al.* (OPAL), Phys. Lett. **B247**, 617 (1990).

[81] W. Dunwoodie *et al.* (BES), Phys. Rev. **D69**, 072002 (2004), [hep-ex/0306055].

[82] D. Buskulic *et al.* (ALEPH), Z. Phys. **C55**, 209 (1992).

[83] A. Heister *et al.* (ALEPH), Eur. Phys. J. **C35**, 457 (2004).

[84] P. Abreu *et al.* (DELPHI), Phys. Lett. **B275**, 231 (1992).

[85] P. Abreu *et al.* (DELPHI), Eur. Phys. J. **C5**, 585 (1998).

[86] P. Abreu *et al.* (DELPHI), Phys. Lett. **B459**, 397 (1999).

[87] M. Acciarri *et al.* (L3), Phys. Lett. **B444**, 569 (1998).

[88] TPC/TWO-GAMMA Collab.: H. Aihara *et al.*, LBL 23737.

[89] B. R. Webber, Phys. Lett. **143B**, 501 (1984).

[90] Y. I. Azimov *et al.*, Z. Phys. **C27**, 65 (1985).

[91] Y. I. Azimov *et al.*, Z. Phys. **C31**, 213 (1986).

[92] I. M. Dremin and J. W. Gary, Phys. Rept. **349**, 301 (2001), [hep-ph/0004215].

[93] I. M. Dremin and V. A. Nechitailo, Mod. Phys. Lett. **A9**, 1471 (1994), [hep-ex/9406002].

[94] S. J. Brodsky and J. F. Gunion, Phys. Rev. Lett. **37**, 402 (1976).

[95] J. Beringer *et al.* (Particle Data Group), Phys. Rev. **D86**, 010001 (2012).

[96] R. Akers *et al.* (OPAL), Z. Phys. **C68**, 203 (1995).

[97] P. D. Acton *et al.* (OPAL), Z. Phys. **C53**, 539 (1992).

[98] D. Buskulic *et al.* (ALEPH), Z. Phys. **C69**, 15 (1995).

[99] P. Abreu *et al.* (DELPHI), Phys. Lett. **B372**, 172 (1996).

[100] P. Abreu *et al.* (DELPHI), Phys. Lett. **B416**, 233 (1998).

[101] P. Abreu *et al.* (DELPHI), Eur. Phys. J. **C18**, 203 (2000), [Erratum: Eur. Phys. J.C25,493(2002)], [hep-ex/0103031].

[102] M. Acciarri *et al.* (L3), Phys. Lett. **B371**, 137 (1996).

[103] M. Acciarri *et al.* (L3), Phys. Lett. **B404**, 390 (1997).

[104] K. Nakabayashi *et al.* (TOPAZ), Phys. Lett. **B413**, 447 (1997).

[105] K. Okabe *et al.* (VENUS), Phys. Lett. **B423**, 407 (1998).

[106] H. Albrecht *et al.* (ARGUS), Z. Phys. **C54**, 13 (1992).

[107] S. Chekanov *et al.* (ZEUS), Phys. Lett. **B510**, 36 (2001), [hep-ex/0104036].

[108] J. Benecke *et al.* (Bonn-Hamburg-Munich), Nucl. Phys. **B76**, 29 (1974).

[109] W. M. Morse *et al.*, Phys. Rev. **D15**, 66 (1977).

[110] W. Thome *et al.* (Aachen-CERN-Heidelberg-Munich), Nucl. Phys. **B129**, 365 (1977).

[111] A. Breakstone *et al.* (Ames-Bologna-CERN-Dortmund-Heidelberg-Warsaw), Phys. Rev. **D30**, 528 (1984).

[112] G. J. Alner *et al.* (UA5), Phys. Rept. **154**, 247 (1987).

[113] R. E. Ansorge *et al.* (UA5), Z. Phys. **C43**, 357 (1989).

[114] C. Albajar *et al.* (UA1), Nucl. Phys. **B335**, 261 (1990).

[115] F. Abe *et al.* (CDF), Phys. Rev. **D41**, 2330 (1990), [,119(1989)].

[116] K. Aamodt *et al.* (ALICE), Eur. Phys. J. **C68**, 89 (2010), [arXiv:1004.3034].

[117] V. Khachatryan *et al.* (CMS), JHEP **02**, 041 (2010), [arXiv:1002.0621].

[118] V. Khachatryan *et al.* (CMS), JHEP **01**, 079 (2011), [arXiv:1011.5531].

[119] V. Khachatryan *et al.* (CMS), Phys. Rev. Lett. **105**, 022002 (2010), [arXiv:1005.3299].

[120] G. Aad *et al.* (ATLAS), Eur. Phys. J. **C76**, 7, 403 (2016), [arXiv:1603.02439].

[121] M. Aaboud *et al.* (ATLAS), Eur. Phys. J. **C76**, 9, 502 (2016), [arXiv:1606.01133].

[122] J. Adam *et al.* (ALICE), Phys. Lett. **B753**, 319 (2016), [arXiv:1509.08734].

[123] J. Adam *et al.* (ALICE), Eur. Phys. J. **C77**, 1, 33 (2017), [arXiv:1509.07541].

[124] P. V. Chliapnikov and V. A. Uvarov, Phys. Lett. **B251**, 192 (1990).

[125] J. F. Grosse-Oetringhaus and K. Reygers, J. Phys. **G37**, 083001 (2010), [arXiv:0912.0023].

[126] E. K. G. Sarkisyan and A. S. Sakharov (2004), [hep-ph/0410324]; E. K. G. Sarkisyan and A. S. Sakharov, AIP Conf. Proc. **828**, 1, 35 (2006), [hep-ph/0510191]; E. K. G. Sarkisyan and A. S. Sakharov, Eur. Phys. J. **C70**, 533 (2010), [arXiv:1004.4390].

[127] S. Hoeche *et al.*, in "HERA and the LHC: A Workshop on the implications of HERA for LHC physics: Proceedings Part A," 288–289 (2005), [hep-ph/0602031]; S. Mrenna and P. Richardson, JHEP **05**, 040 (2004), [hep-ph/0312274]; J. Alwall *et al.*, Eur. Phys. J. **C53**, 473 (2008), [arXiv:0706.2569].

[128] I. Borsa *et al.* (2021), [arXiv:2110.14015].

[129] E. Moffat *et al.* (Jefferson Lab Angular Momentum (JAM)), Phys. Rev. D **104**, 1, 016015 (2021), [arXiv:2101.04664].

[130] V. Bertone *et al.* (NNPDF), Eur. Phys. J. **C77**, 8, 516 (2017), [arXiv:1706.07049].

[131] D. de Florian, R. Sassot and M. Stratmann, Phys. Rev. **D76**, 074033 (2007), [arXiv:0707.1506].

[132] S. Albino, B. A. Kniehl and G. Kramer, Nucl. Phys. **B803**, 42 (2008), [arXiv:0803.2768].

[133] S. Kretzer, E. Leader and E. Christova, Eur. Phys. J. **C22**, 269 (2001), [hep-ph/0108055].

[134] S. Kretzer, Phys. Rev. **D62**, 054001 (2000), [hep-ph/0003177].

[135] L. Bourhis *et al.*, Eur. Phys. J. **C19**, 89 (2001), [hep-ph/0009101].

[136] M. Hirai *et al.*, Phys. Rev. **D75**, 094009 (2007), [hep-ph/0702250].

[137] C. A. Aidala *et al.*, Phys. Rev. **D83**, 034002 (2011), [arXiv:1009.6145].

[138] D. de Florian *et al.*, Phys. Rev. **D91**, 1, 014035 (2015), [arXiv:1410.6027].

[139] D. de Florian *et al.*, Phys. Rev. **D95**, 9, 094019 (2017), [arXiv:1702.06353].

[140] D. de Florian, R. Sassot and M. Stratmann, Phys. Rev. **D75**, 114010 (2007), [hep-ph/0703242].

[141] D. P. Anderle, F. Ringer and M. Stratmann, Phys. Rev. **D92**, 11, 114017 (2015), [arXiv:1510.05845].

[142] E. Leader, A. V. Sidorov and D. B. Stamenov, Phys. Rev. **D93**, 7, 074026 (2016), [arXiv:1506.06381].

Downloaded from https://academic.oup.com/ptep/article/2022/8/083C01/6651666 by KIT Library user on 27 September 2022

[143] R. A. Khalek, V. Bertone and E. R. Nocera (2021), [arXiv:2105.08725].

[144] H. Abdolmaleki *et al.* (xFitter) (2021), [arXiv:2105.11306].

[145] V. Bertone *et al.* (NNPDF), Eur. Phys. J. **C78**, 8, 651 (2018), [arXiv:1807.03310].

[146] R. Barate *et al.* (ALEPH), Eur. Phys. J. **C17**, 1 (2000); R. Akers *et al.* (OPAL), Z. Phys. **C68**, 179 (1995); G. Abbiendi *et al.* (OPAL), Eur. Phys. J. **C11**, 217 (1999), [hep-ex/9903027].

[147] K. Abe *et al.* (SLD), Phys. Rev. **D59**, 052001 (1999), [hep-ex/9805029].

[148] D. Buskulic *et al.* (ALEPH), Z. Phys. **C66**, 355 (1995); H. Albrecht *et al.* (ARGUS), Z. Phys. **C44**, 547 (1989); R. Akers *et al.* (OPAL), Z. Phys. **C63**, 181 (1994).

[149] M. R. Adams *et al.* (E665), Z. Phys. **C61**, 539 (1994).

[150] M. Arneodo *et al.* (European Muon), Z. Phys. **C34**, 283 (1987).

[151] S. Aid *et al.* (H1), Nucl. Phys. **B480**, 3 (1996), [hep-ex/9607010].

[152] J. J. Aubert *et al.* (European Muon), Z. Phys. **C18**, 189 (1983).

[153] A. Airapetian *et al.* (HERMES), Eur. Phys. J. **C21**, 599 (2001), [hep-ex/0104004].

[154] T. P. McPharlin *et al.*, Phys. Lett. **90B**, 479 (1980).

[155] S. S. Adler *et al.* (PHENIX), Phys. Rev. Lett. **91**, 241803 (2003), [hep-ex/0304038].

[156] B. Abelev *et al.* (ALICE), Phys. Lett. **B717**, 162 (2012), [arXiv:1205.5724].

[157] M. Bonesini *et al.* (WA70), Z. Phys. **C38**, 371 (1988).

[158] T. Akesson *et al.* (Axial Field Spectrometer), Sov. J. Nucl. Phys. **51**, 836 (1990), [Yad. Fiz.51,1314(1990)].

[159] C. Kourkoumelis *et al.*, Z. Phys. **C5**, 95 (1980).

[160] L. Apanasevich *et al.* (Fermilab E706), Phys. Rev. **D68**, 052001 (2003), [hep-ex/0204031].

[161] F. Abe *et al.* (CDF), Phys. Rev. Lett. **61**, 1819 (1988).

[162] M. Banner *et al.* (UA2), Phys. Lett. **115B**, 59 (1982).

[163] M. Procura and I. W. Stewart, Phys. Rev. **D81**, 074009 (2010), [Erratum: Phys. Rev.D83,039902(2011)], [arXiv:0911.4980].

[164] A. Jain, M. Procura and W. J. Waalewijn, JHEP **05**, 035 (2011), [arXiv:1101.4953].

[165] M. Procura and W. J. Waalewijn, Phys. Rev. **D85**, 114041 (2012), [arXiv:1111.6605].

[166] F. Arleo *et al.*, JHEP **04**, 147 (2014), [arXiv:1311.7356].

[167] M. Ritzmann and W. J. Waalewijn, Phys. Rev. **D90**, 5, 054029 (2014), [arXiv:1407.3272].

[168] T. Kaufmann, A. Mukherjee and W. Vogelsang, Phys. Rev. **D92**, 5, 054015 (2015), [arXiv:1506.01415].

[169] Y.-T. Chien *et al.*, JHEP **05**, 125 (2016), [arXiv:1512.06851].

[170] F. Abe *et al.* (CDF), Phys. Rev. Lett. **65**, 968 (1990).

[171] T. A. collaboration (ATLAS) (2015).

[172] S. Chatrchyan *et al.* (CMS), JHEP **10**, 087 (2012), [arXiv:1205.5872].

[173] X. Lu (ALICE), Nucl. Phys. **A931**, 428 (2014), [arXiv:1407.8385].

[174] C. Bianchin (ALICE), J. Phys. Conf. Ser. **612**, 1, 012020 (2015).

[175] F. Krizek (ALICE), J. Phys. Conf. Ser. **668**, 1, 012018 (2016), [arXiv:1509.02024].

[176] M. Aaboud *et al.* (ATLAS), Nucl. Phys. **A978**, 65 (2018), [arXiv:1706.02859].

[177] L. Adamczyk *et al.* (STAR), Phys. Rev. **D97**, 3, 032004 (2018), [arXiv:1708.07080].

[178] D. P. Anderle *et al.*, Phys. Rev. **D96**, 3, 034028 (2017), [arXiv:1706.09857].

[179] N. Sato *et al.* (JAM) (2019), [arXiv:1905.03788].

[180] M. Epele *et al.*, Phys. Rev. **D86**, 074028 (2012), [arXiv:1209.3240].

[181] E. Witten, Nucl. Phys. **210**, 189 (1977).

[182] L. Bourhis, M. Fontannaz and J. P. Guillet, Eur. Phys. J. **C2**, 529 (1998), [hep-ph/9704447].

[183] M. Gluck, E. Reya and A. Vogt, Phys. Rev. **D48**, 116 (1993), [Erratum: Phys. Rev.D51,1427(1995)]; Erratum *ibid.* **D51**, 1427 (1995).

[184] G. Abbiendi *et al.* (OPAL), Eur. Phys. J. **C27**, 467 (2003), [hep-ex/0209048].

[185] G. Bocquet *et al.*, Phys. Lett. **B366**, 434 (1996).

[186] T. Kaufmann, A. Mukherjee and W. Vogelsang, Phys. Rev. **D93**, 11, 114021 (2016), [arXiv:1604.07175].

[187] P. Abreu *et al.* (DELPHI), Eur. Phys. J. **C13**, 573 (2000).

[188] B. A. Kniehl, G. Kramer and B. Potter, Phys. Rev. Lett. **85**, 5288 (2000), [hep-ph/0003297].

[189] M. Arneodo *et al.* (European Muon), Z. Phys. **C33**, 167 (1986).

[190] A. Airapetian *et al.* (HERMES), Phys. Rev. **D87**, 074029 (2013), [arXiv:1212.5407].

[191] C. Adolph *et al.* (COMPASS), Phys. Lett. **B764**, 1 (2017), [arXiv:1604.02695].

[192] F. D. Aaron *et al.* (H1), Phys. Lett. **B673**, 119 (2009), [arXiv:0901.0477].

[193] M. Derrick *et al.* (ZEUS), Z. Phys. **C68**, 29 (1995), [hep-ex/9505011].

[194] S. Chekanov *et al.* (ZEUS), Phys. Lett. **B553**, 141 (2003), [hep-ex/0211025].

[195] S. Chekanov *et al.* (ZEUS), Nucl. Phys. **B786**, 181 (2007), [arXiv:0705.3770].

[196] F. D. Aaron *et al.* (H1), Eur. Phys. J. **C61**, 185 (2009), [arXiv:0810.4036].

[197] A. Aktas *et al.* (H1), Eur. Phys. J. **C36**, 413 (2004), [hep-ex/0403056].

[198] P. Dixon, D. Kant and G. Thompson, J. Phys. **G25**, 1453 (1999).

[199] C. Adloff *et al.* (H1), Phys. Lett. **B462**, 440 (1999), [hep-ex/9907030].

[200] D. Graudenz, Fortsch. Phys. **45**, 629 (1997), [hep-ph/9701334].

[201] P. M. Nadolsky, D. R. Stump and C. P. Yuan, Phys. Rev. **D61**, 014003 (2000), [Erratum: Phys. Rev.D64,059903(2001)], [hep-ph/9906280].

[202] D. de Florian *et al.*, Phys. Rev. **D95**, 0334027 (2017).

[203] T. Aaltonen *et al.* (CDF), Phys. Rev. **D79**, 112005 (2009), [Erratum: Phys. Rev.D82,119903(2010)], [arXiv:0904.1098].

[204] G. Aad *et al.* (ATLAS), New J. Phys. **13**, 053033 (2011), [arXiv:1012.5104].

[205] B. I. Abelev *et al.* (STAR), Phys. Rev. **C75**, 064901 (2007), [arXiv:nucl-ex/0607033].

[206] K. Aamodt *et al.* (ALICE), Eur. Phys. J. **C71**, 1655 (2011), [arXiv:1101.4110].

[207] B. B. Abelev *et al.* (ALICE), Phys. Lett. **B736**, 196 (2014), [arXiv:1401.1250].

[208] J. Adam *et al.* (ALICE), Eur. Phys. J. **C75**, 5, 226 (2015), [arXiv:1504.00024].

[209] S. Chatrchyan *et al.* (CMS), Eur. Phys. J. **C72**, 2164 (2012), [arXiv:1207.4724].

Downloaded from https://academic.oup.com/ptep/article/2022/8/083C01/6651666 by KIT Library user on 27 September 2022

[210] A. M. Sirunyan *et al.* (CMS), Phys. Rev. **D96**, 11, 112003 (2017), [arXiv:1706.10194].

[211] G. J. Alner *et al.* (UA5), Z. Phys. **C32**, 153 (1986).

[212] B. Abelev *et al.* (ALICE), Eur. Phys. J. **C73**, 6, 2456 (2013), [arXiv:1208.4968].

[213] G. Antchev *et al.* (TOTEM), EPL **101**, 2, 21004 (2013).

[214] A. M. Sirunyan *et al.* (CMS), JHEP **07**, 161 (2018), [arXiv:1802.02613].

[215] F. Abe *et al.* (CDF), Phys. Rev. **D50**, 5550 (1994).

[216] F. Abe *et al.* (CDF), Phys. Rev. **D50**, 5518 (1994).

[217] S. S. Adler *et al.* (PHENIX), Phys. Rev. **C74**, 024904 (2006), [arXiv:nucl-ex/0603010].

[218] S. Albino *et al.*, Phys. Rev. **D75**, 034018 (2007), [hep-ph/0611029].

[219] I. Borsa, R. Sassot and M. Stratmann, Phys. Rev. **D96**, 9, 094020 (2017), [arXiv:1708.01630].

[220] B. Andersson *et al.*, Phys. Rept. **97**, 31 (1983).

[221] T. Sjostrand and M. Bengtsson, Comput. Phys. Commun. **43**, 367 (1987); T. Sjostrand, Comput. Phys. Commun. **82**, 74 (1994).

[222] P. D. Acton *et al.* (OPAL), Phys. Lett. **B305**, 407 (1993).

[223] J. Breitweg *et al.* (ZEUS), Eur. Phys. J. **C2**, 77 (1998), [hep-ex/9711018].

[224] D. DeProspo *et al.* (E632), Phys. Rev. **D50**, 6691 (1994).

[225] S. Chekanov *et al.* (ZEUS), Eur. Phys. J. **C51**, 1 (2007), [hep-ex/0612023].

[226] G. Grindhammer *et al.*, in: *Proceedings of the Workshop on Monte Carlo Generators for HERA Physics*, Hamburg, Germany, 1998/1999.

[227] N. Brook *et al.*, in: *Proceedings of the Workshop for Future HERA Physics at HERA*, Hamburg, Germany, 1996.

[228] D. Acosta *et al.* (CDF), Phys. Rev. **D72**, 052001 (2005), [hep-ex/0504048].

[229] G. Arnison *et al.* (UA1), Phys. Lett. **118B**, 167 (1982).

[230] M. Banner *et al.* (UA2), Phys. Lett. **122B**, 322 (1983).

[231] M. Banner *et al.* (UA2, Bern-CERN-Copenhagen-Orsay-Pavia-Saclay), Z. Phys. **C27**, 329 (1985).

[232] A. Adare *et al.* (PHENIX), Phys. Rev. **D76**, 051106 (2007), [arXiv:0704.3599].

[233] A. Adare *et al.* (PHENIX), Phys. Rev. **D83**, 032001 (2011), [arXiv:1009.6224].

[234] A. Adare *et al.* (PHENIX), Phys. Rev. **D86**, 092006 (2012), [arXiv:1202.4020].

[235] A. Adare *et al.* (PHENIX), Phys. Rev. **D88**, 3, 032006 (2013), [arXiv:1209.3283].

[236] A. Adare *et al.* (PHENIX), Phys. Rev. **D91**, 3, 032001 (2015), [arXiv:1409.1907].

[237] A. Adare *et al.* (PHENIX), Phys. Rev. **D90**, 7, 072008 (2014), [arXiv:1406.3541].

[238] A. Adare *et al.* (PHENIX), Phys. Rev. **D93**, 1, 011501 (2016), [arXiv:1510.02317].

[239] I. Arsene *et al.* (BRAHMS), Phys. Rev. Lett. **98**, 252001 (2007), [hep-ex/0701041].

[240] J. Adams *et al.* (STAR), Phys. Rev. Lett. **97**, 152302 (2006), [arXiv:nucl-ex/0602011].

[241] J. Adams *et al.* (STAR), Phys. Lett. **B637**, 161 (2006), [arXiv:nucl-ex/0601033].

[242] B. I. Abelev *et al.* (STAR), Phys. Rev. **D80**, 111108 (2009), [arXiv:0911.2773].

[243] G. Agakishiev *et al.* (STAR), Phys. Rev. Lett. **108**, 072302 (2012), [arXiv:1110.0579].

[244] L. Adamczyk *et al.* (STAR), Phys. Rev. **D89**, 1, 012001 (2014), [arXiv:1309.1800].

[245] B. B. Abelev *et al.* (ALICE), Eur. Phys. J. **C73**, 12, 2662 (2013), [arXiv:1307.1093].

[246] L. Apanasevich *et al.* (Fermilab E706), Phys. Rev. Lett. **81**, 2642 (1998), [hep-ex/9711017].

[247] G. Ballocchi *et al.* (UA6), Phys. Lett. **B436**, 222 (1998).

[248] K. Aamodt *et al.* (ALICE), Eur. Phys. J. **C71**, 1594 (2011), [arXiv:1012.3257].

[249] R. Aaij *et al.* (LHCb), Phys. Lett. **B703**, 267 (2011), [arXiv:1107.3935].

[250] G. Aad *et al.* (ATLAS), Phys. Lett. **B758**, 67 (2016), [arXiv:1602.01633].

[251] F. Aversa *et al.*, Nucl. Phys. **B327**, 105 (1989); D. de Florian, Phys. Rev. **D67**, 054004 (2003), [hep-ph/0210442]; B. Jager *et al.*, Phys. Rev. **D67**, 054005 (2003), [hep-ph/0211007].

[252] U. Baur *et al.*, in "QCD and weak boson physics in Run II. Proceedings, Batavia, USA, March 4-6, June 3-4, November 4-6, 1999," 115–164 (2000), [,115(2000)], [hep-ph/0005226], URL `http://lss.fnal.gov/archive/preprint/fermilab-conf-00-411-ae.shtml`.

[253] P. Aurenche *et al.*, Eur. Phys. J. **C13**, 347 (2000), [hep-ph/9910252].

[254] L. Apanasevich *et al.*, Phys. Rev. **D59**, 074007 (1999), [hep-ph/9808467].

[255] U. D'Alesio and F. Murgia, Phys. Rev. **D70**, 074009 (2004), [hep-ph/0408092].

[256] D. de Florian and W. Vogelsang, Phys. Rev. **D71**, 114004 (2005), [hep-ph/0501258].

[257] P. Hinderer *et al.*, Phys. Rev. **D99**, 5, 054019 (2019), [arXiv:1812.00915].

[258] D. d'Enterria *et al.*, Nucl. Phys. **B883**, 615 (2014), [arXiv:1311.1415].

[259] G. Wilk and Z. Wlodarczyk, Eur. Phys. J. **A40**, 299 (2009), [arXiv:0810.2939].

[260] C. Tsallis, J. Statist. Phys. **52**, 479 (1988).

[261] C. Tsallis, Braz. J. Phys. **29**, 1 (1999).

[262] C. Tsallis, Eur. Phys. J. **A40**, 257 (2009), [arXiv:0812.4370].

[263] M. D. Azmi and J. Cleymans, J. Phys. **G41**, 065001 (2014), [arXiv:1401.4835].

[264] G. Wilk and Z. Wlodarczyk, Phys. Rev. Lett. **84**, 2770 (2000), [hep-ph/9908459].

[265] T. Bhattacharyya *et al.*, J. Phys. **G45**, 5, 055001 (2018), [arXiv:1709.07376].

[266] S. Grigoryan, Phys. Rev. **D95**, 5, 056021 (2017), [arXiv:1702.04110].

[267] T. Wibig, Int. J. Mod. Phys. **A29**, 1450021 (2014).

[268] K. Saraswat, P. Shukla and V. Singh, J. Phys. Comm. **2**, 3, 035003 (2018), [arXiv:1706.04860].

[269] K. Urmossy, G. G. Barnafoldi and T. S. Biro, Phys. Lett. **B701**, 111 (2011), [arXiv:1101.3023].

[270] A. S. Parvan, O. V. Teryaev and J. Cleymans, Eur. Phys. J. **A53**, 5, 102 (2017), [arXiv:1607.01956].

[271] K. Adcox *et al.* (PHENIX), Phys. Rev. Lett. **88**, 022301 (2002), [arXiv:nucl-ex/0109003]; C. Adler *et al.* (STAR), Phys. Rev. Lett. **90**, 082302 (2003), [arXiv:nucl-ex/0210033].

[272] V.A. Khoze *et al.*, *Proceedings, Conference on High-Energy Physics, Tbilisi 1976*; J. D. Bjorken, Phys. Rev. **D17**, 171 (1978).

[273] M. Artuso *et al.* (CLEO), Phys. Rev. **D70**, 112001 (2004), [hep-ex/0402040].

[274] R. Seuster *et al.* (Belle), Phys. Rev. **D73**, 032002 (2006), [hep-ex/0506068].

Downloaded from https://academic.oup.com/ptep/article/2022/8/083C01/6651666 by KIT Library user on 27 September 2022

[275] A. Heister *et al.* (ALEPH), Phys. Lett. **B512**, 30 (2001), [hep-ex/0106051]; J. Abdallah *et al.* (DELPHI), Eur. Phys. J. **C71**, 1557 (2011), [arXiv:1102.4748]; G. Abbiendi *et al.* (OPAL), Eur. Phys. J. **C29**, 463 (2003), [hep-ex/0210031]; K. Abe *et al.* (SLD), Phys. Rev. **D65**, 092006 (2002), [Erratum: Phys. Rev.D66,079905(2002)], [hep-ex/0202031].

[276] B. Mele and P. Nason, Phys. Lett. **B245**, 635 (1990); B. Mele and P. Nason, Nucl. Phys. **B361**, 626 (1991), [Erratum: Nucl. Phys.B921,841(2017)].

[277] M. Cacciari and S. Catani, Nucl. Phys. **B617**, 253 (2001), [hep-ph/0107138].

[278] P. Nason and C. Oleari, Phys. Lett. **B418**, 199 (1998), [hep-ph/9709358]; P. Nason and C. Oleari, Phys. Lett. **B447**, 327 (1999), [hep-ph/9811206]; P. Nason and C. Oleari, Nucl. Phys. **B565**, 245 (2000), [hep-ph/9903541].

[279] K. Melnikov and A. Mitov, Phys. Rev. **D70**, 034027 (2004), [hep-ph/0404143].

[280] C. Peterson *et al.*, Phys. Rev. **D27**, 105 (1983).

[281] V. G. Kartvelishvili, A. K. Likhoded and V. A. Petrov, Phys. Lett. **78B**, 615 (1978).

[282] P. D. B. Collins and T. P. Spiller, J. Phys. **G11**, 1289 (1985).

[283] G. Colangelo and P. Nason, Phys. Lett. **B285**, 167 (1992).

[284] M. G. Bowler, Z. Phys. **C11**, 169 (1981).

[285] E. Braaten *et al.*, Phys. Rev. **D51**, 4819 (1995), [hep-ph/9409316].

[286] R. Akers *et al.* (OPAL), Z. Phys. **C67**, 27 (1995).

[287] H. Albrecht *et al.* (ARGUS), Z. Phys. **C52**, 353 (1991).

[288] D. Buskulic *et al.* (ALEPH), Phys. Lett. **B357**, 699 (1995).

[289] J. Chrin, Z. Phys. **C36**, 163 (1987).

[290] R. L. Jaffe and L. Randall, Nucl. Phys. **B412**, 79 (1994), [hep-ph/9306201].

[291] M. Cacciari and E. Gardi, Nucl. Phys. **B664**, 299 (2003), [hep-ph/0301047].

[292] L. Randall and N. Rius, Nucl. Phys. **B441**, 167 (1995), [hep-ph/9405217].

[293] J. C. Collins, Phys. Rev. **D58**, 094002 (1998), [hep-ph/9806259].

[294] B. A. Kniehl *et al.*, Eur. Phys. J. **C41**, 199 (2005), [hep-ph/0502194].

[295] S. Ahmed *et al.* (CLEO), Phys. Rev. **D62**, 112003 (2000), [hep-ex/0008015].

[296] B. Aubert *et al.* (BaBar), Phys. Rev. **D65**, 091104 (2002), [hep-ex/0201041].

[297] D. Bortoletto *et al.* (CLEO), Phys. Rev. **D37**, 1719 (1988), [Erratum: Phys. Rev.D39,1471(1989)].

[298] H. Albrecht *et al.* (ARGUS), Z. Phys. **C54**, 1 (1992).

[299] G. Alexander *et al.* (OPAL), Z. Phys. **C69**, 543 (1996).

[300] A. Heister *et al.* (ALEPH), Phys. Lett. **B561**, 213 (2003), [hep-ex/0302003].

[301] F. D. Aaron *et al.* (H1), Eur. Phys. J. **C65**, 89 (2010), [arXiv:0907.2643].

[302] S. Chekanov *et al.* (ZEUS), JHEP **07**, 074 (2007), [arXiv:0704.3562]; ZEUS Collab: H. Abramowicz *et al.*, JHEP , 1309 (2013); A. Aktas *et al.* (H1), Eur. Phys. J. **C51**, 271 (2007), [hep-ex/0701023]; F. D. Aaron *et al.* (H1), Eur. Phys. J. **C59**, 589 (2009), [arXiv:0808.1003].

[303] B. Adeva *et al.* (L3), Phys. Lett. **B261**, 177 (1991).

[304] O. Biebel, P. Nason and B. R. Webber (2001), [hep-ph/0109282].

[305] H. Evans (ALICE, ATLAS, CMS, LHCb), in "Proceedings, 14th International Conference on Hadron spectroscopy (Hadron 2011): Munich, Germany, June 13-17, 2011," (2011), [arXiv:1110.5294]; E. Aguilo, in "Proceedings, 47th Rencontres de Moriond on QCD and High Energy Interactions: La Thuile, France, March 10-17, 2012," 115–120 (2012), [arXiv:1205.5678]; F. Simonetto, Journal of Physics: Conference Series **347**, 012014 (2012).

[306] V. Khachatryan *et al.* (CMS), JHEP **03**, 136 (2011), [arXiv:1102.3194]; G. Aad *et al.* (ATLAS), Eur. Phys. J. **C71**, 1846 (2011), [arXiv:1109.6833]; S. Chatrchyan *et al.* (CMS), JHEP **04**, 084 (2012), [arXiv:1202.4617]; G. Aad *et al.* (ATLAS), Eur. Phys. J. **C73**, 2, 2301 (2013), [arXiv:1210.0441].

[307] H. Jung *et al.*, Phys. Rev. **D85**, 034035 (2012), [arXiv:1111.1942].

[308] D. Acosta *et al.* (CDF), Phys. Rev. Lett. **91**, 241804 (2003), [hep-ex/0307080]; D. Acosta *et al.* (CDF), Phys. Rev. **D71**, 032001 (2005), [hep-ex/0412071].

[309] M. Cacciari and P. Nason, JHEP **09**, 006 (2003), [hep-ph/0306212]; M. Cacciari *et al.*, JHEP **07**, 033 (2004), [hep-ph/0312132]; B. A. Kniehl *et al.*, Phys. Rev. Lett. **96**, 012001 (2006), [hep-ph/0508129].

[310] H. Abramowicz *et al.* (ZEUS), Eur. Phys. J. **C71**, 1573 (2011), [arXiv:1101.3692].

[311] S. Chekanov *et al.* (ZEUS), Phys. Rev. **D78**, 072001 (2008), [arXiv:0805.4390].

[312] S. Chekanov *et al.* (ZEUS), JHEP **02**, 032 (2009), [arXiv:0811.0894].

[313] F. D. Aaron *et al.* (H1), Eur. Phys. J. **C72**, 2148 (2012), [arXiv:1206.4346].

[314] M. L. Mangano and P. Nason, Phys. Lett. **B285**, 160 (1992).

[315] M. H. Seymour, Nucl. Phys. **B436**, 163 (1995).

[316] D. J. Miller and M. H. Seymour, Phys. Lett. **B435**, 213 (1998), [hep-ph/9805414].

[317] R. Barate *et al.* (ALEPH), Phys. Lett. **B434**, 437 (1998).

[318] P. Abreu *et al.* (DELPHI), Phys. Lett. **B405**, 202 (1997).

[319] M. Acciarri *et al.* (L3), Phys. Lett. **B476**, 243 (2000), [hep-ex/9911016].

[320] G. Abbiendi *et al.* (OPAL), Eur. Phys. J. **C13**, 1 (2000), [hep-ex/9908001].

[321] K. Abe *et al.* (SLD) (1999), [hep-ex/9908028], URL `http://www-public.slac.stanford.edu/sciDoc/docMeta.aspx?slacPubNumber=SLAC-PUB-8157`.

[322] C. Albajar *et al.* (UA1 Collaboration), Z. Phys. C **61**, 41 (1993), URL `http://cds.cern.ch/record/253028`.

[323] R. Aaij *et al.* (LHCb), JHEP **11**, 030 (2017), [arXiv:1708.05994].

[324] M. Aaboud *et al.* (ATLAS), Phys. Rev. **D99**, 5, 052004 (2019), [arXiv:1812.09283].

[325] M. Burkardt and R. L. Jaffe, Phys. Rev. Lett. **70**, 2537 (1993), [hep-ph/9302232].

[326] P. J. Mulders and R. D. Tangerman, Nucl. Phys. **B461**, 197 (1996), [Erratum: Nucl. Phys.B484,538(1997)], [hep-ph/9510301].

[327] R. Jakob, Nucl. Phys. **A711**, 35 (2002), [hep-ph/0206271].

[328] D. de Florian, M. Stratmann and W. Vogelsang, Phys. Rev. Lett. **81**, 530 (1998), [hep-ph/9802432].

[329] D. Buskulic *et al.* (ALEPH), Phys. Lett. **B374**, 319 (1996).

[330] K. Ackerstaff *et al.* (OPAL), Eur. Phys. J. **C2**, 49 (1998), [hep-ex/9708027].

[331] G. Abbiendi *et al.* (OPAL), Phys. Lett. **B444**, 539 (1998), [hep-ex/9808006].

[332] M. Alekseev *et al.* (COMPASS), Eur. Phys. J. **C64**, 171 (2009), [arXiv:0907.0388].

[333] A. Airapetian *et al.* (HERMES), Phys. Rev. **D74**, 072004 (2006), [hep-ex/0607004].

[334] G. Karyan (HERMES), Int. J. Mod. Phys. Conf. Ser. **40**, 1660067 (2016).

[335] J. Adam *et al.* (STAR), Phys. Rev. **D98**, 11, 112009 (2018), [arXiv:1808.07634].

Downloaded from https://academic.oup.com/ptep/article/2022/8/083C01/6651666 by KIT Library user on 27 September 2022

[336] R. L. Jaffe, Phys. Rev. **D54**, 11, R6581 (1996), [hep-ph/9605456].

[337] A. Airapetian *et al.* (HERMES), Phys. Rev. **D76**, 092008 (2007), [arXiv:0704.3133].

[338] A. Moretti (COMPASS), PoS **SPIN2018**, 138 (2018), [arXiv:1901.01735].

[339] L. Gamberg *et al.*, Phys. Lett. B **818**, 136371 (2021), [arXiv:2102.05553].

[340] R. Seidl *et al.* (Belle), Phys. Rev. **D99**, 11, 112006 (2019), [arXiv:1902.01552].

[341] C. Adolph *et al.* (COMPASS), Eur. Phys. J. **C73**, 8, 2531 (2013), [Erratum: Eur. Phys. J.C75,no.2,94(2015)], [arXiv:1305.7317].

[342] A. Signori *et al.*, JHEP **11**, 194 (2013), [arXiv:1309.3507].

[343] M. Anselmino *et al.*, JHEP **04**, 005 (2014), [arXiv:1312.6261].

[344] M. G. Echevarria *et al.*, Phys. Rev. **D89**, 074013 (2014), [arXiv:1401.5078].

[345] M. G. Echevarria, I. Scimemi and A. Vladimirov, Phys. Rev. **D93**, 1, 011502 (2016), [Erratum: Phys. Rev.D94,no.9,099904(2016)], [arXiv:1509.06392].

[346] M. G. Echevarria, I. Scimemi and A. Vladimirov, JHEP **09**, 004 (2016), [arXiv:1604.07869].

[347] A. Bacchetta *et al.*, JHEP **06**, 081 (2017), [Erratum: JHEP06,051(2019)], [arXiv:1703.10157].

[348] M. A. Ebert, B. Mistlberger and G. Vita, JHEP **07**, 121 (2021), [arXiv:2012.07853].

[349] M.-x. Luo *et al.*, JHEP **06**, 115 (2021), [arXiv:2012.03256].

[350] J. C. Collins, Nucl. Phys. **B396**, 161 (1993), [hep-ph/9208213].

[351] J. P. Ralston and D. E. Soper, Nucl. Phys. **B152**, 109 (1979).

[352] H. Avakian *et al.* (CLAS), Phys. Rev. **D69**, 112004 (2004), [hep-ex/0301005].

[353] A. Airapetian *et al.* (HERMES), Phys. Rev. Lett. **84**, 4047 (2000), [hep-ex/9910062].

[354] A. Airapetian *et al.* (HERMES), Phys. Rev. **D64**, 097101 (2001), [hep-ex/0104005].

[355] A. Airapetian *et al.* (HERMES), Phys. Rev. Lett. **94**, 012002 (2005), [hep-ex/0408013].

[356] A. Airapetian *et al.* (HERMES), Phys. Lett. **B693**, 11 (2010), [arXiv:1006.4221].

[357] V. Yu. Alexakhin *et al.* (COMPASS), Phys. Rev. Lett. **94**, 202002 (2005), [hep-ex/0503002].

[358] E. S. Ageev *et al.* (COMPASS), Nucl. Phys. **B765**, 31 (2007), [hep-ex/0610068].

[359] M. Alekseev *et al.* (COMPASS), Phys. Lett. **B673**, 127 (2009), [arXiv:0802.2160].

[360] M. G. Alekseev *et al.* (COMPASS), Phys. Lett. **B692**, 240 (2010), [arXiv:1005.5609].

[361] M. G. Alekseev *et al.* (COMPASS), Eur. Phys. J. **C70**, 39 (2010), [arXiv:1007.1562].

[362] C. Adolph *et al.* (COMPASS), Phys. Lett. **B717**, 376 (2012), [arXiv:1205.5121].

[363] C. Adolph *et al.* (COMPASS), Phys. Lett. **B744**, 250 (2015), [arXiv:1408.4405].

[364] K. Abe *et al.* (Belle), Phys. Rev. Lett. **96**, 232002 (2006), [hep-ex/0507063].

[365] R. Seidl *et al.* (Belle), Phys. Rev. **D78**, 032011 (2008), [Erratum: Phys. Rev.D86,039905(2012)], [arXiv:0805.2975].

[366] J. P. Lees *et al.* (BaBar), Phys. Rev. **D90**, 5, 052003 (2014), [arXiv:1309.5278].

[367] J. P. Lees *et al.* (BaBar), Phys. Rev. **D92**, 11, 111101 (2015), [arXiv:1506.05864].

[368] M. Ablikim *et al.* (BESIII), Phys. Rev. Lett. **116**, 4, 042001 (2016), [arXiv:1507.06824].

[369] M. Anselmino *et al.*, Phys. Rev. **D92**, 11, 114023 (2015), [arXiv:1510.05389].

[370] Z.-B. Kang *et al.*, Phys. Rev. **D93**, 1, 014009 (2016), [arXiv:1505.05589].

[371] F. Yuan, Phys. Rev. Lett. **100**, 032003 (2008), [arXiv:0709.3272].

[372] Z.-B. Kang *et al.*, JHEP **11**, 068 (2017), [arXiv:1705.08443].

[373] K. Konishi, A. Ukawa and G. Veneziano, Phys. Lett. **78B**, 243 (1978).

[374] I. Vendramin, Nuovo Cim. **A66**, 339 (1981).

[375] J. C. Collins, S. F. Heppelmann and G. A. Ladinsky, Nucl. Phys. **B420**, 565 (1994), [hep-ph/9305309].

[376] R. L. Jaffe, X.-m. Jin and J. Tang, Phys. Rev. Lett. **80**, 1166 (1998), [hep-ph/9709322].

[377] R. L. Jaffe, X.-m. Jin and J.-a. Tang, Phys. Rev. **D57**, 5920 (1998), [hep-ph/9710561].

[378] A. Bianconi *et al.*, Phys. Rev. **D62**, 034008 (2000), [hep-ph/9907475].

[379] M. Radici, R. Jakob and A. Bianconi, Phys. Rev. **D65**, 074031 (2002), [hep-ph/0110252].

[380] D. de Florian and L. Vanni, Phys. Lett. **B578**, 139 (2004), [hep-ph/0310196].

[381] A. Bacchetta and M. Radici, Phys. Rev. **D67**, 094002 (2003), [hep-ph/0212300].

[382] A. Vossen *et al.* (Belle), Phys. Rev. Lett. **107**, 072004 (2011), [arXiv:1104.2425].

[383] A. Courtoy *et al.*, Phys. Rev. **D85**, 114023 (2012), [arXiv:1202.0323].

[384] M. Radici *et al.*, JHEP **05**, 123 (2015), [arXiv:1503.03495].

[385] A. Airapetian *et al.* (HERMES), JHEP **06**, 017 (2008), [arXiv:0803.2367].

[386] C. Adolph *et al.* (COMPASS), Phys. Lett. **B713**, 10 (2012), [arXiv:1202.6150].

[387] C. Adolph *et al.* (COMPASS), Phys. Lett. **B736**, 124 (2014), [arXiv:1401.7873].

[388] L. Adamczyk *et al.* (STAR), Phys. Rev. Lett. **115**, 242501 (2015), [arXiv:1504.00415].

[389] A. Bacchetta, A. Courtoy and M. Radici, Phys. Rev. Lett. **107**, 012001 (2011), [arXiv:1104.3855].

[390] A. Bacchetta, A. Courtoy and M. Radici, JHEP **03**, 119 (2013), [arXiv:1212.3568].

[391] M. Radici and A. Bacchetta, Phys. Rev. Lett. **120**, 19, 192001 (2018), [arXiv:1802.05212].

Downloaded from https://academic.oup.com/ptep/article/2022/8/083C01/6651666 by KIT Library user on 27 September 2022

20. High Energy Soft QCD and Diffraction

Written February 2020 by V.A. Khoze (Durham U.), M.G. Ryskin (Petersburg Nuclear Phys. Inst.) and M. Taševský (Prague, Inst. Phys.).

20.1 Introduction

Despite the enormous successes of Quantum Chromodynamics (QCD) (see Section 9 in [1] and [2]) there remain a number of deep questions to be answered in the domain of strong interaction physics. These concern first of all small momentum transfer processes which are generically called soft interactions.

One of the most challenging problems is the high-energy behaviour of hadronic scattering processes. At high collision energies, $\sqrt{s}$, soft interactions play a dominant role. Unfortunately, soft interactions cannot be described in terms of perturbative QCD. These are non-perturbative phenomena related to confinement which are generally considered in the context of the analytic S-matrix, based on *first principles*, such as analyticity, crossing symmetry and unitarity of partial waves, see e.g. [3, 4]. At high energies the most self-consistent way to perform the calculations and to describe the data is the Regge approach (see for example [5–7]), which will be considered below. As discussed in Section 20.5, this formalism could be smoothly matched with perturbative QCD calculations at larger transverse momenta. Therefore, here we will concentrate on the properties of high energy soft interactions that can be expected from the extension of the perturbative QCD domain.

The main aim of this review is to present the well-established theoretical framework, based on Regge theory and QCD, used for describing high-energy collisions. A limited number of some new experimental results, mainly from the LHC, are shown in order to demonstrate that the gross features of the data are in agreement with this approach. We are not focussing on any particular phenomenological or Monte Carlo model, which are covered in the dedicated reviews and books, see e.g. Section 43 in [1], [2, 8–14] and Chapter 2 in [15].

Typically, in multiparticle production, the secondaries[1] fill the whole available rapidity interval.[2] However, there exists an important class of events in which a large interval of rapidity (typically at least 4 units) is devoid of any hadronic activity. Such an interval is called a Large Rapidity Gap (LRG). The most frequent case with a LRG is elastic scattering. There are also events in which one of the incoming protons (or both) is transformed (dissociates) into a set of two or more final state particles with the mass $M \ll \sqrt{s}$ and proton quantum number. All these events have properties similar to those of the well-known from optics pattern of diffraction of a beam of light on an obstacle. By analogy, in high-energy physics, the corresponding processes are usually called diffractive. The classic example is the elastic scattering of hadrons on nuclei (see e.g. [16]), which manifests an angular distribution with a series of minima and maxima, analogous to the diffraction of light on a black disk. At LHC energies diffractive processes constitute up to 40% of the total (pp) cross section, $\sigma_{\rm tot}$. Therefore, we will pay special attention to the description of the elastic scattering amplitude and proton diffractive dissociation. Diffraction dissociation can be considered as a quantum mechanical process caused by the fact that different components of the incoming hadron wave function have different probabilities for interaction with a target [17]. This feature allows us to probe the transverse size of the interaction region.

Note that besides being of a fundamental interest in their own right for understanding the high energy behaviour of the QCD amplitude, there are several reasons why it is important to study soft and diffractive processes. Firstly, soft interactions unavoidably give an underlying component to rare 'hard' events, from which we hope to extract signals for New Physics. Secondly, we should be able to estimate the probability that rapidity gaps, which occur in 'hard' diffractive events, survive rescattering effects, that is, survive the population of the gaps by the secondary particles from the underlying event. Thirdly, an understanding of diffractive processes is very important for evaluation of pile-up backgrounds in high-luminosity pp collisions, which have a direct impact on various experimental measurements. Pile-up corresponds to soft independent interactions in the same bunch crossing whose number rises with increasing instantaneous luminosity. And, finally, studies of diffractive processes should help in the understanding of the structure of high-energy cosmic ray cascades, which requires a very detailed knowledge of the spectra of particles carrying a large fraction x of the incoming momentum in proton-air and nucleus-air interactions, see for instance [18].

Experimentally, diffractive processes are selected using two distinct features:

1. large regions (typically at least $\Delta\eta > 4$) in the detector are devoid of hadronic activity (LRG) and/or
2. one or both incoming particles stay intact after collision and are registered by the dedicated forward detectors placed a few hundred meters from the interaction point. The momentum loss of the initial particle, $\xi = 1 - x$, is typically smaller than 0.15.

Thus, in the case of proton-proton collisions, diffractive events correspond to elastic $pp \to pp$ scattering and to $pp \to p + X$ (Single Dissociation, SD) and $pp \to X + Y$ (Double Dissociation, DD) processes, where the + sign denotes a large rapidity gap. Note that strictly speaking in high energy physics it is impossible to define (and select) rigorously purely diffractive events. We can always have some admixture of events of different origin. As a rule we call 'diffractive' the events with sufficiently large gap (with say $\Delta y > 4$, see above) and the vacuum quantum numbers transferred across the gap. Typically at the LHC the integrated cross sections of diffractive dissociation, $\sigma_{\rm SD}$, $\sigma_{\rm DD}$, are of the order of 5–10 mb depending on the gap size. Schematic diagrams of all discussed processes are shown in Fig. 20.1.

20.2 Regge pole approach

In pre-QCD times, in order to describe the behaviour of scattering amplitudes at high energy, $\sqrt{s}$, and small momentum-transfer squared, $-t$, Regge theory was developed and successfully applied in a wide range of energies. The Regge approach [5–7] is based on the singularities of amplitudes in the complex angular momentum, j, plane.

For instance, the measured $\pi^- p \to \pi^0 n$ amplitude behaves as

$$T_{\pi p}(s,t) \propto s^{\alpha_\rho(t)}, \tag{20.1}$$

where the process is described by the exchange of the ρ-trajectory, $j = \alpha_\rho(t) \simeq 0.5 + 0.9t$ (with $t = (p_{\pi^-} - p_{\pi^0})^2$ in GeV^2). This trajectory passes through the spin-1 ρ-meson resonance in the 'crossed' t-channel $\pi^-\pi^0 \to \bar{p}n$; that is, $\alpha_\rho(t = m_\rho^2) = 1$. The corresponding cross section decreases with increasing s.

On the other hand, high-energy total and elastic pp cross sections are observed to grow slowly with energy (see e.g. Section 53 in [1]) and in terms of Regge theory are dominated by the exchange of a trajectory with vacuum quantum numbers, $\sigma_{\rm tot} \propto s^{j-1}$. The simplest possibility is to assume that the rightmost singularity in the j-plane, which drives the high-energy behaviour of the cross section, is the leading (at $t \le 0$) Regge pole at $j = \alpha(t)$. Then the pp elastic amplitude reads

$$T_{\rm el}(s,t) \propto s^{\alpha_{\mathbb{P}}(t)} \ . \tag{20.2}$$

The total cross section can then be conveniently expressed using the so called optical theorem which states that

$$s\sigma_{\rm tot} = {\rm Im}T_{\rm el}(s, t = 0), \tag{20.3}$$

as illustrated in the upper part of Fig. 20.2, and thus

$$\sigma_{\rm tot} \propto s^{\alpha_{\mathbb{P}}(0)-1}. \tag{20.4}$$

[1] Here and in what follows, we call secondaries the new particles produced in the course of the interaction.

[2] For definition of particle rapidity (pseudorapidity), see Section 49.5.2 in [1]; $y = \frac{1}{2}\ln\frac{E+p_z}{E-p_z}$ ($\eta = -\ln(\tan(\theta/2))$; the correct variable is the rapidity y, however, experimentally it is simpler to use the pseudorapidity η which does not require identifying the particles, setting $m = 0$. For $p_T \gg m$, $\eta \simeq y$.

Downloaded from https://academic.oup.com/ptep/article/2022/8/083C01/6651666 by KIT Library user on 27 September 2022

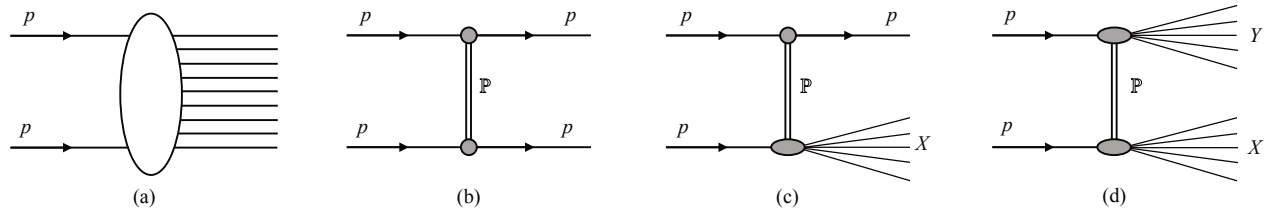

Figure 20.1: Schematic diagrams of soft pp processes. (a) non-diffractive processes, (b) elastic scattering, (c) single dissociation and (d) double dissociation. The double line corresponds to the Pomeron exchange.

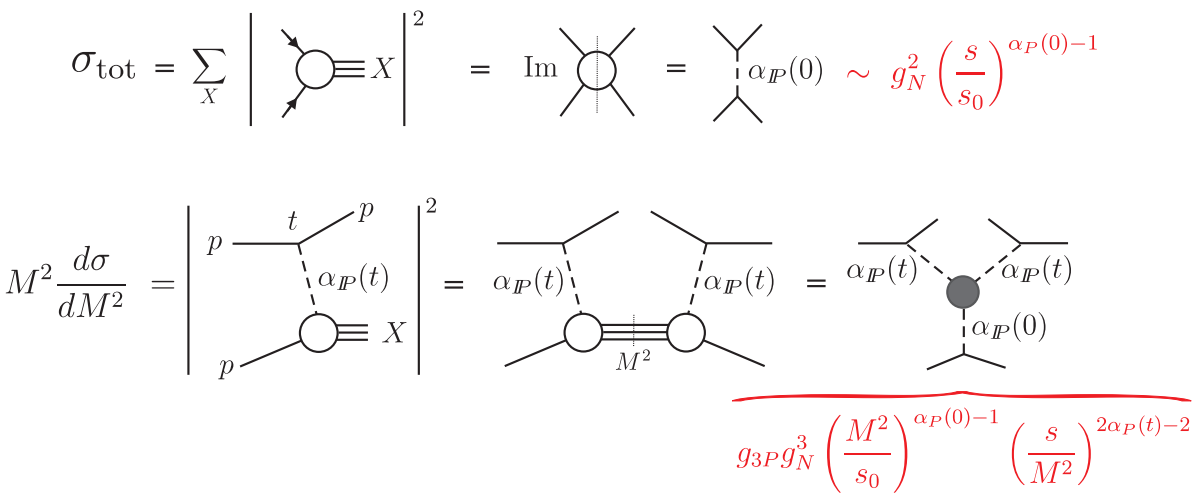

Figure 20.2: Illustration of the optical theorem for the total cross section and for high-mass diffractive dissociation in the absence of absorptive corrections.

The pole with the largest intercept, originally assumed to be $\alpha_{\mathbb{P}}(0) = 1$ since high-energy total cross sections were thought to have a constant asymptotic behaviour, is called the *Pomeron*[3]

Prior to the LHC, the energy behaviour of $pp, p\bar{p}, \pi p, Kp$ cross sections was satisfactorily reproduced by the sum of the Pomeron and secondary Reggeons (the poles at lower values of j, typically with $\alpha_\rho(0) \simeq 0.5$, see [22, 23] and Section 51 in [24]). However, above Tevatron energies the secondary Reggeon contributions (which all have intercepts $\alpha(0) \simeq 0.5$) are highly suppressed, which enables us to study the properties of the Pomeron only.

A popular parameterization of the elastic pp-scattering amplitude by Donnachie-Landshoff (DL) is the Regge form [25]

$$T_{\rm el}(s,t) = \eta_P \sigma_0 F_1^2(t) s^{\alpha_{\mathbb{P}}(t)}, \tag{20.5}$$

where $\sigma_0 = 21.7$ mb [26] and η_P is the signature factor

$$\eta_P = \frac{1 + \exp(-i\pi\alpha_{\mathbb{P}}(t))}{\sin(-\pi\alpha_{\mathbb{P}}(t))}, \tag{20.6}$$

F_1 is the Dirac electromagnetic form factor of the proton and the *effective* Pomeron trajectory

$$\alpha_{\mathbb{P}}(t) = 1 + \Delta + \alpha' t \;\simeq\; 1 + 0.0808 + 0.25t, \tag{20.7}$$

with t given in GeV^2. The intercept $\alpha_{\mathbb{P}}(0)$ just above 1 reproduces the observed slow growth of the total hadron-hadron cross sections at high energies.

However, this simple parameterization is becoming increasingly deficient at higher energies. This is because due to unitarity we have to take into account not only Regge poles, but also the cuts in the j-plane [27, 28], which correspond to the multiple exchange of Regge poles in the t-channel, see for instance [29–31]. A powerful technique to evaluate Reggeon diagrams was developed by Gribov [7, 32] (Reggeon calculus or Reggeon Field Theory (RFT)), which allows us to calculate the multi-Pomeron contributions.

[3]Pomeron pole was named after I. Y. Pomeranchuk. The history of the Pomeron is discussed in [19–21].

20.3 Theoretical description of high-energy diffraction

Diffractive processes (see e.g. reviews [33–37]) represent a rich testing ground for the dynamics of soft interactions as well as Monte Carlo models for soft hadron-hadron physics (see for reviews e.g. [8], Section 43 in [1] and Chapter 2 in [15]).

There is no universally agreed definition of diffractive processes. Theoretically, diffraction is the effect caused by the absorption of the incoming plane-wave in some region of impact parameter, b. After a decomposition of the distorted plane-wave over the outgoing momentum, q, due to absorption we arrive at some set of plane-waves with non-zero transverse momentum, $q_t \neq 0$. Experimentally, we call diffractive the events with large rapidity gaps (LRG) in the distribution of the final state particles. However, this definition is appropriate only for the events with very large gap sizes ($\Delta\eta > 4 - 5$); otherwise gaps can also be caused by fluctuations in the hadronization process [38].

In the case of proton-proton collisions, diffraction corresponds to elastic $pp \to pp$ scattering and to the $pp \to p + X$ and $pp \to X_1 + X_2$ processes where one or both protons are allowed to dissociate into a system X with the quantum numbers of the proton. The $p \to X$ dissociation is caused by the fact that the individual components of the incoming proton wave function interact differently with the target (see Section 20.3.1).

Theoretically, high-energy diffraction may be studied from either the s-channel or the t-channel viewpoint.

20.3.1 *Diffraction from the s-channel viewpoint*

Unitarity plays a central role in diffractive processes. To discuss unitarity effects it is convenient to work in terms of impact parameter, b. The total cross section is closely related to the elastic scattering amplitude and the scattering into inelastic final states via the s-channel unitarity of the S-matrix (see Sections 50 and 53 in [1]), $SS^\dagger = I$, or

$$disc\ T \equiv T - T^\dagger = iT^\dagger T \tag{20.8}$$

Downloaded from https://academic.oup.com/ptep/article/2022/8/083C01/6651666 by KIT Library user on 27 September 2022

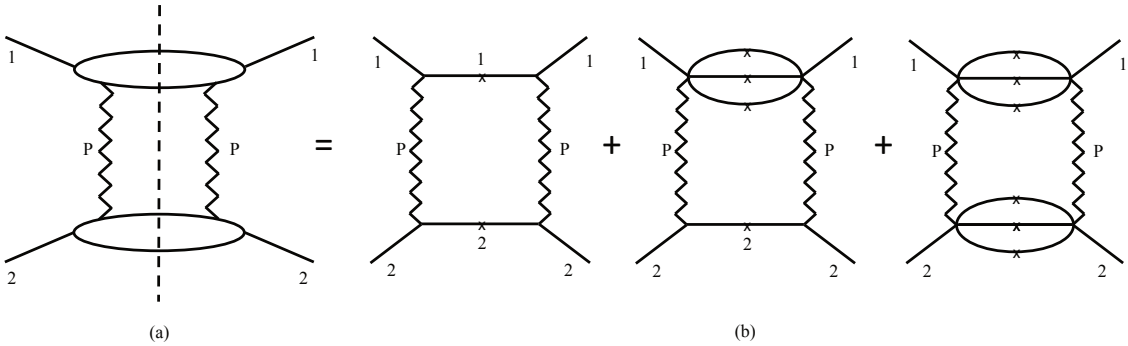

Figure 20.3: Two-Pomeron exchange in the t channel expressed as a sum over all diffractive intermediate states in the s-channel. The crosses indicate that the particles are on the mass shell.

with $S = I + iT$. If we were to focus, for example, on the unitarity for elastic and quasielastic processes, then *disc* T would simply denote a cut in s-channel between incoming and outgoing particles as visualized by crosses in Fig. 20.3.

At high energies, the s-channel unitarity relation is diagonal in the b basis such that

$$2\mathrm{Im}\, T_{\mathrm{el}}(s,b) = |T_{\mathrm{el}}(s,b)|^2 + G_{\mathrm{inel}}(s,b) \tag{20.9}$$

with

$$\sigma_{\mathrm{tot}} = 2\int d^2b\, \mathrm{Im}\, T_{\mathrm{el}}(s,b) \tag{20.10}$$

$$\sigma_{\mathrm{el}} = \int d^2b\, |T_{\mathrm{el}}(s,b)|^2 \tag{20.11}$$

$$\sigma_{\mathrm{inel}} = \int d^2b\, \left[2\mathrm{Im}\, T_{\mathrm{el}}(s,b) - |T_{\mathrm{el}}(s,b)|^2\right]. \tag{20.12}$$

The general solution of Eq. (20.9) is

$$T_{\mathrm{el}}(b) \;=\; i(1 - e^{-\Omega(\mathrm{b})/2}) \tag{20.13}$$

and

$$G_{\mathrm{inel}}(s,b) = 1 - \mathrm{e}^{-\mathrm{Re}\Omega(\mathrm{b})} = 1 - P_{\mathrm{nointer}}(s,b), \tag{20.14}$$

where G_{inel} is the sum over all inelastic intermediate states and P_{nointer} is a probability to have no inelastic interactions. $G_{\mathrm{inel}}(s,b)$ describes the b-profile of inelastic particle collisions. It satisfies the condition $0 \le G_{\mathrm{inel}} \le 1$ and determines how absorptive the interaction region is at a given impact parameter (with $G_{\mathrm{inel}}= 1$ for full absorption and $G_{\mathrm{inel}}= 0$ for the complete dominance of elastic scattering). As seen from Eq. (20.14), $\exp(-\mathrm{Re}\Omega(\mathrm{s},\mathrm{b}))$ is the probability that no inelastic interactions occur at impact parameter b. Ω ($\mathrm{Re}\Omega \ge 0$) is called the opacity (optical density) or eikonal. The quantity

$$S^2(b) \equiv e^{-\mathrm{Re}\Omega(\mathrm{b})} \;=\; P_{\mathrm{nointer}}(b) \tag{20.15}$$

is the so-called survival factor, which enables us to calculate the probability that the LRG survives soft rescattering.

In terms of the opacity the elastic cross section takes the form

$$\begin{aligned}\frac{\mathrm{d}\sigma_{\mathrm{el}}}{\mathrm{d}t} &= \frac{1}{16\pi s^2}\,|T_{\mathrm{el}}(s,t)|^2 = \frac{1}{4\pi}\left|\int \mathrm{d}^2b\; e^{i\vec{q}_t\cdot\vec{b}}(1 - e^{-\Omega(\mathrm{b})/2})\right|^2 \\ &= \pi\left|\int b\mathrm{d}b\; J_0(q_t b)(1 - e^{-\Omega(\mathrm{b})/2})\right|^2,\end{aligned} \tag{20.16}$$

where $q_t = \sqrt{|t|}$ and J_0 is the zeroth-order Bessel function.

To describe the elastic scattering at one fixed energy we can always find an appropriate parameterization for the opacity $\Omega(\mathrm{b})$ and tune the parameters to reproduce the observed $\mathrm{d}\sigma_{\mathrm{el}}/\mathrm{d}t$ cross section. Moreover, we can fix the form of the parameterization, but choose, at each particular energy, the corresponding values of parameters; see, e.g. [39]. Alternatively, we may simply take the Fourier-Bessel transform from the experimental data [33, 40, 41]

$$\mathrm{Im}T_{\mathrm{el}}(b) \;=\; \int \frac{q_t \mathrm{d}q_t}{4\pi}\sqrt{\frac{\mathrm{d}\sigma_{\mathrm{el}}}{\mathrm{d}t}\frac{16\pi}{1+\rho^2}}\; J_0(q_t b), \tag{20.17}$$

where the square root represents $\mathrm{Im}T_{\mathrm{el}}(q_t)$, with $\rho \equiv \mathrm{Re}T_{\mathrm{el}}/\mathrm{Im}T_{\mathrm{el}}$. In this way, we first determine T_{el} from the data for $\mathrm{d}\sigma_{\mathrm{el}}/\mathrm{d}t$, and then calculate $\Omega(\mathrm{b})$ using Eq. (20.13), assuming in accordance with data that ρ is small (or $\rho(t) =$ constant).

At high energies $\rho^2 \ll 1$, which is usually well justified except in the diffractive dip region (see Section 20.3.3.1 for discussion of the dip region).

The value of ρ can be derived via the dispersion relation, see [3]:

$$\begin{aligned}\frac{1}{s}\mathrm{Re}T_{\mathrm{el}}(s) \;&=\; \frac{1}{\pi}\int_{-\infty}^{+\infty}\frac{\mathrm{d}s'}{s'-s}\sigma_{\mathrm{tot}}(|s'|) \\ &=\; \frac{1}{\pi}\int_0^{\infty}\sigma_{\mathrm{tot}}(s')\frac{2s\mathrm{d}s'}{s'^2 - s^2}.\end{aligned} \tag{20.18}$$

Since we consider just the charge-parity C-even amplitude, here for negative s' we put $\sigma_{p\bar{p}} = \sigma_{pp}$. That is, for negative s', which corresponds to the interaction with an *anti*particle, we use the same $\sigma_{pp}(|s'|)$. The major contribution comes from $s' \simeq s$. Thus, with a good accuracy we can evaluate $\rho(t = 0)$ as

$$\rho \;\simeq\; \frac{\pi}{2}\,\frac{\partial \ln \sigma_{\mathrm{tot}}(s)}{\partial \ln s}. \tag{20.19}$$

20.3.2 *Diffractive dissociation*

The elastic cross section probes the optical density of the proton. The well known example of scattering on a black disk, with $G_{\mathrm{inel}} = 1$ for $b < R$, gives $\sigma_{\mathrm{el}} = \sigma_{\mathrm{inel}} = \pi R^2$ and $\sigma_{\mathrm{tot}} = 2\pi R^2$. In general, the absorption of the initial wave (due to inelastic channels) leads, via s-channel unitarity, to elastic scattering.

Inelastic diffraction (i.e. proton dissociation) is a consequence of the *internal structure* of hadrons. This can be conveniently described at high energies, where the lifetimes of each particular Fock component of the incoming hadron/proton wave function (the hadronic fluctuations) are large, $\tau \sim E/m^2$, and during these time intervals the corresponding Fock states can be considered as 'frozen'. Each hadronic constituent can undergo a scattering with its own probability and thus destroys coherence of the fluctuations[4]. As a result, the outgoing superposition of states will be different from the incident particle, and will most likely contain multiparticle states, so we will have *inelastic*, as well as elastic scattering.

[4] At high energies the configurations with different transverse separation, r, between the quarks (valence partons) can serve as an example of such Fock states. An interaction with the QCD Pomeron does not change the value of r, while the cross section $\sigma \propto \alpha_s^2 \cdot r^2$ (see Section 20.4.2 and [42–44]).

Downloaded from https://academic.oup.com/ptep/article/2022/8/083C01/6651666 by KIT Library user on 27 September 2022

To calculate diffractive dissociation we can enlarge the set of intermediate states (p, N_a^*), from just the single elastic channel, and introduce a multichannel eikonal. However, it is more convenient to follow Good and Walker [45], and to introduce states ϕ_k diagonalising the T matrix (which e.g. in the proton case describes different $p \to N^*$, $N_a^* \to N_b^*$ transitions). Such eigenstates only undergo elastic scattering. Since there are no off-diagonal transitions,

$$\langle \phi_i | T | \phi_k \rangle = 0 \qquad \text{for } i \neq k, \tag{20.20}$$

a state k cannot diffractively dissociate into a state $j \neq k$. Working in terms of the Good-Walker eigenstates ϕ_i, we have a simple one-channel eikonal for each state. We denote the orthogonal matrix which diagonalizes T by a, so that

$$T \;=\; aFa^T \qquad \text{with} \qquad \langle \phi_i | F | \phi_k \rangle \;=\; F_k\, \delta_{ik}, \tag{20.21}$$

where F_k is the probability amplitude of the hadronic process proceeding via the diffractive eigenstate ϕ_k.

Now consider the diffractive dissociation of an incoming state $|h\rangle$. We can write

$$|h\rangle \;=\; \sum_k a_{hk}\, |\phi_k\rangle. \tag{20.22}$$

The elastic scattering amplitude satisfies

$$\langle h|T|h\rangle \;=\; \sum_k |a_{hk}|^2\, F_k \;=\; \langle F \rangle, \tag{20.23}$$

where $F_k \equiv \langle \phi_k | F | \phi_k \rangle$ and where the brackets of $\langle F \rangle$ mean that we take the average of F over the initial probability distribution of diffractive eigenstates. After the diffractive scattering described by T_{fh}, the final state $|f\rangle$ will, in general, be a different superposition of eigenstates from that of $|h\rangle$, which was shown in Eq. (20.22). Neglecting the real parts, for the cross sections at a given impact parameter b, we have

$$\begin{aligned}
\frac{\mathrm{d}\sigma_{\mathrm{tot}}}{\mathrm{d}^2 b} &= 2\,\mathrm{Im}\langle h|T|h\rangle \;=\; 2\sum_k |a_{hk}|^2\, \mathrm{Im}F_k \;=\; 2\langle \mathrm{Im}F \rangle \\
\frac{\mathrm{d}\sigma_{\mathrm{el}}}{\mathrm{d}^2 b} &= |\langle h|T|h\rangle|^2 \;=\; \left| \sum_k |a_{hk}|^2\, F_k \right|^2 \;=\; \langle |F| \rangle^2 \\
\frac{\mathrm{d}\sigma_{\mathrm{el+SD}}}{\mathrm{d}^2 b} &= \sum_k |\langle \phi_k|T|h\rangle|^2 \;=\; \sum_k |a_{hk}|^2\, |F_k^2| \;=\; \langle |F^2| \rangle.
\end{aligned} \tag{20.24}$$

It follows that the cross section for the single diffractive dissociation of a proton,

$$\frac{\mathrm{d}\sigma_{\mathrm{SD}}}{\mathrm{d}^2 b} \;=\; \langle |F^2| \rangle \;-\; \langle |F| \rangle^2, \tag{20.25}$$

is given by the statistical dispersion in the absorption probabilities of the diffractive eigenstates. Here the average is taken over the components k of the incoming proton which dissociates. If the averages are taken over the components of both of the incoming particles, then Eq. (20.25) is the sum of the cross sections for single and double dissociation, see Fig. 20.3.

Note that if all the components ϕ_k of the incoming proton $|h\rangle$ were absorbed equally, then the diffracted superposition would be proportional to the incident one and the probability of the inelastic diffraction would be zero. Thus if, at very high energies, the amplitudes F_k at small impact parameters are equal to the black disk limit, $F_k = i$, then diffractive production will be equal to zero in this impact parameter domain, and so will only occur in the peripheral b region where the edge of the disk becomes not completely black. Hence the impact parameter structure of diffractive dissociation and elastic scattering is drastically different in the presence of absorptive s-channel unitarity effects (see the G_{inel} term in Eq. (20.9)). Under the assumption that amplitudes F_k at high energies cannot exceed the black disk limit, $\mathrm{Im}\, F_k \leq 1$, equations 20.24 lead to the following bound

$$\frac{\mathrm{d}\sigma_{\mathrm{el\,+\,SD_1+SD_2+DD}}}{\mathrm{d}^2 b} \leq \frac{1}{2}\,\frac{\mathrm{d}\sigma_{\mathrm{tot}}}{\mathrm{d}^2 b}\,. \tag{20.26}$$

known as the Pumplin bound [46] [5].

20.3.3 *Diffraction from the t-channel viewpoint*

The t-channel approach is based on the Regge model (see Section 20.2), where high-energy diffractive processes are mediated by the exchange of a Pomeron ($\mathbb{P}$). In the case of the elastic pp-scattering amplitude in the eikonal model (see Eq. (20.13)), the opacity corresponding to the exchange of one Pomeron is

$$\Omega(\mathrm{s},\mathrm{b}) = \int \frac{\mathrm{d}^2\mathrm{q_t}}{4ß^2}\; \Omega(\mathrm{s},\mathrm{q_t})\; \mathrm{e}^{\mathrm{i}\bar{\mathrm{q}}_{\mathrm{t}}\cdot\bar{\mathrm{b}}} \tag{20.27}$$

with

$$\Omega(\mathrm{s},\mathrm{q_t}) = \frac{1}{\mathrm{s}}\mathrm{T}'_{\mathrm{el}} = -\mathrm{i}\mathrm{j_P}(\mathrm{t})\mathrm{g_N}(\mathrm{t})\mathrm{g_N}(\mathrm{t})\left(\frac{\mathrm{s}}{\mathrm{s_0}}\right)^{\mathrm{ff}_{\mathbb{P}}(\mathrm{t})-1}, \tag{20.28}$$

where T'_{el} is the two-particle s-channel irreducible elastic amplitude, cf. Eq. (20.5), and $g_N(t)$ is the proton-Pomeron coupling.

If we assume an exponential t-dependence of the coupling, $g_N(t) = g_N(0)\exp(B_0 t)$, and neglect the Pomeron phase, then the opacity is

$$\Omega(\mathrm{s},\mathrm{q_t}) = \mathrm{g_N}(0)\mathrm{g_N}(0)\left(\frac{\mathrm{s}}{\mathrm{s_0}}\right)^{\mathrm{ff}_{\mathbb{P}}(0)-1} \mathrm{e}^{\mathrm{Bt}}, \tag{20.29}$$

with the t-slope given by

$$B \;=\; 2B_0 + \alpha'_{\mathbb{P}}\, \ln\left(\frac{s}{s_0}\right). \tag{20.30}$$

At high energies the opacity has a Gaussian form in the b-space:

$$\Omega(\mathrm{s},\mathrm{b}) = \frac{\mathrm{g_N^2}(0)}{4ß\mathrm{B}}\left(\frac{\mathrm{s}}{\mathrm{s_0}}\right)^{\mathrm{ff}_{\mathbb{P}}(0)-1} \mathrm{e}^{-\mathrm{b}^2/4\mathrm{B}}\,. \tag{20.31}$$

In terms of opacity the effective radius of interaction increases at high energies as $\sqrt{\alpha'_{\mathbb{P}}\ln(s/s_0)}$. This means that with energy increasing the differential cross section becomes steeper (the so called *shrinkage* of the diffractive peak).

If we were to take for the Pomeron the DL parametrisation [25, 26], that is to keep just the first, $T(b) = \Omega(\mathrm{b})/2$, term in the elastic amplitude (Eq. (20.13)) then, at LHC energies, the Gaussian would exceed the black disk limit at small b. However, the eikonal unitarization reduces the power growth of the one-Pomeron exchange cross section. Thus, in Eq. (20.31) $\Omega(\mathrm{s},\mathrm{b}) \propto (\mathrm{s}/\mathrm{s_0})^{\mathrm{ff}_{\mathbb{P}}-1}$ gives an amplitude $\mathrm{Im}\; T_{\mathrm{el}}(s,b) = 1 - e^{-\Omega/2} < 1$. Hence the total cross section is limited by the size of the effective interaction area $\sigma_{\mathrm{tot}} < 2\pi R^2$, where the interaction radius R can be estimated from Eq. (20.31) as the value of b where $\mathrm{Re}\Omega(\mathrm{b})$ becomes ~ 1.

For the parameterization of Eq. (20.31) the corresponding radius grows at very large energies as

$$b^2 = R^2 = 4B\ln\left[\frac{g_N^2(0)}{4\pi B}\left(\frac{s}{s_0}\right)^{\alpha_{\mathbb{P}}(0)-1}\right] \simeq 4\Delta\alpha'_{\mathbb{P}}\ln^2(s/s_0)\,. \tag{20.32}$$

That is for $\Delta = 0.1$ and $\alpha'_{\mathbb{P}}$=0.25 GeV^{-2} we may expect that the cross section increases as

$$\sigma_{\mathrm{tot}} = 2\pi R^2 \simeq c\cdot\ln^2 s\,, \tag{20.33}$$

[5] Strictly speaking the proof of the Pumplin bound is justified only for low mass dissociation. When the masses $M_{1,2}$ become so large (say, $M_i^2 > \sqrt{ss_0}$) that the Good-Walker states $|\phi_i\rangle$, corresponding to two incoming protons overlap, we may face double counting. Therefore, the high mass dissociation will be considered in the next Section, in terms of the multi-Pomeron diagram. Here and in what follows s_0 is a constant which should be defined for a particular theoretical model or fitted from experiment.

Downloaded from https://academic.oup.com/ptep/article/2022/8/083C01/6651666 by KIT Library user on 27 September 2022

with $c = 8\pi\Delta\alpha'_{\mathbb{P}} = 0.24$ mb. This value is close to that obtained by the COMPETE parameterization ($c = 0.27$ mb [22, 24]) but much smaller than the Froissart-Lukaszuk-Martin (FLM) bound [47–49]. With $c^{\rm FLM} = \pi/m_\pi^2 \simeq 60$ mb, see Section 20.7,

$$\sigma_{\rm tot} \leq \frac{\pi}{m_\pi^2} \ln^2\left(\frac{s}{s_0}\right). \tag{20.34}$$

The fact that $c =$(0.24–0.27) mb $\ll c^{\rm FLM} = 60$ mb demonstrates that even at the LHC we are very far from true high-energy asymptotics [6], and the observed growth of the cross section is driven by the interactions at relatively large transverse momenta $k_t \gg m_\pi$ rather than the smallest hadron mass m_π in the denominator of Eq. (20.34).

20.3.3.1 *The t-slope and dip in the elastic cross section*

We first start with a relatively small one-Pomeron amplitude and consider the two-Pomeron contribution corresponding to the Ω^2 term in the expansion of the eikonal $1 - \exp(-\Omega/2)$. In this term the momentum transferred, $q_t = \sqrt{|t|}$, is divided between the two Pomerons so that each Pomeron carries about a momentum $q_t/2$. Correspondingly, the t dependence of the whole 'two-Pomeron' amplitude will be $\exp(2B(t/4)) = \exp(Bt/2)$ [7].

Since the two-Pomeron contribution has an opposite sign in comparison with the one-Pomeron exchange, their interference will result in the appearance of the first diffractive minimum which moves to smaller $|t|$ with energy increasing. Such interference effects are largely responsible for the zero in the imaginary part of the amplitude (with the minimum filled by the real part).

It is worth mentioning that the one-channel eikonal discussed so far is a rather oversimplified approximation. It provides some indications about the behaviour we may expect for the elastic cross section, but clearly it does not give the whole story. Moreover, even within the framework of the one-channel eikonal, the expectation for the elastic slope t-dependence could be masked by other effects. Firstly, there is no reason why the t-dependence of the proton-Pomeron coupling $g_N(t)$ has to be a pure exponent. Next, there exists a two-pion singularity at $t = 4m_\pi^2$ (close to the physical region) in the Pomeron trajectory which generates some curvature in the behaviour of $\mathrm{d}\sigma_{\rm el}/\mathrm{d}t$ [50–52]. So there may be some compensation between the effects caused by the eikonal (arising from the interference between the different multi-Pomeron contributions), and the curvatures coming from the form of the proton-Pomeron coupling and the two-pion singularity of the Pomeron trajectory. However, an exact compensation looks quite non-trivial and a *pure* exponential behaviour of $\mathrm{d}\sigma_{\rm el}/\mathrm{d}t$ looks highly unlikely.

Indeed, the measurements by the TOTEM collaboration at 8 TeV [53] and at 13 TeV [54] clearly demonstrate that the local slope of the elastic pp cross section,

$$B = \mathrm{d}[\ln(\mathrm{d}\sigma_{\rm el}/\mathrm{d}t)]/\mathrm{d}t, \tag{20.35}$$

at $-t \lesssim 0.3$ GeV^2 varies with t.

20.3.3.2 *High mass dissociation*

Let us turn to inelastic diffractive processes that is, to single and double proton dissociations, $pp \to X + p$ and $pp \to X_1 + X_2$, where the + sign denotes the presence of a LRG in the distribution of final state particles. For example, for the diffractive dissociation of a proton into a system of mass M, the rapidity gap between the incoming proton and the remaining hadrons is

$$\Delta y = \ln\left(\frac{s}{M^2}\right) = \ln\left(\frac{1}{\xi}\right), \tag{20.36}$$

where $\xi = 1 - x$ and x is the initial momentum fraction (Feynman variable) carried by the outgoing proton. The masses, M, of the diffractively excited states, produced in high $\sqrt{s}$ collisions, can be large. To separate dissociation from the common inelastic process, usually the condition $M^2 \ll s$ is imposed.

The simplest multi-Pomeron diagram used to describe the diffractive dissociation is the so-called triple-Pomeron graph, shown at the end of Fig. 20.2.

In the Regge pole model, the cross section for the inclusive single diffractive (SD) dissociation process [55–57] can be written in the form (see Fig. 20.2)

$$\frac{\xi \mathrm{d}\sigma_{\rm SD}}{\mathrm{d}t\mathrm{d}\xi} = \frac{M^2 \mathrm{d}\sigma_{\rm SD}}{\mathrm{d}t\mathrm{d}M^2} = \frac{g_{3\mathbb{P}}(t) g_N(0) g_N^2(t)}{16\pi^2} \left(\frac{s}{M^2}\right)^{2\alpha_{\mathbb{P}}(t)-2} \left(\frac{M^2}{s_0}\right)^{\alpha_{\mathbb{P}}(0)-1}, \tag{20.37}$$

where $g_{3\mathbb{P}}(t)$ is the triple-Pomeron coupling. The value of the coupling $g_{3\mathbb{P}}$ is usually obtained from a triple-Regge analysis of lower energy data (see e.g. [34]) .

In an analogous way the cross section for double dissociation reads

$$\frac{\xi_1\xi_2 \mathrm{d}\sigma_{\rm DD}}{\mathrm{d}t\mathrm{d}\xi_1\xi_2} = \frac{M_1^2 M_2^2 \mathrm{d}\sigma_{\rm DD}}{\mathrm{d}t\mathrm{d}M_1^2\mathrm{d}M_2^2} = \frac{g_{3\mathbb{P}}^2(t) g_N^2(0)}{16\pi^3} \left(\frac{s s_0}{M_1^2 M_2^2}\right)^{2\alpha_{\mathbb{P}}(t)-2} \left(\frac{M_1^2 M_2^2}{s_0^2}\right)^{\alpha_{\mathbb{P}}(0)-1}, \tag{20.38}$$

where t is the momentum squared transferred through the LRG. As discussed in Section 20.5, from a microscopic point of view the

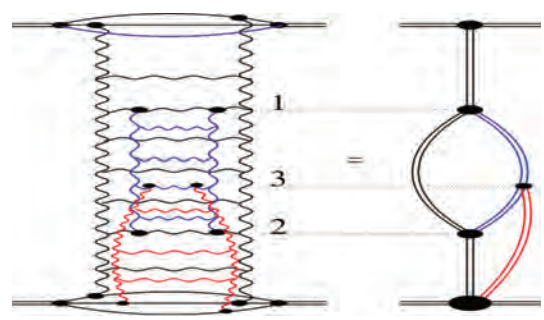

Figure 20.4: Pomeron exchange with schematic diagrams for the enhanced and semi-enhanced exchanges.

Pomeron exchange is described by a set of ladder-type diagrams (see [58–60]), which can lead to a rescattering of the intermediate partons (produced inside this ladder during the evolution), see Fig. 20.4. The left plot shows the Pomeron exchange complemented with the rescattering of partons 1 and 2 and the scattering of a parton 3 on the target. In terms of multi-Pomeron exchanges this corresponds to the diagram on the right hand side, where the Pomeron exchange is shown by the double line of a corresponding colour. The blue one is called "enhanced" (its contribution is integrated over the rapidities of both upper and lower vertices, i.e. of partons 1 and 2). The loop formed by the Pomerons shown in red is called "semi-enhanced" (it is integrated over the rapidity of one intermediate parton).

While the rescattering of the incoming hadron (proton) is already embedded in the eikonal formula (Eq. (20.13)), the rescattering of the intermediate partons in RFT is accounted for by the so-called enhanced diagrams [8] with multi-Pomeron vertices, g_m^n, which couple m to n Pomerons. It is quite a challenging task to resum all the enhanced diagrams, however this was successfully performed within the framework of the QGSJET Monte Carlo [61]. An elegant approach to sum up all enhanced diagrams in the case when each extra effective Pomeron contribution is very

[6] As usual, we assume $s_0 = 1$ GeV^2, but the qualitative conclusion does not depend on any realistic choice of s_0.

[7] The two-Pomeron contribution has a factor of two smaller t-slope, and in terms of the impact parameter, the Ω^2(b) term is concentrated in the domain of a smaller radius. In such a simplified picture, the impact parameters corresponding to an exchange of n Pomerons will rapidly decrease with n increasing.

[8] This contribution is *enhanced* due to the large parton multiplicity.

Downloaded from https://academic.oup.com/ptep/article/2022/8/083C01/6651666 by KIT Library user on 27 September 2022

large was proposed in [62], assuming the analyticity of the g_m^n vertices in n and m in the right half of the complex n- and m-planes. The resulting amplitude becomes a black disk.

The simplest triple-Pomeron vertex $g_2^1 = g_{3\mathbb{P}}$ produces the first multi-Pomeron graph considered above (see the end of Fig. 20.2). However, numerically the multi-Pomeron vertices are relatively small. Note also that the value of $g_{3\mathbb{P}}$, determined from the fit to experimental data (e.g. [63]), is actually an effective vertex with coupling

$$g_{\rm eff} \;=\; g_{3\mathbb{P}}\,\langle S^2\rangle, \tag{20.39}$$

which already includes the survival factor $S^2(b)$, see Eq. (20.15).

Since the opacity Ω increases with energy, at large Ω the number of multiple interactions grows as $N \propto \Omega$, leading to a smaller S^2. An explicit analysis [64] accounting for the survival effects gives a coupling $g_{3\mathbb{P}}$ about a factor of 3 larger than $g_{\rm eff}$, namely $g_{3\mathbb{P}} \simeq 0.2 g_N$.

Recall that the Pomeron exchange simultaneously describes both the elastic scattering amplitude, $T_{\rm el}$, and the multiparticle production cross section, $G_{\rm inel}$. The discontinuity ($disc\ T_{\rm el}$) of the ladder diagram corresponds to the production of secondary particles, practically homogeneously distributed over the whole available rapidity interval covered by the Pomeron, as illustrated by the right-hand diagram in Fig. 20.5.

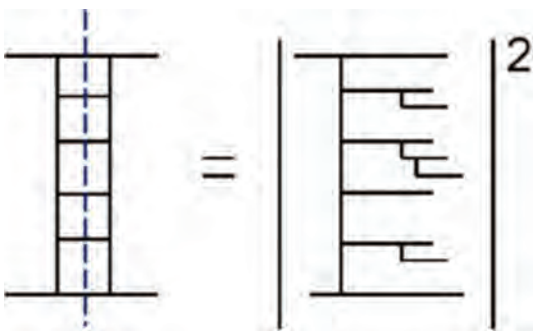

Figure 20.5: Cut Pomeron contribution to the inelastic cross section.

For the one-Pomeron case this discontinuity is called the "cut Pomeron". Correspondingly each multi-Pomeron diagram describes a series of different processes. Cutting k Pomerons in the diagram with n Pomerons we get the inelastic interaction with the multiplicity (density of secondaries) k times larger than that, N_0, produced by one cut Pomeron, $\mathrm{d}N/\mathrm{d}y = k \cdot N_0$. The remaining $n-k$ (elastic) Pomerons account for the absorptive corrections to the subprocess with k cut Pomerons. Indeed, the contribution of the diagram with n Pomerons includes also the processes with larger, $(k+i)\cdot N_0$ multiplicities (cut Pomerons), where $(i = 1, 2, ..., n-k)$. Absorptive corrections, described by the remaining elastic Pomerons, play a role of the survival factor S^2 for the process with the fixed particle density $k \cdot N_0$. They ensure probability conservation (the sum of the probabilities of all possible different channels is equal to one) and restore unitarity. Note that the multi-Pomeron diagrams represent all possible interactions between partons from the protons and partons from the Pomerons. In the case of Monte Carlo generators, the non-enhanced multi-Pomeron contributions are included in terms of the multiple parton interaction (MPI) option, see [13,65] and Section 7.2 in [2]. However, as a rule, this option accounts mainly for the multiple interactions between the partons from the protons (incoming hadrons). The energy-momentum sharing between the various inelastic rescattering processes (including the cut and uncut Pomerons) was performed at the amplitude level within the EPOS Monte Carlo [66].

20.3.3.3 *AGK cutting rules*

The relation between the cross sections of subprocesses with a different number of cut Pomerons within a given diagram with n Pomerons) is given by the AGK (Abramovsky-Gribov-Kancheli [67]) cutting rules. These rules include also the cut *between* the Pomerons with $k = 0$ which corresponds to the contribution of the particular diagram to the elastic cross section. By applying these rules, it is possible to show the self-consistency of the approach, which was lacking in the pure Regge-pole model.

Consider a diagram where the elastic scattering amplitude is mediated by an exchange of n Pomerons. The AGK cutting rules specify the coefficients c_n^k arising when k of these Pomerons are cut. Recall that the Pomeron cut discontinuities give the corresponding inelastic contributions to $\sigma_{\rm tot}$. The terms with $k = 0$ correspond to the diffractive cutting of the diagram (that is, the cut is between the Pomeron exchanges, and not through the Pomerons themselves), while the terms with $k = 1, 2, ...$ describe the processes with k cut Pomerons. The coefficients $c_n^k = \sigma_n^k/|\sigma_{\rm tot}^{(n)}|$ are [9]

$$c_n^{k=0} = (-1)^n(2^{n-1}-1), \qquad c_n^{k\neq 0} \;=\; (-2)^{n-1}\frac{(-1)^{k-1}n!}{k!(n-k)!} \tag{20.40}$$

where $\sigma_{\rm tot}^{(n)}$ denotes the contribution of the n-Pomeron diagram to the total cross section. Note the alternating sign of $\sigma_{\rm tot}^{(n)}$ expressed as $(-1)^{n-1}$.

For the two-Pomeron exchange, $n = 2$, the coefficients are $+1$, -4, or $+2$ according to whether $k = 0$, 1 or 2 Pomerons are cut, respectively. As shown in Fig. 20.6, the amplitude of the two-Pomeron exchange corresponds to a sum of three processes: i) inelastic interaction with particle density twice that caused by one Pomeron (see Fig. 20.6(c)) which enters with the coefficient '2', ii) shadowing (absorptive) correction to the one-Pomeron exchange contribution, which corresponds to events with a single Pomeron density (only one Pomeron is cut), see Fig. 20.6 (b), which enters with a factor '-4', and iii) diffractive elastic scattering or proton dissociation (when different components of the proton wave function correspond to different interaction cross sections), caused by the distortion of the incoming plane wave, see Fig. 20.6(a).

Note that the inclusive cross section is not affected by the multi-Pomeron contribution: $2 \times (2) + 1 \times (-4) = 0$. This is a general property of the AGK rules valid for any number of Pomerons n. Thus in order to calculate the inclusive single-particle cross section, it is sufficient to consider just the *one*-Pomeron exchange diagram.

Let us emphasize that the AGK rules provide a framework to consistently work with multi-Pomeron diagrams, that is, with the Regge cuts, accounting for their contributions to different processes (elastic scattering and diffractive dissociation, inelastic events with different densities, $\mathrm{d}N/\mathrm{d}y$, of secondaries, etc.).

Measurements of diffractive dissociation cross sections have been made in a wide range of pre-LHC energies, see e.g. [68–73]. At the LHC, cross sections of events with a LRG were measured by the ATLAS, CMS and ALICE collaborations at 7 and 8 TeV, see [74–77]. ATLAS [78] and CMS and TOTEM [79] presented first measurements of SD cross sections at 8 TeV with a tagged forward proton. While ATLAS measured inclusive SD cross section, CMS and TOTEM studied SD dijet production. Note that in [78] the measured slope $B = 7.65 \pm 0.34$ GeV^{-2} of the inclusive SD cross section as well as the differential distributions $\frac{\xi \mathrm{d}\sigma_{\rm SD}}{\mathrm{d}t\mathrm{d}\xi}$ for $0.0001 \leq \xi \leq 0.025$ are (within the experimental uncertainties) in a good agreement with the theoretical expectations [29,80]. Moreover a relatively small (in comparison with the $\mathrm{d}\sigma_{\rm el}/\mathrm{d}t$) slope B indicates that the size of the triple-Pomeron vertex is much smaller than the proton size.

20.3.4 *Central Diffractive processes*

Processes $pp \to p + X + p$, where an object X, produced in the central rapidity region, is separated from the outgoing protons by a LRG on each side, are called Central Exclusive Production (CEP). They are described by the double Pomeron exchange (DPE) diagrams. When the mass of the central system, M_X, is large and the interaction in the M_X region can be described by

[9] In their complete form the AGK cutting rules were implemented in the QGSJET Monte Carlo [61].

Downloaded from https://academic.oup.com/ptep/article/2022/8/083C01/6651666 by KIT Library user on 27 September 2022

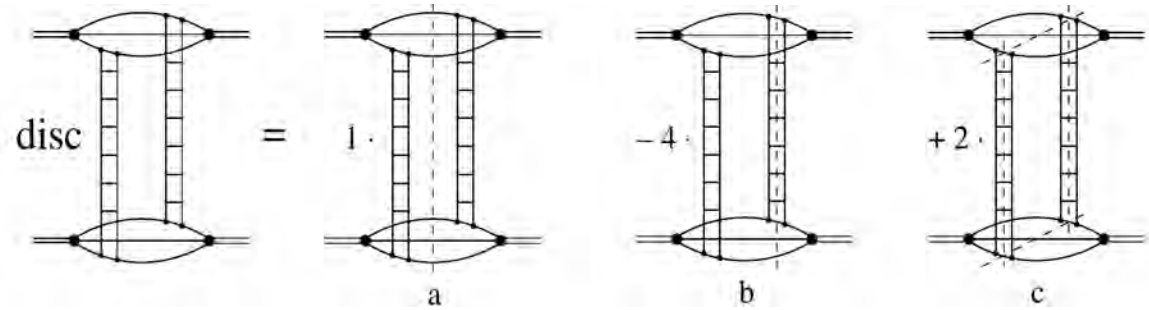

Figure 20.6: Two-Pomeron exchange diagram as a sum of different AGK cuts shown by the dashed lines.

Pomeron exchange, the corresponding cross section reads

$$\frac{\xi_1\xi_2 \mathrm{d}\sigma^{\mathrm{CEP}}}{\mathrm{d}\xi_1 \mathrm{d}t_1 \mathrm{d}\xi_2 \mathrm{d}t_2} = \frac{g_N^2(t_1) g_N^2(t_2)}{(16\pi^2)^2} \left(\frac{1}{\xi_1}\right)^{2\alpha_{\mathbb{P}}(t_1)-2} \left(\frac{1}{\xi_2}\right)^{2\alpha_{\mathbb{P}}(t_2)-2} \times g_{3\mathbb{P}}^2(0) \left(\frac{M_X^2}{s_0}\right)^{\alpha_{\mathbb{P}}(0)-1} . \tag{20.41}$$

If the mass M_X is not too large or for the cases (such as exclusive Higgs boson or dijet production) where the mass M_X is comparable with the corresponding hard scale, the last factor $g_{3\mathbb{P}}^2(0)(M_X^2/s_0)^{\alpha_{\mathbb{P}}(0)-1}$ should be replaced by the corresponding 'Pomeron-Pomeron cross section', see for instance [81, 82].

Note that equations (20.37), (20.38) and (20.41) are written in a simplified way without accounting for absorptive corrections. That is, the cross sections in equations (20.37) (20.38) and (20.41) should be multiplied by the gap survival factor S^2 (see Eq. (20.15)).

Since the QCD Pomeron is built mainly from gluons it is natural to search for glueballs in double Pomeron exchange processes, and in particular, in CEP.

Resonance production in the Pomeron-Pomeron fusion was extensively studied at the CERN ISR at $\sqrt{s}$ from 22 GeV to 63 GeV (see for reviews [82–84]) and, after the ISR closure in 1983, in fixed target experiments at the CERN SPS [85] and E690 at the Tevatron [86, 87]. Glueballs were actively searched for and the properties of the f_0 and f_2 production studied in detail using multiparticle spectrometers, such as the Omega facility at the CERN SPS experiments (WA76, WA91 and WA102), see for a review [85].

An important property of CEP processes, which can be expected from matching with the perturbative QCD LO (leading order) calculation, is the $J_z = 0$ dominance. Perturbatively, for the CEP of a heavy object, the leading contribution comes from a configuration with the projection of this object spin onto the beam axis $J_z = 0$ [81]. Note that the CEP cross section is suppressed at large M_X by a strong bremsstrahlung off the incoming gluons (from the Pomeron) which would violate the 'exclusivity'. The small probability of not having such radiation is described by the Sudakov suppression factor, T_{Sud}, [88], see [81] for details.

20.3.5 *Diffractive parton distributions*

Selecting in Deep Inelastic Scattering (DIS) events with a LRG (see e.g. [89, 90]) or detecting the leading proton (see Section V.C. in the review [91]) we can study the parton (quark and gluon) distributions of the Pomeron [10]. In other words, such events can be treated as DIS on the Pomeron target with the incoming Pomeron flux given by

$$f_{\mathbb{P}}(x_{\mathbb{P}}) = \int \mathrm{d}t \frac{g_N^2(t)}{16\pi^2} x_{\mathbb{P}}^{2(1-\alpha_{\mathbb{P}}(t))} , \tag{20.42}$$

where the proton momentum fraction transferred through the Pomeron $x_{\mathbb{P}} = \xi = M^2/s$.

These Pomeron PDFs were extracted from the HERA measurements of ep scattering with leading protons or a LRG and can be used to describe the inclusive production of high E_T dijets or another hard process based on the collinear factorization theorem in the same way as that in non-diffractive collisions (see [91]). The inclusive measurements of these PDFs are described in [92–94], with the combined H1 and ZEUS data using tagged protons analyzed in [95]. The impact of diffractive jet measurements is addressed e.g. in [96] and the measured charm contribution is presented in [97, 98]. As far as the parton distributions are known, we can calculate the corresponding inelastic cross section of the Pomeron-proton interaction using one of the 'general purpose' Monte Carlo generators (see e.g. [13]), multiply it by the Pomeron flux and compare the obtained result with the Regge formula in Eq. (20.37). This approach provides another way to evaluate the triple-Pomeron vertex $g_{3\mathbb{P}}$. The corresponding analysis was performed in [99] and leads to practically the same (within the error bars) value of $g_{3\mathbb{P}} = 0.2 g_N(0)$.

It is worth mentioning that in DIS at large Q^2 we are dealing with small-size objects and the rescattering effects are small. Therefore, the survival factor $S^2 \simeq 1$ and does not affect the results.

20.4 Experimental data on diffraction at high energies

20.4.1 *Total and elastic cross sections*

The elastic scattering of protons is a process with a special and rather simple experimental signature: the central detector is empty while the incoming protons after the collisions are detected in the dedicated forward proton detectors (FPD) placed far from the interaction point (IP). Elastic scattering data are taken in special runs in order to be able to reach different ranges of t-values and thanks to the very large value of the cross section the data can be collected with a relatively low instantaneous luminosity and hence a negligible pile-up.[11]

These special runs usually have very few proton bunches and differ in the t range covered, which is governed roughly by the relation $t_{\min} \propto d^2/\beta^*$. Here d is the distance, expressed in multiples of the beam size at the detector, from the centre of the LHC beam and β^* is defined as the distance from the IP to the point where the transverse area of the beam is twice as wide as that at the IP (see Section 31 in [1]). Note that if we work at large β^*, the incoming protons have very small angular divergence leading to small average transverse momentum, which allows us to measure very small $|t|$ values. The lowest $|t|$ values measured so far at the LHC are 4×10^{-4} GeV^2 (ALFA) and 6×10^{-4} GeV^2 (TOTEM) reached with the 8 TeV LHC beam configured with β^*=1 km optics. The largest t values of about 4 GeV^2 were measured by TOTEM at 8 and 13 TeV with $\beta^* = 90$ m thanks to special triggers. Other β^* values used in special runs are 3.5 m, 11 m and 2.5 km.

There are four ways to determine the σ_{tot} value:

1. **Elastic and Inelastic.** This method does not require the optical theorem and hence no extrapolation of $\mathrm{d}\sigma_{\mathrm{el}}/\mathrm{d}t$ to $t = 0$ and no ρ (defined below Eq. (20.17)) but rather the

[10] see also Section 18.5 in [1]

[11] The pile-up is formed by additional pp collisions which typically produce low-p_T particles. These may affect the signal sample and worsen various reconstruction and identification efficiencies.

Downloaded from https://academic.oup.com/ptep/article/2022/8/083C01/6651666 by KIT Library user on 27 September 2022

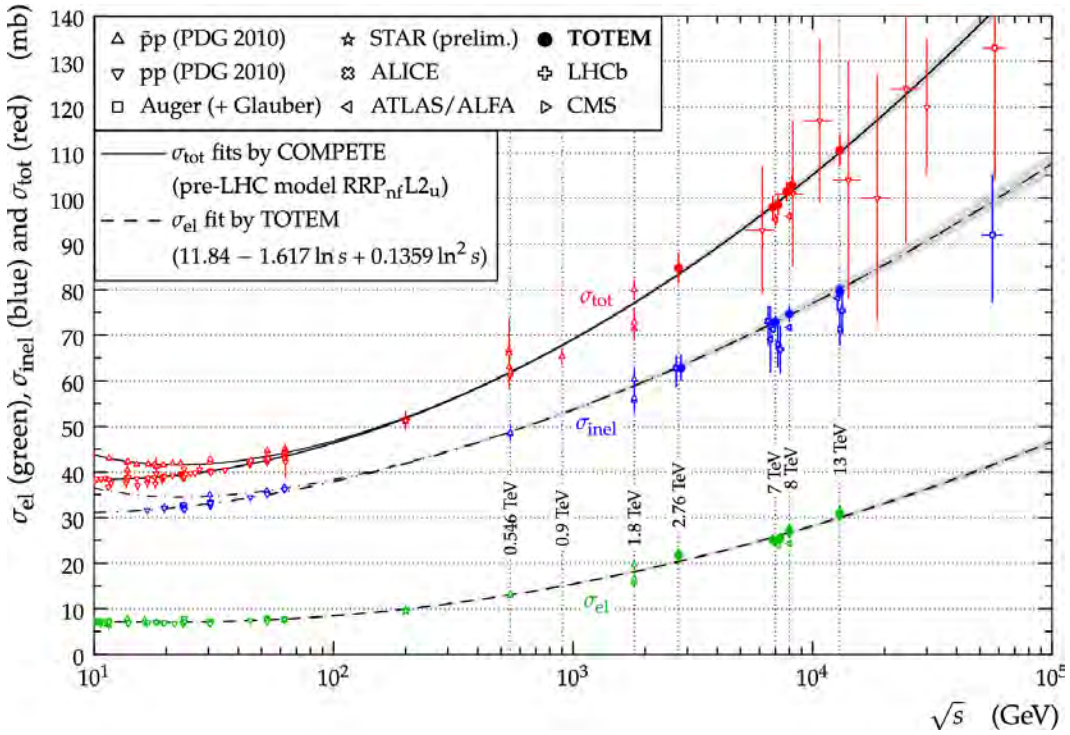

Figure 20.7: Overview of elastic ($\sigma_{\rm el}$), inelastic ($\sigma_{\rm inel}$) and total ($\sigma_{\rm tot}$) cross section data for pp and $p\bar{p}$ collisions as a function of $\sqrt{s}$. The continuous black lines (lower for pp, upper for $p\bar{p}$) represent the best fits of the total cross section data by the COMPETE collaboration [22]. The dashed line is a fit of the elastic cross section data. The dashed-dotted lines refer to the inelastic cross section and are obtained from the difference between the continuous and dashed lines. Figure from Ref. [100].

luminosity and measuring rates $N_{\rm el}$ (elastic) and $N_{\rm inel}$ (inelastic). The total cross section is then simply:

$$\sigma_{\rm tot} = \frac{1}{\mathcal{L}}(N_{\rm el} + N_{\rm inel}). \tag{20.43}$$

Of course, both $N_{\rm el}$ and $N_{\rm inel}$ should be corrected for the detector acceptance and efficiency. This is especially important for $N_{\rm inel}$ since the detectors never cover the whole rapidity region (i.e. the whole 4π).

2. **Elastic only.** This approach necessitates measuring $\mathrm{d}\sigma_{\rm el}/\mathrm{d}t$ and using the optical theorem with a known value of ρ. As explained in Section 20.2, the optical theorem states that $\sigma_{\rm tot} \propto \mathrm{Im}[T_{\rm el}(t \to 0)]$, see Eq. (20.3). Since in practice it is not possible to measure down to $t = 0$, we need to extrapolate. To minimize the model dependence when extrapolating, it is vital to measure down to as low $|t|$ values as possible (i.e. high β^*). This method requires an independent luminosity measurement. Once the luminosity is known, $\mathrm{d}\sigma_{\rm el}/\mathrm{d}t$ can be normalized and used to extract $\sigma_{\rm tot}$ using the formula:

$$\sigma_{\rm tot}^2 = \frac{16\pi}{1+\rho^2}\left.\frac{\mathrm{d}\sigma_{\rm el}}{\mathrm{d}t}\right|_{t\to 0}. \tag{20.44}$$

3. **Coulomb normalization.** Similarly to the previous method, this approach relies on the elastic observables only and requires a measurement of the elastic cross section at very low values of $|t|$, where it is sensitive to the theoretically well known Coulomb QED contribution $4\pi\alpha_{\rm QED}^2/t^2$. The normalization of $\mathrm{d}\sigma_{\rm el}/\mathrm{d}t$ is then determined by fitting the experimental data at very low $|t|$ using a formula including the Coulomb amplitude and its interference with the strongly interacting (the so-called nuclear) term. This method has been successfully used by UA4/2 [101] and TOTEM [102].

4. **Luminosity-independent.** This method does not rely on the knowledge of luminosity but rather on the knowledge of $N_{\rm el}$ and $N_{\rm inel}$ and on the optical theorem: combining equations (20.43) and (20.44) with $\frac{\mathrm{d}\sigma_{\rm el}}{\mathrm{d}t} = \frac{1}{\mathcal{L}}\frac{\mathrm{d}N_{\rm el}}{\mathrm{d}t}$ we get

$$\sigma_{\rm tot} = \frac{16\pi}{1+\rho^2}\frac{\mathrm{d}N_{\rm el}/\mathrm{d}t\big|_{t=0}}{N_{\rm el}+N_{\rm inel}}, \tag{20.45}$$

where $\mathrm{d}N_{\rm el}/\mathrm{d}t\big|_{t=0}$ corresponds to the extrapolation to $t = 0$ of the nuclear term only. By independently and simultaneously measuring $N_{\rm el}$ and $N_{\rm inel}$, and applying the optical theorem, we can also determine the luminosity.

The TOTEM [100, 103–105] and ATLAS [106, 107] collaborations at CERN have covered an energy range from $\sqrt{s}$=2.76 TeV to 13 TeV. A compilation of high energy total pp and $p\bar{p}$ cross section measurements is shown in Fig. 20.7 (for discussion of the pre-LHC elastic scattering data see review [108]).

Despite some tension between the Tevatron CDF [109] and E811 [110] data [12] and to a lesser extent between the TOTEM [104, 105] and ATLAS [106, 107] measurements, the data clearly indicate that in the Tevatron – LHC energy interval the total cross section starts to grow *faster* than the power-law parametrization [26] describing the data below the Tevatron energy. In particular, while the DL fit [26] predicts $\sigma_{\rm tot} = 90.7$ mb at $\sqrt{s} = 7$ TeV, the TOTEM experiment observes 98.6±2.2 mb [104].

A compilation of the high-energy data on the elastic slope is shown in Fig. 20.8. It is clearly seen that in the TeV energy range the slope increases with $\sqrt{s}$ more rapidly than the logarithmic behaviour expected in the case of one-Pomeron exchange, see Eq. (20.30). Such an acceleration of the t-slope derivative, $\mathrm{d}B/\mathrm{d}\ln s$, is a clear manifestation of the increasing role of the multi-Pomeron exchanges, where asymptotically the slope should rise as $\ln^2 s$, see [117]. Finally, Fig. 20.9 illustrates the energy dependence of the differential elastic pp cross section. As expected (see Section 20.3.3.1), the diffractive dip moves to smaller $|t|$ with increasing energy.

[12] The CDF 1.8 TeV point [109] is 2.8 σ higher than the corresponding E811 result [110].

Downloaded from https://academic.oup.com/ptep/article/2022/8/083C01/6651666 by KIT Library user on 27 September 2022

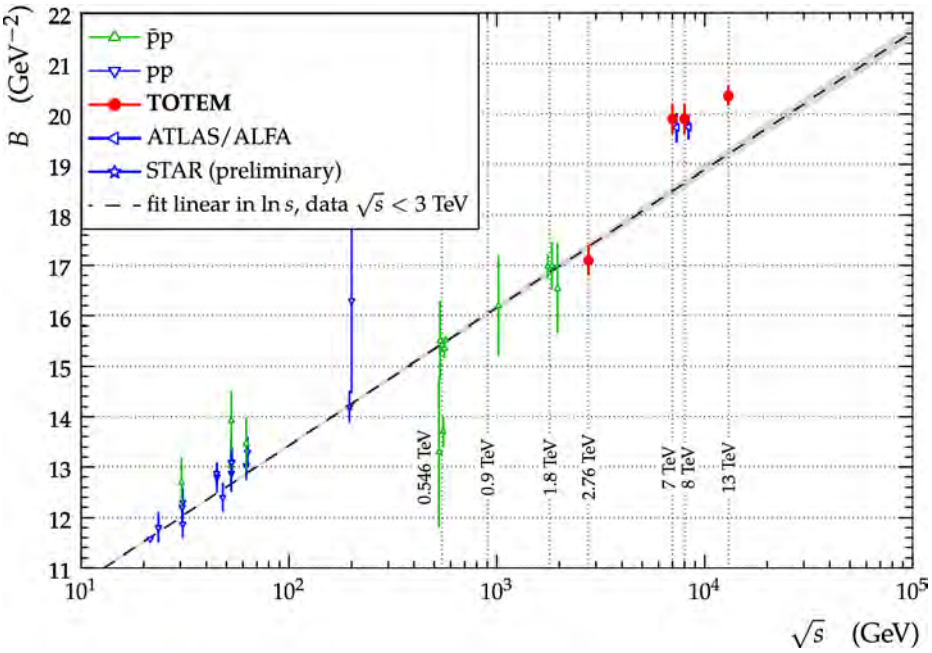

Figure 20.8: The diffractive slope B for pp and $p\bar{p}$ elastic scattering as a function of $\sqrt{s}$. The experimental uncertainties represent the quadratic sum of statistical and systematic uncertainties. The dashed line is a result of a linear fit to data at $\sqrt{s} < 3$ TeV. The data points come from [103–107, 111–113]. Figure from Ref. [100].

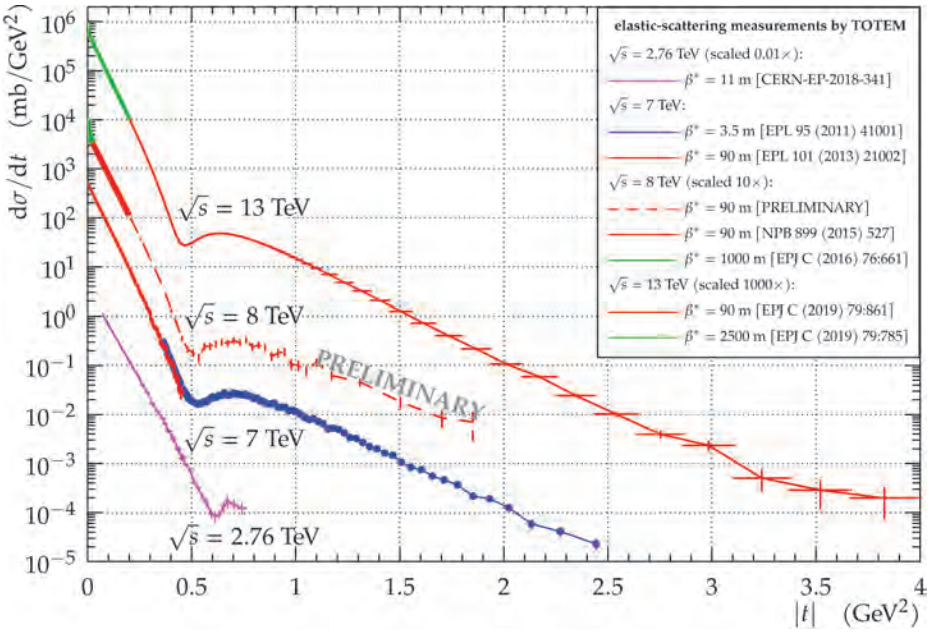

Figure 20.9: The t-dependence of the pp elastic cross section for collision energies $\sqrt{s} = 2.76$ TeV [103], 7 TeV [104, 114], 8 TeV [53,115,116] and 13 TeV [54,102]. The experimental uncertainties represent the quadratic sum of statistical and systematic uncertainties. Figure from Ref. [116].

20.4.2 *Diffractive vector meson production*

The exclusive production of vector mesons was studied in detail at HERA (see for a review [91]). It is well described within the 'dipole model' (see for review and references [120]), where the incoming photon first fluctuates into a quark-antiquark, which then interacts with the target proton and, finally, with the probability given by the overlap integral between the vector meson wave function and the outgoing $q\bar{q}$-pair, the vector meson is produced. The crucial quantity is the value of cross section, $\sigma(q\bar{q} - p)$, of elastic scattering of the $q\bar{q}$-pair on the proton. The energy behaviour of $\sigma(q\bar{q} - p)$ is driven by the intercept, $\alpha_{\rm eff}(0)$, of the effective Pomeron [13] (rightmost singularity in the j-plane), while the value of the cross section depends on the quark separation, r, in the transverse plane, $\sigma(q\bar{q} - p) \propto \alpha_s^2 \langle r^2 \rangle$ [43, 44]. Thus different processes with the same $\langle r^2 \rangle$ are driven by the same $\sigma(q\bar{q} - p)$ cross section.

In the DIS case this separation in turn is controlled by the photon virtuality, Q^2, and the quark mass, m_q: $\langle r^2 \rangle \simeq 1/(z(1-z)Q^2 + m_q^2)$ (z is the photon momentum fraction carried by the quark). Indeed, the cross section of the ρ meson diffractive pro-

[13] Effective Pomeron means that this is not an original pole in the j-plane, but it includes the corrections (renormalizations) caused by the enhanced diagrams (see e.g. [121]).

Downloaded from https://academic.oup.com/ptep/article/2022/8/083C01/6651666 by KIT Library user on 27 September 2022

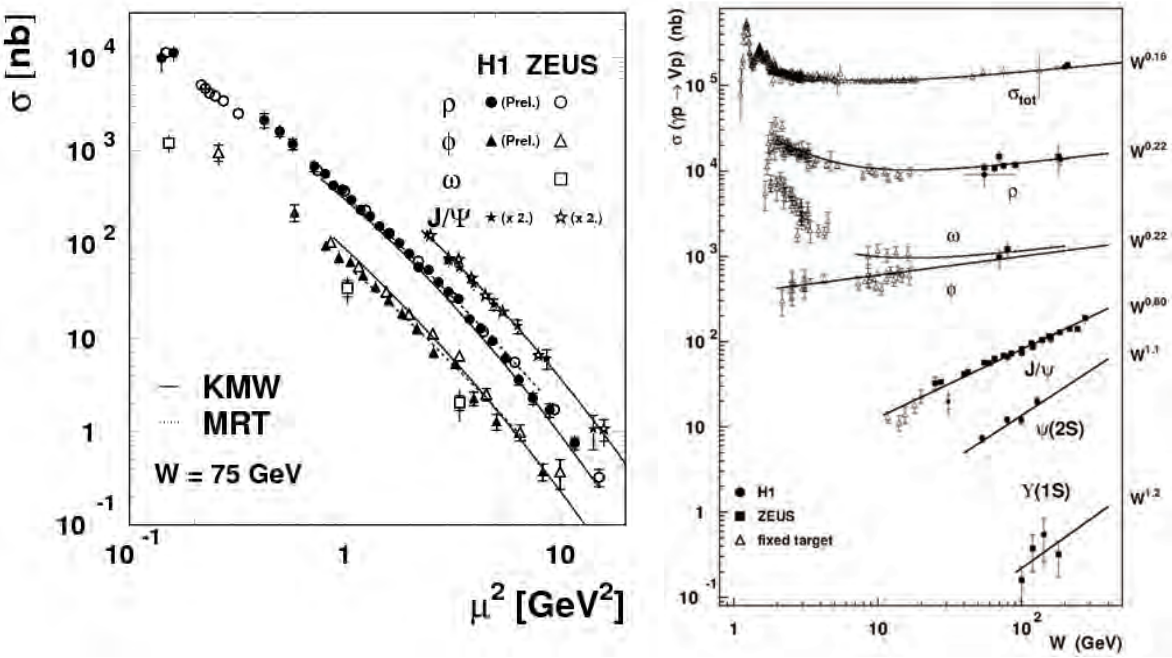

Figure 20.10: (Left) The ρ, ω, ϕ and J/ψ elastic production cross sections as a function of the scale $\mu^2 = (Q^2 + M_V^2)/4$. For readability of the figure, the J/ψ cross sections are multiplied by a factor 2. Figure from Ref. [118]. (Right) Compilation of photoproduction cross section measurements as a function of the γp centre-of-mass energy, W. The total cross section and various vector meson production cross sections are included, with the approximate power law dependences $\sigma \propto W^\delta$ indicated for each process. Figure from Ref. [119].

duction in DIS at $Q^2 = M^2_{J/\psi}$ is close (up to the difference in the quark electric charges) to that for the J/ψ photoproduction, see Fig. 20.10 (Left).

The production cross section depends non-trivially on W, the energy of the $\gamma^* p$ center of mass system. It increases with W as W^n, where $n = 0.2$ for ρ, ω and ϕ (light quark)-mesons but $n = 0.8$ for J/ψ. Note that in the J/ψ case the energy dependence is close to that of the BFKL (Balitsky-Fadin-Kuraev-Lipatov) Pomeron [59,122,123], that is, the singularity calculated within the leading (and next-to-leading) approximation in perturbative QCD. But at lower scales the absorptive (multi-Pomeron) corrections tame the growth which leads to smaller values of n ([124–127]), see Fig. 20.10 (Right).

A similar situation reveals in the dependence of $\alpha_{\rm eff}$ on Q^2, as can be seen in Fig. 47 of [91]. At a large scale $\mu^2 = (Q^2 + M_V^2)/4$ the value of $\alpha_{\rm eff} \simeq 1.3$ is close to the prediction for the QCD Pomeron, while for a smaller scale, the absorptive corrections described by the multi-Pomeron diagrams start to reduce the cross section, and $\alpha_{\rm eff}$ decreases.

20.5 Pomeron in QCD

All features described in the previous Sections were based on *first principles*, such as analyticity (based on causality), unitarity, crossing symmetry, etc. Since QCD theory satisfies all these principles it should reveal a corresponding "Regge" behaviour. Indeed, within perturbative QCD there is a Pomeron: an even-signature singularity in the j-plane with vacuum quantum numbers. While in the old Regge theory the Regge trajectories and their couplings were phenomenological numbers fitted from experiment, perturbative QCD allows one to calculate the positions of the singularities and the corresponding couplings with $O(\alpha_s)$ and even with $O(\alpha_s^2)$ accuracy [59,122,123,128–131].

In terms of Feynman diagrams, the QCD Pomeron may be viewed as a sum of multi-particle ladders built by the exchange of two t-channel (reggeized [14]) gluons, see the left-hand side of Fig. 20.5.

The sum of ladder diagrams of the type of Fig. 20.5 is the simplest multiparticle structure which reproduces the power-like s^α behaviour of the Pomeron pole. In other words it corresponds to a sum of completely inelastic $2 \to n$ processes, that is, to the last term $G_{\rm inel} = 1 - \exp(-\Omega)$ in the unitarity equation (20.9). This set of diagrams was resummed in the limit of a small QCD coupling, $\alpha_s \ll 1$, but large energy, such that $\alpha_s \ln(s/s_0) \sim O(1)$ [59]. The summation results in the rightmost singularity at $j = 1 + \omega_0 > 1$. After accounting for the next-to-leading logarithmic (NLL) corrections, the position of the singularity (Pomeron intercept) corresponds to $\omega_0 = 0.25$–0.3 depending only weakly on the scale [122,123,132–136], whose value is characterized by the transverse momentum, k_t, of gluons in the ladder.

It was demonstrated (see e.g. [137]) that the resummation of the $(\alpha_s \ln(1/x))^n$ terms based on the QCD Pomeron results essentially improves the description of low-x inclusive HERA data within the framework of the NNLO DGLAP evolution.

At this stage the singularity is the cut in the j-plane. However we have to account for the boundary conditions at relatively small k_t. Imposing a reasonable boundary, we arrive at a series of Regge poles in the interval from $j = 1$ to $j = 1 + \omega_0$ instead of the cut [134]. Note that the first (corresponding to the rightmost pole in the j-plane, i.e. to the pole with the largest Re j) eigenfunction consists of gluons with relatively small k_t, while for the next poles the k_t increases. DIS inclusive $\gamma^* p$ cross sections were fitted in [135] using the QCD based approach in which Pomeron is represented by series of Regge poles obtained within the perturbative QCD BFKL approach. It was concluded that the first pole has a small coupling to the proton. It is possible that this small value of the coupling to the proton is related to the fact that the enhanced multi-Pomeron diagrams (i.e. the rescattering of intermediate partons) were neglected in the fit. The main effect of this enhanced contribution is the "renormalization" of the intercept which diminishes the effective value of ω_0. Besides this, the enhanced diagrams provide a saturation by reducing the rise

[14] That is, the virtual loop corrections to the one-gluon exchanges are included. These corrections are important in order to provide infrared stability of the results.

Downloaded from https://academic.oup.com/ptep/article/2022/8/083C01/6651666 by KIT Library user on 27 September 2022

of the parton densities in the (b, k_t, y)-space (see e.g. [138,139]).

Note that perturbative QCD allows us to understand why the values of the phenomenological multi-Pomeron vertices and the shift, ω_0, of the intercept, are small (due to $\alpha_s \ll 1$ and some numerical factors such as N_c and π). Indeed, at the lowest α_s orders we get for the ω_0 value and the simplest multi-Pomeron vertices (see e.g. [59,139,140]):

$$\omega_0 \propto \frac{N_c\alpha_s}{\pi}, \quad g_{3\mathbb{P}} \propto \frac{N_c\alpha_s^2}{(N_c^2-1)\pi^2} \quad \text{and} \quad g_2^2 \propto \frac{N_c\alpha_s}{(N_c^2-1)^2}\ , \tag{20.46}$$

where g_2^2 is the coupling corresponding to the transition of 2 into 2 Pomerons.

20.5.1 *BFKL evolution in the 'dipole' representation*

It was shown in [141–144] that the LO BFKL Pomeron equation [59] can be written in terms of the evolution of the dipole density, $N(x_d, y_d; y)$, in rapidity y (here x_d and y_d are the transverse coordinates of two t-channel gluons which form the colour singlet dipole). Indeed, after the emission of a new gluon at point z_d, the initial colour dipole with coordinates (x_d, y_d) turns into a pair of dipoles (x_d, z_d) and (z_d, y_d). This can be considered as a development of a 'dipole cascade'. Moreover in this formalism it is easy to include the non-linear absorptive corrections (last term in the square brackets in Eq. (20.47)), which accounts for the rescattering of the intermediate partons (gluons) on the target proton. The corresponding contribution is described by the so-called "fan" diagrams and these are the most important corrections to the linear DGLAP (Dokshitzer-Gribov-Lipatov-Altarelli-Parisi) evolution [145] in the case of DIS at not large scales but at very small momentum fraction [139].

The resulting non-linear evolution (Balitsky-Kovchegov equation [146–148]) reads

$$\begin{aligned}\frac{\mathrm{d}}{\mathrm{d}y}N(x_d, y_d; y) = &\frac{\alpha_s N_c}{2\pi^2}\int \mathrm{d}^2 z_d \frac{(x_d-y_d)^2}{(x_d-z_d)^2(y_d-z_d)^2}\\ &\times [N(x_d, z_d; y) + N(y_d, z_d; y) - N(x_d, y_d; y)\\ &-N(x_d, z_d; y)N(y_d, z_d; y)]\ .\end{aligned} \tag{20.47}$$

For a small density N the last term in the square brackets can be neglected, and the first three terms in Eq. (20.47) reproduce the conventional BFKL equation in the coordinate representation. However, for large $N \to 1$ the right-hand side of Eq. (20.47) vanishes and we reach the saturation $N = 1$. It is worth mentioning that, as shown in [149], in terms of 'dipole' formalism, with the triple-Pomeron vertex generated by the 'one dipole to two dipoles' transition, it is possible to relate the Good-Walker approach to high mass diffraction with the triple-Pomeron diagram.

20.5.2 *Distribution of secondaries: theory versus experiment*

As already discussed, in terms of Feynman diagrams the cut Pomeron can be viewed as a set of ladder diagrams corresponding to a sum of completely inelastic $2 \to n$ processes, that is, to the last term $G_{\rm inel} = 1 - \exp(-\Omega)$ in the unitarity equation (20.9). Here $n > 2$ means the production of additional $(n-2)$ gluons which, after hadronization, form minijets. [15] Therefore, in the final state driven by one Pomeron, we expect to observe gluon minijets with a flat rapidity distribution in the central (plateau) rapidity region. This would correspond to a flat pseudorapidity distribution of produced particles if they were massless. A typical pseudorapidity distribution of charged particles in inclusive events (up to $|\eta| = 7$) is shown in Fig. 20.11 (left) [150] (see also Fig. 53.1 in [1]). The central part ($|\eta| < 2.5$) was measured by CMS, while the forward region was covered by TOTEM. The dip observed at $\eta = 0$ is explained by the presence of massive particles (the Jacobian $J(p_T, m, \eta) = p_T/E \to p_T/\sqrt{p_T^2 + m^2}$ at $\eta = 0$). A photon energy spectrum is shown in Fig. 20.11 (right) [151], measured by LHCf inclusively and in events with a diffraction topology, i.e. no charged particles with $p_T > 100$ MeV and $|\eta| < 2.5$ observed by ATLAS. As expected in diffractive events the energy flow decreases with E_γ more slowly than that in the inclusive case.

The energy dependence of the particle density $\mathrm{d}N_{\rm ch}/\mathrm{d}\eta$ at $\eta = 0$ is shown in Fig. 20.12 (left). Neglecting absorptive corrections given by the enhanced diagrams (which mainly change ('renormalize') the effective Pomeron intercept $\alpha_{\rm eff}(0) = 1 + \Delta$ [121]), we conclude that according to the AGK rules the plateau height $\mathrm{d}\sigma/\mathrm{d}\eta \propto s^{\Delta}$ is driven just by the one-Pomeron exchange with effective $\Delta \sim 0.2$ (see Section 20.3.3.3). That is, the density of secondaries observed in the inclusive process increases with increasing energy faster than the total cross section, whose growth is tamed by the multi-Pomeron diagrams. Indeed, as is seen from Fig. 20.12 (left), in the interval of collider energies $\mathrm{d}N_{\rm ch}/\mathrm{d}\eta = (1/\sigma_{\rm inel})\mathrm{d}\sigma/\mathrm{d}\eta \propto s^{0.115}$ (i.e. $\mathrm{d}\sigma/\mathrm{d}\eta \propto s^{0.215}$), while $\sigma_{\rm inel} \propto s^{0.1}$.

Contrary to the 'old' Regge theory where it was *assumed* (based on the experimental data existing in the 1950s and 1960s) that all transverse momenta are limited, in QCD the k_t distributions of jets (charged particles) have a long k_t tail ($\mathrm{d}\sigma/\mathrm{d}k_t^2 \propto \alpha_s^2(k_t^2)/k_t^4$ at large k_t and very large energy $s \gg k_t^2$). An example of the p_T distribution of charged secondaries is shown in Fig. 20.12 (right).

Note that the mean transverse momentum of secondaries, produced via jet fragmentation, slowly increases with collision energy, see Fig. 20.13 (right). This is caused by the stronger absorption (at larger $\sqrt{s}$) of the gluons with a smaller k_t ($\sigma^{\rm abs} \propto 1/k_t^2$). The growth of $\langle p_T \rangle$ with multiplicity (see Fig. 20.13 (left)) can be explained by the fact that events with larger $N_{\rm ch}$ correspond to a smaller impact parameter, b, where the absorption of a low k_t component is stronger and, next, larger multiplicity can be originated by the events with jets/minijets with higher p_T. Since the mean p_T of secondaries grows with $\sqrt{s}$, the increase with $\sqrt{s}$ of transverse energy flow is a bit faster than that of particle density.

The model [162] based on a modification of the classic RFT allows one to trace the smooth transition from the pure perturbative, large k_t, region into the *soft* domain. A strong absorption of the low k_t partons plays a crucial role here since it produces an effective infrared cutoff, $k_{\rm sat}$, and provides the possibility of extending the parton approach, used for 'hard' processes, to also describe high-energy soft and semihard interactions. This approach combines a description of soft physics and diffraction with jet physics in a coherent self-consistent way.

Another way is to include the soft and hard components independently [37, 66, 163, 164]. In this approach the soft part is described in terms of RFT with the phenomenological "soft" Pomeron pole while the hard part is calculated in terms of the parton model for minijet production with the energy dependent cutoff $k_t > k_0(s)$. A combined description of soft and hard processes in hadronic collisions is reached within the QGSJET Monte Carlo model (e.g. [61]) in the framework of the so-called "semihard Pomeron" approach (see e.g. [165]).

In [166] a model was constructed, which incorporated the attractive features of the two successful theoretical approaches to high energy QCD: BFKL Pomeron calculus [59,60] and the Colour Glass Condensate/saturation [167].

20.5.2.1 *Correlations*

All LHC experiments routinely measure tracks with $p_T > p_{\rm min}$, where $p_{\rm min}$ can vary in different studies. Typically, $p_{\rm min} =$ 200 MeV, where tracking reconstruction efficiencies are larger than 70%. In order to identify particle species, each experiment has sophisticated identification procedures usually based on the ionization energy loss, $\mathrm{d}E/\mathrm{d}x$, or other techniques, with different regions of applicability for different particle species. Thanks to usually relatively large cross sections of soft QCD processes, most of the results below come from event samples with very low or negligible pile-up.

Following the notation in [168], symmetrized inclusive particle number densities for q points at $y_1, ..., y_q$ (where y_i represents the 4-momentum of the ith particle), $\rho_q(y_1, ..., y_q)$, are related to the inclusive differential cross section by

[15] Minijets result from hadronization of partons emitted from the cut QCD Pomeron. Typically these are groups of hadrons with comparatively low overall $E_T \lesssim$ 5–10 GeV.

Downloaded from https://academic.oup.com/ptep/article/2022/8/083C01/6651666 by KIT Library user on 27 September 2022

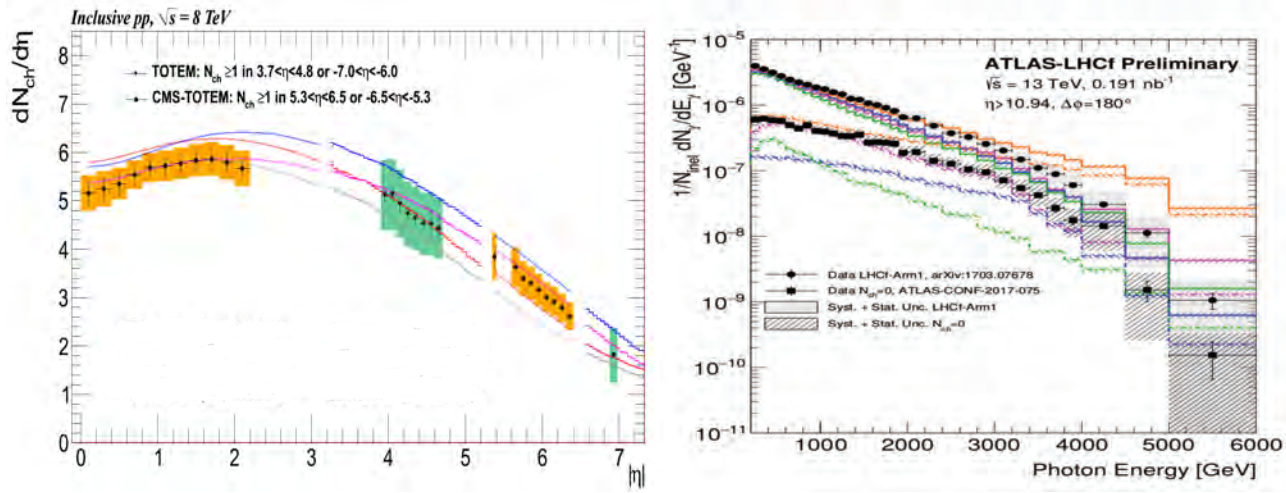

Figure 20.11: (Left) Charged-particle pseudorapidity distribution for inclusive events measured by CMS and TOTEM [150]. The error bars represent the statistical and uncorrelated systematic uncertainties between neighboring bins, while the shaded areas denote the combined statistical and full systematic uncertainties. The coloured lines indicate model predictions. (Right) Photon energy spectrum measured by LHCf at $|\eta|$ >10.94. The filled circles show the inclusive photon spectrum measured by LHCf [152] and filled squares the spectrum for $N_{\rm ch} = 0$ events where no charged particles with $p_T > 100$ MeV and $|\eta|$ <2.5 are observed by ATLAS [153]. The coloured lines indicate model predictions. The error bars correspond to the statistical uncertainties and the shaded areas denote the combined statistical and systematic uncertainties. Figure from Ref. [151].

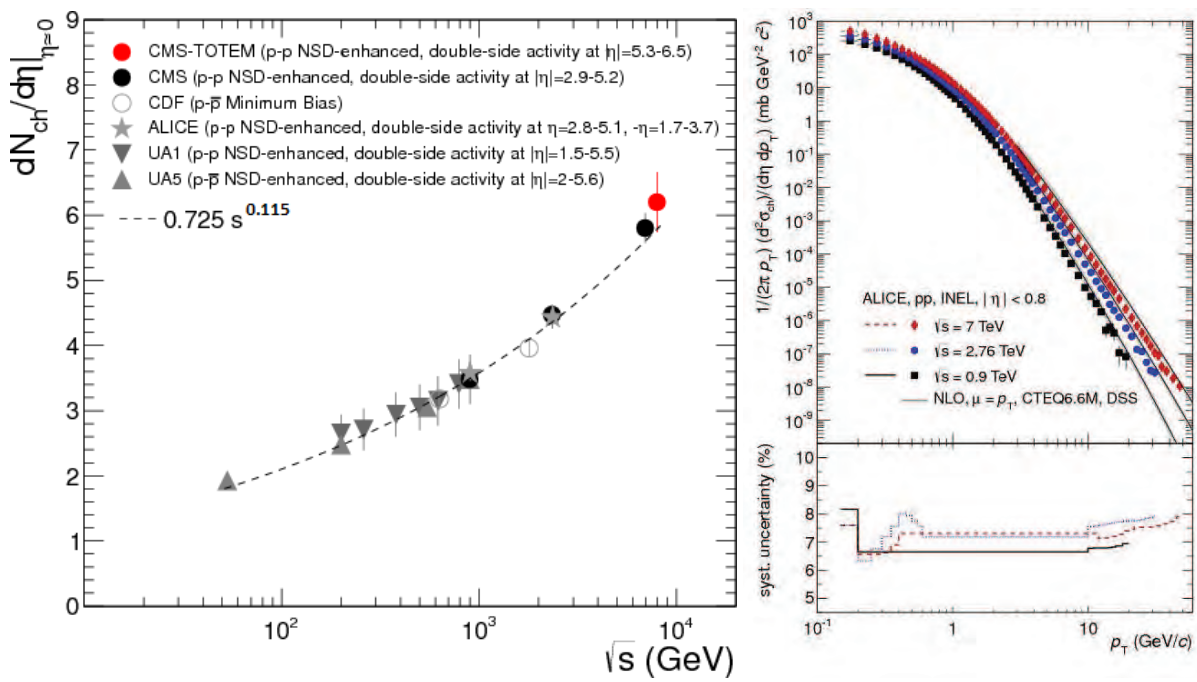

Figure 20.12: (Left) Energy dependence of the charged particle density $\mathrm{d}N_{\rm ch}/\mathrm{d}\eta$ at $\eta \approx 0$ for pp and $p\bar{p}$ collisions. Shown are measurements performed with different Non-SD event selections from UA1 [154], UA5 [155], CDF [156,157], ALICE [158] and CMS [159]. The dashed line is a power-law fit to the data. Figure from Ref. [150]. (Right) Differential cross section of charged particles with $|\eta| < 0.8$ in inelastic pp collisions at $\sqrt{s} = 0.9, 2.76$ and 7 TeV as a function of p_T. Only statistical uncertainties are shown. Figure from Ref. [160].

$$\frac{1}{\sigma_{\rm inel}}\mathrm{d}\sigma = \rho_1(y)\mathrm{d}y, \quad \frac{1}{\sigma_{\rm inel}}\mathrm{d}^2\sigma = \rho_2(y_1, y_2)\mathrm{d}y_1\mathrm{d}y_2 \quad \text{etc.} \tag{20.48}$$

By integrating we get

$$\int \rho_1(y)\mathrm{d}y = \langle n\rangle, \quad \int\int \rho_2(y_1, y_2)\mathrm{d}y_1\mathrm{d}y_2 = \langle n(n-1)\rangle \quad \text{etc.}, \tag{20.49}$$

where the angular brackets denote averaging over the event sample and n is the particle multiplicity.

Since the inclusive q-particle densities in general contain trivial contributions from lower-order densities, it is convenient to consider quantities C_q which vanish when one of their arguments becomes statistically independent of (uncorrelated with) the others. These quantities C_q, called correlation functions (or cumulant

Downloaded from https://academic.oup.com/ptep/article/2022/8/083C01/6651666 by KIT Library user on 27 September 2022

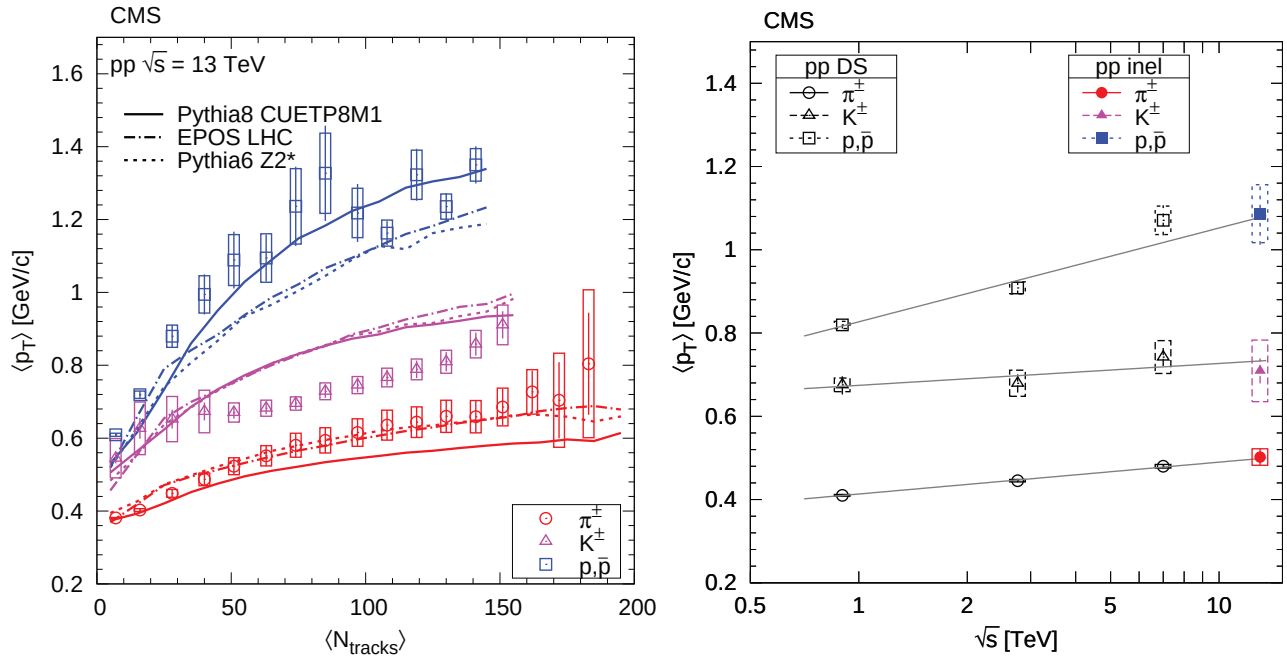

Figure 20.13: Average p_T of pions, kaons and protons in the range $|\eta| < 1.0$ as a function of (left) track multiplicity at $|\eta| < 2.4$ and (right) of center-of-mass energy where the curves show linear fits using $\ln s$. The error bars indicate the uncorrelated combined uncertainties, while the boxes show the uncorrelated systematic uncertainties. Figures from Ref. [161].

functions), are defined as:

$$C_2(1,2) = \rho_2(1,2) - \rho_1(1)\rho_1(2), \quad C_3(1,2,3)$$
$$= \rho_3(1,2,3) - \sum_{(3)} \rho_1(1)\rho_2(2,3) + 2\rho_1(1)\rho_1(2)\rho_1(3),$$
$$C_4(1,2,3,4) = \rho_4(1,2,3,4) - \sum_{(4)} \rho_1(1)\rho_3(1,2,3)$$
$$- \sum_{(3)} \rho_2(1,2)\rho_2(3,4) + 2\sum_{(6)} \rho_1(1)\rho_1(2)\rho_2(3,4)$$
$$- 6\rho_1(1)\rho_1(2)\rho_1(3)\rho_1(4). \tag{20.50}$$

The 2D two-particle correlation function is defined as

$$C(\Delta\eta, \Delta\phi) = \frac{\rho_2(\Delta\eta, \Delta\phi)}{\rho_1(\eta_a, \phi_a)\rho_1(\eta_b, \phi_b)}. \tag{20.51}$$

The distribution $\rho_2(\Delta\eta, \Delta\phi)$ is usually interpreted as a conditional probability to observe a particle a at the phase-space point (η_a, ϕ_a) if a particle b at (η_b, ϕ_b) is observed as well, and $\Delta\eta = \eta_a - \eta_b$ and $\Delta\phi = \phi_a - \phi_b$. The distributions $\rho_1(\eta_a, \phi_a)$ and $\rho_1(\eta_b, \phi_b)$ are probabilities to observe a single particle at (η_a, ϕ_a) and (η_b, ϕ_b), respectively. The denominator of Eq. (20.51) is constructed as a product of two single-particle distributions using an event mixing technique, where each particle in the pair comes from a different event. Experimentally, each reconstructed track is weighted by the inverse of an efficiency factor which accounts for the detector acceptance, the reconstruction and particle identification efficiencies, the contamination by secondary particles and the fraction of misreconstructed tracks.

An example of two-particle correlation functions measured in pp collisions at 7 TeV is shown in Fig. 20.14 for identical-particle pairs (right panel) and for particle–anti-particle pairs (left panel) [169].

We observe two distinct features which can be explained by short-range (in rapidity) correlations: 1) a near-side peak at $\Delta\phi \approx 0$ and 2) an away-side peak or rather a ridge at $\Delta\phi \approx \pi$. The near-side peak is considered to be caused by at least three effects:

- *fragmentation of partons scattered at a hard scale.* These relatively high p_T partons produce showers which after the hadronization form the mini-jets which create a broad structure extending over at least one unit in $\Delta\eta$ and $\Delta\phi$.
- *resonance decays.* The decay of resonances contributes to the near-side peak at $\Delta\eta \sim 0$ and extended in $\Delta\phi$ [170–172], depending on the released kinetic energy of the given resonance. This effect is mostly visible for unlike-sign particle pairs.
- *femtoscopic correlations.* The term "femtoscopic" refers to a length scale of the order of 10^{-15} m. These correlations are present at low relative momenta of the particles in a pair (representing a very small phase-space corner, so they are practically invisible in terms of $(\Delta\eta, \Delta\phi)$) and give rise to an enhancement of the correlation function (due to Bose-Einstein quantum statistics for identical bosons) or its suppression (due to Fermi-Dirac quantum statistics for identical fermions). Besides this, at low relative momenta there are correlations caused by Coulomb and/or other final state interactions. The shape of all these effects in $(\Delta\eta, \Delta\phi)$ space depend strongly on the mass of the particle type as well as on the size of the particle-emitting system. The latter is traditionally measured in Bose-Einstein correlation (BEC) analyses and is not part of this review.

The away-side peak originates from energy-momentum conservation which manifests itself by the quark and the anti-quark going back-to-back in ϕ. In this case the rapidity width of the away-side peak is much larger than the near-side peak since in the original matrix element the quark and the antiquark can be separated by some $\Delta\eta$ interval.

As discussed in Sections 20.3.3.2 and 20.3.3.3, there may be several cut Pomerons in the same event, each giving rise to particle sets which are, in general, independent of each other (except for small Bose-Einstein correlations). This leads to long-range (in rapidity) correlations. Since the density of secondaries, $\mathrm{d}N/\mathrm{d}y$, is proportional to the number of cut Pomerons, k, the probability to observe at least one particle is proportional to $\langle k \rangle$, while the probability to observe simultaneously two particles separated by some (rather large) rapidity interval is proportional to $\langle k^2 \rangle$. Thus the long-range correlations are pedicted to be $C_2 = \langle k^2 \rangle / \langle k \rangle^2 - 1 > 0$ which depends weakly on the separation $\Delta\eta$ between the two particles [173, 174]. In the case of the pure eikonal approach, neglecting the enhanced diagrams and the conservation law effects

Downloaded from https://academic.oup.com/ptep/article/2022/8/083C01/6651666 by KIT Library user on 27 September 2022

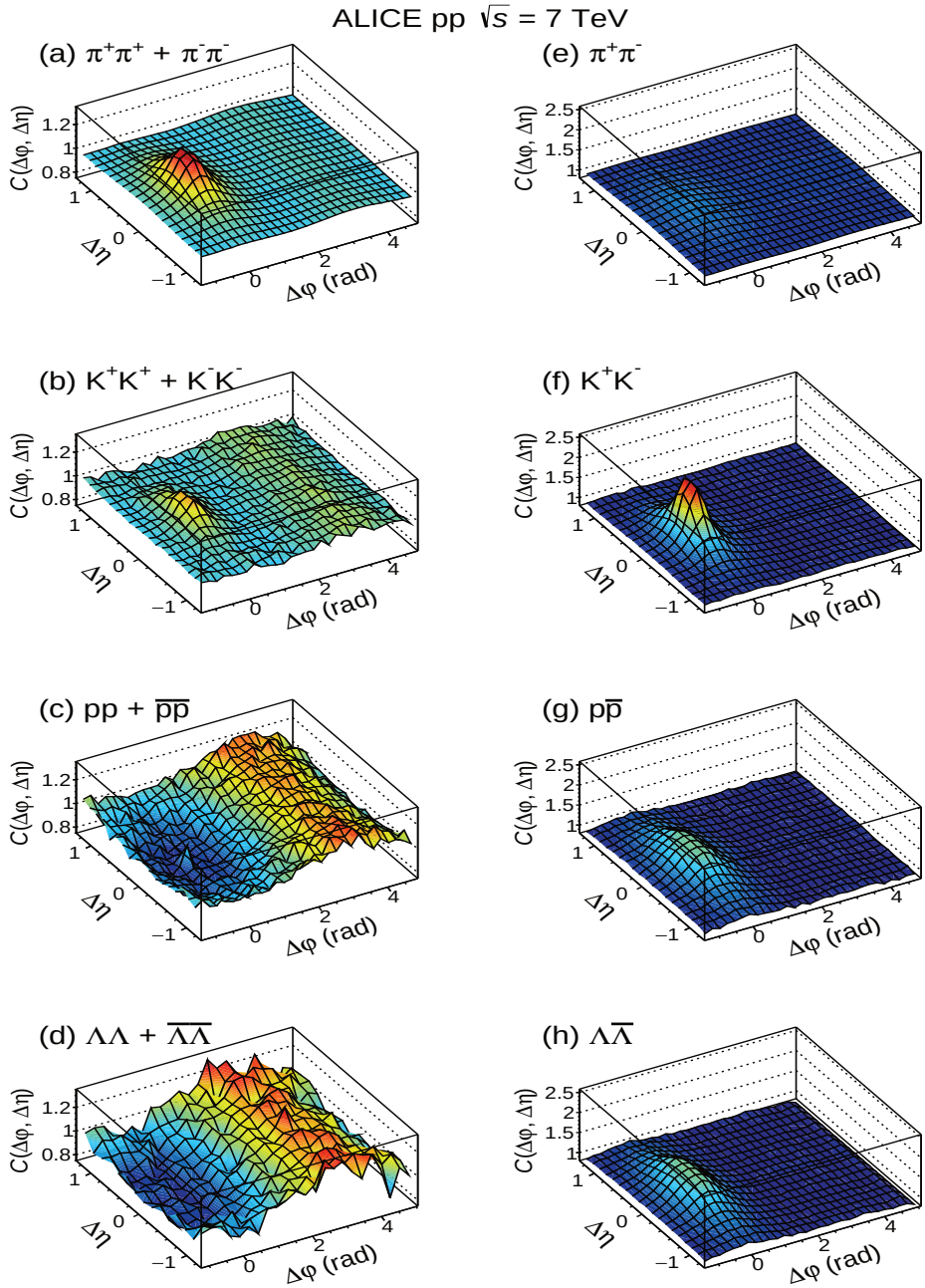

Figure 20.14: Two-particle correlation functions for identical-particle pairs: $\pi^+\pi^+ + \pi^-\pi^-$, $K^+K^+ + K^-K^-$, $pp + \bar{p}\bar{p}$, and $\Lambda\Lambda + \bar{\Lambda}\bar{\Lambda}$ (left panel) and particle–anti-particle pairs: $\pi^+\pi^-$, K^+K^-, $p\bar{p}$ and $\Lambda\bar{\Lambda}$ (right panel). Figure from Ref. [169].

in the proton fragmentation region, we expect that these long-range correlations,

$$C_2(\Delta y) = \frac{\sigma_{\rm inel} {\rm d}^2\sigma/{\rm d}y_1 {\rm d}y_2}{{\rm d}\sigma/{\rm d}y_1 \ {\rm d}\sigma/{\rm d}y_2} - 1 \sim \text{const}, \tag{20.52}$$

do not depend on the rapidity separation, $\Delta y = |y_1 - y_2|$, between the two particles. The contribution of the processes with more cut Pomerons also results in a much wider multiplicity distribution and in a larger density of soft particles coming from the 'underlying event'.

20.5.2.2 *Color reconnection*

In this context, we have to mention also the so-called 'colour reconnection' phenomenon. This is a pure 'soft QCD' effect. The point is that after a number of coloured secondary partons are produced, there are different possibilities to form the colour flow between these partons and to group the partons into colourless clusters. In the process of reconnection, one rearranges the colour flow in such a way as to minimize the size of the clusters. This is especially important when dealing with MPI contributions. The reconnection between the different cut Pomerons diminishes the final multiplicity and can change the form of the $N_{\rm ch}$ distributions (see e.g. Section 43.3.2 of [1] and [2, 13, 177, 178]).

20.5.2.3 *Double parton scattering*

The probability of MPI depends on the spatial distribution of partons in the incoming protons. The effects of MPI are suppressed if the density of partons is low and the partons from the incoming beam particles are separated from each other by a large interval in transverse coordinate space $\vec{x}_t$. Events in which two hard subprocesses, caused by interactions of two different parton pairs (say, $(a_1 b_1)$ and $(a_2 b_2)$), take place simultaneously, are called Double Parton Scattering (DPS). The DPS cross section is driven by the 'double parton distributions', $D(y_{a_1}, y_{a_2}, ...)$, where y_{a_1} and y_{a_2} are momentum fractions carried by the partons from the proton a and the dots denote all other coordinates. As a rule,

Downloaded from https://academic.oup.com/ptep/article/2022/8/083C01/6651666 by KIT Library user on 27 September 2022

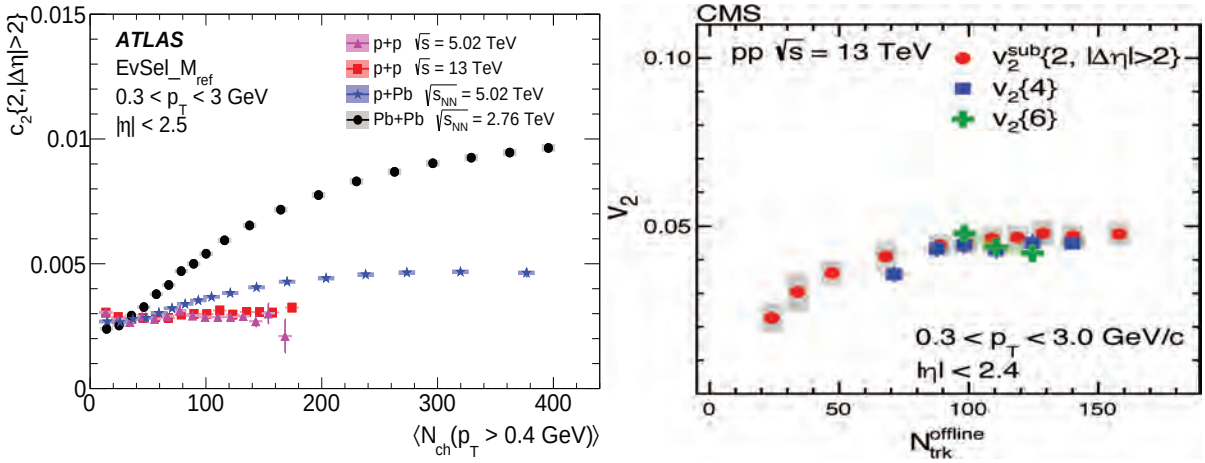

Figure 20.15: (Left) The two-particle cumulant, $c_2\{2, |\Delta\eta| > 2\}$, as a function of $\langle N_{\rm ch}(p_T > 0.4\ {\rm GeV})\rangle$ for pp collisions at $\sqrt{s} = 5.02$ and 13 TeV, pPb collisions at $\sqrt{s_{NN}} = 5.02$ TeV and low-multiplicity $PbPb$ collisions at $\sqrt{s_{NN}} = 2.76$ TeV. The data are constructed from particles with $0.3 < p_T < 3.0$ GeV. Figure from Ref. [175]. (Right) The $v_2\{2, |\Delta\eta| > 2\}$, $v_2\{4\}$ and $v_2\{6\}$ values as a function of number of charged particles, averaged over $0.3 < p_T < 3.0$ GeV and $|\eta| < 2.4$, in pp collisions at $\sqrt{s} = 13$ TeV. Figure from Ref. [176]. The error bars correspond to the statistical uncertainties, while the shaded areas denote the systematic uncertainties.

experiments study DPS processes at relatively small momentum fractions y_i. Here, correlations due to momentum conservation (like $y_{a_1} + y_{a_2} < 1$) are not so important, and with a reasonable accuracy we can assume a factorization

$$D(y_{a_1}, y_{a_2}, ...) \propto F(y_{a_1}) \cdot F(y_{a_2}) \ , \qquad (20.53)$$

where $F(y_{a_i})$ are the single parton distributions. In such a case the DPS cross section takes the form

$$\sigma^{\rm DPS} \ = \ c \cdot \frac{\sigma_{a_1 b_1} \sigma_{a_2 b_2}}{\sigma_{\rm eff}} \ , \qquad (20.54)$$

where $\sigma_{a_1 b_1}$ and $\sigma_{a_2 b_2}$ are cross sections for the two *independent* hard processes, while $\sigma_{\rm eff}$ characterizes the mean area occupied by the partons a_1 and b_1; the constant factor $c = 1/2$ if both hard processes $(a_1 b_1)$ and $(a_2 b_2)$ are identical, otherwise $c = 1$. Thus the DPS cross section is sensitive to the spatial separations between partons in the proton (see Section 7.2.3 in [2] and [179, 180] for more explanations and reviews).

One problem is that within this approach we *assume* that the partons a_1 and a_2 are produced by two independent parton showers (and similarly for the other incoming proton). On the other hand, there is a probability that from the beginning we start with the evolution of a single shower which further splits into two different branches. In this case the separation between the two partons (two shower branches) becomes very small – of the order of the inverse scale ($\sim 1/\sqrt{q^2}$) at which the splitting occurs. The exact value of this 'splitting' scale q^2 depends on the particular kinematics of the DPS process. So, different experiments (with different kinematical conditions) can give somewhat different values of $\sigma_{\rm eff}$. In general, the value of $\sigma_{\rm eff}$ depends on the following features: a) on the measured process since the spatial (b_t) distributions of different incoming partons (light quarks, heavy quarks, gluons) can be different; b) on the splitting scale, $\sqrt{q^2}$, of one parton cascade into two branches. The typically high value of the splitting scale then explains the fact that the experimentally measured values of $\sigma_{\rm eff} \sim 7$–25 mb (see Fig. 4 of [181]) are smaller than $\sigma_{\rm tot}$ or mostly even lower than the proton area $\pi R_p^2 \sim 22$–24 mb (see e.g. [182]); c) on the p_T balance, k_T, in the individual hard process (e.g. for two dijet productions $k_T = |\overrightarrow{p_{T1}} + \overrightarrow{p_{T2}}|$ where p_{T1} and p_{T2} are jet p_T's of the first hard process (similarly for the second hard process). A small value of k_T indicates that there were no splittings or the splitting scale $\sqrt{q^2}$ was small and, therefore, we expect larger $\sigma_{\rm eff}$; d) on the contribution of single parton scatterings misidentified as DPS. For a lower scale of the hard process this contribution is larger (see [183] for more detailed discussion).

20.5.2.4 *Final state interactions*

The formalism of the RFT does not include 'final state interactions' [16]. Therefore, besides the correlations considered in the previous Section 20.5.2.1 we have to expect the correlation caused by partons and hadrons rescattering in the final state. These effects are not crucial at lower energies, but become more important at high LHC energies, in particular in heavy-ion collisions where the particle density is large. For example, the final state interactions (FSI) lead to the formation of the collective flow of secondaries (see e.g. [185] for a review), especially in high-multiplicity events. To study the collective flow experimentally, one has to subtract correlations coming from few-particle sources such as resonance decays, mini-jets, multi-jets and BEC (so called "non-flow"). The non-flow can efficiently be suppressed using the sub-event method, that is by studying the azimuthal correlations between particles separated in η [186], or subtracted using the multi-particle correlation (or cumulant) techniques.

The cumulant method is based on calculating $2k$-particle azimuthal correlations, ${\rm corr}_n\{2k\}$, and cumulants $c_n\{2k\}$ (where $k = 1, 2, ...$), for nth Fourier harmonics. The ${\rm corr}_n\{2k\}$ are defined as [187, 188]:

$$\langle\langle {\rm corr}_n\{2\}\rangle\rangle = \langle\langle e^{in(\phi_1-\phi_2)}\rangle\rangle, \quad \langle\langle {\rm corr}_n\{4\}\rangle\rangle = \langle\langle e^{in(\phi_1+\phi_2-\phi_3-\phi_4)}\rangle\rangle,$$
$$\langle\langle {\rm corr}_n\{6\}\rangle\rangle = \langle\langle e^{in(\phi_1+\phi_2+\phi_3-\phi_4-\phi_5-\phi_6}\rangle\rangle$$

and similarly for higher numbers of correlated particles. The double-brackets $\langle\langle\rangle\rangle$ denote averaging first over particles in an event and then over events within a given event class. For every event, the average is taken over all possible combinations of azimuthal angles ϕ_l $(l = 1, ..., 2k)$ of the $2k$ particles. The cumulants are then obtained from multi-particle azimuthal correlations after subtracting correlations between $2(k-1)$ particles according to the following formulae [187, 188]:

$$c_n\{2\} = \langle\langle {\rm corr}_n\{2\}\rangle\rangle, \ c_n\{4\} = \langle\langle {\rm corr}_n\{4\}\rangle\rangle - 2\langle\langle {\rm corr}_n\{2\}\rangle\rangle^2,$$
$$c_n\{6\} = \langle\langle {\rm corr}_n\{6\}\rangle\rangle - 9\langle\langle {\rm corr}_n\{2\}\rangle\rangle \times \langle\langle {\rm corr}_n\{4\}\rangle\rangle + 12\langle\langle {\rm corr}_n\{2\}\rangle\rangle^3.$$

The cumulants for higher particle multiplicities are calculated in [187, 188]. The cumulants then serve to estimate the Fourier harmonics v_n as follows [187]:

$$v_n\{2\} = \sqrt{c_n\{2\}}, \ v_n\{4\} = \sqrt[4]{-c_n\{4\}}, \ v_n\{6\} = \sqrt[6]{c_n\{6\}/4}.$$

[16] In general, final state interactions can be included into the detailed structure of the multi-Pomeron vertices. However these vertices are phenomenological objects which are not well known experimentally.

Downloaded from https://academic.oup.com/ptep/article/2022/8/083C01/6651666 by KIT Library user on 27 September 2022

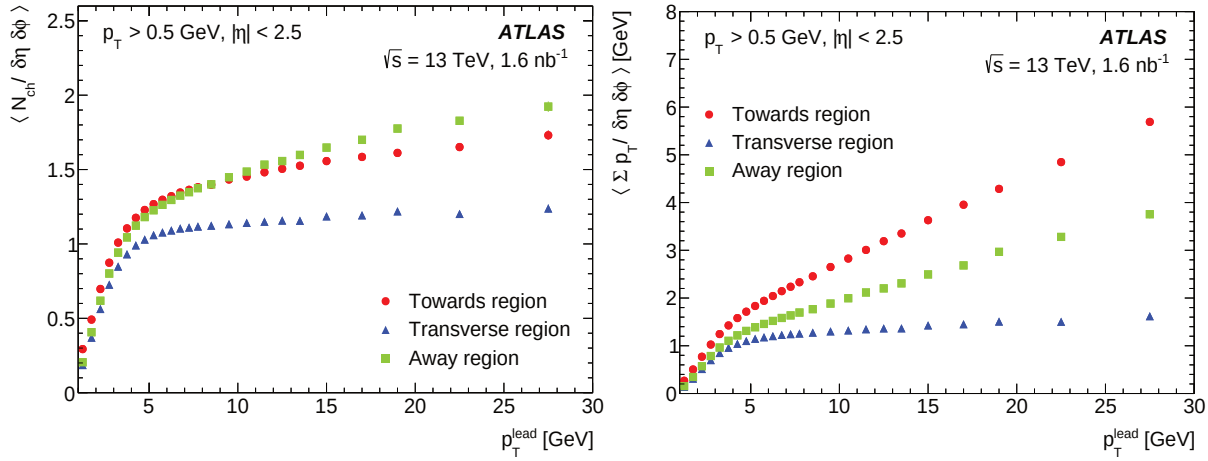

Figure 20.16: Mean charged particle density (left) and the sum of transverse momenta of secondaries (right) in events with the 'leading' high p_T particle as a function of $p_T^{\rm lead}$ in the transverse, towards and away azimuthal regions. Secondaries with $p_T > 0.5$ GeV and $|\eta| < 2.5$ are registered. The error bars (mostly hidden by the data markers) represent combined statistical and systematic uncertainties. Figures from [184].

Some of the long-range correlation ($|\Delta\eta| > 2$) results obtained on a sample of charged particles with $0.3 < p_T < 3.0$ GeV and $|\eta| < 2.4$ are summarized in Fig. 20.15. The left plot shows the cumulant c_2 measured for pp, pPb and $PbPb$ collisions [175], while the right plot shows the elliptical harmonics v_2 measured for pp collisions [176], both as functions of multiplicities of charged particles. The two-particle correlations are observed to be strongest and rising with $N_{\rm ch}$ for $PbPb$ collisions, and weakest and rather flat for pp collisions. The elliptical-flow harmonics for 4- and 6-particle correlations show again a rather flat multiplicity dependence (at least for large multiplicities). Within experimental uncertainties, the values of $v_2\{2\}, v_2\{4\}$ and $v_2\{6\}$ measured in pp collisions at 13 TeV are consistent with each other. The similarity between $v_2\{4\}$ and $v_2\{6\}$ suggests that some collective effects are occurring in pp collisions at high multiplicity and the observations are similar to those in $PbPb$ collisions, where the $v_2\{4\}$ values were measured to be close to $v_2\{6\}$ but they are both lower than $v_2\{2\}$ (not shown here)).

Another example of long-range correlations is the so-called "ridge effect". Here not only the 'back-to-back' jet correlations are registered, but also an excess of particles going in the same (in the azimuthal plane) direction as the leading (relatively high p_T) hadron. Moreover, this excess is seen at the rapidities separated from the leading hadron by a rather large interval (see e.g. [189] for a review).

It is popular to describe such FSI effects within the hydrodynamic model [190], which operates with collective (thermodynamic) variables. In terms of microscopic interactions, the collective flow can be caused by the geometry of a particular collision (the absorption is smaller for the secondaries flying in the direction orthogonal to the impact parameter vector $\vec{b}$ [191, 192]), or by the colour reconnection at the hadronization stage [193], or accounting for the rescattering of secondaries directly, as was done, for example, in the AMPT model [194].

20.5.3 *The underlying event*

Except for the exclusive case, any 'hard' subprocess is accompanied by soft secondaries coming from initial state radiation (ISR), final state radiation (FSR) and multiple parton interaction (MPI), see Subsection 7.2.2 in [2]. These extra particles distort the signal we are looking for. In particular, they affect the isolation criteria applied to photons and charged leptons and the vertex reconstruction efficiency. In general, also the effects of colour reconnection (discussed in Section 20.5.2.2) contribute to the underlying event.

The usual procedure of estimating the amount of underlying event (UE) is to spatially divide tracks in each event according to their azimuthal angle into the Toward region (where the highest p_T jet points), the Away region (opposite to the Toward region) and to two Transverse regions. The standard observables are the average track multiplicity per unit area and the average scalar sum of track p_T per unit area. Figure 20.16 shows the particle density and the sum of p_T for the UE in ATLAS events containing at least one charged particle with $p_T > 0.5$ GeV and $|\eta| < 2.5$ [184].

Note that by construction the largest values of $\langle p_T \rangle$ are observed in the 'Toward' region, while in the 'Away' region we observe a slightly larger density than in the Toward region. These are results of the 'leading' and 'backward' jet fragmentation. In the transverse region, mostly filled by particles from the UE, the particle density and sum of p_T per unit $(\Delta\eta, \Delta\phi)$ area practically do not depend on the $p_T^{\rm lead}$ since these secondaries come from the other cut Pomeron(s), that is, from other 'multiple interactions'. For low $p_T^{\rm lead} < 2$ GeV the distributions in all three regions are close to each other. These events actually do not contain a 'hard' subprocess. Moreover, for a very small $p_T^{\rm lead} \to 1$ GeV we start to select soft events with abnormally low $p_T < p_T^{\rm lead}$ particles. Since only particles with $p_T > 0.5$ GeV are registered, the signal drops fast for $p_T^{\rm lead} \to 1$ GeV. As a function of collision energy $\sqrt{s}$, the energy flow in the transverse region increases as $\sum p_T \sim s^{0.2}$ (as follows from Fig. 7 (right) in [184]) due to the larger number of MPI collisions and larger $\langle p_T \rangle$ in each collision [17]. As follows from this and other UE-dedicated LHC studies [195], from the comparisons of the data to the models with and without MPI, the necessity of MPI is convincingly demonstrated.

20.6 The Odderon

Apart from the even-signature singularity (Pomeron), in QCD with $N_c = 3$ there exists its counterpart, the odd-signature singularity placed at $j \simeq 1$ and formed by three t-channel reggeized gluons connected in colour space by the symmetric d^{abc} tensor of the colour $SU(3)$ group [200, 201]. This object is called the Odderon. The Odderon exchange amplitude has opposite sign for pp and $p\bar{p}$ scatterings. Its intercept is predicted to be very close to $j = 1$ [202–204], while according to perturbative estimates the coupling to the nucleon is rather small [205,206]. The corresponding amplitude is mainly real and is about 100 times smaller than the imaginary part of the Pomeron exchange amplitude. Calculating the elastic amplitude via the eikonal formula (20.13) we have to replace the opacity $\Omega(\mathrm{b})$ by the sum $\Omega = \Omega_{\rm even} + \Omega_{\rm odd}$, where $\Omega_{\rm even}$ is mainly real and $\Omega_{\rm odd}$ is imaginary. Note that at $t = 0$ this QCD Odderon does not couple to mesons, and the t-slope of the Odderon amplitude is expected to be smaller than that for the Pomeron; instead of the singularity at $t = 4m_\pi^2$ in the Pomeron case, the nearest singularity in the Odderon channel is at $t = 9m_\pi^2$, see for instance [204]. Thus, in the impact parameter b space the QCD Odderon occupies an area of a smaller radius, see e.g. [207].

[17] Recall the stronger absorption of the low k_t partons.

Downloaded from https://academic.oup.com/ptep/article/2022/8/083C01/6651666 by KIT Library user on 27 September 2022

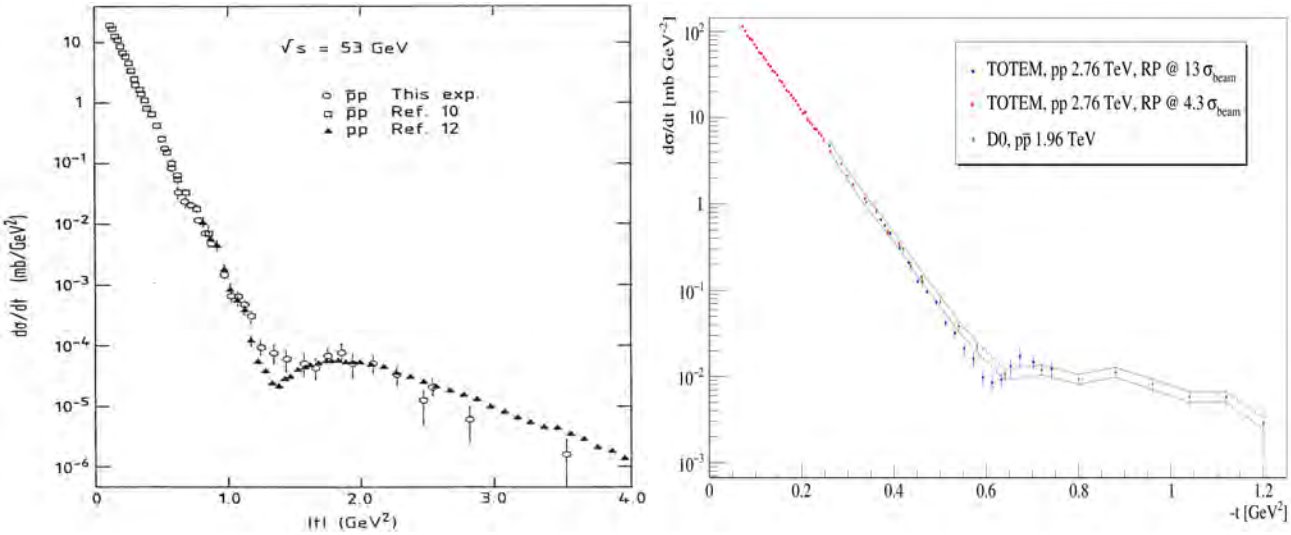

Figure 20.17: Comparison of the t-dependence of the elastic cross sections from pp and $p\bar{p}$ collisions. (Left) Data from the ISR energy of 53 GeV are shown by closed triangles [196] for pp collisions and by open circles [197] and open squares [198] for $p\bar{p}$ collisions. Only t-dependent uncertainties are shown and the systematic scale uncertainty is estimated to be ±30%. Figure from Ref. [197]. (Right) Data from the D0 experiment at 1.96 TeV [199] are compared with data from the TOTEM experiment [103]. The green dashed line indicates the normalization uncertainty of the D0 measurement. Figure from Ref. [103].

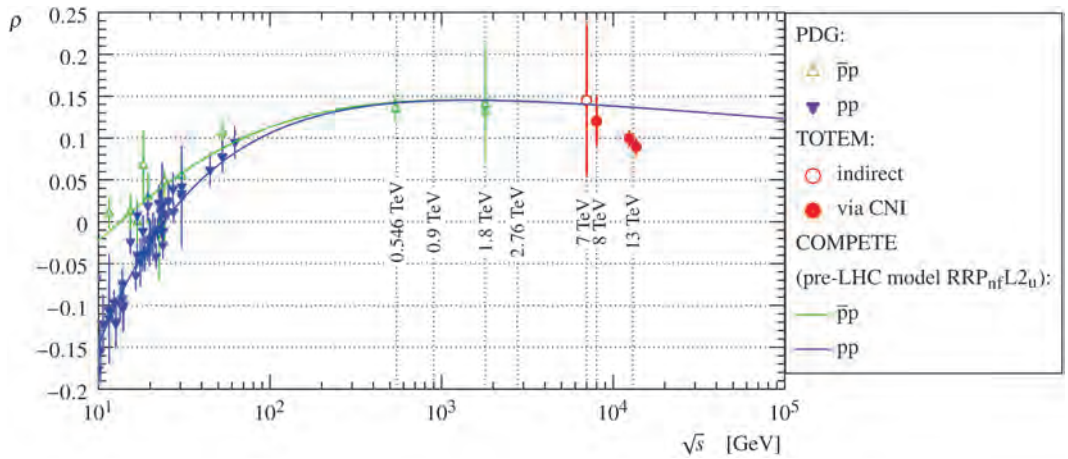

Figure 20.18: The dependence of the ρ parameter on the collision energy. The pp (blue) and $p\bar{p}$ (green) data are taken from [1]. The TOTEM measurements are marked in red. The two points at 13 TeV correspond to two fit cases, discussed in [102], using the same data. The lines represent fits to the data using the COMPETE parameterization [22]. Figure from Ref. [102].

Experimentally an indication in favour of a manifestation of the high energy C-odd amplitude was observed by comparing the elastic pp and $p\bar{p}$ cross sections in the dip region (where the contribution from the C-even amplitude has a minimum) at the CERN-ISR [197], see Fig. 20.17 (left) [18].

To get a better understanding of the Odderon effects it would be very instructive to have the $d\sigma_{el}/dt$ data for both pp and $p\bar{p}$ reactions at the same but higher energy ~ 1 TeV (ideally in the same apparatus) and, in the ideal case, to study the energy dependence.

At the moment we can only compare the pp cross section measured by TOTEM at $\sqrt{s} = 2.76$ TeV [103] with the $d\sigma/dt$ values measured by the D0 collaboration at 1.96 TeV in $p\bar{p}$ collisions [199], see Fig. 20.17 (right).

The situation looks quite intriguing, but needs further investigation. Note that in the TeV energy range the ω, ρ and ωP, ρP exchange contributions, which may be responsible for the difference between the pp and $p\bar{p}$ cross sections in the dip region at the ISR energies, are practically negligible.

Another way to search for the Odderon is to measure the real part of the elastic pp scattering amplitude via the interference with the pure QED one-photon exchange. Since the one-photon exchange amplitude contribution is sizeable only at very small $|t|$, this way we can study the Odderon at or near to $t = 0$. Indeed, the value of the ratio $\rho \equiv \mathrm{Re}T_{\mathrm{el}}/\mathrm{Im}T_{\mathrm{el}}$, obtained by TOTEM at 13 TeV ($\rho = 0.10 \pm 0.01$ [102]), turns out to be smaller than that expected for the pure even-signature amplitude, see Fig. 20.18.

Based on dispersion relations and assuming the C-even contribution only, from the known total cross sections we would rather expect $\rho \simeq 0.13$–0.14. The difference could indicate that the rise of the total cross section at energies above those of the LHC slows down (see the dispersion relation, Eq. (20.19)) or this could be attributed to an Odderon contribution (see e.g. [210]). However, the Odderon exchange amplitude extracted in this analysis has opposite sign to that for the lowest-α_s-order QCD Odderon, see e.g. [205, 206, 211, 212]. Besides this, the Odderon contribution to ρ, obtained in [210], grows with $\sqrt{s}$ (for $\sqrt{s} > 0.5$ TeV), while in QCD we expect that the Odderon contribution to ρ decreases with energy, since the QCD Odderon intercept is smaller than that of

[18] Note that a qualitatively similar behaviour to the $p\bar{p}$ ISR data, namely a filling in of the dip in the t-distribution, was observed by the UA4 collaboration at the CERN $Sp\bar{p}S$ collider at $\sqrt{s}$=546 and 630 GeV(see [208,209] and in particular Fig. 2 in [209]) and by the $D0$ collaboration at the Tevatron at 1.96 TeV [199].

Downloaded from https://academic.oup.com/ptep/article/2022/8/083C01/6651666 by KIT Library user on 27 September 2022

the QCD Pomeron.

It is worth mentioning also that the Odderon contribution is strongly screened by the multi-Pomeron diagrams, which facilitate the falling-off of ρ with energy increasing, see [213, 214]. On the other hand, analyzing the whole ensemble of high energy elastic pp ($p\bar{p}$) low $|t|$ data, a reasonable description can be obtained using the even-signature amplitude only, that is, without the Odderon. In particular, the RR(PL2)qc model/version of the COMPETE parameterization is consistent with the TOTEM 13 TeV data on $\sigma_{\rm tot}$ and ρ within 1σ [19]. Another example is the recent analysis in [212] of the low $|t| < 0.1$ GeV^2 elastic data. Fitting all the low-t pp and $p\bar{p}$ data in the range of $\sqrt{s}$ between 13 GeV and 13 TeV without Odderon, Donnachie and Landshoff [212] succeeded to describe the TOTEM cross section with less than 1σ deviation in each $\mathrm{d}\sigma_{\rm el}/\mathrm{d}t$ point (see Fig. 8 of [212]). Note that in this analysis, they get a larger value of ρ close to 0.14 at 13 TeV.

It was proposed also to search for the Odderon in exclusive C-even meson ($\pi^0, \eta, f_2, \eta_c, ...$) photoproduction (see e.g. [215,216]). However the expected cross sections are small (e.g. for η_c) and in each channel there is a large background caused either by Pomeron-Pomeron fusion (such as CEP of the f_2 meson production in pp or pPb collisions) or due to the vector meson radiative decay (such as $\omega \to \pi^0\gamma$ for the case of pion) [217]. Up to now, no definitive Odderon signal in the C-even meson production has been observed. At the moment there exist only upper limits on the photoproduction cross sections obtained in the measurements at HERA at $\sqrt{s} \simeq 200$ GeV [218–220].

To conclude, let us emphasize that the existence of the C-odd singularity with intercept
$\alpha_{\rm odd}(0) \simeq 1$ is a firm prediction of QCD. At least in the high k_t region there is a well established C-odd three-gluon contribution to the scattering amplitude. However the expected coupling of such an Odderon singularity is numerically very small. Therefore it is quite challenging to observe its manifestation experimentally. Currently it seems to be a bit premature to draw any definite conclusion about an experimental observation of the Odderon signal.

20.7 Asymptotics

The high-energy behaviour of total hadronic cross sections has been one of the oldest problems of strong interactions over many decades, beginning from Heisenberg [221]. The most important bound obtained based on general analytical properties of scattering amplitudes is the FLM bound [47–49]. It states that the growth of the total hadronic cross section with energy does not exceed $\ln^2 s$, see Eq. (20.34).

Recall that we neglected the photon contribution as well as the whole electro-weak sector, and that the parameter in Eq. (20.34) s_0 is an *a priori* unknown scale. However, if we were to assume a reasonable hadronic scale, $s_0 \simeq 1\,\mathrm{GeV}^2$, we would find that Eq. (20.34) implies an unrealistically high upper bound in comparison with the cross sections observed at present collider energies. Nevertheless there is a common trend in the literature (see for instance, reviews [222, 223] and references therein) to fit phenomenologically the total cross section with $\ln^2 s$, keeping in mind the saturation of the FLM bound. Such an asymptotic behaviour is assumed also by the COMPETE collaboration [22], which achieved a comprehensive description of all soft pre-LHC data measured at $\sqrt{s} \geq 4$ GeV as well as total pp cross sections from the LHC available in the first half of 2015 (see Section 51 in [24]).

It is interesting that the Froissart-type $\ln^2 s$ asymptotics of the pp total cross section are also supported by numerical results in lattice QCD [224]. Such a behaviour is also observed in the approach [225] based on Colour Glass Condensate saturation.

Finally, it is worth mentioning that the possibility that *asymptotically* the Pomeron intercept becomes smaller than 1, $\alpha_{\mathbb{P}}(0) < 1$, and at very high energies the total cross section starts to decrease with energy, though highly unlikely, is not yet completely rejected. For instance, such a behaviour is expected in a theory with only the triple-Pomeron coupling, $g_{3\mathbb{P}}$, and which neglects the more complicated multi-Pomeron vertices g^n_m, such as the $2 \to 2$ Pomeron coupling [226, 227].

[19] We thank Jean-Rene Cudell for clarifying this issue.

It was also argued that in the case of an increasing (with energy) cross section the only regime consistent asymptotically with both the s- and the t-channel unitarities is that of a *black* disc whose radius increases as $R = c \cdot \ln s$ [228] (i.e. $R \propto (\ln s)^\gamma$, with $\gamma = 1$ exactly).

20.8 Acknowledgements

It is a pleasure to thank Michael Albrow, Robert Cahn, Robert Ciesielski, Per Grafstrom, Frank Krauss, Paul Newman, Sergey Ostapchenko and Edward Sarkisyan-Grinbaum for discussions, suggestions and comments on this review. Special thanks to Graeme Watt who read the article through and helped to improve the presentation. MT is supported by MEYS of the Czech Republic within project LTT17018. VAK thanks the Institute of Physics of the Czech Academy of Sciences in Prague for hospitality.

References

[1] M. Tanabashi *et al.* (Particle Data Group), Phys. Rev. **D98**, 3, 030001 (2018).

[2] J. Campbell, J. Huston and F. Krauss, *The Black Book of Quantum Chromodynamics*, Oxford University Press (2017), ISBN 9780199652747, `https://doi.org/10.1093/oso/9780199652747.003.0004`.

[3] R. J. Eden *et al.*, *The analytic S-matrix*, Cambridge Univ. Press, Cambridge (1966).

[4] A. Martin, Lect. Notes Phys. **3**, 1 (1969).

[5] P. D. B. Collins, *An Introduction to Regge Theory and High-Energy Physics*, Cambridge Monographs on Mathematical Physics, Cambridge Univ. Press, Cambridge, UK (2009), ISBN 9780521110358, URL `http://www-spires.fnal.gov/spires/find/books/www?cl=QC793.3.R4C695`.

[6] S. Donnachie *et al.*, Camb. Monogr. Part. Phys. Nucl. Phys. Cosmol. **19**, 1 (2002).

[7] V. N. Gribov, *The theory of complex angular momenta: Gribov lectures on theoretical physics*, Cambridge Monographs on Mathematical Physics, Cambridge University Press (2007), ISBN 9780521037037, 9780521818346, 9780511055041, URL `http://www.cambridge.org/uk/catalogue/catalogue.asp?isbn=0521307848`.

[8] S. Ostapchenko, in "25th European Cosmic Ray Symposium (ECRS 2016) Turin, Italy, September 04-09, 2016," (2016), [arXiv:1612.09461].

[9] T. Sjostrand, Int. J. Mod. Phys. **A3**, 751 (1988).

[10] B. Andersson, Camb. Monogr. Part. Phys. Nucl. Phys. Cosmol. **7**, 1 (1997).

[11] W. Kittel and E. A. De Wolf, *Soft multihadron dynamics* (2005), ISBN 9789812562951.

[12] I. M. Dremin and A. B. Kaidalov, Phys. Usp. **49**, 263 (2006), [Usp. Fiz. Nauk176,275(2006)].

[13] A. Buckley *et al.*, Phys. Rept. **504**, 145 (2011), [arXiv:1101.2599].

[14] R. Ciesielski and K. Goulianos, PoS **ICHEP2012**, 301 (2013), [arXiv:1205.1446].

[15] K. Akiba *et al.* (LHC Forward Physics Working Group), J. Phys. **G43**, 110201 (2016), [arXiv:1611.05079].

[16] G. D. Alkhazov, S. L. Belostotsky and A. A. Vorobev, Phys. Rept. **42**, 89 (1978).

[17] E. L. Feinberg and I. Y. Pomeranchuk, Doklady Akad. Nauk SSSR **93**, 439 (1953); E. L. Feinberg and I. Y. Pomeranchuk, Suppl. Nuovo Cimento **III**, serie X, 652 (1956).

[18] R. Engel, D. Heck and T. Pierog, Ann. Rev. Nucl. Part. Sci. **61**, 467 (2011).

[19] M. Gell-Mann, in "High-energy physics. Proceedings, 11th International Conference, ICHEP'62, Geneva, Switzerland, Jul 4-11, 1962," 533–542 (1962).

[20] S. Frautschi, M. Gell-Mann and F. Zachariasen, Phys. Rev. **126**, 6, 2204 (1962).

Downloaded from https://academic.oup.com/ptep/article/2022/8/083C01/6651666 by KIT Library user on 27 September 2022

[21] K. G. Boreskov, A. B. Kaidalov and O. V. Kancheli, Phys. Atom. Nucl. **69**, 1765 (2006), [Yad. Fiz.69,1802(2006)].

[22] J. R. Cudell *et al.* (COMPETE), Phys. Rev. Lett. **89**, 201801 (2002), [hep-ph/0206172].

[23] C. Bourrely, J. Soffer and T. T. Wu, Eur. Phys. J. **C28**, 97 (2003), [hep-ph/0210264].

[24] C. Patrignani *et al.* (Particle Data Group), Chin. Phys. **C40**, 10, 100001 (2016).

[25] A. Donnachie and P. V. Landshoff, Nucl. Phys. **B231**, 189 (1984).

[26] A. Donnachie and P. V. Landshoff, Phys. Lett. **B296**, 227 (1992), [hep-ph/9209205].

[27] S. Mandelstam, Nuovo Cim. **30**, 1148 (1963).

[28] V. N. Gribov, I. Ya. Pomeranchuk and K. A. Ter-Martirosian, Phys. Lett. **9**, 269 (1964).

[29] V. A. Khoze, A. D. Martin and M. G. Ryskin, Int. J. Mod. Phys. **A30**, 08, 1542004 (2015), [arXiv:1402.2778].

[30] E. Gotsman, E. Levin and U. Maor, Int. J. Mod. Phys. **A30**, 08, 1542005 (2015), [arXiv:1403.4531].

[31] S. Ostapchenko, Phys. Rev. **D81**, 114028 (2010), [arXiv:1003.0196].

[32] V. N. Gribov, Sov. Phys. JETP **26**, 414 (1968), [Zh. Eksp. Teor. Fiz.53,654(1967)].

[33] U. Amaldi, M. Jacob and G. Matthiae, Ann. Rev. Nucl. Part. Sci. **26**, 385 (1976).

[34] A. B. Kaidalov, Phys. Rept. **50**, 157 (1979).

[35] V. Barone and E. Predazzi, *High-Energy Particle Diffraction*, volume v.565 of *Texts and Monographs in Physics*, Springer-Verlag, Berlin Heidelberg (2002), ISBN 3540421076, URL `http://www-spires.fnal.gov/spires/find/books/www?cl=QC794.6.C6B37::2002`.

[36] A. B. Kaidalov *et al.*, Acta Phys. Polon. **B34**, 3163 (2003), [hep-ph/0303111].

[37] L. Frankfurt and M. Strikman, in E. M. Henley and S. D. Ellis, editors, "100 Years of Subatomic Physics," 363–423 (2013), [arXiv:1304.4308].

[38] V. A. Khoze *et al.*, Eur. Phys. J. **C69**, 85 (2010), [arXiv:1005.4839].

[39] D. A. Fagundes *et al.*, Phys. Rev. **D88**, 9, 094019 (2013), [arXiv:1306.0452].

[40] R. Fiore *et al.*, Int. J. Mod. Phys. **A24**, 2551 (2009), [arXiv:0810.2902].

[41] I. M. Dremin, Phys. Usp. **56**, 3 (2013), [Usp. Fiz. Nauk 183, 3 (2013)], [arXiv:1206.5474].

[42] L. Frankfurt *et al.*, Phys. Rev. Lett. **101**, 202003 (2008), [arXiv:0808.0182].

[43] G. Bertsch *et al.*, Phys. Rev. Lett. **47**, 297 (1981).

[44] B. Z. Kopeliovich, L. I. Lapidus and A. B. Zamolodchikov, JETP Lett. **33**, 595 (1981), [Pisma Zh. Eksp. Teor. Fiz. 33, 612 (1981)].

[45] M. L. Good and W. D. Walker, Phys. Rev. **120**, 1855 (1960).

[46] J. Pumplin, Phys. Rev. **D8**, 2899 (1973).

[47] M. Froissart, Phys. Rev. **123**, 1053 (1961).

[48] A. Martin, Nuovo Cim. **A42**, 930 (1965).

[49] L. Lukaszuk and A. Martin, Nuovo Cim. **A52**, 122 (1967).

[50] A. A. Anselm and V. N. Gribov, Phys. Lett. **40B**, 487 (1972).

[51] G. Cohen-Tannoudji, V. V. Ilyin and L. L. Jenkovszky, Lett. Nuovo Cim. **5S2**, 957 (1972), [Lett. Nuovo Cim.5,957(1972)].

[52] V. A. Khoze, A. D. Martin and M. G. Ryskin, Eur. Phys. J. **C18**, 167 (2000), [hep-ph/0007359].

[53] G. Antchev *et al.* (TOTEM), Nucl. Phys. **B899**, 527 (2015), [arXiv:1503.08111].

[54] G. Antchev *et al.* (TOTEM), Eur. Phys. J. **C79**, 10, 861 (2019), [arXiv:1812.08283].

[55] L. Caneschi and A. Pignotti, Phys. Rev. Lett. **22**, 1219 (1969).

[56] O. V. Kancheli, JETP Lett. **11**, 267 (1970), [Pisma Zh. Eksp. Teor. Fiz. 11, 397 (1970)].

[57] A. H. Mueller, Phys. Rev. **D4**, 150 (1971).

[58] D. Amati, A. Stanghellini and S. Fubini, Nuovo Cim. **26**, 896 (1962).

[59] V. S. Fadin, E. A. Kuraev and L. N. Lipatov, Phys. Lett. **60B**, 50 (1975); E. A. Kuraev, L. N. Lipatov and V. S. Fadin, Sov. Phys. JETP **44**, 443 (1976), [Zh. Eksp. Teor. Fiz.71,840(1976)]; E. A. Kuraev, L. N. Lipatov and V. S. Fadin, Sov. Phys. JETP **45**, 199 (1977), [Zh. Eksp. Teor. Fiz.72,377(1977)]; I. I. Balitsky and L. N. Lipatov, Sov. J. Nucl. Phys. **28**, 822 (1978), [Yad. Fiz.28,1597(1978)].

[60] B. L. Ioffe, V. S. Fadin and L. N. Lipatov, *Quantum chromodynamics: Perturbative and nonperturbative aspects*, volume 30, Cambridge Univ. Press (2010), ISBN 9781107424753, 9780521631488, 9780511717444, URL `http://www.cambridge.org/de/knowledge/isbn/item2710695`.

[61] S. Ostapchenko, Phys. Rev. **D83**, 014018 (2011), [arXiv:1010.1869].

[62] J. L. Cardy, Nucl. Phys. **B75**, 413 (1974).

[63] A. B. Kaidalov *et al.*, Phys. Lett. **45B**, 493 (1973).

[64] E. G. S. Luna *et al.*, Eur. Phys. J. **C59**, 1 (2009), [arXiv:0807.4115].

[65] T. Sjöstrand, Adv. Ser. Direct. High Energy Phys. **29**, 191 (2018), [arXiv:1706.02166].

[66] K. Werner, F.-M. Liu and T. Pierog, Phys. Rev. **C74**, 044902 (2006), [hep-ph/0506232].

[67] V. A. Abramovsky, V. N. Gribov and O. V. Kancheli, Yad. Fiz. **18**, 595 (1973), [Sov. J. Nucl. Phys. 18, 308 (1974)].

[68] G. Alberi and G. Goggi, Phys. Rept. **74**, 1 (1981).

[69] K. A. Goulianos, Phys. Rept. **101**, 169 (1983).

[70] D. Bernard *et al.* (UA4), Phys. Lett. **B186**, 227 (1987).

[71] R. E. Ansorge *et al.* (UA5), Z. Phys. **C33**, 175 (1986).

[72] N. A. Amos *et al.* (E710), Phys. Lett. **B301**, 313 (1993).

[73] F. Abe *et al.* (CDF), Phys. Rev. **D50**, 5535 (1994).

[74] G. Aad *et al.* (ATLAS), Eur. Phys. J. **C72**, 1926 (2012), [arXiv:1201.2808].

[75] V. Khachatryan *et al.* (CMS), Phys. Rev. **D92**, 1, 012003 (2015), [arXiv:1503.08689].

[76] B. Abelev *et al.* (ALICE), Eur. Phys. J. **C73**, 6, 2456 (2013), [arXiv:1208.4968].

[77] G. Aad *et al.* (ATLAS), Phys. Lett. **B754**, 214 (2016), [arXiv:1511.00502].

[78] G. Aad *et al.* (ATLAS), JHEP **02**, 042 (2020), [arXiv:1911.00453].

[79] A. M. Sirunyan *et al.* (CMS and TOTEM) (2020), [arXiv:2002.12146].

[80] V. A. Khoze, A. D. Martin and M. G. Ryskin, Eur. Phys. J. **C73**, 2503 (2013), [arXiv:1306.2149].

[81] V. A. Khoze, A. D. Martin and M. G. Ryskin, Eur. Phys. J. **C23**, 311 (2002), [hep-ph/0111078].

[82] M. G. Albrow, T. D. Coughlin and J. R. Forshaw, Prog. Part. Nucl. Phys. **65**, 149 (2010), [arXiv:1006.1289].

[83] M. Albrow, Int. J. Mod. Phys. **A29**, 1402006 (2014).

[84] H. G. Fischer, W. Geist and M. Makariev, Int. J. Mod. Phys. **A29**, 28, 1446005 (2014).

[85] A. Kirk, Int. J. Mod. Phys. **A29**, 28, 1446001 (2014), [arXiv:1408.1196].

[86] M. A. Reyes *et al.* (E690), Phys. Rev. Lett. **81**, 4079 (1998).

Downloaded from https://academic.oup.com/ptep/article/2022/8/083C01/6651666 by KIT Library user on 27 September 2022

[87] G. Gutierrez and M. A. Reyes, Int. J. Mod. Phys. **A29**, 28, 1446008 (2014), [arXiv:1409.8243].

[88] Y. L. Dokshitzer, D. Diakonov and S. I. Troian, Phys. Rept. **58**, 269 (1980).

[89] M. Derrick *et al.* (ZEUS), Phys. Lett. **B315**, 481 (1993).

[90] T. Ahmed *et al.* (H1), Nucl. Phys. **B429**, 477 (1994).

[91] P. Newman and M. Wing, Rev. Mod. Phys. **86**, 3, 1037 (2014), [arXiv:1308.3368].

[92] A. Aktas *et al.* (H1), Eur. Phys. J. **C48**, 715 (2006), [hep-ex/0606004].

[93] S. Chekanov *et al.* (ZEUS), Nucl. Phys. **B816**, 1 (2009), [arXiv:0812.2003].

[94] F. D. Aaron *et al.* (H1), Eur. Phys. J. **C72**, 2074 (2012), [arXiv:1203.4495].

[95] F. D. Aaron *et al.* (H1, ZEUS), Eur. Phys. J. **C72**, 2175 (2012), [arXiv:1207.4864].

[96] A. Aktas *et al.* (H1), JHEP **10**, 042 (2007), [arXiv:0708.3217].

[97] A. Aktas *et al.* (H1), Eur. Phys. J. **C50**, 1 (2007), [hep-ex/0610076].

[98] S. Chekanov *et al.* (ZEUS), Nucl. Phys. **B672**, 3 (2003), [hep-ex/0307068].

[99] E. G. de Oliveira, A. D. Martin and M. G. Ryskin, Phys. Lett. **B695**, 162 (2011), [arXiv:1010.1366].

[100] G. Antchev *et al.* (TOTEM), Eur. Phys. J. **C79**, 2, 103 (2019), [arXiv:1712.06153].

[101] C. Augier *et al.* (UA4/2), Phys. Lett. **B316**, 448 (1993).

[102] G. Antchev *et al.* (TOTEM), Eur. Phys. J. **C79**, 9, 785 (2019), [arXiv:1812.04732].

[103] G. Antchev *et al.* (TOTEM), Eur. Phys. J. **C80**, 2, 91 (2020), [arXiv:1812.08610].

[104] G. Antchev *et al.* (TOTEM), EPL **101**, 2, 21002 (2013).

[105] G. Antchev *et al.* (TOTEM), Phys. Rev. Lett. **111**, 1, 012001 (2013).

[106] G. Aad *et al.* (ATLAS), Nucl. Phys. **B889**, 486 (2014), [arXiv:1408.5778].

[107] M. Aaboud *et al.* (ATLAS), Phys. Lett. **B761**, 158 (2016), [arXiv:1607.06605].

[108] M. M. Block and R. N. Cahn, Rev. Mod. Phys. **57**, 563 (1985).

[109] F. Abe *et al.* (CDF), Phys. Rev. **D50**, 5550 (1994).

[110] C. Avila *et al.* (E811), Phys. Lett. **B445**, 419 (1999).

[111] W. Guryn, "Invited talk at the Workshop on Diffraction and Low-x Physics, Reggio Calabria, Italy, August 26th–September 1st, 2018," ; J. Adam *et al.* (STAR), Phys. Lett. B **808**, 135663 (2020), [arXiv:2003.12136].

[112] K. Nakamura *et al.* (Particle Data Group), J. Phys. **G37**, 075021 (2010).

[113] F. J. Nemes, PoS **DIS2017**, 059 (2018).

[114] G. Antchev *et al.* (TOTEM), EPL **95**, 4, 41001 (2011), [arXiv:1110.1385].

[115] G. Antchev *et al.* (TOTEM), Eur. Phys. J. **C76**, 12, 661 (2016), [arXiv:1610.00603].

[116] J. Kaspar, "Invited talk at the meeting of the LHC Working Group on Forward Physics and Diffraction, CERN, Switzerland, December 16-17th, 2019," .

[117] V. A. Schegelsky and M. G. Ryskin, Phys. Rev. **D85**, 094024 (2012), [arXiv:1112.3243].

[118] A. Bruni, X. Janssen and P. Marage, in "Proceedings, HERA and the LHC Workshop Series on the implications of HERA for LHC physics: 2006-2008," 427–439 (2008), [arXiv:0812.0539].

[119] A. Levy, in "Proceedings, 17th International Workshop on Deep-Inelastic Scattering and Related Subjects (DIS 2009): Madrid, Spain, April 26-30, 2009," 177 (2009), [arXiv:0907.2178].

[120] J. R. Forshaw, R. Sandapen and G. Shaw, JHEP **11**, 025 (2006), [hep-ph/0608161].

[121] A. Capella *et al.*, Nucl. Phys. **B593**, 336 (2001), [hep-ph/0005049].

[122] V. S. Fadin and L. N. Lipatov, Phys. Lett. **B429**, 127 (1998), [hep-ph/9802290].

[123] M. Ciafaloni and G. Camici, Phys. Lett. **B430**, 349 (1998), [hep-ph/9803389].

[124] F. D. Aaron *et al.* (H1), JHEP **05**, 032 (2010), [arXiv:0910.5831].

[125] C. Adloff *et al.* (H1), Eur. Phys. J. **C13**, 371 (2000), [hep-ex/9902019].

[126] J. Breitweg *et al.* (ZEUS), Eur. Phys. J. **C6**, 603 (1999), [hep-ex/9808020].

[127] S. Chekanov *et al.* (ZEUS), PMC Phys. **A1**, 6 (2007), [arXiv:0708.1478].

[128] M. Ciafaloni, Nucl. Phys. **B296**, 49 (1988).

[129] S. Catani, F. Fiorani and G. Marchesini, Phys. Lett. **B234**, 339 (1990).

[130] S. Catani, F. Fiorani and G. Marchesini, Nucl. Phys. **B336**, 18 (1990).

[131] G. Marchesini, Nucl. Phys. **B445**, 49 (1995), [hep-ph/9412327].

[132] G. P. Salam, JHEP **07**, 019 (1998), [hep-ph/9806482].

[133] M. Ciafaloni and D. Colferai, Phys. Lett. **B452**, 372 (1999), [hep-ph/9812366].

[134] H. Kowalski, L. N. Lipatov and D. A. Ross, Eur. Phys. J. **C76**, 1, 23 (2016), [arXiv:1508.05744].

[135] H. Kowalski *et al.*, Eur. Phys. J. **C77**, 11, 777 (2017), [arXiv:1707.01460].

[136] S. J. Brodsky *et al.*, JETP Lett. **70**, 155 (1999), [hep-ph/9901229].

[137] R. D. Ball *et al.*, Eur. Phys. J. **C78**, 4, 321 (2018), [arXiv:1710.05935].

[138] E. M. Levin and M. G. Ryskin, Phys. Rept. **189**, 267 (1990).

[139] L. V. Gribov, E. M. Levin and M. G. Ryskin, Phys. Rept. **100**, 1 (1983).

[140] E. M. Levin, M. G. Ryskin and A. G. Shuvaev, Nucl. Phys. **B387**, 589 (1992).

[141] A. H. Mueller, Phys. Rept. **73**, 237 (1981).

[142] A. H. Mueller, Nucl. Phys. **B415**, 373 (1994).

[143] A. H. Mueller and B. Patel, Nucl. Phys. **B425**, 471 (1994), [hep-ph/9403256].

[144] N. N. Nikolaev, B. G. Zakharov and V. R. Zoller, JETP Lett. **59**, 6 (1994), [hep-ph/9312268].

[145] V. N. Gribov and L. N. Lipatov, Sov. J. Nucl. Phys. **15**, 438 (1972), [Yad. Fiz.15,781(1972)]; G. Altarelli and G. Parisi, Nucl. Phys. **B126**, 298 (1977); Y. L. Dokshitzer, Sov. Phys. JETP **46**, 641 (1977), [Zh. Eksp. Teor. Fiz. 73, 1216 (1977)].

[146] I. Balitsky, Nucl. Phys. **B463**, 99 (1996), [hep-ph/9509348].

[147] I. Balitsky, Phys. Rev. **D60**, 014020 (1999), [hep-ph/9812311].

[148] Y. V. Kovchegov, Phys. Rev. **D60**, 034008 (1999), [hep-ph/9901281].

[149] G. Gustafson, Phys. Lett. **B718**, 1054 (2013), [arXiv:1206.1733].

[150] S. Chatrchyan *et al.* (CMS, TOTEM), Eur. Phys. J. **C74**, 10, 3053 (2014), [arXiv:1405.0722].

[151] Q.-D. Zhou (LHCF, ATLAS), EPJ Web Conf. **208**, 05008 (2019).

Downloaded from https://academic.oup.com/ptep/article/2022/8/083C01/6651666 by KIT Library user on 27 September 2022

[152] O. Adriani *et al.* (LHCf), Phys. Lett. **B780**, 233 (2018), [arXiv:1703.07678].

[153] M. Aaboud *et al.* (ATLAS) , ATLAS-CONF-2017-075.

[154] C. Albajar *et al.* (UA1), Nucl. Phys. **B335**, 261 (1990).

[155] G. J. Alner *et al.* (UA5), Z. Phys. **C33**, 1 (1986).

[156] T. Aaltonen *et al.* (CDF), Phys. Rev. **D79**, 112005 (2009), [Erratum: Phys. Rev.D82,119903(2010)], [arXiv:0904.1098].

[157] F. Abe *et al.* (CDF), Phys. Rev. **D41**, 2330 (1990), [,119(1989)].

[158] K. Aamodt *et al.* (ALICE), Eur. Phys. J. **C68**, 89 (2010), [arXiv:1004.3034].

[159] V. Khachatryan *et al.* (CMS), Phys. Rev. Lett. **105**, 022002 (2010), [arXiv:1005.3299].

[160] B. B. Abelev *et al.* (ALICE), Eur. Phys. J. **C73**, 12, 2662 (2013), [arXiv:1307.1093].

[161] A. M. Sirunyan *et al.* (CMS), Phys. Rev. **D96**, 11, 112003 (2017), [arXiv:1706.10194].

[162] M. G. Ryskin, A. D. Martin and V. A. Khoze, Eur. Phys. J. **C71**, 1617 (2011), [arXiv:1102.2844].

[163] X.-N. Wang, Phys. Rept. **280**, 287 (1997), [hep-ph/9605214].

[164] S. Ostapchenko and M. Bleicher, Universe **5**, 5, 106 (2019).

[165] F. M. Liu *et al.*, J. Phys. **G28**, 2597 (2002), [hep-ph/0109104].

[166] E. Gotsman, E. Levin and U. Maor, Acta Phys. Polon. Supp. **8**, 777 (2015).

[167] Y. V. Kovchegov and E. Levin, Camb. Monogr. Part. Phys. Nucl. Phys. Cosmol. **33**, 1 (2012).

[168] E. A. De Wolf, I. M. Dremin and W. Kittel, Phys. Rept. **270**, 1 (1996), [hep-ph/9508325].

[169] J. Adam *et al.* (ALICE), Eur. Phys. J. **C77**, 8, 569 (2017), [arXiv:1612.08975].

[170] V. Khachatryan *et al.* (CMS), JHEP **09**, 091 (2010), [arXiv:1009.4122].

[171] K. Eggert *et al.*, Nucl. Phys. **B86**, 201 (1975).

[172] B. Alver *et al.* (PHOBOS), Phys. Rev. **C75**, 054913 (2007), [arXiv:0704.0966].

[173] E. M. Levin and M. G. Ryskin, Sov. J. Nucl. Phys. **20**, 280 (1975), [Yad. Fiz.20,519(1974)].

[174] A. Capella and A. Krzywicki, Phys. Rev. **D18**, 4120 (1978).

[175] M. Aaboud *et al.* (ATLAS), Eur. Phys. J. **C77**, 6, 428 (2017), [arXiv:1705.04176].

[176] V. Khachatryan *et al.* (CMS), Phys. Lett. **B765**, 193 (2017), [arXiv:1606.06198].

[177] S. Gieseke, "Invited talk at the Workshop on Multiple Partonic Interactions at the LHC, Prague, Czech Republic, November 18th–26th, 2019," .

[178] S. Kundu, B. Mohanty and D. Mallick (2019), [arXiv:1912.05176].

[179] M. Diehl, D. Ostermeier and A. Schafer, JHEP **03**, 089 (2012), [Erratum: JHEP03,001(2016)], [arXiv:1111.0910].

[180] T. Sjostrand and P. Z. Skands, JHEP **03**, 053 (2004), [hep-ph/0402078].

[181] M. Aaboud *et al.* (ATLAS), Phys. Lett. **B790**, 595 (2019), [Phys. Lett.790,595(2019)], [arXiv:1811.11094].

[182] M. G. Ryskin and A. M. Snigirev, Phys. Rev. **D83**, 114047 (2011), [arXiv:1103.3495].

[183] B. Blok *et al.*, Eur. Phys. J. **C74**, 2926 (2014), [arXiv:1306.3763].

[184] M. Aaboud *et al.* (ATLAS), JHEP **03**, 157 (2017), [arXiv:1701.05390].

[185] R. Snellings, New J. Phys. **13**, 055008 (2011), [arXiv:1102.3010].

[186] M. Aaboud *et al.* (ATLAS), Phys. Rev. **C97**, 2, 024904 (2018), [arXiv:1708.03559].

[187] N. Borghini, P. M. Dinh and J.-Y. Ollitrault, Phys. Rev. **C63**, 054906 (2001), [arXiv:nucl-th/0007063].

[188] A. Bilandzic, R. Snellings and S. Voloshin, Phys. Rev. **C83**, 044913 (2011), [arXiv:1010.0233].

[189] W. Li, Mod. Phys. Lett. **A27**, 1230018 (2012), [arXiv:1206.0148].

[190] B. Schenke, J. Phys. **G38**, 124009 (2011), [arXiv:1106.6012].

[191] K. G. Boreskov, A. B. Kaidalov and O. V. Kancheli, Eur. Phys. J. **C58**, 445 (2008), [arXiv:0809.0625].

[192] K. G. Boreskov, A. B. Kaidalov and O. V. Kancheli, Phys. Atom. Nucl. **72**, 361 (2009), [Yad. Fiz.72,390(2009)].

[193] C. Bierlich and J. R. Christiansen, Phys. Rev. **D92**, 9, 094010 (2015), [arXiv:1507.02091].

[194] Z.-W. Lin *et al.*, Phys. Rev. **C72**, 064901 (2005), [arXiv:nucl-th/0411110].

[195] V. Khachatryan *et al.* (CMS) , CMS-PAS-FSQ-16-008.

[196] E. Nagy *et al.*, Nucl. Phys. **B150**, 221 (1979).

[197] A. Breakstone *et al.*, Phys. Rev. Lett. **54**, 2180 (1985).

[198] A. Breakstone *et al.* (AMES-BOLOGNA-CERN-DORTMUND-HEIDELBERG-WARSAW), Nucl. Phys. **B248**, 253 (1984).

[199] V. M. Abazov *et al.* (D0), Phys. Rev. **D86**, 012009 (2012), [arXiv:1206.0687].

[200] J. Bartels, Nucl. Phys. **B175**, 365 (1980).

[201] J. Kwiecinski and M. Praszalowicz, Phys. Lett. **94B**, 413 (1980).

[202] M. A. Braun (1998), [hep-ph/9805394].

[203] J. Bartels, L. N. Lipatov and G. P. Vacca, Phys. Lett. **B477**, 178 (2000), [hep-ph/9912423].

[204] C. Ewerz (2003), [hep-ph/0306137].

[205] M. Fukugita and J. Kwiecinski, Phys. Lett. **83B**, 119 (1979), [,625(1979)].

[206] M. G. Ryskin, Sov. J. Nucl. Phys. **46**, 337 (1987), [Yad. Fiz.46,611(1987)].

[207] J. Bartels, C. Contreras and G. P. Vacca, JHEP **04**, 183 (2020), [arXiv:1910.04588].

[208] M. Bozzo *et al.* (UA4), Phys. Lett. **155B**, 197 (1985).

[209] D. Bernard *et al.* (UA4), Phys. Lett. **B171**, 142 (1986).

[210] E. Martynov and B. Nicolescu, Eur. Phys. J. **C79**, 6, 461 (2019), [arXiv:1808.08580].

[211] A. Donnachie and P. V. Landshoff, Phys. Lett. **123B**, 345 (1983).

[212] A. Donnachie and P. V. Landshoff, Phys. Lett. **B798**, 135008 (2019), [arXiv:1904.11218].

[213] J. Finkelstein *et al.*, Phys. Lett. **B232**, 257 (1989).

[214] V. A. Khoze, A. D. Martin and M. G. Ryskin, Phys. Lett. **B780**, 352 (2018), [arXiv:1801.07065].

[215] W. Kilian and O. Nachtmann, Eur. Phys. J. **C5**, 317 (1998), [hep-ph/9712371].

[216] J. Bartels *et al.*, Eur. Phys. J. **C20**, 323 (2001), [hep-ph/0102221].

[217] L. A. Harland-Lang *et al.*, Phys. Rev. **D99**, 3, 034011 (2019), [arXiv:1811.12705].

[218] J. Olsson (H1), in "New trends in high-energy physics: Experiment, phenomenology, theory. Proceedings, International Conference, Yalta, Crimea, Ukraine, September 22-29, 2001," 79–87 (2001), [hep-ex/0112012].

[219] C. Adloff *et al.* (H1), Phys. Lett. **B544**, 35 (2002), [hep-ex/0206073].

[220] T. Berndt (H1), Acta Phys. Polon. **B33**, 3499 (2002), [,182(2002)].

Downloaded from https://academic.oup.com/ptep/article/2022/8/083C01/6651666 by KIT Library user on 27 September 2022

[221] W. Heisenberg, Z. Phys. **133**, 65 (1952).

[222] G. Pancheri and Y. N. Srivastava, Eur. Phys. J. **C77**, 3, 150 (2017), [arXiv:1610.10038].

[223] M. M. Block, Phys. Rept. **436**, 71 (2006), [hep-ph/0606215].

[224] M. Giordano, E. Meggiolaro and N. Moretti, JHEP **09**, 031 (2012), [arXiv:1203.0961].

[225] E. Ferreiro *et al.*, Nucl. Phys. **A710**, 373 (2002), [hep-ph/0206241].

[226] P. Grassberger and K. Sundermeyer, Phys. Lett. **77B**, 220 (1978).

[227] K. G. Boreskov, in M. Olshanetsky and A. Vainshtein, editors, "Multiple facets of quantization and supersymmetry," 322–351 (2001), [hep-ph/0112325].

[228] V. A. Khoze, A. D. Martin and M. G. Ryskin, Phys. Lett. **B787**, 167 (2018), [arXiv:1809.10406].

Downloaded from https://academic.oup.com/ptep/article/2022/8/083C01/6651666 by KIT Library user on 27 September 2022

Downloaded from https://academic.oup.com/ptep/article/2022/8/083C01/6651666 by KIT Library user on 27 September 2022

Astrophysics and Cosmology

21. Experimental tests of gravitational theory (rev.) 417
22. Big-Bang cosmology (rev.) 430
23. Inflation (rev.) 443
24. Big-Bang nucleosynthesis (rev.) 459
25. Cosmological parameters (rev.) 467
26. Neutrinos in cosmology (rev.) 476
27. Dark matter (rev.) 483
28. Dark energy (rev.) 499
29. Cosmic microwave background (rev.) 509
30. Cosmic rays (rev.) 520

Downloaded from https://academic.oup.com/ptep/article/2022/8/083C01/6651666 by KIT Library user on 27 September 2022

Downloaded from https://academic.oup.com/ptep/article/2022/8/083C01/6651666 by KIT Library user on 27 September 2022

21. Experimental Tests of Gravitational Theory

Revised August 2021 by T. Damour (IHES, Bures-sur-Yvette).

21.1 General Relativity

Einstein's theory of General Relativity (GR), the current "standard" theory of gravitation, describes gravity as a universal deformation of the Minkowski metric:

$$g_{\mu\nu}(x^\lambda) = \eta_{\mu\nu} + h_{\mu\nu}(x^\lambda)\ , \text{ where } \eta_{\mu\nu} = \mathrm{diag}(-1,+1,+1,+1)\ . \tag{21.1}$$

GR is classically defined by two postulates, embodied in the total action defining the theory:

$$S_{\rm tot}[g_{\mu\nu},\psi,A_\mu,H] = c^{-1}\int d^4x(\mathcal{L}_{\rm Ein}+\mathcal{L}_{\rm SM})\,. \tag{21.2}$$

The first postulate that states that the Lagrangian density describing the propagation and self-interaction of the gravitational field is

$$\mathcal{L}_{\rm Ein}[g_{\alpha\beta}] = \frac{c^4}{16\pi G}\sqrt{g}g^{\mu\nu}R_{\mu\nu}(g_{\alpha\beta})\ , \tag{21.3}$$

where G denotes Newton's constant, $g=-\det(g_{\mu\nu})$, $g^{\mu\nu}$ is the matrix inverse of $g_{\mu\nu}$, and where the Ricci tensor $R_{\mu\nu}\equiv R^\alpha{}_{\mu\alpha\nu}$ is the only independent trace of the curvature tensor

$$R^\alpha{}_{\mu\beta\nu} = \partial_\beta\Gamma^\alpha_{\mu\nu} - \partial_\nu\Gamma^\alpha_{\mu\beta} + \Gamma^\alpha_{\sigma\beta}\Gamma^\sigma_{\mu\nu} - \Gamma^\alpha_{\sigma\nu}\Gamma^\sigma_{\mu\beta}\ , \tag{21.4}$$

$$\Gamma^\lambda_{\mu\nu} = \frac{1}{2}g^{\lambda\sigma}(\partial_\mu g_{\nu\sigma}+\partial_\nu g_{\mu\sigma}-\partial_\sigma g_{\mu\nu})\,. \tag{21.5}$$

The second postulate states that $g_{\mu\nu}$ (and its associated connection) couples universally, and minimally, to all the bosonic (respectively fermionic) fields of the Standard Model by replacing everywhere the Minkowski metric $\eta_{\mu\nu}$ (respectively the flat Minkowski connection). Schematically (suppressing matrix indices and labels for the various gauge fields and fermions and for the Higgs doublet),

$$\begin{aligned}&\mathcal{L}_{\rm SM}[\psi,A_\mu,H,g_{\mu\nu}] = \\ &-\frac{1}{4}\sum\sqrt{g}g^{\mu\alpha}g^{\nu\beta}F^a_{\mu\nu}F^a_{\alpha\beta} - \sum\sqrt{g}\,\overline{\psi}\,\gamma^\mu(D_\mu+\frac{1}{4}\omega_{ij\mu}\gamma^{ij})\psi \\ &-\tfrac{1}{2}\sqrt{g}g^{\mu\nu}\overline{D_\mu H}D_\nu H - \sqrt{g}\,V(H) - \sum\lambda\sqrt{g}\,\overline{\psi}\,H\psi\ .\end{aligned} \tag{21.6}$$

Here $F^a_{\mu\nu} = \partial_\mu A^a_\nu - \partial_\nu A^a_\mu + g_A f^a{}_{bc}A^b_\mu A^c_\nu$ and the (representation-dependent) gauge-field covariant derivative $D_\mu = \partial_\mu + g_A A^a_\mu T^{\rm rep}_a$ are defined as in Special Relativity, while the derivative of spin-$\frac{1}{2}$ fermions also includes a coupling to the gravitational "spin-connection" $\omega_{ij\mu} = -\omega_{ji\mu}$, via its contraction with $\gamma^{ij} = \frac{1}{2}(\gamma^i\gamma^j - \gamma^j\gamma^i)$, where $i,j=0,1,2,3$ and $\gamma^i = e^i{}_\mu\gamma^\mu$ are usual (numerical) Dirac matrices satisfying $\gamma^i\gamma^j+\gamma^j\gamma^i = 2\eta^{ij}$. The connection components $\omega_{ij\mu}$ are defined in terms of the local orthonormal frame (vierbein) $e^i{}_\mu$ (such that $g_{\mu\nu} = \eta_{ij}e^i{}_\mu e^j{}_\nu$) used to describe the components of the various fermions ψ, and of its inverse $e_i{}^\mu$ (such that $e_i{}^\mu e^j{}_\mu = \delta^j_i$), by $\omega_{ij\mu} = \frac{1}{2}\left(C_{i[jk]}+C_{j[ki]}-C_{k[ij]}\right)e^k_\mu$ where $C_{i[jk]} = \eta_{is}C^s{}_{[jk]}$, with $C^i{}_{[jk]} \equiv \left(\partial_\mu e^i{}_\nu - \partial_\nu e^i{}_\mu\right)e_j{}^\mu e_k{}^\nu$. From the total action follow Einstein's field equations,

$$R_{\mu\nu} - \tfrac{1}{2}Rg_{\mu\nu} = \frac{8\pi G}{c^4}T_{\mu\nu}\ . \tag{21.7}$$

Here $R = g^{\mu\nu}R_{\mu\nu}$ is the scalar curvature, and $T_{\mu\nu}\equiv g_{\mu\alpha}g_{\nu\beta}T^{\alpha\beta}$ where $T^{\mu\nu} = (2/\sqrt{g})\delta\mathcal{L}_{\rm SM}/\delta g_{\mu\nu}$ is the (symmetric) energy-momentum tensor of the Standard Model matter. The theory is invariant under arbitrary coordinate transformations: $x'^\mu = f^\mu(x^\nu)$ (as well as under arbitrary local SO(3,1) rotations of the vierbein, $e'^i{}_\mu = \Lambda^i{}_j(x)e'^j{}_\mu$). To solve the field equations Eq. (21.7), one needs to fix the coordinate gauge freedom, *e.g.*, the "harmonic gauge" (which is the analogue of the Lorenz gauge, $\partial_\mu A^\mu = 0$, in electromagnetism) corresponds to imposing the condition $\partial_\nu(\sqrt{g}g^{\mu\nu}) = 0$.

In this *Review*, we only consider the classical limit of gravitation (*i.e.* classical matter and classical gravity). Quantum gravitational effects are expected (when considered at low energy) to correct the classical action Eq. (21.2) by additional terms involving quadratic and higher powers of the curvature tensor. This suggests that the validity of classical gravity extends (at most) down to length scales of order the Planck length $L_P = \sqrt{\hbar G/c^3} \simeq 1.62\times10^{-33}$ cm, *i.e.*, up to energy scales of order the Planck energy $E_P = \sqrt{\hbar c^5/G} \simeq 1.22\times10^{19}$ GeV. Considering quantum matter in a classical gravitational background also poses interesting challenges, notably the possibility that the zero-point fluctuations of the matter fields generate a nonvanishing vacuum energy density $\rho_{\rm vac}$, corresponding to a term $-\sqrt{g}\ \rho_{\rm vac}$ in $\mathcal{L}_{\rm SM}$ [1]. This is equivalent to adding a "cosmological constant" term $+\Lambda\, g_{\mu\nu}$ on the left-hand side of Einstein's equations, Eq. (21.7), with $\Lambda = 8\pi G\,\rho_{\rm vac}/c^4$. Recent cosmological observations (see the following *Reviews*) suggest a positive value of Λ corresponding to $\rho_{\rm vac}\approx(2.3\times10^{-3}{\rm eV})^4$. Such a small value has a negligible effect on the non-cosmological tests discussed below.

21.2 Key features and predictions of GR

The definition of GR recalled above makes predictions both about the coupling of gravity to matter, and about the structure of the gravitational field beyond its previously known Newtonian aspects.

21.2.1 *Equivalence Principle*

First, the universal nature of the coupling between $g_{\mu\nu}$ and the Standard Model matter postulated in Eq. (21.6) entails many observable consequences that go under the generic name of "Equivalence Principle".

A first aspect of the Equivalence Principle is that the outcome of a local non-gravitational experiment, referred to local standards, should not depend on where, when, and in which locally inertial frame, the experiment is performed. This means, for instance, that local experiments should neither feel the cosmological evolution of the Universe (constancy of the "constants"), nor exhibit preferred directions in spacetime (isotropy of space, local Lorentz invariance).

A second aspect of the Equivalence Principle is that the kinetic terms, $g^{\mu\nu}\partial_\mu\phi\partial_\nu\phi$ or $\overline{\psi}\gamma^i e_i{}^\mu\partial_\mu\psi$, of all the fields of Nature (including the gravitational field itself) are universally coupled to the same curved spacetime metric $g_{\mu\nu}(x) = \eta_{ij}e^i{}_\mu e^j{}_\nu$. This implies in particular that all massless fields should propagate with the same speed.

A third aspect of the Equivalence Principle is that two (electrically neutral) test bodies dropped at the same location and with the same velocity in an external gravitational field should fall in the same way, independently of their masses and compositions ("universality of free fall" or "Weak Equivalence Principle"). In addition, the study (using the nonlinear structure of GR) of the motion, in an external gravitational field, of bodies having a non-negligible, or even strong, self-gravity (such as planets, neutron stars, or black holes) has shown that the latter property of free-fall universality holds equally well for self-gravitating bodies ("Strong Equivalence Principle").

A last aspect of the Equivalence Principle concerns various universality features of the gravitational redshift of clock rates. GR predicts that, when intercomparing them by means of electromagnetic signals, two (non gravity-based) clocks located along two different spacetime worldlines should exhibit a universal difference in clock rate that depends on their worldlines, but that is independent of their nature and constitution. For instance, two clocks located at two different positions in a static external Newtonian potential $U(\boldsymbol{x}) = \sum Gm/r$ should exhibit, when intercompared by electromagnetic signals, the difference in clock rate, $\tau_1/\tau_2 = \nu_2/\nu_1 = 1 + [U(\boldsymbol{x}_1)-U(\boldsymbol{x}_2)]/c^2 + O(1/c^4)$, ("universal gravitational redshift of clock rates"). Similarly, the comparison of atomic-transition frequencies when observing on Earth a transition that took place on a far-away galaxy should involve (at lowest order in cosmological perturbations) the universal cosmological redshift factor $1+z = a(t_{\rm reception})/a(t_{\rm emission})$ between the Friedmann scale factors $a(t)$ (see below).

Downloaded from https://academic.oup.com/ptep/article/2022/8/083C01/6651666 by KIT Library user on 27 September 2022

21.2.2 *Quasi-stationary, weak-field (post-Newtonian) gravity*

When applied to quasi-stationary, weak-field gravitational fields, Einstein equations, Eq. (21.7), entail a spacetime structure which predicts deviations from Newtonian gravity of the first post-Newtonian (1PN) order, *i.e.*, fractionally smaller than Newtonian effects by a factor $O(v^2/c^2) \sim O(GM/(c^2 r))$. The 1PN-accurate solution of Eq. (21.7) reads (in harmonic gauge)

$$\begin{aligned} g_{00} &= -1 + \frac{2}{c^2}V - \frac{2}{c^4}V^2 + O\left(\frac{1}{c^6}\right) , \\ g_{0i} &= -\frac{4}{c^3}V_i + O\left(\frac{1}{c^5}\right) , \\ g_{ij} &= \delta_{ij}\left[1 + \frac{2}{c^2}V\right] + O\left(\frac{1}{c^4}\right) , \end{aligned} \tag{21.8}$$

where $x^0 = ct$, $i, j = 1, 2, 3$, and where the scalar, V, and vector, V_i, (retarded) potentials are defined in terms of the sources $\sigma = \frac{T^{00}+T^{ii}}{c^2}$, $\sigma_i = \frac{T^{0i}}{c}$ by

$$V = \Box^{-1}_{\rm ret}\left[-4\pi G\sigma\right] \; ; \; V_i = \Box^{-1}_{\rm ret}\left[-4\pi G\sigma_i\right] . \tag{21.9}$$

In GR the gravitational interaction of N moving point masses (labeled by $A = 1, \ldots, N$) is described by a reduced (classical) action that admits a diagrammatic expansion:

$$S_{\rm reduced} = S^{\rm free} + S^{\rm tree-level} + S^{\rm one-loop} + \cdots \tag{21.10}$$

where the free (special-relativistic) action reads

$$\begin{aligned} S^{\rm free} &= -\sum_A \int m_A c\sqrt{-\eta_{\mu\nu}dx^\mu_A dx^\nu_A} \\ &= -\sum_A \int dt m_A c^2 \sqrt{1 - \mathbf{v}_A^2/c^2} , \end{aligned} \tag{21.11}$$

while the tree-level (one-graviton-exchange) interaction term reads

$$S^{\rm tree-level} = -\frac{8\pi G}{c^4}\int d^4x\, T^{\mu\nu}\Box^{-1}(T_{\mu\nu} - \tfrac{1}{2}T\eta_{\mu\nu}) = \int dt L^{(2)} . \tag{21.12}$$

Corresponding to the 1PN-accurate metric of Eq. (21.8), the 1PN-accurate expansion of the latter tree-level, two-body interaction Lagrangian $L^{(2)}$ reads (with $r_{AB} \equiv |\mathbf{x}_A - \mathbf{x}_B|$, $\mathbf{n}_{AB} \equiv (\mathbf{x}_A - \mathbf{x}_B)/r_{AB}$)

$$\begin{aligned} L^{(2)} = \tfrac{1}{2}\sum_{A\neq B} \frac{G\, m_A\, m_B}{r_{AB}} \Big[1 &+ \frac{3}{2c^2}(\boldsymbol{v}_A^2 + \boldsymbol{v}_B^2) - \frac{7}{2c^2}(\boldsymbol{v}_A \cdot \boldsymbol{v}_B) \\ &- \frac{1}{2c^2}(\boldsymbol{n}_{AB}\cdot\boldsymbol{v}_A)(\boldsymbol{n}_{AB}\cdot\boldsymbol{v}_B) + O\left(\frac{1}{c^4}\right)\Big] \end{aligned} \tag{21.13}$$

The two-body interactions, Eq. (21.13), exhibit v^2/c^2 corrections to Newton's $1/r$ potential induced by spin-2 exchange ("gravitomagnetism"). Consistency at the 1PN level, $v^2/c^2 \sim G\,m/rc^2$, requires that one also considers the three-body interactions contained in the one-loop contribution $S^{\rm one-loop}$, corresponding to terms induced by some of the three-graviton vertices and other non-linearities (terms $O(h^2)$ and $O(hT)$ in Eq. (21.15) below), *i.e.*, to the $O(V^2)$ term in Eq. (21.8):

$$L^{(3)} = -\frac{1}{2}\sum_{B\neq A\neq C} \frac{G^2\, m_A\, m_B\, m_C}{r_{AB}\, r_{AC}\, c^2} + O\left(\frac{1}{c^4}\right) . \tag{21.14}$$

21.2.3 *Gravitational Waves in GR*

The linearized approximation to Einstein's field equations, Eq. (21.7), in harmonic gauge $\partial^\nu(h_{\mu\nu} - \frac{1}{2}h\eta_{\mu\nu}) = 0$ (with $h \equiv \eta^{\mu\nu}h_{\mu\nu}$), reads

$$\Box h_{\mu\nu} = -\frac{16\pi G}{c^4}(T_{\mu\nu} - \tfrac{1}{2}T\eta_{\mu\nu}) + O(h^2) + O(hT) . \tag{21.15}$$

Outside of any source (*i.e.*, when $T_{\mu\nu} = 0$), this yields $\Box h_{\mu\nu} = 0$, with $\partial^\nu(h_{\mu\nu} - \frac{1}{2}h\eta_{\mu\nu}) = 0$. The generic linearized solution (modulo the diffeomorphism freedom) of the latter vacuum Einstein equations can be written as (with $k^2 = k\cdot k = \eta_{\mu\nu}k^\mu k^\nu$, $k\cdot x = k_\mu x^\mu$)

$$h_{\mu\nu}(x) = \int d^4k\delta(k^2)\epsilon_{\mu\nu}(k)e^{ik\cdot x} , \tag{21.16}$$

where the polarization tensor $\epsilon_{\mu\nu}(k)$ must be transverse ($\epsilon_{\mu\nu}k^\nu = 0$) and traceless ($\eta^{\mu\nu}\epsilon_{\mu\nu} = 0$). In addition, $\epsilon_{\mu\nu}(k)$ can be freely submitted to the gauge freedom $\epsilon'_{\mu\nu} = \epsilon_{\mu\nu} + \xi_\mu k_\nu + \xi_\nu k_\mu$. This implies that gravitational waves (GW) propagate with the speed of light, and (like electromagnetic waves) have only two independent polarizations. In a frame where, say, $k^\mu = (ck, 0, 0, k)$, the two independent linear polarization tensors can be taken to have components only in the transverse 1-2 plane, of the following form: $\epsilon^+_{11} = -\epsilon^+_{22} = \epsilon^+$, with $\epsilon^+_{12} = \epsilon^+_{21} = 0$; or $\epsilon^\times_{12} = +\epsilon^\times_{21} = \epsilon^\times$, with $\epsilon^\times_{11} = \epsilon^\times_{22} = 0$. Under a little-group rotation of angle θ in the 1-2 plane, the two circular polarization amplitudes $\epsilon^{(\pm)} = \epsilon^+ \mp i\,\epsilon^\times$ vary as $\epsilon'^{(\pm)} = e^{\pm 2i\theta}\epsilon^{(\pm)}$, thereby characterizing the helicity-2 nature of GWs.

When solving the inhomogeneous equation Eq. (21.15), taking into account the nonlinear contributions $O(h^2)+O(hT)$, one finds that, to lowest order, the GW amplitude emitted at large distances by a matter distribution is given by the following "quadrupole formula"

$$h^{\rm TT}_{ij}(T, \mathbf{X}) \approx \frac{2G}{c^4}P^{\rm TT}_{ijab}(\mathbf{N})\frac{\ddot{Q}_{ab}(T - R/c)}{R} , \tag{21.17}$$

where $Q_{ij}(t) = \int d^3x\sigma(t, \mathbf{x})(x^i x^j - \frac{1}{3}\delta_{ij}\mathbf{x^2})$ $(a, b, i, j = 1, 2, 3)$ is the quadrupole moment of the source, $R = |\mathbf{X}|$ the distance to the source, $\mathbf{N} = \mathbf{X}/R$ the unit direction from the source to the observer, and $P^{\rm TT}_{ijab}(\mathbf{N}) = (\delta_{ia} - N_iN_a)(\delta_{jb} - N_jN_b) - \frac{1}{2}(\delta_{ij} - N_iN_j)(\delta_{ab} - N_aN_b)$ the transverse-traceless projector onto the 2-plane orthogonal to $\mathbf{N}$.

21.2.4 *Strong gravitational fields: neutron stars and black holes*

The nonlinear structure of Einstein's equations implies many predictions for strong gravitational fields that distinguish GR from Newtonian gravity. For instance, in Newtonian gravity, there is no upper limit to the dimensionless gravitational potential U/c^2, with U satisfying Poisson's equation $\Delta U = -4\pi G\rho$, where ρ denotes the Newtonian mass density. By contrast, in GR, the dimensionless surface gravitational potential $GM/(c^2R)$ of a spherically symmetric (perfect fluid) body cannot exceed $\frac{4}{9}$ [2].

Given an equation of state $p = f(\rho)$ modeling the interior of a (cold) spherically symmetric body (say a non-rotating neutron star), Einstein equations, Eq. (21.7), with $T^{\mu\nu} = (\rho + p)u^\mu u^\nu + pg^{\mu\nu}$, and

$$g_{\mu\nu}dx^\mu dx^\nu = -e^{2\Phi(r)}c^2dt^2 + \frac{dr^2}{1 - \frac{2GM(r)}{c^2r}} + r^2\left(d\theta^2 + \sin^2\theta d\phi^2\right) , \tag{21.18}$$

yield the following Tolman-Oppenheimer-Volkoff radial equations:

$$p'(r) = -\frac{G(\rho + p/c^2)(M(r) + 4\pi r^3 p/c^2)}{r^2(1 - 2GM(r)/(c^2r))} ; \tag{21.19}$$

$$M'(r) = 4\pi r^2\rho ; \tag{21.20}$$

$$\Phi'(r) = \frac{G(M(r) + 4\pi r^3 p/c^2)}{r^2(1 - 2GM(r)/(c^2r))} . \tag{21.21}$$

In the exterior of the star $(r \geq R)$, the metric takes the Schwarzschild form

$$\begin{aligned} g_{\mu\nu}dx^\mu dx^\nu = &-\left(1 - \frac{2GM}{c^2r}\right)c^2dt^2 + \frac{dr^2}{1 - \frac{2GM}{c^2r}} \\ &+ r^2\left(d\theta^2 + \sin^2\theta d\phi^2\right) , \end{aligned} \tag{21.22}$$

where $M \equiv M(R)$ is the total gravitational mass of the star. GR predicts, for any given $p = f(\rho)$, several (in principle) observable

Downloaded from https://academic.oup.com/ptep/article/2022/8/083C01/6651666 by KIT Library user on 27 September 2022

features of neutron stars, such as: (i) the maximum mass of a neutron star; (ii) the relation between the radius R and the total mass M; (iii) the dimensionless surface gravitational potential $GM/(c^2R)$ (linked to the surface redshift $\sqrt{-g_{00}} = \sqrt{1-\frac{2GM}{c^2R}}$ measured by an observer at infinity); (iv) the moment of inertia; and (v) the Love number (tidal polarizability). The current uncertainty on the equation of state of a neutron star yields the GR-predicted approximate range for the maximum mass of non-rotating neutron stars $1.5\,M_\odot \lesssim M_{\max} \lesssim 2.5\,M_\odot$, and the absolute upper bound $M_{\max} < 3\,M_\odot$ [3]. The surface gravitational potential of a typical neutron star is $GM/c^2R_{\rm NS} \simeq 0.17$, which is a factor $\sim 10^8$ higher than the surface potential of the Earth, and a mere factor 3 below the black hole limit $GM/c^2R_{\rm BH} = \frac{1}{2}$ to be discussed next.

The existence of a maximum mass for a neutron star led Oppenheimer and Snyder [4] to predict that the end point of stellar evolution for sufficiently heavy stars, after exhaustion of all thermonuclear sources of energy, will be what are now called "black holes." The latter are solutions of Einstein's equations whose past structure involves a gravitationally collapsing star, but whose presently observable structure is essentially described (for non-rotating black holes) by the vacuum Schwarzschild solution Eq. (21.22). It took many years for theoretical (and mathematical) physicists to understand that the apparent singularity of the Schwarzschild solution at $r = \frac{2GM}{c^2}$ was a coordinate singularity and that the Schwarzschild spacetime was regular at the "black hole horizon", $R_{\rm BH} \equiv \frac{2GM}{c^2}$. The rotating analog of the Schwarzschild spacetime is the Kerr black hole [5].

Black holes are outstanding consequences of GR which enjoy many remarkable properties, notably: (i) presence of a one-way surface (the horizon) for all waves and particles; (ii) absence of "hair" (*i.e.*, barring a possible electric charge, their structure is fully described by only two parameters, total mass, M, and total angular momentum, $J \leq GM^2/c$); (iii) existence of a spectrum of damped quasi-normal vibrational modes; and (iv) a behavior under external perturbations similar to ordinary physical objects satisfying the laws of (dissipative) thermodynamics. Moreover, though no classical waves or particles can get out of the horizon, black holes are predicted to slowly evaporate via quantum particle creation.

21.2.5 *Cosmology*

To complete our short tour of the main predictions of GR, let us mention that GR offers the current standard framework for describing the large-scale structure of the Cosmos, from the nearly homogeneous Big Bang (and its plausible inflationary beginning) to the current inhomogeneous Universe undergoing an accelerated expansion. The spacetime structure on large (temporal and spatial) scales is well described by a solution of Einstein's equations of the form

$$\begin{aligned} ds^2 = &-\left(1+2\Phi(t,\mathbf{x})\right)c^2dt^2 + 2W_i(t,\mathbf{x})dtdx^i \\ &+ a^2(t)\left(\left(1-2\Psi(t,\mathbf{x})\right)\delta_{ij} + h_{ij}(t,\mathbf{x})\right)dx^idx^j\,, \end{aligned} \tag{21.23}$$

where, after a suitable gauge-fixing [6], $W_i(t,\mathbf{x})$ is transverse, while $h_{ij}(t,\mathbf{x})$ is transverse and traceless. The source $T^{\mu\nu}$ must involve a certain number of postulated ingredients: an inflaton field; the matter of the Standard Model; a dark matter component; and a cosmological constant contribution $T^{\mu\nu}_\Lambda = -\rho_{\rm vac}g^{\mu\nu}$, with $\rho_{\rm vac} \equiv c^4\Lambda/(8\pi G)$. The scale factor $a(t)$ of the Friedmann background metric $ds_0^2 = -c^2dt^2 + a^2(t)\delta_{ij}dx^idx^j$ satisfies the GR-predicted Friedmann equations (with vanishing spatial curvature $k=0$),

$$H^2 \equiv \left(\frac{\dot a}{a}\right)^2 = \frac{8\pi G}{3}\rho_{\rm tot}\,, \tag{21.24}$$

$$\frac{\ddot a}{a} = -\frac{4\pi G}{3}\left(\rho_{\rm tot} + \frac{3}{c^2}p_{\rm tot}\right)\,, \tag{21.25}$$

while the scalar $(\Phi(t,\mathbf{x}),\Psi(t,\mathbf{x}))$, vector $(W_i(t,\mathbf{x}))$, and tensor $(h_{ij}(t,\mathbf{x}))$ inhomogeneous perturbations satisfy some GR-predicted propagation equations (coupled to matter perturbations); see [6] and the following *Reviews*. When the cosmic fluid is well approximated by a perfect fluid, Einstein's equations predict the following link between the scalar perturbations

$$\Phi(t,\mathbf{x}) = \Psi(t,\mathbf{x})\,. \tag{21.26}$$

21.3 A roadmap of parametrizations of deviations from GR, and of modified gravity

As will be discussed below, all currently performed gravitational experiments are compatible with GR. However, similarly to what is done in discussions of precision electroweak experiments, it is useful to quantify the significance of precision gravitational experiments by parameterizing possible deviations from GR. One can distinguish two main approaches to considering, and parameterizing, deviations from GR: (i) theory-agnostic phenomenological approaches; or, (ii) the study of the predictions of specific classes of alternative theories of gravity. Both types have led to useful ways of discussing tests of gravity. Both types also have their limitations. Considering them together leads to cross-fertilization.

21.3.1 *Theory-agnostic phenomenological approaches to parameterizing deviations from GR*

The theory-agnostic phenomenological approach is the oldest, and, arguably, the most robust one. It essentially consists in starting from specific observable predictions within the considered standard theory, and of deforming them by introducing some free parameters measuring either deviations from effects already present within the standard theory, or new effects absent from the standard theory. A classic example is the periastron advance of Mercury (and the other planets). When working within Newtonian gravity as a standard theory of gravity, the rate of periastron advance of Mercury, $\dot\omega$, is (when neglecting the quadrupole moment of the Sun) a calculable function of the masses and semi-major axes of the other planets of the solar system, say $\dot\omega^{\rm Newton}(m_i,a_i)$. However, $\dot\omega$ is also a directly observable quantity, so that one can parameterize the periastron advance of Mercury by writing

$$\dot\omega^{\rm obs} = \dot\omega^{\rm Newton}(m_i,a_i) + \Delta\dot\omega\,. \tag{21.27}$$

Using other observable data to determine some "observed" values of the m_i's and a_i's, one can then measure the anomalous periastron precession $\Delta\dot\omega$ and see whether it is compatible with zero, or not. As is well-known, Leverrier used such a methodology and, in 1859, measured an anomalous periastron precession of about $\Delta\dot\omega \simeq 38$ arcsec/century (later re-estimated at 43 arcsec/century), which was explained in 1915 as a GR prediction. Let us discuss further examples of the use of such theory-agnostic approaches for discussing deviations from GR.

21.3.2 *Parameterized post-Newtonian (PPN) formalism.*

When considering the weak-field slow-motion limit appropriate to describing gravitational experiments in the solar system, it has been traditional to parameterize possible (long-range) deviations from the GR-predicted 1PN metric by introducing extra dimensionless coefficients in the various terms of the metric of Eq. (21.8). The minimal version of the parameterized post-Newtonian (PPN) formalism (essentially due to Eddington) involves only two parameters β and γ, namely

$$g_{00} = -1 + \frac{2}{c^2}V - \frac{2\beta}{c^4}V^2 + O\left(\frac{1}{c^6}\right)\,, \tag{21.28}$$

$$g_{0i} = -\frac{2(\gamma+1)}{c^3}V_i + O\left(\frac{1}{c^5}\right)\,, \tag{21.29}$$

$$g_{ij} = \delta_{ij}\left[1 + \frac{2\gamma}{c^2}V\right] + O\left(\frac{1}{c^4}\right)\,, \tag{21.30}$$

with V and V_i defined by Eq. (21.9), with the same vectorial source $\sigma_i = \frac{T^{0i}}{c}$, but a modified scalar source

$$\sigma^{\rm PPN} = \frac{1}{c^2}\left(\left[1 + (3\gamma - 2\beta - 1)\frac{V}{c^2}\right]T^{00} + \gamma\,T^{ii}\right)\,. \tag{21.31}$$

In GR, $\beta^{\rm GR} = 1$ and $\gamma^{\rm GR} = 1$, so that deviations from GR are parameterized by $\overline{\beta} \equiv \beta - 1$ and $\overline{\gamma} \equiv \gamma - 1$. Richer versions of the

Downloaded from https://academic.oup.com/ptep/article/2022/8/083C01/6651666 by KIT Library user on 27 September 2022

PPN formalism (involving up to ten parameters) were developed in interaction with the study of classes of alternative theories of gravity [7, 8]. This led to parameterizing new types of contributions to the 1PN metric that are absent in the GR framework.

When deriving the 1PN-accurate dynamics of N point masses predicted by the PPN-modified metric, Eq. (21.28), one finds that the free Lagrangian is not modified (because we are considering here a Lorentz-invariant subclass of PPN metrics), while there are modifications of both the two-body Lagrangian, $L^{(2)}$, Eq. (21.13), and the three-body one, $L^{(3)}$, Eq. (21.14). More precisely, denoting $\eta \equiv 4\overline{\beta} - \overline{\gamma}$, the Newtonian interaction energy term in Eq. (21.13) is modified into $G_{AB} m_A m_B / r_{AB}$, with a body-dependent gravitational "constant"

$$G_{AB} = G[1+\eta(E_A^{\rm grav}/m_A c^2 + E_B^{\rm grav}/m_B c^2) + O(1/c^4)] \,, \quad (21.32)$$

where $E_A^{\rm grav}$ denotes the gravitational binding energy of body A. In addition, there is the additional contribution $+\overline{\gamma}(\boldsymbol{v}_A - \boldsymbol{v}_B)^2/c^2$ in the brackets on the right-hand side of $L^{(2)}$, Eq. (21.13). As for the three-body interaction term $L^{(3)}$, Eq. (21.14), it is modified by the overall factor $1 + 2\overline{\beta}$.

These results show how the introduction of the two minimal PPN deviation parameters $\overline{\beta} \equiv \beta - 1$ and $\overline{\gamma} \equiv \gamma - 1$ suffices to introduce many different observable effects. Some of them (the ones linked with $\overline{\gamma}$) concern deviations at the linearized (one-graviton-exchange) level (and affect, for instance, light deflection and time-delay effects), while the deviation parameter $\overline{\beta}$ parameterizes effects linked to the cubic vertex of Einstein's gravity (and affects, for instance, periastron precession). Of particular interest is the fact that Eq. (21.32) shows that the combination $\eta \equiv 4\overline{\beta} - \overline{\gamma}$ parameterizes a violation of the Strong Equivalence Principle, because the gravitational interaction between self-gravitating bodies is seen to be influenced by the gravitational binding energy of each body [9]. As stated above, this effect is absent in GR (where $\eta^{\rm GR} = 0$). This is an example where the fact of contrasting GR with some deviations from it gives physical significance to a null effect in GR (namely the universality of free fall of self-gravitating bodies).

Finally, one can extend the PPN formalism by allowing for a slow, phenomenological time variation of Newton's constant:

$$G(t) = G_0 \left[1 + \frac{\dot{G}_0}{G_0}(t - t_0) \right] . \quad (21.33)$$

Here, one assumes that there exist units in which the masses, m_i, of elementary particles stay constant, and that G is measured in such units. A possible time variation of G then corresponds to a possible common variation of the dimensionless couplings $G m_i^2/(\hbar c)$.

21.3.3 *Parameterized post-Keplerian (PPK) formalism.*

The discovery of pulsars (*i.e.*, rotating neutron stars emitting a beam of radio noise) in gravitationally bound orbits [10, 11] has given us our first experimental handle on a regime of relativistic gravity going significantly beyond the uniformly weak-field, and quasi-stationary regime of solar-system gravity. Binary pulsars allow us to probe some radiative effects, and also some strong-gravitational-field effects. In these systems, the finite speed of propagation of the gravitational interaction between the pulsar and its companion generates damping-like terms at order $(v/c)^5$ in the equations of motion [12]. These damping forces are the local counterparts of the gravitational radiation emitted at infinity by the system ("gravitational radiation reaction"). They cause the binary orbit to shrink and its orbital period P_b to decrease. The remarkable stability of pulsar clocks has allowed one to measure the corresponding very small orbital period decay $\dot{P}_b \equiv dP_b/dt \sim -(v/c)^5 \sim -10^{-12}$–$10^{-14}$ in several binary systems, thereby giving us a direct experimental handle on the propagation properties of the gravitational field. In addition, the large surface gravitational potential of a neutron star allows one to probe the quasi-static strong-gravitational-field regime, as is discussed below.

It is possible to extract phenomenological (theory-independent) tests of gravity from binary pulsar data by using the parameterized post-Keplerian (PPK) formalism [13]. The basis of this formalism is the fact that, after correcting for the Earth's motion around the Sun and for the dispersion due to propagation in the interstellar plasma, the time of arrival of the Nth pulse t_N can be described by a generic, parameterized "timing formula" [13, 14], whose functional form is common to the whole class of tensor-scalar gravitation theories:

$$t_N - t_0 = F[T_N(\nu_p, \dot{\nu}_p, \ddot{\nu}_p) \,;\, \{p^K\} \,;\, \{p^{PK}\}] \,. \quad (21.34)$$

Here, T_N is the pulsar proper time corresponding to the Nth turn given by $N/2\pi = \nu_p T_N + \frac{1}{2}\dot{\nu}_p T_N^2 + \frac{1}{6}\ddot{\nu}_p T_N^3$ (with $\nu_p \equiv 1/P_p$ the spin frequency of the pulsar, *etc.*), $\{p^K\} = \{P_b, T_0, e, \omega_0, x\}$ is the set of "Keplerian" parameters (notably, orbital period P_b, eccentricity e, periastron longitude ω_0 and projected semi-major axis $x = a \sin i/c$), and $\{p^{PK}\} = \{k, \gamma_{\rm timing}, \dot{P}_b, r, s, \delta_\theta, \dot{e}, \dot{x}\}$ denotes the set of (separately measurable) "post-Keplerian" parameters. Most important among these are: the fractional periastron advance per orbit $k \equiv \dot{\omega} P_b/2\pi$; a dimensionful time-dilation parameter $\gamma_{\rm timing}$; the orbital period derivative $\dot{P}_b$; and the "range" and "shape" parameters of the gravitational time delay caused by the companion, r and s.

Without assuming any specific theory of gravity, one can phenomenologically analyze the data from any binary pulsar by least-squares fitting the observed sequence of pulse arrival times to the timing formula of Eq. (21.34). This fit yields the "measured" values of the parameters $\{\nu_p, \dot{\nu}_p, \ddot{\nu}_p\}$, $\{p^K\}$, $\{p^{PK}\}$. Now, each specific relativistic theory of gravity predicts that, for instance, k, $\gamma_{\rm timing}$, $\dot{P}_b$, r, and s (to quote parameters that have been successfully measured from some binary pulsar data) are some theory-dependent functions of the Keplerian parameters and of the (unknown) masses m_1, m_2 of the pulsar and its companion. For instance, in GR, one finds (with $M \equiv m_1 + m_2$, $n \equiv 2\pi/P_b$),

$$\begin{aligned}
k^{\rm GR}(m_1, m_2) =& 3(1-e^2)^{-1}(GMn/c^3)^{2/3} \,, \\
\gamma_{\rm timing}^{\rm GR}(m_1, m_2) =& e n^{-1}(GMn/c^3)^{2/3} m_2(m_1 + 2m_2)/M^2 \,, \\
\dot{P}_b^{\rm GR}(m_1, m_2) =& -(192\pi/5)(1-e^2)^{-7/2}\left(1 + \tfrac{73}{24}e^2 + \tfrac{37}{96}e^4\right) \\
& \times (GMn/c^3)^{5/3} m_1 m_2/M^2 \,, \\
r^{\rm GR}(m_1, m_2) =& G m_2/c^3 \,, \\
s^{\rm GR}(m_1, m_2) =& n x (GMn/c^3)^{-1/3} M/m_2 \,. \qquad (21.35)
\end{aligned}$$

In alternative gravity theories each of the functions $k^{\rm theory}(m_1, m_2)$, $\gamma_{\rm timing}^{\rm theory}(m_1, m_2)$, $\dot{P}_b^{\rm theory}(m_1, m_2)$, *etc.*, is modified by quasi-static strong field effects (associated with the self-gravities of the pulsar and its companion), while the particular function $\dot{P}_b^{\rm theory}(m_1, m_2)$ is further modified by radiative effects [15–18]. If one measures $N > 2$ PPK parameters from the data of a specific binary pulsar, these N measurements determine, for each given theory, N curves (defined by the N equations $k_i^{\rm theory}(m_1, m_2) = k_i^{\rm obs}$) in the two-dimensional mass plane (m_1, m_2). This yields $N - 2$ tests of the specified theory, according to whether the N curves (or strips) have one point in common, as they should.

21.3.4 *Parameterized-post-Friedmannian (PPF) formalisms.*

We have recalled above that, in GR, the two functions, $\Phi(t, \mathbf{x})$, and $\Psi(t, \mathbf{x})$, parameterizing (in the "longitudinal gauge") the scalar perturbations of the background Friedmann metric are related (in absence of anisotropic stresses) by Eq. (21.26). Several authors [19–28] have defined various types of parameterized-post-Friedmannian (PPF) formalisms involving (generally space and time dependent) phenomenological parameters. The simplest versions of these formalisms involve two phenomenological parameters measuring: (i) the ratio between $\Phi(t, \mathbf{x})$, and $\Psi(t, \mathbf{x})$, say (using a parametrization which parallels the usual PPN parametrization)

$$\Psi(t, \mathbf{x}) = \gamma_{\rm cosmo}(t, \mathbf{x}) \Phi(t, \mathbf{x}) \,; \quad (21.36)$$

Downloaded from https://academic.oup.com/ptep/article/2022/8/083C01/6651666 by KIT Library user on 27 September 2022

and (ii) the effective gravitational constant entering the Poisson equation for $\Phi(t,\mathbf{x})$, say

$$\Delta\Phi(t,\mathbf{x}) = 4\pi G_\Phi(t,\mathbf{x})\delta\rho(t,\mathbf{x})\,. \tag{21.37}$$

However, the peculiarities of cosmological observables limit the domain of applicability of such phenomenological approaches [26] (notably because the strong dependence of cosmological probes on epochs and scales obliges one to rely on specific parameterizations of the functions $\gamma_{\rm cosmo}(t,\mathbf{x})$ and $G_\Phi(t,\mathbf{x})$, *e.g.*, [25, 28]). Approaches based on specific classes of modified-gravity theories allow for a more complete treatment involving, in principle, all existing cosmological observables: Big Bang nucleosynthesis, cosmic microwave background, large-scale structure, Hubble diagram, weak lensing, etc. Discussing the current cosmological tests using either such PPF formalisms, or comparisons with the predictions of modified-gravity theories, is beyond the scope of this review. See [29] for a comprehensive recent discussion. The bottom line is that all present cosmological data have been found to be compatible with GR (within the Friedmann-Lemaître-based ΛCDM model). Beyond the quantitative limits on various parameterized theoretical models [29], one should remember the striking (strong-field-type) qualitative verification of GR embodied in the fact that relativistic cosmological models give an accurate picture of the Universe over a period during which the spatial metric has been blown up by a gigantic factor, say $(1+z)^2 \sim 10^{19}$ between Big Bang nucleosynthesis and now.

21.3.5 *Various phenomenological tests of GR from gravitational wave (GW) data*

The observation by the US-based Laser Interferometer Gravitational-wave Observatory (LIGO), later joined by the Europe-based Virgo detector, of gravitational-wave (GW) signals [30–34], has opened up a novel testing ground for relativistic gravity. The first two observing runs of the LIGO-Virgo Collaboration (LVC) have led to the detection of GW signals from ten binary black-hole coalescences, and one binary neutron-star merger [35]. The first six months of the third observing run have led to the detection of thirty nine additional GW candidate events with a false-alarm rate smaller than two per year [36].

Several approaches have been used to either test consistency with GR, or to look for special types of possible deviations. Making accurate predictions for GW signals from coalescing black holes within GR took years of both analytical [37, 38] and numerical [39] work. Some works have started (both analytically [15, 40–44] and numerically [45–47]) to derive the corresponding predictions within some modified-gravity theories. Phenomenological approaches are very useful for parameterizing general, conceivable deviations from GR when analyzing the GW signals emitted by coalescing black holes or neutron stars.

A first phenomenological, global consistency test simply consists of measuring the noise-weighted correlation $\mathcal{C}$ between each detected strain signal and the corresponding best-fit GR-predicted waveform. $\mathcal{C}^{\rm obs}$ should be equal to 1, modulo statistical (and/or systematic) errors.

Various other phenomenological tests of the structure of the GR-predicted waveforms emitted by coalescing compact binaries have been suggested. One general idea [48–50] (dubbed "parameterized post-Einsteinian formalism" in [51]) is to modify the GR-predicted Fourier-domain value $\psi(f)$ of the phase of black-hole coalescence GW signals $h(f) = A(f)e^{i\psi(f)}$ by introducing GR-deviation parameters, say

$$\psi(f) = \sum_i \left[p_i^{\rm GR,NS}(m_1,m_2)(1+\delta\hat{p}_i) + p_i^{\rm GR,S}(m_1,m_2,S_1,S_2)\right] \times u_i(f). \tag{21.38}$$

Here, the $u_i(f)$'s define a basis of functions of the GW frequency f, and the superscript NS refers to the nonspinning contribution, while the superscript S refers to the spinning one. Such a GR-modification directly applies to the phenomenological representation [52] of $\psi(f)$, and can be generalized to any waveform model by adding the non-GR phase term $\sum_i p_i^{\rm GR,NS}(m_1,m_2)\delta\hat{p}_i u_i(f)$ to the corresponding GR-predicted Fourier-domain phase $\psi(f)$ [53]. For instance, the leading-order (LO), quadrupolar term in the GR phase evolution during the early inspiral corresponds to $u_0(f) = f^{-5/3}$ and $p_0^{\rm GR} = \frac{3(m_1+m_2)^2}{128 m_1 m_2}(\pi G(m_1+m_2)/c^3)^{-5/3}$, while the next-to-leading-order (NLO) term is a $O(v^2/c^2)$ correction $p_2^{\rm GR}u_2(f)$ with $u_2(f) = f^{-1}$. In the phenomenological model [52] these terms (as well as the other inspiral contributions) are cut-off beyond the frequency $G(m_1+m_2)f/c^3 = 0.018$.

Each dimensionless parameter $\delta\hat{p}_i$ introduces a fractional deviation from the corresponding individual phasing GR effect having the frequency dependence $u_i(f)$, and can, in principle, be extracted by fitting the inspiral part of the observed waveform to the deformed template of Eq. (21.38). However, one must also use this deformed template for simultaneously extracting the values of m_1, m_2, S_1, and S_2. Together with signal-to-noise ratio (SNR) considerations, and parameter-correlation issues, this limits the applicability of such a test to introducing only one deformation parameter $\delta\hat{p}_i$ at a time. A particularly meaningful test [48] is to leave undeformed the LO and NLO terms $p_0^{\rm GR}u_0(f) + p_2^{\rm GR}u_2(f)$ and to vary the third coefficient p_3 parameterizing the next, "GW tail"-related $O(v^3/c^3)$ correction, with $u_3(f) = f^{-2/3}$. Another well-motivated test [51] is to introduce a new coefficient $\delta\hat{p}_{-2}$, which is absent in GR, and which parameterizes an $O((\frac{v}{c})^{-2})$ fractional correction to the LO, quadrupolar term, thereby allowing for a possible dipolar GW flux (indeed, dipolar GW radiation generally exists in theories containing scalar excitations). As $p_{-2}^{\rm GR}$ vanishes, $\delta\hat{p}_{-2}$ is added as an absolute deviation, scaled by the LO term $p_0^{\rm GR}$.

The coalescence of two black holes, or of a black hole and a neutron star (or of two heavy-enough neutron stars) leads to the formation of a black hole that is initially formed in a perturbed state. The relaxation of the latter perturbed black hole into its stationary, equilibrium state leads to the emission of characteristic (rapidly decaying) ringing GW modes (a.k.a. quasi-normal modes) [54, 55], whose frequencies and decay times are functions of the mass (M_f) and spin ($S_f \equiv GM_f^2 a_f/c$) of the final black hole, say

$$\omega_a = (c^3/GM_f)[2\pi\hat{f}_a^{\rm QNM}(a_f) - i/\hat{\tau}_a^{\rm QNM}(a_f)]\,, \tag{21.39}$$

where $a = 1, 2, \ldots$ labels the various ringing modes, starting from the least-damped one. In principle, if the SNR is large enough, one can directly test for the presence of one or several of these modes in the post-merger signal, and measure both ${\rm Re}(\omega_a)$ and ${\rm Im}(\omega_a)$ in a theory-independent way. These phenomenological measurements then lead to null tests of GR, from which one can extract theoretical information about eventual deviations from GR [56, 57].

As recalled above, GR predicts that GWs propagate (in vacuum) at exactly the same speed as light (*i.e.*, they have the same dispersion law $g^{\mu\nu}k_\mu k_\nu = 0$ in curved spacetime). Deviations from such a universal, scale-free dispersion law can be phenomenologically parameterized in several ways. If one phenomenologically assumes that the graviton dispersion law includes a mass term, say $g^{\mu\nu}k_\mu k_\nu + m_g^2/\hbar^2 = 0$, or some more general type of frequency-dependent modification, such changes affect the phasing of the inspiral GW signal and can be directly tested [58]. When one observes *both* GWs and electromagnetic waves emitted by the same system, one can also directly test whether both types of waves propagate in the same way.

Let us now present some examples of theory-dependent discussions of experimental tests based on considering specific classes of alternative theories. The most conservative deviations from Einstein's pure spin-2 theory are defined by adding new, bosonic, light or massless, macroscopically coupled fields.

21.3.6 *Gravity tests within classes of tensor-scalar theories of gravity*

The possible existence of new gravitational-strength couplings leading to deviations from Einsteinian (and Newtonian) gravity has been suggested by many natural extensions of GR, starting with the classic Kaluza-Klein idea, and continuing up to now with the study of extended supergravity theories, and of (super-)string theory. In particular, a recurrent suggestion of such theories (which dates back to pioneering work by Jordan, and by

Downloaded from https://academic.oup.com/ptep/article/2022/8/083C01/6651666 by KIT Library user on 27 September 2022

Fierz [59]) is the existence of a scalar field φ coupled both to the scalar curvature R and to the various ${F^a_{\mu\nu}}^2$ gauge-field actions. Such fields ("dilaton" or "moduli") generically appear in string theory and are massless at the tree-level, but could acquire a self-interaction potential $V(\varphi)$ beyond the tree-level.

The exchange of such a dilaton-like field leads to several types of observational deviations from GR. For experimental limits on the gravitational inverse-square-law (down to the micrometer range) see Refs. [60–64]. If the potential $V(\varphi)$ is zero or negligible for the considered range, the coupling of φ to ${F^a_{\mu\nu}}^2$ leads to apparent violations of the weak equivalence principle, with rather specific composition-dependence [65]. Next, when neglecting the fractionally small composition-dependent effects, such a field approximately couples to the trace of the energy-momentum tensor $T = g_{\mu\nu}T^{\mu\nu}$. The most general such theory contains (after suitable field redefinitions) two arbitrary functions of the scalar field, namely the self-interaction potential $V(\varphi)$, and a matter-coupling function $a(\varphi)$:

$$\mathcal{L}_{\rm tot}[g_{\mu\nu},\varphi,\psi,A_\mu,H] = \frac{c^4}{16\pi G_*}\sqrt{g}(R(g_{\mu\nu}) - 2g^{\mu\nu}\partial_\mu\varphi\partial_\nu\varphi) - \sqrt{g}V(\varphi) + \mathcal{L}_{\rm SM}[\psi,A_\mu,H,\widetilde{g}_{\mu\nu}]\,. \tag{21.40}$$

Here G_* is a "bare" Newton constant, and the Standard Model matter is coupled not to the "Einstein" (pure spin-2) metric $g_{\mu\nu}$, but to the conformally related ("Jordan-Fierz") metric

$$\widetilde{g}_{\mu\nu} = \exp(2a(\varphi))g_{\mu\nu}. \tag{21.41}$$

The scalar field equation

$$\Box_g\varphi = \frac{4\pi G}{c^4}\left(-\alpha(\varphi)T + \frac{\partial V(\varphi)}{\partial\varphi}\right)\,, \tag{21.42}$$

features

$$\alpha(\varphi) \equiv \partial a(\varphi)/\partial\varphi\,, \tag{21.43}$$

as the basic (field-dependent) coupling between φ and matter [15, 66]. The best-known, special case of these theories is the one-parameter (ω) Jordan-Fierz-Brans-Dicke theory [67], with $V(\varphi) = 0$ and $a(\varphi) = \alpha_0\varphi$, leading to a field-independent coupling $\alpha(\varphi) = \alpha_0$ (with ${\alpha_0}^2 = 1/(2\omega+3)$). More generally, if we consider the massless theories ($V(\varphi) = 0$) with arbitrary (non-linear) coupling function $a(\varphi)$, they modify Einstein's predictions in the weak-field slow-motion limit appropriate to describing gravitational experiments in the solar system (1PN approximation) only through the appearance of exactly the same two "post-Einstein" dimensionless parameters $\overline{\gamma} = \gamma - 1$ and $\overline{\beta} = \beta - 1$ that entered the minimal (Eddington) PPN formalism presented above. However, we now have the following theoretical expressions relating the latter phenomenological parameters to the coupling functions entering the tensor-scalar action Eq. (21.40):

$$\overline{\gamma} = -2\frac{\alpha_0^2}{1+\alpha_0^2}\,; \tag{21.44}$$

$$\overline{\beta} = +\tfrac{1}{2}\frac{\beta_0\alpha_0^2}{(1+\alpha_0^2)^2}\,. \tag{21.45}$$

Here $\alpha_0 \equiv \alpha(\varphi_0)$, and $\beta_0 \equiv \partial\alpha(\varphi_0)/\partial\varphi_0$, with φ_0 denoting the vacuum expectation value (VEV) of φ around the solar system. In addition, the observable value $G^{\rm obs}$ of the gravitational constant is found to be field-dependent and given (at a place where $\varphi = \varphi_0$) by

$$G^{\rm obs} = G(\varphi_0) \equiv G_*\exp[2a(\varphi_0)](1+\alpha_0^2)\,. \tag{21.46}$$

This makes it clear that the parameter $\overline{\gamma}$ is the basic post-Einstein parameter, which measures the admixture of an additional field (here a spin-0 field) to the pure spin-2 GR. One also sees how the parameter $\overline{\beta}$ is linked to non-linear effects (here coupling terms $\beta_0(\varphi-\varphi_0)^2T$ in the action), and how the Nordtvedt parameter $\eta \equiv 4\overline{\beta} - \overline{\gamma}$ is related to the field-dependence of $G^{\rm obs}$ ($\eta = (\alpha_0/(1+\alpha_0^2))\partial\ln G(\varphi_0)/\partial\varphi_0$).

The advantage of a theory-dependent approach, such as Eq. (21.40), over the phenomenological minimal PPN approach of Eq. (21.28), is that it allows one to consistently predict the observational deviations from GR in all possible gravity regimes: the quasi-stationary weak-field regime; the wavelike weak-field regime; the strong-field regime; the cosmological regime, etc. All such observational deviations can be consistently worked out once one chooses specific forms of the coupling function $a(\varphi)$, and of $V(\varphi)$. The simple choice of a two-parameter quadratic coupling function, say $a(\varphi) = \alpha_0(\varphi-\varphi_0) + \frac{1}{2}\beta_0(\varphi-\varphi_0)^2$, has been found useful for describing many possible observable deviations from GR.

The observable consequences for binary pulsar observations of the strong-field and radiative effects linked to the coupling to φ have been explicitly worked out in Refs. [15, 43] in the case where φ is massless (see Ref. [68] for the case where φ is massive). In particular, the strong-field nature of the pulsar tests is demonstrated by the fact that some tensor-scalar theories can be as close as desired to GR in the weak-field regime of the solar-system (*i.e.*, $\overline{\gamma}$ and $\overline{\beta}$ can be as small as desired, or even exactly zero), while developing (via a "spontaneous scalarization" mechanism) differences of order unity with GR in binary pulsar experiments [17, 18].

21.3.7 *Attractor and screening mechanisms in modified gravity*

As will follow from the discussion of experimental data below, the comparison between the predictions of general massless tensor-scalar theories and current data shows that the basic coupling parameter α_0 must be tuned to a small value (especially when allowing for composition-dependent effects). This raises the issue of the naturalness of such small coupling parameters. It has been shown in this respect that, in many tensor-scalar theories, there is an *attractor mechanism* by which the cosmological evolution naturally drives the VEV $\varphi_0(t)$ towards a value for which the coupling parameter $\alpha_0 = \alpha(\varphi_0)$ vanishes, thereby making it natural to expect only small deviations from GR (at least for the weak-field regime) at our current cosmological epoch [69, 70].

There are other theoretical mechanisms (generically called "screening mechanisms") that could explain why a theory of gravity whose theoretical content significantly differs from that of GR could naturally pass all the stringent, GR-compatible experimental limits that will be discussed below. In particular, when considering a self-interacting scalar field ($V(\varphi) \neq 0$), the interplay between the two terms on the right-hand side of Eq. (21.42) tends to drive the local VEV φ_0 of φ to a density-dependent value. In turn, this leads to a corresponding density-dependent effective mass $m_0(\varphi_0) = \sqrt{4\pi G\partial^2V(\varphi_0)/\partial\varphi_0^2}$ of the φ field, and to density-dependent matter couplings [71]. Various choices of the functions $V(\varphi)$ and $a(\varphi)$ can then reduce the φ-induced deviations from GR in dense environments while still allowing for significant deviations in different (*e.g.*, cosmological) regimes [72–76].

Other screening mechanisms have been invoked, based on an environment dependence mediated by (first or second) derivatives of a scalar degree of freedom. Roughly speaking, such mechanisms involve a (possibly effective) scalar degree of freedom φ that satisfies a field equation that is more general than Eq. (21.42) in that the left-hand side, $\Box_g\varphi$, is replaced by a non-linear function of φ, $\partial\varphi$ and $\partial^2\varphi$. The presence of non-linear derivative self-interactions of φ can weaken the effective coupling of φ to matter. A simple toy-model showing this weakening would be to replace Eq. (21.42) by an equation of the form

$$Z(\varphi,\partial\varphi,\partial^2\varphi)\Box_g\varphi = \frac{4\pi G}{c^4}\left(-\alpha(\varphi)T + \frac{\partial V(\varphi)}{\partial\varphi}\right)\,. \tag{21.47}$$

Such an equation is equivalent, at a first level of approximation, to replacing the gravitational constant G entering Eq. (21.42) by $G_{\rm eff}(\varphi_0,\partial\varphi_0,\partial^2\varphi_0) \equiv G/Z_0$, where $Z_0 \equiv Z(\varphi_0,\partial\varphi_0,\partial^2\varphi_0)$. This has a screening effect if $Z_0 \gg 1$. Indeed, the replacement $G \to G_{\rm eff}$ diminishes the strength of the interaction potential due to φ exchange by a factor of $1/Z_0$. In addition, the range of this interaction is also affected: $m_0(\varphi_0) = \sqrt{4\pi G\partial^2V(\varphi_0)/\partial\varphi_0^2} \to m_{0\rm eff}(\varphi_0,\partial\varphi_0,\partial^2\varphi_0) = \sqrt{4\pi G_{\rm eff}\partial^2V(\varphi_0)/\partial\varphi_0^2} = Z_0^{-1/2}m_0$.

Screening mechanisms based on such non-linear derivative self-interactions are often referred to as being "Vainshtein-like" because a similar mechanism was first invoked in Ref. [77] as a con-

Downloaded from https://academic.oup.com/ptep/article/2022/8/083C01/6651666 by KIT Library user on 27 September 2022

jectural way to ensure that the extra degrees of freedom associated with a massive (rather than massless) graviton become effectively weakly coupled to matter within a large domain around gravitational sources. Here, one is considering massive deformations of the massless spin-2 metric field of GR by a very small mass, possibly of cosmological scale: $m_g \sim \hbar H_0 \sim 10^{-33}$ eV. The construction of ghost-free potential terms for a spin-2 field has turned out to be a delicate matter [78]. The phenomenology of a very-low-mass graviton is still partly uncontrolled, both because of the unknown extent to which the Vainshtein screening is really active, and because of subtle constraints linked to an eventual UV completion of the theory beyond the unusually low energy scale where it becomes strongly coupled:

$$\Lambda_{\text{strong coupling}} \sim (M_{\text{Planck}} m_0^2)^{1/3} \sim 10^{-13} \left(\frac{m_0}{\hbar H_0}\right)^{2/3} \text{eV}\,. \tag{21.48}$$

The search for modified gravity theories incorporating an extra scalar degree of freedom potentially able to yield a Vainshtein-like screening led to writing down the following general class of tensor-scalar Lagrangian [79, 80]:

$$\begin{aligned} L_{\text{tot}}[g_{\mu\nu},\varphi,\psi] =& G_2(\varphi,X) - G_3(\varphi,X)\Box_g\varphi + G_4(\varphi,X)R \\ &+ G_{4X}(\varphi,X)[(\Box_g\varphi)^2 - \varphi^{\mu\nu}\varphi_{\mu\nu}] \\ &+ G_5(\varphi,X)G^{\mu\nu}\varphi_{\mu\nu} - \frac{1}{6}G_{5X}(\varphi,X)[(\Box_g\varphi)^3 \\ &- 3\Box_g\varphi\varphi^{\mu\nu} + 2\varphi_{\mu\nu}\varphi^{\mu\lambda}\varphi^{\nu}_{\lambda}] + L_{\text{matter}}[g_{\mu\nu},\psi]\,. \end{aligned} \tag{21.49}$$

Here $g_{\mu\nu}$ denotes the matter-coupled metric, $X \equiv -\frac{1}{2}g^{\mu\nu}\partial_\mu\varphi\partial_\nu\varphi$, $\varphi_{\mu\nu} \equiv \nabla_\mu\nabla_\nu\varphi$, $G^{\mu\nu} \equiv R^{\mu\nu} - \frac{1}{2}Rg^{\mu\nu}$, and the various coefficients $G_n(\varphi,X)$ are arbitrary functions of two variables (with $G_{nX} \equiv \partial G_n/\partial X$). The field equations derived from the Lagrangian of Eq. (21.49) are only of second order in derivatives in spite of the non-linear structure of L_{tot}. This implies that the tensor-scalar theories defined by Eq. (21.49) feature three degrees of freedom, corresponding to a massless spin-2 excitation (GW) and a spin-0 excitation. Contrary to the simpler tensor-scalar theories of Eq. (21.40), it is found that the speed of propagation of GWs implied by Eq. (21.49) is generically different from the speed of light:

$$\frac{c_{\text{GW}}^2}{c^2} = \frac{G_4 - X(\ddot{\varphi}G_{5X} + G_{5\varphi})}{G_4 - 2XG_{4X} - X(H\dot{\varphi}G_{5X} - G_{5\varphi})}\,. \tag{21.50}$$

More general modified gravity models have been proposed (see, *e.g.* Refs. [81, 82]). Apart from the simplest of them, most of these models have a rather artificial flavor, and do not lead to convincing alternative explanations either of dark matter or of dark energy. In addition, many of them do not lead (contrary to GR) to mathematically "well-posed" evolution problems [83–85]. This entails a serious challenge to deriving strong-field predictions for such models. It has been argued that many of these (dark-energy motivated) models should be viewed as effective field theory (EFT) approximations that need some sort of UV completion at an unusually low frequency scale [86]. In spite of these shortcomings, such models are conceptually interesting because they give examples of deviations for various predictions of GR, existing independently from each other, in various regimes. For instance, some special tensor-scalar models lead to black hole solutions modified by scalar-hair [87–89]. For other types of black holes with scalar-hair, see Ref. [90]. This shows the interest of phenomenologically testing, in a democratic and agnostic way, all conceivable deviations from GR.

Let us now turn to briefly presenting current experimental results of various phenomenological tests of the main GR predictions recalled in Section 21.2 above.

21.4 Experimental tests of the Equivalence Principle (*i.e.*, of the matter-gravity coupling)

21.4.1 *Tests of the constancy of constants*

Stringent limits on a possible time variation of the basic coupling constants have been obtained by analyzing a natural fission reactor phenomenon that took place at Oklo, Gabon, two billion years ago [91,92]. These limits are at the 1×10^{-8} level for the fractional variation of the fine-structure constant α_{em} [92], and at the 4×10^{-9} level for the fractional variation of the ratio m_q/Λ_{QCD} between the light quark masses and Λ_{QCD} [93]. The determination of the lifetime of Rhenium 187 from isotopic measurements of some meteorites dating back to the formation of the solar system (about 4.6 Gyr ago) yields comparably strong limits [94]. Measurements of absorption lines in astronomical spectra also give stringent limits on the variability of both α_{em} and $\mu = m_p/m_e$ at cosmological redshifts, *e.g.*,

$$\Delta\alpha_{\text{em}}/\alpha_{\text{em}} = (1.2 \pm 1.7_{\text{stat}} \pm 0.9_{\text{sys}}) \times 10^{-6}\,, \tag{21.51}$$

at redshifts $z = 1.0$–2.4 [95], and

$$|\Delta\mu/\mu| < 4\times10^{-7}(95\%\ \text{C.L.})\,, \tag{21.52}$$

at a redshift $z = 0.88582$ [96]. There are also significant limits on the variation of α_{em} and $\mu = m_p/m_e$ at redshift $z \sim 10^3$ from cosmic microwave background data, *e.g.*, $\Delta\alpha_{\text{em}}/\alpha_{\text{em}} = (3.6 \pm 3.7)\times10^{-3}$ [97]. Direct laboratory limits (based on monitoring the frequency ratio of several different atomic clocks) on the present time variation of α_{em}, $\mu = m_p/m_e$, and m_q/Λ_{QCD} have reached the levels [98]

$$\begin{aligned} d\ln(\alpha_{\text{em}})/dt &= (-2.5 \pm 2.6)\times10^{-17}\text{yr}^{-1}, \\ d\ln(\mu)/dt &= (-1.5 \pm 3.0)\times10^{-16}\text{yr}^{-1}, \\ d\ln(m_q/\Lambda_{\text{QCD}})/dt &= (7.1 \pm 4.4)\times10^{-15}\text{yr}^{-1}. \end{aligned} \tag{21.53}$$

There are also experimental limits on a possible dependence of coupling constants on the gravitational potential [98–100].

Experimental limits on the present time variation of the gravitational constant, Eq. (21.33), have been derived from planetary ephemerides [101], lunar laser ranging [102], and binary-pulsar data [103, 104]. The most stringent limits come from lunar-laser-ranging data [102]:

$$\frac{\dot{G}_0}{G_0} = (7.1 \pm 7.6)\times10^{-14}\ \text{yr}^{-1}\,. \tag{21.54}$$

21.4.2 *Tests of the isotropy of space and of Local Lorentz invariance*

The highest precision tests of the isotropy of space have been performed by looking for possible quadrupolar shifts of nuclear energy levels [105]. The (null) results can be interpreted as testing the fact that the various pieces in the matter Lagrangian, Eq. (21.6), are indeed coupled to the same external metric $g_{\mu\nu}$ to the 10^{-29} level.

Stringent tests of possible violations of local Lorentz invariance in gravitational interactions have been obtained both from solar-system data [8] and pulsar data [106, 107]. For astrophysical constraints on possible Planck-scale violations of Lorentz invariance, see Ref. [108].

21.4.3 *Tests of the universality of free fall (weak, and strong equivalence principles)*

The universality of the acceleration of free fall has been verified, for laboratory bodies, both on the ground [109, 110] (at the 10^{-13} level), and in space [111, 112] (at the 10^{-14} level):

$$\begin{aligned} (\Delta a/a)_{\text{BeTi}} &= (0.3 \pm 1.8)\times10^{-13}\,; \\ (\Delta a/a)_{\text{BeAl}} &= (-0.7 \pm 1.3)\times10^{-13}\,; \\ (\Delta a/a)_{\text{TiPt}} &= (-1 \pm 9(\text{stat}) \pm 9(\text{syst}))\times10^{-15}\,. \end{aligned} \tag{21.55}$$

The universality of free fall has also been verified when comparing the fall of classical and quantum objects (at the 6×10^{-9} level [113]), or of two quantum objects (at the $(0.3\pm5.4)\times10^{-7}$ [114], and $(1\pm1.4)\times10^{-9}$, levels [115]).

The universality of free fall of self-gravitating bodies (strong equivalence principle) has been verified in both the weak-gravity, and the strong-gravity regimes. The gravitational accelerations

Downloaded from https://academic.oup.com/ptep/article/2022/8/083C01/6651666 by KIT Library user on 27 September 2022

of the Earth and the Moon toward the Sun have been checked to agree at the 10^{-13} level [102]

$$(\Delta a/a)_{\rm EarthMoon} = (-3 \pm 5) \times 10^{-14}. \tag{21.56}$$

The latter result constrains the Nordtvedt PPN parameter [9] $\eta \equiv 4\overline{\beta} - \overline{\gamma}$ to the 10^{-4} level:

$$\eta = (-0.2 \pm 1.1) \times 10^{-4}\,. \tag{21.57}$$

See below for strong-field tests of the strong equivalence principle.

Finally, the universality of the gravitational redshift of clock rates has been verified at the 10^{-4} level by comparing a hydrogen-maser clock flying on a rocket up to an altitude of about 10,000 km to a similar clock on the ground [116]. The redshift due to a height change of only 33 cm has been detected by comparing two optical clocks based on $^{27}Al^+$ ions [117]. The gravitational redshift has also been detected in the orbit of a star near the supermassive black hole at the center of our Galaxy [118, 119], and its universality has been verified at the 5% level [120].

21.5 Tests of quasi-stationary, weak-field gravity

All currently performed gravitational experiments in the solar system, including perihelion advances of planetary orbits, the bending and delay of electromagnetic signals passing near the Sun, and very accurate ranging data to the Moon obtained by laser echoes, are compatible with the post-Newtonian results of Eq. (21.15), Eq. (21.13), and Eq. (21.14). The "gravito-magnetic" interactions $\propto v_A v_B$ contained in Eq. (21.13) are involved in many of these experimental tests. They have been particularly tested in lunar-laser-ranging data [121], in the combined LAGEOS-LARES satellite data [122, 123], and in the dedicated Gravity Probe B mission [124].

To assess in a quantitative manner the results of the various solar-system tests of gravity it is convenient to express them in terms of the PPN parameters defined above. The best current limit on the post-Einstein parameter $\overline{\gamma} \equiv \gamma - 1$ is

$$\overline{\gamma} = (2.1 \pm 2.3) \times 10^{-5}\ , \tag{21.58}$$

as deduced from the additional Doppler shift experienced by radio-wave beams connecting the Earth to the Cassini spacecraft when they passed near the Sun [125].

The (cubic-vertex-related) post-Einstein parameter $\overline{\beta} \equiv \beta - 1$ is constrained at the 10^{-4} level both from a study of the global sensitivity of planetary ephemerides to post-Einstein parameters [101],

$$|\overline{\beta}| < 7 \times 10^{-5}\ , \tag{21.59}$$

and from lunar-laser-ranging data [102]

$$\overline{\beta} = (-4.5 \pm 5.6) \times 10^{-5}\ . \tag{21.60}$$

The periastron advance of the star S2 around the Galactic center massive black hole has been observed to agree with GR within 20% [126]. More stringent limits on $\overline{\gamma}$ (*i.e.* the coupling of φ to matter) are obtained in dilaton-like models where scalar couplings violate the Equivalence Principle [127].

21.6 Tests of strong-field gravity (neutron stars and black holes)

Experimental tests of strong-field gravity have been obtained in various physical systems, notably binary pulsars and coalescing binary black holes.

It is convenient to quantitatively express binary-pulsar tests of strong-field gravity by using the PPK formalism defined above. We recall that the measurement of N phenomenological PPK parameters leads to $N-2$ tests of strong-field gravity. In all, *thirteen* tests of strong-field and/or radiative gravity have been obtained in the four different (double neutron-star) binary pulsar systems PSR1913+16 [10, 11, 128], PSR1534+12 [129–131], PSR J1141−6545 [132–135], and PSR J0737−3039 A,B [136–140]. These consist of $N-2 = 5-2 = 3$ tests from PSR1913+16 ; $5-2=3$ tests from PSR1534+12; $4-2=2$ tests from PSR J1141−6545; and $7-2=5$ tests from PSR J0737−3039 (see, also, Ref. [141] for additional, less accurate tests of relativistic gravity). Among these tests, four of them (those involving the measurement of the PPK parameter $\dot{P}_b$) probe radiative effects, and will be discussed in the following section. The four binary pulsar systems PSR1913+16, PSR1534+12, PSR J1141−6545, and PSR J0737−3039 A,B have given nine tests of quasi-static, strong-field gravity. GR passes all these tests within the measurement accuracy. Let us only highlight here some of the most accurate strong-field tests.

In the binary pulsar PSR 1534+12 [129] one has measured *five* post-Keplerian parameters: k, $\gamma_{\rm timing}$, r, s, and (with less accuracy) $\dot{P}_b$ [130, 131]. This yields *three* tests of relativistic gravity. Among these tests, the two involving the measurements of k, $\gamma_{\rm timing}$, r, and s accurately probe strong field gravity, without mixing of radiative effects [130]. The most precise (10^{-3} level) of these pure strong-field tests is the one obtained by combining the measurements of k, $\gamma_{\rm timing}$, and s; namely, [131],

$$\left[\frac{s^{\rm obs}}{s^{\rm GR}[k^{\rm obs}, \gamma^{\rm obs}_{\rm timing}]}\right]_{1534+12} = 1.002 \pm 0.002\ . \tag{21.61}$$

The discovery of the remarkable *double* binary pulsar PSR J0737−3039 A and B [136, 137] has led to the measurement of *seven* independent parameters [138–140]: five of them are the post-Keplerian parameters k, $\gamma_{\rm timing}$, r, s, and $\dot{P}_b$ entering the relativistic timing formula of the fast-spinning pulsar PSR J0737−3039 A; a sixth is the ratio $R = x_B/x_A$ between the projected semi-major axis of the more slowly spinning companion pulsar PSR J0737−3039 B, and that of PSR J0737−3039 A (the theoretical prediction for the ratio $R = x_B/x_A$, considered as a function of the (inertial) masses $m_1 = m_A$ and $m_2 = m_B$, is $R^{\rm theory} = m_1/m_2 + O((v/c)^4)$ [13, 14], independently of the gravitational theory considered). Finally, the seventh parameter $\Omega_{\rm SO,B}$ is the angular rate of (spin-orbit) precession of PSR J0737−3039 B around the total angular momentum vector [139, 140]. These seven measurements give us *five* tests of relativistic gravity [138, 142, 143], four of which are quasi-static, strong-field tests. GR passes all those tests with flying colors [143, 144]. The most accurate is at the 5×10^{-4} level:

$$\left[\frac{s^{\rm obs}}{s^{\rm GR}[k^{\rm obs}, R^{\rm obs}]}\right]_{0737-3039} = 1.0000 \pm 0.0005\ . \tag{21.62}$$

Binary pulsar data on other types of pulsar systems can be used to test strong-field aspects of the "strong equivalence principle," namely the GR prediction that strong-self-gravity objects (such as neutron stars) should fall with the same acceleration as weak-self-gravity objects (such as white-dwarfs) in the (external) gravitational field created by other objects (such as the Galaxy, or another white dwarf). The first binary-pulsar tests of this property have been obtained in nearly circular binary systems (made of a neutron star and a white dwarf) falling in the field of the Galaxy, and have led to strong-field confirmations (at the 2×10^{-3} level) of the strong equivalence principle [104, 145–147]. The remarkable discovery of the pulsar PSR J0337+1715 in a hierarchical triple system [148] has allowed one to derive a much more accurate test of the strong equivalence principle because the inner binary (comprising a pulsar and a close white-dwarf companion) falls toward the outer white-dwarf companion with an acceleration that is 10^8 times larger than the Galactic acceleration. This leads to a 95% confidence level limit on a possible fractional difference in free-fall acceleration of the pulsar and its close companion of [149, 150]

$$|\Delta a/a| < 2.05 \times 10^{-6}\ (95\%\ \text{C.L.})\,. \tag{21.63}$$

.. This limit yields strong constraints on tensor-scalar gravity models.

Measurements over several years of the pulse profiles of various pulsars have detected secular changes compatible with the prediction [151] that the general relativistic spin-orbit coupling should cause a secular change in the orientation of the pulsar beam with respect to the line of sight ("geodetic precession"). Such confirmations of general-relativistic spin-orbit effects were obtained in

Downloaded from https://academic.oup.com/ptep/article/2022/8/083C01/6651666 by KIT Library user on 27 September 2022

PSR 1913+16 [152], PSR B1534+12 [131], PSR J1141−6545 [153], PSR J0737−3039 [139, 140], and PSR J1906+0746 [154, 155]. In some cases (notably PSR 1913+16 and PSR J1906+0746) the secular change in the orientation of the pulsar beam is expected to lead to the disappearance of the beam (as seen on the Earth) on a human time scale (the second pulsar in the double system PSR J0737−3039 already disappeared in March 2008 and is expected to reappear around 2035 [140]).

Recently, the ultimate strong-field regime of black holes has started to be quantitatively probed via GW observations. The LIGO-Virgo collaboration has detected (starting in September 2015) GW signals [156], which, besides testing the radiative structure of gravity (see next section), are in excellent qualitative and quantitative agreement with the structure and dynamics of black-hole horizons in GR. Because of the mixing of strong-field effects with radiative effects during the coalescence of two black holes, and because of the lack of detailed alternative-theory predictions for this process (see, however, Refs. [45–47]), it is not easy to set quantitative limits on possible strong-field deviations from GR, independently of radiative effects. Direct tests of the existence of black-hole horizons are scarce (see, however, Sec. VIIB of [157] which reports the lack of any statistical evidence for GW echoes).

Let us also mention that the Event Horizon Telescope collaboration has obtained event-horizon-scale images of the supermassive black hole candidate in the center of the giant elliptical galaxy M87 that are "consistent with expectations for the shadow of a Kerr black hole as predicted by general relativity" [158]. For discussions of the corresponding constraints on the black hole geometry in the vicinity of the light ring see Refs. [159, 160].

21.7 Tests of radiative gravity (both in binary-pulsar data and in GW data)

Experimental confirmations of the GR predictions for the radiative structure of gravity have been obtained both in binary-pulsar data and in the observation of GW signals from coalescing compact binaries (binary black holes and binary neutron stars).

Binary-pulsar observations involving the measurement of the orbital period derivative $\dot{P}_b$ give *direct* experimental tests of the reality of gravitational radiation, and, in particular, an experimental confirmation that the speed of propagation of gravity c_g is equal to the speed of light c (indeed, as recalled above, $\dot{P}_b$ is a consequence of the propagation of the gravitational interaction between the two neutron stars [12]). Even in the presence of screening mechanisms within the binary system, the value of $\dot{P}_b$ yields a measurement of the speed of propagation of GWs at the 10^{-2} level [161]. The currently most accurate binary-pulsar tests of the radiative properties of gravity come from the binary neutron-star systems PSR1913+16 and PSR J0737−3039 A,B, as well as from several neutron-star-white-dwarf systems, notably PSR J1738+0333.

After subtracting a small ($\sim 10^{-14}$ level in $\dot{P}_b^{\rm obs} = (-2.423 \pm 0.001) \times 10^{-12}$), but significant, "Galactic" perturbing effect (linked to Galactic accelerations and to the pulsar proper motion) [162], one finds that the phenomenological test obtained by combining the measurements of the three PPK parameters $(k - \gamma_{\rm timing} - \dot{P}_b)_{1913+16}$ is passed by GR with complete success [128]:

$$\left[\frac{\dot{P}_b^{\rm obs} - \dot{P}_b^{\rm gal}}{\dot{P}_b^{\rm GR}[k^{\rm obs}, \gamma_{\rm timing}^{\rm obs}]}\right]_{1913+16} = 0.9983 \pm 0.0016 \ . \qquad (21.64)$$

Here $\dot{P}_b^{\rm GR}[k^{\rm obs}, \gamma_{\rm timing}^{\rm obs}]$ is the result of inserting in $\dot{P}_b^{\rm GR}(m_1, m_2)$ the values of the masses predicted by the two equations $k^{\rm obs} = k^{\rm GR}(m_1, m_2)$, and $\gamma_{\rm timing}^{\rm obs} = \gamma_{\rm timing}^{\rm GR}(m_1, m_2)$. This yields experimental evidence for the reality of gravitational radiation damping forces at the $(-1.7 \pm 1.6) \times 10^{-3}$ level.

Similarly, the combined measurement in PSR J0737−3039 A,B of the three parameters k, $R \equiv x_B/x_A$, and $\dot{P}_b$ yields another experimental test of the radiative structure of gravity at the 10^{-3} level [138–140]:

$$\left[\frac{\dot{P}_b^{\rm obs}}{\dot{P}_b^{\rm GR}[k^{\rm obs}, R^{\rm obs}]}\right]_{0737-3039} = 1.000 \pm 0.001 \ . \qquad (21.65)$$

In addition to the above tests, further very stringent tests of radiative gravity follow from the measurement of the orbital period decay $\dot{P}_b$ of low-eccentricity pulsar-white dwarf systems. Notably, the system PSR J1738+0333 yields an intrinsic orbital decay of [163]

$$\left[\dot{P}_b^{\rm obs} - \dot{P}_b^{\rm gal}\right]_{1738+0333} = (-25.9 \pm 3.2) \times 10^{-15} \ , \qquad (21.66)$$

to be compared to

$$\left[\dot{P}_b^{\rm GR}\right]_{1738+0333} = (-27.7^{+1.5}_{-1.9}) \times 10^{-15} \ . \qquad (21.67)$$

The fractional agreement between the (corrected) observed period decay and the GR-predicted one seems to be quantitatively less impressive than the double-neutron-star results cited above, but the crucial point is that asymmetric binary systems (such as neutron-star-white-dwarf ones) are strong emitters of dipolar gravitational radiation in tensor-scalar theories, with $\dot{P}_b$ scaling (modulo matter-scalar couplings) like $m_1 m_2/(m_1 + m_2)^2 (v/c)^3$, instead of the parametrically smaller GR-predicted quadrupolar radiation $\dot{P}_b \sim (v/c)^5$ [7, 15]. In view of the very small absolute value of $\dot{P}_b$, this makes such systems (and notably PSR J1738+0333) very sensitive probes of tensor-scalar gravity [103, 144, 163–166]. It is then useful to turn to a theory-dependent analysis of pulsar data. Such an analysis (see, *e.g.*, [17, 130, 144, 163, 166]) leads to excluding a large portion of the parameter space of tensor-scalar gravity allowed by solar-system tests. As a result, the basic matter-scalar coupling α_0^2 is more strongly constrained, over most of the parameter space, than the best current solar-system limits of Eq. (21.58) (namely below the 10^{-5} level) [163, 166].

We now turn to the tests of radiative gravity that can be deduced from the GW data gathered from the first two observing runs of the LIGO-Virgo collaboration (LVC), and the first half of the third observing run (*i.e.* about fifty GW signals). All currently detected GW signals are consistent with GR predictions. Several phenomenological approaches were used and led to setting limits on possible deviations from GR [50, 157, 167].

A theory-agnostic quantitative assessment on possible deviations from GR is given by measuring the agreement between the full observed GW signal of coalescing binary black holes, and the GR-predicted one. The strongest such result was obtained with the first event: GW150914, which had an SNR of 24. The noise-weighted correlation between the GW150914 signal and the best-fit GR-predicted waveform was found to be $\geq 97\%$ [50, 167]. In other words, GR-violation effects that cannot be reabsorbed in a redefinition of physical parameters are limited (in a noise-weighted sense) to less than 3%.

Besides checking the agreement between the *full* observed GW signals and the corresponding best-fit full signals predicted by GR, one also tested the consistency between separate parts of the signals. A first approach [157, 167] separates: (i) the lower-frequency signal emitted during the *inspiral* phase (considered up to the innermost stable circular orbit); and (ii) the higher-frequency remaining signal emitted during the *postinspiral* phase, comprising the late-inspiral, the merger, and the ringdown. Separately fitting each of these partial signals to GR-based templates then yields separate estimates of the binary's parameters, leading to separate estimates of the mass M_f and dimensionless spin parameter $a_f = J_f/(GM_f^2)$ of the final black hole that would be formed (in GR) by the coalescence of the two initial black holes. The consistency with GR then consists in testing whether the two estimates $(M_f, a_f)_{\rm insp}$ and $(M_f, a_f)_{\rm postinsp}$ are compatible with each other. They were found to be compatible for all events whose corresponding separate SNRs made such an analysis meaningful (see Figs. 3 and 4 in [157]). Quantitatively, the (population-marginalized) fractional differences

$$\frac{\Delta M_f}{\bar{M}_f} = 2\frac{M_f^{\rm insp} - M_f^{\rm postinsp}}{M_f^{\rm insp} + M_f^{\rm postinsp}} ,$$
$$\frac{\Delta a_f}{\bar{a}_f} = 2\frac{a_f^{\rm insp} - a_f^{\rm postinsp}}{a_f^{\rm insp} + a_f^{\rm postinsp}} , \qquad (21.68)$$

Downloaded from https://academic.oup.com/ptep/article/2022/8/083C01/6651666 by KIT Library user on 27 September 2022

between the two estimates were found to be consistent with zero (*i.e.* with GR) [157]

$$\frac{\Delta M_f}{\bar{M}_f} = 0.02^{+0.20}_{-0.17},$$
$$\frac{\Delta a_f}{\bar{a}_f} = -0.05^{+0.36}_{-0.41}. \tag{21.69}$$

A second approach [168, 169] considers the signal of coalescing black holes in the time domain, and separates it in its *premerger*, and *postmerger* parts, the dividing line being the (inferred) peak of the waveform. Using various models of the postmerger signal (including either one or two black-hole ringing modes) leads to estimates of the mass and spin of the final black hole, $(M_f, a_f)_{\rm postmerger}$. The application of this time-domain analysis to the (high SNR) first event GW150914 has shown consistency between $(M_f, a_f)_{\rm postmerger}$, $(M_f, a_f)_{\rm premerger}$ and $(M_f, a_f)_{\rm full\,signal}$ (see Fig. 4 and Table I in [169]). This consistency confirms Hawking's area-increase theorem with 97 % probability [169]. Applying such an analysis to the data of the second LIGO-Virgo transient catalog allows one to constrain possible deviations away from the GR-predicted frequencies and damping times of the first two quadrupolar ringing modes [157]. For instance, the population-marginalized constraint on the fractional deviation of the fundamental 220 ringing mode was found to be $\delta\hat{f}_{220} = 0.03^{+0.38}_{-0.35}$ [157] (see also Fig. 14 there). Applying the different analysis advocated in Ref. [170] allows one to derive a stronger constraint on $\delta\hat{f}_{220}$, namely $\delta\hat{f}_{220} = -0.05^{+0.05}_{-0.05}$ [171].

The parametrization of Eq. (21.38) for possible deviations in the frequency dependence of the Fourier-domain phase $\psi(f)$ of the black hole coalescence GW signal was used to measure best-fit values for each fractional deviation parameter $\delta\hat{p}_i$, considered separately (the other ones being set to zero). In all cases, the posterior distribution for each $\delta\hat{p}_i$ is consistent with the GR value, *i.e.*, $\delta\hat{p}_i^{\rm GR} = 0$ (see Fig. 6 in [157]). The current limits on $\delta\hat{p}_i$ are (roughly) of order unity, except for the two parameters highlighted above: $\delta\hat{p}_3$ (parameterizing the $O((\frac{v}{c})^3)$ fractional correction to the LO, quadrupolar term); and $\delta\hat{p}_{-2}$ (parameterizing a possible dipolar-radiation-related $O((\frac{v}{c})^{-2})$ fractional correction to the LO, quadrupolar term). The current [157] 90%-credible interval for $\delta\hat{p}_3$ is $-0.02^{+0.11}_{-0.10}$ (when using a phenomenological model [52]), and $-0.01^{+0.10}_{-0.11}$ (when using an effective one-body model [37]). The corresponding 90%-credible intervals for a possible dipolar term $\delta\hat{p}_{-2}$ are, respectively, $(-1.0^{+4.5}_{-4.0}) \times 10^{-3}$ and $(-0.5^{+3.5}_{-3.5}) \times 10^{-3}$ [157]. For examples of the translation of these phenomenological constraints into bounds on specific gravitational theories see Refs. [172, 173].

As recalled above, GR predicts that the polarization content of GWs is pure helicity-2, *i.e.* described by the two independent components of a traceless tensor transverse to the propagation direction. A (massless) scalar excitation would add a pure-trace "breathing mode" in the plane transverse to the propagation direction. A phenomenological approach to generic metric theories of gravity would allow for up to six polarizations for a GW [174], namely two tensor, two vector and two scalar modes. The LVC tested possible polarization deviations from GR in the following way [33, 167]: they assumed that the phase evolution of the GW signal was the one predicted by GR, but they replaced the polarization structure of the signal either by a generic vector-like one, or by a generic scalar-like one. The best polarization constraints have been obtained from the GW170817 event. The latter very long (~ 100 s) and very loud (SNR $\simeq 33$) event was convincingly interpreted as coming from a binary neutron star inspiral (~ 40 Mpc away), and was associated with a subsequent γ-ray burst, followed by transient counterparts across the electromagnetic spectrum [175]. The polarization analysis of the GW170817 data has given overwhelming evidence in favor of pure tensor polarization modes in comparison to pure vector or pure scalar modes with a base-ten logarithm of the Bayes factor of $+20.81 \pm 0.08$ and $+23.09 \pm 0.08$, respectively [167]. See also Sec. VIII of [157] for an analysis that does not rely on specific waveform models.

GR also predicts that GWs are non dispersive, and propagate at the same speed as light. One can phenomenologically modify the GR-predicted GW phase evolution by adding the putative effect of an anomalous dispersion relation of the form $E^2 = p^2c^2 + Ap^\alpha c^\alpha$. GW data have been used to set bounds on the anomalous coefficient A for various values of the exponent α. The case $\alpha = 0$ is equivalent to assuming that gravitons disperse as a massive particle [58]. Combined GW data from the second GW transient catalog lead to the following (90%-credibility) phenomenological limit on the graviton mass: $m_g \leq 1.76 \times 10^{-23}{\rm eV}/c^2$ [157]. This limit is 1.8 times more stringent than the most recent Solar System bound [64].

Finally, a very constraining bound on the speed of propagation of gravity $c_{\rm GW}$ was derived from the observed time delay of 1.7 s between GW170817 and the associated γ-ray burst. Namely, the fractional difference between $c_{\rm GW}$ and $c_{\rm light} \equiv c$ is constrained to be [176]

$$-3 \times 10^{-15} < \frac{c_{\rm GW} - c}{c} < +7 \times 10^{-16}\,. \tag{21.70}$$

When comparing the latter bound to the prediction Eq. (21.50) from general second-order tensor-scalar theories, Eq. (21.49), one is led to conclude that the coupling function $G_5(\varphi, X)$ has to be ignored and that the coupling function $G_4(\varphi, X)$ has to be restricted to depend only on φ. This drastically reduces the viable tensor-scalar modified-gravity models [177–180].

21.8 Conclusions

All present experimental tests are compatible with the predictions of the current "standard" theory of gravitation, Einstein's General Relativity. Let us recap the main tests. The universality of the coupling between matter and gravity (Equivalence Principle) has been verified at around the 10^{-14} level. Solar system experiments have tested the weak-field predictions of Einstein's theory at the few times 10^{-5} level. The propagation properties (in the near zone) of relativistic gravity, as well as several of its static strong-field aspects, have been verified at the 10^{-3} level (or better) in several binary pulsar experiments. Interferometric detectors of gravitational radiation have given direct observational proofs of the existence, and properties, of gravitational waves (in the wave zone), and of the existence of coalescing black holes, and they have already set strong limits on possible deviations; in particular: an upper bound $|\delta\hat{p}_{-2}| \lesssim 4 \times 10^{-3}$ on a possible dipolar contribution to the GW flux; the $O(10^{-15})$ bound of Eq. (21.70) on the speed of gravity; and evidence for the tensor polarization structure of gravitational waves. In addition, laboratory experiments have set strong constraints on sub-millimeter modifications of Newtonian gravity, while many different cosmological data sets have been used to set limits on possible GR deviations on cosmological scales [29]. In spite of the uneasiness of having to assume the existence of dark matter, and the presence of an unnaturally small cosmological constant (as dark energy), General Relativity stands out as a uniquely successful description of gravity on all the scales that have been explored so far. There are no modified-gravity models which naturally pass all existing experimental tests, while either explaining away the need for dark matter or for dark energy.

References

[1] S. Weinberg, Rev. Mod. Phys. **61**, 1 (1989).

[2] H. A. Buchdahl, Phys. Rev. **116**, 1027 (1959).

[3] N. Chamel *et al.*, Int. J. Mod. Phys. **E22**, 1330018 (2013), [arXiv:1307.3995].

[4] J. R. Oppenheimer and H. Snyder, Phys. Rev. **56**, 455 (1939).

[5] R. P. Kerr, Phys. Rev. Lett. **11**, 237 (1963).

[6] V. F. Mukhanov, H. A. Feldman and R. H. Brandenberger, Phys. Rept. **215**, 203 (1992).

[7] C. M. Will, *Theory and Experiment in Gravitational Physics*, Cambridge University Press (2018).

[8] C. M. Will, Living Rev. Rel. **17**, 4 (2014), [arXiv:1403.7377].

[9] K. Nordtvedt, Phys. Rev. **170**, 1186 (1968).

Downloaded from https://academic.oup.com/ptep/article/2022/8/083C01/6651666 by KIT Library user on 27 September 2022

[10] R. A. Hulse, Rev. Mod. Phys. **66**, 699 (1994).

[11] J. H. Taylor, Rev. Mod. Phys. **66**, 711 (1994).

[12] T. Damour and N. Deruelle, Phys. Lett. **A87**, 81 (1981); T. Damour, C.R. Acad. Sci. Paris **294**, 1335 (1982).

[13] T. Damour and J. H. Taylor, Phys. Rev. **D45**, 1840 (1992).

[14] T. Damour and N. Deruelle, Ann. Inst. H. Poincare A, **44**, 263 (1986).

[15] T. Damour and G. Esposito-Farese, Class. Quant. Grav. **9**, 2093 (1992).

[16] C. M. Will and H. W. Zaglauer, Astrophys. J. **346**, 366 (1989).

[17] T. Damour and G. Esposito-Farese, Phys. Rev. **D54**, 1474 (1996), [arXiv:gr-qc/9602056].

[18] T. Damour and G. Esposito-Farese, Phys. Rev. **D58**, 042001 (1998), [arXiv:gr-qc/9803031].

[19] J.-P. Uzan, Gen. Rel. Grav. **39**, 307 (2007), [arXiv:astro-ph/0605313].

[20] R. Caldwell, A. Cooray and A. Melchiorri, Phys. Rev. **D76**, 023507 (2007), [arXiv:astro-ph/0703375].

[21] P. Zhang *et al.*, Phys. Rev. Lett. **99**, 141302 (2007), [arXiv:0704.1932].

[22] L. Amendola, M. Kunz and D. Sapone, JCAP **0804**, 013 (2008), [arXiv:0704.2421].

[23] W. Hu and I. Sawicki, Phys. Rev. **D76**, 104043 (2007), [arXiv:0708.1190].

[24] S. F. Daniel *et al.*, Phys. Rev. **D77**, 103513 (2008), [arXiv:0802.1068].

[25] G.-B. Zhao *et al.*, Phys. Rev. **D79**, 083513 (2009), [arXiv:0809.3791].

[26] J.-P. Uzan, Gen. Rel. Grav. **42**, 2219 (2010), [arXiv:0908.2243].

[27] E. Bertschinger, Phil. Trans. Roy. Soc. Lond. **A369**, 4947 (2011), [arXiv:1111.4659].

[28] T. Baker, P. G. Ferreira and C. Skordis, Phys. Rev. **D87**, 2, 024015 (2013), [arXiv:1209.2117].

[29] M. Ishak, Living Rev. Rel. **22**, 1, 1 (2019), [arXiv:1806.10122].

[30] B. P. Abbott *et al.* (LIGO Scientific, Virgo), Phys. Rev. Lett. **116**, 6, 061102 (2016), [arXiv:1602.03837].

[31] B. P. Abbott *et al.* (LIGO Scientific, Virgo), Phys. Rev. Lett. **116**, 24, 241103 (2016), [arXiv:1606.04855].

[32] B. P. Abbott *et al.* (LIGO Scientific, VIRGO), Phys. Rev. Lett. **118**, 22, 221101 (2017), [Erratum: Phys. Rev. Lett.121,no.12,129901(2018)], [arXiv:1706.01812].

[33] B. P. Abbott *et al.* (LIGO Scientific, Virgo), Phys. Rev. Lett. **119**, 14, 141101 (2017), [arXiv:1709.09660].

[34] B. P. Abbott *et al.* (LIGO Scientific, Virgo), Phys. Rev. Lett. **119**, 16, 161101 (2017), [arXiv:1710.05832].

[35] B. P. Abbott *et al.* (LIGO Scientific, Virgo), Phys. Rev. **X6**, 4, 041015 (2016), [erratum: Phys. Rev.X8,no.3,039903(2018)], [arXiv:1606.04856].

[36] R. Abbott *et al.* (LIGO Scientific, Virgo), Phys. Rev. X **11**, 021053 (2021), [arXiv:2010.14527].

[37] A. Buonanno and T. Damour, Phys. Rev. **D62**, 064015 (2000), [arXiv:gr-qc/0001013].

[38] L. Blanchet, Living Rev. Rel. **17**, 2 (2014), [arXiv:1310.1528].

[39] F. Pretorius, Phys. Rev. Lett. **95**, 121101 (2005), [arXiv:gr-qc/0507014]; M. Campanelli *et al.*, Phys. Rev. Lett. **96**, 111101 (2006), [arXiv:gr-qc/0511048]; J. G. Baker *et al.*, Phys. Rev. Lett. **96**, 111102 (2006), [arXiv:gr-qc/0511103].

[40] K. Yagi *et al.*, Phys. Rev. **D85**, 064022 (2012), [Erratum: Phys. Rev.D93,no.2,029902(2016)], [arXiv:1110.5950].

[41] K. Yagi, L. C. Stein and N. Yunes, Phys. Rev. **D93**, 2, 024010 (2016), [arXiv:1510.02152].

[42] K. Prabhu and L. C. Stein, Phys. Rev. **D98**, 2, 021503 (2018), [arXiv:1805.02668].

[43] L. Bernard, Phys. Rev. **D98**, 4, 044004 (2018), [arXiv:1802.10201].

[44] F.-L. Julié and E. Berti, Phys. Rev. D **100**, 10, 104061 (2019), [arXiv:1909.05258].

[45] M. Okounkova *et al.*, Phys. Rev. **D96**, 4, 044020 (2017), [arXiv:1705.07924].

[46] H. Witek *et al.*, Phys. Rev. **D99**, 6, 064035 (2019), [arXiv:1810.05177].

[47] M. Okounkova *et al.* (2019), [arXiv:1906.08789].

[48] L. Blanchet and B. S. Sathyaprakash, Phys. Rev. Lett. **74**, 1067 (1995).

[49] K. G. Arun *et al.*, Phys. Rev. **D74**, 024006 (2006), [arXiv:gr-qc/0604067].

[50] B. P. Abbott *et al.* (LIGO Scientific, Virgo), Phys. Rev. Lett. **116**, 22, 221101 (2016), [Erratum: Phys. Rev. Lett.121,no.12,129902(2018)], [arXiv:1602.03841].

[51] N. Yunes and F. Pretorius, Phys. Rev. **D80**, 122003 (2009), [arXiv:0909.3328].

[52] S. Khan *et al.*, Phys. Rev. **D93**, 4, 044007 (2016), [arXiv:1508.07253].

[53] B. P. Abbott *et al.* (LIGO Scientific, Virgo), Phys. Rev. Lett. **123**, 1, 011102 (2019), [arXiv:1811.00364].

[54] C. V. Vishveshwara, Nature **227**, 936 (1970).

[55] S. L. Detweiler, Astrophys. J. **239**, 292 (1980).

[56] V. Cardoso *et al.*, Phys. Rev. **D99**, 10, 104077 (2019), [arXiv:1901.01265].

[57] R. McManus *et al.*, Phys. Rev. **D100**, 4, 044061 (2019), [arXiv:1906.05155].

[58] C. M. Will, Phys. Rev. **D57**, 2061 (1998), [arXiv:gr-qc/9709011].

[59] M. Fierz, Helv. Phys. Acta **29**, 128 (1956).

[60] E. G. Adelberger, B. R. Heckel and A. E. Nelson, Ann. Rev. Nucl. Part. Sci. **53**, 77 (2003), [hep-ph/0307284].

[61] D. J. Kapner *et al.*, Phys. Rev. Lett. **98**, 021101 (2007), [hep-ph/0611184].

[62] A. O. Sushkov *et al.*, Phys. Rev. Lett. **107**, 171101 (2011), [arXiv:1108.2547].

[63] W.-H. Tan *et al.*, Phys. Rev. Lett. **124**, 5, 051301 (2020).

[64] L. Bernus *et al.*, Phys. Rev. D **102**, 2, 021501 (2020), [arXiv:2006.12304].

[65] T. Damour and J. F. Donoghue, Phys. Rev. **D82**, 084033 (2010), [arXiv:1007.2792].

[66] R. V. Wagoner, Phys. Rev. **D1**, 3209 (1970).

[67] C. Brans and R. H. Dicke, Phys. Rev. **124**, 925 (1961), [,142(1961)].

[68] J. Alsing *et al.*, Phys. Rev. **D85**, 064041 (2012), [arXiv:1112.4903].

[69] T. Damour and K. Nordtvedt, Phys. Rev. Lett. **70**, 2217 (1993).

[70] T. Damour and A. M. Polyakov, Nucl. Phys. **B423**, 532 (1994), [hep-th/9401069].

[71] K. A. Olive and M. Pospelov, Phys. Rev. **D77**, 043524 (2008), [arXiv:0709.3825].

[72] J. Khoury and A. Weltman, Phys. Rev. Lett. **93**, 171104 (2004), [arXiv:astro-ph/0309300].

[73] K. Hinterbichler and J. Khoury, Phys. Rev. Lett. **104**, 231301 (2010), [arXiv:1001.4525].

[74] P. Brax *et al.*, Phys. Rev. **D82**, 063519 (2010), [arXiv:1005.3735].

Downloaded from https://academic.oup.com/ptep/article/2022/8/083C01/6651666 by KIT Library user on 27 September 2022

[75] A. Joyce *et al.*, Phys. Rept. **568**, 1 (2015), [arXiv:1407.0059].

[76] C. Burrage and J. Sakstein, Living Rev. Rel. **21**, 1, 1 (2018), [arXiv:1709.09071].

[77] A. I. Vainshtein, Phys. Lett. **39B**, 393 (1972).

[78] C. de Rham, Living Rev. Rel. **17**, 7 (2014), [arXiv:1401.4173].

[79] G. W. Horndeski, Int. J. Theor. Phys. **10**, 363 (1974).

[80] C. Deffayet *et al.*, Phys. Rev. **D84**, 064039 (2011), [arXiv:1103.3260].

[81] L. Heisenberg, Phys. Rept. **796**, 1 (2019), [arXiv:1807.01725].

[82] T. Kobayashi, Rept. Prog. Phys. **82**, 8, 086901 (2019), [arXiv:1901.07183].

[83] G. Papallo and H. S. Reall, Phys. Rev. **D96**, 4, 044019 (2017), [arXiv:1705.04370].

[84] L. Bernard, L. Lehner and R. Luna, Phys. Rev. **D100**, 2, 024011 (2019), [arXiv:1904.12866].

[85] A. D. Kovács, Phys. Rev. **D100**, 2, 024005 (2019), [arXiv:1904.00963].

[86] C. de Rham and S. Melville, Phys. Rev. Lett. **121**, 22, 221101 (2018), [arXiv:1806.09417].

[87] D. D. Doneva and S. S. Yazadjiev, Phys. Rev. Lett. **120**, 13, 131103 (2018), [arXiv:1711.01187].

[88] H. O. Silva *et al.*, Phys. Rev. Lett. **120**, 13, 131104 (2018), [arXiv:1711.02080].

[89] G. Antoniou *et al.*, Phys. Rev. D **104**, 4, 044002 (2021), [arXiv:2105.04479].

[90] C. A. R. Herdeiro and E. Radu, Int. J. Mod. Phys. **D24**, 09, 1542014 (2015), [arXiv:1504.08209].

[91] A.I. Shlyakhter, Nature **264**, 340 (1976).

[92] T. Damour and F. Dyson, Nucl. Phys. **B480**, 37 (1996), [hep-ph/9606486]; C. R. Gould, E. I. Sharapov and S. K. Lamoreaux, Phys. Rev. **C74**, 024607 (2006), [arXiv:nucl-ex/0701019]; E. D. Davis and L. Hamdan, Phys. Rev. **C92**, 1, 014319 (2015), [arXiv:1503.06011]; Yu. V. Petrov *et al.*, Phys. Rev. **C74**, 064610 (2006), [hep-ph/0506186].

[93] V. V. Flambaum and R. B. Wiringa, Phys. Rev. **C79**, 034302 (2009), [arXiv:0807.4943].

[94] K. A. Olive *et al.*, Phys. Rev. **D69**, 027701 (2004), [arXiv:astro-ph/0309252].

[95] M. T. Murphy, A. L. Malec and J. X. Prochaska, Mon. Not. Roy. Astron. Soc. **461**, 3, 2461 (2016), [arXiv:1606.06293].

[96] N. Kanekar *et al.*, Mon. Not. Roy. Astron. Soc. **448**, 1, L104 (2015), [arXiv:1412.7757].

[97] P. A. R. Ade *et al.* (Planck), Astron. Astrophys. **580**, A22 (2015), [arXiv:1406.7482].

[98] T. Rosenband *et al.*, Science **319**, 1808 (2008); J. Guena *et al.*, Phys. Rev. Lett. **109**, 080801 (2012); R. M. Godun *et al.*, Phys. Rev. Lett. **113**, 21, 210801 (2014), [arXiv:1407.0164].

[99] T. M. Fortier *et al.*, Phys. Rev. Lett. **98**, 070801 (2007).

[100] R. Lange *et al.*, Phys. Rev. Lett. **126**, 1, 011102 (2021), [arXiv:2010.06620]; S. Blatt *et al.*, Phys. Rev. Lett. **100**, 140801 (2008), [arXiv:0801.1874]; T. Dent, Phys. Rev. Lett. **101**, 041102 (2008), [arXiv:0805.0318].

[101] A. Fienga *et al.*, Cel. Mech. Dyn. Astr. **123**, Issue 2, 1 (2015).

[102] F. Hofmann and J. Müller, Class. Quant. Grav. **35**, 3, 035015 (2018).

[103] K. Lazaridis *et al.*, Mon. Not. R. Astron. Soc. **400**, 805 (2009), [arXiv:0908.0285].

[104] W. W. Zhu *et al.*, Mon. Not. Roy. Astron. Soc. **482**, 3, 3249 (2019), [arXiv:1802.09206].

[105] M. Smiciklas *et al.*, Phys. Rev. Lett. **107**, 171604 (2011), [arXiv:1106.0738].

[106] J. F. Bell and T. Damour, Class. Quant. Grav. **13**, 3121 (1996), [arXiv:gr-qc/9606062].

[107] L. Shao and N. Wex, Class. Quant. Grav. **29**, 215018 (2012), [arXiv:1209.4503].

[108] S. Liberati, J. Phys. Conf. Ser. **631**, 1, 012011 (2015).

[109] S. Schlamminger *et al.*, Phys. Rev. Lett. **100**, 041101 (2008), [arXiv:0712.0607].

[110] T. A. Wagner *et al.*, Class. Quant. Grav. **29**, 184002 (2012), [arXiv:1207.2442].

[111] P. Touboul *et al.*, Phys. Rev. Lett. **119**, 23, 231101 (2017), [arXiv:1712.01176].

[112] P. Touboul *et al.* (MICROSCOPE), Class. Quant. Grav. **36**, 22, 225006 (2019), [arXiv:1909.10598].

[113] S. Merlet *et al.*, Metrologia, **47**, L9-L11 (2010).

[114] D. Schlippert *et al.*, Phys. Rev. Lett. **112**, 203002 (2014), [arXiv:1406.4979].

[115] G. Rosi *et al.*, Nature Commun. **8**, 5529 (2017), [arXiv:1704.02296].

[116] R.F.C. Vessot and M.W. Levine, Gen. Rel. Grav. **10**, 181 (1978); R. F. C. Vessot *et al.*, Phys. Rev. Lett. **45**, 2081 (1980).

[117] C. W. Chou *et al.*, Science **329**, 1630 (2010).

[118] R. Abuter *et al.* (GRAVITY), Astron. Astrophys. **615**, L15 (2018), [arXiv:1807.09409].

[119] T. Do *et al.*, Science **365**, 6454, 664 (2019), [arXiv:1907.10731].

[120] A. Amorim *et al.* (GRAVITY), Phys. Rev. Lett. **122**, 10, 101102 (2019), [arXiv:1902.04193].

[121] J.G. Williams, S.G. Turyshev, and D.H. Boggs, Class. Quantum Grav. **29**, 184004 (2012).

[122] I. Ciufolini and E. C. Pavlis, Nature **431**, 958 (2004).

[123] I. Ciufolini *et al.*, Eur. Phys. J. **C76**, 3, 120 (2016), [arXiv:1603.09674].

[124] C. W. F. Everitt *et al.*, Phys. Rev. Lett. **106**, 221101 (2011), [arXiv:1105.3456].

[125] B. Bertotti, L. Iess and P. Tortora, Nature **425**, 374 (2003).

[126] R. Abuter *et al.* (GRAVITY), Astron. Astrophys. **636**, L5 (2020), [arXiv:2004.07187].

[127] J. Bergé *et al.*, Phys. Rev. Lett. **120**, 14, 141101 (2018), [arXiv:1712.00483].

[128] J. M. Weisberg and Y. Huang, Astrophys. J. **829**, 1, 55 (2016), [arXiv:1606.02744].

[129] A. Wolszczan, Nature **350**, 688 (1991).

[130] J. N. Taylor, A. Wolszczan and T. Damour, Nature **355**, 132 (1993).

[131] E. Fonseca, I. H. Stairs and S. E. Thorsett, Astrophys. J. **787**, 82 (2014), [arXiv:1402.4836].

[132] V. M. Kaspi *et al.*, Astrophys. J. **528**, 445 (2000), [arXiv:astro-ph/9906373].

[133] S. M. Ord, M. Bailes and W. van Straten, Astrophys. J. **574**, L75 (2002), [arXiv:astro-ph/0204421].

[134] M. Bailes *et al.*, Astrophys. J. **595**, L49 (2003), [arXiv:astro-ph/0307468].

[135] N. D. R. Bhat, M. Bailes and J. P. W. Verbiest, Phys. Rev. **D77**, 124017 (2008), [arXiv:0804.0956].

[136] M. Burgay *et al.*, Nature **426**, 531 (2003), [arXiv:astro-ph/0312071].

[137] A. G. Lyne *et al.*, Science **303**, 1153 (2004), [arXiv:astro-ph/0401086].

[138] M. Kramer *et al.*, Science **314**, 97 (2006), [arXiv:astro-ph/0609417].

Downloaded from https://academic.oup.com/ptep/article/2022/8/083C01/6651666 by KIT Library user on 27 September 2022

[139] R. P. Breton *et al.*, Science **321**, 104 (2008), [arXiv:0807.2644].

[140] B. Perera *et al.*, Astrophys. J. **721**, 1193 (2010), [arXiv:1008.1097].

[141] R. D. Ferdman *et al.*, Mon. Not. Roy. Astron. Soc. **443**, 3, 2183 (2014), [arXiv:1406.5507].

[142] M. Kramer and N. Wex, Class. Quant. Grav. **26**, 073001 (2009).

[143] M. Kramer, in *Neutron Stars and Pulsars: Challenges and Opportunities after 80 Years*; M. Kramer, IAU Symp. **291**, 19 (2013), [arXiv:1211.2457].

[144] N. Wex and M. Kramer, Universe **6**, 9, 156 (2020).

[145] T. Damour and G. Schaefer, Phys. Rev. Lett. **66**, 2549 (1991).

[146] M. E. Gonzalez *et al.*, Astrophys. J. **743**, 102 (2011), [arXiv:1109.5638].

[147] P. C. C. Freire, M. Kramer and N. Wex, Class. Quant. Grav. **29**, 184007 (2012), [arXiv:1205.3751].

[148] S. M. Ransom *et al.*, Nature **505**, 520 (2014), [arXiv:1401.0535].

[149] A. M. Archibald *et al.*, Nature **559**, 7712, 73 (2018), [arXiv:1807.02059].

[150] G. Voisin *et al.*, Astron. Astrophys. **638**, A24 (2020), [arXiv:2005.01388].

[151] T. Damour and R. Ruffini, C. R. Acad. Sc. Paris **279**, série A, 971 (1974); B. M. Barker and R. F. O'Connell, Phys. Rev. **D12**, 329 (1975).

[152] M. Kramer, Astrophys. J. **509**, 856 (1998), [arXiv:astro-ph/9808127]; J. M. Weisberg and J. H. Taylor, Astrophys. J. **576**, 942 (2002), [arXiv:astro-ph/0205280].

[153] R. N. Manchester *et al.*, Astrophys. J. **710**, 1694 (2010), [arXiv:1001.1483].

[154] J. van Leeuwen *et al.*, Astrophys. J. **798**, 2, 118 (2015), [arXiv:1411.1518].

[155] G. Desvignes *et al.*, Science **365**, 6457, 1013 (2019).

[156] B. P. Abbott *et al.* (LIGO Scientific, Virgo), Phys. Rev. **X9**, 3, 031040 (2019), [arXiv:1811.12907].

[157] R. Abbott *et al.* (LIGO Scientific, Virgo), Phys. Rev. D **103**, 12, 122002 (2021), [arXiv:2010.14529].

[158] K. Akiyama *et al.* (Event Horizon Telescope), Astrophys. J. **875**, 1, L1 (2019), [arXiv:1906.11238].

[159] D. Psaltis *et al.* (Event Horizon Telescope), Phys. Rev. Lett. **125**, 14, 141104 (2020), [arXiv:2010.01055].

[160] S. H. Völkel *et al.* (2020), [arXiv:2011.06812].

[161] J. Beltran Jimenez, F. Piazza and H. Velten, Phys. Rev. Lett. **116**, 6, 061101 (2016), [arXiv:1507.05047].

[162] T. Damour and J. H. Taylor, Astrophys. J. **366**, 501 (1991).

[163] P. C. C. Freire *et al.*, Mon. Not. Roy. Astron. Soc. **423**, 3328 (2012), [arXiv:1205.1450].

[164] J. Antoniadis *et al.*, Science **340**, 6131 (2013), [arXiv:1304.6875].

[165] W. W. Zhu *et al.*, Astrophys. J. **809**, 1, 41 (2015), [arXiv:1504.00662].

[166] L. Shao *et al.*, Phys. Rev. **X7**, 4, 041025 (2017), [arXiv:1704.07561].

[167] B. P. Abbott *et al.* (LIGO Scientific, Virgo), Phys. Rev. D **100**, 10, 104036 (2019), [arXiv:1903.04467].

[168] M. Isi *et al.*, Phys. Rev. Lett. **123**, 11, 111102 (2019), [arXiv:1905.00869].

[169] M. Isi *et al.*, Phys. Rev. Lett. **127**, 1, 011103 (2021), [arXiv:2012.04486].

[170] A. Maselli *et al.*, Phys. Rev. D **101**, 2, 024043 (2020), [arXiv:1910.12893].

[171] G. Carullo, Phys. Rev. D **103**, 12, 124043 (2021), [arXiv:2102.05939].

[172] S. E. Perkins *et al.*, Phys. Rev. D **104**, 2, 024060 (2021), [arXiv:2104.11189].

[173] P. K. Gupta *et al.* (2021), [arXiv:2107.12111].

[174] D. M. Eardley, D. L. Lee and A. P. Lightman, Phys. Rev. **D8**, 3308 (1973).

[175] B. P. Abbott *et al.*, Astrophys. J. **848**, 2, L12 (2017), [arXiv:1710.05833].

[176] B. P. Abbott *et al.* (LIGO Scientific, Virgo, Fermi-GBM, INTEGRAL), Astrophys. J. **848**, 2, L13 (2017), [arXiv:1710.05834].

[177] T. Baker *et al.*, Phys. Rev. Lett. **119**, 25, 251301 (2017), [arXiv:1710.06394].

[178] P. Creminelli and F. Vernizzi, Phys. Rev. Lett. **119**, 25, 251302 (2017), [arXiv:1710.05877].

[179] J. Sakstein and B. Jain, Phys. Rev. Lett. **119**, 25, 251303 (2017), [arXiv:1710.05893].

[180] J. M. Ezquiaga and M. Zumalacárregui, Phys. Rev. Lett. **119**, 25, 251304 (2017), [arXiv:1710.05901].

Downloaded from https://academic.oup.com/ptep/article/2022/8/083C01/6651666 by KIT Library user on 27 September 2022

22. Big-Bang Cosmology

Revised August 2021 by K.A. Olive (Minnesota U.) and J.A. Peacock (Edinburgh U.).

22.1 Introduction to the standard big-bang model

The observed expansion of the Universe [1–3] is a natural (almost inevitable) result of any homogeneous and isotropic cosmological model based on general relativity. However, by itself, the Hubble expansion does not provide sufficient evidence for what we generally refer to as the Big-Bang model of cosmology. While general relativity is in principle capable of describing the cosmology of any given distribution of matter, it is extremely fortunate that our Universe appears to be homogeneous and isotropic on large scales. Together, homogeneity and isotropy allow us to extend the Copernican Principle to the Cosmological Principle, stating that all spatial positions in the Universe are essentially equivalent.

The formulation of the Big-Bang model began in the 1940s with the work of George Gamow and his collaborators, Ralph Alpher and Robert Herman. In order to account for the possibility that the abundances of the elements had a cosmological origin, they proposed that the early Universe was once very hot and dense (enough so as to allow for the nucleosynthetic processing of hydrogen), and has subsequently expanded and cooled to its present state [4, 5]. In 1948, Alpher and Herman predicted that a direct consequence of this model is the presence of a relic background radiation with a temperature of order a few K [6, 7]. Of course this radiation was observed 16 years later as the Cosmic Microwave Background (CMB) [8]. Indeed, it was the observation of this radiation that singled out the Big-Bang model as the prime candidate to describe our Universe. Subsequent work on Big-Bang nucleosynthesis further confirmed the necessity of our hot and dense past. (See Sec. 22.3.7 for a brief discussion of BBN and the review on BBN – Sec. 24 of this *Review* for a detailed discussion of BBN.) These relativistic cosmological models face severe problems with their initial conditions, to which the best modern solution is inflationary cosmology, discussed in Sec. 22.3.5 and in – Sec. 23 of this *Review*. If correct, these ideas would strictly render the term 'Big Bang' redundant, since it was first coined by Hoyle to represent a criticism of the lack of understanding of the initial conditions.

22.1.1 *The Robertson-Walker Universe*

The observed homogeneity and isotropy enable us to describe the overall geometry and evolution of the Universe in terms of two cosmological parameters accounting for the spatial curvature and the overall expansion (or contraction) of the Universe. These two quantities appear in the most general expression for a space-time metric that has a (3D) maximally symmetric subspace of a 4D space-time, known as the Robertson-Walker metric:

$$ds^2 = dt^2 - R^2(t)\left[\frac{dr^2}{1-kr^2} + r^2\left(d\theta^2 + \sin^2\theta\, d\phi^2\right)\right]. \qquad (22.1)$$

Note that we adopt $c = 1$ throughout. By rescaling the radial coordinate, we can choose the curvature constant k to take only the discrete values $+1$, -1, or 0 corresponding to closed, open, or spatially flat geometries. In this case, it is often more convenient to re-express the metric as

$$ds^2 = dt^2 - R^2(t)\left[d\chi^2 + S_k^2(\chi)\left(d\theta^2 + \sin^2\theta\, d\phi^2\right)\right], \qquad (22.2)$$

where the function $S_k(\chi)$ is $(\sin\chi, \chi, \sinh\chi)$ for $k = (+1, 0, -1)$. The coordinate r [in Eq. (22.1)] and the 'angle' χ [in Eq. (22.2)] are both dimensionless; the dimensions are carried by the cosmological scale factor, $R(t)$, which determines proper distances in terms of the comoving coordinates. A common alternative is to define a dimensionless scale factor, $a(t) = R(t)/R_0$, where $R_0 \equiv R(t_0)$ is R at the present epoch. It is also sometimes convenient to define a dimensionless or conformal time coordinate, η, by $d\eta = dt/R(t)$. Along constant spatial sections, the proper time is defined by the time coordinate, t. Similarly, for $dt = d\theta = d\phi = 0$, the proper distance is given by $R(t)\chi$. For standard texts on cosmological models see *e.g.*, Refs. [9–16].

22.1.2 *The redshift*

The cosmological redshift is a direct consequence of the Hubble expansion, determined by $R(t)$. A local observer detecting light from a distant emitter sees a redshift in frequency. We can define the redshift as

$$z \equiv \frac{\nu_1 - \nu_2}{\nu_2} \simeq v_{12}, \qquad (22.3)$$

where ν_1 is the frequency of the emitted light, ν_2 is the observed frequency, and v_{12} is the relative velocity between the emitter and the observer. While the definition, $z = (\nu_1 - \nu_2)/\nu_2$ is valid in general, relating the redshift to a simple relative velocity is only correct on small scales (*i.e.*, less than cosmological scales) such that the expansion velocity is non-relativistic. For light signals, we can use the metric given by Eq. (22.1) and $ds^2 = 0$ to write

$$v_{12} = \dot{R}\,\delta r = \frac{\dot{R}}{R}\,\delta t = \frac{\delta R}{R} = \frac{R_2 - R_1}{R_1}, \qquad (22.4)$$

where $\delta r(\delta t)$ is the radial coordinate (temporal) separation between the emitter and observer. Noting that physical distance, D, is $R\delta r$ or δt, Eq. (22.4) gives us Hubble's law, $v = HD$. In addition, we obtain the simple relation between the redshift and the scale factor

$$1 + z = \frac{\nu_1}{\nu_2} = \frac{R_2}{R_1}. \qquad (22.5)$$

This result does not depend on the non-relativistic approximation.

22.1.3 *The Friedmann equations of motion*

The cosmological equations of motion are derived from Einstein's equations

$$\mathcal{R}_{\mu\nu} - \tfrac{1}{2}g_{\mu\nu}\mathcal{R} = 8\pi G_{\rm N} T_{\mu\nu} + \Lambda g_{\mu\nu} \qquad (22.6)$$

Gliner [17] and Zeldovich [18] have pioneered the modern view, in which the Λ term is set on the rhs and interpreted as an effective energy – momentum tensor $T_{\mu\nu}$ for the vacuum of $\Lambda g_{\mu\nu}/8\pi G_{\rm N}$. It is common to assume that the matter content of the Universe is a perfect fluid, for which

$$T_{\mu\nu} = -p g_{\mu\nu} + (p + \rho)\, u_\mu u_\nu, \qquad (22.7)$$

where $g_{\mu\nu}$ is the space-time metric described by Eq. (22.1), p is the isotropic pressure, ρ is the energy density and $u = (1, 0, 0, 0)$ is the velocity vector for the isotropic fluid in co-moving coordinates. With the perfect fluid source, Einstein's equations lead to the Friedmann equations

$$H^2 \equiv \left(\frac{\dot{R}}{R}\right)^2 = \frac{8\pi\, G_{\rm N}\, \rho}{3} - \frac{k}{R^2} + \frac{\Lambda}{3}, \qquad (22.8)$$

and

$$\frac{\ddot{R}}{R} = \frac{\Lambda}{3} - \frac{4\pi G_{\rm N}}{3}\,(\rho + 3p), \qquad (22.9)$$

where $H(t)$ is the Hubble parameter and Λ is the cosmological constant. The first of these is sometimes called the Friedmann equation. Energy conservation via $T^{\mu\nu}_{;\mu} = 0$, leads to a third useful equation [which can also be derived from Eq. (22.8) and Eq. (22.9)]

$$\dot{\rho} = -3H\,(\rho + p)\,. \qquad (22.10)$$

Eq. (22.10) can also be simply derived as a consequence of the first law of thermodynamics.

Eq. (22.8) has a simple classical mechanical analog if we neglect (for the moment) the cosmological term Λ. By interpreting $-k/R^2$ Newtonianly as a 'total energy', then we see that the evolution of the Universe is governed by a competition between the potential energy, $8\pi G_{\rm N}\rho/3$, and the kinetic term $(\dot{R}/R)^2$. For $\Lambda = 0$, it is clear that the Universe must be expanding or contracting (except at the turning point prior to collapse in a closed Universe). The ultimate fate of the Universe is determined by the curvature constant k. For $k = +1$, the Universe will recollapse in a finite time, whereas for $k = 0, -1$, the Universe will expand indefinitely. These simple conclusions can be altered when $\Lambda \neq 0$ or more generally with some component with $(\rho + 3p) < 0$.

Downloaded from https://academic.oup.com/ptep/article/2022/8/083C01/6651666 by KIT Library user on 27 September 2022

22.1.4 *Definition of cosmological parameters*

In addition to the Hubble parameter, it is useful to define several other measurable cosmological parameters. The Friedmann equation can be used to define a critical density such that $k = 0$ when $\Lambda = 0$,

$$\rho_c \equiv \frac{3H^2}{8\pi G_N} = 1.88 \times 10^{-26}\, h^2 \text{ kg m}^{-3} = 1.05 \times 10^{-5}\, h^2 \text{ GeV cm}^{-3}, \tag{22.11}$$

where the scaled Hubble parameter, h, is defined by

$$H \equiv 100\, h \text{ km s}^{-1} \text{ Mpc}^{-1} \Rightarrow H^{-1} = 9.778\, h^{-1} \text{ Gyr} = 2998\, h^{-1} \text{ Mpc}. \tag{22.12}$$

The cosmological density parameter $\Omega_{\rm tot}$ is defined as the energy density relative to the critical density,

$$\Omega_{\rm tot} = \rho/\rho_c. \tag{22.13}$$

Note that one can now rewrite the Friedmann equation as

$$k/R^2 = H^2(\Omega_{\rm tot} - 1)\ . \tag{22.14}$$

From Eq. (22.14), one can see that when $\Omega_{\rm tot} > 1$, $k = +1$ and the Universe is closed, when $\Omega_{\rm tot} < 1$, $k = -1$ and the Universe is open, and when $\Omega_{\rm tot} = 1$, $k = 0$, and the Universe is spatially flat.

It is often necessary to distinguish different contributions to the density. It is therefore convenient to define present-day density parameters for pressureless matter ($\Omega_{\rm m}$) and relativistic particles ($\Omega_{\rm r}$), plus the quantity $\Omega_\Lambda = \Lambda/3H^2$. In more general models, we may wish to drop the assumption that the vacuum energy density is constant, and we therefore denote the present-day density parameter of the vacuum by $\Omega_{\rm v}$. The Friedmann equation then becomes

$$k/R_0^2 = H_0^2(\Omega_{\rm m} + \Omega_{\rm r} + \Omega_{\rm v} - 1), \tag{22.15}$$

where the subscript 0 indicates present-day values. Thus, it is the sum of the densities in matter, relativistic particles, and vacuum that determines the overall sign of the curvature. Note that the quantity $-k/R_0^2H_0^2$ is sometimes referred to as Ω_K. This usage is unfortunate: it encourages one to think of curvature as a contribution to the energy density of the Universe, which is not correct.

22.1.5 *Standard Model solutions*

Much of the history of the Universe in the standard Big-Bang model can be easily described by assuming that either matter or radiation dominates the total energy density. During inflation and again today the expansion rate for the Universe is accelerating, and domination by a cosmological constant or some other form of dark energy should be considered. In the following, we shall delineate the solutions to the Friedmann equation when a single component dominates the energy density. Each component is distinguished by an equation of state parameter $w = p/\rho$. We concentrate on solutions that expand at early times, although the Friedmann equation also permits a time-reversed contracting solution.

22.1.5.1 *Solutions for a general equation of state*

Let us first assume a general equation of state parameter for a single component, w, which is constant. In this case, Eq. (22.10) can be written as $\dot\rho = -3(1+w)\rho\dot R/R$ and is easily integrated to yield

$$\rho \propto R^{-3(1+w)}. \tag{22.16}$$

Note that at early times when R is small, the less singular curvature term k/R^2 in the Friedmann equation can be neglected so long as $w > -1/3$. Curvature domination occurs at rather late times (if a cosmological constant term does not dominate sooner). For $w \neq -1$, one can insert this result into the Friedmann equation Eq. (22.8), and if one neglects the curvature and cosmological constant terms, it is easy to integrate the equation to obtain,

$$R(t) \propto t^{2/[3(1+w)]}. \tag{22.17}$$

22.1.5.2 *A Radiation-dominated Universe*

In the early hot and dense Universe, it is appropriate to assume an equation of state corresponding to a gas of radiation (or relativistic particles) for which $w = 1/3$. In this case, Eq. (22.16) becomes $\rho \propto R^{-4}$. The 'extra' factor of $1/R$ is due to the cosmological redshift; not only is the number density of particles in the radiation background decreasing as R^{-3} since volume scales as R^3, but in addition each particle's energy is decreasing as $E \propto \nu \propto R^{-1}$. Similarly, one can substitute $w = 1/3$ into Eq. (22.17) to obtain

$$R(t) \propto t^{1/2}; \qquad H = 1/2t. \tag{22.18}$$

22.1.5.3 *A Matter-dominated Universe*

At relatively late times, non-relativistic matter eventually dominates the energy density over radiation [see Eq. (22.3.8)]. A pressureless gas ($w = 0$) leads to the expected dependence $\rho \propto R^{-3}$ from Eq. (22.16) and, if $k = 0$, we obtain

$$R(t) \propto t^{2/3}; \qquad H = 2/3t. \tag{22.19}$$

22.1.5.4 *A Universe dominated by vacuum energy*

If there is a dominant source of vacuum energy, V_0, it would act as a cosmological constant with $\Lambda = 8\pi G_N V_0$ and equation of state $w = -1$. In this case, the solution to the Friedmann equation when curvature is neglected is particularly simple and leads to an exponential expansion of the Universe:

$$R(t) \propto e^{\sqrt{\Lambda/3}\, t}. \tag{22.20}$$

More generally we could write

$$a(t) = \sinh^{2/3}(\sqrt{3\Lambda}t/2), \tag{22.21}$$

which describes a flat Universe containing both matter and vacuum energy, with $a(t)$ being the scale factor normalized to unity when both components are equal.

A key parameter is the equation of state of the vacuum, $w \equiv p/\rho$: this need not be the $w = -1$ of Λ, and may not even be constant [19–21]. There is much interest in the more general possibility of a dynamically evolving vacuum energy, for which the name 'dark energy' has become commonly used. A variety of techniques exist whereby the vacuum density as a function of time may be measured, usually expressed as the value of w as a function of epoch [22, 23]. The best current measurement for the equation of state (assumed constant, but without assuming zero curvature) is $w = -1.028 \pm 0.031$ [24]. Unless stated otherwise, we will assume that the vacuum energy is a cosmological constant with $w = -1$ exactly.

The presence of vacuum energy can dramatically alter the fate of the Universe. For example, if $\Lambda < 0$, the Universe will eventually recollapse independent of the sign of k. For large values of $\Lambda > 0$ (larger than the Einstein static value needed to halt any cosmological expansion or contraction), even a closed Universe will expand forever. One way to quantify this is the deceleration parameter, q_0, defined as

$$q_0 = -\left.\frac{R\ddot R}{\dot R^2}\right|_0 = \frac{1}{2}\Omega_{\rm m} + \Omega_{\rm r} + \frac{(1+3w)}{2}\Omega_{\rm v}. \tag{22.22}$$

This equation shows us that $w < -1/3$ for the vacuum may lead to an accelerating expansion. To the continuing astonishment of cosmologists, such an effect has been observed; one piece of direct evidence is the supernova Hubble diagram [25–30] (see Fig. 22.1 below). Current data indicate that vacuum energy is indeed the largest contributor to the cosmological density budget, with $\Omega_{\rm v} = 0.685 \pm 0.007$ and $\Omega_{\rm m} = 0.315 \pm 0.007$ if $k = 0$ is assumed [24].

The existence of this constituent is without doubt the greatest puzzle raised by the current cosmological model; the final section of this review discusses some of the ways in which the vacuum-energy problem is being addressed. For more details, see the review on Dark Energy – Sec. 28.

Downloaded from https://academic.oup.com/ptep/article/2022/8/083C01/6651666 by KIT Library user on 27 September 2022

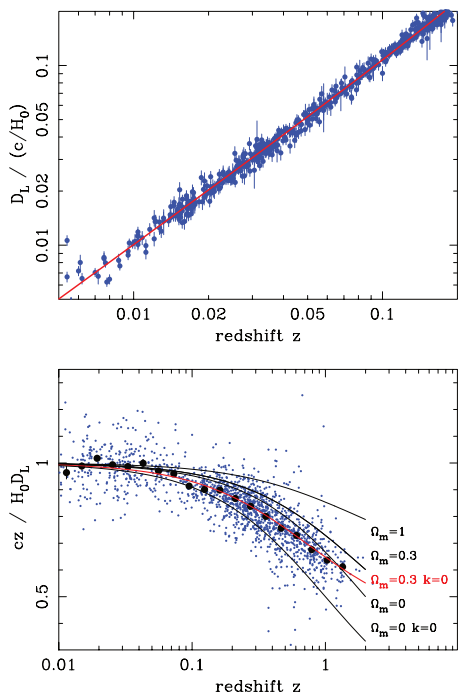

Figure 22.1: The type Ia supernova Hubble diagram, based on 1650 publicly available supernova distance estimates [28–30]. The first panel shows that for $z \ll 1$ the large-scale Hubble flow is indeed linear and uniform; the second panel shows an expanded scale, with the linear trend divided out, and with the redshift range extended to show how the Hubble law becomes nonlinear. ($\Omega_r = 0$ is assumed.) Larger points with errors show median values in redshift bins. Comparison with the prediction of Friedmann models favors a vacuum-dominated Universe.

22.2 Introduction to observational cosmology

22.2.1 *Fluxes, luminosities, and distances*

The key quantities for observational cosmology can be deduced quite directly from the metric.

(1) The *proper* transverse size of an object seen by us to subtend an angle $d\psi$ is its comoving size $d\psi\, S_k(\chi)$ times the scale factor at the time of emission:

$$d\ell = d\psi\; R_0 S_k(\chi)/(1+z). \tag{22.23}$$

(2) The apparent flux density of an object is deduced by allowing its photons to flow through a sphere of current radius $R_0 S_k(\chi)$; but photon energies and arrival rates are redshifted, and the bandwidth $d\nu$ is reduced. The observed photons at frequency ν_0 were emitted at frequency $\nu_0(1+z)$, so the flux density is the luminosity at this frequency, divided by the total area, divided by $1+z$:

$$S_\nu(\nu_0) = \frac{L_\nu([1+z]\nu_0)}{4\pi R_0^2 S_k^2(\chi)(1+z)}. \tag{22.24}$$

These relations lead to the following common definitions:

$$\begin{aligned} \text{angular-diameter distance:}\quad & D_A = (1+z)^{-1} R_0 S_k(\chi) \\ \text{luminosity distance:}\quad & D_L = (1+z)\; R_0 S_k(\chi)\;. \end{aligned} \tag{22.25}$$

These distance-redshift relations are expressed in terms of observables by using the equation of a null radial geodesic ($R(t)d\chi = dt$) plus the Friedmann equation:

$$\begin{aligned} R_0 d\chi = \frac{1}{H(z)}\, dz = \frac{1}{H_0}\, \big[& (1-\Omega_m-\Omega_v-\Omega_r)(1+z)^2 \\ & + \Omega_v(1+z)^{3+3w} + \Omega_m(1+z)^3 \\ & + \Omega_r(1+z)^4 \big]^{-1/2}\, dz. \end{aligned} \tag{22.26}$$

The main scale for the distance here is the Hubble length, $1/H_0$. The flux density is the product of the specific intensity I_ν and the solid angle $d\Omega$ subtended by the source: $S_\nu = I_\nu\, d\Omega$. Combining the angular size and flux-density relations thus gives the relativistic version of surface-brightness conservation:

$$I_\nu(\nu_0) = \frac{B_\nu([1+z]\nu_0)}{(1+z)^3}, \tag{22.27}$$

where B_ν is surface brightness (luminosity emitted into unit solid angle per unit area of source). We can integrate over ν_0 to obtain the corresponding total or bolometric formula:

$$I_{\rm tot} = \frac{B_{\rm tot}}{(1+z)^4}. \tag{22.28}$$

This cosmology-independent form expresses Liouville's Theorem: photon phase-space density is conserved along rays.

22.2.2 *Distance data and geometrical tests of cosmology*

In order to confront these theoretical predictions with data, we have to bridge the divide between two extremes. Nearby objects may have their distances measured quite easily, but their radial velocities are dominated by deviations from the ideal Hubble flow, which typically have a magnitude of several hundred $\mathrm{km\,s^{-1}}$. On the other hand, objects at redshifts $z \gtrsim 0.01$ will have observed recessional velocities that differ from their ideal values by $\lesssim 10\%$, but absolute distances are much harder to supply in this case. The traditional solution to this problem is the construction of the distance ladder: an interlocking set of methods for obtaining relative distances between various classes of object, which begins with absolute distances at the 10 to 100 pc level, and terminates with galaxies at significant redshifts. This is discussed in the article on Cosmological Parameters – Sec. 25 of this *Review*.

One of the key developments in this area has been the use of type Ia supernovae (SNe), which now allow measurement of relative distances with 5% precision. In combination with improved Cepheid data from the HST plus improved measurements of the distance to the LMC (or alternatively a direct geometrical distance to the maser galaxy NGC4258), SNe results extend the distance ladder to the point where deviations from uniform expansion are negligible, leading to the best existing Cepheid-based value for H_0: $73.2\pm1.3\,\mathrm{km\,s^{-1}Mpc^{-1}}$ [31]. Better still, the analysis of high-z SNe has allowed a simple and direct test of cosmological geometry to be carried out: as shown in Fig. 22.1 and Fig. 22.2, supernova data and measurements of CMB anisotropies strongly favor a $k=0$ model dominated by vacuum energy. It is worth noting that there is some tension (4.2σ) between the Cepheid and CMB determinations of H_0 (the latter is 67.4 ± 0.5 [24]. While it is remarkable that the two very different methods give such similar results, the formal disagreement shows that either there are unidentified systematic errors or that some new post-CDM physics is required; there is no current consensus in the community on these alternatives. We do note that a recent analysis of SNe Ia with a calibration of the tip of the red-giant branch gives a result close to that of the CMB: $69.8\pm0.6\,(\mathrm{stat.})\pm1.6\,(\mathrm{sys.})\,\mathrm{km\,s^{-1}Mpc^{-1}}$ [32,33]. (See the review on Cosmological Parameters – Sec. 25 of this *Review* for a more comprehensive review of Hubble parameter determinations.)

22.2.3 *Age of the Universe*

The most striking conclusion of relativistic cosmology is that the Universe has not existed forever. The dynamical result for the age of the Universe may be written as

$$\begin{aligned} H_0 t_0 &= \int_0^\infty \frac{dz}{(1+z)H(z)} \\ &= \int_0^\infty \frac{dz}{(1+z)\,\left[(1+z)^2(1+\Omega_m z) - z(2+z)\Omega_v\right]^{1/2}}, \end{aligned} \tag{22.29}$$

where we have neglected Ω_r and chosen $w=-1$. Over the range of interest ($0.1 \lesssim \Omega_m \lesssim 1$, $|\Omega_v| \lesssim 1$), this exact answer may be approximated to a few per cent accuracy by

$$H_0 t_0 \simeq \tfrac{2}{3}\,(0.7\Omega_m + 0.3 - 0.3\Omega_v)^{-0.3}. \tag{22.30}$$

Downloaded from https://academic.oup.com/ptep/article/2022/8/083C01/6651666 by KIT Library user on 27 September 2022

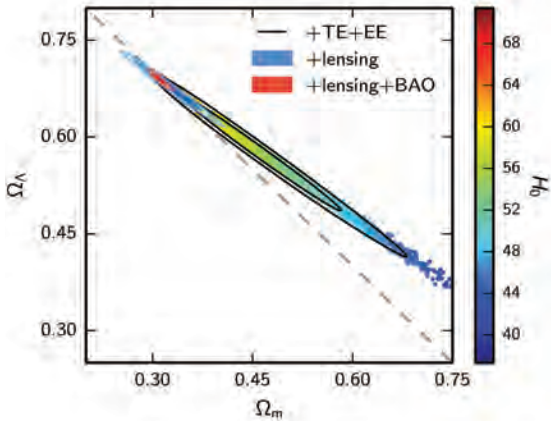

Figure 22.2: Likelihood-based probability densities over the plane Ω_Λ (*i.e.*, Ω_v assuming $w = -1$) vs Ω_m. The colored locus derives from *Planck* [34] and shows that the CMB alone requires a flat Universe $\Omega_v + \Omega_m \simeq 1$ if the Hubble constant is not too high. The SNe Ia results [35] very nearly constrain the orthogonal combination $\Omega_v - \Omega_m$, and the intersection of these constraints directly favors a flat model with $\Omega_m \simeq 0.3$, as does the measurement of the Baryon Acoustic Oscillation lengthscale (for which a joint constraint is shown on this plot). The CMB alone is capable of breaking the degeneracy with H_0 by using the measurements of gravitational lensing that can be made with modern high-resolution CMB data.

For the special case that $\Omega_m + \Omega_v = 1$, the integral in Eq. (22.29) can be expressed analytically as

$$H_0 t_0 = \frac{2}{3\sqrt{\Omega_v}} \ln \frac{1+\sqrt{\Omega_v}}{\sqrt{1-\Omega_v}} \quad (\Omega_m < 1). \tag{22.31}$$

The most accurate means of obtaining ages for astronomical objects is based on the natural clocks provided by radioactive decay. The use of these clocks is complicated by a lack of knowledge of the initial conditions of the decay. In the Solar System, chemical fractionation of different elements helps pin down a precise age for the pre-Solar nebula of 4.6 Gyr, but for stars it is necessary to attempt an a priori calculation of the relative abundances of nuclei that result from supernova explosions. In this way, a lower limit for the age of stars in the local part of the Milky Way of about 11 Gyr is obtained [36, 37].

The other major means of obtaining cosmological age estimates is based on the theory of stellar evolution. In principle, the main-sequence turnoff point in the color-magnitude diagram of a globular cluster should yield a reliable age. But these have been controversial, owing to theoretical uncertainties in the evolution model – as well as observational uncertainties in the distance, dust extinction, and metallicity of clusters. The present consensus favors ages for the oldest clusters of about 13 Gyr [38].

These methods are all consistent with the age deduced from studies of structure formation, using the microwave background and large-scale structure: $t_0 = 13.80 \pm 0.02$ Gyr [24], where the extra accuracy comes at the price of assuming the simple 6-parameter ΛCDM model to be true.

22.2.4 *Horizon, isotropy, flatness problems*

For photons, the radial equation of motion is just $c\,dt = R\,d\chi$. How far can a photon get in a given time? The answer is clearly

$$\Delta\chi = \int_{t_1}^{t_2} \frac{dt}{R(t)} \equiv \Delta\eta, \tag{22.32}$$

i.e., just the interval of conformal time. We can replace dt by $dR/\dot{R}$, which the Friedmann equation says is $\propto dR/\sqrt{\rho R^2}$ at early times. Thus, this integral converges if $\rho R^2 \to \infty$ as $t_1 \to 0$, otherwise it diverges. Provided the equation of state is such that ρ changes faster than R^{-2}, light signals can only propagate a finite distance between the Big Bang and the present; there is then said to be a particle horizon. Such a horizon therefore exists in conventional Big-Bang models, which are dominated by radiation ($\rho \propto R^{-4}$) at early times.

At late times, the integral for the horizon is largely determined by the matter-dominated phase, for which

$$D_H = R_0\,\chi_H \equiv R_0 \int_0^{t(z)} \frac{dt}{R(t)} \simeq \frac{6000}{\sqrt{\Omega_m z}}\, h^{-1}\,\mathrm{Mpc} \quad (z \gg 1). \tag{22.33}$$

The horizon at the time of formation of the microwave background ('last scattering': $z \simeq 1100$) was thus of order 100 Mpc in size, subtending an angle of about 1°. Why then are the large number of causally disconnected regions we see on the microwave sky all at the same temperature? The Universe is very nearly isotropic and homogeneous, even though the initial conditions appear not to permit such a state to be constructed.

A related problem is that the $\Omega = 1$ Universe is unstable:

$$\Omega(a) - 1 = \frac{\Omega - 1}{1 - \Omega + \Omega_v a^2 + \Omega_m a^{-1} + \Omega_r a^{-2}}\,, \tag{22.34}$$

where Ω with no subscript is the total density parameter, and $a(t) = R(t)/R_0$. This requires $\Omega(t)$ to be unity to arbitrary precision as the initial time tends to zero; a Universe of non-zero curvature today requires very finely tuned initial conditions.

22.3 The Hot Thermal Universe

22.3.1 *Thermodynamics of the early Universe*

As alluded to above, we expect that much of the early Universe can be described by a radiation-dominated equation of state. In addition, through much of the radiation-dominated period, thermal equilibrium is established by the rapid rate of particle interactions relative to the expansion rate of the Universe (see Sec. 22.3.3 below). In equilibrium, it is straightforward to compute the thermodynamic quantities, ρ, p, and the entropy density, s. In general, the energy density for a given particle type i can be written as

$$\rho_i = \int E_i\, dn_{q_i}, \tag{22.35}$$

with the density of states given by

$$dn_{q_i} = \frac{g_i}{2\pi^2} \left(\exp[(E_{q_i} - \mu_i)/T_i] \pm 1\right)^{-1} q_i^2\, dq_i, \tag{22.36}$$

where g_i counts the number of degrees of freedom for particle type i, $E_{q_i}^2 = m_i^2 + q_i^2$, μ_i is the chemical potential, and the $\pm$ corresponds to either Fermi or Bose statistics. Similarly, we can define the pressure of a perfect gas as

$$p_i = \frac{1}{3} \int \frac{q_i^2}{E_i}\, dn_{q_i}. \tag{22.37}$$

The number density of species i is simply

$$n_i = \int dn_{q_i}, \tag{22.38}$$

and the entropy density is

$$s_i = \frac{\rho_i + p_i - \mu_i n_i}{T_i}\,. \tag{22.39}$$

In the Standard Model, a chemical potential is often associated with baryon number, and since the net baryon density relative to the photon density is known to be very small (of order 10^{-9}), we can neglect any such chemical potential when computing total thermodynamic quantities.

For photons, we can compute all of the thermodynamic quantities rather easily. Taking $g_i = 2$ for the 2 photon polarization states, we have (in units where $\hbar = k_B = 1$)

$$\rho_\gamma = \frac{\pi^2}{15} T^4, \quad p_\gamma = \frac{1}{3}\rho_\gamma, \quad s_\gamma = \frac{4\rho_\gamma}{3T}, \quad n_\gamma = \frac{2\zeta(3)}{\pi^2} T^3, \tag{22.40}$$

Downloaded from https://academic.oup.com/ptep/article/2022/8/083C01/6651666 by KIT Library user on 27 September 2022

with $2\zeta(3)/\pi^2 \simeq 0.2436$. Note that Eq. (22.10) can be converted into an equation for entropy conservation. Recognizing that $\dot{p} = s\dot{T}$, Eq. (22.10) becomes

$$d(sR^3)/dt = 0. \tag{22.41}$$

For radiation, this corresponds to the relationship between expansion and cooling, $T \propto R^{-1}$ in an adiabatically expanding Universe. Note also that both s and n_γ scale as T^3.

22.3.2 *Radiation content of the Early Universe*

At the very high temperatures associated with the early Universe, massive particles are pair produced, and are part of the thermal bath. If for a given particle species i we have $T \gg m_i$, then we can neglect the mass in Eq. (22.35) to Eq. (22.39), and the thermodynamic quantities are easily computed as in Eq. (22.40). In general, we can approximate the energy density (at high temperatures) by including only those particles with $m_i \ll T$. In this case, we have

$$\rho = \left(\sum_{\rm B} g_{\rm B} + \frac{7}{8} \sum_{\rm F} g_{\rm F} \right) \frac{\pi^2}{30} T^4 \equiv \frac{\pi^2}{30} N(T)\, T^4, \tag{22.42}$$

where $g_{\rm B(F)}$ is the number of degrees of freedom of each boson (fermion) and the sum runs over all boson and fermion states with $m \ll T$. The factor of 7/8 is due to the difference between the Fermi and Bose integrals. Eq. (22.42) defines the effective number of degrees of freedom, $N(T)$, by taking into account new particle degrees of freedom as the temperature is raised. This quantity, calculated from high temperature lattice QCD, is plotted in Fig. 22.3 [39]. Near the QCD transition, there is a slight difference between the coefficient of T^4 for ρ and the coefficient of T^3 for the entropy density $s = (2\pi^2/45)N_s(T)T^3$ [40], as seen in the figure.

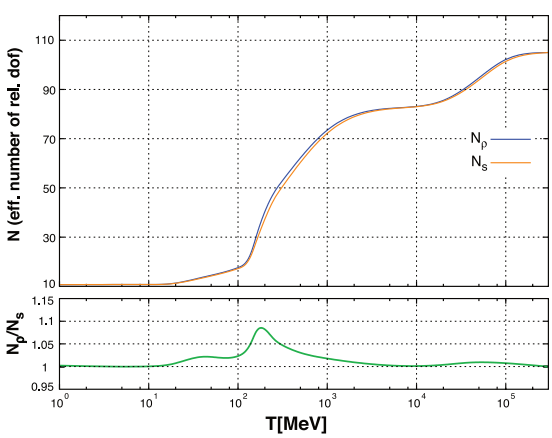

Figure 22.3: The effective numbers of relativistic degrees of freedom as a function of temperature. The sharp drop corresponds to the quark-hadron transition. The bottom panel shows the relative ratio between the number of degrees of freedom characterizing the energy density and the entropy.

The value of $N(T)$ at any given temperature depends on the particle physics model. In the standard SU(3) × SU(2) × U(1) model, we can specify $N(T)$ up to temperatures of $O(100)$ GeV. The change in N (ignoring mass effects) can be seen in the table below.

Temperature	New Particles	$4N(T)$
$T < m_e$	γ's + ν's	29
$m_e < T < m_\mu$	$e^\pm$	43
$m_\mu < T < m_\pi$	$\mu^\pm$	57
$m_\pi < T < T_c$ †	π's	69
$T_c < T < m_{\rm strange}$	π's + $u, \bar{u}, d, \bar{d}$ + gluons	205
$m_s < T < m_{\rm charm}$	$s, \bar{s}$	247
$m_c < T < m_\tau$	$c, \bar{c}$	289
$m_\tau < T < m_{\rm bottom}$	$\tau^\pm$	303
$m_b < T < m_{\rm W,Z}$	$b, \bar{b}$	345
$m_{W,Z} < T < m_{\rm Higgs}$	$W^\pm, Z$	381
$m_H < T < m_{\rm top}$	H^0	385
$m_t < T$	$t, \bar{t}$	427

† T_c corresponds to the confinement-deconfinement transition between quarks and hadrons.

At higher temperatures, $N(T)$ will be model-dependent. For example, in the minimal SU(5) model, one needs to add 24 states to $N(T)$ for the charged and colored X and Y gauge bosons, another 24 from the adjoint Higgs, and another 6 scalar degrees of freedom (in addition to the 4 associated with the complex Higgs doublet already counted in the longitudinal components of $W^\pm$ and Z, and in H) from the $\bar{5}$ of Higgs. Hence for $T > m_{\rm X}$ in minimal SU(5), $N(T) = 160.75$. In a supersymmetric model this would at least double.

In the radiation-dominated epoch, Eq. (22.10) can be integrated (neglecting the T-dependence of N) giving us a relationship between the age of the Universe and its temperature

$$t = \left(\frac{90}{32\pi^3 G_{\rm N} N(T)} \right)^{1/2} T^{-2}\,. \tag{22.43}$$

Put into a more convenient form

$$t\, T_{\rm MeV}^2 = 2.4[N(T)]^{-1/2}, \tag{22.44}$$

where t is measured in seconds and $T_{\rm MeV}$ in units of MeV.

22.3.3 *Neutrinos and equilibrium*

Due to the expansion of the Universe, certain rates may be too slow to either establish or maintain equilibrium. Quantitatively, for each particle i, as a minimal condition for equilibrium, we will require that some rate Γ_i involving that type be larger than the expansion rate of the Universe, or

$$\Gamma_i > H. \tag{22.45}$$

Recalling that the age of the Universe is determined by H^{-1}, this condition is equivalent to requiring that on average, at least one interaction has occurred over the lifetime of the Universe.

A good example for a process that goes in and out of equilibrium is the weak interaction of neutrinos. On dimensional grounds, one can estimate the thermally averaged scattering cross-section:

$$\langle \sigma v \rangle \sim O(10^{-2}) T^2/m_{\rm W}^4 \tag{22.46}$$

for $T \lesssim m_{\rm W}$. Recalling that the number density of leptons is $n \propto T^3$, we can compare the weak interaction rate, $\Gamma_{\rm wk} \sim n\langle \sigma v \rangle$, with the expansion rate,

$$\begin{aligned} H = \left(\frac{8\pi G_{\rm N} \rho}{3} \right)^{1/2} &= \left(\frac{8\pi^3}{90} N(T) \right)^{1/2} T^2/M_{\rm P} \\ &\simeq 1.66 N(T)^{1/2} T^2/M_{\rm P}, \end{aligned} \tag{22.47}$$

where the Planck mass $M_{\rm P} = G_{\rm N}^{-1/2} = 1.22 \times 10^{19}$ GeV.

Neutrinos will be in equilibrium when $\Gamma_{\rm wk} > H$ or

$$T > (500\, m_{\rm W}^4/M_{\rm P})^{1/3} \sim 1 \text{ MeV}. \tag{22.48}$$

However, this condition assumes $T \ll m_{\rm W}$; for higher temperatures, we should write $\langle \sigma v \rangle \sim O(10^{-2})/T^2$, so that $\Gamma \sim 10^{-2} T$. Thus, in the very early stages of expansion, at temperatures $T \gtrsim 10^{-2} M_{\rm P}/\sqrt{N}$, equilibrium will not have been established.

Having attained a quasi-equilibrium stage, the Universe then cools further to the point where the interaction and expansion

Downloaded from https://academic.oup.com/ptep/article/2022/8/083C01/6651666 by KIT Library user on 27 September 2022

timescales match once again. The temperature at which these rates are equal is commonly referred to as the neutrino decoupling or freeze-out temperature and is defined by $\Gamma_{\rm wk}(T_d) = H(T_d)$. For $T < T_d$, neutrinos drop out of equilibrium. The Universe becomes transparent to neutrinos and their momenta simply redshift with the cosmic expansion. The effective neutrino temperature will simply fall with $T \sim 1/R$.

Soon after decoupling, $e^\pm$ pairs in the thermal background begin to annihilate (when $T \lesssim m_e$). Because the neutrinos are decoupled, the energy released due to annihilation heats up the photon background relative to the neutrinos. The change in the photon temperature can be easily computed from entropy conservation. The neutrino entropy must be conserved separately from the entropy of interacting particles. A straightforward computation yields

$$T_\nu = (4/11)^{1/3}\, T_\gamma \simeq 1.9 \text{ K}. \tag{22.49}$$

The total entropy density is therefore given by the contribution from photons and 3 flavors of neutrinos

$$s = \frac{4}{3}\frac{\pi^2}{30}\left(2 + \frac{21}{4}(T_\nu/T_\gamma)^3\right) T_\gamma^3 = \frac{4}{3}\frac{\pi^2}{30}\left(2 + \frac{21}{11}\right) T_\gamma^3 = 7.04\, n_\gamma. \tag{22.50}$$

Similarly, the total relativistic energy density is given by

$$\rho_r = \frac{\pi^2}{30}\left[2 + \frac{21}{4}(T_\nu/T_\gamma)^4\right] T_\gamma^4 \simeq 1.68\rho_\gamma. \tag{22.51}$$

In practice, a small correction is needed to this, since neutrinos are not totally decoupled at $e^\pm$ annihilation: the effective number of massless neutrino species is 3.044, rather than 3 [41].

This expression ignores neutrino rest masses, but current oscillation data require at least one neutrino eigenstate to have a mass exceeding 0.05 eV. In this minimal case, $\Omega_\nu h^2 = 6 \times 10^{-4}$, so the neutrino contribution to the matter budget would be negligibly small (which is our normal assumption). However, a nearly degenerate pattern of mass eigenstates could allow larger densities, since oscillation experiments only measure differences in m^2 values. Note that a 0.05-eV neutrino has $T_\nu = m_\nu$ at $z \simeq 296$, so the above expression for the total present relativistic density is really only an extrapolation. However, neutrinos are almost certainly relativistic at all epochs where the radiation content of the Universe is dynamically significant.

22.3.4 *Field theory and phase transitions*

It is very likely that the Universe has undergone one or more phase transitions during the course of its evolution [42–45]. Our current vacuum state is described by $\mathrm{SU}(3)_c\times\ \mathrm{U}(1)_{\rm em}$, which in the Standard Model is a remnant of an unbroken $\mathrm{SU}(3)_c\times\ \mathrm{SU}(2)_L\times\ \mathrm{U}(1)_Y$ gauge symmetry. Symmetry breaking occurs when a non-singlet gauge field (the Higgs field in the Standard Model) picks up a non-vanishing vacuum expectation value, determined by a scalar potential. For example, a simple (non-gauged) potential describing symmetry breaking is $V(\phi) = \frac{1}{4}\lambda\phi^4 - \frac{1}{2}\mu^2\phi^2 + V(0)$. The resulting expectation value is simply $\langle\phi\rangle = \mu/\sqrt{\lambda}$.

In the early Universe, finite temperature radiative corrections typically add terms to the potential of the form $\phi^2 T^2$. Thus, at very high temperatures, the symmetry is restored and $\langle\phi\rangle = 0$. As the Universe cools, depending on the details of the potential, symmetry breaking will occur via a first-order phase transition in which the field tunnels through a potential barrier, or via a second-order transition in which the field evolves smoothly from one state to another (as would be the case for the above example potential).

The evolution of scalar fields can have a profound impact on the early Universe. The equation of motion for a scalar field ϕ can be derived from the energy-momentum tensor

$$T_{\mu\nu} = \partial_\mu\phi\partial_\nu\phi - \frac{1}{2}g_{\mu\nu}\partial_\rho\phi\partial^\rho\phi - g_{\mu\nu}V(\phi). \tag{22.52}$$

By associating $\rho = T_{00}$ and $p = R^{-2}(t)T_{ii}$ we have

$$\begin{aligned} \rho &= \frac{1}{2}\dot\phi^2 + \frac{1}{2}R^{-2}(t)(\nabla\phi)^2 + V(\phi) \\ p &= \frac{1}{2}\dot\phi^2 - \frac{1}{6}R^{-2}(t)(\nabla\phi)^2 - V(\phi)\ , \end{aligned} \tag{22.53}$$

and from Eq. (22.10) we can write the equation of motion (by considering a homogeneous region, we can ignore the gradient terms)

$$\ddot\phi + 3H\dot\phi = -\partial V/\partial\phi. \tag{22.54}$$

22.3.5 *Inflation*

In Sec. 22.2.4, we discussed some of the problems associated with the standard Big-Bang model. However, during a phase transition, our assumptions of an adiabatically expanding Universe are generally not valid. If, for example, a phase transition occurred in the early Universe such that the field evolved slowly from the symmetric state to the global minimum, the Universe may have been dominated by the vacuum energy density associated with the potential near $\phi \simeq 0$. During this period of slow evolution, the energy density due to radiation will fall below the vacuum energy density, $\rho \ll V(0)$. When this happens, the expansion rate will be dominated by the constant V(0), and we obtain the exponentially expanding solution given in Eq. (22.20). When the field evolves towards the global minimum it will begin to oscillate about the minimum, energy will be released during its decay, and a hot thermal Universe will be restored. If released fast enough, it will produce radiation at a temperature $N{T_{\rm R}}^4 \lesssim V(0)$. In this reheating process, entropy has been created and the final value of RT is greater than the initial value of RT. Thus, we see that, during a phase transition, the relation $RT \sim$ constant need not hold true. This is the basis of the inflationary Universe scenario [46–48].

If, during the phase transition, the value of RT changed by a factor of $O(10^{29})$, the cosmological problems discussed above would be solved. The observed isotropy would be generated by the immense expansion; one small causal region could get blown up, and thus our entire visible Universe would have been in thermal contact some time in the past. In addition, the density parameter Ω would have been driven to 1 (with exponential precision). Density perturbations will be stretched by the expansion, $\lambda \sim R(t)$. Thus it will appear that $\lambda \gg H^{-1}$ or that the perturbations have left the horizon, where in fact the size of the causally connected region is now no longer simply H^{-1}. However, not only does inflation offer an explanation for large scale perturbations, it also offers a source for the perturbations themselves through quantum fluctuations.

Problems with early models of inflation based on either a first-order [49] or second-order [50, 51] phase transition of a Grand Unified Theory led to models invoking a completely new scalar field: the inflaton, ϕ. The potential of this field, $V(\phi)$, needs to have a very low gradient and curvature in order to match observed metric fluctuations. For a more thorough discussion of the problems of early models and a host of current models being studied see the review on inflation – Sec. 23 of this *Review*. In most current inflation models, reheated bubbles typically do not percolate, so inflation is 'eternal' and continues with exponential expansion in the region outside bubbles. These causally disconnected bubble Universes constitute a 'multiverse', where low-energy physics can vary between different bubbles. This has led to a controversial 'anthropic' approach to cosmology [52–54], where observer selection within the multiverse can be introduced as a means of understanding e.g. why the observed level of vacuum energy is so low (because larger values suppress growth of structure).

22.3.6 *Baryogenesis*

The Universe appears to be populated exclusively with matter rather than antimatter. Indeed antimatter is only detected in accelerators or in cosmic rays. However, the presence of antimatter in the latter is understood to be the result of collisions of primary particles in the interstellar medium. There is in fact strong evidence against primary forms of antimatter in the Universe. Furthermore, the density of baryons compared to the density of photons is extremely small, $\eta \sim 10^{-9}$.

Downloaded from https://academic.oup.com/ptep/article/2022/8/083C01/6651666 by KIT Library user on 27 September 2022

The production of a net baryon asymmetry requires baryon number violating interactions, C and CP violation, and a departure from thermal equilibrium [55]. The first two of these ingredients are expected to be contained in Grand Unified Theories (GUTs) as well as in the non-perturbative sector of the Standard Model; the third can be realized in an expanding Universe where, as we have seen, interactions come in and out of equilibrium.

There are several interesting and viable mechanisms for the production of the baryon asymmetry. While we can not review any of them here in any detail, we mention some of the important scenarios. In all cases, all three ingredients listed above are incorporated. One of the first mechanisms was based on the out of equilibrium decay of a massive particle such as a superheavy GUT gauge or Higgs boson [56, 57]. A novel mechanism involving the decay of flat directions in supersymmetric models is known as the Affleck-Dine scenario [58]. There is also the possibility of generating the baryon asymmetry at the electro-weak scale using the non-perturbative interactions of sphalerons [59]. Because these interactions conserve the sum of baryon and lepton number, $B+L$, it is possible to first generate a lepton asymmetry (*e.g.*, by the out-of-equilibrium decay of a superheavy right-handed neutrino), which is converted to a baryon asymmetry at the electro-weak scale [60]. This mechanism is known as lepto-baryogenesis, or simply leptogenesis.

22.3.7 *Nucleosynthesis*

An essential element of the standard cosmological model is Big-Bang nucleosynthesis (BBN), the theory that predicts the abundances of the light element isotopes D, ^{3}He, ^{4}He, and ^{7}Li. Nucleosynthesis takes place at a temperature scale of order 1 MeV. The nuclear processes lead primarily to ^{4}He, with a primordial mass fraction of about 25%. Lesser amounts of the other light elements are produced: about 10^{-5} of D and ^{3}He and about 10^{-10} of ^{7}Li by number relative to H. The abundances of the light elements depend almost solely on one key parameter, the baryon-to-photon ratio, η. The nucleosynthesis predictions can be compared with observational determinations of the abundances of the light elements. Consistency between theory and observations driven primarily by recent D/H measurements [61, 62] leads to a range of

$$5.8 \times 10^{-10} < \eta < 6.5 \times 10^{-10}. \tag{22.55}$$

η is related to the fraction of Ω contained in baryons:

$$\Omega_{\rm b} = 3.66 \times 10^7 \eta\, h^{-2}, \tag{22.56}$$

or $10^{10}\eta = 274\Omega_{\rm b}h^2$. The *Planck* result [24] for $\Omega_{\rm b}h^2$ of 0.0224 $\pm$ 0.0002 translates into a value of $\eta = 6.12 \pm 0.04$. This result can be used to 'predict' the light element abundances, which can in turn be compared with observation [63]. The resulting D/H abundance is in excellent agreement with that found in quasar absorption systems. It is in reasonable agreement with the helium abundance observed in extragalactic HII regions (once systematic uncertainties are accounted for), but is in poor agreement with the Li abundance observed in the atmospheres of halo dwarf stars [64]. See the review on BBN – Sec. 24 of this *Review* for a detailed discussion of BBN or references [65–69].

22.3.8 *The transition to a matter-dominated Universe*

In the Standard Model, the temperature (or redshift) at which the Universe undergoes a transition from a radiation-dominated to a matter-dominated Universe is determined by the amount of dark matter. Assuming three nearly massless neutrinos, the energy density in radiation at temperatures $T \ll 1$ MeV, is given by

$$\rho_{\rm r} = \frac{\pi^2}{30}\left[2 + \frac{21}{4}\left(\frac{4}{11}\right)^{4/3}\right] T^4. \tag{22.57}$$

In the absence of non-baryonic dark matter, the matter density can be written as

$$\rho_{\rm m} = m_{\rm N}\eta\, n_\gamma, \tag{22.58}$$

where $m_{\rm N}$ is the nucleon mass. Recalling that $n_\gamma \propto T^3$ [cf. Eq. (22.40)], we can solve for the temperature or redshift at the matter-radiation equality when $\rho_{\rm r} = \rho_{\rm m}$,

$$T_{\rm eq} = 0.22\, m_{\rm N}\, \eta \qquad \text{or} \qquad (1+z_{\rm eq}) = 0.22\, \eta \frac{m_{\rm N}}{T_0}, \tag{22.59}$$

where T_0 is the present temperature of the microwave background. For $\eta = 6.1 \times 10^{-10}$, this corresponds to a temperature $T_{\rm eq} \simeq 0.13$ eV or $(1+z_{\rm eq}) \simeq 550$. A transition this late would be problematic for structure formation (see Sec. 22.4.5).

The redshift of matter domination can be pushed back significantly if non-baryonic dark matter is present. If instead of Eq. (22.58), we write

$$\rho_{\rm m} = \Omega_{\rm m}\rho_{\rm c}\left(\frac{T}{T_0}\right)^3, \tag{22.60}$$

we find that

$$T_{\rm eq} = 0.9\frac{\Omega_{\rm m}\rho_{\rm c}}{T_0^3} \qquad \text{or} \qquad (1+z_{\rm eq}) = 2.4 \times 10^4 \Omega_{\rm m} h^2. \tag{22.61}$$

22.4 The Universe at late times

22.4.1 *The CMB*

One form of the infamous Olbers' paradox says that, in Euclidean space, surface brightness is independent of distance. Every line of sight will terminate on matter that is hot enough to be ionized and so scatter photons: $T \gtrsim 10^3$ K, and the sky should therefore shine as brightly as the surface of the Sun. The reason the night sky is dark is entirely due to the expansion, which cools the radiation temperature to 2.73 K. This gives a Planck function peaking at around 1 mm to produce the CMB.

The CMB spectrum is a very accurate match to a Planck function [70]. (See the review on CMB – Sec. 29 of this *Review*.) The COBE estimate of the temperature is [71]

$$T = 2.7255 \pm 0.0006\,{\rm K}. \tag{22.62}$$

The lack of any distortion of the Planck spectrum is a strong physical constraint. It is very difficult to account for in any expanding Universe other than one that passes through a hot stage. Alternative schemes for generating the radiation, such as thermalization of starlight by dust grains, inevitably generate a superposition of temperatures. What is required in addition to thermal equilibrium is that $T \propto 1/R$, so that radiation from different parts of space arrive at an observer with the same apparent temperature.

Although it is common to speak of the CMB as originating at 'recombination', a more accurate terminology is the era of 'last scattering'. In practice, this takes place at $z \simeq 1100$, almost independently of the main cosmological parameters, at which time the fractional ionization is very small. This occurred when the age of the Universe was about 370,000 years. But the CMB photons themselves were not generated at this point, and were the result of thermalization at $z \sim 10^7$. (See the review on CMB – Sec. 29 of this *Review* for a full discussion of the CMB.)

22.4.2 *Matter in the Universe*

One of the main tasks of cosmology is to measure the density of the Universe, and how this is divided between dark matter and baryons. The baryons consist partly of stars, with $0.002 \lesssim \Omega_* \lesssim 0.003$ [72] but mainly inhabit the intergalactic medium (IGM). One powerful way in which this can be studied is via the absorption of light from distant luminous objects such as quasars. Even very small amounts of neutral hydrogen can absorb rest-frame UV photons (the Gunn-Peterson effect), and should suppress the continuum by a factor $\exp(-\tau)$, where

$$\tau \simeq 10^{4.62} h^{-1}\left[\frac{n_{\rm HI}(z)/{\rm m}^{-3}}{(1+z)\sqrt{1+\Omega_{\rm m} z}}\right], \tag{22.63}$$

and this expression applies while the Universe is matter dominated ($z \gtrsim 1$ in the $\Omega_{\rm m} = 0.3$ $\Omega_{\rm v} = 0.7$ model). At $z < 6$, the dominant effect on quasar spectra is a 'forest' of narrow absorption lines, which produce a mean $\tau = 1$ in the Lyα forest at about $z = 3$, and so we have $\Omega_{\rm HI} \simeq 10^{-6.7} h^{-1}$. This is such a small number that the IGM must be very highly ionized at these redshifts, apart

Downloaded from https://academic.oup.com/ptep/article/2022/8/083C01/6651666 by KIT Library user on 27 September 2022

from a few high-density clumps. But at $z > 6$ there is good evidence for a 'reionization' era at which the general IGM is not so strongly ionized [73]. As discussed below, this ionized IGM at low z is also detectable via the secondary Compton scattering of CMB photons.

The Lyα forest is of great importance in pinning down the abundance of deuterium. Because electrons in deuterium differ in reduced mass by about 1 part in 4000 compared to hydrogen, each absorption system in the Lyα forest is accompanied by an offset deuterium line. By careful selection of systems with an optimal HI column density, a measurement of the D/H ratio can be made. This has now been done with high accuracy in 10 quasars, with consistent results [61]. Combining these determinations with the theory of primordial nucleosynthesis yields a baryon density of $\Omega_{\rm b}h^2 = 0.021 - 0.024$ (95% confidence) in excellent agreement with the Planck result. (See also the review on BBN – Sec. 24 of this *Review*.)

Ionized IGM can also be detected in emission when it is densely clumped, via bremsstrahlung radiation. This generates the spectacular X-ray emission from rich clusters of galaxies. Studies of this phenomenon allow us to achieve an accounting of the total baryonic material in clusters. Within the central $\simeq 1$ Mpc, the masses in stars, X-ray emitting gas, and total dark matter can be determined with reasonable accuracy (perhaps 20% rms), and this allows a minimum baryon fraction to be determined [74, 75]:

$$\frac{M_{\rm baryons}}{M_{\rm total}} \gtrsim 0.009 + (0.066 \pm 0.003)\, h^{-3/2}. \tag{22.64}$$

Because clusters are the largest collapsed structures, it is reasonable to take this as applying to the Universe as a whole. This equation implies a minimum baryon fraction of perhaps 12% (for reasonable h), which is too high for $\Omega_{\rm m} = 1$ if we take $\Omega_{\rm b}h^2 \simeq 0.02$ from nucleosynthesis. This is therefore one of the more robust arguments in favor of $\Omega_{\rm m} \simeq 0.3$. (See the review on Cosmological Parameters – Sec. 25 of this *Review*.) This argument is also consistent with the inference on $\Omega_{\rm m}$ that can be made from Fig. 22.2.

This method is much more robust than the older classical technique for weighing the Universe: '$L \times M/L$'. The overall light density of the Universe is reasonably well determined from redshift surveys of galaxies, so that a good determination of mass M and luminosity L for a single object suffices to determine $\Omega_{\rm m}$ – but only *if* the mass-to-light ratio were universal.

22.4.3 *Gravitational lensing*

A robust method for determining masses in cosmology is to use gravitational light deflection. Most systems can be treated as a geometrically thin gravitational lens, where the light bending is assumed to take place only at a single distance. Simple geometry then determines a mapping between the coordinates in the intrinsic source plane (S) and the observed image plane (I):

$$\alpha(D_{\rm L}\theta_{\rm I}) = \frac{D_{\rm S}}{D_{\rm LS}}(\theta_{\rm I} - \theta_{\rm S}), \tag{22.65}$$

where the angles $\theta_{\rm I}, \theta_{\rm S}$, and α are in general two-dimensional vectors on the sky. The distances $D_{\rm LS}$ etc. are given by an extension of the usual distance-redshift formula:

$$D_{\rm LS} = \frac{R_0 S_k(\chi_{\rm S} - \chi_{\rm L})}{1 + z_{\rm S}}. \tag{22.66}$$

This is the angular-diameter distance for objects on the source plane as perceived by an observer on the lens.

Solutions of this equation divide into weak lensing, where the mapping between source plane and image plane is one-to-one, and strong lensing, in which multiple imaging is possible. For circularly-symmetric lenses, an on-axis source is multiply imaged into a 'caustic' ring, whose radius is the Einstein radius:

$$\begin{aligned}\theta_{\rm E} &= \left(4GM\,\frac{D_{\rm LS}}{D_{\rm L}D_{\rm S}}\right)^{1/2} \\ &= \left(\frac{M}{10^{11.09}M_\odot}\right)^{1/2}\left(\frac{D_{\rm L}D_{\rm S}/D_{\rm LS}}{\rm Gpc}\right)^{-1/2} \quad \text{arcsec}\ .\end{aligned} \tag{22.67}$$

The observation of 'arcs' (segments of near-perfect Einstein rings) in rich clusters of galaxies has thus given very accurate masses for the central parts of clusters – generally in good agreement with other indicators, such as analysis of X-ray emission from the cluster IGM [76, 77].

Gravitational lensing has also developed into a particularly promising probe of cosmological structure on 10-Mpc to 100-Mpc scales. Weak image distortions manifest themselves as an additional ellipticity of galaxy images ('shear'), which can be observed by averaging many images together (the corresponding flux amplification is less readily detected). The result is a 'cosmic shear' field of order 1% ellipticity, coherent over scales of around 30 arcmin, which is directly related to the cosmic mass field. For this reason, weak lensing is seen as potentially the cleanest probe of matter fluctuations, next to the CMB. Already, impressive results have been obtained in measuring cosmological parameters, based on survey data from only $\sim 10^3$ deg^2 [78, 79]. A particular strength of lensing is its ability to measure the amplitude of mass fluctuations; this can be deduced from the amplitude of CMB fluctuations, but only with low precision on account of the poorly-known optical depth due to Compton scattering after reionization. However, the effect of weak lensing on the CMB map itself can be detected via the induced non-Gaussian signal, and this gives the CMB greater internal power [80]. The main difficulty of principle with lensing is that part of the signal is generated by small-scale density fluctuations; thus a model is required for nonlinear evolution, including astrophysical effects that separate baryons and dark matter. In this respect, the CMB is a cleaner probe of the primordial fluctuations.

22.4.4 *Density fluctuations*

The overall properties of the Universe are very close to being homogeneous; and yet telescopes reveal a wealth of detail on scales varying from single galaxies to large-scale structures of size exceeding 100 Mpc. The existence of these structures must be telling us something important about the initial conditions of the Big Bang, and about the physical processes that have operated subsequently. This motivates the study of the density perturbation field, defined as

$$\delta(\mathbf{x}) \equiv \frac{\rho(\mathbf{x}) - \langle\rho\rangle}{\langle\rho\rangle}. \tag{22.68}$$

A critical feature of the δ field is that it inhabits a Universe that is isotropic and homogeneous in its large-scale properties. This suggests that the statistical properties of δ should also be statistically homogeneous – *i.e.*, it is a stationary random process.

It is often convenient to describe δ as a Fourier superposition:

$$\delta(\mathbf{x}) = \sum \delta_{\mathbf{k}} e^{-i\mathbf{k}\cdot\mathbf{x}}. \tag{22.69}$$

We avoid difficulties with an infinite Universe by applying periodic boundary conditions in a cube of some large volume V. The cross-terms vanish when we compute the variance in the field, which is just a sum over modes of the power spectrum:

$$\langle\delta^2\rangle = \sum |\delta_{\mathbf{k}}|^2 \equiv \sum P(k). \tag{22.70}$$

Note that the statistical nature of the fluctuations must be isotropic, so we write $P(k)$ rather than $P(\mathbf{k})$. The $\langle\ldots\rangle$ average here is a volume average. Cosmological density fields are an example of an ergodic process, in which the average over a large volume tends to the same answer as the average over a statistical ensemble.

The statistical properties of discrete objects sampled from the density field are often described in terms of N-point correlation functions, which represent the excess probability over random for finding one particle in each of N boxes in a given configuration. For the 2-point case, the correlation function is readily shown to be identical to the autocorrelation function of the δ field: $\xi(r) = \langle\delta(x)\delta(x+r)\rangle$.

The power spectrum and correlation function are Fourier conjugates, and thus are equivalent descriptions of the density field

Downloaded from https://academic.oup.com/ptep/article/2022/8/083C01/6651666 by KIT Library user on 27 September 2022

(similarly, k-space equivalents exist for the higher-order correlations). It is convenient to take the limit $V \to \infty$ and use k-space integrals, defining a dimensionless power spectrum, which measures the contribution to the fractional variance in density per unit logarithmic range of scale, as $\Delta^2(k) = d\langle\delta^2\rangle/d\ln k = Vk^3P(k)/2\pi^2$:

$$\xi(r) = \int \Delta^2(k)\,\frac{\sin kr}{kr}\,d\ln k; \quad \Delta^2(k) = \frac{2}{\pi}k^3\int_0^\infty \xi(r)\,\frac{\sin kr}{kr}\,r^2\,dr. \tag{22.71}$$

For many years, an adequate approximation to observational data on galaxies was $\xi = (r/r_0)^{-\gamma}$, with $\gamma \simeq 1.8$ and $r_0 \simeq 5\,h^{-1}$ Mpc. Modern surveys are now able to probe into the large-scale linear regime where unaltered traces of the curved post-recombination spectrum can be detected [81–83].

22.4.5 *Formation of cosmological structure*

The simplest model for the generation of cosmological structure is gravitational instability acting on some small initial fluctuations (for the origin of which a theory such as inflation is required). If the perturbations are adiabatic (*i.e.*, fractionally perturb number densities of photons and matter equally), the linear growth law for matter perturbations is simple:

$$\delta \propto \begin{cases} a^2(t) & \text{(radiation domination; } \Omega_\mathrm{r} = 1); \\ a(t) & \text{(matter domination; } \Omega_\mathrm{m} = 1)\ . \end{cases} \tag{22.72}$$

For low-density Universes, the growth is slower:

$$d\ln\delta/d\ln a \simeq \Omega_\mathrm{m}^\gamma(a), \tag{22.73}$$

where the parameter γ is close to 0.55 independent of the vacuum density [84, 85].

The alternative perturbation mode is isocurvature: only the equation of state changes, and the total density is initially unperturbed. These modes perturb the total entropy density, and thus induce additional large-scale CMB anisotropies [86]. Although the character of perturbations in the simplest inflationary theories are purely adiabatic, correlated adiabatic and isocurvature modes are predicted in many models; the simplest example is the curvaton, which is a scalar field that decays to yield a perturbed radiation density. If the matter content already exists at this time, the overall perturbation field will have a significant isocurvature component. Such a prediction is inconsistent with current CMB data [87], and most analyses of CMB and large-scale structure (LSS) data assume the adiabatic case to hold exactly.

Linear evolution preserves the shape of the power spectrum. However, a variety of processes mean that growth actually depends on the matter content.

1. Pressure opposes gravity effectively for wavelengths below the horizon length while the Universe is radiation dominated. The *comoving* horizon size at z_eq is therefore an important scale:

$$D_\mathrm{H}(z_\mathrm{eq}) = \frac{2(\sqrt{2}-1)}{(\Omega_\mathrm{m}z_\mathrm{eq})^{1/2}H_0} = \frac{16.0}{\Omega_\mathrm{m}h^2}\ \mathrm{Mpc}\ . \tag{22.74}$$

2. At early times, dark matter particles will undergo free streaming at the speed of light, and so erase all scales up to the horizon – a process that only ceases when the particles go nonrelativistic. For light massive neutrinos, this happens at z_eq; all structure up to the horizon-scale power-spectrum break is in fact erased. Hot(cold) dark matter models are thus sometimes dubbed large(small)-scale damping models.
3. A further important scale arises where photon diffusion can erase perturbations in the matter – radiation fluid; this process is named Silk damping.

The overall effect is encapsulated in the transfer function, which gives the ratio of the late-time amplitude of a mode to its initial value (see Fig. 22.4). The overall power spectrum is thus the primordial scalar-mode power law, times the square of the transfer function:

$$P(k) \propto k^{n_\mathrm{s}}\,T_k^2. \tag{22.75}$$

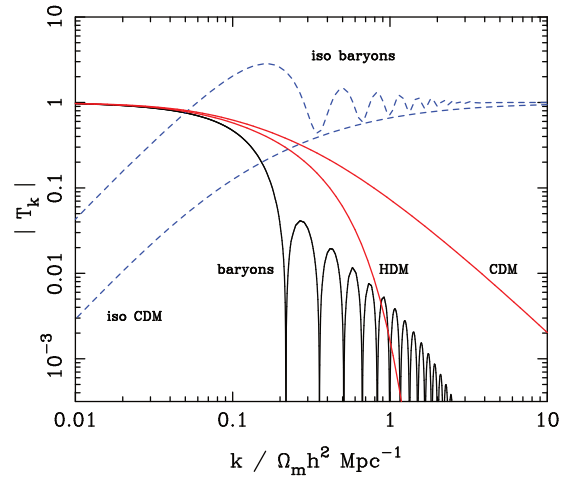

Figure 22.4: A plot of transfer functions for various models. For adiabatic models, $T_k \to 1$ at small k, whereas the opposite is true for isocurvature models. For dark-matter models, the characteristic wavenumber scales proportional to $\Omega_\mathrm{m}h^2$. The scaling for baryonic models does not obey this exactly; the plotted cases correspond to $\Omega_\mathrm{m} = 1$, $h = 0.5$.

The most generic power-law index is $n_\mathrm{s} = 1$: the 'Zeldovich' or 'scale-invariant' spectrum. Inflationary models tend to predict a small 'tilt:' $|n_\mathrm{s} - 1| \lesssim 0.05$ [12, 13]. On the assumption that the dark matter is cold, the power spectrum then depends on 5 parameters: n_s, h, Ω_b, Ω_c ($\equiv \Omega_\mathrm{m} - \Omega_\mathrm{b}$), and an overall amplitude. The latter is often specified as σ_8, the linear-theory fractional rms in density when a spherical filter of radius $8\,h^{-1}$ Mpc is applied in linear theory. This scale can be probed directly via weak gravitational lensing, and also via its effect on the abundance of rich galaxy clusters. The normalization derived from samples of X-ray clusters has been given variously as [88, 89]

$$\sigma_8 = [0.746 \pm 0.012(\mathrm{stat.}) \pm 0.022(\mathrm{sys.})](\Omega_m/0.3)^{-0.47}; \tag{22.76}$$

$$\sigma_8 = [0.81 \pm 0.03](\Omega_m/0.3)^{-0.17}. \tag{22.77}$$

The higher figure is well consistent with *Planck*, whereas the lower is rather similar to the normalization inferred from weak lensing: $\sigma_8 \simeq [0.737^{+0.040}_{-0.036}](\Omega_\mathrm{m}/0.3)^{-0.5}$ [78]; or $[0.759^{+0.025}_{-0.023}](\Omega_\mathrm{m}/0.3)^{-0.5}$ [79]. These figures are both in 2.3σ tension with the *Planck* values of $(\sigma_8, \Omega_\mathrm{m}) = (0.811 \pm 0.006, 0.315 \pm 0.007)$. If real, such a discrepancy could indicate interesting new physics; but the current evidence is not strong enough to make such a claim. However, it is worth noting that the CMB requires an almost perfect degeneracy, $\Omega_m h^3 = \mathrm{const}$ for flat models, so that raising h as far as allowed by the CMB would require a lower density, which would reduce the tension with the amplitude of the lensing measurements.

A direct measure of mass inhomogeneity is valuable, since the galaxies inevitably are biased with respect to the mass. This means that the fractional fluctuations in galaxy number, $\delta n/n$, may differ from the mass fluctuations, $\delta\rho/\rho$. It is commonly assumed that the two fields obey some proportionality on large scales where the fluctuations are small, $\delta n/n = b\delta\rho/\rho$, but even this is not guaranteed [90].

The main shape of the transfer function is a break around the horizon scale at z_eq, which depends just on $\Omega_\mathrm{m}h$ when wavenumbers are measured in observable units ($h\,\mathrm{Mpc}^{-1}$). For reasonable baryon content, weak oscillations in the transfer function are also expected, and these BAOs (Baryon Acoustic Oscillations) have been clearly detected [91, 92]. As well as directly measuring the baryon fraction, the scale of the oscillations directly measures the acoustic horizon at decoupling; this can be used as an additional standard ruler for cosmological tests, and the BAO signature has become one of the most important applications of large galaxy surveys. Overall, current power-spectrum data [81–83] fa-

Downloaded from https://academic.oup.com/ptep/article/2022/8/083C01/6651666 by KIT Library user on 27 September 2022

vor $\Omega_{\rm m}h \simeq 0.20$ and a baryon fraction of about 0.15 for $n_{\rm s} \simeq 1$ (see Fig. 22.5).

In principle, accurate data over a wide range of k could determine both $\Omega_{\rm m}h$ and n, but in practice there is a strong degeneracy between these. In order to constrain $n_{\rm s}$ itself, it is necessary to examine data on anisotropies in the CMB.

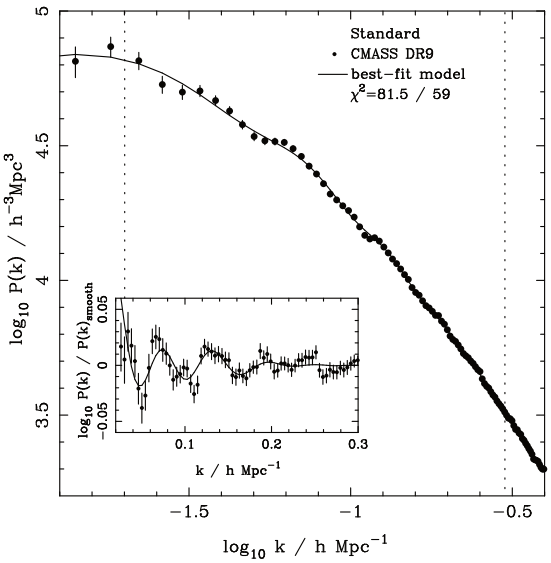

Figure 22.5: The galaxy power spectrum from the SDSS BOSS survey [83]. The solid points with error bars show the power estimate. The solid line shows a standard ΛCDM model with $\Omega_{\rm b}h^2 \simeq 0.02$ and $\Omega_{\rm m}h \simeq 0.2$. The inset amplifies the region where BAO features are visible. The fact that these perturb the power by $\sim 20\%$ rather than order unity is direct evidence that the matter content of the Universe is dominated by collisionless dark matter.

22.4.6 *CMB anisotropies*

The CMB has a clear dipole anisotropy, of magnitude 1.23×10^{-3}. This is interpreted as being due to the Earth's motion, which is equivalent to a peculiar velocity for the Milky Way of

$$v_{\rm MW} \simeq 600\,{\rm km\,s^{-1}} \quad \text{towards} \quad (\ell, b) \simeq (270^\circ, 30^\circ). \tag{22.78}$$

A continuing challenge in cosmology is to demonstrate that this dipole is indeed kinematic, as opposed to representing a violation of large-scale isotropy. Galaxy surveys have attempted to identify the accelerating superclusters responsible for the motion [93], but there are also claims that the observed matter distribution contains an intrinsic dipole, which would be incompatible with the standard interpretation [94].

All higher-order multipole moments of the CMB are however much smaller (of order 10^{-5}), and interpreted as signatures of density fluctuations at last scattering ($\simeq 1100$). To analyze these, the sky is expanded in spherical harmonics as explained in the review on the CMB – Sec. 29 of this *Review*. The dimensionless power per ln k or 'bandpower' for the CMB is defined as

$$\mathcal{T}^2(\ell) = \frac{\ell(\ell+1)}{2\pi}\, C_\ell. \tag{22.79}$$

This function encodes information from the three distinct mechanisms that cause CMB anisotropies:

- (1) Gravitational (Sachs – Wolfe) perturbations. Photons from high-density regions at last scattering have to climb out of potential wells, and are thus redshifted.
- (2) Intrinsic (adiabatic) perturbations. In high-density regions, the coupling of matter and radiation can compress the radiation also, giving a higher temperature.
- (3) Velocity (Doppler) perturbations. The plasma has a non-zero velocity at recombination, which leads to Doppler shifts in frequency and hence shifts in brightness temperature.

Because the potential fluctuations obey Poisson's equation, $\nabla^2\Phi = 4\pi G\rho\delta$, and the velocity field satisfies the continuity equation $\nabla\cdot\mathbf{u} = -\dot\delta$, the resulting different powers of k ensure that the Sachs-Wolfe effect dominates on large scales and adiabatic effects on small scales.

The relation between angle and comoving distance on the last-scattering sphere requires the comoving angular-diameter distance to the last-scattering sphere; because of its high redshift, this is effectively identical to the horizon size at the present epoch, $D_{\rm H}$:

$$\begin{aligned} D_{\rm H} &= \frac{2}{\Omega_{\rm m}H_0} \quad (\Omega_{\rm v} = 0) \\ D_{\rm H} &\simeq \frac{2}{\Omega_{\rm m}^{0.4}H_0} \quad (\text{flat} : \Omega_{\rm m} + \Omega_{\rm v} = 1)\ . \end{aligned} \tag{22.80}$$

These relations show how the CMB is strongly sensitive to curvature: the horizon length at last scattering is $\propto 1/\sqrt{\Omega_{\rm m}}$, so that this subtends an angle that is virtually independent of $\Omega_{\rm m}$ for a flat model. Observations of a peak in the CMB power spectrum at relatively large scales ($\ell \simeq 221$) are thus strongly inconsistent with zero-Λ models with low density: current CMB + BAO + lensing data require $\Omega_{\rm m} + \Omega_{\rm v} = 0.999 \pm 0.004$ (95%) [24]. (See *e.g.*, Fig. 22.2).

In addition to curvature, the CMB encodes information about several other key cosmological parameters. Within the compass of simple adiabatic CDM models, there are 9 of these:

$$\omega_{\rm c},\ \omega_{\rm b},\ \Omega_{\rm tot},\ h,\ \tau,\ n_{\rm s},\ n_{\rm t},\ r,\ Q. \tag{22.81}$$

The symbol ω denotes the physical density, Ωh^2: the transfer function depends only on the densities of CDM ($\omega_{\rm c}$) and baryons ($\omega_{\rm b}$). Transcribing the power spectrum at last scattering into an angular power spectrum brings in the total density parameter ($\Omega_{\rm tot} \equiv \Omega_{\rm m} + \Omega_{\rm v} = \Omega_{\rm c} + \Omega_{\rm b} + \Omega_{\rm v}$) and h: there is a near-exact geometrical degeneracy [95] between these that keeps the angular-diameter distance to last scattering invariant, so that models with substantial spatial curvature and large vacuum energy cannot be ruled out without prior knowledge of the Hubble parameter. Alternatively, the CMB alone cannot measure the Hubble parameter without taking into account the line-of-sight information from CMB lensing.

A further possible degeneracy involves the tensor contribution to the CMB anisotropies. These are important at large scales (up to the horizon scales); for smaller scales, only scalar fluctuations (density perturbations) are important. Each of these components is characterized by a spectral index, n, and a ratio between the power spectra of tensors and scalars (r). See the review on Cosmological Parameters – Sec. 25 of this *Review* for a technical definition of the r parameter. Finally, the overall amplitude of the spectrum must be specified (Q), together with the optical depth to Compton scattering owing to recent reionization (τ). Adding a large tensor contribution reduces the contrast between low ℓ and the peak at $\ell \simeq 221$ (because the tensor spectrum has no acoustic component). The previous relative height of the peak can be recovered by increasing $n_{\rm s}$ to increase the small-scale power in the scalar component; this in turn over-predicts the power at $\ell \sim 1000$, but this effect can be counteracted by raising the baryon density [96]. This approximate 3-way degeneracy is broken as we increase the range of multipoles sampled.

The reason the tensor component is introduced, and why it is so important, is that it is the only non-generic prediction of inflation. Slow-roll models of inflation involve two dimensionless parameters:

$$\epsilon \equiv \frac{M_{\rm P}^2}{16\pi}\left(\frac{V'}{V}\right)^2, \qquad \eta \equiv \frac{M_{\rm P}^2}{8\pi}\left(\frac{V''}{V}\right), \tag{22.82}$$

where V is the inflaton potential, and dashes denote derivatives with respect to the inflation field. In terms of these, the tensor-to-scalar ratio is $r \simeq 16\epsilon$, and the spectral indices are $n_{\rm s} = 1 - 6\epsilon + 2\eta$ and $n_{\rm t} = -2\epsilon$. The natural expectation of inflation is that the quasi-exponential phase ends once the magnitudes of the slow-roll parameters become of order unity, so that both $n_{\rm s} \neq 1$ and a significant tensor component are expected. These predictions can

Downloaded from https://academic.oup.com/ptep/article/2022/8/083C01/6651666 by KIT Library user on 27 September 2022

be avoided in some models, but it is undeniable that observation of such features would be a great triumph for inflation. Cosmology therefore stands at a fascinating point given that the most recent CMB data reject the zero-tensor $n_s = 1$ model at more than 8σ: $n_s = 0.965 \pm 0.004$ [24]. This rejection is strong enough that it is also able to break the tensor degeneracy, so that no model with $n_s = 1$ is acceptable, whatever the value of r.

The current limit on r is < 0.036 at 95% confidence [97,98]. In conjunction with the measured value of n_s, this upper limit sits close to the prediction of a linear potential (i.e. $|\eta| \ll |\epsilon|$). Any further reduction in the limit on r will force η to be negative – i.e. a convex potential at the point where LSS scales were generated (sometimes called a 'hilltop'), in contrast to simple early models such as $V(\phi) = m^2\phi^2$ or $\lambda\phi^4$, which are now excluded. Examples of models that are currently in excellent agreement with the Planck results are the Starobinsky model of $\mathcal{R}+\mathcal{R}^2$ gravity [99], or the Higgs-inflation model where the Higgs field is non-minimally coupled [100]. Assuming 55 e-foldings of inflation, these models predict $n_s = 0.965$ and $r = 0.0035$. Assuming that no systematic error in the CMB data can be identified, cosmology has thus passed a critical hurdle in rejecting scale-invariant fluctuations. The years ahead will be devoted to the task of searching for the tensor fluctuations – for which the main tool will be the polarization of the CMB [14].

22.4.6.1 *CMB foregrounds*

As the quality of CMB data improves, there is a growing interest in effects that arise along the line of sight. The CMB temperature is perturbed by dark-matter structures and by Compton scattering from ionized gas. In the former case, we have the integrated Sachs-Wolfe effect, which is sensitive to the time derivative of the gravitational potential. In the linear regime, this is damped when the Universe becomes Λ-dominated, and this is an independent way of detecting Λ [101]. The potential also causes gravitational lensing of the CMB: structures at $z \simeq 1-2$ displace features on the CMB sky by about 2 arcmin over coherent degree-scale patches. Detection of these distortions allows a map to be made of overdensity projected from $z = 0$ to 1100 [80]. This is a very powerful calibration for direct studies of gravitational lensing using galaxies. Finally, Comptonization affects the CMB in two ways: the thermal Sunyaev-Zel'dovich effect measures the blurring of photon energies by hot gas, and the kinetic Sunyaev-Zel'dovich effect is sensitive to the bulk velocity of the gas. Both these effects start to dominate over the intrinsic CMB fluctuations at multipoles $\ell \gtrsim 2000$ [102].

22.4.7 *Probing dark energy and the nature of gravity*

The most radical element of our current cosmological model is the dark energy that accelerates the expansion. The energy density of this component is approximately $(2.2\,\mathrm{meV})^4$ (for $w = -1$, $\Omega_v = 0.68$, $h = 0.67$), or roughly $10^{-123} M_P^4$, and such an unnaturally small number is hard to understand. Various quantum effects (most simply, zero-point energy) should make contributions to the vacuum energy density. These may be truncated by new physics at high energy, but this presumably occurs at $> 1\,\mathrm{TeV}$ scales, not meV; thus the apparent energy scale of the vacuum is at least 10^{15} times smaller than its natural value. A classic review of this situation is given by Weinberg [52], which lists extreme escape routes – especially the multiverse viewpoint, according to which low values of Λ are rare, but high values suppress the formation of structure and observers. It is certainly impressive that Weinberg used such reasoning to predict the value of Λ before any data strongly indicated a non-zero value.

But it may be that the phenomenon of dark energy is entirely illusory. The necessity for this constituent arises from using the Friedmann equation to describe the evolution of the cosmic expansion; if this equation is incorrect, it would require the replacement of Einstein's relativistic theory of gravity with some new alternative. A frontier of current cosmological research is to distinguish these possibilities [103,104]. We also note that it has been suggested that dark energy might be an illusion even within general relativity, owing to an incorrect treatment of averaging in an inhomogeneous Universe [105,106]. Most would argue that a standard Newtonian treatment of such issues should be adequate inside the cosmological horizon, but debate on this issue continues.

Dark Energy can differ from a classical cosmological constant in being a dynamical phenomenon [107,108], *e.g.*, a rolling scalar field (sometimes dubbed 'quintessence'). Empirically, this means that it is endowed with two thermodynamic properties that astronomers can try to measure: the bulk equation of state, and the sound speed. If the sound speed is close to the speed of light, the effect of this property is confined to very large scales, and mainly manifests itself in the large-angle multipoles of the CMB anisotropies [109]. The equation of state parameter governs the rate of change of the vacuum density: $d\ln\rho_v/d\ln a = -3(1+w)$, so it can be accessed via the evolving expansion rate, $H(a)$. This can be measured most cleanly by using the inbuilt natural ruler of large-scale structure: the BAO horizon scale [110]:

$$D_{\mathrm{BAO}} \simeq 147.0\,(\Omega_m h^2/0.1424)^{-0.253}(\Omega_b h^2/0.0224)^{-0.128}\ \mathrm{Mpc}. \tag{22.83}$$

Observing the equivalent acoustic scale at last scattering in the CMB yields the precise geometrical degeneracy $\Omega_m h^3 = 0.09633 \pm 0.00029$ [24].

$H(a)$ is measured by radial clustering, since $dr/dz = c/H$; clustering in the plane of the sky measures the integral of this. The expansion rate is also measured by the growth of density fluctuations, where the pressure-free growth equation for the density perturbation is $\ddot{\delta} + 2H(a)\dot{\delta} = 4\pi G\rho_0\,\delta$. Thus, both the scale and amplitude of density fluctuations are sensitive to $w(a)$ – but only weakly. These observables change by only typically 0.2% for a 1% change in w. Current constraints [24] place a constant w to within 5–10% of -1, depending on the data combination chosen. A substantial improvement in this precision will require us to limit systematics in data to a few parts in 1000.

Testing whether theories of gravity require revision can also be done using data on cosmological inhomogeneities. Two separate issues arise, concerning the metric perturbation potentials Ψ and Φ, which affect respectively the time and space parts of the metric. In Einstein gravity, these potentials are both equal to the Newtonian gravitational potential, which satisfies Poisson's equation: $\nabla^2\Phi/a^2 = 4\pi G\bar{\rho}\delta$. Empirically, modifications of gravity require us to explore a change with scale and with time of the 'slip' (Ψ/Φ) and the effective G on the rhs of the Poisson equation. The former aspect can only be probed via gravitational lensing, whereas the latter can be addressed on 10–100 Mpc scales via the growth of clustering. Various schemes for parameterising modified gravity exist, but a practical approach is to assume that the growth rate can be tied to the density parameter: $d\ln\delta/d\ln a = \Omega_m^\gamma(a)$ [84,85]. The parameter γ is close to 0.55 for standard relativistic gravity, but can differ by around 0.1 from this value in many non-standard models. Clearly this parameterization is incomplete, since it explicitly rejects the possibility of early dark energy ($\Omega_m(a) \to 1$ as $a \to 0$), but it is a convenient way of capturing the power of various experiments. Current data are consistent with standard ΛCDM [111], and exclude variations in slip or effective G of larger than a few times 10%.

Current planning envisages a set of satellite probes that, a decade hence, will have pursued these fundamental tests via gravitational lensing measurements over thousands of square degrees, $> 10^8$ redshifts, and photometry of > 1000 supernovae (Euclid in Europe, Roman Space Telescope in the USA) [22,23]. These experiments will measure both w and the perturbation growth rate to an accuracy of around 1%. The outcome will be either a validation of the standard relativistic vacuum-dominated Big Bang cosmology at a level of precision far beyond anything attempted to date, or the opening of entirely new directions in cosmological models. For a more complete discussion of dark energy and future probes see the review on Dark Energy – Sec. 28

References

[1] V.M. Slipher, Pop. Astr. **23**, 21 (1915).

[2] K. Lundmark, Mon. Not. R. Astron. Soc **84**, 747 (1924).

[3] E. Hubble and M. L. Humason, Astrophys. J. **74**, 43 (1931).

[4] G. Gamow, Phys. Rev. **70**, 572 (1946).

[5] R. A. Alpher, H. Bethe and G. Gamow, Phys. Rev. **73**, 803 (1948).

Downloaded from https://academic.oup.com/ptep/article/2022/8/083C01/6651666 by KIT Library user on 27 September 2022

[6] R.A. Alpher and R.C. Herman, Phys. Rev. **74**, 1737 (1948).

[7] R.A. Alpher and R.C. Herman, Phys. Rev. **75**, 1089 (1949).

[8] A. A. Penzias and R. W. Wilson, Astrophys. J. **142**, 419 (1965).

[9] P.J.E. Peebles, *Principles of Physical Cosmology*, Princeton University Press (1993) .

[10] G. Börner, *The Early Universe: Facts and Fiction*, Springer-Verlag (1988).

[11] E.W. Kolb and M.S. Turner, *The Early Universe*, Addison-Wesley (1990).

[12] J.A. Peacock, *Cosmological Physics*, Cambridge Univ. Press (1999).

[13] A.R. Liddle and D. Lyth, *Cosmological Inflation and Large-Scale Structure*, Cambridge University Press (2000).

[14] S. Dodelson, *Modern Cosmology*, Academic Press (2003).

[15] V. Mukhanov, *Physical Foundations of Cosmology*, Cambridge University Press (2005).

[16] S. Weinberg, *Cosmology*, Oxford Press (2008).

[17] E.B. Gliner, Sov. Phys. JETP **22**, 378 (1966).

[18] Ya. B. Zel'dovich, A. Krasinski and Ya. B. Zeldovich, Sov. Phys. Usp. **11**, 381 (1968), [Usp. Fiz. Nauk95,209(1968)].

[19] P.M. Garnavich *et al.*, Astrophys. J. **507**, 74 (1998), [arXiv:astro-ph/9806396].

[20] S. Perlmutter, M. S. Turner and M. J. White, Phys. Rev. Lett. **83**, 670 (1999), [arXiv:astro-ph/9901052].

[21] I. Maor *et al.*, Phys. Rev. **D65**, 123003 (2002), [arXiv:astro-ph/0112526].

[22] A. Albrecht *et al.* (2006), [arXiv:astro-ph/0609591].

[23] J. A. Peacock *et al.* (2006), [arXiv:astro-ph/0610906].

[24] N. Aghanim *et al.* (Planck), Astron. Astrophys. **641**, A6 (2020), [arXiv:1807.06209].

[25] A.G. Riess *et al.*, Astrophys. J. **116**, 1009 (1998), [arXiv:astro-ph/9805201].

[26] S. Perlmutter *et al.* (Supernova Cosmology Project), Astrophys. J. **517**, 565 (1999), [arXiv:astro-ph/9812133].

[27] A. G. Riess, Publ. Astron. Soc. Pac. **112**, 1284 (2000), [arXiv:astro-ph/0005229].

[28] J. L. Tonry *et al.* (Supernova Search Team), Astrophys. J. **594**, 1 (2003), [arXiv:astro-ph/0305008].

[29] N. Suzuki *et al.*, Astrophys. J. **746**, 85 (2012), [arXiv:1105.3470].

[30] D. M. Scolnic *et al.*, Astrophys. J. **859**, 101 (2018), [arXiv:1710.00845].

[31] A. G. Riess *et al.*, Astrophys. J. Lett. **908**, 1, L6 (2021), [arXiv:2012.08534].

[32] W. L. Freedman *et al.*, Astrophys. J. **882**, 34 (2019), [arXiv:1907.05922].

[33] W. L. Freedman (2021), [arXiv:2106.15656].

[34] Planck Collab. 2015 Results XIII, Astron. & Astrophys. **594**, A13 (2016), [arXiv:1502.10589].

[35] P. Astier *et al.*, Astron. & Astrophys. **447**, 31 (2006), [arXiv:astro-ph/0510447].

[36] J. A. Johnson and M. Bolte, Astrophys. J. **554**, 888 (2001), [arXiv:astro-ph/0103299].

[37] R. Cayrel *et al.*, Nature **409**, 691 (2001), [arXiv:astro-ph/0104357].

[38] D. A. Vandenberg *et al.*, Astrophys. J. **775**, 134 (2013), [arXiv:1308.2257].

[39] S. Borsanyi *et al.*, Nature **539**, 7627, 69 (2016), [arXiv:1606.07494].

[40] M. Srednicki, R. Watkins and K. A. Olive, Nucl. Phys. **B310**, 693 (1988), [,247(1988)].

[41] J. J. Bennett *et al.*, JCAP **04**, 073 (2021), [arXiv:2012.02726].

[42] A. D. Linde, Phys. Rev. **D14**, 3345 (1976).

[43] A. Linde, Rept. on Prog. in Phys. **42**, 389 (1979).

[44] C.E. Vayonakis, Surv. High Energy Physics **5**, 87 (1986).

[45] S.A. Bonometto and A. Masiero, Nuovo Cimento **9N5**, 1 (1986).

[46] A. Linde, *Particle Physics And Inflationary Cosmology*, Harwood (1990).

[47] K. A. Olive, Phys. Rept. **190**, 307 (1990).

[48] D. H. Lyth and A. Riotto, Phys. Rept. **314**, 1 (1999), [hep-ph/9807278].

[49] A. H. Guth, Phys. Rev. **D23**, 347 (1981), [Adv. Ser. Astrophys. Cosmol.3,139(1987)].

[50] A. D. Linde, Phys. Lett. **108B**, 389 (1982), [Adv. Ser. Astrophys. Cosmol.3,149(1987)].

[51] A. Albrecht and P. J. Steinhardt, Phys. Rev. Lett. **48**, 1220 (1982), [Adv. Ser. Astrophys. Cosmol.3,158(1987)].

[52] S. Weinberg, Rev. Mod. Phys. **61**, 1 (1989).

[53] L. Susskind 247–266 (2003), [hep-th/0302219].

[54] B. Carr, *Universe or multiverse?* C.U.P. (2007).

[55] A. D. Sakharov, Pisma Zh. Eksp. Teor. Fiz. **5**, 32 (1967), [Usp. Fiz. Nauk161,no.5,61(1991)].

[56] S. Weinberg, Phys. Rev. Lett. **42**, 850 (1979).

[57] D. Toussaint *et al.*, Phys. Rev. **D19**, 1036 (1979).

[58] I. Affleck and M. Dine, Nucl. Phys. **B249**, 361 (1985).

[59] V. A. Kuzmin, V. A. Rubakov and M. E. Shaposhnikov, Phys. Lett. **155B**, 36 (1985).

[60] M. Fukugita and T. Yanagida, Phys. Lett. **B174**, 45 (1986).

[61] S. Riemer-Sorensen and S. Jenssen, Universe **3**, 44 (2017), [arXiv:1502.10589].

[62] R. J. Cooke, M. Pettini and C. C. Steidel, Astrophys. J. **855**, 2, 102 (2018), [arXiv:1710.11129].

[63] R. H. Cyburt, B. D. Fields and K. A. Olive, Phys. Lett. **B567**, 227 (2003), [arXiv:astro-ph/0302431].

[64] R. H. Cyburt, B. D. Fields and K. A. Olive, JCAP **0811**, 012 (2008), [arXiv:0808.2818].

[65] K. A. Olive, G. Steigman and T. P. Walker, Phys. Rept. **333**, 389 (2000), [arXiv:astro-ph/9905320].

[66] F. Iocco *et al.*, Phys. Rept. **472**, 1 (2009), [arXiv:0809.0631].

[67] R. H. Cyburt *et al.*, Rev. Mod. Phys. **88**, 015004 (2016), [arXiv:1505.01076].

[68] C. Pitrou *et al.*, Phys. Rept. **754**, 1 (2018), [arXiv:1801.08023].

[69] B. D. Fields *et al.*, JCAP **03**, 010 (2020), [Erratum: JCAP 11, E02 (2020)], [arXiv:1912.01132].

[70] D. J. Fixsen *et al.*, Astrophys. J. **473**, 576 (1996), [arXiv:astro-ph/9605054].

[71] J. C. Mather *et al.*, Astrophys. J. **512**, 511 (1999), [arXiv:astro-ph/9810373].

[72] S. Cole *et al.* (2dFGRS), Mon. Not. Roy. Astron. Soc. **326**, 255 (2001), [arXiv:astro-ph/0012429].

[73] J. Schroeder, A. Mesinger and Z. Haiman, Mon. Not. R. Astron. Soc **428**, 3058 (2013), [arXiv:1204.2838].

[74] S. D. M. White *et al.*, Nature **366**, 429 (1993).

[75] S. W. Allen, R. W. Schmidt and A. C. Fabian, Mon. Not. Roy. Astron. Soc. **334**, L11 (2002), [arXiv:astro-ph/0205007].

[76] S. W. Allen, Mon. Not. Roy. Astron. Soc. **296**, 392 (1998), [arXiv:astro-ph/9710217].

[77] G. P. Smith *et al.*, Mon. Not. Roy. Astron. Soc. **456**, 1, L74 (2016), [arXiv:1511.01919].

Downloaded from https://academic.oup.com/ptep/article/2022/8/083C01/6651666 by KIT Library user on 27 September 2022

[78] H. Hildebrandt *et al.*, Astron. Astrophys. **633**, A69 (2020), [arXiv:1812.06076].

[79] A. Amon *et al.*, arXiv e-prints (2021), [arXiv:2105.13543].

[80] Planck Collab. 2015 Results XV, Astron. & Astrophys. **594**, A15 (2016), [arXiv:1502.01591].

[81] S. Cole *et al.* (2dFGRS), Mon. Not. Roy. Astron. Soc. **362**, 505 (2005), [arXiv:astro-ph/0501174].

[82] W. J. Percival *et al.*, Astrophys. J. **657**, 645 (2007), [arXiv:astro-ph/0608636].

[83] L. Anderson *et al.*, Mon. Not. Roy. Astron. Soc. **427**, 4, 3435 (2013), [arXiv:1203.6594].

[84] E. Linder, Phys. Rev. **D72**, 43529 (2005), [arXiv:astro-ph/0507263].

[85] D. Polarski and R. Gannouji, Phys. Lett. **B660**, 439 (2008), [arXiv:0710.1510].

[86] G. Efstathiou and J. R. Bond, Mon. Not. Roy. Astron. Soc. **218**, 1, 103 (1986).

[87] C. Gordon and A. Lewis, Phys. Rev. **D67**, 123513 (2003), [arXiv:astro-ph/0212248].

[88] A. Vikhlinin *et al.*, Astrophys. J. **692**, 1060 (2009), [arXiv:0812.2720].

[89] A. Mantz *et al.*, Mon. Not. Roy. Astron. Soc. **446**, 2205 (2015), [arXiv:1407.4516].

[90] A. Dekel and O. Lahav, Astrophys. J. **520**, 24 (1999), [arXiv:astro-ph/9806193].

[91] W. J. Percival *et al.*, Mon. Not. Roy. Astron. Soc. **381**, 1053 (2007), [arXiv:0705.3323].

[92] W. J. Percival *et al.* (SDSS), Mon. Not. Roy. Astron. Soc. **401**, 2148 (2010), [arXiv:0907.1660].

[93] G. Lavaux *et al.*, Astrophys. J. **709**, 483 (2010), [arXiv:0810.3658].

[94] N. J. Secrest *et al.*, Astrophys. J. **908**, L51 (2021), [arXiv:2009.14826].

[95] G. Efstathiou and J. R. Bond, Mon. Not. Roy. Astron. Soc. **304**, 75 (1999), [arXiv:astro-ph/9807103].

[96] G. Efstathiou *et al.* (2dFGRS), Mon. Not. Roy. Astron. Soc. **330**, L29 (2002), [arXiv:astro-ph/0109152].

[97] M. Tristram *et al.*, Astron. Astrophys. **647**, A128 (2021), [arXiv:2010.01139].

[98] P. A. R. Ade *et al.* (BICEP/Keck), Phys. Rev. Lett. **127**, 15, 151301 (2021), [arXiv:2110.00483].

[99] A. A. Starobinsky, Phys. Lett. **B91**, 99 (1980), [,771(1980)].

[100] F. Bezrukov and M. Shaposhnikov, JHEP **07**, 089 (2009), [arXiv:0904.1537].

[101] Planck Collab. 2015 Results XXI, Astron. & Astrophys. **594**, A21 (2016), [arXiv:1502.01595].

[102] Planck Collab. 2015 Results XXII, Astron. & Astrophys. **594**, A22 (2016), [arXiv:1502.01596].

[103] W. Hu and I. Sawicki, Phys. Rev. **D76**, 4043 (2007), [arXiv:0708.1190].

[104] B. Jain and P. Zhang, Phys. Rev. **D78**, 3503 (2008), [arXiv:0709.2375].

[105] D. L. Wiltshire, Phys. Rev. Lett. **99**, 251101 (2007), [arXiv:0709.0732].

[106] T. Buchert, Gen. Rel. Grav. **40**, 467 (2008), [arXiv:0707.2153].

[107] I. Zlatev, L.-M. Wang and P. J. Steinhardt, Phys. Rev. Lett. **82**, 896 (1999), [arXiv:astro-ph/9807002].

[108] C. Armendariz-Picon, V. Mukhanov, and P.J. Steinhardt, Phys. Rev. **D63**, 3510 (2001), [arXiv:astro-ph/0006373].

[109] S. DeDeo, R.R. Caldwell, and P.J. Steinhardt, Phys. Rev. **D67**, 3509 (2003), [arXiv:astro-ph/0301284].

[110] É. Aubourg *et al.*, Phys. Rev. **D92**, 123516 (2015), [arXiv:1411.1074].

[111] S. F. Daniel *et al.*, Phys. Rev. **D81**, 123508 (2010), [arXiv:1002.1962].

Downloaded from https://academic.oup.com/ptep/article/2022/8/083C01/6651666 by KIT Library user on 27 September 2022

23. Inflation

Revised August 2021 by J. Ellis (King's Coll. London; CERN) and D. Wands (Portsmouth U.).

23.1 Motivation and Introduction

The standard Big-Bang model of cosmology provides a successful framework in which to understand the thermal history of our Universe and the growth of cosmic structure, but it is essentially incomplete. As described in Sec. 22.2.4, Big-Bang cosmology requires very specific initial conditions. It postulates a uniform cosmological background, described by a spatially-flat, homogeneous and isotropic Robertson-Walker (RW) metric (Eq. (22.1) in "Big Bang Cosmology" review), with scale factor $R(t)$. Within this setting, it also requires an initial almost scale-invariant distribution of primordial density perturbations as seen, for example, in the cosmic microwave background (CMB) radiation (described in Chap. 29, "Cosmic Microwave Background" review), on scales far larger than the causal horizon at the time the CMB photons last scattered.

The Hubble expansion rate, $H \equiv \dot{R}/R$, in a RW cosmology is given by the Friedmann constraint equation (Eq. (22.8) in "Big Bang Cosmology" review)

$$H^2 = \frac{8\pi\rho}{3M_P^2} + \frac{\Lambda}{3} - \frac{k}{R^2}\,, \tag{23.1}$$

where k/R^2 is the intrinsic spatial curvature. We use natural units such that the speed of light $c = 1$ and hence we have the Planck mass $M_P = G_N^{-1/2} \simeq 10^{19}$ GeV (see "Astrophysical Constants and Parameters"). A cosmological constant, Λ, of the magnitude required to accelerate the Universe today (see Chap. 28, "Dark Energy" review) would have been completely negligible in the early Universe where the energy density $\rho \gg M_P^2\Lambda \sim 10^{-12}(\mathrm{eV})^4$. The standard early Universe cosmology, described in Sec. 22.1.5 in "Big Bang Cosmology" review, is thus dominated by non-relativistic matter ($p_m \ll \rho_m$) or radiation ($p_r = \rho_r/3$ for an isotropic distribution). This leads to a decelerating expansion with $\ddot{R} < 0$.

The hypothesis of inflation [1,2] postulates a period of accelerated expansion, $\ddot{R} > 0$, in the very early Universe, preceding the standard radiation-dominated era, which offers a physical model for the origin of these initial conditions, as reviewed in [3–7]. Such a period of accelerated expansion (i) drives a curved Robertson-Walker spacetime (with spherical or hyperbolic spatial geometry) towards spatial flatness, and (ii) it also expands the causal horizon beyond the present Hubble length, so as to encompass all the scales relevant to describe the large-scale structure observed in our Universe today, via the following two mechanisms.

1. A spatially-flat Universe with vanishing spatial curvature, $k = 0$, has the dimensionless density parameter $\Omega_{tot} = 1$, where we define (Eq. (22.13) in "Big Bang Cosmology" review; see Chap. 25, "Cosmological Parameters" review for more complete definitions)

$$\Omega_{tot} \equiv \frac{8\pi\rho_{tot}}{3M_P^2 H^2}\,, \tag{23.2}$$

with $\rho_{tot} \equiv \rho + \Lambda M_P^2/8\pi$. If we re-write the Friedmann constraint (Eq. (23.1)) in terms of Ω_{tot} we have

$$1 - \Omega_{tot} = -\frac{k}{\dot{R}^2}\,. \tag{23.3}$$

Observations require $|1-\Omega_{tot,0}| < 0.005$ today [8], where the subscript 0 denotes the present-day value. Taking the time derivative of Eq. (23.3) we obtain

$$\frac{d}{dt}\left(1 - \Omega_{tot}\right) = -2\frac{\ddot{R}}{\dot{R}}\left(1 - \Omega_{tot}\right)\,. \tag{23.4}$$

Thus in a decelerating expansion, $\dot{R} > 0$ and $\ddot{R} < 0$, any small initial deviation from spatial flatness grows, $(d/dt)|1-\Omega_{tot}| > 0$. A small value such as $|1-\Omega_{tot,0}| < 0.005$ today requires an even smaller value at earlier times, e.g., $|1 - \Omega_{tot}| < 10^{-5}$ at the last scattering of the CMB, which appears unlikely, unless for some reason space is exactly flat. However, an extended period of accelerated expansion in the very early Universe, with $\dot{R} > 0$ and $\ddot{R} > 0$ and hence $(d/dt)|1 - \Omega_{tot}| < 0$, can drive Ω_{tot} sufficiently close to unity, so that $|1 - \Omega_{tot,0}|$ remains unobservable small today, even after the radiation- and matter-dominated eras, for a wide range of initial values of Ω_{tot}.

2. The comoving distance (the present-day proper distance) traversed by light between cosmic time t_1 and t_2 in an expanding Universe can be written, (see Eq. (22.32) in "Big Bang Cosmology" review), as

$$D_0(t_1, t_2) = R_0 \int_{t_1}^{t_2} \frac{dt}{R(t)} = R_0 \int_{\ln R_1}^{\ln R_2} \frac{d(\ln R)}{\dot{R}}\,. \tag{23.5}$$

In standard decelerated (radiation- or matter-dominated) cosmology the integrand, $1/\dot{R}$, decreases towards the past, and there is a finite comoving distance traversed by light (a particle horizon) since the Big Bang ($R_1 \to 0$). For example, the comoving size of the particle horizon at the CMB last-scattering surface ($R_2 = R_{lss}$) corresponds to $D_0 \sim 100\,\mathrm{Mpc}$, or approximately 1° on the CMB sky today (see Sec. 22.2.4 in "Big Bang Cosmology" review). However, during a period of inflation, $1/\dot{R}$ increases towards the past, and hence the integral (Eq. (23.5)) diverges as $R_1 \to 0$, allowing an arbitrarily large causal horizon, dependent only upon the duration of the accelerated expansion. Assuming that the Universe inflates with a finite Hubble rate H_* at $t_1 = t_*$, ending with $H_{end} < H_*$ at $t_2 = t_{end}$, we have

$$D_0(t_*, t_{end}) > \left(\frac{R_0}{R_{end}}\right) H_*^{-1}\left(e^{N_*} - 1\right)\,, \tag{23.6}$$

where $N_* \equiv \ln(R_{end}/R_*)$ describes the duration of inflation, measured in terms of the logarithmic expansion (or "e-folds") from $t_1 = t_*$ up to the end of inflation at $t_2 = t_{end}$, and R_0/R_{end} is the subsequent expansion from the end of inflation to the present day. If inflation occurs above the TeV scale, the comoving Hubble scale at the end of inflation, $(R_0/R_{end})H_{end}^{-1}$, is less than one astronomical unit ($\sim 10^{11}$ m), and a causally-connected patch can encompass our entire observable Universe today, which has a size $D_0 > 30$ Gpc, if there were more than 40 e-folds of inflation ($N_* > 40$). If inflation occurs at the GUT scale (10^{15} GeV) then we require more than 60 e-folds.

Producing an accelerated expansion in general relativity requires an energy-momentum tensor with negative pressure, $p < -\rho/3$ (see Eq. (22.9) in "Big Bang Cosmology" review and Chap. 28, "Dark Energy" review), quite different from the hot dense plasma of relativistic particles in the hot Big Bang. However a positive vacuum energy $V > 0$ does exert a negative pressure, $p_V = -\rho_V$. The work done by the cosmological expansion must be negative in this case so that the local vacuum energy density remains constant in an expanding Universe, $\dot{\rho}_V = -3H(\rho_V + p_V) = 0$. Therefore, a false vacuum state can drive an exponential expansion, corresponding to a de Sitter spacetime with a constant Hubble rate $H^2 = 8\pi\rho_V/3M_P^2$ on spatially-flat hypersurfaces.

A constant vacuum energy V, equivalent to a cosmological constant Λ in the Friedmann equation Eq. (23.1), cannot provide a complete description of inflation in the early Universe, since inflation must necessarily have come to an end in order for the standard Big-Bang cosmology to follow. A phase transition to the present true vacuum is required to release the false vacuum energy into the energetic plasma of the hot Big Bang and produce the large total entropy of our observed Universe today. Thus, we must necessarily study dynamical models of inflation, where the time-invariance of the false vacuum state is broken by a time-dependent field. A first-order phase transition would produce a very inhomogeneous Universe [9] unless a time-dependent scalar field leads to a rapidly changing percolation rate [10–12]. However,

Downloaded from https://academic.oup.com/ptep/article/2022/8/083C01/6651666 by KIT Library user on 27 September 2022

a second-order phase transition [13, 14], controlled by a slowly-rolling scalar field, can lead to a smooth classical exit from the vacuum-dominated phase.

As a spectacular bonus, quantum fluctuations in that scalar field could provide a source of almost scale-invariant density fluctuations [15, 16], as detected in the CMB (see Chap. 29), which are thought to be the origin of the structures seen in the Universe today.

Accelerated expansion and primordial perturbations can also be produced in some modified gravity theories (e.g., [1, 17]), which introduce additional non-minimally coupled degrees of freedom. Such inflation models can often be conveniently studied by transforming variables to an 'Einstein frame' in which Einstein's equations apply with minimally coupled scalar fields [18–20].

In the following we will review scalar field cosmology in general relativity and the spectra of primordial fluctuations produced during inflation, before studying selected inflation models.

23.2 Scalar Field Cosmology

The energy-momentum tensor for a canonical scalar field ϕ with self-interaction potential $V(\phi)$ is given in Eq. (22.52) in "Big Bang Cosmology" review. In a homogeneous background this corresponds to a perfect fluid with density

$$\rho = \frac{1}{2}\dot{\phi}^2 + V(\phi)\,, \tag{23.7}$$

and isotropic pressure

$$p = \frac{1}{2}\dot{\phi}^2 - V(\phi)\,, \tag{23.8}$$

while the 4-velocity is proportional to the gradient of the field, $u^\mu \propto \nabla^\mu \phi$.

A field with vanishing potential energy acts like a stiff fluid with $p = \rho = \dot{\phi}^2/2$, whereas if the time-dependence vanishes we have $p = -\rho = -V$ and the scalar field is uniform in time and space. Thus a classical, potential-dominated scalar-field cosmology, with $p \simeq -\rho$, can naturally drive a quasi-de Sitter expansion; the slow time-evolution of the energy density weakly breaks the exact $O(1,3)$ symmetry of four-dimensional de Sitter spacetime down to a Robertson-Walker (RW) spacetime, where the scalar field plays the role of the cosmic time coordinate.

In a scalar-field RW cosmology the Friedmann constraint equation (Eq. (23.1)) reduces to

$$H^2 = \frac{8\pi}{3M_P^2}\left(\frac{1}{2}\dot{\phi}^2 + V\right) - \frac{k}{R^2}\,, \tag{23.9}$$

while energy conservation (Eq. (22.10) in "Big Bang Cosmology" review) for a homogeneous scalar field reduces to the Klein-Gordon equation of motion (Eq. (22.54) in "Big Bang Cosmology" review)

$$\ddot{\phi} = -3H\dot{\phi} - V'(\phi)\,. \tag{23.10}$$

The evolution of the scalar field is thus driven by the potential gradient $V' = dV/d\phi$, subject to damping by the Hubble expansion $3H\dot{\phi}$.

If we define the Hubble slow-roll parameter

$$\epsilon_H \equiv -\frac{\dot{H}}{H^2}\,, \tag{23.11}$$

then we see that inflation ($\ddot{R} > 0$ and hence $\dot{H} > -H^2$) requires $\epsilon_H < 1$. In this case the spatial curvature decreases relative to the scalar field energy density as the Universe expands. Hence, in the following we drop the spatial curvature and consider a spatially-flat RW cosmology, assuming that inflation has lasted sufficiently long that our observable Universe is very close to spatially flatness. However, we note that bubble nucleation, leading to a first-order phase transition during inflation, can lead to homogeneous hypersurfaces with a hyperbolic ('open') geometry, effectively resetting the spatial curvature inside the bubble [21]. This is the basis of so-called open inflation models [22–24], where inflation inside the bubble has a finite duration, leaving a finite negative spatial curvature.

In a scalar field-dominated cosmology (Eq. (23.11)) gives

$$\epsilon_H = \frac{3\dot{\phi}^2}{2V + \dot{\phi}^2}\,, \tag{23.12}$$

in which case we see that inflation requires a potential-dominated expansion, $\dot{\phi}^2 < V$.

23.2.1 *Slow-Roll Inflation*

It is commonly assumed that the field acceleration term, $\ddot{\phi}$, in (Eq. (23.10)) can be neglected, in which case one can give an approximate solution for the inflationary attractor [25]. This slow-roll approximation reduces the second-order Klein-Gordon equation (Eq. (23.10)) to a first-order system, which is over-damped, with the potential gradient being approximately balanced against to the Hubble damping:

$$3H\dot{\phi} \simeq -V'\,, \tag{23.13}$$

and at the same time that the Hubble expansion (Eq. (23.9)) is dominated by the potential energy

$$H^2 \simeq \frac{8\pi}{3M_P^2}V(\phi)\,, \tag{23.14}$$

corresponding to $\epsilon_H \ll 1$.

A necessary condition for the validity of the slow-roll approximation is that the potential slow-roll parameters

$$\epsilon \equiv \frac{M_P^2}{16\pi}\left(\frac{V'}{V}\right)^2\,, \quad \eta \equiv \frac{M_P^2}{8\pi}\left(\frac{V''}{V}\right)\,, \tag{23.15}$$

are small, i.e., $\epsilon \ll 1$ and $|\eta| \ll 1$, requiring the potential to be correspondingly flat. If we identify V'' with the effective mass of the field, we see that the slow-roll approximation requires that the mass of the scalar field must be small compared with the Hubble scale. We note that the Hubble slow-roll parameter (Eq. (23.11)) coincides with the potential slow-roll parameter, $\epsilon_H \simeq \epsilon$, to leading order in the slow-roll approximation.

The slow-roll approximation allows one to determine the Hubble expansion rate as a function of the scalar field value, and vice versa. In particular, we can express, in terms of the scalar field value during inflation, the total logarithmic expansion, or number of "e-folds":

$$\begin{aligned} N_* &\equiv \ln\left(\frac{R_{end}}{R_*}\right) \\ &= \int_{t_*}^{t_{end}} H dt \simeq -\int_{\phi_*}^{\phi_{end}} \sqrt{\frac{4\pi}{\epsilon}}\frac{d\phi}{M_P} \text{ for } V' > 0\,. \end{aligned} \tag{23.16}$$

Given that the slow-roll parameters are approximately constant during slow-roll inflation, $d\epsilon/dN \simeq 2\epsilon(\eta - 2\epsilon) = \mathcal{O}(\epsilon^2)$, we have

$$N_* \simeq \frac{4}{\sqrt{\epsilon}}\frac{\Delta\phi}{M_P}\,. \tag{23.17}$$

Since we require $N > 40$ to solve the flatness, horizon and entropy problems of the standard Big Bang cosmology, we require either very slow roll, $\epsilon < 0.01$, or a large change in the value of the scalar field relative to the Planck scale, $\Delta\phi > M_P$.

23.2.2 *Reheating*

Slow-roll inflation can lead to an exponentially large Universe, close to spatial flatness and homogeneity, but the energy density is locked in the potential energy of the scalar field, and needs to be converted to particles and thermalised to recover a hot Big Bang cosmology at the end of inflation [26, 27]. This process is usually referred to as reheating, although there was not necessarily any preceding thermal era. Reheating can occur when the scalar field evolves towards the minimum of its potential, converting the potential energy first to kinetic energy. This can occur either through the breakdown of the slow-roll condition in single-field models, or due to an instability triggered by the inflaton reaching

Downloaded from https://academic.oup.com/ptep/article/2022/8/083C01/6651666 by KIT Library user on 27 September 2022

a critical value, in multi-field models known as hybrid inflation models [28].

Close to a simple minimum, the scalar field potential can be described by a quadratic function, $V = m^2\phi^2/2$, where m is the mass of the field. We can obtain slow-roll inflation in such a potential at large field values, $\phi \gg M_P$. However, for $\phi \ll M_P$ the field approaches an oscillatory solution:

$$\phi(t) \simeq \frac{M_P}{\sqrt{3\pi}} \frac{\sin(mt)}{mt} \,. \tag{23.18}$$

For $|\phi| < M_P$ the Hubble rate drops below the inflaton mass, $H < m$, and the field oscillates many times over a Hubble time. Averaging over several oscillations, $\Delta t \gg m^{-1}$, we find $\langle \dot{\phi}^2/2 \rangle_{\Delta t} \simeq \langle m^2\phi^2/2 \rangle_{\Delta t}$ and hence

$$\langle \rho \rangle_{\Delta t} \simeq \frac{M_P^2}{6\pi t^2} \,, \quad \langle p \rangle_{\Delta t} \simeq 0 \,. \tag{23.19}$$

This coherent oscillating field corresponds to a condensate of non-relativistic massive inflaton particles, driving a matter-dominated era at the end of inflation, with scale factor $R \propto t^{2/3}$.

The inflaton condensate can lose energy through perturbative decays due to terms in the interaction Lagrangian, such as

$$\mathcal{L}_{int} \subset -\lambda_i \sigma \phi \chi_i^2 - \lambda_j \phi \bar{\psi}_j \psi_j \tag{23.20}$$

that couple the inflation to scalar fields χ_i or fermions ψ_j, where σ has dimensions of mass and the λ_i are dimensionless couplings. When the mass of the inflaton is much larger than the decay products, the decay rate is given by [29]

$$\Gamma_i = \frac{\lambda_i^2 \sigma^2}{8\pi m} \,, \quad \Gamma_j = \frac{\lambda_j^2 m}{8\pi} \,. \tag{23.21}$$

These decay products must in turn thermalise with Standard Model particles before we recover conventional hot Big Bang cosmology. An upper limit on the reheating temperature after inflation is given by [27]

$$T_{rh} = 0.2 \left(\frac{100}{g_*}\right)^{1/4} \sqrt{M_P \Gamma_{tot}} \,, \tag{23.22}$$

where g_* is the effective number of degrees of freedom and Γ_{tot} is the total decay rate for the inflaton, which is required to be less than m for perturbative decay.

The baryon asymmetry of the Universe must be generated after the main release of entropy during inflation, which is an important constraint on possible models. Also, the fact that the inflaton mass is much larger than the mass scale of the Standard Model opens up the possibility that it may decay into massive stable or metastable particles that could be connected with dark matter, constraining possible models. For example, in the context of supergravity models the reheat temperature is constrained by the requirement that gravitinos are not overproduced, potentially destroying the successes of Big Bang nucleosynthesis. For a range of gravitino masses one must require $T_{rh} < 10^9$ GeV [30, 31].

The process of inflaton decay and reheating can be significantly altered by interactions leading to space-time dependences in the effective masses of the fields. In particular, parametric resonance can lead to explosive, non-perturbative decay of the inflaton in some cases, a process often referred to as preheating [26, 32]. For example, an interaction term of the form

$$\mathcal{L}_{int} \subset -\lambda^2 \phi^2 \chi^2 \,, \tag{23.23}$$

leads to a time-dependent effective mass for the χ field as the inflaton ϕ oscillates. This can lead to non-adiabatic particle production if the bare mass of the χ field is small for large couplings or for rapid changes of the inflaton field. The process of preheating is highly model-dependent, but it highlights the possible role of non-thermal particle production after and even during inflation.

23.3 Primordial Perturbations from Inflation

Although inflation was originally discussed as a solution to the problem of initial conditions required for homogeneous and isotropic hot Big Bang cosmology, it was soon realised that inflation also offered a mechanism to generate the inhomogeneous initial conditions required for the formation of large-scale structure [15–17, 33].

23.3.1 *Metric Perturbations*

In a homogeneous classical inflationary cosmology driven by a scalar field, the inflaton field is uniform on constant-time hypersurfaces, $\phi = \phi_0(t)$. However, quantum fluctuations inevitably break the spatial symmetry leading to an inhomogeneous field:

$$\phi(t, x^i) = \phi_0(t) + \delta\phi(t, x^i) \,. \tag{23.24}$$

At the same time, one should consider inhomogeneous perturbations of the RW spacetime metric (see, e.g., [34–36]):

$$\begin{aligned} ds^2 = (1+2A)dt^2 - 2RB_i dt dx^i \\ - R^2 \left[(1+2C)\delta_{ij} + \partial_i\partial_j E + h_{ij}\right] dx^i dx^j \,, \end{aligned} \tag{23.25}$$

where A, B, E and C are scalar perturbations while h_{ij} represents transverse and tracefree, tensor metric perturbations. Vector metric perturbations can be eliminated using Einstein constraint equations in a scalar field cosmology.

The tensor perturbations remain invariant under a temporal gauge transformation $t \to t + \delta t(t, x^i)$, but both the scalar field and the scalar metric perturbations transform. For example, we have

$$\delta\phi \to \delta\phi - \dot{\phi}_0 \delta t \,, \quad C \to C - H\delta t \,. \tag{23.26}$$

However, there are gauge invariant combinations, such as [37]

$$Q = \delta\phi - \frac{\dot{\phi}_0}{H} C \,, \tag{23.27}$$

which describes the scalar field perturbations on spatially-flat ($C = 0$) hypersurfaces. This is simply related to the curvature perturbation on uniform-field ($\delta\phi = 0$) hypersurfaces:

$$\mathcal{R} = C - \frac{H}{\dot{\phi}_0}\delta\phi = -\frac{H}{\dot{\phi}_0} Q \,, \tag{23.28}$$

which coincides in slow-roll inflation, $\rho \simeq \rho(\phi)$, with the curvature perturbation on uniform-density hypersurfaces [16]

$$\zeta = C - \frac{H}{\dot{\rho}_0}\delta\rho \,. \tag{23.29}$$

Thus scalar field and scalar metric perturbations are coupled by the evolution of the inflaton field.

23.3.2 *Gravitational waves from inflation*

The tensor metric perturbation, h_{ij} in Eq. (23.25), is gauge-invariant and decoupled from the scalar perturbations at first order. This represents the free excitations of the spacetime, i.e., gravitational waves, which are the simplest metric perturbations to study at linear order.

Each tensor mode, with wavevector $\vec{k}$, has two linearly-independent transverse and trace-free polarization states:

$$h_{ij}(\vec{k}) = h_{\vec{k}} q_{ij} + \bar{h}_{\vec{k}} \bar{q}_{ij} \,. \tag{23.30}$$

The linearised Einstein equations then yield the same evolution equation for the amplitude as that for a massless field in RW spacetime:

$$\ddot{h}_{\vec{k}} + 3H\dot{h}_{\vec{k}} + \frac{k^2}{R^2} h_{\vec{k}} = 0 \,, \tag{23.31}$$

(and similarly for $\bar{h}_{\vec{k}}$). This can be re-written in terms of the conformal time, $\eta = \int dt/R$, and the conformally rescaled field:

$$u_{\vec{k}} = \frac{M_P R h_{\vec{k}}}{\sqrt{32\pi}} \,. \tag{23.32}$$

Downloaded from https://academic.oup.com/ptep/article/2022/8/083C01/6651666 by KIT Library user on 27 September 2022

This conformal field then obeys the wave equation for a canonical scalar field in Minkowski spacetime with a time-dependent mass:

$$u''_{\vec{k}} + \left(k^2 - \frac{R''}{R}\right) u_{\vec{k}} = 0\,. \tag{23.33}$$

During slow-roll

$$\frac{R''}{R} \simeq (2-\epsilon)R^2H^2\,. \tag{23.34}$$

This makes it possible to quantise the linearised metric fluctuations, $u_{\vec{k}} \to \hat{u}_{\vec{k}}$, on sub-Hubble scales, $k^2/R^2 \gg H^2$, where the background expansion can be neglected.

Crucially, in an inflationary expansion, where $\ddot{R} > 0$, the comoving Hubble length $H^{-1}/R = 1/\dot{R}$ decreases with time. Thus, all modes start inside the Hubble horizon and it is possible to take the initial field fluctuations to be in a vacuum state at early times or on small scales:

$$\langle u_{\vec{k}_1} u_{\vec{k}_2}\rangle = \frac{i}{2}(2\pi)^3\delta^{(3)}\left(\vec{k}_1+\vec{k}_2\right)\,. \tag{23.35}$$

In terms of the amplitude of the tensor metric perturbations, this corresponds to

$$\langle h_{\vec{k}_1} h_{\vec{k}_2}\rangle = \frac{1}{2}\frac{\mathcal{P}_t(k_1)}{4\pi k_1^3}(2\pi)^3\delta^{(3)}\left(\vec{k}_1+\vec{k}_2\right)\,, \tag{23.36}$$

where the factor 1/2 appears due to the two polarization states that contribute to the total tensor power spectrum:

$$\mathcal{P}_t(k) = \frac{64\pi}{M_P^2}\left(\frac{k}{2\pi R}\right)^2\,. \tag{23.37}$$

On super-Hubble scales, $k^2/R^2 \ll H^2$, we have the growing mode solution to Eq. (23.33), $u_{\vec{k}} \propto R$, corresponding to $h_{\vec{k}} \to$ constant, i.e., tensor modes are frozen-in on super-Hubble scales, both during and after inflation. Thus, connecting the initial vacuum fluctuations on sub-Hubble scales to the late-time power spectrum for tensor modes at Hubble exit during inflation, $k = R_*H_*$, we obtain

$$\mathcal{P}_t(k) \simeq \frac{64\pi}{M_P^2}\left(\frac{H_*}{2\pi}\right)^2\,. \tag{23.38}$$

In the de Sitter limit, $\epsilon \to 0$, the Hubble rate becomes time-independent and the tensor spectrum on super-Hubble scales becomes scale-invariant [39]. However slow-roll evolution leads to weak time dependence of H_* and thus a scale-dependent spectrum on large scales, with a spectral tilt

$$n_t \equiv \frac{d\ln\mathcal{P}_T}{d\ln k} \simeq -2\epsilon_*\,. \tag{23.39}$$

23.3.3 *Density Perturbations from single-field inflation*

The inflaton field fluctuations on spatially-flat hypersurfaces are coupled to scalar metric perturbations at first order, but these can be eliminated using the Einstein constraint equations to yield an evolution equation

$$\ddot{Q}_{\vec{k}} + 3H\dot{Q}_{\vec{k}} + \left[\frac{k^2}{R^2} + V'' - \frac{8\pi}{M_P^2R^3}\frac{d}{dt}\left(\frac{R^3\dot{\phi}^2}{H}\right)\right]Q_{\vec{k}} = 0\,. \tag{23.40}$$

Terms proportional to M_P^{-2} represent the effect on the field fluctuations of gravity at first order. As can be seen, this vanishes in the limit of a constant background field, and hence is suppressed in the slow-roll limit, but it is of the same order as the effective mass, $V'' = 3\eta H^2$, so must be included if we wish to model deviations from exact de Sitter symmetry.

This wave equation can also be written in the canonical form for a free field in Minkowski spacetime if we define [37]

$$v_{\vec{k}} \equiv RQ_{\vec{k}}\,, \tag{23.41}$$

to yield

$$v''_{\vec{k}} + \left(k^2 - \frac{z''}{z}\right)v_{\vec{k}} = 0\,, \tag{23.42}$$

where we define

$$z \equiv \frac{R\dot{\phi}}{H}\,, \qquad \frac{z''}{z} \simeq (2+5\epsilon-3\eta)R^2H^2\,, \tag{23.43}$$

where the last approximate equality holds to leading order in the slow-roll approximation.

As previously done for gravitational waves, we quantise the linearised field fluctuations $v_{\vec{k}} \to \hat{v}_{\vec{k}}$ on sub-Hubble scales, $k^2/R^2 \gg H^2$, where the background expansion can be neglected. Thus, we impose

$$\langle v_{\vec{k}_1} v'_{\vec{k}_2}\rangle = \frac{i}{2}\delta^{(3)}\left(\vec{k}_1+\vec{k}_2\right)\,. \tag{23.44}$$

In terms of the field perturbations, this corresponds to

$$\langle Q_{\vec{k}_1} Q_{\vec{k}_2}\rangle = \frac{\mathcal{P}_Q(k_1)}{4\pi k_1^3}(2\pi)^3\delta^{(3)}\left(\vec{k}_1+\vec{k}_2\right)\,, \tag{23.45}$$

where the power spectrum for vacuum field fluctuations on sub-Hubble scales, $k^2/R^2 \gg H^2$, is simply

$$\mathcal{P}_Q(k) = \left(\frac{k}{2\pi R}\right)^2\,, \tag{23.46}$$

yielding the classic result for the vacuum fluctuations for a massless field in de Sitter at Hubble exit, $k = R_*H_*$:

$$\mathcal{P}_Q(k) \simeq \left(\frac{H}{2\pi}\right)^2_*\,. \tag{23.47}$$

In practice there are slow-roll corrections due to the small but finite mass (η) and field evolution (ϵ) [40].

Slow-roll corrections to the field fluctuations are small on sub-Hubble scales, but can become significant as the field and its perturbations evolve over time on super-Hubble scales. Thus, it is helpful to work instead with the curvature perturbation, ζ defined in equation (Eq. (23.29)), which remains constant on super-Hubble scales for adiabatic density perturbations both during and after inflation [16,41]. Thus we have an expression for the primordial curvature perturbation on super-Hubble scales produced by single-field inflation:

$$\mathcal{P}_\zeta(k) = \left[\left(\frac{H}{\dot{\phi}}\right)^2\mathcal{P}_Q(k)\right]_* \simeq \frac{4\pi}{M_P^2}\left[\frac{1}{\epsilon}\left(\frac{H}{2\pi}\right)^2\right]_*\,. \tag{23.48}$$

Comparing this with the primordial gravitational wave power spectrum (Eq. (23.38)) we obtain the tensor-to-scalar ratio for single-field slow-roll inflation

$$r \equiv \frac{\mathcal{P}_t}{\mathcal{P}_\zeta} \simeq 16\epsilon_*\,. \tag{23.49}$$

Note that the scalar amplitude is boosted by a factor $1/\epsilon_*$ during slow-roll inflation, because small scalar field fluctuations can lead to relatively large curvature perturbations on hypersurfaces defined with respect to the density if the potential energy is only weakly dependent on the scalar field, as in slow-roll. Indeed, the de Sitter limit is singular, since the potential energy becomes independent of the scalar field at first order, $\epsilon \to 0$, and the curvature perturbation on uniform-density hypersurfaces becomes ill-defined.

We note that in single-field inflation the tensor-to-scalar ratio and the tensor tilt (Eq. (23.39)) at the same scale are both determined by the first slow-roll parameter at Hubble exit, ϵ_*, giving rise to an important consistency test for single-field inflation:

$$n_t = -\frac{r}{8}\,. \tag{23.50}$$

This may be hard to verify if r is small, making any tensor tilt n_t difficult to measure. On the other hand, it does offer a way to rule out single-field slow-roll inflation if either r or n_t is large.

Given the relatively large scalar power spectrum, it has proved easier to measure the scalar tilt, conventionally defined as $n_s - 1$.

Downloaded from https://academic.oup.com/ptep/article/2022/8/083C01/6651666 by KIT Library user on 27 September 2022

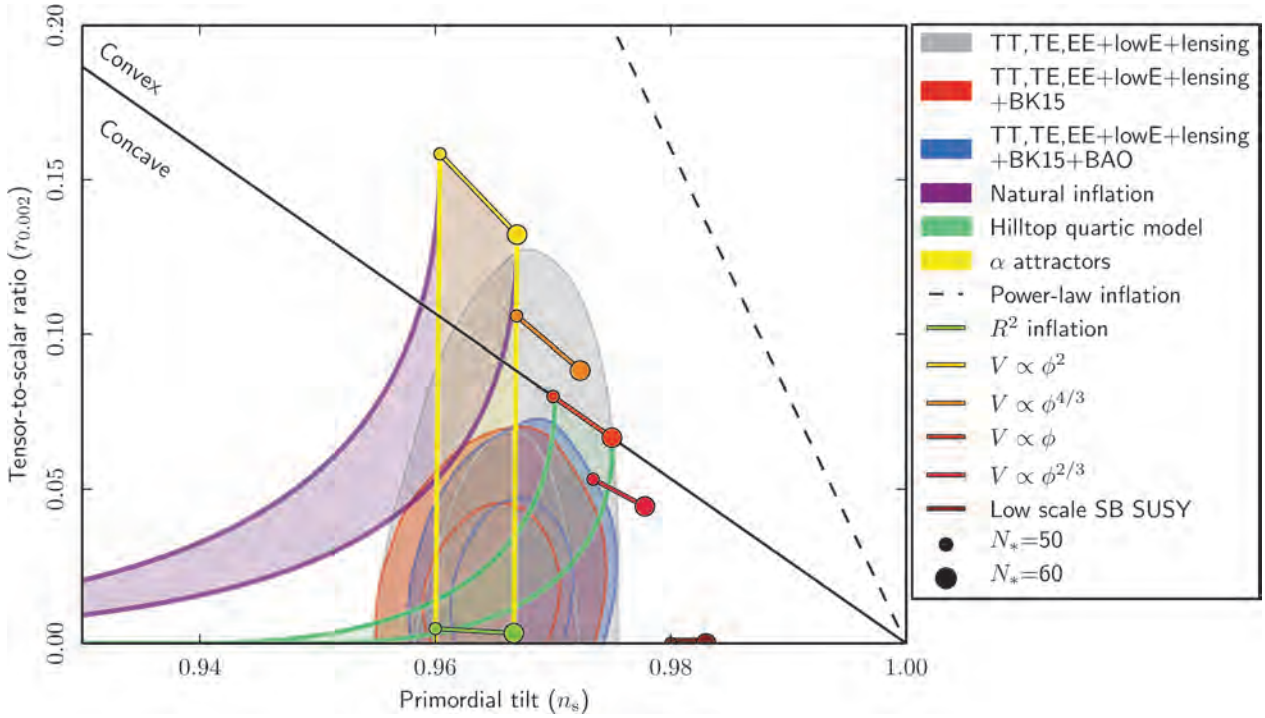

Figure 23.1: The marginalized joint 68 and 95% CL regions for the tilt in the scalar perturbation spectrum, n_s, and the relative magnitude of the tensor perturbations, r, obtained from the *Planck* 2018 and lensing data alone, and their combinations with BICEP2/Keck Array (BK15) and (optionally) BAO data, confronted with the predictions of some of the inflationary models discussed in this review. This figure is taken from [38].

Slow-roll corrections lead to slow time-dependence of both H_* and ϵ_*, giving a weak scale-dependence of the scalar power spectrum:

$$n_s - 1 \equiv \frac{d\ln \mathcal{P}_\zeta}{d\ln k} \simeq -6\epsilon_* + 2\eta_* \,, \tag{23.51}$$

and a running of this tilt at second-order in slow-roll:

$$\frac{dn_s}{d\ln k} \simeq -8\epsilon_*(3\epsilon_* - 2\eta_*) - 2\xi_*^2 \,, \tag{23.52}$$

where the running introduces a new slow-roll parameter at second-order:

$$\xi^2 = \frac{M_P^4}{64\pi^2}\frac{V'V'''}{V^2} \,. \tag{23.53}$$

23.3.4 *Observational Bounds*

The observed scale-dependence of the power spectrum makes it necessary to specify the comoving scale, k, at which quantities are constrained and hence the Hubble-exit time, $k = a_* H_*$, when the corresponding theoretical quantities are calculated during inflation. This is usually expressed in terms of the number of e-folds from the end of inflation [42]:

$$N_*(k) \simeq 67 - \ln\left(\frac{k}{a_0 H_0}\right) + \frac{1}{4}\ln\left(\frac{V_*^2}{M_P^4 \rho_{end}}\right) + \frac{1}{12}\ln\left(\frac{\rho_{rh}}{\rho_{end}}\right) - \frac{1}{12}\ln(g_*), \tag{23.54}$$

where H_0^{-1}/a_0 is the present comoving Hubble length. Different models of reheating and and thus different reheat temperatures and densities, ρ_{rh} in Eq. (23.54), lead to a range of possible values for N_* corresponding to a fixed physical scale, and hence we have a range of observational predictions for a given inflation model, as seen in Fig. 23.1.

The *Planck* 2018 temperature and polarization data (see Chap. 29, "Cosmic Microwave Background" review) are consistent with a smooth featureless power spectrum over a range of comoving wavenumbers, $0.008\ h^{-1}\ \mathrm{Mpc}^{-1} \le k \le 0.1\ h\ \mathrm{Mpc}^{-1}$. In the absence of running, the data measure the spectral index to be [38]

$$n_s = 0.9649 \pm 0.0042 \,, \tag{23.55}$$

corresponding to a deviation from scale-invariance exceeding the 7σ level. If running of the spectral tilt is included in the model, this is constrained to be [38]

$$\frac{dn_s}{d\ln k} = -0.0045 \pm 0.0067 \tag{23.56}$$

at the 95% CL, assuming no running of the running. The most recent analysis [43] of the BICEP, Keck Array and Planck data places an upper bound on the tensor-to-scalar ratio

$$r < 0.036 \,, \tag{23.57}$$

at the 95% CL.

These observational bounds can be converted into bounds on the slow-roll parameters and hence the potential during slow-roll inflation. Setting higher-order slow-roll parameters (beyond second-order in horizon-flow parameters [44]) to zero, the *Planck* collaboration obtain the following 95% CL bounds when lensing and BK15 data are included [38]

$$\epsilon < 0.0044 \,, \tag{23.58}$$

$$\eta = -0.015 \pm 0.006 \,, \tag{23.59}$$

$$\xi^2 = 0.0029^{+0.0073}_{-0.0069} \,, \tag{23.60}$$

which can be used to constrain models, as discussed in the next Section.

Fig. 23.1, which is taken from [38], compares observational CMB constraints on the tilt, n_s, in the spectrum of scalar perturbations and the ratio, r, between the magnitudes of tensor and scalar perturbations. Important rôles are played by data from the *Planck* satellite and on lensing, the BICEP2/Keck Array (BK15) and measurements of baryon acoustic oscillations (BAO). The reader is referred to [38] for technical details. These experimental constraints are compared with the predictions of some

Downloaded from https://academic.oup.com/ptep/article/2022/8/083C01/6651666 by KIT Library user on 27 September 2022

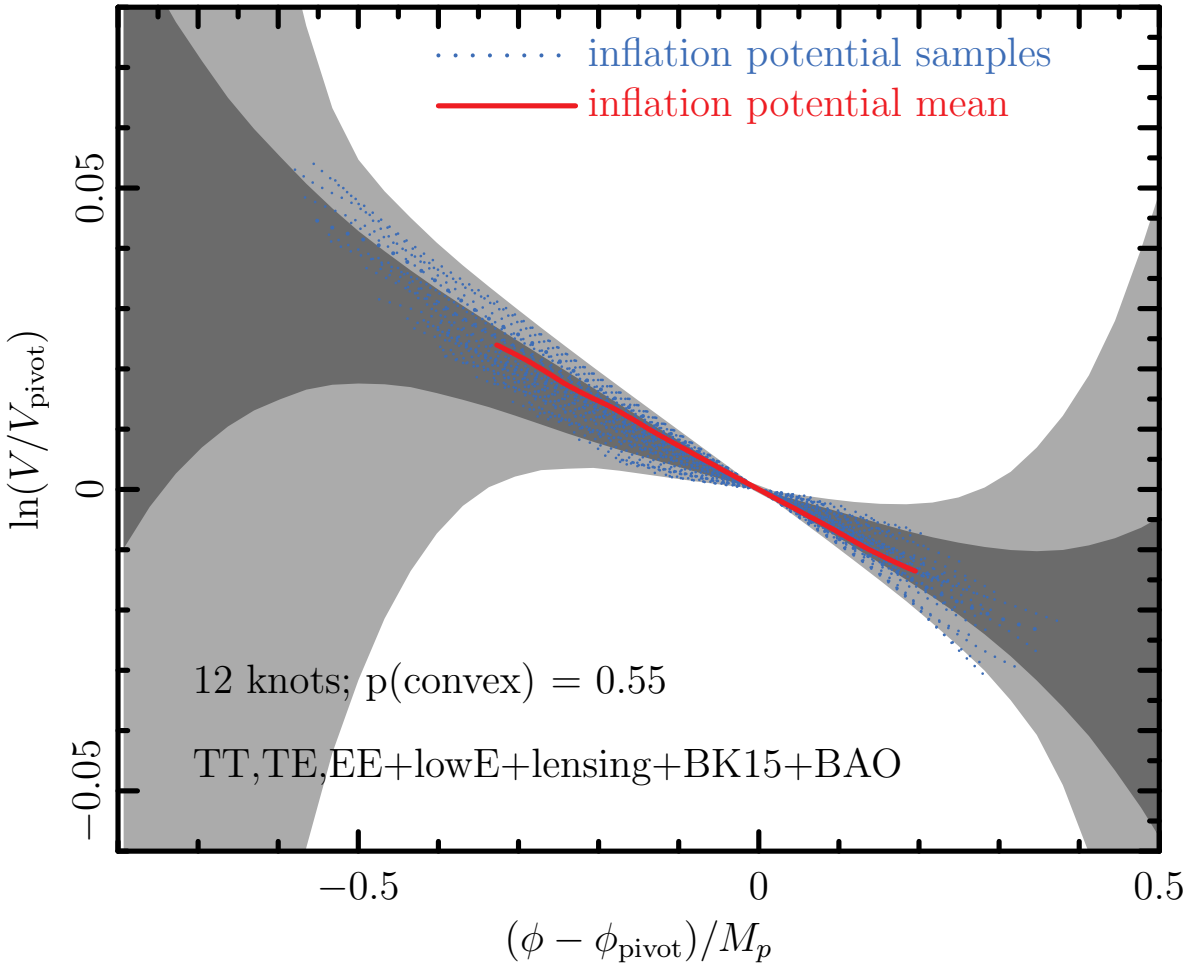

Figure 23.2: The result of reconstructing a single-field inflaton potential using a cubic-spline power-spectrum mode expansion and the the full *Planck*, lensing, BK15 and BAO data set. This figure is taken from [38].

of the inflationary models discussed in this review. Generally speaking, models with a concave potential are favored over those with a convex potential, and models with power-law inflation are now excluded, as opposed to models with de Sitter-like (quasi-)exponential expansion.

There is no significant evidence for local features within the range of inflaton field values probed by the data [38]. However, the data may be used to reconstruct partially the effective inflationary potential over a range of inflaton field values, assuming that it is suitably smooth. The result of one such exercise by the *Planck* collaboration [38] in the framework of a generic single-field inflaton potential is shown in Fig. 23.2. This reconstruction assumes a cubic-spline power-spectrum mode expansion and employs the full *Planck*, lensing, BK15 and BAO data set. The reader is again referred to [38] for technical details. We see that the effective inflaton potential is relatively well reconstructed over field values ϕ within ± 0.5 of the chosen pivot value, but the potential is only very weakly constrained for larger values of $|\phi - \phi_{pivot}|$, providing wide scope for inflationary model-builders.

23.4 Models

23.4.1 *Pioneering Models*

The paradigm of the inflationary Universe was proposed in [2], where it was pointed out that an early period of (near-)exponential expansion, in addition to resolving the horizon and flatness problems of conventional Big-Bang cosmology as discussed above (the possibility of a de Sitter phase in the early history of the Universe was also proposed in the non-minimal gravity model of [1], with the motivation of avoiding an initial singularity), would also dilute the prior abundance of any unseen heavy, (meta-)stable particles, as exemplified by monopoles in grand unified theories (GUTs; see Chap. 93, "Grand Unified Theories" review). The original proposal was that this inflationary expansion took place while the Universe was in a metastable state (a similar suggestion was made in [45, 46], where in [45] it was also pointed out that such a mechanism could address the horizon problem) and was terminated by a first-order transition due to tunnelling though a potential barrier. However, it was recognized already in [2] that this 'old inflation' scenario would need modification if the transition to the post-inflationary Universe were to be completed smoothly without generating unacceptable inhomogeneities.

This 'graceful exit' problem was addressed in the 'new inflation' model of [13] (see also [14] and footnote [39] of [2]), which studied models based on an SU(5) GUT with an effective potential of the Coleman-Weinberg type (i.e., dominated by radiative corrections), in which inflation could occur during the roll-down from the local maximum of the potential towards a global minimum. However, it was realized that the Universe would evolve to a different minimum from the Standard Model [47], and it was also recognized that density fluctuations would necessarily be too large [15], since they were related to the GUT coupling strength.

These early models of inflation assumed initial conditions enforced by thermal equilibrium in the early Universe. However, this assumption was questionable: indeed, it was not made in the model of [1], in which a higher-order gravitational curvature term was assumed to arise from quantum corrections, and the assumption of initial thermal equilibrium was jettisoned in the 'chaotic' inflationary model of [48]. These are the inspirations for much recent inflationary model building, so we now discuss them in more detail, before reviewing contemporary models.

Downloaded from https://academic.oup.com/ptep/article/2022/8/083C01/6651666 by KIT Library user on 27 September 2022

In this section we will work in natural units where we set the reduced Planck mass to unity, i.e., $8\pi/M_P^2 = 1$. All masses are thus relative to the reduced Planck scale.

23.4.2 R^2 *Inflation*

The first-order Einstein-Hilbert action, $(1/2)\int d^4x\sqrt{-g}R$, where R is the Ricci scalar curvature, is the minimal possible theory consistent with general coordinate invariance. However, it is possible that there might be non-minimal corrections to this action, and the unique second-order possibility is

$$S = \frac{1}{2}\int d^4x\sqrt{-g}\left(R + \frac{R^2}{6M^2}\right) . \tag{23.61}$$

It was pointed out in [1] that an R^2 term could be generated by quantum effects, and that (Eq. (23.61)) could lead to de Sitter-like expansion of the Universe. Scalar density perturbations in this model were calculated in [17]. Because the initial phase was (almost) de Sitter, these perturbations were (approximately) scale-invariant, with magnitude $\propto M$. It was pointed out in [17] that requiring the scalar density perturbations to lie in the range 10^{-3} to 10^{-5}, consistent with upper limits at that time, would require $M \sim 10^{-3}$ to 10^{-5} in Planck units, and it was further suggested in that these perturbations could lead to the observed large-scale structure of the Universe, including the formation of galaxies.

Although the action (Eq. (23.61)) does not contain an explicit scalar field, [17] reduced the calculation of density perturbations to that of fluctuations in the scalar curvature R, which could be identified (up to a factor) with a scalar field of mass M. The formal equivalence of R^2 gravity (Eq. (23.61)) to a theory of gravity with a massive scalar ϕ had been shown in [18], see also [19]. The effective scalar potential for what we would nowadays call the 'inflaton' [49] takes the form

$$S = \frac{1}{2}\int d^4x\sqrt{-g}\left[R + (\partial_\mu\phi)^2 - \frac{3}{2}M^2(1 - e^{-\sqrt{2/3}\phi})^2\right] \tag{23.62}$$

when the action is written in the Einstein frame, and the potential is shown as the solid black line in Fig. 23.3. Using (Eq. (23.48)), one finds that the amplitude of the scalar density perturbations in this model is given by

$$\Delta_{\mathcal{R}} = \frac{3M^2}{8\pi^2}\sinh^4\left(\frac{\phi}{\sqrt{6}}\right) , \tag{23.63}$$

The measured magnitude of the density fluctuations in the CMB requires $M \simeq 1.3 \times 10^{-5}$ in Planck units (assuming $N_* \simeq 55$), so one of the open questions in this model is why M is so small. Obtaining $N_* \simeq 55$ also requires an initial value of $\phi \simeq 5.5$, i.e., a super-Planckian initial condition, and another issue for this and many other models is how the form of the effective potential is protected and remains valid at such large field values. Using Eq. (23.51) one finds that $n_s \simeq 0.965$ for $N_* \simeq 55$ and using (Eq. (23.49)) one finds that $r \simeq 0.0035$. These predictions are consistent with the present data from *Planck* and other experiments, as seen in Fig. 23.1.

23.4.3 *Chaotic Models with Power-Law Potentials*

As has already been mentioned, a key innovation in inflationary model-building was the suggestion to abandon the questionable assumption of a thermal initial state, and consider 'chaotic' initial conditions with very general forms of potential [48]. (Indeed, the R^2 model discussed above can be regarded as a prototype of this approach.) The chaotic approach was first proposed in the context of a simple power-law potential of the form $\mu^{4-\alpha}\phi^\alpha$, and the specific example of $\lambda\phi^4$ was studied in [48]. Such models make the following predictions for the slow-roll parameters ϵ and η:

$$\epsilon \;=\; \frac{1}{2}\left(\frac{\alpha}{\phi}\right)^2 , \;\; \eta \;=\; \frac{\alpha(\alpha-1)}{\phi^2} , \tag{23.64}$$

leading to the predictions

$$r \;\approx\; \frac{4\alpha}{N_*} , \qquad n_s - 1 \;\approx\; -\frac{\alpha+2}{2N_*} , \tag{23.65}$$

which are shown in Fig. 23.1 for some illustrative values of α. We note that the prediction of the original ϕ^4 model lies out of the frame, with values of r that are too large and values of n_s that are too small. The ϕ^3 model has similar problems, and would in any case require modification in order to have a well-defined minimum. The simplest possibility is ϕ^2, but this is now also disfavored by the data, at the 95% CL if only the *Planck* data are considered, and more strongly if other data are included, as seen in Fig. 23.1. (For non-minimal models of quadratic inflation that avoid this problem, see, e.g., [51].)

Indeed, as can be seen in Fig. 23.1, all single-field models with a convex potential (i.e., one curving upwards) are disfavored compared to models with a concave potential.

23.4.4 *Hilltop Models*

This preference for a concave potential motivates interest in 'hilltop' models [52], whose starting-point is a potential of the form

$$V(\phi) \;=\; \Lambda^4\left[1 - \left(\frac{\phi}{\mu}\right)^p + \ldots\right] , \tag{23.66}$$

where the ... represent extra terms that yield a positive semi-definite potential. To first order in the slow-roll parameters, when $x \equiv \phi/\mu$ is small, one has

$$n_s \;\simeq\; 1 - p(p-1)\mu^{-2}\frac{x^{p-2}}{(1-x^p)} - \frac{3}{8}r , \qquad r \;\simeq\; 8p^2\mu^{-2}\frac{x^{2p-2}}{(1-x^p)^2} . \tag{23.67}$$

As seen in Fig. 23.1, a hilltop model with $p = 4$ can be compatible with the *Planck* and other measurements, if $\mu \gg M_P$.

23.4.5 *D-Brane Inflation*

Many scenarios for inflation involving extra dimensions have been proposed, e.g., the possibility that observable physics resides on a three-dimensional brane, and that there is an inflationary potential that depends on the distance between our brane and an antibrane, with a potential of the form [53]

$$V(\phi) \;=\; \Lambda^4\left[1 - \left(\frac{\mu}{\phi}\right)^p + \ldots\right] . \tag{23.68}$$

In this scenario the effective potential vanishes in the limit $\phi \to \infty$, corresponding to complete separation between our brane and the antibrane. The predictions for n_s and r in this model can be obtained from (Eq. 23.67) by exchanging $p \leftrightarrow -p$, and are also consistent with the *Planck* and other data.

23.4.6 *Natural Inflation*

Also seen in Fig. 23.1 are the predictions of 'natural inflation' [54], in which one postulates a non-perturbative shift symmetry that suppresses quantum corrections, so that a hierarchically small scale of inflation, $H \ll M_P$, is technically natural. In the simplest models, there is a periodic potential of the form

$$V(\phi) \;=\; \Lambda^4\left[1 + \cos\left(\frac{\phi}{f}\right)\right] , \tag{23.69}$$

where f is a dimensional parameter reminiscent of an axion decay constant (see the next subsection) [55], which must have a value $> M_P$. Natural inflation can yield predictions similar to quadratic inflation (which are no longer favored, as already discussed), but can also yield an effective convex potential. Thus, it may lead to values of r that are acceptably small, but for values of n_s that are in tension with the data, as seen in Fig. 23.1.

23.4.7 *Axion Monodromy Models*

The effective potentials in stringy models [56, 57] motivated by axion monodromy may be of the form

$$V(\phi) \;=\; \mu^{4-\alpha}\phi^\alpha + \Lambda^4 e^{-C\left(\frac{\phi}{\phi_0}\right)^{p_\Lambda}}\cos\left[\gamma + \frac{\phi}{f}\left(\frac{\phi}{\phi_0}\right)^{p_f+1}\right] , \tag{23.70}$$

where μ, Λ, f and ϕ_0 are parameters with the dimension of mass, and C, p, p_Λ, p_f and γ are dimensionless constants, generalizing the potential ([54]) in the simplest models of natural inflation. The oscillations in (Eq. 23.70) are associated with the axion field, and powers $p_\Lambda, p_f \neq 0$ may arise from ϕ-dependent evolutions of

Downloaded from https://academic.oup.com/ptep/article/2022/8/083C01/6651666 by KIT Library user on 27 September 2022

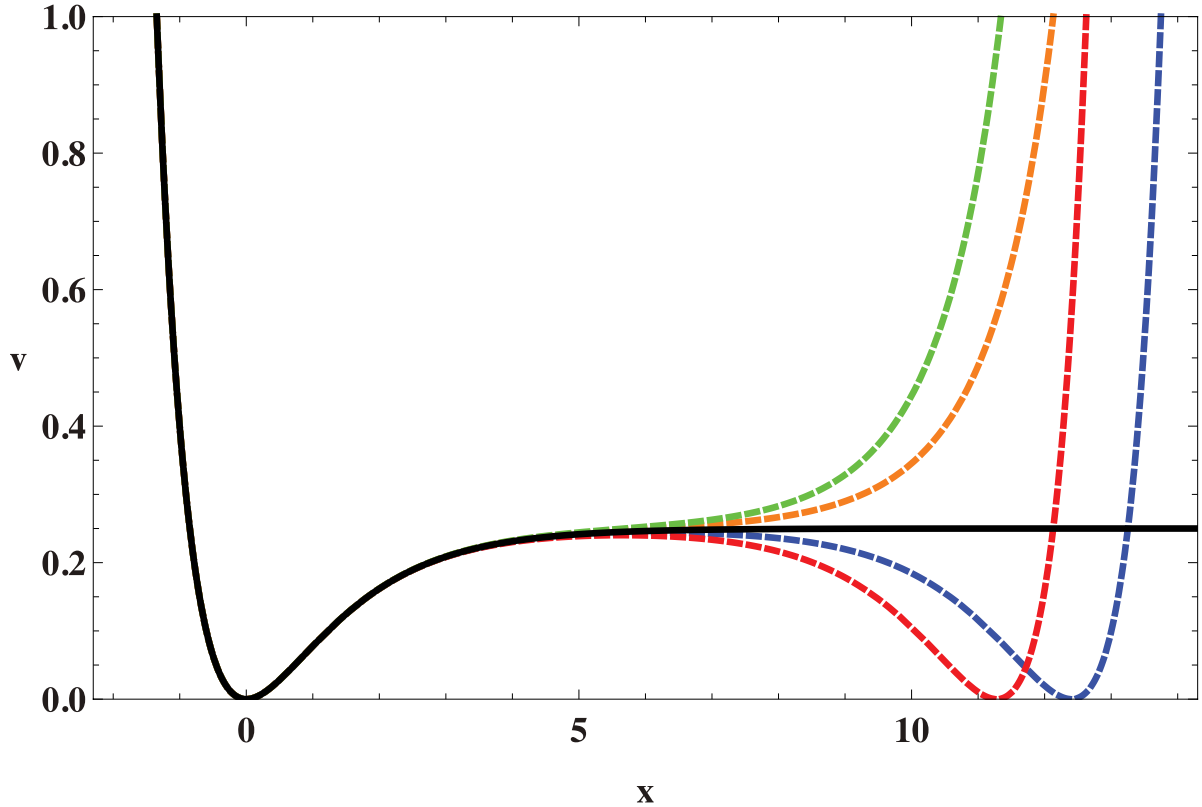

Figure 23.3: The inflationary potential V in the R^2 model (solid black line) compared with its form in various no-scale models discussed in detail in [50] (dashed coloured lines).

string moduli. Since the exponential prefactor in (Eq. 23.70) is due to non-perturbative effects that may be strongly suppressed, the oscillations may be unobservable small. Specific string models having ϕ^α with $\alpha = 4/3, 1$ or $2/3$ have been constructed in [56,57], providing some motivation for the low-power models mentioned above.

As seen in Fig. 23.1, the simple axion monodromy models with the power $\alpha = 4/3$ or 1 are no longer compatible with the current CMB data at the 95% CL, while $\alpha = 2/3$ is only marginally compatible at 95% CL. The *Planck* Collaboration has also searched for characteristic effects associated with the second term in (Eq. (23.70)), such as a possible drift in the modulation amplitude (setting $p_\Lambda = C = 0$), and a possible drifting frequency generated by $p_f \neq 0$, without finding any compelling evidence [38].

23.4.8 *Higgs Inflation*

Since the energy scale during inflation is commonly expected to lie between the Planck and TeV scales, it may serve as a useful bridge with contacts both to string theory or some other quantum theory of gravity, on the one side, and particle physics on the other side. However, as the above discussion shows, much of the activity in building models of inflation has been largely independent of specific connections with these subjects, though some examples of string-motivated models of inflation were mentioned above.

The most economical scenario for inflation might be to use as inflaton the only established scalar field, namely the Higgs field (see Chap.11, "Status of Higgs boson physics" review). A specific model assuming a non-minimal coupling of the Higgs field h to gravity was constructed in [58]. Its starting-point is the action

$$S = \int d^4x\sqrt{-g}\left[\frac{M^2+\xi h^2}{2}R + \frac{1}{2}\partial_\mu h\partial^\mu h - \frac{\lambda}{4}(h^2-v^2)^2\right], \tag{23.71}$$

where v is the Higgs vacuum expectation value. The model requires $\xi \gg 1$, in which case it can be rewritten in the Einstein frame as

$$S = \int d^4x\sqrt{-g}\left[\frac{1}{2}R + \frac{1}{2}\partial_\mu\chi\partial^\mu\chi - U(\chi)\right], \tag{23.72}$$

where the effective potential for the canonically-normalized inflaton field χ has the form

$$U(\chi) = \frac{\lambda}{4\xi^2}\left[1+\exp\left(-\frac{2\chi}{\sqrt{6}M_P}\right)\right]^{-2}, \tag{23.73}$$

which is similar to the effective potential of the R^2 model at large field values. As such, the model inflates successfully if $\xi \simeq 5\times 10^4\ m_h/(\sqrt{2}v)$, with predictions for n_s and r that are indistinguishable from the predictions of the R^2 model shown in Fig. 23.1.

This model is very appealing, but must confront several issues. One is to understand the value of ξ, and another is the possibility of unitarity violation. However, a more fundamental issue is whether the effective quartic Higgs coupling is positive at the scale of the Higgs field during inflation. Extrapolations of the effective potential in the Standard Model using the measured values of the masses of the Higgs boson and the top quark indicate that probably $\lambda < 0$ at this scale [59], though there are still significant uncertainties associated with the appropriate input value of the top mass and the extrapolation to high renormalization scales.

23.4.9 *Supersymmetric Models of Inflation*

Supersymmetry [60] is widely considered to be a well-motivated possible extension of the Standard Model that might become apparent at the TeV scale. It is therefore natural to consider supersymmetric models of inflation. These were originally proposed because of the problems of the new inflationary theory [13, 14] based on the one-loop (Coleman-Weinberg) potential for breaking SU(5). Several of these problems are related to the magnitude of the effective potential parameters: in any model of inflation based on an elementary scalar field, some parameter in the effective potential must be small in natural units, e.g., the quartic

Downloaded from https://academic.oup.com/ptep/article/2022/8/083C01/6651666 by KIT Library user on 27 September 2022

coupling λ in a chaotic model with a quartic potential, or the mass parameter μ in a model of chaotic quadratic inflation. These parameters are renormalized multiplicatively in a supersymmetric theory, so that the quantum corrections to small values would be under control. Hence, it was suggested that inflation cries out for supersymmetry [61], though non-supersymmetric resolutions of the problems of Coleman-Weinberg inflation are also possible: see, e.g., Ref. [62].

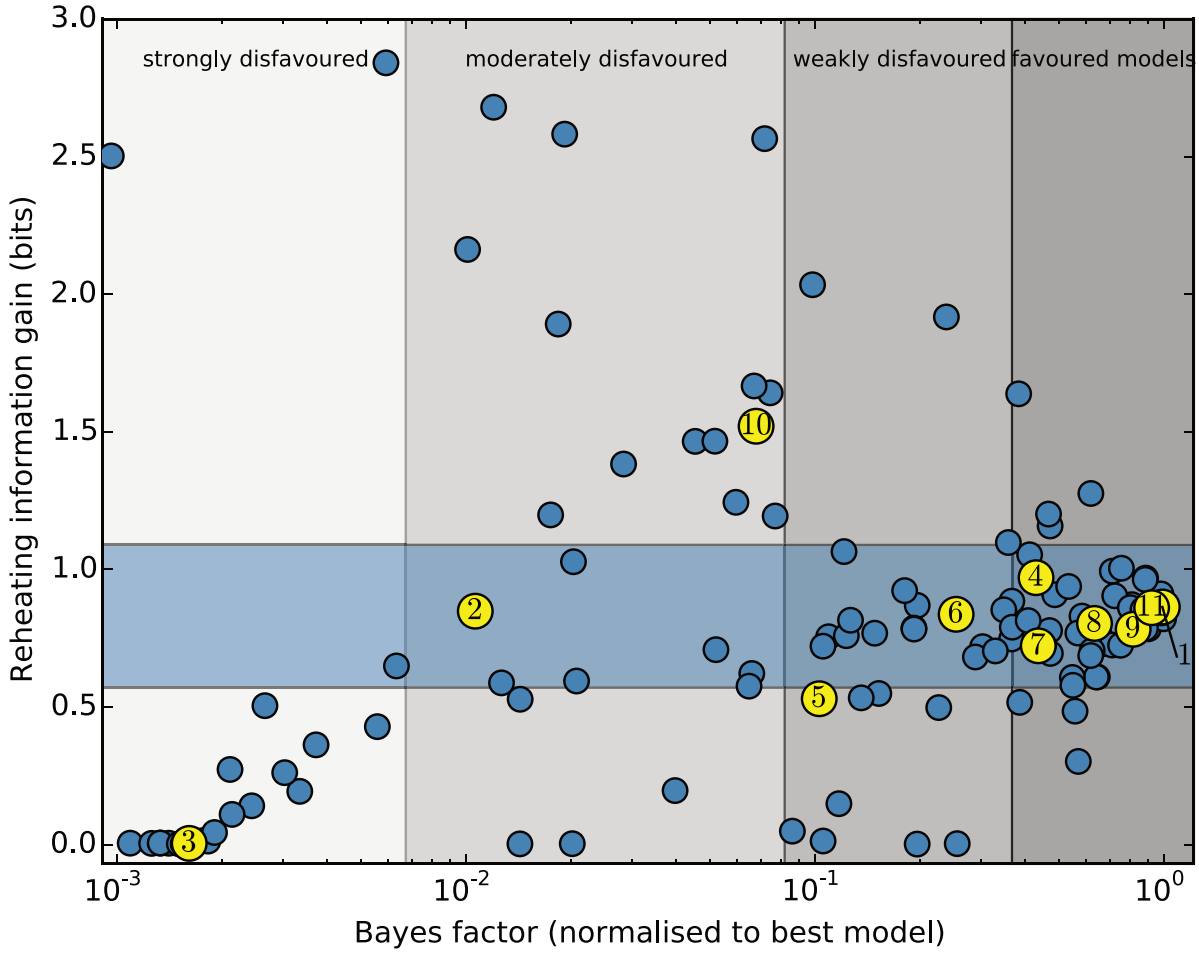

Figure 23.4: The Bayes factors calculated in [63] for a large sample of inflationary models using *Planck* 2015 data [64]. Those highlighted in yellow are featured in this review, according to the numbers listed in the text.

In the Standard Model there is only one scalar field that could be a candidate for the inflaton, namely the Higgs field discussed above, but even the minimal supersymmetric extension of the Standard Model (MSSM) contains many scalar fields. However, none of these is a promising candidate for the inflaton. The minimal extension of the MSSM that may contain a suitable candidate is the supersymmetric version of the minimal seesaw model of neutrino masses, which contains the three supersymmetric partners of the heavy singlet (right-handed) neutrinos. One of these singlet sneutrinos $\tilde{\nu}$ could be the inflaton [65]: it would have a quadratic potential, the mass coefficient required would be $\sim 10^{13}$ GeV, very much in the expected ball-park for singlet (right-handed) neutrino masses, and sneutrino inflaton decays also could give rise to the cosmological baryon asymmetry via leptogenesis. However, as seen in Fig. 23.1 and already discussed, a purely quadratic inflationary potential is no longer favored by the data. This difficulty could in principle be resolved in models with multiple sneutrinos [66], or by postulating a trilinear sneutrino coupling and hence a superpotential of Wess-Zumino type [67], which can yield successful inflation with predictions intermediate between those of natural inflation and hilltop inflation in Fig. 23.1.

Finally, we note that it is also possible to obtain inflation via supersymmetry breaking, as in the model [68] whose predictions are illustrated in Fig. 23.1.

23.4.10 *Supergravity Models*

Any model of early-Universe cosmology, and specifically inflation, must necessarily incorporate gravity. In the context of supersymmetry this requires an embedding in some supergravity theory [69, 70]. An $\mathcal{N} = 1$ supergravity theory is specified by three functions: a Hermitian function of the matter scalar fields ϕ^i, called the Kähler potential K, that describes its geometry, a holomorphic function of the superfields, called the superpotential W, which describes their interactions, and another holomorphic function $f_{\alpha\beta}$, which describes their couplings to gauge fields V_α [71].

The simplest possibility is that the Kähler metric is flat:

$$K = \phi^i \phi_i^* \,, \tag{23.74}$$

where the sum is over all scalar fields in the theory, and the simplest inflationary model in minimal supergravity had the superpotential [72]

$$W = m^2 (1 - \phi)^2 \,, \tag{23.75}$$

Where ϕ is the inflaton. However, this model predicts a tilted scalar perturbation spectrum, $n_s = 0.933$, which is now in serious disagreement with the data from *Planck* and other experiments shown in Fig. 23.1.

Moreover, there is a general problem that arises in any supergravity theory coupled to matter, namely that, since its ef-

Downloaded from https://academic.oup.com/ptep/article/2022/8/083C01/6651666 by KIT Library user on 27 September 2022

fective scalar potential contains a factor of e^K, scalars typically receive squared masses $\propto H^2 \sim V$, where H is the Hubble parameter [73], an issue called the 'η problem'. The theory given by (Eq. (23.75)) avoids this η problem, but a generic supergravity inflationary model encounters this problem of a large inflaton mass. Moreover, there are additional challenges for supergravity inflation associated with the spontaneous breaking of local supersymmetry [74–76].

Various approaches to the η problem in supergravity have been proposed, including the possibility of a shift symmetry [77], and one possibility that has attracted renewed attention recently is no-scale supergravity [78,79]. This is a form of supergravity with a Kähler potential that can be written in the form [80]

$$K \;=\; -3\ln\left(T + T^* - \frac{\sum_i |\phi^i|^2}{3}\right)\,, \tag{23.76}$$

which has the special property that it naturally has a flat potential, at the classical level and before specifying a non-trivial superpotential. As such, no-scale supergravity is well-suited for constructing models of inflation. Adding to its attraction is the feature that compactifications of string theory to supersymmetric four-dimensional models yield effective supergravity theories of the no-scale type [81]. There are many examples of superpotentials that yield effective inflationary potentials for either the T field (which is akin to a modulus field in some string compactification) or a ϕ field (generically representing matter) that are of the same form as the effective potential of the R^2 model (Eq. (23.62)) when the magnitude of the inflaton field $\gg 1$ in Planck units, as required to obtain sufficiently many e-folds of inflation, N_* [82, 83]. This framework also offers the possibility of using a suitable superpotential to construct models with effective potentials that are similar, but not identical, to the R^2 model, as shown by the dashed coloured lines in Fig. 23.3.

23.4.11 *Other Exponential Potential Models*

This framework also offers the possibility [82] of constructing models in which the asymptotic constant value of the potential at large inflaton field values is approached via a different exponentially-suppressed term:

$$V(\phi) \;=\; A\left[1 - \delta e^{-B\phi} + \mathcal{O}(e^{-2B\phi})\right]\,, \tag{23.77}$$

where the magnitude of the scalar density perturbations fixes A, but δ and B are regarded as free parameters. In the case of R^2 inflation $\delta = 2$ and $B = \sqrt{2/3}$. In a model such as (Eq. (23.77)), one finds at leading order in the small quantity $e^{-B\phi}$ that

$$\begin{aligned} n_s &= 1 - 2B^2\delta e^{-B\phi}\,,\\ r &= 8B^2\delta^2 e^{-2B\phi}\,,\\ N_* &= \frac{1}{B^2\delta}e^{+B\phi}\,. \end{aligned} \tag{23.78}$$

yielding the relations

$$n_s \;=\; 1 - \frac{2}{N_*}\,, r \;=\; \frac{8}{B^2 N_*^2}\,. \tag{23.79}$$

This model leads to the class of predictions labeled by 'α attractors' [84] in Fig. 23.1. There are generalizations of the simplest no-scale model (Eq. (23.76)) with prefactors before the $\ln(\ldots)$ that are 1 or 2, leading to larger values of $B = \sqrt{2}$ or 1, respectively, and hence smaller values of r than in the R^2 model.

23.5 Model Comparison

Given a particular inflationary model, one can obtain constraints on the model parameters, informed by the likelihood, corresponding to the probability of the data given a particular choice of parameters (see Sec. 40, "Statistics" review). In the light of the detailed constraints on the statistical distribution of primordial perturbations now inferred from high-precision observations of the cosmic microwave background, it is also possible to make quantitative comparison of the statistical evidence for or against different inflationary models. This can be done either by comparing the logarithm of the maximum likelihood that can be obtained for the data using each model, i.e., the minimum χ^2 (with some correction for the number of free parameters in each model), or by a Bayesian model comparison [85] (see also Sec. 40.3.3 in "Statistics" review).

In such a Bayesian model comparison one computes [7] the evidence, $\mathcal{E}(\mathcal{D}|\mathcal{M}_A)$ for a model, $\mathcal{M}_A$, given the data $\mathcal{D}$. This corresponds to the likelihood, $\mathcal{L}(\theta_{Aj}) = p(\mathcal{D}|\theta_{Aj}, \mathcal{M}_A)$, integrated over the assumed prior distribution, $\pi(\theta_{Aj}|\mathcal{M}_A)$, for all the model parameters θ_{Aj}:

$$\mathcal{E}(\mathcal{D}|\mathcal{M}_A) = \int \mathcal{L}(\theta_{Aj})\pi(\theta_{Aj}|\mathcal{M}_A)d\theta_{Aj}\,. \tag{23.80}$$

The posterior probability of the model given the data follows from Bayes' theorem

$$p(\mathcal{M}_A|\mathcal{D}) = \frac{\mathcal{E}(\mathcal{D}|\mathcal{M}_A)\pi(\mathcal{M}_A)}{p(\mathcal{D})}\,, \tag{23.81}$$

where the prior probability of the model is given by $\pi(\mathcal{M}_A)$. Assuming that all models are equally likely a priori, $\pi(\mathcal{M}_A) = \pi(\mathcal{M}_B)$, the relative probability of model A relative to a reference model, in the light of the data, is thus given by the Bayes factor

$$B_{A,ref} = \frac{\mathcal{E}(\mathcal{D}|\mathcal{M}_A)}{\mathcal{E}(\mathcal{D}|\mathcal{M}_{ref})}\,. \tag{23.82}$$

Computation of the multi-dimensional integral (Eq. (23.80)) is a challenging numerical task. Even using an efficient sampling algorithm requires hundreds of thousands of likelihood computations for each model, though slow-roll approximations can be used to calculate rapidly the primordial power spectrum using the APSIC numerical library [7] for a large number of single-field, slow-roll inflation models.

The change in χ^2 for selected slow-roll models relative to the Starobinsky R^2 inflationary model, used as a reference, is given in Table 23.1 (taken from [38]). All the other inflation models require a substantial amplitude of tensor modes, and so have an increased χ^2 with respect to the Starobinsky and other models with a scalar tilt but small tensor modes. Table 23.1 also shows the Bayesian evidence for ($\ln B_{A,ref} > 0$) or against ($\ln B_{A,ref} < 0$) a selection of inflation models using the *Planck* analysis priors [38]. The Starobinsky R^2 inflationary model may be chosen as a reference [38] that provides a good fit to current data. Higgs inflation [58] is indistinguishable using current data, making the model comparison "inconclusive" on the Jeffrey's scale ($|\ln B_{A,ref}| < 1$). (Recall, though, that this model is disfavored by the measured values of the Higgs and top quark masses [59].) We note that although α-attractor models can provide a good fit to the data, they are disfavored relative to the Starobinsky model due to their larger prior volume. There is now strong evidence ($|\ln B_{A,ref}| > 5$) against large-field models such as chaotic inflation with a quadratic or a quartic potential. Indeed, over 30% of the slow-roll inflation models considered in Ref. [7] are strongly disfavored by the *Planck* data.

Table 23.1: Observational evidence for and against selected inflation models: $\Delta\chi^2$ and the Bayes factors are calculated relative to the Starobinsky R^2 inflationary model, which is treated as a reference. Results from *Planck* 2018 analysis [38].

Model	$\Delta\chi^2$	$\ln B_{A,ref}$
R^2 inflation	0	0
Power-law potential $\phi^{2/3}$	+4.0	−4.6
Power-law potential ϕ^2	+21.6	< -10
Power-law potential ϕ^4	+75.3	< -10
Natural inflation	+9.9	−6.6
Hilltop quartic model	-0.3	−1.4

The Bayes factors for a wide selection of slow-roll inflationary models are displayed in Fig. 23.4, which is adapted from Fig. 3

Downloaded from https://academic.oup.com/ptep/article/2022/8/083C01/6651666 by KIT Library user on 27 September 2022

in [63], where more complete descriptions of the models and the calculations of the Bayes factors using *Planck* 2015 data [64] are given. Models discussed in this review are highlighted in yellow, and numbered as follows: (1) R^2 inflation (Sec. 23.4.2) and models with similar predictions, such as Higgs inflation (Sec. 23.4.8) and no-scale supergravity inflation (Sec. 23.4.10); chaotic inflation models (2) with a ϕ^2 potential; (3) with a ϕ^4 potential; (4) with a $\phi^{2/3}$ potential, and (5) with a ϕ^p potential marginalising over $p \in [0.2, 6]$ (Sec. 23.4.3); hilltop inflation models (6) with $p = 2$; (7) with $p = 4$ and (8) marginalising over p (Sec. 23.4.4); (9) brane inflation (Sec. 23.4.5); (10) natural inflation (Sec. 23.4.6); (11) exponential potential models such as α-attractors (Sec. 23.4.11). As seen in Fig. 23.4 and discussed in the next Section, constraints on reheating are starting to provide additional information about models of inflation.

23.6 Constraints on Reheating

One connection between inflation and particle physics is provided by inflaton decay, whose products are expected to have thermalized subsequently. As seen in (Eq. (23.54)), the number of e-folds required during inflation depends on details of this reheating process, including the matter density upon reheating, denoted by ρ_{th}, which depends in turn on the inflaton decay rate Γ_ϕ. We see in Fig. 23.1 that, within any specific inflationary model, both n_s and particularly r are sensitive to the value of N_*. In particular, the one-σ uncertainty in the experimental measurement of n_s is comparable to the variation in many model predictions for $N_* \in [50, 60]$. This implies that the data start to constrain scenarios for inflaton decay in many models. For example, it is clear from Fig. 23.1 that $N_* = 60$ would be preferred over $N_* = 50$ in a chaotic inflationary model with a quadratic potential.

As a specific example, let us consider R^2 models and related models such as Higgs and no-scale inflation models that predict small values of r [86]. As seen in Fig. 23.1, within these models the combination of *Planck*, BICEP2/Keck Array and BAO data would require a limited range of n_s, corresponding to a limited range of N_*, as seen by comparing the left and right vertical axes in Fig. 23.5:

$$N_* \gtrsim 52 \quad (68\%\ \mathrm{CL}), \quad N_* \gtrsim 44 \quad (95\%\ \mathrm{CL})\,. \tag{23.83}$$

Within any specific model for inflaton decay, these bounds can be translated into constraints on the effective decay coupling. For example, if one postulates a two-body inflaton decay coupling y, the bounds (Eq. (23.83)) can be translated into bounds on y. This is illustrated in Fig. 23.5, where any value of N_* (on the left vertical axis), projected onto the diagonal line representing the correlation predicted in R^2-like models, corresponds to a specific value of the inflaton decay rate Γ_ϕ/m (lower horizontal axis) and hence y (upper horizontal axis):

$$y \gtrsim 10^{-5} \quad (68\%\ \mathrm{CL}), \quad y \gtrsim 10^{-15} \quad (95\%\ \mathrm{CL})\,. \tag{23.84}$$

These bounds are not very constraining – although the 68% CL lower bound on y is already comparable with the electron Yukawa coupling – but can be expected to improve significantly in the coming years and thereby provide significant information on the connections between inflation and particle physics.

23.7 Beyond Single-Field Slow-Roll Inflation

There are numerous possible scenarios beyond the simplest single-field models of slow-roll inflation. These include theories in which non-canonical fields are considered, such as k-inflation [87] or DBI inflation [88], and multiple-field models, such as the curvaton scenario [89]. As well as altering the single-field predictions for the primordial curvature power spectrum (Eq. (23.48)) and the tensor-scalar ratio (Eq. (23.49)), they may introduce new quantities that vanish in single-field slow-roll models, such as isocurvature matter perturbations, corresponding to entropy fluctuations in the photon-to-matter ratio, at first order:

$$S_m = \frac{\delta n_m}{n_m} - \frac{\delta n_\gamma}{n_\gamma} = \frac{\delta \rho_m}{\rho_m} - \frac{3}{4}\frac{\delta \rho_\gamma}{\rho_\gamma}\,. \tag{23.85}$$

Another possibility is non-Gaussianity in the distribution of the primordial curvature perturbation (see Chap. 29, "Cosmic Microwave Background" review), encoded in higher-order correlators such as the primordial bispectrum [90]

$$\langle \zeta(\mathbf{k})\zeta(\mathbf{k}')\zeta(\mathbf{k}'')\rangle \;\equiv\; (2\pi)^3\delta(\mathbf{k}+\mathbf{k}'+\mathbf{k}'')B_\zeta(k,k',k'')\,, \tag{23.86}$$

which is often expressed in terms of a dimensionless non-linearity parameter

$$f_{NL} \propto B_\zeta(k,k',k'')/P_\zeta(k)P_\zeta(k').$$

The three-point function (Eq. (23.86)) can be thought of as defined on a triangle whose sides are $\mathbf{k}, \mathbf{k}', \mathbf{k}''$, of which only two are independent, since they sum to zero. Further assuming statistical isotropy ensures that the bispectrum depends only on the magnitudes of the three vectors, k, k' and k''. The search for f_{NL} and other non-Gaussian effects was a prime objective of the *Planck* data analysis [91, 92].

23.7.1 *Effective Field Theory of Inflation*

Since slow-roll inflation is a phase of accelerated expansion with an almost constant Hubble parameter, one may think of inflation in terms of an effective theory where the de Sitter spacetime symmetry is spontaneously broken down to RW symmetry by the time-evolution of the Hubble rate, $\dot{H} \neq 0$. There is then a Goldstone boson, π, associated with the spontaneous breaking of time-translation invariance, which can be used to study model-independent properties of inflation. The Goldstone boson describes a spacetime-dependent shift of the time coordinate, corresponding to an adiabatic perturbation of the matter fields:

$$\delta\phi_i(t,\vec{x}) = \phi_i(t + \pi(t,\vec{x})) - \phi_i(t)\,. \tag{23.87}$$

Thus adiabatic field fluctuations can be absorbed into the spatial metric perturbation, $\mathcal{R}$ in Eq. (23.28) at first order, in the comoving gauge:

$$\mathcal{R} = -H\pi\,, \tag{23.88}$$

where we define π on spatially-flat hypersurfaces. In terms of inflaton field fluctuations, we can identify $\pi \equiv \delta\phi/\dot{\phi}$, but in principle this analysis is not restricted to inflation driven by scalar fields.

The low-energy effective action for π can be obtained by writing down the most general Lorentz-invariant action and expanding in terms of π. The second-order effective action for the free-field wave modes, π_k, to leading order in slow roll is then

$$S_\pi^{(2)} = -\int d^4x\sqrt{-g}\frac{M_P^2\dot{H}}{c_s^2}\left[\dot{\pi}_k^2 - \frac{c_s^2}{R^2}(\nabla\pi)^2\right]\,, \tag{23.89}$$

where ϵ_H is the Hubble slow-roll parameter (Eq. (23.11)). We identify c_s^2 with an effective sound speed, generalising canonical slow-roll inflation, which is recovered in the limit $c_s^2 \to 1$.

The scalar power spectrum on super-Hubble scales (Eq. (23.48)) is enhanced for a reduced sound speed, leading to a reduced tensor-scalar ratio (Eq. (23.49))

$$\mathcal{P}_\zeta(k) \simeq \frac{4\pi}{M_P^2}\frac{1}{c_s^2\epsilon}\left(\frac{H}{2\pi}\right)_*^2\,, \qquad r \simeq 16(c_s^2\epsilon)_*\,. \tag{23.90}$$

At third perturbative order and to lowest order in derivatives, one obtains [94]

$$S_\pi^{(3)} = \int d^4x\sqrt{-g}\frac{M_P^2(1-c_s^2)\dot{H}}{c_s^2}\left[\frac{\dot{\pi}(\nabla\pi)^2}{R^2} - \left(1+\frac{2}{3}\frac{\tilde{c}_3}{c_s^2}\right)\dot{\pi}^3\right]\,. \tag{23.91}$$

Note that this expression vanishes for canonical fields with $c_s^2 = 1$. For $c_s^2 \neq 1$ the cubic action is determined by the sound speed and an additional parameter $\tilde{c}_3$. Both terms in the cubic action give rise to primordial bispectra that are well approximated by equilateral bispectra. However, the shapes are not identical, so one can find a linear combination for which the equilateral bispectra of each term cancel, giving rise to a distinctive orthogonal-type bispectrum [94].

Analysis based on *Planck* 2018 temperature and polarization data has placed bounds on several bispectrum shapes including

Downloaded from https://academic.oup.com/ptep/article/2022/8/083C01/6651666 by KIT Library user on 27 September 2022

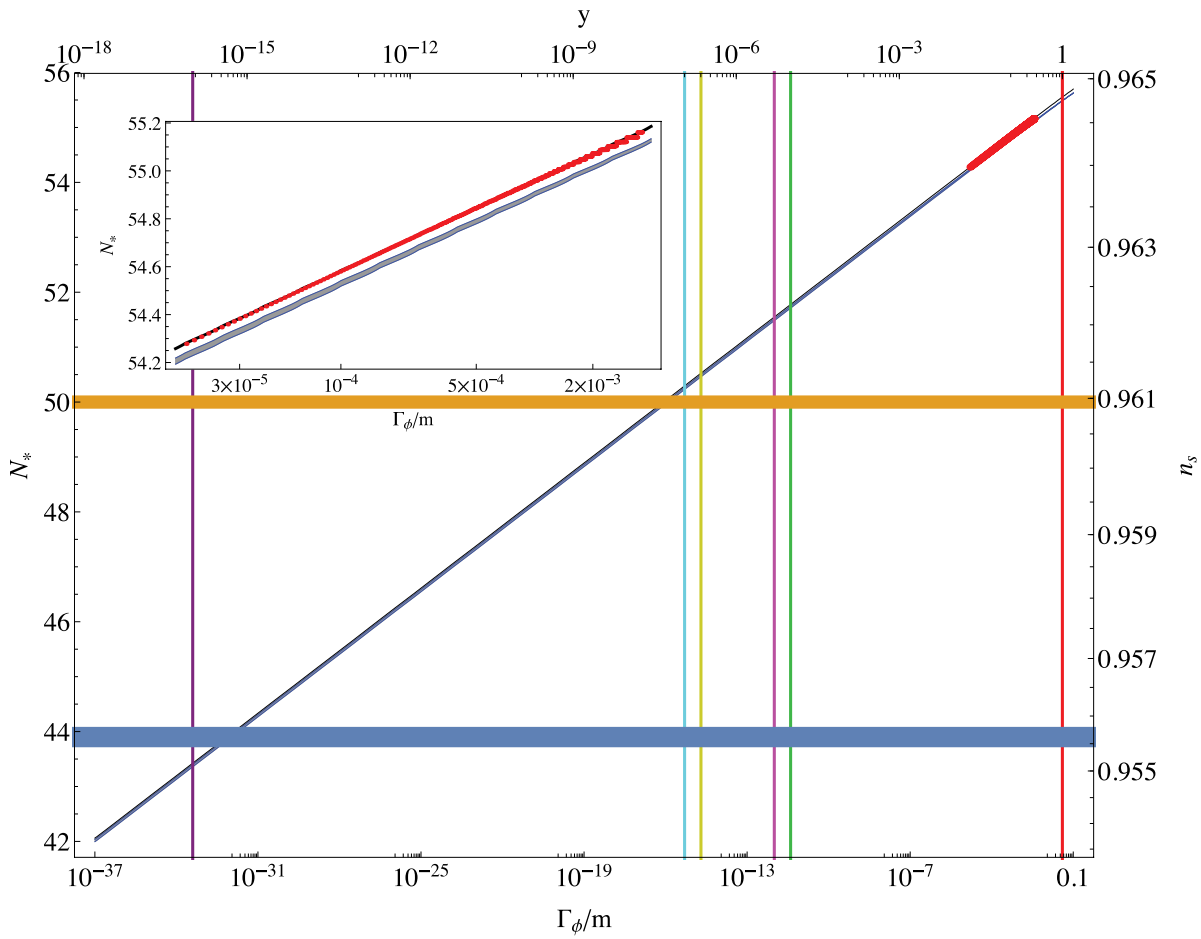

Figure 23.5: The values of N_* (left axis) and n_s (right axis) in R^2 inflation and related models for a wide range of decay rates, Γ_ϕ/m, (bottom axis) and corresponding two-body couplings, y (top axis). The diagonal red line segment shows full numerical results over a restricted range of Γ_ϕ/m (which are shown in more detail in the insert), while the diagonal blue strip represents an analytical approximation described in [86]. The difference between these results is indistinguishable in the main plot, but is visible in the insert. The horizontal yellow and blue lines show the 68 and 95% CL lower limits from the *Planck* 2015 data [64], and the vertical coloured lines correspond to specific models of inflaton decay. Figure taken from [93].

equilateral and orthogonal shapes [92]:

$$f_{NL}^{equil} = -26 \pm 47\,, \qquad f_{NL}^{orthog} = -38 \pm 24 \quad (68\%\ \text{CL})\,. \tag{23.92}$$

For the simplest case of a constant sound speed, and marginalising over $\tilde{c}_3$, this provides a bound on the inflaton sound speed [92]

$$c_s \geq 0.021 \quad (95\%\ \text{CL})\,. \tag{23.93}$$

For a specific model such as DBI inflation [88], corresponding to $\tilde{c}_3 = 3(1-c_s^2)/2$, one obtains a tighter bound [92]:

$$c_s^{DBI} \geq 0.086 \quad (95\%\ \text{CL})\,. \tag{23.94}$$

The *Planck* team have analysed a wide range of non-Gaussian templates from different inflation models, including tests for deviations from an initial Bunch-Davies vacuum state, direction-dependent non-Gaussianity, and feature models with oscillatory bispectra [92]. No individual feature or resonance is above the three-σ significance level after accounting for the look-elsewhere effect. These results are consistent with the simplest canonical, slow-roll inflation models, but do not rule out most alternative models; rather, bounds on primordial non-Gaussianity place important constraints on the parameter space for non-canonical models.

23.7.2 *Multi-Field Fluctuations*

There is a very large literature on two- and multi-field models of inflation, most of which lies beyond the scope of this review [95, 96]. However, two important general topics merit being mentioned here, namely residual isocurvature perturbations and the possibility of non-Gaussian effects in the primordial perturbations.

One might expect that other scalar fields besides the inflaton might have non-negligible values that evolve and fluctuate in parallel with the inflaton, without necessarily making the dominant contribution to the energy density during the inflationary epoch. However, the energy density in such a field might persist beyond the end of inflation before decaying, at which point it might come to dominate (or at least make a non-negligible contribution to) the total energy density. In such a case, its perturbations could end up generating the density perturbations detected in the CMB. This could occur due to a late-decaying scalar field [89] or a field fluctuation that modulates the end of inflation [97] or the inflaton decay [98].

23.7.2.1 *Isocurvature Perturbations*

Primordial perturbations arising in single-field slow-roll inflation are necessarily adiabatic, i.e., they affect the overall density without changing the ratios of different contributions, such as the photon-matter ratio, $\delta(n_\gamma/n_m)/(n_\gamma/n_m)$. This is because inflaton perturbations represent a local shift of the time, as described in section Sec. 23.7.1:

$$\pi = \frac{\delta n_\gamma}{\dot{n}_\gamma} = \frac{\delta n_m}{\dot{n}_m}\,. \tag{23.95}$$

However, any light scalar field (i.e., one with effective mass less than the Hubble scale) acquires a spectrum of nearly scale-

Downloaded from https://academic.oup.com/ptep/article/2022/8/083C01/6651666 by KIT Library user on 27 September 2022

invariant perturbations during inflation. Fluctuations orthogonal to the inflaton in field space are decoupled from the inflaton at Hubble-exit, but can affect the subsequent evolution of the density perturbation. In particular, they can give rise to local variations in the equation of state (non-adabatic pressure perturbations) that can alter the primordial curvature perturbation ζ on super-Hubble scales. Since these fluctuations are statistically independent of the inflaton perturbations at leading order in slow-roll [96], non-adiabatic field fluctuations can only increase the scalar power spectrum with respect to adiabatic perturbations at Hubble exit, while leaving the tensor modes unaffected at first perturbative order. Thus, the single-field result for the tensor-scalar ratio (Eq. (23.49)) becomes an inequality [99]

$$r \leq 16\epsilon_* \,. \tag{23.96}$$

Hence, an observational upper bound on the tensor-scalar ratio does not bound the slow-roll parameter ϵ in multi-field models.

If all the scalar fields present during inflation eventually decay completely into fully thermalized radiation, these field fluctuations are converted fully into adiabatic perturbations in the primordial plasma [100]. On the other hand, non-adiabatic field fluctuations can also leave behind primordial isocurvature perturbations (Eq. (23.85)) after inflation. In multi-field inflation models it is thus possible for non-adiabatic field fluctuations to generate both curvature and isocurvature perturbations leading to correlated primordial perturbations [101].

The amplitudes of any primordial isocurvature perturbations (Eq. (23.85)) are strongly constrained by the current CMB data, especially on large angular scales. Using temperature and low-ℓ polarization data yields the following bound on the amplitude of cold dark matter isocurvature perturbations at scale $k = 0.002h^{-1}\mathrm{Mpc}^{-1}$ (marginalising over the correlation angle and in the absence of primordial tensor perturbations) [38]:

$$\frac{\mathcal{P}_{S_m}}{\mathcal{P}_\zeta + \mathcal{P}_{S_m}} < 0.025 \text{ (95\% CL)} \,. \tag{23.97}$$

For fully (anti-)correlated isocurvature perturbations, corresponding to a single isocurvature field providing a source for both the curvature and residual isocurvature perturbations, the bounds become significantly tighter [38]:

$$\frac{\mathcal{P}_{S_m}}{\mathcal{P}_\zeta + \mathcal{P}_{S_m}} < 0.0002 \text{ (95\% CL), correlated} \,, \tag{23.98}$$

$$\frac{\mathcal{P}_{S_m}}{\mathcal{P}_\zeta + \mathcal{P}_{S_m}} < 0.003 \text{ (95\% CL), anti-correlated} \tag{23.99}$$

23.7.2.2 *Local-Type Non-Gaussianity*

Since non-adiabatic field fluctuations in multi-field inflation may lead the to evolution of the primordial curvature perturbation at all orders, it becomes possible to generate significant non-Gaussianity in the primordial curvature perturbation. Non-linear evolution on super-Hubble scales leads to local-type non-Gaussianity, where the local integrated expansion is a non-linear function of the local field values during inflation, $N(\phi_i)$. While the field fluctuations at Hubble exit, $\delta\phi_{i*}$, are Gaussian in the slow-roll limit, the curvature perturbation, $\zeta = \delta N$, becomes a non-Gaussian distribution [102]:

$$\zeta = \sum_i \frac{\partial N}{\partial \phi_i}\delta\phi_i + \frac{1}{2}\sum_{i,j}\frac{\partial^2 N}{\partial\phi_i\partial\phi_j}\delta\phi_i\delta\phi_j + \ldots \tag{23.100}$$

with non-vanishing bispectrum in the squeezed limit ($k_1 \approx k_2 \gg k_3$):

$$B_\zeta(k_1,k_2,k_3) \approx \frac{12}{5} f_{NL}^{local} \frac{\mathcal{P}_\zeta(k_1)}{4\pi k_1^3}\frac{\mathcal{P}_\zeta(k_3)}{4\pi k_3^3} \,, \tag{23.101}$$

where

$$\frac{6}{5} f_{NL}^{local} = \frac{\sum_{i,j}\frac{\partial^2 N}{\partial\phi_i\partial\phi_j}}{\left(\sum_i \frac{\partial N}{\partial\phi_i}\right)^2} \,. \tag{23.102}$$

Both equilateral and orthogonal bispectra, discussed above in the context of generalised single field inflation, vanish in the squeezed limit, enabling the three types of non-Gaussianity to be distinguished by observations, in principle.

Non-Gaussianity during multi-field inflation is highly model dependent, though f_{NL}^{local} can often be smaller than unity in multi-field slow-roll inflation [103]. Scenarios where a second light field plays a role during or after inflation can make distinctive predictions for f_{NL}^{local}, such as $f_{NL}^{local} = -5/4$ in some curvaton scenarios [102, 104] or $f_{NL}^{local} = 5$ in simple modulated reheating scenarios [98, 105]. By contrast the constancy of ζ on super-Hubble scales in single-field slow-roll inflation leads to a very small non-Gaussianity [106, 107], and in the squeezed limit we have the simple result $f_{NL}^{local} = 5(1-n_S)/12$ [108, 109].

A combined analysis of the *Planck* 2018 temperature and polarization data [92] yields the following range for f_{NL}^{local} defined in (Eq. (23.102)):

$$f_{NL}^{local} \;=\; -1 \pm 5 \quad (68\% \text{ CL}) \,. \tag{23.103}$$

This sensitivity is sufficient to rule out parameter regimes giving rise to relatively large non-Gaussianity, but insufficient to probe $f_{NL}^{local} = \mathcal{O}(\epsilon)$, as expected in single-field models, or the range $f_{NL}^{local} = \mathcal{O}(1)$ found in the simplest two-field models.

Local-type primordial non-Gaussianity can also give rise to a striking scale-dependent bias in the distribution of collapsed dark matter halos and thus the galaxy distribution [110, 111]. Bounds from high-redshift galaxy surveys are not currently competitive with the best CMB constraints. The most recent analysis [112] based on the clustering of quasars in the final data release (DR16) of the extended Baryon acoustic Oscillation Spectroscopic Survey (eBOSS) yields

$$f_{NL}^{local} \;=\; -12 \pm 21 \quad (68\% \text{ CL}) \,. \tag{23.104}$$

23.8 Initial Conditions and Fine-tuning

This review is based on the assumption that the inflationary paradigm is valid. However, it remains the object of many criticisms (see, e.g., [113]), many of them related to the perceived unnaturalness of the required initial conditions.

Most work on inflation is done in the context of RW cosmology, which assumes a high degree of symmetry, or small inhomogeneous perturbations (usually first order) about an RW cosmology. The isotropic RW space-time is an attractor for many homogeneous but anisotropic cosmologies in the presence of a false vacuum energy density [114], or a scalar field with suitable self-interaction potential energy [115, 116]. However it is much harder to establish the range of highly inhomogeneous initial conditions that yield a successful RW Universe, with only limited studies initially (see, e.g., [117, 118]). A related open question is the general nature of the pre-inflationary state of the inflaton and other fields that could have provided initial conditions suitable for inflation [113]. They would need to have satisfied non-trivial homogeneity and isotropy conditions, and one may ask how these could have arisen, whether these are plausible, and whether there may be some observable signature of the pre-inflationary state. These and other criticisms of inflation were addressed in [119], which presented studies of the sensitivity of inflation to the initial conditions. Complementing the studies reported in [119], there have been numerical relativity investigations of highly inhomogeneous initial conditions [120–122]. The general conclusion is that inflation is rather robust with respect to inhomogeneities in the initial conditions in both the scalar field profile and the extrinsic curvature, including large tensor perturbations.

To quantify the fine-tuning of initial conditions requires a measure in the space of possible cosmologies [123], however it has been argued that some of the measures historically used to frame this problem are formally invalid [124]. It is sometimes also objected that inflationary models predict the existence of a multiverse, and potentially a loss of predictive power [125], if it undergoes the process termed eternal inflation [126–128]. However, whether this is actually a bug or a feature remains a topic of debate [129, 130]. The existence of the multiverse is a purely philosophical problem, unless it has observable consequences, e.g., in the CMB.

Downloaded from https://academic.oup.com/ptep/article/2022/8/083C01/6651666 by KIT Library user on 27 September 2022

One might expect signatures of any pre-inflationary state to appear at large angular scales, i.e., low multipoles ℓ. Indeed, various anomalies have been noted in the large-scale CMB anisotropies, as also discussed in Chap. 29, the "Cosmic Microwave Background" review, including a possible suppression of the quadrupole and other very large-scale anisotropies, an apparent feature in the range $\ell \approx 20$ to 30, and a possible hemispheric asymmetry. However, none of these are highly significant statistically, in view of the limitations due to cosmic variance [64]. They cannot yet be regarded as signatures of initial conditions, the multiverse or some pre-inflationary dynamics, such as might emerge from string theory.

A different kind of initial condition problem, called the trans-Planckian problem [131], is that the perturbations now seen in the CMB would have had wavelengths shorter than the Planck length at the onset of inflation. However, under quite general and conservative assumptions the usual inflationary predictions would be quite robust [132], with the possibility of $\mathcal{O}((H/m_P)^n)$ corrections that might have interesting signatures in the CMB [133].

When inflation was first proposed [1] [2] there was no evidence for the existence of scalar fields or the accelerated expansion of the Universe. The situation has changed dramatically in recent years with the observational evidence that the cosmic expansion is currently accelerating and with the discovery of a scalar particle, namely the Higgs boson (see Chap. 11, "Status of Higgs boson physics" review). Combined with the lack of any widely accepted alternative model for the origin of cosmic structure, these discoveries have lent support to the idea of a primordial accelerated expansion driven by a scalar field, i.e., cosmological inflation. In parallel, successive CMB experiments have been consistent with generic predictions of inflationary models, although without yet providing irrefutable evidence. It was concluded in [119] that the inflationary paradigm is not currently in trouble. However, we note that inflation via a formally elementary scalar inflaton should probably only be regarded as an effective field theory valid at energy densities hierarchically smaller than the Planck scale. It should eventually be embedded in a suitable ultraviolet completion, on which inflationary dynamics may be our clearest window.

23.9 Future Probes of Inflation

Prospective future CMB experiments, both ground- and space-based are reviewed in the separate PDG "Cosmic Microwave Background" review, Chap. 29. The main emphasis in CMB experiments in the coming years will be on ground-based experiments providing improved measurements of B-mode polarization and greater sensitivity to the tensor-to-scalar ratio r, and more precise measurements at higher ℓ that will constrain n_s better. As is apparent from Fig. 23.1 and the discussion of models such as R^2 inflation, there is a strong incentive to reach a 5-σ sensitivity to $r \sim 3$ to 4×10^{-3}. This could be achieved with a moderately-sized space mission with large sky coverage [134], improvements in delensing and foreground measurements. The discussion in Sec. 23.3 (see also Fig. 23.5), also brought out the importance of reducing the uncertainty in n_s, as a way to constrain post-inflationary reheating and the connection to particle physics. CMB temperature anisotropies probe primordial density perturbations down to comoving scales of order 50 Mpc, beyond which scale secondary sources of anisotropy dominate. CMB spectral distortions could potentially constrain the amplitude and shape of primordial density perturbations on comoving scales from Mpc to kpc due to distortions caused by the Silk damping of pressure waves in the radiation dominated era, before the last scattering of the CMB photons but after the plasma can be fully thermalised [135].

Improved sensitivity to non-Gaussianities is also a priority. In addition to CMB measurements, future large-scale structure surveys will also have roles to play as probes into models of inflation, for which there are excellent prospects. High-redshift galaxy surveys are sensitive to local-type non-Gaussianity due to the scale-dependent bias induced on large scales. Upcoming surveys such as DESI may reach $\Delta f_{NL} \sim 4$ [136] comparable with the *Planck* sensitivity. In the future, radio surveys such as SKA will measure large-scale structure out to redshift $z \sim 3$ [137], initially through mapping the intensity of the neutral hydrogen 21-cm line, and eventually through radio galaxy surveys which will probe local-type non-Gaussianity to $f_{NL} \sim 1$.

Galaxy clustering using DESI and *Euclid* satellite data could also constrain the running of the scalar tilt to a precision of $\Delta\alpha_s \approx 0.0028$, a factor of 2 improvement on *Planck* constraints, or a precision of 0.0016 using LSST data [136].

As an example of a proposed future satellite mission, *SPHEREx* [138] will use measurements of the galaxy power spectrum to target a measurement of the running of the scalar spectral index with a sensitivity $\Delta\alpha_s \sim 10^{-3}$ and local-type primordial non-Gaussianity, $\Delta f_{NL} \sim 1$. Including information from the galaxy bispectrum one might reduce the measurement error on non-Gaussianity to $\Delta f_{NL} \sim 0.2$, making it possible to distinguish between single-field slow-roll models and alternatives such as the curvaton scenario for the origin of structure, which generate $f_{NL} \sim 1$.

Acknowledgements

The authors are grateful to Vincent Vennin for his careful reading of this manuscript and preparing Fig. 23.4 for this review. The work of J.E. was supported in part by the UK STFC via the research grant ST/L000258/1 and in part by the Estonian Research Council via a Mobilitas Pluss grant. The work of D.W. was supported in part by the UK STFC research grant ST/S000550/1.

References

[1] A. A. Starobinsky, Phys. Lett. **B91**, 99 (1980), [Adv. Ser. Astrophys. Cosmol.3,130(1987)].

[2] A. H. Guth, Phys. Rev. **D23**, 347 (1981), [Adv. Ser. Astrophys. Cosmol.3,139(1987)].

[3] K. A. Olive, Phys. Rept. **190**, 307 (1990).

[4] D. H. Lyth and A. Riotto, Phys. Rept. **314**, 1 (1999), [hep-ph/9807278].

[5] A.R. Liddle and D.H. Lyth, *Cosmological inflation and large-scale structure* (Cambridge University Press, 2000).

[6] D. Baumann, in "Physics of the large and the small, TASI 09, proceedings of the Theoretical Advanced Study Institute in Elementary Particle Physics, Boulder, Colorado, USA, 1-26 June 2009," 523–686 (2011), [arXiv:0907.5424].

[7] J. Martin, C. Ringeval and V. Vennin, Phys. Dark Univ. **5-6**, 75 (2014), [arXiv:1303.3787]; J. Martin *et al.*, JCAP **1403**, 039 (2014), [arXiv:1312.3529]; J. Martin, Astrophys. Space Sci. Proc. **45**, 41 (2016), [arXiv:1502.05733].

[8] P. A. R. Ade *et al.* (Planck), Astron. Astrophys. **594**, A13 (2016), [arXiv:1502.01589].

[9] A. H. Guth and E. J. Weinberg, Nucl. Phys. **B212**, 321 (1983).

[10] D. La and P. J. Steinhardt, Phys. Rev. Lett. **62**, 376 (1989), [Erratum: Phys. Rev. Lett.62,1066(1989)].

[11] A. D. Linde, Phys. Lett. **B249**, 18 (1990).

[12] F. C. Adams and K. Freese, Phys. Rev. **D43**, 353 (1991), [hep-ph/0504135].

[13] A. D. Linde, Phys. Lett. **108B**, 389 (1982), [Adv. Ser. Astrophys. Cosmol.3,149(1987)].

[14] A. Albrecht and P. J. Steinhardt, Phys. Rev. Lett. **48**, 1220 (1982), [Adv. Ser. Astrophys. Cosmol.3,158(1987)].

[15] W. H. Press, Phys. Scripta **21**, 702 (1980); S. W. Hawking, Phys. Lett. **115B**, 295 (1982); A. A. Starobinsky, Phys. Lett. **117B**, 175 (1982); A. H. Guth and S. Y. Pi, Phys. Rev. Lett. **49**, 1110 (1982).

[16] J. M. Bardeen, P. J. Steinhardt and M. S. Turner, Phys. Rev. **D28**, 679 (1983).

[17] V. F. Mukhanov and G. V. Chibisov, JETP Lett. **33**, 532 (1981), [Pisma Zh. Eksp. Teor. Fiz.33,549(1981)].

[18] K. S. Stelle, Gen. Rel. Grav. **9**, 353 (1978).

[19] B. Whitt, Phys. Lett. **145B**, 176 (1984).

[20] D. Wands, Class. Quant. Grav. **11**, 269 (1994), [arXiv:gr-qc/9307034].

[21] S. R. Coleman and F. De Luccia, Phys. Rev. **D21**, 3305 (1980).

Downloaded from https://academic.oup.com/ptep/article/2022/8/083C01/6651666 by KIT Library user on 27 September 2022

[22] M. Sasaki *et al.*, Phys. Lett. **B317**, 510 (1993).

[23] M. Bucher, A. S. Goldhaber and N. Turok, Phys. Rev. **D52**, 3314 (1995), [hep-ph/9411206].

[24] A. D. Linde and A. Mezhlumian, Phys. Rev. **D52**, 6789 (1995), [arXiv:astro-ph/9506017].

[25] A. R. Liddle, P. Parsons and J. D. Barrow, Phys. Rev. **D50**, 7222 (1994), [arXiv:astro-ph/9408015].

[26] L. Kofman, A. D. Linde and A. A. Starobinsky, Phys. Rev. **D56**, 3258 (1997), [hep-ph/9704452].

[27] B. A. Bassett, S. Tsujikawa and D. Wands, Rev. Mod. Phys. **78**, 537 (2006), [arXiv:astro-ph/0507632].

[28] A. D. Linde, Phys. Rev. **D49**, 748 (1994), [arXiv:astro-ph/9307002].

[29] A. D. Dolgov and A. D. Linde, Phys. Lett. **116B**, 329 (1982).

[30] J. R. Ellis *et al.*, Nucl. Phys. **B238**, 453 (1984), [,223(1983)].

[31] M. Kawasaki and T. Moroi, Prog. Theor. Phys. **93**, 879 (1995), [hep-ph/9403364].

[32] J. H. Traschen and R. H. Brandenberger, Phys. Rev. **D42**, 2491 (1990).

[33] G. V. Chibisov and V. F. Mukhanov, Mon. Not. Roy. Astron. Soc. **200**, 535 (1982).

[34] H. Kodama and M. Sasaki, Prog. Theor. Phys. Suppl. **78**, 1 (1984).

[35] V.F. Mukhanov, H.A. Feldman and R.H. Brandenberger, Phys. Rept. **215**, 203 (1992).

[36] K. A. Malik and D. Wands, Phys. Rept. **475**, 1 (2009), [arXiv:0809.4944].

[37] V. F. Mukhanov, Sov. Phys. JETP **67**, 1297 (1988), [Zh. Eksp. Teor. Fiz.94N7,1(1988)].

[38] Y. Akrami *et al.* (Planck), Astron. Astrophys. **641**, A10 (2020), [arXiv:1807.06211].

[39] A. A. Starobinsky, JETP Lett. **30**, 682 (1979), [,767(1979)].

[40] E. D. Stewart and D. H. Lyth, Phys. Lett. **B302**, 171 (1993), [arXiv:gr-qc/9302019].

[41] D. Wands *et al.*, Phys. Rev. **D62**, 043527 (2000), [arXiv:astro-ph/0003278].

[42] A. R. Liddle and S. M. Leach, Phys. Rev. **D68**, 103503 (2003), [arXiv:astro-ph/0305263].

[43] P. A. R. Ade *et al.* (BICEP/Keck), Phys. Rev. Lett. **127**, 15, 151301 (2021), [arXiv:2110.00483].

[44] S.M. Leach, A.R. Liddle, J. Martin, and D.J. Schwarz, Phys. Rev. **D66**, 23515 (2002).

[45] D. Kazanas, Astrophys. J. **241**, L59 (1980).

[46] K. Sato, Mon. Not. Roy. Astron. Soc. **195**, 467 (1981).

[47] A. Billoire and K. Tamvakis, Nucl. Phys. **B200**, 329 (1982); J. D. Breit, S. Gupta and A. Zaks, Phys. Rev. Lett. **51**, 1007 (1983).

[48] A. D. Linde, Phys. Lett. **129B**, 177 (1983).

[49] D. V. Nanopoulos, K. A. Olive and M. Srednicki, Phys. Lett. **127B**, 30 (1983).

[50] J. Ellis, D. V. Nanopoulos and K. A. Olive, Phys. Rev. Lett. **111**, 111301 (2013), [Erratum: Phys. Rev. Lett.111,no.12,129902(2013)], [arXiv:1305.1247].

[51] T. S. Koivisto and F. R. Urban, JCAP **1503**, 03, 003 (2015), [arXiv:1407.3445].

[52] L. Boubekeur and D. H. Lyth, JCAP **0507**, 010 (2005), [hep-ph/0502047].

[53] G. R. Dvali, Q. Shafi and S. Solganik, in "4th European Meeting From the Planck Scale to the Electroweak Scale (Planck 2001) La Londe les Maures, Toulon, France, May 11-16, 2001," (2001), [hep-th/0105203]; J. Garcia-Bellido, R. Rabadan and F. Zamora, JHEP **01**, 036 (2002), [hep-th/0112147]; S. Kachru *et al.*, JCAP **0310**, 013 (2003), [hep-th/0308055].

[54] F. C. Adams *et al.*, Phys. Rev. **D47**, 426 (1993), [hep-ph/9207245].

[55] E. Pajer and M. Peloso, Class. Quant. Grav. **30**, 214002 (2013), [arXiv:1305.3557].

[56] E. Silverstein and A. Westphal, Phys. Rev. **D78**, 106003 (2008), [arXiv:0803.3085].

[57] L. McAllister, E. Silverstein and A. Westphal, Phys. Rev. **D82**, 046003 (2010), [arXiv:0808.0706].

[58] F. L. Bezrukov and M. Shaposhnikov, Phys. Lett. **B659**, 703 (2008), [arXiv:0710.3755].

[59] D. Buttazzo *et al.*, JHEP **12**, 089 (2013), [arXiv:1307.3536].

[60] H. P. Nilles, Phys. Rept. **110**, 1 (1984); H. E. Haber and G. L. Kane, Phys. Rept. **117**, 75 (1985).

[61] J.R. Ellis *et al.*, Phys. Lett. **118B**, 335 (1982).

[62] N. Okada and Q. Shafi (2013), [arXiv:1311.0921].

[63] J. Martin, C. Ringeval and V. Vennin, Phys. Rev. **D93**, 10, 103532 (2016), [arXiv:1603.02606].

[64] P. A. R. Ade *et al.* (Planck), Astron. Astrophys. **594**, A20 (2016), [arXiv:1502.02114].

[65] H. Murayama *et al.*, Phys. Rev. Lett. **70**, 1912 (1993).

[66] J. Ellis, M. Fairbairn and M. Sueiro, JCAP **1402**, 044 (2014), [arXiv:1312.1353].

[67] D. Croon, J. Ellis and N. E. Mavromatos, Phys. Lett. **B724**, 165 (2013), [arXiv:1303.6253].

[68] G. R. Dvali, Q. Shafi and R. K. Schaefer, Phys. Rev. Lett. **73**, 1886 (1994), [hep-ph/9406319].

[69] D. V. Nanopoulos *et al.*, Phys. Lett. **123B**, 41 (1983).

[70] A. B. Goncharov and A. D. Linde, Phys. Lett. **139B**, 27 (1984).

[71] E. Cremmer *et al.*, Nucl. Phys. **B212**, 413 (1983), [,413(1982)].

[72] R. Holman, P. Ramond and G. G. Ross, Phys. Lett. **137B**, 343 (1984).

[73] E. J. Copeland *et al.*, Phys. Rev. **D49**, 6410 (1994), [arXiv:astro-ph/9401011]; E. D. Stewart, Phys. Rev. **D51**, 6847 (1995), [hep-ph/9405389].

[74] G. D. Coughlan *et al.*, Phys. Lett. **131B**, 59 (1983); A. S. Goncharov, A. D. Linde and M. I. Vysotsky, Phys. Lett. **147B**, 279 (1984); T. Banks, D. B. Kaplan and A. E. Nelson, Phys. Rev. **D49**, 779 (1994), [hep-ph/9308292]; B. de Carlos *et al.*, Phys. Lett. **B318**, 447 (1993), [hep-ph/9308325]; M. Kawasaki, T. Moroi and T. Yanagida, Phys. Lett. **B370**, 52 (1996), [hep-ph/9509399].

[75] J. R. Ellis, D. V. Nanopoulos and M. Quiros, Phys. Lett. **B174**, 176 (1986).

[76] T. Moroi, M. Yamaguchi and T. Yanagida, Phys. Lett. **B342**, 105 (1995), [hep-ph/9409367].

[77] M. Kawasaki, M. Yamaguchi and T. Yanagida, Phys. Rev. Lett. **85**, 3572 (2000), [hep-ph/0004243]; K. Nakayama, F. Takahashi and T. T. Yanagida, JCAP **1308**, 038 (2013), [arXiv:1305.5099].

[78] E. Cremmer *et al.*, Phys. Lett. **133B**, 61 (1983).

[79] A. S. Goncharov and A. D. Linde, Class. Quant. Grav. **1**, L75 (1984); C. Kounnas and M. Quiros, Phys. Lett. **151B**, 189 (1985).

[80] J. R. Ellis, C. Kounnas and D. V. Nanopoulos, Nucl. Phys. **B247**, 373 (1984).

[81] E. Witten, Phys. Lett. **155B**, 151 (1985).

[82] J. Ellis, D. V. Nanopoulos and K. A. Olive, JCAP **1310**, 009 (2013), [arXiv:1307.3537].

[83] J. Ellis *et al.*, Class. Quant. Grav. **33**, 9, 094001 (2016), [arXiv:1507.02308].

[84] R. Kallosh, A. Linde and D. Roest, JHEP **11**, 198 (2013), [arXiv:1311.0472].

Downloaded from https://academic.oup.com/ptep/article/2022/8/083C01/6651666 by KIT Library user on 27 September 2022

[85] A. R. Liddle, Mon. Not. Roy. Astron. Soc. **377**, L74 (2007), [arXiv:astro-ph/0701113].

[86] C. T. Byrnes and E. R. M. Tarrant, JCAP **1507**, 007 (2015), [arXiv:1502.07339].

[87] C. Armendariz-Picon, T. Damour and V. F. Mukhanov, Phys. Lett. **B458**, 209 (1999), [hep-th/9904075].

[88] M. Alishahiha, E. Silverstein and D. Tong, Phys. Rev. **D70**, 123505 (2004), [hep-th/0404084].

[89] K. Enqvist and M. S. Sloth, Nucl. Phys. **B626**, 395 (2002), [hep-ph/0109214]; D. H. Lyth and D. Wands, Phys. Lett. **B524**, 5 (2002), [hep-ph/0110002]; T. Moroi and T. Takahashi, Phys. Lett. **B522**, 215 (2001), [Erratum: Phys. Lett.B539,303(2002)], [hep-ph/0110096].

[90] N. Bartolo *et al.*, Phys. Rept. **402**, 103 (2004), [arXiv:astro-ph/0406398].

[91] P. A. R. Ade *et al.* (Planck), Astron. Astrophys. **594**, A17 (2016), [arXiv:1502.01592].

[92] Y. Akrami *et al.* (Planck), Astron. Astrophys. **641**, A9 (2020), [arXiv:1905.05697].

[93] J. Ellis *et al.*, JCAP **1507**, 07, 050 (2015), [arXiv:1505.06986].

[94] L. Senatore, K. M. Smith and M. Zaldarriaga, JCAP **1001**, 028 (2010), [arXiv:0905.3746].

[95] C. Gordon *et al.*, Phys. Rev. **D63**, 023506 (2001), [arXiv:astro-ph/0009131]; R. Easther *et al.*, Phys. Rev. Lett. **112**, 161302 (2014), [arXiv:1312.4035]; J. Ellis *et al.*, JCAP **1501**, 010 (2015), [arXiv:1409.8197]; S. Renaux-Petel and K. Turzynski, JCAP **1506**, 06, 010 (2015), [arXiv:1405.6195].

[96] C. T. Byrnes and D. Wands, Phys. Rev. **D74**, 043529 (2006), [arXiv:astro-ph/0605679].

[97] D. H. Lyth, JCAP **0511**, 006 (2005), [arXiv:astro-ph/0510443].

[98] G. Dvali, A. Gruzinov and M. Zaldarriaga, Phys. Rev. **D69**, 023505 (2004), [arXiv:astro-ph/0303591].

[99] D. Wands *et al.*, Phys. Rev. **D66**, 043520 (2002), [arXiv:astro-ph/0205253].

[100] S. Weinberg, Phys. Rev. **D67**, 123504 (2003), [arXiv:astro-ph/0302326].

[101] D. Langlois, Phys. Rev. **D59**, 123512 (1999), [arXiv:astro-ph/9906080].

[102] D. H. Lyth and Y. Rodriguez, Phys. Rev. Lett. **95**, 121302 (2005), [arXiv:astro-ph/0504045].

[103] F. Vernizzi and D. Wands, JCAP **0605**, 019 (2006), [arXiv:astro-ph/0603799].

[104] M. Sasaki, J. Valiviita and D. Wands, Phys. Rev. **D74**, 103003 (2006), [arXiv:astro-ph/0607627].

[105] G. Dvali, A. Gruzinov and M. Zaldarriaga, Phys. Rev. **D69**, 083505 (2004), [arXiv:astro-ph/0305548].

[106] D. S. Salopek and J. R. Bond, Phys. Rev. **D43**, 1005 (1991).

[107] A. Gangui *et al.*, Astrophys. J. **430**, 447 (1994), [arXiv:astro-ph/9312033].

[108] J. M. Maldacena, JHEP **05**, 013 (2003), [arXiv:astro-ph/0210603].

[109] V. Acquaviva *et al.*, Nucl. Phys. **B667**, 119 (2003), [arXiv:astro-ph/0209156].

[110] N. Dalal *et al.*, Phys. Rev. **D77**, 123514 (2008), [arXiv:0710.4560].

[111] S. Matarrese and L. Verde, Astrophys. J. **677**, L77 (2008), [arXiv:0801.4826].

[112] E.-M. Mueller *et al.* (2021), [arXiv:2106.13725].

[113] A. Ijjas, P. J. Steinhardt and A. Loeb, Phys. Lett. **B723**, 261 (2013), [arXiv:1304.2785].

[114] R. M. Wald, Phys. Rev. **D28**, 2118 (1983).

[115] M. Heusler, Phys. Lett. **B253**, 33 (1991).

[116] Y. Kitada and K.-i. Maeda, Phys. Rev. **D45**, 1416 (1992).

[117] D. S. Goldwirth and T. Piran, Phys. Rept. **214**, 223 (1992).

[118] T. Vachaspati and M. Trodden, Phys. Rev. **D61**, 023502 (1999), [arXiv:gr-qc/9811037].

[119] D. Chowdhury *et al.*, Phys. Rev. D **100**, 8, 083537 (2019), [arXiv:1902.03951].

[120] W. E. East *et al.*, JCAP **1609**, 09, 010 (2016), [arXiv:1511.05143].

[121] K. Clough *et al.*, JCAP **1709**, 09, 025 (2017), [arXiv:1608.04408].

[122] K. Clough, R. Flauger and E. A. Lim, JCAP **1805**, 05, 065 (2018), [arXiv:1712.07352].

[123] G. W. Gibbons, S. W. Hawking and J. M. Stewart, Nucl. Phys. **B281**, 736 (1987).

[124] J. S. Schiffrin and R. M. Wald, Phys. Rev. **D86**, 023521 (2012), [arXiv:1202.1818].

[125] A. Ijjas, P. J. Steinhardt and A. Loeb, Phys. Lett. **B736**, 142 (2014), [arXiv:1402.6980].

[126] A. Vilenkin, Phys. Rev. **D27**, 2848 (1983).

[127] A. D. Linde, Phys. Lett. **B175**, 395 (1986).

[128] A. S. Goncharov, A. D. Linde and V. F. Mukhanov, Int. J. Mod. Phys. **A2**, 561 (1987).

[129] A. H. Guth, D. I. Kaiser and Y. Nomura, Phys. Lett. **B733**, 112 (2014), [arXiv:1312.7619].

[130] A. Linde, in "Proceedings, 100th Les Houches Summer School: Post-Planck Cosmology: Les Houches, France, July 8 - August 2, 2013," 231–316 (2015), [arXiv:1402.0526].

[131] J. Martin and R. H. Brandenberger, Phys. Rev. **D63**, 123501 (2001), [hep-th/0005209].

[132] R. H. Brandenberger and J. Martin, Mod. Phys. Lett. **A16**, 999 (2001), [arXiv:astro-ph/0005432].

[133] J. Martin and R. H. Brandenberger, in "Recent developments in theoretical and experimental general relativity, gravitation and relativistic field theories. Proceedings, 9th Marcel Grossmann Meeting, MG'9, Rome, Italy, July 2-8, 2000. Pts. A-C," 2001–2002 (2000), [arXiv:astro-ph/0012031].

[134] A. Kogut *et al.*, JCAP **1107**, 025 (2011), [arXiv:1105.2044].

[135] J. Chluba, J. Hamann and S. P. Patil, Int. J. Mod. Phys. **D24**, 10, 1530023 (2015), [arXiv:1505.01834].

[136] A. Font-Ribera *et al.*, JCAP **1405**, 023 (2014), [arXiv:1308.4164].

[137] R. Maartens *et al.* (SKA Cosmology SWG), PoS **AASKA14**, 016 (2015), [arXiv:1501.04076].

[138] O. Doré *et al.* (2014), [arXiv:1412.4872].

Downloaded from https://academic.oup.com/ptep/article/2022/8/083C01/6651666 by KIT Library user on 27 September 2022

24. Big Bang Nucleosynthesis

Revised August 2021 by B.D. Fields (Astronomy, Illinois U.; Physics, Illinois U.), P. Molaro (INAF-OATS Trieste; IFPU) and S. Sarkar (Rudolf Peierls, Oxford U.).

24.1 Abstract

Big-Bang nucleosynthesis (BBN) offers the deepest reliable probe of the early Universe, being based on well-understood Standard Model physics [1]. Predictions of the abundances of the light elements, D, ^{3}He, ^{4}He, and ^{7}Li, synthesized at the end of the *first three minutes*, are in good overall agreement with the primordial abundances inferred from observational data, thus validating the standard hot Big-Bang cosmology (see [2–5] for reviews). This is particularly impressive given that these abundances span nine orders of magnitude – from ^{4}He/H~ 0.08 down to ^{7}Li/H$\sim 10^{-10}$ (ratios by number). Thus BBN provides powerful constraints on possible deviations from the standard cosmology, and on new physics beyond the Standard Model [6–9].

24.2 Theory

The synthesis of the light elements is sensitive to physical conditions in the early radiation-dominated era at a temperature $T \sim 1$ MeV, corresponding to an age $t \sim 1$ s. At higher temperatures, weak interactions were in thermal equilibrium, thus fixing the ratio of the neutron and proton number densities to be $n/p = \mathrm{e}^{-Q/T}$, where $Q = 1.293$ MeV is the neutron-proton mass difference. As the temperature dropped, the neutron-proton inter-conversion rate per nucleon, $\Gamma_{n\leftrightarrow p} \sim G_{\mathrm{F}}^2 T^5$, fell faster than the Hubble expansion rate, $H \sim \sqrt{g_* G_{\mathrm{N}}}\ T^2$, where g_* counts the number of relativistic particle species determining the energy density in radiation (see 'Big Bang Cosmology' — Sec. 22 of this *Review*). This resulted in departure from chemical equilibrium (*freeze-out*) at $T_{\mathrm{fr}} \sim (g_* G_{\mathrm{N}}/G_{\mathrm{F}}^4)^{1/6} \simeq 1$ MeV. The neutron fraction at this time, $n/p = \mathrm{e}^{-Q/T_{\mathrm{fr}}} \simeq 1/6$, is thus sensitive to every known physical interaction, since Q is determined by both strong and electromagnetic interactions while T_{fr} depends on the weak as well as gravitational interactions. Moreover, the sensitivity to the Hubble expansion rate affords a probe of, *e.g.,* the number of relativistic neutrino species [10]. After freeze-out, the neutrons were free to β-decay, so the neutron fraction dropped to $n/p \simeq 1/7$ by the time nuclear reactions began. A simplified analytic model of freeze-out yields the n/p ratio to an accuracy of $\sim 1\%$ [11,12].

The rates of these reactions depend on the density of baryons (strictly speaking, nucleons), which is usually expressed normalized to the relic blackbody photon density as $\eta \equiv n_b/n_\gamma$. As we shall see, all the light-element abundances can be explained with $\eta_{10} \equiv \eta \times 10^{10}$ in the range 6.143 ± 0.190. With n_γ fixed by the present CMB temperature 2.7255 K (see 'Cosmic Microwave Background' — Sec. 29 of this *Review*), this can be stated as the allowed range for the baryon mass density today, $\rho_{\mathrm{b}} = (4.2\pm0.1)\times10^{-31}\ \mathrm{g\,cm^{-3}}$, or as the baryonic fraction of the critical density, $\Omega_{\mathrm{b}} = \rho_b/\rho_{\mathrm{crit}} \simeq \eta_{10} h^{-2}/274 = (0.02244 \pm 0.00069)h^{-2}$, where $h \equiv H_0/100\ \mathrm{km\,s^{-1}\,Mpc^{-1}}$ is the present Hubble parameter (see 'The Cosmological Parameters' — Sec. 25 of this *Review*).

The nucleosynthesis chain begins with the formation of deuterium in the process $p(n,\gamma)$D. However, photo-dissociation by the high number density of photons delays production of deuterium (and other complex nuclei) until well after T drops below the binding energy of deuterium, $\Delta_{\mathrm{D}} = 2.23$ MeV. The quantity $\eta^{-1}\mathrm{e}^{-\Delta_{\mathrm{D}}/T}$, *i.e.,* the number of photons per baryon above the deuterium photo-dissociation threshold, falls below unity at $T \simeq 0.1$ MeV; nuclei can then begin to form without being immediately photo-dissociated again. Only 2-body reactions, such as $\mathrm{D}(p,\gamma)^3\mathrm{He}$ and $^3\mathrm{He}(\mathrm{D},p)^4\mathrm{He}$ are important because the density by this time has become rather low – comparable to that of air!

Nearly all neutrons end up bound in the most stable light element ^{4}He. Heavier nuclei do not form in any significant quantity both because of the absence of stable nuclei with mass number 5 or 8 (which impedes nucleosynthesis via n^4He, p^4He or ^{4}He^{4}He reactions), and the large Coulomb barriers for reactions such as $^3\mathrm{He}(^4\mathrm{He},\gamma)^7\mathrm{Li}$ and $^3\mathrm{He}(^4\mathrm{He},\gamma)^7\mathrm{Be}$. Hence the primordial mass fraction of ^{4}He, $Y_{\mathrm{p}} \equiv \rho(^4\mathrm{He})/\rho_{\mathrm{b}}$, can be estimated by the simple counting argument

$$Y_{\mathrm{p}} = \frac{2(n/p)}{1+n/p} \simeq 0.25 \tag{24.1}$$

where strictly speaking this gives the baryon fraction in ^{4}He, which is what we will quote throughout. This differs slightly from the mass fraction due to small binding energy corrections.

There is little sensitivity here to the actual nuclear reaction rates for the production of ^{4}He. Nuclear rates are, however, critically important in determining the other 'left-over' abundances: D and ^{3}He at the level of a few times 10^{-5} by number relative to H, and ^{7}Li/H at the level of about 10^{-10} (when η_{10} is in the range 1–10). These values can be understood in terms of approximate analytic arguments [12,13].

The elemental abundances shown in Fig. 24.1 as a function of η_{10} were calculated using an updated version [14] of the Wagoner code [1]; other versions [15–17] too are publicly available. The ^{4}He curve includes small corrections due to radiative processes at zero and finite temperatures [18], non-equilibrium neutrino heating during $e^\pm$ annihilation [19], and finite nucleon mass effects [20]; the range primarily reflects the 2σ uncertainty in the neutron lifetime. The spread in the curves for D, ^{3}He, and ^{7}Li corresponds to the 2σ uncertainties in nuclear cross sections, as estimated by Monte Carlo methods [21–24]. The input nuclear data have been carefully reassessed [2,14,21–31], leading to improved precision for the abundance predictions. In particular, the uncertainty in ^{7}Li/H at interesting values of η has been reduced recently by a factor ~ 2, a consequence of a similar reduction in the error budget [32] for the dominant mass-7 production channel $^3\mathrm{He}(^4\mathrm{He},\gamma)^7\mathrm{Be}$. Polynomial fits to the predicted abundances and the error correlation matrix have been given in refs. [23,33]. The boxes in Fig 24.1 show the observationally inferred primordial abundances with their associated uncertainties, as discussed below.

The nuclear reaction cross sections important for BBN have all been measured at the relevant energies. Recently however there have been substantial advances in the precision of light element observations (e.g., D/H) and in the determination of cosmological parameters (e.g., from *Planck*). This motivates corresponding improvement in BBN predictions and thus in the key reaction cross sections. Recent measurements of $\mathrm{D}(p,\gamma)^3\mathrm{He}$ by the LUNA collaboration have significantly improved the precision of D/H predictions [34]. Even so, the nuclear uncertainties still leave D/H prediction errors larger than those of the observations [14,30,31]. The $\mathrm{D}(\mathrm{D},n)^3\mathrm{He}$ and $\mathrm{D}(\mathrm{D},p)^3H$ reactions now not only dominate the uncertainty budget, but they can give significantly different D/H predictions depending on whether one uses just the empirical determination of the cross sections, or also uses theory to guide the functional form. Clearly, more experimental data is needed.

An additional experimental parameter important in determining the light element abundances is the neutron lifetime, τ_n, which normalizes (the inverse of) $\Gamma_{n\leftrightarrow p}$. Its value has been revised downwards to $\tau_n = 879.4 \pm 0.6$ s (see *N* Baryons Listing).

24.3 Observations: the Light Element Abundances

BBN theory predicts the universal abundances of D, ^{3}He, ^{4}He, and ^{7}Li which are essentially fixed by $t \sim 180$ s. However, abundances are *derived* at much later epochs, after stellar nucleosynthesis commenced. Stars produce heavy elements such as C, N, O, and Fe ("metals"), while the ejected remains of stellar processing alters the light element abundances from their primordial values. Thus, one seeks astrophysical sites with low metal abundances to measure light element abundances that are closer to primordial.

BBN is the only significant source of deuterium which is entirely destroyed when it is cycled into stars [35]. Thus, any detection provides a lower limit to primordial D/H, and an upper limit on η_{10}. The best proxy to the primordial value of D is its measure in distant and chemically unprocessed matter, where stellar processing (astration) is minimal [35]. This has become possible with the advent of large telescopes, but after nearly three decades of observational efforts we have only 16 determinations listed in Table

Downloaded from https://academic.oup.com/ptep/article/2022/8/083C01/6651666 by KIT Library user on 27 September 2022

24.1 [36–49].

High-resolution spectra reveal the presence of D in high-redshift, low-metallicity quasar absorption systems via its isotope-shifted Lyman-α absorption features, though, unfortunately, these are often obscured or contaminated by the hydrogen features of the Lyman-α forest.

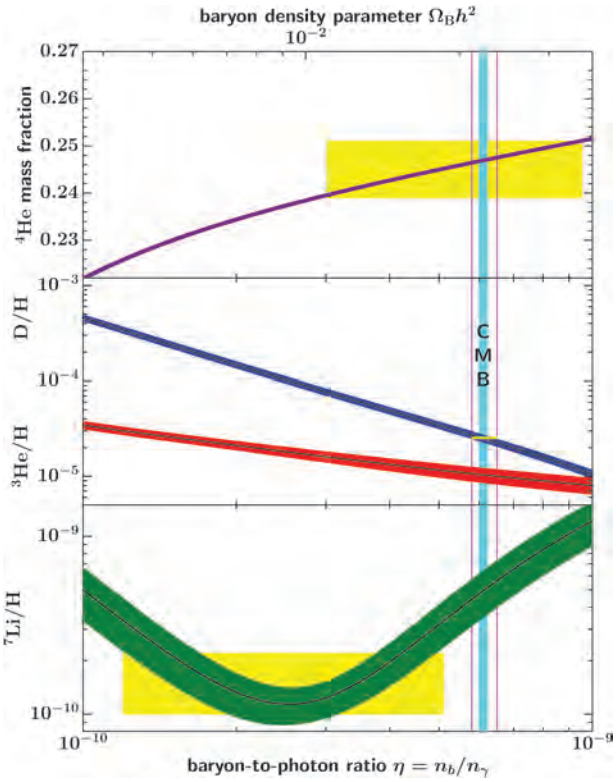

Figure 24.1: The primordial abundances of ^{4}He, D, ^{3}He, and ^{7}Li as predicted by the standard model of Big-Bang nucleosynthesis — the bands show the 95% CL range [50]. Boxes indicate the observed light element abundances. The narrow vertical band indicates the CMB measure of the cosmic baryon density, while the wider band indicates the BBN D+^{4}He concordance range (both at 95% CL).

A few DLA systems show D lines resolved up to the higher members of the Lyman series. Recent determinations [40,42] and re-analyses [41,49,51] provide strikingly improved precision over earlier work. The weighted mean of the 11 most precise measurements in Table 24.1 is (with 1% precision):

$$\mathrm{D/H}|_{\mathrm{p}} \times 10^6 = (25.47 \pm 0.25). \tag{24.2}$$

Considering all the 16 extant determinations, the weighted mean is $\mathrm{D/H}|_{\mathrm{p}} \times 10^6 = (25.36 \pm 0.26)$, while different selections provide $\mathrm{D/H}|_{\mathrm{p}} \times 10^6 = (25.27 \pm 0.30)$ [51] or $\mathrm{D/H}|_{\mathrm{p}} \times 10^6 = (25.45 \pm 0.25)$ [52], all consistent with each other. Metallicities of the absorbers are $(0.001 - 0.03)\times$ Solar, i.e. at a level where no significant astration is expected [37,53]. D/H shows no correlation with metallicity, redshift, or the neutral hydrogen column density $N(\mathrm{HI})$ ($= \int_{\mathrm{los}} n_{\mathrm{HI}}\, ds$) integrated over the line-of-sight through the absorber. In the Galaxy D/H measurements are anti-correlated with metal abundances, which suggests that interstellar D partly resides in dust particles [54]. However, in the absorbers where deuterium is measured, the dust content is quite small as implied by Solar proportions of the abundances of refractory and non refractory elements. This is consistent with the measured D/H being truly representative of the primordial value.

The primordial ^{4}He abundance is best determined through recombination emission lines of He and H in the most metal-poor extragalactic HII (ionized) regions, *viz.* blue compact galaxies, generally found at low redshift. There is now a large body of data on ^{4}He and CNO in these galaxies, with over 1000 such systems in the Sloan Digital Sky Survey alone [59]. These data confirm that the stellar contribution to the helium abundance is positively correlated with metal production, so extrapolation to zero metallicity gives the primordial ^{4}He abundance Y_{p}. However, HII regions are complex systems and several physical parameters enter in the He/H determination, notably the electron density and temperature, as well as reddening. Thus, systematic effects dominate the uncertainties in the abundance determination [60, 61]. A major step forward has been the inclusion of the He λ10830 infrared emission line which shows a strong dependence on the electron density and is thus useful to break the degeneracy with the temperature, allowing for a more robust helium abundance determination. In recent works the underlying ^{4}He stellar absorption, and/or the newly derived values of the HeI-recombination and H-excitation-collisional coefficients are adressed and the ^{4}He abundances have increased significantly. Some recent results are reported in Table 24.2.

There is a reassuring convergence towards the value of $Y_{\mathrm{p}} = 0.245$ between detailed analyses of specific extragalactic HII regions with other (statistically more significant) analyses of many systems. Thus our recommended ^{4}He abundance is:

$$Y_{\mathrm{p}} = 0.245 \pm 0.003. \tag{24.3}$$

The central value is close to the mean/weighted average of the values in Table 24.2, however we caution that combining these partially overlapping data sets is not straightforward. The uncertainty reflects the combined statistical and systematic errors, with the latter, estimated to be ± 0.002 [67], being dominant.

The best suited objects for the determination of primordial ^{7}Li are metal-poor stars in the Galactic halo, which have metallicities going down to 10^{-6} of the Solar value [68]. Observations have long shown [69–72] that ^{7}Li does not vary significantly in halo dwarfs with metallicities $\lesssim 1/30$ of Solar — the *Spite plateau* [69, 73]. Recent observations show a puzzling drop in the Li/H abundance in metal-poor stars with $[\mathrm{Fe/H}] < -3.0$ [74–76]. This becomes particularly acute at the very low metallicity end where only one star out of the seven dwarfs with metallicities $[\mathrm{Fe/H}] \lesssim -4.5$ shows a ^{7}Li abundance close to the Spite Plateau, while in the others where it ought to be present it is either lower or totally absent [68,77]. The reason for the increase in scatter at low metallicity is unknown and prevents derivation of the primordial ^{7}Li value by extrapolation to zero metallicity [75, 76].

To estimate the primordial ^{7}Li value we consider only stars with metallicity in the range $-2.8 < [\mathrm{Fe/H}] < -1.5$ [76], where no scatter in excess of the observational errors is observed. This yields:

$$\mathrm{Li/H}|_{\mathrm{p}} = (1.6 \pm 0.3) \times 10^{-10}. \tag{24.4}$$

Strictly speaking the suggested primordial ^{7}Li abundance should be considered a *lower bound* rather than a measure. In fact, ^{7}Li in Pop II stars may have been partially destroyed due to mixing of the outer layers with the hotter interior [78]. Such processes can be constrained by the absence of significant scatter in ^{7}Li versus T_{eff} [71], but ^{7}Li depletion by a factor as large as ~ 1.8 may have occurred [71, 79]. Stellar determination of Li abundances typically sum over both ^{6}Li and ^{7}Li isotopes. however, high-precision measurements indicate $^6\mathrm{Li}/^7\mathrm{Li} \leq 0.05$, thus confirming that ^{7}Li is dominant [80].

The primordial abundance of ^{3}He has the poorest observational determination of all of the light nuclides. The only data available come from the Solar system and from solar-metallicity HII regions in the Galaxy [81]. Therefore, inferring the primordial ^{3}He abundance is problematic, compounded by the fact that stellar nucleosynthesis models for ^{3}He are in conflict with observations. Consequently, we consider it inappropriate to use ^{3}He (and also D+^{3}He) as a cosmological probe.

Downloaded from https://academic.oup.com/ptep/article/2022/8/083C01/6651666 by KIT Library user on 27 September 2022

Table 24.1: D/H measurements. For systems with multiple measurements we used the most recent one which is generally more precise.

QSO	$z_{\rm em}$	$z_{\rm abs}$	$\log N$((HI))	[X/H]	(D/H) $\times 10^6$	Ref
QSO 2206−199	2.56	2.076	20.436±0.008	-2.04	16.5 ± 3.5	[55]
QSO 0347−3819	3.22	3.025	20.63±0.09	-1.25	22.4 ± 6.7	[56]
SDSS J1134+5742	3.52	3.411	17.95±0.05	<-4.2	20.4 ± 6.1	[44]
QSO CTQ 247	3.02	2.621	20.45±0.10	-1.99	28.0 ± 8.0	[46]
SDSS 1337+3152	3.17	3.168	20.41±0.15	-2.68	12.0 ± 5.0	[57]
SDSS J1419+0829	3.03	3.049	20.392±0.003	-1.92	25.1 ± 0.5	[39]
HS 0105+1619	2.65	2.536	19.40±0.01	-1.77	25.8 ± 1.5	[39]
QSO B0913+0715	2.78	2.618	20.312±0.008	-2.40	25.3 ± 1.0	[39]
SDSS J1358+0349	2.89	2.853	20.524±0.006	-2.33	26.2 ± 0.7	[40]
SDSS J1358+6522	3.17	3.067	20.50±0.01	-2.33	25.8 ± 1.0	[39]
SDSS J1558−0031	2.82	2.702	20.75±0.03	-1.55	24.0 ± 1.4	[39]
PKS 1937−1009	3.78	3.256	18.09±0.03	-1.87	24.5 ± 2.8	[58]
QSO J1444+2919	2.66	2.437	19.983±0.010	-2.04	19.7 ± 3.3	[42]
PKS 1937−1009	3.78	3.572	17.925±0.006	-2.26	26.2 ± 0.5	[49]
QSO 1009+2956	2.63	2.504	17.362±0.005	-2.50	24.8 ± 4.1	[52]
QSO 1243+307	2.55	2.525	19.761±0.026	-2.77	23.9 ± 1.0	[51]
Weighted mean of all 16					25.38 ± 0.25	
Weighted mean of the most recent 11					25.47 ± 0.25	

Table 24.2: Recent primordial ^{4}He measurements in extragalactic HII regions.

$Y_{\rm p}(^4{\rm He})$	$\pm 1\sigma_{\rm stat}$	$\pm 1\sigma_{\rm sys}$	$\pm 1\sigma_{\rm tot}$	# systems	Ref
0.2453	0.0034			16	[62]
0.2451	0.0019	0.0018	0.0026	1	[63]
0.243	0.005			16	[64]
0.2462	0.0022			120	[65]
0.2436	0.0040			54	[66]
0.2448	0.0027	0.0018	0.0033	7	[67]

24.4 Concordance, Dark Matter, and the CMB

We now use the observed light element abundances to test the theory. We first consider standard BBN, which is based on Standard Model physics alone, so $N_\nu = 3$ and the only free parameter is the baryon-to-photon ratio η. (The implications of BBN for physics beyond the Standard Model will be considered below). Thus, any abundance measurement determines η, and additional measurements overconstrain the theory and thereby provide a consistency check.

While the η ranges spanned by the boxes in Fig 24.1 do not all overlap, they are all within a factor ~ 2 of each other. In particular, the lithium abundance corresponds to η values that are inconsistent with that of the (now very precise) D/H abundance as well as the less-constraining ^{4}He abundance. This discrepancy marks the *lithium problem*. The problem could simply reflect difficulty in determining the primordial lithium abundance, or could hint at a more fundamental omission in the theory. The possibility that lithium reveals new physics is addressed in detail in the next section. If however we exclude the lithium constraint because its inferred abundance suffers from systematic uncertainties, then D/H and ^{4}He are in agreement. The concordant η range is essentially determined by D/H, and yields [50]

$$\eta_{10} = 6.143 \pm 0.190 \tag{24.5}$$

where the errors are 1σ. Despite the lithium problem, the overall concordance remains remarkable: using only well-established microphysics we can extrapolate back to $t \sim 1$ s to predict light element abundances spanning nine orders of magnitude, in approximate agreement with observation. This is a major success for the standard cosmology, and inspires confidence in extrapolation back to such early times.

This concordance provides a measure of the baryon content:

$$\Omega_{\rm b}{\rm h}^2 = 0.02244 \pm 0.00069 \tag{24.6}$$

where again errors are 1σ, a result that plays a key role in our understanding of the matter budget of the Universe. First of all $\Omega_{\rm b} \ll 1$, *i.e.*, baryons cannot close the Universe [82]. Furthermore, the cosmic density of (optically) luminous matter is $\Omega_{\rm lum} \simeq 0.0024{\rm h}^{-1}$ [83], so that $\Omega_{\rm b} \gg \Omega_{\rm lum}$: most baryons are optically dark, probably in the form of a diffuse intergalactic medium [84]. Finally, given that $\Omega_{\rm m} \sim 0.3$ (see the 'Dark Matter' and 'Cosmological Parameters' reviews), we infer that most matter in the Universe is not only dark, but also takes some non-baryonic (more precisely, non-nucleonic) form.

The BBN prediction for the cosmic baryon density can be tested through precision measurements of CMB temperature fluctuations (see the 'Cosmic Microwave Background' review). One can determine η from the amplitudes of the acoustic peaks in the CMB angular power spectrum [85], making it possible to compare two measures of η using very different physics, at two widely separated epochs. In the standard cosmology, there is no change in η between BBN and CMB decoupling, thus, a comparison of $\eta_{\rm BBN}$ and $\eta_{\rm CMB}$ is a key test. Agreement would endorse the standard picture, while disagreement could point to new physics during/-between the BBN and CMB epochs.

The analysis described in the Cosmic Microwave Background review (Sec.29), based on *Planck* TT, TE, EE + lowE data and lensing, yields $\Omega_{\rm b}{\rm h}^2 = 0.02237 \pm 0.00015$ [86], which corresponds to $\eta_{10} = 6.12 \pm 0.04$ [87]. This result depends weakly on the primordial helium abundance, and the fiducial *Planck* analysis uses BBN theory to fix $Y_{\rm p}(\eta)$. Without BBN theory, the *Planck* TT, TE, EE + lowE data plus lensing give $\Omega_{\rm b}{\rm h}^2 = 0.02230 \pm 0.00021$, corresponding to $\eta_{10} = 6.104 \pm 0.058$. As shown in Fig. 24.1, this CMB estimate of the baryon density (narrow vertical band) is consistent with the BBN range, *i.e.*, in good agreement with the value inferred from high-redshift D/H measurements and local ^{4}He determinations; together these observations span diverse environments from redshifts $z \sim 1000$ to the present. Combining the CMB and BBN sharpens the baryon measures to $\eta_{10} = 6.129 \pm 0.039$ and $\Omega_{\rm b}h^2 = 0.02239 \pm 0.00014$.

Downloaded from https://academic.oup.com/ptep/article/2022/8/083C01/6651666 by KIT Library user on 27 September 2022

The ^{4}He abundance is proportional to the n/p ratio when the weak-interaction rate falls behind the Hubble expansion rate at $T_{\rm fr} \sim 1$ MeV. The presence of additional neutrino flavors (or of any other relativistic species) at this time increases g_*, hence the expansion rate, leading to a larger value of $T_{\rm fr}$, n/p, and therefore $Y_{\rm P}$ [10, 88]. In the Standard Model at $T = 1$ MeV, $g_* = 5.5 + \frac{7}{4}N_\nu$, where N_ν is the *effective* number of (nearly) massless neutrino flavors. The helium curves in 24.1 were computed taking $N_\nu = 3$; small corrections for non-equilibrium neutrino heating [19] are included in the thermal evolution and lead to an effective $N_\nu = 3.044$ compared to assuming instantaneous neutrino freezeout (see 'Big Bang Cosmology' — Sec. 22 of this *Review*). The computed ^{4}He abundance scales as $\Delta Y_{\rm P} \simeq 0.013\Delta N_\nu$ [11]. Clearly the central value for N_ν from BBN will depend on η, which is independently determined (with weaker sensitivity to N_ν) by the adopted D or ^{7}Li abundance. For example, if the best value for the observed primordial ^{4}He abundance is 0.249, then, for $\eta_{10} \sim 6$, the central value for N_ν is very close to 3. A maximum likelihood analysis on η and N_ν based on ^{4}He and D abundances nearly identical to those above finds the (correlated) 95% CL ranges to be $\eta_{10} = 6.090 \pm 0.055$ and $N_\nu = 2.843 \pm 0.154$ [50, 89]. Identical results are obtained using a simpler method to extract such bounds based on χ^2 statistics, given a set of input abundances [90].

The CMB damping tail is sensitive to the primordial ^{4}He abundance independently of both BBN and local ^{4}He measurements [91]. The *Planck* analysis using TT, TE, EE+lowE and lensing but not the BBN $Y_{\rm P}(\eta)$ relation gives a ^{4}He mass fraction $0.239^{+0.024}_{-0.025}$, and nucleon fraction $Y_{\rm P} = 0.240^{+0.24}_{-0.25}$, both at 95% CL [86]. This is consistent with the HII region helium abundance determination. Moreover, this value is consistent with the Standard ($N_\nu = 3$) BBN prediction for $Y_{\rm P}$ with the *Planck*-determined baryon density. This concordance represents a successful CMB-only test of BBN.

The precision determination of the baryon density using the CMB motivates using this as an input to BBN calculations. Within the context of the Standard Model, BBN then becomes a zero-parameter theory, and the light element abundances are completely determined to within the uncertainties in $\eta_{\rm CMB}$ and the BBN theoretical errors. Comparison with the observed abundances then can be used to test the astrophysics of post-BBN light element evolution [92]. Alternatively, one can consider possible physics beyond the Standard Model (*e.g.*, which might change the expansion rate during BBN) and then use all of the abundances to test such models; this is discussed in 23.6 below.

24.5 The Lithium Problem

As Fig. 24.1 shows, stellar Li/H measurements are inconsistent with the D/H (and CMB), given the error budgets we have quoted. Recent updates in nuclear cross sections and stellar abundance systematics *increase* the discrepancy to over 5σ, depending on the stellar abundance analysis adopted [25]. For instance, the value of $\mathrm{Li/H}|_{\rm P} = (4.72 \pm 0.7) \times 10^{-10}$ [50] is a factor 3.1 higher than in eq.24.4 which is a 4.4 σ discrepancy.

Stars that have been accreted by the Milky Way about 10 Gyrs ago from the Gaia-Enceladus-Sausage galaxy have the same abundances as those in the Milky Way, showing that the Li problem is universal [93, 94]. The question then becomes pressing as to whether this mismatch comes from systematic errors in the observed abundances, and/or uncertainties in stellar astrophysics or nuclear inputs, or whether there might be new physics at work [9]. Nuclear inputs (cross sections) for BBN reactions are constrained by extensive laboratory measurements; to increase ^{7}Be destruction requires enhancement of otherwise subdominant processes that can be attained by missed resonances in a few reactions such as $^7\mathrm{Be}(d,p)2\alpha$ if the compound nuclear state properties are particularly favorable [29, 95–97]. However, experimental searches have now closed off these possibilities [98–100], making a *nuclear fix* increasingly unlikely.

Another means to solve the lithium problem is by *in situ* destruction over the long lifetimes of the host halo stars. Stellar depletion mechanisms include diffusion, rotationally induced mixing, or pre-main-sequence depletion. These effects certainly occur, but to reduce lithium to the required levels generally requires some *ad hoc* mechanism and fine tuning of the initial stellar parameters [79, 101–103]. General features of diffusive models are a dispersion in the Li abundances and a pronounced downturn in the Li abundances at the hot end of the Li plateau. Some extra turbulence needs to be invoked to limit diffusion in the hotter stars and to restore uniform Li abundance along the Spite plateau [103]. Li abundances for over 100 000 field stars have been obtained in the GALAH (Galactic Archeology with HERMES) survey. Warm stars with [Fe/H] in between -1.0 and -0.5 form an elevated plateau consistent with the BBN prediction and it has been suggested that this could have been also true for the more metal poor stars which have evolved further [104]. Li destruction in the pre-Main sequence phase has been also proposed [102].

Observations of interstellar lithium in low-metallicity systems probe lithium abundances not subject to stellar depletion. Measurements of interstellar Li/H in the Small Magellanic Cloud lie near the primordial level, but also are consistent with Milky Way stellar abundances at that metallicity ($\sim 1/4$ solar) [105]. Additional such measurements in more metal-poor systems would be of great interest.

As nuclear and astrophysical solutions to the lithium problem become increasingly constrained, the possibility of new physics arises. Nucleosynthesis models in which the baryon-to-photon ratio is inhomogeneous can alter abundances for a given $\eta_{\rm BBN}$, but will overproduce ^{7}Li [106]. Entropy generation by some non-standard process could have decreased η between the BBN era and CMB decoupling, however the lack of spectral distortions in the CMB rules out any significant energy injection up to a redshift $z \sim 10^7$ [107]. The most intriguing resolution of the lithium problem thus involves new physics during BBN [7–9]

We summarize the general features of such solutions here, and later consider examples in the context of specific particle physics models. Many proposed solutions introduce perturbations to light-element formation during BBN; while all element abundances may suffer perturbations, the interplay of ^{7}Li and D is often the most important *i.e.* observations of D often provide the strongest constraints on the allowed perturbations to ^{7}Li. In this connection it is important to note that the new, very precise determination of D/H will significantly constrain the ability of such models to ameliorate or solve the lithium problem.

A well studied class of models invokes the injection of suprathermal hadronic or electromagnetic particles due to decays of dark matter particles. The effects are complex and depend on the nature of the decaying particles and their branchings and spectra. However, the models that most successfully solve the lithium problem generally feature non-thermal nucleons, which dissociate all light elements. Dissociation of even a small fraction of ^{4}He introduces a large abundance of free neutrons, which quickly thermalize. The thermal neutrons drive the $^7\mathrm{Be}(n,p)^7\mathrm{Li}$ conversion of ^{7}Be. The resulting ^{7}Li has a lower Coulomb barrier relative to ^{7}Be and is readily destroyed via $^7\mathrm{Li}(p,\alpha)^4\mathrm{He}$ [108, 109]]. But ^{4}He dissociation also produces D directly as well as via nonthermal neutron $n(p,\gamma)d$ reactions. This introduces a tension between Li/H reduction and D/H enhancement that becomes increasingly restrictive with the increasing precision of deuterium observations. Indeed, this now forces particle injection scenarios to make very small ^{7}Li perturbations — far short of the level needed. An exception is a recent model wherein MeV-scale decays by construction avoid ^{4}He dissociation and associated D/H overproduction, instead *borrowing* neutrons by dissociating only deuterons [110].

Another important class of models retains the standard cosmic particle content, but changes their interactions via time variations in the fundamental constants [111–117]. Here too, the details are model-dependent, but scenarios that solve or alleviate the lithium problem often feature perturbations to the deuteron binding energy. A weaker D binding leads to the D bottleneck being overcome later, so that element formation commences at a lower temperature and lower density. This leads in turn to slower nuclear rates that freeze out earlier. The net result is a *higher* final D/H, due to less efficient processing into ^{4}He, but also *lower* Li, due to suppressed production via $^3\mathrm{He}(\alpha,\gamma)^7\mathrm{Be}$.

The *cosmological lithium problem* remains an unresolved issue

Downloaded from https://academic.oup.com/ptep/article/2022/8/083C01/6651666 by KIT Library user on 27 September 2022

in BBN. Nevertheless, the remarkable concordance between the CMB and the D (as well as ^{4}He) abundance, is a non-trivial success, and provides important constraints on the early Universe.

24.6 Beyond the Standard Model

Given the simple physics underlying BBN, it is remarkable that it still provides the most effective test for the cosmological viability of ideas concerning physics beyond the Standard Model. Although baryogenesis and inflation must have occurred at higher temperatures in the early Universe, we do not as yet have 'standard models' for these, so BBN still marks the boundary between the established and the speculative in Big Bang cosmology. It might appear possible to push the boundary back to the quark-hadron transition at $T \sim \Lambda_{\rm QCD}$, or electroweak symmetry breaking at $T \sim 1/\sqrt{G_{\rm F}}$; however, so far no observable relics of these epochs have been identified, either theoretically or observationally. Thus, although the Standard Model provides a precise description of physics up to the Fermi scale, cosmology cannot be traced in detail before the BBN era.

The CMB power spectrum in the damping tail is independently sensitive to N_ν (*e.g.* [118]). The CMB value $N_\nu^{\rm CMB}$ probes the cosmic radiation content at (re)combination, so a discrepancy would imply new physics or astrophysics. Indeed, observations by the South Pole Telescope implied $N_\nu^{\rm CMB} = 3.85 \pm 0.62$ [119], prompting discussion of *dark radiation* such as sterile neutrinos [120]. However, *Planck* 2018 results give $N_\nu^{\rm CMB} = 2.92^{+0.36}_{+0.37}$, 95% CL, when using Planck TT, TE, EE+lowE, a result quite consistent with 3 Standard Model neutrinos [86] (and adjusting for the CMB's measurement of $N_{\rm eff} = 3.044$ due to neutrino heading effects [121–123]).

Just as one can use the measured helium abundance to place limits on g_* [88, 112, 124–126], any changes in the strong, weak, electromagnetic, or gravitational coupling constants, arising *e.g.*, from the dynamics of new dimensions, can be similarly constrained [127], as can any speed-up of the expansion rate in, *e.g.*, scalar-tensor theories of gravity [128].

The limits on N_ν can be translated into limits on other types of particles or particle masses that would affect the expansion rate of the Universe during nucleosynthesis. For example, consider *sterile* neutrinos with only right-handed interactions of strength $G_{\rm R} < G_{\rm F}$. Such particles would decouple at higher temperature than (left-handed) neutrinos, so their number density ($\propto T^3$) relative to neutrinos would be reduced by any subsequent entropy release, *e.g.*, due to annihilations of massive particles that become non-relativistic between the two decoupling temperatures. Thus, (relativistic) particles with less than full strength weak interactions contribute less to the energy density than particles that remain in equilibrium up to the time of nucleosynthesis [129]. If we impose $N_\nu < 4$ as an illustrative constraint, then the three right-handed neutrinos must have a temperature $3(T_{\nu_{\rm R}}/T_{\nu_{\rm L}})^4 < 1$. Since the temperature of the decoupled $\nu_{\rm R}$ is determined by entropy conservation (see 'Big Bang Cosmology' — Sec. 22 of this *Review*), $T_{\nu_{\rm R}}/T_{\nu_{\rm L}} = [(43/4)/g_*(T_{\rm d})]^{1/3} < 0.76$, where $T_{\rm d}$ is the decoupling temperature of the $\nu_{\rm R}$. This requires $g_*(T_{\rm d}) > 24$, so decoupling must have occurred at $T_{\rm d} > 140$ MeV. The decoupling temperature is related to $G_{\rm R}$ through $(G_{\rm R}/G_{\rm F})^2 \sim (T_{\rm d}/3\,{\rm MeV})^{-3}$, where 3 MeV is the decoupling temperature for $\nu_{\rm L}$s. This yields a limit $G_{\rm R} \lesssim 10^{-2} G_{\rm F}$. The above argument sets lower limits on the masses of new Z' gauge bosons to which right-handed neutrinos would be coupled in models of superstrings [130], or extended technicolour [131]. Similarly a Dirac magnetic moment for neutrinos, which would allow the right-handed states to be produced through scattering and thus increase g_*, can be significantly constrained [132], as can any new interactions for neutrinos that have a similar effect [133–135]. Right-handed states can be populated directly by helicity-flip scattering if the neutrino mass is large enough, and this property has been used to infer a bound of $m_{\nu_\tau} \lesssim 1$ MeV (taking $N_\nu < 4$) [136]. If there is mixing between active and sterile neutrinos then the effect on BBN is more complicated [137, 138].

BBN limits on the cosmic expansion rate constrain supersymmetric scenarios in which the neutralino or gravitino are very light, so that they contribute to g_* [139]. A gravitino in the mass range $\sim 10^{-4} - 10$ eV will affect the expansion rate of the Universe similarly to a light neutralino (which is however now probably ruled out by collider data, especially the decays of the Higgs-like boson). The net contribution to N_ν then ranges between 0.74 and 1.69, depending on the gravitino and slepton masses [140].

The limit on the expansion rate during BBN can also be translated into bounds on the mass/lifetime of non-relativistic particles that decay during BBN. This results in an even faster speed-up rate, and typically also changes the entropy [141–143]. If the decays include Standard Model particles, the resulting electromagnetic [144] [92, 130, 145] and/or hadronic [146, 147] cascades can strongly perturb the light elements, which leads to even stronger constraints. Such arguments have been applied to rule out an MeV mass for ν_τ, which decays during nucleosynthesis [148].

Decaying-particle arguments have proved very effective in probing supersymmetry. Light-element abundances generally are complementary to accelerator data in constraining SUSY parameter space, with BBN reaching to values kinematically inaccessible to the LHC. Much recent interest has focused on the case in which the next-to-lightest supersymmetric particle is metastable and decays during or after BBN. The constraints on unstable particles discussed above imply stringent bounds on the allowed abundance of such particles [108]; if the metastable particle is charged (*e.g.*, the stau), then it is possible for it to form atom-like electromagnetic bound states with nuclei, and the resulting impact on light elements can be quite complex [8, 95, 149]. Moreover, SUSY decays can destroy ^{7}Li and/or produce ^{6}Li, leading to a possible supersymmetric solution to the lithium problems noted above [150] (see [7] for a review).

These arguments impose powerful constraints on supersymmetric inflationary cosmology [92, 130, 145–147], particularly thermal leptogenesis [151]. These limits can be evaded only if the gravitino is massive enough to decay before BBN, i.e., $m_{3/2} \gtrsim 50$ TeV [152] (which would be unnatural), or if it is in fact the lightest supersymmetric particle and thus stable [130, 145, 153, 154]. Similar constraints apply to moduli – very weakly coupled fields in string theory that obtain an electroweak-scale mass from supersymmetry breaking [155].

Finally, we mention that BBN places powerful constraints on the possibility that there are new large dimensions in nature, perhaps enabling the scale of quantum gravity to be as low as the electroweak scale [156]. Thus, Standard Model fields may be localized on a *brane*, while gravity alone propagates in the *bulk*. It has been further noted that the new dimensions may be non-compact, even infinite [157], and the cosmology of such models has attracted considerable attention. The expansion rate in the early Universe can be significantly modified, so BBN is able to set interesting constraints on such possibilities [158, 159].

References

[1] R. V. Wagoner, W. A. Fowler and F. Hoyle, Astrophys. J. **148**, 3 (1967).

[2] D. N. Schramm and M. S. Turner, Rev. Mod. Phys. **70**, 303 (1998), [arXiv:astro-ph/9706069].

[3] G. Steigman, Ann. Rev. Nucl. Part. Sci. **57**, 463 (2007), [arXiv:0712.1100].

[4] F. Iocco *et al.*, Phys. Rept. **472**, 1 (2009), [arXiv:0809.0631].

[5] R. H. Cyburt *et al.*, Rev. Mod. Phys. **88**, 015004 (2016), [arXiv:1505.01076].

[6] S. Sarkar, Rept. on Prog. in Phys. **59**, 1493 (1996).

[7] K. Jedamzik and M. Pospelov, New J. Phys. **11**, 105028 (2009), [arXiv:0906.2087].

[8] M. Pospelov and J. Pradler, Ann. Rev. Nucl. Part. Sci. **60**, 539 (2010), [arXiv:1011.1054].

[9] B. D. Fields, Ann. Rev. Nucl. Part. Sci. **61**, 47 (2011), [arXiv:1203.3551].

[10] P.J.E. Peebles, Phys. Rev. Lett. **16**, 411 (1966).

[11] J. Bernstein, L. S. Brown and G. Feinberg, Rev. Mod. Phys. **61**, 25 (1989).

[12] S. Mukhanov, Int. J. Theor. Phys. **143**, 669 (2004).

[13] R. Esmailzadeh, G. D. Starkman and S. Dimopoulos, Astrophys. J. **378**, 504 (1991).

Downloaded from https://academic.oup.com/ptep/article/2022/8/083C01/6651666 by KIT Library user on 27 September 2022

[14] T.-H. Yeh, K. A. Olive and B. D. Fields, JCAP **03**, 046 (2021), [arXiv:2011.13874].

[15] L. Kawano, Technical report (1992), URL `https://ui.adsabs.harvard.edu/abs/1992STIN...9225163K`.

[16] A. Arbey *et al.*, Comput. Phys. Commun. **248**, 106982 (2020), [arXiv:1806.11095].

[17] R. Consiglio *et al.*, Computer Physics Communications **233**, 237 (2018), [arXiv:1712.04378].

[18] S. Esposito *et al.*, Nucl. Phys. **B568**, 421 (2000), [arXiv:astro-ph/9906232].

[19] S. Dodelson and M. S. Turner, Phys. Rev. **D46**, 3372 (1992).

[20] D. Seckel (1993), [hep-ph/9305311].

[21] R. H. Cyburt, B. D. Fields and K. A. Olive, New Astron. **6**, 215 (2001), [arXiv:astro-ph/0102179].

[22] M. S. Smith, L. H. Kawano and R. A. Malaney, Astrophys. J. Suppl. **85**, 219 (1993).

[23] G. Fiorentini *et al.*, Phys. Rev. **D58**, 063506 (1998), [arXiv:astro-ph/9803177].

[24] A. Coc *et al.*, Astrophys. J. **744**, 158 (2012), [arXiv:1107.1117].

[25] R. H. Cyburt, B. D. Fields and K. A. Olive, JCAP **0811**, 012 (2008), [arXiv:0808.2818].

[26] K. M. Nollett and S. Burles, Phys. Rev. **D61**, 123505 (2000), [arXiv:astro-ph/0001440].

[27] R. H. Cyburt, Phys. Rev. **D70**, 023505 (2004), [arXiv:astro-ph/0401091].

[28] P. D. Serpico *et al.*, JCAP **0412**, 010 (2004), [arXiv:astro-ph/0408076].

[29] R. N. Boyd *et al.*, Phys. Rev. **D82**, 105005 (2010), [arXiv:1008.0848].

[30] C. Pitrou *et al.*, Mon. Not. Roy. Astron. Soc. **502**, 2, 2474 (2021), [arXiv:2011.11320].

[31] O. Pisanti *et al.*, JCAP **04**, 020 (2021), [arXiv:2011.11537].

[32] R.H. Cyburt and B. Davids, Phys. Rev. **C78**, 012 (2008).

[33] S. Burles, K. M. Nollett and M. S. Turner, Astrophys. J. **552**, L1 (2001), [arXiv:astro-ph/0010171].

[34] V. Mossa *et al.*, Nature **587**, 7833, 210 (2020).

[35] R. I. Epstein, J. M. Lattimer and D. N. Schramm, Nature **263**, 198 (1976).

[36] S. D'Odorico *et al.*, Astron. & Astrophys. **368**, L21 (2001).

[37] D. Romano *et al.*, Mon. Not. Roy. Astron. Soc. **369**, 295 (2006), [arXiv:astro-ph/0603190].

[38] M. Pettini and D. V. Bowen, Astrophys. J. **560**, 41 (2001), [arXiv:astro-ph/0104474].

[39] R. Cooke *et al.*, Astrophys. J. **781**, 1, 31 (2014), [arXiv:1308.3240].

[40] R. J. Cooke *et al.*, Astrophys. J. **830**, 2, 148 (2016), [arXiv:1607.03900].

[41] E.O. Zavarygin *et al.*, `arXiv:1706.09512`(2017).

[42] S. A. Balashev *et al.*, Mon. Not. Roy. Astron. Soc. **458**, 2, 2188 (2016), [arXiv:1511.01797].

[43] S. A. Levshakov *et al.*, Astrophys. J. **565**, 696 (2002), [arXiv:astro-ph/0105529].

[44] M. Fumagalli, J. M. O'Meara and J. X. Prochaska, Science **334**, 1245 (2011), [arXiv:1111.2334].

[45] R. Srianand *et al.*, Mon. Not. Roy. Astron. Soc. **405**, 1888 (2010), [arXiv:1002.4620].

[46] P. Noterdaeme *et al.*, Astron. Astrophys. **542**, L33 (2012), [arXiv:1205.3777].

[47] M. Pettini and R. Cooke, Mon. Not. Roy. Astron. Soc. **425**, 2477 (2012), [arXiv:1205.3785].

[48] S. Riemer-Sørensen *et al.*, Mon. Not. Roy. Astron. Soc. **447**, 2925 (2015), [arXiv:1412.4043].

[49] S. Riemer-Sørensen *et al.*, Mon. Not. Roy. Astron. Soc. **468**, 3, 3239 (2017), [arXiv:1703.06656].

[50] B. D. Fields *et al.*, JCAP **2020**, 3, 010 (2020), [arXiv:1912.01132].

[51] R. J. Cooke, M. Pettini and C. C. Steidel, Astrophys. J. **855**, 2, 102 (2018), [arXiv:1710.11129].

[52] E. O. Zavarygin *et al.*, Mon. Not. Roy. Astron. Soc. **477**, 4, 5536 (2018), [arXiv:1706.09512].

[53] F. van de Voort *et al.*, Mon. Not. Roy. Astron. Soc. **477**, 1, 80 (2018), [arXiv:1704.08254].

[54] J. L. Linsky *et al.*, Astrophys. J. **647**, 1106 (2006), [arXiv:astro-ph/0608308].

[55] M. Pettini and D. V. Bowen, Astrophys. J. **560**, 1, 41 (2001), [arXiv:astro-ph/0104474].

[56] S. D'Odorico, M. Dessauges-Zavadsky and P. Molaro, Astron. Astrophys. **368**, L21 (2001), [arXiv:astro-ph/0102162].

[57] R. Srianand *et al.*, Mon. Not. Roy. Astron. Soc. **405**, 3, 1888 (2010), [arXiv:1002.4620].

[58] S. Riemer-Sørensen *et al.*, Mon. Not. Roy. Astron. Soc. **447**, 3, 2925 (2015), [arXiv:1412.4043].

[59] Y. I. Izotov, T. X. Thuan and N. G. Guseva, Mon. Not. Roy. Astron. Soc. **445**, 1, 778 (2014), [arXiv:1408.6953].

[60] Y. I. Izotov *et al.*, Astrophys. J. **527**, 757 (1999), [arXiv:astro-ph/9907228].

[61] K. A. Olive and E. D. Skillman, Astrophys. J. **617**, 29 (2004), [arXiv:astro-ph/0405588].

[62] E. Aver *et al.*, JCAP **2021**, 3, 027 (2021), [arXiv:2010.04180].

[63] M. Valerdi *et al.*, Astrophys. J. **876**, 2, 98 (2019), [arXiv:1904.01594].

[64] V. Fernández *et al.*, Mon. Not. Roy. Astron. Soc. **487**, 3, 3221 (2019), [arXiv:1905.09215].

[65] O. A. Kurichin *et al.*, Mon. Not. Roy. Astron. Soc. **502**, 2, 3045 (2021), [arXiv:2101.09127].

[66] T. Hsyu *et al.*, Astrophys. J. **896**, 1, 77 (2020), [arXiv:2005.12290].

[67] M. Valerdi, A. Peimbert and M. Peimbert, Mon. Not. Roy. Astr. Soc. **505**, 3, 3624 (2021), [arXiv:2105.12260].

[68] D. S. Aguado *et al.*, Astrophys. J. Lett. **874**, 2, L21 (2019), [arXiv:1904.04892].

[69] M. Spite and F. Spite, Nature **297**, 483 (1982).

[70] E. Vangioni-Flam *et al.*, New Astron. **4**, 245 (1999), [arXiv:astro-ph/9811327].

[71] S. G. Ryan *et al.*, Astrophys. J. **530**, L57 (2000), [arXiv:astro-ph/9905211].

[72] P. Bonifacio and P. Molaro, Mon. Not. Roy. Astron. Soc. **285**, 847 (1997), [arXiv:astro-ph/9611043].

[73] R. Rebolo, P. Molaro and J. E. Beckman, Astron. Astrophys. **192**, 192 (1988).

[74] P. Bonifacio *et al.*, Astron. & Astrophys. **462**, 851 (2007).

[75] W. Aoki *et al.*, Astrophys. J. **698**, 1803 (2009), [arXiv:0904.1448].

[76] L. Sbordone *et al.*, Astron. & Astrophys. **522**, A26 (2010).

[77] P. Bonifacio *et al.*, Astron. Astrophys. **612**, A65 (2018), [arXiv:1801.03935].

[78] M.H. Pinsonneault *et al.*, Astrophys. J. **574**, 389 (2002).

[79] A. J. Korn *et al.*, Nature **442**, 657 (2006), [arXiv:astro-ph/0608201].

[80] R. Cayrel *et al.*, Astron. & Astrophys. **473**, L37 (2007).

[81] D. S. Balser and T. M. Bania, Astrophys. J. **156**, 6, 280 (2018), [arXiv:1810.09422].

[82] H. Reeves *et al.*, Astrophys. J. **179**, 909 (1973).

Downloaded from https://academic.oup.com/ptep/article/2022/8/083C01/6651666 by KIT Library user on 27 September 2022

[83] M. Fukugita and P. J. E. Peebles, Astrophys. J. **616**, 643 (2004), [arXiv:astro-ph/0406095].

[84] R. Cen and J. P. Ostriker, Astrophys. J. **514**, 1 (1999), [arXiv:astro-ph/9806281].

[85] G. Jungman *et al.*, Phys. Rev. **D54**, 1332 (1996), [arXiv:astro-ph/9512139].

[86] Planck Collaboration *et al.*, arXiv e-prints arXiv:1807.06209 (2018), [arXiv:1807.06209].

[87] P.A.R. Ade *et al.*, Astron. & Astrophys. **594**, A13 (2016).

[88] G. Steigman, D. N. Schramm and J. E. Gunn, Phys. Lett. **B66**, 202 (1977), [,159(1977)].

[89] B. D. Fields *et al.*, JCAP **2020**, 11, E02 (2020).

[90] E. Lisi, S. Sarkar and F. L. Villante, Phys. Rev. **D59**, 123520 (1999), [hep-ph/9901404].

[91] R. Trotta and S. H. Hansen, Phys. Rev. **D69**, 023509 (2004), [arXiv:astro-ph/0306588].

[92] R. H. Cyburt, B. D. Fields and K. A. Olive, Phys. Lett. **B567**, 227 (2003), [arXiv:astro-ph/0302431].

[93] P. Molaro, G. Cescutti and X. Fu, Mon. Not. Roy. Astron. Soc. **496**, 3, 2902 (2020), [arXiv:2006.00787].

[94] J. D. Simpson *et al.*, Mon. Not. Roy. Astron. Soc. (2021).

[95] R. H. Cyburt *et al.*, JCAP **1305**, 014 (2013), [arXiv:1303.0574].

[96] N. Chakraborty, B. D. Fields and K. A. Olive, Phys. Rev. **D83**, 063006 (2011), [arXiv:1011.0722].

[97] C. Broggini *et al.*, JCAP **1206**, 030 (2012), [arXiv:1202.5232].

[98] P. D. O'Malley *et al.*, Phys. Rev. **C84**, 042801 (2011).

[99] F. Hammache *et al.*, Phys. Rev. **C88**, 6, 062802 (2013), [arXiv:1312.0894].

[100] M. W. Paris *et al.*, Nucl. Data Sheets **120**, 184 (2014), [arXiv:1304.3153].

[101] P. Molaro *et al.*, Memorie della Soc. Astronomica Italiana Supp. **22**, 233 (2012).

[102] X. Fu *et al.*, Mon. Not. R. Astron. Soc **452**, 325 (2015).

[103] O. Richard, G. Michaud and J. Richer, Astrophys. J. **619**, 538 (2005), [arXiv:astro-ph/0409672].

[104] X. Gao *et al.*, Mon. Not. Roy. Astron. Soc. **497**, 1, L30 (2020), [arXiv:2006.05173].

[105] J. C. Howk *et al.*, Nature **489**, 7414, 121 (2012), [arXiv:1207.3081].

[106] K. Jedamzik and J. B. Rehm, Phys. Rev. **D64**, 023510 (2001), [arXiv:astro-ph/0101292].

[107] D. J. Fixsen *et al.*, Astrophys. J. **473**, 576 (1996), [arXiv:astro-ph/9605054].

[108] M. Kawasaki, K. Kohri and T. Moroi, Phys. Rev. **D71**, 083502 (2005), [arXiv:astro-ph/0408426].

[109] K. Jedamzik, Phys. Rev. **D70**, 063524 (2004), [arXiv:astro-ph/0402344].

[110] A. Goudelis, M. Pospelov and J. Pradler, Phys. Rev. Lett. **116**, 21, 211303 (2016), [arXiv:1510.08858].

[111] J. D. Barrow, Phys. Rev. **D35**, 1805 (1987).

[112] B. A. Campbell and K. A. Olive, Phys. Lett. **B345**, 429 (1995), [hep-ph/9411272].

[113] L. Bergstrom, S. Iguri and H. Rubinstein, Phys. Rev. **D60**, 045005 (1999), [arXiv:astro-ph/9902157].

[114] V. V. Flambaum and E. V. Shuryak, Phys. Rev. **D65**, 103503 (2002), [hep-ph/0201303].

[115] A. Coc *et al.*, Phys. Rev. **D76**, 023511 (2007), [arXiv:astro-ph/0610733].

[116] J. C. Berengut *et al.*, Phys. Rev. **D87**, 8, 085018 (2013), [arXiv:1301.1738].

[117] C. J. A. P. Martins, Astron. Astrophys. **646**, A47 (2021), [arXiv:2012.10505].

[118] Z. Hou *et al.*, Phys. Rev. **D87**, 083008 (2013), [arXiv:1104.2333].

[119] R. Keisler *et al.*, Astrophys. J. **743**, 28 (2011), [arXiv:1105.3182].

[120] J. Hamann *et al.*, Phys. Rev. Lett. **105**, 181301 (2010), [arXiv:1006.5276].

[121] K. Akita and M. Yamaguchi, JCAP **2020**, 8, 012 (2020), [arXiv:2005.07047].

[122] J. Froustey, C. Pitrou and M. C. Volpe, JCAP **2020**, 12, 015 (2020), [arXiv:2008.01074].

[123] J. J. Bennett *et al.*, JCAP **04**, 073 (2021), [arXiv:2012.02726].

[124] F. S. Accetta, L. M. Krauss and P. Romanelli, Phys. Lett. **B248**, 146 (1990).

[125] K. M. Nollett and R. E. Lopez, Phys. Rev. **D66**, 063507 (2002), [arXiv:astro-ph/0204325].

[126] C. Bambi, M. Giannotti and F. L. Villante, Phys. Rev. **D71**, 123524 (2005), [arXiv:astro-ph/0503502].

[127] E. W. Kolb, M. J. Perry and T. P. Walker, Phys. Rev. **D33**, 869 (1986).

[128] A. Coc *et al.*, Phys. Rev. **D73**, 083525 (2006), [arXiv:astro-ph/0601299].

[129] K. A. Olive, D. N. Schramm and G. Steigman, Nucl. Phys. **B180**, 497 (1981).

[130] J. R. Ellis *et al.*, Phys. Lett. **167B**, 457 (1986).

[131] L. M. Krauss, J. Terning and T. Appelquist, Phys. Rev. Lett. **71**, 823 (1993), [hep-ph/9305265].

[132] J. A. Morgan, Phys. Lett. **102B**, 247 (1981).

[133] E. W. Kolb, M. S. Turner and T. P. Walker, Phys. Rev. **D34**, 2197 (1986).

[134] J. A. Grifols and E. Masso, Mod. Phys. Lett. **A2**, 205 (1987).

[135] K. S. Babu, R. N. Mohapatra and I. Z. Rothstein, Phys. Rev. Lett. **67**, 545 (1991).

[136] A. D. Dolgov, S. H. Hansen and D. V. Semikoz, Nucl. Phys. **B524**, 621 (1998), [hep-ph/9712284].

[137] K. Enqvist, K. Kainulainen and M. J. Thomson, Nucl. Phys. **B373**, 498 (1992).

[138] A. D. Dolgov, Phys. Rept. **370**, 333 (2002), [hep-ph/0202122].

[139] J. A. Grifols, R. N. Mohapatra and A. Riotto, Phys. Lett. **B400**, 124 (1997), [hep-ph/9612253].

[140] H. K. Dreiner *et al.*, Phys. Rev. **D85**, 065027 (2012), [arXiv:1111.5715].

[141] K. Sato and M. Kobayashi, Prog. Theor. Phys. **58**, 1775 (1977).

[142] D. A. Dicus *et al.*, Phys. Rev. **D17**, 1529 (1978).

[143] R. J. Scherrer and M. S. Turner, Astrophys. J. **331**, 19 (1988), [Astrophys. J.331,33(1988)].

[144] D. Lindley, Mon. Not. R. Astron. Soc **188**, 15 (1979).

[145] J. R. Ellis *et al.*, Nucl. Phys. **B373**, 399 (1992).

[146] M. H. Reno and D. Seckel, Phys. Rev. **D37**, 3441 (1988).

[147] S. Dimopoulos *et al.*, Nucl. Phys. **B311**, 699 (1989).

[148] S. Sarkar and A. M. Cooper-Sarkar, Phys. Lett. **148B**, 347 (1984).

[149] M. Kawasaki, K. Kohri and T. Moroi, Phys. Lett. **B649**, 436 (2007), [hep-ph/0703122].

[150] K. Jedamzik *et al.*, JCAP **0607**, 007 (2006), [hep-ph/0512044].

[151] S. Davidson *et al.*, Phys. Rev. **466**, 105 (2008).

[152] S. Weinberg, Phys. Rev. Lett. **48**, 1303 (1982).

Downloaded from https://academic.oup.com/ptep/article/2022/8/083C01/6651666 by KIT Library user on 27 September 2022

[153] R. H. Cyburt *et al.*, Phys. Rev. **D67**, 103521 (2003), [arXiv:astro-ph/0211258].

[154] M. Bolz, A. Brandenburg and W. Buchmuller, Nucl. Phys. **B606**, 518 (2001), [Erratum: Nucl. Phys.B790,336(2008)], [hep-ph/0012052].

[155] G. D. Coughlan *et al.*, Physics Letters B **131**, 1-3, 59 (1983).

[156] N. Arkani-Hamed, S. Dimopoulos and G. R. Dvali, Phys. Rev. **D59**, 086004 (1999), [hep-ph/9807344].

[157] L. Randall and R. Sundrum, Phys. Rev. Lett. **83**, 3370 (1999), [hep-ph/9905221].

[158] J. M. Cline, C. Grojean and G. Servant, Phys. Rev. Lett. **83**, 4245 (1999), [hep-ph/9906523].

[159] P. Binetruy *et al.*, Phys. Lett. **B477**, 285 (2000), [hep-th/9910219].

Downloaded from https://academic.oup.com/ptep/article/2022/8/083C01/6651666 by KIT Library user on 27 September 2022

25. Cosmological Parameters

Revised September 2021 by O. Lahav (UCL) and A.R. Liddle (ULisboa).

25.1 Parametrizing the Universe

Rapid advances in observational cosmology have led to the establishment of a precision cosmological model, with many of the key cosmological parameters determined to one or two significant figure accuracy. Particularly prominent are measurements of cosmic microwave background (CMB) anisotropies, with the highest precision observations being those of the *Planck* Satellite [1, 2] which supersede the landmark *WMAP* results [3, 4]. However the most accurate model of the Universe requires consideration of a range of observations, with complementary probes providing consistency checks, lifting parameter degeneracies, and enabling the strongest constraints to be placed.

The term 'cosmological parameters' now has a wide scope, and may include the parameterization of some functions as well as simple numbers describing properties of the Universe. The original usage referred to the parameters describing the global dynamics of the Universe, such as its expansion rate and curvature. Now we wish to know how the matter budget of the Universe is built up from its constituents: baryons, photons, neutrinos, dark matter, and dark energy. We also need to describe the nature of perturbations in the Universe, through global statistical descriptors such as the matter and radiation power spectra. There may be additional parameters describing the physical state of the Universe, such as the ionization fraction as a function of time during the era since recombination. Typical comparisons of cosmological models with observational data now feature between five and ten parameters.

25.1.1 *The global description of the Universe*

Ordinarily, the Universe is taken to be a perturbed Robertson–Walker space-time, with dynamics governed by Einstein's equations. This is described in detail in the Big-Bang Cosmology chapter in this volume. Using the density parameters Ω_i for the various matter species and Ω_Λ for the cosmological constant, the Friedmann equation can be written

$$\sum_i \Omega_i + \Omega_\Lambda - 1 = \frac{k}{R^2 H^2}\,, \tag{25.1}$$

where the sum is over all the different species of material in the Universe. This equation applies at any epoch, but later in this article we will use the symbols Ω_i and Ω_Λ to refer specifically to the present-epoch values.

The complete present-epoch state of the homogeneous Universe can be described by giving the current-epoch values of all the density parameters and the Hubble constant h (the present-day Hubble parameter being written $H_0 = 100h\,\mathrm{km\,s^{-1}\,Mpc^{-1}}$). A typical collection would be baryons Ω_b, photons Ω_γ, neutrinos Ω_ν, and cold dark matter Ω_c (given charge neutrality, the electron density is guaranteed to be too small to be worth considering separately and is effectively included with the baryons). The spatial curvature can then be determined from the other parameters using Eq. (25.1). The total present matter density $\Omega_\mathrm{m} = \Omega_\mathrm{c} + \Omega_\mathrm{b}$ may be used in place of the cold dark matter density Ω_c.

These parameters also allow us to track the history of the Universe, at least back until an epoch where interactions allow interchanges between the densities of the different species; this is believed to have last happened at neutrino decoupling, shortly before Big-Bang Nucleosynthesis (BBN). To probe further back into the Universe's history requires assumptions about particle interactions, and perhaps about the nature of physical laws themselves.

The standard neutrino sector has three flavors. For neutrinos of mass in the range $5\times10^{-4}\,\mathrm{eV}$ to $1\,\mathrm{MeV}$, the density parameter in neutrinos is predicted to be

$$\Omega_\nu h^2 = \frac{\sum m_\nu}{93.14\,\mathrm{eV}}\,, \tag{25.2}$$

where the sum is over all families with mass in that range (higher masses need a more sophisticated calculation). We use units with $c = 1$ throughout. Results on atmospheric and Solar neutrino oscillations [5] imply non-zero mass-squared differences between the three neutrino flavors. These oscillation experiments cannot tell us the absolute neutrino masses, but within the normal assumption of a mass hierarchy suggest a lower limit of approximately $0.06\,\mathrm{eV}$ for the sum of the neutrino masses (see the Neutrino chapter).

Even a mass this small has a potentially observable effect on the formation of structure, as neutrino free-streaming damps the growth of perturbations. Analyses commonly now either assume a neutrino mass sum fixed at this lower limit, or allow the neutrino mass sum to be a variable parameter. To date there is no decisive evidence of any effects from either neutrino masses or an otherwise non-standard neutrino sector, and observations impose quite stringent limits; see the Neutrinos in Cosmology chapter. However, we note that the inclusion of the neutrino mass sum as a free parameter can affect the derived values of other cosmological parameters.

25.1.2 *Inflation and perturbations*

A complete model of the Universe must include a description of deviations from homogeneity, at least statistically. Indeed, the most powerful probes of the parameters described above come from the evolution of perturbations, so their study is naturally intertwined with the determination of cosmological parameters.

There are many different notations used to describe the perturbations, both in terms of the quantity used to and the definition of the statistical measure. We use the dimensionless power spectrum Δ^2 as defined in the Big Bang Cosmology section (also denoted $\mathcal{P}$ in some of the literature). If the perturbations obey Gaussian statistics, the power spectrum provides a complete description of their properties.

From a theoretical perspective, a useful quantity to describe the perturbations is the curvature perturbation $\mathcal{R}$, which measures the spatial curvature of a comoving slicing of the space-time. A simple case is the Harrison–Zeldovich spectrum, which corresponds to a constant $\Delta^2_\mathcal{R}$. More generally, one can approximate the spectrum by a power law, writing

$$\Delta^2_\mathcal{R}(k) = \Delta^2_\mathcal{R}(k_*)\left[\frac{k}{k_*}\right]^{n_\mathrm{s}-1}\,, \tag{25.3}$$

where n_s is known as the spectral index, always defined so that $n_\mathrm{s} = 1$ for the Harrison–Zeldovich spectrum, and k_* is an arbitrarily chosen scale. The initial spectrum, defined at some early epoch of the Universe's history, is usually taken to have a simple form such as this power law, and we will see that observations require n_s close to one. Subsequent evolution will modify the spectrum from its initial form.

The simplest mechanism for generating the observed perturbations is the inflationary cosmology, which posits a period of accelerated expansion in the Universe's early stages [6, 7]. It is a useful working hypothesis that this is the sole mechanism for generating perturbations, and it may further be assumed to be the simplest class of inflationary model, where the dynamics are equivalent to that of a single scalar field ϕ with canonical kinetic energy slowly rolling on a potential $V(\phi)$. One may seek to verify that this simple picture can match observations and to determine the properties of $V(\phi)$ from the observational data. Alternatively, more complicated models, perhaps motivated by contemporary fundamental physics ideas, may be tested on a model-by-model basis (see more in the Inflation chapter in this volume).

Inflation generates perturbations through the amplification of quantum fluctuations, which are stretched to astrophysical scales by the rapid expansion. The simplest models generate two types, density perturbations that come from fluctuations in the scalar field and its corresponding scalar metric perturbation, and gravitational waves that are tensor metric fluctuations. The former experience gravitational instability and lead to structure formation, while the latter can influence the CMB anisotropies. Defining slow-roll parameters (with primes indicating derivatives with respect to the scalar field, and $m_\mathrm{Pl} \equiv \sqrt{\hbar c/G}$ the Planck mass) as

$$\epsilon = \frac{m_\mathrm{Pl}^2}{16\pi}\left(\frac{V'}{V}\right)^2 \quad , \quad \eta = \frac{m_\mathrm{Pl}^2}{8\pi}\frac{V''}{V}\,, \tag{25.4}$$

Downloaded from https://academic.oup.com/ptep/article/2022/8/083C01/6651666 by KIT Library user on 27 September 2022

which should satisfy $\epsilon, |\eta| \ll 1$, the spectra can be computed using the slow-roll approximation as

$$\Delta^2_{\mathcal{R}}(k) \simeq \frac{8}{3m_{\rm Pl}^4}\frac{V}{\epsilon}\bigg|_{k=aH} \quad , \quad \Delta^2_{\rm t}(k) \simeq \frac{128}{3m_{\rm Pl}^4}V\bigg|_{k=aH} \, . \tag{25.5}$$

In each case, the expressions on the right-hand side are to be evaluated when the scale k is equal to the Hubble radius during inflation. The symbol '$\simeq$' here indicates use of the slow-roll approximation, which is expected to be accurate to a few percent or better.

From these expressions, we can compute the spectral indices [8]:

$$n_{\rm s} \simeq 1 - 6\epsilon + 2\eta \quad ; \quad n_{\rm t} \simeq -2\epsilon \, . \tag{25.6}$$

Another useful quantity is the ratio of the two spectra, defined by

$$r \equiv \frac{\Delta^2_{\rm t}(k_*)}{\Delta^2_{\mathcal{R}}(k_*)} \, . \tag{25.7}$$

We have

$$r \simeq 16\epsilon \simeq -8n_{\rm t} \, , \tag{25.8}$$

which is known as the consistency equation.

One could consider corrections to the power-law approximation, which we discuss later. However, for now we make the working assumption that the spectra can be approximated by such power laws. The consistency equation shows that r and $n_{\rm t}$ are not independent parameters, and so the simplest inflation models give initial conditions described by three parameters, usually taken as $\Delta^2_{\mathcal{R}}$, $n_{\rm s}$, and r, all to be evaluated at some scale k_*, usually the 'statistical center' of the range explored by the data. Alternatively, one could use the parametrization V, ϵ, and η, all evaluated at a point on the putative inflationary potential.

After the perturbations are created in the early Universe, they undergo a complex evolution up until the time they are observed in the present Universe. When the perturbations are small, this can be accurately followed using a linear theory numerical code such as `CAMB` or `CLASS` [9]. This works right up to the present for the CMB, but for density perturbations on small scales nonlinear evolution is important and can be addressed by a variety of semi-analytical and numerical techniques. However the analysis is made, the outcome of the evolution is in principle determined by the cosmological model and by the parameters describing the initial perturbations, and hence can be used to determine them.

Of particular interest are CMB anisotropies. Both the total intensity and two independent polarization modes are predicted to have anisotropies. These can be described by the radiation angular power spectra C_ℓ as defined in the CMB article in this volume, and again provide a complete description if the density perturbations are Gaussian.

25.1.3 *The standard cosmological model*

We now have most of the ingredients in place to describe the cosmological model. Beyond those of the previous subsections, we need a measure of the ionization state of the Universe. The Universe is known to be highly ionized at redshifts below 5 or so (otherwise radiation from distant quasars would be heavily absorbed in the ultra-violet), and the ionized electrons can scatter microwave photons, altering the pattern of observed anisotropies. The most convenient parameter to describe this is the optical depth to scattering τ (*i.e.*, the probability that a given photon scatters once); in the approximation of instantaneous and complete reionization, this could equivalently be described by the redshift of reionization $z_{\rm i}$.

As described in Sec. 25.4, models based on these parameters are able to give a good fit to the complete set of high-quality data available at present, and indeed some simplification is possible. Observations are consistent with spatial flatness, and the inflation models so far described automatically generate negligible spatial curvature, so we can set $k = 0$; the density parameters then must sum to unity, and so one of them can be eliminated. The neutrino energy density is often not taken as an independent parameter; provided that the neutrino sector has the standard interactions, the neutrino energy density, while relativistic, can be related to the photon density using thermal physics arguments, and a minimal assumption takes the neutrino mass sum to be that of the lowest mass solution to the neutrino oscillation constraints, namely 0.06 eV. In addition, there is no observational evidence for the existence of tensor perturbations (with the upper limits now starting to become constraining on models), and so r could be set to zero. This leaves seven parameters, which is the smallest set that can usefully be compared to the present cosmological data. This model is referred to by various names, including ΛCDM, the concordance cosmology, and the standard cosmological model.

Of these parameters, only Ω_γ is accurately measured directly. The radiation density is dominated by the energy in the CMB, and the COBE satellite FIRAS experiment determined its temperature to be $T = 2.7255 \pm 0.0006\,{\rm K}$ [10],[1] corresponding to $\Omega_\gamma = 2.47 \times 10^{-5} h^{-2}$. It typically can be taken as fixed when fitting other data. Hence the minimum number of cosmological parameters varied in fits to data is six, though as described below there may additionally be many 'nuisance' parameters necessary to describe astrophysical processes influencing the data.

In addition to this minimal set, there is a range of other parameters that might prove important in future as the data-sets further improve, but for which there is so far no direct evidence, allowing them to be set to specific values for now. We discuss various speculative options in the next section. For completeness at this point, we mention one other interesting quantity, the helium fraction, which is a non-zero parameter that can affect the CMB anisotropies at a subtle level. It is usually fixed in microwave anisotropy studies, but the data are approaching a level where allowing its variation may become mandatory.

In conventional parameter estimation, a set of parameters is chosen by hand and the aim is to constrain their values. The higher-level inference problem of model selection instead compares different choices of parameter sets, as is necessary to assess whether observations are pointing towards inclusion of new physical effects. Bayesian inference offers an attractive framework for cosmological model selection, setting a tension between model predictiveness and ability to fit the data [11], and its use is becoming widespread.

25.1.4 *Derived parameters*

The parameter list of the previous subsection is sufficient to give a complete description of cosmological models that agree with observational data. However, it is not a unique parameterization, and one could instead use parameters derived from that basic set. Parameters that can be obtained from the set given above include the age of the Universe, the present horizon distance, the present neutrino background temperature, the epoch of matter–radiation equality, the epochs of recombination and decoupling, the epoch of transition to an accelerating Universe, the baryon-to-photon ratio, and the baryon-to-dark-matter density ratio. In addition, the physical densities of the matter components, $\Omega_i h^2$, are often more useful than the density parameters. The density perturbation amplitude can be specified in many different ways other than the large-scale primordial amplitude, for instance, in terms of its effect on the CMB, or by specifying a short-scale quantity, a common choice being the present linear-theory mass dispersion on a radius of $8\,h^{-1}$Mpc, known as σ_8.

Different types of observation are sensitive to different subsets of the full cosmological parameter set, and some are more naturally interpreted in terms of some of the derived parameters of this subsection than on the original base parameter set. In particular, most types of observation feature degeneracies whereby they are unable to separate the effects of simultaneously varying specific combinations of several of the base parameters.

25.2 Extensions to the standard model

At present, there is no positive evidence in favor of extensions of the standard model. These are becoming increasingly constrained

[1] All quoted uncertainties in this article are $1\sigma/68\%$ confidence and all upper limits are 95% confidence. Cosmological parameters sometimes have significantly non-Gaussian uncertainties. Throughout we have rounded central values, and especially uncertainties, from original sources, in cases where they appear to be given to excessive precision.

Downloaded from https://academic.oup.com/ptep/article/2022/8/083C01/6651666 by KIT Library user on 27 September 2022

by the data, though there always remains the possibility of trace effects at a level below present observational capability.

25.2.1 *More general perturbations*

The standard cosmology assumes adiabatic, Gaussian perturbations. Adiabaticity means that all types of material in the Universe share a common perturbation, so that if the space-time is foliated by constant-density hypersurfaces, then all fluids and fields are homogeneous on those slices, with the perturbations completely described by the variation of the spatial curvature of the slices. Gaussianity means that the initial perturbations obey Gaussian statistics, with the amplitudes of waves of different wavenumbers being randomly drawn from a Gaussian distribution of width given by the power spectrum. Note that gravitational instability generates non-Gaussianity; in this context, Gaussianity refers to a property of the initial perturbations, before they evolve.

The simplest inflation models, based on one dynamical field, predict adiabatic perturbations and a level of non-Gaussianity that is too small to be detected by any experiment so far conceived. For present data, the primordial spectra are usually assumed to be power laws.

25.2.1.1 *Non-power-law spectra*

For typical inflation models, it is an approximation to take the spectra as power laws, albeit usually a good one. As data quality improves, one might expect this approximation to come under pressure, requiring a more accurate description of the initial spectra, particularly for the density perturbations. In general, one can expand $\ln \Delta^2_{\mathcal{R}}$ as

$$\ln \Delta^2_{\mathcal{R}}(k) = \ln \Delta^2_{\mathcal{R}}(k_*) + (n_{\mathrm{s},*} - 1) \ln \frac{k}{k_*} + \frac{1}{2} \left. \frac{dn_{\mathrm{s}}}{d \ln k} \right|_* \ln^2 \frac{k}{k_*} + \cdots , \tag{25.9}$$

where the coefficients are all evaluated at some scale k_*. The term $dn_{\mathrm{s}}/d\ln k|_*$ is often called the running of the spectral index [12]. Once non-power-law spectra are allowed, it is necessary to specify the scale k_* at which the spectral index is defined.

25.2.1.2 *Isocurvature perturbations*

An isocurvature perturbation is one that leaves the total density unperturbed, while perturbing the relative amounts of different materials. If the Universe contains N fluids, there is one growing adiabatic mode and $N-1$ growing isocurvature modes (for reviews see Ref. [7] and Ref. [13]). These can be excited, for example, in inflationary models where there are two or more fields that acquire dynamically-important perturbations. If one field decays to form normal matter, while the second survives to become the dark matter, this will generate a cold dark matter isocurvature perturbation.

In general, there are also correlations between the different modes, and so the full set of perturbations is described by a matrix giving the spectra and their correlations. Constraining such a general construct is challenging, though constraints on individual modes are beginning to become meaningful, with no evidence that any other than the adiabatic mode must be non-zero.

25.2.1.3 *Seeded perturbations*

An alternative to laying down perturbations at very early epochs is that they are seeded throughout cosmic history, for instance by topological defects such as cosmic strings. It has long been excluded that these are the sole original of structure, but they could contribute part of the perturbation signal, current limits being just a few percent [14]. In particular, cosmic defects formed in a phase transition ending inflation is a plausible scenario for such a contribution.

25.2.1.4 *Non-Gaussianity*

Multi-field inflation models can also generate primordial non-Gaussianity (reviewed, *e.g.*, in Ref. [7]). The extra fields can either be in the same sector of the underlying theory as the inflaton, or completely separate, an interesting example of the latter being the curvaton model [15]. Current upper limits on non-Gaussianity are becoming stringent, but there remains strong motivation to push down those limits and perhaps reveal trace non-Gaussianity in the data. If non-Gaussianity is observed, its nature may favor an inflationary origin, or a different one such as topological defects.

25.2.2 *Dark matter properties*

Dark matter properties are discussed in the Dark Matter chapter in this volume. The simplest assumption concerning the dark matter is that it has no significant interactions with other matter, and that its particles have a negligible velocity as far as structure formation is concerned. Such dark matter is described as 'cold,' and candidates include the lightest supersymmetric particle, the axion, and primordial black holes. As far as astrophysicists are concerned, a complete specification of the relevant cold dark matter properties is given by the density parameter Ω_{c}, though those seeking to detect it directly need also to know its interaction properties.

Cold dark matter is the standard assumption and gives an excellent fit to observations, except possibly on the shortest scales where there remains some controversy concerning the structure of dwarf galaxies and possible substructure in galaxy halos. It has long been excluded for all the dark matter to have a large velocity dispersion, so-called 'hot' dark matter, as it does not permit galaxies to form; for thermal relics the mass must be above about 1 keV to satisfy this constraint, though relics produced non-thermally, such as the axion, need not obey this limit. However, in future further parameters might need to be introduced to describe dark matter properties relevant to astrophysical observations. Suggestions that have been made include a modest velocity dispersion (warm dark matter) and dark matter self-interactions. There remains the possibility that the dark matter is comprized of two separate components, *e.g.*, a cold one and a hot one, an example being if massive neutrinos have a non-negligible effect.

25.2.3 *Relativistic species*

The number of relativistic species in the young Universe (omitting photons) is denoted N_{eff}. In the standard cosmological model only the three neutrino species contribute, and its baseline value is assumed fixed at 3.044 (the small shift from 3 is because of a slight predicted deviation from a thermal distribution [16]). However other species could contribute, for example an extra neutrino, possibly of sterile type, or massless Goldstone bosons or other scalars. It is hence interesting to study the effect of allowing this parameter to vary, and indeed although 3.044 is consistent with the data, most analyses currently suggest a somewhat higher value (*e.g.*, Ref. [17]).

25.2.4 *Dark energy and modified gravity*

While the standard cosmological model given above features a cosmological constant, in order to explain observations indicating that the Universe is presently accelerating, further possibilities exist under the general headings of 'dark energy' and 'modified gravity'. These topics are described in detail in the Dark Energy chapter in this volume. This article focuses on the case of the cosmological constant, since this simple model is a good match to existing data. We note that more general treatments of dark energy/modified gravity will lead to weaker constraints on other parameters.

25.2.5 *Complex ionization history*

The full ionization history of the Universe is given by the ionization fraction as a function of redshift z. The simplest scenario takes the ionization to have the small residual value left after recombination up to some redshift z_{i}, at which point the Universe instantaneously reionizes completely. Then there is a one-to-one correspondence between τ and z_{i} (that relation, however, also depending on other cosmological parameters). An accurate treatment of this process will track separate histories for hydrogen and helium. While currently rapid ionization appears to be a good approximation, as data improve a more complex ionization history may need to be considered.

25.2.6 *Varying 'constants'*

Variation of the fundamental constants of Nature over cosmological times is another possible enhancement of the standard cosmology. There is a long history of study of variation of the gravitational constant G_{N}, and more recently attention has been

Downloaded from https://academic.oup.com/ptep/article/2022/8/083C01/6651666 by KIT Library user on 27 September 2022

drawn to the possibility of small fractional variations in the fine-structure constant. There is presently no observational evidence for the former, which is tightly constrained by a variety of measurements. Evidence for the latter has been claimed from studies of spectral line shifts in quasar spectra at redshift $z \simeq 2$ [18], but this is presently controversial and in need of further observational study.

25.2.7 *Cosmic topology*

The usual hypothesis is that the Universe has the simplest topology consistent with its geometry, for example that a flat Universe extends forever. Observations cannot tell us whether that is true, but they can test the possibility of a non-trivial topology on scales up to roughly the present Hubble scale. Extra parameters would be needed to specify both the type and scale of the topology; for example, a cuboidal topology would need specification of the three principal axis lengths and orientation. At present, there is no evidence for non-trivial cosmic topology [19].

25.3 Cosmological Probes

The goal of the observational cosmologist is to utilize astronomical information to derive cosmological parameters. The transformation from the observables to the parameters usually involves many assumptions about the nature of the data, as well as of the dark sector. Below we outline the physical processes involved in each of the major probes, and the main recent results. The first two subsections concern probes of the homogeneous Universe, while the remainder consider constraints from perturbations.

In addition to statistical uncertainties we note three sources of systematic uncertainties that will apply to the cosmological parameters of interest: (i) due to the assumptions on the cosmological model and its priors (*i.e.*, the number of assumed cosmological parameters and their allowed range); (ii) due to the uncertainty in the astrophysics of the objects (*e.g.*, light-curve fitting for supernovae or the mass–temperature relation of galaxy clusters); and (iii) due to instrumental and observational limitations (*e.g.*, the effect of 'seeing' on weak gravitational lensing measurements, or beam shape on CMB anisotropy measurements).

These systematics, the last two of which appear as 'nuisance parameters', pose a challenging problem to the statistical analysis. We attempt a statistical fit to the whole Universe with 6 to 12 parameters, but we might need to include hundreds of nuisance parameters, some of them highly correlated with the cosmological parameters of interest (for example time-dependent galaxy biasing could mimic the growth of mass fluctuations). Fortunately, there is some astrophysical prior knowledge on these effects, and a small number of physically-motivated free parameters would ideally be preferred in the cosmological parameter analysis.

25.3.1 *Measures of the Hubble constant*

In 1929, Edwin Hubble discovered the law of expansion of the Universe by measuring distances to nearby galaxies. The slope of the relation between the distance and recession velocity is defined to be the present-epoch Hubble constant, H_0. Astronomers argued for decades about the systematic uncertainties in various methods and derived values over the wide range $40\,\mathrm{km\,s^{-1}\,Mpc^{-1}} \lesssim H_0 \lesssim 100\,\mathrm{km\,s^{-1}\,Mpc^{-1}}$.

One of the most reliable results on the Hubble constant came from the Hubble Space Telescope (HST) Key Project [20]. This study used the empirical period–luminosity relation for Cepheid variable stars, and calibrated a number of secondary distance indicators: Type Ia Supernovae (SNe Ia), the Tully–Fisher relation, surface-brightness fluctuations, and Type II Supernovae. This approach has been further extended. Based on HST photometry of 75 Milky Way Cepheids and Gaia EDR3 parallaxes, the SH0ES team derived $H_0 = 73.2 \pm 1.3\,\mathrm{km\,s^{-1}\,Mpc^{-1}}$ [21].

Three other methods have been used recently. One is a calibration of the tip of the red-giant branch applied to Type Ia supernovae, the Carnegie–Chicago Hubble Programme (CCHP) finding $H_0 = 69.8 \pm 0.6$ (stat.) ± 1.6 (sys.) $\mathrm{km\,s^{-1}\,Mpc^{-1}}$ [22]. The second uses the method of time delay in gravitationally-lensed quasars; Birrer et al. [23] find $H_0 = 67.4^{+4.1}_{-3.2}\,\mathrm{km\,s^{-1}\,Mpc^{-1}}$ from a sample of 40 lenses (which includes as a subset the six systems previously used by the HOLiCOW collaboration [24] who obtained a higher value). A third method that came to fruition recently is based on gravitational waves; the 'bright standard siren' method applied to the binary neutron star GW170817 yields $H_0 = 70^{+12}_{-8}\,\mathrm{km\,s^{-1}\,Mpc^{-1}}$ [25]. Adding two 'dark standard siren' systems shifts this to $H_0 = 72^{+12}_{-8}\,\mathrm{km\,s^{-1}\,Mpc^{-1}}$ [26], still dominated by the single bright siren system. When many more gravitational-wave events have been acquired, the future uncertainties on H_0 from standard sirens will get smaller.

The determination of H_0 by the *Planck* Collaboration [2] gives a lower value than most of the above methods, $H_0 = 67.4 \pm 0.5\,\mathrm{km\,s^{-1}\,Mpc^{-1}}$. As they discuss, there is strong degeneracy of H_0 with other parameters, particularly Ω_m and the neutrino mass. It is worth noting that using the 'inverse distance ladder' method gives a result $H_0 = 67.8 \pm 1.3\,\mathrm{km\,s^{-1}\,Mpc^{-1}}$ [27], close to the *Planck* result. The inverse distance ladder relies on absolute-distance measurements from baryon acoustic oscillations (BAOs) to calibrate the intrinsic magnitude of the SNe Ia (rather than nearby Cepheids and parallax). This measurement was derived from 207 spectroscopically-confirmed Type Ia supernovae from the Dark Energy Survey (DES), an additional 122 low-redshift SNe Ia, and measurements of BAOs. A combination of DES Year 3 (Y3) clustering and weak lensing with BAO and BBN (assuming ΛCDM) gives $H_0 = 67.6 \pm 0.9\,\mathrm{km\,s^{-1}\,Mpc^{-1}}$ [28]. The completed Extended Baryon Oscillation Spectroscopic Survey (eBOSS) [29] inverse distance ladder result, within an assumed extended cosmological model, is $H_0 = 68.2 \pm 0.8\,\mathrm{km\,s^{-1}\,Mpc^{-1}}$, also close to the *Planck* value.

The tension between the H_0 values from *Planck* and the traditional cosmic distance ladder methods, with the SH0ES result deviating from *Planck* by 4.2σ, is under intense investigation for potential systematic effects. There is possibly a trend for higher H_0 derived from the nearby Universe and a lower H_0 from the early Universe, which has led some researchers to propose a time-variation of the dark energy component or other exotic scenarios. Ongoing studies are addressing the question of whether the Hubble tension is due to systematics in at least one of the probes, or a signature of new physics.

Figure 25.1 shows a selection of recent H_0 values, summarizing the current status of the Hubble constant tension. We note that while the tension remains highly significant, its severity has somewhat lessened compared to our assessment in the previous edition of this article two years ago.

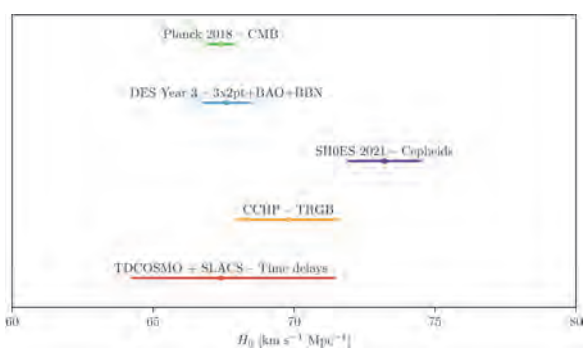

Figure 25.1: A selection of recent H_0 measurements from the various projects as described in the text. The standard-siren determinations are omitted as they are too wide for the plot. Figure courtesy of Pablo Lemos.

25.3.2 *Supernovae as cosmological probes*

Empirically, the peak luminosity of SNe Ia can be used as an efficient distance indicator (*e.g.*, Ref. [30]), thus allowing cosmology to be constrained via the distance–redshift relation. The favorite theoretical explanation for SNe Ia is the thermonuclear disruption of carbon–oxygen white dwarfs. Although not perfect 'standard candles', it has been demonstrated that by correcting for a relation between the light-curve shape, color, and luminosity at max-

Downloaded from https://academic.oup.com/ptep/article/2022/8/083C01/6651666 by KIT Library user on 27 September 2022

imum brightness, the dispersion of the measured luminosities can be greatly reduced. There are several possible systematic effects that may affect the accuracy of the use of SNe Ia as distance indicators, *e.g.*, evolution with redshift and interstellar extinction in the host galaxy and in the Milky Way.

Two major studies, the Supernova Cosmology Project and the High-z Supernova Search Team, found evidence for an accelerating Universe [31], interpreted as due to a cosmological constant or a dark energy component. When combined with the CMB data (which indicate near flatness, *i.e.*, $\Omega_{\rm m} + \Omega_\Lambda \simeq 1$), the best-fit values were $\Omega_{\rm m} \simeq 0.3$ and $\Omega_\Lambda \simeq 0.7$. Most results in the literature are consistent with the $w = -1$ cosmological constant case. The most-used sample currently is the Pantheon compilation [32]. This sample of 1048 spectroscopically-confirmed SNe Ia gives $\Omega_{\rm m} = 0.298 \pm 0.022$ (stat+sym) for an assumed flat ΛCDM model. In combination with the CMB, for a flat wCDM model these data give $w = -1.03 \pm 0.04$ and $\Omega_{\rm m} = 0.307 \pm 0.012$. For comparison, an analysis of a sample of 207 spectroscopically-confirmed DES SNe Ia combined with 122 low-redshift SNe [33] yielded $\Omega_{\rm m} = 0.331 \pm 0.038$ for an assumed flat ΛCDM model. Future experiments will refine constraints on the cosmic equation of state $w(z)$.

25.3.3 *Cosmic microwave background*

The physics of the CMB is described in detail in the CMB chapter in this volume. Before recombination, the baryons and photons are tightly coupled, and the perturbations oscillate in the potential wells generated primarily by the dark matter perturbations. After decoupling, the baryons are free to collapse into those potential wells. The CMB carries a record of conditions at the time of last scattering, often called primary anisotropies. In addition, it is affected by various processes as it propagates towards us, including the effect of a time-varying gravitational potential (the integrated Sachs-Wolfe effect), gravitational lensing, and scattering from ionized gas at low redshift.

The primary anisotropies, the integrated Sachs–Wolfe effect, and the scattering from a homogeneous distribution of ionized gas, can all be calculated using linear perturbation theory. Available codes include `CAMB` and `CLASS` [9], the former widely used embedded within the analysis package `CosmoMC` [34] and in higher-level analysis packages such as `CosmoSIS` [35] and `CosmoLike` [36]. Gravitational lensing is also calculated in these codes. Secondary effects, such as inhomogeneities in the reionization process, and scattering from gravitationally-collapsed gas (the Sunyaev–Zeldovich or SZ effect), require more complicated, and more uncertain, calculations.

The upshot is that the detailed pattern of anisotropies depends on all of the cosmological parameters. In a typical cosmology, the anisotropy power spectrum [usually plotted as $\ell(\ell+1)C_\ell$] features a flat plateau at large angular scales (small ℓ), followed by a series of oscillatory features at higher angular scales, the first and most prominent being at around one degree ($\ell \simeq 200$). These features, known as acoustic peaks, represent the oscillations of the photon–baryon fluid around the time of decoupling. Some features can be closely related to specific parameters—for instance, the location in multipole space of the set of peaks probes the spatial geometry, while the relative heights of the peaks probe the baryon density—but many other parameters combine to determine the overall shape.

The 2018 data release from the *Planck* satellite [1] gives the most powerful results to date on the spectrum of CMB temperature anisotropies, with a precision determination of the temperature power spectrum to beyond $\ell = 2000$. The Atacama Cosmology Telescope (ACT) and South Pole Telescope (SPT) experiments extend these results to higher angular resolution, though without full-sky coverage. *Planck* and the polarization-sensitive versions of ACT and SPT give the state of the art in measuring the spectrum of E-polarization anisotropies and the correlation spectrum between temperature and polarization. These are consistent with models based on the parameters we have described, and provide accurate determinations of many of those parameters [2]. Primordial B-mode polarization has not been detected (although the gravitational lensing effect on B modes has been measured).

The data provide an exquisite measurement of the location of the set of acoustic peaks, determining the angular-diameter distance of the last-scattering surface. In combination with other data this strongly constrains the spatial geometry, in a manner consistent with spatial flatness and excluding significantly-curved Universes. CMB data give a precision measurement of the age of the Universe. The CMB also gives a baryon density consistent with, and at higher precision than, that coming from BBN. It affirms the need for both dark matter and dark energy. It shows no evidence for dynamics of the dark energy, being consistent with a pure cosmological constant ($w = -1$). The density perturbations are consistent with a power-law primordial spectrum, and there is no indication yet of tensor perturbations. The current best-fit for the reionization optical depth from CMB data, $\tau = 0.054$, is in line with models of how early structure formation induces reionization.

Planck has also made the first all-sky map of the CMB lensing field, which probes the entire matter distribution in the Universe and adds some additional constraining power to the CMB-only data-sets. These measurements are compatible with the expected effect in the standard cosmology.

25.3.4 *Galaxy clustering*

The power spectrum of density perturbations is affected by the nature of the dark matter. Within the ΛCDM model, the power spectrum shape depends primarily on the primordial power spectrum and on the combination $\Omega_{\rm m}h$, which determines the horizon scale at matter–radiation equality, with a subdominant dependence on the baryon density. The matter distribution is most easily probed by observing the galaxy distribution, but this must be done with care since the galaxies do not perfectly trace the dark matter distribution. Rather, they are a 'biased' tracer of the dark matter [37]. The need to allow for such bias is emphasized by the observation that different types of galaxies show bias with respect to each other. In particular, scale-dependent and stochastic biasing may introduce a systematic effect on the determination of cosmological parameters from redshift surveys [38]. Prior knowledge from simulations of galaxy formation or from gravitational lensing data could help to quantify biasing. Furthermore, the observed 3D galaxy distribution is in redshift space, *i.e.*, the observed redshift is the sum of the Hubble expansion and the line-of-sight peculiar velocity, leading to linear and non-linear dynamical effects that also depend on the cosmological parameters. On the largest length scales, the galaxies are expected to trace the location of the dark matter, except for a constant multiplier b to the power spectrum, known as the linear bias parameter. On scales smaller than 20 Mpc or so, the clustering pattern is 'squashed' in the radial direction due to coherent infall, which depends approximately on the parameter $\beta \equiv \Omega_{\rm m}^{0.6}/b$ (on these shorter scales, more complicated forms of biasing are not excluded by the data). On scales of a few Mpc, there is an effect of elongation along the line of sight (colloquially known as the 'finger of God' effect) that depends on the galaxy velocity dispersion.

25.3.4.1 *Baryon acoustic oscillations*

The power spectra of the 2-degree Field (2dF) Galaxy Redshift Survey and the Sloan Digital Sky Survey (SDSS) are well fit by a ΛCDM model and both surveys showed first evidence for baryon acoustic oscillations (BAOs) [39, 40]. When eBOSS is combined with *Planck*, Pantheon Type Ia Supernovae and other probes the result is $w_p = -1.020 \pm 0.032$ at the pivot redshift $z_p = 0.29$ [29]. Similar results for w were obtained e.g. by the WiggleZ survey [41].

25.3.4.2 *Redshift distortion*

There is continuing interest in the 'redshift distortion' effect. This distortion depends on cosmological parameters [42] via the perturbation growth rate in linear theory $f(z) = d\ln\delta/d\ln a \simeq \Omega_{\rm m}^{\gamma}(z)$, where $\gamma \simeq 0.55$ for the ΛCDM model and may be different for modified gravity models. By measuring $f(z)$ it is feasible to constrain γ and rule out certain modified gravity models [43, 44]. We note the degeneracy of the redshift-distortion pattern and the geometric distortion (the so-called Alcock–Paczynski effect [45]), *e.g.*, as illustrated by the WiggleZ survey [46] and eBOSS [29].

Downloaded from https://academic.oup.com/ptep/article/2022/8/083C01/6651666 by KIT Library user on 27 September 2022

25.3.4.3 *Limits on neutrino mass from galaxy surveys and other probes*

Large-scale structure data place constraints on Ω_ν due to the neutrino free-streaming effect [47]. Presently there is no clear detection, and upper limits on neutrino mass are commonly estimated by comparing the observed galaxy power spectrum with a four-component model of baryons, cold dark matter, a cosmological constant, and massive neutrinos. Such analyses also assume that the primordial power spectrum is adiabatic, scale-invariant, and Gaussian. Potential systematic effects include biasing of the galaxy distribution and non-linearities of the power spectrum. An upper limit can also be derived from CMB anisotropies alone, while combination with additional cosmological data-sets can improve the results.

The most recent results on neutrino mass upper limits and other neutrino properties are summarized in the Neutrinos in Cosmology chapter in this volume. The latest cosmological data constrain the sum of neutrino masses to be below 0.2 eV or even 0.1 eV depending on the assumed priors and systematics (e.g. Refs. [2,29].) Since the lower limit on this sum from oscillation experiments (assuming normal hierarchy) is 0.06 eV it is expected that future cosmological surveys will soon detect effects from the neutrino mass. Also, current cosmological datasets are in good agreement with the standard value for the effective number of neutrino species $N_{\rm eff} = 3.044$.

25.3.5 *Clustering in the inter-galactic medium*

It is commonly assumed, based on hydrodynamic simulations, that the neutral hydrogen in the inter-galactic medium (IGM) can be related to the underlying mass distribution. It is then possible to estimate the matter power spectrum from the absorption observed in quasar spectra, the so-called Lyman-α forest. The usual procedure is to measure the power spectrum of the transmitted flux, and then to infer the mass power spectrum. Photoionization heating by the ultraviolet background radiation and adiabatic cooling by the expansion of the Universe combine to give a simple power-law relation between the gas temperature and the baryon density. It also follows that there is a power-law relation between the optical depth τ and $\rho_{\rm b}$. Therefore, the observed flux $F = \exp(-\tau)$ is strongly correlated with $\rho_{\rm b}$, which itself traces the mass density. The matter and flux power spectra can be related by a biasing function that is calibrated from simulations. There are two variants of Lyman-alpha analyses: 1-dimensional power spectra from individual lines-of-sight that probe small ($\sim$Mpc) scales, and 3-dimensional Lyman-alpha BAO analyses that measure large-scale correlations (over $\sim$100 Mpc scales) using neighbouring quasar lines-of-sight.

The latest BOSS and eBOSS datasets have provided measurements of the BAO scale both in the Lyman-α absorption and in its cross correlation with quasars at an effective redshift $z = 2.3$ [29, 48]. The results agree within 1.5-σ with the *Planck* CMB flat-Λ estimation for BAO scale. Such measurements will improve with the Dark Energy Spectroscopic Instrument (DESI) and other future spectroscopic surveys. The Lyman-α flux power spectrum has also been used to constrain the nature of dark matter, for example limiting the amount of warm dark matter [49].

25.3.6 *Weak gravitational lensing*

Images of background galaxies are distorted by the gravitational effect of mass variations along the line of sight. Deep gravitational potential wells, such as galaxy clusters, generate 'strong lensing' leading to arcs, arclets, and multiple images, while more moderate perturbations give rise to 'weak lensing'. Weak lensing is now widely used to measure the mass power spectrum in selected regions of the sky (see Ref. [50] for reviews). Since the signal is weak, the image of deformed galaxy shapes (the 'shear map') must be analyzed statistically to measure the power spectrum, higher moments, and cosmological parameters. There are various systematic effects in the interpretation of weak lensing, *e.g.*, due to atmospheric distortions during observations, the redshift distribution of the background galaxies (usually depending on the accuracy of photometric redshifts), the intrinsic correlation of galaxy shapes, and non-linear modeling uncertainties.

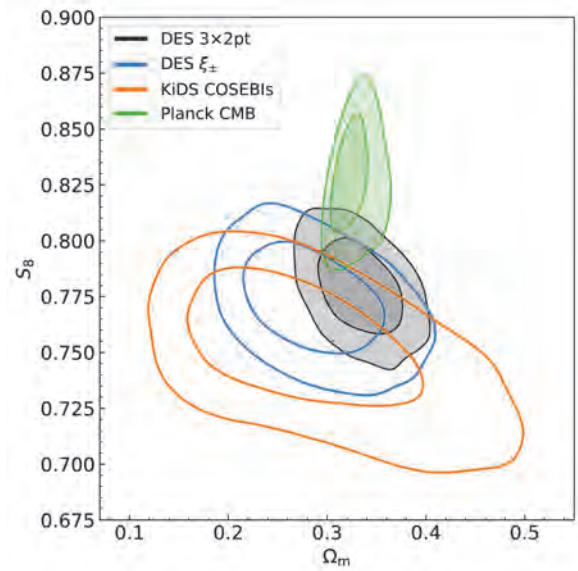

Figure 25.2: Marginalized posterior contours (inner 68% confidence level, outer 95% confidence level) in the $\Omega_{\rm m}$–S_8 plane. The plot shows a subset of the cases shown in Figure 19 of Ref. [28]: KiDS weak lensing alone, DES Y3 weak lensing alone, DES Y3 combined weak lensing and galaxy clustering (3x2pt), and Planck CMB. Figure courtesy of Michael Troxel and the DES collaboration.

Weak-lensing measurements from the Kilo-Degree Survey (KiDS) [51], the Subaru Hyper-Suprime-Cam (HSC) [52], and DES Y3 [53] have constrained the clumpiness parameter $S_8 \equiv \sigma_8(\Omega_{\rm m}/0.3)^{0.5}$. Each of these surveys has yielded S_8 lower by about 2σ than S_8 derived from *Planck*. This tension is not yet resolved. Figure 25.2 shows the $\Omega_{\rm m}$–S_8 constraints derived from of KiDS (weak lensing) and DES Y3 (weak lensing with and without galaxy clustering) versus the CMB constraint from *Planck*. Results from weak lensing from DES, combined with other probes, are described in the next section.

25.3.7 *Other probes*

Other probes that have been used to constrain cosmological parameters, but that are not presently competitive in terms of accuracy, are the integrated Sachs-Wolfe effect [54,55], the number density or composition of galaxy clusters [56], and galaxy peculiar velocities which probe the mass fluctuations in the local Universe [57].

25.4 Bringing probes together

Although it contains two ingredients—dark matter and dark energy—which have not yet been verified by laboratory experiments, the ΛCDM model is almost universally accepted by cosmologists as the best description of the present data. The approximate values of some of the key parameters are $\Omega_{\rm b} \simeq 0.05$, $\Omega_{\rm c} \simeq 0.25$, $\Omega_\Lambda \simeq 0.70$, and a Hubble constant $h \simeq 0.70$. The spatial geometry is very close to flat (and usually assumed to be precisely flat), and the initial perturbations Gaussian, adiabatic, and nearly scale-invariant.

The most powerful data source is the CMB, which on its own supports all these main tenets. Values for some parameters, as given in Ref. [2], are reproduced in Table 25.1. These particular results presume a flat Universe. The constraints are somewhat strengthened by adding additional data-sets, BAO being shown in the Table as an example, though most of the constraining power resides in the CMB data. Similar constraints at lower precision were previously obtained by the *WMAP* collaboration.

If the assumption of spatial flatness is lifted, it turns out that the primary CMB on its own constrains the spatial curvature fairly weakly, due to a parameter degeneracy in the angular-diameter distance. However, inclusion of other data readily re-

Downloaded from https://academic.oup.com/ptep/article/2022/8/083C01/6651666 by KIT Library user on 27 September 2022

Table 25.1: Parameter constraints reproduced from Ref. [2] (Table 2, column 5), with some additional rounding. Both columns assume the ΛCDM cosmology with a power-law initial spectrum, no tensors, spatial flatness, a cosmological constant as dark energy, and the sum of neutrino masses fixed to 0.06 eV. Above the line are the six parameter combinations actually fit to the data ($\theta_{\rm MC}$ is a measure of the sound horizon at last scattering); those below the line are derived from these. The first column uses *Planck* primary CMB data plus the *Planck* measurement of CMB lensing. This column gives our present recommended values. The second column adds in data from a compilation of BAO measurements described in Ref. [2]. The perturbation amplitude $\Delta^2_{\mathcal{R}}$ (denoted $A_{\rm s}$ in the original paper) is specified at the scale $0.05\,{\rm Mpc}^{-1}$. Uncertainties are shown at 68% confidence.

	Planck TT,TE,EE+lowE+lensing	+BAO
$\Omega_{\rm b}h^2$	0.02237 ± 0.00015	0.02242 ± 0.00014
$\Omega_{\rm c}h^2$	0.1200 ± 0.0012	0.1193 ± 0.0009
$100\,\theta_{\rm MC}$	1.0409 ± 0.0003	1.0410 ± 0.0003
$n_{\rm s}$	0.965 ± 0.004	0.966 ± 0.004
τ	0.054 ± 0.007	0.056 ± 0.007
$\ln(10^{10}\Delta^2_{\mathcal{R}})$	3.044 ± 0.014	3.047 ± 0.014
h	0.674 ± 0.005	0.677 ± 0.004
σ_8	0.811 ± 0.006	0.810 ± 0.006
$\Omega_{\rm m}$	0.315 ± 0.007	0.311 ± 0.006
Ω_Λ	0.685 ± 0.007	0.689 ± 0.006

moves this degeneracy. Simply adding the *Planck* lensing measurement, and with the assumption that the dark energy is a cosmological constant, yields a 68% confidence constraint on $\Omega_{\rm tot} \equiv \sum \Omega_i + \Omega_\Lambda = 1.011 \pm 0.006$ and further adding BAO makes it 0.9993 ± 0.0019 [2]. Results of this type are normally taken as justifying the restriction to flat cosmologies.

One derived parameter that is very robust is the age of the Universe, since there is a useful coincidence that for a flat Universe the position of the first peak is strongly correlated with the age. The CMB data give 13.797 ± 0.023 Gyr (assuming flatness). This is in good agreement with the ages of the oldest globular clusters and with radioactive dating.

The baryon density $\Omega_{\rm b}$ is now measured with high accuracy from CMB data alone, and is consistent with and more precise than the determination from BBN. The value quoted in the Big-Bang Nucleosynthesis chapter in this volume is $\Omega_{\rm b}h^2 = 0.0224 \pm 0.0007$.

While Ω_Λ is measured to be non-zero with very high confidence, there is no evidence of evolution of the dark energy density. As described in the Dark Energy chapter in this volume a combination of CMB, SN, and BAO measurements, assuming a flat Universe, found $w = -1.03 \pm 0.03$ [29], consistent with the cosmological constant case $w = -1$. Allowing more complicated forms of dark energy weakens the limits.

The data provide strong support for the main predictions of the simplest inflation models: spatial flatness and adiabatic, Gaussian, nearly scale-invariant density perturbations. But it is disappointing that there is no sign of primordial gravitational waves; combining *Planck* and *WMAP* with BICEP2/Keck Array BK18 data (plus BAO data to help constrain $n_{\rm s}$) gives a 95% confidence upper limit of $r < 0.036$ at the scale $0.05\,{\rm Mpc}^{-1}$ [58]. The density perturbation spectral index is clearly required to be less than one by current data, though the strength of that conclusion can weaken if additional parameters are included in the model fits.

Tests have been made for various types of non-Gaussianity, a particular example being a parameter $f_{\rm NL}$ that measures a quadratic contribution to the perturbations. Various non-Gaussian shapes are possible (see Ref. [59] for details), and current constraints on the popular 'local', 'equilateral', and 'orthogonal' types (combining CMB temperature and polarization data) are $f_{\rm NL}^{\rm local} = -1 \pm 5$, $f_{\rm NL}^{\rm equil} = -26 \pm 47$, and $f_{\rm NL}^{\rm ortho} = -38 \pm 24$ respectively (these look weak, but prominent non-Gaussianity requires the product $f_{\rm NL}\Delta_{\mathcal{R}}$ to be large, and $\Delta_{\mathcal{R}}$ is of order 10^{-5}). Clearly none of these give any indication of primordial non-Gaussianity.

While the above results come from the CMB alone, other probes are becoming competitive (especially when considering more complex cosmological models), and so combination of data from different sources is of growing importance. We note that it has become fashionable to combine probes at the level of power-spectrum data vectors, taking into account nuisance parameters in each type of measurement. Discussions on 'tension' in resulting cosmological parameters depend on the statistical approaches used. Commonly the cosmology community works within the Bayesian framework, and assesses agreement amongst data sets with respect to a model via Bayesian Evidence, essentially the denominator in Bayes's theorem.

As an example of results, combining DES Y3 (position–position clustering, galaxy–galaxy lensing, and weak lensing shear) with *Planck*, BAO and RSD measurements from eBOSS, and type Ia supernovae from the Pantheon dataset compilation has shown the datasets to be mutually compatible and yields very tight constraints on cosmological parameters: $S_8 \equiv \sigma_8(\Omega_{\rm m}/0.3)^{0.5} = 0.812 \pm 0.008$, and $\Omega_{\rm m} = 0.306^{+0.004}_{-0.005}$ in ΛCDM, and $w = -1.03 \pm 0.03$ in wCDM [28] matching the constraint in Ref. [29]. The combined measurement of the Hubble constant within ΛCDM gives $H_0 = 68.0^{+0.4}_{-0.3}\,{\rm km\,s^{-1}\,Mpc^{-1}}$, still leaving substantial tension with the SH0ES measurement described earlier. Future analyses and the next generation of surveys will test for deviations from ΛCDM, for example epoch-dependent $w(z)$ and modifications to General Relativity.

25.5 Outlook for the future

The concordance model is now well-established, and there seems little room left for any dramatic revision of this paradigm. A measure of the strength of that statement is how difficult it has proven to formulate convincing alternatives.

Should there indeed be no major revision of the current paradigm, we can expect future developments to take one of two directions. Either the existing parameter set will continue to prove sufficient to explain the data, with the parameters subject to ever-tightening constraints, or it will become necessary to deploy new parameters. The latter outcome would be very much the more interesting, offering a route towards understanding new physical processes relevant to the cosmological evolution. There are many possibilities on offer for striking discoveries, for example:

- the cosmological effects of a neutrino mass may be unambiguously detected, shedding light on fundamental neutrino properties;
- detection of primordial non-Gaussianities would indicate that non-linear processes influence the perturbation generation mechanism;
- detection of variation in the dark-energy density (*i.e.*, $w \neq -1$) would provide much-needed experimental input into its nature.

These provide more than enough motivation for continued efforts to test the cosmological model and improve its accuracy. Over the coming years, there are a wide range of new observations that will bring further precision to cosmological studies. Indeed, there are far too many for us to be able to mention them all here, and so we will just highlight a few areas.

The CMB observations will improve in several directions. A current frontier is the study of polarization, for which power spectrum measurements have now been made by several experiments. Detection of primordial B-mode anisotropies is the next major goal and a variety of projects are targeting this, though theory gives little guidance as to the likely signal level. Future CMB projects that are approved include *LiteBIRD* and the Simons Observatory.

An impressive array of cosmology surveys are already operational, under construction, or proposed, including the ground-

Downloaded from https://academic.oup.com/ptep/article/2022/8/083C01/6651666 by KIT Library user on 27 September 2022

based Hyper Suprime Camera (HSC) and Rubin-LSST imaging surveys, spectroscopic surveys such as DESI and space missions *Euclid* and the Roman Wide-Field Infrared Survey (WFIRST).

An exciting area for the future is radio surveys of the redshifted 21-cm line of hydrogen. Because of the intrinsic narrowness of this line, by tuning the bandpass the emission from narrow redshift slices of the Universe will be measured to extremely high redshift, probing the details of the reionization process at redshifts up to perhaps 20, as well as measuring large-scale features such as the BAOs. LOFAR and CHIME are the first instruments able to do this and have begun operations. In the longer term, the Square Kilometre Array (SKA) will take these studies to a precision level.

The development of the first precision cosmological model is a major achievement. However, it is important not to lose sight of the motivation for developing such a model, which is to understand the underlying physical processes at work governing the Universe's evolution. From that perspective, progress has been much less dramatic. For instance, there are many proposals for the nature of the dark matter, but no consensus as to which is correct. The nature of the dark energy remains a mystery. Even the baryon density, now measured to an accuracy of a percent, lacks an underlying theory able to predict it within orders of magnitude. Precision cosmology may have arrived, but at present many key questions remain to motivate and challenge the cosmology community.

References

[1] Planck Collab. 2018 Results I, Astron. Astrophys. **641**, A1 (2020), [arXiv:1807.06205].

[2] Planck Collab. 2018 Results VI, Astron. Astrophys. **641**, A6 (2020), [arXiv:1807.06209].

[3] C. L. Bennett *et al.* (WMAP), Astrophys. J. Suppl. **208**, 20 (2013), [arXiv:1212.5225].

[4] G. Hinshaw *et al.* (WMAP), Astrophys. J. Suppl. **208**, 19 (2013), [arXiv:1212.5226].

[5] S. Fukuda *et al.* (Super-Kamiokande), Phys. Rev. Lett. **85**, 3999 (2000), [hep-ex/0009001]; Q. R. Ahmad *et al.* (SNO), Phys. Rev. Lett. **87**, 071301 (2001), [arXiv:nucl-ex/0106015].

[6] E.W. Kolb and M.S. Turner, *The Early Universe*, Addison–Wesley (Redwood City, 1990).

[7] D.H. Lyth and A.R. Liddle, *The Primordial Density Perturbation*, Cambridge University Press (2009).

[8] A. R. Liddle and D. H. Lyth, Phys. Lett. **B291**, 391 (1992), [arXiv:astro-ph/9208007].

[9] A. Lewis, A. Challinor and A. Lasenby, Astrophys. J. **538**, 473 (2000), [arXiv:astro-ph/9911177]; D. Blas, J. Lesgourgues and T. Tram, JCAP **1107**, 034 (2011), [arXiv:1104.2933].

[10] D. J. Fixsen, Astrophys. J. **707**, 916 (2009), [arXiv:0911.1955].

[11] M. Hobson et al. (eds). *Bayesian Methods in Cosmology*, Cambridge University Press (2009).

[12] A. Kosowsky and M. S. Turner, Phys. Rev. **D52**, R1739 (1995), [arXiv:astro-ph/9504071].

[13] K. A. Malik and D. Wands, Phys. Rept. **475**, 1 (2009), [arXiv:0809.4944].

[14] Planck Collab. 2013 Results XXV, Astron. Astrophys. **571**, A25 (2014), [arXiv:1303.5085].

[15] D. H. Lyth and D. Wands, Phys. Lett. **B524**, 5 (2002), [hep-ph/0110002]; K. Enqvist and M. S. Sloth, Nucl. Phys. **B626**, 395 (2002), [hep-ph/0109214]; T. Moroi and T. Takahashi, Phys. Lett. **B522**, 215 (2001), [Erratum: Phys. Lett.B539,303(2002)], [hep-ph/0110096].

[16] J. J. Bennett *et al.*, JCAP **04**, 073 (2021), [arXiv:2012.02726].

[17] S. Riemer-Sorensen, D. Parkinson and T. M. Davis, Publ. Astron. Soc. Austral. **30**, e029 (2013), [arXiv:1301.7102].

[18] J. K. Webb *et al.*, Phys. Rev. Lett. **107**, 191101 (2011), [arXiv:1008.3907]; J. A. King *et al.*, Mon. Not. Roy. Astron. Soc. **422**, 3370 (2012), [arXiv:1202.4758]; P. Molaro *et al.*, Astron. & Astrophys. **555**, 68 (2013).

[19] Planck Collab. 2015 Results XVIII, Astron. Astrophys. **594**, A18 (2016), [arXiv:1502.01593].

[20] W. L. Freedman *et al.* (HST), Astrophys. J. **553**, 47 (2001), [arXiv:astro-ph/0012376].

[21] A. G. Riess *et al.*, Astrophys. J. Lett. **908**, 1, L6 (2021), [arXiv:2012.08534].

[22] W. L. Freedman (2021), [arXiv:2106.15656].

[23] S. Birrer *et al.*, Astron. Astrophys. **643**, A165 (2020), [arXiv:2007.02941].

[24] K. C. Wong *et al.* (2019), [arXiv:1907.04869].

[25] B. P. Abbott *et al.* (LIGO Scientific, Virgo, 1M2H, Dark Energy Camera GW-E, DES, DLT40, Las Cumbres Observatory, VINROUGE, MASTER), Nature **551**, 7678, 85 (2017), [arXiv:1710.05835].

[26] A. Palmese *et al.* (DES), Astrophys. J. Lett. **900**, 2, L33 (2020), [arXiv:2006.14961].

[27] E. Macaulay *et al.* (DES), Mon. Not. Roy. Astron. Soc. **486**, 2, 2184 (2019), [arXiv:1811.02376].

[28] T. M. C. Abbott *et al.* (DES) (2021), [arXiv:2105.13549].

[29] S. Alam *et al.* (eBOSS), Phys. Rev. D **103**, 8, 083533 (2021), [arXiv:2007.08991].

[30] B. Leibundgut, Ann. Rev. Astron. Astrophys. **39**, 67 (2001).

[31] A. G. Riess *et al.* (Supernova Search Team), Astron. J. **116**, 1009 (1998), [arXiv:astro-ph/9805201]; P. M. Garnavich *et al.* (Supernova Search Team), Astrophys. J. **509**, 74 (1998), [arXiv:astro-ph/9806396]; S. Perlmutter *et al.* (Supernova Cosmology Project), Astrophys. J. **517**, 565 (1999), [arXiv:astro-ph/9812133].

[32] D. M. Scolnic *et al.*, Astrophys. J. **859**, 2, 101 (2018), [arXiv:1710.00845].

[33] T. M. C. Abbott *et al.* (DES), Astrophys. J. **872**, 2, L30 (2019), [arXiv:1811.02374].

[34] A. Lewis and S. Bridle, Phys. Rev. **D66**, 103511 (2002), [arXiv:astro-ph/0205436].

[35] J. Zuntz *et al.*, Astron. Comput. **12**, 45 (2015), [arXiv:1409.3409].

[36] E. Krause and T. Eifler, Mon. Not. Roy. Astron. Soc. **470**, 2, 2100 (2017), [arXiv:1601.05779].

[37] N. Kaiser, Astrophys. J. **284**, L9 (1984).

[38] A. Dekel and O. Lahav, Astrophys. J. **520**, 24 (1999), [arXiv:astro-ph/9806193].

[39] D. J. Eisenstein *et al.* (SDSS), Astrophys. J. **633**, 560 (2005), [arXiv:astro-ph/0501171].

[40] S. Cole *et al.* (2dFGRS), Mon. Not. Roy. Astron. Soc. **362**, 505 (2005), [arXiv:astro-ph/0501174].

[41] D. Parkinson *et al.*, Phys. Rev. **D86**, 103518 (2012), [arXiv:1210.2130].

[42] N. Kaiser, Mon. Not. Roy. Astron. Soc. **227**, 1 (1987).

[43] L. Guzzo *et al.*, Nature **451**, 541 (2008), [arXiv:0802.1944].

[44] A. Nusser and M. Davis, Astrophys. J. **736**, 93 (2011), [arXiv:1101.1650].

[45] C. Alcock and B. Paczynski, Nature **281**, 358 (1979).

[46] C. Blake *et al.*, Mon. Not. Roy. Astron. Soc. **425**, 405 (2012), [arXiv:1204.3674].

[47] J. Lesgourgues and S. Pastor, Phys. Rept. **429**, 307 (2006), [arXiv:astro-ph/0603494].

[48] H. du Mas des Bourboux *et al.*, Astrophys. J. **901**, 2, 153 (2020), [arXiv:2007.08995].

[49] M. Viel *et al.*, Phys. Rev. **D88**, 043502 (2013), [arXiv:1306.2314].

[50] A. Refregier, Ann. Rev. Astron. Astrophys. **41**, 645 (2003), [arXiv:astro-ph/0307212]; R. Massey *et al.*, Nature **445**, 286 (2007), [arXiv:astro-ph/0701594]; H. Hoekstra and B. Jain, Ann. Rev. Nucl. Part. Sci. **58**, 99 (2008), [arXiv:0805.0139].

Downloaded from https://academic.oup.com/ptep/article/2022/8/083C01/6651666 by KIT Library user on 27 September 2022

[51] M. Asgari *et al.* (KiDS), Astron. Astrophys. **645**, A104 (2021), [arXiv:2007.15633].

[52] C. Hikage *et al.* (HSC), Publ. Astron. Soc. Jap. **71**, 2, 43 (2019), [arXiv:1809.09148].

[53] L. F. Secco *et al.* (DES) (2021), [arXiv:2105.13544].

[54] R. G. Crittenden and N. Turok, Phys. Rev. Lett. **75**, 2642 (1995), [arXiv:astro-ph/9505120].

[55] Planck Collab. 2015 Results XXI, Astron. Astrophys. **594**, A21 (2016), [arXiv:1502.01595].

[56] Planck Collab. 2015 Results XXIV, Astron. Astrophys. **594**, A24 (2016), [arXiv:1502.01597].

[57] A. Dekel, Ann. Rev. Astron. Astrophys. **32**, 371 (1994), [arXiv:astro-ph/9401022].

[58] P. A. R. Ade *et al.* (BICEP/Keck), Phys. Rev. Lett. **127**, 15, 151301 (2021), [arXiv:2110.00483].

[59] Planck Collab. 2018 Results IX, Astron. Astrophys. **641**, A9 (2020), [arXiv:1905.05697].

Downloaded from https://academic.oup.com/ptep/article/2022/8/083C01/6651666 by KIT Library user on 27 September 2022

26. Neutrinos in Cosmology

Revised August 2021 by J. Lesgourgues (TTK, RWTH) and L. Verde (ICC, U. of Barcelona; ICREA, Barcelona).

26.1 Standard neutrino cosmology

Neutrinos leave detectable imprints on cosmological observations that can then be used to constrain neutrino properties. This is a great example of the remarkable interconnection and interplay between nuclear physics, particle physics, astrophysics and cosmology (for general reviews see *e.g.*, [1–4]). Present cosmological data are already providing constraints on neutrino properties not only complementary but also competitive with terrestrial experiments; for instance, upper bounds on the total neutrino mass have shrinked by a factor of about 20 in the past 19 years. Forthcoming cosmological data may soon provide key information, not obtainable in other ways like *e.g.*, a measurement of the absolute neutrino mass scale.

A relic neutrino background pervading the Universe (the Cosmic Neutrino background, CνB) is a generic prediction of the standard hot Big Bang model (see Big Bang Nucleosynthesis – Chap. 24 of this *Review*). While it has not yet been detected directly, it has been indirectly confirmed by the accurate agreement of predictions and observations of: *a*) the primordial abundance of light elements (see Big Bang Nucleosynthesis – Chap. 24) of this *Review*; *b*) the power spectrum of Cosmic Microwave Background (CMB) anisotropies (see Cosmic Microwave Background – Chap. 29 of this *Review*); and *c*) the large scale clustering of cosmological structures. Within the hot Big Bang model such good agreement would fail dramatically without a CνB with properties matching closely those predicted by the standard neutrino decoupling process (*i.e.*, involving only weak interactions).

We will illustrate below that cosmology is sensitive to the following neutrino properties: their density, related to the number of active (*i.e.*, left-handed, see Neutrino Mass, Mixing, and Oscillations - Chap. 14 of this *Review*) neutrino species, and their masses. At first order, cosmology is sensitive to the total neutrino mass, but is blind to the mixing angles and CP violation phase as discussed in Neutrino Mass, Mixing, and Oscillations (Chap. 14 of this *Review*). This makes cosmological constraints nicely complementary to measurements from terrestrial neutrino experiments.

The minimal cosmological model, ΛCDM, currently providing a good fit to most cosmological data sets (with the exception of some data in tension, discussed in The Cosmological Parameters Chap. 25 of this *Review*), assumes that the only massless or light (sub-keV) relic particles since the Big Bang Nucleosynthesis (BBN) epoch are photons and active neutrinos. Extended models with light sterile neutrinos, light thermal axions or other light relics – sometimes referred to as "dark radiation"– would produce effects similar to, and potentially degenerate with, those of active neutrinos. Thus neutrino bounds are often discussed together with limits on such scenarios. In case of anomalies in cosmological data, it might not be obvious to discriminate between interpretation in terms of active neutrinos with non-standard decoupling, additional production mechanisms, non-standard interactions, etc., or in terms of some additional light particles. Such extensions have been recently explored as a possible way to resolve the H_0 tension between late and early Universe determinations [5–8], but are not widely favoured [9–11].

Hence neutrino density and mass bounds can be derived under the assumption of no additional massless or light relic particles, and the neutrino density measured in that way provides a test of standard (*i.e.*, involving only weak interactions) neutrino decoupling.

In that model, the three active neutrino types thermalize in the early Universe, with a negligible leptonic asymmetry. Then they can be viewed as three propagating mass eigenstates sharing the same temperature and identical Fermi-Dirac distributions, thus with no visible effects of flavour oscillations. Neutrinos decouple gradually from the thermal plasma at temperatures $T \sim 2\,\mathrm{MeV}$. In the instantaneous neutrino decoupling limit, *i.e.*, assuming that neutrinos were fully decoupled at the time when electron-positrons annihilate and release entropy in the thermal bath, the neutrino-to-photon density ratio between the time of electron-positron annihilation and the non-relativistic transition of neutrinos would be given by

$$\frac{\rho_\nu}{\rho_\gamma} = \frac{7}{8} N_{\rm eff} \left(\frac{4}{11}\right)^{4/3} , \tag{26.1}$$

with $N_{\rm eff} = 3$, and the last factor comes from the fourth power of the temperature ratio $T_\nu/T_\gamma = (4/11)^{1/3}$ (see Big Bang Cosmology – Chap. 22 in this *Review*). In the above formula, $N_{\rm eff}$ is called the effective number of neutrino species because it can be viewed as a convenient parametrisation of the relativistic energy density of the Universe beyond that of photons, in units of one neutrino in the instantaneous decoupling limit. Precise simulations of neutrino decoupling and electron-positron annihilation, taking into account flavor oscillations, provide precise predictions for the actual phase-space distribution of relic neutrinos [12–15]. These distributions differ from the instantaneous decoupling approximation through a combination of a small shift in the photon temperature and small non-thermal distortions, all at the percent level. The final result for the density ratio ρ_ν/ρ_γ in the relativistic regime can always be expressed as in Eq. (26.1), but with a different value of $N_{\rm eff}$. The most recent analyses, that includes the effect of neutrino oscillations with the present values of the mixing parameters, an improved calculation of the collision terms and the most recent results on plasma thermodynamics QED corrections, gives $N_{\rm eff} = 3.044$ [16, 17]. The precise number density ratio n_ν/n_γ can also be derived from such studies, and is important for computing the ratio $\Omega_\nu h^2/\sum_i m_i$ (ratio of the physical density of neutrinos in units of the critical density to the sum of neutrino masses) in the non-relativistic regime.

The neutrino temperature today, $T_\nu^0 \simeq 1.7 \times 10^{-4}$ eV $\simeq 1.9$ K, is smaller than at least two of the neutrino masses, since the two squared-mass differences are $|\Delta m^2_{31}|^{1/2} > |\Delta m^2_{21}|^{1/2} > T_\nu^0$ (see Neutrino mass, Mixing, and oscillations – Chap. 14 of this *Review*). Thus at least two neutrino mass eigenstates are non-relativistic today and behave as a small "hot" fraction of the total dark matter (they cannot be all the dark matter, as explained in Chap. 27 in this *Review*). This fraction of hot dark matter can be probed by cosmological experiments, for two related reasons, as we now describe.

First, neutrinos are the only known particles behaving as radiation at early times (during the CMB acoustic oscillations) and dark matter at late times (during structure formation), which has consequences on the background evolution. Neutrinos become non-relativistic when their mass is equal to their average momentum, given for any Fermi-Dirac-distributed particle by $\langle p \rangle = 3.15\,T$. Thus the redshift of the non-relativistic transition is given by $z_i^{\rm nr} = m_i/(3.15\,T_\nu^0) - 1 = m_i/[0.53\,\mathrm{meV}] - 1$ for each eigenstate of mass m_i, giving for instance $z_i^{\rm nr} = 110$ for $m_i = 60\,\mathrm{meV}$, corresponding to a time deep inside the matter-dominated regime. Second, until the non-relativistic transition, neutrinos travel at the speed of light, and later on they move at a typical velocity $\langle v_i/c \rangle = 3.15\,T_\nu(z)/m_i = 0.53(1+z)\,\mathrm{meV}/m_i$, which is several orders of magnitude larger than that of the dominant cold (or even of possibly warm) dark matter component(s). This brings their characteristic diffusion scale, called the "free-streaming length", to cosmological relevant values, with consequences on gravitational clustering and the growth of structure.

Once neutrinos are non-relativistic, their energy density is given by $\rho_\nu \simeq \sum m_i n_i$. Since the number densities n_i are equal to each other (up to negligible corrections coming from flavour effects in the decoupling phase), the total mass $(\sum m_\nu) = m_1 + m_2 + m_3$ can be factorized out. It is possible that the lightest neutrino is still relativistic today, in which case this relation is slightly incorrect, but given that the total density is always strongly dominated by that of non-relativistic neutrinos, the error made is completely negligible. Using the expression for n_i/n_γ obtained from precise neutrino decoupling studies, and knowing n_γ from the measurement of the CMB temperature, one can compute ρ_ν^0, the total neutrino density today, in units of the critical density $\rho_{\rm crit}^0$ [15]:

$$\Omega_\nu = \frac{\rho_\nu^0}{\rho_{\rm crit}^0} = \frac{\sum m_\nu}{93.14 h^2\,\mathrm{eV}} , \tag{26.2}$$

Downloaded from https://academic.oup.com/ptep/article/2022/8/083C01/6651666 by KIT Library user on 27 September 2022

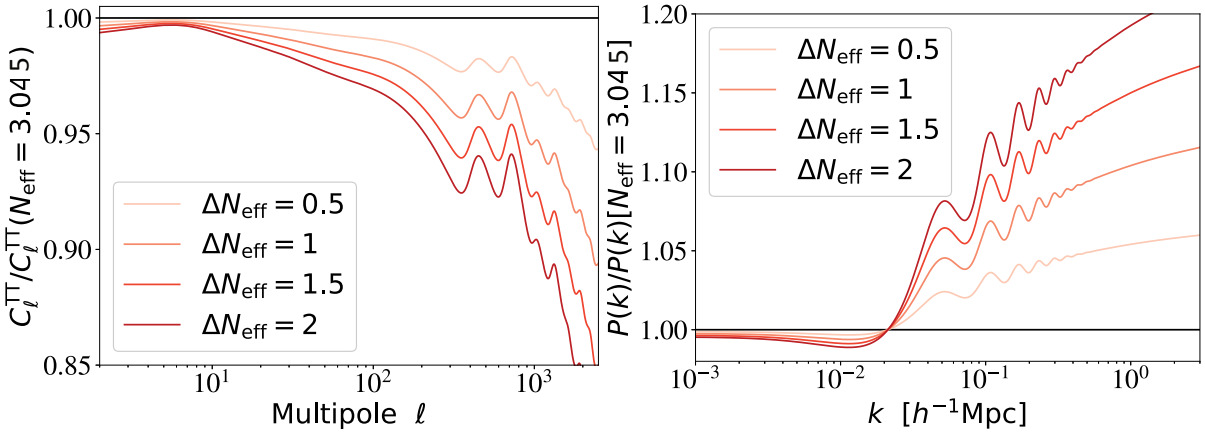

Figure 26.1: Ratio of the CMB C_ℓ^{TT} (left, including lensing effects) and matter power spectrum $P(k)$ (right, computed for each model in units of $(h^{-1}\mathrm{Mpc})^3$) for different values of $\Delta N_{\rm eff} \equiv N_{\rm eff} - 3.044$ over those of a reference model with $\Delta N_{\rm eff} = 0$. In order to minimize and better characterise the effect of $N_{\rm eff}$ on the CMB, the parameters that are kept fixed are $\{z_{\rm eq},\, z_\Lambda,\, \omega_{\rm b},\, \tau\}$ and the primordial spectrum parameters. Fixing $\{z_{\rm eq},\, z_\Lambda\}$ is equivalent to fixing the fractional density of total radiation, of total matter and of cosmological constant $\{\Omega_{\rm r}, \Omega_{\rm m}, \Omega_\Lambda\}$ while increasing the Hubble parameter as a function of $N_{\rm eff}$. The statistical errors on the C_ℓ are $\sim 1\%$ for a band power of $\Delta\ell = 30$ at $\ell \sim 1000$. The error on $P(k)$ is estimated to be of the order of 5%.

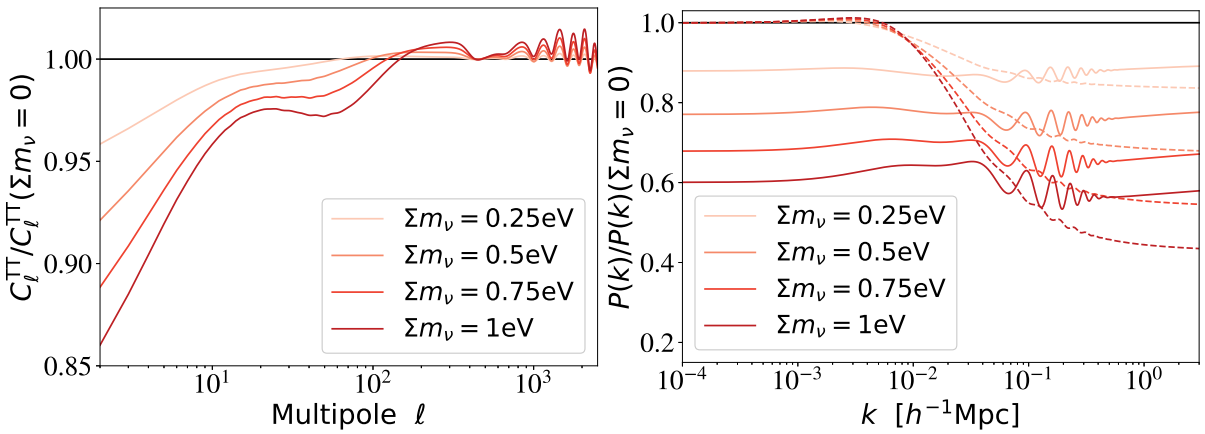

Figure 26.2: Ratio of the CMB C_ℓ^{TT} and matter power spectrum $P(k)$ (computed for each model in units of $(h^{-1}\mathrm{Mpc})^3$) for different values of $\sum m_\nu$ over those of a reference model with massless neutrinos. In order to minimize and better characterise the effect of $\sum m_\nu$ on the CMB, the parameters that are kept fixed are $\omega_{\rm b}$, $\omega_{\rm c}$, τ, the angular scale of the sound horizon $\theta_{\rm s}$ and the primordial spectrum parameters (solid lines). This implies that we are increasing the Hubble parameter h as a function of $\sum m_\nu$. For the matter power spectrum, in order to single out the effect of neutrino free-streaming on $P(k)$, the dashed lines show the spectrum ratio when $\{\omega_{\rm m}, \omega_{\rm b}, \Omega_\Lambda\}$ are kept fixed. For comparison, the error on $P(k)$ is of the order of 5% with current observations, and the fractional C_ℓ errors are of the order of $1/\sqrt{\ell}$ at low ℓ.

and the total neutrino average number density today: n_ν^0 =339.5 cm^{-3}. Here h is the Hubble constant in units of 100 km s^{-1} Mpc^{-1}.

26.2 Effects of neutrino properties on cosmological observables

As long as they are relativistic, *i.e.*, until some time deep inside the matter-dominated regime for neutrinos with a mass $m_i \ll 3.15\, T_\nu^{\rm eq} \sim 1.5$ eV (see Big Bang Cosmology, Chap. 22 in this *Review*), neutrinos enhance the density of radiation: this effect is parameterised by $N_{\rm eff}$ and can be discussed separately from the effect of the mass that will be described later in this section. Increasing $N_{\rm eff}$ impacts the observable spectra of CMB anisotropies and matter fluctuations through background and perturbation effects.

26.2.1 *Effect of* $N_{\rm eff}$ *on the CMB*

The background effects depend on what is kept fixed when increasing $N_{\rm eff}$. If the densities of other species are kept fixed, a higher $N_{\rm eff}$ implies a smaller redshift of radiation-to-matter equality, with very strong effects on the CMB spectrum: when the amount of expansion between radiation-to-matter equality and photon decoupling is larger, the CMB peaks are suppressed. This effect is not truly characteristic of the neutrino density, since it can be produced by varying several other parameters. Hence, to characterise the effect of $N_{\rm eff}$, it is more useful and illuminating to enhance the density of total radiation, of total matter and of Λ by exactly the same amount, in order to keep the redshift of radiation-to-matter equality $z_{\rm eq}$ and matter-to-Λ equality z_Λ fixed [18–20]. The primordial spectrum parameters, the baryon density $\omega_{\rm b} \equiv \Omega_{\rm b} h^2$ and the optical depth to reionization τ can be kept fixed at the same time, since we can simply vary $N_{\rm eff}$ together with the Hubble parameter h with fixed $\{\omega_{\rm b},\, \Omega_{\rm c},\, \Omega_\Lambda\}$. The impact of such a transformation is shown in Fig. 26.1 for the CMB temperature spectrum C_ℓ^{TT} (defined in Chap. 29 in this *Review*) and for the matter power spectrum $P(k)$ (defined in Chap. 22 in this *Review*) for several representative values of $N_{\rm eff}$. These effects are within the reach of cosmological observations given current error bars, as discussed in Section 26.3.1 (for instance, with the *Planck* satellite data, the statistical error on the C_ℓ's is of the order of one per cent for a band power of $\Delta\ell = 30$ at $\ell \sim 1000$).

With this transformation, the main background effect of $N_{\rm eff}$

Downloaded from https://academic.oup.com/ptep/article/2022/8/083C01/6651666 by KIT Library user on 27 September 2022

is an increase in the diffusion scale (or Silk damping scale, see Cosmic Microwave Background – Chap. 29 in this *Review*) at the time of decoupling, responsible for the decrease in C_ℓ^{TT} at high ℓ, plus smaller effects coming from a slight increase in the redshift of photon decoupling [18–20]. At the level of perturbations, a higher $N_{\rm eff}$ implies that photons feel gravitational forces from a denser neutrino component; this tends to decrease the acoustic peaks (because neutrinos are distributed in a smoother way than photons) and to shift them to larger scales / smaller multipoles (because photon perturbations traveling at the speed of sound in the photon-baryon fluid feel some dragging effect from neutrino perturbations travelling at the speed of light) [18,20,21]. The effect of increasing $N_{\rm eff}$ on the polarization spectrum features are the same as on the temperature spectrum: an increased Silk damping, and a shift in the acoustic peak amplitude and location - the latter effect is even more clear in the polarization spectrum, in which the location of acoustic peaks does not get further influenced by a Doppler effect like for temperature. The combination of these effects is truly characteristic of the radiation density parameter $N_{\rm eff}$ and cannot be mimicked by other parameters; thus $N_{\rm eff}$ can be accurately measured from the CMB alone. However, there are correlations between $N_{\rm eff}$ and other parameters. In particular, we have seen (Fig. 26.1) that in order to minimise the effect of $N_{\rm eff}$ on the CMB spectrum, one should vary h at the same time, hence there is a correlation between $N_{\rm eff}$ and h, which implies that independent measurements reducing the error bar on h also reduce that on $N_{\rm eff}$. Note that this correlation is not equivalent to a perfect degeneracy, so both parameters can anyway be constrained with CMB data alone.

26.2.2 *Effect of $N_{\rm eff}$ on the matter spectrum*

We have discussed the effect of increasing $N_{\rm eff}$ while keeping $z_{\rm eq}$ and $\omega_{\rm b}$ fixed, because the latter two quantities are very accurately constrained by CMB data. This implies that $\omega_{\rm c}$ increases with $N_{\rm eff}$, and that the ratio $\omega_{\rm b}/\omega_{\rm c} = \Omega_{\rm b}/\Omega_{\rm c}$ decreases. However, the ratio of baryonic-to-dark matter has a strong impact on the shape of the matter power spectrum, because until the time of decoupling of the baryons from the photons, CDM experiences gravitational collapse, while baryons are kept smoothly distributed by photon pressure and affected by acoustic oscillations. The decrease of $\Omega_{\rm b}/\Omega_{\rm c}$ following from the increase of $N_{\rm eff}$ gives more weight to the most clustered of the two components, namely the dark matter one, and produces an enhancement of the small-scale matter power spectrum and a damping of the amplitude of baryon acoustic oscillations (BAOs), clearly visible in Fig. 26.1 (right plot). The scale of BAOs is also slightly shifted by the same neutrino dragging effect as for CMB peaks [24].

The increase in the small-scale matter power spectrum is also responsible for a last effect on the CMB spectra: the CMB last scattering surface is slightly more affected by weak lensing from large-scale structures. This tends to smooth the maxima, the minima, and the damping scale of the CMB spectra [25].

26.2.3 *Effect of neutrino masses on the CMB*

Neutrino eigenstates with a mass $m_i \ll 0.6$ eV become non-relativistic after photon decoupling. They contribute to the non-relativistic matter budget today, but not at the time of equality or recombination. If we increase the neutrino mass while keeping fixed the density of baryons and dark matter ($\omega_{\rm b}$ and $\omega_{\rm c}$), the early cosmological evolution remains fixed and independent of the neutrino mass, until the time of the non-relativistic transition. Thus one might expect that the CMB temperature and polarization power spectra are left invariant. This is not true for four reasons.

First, the neutrino density enhances the total non-relativistic density at late times, $\omega_{\rm m} = \omega_{\rm b} + \omega_{\rm c} + \omega_\nu$, where $\omega_\nu \equiv \Omega_\nu h^2$ is given as a function of the total mass $\sum m_\nu$ by Eq. (26.2). The late background evolution impacts the CMB spectrum through the relation between scales on the last scattering surface and angles on the sky, and through the late ISW effect (see Cosmic Microwave Background – Chap. 29 of this *Review*). These two effects depend respectively on the angular diameter distance to recombination, $d_A(z_{\rm rec})$, and on the redshift of matter-to-Λ equality. Increasing $\sum m_\nu$ tends to modify these two quantities. By playing with h and Ω_Λ, it is possible to keep one of them fixed, but not both at the same time. Since the CMB measures the angular scale of acoustic oscillations with exquisite precision, and is only loosely sensitive to the late ISW effect due to cosmic variance, we choose in Fig. 26.2 to play with the Hubble parameter in order to maintain a fixed scale $d_A(z_{\rm rec})$. With such a choice, an increase in neutrino mass comes together with a decrease in the late ISW effect explaining the depletion of the CMB spectrum for $l \leq 20$. The fact that both $\sum m_\nu$ and h enter the expression of $d_A(z_{\rm rec})$ implies that measurements of the neutrino mass from CMB data are strongly correlated with h. Second, the non-relativistic transition of neutrinos affects the total pressure-to-density ratio of the Universe, and causes a small variation of the metric fluctuations. If this transition takes place not too long after photon decoupling, this variation is observable through the early ISW effect [20,26,27]. It is responsible for the dip seen in Fig. 26.2 for $20 \leq \ell \leq 200$. Third, when the neutrino mass is higher, the CMB spectrum is less affected by the weak lensing effect induced by the large-scale structure at small redshift. This is due to a decrease in the matter power spectrum described in the next paragraphs. This reduced lensing effect is responsible for most of the oscillatory patterns visible in Fig. 26.2 (left plot) for $\ell \geq 200$. Fourth, the neutrinos with the smallest momenta start to be non-relativistic earlier than the average ones. The photon perturbations feel this through their gravitational coupling with neutrinos. This leads to a small enhancement of C_l^{TT} for $\ell \geq 500$, hardly visible on Fig. 26.2 because it is balanced by the lensing effect.

26.2.4 *Effect of neutrino masses on the matter spectrum*

The physical effect of neutrinos on the matter power spectrum is related to their velocity dispersion. Neutrinos free-stream over large distances without falling into small potential wells. The free-streaming scale is roughly defined as the distance travel by neutrinos over a Hubble time scale $t_{\rm H} = (a/\dot{a})$, and approximates the scale below which neutrinos remain very smooth. On larger scales, they cluster in the same way as cold dark matter. The power spectrum of total matter fluctuations, related to the squared fluctuation $\delta_{\rm m}^2$ with $\delta_{\rm m} \equiv \delta_{\rm b} + \delta_{\rm c} + \delta_\nu$, gets a negligible contribution from the neutrino component on small scales, and is reduced by a factor $(1 - 2f_\nu)$, where $f_\nu = \omega_\nu/\omega_{\rm m}$. Additionally, on scales below the free-streaming scale, the growth of ordinary cold dark matter and baryon fluctuations is modified by the fact that neutrinos contribute to the background density, but not to the density fluctuations. This changes the balance between the gravitational forces responsible for clustering, and the Hubble friction term slowing it down. Thus the growth rate of CDM and baryon fluctuations is reduced [28]. This results today in an additional suppression of the small-scale linear matter power spectrum by approximately $(1 - 6f_\nu)$. These two effects sum up to a factor $(1 - 8f_\nu)$ [29] (more precise approximations can be found in [2, 20]). The non-linear spectrum is even more suppressed on mildly non-linear scales [3, 30–34].

This effect is often illustrated by plots of the matter power spectrum ratio with fixed parameters $\{\omega_{\rm m}, \omega_{\rm b}, \Omega_\Lambda\}$ and varying f_ν, *i.e.*, with the CDM density adjusted to get a fixed total dark matter density [2, 20, 29] (see Fig. 26.2, right plot, dashed lines). This transformation does not leave the redshift of equality $z_{\rm eq}$ invariant, and has very large effects on the CMB spectra. If one follows the logic of minimizing CMB variations and fixing $z_{\rm eq}$ like in the previous paragraphs, the increase in $\sum m_\nu$ must take place together with an increase of h, which tends to suppress the large-scale power spectrum, by approximately the same amount as the neutrino free-streaming effect [35]. In that case, the impact of neutrino masses on the matter power spectrum appears as an overall amplitude suppression, which can be seen in Fig. 26.2 (right plot, solid lines). The oscillations on intermediate wavenumbers come from a small shift in the BAO scale [35]. This global effect is not degenerate with a variation of the primordial spectrum amplitude $A_{\rm s}$, because it only affects the matter power spectrum, and not the CMB spectra. However, the amplitude of the CMB temperature and polarization spectrum is given by the combination $A_{\rm s}e^{-2\tau}$. Hence a measurement of τ is necessary in order to fix $A_{\rm s}$ from CMB data, and avoid a parameter degeneracy between $\sum m_\nu$ and $A_{\rm s}$ [35–37].

Downloaded from https://academic.oup.com/ptep/article/2022/8/083C01/6651666 by KIT Library user on 27 September 2022

Table 26.1: Summary of $N_{\rm eff}$ constraints.

	Model	95%CL	Ref.
CMB alone			
Pl18[TT,TE,EE+lowE]	ΛCDM+$N_{\rm eff}$	$2.92^{+0.36}_{-0.37}$	[22]
CMB + background evolution + LSS			
Pl18[TT,TE,EE+lowE+lensing] + BAO	ΛCDM+$N_{\rm eff}$	$2.99^{+0.34}_{-0.33}$	[22]
" + BAO + R21	ΛCDM+$N_{\rm eff}$	3.34 ± 0.14 (68%CL)	[11]
"	" +5-params.	2.85 ± 0.23 (68%CL)	[23]

A few of the neutrino mass effects described above –free-streaming scale, early ISW– depend on individual masses m_i, but most of them depend only on the total mass through f_ν – suppression of the matter power spectrum, CMB lensing, shift in angular diameter distance–. Because the latter effects are easier to measure, cosmology is primarily sensitive to the total mass $\sum m_\nu$ [38,39]. The possibility that future data sets might be able to measure individual masses or the mass hierarchy, despite systematic errors and parameter degeneracies, has recently become a subject of investigation [40,41].

26.3 Cosmological Constraints on neutrino properties

In this review we focus on cosmological constraints on the abundance and mass of ordinary active neutrinos. Several stringent but model-dependent constraints on non-standard neutrinos (*e.g.*, sterile neutrinos, active neutrinos with interactions beyond the weak force, unstable neutrinos with invisible decay, etc.) can also be found in the literature.

26.3.1 *Neutrino abundance*

Table 26.1 shows a list of constraints on $N_{\rm eff}$ obtained with several combination of data sets. 'Pl18' denotes the *Planck* 2018 data, composed of a high-ℓ temperature+polarization likelihood (TT,TE,EE), low-ℓ polarization (low E) and CMB lensing spectrum likelihood (lensing) based on lensing extraction from quadratic estimators [22]. 'BAO' refers to measurements of the BAO scale (and hence of the angular diameter distance) from various recent data sets, described in detail in the references given in the table. 'R21' refers to the distance ladder local measurement of the Hubble scale from cepheids and supernovae [42].

Within the framework of a 7-parameter cosmological model (ΛCDM+$N_{\rm eff}$), the constraint on $N_{\rm eff}$ from the *Planck* 2018 data release [TT,TE,EE+lowE] is $N_{\rm eff} = 2.92^{+0.36}_{-0.37}$ (95%CL). This number is perfectly compatible with the prediction of the standard neutrino decoupling model, $N_{\rm eff} = 3.044$, and can be viewed as a proof of self-consistency of the cosmological model.

The bounds can be tightened by adding information on the low-redshift background expansion from BAOs, or local H_0 measurements. Finally, one can also add information on large scale structure (LSS), *i.e.*, on the growth rate and clustering amplitude of matter as a function of scale. However, LSS data are not very constraining for the $N_{\rm eff}$ parameter, and the only LSS data included in Table 26.1 is the measurement of the CMB lensing spectrum. All combinations of *Planck* 2018 data with BAO or CMB lensing constraints return measurements consistent with the standard expectation.

The situation is different with the inclusion of the low-redshift measurement of H_0 by R21 [42], known to be in tension with *Planck* in the ΛCDM framework. As explained in Section 26.2, the positive correlation between $N_{\rm eff}$ and h means that inclusion of the H_0 measurement pushes $N_{\rm eff}$ to higher values, $N_{\rm eff} = 3.34 \pm 0.14$ (68%CL, Pl18[TT,TE,EE+lowE+lensing] + BAO + R21) [11], compatible with the standard expectation at the $\sim 2.1\sigma$ level. However, the $N_{\rm eff}$ extension to the ΛCDM model does not reduce the tension significantly enough to be an appealing solution. It remains to be seen whether the $> 4.2\sigma$ tension between CMB data and direct measurements of H_0 results from systematics, or from a departure from the ΛCDM model [11,46–49].

The error bars on $N_{\rm eff}$ degrade mildly when the data are analysed in the context of more extended cosmological scenarios. Adding only the total neutrino mass as an 8th free parameter has a negligible impact on the bounds.

The authors of Ref. [23] take a more extreme point of view and fit a 12-parameter model to Pl18[TT,TE,EE+lowE+lensing] data; they obtain $N_{\rm eff} = 2.95 \pm 0.24$ (68% CL), showing that it is very difficult with current cosmological data to accommodate shifts of more than 0.5 from the standard $N_{\rm eff}$ value, and to obtain good fits with, for instance, a fourth (sterile) thermalized neutrino. This is interesting since the anomalies in some oscillation data could be interpreted as evidence for at least one sterile neutrino with a large mixing angle, which would need to be thermalised unless non-standard interactions come into play [5]. In other words cosmology disfavours the explanation of the oscillations anomalies in terms of extra neutrinos if they are thermalized.

26.3.2 *Are they really neutrinos, as expected?*

While a value of $N_{\rm eff}$ significantly different from zero (at more than 15σ) and consistent with the expected number 3.044 yields a powerful indirect confirmation of the CνB, departures from standard $N_{\rm eff}$ could be caused by any ingredient affecting the early-time expansion rate of the Universe. Extra relativistic particles (either decoupled, self-interacting, or interacting with a dark sector), a background of gravitational waves, an oscillating scalar field with quartic potential, departures from Einstein gravity, or large extra dimensions are some of the possibilities for such ingredients. In principle one could even assume that the cosmic neutrino background never existed or has decayed (like in the "neutrinoless Universe" model of [50]) while another dark radiation component is responsible for $N_{\rm eff}$. At least, cosmological data allow to narrow the range of possible interpretations of $N_{\rm eff} \simeq 3$ to the presence of decoupled relativistic relics like standard neutrinos. Indeed, free-streaming particles leave specific signatures in the CMB and LSS spectra, because their density and pressure perturbations, bulk velocities and anisotropic stress also source the metric perturbations. These signatures can be tested in several ways.

A first approach consists of introducing a self-interaction term in the neutrino equations [6,7]. Ref. [8] finds that current CMB and BAO data are compatible with no self-interactions. The upper limit to the effective coupling constant $G_{\rm eff}$ for a Fermi-like four-fermions interaction at 95% confidence is $\log_{10}(G_{\rm eff}{\rm MeV}^2) < -0.8$ for Pl15+BAO. Note however that neutrino self-interactions as strong as $\log_{10}(G_{\rm eff}{\rm MeV}^2) \simeq -1.4$ could reconcile CMB temperature and BAO data with the direct H_0 measurement of Ref [42], but such interactions seem to be hardly compatible with BBN, laboratory constraints [10] and CMB polarization [9,11].

A second approach consists of introducing two phenomenological parameters, $c_{\rm eff}$ and $c_{\rm vis}$ (see *e.g.*, [51–53]): $c^2_{\rm eff}$ generalizes the linear relation between isotropic pressure perturbations and density perturbations, while $c^2_{\rm vis}$ modifies the neutrino anisotropic stress equation. While relativistic free-streaming species have $(c^2_{\rm eff}, c^2_{\rm vis}) = (1/3, 1/3)$, a perfect relativistic fluid would have $(c^2_{\rm eff}, c^2_{\rm vis}) = (1/3, 0)$. Other values do not necessarily refer to a concrete model, but make it possible to interpolate between these limits. *Planck* data strongly suggests $(c^2_{\rm eff}, c^2_{\rm vis}) = (1/3, 1/3)$ [54,55].

Finally, Ref. [21] (resp. [24]) shows that current data are precise enough to detect the "neutrino drag" effect mentioned in Sec. 26.2 through the measurement of the CMB peak (resp. BAO) scale. These findings show that current cosmological data are able to detect not just the average density of some relativistic relics, but also their anisotropies.

Downloaded from https://academic.oup.com/ptep/article/2022/8/083C01/6651666 by KIT Library user on 27 September 2022

Table 26.2: Summary of $\sum m_\nu$ constraints.

	Model	95% CL (eV)	Ref.
CMB alone			
Pl18[TT+lowE]	ΛCDM+$\sum m_\nu$	< 0.54	[22]
Pl18[TT,TE,EE+lowE]	ΛCDM+$\sum m_\nu$	< 0.26	[22]
CMB + probes of background evolution			
Pl18[TT+lowE] + BAO	ΛCDM+$\sum m_\nu$	< 0.13	[43]
Pl18[TT,TE,EE+lowE]+BAO	ΛCDM+$\sum m_\nu$+5 params.	< 0.515	[23]
CMB + LSS			
Pl18[TT+lowE+lensing]	ΛCDM+$\sum m_\nu$	< 0.44	[22]
Pl18[TT,TE,EE+lowE+lensing]	ΛCDM+$\sum m_\nu$	< 0.24	[22]
CMB + probes of background evolution + LSS			
Pl18[TT,TE,EE+lowE] + BAO + RSD	ΛCDM+$\sum m_\nu$	< 0.10	[43]
Pl18[TT+lowE+lensing] + BAO + Lyman-α	ΛCDM+$\sum m_\nu$	< 0.087	[44]
Pl18[TT,TE,EE+lowE] + BAO + RSD + Pantheon + DES	ΛCDM+$\sum m_\nu$	< 0.13	[45]

26.3.3 *Neutrino masses*

Table 26.2 shows a list of constraints on $\sum m_\nu$ obtained with several combinations of data sets. The acronyms "Pl18" and "BAO" have been described in the previous subsection, while "Pantheon" refers to the supernovae Type Ia compilation of [56], "RSD" to Redshift Space Distorsions in the eBOSS galaxy survey [43], and "Lyman-α" to the one-dimensional flux power spectrum of eBOSS quasars [44].

Given that most determinations of $N_{\rm eff}$ are compatible with the standard prediction, $N_{\rm eff} = 3.044$, it is reasonable to adopt this value as a theoretical prior and to investigate neutrino mass constraints in the context of a minimal 7-parameter model, ΛCDM+$\sum m_\nu$. Under this assumption, the most robust constraints come from *Planck* 2018 temperature and polarization data alone: $\sum m_\nu < 0.26$ eV (95%CL) [22]. Among the four effects of neutrino masses on the CMB spectra described before, current bounds are dominated by the first and the third effects (modified late background evolution, and distortions of the temperature and polarization spectra through weak lensing).

Adding measurements of the BAO scale is crucial, since the determination of the angular diameter distance at small redshift allows us to break parameter degeneracies, for instance between $\sum m_\nu$ and h. The combination of Pl18[TT,TE,EE+lowE] with the most recent BAO measurements, including the eBOSS Data Release 16 (DR16), gives $\sum m_\nu < 0.13$ eV (95%CL) [43]. Supernovae data are less constraining than BAO data for the neutrino mass determination.

Because the parameter correlation between $\sum m_\nu$ and H_0 is negative, the inclusion of distance ladder data provides stronger bounds on neutrinos masses, down to $\sum m_\nu < 0.097$ eV (95% CL) when including Pl18[TT,TE,EE+lowE]+R18 [22], where R18 refers to the 2018 estimate of the Hubble rate by [57]. However, such bounds are subject to caution, since they come from a combination of discrepant data sets (at the $> 3\sigma$ level).

It is interesting to add LSS data sets, sensitive to the small-scale suppression of the matter power spectrum due to neutrino free-streaming. Some conservative LSS information comes from the eBOSS survey, which infers the growth rate of structures from Redshift Space Distorsions (RSD) and tigthens the bound down to $\sum m_\nu < 0.10$ eV (95%CL) [43]. This already challenges the inverted hierarchy mass scheme, which predicts $\sum m_\nu \geq 0.11$ eV. The inclusion of CMB lensing data from *Planck* 18 improves the CMB-only bound, but hardly affects the latest joint CMB+BAO+RSD bounds [58]. The most recent Lyα forest data from eBOSS combined with Pl18[TT,TE,EE+lowE+lensing] and BAO data provides the strongest bound to date, $\sum m_\nu < 0.087$ eV (95% CL). It should however be noticed that the full DES 3-year data prefer a lower σ_8 value than the *Planck* best fit, relaxing the bound to $\sum m_\nu < 0.13$ eV (95%CL, Pl18[TT,TE,EE+lowE+lensing]+BAO+RSD+Pantheon+DES) [45].

Upper bounds on neutrino masses become weaker when the data are analysed in the context of extended cosmological models, but only by a small amount. Floating $N_{\rm eff}$ instead of fixing it to 3.044 has no significant impact on the neutrino mass bounds reported in the previous paragraphs. Even in the extreme case considered by Ref. [23], with 12 free cosmological parameters, one can see in Table 26.2 that the bound from *Planck* 2018 (without lensing) + BAO increases from 0.13 eV to 0.52 eV (95% CL) only. This shows that current cosmological data are precise enough to disentangle the effect of several extended cosmological parameters, and that neutrino mass bounds are becoming increasingly robust.

26.4 Future prospects and outlook

The cosmic neutrino background has been detected indirectly at very high statistical significance. Direct detection experiments are now being planned, *e.g.*, at the Princeton Tritium Observatory for Light, Early Universe, Massive-neutrino Yield (PTOLEMY) [59]. The detection prospects crucially depend on the exact value of neutrino masses and on the enhancement of their density at the location of the Earth through gravitational clustering in the Milky Way and its sub-halos – an effect however expected to be small [60–62].

Over the past few years the upper limit on the sum of neutrino masses has become increasingly stringent, first indicating that the mass ordering is hierarchical and recently putting the inverted hierarchy under pressure and favouring the normal hierarchy (although quantitative estimates of how disfavoured the inverted hierarchy is vary depending on assumptions, see *e.g.* [63–65]) which has consequences for planning future double beta decay experiments.

Neutrino mass and density bounds are expected to keep improving significantly over the next years, thanks to new LSS experiments like DESI [66], Euclid [67], LSST [68], SPHEREx [69] and SKA [70], in combinations with new CMB experiments like Simons Observatory [71], CMB-S4 [72] or LiteBird [73]. If the ΛCDM model is confirmed, and if neutrinos have standard properties, the total neutrino mass should be detected at the level of at least 3–4σ even at the minimum level allowed by oscillations. This is the conclusion reached by several independent studies, using different dataset combinations (see *e.g.*, [37, 74–79]). One should note that at the minimum level allowed by oscillations $\sum m_\nu \sim 0.06$, neutrinos constitute $\sim 0.5\%$ of the Universe matter density, and their effects on the matter power spectrum is only at the 5% level, implying that exquisite control of systematic errors will be crucial to achieve the required accuracy. At this level, the information coming from the power spectrum shape is more powerful than that coming from geometrical measurements (e.g., BAO). But exploiting the shape information requires improved understanding of the non-linear regime, and of galaxy bias for galaxy surveys. The fact that different surveys and different data set combinations have enough statistical power to reach this level, offers a much needed redundancy and the possibility to perform consistency checks which in turns helps immensely with the control of systematic errors and in making the measurement robust. Using the entire Universe as a particle detector, the on-going and future observational efforts hold the exciting prospect to provide a measurement of the sum of neutrino masses and possibly indication of their mass hierarchy.

Downloaded from https://academic.oup.com/ptep/article/2022/8/083C01/6651666 by KIT Library user on 27 September 2022

References

[1] A. D. Dolgov, Phys. Rept. **370**, 333 (2002), [hep-ph/0202122].

[2] J. Lesgourgues and S. Pastor, Phys. Rept. **429**, 307 (2006), [arXiv:astro-ph/0603494].

[3] S. Hannestad, Prog. Part. Nucl. Phys. **65**, 185 (2010), [arXiv:1007.0658].

[4] J. Lesgourgues *et al.*, *Neutrino Cosmology*, Cambridge University Press (2013), ISBN 978-1-108-70501-1, 978-1-139-60341-6.

[5] M. Archidiacono *et al.*, JCAP **1608**, 08, 067 (2016), [arXiv:1606.07673].

[6] L. Lancaster *et al.*, JCAP **1707**, 07, 033 (2017), [arXiv:1704.06657].

[7] I. M. Oldengott *et al.*, JCAP **1711**, 11, 027 (2017), [arXiv:1706.02123].

[8] M. Park *et al.*, Phys. Rev. D **100**, 6, 063524 (2019), [arXiv:1904.02625].

[9] C. D. Kreisch, F.-Y. Cyr-Racine and O. Doré, Phys. Rev. D **101**, 12, 123505 (2020), [arXiv:1902.00534].

[10] N. Blinov *et al.*, Phys. Rev. Lett. **123**, 19, 191102 (2019), [arXiv:1905.02727].

[11] N. Schöneberg *et al.* (2021), [arXiv:2107.10291].

[12] J. Birrell, C.-T. Yang and J. Rafelski, Nucl. Phys. **B890**, 481 (2014), [arXiv:1406.1759].

[13] G. Mangano *et al.*, Nucl. Phys. **B729**, 221 (2005), [hep-ph/0506164].

[14] E. Grohs *et al.*, Phys. Rev. **D93**, 8, 083522 (2016), [arXiv:1512.02205].

[15] P. F. de Salas and S. Pastor, JCAP **1607**, 07, 051 (2016), [arXiv:1606.06986].

[16] J. Froustey, C. Pitrou and M. C. Volpe, JCAP **12**, 015 (2020), [arXiv:2008.01074].

[17] J. J. Bennett *et al.*, JCAP **04**, 073 (2021), [arXiv:2012.02726].

[18] S. Bashinsky and U. Seljak, Phys. Rev. **D69**, 083002 (2004), [arXiv:astro-ph/0310198].

[19] Z. Hou *et al.*, Phys. Rev. **D87**, 083008 (2013), [arXiv:1104.2333].

[20] J. Lesgourgues *et al.*, *Neutrino cosmology* (Cambridge University Press, 2013).

[21] B. Follin *et al.*, Phys. Rev. Lett. **115**, 9, 091301 (2015), [arXiv:1503.07863].

[22] N. Aghanim *et al.* (Planck) (2018), [arXiv:1807.06209].

[23] E. Di Valentino, A. Melchiorri and J. Silk, JCAP **01**, 013 (2020), [arXiv:1908.01391].

[24] D. Baumann *et al.*, Nature Phys. **15**, 465 (2019), [arXiv:1803.10741].

[25] A. Lewis and A. Challinor, Phys. Rept. **429**, 1 (2006), [arXiv:astro-ph/0601594].

[26] J. Lesgourgues and S. Pastor, Adv. High Energy Phys. **2012**, 608515 (2012), [arXiv:1212.6154].

[27] Z. Hou *et al.*, Astrophys. J. **782**, 74 (2014), [arXiv:1212.6267].

[28] J. R. Bond, G. Efstathiou and J. Silk, Phys. Rev. Lett. **45**, 1980 (1980), [,61(1980)].

[29] W. Hu, D. J. Eisenstein and M. Tegmark, Phys. Rev. Lett. **80**, 5255 (1998), [arXiv:astro-ph/9712057].

[30] S. Bird, M. Viel and M. G. Haehnelt, Mon. Not. Roy. Astron. Soc. **420**, 2551 (2012), [arXiv:1109.4416].

[31] C. Wagner, L. Verde and R. Jimenez, Astrophys. J. **752**, L31 (2012), [arXiv:1203.5342].

[32] C. J. Todero Peixoto, V. de Souza and P. L. Biermann, JCAP **1507**, 07, 042 (2015), [arXiv:1502.00305].

[33] J. Brandbyge and S. Hannestad, JCAP **1710**, 10, 015 (2017), [arXiv:1706.00025].

[34] J. Adamek, R. Durrer and M. Kunz, JCAP **1711**, 11, 004 (2017), [arXiv:1707.06938].

[35] M. Archidiacono *et al.*, JCAP **1702**, 02, 052 (2017), [arXiv:1610.09852].

[36] A. Liu *et al.*, Phys. Rev. **D93**, 4, 043013 (2016), [arXiv:1509.08463].

[37] R. Allison *et al.*, Phys. Rev. **D92**, 12, 123535 (2015), [arXiv:1509.07471].

[38] J. Lesgourgues, S. Pastor and L. Perotto, Phys. Rev. **D70**, 045016 (2004), [hep-ph/0403296].

[39] A. Slosar, Phys. Rev. **D73**, 123501 (2006), [arXiv:astro-ph/0602133].

[40] R. Jimenez *et al.*, JCAP **1005**, 035 (2010), [arXiv:1003.5918].

[41] R. Jimenez, C. P. Garay and L. Verde, Phys. Dark Univ. **15**, 31 (2017), [arXiv:1602.08430].

[42] A. G. Riess *et al.*, Astrophys. J. Lett. **908**, 1, L6 (2021), [arXiv:2012.08534].

[43] S. Alam *et al.* (eBOSS), Phys. Rev. D **103**, 8, 083533 (2021), [arXiv:2007.08991].

[44] N. Palanque-Delabrouille *et al.*, JCAP **04**, 038 (2020), [arXiv:1911.09073].

[45] T. M. C. Abbott *et al.* (DES) (2021), [arXiv:2105.13549].

[46] J. L. Bernal, L. Verde and A. G. Riess, JCAP **1610**, 10, 019 (2016), [arXiv:1607.05617].

[47] L. Verde, T. Treu and A. G. Riess, Nature Astron. **3**, 891 (2019), [arXiv:1907.10625].

[48] J. L. Bernal *et al.*, Phys. Rev. D **103**, 10, 103533 (2021), [arXiv:2102.05066].

[49] E. Di Valentino *et al.*, Class. Quant. Grav. **38**, 15, 153001 (2021), [arXiv:2103.01183].

[50] J. F. Beacom, N. F. Bell and S. Dodelson, Phys. Rev. Lett. **93**, 121302 (2004), [arXiv:astro-ph/0404585].

[51] W. Hu, Astrophys. J. **506**, 485 (1998), [arXiv:astro-ph/9801234].

[52] W. Hu *et al.*, Phys. Rev. **D59**, 023512 (1999), [arXiv:astro-ph/9806362].

[53] M. Gerbino, E. Di Valentino and N. Said, Phys. Rev. **D88**, 6, 063538 (2013), [arXiv:1304.7400].

[54] B. Audren *et al.*, JCAP **1503**, 036 (2015), [arXiv:1412.5948].

[55] P. A. R. Ade *et al.* (Planck), Astron. Astrophys. **594**, A13 (2016), [arXiv:1502.01589].

[56] D. M. Scolnic *et al.*, Astrophys. J. **859**, 2, 101 (2018), [arXiv:1710.00845].

[57] A. G. Riess *et al.*, Astrophys. J. **855**, 2, 136 (2018), [arXiv:1801.01120].

[58] E. Di Valentino, S. Gariazzo and O. Mena (2021), [arXiv:2106.15267].

[59] S. Betts *et al.*, in "Proceedings, 2013 Community Summer Study on the Future of U.S. Particle Physics: Snowmass on the Mississippi (CSS2013): Minneapolis, MN, USA, July 29-August 6, 2013," (2013), [arXiv:1307.4738], URL `http://www.slac.stanford.edu/econf/C1307292/docs/submittedArxivFiles/1307.4738.pdf`.

[60] A. Ringwald and Y. Y. Y. Wong, JCAP **0412**, 005 (2004), [hep-ph/0408241].

[61] F. Villaescusa-Navarro *et al.*, JCAP **1303**, 019 (2013), [arXiv:1212.4855].

[62] P. F. de Salas *et al.*, JCAP **1709**, 09, 034 (2017), [arXiv:1706.09850].

[63] F. Simpson *et al.*, JCAP **1706**, 06, 029 (2017), [arXiv:1703.03425].

Downloaded from https://academic.oup.com/ptep/article/2022/8/083C01/6651666 by KIT Library user on 27 September 2022

[64] S. Hannestad and T. Schwetz, JCAP **1611**, 11, 035 (2016), [arXiv:1606.04691].

[65] S. Roy Choudhury and S. Hannestad (2019), [arXiv:1907.12598].

[66] A. Aghamousa *et al.* (DESI) (2016), [arXiv:1611.00036].

[67] R. Laureijs *et al.* (EUCLID) (2011), [arXiv:1110.3193].

[68] Paul A. Abell *et al.*, LSST Science and LSST Project Collaborations, `http://lss.fnal.gov/archive/test-tm/2000/fermilab-tm-2495-a.pdf` (2009) `arXiv:0912.0201`.

[69] J. Bock and SPHEREx Science Team, in "American Astronomical Society Meeting Abstracts #231," volume 231 of *American Astronomical Society Meeting Abstracts*, 354.21 (2018).

[70] `http://www.skatelescope.org`.

[71] P. Ade *et al.* (Simons Observatory), JCAP **02**, 056 (2019), [arXiv:1808.07445].

[72] K. N. Abazajian *et al.* (CMB-S4) (2016), [arXiv:1610.02743].

[73] M. Hazumi *et al.*, J. Low Temp. Phys. **194**, 5-6, 443 (2019).

[74] C. Carbone *et al.*, JCAP **1103**, 030 (2011), [arXiv:1012.2868].

[75] J. Hamann, S. Hannestad and Y. Y. Y. Wong, JCAP **1211**, 052 (2012), [arXiv:1209.1043].

[76] B. Audren *et al.*, JCAP **1301**, 026 (2013), [arXiv:1210.2194].

[77] R. Pearson and O. Zahn, Phys. Rev. **D89**, 4, 043516 (2014), [arXiv:1311.0905].

[78] F. Villaescusa-Navarro, P. Bull and M. Viel, Astrophys. J. **814**, 2, 146 (2015), [arXiv:1507.05102].

[79] T. Brinckmann *et al.*, JCAP **1901**, 059 (2019), [arXiv:1808.05955].

Downloaded from https://academic.oup.com/ptep/article/2022/8/083C01/6651666 by KIT Library user on 27 September 2022

27. Dark Matter

Revised August 2021 by L. Baudis (Zurich U.) and S. Profumo (UC Santa Cruz).

27.1 The case for dark matter

Modern cosmological models invariably include an electromagnetically close-to-neutral, non-baryonic matter species with negligible velocity from the standpoint of structure formation, generically referred to as "cold dark matter" (CDM; see The Big-Bang Cosmology—Sec. 22 of this *Review*). For the benchmark ΛCDM cosmology adopted in the Cosmological Parameters—Sec. 25 of this *Review*, the DM accounts for 26.4% of the critical density in the universe, or 84.4% of the total matter density. The nature of only a small fraction, between at least 0.5% (given neutrino oscillations) and at most 1.6% (from combined cosmological constraints), of the non-baryonic matter content of the universe is known: the three Standard Model neutrinos (see the Neutrino Masses, Mixing, and Oscillations—Sec. 14 of this *Review*)). The fundamental makeup of the large majority of the DM is, as of yet, unknown.

Assuming the validity of General Relativity, DM is observed to be ubiquitous in gravitationally collapsed structures of size ranging from the smallest known galaxies [1] to galaxies of size comparable to the Milky Way [2], to groups and clusters of galaxies [3]. The mass-to-light ratio is observed to saturate at the largest collapsed scales to a value indicative, and close to, what inferred from other cosmological observations for the universe as a whole [4]. In such collapsed structures, the existence of DM is inferred directly using tracers of mass enclosed within a certain radius such as stellar velocity dispersion, rotation curves in axisymmetric systems, the virial theorem, gravitational lensing, and measures of the amount of non-dark, i.e. baryonic, mass such as stellar number counts and tracers of gas density such as X-ray emission [5]. The global DM abundance as determined from cosmological probes is discussed in Sec. 22.

The picture of structure formation in modern cosmology heavily relies on, and can be considered an independent and exceptionally strong motivation for, DM. Baryonic density fluctuations at CMB decoupling are observed to be at most on the order of $\delta\rho_b/\rho_b|_{\rm rec} \approx 10^{-5}$; since density perturbations grow linearly with the scale factor in the linear regime, absent any other matter fluid, one would predict that

$$\delta\rho_b/\rho_b|_{\rm today} \approx \frac{\delta\rho_b/\rho_b|_{\rm rec}}{a_{\rm rec}} \approx 10^{-2}, \qquad (27.1)$$

at odds with the observed highly non-linear structures in the universe, $\delta\rho_b/\rho_b|_{\rm obs} \gg 1$. The presence of a dominant non-relativistic ("cold") pressure-less matter component decoupled from the thermal bath well before recombination allows instead for the prediction of a matter power spectrum in remarkable agreement with observations [6].

Assuming deviations of gravitational interactions on large scales from general relativity or from its Newtonian limit, certain effects, attributed in the standard scenario to DM, can be explained by modified gravity [7]. Usually such theories mimic the effects otherwise attributed to DM on a limited range of scales, but fail globally, and especially at the largest scales. Key issues that at present appear highly problematic in the framework of theories of modified gravity without DM include (i) predicting the correct spectrum of density perturbations, (ii) predicting the observed anisotropy power spectrum of the CMB, and (iii) explaining weak lensing and X-ray observations of merging clusters such as 1E 0657-558 (the "Bullet" cluster) [8]. The inferred relative speed of gravitational and electromagnetic radiation in GW170817 additionally excludes a significant swath of modified theories of gravity where the two speeds (of gravitational and electromagnetic waves) differ [9].

27.2 Properties of dark matter candidates

Electric charge: The "darkness" of DM can be quantified based on constraints from the CMB and large-scale structure: if the DM is charged, or "milli-charged" (for instance via a kinetic mixing with a dark photon field, producing an effective suppressed coupling to the visible photon field), it might impact the baryon-photon plasma during recombination; in turn, DM density fluctuations can be suppressed by radiation pressure and photon diffusion, additionally altering the baryon acoustic peak structure. [10] finds that the most stringent constraints stem from the requirement that the DM be completely decoupled from the baryon-photon plasma at recombination, yielding a maximal "milli-electric" charge, in units of the electron charge, of $3.5\times10^{-7}(m_{\rm DM}/1\ {\rm GeV})^{0.58}$ for $m_{\rm DM} > 1$ GeV, and of $4.0\times10^{-7}(m_{\rm DM}/1\ {\rm GeV})^{0.35}$ for $m_{\rm DM} < 1$ GeV. Limits also exist from structure formation on how optically dark and dissapationaless the DM should be.

Self-interactions: Observations of merging clusters [8] and of the ellipticity of certain galaxies as inferred from X-rays [11] constrain the level of DM-DM self interactions. The figure of merit is the ratio of the DM-DM cross section and the DM mass [12] (see Ref. [13] for a review), $\sigma_{\rm DM-DM}/m_{\rm DM} < 0.47\ {\rm cm}^2/{\rm g} \simeq 0.84$ barn/GeV at 95% C.L.. Assuming a velocity dependence in $\sigma_{\rm DM-DM}$, "self-interacting DM" has been advocated as a possible solution to certain possible small-scale structure issues in the standard non-collisional ($\sigma_{\rm DM-DM} \simeq 0$) setup [13, 14] (see Sec. 27.4).

Mass: Lower Limits: Model-independent lower limits for very small DM masses are due to quantum effects: for fermionic DM particles, the phase-space density $f(\vec{x},\vec{p})$ is bounded from above due to Pauli's exclusion principle, $f < gh^{-3}$, with g the number of internal degrees of freedom and h Planck's constant; observations of the velocity dispersion (or, equivalently, measures of the enclosed mass) and physical density in dwarf galaxies, lead to a lower limit on fermionic DM masses, sometimes known as the Tremaine-Gunn limit [15]. Using the Fornax dwarf, Ref. [16] finds $m_F > 70$ eV. More stringent limits can be drawn from Lyman-α observations, although such limits depend on the thermal history of the DM. In the case of bosonic DM, the Compton wavelength of an ultra-light species might erase small-scale structure, in conflict with CMB and large-scale structure [17], Lyman-α observations [18,19], and measurements of high-redshift galaxy luminosity functions and the Milky Way satellite luminosity function [20–22]: these observations indicate that $m_B \gtrsim 10^{-22}$ eV.

Mass: Upper Limits: General upper limits exist on the mass of the DM constituent from the stability against tidal disruption of structures immersed in DM halos, such as galactic disks and globular clusters, and of individual small galaxies. The most stringent limits can be derived using wide halo binaries [23] and the stability of the star cluster within Eridanus II [24]. Such limits constrain an individual, point-like DM constituent, assuming it makes up 100% of the DM, to be lighter than around 5 $M_\odot$. (Notice that the mass limits discussed here do not assume any specific production mechanism, and do not depend on the observed cosmological DM density).

Stability: The DM lifetime must be long compared to cosmological timescales [25].

27.3 Genesis of dark matter

The generation of DM in the early universe can proceed via thermal or non-thermal production, or both, or it may result from a particle-antiparticle asymmetry.

Freeze-out: The process of chemical decoupling from the high-temperature, high-density thermal bath (freeze-out) as a paradigm for particle production in the early universe is both a predictive and a successful one. The possibility that just like light elements, neutrinos, and CMB photons, particle DM also originated from a thermal decoupling process has thus garnered significant attention.

A particle species *chemically* decouples when the rate Γ for the species' number-changing processes drops below the Hubble rate H. Rough estimates for the abundance of relics can be obtained by (i) calculating the freeze-out (i.e. "decoupling") temperature $T_{\rm f.o.}$, corresponding to $H(T_{\rm f.o.}) \sim \Gamma(T_{\rm f.o.})$, (ii) equating the comoving number density at freeze-out and today, eventually (iii) obtaining the physical density of relic particles today. This procedure assumes that entropy is conserved between $T_{\rm f.o.}$ and today, an assumption that could well be violated, especially for

Downloaded from https://academic.oup.com/ptep/article/2022/8/083C01/6651666 by KIT Library user on 27 September 2022

heavy relics that decouple early, for instance by entropy injection episodes [26]. Notice also that the freeze-out calculation strongly depends on the assumed background cosmology, and changes e.g. if the early universe is not radiation-dominated around DM decoupling.

The calculation of the freeze-out relic abundance hinges on a Boltzmann equation relating the Liouville operator to the collision operator acting on the phase space density. Under a variety of simplifying assumptions including homogeneity and isotropy, it is possible to reduce the relevant equation for the number density n of a single species pair-annihilating with particles in the thermal bath via 2-to-2 processes to

$$\frac{dn}{dt} - 3Hn = -\langle \sigma v \rangle \left(n^2 - n_{\rm eq}^2 \right), \tag{27.2}$$

where $\langle \sigma v \rangle$ is the thermally-averaged pair-annihilation cross section times relative velocity (see Ref. [27]), and $n_{\rm eq}$ is the equilibrium number density. Relics for which the freeze-out temperature is much larger than the particle mass (and thus that freeze-out as ultra-reltivistic) are called *hot* relics; if the opposite is true, the relic is instead considered *cold*.

A straightforward calculation shows that to leading order the frozen-out density of *hot* relics is *linearly proportional to the relic particle mass*. The comoving number density $Y = n/s$, where s is the entropy density, for a hot relic is approximately given by its equilibrium value,

$$Y_{\rm f.o.} \simeq Y_{\rm eq} \simeq 0.278 \frac{g_{\rm eff}}{g_{*s}}, \tag{27.3}$$

where $g_{\rm eff}$ is the relic's effective number of degrees of freedom, and g_{*s} is the number of entropic relativistic degrees of freedom, both calculated at $T_{\rm f.o.}$. The resulting relic abundance, assuming an iso-entropic expansion, is

$$\Omega_{\rm hot} h^2 = \frac{m Y_{\rm f.o.} s_0 h^2}{\rho_c} \simeq \frac{m}{93 \text{ eV}}, \tag{27.4}$$

with s_0 the entropy density today, and with the latter equality holding for the case of SM neutrinos, with a freeze-out temperature around 1 MeV (which enters in the final relic abundance through the degrees of freedom dependence on the right-hand-side of Eq. (27.3)).

For *cold* relics, the leading-order dependence of the relic abundance on the DM particle properties is an *inverse proportionality relation to the pair-annihilation cross section*,

$$\Omega_{\rm cold} h^2 \simeq 0.1 \left(\frac{x_{\rm f.o.}}{20} \right) \left(\frac{10^{-8} \text{ GeV}^{-2}}{\sigma_{DM+DM \leftrightarrow \rm anything}} \right), \tag{27.5}$$

where $x \equiv m_{\rm DM}/T$. In turn, the freeze-out temperature is approximately given by the solution to the equation

$$\sqrt{x} \cdot e^{-x} = \left(m_{\rm DM} \cdot M_P \cdot \sigma_{DM+DM \leftrightarrow \rm anything} \right)^{-1}, \tag{27.6}$$

where $M_P \simeq 2.435 \times 10^{18}$ GeV is the reduced Planck mass. As a result, $T_{\rm f.o.} \simeq m_{\rm DM}/x_{\rm f.o.}$, with $x_{\rm f.o.}$ a number between 10 and 50, depending on the cross section, with only a logarithmic dependence on the DM mass. Since for electroweak-scale cross sections and masses $\sigma_{DM+DM} \simeq 10^{-8}$ GeV^{-2}, "weakly-interacting massive particles", or WIMPs have gained exceptional popularity. Notice that Eq. (27.5) bears, however, no connection to the weak scale [28], despite the relation being known as "WIMP miracle".

Numerous scenarios exist, including notably supersymmetry [29,30] and models with universal extra dimensions [31,32] where the relic abundance of the DM is controlled by processes involving a slightly heavier, unstable, co-annihilating species [33]. In this case the calculation of the abundance of the stable species proceeds similarly to what outlined above, with an effective pair-annihilation cross section that captures the effects of co-annihilation replacing the pair-annihilation cross section [30].

Freeze-in: Collisional processes can lead to the production of out-of-equilibrium particles that progressively accumulate over cosmic time, a process sometimes called *freeze-in*. The abundance of the frozen-in particles produced at a given redshift depends on the product of the production rate times the Hubble time at that redshift. Freeze-in generally implies that the lightest observable-sector particles decay to the DM with relatively long lifetimes, giving peculiar signals at colliders (see e.g. [34]). Gravitinos are an example of DM candidates possibly produced via a freeze-in type scenario, albeit the portal coupling is in that case via a higher dimensional, Planck-suppressed operator [35].

Cannibalization and other dark-sector number-changing processes: Thermal processes can drive the abundance of the DM beyond simple 2-to-2 number-changing interactions. For instance, DM can "cannibalize" [36, 37] itself if $n \to 2$ processes exist. In this case, a critical aspect is whether or not the DM sector is in thermal contact with the Standard Model thermal bath. If it is, $n \to 2$ processes can drive the relic abundance, e.g. in the Strongly Interacting Massive Particles (SIMP) scenario [38]. Models exist where the *kinetic decoupling* (i.e. the decoupling from the *thermal equilibrium velocity distribution*) of the two sectors drives the abundance of the DM (elastically decoupling relics, or ELDERs [39]). When the two sectors are not in thermal contact, $n \to 2$ processes heat the DM sector dramatically, rapidly affecting the temperature ratio between the visible and dark sectors [36, 38]. If the relevant cross sections are large enough, and the DM mass light enough, significant effects can arise in structure formation [36].

Non-thermal production: DM production can proceed via processes out of thermal equilibrium ("non-thermal" production). These include DM production via the decay of a "mother" particle [40,41] (or of topological defects [42], moduli [43] etc.) to the DM, or production via gravitational effects.

Asymmetric DM: An enticing alternative possibility for DM production is that of *asymmetric* DM [44,45]: the relic DM abundance arises from an asymmetry between anti-DM and DM. This asymmetry may or may not be related to the baryon-antibaryon asymmetry. If it is, then depending on the model and its thermal history, a relation exists between the mass of the DM and the proton mass. A variety of proposals have been put forward where alternately baryogenesis is explained from a DM sector asymmetry, or vice-versa (see e.g. Ref. [46] for a review).

Primordial Black Holes production: A qualitatively stand-alone class of DM candidates, primordial black holes (PBHs), arises from entirely different mechanisms from what reviewed above. PBHs are thought to originate from gravitational collapse of large density fluctuations in the early universe [47, 48]. The over-densities could be produced in a variety of ways, such as topological defects like cosmic strings, necklaces or domain walls, curvature fluctuations from a period of ultra-slow-roll, a sound speed "resonance" , an early phase of matter domination, or sub-horizon phenomena including a phase transition and preheating.Albeit the calculation depends on the details of gravitational collapse, the formation time is connected to the PBH mass via $M = \gamma M_{PBH} \simeq 2 \times 10^5 \gamma \left(\frac{t}{1 \text{ s}} \right) M_\odot$, with $\gamma \simeq (1/\sqrt{3})^3$ during radiation domination [49].

27.4 Density and velocity distribution of dark matter

27.4.1 *Local density and velocity distribution*

The density and distribution of DM in the Milky Way encipher relevant dynamical information about our Galaxy, and are particularly important for direct and indirect detection experiments. The *local density* (ρ_0) is an average over a volume of a few hundred parsecs in the Solar neighbourhood.

To determine the local density from observations, two classes of methods are used [50]. So-called *local measures* rely on the vertical motion of tracer stars in the vicinity of the Sun, while *global measures* extrapolate ρ_0 from the measured rotation curve, with additional assumptions about the Galactic halo shape. Conversely, by comparing the extrapolated local density with the one obtained from local measures, one can constrain the local shape of the Milky Way halo. A major source of uncertainty on ρ_0 is the contribution of baryons (stars, gas, stellar remnants) to the local dynamical mass. For instance, the motion of tracer stars used in local measures is dictated by the total potential generated by

Downloaded from https://academic.oup.com/ptep/article/2022/8/083C01/6651666 by KIT Library user on 27 September 2022

baryons and DM, and a robust baryonic census must be available to infer the additional contribution from DM. Recent determinations from global methods lie in the range $(0.2-0.6)\,\mathrm{GeV/cm^3}$, while new studies of the local DM density from *Gaia* satellite data yield $(0.3-1.5)\,\mathrm{GeV/cm^3}$, depending on the type of stars used in the study.

Other observational quantities that enter in the phase space distribution of DM, and provide constraints on mass models of the Milky Way are the local circular speed v_c and the escape velocity v_{esc}. The local circular speed is measured by various methods, roughly divided into measurements of the Sun's velocity with respect to an object assumed to be at rest with respect to the Galactic centre or direct measurements of the local radial force. These methods yield values of $v_c = (218-246)\,\mathrm{km/s}$. A recent estimate of the escape velocity, defined as the speed above which objects are not gravitationally bound to our galaxy, is v_{esc}=533^{+54}_{-41} km/s [51].

The local velocity distribution of DM particles can not be measured directly at present, and is mostly derived from simulations. In general, experiments use the simplest, so-called *Standard Halo Model (SHM)* for their data analysis. It assumes an isotropic, isothermal sphere of DM particles with a density profile of $\rho(r) \propto r^{-2}$, for which the velocity distribution is Maxwellian, with a velocity dispersion $\sigma_v = v_c/\sqrt{2}$. This distribution, which formally extends to infinity, is truncated at v_{esc} [52]. Earlier high resolution, dark-matter-only simulations found velocity distributions that markedly deviated from a Maxwell-Boltzmann distribution and in addition revealed components above the dominant smooth distribution, including narrow spikes due to tidal streams. Recent hydrodynamical simulations of Milky Way-like galaxies including baryons, which have a non-negligible effect on the DM distribution in the Solar neighbourhood, find velocity distributions that are indeed close to Maxwellian, arguing that the SHM is a good approximation.

Ultimately the goal is to determine the velocity distribution from observations (for example by studying the motion of stars that share the same kinematics as the DM), and the *Gaia* satellite data offers a unique opportunity to study the various stellar populations. Recently it was revealed that the local stellar halo has two components: a quasi-spherical, weakly rotating structure with metal-poor stars, and a flattened, radially anisotropic structure of metal-rich stars, which arose due to accretion of a large $(10^{11-12}\,\mathrm{M_\odot})$ dwarf galaxy around (8-10)$\times 10^9$ y ago [53]. The expectation is that the local DM halo shows a similar bimodal structure, and first velocity distributions of the two components - using the stellar populations as tracers - were inferred in [54]. In Ref. [55], an updated halo model is introduced: it includes the anisotropic structure seen in the *Gaia* data and provides an analytic expression for the velocity distribution. The value of the local DM density is updated to $(0.55 \pm 0.17)\,\mathrm{GeV/cm^3}$, where the 30% error accounts for the systematics. The circular rotation and the escape speeds are updated to $v_c = (233 \pm 3)\,\mathrm{km/s}$ and v_{esc}=528^{+24}_{-25} km/s.

27.4.2 *Small-scale challenges*

The ΛCDM framework is tremendously successful at explaining the observed large-scale structures of the Universe (corresponding to distances $\geq$1 Mpc, the typical inter-galactic distance), as well as the main properties of galaxies that form within DM haloes, see the comprehensive review in Ref. [56]. The observed large-scale structure is consistent with point-like, cold DM particles that interact purely via the gravitational force. But in the past decades, observations at scales below $\sim$1 Mpc, where structure formation becomes strongly nonlinear, turned out more problematic to be described within the ΛCDM model. The main *small-scale challenges* are known as: the missing satellites problem, the cusp-core problem and the too-big-to-fail problem. Initially these issues, which are not all independent of one another, arose by comparing theoretical predictions from dark-matter-only simulations to observation. While their most likely solutions are in dissipative, baryonic physics (such gas cooling, star formation, supernovae feedback), see the recent review in Ref. [57], the small-scale problems could in addition call for a modification or an extension of the ΛCDM paradigm. Most importantly, the ever increasing amount of data on the satellites of the MW and M31 are used to constrain alternative DM models.

The missing satellites problem: High-resolution cosmological simulations of DM haloes the size of the MW predict hundreds or thousands of subhaloes with masses that are in principle large enough to allow for galaxy formation ($> 10^7\,\mathrm{M_\odot}$). Yet less than $\sim$100 satellite galaxies with masses down to $\sim$300 $\mathrm{M_\odot}$ are known to orbit our galaxy within 300 kpc. Galaxies in the field show a similar under-abundance. One solution could be that galaxy formation becomes increasingly inefficient as the halo mass drops, and thus the smallest DM haloes have naturally failed to form galaxies.

The cusp-core problem: The mass density profiles of DM haloes in ΛCDM simulations rise steeply at small radii, $\rho(r) \propto r^{-\gamma}$, with $\gamma \simeq 0.8-1.4$. This is in contrast to the observed density profiles of many low-mass galaxies (albeit not all), the rotation curves of which are best fit with constant-density cores, $\gamma \simeq 0-0.5$. A related issue is that simulations predict more DM than measured in the central regions of galaxies (also known as the central density problem). A likely solution is that baryonic feedback modifies the structure of DM haloes. Hydrodynamic simulations which include the effects of baryons on galaxy formation have shown that baryonic feedback (e.g., supernova-driven blowouts) can erase the central cusps and produce core-like density profiles.

The too-big-to-fail problem: This problem is related to the fact that the local Universe contains fewer galaxies with large central densities ($\simeq 10^{10}\,\mathrm{M_\odot}$) compared to ΛCDM predictions. DM haloes of such masses are thought to be too massive to have failed to form stars (hence the name of the problem), especially if lower-mass subhaloes are capable of doing so. The bright MW satellites are generally associated with subhaloes (e.g., from the Aquarius and Via Lactea II ΛCDM simulations), however not with the most massive ones. A similar issue is present in Andromeda and in field galaxies outside the Local Group.

The solutions that were briefly mentioned above do not require modifications to the ΛCDM framework. Other solutions involve either modifications of linear theory predictions (via the nature of the DM particle, e.g., Warm DM - WDM) or modifications of nonlinear predictions (via DM models that involve a self-interaction of DM particles - SIDM). WDM models postulate particles with masses at the keV-scale, and the observed number of dark-matter-dominated satellites is used to set a lower limit on the number of subhaloes in the MW and thus a lower limit on the particle's mass [57]. Current constraints are in the range $m_{WDM} > (1.6-2.3)\,\mathrm{keV}$. Cosmological simulations with SIDM find that $\sigma/m_{SIDM} \simeq$(0.5-10) $\mathrm{cm^2/g}$ can alleviate the cusp-core and too-big-to-fail problems, giving rise to DM cores in dwarf galaxies with sizes of (0.3-1.5) kpc [13]. Galaxy clusters provide important constraints, and their large central DM densities prefer models with $\sigma/m_{\mathrm{DM}} \lesssim 0.1\,\mathrm{cm^2/g}$ [58]. Thus, if SIDM is to solve the small-scale CDM problems and obey the constraints observed on the scales of clusters, σ must depend on the velocity of the particle: it must increase as the rms speed of the particle decreases from the scale of clusters ($v \sim 10^3$ km/s) to the scale of dwarf galaxies ($v \sim 10$ km/s).

27.5 Dark matter models

Particle DM model building is deeply intertwined with the question of the nature of physics beyond the Standard Model (BSM) of particle physics[1]. Directions in this area have followed a few strategies, including, but not limited to

(1) pursuing DM candidates embedded in frameworks that include solutions to other open issues in particle physics, for example WIMPs in connection with electroweak-scale new physics that addresses the hierarchy problem, such as supersymmetry (see the Supersymmetry reviews Sec. 88 and 88); axions in connection with frameworks that address the strong CP problem (see Axions and Other Similar Particles—Sec. 90); sterile neutrinos in connection with the problem of neutrino masses and mixing (see

[1] Notice that this includes the case of PBHs, as successful formation of the correct number density of PBHs involves new ingredients beyond standard cosmology and particle physics

Downloaded from https://academic.oup.com/ptep/article/2022/8/083C01/6651666 by KIT Library user on 27 September 2022

the Neutrino Masses, Mixing, and Oscillations—Sec. 14); or (2) *ad hoc*, or *bottom-up* models built with the intent of addressing or explaining a putative experimental (e.g. particle physical anomalies) or observational (e.g. astronomical) signal.

WIMPs: The WIMP paradigm has been a preferred framework chiefly because it often arises in beyond the Standard Model scenarios that address the hierarchy problem whilst also providing a simple mechanism to explain the observed relic abundance via the "WIMP miracle" described above. Perhaps the most notable example of a framework containing a paradigmatic WIMP is the minimal supersymmetric extension to the Standard Model, if the lightest supersymmetric particle is a neutralino (the mass eigenstate resulting from the mixing of the supersymmetric partners to the Higgses and to the SU(2) and hypercharge gauge bosons, and, possibly, of additional singlet scalars); purely SU(2) sneutrinos have long been ruled out by direct detection, but with suitable mixing with "inert" (gauge-singlet) sneutrinos they can also play the role of WIMP candidates. For more details see the the Supersymmetry—Sec. 88 and 89 in this *Review*. Other non-superysmmetric WIMP models include models with a Higgs or Z (or Z') portal, universal extra dimensions [32], and other models with extra (warped or flat) dimensions, little Higgs theories, technicolor and composite Higgs theories, among others (see e.g. the review in [59]).

Axions and axion-like particles: Axions are an especially compelling example of a broad category of DM candidates encompassing very light scalar or pseudoscalar fields. The QCD axion provides a solution to the strong CP problem, and is at present a viable DM candidate (see Sec. 90 for details on motivations, production mechanisms, and detection prospects for the QCD axion). Ultra-light, bosonic DM generally implies the imprint of quantum effects on macroscopic scales (hence the name of *wave* or *fuzzy* DM). Specifically, some of the small-scale issues mentioned in sec. 27.4 can be addressed if the de Broglie wavelength of the DM, of mass m_a and velocity v_a,

$$\frac{\lambda}{2\pi} = \frac{\hbar}{m_a v_a} \simeq 1.9 \text{ kpc} \left(\frac{10^{-22} \text{ eV}}{m_a}\right) \left(\frac{10 \text{ km/s}}{v_a}\right) \tag{27.7}$$

is comparable to the size of the smallest observed gravitationally collapsed structures, roughly, for a self-gravitating system of mass M, a scale $r \simeq GM/v^2$. The typical expectation is the formation of a soliton-like core in the DM density profile of size λ, thus inversely proportional to the DM mass, with an upper limit on the central density of around

$$\rho_s \lesssim 7 \ M_\odot/\text{pc}^3 \left(\frac{m_a}{10^{-22} \text{ eV}}\right)^6 \left(\frac{M}{10^9 \ M_\odot}\right) \tag{27.8}$$

for a halo of virial mass M. Additionally, wave DM predicts that halos lighter than around $10^7(m_a/10^{-22} \text{ eV})^{-3/2} M_\odot$ should not exist [60], and that the number of halos in the local universe with a mass at or less $10^9(m_a/10^{-22} \text{ eV})^{-4/3} M_\odot$ [61] be significantly depleted, addressing in part the too big to fail and missing satellite problems (see Sec. 27.4 above). Light bosonic DM is necessarily produced non-thermally [62], and the connection with the visible sector need not, but might, exist.

Dark photons: Light *vector* bosons such as a "dark photon" V with a mass below $m_V < 2m_e$, can be cosmologically stable (depending upon its kinetic mixing coupling with the visible photon) and be a viable DM candidate. Light dark photons can be produced in the early universe through scattering or annihilation via processes such as $\gamma e^\pm \to V e^\pm$ or $e^+e^- \to V\gamma$, or via resonant photon-dark photon conversion, or from a condensate seeded by inflationary perturbations [63], or from a misalignment mechanism similar to the one commonly invoked for axion production; constraints on the parameter space stem from a combination of direct detection experiments, where the dark photon is absorbed and leads to a large ionization signal, from stellar cooling constraints from the Sun, horizontal branch stars, and red giants, and from CMB and the diffuse radiation from the $V \to 3\gamma$ decay mode. More broadly, light dark (pseudo-)scalars and vectors can be best constrained with experiments that rely on their wave-like behaviour and/or on their possible "portal" with the visible sector. A broad assortment of experiments is sensitive to the range of masses between 10^{-22} eV and 10^{-2} eV. Among these experimental efforts, the lowest masses are probed by torsion balance experiments [64, 65], atom interferometry [66], comagnetometers [67, 68], and even gravitational wave detectors [69]; at increasing masses, if the light bosons couple electromagnetically, they can generate effective currents which are detectable with different apparata depending on the relevant, mass-dependent target frequency. The experimental portfolio includes the broadband axion search ABRACADABRA [70,71], the LC resonator DM Radio [72], lumped-element LC resonators [73], and cavity resonators such as HAYSTAC [74] and ADMX [75] .

Sterile Neutrinos: Sterile (gauge-singlet) neutrinos, assumed to share a Dirac mass term with ordinary, $\text{SU}(2)_L$-active neutrinos, have long been considered viable DM candidates [76]. The mostly-sterile mass eigenstate participates in $\text{SU}(2)_L$ interactions via a mixing parameter $\theta \ll 1$ that controls much of the particle's phenomenology. In particular, the sterile neutrino possesses an inverse-lifetime on the order of $\tau^{-1} \sim G_F^2 m_\nu^5 \theta^2$, forcing the mixing to not exceed

$$\theta < 3.3 \times 10^{-4} \left(\frac{10 \text{ keV}}{m_\nu}\right)^5 \tag{27.9}$$

in order for the lifetime to exceed the age of the universe. While the main decay channel is to three active neutrinos, observationally the radiative decay mode to one neutrino plus a photon is much more relevant, giving rise to a quasi-monochromatic photon line at half the sterile neutrino mass. A recent tentative signal at 3.5 keV was reported from stacked observations of clusters of galaxies, individual clusters [77, 78], and the Galactic center [79] with both the XMM and Chandra X-ray observatories. The signal however was not detected in a large sample of galaxies and groups of galaxies [80] and dwarf galaxies [81], and especially Draco [82], shedding strong doubts on its sterile neutrino decay origin. Future observations with increased energy resolution might conclusively pinpoint the origin of the 3.5 keV emission [83].

Models with rich dark sectors: The absence of any conclusive signals from DM as a particle thus far motivates the hypothesis that the DM be charged under some new "hidden" dark-sector force, an idea that dates back many decades [84], including in the guise of "mirror DM" (more recently in the context of "neutral naturalness"). Top-down motivation for hidden-sector DM comes from string theory [85], although TeV-scale BSM framework such as supersymmetry and composite Higgs models can also naturally accommodate hidden sectors [86]. Although no coupling of the visible sector to the hidden sector need exist in principle, there are a few reasons to expect it [87].The mass scale for hidden-sector DM is broader than, but overlapping with, that for WIMPs (this latter being limited to roughly between a few GeV and a few TeV). In particular, while some motivation exists for electroweak-scale hidden sectors, light, sub-GeV hidden sectors have a strong theoretical underpinning, and offer novel detection avenues and opportunities. The phenomenology of hidden-sector DM depends primarily on the nature of the force and its force carrier. The most-widely considered cases are (pseudo-)scalar and (axial-)vector mediators. Among the structures for the mediators' coupling to the visible sector, renormalizable "portals" include the $H^\dagger H$ operator, through Lagrangian terms of the type $(\mu\phi + \lambda\phi^2)H^\dagger H$, coupling to the hypercharge field strength $B^{\mu\nu}$ via kinetic mixing, $\epsilon' B_{\mu\nu} F'^{\mu\nu}$, and the "neutrino" portal, $y_n LHN$, where L is the lepton doublet of any generation, N is a right-handed neutrino, H is the SM Higgs doublet, and y_n the Yukawa coupling. Other possibilities are for instance a vector mediator directly coupled to SM fermions charged under its corresponding symmetry [88], or a Z' associated to $\text{U}(1)_{B-L}$.Additional possibilities, arising for instance from vector couplings to anomalous global symmetries of the SM like baryon or lepton number, also exist [87]. The accelerator program necessary to probe hidden-sector DM often involves small-scale colliders and fixed-target experiments, with experiments utilizing missing energy and momentum offering the best sensitivity. Beam-dump experiments can test large ranges of DM-mediator couplings as long as mediators decay or scatter inside the detector (see e.g. the recent review [89]). Such exper-

Downloaded from https://academic.oup.com/ptep/article/2022/8/083C01/6651666 by KIT Library user on 27 September 2022

iments can also probe dark sectors with light vectors coupled to visible matter besides gauge kinetic mixing: an instance are neutrino trident scattering used to place bounds on e.g. $L_\mu - L_\tau$ Z' gauge bosons. Being virtually unconstrained, the phenomenology of dark sectors can be arbitrarily rich, with possibilities ranging from dark non-Abelian gauge interactions creating non-trivial self-interacting and/or particle number-changing dynamics, to models of "dynamical" DM, with multi-component, unstable DM candidates and a time-variable effective total DM abundance and equation of state [90].

27.6 Laboratory detection of dark matter

Laboratory searches for DM particles can be roughly classified in direct detection experiments, axion searches (see Axions and Other Similar Particles—Sec. 90), and searches at accelerators and colliders.

27.6.1 *Searches at Accelerators and Colliders*

Various searches for dark matter have been carried out by the CMS and ATLAS collaborations at the LHC in pp collisions [91–95]. In general, these assume that dark matter particles escape the detector without interacting leading to significant amounts of missing energy and momentum.

Searches for DM with the LHC and other colliders have targeted DM models that interact with the SM via Higgs or Z boson exchange, effective field theories with heavy mediators, UV-complete models such as supersymmetry, models with long-lived particles, and models with rich dark sectors. The experimental program correspondingly includes searches for invisible-particle production mediated by a SM boson, generic searches for invisible particles produced via new particle mediators, and specific searches for complete models.

There are a variety of types of signals for DM, as noted by Ref. [91]:

(a) the imbalance in the transverse momentum in an event due to the presence of DM particles, produced together with one Standard Model particle,

(b) a bump in the di-jet or di-lepton invariant mass distributions, or

(c) an excess of events in the di-jet angular distribution, produced by a dark matter mediator. No signal for DM has been observed in the LHC experiments so far. Instead, limits are set on masses, couplings, and cross-sections. The latter can be compared, generally in a model-dependent way, with direct detection experiments.

Searches strategies are designed to optimize signal-to-noise by selecting search-specific cuts: a model-independent instance is initial-state electromagnetic or strong-interaction radiation plus missing transverse energy. Collider searches for DM inform, and are informed, by DM searches through direct or indirect detection (see below), and, if possible, by the inferred thermal relic DM abundance. The collider searches alone cannot prove that a discovery is of dark matter.

In the latter category, searches for DM with the LHC and other colliders have targeted DM models that interact with the SM via Higgs or Z boson exchange, effective field theories with heavy mediators, UV-complete models such as supersymmetry, models with long-lived particles, and models with rich dark sectors. The experimental program correspondingly includes searches for invisible-particle production mediated by a SM boson, generic searches for invisible particles produced via new particle mediators, and specific searches for complete models. Searches strategies are designed to optimize signal-to-noise by selecting specific search-specific cuts: a model-independent instance is initial-state electromagnetic or strong-interaction radiation plus missing transverse energy.

New fixed-target experiments are increasingly probing lighter, sub-GeV dark sectors; thermal, or quasi-thermal relics (such as asymmetric, SIMP, ELDER DM models) provide sharp, largely model-independent experimental targets in the case of direct annihilation to Standard Model particles; even "secluded" annihilation to dark-sector particles can be probed with fixed-target experiments, albeit with some model-dependent caveats. Accelerator searches provide unique ways to test light DM models in that they present a lower dependence on the DM particle nature, that could e.g. drive suppressed velocity-dependent direct detection cross sections, and on kinematic thresholds that can similarly suppress rates with other search strategies; additionally, accelerator searches offer opportunities to explore dark sectors in greater detail than other search strategies [87].

Experimental approaches to explore scenarios with a light DM χ and mediator A' include (i) searches for missing mass in exclusive reactions such as $e^+e^- \to \gamma(A'\chi\bar{\chi})$ or $e^-p \to e^-p(A'\chi\bar{\chi})$, (ii) missing momentum/energy, e.g. in fixed-target reactions such as $eZ \to eZ(A'\chi\bar{\chi})$, (iii) electron and proton beam dump, where the DM particle is detected from scattering in a downstream detector after being produced in the beam dump, (iv) direct dark photon searches, when the mediator cannot decay to the dark matter, $m_{A'} < 2m_\chi$. Current facilities actively probing the methods listed above include APEX and HPS and JLab, MiniBooNE at Fermilab, NA64 at CERN, and TREK at J-PARC. Future experiments that will eventually contribute to covering the mentioned thermal targets include Belle-II at KEK, MAGIX at MESA, PADME at LNF, SHIP at CERN, VEPP3 at BINP, BDX at JLab, COHERENT at ORNL, DarkLight at JLab, LDMX at SLAC or JLab, MMAPS at Cornell, SBN at Fermilab, and SeaQuest [87].

27.6.2 *Direct detection formalism*

Direct detection experiments mostly aim to observe elastic or inelastic scatters of Galactic DM particles with atomic nuclei, or with electrons in the detector material. Predicted event rates assume a certain mass and scattering cross section, as well as a set of astrophysical parameters: the local density ρ_0, the velocity distribution $f(\vec{v})$, and the escape velocity v_{esc} (see Sec. 27.4).

Interactions with atomic nuclei: For DM scattering off nuclei, the differential scattering rate R as a function of nuclear recoil energy E_R is

$$\frac{dR(E_R,t)}{dE_R} = N_T \frac{\rho_0}{m_{\rm DM}} \int_{v>v_{min}} v f(\vec{v}+\vec{v}_E(t)) \frac{d\sigma(E_R,v)}{dE_R} d^3v, \tag{27.10}$$

where N_T is the number of target nuclei, $m_{\rm DM}$ is the mass of the DM particles, $v = |\vec{v}|$ is the speed of the particle in the experiment's rest frame, $f(\vec{v}+\vec{v}_E(t))$ is the velocity distribution in the Earth's frame, v_{min} is the minimum speed of the DM particles that can cause a recoil energy E_R and σ is the scattering cross section on the nucleus [29, 114]. For elastic scattering, the minimum velocity is $v_{min} = (m_N E_R/2m_r^2)^{1/2}$, with m_N being the mass of the nucleus, and $m_r = (m_N m_{\rm DM})/(m_N + m_{\rm DM})$ the reduced mass of the nucleus-DM system. In case of inelastic scattering, the minimum speed becomes $v_{min} = (m_N E_R/2m_r^2)^{1/2} + E^*/(2m_N E_R)^{1/2}$, with the nuclear excitation energy E^*, for part of the kinetic energy of the incoming particle will be spent on exciting the nucleus. The prompt de-excitation energy, if observed in addition to the nuclear recoil energy, will boost the region-of-interest to higher energies [115].

If one assumes the standard, leading order spin-independent (SI) and spin-dependent (SD) interactions, which couple to the charge/mass and spin of the nucleus, respectively, the differential cross section is proportional to the inverse squared speed of the DM particle, $d\sigma/dE_R \propto v^{-2}$, and the dependence on the velocity distribution can be expressed as:

$$g(v_{min},t) = \int_{v>v_{min}} \frac{f(\vec{v}+\vec{v}_E(t))}{v} d^3v. \tag{27.11}$$

This functions allows for the comparison of various experimental results independently of the underlying velocity distribution [116], for a given DM mass. The time-integrated differential cross section is the sum of the SI and SD contributions:

$$\frac{d\sigma(E_R,v)}{dE_R} = \frac{m_N}{2m_r^2 v^2} \left(\sigma_0^{SI} F_{SI}^2(E_R) + \sigma_0^{SD} F_{SD}^2(E_R)\right), \tag{27.12}$$

where $F^2(E_R)$ are the nuclear form factors and σ_0 the cross sections in the limit of zero momentum transfer. Since the in-

Downloaded from https://academic.oup.com/ptep/article/2022/8/083C01/6651666 by KIT Library user on 27 September 2022

Table 27.1: Best constraints from direct detection experiments on the SI (at high >5 GeV and low < 5 GeV masses) and SD DM-nucleon couplings.

Experiment	Target	Fiducial mass [kg]	Cross section [cm^2]	DM mass [GeV]	Ref.
		Spin independent high mass (>5 GeV)			
XENON1T	Xe	1042	4.1×10^{-47}	30	[96]
PandaX-II	Xe	364	2.2×10^{-46}	30	[97]
LUX	Xe	118	1.1×10^{-46}	50	[98]
SuperCDMS	Ge	12	1.0×10^{-44}	46	[99]
DarkSide-50	Ar	46	1.14×10^{-44}	100	[100]
DEAP-3600	Ar	2000	3.9×10^{-45}	100	[101]
		Spin independent low mass (<5 GeV)			
LUX (Migdal)	Xe	118	6.9×10^{-38}	2	[102]
XENON1T (Migdal)	Xe	1042	3×10^{-40}	2	[103]
XENON1T (ionisation only)	Xe	1042	3.6×10^{-41}	3	[104]
DarkSide-50 (ionisation only)	Ar	20	1×10^{-41}	2	[105]
SuperCDMS (CDMSlite)	Ge	0.6	2×10^{-40}	2	[106]
CRESST	$CaWO_4$ - O	0.024	1×10^{-39}	2	[107]
NEWS-G	Ne	0.3	1×10^{-38}	2	[108]
DAMIC	Si	0.3	1×10^{-41}	7	[109]
		Spin dependent proton			
PICO60	C_3F_8 - F	49	3.2×10^{-41}	25	[110]
		Spin dependent neutron			
XENON1T	Xe	1042	6.3×10^{-42}	30	[111]
PandaX-II	Xe	364	1.6×10^{-41}	40	[112]
LUX	Xe	118	1.6×10^{-41}	35	[113]

coming particle velocity is $v/c \sim 10^{-3}$, the nuclear recoil energy is at most tens of keV (much smaller than typical nuclear binding energies per nucleon), and the momentum transfer $q = (2m_N E_R)^{1/2} \sim \mathcal{O}(10\text{-}100\,\text{MeV})$. This implies that $1/q$ can be of the same order as nuclear radii $R \sim A^{1/3}$ fm, and that nuclei are not point-like from the perspective of a DM particle. The cross sections will thus involve nuclear form factors. These were calculated in [117] and [118] for the SI and SD case, respectively, for specific target nuclei, while the cross sections are often expressed in terms of single-nucleon cross sections and effective couplings of the DM particle to protons and neutrons. In the SI case, all the nucleons in the nucleus contribute coherently to the cross section (under the assumption of iso-spin independence in the DM couplings). Dominant sources of uncertainty are the nucleon sigma terms, especially for Higgs-dominated interactions, where the couplings are proportional to the quark masses. An overview is presented in Ref. [119]. For SD scattering, the nuclear spin contents due to the protons and neutrons must be considered.

The interactions of DM particles with nuclei can be treated in a non-relativistic effective field theory (NR-EFT) approach, which considers more general DM scenarios based on the lowest-order, four-field operators that describe the couplings to nucleons. These operators, which correspond to different types of interactions between the DM and quark fields, can be momentum- and velocity-dependent, and might be leading when momentum-independent interactions are suppressed, or even vanish in the limit of zero momentum [120, 121]. In Ref. [121, 122] all 15 operators (arising from 20 possible bilinear combinations between the DM and nucleon fields) which obey Galilean-invariance, T-symmetry and are Hermitian are written out up to quadratic order in q, and the nuclear response functions evaluated in shell-model calculations for DM targets made of F, Na, Ge, I and Xe isotopes. The connection to particle physics within the context of *simplified DM models* is made in Ref. [123, 124], where the simplified models assume a single DM particle with one mediator which couples it to quarks. More recently the DM-nucleus scattering was also analysed in the framework of chiral effective field theory (Ch-EFT), a low-energy effective theory of QCD, which allows for a consistent derivation of the nuclear responses beyond the leading-order expressions [125, 126]. Ch-EFT preserves the QCD symmetries, and predicts DM couplings to two nucleons (e.g., when the hypothetical particle couples to a virtual pion exchanged between the nucleons). It also provides a power counting that suggests a hierarchy of the various NR-EFT operators, which is however approximate given that the couplings between the DM and the Standard Model fields are not known. The generalized SI structure factors for spin-1/2 and spin-0 DM particles and various isotopes of F, Si, Ar, Ge and Xe employed in direct detection experiments are provided in Ref. [126].

Scattering off bound electrons and absorption: For DM particle masses below the GeV-scale, most searches for DM-nucleus scattering rapidly lose sensitivity, due to energy thresholds around a few 100 eV - few keV. As an example, a light DM particle with a mass of 100 MeV and $v \propto 10^{-3}c$ will induce a nuclear recoil energy of about 0.5 eV in a target made of argon. Another strategy is to search for DM scattering off bound electrons, allowing for all of the kinetic energy (50 eV in the above case) to be transferred to the material [127]. The leading possibilities are ionisation, excitation, and molecular dissociation processes, which typically require energies of (1-10) eV, and thus allow to probe scattering of DM particles with masses down to the $\mathcal{O}$(MeV) range.

For a bound electron with binding energy E_B DM particle masses of $m_{\rm DM} \geq 250\,\text{keV} \times \text{E}_\text{B}/1$ eV can in principle be probed. The signal depends on the material, and can consist of one or more electrons (in semiconductors, noble liquids, graphene), one or more photons (in scintillators) or phonons (in superconductors and superfluids) and quasiparticles (in superconductors). As an example, the differential event rate for ionization in atoms is given by

$$\frac{dR_{ion}}{d\ln E_R} = N_T \frac{\rho_0}{m_{\rm DM}} \frac{d\langle\sigma_{ion} v\rangle}{d\ln E_R}, \tag{27.13}$$

where E_R is the recoil energy transferred to the electron, $\langle\sigma_{ion} v\rangle$ is the thermally averaged ionization cross section and N_T is the number of target atoms per unit mass. The cross section is related to the non relativistic DM-electron elastic scattering cross section (σ_e):

$$\frac{dR_{ion}}{d\ln E_R} = \frac{6.2}{A}\left(\frac{\rho_0}{0.4\,\text{GeV}\,\text{cm}^{-3}}\right)\left(\frac{\sigma_e}{10^{-40}\text{cm}^2}\right)\left(\frac{10\,\text{MeV}}{m_{\rm DM}}\right) \times \frac{d\langle\sigma_{ion} v\rangle/d\ln E_R}{10^{-3}\sigma_e}\,\frac{\text{events}}{\text{kg d}} \tag{27.14}$$

Predicted differential rates in various materials (He, Ar, Ge, Xe) and for different particle masses are shown in [127], together

Downloaded from https://academic.oup.com/ptep/article/2022/8/083C01/6651666 by KIT Library user on 27 September 2022

with cross section sensitivities as a function of mass and expected background rates from neutrinos.

Two classes of DM candidates, axion-like-particles (ALPs) and dark (or hidden) photons (see Sec. 27.5), can be absorbed in a target material by interactions with bound electrons via the axioelectric effect, which is analogous to the photoelectric effect: a boson is absorbed by a bound electron, which is then ejected from the atom [63,128,129]. The dark photon arises in extensions of the SM by a new massive or massless U(1)' field, coupled to the SM $U(1)_Y$ via a kinetic mixing term κ, see Sec. 27.5. The absorption cross section of a massive, NR particle m_V with coupling $e' = e\kappa$ to electrons is (in natural units, and for energies $E_V \ll m_e$)

$$\sigma_{abs} = \frac{\alpha'}{\alpha}\left(\frac{E_V}{2m_e}\right)^2 \sigma_{pe}, \tag{27.15}$$

where σ_{pe} is the photoelectric cross section, and an analogue to the electromagnetic fine structure constant α is introduced, $\alpha' = (e\kappa)^2/4\pi$. The rate per atom is

$$R \simeq \frac{\rho_0}{m_V} \times \kappa^2 \sigma_{pe}. \tag{27.16}$$

Since the kinetic energy of the dark photon is negligible compared to its rest energy, a mono-energetic peak at its mass is expected in the spectrum of a direct detection experiment. Dark photons with a thermally generated abundance are excluded by direct detection experiments [63], however non-thermal mechanisms (e.g., via perturbations during inflation) could create the relic abundance, see Section 27.3.

Similarly to axions, ALPs arise in the spontaneous breaking of a global symmetry, and are phenomenologically described by a mass m_a and a decay constant f_a. Unlike for QCD axions, however, there is no strict relation between m_a and f_a. The coupling strength to electrons with mass m_e is parameterised by $g_{ae} = 2m_e/f_a$, and the absorption cross section of a particle with incoming velocity v_a is related to the cross section for the photoelectric effect as

$$\sigma_{abs} v_a \simeq \frac{3E_a^2}{4\pi\alpha f_a^2}\sigma_{pe} = \frac{3g_{ae}^2}{4\pi\alpha}\left(\frac{E_a}{2m_e}\right)^2 \sigma_{pe}. \tag{27.17}$$

As in the case of the dark photon, the signature is a mono-energetic peak at the mass of the particle, broadened by the energy resolution of the detector. Constraints on the couplings of ALPs and dark photons to electrons from direct detection experiments in m_a and m_V mass ranges from $\sim (1 - 10^4)$ eV were derived in Ref. [130, 131], and compared to indirect limits from anomalous energy losses in the Sun, in red-giant and horizontal-branch stars. For a detailed discussion of axion and ALP searches, we refer to the *Axion* review.

27.6.3 *Current and future direct detection technologies*

Direct detection experiments aim to observe the small (keV-scale and below) and rare (fewer than $\sim$1 event/(kg y)) signals which are induced by DM particle scatters in a detector, mostly in the form of ionisation, scintillation or lattice vibrations. A majority of experiments detects more than one signal, which allows to distinguish between scattering off of electrons (electronic recoils, ER) and off of atomic nuclei (nuclear recoils, NR). A 3D position resolution is required to define central detector regions (or fiducial volumes) with low background rates from surrounding materials, and the distinction between single- versus multiple-scatters rejects a significant fraction of backgrounds, given that DM will scatter at most once. We refer to [132,133] for recent reviews of the field.

Specific signatures: For NRs, the shape of the differential recoil spectrum is exponentially falling with recoil energy, and depends on the mass of the particle and on the nuclear mass. Unless $m_{\rm DM} \gg m_N$, $m_{\rm DM}$ can in principle be determined from the measured recoil spectrum, where multiple targets will provide tighter constraints [134]. The Earth's motion through the MW induces a seasonal variation of the total event rate and a forward-backward asymmetry in a directional signal [135, 136]. The annual modulation is due to the Earth's motion in the Galactic rest frame, which is a superposition of the Earth's rotation around the Sun and the Sun's rotation around the Galactic center. Since the Earth's orbital speed is much smaller than the Sun's speed, the expected amplitude of the modulation is $\simeq 5\%$. In the SHM, the period is one year, and the phase is 150 d (June 2), when both speeds add up maximally. This expectation is modified for different DM distributions, e.g. in the case of sub-structures such as clumps and streams [137, 138] and a DM disc [139]. In addition, the modulation changes phase at a specific recoil energy (known as crossing-energy) [140], which depends on the DM and nuclear mass, allowing to in principle determine $m_{\rm DM}$ if low energy thresholds can be achieved. A powerful signature is provided by the ability to detect the axis and direction of the recoiling nucleus. Since the DM flux in the laboratory frame is peaked in the direction of motion of the Sun towards the constellation Cygnus, the recoil spectrum is peaked in the opposite direction. The observation of such a dipole feature would provide a 'smoking-gun' evidence for DM, where the forward-backward rates can differ by a factor of $\sim$10, depending on the energy threshold. Ref. [141] provides a recent review of the theoretical framework and of the discovery reach of directional detectors.

Backgrounds, including neutrinos: Early direct detection experiments employing low-background Ge spectrometers featured background levels around 2 events/(kg d keV), while the latest generation of liquid Xe experiments reduced this noise by four orders of magnitude, to 2×10^{-4} events/(kg d keV). Nonetheless, the measured energy spectra are still dominated by interactions due to the radioactivity of detector components, followed by cosmic muons and their secondaries such as fast neutrons. The cosmic and environmental radiation are suppressed by going deep underground and surrounding the experiments with appropriate shielding structures (mainly large water Cherenkov detectors for the current and next-generation detectors). Activation of materials via cosmic-ray interactions produce long-lived radio-nuclides (e.g., ^{39}Ar, ^{60}Co, ^{68}Ge, ^{32}Si, etc), while long-lived, human-made isotopes (^{85}Kr, ^{137}Cs, etc) can mix with detector materials or generate surface backgrounds. For details, we refer to *Section 36.6* of this *Review*.

The final backgrounds will be due to the irreducible neutrino flux from the Sun, the atmosphere and the diffuse supernovae background [142]. Solar pp-neutrinos will dominate the electronic recoil background due to elastic neutrino-electron scatters, at a level of $\sim (10-25)$ events/(t y) below energies of $\sim$100 keV, while coherent elastic neutrino-nucleus scatters (CEνNS) from ^{8}B solar neutrinos will induce up to $\sim 10^3$ events/(t y) for high-A targets, at nuclear recoil energies below $\sim$few keV. Nuclear recoils from atmospheric neutrinos and the diffuse supernovae neutrino background will yield event rates in the range $(1-5)$ events/(100 t y), depending on the detector material. In general, ^{8}B and atmospheric neutrinos will impact light (≤ 6 GeV) and heavy (100 GeV and above) DM searches for cross sections on nucleons below $\sim 10^{-45}$ cm^2 and $\sim 10^{-49}$ cm^2, respectively. The precise cross sections where neutrinos constitute a dominant background depend however on the uncertainties on the flux of each neutrino source, and on the astrophysical parameters that enter in the DM signal models [143]. For very low energy thresholds to nuclear recoils, e.g. 10-30 eV in Ge and Si detectors, CEνNS due to the ^{7}Be neutrino flux become relevant for exposures of $\sim$50 kg y [144]. For DM searches with electron recoils via DM-electron scattering and dark photon or ALP absorption, solar neutrinos will also limit the sensitivity to DM masses in the range $\sim$(1-10^3) MeV and $\sim$(1-10^3) eV, respectively, for large exposures $\sim$1 t y, as shown in Ref. [145].

Solid-state cryogenic detectors: Current experiments using the bolometric technique (see *Section 36.5* of this *Review*), together with either charge or light readout, are SuperCDMS (Si, Ge) at Soudan, EDELWEISS (Ge) at the Laboratoire Souterrain de Modane (LSM) and CRESST ($CaWO_4$) at the Laboratori Nazionali del Gran Sasso (LNGS). These experiments are optimised for low-mass DM searches, and can probe masses down to $\sim$0.2 GeV. CDMSlite also operates detectors at higher bias voltages to amplify the phonon signals produced by drifting charges and thus have access to light DM around 1.5 GeV. The goal of their future phases is to probe the low-mass region down to cross

Downloaded from https://academic.oup.com/ptep/article/2022/8/083C01/6651666 by KIT Library user on 27 September 2022

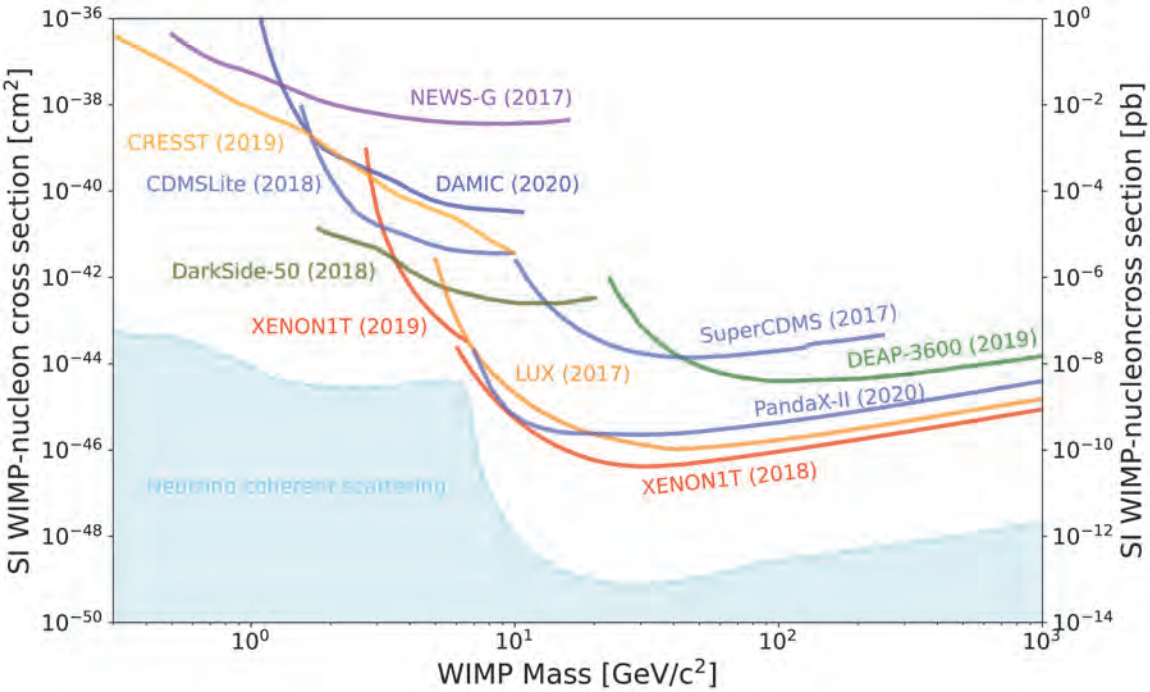

Figure 27.1: Upper limits on the SI DM-nucleon cross section as a function of DM mass.

sections of 10^{-43}-10^{-44} cm^2. Much smaller, gram-scale versions of cryogenic detectors can have single-charge resolution and thus probe low-mass DM via inelastic electron recoils. A SuperCDMS single-charge sensitive Si detector placed upper limits on DM interacting with electrons for masses between $(0.5 - 10^4)$ MeV, as well as on dark photon kinetic mixing for dark photon masses in the range $(1.5 - 40)$ eV. With Ge crystals operated at Soudan, SuperCDMS constrained dark photons and ALPs in the mass range 40 eV to 500 keV.

Germanium ionisation detectors operated at 77 K can reach sub-keV energy thresholds and low backgrounds, but lack the ability to distinguish electronic from nuclear recoils. The CDEX-10 experiment, located at the China Jinping Underground Laboratory (CJPL), uses p-type, point-contact Ge detectors operated in liquid nitrogen, and probes DM masses down to 3 GeV. It also reported constraints on the kinetic mixing of dark photons in the mass range 0.1-4.0 keV. The neutrinoless double beta experiments Majorana Demonstrator and GERDA have obtained constraints on the couplings of ALPs and dark photons to electrons, with masses between (6-100) keV and (60-1000) keV, respectively.

Noble liquids: Liquid argon (LAr) and liquid xenon (LXe) are employed as DM targets, while R&D on liquid helium and neon is ongoing. We refer to Ref. [146] for a review of the liquid noble gas detector technology in low-energy physics, as well to *Section 36.4* of this *Review*. At present the best constraints on DM-nucleus interactions come from experiments using xenon: the LUX experiment which was operated at SURFi, PandaX-II at CJPL and XENON1T at LNGS. These experiments probe particle masses down to ~6 GeV (when using both light and charge signals) and the SI DM-nucleon cross section down to 4.1×10^{-47} cm^2 (at 30 GeV). LAr experiments use the powerful pulse shape discrimination (PSD) that allows for distinguishing between ER and NR events, at the expense of higher energy thresholds than in LXe. The DarkSide-50 TPC at LNGS sets a minimum upper limit on the SI, DM-nucleon cross section of 1.09×10^{-44} cm^2 at 126 GeV, while the single-phase experiment DEAP-3600 at SNOLAB constrains the SI cross section to values below 3.9×10^{-45} cm^2 at 100 GeV.

In noble liquids, sub-GeV DM particles can be searched for by observing inelastic, ER processes following a low-energy nuclear recoil: excitation and ionisation of the recoiling atom (the hypothetical Migdal effect) and a bremsstrahlung photon [147]. As an example, LUX and XENON1T constrained DM particle masses between $(0.3 - 5)$ GeV via bremsstrahlung photons and Migdal electrons. Even lower masses are accessible when using the amplified, charge signal only, at the expense of giving up discrimination between ERs and NRs. XENON1T probed particle masses down to 60 MeV, while DarkSide-50 published constraints on WIMP masses as low as 1.8 GeV. DM masses at the MeV-scale can also be probed by exploiting the scattering off electrons. The XENON1T experiment presented a light DM search with ionisation signals, with a background level of <1 event(t d keV) above 0.4 keV. LXe TPCs also search for solar axions, Galactic ALPs and dark photons. PandaX-II and LUX set upper limits on the axion-electron coupling of 3.5×10^{-12} in the mass range $(10^{-5} - 1)$ eV for solar axions, and probe couplings around 4×10^{-13} in the mass range $(1 - 10)$ keV for Galactic ALPs [148, 149]. XENON1T observed an excess of events over known backgrounds at energies below 7 keV, which can be explained by solar axions ($3.4\,\sigma$) or bosonic dark matter with a mass around 2.3 keV ($3.0\,\sigma$), where the former is in strong tension with stellar constraints [150].

The next generation of liquefied noble gas detectors are in construction (DarkSide-20k), commissioning (LZ), operation (PandaX-4T and XENONnT) or at the design and R&D stage (ARGO, DARWIN). These will increase the sensitivity to various DM candidates by 1-2 orders of magnitude, with the ultimate goal of exploring the experimentally accessible parameter space, until the backgrounds from neutrinos will start dominating the event rates.

Room temperature scintillators: Several large DM experiments using high-purity NaI(Tl) crystals are acquiring data in various underground laboratories. Of these, DAMA/LIBRA at LNGS has the highest mass, 250 kg, and the largest exposure: 1.33 t y with an energy threshold of 1 keV and 2.46 t y with an energy threshold of 2 keV. It is the only experiment in the field that reported an annually modulated event rate with a statistical significance of $12.9\,\sigma$ C.L. (20 annual cycles), with a modulation amplitude around 0.02 events/(kg d keV) in the energy region (1-4) keV. These findings were interpreted as due to DM interactions via nuclear or electronic recoils. The ANAIS experiment at Canfranc operates 112.5 kg of NaI(Tl) scintillators with an energy threshold of 1 keV and a background rate of 3.6 events/(kg d keV) in the (1-6) keV region. A blind analysis of 3 y of data, for an exposure of 314 kg y is consistent with an absence of mod-

Downloaded from https://academic.oup.com/ptep/article/2022/8/083C01/6651666 by KIT Library user on 27 September 2022

ulation at $3.3\,\sigma$. The COSINE-100 experiment, located at the Yangyang Underground Laboratory, operates 106 kg of NaI(Tl) crystals in a liquid scintillator, with an energy threshold of 2 keV and a background rate of 3.6 events/(kg d keV). Results from a 97.7 kg y exposure in the (2-6) keV energy range are consistent, at 68.3%C.L., with both the null hypothesis and DAMA/LIBRA's best fit value in the same energy range. A larger exposure and a reduced energy threshold are required to test DAMA/LIBRA for $3\,\sigma$ coverage. The SABRE experiment plans to operate a total of 50 kg of NaI(Tl) crystals, focussing on reaching a background level of 0.1 events/(kg d keV), an order of magnitude below DAMA/LIBRA. Twin detectors will be installed at LNGS and at the Stawell Underground Physics Laboratory in the Southern hemisphere. While a DM-induced signal is expected to have the same phase in both hemispheres, seasonal or site-related effects would show different amplitudes and phases in the twin detectors. The COSINUS R&D project aims to develop a cryogenic scintillating bolometer with undoped NaI crystals with phonon and light readout, the ratio of which allows for particle discrimination. The hope is that it will shed light on the type of interactions responsible for the modulated signal.

Room temperature ionisation detectors: Silicon charged-coupled devices (CCDs) are employed for low-mass DM searches, as well as for hidden photon searches in the eV-mass range. Ionisation events induced in bulk silicon of high-resistivity, fully depleted CCDs are observed with charge resolutions around 1-2 e^- and extremely low leakage currents, at the level of few $e^-\,mm^{-2}d^{-1}$. The position of an energy deposit is reconstructed in 3 dimensions and the particle type (electron, neutron, muon, α-particles, etc) is reconstructed based on the recorded track pattern.

The DAMIC experiment at SNOLAB yielded new constraints on DM-electron scattering, and on the hidden-photon kinetic mixing parameter in the mass range (1-30) eV with an exposure of 7.6 kg d and on low-mass WIMPs with an exposure of 11 kg d. The SENSEI projects employs the skipper technology to achieve single-electron sensitivity. A run with a 2 g detector in the MINOS cavern at Fermilab yielded world-leading constraints on DM-electron scattering for a large range of sub-GeV dark matter masses. The skipper technology will also be employed in the next stage of the DAMIC programme, DAMIC-M at LSM, which plans for a kg-size mass. The goal is to achieve thresholds of 2-3 electrons and to probe the DM-nucleon cross section down to few$\times 10^{-43}$cm^2 around 2-3 GeV and the DM-electron cross section down to 2×10^{-41}cm^2 at 10 MeV mass.

The NEWS-G collaboration operates spherical proportional counters filled with a noble gas. Advantages of this technology are the low intrinsic electronic noise and a high amplification gain, allowing for low energy thresholds down to single-electron detection, and the possibility to use different light targets (He, Ne, etc). A 60 cm diameter chamber operated at LSM with a gas mixture of Ne + CH_4 (0.7%) at 3.1 bar, excluded SI, WIMP-nucleon cross sections above 4.4×10^{-37}cm^2 at 0.5 GeV after an exposure of 9.6 kg d with an energy threshold $\sim$100 eV. The next iteration, a 140 cm sphere detector made of very low radioactivity copper (few μBq/kg of ^{238}U and ^{232}Th) is under construction at SNOLAB.

Superheated liquid detectors: Investigation of the spin-dependent interaction channel calls for target nuclei with uneven total angular momentum. A particularly favourable candidate is ^{19}F, the spin of which is carried mostly by the unpaired proton, yielding a cross section which is almost a factor of ten higher than of other employed nuclei with spin (e.g., ^{23}Na, ^{73}Ge, ^{127}I, ^{129}Xe, ^{131}Xe). Fluorine is part of the target of experiments using superheated liquids, such as the ones operated by the PICO and MOSCAB collaborations. A search in the PICO-60 C_3F_6 bubble chamber at SNOLAB with an exposure of 1404 kg d and an energy threshold of 2.45 keV, yielded the most stringent constraint on the DM-proton SD cross section at 3.2×10^{-41}cm^2 for a 25 GeV particle mass. In construction is a ton-scale detector (PICO-500) to be deployed in the cube area hall of SNOLAB. MOSCAB successfully built and tested a geyser-concept bubble chamber, the operation of which is based on a continuous process of evaporation and condensation, with the detector recovering its superheated state automatically after each event. After first results in a surface laboratory, the detector was moved underground to LNGS for science data taking.

Directional detectors: Detectors capable of measuring the direction of the recoiling nucleus would unequivocally confirm the Galactic origin of a signal and could probe the region below the neutrino floor [151, 152]. Because nuclear recoils have a range which is about 10 times smaller than the one of Compton recoils of the same energy, gaseous detectors have an excellent intrinsic background rejection if they can measure the range of events precisely. Several directional detectors are presently in operation, where a 1 m^3 detector has a typical mass of a few 100 g and can measure the sense of an incoming nuclear recoil above a few tens of keV. Cygnus is a proto-collaboration which coordinates the R&D efforts for gas based TPCs with 1 keV threshold.

A new technique is based on fine-grained nuclear emulsions (solid-state detectors with silver halide crystals uniformly dispersed in a gelatine film, where each crystal works as a sensor for charged particles), as proposed by the NEWSdm collaboration. These act as target and nanometric tracking device, and the expected NR tracks are sub-μm in size. Due to the small crystal size and larger number density, a superior spatial resolution compared to gaseous detectors is obtained. Simulations show that to reach the neutrino floor, exposures of 10 t y and 100 t y are required if a 30 nm and 50 nm threshold for detecting the track length is reached. This requires further R&D, since current emulsions allow for 100 nm tracking and target masses are around 1 kg, with 10 kg y exposures planned. A proposed approach for the directional detection of sub-GeV DM is to use two-dimensional materials such as monolayer graphene [153], from which the DM particle can eject electrons. Their energy and direction, correlated with the direction of the incoming DM, can be measured for instance with the proposed PTOLEMY experiment.

New techniques: To probe light (sub-GeV) DM particles, either via scatters off electrons or via couplings to phonons, new techniques beyond the ones discussed above are proposed. The DM particle mass that can be accessed in DM-electron scattering in noble liquids and semiconductors is limited by the minimum ionisation/excitation energy and the size of the band gap, respectively (at the $\sim$eV-scale). To reach lower energy thresholds, materials with smaller band gaps for electron excitations ($\sim$meV), such as superconductors and superfluids, as well as Dirac materials were recently proposed [154]. These would in principle allow for the detection of keV-scale DM. Other ideas to detect keV-MeV scale DM are to observe NRs in superfluid He, via collective excitation modes in the fluid [155], or based on the breaking of chemical bonds between atoms [156].

Even lighter DM, with masses in the meV-eV range, could be detected via absorption on a conduction electron in a superconductor, followed by the emission of an athermal phonon [157]. Another proposed target for light DM are polar materials (for example GaAs, sapphire), which are especially sensitive for scattering through an ultralight dark photon, via excitation of single optical phonons [158]. If an anisotropic crystal such as sapphire is employed, a daily modulation interaction rate could be established [159]. A new class of detectors for bosonic DM, based on resonant absorption onto a gas of small polyatomic molecules, is proposed in [160]. The DM would effectively act as a laser that resonantly excites transitions in molecules when its mass closely matches the transition energy. While DM with SI couplings can efficiently excite phonons, it has been shown in [161] that if DM couples to the electron spin, magnon excitations (quanta of collective spin wave excitations) in materials with magnetic dipole order may also offer a promising detection avenue. Yet another approach for sub-GeV DM is to employ superconducting nanowires as both target and sensor, and first bounds on DM-electron interactions were already placed from a 4.3 ng tungsten-silicide prototype with a 0.8 eV energy threshold [162].

The detection of light DM via collective excitations in condensed matter systems and other methods is a rapidly evolving field, and a growing area of research at the interface of DM physics, condensed matter and materials science. We refer to Ref. [87,163]

Downloaded from https://academic.oup.com/ptep/article/2022/8/083C01/6651666 by KIT Library user on 27 September 2022

for discussions of some of these new directions and models. Critical challenges are to detect these very small energy depositions, and to reliably asses the background noise.

Table 27.1 summarises the most stringent constraints on the DM-nucleon SI and SD cross sections, and Figure 27.1 shows the best constraints for SI couplings in the cross section versus DM mass parameter space, above masses of 0.3 GeV.

27.7 Astrophysical detection of dark matter

DM as a microscopic constituent can have measurable, macroscopic effects on astrophysical systems. Indirect DM detection refers to the search for the annihilation or decay debris from DM particles, resulting in detectable species, including especially gamma rays, neutrinos, and antimatter particles. The production rate of such particles depends on (i) the annihilation (or decay) rate (ii) the density of pairs (respectively, of individual particles) in the region of interest, and (iii) the number of final-state particles produced in one annihilation (decay) event. In formulae, the rate for production of a final state particle f per unit volume from DM annihilation can be cast as

$$\Gamma_f^A = c\frac{\rho_{\rm DM}^2}{m_{\rm DM}^2}\langle\sigma v\rangle N_f^A, \tag{27.18}$$

where $\langle\sigma v\rangle$ indicates the thermally-averaged cross section for DM annihilation times relative velocity [27], calculated at the appropriate temperature, $\rho_{\rm DM}$ is the physical density of DM, and N_f^A is the number of final state particles f produced in one individual annihilation event. The constant c depends on whether the DM is its on antiparticle, in which case $c = 1/2$, or if there is a mixture of DM particles and antiparticles (in case there is no asymmetry, $c = 1/4$). The analog for decay is

$$\Gamma_f^D = \frac{\rho_{\rm DM}}{m_{\rm DM}}\frac{1}{\tau_{\rm DM}}N_f^D, \tag{27.19}$$

with the same conventions for the symbols, and where $\tau_{\rm DM}$ is the DM's lifetime.

Gamma Rays: DM annihilation to virtually any final state produces gamma rays: emission processes include the dominant two-photon decay mode of neutral pions resulting from the hadronization of strongly-interacting final states; final state radiation; and internal bremsstrahlung, the latter two including, possibly, the emission of massive gauge or Higgs bosons subsequently producing photons via their decay products. Similarly, neutrinos are produced from charged pion decay and from radiative processes. The flux of gamma rays and neutrinos is calculated integrating the rate Γ_f per steradian (simply meaning, for isotropic emission, $\Gamma_f/(4\pi)$) along the line of sight within the appropriate angular region (the *differential* flux is obtained in the same way by simply replacing N_f with the differential flux at production, at the appropriate redshift in the case of cosmologically distant sources),

$$\phi_f = \int_{\Delta\Omega} d\Omega \int_{\rm l.o.s.} dl\frac{\Gamma_f}{4\pi}. \tag{27.20}$$

It is customary to factor out, in the expression for the rate, a *particle physics* factor, depending upon the DM particle mass and its annihilation or decay rate, and an *astrophysical* factor, which only depends on the observational target. The latter is sometimes denoted with $J_{\Delta\Omega}(\psi)$ with ψ indicating the direction of the line of sight. Although different conventions are in use, a common choice is to define

$$J_{\Delta\Omega}(\psi) = \int_{\Delta\Omega}\int_{\rm l.o.s.(\psi)} \rho_{\rm DM}^2(l,\Omega)\ dl d\Omega. \tag{27.21}$$

For a target with uniform density ρ and radius r at a distance $d \gg r$, such that the target is entirely within the solid angle $\Delta\Omega$,

$$J \simeq \frac{4\pi r^3\bar{\rho}_{\rm DM}^2}{3d^2}. \tag{27.22}$$

Searches for gamma-ray emission from DM annihilation have focused on targets chosen based on a variety of considerations, primarily intended to maximize signal to noise. Nearby dwarf spheroidal galaxies contain very small amounts of gas, and do not host any significant astrophysical background at gamma-ray or X-ray frequencies, and are thus an optimal target choice for DM searches. An accurate determination of the DM density profile in these objects results in somewhat large systematics when deriving constraints from the non-observation of emission from DM; future optical surveys will help pinpoint with greater accuracy stellar kinematics and thus reduce such uncertainty; a second target is the inner region of the Milky Way: while nearby and potentially hosting a large density of DM, the Galactic center region is however very bright at almost any wavelength, making the extraction of a signal highly problematic; nearby clusters of galaxies are also known to host significant astrophysical emission, but are potentially ideally suited to constrain DM decay. Finally, putative nearby DM clumps are also a possible source of a bright DM signal (albeit from an unknown direction), as is the annihilation of DM in all halos at all redshifts.

DM annihilation and decay can lead to striking spectral features. Since the process happens typically at very low particle velocities, if the DM pair-annihilates e.g. to two photons or two neutrinos, the final-state particles will be nearly monoenergetic, with an energy close to the DM particle mass and a width proportional to the DM velocity in units of c (if a $\gamma\gamma$ line is present electroweak symmetry also implies a $Z\gamma$ line, if kinematically allowed). No astrophysical processes are known to produce lines at gamma-ray or neutrino energies in the GeV and above (with, perhaps, the possible exception of cold pulsar winds [164]) making this channel virtually background-free. At lower energy, lines are expected from radiative decay modes of candidates such as sterile neutrinos (see Sec. 27.5).DM annihilation or decay can lead to additional spectral features besides lines. These include (one or more) "boxes" [165], produced by boosted final states decaying to monochromatic photons (such as e.g. neutral pions), or combinations thereof. Processes occurring at higher redshift can distort these spectral features by smearing them to lower energies. Neglecting gamma-ray attenuation, the flux of gamma rays from all redshift can be cast as

$$\frac{dN_\gamma}{dE_\gamma}(E_\gamma) = \frac{c}{8\pi}\int \frac{\langle\sigma v\rangle\rho_{\rm DM}(z)dz}{H(z)(1+z)^3 m_{\rm DM}^2}\left(\frac{dN_\gamma}{dE'}\right)_{E'=E_\gamma(1+z)}. \tag{27.23}$$

While the calculation of the differential spectrum of gamma rays from a given final state f, dN_γ^f/dE_γ, is carried out using numerical tools, such as Pythia [166] that reproduce hadronization and particle decay for masses well above a few GeV, in the sub-GeV range gamma-ray production follows primarily from meson decay and radiative processes well outside the range of applicability of the Altarelli-Parisi splitting function. The MeV gamma-ray range will soon be probed with forthcoming satellites [167]. Recently a code that provides the expected gamma-ray spectrum for sub-GeV DM, `Hazma`, has become available [168].

Observations with the Fermi Large Area Telescope (LAT) and with ground-based facilities such as HESS, VERITAS, MAGIC, and HAWC have provided an unprecedented picture of the gamma-ray sky ideally suited to look for a signal from DM annihilation or decay for DM particles from a few GeV mass up to several TeV. The LAT has provided some of the most stringent constraints to-date on DM pair-annihilation for a variety of annihilation final states, chiefly from stacked observations of nearby satellite dwarf spheroidal galaxies [169]. Excesses of gamma rays over the expected diffuse and point-source background have been claimed, most importantly from the direction of the inner Galaxy, where a signal from DM annihilation might be especially bright [170,171]. The nature of this excess is quite controversial: while the morphology and spectrum fall within what expected for a standard WIMP with a mass of a few tens of GeV [172], unresolved point sources, including especially an (expected) population of millisecond pulsars (MSPs) have been advocated as a possible plausible counterpart [173]. Statistical methods to discriminate between DM and MSPs have been utilized [174,175], but recent studies indicate that such results might not be conclusive [176]. Large uncertainties in the Galactic diffuse background emission model are addition-

Downloaded from https://academic.oup.com/ptep/article/2022/8/083C01/6651666 by KIT Library user on 27 September 2022

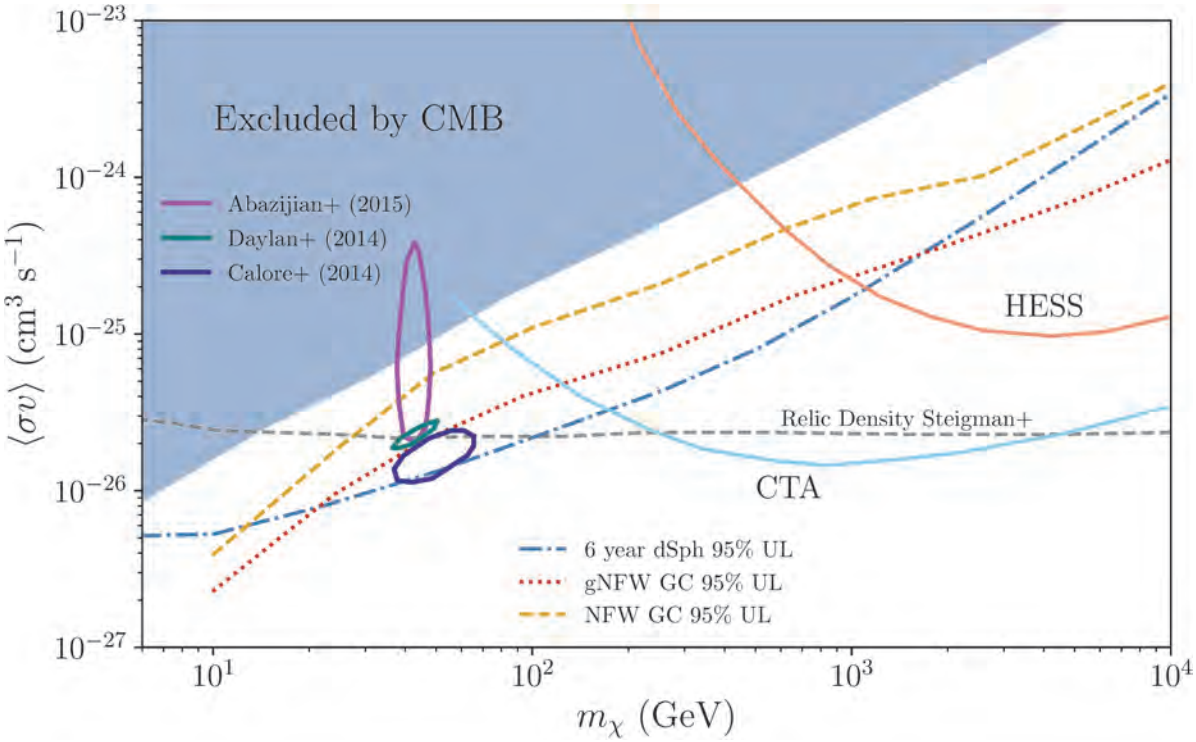

Figure 27.2: Upper limits and projected sensitivity from CTA on the pair-annihilation rate versus the DM mass from gamma-ray and CMB observations (figure courtesy of Logan Morrison).

ally known to exist, and possible plague the morphological and spectral information [177, 178].Other notable potential gamma-ray excesses include a diffuse emission from the Andromeda galaxy (M31) [179–181], possibly in excess of what expected from cosmic-ray models [182]; and a diffuse emission at 511 keV energy in the inner Galaxy from Integral-SPI observations [183]; such emission has known astrophysical counterparts [184], as well as several proposed DM explanations (e.g. [185]).

While DM annihilation and decay typically occurs at low velocities, the possibility of "boosted" DM has also been considered [186]. In this case, the DM particle might dominantly pair-annihilate to a lighter dark species, which does interact with Standard Model particle, and could be detected with neutrino telescopes or direct detection experiments. Future facilities that promise to widen the reach of gamma-ray searches for DM include especially the Cherenkov Telescope Array (CTA), see fig. 27.2.

Neutrinos: DM can be captured in celestial bodies in significant amounts, depending on the DM scattering cross section off of nucleons, the DM mass, and the DM flux incident on the celestial body of interest. For DM masses at or around the GeV scale, evaporation from the celestial body plays an important role [187]. If enough DM accumulates, DM annihilation inside the celestial body can then lead to the production of Standard Model particles. Such particles can heat up the body, if they lose most of their energy before escaping. Utilizing models for heat production in planets, or stellar interior models in the case of stars, constraints can be put on DM particle properties. Of note are constraints from anomalous warming of cold planets such as Uranus [188], alterations to the stellar structure or the Sun's seismic activity [189], and anomalous Earth heat flow [190]. Alternately, DM annihilation in celestial bodies can result in the production of particles that can escape the body. Within the Standard Model, the only such instance is annihilation to neutrinos, but, similarly to the boosted DM case the DM can annihilate to a (stable or unstable) dark-sector particles, whose decay or interactions can be detected on Earth [191,192]. For direct annihilation to neutrinos, given the lower limit on the DM mass from evaporation, the typical neutrino energies usually exceed the energy of neutrinos from the Sun, the best target for this type of searches, making this a virtually background-free DM search. Significant neutrino fluxes can only be achieved, however, if near-equilibration is reached between the capture and annihilation rates. In turn, this requires large-enough DM-nucleon scattering cross sections, to-date very close to the limits from direct detection (see sec. 27.6). Only spin-dependent cross section, and capture in the Sun usually provide large-enough neutrino fluxes. IceCube and ANTARES searches for an anomalous flux of high-energy neutrinos from the Sun yielded null results, which can be interpreted as constraints on spin-dependent nucleon-DM interactions under the assumption of equilibration and of specific annihilation final states [193,194]. Lower-threshold detectors, including DeepCore [195] and PINGU [196], can produce interesting limits on lower-mass DM candidates above the evaporation threshold.

Cosmic-ray Antimatter: Stable charged particles produced by decays of products of, or directly from DM annihilation or decay, populate the cosmic radiation and are a prime target for indirect DM searches. To maximize signal to noise, searches focus on relatively rare particle species, such as positrons, antiprotons, and antinuclei. While in certain models the production of particles and antiparticles is not symmetric [197], generally DM annihilation or decay produces as many particles as antiparticles in the final state. Charged particles produced by DM propagate and lose energy prior to reaching detectors. The transport of charged particles is customarily carried out in the context of diffusion models such as the Galactic "leaky box" setup, see e.g. [198]. While progress in constraining the uncertain propagation and energy-loss processes has been steady with improved data from new detectors such as PAMELA [199] and AMS-02 [200], the calculation of the particle flux at Earth from that at production suffers from significant uncertainties [198].

An excess of high-energy positrons over the standard secondary production from inelastic cosmic-ray interactions has been firmly established by several experiments, most recently and with the highest statistics by AMS-02 [201]. The excess has been ascribed to DM annihilation, although strong constraints from the non-observation of corresponding anomalies in other channels, such as antiprotons and gamma rays, and the peculiar spectral shape, force DM models to be quite convoluted (see e.g. [202]). Alter-

Downloaded from https://academic.oup.com/ptep/article/2022/8/083C01/6651666 by KIT Library user on 27 September 2022

nately, excess *primary* positrons can be produced in the magnetosphere of nearby pulsars [203, 204]. This latter explanation was questioned in [205] in connection with the detection of a TeV halo around two candidate pulsars, leading to the determination of a highly suppressed diffusion coefficient within the pulsar nebula; with such low diffusion coefficient, positrons from the pulsars would not contribute significantly to the flux at Earth; Ref. [206], however, showed that likely the diffusion coefficient is not constant, and that if it increases outside the nebula, as expected from other cosmic-ray measurements, pulsars can still be considered as the counterpart to the positron excess. Other explanations for the excess, albeit somewhat controversial, and increasingly constrained by data, also exist [207, 208].

The antiproton spectrum in the cosmic radiation as measured by AMS-02 [200] also exhibits features that might be considered as excess flux between 10 and 20 GeV, and energies above 100 GeV [209], which have been interpreted as possible signal of DM annihilation; more realistically, however, systematic uncertainties in the antiproton production cross section, in cosmic-ray transport, reacceleration at high energy and, at low energy, solar modulation make it extremely difficult to assess the robustness of the excesses [210, 211].

Antinuclei such as anti-deuterium and anti-helium could also form as a result of DM annihilation or decay. While baryon number conservation forces the typical kinetic energy of antinuclei produced in inelastic cosmic-ray processes to large values, antinuclei arising from hadronization of DM-initiated jets have low energy, offering optimal signal-to-noise when a low-energy cut on the antinucleus kinetic energy is used [212–216]. Specific detector designs have been developed to single out low-energy cosmic-ray antinuclei (e.g. $E < 0.25$ GeV/nucleon in the case of the General Antiparticle Spectrometer, or GAPS [217]). The detection of even a single antinucleus would have considerable importance as a possible sign of new physics [218].

Multi-wavelength studies: Electrons and positrons from DM lose energy quite efficiently, radiating at a variety of wavelengths. This *secondary* radiative emission presents spectral and morphological features that might provide an important additional indirect detection channel. The most efficient energy loss mechanisms for high-energy electrons and positrons are inverse Compton (IC) up-scattering of background photons, and synchrotron radiation in the presence of magnetic fields. Depending on the DM mass, the emitted light from synchrotron peaks at MHz-GHz frequencies, while the IC emission at X-ray to gamma-ray frequencies, depending on the energy of the background radiation, typically ranging from CMB photons up to starlight photons [219–221]. The calculation of the secondary emission from DM entails both solving the transport of the electrons and positrons from DM, and for the radiative emission; codes exist that perform these calculations for certain astrophysical environments [222–224], with diffusion playing an increasingly critical role in smaller and smaller structures such as dwarf galaxies [220]. It has been demonstrated that for large magnetic fields and for certain final states, the synchrotron emission is more constraining than the gamma-ray emission [225].

Stellar Physics: Microscopic properties of the DM can meaningfully alter, and thus be constrained by, several astrophysical environments, from planets and stars, up to the universe as a whole. DM particles light enough to be produced in collisional processes inside stars, with typically temperatures in the keV, or supernovae, with energy scales in the MeV, lead to an additional energy-loss mechanism, if capable of escaping the system. If this is the case, the increased needed energy output would also result in an increased neutrino flux, leading to constraints on the masses and couplings of the DM, see e.g. [226] for a comprehensive review. DM annihilation can even have fueled early stages of stellar evolution, perhaps with measurable consequences [227]. DM capture in neutron stars could lead to the collapse of the star into black holes; the existence of neutron stars in DM-rich environments can thus be used to constrain the mass and interaction cross section of DM with nucleons [228] and even relatively light, but stable, primordial black holes [229].

Cosmology: Energy injection from DM processes in the early universe, as well as the contribution of DM to the effective relativistic degrees of freedom, are severely constrained from data on Big Bang Nucleosynthesis (see Sec. 24 in this *Review*) and on the energy and anisotropy power spectrum of the CMB (see Sec. 29). Codes exist that perform the calculation of the constraints on particle DM models [168, 230].

PBH Detection: Macroscopic DM candidates can gravitationally perturb structure and compromise the stability of, for instance, globular clusters such as Eridanus II [24], and/or disrupt wide binaries [231]. This constrains the maximal mass of a macroscopic DM candidate to not much more than 5 $M_\odot$ [231] (see also [24]). In the specific case or primordial black holes, strong constraints also stem from the acceleration of charged particles around and after recombination, with significant effects on the CMB [232], albeit a lively debate exists over the accretion efficiency around such objects at high redshift [233, 234]. Whether or not PBH in the solar-mass range can be 100% of the DM is therefore disputed at present. Other effects produced by macroscopic, massive DM candidates are the microlensing of stars [235, 236] and quasars [237], femtolensing of gamma-ray bursts [238], and neutron star capture [229]. It is important to note that recently constraints from both microlensing and femtolensing have been corrected after the realization of important finite-size source and wave effects [236, 239, 240], leaving a substantial window, at PBH masses $10^{17} \lesssim M_{\rm BH}/{\rm g} \lesssim 10^{21}$ where PBH can be 100% of the DM. Light black holes, $M_{\rm BH} \lesssim 10^{17}$ g, are also constrained by the non-detection of products of evaporation [241]; future MeV gamma-ray detectors are slated to significantly improve such constraints and to enable the direct detection of Hawking radiation [242]. If evaporation shuts down at or near the Planck scale, Planck-scale relic PBH are generally expected to carry electric charge and to be detectable with direct detection and neutrino experiments, or with paleo-detectors [243].

References

[1] J. D. Simon, arXiv e-prints arXiv:1901.05465 (2019), [arXiv:1901.05465].

[2] P. Salucci, Astron. Astrophys. Rev. **27**, 1, 2 (2019), [arXiv:1811.08843].

[3] S. W. Allen, A. E. Evrard and A. B. Mantz, Ann. Rev. Astron. Astrophys. **49**, 409 (2011), [arXiv:1103.4829].

[4] N. A. Bahcall *et al.*, ApJ **541**, 1 (2000).

[5] S. D. M. White, G. Efstathiou and C. S. Frenk, Mon. Not. Roy. Astron. Soc. **262**, 1023 (1993).

[6] A. J. S. Hamilton and M. Tegmark, Mon. Not. Roy. Astron. Soc. **330**, 506 (2002), [arXiv:astro-ph/0008392].

[7] B. Famaey and S. McGaugh, Living Rev. Rel. **15**, 10 (2012), [arXiv:1112.3960].

[8] S. W. Randall *et al.*, Astrophys. J. **679**, 1173 (2008), [arXiv:0704.0261].

[9] R. H. Sanders, Int. J. Mod. Phys. **D27**, 14, 14 (2018), [arXiv:1805.06804].

[10] S. D. McDermott, H.-B. Yu and K. M. Zurek, Phys. Rev. **D83**, 063509 (2011), [arXiv:1011.2907].

[11] D. A. Buote *et al.*, Astrophys. J. **577**, 183 (2002), [arXiv:astro-ph/0205469].

[12] D. Harvey *et al.*, Science **347**, 1462 (2015), [arXiv:1503.07675].

[13] S. Tulin and H.-B. Yu, Phys. Rept. **730**, 1 (2018), [arXiv:1705.02358].

[14] D. N. Spergel and P. J. Steinhardt, Phys. Rev. Lett. **84**, 3760 (2000), [arXiv:astro-ph/9909386].

[15] S. Tremaine and J. E. Gunn, Phys. Rev. Lett. **42**, 407 (1979), [,66(1979)].

[16] L. Randall, J. Scholtz and J. Unwin, Mon. Not. Roy. Astron. Soc. **467**, 2, 1515 (2017), [arXiv:1611.04590].

[17] R. Hlozek *et al.*, Phys. Rev. **D91**, 10, 103512 (2015), [arXiv:1410.2896].

Downloaded from https://academic.oup.com/ptep/article/2022/8/083C01/6651666 by KIT Library user on 27 September 2022

[18] E. Armengaud *et al.*, Mon. Not. Roy. Astron. Soc. **471**, 4, 4606 (2017), [arXiv:1703.09126].

[19] M. Nori *et al.*, Mon. Not. Roy. Astron. Soc. **482**, 3, 3227 (2019), [arXiv:1809.09619].

[20] B. Bozek *et al.*, Mon. Not. Roy. Astron. Soc. **450**, 1, 209 (2015), [arXiv:1409.3544].

[21] H.-Y. Schive *et al.*, Astrophys. J. **818**, 1, 89 (2016), [arXiv:1508.04621].

[22] E. O. Nadler *et al.*, Astrophys. J. **878**, 2, L32 (2019), [Astrophys. J. Lett.878,32(2019)], [arXiv:1904.10000].

[23] M. A. Monroy-Rodríguez and C. Allen, ApJ **790**, 2, 159 (2014), [arXiv:1406.5169].

[24] T. D. Brandt, Astrophys. J. **824**, 2, L31 (2016), [arXiv:1605.03665].

[25] B. Audren *et al.*, JCAP **1412**, 12, 028 (2014), [arXiv:1407.2418].

[26] M. Dutra *et al.*, JCAP **1803**, 037 (2018), [arXiv:1801.05447].

[27] P. Gondolo and G. Gelmini, Nucl. Phys. **B360**, 145 (1991).

[28] J. L. Feng and J. Kumar, Phys. Rev. Lett. **101**, 231301 (2008), [arXiv:0803.4196].

[29] G. Jungman, M. Kamionkowski and K. Griest, Phys. Rept. **267**, 195 (1996), [hep-ph/9506380].

[30] J. Edsjo *et al.*, JCAP **0304**, 001 (2003), [hep-ph/0301106].

[31] G. Servant and T. M. P. Tait, Nucl. Phys. **B650**, 391 (2003), [hep-ph/0206071].

[32] D. Hooper and S. Profumo, Phys. Rept. **453**, 29 (2007), [hep-ph/0701197].

[33] K. Griest and D. Seckel, Phys. Rev. **D43**, 3191 (1991).

[34] R. T. Co *et al.*, JCAP **1512**, 12, 024 (2015), [arXiv:1506.07532].

[35] V. S. Rychkov and A. Strumia, Phys. Rev. **D75**, 075011 (2007), [hep-ph/0701104].

[36] E. D. Carlson, M. E. Machacek and L. J. Hall, Astrophys. J. **398**, 43 (1992).

[37] D. Pappadopulo, J. T. Ruderman and G. Trevisan, Phys. Rev. **D94**, 3, 035005 (2016), [arXiv:1602.04219].

[38] Y. Hochberg *et al.*, Phys. Rev. Lett. **113**, 171301 (2014), [arXiv:1402.5143].

[39] E. Kuflik *et al.*, Phys. Rev. Lett. **116**, 22, 221302 (2016), [arXiv:1512.04545].

[40] W. B. Lin *et al.*, Phys. Rev. Lett. **86**, 954 (2001), [arXiv:astro-ph/0009003].

[41] G. B. Gelmini and P. Gondolo, Phys. Rev. **D74**, 023510 (2006), [hep-ph/0602230].

[42] M. Hindmarsh, R. Kirk and S. M. West, JCAP **1403**, 037 (2014), [arXiv:1311.1637].

[43] T. Moroi and L. Randall, Nucl. Phys. **B570**, 455 (2000), [hep-ph/9906527].

[44] P. Hut and K. A. Olive, Phys. Lett. **87B**, 144 (1979).

[45] S. Nussinov, Phys. Lett. **165B**, 55 (1985).

[46] K. M. Zurek, Phys. Rept. **537**, 91 (2014), [arXiv:1308.0338].

[47] Y. B. Zel'dovich and I. D. Novikov, Soviet Ast. **10**, 602 (1967).

[48] S. Hawking, Mon. Not. Roy. Astron. Soc. **152**, 75 (1971).

[49] B. J. Carr, ApJ **201**, 1 (1975).

[50] J. I. Read, J. Phys. **G41**, 063101 (2014), [arXiv:1404.1938].

[51] T. Piffl *et al.*, Astron. Astrophys. **562**, A91 (2014), [arXiv:1309.4293].

[52] A. M. Green, J. Phys. **G44**, 8, 084001 (2017), [arXiv:1703.10102].

[53] A. Helmi *et al.*, Nature **7729**, 985 (2018).

[54] L. Necib, M. Lisanti and V. Belokurov (2018), [arXiv:1807.02519].

[55] N. W. Evans, C. A. J. O'Hare and C. McCabe, Phys. Rev. **D99**, 2, 023012 (2019), [arXiv:1810.11468].

[56] J. S. Bullock and M. Boylan-Kolchin, Ann. Rev. Astron. Astrophys. **55**, 343 (2017), [arXiv:1707.04256].

[57] J. Zavala and C. S. Frenk (2019), [arXiv:1907.11775].

[58] K. E. Andrade *et al.* (2019), [arXiv:1901.00507].

[59] G. Servant, in "Particle dark matter," 164–189 (2010).

[60] L. Hui *et al.*, Phys. Rev. **D95**, 4, 043541 (2017), [arXiv:1610.08297].

[61] A. Fattahi *et al.* (2016), [arXiv:1607.06479].

[62] D. J. E. Marsh, Phys. Rept. **643**, 1 (2016), [arXiv:1510.07633].

[63] H. An *et al.*, Phys. Lett. **B747**, 331 (2015), [arXiv:1412.8378].

[64] P. W. Graham and S. Rajendran, Phys. Rev. **D88**, 035023 (2013), [arXiv:1306.6088].

[65] P. W. Graham *et al.*, Phys. Rev. **D93**, 7, 075029 (2016), [arXiv:1512.06165].

[66] A. Arvanitaki *et al.*, Phys. Rev. **D97**, 7, 075020 (2018), [arXiv:1606.04541].

[67] P. W. Graham *et al.*, Phys. Rev. **D97**, 5, 055006 (2018), [arXiv:1709.07852].

[68] I. M. Bloch *et al.* (2019), [arXiv:1907.03767].

[69] A. Pierce, K. Riles and Y. Zhao, Phys. Rev. Lett. **121**, 6, 061102 (2018), [arXiv:1801.10161].

[70] Y. Kahn, B. R. Safdi and J. Thaler, Phys. Rev. Lett. **117**, 14, 141801 (2016), [arXiv:1602.01086].

[71] R. Henning *et al.* (ABRACADABRA), in "Proceedings, 13th Patras Workshop on Axions, WIMPs and WISPs, (PATRAS 2017): Thessaloniki, Greece, 15 May 2017 - 19, 2017," 28–31 (2018).

[72] S. Chaudhuri *et al.*, Phys. Rev. **D92**, 7, 075012 (2015), [arXiv:1411.7382].

[73] P. Sikivie, N. Sullivan and D. B. Tanner, Phys. Rev. Lett. **112**, 13, 131301 (2014), [arXiv:1310.8545].

[74] B. M. Brubaker *et al.*, Phys. Rev. **D96**, 12, 123008 (2017), [arXiv:1706.08388].

[75] G. Rybka (ADMX), Phys. Dark Univ. **4**, 14 (2014).

[76] S. Dodelson and L. M. Widrow, Phys. Rev. Lett. **72**, 17 (1994), [hep-ph/9303287].

[77] E. Bulbul *et al.*, Astrophys. J. **789**, 13 (2014), [arXiv:1402.2301].

[78] A. Boyarsky *et al.*, Phys. Rev. Lett. **113**, 251301 (2014), [arXiv:1402.4119].

[79] T. E. Jeltema and S. Profumo, Mon. Not. Roy. Astron. Soc. **450**, 2, 2143 (2015), [arXiv:1408.1699].

[80] M. E. Anderson, E. Churazov and J. N. Bregman, Mon. Not. Roy. Astron. Soc. **452**, 4, 3905 (2015), [arXiv:1408.4115].

[81] D. Malyshev, A. Neronov and D. Eckert, Phys. Rev. **D90**, 103506 (2014), [arXiv:1408.3531].

[82] T. E. Jeltema and S. Profumo, Mon. Not. Roy. Astron. Soc. **458**, 4, 3592 (2016), [arXiv:1512.01239].

[83] F. A. Aharonian *et al.* (Hitomi), Astrophys. J. **837**, 1, L15 (2017), [arXiv:1607.07420].

[84] I. Yu. Kobzarev, L. B. Okun and I. Ya. Pomeranchuk, Sov. J. Nucl. Phys. **3**, 6, 837 (1966), [Yad. Fiz.3,1154(1966)].

[85] M. J. Strassler and K. M. Zurek, Phys. Lett. **B651**, 374 (2007), [hep-ph/0604261].

[86] M. J. Strassler (2006), [hep-ph/0607160].

[87] M. Battaglieri *et al.*, in "U.S. Cosmic Visions: New Ideas in Dark Matter," (2017), [arXiv:1707.04591].

Downloaded from https://academic.oup.com/ptep/article/2022/8/083C01/6651666 by KIT Library user on 27 September 2022

[88] Y. Kahn *et al.*, JHEP **05**, 002 (2017), [arXiv:1609.09072].

[89] J. Alexander *et al.* (2016), [arXiv:1608.08632], URL `http://lss.fnal.gov/archive/2016/conf/fermilab-conf-16-421.pdf`.

[90] K. R. Dienes and B. Thomas, Phys. Rev. **D85**, 083523 (2012), [arXiv:1106.4546].

[91] N. Trevisani (ATLAS, CMS), Universe **4**, 11, 131 (2018).

[92] E. Tolley (ATLAS), PoS **ICHEP2018**, 171 (2019).

[93] W. C. Kalderon (ATLAS), PoS **DIS2018**, 085 (2018).

[94] D. Vannerom (CMS), PoS **DIS2019**, 111 (2019).

[95] G. Gómez-Ceballos (CMS), PoS **EDSU2018**, 014 (2018).

[96] E. Aprile *et al.* (XENON), Phys. Rev. Lett. **121**, 11, 111302 (2018), [arXiv:1805.12562].

[97] Q. Wang *et al.* (PandaX-II), Chin. Phys. C **44**, 12, 125001 (2020), [arXiv:2007.15469].

[98] D. S. Akerib *et al.* (LUX), Phys. Rev. Lett. **118**, 2, 021303 (2017), [arXiv:1608.07648].

[99] R. Agnese *et al.* (SuperCDMS), Phys. Rev. Lett. **120**, 6, 061802 (2018), [arXiv:1708.08869].

[100] P. Agnes *et al.* (DarkSide), Phys. Rev. **D98**, 10, 102006 (2018), [arXiv:1802.07198].

[101] R. Ajaj *et al.* (DEAP), Phys. Rev. **D100**, 022004 (2019), [arXiv:1902.04048].

[102] D. S. Akerib *et al.* (LUX), Phys. Rev. Lett. **122**, 13, 131301 (2019), [arXiv:1811.11241].

[103] E. Aprile *et al.* (XENON) (2019), [arXiv:1907.12771].

[104] E. Aprile *et al.* (2019), [arXiv:1907.11485].

[105] P. Agnes *et al.* (DarkSide), Phys. Rev. Lett. **121**, 8, 081307 (2018), [arXiv:1802.06994].

[106] R. Agnese *et al.* (SuperCDMS), Phys. Rev. **D99**, 6, 062001 (2019), [arXiv:1808.09098].

[107] A. H. Abdelhameed *et al.* (CRESST) (2019), [arXiv:1904.00498].

[108] Q. Arnaud *et al.* (NEWS-G), Astropart. Phys. **97**, 54 (2018), [arXiv:1706.04934].

[109] A. Aguilar-Arevalo *et al.* (DAMIC), Phys. Rev. Lett. **125**, 241803 (2020), [arXiv:2007.15622].

[110] C. Amole *et al.* (PICO), Phys. Rev. **D100**, 2, 022001 (2019), [arXiv:1902.04031].

[111] E. Aprile *et al.* (XENON), Phys. Rev. Lett. **122**, 14, 141301 (2019), [arXiv:1902.03234].

[112] J. Xia *et al.* (PandaX-II), Phys. Lett. **B792**, 193 (2019), [arXiv:1807.01936].

[113] D. S. Akerib *et al.* (LUX), Phys. Rev. Lett. **118**, 25, 251302 (2017), [arXiv:1705.03380].

[114] J. D. Lewin and P. F. Smith, Astropart. Phys. **6**, 87 (1996).

[115] J. R. Ellis, R. A. Flores and J. D. Lewin, Phys. Lett. **B212**, 375 (1988).

[116] P. J. Fox, J. Liu and N. Weiner, Phys. Rev. **D83**, 103514 (2011), [arXiv:1011.1915].

[117] L. Vietze *et al.*, Phys. Rev. **D91**, 4, 043520 (2015), [arXiv:1412.6091].

[118] P. Klos *et al.*, Phys. Rev. **D88**, 8, 083516 (2013), [Erratum: Phys. Rev.D89,no.2,029901(2014)], [arXiv:1304.7684].

[119] J. Ellis, N. Nagata and K. A. Olive, Eur. Phys. J. **C78**, 7, 569 (2018), [arXiv:1805.09795].

[120] J. Fan, M. Reece and L.-T. Wang, JCAP **1011**, 042 (2010), [arXiv:1008.1591].

[121] A. L. Fitzpatrick *et al.*, JCAP **1302**, 004 (2013), [arXiv:1203.3542].

[122] N. Anand, A. L. Fitzpatrick and W. C. Haxton, Phys. Rev. **C89**, 6, 065501 (2014), [arXiv:1308.6288].

[123] M. I. Gresham and K. M. Zurek, Phys. Rev. **D89**, 12, 123521 (2014), [arXiv:1401.3739].

[124] J. B. Dent *et al.*, Phys. Rev. **D92**, 6, 063515 (2015), [arXiv:1505.03117].

[125] D. Gazda, R. Catena and C. Forssén, Phys. Rev. **D95**, 10, 103011 (2017), [arXiv:1612.09165].

[126] M. Hoferichter *et al.*, Phys. Rev. **D99**, 5, 055031 (2019), [arXiv:1812.05617].

[127] R. Essig, J. Mardon and T. Volansky, Phys. Rev. **D85**, 076007 (2012), [arXiv:1108.5383].

[128] F. T. Avignone, III *et al.*, Phys. Rev. **D35**, 2752 (1987).

[129] M. Pospelov, A. Ritz and M. B. Voloshin, Phys. Rev. **D78**, 115012 (2008), [arXiv:0807.3279].

[130] I. M. Bloch *et al.*, JHEP **06**, 087 (2017), [arXiv:1608.02123].

[131] Y. Hochberg, T. Lin and K. M. Zurek, Phys. Rev. **D95**, 2, 023013 (2017), [arXiv:1608.01994].

[132] M. Schumann (2019), [arXiv:1903.03026].

[133] J. Billard *et al.* (2021), [arXiv:2104.07634].

[134] M. Pato *et al.*, Phys. Rev. **D83**, 083505 (2011), [arXiv:1012.3458].

[135] A. K. Drukier, K. Freese and D. N. Spergel, Phys. Rev. **D33**, 3495 (1986).

[136] D. N. Spergel, Phys. Rev. **D37**, 1353 (1988).

[137] D. Stiff, L. M. Widrow and J. Frieman, Phys. Rev. **D64**, 083516 (2001), [arXiv:astro-ph/0106048].

[138] K. Freese *et al.*, Phys. Rev. Lett. **92**, 111301 (2004), [arXiv:astro-ph/0310334].

[139] T. Bruch *et al.*, Astrophys. J. **696**, 920 (2009), [arXiv:0804.2896].

[140] M. J. Lewis and K. Freese, Phys. Rev. **D70**, 043501 (2004), [arXiv:astro-ph/0307190].

[141] F. Mayet *et al.*, Phys. Rept. **627**, 1 (2016), [arXiv:1602.03781].

[142] L. E. Strigari, New J. Phys. **11**, 105011 (2009), [arXiv:0903.3630].

[143] C. A. J. O'Hare, Phys. Rev. **D94**, 6, 063527 (2016), [arXiv:1604.03858].

[144] L. E. Strigari, Phys. Rev. **D93**, 10, 103534 (2016), [arXiv:1604.00729].

[145] R. Essig, M. Sholapurkar and T.-T. Yu, Phys. Rev. **D97**, 9, 095029 (2018), [arXiv:1801.10159].

[146] V. Chepel and H. Araujo, JINST **8**, R04001 (2013), [arXiv:1207.2292].

[147] M. J. Dolan, F. Kahlhoefer and C. McCabe, Phys. Rev. Lett. **121**, 10, 101801 (2018), [arXiv:1711.09906].

[148] C. Fu *et al.* (PandaX), Phys. Rev. Lett. **119**, 18, 181806 (2017), [arXiv:1707.07921].

[149] D. S. Akerib *et al.* (LUX), Phys. Rev. Lett. **118**, 26, 261301 (2017), [arXiv:1704.02297].

[150] E. Aprile *et al.* (XENON), Phys. Rev. D **102**, 7, 072004 (2020), [arXiv:2006.09721].

[151] P. Grothaus, M. Fairbairn and J. Monroe, Phys. Rev. **D90**, 5, 055018 (2014), [arXiv:1406.5047].

[152] C. A. J. O'Hare *et al.*, Phys. Rev. **D92**, 6, 063518 (2015), [arXiv:1505.08061].

[153] Y. Hochberg *et al.*, Phys. Lett. **B772**, 239 (2017), [arXiv:1606.08849].

[154] Y. Hochberg *et al.*, Phys. Rev. **D97**, 1, 015004 (2018), [arXiv:1708.08929].

[155] S. Knapen, T. Lin and K. M. Zurek, Phys. Rev. **D95**, 5, 056019 (2017), [arXiv:1611.06228].

[156] R. Essig *et al.*, Phys. Rev. **D95**, 5, 056011 (2017), [arXiv:1608.02940].

Downloaded from https://academic.oup.com/ptep/article/2022/8/083C01/6651666 by KIT Library user on 27 September 2022

[157] Y. Hochberg, T. Lin and K. M. Zurek, Phys. Rev. **D94**, 1, 015019 (2016), [arXiv:1604.06800].

[158] S. Knapen *et al.*, Phys. Lett. **B785**, 386 (2018), [arXiv:1712.06598].

[159] S. Griffin *et al.*, Phys. Rev. **D98**, 11, 115034 (2018), [arXiv:1807.10291].

[160] A. Arvanitaki, S. Dimopoulos and K. Van Tilburg, Phys. Rev. **X8**, 4, 041001 (2018), [arXiv:1709.05354].

[161] T. Trickle, Z. Zhang and K. M. Zurek (2019), [arXiv:1905.13744].

[162] Y. Hochberg *et al.*, Phys. Rev. Lett. **123**, 15, 151802 (2019), [arXiv:1903.05101].

[163] T. Lin, PoS **333**, 009 (2019), [arXiv:1904.07915].

[164] F. Aharonian, D. Khangulyan and D. Malyshev, Astron. Astrophys. **547**, A114 (2012), [arXiv:1207.0458].

[165] K. K. Boddy *et al.*, Phys. Rev. **D94**, 9, 095027 (2016), [arXiv:1606.07440].

[166] T. Sjöstrand (2019), [arXiv:1907.09874].

[167] M. Tavani *et al.* (e-ASTROGAM), JHEAp **19**, 1 (2018), [arXiv:1711.01265].

[168] A. Coogan, L. Morrison and S. Profumo (2019), [arXiv:1907.11846].

[169] M. Ackermann *et al.* (Fermi-LAT), Phys. Rev. Lett. **115**, 23, 231301 (2015), [arXiv:1503.02641].

[170] D. Hooper and L. Goodenough, Phys. Lett. **B697**, 412 (2011), [arXiv:1010.2752].

[171] M. Ackermann *et al.* (Fermi-LAT), Astrophys. J. **840**, 1, 43 (2017), [arXiv:1704.03910].

[172] F. Calore, I. Cholis and C. Weniger, JCAP **1503**, 038 (2015), [arXiv:1409.0042].

[173] K. N. Abazajian and M. Kaplinghat, Phys. Rev. **D86**, 083511 (2012), [Erratum: Phys. Rev. **D87**, 129902 (2013)], [arXiv:1207.6047].

[174] S. K. Lee, M. Lisanti and B. R. Safdi, JCAP **1505**, 05, 056 (2015), [arXiv:1412.6099].

[175] T. Daylan *et al.*, Phys. Dark Univ. **12**, 1 (2016), [arXiv:1402.6703].

[176] R. K. Leane and T. R. Slatyer (2019), [arXiv:1904.08430].

[177] E. Carlson, T. Linden and S. Profumo, Phys. Rev. Lett. **117**, 11, 111101 (2016), [arXiv:1510.04698].

[178] M. Ajello *et al.* (Fermi-LAT), Astrophys. J. **819**, 1, 44 (2016), [arXiv:1511.02938].

[179] M. Ackermann *et al.* (Fermi-LAT), Astrophys. J. **836**, 2, 208 (2017), [arXiv:1702.08602].

[180] A. McDaniel, T. Jeltema and S. Profumo, Phys. Rev. **D97**, 10, 103021 (2018), [arXiv:1802.05258].

[181] C. Karwin *et al.* (2019), [arXiv:1903.10533].

[182] A. McDaniel, T. Jeltema and S. Profumo, Phys. Rev. **D100**, 2, 023014 (2019), [arXiv:1903.06833].

[183] R. L. Kinzer *et al.*, Astrophys. J. **559**, 282 (2001).

[184] R. M. Bandyopadhyay *et al.*, Mon. Not. Roy. Astron. Soc. **392**, 1115 (2009), [arXiv:0810.3674].

[185] D. P. Finkbeiner and N. Weiner, Phys. Rev. **D76**, 083519 (2007), [arXiv:astro-ph/0702587].

[186] K. Agashe *et al.*, JCAP **1410**, 10, 062 (2014), [arXiv:1405.7370].

[187] T. Damour and L. M. Krauss, Phys. Rev. Lett. **81**, 5726 (1998), [arXiv:astro-ph/9806165].

[188] S. L. Adler, Phys. Lett. **B671**, 203 (2009), [arXiv:0808.2823].

[189] J. Casanellas and I. Lopes, Astrophys. J. **765**, L21 (2013), [arXiv:1212.2985].

[190] G. D. Mack, J. F. Beacom and G. Bertone, Phys. Rev. **D76**, 043523 (2007), [arXiv:0705.4298].

[191] J. Smolinsky and P. Tanedo, Phys. Rev. **D95**, 7, 075015 (2017), [Erratum: Phys. Rev.D96,no.9,099902(2017)], [arXiv:1701.03168].

[192] C. Niblaeus, A. Beniwal and J. Edsjo (2019), [arXiv:1903.11363].

[193] M. G. Aartsen *et al.* (IceCube), JCAP **1604**, 04, 022 (2016), [arXiv:1601.00653].

[194] S. Adrian-Martinez *et al.* (ANTARES), Phys. Lett. **B759**, 69 (2016), [arXiv:1603.02228].

[195] C. R. Das *et al.*, Phys. Lett. **B725**, 297 (2013), [arXiv:1110.5095].

[196] M. G. Aartsen *et al.* (IceCube), J. Phys. **G44**, 5, 054006 (2017), [arXiv:1607.02671].

[197] Y. Zhao and K. M. Zurek, JHEP **07**, 017 (2014), [arXiv:1401.7664].

[198] A. W. Strong, I. V. Moskalenko and V. S. Ptuskin, Ann. Rev. Nucl. Part. Sci. **57**, 285 (2007), [arXiv:astro-ph/0701517].

[199] O. Adriani *et al.* (PAMELA), Phys. Rev. Lett. **111**, 081102 (2013), [arXiv:1308.0133].

[200] M. Aguilar *et al.* (AMS), Phys. Rev. Lett. **117**, 9, 091103 (2016).

[201] M. Aguilar *et al.* (AMS), Phys. Rev. Lett. **110**, 141102 (2013).

[202] S. Profumo, F. Queiroz and C. Siqueira (2019), [arXiv:1903.07638].

[203] D. Hooper, P. Blasi and P. D. Serpico, JCAP **0901**, 025 (2009), [arXiv:0810.1527].

[204] S. Profumo, Central Eur. J. Phys. **10**, 1 (2011), [arXiv:0812.4457].

[205] A. U. Abeysekara *et al.* (HAWC), Science **358**, 6365, 911 (2017), [arXiv:1711.06223].

[206] S. Profumo *et al.*, Phys. Rev. **D97**, 12, 123008 (2018), [arXiv:1803.09731].

[207] R. Cowsik, B. Burch and T. Madziwa-Nussinov, Astrophys. J. **786**, 124 (2014), [arXiv:1305.1242].

[208] K. Blum, B. Katz and E. Waxman, Phys. Rev. Lett. **111**, 21, 211101 (2013), [arXiv:1305.1324].

[209] M.-Y. Cui *et al.*, Phys. Rev. Lett. **118**, 19, 191101 (2017), [arXiv:1610.03840].

[210] A. Reinert and M. W. Winkler, JCAP **1801**, 01, 055 (2018), [arXiv:1712.00002].

[211] M. W. Winkler, JCAP **1702**, 02, 048 (2017), [arXiv:1701.04866].

[212] F. Donato, N. Fornengo and P. Salati, Phys. Rev. **D62**, 043003 (2000), [hep-ph/9904481].

[213] K. Mori *et al.*, Astrophys. J. **566**, 604 (2002), [arXiv:astro-ph/0109463].

[214] H. Baer and S. Profumo, JCAP **0512**, 008 (2005), [arXiv:astro-ph/0510722].

[215] E. Carlson *et al.*, Phys. Rev. **D89**, 7, 076005 (2014), [arXiv:1401.2461].

[216] M. Cirelli *et al.*, JHEP **08**, 009 (2014), [arXiv:1401.4017].

[217] R. Bird *et al.*, in "36th International Cosmic Ray Conference (ICRC 2019) Madison, Wisconsin, USA, July 24-August 1, 2019," (2019), [arXiv:1908.03154].

[218] A. Coogan and S. Profumo, Phys. Rev. **D96**, 8, 083020 (2017), [arXiv:1705.09664].

[219] S. Colafrancesco, S. Profumo and P. Ullio, Astron. Astrophys. **455**, 21 (2006), [arXiv:astro-ph/0507575].

[220] S. Colafrancesco, S. Profumo and P. Ullio, Phys. Rev. **D75**, 023513 (2007), [arXiv:astro-ph/0607073].

[221] S. Profumo and P. Ullio (2010), [arXiv:1001.4086].

Downloaded from https://academic.oup.com/ptep/article/2022/8/083C01/6651666 by KIT Library user on 27 September 2022

[222] T. E. Jeltema and S. Profumo, JCAP **0811**, 003 (2008), [arXiv:0808.2641].

[223] M. Cirelli *et al.*, JCAP **1103**, 051 (2011), [Erratum: JCAP1210,E01(2012)], [arXiv:1012.4515].

[224] A. McDaniel *et al.*, JCAP **1709**, 09, 027 (2017), [arXiv:1705.09384].

[225] E. Storm *et al.*, Astrophys. J. **768**, 106 (2013), [arXiv:1210.0872].

[226] G. G. Raffelt, *Stars as laboratories for fundamental physics* (1996), ISBN 9780226702728, URL `http://wwwth.mpp.mpg.de/members/raffelt/mypapers/199613.pdf`.

[227] D. Spolyar, K. Freese and P. Gondolo, Phys. Rev. Lett. **100**, 051101 (2008), [arXiv:0705.0521].

[228] S. Dimopoulos, J. Preskill and F. Wilczek, Phys. Lett. **119B**, 320 (1982).

[229] P. Pani and A. Loeb, JCAP **1406**, 026 (2014), [arXiv:1401.3025].

[230] H. Liu, G. W. Ridgway and T. R. Slatyer (2019), [arXiv:1904.09296].

[231] M. A. Monroy-Rodríguez and C. Allen, Astrophys. J. **790**, 2, 159 (2014), [arXiv:1406.5169].

[232] M. Ricotti, J. P. Ostriker and K. J. Mack, Astrophys. J. **680**, 829 (2008), [arXiv:0709.0524].

[233] S. Bird *et al.*, Phys. Rev. Lett. **116**, 20, 201301 (2016), [arXiv:1603.00464].

[234] V. Poulin *et al.*, Phys. Rev. **D96**, 8, 083524 (2017), [arXiv:1707.04206].

[235] P. Tisserand *et al.* (EROS-2), Astron. Astrophys. **469**, 387 (2007), [arXiv:astro-ph/0607207].

[236] H. Niikura *et al.*, Nat. Astron. **3**, 6, 524 (2019), [arXiv:1701.02151].

[237] E. Mediavilla *et al.*, Astrophys. J. **706**, 1451 (2009), [arXiv:0910.3645].

[238] A. Barnacka, J. F. Glicenstein and R. Moderski, Phys. Rev. **D86**, 043001 (2012), [arXiv:1204.2056].

[239] A. Katz *et al.*, JCAP **1812**, 005 (2018), [arXiv:1807.11495].

[240] N. Smyth *et al.* (2019), [arXiv:1910.01285].

[241] B. J. Carr *et al.*, Phys. Rev. **D81**, 104019 (2010), [arXiv:0912.5297].

[242] A. Coogan, L. Morrison and S. Profumo, Phys. Rev. Lett. **126**, 17, 171101 (2021), [arXiv:2010.04797].

[243] B. V. Lehmann *et al.*, JCAP **10**, 046 (2019), [arXiv:1906.06348].

Downloaded from https://academic.oup.com/ptep/article/2022/8/083C01/6651666 by KIT Library user on 27 September 2022

28. Dark Energy

Revised August 2021 by D.H. Weinberg (Ohio State U.) and M. White (UC Berkeley; LBNL).

28.1 Repulsive Gravity and Cosmic Acceleration

In the first modern cosmological model, Einstein [1] modified his field equation of General Relativity (GR), introducing a "cosmological term" that enabled a solution with time-independent, spatially homogeneous matter density $\rho_{\rm m}$ and constant positive space curvature. Although Einstein did not frame it this way, one can view the "cosmological constant" Λ as representing a constant energy density of the vacuum [2], whose repulsive gravitational effect balances the attractive gravity of matter and thereby allows a static solution. After the development of dynamic cosmological models [3,4] and the discovery of cosmic expansion [5], the cosmological term appeared unnecessary, and Einstein and de Sitter [6] advocated adopting an expanding, homogeneous and isotropic, spatially flat, matter-dominated Universe as the default cosmology until observations dictated otherwise. Such a model has matter density equal to the critical density, $\Omega_{\rm m} \equiv \rho_{\rm m}/\rho_{\rm c} = 1$, and negligible contribution from other energy components [7].

By the mid-1990s, the Einstein-de Sitter model was showing numerous cracks, under the combined onslaught of data from the cosmic microwave background (CMB), large-scale galaxy clustering, and direct estimates of the matter density, the expansion rate (H_0), and the age of the Universe. As noted in a number of papers from this time, introducing a cosmological constant offered a potential resolution of many of these tensions, yielding the most empirically successful version of the inflationary cold dark matter scenario. In the late 1990s, supernova surveys by two independent teams provided direct evidence for accelerating cosmic expansion [8,9], establishing the cosmological constant model (with $\Omega_{\rm m} \simeq 0.3$, $\Omega_\Lambda \simeq 0.7$) as the preferred alternative to the $\Omega_{\rm m} = 1$ scenario. Shortly thereafter, CMB evidence for a spatially flat Universe [10,11], and thus for $\Omega_{\rm tot} \simeq 1$, cemented the case for cosmic acceleration by firmly eliminating the free-expansion alternative with $\Omega_{\rm m} \ll 1$ and $\Omega_\Lambda = 0$. Today, the accelerating Universe is well established by multiple lines of independent evidence from a tight web of precise cosmological measurements.

As discussed in the Big Bang Cosmology article of this *Review* (Sec. 22), the scale factor $R(t)$ of a homogeneous and isotropic Universe governed by GR grows at an accelerating rate if the pressure $p < -\frac{1}{3}\rho$ (in $c = 1$ units). A cosmological constant has $\rho_\Lambda =$ constant and pressure $p_\Lambda = -\rho_\Lambda$ (see Eq. 22.10), so it will drive acceleration if it dominates the total energy density. However, acceleration could arise from a more general form of "dark energy" that has negative pressure, typically specified in terms of the equation-of-state-parameter $w = p/\rho$ ($= -1$ for a cosmological constant). Furthermore, the conclusion that acceleration requires a new energy component beyond matter and radiation relies on the assumption that GR is the correct description of gravity on cosmological scales. The title of this article follows the common but inexact usage of "dark energy" as a catch-all term for the origin of cosmic acceleration, regardless of whether it arises from a new form of energy or a modification of GR. Our account here draws on the much longer review of cosmic acceleration by Ref. [12], which provides background explanation and extensive literature references for the discussion in Secs. 28.2 and 28.3.

Below we will use the abbreviation ΛCDM to refer to a model with cold dark matter, a cosmological constant, inflationary initial conditions, standard radiation and neutrino content, and a flat Universe with $\Omega_{\rm tot} = 1$ (though we will sometimes describe this model as "flat ΛCDM" to emphasize this last restriction). We will use wCDM to denote a model with the same assumptions but a free, constant value of w. Models with the prefix "o" (*e.g.*, `owCDM`) allow non-zero space curvature.

28.2 Theories of Cosmic Acceleration

28.2.1 *Dark Energy or Modified Gravity?*

A cosmological constant is the mathematically simplest, and perhaps the physically simplest, theoretical explanation for the accelerating Universe. The problem is explaining its unnaturally small magnitude, as discussed in Sec. 22.4.7of this *Review*. An alternative (which still requires finding a way to make the cosmological constant zero or at least negligibly small) is that the accelerating cosmic expansion is driven by a new form of energy such as a scalar field [13] with potential $V(\phi)$. The energy density and pressure of the field $\phi(\mathbf{x})$ take the same forms as for inflationary scalar fields, given in Eq. (22.52) of the Big Bang Cosmology article. In the limit that $\frac{1}{2}\dot\phi^2 \ll |V(\phi)|$, the scalar field acts like a cosmological constant, with $p_\phi \simeq -\rho_\phi$. In this scenario, today's cosmic acceleration is closely akin to the epoch of inflation, but with radically different energy and timescale.

More generally, the value of $w = p_\phi/\rho_\phi$ in scalar field models evolves with time in a way that depends on $V(\phi)$ and on the initial conditions $(\phi_i, \dot\phi_i)$; some forms of $V(\phi)$ have attractor solutions in which the late-time behavior is insensitive to initial values. Many forms of time evolution are possible, including ones where w is approximately constant and broad classes where w "freezes" towards or "thaws" away from $w = -1$, with the transition occurring when the field comes to dominate the total energy budget. If ρ_ϕ is even approximately constant, then it becomes dynamically insignificant at high redshift, because the matter density scales as $\rho_{\rm m} \propto (1+z)^3$. "Early dark energy" models are ones in which ρ_ϕ is a small but not negligible fraction (*e.g.*, a few percent) of the total energy throughout the matter- and radiation-dominated eras, tracking the dominant component before itself coming to dominate at low redshift.

Instead of introducing a new energy component, one can attempt to modify gravity in a way that leads to accelerated expansion [14]. One option is to replace the Ricci scalar $\mathcal{R}$ with a function $\mathcal{R} + f(\mathcal{R})$ in the gravitational action [15]. Other changes can be more radical, such as introducing extra dimensions and allowing gravitons to "leak" off the brane that represents the observable Universe (the "DGP" model [16]). The DGP example has inspired a more general class of "galileon" and massive gravity models. Constructing viable modified gravity models is challenging, in part because it is easy to introduce theoretical inconsistencies (such as "ghost" fields with negative kinetic energy), but above all because GR is a theory with many high-precision empirical successes on solar system scales [17]. Modified gravity models typically invoke screening mechanisms that force model predictions to approach those of GR in regions of high density or strong gravitational potential. Screening offers potentially distinctive signatures, as the strength of gravity (*i.e.*, the effective value of $G_{\rm N}$) can vary by order unity in environments with different gravitational potentials.

More generally, one can search for signatures of modified gravity by comparing the history of cosmic structure growth to the history of cosmic expansion. Within GR, these two are linked by a consistency relation, as described below (Eq. (28.2)). Modifying gravity can change the predicted rate of structure growth, and it can make the growth rate dependent on scale or environment. In some circumstances, modifying gravity alters the combinations of potentials responsible for gravitational lensing and the dynamics of non-relativistic tracers (such as galaxies or stars) in different ways (see Sec. 22.4.7 in this *Review*), leading to order unity mismatches between the masses of objects inferred from lensing and those inferred from dynamics in unscreened environments.

At present there are no fully realized and empirically viable modified gravity theories that explain the observed level of cosmic acceleration. The constraints on $f(\mathcal{R})$ models now force them so close to GR that they cannot produce acceleration without introducing a separate dark energy component [18]. The DGP model is empirically ruled out by several tests, including the expansion history, the integrated Sachs-Wolfe effect, and redshift-space distortion measurements of the structure growth rate [19]. The near-simultaneous arrival of gravitational waves and electromagnetic signals from the neutron star merger event GW170817, which shows that gravitational waves travel at almost exactly the speed of light, is a further strong constraint on modified gravity theories [20]. The elimination of models should be considered an important success of the program to empirically test theories of cosmic acceleration. However, it is worth recalling that there was no fully realized gravitational explanation for the precession of Mercury's orbit prior to the completion of GR in 1915, and the fact that no complete and viable modified gravity theory exists

Downloaded from https://academic.oup.com/ptep/article/2022/8/083C01/6651666 by KIT Library user on 27 September 2022

today does not mean that one will not arise in the future. In the meantime, we can continue empirical investigations that can tighten restrictions on such theories or perhaps point towards the gravitational sector as the origin of accelerating expansion.

28.2.2 *Expansion History and Growth of Structure*

The main line of empirical attack on dark energy is to measure the history of cosmic expansion and the history of matter clustering with the greatest achievable precision over a wide range of redshift. Within GR, the expansion rate $H(z)$ is governed by the Friedmann equation (see the articles on Big Bang Cosmology and Cosmological Parameters—Secs. 22 and 25 in this *Review*). For dark energy with an equation of state $w(z)$, the cosmological constant contribution to the expansion, Ω_Λ, is replaced by a redshift-dependent contribution. The evolution of the dark energy density follows from Eq. (22.10),

$$\Omega_{\rm de}\frac{\rho_{\rm de}(z)}{\rho_{\rm de}(z=0)} = \Omega_{\rm de}\exp\left[3\int_0^z [1+w(z')]\frac{dz'}{1+z'}\right] = \Omega_{\rm de}(1+z)^{3(1+w)}, \tag{28.1}$$

where the second equality holds for constant w. If $\Omega_{\rm m}$, $\Omega_{\rm r}$, and the present value of $\Omega_{\rm tot}$ are known, then measuring $H(z)$ pins down $w(z)$. (Note that $\Omega_{\rm de}$ is the same quantity denoted $\Omega_{\rm v}$ in Sec. 22, but we have adopted the 'de' subscript to avoid implying that dark energy is necessarily a vacuum effect.)

While some observations can probe $H(z)$ directly, others measure the distance-redshift relation. The basic relations between angular diameter distance or luminosity distance and $H(z)$ are given in Ch. 22 —and these are generally unaltered in time-dependent dark energy or modified gravity models. For convenience, in later sections, we will sometimes refer to the comoving angular distance, $D_{\rm A,c}(z) = (1+z)D_{\rm A}(z)$.

In GR-based linear perturbation theory, the density contrast $\delta(\mathbf{x},t) \equiv \rho(\mathbf{x},t)/\bar\rho(t) - 1$ of pressureless matter grows in proportion to the linear growth function $G(t)$ (not to be confused with the gravitational constant $G_{\rm N}$), which follows the differential equation

$$\ddot G + 2H(z)\dot G - \frac{3}{2}\Omega_{\rm m}H_0^2(1+z)^3 G = 0\ . \tag{28.2}$$

To a good approximation, the logarithmic derivative of $G(z)$ is

$$f(z) \equiv -\frac{d\ln G}{d\ln(1+z)} \simeq \left[\Omega_{\rm m}(1+z)^3\frac{H_0^2}{H^2(z)}\right]^\gamma\ , \tag{28.3}$$

where $\gamma \simeq 0.55$ for relevant values of cosmological parameters [21]. In an $\Omega_{\rm m} = 1$ Universe, $G(z) \propto (1+z)^{-1}$, but growth slows when $\Omega_{\rm m}$ drops significantly below unity. One can integrate Eq. (28.3) to get an approximate integral relation between $G(z)$ and $H(z)$, but the full (numerical) solution to Eq. (28.2) should be used for precision calculations. Even in the non-linear regime, the amplitude of clustering is determined mainly by $G(z)$, so observations of non-linear structure can be used to infer the linear $G(z)$, provided one has good theoretical modeling to relate the two.

In modified gravity models the growth rate of gravitational clustering may differ from the GR prediction. A general strategy to test modified gravity, therefore, is to measure both the expansion history and the growth history to see whether they yield consistent results for $H(z)$ or $w(z)$.

28.2.3 *Parameters*

Constraining a general history of $w(z)$ is nearly impossible, because the dark energy density, which affects $H(z)$, is given by an integral over $w(z)$, and distances and the growth factor involve a further integration over functions of $H(z)$. Oscillations in $w(z)$ over a range $\Delta z/(1+z) \ll 1$ are therefore extremely difficult to constrain. It has become conventional to phrase constraints or projected constraints on $w(z)$ in terms of a linear evolution model,

$$w(a) = w_0 + w_{\rm a}(1-a) = w_{\rm p} + w_{\rm a}(a_{\rm p} - a), \tag{28.4}$$

where $a \equiv (1+z)^{-1}$, w_0 is the value of w at $z = 0$, and $w_{\rm p}$ is the value of w at a "pivot" redshift $z_{\rm p} \equiv a_{\rm p}^{-1} - 1$, where it is best constrained by a given set of experiments. For typical data combinations, $z_{\rm p} \simeq 0.5$. This simple parameterization can provide a good approximation to the predictions of many physically motivated models for observables measured with percent-level precision. A widely used "Figure of Merit" (FoM) for dark energy experiments [22] is the projected combination of errors $[\sigma(w_{\rm p})\sigma(w_{\rm a})]^{-1}$. Ambitious future experiments with 0.1–0.3% precision on observables can constrain richer descriptions of $w(z)$, which can be characterized by principal components.

There has been less convergence on a standard parameterization for describing modified gravity theories. Deviations from the GR-predicted growth rate can be described by a deviation $\Delta\gamma$ in the index of Eq. (28.3), together with an overall multiplicative offset relative to the $G(z)$ expected from extrapolating the CMB-measured fluctuation amplitude to low redshift. However, these two parameters may not accurately capture the growth predictions of all physically interesting models. Another important parameter to constrain is the ratio of the gravitational potentials governing space curvature and the acceleration of non-relativistic test particles. The possible phenomenology of modified gravity models is rich [23], which enables many consistency tests but complicates the task of constructing parameterized descriptions.

The more general set of cosmological parameters is discussed elsewhere in this *Review* (Sec. 25), but here we highlight a few that are particularly important to the dark energy discussion.

- The dimensionless Hubble parameter $h \equiv H_0/100\ {\rm km\,s^{-1}\,Mpc^{-1}}$ determines the present day value of the critical density and the overall scaling of distances inferred from redshifts.
- $\Omega_{\rm m}$ and $\Omega_{\rm tot}$ affect the expansion history and the distance-redshift relation.
- The sound horizon $r_{\rm s} = \int_0^{t_{\rm rec}} c_{\rm s}(t)dt/a(t)$, the comoving distance that pressure waves can propagate between $t = 0$ and recombination, determines the physical scale of the acoustic peaks in the CMB and the baryon acoustic oscillation (BAO) feature in low-redshift matter clustering [24].
- The amplitude of matter fluctuations, conventionally represented by the quantity $\sigma_8(z)$, scales the overall amplitude of growth measures such as weak lensing or redshift-space distortions (discussed in the next section).

Specifically, $\sigma_8(z)$ refers to the rms fluctuation of the matter overdensity $\rho/\bar\rho$ in spheres of radius $8\,h^{-1}$Mpc, computed from the linear theory matter power spectrum at redshift z, and σ_8 on its own refers to the value at $z = 0$ (just like our convention for $\Omega_{\rm m}$).

While discussions of dark energy are frequently phrased in terms of values and errors on quantities like $w_{\rm p}$, $w_{\rm a}$, $\Delta\gamma$, and $\Omega_{\rm tot}$, parameter precision is the means to an end, not an end in itself. The underlying goal of empirical studies of cosmic acceleration is to address two physically profound questions:

- 1. Does acceleration arise from a breakdown of GR on cosmological scales or from a new energy component that exerts repulsive gravity within GR?
- 2. If acceleration is caused by a new energy component, is its energy density constant in space and time, as expected for a fundamental vacuum energy, or does it show variations that indicate a dynamical field?

Substantial progress towards answering these questions, in particular any definitive rejection of the cosmological constant "null hypothesis," would be a major breakthrough in cosmology and fundamental physics.

28.3 Observational Probes

We briefly summarize the observational probes that play the greatest role in current constraints on dark energy. Further discussion can be found in other articles of this *Review*, in particular Secs. 25 (Cosmological Parameters) and 29 (The Cosmic Microwave Background), and in Ref. [12], which provides extensive references to background literature. Recent observational results from these methods are discussed in Sec. 28.4.

Downloaded from https://academic.oup.com/ptep/article/2022/8/083C01/6651666 by KIT Library user on 27 September 2022

28.3.1 *Methods, Sensitivity, Systematics*

Cosmic Microwave Background Anisotropies: Although CMB anisotropies provide limited information about dark energy on their own, CMB constraints on the geometry, matter content, and radiation content of the Universe play a critical role in dark energy studies when combined with low-redshift probes. In particular, CMB data supply measurements of $\theta_{\rm s} = r_{\rm s}/D_{\rm A,c}(z_{\rm rec})$, the angular size of the sound horizon at recombination, from the angular location of the acoustic peaks, measurements of $\Omega_{\rm m}h^2$ and $\Omega_{\rm b}h^2$ from the heights of the peaks, and normalization of the amplitude of matter fluctuations at $z_{\rm rec}$ from the amplitude of the CMB fluctuations themselves. *Planck* data yield a 0.18% determination of $r_{\rm s}$, which scales as $(\Omega_{\rm m}h^2)^{-0.25}$ for cosmologies with standard matter and radiation content. The uncertainty in the matter fluctuation amplitude at the epoch of recombination is 0.5%. Secondary anisotropies, including the integrated Sachs-Wolfe effect, the Sunyaev-Zel'dovich (SZ, [25]) effect, and weak lensing of primary anisostropies, provide additional information about dark energy by constraining low-redshift structure growth.

Type Ia Supernovae (SN): Type Ia supernovae, produced by the thermonuclear explosions of white dwarfs, exhibit 10–15% scatter in peak luminosity after correction for light curve duration (the time to rise and fall) and color (which is a diagnostic of dust extinction). Since the peak luminosity is not known *a priori*, supernova surveys constrain ratios of luminosity distances at different redshifts. If one is comparing a high-redshift sample to a local calibrator sample measured with much higher precision (and distances inferred from Hubble's law), then one essentially measures the luminosity distance in h^{-1}Mpc, constraining the combination $hD_{\rm L}(z)$. With distance uncertainties of 5–8% per well observed supernova, a sample of around 100 SNe is sufficient to achieve sub-percent statistical precision. The 1–2% systematic uncertainties in current samples are dominated by uncertainties associated with photometric calibration and dust extinction corrections plus the observed dependence of luminosity on host galaxy properties. Another potential systematic is redshift evolution of the supernova population itself, which can be tested by analyzing subsamples grouped by spectral properties or host galaxy properties to confirm that they yield consistent results.

Baryon Acoustic Oscillations (BAO):

Pressure waves that propagate in the pre-recombination photon-baryon fluid imprint a characteristic scale in the clustering of matter and galaxies, which appears in the galaxy correlation function as a localized peak at the sound horizon scale $r_{\rm s}$, or in the power spectrum as a series of oscillations. Since observed galaxy coordinates consist of angles and redshifts, measuring this "standard ruler" scale in a galaxy redshift survey determines the angular diameter distance $D_{\rm A}(z)$ and the expansion rate $H(z)$, which convert coordinate separations to comoving distances. Errors on the two quantities are correlated, and in existing galaxy surveys the best determined combination is approximately $D_{\rm V}(z) = [czD^2_{\rm A,c}(z)/H(z)]^{1/3}$. As an approximate rule of thumb, a survey that fully samples structures at redshift z over a comoving volume V, and is therefore limited by cosmic variance rather than shot noise, measures $D_{\rm A,c}(z)$ with a fractional error of $0.005(V/10\,{\rm Gpc}^3)^{-1/2}$ and $H(z)$ with a fractional error 1.6–1.8 times higher. The most precise BAO measurements to date come from large galaxy redshift surveys probing $z < 0.8$, and these will be extended to higher redshifts by future projects. At redshifts $z > 2$, BAO can also be measured in the Lyman-α forest of intergalactic hydrogen absorption towards background quasars, where the fluctuating absorption pattern provides tens or hundreds of samples of the density field along each quasar sightline. For Lyman-α forest BAO, the best measured parameter combination is more heavily weighted towards $H(z)$ because of strong redshift-space distortions that enhance clustering in the line-of-sight direction. Radio intensity mapping, which maps large-scale structure in redshifted 21-cm hydrogen emission without resolving individual galaxies, offers a potentially promising route to measuring BAO over large volumes at relatively low cost, but the technique is still under development. Photometric redshifts in optical imaging surveys can be used to measure BAO in the angular direction, though the typical distance precision is a factor of 3–4 lower compared to a well sampled spectroscopic survey of the same area, and angular BAO measurements do not directly constrain $H(z)$. BAO distance measurements complement SN distance measurements by providing absolute rather than relative distances (with precise calibration of $r_{\rm s}$ from the CMB) and by having greater achievable precision at high redshift thanks to the increasing comoving volume available. Theoretical modeling suggests that BAO measurements from even the largest feasible redshift surveys will be limited by statistical rather than systematic uncertainties.

Weak Gravitational Lensing: Gravitational light bending by a clustered distribution of matter shears the shapes of higher redshift background galaxies in a spatially coherent manner, producing a correlated pattern of apparent ellipticities. By studying the weak lensing signal for source galaxies binned by photometric redshift (estimated from broad-band colors), one can probe the history of structure growth. "Cosmic shear" weak lensing uses the correlation of source ellipticities to deduce the clustering of intervening matter. "Galaxy-galaxy lensing" (GGL) uses the correlation between a shear map and a foreground galaxy sample to measure the average mass profile around the foreground galaxies, which can be combined with galaxy clustering to constrain total matter clustering. For a specified expansion history, the predicted signals scale approximately as $\sigma_8\Omega_{\rm m}^{\alpha}$, with $\alpha \simeq 0.3$–0.5. The predicted signals also depend on the distance-redshift relation, so weak lensing becomes more powerful in concert with SN or BAO measurements that can pin this relation down independently. The most challenging systematics are shape measurement biases, biases in the distribution of photometric redshifts, and intrinsic alignments of galaxy orientations that could contaminate the lensing-induced signal. Weak lensing of CMB anisotropies is an increasingly powerful tool, in part because it circumvents many of these observational and astrophysical systematics. Predicting the large-scale weak lensing signal is straightforward in principle, but the number of independent modes on large scales is small, and the inferences are therefore dominated by sample variance. Exploiting small-scale measurements, for tighter constraints, requires modeling the effects of complex physical processes such as star formation and feedback on the matter power spectrum. Strong gravitational lensing can also provide constraints on dark energy, either through time delay measurements that probe the absolute distance scale, or through measurements of multiple-redshift lenses that constrain distance ratios. The primary uncertainty for strong lensing constraints is modeling the mass distribution of the lens systems.

Clusters of Galaxies: Like weak lensing, the abundance of massive dark-matter halos probes structure growth by constraining $\sigma_8\Omega_{\rm m}^{\alpha}$, where $\alpha \simeq 0.3$–0.5. These halos can be identified as dense concentrations of galaxies or through the signatures of hot (10^7–10^8 K) gas in X-ray emission or SZ distortion of the CMB. The critical challenge in cluster cosmology is calibrating the relation $P(M_{\rm halo}|O)$ between the halo mass as predicted from theory and the observable O used for cluster identification. Measuring the stacked weak lensing signal from clusters has emerged as a promising approach to achieve percent-level accuracy in calibration of the mean relation, which is required for clusters to remain competitive with other growth probes. This method requires accurate modeling of completeness and contamination of cluster catalogs, projection effects on cluster selection and weak lensing measurements, and possible baryonic physics effects on the mass distribution within clusters.

Redshift-Space Distortions (RSD) and the Alcock-Paczynksi (AP) Effect: Redshift-space distortions of galaxy clustering, induced by peculiar motions, probe structure growth by constraining the parameter combination $f(z)\sigma_8(z)$, where $f(z)$ is the growth rate defined by Eq. (28.3). Uncertainties in theoretical modeling of non-linear gravitational evolution and the non-linear bias between the galaxy and matter distributions currently limit application of the method to large scales (comoving separations $r \gtrsim 10\,h^{-1}$Mpc or wavenumbers $k \lesssim 0.2h\,{\rm Mpc}^{-1}$). A second source of anisotropy arises if one adopts the wrong cosmological metric to convert angles and redshifts into comoving separations, a phenomenon known as the Alcock-Paczynksi effect [27]. Demanding isotropy

Downloaded from https://academic.oup.com/ptep/article/2022/8/083C01/6651666 by KIT Library user on 27 September 2022

Table 28.1: A selection of major dark-energy experiments, based on Ref. [26]. Abbreviations in the "Data" column refer to optical (Opt) or near-infrared (NIR) imaging (I) or spectroscopy (S). For spectroscopic experiments, the "Spec-z" column lists the primary redshift range for galaxies (gals), quasars (QSOs), or the Lyman-α forest (LyαF). Abbreviations in the "Methods" column are weak lensing (WL), clusters (CL), supernovae (SN), baryon acoustic oscillations (BAO), and redshift-space distortions (RSD).

Project	Dates	Area/deg^2	Data	Spec-z Range	Methods
BOSS	2008–2014	10,000	Opt-S	0.3–0.7 (gals)	BAO/RSD
				2–3.5 (LyαF)	
KiDS	2011–2019	1350	Opt-I	——	WL/CL
DES	2013–2019	5000	Opt-I	——	WL/CL
					SN/BAO
eBOSS	2014–2018	7500	Opt-S	0.6–2.0 (gal/QSO)	BAO/RSD
				2–3.5 (LyαF)	
SuMIRE	2014–2024	1500	Opt-I		WL/CL
			Opt/NIR-S	0.8–2.4 (gals)	BAO/RSD
HETDEX	2017–2023	450	Opt-S	$1.9 < z < 3.5$ (gals)	BAO/RSD
DESI	2021–2026	14,000	Opt-S	0–1.7 (gals)	BAO/RSD
				2–3.5 (LyαF)	
VRO/LSST	2022–2032	20,000	Opt-I	——	WL/CL
					SN/BAO
Euclid	2022–2028	15,000	Opt-I		WL/CL
			NIR-S	0.7–2.2 (gals)	BAO/RSD
Roman	2026–2031	2200	NIR-I		WL/CL/SN
			NIR-S	1.0–3.0 (gals)	BAO/RSD

of clustering at redshift z constrains the parameter combination $H(z)D_{\rm A}(z)$. The main challenge for the AP method is correcting for the anisotropy induced by peculiar velocity RSD.

Low Redshift Measurement of H_0: The value of H_0 sets the current value of the critical density $\rho_{\rm c} = 3H_0^2/8\pi G_{\rm N}$, and combination with CMB measurements provides a long lever arm for constraining the evolution of dark energy. The challenge in conventional H_0 measurements is establishing distances to galaxies that are "in the Hubble flow," *i.e.*, far enough away that their peculiar velocities are small compared to the expansion velocity $v = H_0 d$. This can be done by building a ladder of distance indicators tied to stellar parallax on its lowest rung, or by using gravitational-lens time delays or geometrical measurements of maser data to circumvent this ladder.

28.3.2 *Dark Energy Experiments*

Most observational applications of these methods now take place in the context of large cosmological surveys, for which constraining dark energy and modified gravity theories is a central objective. Table 28.1 lists a selection of recent, ongoing, and planned dark-energy experiments, taken originally from the Snowmass 2013 Dark Energy Facilities review [26], which focused on projects in which the U.S. has either a leading role or significant participation. References and links to further information about these projects can be found in Ref. [26]. We have adjusted some of the dates in this Table relative to those in Ref. [26] and added the European-led KiloDegree Survey (KiDS). Dates in the Table correspond to the duration of survey observations, and the final cosmological results frequently require 1–3 years of analysis and modeling beyond the end of data taking.

Beginning our discussion with imaging surveys, the Dark Energy Survey (DES) has observed 1/8 of the sky to a depth roughly 2 magnitudes deeper than the Sloan Digital Sky Survey (SDSS), enabling weak lensing measurements with much greater statistical precision, cluster measurements calibrated by weak lensing, and angular BAO measurements based on photometric redshifts. With repeated imaging of selected fields, DES has identified thousands of Type Ia SNe, which together with spectroscopic follow-up data enable significant improvements on the current state-of-the-art for supernova (SN) cosmology. Cosmological results from weak lensing and galaxy clustering analyses of the 3-year (Y3) DES data set are presented in Ref. [28] and discussed further below, while the first cosmological results from the DES supernova survey are presented in Ref. [29]. KiDS and the Subaru Hyper-Suprime Camera (HSC) collaboration are carrying out optical imaging surveys similar to the DES weak lensing survey, smaller in area but with greater depth and sharper image quality. Weak lensing cosmology results from 1000 deg^2 of KiDS imaging are reported by Refs. [30,31] and from the first year of HSC imaging by Refs. [32,33], all discussed further below. The HSC survey is one component of the Subaru Measurement of Images and Redshifts (SuMIRE) project. Beginning in the early 2020s, the Legacy Survey of Space and Time (LSST) of the Vera Rubin Observatory (VRO) will scan the southern sky to SDSS-like depth every four nights. LSST imaging co-added over its decade-long primary survey will reach extraordinary depth, enabling weak lensing, cluster, and photometric BAO studies from billions of galaxies. Additionally, LSST time-domain monitoring will identify and measure light curves for thousands of Type Ia SNe per year.

Turning to spectroscopic surveys, the Baryon Oscillation Spectroscopic Survey (BOSS) and its successor eBOSS used fiber-fed optical spectrographs to map the redshift-space distributions of millions of galaxies and quasars. These 3-dimensional maps enable BAO and RSD measurements, and Lyman-α forest spectra of high-redshift quasars extend these measurements to redshifts $z > 2$. As discussed below, the eBOSS Collaboration has now published BAO and RSD analyses from the final data sets of the BOSS and eBOSS programs. The Hobby-Eberly Telescope Dark Energy Experiment (HETDEX) uses integral field spectrographs to detect Lyman-α emission-line galaxies at $z \simeq 1.9$–3.5, probing a small sky area but a substantial comoving volume. The Dark Energy Spectroscopic Instument (DESI) follows a strategy similar to BOSS/eBOSS but on a much grander scale, using a larger telescope (4-m vs. 2.5-m) and a much higher fiber multiplex (5000 vs. 1000) to survey an order-of-magnitude more galaxies. After commissioning and survey validation observations, DESI began full operations in May 2021, and it has already measured more galaxy redshifts than BOSS and eBOSS combined. A new Prime Focus Spectrograph (PFS) for the Subaru telescope will enable the spectroscopic component of SuMIRE, with the large telescope aperture and wavelength sensitivity that extends to the near-infrared (NIR) allowing it to probe a higher redshift galaxy population than DESI, over a smaller area of sky.

Compared to ground-based observations, space observations afford higher angular resolution and a far lower NIR sky background. The *Euclid* mission and the *Nancy Grace Roman Space Telescope* (formerly *WFIRST*) will exploit these advantages, conducting large area imaging surveys for weak lensing and cluster studies and slitless spectroscopic surveys of emission-line galaxies for BAO and RSD studies. *Roman* will also incorporate an imag-

Downloaded from https://academic.oup.com/ptep/article/2022/8/083C01/6651666 by KIT Library user on 27 September 2022

ing and spectrophotometric supernova (SN) survey, extending to redshift $z \simeq 1.7$. Survey details are likely to evolve prior to launch, but in the current designs one can roughly characterize the difference between the *Euclid* and *Roman* dark-energy experiments as "wide vs. deep," with planned survey areas of 15,000 deg^2 and 2200 deg^2, respectively. For weak lensing shape measurements, *Euclid* will use a single wide optical filter, while *Roman* will use three NIR filters. The *Euclid* galaxy redshift survey will cover a large volume at relatively low space density, while the *Roman* survey will provide denser sampling of structure in a smaller volume. There are numerous synergies among the LSST, *Euclid*, and *Roman* dark energy programs, as discussed in Ref. [34].

28.4 Current Constraints on Expansion, Growth, and Dark Energy

The last decade has seen dramatic progress in measurements of the cosmic expansion history and structure growth, leading to much tighter constraints on the parameters of dark energy models. CMB data from the *WMAP* and *Planck* satellites and from higher resolution ground-based experiments have provided an exquisitely detailed picture of structure at the recombination epoch and the first CMB-based measures of low-redshift structure through lensing and SZ cluster counts. Cosmological supernova samples have increased in size from tens to many hundreds, with continuous coverage from $z = 0$ to $z \simeq 1.4$, alongside major improvements in data quality, analysis methods, and detailed understanding of local populations. BAO measurements have advanced from the first detections to 1–2% precision at multiple redshifts, with increasingly sophisticated methods for testing systematics, fitting models, and evaluating statistical errors. Advances in X-ray, SZ, and weak-lensing observations of large samples of galaxy clusters allow a multi-faceted approach to mass calibration, improving statistical precision but also revealing sources of astrophysical uncertainty. Cluster constraints have been joined, and for the present superseded, by the first precise matter-clustering constraints from cosmic-shear weak lensing and galaxy-galaxy lensing, and by redshift-space distortion measurements that probe different aspects of structure growth at (presently) lower precision. The precision of low-redshift H_0 measurements has sharpened from the roughly 10% error of the *HST* Key Project [35] to 2–3% in recent analyses.

As an illustration of current measurements of the cosmic expansion history, Fig. 28.1 compares distance-redshift measurements from SN and BAO data to the predictions for a flat Universe with a cosmological constant. SN cosmology relies on compilation analyses that try to bring data from different surveys probing distinct redshift ranges to a common scale. Here we use the "joint light curve analysis" (JLA) sample of Ref. [37], who carried out a careful intercalibration of the 3-year Supernova Legacy Survey (SNLS3, [39]) and the full SDSS-II Supernova Survey [3] data in combination with several local supernova samples and high-redshift supernovae from *HST*. Results from the Union2.1 sample [40], which partly overlaps JLA but has different analysis procedures, would be similar. Other state-of-the-art supernova data sets include the Pan-STARRS1 sample incorporated in the PANTHEON compilation [41] and the sample of spectroscopically confirmed supernovae from DES [29]. For illustration purposes, we have binned the JLA data in redshift and plotted the diagonal elements of the covariance matrix as error bars, and we have converted the SN luminosity distances to an equivalent comoving angular diameter distance. Because the peak luminosity of a fiducial SN Ia is an unknown free parameter, the SN distance measurements could all be shifted up and down by a constant multiplicative factor; cosmological information resides in the relative distances as a function of redshift. The normalization used here corresponds to a Hubble parameter $h = 0.674$.

For the BAO data points in Fig. 28.1 we have used the compilation in Table 3 (the "BAO-only" row) from the summary cosmology paper by the eBOSS collaboration [38], where one can find references for the original data sources. The individual BAO measurements come (in order of increasing redshift) from the SDSS-II main galaxy sample and from luminous red galaxies, emission line galaxies, and quasars mapped by BOSS and eBOSS. The two high-

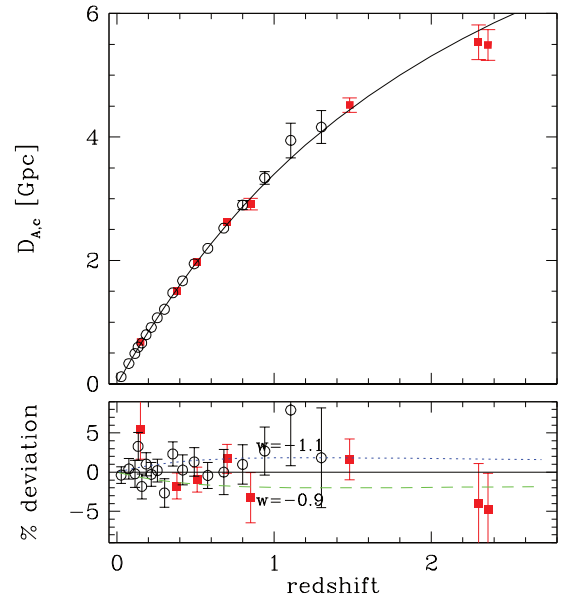

Figure 28.1: Distance-redshift relation measured from Type Ia SNe and BAO compared to the predictions (black curve) of a flat ΛCDM model with $\Omega_m = 0.315$ and $h = 0.674$, the best-fit parameters inferred from *Planck* CMB data [36]. Circles show binned luminosity distances from the JLA SN sample [37], multiplied by $(1+z)^{-1}$ to convert to comoving angular diameter distance. Red squares show BAO distance measurements from the SDSS-II, BOSS, and eBOSS surveys as compiled in Ref. [38]. The lower panel plots residuals from the ΛCDM prediction, with dashed and dotted curves that show the effect of changing w by ±0.1 while all other parameters are held fixed. Note that the SN data points can be shifted up or down by a constant factor to account for freedom in the peak luminosity, while the BAO points are calibrated to 0.2% precision by the sound horizon scale computed from *Planck* data. The errors on the BAO data points are approximately independent, but not entirely so. In the upper panel, error bars are plotted only at $z > 0.7$ to avoid visual confusion. The two Lyman-α forest data points are slightly offset from their effective redshift of $z = 2.33$ for clarity.

est redshift points, both with an effective $z \approx 2.3$, come from the auto-correlation of the Lyman-α forest in high-redshift ($z > 2$) quasars from BOSS and eBOSS and from the cross-correlation of the Lyman-α forest with the quasars themselves. The BAO measurements are converted to absolute distances using the sound horizon scale $r_s = 147.09$ Mpc from *Planck* 2018 CMB data, whose 0.18% uncertainty is small compared to the current BAO measurement errors. For the $z = 0.15$ and $z = 1.5$ data points we have converted values of D_V to $D_{A,c}$, while for other redshifts we use the $D_{A,c}$ determinations measured directly by the transverse BAO. The galaxy and Lyman-α forest analyses also measure $H(z)$ at the same redshifts, providing further leverage on expansion history that is not captured in Fig. 28.1.

The plotted cosmological model has $\Omega_m = 0.315$ and $h = 0.674$, the best-fit values from *Planck* (TT+TE+EE+lowE+lensing) assuming $w = -1$ and $\Omega_{tot} = 1$ [36]. The SN, BAO, and CMB data sets, probing a wide range of redshifts with radically different techniques, are for the most part mutually consistent with the predictions of a flat ΛCDM cosmology. This consistency has held steady or improved as the measurements themselves have improved over the past decade. Dotted and dashed curves in the lower panel of Fig. 28.1 show the effect of changing w by ±0.1 with all other parameters held fixed, which leads to significantly worse agreement with the data. However, such a single-parameter comparison does not capture the impact of parameter degeneracies or the ability of complementary data sets to break them, and if one instead forced a match to CMB data by changing h and Ω_m when changing w then the predicted BAO distances would diverge at

Downloaded from https://academic.oup.com/ptep/article/2022/8/083C01/6651666 by KIT Library user on 27 September 2022

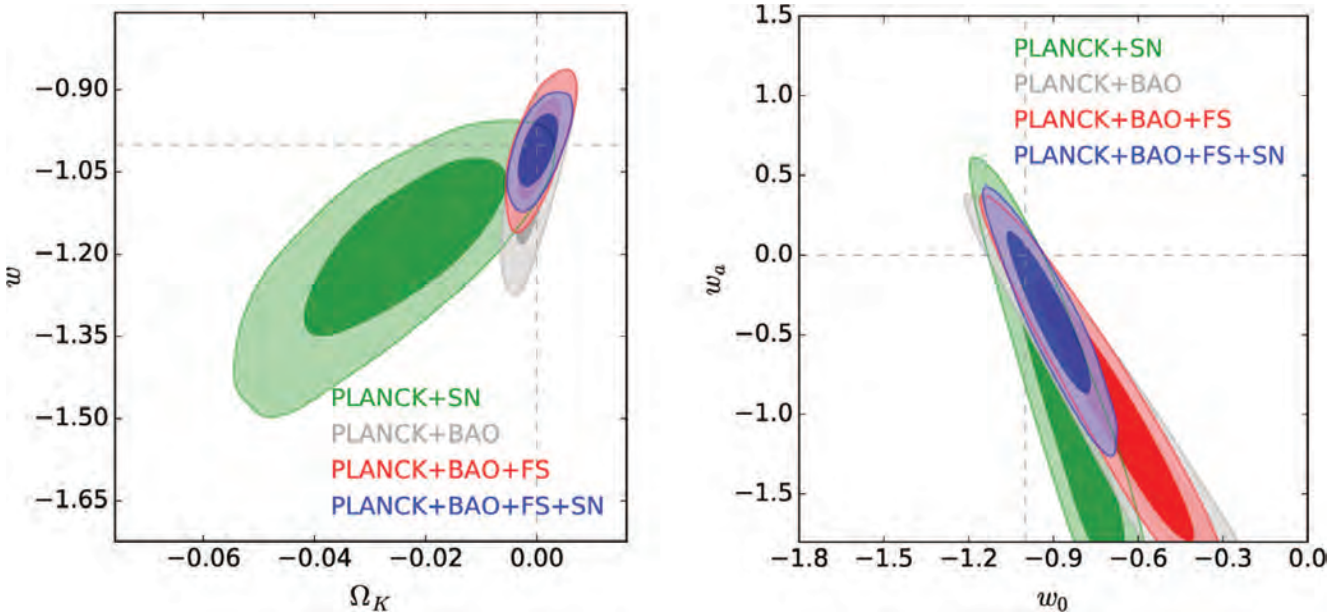

Figure 28.2: Constraints on dark energy model parameters from combinations of CMB, BAO, galaxy clustering, and supernova (SN) data, taken from Ref. [42]. The left panel shows 68% and 95% confidence contours in the `owCDM` model, with constant equation-of-state parameter w and non-zero space curvature $\Omega_K \equiv 1 - \Omega_{\rm tot}$. Green and gray contours show the combination of *Planck* CMB data with SN or BAO data, respectively. Red contours combine CMB, BAO, and the full shape (FS) of redshift-space galaxy clustering. Blue contours add SN data to this combination. The right panel shows confidence contours for the same data combinations in the $\mathtt{w_0w_aCDM}$ model, which assumes a flat Universe and an evolving equation of state with $w(a) = w_0 + w_{\rm a}(1-a)$.

$z = 0$ rather than converging there. Other good representations of recent observational constraints on the cosmic expansion history include Fig. 11 of Ref. [41] for SNIa and Fig. 2 of Ref. [38] for BAO.

Fig. 28.2, taken from Ref. [42], presents constraints on models that allow a free but constant value of w with non-zero space curvature (`owCDM`, left panel) or the evolving equation of state of Eq. (28.4) in a flat Universe ($\mathtt{w_0w_aCDM}$, right panel). Green contours show constraints from the combination of *Planck* 2015 CMB data and the JLA supernova sample. Gray contours show the combination of *Planck* with BAO measurements from BOSS, 6dFGS [43], and SDSS-II [44]. Red contours adopt a more aggressive analysis of the BOSS galaxy data that uses the full shape (FS) of the redshift-space power spectrum and correlation function, modeled via perturbation theory, in addition to the measurement of the BAO scale itself. The full shape analysis improves the constraining power of the data, primarily because measurement of the Alcock-Paczynski effect on sub-BAO scales helps to break the degeneracy between $D_{\rm A,c}(z)$ and $H(z)$. Blue contours show constraints from the full combination of CMB, BAO+FS, and SN data. Supernovae provide fine-grained relative distance measurements with good bin-by-bin precision at $z < 0.7$ (see Fig. 28.1), which is complementary to BAO for constraining redshift evolution of w. In both classes of model, the flat ΛCDM parameters ($w = w_0 = -1$, $\Omega_{\rm K} = w_{\rm a} = 0$) lie within the 68% confidence contour. Many recent papers feature constraint diagrams analogous to Fig. 28.2, and the constraints within this parameter space have tightened moderately with new data while remaining consistent with flat ΛCDM.

The precision on dark energy parameters depends, of course, on both the data being considered and the flexibility of the model being assumed. For `wCDM`, Ref. [38] find $w = -1.026 \pm 0.033$ using *Planck* CMB data, BAO measurements from SDSS-II and BOSS/eBOSS, and SN measurements from the Pantheon compilation. With the addition of eBOSS RSD data and DES 3×2pt measurements, they constrain a more flexible model ($\mathtt{ow_0w_aCDM}$) that allows non-zero curvature and an evolving equation-of-state (Eq. 28.4), finding

$$w_p = -1.020 \pm 0.032 \tag{28.5}$$

at a pivot redshift $z_p = 0.29$, a tight constraint on curvature

$$1 - \Omega_{\rm tot} = -0.0023 \pm 0.0022 \tag{28.6}$$

but only a loose constraint on the evolution parameter

$$w_a = -0.48^{+0.36}_{-0.30}. \tag{28.7}$$

Obtaining a tight constraint on w_p in such a flexible cosmological model requires measurements that have complementary sensitivity to its multiple free parameters, and the precision of Eq. (28.5) is a testament to the remarkable improvements in cosmological measurements over the past decade.

A flat ΛCDM model fit to *Planck* CMB data alone predicts $H_0 = 67.4 \pm 0.5$ km s^{-1} Mpc^{-1} (see Chapter 29 of this *Review*). This prediction and its error bar are sensitive to the assumptions of constant dark energy and a flat Universe. However, by adding BAO and supernova data one can construct an "inverse distance ladder" to measure H_0 precisely, even with a general dark energy model and free curvature [45]. Ref. [38] applies this approach to obtain $H_0 = 68.2 \pm 0.81$ km s^{-1} Mpc^{-1}. As discussed in Sec. 25.3.1of this *Review*, some recent measurements from low-redshift data yield higher values of H_0. Fig. 28.3 compares the CMB-anchored H_0 estimates cited above to distance-ladder estimates that use Cepheid [46] or tip-of-the-red-giant-branch (TRGB) [47] stars to calibrate Type Ia supernova luminosities, and to an entirely independent estimate that uses gravitational-lens time delays [48]. The Cepheid estimate is discrepant with the CMB-anchored estimates at a statistically significant level (Ref. [46] quotes 4.2σ relative to *Planck* ΛCDM), while the TRGB calibration yields an intermediate result that is consistent with either the "high" or "low" values of H_0. Strong lensing inferences of H_0 depend on the mass profiles of the lensing galaxies and halos. The two strong lensing values in Fig. 28.3, both from Ref. [48], use the same lensing time delay data but either a loose prior or an independent dynamical constraint on these profiles. Earlier strong lensing analyses made stronger assumptions about mass profiles and inferred smaller H_0 uncertainties [49].

The tension in H_0 could reflect some combination of statistical flukes and systematic errors in one or more of the data sets employed in these analyses. However, if the resolution lies in new physics rather than measurement errors, then this is probably

Downloaded from https://academic.oup.com/ptep/article/2022/8/083C01/6651666 by KIT Library user on 27 September 2022

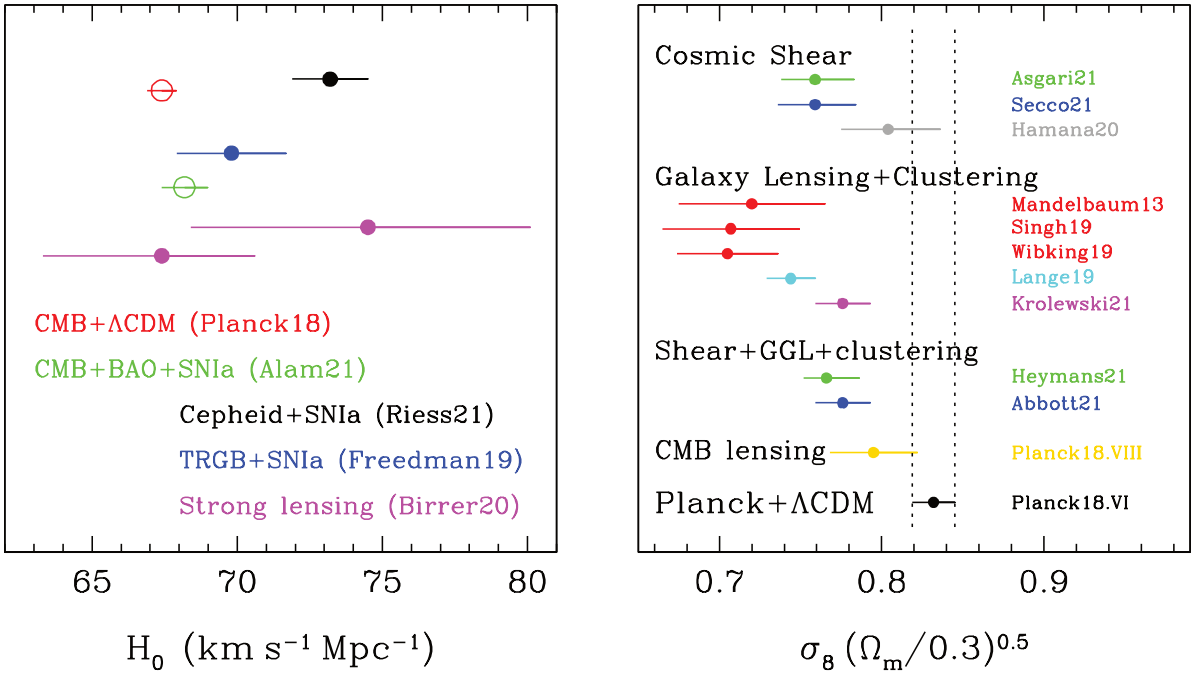

Figure 28.3: Tensions between low-redshift cosmological measurements and the predictions of a CMB-normalized ΛCDM model. All error bars are 1σ; see text for observational references. *(Left)* Open circles show values of H_0 for flat ΛCDM with *Planck* parameters (red) or a general dark energy model constrained by a combination of CMB, BAO, and supernova data (green). Filled circles show distance-ladder estimates based on Cepheid (black) or TRGB (blue) calibration of SNIa luminosities, or an independent estimate using gravitational-lens time delays with two alternative constraints on lens mass profiles (magenta). *(Right)* Matter clustering characterized by the parameter combination $\sigma_8(\Omega_m/0.3)^{0.5}$, as predicted by a *Planck*-normalized ΛCDM model (vertical dotted lines, black hexagon) and estimated from weak gravitational lensing using: cosmic shear from KiDS-1000 (green), DES Y3 (blue) or HSC Y1 (gray), galaxy clustering and galaxy-galaxy lensing of SDSS galaxies (red, cyan) or galaxy clustering and CMB lensing of WISE galaxies (magenta), and the "3 × 2pt" analyses of KiDS-1000 (green) and DES Y3 (blue). Points of the same color are based on the same weak-lensing data. The "CMB lensing" point (gold) shows the value of σ_8 for $\Omega_m = 0.3$ inferred from *Planck* CMB lensing, a measurement that is independent of the "Planck+ΛCDM" prediction and weighted to somewhat higher redshift than the other weak-lensing points.

physics that operates in the *pre-recombination* Universe, rescaling the BAO standard ruler in a way that shifts the ΛCDM and inverse-distance-ladder values upward. Models with extra relativistic degrees of freedom or dark energy that is dynamically significant in the early Universe can achieve this effect by increasing the early expansion rate, but they are tightly constrained by the damping tail of CMB anisotropies and by the shape of the galaxy power spectrum. A finely tuned model in which early dark energy decays rapidly after recombination can mitigate the tension between CMB data and local H_0 measurements [50], though it still prefers H_0 values below those of Ref. [46]. Numerous theory papers have examined possible physical solutions to the H_0 tension, all of which involve significant modifications to the ΛCDM scenario.

The amplitude of CMB anisotropies is proportional to the amplitude of density fluctuations present at recombination, and by assuming GR and a specified dark energy model one can extrapolate the growth of structure forward to the present day to predict σ_8. Probes of low-redshift structure yield constraints in the (σ_8, Ω_m) plane, which can be summarized in terms of the parameter combination $S_8 \equiv \sigma_8(\Omega_m/0.3)^{0.5}$. As discussed in earlier editions of this *Review*, many but not all weak-lensing and cluster studies to date yield S_8 values lower than those predicted for *Planck*-normalized ΛCDM. The right panel of Fig. 28.3 illustrates the current state-of-play, comparing a selection of recently published S_8 estimates to the *Planck*+ΛCDM prediction of $S_8 = 0.832 \pm 0.013$.

The first three points show recent cosmic-shear weak-lensing estimates from KiDS [30], DES [51], and HSC [33]. The next four points use galaxy-galaxy lensing in combination with galaxy clustering. Ref. [52] used weak-lensing data from SDSS imaging and the SDSS main galaxy redshift catalog, restricting the analysis to scales well described by perturbation theory. Refs. [53] and [54] used the same weak-lensing data but the BOSS LOWZ galaxy sample, and they employed two quite different approaches to model the clustering and lensing signals into the strongly non-linear regime ($r \approx 1\,h^{-1}$Mpc) so that they could fully exploit the constraining power of the data. Ref. [55] found a strong discrepancy on these non-linear scales between the predictions of a *Planck*-normalized ΛCDM model and the galaxy-galaxy lensing of BOSS CMASS galaxies, measured from 250 deg^2 of deep imaging from the Canada-France-Hawaii Telescope. Ref. [56], plotted in Fig. 28.3, revisited these data with a more general modeling approach and showed that the discrepancy persists over a range of redshift and galaxy stellar mass. The last point in this group, from Ref. [57], uses the clustering of galaxies in the WISE satellite's all-sky infrared survey and the cross-correlation of these galaxies with *Planck* CMB-lensing, with galaxy redshifts estimated from photometry.

The third set of points in this panel shows S_8 estimates that combine cosmic shear with galaxy-galaxy lensing and galaxy clustering (a.k.a. "3 × 2" analyses because they combine three 2-point correlations), restricted to fairly large scales in the perturbative regime. These points come from analyses of the KiDS-1000 data set [31] and the DES Y3 data set [28]. The "CMB lensing" point shows the matter-clustering amplitude inferred from *Planck* CMB lensing; we have evaluated Eq. (38) of Ref. [58] at $\Omega_m = 0.3$ and adopted the same fractional error. Although the background being lensed is the CMB, this is still a measurement of low-redshift clustering, albeit with an effective redshift that is higher than that of the other weak lensing analyses. For multipoles $l > 100$ roughly half of the expected signal comes from structure at $z < 2$ and nearly all from $z < 10$ [59].

The HSC cosmic shear and *Planck* CMB lensing measurements are both consistent with the *Planck*+ΛCDM prediction at $\sim 1\sigma$, and most but not all of the remaining points are individually

Downloaded from https://academic.oup.com/ptep/article/2022/8/083C01/6651666 by KIT Library user on 27 September 2022

consistent at $\sim 2\sigma$. However, it is clear that the low redshift data prefer a value of S_8 below the predicted value. As a simple (but arguably appropriate) characterization of these measurements, we have averaged together estimates from the same weak lensing experiment (*i.e.*, points of the same color), then averaged the values from the seven experiments to obtain the mean estimate $S_8 = 0.766 \pm 0.012$, where the quoted uncertainty is simply the dispersion of the seven estimates divided by $\sqrt{N-1} = \sqrt{6}$. The $\sim 8\%$ discrepancy with the predicted $S_8 = 0.832 \pm 0.013$ is thus statistically significant if we assume that the errors (both statistical and systematic) of each measurement are independent. Using a much more sophisticated approach to data combination, but before the availability of the DES Y3 results, Ref. [60] found a slightly higher central value and slightly tighter error bar, $S_8 = 0.7769 \pm 0.0095$. However, common systematics might affect multiple weak lensing measurements, and any downward revision of the *Planck*+ΛCDM central value would weaken the tension.

In the two years since the last edition of this *Review*, the precision and systematics tests of the weak lensing measurements have improved significantly. The evidence for a discrepancy between the predicted and inferred values of S_8 has not become obviously stronger or obviously weaker as a result of these improvements. It remains possible that the tension seen in Fig. 28.3 represents a true deviation between the clustering growth extrapolated forward from the early Universe and the clustering of matter at late times. Because the expansion history is well constrained by BAO and SN data, it is difficult to change low-redshift matter clustering by simply changing the equation of state of dark energy. Instead, a deviation between predicted and observed clustering might point towards modified gravity, decaying dark matter, or coupling between dark matter and dark energy.

Final results from KiDS, DES, and HSC may clarify this situation over the next two years. Cluster weak lensing from the same surveys can achieve S_8 constraints with comparable statistical power, though systematic biases associated with cluster selection have thus far been a limiting factor. CMB lensing constraints will improve with higher angular resolution data from the South Pole Telescope and the Atacama Cosmology Telescope and their successors. The DESI survey will soon allow the first RSD-based measurements of structure growth at the 1–2% level, providing an entirely distinct route to probe the clustering tension hinted at by weak lensing data.

28.5 Summary and Outlook

Figure 28.2 focuses on model parameter constraints, but to describe the observational situation it is more useful to characterize the precision, redshift range, and systematic uncertainties of the basic expansion and growth measurements. At present, supernova surveys constrain distance ratios at the 1–2% level in redshift bins of width $\Delta z = 0.1$ out to $z \approx 0.8$, with larger but still interesting error bars out to $z \simeq 1.3$. Estimated systematic uncertainties are comparable to statistical uncertainties and include effects of photometric calibration, dust reddening, host-galaxy correlations, and possible evolution of the SN population. BAO surveys have measured the angular diameter distance $D_{\rm A,c}(z)$ and the expansion rate $H(z)$ over the range $0 < z < 2.5$, calibrated to absolute units using the CMB-based value of the sound horizon r_s. For $D_{\rm A,c}(z)$, the final analyses of BOSS/eBOSS achieve precision of 1.6–1.8% in three overlapping redshift bins from luminous galaxies at $z = 0.2 - 1.0$, 2.6% from quasars at $z \approx 1.5$, and 2.9% from the Lyman-α forest at $z \approx 2.3$. For $H(z)$, the precision at the same redshifts is 2.6–3.0%, 4.1%, and 2.1%, respectively. SDSS, DES, KiDS, and HSC have used combinations of weak lensing and galaxy clustering to measure the parameter combination $S_8 = \sigma_8(\Omega_{\rm m}/0.3)^{0.5}$ with estimated precision of 2-4%, and the cross-correlation of WISE galaxies with *Planck* CMB lensing achieves similar precision. These estimates account for identified systematic uncertainties, but the measurements and modeling are challenging, and it is possible that the systematics are underestimated. Our simple average of these measurements, treating them as independent and using their dispersion as an empirical estimate of uncertainty, yields an error on the mean of 1.5%. The statistical power of these weak lensing surveys is concentrated at $z \approx 0.2 - 0.8$, and they provide useful constraints at lower precision on redshift evolution over this range and on individual values of $\Omega_{\rm m}$ and σ_8. RSD measurements constrain the similar parameter combination $f(z)\sigma_8(z)$, but they do not yet have precision competitive with that of weak lensing measurements. Distance-ladder estimates of H_0 now span a small range, using overlapping data but distinct treatments of key steps; individual studies quote uncertainties of 2–3%, with similar statistical and systematic contributions.

Planck data and higher resolution ground-based experiments now measure CMB anisotropies with exquisite precision; for example, CMB measurements now constrain the physical size of the BAO sound horizon to 0.2% and the angular scale of the sound horizon to 0.01%. A flat ΛCDM model with standard radiation and neutrino content can fit the CMB data and the BAO and SN distance measurements to within their estimated uncertainties. The value of H_0 implied by this model disagrees with recent Cepheid+SNIa distance-ladder measurements of H_0 at a $\sim 4\sigma$ level. This disagreement persists in models that allow non-zero curvature and low redshift evolution of $w(z)$, provided one assumes standard pre-recombination physics to compute the sound horizon r_s. The discrepancy could reflect underestimated systematic uncertainties in the Cepheid-based H_0 estimate, or it could be a sign of new physics in the early Universe that rescales r_s. Over the next few years, improved parallax data from *HST* and *Gaia*, discovery of new SNIa in nearby galaxies, and observing programs on the *James Webb Space Telescope* (*JWST*) should allow further improvements and systematics checks in the Cepheid distance ladder. It will be equally important to bring the TRGB calibration method to a comparable level of precision and systematics control, and to understand any differences between the Cepheid and TRGB distance scales. Strong lensing time delays and gravitational wave standard sirens may provide useful independent tests if their systematic uncertainties can be sufficiently well controlled. Improving measurements of the CMB damping tail from ground-based experiments will provide increasingly strong constraints on resolutions of the H_0-tension that invoke novel pre-recombination physics.

Extrapolating forward from the CMB anisotropies measured by *Planck* implies a low redshift value of S_8 that is higher than recent direct estimates from weak gravitational lensing and galaxy clustering. Comparing the Planck central value to the simple average of recent experiments discussed in §28.4 implies a difference of 8.6%: $S_8 = 0.832 \pm 0.013$ vs. $S_8 = 0.766 \pm 0.012$. This disagreement could reflect a common systematic that biases several of the weak lensing analyses in the same direction, and it would be weakened if the *Planck* S_8 value were high because of an unlucky statistical fluctuation or a residual systematic. If real, this discrepancy could point towards modified gravity, decaying dark matter, or coupling between dark matter and dark energy.

Analyses of the final (6-year) DES data could plausibly achieve a factor of two or more improvement on current uncertainties, along with more stringent internal cross-checks, from a combination of deeper imaging, improved weak lensing calibration, and modeling that exploits measurements in the non-linear clustering regime. The final KiDS and HSC data sets will be smaller than DES, but still large enough to achieve competitive precision with independent observations and analyses. Higher signal-to-noise CMB lensing maps cross-correlated with galaxies will provide independent tests that avoid some of the systematic uncertainties of optical weak lensing. Collectively these efforts could achieve an unambiguous determination of the amplitude of low redshift matter clustering at the 1–2% level.

The DESI galaxy redshift survey will soon exceed the size of the existing SDSS and BOSS/eBOSS surveys, ultimately by a factor of ~ 10. DESI will enable high precision BAO measurements of expansion history at $z \approx 0.7$–1.4 and, for the first time, percent-level measurements of structure growth through RSD. Cross-correlation of DESI galaxies with cosmic shear or CMB lensing maps will achieve high precision while sidestepping many of the systematics that affect pure imaging surveys. Precise BAO and RSD measurements at higher redshifts will come from DESI Lyman-α forest maps and the HETDEX and Subaru PFS galaxy surveys. The BAO measurements will complement increasingly

Downloaded from https://academic.oup.com/ptep/article/2022/8/083C01/6651666 by KIT Library user on 27 September 2022

precise measurements of the relative distance scale at $z < 1$ from the DES photometric supernova sample and from improved local supernova samples ($z < 0.1$) that provide a low-redshift anchor. Large galaxy samples will also enable more powerful applications of the Alcock-Paczynski effect and parameter measurements based on voids or higher order clustering statistics.

The next five years will see another major leap in observational capabilities with the advent of LSST, *Euclid*, and *Roman*. LSST will be the ultimate ground-based optical weak-lensing experiment, measuring several billion galaxy shapes over 20,000 deg^2 of the southern hemisphere sky, and it will detect and monitor many thousands of SNe per year. *Euclid* and *Roman* also have weak lensing as a primary science goal, taking advantage of the high angular resolution and extremely stable image quality achievable from space. Both missions plan large spectroscopic galaxy surveys, which will provide better sampling at high redshifts than DESI or PFS because of the lower infrared sky background above the atmosphere. *Roman* is also designed to carry out what should be the ultimate supernova cosmology experiment, with deep, high resolution, near-IR observations and the stable calibration achievable with a space platform. The 2020s will also see dramatic advances in CMB lensing from the Simons Observatory and, potentially, CMB-S4 and/or a space-based probe; cross-correlation with galaxy surveys allows precise tomographic measurements of clustering as a function of redshift.

If the anomalies suggested in Fig. 28.3 are real, then the experiments of the 2020s will map out their redshift, scale, and environment dependence in great detail, providing detailed empirical constraints on dynamical dark energy or modified gravity models. If these tensions dissipate with improved measurements, then the experiments of the 2020s will achieve much more stringent tests of the ΛCDM paradigm, with the potential to reveal deviations that are still within the statistical uncertainties of current data. The critical clue to the origin of cosmic acceleration could also come from a surprising direction, such as laboratory, solar-system, or gravitational wave tests that challenge GR, time variation of fundamental "constants," or anomalous behavior of gravity in some astronomical environments. Experimental advances along these multiple axes could confirm today's relatively simple, but frustratingly incomplete, "standard model" of cosmology, or they could force yet another radical revision in our understanding of energy, or gravity, or the spacetime structure of the Universe.

References

[1] A. Einstein, Sitzungsber. Preuss. Akad. Wiss. Berlin (Math. Phys.), 142 (1917).

[2] Ya. B. Zel'dovich, A. Krasinski and Ya. B. Zeldovich, Sov. Phys. Usp. **11**, 381 (1968), [Gen. Rel. Grav.40,1557(2008); Usp. Fiz. Nauk95,209(1968)].

[3] A. Friedman, Z. Phys. **10**, 377 (1922), [Gen. Rel. Grav.31,1991(1999)].

[4] G. Lemaître, Annales de la Societe Scietifique de Bruxelles **47**, 49 (1927).

[5] E. Hubble, Proc. Nat. Acad. Sci. **15**, 168 (1929).

[6] A. Einstein and W. de Sitter, Proc. Nat. Acad. Sci. **18**, 213 (1932).

[7] For background and definitions, see Big-Bang Cosmology – Sec. 22 of this *Review*.

[8] A. G. Riess *et al.* (Supernova Search Team), Astron. J. **116**, 1009 (1998), [arXiv:astro-ph/9805201].

[9] S. Perlmutter *et al.* (Supernova Cosmology Project), Astrophys. J. **517**, 565 (1999), [arXiv:astro-ph/9812133].

[10] P. de Bernardis *et al.* (Boomerang), Nature **404**, 955 (2000), [arXiv:astro-ph/0004404].

[11] S. Hanany *et al.*, Astrophys. J. **545**, L5 (2000), [arXiv:astro-ph/0005123].

[12] D. H. Weinberg *et al.*, Phys. Rept. **530**, 87 (2013), [arXiv:1201.2434].

[13] C. Wetterich, Nucl. Phys. **B302**, 668 (1988), [arXiv:1711.03844].

[14] A. Joyce *et al.*, Phys. Rept. **568**, 1 (2015), [arXiv:1407.0059].

[15] S. M. Carroll *et al.*, Phys. Rev. **D70**, 043528 (2004), [arXiv:astro-ph/0306438].

[16] G. R. Dvali, G. Gabadadze and M. Porrati, Phys. Lett. **B485**, 208 (2000), [hep-th/0005016].

[17] C.M. Will, Living Reviews in Relativity, **9**, 3 (2006). See also the chapter on Experimental Tests of Gravitational Theory — in this *Review*.

[18] J. Wang, L. Hui and J. Khoury, Phys. Rev. Lett. **109**, 241301 (2012), [arXiv:1208.4612].

[19] M. Fairbairn and A. Goobar, Phys. Lett. **B642**, 432 (2006), [arXiv:astro-ph/0511029]; Y.-S. Song, I. Sawicki and W. Hu, Phys. Rev. **D75**, 064003 (2007), [arXiv:astro-ph/0606286]; C. Blake *et al.*, Mon. Not. Roy. Astron. Soc. **415**, 2876 (2011), [arXiv:1104.2948].

[20] T. Baker *et al.*, Phys. Rev. Lett. **119**, 25, 251301 (2017), [arXiv:1710.06394].

[21] E. V. Linder, Phys. Rev. **D72**, 043529 (2005), [arXiv:astro-ph/0507263].

[22] This is essentially the FoM proposed in the Dark Energy Task Force (DETF) report, A. Albrecht *et al.*, `astro-ph/0609591`,though they based their FoM on the area of the 95 in the $w_0 - w_a$ plane.

[23] T. Baker *et al.*, Rev. Mod. Phys. **93**, 1, 015003 (2021), [arXiv:1908.03430].

[24] For high accuracy, the impact of acoustic oscillations must be computed with a full Boltzmann code, but the simple integral for r_s captures the essential physics and the scaling with cosmological parameters.

[25] R. A. Sunyaev and Ya. B. Zeldovich, Astrophys. Space Sci. **7**, 3 (1970).

[26] D. Weinberg *et al.* (2013), [arXiv:1309.5380].

[27] C. Alcock and B. Paczynski, Nature **281**, 358 (1979).

[28] T. M. C. Abbott *et al.* (DES) (2021), [arXiv:2105.13549].

[29] T. M. C. Abbott *et al.* (DES), Astrophys. J. **872**, 2, L30 (2019), [arXiv:1811.02374].

[30] M. Asgari *et al.* (KiDS), Astron. Astrophys. **645**, A104 (2021), [arXiv:2007.15633].

[31] C. Heymans *et al.*, Astron. Astrophys. **646**, A140 (2021), [arXiv:2007.15632].

[32] C. Hikage *et al.* (HSC), Publ. Astron. Soc. Jap. **71**, 2, Publications of the Astronomical Society of Japan, Volume 71, Issue 2, April 2019, 43, https://doi.org/10.1093/pasj/psz010 (2019), [arXiv:1809.09148].

[33] T. Hamana *et al.*, Publ. Astron. Soc. Jap. **72**, 1, Publications of the Astronomical Society of Japan, Volume 72, Issue 1, February 2020, 16, https://doi.org/10.1093/pasj/psz138 (2020), [arXiv:1906.06041].

[34] B. Jain *et al.* (2015), [arXiv:1501.07897].

[35] W. L. Freedman *et al.* (HST), Astrophys. J. **553**, 47 (2001), [arXiv:astro-ph/0012376].

[36] N. Aghanim *et al.* (Planck) (2018), [arXiv:1807.06209].

[37] M. Betoule *et al.*, Astron. & Astrophys. **568**, 22 (2014).

[38] S. Alam *et al.* (eBOSS), Phys. Rev. D **103**, 8, 083533 (2021), [arXiv:2007.08991].

[39] M. Sullivan *et al.* (SNLS), Astrophys. J. **737**, 102 (2011), [arXiv:1104.1444].

[40] N. Suzuki *et al.* (Supernova Cosmology Project), Astrophys. J. **746**, 85 (2012), [arXiv:1105.3470].

[41] D. M. Scolnic *et al.*, Astrophys. J. **859**, 2, 101 (2018), [arXiv:1710.00845].

[42] S. Alam *et al.* (BOSS), Mon. Not. Roy. Astron. Soc. **470**, 3, 2617 (2017), [arXiv:1607.03155].

[43] F. Beutler *et al.*, Mon. Not. Roy. Astron. Soc. **416**, 3017 (2011), [arXiv:1106.3366].

Downloaded from https://academic.oup.com/ptep/article/2022/8/083C01/6651666 by KIT Library user on 27 September 2022

[44] A. J. Ross *et al.*, Mon. Not. Roy. Astron. Soc. **449**, 1, 835 (2015), [arXiv:1409.3242].

[45] E. Aubourg *et al.*, Phys. Rev. **D92**, 12, 123516 (2015), [arXiv:1411.1074].

[46] A. G. Riess *et al.*, Astrophys. J. Lett. **908**, 1, L6 (2021), [arXiv:2012.08534].

[47] W.L. Friedman, Astron. J. **882** (2019) 34.

[48] S. Birrer *et al.*, Astron. Astrophys. **643**, A165 (2020), [arXiv:2007.02941].

[49] K. C. Wong *et al.* (2019), [arXiv:1907.04869].

[50] V. Poulin *et al.*, Phys. Rev. Lett. **122**, 22, 221301 (2019), [arXiv:1811.04083].

[51] L. F. Secco *et al.* (DES) (2021), [arXiv:2105.13544].

[52] R. Mandelbaum *et al.*, Mon. Not. Roy. Astron. Soc. **432**, 1544 (2013), [arXiv:1207.1120].

[53] S. Singh *et al.*, Mon. Not. Roy. Astron. Soc. **491**, 1, 51 (2020), [arXiv:1811.06499].

[54] B. D. Wibking *et al.*, Mon. Not. Roy. Astron. Soc. **492**, 2, 2872 (2020), [arXiv:1907.06293].

[55] A. Leauthaud *et al.*, Mon. Not. Roy. Astron. Soc. **467**, 3, 3024 (2017), [arXiv:1611.08606].

[56] J. U. Lange *et al.*, Mon. Not. Roy. Astron. Soc. **488**, 4, 5771 (2019), [arXiv:1906.08680].

[57] A. Krolewski, S. Ferraro and M. White (2021), [arXiv:2105.03421].

[58] N. Aghanim *et al.* (Planck) (2018), [arXiv:1807.06210].

[59] A. Lewis and A. Challinor, Phys. Rept. **429**, 1 (2006), [arXiv:astro-ph/0601594].

[60] C. García-García *et al.* (2021), [arXiv:2105.12108].

Downloaded from https://academic.oup.com/ptep/article/2022/8/083C01/6651666 by KIT Library user on 27 September 2022

29. Cosmic Microwave Background

Revised August 2021 by D. Scott (U. of British Columbia) and G.F. Smoot (HKUST; UC Berkeley; LBNL; DIPC; Paris U.).

29.1 Introduction

The energy content in electromagnetic radiation from beyond our Galaxy is dominated by the cosmic microwave background (CMB), discovered in 1965 [1]. The spectrum of the CMB is well described by a blackbody function with $T = 2.7255\,\mathrm{K}$. This spectral form is a main supporting pillar of the hot Big Bang model for the Universe. The lack of any observed deviations from a blackbody spectrum constrains physical processes over cosmic history at redshifts $z \lesssim 10^7$ (see earlier versions of this review).

Currently the key CMB observable is the angular variation in temperature (or intensity) correlations, and to a growing extent polarization [2]. Since the first detection of these anisotropies by the Cosmic Background Explorer (*COBE*) satellite in 1992 [3], there has been intense activity to map the sky at increasing levels of sensitivity and angular resolution by ground-based and balloon-borne measurements. These were joined in 2003 by the first results from NASA's Wilkinson Microwave Anisotropy Probe (*WMAP*) [4], which were improved upon by analyses of data added every 2 years, culminating in the 9-year results [5]. In 2013 we had the first results [6] from the third generation CMB satellite, ESA's *Planck* mission [7], which were enhanced by results from the 2015 *Planck* data release [8, 9], and then the final 2018 *Planck* data release [10, 11]. Additionally, CMB anisotropies have been extended to smaller angular scales by ground-based experiments, particularly the Atacama Cosmology Telescope (ACT) [12] and the South Pole Telescope (SPT) [13]. Together these observations have led to a stunning confirmation of the 'Standard Model of Cosmology.' In combination with other astrophysical data, the CMB anisotropy measurements place quite precise constraints on a number of cosmological parameters, and have launched us into an era of precision cosmology. With the CMB now having been studied for more than half a century, the program to map temperature anisotropies is effectively wrapping up, and attention is increasingly focussing on polarization measurements as the future arena in which to test fundamental physics.

29.2 CMB Spectrum

It is well-known that the spectrum of the microwave background is very precisely that of blackbody radiation, whose temperature evolves with redshift as $T(z) = T_0(1+z)$ in an expanding Universe. As a direct test of its cosmological origin, this relationship has been tested by measuring the strengths of emission and absorption lines in high-redshift systems [14].

Measurements of the spectrum are consistent with a blackbody distribution over more than three decades in frequency (there is a claim by ARCADE [15] of a possible unexpected extragalactic emission signal at low frequency, but the interpretation is debated [16]). All viable cosmological models predict a very nearly Planckian spectrum to within the current observational limits. Because of this, measurements of deviations from a blackbody spectrum have received little attention in recent years, with only a few exceptions. However, that situation will eventually change, since proposed experiments [17] have the potential to dramatically improve the constraints on energy release in the early Universe. It now seems feasible to probe spectral distortion mechanisms that are *required* in the standard picture, such as those arising from the damping and dissipation of relatively small-scale primordial perturbations, or the average effect of inverse Compton scattering. A more ambitious goal would be to reach the precision needed to detect the residual lines from the cosmological recombination of hydrogen and helium and hence test whether conditions at $z \gtrsim 1000$ accurately follow those in the standard picture [18].

29.3 Description of CMB Anisotropies

Observations show that the CMB contains temperature anisotropies at the 10^{-5} level and polarization anisotropies at the 10^{-6} (and lower) level, over a wide range of angular scales. These anisotropies are usually expressed using a spherical harmonic expansion of the CMB sky:

$$T(\theta,\phi) = \sum_{\ell m} a_{\ell m} Y_{\ell m}(\theta,\phi) \tag{29.1}$$

(with the linear polarization pattern written in a similar way using the so-called spin-2 spherical harmonics). Increasing angular resolution requires that the expansion goes to higher multipoles. Because there are only very weak phase correlations seen in the CMB sky and since we notice no preferred direction, the vast majority of the cosmological information is contained in the temperature 2-point function, *i.e.*, the variance as a function only of angular separation. Equivalently, the anisotropy power per unit $\ln \ell$ is $\ell \sum_m |a_{\ell m}|^2 / 4\pi$.

29.3.1 *The Monopole*

The CMB has a mean temperature of $T_\gamma = 2.7255 \pm 0.0006\,\mathrm{K}$ (1σ) [19], which can be considered as the monopole component of CMB maps, a_{00}. Since all mapping experiments involve difference measurements, they are insensitive to this average level; monopole measurements can only be made with absolute temperature devices, such as the FIRAS instrument on the *COBE* satellite [20]. The measured kT_γ is equivalent to $0.234\,\mathrm{meV}$ or $4.60 \times 10^{-10}\, m_e c^2$. A blackbody of the measured temperature has a number density $n_\gamma = (2\zeta(3)/\pi^2)\, T_\gamma^3 \simeq 411\,\mathrm{cm}^{-3}$, energy density $\rho_\gamma = (\pi^2/15)\, T_\gamma^4 \simeq 4.64 \times 10^{-34}\,\mathrm{g\,cm}^{-3} \simeq 0.260\,\mathrm{eV\,cm}^{-3}$, and a fraction of the critical density $\Omega_\gamma \simeq 5.38 \times 10^{-5}$.

29.3.2 *The Dipole*

The largest anisotropy is in the $\ell = 1$ (dipole) first spherical harmonic, with amplitude $3.3621 \pm 0.0010\,\mathrm{mK}$ [10]. The dipole is interpreted to be the result of the Doppler boosting of the monopole caused by the Solar System motion relative to the nearly isotropic blackbody field, as broadly confirmed by measurements of the radial velocities of local galaxies (*e.g.*, Ref. [21]); the intrinsic part of the signal is expected to be 2 orders of magnitude smaller (and fundamentally difficult to distinguish). The motion of an observer with velocity $\beta \equiv v/c$ relative to an isotropic Planckian radiation field of temperature T_0 produces a Lorentz-boosted temperature pattern

$$\begin{aligned} T(\theta) &= T_0 (1-\beta^2)^{1/2} / (1 - \beta\cos\theta) \\ &\simeq T_0 \left[1 + \beta\cos\theta + \left(\beta^2/2\right)\cos 2\theta + \mathrm{O}\left(\beta^3\right) \right] . \end{aligned} \tag{29.2}$$

At every point in the sky, one observes a blackbody spectrum, with temperature $T(\theta)$. The spectrum of the dipole has been confirmed to be the differential of a blackbody spectrum [22]. At higher order there are additional effects arising from aberration and from modulation of the anisotropy pattern, which have also been observed [23].

The implied velocity for the Solar System barycenter is $v = 369.82 \pm 0.11\,\mathrm{km\,s}^{-1}$, assuming a value $T_0 = T_\gamma$, towards $(l, b) = (264.021^\circ \pm 0.011^\circ, 48.253^\circ \pm 0.005^\circ)$ [10]. Such a Solar System motion implies a velocity for the Galaxy and the Local Group of galaxies relative to the CMB. The derived value is $v_{\mathrm{LG}} = 620 \pm 15\,\mathrm{km\,s}^{-1}$ towards $(l, b) = (271.9^\circ \pm 2.0^\circ, 29.6^\circ \pm 1.4^\circ)$ [10], where most of the error comes from uncertainty in the velocity of the Solar System relative to the Local Group.

The dipole is a frame-dependent quantity, and one can thus determine the 'CMB frame' (in some sense this is a special frame) as that in which the CMB dipole would be zero. Any velocity of the receiver relative to the Earth and the Earth around the Sun is removed for the purposes of CMB anisotropy studies, while our velocity relative to the Local Group of galaxies and the Local Group's motion relative to the CMB frame are normally removed for cosmological studies. The dipole is now routinely used as a primary calibrator for mapping experiments, either via the time-varying orbital motion of the Earth, or through the cosmological dipole measured by satellite experiments.

29.3.3 *Higher-Order Multipoles*

The variations in the CMB temperature maps at higher multipoles ($\ell \geq 2$) are interpreted as being mostly the result of per-

Downloaded from https://academic.oup.com/ptep/article/2022/8/083C01/6651666 by KIT Library user on 27 September 2022

turbations in the density of the early Universe, manifesting themselves at the epoch of the last scattering of the CMB photons. In the hot Big Bang picture, the expansion of the Universe cools the plasma so that by a redshift $z \simeq 1100$ (with little dependence on the details of the model), the hydrogen and helium nuclei can bind electrons into neutral atoms, a process usually referred to as 'recombination' [24]. Before this epoch, the CMB photons were tightly coupled to the baryons, while afterwards they could freely stream towards us. By measuring the $a_{\ell m}$s we are thus learning directly about physical conditions in the early Universe.

A statistically-isotropic sky means that all ms are equivalent, *i.e.*, there is no preferred axis, so that the temperature correlation function between two positions on the sky depends only on angular separation and not orientation. Together with the assumption of Gaussian statistics (*i.e.*, no correlations between the modes), the 2-point function of the temperature field (or equivalently the power spectrum in ℓ) then fully characterizes the anisotropies. The power summed over all ms at each ℓ is $(2\ell+1)C_\ell/(4\pi)$, where $C_\ell \equiv \left\langle |a_{\ell m}|^2 \right\rangle$. Thus, averages of $a_{\ell m}$s over m can be used as estimators of the C_ℓs to constrain their expectation values, which are the quantities predicted by a theoretical model. For an idealized full-sky observation, the variance of each measured C_ℓ (*i.e.*, the variance of the variance) is $[2/(2\ell+1)]C_\ell^2$. This sampling uncertainty (known as 'cosmic variance') comes about because each C_ℓ is χ^2 distributed with $(2\ell+1)$ degrees of freedom for our observable volume of the Universe. For fractional sky coverage, $f_{\rm sky}$, this variance is increased by $1/f_{\rm sky}$ and the modes become partially correlated.

It is important to understand that theories predict the expectation value of the power spectrum, whereas our sky is a single realization. Hence, the cosmic variance is an unavoidable source of uncertainty when constraining models; it dominates the scatter at lower ℓs, while the effects of instrumental noise and resolution dominate at higher ℓs [25].

Theoretical models generally predict that the $a_{\ell m}$ modes are Gaussian random fields to high precision, matching the empirical tests, *e.g.*, standard slow-roll inflation's non-Gaussian contribution is expected to be at least an order of magnitude below current observational limits [26]. Although non-Gaussianity of various forms is possible in early Universe models, tests show that Gaussianity is an extremely good simplifying approximation [27]. The only current indications of any non-Gaussianity or statistical anisotropy are some relatively weak signatures at large scales, seen in both *WMAP* [28] and *Planck* data [29], but not of high enough significance to reject the simplifying assumption. Nevertheless, models that deviate from the inflationary slow-roll conditions can have measurable non-Gaussian signatures. So while the current observational limits make the power spectrum the dominant probe of cosmology, it is worth noting that higher-order correlations are becoming a tool for constraining otherwise viable theories.

29.3.4 *Angular Resolution and Binning*

There is no one-to-one conversion between multipole ℓ and the angle subtended by a particular spatial scale projected onto the sky. However, crudely speaking, a single spherical harmonic $Y_{\ell m}$ corresponds to angular variations of $\theta \sim \pi/\ell$. CMB maps contain anisotropy information from the size of the map (or in practice some fraction of that size) down to the beam-size of the instrument, σ (the standard deviation of the beam, in radians). One can think of the effect of a Gaussian beam as rolling off the power spectrum with the function $\mathrm{e}^{-\ell(\ell+1)\sigma^2}$.

For less than full sky coverage, the ℓ modes become correlated. Hence, experimental results are usually quoted as a series of 'band powers,' defined as estimators of $\ell(\ell+1)C_\ell/2\pi$ over different ranges of ℓ. Because of the strong foreground signals in the Galactic plane, even 'all-sky' surveys, such as *WMAP* and *Planck*, involve a cut sky. The amount of binning required to obtain uncorrelated estimates of power also depends on the map size.

29.4 Cosmological Parameters

The current 'Standard Model' of cosmology contains around 10 free parameters, only six of which are required to have non-null values (see The Cosmological Parameters—Sec. 25 of this *Review*). The basic framework is the Friedmann-Robertson-Walker (FRW) metric (*i.e.*, a Universe that is approximately homogeneous and isotropic on large scales), with density perturbations laid down at early times and evolving into today's structures (see Big-Bang cosmology—Sec. 22 of this *Review*). The most general possible set of density variations is a linear combination of an adiabatic density perturbation and some isocurvature perturbations. Adiabatic means that there is no change to the entropy per particle for each species, *i.e.*, $\delta\rho/\rho$ for matter is $(3/4)\delta\rho/\rho$ for radiation. Isocurvature means that the set of individual density perturbations adds to zero, for example, matter perturbations compensate radiation perturbations so that the total energy density remains unperturbed, *i.e.*, $\delta\rho$ for matter is $-\delta\rho$ for radiation. These different modes give rise to distinct (temporal) phases during growth, with those of the adiabatic scenario being fully consistent with the data. Models that generate mainly isocurvature type perturbations (such as most topological defect scenarios) are not viable. However, an admixture of the adiabatic mode with up to 1.7% isocurvature contribution (depending on details of the mode) is still allowed [30].

29.4.1 *Initial Condition Parameters*

Within the adiabatic family of models, there is, in principle, a free function describing the variation of comoving curvature perturbations, $\mathcal{R}(\mathbf{x}, t)$. The great virtue of $\mathcal{R}$ is that, on large scales, it is constant in time on super-horizon scales for a purely adiabatic perturbation. There are physical reasons to anticipate that the variance of these perturbations will be described well by a power law in scale, *i.e.*, in Fourier space $\left\langle |\mathcal{R}|_k^2 \right\rangle \propto k^{n_{\rm s}-4}$, where k is wavenumber and $n_{\rm s}$ is the spectral index as usually defined. So-called 'scale-invariant' initial conditions (meaning gravitational potential fluctuations that are independent of k) correspond to $n_{\rm s} = 1$. In inflationary models [31] (see Inflation—Sec. 23 of this *Review*), perturbations are generated by quantum fluctuations, which are set by the energy scale of inflation, together with the slope and higher derivatives of the inflationary potential. One generally expects that the Taylor series expansion of $\ln \mathcal{R}_k(\ln k)$ has terms of steadily decreasing size. For the simplest models, there are thus two parameters describing the initial conditions for density perturbations, namely the amplitude and slope of the power spectrum. These can be explicitly defined, for example, through

$$\mathcal{P}_{\mathcal{R}}^2 \equiv k^3 \left\langle |\mathcal{R}|_k^2 \right\rangle / 2\pi^2 \simeq A_{\rm s}\,(k/k_0)^{n_{\rm s}-1}\,, \qquad (29.3)$$

with $A_{\rm s} \equiv \mathcal{P}_{\mathcal{R}}^2(k_0)$ and $k_0 = 0.05\,\mathrm{Mpc}^{-1}$, say. There are other equally valid definitions of the amplitude parameter (see also Secs. 22, 23, and 25 of this *Review*), and we caution that the relationships between some of them can be cosmology-dependent. In slow-roll inflationary models, this normalization is proportional to the combination $V^3/(V')^2$, for the inflationary potential $V(\phi)$. The slope $n_{\rm s}$ also involves V'', and so the combination of $A_{\rm s}$ and $n_{\rm s}$ can constrain potentials.

Inflation generates tensor (gravitational wave) modes, as well as scalar (density perturbation) modes. This fact introduces another parameter, measuring the amplitude of a possible tensor component, or equivalently the ratio of the tensor to scalar contributions. The tensor amplitude is $A_{\rm t} \propto V$, and thus one expects a larger gravitational wave contribution in models where inflation happens at higher energies. The tensor power spectrum also has a slope, often denoted $n_{\rm t}$, but since this seems unlikely to be measured in the near future (and there is also a consistency relation with tensor amplitude), it is sufficient for now to focus only on the amplitude of the gravitational wave component. It is most common to define the tensor contribution through r, the ratio of tensor to scalar perturbation spectra at some fixed value of k (*e.g.*, $k = 0.002\,\mathrm{Mpc}^{-1}$ or $k = 0.05\,\mathrm{Mpc}^{-1}$, although it was historically defined in terms of the ratio of contributions at $\ell = 2$). Different inflationary potentials will lead to different predictions, *e.g.*, for 50 e-folds, $\lambda\phi^4$ inflation gives $r = 0.32$ and $m^2\phi^2$ inflation gives $r = 0.16$ (both now strongly disfavored by the data), while other models can have arbitrarily small values of r. In any case, whatever the specific definition, and whether they come from inflation or something else, the 'initial conditions' give rise to a minimum of three parameters, $A_{\rm s}$, $n_{\rm s}$, and r.

Downloaded from https://academic.oup.com/ptep/article/2022/8/083C01/6651666 by KIT Library user on 27 September 2022

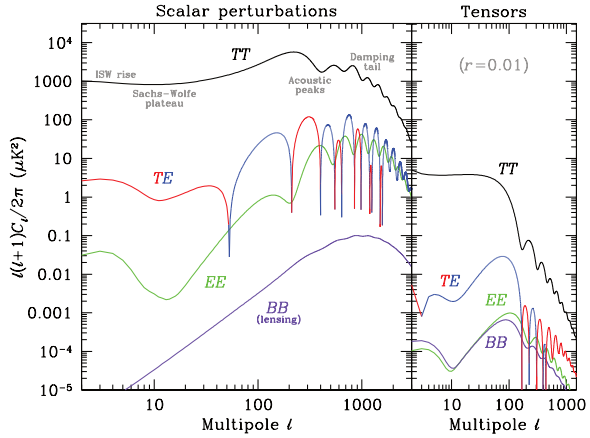

Figure 29.1: Theoretical CMB anisotropy power spectra, using the best-fitting ΛCDM model from *Planck*, calculated using `CAMB`. The panel on the left shows the theoretical expectation for scalar perturbations, while the panel on the right is for tensor perturbations, with an amplitude set to $r = 0.01$ for illustration. Note that the horizontal axis is logarithmic here. For the well-measured scalar TT spectrum, the regions, each covering roughly a decade in ℓ, are labeled as in the text: the ISW rise; Sachs-Wolfe plateau; acoustic peaks; and damping tail. The TE cross-correlation power spectrum changes sign, indicated here by plotting the absolute value, but switching color for the negative parts.

29.4.2 *Background Cosmology Parameters*

The FRW cosmology requires an expansion parameter (the Hubble constant, H_0, often represented through $H_0 = 100\,h\,\mathrm{km\,s^{-1}Mpc^{-1}}$) and several parameters to describe the matter and energy content of the Universe. These are usually given in terms of the critical density, *i.e.*, for species 'x,' $\Omega_\mathrm{x} \equiv \rho_\mathrm{x}/\rho_\mathrm{crit}$, where $\rho_\mathrm{crit} \equiv 3H_0^2/8\pi G$. Since physical densities $\rho_\mathrm{x} \propto \Omega_\mathrm{x} h^2 \equiv \omega_\mathrm{x}$ are what govern the physics of the CMB anisotropies, it is these ωs that are best constrained by CMB data. In particular, CMB observations constrain $\Omega_\mathrm{b}h^2$ for baryons and $\Omega_\mathrm{c}h^2$ for cold dark matter (with $\rho_\mathrm{m} = \rho_\mathrm{c} + \rho_\mathrm{b}$ for the sum).

The contribution of a cosmological constant Λ (or other form of dark energy, see Dark Energy—Sec. 28) is usually included, together with a parameter that quantifies the curvature, $\Omega_K \equiv 1 - \Omega_\mathrm{tot}$, where $\Omega_\mathrm{tot} = \Omega_\mathrm{m} + \Omega_\Lambda$. The radiation content, while in principle a free parameter, is precisely enough determined by the measurement of T_γ that it can be considered fixed, and makes a $< 10^{-4}$ contribution to Ω_tot today.

Astrophysical processes at relatively low redshift can also affect the C_ℓs, with a particularly significant effect coming through reionization. The Universe became reionized at some redshift z_i, long after recombination, affecting the CMB through the integrated Thomson scattering optical depth:

$$\tau = \int_0^{z_\mathrm{i}} \sigma_\mathrm{T} n_\mathrm{e}(z) \frac{dt}{dz} dz, \tag{29.4}$$

where σ_T is the Thomson cross-section, $n_\mathrm{e}(z)$ is the number density of free electrons (which depends on astrophysics), and dt/dz is fixed by the background cosmology. In principle, τ can be determined from the small-scale matter power spectrum, together with the physics of structure formation and radiative feedback processes; however, this is a sufficiently intractable calculation that in practice τ needs to be considered as a free parameter.

Thus, we have eight basic cosmological parameters, namely A_s, n_s, r, h, $\Omega_\mathrm{b}h^2$, $\Omega_\mathrm{c}h^2$, Ω_tot, and τ. One can add additional parameters to this list, particularly when using the CMB in combination with other data sets. The next most relevant ones might be: $\Omega_\nu h^2$, the massive neutrino contribution; w ($\equiv p/\rho$), the equation of state parameter for the dark energy; and $dn_\mathrm{s}/d\ln k$, measuring deviations from a constant spectral index. To these 11 one could of course add further parameters describing additional physics, such as details of the reionization process, features in the initial power spectrum, a sub-dominant contribution of isocurvature modes, *etc.*

As well as these underlying parameters, there are other (dependent) quantities that can be obtained from them. Such derived parameters include the actual Ωs of the various components (*e.g.*, Ω_m), the variance of density perturbations at particular scales (*e.g.*, σ_8), the angular scale of the sound horizon (θ_*), the age of the Universe today (t_0), the age of the Universe at recombination, reionization, *etc.* (see The Cosmological Parameters—Sec. 25).

29.5 Physics of Anisotropies

The cosmological parameters affect the anisotropies through the well understood physics of the evolution of linear perturbations within a background FRW cosmology. There are very effective, fast, and publicly-available software codes for computing the CMB temperature, polarization, and matter power spectra, *e.g.*, `CMBFAST` [32], `CAMB` [33], and `CLASS` [34]. These have been tested over a wide range of cosmologies and are considered to be accurate to much better than the 1% level [35], so that numerical errors are less than 10% of the parameter uncertainties for *Planck* [6].

For pedagogical purposes, it is easiest to focus on the temperature anisotropies, before moving to the polarization power spectra. A description of the physics underlying the C_ℓ^{TT}s can be separated into four main regions (the first two combined below), as shown in the top left part of Fig. 29.1.

29.5.1 *The ISW Rise,* $\ell \lesssim 10$*, and Sachs-Wolfe Plateau,* $10 \lesssim \ell \lesssim 100$

The horizon scale (or more precisely, the angle subtended by the Hubble radius) at last scattering corresponds to $\ell \simeq 100$. Anisotropies at larger scales have not evolved significantly, and hence directly reflect the 'initial conditions.' Temperature variations are $\delta T/T = -(1/5)\mathcal{R}(\mathbf{x}_\mathrm{LSS}) \simeq (1/3)\delta\phi/c^2$, where $\delta\phi$ is the perturbation to the gravitational potential, evaluated on the last-scattering surface (LSS). This is a result of the combination of gravitational redshift and intrinsic temperature fluctuations, and is usually referred to as the Sachs-Wolfe effect [36].

Assuming that a nearly scale-invariant spectrum of curvature (and corresponding density) perturbations was laid down at early times (*i.e.*, $n_\mathrm{s} \simeq 1$, meaning equal power per decade in k), then $\ell(\ell+1)C_\ell \simeq$ constant at low ℓs. This effect is hard to see unless the multipole axis is plotted logarithmically (as in Fig. 29.1, and part of Fig. 29.2).

Time variation of the potentials (*i.e.*, time-dependent metric perturbations) at late times leads to an upturn in the C_ℓs in the lowest several multipoles; any deviation from a total equation of state $w = 0$ has such an effect. So the dominance of the dark energy at low redshift (see Dark Energy—Sec. 28) makes the lowest ℓs rise above the plateau. This is usually called the integrated Sachs-Wolfe effect (or ISW rise), since it comes from the line integral of $\dot{\phi}$; it has been confirmed through correlations between the large-angle anisotropies and large-scale structure [37]. Specific models can also give additional contributions at low ℓ (*e.g.*, perturbations in the dark-energy component itself [38]), but typically these are buried in the cosmic variance.

In principle, the mechanism that produces primordial perturbations could generate scalar, vector, and tensor modes. However, the vector (vorticity) modes decay with the expansion of the Universe. The tensors (transverse trace-free perturbations to the metric) generate temperature anisotropies through the integrated effect of the locally-anisotropic expansion of space. Since the tensor modes also redshift away after they enter the horizon, they contribute only to angular scales above about 1° (see Fig. 29.1). Hence, some fraction of the low-ℓ signal could be due to a gravitational wave contribution, although small amounts of tensors are essentially impossible to discriminate from other effects that might raise the level of the plateau. Nevertheless, the tensors *can* be distinguished using polarization information (see Sec. 29.7).

29.5.2 *The Acoustic Peaks,* $100 \lesssim \ell \lesssim 1000$

On sub-degree scales, the rich structure in the anisotropy spectrum is the consequence of gravity-driven acoustic oscillations oc-

Downloaded from https://academic.oup.com/ptep/article/2022/8/083C01/6651666 by KIT Library user on 27 September 2022

curring before the atoms in the Universe became neutral [39]. Perturbations inside the horizon at last scattering have been able to evolve causally and produce anisotropy at the last-scattering epoch, which reflects this evolution. The frozen-in phases of these sound waves imprint a dependence on the cosmological parameters, which gives CMB anisotropies their great constraining power.

The underlying physics can be understood as follows. Before the Universe became neutral, the proton-electron plasma was tightly coupled to the photons, and these components behaved as a single 'photon-baryon fluid.' Perturbations in the gravitational potential, dominated by the dark-matter component, were steadily evolving. They drove oscillations in the photon-baryon fluid, with photon pressure providing most of the restoring force and baryons giving some additional inertia. The perturbations were quite small in amplitude, $\mathcal{O}(10^{-5})$, and so evolved linearly. That means each Fourier mode developed independently, and hence can be described as a driven harmonic oscillator, with frequency determined by the sound speed in the fluid. Thus, the fluid density underwent oscillations, giving time variations in temperature. These combine with a velocity effect, which is $\pi/2$ out of phase and has its amplitude reduced by the sound speed.

After the Universe recombined, the radiation decoupled from the baryons and could travel freely towards us. At that point, the (temporal) phases of the oscillations were frozen-in, and became projected on the sky as a harmonic series of peaks and troughs in power. The main peak is the mode that went through 1/4 of a period, reaching maximal compression. The even peaks are maximal *under*-densities, which are generally of smaller amplitude because the rebound has to fight against the baryon inertia. The troughs, which do not extend to zero power, are partially filled by the Doppler effect because they are at the velocity maxima.

The physical length scale associated with the peaks is the sound horizon at last scattering, which can be straightforwardly calculated. This length is projected onto the sky, leading to an angular scale that depends on the geometry of space, as well as the distance to last scattering. Hence, the angular position of the peaks is a sensitive probe of a particular combination of cosmological parameters. In fact, the angular scale, θ_*, is the most precisely measured observable, and hence is usually treated as an element of the cosmological parameter set.

One additional effect arises from reionization at redshift $z_{\rm i}$. A fraction of photons (τ) will be isotropically scattered at $z < z_{\rm i}$, partially erasing the anisotropies at angular scales smaller than those subtended by the Hubble radius at $z_{\rm i}$. This corresponds typically to ℓs above about 10, depending on the specific reionization model. The acoustic peaks are therefore reduced by a factor $e^{-2\tau}$ relative to the plateau.

These peaks were a clear theoretical prediction going back to about 1970 [40]. One can think of them as a snapshot of stochastic standing waves. Since the physics governing them is simple and their structure rich, one can see how they encode extractable information about the cosmological parameters. Their empirical existence started to become clear around 1994 [41], and the emergence, over the following decade, of a coherent series of acoustic peaks and troughs is a triumph of modern cosmology. This picture has received further confirmation with the detection in the power spectrum of galaxies (at redshifts $z \lesssim 1$) of the imprint of these same acoustic oscillations in the baryon component [42], as well as through detection of the expected oscillations in CMB polarization power spectra (see Sec. 29.7).

29.5.3 *The Damping Tail,* $\ell \gtrsim 1000$

The recombination process is not instantaneous, which imparts a thickness to the LSS. This leads to a damping of the anisotropies at the highest ℓs, corresponding to scales smaller than that subtended by this thickness. One can also think of the photon-baryon fluid as having imperfect coupling, so that there is diffusion between the two components, and hence the amplitudes of the oscillations decrease with time. These effects lead to a damping of the C_ℓs, sometimes called 'Silk damping' [43], which cuts off the anisotropies at multipoles above about 2000. So, although in principle it is possible to measure to ever smaller scales, this becomes increasingly difficult in practice.

29.5.4 *Gravitational Lensing Effects*

An extra effect at high ℓs comes from gravitational lensing, caused by structures at low redshift along the line of sight to the LSS. The C_ℓs are convolved with a smoothing function in a calculable way, partially flattening the peaks and troughs, generating a power-law tail at the highest multipoles, and complicating the polarization signal [44]. The expected effects of lensing on the CMB have been definitively detected through the 4-point function, which correlates temperature gradients and small-scale anisotropies (enabling a map of the lensing potential to be constructed [45]), as well as through the smoothing effect on the shape of the C_ℓs. Lensing is important because it gives an independent estimate of $A_{\rm s}$, breaking the parameter combination $A_{\rm s}{\rm e}^{-2\tau}$ that is largely degenerate in the temperature anisotropy power spectra. Lensing is an example of a 'secondary effect,' *i.e.*, the processing of anisotropies due to relatively nearby structures (see Sec. 29.8.2). Galaxies and clusters of galaxies give several such effects; all are expected to be of low amplitude, but are increasingly important at the highest ℓs. Such effects carry additional cosmological information (about evolving gravitational potentials in the low-redshift Universe) and are receiving more attention as experiments push to higher sensitivity and angular resolution. The lensing power spectrum can potentially constrain dark-energy evolution, while future measurements at high ℓ are a particularly sensitive probe of the sum of the neutrino masses [46].

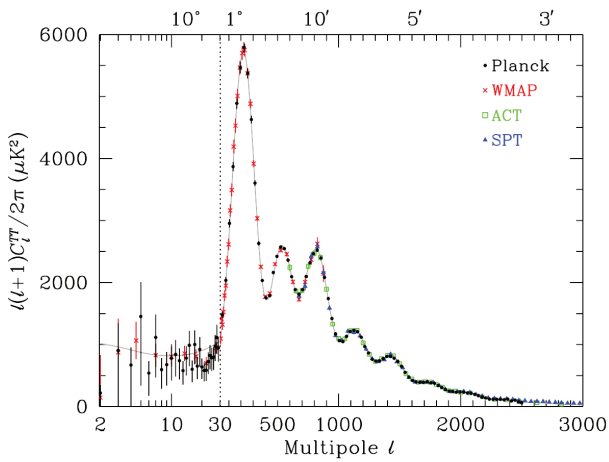

Figure 29.2: CMB temperature anisotropy band-power estimates from the *Planck*, *WMAP*, ACT, and SPT experiments. Note that the widths of the multipole bands vary between experiments and have not been plotted. This figure represents only a selection of the most recent available experimental results, and some points with large error bars have been omitted. At the higher multipoles these band-powers involve subtraction of particular foreground models, and so proper analysis requires simultaneous fitting of CMB and foregrounds over multiple frequencies. The horizontal axis here is logarithmic for the lowest multipoles, to show the Sachs-Wolfe plateau, and linear for the other multipoles. The acoustic peaks and damping region are very clearly observed, with no need for a theoretical line to guide the eye; however, the curve plotted is the best-fit *Planck* ΛCDM model.

29.6 Current Temperature Anisotropy Data

There has been a steady improvement in the quality of CMB data that has led to the development of the present-day cosmological model. The most robust constraints currently available come from *Planck* satellite [47,48] data (together with constraints from non-CMB cosmological data sets), although smaller-scale results from the ACT [49] and SPT [50] experiments are beginning to add useful constraining power. We plot power spectrum estimates from these experiments in Fig. 29.2, along with *WMAP* data [5] to show the consistency (see previous versions of this review for data from earlier experiments). Comparisons among data sets show consistency, both in maps and in derived power spectra (up

Downloaded from https://academic.oup.com/ptep/article/2022/8/083C01/6651666 by KIT Library user on 27 September 2022

to systematic uncertainties in the overall calibration for some experiments). This makes it clear that systematic effects are largely under control.

The band-powers shown in Fig. 29.2 are in very good agreement with a 'ΛCDM' model. As described earlier, several (at least seven) of the peaks and troughs are quite apparent. For details of how these estimates were arrived at, the strength of correlations between band-powers, and other information required to properly interpret them, the original papers should be consulted.

29.7 CMB Polarization

Thomson scattering of an anisotropic radiation field also generates linear polarization and the CMB is predicted to be polarized, at the level of roughly 5% of the temperature anisotropies [51]. Polarization is a spin-2 field on the sky, and the algebra of the modes in multipole space is strongly analogous to spin-orbit coupling in quantum mechanics [52]. The linear polarization pattern can be decomposed in a number of ways, with two quantities required for each pixel in a map, often given as the Q and U Stokes parameters. However, the most intuitive and physical decomposition is a geometrical one, splitting the polarization pattern into a part that comes from a divergence (often referred to as the 'E mode') and a part with a curl (called the 'B mode') [53]. More explicitly, the modes are defined in terms of second derivatives of the polarization amplitude, with the Hessian for the E modes having principal axes in the same sense as the polarization, while the B-mode pattern can be thought of as a 45° rotation of the E-mode pattern. Globally one sees that the E modes have $(-1)^\ell$ parity (like the spherical harmonics), while the B modes have $(-1)^{\ell+1}$ parity.

The existence of this linear polarization allows for six different cross-power spectra to be determined from data that measure the full temperature and polarization anisotropy information. Parity considerations make two of these zero, and we are left with four potential observables, C_ℓ^{TT}, C_ℓ^{TE}, C_ℓ^{EE}, and C_ℓ^{BB} (see Fig. 29.1). Because scalar perturbations have no handedness, the B-mode power spectrum can only be sourced by vectors or tensors. Moreover, since inflationary scalar perturbations give only E modes, while tensors generate roughly equal amounts of E and B, then the determination of a non-zero B-mode signal is a way to measure the gravitational-wave contribution (and thus potentially derive the energy scale of inflation). However, since the signal is expected to be rather weak, one must first eliminate the foreground contributions and other systematic effects down to very low levels. In addition, CMB lensing creates B modes from E modes, further complicating the extraction of a tensor signal.

Like with temperature, the polarization C_ℓs exhibit a series of acoustic peaks generated by the oscillating photon-baryon fluid. The main 'EE' power spectrum has peaks that are out of phase with those in the 'TT' spectrum because the polarization anisotropies are sourced by the fluid velocity. The 'TE' part of the polarization and temperature patterns comes from correlations between density and velocity perturbations on the last-scattering surface, which can be both positive and negative, and is of larger amplitude than the EE signal. There is no polarization Sachs-Wolfe effect, and hence no large-angle plateau. However, scattering during a recent period of reionization can create a polarization 'bump' at large angular scales.

Because the polarization anisotropies have only a small fraction of the amplitude of the temperature anisotropies, they took longer to detect. The first measurement of a polarization signal came in 2002 from the DASI experiment [54], which provided a convincing detection, confirming the general paradigm, but of low enough significance that it lent no real constraint to models. Despite dramatic progress since then, it is still the case that polarization data mainly support the basic paradigm, while reducing error bars on parameters by only around 20%. However, there are exceptions to this, specifically in the reionization optical depth, and the potential to constrain primordial gravitational waves. Moreover the situation is expected to change dramatically as more of the available polarization modes are measured.

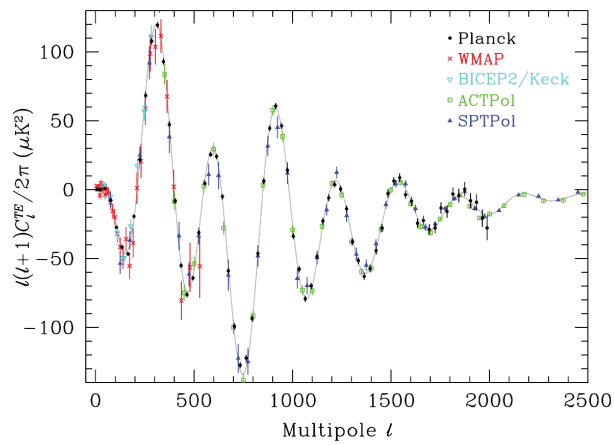

Figure 29.3: Cross-power spectrum band-powers of the temperature anisotropies and E-mode polarization signal from *Planck* (the low multipole data have been binned here), as well as *WMAP*, BICEP2/Keck, ACTPol, and SPTPol. The curve is the best fit to the *Planck* temperature, polarization, and lensing band-powers. Note that each data point is an average over a band of multipoles, and hence to compare in detail with a model one has to integrate the theoretical curve through the band.

29.7.1 *T–E Power Spectrum*

Since the T and E skies are correlated, one has to measure the TE power spectrum, as well as TT and EE, in order to extract all the cosmological information. This TE signal has now been mapped out extremely accurately by *Planck* [48], and these band-powers are shown in Fig. 29.3, along with those from *WMAP* [55] and BICEP2/Keck [56], with ACTPol [57] and SPTPol [58] extending to smaller angular scales. The anti-correlation at $\ell \simeq 150$ and the peak at $\ell \simeq 300$ were the first features to become distinct, but now a whole series of oscillations is clearly seen in this power spectrum (including at least six peaks and troughs [10]). The measured shape of the cross-correlation power spectrum provides supporting evidence for the general cosmological picture, as well as directly constraining the thickness of the last-scattering surface. Since the polarization anisotropies are generated in this scattering surface, the existence of correlations at angles above about a degree demonstrates that there were super-Hubble fluctuations at the recombination epoch. The sign of this correlation also confirms the adiabatic paradigm.

The overall picture of the source of CMB polarization and its oscillations has also been confirmed through tests that average the maps around both temperature hot spots and cold spots [59]. One sees precisely the expected patterns of radial and tangential polarization configurations, as well as the phase shift between polarization and temperature. This leaves no doubt that the oscillation picture is the correct one and that the polarization is coming from Thomson scattering at $z \simeq 1100$.

29.7.2 *E–E Power Spectrum*

Experimental band-powers for C_ℓ^{EE} from *Planck*, *WMAP*, BICEP2/Keck Array [56], ACTPol [57], and SPTPol [58] are shown in Fig. 29.4. Without the benefit of correlating with the temperature anisotropies (*i.e.*, measuring C_ℓ^{TE}), the polarization anisotropies are very weak and challenging to measure. Nevertheless, the oscillatory pattern is now well established and the data closely match the TT-derived theoretical prediction. In Fig. 29.4 one can clearly see the 'shoulder' expected at $\ell \simeq 140$, the first main peak at $\ell \simeq 400$ (corresponding to the first trough in C_ℓ^{TT}), and the series of oscillations that is out of phase with those of the temperature anisotropy power spectrum (including four or five peaks and troughs [10]).

Perhaps the most unique result from the polarization measurements is at the largest angular scales ($\ell < 10$) in C_ℓ^{TE} and C_ℓ^{EE}, where there is evidence for an excess signal (not visible in

Downloaded from https://academic.oup.com/ptep/article/2022/8/083C01/6651666 by KIT Library user on 27 September 2022

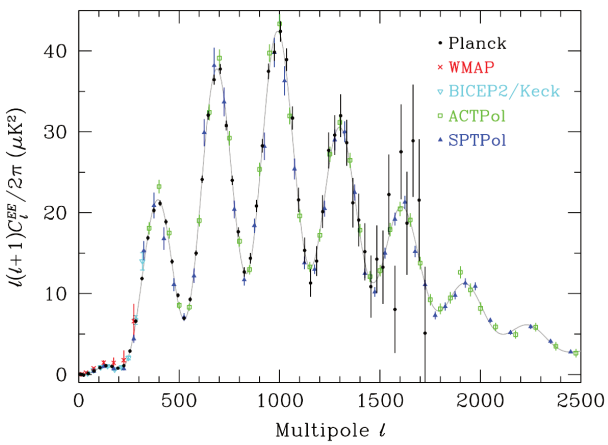

Figure 29.4: Power spectrum of E-mode polarization from *Planck*, together with *WMAP*, BICEP2/Keck, ACTPol, and SPTPol. Note that some band-powers with larger uncertainties have been omitted and that the unbinned *Planck* low-ℓ data have been binned here. Also plotted is the best-fit theoretical model from *Planck* temperature, polarization, and lensing data.

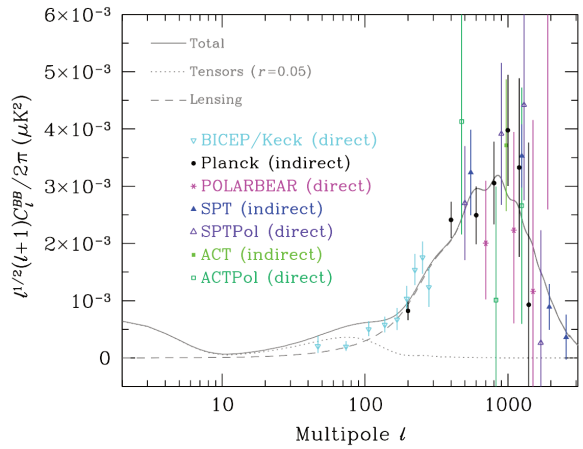

Figure 29.5: Power spectrum of B-mode polarization, including results from the BICEP2/BICEP3/Keck Array combined analysis, *Planck*, POLARBEAR, SPT, and ACT. Note that some of the measurements are direct estimates of B modes on the sky, while others are only sensitive to the lensing signal and come from combining E-mode and lensing potential measurements. Several earlier experiments reported upper limits, which are all off the top of this plot. A logarithmic horizontal axis is adopted here and the y-axis has been divided by a factor of $\sqrt{\ell}$ in order to show all three theoretically expected contributions: the low-ℓ reionization bump; the $\ell \simeq 100$ recombination peak; and the high-ℓ lensing signature. The dotted line is for a tensor (primordial gravitational wave) fraction $r = 0.05$, simply as an example, with all other cosmological parameters set at the best *Planck*-derived values, for which model the expected lensing B modes have also been shown with a dashed line.

Fig. 29.4) compared to that expected from the temperature power spectrum alone. This is precisely the signal anticipated from an early period of reionization, arising from Doppler shifts during the partial scattering at $z < z_{\rm i}$. The amplitude of the signal indicates that the first stars, presumably the source of the ionizing radiation, formed around $z \simeq 8$ (although the uncertainty is still quite large). Since this corresponds to a scattering optical depth $\tau \simeq 0.06$, then roughly 6% of CMB photons were re-scattered at the reionization epoch, with the other 94% last scattering at $z \simeq 1100$. However, estimates of the amplitude of this reionization excess have come down since the first measurements by *WMAP* (indicating that this is an extremely difficult measurement to make) and the latest *Planck* results have reduced the value further [11, 60].

29.7.3 *B–B Power Spectrum*

The expected amplitude of C_ℓ^{BB} is very small, and so measurements of this polarization curl-mode are extremely challenging. The first indication of the existence of the BB signal came from the detection of the expected conversion of E modes to B modes by gravitational lensing, through a correlation technique using the lensing potential and polarization measurements from SPT [61]. However, the real promise of B modes lies in the detection of primordial gravitational waves at larger scales. This tensor signature could be seen either in the 'recombination bump' at around $\ell = 100$ (caused by an ISW effect as gravitational waves redshift away at the last-scattering epoch) or the 'reionization bump' at $\ell \lesssim 10$ (from additional scattering at low redshifts).

Results from the BICEP2 experiment [62] in 2014 suggested a detection of the primordial B-mode signature around the recombination peak. BICEP2 mapped a small part of the CMB sky with the best sensitivity level reached at that time (below 100 nK), but at a single frequency. Higher frequency data from *Planck* indicated that much of the BICEP2 signal was due to dust within our Galaxy, and a combined analysis by the BICEP2, Keck Array, and *Planck* teams [63] indicated that the data are consistent with no primordial B modes. The current constraint from *Planck* data alone is $r < 0.069$ (95% at $k = 0.05\,{\rm Mpc}^{-1}$ [11, 60]) using all CMB power spectra, and this limit is reduced to $r < 0.044$ with the inclusion of BICEP2/Keck Array data [60, 64]. The most constraining limit is $r < 0.036$ from a combination of BICEP2, Keck Array, and BICEP3 data, using *WMAP* and *Planck* maps to help remove foregrounds [65].

Several experiments are continuing to push down the sensitivity of B-mode measurements, motivated by the enormous importance of a future detection of this telltale signature of inflation (or other physics at the highest energies). A compilation of experimental results for C_ℓ^{BB} is shown in Fig. 29.5, coming from a combination of direct estimates of the B modes (BICEP2/BICEP3/Keck Array [65], POLARBEAR [66], SPTPol [67], and ACTPol [57]) and indirect determinations of the lensing B modes based on estimating the effect of measured lensing on measured E modes (*Planck* [68], SPT [61], and ACT [69]). Additional band-power estimates are expected from these and other experiments in the near future, with the Simons Observatory [70], the so-called 'Stage 4' CMB project [71] and the *LiteBIRD* satellite [72], holding great promise for pushing down to the $r \sim 0.001$ level.

29.7.4 *ϕ–ϕ Power Spectrum*

One further CMB observable that can be measured is the gravitational lensing deflection, leading to the construction of a map of the lensing potential. The latest *Planck* results [73] give a map that is detected at the 40σ level using a minimum-variance procedure from the 4-point function of temperature and polarization data. From this, estimates can be constructed of $C_\ell^{\phi\phi}$, the lensing-potential power spectrum, which is found to be consistent with predictions from the best-fit temperature and polarization model.

We can think of each sky pixel as possessing three independent quantities that can be measured, namely T, E, and ϕ (and potentially B, if that becomes detectable). Determining the constraining power comes down to counting $Y_{\ell m}$ modes [74], as well as appreciating that some modes help to break particular parameter degeneracies. We have only scratched the surface of CMB lensing so far, and it is expected that future small-scale experiments will be able to extract more of the cosmological information. Further constraints can also be derived on the lower-z Universe by cross-correlating CMB lensing with other cosmological tracers of large-scale structure. Additionally, small-scale lensing, combined with E-mode measurements, can be used to 'delens' CMB B-mode data, which will be important for pushing down into the $r \lesssim 0.01$ regime [75].

Downloaded from https://academic.oup.com/ptep/article/2022/8/083C01/6651666 by KIT Library user on 27 September 2022

29.8 Complications

There are a number of issues that complicate the interpretation of CMB anisotropy data (and are considered to be *signal* by many astrophysicists), some of which we sketch out below.

29.8.1 *Foregrounds*

The microwave sky contains significant emission from our Galaxy and from extragalactic sources [76]. Fortunately, the frequency dependence of these various sources is in general substantially different from that of the CMB anisotropy signals. The combination of Galactic synchrotron, bremsstrahlung, and dust emission reaches a minimum at a frequency of roughly 100 GHz (or wavelength of about 3 mm). As one moves to greater angular resolution, the minimum moves to slightly higher frequencies, but becomes more sensitive to unresolved (point-like) sources.

At frequencies around 100 GHz, and for portions of the sky away from the Galactic plane, the foregrounds are typically 1 to 10% of the CMB anisotropies. By making observations at multiple frequencies, it is relatively straightforward to separate the various components and determine the CMB signal to the few per cent level. For greater sensitivity, it is necessary to use the spatial information and statistical properties of the foregrounds to separate them from the CMB. Furthermore, at higher ℓs it is essential to carefully model extragalactic foregrounds, particularly the clustering of infrared-emitting galaxies, which dominate the measured power spectrum as we move into the damping tail.

The foregrounds for CMB polarization follow a similar pattern to those for temperature, but are intrinsically brighter relative to CMB anisotropies. *WMAP* showed that the polarized foregrounds dominate at large angular scales, and that they must be well characterized in order to be discriminated [77]. *Planck* has shown that it is possible to characterize the foreground polarization signals, with synchrotron dominating at low frequencies and dust at high frequencies [78]. On smaller scales there are no strongly-polarized foregrounds, and hence it is in principle easier to measure foreground-free modes at high multipoles in polarization than in temperature. Although foreground contamination will no doubt become more complicated as we push down in sensitivity, making analysis more difficult, for the time being, foreground contamination is not a fundamental limit for CMB experiments.

29.8.2 *Secondary Anisotropies*

With increasingly precise measurements of the primary anisotropies, there is growing theoretical and observational interest in 'secondary anisotropies,' pushing experiments to higher angular resolution and sensitivity. These secondary effects arise from the processing of the CMB due to ionization history and the evolution of structure, including gravitational lensing (which was already discussed) and patchy reionization effects [79]. Additional information can thus be extracted about the Universe at $z \ll 1000$. This tends to be most effectively done through correlating CMB maps with other cosmological probes of structure. Secondary signals are also typically non-Gaussian, unlike the primary CMB anisotropies.

A secondary signal of great current interest is the Sunyaev-Zeldovich (SZ) effect [80], which is Compton scattering ($\gamma e \to \gamma' e'$) of the CMB photons by hot electrons in intergalactic plasma. This creates spectral distortions by transferring energy from the electrons to the photons. It is particularly important for clusters of galaxies, through which one observes a partially Comptonized spectrum, resulting in a decrement at radio wavelengths and an increment in the submillimeter.

The imprint on the CMB sky is of the form $\Delta T/T = y\, f(x)$, with the y parameter being the integral of Thomson optical depth times $kT_{\rm e}/m_{\rm e}c^2$ through the cluster, and $f(x)$ describing the frequency dependence. This is simply $x \coth(x/2) - 4$ for a non-relativistic gas (the electron temperature in a cluster is typically a few keV), where the dimensionless frequency $x \equiv h\nu/kT_\gamma$. As well as this 'thermal' SZ effect, there is also a smaller 'kinetic' effect due to the bulk motion of the cluster gas, giving $\Delta T/T \sim \tau(v/c)$, with either sign, but having the same spectrum as the primary CMB anisotropies.

A significant advantage in finding galaxy clusters via the SZ effect is that the signal is largely independent of redshift, so in principle clusters can be found to arbitrarily large distances. The SZ effect can be used to find and study individual clusters, and to obtain estimates of the Hubble constant. There is also the potential to constrain cosmological parameters, such as the clustering amplitude σ_8 and the equation of state of the dark energy, through counts of detected clusters as a function of redshift. The promise of the method has been realized through detections of clusters purely through the SZ effect by SPT [81], ACT [82], and *Planck* [83]. Results from *Planck* clusters [84] suggest a somewhat lower value of σ_8 than inferred from CMB anisotropies, but there are still systematic uncertainties that might encompass the difference, and a more recent analysis of SPT-detected clusters shows better agreement [85]. Further analysis of scaling relations among cluster properties should enable more robust cosmological constraints to be placed in future, so that we can understand whether this 'tension' might be a sign of new physics.

29.8.3 *Higher-order Statistics*

Although most of the CMB anisotropy information is contained in the power spectra, there will also be weak signals present in higher-order statistics. These can measure any primordial non-Gaussianity in the perturbations, as well as non-linear growth of the fluctuations on small scales and other secondary effects (plus residual foreground contamination of course). There are an infinite variety of ways in which the CMB could be non-Gaussian [26]; however, there is a generic form to consider for the initial conditions, where a quadratic contribution to the curvature perturbations is parameterized through a dimensionless number $f_{\rm NL}$. This weakly non-linear component can be constrained in several ways, the most popular being through measurements of the bispectrum (or 3-point function).

The constraints depend on the shape of the triangles in harmonic space, and it has become common to distinguish the 'local' or 'squeezed' configuration (in which one side is much smaller than the other two) from the 'equilateral' configuration. Other configurations are also relevant for specific theories, such as 'orthogonal' non-Gaussianity, which has positive correlations for $k_1 \simeq 2k_2 \simeq 2k_3$, and negative correlations for the equilateral configuration. The latest results from the *Planck* team [86] are $f_{\rm NL}^{\rm local} = 1 \pm 5$, $f_{\rm NL}^{\rm equil} = -26 \pm 47$, and $f_{\rm NL}^{\rm ortho} = -38 \pm 24$.

These results are consistent with zero, but are at a level that is now interesting for model predictions. The amplitude of $f_{\rm NL}$ expected is small, so that a detection of $f_{\rm NL} \gg 1$ would rule out all single-field, slow-roll inflationary models. It is still possible to improve upon these *Planck* results, and it certainly seems feasible that a measurement of primordial non-Gaussianity may yet be within reach. *Non*-primordial detections of non-Gaussianity from expected signatures have already been made. For example, the bispectrum and trispectrum contain evidence of gravitational lensing, the ISW effect, and Doppler boosting. For now the primordial signal is elusive, but should it be detected, then detailed measurements of non-Gaussianity will become a unique probe of inflationary-era physics. Because of that, much effort continues to be devoted to honing predictions and measurement techniques, with the expectation that we will need to go beyond the CMB (*e.g.*, 3D galaxy surveys) to dramatically improve the constraints.

29.8.4 *Anomalies*

Several features seen in the *Planck* data [29,59,87] confirm those found earlier with *WMAP* [28], showing mild deviations from a simple description of the sky; these are often referred to as 'anomalies.' One such feature is the lack of power in the multipole range $\ell \simeq 20$–30 [11,48]. Other examples involve the breaking of statistical anisotropy, caused by alignment of the lowest multipoles, as well as a somewhat excessive cold spot and a power asymmetry between hemispheres. No such feature is significant at more than the roughly 3σ level, and the importance of '*a posteriori*' statistics here has been emphasized by many authors. Since these effects are at large angular scales, where cosmic variance dominates, the results will not increase in significance with more data, although there is the potential for more sensitive polarization measurements to provide independent tests.

Downloaded from https://academic.oup.com/ptep/article/2022/8/083C01/6651666 by KIT Library user on 27 September 2022

29.9 Constraints on Cosmological Parameters

The most striking outcome of the last couple of decades of experimental results is that the standard cosmological paradigm continues to be in very good shape. A large amount of high-precision data on the power spectrum is adequately fit with fewer than 10 free parameters (and only six need non-trivial values). The framework is that of FRW models, which have nearly flat geometry, containing dark matter and dark energy, and with adiabatic perturbations having close to scale-invariant initial conditions.

Within this basic picture, the values of the cosmological parameters can be constrained. Of course, more stringent bounds can be placed on models that cover a restricted parameter space, *e.g.*, assuming that $\Omega_{\rm tot} = 1$ or $r = 0$. More generally, the constraints depend upon the adopted prior probability distributions, even if they are implicit, for example by restricting the parameter freedom or their ranges (particularly where likelihoods peak near the boundaries), or by using different choices of other data in combination with the CMB. As the data become even more precise, these considerations will be less important, but for now we caution that restrictions on model space and choice of non-CMB data sets and priors need to be kept in mind when adopting specific parameter values and uncertainties.

There are some combinations of parameters that fit the CMB anisotropies almost equivalently. For example, there is a nearly exact geometric degeneracy, where any combination of $\Omega_{\rm m}$ and Ω_Λ that provides the same angular-diameter distance to last scattering will give nearly identical C_ℓs. There are also other less exact degeneracies among the parameters. Such degeneracies can be broken when using the CMB results in combination with other cosmological data sets. Particularly useful are complementary constraints from baryon acoustic oscillations, galaxy clustering, the abundance of galaxy clusters, weak gravitational lensing measurements, and Type Ia supernova distances. For an overview of some of these other cosmological constraints, see The Cosmological Parameters—Sec. 25 of this *Review*.

Within the context of a 6-parameter family of models (which fixes $\Omega_{\rm tot} = 1$, $dn_{\rm s}/d\ln k = 0$, $r = 0$, and $w = -1$) the *Planck* results for TT, together with TE, EE, and CMB lensing, yield [11]: $\ln(10^{10}A_{\rm s}) = 3.044 \pm 0.014$; $n_{\rm s} = 0.965 \pm 0.004$; $\Omega_{\rm b}h^2 = 0.02237 \pm 0.00015$; $\Omega_{\rm c}h^2 = 0.1200 \pm 0.0012$; $100\theta_* = 1.04092 \pm 0.00031$; and $\tau = 0.054 \pm 0.007$. Other parameters can be derived from this basic set, including $h = 0.674 \pm 0.005$, $\Omega_\Lambda = 0.685 \pm 0.007$ $(= 1 - \Omega_{\rm m})$ and $\sigma_8 = 0.811 \pm 0.006$. Somewhat different (although consistent) values are obtained using other data combinations, such as including BAO, supernova, H_0, or weak-lensing constraints (see Sec. 25 of this *Review*). However, the results quoted above are currently the best available from CMB data alone.

The standard cosmological model still fits the data well, with the error bars on the parameters continuing to shrink. Improved measurement of higher acoustic peaks has dramatically reduced the uncertainty in the θ_* parameter, which is now detected at $> 3000\sigma$. The evidence for $n_{\rm s} < 1$ is now at the 8σ level from *Planck* data alone. The value of the reionization optical depth has decreased compared with earlier estimates; it is convincingly detected, but still not at very high significance.

Constraints can also be placed on parameters beyond the basic six, particularly when including other astrophysical data sets. Relaxing the flatness assumption, the constraint on $\Omega_{\rm tot}$ is 1.011 ± 0.006. Note that for h, the CMB data alone provide only a very weak constraint if spatial flatness is not assumed. However, with the addition of other data (particularly powerful in this context being a compilation of BAO measurements; see Sec. 25 of this *Review*), the constraints on the Hubble constant and curvature improve considerably, leading to $\Omega_{\rm tot} = 0.9993 \pm 0.0019$ [11].

For $\Omega_{\rm b}h^2$ the CMB-derived value is generally consistent with completely independent constraints from Big Bang nucleosynthesis (see Sec. 24 of this *Review*). Related are constraints on additional neutrino-like relativistic degrees of freedom, which lead to $N_{\rm eff} = 2.99 \pm 0.17$ (including BAO), *i.e.*, no evidence for extra neutrino species.

The best published limit on the tensor-to-scalar ratio is $r < 0.036$ (measured at $k = 0.05\,{\rm Mpc}^{-1}$) from BICEP/Keck Array [65]. The detailed limit will depend on how the slope $n_{\rm t}$ is restricted and whether $dn_{\rm s}/d\ln k \neq 0$ is allowed. The joint constraints on $n_{\rm s}$ and r allow specific inflationary models to be tested [30,88]. Looking at the $(n_{\rm s}, r)$ plane, this means that $m^2\phi^2$ (mass-term quadratic) inflation is disfavored by the data, as well as $\lambda\phi^4$ (self-coupled) inflation.

The addition of the dark-energy equation of state w adds the partial degeneracy of being able to fit a ridge in (w, h) space, extending to low values of both parameters. This degeneracy is broken when the CMB is used in combination with other data sets, *e.g.*, adding a compilation of BAO and supernova data gives $w = -1.028 \pm 0.031$. Constraints can also be placed on more general dark energy and modified-gravity models [89]. However, when extending the search space, one needs to be careful not to over-interpret some tensions between data sets as evidence for new physics.

For the reionization optical depth, a reanalysis of *Planck* data in 2016 resulted in a reduction in the value of τ, with the tightest result giving $\tau = 0.055 \pm 0.009$, and the newest analysis gives similar numbers. This corresponds to $z_{\rm i} = 7.8$–8.8 (depending on the functional form of the reionization history), with an uncertainty of ± 0.9 [90]. This redshift is only slightly higher that that suggested from studies of absorption lines in high-z quasar spectra [91] and Ly α-emitting galaxies [92], perhaps hinting that the process of reionization was not as complex as previously suspected. The important constraint provided by CMB polarization, in combination with astrophysical measurements, thus allows us to investigate how the first stars formed and brought about the end of the cosmic dark ages.

29.10 Particle Physics Constraints

CMB data place limits on parameters that are directly relevant for particle physics models. For example, there is a limit on the sum of the masses of the neutrinos, $\Sigma m_\nu < 0.12\,{\rm eV}$ (95%) [11] coming from *Planck* together with BAO measurements (although limits are weaker when considering both $N_{\rm eff}$ and Σm_ν as free parameters). This assumes the usual number density of fermions, which decoupled when they were relativistic. The limit is tantalizingly only a factor of a few higher than the minimum value coming from neutrino mixing experiments (see Neutrino Mixings—Secs. 14 and 26). As well as being an indirect probe of the neutrino background, *Planck* data also require that the neutrino background has perturbations, *i.e.*, that it possesses a sound speed $c_{\rm s}^2 \simeq 1/3$, as expected [9].

The current suite of data suggests that $n_{\rm s} < 1$, with a best-fitting value about 0.035 below unity. This is already quite constraining for inflationary models, particularly along with r limits. There is no current evidence for running of the spectral index, with $dn_{\rm s}/d\ln k = -0.004 \pm 0.007$ from *Planck* alone [11] (with a similar value when BAO data are included), although this is less of a constraint on models. Similarly, primordial non-Gaussianity is being probed to interesting levels, although tests of simple inflationary models will only come with significant reductions in uncertainty.

The large-angle anomalies, such as the hemispheric modulation of power and the dip in power at $\ell \simeq 20$–30, have the potential to be hints of new physics. Such effects might be expected in a Universe that has a large-scale power cut-off, or anisotropy in the initial power spectrum, or is topologically non-trivial. However, cosmic variance and *a posteriori* statistics limit the significance of these anomalies, absent the existence of a model that naturally yields some of these features (and ideally also predicting other phenomena that can be tested).

Constraints on 'cosmic birefringence' (*i.e.*, rotation of the plane of CMB polarization that generates non-zero TB and EB power) can be used to place limits on theories involving parity violation, Lorentz violation, or axion-photon mixing [93].

It is possible to place limits on additional areas of physics [94], for example annihilating dark matter [9, 9], primordial magnetic fields [95], and time variation of the fine-structure constant [96], as well as the neutrino chemical potential, a contribution of warm dark matter, topological defects, or physics beyond general relativity. Further particle physics constraints will follow as the

Downloaded from https://academic.oup.com/ptep/article/2022/8/083C01/6651666 by KIT Library user on 27 September 2022

smaller-scale and polarization measurements continue to improve.

The CMB anisotropy measurements precisely pin down physics at the time of last-scattering, and so any change of physics can be constrained if it affects the relevant energies or timescales. Future, higher sensitivity measurements of the CMB frequency spectrum will push the constraints back to cover energy injection at much earlier times (~ 1 year). Comparison of CMB and BBN observables extend these constraints to timescales of order seconds, and energies in the MeV range. And to the extent that inflation provides an effective description of the generation of perturbations, the inflationary observables may constrain physics at GUT-type energy scales.

More generally, careful measurement of the CMB power spectra and non-Gaussianity can in principle put constraints on physics at the highest energies, including ideas of string theory, extra dimensions, colliding branes, *etc.* At the moment any calculation of predictions appears to be far from definitive. However, there is a great deal of activity on implications of string theory for the early Universe, and hence a chance that there might be observational implications for specific scenarios.

29.11 Fundamental Lessons

More important than the precise values of parameters is what we have learned about the general features that describe our observable Universe. Beyond the basic hot Big Bang picture, the CMB has taught us that:

- the (observable) Universe is very close to isotropic;
- the Universe recombined at $z \sim 1000$ and started to become ionized again at $z \sim 10$;
- the geometry of the Universe is close to flat;
- both dark matter and dark energy are required;
- gravitational instability is sufficient to grow all of the observed large structures in the Universe;
- topological defects were not important for structure formation;
- there were 'synchronized' super-Hubble modes generated in the early Universe;
- the initial perturbations were predominantly adiabatic in nature;
- the primordial perturbation spectrum has a slightly red tilt;
- the perturbations had close to Gaussian (*i.e.*, maximally random) initial conditions.

These features form the basis of the cosmological standard model, ΛCDM, for which it is tempting to make an analogy with the Standard Model of particle physics (see earlier Sections of this *Review*). The cosmological model is much further from any underlying 'fundamental theory,' which might ultimately provide the values of the parameters from first principles. Nevertheless, any genuinely complete 'theory of everything' must include an explanation for the values of these cosmological parameters in addition to the parameters of the Standard Model of particle physics.

29.12 Future Directions

Given the significant progress in measuring the CMB sky, which has been instrumental in tying down the cosmological model, what can we anticipate for the future? There will be a steady improvement in the precision and confidence with which we can determine the appropriate cosmological parameters. Ground-based experiments operating at smaller angular scales will continue to place tighter constraints on the damping tail, lensing, and cross-correlations. New polarization experiments at small scales will probe further into the damping tail, without the limitation of extragalactic foregrounds. And polarization experiments at large angular scales will push down the limits on primordial B modes.

Planck, the third generation CMB satellite mission, was launched in May 2009, and produced a large number of papers, including a set of cosmological studies based on the first two full surveys of the sky (accompanied by a public release of data products) in 2013, a further series coming from analysis of the full mission data release in 2015 (eight surveys for the Low Frequency Instrument and five surveys for the High Frequency Instrument), and a third series derived from a final analysis of the 2018 data release, including full constraints from polarization data. *Planck* data currently dominate constraints on models (but that situation will change soon).

A set of cosmological parameters is now known to percent-level accuracy, and that may seem sufficient for many people. However, we should certainly demand more of measurements that describe *the entire observable Universe!* Hence a lot of activity in the coming years will continue to focus on determining those parameters with increasing precision. This necessarily includes testing for consistency among different predictions of the cosmological Standard Model, and searching for signals that might require additional physics.

A second area of focus will be the smaller-scale anisotropies and 'secondary effects.' There is a great deal of information about structure formation at $z \ll 1000$ encoded in the CMB sky. This may involve higher-order statistics and cross-correlations with other large-scale structure tracers, as well as spectral signatures, with many experiments targeting the galaxy cluster SZ effect. The current status of CMB lensing is similar (in terms of total signal-to-noise) to the quality of the first CMB anisotropy measurements by *COBE*, and thus we can expect that experimental probes of lensing will improve dramatically in the coming years. All of these investigations can provide constraints on the dark-energy equation of state, for example, which is a major area of focus for several future cosmological surveys at optical wavelengths. CMB lensing also promises to yield a measurement of the sum of the neutrino masses.

A third direction is increasingly sensitive searches for specific signatures of physics at the highest energies. The most promising of these may be the primordial gravitational wave signals in C_ℓ^{BB}, which could be a probe of the $\sim 10^{16}$ GeV energy range. There are several ground- and balloon-based experiments underway that are designed to search for the polarization B modes. Additionally, non-Gaussianity holds the promise of constraining models beyond single-field slow-roll inflation.

Anisotropies in the CMB have proven to be the premier probe of cosmology and the early Universe. Theoretically the CMB involves well-understood physics in the linear regime, and is under very good calculational control. A substantial and improving set of observational data now exists. Systematics appear to be under control and are not currently a limiting factor. And so for the next several years we can expect an increasing amount of cosmological information to be gleaned from CMB anisotropies, with the prospect also of some genuine surprises.

References

[1] A. A. Penzias and R. W. Wilson, Astrophys. J. **142**, 419 (1965); R. H. Dicke *et al.*, Astrophys. J. **142**, 414 (1965).

[2] M. White, D. Scott and J. Silk, Ann. Rev. Astron. Astrophys. **32**, 319 (1994); W. Hu and S. Dodelson, Ann. Rev. Astron. Astrophys. **40**, 171 (2002), [arXiv:astro-ph/0110414]; A. Challinor and H. Peiris, in M. Novello and S. Perez, editors, "American Institute of Physics Conference Series," volume 1132, 86–140 (2009), [arXiv:0903.5158].

[3] G. F. Smoot *et al.*, Astrophys. J. Lett. **396**, L1 (1992).

[4] C. L. Bennett *et al.*, Astrophys. J. Supp. **148**, 1 (2003), [arXiv:astro-ph/0302207].

[5] G. Hinshaw *et al.*, Astrophys. J. Supp. **208**, 19 (2013).

[6] Planck Collab. 2013 Results XVI, Astron. Astrophys. **571**, A16 (2014).

[7] J. A. Tauber *et al.*, Astron. Astrophys. **520**, A1 (2010); Planck Collab. 2013 Results I, Astron. Astrophys. **571**, A1 (2014), [arXiv:1303.5062].

[8] Planck Collab. 2015 Results I, Astron. Astrophys. **594**, A1 (2016), [arXiv:1502.01582].

[9] Planck Collab. 2015 Results XIII, Astron. Astrophys. **594**, A13 (2016), [arXiv:1502.01589].

[10] Planck Collab. 2018 Results I, Astron. Astrophys. **641**, A1 (2020), [arXiv:1807.06205].

Downloaded from https://academic.oup.com/ptep/article/2022/8/083C01/6651666 by KIT Library user on 27 September 2022

[11] Planck Collab. 2018 Results VI, Astron. Astrophys. **641**, A6 (2020), [arXiv:1807.06209].

[12] D. S. Swetz *et al.*, Astrophys. J. Supp. **194**, 41 (2011), [arXiv:1007.0290].

[13] J. E. Carlstrom *et al.*, Proc. Astron. Soc. Pacific **123**, 568 (2011), [arXiv:0907.4445].

[14] P. Noterdaeme *et al.*, Astron. Astrophys. **526**, L7 (2011), [arXiv:1012.3164]; S. Muller *et al.*, Astron. Astrophys. **551**, A109 (2013), [arXiv:1212.5456].

[15] D. J. Fixsen *et al.*, Astrophys. J. **734**, 5 (2011), [arXiv:0901.0555].

[16] J. Singal *et al.*, Proc. Astron. Soc. Pacific **130**, 985, 036001 (2018), [arXiv:1711.09979].

[17] A. Kogut *et al.*, J. Cosmology Astropart. Phys. **2011**, 7, 025 (2011), [arXiv:1105.2044]; P. André *et al.*, J. Cosmology Astropart. Phys. **2014**, 2, 006 (2014), [arXiv:1310.1554]; J. Delabrouille *et al.*, Experimental Astronomy, in press (2021), [arXiv:1909.01591].

[18] V. Desjacques *et al.*, Mon. Not. R. Astron. Soc. **451**, 4460 (2015), [arXiv:1503.05589].

[19] D. J. Fixsen, Astrophys. J. **707**, 916 (2009), [arXiv:0911.1955].

[20] J. C. Mather *et al.*, Astrophys. J. **512**, 511 (1999), [arXiv:astro-ph/9810373].

[21] Y. Hoffman, H. M. Courtois and R. B. Tully, Mon. Not. R. Astron. Soc. **449**, 4494 (2015), [arXiv:1503.05422].

[22] D. J. Fixsen *et al.*, Astrophys. J. **420**, 445 (1994).

[23] Planck Collab. 2013 Results XXVII, Astron. Astrophys. **571**, A27 (2014), [arXiv:1303.5087].

[24] S. Seager, D. D. Sasselov and D. Scott, Astrophys. J. Supp. **128**, 407 (2000), [arXiv:astro-ph/9912182].

[25] L. Knox, Phys. Rev. **D52**, 4307 (1995), [arXiv:astro-ph/9504054].

[26] N. Bartolo *et al.*, Phys. Rep. **402**, 103 (2004), [arXiv:astro-ph/0406398].

[27] Planck Collab. 2013 Results XXIV, Astron. Astrophys. **571**, A24 (2014), [arXiv:1303.5084].

[28] C. L. Bennett *et al.*, Astrophys. J. Supp. **192**, 17 (2011), [arXiv:1001.4758].

[29] Planck Collab. 2013 Results XXIII, Astron. Astrophys. **571**, A23 (2014), [arXiv:1303.5083].

[30] Planck Collab. 2018 Results X, Astron. Astrophys. **641**, A10 (2020), [arXiv:1807.06211].

[31] A. R. Liddle and D. H. Lyth, *Cosmological Inflation and Large-Scale Structure*, Cambridge University Press, Cambridge (2000).

[32] U. Seljak and M. Zaldarriaga, Astrophys. J. **469**, 437 (1996), [arXiv:astro-ph/9603033].

[33] A. Lewis, A. Challinor and A. Lasenby, Astrophys. J. **538**, 473 (2000), [arXiv:astro-ph/9911177].

[34] D. Blas, J. Lesgourgues and T. Tram, J. Cosmology Astropart. Phys. **7**, 034 (2011), [arXiv:1104.2933].

[35] U. Seljak *et al.*, Phys. Rev. **D68**, 083507 (2003), [arXiv:astro-ph/0306052].

[36] R. K. Sachs and A. M. Wolfe, Astrophys. J. **147**, 73 (1967).

[37] R. G. Crittenden and N. Turok, Phys. Rev. Lett. **76**, 575 (1996), [arXiv:astro-ph/9510072]; Planck Collab. 2015 Results XXI, Astron. Astrophys. **594**, A21 (2016), [arXiv:1502.01595].

[38] W. Hu *et al.*, Phys. Rev. **D59**, 2, 023512 (1998), [arXiv:astro-ph/9806362].

[39] W. Hu, N. Sugiyama and J. Silk, Nature **386**, 37 (1997), [arXiv:astro-ph/9604166].

[40] P. J. E. Peebles and J. T. Yu, Astrophys. J. **162**, 815 (1970); Sunyaev, R. A. and Zeldovich, Ya. B., Astron. Astrophys. Supp. **7**, 3 (1970).

[41] D. Scott, J. Silk and M. White, Science **268**, 829 (1995), [arXiv:astro-ph/9505015].

[42] D. J. Eisenstein, New Astron. Rev. **49**, 360 (2005).

[43] J. Silk, Astrophys. J. **151**, 459 (1968).

[44] M. Zaldarriaga and U. Seljak, Phys. Rev. **D58**, 023003 (1998), [arXiv:astro-ph/9803150].

[45] Planck Collab. 2013 Result XVII, Astron. Astrophys. **571**, A17 (2014), [arXiv:1303.5077].

[46] M. Kaplinghat, L. Knox and Y.-S. Song, Phys. Rev. Lett. **91**, 24, 241301 (2003), [arXiv:astro-ph/0303344].

[47] Planck Collab. 2013 Results XV, Astron. Astrophys. **571**, A15 (2014), [arXiv:1303.5075].

[48] Planck Collab. 2018 Results V, Astron. Astrophys. **641**, A5 (2020), [arXiv:1907.12875].

[49] S. Das *et al.*, J. Cosmology Astropart. Phys. **4**, 014 (2014), [arXiv:1301.1037].

[50] K. T. Story *et al.*, Astrophys. J. **779**, 86 (2013), [arXiv:1210.7231].

[51] W. Hu and M. White, New Astron. **2**, 323 (1997), [arXiv:astro-ph/9706147].

[52] W. Hu and M. J. White, Phys. Rev. **D56**, 596 (1997), [arXiv:astro-ph/9702170].

[53] M. Zaldarriaga and U. Seljak, Phys. Rev. **D55**, 1830 (1997), [arXiv:astro-ph/9609170]; M. Kamionkowski, A. Kosowsky and A. Stebbins, Phys. Rev. **D55**, 7368 (1997), [arXiv:astro-ph/9611125].

[54] J. M. Kovac *et al.*, Nature **420**, 772 (2002), [arXiv:astro-ph/0209478].

[55] D. Larson *et al.*, Astrophys. J. Supp. **192**, 16 (2011), [arXiv:1001.4635].

[56] Keck Array and BICEP2 Collabs. V, Astrophys. J. **811**, 126 (2015), [arXiv:1502.00643].

[57] S. K. Choi *et al.*, J. Cosmology Astropart. Phys. **2020**, 12, 045 (2020), [arXiv:2007.07289].

[58] A. T. Crites *et al.*, Astrophys. J. **805**, 36 (2015), [arXiv:1411.1042].

[59] Planck Collab. 2018 Results VII, Astron. Astrophys. **641**, A7 (2020), [arXiv:1906.02552].

[60] M. Tristram *et al.*, Astron. Astrophys. **647**, A128 (2021), [arXiv:2010.01139].

[61] D. Hanson *et al.*, Phys. Rev. Lett. **111**, 14, 141301 (2013), [arXiv:1307.5830].

[62] BICEP2 Collab., Phys. Rev. Lett. **112**, 24, 241101 (2014), [arXiv:1403.3985].

[63] BICEP2/Keck and Planck Collabs., Phys. Rev. Lett. **114**, 10, 101301 (2015), [arXiv:1502.00612].

[64] BICEP2 and Keck Array Collab., Phys. Rev. Lett. **121**, 22, 221301 (2018), [arXiv:1810.05216].

[65] BICEP/Keck Collab., Phys. Rev. Lett. **127**, 151301 (2021), [arXiv:2110.00483].

[66] POLARBEAR Collab., Astrophys. J. **848**, 121 (2017), [arXiv:1705.02907].

[67] R. Keisler *et al.*, Astrophys. J. **807**, 151 (2015), [arXiv:1503.02315].

[68] Planck Collab. 2015 Results XV, Astron. Astrophys. **594**, A15 (2016), [arXiv:1502.01591].

[69] A. van Engelen *et al.*, Astrophys. J. **808**, 7 (2015), [arXiv:1412.0626].

[70] P. Ade *et al.* (Simons Observatory Collab.), J. Cosmology Astropart. Phys. **2019**, 2, 056 (2019), [arXiv:1808.07445].

Downloaded from https://academic.oup.com/ptep/article/2022/8/083C01/6651666 by KIT Library user on 27 September 2022

[71] K. N. Abazajian *et al.*, ArXiv e-prints (2016), [arXiv:1610.02743].

[72] M. Hazumi *et al.*, in "S.P.I.E. Conf. Ser.", volume 11443, 114432F (2020), [arXiv:2101.12449].

[73] Planck Collab. 2018 Results VIII, Astron. Astrophys. **641**, A8 (2020), [arXiv:1807.06210].

[74] D. Scott *et al.*, J. Cosmology Astropart. Phys. **2016**, 6, 046 (2016), [arXiv:1603.03550].

[75] L. Knox and Y.-S. Song, Phys. Rev. Lett. **89**, 1, 011303 (2002), [arXiv:astro-ph/0202286]; M. Kesden, A. Cooray and M. Kamionkowski, Phys. Rev. Lett. **89**, 011304 (2002), [arXiv:astro-ph/0202434]; C. M. Hirata and U. Seljak, Phys. Rev. **D68**, 8, 083002 (2003), [arXiv:astro-ph/0306354].

[76] Planck Collab. 2013 Results XII, Astron. Astrophys. **571**, A12 (2014), [arXiv:1303.5072]; Planck Collab. 2015 Results X, Astron. Astrophys. **594**, A10 (2016), [arXiv:1502.01588]; Planck Collab. 2018 Results IV, Astron. Astrophys. **641**, A4 (2020), [arXiv:1807.06208].

[77] B. Gold *et al.*, Astrophys. J. Supp. **192**, 15 (2011), [arXiv:1001.4555].

[78] Planck Collab. Interm. Results XXX, Astron. Astrophys. **586**, A133 (2016), [arXiv:1409.5738].

[79] M. Millea *et al.*, Astrophys. J. **746**, 4 (2012), [arXiv:1102.5195].

[80] Sunyaev, R. A. and Zeldovich, Ya. B., Ann. Rev. Astron. Astrophys. **18**, 537 (1980).

[81] R. Williamson *et al.*, Astrophys. J. **738**, 139 (2011), [arXiv:1101.1290].

[82] M. Hilton *et al.*, Astrophys. J. Supp. **253**, 1, 3 (2021), [arXiv:2009.11043].

[83] Planck Collab. Early Results VIII, Astron. Astrophys. **536**, A8 (2011), [arXiv:1101.2024].

[84] Planck Collab. 2013 Results XX, Astron. Astrophys. **571**, A20 (2014), [arXiv:1303.5080].

[85] T. de Haan *et al.*, Astrophys. J. **832**, 95 (2016), [arXiv:1603.06522].

[86] Planck Collab. 2018 Results IX, Astron. Astrophys. **641**, A9 (2020), [arXiv:1905.05697].

[87] Planck Collab. 2015 Results XVI, Astron. Astrophys. **594**, A16 (2016), [arXiv:1506.07135].

[88] Planck Collab. 2013 Results XXII, Astron. Astrophys. **571**, A22 (2014), [arXiv:1303.5082]; Planck Collab. 2015 Results XX, Astron. Astrophys. **594**, A20 (2016), [arXiv:1502.02114].

[89] Planck Collab. 2015 Results XIV, Astron. Astrophys. **594**, A14 (2016), [arXiv:1502.01590].

[90] Planck Collab. Interm. Results XLVI, Astron. Astrophys. **596**, A107 (2016), [arXiv:1605.02985].

[91] X. Fan, C. L. Carilli and B. Keating, Ann. Rev. Astron. Astrophys. **44**, 415 (2006), [arXiv:astro-ph/0602375].

[92] C. A. Mason *et al.*, Astrophys. J. **856**, 1, 2 (2018), [arXiv:1709.05356].

[93] Planck Collab. Interm. Results XLIX, Astron. Astrophys. **596**, A110 (2016), [arXiv:1605.08633].

[94] M. Kamionkowski and A. Kosowsky, Ann. Rev. Nucl. Part. Sci. **49**, 77 (1999), [arXiv:astro-ph/9904108].

[95] Planck Collab. 2015 Results XIX, Astron. Astrophys. **594**, A19 (2016), [arXiv:1502.01594].

[96] Planck Collab. Interm. Results XXIV, Astron. Astrophys. **580**, A22 (2015), [arXiv:1406.7482].

Downloaded from https://academic.oup.com/ptep/article/2022/8/083C01/6651666 by KIT Library user on 27 September 2022

30. Cosmic Rays

Revised October 2021 by J.J. Beatty (Ohio State U.), J. Matthews (Louisiana State U.) and S.P. Wakely (Chicago U.; Chicago U., Kavli Inst.).

Cosmic rays are a population of energetic elementary particles and nuclei with a steeply falling, nearly power-law spectrum extending from a few MeV to tens of J per particle. Primary cosmic rays can be measured directly by experiments in space or on balloons at energies where there is sufficient flux (§30.1). Atmospheric interactions of primary cosmic rays produce fluxes of secondary elementary particles which can be detected in the atmosphere (§30.2), at the Earth's surface (§30.3), and underground (§30.4). At high energies, air showers of particles generated by a single primary can be detected (§30.5). These showers can be reconstructed to determine the energy, direction, and composition of the incident particle. Gamma-ray photons are observed both as diffuse fluxes and as steady-state and transient emission from sources (§30.6). Energetic neutrinos are closely linked to high energy protons and nuclei, both through production at astrophysical sites of particle acceleration and by production during propagation of extremely high energy particles (§30.7).

30.1 Primary Spectra from Direct Measurements

The cosmic radiation incident at the top of the terrestrial atmosphere includes all stable charged particles and nuclei with lifetimes of order 10^6 years or longer. When discussing the astrophysical origin of cosmic rays, "primary" cosmic rays are those particles accelerated at astrophysical sources and "secondaries" are those particles produced in interaction of the primaries with interstellar gas[1]. Thus electrons, protons and helium, as well as carbon, oxygen, iron, and other nuclei synthesized in stars, are primaries. Nuclei such as lithium, beryllium, and boron (which are not abundant end-products of stellar nucleosynthesis) are secondaries. Antiprotons and positrons are also in large part secondary. Whether a small fraction of these particles may be primary is a question of current interest.

There are four different ways to describe the spectra of the components of the cosmic radiation: (1) By particles per unit rigidity. Propagation (and probably also acceleration) through cosmic magnetic fields depends on the gyroradius or *magnetic rigidity, R*, which is the gyroradius multiplied by the magnetic field strength:

$$R = \frac{p\,c}{Z\,e} = r_L\,B \tag{30.1}$$

(2) By particles per energy-per-nucleon. Fragmentation of nuclei propagating through the interstellar gas depends on the energy per nucleon, since that quantity is approximately conserved when a nucleus breaks up on interaction with the gas. (3) By nucleons per energy-per-nucleon. Production of secondary cosmic rays in the atmosphere depends on the intensity of nucleons per energy-per-nucleon, approximately independently of whether the incident nucleons are free protons or bound in nuclei. (4) By particles per energy-per-nucleus. Air shower experiments that use the atmosphere as a calorimeter generally measure a quantity that is related to total energy per particle.

The units of differential intensity I are $[\mathrm{m}^{-2}\,\mathrm{s}^{-1}\mathrm{sr}^{-1}\mathcal{E}^{-1}]$, where $\mathcal{E}$ represents the units of one of the four variables listed above.

Apart from particles associated with solar flares[2], the cosmic radiation comes from outside the solar system. The incoming charged particles are "modulated" by the solar wind, the expanding magnetized plasma generated by the Sun, which decelerates and partially excludes the lower energy Galactic cosmic rays from the inner solar system. There is a significant anti-correlation between solar activity (which has an alternating eleven-year cycle) and the intensity of the cosmic rays with rigidities below about 10 GV. In addition, the lower-energy cosmic rays are affected by the geomagnetic field, which they must penetrate to reach the top of the atmosphere. Thus the intensity of any component of the cosmic radiation in the GeV range depends both on the location and time.

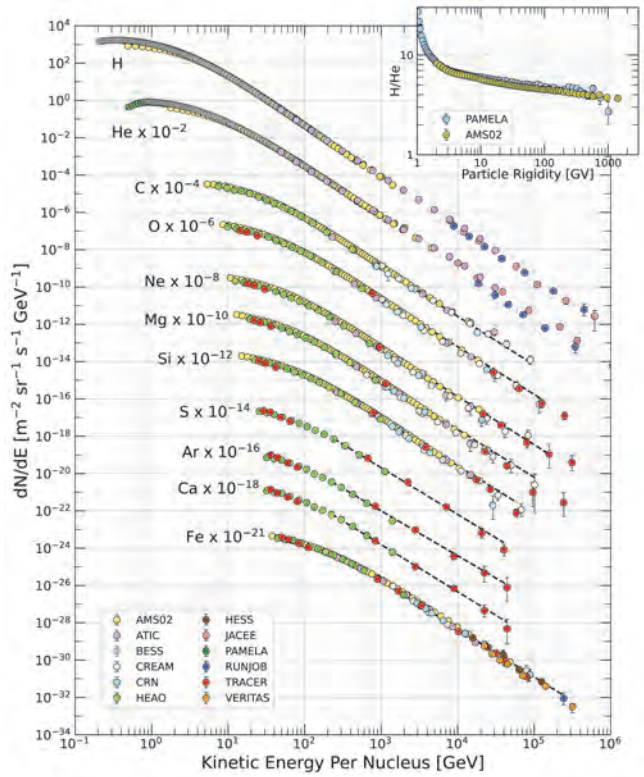

Figure 30.1: Fluxes of nuclei of the primary cosmic radiation in particles per energy-per-nucleus are plotted vs energy-per-nucleus using data from Refs. [1–15] The inset shows the H/He ratio as a function of rigidity [1, 3].

The intensity of primary nucleons in the energy range from several GeV to somewhat beyond 100 TeV is given approximately by

$$I_N(E) \;\approx\; 1.8\times10^4\;(E/1\;\mathrm{GeV})^{-\alpha}\;\frac{\mathrm{nucleons}}{\mathrm{m}^2\;\mathrm{s\;sr\;GeV}}, \tag{30.2}$$

where E is the energy-per-nucleon (including rest mass energy), α $(\equiv \gamma+1) \approx 2.7$ is the differential spectral index of the cosmic-ray flux, and γ is the integral spectral index. About 74% of the primary nucleons are free protons and about 70% of the rest are nucleons bound in helium nuclei. The fractions of the primary nuclei are nearly constant over this energy range. Fractions of both primary and secondary incident nuclei are listed in Table 30.1. Figure 30.1 shows the major nuclear components for kinetic energies greater than 0.22 GeV/nucleus. Figure 30.2 shows the relative abundances of low-energy ($\tilde{0}$.2 GeV/nucleon) cosmic rays compared to the present-day solar system. Secondary cosmic rays contribute to increased abundances of rare elements and a reduced even-odd effect. A useful compendium of experimental data for cosmic-ray nuclei and electrons is described in [16].

The composition and energy spectra of nuclei are typically interpreted in the context of propagation models, in which the sources of the primary cosmic radiation are located within the Galaxy [23]. The ratio of secondary to primary nuclei is observed to decrease with increasing energy, a fact often interpreted to mean that the lifetime of cosmic rays in the Galaxy decreases with energy. Measurements of radioactive "clock" isotopes in the low energy cosmic radiation are consistent with a lifetime in the Galaxy of about 15 Myr [24].

Cosmic rays are nearly isotropic at most energies due to diffu-

[1] 'Primary' and 'secondary' are used in a different but analogous sense when discussing cosmic ray interactions in the atmosphere.

[2] Energetic particles accelerated by the Sun and at other sites within the heliosphere and at its boundary are outside the scope of this review.

Downloaded from https://academic.oup.com/ptep/article/2022/8/083C01/6651666 by KIT Library user on 27 September 2022

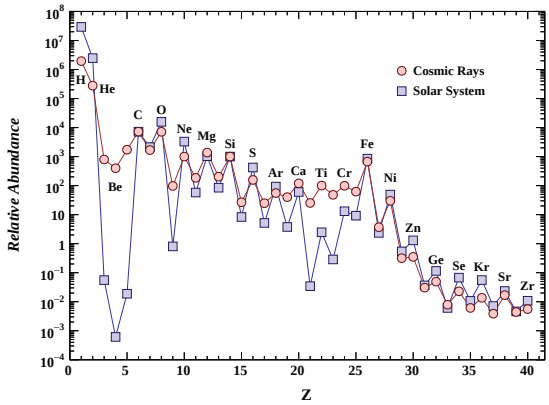

Figure 30.2: Cosmic ray elemental abundances compared to abundances in present-day solar system material. Abundances are normalised to Si=10^3. Cosmic ray abundances are from AMS-02 (H,He) [3, 17], ACE/CRIS (Li-Ni) [18, 19], and TIGER/Super-TIGER (Cu-Zr) [20, 21]. Solar system abundances are from Table 6 of Ref. [22].

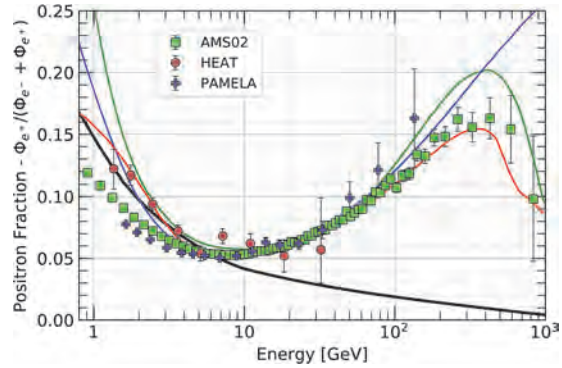

Figure 30.4: The positron fraction (ratio of the flux of e^+ to the total flux of e^+ and e^-) [33, 41–43]. The heavy black line is a model of pure secondary production [44] and the three thin lines show three representative attempts to model the positron excess with different phenomena: green: dark matter decay [45]; blue: propagation physics [46]; red: production in pulsars [47]. The ratio below 10 GeV is dependent on the intensity and polarity of the solar magnetic field.

sive propagation in the Galactic magnetic field. Several collaboratiions [25–29] have observed anisotropy on various angular scales at the level of about 10^{-3} for cosmic rays with energy of a few TeV, possibly due the direction of local Galactic magnetic fields, motion of the solar system in the Galaxy, and to the distribution of sources [30].

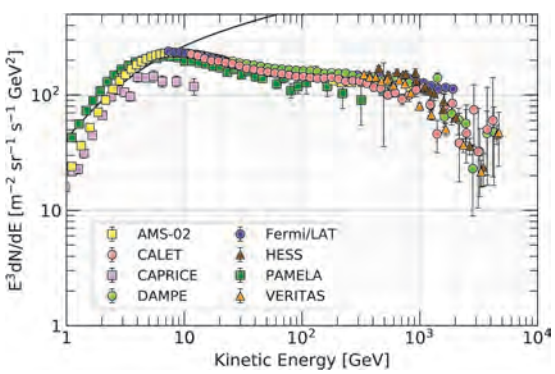

Figure 30.3: Differential spectrum of electrons plus positrons (except PAMELA data, which are electrons only) multiplied by E^3 [31–39] The line shows the proton spectrum [40] multiplied by 0.01.

The spectrum of electrons and positrons incident at the top of the atmosphere is generally expected to steepen by one power of E above an energy of 5 GeV because of radiative energy loss effects in the Galaxy. Most modern measurements of the combined electron+positron spectrum at high energy, which includes data from spectrometers, calorimeters, and ground-based air Cherenkov telescopes, reveal a relatively smooth spectrum to approximately 1 TeV, where evidence of a cutoff has been reported [35, 37, 39].

The PAMELA [41, 42] and AMS-02 [48, 49] satellite experiments measured the positron to electron ratio to increase above 10 GeV instead of the expected decrease [44] at higher energy, confirming earlier hints seen by the HEAT balloon-borne experiment [43]. The structure in the electron spectrum, as well as the increase in the positron fraction, may be related to contributions from individual nearby sources (supernova remnants or pulsars) emerging above a background suppressed at high energy by synchrotron losses [50]. Other explanations have invoked propagation effects [46] or dark matter decay/annihilation processes (see, e.g., [45]). The significant disagreement in the ratio below ∼10 GeV is attributable to differences in charge-sign dependent solar modulation effects present near Earth at the times of measurement.

The ratio of antiprotons to protons is $\sim 2\times10^{-4}$ [51] at around 10–20 GeV, and there is clear evidence [52] for the kinematic suppression at lower energy that is the signature of secondary antiprotons. The $\overline{p}/p$ ratio also shows a strong dependence on the phase and polarity of the solar cycle [53] in the opposite sense to that of the positron fraction. There is at this time no evidence for a significant primary component of antiprotons. No antihelium or antideuteron has been found in the cosmic radiation. The best measured upper limit on the ratio antihelium/helium is currently approximately 1×10^{-7} [54] The upper limit on the flux of antideuterons around 1 GeV/nucleon is approximately 2×10^{-4} (m^2 s sr GeV/nucleon)$^{-1}$ [55].

A useful method for calculating the effect of solar modulation including time, charge-sign, and rigidity-dependent effects is given in Ref. [56].

Table 30.1: Relative abundances F of cosmic-ray nuclei at 10.6 GeV/nucleon normalized to oxygen (≡ 1) [9]. The oxygen flux at kinetic energy of 10.6 GeV/nucleon is 3.29×10^{-2} (m^2 s sr GeV/nucleon)$^{-1}$. Abundances of hydrogen and helium are from Refs. [2–4]. Note that one can not use these values to extend the cosmic-ray flux to high energy because the power law indices for each element may differ slightly.

Z	Element	F	Z	Element	F
1	H	550	13–14	Al-Si	0.19
2	He	34	15–16	P-S	0.03
3–5	Li-B	0.40	17–18	Cl-Ar	0.01
6–8	C-O	2.20	19–20	K-Ca	0.02
9–10	F-Ne	0.30	21–25	Sc-Mn	0.05
11–12	Na-Mg	0.22	26–28	Fe-Ni	0.12

30.2 Cosmic Rays in the Atmosphere

Figure 30.5 shows the vertical fluxes of the major cosmic-ray components in the atmosphere in the energy region where the particles are most numerous (except for electrons, which are most numerous near their critical energy, which is about 81 MeV in air). Except for protons and electrons near the top of the atmosphere, all particles are produced in interactions of the primary[3] cosmic rays in the air. Muons and neutrinos are products of the decay chain of charged mesons, while electrons and photons originate in

[3] When discussing cosmic rays in the atmosphere, 'primary' is used to denote the original particle and 'secondary' to denote the particles produced in interactions.

Downloaded from https://academic.oup.com/ptep/article/2022/8/083C01/6651666 by KIT Library user on 27 September 2022

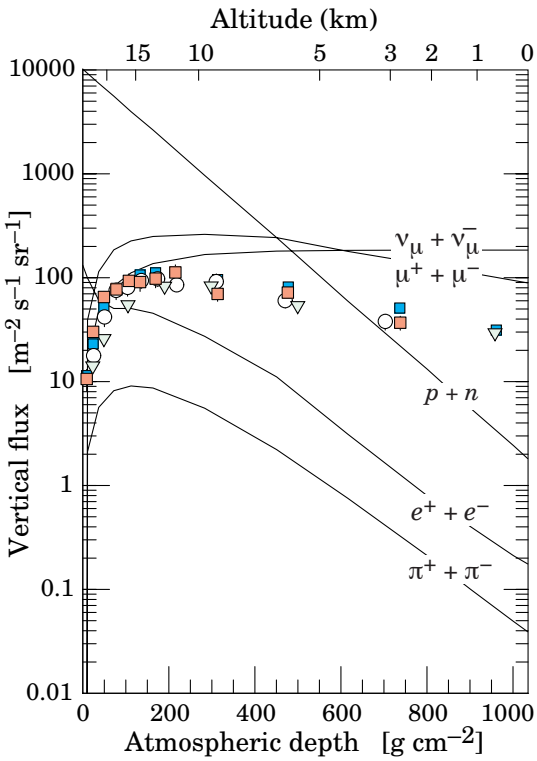

Figure 30.5: Vertical fluxes of cosmic rays in the atmosphere with $E > 1$ GeV estimated from the nucleon flux of Eq. (30.2). The experimental points show measurements of negative muons with $E_\mu > 1$ GeV [57–62].

decays of neutral mesons.

Most measurements are made at ground level or near the top of the atmosphere, but there are also measurements of muons and electrons from airplanes and balloons. Fig. 30.5 shows measurements of negative muons [57–62]. Since $\mu^+(\mu^-)$ are produced in association with $\nu_\mu(\overline{\nu}_\mu)$, the measurement of muons near the maximum of the intensity curve for the parent pions serves to calibrate the atmospheric $\nu_\mu(\overline{\nu}_\mu)$ beam [63]. Because muons typically lose almost 2 GeV in passing through the atmosphere, the comparison near the production altitude is important for the sub-GeV range of $\nu_\mu(\overline{\nu}_\mu)$ energies.

The flux of cosmic rays through the atmosphere is described by a set of coupled cascade equations with boundary conditions at the top of the atmosphere to match the primary spectrum. Numerical or Monte Carlo calculations are needed to account accurately for decay and energy-loss processes, and for the energy-dependences of the cross sections and of the primary spectral index γ. Approximate analytic solutions are, however, useful in limited regions of energy [64, 65]. For example, the vertical intensity of charged pions with energy $E_\pi \ll \epsilon_\pi = 115$ GeV is

$$I_\pi(E_\pi, X) \approx \frac{Z_{N\pi}}{\lambda_N} I_N(E_\pi, 0)\, e^{-X/\Lambda \frac{X E_\pi}{\epsilon_\pi}} \tag{30.3}$$

where Λ is the characteristic length for exponential attenuation of the parent nucleon flux in the atmosphere. This expression has a maximum at $X = \Lambda \approx 121 \pm 4$ g cm^{-2} [66], which corresponds to an altitude of 15 kilometers. The quantity $Z_{N\pi}$ is the spectrum-weighted moment that characterizes the inclusive distribution of charged pions in interactions of a spectrum of nucleons with nuclei of the atmosphere. The intensity of low-energy pions is much less than that of nucleons because $Z_{N\pi} \approx 0.079$ is small and because most pions with energy much less than the critical energy ϵ_π decay rather than interact.

30.3 Cosmic rays at the surface

30.3.1 *Muons*

Muons are the most numerous charged particles at sea level (see Fig. 30.5). Most muons are produced high in the atmosphere (typically 15 km) and lose about 2 GeV to ionization before reaching the ground. Their energy and angular distribution reflect a convolution of the production spectrum, energy loss in the atmosphere, and decay. For example, 2.4 GeV muons have a decay length of 15 km, which is reduced to 8.7 km by energy loss. The mean energy of muons at the ground is ≈ 4 GeV. The energy spectrum is almost flat below 1 GeV, steepens gradually to reflect the primary spectrum in the 10–100 GeV range, and steepens further at higher energies because pions with $E_\pi > \epsilon_\pi$ tend to interact in the atmosphere before they decay. Asymptotically ($E_\mu \gg 1$ TeV), the energy spectrum of atmospheric muons is one power steeper than the primary spectrum. The integral intensity of vertical muons above 1 GeV/c at sea level is ≈ 70 m^{-2}s^{-1}sr^{-1} [67, 68], with recent measurements [62, 69, 70] favoring a lower normalization by 10-15%. Experimentalists are familiar with this number in the form $I \approx 1$ cm^{-2} min^{-1} for horizontal detectors. The overall angular distribution of muons at the ground as a function of zenith angle θ is $\propto \cos^2\theta$, which is characteristic of muons with $E_\mu \sim 3$ GeV. At lower energy the angular distribution becomes increasingly steep, while at higher energy it flattens, approaching a $\sec\theta$ distribution for $E_\mu \gg \epsilon_\pi$ and $\theta < 70°$.

Figure 30.6 shows the muon energy spectrum at sea level for two angles. At large angles low energy muons decay before reaching the surface and high energy pions decay before they interact, thus the average muon energy increases. An approximate extrapolation formula valid when muon decay is negligible ($E_\mu > 100/\cos\theta$ GeV) and the curvature of the Earth can be neglected ($\theta < 70°$) is

$$\frac{dN_\mu}{dE_\mu d\Omega} \approx \frac{0.14\, E_\mu^{-2.7}}{\text{cm}^2\ \text{s sr GeV}} \times \left\{ \frac{1}{1 + \frac{1.1 E_\mu \cos\theta}{115\ \text{GeV}}} + \frac{0.054}{1 + \frac{1.1 E_\mu \cos\theta}{850\ \text{GeV}}} \right\} \tag{30.4}$$

where the two terms give the contribution of pions and charged kaons. Eq. (30.4) neglects a small contribution from charm and heavier flavors which is negligible except at very high energy [75].

The muon charge ratio reflects the excess of π^+ over π^- and K^+ over K^- in the forward fragmentation region of proton initiated interactions together with the fact that there are more free and bound protons than free and bound neutrons in the primary spectrum. The increase with energy of μ^+/μ^- shown in Fig. 30.7 reflects the increasing importance of kaons in the TeV range [76] and indicates a significant contribution of associated production by cosmic-ray protons ($p \to \Lambda + K^+$). The same process is even more important for atmospheric neutrinos at high energy.

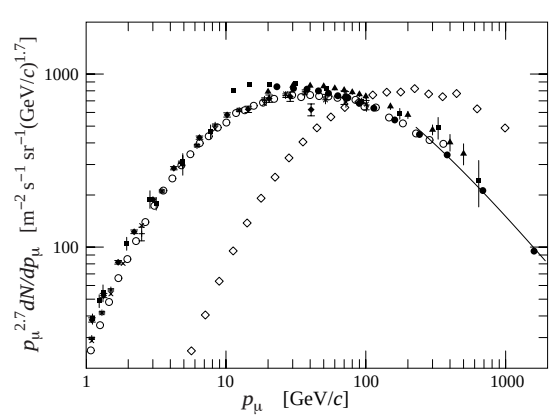

Figure 30.6: Spectrum of muons at $\theta = 0°$ (♦ [67], ■ [71], ▼ [72], ▲ [73], ×, + [69], ○ [62], and ● [70] and $\theta = 75°$ ◊ [74]). The line plots the result from Eq. (30.4) for vertical showers.

Downloaded from https://academic.oup.com/ptep/article/2022/8/083C01/6651666 by KIT Library user on 27 September 2022

30.3.2 *Electromagnetic component*

At the ground, this component consists of electrons, positrons, and photons primarily from cascades initiated by decay of neutral and charged mesons. Muon decay is the dominant source of low-energy electrons at sea level. Decay of neutral pions is more important at high altitude or when the energy threshold is high. Knock-on electrons also make a small contribution at low energy [77]. The integral vertical intensity of electrons plus positrons is very approximately 30, 6, and 0.2 $\mathrm{m^{-2}s^{-1}sr^{-1}}$ above 10, 100, and 1000 MeV respectively [68, 78], but the exact numbers depend sensitively on altitude, and the angular dependence is complex because of the different altitude dependence of the different sources of electrons [77, 79]. The ratio of photons to electrons plus positrons is approximately 1.3 above 1 GeV and 1.7 below the critical energy [79].

30.3.3 *Nucleons*

Nucleons above 1 GeV/c at ground level are degraded remnants of the primary cosmic radiation. The intensity is approximately $I_N(E,0)\times\exp(-X/\cos\theta\Lambda)$ for $\theta < 70°$. At sea level, about 1/3 of the nucleons in the vertical direction are neutrons (up from $\approx 10\%$ at the top of the atmosphere as the n/p ratio approaches equilibrium). The integral intensity of vertical protons above 1 GeV/c at sea level is ≈ 0.9 $\mathrm{m^{-2}s^{-1}sr^{-1}}$ [68, 80].

30.4 Cosmic Rays Underground

Only muons and neutrinos penetrate to significant depths underground. The muons produce tertiary fluxes of photons, electrons, and hadrons.

30.4.1 *Muons*

As discussed in Section 34.6 of this *Review*, muons lose energy by ionization and by radiative processes: bremsstrahlung, direct production of e^+e^- pairs, and photonuclear interactions. The total muon energy loss may be expressed as a function of the amount of matter traversed as

$$-\frac{dE_\mu}{dX} = a + b\,E_\mu \tag{30.5}$$

where a is the ionization loss and b is the fractional energy loss by the three radiation processes. Both are slowly varying functions of energy. The quantity $\epsilon \equiv a/b$ (≈ 500 GeV in standard rock) defines a critical energy below which continuous ionization loss is more important than radiative losses. Table 30.2 shows a and b values for standard rock, and b for ice, as a function of muon energy. The second column of Table 30.2 shows the muon range in standard rock ($A = 22$, $Z = 11$, $\rho = 2.65$ g cm^{-3}). These parameters are quite sensitive to the chemical composition of the rock, which must be evaluated for each location.

The intensity of muons underground can be estimated from the muon intensity in the atmosphere and their rate of energy loss. To the extent that the mild energy dependence of a and b can be neglected, Eq. (30.5) can be integrated to provide the following relation between the energy $E_{\mu,0}$ of a muon at production in the atmosphere and its average energy E_μ after traversing a thickness X of rock (or ice or water):

$$E_{\mu,0} = (E_\mu + \epsilon)e^{bX} - \epsilon\ . \tag{30.6}$$

Especially at high energy, however, fluctuations are important and an accurate calculation requires a simulation that accounts for stochastic energy-loss processes [83].

There are two depth regimes for which Eq. (30.6) can be simplified. For $X \ll b^{-1} \approx 2.5$ km water equivalent, $E_{\mu,0} \approx E_\mu(X) + aX$, while for $X \gg b^{-1}$ $E_{\mu,0} \approx (\epsilon + E_\mu(X))\exp(bX)$. Thus at shallow depths the differential muon energy spectrum is approximately constant for $E_\mu < aX$ and steepens to reflect the surface muon spectrum for $E_\mu > aX$, whereas for $X > 2.5$ km-water-equvalent (km.w.e.)] the differential spectrum underground is again constant for small muon energies but steepens to reflect the surface muon spectrum for $E_\mu > \epsilon \approx 0.5$ TeV. In the deep regime the shape is independent of depth although the intensity decreases exponentially with depth. In general the muon spectrum at slant depth X is

$$\frac{dN_\mu(X)}{dE_\mu} = \frac{dN_\mu}{dE_{\mu,0}}\frac{dE_{\mu,0}}{dE_\mu} = \frac{dN_\mu}{dE_{\mu,0}}\,e^{bX} \tag{30.7}$$

where $E_{\mu,0}$ is the solution of Eq. (30.6) in the approximation neglecting fluctuations.

Fig. 30.8 shows the vertical muon intensity versus depth. In constructing this "depth-intensity curve," each group has taken account of the angular distribution of the muons in the atmosphere, the map of the overburden at each detector, and the properties of the local medium in connecting measurements at various slant depths and zenith angles to the vertical intensity. Use of data from a range of angles allows a fixed detector to cover a wide range of depths. The flat portion of the curve is due to muons produced locally by charged-current interactions of ν_μ. The inset shows the vertical intensity curve for water and ice [90–93]. It is not as steep as the one for rock because of the lower muon energy loss in water.

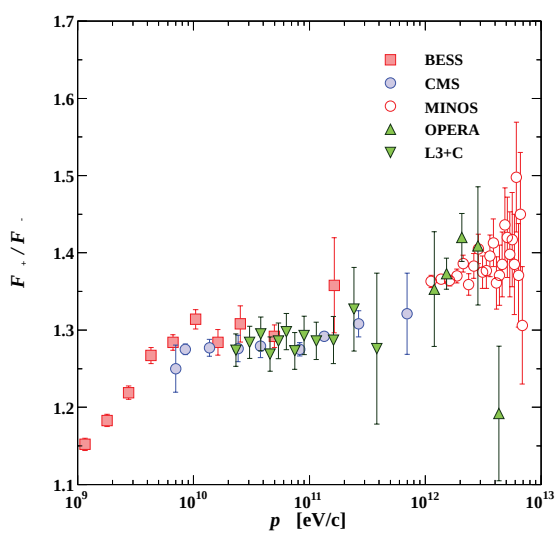

Figure 30.7: Muon charge ratio as a function of the muon momentum from Refs. [62, 70, 76, 81, 82].

Table 30.2: Average muon range R and energy loss parameters calculated for standard rock. Range is given in km-water-equivalent, or 10^5 g cm^{-2}.

E_μ GeV	R km.w.e.	a $\frac{\text{MeV cm}^2}{\text{g}}$	b_{brems}	b_{pair}	b_{nucl}	$\sum b_i$	$\sum b_{\text{ice}}$
			10^{-6} g^{-1} cm^2				
10	0.05	2.17	0.70	0.70	0.50	1.90	1.66
10^2	0.41	2.44	1.10	1.53	0.41	3.04	2.51
10^3	2.45	2.68	1.44	2.07	0.41	3.92	3.17
10^4	6.09	2.93	1.62	2.27	0.46	4.35	3.78

30.4.2 *Atmospheric Neutrinos*

Because neutrinos have small interaction cross sections, measurements of atmospheric neutrinos require a deep detector to avoid backgrounds. There are two types of measurements: contained (or semi-contained) events, in which the vertex is determined to originate inside the detector, and neutrino-induced muons. The latter are muons that enter the detector from zenith angles so large (*e.g.*, nearly horizontal or upward) that they cannot be muons produced in the atmosphere. In neither case is the neutrino flux measured directly. What is measured is a convolution of the neutrino flux and cross section with the properties of the detector (which includes the surrounding medium in the case of entering muons). This section focuses on neutrinos below about 1 TeV. For discussion of atmospheric neutrinos in the TeV–PeV region including a prompt component produced by charmed meson decays, see Ref. [64].

Downloaded from https://academic.oup.com/ptep/article/2022/8/083C01/6651666 by KIT Library user on 27 September 2022

Table 30.3: Measured fluxes (10^{-9} m^{-2} s^{-1} sr^{-1}) of neutrino-induced muons as a function of the effective minimum muon energy E_μ.

$E_\mu >$	1 GeV	1 GeV	1 GeV	2 GeV	3 GeV	3 GeV
Ref.	CWI [95]	Baksan [96]	MACRO [97,98]	IMB [99,100]	Kam [101]	SuperK [102]
F_μ	2.17±0.21	2.77±0.17	2.29 ± 0.15	2.26±0.11	1.94±0.12	1.74±0.07

Contained and semi-contained events reflect neutrinos in the sub-GeV to multi-GeV region where the product of increasing cross section and decreasing flux is maximum. In the GeV region the neutrino flux and its angular distribution depend on the geomagnetic location of the detector and, to a lesser extent, on the phase of the solar cycle. Naively, we expect $\nu_\mu/\nu_e = 2$ from counting neutrinos of the two flavors coming from the chain of pion and muon decays. Contrary to expectation, however, the numbers of the two classes of events are similar rather than different by a factor of two. This is now understood to be a consequence of neutrino flavor oscillations [103]. (See the article on neutrino properties in this *Review*.)

Two well-understood properties of atmospheric cosmic rays provide a standard for comparison of the measurements of atmospheric neutrinos to expectation. These are the "$\sec\theta$ effect" and the "east-west effect" due to the Earth's magnetic field [104]. The former refers originally to the enhancement of the flux of > 10 GeV muons (and neutrinos) at large zenith angles because the parent pions propagate more in the low density upper atmosphere where decay is enhanced relative to interaction. For neutrinos from muon decay, the enhancement near the horizontal becomes important for $E_\nu > 1$ GeV and arises mainly from the increased pathlength through the atmosphere for muon decay in flight. Fig. 14.4 from Ref. [105] shows a comparison between measurement and expectation for the zenith angle dependence of multi-GeV electron-like (mostly ν_e) and muon-like (mostly ν_μ) events separately. The ν_e show an enhancement near the horizontal and approximate equality for nearly upward ($\cos\theta \approx -1$) and nearly downward ($\cos\theta \approx 1$) events. There is, however, a very significant deficit of upward ($\cos\theta < 0$) ν_μ events, which have long pathlengths comparable to the radius of the Earth. This feature is the principal signature for atmospheric neutrino oscillations [103].

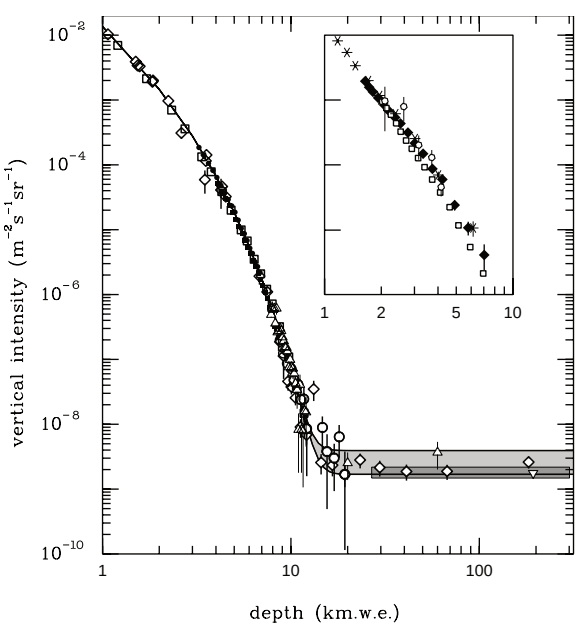

Figure 30.8: Vertical muon intensity vs depth (1 km.w.e. = 10^5 g cm^{-2} of standard rock). The experimental data are from: ◊: the compilations of Crouch [84], □: Baksan [85], ○: LVD [86], •: MACRO [87], ■: Frejus [88], and △: SNO [89]. The shaded area at large depths represents neutrino-induced muons of energy above 2 GeV. The upper line is for horizontal neutrino-induced muons, the lower one for vertically upward muons. Darker shading shows the muon flux measured by the SuperKamiokande experiment. The inset shows the vertical intensity curve for water and ice published in Refs. [90–93]. Additional data extending to slant depths of 13 km are available in [94].

Muons that enter the detector from outside after production in charged-current interactions of neutrinos naturally reflect a higher energy portion of the neutrino spectrum than contained events because the muon range increases with energy as well as the cross section. The relevant energy range is $\sim 10 < E_\nu < 1000$ GeV, depending somewhat on angle. Neutrinos in this energy range show a $\sec\theta$ effect similar to muons (see Eq. (30.4)). This causes the flux of horizontal neutrino-induced muons to be approximately a factor two higher than the vertically upward flux. The upper and lower edges of the horizontal shaded region in Fig. 30.8 correspond to horizontal and vertical intensities of neutrino-induced muons. Table 30.3 gives the measured fluxes of upward-moving neutrino-induced muons averaged over the lower hemisphere. Generally the definition of minimum muon energy depends on where it passes through the detector. The tabulated effective minimum energy estimates the average over various accepted trajectories.

30.5 Air Showers

So far we have discussed inclusive or uncorrelated fluxes of various components of the cosmic radiation. An air shower is caused by a single cosmic ray with energy high enough for the cascade that it creates in the atmosphere to be detectable at the ground. The shower has a hadronic core, which acts as a collimated source of electromagnetic sub-showers, generated mostly from $\pi^0 \to \gamma\gamma$ decays. The resulting electrons and positrons are the most numerous charged particles in the shower, and are accompanied by about ten times as many photons with a mean energy of ~ 10 MeV. The number of muons, produced by decays of charged mesons, is an order of magnitude lower. Air showers spread over a large area on the ground, and arrays of detectors operated for long times are important for studying cosmic rays with primary energy $E_0 > 100$ TeV, where the low flux makes measurements with small detectors in balloons and satellites impractical.

Greisen [120] gives the following approximate analytic expressions for the numbers and lateral distributions of particles in showers at ground level. The total number of muons N_μ with energies above 1 GeV is

$$N_\mu(> 1\text{GeV}) \approx 0.95 \times 10^5 \left(N_e/10^6\right)^{3/4} , \qquad (30.8)$$

where N_e is the total number of charged particles in the shower (not just $e^\pm$). The number of muons per square meter, ρ_μ, as a function of the lateral distance r (in meters) from the center of the shower is

$$\rho_\mu = \frac{1.25 N_\mu}{2\pi\Gamma(1.25)} \left(\frac{1}{320}\right)^{1.25} r^{-0.75} \left(1 + \frac{r}{320}\right)^{-2.5} , \qquad (30.9)$$

where Γ is the gamma function. The number density of charged particles is

$$\rho_e = C_1(s,d,C_2) x^{(s-2)} (1+x)^{(s-4.5)} (1 + C_2 x^d) . \qquad (30.10)$$

Here s, d, and C_2 are parameters in terms of which the overall normalization constant $C_1(s,d,C_2)$ is given by

$$C_1(s,d,C_2) = \frac{N_e}{2\pi r_1^2} \left[B(s, 4.5-2s) C_2 B(s+d,\, 4.5-d-2s) \right]^{-1} , \qquad (30.11)$$

where $B(m,n)$ is the beta function. The values of the parameters depend on shower size (N_e), depth in the atmosphere, identity of the primary nucleus, etc. For showers with $N_e \approx 10^6$ at sea level,

Downloaded from https://academic.oup.com/ptep/article/2022/8/083C01/6651666 by KIT Library user on 27 September 2022

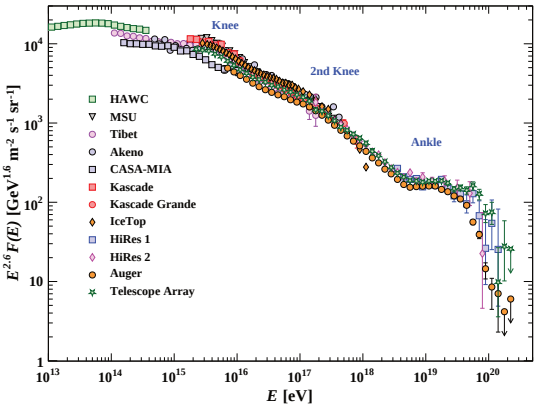

Figure 30.9: The all-particle spectrum as a function of E (energy-per-nucleus) from air shower measurements [106–119]

Greisen uses $s = 1.25$, $d = 1$, and $C_2 = 0.088$. For showers with average $N_e \approx 6 \times 10^7$ at the Akeno array [109], $d = 1.3$, $C_2 = 0.2$ and s is fitted for each shower with typical values between 0.95 and 1.15. Finally, x is r/r_1, where r_1 is the Molière radius, which depends on the density of the atmosphere and hence on the altitude at which showers are detected. At sea level $r_1 \approx 78$ m, and it increases with altitude as the air density decreases. (See the section on electromagnetic cascades in the article on the passage of particles through matter in this *Review*).

The lateral spread of a shower is determined largely by Coulomb scattering of the many low-energy electrons and is characterized by the Molière radius, which depends on density and thus on temperature and pressure. The lateral spread of the muons (ρ_μ) is larger and depends on the transverse momenta of the muons at production as well as multiple scattering.

There are large fluctuations in development from shower to shower, even for showers initiated by primaries of the same energy and mass—especially for small showers, which are usually well past maximum development when observed at the ground. Thus the shower size N_e and primary energy E_0 are only related in an average sense, and even this relation depends on depth in the atmosphere. One estimate of the relation is [109]

$$E_0 \sim 3.9 \times 10^6 \mathrm{GeV}(N_e/10^6)^{0.9} \tag{30.12}$$

for vertical showers with $10^{14} < E < 10^{17}$ eV at 920 g cm^{-2} (965 m above sea level). As E_0 increases, the shower maximum (on average) moves down into the atmosphere and the relation between N_e and E_0 changes. Moreover, because of fluctuations, N_e as a function of E_0 is not correctly obtained by inverting Eq. (30.12). At the maximum of shower development, there are approximately 0.66 particles per GeV of primary energy.

The muon and electron lateral distributions used in reconstructing experimental data must be adapted taking into consideration the altitude of the observations and the characteristics of the detectors used. Useful examples include the Akeno [109] and Volcano Ranch [121] arrays. Compilations of useful lateral distribution functions and discussion of their applications are given in Refs. [122, 123].

Cosmic ray shower development is sensitive to hadronic physics in the forward region above energies that can be probed at accelerators. Specialized simulation codes such as CORSIKA [124] include both the relevant physics and methods for efficiently dealing with the large number of particles in high energy air showers. Hadronic interaction models used to interpret air shower measurements now incorporate data from the LHC, reducing the extrapolation required. However, differences between the simulated and observed properties of showers remain. Most notably, the observed muon content of showers near 10^{19} eV exceeds that given by models by 30–60% [125].

There are three common types of air shower detectors: shower arrays that measure a ground parameter related to shower size N_e and muon number N_μ as well as the lateral distribution on the ground, optical Cherenkov and radio detectors that detect forward-beamed emission by the charged particles of the shower, and 'fluorescence' detectors that measure nitrogen scintillation excited by the charged particles in the shower. The fluorescence light is emitted isotropically so the showers can be observed from the side. Detection of radiofrequency emission from showers via geomagnetic and Askaryan mechanisms has been successfully employed in recent experiments [126]. Detailed simulations and cross-calibrations between different types of detectors are necessary to establish the primary energy spectrum from air-shower experiments.

Figure 30.9 shows the "all-particle" spectrum. The differential energy spectrum has been multiplied by $E^{2.6}$ in order to display the features of the steep spectrum that are otherwise difficult to discern. The steepening that occurs between 10^{15} and 10^{16} eV is known as the *knee* of the spectrum. Another steepening occurs around 10^{17} eV, known as the *second knee*. The feature around $10^{18.5}$ eV is called the *ankle* of the spectrum.

Cosmic ray experiments have systematic differences in their energy scales. For ground-based air-shower arrays, these are dependent on an assumed composition and on the hadronic interaction model used when interpreting the data. Systematic errors in energy scale are simplest when plotting $\frac{dN}{d\ln E} = E\frac{dN}{dE}$. When the spectrum is multiplied by a different power of energy, systematic errors in energy scale result in an apparent shift in the normalization of the spectrum; for example, when the spectrum is multiplied by $E^{2.6}$ a systematic shift of 10% in the energy scale results in a 16% change in the normalization of the plotted flux. See Ref. [64],§2.5.2 for further discussion of this issue.

In the energy range above 10^{17} eV, the fluorescence technique [127] is particularly useful because it can establish the primary energy in a nearly model-independent way by observing most of the longitudinal development of each shower, from which E_0 is obtained by integrating the energy deposition in the atmosphere. The result, however, depends strongly on the light absorption in the atmosphere and the calculation of the aperture of the detector.

Assuming the cosmic-ray spectrum below 10^{18} eV is of Galactic origin, the knee could indicate that most cosmic accelerators in the Galaxy have reached their maximum energy for acceleration of protons. Some types of expanding supernova remnants, for example, are estimated not to be able to accelerate protons above energies in the range of 10^{15} eV. Further observations of the PeV gamma-ray sources recently detected by LHAASO [128] may provide insight into the types of objects that act as Galactic sources near the knee and energies to which they can accelerate cosmic rays. Effects of propagation and confinement in the Galaxy [129] also need to be considered. A discussion of models of the knee may be found in Ref. [130].

The second knee may have a similar origin to the knee, but corresponding to steepening of the spectrum of heavy nuclei, particularly iron. The Kascade-Grande experiment has reported observation of a second steepening of the spectrum near 8×10^{16} eV, with evidence that this structure is accompanied by a transition to electron-poor showers resulting from heavy primaries [112]. Kascade Grande has also reported that the spectrum of light nuclei is steeper than the all-particle spectrum below the second knee and flattens in the vicinity of the second knee [131]. IceCube has performed a composition analysis using coincident surface (IceTop) and in-ice data, and finds that the mean logarithmic mass increases between 5×10^{15} eV and 10^{17} eV [132]. Together, these data are suggestive that the knee and second knee may result from a *Peters cycle*, with a steepening of the spectrum of each primary element taking place at the same rigidity but different energy per particle [133].

The Auger Observatory and Telescope Array (TA) have studied composition using the depth of shower maximum X_{max}, a quantity that correlates strongly with $\ln E/A$ and with the interaction cross section of the primary particle. The Auger Collaboration [134], using a post-LHC hadronic interaction model, reports a light composition below 2×10^{18} eV and becoming heavier above that energy, with the mean mass intermediate between protons and iron at 3×10^{19} eV. The TA Collaboration [135], using a different post-LHC model, has interpreted their data as implying a

Downloaded from https://academic.oup.com/ptep/article/2022/8/083C01/6651666 by KIT Library user on 27 September 2022

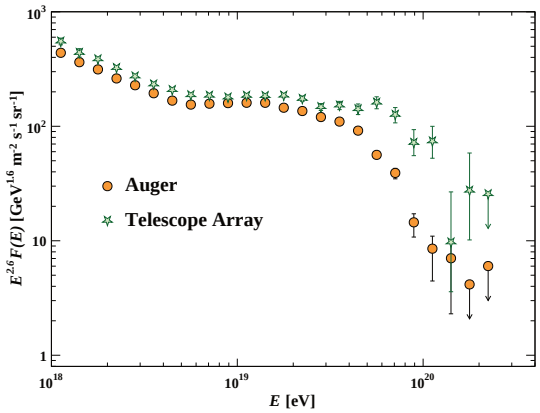

Figure 30.10: Expanded view of the highest energy portion of the cosmic-ray spectrum from data of the Pierre Auger Observatory [115–117, 139] and the Telescope Array [118, 119]. The small difference in the normalization of the spectra corresponds to a difference in energy scale of 9%.

light primary composition (mainly p and He) of ultrahigh-energy cosmic-rays (UHECR) from 1.3×10^{18} to 4×10^{19} eV. The Auger and TA Collaborations have also conducted a thorough joint analysis [136] and state that, at the current level of statistics and understanding of systematics, both data sets are compatible with being drawn from the same parent distribution, and that the TA data is compatible both with a light composition below 10^{19} eV and with the mixed composition above 10^{19} eV as reported by the Auger Collaboration.

Possible contributions to the origin of the ankle include a higher energy population of particles overtaking a lower energy population, for example an extragalactic flux beginning to dominate over the Galactic flux (e.g. Ref. [127]). Another proposed mechanism is that the dip structure in the region of the ankle is due to $p\gamma \to e^+ + e^-$ energy losses of extragalactic protons on the 2.7 K cosmic microwave radiation (CMB) [137]. The latter mechanism requires that the composition in this energy range is predominantly protons. A study of the correlation between the depth of shower maximum and the surface detector singal in hybrid showers by the Auger Collaboration favors a mixed composition at the ankle, disfavoring the dip model [138].

The propagation of the highest energy cosmic rays over extragalactic distances is predicted to result in a rapid steepening of the spectrum (called the GZK feature) around 5×10^{19} eV, resulting from the onset of inelastic interactions of UHE cosmic rays with the cosmic microwave background [140, 141]. Photo-dissociation of heavy nuclei in the mixed composition model [142] would have a similar effect. The HiRes detector, Auger Observatory, and the Telescope Array have all detected evidence of a suppression consistent with the GZK effect [114–116, 118, 143], with a steepened spectrum extending beyond 10^{20} eV. The differential energy spectra measured by the TA and Auger collaborations agree within systematic errors except at the very highest energies (Fig. 30.10). Both collaborations have also reported evidence for a steepening of the spectrum around $10^{19.2}$ eV, dubbed the 'instep' [115, 144].

Cosmic rays above 5×10^{19} eV are predominantly from nearby sources (< 100 Mpc). Differences between the Auger Observatory and Telescope Array spectra above this energy may reflect differences in the spectra between the northern and southern hemispheres. The Auger Collaboration has reported the observation of a dipole of amplitude $6.6\,^{+1.2}_{-0.8}\,\%$ for cosmic rays with energies above 8×10^{18} eV. The direction of the dipole indicates an extragalactic origin for these particles [145–147]. There are also hints of structure at smaller angular scales. TA has reported a 'hot spot' in the Northern Hemisphere at energies above 5.7×10^{19} eV of radius $\sim 20^\circ$ with a chance probability of this excess with respect to an isotropic distribution of 3.7×10^{-4} [148]. The Auger Collaboration has also reported an excess of events above 3.7×10^{19} eV in a region near the radio-loud active galaxy Centaurus A with a post-trial significance of 3.9σ, and a correlation of the distribution of ultrahigh energy events with several catalogs of nearby astrophysical objects, with starburst galaxies giving the highest significance at 4.5σ [149]. TA has also observed a similar correlation of cosmic arrival directions above 4.9×10^{19} eV with starburst galixies with a significance of 4.3σ [148].

30.6 Gamma Rays

There is a well-studied flux of cosmic gamma rays (gamma rays defined here as having energy greater than 1 MeV) present at the top of the atmosphere. This flux has been measured with multiple space and ground-based instruments [Cite PDG 36.2.2] across a broad range of energies.

Contributions to the flux include steady and transient emissions from numerous Galactic and extragalactic sources, as well as diffuse components originating from both inside and outside the Galaxy. The source-associated contributions include photons from a range of objects and phenomena such as supernova remnants, pulsars, active galactic nuclei, GRBs, and more. These contributions have been well documented in reviews (e.g., [150]) and in catalogs in the MeV [151, 152] GeV [153] and TeV [154] energy ranges. LHAASO has recently observed photon spectra from several sources extending to ~ 1 PeV and beyond [128, 155].

The majority of photons detected at higher energies are characterized as diffuse emission unassociated with discrete sources. The Large Area Telescope (LAT) of the Fermi Gamma-Ray Space Telescope has examined this radiation in detail for energies above 50 MeV [156]. The dominant component comes from the plane of the Galaxy (i.e., $|b| \lesssim 10$ deg) and is referred to as the Galactic diffuse emission. It can be attributed largely to interactions of high energy cosmic hadrons and electrons with interstellar matter and photon fields, leading to emission from π^0 decay, inverse Compton scattering and bremsstrahlung [153, 157]. Ground-based all-sky gamma detectors have extended these measurements to TeV energies and beyond in certain regions of the Galactic Plane [158–160].

In addition to the Galactic flux, there is a lower-intensity component to the diffuse emission that appears to be isotropic across the sky. This is thought to be extragalactic in origin and is often referred to as the isotropic gamma-ray background (IGRB). The IGRB has been measured by the LAT above 100 MeV and has an energy spectrum that can be described by a power-law with index -2.3 and an exponential cutoff at approximately 280 GeV, with a total intensity of $(7.2 \pm 0.6) \times 10^{-6}\mathrm{cm}^{-2}\mathrm{s}^{-1}\mathrm{sr}^{-1}$ [161]. Above energies of tens of TeV most emission is likely of local origin, due to Mpc and shorter attenuation lengths for interactions with cosmic microwave and infrared photons fields - this is referred to as the gamma-ray horizon [162, 163].

30.7 High-Energy Astrophysical Neutrinos

Neutrinos are expected to be produced in hadronic interactions in a variety of astrophysical objects. IceCube has reported a population of astrophysical neutrino events extending from tens of TeV to beyond ten PeV [164, 173, 174]. Multimessenger observations of the flaring blazar TXS 0506+056 have identified this object as a high-energy neutrino source [175, 176].

There is also expected to be a neutrino flux produced in cosmic ray GZK interactions. Measuring this *cosmogenic*[4] neutrino flux above 10^{18} eV would help resolve the UHECR uncertainties mentioned above. One half of the energy that UHECR protons lose in photoproduction interactions that cause the GZK effects ends up in neutrinos [177]. Heavier nuclei produce lower energy neutrinos due to the lower energy of their constituent nucleons. The magnitude of the cosmogenic neutrino flux depends strongly on the cosmic-ray spectrum at acceleration, the cosmic-ray composition, the cosmological evolution of the cosmic-ray sources, and the energy of the Galactic-extragalactic transition.

The expected rate of cosmogenic neutrinos is lower than current limits obtained by IceCube [164],the Auger Observatory [167], RICE [166, 178], and ANITA [168], which are shown in Fig. 30.11 together with a models for cosmogenic neutrino production [171, 172] and the Waxman-Bahcall benchmark flux of

[4] Here we use cosmogenic to denote neutrinos produced by photoproduction during propagation, and astrophysical to denote neutrinos produced by other mechanisms or close to sources.

Downloaded from https://academic.oup.com/ptep/article/2022/8/083C01/6651666 by KIT Library user on 27 September 2022

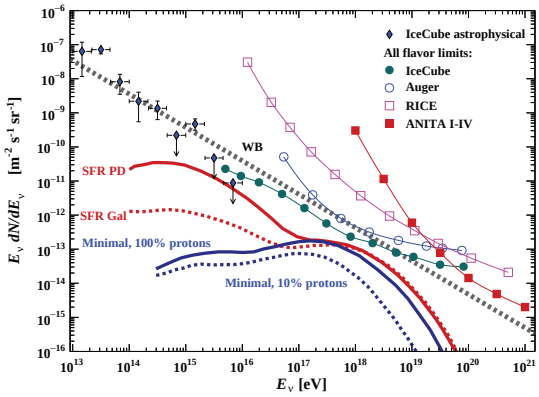

Figure 30.11: The best-fit IceCube *astrophysical* all-flavor neutrino flux [164]. Also shown are differential limits on the flux of *cosmogenic* neutrinos set by four experiments [165–168] The IceCube limit on cosmogenic neutrinos accounts for a nuisance background of astrophysical neutrinos. The curves show the Waxman-Bahcall benchmark flux (solid grey) [169,170], cosmogenic models with cosmic ray sources with maximum proton energy of $10^{20.5}$ eV evolving with the star-formation rate in proton dip (solid red) and Galactic composition (dashed red) scenarios [171], and 'minimal' cosmogenic models with protons constituting 100% (solid blue) and 10% (dashed red) of the cosmic rays [172].

neutrinos produced in cosmic ray sources [169, 170]. At production, the dominant component of neutrinos comes from $\pi^{\pm}$ decays and has flavor content ν_e:ν_μ:ν_τ = 1:2:0. After oscillations, the arriving cosmogenic neutrinos are expected to be a 1:1:1 mixture of flavors. The sensitivity of each experiment depends on neutrino flavor, and all limits are expressed as three-flavor limits assuming a 1:1:1 mixture.

References

[1] O. Adriani *et al.* (PAMELA), Science **332**, 69 (2011).

[2] M. Aguilar *et al.* (AMS), Phys. Rev. Lett. **114**, 171103 (2015).

[3] M. Aguilar *et al.* (AMS), Phys. Rev. Lett. **115**, 21, 211101 (2015).

[4] K. Abe *et al.*, Astrophys. J. **822**, 2, 65 (2016).

[5] M. J. Christ *et al.*, Astrophys. J. **502**, 278 (1998).

[6] A.D. Panov *et al.* (ATIC Collab.), Bull. Russian Acad. of Science, Physics, **73**, 564 (2009).

[7] V. A. Derbina *et al.* (RUNJOB), Astrophys. J. **628**, L41 (2005).

[8] H. S. Ahn *et al.*, Astrophys. J. **707**, 593 (2009).

[9] J.J. Engelmann *et al.* (HEAO3-C2 Collab.), Astron. & Astrophys. **233**, 96 (1990).

[10] D. Müller *et al.* (CRN Collab.), Astrophys. J. **374**, 356 (1991).

[11] M. Ave *et al.*, Astrophys. J. **678**, 262 (2008).

[12] F. Aharonian *et al.* (H.E.S.S.), Phys. Rev. **D75**, 042004 (2007).

[13] A. Archer *et al.* (VERITAS), Phys. Rev. **D98**, 2, 022009 (2018).

[14] M. Aguilar *et al.*, Phys. Rev. Lett. **124**, 21, 211102 (2020).

[15] M. Aguilar *et al.*, Phys. Rev. Lett. **126**, 4, 041104 (2021).

[16] D. Maurin *et al.*, Astron. & Astrophys. **569**, A32 (2014).

[17] M. Aguilar *et al.* (AMS), Phys. Rev. Lett. **119**, 25, 251101 (2017).

[18] K. Lave *et al.*, Astrophys. J. **770**, 117 (2013).

[19] G. DeNolfo *et al.*, Adv. Space Res. **38**, 1558 (2006).

[20] R. Murphy *et al.*, Astrophys. J. **831**, 148 (2016).

[21] B. Rauch *et al.*, Astrophys. J. **697**, 2083 (2009).

[22] K. Lodders, H. Palme and H.P.Gail, *Landolt-Börnstein, New Series*, volume VI/4b, chapter 4.4, 560, Springer-Verlag (2009).

[23] A. W. Strong, I. V. Moskalenko and V. S. Ptuskin, Ann. Rev. Nucl. Part. Sci. **57**, 285 (2007).

[24] R.A. Mewaldt *et al.*, Space Science Reviews 99,27(2001).

[25] A. A. Abdo *et al.*, Astrophys. J. **698**, 2121 (2009).

[26] A. U. Abeysekara *et al.* (HAWC, IceCube), Astrophys. J. **871**, 1, 96 (2019).

[27] M. Amenomori *et al.*, Astrophys. J. **711**, 119 (2010).

[28] M. G. Aartsen *et al.*, Astrophys. J. **826**, 2, 220 (2016), [arXiv:1603.01227].

[29] M. Amenomori *et al.*, Astrophys. J. **836**, 2, 153 (2017), [arXiv:1701.07144].

[30] M. Ahlers and P. Mertsch, Progr. Part. and Nucl. Phys. **94**, 184 (2017), [arXiv:1612.01873].

[31] O. Adriani *et al.* (PAMELA), Phys. Rev. Lett. **106**, 201101 (2011).

[32] M. Boezio *et al.*, Astrophys. J. **532**, 653 (2000).

[33] M. Aguilar *et al.* (AMS), Phys. Rev. Lett. **122**, 10, 101101 (2019).

[34] S. Abdollahi *et al.* (Fermi-LAT), Phys. Rev. **D95**, 8, 082007 (2017).

[35] G. Ambrosi *et al.* (DAMPE), Nature **552**, 63 (2017).

[36] O. Adriani *et al.* (CALET), Phys. Rev. Lett. **122**, 18, 181102 (2019).

[37] F. Aharonian *et al.* (H.E.S.S.), Phys. Rev. Lett. **101**, 261104 (2008).

[38] F. Aharonian *et al.* (H.E.S.S.), Astron. Astrophys. **508**, 561 (2009).

[39] A. Archer *et al.* (VERITAS), Phys. Rev. **D98**, 6, 062004 (2018).

[40] Y. Shikaze *et al.*, Astropart. Phys. **28**, 154 (2007).

[41] O. Adriani *et al.* (PAMELA), Nature **458**, 607 (2009).

[42] O. Adriani *et al.*, Phys. Rev. Lett. **102**, 051101 (2009).

[43] J.J. Beatty *et al.*, Phys. Rev. Lett. **93**, 24112 (2004).

[44] I. V. Moskalenko and A. W. Strong, Astrophys. J. **493**, 694 (1998).

[45] A. Ibarra, D. Tran and C. Weniger, Int. J. Mod. Phys. **A28**, 1330040 (2013).

[46] D. Gaggero *et al.*, Phys. Rev. Lett. **111**, 021102 (2013).

[47] P.-F. Yin *et al.*, Phys. Rev. **D88**, 2, 023001 (2013).

[48] M. Aguilar *et al.* (AMS), Phys. Rev. Lett. **110**, 141102 (2013).

[49] L. Accardo *et al.* (AMS), Phys. Rev. Lett. **113**, 121101 (2014).

[50] J. Nishimura *et al.*, Adv. Space Research **19**, 767 (1997).

[51] A. S. Beach *et al.*, Phys. Rev. Lett. **87**, 271101 (2001).

[52] A. Yamamoto *et al.*, Adv. Space Research**42**, 443(2008).

[53] Y. Asaoka *et al.*, Phys. Rev. Lett. **88**, 51101 (2002).

[54] K. Abe *et al.*, Phys. Rev. Lett. **108**, 131301 (2012).

[55] H. Fuke *et al.*, Phys. Rev. Lett. **95**, 081101 (2005).

[56] I. Cholis, D. Hooper and T. Linden, Phys. Rev. **D93**, 4, 043016 (2016).

[57] R. Bellotti *et al.*, Phys. Rev. **D53**, 35 (1996).

[58] R. Bellotti *et al.* (WiZard/MASS2), Phys. Rev. **D60**, 052002 (1999).

[59] M. Boezio *et al.* (WiZard/CAPRICE), Phys. Rev. **D62**, 032007 (2000).

[60] M. Boezio *et al.*, Phys. Rev. **D67**, 072003 (2003).

[61] S. Coutu *et al.*, Phys. Rev. **D62**, 032001 (2000).

Downloaded from https://academic.oup.com/ptep/article/2022/8/083C01/6651666 by KIT Library user on 27 September 2022

[62] S. Haino *et al.*, Phys. Lett. **B594**, 35 (2004).

[63] T. Sanuki *et al.*, Phys. Rev. **D75**, 043005 (2007).

[64] T.K. Gaisser, R. Engel, and E. Resconi, *Cosmic Rays and Particle Physics (second edition)*, Cambridge University Press (2016).

[65] P. Lipari, Astropart. Phys. **1**, 195 (1993).

[66] E. Mocchiutti *et al.*, in *Proc. 28th Int. Cosmic Ray Conf.*, Tsukuba, 1627 (2003). [http://adsabs.harvard.edu/abs/2003ICRC....3.1627M].

[67] M. P. De Pascale *et al.*, J. Geophys. Res. **98**, A3, 3501 (1993).

[68] P.K.F. Grieder, *Cosmic Rays at Earth*, Elsevier Science (2001).

[69] J. Kremer *et al.*, Phys. Rev. Lett. **83**, 4241 (1999).

[70] P. Achard *et al.* (L3), Phys. Lett. **B598**, 15 (2004).

[71] O. C. Allkofer, K. Carstensen and D. W. Dau, Phys. Lett. **36B**, 425 (1971).

[72] B. C. Rastin, J. Phys. **G10**, 1609 (1984).

[73] C. A. Ayre *et al.*, J. Phys. **G1**, 584 (1975).

[74] H. Jokisch *et al.*, Phys. Rev. **D19**, 1368 (1979).

[75] C. G. S. Costa, Astropart. Phys. **16**, 193 (2001).

[76] P. Adamson *et al.* (MINOS), Phys. Rev. **D76**, 052003 (2007).

[77] S. Hayakawa, *Cosmic Ray Physics*, Wiley, Interscience, New York (1969).

[78] R.R. Daniel and S.A. Stephens, Revs. Geophysics & Space Sci. **12**, 233 (1974).

[79] K.P. Beuermann and G. Wibberenz, Can. J. Phys. **46**, S1034 (1968).

[80] I. S. Diggory *et al.*, J. Phys. **A7**, 741 (1974).

[81] V. Khachatryan *et al.* (CMS), Phys. Lett. **B692**, 83 (2010).

[82] N. Agafonova *et al.* (OPERA), Eur. Phys. J. **C67**, 25 (2010).

[83] P. Lipari and T. Stanev, Phys. Rev. **D44**, 3543 (1991).

[84] M. Crouch, in *Proc. 20th Int. Cosmic Ray Conf.*, Moscow, **6**, 165 (1987) [http://adsabs.harvard.edu/abs/1987ICRC....6..165C].

[85] Yu.M. Andreev, V.I. Gurentzov, and I.M. Kogai, in *Proc. 20th Int. Cosmic Ray Conf.*, Moscow, **6**, 200 (1987), [http://adsabs.harvard.edu/abs/1987ICRC....6..200A].

[86] M. Aglietta *et al.* (LVD), Astropart. Phys. **3**, 311 (1995).

[87] M. Ambrosio *et al.* (MACRO), Phys. Rev. **D52**, 3793 (1995).

[88] C. Berger *et al.* (FREJUS), Phys. Rev. **D40**, 2163 (1989).

[89] C. Waltham *et al.*, in *Proc. 27th Int. Cosmic Ray Conf.*, Hamburg, 991 (2001), [http://adsabs.harvard.edu/abs/2001ICRC....3..991W].

[90] I. A. Belolaptikov *et al.* (BAIKAL), Astropart. Phys. **7**, 263 (1997).

[91] J. Babson *et al.* (DUMAND), Phys. Rev. **D42**, 3613 (1990).

[92] P. Desiati *et al.*, in *Proc. 28th Int. Cosmic Ray Conf.*, Tsukuba, 1373 (2003) [http://adsabs.harvard.edu/abs/2003ICRC....3.1373D].

[93] T. Pradier (ANTARES), in "Proceedings, 43rd Rencontres de Moriond on Electroweak Interactions and Unified Theories: La Thuile, Italy, March 1-8, 2008," 423–430 (2008).

[94] S. Aiello *et al.* (NEMO), Astropart. Phys. **66**, 1 (2015).

[95] F. Reines *et al.*, Phys. Rev. Lett. **15**, 429 (1965).

[96] M.M. Boliev *et al.*, in *Proc. 3rd Int. Workshop on Neutrino Telescopes* (ed. Milla Baldo Ceolin), 235 (1991).

[97] M. Ambrosio *et al.* (MACRO), Phys. Lett. **B434**, 451 (1998).

[98] F. Ronga (MACRO), in "Proceedings, 26th International Cosmic Ray Conference (ICRC), August 17-25, 1999, Salt Lake City: Invited, Rapporteur, and Highlight Papers," volume 2, 172 (1999), URL http://krusty.physics.utah.edu/~icrc1999/root/vol2/h4_1_07.pdf.

[99] R. Becker-Szendy *et al.*, Phys. Rev. Lett. **69**, 1010 (1992).

[100] *Proc. 25th Int. Conf. High-Energy Physics*, Singapore (eds. K.K. Phua and Y. Yamaguchi, World Scientific), 662 1991.

[101] S. Hatakeyama *et al.* (Kamiokande), Phys. Rev. Lett. **81**, 2016 (1998).

[102] Y. Fukuda *et al.* (Super-Kamiokande), Phys. Rev. Lett. **82**, 2644 (1999).

[103] Y. Fukuda *et al.* (Super-Kamiokande), Phys. Rev. Lett. **81**, 1562 (1998).

[104] T. Futagami *et al.* (Super-Kamiokande), Phys. Rev. Lett. **82**, 5194 (1999).

[105] Y. Ashie *et al.* (Super-Kamiokande), Phys. Rev. **D71**, 112005 (2005).

[106] R. Alfaro *et al.* (HAWC), Phys. Rev. **D96**, 12, 122001 (2017).

[107] Yu. A. Fomin *et al.*, *Proc. 22nd Int. Cosmic Ray Conf.*, Dublin, **2**, 85 (1991) [http://adsabs.harvard.edu/abs/1991ICRC....2...85F].

[108] M. Amenomori *et al.*, Astrophys. J. **268**, 1165 (2008).

[109] M. Nagano *et al.*, J. Phys. **G10**, 1295 (1984).

[110] M. A. K. Glasmacher *et al.*, Astropart. Phys. **10**, 291 (1999).

[111] T. Antoni *et al.* (KASCADE), Astropart. Phys. **24**, 1 (2005).

[112] W. D. Apel *et al.* (KASCADE Grande), Phys. Rev. Lett. **107**, 171104 (2011).

[113] K. Andeen, M. Plum *et al.*, (IceCube Collab.), *Proceedings of Science* (ICRC2019), 172 (2019).

[114] R. U. Abbasi *et al.* (HiRes), Phys. Rev. Lett. **100**, 101101 (2008).

[115] A. Aab *et al.* (Pierre Auger), Phys. Rev. Lett. **125**, 12, 121106 (2020), [arXiv:2008.06488].

[116] A. Aab *et al.* (Pierre Auger), Phys. Rev. D **102**, 6, 062005 (2020), [arXiv:2008.06486].

[117] P. Abreu *et al.*, Eur. Phys, J. C **81** (2021).

[118] D. Ivanov *et al.*, (Telescope Array Collab.), *Proceedings of Science* (ICRC2019), 298 (2019).

[119] R. U. Abbasi *et al.* (Telescope Array), Astrophys. J. **865**, 1, 74 (2018), [arXiv:1803.01288].

[120] K. Greisen, Ann. Rev. Nucl. Sci. **10**, 63 (1960).

[121] J. Linsley, *Proc. 15th. Internat. Cosmic Ray Conf. (Plovdiv)*, **12**, 56-65, 89-96. (Available from ADS).

[122] M. Nagano and A. Watson, Rev. Mod. Phys. **72**, 689 (2000).

[123] A. Haungs *et al.*, Rep. Prog. Phys. (2003).

[124] Https://www.iap.kit.edu/corsika/.

[125] A. Aab *et al.* (Pierre Auger), Phys. Rev. Lett. **117**, 19, 192001 (2016).

[126] T. Huege, Phys. Rept. **620**, 1 (2016).

[127] D. J. Bird *et al.* (HiRes), Astrophys. J. **424**, 491 (1994).

[128] Z. Cao *et al.*, Nature **594**, 7861, 33 (2021).

[129] V.S. Ptuskin *et al.*, Astron. & Astrophys. **268**, 726 (1993).

[130] J. R. Hoerandel, Astropart. Phys. **21**, 241 (2004).

[131] W. D. Apel *et al.*, Phys. Rev. **D87**, 081101 (2013), [arXiv:1304.7114].

[132] M. G. Aartsen *et al.* (IceCube) (2019), [arXiv:1906.04317].

[133] B. Peters, Nuovo Cimento **XXII**, 800 (1961).

[134] J. Bellido *et al.* (Auger Collab.), Proceedings of Science(ICRC2017), 506 (2017).

Downloaded from https://academic.oup.com/ptep/article/2022/8/083C01/6651666 by KIT Library user on 27 September 2022

[135] D. Ikeda *et al.* (TA Collab.), Proceedings of Science(ICRC2017), 515 (2017).

[136] V. de Souza *et al.* (TA and Auger Collabs.), Proceedings of Science(ICRC2017), 522 (2017).

[137] V. Berezinsky, A. Z. Gazizov and S. I. Grigorieva, Phys. Rev. **D74**, 043005 (2006).

[138] A. Aab *et al.* (Pierre Auger), Phys. Lett. B **762**, 288 (2016), [arXiv:1609.08567].

[139] V. Novotny *et al.*, (Auger Collab.), *Proceedings of Science* (ICRC2021), 324 (2021).

[140] K. Greisen, Phys. Rev. Lett. **16**, 748 (1966).

[141] G. T. Zatsepin and V. A. Kuzmin, JETP Lett. **4**, 78 (1966), [Pisma Zh. Eksp. Teor. Fiz.4,114(1966)].

[142] D. Allard *et al.*, Astron. & Astrophys. **443**, L29 (2005).

[143] R. U. Abbasi *et al.* (HiRes), Astropart. Phys. **32**, 53 (2009).

[144] D. Ivanov *et al.*, *Proceedings of Science* (ICRC2021), 341(2021).

[145] A. Aab *et al.*, Science **357**, 1266 (2017).

[146] A. Aab *et al.*, Astrophys. J. **868**, 1 (2018).

[147] E. Roulet *et al.*, (Auger Collab.), *Proceedings of Science* (ICRC2019), 408 (2019.

[148] T. Fujii*et al.*, (Telescope Array Collab.), *Proceedings of Science* (ICRC2021), 392 (2021).

[149] L. Caccianiga *et al.*, (Auger Collab.), *Proceedings of Science* (ICRC2019), 206 (2019).

[150] A. De Angelis and M. Mallamaci, European Physical Journal Plus **133**, 8, 324 (2018), [arXiv:1805.05642].

[151] V. Schönfelder *et al.*, Astron. Astrophys. Suppl. **143**, 145 (2000), [arXiv:astro-ph/0002366].

[152] I. S. D. Centre, "Integral general reference catalog," `https://www.isdc.unige.ch/integral/science/catalogue`.

[153] S. Abdollahi *et al.*, Astrophys. J. Suppl. **247**, 1, 33 (2020), [arXiv:1902.10045].

[154] S. Wakely and D. Horan, "Tevcat," `http://tevcat.uchicago.edu`.

[155] Z. Cao *et al.*, Science **373**, 6553, 425 (2021).

[156] M. Ackermann *et al.*, Astrophys. J. **750**, 1, 3 (2012), [arXiv:1202.4039].

[157] F. Acero *et al.*, Astrophys. J. Suppl. **223**, 2, 26 (2016), [arXiv:1602.07246].

[158] R. Atkins *et al.*, Phys. Rev. Lett. **95**, 25, 251103 (2005), [arXiv:astro-ph/0502303].

[159] B. Bartoli *et al.*, Astrophys. J. **806**, 1, 20 (2015), [arXiv:1507.06758].

[160] M. Amenomori *et al.*, Phys. Rev. Lett. **126**, 14, 141101 (2021), [arXiv:2104.05181].

[161] M. Ackermann *et al.*, Astrophys. J. **799**, 1, 86 (2015), [arXiv:1410.3696].

[162] T. M. Kneiske, K. Mannheim and D. H. Hartmann, in S. Ritz, N. Gehrels and C. R. Shrader, editors, "Gamma 2001: Gamma-Ray Astrophysics," volume 587 of *American Institute of Physics Conference Series*, 358–362 (2001).

[163] S. P. Wakely, in S. R. Magill and R. Yoshida, editors, "Calorimetry in High Energy Physics: XII," volume 867 of *American Institute of Physics Conference Series*, 139–147 (2006).

[164] M. G. Aartsen *et al.* (IceCube), Astrophys. J. **809**, 1, 98 (2015).

[165] M. G. Aartsen *et al.* (IceCube), Phys. Rev. **D98**, 6, 062003 (2018).

[166] I. Kravchenko *et al.*, Phys. Rev. **D85**, 062004 (2012).

[167] F. Pedriera *et al.*, (Auger Collab.), *Proceedings of Science* (ICRC2019), 172 (2019).

[168] C. Deaconu *et al.*, (ANITA Collab.), *Proceedings of Science* (ICRC2019), 867 (2019).

[169] E. Waxman and J. N. Bahcall, Phys. Rev. **D59**, 023002 (1999).

[170] E. Waxman, *The Origin of IceCube's Neutrinos: Cosmic Ray Accelerators Embedded in Star Forming Calorimeters* (2017), [arXiv:1511.00815].

[171] K. Kotera, D. Allard and A. V. Olinto, JCAP **1010**, 013 (2010).

[172] M. Ahlers and F. Halzen, Phys. Rev. **D86**, 083010 (2012).

[173] M. G. Aartsen *et al.* (IceCube), Science **342**, 1242856 (2013).

[174] M. G. Aartsen *et al.* (IceCube), Phys. Rev. Lett. **113**, 101101 (2014).

[175] M. G. Aartsen *et al.* (IceCube, Fermi-LAT, MAGIC, AGILE, ASAS-SN, HAWC, H.E.S.S., INTEGRAL, Kanata, Kiso, Kapteyn, Liverpool Telescope, Subaru, Swift NuSTAR, VERITAS, VLA/17B-403), Science **361**, eaat1378 (2018).

[176] M. G. Aartsen *et al.* (IceCube), Science **361**, 6398, 147 (2018).

[177] V. S. Berezinsky and G. T. Zatsepin, Phys. Lett. **28B**, 423 (1969).

[178] I. Kravchenko *et al.*, Phys. Rev. **D73**, 082002 (2006).

Downloaded from https://academic.oup.com/ptep/article/2022/8/083C01/6651666 by KIT Library user on 27 September 2022

Downloaded from https://academic.oup.com/ptep/article/2022/8/083C01/6651666 by KIT Library user on 27 September 2022

Experimental Methods and Colliders

31. Accelerator physics of colliders (rev.) 533
32. High-energy collider parameters (rev.) 543
33. Neutrino beam lines at high-energy proton synchrotrons (rev.) 548
34. Passage of particles through matter (rev.) 549
35. Particle detectors at accelerators (rev.) 565
36. Particle detectors for non-accelerator phys. (rev.) 618
37. Radioactivity and radiation protection (rev.) 646
38. Commonly used radioactive sources (rev.) 652

Downloaded from https://academic.oup.com/ptep/article/2022/8/033C01/6651666 by KIT Library user on 27 September 2022

Downloaded from https://academic.oup.com/ptep/article/2022/8/083C01/6651666 by KIT Library user on 27 September 2022

31. Accelerator Physics of Colliders

Revised August 2021 by V. Shiltsev (FNAL) and F. Zimmermann (CERN).

This article provides background for the High-Energy Collider Parameter Tables that follow and some additional information; see in-depth review and a comprehensive list of references in [1]; citations below are limited to widely used textbooks and open access seminal papers and reviews.

31.1 Energy and Luminosity

Collisions of two beams of particles accelerated to high energies $E_{1,2}$ provide access to center-of-mass energies (c.m.e.) $E_{\rm cme} \approx 2\sqrt{E_1 E_2}$, assuming a typically small or zero crossing angle. Most of the 31 colliders that have ever reached the operational stage (seven are operational now) used equal masses and energies of colliding particles, with c.m.e. equal to twice the beam energy $E_{\rm cme} = 2E_{\rm b}$. Other machines collide beams of unequal energies, such as electron-proton or electron-ion colliders, or asymmetric B-factories, that produce new short-lived particles, whose decays are more easily detected and analyzed with a Lorentz boost.

In an accelerator, charged particles gain energy from an electric field, which usually varies in time at a high frequency ranging from 100s of kHz to 10s of GHz. With proper phasing to the RF field over distance l, the energy gain of a particle with charge Ze is proportional to the average accelerating gradient G, i.e. $\Delta E_{\rm b} = ZeGl$. In principle, the highest beam accelerating gradients achieved to date in operational machines or beam test facilities ($G \approx 100$ MV/m in 12 GHz normal-conducting RF cavities and 31.5 MV/m in 1.3 GHz superconducting ones) allow accessing high energies over reasonably long linear accelerators (linacs), but cost considerations often call for minimization of RF acceleration via repeated use of the same RF system which, in that case, would boost the energy in small portions $\Delta E_{\rm b} = ZeV_{\rm RF}$ per turn every time a particle passes through the total cavity voltage $V_{\rm RF}$. Such an arrangement can be realized either in the form of storage-ring circular colliders or also through novel schemes based on, e.g., recirculating linear accelerators (RLAs) with or without energy recovery. Circular colliders are by far the most common; here, the momentum and energy of ultra-relativistic particles are determined by the bending radius inside the dipole magnets, ρ, and by the average magnetic field B of these magnets:

$$p = ZeB\rho \quad \text{or} \quad E_{\rm b}\ [\text{GeV}] = 0.3Z(B\rho)\ [\text{Tm}]\ . \tag{31.1}$$

Such *synchrotron condition* assures approximately constant radius of the beam orbit during acceleration. Transverse focusing by quadrupole magnets is needed to keep particles inside the rather limited space provided by the accelerator beam pipe passing through the magnet apertures. The maximum field of normal-conducting (NC) magnets is about 2 T, due to the saturation of ferromagnetic materials, and, while this is sufficient for lower energy colliders, such as most e^+e^- storage rings, it is not adequate for frontier-energy hadron (or muon) beams, because of the implied need for excessively long accelerator tunnels and prohibitively high total magnet power consumption. The development of superconducting (SC) magnets that employ high electric current carrying Nb-Ti wires cooled by liquid helium below 5 K, opened up the way towards higher fields and to hadron colliders at record energies [2]. For example, the 14 TeV c.m.e. LHC at CERN, uses double-bore SC magnets with a maximum field of 8.3 T at a temperature of 1.9 K, in a tunnel of $C = 26.7$ km circumference (dipole-magnet bending radius $\rho = 2800$ m). The double-bore design allows acceleration of the same particle type in opposite directions and also the operation with different particle species (e.g., protons and heavy ions) in the two apertures, while a single bore magnet implies the use of particles and antiparticles for the collider application. As the production of anti-particles is energy consuming and therefore limited, this concept opens the door to high-performance hadron colliders.

The exploration of rare nuclear and high energy particle physics phenomena requires not only an appropriately high energy, but also a sufficiently large number of detectable reactions. The number of events of interest N_{exp} is given by the product of the cross section of the reaction under study, $\sigma_{\rm exp}$, and the time integral over the instantaneous *luminosity*, $\mathcal{L}$:

$$N_{\rm exp} = \sigma_{\rm exp} \cdot \int \mathcal{L}(t)dt. \tag{31.2}$$

In the Tables, luminosity is stated in the units of cm^{-2}s^{-1}. The integral on the right is referred to as integrated luminosity $\mathcal{L}_{\rm int}$, and, reflecting the smallness of typical particle-interaction cross-sections is often reported in units of inverse femto- or attobarn, e.g., 1 ab^{-1}=10^{42} cm^2. Colliders usually employ bunched beams of particles with approximately Gaussian distributions, and for two bunches containing N_1 and N_2 particles colliding head-on with frequency $f_{\rm coll}$, a basic expression for the luminosity is

$$\mathcal{L} = f_{\rm coll}\frac{N_1 N_2}{4\pi\sigma_x^*\sigma_y^*}\mathcal{F} \tag{31.3}$$

where σ_x^* and σ_y^* characterize the rms transverse beam sizes in the horizontal and vertical directions at the interaction point, and $\mathcal{F}$ is a factor of order 1, that takes into account inefficient geometric overlapping of the beams due to a crossing angle and finite bunch length, and dynamic effects, such as the mutual focusing of the two beam during the collision (see below). Having $n_{\rm b}$ bunches per beam increases the frequency of collisions $f_{\rm coll} = n_{\rm b} f_0$ where f_0 is either the revolution frequency of a circular collider or the repetition rate of a linear one. To achieve a high luminosity, one, therefore, has to maximize the population and number of bunches, either producing these narrowly or focusing them tightly, and colliding them at high frequencies at dedicated locations, where products of their reactions can be registered by particle detectors.

Subsequent sections in this report briefly expand on the beam dynamics behind collider design, comment on the realization of collider performance in a selection of today's facilities, and end with some remarks on future possibilities.

31.2 Beam Dynamics

Given the enormous and highly concentrated power carried by modern high energy particle beams, the main concern of beam dynamics in colliders is stability of motion of i) individual particles in accelerators, ii) single high-intensity beams of many particles moving together, and iii) colliding beams [3–5].

31.2.1 *Single Particle Dynamics*

While a reference particle at the nominal energy proceeds along the design trajectory (reference orbit) mostly determined by transverse magnetic dipole fields, other particles in the bunch are kept close by through the focusing effect of quadrupole fields. Assume that the reference particle carries a right-handed Cartesian coordinate system, with the co-moving z-coordinate pointed in the direction of motion along the reference trajectory, $z = s - vt$ (with v the reference particle velocity, and t time). The independent variable is the distance s of the reference particle along this trajectory, rather than time t, and for simplicity this reference path is taken to be planar. The transverse coordinates are x (horizontal) and y (vertical), where $\{x, z\}$ defines the plane of the reference trajectory.

Several time scales are involved, and this is reflected in the approximations used in formulating the equations of motion. All of today's high-energy colliders are alternating gradient synchrotrons or, respectively, storage rings and the shortest time scale is set by so-called *betatron oscillations*. The linearized equations of motion of a particle displaced from the reference trajectory are:

$$\begin{aligned} &x'' + K_x(s)x = 0\ , y'' + K_y(s)y = 0\ ,\ z' = -x/\rho(s)\ , \\ &\text{with}\ \ K_x \equiv \frac{Ze}{p}\frac{\partial B_y}{\partial x} + \frac{1}{\rho^2}\ \text{and}\ K_y \equiv -\frac{Ze}{p}\frac{\partial B_y}{\partial x} \end{aligned} \tag{31.4}$$

where $\rho = p/ZeB_y$ is the radius of curvature due to the field on the reference orbit. The prime denotes d/ds and the Maxwell equation in vacuum $\nabla \times \mathbf{B} = \mathbf{0}$ helps to eliminate $B_x(s)$ using the relation $\partial B_x/\partial y = \partial B_y/\partial x$. In this linear approximation, the vertical magnetic field $B_y(s)$ in the (x, z)-plane contains only

Downloaded from https://academic.oup.com/ptep/article/2022/8/083C01/6651666 by KIT Library user on 27 September 2022

dipole and quadrupole terms, which are treated as static in time, but s-dependent.

The solutions of the Hill's equations (31.4) for x and y with a restoring force periodic in s are those of quasi-harmonic oscillators:

$$x(s) = \sqrt{2J_x\beta_x}\ \cos\psi_x\ ,\ \ x'(s) = -\sqrt{\frac{2J_x}{\beta_x}}\,[\alpha_x\cos\psi_x + \sin\psi_x]\ , \tag{31.5}$$

where the *action* J_x is a constant of integration, $\alpha_x = \alpha_x(s) \equiv -(1/2)d\beta_x(s)/ds$, and the envelope of oscillations is modulated by the *beta-function* $\beta_x(s)$. A solution of the same form describes the motion in y. The betatron oscillation phase advances according to $d\psi_x/ds = 1/\beta_x$; that is, $2\pi\beta_x$ also plays the role of a local wavelength of oscillations along the orbit. An extremely important parameter for circular machines is the *tune*, Q_x, which is the number of such oscillations per turn about the closed path:

$$Q_x = \frac{1}{2\pi}\oint d\psi_x = \frac{1}{2\pi}\oint\frac{ds}{\beta_x(s)}. \tag{31.6}$$

While the integer part of the tune $[Q_{x,y}]$ generally characterizes the extent of the focusing lattice, it is the fractional part of the tune $\{Q_{x,y}\}$ that needs to be well defined and controlled by the machine operators in order to stay away from potentially detrimental resonances, which may occur under conditions of $kQ_x + lQ_y = m$, where k, l, and m are integers. For example, for the LHC a combination of horizontal and vertical tunes — also called the *working point* — equal to (Q_x, Q_y)=(64.31, 59.32) has been selected, such that resonances up to the order of $|k|+|l| = 10$ or 12 are avoided. These resonances are driven by high order multipole components of the fields in the magnets, or by self-fields of the beam, or by the electromagnetic fields of the opposite bunch. Normally, the nonlinear components are very weak compared to linear ones, nevertheless, when the nonlinear resonance condition is encountered, the amplitudes of particle oscillations could grow over the beam lifetime, resulting in the escape of the particles to the machine aperture, in the increase of the average beam size, or in both; either of these is highly undesirable phenomena. Careful analysis of nonlinear beam dynamics is instrumental in determining and optimizing the *dynamic aperture*, which is defined as the maximum amplitude of a bounded particle motion.

Neglecting for now all nonlinear effects and usually small $x-y$ coupling, and considering only the linear dynamics, the beta-function is well defined and satisfies the following equation:

$$2\beta_x\beta_x'' - \beta_x'^2 + 4\beta_x^2K_x = 4\,. \tag{31.7}$$

In a region free of magnetic fields, such as in the neighborhood of a collider interaction point (IP), usually occupied by particle detectors, a symmetric solution of Eq. (31.7) is a parabola:

$$\beta_x(s) = \beta_x^* + \frac{s^2}{\beta_x^*}\,, \tag{31.8}$$

where, in this case, s denotes the longitudinal distance from the IP. The location of the beam waist usually coincides with the IP and corresponds to the minimum value of the beta-function β_x^*; the asterisk is used to indicate IP parameters.

Note that individual quadrupole magnet focuses particles in one plane and defocuses in another, see Eq.(31.4), and a standard way to provide focusing in both planes is to employ an alternating gradient periodic focusing lattice, consisting of a sequence of equally-spaced quadrupoles with a magnetic field gradient equal in magnitude, but alternating in sign ("focusing quadrupole - drift space - defocusing quadrupole - drift space" – known as a *FODO cell*), Eq. (31.7) has stable periodic solutions $\beta_x(s), \beta_y(s)$ in both planes provided that the focal length of the quadrupoles is longer than half the focusing-lens spacing L, i.e., $f = p/(eB_2l) > L/2$ (where l is the length of a quadrupole magnet, here assumed to be short $l \ll L$, and $B_2 \equiv |\partial B_y/\partial x|$ the quadrupoles' field gradient). In that case, the beta-functions have maxima at the focusing quadrupoles and minima at the defocusing ones, equal to, for example, $\beta_{\rm max,min} = (2 \pm \sqrt{2})L$ in the case of $f = L/\sqrt{2}$, which corresponds to a betatron phase advance $\Delta\psi_{x,y} = 90°$ per FODO cell.

Expressing the invariant J_x in terms of $x,\ x'$ yields

$$J_x = \frac{1}{2}\left(\gamma_x x^2 + 2\alpha_x x x' + \beta_x x'^2\right) = \frac{x^2 + (\alpha_x x + \beta_x x')^2}{2\beta_x} \tag{31.9}$$

with $\gamma_x = \gamma_x(s) \equiv (1 + \alpha_x^2(s))/\beta_x(s)$. In a periodic system, these *Courant-Snyder parameters* [6] or *Twiss parameters* $\alpha(s)$, $\beta(s)$, $\gamma(s)$ are usually defined by the focusing lattice; in a single pass system such as a linac, the parameters may be selected to match the x-x' distribution of the input beam. For a given position s in the ring, the transverse particle motion in $\{x, x' \equiv dx/ds\}$ phase space describes an ellipse, the area of which is $2\pi J_x$, where the horizontal action J_x is a constant of motion and independent of s. If the interior of that ellipse is populated by an ensemble of non-interacting and non-radiating particles, that area, given the name *emittance*, is constant over the trajectory as well and would only change with energy. In a typical case of the particle's energy change rate being much slower than betatron motion, and considering a Hamiltonian system (i.e., a hadron collider or a linear collider, either without significant synchrotron radiation), the adiabatic invariant $\int p_x dx$ is conserved, and given that for small angles $p_x = x' \cdot \beta\gamma mc^2$, it is common practice to consider an energy-independent *normalized emittance* that is equal to the product of the emittance and relativistic factor $\beta\gamma/\pi$ and denoted by $\varepsilon_{\rm n}$. For a beam with a Gaussian distribution in $\{x, x'\}$, average action value $\langle J_x\rangle$ and standard deviations σ_x, and $\sigma_{x'}$, the definition of the normalized rms emittance is

$$\varepsilon_{\rm n}x \equiv \beta\gamma\langle J_x\rangle = \beta\gamma\frac{\sigma_x^2(s)}{\beta_x(s)} = \beta\gamma\frac{\sigma_{x'}^2(s)}{\gamma_x(s)}\,, \tag{31.10}$$

with a corresponding expression for the other transverse direction, y. The angular brackets denote an average over the beam distribution. For 1D Gaussian beam, 95% of the particles are contained within $\{x, x'\}$ phase space area of $6\pi\varepsilon_{\rm n}/(\beta\gamma)$. Normalized beam emittances are conserved over the acceleration cycle in linear, static focusing lattices $K_{x,y}(s)$, and consequently, one would expect the same $\varepsilon_{\rm n}$ at the hadron (or linear) collider top energy as the one coming from the very initial low energy particle source. Unfortunately, that is rarely the case as many time-varying or nonlinear phenomena come into play. In an e^-/e^+ storage ring, the normalized emittance is not preserved during acceleration, but at each energy the beam's equilibrium emittance is determined by the effect of synchrotron radiation as a balance between radiation damping and quantum excitation [7]. In such a ring, for a given accelerator optics, the normalized equilibrium emittance increases with the third power of the beam energy [8].

As for the description of a particle's longitudinal motion, one takes the fractional momentum deviation $\Delta p/p$ from that of the reference particle as the variable conjugate to z. The factors $K_{x,y}$ and ρ in Hill's equations (31.4) are dependent on momentum p, leading to a number of effects: first, the trajectory of off-momentum particles deviates by $\Delta x(s) = D_x(s)(\Delta p/p)$, where the *dispersion function* $D_x(s)$ is determined by the magnetic lattice and is usually positive, periodic, and of the order of $\sim \rho/Q_x^2$. Second, the radius of curvature and orbit path-length C vary with the momentum and, to first order, are characterized by the momentum compaction factor $\alpha_{\rm c}$,

$$\alpha_{\rm c} \equiv \frac{\Delta C/C}{\Delta p/p} = \frac{1}{C}\oint\frac{D_x(s)}{\rho(s)}ds\,, \tag{31.11}$$

which typically is of order $1/Q_x^2$. Energy deviations also result in changes of machine focusing lattice properties and variations of the particle tunes, characterized by the *chromaticity* $Q'_{x,y} \equiv \Delta Q_{x,y}/(\Delta p/p)$. The natural chromaticity due to momentum dependence of the quadrupole focusing is negative and large $\sim -Q_{x,y}$. Corresponding chromatic tune variations can, therefore, become unacceptably large even for relatively small energy deviations $(\Delta p/p) \sim (0.1 - 1)\cdot 10^{-3}$. To assure transverse particle stability, usually, the chromaticity is partially or fully com-

Downloaded from https://academic.oup.com/ptep/article/2022/8/083C01/6651666 by KIT Library user on 27 September 2022

pensated by additional sextupole magnets placed at locations of non-zero dispersion.

Radiofrequency electric fields in s direction provide a longitudinal focusing effect, allowing a stable increase of particle energy. The frequency f_s of such longitudinal *synchrotron oscillations* is (expressed in units of revolution frequency f_0, to become the synchrotron tune Q_s)

$$Q_s \equiv \frac{f_s}{f_0} = \sqrt{\frac{(\alpha_c - 1/\gamma^2) hZeV_{\rm RF}\sin(\phi_s)}{2\pi\beta cp}}\,, \tag{31.12}$$

where $h = f_{RF}/f_0$ denotes the RF harmonic number, $V_{\rm RF}$ the RF voltage, and $\phi_s = \cos^{-1}(\Delta E/ZeV_{\rm RF})$ the synchronous phase, with ΔE the average energy loss per turn (e.g. due to synchrotron radiation and impedance). The synchrotron tune Q_s determines the amplitude of longitudinal oscillations for a particle with an initial momentum offset, e.g., the rms bunch length σ_z relates to the rms momentum spread $\delta p/p$ as:

$$\sigma_z = \frac{c(\alpha_c - 1/\gamma^2)}{2\pi Q_s f_0}\left(\frac{\delta p}{p}\right). \tag{31.13}$$

Similarly to the case of transverse oscillations, the area of the longitudinal phase space $\{\Delta E, \Delta t\}$, or $\{\gamma\beta\delta p/p = (1/\beta)\Delta\gamma, z = \beta c\Delta t\}$, encircled by a moving particle is an adiabatic invariant, and the corresponding normalized *longitudinal emittance* $\varepsilon_{{\rm n},L} = \beta\gamma mc\sigma_z(\delta p/p)$ is a generally conserved quantity in hadron accelerators and also in linear accelerators. In the case of lepton storage rings, synchrotron radiation determines the equilibrium relative momentum spread, which grows linearly with beam energy [7, 8], and the corresponding bunch length follows from Eq. (31.13). In hadron synchrotrons, the longitudinal emittance sometimes is intentionally blown up during acceleration, so as to preserve longitudinal beam stability.

Longitudinal oscillations are the slowest of all the periodic processes which take place in the accelerators. For example, in the LHC, the frequency of synchrotron oscillations at the top energy of 7 TeV is about f_s = 23 Hz, the revolution frequency is f_0 =11.3 kHz, the frequency of betatron oscillations is about $Q_{x,y}f_{\rm rev} \simeq 700$ kHz and the RF frequency is $f_{\rm RF}$ = 400.8 MHz ($h = 35640$). It should be noted that longitudinal motion is practically absent in linacs. In the absence of bending dipoles, dispersion $D_x(s)$ is zero and so are the momentum compaction factor α_c and the synchrotron tune Q_s. As a result, ultrarelativistic particles in a linac barely change their relative positions during acceleration despite significant energy spread.

Highest-energy circular colliders face a serious impediment in the form of synchrotron radiation (SR) that causes an energy loss per turn of

$$\Delta E_{\rm SR} = \frac{1}{3\varepsilon_0}\frac{Z^2e^2\beta^3\gamma^4}{\rho}\,, \tag{31.14}$$

here, ε_0 is the permittivity of vacuum. For electrons and positrons it is equal to $\Delta E_{\rm SR}$ = 88.5 [keV/turn] $E_{\rm b}^4$[GeV]/ρ[m] and requires correspondingly high total RF voltage per turn to replenish the loss. Above a few hundred GeV, the SR energy loss becomes comparable to beam energy $\Delta E_{\rm SR} \sim E_{\rm b}$, which makes circular e^+e^- colliders impractical for c.m.e. above $\sim$ 500 GeV.

Dynamics of the particle spin and sophisticated methods to maintain beam polarization along the acceleration chain, from the polarized sources to collisions, dedicated spin matching procedures to enable self polarization in e^+/e^- storage rings and the *resonant depolarization* method of ultra-precise c.m.e. calibration are described in [9].

31.2.2 *High Intensity Beams*

Ultimate collider luminosity calls for high beam currents $I_{\rm b} = Zef_0n_{\rm b}N$. Three related major difficulties include growing RF demands to compensate the synchrotron-radiation power loss $P = I_{\rm b}\Delta E_{\rm SR}$ in e^+/e^- beams, the advent of so-called *coherent* or *(collective) beam instabilities*, and growing demands for minimization of radiation due to inevitable particle losses. Many types of single- and multi-bunch instabilities are caused by beam interactions with electromagnetic fields induced by the beam itself due to the *impedance* of the vacuum chambers and RF cavities [4], or caused by unstable clouds of secondary particles, like electrons or ions, which are formed around the circulating beams [10]. These instabilities can develop as quickly as within tens to thousands of turns and need to be controlled. Mechanisms that are routinely employed to avoid coherent instabilities include the use of nonlinear magnets to generate sufficient spread of the tunes and therefore, provide *Landau damping*, fast beam-based transverse and longitudinal feedback systems, and electron/ion clearing (either by weak magnetic or electric fields or by modulation of the primary beam current profile rendering secondaries unstable, or by reducing the yield of secondary electrons via either a special coating or extensive *beam scrubbing* of the vacuum chamber walls).

High current beam operation is sensitive to even minuscule fractional intensity losses caused by particles' scattering at a large angle or with a large energy loss, sufficient for either the particle amplitudes $\sqrt{2J_{x,y}\beta_{x,y}(s)}$, or their dispersive position deviations $\Delta x = D_x(s)(\delta p/p)$ to exceed the available transverse aperture, usually set by collimators (otherwise, by the vacuum chamber and magnet apertures). This can be due to residual vacuum molecules near the beam orbit or Compton scattering off thermal photons, due to Coulomb scattering off other particles within the same bunch (*Touschek effect*), or due to collisions with opposite beam particles and fields, such as inelastic interaction of protons, Bhabha scattering $e^+e^- \to e^+e^-$, or radiative Bhabha scattering $e^+e^- \to e^+e^-\gamma$ (see corresponding chapters in [11]).

Particles can also get lost on the aperture as a result of much slower mechanisms of diffusion caused either by the above processes with smaller scattering amplitudes, but stochastically repeated many times, such as intensity-dependent multiple Coulomb *intrabeam scattering* [12], by external noises such as ground motion or magnetic field fluctuations, or via chaotic mechanisms like Arnold diffusion, modulational diffusion, or resonance streaming in nonlinear fields, enhanced by minor tune modulations. Diffusion leads to a slow evolution of the beam distribution function and appearance of highly unwanted large-amplitude tails and beam emittance growth. The only way to counteract it is to arrange *beam cooling* (damping of particle oscillations). The cooling requires a reaction force opposite to particle momentum arranged such that, on average, the corresponding dissipative particle energy loss is compensated for by external power [13, 14].

In the case of electron or positron storage rings, such cooling occurs naturally due to synchrotron radiation and provides an automatic route to achieve small equilibrium emittances through a balance between radiation damping and excitation of oscillations by random radiation of individual photons. Fast radiation damping allows *top-up injection* of new particles without removing existing ones, a useful method to maximize the integrated luminosity of circular e^+e^- colliders. Synchrotron radiation damping will also be an important cooling mechanism for future energy-frontier hadron colliders, like the proposed FCC-hh and SppC (see below).

Four other methods of beam cooling have been developed and successfully employed to attain low emittances, namely *electron cooling* and *stochastic cooling* of heavy particles (ions and antiprotons), *laser cooling* of ion beams, and the *ionization cooling* of muons.

To avoid damage or excessive irradiation of accelerator components so that these remain accessible for maintenance in the tunnel, sophisticated collimation systems are utilized. These systems usually employ a series of targets or primary collimators which scatter the halo particles, and numerous absorbers (sometimes as many as a hundred, which intercept particles in dedicated locations) [15, Ch.9.7]. In the highest energy modern and future colliders, extreme total beam energies $n_{\rm b}NE_{\rm b}$ ranging from MJs to GJs and impacting energy surface densities reaching many GJ/mm^2 pose one of the biggest challenges for high efficiency and robust particle collimation.

31.2.3 *High Luminosity Collisions*

Eq. (31.3) for luminosity can be recast in terms of normalized transverse emittances Eq. (31.10) and the beta-functions β^* at

Downloaded from https://academic.oup.com/ptep/article/2022/8/083C01/6651666 by KIT Library user on 27 September 2022

the IP as:

$$\mathcal{L} = f_0 \gamma n_{\rm b} \frac{N^2}{4\pi\sqrt{\varepsilon_{\rm nx}\beta_x^*\varepsilon_{\rm ny}\beta_y^*}}\mathcal{F}\,. \tag{31.15}$$

Here, equal bunch populations N are assumed in two Gaussian beams with the same emittances. Naturally, to achieve a high luminosity, one has to maximize the total beam populations $n_{\rm b}N$ within the lowest possible emittances, and collide the beams at high frequency at locations where the focusing beam optics provides the lowest possible values of the amplitude functions β^*, the so-called *low-beta insertion*. The latter requires sophisticated systems of strong focusing elements, sometimes occupying quite a significant fraction of the collider's total length. The lowest $\beta^*_{x,y}$ is determined by the maximum field gradients and apertures in the interaction region (IR) magnets and the effectiveness of compensation of chromatic and nonlinear aberrations.

The typical geometric reduction factor is $\mathcal{F} \approx 1$, and it rarely drops below 0.5 for the majority of colliders, unless this is specifically required by physics processes under study. The reduction due to the *hourglass effect* is caused by the increase in transverse beam sizes as one proceeds away from the IP, where $\beta(s)$ grows parabolically, as in Eq. (31.8). For long round bunches the effect scales as $\mathcal{F} \approx \sqrt{\pi}A\exp(A^2){\rm erfc}(A)$, where $A = \beta^*/\sigma_z$. Nonzero beam crossing angles $\theta_{\rm c}$ in the horizontal plane and long bunches (rms bunch length σ_z) will reduce the luminosity, too, by a factor $\mathcal{F} \approx 1/(1+\Phi^2)^{1/2}$, where the parameter $\Phi = \sigma_z \tan(\theta_{\rm c}/2)/\sigma_x^*$ is known as the *Piwinski angle*.

One of the most common limits to producing high luminosity arises from electric and magnetic forces of the opposite bunch at the IPs, characterized by a dimensionless *beam-beam parameter* :

$$\xi_{x,y} = \frac{r_0 N \beta^*_{x,y}}{2\pi\gamma\sigma^*_{x,y}(\sigma^*_x + \sigma^*_y)}\,, \tag{31.16}$$

where $r_0 = Z^2e^2/(4\pi\varepsilon_0 mc^2)$ is the classical radius of the colliding particle (with charge Ze and mass m). From Eqs. (31.3) or (31.15) and (31.16), one can note that the path to higher luminosity via higher beam intensity and smaller beam sizes almost automatically calls for a higher beam-beam parameter as $\mathcal{L} \propto \xi$. Cited in the Tables, the beam-beam parameter is roughly equal to the betatron tune shift experienced by small-amplitude particles – positive in the case of opposite charge beams, like e^+e^-, and negative for same charge beams as in pp collisions. Beam-beam forces can lead to coherent effects, such as unstable beam oscillations or blow-up of one beam's size while the other beam remains small or even shrinks (*flip-flop effect*). The tune spread arising from ξ and the nonlinear nature of beam-beam interactions results in strong diffusion along high-order transverse resonances $kQ_x + lQ_y = m$ and, ultimately, in beam size growth and beam losses. Operational experience indicates that the aforementioned effects are tolerable below certain *beam-beam limit* of $\xi_{x,y} \approx 0.003 - 0.012$ in hadron colliders [16], and – due to strong synchrotron radiation damping – an order of magnitude higher one in e^+e^- colliders, with maximum $\xi_{x,y} \approx 0.03 - 0.12$ [17, 18]. The accessible beam-beam parameter range can also be restricted by coherent beam-beam instabilities. These various limits translate into a maximum allowed single bunch intensity N and call for an increase of the number of bunches n_b to achieve higher luminosities.

In linear colliders, where each bunch collides only once, with typically much smaller beam size and experiencing much stronger forces, the strength of the collision is measured by the ratio of the rms bunch length σ_z to the beam-beam focal length. This ratio, called *disruption parameter* D_y, is related to ξ_y via $D_y = 4\pi\sigma_z\xi_y/\beta^*_y$. Significant disruption leads to effectively smaller beam size and a resulting luminosity enhancement; it also makes the collision more sensitive to small offsets, resulting in a *kink instability*. Additional beam-beam effects arising in the collisions at linear colliders are the emission of *beamstrahlung* (synchrotron radiation in the field of the opposing beam), along with e^+e^- pair creation, and depolarization by various mechanisms.

Beamstrahlung is relevant for both linear colliders, where it may significantly degrade the luminosity spectrum, and for future highest-energy circular colliders, where it may limit the beam lifetime, and also increases the energy spread and bunch length of the stored beam. For both types of colliders, the beamstrahlung is mitigated by making the colliding beams as flat as possible at the interaction point ($\sigma^*_x \gg \sigma^*_y$). The photon energy spectrum of the beamstrahlung is characterized by the parameter $\Upsilon = (2/3)\hbar\omega_{\rm c}/E_{\rm b}$ [19], with $\hbar\omega_{\rm c}$ denoting the critical photon energy. The spectrum strongly deviates from the classical synchrotron radiation spectrum for Υ approaching or exceeding 1.

For hadron colliders, two fundamental luminosity limits are the beam lifetime, determined by burn-off in the collisions due to inelastic pp interaction $dN/dt = -\mathcal{L}\sigma_{\rm in}$, and the radiation from the collision debris, which may induce "quenches" (transitions to the normal-conducting state) of the superconducting final quadrupole magnets, and, in the long term, affect the equipment lifetime. Another limit on the achievable integrated luminosity in circular colliders is set by the minimum or average turnaround time (the time between the beam abort at the end of a physics fill and the start of the next physics collisions). Achieving practical filling times with many bunches in the collider requires either fast cycling injector machines and/or the top-up injection operation. The latter makes the average luminosity of circular electron-positron colliders approximately equal to the peak luminosity.

31.3 Recent High Energy Colliders

In this and the following section, elaboration is made on various issues associated with some of the recently operating colliders, particularly factors which impact integrated luminosity. Only general references are provided, where further information can be obtained. A more complete list of recent colliders and their parameters can be found in the High-Energy Collider Parameters tables.

31.3.1 *Tevatron*

The first superconducting synchrotron in history, the Tevatron [20] was converted into a proton-antiproton collider in 1985. Its 4.4 T dipole magnets employed Nb-Ti superconducting cable operating at 4.5 K, requiring what was then the world's largest cryogenic system. With $\sqrt{s}$ up to 1.96 TeV it was the highest energy collider for 25 years and delivered more than 12 fb^{-1} of the integrated luminosity to each $p\bar{p}$ detector experiments (CDF and D0) before being shut off in 2011. The route to high integrated luminosity in the Tevatron was governed by the antiproton production rate, the turn-around time to produce another store, and the resulting optimization of store time [21]. The antiproton production complex consisted of three 8 GeV $\bar{p}$ accelerators (the Accumulator, Debuncher, and Recycler – the latter was the first high energy accelerator built with permanent magnets), and employed 25 independent stochastic cooling systems and one pioneering high-energy electron cooling set-up to accumulate up to a record high value of $25{\cdot}10^{10}$ $\bar{p}$ per hour. Despite severe parasitic long-range interactions of the two beams, each consisting of 36 bunches placed on helical orbits by two dozen ±150 kV high-voltage (HV) separators, a total beam-beam tune shift parameter of $n_{\rm IP}\xi$ ≈0.025-0.03 was achieved, a record for hadron beams, with $n_{\rm IP} = 2$ primary collision points. Other notable advances in the accelerator science and technology included advanced longitudinal beam manipulation techniques of *slip-stacking* and *momentum mining* and the first operational use of *electron lenses* for beam collimation and for compensation of long-range beam-beam effects [22]. The Tevatron ultimately achieved luminosities a factor of 430 higher than the original design specification.

31.3.2 *HERA*

The first lepton-proton collider, the 6.4 km long Hadron-Elektron-Ring-Anlage (HERA) at DESY in Germany [23], operated between 1992 and 2007 and delivered nearly 1 fb^{-1} of integrated luminosity at $\sqrt{s}$ of about 320 GeV to the electron-proton collider experiments H1 and ZEUS [24, Ch.10.5]. It was the first facility to employ both applications of superconductivity: 5 T magnets in the 920 GeV proton ring and SRF accelerating structures to provide about 12 MW of RF power to compensate for synchrotron radiation losses of 30 GeV lepton beams (positrons or electrons, in a conventional-magnet ring). With proper orbit and

Downloaded from https://academic.oup.com/ptep/article/2022/8/083C01/6651666 by KIT Library user on 27 September 2022

optics control, the HERA lepton beam would naturally become transversely polarized to about 60% (within about 40 minutes) thanks to the *Sokolov-Ternov effect*. Special magnets called *spin rotators* were implemented on either side of the collider IPs to produce 30–45% longitudinal polarization at the experiments.

31.3.3 *LEP*

Installed in a tunnel of 26.7 km circumference, LEP [25] was the largest circular e^+e^- collider built so far. LEP was operated from 1989 to 2000 with beam energies ranging from 45.6 to 104.5 GeV. The synchrotron radiation loss per turn reached some 3% of beam energy and it was the total available RF voltage and power, respectively, that determined LEP maximum energy and luminosity of 10^{32} cm^{-2}s^{-1}. At a beam energy of 98 GeV, LEP operated with a beam-beam parameter $\xi \approx 0.083$, i.e., the total beam-beam tune shift for four interaction points was $n_{\rm IP}\xi \approx 0.33$. In the last year of operation, 288 SRF cavities were powered by 36 klystrons with an average power of 0.6 MW each and provided $V_{\rm RF}$= 3.63 GV. Up to about 60 GeV, LEP used resonant depolarization to measure the beam energy with 0.001% accuracy.

31.3.4 *SLC*

Based on an existing 3-km long 2.85 GHz warm RF linac, the SLC [26] was the first and only linear collider. It was operated from 1987 to 1998 with a constant beam energy of 45.6 GeV, up to about 80% electron-beam polarization, quasi-flat beams, a final-focus optics with local chromatic correction based on four interleaved sextupoles and $\beta_y^* \approx 1$ mm. In its last year, SLC achieved a peak luminosity of about 3×10^{30} cm^{-2}s^{-1}, roughly half of the design value. The SLC had a high-efficiency positron source providing 5×10^{12} e^+ per s for 120 Hz injection into the linac. It also employed the *BNS damping* to suppress the single-bunch beam break up instability, and also demonstrated an about 2-fold increase of luminosity from *disruption enhancement* due to the mutual focusing of the colliding electron and positron bunches at the interaction point,

31.4 Presently Operating Colliders

31.4.1 *LHC*

With a beam energy of 6.5 TeV (to be raised, first, to 6.8 TeV and, then, to the design value of 7 TeV, through consolidation and magnet training), the superconducting Large Hadron Collider [27] presently is the world's highest energy collider. In the latest runs, peak luminosities of up to 2.1×10^{34} cm^{-2}s^{-1} have been achieved - more than twice the design value (the current status is best checked at the Web site [28]). To meet its luminosity goals, the LHC operates with a high beam current of approximately 0.5 A, leading to stored energies of about 330 MJ per beam. Controlled energy deposition and component protection are given a high priority and a sophisticated highly efficient system of more than 100 beam collimators is employed [29]. At the energy of 6.5 or 7 TeV per particle, synchrotron radiation poses a challenge, as the cryogenic system must remove roughly 7 kW due to synchrotron radiation, intercepted with a specially designed *beamscreen* inside the vacuum chamber, at a temperature of about 5–20 K, to be compared with a temperature of 1.9 K for the magnet cold bore. The elevated temperature allows for a more energy-efficient removal of beam-induced heat. The beamscreen also provides an effective cryo-pump for the vacuum system. When synchrotron-radiation photons hit the beamscreen, they can generate photoelectrons. These photoelectrons, and also any other electrons generated in the vacuum system, e.g. by residual-gas ionization, are accelerated in the electric field of the beam and may multiply via secondary-electron emission, with consequent electron cloud development. To mitigate this issue, the beamscreen is regularly subjected to beam-induced surface conditioning (*scrubbing*), thereby lowering the secondary emission yield. The two proton beams of 2556 bunches spaced by 25 ns are contained in separate pipes throughout most of the circumference and are brought together into a single 130 m long beam pipe at the interaction points. To avoid approximately 30 head-on collisions a small crossing angle of about 0.3 mrad is employed, which reduces the luminosity by about 15%. Still, the bunches moving in one direction experience multiple long-range encounters with the counter-rotating bunches and the resulting perturbations of the particle motion substantially contribute to the beam lifetime reduction. The dominant source of approximately 8 hour characteristic luminosity decay time is proton burn-off due to inelastic *pp* interaction with $\sigma_{\rm in} \approx 81$ mbarn, corresponding to *pile-up* of up to 50 (number of events per individual bunch crossing). In special physics runs with a few bunches and large β^*, the LHC achieved a head-on beam-beam tune shift of $n_{\rm IP}|\xi| \approx 0.02$ with $n_{\rm IP} = 2$ [30], about twice as high as in regular operation.

The Tables also show the LHC luminosity performance in Pb-Pb collisions, which for the ATLAS and CMS experiments well exceeded the design value, while for the ALICE experiment, the luminosity is *levelled* near the Pb-Pb design value of 10^{27} cm^{-2}s^{-1}. The LHC can also provide Pb-p collisions as it did in 2013 and 2016, and other ion-ion or ion-proton collisions, at different energies.

In the coming years, an ambitious upgrade program, HL-LHC [31], with the accompanying LHC Injectors Upgrade [32], has as its target an order-of-magnitude increase in integrated luminosity through doubling the proton beam current, the utilization of new larger aperture Nb_3Sn superconducting final quadrupoles to allow squeezing the β^* to as low as 10 cm, superconducting compact *crab cavities* and luminosity leveling also for ATLAS and CMS as its key ingredients.

31.4.2 *Electron-Positron Rings*

Asymmetric energies of the two beams allow for the enhancement of *B*-physics research and for interesting interaction region designs. SuperKEKB operates with 7 GeV electron and 4 GeV positron beams since 2018 and is aiming for luminosities of 8×10^{35} cm^{-2}s^{-1} [33]. By summer 2021, a world record luminosity in excess of 3×10^{34} cm^{-2}s^{-1} has been reached, still at rather low beam currents. Vertical beam-beam tune shifts of $\xi_y \approx 0.5$ for the 4 GeV positron beam, and $\xi_y \approx 0.03$ for the 7 GeV electron beam have been achieved. These values are still about a factor of two lower than at the previous KEKB. Since 2020 SuperKEKB operates with a virtual *crab-waist* collision scheme, first developed for the FCC-ee design [34]. The original crab-waist scheme, based on additional sextupole magnets, was earlier implemented at DAΦNE [35]. The general crab-waist concept combines a large Piwinski angle Φ, and an extremely low β_y^* ($\ll \sigma_z$) with the cancellation of the transverse betatron resonances which occur under conditions of $kQ_x + lQ_y = n$, where k, l, n are integers. The latter is achieved by means of existing or additional electromagnetic sextupoles with special betatron phase advances to the collision point [36]. The crab-waist collision scheme has become a design choice for all proposed future e^+e^- circular colliders.

Beside SuperKEKB and DAΦNE, three other e^+e^- ring colliders currently in operation are VEPP-2000 with $\sqrt{s}$ up to 2.0 GeV, BEPC-II with $\sqrt{s}$ up to 4.6 GeV and VEPP-4M with maximum c.m.e. of 12 GeV [1].

31.4.3 *RHIC*

The Relativistic Heavy Ion Collider [37] employs 3.45 T Nb-Ti superconducting magnets, and collides combinations of fully-stripped ions such as H-H ($p-p$), *p*-Al, *p*-Au, *d*-Au, *h*-Au, Cu-Cu, Cu-Au, Zr-Zr, Ru-Ru, Au-Au, and U-U over a wide energy range. The high charge per particle (+79 for gold, for instance) makes intra-beam scattering of particles within the bunch a special concern, even for seemingly moderate bunch intensities. In 2012, 3-D stochastic cooling was successfully implemented in RHIC [38] and is now routinely used. With stochastic cooling, steady increases in the bunch intensity, and numerous other upgrades, RHIC now operates at 44 times the Au-Au design average luminosity. Unique among high energy colliders, RHIC heavy ions beams cross the *transition energy* $\gamma_{rmt} = 1/\sqrt{\alpha_c}$ during acceleration – see Eqs.(31.11, 31.12) – a point where the derivative with respect to momentum of the revolution period is zero. This period of time is kept as short as allowed by the magnet ramp rate and must be dealt with carefully.

RHIC is also unique in its ability to accelerate and collide polarized proton beams. As proton beam polarization must be maintained from its low-energy source, successful acceleration through the myriad of depolarizing resonance conditions in high energy

Downloaded from https://academic.oup.com/ptep/article/2022/8/083C01/6651666 by KIT Library user on 27 September 2022

circular accelerators has taken years to accomplish [39]. An energy of 255 GeV per proton with 60% final polarization per beam has been realized. As part of a scheme to compensate the head-on beam-beam effect, electron lenses operated routinely during the record high beam-beam parameter polarized proton operation at 100 GeV energy in 2015 [40].

31.5 Future High Energy Colliders and Prospects

Modern nuclear physics and high energy particle physics face critical questions which require next-generation high-energy and high-intensity experiments using hadron-hadron, lepton-lepton, and lepton-proton colliding-beam facilities. Understanding the structure of the proton and neutron directly from the dynamics of their quarks and gluons governed by the quantum chromodynamics calls for new ion-ion and electron-ion colliders. Two types of colliders are generally aspired by the HEP community [41]: i) Higgs factories with a c.m.e. of 240–250 GeV in e^+e^- collisions for precision studies of the Higgs boson ($m_H = 125$ GeV) and exploration of the Higgs sector in greater detail, including measurements of Higgs couplings to fermions and vector bosons, self-coupling, rare decays, mass and width, that can also deliver other electroweak precision physics, e.g. on the Z-pole (91 GeV c.m.e.), at the W-pair threshold (about 160 GeV), and when run as a top quark factory (365–380 GeV); and ii) colliders to explore the energy frontier for potential discoveries through direct searches with c.m.e. levels significantly beyond those of the LHC in pp, $\mu\mu$ and e^+e^- interactions. In addition, precision physics at future high-luminosity factories operating at the τ-charm energy also provides sensitivity to new physics at multi-TeV energies and beyond. A comprehensive review of the future colliders' projects, ideas, and R&D activities can be found in Ref. [1]. Below we only briefly summarize leading collider proposals for construction over the next several decades which rely mostly on currently available technologies, such as normal-conducting (NC) or SC RF and/or NC or SC magnets, some of them requiring reasonable scope and duration mission-oriented development programs, as well as advanced schemes based on plasma acceleration and other innovative ideas. Tentative parameters of some of the colliders discussed, or mentioned, in this section are summarized in Table 31.1 and Table 31.2.

31.5.1 *Ion-Ion and Electron-Ion Colliders*

NICA (Nuclotron-based Ion Collider fAcility) is a new accelerator complex under construction at the Joint Institute for Nuclear Research (JINR, Dubna, Russia) to study properties of hot and dense baryonic matter, strong interactions between quarks and gluons, and spin physics [42]. NICA will provide a variety of beam species, ranging from protons and polarized deuterons to massive gold ions. The 500 m circumference SC magnet based collider is designed for average luminosity in heavy ion and light ion interactions at $\sqrt{s_{NN}}$=4–11 GeV of $1\times10^{27}\mathrm{cm}^{-2}\mathrm{s}^{-1}$ for a variety of nuclei up to $^{197}\mathrm{Au}^{79+}$, and for polarized proton and deuteron collisions at $\sqrt{s}$=12–27 GeV with $\mathcal{L}$=(1–10)$\times10^{31}\mathrm{cm}^{-2}\mathrm{s}^{-1}$. NICA major accelerator challenges include strong intrabeam scattering and space-charge effects which will be mitigated by extensive use of electron and stochastic cooling systems.

The recently announced Electron-Ion Collider (EIC) for nuclear physics research will be built at Brookhaven National Laboratory in the US and arrange collisions between an the reconfigured RHIC with a 41–275 GeV proton beam and a 5-18 GeV electron beam stored in a new ring (eRHIC) [43]. The EIC physics requirements [44], include highly polarized ($P_{e,n}$ ~70%) electron and nucleon beams (as the precision of measurements of interest scales as $\mathcal{L}P_e^2P_n^2$), a spectrum of ion beams from deuterons to the heaviest nuclei (U or Pb), variable c.m.e. values from $\sqrt{s}$ =20 GeV to 140 GeV, high luminosities of up to 10^{33-34} $\mathrm{cm}^{-2}\mathrm{s}^{-1}$, as well as possibilities of having more than one interaction region. Main accelerator design challenges on the path to the required energy, luminosity, and polarization, include the development of SRF crab-cavities and advanced SC magnets for interaction region focusing, energy-recovery linac (ERL) based electron cooling of hadron beams, essential to attain luminosities two orders of magnitude beyond the predecessor HERA *ep* collider, and high intensity polarized particle sources, augmented by the development of special magnets and operational techniques to preserve the polarization through the acceleration process to the collisions, including swap-out injection.

31.5.2 *Higgs/Electroweak Factories*

Higgs factory proposals generally aim at improving the precision of coupling measurements of Higgs boson, top quark, W and Z by an order of magnitude or more compared with previous studies. Two proposals for ~100 km circumference circular e^+e^- colliders have recently gained momentum: the Future Circular Collider (FCC-ee) at CERN [34] and the Circular Electron-Positron Collider (CEPC) in China [45]. Design philosophy of these machines assumes use of the maximum RF power available to compensate O(100 MW) synchrotron radiation losses $P_{SR} = 2I \cdot \Delta E_{SR}$ and operation at the beam-beam limit ξ_y that yields peak luminosity:

$$\mathcal{L} = \frac{3}{16\pi r_0^2(m_e c^2)} \frac{P_{\mathrm{SR}}\xi_y\rho}{\beta_y^*\gamma^3}\,, \tag{31.17}$$

that scales approximately as $1/E_{\mathrm{b}}^{3.5}$ for practical limits on P, ξ_y and β_y^*. The short beam lifetime at the high target luminosity, due to radiative Bhabha scattering, requires these machines to be constructed with a full-energy injector ring installed in the same tunnel to *top off* the electron and positron currents in the collider rings operating at constant energy. Beamstrahlung introduces an additional beam lifetime limitation depending on momentum acceptance (so that achieving sufficient off-momentum dynamic aperture becomes one of the design challenges), as well as some bunch lengthening.

These ambitious, large-scale projects based on well-established technologies are not extendable to TeV or multi-TeV energies, but they offer several important advantages that include the potential for much higher luminosities and, thus, higher precision, the ability to operate multiple experiments simultaneously, and their 100 km circular tunnels that could later house O(100 TeV) hadron colliders.

For more than four decades, efforts have been devoted to developing high-gradient RF technology linear e^+e^- colliders in order to overcome the synchrotron radiation limitations of circular e^+e^- machines. The International Linear Collider (ILC), with a c.m.e. of 250 GeV in e^+e^- collisions, has been under consideration for more than two decades and could potentially be upgraded to $\sqrt{s}$=500 GeV and further to 1 TeV. CERN's Compact Linear Collider (CLIC) design, developed since the mid-1980s, also includes possible upgrades, from an initial 380 GeV c.m.e. to ultimately 3 TeV, which would enable searches for new particles of significantly higher masses.

The primary challenge confronting a high energy, high luminosity single pass collider design is the beam power requirement, so that measures must be taken to keep the demand within bounds as illustrated in a transformed Eq.(31.15):

$$\mathcal{L} = \frac{1}{8\pi\alpha r_0}\,\frac{P_{\mathrm{wall}}}{\sqrt{s}}\,\frac{\eta}{\sigma_y^*}\,N_\gamma\,H_{\mathrm{D}}\,. \tag{31.18}$$

Here, P_{wall} is the total wall-plug power of the collider, to be converted into beam power $P_{\mathrm{b}} = 2f_0NE_{\mathrm{b}}$ with efficiency η, $N_\gamma \approx 2\alpha r_0 N/\sigma_x^*$ is the number of beamstrahlung photons emitted per $e^\pm$ (α denotes the fine-structure constant), and the last factor H_{D}, typically between 1 and 2, represents the enhancement of luminosity due to the *pinch effect*, the additional focusing occurring during the collision of oppositely charged bunches. The management of P_{wall} leads to an upward push on the bunch population N with an attendant rise in the energy radiated due to the electromagnetic field of one bunch acting on the particles of the other (beamstrahlung). Keeping a significant fraction of the luminosity close to the nominal energy represents a design goal, which is met if N_γ does not exceed a value of about 1. A consequence is the use of flat beams, where N_γ is managed by the beam width, and luminosity adjusted by the beam height, thus the explicit appearance of the vertical beam size σ_y^*.

The ILC [46, 47] is based on 1.3 GHz superconducting accelerating structures with 31.5 MV/m average gradient, up to 8 nm

Downloaded from https://academic.oup.com/ptep/article/2022/8/083C01/6651666 by KIT Library user on 27 September 2022

Table 31.1: Tentative parameters of selected future e^+e^- high-energy colliders. Parameters associated with different beam energy scenarios are comma-separated; H and V indicate horizontal and vertical directions.

	FCC-ee	CEPC	ILC	CLIC
Species	e^+e^-	e^+e^-	e^+e^-	e^+e^-
Beam energy E_b (GeV)	46, 120, 183	46, 120	125, 250	190, 1500
Circumference or length (km)	97.75	100	20.5, 31	11, 50
Interaction regions	2	2	1	1
Est. integrated luminosity per experiment (ab^{-1}/year)	26, 0.9, 0.17	4, 0.4	0.2, 0.3	0.1, 0.6
Peak lumi. $\mathcal{L}$ (10^{34}cm^{-2}s^{-1})	230, 8.5, 1.55	32, 3	1.4, 1.8	1.5, 6
Rep.rate (Hz, f_rev for rings)	3067	3000	5	50
Polarization (%)	$\geq$10, 0, 0	5–10, 0	80/30 (e^-/e^+)	80/0 (e^-/e^+)
Time between collisions (μs)	0.02, 0.99, 3.4	0.025, 0.68	0.55	0.0005
Energy spread (rms, 10^{-3})	1.3, 1.65, 2.0	0.8, 1.3	e^-: 1.9, 1.2 e^+: 1.5, 0.7	3.5
Bunch length σ_z (rms, mm)	12.1, 5.3, 2.5	8.5, 4.4	0.3	0.07, 0.044
IP beam size σ^* (rms, μm)	H: 6.4, 14, 38 V: 0.03, 0.04, 0.07	H: 6.0, 21 V: 0.04, 0.06	H: 0.52, 0.47 V: 0.008, 0.006	H: 0.15, 0.04 V: 0.003, 0.001
Emittance, ε_n (rms, μm)	H: 24, 148, 520 V: 0.09, 0.3, 1.0	H: 16, 284 V: 0.14, 0.6	H: 5, 10 V: 0.035, 0.035	H: 0.95, 0.66 V: 0.03, 0.02
β^* at interaction point (cm)	H: 15, 30, 100 V: 0.08, 0.1, 0.16	H: 20, 36 V: 0.1, 0.15	H: 1.3, 1.1 V: 0.041, 0.048	H: 0.8, 0.69 V: 0.01, 0.0068
Full crossing angle θ_c (mrad)	30	33	14	20
Crossing scheme	crab waist	crab waist	crab crossing	crab crossing
Piwinski angle $\Phi = \sigma_z\theta_\mathrm{c}/(2\sigma_x^*)$	28.5, 5.8, 1.0	23.8, 3.5	0	0
Beam-beam param. ξ_y (10^{-3})	133, 118, 126	79, 109	n/a	n/a
Disruption parameter D_y	0.9, 1.3, 1.1	0.4, 1.1	35, 25	13, 8
Average Upsilon Υ (10^{-2})	0.02, 0.05, 0.08	0.01, 0.04	3, 6	17, 500
RF frequency f_RF (MHz)	400, 400, 800	650	1300	11994
Particles per bunch N (10^{10})	17, 18, 23	8, 15	2	0.52, 0.37
Bunches per beam n_b	16640, 328, 48	12000, 242	1312 (pulse)	352, 312 (trains at 50 Hz)
Average beam current I_b (mA)	1390, 29, 5.4	461, 17.4	0.021	0.014, 0.009
Injection energy (GeV)	on E_b (top off)	on E_b (top off)	5.0 (linac)	9.0 (linac)
RF gradient G (MV/m)	1.3, 9.8, 19.8	3.6, 19.7	31.5	72, 100
Total SR power loss (MW)	100	33, 60	n/a	n/a
Total beam power (MW)	n/a	n/a	5.3, 10.5	5.6, 28
Key technology	—	—	high grad. SC RF	two-beam accel.

vertical beam size at the IP, and luminosity comparable to the LHC. Progress toward higher field gradients and Q values continues to be made, with nitrogen-doping techniques being a recent example [48]. CLIC is based on a novel two-beam acceleration scheme [49]. Here, NC copper high-gradient 12 GHz accelerating structures are powered by a high-current 1.9 GeV drive beam to efficiently enable accelerating gradients of up to 100 MV/m (though optimal G=70 MV/m for the first CLIC stage at $\sqrt{s}$=380 GeV, and for this stage an alternative RF power drive option with 12 GHz klystrons powering is also being considered). To reach their design luminosities, both CLIC and ILC require unprecedented rates of positron production about 40 times the world record set by the SLC positron source, and very tight control of imperfections, such as $O(10\ \mu\mathrm{m})$ accuracy of pre-alignment of the main linac and beam delivery system components at the level, suppression of fast vibrations of the quadrupoles due to ground motion to $O(1\ \mathrm{nm})$ level at frequencies above 1 Hz, advanced beam-based trajectory tuning, and mitigation of the effect of wakefields [50].

There are a number of alternative ideas proposed for studies of the Higgs/Electroweak physics, such as high-energy, high-luminosity e^+e^- collider in a 100 km tunnel using ERLs to accelerate particles to collision energy in 4 to 6 passes and return up to 81% of the energy back into the SRF cavities on deceleration turns, thus, lowering the required facility power several-fold [51]; similar power recovery in one pass can greatly improve efficiency of linear colliders [52–54]; an arrangement of $\gamma\gamma$ collision through near-IP conversion of high energy electron beams into intense photon beams by backward Compton scattering off a high-power laser [55] or off an FEL photon pulse [56]; $\mu\mu$ Higgs factory with unprecedented 0.004% energy resolution [57], and a high-energy lepton-hadron collider bringing into collision a 60-GeV electron beam from an ERL with the 7 TeV protons circulating in the LHC (LHeC) [58]. At lower energies, Super Tau-Charm Factory proposals aim at the production and precise study of charmonium states and of the tau lepton [59].

31.5.3 *Energy Frontier Circular Colliders*

Several hadron and lepton colliders have been proposed to extend the energy reach beyond the LHC. As noted above, ambitious plans have been proposed to upgrade the FCC and CEPC to hadron colliders – FCC-hh at CERN and Super Proton Proton Collider (SPPC) in China, respectively – by means of next- or next-next generation SC magnets installed in the arc sections of the 100 km rings, so as to enable $\sqrt{s}$ of the order 100 TeV or above [60, 61]. Comparable discovery reach is expected for a circular 10–14 TeV muon collider [62], significantly beyond that of practical e^+e^- linear colliders.

The maximum beam energy Eq.(31.1) is directly proportional to the magnetic field and to the ring circumference, hence, the hadron colliders rely on the development of the technology of 16T Nb_3Sn dipole magnets (FCC-hh) [63] or 12 T iron-based superconducting magnets (SPPC) [64]. Though higher fields are possible with high-temperature superconductors (HTS), more cost-effective might be hybrid magnet designs incorporating Nb-Ti, Nb_3Sn, and an inner layer of HTS and providing fields of about 20 T. Another important technology is the cryogenic beam vacuum system, which has to cope with unusually high levels of synchrotron radiation (up to 5 MW in total, for FCC-hh) in a cold environment. The beam-screen intercepting the radiation inside the cold bore of the magnets should operate at 50 K — significantly higher temperature than in the LHC.

Design luminosities of these hadron colliders $O(10^{35}\ \mathrm{cm}^{-2}\mathrm{s}^{-1})$

Downloaded from https://academic.oup.com/ptep/article/2022/8/083C01/6651666 by KIT Library user on 27 September 2022

Table 31.2: Tentative parameters of selected future high-energy hadronic colliders. Parameters associated with different particle species for NICA and EIC, and different beam-energy scenarios for a muon collider, are comma-separated. Quantities are, where appropriate, r.m.s.; unless noted otherwise, energies refer to beam energy; H and V indicate horizontal and vertical directions. Parameters of HL-LHC can be found in the High-Energy Collider Parameters review tables.

	NICA	EIC	FFC-hh	SPPC	$\mu\mu$ collider
Species	ion-ion, pp	ep, e-ion	pp	pp	$\mu^+\mu^-$
Beam energy E_b (TeV)	$10^{-3}\cdot$(4.5/u, 13)	0.01(e),0.275(p)	50	37.5	0.063, 5
Circumference C (km)	0.503	3.834	97.75	100	0.3, 10
Interaction regions	2	1(2)	4	2	1, 2
Est. integr. luminosity per exp. (ab^{-1}/year)	$10^{-8,-3}$ (ii, pp)	0.1	0.2–1.0	0.4	0.001, 2.0
Peak luminosity $\mathcal{L}$ (10^{34}cm^{-2}s^{-1})	$10^{-7,-2}$ (ii, pp)	1.05	5–30	10	0.008, 20
Rep.rate (Hz, f_rev for rings)	$5.9\cdot10^5$	$7.8\cdot10^4$	3067	3000	15, 5
Time between collisions (μs)	0.077	0.009	0.025	0.025	1, 33
Energy spread (rms, 10^{-3})	1.6 (Au)	0.6 (e), 0.7 (p)	0.1	0.2	0.04, 1
Bunch length σ_z (rms, mm)	600	7 (e), 60 (p)	80	75.5	63, 1.5
IP beam size σ^* (H/V rms, μm)	360	95/8.5	6.7-3.5 (init.)	6.8 (init.)	75, 0.9
Emittance ε_n (H/V rms, mm mrad)	1.1	11.3/1.0 (e), 9.2/1.6 (p)	2.2 (init.)	2.4 (init.)	200, 25
Beta function at IP β^* (H/V cm)	60	45/5.6 (e), 80/7.2 (p)	110–30	75	1.7, 0.15
Beam-beam param. ξ (10^{-3} H/V)	25	72/100 (e),12 (p)	5–15	7.5	22, 78
RF frequency f_RF (MHz)	13/39	591	400	400/200	805/1300
Particles per bunch N (10^{10})	0.23	17.2(e), 6.9(p)	10	15	400, 180
Bunches per beam n_b	22	1160	10400	10080	1
Average beam current I_b (mA)	480	2500(e),1000 (p)	500	730	640, 9 (peak)
Injection energy (GeV)	1-3.8	on E_b (e), 25 (p)	3300	2100	on E_b
Peak magnetic field B (T)	1.8	0.248 (e), 3.80 (p)	16	12	10
Polarization (%)	0(i), >50(p)	> 70(e), >70(p)	0	0	0
SR power loss/beam (MW)	10^{-6}	10(e), $< 10^{-6}$(p)	2.4	1.1	10^{-3}, 0.16
Key technology	electron and stoch. cooling	strong hadron cooling	16 T Nb_3Sn magnets	HTS magnets	muon prod. & cooling

will result in a pile-up of events per crossing $O(500)$ (from up to 50 in LHC) and fast intensity drop due to burn-off. Significant radiation damping of beam emittances will naturally level luminosity evolution, though the total beam-beam tune shift $n_\mathrm{IP}\xi \sim (0.01 - 0.03)$ might need a special control as it will increase during the store [65].

Future hadron colliders are characterized by record high stored beam energy – 8.4 GJ in FCC-hh – rendering machine protection a paramount concern. A very challenging multi-stage collimation system is needed to avoid local beam loss spikes near cold magnets, which would induce magnet quenches. The primary and secondary collimators of the LHC are based on carbon-carbon composite material. For the future hadron colliders, ever stronger materials are being developed and examined, which also feature higher conductivity and, hence, lower impedance. More advanced options include the use of short bent crystals as primary collimators [66] and the deployment of hollow electron-beam lenses as non-destructible collimators [67].

It is noteworthy that machines like FCC-hh or SPPC can additionally be used for ion-ion/ion-proton collisions; their high-energy proton beams can also be collided with high-intensity $O(60$ GeV) electrons from an ERL resulting in c.m.e. of 3.5 TeV.

The lifetime of the muon, $\gamma\tau_0$ where τ_0=2.2μs, is sufficient to allow fast acceleration to high energy before most, or all, of the muons decay, and storage for some 300B turns in a ring with an average bending magnets field of B (in units of Tesla). The muon to electron mass ratio of 210 implies removal of the synchrotron radiation barrier and possibility of a muon collider facility scale to a level compatible with on-site placement at existing accelerator laboratories. High-energy muon colliders, as presently conceived, are predicted to be more compact, more power-efficient and significantly less expensive than the equivalent energy-frontier hadron or e^+e^- machines [68], and a neutrino factory could potentially be realized in the course of their construction [69]. The Higgs production cross-section in the s-channel is enhanced by a factor of $(m_\mu/m_e)^2$ compared to that in e^+e^- collisions.

The average luminosity of a muon collider,

$$\langle\mathcal{L}\rangle = f_0\gamma^2\frac{c\tau_0}{2C}\frac{n_\mathrm{b}N^2}{4\pi\varepsilon_\mathrm{n}\beta^*}\mathcal{F} = BP_\mathrm{b}\frac{Nr_0}{4\pi\varepsilon_\mathrm{n}}\frac{\gamma}{\beta^*}\left(\frac{c\tau_0\mathcal{F}}{8\pi e}\right), \qquad (31.19)$$

scales with B, the total beam power P_b, and the beam brightness – the third factor above is nothing but the muon beam-beam tune shift Eq. (31.16). There is an obvious incentive to have all the particles in just one bunch per beam. The beta-function at the two IPs $\beta^* \approx \sigma_z$ scales as $1/\gamma$ within certain range of energies, giving overall scaling $\langle\mathcal{L}\rangle \propto \gamma^2$ with other limiting parameters fixed. The main challenges to luminosity achievement with decaying particles are related to production and fast cooling and acceleration of $O(10^{12})$ muons per bunch without emittance degradation. A multi-TeV c.m.e. high luminosity $O(10^{34}$ cm^{-2}s$^{-1})$ muon collider would consist of [70] : (i) a high power proton driver (e.g., 8 GeV 2-4 MW H$^-$ SRF linac), (ii) pre-target accumulation and compressor rings, in which high intensity 1-3 ns long proton bunches are formed, (iii) a liquid-mercury or other high-power target for converting the proton beam into a tertiary muon beam with energy of about 200 MeV, (iv) a multi-stage ionization cooling section that reduces transverse and longitudinal emittances by several orders of magnitude and creates a low emittance beam, similarly to that recently demonstrated [71], (v) a multistage acceleration system, possibly employing either rapid cycling synchrotrons or RLAs to accelerate muons in a modest number of turns up to the final energy using superconducting RF technology, and, finally, (vi) a 3–14 km diameter collider ring, where counter-propagating muon beams are stored and collide over the roughly 3000 turns corresponding to the muon lifetime.

The intense neutrino flux originating from the multi-TeV muon beams decaying in the collider poses another challenge — the need

Downloaded from https://academic.oup.com/ptep/article/2022/8/083C01/6651666 by KIT Library user on 27 September 2022

to minimize the environmental impact. The collider complex is usually located underground and when the produced neutrinos emerge at the surface, a small fraction interacts with the rock (and other material) and produces ionizing radiation dose scaling as γ^3. The impact of this neutrino-induced radiation can be mitigated, for example, by continually adjusting the orbits of the beams to spread them out on a wider area, by deeper collider tunnels or with a further reduced emittance of the muon beam so that the required luminosity could be obtained using a substantially smaller number of muons.

31.5.4 *Plasma Acceleration and Other Advanced Concepts*

Since about the mid-1950s, it has been understood that collective plasma-based accelerators promise extremely large accelerating gradients, approximately three orders of magnitude greater than ∼100 MV/m obtained in conventional breakdown limited RF structures [72]. Ionized plasmas can sustain electron plasma density waves with electric fields in excess of $E_0 = cm_e\omega_\mathrm{p}/e$ or

$$E_0 \approx 96\,[\mathrm{V/m}]\,\sqrt{n_0[\mathrm{cm}^{-3}]}, \tag{31.20}$$

where n_0 denotes the ambient electron number density and $\omega_\mathrm{p} = \sqrt{e^2 n_0/(m_e\varepsilon_0)}$ is the electron plasma frequency [73].

Such gradients can be effectively excited by either powerful external pulses of laser light or by electron bunches if they are shorter than the plasma wavelength $\lambda_\mathrm{p} = c/\omega_\mathrm{p} \approx 1\ \mathrm{mm}\times\sqrt{10^{15}\,\mathrm{cm}^{-3}/n_0}$, or by longer beams of protons if their charge density is modulated with the period of λ_p. In the past decade, we have seen impressive progress in the plasma wakefield acceleration of high-quality beams. Laser-driven electron energy gain of about 8 GeV over 20 cm of plasma with density $3\times10^{17}\mathrm{cm}^{-3}$ has been demonstrated at the BELLA facility at the Lawrence Berkeley National Laboratory (LBNL) [74]. Short electron bunches were used to boost the energy of externally injected electron bunches by 9 GeV over 1.3 m of $\sim10^{17}\mathrm{cm}^{-3}$ plasma at the FACET facility in SLAC [75]. The AWAKE experiment at CERN used self-modulating long 450 GeV proton bunches to accelerate electrons to 2 GeV over 10 m of 10^{15} cm^{-3} plasma [76].

Whether plasma acceleration will find application in an HEP facility is not yet clear, given the necessity of staging and phase-locking acceleration in multiple plasma chambers. Another critical issue is the power efficiency η for a collider based on plasma acceleration, whose luminosity would still be described by Eq.(31.18). In addition, many novel ideas and approaches have been proposed to extend the energy reach of future particle colliders, reduce their cost, and improve their luminosity or energy efficiency. Those include: i) *cold normal–conducting RF* based TeV-class linear e^+e^- collider operating copper accelerating cavities at liquid nitrogen temperature and promising significantly lower linac cost and power per GeV than in the ILC (SRF cavities at 2 K) and CLIC (room temperature RF structures) [77]; ii) *dielectric wakefield accelerators* in which resonant dielectric accelerating structures are fed by ultra-short RF pulses of wakefields driven by either collinear or preceding high charge electron bunches and withstand 270 MV/m operational accelerating gradients [78]; iii) *dielectric laser accelerators* – micron-size dielectric accelerating structures driven by a laser and supporting O(1 GV/m) accelerating fields [79]; iv) compact *linear muon crystal colliders* with ultimate energies O(1–10 PeV) [80] based on 1–10 TeV/m wakefield acceleration of muons (instead of electrons or hadrons) channeling between the planes in crystals or inside carbon nanotubes (CNT) with charge carrier density $\sim10^{20-22}$ cm^{-3} [81]; v) the *Gamma Factory* concept [82], where frequent bursts of gamma rays are generated by repeatedly colliding a partially stripped heavy-ion beam circulating in the LHC, or in a future higher-energy hadron storage ring like the FCC-hh, with a conventional laser pulse, profiting from two Lorentz boosts. Active R&D programs are presently underway worldwide to determine the suitability of novel technologies for use in future high-energy colliders.

References

[1] V. Shiltsev and F. Zimmermann, Reviews of Modern Physics **93**, 1, 015006 (2021).

[2] A. Tollestrup and E. Todesco, in "Reviews Of Accelerator Science And Technology: Volume 1," 185–210, World Scientific (2008).

[3] D. A. Edwards and M. J. Syphers, *An introduction to the physics of high energy accelerators*, John Wiley & Sons, New York, NY (2008).

[4] A. W. Chao, *Physics of collective beam instabilities in high energy accelerators*, Wiley, New York, NY (1993), URL `https://cds.cern.ch/record/246480`.

[5] S.-Y. Lee, *Accelerator physics*, World Scientific, Singapore (2018).

[6] E. D. Courant and H. S. Snyder, Annals of physics **3**, 1, 1 (1958).

[7] H. Wiedemann, *Particle accelerator physics*, Springer Nature (2015), URL `https://library.oapen.org/handle/20.500.12657/23641`.

[8] M. Sands, Conf. Proc. C **6906161**, 257 (1969).

[9] S.-Y. Lee, *Spin dynamics and snakes in synchrotrons*, World Scientific Publishing Company (1997).

[10] F. Zimmermann, Physical Review Special Topics-Accelerators and Beams **7**, 12, 124801 (2004).

[11] A. W. Chao *et al.*, editors, *Handbook of accelerator physics and engineering*, World Scientific, Hackensack, USA (2013), ISBN 9789814415842, URL `http://www.worldscientific.com/worldscibooks/10.1142/8543`.

[12] A. Piwinski, J. D. Bjorken and S. K. Mtingwa, Physical Review Accelerators and Beams **21**, 11, 114801 (2018).

[13] V. Parkhomchuk and A. Skrinsky, Reviews of Accelerator Science and Technology **1**, 01, 237 (2008).

[14] M. Minty and F. Zimmermann, *Measurement and control of charged particle beams*, Springer Nature (2003), URL `https://library.oapen.org/handle/20.500.12657/23642`.

[15] S. Myers, *Particle Physics Reference Library: Volume 3: Accelerators and Colliders*, volume 3, Springer Nature (2020), URL `https://library.oapen.org/handle/20.500.12657/39571`.

[16] V. Shiltsev *et al.*, Physical Review Special Topics-Accelerators and Beams **8**, 10, 101001 (2005).

[17] J. T. Seeman, *Observations of the beam-beam interaction*, Springer (1986).

[18] R. Assmann, M. Lamont and S. Myers, Nucl. Phys. B Proc. Suppl. **109**, 17 (2002).

[19] K. Yokoya and P. Chen, Lect. Notes Phys. **400**, 415 (1992).

[20] H. T. Edwards, Annual Review of Nuclear and Particle Science **35**, 1, 605 (1985).

[21] V. Lebedev and V. Shiltsev, *Accelerator physics at the Tevatron collider*, Springer (2014).

[22] S. D. Holmes and V. D. Shiltsev, Annual Review of Nuclear and Particle Science **63**, 435 (2013).

[23] G. Voss and B. Wiik, Annual Review of Nuclear and Particle Science **44**, 1, 413 (1994).

[24] S. Myers and H. Schopper, Landolt Börnstein **21** (2013).

[25] D. Brandt *et al.*, Reports on Progress in Physics **63**, 6, 939 (2000).

[26] N. Phinney, eConf **C00082**, MO102 (2000), [arXiv:physics/0010008].

[27] L. Evans, Annual Review of Nuclear and Particle Science **61**, 435 (2011).

[28] CERN, "The Large Hadron Collider web site: http://lhc.web.cern.ch/lhc/," .

[29] G. Valentino *et al.*, Physical Review Special Topics-Accelerators and Beams **15**, 5, 051002 (2012).

[30] J. Wenninger (2019), URL `https://cds.cern.ch/record/2668326`.

Downloaded from https://academic.oup.com/ptep/article/2022/8/083C01/6651666 by KIT Library user on 27 September 2022

[31] G. Apollinari *et al.*, Technical Report CERN Yellow Report: Monograph 2017-007-M (2017).

[32] H. Damerau *et al.*, *LHC Injectors Upgrade, Technical Design Report* (2014), URL `https://cds.cern.ch/record/1976692`.

[33] Y. Ohnishi *et al.*, Progress of Theoretical and Experimental Physics **2013(3)**, 3 (2013).

[34] M. Benedikt *et al.*, The European Physical Journal Special Topics **228**, 2, 261 (2019).

[35] M. Zobov *et al.*, Physical Review Letters **104**, 17, 174801 (2010).

[36] P. Raimondi, D. N. Shatilov and M. Zobov (2007), [arXiv:physics/0702033].

[37] M. Harrison, S. Peggs and T. Roser, Annual Review of Nuclear and Particle Science **52**, 1, 425 (2002).

[38] M. Blaskiewicz, J. M. Brennan and K. Mernick, Phys. Rev. Lett. **105**, 094801 (2010).

[39] M. Bai *et al.*, Physical Review Letters **96**, 17, 174801 (2006).

[40] W. Fischer *et al.*, Phys. Rev. Lett. **115**, 26, 264801 (2015).

[41] 2020 Update of the European Strategy for Particle Physics by the European Strategy Group, `https://home.cern/sites/home.web.cern.ch/files/2020-06/2020UpdateEuropeanStrategy.pdf` (2020), accessed: June 20, 2020.

[42] V. Kekelidze *et al.*, The European Physical Journal A **52**, 8, 211 (2016).

[43] E. Beebe-Wang (ed.) et al., Technical Report BNL Formal Report BNL-211943-2019-FORE, Brookhaven (2019).

[44] A. Accardi *et al.*, The European Physical Journal A **52**, 9, 268 (2016).

[45] CEPC Study Group (2018), [arXiv:1809.00285].

[46] C. Adolphsen *et al.*, Technical Report arXiv:1306.6328. CERN-ATS-2013-037. IHEP-AC-ILC-2013-001. ILC-REPORT-2013-040. INFN-13-04-LNF. JINR-E9-2013-35. JLAB-R-2013-01. LLNL-TR-635539. comments: See also http://www.linearcollider.org/ILC/TDR . The full list of signatories is inside the Report, URL `http://cds.cern.ch/record/1601969`.

[47] L. Evans and S. Michizono (Linear Collider) (2017), [arXiv:1711.00568].

[48] A. Grassellino *et al.*, Supercond. Sci. Technol. **26**, 102001 (2013), [arXiv:1306.0288].

[49] T. K. Charles *et al.* (CLICdp, CLIC), CERN Yellow Rep. Monogr. **1802**, 1 (2018), [arXiv:1812.06018].

[50] T. O. Raubenheimer, Physical Review Special Topics-Accelerators and Beams **3**, 12, 121002 (2000).

[51] V. N. Litvinenko, T. Roser and M. Chamizo-Llatas, Physics Letters B **804**, 135394 (2020), ISSN 0370-2693, URL `http://www.sciencedirect.com/science/article/pii/S0370269320301982`.

[52] M. Tigner, Il Nuovo Cimento (1955-1965) **37**, 3, 1228 (1965).

[53] U. Amaldi, Physics Letters B **61**, 3, 313 (1976).

[54] V. I. Telnov, JINST **16**, 12, P12025 (2021), [arXiv:2105.11015].

[55] V. Telnov, Journal of Instrumentation **9**, 09, C09020 (2014).

[56] The ERL Study Group — Angal-Kalinin, Deepa and others, A Contribution to the European Strategy for Particle Physics (2021).

[57] Y. Alexahin, E. Gianfelice-Wendt and V. Kapin, Journal of Instrumentation **13**, 11, P11002 (2018).

[58] P. Agostini *et al.*, "The Large Hadron-Electron Collider at the HL-LHC," (2020), [arXiv:2007.14491].

[59] P. Piminov, Physics of Particles and Nuclei Letters **15**, 7, 732 (2018).

[60] M. Benedikt *et al.*, The European Physical Journal Special Topics **228**, 4, 755 (2019), ISSN 1951-6401, URL `https://doi.org/10.1140/epjst/e2019-900087-0`.

[61] CEPC Study Group (2018), [arXiv:1809.00285].

[62] H. Al Ali *et al.* (2021), [arXiv:2103.14043].

[63] D. Schoerling and A. V. Zlobin, *Nb3Sn Accelerator Magnets: Designs, Technologies and Performance*, Springer Nature (2019).

[64] E. Kong *et al.*, International Journal of Modern Physics A **34**, 13n14, 1940003 (2019).

[65] M. Benedikt, D. Schulte and F. Zimmermann, Phys. Rev. ST Accel. Beams **18**, 101002 (2015).

[66] W. Scandale and A. Taratin, Physics Reports **815**, 1 (2019).

[67] V. Shiltsev, Journal of Instrumentation **16**, 03, P03039 (2021).

[68] K. R. Long *et al.*, Nature Physics **17**, 3, 289 (2021).

[69] S. Geer, Annual Review of Nuclear and Particle Science **59**, 347 (2009).

[70] C. Ankenbrandt *et al.*, Physical Review Special Topics-Accelerators and Beams **2**, 8, 081001 (1999).

[71] M. Bogomilov *et al.*, Nature **578**, 53 (2020).

[72] V. Veksler, The Soviet Journal of Atomic Energy **2**, 5, 525 (1957).

[73] T. Tajima and J. M. Dawson, Physical Review Letters **43**, 4, 267 (1979).

[74] A. Gonsalves *et al.*, Physical Review Letters **122**, 8, 084801 (2019).

[75] M. Litos *et al.*, Plasma Physics and Controlled Fusion **58**, 3, 034017 (2016).

[76] E. Adli *et al.*, Nature **561**, 7723, 363 (2018).

[77] K. L. Bane *et al.* (2018), [arXiv:1807.10195].

[78] C. Jing, Reviews of Accelerator Science and Technology **9**, 127 (2016).

[79] E. Peralta *et al.*, Nature **503**, 7474, 91 (2013).

[80] V. D. Shiltsev, Physics-Uspekhi **55**, 10, 965 (2012).

[81] T. Tajima and M. Cavenago, Physical Review Letters **59**, 13, 1440 (1987).

[82] M. W. Krasny (2015), [arXiv:1511.07794].

Downloaded from https://academic.oup.com/ptep/article/2022/8/083C01/6651666 by KIT Library user on 27 September 2022

32. High-Energy Collider Parameters

High-Energy Collider Parameters: e^+e^- Colliders (I)

Table 32.1: Updated in March 2022 with numbers received from representatives of the colliders (contact E. Pianori, LBNL). The table shows the parameter values achieved. Quantities are, where appropriate, r.m.s.; unless noted otherwise, energies refer to beam energy; H and V indicate horizontal and vertical directions; s.c. stands for superconducting. Parameters for the defunct SPEAR, DORIS, PETRA, PEP, TRISTAN, and VEPP-2M colliders may be found in our 1996 edition (Phys. Rev. **D54**, 1 July 1996, Part I).

	VEPP-2000 (Novosibirsk)	VEPP-4M (Novosibirsk)	BEPC (China)	BEPC-II (China)	DAΦNE (Frascati)
Physics start date	2010	1994	1989	2008	1999
Physics end date	—	—	2005	—	—
Maximum beam energy (GeV)	1.0	6	2.5	1.89 (2.474 max)	0.510
Delivered integrated luminosity per exp. (fb^{-1})	0.25	0.05	0.11	34.5	$\approx$ 4.7 in 2001-2007 $\approx$ 2.7 w/crab-waist $\approx$ 6.8 since Nov 2014
Luminosity (10^{30} $\mathrm{cm}^{-2}\mathrm{s}^{-1}$)	50	20	12.6 at 1.843 GeV 5 at 1.55 GeV	1000	453
Time between collisions (μs)	0.04	0.6	0.8	0.008	0.0027
Full crossing angle (μ rad)	0	0	0	2.2×10^4	5×10^4
Energy spread (units 10^{-3})	0.71	1	0.58 at 2.2 GeV	0.52	0.40
Bunch length (cm)	4	5	$\approx$ 5	$\approx$ 1.2	low current: 1 at 15mA: 2
Beam radius (10^{-6} m)	125 (round)	H:1000 V:30	H:890 V:37	H:347 V:4.5	H:260 V:4.8
Free space at interaction point (m)	$\pm$0.5	$\pm$2	$\pm$2.15	$\pm$0.63	$\pm$0.295
Luminosity lifetime (hr)	continuous	2	7–12	1.5	0.2
Turn-around time (min)	continuous	18	32	4 (topping up)	2 (topping up)
Injection energy (GeV)	0.2–1.0	1.8	1.55	1.89	on energy
Transverse emittance (10^{-9} m)	H:150 V:150	H:200 V:20	H:660 V:28	H:121 V:1.56	H:260 V:2.6
β^*, amplitude function at interaction point (m)	H:0.05 - 0.11 V:0.05 - 0.11	H:0.75 V:0.05	H:1.2 V:0.05	H:1.0 V:0.0129	H:0.26 V:0.009
Beam-beam tune shift per crossing (units 10^{-4})	H:850 V:850	500	350	383	440/894 (crab-waist run/test)
RF frequency (MHz)	172	180	199.53	499.8	368.667
Particles per bunch (units 10^{10})	8	15	20 at 2 GeV 11 at 1.55 GeV	3.8	e^-: 3.2 e^+: 2.1
Bunches per ring per species	1	2	1	119	100 to 110 (120 buckets)
Average beam current per species (mA)	160	80	40 at 2 GeV 22 at 1.55 GeV	851	e^-: 1250 e^+: 800
Circumference or length (km)	0.024	0.366	0.2404	0.23753	0.098
Interaction regions	2	1	2	1	1
Magnetic length of dipole (m)	1.1	2	1.6	outer ring: 1.6 inner ring: 1.41	outer ring: 1.2 inner ring: 1
Length of standard cell (m)	12	7.2	6.6	outer ring: 6.6 inner ring: 6.2	n/a
Phase advance per cell (deg)	H:745 V:385	65	$\approx$ 60	60–90 non-standard cells	—
Dipoles in ring	8	78	40 + 4 weak	84 + 8 weak	8
Quadrupoles in ring	24 + 4 s.c.	150	68	134+2 s.c.	48
Peak magnetic field (T)	2.4	0.6	0.903 at 2.8 GeV	outer ring: 0.677 inner ring: 0.766	1.2

Downloaded from https://academic.oup.com/ptep/article/2022/8/083C01/6651666 by KIT Library user on 27 September 2022

High-Energy Collider Parameters: e^+e^- Colliders (II)

Table 32.2: Updated in March 2020 with numbers received from representatives of the colliders (contact E. Pianori, LBNL). The table shows the parameter values achieved. Quantities are, where appropriate, r.m.s.; unless noted otherwise, energies refer to beam energy; H and V indicate horizontal and vertical directions; s.c. stands for superconducting. ILC and CLIC parameters are documented in the Accelerator physics of colliders review.

	CESR (Cornell)	CESR-C (Cornell)	LEP (CERN)	SLC (SLAC)
Physics start date	1979	2002	1989	1989
Physics end date	2002	2008	2000	1998
Maximum beam energy (GeV)	6	6	100 - 104.6	50
Delivered integrated luminosity per experiment (fb^{-1})	41.5	2.0	0.221 at Z peak 0.501 at 65 – 100 GeV 0.275 at >100 GeV	0.022
Luminosity (10^{30} $\mathrm{cm}^{-2}\mathrm{s}^{-1}$)	1280 at 5.3 GeV	76 at 2.08 GeV	24 at Z peak 100 at > 90 GeV	2.5
Time between collisions (μs)	0.014 to 0.22	0.014 to 0.22	22	8300
Full crossing angle (μ rad)	±2000	±3300	0	0
Energy spread (units 10^{-3})	0.6 at 5.3 GeV	0.82 at 2.08 GeV	0.7→1.5	1.2
Bunch length (cm)	1.8	1.2	1.0	0.1
Beam radius (μm)	H:460 V:4	H:340 V:6.5	H:200→300 V:2.5→8	H:1.5 V:0.5
Free space at interaction point (m)	±2.2 (±0.6 to REC quads)	±2.2 (±0.3 to PM quads)	±3.5	±2.8
Luminosity lifetime (hr)	2–3	2–3	20 at Z peak 10 at > 90 GeV	—
Turn-around time (min)	5 (topping up)	1.5 (topping up)	50	120 Hz (pulsed)
Injection energy (GeV)	1.8–6	1.5–6	22	45.64
Transverse emittance (10^{-9} m)	210 1	120 3.5	H:20–45 V:0.25→1	H:0.5 V:0.05
β^*, amplitude function at interaction point (m)	1.0 0.018	0.94 0.012	1.5 0.05	0.0025 0.0015
Beam-beam tune shift per crossing (10^{-4}) or disruption	250 620	e^-: 420 (H), 280 (V) e^+: 410 (H), 270 (V)	830	0.75 (H) 2.0 (V)
RF frequency (MHz)	500	500	352.2	2856
Particles per bunch (units 10^{10})	1.15	4.7	45 in collision 60 in single beam	4.0
Bunches per ring per species	9 trains of 5 bunches	8 trains of 3 bunches	4 trains of 1 or 2	1
Average beam current per species (mA)	340	72	4 at Z peak 4→6 at > 90 GeV	0.0008
Beam polarization (%)	—	—	55 at 45 GeV 5 at 61 GeV	e^-: 80
Circumference or length (km)	0.768	0.768	26.66	1.45 +1.47
Interaction regions	1	1	4	1
Magnetic length of dipole (m)	1.6–6.6	1.6–6.6	11.66/pair	2.5
Length of standard cell (m)	16	16	79	5.2
Phase advance per cell (deg)	45–90 (no standard cell)	45–90 (no standard cell)	102/90	108
Dipoles in ring	86	84	3280 + 24 inj. + 64 weak	460+440
Quadrupoles in ring	101 + 4 s.c.	101 + 4 s.c.	520 + 288 + 8 s.c.	—
Peak magnetic field (T)	0.3 / 0.8 at 8 GeV	0.3 / 0.8 at 8 GeV, 2.1 wigglers at 1.9 GeV	0.135	0.597

Downloaded from https://academic.oup.com/ptep/article/2022/8/083C01/6651666 by KIT Library user on 27 September 2022

High-Energy Collider Parameters: e^+e^- Colliders (III)

Table 32.3: Updated in March 2022 with numbers received from representatives of the colliders (contact E. Pianori, LBNL). The table shows the parameter values achieved. Design parameters for SuperKEKEB may be found in our 2018 edition (Phys. Rev. **D98**, 030001 (2018)) Quantities are, where appropriate, r.m.s.; unless noted otherwise, energies refer to beam energy; H and V indicate horizontal and vertical directions; s.c. stands for superconducting.

	KEKB (KEK)	PEP-II (SLAC)	SuperKEKB (KEK)
Physics start date	1999	1999	2018
Physics end date	2010	2008	—
Maximum beam energy (GeV)	e^-: 8.33 (8.0 nominal) e^+: 3.64 (3.5 nominal)	e^-: 7–12 (9.0 nominal) e^+: 2.5–4 (3.1 nominal)	e^-: 7 e^+: 4
Delivered integrated luminosity per exp. (fb^{-1})	1040	557	307
Luminosity (10^{30} $\mathrm{cm}^{-2}\mathrm{s}^{-1}$)	21083	12069 (design: 3000)	3.81×10^4
Time between collisions (μs)	0.00590 or 0.00786	0.0042	0.0065
Full crossing angle (μ rad)	$\pm 11000^*$	0	± 41500
Energy spread (units 10^{-3})	0.7	e^-/e^+: 0.61/0.77	e^-/e^+: 0.64/0.81
Bunch length (cm)	0.65	e^-/e^+: 1.1/1.0	e^-/e^+: 0.6/0.6
Beam radius (μm)	H: 124 (e^-), 117 (e^+) V: 1.9	157 4.7	e^-: 16.6 (H), 0.24 (V) e^+: 17.9 (H), 0.24 (V)
Free space at interaction point (m)	+0.75/−0.58 (+300/−500) mrad cone	±0.2, ±300 mrad cone	$e^- : +1.20/-1.28, e^+ : +0.78/-0.73$ (+300/−500) mrad cone
Luminosity lifetime (hr)	continuous	continuous	continuous
Turn-around time (min)	continuous	continuous	continuous
Injection energy (GeV)	e^-/e^+ : 8.0/3.5 (nominal)	e^-/e^+ : 9.0/3.1 (nominal)	e^-/e^+ : 7/4
Transverse emittance (10^{-9} m)	e^-: 24 ($57^\dagger$) (H), 0.61 (V) e^+: 18 ($55^\dagger$) (H), 0.56 (V)	e^-: 48 (H), 1.8 (V) e^+: 24 (H), 1.8 (V)	e^-: 4.6 (H), 0.058 (V) e^+: 4.0 (H), 0.058 (V)
β^*, amplitude function at interaction point (m)	e^-: 1.2 ($0.27^\dagger$) (H), 0.0059 (V) e^+: 1.2 ($0.23^\dagger$) (H), 0.0059 (V)	e^-: 0.50 (H), 0.012 (V) e^+: 0.50 (H), 0.012 (V)	e^-: 0.060 (H), 1×10^{-3} (V) e^+: 0.080 (H), 1×10^{-3} (V)
Beam-beam tune shift per crossing (units 10^{-4})	e^-: 1020 (H), 900 (V) e^+: 1270 (H), 1290 (V)	e^-: 703 (H), 498 (V) e^+: 510 (H), 727 (V)	e^-: 15 (H), 315 (V) e^+: 27 (H), 433 (V)
RF frequency (MHz)	508.887	476	508.887
Particles per bunch (units 10^{10})	e^-/e^+: 4.7/6.4	e^-/e^+: 5.2/8.0	e^-/e^+: 2.76/3.52
Bunches per ring per species	1585	1732	1476
Average beam current per species (mA)	e^-/e^+: 1188/1637	e^-/e^+: 1960/3026	e^-/e^+: 640/819
Beam polarization (%)	—	—	—
Circumference or length (km)	3.016	2.2	3.016
Interaction regions	1	1	1
Magnetic length of dipole (m)	e^-/e^+ : 5.86/0.915	e^-/e^+: 5.4/0.45	e^-/e^+ : 5.9/4.0
Length of standard cell (m)	e^-/e^+ : 75.7/76.1	15.2	e^-/e^+ : 75.7/76.1
Phase advance per cell (deg)	450	e^-/e^+: 60/90	450
Dipoles in ring	e^-/e^+ : 116/112	e^-/e^+: 192/192	e^-/e^+ : 116/112
Quadrupoles in ring	e^-/e^+ : 452/452	e^-/e^+: 290/326	e^-/e^+ : 466/460
Peak magnetic field (T)	e^-/e^+ : 0.25/0.72	e^-/e^+: 0.18/0.75	e^-/e^+ : 0.22/0.19

*KEKB was operated with crab crossing from 2007 to 2010.
†With dynamic beam-beam effect.

Downloaded from https://academic.oup.com/ptep/article/2022/8/083C01/6651666 by KIT Library user on 27 September 2022

High-Energy Collider Parameters: ep, $\bar{\text{p}}$p, pp Colliders

Table 32.4: Updated in March 2022 with numbers received from representatives of the colliders (contact E. Pianori, LBNL). The table shows the parameter values achieved. Parameters for the defunct S$p\bar{p}$S collider may be found in our 2002 edition (Phys. Rev. **D66**, 010001 (2002)). Quantities are, where appropriate, r.m.s.; unless noted otherwise, energies refer to beam energy; H and V indicate horizontal and vertical directions; s.c. stands for superconducting.

	HERA (DESY)	TEVATRON* (Fermilab)	RHIC Brookhaven	LHC (CERN)		
Physics start date	1992	1987	2001	2009	2015	2029 (HL-LHC)
Physics end date	2007	2011	—	—		
Particles collided	ep	$p\bar{p}$	pp (polarized)	pp		
Maximum beam energy (TeV)	e: 0.030 p: 0.92	0.980	0.255 55% polarization	4.0	6.5	7.0
Max. delivered integrated luminosity per exp. (fb^{-1})	0.8	12	0.38 at 100 GeV 1.3 at 250/255 GeV	23.3 at 4.0 TeV 6.1 at 3.5 TeV	160	250/y
Luminosity (10^{30} cm^{-2}s^{-1})	75	431	245 (pk) 160 (avg)	7.7×10^3	2.1×10^4	5.0×10^4 (leveled)
Time between collisions (ns)	96	396	107	49.90	24.95	24.95
Full crossing angle (μ rad)	0	0	0	290	320 $\rightarrow$ 260†	500
Energy spread (units 10^{-3})	e: 0.91 p: 0.2	0.14	0.15	0.1445	0.105	0.129
Bunch length (cm)	e: 0.83 p: 8.5	p: 50 $\bar{p}$: 45	60	9.4	8	9
Beam radius (10^{-6} m)	e: 110 (H), 30 (V) p: 111 (H), 30 (V)	p: 28 $\bar{p}$: 16	85	18.8	8.5‡	7‡
Free space at interaction point (m)	±2	±6.5	16	38	38	38
Initial luminosity decay time, $-L/(dL/dt)$ (hr)	10	6 (avg)	7.5	≈ 6	≈ 8	≈ 7.5 (leveled)
Turn-around time (min)	e: 75, p: 135	90	25	180	150	145
Injection energy (TeV)	e: 0.012 p:0.040	0.15	0.023	0.450	0.450	0.450
Transverse emittance (10^{-9} m)	e: 20 (H), 3.5 (V) p: 5 (H), 5 (V)	p: 3 $\bar{p}$: 1	11	0.59	0.29	0.33
β^*, ampl. function at interaction point (m)	e: 0.6 (H), 0.26 (V) p: 2.45 (H), 0.18 (V)	0.28	0.65	0.6	0.3 $\rightarrow$ 0.25§	0.6 $\rightarrow$ 0.15§
Beam-beam tune shift per crossing (units 10^{-4})	e:190 (H), 450 (V) p: 12 (H), 9 (V)	p: 120 $\bar{p}$: 120	73	72	45	86
RF frequency (MHz)	e:499.7 p: 208.2/52.05	53	accel: 9 store: 28	400.8	400.8	400.8
Particles per bunch (units 10^{10})	e:3 p:7	p:26 $\bar{p}$:9	18.5	16	11	22
Bunches per ring per species	e: 189 p: 180	36	111	1380	2556 2544 (i.r. 1/5¶)	2760 2748 (i.r. 1/5¶)
Average beam current per species (mA)	e:40 p:90	p:70 $\bar{p}$:24	257	400	510	1100
Circumference (km)	6.336	6.28	3.834	26.659		
Interaction regions	2 colliding beams 1 fixed target (e beam)	2 high $\mathfrak{L}$	6 total, 2 high $\mathfrak{L}$	4 total, 2 high $\mathfrak{L}$		
Magnetic length of dipole (m)	e:9.185; p: 8.82	6.12	9.45	14.3		
Length of standard cell (m)	e:23.5 p:47	59.5	29.7	106.90		
Phase advance per cell (deg)	e:60 p:90	67.8	84	90		
Dipoles in ring	e: 396 p: 416	774	192 per ring + 12 common	1232 main dipoles		
Quadrupoles in ring	e:580 p:280	216	246 per ring	482 2-in-1 24 1-in-1		
Magnet types	e: C-shaped p: s.c., col., warm iron	s.c., $\cos\theta$ warm iron	s.c., $\cos\theta$ cold iron	s.c., 2-in-1 cold iron		
Peak magnetic field (T)	e: 0.274; p: 5	4.4	3.5	8.3‖		

*Other TEVATRON parameters: $\bar{p}$ source accum. rate: 25×10^{10} hr^{-1}; max. no. of $\bar{p}$ stored: 3.4×10^{12} (Accumulator), 6.1×10^{12} (Recycler).
†Variable crossing angle decreasing during the fill with the reduction in bunch population
‡Minimum beam radius during levelling
§β^* levelling
¶Number of bunches colliding at the interaction regions (i.r.) 1 (ATLAS) and 5 (CMS).
‖Value for design beam energy of 7 TeV.

Downloaded from https://academic.oup.com/ptep/article/2022/8/083C01/6651666 by KIT Library user on 27 September 2022

High-Energy Collider Parameters: Heavy Ion Colliders

Table 32.5: Updated in March 2022 with numbers received from representatives of the collider (contact E. Pianori, LBNL) The table shows the parameter values achieved. For the LHC, only maximum values for the ATLAS and CMS experiments are provided (ALICE and LHCb have different requirements for energy and luminosity). Design values for a high-luminosity upgrade are also given. Quantities are, where appropriate, r.m.s.; unless noted otherwise, energies refer to beam energy; s.c. stands for superconducting. pk and avg denote peak and average values.

	RHIC (Brookhaven)		LHC (CERN)			
Physics start date	2000	2012 / 2018 / 2018 / 2012 / 2004 2021 / 2014 / 2002 / 2015 / 2015	2010	2012	2017	$\geq$ 2022 (high lum.)*
Physics end date	—		—			
Particles collided	Au Au	U U / Zr Zr / Ru Ru / Cu Au / Cu Cu O O / h Au / d Au / p Au / p Al	Pb Pb	p Pb	Xe Xe	Pb Pb
Max. beam energy (TeV/n)	0.1	0.1	2.51	p:6.5 Pb:2.56	2.72	2.76
$\sqrt{s_{NN}}$ (TeV)	0.2	0.2	5.02	8.16	5.44	5.5
Max. delivered int. nucleon-pair lumin. per exp. (pb^{-1})	2639 (at 100 GeV/n)	21 / 36 / 36.9 / 167 / 60 8.2 / 43 / 169 / 124 / 63 (all at 100 GeV/n)	77.8	194	0.05	$\approx 121/y$
Luminosity (10^{27} $\mathrm{cm}^{-2}\mathrm{s}^{-1}$)	pk: 15.5 avg: 8.7	pk: 0.4 / 4.8 / 3.8 / 12 / 21 450 / 170 / 850 / 880 / 7600 avg: 0.6 / 2.2 / 2.1 / 10 / 8 230 / 100 / 500 / 450 / 3800	6.1	900	0.4	6.4 (leveled)
Time between collisions (ns)	107	107 / 107 / 107/ 107 / 321 107 / 107 / 107 / 107 / 107	74.9 / 149.7	99.8 / 149.7	$\approx$ 5500	49.9
Full crossing angle (μ rad)	0	0	320	280	300	340
Energy spread (units 10^{-3})	0.75	0.75	0.11	0.11	0.11	0.11
Bunch length (cm)	30	30	8.0	p / Pb: 9 / 11.5	11	7.9
Beam radius (10^{-6} m)	114†	123† / 87† / 88† / 163† / 145† 100† / 136† / 124† / 147† / 128†	21	19	12	17
Free space at inter. point (m)	16	16	38	38	38	38
Initial luminosity decay time, $-L/(dL/dt)$ (hr)	1	-0.35‡ / ∞§ / ∞§ / ∞‡ / 1.8 ∞ / 0.6 / ∞‡ / 0.5 / 0.25	3.3	≈ 2	≈ 6	∞
Turn-around time (min)	30	60¶ / 40¶ / 40¶ / 160¶ / 90¶ 45¶/ 45¶ / 90¶ / 60¶ / 50¶	$\approx$ 180	150	180	$\approx$ 200
Injection energy (TeV/n)	0.011	0.011	0.177	p / Pb: 0.45 / 0.177	0.188	0.177
Transverse emittance (10^{-9} m)	19†	22† /10.7† / 11.2† / 38† / 23† 12 † / 19† / 22† / 26† / 21†	0.85	0.29	0.3	0.5
β^*, ampl. function at interaction point (m)	0.7	0.7 / 0.7 /0.7 / 0.7 / 0.9 0.7 / 1.0 / 0.7 / 0.8 / 0.8	0.5	0.5	0.4	0.5
Beam-beam tune shift per crosssing (units 10^{-4})	39†	6† / 18† /21† / 14†, 14† / 30† / 34† 42†, 22† / 40†, 27† / 53†, 41† / 80†, 59†	15	15	$\approx$ 10	4.3
RF frequency (MHz)	accel: 28, store: 197		400.8	400.8	400.8	400.8
Particles per bunch (units 10^{10})	0.20	0.03 / 0.1 / 0.1 / 0.4, 0.13 / 0.45 / 0.85 4.5, 0.13 / 13, 0.20 / 22.5, 0.16 / 24, 1.1	0.022 (r.m.s.)	p:2.6 Pb:0.022	0.027	0.018
Bunches per ring per species	111	111 / 111 / 111/ 111 / 37 106 / 111 /111 / 111 / 111	733	p:540 Pb:684	16	1240
Average beam current per species (mA)	224	38 / 56 / 61 / 160,138 / 60 / 95 125,143 / 181,213 / 313,176 / 334,199	23.8	p:16 Pb:15	0.54	33
Circumference (km)	3.834		26.659			
Interaction regions	6 total, 2 high $\mathfrak{L}$		4 total, 3 high $\mathfrak{L}$			
Magnetic length of dipole (m)	9.45		14.3			
Length of standard cell (m)	29.7		106.90			
Phase advance per cell (deg)	93	84 /84 / 84 / 84 / 84 / 84 93 / 84(d), 93 / 84(p), 93 / 84(p), 93	90			
Dipoles in ring	192 per ring, + 12 common		1232, main dipoles			
Quadrupoles in ring	246 per ring		482 2-in-1, 24 1-in-1			
Magnet Type	s.c. $\cos\theta$, cold iron		s.c., 2 in 1, cold iron			
Peak magnetic field (T)	3.5		8.3			

*High luminosity upgrade expected >= 2022; will extend throughout HL-LHC running. Very preliminary, conservative estimates.
†Initial value, increases (descreases) without (with) cooling
‡Negative or infinite decay time is effect of cooling.
§luminosity leveled to flat after set to target value, with cooling
¶measured minimum, not theoretical

Downloaded from https://academic.oup.com/ptep/article/2022/8/083C01/6651666 by KIT Library user on 27 September 2022

33. Neutrino Beam Lines at High-Energy Proton Synchrotrons

Revised August 2021 with numbers verified by representatives of the synchrotrons (contact C.-J. Lin, LBNL). For existing (future) neutrino beam lines the latest achieved (design) values are given.

The main source of neutrinos at proton synchrotrons is from the decay of pions and kaons produced by protons striking a nuclear target. There are different schemes to focus the secondary particles to enhance neutrino flux and/or tune the neutrino energy profile. In wide-band beams (WBB), the neutrino parent mesons are focused over a wide momentum range to obtain maximum neutrino intensity. In narrow-band beams (NBB), the secondary particles are first momentum-selected to produce a monochromatic parent beam. Another approach to generate a narrow-band neutrino spectrum is to select neutrinos that are emitted off-axis relative to the momentum of the parent mesons. For a comprehensive review of the topic, including other historical neutrino beam lines, see the article by S. E. Kopp, "Accelerator-based neutrino beams," Phys. Rept. **439**, 101 (2007).

	PS (CERN)				SPS (CERN)				PS (KEK)	Main Ring (JPARC)
Date	1963	1969	1972	1983	1977	1977	1995	2006	1999	2021
Proton Kinetic Energy (GeV)	20.6	20.6	26	19	350	350	450	400	12	30 (50)
Protons per Cycle (10^{12})	0.7	0.6	5	5	10	10	36	48	6	270 (330)
Cycle Time (s)	3	2.3	-	-	-	-	14.4	6	2.2	2.48 (2.1)
Beam Power (kW)	0.8	0.9	-	-	-	-	180	510	5	515 (750)
Target	-	-	-	-	-	-	Be	Graphite	Al	Graphite
Target Length (cm)	-	-	-	-	-	-	290	130	66	91
Secondary Focussing	1-horn WBB	3-horn WBB	2-horn WBB	bare target	dichromatic NBB	2-horn WBB	2-horn WBB	2-horn WBB	2-horn WBB	3-horn off-axis
Decay Pipe Length (m)	-	-	-	-	-	-	110	1090	200	96
$\langle E_\nu \rangle$ (GeV)	1.5	1.5	1.5	1	50,150†	20	24.3	17	1.3	0.6
Experiments	HLBC, Spark Ch.	HLBC, Spark Ch.	GGM, Aachen-Padova	CDHS, CHARM	CDHS, CHARM, BEBC	GGM,CDHS, CHARM, BEBC	NOMAD, CHORUS	OPERA, ICARUS	K2K	T2K

	Main Ring (Fermilab)					Booster (Fermilab)	Main Injector (Fermilab)			
Date	1974	1979	1976	1991	1998	2002, (2022)	2005	2017	2021	(2026)
Proton Kinetic Energy (GeV)	300	400	350	800	800	8	120	120	120	(60 – 120)
Protons per Cycle (10^{12})	10	10	13	10	12	4.5	37	54	55 (65)	(75)
Cycle Time (s)	-	-	-	60	60	0.2	2	1.333	1.2	(1.2)
Beam Power (kW)	-	-	-	20	25	29	350	720	840 (1000)	(1200)
Target	-	-	-	-	BeO	Be	Graphite	Graphite	Graphite	(Graphite)
Target Length (cm)	-	-	-	-	31	71	95	120	120	(150-220)
Secondary Focussing	dichromatic NBB	2-horn WBB	1-horn WBB	quad trip.	SSQT WBB	1-horn WBB	2-horn WBB	2-horn off-axis	2-horn off-axis	(3-horn WBB)
Decay Pipe Length (m)	400	400	400	400	400	50	675	675	675	(220)
$\langle E_\nu \rangle$ (GeV)	50,180†	25	100	90,260	70,180	1	3-20‡	2	2	(2.5)
Experiments	CITF, HPWF, 15' BC	15' BC	HPWF 15' BC	15' BC, CCFRR	NuTeV	MiniBooNE, SciBooNE, MicroBooNE, (SBND,ICARUS)	MINOS, MINERνA	NOνA, MINERνA, MINOS+	NOνA	LBNF/ DUNE

†Pion and kaon peaks in the momentum-selected channel.

‡Tunable WBB energy spectrum.

Downloaded from https://academic.oup.com/ptep/article/2022/8/083C01/6651666 by KIT Library user on 27 September 2022

34. Passage of Particles Through Matter

Revised August 2021 by D.E. Groom (LBNL) and S.R. Klein (NSD LBNL; UC Berkeley).

34.1 Notation . . . 549
34.2 Electronic energy loss by heavy particles . . . 549
34.2.1 Moments and cross sections . . . 549
34.2.2 Maximum energy transfer to an electron in a single collision . . . 550
34.2.3 Stopping power at intermediate energies . . . 550
34.2.4 Mean excitation energy . . . 550
34.2.5 Density effect . . . 550
34.2.6 Energy loss at low energies . . . 551
34.2.7 Energetic knock-on electrons (δ rays) . . . 553
34.2.8 Restricted energy loss rates for relativistic ionizing particles . . . 553
34.2.9 Fluctuations in energy loss . . . 553
34.2.10 Energy loss in mixtures and compounds . . . 554
34.2.11 Ionization yields . . . 554
34.3 Multiple scattering through small angles . . . 554
34.4 Photon and electron interactions in matter . . . 555
34.4.1 Collision energy losses by $e^{\pm}$ . . . 555
34.4.2 Radiation length . . . 556
34.4.3 Bremsstrahlung energy loss by $e^{\pm}$ . . . 556
34.4.4 Critical energy . . . 556
34.4.5 Energy loss by photons . . . 557
34.4.6 Bremsstrahlung and pair production at very high energies . . . 558
34.4.7 Photonuclear and electronuclear interactions at still higher energies . . . 559
34.5 Electromagnetic cascades . . . 559
34.6 Muon energy loss at high energy . . . 560
34.7 Cherenkov and transition radiation . . . 561
34.7.1 Optical Cherenkov radiation . . . 561
34.7.2 Coherent radio Cherenkov radiation . . . 562
34.7.3 Transition radiation . . . 562

This review covers the interactions of photons and electrically charged particles in matter, concentrating on energies of interest for high-energy physics and astrophysics and processes of interest for particle detectors (ionization, Cherenkov radiation, transition radiation). Much of the focus is on particles heavier than electrons ($\pi^{\pm}$, p, etc.). Although the charge number z of the projectile is included in the equations, only $z = 1$ is discussed in detail. Muon radiative losses are discussed, as are photon/electron interactions at high to ultrahigh energies. Neutrons are not discussed.

34.1 Notation

The notation and important numerical values are shown in Table 34.1.

Table 34.1: Summary of variables used in this section. The kinematic variables β and γ have their usual relativistic meanings.

Symb.	Definition	Value or (usual) units
$m_e c^2$	electron mass $\times\, c^2$	0.510 998 950 00(15) MeV
r_e	classical electron radius $e^2/4\pi\epsilon_0 m_e c^2$	2.817 940 3227(19) fm
α	fine structure constant $e^2/4\pi\epsilon_0\hbar c$	1/137.035 999 139(31)
N_A	Avogadro's number	6.022 140 857(74) $\times 10^{23}$ mol^{-1}
ρ	density	g cm^{-3}
x	mass per unit area	g cm^{-2}
M	incident particle mass	MeV/c^2
E	incident part. energy γMc^2	MeV
T	kinetic energy, $(\gamma - 1)Mc^2$	MeV
W	energy transfer to an electron in a single collision	MeV
$W_{\max}$	Maximum possible energy transfer to an electron in a single collision	MeV
k	bremsstrahlung photon energy	MeV
z	charge number of incident particle	
Z	atomic number of absorber	
A	atomic mass of absorber	g mol^{-1}
K	$4\pi N_A r_e^2 m_e c^2$ (Coefficient for dE/dx)	0.307 075 MeV mol^{-1} cm^2
I	mean excitation energy	eV (*Nota bene!*)
$\delta(\beta\gamma)$	density effect correction to ionization energy loss	
$\hbar\omega_p$	plasma energy $\sqrt{4\pi N_e r_e^3}\; m_e c^2/\alpha$	$\sqrt{\rho\,\langle Z/A\rangle} \times 28.816$ eV, $\hookrightarrow \rho$ in g cm^{-3}
N_e	electron density	(units of r_e)$^{-3}$
w_j	weight fraction of the jth element in a compound or mixt.	
n_j	$\propto$ number of jth kind of atoms in a compound or mixture	
X_0	radiation length	g cm^{-2}
E_c	critical energy for electrons	MeV
$E_{\mu c}$	critical energy for muons	GeV
E_s	scale energy $\sqrt{4\pi/\alpha}\; m_e c^2$	21.2052 MeV
R_M	Molière radius	g cm^{-2}

34.2 Electronic energy loss by heavy particles

34.2.1 *Moments and cross sections*

The electronic interactions of fast charged particles with speed $v = \beta c$ occur in *single collisions with energy losses* W [1], leading to ionization, atomic, or collective excitation. Most frequently the energy losses are small (for 90% of all collisions the energy losses are less than 100 eV). In thin absorbers few collisions will take place and the total energy loss will show a large variance [1]; also see Sec. 34.2.9 below. For particles with charge ze more massive than electrons ("heavy" particles), scattering from free electrons is adequately described by the Rutherford differential cross section [2,3].

$$\frac{d\sigma_R(W;\beta)}{dW} = \frac{2\pi r_e^2 m_e c^2 z^2}{\beta^2}\,\frac{(1-\beta^2 W/W_{\max})}{W^2}\ , \qquad (34.1)$$

where $W_{\max}$, the maximum energy transfer possible in a single collision, is discussed below. It differs from the classical cross section by the factor $(1 - \beta^2 W/W\max)$, which arises when the spin of the target electrons is taken into account.

Bethe's original theory applied only to energies above which atomic effects are not important. The free-electron cross section (Eq. (34.1)) was used to extend the cross section to $W_{\max}$. This free-electron approximation is not valid if W is not large compared to electron binding energies. For this energy regime Bethe [4,5] used "Born Theorie" to obtain the differential cross section

$$\frac{d\sigma_B(W;\beta)}{dW} = \frac{d\sigma_R(W,\beta)}{dW} B(W)\ . \qquad (34.2)$$

Electronic binding is accounted for by the correction factor $B(W)$. Examples of $B(W)$ and $d\sigma_B/dW$ can be seen in Figs. 5 and 6 of Ref. [1]. For a given material, the correction results in introducing an *effective ionization energy* I "which is a geometric average of the excitation energies of the medium weighed by the corresponding oscillator strength." [6]. The nontrivial task of finding these values is discussed in Sec. 34.2.4.

At high energies the stopping power is further modified by polarization of the medium, and this "density effect," discussed in Sec. 34.2.5, must also be included.

The mean number of collisions with energy loss between W and $W + dW$ occurring in a distance δx is $N_e \delta x\,(d\sigma/dW)dW$, where $d\sigma(W;\beta)/dW$, where the cross section is the Rutherford formula if free electrons can be assumed and the Bethe form where binding energy is important. It is convenient to define the moments

$$M_j(\beta) = N_e\,\delta x \int W^j\,\frac{d\sigma(W;\beta)}{dW}dW\ , \qquad (34.3)$$

Downloaded from https://academic.oup.com/ptep/article/2022/8/083C01/6651666 by KIT Library user on 27 September 2022

so that M_0 is the mean number of collisions in δx, M_1 is the mean energy loss in δx, $(M_2 - M_1)^2$ is the variance, *etc.* The number of collisions is Poisson-distributed with mean M_0. N_e is either measured in electrons/g ($N_e = N_A Z/A$) or electrons/cm^3 ($N_e = N_A \rho Z/A$). The former is used throughout this chapter, since quantities of interest (dE/dx, X_0, *etc.*) vary smoothly with composition when there is no density dependence.

34.2.2 *Maximum energy transfer to an electron in a single collision*

For a point-like particle with mass $M >> m_e$,

$$W_{\max} = \frac{2m_e c^2 \beta^2\gamma^2}{1 + 2\gamma m_e/M + (m_e/M)^2} \ . \tag{34.4}$$

In older references [2, 9] the "low-energy" approximation $W_{\max} = 2m_e c^2 \beta^2\gamma^2$, valid for $2\gamma m_e \ll M$, is often implicit. For a pion in copper, the error thus introduced into dE/dx is greater than 6% at 100 GeV. For $2\gamma m_e \gg M$, $W_{\max} = Mc^2 \beta^2\gamma$.

At energies of order 100 GeV, the maximum 4-momentum transfer to the electron can exceed 1 GeV/c, where hadronic structure effects modify the cross sections. This problem has been investigated by J.D. Jackson [10], who concluded that for incident hadrons (but not for large nuclei) corrections to dE/dx are negligible below energies where radiative effects dominate. While the cross section for rare hard collisions is modified, the average stopping power, dominated by many softer collisions, is almost unchanged.

34.2.3 *Stopping power at intermediate energies*

The mean rate of energy loss by moderately relativistic charged heavy particles is well described by the "Bethe equation" [2,4,5,9],

$$\left\langle -\frac{dE}{dx} \right\rangle = Kz^2 \frac{Z}{A} \frac{1}{\beta^2} \left[\frac{1}{2} \ln \frac{2m_e c^2 \beta^2\gamma^2 W_{\max}}{I^2} - \beta^2 - \frac{\delta(\beta\gamma)}{2} \right] . \tag{34.5}$$

Eq. (34.5) is valid in the region $0.1 \lesssim \beta\gamma \lesssim 1000$ with an accuracy of a few percent. At $\beta\gamma \sim 0.1$ the projectile speed is comparable to atomic electron "speed," and at $\beta\gamma \sim 1000$ radiative effects begin to be important (Sec. 34.6). Both limits are Z dependent. A minor dependence on M at high energies is introduced through $W_{\max}$, but for all practical purposes the stopping power in a given material is a function of β alone. Small corrections are discussed in Sec. 34.2.6.[1,2]

This is the *mass stopping power*; with the symbol definitions and values given in Table 34.1, the units are MeV g^{-1}cm^2. As can be seen from Fig. 34.2, dE/dx defined in this way is about the same for most materials, decreasing slowly with Z. The *linear stopping power*, in MeV/cm, is $\rho\, dE/dx$, where ρ is the density in g/cm^3.

The stopping power at first falls as $1/\beta^\alpha$ where $\alpha \approx 1.7$–1.5, decreasing with increasing Z, and reaches a broad minimum at $\beta\gamma = 3.8$–3.0 as Z rises from 6 to 82. It then inexorably rises as the argument of the logarithmic term increases. Two independent mechanisms contribute. Two thirds of the rise is produced by the explicit $\beta^2\gamma^2$ dependence through the relativistic flattening and extension of the particle's electric field. Rather than producing ionization at greater and greater distances, the field polarizes the medium, cancelling the increase in the logarithmic term at high energies. This is taken into account by the density-effect correction $\delta(\beta\gamma)$. The other third is introduced by the $\beta^2\gamma$ dependence of $W_{\max}$, the maximum possible energy transfer to a recoil electron. "Hard collision" events increasingly extend the tail of the energy loss distribution, increasing the mean but with little effect on the position of the maximum, the most probable energy loss.

Few concepts in high-energy physics are as misused as dE/dx, since the mean is weighted by rare events with large single-collision energy losses. Even with samples of hundreds of events in a typical detector, the mean energy loss cannot be obtained dependably. Far better and more easily measured is the most probable energy loss, discussed in Sec. 34.2.9. The most probable energy loss in a typical detector is considerably smaller than the mean given by the Bethe equation. It does not continue to rise with the mean stopping power, but approaches a "Fermi plateau."

In analysing TPC data (Sec. 35.6.5), the same end is often accomplished by using a restricted energy loss, the mean of 50%–70% of the samples with the smallest signals as the estimator.

Although it must be used with cautions and caveats, dE/dx as described in Eq. (34.5) still forms the basis of much of our understanding of energy loss by charged particles. Extensive tables are available [6, 7] and `pdg.lbl.gov/current/AtomicNuclearProperties/`.

For heavy projectiles, like ions, additional terms are required to account for higher-order photon coupling to the target, and to account for the finite target radius. These can change dE/dx by a factor of two or more for the heaviest nuclei in certain kinematic regimes [11].

The function as computed for muons on copper is shown as the "Bethe" region of Fig. 34.1. Mean energy loss behavior below this region is discussed in Sec. 34.2.6, and the radiative effects at high energy are discussed in Sec. 34.6. Only in the Bethe region is it a function of β alone; the mass dependence is more complicated elsewhere. The stopping power in several other materials is shown in Fig. 34.2. Except in hydrogen, particles with the same speed have similar rates of energy loss in different materials, although there is a slow decrease in the rate of energy loss with increasing Z. The qualitative behavior difference at high energies between a gas (He in the figure) and the other materials shown in the figure is due to the density-effect correction, $\delta(\beta\gamma)$, discussed in Sec. 34.2.5. The stopping power functions are characterized by broad minima whose position drops from $\beta\gamma = 3.5$ to 3.0 as Z goes from 7 to 100. The values of minimum ionization as a function of atomic number are shown in Fig. 34.3.

In practical cases, most relativistic particles (*e.g.*, cosmic-ray muons) have mean energy loss rates close to the minimum; they are "minimum-ionizing particles," or mip's.

Eq. (34.5) may be integrated to find the total (or partial) "continuous slowing-down approximation" (CSDA) range R for a particle which loses energy only through ionization and atomic excitation. Since dE/dx depends only on β, R/M is a function of E/M or pc/M. In practice, range is a useful concept only for low-energy hadrons ($R \lesssim \lambda_I$, where λ_I is the nuclear interaction length), and for muons below a few hundred GeV (above which radiative effects dominate). Fig. 34.4 shows R/M as a function of $\beta\gamma$ ($= p/Mc$) for a variety of materials.

The mass scaling of dE/dx and range is valid for the electronic losses described by the Bethe equation, but not for radiative losses.

34.2.4 *Mean excitation energy*

"The determination of the mean excitation energy is the principal non-trivial task in the evaluation of the Bethe stopping-power formula" [15]. Recommended values have varied substantially with time. Estimates based on experimental stopping-power measurements for protons, deuterons, and alpha particles and on oscillator-strength distributions and dielectric-response functions were given in ICRU 49 [6]. See also ICRU 37 [12]. These values, shown in Fig. 34.5, have since been widely used. Machine-readable versions can also be found [16].

34.2.5 *Density effect*

As the particle energy increases, its electric field flattens and extends, so that the distant-collision contribution to the logarithmic term in Eq. (34.5) increases as $\beta^2\gamma^2$. However, real media become polarized, limiting the field extension and effectively truncating this part of the logarithmic rise [2,3,6,17,18]. At very high energies,

$$\delta(\beta\gamma)/2 \to \ln(\hbar\omega_p/I) + \ln\beta\gamma - 1/2 \ , \tag{34.6}$$

where $\delta(\beta\gamma)/2$ is the density effect correction introduced in Eq. (34.5) and $\hbar\omega_p$ is the plasma energy defined in Table 34.1. A comparison with Eq. (34.5) shows that dE/dx then grows as

[1] For incident spin 1/2 particles, $(W_{\max}/E)^2/4$ is included in the square brackets. Although this correction is within the uncertainties in the total stopping power, its inclusion avoids a systematic bias.

[2] In this section, "dE/dx" will be understood to mean the mass stopping power "$\langle -dE/dx \rangle$."

Downloaded from https://academic.oup.com/ptep/article/2022/8/083C01/6651666 by KIT Library user on 27 September 2022

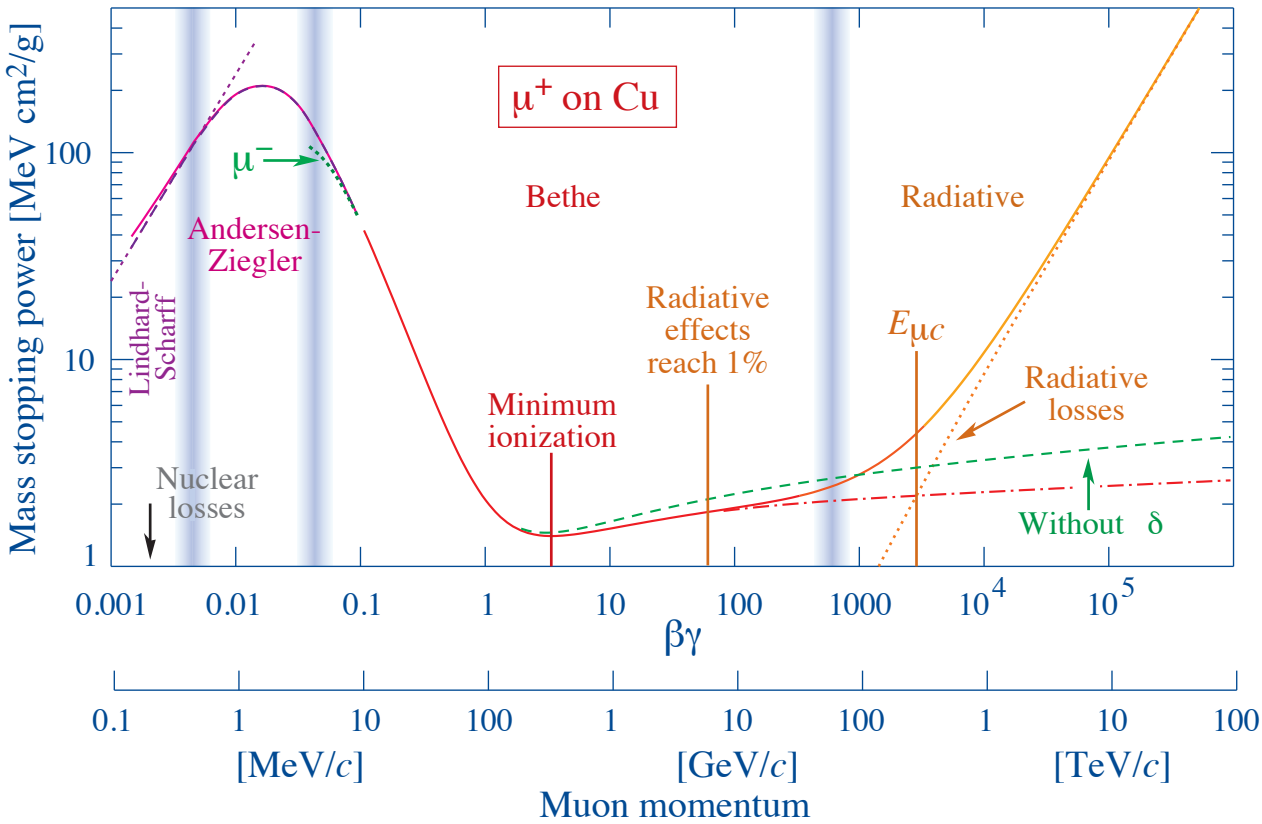

Figure 34.1: Mass stopping power (dE/dx) for positive muons in copper as a function of $\beta\gamma = p/Mc$ over nine orders of magnitude in momentum (12 orders of magnitude in kinetic energy). Solid curves indicate the total stopping power. Data below the break at $\beta\gamma \approx 0.1$ are taken from ICRU 49 [6] assuming only β dependence, and data at higher energies are from [7]. Vertical bands indicate boundaries between different approximations discussed in the text. The short dotted lines labeled "μ^-" illustrate the "Barkas effect," the dependence of stopping power on projectile charge at very low energies [8]. dE/dx in the radiative region is not simply a function of β.

$\ln T_{\max}$ rather than $\ln \beta^2\gamma^2 T_{\max}$, and that the mean excitation energy I is replaced by the plasma energy $\hbar\omega_p$. An example of the ionization stopping power as calculated with and without the density effect correction is shown in Fig. 34.1. Since the plasma frequency scales as the square root of the electron density, the correction is much larger for a liquid or solid than for a gas, as is illustrated in Fig. 34.2.

The density effect correction is usually computed using Sternheimer's parameterization [17]:

$$\delta(\beta\gamma) = \begin{cases} 2(\ln 10)x - \overline{C} & \text{if } x \geq x_1; \\ 2(\ln 10)x - \overline{C} + a(x_1 - x)^k & \text{if } x_0 \leq x < x_1; \\ 0 & \text{if } x < x_0 \text{ (nonconductors)}; \\ \delta_0 10^{2(x-x_0)} & \text{if } x < x_0 \text{ (conductors)} \end{cases} \tag{34.7}$$

Here $x = \log_{10}\beta\gamma = \log_{10}(p/Mc)$. $\overline{C}$ (the negative of the C used in Ref. [17]) is obtained by equating the high-energy case of Eq. (34.7) with the limit given in Eq. (34.6). The other parameters are adjusted to give a best fit to the results of detailed calculations for momenta below $Mc\exp(x_1)$. For nonconductors the correction is 0 below $\beta\gamma = 10^{x_0}$, corresponding to 100–200 MeV for pions and 1–2 GeV for protons. For conductors it decreases rapidly below this point. Parameters for the elements and nearly 200 compounds and mixtures of interest are published in a variety of places, notably in Ref. [18]. A recipe for finding the coefficients for nontabulated materials is given by Sternheimer and Peierls [19] and is summarized in Ref. [7].

The remaining relativistic rise comes from the $\beta^2\gamma$ growth of $W_{\max}$, which in turn is due to (rare) large energy transfers to a few electrons. When these events are excluded, the energy deposit in an absorbing layer approaches a constant value, the Fermi plateau (see Sec. 34.2.8 below). At even higher energies (*e.g.*, > 332 GeV for muons in iron, and at a considerably higher energy for protons in iron), radiative effects are more important than ionization losses. These are especially relevant for high-energy muons, as discussed in Sec. 34.6.

34.2.6 *Energy loss at low energies*

The theory of energy loss by ionization and excitation as given by Bethe is based on a first-order Born approximation. It assumes free electrons, and should be valid when the projectile's speed is large compared to that of the atomic electrons. This presents a problem at low energies, where $W_{\max}$ is less than the K shell binding energy. However, Mott showed that the Born approximation can be applied at energies much smaller than atomic binding energies [20]; the incident particle can be treated by classical mechanics since its wavelength is shorter than atomic dimensions. The Born method is actually better justified when its speed is not large compared to the K electron speed [5].

Higher-order corrections must still be made to extend the Bethe equation (Eq. (34.5)) to low energies. An improved approximation for the terms in the square brackets of Eq. (34.5) at low energies is obtained with

$$L(\beta) = L_a(\beta) - \frac{C(\beta)}{Z} + zL_1(\beta) + z^2L_2(\beta)\ . \tag{34.8}$$

Here L_a is the square-bracketed terms of Eq. (34.5), C/Z is the sum of shell corrections and zL_1 and z^2L_2 are Barkas and Bloch correction terms [6, 21]. With these corrections, the Bethe treatment is accurate to about 1% down to $\beta \approx 0.05$, or about 1 MeV for protons (0.13 MeV for muons). Values of L_a, C/Z, L_1, and L_2 in the range $T = 0.3$–30 MeV for a proton traversing aluminum can be found in Table I of Ref. [21].

Shell correction $-C/Z$. As the speed of the projectile decreases, the contribution to the stopping power from K shell electrons de-

Downloaded from https://academic.oup.com/ptep/article/2022/8/083C01/6651666 by KIT Library user on 27 September 2022

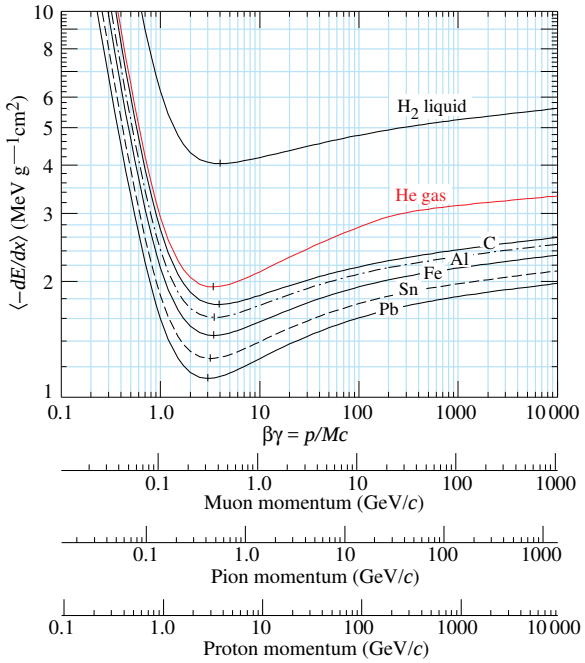

Figure 34.2: Mean energy loss rate in liquid (bubble chamber) hydrogen, gaseous helium, carbon, aluminum, iron, tin, and lead. Radiative effects, relevant for muons and pions, are not included. These become significant for muons in iron for $\beta\gamma \gtrsim 1000$, and at lower momenta for muons in higher-Z absorbers. See Fig. 34.23.

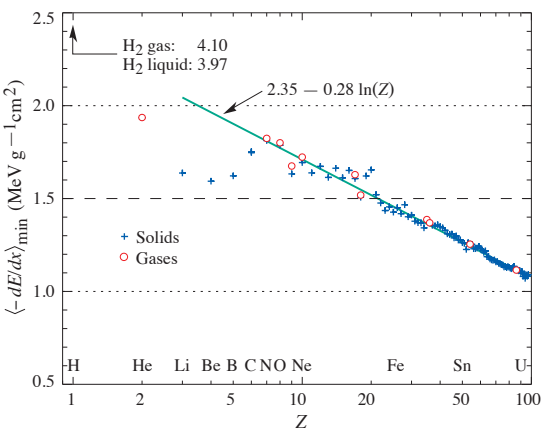

Figure 34.3: Mass stopping power at minimum ionization for the chemical elements. The straight line is fitted for $Z > 6$. A simple functional dependence on Z is not to be expected, since dE/dx also depends on other variables.

creases, and at even lower velocities contributions from L and higher shells further reduce it. The correction $(C_{\rm K} + C_{\rm L} + \ldots)/Z$ is should be included in the square brackets of Eq. (34.5). It is calculated and tabulated (for a few common materials) in a number of places; Refs. [6,12,21] are especially useful. As an example, the shell correction for a 30 MeV proton traversing aluminum is 0.6%, increasing to 9.9% as the proton's energy decreases to 0.3 MeV.

Barkas correction zL_1. Qualitatively, one might imagine an atom's electron cloud slightly recoiling at the approach of a negative projectile and being attracted toward an approaching positive projectile. Hence the stopping power for negative particles should be slightly smaller than the stopping power for positive particles. In a 1956 paper, Barkas *et al.* noted that negative pions possibly had a longer range than positive pions [8]. The effect has been measured for a number of negative/positive particle pairs, and more recently in detailed studies with antiprotons at the CERN LEAR facility [22]. Since no complete theory exists, an empirical

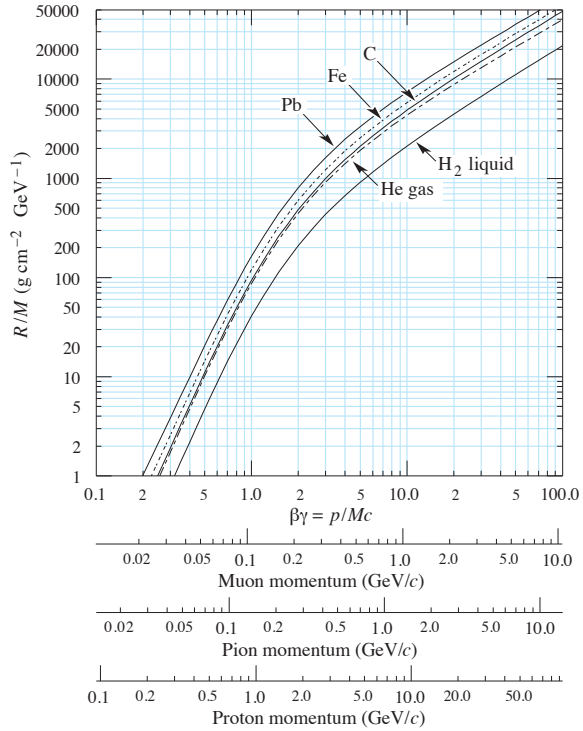

Figure 34.4: Range of heavy charged particles in liquid (bubble chamber) hydrogen, helium gas, carbon, iron, and lead. For example: For a K^+ whose momentum is 700 MeV/c, $\beta\gamma = 1.42$. For lead we read $R/M \approx 396$, and so the range is 195 g cm^{-2} (17 cm).

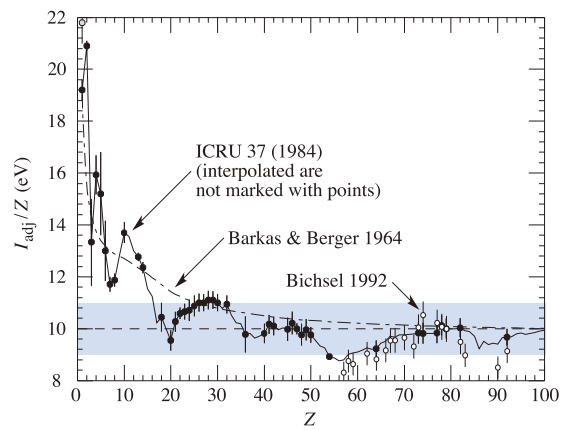

Figure 34.5: Mean excitation energies (divided by Z) as adopted by the ICRU [12]. Those based on experimental measurements are shown by symbols with error flags; the interpolated values are simply joined. The grey point is for liquid H_2; the black point at 19.2 eV is for H_2 gas. The open circles show more recent determinations by Bichsel [13]. The dash-dotted curve is from the approximate formula of Barkas [14] used in early editions of this *Review*.

approach is necessary. A 1972 harmonic-oscillator model by Ashley *et al.* [23] is often used; it has two parameters determined by experimental data. For protons in aluminum, L_1/L_a is less than 0.1% at 30 MeV, but increases to 17% as T decreases to 0.3 MeV. This correction is indicated in Fig. 34.1.

Bloch correction z^2L_2. Bloch's extension of Bethe's theory introduced a low-energy correction that takes account of perturbations of the atomic wave functions. The form obtained by Lindhard and Sørensen [11] is used *e.g.* in Refs. [6,21]. For protons in aluminum, $-L_2/L_|$ is less than 0.3% at 3.0 MeV, but rises to 7%

Downloaded from https://academic.oup.com/ptep/article/2022/8/083C01/6651666 by KIT Library user on 27 September 2022

when the energy has fallen to 0.3 MeV.

For the interval $0.01 < \beta < 0.05$ there is no satisfactory theory. For protons, one usually relies on the phenomenological fitting formulae developed by Andersen and Ziegler [6, 24]. As tabulated in ICRU 49 [6], the nuclear plus electronic proton stopping power in copper is 113 MeV cm^2 g^{-1} at $T = 10$ keV ($\beta\gamma = 0.005$), rises to a maximum of 210 MeV cm^2 g^{-1} at $T \approx 120$ keV ($\beta\gamma = 0.016$), then falls to 118 MeV cm^2 g^{-1} at $T = 1$ MeV ($\beta\gamma = 0.046$). Above 0.5–1.0 MeV the corrected Bethe theory is adequate.

For particles moving more slowly than $\approx 0.01c$ (more or less the speed of the outer atomic electrons), Lindhard has been quite successful in describing electronic stopping power, which is proportional to β [25]. Finally, we note that at even lower energies, *e.g.*, for protons of less than several hundred eV, non-ionizing nuclear recoil energy loss dominates the total energy loss [6, 25, 26].

34.2.7 *Energetic knock-on electrons (δ rays)*

The distribution of secondary electrons with kinetic energies $T \gg I$ is [2]

$$\frac{d^2N}{dTdx} = \frac{1}{2}\,Kz^2\frac{Z}{A}\,\frac{1}{\beta^2}\,\frac{F(T)}{T^2} \tag{34.9}$$

for $I \ll T \leq W_{\max}$, where $W_{\max}$ is given by Eq. (34.4). Here β is the speed of the primary particle. The factor F is spin-dependent, but is about unity for $T \ll W_{\max}$. For spin-0 particles $F(T) = (1-\beta^2 T/W_{\max})$; forms for spins 1/2 and 1 are also given by Rossi [2] (Sec. 2.3, Eqs. 7 and 8). Additional formulae are given in [27]. Equation Eq. (34.9) is inaccurate for T close to I [28].

δ rays of even modest energy are rare. For a $\beta \approx 1$ particle, for example, on average only one collision with $T_e > 10$ keV will occur along a path length of 90 cm of argon gas [1].

A δ ray with kinetic energy T_e and corresponding momentum p_e is produced at an angle θ given by

$$\cos\theta = (T_e/p_e)(p_{\max}/W_{\max})\ , \tag{34.10}$$

where $p_{\max}$ is the momentum of an electron with the maximum possible energy transfer $W_{\max}$.

34.2.8 *Restricted energy loss rates for relativistic ionizing particles*

Further insight can be obtained by examining the mean energy deposit by an ionizing particle when energy transfers are restricted to $T \leq W_{\rm cut} \leq W_{\max}$. The restricted energy loss rate is

$$-\frac{dE}{dx}\bigg|_{T<W_{\rm cut}} = Kz^2\frac{Z}{A}\frac{1}{\beta^2}\left[\frac{1}{2}\ln\frac{2m_ec^2\beta^2\gamma^2W_{\rm cut}}{I^2} - \frac{\beta^2}{2}\left(1+\frac{W_{\rm cut}}{W_{\max}}\right) - \frac{\delta}{2}\right]. \tag{34.11}$$

This form approaches the normal Bethe function (Eq. (34.5)) as $W_{\rm cut} \to W_{\max}$. It can be verified that the difference between Eq. (34.5) and Eq. (34.11) is equal to $\int_{W_{\rm cut}}^{W_{\max}} T(d^2N/dTdx)dT$, where $d^2N/dTdx$ is given by Eq. (34.9).

Since $W_{\rm cut}$ replaces $W_{\max}$ in the argument of the logarithmic term of Eq. (34.5), the $\beta\gamma$ term producing the relativistic rise in the close-collision part of dE/dx is replaced by a constant, and $|dE/dx|_{T<W_{\rm cut}}$ approaches the constant "Fermi plateau." (The density effect correction δ eliminates the explicit $\beta\gamma$ dependence produced by the distant-collision contribution.) This behavior is illustrated in Fig. 34.6, where restricted loss rates for two examples of $W_{\rm cut}$ are shown in comparison with the full Bethe dE/dx and the Landau-Vavilov most probable energy loss (to be discussed in Sec. 34.2.9 below).

"Restricted energy loss" is cut at the total mean energy, not the single-collision energy above $W_{\rm cut}$ It is of limited use. The most probable energy loss, discussed in the next Section, is far more useful in situations where single-particle energy loss is observed.

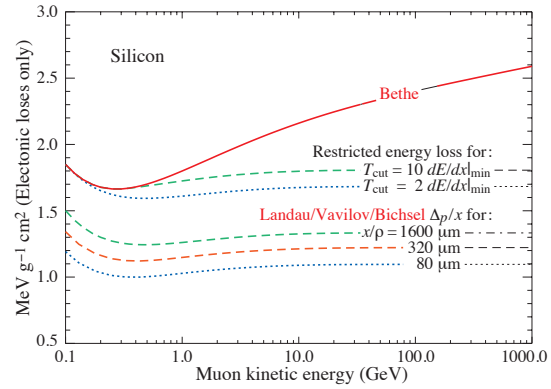

Figure 34.6: Bethe dE/dx, two examples of restricted energy loss, and the Landau most probable energy per unit thickness in silicon. The change of $\Delta_{\rm p}/{\rm x}$ with thickness x illustrates its $a\ln x + b$ dependence. Minimum ionization ($dE/dx|_{\rm min}$) is 1.664 MeV g^{-1} cm^2. Radiative losses are excluded. The incident particles are muons.

34.2.9 *Fluctuations in energy loss*

For detectors of moderate thickness x (*e.g.* scintillators or LAr cells),[3] the energy loss probability distribution $f(\Delta;\beta\gamma,x)$ is adequately described by the highly-skewed Landau (or Landau-Vavilov) distribution [29, 30].

The most probable energy loss is [31][4]

$$\Delta_p = \xi\left[\ln\frac{2mc^2\beta^2\gamma^2}{I} + \ln\frac{\xi}{I} + j - \beta^2 - \delta(\beta\gamma)\right]\ , \tag{34.12}$$

where $\xi = (K/2)\,\langle Z/A\rangle\, z^2(x/\beta^2)$ MeV for a detector with a thickness x in g cm^{-2}, and $j = 0.200$ [31].[5] While dE/dx is independent of thickness, Δ_p/x scales as $a\ln x + b$. The density correction $\delta(\beta\gamma)$ was not included in Landau's or Vavilov's work, but it was later included by Bichsel [31]. The high-energy behavior of $\delta(\beta\gamma)$ (Eq. (34.6)) is such that

$$\Delta_p \underset{\beta\gamma\gtrsim 100}{\longrightarrow} \xi\left[\ln\frac{2mc^2\xi}{(\hbar\omega_p)^2} + j\right]\ . \tag{34.13}$$

Thus the Landau-Vavilov most probable energy loss, like the restricted energy loss, reaches a Fermi plateau. The Bethe dE/dx and Landau-Vavilov-Bichsel Δ_p/x in silicon are shown as a function of muon energy in Fig. 34.6. The energy deposit in the 1600 μm case is roughly the same as in a 3 mm thick plastic scintillator.

The distribution function for the energy deposit by a 10 GeV muon going through a detector of about this thickness is shown in Fig. 34.7. In this case the most probable energy loss is 62% of the mean ($M_1(\langle\Delta\rangle)/M_1(\infty)$). Folding in experimental resolution displaces the peak of the distribution, usually toward a higher value. 90% of the collisions ($M_1(\langle\Delta\rangle)/M_1(\infty)$) contribute to energy deposits below the mean. It is the very rare high-energy-transfer collisions, extending to $W_{\max}$ at several GeV, that drives the mean into the tail of the distribution. The large weight of these rare events makes the mean of an experimental distribution consisting of a few hundred events subject to large fluctuations and sensitive to cuts. *The mean of the energy loss given by the Bethe equation, Eq. (34.5), is thus ill-defined experimentally and*

[3] "Moderate thickness" means $G \lesssim 0.05$–0.1, where G is given by Rossi Ref. [2], Eq. 2.7(10). It is Vavilov's κ [29]. G is proportional to the absorber's thickness, and as such parameterizes the constants describing the Landau distribution. These are fairly insensitive to thickness for $G \lesssim 0.1$, the case for most detectors.

[4] Practical calculations can be expedited by using the tables of δ and β from the text versions of the muon energy loss tables to be found at `pdg.lbl.gov/curremt/AtomicNuclearProperties`.

[5] Rossi [2], Talman [32], and others give somewhat different values for j. The most probable loss is not sensitive to its value.

Downloaded from https://academic.oup.com/ptep/article/2022/8/083C01/6651666 by KIT Library user on 27 September 2022

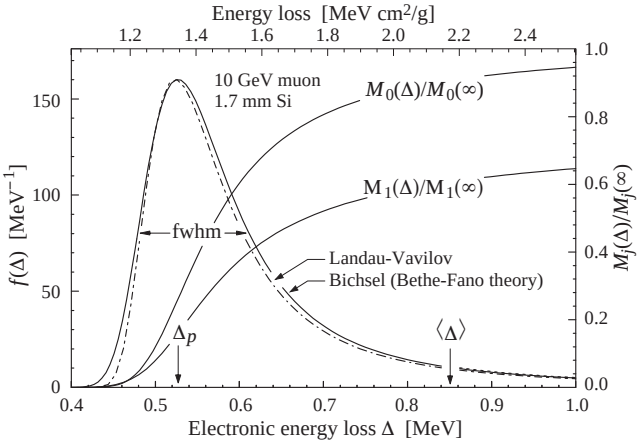

Figure 34.7: Electronic energy deposit distribution for a 10 GeV muon traversing 1.7 mm of silicon, the stopping power equivalent of about 0.3 cm of PVT-based scintillator [1, 13, 33]. The Landau-Vavilov function (dot-dashed) uses a Rutherford cross section without atomic binding corrections but with a kinetic energy transfer limit of $W_{\max}$. The solid curve was calculated using Bethe-Fano theory. $M_0(\Delta)$ and $M_1(\Delta)$ are the cumulative 0th moment (mean number of collisions) and 1st moment (mean energy loss) in crossing the silicon. (See Sec. 34.2.1). The fwhm of the Landau-Vavilov function is about 4ξ for detectors of moderate thickness. Δ_p is the most probable energy loss, and $\langle\Delta\rangle$ divided by the thickness is the Bethe dE/dx.

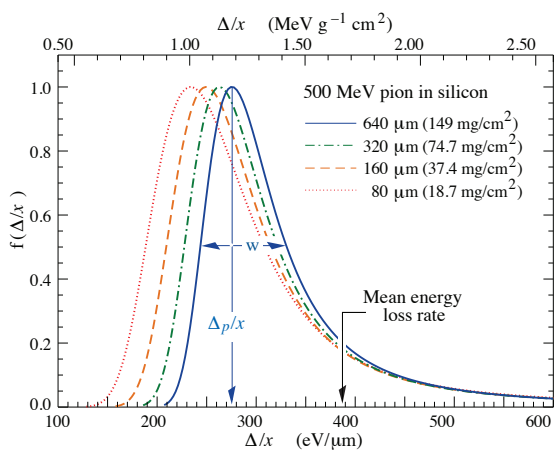

Figure 34.8: Straggling functions in silicon for 500 MeV pions, normalized to unity at the most probable value Δ_p/x. The width w is the full width at half maximum.

is not useful for describing energy loss by single particles.[6] It rises as $\ln\gamma$ because $W_{\max}$ increases as γ at high energies. *The most probable energy loss should be used.*

A practical example: For muons traversing 0.25 inches (0.64 cm) of PVT (polyvinyltolulene) based plastic scintillator, the ratio of the most probable E loss rate to the mean loss rate via the Bethe equation is $[0.69, 0.57, 0.49, 0.42, 0.38]$ for $T_\mu = [0.01, 0.1, 1, 10, 100]$ GeV. Radiative losses add less than 0.5% to the total mean energy deposit at 10 GeV, but add 7% at 100 GeV. The most probable E loss rate rises slightly beyond the minimum ionization energy, then is essentially constant.

The Landau distribution fails to describe energy loss in thin absorbers such as gas TPC cells [1] and Si detectors [31], as can be seen *e.g.* in Fig. 1 of Ref. [1] for an argon-filled TPC cell. Also see Talman [32]. While Δ_p/x may be calculated adequately with Eq. (34.12), the distributions are significantly wider than the Landau width $w = 4\xi$ Ref. [31], Fig. 15. Examples for 500 MeV pions incident on thin silicon detectors are shown in Fig. 34.8. For very thick absorbers the distribution is less skewed but never approaches a Gaussian.

The most probable energy loss, scaled to the mean loss at minimum ionization, is shown in Fig. 34.9 for several silicon detector thicknesses.

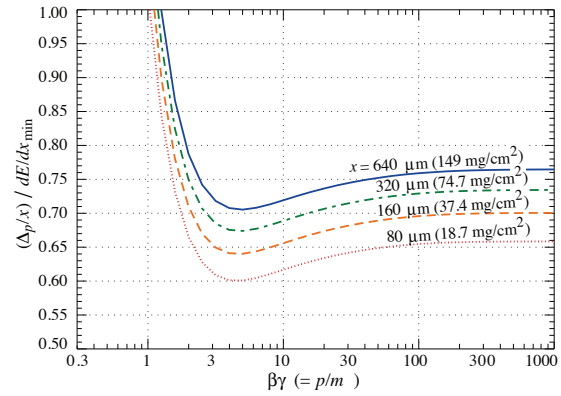

Figure 34.9: Most probable energy loss in silicon, scaled to the mean loss of a minimum ionizing particle, 388 eV/μm (1.66 MeV g^{-1}cm^2).

34.2.10 *Energy loss in mixtures and compounds*

A mixture or compound can be thought of as made up of thin layers of pure elements in the right proportion (Bragg additivity). In this case,

$$\left\langle \frac{dE}{dx} \right\rangle = \sum w_j \left\langle \frac{dE}{dx} \right\rangle_j , \tag{34.14}$$

where $dE/dx|_j$ is the mean rate of energy loss (in MeV g cm^{-2}) in the jth element. Eq. (34.5) can be inserted into Eq. (34.14) to find expressions for $\langle Z/A\rangle$, $\langle I\rangle$, and $\langle\delta\rangle$; for example, $\langle Z/A\rangle = \sum w_j Z_j/A_j = \sum n_j Z_j / \sum n_j A_j$. However, $\langle I\rangle$ as defined this way is an underestimate, because in a compound electrons are more tightly bound than in the free elements, and $\langle\delta\rangle$ as calculated this way has little relevance, because it is the electron density that matters. If possible, one uses the tables given in Refs. [18, 34], or the recipes given in [19] (repeated in Ref. [7]), that include effective excitation energies and interpolation coefficients for calculating the density effect correction for the chemical elements and nearly 200 mixtures and compounds. Otherwise, use the recipe for δ given in Refs. [7, 19], and calculate $\langle I\rangle$ following the discussion in Ref. [15]. (Note the "13%" rule!)

34.2.11 *Ionization yields*

The Bethe equation describes energy loss via excitation and ionization. Many gaseous detectors (proportional counters or TPCs) or liquid ionization detectors count the number of electrons or positive ions from ionization, rather than the ionization energy. As a further complication, the electron liberated in the initial ionization often has enough energy to ionize other atoms or molecules; this process can happen several times. The number of electron-ion pairs per unit length is typically three or more times the original number. Ion or electron counting is a proxy for a direct dE/dx measurement. Calibrations link the number of observed ions to the traversing particle's dE/dx.

The details depend on the gases (or liquids) and the particular detector involved. A useful discussion of the physics is provided in Sec.35.6 of this Review.

34.3 Multiple scattering through small angles

A charged particle traversing a medium is deflected by many small-angle scatters. Most of this deflection is due to Coulomb scattering from nuclei as described by the Rutherford cross section. (However, for hadronic projectiles, the strong interactions also contribute to multiple scattering.) For many small-angle scatters the net scattering and displacement distributions are Gaussian via the central limit theorem. Less frequent "hard" scatters

[6] It does find application in dosimetry, where only bulk deposit is relevant.

Downloaded from https://academic.oup.com/ptep/article/2022/8/083C01/6651666 by KIT Library user on 27 September 2022

produce non-Gaussian tails. These Coulomb scattering distributions are well-represented by the theory of Molière [35]. Accessible discussions are given by Rossi [2] and Jackson [3], and exhaustive reviews have been published by Scott [36] and Motz *et al.* [37]. Experimental measurements have been published by Bichsel [38] (low energy protons) and by Shen *et al.* [39] (relativistic pions, kaons, and protons).[7]

If we define

$$\theta_0 = \theta^{\,\mathrm{rms}}_{\,\mathrm{plane}} = \frac{1}{\sqrt{2}}\,\theta^{\mathrm{rms}}_{\mathrm{space}}\ , \tag{34.15}$$

then it is sufficient for many applications to use a Gaussian approximation for the central 98% of the projected angular distribution, with an rms width given by Lynch & Dahl [40]:

$$\begin{aligned}\theta_0 &= \frac{13.6\ \mathrm{MeV}}{\beta cp}\ z\ \sqrt{\frac{x}{X_0}}\left[1 + 0.088\log_{10}(\frac{x\,z^2}{X_0\beta^2})\right]\\ &= \frac{13.6\ \mathrm{MeV}}{\beta cp}\ z\ \sqrt{\frac{x}{X_0}}\left[1 + 0.038\ln(\frac{x\,z^2}{X_0\beta^2})\right]\end{aligned} \tag{34.16}$$

Here p, βc, and z are the momentum, speed, and charge number of the incident particle, and x/X_0 is the thickness of the scattering medium in radiation lengths (defined below). This takes into account the p and z dependence quite well at small Z, but for large Z and small x the β-dependence is not well represented. Further improvements are discussed in Ref. [40].

Eq. (34.16) describes scattering from a single material, while the usual problem involves the multiple scattering of a particle traversing many different layers and mixtures. Since it is from a fit to a Molière distribution, it is incorrect to add the individual θ_0 contributions in quadrature; the result is systematically too small. It is much more accurate to apply Eq. (34.16) once, after finding x and X_0 for the combined scatterer.

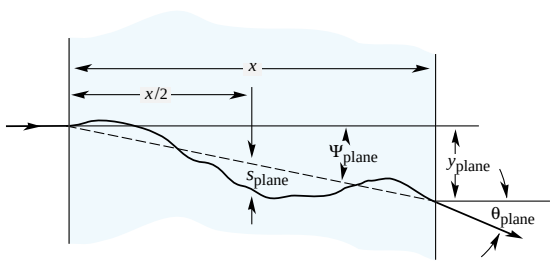

Figure 34.10: Quantities used to describe multiple Coulomb scattering. The particle is incident in the plane of the figure.

The nonprojected (space) and projected (plane) angular distributions are given approximately by [35]

$$\frac{1}{2\pi\,\theta_0^2}\ \exp\left(-\frac{\theta^2_{\mathrm{space}}}{2\theta_0^2}\right)\ d\Omega, \tag{34.17}$$

$$\frac{1}{\sqrt{2\pi}\,\theta_0}\ \exp\left(-\frac{\theta^2_{\mathrm{plane}}}{2\theta_0^2}\right)\ d\theta_{\mathrm{plane}}, \tag{34.18}$$

where θ is the deflection angle. In this approximation, $\theta^2_{\mathrm{space}} \approx (\theta^2_{\mathrm{plane},x} + \theta^2_{\mathrm{plane},y})$, where the x and y axes are orthogonal to the direction of motion, and $d\Omega \approx d\theta_{\mathrm{plane},x}\,d\theta_{\mathrm{plane},y}$. Deflections into $\theta_{\mathrm{plane},x}$ and $\theta_{\mathrm{plane},y}$ are independent and identically distributed. Fig. 34.10 shows these and other quantities sometimes used to describe multiple Coulomb scattering. They are

$$\psi^{\,\mathrm{rms}}_{\,\mathrm{plane}} = \frac{1}{\sqrt{3}}\,\theta^{\,\mathrm{rms}}_{\,\mathrm{plane}} \quad = \frac{1}{\sqrt{3}}\,\theta_0, \tag{34.19}$$

$$y^{\,\mathrm{rms}}_{\,\mathrm{plane}} = \frac{1}{\sqrt{3}}\,x\,\theta^{\,\mathrm{rms}}_{\,\mathrm{plane}} \quad = \frac{1}{\sqrt{3}}\,x\,\theta_0, \tag{34.20}$$

$$s^{\,\mathrm{rms}}_{\,\mathrm{plane}} = \frac{1}{4\sqrt{3}}\,x\,\theta^{\,\mathrm{rms}}_{\,\mathrm{plane}} = \frac{1}{4\sqrt{3}}\,x\,\theta_0. \tag{34.21}$$

All the quantitative estimates in this section apply only in the limit of small $\theta^{\,\mathrm{rms}}_{\,\mathrm{plane}}$ and in the absence of large-angle scatters. The random variables s, ψ, y, and θ in a given plane are correlated. Obviously, $y \approx x\psi$. In addition, y and θ have the correlation coefficient $\rho_{y\theta} = \sqrt{3}/2 \approx 0.87$. For Monte Carlo generation of a joint $(y_{\,\mathrm{plane}}, \theta_{\mathrm{plane}})$ distribution, or for other calculations, it may be most convenient to work with independent Gaussian random variables (z_1, z_2) with mean zero and variance one, and then set

$$y_{\mathrm{plane}} = z_1\,x\,\theta_0(1-\rho^2_{y\theta})^{1/2}/\sqrt{3} + z_2\,\rho_{y\theta}x\,\theta_0/\sqrt{3} \tag{34.22a}$$

$$= z_1\,x\,\theta_0/\sqrt{12} + z_2\,x\,\theta_0/2; \tag{34.22b}$$

$$\theta_{\mathrm{plane}} = z_2\,\theta_0. \tag{34.22c}$$

Note that the second term for $y_{\,\mathrm{plane}}$ equals $x\,\theta_{\mathrm{plane}}/2$ and represents the displacement that would have occurred had the deflection θ_{plane} all occurred at the single point $x/2$.

For heavy ions the multiple Coulomb scattering has been measured and compared with various theoretical distributions [41].

34.4 Photon and electron interactions in matter

At low energies electrons and positrons primarily lose energy by ionization, although other processes (Møller scattering, Bhabha scattering, e^+ annihilation) contribute, as shown in Fig. 34.11. While ionization loss rates rise logarithmically with energy, bremsstrahlung losses rise nearly linearly (fractional loss is nearly independent of energy), and dominates above the critical energy (Sec. 34.4.4 below), a few tens of MeV in most materials.

34.4.1 *Collision energy losses by* $e^{\pm}$

Stopping power differs somewhat for electrons and positrons, and both differ from stopping power for heavy particles because of the kinematics, spin, charge, and the identity of the incident electron with the electrons that it ionizes. Complete discussions and tables can be found in Refs. [12, 15, 34].

For electrons, large energy transfers to atomic electrons (taken as free) are described by the Møller cross section. From Eq. (34.4), the maximum energy transfer in a single collision should be the entire kinetic energy, $W_{\max} = m_e c^2(\gamma - 1)$, but because the particles are identical, the maximum is half this, $W_{\max}/2$. (The results are the same if the transferred energy is ϵ or if the transferred energy is $W_{\max} - \epsilon$. The stopping power is by convention calculated for the faster of the two emerging electrons.) The first moment of the Møller cross section [27] (divided by dx) is the stopping power:

$$\begin{aligned}\left\langle -\frac{dE}{dx}\right\rangle = \frac{1}{2}K\frac{Z}{A}\frac{1}{\beta^2}\Bigg[&\ln\frac{m_e c^2\beta^2\gamma^2\{m_e c^2(\gamma-1)/2\}}{I^2} + (1-\beta^2)\\ &- \frac{2\gamma-1}{\gamma^2}\ln 2 + \frac{1}{8}\left(\frac{\gamma-1}{\gamma}\right)^2 - \delta\Bigg]\end{aligned} \tag{34.23}$$

The logarithmic term can be compared with the logarithmic term in the Bethe equation (Eq. (34.2)) by substituting $W_{\max} = m_e c^2(\gamma-1)/2$. Electron-positron scattering is described by the fairly complicated Bhabha cross section [27]. There is no identical particle problem, so $W_{\max} = m_e c^2(\gamma - 1)$. The first moment of the Bhabha equation yields

$$\begin{aligned}\left\langle -\frac{dE}{dx}\right\rangle = \frac{1}{2}K\frac{Z}{A}\frac{1}{\beta^2}\Bigg[&\ln\frac{m_e c^2\beta^2\gamma^2\{m_e c^2(\gamma-1)\}}{2I^2} + 2\ln 2\\ &-\frac{\beta^2}{12}\left(23 + \frac{14}{\gamma+1} + \frac{10}{(\gamma+1)^2} + \frac{4}{(\gamma+1)^3}\right) - \delta\Bigg]\ .\end{aligned} \tag{34.24}$$

Following ICRU 37 [12], the density effect correction δ has been added to Uehling's equations [27] in both cases.

For heavy particles, shell corrections were developed assuming that the projectile is equivalent to a perturbing potential whose center moves with constant speed. This assumption has no sound

[7] Shen *et al.*'s measurements show that Bethe's simpler methods of including atomic electron effects agrees better with experiment than does Scott's treatment.

Downloaded from https://academic.oup.com/ptep/article/2022/8/083C01/6651666 by KIT Library user on 27 September 2022

theoretical basis for electrons. The authors of ICRU 37 [12] estimated the possible error in omitting it by assuming the correction was twice as great as for a proton of the same speed. At $T = 10$ keV, the error was estimated to be ≈2% for water, ≈9% for Cu, and ≈21% for Au.

As shown in Fig. 34.11, stopping powers for e^-, e^+, and heavy particles are not dramatically different. In silicon, the minimum value for electrons is 1.50 MeV cm^2/g (at $\gamma = 3.3$); for positrons, 1.46 MeV cm^2/g (at $\gamma = 3.7$), and for muons, 1.66 MeV cm^2/g (at $\gamma = 3.58$).

34.4.2 *Radiation length*

High-energy electrons predominantly lose energy in matter by bremsstrahlung, and high-energy photons by e^+e^- pair production. The characteristic amount of matter traversed for these related interactions is called the radiation length X_0, usually measured in g cm^{-2}. It is the mean distance over which a high-energy electron loses all but $1/e$ of its energy by bremsstrahlung. It is also the appropriate scale length for describing high-energy electromagnetic cascades. X_0 has been calculated and tabulated by Y.S. Tsai [42]:

$$\frac{1}{X_0} = 4\alpha r_e^2 \frac{N_A}{A}\left\{Z^2\left[L_{\rm rad} - f(Z)\right] + Z\,L'_{\rm rad}\right\}\,. \tag{34.25}$$

For $A = 1$ g mol^{-1}, $4\alpha r_e^2 N_A/A = (716.408\ \text{g cm}^{-2})^{-1}$. $L_{\rm rad}$ and $L'_{\rm rad}$ are given in Table 34.2. The function $f(Z)$ is an infinite sum, but for elements up to uranium can be represented to 4-place accuracy by

$$f(Z) = a^2\Big[(1+a^2)^{-1} + 0.20206 - 0.0369\,a^2 + 0.0083\,a^4 - 0.002\,a^6\Big], \tag{34.26}$$

where $a = \alpha Z$ [43].

Table 34.2: Tsai's $L_{\rm rad}$ and $L'_{\rm rad}$, for use in calculating the radiation length in an element using Eq. (34.25).

Element	Z	$L_{\rm rad}$	$L'_{\rm rad}$
H	1	5.31	6.144
He	2	4.79	5.621
Li	3	4.74	5.805
Be	4	4.71	5.924
Others	> 4	$\ln(184.15\,Z^{-1/3})$	$\ln(1194\,Z^{-2/3})$

The radiation length in a mixture or compound may be approximated by

$$1/X_0 = \sum w_j/X_j, \tag{34.27}$$

where w_j and X_j are the fraction by weight and the radiation length for the jth element.

34.4.3 *Bremsstrahlung energy loss by* $e^\pm$

At very high energies and except at the high-energy tip of the bremsstrahlung spectrum, the cross section can be approximated in the "complete screening case" as [42]

$$d\sigma/dk = (1/k)4\alpha r_e^2\Big\{(\tfrac{4}{3} - \tfrac{4}{3}y + y^2)[Z^2(L_{\rm rad} - f(Z)) + Z\,L'_{\rm rad}] + \tfrac{1}{9}(1-y)(Z^2+Z)\Big\}\,, \tag{34.28}$$

where $y = k/E$ is the fraction of the electron's energy transferred to the radiated photon. At small y (the "infrared limit") the term on the second line ranges from 1.7% (low Z) to 2.5% (high Z) of the total. If it is ignored and the first line simplified with the definition of X_0 given in Eq. (34.25), we have

$$\frac{d\sigma}{dk} = \frac{A}{X_0 N_A k}\left(\tfrac{4}{3} - \tfrac{4}{3}y + y^2\right)\,. \tag{34.29}$$

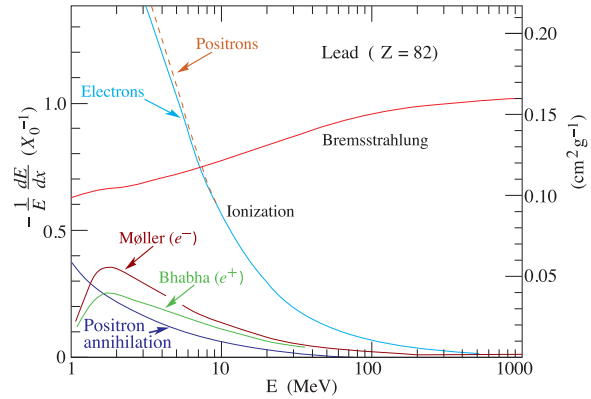

Figure 34.11: Fractional energy loss per radiation length in lead as a function of electron or positron energy. Electron (positron) scattering is considered as ionization when the energy loss per collision is below 0.255 MeV, and as Møller (Bhabha) scattering when it is above. Adapted from Fig. 3.2 from Messel and Crawford, *Electron-Photon Shower Distribution Function Tables for Lead, Copper, and Air Absorbers*, Pergamon Press, 1970. Messel and Crawford use X_0(Pb) = 5.82 g/cm^2, but we have modified the figures to reflect the value given in the Table of Atomic and Nuclear Properties of Materials (X_0(Pb) = 6.37 g/cm^2).

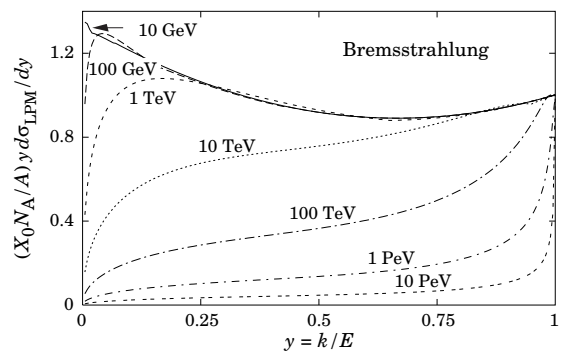

Figure 34.12: The normalized bremsstrahlung cross section $k\,d\sigma_{LPM}/dk$ in lead versus the fractional photon energy $y = k/E$. The vertical axis has units of photons per radiation length.

This cross section (times k) is shown by the top curve in Fig. 34.12.

This formula is accurate except near $y = 1$, where screening may become incomplete, and near $y = 0$, where the infrared divergence is removed by the interference of bremsstrahlung amplitudes from nearby scattering centers (the LPM effect) [44, 45] and dielectric suppression [46, 47]. These and other suppression effects in bulk media are discussed in Sec. 34.4.6.

With decreasing energy ($E \lesssim 10$ GeV) the high-y cross section drops and the curves become rounded as $y \to 1$. Curves of this familar shape can be seen in Rossi [2] (Figs. 2.11.2,3); see also the review by Koch & Motz [48].

Except at these extremes, and still in the complete-screening approximation, the number of photons with energies between $k_{\rm min}$ and $k_{\rm max}$ emitted by an electron travelling a distance $d \ll X_0$ is

$$N_\gamma = \frac{d}{X_0}\left[\frac{4}{3}\ln\left(\frac{k_{\rm max}}{k_{\rm min}}\right) - \frac{4(k_{\rm max} - k_{\rm min})}{3E} + \frac{k_{\rm max}^2 - k_{\rm min}^2}{2E^2}\right]\,. \tag{34.30}$$

34.4.4 *Critical energy*

An electron loses energy by bremsstrahlung at a rate nearly proportional to its energy, while the ionization loss rate varies only logarithmically with the electron energy. The *critical energy* E_c is sometimes defined as the energy at which the two loss rates are equal [49]. Among alternate definitions is that of Rossi [2], who defines the critical energy as the energy at which the ion-

Downloaded from https://academic.oup.com/ptep/article/2022/8/083C01/6651666 by KIT Library user on 27 September 2022

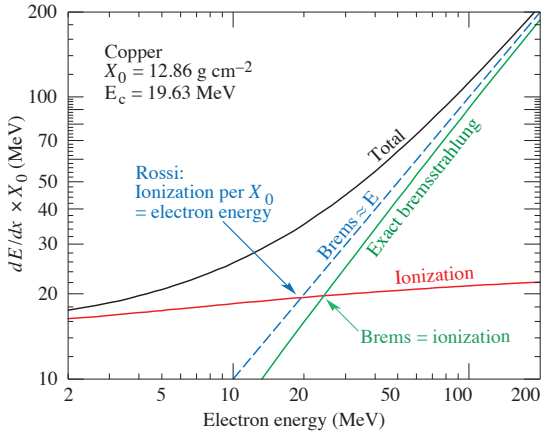

Figure 34.13: Two definitions of the critical energy E_c.

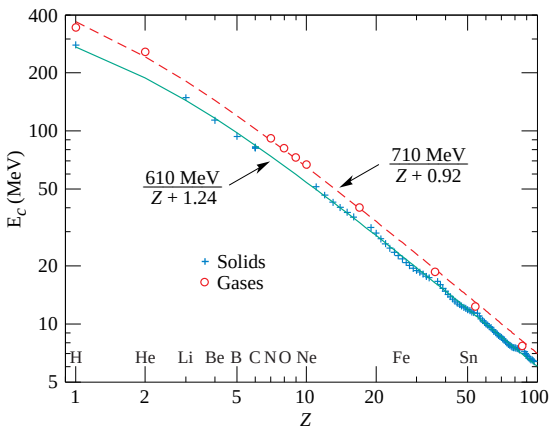

Figure 34.14: Electron critical energy for the chemical elements, using Rossi's definition [2]. The fits shown are for solids and liquids (solid line) and gases (dashed line). The rms deviation is 2.2% for the solids and 4.0% for the gases.

ization loss per radiation length is equal to the electron energy. Equivalently, it is the same as the first definition with the approximation $|dE/dx|_{\text{brems}} \approx E/X_0$. This form has been found to describe transverse electromagnetic shower development more accurately (see below). These definitions are illustrated in the case of copper in Fig. 34.13.

The accuracy of approximate forms for E_c has been limited by the failure to distinguish between gases and solid or liquids, where there is a substantial difference in ionization at the relevant energy because of the density effect. We distinguish these two cases in Fig. 34.14. Fits were also made with functions of the form $a/(Z+b)^\alpha$, but α was found to be essentially unity. Since E_c also depends on A, I, and other factors, such forms are at best approximate.

Values of E_c for both electrons and positrons in more than 300 materials at
`pdg.lbl.gov/current/AtomicNuclearProperties.`

34.4.5 *Energy loss by photons*

Contributions to the photon cross section in a light element (carbon) and a heavy element (lead) are shown in Fig. 34.15. At low energies it is seen that the photoelectric effect dominates, although Compton scattering, Rayleigh scattering, and photonuclear absorption also contribute. The photoelectric cross section is characterized by discontinuities (absorption edges) as thresholds for photoionization of various atomic levels are reached. Photon attenuation lengths for a variety of elements are shown in Fig. 34.16, and data for 30 eV$< k <$100 GeV for all elements are available from the web pages given in the caption. Here k is the photon energy.

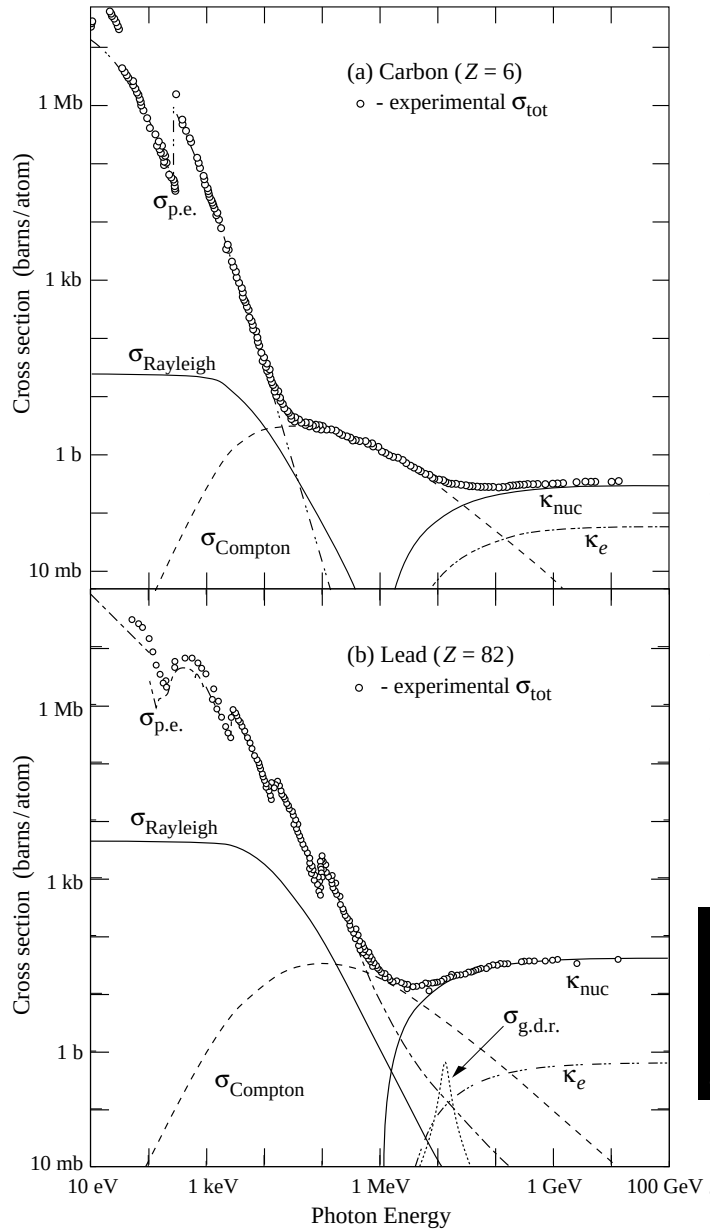

Figure 34.15: Photon total cross sections as a function of energy in carbon and lead, showing the contributions of different processes [50]:

$\sigma_{\text{p.e.}}$ = Atomic photoelectric effect (electron ejection, photon absorption)
σ_{Rayleigh} = Rayleigh (coherent) scattering–atom neither ionized nor excited
σ_{Compton} = Incoherent scattering (Compton scattering off an electron)
κ_{nuc} = Pair production, nuclear field
κ_e = Pair production, electron field
$\sigma_{\text{g.d.r.}}$ = Photonuclear interactions, most notably the Giant Dipole Resonance [51]. In these interactions, the target nucleus is usually broken up.

Original figures through the courtesy of John H. Hubbell (NIST).

The increasing domination of pair production as the energy increases is shown in Fig. 34.17. Using approximations similar to those used to obtain Eq. (34.29), Tsai's formula for the differential cross section [42] reduces to

$$\frac{d\sigma}{dx} = \frac{A}{X_0 N_A}\left[1 - \tfrac{4}{3}x(1-x)\right] \tag{34.31}$$

Downloaded from https://academic.oup.com/ptep/article/2022/8/083C01/6651666 by KIT Library user on 27 September 2022

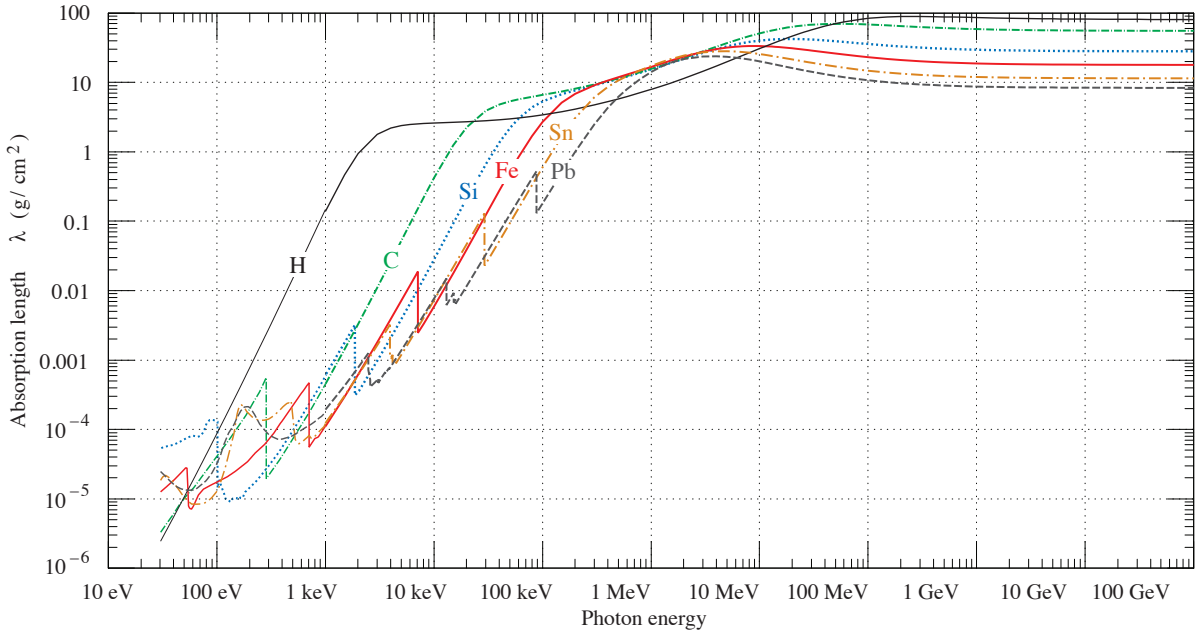

Figure 34.16: The photon mass attenuation length (or mean free path) $\lambda = 1/(\mu/\rho)$ for various elemental absorbers as a function of photon energy. The mass attenuation coefficient is μ/ρ, where ρ is the density. The intensity I remaining after traversal of thickness t (in mass/unit area) is given by $I = I_0 \exp(-t/\lambda)$. The accuracy is a few percent. For a chemical compound or mixture, $1/\lambda_{\rm eff} \approx \sum_{\rm elements} w_Z/\lambda_Z$, where w_Z is the proportion by weight of the element with atomic number Z. The processes responsible for attenuation are given in Fig. 34.11. Since coherent processes are included, not all these processes result in energy deposition. The data for 30 eV $< E <$ 1 keV are from Ref. [52], those for 1 keV $< E <$ 100 GeV from Ref. [53].

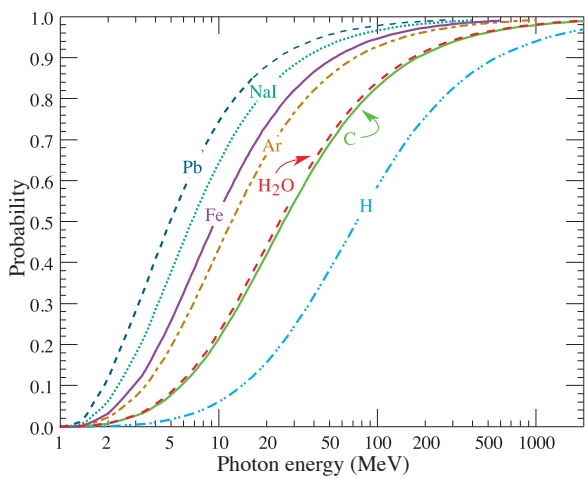

Figure 34.17: Probability P that a photon interaction will result in conversion to an e^+e^- pair. Except for a few-percent contribution from photonuclear absorption around 10 or 20 MeV, essentially all other interactions in this energy range result in Compton scattering off an atomic electron. For a photon attenuation length λ (Fig. 34.16), the probability that a given photon will produce an electron pair (without first Compton scattering) in thickness t of absorber is $P[1 - \exp(-t/\lambda)]$.

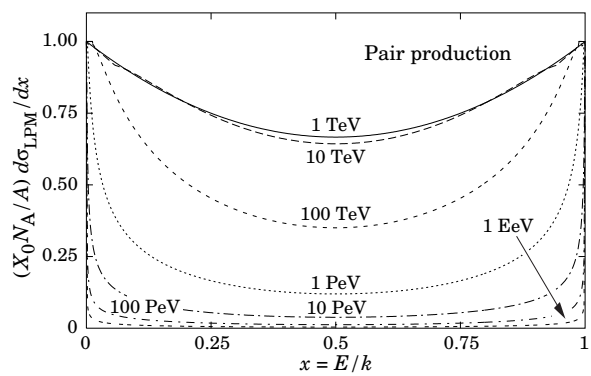

Figure 34.18: The normalized pair production cross section $d\sigma_{LPM}/dx$, versus fractional electron energy $x = E/k$.

in the complete-screening limit valid at high energies. Here $x = E/k$ is the fractional energy transfer to the pair-produced electron (or positron), and k is the incident photon energy. The cross section is very closely related to that for bremsstrahlung, since the Feynman diagrams are variants of one another. The cross section is of necessity symmetric between x and $1 - x$, as can be seen by the solid curve in Fig. 34.18. See the review by Motz, Olsen, & Koch for a more detailed treatment [54]. Eq. (34.31) may be integrated to find the high-energy limit for the total e^+e^- pair-production cross section:

$$\sigma = \tfrac{7}{9}(A/X_0 N_A). \tag{34.32}$$

Equation Eq. (34.32) is accurate to within a few percent down to energies as low as 1 GeV, particularly for high-Z materials.

34.4.6 *Bremsstrahlung and pair production at very high energies*

At ultrahigh energies, Eqns. 34.28–34.32 will fail because of quantum mechanical interference between amplitudes from different scattering centers. Since the longitudinal momentum transfer to a given center is small ($\propto k/E(E-k)$, in the case of bremsstrahlung), the interaction is spread over a comparatively long distance called the formation length ($\propto E(E-k)/k$) via the uncertainty principle. In alternate language, the formation length is the distance over which the highly relativistic electron and the photon "split apart." The interference is usually destructive. Calculations of the "Landau-Pomeranchuk-Migdal" (LPM) effect may be made semi-classically based on the average multiple scattering, or more rigorously using a quantum transport approach [44, 45].

Downloaded from https://academic.oup.com/ptep/article/2022/8/083C01/6651666 by KIT Library user on 27 September 2022

In amorphous media, bremsstrahlung is suppressed if the photon energy k is less than $E^2/(E + E_{LPM})$ [45], where[8]

$$E_{LPM} = (m_e c^2)^2 \alpha \frac{X_0}{4\pi\hbar c\rho} = (7.7 \text{ TeV/cm}) \times \frac{X_0}{\rho} \ . \qquad (34.33)$$

Since physical distances are involved, X_0/ρ, in cm, appears. The energy-weighted bremsstrahlung spectrum for lead, $k\, d\sigma_{LPM}/dk$, is shown in Fig. 34.12. With appropriate scaling by X_0/ρ, other materials behave similarly.

For photons, pair production is reduced for $E(k - E) > k\, E_{LPM}$. The pair-production cross sections for different photon energies are shown in Fig. 34.18.

If $k \ll E$, several additional mechanisms can also produce suppression. When the formation length is long, even weak factors can perturb the interaction. For example, the emitted photon can coherently forward scatter off of the electrons in the media. Because of this, for $k < \omega_p E/m_e \sim 10^{-4}$, bremsstrahlung is suppressed by a factor $(k m_e/\omega_p E)^2$ [47]. Magnetic fields can also suppress bremsstrahlung.

In crystalline media, the situation is more complicated, with coherent enhancement or suppression possible. The cross section depends on the electron and photon energies and the angles between the particle direction and the crystalline axes [56].

34.4.7 *Photonuclear and electronuclear interactions at still higher energies*

At still higher photon and electron energies, where the bremsstrahlung and pair production cross-sections are heavily suppressed by the LPM effect, photonuclear and electronuclear interactions predominate over electromagnetic interactions.

At photon energies above about 10^{20} eV, for example, photons usually interact hadronically. The exact cross-over energy depends on the model used for the photonuclear interactions. These processes are illustrated in Fig. 34.19. At still higher energies ($\gtrsim 10^{23}$ eV), photonuclear interactions can become coherent, with the photon interaction spread over multiple nuclei. Essentially, the photon coherently converts to a ρ^0, in a process that is somewhat similar to kaon regeneration [57].

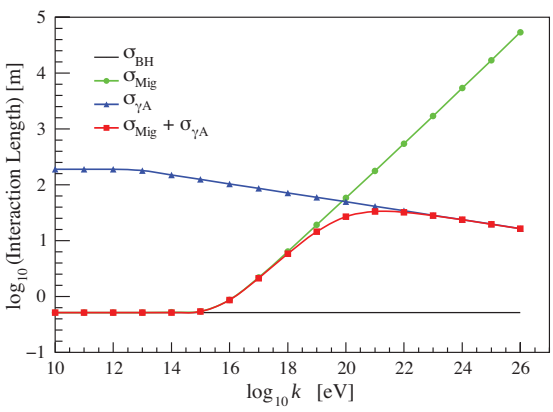

Figure 34.19: Interaction length for a photon in ice as a function of photon energy for the Bethe-Heitler (BH), LPM (Mig) and photonuclear (γA) cross sections [57]. The Bethe-Heitler interaction length is $9X_0/7$, and X_0 is 0.393 m in ice.

Similar processes occur for electrons. As electron energies increase and the LPM effect suppresses bremsstrahlung, electronuclear interactions become more important. At energies above 10^{21}eV, these electronuclear interactions dominate electron energy loss [57].

34.5 Electromagnetic cascades

When a high-energy electron or photon is incident on a thick absorber, it initiates an electromagnetic cascade as pair production and bremsstrahlung generate more electrons and photons with lower energy. The longitudinal development is governed by the high-energy part of the cascade, and therefore scales as the radiation length in the material. Electron energies eventually fall below the critical energy, and then dissipate their energy by ionization and excitation rather than by the generation of more shower particles. In describing shower behavior, it is therefore convenient to introduce the scale variables

$$t = x/X_0, \qquad y = E/E_c, \qquad (34.34)$$

so that distance is measured in units of radiation length and energy in units of critical energy.

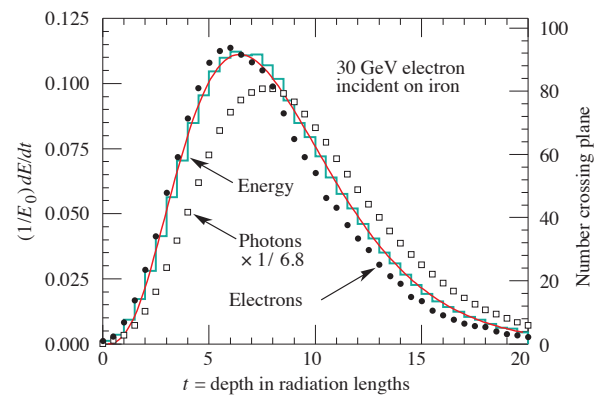

Figure 34.20: An EGS4 simulation of a 30 GeV electron-induced cascade in iron. The histogram shows fractional energy deposition per radiation length, and the curve is a gamma-function fit to the distribution. Circles indicate the number of electrons with total energy greater than 1.5 MeV crossing planes at $X_0/2$ intervals (scale on right) and the squares the number of photons with $E \geq$ 1.5 MeV crossing the planes (scaled down to have same area as the electron distribution).

Longitudinal profiles from an EGS4 [58] simulation of a 30 GeV electron-induced cascade in iron are shown in Fig. 34.20. The number of particles crossing a plane (very close to Rossi's Π function [2]) is sensitive to the cutoff energy, here chosen as a total energy of 1.5 MeV for both electrons and photons. The electron number falls off more quickly than energy deposition. This is because, with increasing depth, a larger fraction of the cascade energy is carried by photons. Exactly what a calorimeter measures depends on the device, but it is not likely to be exactly any of the profiles shown. In gas counters it may be very close to the electron number, but in glass Cherenkov detectors and other devices with "thick" sensitive regions it is closer to the energy deposition (total track length). In such detectors the signal is proportional to the "detectable" track length T_d, which is in general less than the total track length T. Practical devices are sensitive to electrons with energy above some detection threshold E_d, and $T_d = T\, F(E_d/E_c)$. An analytic form for $F(E_d/E_c)$ obtained by Rossi [2] is given by Fabjan in Ref. [59]; see also Amaldi [60].

The mean longitudinal profile of the energy deposition in an electromagnetic cascade is reasonably well described by a gamma distribution [61]:

$$\frac{dE}{dt} = E_0\, b\, \frac{(bt)^{a-1} e^{-bt}}{\Gamma(a)} \qquad (34.35)$$

The maximum $t_{\max}$ occurs at $(a-1)/b$. We have made fits to shower profiles in elements ranging from carbon to uranium, at energies from 1 GeV to 100 GeV. The energy deposition profiles are well described by Eq. (34.35) with

$$t_{\max} = (a-1)/b = 1.0 \times (\ln y + C_j), \qquad j = e, \gamma, \qquad (34.36)$$

where $C_e = -0.5$ for electron-induced cascades and $C_\gamma = +0.5$ for photon-induced cascades. To use Eq. (34.35), one finds $(a-1)/b$ from Eq. (34.36) and Eq. (34.34), then finds a either by assuming

[8] This definition differs from that of Ref. [55] by a factor of two. E_{LPM} scales as the 4th power of the mass of the incident particle, so that $E_{LPM} = (1.4 \times 10^{10}$ TeV/cm$) \times X_0/\rho$ for a muon.

Downloaded from https://academic.oup.com/ptep/article/2022/8/083C01/6651666 by KIT Library user on 27 September 2022

$b \approx 0.5$ or by finding a more accurate value from Fig. 34.21. The results are very similar for the electron number profiles, but there is some dependence on the atomic number of the medium. A similar form for the electron number maximum was obtained by Rossi in the context of his "Approximation B," [2] (see Fabjan's review in Ref. [59]), but with $C_e = -1.0$ and $C_\gamma = -0.5$; we regard this as superseded by the EGS4 result.

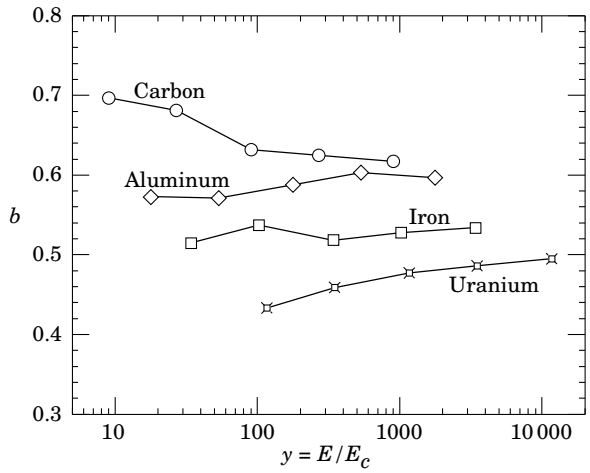

Figure 34.21: Fitted values of the scale factor b for energy deposition profiles obtained with EGS4 for a variety of elements for incident electrons with $1 \leq E_0 \leq 100$ GeV. Values obtained for incident photons are essentially the same.

The "shower length" $X_s = X_0/b$ is less conveniently parameterized, since b depends upon both Z and incident energy, as shown in Fig. 34.21. As a corollary of this Z dependence, the number of electrons crossing a plane near shower maximum is underestimated using Rossi's approximation for carbon and seriously overestimated for uranium. Essentially the same b values are obtained for incident electrons and photons. For many purposes it is sufficient to take $b \approx 0.5$.

The length of showers initiated by ultra-high energy photons and electrons is somewhat greater than at lower energies since the first or first few interaction lengths are increased via the mechanisms discussed above.

The gamma function distribution is very flat near the origin, while the EGS4 cascade (or a real cascade) increases more rapidly. As a result Eq. (34.35) fails badly for about the first two radiation lengths; it was necessary to exclude this region in making fits.

Because fluctuations are important, Eq. (34.35) should be used only in applications where average behavior is adequate. Grindhammer *et al.* have developed fast simulation algorithms in which the variance and correlation of a and b are obtained by fitting Eq. (34.35) to individually simulated cascades, then generating profiles for cascades using a and b chosen from the correlated distributions [62].

The transverse development of electromagnetic showers in different materials scales fairly accurately with the *Molière radius* R_M, given by [63, 64]

$$R_M = X_0\, E_s/E_c, \tag{34.37}$$

where $E_s \approx 21$ MeV (Table 34.1), and the Rossi definition of E_c is used.

In a material containing a weight fraction w_j of the element with critical energy E_{cj} and radiation length X_j, the Molière radius is given by

$$\frac{1}{R_M} = \frac{1}{E_s} \sum \frac{w_j\, E_{cj}}{X_j}\ . \tag{34.38}$$

Measurements of the lateral distribution in electromagnetic cascades are shown in Refs. [63, 64]. On the average, only 10% of the energy lies outside the cylinder with radius R_M. About 99% is contained inside of $3.5R_M$, but at this radius and beyond composition effects become important and the scaling with R_M fails. The distributions are characterized by a narrow core, and broaden as the shower develops. They are often represented as the sum of two Gaussians.

At high enough energies, the LPM effect (Sec. 34.4.6) reduces the cross sections for bremsstrahlung and pair production, and hence can cause significant elongation of electromagnetic cascades [45].

34.6 Muon energy loss at high energy

At sufficiently high energies, radiative processes become more important than ionization for all charged particles. For muons and pions in materials such as iron, this "critical energy" occurs at several hundred GeV. (There is no simple scaling with particle mass, but for protons the "critical energy" is much, much higher.) Radiative effects dominate the energy loss of energetic muons found in cosmic rays or produced at the newest accelerators. These processes are characterized by small cross sections, hard spectra, large energy fluctuations, and the associated generation of electromagnetic and (in the case of photonuclear interactions) hadronic showers [65–73] As a consequence, at these energies the treatment of energy loss as a uniform and continuous process is for many purposes inadequate.

It is convenient to write the average rate of muon energy loss as [74]

$$\langle -dE/dx \rangle = a(E) + b(E)\, E. \tag{34.39}$$

Here $a(E)$ is the ionization energy loss given by Eq. (34.5), and $b(E)$ is the sum of e^+e^- pair production, bremsstrahlung, and photonuclear contributions. To the approximation that these slowly-varying functions are constant, the mean range x_0 of a muon with initial energy E_0 is given by

$$x_0 \approx (1/b) \ln(1 + E_0/E_{\mu c}), \tag{34.40}$$

where $E_{\mu c} = a/b$.

Fig. 34.22 shows contributions to $b(E)$ for iron. Since $a(E) \approx 0.002$ GeV g^{-1} cm^2, $b(E)E$ dominates the energy loss above several hundred GeV, where $b(E)$ is nearly constant. The rates of energy loss for muons in hydrogen, uranium, and iron are shown in Fig. 34.23 [7].

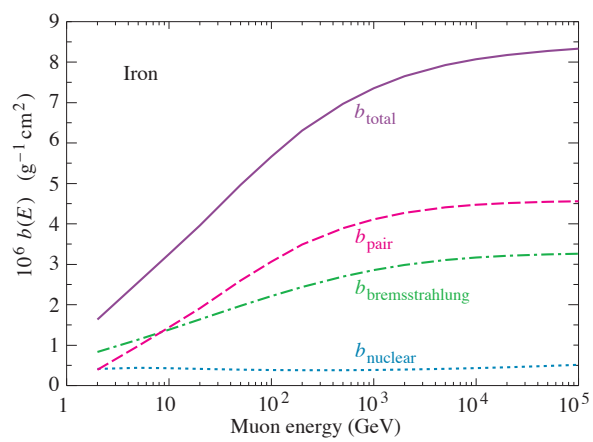

Figure 34.22: Contributions to the fractional energy loss by muons in iron due to e^+e^- pair production, bremsstrahlung, and photonuclear interactions, as obtained from Groom *et al.* [7] except for post-Born corrections to the cross section for direct pair production from atomic electrons.

The "muon critical energy" $E_{\mu c}$ can be defined more exactly as the energy at which radiative and ionization losses are equal, and can be found by solving $E_{\mu c} = a(E_{\mu c})/b(E_{\mu c})$. This definition corresponds to the solid-line intersection in Fig. 34.13, and is different from the Rossi definition we used for electrons. It serves the same function: below $E_{\mu c}$ ionization losses dominate, and above $E_{\mu c}$ radiative effects dominate. The dependence of $E_{\mu c}$ on atomic number Z is shown in Fig. 34.24.

The radiative cross sections are expressed as functions of the fractional energy loss ν. The bremsstrahlung cross section goes

Downloaded from https://academic.oup.com/ptep/article/2022/8/083C01/6651666 by KIT Library user on 27 September 2022

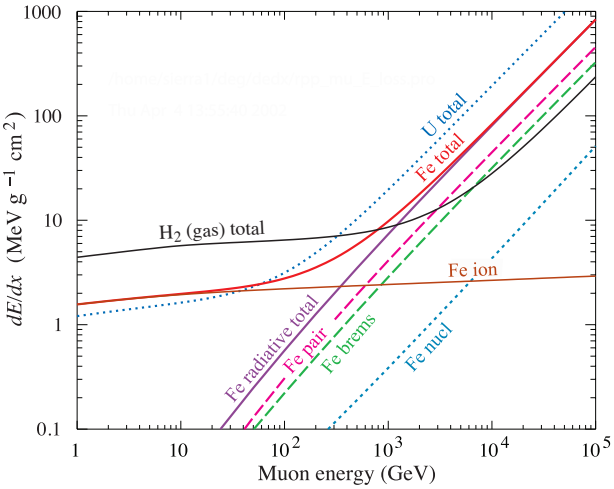

Figure 34.23: The average energy loss of a muon in hydrogen, iron, and uranium as a function of muon energy. Contributions to dE/dx in iron from ionization and pair production, bremsstrahlung and photonuclear interactions are also shown.

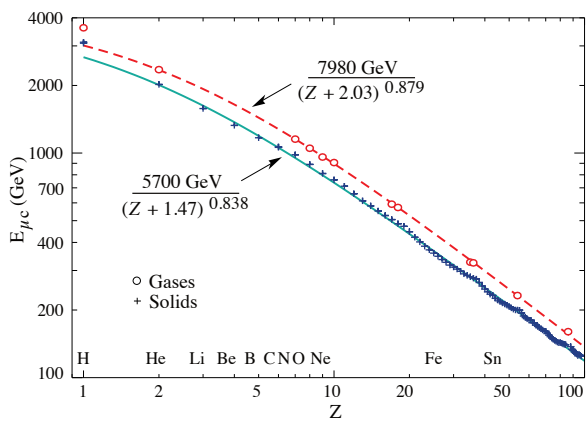

Figure 34.24: Muon critical energy for the chemical elements, defined as the energy at which radiative and ionization energy loss rates are equal [7]. The equality comes at a higher energy for gases than for solids or liquids with the same atomic number because of a smaller density effect reduction of the ionization losses. The fits shown in the figure exclude hydrogen. Alkali metals fall 3–4% above the fitted function, while most other solids are within 2% of the function. Among the gases the worst fit is for radon (2.7% high).

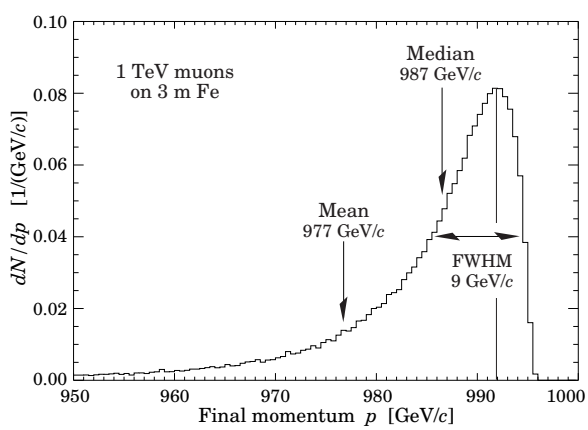

Figure 34.25: The momentum distribution of 1 TeV/c muons after traversing 3 m of iron as calculated by S.I. Striganov [7].

roughly as $1/\nu$ over most of the range, while for the pair production case the distribution goes as ν^{-3} to ν^{-2} [75]. "Hard" losses are therefore more probable in bremsstrahlung, and in fact energy losses due to pair production may very nearly be treated as continuous. The simulated momentum distribution of an incident 1 TeV/c muon beam after it crosses 3 m of iron is shown in Fig. 34.25 [7]. The most probable loss is 8 GeV, or 3.4 MeV $g^{-1}cm^2$. The full width at half maximum is 9 GeV/c, or 0.9%. The radiative tail is almost entirely due to bremsstrahlung, although most of the events in which more than 10% of the incident energy lost experienced relatively hard photonuclear interactions. The latter can exceed detector resolution [76], necessitating the reconstruction of lost energy. Tables in Ref. [7] list the stopping power as 9.82 MeV $g^{-1}cm^2$ for a 1 TeV muon, so that the mean loss should be 23 GeV ($\approx$ 23 GeV/c), for a final momentum of 977 GeV/c, far below the peak. This agrees with the indicated mean calculated from the simulation. Electromagnetic and hadronic cascades in detector materials can obscure muon tracks in detector planes and reduce tracking efficiency [77].

34.7 Cherenkov and transition radiation [3, 78, 79]

A charged particle radiates if its speed is greater than the local phase speed of light (Cherenkov radiation) or if it crosses suddenly from one medium to another with different optical properties (transition radiation). Neither process is important for energy loss, but both are used in high-energy and cosmic-ray physics detectors.

34.7.1 *Optical Cherenkov radiation*

The angle θ_c of Cherenkov radiation, relative to the particle's direction, for a particle with speed βc in a medium with index of refraction n is

$$\begin{aligned} &\cos\theta_c = (1/n\beta) \\ \text{or}\quad &\tan\theta_c = \sqrt{\beta^2 n^2 - 1} \\ &\approx \sqrt{2(1-1/n\beta)} \quad \text{for small } \theta_c, \textit{e.g.} \text{ in gases.} \end{aligned} \tag{34.41}$$

The threshold speed β_t is $1/n$, and $\gamma_t = 1/(1-\beta_t^2)^{1/2}$. Therefore, $\beta_t\gamma_t = 1/(2\delta+\delta^2)^{1/2}$, where $\delta = n-1$. Values of δ for various commonly used gases are given as a function of pressure and wavelength in Ref. [80]. See its Table 6.1 for values at atmospheric pressure. Data for other commonly used materials are given in Ref. [81].

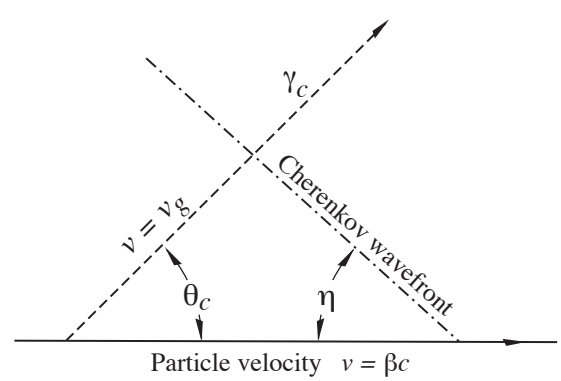

Figure 34.26: Cherenkov light emission and wavefront angles. In a dispersive medium, $\theta_c + \eta \neq 90^0$.

Practical Cherenkov radiator materials are dispersive. Let ω be the photon's frequency, and let $k = 2\pi/\lambda$ be its wavenumber. The photons propage at the group speed $v_g = d\omega/dk = c/[n(\omega) + \omega(dn/d\omega)]$. In a non-dispersive medium, this simplies to $v_g = c/n$.

In his classical paper, Tamm [82] showed that for dispersive media the radiation is concentrated in a thin conical shell whose

Downloaded from https://academic.oup.com/ptep/article/2022/8/083C01/6651666 by KIT Library user on 27 September 2022

vertex is at the moving charge, and whose opening half-angle η is

$$\cot\eta = \left[\frac{d}{d\omega}(\omega\tan\theta_c)\right]_{\omega_0} = \left[\tan\theta_c + \beta^2\omega\, n(\omega)\,\frac{dn}{d\omega}\cot\theta_c\right]_{\omega_0}, \qquad (34.42)$$

where ω_0 is the central value of the small frequency range under consideration. (See Fig. 34.26.) This cone has a opening half-angle η, and, unless the medium is non-dispersive ($dn/d\omega = 0$), $\theta_c + \eta \neq 90^0$. The Cherenkov wavefront 'sideslips' along with the particle [83]. This effect has timing implications for ring imaging Cherenkov counters [84], but it is probably unimportant for most applications.

The number of photons produced per unit path length of a particle with charge ze and per unit energy interval of the photons is

$$\frac{d^2N}{dEdx} = \frac{\alpha z^2}{\hbar c}\sin^2\theta_c = \frac{\alpha^2 z^2}{r_e\, m_e c^2}\left(1 - \frac{1}{\beta^2 n^2(E)}\right) \approx 370\,\sin^2\theta_c(E)\ \mathrm{eV}^{-1}\mathrm{cm}^{-1} \qquad (z=1)\,, \qquad (34.43)$$

or, equivalently,

$$\frac{d^2N}{dxd\lambda} = \frac{2\pi\alpha z^2}{\lambda^2}\left(1 - \frac{1}{\beta^2 n^2(\lambda)}\right)\,. \qquad (34.44)$$

The index of refraction n is a function of photon energy $E = \hbar\omega$, as is the sensitivity of the transducer used to detect the light. For practical use, Eq. (34.43) must be multiplied by the the transducer response function and integrated over the region for which $\beta\, n(\omega) > 1$. Further details are given in the discussion of Cherenkov detectors in the Particle Detectors section (Sec. 35.5 of this *Review*).

When two particles are close together (lateral separation $\lesssim 1$ wavelength), the electromagnetic fields from the particles may add coherently, affecting the Cherenkov radiation. Because of their opposite charges, the radiation from an e^+e^- pair at close separation is suppressed compared to two independent leptons [85].

34.7.2 *Coherent radio Cherenkov radiation*

Coherent Cherenkov radiation is produced by many charged particles with a non-zero net charge moving through matter on an approximately common "wavefront"—for example, the electrons and positrons in a high-energy electromagnetic cascade. The signals can be visible for energies above 10^{16} eV; see Sec. 36.3.3 for more details. The phenomenon is called the Askaryan effect [86]. Near the end of a shower, when typical particle energies are below E_c (but still relativistic), a charge imbalance develops. Photons can Compton-scatter atomic electrons, and positrons can annihilate with atomic electrons to contribute even more photons which can in turn Compton scatter. These processes result in a roughly 20% excess of electrons over positrons in a shower. The net negative charge leads to coherent radio Cherenkov emission. The radiation includes a component from the decelerating charges (as in bremsstrahlung). Because the emission is coherent, the electric field strength is proportional to the shower energy, and the signal power increases as its square. The electric field strength also increases linearly with frequency, up to a maximum frequency determined by the lateral spread of the shower. This cutoff occurs at about 1 GHz in ice, and scales inversely with the Moliere radius. At low frequencies, the radiation is roughly isotropic, but, as the frequency rises toward the cutoff frequency, the radiation becomes increasingly peaked around the Cherenkov angle. The radiation is linearly polarized in the plane containing the shower axis and the photon direction. A measurement of the signal polarization can be used to help determine the shower direction. The characteristics of this radiation have been nicely demonstrated in a series of experiments at SLAC [87]. A detailed discussion of the radiation can be found in Ref. [88].

34.7.3 *Transition radiation*

The energy radiated when a particle with charge ze crosses the boundary between vacuum and a medium with plasma frequency ω_p is

$$I = \alpha z^2\gamma\hbar\omega_p/3, \qquad (34.45)$$

where

$$\hbar\omega_p = \sqrt{4\pi N_e r_e^3}\; m_e c^2/\alpha = \sqrt{\rho\ (\text{in g/cm}^3)\ \langle Z/A\rangle} \times 28.81\ \text{eV}. \qquad (34.46)$$

For styrene and similar materials, $\hbar\omega_p \approx 20$ eV; for air it is 0.7 eV.

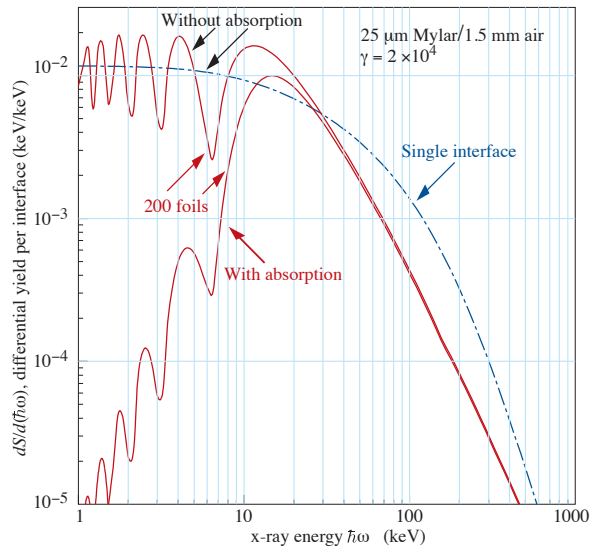

Figure 34.27: X-ray photon energy spectra for a radiator consisting of 200 25 μm thick foils of Mylar with 1.5 mm spacing in air (solid lines) and for a single surface (dashed line). Curves are shown with and without absorption. Adapted from Ref. [89].

The number spectrum $dN_\gamma/d(\hbar\omega$ diverges logarithmically at low energies and decreases rapidly for $\hbar\omega/\gamma\hbar\omega_p > 1$. About half the energy is emitted in the range $0.1 \le \hbar\omega/\gamma\hbar\omega_p \le 1$. Inevitable absorption in a practical detector removes the divergence. For a particle with $\gamma = 10^3$, the radiated photons are in the soft x-ray range 2 to 40 keV. The γ dependence of the emitted energy thus comes from the hardening of the spectrum rather than from an increased quantum yield.

The number of photons with energy $\hbar\omega > \hbar\omega_0$ is given by the answer to problem 13.15 in Ref. [3],

$$N_\gamma(\hbar\omega > \hbar\omega_0) = \frac{\alpha z^2}{\pi}\left[\left(\ln\frac{\gamma\hbar\omega_p}{\hbar\omega_0} - 1\right)^2 + \frac{\pi^2}{12}\right], \qquad (34.47)$$

within corrections of order $(\hbar\omega_0/\gamma\hbar\omega_p)^2$. The number of photons above a fixed energy $\hbar\omega_0 \ll \gamma\hbar\omega_p$ thus grows as $(\ln\gamma)^2$, but the number above a fixed fraction of $\gamma\hbar\omega_p$ (as in the example above) is constant. For example, for $\hbar\omega > \gamma\hbar\omega_p/10$, $N_\gamma = 2.519\,\alpha z^2/\pi = 0.59\% \times z^2$.

The particle stays "in phase" with the x ray over a distance called the formation length, $d(\omega) = (2c/\omega)(1/\gamma^2 + \theta^2 + \omega_p^2/\omega^2)^{-1}$. Most of the radiation is produced in this distance. Here θ is the x-ray emission angle, characteristically $1/\gamma$. For $\theta = 1/\gamma$ the formation length has a maximum at $d(\gamma\omega_p/\sqrt{2}) = \gamma c/\sqrt{2}\,\omega_p$. In practical situations it is tens of μm.

Since the useful x-ray yield from a single interface is low, in practical detectors it is enhanced by using a stack of N foil radiators—foils L thick, where L is typically several formation lengths—separated by gas-filled gaps. The amplitudes at successive interfaces interfere to cause oscillations about the single-interface spectrum. At increasing frequencies above the position of the last interference maximum ($L/d(w) = \pi/2$), the formation zones, which have opposite phase, overlap more and more and the

Downloaded from https://academic.oup.com/ptep/article/2022/8/083C01/6651666 by KIT Library user on 27 September 2022

spectrum saturates, $dI/d\omega$ approaching zero as $L/d(\omega) \to 0$. This is illustrated in Fig. 34.27 for a realistic detector configuration.

For regular spacing of the layers fairly complicated analytic solutions for the intensity have been obtained [89, 90]. Although one might expect the intensity of coherent radiation from the stack of foils to be proportional to N^2, the angular dependence of the formation length conspires to make the intensity $\propto N$.

References

[1] H. Bichsel, Nucl. Instrum. Meth. **A562**, 154 (2006).

[2] B. Rossi, *High Energy Particles*, Prentice-Hall, Inc., Englewood Cliffs, NJ, 1952.

[3] J.D. Jackson, *Classical Electrodynamics*, 3rd edition, (John Wiley and Sons, New York, 1998).

[4] H.A. Bethe, *Zur Theorie des Durchgangs schneller Korpuskularstrahlen durch Materie,* H. Bethe, Ann. Phys. **5**, 325 (1930).

[5] M. S. Livingston and H. A. Bethe, Rev. Mod. Phys. **9**, 245 (1937).

[6] "Stopping Powers and Ranges for Protons and Alpha Particles," ICRU Report No. 49 (1993); Tables and graphs are available at
`physics.nist.gov/PhysRefData/Star/Text/PSTAR.html`
and
`physics.nist.gov/PhysRefData/Star/Text/ASTAR.html`.

[7] D.E. Groom, N.V. Mokhov, and S.I. Striganov, "Muon stopping-power and range tables: 10 MeV–100 TeV," Atomic Data and Nuclear Data Tables **78**, 183–356 (2001). Since submission of this paper it has become likely that post-Born corrections to the direct pair production cross section should be made. Code used to make Figs. 34.22–34.24 included these corrections [D.Yu. Ivanov *et al.*, Phys. Lett. **B442**, 453 (1998)]. The effect is negligible except at high Z. (It is less than 1% for iron.); The introductory text of the paper can be found at
`pdg.lbl.gov/current/AtomicNuclearProperties/adndt.pdf`

Extensive printable and machine-readable tables for muons are given at
`pdg.lbl.gov/current/AtomicNuclearProperties/`.

[8] W. H. Barkas, W. Birnbaum and F. M. Smith, Phys. Rev. **101**, 778 (1956).

[9] U. Fano, Ann. Rev. Nucl. Part. Sci. **13**, 1 (1963).

[10] J. D. Jackson, Phys. Rev. **D59**, 017301 (1999).

[11] J. Lindhard and A. H. Sørensen, Phys. Rev. **A53**, 2443 (1996).

[12] "Stopping Powers for Electrons and Positrons," ICRU Report No. 37 (1984); Tables and graphs are available at
`physics.nist.gov/PhysRefData/Star/Text/ESTAR.html` .

[13] H. Bichsel, Phys. Rev. **A46**, 5761 (1992).

[14] W.H. Barkas and M.J. Berger, *Tables of Energy Losses and Ranges of Heavy Charged Particles*, NASA-SP-3013 (1964).

[15] S.M. Seltzer and M.J. Berger, Int. J. of Applied Rad. **33**, 1189 (1982).

[16] `physics.nist.gov/PhysRefData/XrayMassCoef/tab1.html`.

[17] R. M. Sternheimer, Phys. Rev. **88**, 851 (1952).

[18] R. M. Sternheimer, M. J. Berger and S. M. Seltzer, Atom. Data Nucl. Data Tabl. **30**, 261 (1984); Minor errors are corrected in Ref. 5. Chemical composition for the tabulated materials is given in Ref. 10.

[19] R. M. Sternheimer and R. F. Peierls, Phys. Rev. **B3**, 3681 (1971).

[20] N. F. Mott, Proceedings of the Cambridge Philosophical Society **27**, 553 (1931).

[21] H. Bichsel, Phys. Rev. **A65**, 5, 052709 (2002).

[22] S. P. Møller *et al.*, Phys. Rev. **A56**, 4, 2930 (1997).

[23] J. C. Ashley, R. H. Ritchie and W. Brandt, Phys. Rev. B **5**, 2393 (1972).

[24] H.H. Andersen and J.F. Ziegler, *Hydrogen: Stopping Powers and Ranges in All Elements.* Vol. 3 of *The Stopping and Ranges of Ions in Matter* (Pergamon Press 1977).

[25] J. Lindhard, Kgl. Danske Videnskab. Selskab, Mat.-Fys. Medd. **28**, No. 8 (1954); J. Lindhard, M. Scharff, and H.E. Schiøtt, Kgl. Danske Videnskab. Selskab, Mat.-Fys. Medd. **33**, No. 14 (1963).

[26] J.F. Ziegler, J.F. Biersac, and U. Littmark, *The Stopping and Range of Ions in Solids*, Pergamon Press 1985.

[27] E.A. Uehling, Ann. Rev. Nucl. Sci. **4**, 315 (1954) (For heavy particles with unit charge, but $e^{\pm}$ cross sections and stopping powers are also given).

[28] N.F. Mott and H.S.W. Massey, *The Theory of Atomic Collisions*, Oxford Press, London, 1965.

[29] P. V. Vavilov, Sov. Phys. JETP **5**, 749 (1957), [Zh. Eksp. Teor. Fiz.32,920(1957)].

[30] L.D. Landau, J. Exp. Phys. (USSR) **8**, 201 (1944).

[31] H. Bichsel, Rev. Mod. Phys. **60**, 663 (1988).

[32] R. Talman, Nucl. Instrum. Meth. **159**, 189 (1979).

[33] H. Bichsel, Ch. 87 in the Atomic, Molecular and Optical Physics Handbook, G.W.F. Drake, editor (Am. Inst. Phys. Press, Woodbury NY, 1996).

[34] S.M. Seltzer and M.J. Berger, Int. J. of Applied Rad. **35**, 665 (1984). This paper corrects and extends the results of Ref. [15].

[35] H. A. Bethe, Phys. Rev. **89**, 1256 (1953).

[36] W. T. Scott, Rev. Mod. Phys. **35**, 231 (1963).

[37] J. W. Motz, H. Olsen and H. W. Koch, Rev. Mod. Phys. **36**, 881 (1964).

[38] H. Bichsel, Phys. Rev. **112**, 182 (1958).

[39] G. Shen *et al.*, Phys. Rev. **D20**, 1584 (1979).

[40] G. R. Lynch and O. I. Dahl, Nucl. Instrum. Meth. **B58**, 6 (1991).

[41] M. Wong *et al.*, Med. Phys. **17**, 163 (1990).

[42] Y.-S. Tsai, Rev. Mod. Phys. **46**, 815 (1974), [Erratum: Rev. Mod. Phys.49,521(1977)].

[43] H. Davies, H. A. Bethe and L. C. Maximon, Phys. Rev. **93**, 788 (1954).

[44] L. D. Landau and I. Pomeranchuk, Dokl. Akad. Nauk Ser. Fiz. **92**, 535 (1953); **92**, 735 (1953). These papers are available in English in L. Landau, *The Collected Papers of L.D. Landau*, Pergamon Press, 1965; A. B. Migdal, Phys. Rev. **103**, 1811 (1956).

[45] S. Klein, Rev. Mod. Phys. **71**, 1501 (1999).

[46] M.L. Ter-Mikaelian, SSSR **94**, 1033 (1954); M.L. Ter-Mikaelian, *High Energy Electromagnetic Processes in Condensed Media* (John Wiley and Sons, New York, 1972).

[47] P. L. Anthony *et al.*, Phys. Rev. Lett. **76**, 3550 (1996).

[48] H. W. Koch and J. W. Motz, Rev. Mod. Phys. **31**, 920 (1959).

[49] M.J. Berger and S.M. Seltzer, "Tables of Energy Losses and Ranges of Electrons and Positrons," National Aeronautics and Space Administration Report NASA-SP-3012 (Washington DC 1964).

[50] Curves for these and other elements, compounds, and mixtures may be obtained from
`nist.gov/pml/xcom-photon-cross-sections-database`.
The photon total cross section is approximately flat for at least two decades beyond the energy range shown.

[51] B. L. Berman and S. C. Fultz, Rev. Mod. Phys. **47**, 713 (1975).

[52] `www.cxro.lbl.gov/optical_constants/pert_form.html`.

[53] `physics.nist.gov/PhysRefData/XrayMassCoef/tab3.html`.

[54] J. W. Motz, H. A. Olsen and H. W. Koch, Rev. Mod. Phys. **41**, 581 (1969).

Downloaded from https://academic.oup.com/ptep/article/2022/8/083C01/6651666 by KIT Library user on 27 September 2022

[55] P. L. Anthony *et al.*, Phys. Rev. Lett. **75**, 1949 (1995).

[56] U. I. Uggerhøj, Rev. Mod. Phys. **77**, 1131 (2005).

[57] L. Gerhardt and S. R. Klein, Phys. Rev. **D82**, 074017 (2010).

[58] W.R. Nelson, H. Hirayama, and D.W.O. Rogers, "The EGS4 Code System," SLAC-265, Stanford Linear Accelerator Center (Dec. 1985).

[59] *Experimental Techniques in High Energy Physics*, ed. T. Ferbel (Addison-Wesley, Menlo Park CA 1987).

[60] U. Amaldi, Phys. Scripta **23**, 409 (1981).

[61] E. Longo and I. Sestili, Nucl. Instrum. Meth. **128**, 283 (1975), [Erratum: Nucl. Instrum. Meth.135,587(1976)].

[62] G. Grindhammer *et al.*, in *Proceedings of the 1988 Summer Study on High Energy Physics in the 1990's*, Snowmass, CO, June 27 – July 15, 1990, edited by F.J. Gilman and S. Jensen, (World Scientific, Teaneck, NJ, 1989) p. 151.

[63] W. R. Nelson *et al.*, Phys. Rev. **149**, 201 (1966).

[64] G. Bathow *et al.*, Nucl. Phys. **B20**, 592 (1970).

[65] H. Bethe and W. Heitler, Proc. Roy. Soc. Lond. **A146**, 83 (1934); H.A. Bethe, *Proc. Cambridge Phil. Soc.* **30**, 542 (1934).

[66] A.A. Petrukhin and V.V. Shestakov, Can. J. Phys. **46**, S377 (1968).

[67] V.M. Galitskii and S.R. Kel'ner, Sov. Phys. JETP **25**, 948 (1967).

[68] S.R. Kel'ner and Yu.D. Kotov, Sov. J. Nucl. Phys. **7**, 237 (1968).

[69] R.P. Kokoulin and A.A. Petrukhin, in *Proceedings of the International Conference on Cosmic Rays*, Hobart, Australia, August 16–25, 1971, Vol. **4**, p. 2436 .

[70] A. I. Nikishov, Sov. J. Nucl. Phys. **27**, 677 (1978), [Yad. Fiz.27,1281(1978)].

[71] Yu. M. Andreev, L. B. Bezrukov and E. V. Bugaev, Phys. Atom. Nucl. **57**, 2066 (1994), [Yad. Fiz.57,2146(1994)].

[72] L. B. Bezrukov and E. V. Bugaev, Yad. Fiz. **33**, 1195 (1981), [Sov. J. Nucl. Phys.33,635(1981)].

[73] N.V. Mokhov and C.C. James, The MARS Code System User's Guide, Fermilab-FN-1058-APC (2018), `mars.fnal.gov/`; N. Mokhov *et al.*, Prog. Nucl. Sci. Tech. **4**, 496 (2014).

[74] P. H. Barrett *et al.*, Rev. Mod. Phys. **24**, 3, 133 (1952).

[75] A. Van Ginneken, Nucl. Instrum. Meth. **A251**, 21 (1986).

[76] U. Becker *et al.*, Nucl. Instrum. Meth. **A253**, 15 (1986).

[77] J.J. Eastman and S.C. Loken, in *Proceedings of the Workshop on Experiments, Detectors, and Experimental Areas for the Supercollider*, Berkeley, CA, July 7–17, 1987, edited by R. Donaldson and M.G.D. Gilchriese (World Scientific, Singapore, 1988), p. 542.

[78] *Methods of Experimental Physics*, L.C.L. Yuan and C.-S. Wu, editors, Academic Press, 1961, Vol. 5A, p. 163.

[79] W.W.M. Allison and P.R.S. Wright, "The Physics of Charged Particle Identification: dE/dx, Cherenkov Radiation, and Transition Radiation," p. 371 in *Experimental Techniques in High Energy Physics*, T. Ferbel, editor, (Addison-Wesley 1987).

[80] E.R. Hayes, R.A. Schluter, and A. Tamosaitis, "Index and Dispersion of Some Cherenkov Counter Gases," ANL-6916 (1964).

[81] T. Ypsilantis, in "Proceedings of the Symposium on Particle Identification at High Luminosity Hadron Colliders, Apr 5-7, 1989 Batavia, Ill.", 0661–676 (1989).

[82] I. Tamm, J. Phys. U.S.S.R., **1**, 439 (1939).

[83] H. Motz and L.I. Schiff, Am. J. Phys. **21**, 258 (1953).

[84] B. N. Ratcliff, Nucl. Instrum. Meth. **A502**, 211 (2003).

[85] S. K. Mandal, S. R. Klein and J. D. Jackson, Phys. Rev. **D72**, 093003 (2005).

[86] G. A. Askar'yan, Sov. Phys. JETP **14**, 2, 441 (1962), [Zh. Eksp. Teor. Fiz.41,616(1961)].

[87] P. W. Gorham *et al.*, Phys. Rev. **D72**, 023002 (2005).

[88] E. Zas, F. Halzen and T. Stanev, Phys. Rev. **D45**, 362 (1992).

[89] M. L. Cherry *et al.*, Phys. Rev. **D10**, 3594 (1974); M. L. Cherry, Phys. Rev. **D17**, 2245 (1978).

[90] B. Dolgoshein, Nucl. Instrum. Meth. **A326**, 434 (1993).

Downloaded from https://academic.oup.com/ptep/article/2022/8/083C01/6651666 by KIT Library user on 27 September 2022

35. Particle Detectors at Accelerators

Revised 2021. See the various sections for authors.

35.1 Introduction . . . 565
35.2 Photon detectors . . . 565
35.2.1 Vacuum photodetectors . . . 566
35.2.2 Gaseous photon detectors . . . 567
35.2.3 Solid-state photon detectors . . . 567
35.2.4 Superconducting photon detectors . . . 568
35.3 Organic scintillators . . . 568
35.3.1 Scintillation mechanism . . . 568
35.3.2 Plastic scintillator practicalities . . . 569
35.3.3 Liquid scintillator practicalities . . . 569
35.4 Inorganic scintillators . . . 570
35.5 Cherenkov detectors . . . 572
35.6 Gaseous detectors . . . 574
35.6.1 Energy loss and charge transport in gases . 574
35.6.2 Multi-Wire Proportional and Drift Chambers 577
35.6.3 High Rate Effects . . . 578
35.6.4 Micro-Pattern Gas Detectors . . . 578
35.6.5 Time-projection chambers . . . 581
35.6.6 Transition radiation detectors (TRD's) . . . 582
35.6.7 Resistive-plate chambers . . . 584
35.7 LAr Time Projection Chamber . . . 586
35.7.1 Introduction . . . 586
35.7.2 A Mass of ultra-pure Liquid Argon . . . 587
35.7.3 Charge and Light Signals . . . 587
35.7.4 LAr TPC topologies . . . 588
35.7.5 Prospect - written October 2021 . . . 589
35.7.6 Acknowledgement . . . 589
35.8 Semiconductor detectors . . . 589
35.8.1 Signal generation . . . 590
35.8.2 Typical detectors . . . 591
35.8.3 Radiation Damage . . . 592
35.9 Low-noise detector readout . . . 593
35.9.1 Principal noise origins . . . 594
35.9.2 Equivalent noise analysis . . . 594
35.9.3 Timing measurements . . . 596
35.9.4 Digital signal processing . . . 596
35.9.5 What to use when? . . . 596
35.10 Calorimeters . . . 597
35.10.1 Introduction . . . 597
35.10.2 Electromagnetic calorimeters . . . 599
35.10.3 Hadronic calorimeters . . . 600
35.10.4 Free electron drift velocities in liquid ionization chambers . . . 604
35.11 Accelerator-based neutrino detectors . . . 605
35.11.1 Introduction . . . 605
35.11.2 Signals and Backgrounds . . . 605
35.11.3 Instances of Neutrino Detector Technology 606
35.11.4 Outlook . . . 608
35.12 Superconducting magnets for collider detectors . 609
35.12.1 Solenoid Magnets . . . 609
35.12.2 Properties of collider detector magnets . . 609
35.12.3 Toroidal magnets . . . 609
35.13 Measurement of particle momenta in a uniform magnetic field . . . 610

35.1 Introduction

This review summarizes the detector technologies employed at accelerator particle physics experiments. Several of these detectors are also used in a non-accelerator context and examples of such applications will be provided. The detector techniques which are specific to non-accelerator particle physics experiments are the subject of Chap. 36. More detailed discussions of detectors and their underlying physics can be found in books by Kolanoski & Wermes [1], Ferbel [2], Kleinknecht [3], Knoll [4], Green [5], Leroy & Rancoita [6], and Grupen [7].

In Table 35.1 are given typical resolutions and deadtimes of common charged particle detectors. The quoted numbers are usually based on typical devices, and should be regarded only as rough approximations for new designs. The spatial resolution refers to the intrinsic detector resolution, i.e. without multiple scattering. We note that analog detector readout can provide better spatial resolution than digital readout by measuring and averaging the deposited charge in neighboring channels. Quoted ranges attempt to be representative of both possibilities. The time resolution is defined by how accurately the time at which a particle crossed the detector can be determined. The deadtime is the minimum separation in time between two resolved hits on the same channel. Typical performance of calorimetry and particle identification are provided in the relevant sections below.

Table 35.1: Typical resolutions and deadtimes of common charged particle detectors. Revised November 2021.

Detector Type	Intrinsinc Spatial Resolution (rms)	Time Resolution	Dead Time
Resistive plate chamber	50μm	50–1000 ps*	10 ns†
Liquid argon TPC	0.5–1 mm‡	0.01-1 μs§	—¶
Scintillation tracker	∼100 μm	100 ps/n‖	10 ns
Bubble chamber	10–150 μm	1 ms	50 ms**
Wire chambers (proportional & drift chambers)	50–100 μm	5–10 ns††	2–200 ns‡‡
Micro-pattern gas detect.	30–40 μm	5–10 ns††	2–200 ns‡‡
Silicon strips/pixels	$\lesssim 10\,\mu$m§§	few ns¶¶ ‡‡	$\lesssim 50$ ns‡‡

*LHC: ∼ 2mm gap, ∼1ns. HL-LHC: ∼ 1mm gap, ∼350ps. Timing RPC: ∼50ps
†Limited by amplifier and discriminator bandwidth, usually around 100MHz
‡Detector geometry dependent
§Using the scintillation signal
¶No deadtime for medium
‖n = index of refraction.
**Multiple pulsing time.
††For fast particles
‡‡Depending/limited by the amplifying electronics [8]
§§Depending on electrode pitch, best values around 2–4 μm have been achieved
¶¶Resolutions < 100 ps are reached in dedicated pixel developments

35.2 Photon detectors

Revised August 2021 by P. Križan (Ljubljana U; Jozef Stefan Inst.).

Most detectors in high-energy, nuclear, and astrophysics rely on the detection of photons in or near the visible range, $100\,\text{nm} \lesssim \lambda \lesssim 1000\,\text{nm}$, or $1\,\text{eV} \lesssim E \lesssim 10\,\text{eV}$. This range covers scintillation and Cherenkov radiation as well as the light detected in many astronomical observations.

Generally, photodetection involves generating a detectable electrical signal proportional to the (usually very small) number of incident photons. The process involves three distinct steps:

1. generation of a primary photoelectron or electron-hole (e-h) pair by an incident photon by the photoelectric or photoconductive effect,
2. multiplication of the photoelectron or electron-hole pair signal to detectable levels, usually by one or more multiplicative bombardment steps and/or an avalanche process, and,
3. detection of charges induced by secondary electrons.

The important characteristics of a photodetector include the following:

1. quantum efficiency (QE or ϵ_Q): the average number of primary photoelectrons generated per incident photon ($0 \leq \epsilon_Q \leq 1$; in silicon more than one e-h pair per incident photon can be generated for $\lambda \lesssim 165$ nm),
2. collection efficiency (CE or ϵ_C): the overall acceptance factor other than the generation of photoelectrons ($0 \leq \epsilon_C \leq 1$),
3. gain (G): the number of electrons collected for each photoelectron generated,

Downloaded from https://academic.oup.com/ptep/article/2022/8/083C01/6651666 by KIT Library user on 27 September 2022

4. dark current or dark noise: the electrical signal when there is no incident photon,
5. precision of measuring the intensity I of the incoming light: electronic noise (ENC or N_e) and statistical fluctuations in the amplification process compound the Poisson distribution of n_γ photons from a given source:

$$\frac{\sigma(I)}{\langle I\rangle} = \sqrt{\frac{f_N}{n_\gamma \epsilon_Q \epsilon_C} + \left(\frac{N_e}{G n_\gamma \epsilon_Q \epsilon_C}\right)^2}, \qquad (35.1)$$

   where f_N, or the excess noise factor (ENF), is the contribution to the intensity distribution variance due to multiplication statistics [9],
6. dynamic range, linearity and saturation: relation between the number of incident photons and the sensor output in the pulsed mode,
7. time dependence of the response: this includes the transit time, which is the time between the arrival of the photon and the electrical pulse, and the transit time spread, and
8. rate capability: maximal rate of light pulses at which detection is still possible.

The QE is a strong function of the photon wavelength (λ), and is usually quoted at maximum, together with a range of λ where the QE is comparable to its maximum. Spatial uniformity and linearity with respect to the number of photons are highly desirable in a photodetector response.

Optimization of these factors involves many trade-offs and varies widely between applications. For example, while a large gain is desirable, attempts to increase the gain for a given device also increases the ENF and after-pulsing ("echos" of the main pulse). In solid-state devices, a higher QE often requires a compromise in the timing properties. In other types, coverage of large areas by focusing photoelectrons increases the transit time spread.

Other important considerations also are highly application-specific. These include the photon flux and wavelength range, the total area to be covered, and the efficiency required, the volume available to accommodate the detectors, characteristics of the environment such as chemical composition, temperature, magnetic field, ambient background, as well as ambient radiation of different types, mode of operation (continuous or triggered), bias (high-voltage) requirements, power consumption, calibration needs, aging, cost, and so on. Several technologies employing different phenomena for the three steps described above, and many variants within each, offer a wide range of solutions to choose from. The salient features of the main technologies and the common variants are described below. Some key characteristics are summarized in Table 35.2.

35.2.1 *Vacuum photodetectors*

Vacuum photodetectors can be broadly subdivided into three types: photomultiplier tubes, microchannel plate photomultiplier tubes, and hybrid photodetectors.

35.2.1.1 *Photomultiplier tubes*

A versatile class of photon detectors, vacuum photomultiplier tube (PMT) has been employed by a vast majority of all particle physics experiments to date [9]. Both "transmission-" and "reflection-type" PMTs are widely used. In the former, the photocathode material is deposited on the inside of a transparent window through which the photons enter, while in the latter, the photocathode material rests on a separate surface that the incident photons strike. The cathode material has a low work function, chosen for the wavelength band of interest. When a photon hits the cathode and liberates an electron (the photoelectric effect), the latter is accelerated and guided by electric fields to impinge on a secondary-emission electrode, or dynode, which then emits several($\sim$ 5) secondary electrons. The multiplication process is repeated typically about 10 times in series to generate a sufficient number of electrons, which are collected at the anode for delivery to the external circuit. The total gain of a PMT depends on the applied high voltage V as $G = AV^{kn}$, where $k \approx 0.7$–0.8 (depending on the dynode material), n is the number of dynodes in the chain, and A a constant (which also depends on n). Typically, G is in the range of 10^5–10^7; time resolution is $O(1ns)$ but can be as good as $\approx$ 100 ps for certain PMT types.

A large variety of PMTs covers a wide span of wavelength ranges from infrared (IR) to extreme ultraviolet (XUV) [10]. They are categorized by the window materials, photocathode materials, dynode structures, and anode configurations. Common window materials are borosilicate glass for IR to near-UV, fused quartz and sapphire (Al_2O_3) for UV, and MgF_2 or LiF for XUV. The choice of photocathode materials include a variety of mostly Cs- and/or Sb-based compounds such as CsI, CsTe, bi-alkali (SbRbCs, SbKCs), multi-alkali (SbNaKCs), GaAs(Cs), GaAsP(Cs), *etc.* Sensitive wavelengths and peak quantum efficiencies for these materials are summarized in Table-35.3. Typical dynode structures used in PMTs are circular cage, line focusing, box-and-grid, venetian blind, and fine mesh.

Multianode PMTs (MaPMTs) of up to 5×5 cm^2 in size are based on the parallel (side-by-side) arrangement of several dynode channels and anodes in the same tube, requiring advanced micro-machining and processing techniques. Fast PMTs with very large windows—measuring up to 508 mm across—have been developed for detection of Cherenkov radiation in neutrino experiments such as Super-Kamiokande and KamLAND among many others. Specially prepared low-radioactivity glass is used to make these PMTs, and they are also able to withstand the high pressure of the surrounding liquid.

PMTs are vulnerable to magnetic fields—sometimes even the geomagnetic field causes large orientation-dependent gain changes. A high-permeability metal shield is often necessary. However, proximity-focused PMTs, *e.g.* the fine-mesh types, can be used even in a high magnetic field ($\geq$ 1 T) if the direction of electric field of the tube is close to the direction of the external magnetic field. CMS uses custom-made vacuum phototriodes (VPT) mounted on the back face of projective lead tungstate crystals to detect scintillation light in the endcap sections of its electromagnetic calorimeters, which are inside a 3.8 T superconducting solenoid. A VPT employs a single dynode (thus, $G \approx 10$) placed close to the photocathode, and a mesh anode plane between the two, to help it cope with the strong magnetic field, which is not too unfavorably oriented with respect to the photodetector axis in the endcaps (within 25°), but where the radiation level is too high for Avalanche Photodiodes (APDs) like those used in the barrel section.

35.2.1.2 *Microchannel plate photomultiplier tubes*

A typical microchannel plate photomultiplier tube (MCP-PMT) consists of two or more $\sim$1 mm thick glass plates with densely packed $O(10\ \mu\text{m})$-diameter cylindrical holes, or "microchannels", sitting between the transmission-type photocathode and anode planes, separated by $O(1$ mm$)$ gaps. Instead of discrete dynodes, the inner surface of each cylindrical hole with a length-to-diameter ratio of 40-100 serves as a continuous dynode for the entire cascade of multiplicative bombardments initiated by a photoelectron. Gain fluctuations are reduced by operating each of the MCPs in the saturation mode. MCPs are stacked in a "chevron" configuration that alternates their bias angle; this reduces ion and photon feed-back effects and optimizes the overall amplification gain.

MCP-PMTs are thin, offer good spatial resolution, have excellent time resolution ($\sim$20 ps), and can tolerate magnetic fields up to 0.1 T and axial fields up to $1-2$ T. The technology has significantly evolved over the past 10 years [11]. A main breakthrough was the introduction of the atomic layer deposition (ALD) coatings on the MCP surfaces to increase the lifetime (>20 C/cm^2 of charge accumulated on the anode) and gain. The Large Area Picosecond Photo-Detector (LAPPD) project [12] is an important attempt to produce at a reasonable cost large (20 by 20 cm^2) sensors with a transit time spread of 50-70 ps.

35.2.1.3 *Hybrid photon detectors*

Hybrid photon detectors (HPD) combine the sensitivity of a vacuum PMT with the excellent spatial and energy resolutions of a silicon sensor [13]. A single photoelectron ejected from the photocathode is accelerated through a large potential difference of

Downloaded from https://academic.oup.com/ptep/article/2022/8/083C01/6651666 by KIT Library user on 27 September 2022

Table 35.2: Representative characteristics of some photodetectors commonly used in particle physics.

Type	λ (nm)	$\epsilon_Q\,\epsilon_C$	Gain	Risetime (ns)	Single photon time resol. (ps)	Area (mm^2)	1-p.e noise (Hz)	HV (V)
PMT *	115–1700	0.15–0.25	10^5–10^7	0.7–10	∼200	10^2–10^5	10–10^4	500–3000
MCP-PMT*	115–650	0.01–0.10	10^3–10^7	0.15–0.3	∼20	10^2–10^4	0.1–200	500–3500
HPD*	115–850	0.1–0.3	10^3–10^4	$O(1)$	∼1000	10^2–10^5	10–10^3	$\sim 2\times 10^4$
HAPD*	115–850	0.1–0.3	10^4–10^5	$O(1)$	∼30	10^2–10^5	10–10^3	$\sim 1\times 10^4$
GPD*	115–500	0.15–0.3	10^3–10^6	$O(0.1)$	∼100	$O(10)$	10–10^3	300–2000
APD	300–1700	∼0.7	10–10^8	$O(1)$	- †	10–10^3	1–10^3	400–1400
SiPM	125–1000	0.15–0.4	10^5–10^6	∼ 1	∼50	1–10	$O(10^5)$	30–60

*These devices often come in multi-anode configurations. In such cases, area and noise are to be considered on a "per readout-channel" basis.
†No single photon detection possible.

∼20 kV before it impinges on the silicon sensor/anode. The gain nearly equals the maximum number of *e*-*h* pairs that could be created from the entire kinetic energy of the accelerated electron: $G \approx \mathrm{eV}/w$, where e is the electronic charge, V is the applied potential difference, and $w \approx 3.7$ eV is the mean energy required to create an *e*-*h* pair in Si at room temperature. Since the gain is achieved in a single step, one can expect to have the excellent resolution of a simple Poisson statistic with large mean, but in fact it is even better, thanks to the Fano effect discussed in Sec. 35.8.

Low-noise electronics must be used to read out HPDs if one intends to take advantage of the low fluctuations in gain, *e.g.* when counting small numbers of photons. HPDs can have the same $\epsilon_Q\,\epsilon_C$ and window geometries as PMTs and can be segmented down to ∼50 μm. However, they require rather high biases and will not function in a magnetic field. The exception is proximity-focused devices (⇒ no (de)magnification) in an axial field. With time resolutions of ∼10 ps and superior rate capability, proximity-focused HPDs can be an alternative to MCP-PMTs. Applications of HPDs include the CMS hadronic calorimeter and the RICH detector in LHCb. Large-size HPDs with sophisticated focusing may be suitable for future water Cherenkov experiments.

Hybrid APDs (HAPDs) add an avalanche multiplication step following the electron bombardment to boost the gain by a factor of ∼50. This affords a higher gain and/or a lower bias voltage, but also increases the detector capacitance and fluctuations in multiplication. The forward RICH detector of Belle II uses a 144-channel device of this type [14].

Table 35.3: Properties of photocathode and window materials commonly used in vacuum photodetectors. [10]

Photocathode material	λ (nm)	Window material	Peak ϵ_Q (λ/nm)
CsI	115–200	MgF_2	0.13 (130)
CsTe	115–320	MgF_2	0.17 (200)
Bi-alkali	300–650	Borosilicate	0.27 (390)
	160-650	Synthetic Silica	0.27 (390)
"Ultra Bi-alkali"	300–650	Borosilicate	0.43 (350)
	160-650	Synthetic Silica	0.43 (350)
Multi-alkali	300–850	Borosilicate	0.20 (375)
	160-850	Synthetic Silica	0.25 (380)
GaAsP(Cs)	280-720	Borosilicate	0.40 (480-530)

35.2.2 *Gaseous photon detectors*

In a gaseous photon detector (GPD) a photoelectron in a suitable gas mixture initiates an avalanche in a high-field region, producing a large number of secondary impact-ionization electrons. In principle the charge multiplication and collection processes are identical to those employed in gaseous tracking detectors such as multiwire proportional chambers (MWPC), micromesh gaseous detectors (Micromegas), or gas electron multipliers (GEM). These are discussed in Sec. 35.6.4.

The devices can be divided into two types depending on the photosensitive material. One type uses solid photocathode materials much in the same way as PMTs. Since it is resistant to gas mixtures typically used in tracking chambers, CsI is a common choice. In the other type, photoionization occurs on suitable molecules vaporized and mixed in the drift volume. Most gases have photoionization work functions in excess of 10 eV, which would limit their sensitivity to wavelengths far too short. However, vapors of tetrakis dimethyl-amine ethylene (TMAE) or triethyl-amine (TEA), which have smaller work functions (5.3 eV for TMAE and 7.5 eV for TEA), are suited for XUV photon detection [15]. Since devices like GEMs offer sub-mm spatial resolution, GPDs are often used as position-sensitive photon detectors. They can be made into flat panels to cover large areas ($O(1\ \mathrm{m}^2)$), can operate in high magnetic fields, and are relatively inexpensive. Many of the ring imaging Cherenkov (RICH) detectors have used GPDs for the detection of Cherenkov light [16–19]. Special care must be taken to suppress the ion-feedback and photon-feedback processes in GPDs. It is also important to maintain high purity of the gas as minute traces of O_2 or H_2O can significantly degrade the detection efficiency.

35.2.3 *Solid-state photon detectors*

In a phase of rapid development, solid-state photodetectors are competing with vacuum- or gas-based devices for many existing applications and making way for a multitude of new ones. Compared to traditional vacuum- and gaseous photodetectors, solid-state devices are more compact, lightweight, rugged, tolerant to magnetic fields, and often cheaper. They also allow fine pixelization, are easy to integrate into large systems, and can operate at low electric potentials, while matching or exceeding most performance criteria.

Silicon photodiodes (PD) are widely used in high-energy physics as particle detectors and in a large number of applications as photon detectors. The structure is discussed in some detail in Sec. 35.8. In its simplest form, the PD is a reverse-biased *p*-*n* junction. Photons with energies above the indirect bandgap energy (wavelengths shorter than about 1050 nm, depending on the temperature) can create *e*-*h* pairs (the photoconductive effect), which are collected on the p and n sides, respectively. Often, as in the PDs used for crystal scintillator readout in CLEO, L3, Belle, BaBar, and GLAST, intrinsic silicon is doped to create a *p*-*i*-*n* structure. The reverse bias increases the thickness of the depleted region; in the case of these particular detectors, to full depletion at a depth of about 100 μm. Increasing the depletion depth decreases the capacitance (and hence electronic noise) and extends the red response. Quantum efficiency can exceed 90%, but falls toward the red because of the decrease of the light absorption probability in silicon; the absorption length reaches 100 μm at 985 nm. However, since $G = 1$, electronic signal amplification is necessary. Optimal low-noise amplifiers are slow, but, even so, noise limits the minimum detectable signal in room-temperature devices to several hundred photons.

In APDs, an exponential cascade of impact ionizations initiated by the original photogenerated *e*-*h* pair under a large reverse-bias voltage leads to an avalanche multiplication [20–23], and eventually to breakdown in Geiger-mode APDs. As a result, de-

Downloaded from https://academic.oup.com/ptep/article/2022/8/083C01/6651666 by KIT Library user on 27 September 2022

tectable electrical response can be obtained from low-intensity optical signals down to single photons. Excellent junction uniformity is critical, and a guard ring is generally used as a protection against edge breakdown. Well-designed APDs, such as those used in CMS crystal-based electromagnetic calorimeter, have achieved $\epsilon_Q\,\epsilon_C \approx 0.7$ with sub-ns response time. The sensitive wavelength window and gain depend on the semiconductor used. The gain is typically 10–200 in linear and up to 10^8 in Geiger mode of operation. Stability and close monitoring of the operating temperature are important for linear-mode operation, and substantial cooling is often necessary.

One of the most promising recent developments in the field is SiPMs ("Silicon Photomultiplier"), a device consisting of large arrays ($O(10^3)$) of tiny APDs packed over a small area ($O(1\ \mathrm{mm}^2)$) and operated in a limited Geiger mode [24–26]. Although each cell only offers a binary output, linearity with respect to the number of photons is achieved by summing the cell outputs. The sum of all cells is proportional to the number of photons received so long as the probability of an individual cell receiving multiple photons during a single time gate is negligible. SiPMs are being adopted as the preferred solution for various purposes including medical imaging, *e.g.* positron emission tomography (PET). These compact, rugged, and economical devices allow auto-calibration through decent separation of photoelectron peaks and offer gains of $O(10^6)$ at a moderate bias voltage ($\sim$30 V). However, the single-photoelectron noise of a SiPM, being the logical "or" of $O(10^3)$ Geiger APDs, is rather large: O(10-100 kHz/mm^2) at room temperature. Intensive R&D in recent years [27] led to a substantial reduction in dark count rates and in correlated noise levels, resulting in coverage of larger areas and in a wider range of applications. One way to further improve the signal-to-noise ratio in SiPMs is by using dedicated light collectors, either as quartz Winston cone like arrays [28] or suitably designed meta-materials [29]. In this way, photons propagate from a larger entry window to a considerably smaller semiconductor sensor, resulting in an improved signal photon to dark-count ratio. Intense R&D is expected to improve radiation hardness of these sensors. The fabrication of the sensors and the front-end electronics combined in the same process with the goal of making SiPMs extremely easy to use has already been successful (digital SiPMs) [30], and remains a topic of intense R&D.

More solid-state light sensors have either been developed or are potentially interesting for use in HEP experiments. The Run 2 DØ detector used 86000 Visible-light photon counters (VLPC) to read the optical signal from its scintillating-fiber tracker and scintillator-strip preshower detectors. These light sensors utilize the formation of an impurity band only 50 meV below the conduction band in As-doped Si to generate strong ($G \approx 5 \times 10^4$) yet sharp response to single photons with $\epsilon_Q \approx 0.9$ [31–33]. Only a very small bias ($\sim$7 V) is needed, but high sensitivity to infrared photons requires cooling below 10 K. Another interesting light sensor that has not yet found its use in HEP instrumentation are quantum dots, realized by nanometer-sized semiconductor 'particles' embedded in a semiconductor bulk.

35.2.4 *Superconducting photon detectors*

In this rapidly developing technology field, three most established technologies are the superconducting nano-wire single photon detector (SNSPD), the transition edge sensor (TES), and the microwave kinetic inductance detector (MKID). An SNSPD consists of a thin (4 nm) and narrow (100-250 nm) superconducting nanostrip that is current-biased just below its critical current. Absorption of a photon generates a resistive domain in the superconducting nanostrip, which leads to a transient voltage signal that can be detected. SNSPDs offer a unique combination of speed, both in terms of count rate ($\sim$GHz) and low timing jitter ($<$ 3 ps [34]), large range of wavelength sensitivity from VUV (120 nm) to mid-IR (10 μm), high detection efficiencies (approaching 100% for UV to near-IR), and low dark count rates ($\sim$5-10 Hz), making them appealing for a wide variety of demanding applications.

Examples of present use in particle physics are small nanowire detectors for dark matter and dark photons. Work is in progress that could make these sensors relevant to HEP applications by increasing the area (using 300 mm wafers and larger) and pixel size, coupling via windows to cryogenic stages, and readout of arrays (superconducting electronics for data processing). While the performance of these sensors is impressive, an application in large accelerator-based detectors would require an extensive R&D program because of the severe cryogenic requirements.

35.3 Organic scintillators

Written August 2021 by S. C. Eno (U. Maryland) and Matthieu Hamel (Paris-Saclay U. CEA, LIST).

Organic scintillators produce light when transversed by a charged particle. They can be broadly categorized into four types: single crystal, liquid, plastic, and a recently emerged glass [35]. The most useful scintillators produce photons with wavelengths between 370-750 nm (blue to red), typically peaking at 425 nm [36] via a series of processes that are initialized when charged particles interact with the material via both excitation and ionization/recombination (see Sec. 34.2 of this *Review*). Typical photon yields are about 1 photon per 100 eV of energy deposit [37], although the collected and transduced signal can be much lower. Methods to guide the light towards the photon-electron converter, such as diffusive paint, reflectors, photonic crystals, or light guides, may be required to optimize light yield.

Organic scintillators have found use in a wide variety of detectors [38]. Plastics are mostly used in collider detectors, and liquids in neutrino experiments. Ease of fabrication into desired shapes and low cost has made plastic scintillator ideal for large detectors. In the form of scintillating fiber, it has found widespread use in tracking and calorimetry. Demand for large volume detectors (e.g. neutrino detectors: MiniBooNE, NOvA) has led to increased use of liquid scintillator, which can be very low cost.

35.3.1 *Scintillation mechanism*

Plastic and liquid scintillators are based on an aromatic "matrix" such as benzene. The p electrons form both "pi" and "sigma" bonds between the atoms; the pi bonds are responsible for scintillation. Scintillation is produced via standard photophysical interactions, shown schematically in Fig. 35.1. While there have been claims of delayed light production on long time scales (labeled "phosphorescence" in the figure), this is still a subject of active debate in the community. As aromatic molecules scintillate in the ultraviolet (UV), useful scintillators have one or several fluorophores dissolved into the matrix as dopants. Common fluorophores include 2,5-diphenyloxazole, *p*-terphenyl, 9,10-diphenylanthracene (9,10-DPA), 1,4-bis(2-methylstyryl)benzene (bis-MSB) and 1,4-bis(5-phenyl-2-oxazolyl)benzene (POPOP). Each molecule has its own role: the matrix (whether liquid or plastic) is where most of the radiation/matter interaction occurs. After radiation interaction, ions may recombine giving birth to excited molecules (excitons). Excitons in the matrix are transferred to a "primary fluorophore", whose concentration is typically 1-3 weight % in commercial plastic and liquid scintillators. This concentration is large enough to ensure exciton transfer is primarily via the Förster mechanism, a resonant dipole-dipole interaction which decreases at sixth the power of the distance between molecules. The concentration, however, can be up to the solubility limit. Transfer via the Förster mechanism increases both speed and light output of the organic scintillator. To reduce reabsorption of the emitted light by the matrix or the primary fluorophore, and the resulting shortened attenuation length, a "secondary fluorophore" is also used to shift the light to longer wavelengths. Transfer from the primary to the secondary is generally radiative. Typical secondary concentrations in plastic and liquids are 0.01-0.2 weight %. The chain of emission and absorption from the matrix to the subsequent flurophores is shown in Fig. 35.2. Scintillators with two fluorophores typically have absorption lengths of several meters. The longest attenuation lengths require a third fluorophore: when the matrix is transparent up to 1 cm, adding a primary fluorophore increases the light transmission up to $\approx$ 10 cm, whereas the ternary cocktail is transparent up to 2 m and longer [39].

For most scintillators, decay times are in the ns range; rise times are much faster. Sub-ns timing resolutions have been achieved [40].

Downloaded from https://academic.oup.com/ptep/article/2022/8/083C01/6651666 by KIT Library user on 27 September 2022

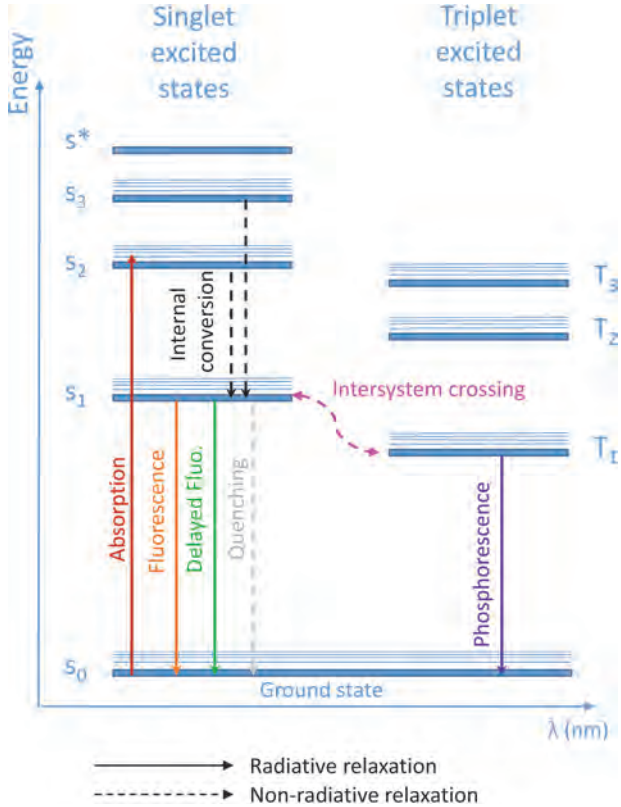

Figure 35.1: Schematic of scintillation mechanism. Schematic of typical excitation and de-excitation of matrix modules.

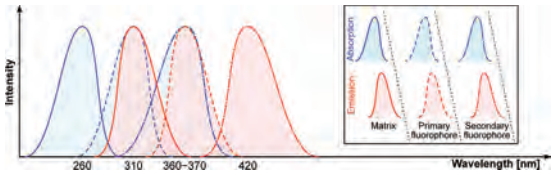

Figure 35.2: Schematic of scintillation mechanism. Typical emission and absorption spectra for the matrix, the primary, and the secondary fluorophore

Organic scintillators do not respond linearly to the ionization density. Very dense ionization tracks, with large dE/dx, emit less light than expected compared to minimum-ionizing particles. A widely used semi-empirical model by Birks posits that recombination and quenching effects between the excited molecules reduce the light yield [41]. These effects are more pronounced the greater the density of the excited molecules. Birks' formula is

$$\frac{d\mathcal{L}}{dx} = \mathcal{L}_0 \frac{dE/dx}{1 + kB\, dE/dx}, \tag{35.2}$$

where $\mathcal{L}$ is the luminescence, $\mathcal{L}_0$ is the luminescence at low specific ionization density, and the product kB is known as Birks' constant, which must be determined for each scintillator by measurement. The value of kB for polystyrene is 0.126 mm/MeV, which is large enough to play an important role in compensation in scintillator-based calorimetry. The high hydrogen content of plastic, which enhances the neutron interaction cross section, as well as the its large mass stopping power, also contributes to calorimetery compensation. In the case of large dE/dx values (e.g. with alpha particles), ion recombination may lead to the creation of triplet excited states instead of singlet excited states. If two triplet states are close enough (typically in the order of 10Å), then triplet-triplet annihilation may occur following the Dexter process [42], leading to delayed fluorescence. This phenomenon is useful for α/β or neutron/γ discrimination.

Extensive research searching for new efficient molecules that can act as matrix, primary, or secondary fluorophores, is ongoing [43]. Other chemical modifications can affect the scintillator emission wavelength and decay time, or be used *e.g.* as stabilizers or to enhance thermal neutron sensitivity. Other parameters that can be modified are the density and the effective atomic number.

35.3.2 *Plastic scintillator practicalities*

Most commercial plastic scintillators use either polystyrene (PS) or poly(vinyltoluene) (PVT) as matrix. A variety of manufacturing techniques [43] are used in the production of plastic scintillator. Cast plastic has the highest light yield, while extruded scintillator is less expensive and allows creation of the scintillator and coating with a diffusive reflector in a single process. 3D printing of plastic scintillator is being actively pursued [44]. Plastic scintillator is also used to produce scintillating, wavelength-shifting, and clear fibers. These fibers can be useful to guide light to photodetectors, and as the active element in the type of calorimeter pioneered by the RD52/DREAM collaboration [45]. They have even been used in the construction of trackers [46,47].

Plastic scintillators are reliable, robust, and convenient. However, exposure to solvent vapors, high temperatures, mechanical flexing, irradiation, or rough handling will cause degradation. The surface is a particularly fragile region and can "craze" – develop microcracks which degrade transmission of light by total internal reflection. Crazing is particularly likely where oils, solvents, or fingerprints have contacted the surface or when mechanical stresses are present. The light yield is influenced by several environmental factors: it decreases with the partial pressure of oxygen [48] and increases with increasing magnetic field. Water vapour can also diffuse into plastic and cause clouding.

Plastics are susceptible to radiation damage [49]. At high enough dose, the visible color of the plastic can change to yellow or (at high enough dose) even brown. During irradiation, broken molecular bonds ("radicals") absorb light, generally strongly in the UV, with tails to longer wavelengths. Because of this, shifting the light to longer wavelengths reduces the decrease in light output and in attenuation length due to radiation effects. Radicals produce mostly temporary damage that "anneals" when the irradiation ends, as the bonds can reform. Radicals can also polymerize via cross linking, and this leads to a permanent reduction in light yield [50]. In an inert atmosphere at room temperature, the bond reformation timescale is on the order of a month. Oxygen, which diffuses into the plastic during radiation to a depth that scales as the inverse square root of dose rate, can quickly bind to the radicals, reducing but not eliminating temporary damage at the price of a small increased permanent damage [51–53]. After irradiation, oxygen, if present, will diffuse through the entire sample, leading to oxide formation and speeding the annealing process. The decrease in light output due to permanent damage depends on the dose rate. Lower dose rates show large light losses for the same dose. The ratio of the light output to the unirradiated light output can roughly be parameterized as an exponential. For dose rates typical of current collider detectors at the Large Hadron Collider (from a few 10^{-3} to 10 Gy/hr), an exponential dose constant of tens of kGy is observed.

35.3.3 *Liquid scintillator practicalities*

Liquid scintillators have been used in large scale neutrino experiments 36.3.1.1 due to their low cost. They can hermetically fill any vessel shape. Liquid scintillators are also, due to the mobility of the molecules, much less susceptible to radiation damage.

Care must be taken to avoid dissolved water, solvents such as isopropyl alcohol, and oxygen, which reduce light yield. As they can dissolve many materials (e.g. plastics, adhesives, paints..) care must be taken in their handling. Flammability concerns limit their use in practical experiments in intense radiation fields.

Downloaded from https://academic.oup.com/ptep/article/2022/8/083C01/6651666 by KIT Library user on 27 September 2022

35.4 Inorganic scintillators

Revised August 2021 by C.L. Woody (BNL) and R.-Y. Zhu (HEP California Inst. of Technology).

Inorganic crystals form a class of scintillating materials with much higher densities than organic plastic scintillators (typically $\sim$ 4–8 g/cm^3) with a variety of different properties for use as scintillation detectors. Due to their high density and high effective atomic number, they can be used in applications where high stopping power or a high conversion efficiency for electrons or photons is required. These include total absorption electromagnetic calorimeters (see Sec. 35.10.2), which consist of a totally active absorber (as opposed to a sampling calorimeter), as well as serving as gamma ray detectors over a wide range of energies. Many of these crystals also have very high light output, and can therefore provide excellent energy resolution down to very low energies ($\sim$ few hundred keV).

Some crystals are intrinsic scintillators in which the luminescence is produced by a part of the crystal lattice itself. However, other crystals require the addition of a dopant, typically fluorescent ions such as thallium (Tl) or cerium (Ce) which is responsible for producing the scintillation light. However, in both cases, the scintillation mechanism is the same. Energy is deposited in the crystal by ionization, either directly by charged particles, or by the conversion of photons into electrons or positrons which subsequently produce ionization. This energy is transferred to the luminescent centers which then radiate scintillation photons. The light yield L in terms of the number of scintillation photons produced per MeV of energy deposit in the crystal can be expressed as [54]

$$L = 10^6 \ S \cdot Q/(\beta \cdot E_g), \tag{35.3}$$

where $\beta \cdot E_g$ is the energy required to create an e-h pair expressed as a multiple of the band gap energy Eg (eV), S is the efficiency of energy transfer to the luminescent center and Q is the quantum efficiency of the luminescent center. The values of β, S and Q are crystal dependent and are the main factors in determining the intrinsic light yield of the scintillator. The decay time of the scintillator is mainly dominated by the decay time of the luminescent center.

Table-35.4 lists the basic properties of some commonly used inorganic crystals. NaI(Tl) is one of the most common and widely used scintillators, with an emission that is well matched to a bialkali photomultiplier tube, but it is highly hygroscopic and difficult to work with, and has a rather low density. CsI(Tl) and CsI(Na) have high light yield, low cost, and are mechanically robust (high plasticity and resistance to cracking). However, they need careful surface treatment and are slightly and highly hygroscopic respectively. Pure CsI has identical mechanical properties as CsI(Tl), but a faster emission at shorter wavelength and a much lower light output.

Undoped BaF_2 has a fast component with a less than 0.6 ns decay time, and is the fastest known scintillator. However, it also has a slow component with a much longer decay time ($\sim$ 630 ns). Bismuth gemanate ($Bi_4Ge_3O_{12}$ or BGO) has a high density, and consequently a short radiation length X_0 and Molière radius R_M. Similar to CsI(Tl), BGO's emission is well-matched to the spectral sensitivity of photodiodes, and it is easy to handle and not hygroscopic. Lead tungstate ($PbWO_4$ or PWO) has a very high density, with a very short X_0 and R_M, but its intrinsic light yield is rather low.

Cerium doped lutetium oxyorthosilicate (Lu_2SiO_5:Ce, or LSO:Ce) [55] and cerium doped lutetium-yttrium oxyorthosilicate ($Lu_{2(1-x)}Y_{2x}SiO_5$, LYSO:Ce) [56] are dense crystal scintillators which have a high light yield and a fast decay time. Only the properties of LSO:Ce are listed in Table-35.4 since the properties of LYSO:Ce are similar to that of LSO:Ce except a slightly lower density than LSO:Ce depending on the yttrium fraction (typically 5 to 10%) in LYSO:Ce. This material is also featured with excellent radiation hardness [57, 58], so is expected to be used where extraordinary radiation hardness is required.

Also listed in Table-35.4 are other fluoride crystals such as PbF_2 as a Cherenkov material and CeF_3, which have been shown to provide excellent energy resolution in calorimeter applications. Table-35.4 also includes cerium doped lanthanum tri-halides, such as $LaBr_3$ [59] and $CeBr_3$ [60], which are brighter and faster than LSO:Ce, but they are highly hygroscopic and have a lower density. The FWHM energy resolution measured for these materials coupled to a PMT with bi-alkali photocathode for 0.662 MeV γ-rays from a ^{137}Cs source is about 3%, and has recently been improved to 2% by co-doping with cerium and strontium [61], which is the best among all inorganic crystal scintillators. For this reason, $LaBr_3$ and $CeBr_3$ are expected to be used in applications where a good energy resolution for low energy photons are required, such as homeland security.

Beside the crystals listed in Table-35.4, a number of new crystals are being developed that may have potential applications in high energy or nuclear physics. Of particular interest is the family of yttrium and lutetium perovskites and garnet, which include YAP ($YAlO_3$:Ce), LuAP ($LuAlO_3$:Ce), YAG ($Y_3Al_5O_{12}$:Ce) and LuAG ($Lu_3Al_5O_{12}$:Ce) and their mixed compositions. These have been shown to be linear over a large energy range [62], and have the potential for providing good intrinsic energy resolution.

Aiming at the best jet-mass resolution inorganic scintillators are being investigated for HEP calorimeters with dual readout for both Cherenkov and scintillation light to be used at future linear lepton colliders. These materials may be used for an electromagnetic calorimeter [63] or a homogeneous hadronic calorimetry (HHCAL) detector concept, including both electromagnetic and hadronic parts [64, 65]. Because of the unprecedented volume (70 to 100 m^3) foreseen for the HHCAL detector concept the materials must be (1) dense (to minimize the leakage) and (2) cost-effective. It should also be UV transparent (for effective collection of the Cherenkov light) and allow for a clear discrimination between the Cherenkov and scintillation light. The preferred scintillation light is thus at a longer wavelength, and not necessarily bright or fast. Dense crystals, scintillating glasses and ceramics offer a very attractive implementation for this detector concept [66].

The fast scintillation light provides timing information about electromagnetic interactions and showers, which may be used to mitigate pile-up effects and/or for particle identification since the time development of electromagnetic and hadronic showers, as well as minimum ionizing particles, are different. The timing information is primarily determined by the scintillator rise time and decay time, and the number of photons produced. For fast timing, it is important to have a large number of photons emitted in the initial part of the scintillation pulse, e.g. in the first ns, since one is often measuring the arrival time of the particle in the crystal using the leading edge of the light pulse. A good example of this is BaF_2, which has $\sim$ 10% of its light in its fast component with a decay time of less than 0.6 ns. Recent investigation shows that doping with yttrium in BaF_2 reduces its slow component significantly, while keeping its ultrafast scintillation component unchanged [67, 68]. The light propagation can spread out the arrival time of the scintillation photons at the photodetector due to time dispersion [69]. The time response of the photodetector also plays a major role in achieving good time resolution with fast scintillating crystals.

Table-35.4 gives the light output of other crystals relative to NaI(Tl) and their dependence to the temperature variations measured for 1.5 X_0 cube crystal samples with a Tyvek paper wrapping and a full end face coupled to a photodetector [70]. The quantum efficiency of the photodetector is taken out to facilitate a direct comparison of crystal's light output. However, the useful signal produced by a scintillator is usually quoted in terms of the number of photoelectrons per MeV produced by a given photodetector. The relationship between the light yield (LY) in number of photons/MeV produced (N_{photons}/MeV) and the light output in number of photoelectrons/MeV detected involves the factors for the light collection efficiency (LC) and the quantum efficiency (QE) of the photodetector:

$$N_{\text{p.e.}}/\text{MeV} = LY \cdot LC \cdot QE. \tag{35.4}$$

LC depends on the size and shape of the crystal, and includes effects such as the transmission of scintillation light within the crystal (i.e., the bulk attenuation length of the material), scattering from within the crystal, reflections and scattering from the

Downloaded from https://academic.oup.com/ptep/article/2022/8/083C01/6651666 by KIT Library user on 27 September 2022

Table 35.4: Properties of several inorganic crystals. Most of the notation is defined in Sec. 6 of this *Review*.

Parameter:	ρ	MP	X_0*	R_M*	dE/dx*	λ_I*	$\tau_{\rm decay}$	$\lambda_{\rm max}$	$n^\dagger$	Relative output‡	Hygro-scopic?	$d(\mathrm{LY})/dT$
Units:	g/cm^3	°C	cm	cm	MeV/cm	cm	ns	nm				%/°C§
NaI(Tl)	3.67	651	2.59	4.13	4.8	42.9	245	410	1.85	100	yes	−0.2
BGO	7.13	1050	1.12	2.23	9.0	22.8	300	480	2.15	21	no	−0.9
BaF_2	4.89	1280	2.03	3.10	6.5	30.7	650^s	300^s	1.50	36^s	no	-1.9^s
							$<0.6^f$	220^f		4.1^f		0.1^f
CsI(Tl)	4.51	621	1.86	3.57	5.6	39.3	1220	550	1.79	165	slight	0.4
CsI(Na)	4.51	621	1.86	3.57	5.6	39.3	690	420	1.84	88	yes	0.4
CsI(pure)	4.51	621	1.86	3.57	5.6	39.3	30^s	310	1.95	3.6^s	slight	−1.4
							6^f			1.1^f		
$PbWO_4$	8.30	1123	0.89	2.00	10.1	20.7	30^s	425^s	2.20	0.3^s	no	−2.5
							10^f	420^f		0.077^f		
LSO(Ce)	7.40	2050	1.14	2.07	9.6	20.9	40	402	1.82	85	no	−0.2
PbF_2	7.77	824	0.93	2.21	9.4	21.0	-	-	-	Cherenkov	no	-
CeF_3	6.16	1460	1.70	2.41	8.42	23.2	30	340	1.62	7.3	no	0
$LaBr_3$(Ce)	5.29	783	1.88	2.85	6.90	30.4	20	356	1.9	180	yes	0.2
$CeBr_3$	5.23	722	1.96	2.97	6.65	31.5	17	371	1.9	165	yes	−0.1

*Numerical values calculated using formulae in this review.

†Refractive index at the wavelength of the emission maximum.

‡Relative light output measured for samples of 1.5 X_0 cube with a Tyvek paper wrapping and a full end face coupled to a photodetector. The quantum efficiencies of the photodetector are taken out.

§Variation of light yield with temperature evaluated at the room temperature.

f = fast component, s = slow component

crystal surfaces, and re-bouncing back into the crystal by wrapping materials. These factors can vary considerably depending on the sample, but can be in the range of ∼10–60%. The internal light transmission depends on the intrinsic properties of the material, e.g. the density and type of the scattering centers and defects that can produce internal absorption within the crystal, and can be highly affected by factors such as radiation damage, as discussed below.

The quantum efficiency depends on the type of photodetector used to detect the scintillation light, which is typically ∼15–30% for photomultiplier tubes and ∼70% for silicon photodetectors for visible wavelengths. The quantum efficiency of the detector is usually highly wavelength dependent and should be matched to the particular crystal of interest to give the highest quantum yield at the wavelength corresponding to the peak of the scintillation emission. Fig. 35.3 shows the quantum efficiencies of two photodetectors, a Hamamatsu R2059 PMT with bi-alkali cathode and quartz window and a Hamamatsu S8664 avalanche photodiode (APD) as a function of wavelength. Also shown in the figure are emission spectra of three crystal scintillators, BGO, LSO:Ce/LYSO:Ce and CsI(Tl), and the numerical values of the emission weighted quantum efficiency. The area under each emission spectrum is proportional to crystal's light yield, as shown in Table-35.4, where the quantum efficiencies of the photodetector has been taken out. Results with different photodetectors can be significantly different. For example, the response of CsI(Tl) relative to NaI(Tl) with a standard photomultiplier tube with a bi-alkali photo-cathode, e.g. Hamamatsu R2059, would be 45 rather than 165 because of the photomultiplier's low quantum efficiency at longer wavelengths. For scintillators which emit in the UV, a detector with a quartz window should be used.

For very low energy applications (typically below 1 MeV), non-proportionality of the scintillation light yield may be important. It has been known for a long time that the conversion factor between the energy deposited in a crystal scintillator and the number of photons produced is not constant. It is also known that the energy resolution measured by all crystal scintillators for low energy γ-rays is significantly worse than the contribution from photo-electron statistics alone, indicating an intrinsic contribution from the scintillator itself. Precision measurement using low energy electron beam shows that this non-proportionality is crystal dependent [71]. Recent study on this issue also shows that this effect is also sample dependent even for the same crystal [72]. Further work is therefore needed to fully understand this subject.

One important issue related to the application of a crystal scintillator is its radiation hardness. Stability of its light output, or the ability to track and monitor the variation of its light output in a radiation environment, is required for high resolution and precision calibration [73]. All known crystal scintillators suffer from ionization dose induced radiation damage [74], where a common damage phenomenon is the appearance of radiation induced absorption caused by the formation of color centers originated from the impurities or point defects in the crystal. This radiation induced absorption reduces the light attenuation length in the crystal, and hence its light output. For crystals with high defect density, a severe reduction of light attenuation length may cause a distortion of the light response uniformity, leading to a degradation of the energy resolution. Additional radiation damage effects may include a reduced intrinsic scintillation light yield (damage to the luminescent centers) and an increased phosphorescence (afterglow). For crystals to be used in a high precision calorimeter in a radiation environment, its scintillation mechanism must not

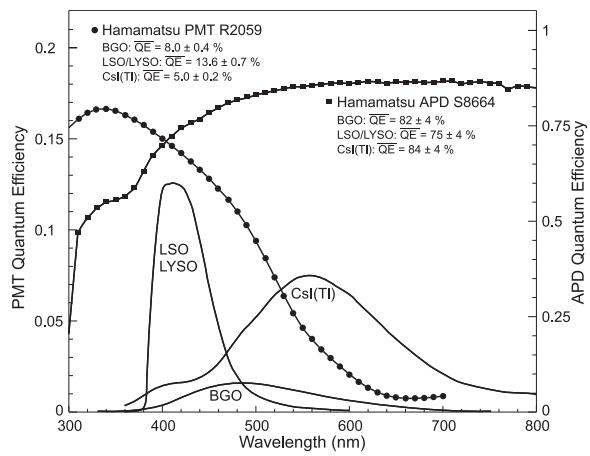

Figure 35.3: The quantum efficiencies of two photodetectors, a Hamamatsu R2059 PMT with bi-alkali cathode and a Hamamatsu S8664 avalanche photodiode (APD), are shown as a function of wavelength. Also shown in the figure are emission spectra of three crystal scintillators, BGO, LSO and CsI(Tl), and the numerical values of the emission weighted quantum efficiencies. The area under each emission spectrum is proportional to crystal's light yield.

Downloaded from https://academic.oup.com/ptep/article/2022/8/083C01/6651666 by KIT Library user on 27 September 2022

be damaged and its light attenuation length in the expected radiation environment must be long enough so that its light response uniformity, and thus its energy resolution, does not change.

While radiation damage induced by ionization dose is well understood [75], investigation is on-going to understand radiation damage caused by hadrons, including both charged hadrons [76] and neutrons [77]. Two additional fundamental processes may cause defects by hadrons: displacement damage and nuclear breakup. While charged hadrons can produce all three types of damage (and it's often difficult to separate them), neutrons can produce only the last two, and electrons and photons only produce ionization damage. Studies on hadron induced radiation damage to lead tungstate [78] show a proton-specific damage component caused by fragments from fission induced in lead and tungsten by particles in the hadronic shower. The fragments cause a severe, local damage to the crystalline lattice due to their extremely high energy loss over a short distance [78]. Recent investigation also sees evidence of neutron-specfic damage in various crystals [77].

Most of the crystals listed in Table-35.4 have been used in high energy or nuclear physics experiments when the ultimate energy resolution for electrons and photons is desired. Examples are the Crystal Ball NaI(Tl) calorimeter at SPEAR, the L3 BGO calorimeter at LEP, the CLEO CsI(Tl) calorimeter at CESR, the KTeV CsI calorimeter at the Tevatron, and the BaBar, BELLE and BES III CsI(Tl) calorimeters at PEP-II, KEK and BEPC II, respectively. Because of their high density and relative low cost, PWO calorimeters are used by CMS and ALICE at LHC, by CLAS and PrimEx at CEBAF and by PANDA at GSI. Similarly, PbF_2 calorimeters are used by the A4 experiment at MAINZ and by the g-2 experiment at Fermilab. A CsI calorimeter is being built for the Mu2e experiment at Fermilab. An LYSO:Ce calorimeter is being built for the COMET experiment at J-PARC, and an LYSO:Ce crystal-based precision timing layer is being built for the CMS experiment at the HL-LHC.

35.5 Cherenkov detectors

Revised July 2021 by J. Schwiening (GSI Darmstadt).

Although devices using Cherenkov radiation are often thought of as only particle identification (PID) detectors, in practice they are used over a much broader range of applications including; (1) fast particle counters; (2) hadronic PID; (3) electromagnetic calorimeters (EMC); and (4) tracking detectors performing complete event reconstruction. Examples of applications from each category include; (1) the BaBar luminosity detector [79] and the Quartic fast timing counter for the ATLAS Forward Proton Detector, designed to measure small angle scatters at the LHC [80]; (2) the hadronic PID detectors at the B factory detectors—DIRC in BaBar [81], and the modern Imaging Aerogel and TOP counters at Belle II [82]; (3) the CMS Hadron Forward calorimeter based on Cherenkov light emitted in quartz fibers embedded in a steel absorber [83]; and (4) large water Cherenkov counters such as Super-Kamiokande [84].

Cherenkov counters contain two main elements; (1) a radiator through which the charged particle passes, and (2) a photodetector. As Cherenkov radiation is a weak source of photons, light collection and detection must be as efficient as possible. The refractive index n and the particle's path length through the radiator L appear in the Cherenkov relations allowing the tuning of these quantities for particular applications. One or more of the properties of Cherenkov radiation discussed in the Passages of Particles through Matter section (Sec. 34 of this *Review*) are utilized in Cherenkov detectors: the prompt emission of a light pulse; the existence of a velocity threshold for radiation; and the dependence of the Cherenkov cone half-angle θ_c and the number of emitted photons on the velocity of the particle v_p and the refractive index n of the medium. The Cherenkov angle can be calculated as

$$\cos\theta_c = \frac{1}{n(E)\beta}, \tag{35.5}$$

where $\beta = v_p/c$ with c being the speed of light, and E the photon energy. The number of photoelectrons ($N_{\text{p.e.}}$) detected in a given device with radiator of length L is

$$N_{\text{p.e.}} = L\frac{\alpha^2 z^2}{r_e\, m_e c^2}\int \epsilon(E)\,\sin^2\theta_c(E)dE, \tag{35.6}$$

where $\epsilon(E)$ is the efficiency for collecting the Cherenkov light and transducing it into photoelectrons, and $\alpha^2/(r_e\, m_e c^2) = 370\ \text{cm}^{-1}\text{eV}^{-1}$. The quantities ϵ and θ_c are functions of the photon energy. As the typical energy dependent variation of the index of refraction is modest, a quantity called the *Cherenkov detector quality factor* N_0 can be defined as

$$N_0 = \frac{\alpha^2 z^2}{r_e\, m_e c^2}\int \epsilon\, dE, \tag{35.7}$$

so that, taking the charge number $z = 1$ (the usual case in high-energy physics),

$$N_{\text{p.e.}} \approx L N_0 \langle\sin^2\theta_c\rangle. \tag{35.8}$$

This definition of the quality factor N_0 is not universal, nor, indeed, very useful for those common situations where ϵ factorizes as $\epsilon = \epsilon_{\text{coll}}\epsilon_{\text{det}}$ with the geometrical photon collection efficiency (ϵ_{coll}) varying substantially for different tracks while the photon detector efficiency (ϵ_{det}) remains nearly track independent. In this case, it can be useful to explicitly remove (ϵ_{coll}) from the definition of N_0. A typical value of N_0 for a photomultiplier (PMT) detection system working in the visible and near UV, and collecting most of the Cherenkov light, is about 100 cm^{-1}. Practical counters, utilizing a variety of different photodetectors, have values ranging between about 30 and 180 cm^{-1}. Radiators can be chosen from a variety of transparent materials (Sec. 34 of this *Review* and Table 6). In addition to refractive index, the choice requires consideration of factors such as material density, radiation length and radiation hardness, transmission bandwidth, absorption length, chromatic dispersion, optical workability (for solids), availability, and cost. When the momenta of particles to be identified is high, the refractive index must be set close to one, so that the photon yield per unit length is low and a long particle path in the radiator is required. Recently, the gap in refractive index that has traditionally existed between gases and liquid or solid materials has been partially closed with transparent *silica aerogels* with indices that range between about 1.007 and 1.13.

Cherenkov counters may be classified as either *imaging* or *threshold* types, depending on whether they do or do not make use of Cherenkov angle (θ_c) information. Imaging counters may be used to track particles as well as identify them. The recent development of very fast photodetectors such as micro-channel plate PMTs (MCP-PMT) (see 35.2 of this *Review*) also potentially allows very fast Cherenkov based time of flight (TOF) detectors of either class [85]. The track timing resolution of imaging detectors can be extremely good as it scales approximately as $\frac{1}{\sqrt{N_{\text{p.e.}}}}$.

Threshold Cherenkov detectors [86], in their simplest form, make a yes/no decision based

on whether the particle is above or below the Cherenkov threshold velocity $\beta_t = 1/n$. A straightforward enhancement of such detectors uses the number of observed photoelectrons (or a calibrated pulse height) to discriminate between species or to set probabilities for each particle species [87]. This strategy can increase the momentum range of particle separation by a modest amount (to a momentum some 20% above the threshold momentum of the heavier particle in a typical case).

Careful designs give $\langle\epsilon_{\text{coll}}\rangle \gtrsim 90\%$. For a photomultiplier with a typical bialkali cathode, $\int \epsilon_{\text{det}} dE \approx 0.27$ eV, so that

$$N_{\text{p.e.}}/L \approx 90\ \text{cm}^{-1}\,\langle\sin^2\theta_c\rangle \qquad (\textit{i.e.},\ N_0 = 90\ \text{cm}^{-1}). \tag{35.9}$$

Suppose, for example, that n is chosen so that the threshold for species a is p_t; that is, at this momentum species a has velocity $\beta_a = 1/n$. A second, lighter, species b with the same momentum has velocity β_b, so $\cos\theta_c = \beta_a/\beta_b$, and

$$N_{\text{p.e.}}/L \approx 90\ \text{cm}^{-1}\,\frac{m_a^2 - m_b^2}{p_t^2 + m_a^2}. \tag{35.10}$$

Downloaded from https://academic.oup.com/ptep/article/2022/8/083C01/6651666 by KIT Library user on 27 September 2022

For K/π separation at $p = p_t = 1(5)$ GeV/c, $N_{\rm p.e.}/L \approx 16(0.8)$ cm^{-1} for π's and (by design) 0 for K's.

For limited path lengths $N_{\rm p.e.}$ will usually be small. The overall efficiency of the device is controlled by Poisson fluctuations, which can be especially critical for separation of species where one particle type is dominant. Moreover, the effective number of photoelectrons is often less than the average number calculated above due to additional equivalent noise from the photodetector (see the discussion of the excess noise factor in 35.2 of this *Review*). It is common to design for at least 10 photoelectrons for the high velocity particle in order to obtain a robust counter. As rejection of the particle that is below threshold depends on *not* seeing a signal, electronic and other background noise, especially overlapping tracks, can be important. Physics sources of light production for the below threshold particle, such as decay to an above threshold particle, scintillation light, or the production of delta rays in the radiator, often limit the separation attainable, and need to be carefully considered. Well designed, modern multi-channel counters, such as the ACC at Belle [88], can attain adequate particle separation performance over a substantial momentum range.

Imaging counters make the most powerful use of the information available by measuring the ring-correlated angles of emission of the individual Cherenkov photons. They typically provide positive ID information both for the "wanted" and the "unwanted" particles, thus reducing mis-identification substantially. Since low-energy photon detectors can measure only the position (and, perhaps, a precise detection time) of the individual Cherenkov photons (not the angles directly), the photons must be "imaged" onto a detector so that their angles can be derived [89]. Typically the optics map the Cherenkov cone onto (a portion of) a distorted "circle" at the photodetector. Though the imaging process is directly analogous to familiar imaging techniques used in telescopes and other optical instruments, there is a somewhat bewildering variety of methods used in a wide variety of counter types with different names. Some of the imaging methods used include (1) focusing by a lens or mirror; (2) proximity focusing (i.e., focusing by limiting the emission region of the radiation); and (3) focusing through an aperture (a pinhole). In addition, the prompt Cherenkov emission coupled with the speed of some modern photon detectors allows the use of (4) time imaging, a method which is little used in conventional imaging technology, and may allow some separation with particle TOF. Finally, (5) correlated tracking (and event reconstruction) can be performed in large water counters by combining the individual space position and time of each photon together with the constraint that Cherenkov photons are emitted from each track at the same polar angle (Sec. 36.3.1of this *Review*).

In a simple model of an imaging PID counter, the fractional error on the particle velocity (δ_β) is given by

$$\delta_\beta = \frac{\sigma_\beta}{\beta} = \tan\theta_c \sigma(\theta_c) \ , \tag{35.11}$$

where

$$\sigma(\theta_c) = \frac{\langle\sigma(\theta_i)\rangle}{\sqrt{N_{\rm p.e.}}} \oplus C, \tag{35.12}$$

and $\langle\sigma(\theta_i)\rangle$ is the average single photoelectron resolution, as defined by the optics, detector resolution and the intrinsic chromaticity spread of the radiator index of refraction averaged over the photon detection bandwidth. C combines a number of other contributions to resolution including, (1) correlated terms such as tracking, alignment, and multiple scattering, (2) hit ambiguities, (3) background hits from random sources, and (4) hits coming from other tracks. The actual separation performance is also limited by physics effects such as decays in flight and particle interactions in the material of the detector. In many practical cases, the performance is limited by these effects.

For a $\beta \approx 1$ particle of momentum (p) well above threshold entering a radiator with index of refraction (n), the number of σ separation (N_σ) between particles of mass m_1 and m_2 is approximately

$$N_\sigma \approx \frac{|m_1^2 - m_2^2|}{2p^2\sigma(\theta_c)\sqrt{n^2-1}}. \tag{35.13}$$

In practical counters, the angular resolution term $\sigma(\theta_c)$ varies between about 0.1 and 5 mrad depending on the size, radiator, and photodetector type of the particular counter. The range of momenta over which a particular counter can separate particle species extends from the point at which the number of photons emitted becomes sufficient for the counter to operate efficiently as a threshold device ($\sim$20% above the threshold for the lighter species) to the value in the imaging region given by the equation above. For example, for $\sigma(\theta_c)$ =2 mrad, a fused silica radiator ($n = 1.474$), or a fluorocarbon gas radiator (C_5F_{12}, $n = 1.0017$), would separate π/K's from the threshold region starting around 0.15(3) GeV/c through the imaging region up to about 4.2(18) GeV/c at better than 3σ.

Many different imaging counters have been built during the last several decades [85]. Among the earliest examples of this class of counters are the very limited acceptance

Differential Cherenkov detectors, designed for particle selection in high momentum beam lines. These devices use optical focusing and/or geometrical masking to select particles having velocities in a specified region. With careful design, a velocity resolution of $\sigma_\beta/\beta \approx 10^{-4}$–$10^{-5}$ can be obtained [86].

Practical multi-track *Ring-Imaging Cherenkov detectors* (generically called RICH counters) are a more recent development. RICH counters are sometimes further classified by 'generations' that differ based on historical timing, performance, design, and photodetection techniques. Prototypical examples of first generation RICH counters are those used in the DELPHI and SLD detectors at the LEP and SLC Z factory e^+e^- colliders [85]. They have both liquid (C_6F_{14}, $n = 1.276$) and gas (C_5F_{12}, $n = 1.0017$) radiators, the former being proximity imaged with the latter using mirrors. The phototransducers are a TPC/wire-chamber combination. They are made sensitive to photons by doping the TPC gas (usually, ethane/methane) with $\sim$ 0.05% TMAE (tetrakis(dimethylamino)ethylene). Great attention to detail is required, (1) to avoid absorbing the UV photons to which TMAE is sensitive, (2) to avoid absorbing the single photoelectrons as they drift in the long TPC, and (3) to keep the chemically active TMAE vapor from interacting with materials in the system. In spite of their unforgiving operational characteristics, these counters attained good $e/\pi/K/p$ separation over wide momentum ranges (from about 0.25 to 20 GeV/c) during several years of operation at LEP and SLC. Related but smaller acceptance devices include the OMEGA RICH at the CERN SPS, and the RICH in the balloon-borne CAPRICE detector [85].

Later generation counters [85] generally operate at much higher rates, with more detection channels, than the first generation detectors just described. They also utilize faster, more forgiving photon detectors, covering different photon detection bandwidths. Radiator choices have broadened to include materials such as lithium fluoride, fused silica, and aerogel. Vacuum-based photodetection systems (*e.g.*, single or multi anode PMTs, MCP-PMTs, or hybrid photodiodes (HPD)) have become increasingly common (see 35.2 of this *Review*). They handle high rates, and can be used with a wide choice of radiators. Examples include (1) the SELEX RICH at Fermilab, which mirror focuses the Cherenkov photons from a neon radiator onto a camera array made of $\sim$ 2000 PMTs to separate hadrons over a wide momentum range (to well above 200 GeV/c for heavy hadrons);(2) the NA62 RICH at CERN, which uses a 17 m long tank filled with neon gas as radiator and spherical mirrors to focus the photons on two arrays of 2 000 PMTs to separate pions from muons for momenta between 15 and 35 GeV/c; (3) the CBM RICH under construction at FAIR where the Cherenkov photons, produced in about 30 m^3 of CO_2 radiator gas, are mirror-focused on arrays of multi-anode PMTs (MaPMTs) with a total of about 55,000 pixels, to identify electrons with momenta up to 10 GeV/c; and (4) the LHCb detector now running at the LHC. It uses two separate counters. One volume contains C_4F_{10} (originally in combination with aerogel, which was removed in 2015) while the second volume contains CF_4. Photons are mirror-focused onto detector arrays of HPDs to cover a π/K separation momentum range between 1 and 150 GeV/c. Further upgrades, including the replacement of the

Downloaded from https://academic.oup.com/ptep/article/2022/8/083C01/6651666 by KIT Library user on 27 September 2022

HPDs by MaPMTs and improved readout electronics, are necessary to deal with increases in luminosity.

Other fast detection systems that use solid cesium iodide (CsI) photocathodes or triethylamine (TEA) doping in proportional chambers are useful with certain radiator types and geometries. Examples include (1) the CLEO-III RICH at CESR that uses a LiF radiator with TEA doped proportional chambers; (2) the ALICE detector at the LHC that uses proximity focused liquid (C_6F_{14} radiators and solid CsI photocathodes (similar photodectors have been used for several years by the HADES and COMPASS detectors), and the hadron blind detector (HBD) in the PHENIX detector at RHIC that couples a low index CF_4 radiator to a photodetector based on electron multiplier (GEM) chambers with reflective CsI photocathodes [85].

Recent technological advances in the production of aerogel with improved transparency in the UV range and finely tuned refractive indices enable several new RICH designs. The innovative hybrid geometry of the CLAS12 RICH, with complex photon paths that feature multiple passes through the aerogel tiles, is only possible due to the improved scattering length of the aerogel. It minimizes the material inside of the detector acceptance as well as the cost of the photon sensor array. Beam tests have demonstrated that the counter will be able to provide clean π/K separation up to 8 GeV/c. The forward endcap Aerogel RICH (ARICH) for the Belle II upgrade at KEKB, designed to provide clean π/K separation for momenta up to 3.5 GeV/c, is an example of the so-called focusing aerogel approach [90]. The radiator is a dual-layer aerogel, with a thickness of 20 mm for each layer and increasing refractive indices of $n = 1.045$ and $n = 1.055$ along the particle path. The Cherenkov ring images from the two layers overlap on the array of Hybrid Avalanche Photo Detectors (HAPDs), which provide efficient single photon detection in the 1.5 T magnetic field.

A DIRC (Detection [of] Internally Reflected Cherenkov [light]) is a distinctive, compact RICH subtype first used in the BaBar detector [81]. A DIRC "inverts" the usual RICH principle for use of light from the radiator by collecting and imaging the total internally reflected light rather than the transmitted light. It utilizes the optical material of the radiator in two ways, simultaneously: as a Cherenkov radiator and as a light pipe. The magnitudes of the photon angles are preserved during transport by the flat, rectangular cross section radiators, allowing the photons to be efficiently transported to a detector outside the path of the particle where they may be imaged in up to three independent dimensions (the usual two in space and, due to the long photon paths lengths, one in time). Because the index of refraction in the radiator is large ($n \sim 1.47$ for fused silica), the momentum range with good π/K separation goes up to 4–5 GeV/c. It is plausible, but difficult, to extend it up to about 10 GeV/c with an improved design.

The BaBar experiment at the asymmetric PEP-II e^+e^- collider studied CP violation in $\Upsilon(4S)$ decays. Excellent pion/kaon separation for particle momenta up to 4 GeV/c was required. The BaBar DIRC used 4.9 m long, rectangular bars made from synthetic fused silica as radiator and light guide. The photons were imaged via a "pin-hole" through an expansion region filled with 6 000 liters of purified water onto an array of 10 752 densely packed photomultiplier tubes placed at a distance of about 1.2 m from the bar end. During more than 8 years of operation, the BaBar DIRC achieved π/K separation of 2.5 standard deviations or more up to 4 GeV/c momentum. For a pion identification rate around 85% the DIRC provided a kaon misidentification rate well below 1% up to 3 GeV/c.

The next generation of DIRC detectors [91] takes advantage of the new, very fast, pixelated photodetectors becoming available, such as MaPMTs and MCP-PMTs. They typically utilize either time imaging or lens/mirror-focused optics, or both, leading not only to a precision measurement of the Cherenkov angle, but in some cases, to a precise measurement of the particle time of flight, and/or to correction of the chromatic dispersion in the radiator. Examples [85] include (1) the Belle II Time of Propagation (TOP) counter that emphasizes precision timing for both Cherenkov imaging and TOF to perform π/K separation of at least 3 standard deviations up to 4 GeV/c; (2) the DIRC upgrade of the GlueX experiment at Jefferson Lab that places four decommissioned BaBar DIRC modules, coupled to upgraded optics and readout, perpendicular to the beamline, the first application of a DIRC in a detector endcap; (3) the PANDA Barrel DIRC at FAIR, to be installed in 2025, that will be the first DIRC counter to use lens focusing and is expected to provide more than 3 standard deviations π/K separation up to 3.5 GeV/c; and (4) the TORCH proposal being developed for an LHCb upgrade in 2027 which uses DIRC imaging for individual photons with fast photon detectors to provide particle separation via particle TOF with a precision of 10-15 ps per track over a flight path length of 9.5m.

35.6 Gaseous detectors

35.6.1 *Energy loss and charge transport in gases*

Revised November 2021 by F. Sauli (CERN) and M. Titov (IRFU, CEA, Université Paris-Saclay).

Gas-filled detectors use the localized ionization produced by charged particles, generally after charge multiplication. The statistics of ionization processes, having asymmetries in the ionization trails, affect the coordinate determination deduced from the measurement of drift time, or of the center of gravity of the collected charge. For thin gas layers, the width of the energy loss distribution can be larger than its average, requiring multi-sampling devices or truncated mean analysis to achieve good particle identification. In the truncated mean method for calculating $\langle dE/dx \rangle$, the ionization measurements along the track length are broken into many samples and then a fixed fraction of high-side (and sometimes also low-side) values are rejected [92].

Table 35.5: Properties of noble and molecular gases at normal temperature and pressure (NTP: 20° C, one atm). E_X, E_I: first excitation, ionization energy; W_I: average energy for creation of ion pair; $dE/dx|_{\rm min}$, N_P, N_T: differential energy loss, primary and total number of electron-ion pairs per cm, for unit charge minimum ionizing particles. Values often differ, depending on the source, and those in the table should be taken only as approximate.

Gas	Density, mg cm^{-3}	E_x eV	E_I eV	W_I eV	$dE/dx\|_{\rm min}$ keV cm^{-1}	N_P cm^{-1}	N_T cm^{-1}
H_2	0.084	10.8	13.6	37	0.34	5.2	9.2
He	0.179	19.8	24.6	41.3	0.32	3.5	8
Ne	0.839	16.7	21.6	37	1.45	13	40
Ar	1.66	11.6	15.7	26	2.53	25	97
Xe	5.495	8.4	12.1	22	6.87	41	312
CH_4	0.667	8.8	12.6	30	1.61	28	54
C_2H_6	1.26	8.2	11.5	26	2.91	48	112
iC_4H_{10}	2.49	6.5	10.6	26	5.67	90	220
CO_2	1.84	7.0	13.8	34	3.35	35	100
CF_4	3.78	10.0	16.0	35-52	6.38	52-63	120

The energy loss of charged particles and photons in matter is discussed in Sec. 34. Every ionization process is a quantum mechanical transition initiated by the Coulomb field of the particle and the field created by neighbouring polarizable atoms; the average energy losses are described by the Bethe-Bloch formula with Sternheimer's density effect corrections. The fluctuations caused by Rutherford scattering on quasi-free electrons follow a Landau distribution and the influence of atomic shells is described by the photoabsorption ionization (PAI) model, which allows simulation of each energy transfer [93], with relaxation cascades and simulation of delta-electrons [94]. Table 35.5 provides values of relevant parameters in some commonly used gases at NTP for unit-charge minimum-ionizing particles (MIPs) [95] [96]. When an ionizing particle passes through the gas it creates electron-ion pairs; often the ejected electrons have sufficient energy to further ionize the medium. The number of pairs is known as cluster-size distribution, because the secondary electrons are created in the immedi-

Downloaded from https://academic.oup.com/ptep/article/2022/8/083C01/6651666 by KIT Library user on 27 September 2022

ate vicinity of the primary encounter and, together with the primary electrons, form clusters of one, several, or sometimes many, electron-ion pairs. As shown in Table 35.5, the total number of pairs (N_T) is a few times larger than the number of primaries (N_P). For different conditions and for mixtures, and neglecting energy transfer processes (*e.g.* Penning effect), one can scale the density, N_P, and N_T with temperature and pressure assuming a perfect gas law.

The probability for a released electron to have an energy E or larger follows an approximate $1/E^2$ dependence (Rutherford law), shown in Fig. 35.4 for Ar at NTP (dotted line, left scale). More detailed estimates taking into account the electronic structure of the medium are shown in the figure, for three values of the particle velocity factor $\beta\gamma$ [97]. The dot-dashed line provides, on the right scale, the practical range of electrons (including scattering) of energy E. As an example, about 0.6% of released electrons have 1 keV or more energy, substantially increasing the total ionization loss. The practical range of 1 keV electrons in argon (dot-dashed line, right scale) is 70 μm and this can contribute to the error in the coordinate determination.

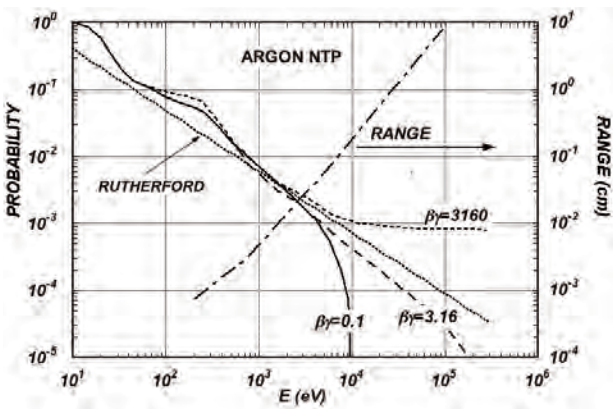

Figure 35.4: Probability of single collisions in which released electrons have an energy E or larger (left scale) and practical range of electrons in Ar at NTP (dot-dashed curve, right scale) [97].

Garfield^{++} [98], together with HEED [94], Degrad [99], Magboltz [100, 101], SRIM, ANSYS, COMSOL, and neBEM [102] software packages represent the core simulation tools for microscopic modelling of gaseous detector response. The number of electron-ion pairs per primary ionization, or cluster size depends little on the medium; it can be computed with the programs mentioned above or experimentally measured. For example, there is about 1% probability for primary clusters to contain ten or more electron-ion pairs in argon [103].

Once released in the gas, and under the influence of an applied electric field, electrons and ions drift in opposite directions and diffuse towards the electrodes. The electron-molecule collision cross sections are determined by the details of atomic and molecular structure and depends strongly on the electron energy and therefore on the electric field **E** for most gases. High values of the total electron scattering cross section reduce the electron diffusion and increase the drift velocity; a large inelasticity implies that high fields are required to raise the electron energy. For noble gases, the inelastic cross section is zero until the electrons reach the first excitation and ionization energies $\mathcal{O}(10\ eV)$; on the contrary, for molecular gases, like CH_4, inelastic channels, involving rotational and vibrational levels, open up at energies above ~ 0.1 eV. Large drift velocities are achieved by adding polyatomic gases (usually hydrocarbons C_xH_y, CO_2, CF_4) having large inelastic component at moderate energies of a few eV; this results in the electron "cooling" into the energy range of the Ramsauer-Townsend minimum (at $\sim$0.5 eV) of the elastic ("momentum-transfer") cross-section in Ar [96]. Under these circumstances, it is not surprising that the addition of very small quantities of one gas to another can dramatically modify the average electron energy and alter the dependence of the drift velocity (v_d) on **E/P** and temperature; this has a particularly strong effect for noble gases, as illustrated in Fig. 35.5 for Ar. Carbon tetrafluoride (CF_4) has the largest drift velocity and the lowest electron diffusion among known gases due to the sizeable Ramsauer-Townsend dip in the elastic cross-section which coincides with a very large vibrational modes. Another principal role of the polyatomic gas is to absorb the ultraviolet photons emitted by the excited noble gas atoms. Addition of molecular gases (hydrocarbons or CO_2 are widely used in the proportional counters as a quencher) to noble gas allows to dissipate a good fraction of energy through rotational and vibrational radiationless transitions without the creation of photons or ions. On the contrary, CF_4 has a small quenching cross-section of excited Ar states and light emission in CF_4 (from the far UV to the visible light) is a complex process, involving the creation of CF_3^+ excited states [104].

Extensive collections of experimental data [105] and theoretical calculations based on transport theory permit evaluation of drift and diffusion properties in pure gases and their mixtures; modern compilations of the electron-molecule cross sections are available at the open-access website LXCAT [106]. Fig. 35.5 and Fig. 35.6 show drift velocity and transverse diffusion for some commonly used gases at NTP, computed with the Magboltz program [100,101]. For different conditions, the horizontal axis must be scaled inversely with the gas density. Standard deviations for longitudinal (σ_L) and transverse diffusion (σ_T) are given for one cm of drift, and scale with the the square root of the drift distance.

In a simple approximation, gas kinetic theory provides the drift velocity v_d as a function of the mean collision time τ and the electric field **E**: $v_d = eE\tau/m_e$ (Townsend's expression). In the presence of an external magnetic field, the Lorentz force acting on electrons between collisions deflects the drifting electrons and modifies the drift properties. The electron trajectories, velocities and diffusion parameters can be computed with Magboltz. The friction force model provides an approximate expression for the vector drift velocity $\boldsymbol{v}$ as a function of electric and magnetic field vectors $\boldsymbol{E}$ and $\boldsymbol{B}$, of the Larmor frequency $\omega = eB/m_e$, and of the mean collision time τ (more precise calculation is available in Magboltz, which computes drift velocity by tracing electrons at the microscopic level through numerous collisions with gas molecules):

$$\boldsymbol{v} = \frac{e}{m_e}\frac{\tau}{1+\omega^2\tau^2}\left(\boldsymbol{E} + \frac{\omega\tau}{B}(\boldsymbol{E}\times\boldsymbol{B}) + \frac{\omega^2\tau^2}{B^2}(\boldsymbol{E}\cdot\boldsymbol{B})\boldsymbol{B}\right) \quad (35.14)$$

To a good approximation, and for moderate fields, one can assume that the energy of the electrons is not affected by B, and use for τ the values deduced from the drift velocity at $B = 0$ (the Townsend expression). For $\boldsymbol{E}$ perpendicular to $\boldsymbol{B}$, the drift angle relative to the electric field vector is $\tan\theta_B = \omega\tau$ and $v = (E/B)(\omega\tau/\sqrt{1+\omega^2\tau^2})$. For parallel electric and magnetic fields, drift velocity and longitudinal diffusion are not affected, while the transverse diffusion can be strongly reduced: $\sigma_T(B) = \sigma_T(B=0)/\sqrt{1+\omega^2\tau^2}$. As an example, the dotted line in Fig. 35.6 represents σ_T for the classic Ar/CH_4 (90:10) mixture at 4 T. Large values of $\omega\tau \sim 20$ at 5 T are consistent with the measurement of diffusion coefficient in $Ar/CF_4/iC_4H_{10}$ (95:3:2). This reduction is exploited to substantially improve spatial resolution in the Drift (Sec. 35.6.2) and Time Projection Chambers (Sec. 35.6.5).

In some mixtures containing molecules with electronic affinity, electrons can be captured to form negative ions. Capture cross sections vary considerably with an energy and, hence, the electric field; as a consequence, the three-body electron attachment coefficients may differ significantly for the same additive in different mixtures. As an example, at moderate fields (up to 1 kV/cm) the addition of 0.1% of oxygen to an Ar/CO_2 mixture results in an electron capture probability about twenty times larger than in Ar/CH_4. Among common molecules, the largest electron affinities are found for the halogenides, O_2 and H_2O. The attachment probability in O_2 or H_2O is large at low fields and electron energies close to thermal, but decreases at increasing fields. On the contrary, CF_4 is not electronegative at low and moderate fields, but has a large electron capture cross section at fields above $\sim$8 kV/cm, before reaching the avalanche field strengths. Depending on the mixture and detector geometry, some signal reduction and energy resolution loss is expected in this gas.

Downloaded from https://academic.oup.com/ptep/article/2022/8/083C01/6651666 by KIT Library user on 27 September 2022

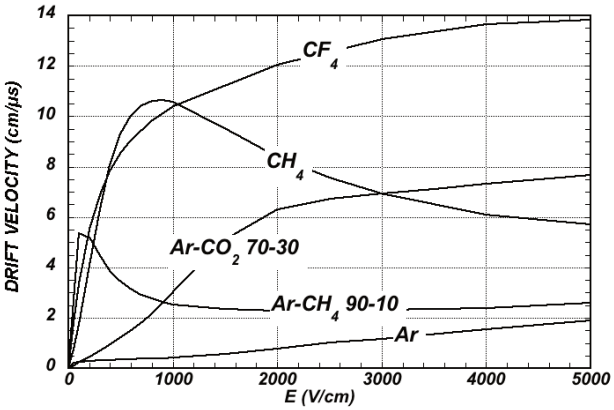

Figure 35.5: Computed electron drift velocity as a function of electric field in several gases at NTP and $B = 0$ [100, 101].

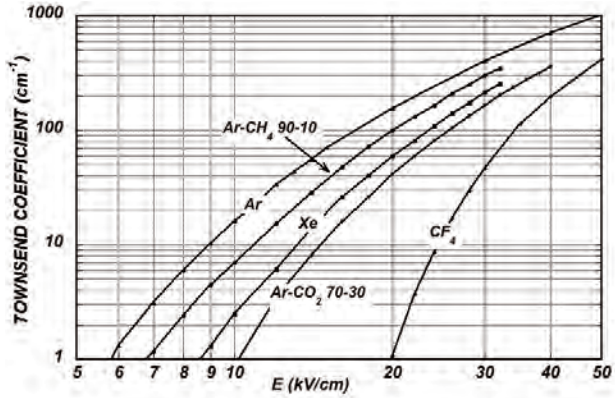

Figure 35.7: Computed first Townsend coefficient α as a function of electric field in several gases at NTP [100, 101].

If the electric field is increased sufficiently, electrons gain enough energy between collisions to excite and ionize molecules. Above a gas-dependent threshold, the mean free path for ionization, λ_i, decreases exponentially with the field; its inverse, $\alpha = 1/\lambda_i$, is named the first Townsend coefficient. In wire chambers, most of the increase of avalanche particle density occurs very close to the anode wires, and a simple electrostatic consideration shows that the largest fraction of the detected signal is due to the motion of positive ions receding from the wires. The electron component, although very fast, contributes very little to the signal. This determines the characteristic shape of the detected signals in the proportional mode: a fast rise followed by a gradual increase. The slow component, the so-called "ion tail" that limits the time resolution of the detector, is usually removed by differentiation of the signal. In uniform fields, N_0 initial electrons multiply over a length x forming an electron avalanche of size $N = N_0\, e^{\alpha x}$; N/N_0 is the gain of the detector. Fig. 35.7 shows examples of Townsend coefficients for several gas mixtures, computed with Magboltz [100, 101].

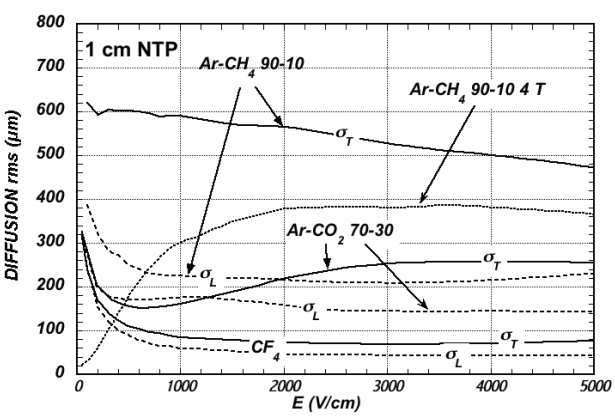

Figure 35.6: Electron longitudinal diffusion (σ_L) (dashed lines) and transverse diffusion (σ_T) (full lines) for 1 cm of drift at NTP and $B = 0$. The dotted line shows σ_T for the P10 mixture at 4 T [100, 101].

Additional ionizing energy transfer mechanisms due to the excited noble gas atoms, called collisional Penning energy transfers, occur when the excitation energy of a noble gas is higher than the ionization potential of an admixture gas. The energy transfer rate, probability that an excited atom ionizes a quenching agent, is a priori not known for a mixture but can be extracted from the fits of the experimental gas gain data [107] using the Magboltz simulations [100, 101]. In the gain calculations, the Penning adjusted Townsend coefficient is defined in terms of the total production frequencies of the noble gas excitations and direct ionizations of the mixture. Systematic gas gain measurements for varying mixing ratios and pressures are critical for determining the efficiency of the different mechanisms involved in the transfers. Collisional energy transfer mostly scales linearly with the gas pressure and the fraction of quenching gas in the mixture, while ionization by photons emitted from excitations is independent of the medium [108]. In addition, collisional Penning transfers of some higher excited states can occur before they decay at atmopheric pressure and are not restricted to metastable states of the excited noble gas. For example, the impact of the Penning effect on gas gain is roughly a factor 10 in Ar-CO_2 mixtures and exceeding a factor of 100 in Ar-C_2H_2 mixtures [108].

Positive ions released by the primary ionization or produced in the avalanches drift and diffuse under the influence of the electric field. Negative ions may also be produced by electron attachment to gas molecules. The drift velocity of ions in the fields encountered in gaseous detectors (up to few kV/cm) is typically about three orders of magnitude smaller than for electrons. The ion mobility μ, the ratio of drift velocity to electric field, is constant for a given ion type up to very high fields. Values of ions mobility at NTP are given in Table 35.6 [109]. For different temperatures and pressures, the mobility can be scaled inversely with the density assuming an ideal gas law. Both the longitudinal and transverse diffusion of ions are proportional to the square root of the drift time, with a coefficient that depends on temperature but not on the ion mass. It has been historically assumed that, due to a very effective charge transfer mechanism, only ions with the lowest ionization potential survive after a short path in the mixture. However, recent experimental data suggests that the signal ions, in e.g. CO_2-quenched mixtures of Ar and Ne are $CO_2^+\cdot(CO2)_n$ cluster ions, and not CO_2^+ or noble gas ions [110]. Since the cluster ions are slower than the initial ions, the signals induced by ion motion are altered. The effect can be present in constant-field detectors and TPCs (see Sec. 35.6.5), and might affect devices such as Micromegas (see Sec. 35.6.4) and drift tubes. A negative-ion TPC can be used to expand the reach of directional dark matters searches [111].

Table 35.6: Mobility of ions in gases and mixtures at NTP [109].

Gas	Mobility μ ($cm^2\ V^{-1}\ s^{-1}$)
He	10.4
Ne	4.7
Ar	1.54
Ar/CH_4	1.87
Ar/CO_2	1.72
CH_4	2.26
CO_2	1.09

Downloaded from https://academic.oup.com/ptep/article/2022/8/083C01/6651666 by KIT Library user on 27 September 2022

35.6.2 *Multi-Wire Proportional and Drift Chambers*

Revised November 2021 by F. Sauli (CERN) and M. Titov (IRFU, CEA, Université Paris-Saclay).

Single-wire counters that detect the ionization produced in a gas by a charged particle, followed by charge multiplication and collection around a thin (typically 20 – 50 μm diameter) wire, have been used for decades. Good energy resolution is obtained in the proportional amplification mode, while very large saturated pulses can be detected in the streamer and Geiger modes [112].

Modern fully electronic devices, multiwire proportional chambers (MWPCs) [113,114] introduced in the late 1960's, detect, localize and measure energy deposit by charged particles over large areas. A mesh of parallel anode wires at a suitable potential, inserted between two cathodes, acts almost as a set of independent proportional counters (see Fig. 35.8a). Electrons released in the gas volume drift towards the anodes and produce avalanches in the increasing field. Analytic expressions for the electric field can be found in many textbooks. The fields close to the wires $E(r)$, in the drift region E_D, and the capacitance C per unit length of anode wire are approximately given by

$$E(r) = \frac{CV_0}{2\pi\epsilon_0}\,\frac{1}{r} \qquad E_D = \frac{CV_0}{2\epsilon_0 s} \qquad C = \frac{2\pi\epsilon_0}{\pi(\ell/s) - \ln(2\pi a/s)}\ , \tag{35.15}$$

where r is the distance from the center of the anode, s the wire spacing, ℓ and V_0 the distance and potential difference between anode and cathode, and a the anode wire radius.

Because of electrostatic forces, anode wires are in equilibrium only for a perfect geometry. Small deviations result in forces displacing the wires alternatively below and above the symmetry plane, sometimes with catastrophic results [115]. These displacement forces are countered by the mechanical tension of the wire, up to a maximum unsupported stable length, L_M [116], above which the wire displaces:

$$L_M = \frac{s}{CV_0}\sqrt{4\pi\epsilon_0 T_M} \tag{35.16}$$

The maximum tension T_M depends on the wire diameter and modulus of elasticity. Table 35.7 gives approximate values for tungsten and the corresponding maximum stable wire length under reasonable assumptions for the operating voltage ($V_0 = 5\,\mathrm{kV}$) [117]. Internal supports and spacers can be used in the construction of longer detectors to overcome limits on the wire length imposed by Eq. (35.16).

Table 35.7: Maximum tension T_M and stable unsupported length L_M for tungsten wires with spacing s, operated at $V_0 = 5$ kV. No safety factor is included.

Wire diameter (μm)	T_M (newton)	s (mm)	L_M (cm)
10	0.16	1	25
20	0.65	2	85

Traditionally, several simplifying assumptions are made in such analytical calculations: electrostatic force acting on the wire does not change during wire movements, or varies linearly with the displacement, the wire shape is parabolic; only one wire moves at a time. Therefore, for complicated electrode geometries the approximations listed above are not applicable. The advantage of numerical integrations using Garfield^{++} program is to simulate the collective movement of all wires, which are difficult analytically, and to consider all forces acting on a wire: forces between anode wire and other electrodes (wires, cathode) and a gravitational force [118].

Detection of charge on the wires over a predefined threshold provides the transverse coordinate to the wire with an accuracy comparable to that of the wire spacing. The coordinate along each wire can be obtained by measuring the ratio of collected charge at the two ends of resistive wires. The cathode planes can be fabricated in the form of group of wires or isolated strips, which are often patterned in orthogonal directions. Making use of

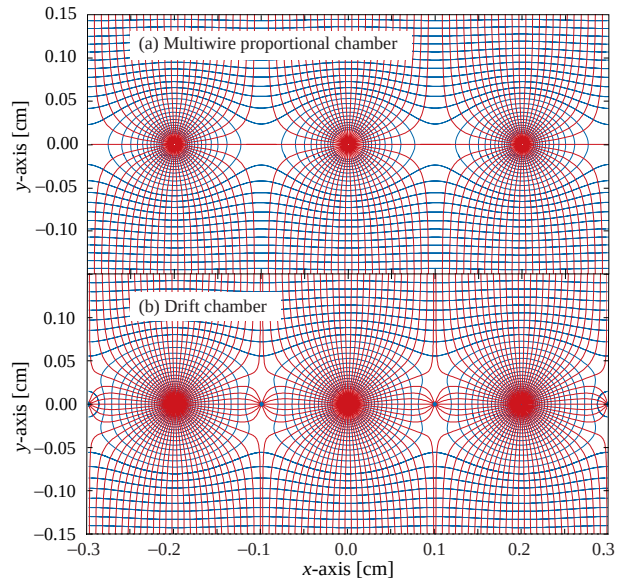

Figure 35.8: Electric field lines and equipotentials in (a) a multiwire proportional chamber and (b) a drift chamber.

the charge profile induced by avalanches on segmented cathodes, the so-called electronic center-of-gravity (COG) method allows localization of tracks to sub-mm accuracy. Due to the statistics of energy loss and asymmetric ionization clusters, the position accuracy is $\sim$ 50 μm rms for fast particles perpendicular to the wire plane, but degrades to $\sim$ 250 μm at 30° to the normal [119].

Drift chambers, developed in the early '70's, can be used to estimate the space coordinate perpendicular to the wires by exploiting the arrival time of electrons at the anodes if the time of interaction is known [120]. The distance between anode wires (e.g. Au-plated W) is usually several cm, allowing coverage of large areas at reduced cost. In the original design, a thicker wire (the field wire, often from Cu-Be or Al) at the proper voltage, placed between the anode wires, removes the low-field region at the midpoint between anodes and improves charge collection (Fig. 35.8b). In some drift chamber designs, and with the help of suitable voltages applied to field-shaping electrodes, the electric field structure is adjusted to improve the linearity of space-to-drift-time relation, resulting in better spatial resolution [121].

Drift chambers can reach a longitudinal spatial resolution from timing measurement of order 100 μm (rms) or better for minimum ionizing particles, depending on the geometry and operating conditions. However, a degradation of resolution is observed [122] due to primary ionization statistics for tracks close to the anode wires, caused by the spread in arrival time of the nearest ionization clusters. The effect can be reduced by operating the detector at higher pressures. Sampling the drift time on rows of anodes led to the concept of multiple arrays such as the multi-drift module [123] and the JET chamber [124]. A measurement of drift time, together with the recording of charge sharing from the two ends of the anode wires provides the coordinates of segments of tracks. An ultimate drift chamber design is the Time Projection Chamber (TPC) concept [125], which provides 3D precision tracking with low material budget and enables particle identification through differential energy loss dE/dx measurement or cluster counting $\mathrm{dN}_{cl}/\mathrm{dx}$ techniques. In all cases, a good knowledge of electron drift velocity and diffusion properties is required. This has to be combined with the knowledge of the electric fields in the structures [101]. Accumulation of ions in the gas volume may induce gain reduction and field distortions, especially for long drift distances in TPC (see Sec. 35.6.5). An important major innovation is related to the replacement of MWPC with Micro-Pattern Gaseous Detectors (MPGD) (see Sec. 35.6.4) for the TPC endplate readout, which offers many advantages: reduced track-angle, and negligible E × B track distortion effects, narrower pad

Downloaded from https://academic.oup.com/ptep/article/2022/8/083C01/6651666 by KIT Library user on 27 September 2022

response function (PRF), and intrinsic suppression of Ion Back Flow (IBF). For an overview of detectors exploiting the drift time for coordinate measurement see Refs. [116, 126].

Multiwire and drift chambers have been operated with a variety of gas fillings and operating modes, depending on experimental requirements. The so-called "Magic Gas," a mixture of argon, isobutane and Freon [114], permits very high and saturated gains ($\sim 10^6$). This gas mixture was used in early wire chambers, but was found to be susceptible to severe aging processes. DAFNE's KLOE Drift Chamber and the recent version of it developed for the MEG2 experiment [127] are the precursors of the next generation of ultralight central trackers for future colliders. Since the main contribution in terms of radiation length is related to tungsten wires, high transparency can be achieved thanks to the development of new wire materials (e.g. carbon monofilaments) and novel approaches for the wiring and assembly procedures. Drift chambers have been operated with a light helium/hydrocarbon mixtures, which are not reliable for long-term, high-rate operation [128]. Dedicated R&D is necessary to find an alternative hydrocarbon-free mixture adapted to the desired performance at future colliders.

Although very powerful in terms of performance, multi-wire structures have reliability problems when used in harsh or hard-to-access environments, since a single broken wire can disable the entire detector. Introduced in the 1980s, straw and drift tube systems make use of large arrays of proportional counters encased in individual enclosures, each acting as an independent wire counter [129]. Techniques for low-cost mass production of these detectors have been developed for large experiments, such as the Transition Radiation Tracker and the Drift Tubes arrays for CERN's LHC experiments [130]. The state-of-the-art NA62 straw tracker utilizes new construction techniques of ultrasonic welding to close the straw and to keep them straight and withstand the vacuum pressure without breaking [131]. Future efforts for straw detectors, e.g. COMET Phase-II at JPARC or Mu2e-II at Fermilab, will focus on ultra-thin wall development, long and thin wire handling, precise mechanics and innovative designs.

35.6.3 *High Rate Effects*

Revised November 2021 by F. Sauli (CERN) and M. Titov (IRFU, CEA, Université Paris-Saclay).

The production of positive ions in the avalanches and their slow drift before neutralization result in a rate-dependent accumulation of positive charge in the detector. This may result in significant field distortion, gain reduction and degradation of spatial resolution. As shown in Fig. 35.9 [132], the proportional gain drops above a charge production rate around 10^9 electrons per second and mm of wire, independently of the avalanche size. For a proportional gain of 10^4 and 100 electrons per track, this corresponds to a particle flux of $10^3\,\mathrm{s}^{-1}\mathrm{mm}^{-1}$ (1 kHz/mm^2 for 1 mm wire spacing). For the description of rate effects in MPGD, see Sec. 35.6.4.

Although almost any gas can be used to operate wire chambers, CF_4-based mixtures have been preferred due to their properties. Their main advantage for the use in large volume detectors are high drift velocity, low diffusion, non-flammability and low sensitivity to neutrons; also they do not form polymers in avalanches.

However, the problem of greenhouse gases, such as CF_4, could become a fundamental limitation for their future applications in gaseous detectors; due to the EU regulations their prices might go up and future availability is unknown. Performance studies of several eco-friendly mixtures have been initiated, together with a better understanding of their long-term ageing effects [133] (see also Sec. 35.6.4).

Ageing phenomena (formation of polymer deposits on the electrodes) constitute one of the most complex and serious potential problems which could limit or severely impair the use of gaseous detectors in unprecedented harsh radiation environments and lead to operational instabilities [134] [128]. The process has been extensively investigated, often with conflicting results. Several causes have been identified, including organic pollutants and silicone oils. Addition of small amounts of water in many (but not all) cases has been shown to extend the lifetime of the detectors.

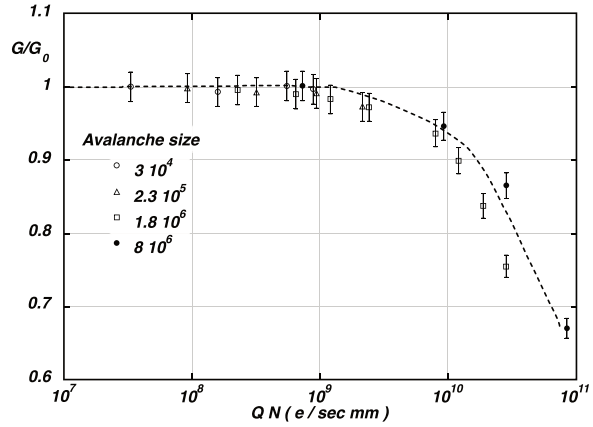

Figure 35.9: Charge rate dependence of normalized gas gain G/G_0 (relative to zero counting rate) in proportional thin-wire detectors [132]. Q is the total charge in single avalanche; N is the particle rate per wire length.

Addition of fluorinated gases (*e.g.*, CF_4) or oxygen may result in an etching action that can overcome polymer formation, or even eliminate already existing deposits. However, the issue of long-term survival of gas detectors with these gases is controversial. Under optimum operating conditions, a total collected charge of a few coulombs per cm of wire can usually be reached before noticeable degradation occurs. This corresponds, for one mm spacing and at a gain of 10^4, to a total particle flux of $\sim 10^{14}$ MIPs/cm^2.

35.6.4 *Micro-Pattern Gas Detectors*

Revised November 2021 by F. Sauli (CERN) and M. Titov (IRFU, CEA, Université Paris-Saclay).

Despite various improvements, position-sensitive detectors based on wire structures are limited by basic diffusion processes and space charge effects to localization accuracies of 50–100 μm [135]. Industrial advances in microelectronics and photolithographic technology on flexible and standard PCB substrates has favored the invention, in the last years of the 20th century, of novel Micro-Pattern Gaseous Detectors (MPGD) [136–138]. Since the very beginning, the goal was the development of novel devices with high rate capability (up to 10^6 Hz/mm^2) and excellent spatial resolution (down to 30 μm), single photo-electron time resolution in the ns-range, large sensitive area and dynamic range, superior radiation hardness and low-cost for large area coverage. Nowadays, a broad family of MPGD technologies are being developed and optimized for numerous applications, such as [139, 140]: Micro-Strip Gas Chamber (MSGC), Gas Electron Multiplier (GEM), Micro-Mesh Gaseous Structure (Micromegas), THick GEMs (THGEM), also referred to in the literature as Large Electron Multipliers (LEM), Resistive Plate WELL (RPWELL), GEM-derived architecture (μ-RWELL), Micro-Pixel Gas Chamber (μ-PIC), and an integrated readout of gaseous detectors (Gridpix) using solid-state pixel chips (e.g. Medipix or Timepix).

The MSGC concept, invented in 1988, was the first of the microstructure gas chambers [136]. It consists of a set of tiny parallel metal strips laid on a thin resistive support, alternatively connected as anodes and cathodes and resembles a multi-anode proportional counter. Through an accurate and simple photolithography process, the anode strips can be made very narrow ($\sim 10\ \mu m$) with a typical pitch (distance between strips) of $\sim 100\ \mu m$. When appropriate potentials are applied to the electrodes, electrons released in the drift volume move toward the strips and multiply in the high-field region. Owing to the small anode-to-cathode distance, the fast removal of positive ions by nearby cathode strips reduces space charge build-up, and improves siginicantly the rate capability, compared to wire counter. Despite their promising performance, experience with MSGCs has raised serious concerns about their long-term behavior. There are several major processes, particularly at high rates, leading to the MSGC operational instabilities: substrate charging-up and time-dependent distor-

Downloaded from https://academic.oup.com/ptep/article/2022/8/083C01/6651666 by KIT Library user on 27 September 2022

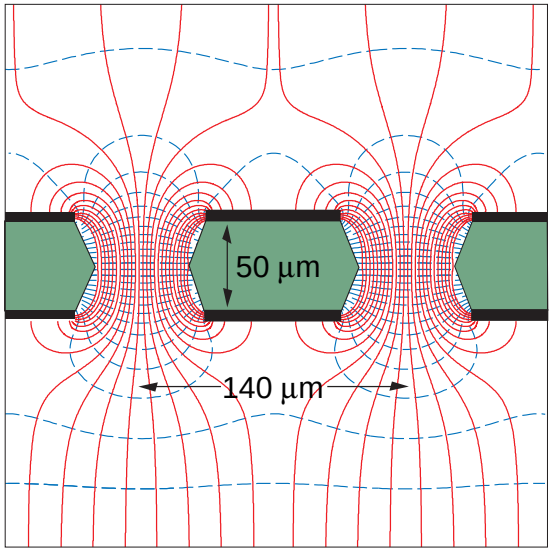

Figure 35.10: Schematic view and typical dimensions of the hole structure in the GEM amplification cell. Electric field lines (solid) and equipotentials (dashed) are shown. Electron trajectories do not strictly follow the field lines as drifting electrons scatter isotropically with gas molecules and diffuse transversally.

tions of the electric field, surface deposition of polymers ("aging") during sustained irradiation, and destructive micro-discharges under exposure to heavily ionizing particles [141]. The physical parameters used to manufacture and operate these detectors (substrate material, metal of strips, type and purity of the gas mixture) appeared to play dominant roles in determining the medium- and long-term stability. The problems encountered inspired the development of novel structures, using modern photolithographic processes: GEM, Micromegas and others, having increased reliability and radiation hardness.

A GEM detector consists of a thin-foil copper-insulator-copper sandwich chemically perforated to obtain a high density of holes in which avalanches occur [137, 142]. The hole diameter is typically between 25 μm and 150 μm, while the corresponding distance between holes varies between 50 μm and 200 μm. The central insulator is usually (in the original design) a polyimid foil, with a thickness of 50 μm. Application of a potential difference between the two metal sides of the GEM generates the electric fields indicated in Fig. 35.10. Each hole acts as an independent proportional counter. Electrons released by the primary ionization particle in the upper conversion region (above the GEM foil) drift into the holes, where charge multiplication occurs in the high electric field (50–70 kV/cm), and are transferred into the gap below the GEM. Systematic measurements with cascaded multi-GEM structures confirm that the gains and charge transfer processes are predictable from electrostatic considerations and avalanche development models; an overall gas gain well above 10^4 can be reached in the presence of highly ionizing particles, while strongly reducing the risk of discharges [143]. Other important parameters such as attachment, diffusion depend on the gas mixture composition and E/P. The majority of the charges created in the avalanche process follow the field lines and are collected by the metallic electrodes; owing however to diffusion, some may deposit on the dielectric surfaces, modifying the field and affecting gain and transparency of the structures [144]. This effect is known as "charging-up" effect; its time constant and amplitude depend largely on the shape of the holes.

The micro-mesh gaseous structure (Micromegas) is a thin parallel-plate avalanche counter, as shown in Fig. 35.11 [138]. It consists of a drift region and a narrow multiplication gap (25–150 μm) between a thin metal grid (micromesh) and the readout electrode (strips or pads of conductor printed on an insulator board). Electrons from the primary ionization drift through the mesh into the narrow multiplication gap, where they are amplified. The electric field is mostly homogeneous in both the drift (electric field $\sim$1 kV/cm) and amplification (50–70 kV/cm) regions and exhibits a funnel-like shape close to the openings of the micromesh: field lines are compressed into a small diameter of the order of a few microns, depending on the electric field ratio between the two gaps. In the narrow multiplication region, small variations of the amplification gap are approximately compensated by an inverse variation of the Townsend coefficient from the electric field, resulting in a more uniform gain. The transverse size of the electron avalanche due to diffusion is of the order of 10–15 μm, depending on the gas mixture, the electric field, and the gap width, giving rise to excellent spatial resolution (12 μm for MIPs) [145]. Most positive ions are quickly removed by the micromesh; this prevents space-charge accumulation and induces very fast signals ($\sim$ 100 ns length) due to electrons with a (fast) tail due to ions. Efforts have been also focused on producing Micromegas detector using innovative manufacturing techniques - the "Bulk" and "'MicroBulk" technologies [146].

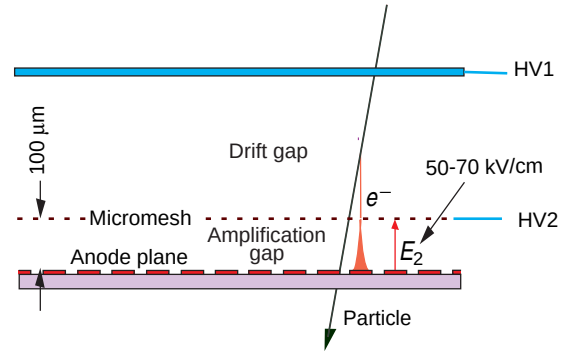

Figure 35.11: Schematic drawing of the Micromegas detector.

The absence of space-charge effects in GEMs at the highest rates reached so far, thanks to its fine-pitch structure of a few hundred microns, improves the maximum rate capability by more than two orders of magnitude compared to MWPC (see Fig.35.12) [147] [148]. Even larger rate capability has been reported for Micromegas [149].

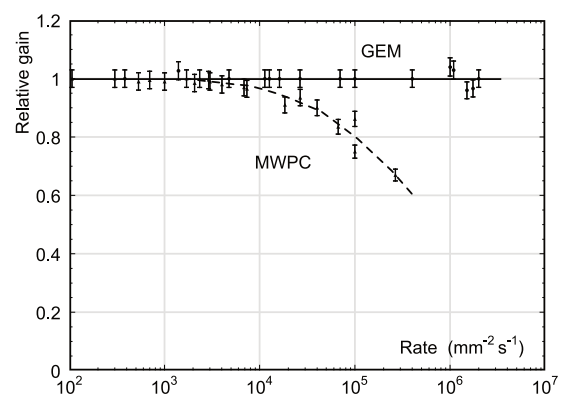

Figure 35.12: Normalized gas gain as a function of particle rate for MWPC [147] and GEM [148].

The fine granularity and high-rate capability of GEM and Micromegas can be fully exploited by using high-density pixel readout with a size corresponding to the intrinsic width of the detected avalanche charge. An elegant solution is the use of a CMOS pixel ASIC, assembled directly below the GEM or Micromegas amplification structure. Modern wafer post-processing technology allows an integration of a small-scale micromesh grid directly on top of a Timepix chip, thus forming an integrated MPGD readout, called GridPix concept (see Fig.35.13) [150]. With this arrangement, avalanche electrons are collected on the metalized input pads, exposed to the gas and signals are induced at the input gate of a charge-sensitive preamplifier. Every pixel is then directly con-

Downloaded from https://academic.oup.com/ptep/article/2022/8/083C01/6651666 by KIT Library user on 27 September 2022

nected to the amplification and digitization circuits, integrated in the underlying CMOS layers. A thin insulating layer, e.g. a few μm of silicon nitride, is usually deposited on top of CMOS ASIC to protect against destructive discharges across the $\mathcal{O}(50\ \mu m)$ amplification gap. The GridPix concept provides the high granularity needed to resolve individual electron clusters (separated by an average distance of a few hundred microns) and to determine energy loss by the cluster counting technique, rather than by the charge measurement, with a precision of better than 3 %. Despite the enormous challenges, real breakthrough was the development of the TPC readout endplate with a 160 GridPix ASICs, each 2 cm^2, corresponding to 10.5 million pixels, demonstrating for the first time the feasibility of large-area MPGD with CMOS pixel readout [151]. New structures, where a GEM foil is facing the Medipix chip, forming the GEMpix detector, are in use for medical applications [152] as well as for monitoring the radioactive waste [153].

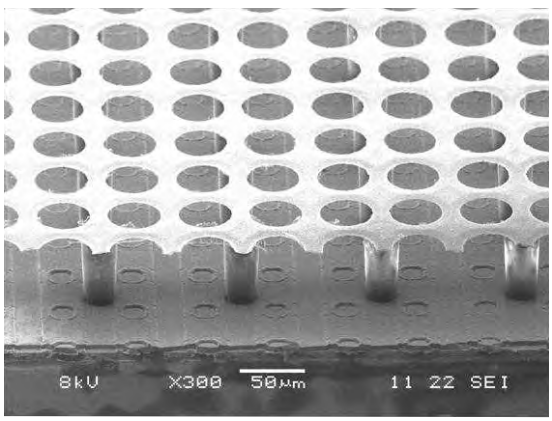

Figure 35.13: Photo of the Micromegas ('GridPix") detector. The grid holes can be accurately aligned with readout pixels of Timepix CMOS chip. The insulating pillars are centered between the grid holes, thus avoiding dead regions.

Gaseous detectors represent the most cost-effective solution to cover very large areas with photosensitive elements. MPGD-based gaseous photomultipliers, conceived with the aim to overcome the limitations of MWPCs, with semi-transparent or reflective photocathodes (PC), allow to minimize PC aging due to the ion and photon feedback and to avoid secondary effects causing electrical instability. For RICH applications requiring large-area coverage and moderate spatial resolution, coarser macro-patterned structures (e.g. THGEM with typical thickness of 0.4–1 mm and hole spacing of 0.7–1.2 mm) offer an interesting cheaper solution [154]. These are derived from the GEM design, scaling up $\sim$ 10-fold geometrical parameters, and can be mass-produced with standard PCB technology and mechanical drilling of large number of holes: some millions per square meter. Systematic studies to find the optimal electrostatic configuration revealed that the presence of a rim, a circular region around the holes where metal is etched away, plays a major role in THGEM performance. A small or zero rim allows to achieve better gain stability in time and under irradiation, while large rims permit to attain larger maximum gain and to reduce discharges, at the cost of significant charging up of the insulating surface, which modify the electric field. Therefore, in spite of the enhanced gain performance, the use of large rim THGEMs must be avoided to guarantee stable detector performance [155]. MPGDs are now in operation for single photon detection in the COMPASS RICH where a hybrid architecture formed by two THGEM layers (one covered by CsI-PC) and a Micromegas, acting as a third amplification stage, has been adopted.

Lately, closed geometry THGEM-based structures (RPWELL) [156], in common with some MPGDs invented at the end of the last century – C.A.T. and WELL, with resistive anodes have been developed, combining THGEM and RPC properties. This concept consists of a single-faced THGEM, copper-clad on its top side only, mounted directly on top of a resistive film deposited on a thin insulating sheet. Compared to THGEM with an induction gap, higher gains could be achieved in RPWELL for lower applied voltage across the THGEM electrode, due to the larger electric field within the closed holes. Another promising GEM-derived architecture is that of the μ-RWELL [157], with its $\sim$ seven-fold smaller pitch with respect to the RPWELL. Two different layouts for resistive stage have been studied: the simplest one is based on a single-resistive Diamong-Like Carbon (DLC) layer, and grounding by edges (2D charge evacuation for low-rates $\mathcal{O}(\mathrm{kHz/cm^2})$) and a more sophisticated scheme using double-resistive layer with a through-vias between them and the grounding done by means of the readout electrodes (3D charge evacuation for high-rate $\mathcal{O}(\mathrm{MHz/cm^2})$ applications) [158]. The μ-PIC structure is an industrially produced PCB including anode strips on one side and orthogonal cathode strips on the other one. A regular pattern of uncoated regions is present along the cathode strips; an electric conductor buried in the thin PCB substrate transfers the anode voltage to a "dot" at the center of each of the uncoated cathode zones. Electron avalanches occur under the high-electric field around the point-like anodes; the electric field near cathode edges is weaker than in MSGCs, resulting in a lower discharge probability. A resistive coating of the cathode strips (e.g. using DLC layers) ensures tolerance to occasional discharges [159].

A big step in the direction of large-size applications has been obtained both with conceptual consolidation and industrial and cost-effective manufacturing of MPGDs by developing new fabrication techniques: resistive Micromegas (to suppress destructive sparks in hadron environments) [160] and single-mask and self-stretching GEM techniques (to enable production of large-size foils and significantly reduce detector assembly time) [161]. Scaling up of MPGDs to very large single unit detectors of $\mathcal{O}(\mathrm{m^2})$, has facilitated their use in the High Luminosity LHC upgrades: Micromegas will instrument an area of $\mathcal{O}(1000\,\mathrm{m^2})$ in the New Small Wheel of the ATLAS Muon endcaps, while GEMs be used in the CMS Muon system and for the ALICE TPC readout. Exploiting the Micromegas, GEM, and μ-RWELL ability to measure both position and arrival time of the charge released in the drift gap, a novel μ-TPC concept has been developed; it permits achieving nearly constant spatial resolution over a wide range of particle incident angles and allows 3D track reconstruction with a single MPGD layer [162]. Although normally used as planar detectors, GEM, Micromegas, and μ-RWELL can be bent to form cylindrically curved ultra-light inner tracking systems, without support and cooling structures [163].

The consolidation of the better-established technologies has been accompanied with flourishing of novel ones, often specific to well-defined applications. Modern technologies have been also derived from Micromegas and GEM concepts, hybrid approaches combining different elements in a single device, gaseous with non-gaseous detectors, as is the case for optical read-out. MPGD hybridization, a strategy aiming to strengthen the detector performance, remains a valid asset for addressing future experimental challenges such as high granularity and picosecond-precision timing (e.g. PICOSEC-Micromegas concept [164]). A clear direction for future developments is that of resistive materials and related detector architectures. Their usage improves detector stability, making possible a higher gain in a single multiplication layer. Recent DLC resistive layers studies are the key ingredients for increasing the rate capability of MPGDs [165]. Future developments call for novel materials as well as for new fabrication techniques. Contributions to the detector concepts are required in several domains: resistive materials, solid-state photon and neutron converters, innovative nanotechnology components. Material studies can contribute to requirements related to low out-gassing, radiation hardness, radio-purity, converter robustness, and eco-friendly gases. The development of the next generation of MPGDs can largely profit from emerging technologies as those related to MicroElectroMechanical Systems (MEMS), sputtering, novel photoconverters, 3D printing of amplifying structures and cooling circuits, etc. Nowadays, many intensive MPGD R&D activities and their diversified applications are pursued within the world-wide CERN-RD51 collaboration [166].

Downloaded from https://academic.oup.com/ptep/article/2022/8/083C01/6651666 by KIT Library user on 27 September 2022

35.6.5 *Time-projection chambers*

Revised July 2021 by C. Lippmann (GSI Darmstadt).

The Time Projection Chamber (TPC) concept was invented by David Nygren in the 1970's [167]. It consists of a cylindrical or square field cage that is filled with a gaseous (or liquid) detection medium. Charged particles produce tracks of ionization electrons that drift in a uniform electric field towards a position-sensitive amplification stage which provides a 2D projection of the particle trajectories. The third coordinate can be calculated from the arrival times of the drifted electrons. The start for this drift time measurement is usually derived from an external detector, e.g. a fast interaction trigger detector.

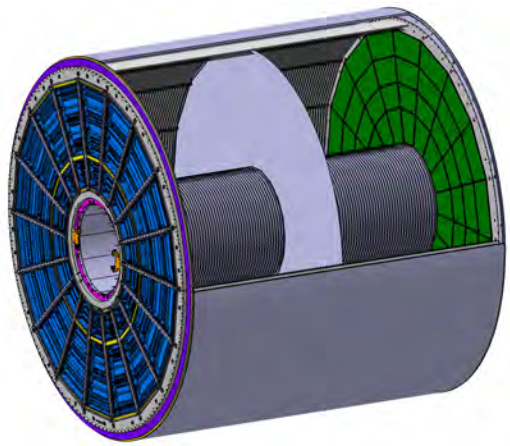

Figure 35.14: Schematic view of the ALICE TPC [168, 169]. The drift volume with 5 m diameter is divided into two halves, each providing 2.5 m drift length. The amplification stage has recently been upgraded from wire planes to GEMs.

This section focuses on the gas-filled TPCs that are often used in particle or nuclear physics experiments at accelerators on account of their low material budget. For neutrino physics (Sec. 35.11) or for detecting rare events (Sec. 36.4), on the contrary, usually high density and large active mass are required, and a liquid detection medium is favored.

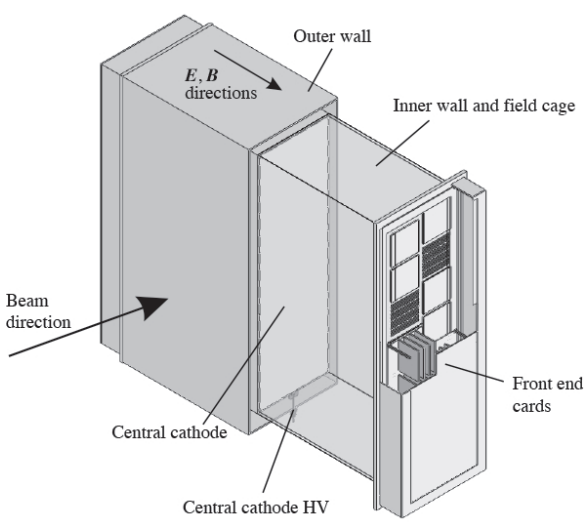

Figure 35.15: One of the 3 TPC modules for the near detector of the T2K experiment [170]. The size is $2 \times 2 \times 0.8\,\mathrm{m}^3$. Micromegas devices are used for gas amplification and readout.

The TPC enables full 3D measurements of charged particle tracks, which gives it a distinct advantage over other tracking detector designs which record information only in two-dimensional detector planes and have less overall segmentation. The track points recorded in a TPC are basically adjacent, which facilitates the track finding enormously. This advantage is often exploited for pattern recognition in events with large numbers of particles, e.g. heavy-ion collisions. Two examples of modern large-volume gaseous TPCs are shown in (Figure 35.14) and (Figure 35.15).

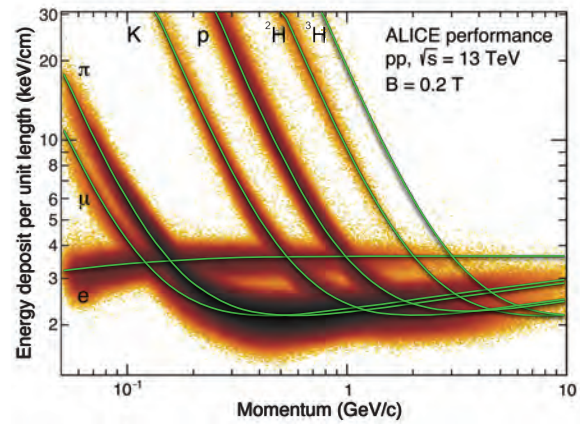

Figure 35.16: Energy deposit versus momentum measured in the ALICE TPC.

Identification of the charged particles crossing the TPC is possible by simultaneously measuring their momentum and specific energy deposit through ionisation ($\mathrm{d}E/\mathrm{d}x$). The momentum, as well as the charge sign, are calculated from a helix fit to the particle trajectory in the presence of a magnetic field (typically parallel to the drift field). For this application, precise spatial measurements in the plane transverse to the magnetic field are most important. The specific energy deposit is estimated from many charge measurements along the particle trajectory (e.g. one measurement per anode wire or per row of readout pads). As the charge collected per readout segment depends on the track angle and on the ambient conditions, the measured values are corrected for the effective length of the track segments and for variations of the gas temperature and pressure. The most probable value of the corrected signal amplitudes for a given track provides the best estimator for the specific energy deposit (see Sec. 34.2.3); it is usually approximated by the truncated mean, i.e. the average of the 50%–70% smallest values. The resulting particle identification performance is illustrated in (Figure 35.16), for the ALICE TPC.

The dependence of the achievable energy resolution on the number of measurements N, on the thickness of the sampling layers t, and on the gas pressure P can be estimated using an empirical formula [171]:

$$\sigma_{dE/dx} = 0.41\ N^{-0.43}(t\,P)^{-0.32}. \tag{35.17}$$

Typical values at nominal pressure are $\sigma_{dE/dx} = 4.5$ to 7.5%, with $t = 0.4$ to 1.5 cm and $N = 40$ up to more than 300. The record, with an unprecedented energy resolution of 3%, is held by the PEP-4/9 TPC [172], due to the high gas pressure of 8.5 bar.

The greatest challenges for a large TPC are due to the length of the drift of up to a few meters. In particular, it can make the device sensitive to small distortions in the electric field. Such distortions can arise from a number of sources, e.g. imperfections in the field cage construction or the presence of ions in the drift volume. The electron drift in a TPC in the presence of a magnetic field is defined by Eq. (35.14). The $E \times B$ term of Eq. (35.14) vanishes for perfectly aligned electric and magnetic fields, which can be difficult to achieve in practice. Furthermore, the electron drift depends on the $\omega\tau$ factor, which is defined by the gas mixture and the magnetic field strength. The electrons will tend to follow the magnetic field lines for $\omega\tau > 1$, or the electric field lines for $\omega\tau < 1$. The former mode of operation makes the TPC less

Downloaded from https://academic.oup.com/ptep/article/2022/8/083C01/6651666 by KIT Library user on 27 September 2022

sensitive to non-uniformities of the electric field, which is usually desirable.

The drift of the ionization electrons is superposed with a random diffusion motion which degrades their position information. The ultimate resolution of a single position measurement is limited to around

$$\sigma_x = \frac{\sigma_D \sqrt{L}}{\sqrt{n}}\,, \tag{35.18}$$

where σ_D is the transverse diffusion coefficient for 1 cm drift, L is the drift length in cm and n is the effective number of electrons collected. Without a magnetic field, $\sigma_{D,B=0}\sqrt{L}$ is typically a few mm after a drift of $L = 100\,\mathrm{cm}$. However, in a strong magnetic field parallel to the drift field, a large value of $\omega\tau$ can significantly reduce diffusion:

$$\frac{\sigma_{D,B>0}}{\sigma_{D,B=0}} = \frac{1}{\sqrt{1+\omega^2\tau^2}}\,. \tag{35.19}$$

This factor can reach values of up to 10. In practice, the final resolution limit due to diffusion typically lies around $\sigma_x = 100\,\mu\mathrm{m}$.

The drift and diffusion of electrons depend strongly on the gas mixture. The optimal gas mixture varies according to the environment in which the TPC will operate. In all cases, the oxygen concentration must be kept very low (few ten parts per million in a large TPC) in order to avoid electron loss through attachment.

Ideally, the drift velocity should depend only weakly on the electric field at the nominal operating condition. The classic Ar/CH_4 (90:10) mixture, known as P10, has a drift velocity maximum of $5\,\mathrm{cm}/\mu\mathrm{s}$ at an electric field of only $125\,\mathrm{V/cm}$ (Figure 35.5). In this regime, the electron arrival time is not affected by small variations in the ambient conditions. Moreover, low electric fields simplify the design and operation of the field cage. The mixture has a large transverse diffusion at $B = 0$, but this can be reduced significantly in a strong magnetic field due to the relatively large value of $\omega\tau$.

For some applications organic gases like CH_4 are not desirable since they may cause aging. An alternative is to replace CH_4 with CO_2. An Ar/CO_2 (90:10) mixture has a low transverse diffusion at all magnetic field strengths, but does not provide a saturated drift velocity for the typical electric fields used in TPCs (up to a few $100\,\mathrm{V/cm}$). As a consequence, it is quite sensitive to the ambient conditions. Freon admixtures like CF_4 can be an attractive option for a TPC as well, since the resulting gas mixtures provide high drift velocities at low electric fields. However, the use of CF_4 always needs to be thoroughly validated for compatibility with all materials of the detector and the gas system.

Historically, the amplification stages used in gaseous TPCs have been planes of anode wires operated in proportional mode. The performance is limited by effects related to the feature size (wire spacing) of a few mm. Since near the wires the electric and magnetic fields are not parallel, the incoming ionisation electrons are displaced in the direction of the wires ("wire $E \times B$ effect"), which degrades the resolution. The smaller feature sizes of Micro-Pattern Gas Detectors (MPGDs) like GEMs and Micromegas lead to many advantages as compared to wire planes (see Sec. 35.6.4). In particular, $E \times B$ effects in the amplification stage are much smaller. Moreover, the signal induction process in MPGDs leads to a very narrow pad response, allowing for a much finer segmentation, which improves the separation for two very close tracks. Combinations of MPGDs with silicon sensors have resulted in the highest granularity readout systems so far (see Sec. 35.6.4). These devices make it possible to count the number of ionization clusters along the length of a track, which can, in principle, improve the particle identification capability. However, the big challenge for such a system is the huge number of readout channels for a TPC of a typical size.

The accumulation of the positive ions created by the ionization from the particle tracks can lead to time-dependent distortions of the drift field. Due to their low drift velocity, ions from many events may coexist in the drift volume. To reduce the effect of such a build-up of space charge, Argon can be replaced by Neon as the main component of the gas mixture. Neon features a lower number of ionisation electrons per unit of track length (see 35.5) and a higher ion mobility (see 35.6).

Of greater concern are the ions produced in the gas amplification stage. In order to prevent them from entering the drift volume, large TPCs built until now have a gating grid. The gating grid can be switched to transparent mode (usually in the presence of an interaction trigger) to allow the ionization electrons to pass into the amplification region. After all electrons have reached the amplification region, it is usually closed such that it is rendered opaque to electrons and ions. However, a gating grid implies a principal rate limitation to a few kHz. Different groups are therefore working towards the goal of continuous readout, for applications where a triggered operation would lead to inacceptable data loss (e.g. ALICE [169], sPHENIX [173]). The employed readout schemes are based on MPGDs, as these can be optimised in order to drastically reduce the ion back-flow at the same effective gain as MWPCs. Extensive work has been carried out during the 2010's to design such readout structures. In ALICE and sPHENIX ion back-flow values below 1 % are achieved with a thorough adjustment of the various fields in a quadruple GEM system. Similar levels of ion back-flow can be reached with Micromegas detectors [174]. For triggered operation, on the other hand, a combination of a MPGD and a gating structure may be an attractive solution.

35.6.6 *Transition radiation detectors (TRD's)*

Revised July 2021 by P. Nevski (BNL) and A. Romaniouk (Insbruck U.; MEPhI Moscow).

Transition radiation (TR) x-rays are produced when a highly relativistic particle ($\gamma \gtrsim 10^3$) crosses a refractive index interface, as discussed in Sec. 34.7. Since the TR yield is about a few % per boundary crossing, radiation from multiple surface crossings (e.g., a stack of foils) is used in practical detectors. The x-rays, ranging from a few keV to a few dozen keV or more, are emitted in a forward direction at small angles (within few mrad) to the particle trajectory. The TR intensity for a single boundary crossing always increases with γ, but, for multiple boundary crossings, interference leads to saturation above a Lorentz factor $\gamma_{\mathrm{sat}} = 0.6\,\omega_1\sqrt{\ell_1\ell_2}/c$ [175], where ω_1 is the radiator material plasma frequency, ℓ_1 is its thickness, and ℓ_2 the spacing between material elements. The probability density function of TR is a fairly complex function of γ, radiator parameters, photon energy (ω) and its emission angle (θ). For well defined radiator parameters a measured two-dimensional distribution of photon energy vs its reconstructed emission angle is in very good agreement with the theory predictions [176].

Integration over the angle yields the TR spectrum, which typically features many maxima (see Sec. 34.7). Most of the TR energy is emitted near the last maximum of the spectra determined by radiator material parameters at $\omega_{max} = \ell_1\omega_1^2/2\pi c$. The effective TR photon emission starts at about $\gamma_{thr} = \ell_1\omega_1/c$. By varying radiator parameters one may optimize the particle separation for a given range of the γ-factor. The angular distribution of TR photons has a few maxima and extends up to $\theta_{max} = (1/\gamma^2 + \omega_1^2/\omega^2)^{1/2}$ [177]. For a single foil the largest part of the TR energy is emitted around the most probable angle $\theta = (1/\gamma^2 + \omega_2^2/\omega^2)^{1/2}$, where ω_2 is the plasma frequency of the gas surrounding the radiator material elements. However, in case of multiple interfaces, interference effects may significantly change this angle and more realistic expression for the angle which corresponds to the last interference maximum of the energy spectra is $\theta \approx \sqrt{1.4\pi^2/\gamma_{\mathrm{sat}}^2 - 1/\gamma^2}$ [176]. The higher is the gamma-factor, the larger is the angle of the first interference maximum. It reaches almost its asymptotic limit at $\gamma = \gamma_{sat}$. This effect is illustrated in Fig. 35.17 [176] which shows two-dimensional distribution of the TR photon energy versus the reconstructed production angle obtained in 20 GeV electron beam with the radiator containing a stack of foils of 15.5 μm thickness spaced by 210 μm (the left plot) using a Si-pixel detector. TR produced by 20 GeV electrons is emitted mostly around $\theta \sim 0.9$ mrad. All features of this distribution are well reproduced with MC simulations (the right plot).

The simplified numerical expressions can be used for practical

Downloaded from https://academic.oup.com/ptep/article/2022/8/083C01/6651666 by KIT Library user on 27 September 2022

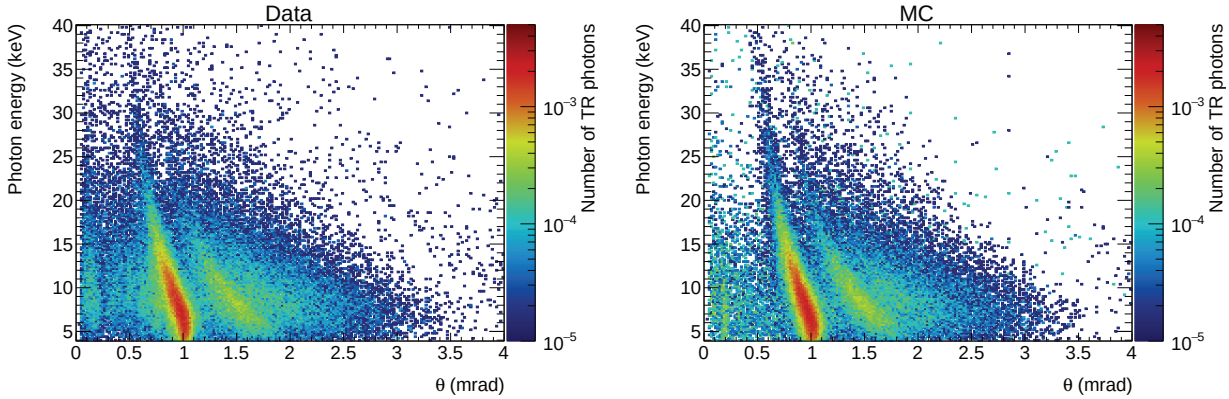

Figure 35.17: Two dimensional distributions of photon energy versus reconstructed production angle obtained with the polypropylene radiator with 20 GeV/c electron beam. Data - the left plot, MC - the right plot. Z-axis is a number of photons per particle [176]

estimation of the main TR production parameters [176]: $\theta \sim 1.2/\omega_1\sqrt{l_1 l_2}$, $\gamma_{thr} \sim 3\times10^3\ \omega_1\ell_1$, $\gamma_{\rm sat} \sim 3\times10^3\ \omega_1\sqrt{\ell_1\ell_2}$ and $\omega_{max} = 0.65\ \ell_1\omega_1^2$, where θ in mrad, ω_1 in eV, ω_{max} in keV and l_1 and l_2 in mm.

In the simplest concept, a detector module might consist of a low-Z TR radiator followed by a high-Z active layer made of proportional counters filled with a Xe-rich gas mixture. The atomic number considerations follow from the dominant photoelectric absorption cross section per atom going roughly as Z^n/ω^3, where n varies between 4 and 5 over the region of interest.[1] To minimize self-absorption, materials such as polypropylene, Mylar, carbon, and (rarely) lithium in the form of foils, fibers or foams are used as radiators. The TR signal in the active regions is in most cases superimposed upon the particle ionization losses, which are proportional to Z. In most of the detectors used in particle physics the radiator parameters are chosen to provide $\gamma_{\rm sat} \approx 3000$. Those detectors normally work as threshold devices, ensuring the best electron/pion separation in the momentum range 1 GeV/$c \lesssim p \lesssim 150$ GeV/c.

One can distinguish two design concepts—"thick" and "thin" detectors. In "thick" detectors the radiator, optimized for a fixed total radiation length at maximum TR yield and maximum TR absorption in the detector, consists of few hundred foils (for instance 300 20 μm thick polypropylene foils). Most of the TR photons are absorbed in the radiator itself. To maximise the number of TR photons reaching the detector, part of the radiator far from the active layers is often made of thicker foils, which shifts the x-ray spectrum to higher energies. The detector thickness, about 2-4 cm for Xe-filled gas chambers, is optimized to absorb most of the incoming x-ray spectrum. A classical detector is composed of several similar modules which respond nearly independently. Such detectors were used in the UA2, NA34 and other experiments [178], are being used in the ALICE experiment [179, 180] and are built for the CBM experiment [181]. In another TRD concept a fine granular radiator/detector structure exploits the soft part of the TR spectrum more efficiently. This can be achieved, for instance, by distributing small-diameter straw-tube detectors uniformly or in thin layers throughout the radiator material. This approach allows to realise a TRD as an integral part of a tracking detector providing many points of measurements on the particle track. Even with a relatively thin radiator stack, radiation below 4 keV is mostly lost in the radiators themselves. However, for photon energies above this value, the absorption is reduced and the radiation can be registered by several consecutive detector layers, thus creating a strong TR build-up effect. Descriptions of detectors using this approach in both accelerator and space experiments can be found in [179, 182–185]. For example, in the ATLAS TR tracker (TRT), charged particles on average cross about 35 straw tube layers embedded in the radiator material [182]. The effective thickness of the Xe gas per straw is about 2.5 mm and the average number of foils per straw is about 40 with an effective foil thickness of about 18 μm. In this approach straw walls also act as radiator and make some contribution to the TR spectrum.

Although the values mentioned above are typical for most of the plastic radiators used with Xe-based detectors, they vary significantly depending on the detector requirements. Careful simulations are usually needed to build a detector optimized for a particular application. For TRD simulations the codes are based on well understood TR emission formulas (see for instance [177] for regular radiators and [186] for irregular radiators). They are realised as the stand-alone simulation programs [176,187,188] or GEANT4 based ones [189] and give both a good agreement of the TR energy spectra and of the angular distributions with data [176, 190, 191].

The discrimination between electrons and pions can be based on the charge deposition measured in each detection module, on the number of clusters – energy depositions observed above an optimal threshold (usually it is 5–7 keV), or on more sophisticated methods such as analyzing the pulse shape as a function of time. The total energy measurement technique is more suitable for thick gas volumes, which absorb most of the TR radiation and where the ionization loss fluctuations are relatively small. The cluster-counting method works better for detectors with thin gas layers, where the fluctuations of the ionization losses are bigger. Cluster-counting replaces the Landau-Vavilov distribution of background ionization energy losses with the Poisson statistics of δ-electrons, responsible for the distribution tails. The latter distribution is narrower than the Landau-Vavilov distribution. In practice, most of the experiments use a likelihood method, which exploits detailed knowledge of the detector response for different particles and gives the best separation. The more parameters are considered, the better achievable separation power. The neural network method is the most powerful tool. When it used by the ALICE TRD (ALICE point in Fig. 35.18) it lead to an increase of the rejection power by another factor of 2–3 with respect to the likelihood method [179].

The major factor in the performance of any TRD is its overall length. This is illustrated in Fig. 35.18, which shows, for a variety of detectors, the pion efficiency at a fixed electron efficiency of 90% as a function of the overall detector length. As TRD performance depends on particle energy, the experimental data in this figure covering a range of particle energies from 1 GeV to 40 GeV, are rescaled to an energy of 10 GeV when possible. Phenomenologically, the rejection power against pions increases as $5\cdot10^{L/38}$, where the range of validity is $L \approx 20$–100 cm. Apart from the beam energy variations, the observed scattering of the points in the plot reflects how effectively the detector space is used and how well the exact response to different particles is taken into account in the analysis. For instance, the ATLAS TRT was built as a compromise between TR and tracking requirements; that is why the test-beam prototype result (lower point) is better than the real End-Cap TRT performance at the LHC shown in Fig. 35.18

[1] Photon absorption coefficients for the elements (via a NIST link), and $dE/dx|_{\rm min}$ and plasma energies for many materials are given in https://pdg.lbl.gov/current/AtomicNuclearProperties.

Downloaded from https://academic.oup.com/ptep/article/2022/8/083C01/6651666 by KIT Library user on 27 September 2022

for different regions in the detector (in agreement with MC).

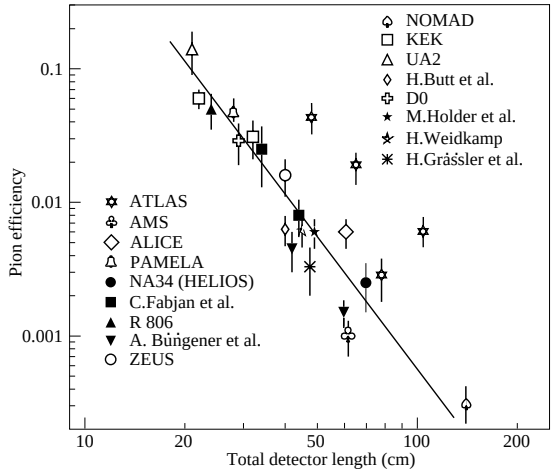

Figure 35.18: Pion efficiency measured (or predicted) for different TRDs as a function of the detector length for a fixed electron efficiency of 90%. The plot is based on the table given in [178]. Results from more recent detectors are added from [179, 183–185, 192].

In most cases, recent TRDs combine particle identification with charged-track measurement in the same detector [179, 181, 184]. This is particularly important for collider experiments, where the available space for the inner detector is very limited. For a modest increase of the radiation length due to the radiator (∼4% X0), a significant enhancement of the electron identification was obtained in the case of the ATLAS TRT. Here, the combination of the two detector functions provides a powerful tool for electron identification even at very high particle densities.

In addition to the enhancement of the electron identification during offline data analysis, TRD signatures are often used in the trigger algorithms at collider experiments. The ALICE experiment [180] is a good example for the use of the TRD in a First Level Trigger. In the ATLAS experiment, the TRT information is used in the High Level Trigger (HLT) algorithms. At increasing luminosities, the electron trigger output rate becomes so high, that a significant increase of the calorimeter energy threshold is required to keep it at an acceptable level. This may affect the trigger efficiency of very important physics channels (e.g. $W \to e\nu$ inclusive decay). Even a very soft TR cut at the HLT level, which preserves high electron efficiency (98%), allows to suppress a significant part of fake triggers and enhance the purity for physics events with electrons in a final state. The TRT also plays a crucial role in the studies where an electron suppression is required (e.g. hadronic mode of τ–decays). TR information is a completely independent tool for electron identification and allows to study systematic uncertainties of other electron reconstruction methods.

Electron identification is not the only TRD application. Some TRDs for particle astrophysics are designed to directly measure the Lorentz factor of high-energy nuclei by using the quadratic dependence of the TR yield on nuclear charge; see, for instance, in [193]. The radiator configuration (ℓ_1, ℓ_2) is tuned to extend the TR yield rise up to $\gamma \approx 10^5$ using the more energetic part of the TR spectrum (up to 100 keV). High density radiator materials (such as Al) are the best for this purpose. Direct absorption of the TR-photons of these energies with thin detectors becomes problematic and TR detection methods based on Compton scattering have been proposed, see in [194].

The high granularity of the semiconductor pixel or microstrip detectors provides spatial separation of the TR photons and dE/dx losses at relatively modest distances between radiator and detector. These detectors may be the basis for novel devices which combine precise tracking and PID properties [176, 188, 195]. Use of the TR production angle in addition to its energy can help to improve PID properties of the TRD. The presence of a magnetic field could enhance the separation between TR photons and dE/dx losses [196]. New detector techniques for TRDs are also under consideration. GasPixel detectors allow to reconstruct a track segment with a space point accuracy of $< 30\ \mu m$ and exploit all details of the particle tracks to highlight individual TR clusters in the gas, see in [197]. Thin films of heavy scintillators might be a very attractive option for non-gas based TRD [198].

35.6.7 *Resistive-plate chambers*

Revised August 2021 by G. Aielli (Rome U. Tor Vergata).

The resistive-plate chamber (RPC) is a gaseous detector working at atmospheric pressure developed by R. Santonico and R. Cardarelli in the early 1980's [199]. A precursor of the RPC is the Pestov spark chamber [200] [201] having a metallic plate cathode and a thick glass plate anode, designed to work at 12 bars to obtain an outstanding 0.1 ns time resolution. Although the original purpose of RPCs was to provide a competitive alternative to large scintillator counters, the RPC's potential for timing tracker systems was quickly recognized given its high detection efficiency (>95%), excellent temporal and spatial resolutions and ease of constructing large-format single frame detectors. The RPC, as sketched in Fig. 35.19, is a large planar capacitor with two parallel high bulk resistivity electrode plates (10^9–10^{13} Ω·cm) separated by a set of insulating spacers. The spacers define a gap in the range from a few millimeters down to 0.1 mm with a precision of a few μm. The gap is filled with a suitable atmospheric-pressure gas mixture which serves as a target for ionizing radiation. The gas gap thickness practically determines the time resolution of the RPC, on the other side the limit for reaching full detection efficiency at atmospheric pressure is typically 1 mm (also influenced by the gas molecular weight). Since the primary ionization for sub-millimeter gas gaps is limited, multiple gaps can be combined to effectively obtain a very high detection efficiency [202]. The electrodes are most commonly made of high pressure phenolic-melaminic laminate (HPL), commonly referred to as "bakelite",

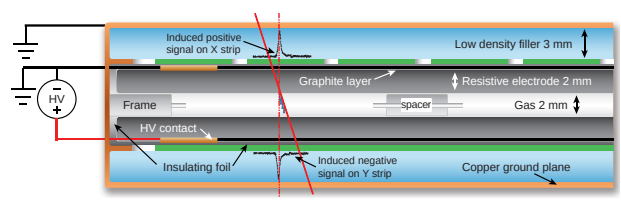

Figure 35.19: Schematic cross section of a generic single gap RPC.

or glass. An uniform electric field of several kV/mm, is established on the gas gap, sufficient to promptly multiply the primary ionization. This is realized through a moderately conductive coating ($\sim 10^5\ \Omega/\square$) placed on the external faces of the electrodes. The conductivity sufficiently low to be transparent to the fast avalanche signal transients, and high enough to suppress field gradients. Due to the high electrode resistivity in RPCs, the time constant of the equivalent RC circuit ($\tau = \rho\epsilon_r$ being ρ the electrode resistivity and ϵ_r its dielectric constant) is much longer than discharge processes. Therefore only the locally-stored electrostatic energy contributes to the discharge, preventing the formation of sparks and leaving the rest of the detector field unaffected. The gas-facing surface of HPL electrodes are commonly coated with a few μm-thick layer of polymerized linseed oil [203] with the function of smoothing the electrode surface, improving the electric field uniformity. It also has the function of protecting the electrode from the being eventually etched by free radicals generated in the discharge e.g. in presence of fluorocarbons. It is generally assumed that the linseed oil layer has a resistivity comparable to the electrode's one, due to the absence of the Malter effect. In the early stage of the avalanche multiplication, the uniform electric field of RPCs exponentially amplifies each primary ionization cluster in function of its distance from the location of the primary ionization. Therefore RPC signals spectrum would be broad and exponentially distributed (unlike gaseous detectors where ionization and amplification occur in separate regions) having the most probable amplitude close the zero. For increasingly

Downloaded from https://academic.oup.com/ptep/article/2022/8/083C01/6651666 by KIT Library user on 27 September 2022

larger avalanches, the space-charge progressively saturates the avalanche growth from exponential to linear, producing a peaked signal spectrum, essential to efficiently separate the signal from the noise [204]. For gains exceeding the Meek limit, the avalanche undergoes a transition to "streamer", connecting the electrodes with a plasma filament which exhausts all the locally-available energy [205], generating an almost fixed amplitude signal. This prevents any further evolution of the discharge. The streamer mode was the first ever used by RPCs, until the introduction of very electronegative gases and more sensitive front end electronics, permitted to detect the precursor avalanche independently on the streamer [206, 207] Any of this operating regimes can be used in RPC detectors, depending on the applications.

As with other gaseous detectors, the gas mixture is optimized for each specific application. In general it needs to contain a UV photons quencher to limit the occurrence of photon feedback from the avalanches to the cathode, suppressing the spurious counts, and one or more electronegative components, to extend the avalanche growth, free from streamers, to as high as possible electric fields [208]. The role of the electronegative molecule is to capture slow electrons preventing their recombination with emission of photons, known to be the mediators for the transition to streamer. As a reference, the mixture for stable avalanche operation in ATLAS and CMS is $C_2H_2F_4$/i-C_4H_10/SF_6=94.5%/5%/0.3%.

The avalanche induces a fast electron signal on a set of metallic readout electrodes (e.g. pads or strips) commonly placed externally and insulated from the resistive electrodes. The signal is isotropically distributed with respect to the field direction and present with equal but opposite amplitude on both electrodes. This feature allows to place readout electrodes on both RPC sides with equivalent performance. The induced charge density can be ideally calculated for a simplified RPC model [209] [210] as: $\sigma(x) = A/\cosh[(r)/\delta]$ where A is a normalization constant, r is the distance from the center of the avalanche axis and $\delta = (g + 2d)/\pi$ depends on the gap and electrode width (g and d, respectively). Depending on the specific RPC layout and geometry, the interplay between graphite and pick-up electrodes typically broadens, by means of a diffusion-like process, such distribution [210] [211]. This effect mostly preserves the impact position information, which can be obtained using the charge centroid method, with the drawback of increasing the signal space occupancy. Sensitivity to the high-frequency spectrum of electron avalanche signals over large RPC areas, requires a correspondingly adequate Faraday cage and readout design. At the same time, to preserve the excellent timing features of the RPC signal, the front end electronics should have a short rise time (ideally $\ll$ than the signal rise time)and low noise, although these requirements could be in competition [212].

35.6.7.1 *RPC types and applications*

RPCs are generally classified in two categories depending on the gas gap structure: single gap RPCs (described above) and multiple gap RPCs [202] (typically referred as mRPCs or timing RPCs). While they are both based on the same principle they have different construction techniques, performance and limitations, making them suitable for different applications. Due to its simplicity and robustness, the single gap RPC is ideal for covering very large surfaces. Typical detector systems can have sensitive surface areas up to $\sim 10^4$ m^2, with single module areas of a few m^2, and a space-time resolution down to $\sim$0.4 ns $\times$ 100 μm [213] [214].

Representative examples are the muon systems of ATLAS [215] and CMS [216] or ground and underground based cosmic rays [217] and neutrino arrays [218]. Interesting to note that CMS implements a bi-gap structure, i.e. the pickup signal is sandwiched by 2 single gas gaps, both contributing to the signal induction, improving efficiency and time resolution with respect to the single gas gap. Relevant new trends for single gap RPC applications are represented by new Dark Matter search experiments such as CODEX-B [219] and ANUBIS [220], in both cases exploiting RPCs to enclose and instrument large detection volumes with a good space-time tracker. Single gap RPCs have also recently demonstrated good candidates for application in tracking calorimetry [221].

The mRPC [222], as sketched in Fig. 35.20, segments the sensitive target by means of a stack of floating glass electrodes separated by a monofilament (i.e. fishing line), sandwiched between two external electrodes providing the high-voltage bias. The electrically-floating glass electrodes assume a potential determined by the avalanche processes occurring between them. An extensive description can be found in [223]. It has been observed that higher time resolution is inversely correlated to the gas gap size so this configuration allows for smaller gas thicknesses while maintaining a sufficient total gas thickness. This tends to separate primary clusters avalanches in different gas gaps, treating them independently, and determines a shorter avalanche growth time, increasing time resolution by one order of magnitude with respect to the classic RPCs [224]. The mechanical fragility of sub-mm-gap structures makes this technique less suitable for very large detector areas. Moreover the only material nowadays practically suitable for building such structures is soda-lime glass with resistivity above 10^{12} Ω·cm, limiting the rate capability to about 500 Hz/cm^2 [225].

mRPCs have been largely used in Time Of Flight systems such as ALICE [226], HADES [227], FOPI [228] and BESSIII [229], and in applications such as timing PET [230]. In perspective mRPC will be used for upgraded and new nuclear physics experiments such as CBM@FAIR [231] and SoLID [232].

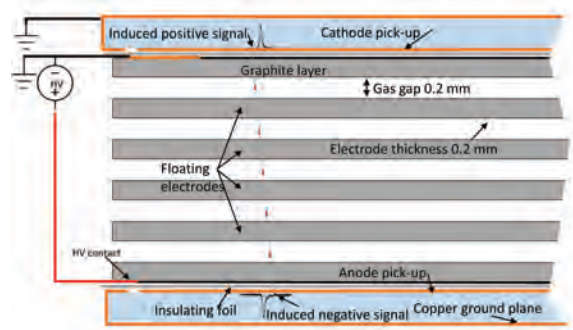

Figure 35.20: Schematic cross section of a generic multi gap RPC.

35.6.7.2 *Time and space resolution*

Space-time uncertainties in RPCs are determined by the statistical fluctuations of the primary and secondary ionization, the avalanche multiplication rate which is function of the electric field, and on the Signal/Noise ratio of the front-end electronics. The intrinsic signal latency is commonly in a few ns range (avalanche growth time to produce a detectable signal), making the RPC suitable for applications where a low latency is essential.

The gas gap size is a crucial feature for the RPC timing performance: producing the same total charge (for a detectable signal) in a smaller gas gap implies the necessity of increasing the Townsend coefficient by increasing the electric field, reducing at the same time the total signal duration and the related time fluctuations; moreover the chance of having multiple clusters in the same gas gap reduces with the gaps size, suppressing the charge collection fluctuations [233], which can be relevant for gas gap size $\gtrsim$ 500μm. Typical timing performances range from around 1 ns with a 2 mm gas gap, down to 20 ps for a stack of several 0.1 mm gaps [234].

The intrinsic position sensitivity of an RPC is in the range of tens of μm depending on the avalanche footprint fluctuations, influenced also by the gap size. In typical RPC applications the pick up electrodes pitch L ($\sim$1 cm) is much broader than the intrinsic resolution, and being readout via a discriminator, the spatial resolution is limited in the range of L/$\sqrt{12}$. A much better result is obtained by using a finer electrodes granularity and measuring the charge in each strip collecting the avalanche charge, so to reconstruct the charge centroid. It has been demonstrated recently, through charge centroid techniques, that the RPC avalanche space-time localization is better than $\sim$50 ps $\times$ 40 μm [235] [236].

Downloaded from https://academic.oup.com/ptep/article/2022/8/083C01/6651666 by KIT Library user on 27 September 2022

35.6.7.3 *Rate capability and ageing*

RPC rate capability is limited by the voltage drop on resistive electrodes, $\Delta V = V_a - V_{gas} = I \cdot R$ [237]. Here V_a is the applied voltage, V_{gas} is the effective voltage on the gas, $R = \rho \cdot d/S$ is the total electrode resistance, ρ being the resistivity and d,S the sample thickness and surface respectively, and I is the working current. Assuming uniform irradiation we can express $I = \phi \cdot S \cdot \langle Q \rangle$ where ϕ is the particle fluence and $\langle Q \rangle$ is average charge per avalanche. So we obtain a state equation for the RPC rate capability:

$$\Delta V/\phi = \rho \cdot d \cdot \langle Q \rangle$$

A large I not only limits the rate capability but also affects the long term performance of the detector since the working current, associated to discharges, depletes the conductive properties of HPL electrodes [238]. In presence of fluorocarbons and water, discharges generate hydrofluoric acid (HF) which damages internal detector surfaces, especially if made of glass, known to be not resistant to HF [239]. The practical way to suppress HF formation in glass RPCs is preventing water vapor contamination. Conversely, HPL electrodes, coated with linseed oil, are relatively resistant to HF, but the presence water can not be avoided since it mediates the HPL conduction. In this case the HF damage is mitigated by removing it with a forced flow of gas through the gas gap. Operating in the streamer regime puts low requirements on the front end electronics sensitivity, but generally limits the counting rate capability to ∼100 Hz/cm^2. Higher-rate operation can be achieved by reducing gas gain in favor of electronic amplification, operating the detector in avalanche mode. Increasing concentrations of electronegative gases, such as $C_2H_2F_4$ and SF_6 [208], shifts the streamer transition to higher gains. The avalanche signal has a higher dynamic range, a drawback which puts a further stress on the performance request on the front-end electronics. With these techniques, stable performance at high rates (e.g. 10 kHz/cm^2) has been achieved for large area single gap RPCs [212]. Two complementary strategies rely either on the natural redundancy and higher signal yield of multiple micro gap structures [240] or on electrodes made with lower resistivity materials [241]. Lowering the electrode resistivity in presence of high uniform field, finds a limit in the increasing probability of larger discharge events and overall noise. In this case, to safely lower the electrode resistivity, a safety margin would be given by operating with a lower electric field, and a correspondingly lower average charge per count.

35.6.7.4 *A new detector: the **R**esistive **C**ylindrical **C**ounter*

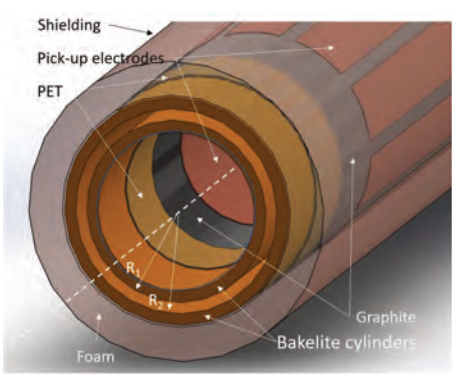

Figure 35.21: Schematic drawing of an RCC.

The RCC, illustrated in fig. 35.20, has been recently proposed as an evolution of the RPC [242] and is essentially an RPC warped to a cylindrical shape. The idea is to combine the advantages of parallel plate geometry and high pressure drift tubes in a single detector. The electric field $E(r)$, which is uniform in RPCs, here depends instead on the distance from the axis r, according to $E(r) = -\frac{V}{r \ln(R_1/R_2)}$. By choosing appropriate values for R_1, R_2, V and its polarization (the innermost cylinder is the cathode), it is possible to virtually segment the cylindrical gap in a innermost sensitive layer, where the field is sufficiently high to start the avalanche multiplication, and an outermost layer where the drift happens, increasing the induced signal with lower or no multiplication at all. This effect is called geometrical quenching and limits the avalanche growth without the necessity of electronegative gases. Moreover a geometrically quenched avalanche would have a much better prompt to total charge ratio, lowering the total operative current, hence increasing the rate capability. The cylindrical structure has a further major advantage with respect to the planar one, it can be easily pressurized overcoming the RPC limitation of working at atmospheric pressure only. Pressurization on one side increases the gaseous target density, thus increasing the efficiency of narrow gaps, on the other, it could largely improve RPC time resolution since the Townsend coefficient $\alpha = A\ p \cdot \exp(-Bp/E)$ (where p is the pressure, E the electric field and A,B are constants), as we learn from the RPC precursor, the Pestov spark chamber [201]. RCC concept can be exploited to reach ∼ps resolution and counting rates sufficient for many FCC applications. On the other side, being insensitive to the environmental pressure, potentially extends its range to space and under water applications.

35.7 LAr Time Projection Chamber

Written August 2021 by F. Pietropaolo (CERN; INFN, Padua) and S. Pordes (FNAL).

35.7.1 *Introduction*

Liquid argon is an attractive material for particle detection. Energy deposition in the argon produces scintillation light and ionization electrons; in the presence of a moderate electric field, a significant fraction of the electrons escape recombination, making them available for detection as a charge signal. Typical values for a minimum ionizing particle are ∼ 40,000 photons/MeV at zero field (lower at finite fields) and ∼ 30,000 electrons/MeV at a field of 500 V/cm. That the liquid has a relative density of 1.4 and that the free electrons can be drifted many meters with minimal dispersion makes it particularly attractive for use in massive time-projection chambers (TPC) to study rare processes, as realized in [243] and [244]. Since that time, the liquid argon TPC (LAr TPC) has been developed into a detector that combines mm^3 resolution with particle identification, calorimetry, and 100% live time. Detectors with masses up to 600 tons have been built and operated and detectors of 10's of kilotons are being planned.

The operation of a liquid argon time projection chamber requires

1. a cryostat and cryogenic system to maintain a mass of ultra-pure liquid argon clean, cold and calm,
2. an electric field that permeates the volume of liquid argon and allows electrons liberated by deposition of energy in the argon to escape recombination, and drifts them to the charge sensors,
3. an array of charge sensors and associated electronics to amplify and digitize the charge signals,
4. sensors to detect the scintillation light, and associated electronics,
5. a data-acquisition system to read out and record the data,
6. software to reconstruct and interpret the data.

Surveys of previous, present and proposed detectors are described in the literature - see references [245] and [246] and detailed descriptions of detectors which have operated in experiments are given in descriptions [247–253].

This article provides a description of some of the challenges in achieving items 1 to 4 and of some of the solutions presently adopted. Topics 5 and 6 are not discussed. They are crucial to the successful exploitation of the LAr TPC technology and the subject of intense activity; interested readers may note the references. [254–256]. References are also given for a number of ancillary devices - cameras that can operate in the liquid argon [253], monitors to provide a rapid measurement of the purity of the argon [257, 258], ionization lasers to measure distortions of the drift field due to space charge or electrical problems [259] - that have been developed to improve performance. A list of experiments with their masses is also given in 35.14.

Downloaded from https://academic.oup.com/ptep/article/2022/8/083C01/6651666 by KIT Library user on 27 September 2022

35.7.2 *A Mass of ultra-pure Liquid Argon*

Argon is abundant in the atmosphere (0.93% by volume, 1.3% by mass) as a result of the decay of ^{40}K in the earth's surface. The stable isotopes of argon are ^{40}Ar (99.6%), ^{36}Ar (0.33%) and ^{38}Ar (0.06%). Argon in the atmosphere is exposed to cosmic rays, forming the unstable isotope ^{39}Ar (lifetime 388 yr, β^-, endpoint 565 keV) at the level of 1 Bq/kg [260, 261]. Liquid argon is commercially available as a by-product in the distillation of air to produce nitrogen and oxygen. Some properties of argon are given in table 35.8; for many more see [262].

Table 35.8: Some physical properties of liquid argon from [263].

Property	Unit	Value
Boiling Point *(BP)* at 1013 hPa	K	87.3
Density (ρ) at 1013 hPa	kg m^{-3}	1395
d*(BP)*/dP	K hPa^{-1}	9×10^{-3}
dρ/dT	kg m^{-3} K^{-1}	-6.2
Latent Heat of Evaporation	kJ kg^{-1}	161
Freezing Point (1013 hPa)	K	83.8

Critical to any LAr TPC are the cryostat and the cryogenic and purification system to maintain the argon liquid, ultra-clean and calm. Evacuable double-walled vacuum cryostats are practical for detectors with a mass of O(100) t. Larger evacuable cryostats would not be feasible and given the demonstration that ultra-clean argon can be achieved without initial evacuation [258], current and proposed mid-size and larger detectors sit in foam-insulated non-evacuable cryostats based on a technology used in liquefied natural gas transport [253]. A convenient feature of these cryostats is that their components (inner walls, insulation, outer structures) are modular and of a size suited to assembly underground.

The absence of electronegative contaminants from the liquid argon is crucial to ensure the ionization electrons drift from their point of production to the charge sensors without being captured and their drift motion becoming too slow to detect. The major potential contaminants are environmental oxygen, nitrogen and water. Oxygen and water capture electrons; the scintillation light is affected by all three but at much higher levels of contamination. The loss of the charge signal depends on the product of the concentration of contaminant, the cross section for electron capture, and the time taken to reach the sensors. This combination leads to the quality of the argon being described in terms of 'electron lifetime', τ. To set a scale, the electron capture time in liquid argon with a concentration of oxygen of 1 ppb (part per billion by volume - all concentrations here are by volume) is ~ 300 μs [264, 265], largely independent of electric field in our range of interest. For detectors with electron drift times in the milliseconds, the oxygen level must be well below 0.1 ppb to avoid losing most of the signal. The capture time for water has not been measured directly; the one indirect measurement in the literature [266] suggests water is more potent than oxygen. Nitrogen does not affect the free electron lifetime at levels up to many ppm but it does affect light production [267] and transmission [268] at the few ppm level. Oxygen at the ppm level affects light production [269]; its effect in TPCs is usually ignored given the requirements for electron drift.

The atmosphere is removed from the cryostat volume either by evacuation or a controlled purging with argon [270]; purging achieves ppm levels of oxygen and nitrogen gas which on dilution in the liquid present a negligible (ppb) level compared to the levels in the commercially provided argon. With the cryostat ready for cooldown and filling, a purification system is required to purify the commercial argon delivered from its typical ppm oxygen and water levels to the level required for TPC operation. Commercial argon is available with acceptable levels of nitrogen ($<$ 2ppm) and typically no further reduction of the nitrogen level is provided. Molecular sieve and activated copper on alumina [271] are commonly used to remove water and oxygen, respectively. This purification is performed in the liquid phase and the discovery that purification with standard materials is effective at cryogenic temperatures [272] allowed for an enormous gain in throughput compared to purification in the gas phase. The purification system delivers essentially pure argon - which then mixes with any contaminants from outgassing or leaks that escaped the stringent leak-check. To avoid the build-up of contaminants, many small systems recirculate the boil-off gas through purifying filters, while all large systems circulate the liquid and boil-off gas continuously through the purification system. Schematics of experiment cryogenics systems are shown in [248, 250, 253]. While reconstructed tracks eventually determine the argon quality, so-called 'purity monitors', double-gridded ionization chambers, are often installed to give rapid feedback on the purity of the liquid [253].

35.7.3 *Charge and Light Signals*

Figure 35.22 (left) shows how the electron and scintillation yields for a minimum ionizing particle (m.i.p.) change with electric field. The free electron yield from the passage of a charged particle can be calculated from 'W$_{el}$' = 23.6 eV [273], the energy deposit that generates one ion-electron pair, the dE/dx of the particle, and 'R' the (unfortunately labeled) fraction of electrons that escape recombination - see figure 35.22 (left). Measurements of electron yield have been made at various electric fields and at different ionization densities [274–278] and show good consistency. Of the models proposed to predict recombination [279, 280], none is fully successful; the so-called 'box model' [281] which considers the situation of mobile electrons and stationary ions makes more realistic assumptions than previous models and its form is commonly used. The data from [277] which are some of the most comprehensive are described by the form $R = \frac{0.8}{(1+0.049(dE/dx)/\rho\mathcal{E})}$ where dE/dx is in MeV g^{-1} cm^2 and $\mathcal{E}$ in kV/cm. At a drift field of 500 V/cm, R for a minimum ionizing particle is $\sim 70\%$. A comprehensive summary and analysis of charge yield is given in [282].

The movement of the free electron charge towards the charge sensors is characterized by the drift velocity, the charge loss due to impurities, and the diffusion. The drift velocity depends on the strength of the electric field and slightly on the argon temperature (see table 35.9); a measurement of drift velocity vs electric field from [283] with a fit from [284] is shown in 35.22 (right). At an electric field of 500 V/cm, the drift velocity is ~ 1.55 m/ms at 89 K. The charge loss depends on the purity of the liquid. For a drift of duration, t, the fraction of charge that survives to the sense electrodes is $e^{-t/\tau}$ where τ is the electron lifetime. Values of τ exceeding tens of ms have been achieved [285–287]. Diffusion broadens the charge distribution as it travels to the sensor. The diffusion coefficient, D, defines the contribution to the spatial distribution of the charge at the sensor from diffusion after a drift of time, t, via $\sigma_D^2 = 2Dt$. Several measurements of the longitudinal diffusion component, D_L, have been made with a typical value around 0.4 mm^2/ms [276, 288–290]. For a 3 ms drift, this gives a contribution of $(0.4 \cdot 6)^{1/2}$ mm, ~ 1.5 mm, to the spread of the charge.

The scintillation light comes from the decay of excited argon dimers, Ar$_2^*$, (excimers) produced through direct excitation and through recombination of ionized argon ions and electrons [303]. The contribution of the latter process is reduced in the presence of an electric field as shown in figure 35.22, (left). The excimer is produced either in a singlet ('allowed' decay) or in a triplet spin state ('forbidden' (spin-flip) decay), with lifetimes of ~ 6 ns and ~ 1.5 μs respectively. The states are almost degenerate and photons are emitted, somewhat inconveniently [304], in the VUV with a spectrum peaked at 128 nm with a ± 8 nm (FWHM) spread [295]. The relative populations of the two states depends on the ionization density; typically 1:3 (singlet:triplet) for minimum ionizing and 3:1 for highly ionizing nuclear fragments [299]. As described in Section 36.4.1, this effect is exploited in argon-based WIMP dark matter searches to distinguish electromagnetic background from the nuclear recoil candidate signal. The long lifetime of the triplet state makes it sensitive to quenching impurities such as nitrogen or oxygen to which the excitation energy of the dimer can be transferred without the subsequent emission of a visible photon [267, 269].

The propagation of the scintillation is affected by two processes: absorption and Rayleigh scattering. While the large Stokes shift [305] makes pure LAr transparent to its own scintillation light, methane at the few ppb level [306] and nitrogen at the few ppm [268] level lead to light absorption. Rayleigh scattering

Downloaded from https://academic.oup.com/ptep/article/2022/8/083C01/6651666 by KIT Library user on 27 September 2022

Table 35.9: Some Detector Relevant Properties of liquid argon.

Property	Unit	Value
Stopping Power (m.i.p.)	MeV g^{-1} cm^2	1.51
Radiation Length	g cm^{-2}	19.6
Nuclear Interaction / Collision Length	g cm^{-2}	120 / 76
W_{el}, Energy to form one electron-ion pair	eV	23.6 ($\pm$0.3) [273, 291]
Ion mobility	cm^2 V^{-1} s^{-1}	1.6 $\times 10^{-3}$ [292]
Temperature dependence of drift velocity	% K^{-1}	-1.7 [284]
Longitudinal diffusion coefficient, D_L	mm^2 ms^{-1}	0.4 (see text)
W_{ph}, Energy to produce one scint. photon (m.i.p.)	eV	25 [293, 294]
Scintillation photon wavelength (vacuum)	nm	128 $\pm$8 (FWHM) [295]
Scintillation light inverse velocity	ns m^{-1}	7.46 ($\pm$0.08) [296]
Rayleigh scattering length (predicted)	m	0.9 ($\pm$0.2) [296–298]
Scintillation Decay times fast/slow	ns	6 ($\pm$1)/1500 ($\pm$100) [267, 299, 300]
Dielectric strength	kV cm^{-1}	>40 [301, 302]

increases the effective travel distance of photons between their production point and their detection and for detectors where the distance between origin and detection covers a range of many meters, the short Rayleigh scattering length for argon scintillation has a serious effect on the uniformity of detection. In this situation, the long lifetime of the triplet state can be exploited by the use of dopants to which the argon dimers can transfer their excitation energy with subsequent photon emission. Xenon, where almost complete transfer of the long-lived state energy is achieved at a concentration of 10's of ppm (mass), is a leading candidate. [307, 308].

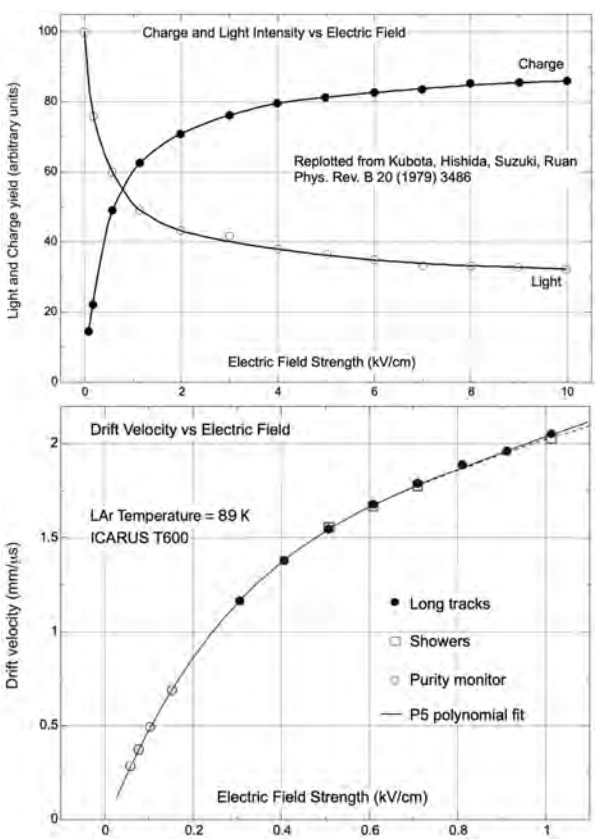

Figure 35.22: (*top*) the form of the light yield and the charge yield vs electric field redrawn from [303]; (*bottom*) electron drift velocity vs electric field redrawn from [283].

35.7.4 *LAr TPC topologies*

There are two basic LAr TPC formats: the single-phase design where all the detector elements are in the liquid, and the dual-phase design which drifts the electrons upwards and extracts them from the liquid into a thin layer of argon gas above the liquid to allow amplification of the signal [309]. (Charge amplification in the liquid is difficult to achieve given that there is no equivalent to the Ramsauer minimum that occurs in the gas phase [310, 311].) The dual-phase format is popular in dark matter searches where electroluminescence produced by the extracted electrons in the argon gas is exploited (see Chapter 36.4); scaling up detectors with charge gain ([312, 313] to kilotons for neutrino experiments has not yet proved successful. In single-phase detectors, the drift direction can be either horizontal or vertical. Currently operating detectors come in a range of sizes but the basic form of a cathode and field cage generating a field which drives the ionization electrons to planes of charge sensors at ground potential is universal. A standard criterion is to make the TPC drift as long as considered possible to maximize the detector mass for a given channel count; this can result in a single drift volume; two drift volumes with a common cathode, or multiple drift volumes with multiple common cathodes. An exception is the DUNE near detector TPC; it is segmented into many small TPCs to help resolve the large interaction rate [314].

The drift field is produced by a planar cathode at -HV, a graded field-cage surrounding the active volume, and the sensing electrodes at a potential near ground which form the anode. The field cage is designed to produce a uniform electric field throughout the drift region although for detectors at surface, the slow-moving positive ions generated by the flux of cosmic rays distort the field, particularly for TPCs with long drift [282, 287, 315–317]. Particular challenges in the drift field system are the feed-through [248, 318] that brings the voltage from the HV supply outside the cryostat to the cathode (the cathode can sit at (-ve) voltages up to 300 kV), avoiding damage to the electronics from a potential cathode discharge [253], and ensuring the integrity of the field-cage resistor chain [319]. Avoiding discharge and current draw in a medium chosen because it allows electron flow is possibly the hardest challenge in the technology.

To date, the sensor arrangement for large detectors has used vertical planes of wires as sense electrodes and a horizontal electric field. A schematic is shown in figure 35.23.

The sense planes are perpendicular to the drift direction and arranged in a stack with the wires in each plane oriented at a different angle. (While the schematic shows three planes, in principle only two are needed.) The wire-pitch, p, is a few mm and the plane spacing is similar. As indicated in figure 35.23, the planes are biased such that all field lines from the drift region pass through the intermediate planes and terminate on the final plane as shown in 35.23. (The condition for transparency across one plane is derived in [320].) The drift electrons follow the field lines, inducing bi-polar current pulses on the first two planes, and terminate on the last one, the collection plane, producing a unipolar signal [321].

The raw signal rise and fall times are a few μs as determined by the electron drift velocity and the plane spacing, and any geometric effects from the track angles. The signals from each wire

Downloaded from https://academic.oup.com/ptep/article/2022/8/083C01/6651666 by KIT Library user on 27 September 2022

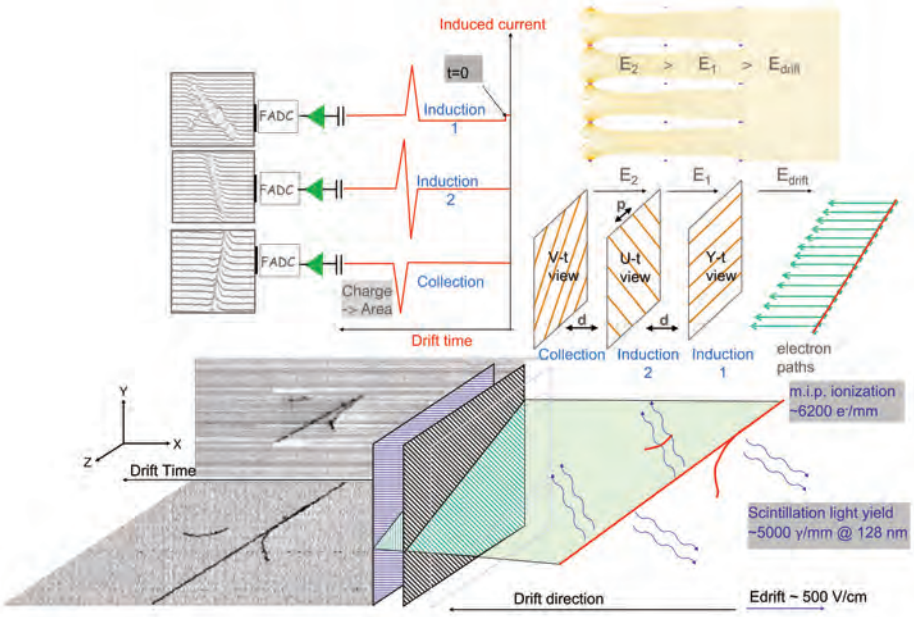

Figure 35.23: Schematic of an event in the ICARUS 3 t LAr TPC; *Top (from right to left)*: field lines from drift region to collection wires, electron flow & arrangement of wire-planes, signal shapes on the wires, and wave-forms from the continuous readout and digitization; *Bottom*: the passage of a muon. The gray scale on the track indicates the ionization density.

are recorded as wave-forms spanning the maximum drift time at typically 2 or 2.5 MHz sampling rate. The intersection of wires on different planes which record signals at the same time, and the drift time converted to a distance knowing the drift velocity give the position of the charge source.

The design of large (> kiloton) detectors faces an intrinsic electrical challenge in that long (> few m) cables from the sense electrodes to the first-stage amplifier will introduce an unacceptable amount of noise through their capacitance, and attempts to avoid such cables leads to impractical constraints on the charge sensor geometry; both of these are emphasized in [321]. To address this problem, CMOS based ASIC amplifiers that operate in the cold and can be placed next to the charge sensor (wire or strip or pixel) have been developed, their design rules and robustness validated, and successfully deployed [322,323]. The subsequent problem that individual feed-throughs for each signal in a detector with hundreds of thousands of channels complicate the cryostat structure and raise the specter of leaks has been resolved by the development of flash-ADC and signal multiplexers [324] that also operate in the liquid. These implementations have resulted in equivalent noise charge levels of a few hundred electrons [287, 325] to be compared with a charge yield for a m.i.p of 30,000 e/MeV. With such low noise, energy depositions well below 1 MeV are quite accessible.

Large LAr detectors usually contain a system to detect the primary scintillation light. These provide an event time for drift time measurement [326], a trigger [327,328], calorimetry that can be independent of and complementary to the charge [287], and event position information [254]. Given the VUV nature of the scintillation, a wavelength shifter is typically used to move the light into the visible [304]. Photo-multiplier tubes that operate in liquid argon were developed under the ICARUS program [329], while some recent systems are based on Silicon Photo-Multipliers. This latter approach separates the light collection from the light-to-electrical signal transducer, and many designs for the first task are being pursued [253,330,331].

35.7.5 *Prospect - written October 2021*

The successful operation [332] of the ICARUS T600 TPC served as clear demonstration of the feasibility of the liquid argon TPC technology on a massive scale. Since this milestone, the liquid argon TPC community has expanded and the technology has continued to evolve. Notable developments include in-liquid electronics, the adoption of Silicon Photo-Multipliers and new light collection technologies, the use of dopants in the argon to improve the light performance, improved techniques for wavelength shifting, the adoption of a cryostat technology which permits detector masses of tens of kilotons and, in a major change to the standard single-phase topology, the implementation of pixelated readout to replace projective geometry in busy environments [333]. Technical R&D is continuing; as examples, the vertical-drift single-phase design for the second DUNE far-detector that uses strips on perforated printed circuit boards as charge sensors [334], a dual-phase TPC readout [335] using fast cameras to read out the scintillation light produced in the gas region in place of a charge readout; a light detection system powered and readout using optical fiber allowing the readout to operate at any potential and therefore anywhere in the TPC (including on the cathode), and plans to replace the classic HV feed-through and filter with continuous semi-conductive cable. An abundance of data from recent experiments is encouraging insights into the liquid argon medium as in [282,336] and revealing new phenomena. For a taste, see [337]. The ground is fertile, busy, and full of opportunity.

35.7.6 *Acknowledgement*

We thank Drs Thorsten Lux and Stefania Bordoni for their enormous and invaluable help.

35.8 Semiconductor detectors

Revised August 2021 by N. Wermes (Bonn U.).

Semiconductor detectors provide outstanding detection opportunities in terms of position, energy and also time resolution, often in combination. In accelerator experiments they are most widely used as position sensing devices or as photodetectors (Sec. 35.2), for example in calorimeters (Sec. 35.10) or in imaging Cherenkov detectors (Sec. 35.5). Comparing in particular with gaseous detectors, main features are high density and low ionization threshold, providing in high resistivity substrates comparatively large signals without intrinsic amplification. Silicon detectors with active layers only 100–300 μm thick provide adequately large and fast signals (of order nanoseconds). Challenges are the purity of a semiconductor material, characterized by its mobility-lifetime product and its radiation resistance. Modern semiconductor detectors are strongly connected with integrated circuit technology allowing on one hand for the formation of high-density micron-scale electrodes

Downloaded from https://academic.oup.com/ptep/article/2022/8/083C01/6651666 by KIT Library user on 27 September 2022

on large wafers (6–8 in $\approx$ 15–20 cm diameter sensor wafers) and for amplification and readout circuits connected to them on the other (a typical CMOS wafer reticle is 26×33 mm^2) .

Some important material properties of common semiconductors used as detectors are summarized in Tab. 35.10. While for particle tracking the excellent position resolution is the main (but not the only) interest, high stopping power and high energy resolution are key parameters in X-ray, gamma-ray, and β spectroscopy, *e.g.*, in neutrinoless double beta decay searches. Due to its small bandgap germanium excels in energy resolution, but needs to be operated at very low temperatures to reduce thermally generated reverse bias current. GaAs, CdTe and CdZnTe (CZT, with the bandgap depending on the Cd to Zn ratio) also feature high atomic numbers and hence much higher stopping power which is important especially for X-ray absorption. Diamond, fabricated by chemical vapor deposition (CVD) and strictly speaking classifying as an insulator, features low Z and large radiation length X_0. It is used for particle detection especially in environments with high particle flux thanks to its radiation hardness (Sec. 35.8.3), especially regarding its low leakage current.

Materials R&D for radiation sensors extends to other bulk semiconductors as well, as for example ZnS, SiC or InP, and also to new material structures. Examples are semiconductor Quantum Dots - realized by nanometer-sized semiconductor 'particles' embedded in a semiconductor bulk, or Graphene, which – as a zero bandgap 2D material – features extraordinarily high conductivity (electrical and thermal). A bandgap can be introduced by structuring, doping, and other means, hence rendering transistor and sensor realizations possible. The interested reader is referred to reference [338] or [339], for example.

Operating without intrinsic amplification, semiconductor detectors crucially depend on low-noise electronics (see Sec. 35.9), so the detection sensitivity is determined largely by signal charge and input capacitance. Reviews of semiconductor detectors and electronics can be found for example in Refs. [1, 8, 340, 341]

35.8.1 *Signal generation*

35.8.1.1 *Creation of charges*

Semiconductor detectors are solid state ionization chambers. Absorbed energy forms electron-hole (e-h) pairs, *i.e.*, negative and positive charge carriers, which induce a signal current on electrodes when moving under an applied electric field (see Sec. 35.8.1.2). In order for the signal charge carriers to (freely) drift in the electric field and to become detectable, semiconductors must feature small intrinsic charge carrier densities (as *e.g.* in GaAs, CZT or diamond) or they must be depleted by reverse bias junction configurations (as for Si or Ge). In addition, they should feature low intrinsic density of defects which can act as trapping or generation/recombination centers (see Sec. 35.8.3).

The minimum energy required to form an e-h pair is the bandgap energy (1.12 eV in Si, 0.66 eV in Ge). However, impinging radiation or particles also release energy into lattice vibrations (phonons). In an "indirect" semiconductor like Si the valance band maximum is not at the same position in k-space (crystal-momentum space) as the conduction-band minimum and additional momentum transfer is required for a band transition to occur. For few-eV photons this momentum kick must come from lattice phonons which are Bose-Einstein distributed and hence cause a steep rise of photon absorption probability between 1.12 eV and about 3.4 eV, which is the "direct" energy gap without k-transfer. For much larger energy deposits the mean energy $w_{\rm i}$ required to produce an e-h pair assumes a constant value of 3.65 eV at room temperature; for other semiconductors consult Tab. 35.10.

For minimum-ionizing particles, the most probable charge deposition in a 300 µm thick silicon detector is about 3.7 fC ($\sim$23 000 electrons). In tracking detectors a particle's energy loss and scattering in the detector material should be minimal (large X_0), whereas for energy spectroscopy, *e.g.* of X-ray photons, the stopping power should be maximized by choosing high-Z semiconductors. A smaller bandgap produces a larger signal and improves energy resolution, but also (exponentially) increases thermally excited carrier generation, following the Fermi-Dirac distribution law. In order to cope with excessive leakage currents at room temperature, Ge diodes are typically operated at liquid nitrogen temperature (77 K). In pure Si at 300 K the carrier concentration is $n \simeq 10^{10}\,\mathrm{cm}^{-3}$ (Tab. 35.10), corresponding to a resistivity in the order of $\rho \simeq (e\mu n)^{-1} \approx 400\,\mathrm{k\Omega\,cm}$. In reality, crystal imperfections and minute impurity concentrations limit Si carrier concentrations to about $10^{11}\,\mathrm{cm}^{-3}$ at 300 K ($\rho \approx 40\,\mathrm{k\Omega\,cm}$). In practice, wafer resistivities up to 20 kΩ cm are available, with mass production ranging from 1 to 10 kΩ cm.

Since both electronic and lattice excitations are involved in digesting absorbed energy (in a correlated way), the variance in the number of charge carriers $N = E/w_i$ produced by fixed absorbed energy E (for example by an X-ray photon) follows binomial statistics and is, due to the energy constraint, reduced by the Fano factor F (about 0.1 in Si and Ge) relative to Poisson statistics. Thus, $\sigma_N = \sqrt{FN}$ and the energy resolution is $\sigma_E/E = \sqrt{Fw_i/E}$. However, the measured signal fluctuations are usually dominated by electronic noise or energy-loss fluctuations deposited in the detector. The electronic noise contributions depend on the detector leakage current and the electrode capacitance as well as on pulse shaping (shaping time) in the signal processing electronics (see Sec. 35.9).

Electric field strength and shape inside the semiconductor bulk are important for efficient signal charge collection, governed by the applied external voltage as well as by space charges. The latter naturally exists in junction detectors (see Sec. 35.8.2.1) leading (for constant space charge) to a linear decrease of the field strength from the junction boundary into the space charge region. Space charge can also occur from ionized lattice defects, either naturally existent as for example in GaAs or created by irradiation in any semiconductor material. This can lead to low field regions as well as to changes in the field's shape (deviating from linear), both of which usually deteriorate the charge collection properties of a detector.

For X-ray detection a major effort is to find high-Z materials with a bandgap that is sufficiently large to allow for room-temperature operation while still providing good energy resolution. Compound semiconductors, *e.g.* CZT, can allow this, but typically suffer from charge collection problems, characterized by the product $\mu\tau$ of mobility and carrier lifetime. In Si and Ge $\mu\tau$ is orders of magnitude larger than in compound semiconductors (see Tab. 35.10) for both electrons and holes. Since for holes $\mu\tau$ is typically much smaller than for electrons, detector configurations where the electron contribution to the charge signal near the readout electrode dominates—*e.g.*, strip or pixel structures with electron collection—can provide better performance (see also next section).

35.8.1.2 *Signal Formation*

The signal and its pulse shape depend on the instantaneous carrier velocity $\vec{v}(\vec{x}) = \mu\vec{E}(\vec{x})$ and the electrode geometry, which determine the distribution of induced current according to the Shockley-Ramo theorem

$$i_S(t) = Ne\,\vec{E}_w(\vec{x})\,\vec{v}(\vec{x}(t))\,, \tag{35.20}$$

where Ne represents a drifting charge cloud of N elementary charges, $\vec{E}_w(\vec{x})$ is the "weighting field", which accounts for the coupling of the charge to a specific electrode, and $\vec{v}$ is the drift velocity. Note that the mobility is in general field dependent, $\mu = \mu(E)$, with $v \approx const$ at high fields (velocity saturation, in Si approaching 10^7cm/s at $E > 10^4$ V/cm). Both, electron and hole movements contribute to an electrode's signal. Hence, if the carrier mobility is very different for electrons and holes, like *e.g.* in CdTe where $\mu_h \ll \mu_e$, a photon signal, for example, becomes absorption-point dependent. Integration of the induced current signal on an electrode yields the "collected charge". For a simple parallel-plate geometry with two electrodes the weighting field is constant, whereas for structured electrode geometries, like for example strips or pixels, E_w is position dependent which for small electrodes (compared to the sensor dimensions) strongly enhances the contribution of the movement close to the electrode ("small-pixel effect"). More details and practical accounts on the Shockley-Ramo theorem and its usage can be found in [1, 8] and references therein.

During the movement the charge cloud spreads due to diffusion

Downloaded from https://academic.oup.com/ptep/article/2022/8/083C01/6651666 by KIT Library user on 27 September 2022

widecaptionscale=1,tabularstretch=1.2]

Table 35.10: Properties of some detector-relevant semiconductors; temperature-dependent quantities given at 300 K (from [1] and references therein).

Property	Si	Ge	GaAs	CdTe (CZT)	Diamond
atomic number (Z)	14	32	31/33	48/(30)/52	6
density ρ (g/cm^3)	2.328	5.327	5.32	5.85	3.51
semiconductor type	indirect	indirect	direct	direct	indirect
bandgap E_G (eV)	1.12	0.66	1.424	1.44(1.44–2.2)	5.5
intr. carrier density (cm^{-3})	1.01×10^{10}	2.4×10^{13}	2.1×10^{6}	10^7	≈ 0
radiation length X_0 (cm)	9.36	2.30	2.29	1.52	12.15
average energy w_i for (e/h) creation (eV)	3.65	2.96	4.35	4.43	13.1
mobility (cm^2/Vs)					
electrons μ_n	1450	3900	8500	1050	≈1800*
holes μ_h	500	1800	400	90	≈2300*
lifetime					
electrons τ_e	>100 µs	∼ms	1–10 ns	0.1–2 µs	≈100 ns
holes τ_h	>100 µs	∼ms	20 ns	0.1–1 µs	≈ 50 ns

*Approximate averages. Values quoted in the literature for the mobility in diamond vary strongly.

(typically 5 µm for 300 µm thickness) such that more than one electrode might collect charge ("charge sharing"), an effect that usually improves position resolution. Charge collection time decreases with increasing bias voltage (*i.e.* field strength), and can be reduced further by operating the detector with "overbias", *i.e.*, a bias voltage exceeding the value required to fully deplete the device. Note that in partial depletion the electric field goes to zero at the end of the depletion zone, whereas overbias adds a constant electric field component. At an average field of $E = 10^4$ V/cm, the onset of velocity saturation, the collection times for Si are about 15 ps/µm for electrons and 30 ps/µm for holes. In typical fully-depleted detectors, 200–300 µm thick, electrons are collected within about 5–10 ns, and holes within about 15–25 ns.

Position resolution is ultimately limited by transverse diffusion and by the emission of δ electrons. Performance also depends on optimal usage of charge sharing between neighboring electrodes and on noise. Resolutions of 2–4 µm (rms) have been obtained. In magnetic fields, Lorentz drift deflects the electron and hole trajectories increasing the spatial spreading. Total spreading and hence charge sharing between electrodes can be tuned (increased or decreased) by tilting the detector relative to the incoming (average) particle direction.

35.8.2 *Typical detectors*

35.8.2.1 *Junction detectors*

A p-n junction operated in reverse bias forms a sensitive region depleted of mobile charges and sets up an electric field that sweeps charge liberated by radiation to the electrodes. Detectors typically use an asymmetric structure, for example a highly doped p electrode and a lightly doped n region – or vice versa, so that the depletion region extends predominantly into the lightly doped bulk volume.

In a planar Si (or Ge) device the thickness of the depleted region is

$$d = \sqrt{2\epsilon\,(V+V_{bi})/Ne} = \sqrt{2\rho\mu\epsilon(V+V_{bi})} \qquad (35.21)$$

$$\approx \frac{0.5}{\mu\text{m}} \times \sqrt{\frac{\rho\,V}{\Omega\,\text{cm}\cdot\text{V}}} \qquad \text{for } n\text{-type Si}$$

$$\approx \frac{0.3}{\mu\text{m}} \times \sqrt{\frac{\rho\,V}{\Omega\,\text{cm}\cdot\text{V}}} \qquad \text{for } p\text{-type Si}$$

with (values for Si)

V = external bias voltage
V_{bi} = "built-in" voltage (≈ 0.5 V for typically used resistivities)
N = doping concentration
e = elementary charge
ϵ = dielectric constant = $11.9\,\epsilon_0 \approx 1$ pF/cm
ρ = resistivity (typically 1–10 kΩ cm)
μ = charge carrier mobility (∼1450 cm^2/Vs (electrons), ∼500 cm^2/Vs (holes) [342])

The conductive p and n regions together with the depleted volume form a capacitor with capacitance per unit area

$$C = \frac{\epsilon}{d} \approx \frac{1\,\text{pF/cm}}{d} \qquad \text{in Si.} \qquad (35.22)$$

In strip and pixel detectors (see next section) the capacitance is dominated by the fringing capacitance to neighboring electrodes as the electrode pitch is usually much smaller than the sensor thickness. For example, the strip-to-strip Si fringing capacitance is about 1–1.5 pF per cm of strip length at a strip pitch of 25–50 µm.

Large volume ($\sim 10^2 - 10^3$ cm^3) germanium detectors are commonly configured cylindrical, for example, a cylindrical n-type crystal with 5–10 cm diameter and 10 cm length with an inner 5–10 mm diameter n$^+$ electrode and an outer p$^+$ layer forming the diode junction. Germanium can be grown with fairly low impurity levels, 10^9–10^{10} cm^{-3} (HPGe, high-purity germanium), so these large volumes can be depleted with several kilovolts.

Diamond, featuring free charge carrier densities close to zero, needs no depletion and is operated as a parallel plate capacitor with insulator dielectrics. Still, substantial bias voltage is required to overcome charge trapping.

35.8.2.2 *Detectors with structured electrodes*

In HEP experiments semiconductor detectors usually aim at good position resolution achieved with electrodes patterned in "strips" or "pixels" with typical dimension scales (electrode pitch) of 50–100 µm, or in "pads" (mm^2–cm^2) if coarser granularity is affordable for the benefit of fewer channels.

Electrodes are usually placed "planar", *i.e.*, at the surface of the sensing Si bulk, or can sometimes be shaped as columns or trenches running normal to the surface and hence parallel to the average direction of impinging particles, which increases radiation tolerance due to the shorter drift distances [343] (see also Sec. 35.8.3).

Various readout structures have been developed for pixels, *e.g.*, CCDs, DEPFETs as well as hybrid or monolithic pixels that either split or rather merge the sensing and readout IC functionality, as is illustrated in Fig. 35.24. Hybrid pixel devices utilize separate sensors and readout ICs connected by two-dimensional arrays of solder or indium bumps (for more details see *e.g.* [340, 344]). Monolithic pixel detectors combine sensing and readout in one chip with proper shielding of either function by exploiting multi-well IC technology.

Downloaded from https://academic.oup.com/ptep/article/2022/8/083C01/6651666 by KIT Library user on 27 September 2022

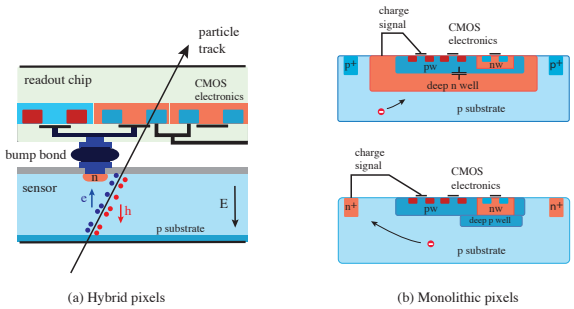

(a) Hybrid pixels (b) Monolithic pixels

Figure 35.24: Pixel detectors: (a) hybrid pixels (one cell); (b) monolithic pixels (one cell): (top) DMAPS with large collection electrode, (bottom) DMAPS with small collection electrode.

The hybrid approach excels in optimally utilizing chip and sensor technologies (see *e.g.* [345]); its disadvantage is complex and cost intensive assembly. Monolithic pixels, on the contrary, combine sensing and readout functionalities. Realized as MAPS (monolithic active pixel sensors) standard CMOS wafers are used with a Si epitaxial layer usually as the sensitive part, where charge collection is largely governed by slow and non-directional charge diffusion. Depleted MAPS (DMAPS) exploit non-standard high resistivity wafers (typically $>1\,\mathrm{k\Omega\,cm}$) and high bias voltage (up to $\sim$300 V) resulting in charge collection by directed drift motion. Charge collecting electrodes are deep wells (n-wells in Fig. 35.24(b)), either formed as large structures to fully contain the CMOS circuitry (top) or as small nodes, set aside the electronics (bottom), with obvious pros and cons resulting from shorter average drift distance (large electrode) versus much smaller capacitance (small electrode). The former benefits radiation tolerance, whereas the latter allows for smaller pixels and benefits from small sensor capacitance in noise and timing performance. However, in both approaches radiation tolerance levels to the order of $10^{15}\,\mathrm{n_{eq}/cm^2}$ (fluence) and 1 MGy (ion. dose) have been demonstrated.

A high spatial resolution, but less radiation-tolerant variant of the monolithic approach are SOI (silicon on insulator) pixels (see *e.g.* [346]), where a high-resistivity supporting wafer, employed for particle sensing, connects through an embedded insulator (a buried oxide layer, BOX) to the CMOS circuitry. The BOX separates the sensing volume from the electronics layer and provides shielding.

DEPFET pixels (see *e.g.* [347]) contain one transistor in every cell which—apart from a normal (external) gate electrode—is controlled by an "internal gate" (a local n-implant) about 1 µm underneath the surface. By appropriately biasing from two diode structures on either side of the bulk together with the internal gate, a local potential minimum for electrons is created underneath the transistor channel which gathers the released ionization electrons, thus modulating the transistor's channel current by about 0.5 nA per collected electron. Very thin sensors and $\mathcal{O}$(µm) spatial resolutions have been achieved.

35.8.2.3 *Timing with silicon detectors*

Essential for precision timing (<100 ps) are steep signal rise and low noise (see Eq. (35.37) in Section 35.9). Thin detectors with high E-fields and short amplifier rise times are necessary to achieve the required small collection times and fast amplification. Columnar electrodes (normal to the surface) with small diameter and small pitch are a suitable choice by design but they require non-standard fabrication processes. Planar electrode geometries that include an implanted low-gain ($g = 10$–50) amplification structure on either top or bottom electrode side to maximize the slew rate (dS/dt, with S="signal", *e.g.* an induced current or a voltage), are employed in so-called LGADs (low gain avalanche diodes, Fig. 35.25). Electrons created from ionizing traversing particles are accelerated in a high field towards an amplification layer near the top electrode, where they create a multitude of e-h pairs. They induce a very fast and large signal rise, mainly governed by the holes' movement away from the amplification layer. Sufficiently low amplification gain minimizes excess noise contributions and avoids creation of hole-induced avalanches moving in opposite direction to electron avalanches.

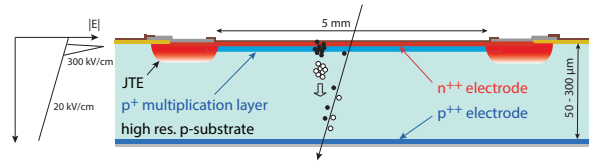

Figure 35.25: LGAD amplification structure for precision timing. Amplification occurs inside the structure boundaries in a highly doped p-n junction near the surface (JTE = Junction Termination Extension, deep n-well).

The achievable time resolution has several contributions:

$$\sigma_t^2 = \left(\frac{\sigma_S^{thr}}{dS/dt}\right)^2 + \left(\frac{\sigma_n}{dS/dt}\right)^2 + \sigma_{\mathrm{arrival}}^2 + \sigma_{\mathrm{dist}}^2 + \sigma_{\mathrm{TDC}}^2\,. \quad (35.23)$$

The first term represents "time walk" coming from Landau fluctuations, defined as originating from number and energy transfer fluctuations in the energy loss process (see *e.g.* [1]) with σ_S^{thr} being the signal height variations at discriminator threshold. This term can be kept minimal, *e.g.*, by employing constant fraction discrimination or by applying corrections using amplitude information. The second term is noise jitter, which can also be expressed as t_r/SNR with t_r = rise time, SNR = signal-to-noise ratio. Both first terms are made small by large signal slew rates. An irreducible contribution comes from fluctuations in non-uniform depositions of charge along the particle path (including fluctuations in the amplification process) which causes an intrinsic jitter in the arrival time (third term)[2]. The thinner the detector the less disturbing is this effect. The fourth contribution is signal distortion due to non-uniform weighting field regions and variations in (non-saturated) drift velocities. The final term denotes time fluctuations due to uncertainties in the digitization, which can, however, be made negligible with GHz TDCs. Timing precisions of order 30 ps have been reached. More elaborate discussions on timing in silicon detectors can be found *e.g.* in [348]; more details on LGADs are given in [349].

35.8.3 *Radiation Damage*

High channel density and response times in the nanosecond range renders micro-patterned semiconductor detectors particularly suited for high particle rates. This is usually accompanied by high radiation causing damage of sensors and front-end electronics. Radiation damage occurs through two basic mechanisms:

1. *Bulk damage* due to displacement of atoms from their lattice sites resulting in defect energy levels inside the band gap. This leads to increased leakage current, carrier trapping, and build-up of space charge that changes the required operating voltage. Displacement damage results from non-ionizing energy loss (NIEL) and the energy imparted to the recoil atoms can initiate a chain of subsequent displacements including "damage clusters". Hence, it is critical to consider both, particle type and energy. Conventionally, for silicon the received NIEL is normalized to the damage level caused by 1 MeV neutrons and specified in units of neutron-equivalent fluence Φ_{eq} with units n_{eq}/cm^2.
2. *Surface damage* due to charge build-up in surface layers and formation of interface traps at *e.g.* Si–SiO_2 boundaries. These cause thin charge carrier layers at the silicon surface, leading to increased surface leakage currents in sensors or circuits affecting electrode isolation or transistor characteristics, respectively. The effects of charge build-up are strongly dependent on the device structure and on fabrication details. The damage is dominantly due to ionizing energy loss (IEL)

[2] In LGAD literature these fluctuations are sometimes also referred to as "Landau fluctuations".

Downloaded from https://academic.oup.com/ptep/article/2022/8/083C01/6651666 by KIT Library user on 27 September 2022

and hence proportional to the absorbed total ionization dose (TID) measured in Gy (or rad), independent of particle type.

The increase in reverse bias generation current due to bulk damage is $\Delta I_L = \alpha \Phi_{eq} V$, where V is the volume under an electrode and $\alpha \simeq 4 \times 10^{-17}$ A/cm, a universal constant when normalized to temperature (conventionally 20°C), and given after annealing for 80 min at 60°C. Note that for devices with intrinsic amplification, generation current is amplified accordingly. The reverse bias leakage current depends strongly on temperature

$$I_L(T) \propto T^2 \exp\left(-\frac{E_a}{2kT}\right) , \qquad (35.24)$$

where $E_a \approx 1.2$ eV (activation energy), so rather modest cooling can reduce the current substantially (∼6-fold reduction in cooling from room temperature to 0°C).

For bulk damage in silicon the *NIEL hypothesis* is a good first order description of the observed damage (especially regarding I_L). It states that all lattice radiation damage in silicon linearly scales with NIEL and can be traced back to the abundance of primary defects (point defects and clusters), irrespective of their initial distribution over energy and space, that is, regardless of topology and origin of the damage. Under the NIEL hypothesis, the observed differences in damage caused by neutrons, protons, pions and electrons are hence usually scaled to each other.

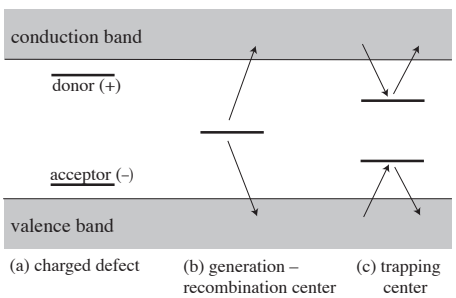

Figure 35.26: Characteristic locations of energy levels caused by bulk radiation damage and their main effects on device operation.

Three main bulk displacement damage effects are sketched in Figure 35.26: (a) defects acting as charged donors/acceptors, (b) deep defects (near the middle of the bandgap) causing increased leakage current, and (c) carrier trapping centers. Damage effects are not constant with time; for example, the negative space charge first anneals reaching a stable damage minimum (beneficial annealing) and then electrically active defects (negative space charge) build up on the time scale of months (reverse annealing).

Acceptor- (typically dominant) or donor-like states, when ionized, build up space charge, which in turn requires an increase in the applied voltage to sweep signal charge through the detector thickness. For n-type silicon, acceptor buildup with fluence initially leads to a decrease in the required bias voltage until (effective) positive and negative space charges balance; only little bias voltage is required for operation (point of effective space charge inversion, also called "type" inversion). At larger fluences the negative space charge dominates, and the required operating voltage increases proportional to the increasing effective space charge density $N_{\rm eff}$, also called effective doping concentration. Today, p-type silicon is the preferred choice for sensors operating in high radiation environments for reasons of cost-effectiveness in production and high radiation hardness due to electron collection in high electric- and high weighting-field regions at segmented n^+ electrodes. Dopant removal, *e.g.*, through phosphorous or boron reactions with crystal defects, also plays an important role in more complex sensor structures like for example DMAPS or LGADs. Various techniques have been applied to neutralize "active" damage sites, for example by oxygen or carbon enrichment for n-type/p-type substrates with different successes (for more details see *e.g.* [350, 351]).

Deep level defects (Fig. 35.26(b)) typically are the origin of leakage current increase, whereas trapping centers (Fig. 35.26(c)) dominate carrier lifetime and signal loss at high fluences beyond 10^{15} $\mathrm{n_{eq}/cm^2}$. The safe limit on operating voltage ultimately limits the detector lifetime. Strip and pixel detectors specifically designed for high voltages have been extensively operated at bias voltages of 500–600 V.

Strip and pixel detectors have remained functional in large detectors even at particle fluences beyond 10^{15} $\mathrm{n_{eq}/cm^2}$ where charge loss due to recombination and trapping becomes significant. The high SNR obtainable with low capacitance pixel structures extends detector lifetime. The higher mobility of electrons makes them less sensitive to carrier lifetime than holes, so detector configurations that emphasize the electron contribution to the charge signal are advantageous, *e.g.*, n^+ strips or pixels on a p- or n-substrate. The occupancy of the defect charge states is strongly temperature dependent; competing processes can increase or decrease space charge and the required operating voltage. It is critical to choose the operating temperature judiciously (−30 °C to 0 °C in typical collider detectors) and to limit warm-up periods during maintenance. Detailed discussions of the current understanding of radiation effects can be found in [350, 351].

Tolerance against surface damage, especially in SiO_2 layers and in trenches of CMOS transistor structures, largely depends on the feature size of a technology and on appropriately designed circuitry. Deep submicron technology nodes of 130 nm and 65 nm sustain total ionization doses of up to 5 MGy (500 Mrad), corresponding to fluences of up to 5×10^{15} $\mathrm{cm^{-2}}$ of minimum ionizing pions or protons.

35.9 Low-noise detector readout

Revised November 2021 by N. Wermes (Bonn U.), revised November 2013 by H. Spieler (LBNL).

Many detectors rely critically on low-noise readout electronics, for best energy resolution or to allow low thresholds for high detection efficiencies. A typical detector front-end is shown in Fig. 35.27.

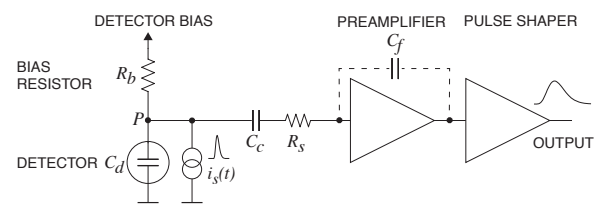

Figure 35.27: Typical detector front-end. The dashed circuit part is a charge-sensitive amplifier (CSA) realization.

In a model relevant for most readout applications, the detector, represented by a capacitance C_d, delivers a delta-function-shaped current signal, represented by a current source in parallel. Bias voltage is applied through resistor R_b and the signal is (often) coupled to the amplifier through a blocking capacitor C_c. The series resistance R_s represents the sum of all resistances present in the input signal path, *e.g.*, the electrode resistance, any input protection networks, and parasitic resistances in the input transistor. The amplification stage contains the preamplifier providing gain and a pulse shaper (characterized by a shaping time τ), which tailors the overall frequency response to optimize the signal-to-noise ratio (SNR) while limiting the duration of the signal pulse to accommodate the signal pulse rate. For a given input signal, purely random noise leads to a gaussianly smeared signal distribution behind the shaper. Even if not explicitly stated, all amplifiers provide some form of pulse shaping due to their limited frequency response.

It is useful to distinguish between noise inherent to a detector's signal amplification and processing circuitry (per channel) on the one hand, depending on the detector specifics and the experimental environment (*e.g.* the data rate), and — on the other hand — external noise sources introduced *e.g.* by systems external to a specific readout circuit often resulting in "common-mode" noise, *i.e.* common to all channels. External noise can be introduced for

Downloaded from https://academic.oup.com/ptep/article/2022/8/083C01/6651666 by KIT Library user on 27 September 2022

example from power supplies, digital signal switching, RF pick-up, or can come from effects due to "common grounding" allowing noise to couple to the current loop connecting the detector to the preamplifier. These noise sources differ from setup to setup and must be dealt with – and should at best be eliminated – individually. In the following, therefore, only the noise inherent to typical detector signal processing is discussed.

35.9.1 *Principal noise origins*

As principal noise origins in circuit elements we mainly distinguish "thermal noise" resulting from velocity fluctuations of charge carriers (Brownian motion), as well as "shot noise" and "$1/f$ noise", both resulting from charge carrier number fluctuations. Shot noise is due to emission statistics of electrons crossing a barrier, $1/f$ noise is often — especially in MOSFETs — due to charge trapping–detrapping processes leading to a spectral behavior as $1/f^\alpha$ with $\alpha = 0.5\ldots2$. Further noise nomenclature, like for example RTS (random telegraph signal) noise, also called "burst noise" or "popcorn noise", is in its origin like $1/f$ noise usually related to trapping/detrapping processes. The popping-up nature of individual RTS bursts eventually leads to the $1/f$ noise spectral density when noise of several traps with (very) different trapping times are superimposed. RTS noise is omitted in the following for simplicity reasons.

35.9.2 *Equivalent noise analysis*

The equivalent circuit for noise analysis (Fig. 35.28) shows contributions of the mentioned noise sources at several circuit points. Originating from fluctuations, noise is expressed as the variance $\langle i^2\rangle$ or $\langle v^2\rangle$ of a noise current or voltage distribution. Shot noise, such as that produced in a semiconductor detector by leakage current fluctuations, is represented by a current noise generator in parallel with the detector and the amplifier input. The statistical fluctuations in a charge measurement will scale with the square root of the total number of recorded charges, so this noise contribution increases with the measurement (shaping) time. Thermal noise in resistors produces a white noise, *i.e.* a noise power density independent of frequency. Hence limiting the bandwidth by a shaper, *i.e.*, increasing the shaping time, will decrease the noise at the expense of slowing down the detector response. Usually, resistors shunting the input act as noise current sources and resistors in series with the amplifier input act as noise voltage sources, so that they are often referred to as "parallel" and "series" noise. Thermal fluctuations in the bias resistor result in fluctuations of the voltage at point P in Fig. 35.27 and its noise current source $\langle i_b^2\rangle$ has the same effect as the shot noise current $\langle i_d^2\rangle$ from the detector. Conversely, the series resistor R_s acts as a voltage noise generator $\langle v_s^2\rangle$ for the amplifier input.

Shot noise and thermal noise have a "white" frequency distribution, *i.e.*, the (power) spectral densities (f = frequency) $d\langle i^2\rangle/df$ and $d\langle v^2\rangle/df$ are constant with magnitudes

$$\begin{aligned} d\langle i_d^2\rangle &= 2eI_d\,df\,,\\ d\langle i_b^2\rangle &= \frac{4kT}{R_b}\,df\,,\\ d\langle v_s^2\rangle &= 4kTR_s\,df\,, \end{aligned} \tag{35.25}$$

where e is the elementary charge, I_d the detector leakage current, and k,T Boltzmann constant and temperature. Hence, in a 1 kΩ resistor at room temperature, for example, one finds a current-independent thermal noise of $\sqrt{d\langle i^2\rangle/df} = 4\,\mathrm{pA}/\sqrt{\mathrm{Hz}}$ or $\sqrt{d\langle v^2\rangle/df} = 4\,\mathrm{nV}/\sqrt{\mathrm{Hz}}$, respectively. For $1/f$ noise, by contrast, the spectral power density is proportional to $1/f^\alpha$ ($\alpha = 0.5$–2) with a device specific proportionality constant. In what follows, we will assume $\alpha = 1$ for simplicity reasons, noting though that more complex models exist.

An important noise source is the preamplifier input stage, very often dominated by the first amplification transistor. In what follows we assume a MOSFET at this point, as the large majority of amplification circuits is based on MOS transistors. Noise sources in bipolar amplification is shortly mentioned at the end of this section. A MOS transistor's channel features thermal noise with "resistance" $1/g_m$, where $g_m = \partial I/\partial V$ is the transconductance. Correction factor(s) for parametrization depend on the transistor

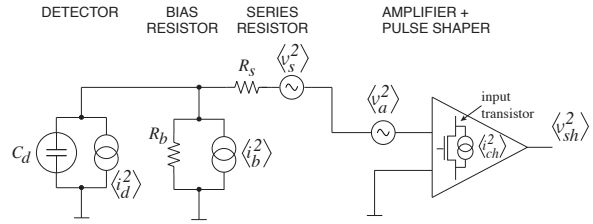

Figure 35.28: Equivalent circuit for noise analysis.

operation point. Conventionally, a factor γ is applied varying between 0.5 and 1 when temperature dependence is implicit, but is commonly taken as $\gamma \approx 2/3$ for operation in strong inversion and 0.5 in weak inversion.

In addition, especially in MOSFETs, there is $1/f$ noise originating from trapping/detrapping processes of charge carriers at the channel's Si–SiO_2 interface. The channel's current noise is equivalent to a voltage noise at the transistor input (the gate) via

$$\langle i_{ch}^2\rangle = \langle (g_m v_a)^2\rangle \tag{35.26}$$

leading to respective noise power spectral densities of

$$\frac{d\langle v_a^2\rangle}{df} = 4kT\gamma\frac{1}{g_m} + K_f\frac{1}{C'_{ox}WL}\frac{1}{f}\,, \tag{35.27}$$

where the individual (uncorrelated) noise contributions add in quadrature. The "$1/f$ noise constant" K_f has magnitude in the order of $10^{-24} - 10^{-26}$J depending on the device type and the technology[3]. C'_{ox} is the oxide capacitance per unit area, and W, L are width and length of the gate.

Particle and radiation detectors typically convert the deposited energy into charge (usually e-ion or e-h pairs) which can be measured by integrating the current induced on an electrode by the drifting charge pairs (see *e.g.* Sec. 35.8) employing a "charge-sensitive (pre)amplifier" (CSA), realized by feeding back the preamp's output to the input through capacitor C_f (dashed circuit part of Fig. 35.27). The feedback capacitance must be discharged for the next pulse to appear, for example by a resistor, a (constant) current source or a switch. Noise contributions from such components can usually be kept small in comparison.

For a CSA the noise output voltage after the preamplifier $\langle v_{pa}^2\rangle$ relates to the input (current or voltage) noise sources via the transimpedance $1/\omega C_f$ as

$$\left\langle v_{pa}^2\right\rangle = \left\langle i_{in}^2\right\rangle\left(\frac{1}{\omega C_f}\right)^2 \qquad \text{or} \qquad \left\langle v_{pa}^2\right\rangle = \left\langle v_{in}^2\right\rangle\left(\frac{\omega C_D}{\omega C_f}\right)^2 \tag{35.28}$$

with $\omega = 2\pi f$. The capacitance C_D includes the detector capacitance C_d plus all capacitances shunting the input. Considering only the (usually) dominant noise sources, being the detector shot noise as well as the transistor channel noise, and neglecting the resistor parallel and serial noise sources of (35.25) by choosing R_b large and keeping R_s small, one obtains

$$\frac{d\left\langle v_{pa}^2\right\rangle}{d\omega} = \sum_{k=-2}^{0} c_k\,\omega^k \tag{35.29}$$

with

$$c_{-2} = \frac{e}{\pi}I_d\frac{1}{C_f^2}\,,\quad c_{-1} = K_f\frac{1}{C'_{ox}WL}\frac{C_D^2}{C_f^2}\,,\quad c_0 = \frac{2\gamma}{\pi}kT\frac{1}{g_m}\frac{C_D^2}{C_f^2}\,, \tag{35.30}$$

which correspond to the discussed main noise components, c_{-2}: shot noise, c_{-1}: $1/f$ noise, c_0: thermal noise, respectively.

The filtering effect of the shaper limits the bandwidth of the system and is generally described by a transfer function $H(\omega)$ for

[3] Other $1/f$ noise parametrizations also exist with correspondingly different numerical values for K_f.

Downloaded from https://academic.oup.com/ptep/article/2022/8/083C01/6651666 by KIT Library user on 27 September 2022

$\langle v_{pa}^2 \rangle$ integrated over the full bandwidth

$$\left\langle v_{\rm sh}^2 \right\rangle = \int_0^\infty \frac{d\langle v_{\rm pa}^2 \rangle}{d\omega} \, |H(\omega)|^2 \, d\omega \tag{35.31}$$

with $\langle v_{sh}^2 \rangle$ being the shaper output voltage noise. $H(\omega)$ depends on the filter circuit, *i.e.* the shape of the pulse formed by the shaper, and is characterized by a characteristic time τ, the shaping time, which can, for example, be the peaking time of a semi-gaussian pulse or the sampling interval in a correlated double-sampler (see *e.g.* [8]). The peaking time is an important quantity for readout systems since for peaking times large compared to the duration of the input signal the amplitude at peaking time corresponds to the total input charge.

For a simple time-invariant CR–RC filter, consisting of a high-pass followed by a low-pass filter with equal time constants, the transfer function is

$$|H(\omega)|^2 = A^2 \left(\frac{\omega\tau}{1+\omega^2\tau^2} \right)^2 \tag{35.32}$$

and (35.29) becomes

$$\left\langle v_{\rm sh}^2 \right\rangle = \frac{\pi}{4} A^2 \left(c_{-2}\,\tau + \frac{2}{\pi} c_{-1} + c_0 \frac{1}{\tau} \right) \tag{35.33}$$

with A being an overall gain factor.

The system noise for a charge measurement is conveniently expressed as an equivalent noise charge (ENC) referring the noise to the equivalent signal of one electron at the input:

$$\mathrm{ENC}^2 = \frac{\langle v_{\rm sh}^2 \rangle}{v_{\rm signal}^2 (1e^-)} \, . \tag{35.34}$$

While being dimensionless by definition, ENC is commonly expressed as an equivalent number of electrons (e^-) at the input or alternatively as equivalent Coulombs (C) when multiplying by the elementary charge or as equivalent deposited energy (eV), where $1e^-$ equivalent charge corresponds to 3.65 eV of equivalent deposited energy in Si.

A charge of one electron at the input yields a voltage signal (peak) behind the shaper of $v_{\rm signal} = \dfrac{A}{2.71}\dfrac{e}{C_f}$. Hence with (35.34) and (35.33) one obtains:

$$\begin{aligned} \mathrm{ENC}^2\,(e^{-2}) &= \frac{(2.71)^2}{4e^2} \left(e I_d \tau + 2 C_D^2\, K_f \frac{1}{C'_{ox} W L} + \gamma \frac{2kT}{g_m} \frac{C_D^2}{\tau} \right) \\ &= a_{\rm shot}\,\tau + a_{1/f}\, C_D^2 + a_{\rm therm}\, \frac{C_D^2}{\tau} \, , \end{aligned} \tag{35.35}$$

where 2.71 is Euler's number resulting from the amplitude peak value behind the (CR–RC) shaper (for $t = \tau$), while e is the elementary charge and (e^-) explicitly denotes equivalent number of electrons.

Equation (35.35) accentuates the main noise dependencies of the system. The contribution from parallel current shot noise (*i.e.* detector leakage) increases with shaping time, *i.e.* with pulse duration, whereas thermal noise (here serial voltage noise at the gate, originating from transistor channel noise) decreases with increasing shaping time, *i.e.* with reduced bandwidth. Noise with a $1/f$ spectrum depends only on the ratio of upper to lower cutoff frequencies (low pass to high pass time constants) and is hence independent of τ for a given shaper topology. Furthermore, the contribution of serial noise voltage ($1/f$ and thermal noise) to ENC increases with input (detector) capacitance C_D. Pulse shapers can be designed to optimize the noise performance of a system or to mitigate operation variations with time (*e.g.* due to radiation damage) deteriorating the performance, at the expense of loss of simplicity. For example, a shaper with one high-pass filter followed by four cascaded low-pass filters, increases the pulse symmetry and tends to decrease the current noise, but increases the voltage noise contributions for the circuit of Fig. 35.28, if the same peaking time is assured by adjusting the individual time constants of the filter stages. If instead the low-pass filters cause the peaking time of the pulse to increase, the opposite can be true. More details about shaping filters can be found *e.g.* in [8, 352–354].

Figure 35.29 shows a typical example of eq. (35.35) displaying ENC as a function of shaping time τ for a system. At short shaping times, thermal noise dominates, whereas for longer shaping times the shot noise contribution takes over. The total noise has a minimum at a shaping time where shot and thermal noise contributions are equal. The minimum is flattened by the presence of $1/f$ noise. Increasing the detector capacitance increases the thermal and $1/f$ contributions and shifts the noise minimum to larger shaping times. One can hence exploit the shaping time dependence of the total noise to determine the individual noise contributions of a system.

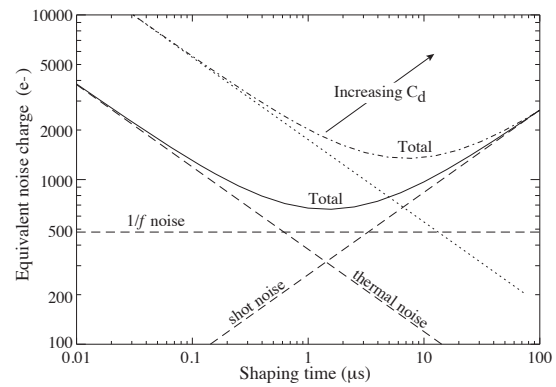

Figure 35.29: Equivalent noise charge *vs* shaping time. Changing the detector capacitance C_D affects thermal and $1/f$ noise contributions and moves the noise minimum as indicated by the dotted and dash-dotted lines. The $1/f$ noise contribution is small for the chosen parameters ($C_D = 20\,\mathrm{pF}$, $I_d = 10\,\mathrm{nA}$, $g_m = 1\,\mathrm{mS}$) in this example.

For quick estimates (35.35) is cast into a useful equation for a typical CSA-shaper system [1]:

$$\begin{aligned} \mathrm{ENC}^2\,(e^{-2}) = 11\, \frac{I_d}{\mathrm{nA}}\, \frac{\tau}{\mathrm{ns}} + 740\, \frac{1}{WL/(\mu\mathrm{m}^2)}\, \frac{C_D^2}{(100\,\mathrm{fF})^2} \\ + 4000\, \frac{1}{g_m/\mathrm{mS}}\, \frac{C_D^2/(100\,\mathrm{fF})^2}{\tau/\mathrm{ns}} \, , \end{aligned} \tag{35.36}$$

where $\gamma = 2/3$, $K_f = 33 \times 10^{-25}\,\mathrm{J}$, and $C'_{ox} = 6\,\mathrm{fF}/\mu\mathrm{m}^2$ has been used, the latter being typical for CMOS technologies as employed for example for the detector readout chips of the LHC experiments and their upgrades. Generally, noise performance is improved by reducing the detector capacitance and leakage current, judiciously selecting all resistances in the input circuit, and by choosing the optimum shaping time constant. Another noise contribution to consider is the fact that noise can cross-couple from the neighboring front-ends in detectors with structured electrodes through the inter-electrode capacitance.

As mentioned, the noise parameters of the amplifier depend primarily on the input device (input transistor(s)). In field-effect transistors, the input noise current contribution of the transistor itself is very small. Hence, if the experiment's time structure permits, reducing the detector leakage current and increasing the bias resistance will allow long shaping times with correspondingly lower noise. For amplifiers employing bipolar transistors, shot noise sources originate from both, base-emitter and collector-base, junctions and from the series resistance at the base which is especially important for small structures optimized for radiation hardness. For the shot-noise contribution, the input base current I_B sets a lower bound on the noise current, such that these devices are best at short shaping times.

35.9.2.0.1 Examples Using (35.36) one finds for a typical pixel detector (before heavy irradiation) with $C_D = 200\,\mathrm{fF}$, $I_d =$

Downloaded from https://academic.oup.com/ptep/article/2022/8/083C01/6651666 by KIT Library user on 27 September 2022

1 nA, $\tau = 50$ ns, $W = 20\,\mu$m, $L = 0.5\,\mu$m, $g_m = 0.5$ mS:

$$\mathrm{ENC}^2 \approx (24\,e^-)^2\Big|_{\mathrm{shot}} + (17\,e^-)^2\Big|_{1/\mathrm{f}} + (25\,e^-)^2\Big|_{\mathrm{therm}} \approx (40\,e^-)^2\,.$$

For a typical silicon microstrip detector after radiation damage (fluence $\gtrsim 10^{14}\mathrm{n_{eq}/cm^2}$, assuming no degradation of the front-end electronics due to radiation) one obtains for $C_D = 20$ pF, $I_d = 1\,\mu$A, $\tau = 50$ ns, $W = 2000\,\mu$m, $L = 0.4\,\mu$m, $g_m = 5$ mS:

$$\mathrm{ENC}^2 \approx (750\,e^-)^2\Big|_{\mathrm{shot}} + (200\,e^-)^2\Big|_{1/\mathrm{f}} + (800\,e^-)^2\Big|_{\mathrm{therm}} \approx (1100\,e^-)^2.$$

Apart from the larger leakage current, the larger capacitance of strips compared to pixels leads to a much worse noise performance which can only be partially compensated by allowing more power in the amplification transistor, *i.e.*, by increasing g_m.

A liquid argon calorimeter cell is a suitable example of a detector with a large electrode capacitance with typical parameters (similar to the ATLAS central electromagnetic calorimeter, see Sec. 35.10). Using $C_D = 1.5$ nF, $I_d = < 2\,\mu$A, $\tau = 50$ ns, $W = 3000\,\mu$m, $L = 0.25\,\mu$m, $g_m = 100$ mS, one obtains:

$$\mathrm{ENC}^2 \approx (1000\,e^-)^2\Big|_{\mathrm{shot}} + (15000\,e^-)^2\Big|_{1/\mathrm{f}} + (13500\,e^-)^2\Big|_{\mathrm{therm}} \approx (20200\,e^-)^2\,.$$

Here only a small (negligible) parallel shot noise (leakage current) contribution is assumed, which is typical for liquid argon calorimeters.

Practical noise levels range from $\sim 1e^-$ for CCD's at long shaping times to $\sim 10^4\,e^-$ in high-capacitance liquid argon calorimeters. Gaseous micropattern detectors like GEMs or MicroMegas (see Sec. 35.6.4) typically feature noise levels between $1000\,e^-$ and $1500\,e^-$, depending on the ability to correct for common-mode noise. Silicon strip detectors typically operate at levels of $\sim 10^3\,e^-$, whereas pixel detectors with fast readout typically have noise levels below about 100 electrons.

35.9.3 *Timing measurements*

In timing measurements, the slope-to-noise ratio must be optimized, rather than the signal-to-noise ratio alone, so the rise time t_r of the pulse is important. The "jitter" σ_t of the timing distribution is

$$\sigma_t = \frac{\sigma_n}{(dS/dt)_{\mathrm{trig}}} \approx \frac{t_r}{SNR}, \tag{35.37}$$

where σ_n is the rms noise, SNR the signal-to-noise ratio and the "slew rate" dS/dt, *i.e.* the derivative of the signal, is evaluated at the trigger level. The rise-time of a CSA again depends on the detector and feedback capacitances and on the amplifier transconductance

$$t_r \propto \frac{C_D}{C_f \cdot g_m}\,. \tag{35.38}$$

To increase dS/dt without incurring excessive noise, the amplifier bandwidth should match the rise-time of the detector signal. The 10% to 90% rise time of an amplifier with bandwidth f_U is $0.35/f_U$. For example, an oscilloscope with 350 MHz bandwidth has a 1 ns rise time. For cascaded amplifiers the individual rise times add in quadrature to first order.

As increasing SNR also improves the time resolution, minimizing the total input capacitance is extremely important for timing measurements (see also Sec. 35.8). At high signal-to-noise ratios, the time jitter can be much smaller than the rise time. The time-mark distribution of pulses may shift with the signal level ("time walk"), but this can be corrected by various means, either in hardware or in software.

For applications aiming at extreme time resolution a charge sensitive (integrating) amplification is not optimal. Transimpedance or voltage amplifiers converting current/voltage to voltage are preferred. Also, when aiming for picosecond timing using voltage amplifiers, *e.g.*, with LGAD detectors having C_D of $\mathcal{O}$(pF) (see Sec. 35.8), not only the preamplifier rise time t_r but also the signal pulse duration t_d at the preamplifier input is important, *i.e.*, the preamplifier must react draining the charge from C_D before the input voltage $v_{in} = Q_S/C_D$ (Q_S = signal charge) reaches its peak. Both times must reasonably match, $t_r \approx t_d$, resulting in a time jitter of [355]

$$\sigma_t^2 \approx \frac{C_D^2}{Q_S^2}\frac{d\langle v_n^2\rangle}{df}\,t_d\,, \tag{35.39}$$

where $d\langle v_n^2\rangle/df$ is the voltage noise spectral density.

35.9.4 *Digital signal processing*

The filtering principles apply to both analog and digital signal processing. In digital signal processing the pulse shaper shown in Fig. 35.27 is replaced by an analog to digital converter (ADC) followed by a digital processor that determines the pulse shape. Digital signal processing allows great flexibility in implementing filtering functions. The software can be changed readily to adapt to a wide variety of operating conditions and it is possible to implement filters that are impractical or even impossible using analog circuitry. However, this comes at the expense of increased circuit complexity and increased demands on the ADC compared to analog shaping.

If the sampling rate of the ADC is too low, high frequency components will be transferred to lower frequencies ("aliasing"). The sampling rate of the ADC must be high enough to capture the maximum frequency component of the input signal. Apart from missing information on the fast components of the pulse, undersampling introduces spurious artifacts. If the frequency range of the input signal is much larger than the sampling rate, the noise at the higher frequencies will be transferred to lower frequencies and will increase the noise level in the frequency range of pulses formed in the subsequent digital shaper. The Nyquist criterion states that the sampling frequency must be at least twice the maximum relevant input frequency. This requires that the bandwith of the circuitry preceding the ADC must be limited. The most reliable technique is to insert a low-pass filter.

The digitization process also introduces inherent noise, since the voltage range ΔV corresponding to a minimum bit step introduces quasi-random fluctuations relative to the exact amplitude

$$\sigma_n = \frac{\Delta V}{\sqrt{12}}\,. \tag{35.40}$$

When the Nyquist condition is fulfilled the noise bandwidth Δf_n is spread nearly uniformly and extends to 1/2 the sampling frequency f_S, so the spectral noise density is

$$\frac{\sigma_n}{\sqrt{\Delta f_n}} = \frac{\Delta V}{\sqrt{12}}\cdot\frac{1}{\sqrt{f_S/2}} = \frac{\Delta V}{\sqrt{6 f_S}}\,. \tag{35.41}$$

Sampling at a higher frequency spreads the total noise over a larger frequency range, so oversampling can be used to increase the effective resolution. In practice, this quantization noise is increased by the ADC's differential non-linearity. Furthermore, the equivalent input noise of ADCs is often rather high, so the overall gain of the stages preceding the ADC must be sufficiently large for the preamplifier to override the ADC input noise.

35.9.5 *What to use when?*

When implemented properly, digital signal processing provides significant advantages in systems where the shape of detector signal pulses changes greatly, for example in large semiconductor detectors for gamma rays or in gaseous detectors (*e.g.* TPCs) where the duration of the current pulse varies with drift time, which can range over orders of magnitude. Analog signal processing is best or most efficient in systems that require fast time response, but the high power requirements of high-speed ADCs are prohibitive. Systems that are not sensitive to pulse shape can use fixed shaping time constants and rather simple filters (like CR–RC), which can be either continuous or sampled. In high density systems that require small circuit area and low power (*e.g.*, in strip and pixel detectors), analog filtering often yields the required response and tends to be most efficient.

As stressed already in the introduction, it is important to consider that additional noise is often introduced externally. Recognizing additional noise sources and minimizing cross-coupling

Downloaded from https://academic.oup.com/ptep/article/2022/8/083C01/6651666 by KIT Library user on 27 September 2022

to the detector current loop is often essential to obtain the best overall noise performance. Understanding basic physics and its practical effects is important in forming a broad view of the detector system and recognizing potential problems (*e.g.* modified data), rather than merely following standard recipes.

More comprehensive treatments of low noise detector readout and signal processing can be found, for example, in [8, 352, 354] and in [1, 344].

35.10 Calorimeters

35.10.1 *Introduction*

Revised August 2021 by F. Sefkow (DESY, Hamburg) and F. Simon (Werner-Heisenberg-Inst.).

A calorimeter measures the energy and direction of particles by absorption in the detector material and registration of the energy deposited in an (ideally) contained electromagnetic (EM) or hadronic shower. Calorimeters are central components of modern high energy physics experiments, due to their ability to measure not only the energy of charged particles (with the exception of muons), but also of photons and neutral hadrons, thus enabling the reconstruction of π^0 and η decays and of exclusive final states involving long-lived neutral kaons, or neutrons. They are indispensable for the measurement of particle jets and for the reconstruction of total event properties, which, via the measurement of missing energy (or missing transverse energy in hadron colliders). enable the detection of the presence of "invisible" particles such as neutrinos and hypothetical particles such as dark-matter candidates. Calorimeters are also important for the identification of particle species, using information on the longitudinal and transverse shape of the energy deposition to separate electrons, photons, hadrons and muons. While the performance of calorimeters is typically assessed by the quality of their energy measurements, position resolution, both for EM and hadronic showers, is also highly relevant, for example for the reconstruction of effective jet masses. The capability to measure high-level observables that serve to classify events, such as particle and jet energies, missing energy and isolated leptons, makes calorimeters central components of the trigger systems in high-energy physics experiments.

In collider experiments, the importance of calorimeters tends to increase with increasing collision energies since the relative energy resolution improves with increasing particle energy while the depth required for full containment of the showers shows only logarithmic growth with energy. This is in contrast to the precision of track-based measurements, which is decreasing with increasing momentum. With recent advances in timing capabilities calorimeters are also contributing to the rejection of pile-up from multiple interactions within the same bunch crossings at colliders.

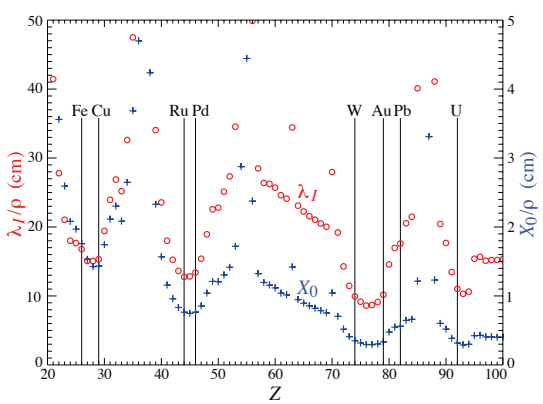

Figure 35.30: Nuclear interaction length λ_I/ρ (circles) and radiation length X_0/ρ (+'s) in cm for the chemical elements with $Z > 20$ and $\lambda_I < 50$ cm.

The characteristic length scale for EM showers is the radiation length X_0, which ranges from 1.8 cm (13.8 g cm^{-2}) in iron to 3.2 mm (6.0 g cm^{-2}) in uranium for materials used to generate showers in calorimeters.[4] Similarly, the characteristic nuclear interaction length λ_I varies from 16.8 cm (132.1 g cm^{-2}) (Fe) to 11.0 cm (209 g cm^{-2}) (U).[5] There is a premium on small λ_I/ρ and X_0/ρ (both with units of length). These quantities are shown for elements with $Z > 20$ in Fig. 35.30. The minima for both X_0 and λ_I correspond to elements between W and Au. Some of these elements are very difficult to work with (e.g. W) or expensive (e.g. Au), so, depending on the application (size of the required calorimeter) other materials, such as Fe, Cu, Pb, and different alloys like brass and CuW are often chosen. For EM calorimeters high Z is preferred; here Pb is a popular choice, while W provides even higher density and is generally affordable due to the limited volume of EM systems.

Most existing calorimeters are subdivided into a front EM section (ECAL) and a hadronic part (HCAL) behind; electrons and photons are measured in the ECAL, while hadrons and jets are measured in the combined ECAL and HCAL system. The detailed design depends on energy range and performance requirements as well as on size and cost constraints for the entire system. EM calorimeters tend to be 15–30 X_0 deep, while hadronic calorimeters are usually optimised for cost and performance at 5–8 λ_I. The depth of the ECAL typically corresponds to approximately 1 λ_I, with the exact value depending on the material. This means that approximately 70% of all hadronic showers will already begin in the electromagnetic calorimeter, making its response to a hadronic cascade highly relevant for the overall performance of the system. The choice of the calorimeter technology for the ECAL is thus a result of simultaneous optimisation for EM and hadronic performance of the overall system.

Sampling calorimeters consist of a high-density, normally metallic absorber sandwiched (or threaded) with an active material which generates a signal in response to shower particles. The active medium may be a scintillator, a noble liquid, a gas, silicon, or a Cherenkov radiator. These active media all have a relatively low Z, a significantly lower density, and larger X_0 and λ_I values than typical absorber materials. The average radiation and interaction lengths in the full detector are thus larger than those of the absorber alone.

There are also *homogeneous calorimeters*, in which the entire volume contributes to the signal. Homogeneous calorimeters may be built with inorganic heavy scintillating crystals or non-scintillating Cherenkov radiators such as lead glass and lead fluoride. Nuclear interaction lengths in inorganic crystals range from 17.8 cm ($LuAlO_3$) to 42.2 cm (NaI). Materials with low X_0 used in large systems are for example BGO with $\lambda_I = 22.3$ cm and $X_0 = 1.12$ cm, and $PbWO_4$ (20.3 cm and 0.89 cm). Properties of these and other commonly used inorganic crystal scintillators can be found in Table 35.4. Cryogenic noble liquids, where scintillation light and/or inonization can be detected, are also suitable materials for homogeneous detectors.

Homogeneous calorimeters at colliders are usually only used for the EM section. For the use of homogeneous calorimeters for hadron energy measurement, the large differences in the response to EM and hadronic parts of the shower are a significant challenge, as is the three-dimensional segmentation. This is still requiring substantial R&D, including the search for affordable materials. In non-accelerator physics experiments or at neutrino beams, homogeneous calorimeters, where the sensitive medium can be water or ice, scintillator, a noble liquid or the atmosphere itself, are used to detect both EM and hadronic showers.

Comprehensive tables of particle-physics calorimeters are given as Appendix C in Ref. [356].

35.10.1.1 *Energy Resolution and System Performance*

The energy resolution of calorimeters is a complex observable, due to the variety of contributing processes with different energy dependencies, and response functions often not perfectly Gaussian. Nevertheless, a simplified picture is useful in practice, and in particular for EM calorimeters also numerically accurate. For hadronic calorimeters additional complications must be taken into

[4] $X_0 = 120$ g cm^{-2} $Z^{-2/3}$ to better than 5% for $Z > 23$.
[5] $\lambda_I = 37.8$ g cm^{-2} $A^{0.312}$ to within 0.8% for $Z > 15$.
See https://pdg.lbl.gov/current/AtomicNuclearProperties for actual values.

Downloaded from https://academic.oup.com/ptep/article/2022/8/083C01/6651666 by KIT Library user on 27 September 2022

account. In such a simplified picture, due to the stochastic nature of shower evolution, the intrinsic calorimeter energy resolution, σ, is proportional to $\sqrt{E}$, as the number of charged particles, or the total ionising track length in a shower are on average proportional to the incident particle energy E. The relative resolution σ/E therefore improves with $A/\sqrt{E}$, where A denotes the so-called *stochastic term*. The readout system of the active medium will contribute noise to the resolution, $\sigma_N = B$, which in general is not energy-dependent. Effects that are proportional to the total deposited energy result in a *constant term*, $\sigma_C = C \cdot E$. Different sources contribute to this term, depending on the type of calorimeter. For both EM and hadronic calorimeters, imperfections of the detector, inhomogeneities such as density variations or those introduced by the detector mechanics, instabilities in time, imperfections of the readout or incorrect calibration of channels contribute. Shower leakage, which depends on particle energy, also contributes to the resolution with approximately linear dependence on energy. In non-compensating hadronic calorimeters, fluctuations of the EM fraction f_{em} from shower to shower, together with the energy dependence of the average f_{em} value, can lead to a significant constant term that often dominates over the instrumental effects. Adding up all contributions in quadrature yields the standard parameterisation of the relative energy resolution of a calorimeter:

$$\frac{\sigma}{E} = \frac{A}{\sqrt{E}} \oplus \frac{B}{E} \oplus C\,. \tag{35.42}$$

In particular the effects specific to hadronic showers give rise to non-Gaussian distributions of the energy response. Therefore care must be used in performance comparisons, as different parameterisations of the line shape and different definitions of the resolution are in use. In some cases, a linear rather than a quadratic addition of the stochastic and constant term may provide a better description of the energy resolution as a function of energy. It should be noted that the individual terms then lose the simplified interpretation discussed above, and care has to be taken when comparing performance based on fits to the energy dependence of the resolution.

Typically, primarily the stochastic term — which is determined by the calorimeter design in terms of material and geometry — is considered in order to describe the overall properties of a calorimeter. For the calorimeters of the multi-purpose experiments at the LHC, the stochastic terms are $3 - 10\%$ for electromagnetic and $50 - 80\%$ for hadronic calorimeters. In practice, the energy resolution of a calorimeter at high energies is limited by the constant term C, which in the EM case mainly reflects the precision and stability of the mechanical construction, electronic readout system and calibration. Typical constant terms are a few per-mil for EM and a few percent for hadronic calorimeters. For concrete examples and references see Tables 35.11 and 35.13.

For sampling calorimeters, the stochastic term depends on the *sampling fraction* $f_{\rm samp}$, i.e. the ratio of energies deposited in the active and passive material. Also the *sampling frequency* enters, which is determined by the number N of different sampling elements present in the region in which the shower develops. The stochastic term A scales approximately with $1/\sqrt{f_{\rm samp}}$, and for given $f_{\rm samp}$ and total depth, with $1/\sqrt{N}$.

While the energy resolution for single hadrons (most commonly pions) is often used as the key performance criterion for a hadronic calorimeter, it has to be noted that this value is only of limited relevance in high-energy physics experiments. In most experiments, the calorimetric measurement of hadrons is based on the combined system consisting of ECAL and HCAL. Moreover, for the physics capabilities of a detector at a high-energy particle collider, also the combined calorimetric resolution for single hadrons is not a sufficient criterion to fully characterise hadronic performance, but rather the jet energy resolution, the resolution for missing (transverse) energy, and the capability to cope with high background and pile-up levels. These quantities cannot be measured directly with prototypes in beam tests, and strongly depend on overall system aspects and reconstruction tools. However, the performance in these observables can be reliably inferred from system simulations once the simulated response to single particles and the simulated topology of showers has been validated in detail by beam tests.

Besides energy resolution, response linearity is an important factor in the design of calorimeters. While a non-linear response for single particles can be corrected for if appropriate calibration measurements exist, such corrections deteriorate the energy resolution, in particular in the case of superposition of several showers, as it often occurs in jets. Sources for non-linearities can be intrinsic to the design, for example due to saturation effects in the active medium with increasing energy density, due to leakage, or connected to shower physics as discussed in section 35.10.3.

The energy resolution for hadrons is intrinsically limited by large event-to-event fluctuations of the shower evolution and of "invisible" components not contributing to the detector signal. It remains the limiting factor for single particles and for the high-level performance for jets and total event properties. This has motivated intense research in the past decades. One direction aims at improving the hadronic resolution by extracting additional signals to disentangle the shower composition, e.g.with so-called dual read-out methods, and is explained in the hadron calorimeter section 35.10.3. Another, so-called "particle flow" approach described below optimises the combination of measurements of individual particles in different detector components. Ideally, both methods can be combined.

35.10.1.2 *Role of Simulations*

Simulations have become indispensable for the design of detectors and the development of reconstruction algorithms. Since event-to-event fluctuations drive calorimeter performance, Monte Carlo techniques that accurately model the evolution of particle cascades in material are required. By far the most common computer code in use today is the *GEANT4* toolkit [357, 358], which provides a step-based simulation of the passage of particles through matter. Thanks to the relative simplicity of EM cascades, simulations of EM showers are typically highly accurate. The modelling of hadronic showers is more complex, and suffers from larger uncertainties. Significant improvement has been achieved in this area, moving from simpler parameterised models to physics-driven interaction models. From early on, detailed codes and data describing nuclear break-up and neutron transport like *CALOR* [359] or *FLUKA* [360, 361] contributed crucially to the understanding of hadron calorimetry. The simulations reproduce the general features of the substructure of hadronic showers, characterised by dense shower activity and sparser ionising track segments, and their accuracy is adequate for most purposes of quantitative design optimisations. Details of the implementation of physics models in *GEANT4* are discussed in [362].

35.10.1.3 *Particle flow approach*

In a typical collider experiment, the EM and hadronic calorimeter system surrounds a charged-particle tracking volume devised for momentum measurement in a magnetic field. Matching tracks to calorimetric energy deposits provides corrections for the magnetic deflection of the charged particles, necessary for the reconstruction of invariant masses in multi-jet final states, or of the total momentum imbalance. Furthermore, for charged particles the track-based measurements are far more precise for particles in jets with energies of up to several hundred GeV, so using these instead of calorimeter energies may optimise the jet energy resolution. This so-called "particle flow" approach aims at reconstructing each particle individually, using a combination of the best measurements from the detector.

About 60% of the energy in a typical jet is carried by charged particles, predominantly hadrons, 30% by photons and only 10% by long-lived neutral hadrons (K_L^0 and n), for which hadronic calorimetry is unavoidable. Assuming, as motivated by detector designs proposed for a future Higgs factory, $15\%/\sqrt{E(\mathrm{GeV})}$ for photons and $55\%/\sqrt{E(\mathrm{GeV})}$ for hadrons, then, in the ideal case, where each particle is resolved, a jet energy resolution of $19\%/\sqrt{E(\mathrm{GeV})}$ could be obtained. Here the dominant part ($18\%/\sqrt{E(\mathrm{GeV})}$) is still due to the calorimeter resolution for the neutral hadrons.

The particle flow method places high demands on the imaging

Downloaded from https://academic.oup.com/ptep/article/2022/8/083C01/6651666 by KIT Library user on 27 September 2022

capabilities of the calorimeters, and on the pattern recognition performance of the reconstruction algorithms. Only energy deposits not associated with charged particles and not identified as photons, will be interpreted as neutral hadrons. In practice, this cannot always be done unambiguously, and mis-assignments give rise to an additional measurement uncertainty, which is called *confusion*. For simulated detectors at proposed future Higgs factories jet energy resolutions of 3-4% have been demonstrated, significantly larger than in the ideal case, but sufficient for the required efficient separation of W and Z hadronic final states.

Particle flow-like techniques were first applied in the ALEPH detector [363], which achieved a jet energy resolution of $60\%/\sqrt{E}$, or 6.2 GeV for hadronic Z decays. More recently, particle flow techniques are successfully used in the CMS experiment [364], for example improving the missing energy resolution by one third over a wide range.

The Pandora particle flow algorithm (PFA) [365] is the most developed and best performing today in the context of future lepton colliders. The algorithms make use of topological information, including the sub-structure of showers, as well as the compatibility of calorimetric and track-based measurements. In this way the purely calorimetric performance for the jet is either retained or improved. In the framework of studies for CLIC [366], it was shown that the required jet energy resolution of 3.5% can be achieved with the PF technique for jet energies up to 1500 GeV.

For the use of energy-momentum matching in the assignment of energy depositions, and for energy flow treatment of dense jets, particle flow calorimeters with their emphasis on imaging must still feature a good energy resolution. Furthermore, the neutral hadron energy uncertainty is the dominant contribution to the jet resolution for low energy jets, where particles are well separated, while at higher energies the confusion effects take over.

High granularity in all three space dimensions comparable to or smaller than the length scales of particle showers given by X_0 and ρ_M for both ECAL and HCAL brings additional advantages; for example it offers ideal conditions for the application of software compensation methods, which improves the intrinsic resolution and also reduces "confusion" [367]. A particular strength is the possibility to use topological information such as the reconstructed starting point of the shower for the estimation of leakage. Moreover, the combination of fine-grained topological reconstruction and cuts on cluster-wise timing with a precision of few tens of pico-seconds allows for powerful pile-up rejection. This extends the application range of particle flow methods towards collider environments with less benign background conditions, like multi-TeV e^+e^- collisions, and it is an asset on its own for high-intensity hadron colliders, even if particle flow methods are difficult to apply.

The performance of highly granular calorimeters depends, among others, on the particle separation and pattern recognition capabilities and on the single particle energy and timing resolution. They are thus not only optimised for energy measurement, but also for multi-dimensional shower reconstruction and particle separation in space and time.

35.10.2 *Electromagnetic calorimeters*

Revised October 2021 by C.L. Woody (BNL) and R.-Y. Zhu (HEP California Inst. of Technology).

The development of electromagnetic showers is discussed in the section on "Passage of Particles Through Matter" (Sec. 34 of this *Review*). Formulae are given which approximately describe average showers, but since the physics of electromagnetic showers is well understood, a detailed and reliable Monte Carlo simulation is possible. EGS4 [368] and GEANT [357] have emerged as the standards.

Electromagnetic calorimeters are devices that are designed to measure the total energy of electrons and photons by total absorption. They come in two general categories: homogeneous and sampling. In a homogeneous calorimeter, all of the particle's energy is deposited in the active detector volume and is used to produce a measurable signal (either scintillation light, Cherenkov light or charge). Homogeneous electromagnetic calorimeters are typically constructed using high density, high Z inorganic scintillating crystals such as BaF_2, BGO, CsI, CsI(Tl), LYSO, NaI(Tl) and PWO, non-scintillating Cherenkov radiators such as lead glass and lead fluoride (PbF_2), or ionizing noble liquids such as liquid argon, liquid krypton or liquid xenon. The properties of some commonly used inorganic crystal scintillators can be found in Table 35.4. Total absorption homogeneous calorimeters such as those built with heavy crystal scintillators provide the best energy resolution for measuring electromagnetic showers and are generally used when the best possible performance is required, particularly at lower energies. Attention, however, needs to be paid to radiation damage in inorganic scintillators when exposed to the typical environment of high luminosity proton colliders, as discussed below and in Section 35.4.

A sampling calorimeter consists of an active medium which generates a signal and a passive medium which functions as an absorber. In this case, most of the particle's energy is deposited in the absorber and only a fraction of the energy is detected in the active medium. The ratio of energy in the sampling medium to the total enegy in calorimeter is called the sampling fraction. The active medium may be a scintillator, an ionizing noble liquid, a semiconductor, or a gas ionization detector. The absorber is typically a heavy metal with a high Z such as lead, tungsten, iron, copper, or depleted uranium. The active material is interspersed with the passive absorber in a variety of ways, e.g. by using alternating plates of active material and absorber or embedding the active material, such as scintillating fibers, into the absorber. The main difficulty in this approach is extracting the signal from the active material. One possibility is a simple stack of alternating absorber and active material, which, however, usually leads to gaps for services and hence non-uniformities. This can be improved by using a so-called "spaghetti" design, where scintillating fibers are brought to the front or back of the detector and read out. This can also be done with either wavelength shifting plates or fibers, such as in a so-called "shashlik" design where wavelength shifting fibers run through the stack of alternating scintillator and absorber plates and are read out at one end, or embedding wavelength shifting fibers in the scintillating plates which are then brought out to the edges or back of the detector and read out. For ionization detectors, there is also an "accordion" design which avoids all gaps for services and where the absorber plates are folded into an accordion shape along with interspersed electrodes to collect the ionization charge [369]. While these readout schemes are generally more complicated than those for homogeneous calorimeters, the sampling calorimeter design allows the construction of large calorimeters at much lower cost than homogeneous calorimeters.

The energy resolution σ_E/E of a calorimeter can be parameterized as $a/\sqrt{E} \oplus b \oplus c/E$, where $\oplus$ represents addition in quadrature and E and σ_E are in GeV. The stochastic term a represents statistics-related fluctuations such as intrinsic shower fluctuations, photoelectron statistics, dead material at the front of the calorimeter, and sampling fluctuations for minimum ionizing particles. For a fixed number of radiation lengths, the stochastic term a for a sampling calorimeter is expected to be proportional to $\sqrt{t/f}$, where t is plate thickness and f is sampling fraction [370–372]. The stochastic term a is typically of the order of a few percent for a homogeneous calorimeter, and is generally in the range of 8 to 20% for sampling calorimeters, depending on the sampling fraction.

The main contributions to the systematic, or constant, term b are detector non-uniformity and calibration uncertainties. In the case of hadronic cascades discussed below, non-compensation also contributes deviations from $\sqrt{E}$ scaling. Another important contribution to the energy resolution of calorimeters that are used in high radiation environments such as high lumnosity colliders is radiation damage of the active medium. Radiation damage can induce optical absorption in scintillating materials which reduces the measured light output and produces non-uniformities in light collection. This can be mitigated by developing radiation-hard active media [373], by reducing the signal path length [374] and by frequent *in situ* calibration and monitoring [73, 372]. With effort, the constant term b can be reduced to below one percent. The term c is due mainly to electronic noise summed over the readout

Downloaded from https://academic.oup.com/ptep/article/2022/8/083C01/6651666 by KIT Library user on 27 September 2022

Table 35.11: Resolution of typical electromagnetic calorimeters. E is in GeV.

Technology (Experiment)	Depth	Energy resolution	Date
NaI(Tl) (Crystal Ball)	$20X_0$	$2.7\%/\mathrm{E}^{1/4}$	1983
$Bi_4Ge_3O_{12}$ (BGO) (L3)	$22X_0$	$2\%/\sqrt{E} \oplus 0.7\%$	1993
CsI (KTeV)	$27X_0$	$2\%/\sqrt{E} \oplus 0.45\%$	1996
CsI(Tl) (BaBar)	16–$18X_0$	$2.3\%/E^{1/4} \oplus 1.4\%$	1999
CsI(Tl) (BELLE)	$16X_0$	1.7% for $E_\gamma > 3.5$ GeV	1998
CsI(Tl) (BES III)	$15X_0$	2.5% for $E_\gamma = 1$ GeV	2010
$PbWO_4$ (PWO) (CMS)	$25X_0$	$3\%/\sqrt{E} \oplus 0.5\% \oplus 0.2/E$	1997
$PbWO_4$ (PWO) (ALICE)	$19X_0$	$3.6\%/\sqrt{E} \oplus 1.2\%$	2008
Lead glass (OPAL)	$20.5X_0$	$5\%/\sqrt{E}$	1990
Liquid Kr (NA48)	$27X_0$	$3.2\%/\sqrt{E} \oplus 0.42\% \oplus 0.09/E$	1998
Scintillator/depleted U (ZEUS)	20–$30X_0$	$18\%/\sqrt{E}$	1988
Scintillator/Pb (CDF)	$18X_0$	$13.5\%/\sqrt{E}$	1988
Scintillator fiber/Pb spaghetti (KLOE)	$15X_0$	$5.7\%/\sqrt{E} \oplus 0.6\%$	1995
Liquid Ar/Pb (NA31)	$27X_0$	$7.5\%/\sqrt{E} \oplus 0.5\% \oplus 0.1/E$	1988
Liquid Ar/Pb (SLD)	$21X_0$	$8\%/\sqrt{E}$	1993
Liquid Ar/Pb (H1)	20–$30X_0$	$12\%/\sqrt{E} \oplus 1\%$	1998
Liquid Ar/depl. U (DØ)	$20.5X_0$	$16\%/\sqrt{E} \oplus 0.3\% \oplus 0.3/E$	1993
Liquid Ar/Pb accordion (ATLAS)	$25X_0$	$10\%/\sqrt{E} \oplus 0.4\% \oplus 0.3/E$	1996

channels required to measure the shower energy (typically a few Molière radii).

The position resolution depends on the effective Molière radius and the transverse granularity of the calorimeter. Like the energy resolution, it can be factored as $a/\sqrt{E} \oplus b$, where a is the stochastic term, typically of the order of a few mm to 20 mm, and b can be as small as a fraction of mm for a dense calorimeter with fine granularity. Fine granularity also helps particle flow analysis discussed in the hadron calorimeters section below.

Electromagnetic calorimeters may also provide angular measurements for electrons and photons. This is particularly important for photon-related physics to identify the correct primary vertex, since photons are not detected by the tracking system of the overall experiment. The typical photon angular resolution is about 45 mrad/$\sqrt{E}$, which can be achieved by implementing longitudinal segmentation [369] for a sampling calorimeter or by adding a preshower detector [375] for a homogeneous calorimeter without longitudinal segmentation.

There have been many electromagnetic calorimeters built and used in particle physics experiments for a variety of applications. Table 35.11 provides a short list of the major ones used in some of the larger experiments. Also listed are calorimeter depths in radiation lengths (X_0) and the achieved energy resolution. Whenever possible, the performance of the calorimeters *in situ* is quoted, which is usually in good agreement with prototype test beam results as well as EGS or GEANT simulations, provided that all systematic effects are properly included. Details about detector design and performance can be found in Appendix C of reference [372] and Proceedings of the International Conference series on Calorimetry in High Energy Physics.

35.10.3 *Hadronic calorimeters*

Revised August 2021 by F. Sefkow (DESY, Hamburg) and F. Simon (Werner-Heisenberg-Inst.).

Hadronic calorimetry [356, 376, 377] is considerably more complex than electromagnetic (EM) calorimetry due to the wider range and different nature of physical processes contributing to shower development and energy deposition, which in turn are characterised by different length and time scales. Hadronic showers are initiated by inelastic strong interactions of highly-energetic charged and neutral hadrons with atomic nuclei. These interactions result in the production of secondary particles, which drive the development of the shower. Among these are energetic hadrons, as well as lower-energy nucleons, photons and nuclear fragments. Energy transferred to nuclear break-up, excitation or recoil does not, in general, produce a signal, but remains *invisible*, and event-to-event fluctuations of this invisible energy deposit ultimately limit the resolution of hadronic calorimeters (HCALs).

The length scale of the interaction of relativistic hadrons is given by the nuclear interaction length λ_I. As discussed in Section 35.10.1, λ_I is a factor 10 to 30 larger than X_0 for common materials used in the construction of calorimeters. HCALs thus require a significantly larger geometrical depth for full containment than electromagnetic calorimeters (ECALs), albeit not by the factor suggested by the ratio of λ_I/X_0 due to the different nature of the showers. A key role is played by the production of π^0s and their subsequent decay into two photons. These result in the formation of electromagnetic sub-showers which evolve on the scale given by the radiation length X_0, and thus require sufficiently fine sampling of the shower activity to capture also this electromagnetic component. The two different length scales occurring in hadronic showers, and the large fluctuations of hadronic, electromagnetic and invisible activity, result in significant event-to-event variations of the energy response and of the shower topology. This topology is characterized by a lumpy structure, with compact regions of high local energy density originating from electromagnetic sub-showers, and sparser hadronic activity with minimum-ionizing hadrons.

Figure 35.31 (left) shows the distribution of the longitudinal position of the first inelastic interaction measured for pion-induced hadronic showers with the highly-granular scintillator-steel HCAL of the CALICE collaboration [378]. The figure illustrates the exponential distribution, with a slope consistent with the pion interaction length expected from the geometry and material composition of the calorimeter. This distribution is well reproduced by simulations using GEANT4 [357, 362]. Figure 35.31 (right) shows the mean longitudinal shower profile, given by the mean energy deposition in each calorimeter layer, both relative to the front face of the calorimeter (dots, without corrections for dead cells) and relative to the measured shower starting point given by the first inelastic interaction (filled histogram). The latter is much more compact than the former, which is a convolution of the latter with the distribution of shower starting point shown in the left panel of the figure. This shows that the detector depth required for adequate shower containment is significantly influenced by the fluctuations of the position of the first hadronic interaction. Detection of this position allows for an estimate of leakage from a finite calorimeter volume, and it enables stringent tests of shower evolution models. In the past years, motivated by precision needs at the next generation of e^+e^- colliders, the CALICE

Downloaded from https://academic.oup.com/ptep/article/2022/8/083C01/6651666 by KIT Library user on 27 September 2022

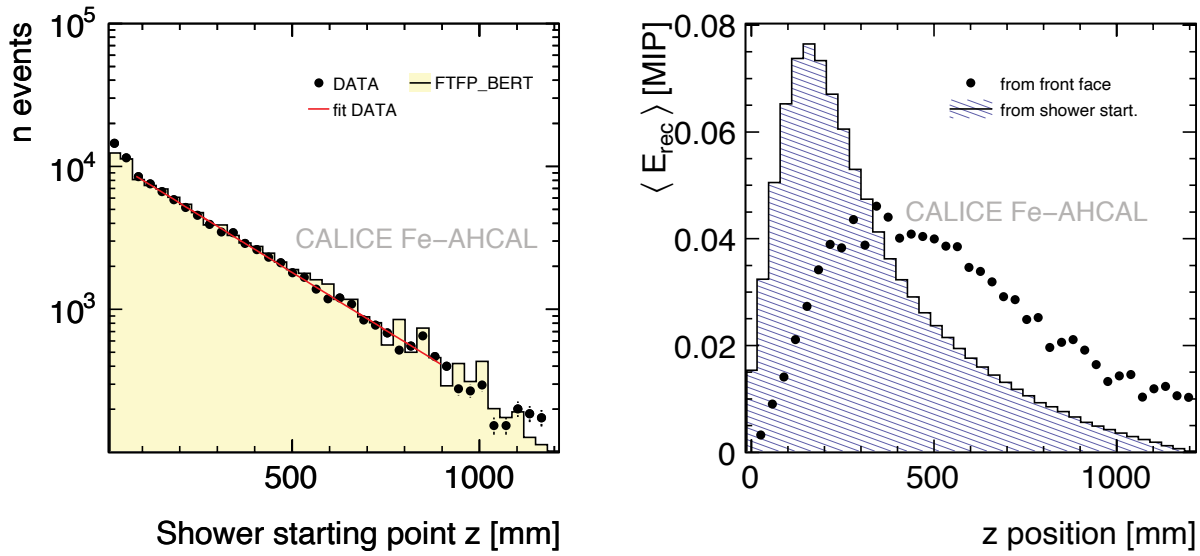

Figure 35.31: Longitudinal profile of hadronic showers induced by 45 GeV negative pions measured in he CALICE highly-granular steel-scintillator sampling calorimeter [378]. Left: Reconstructed position of the first inelastic interaction, compared to simulations (GEANT4 9.4p03, FTFP_BERT), and an exponential fit yielding a slope consistent with the expected pion interaction length. Right: Longitudinal shower profile measured from the front face of the calorimeter (dots, without corrections for dead cells) and relative to the position of the shower start given by the first inelastic interaction (filled histogram). The visible energy is given in units of the most probable energy loss of a minimum-ionizing particle (MIP). The integrals of the distributions are normalized to unity.

collaboration has constructed a number of prototypes with high 3-dimensional spatial granularity and recorded large sets of data at test beams, allowing for studies of shower evolution processes in unprecedented detail. The refined simulations support the trend to proceed from research focused on understanding the global intrinsic properties of showers, e.g. for the purpose of compensation, towards the study of detailed information, in space, time, and energy deposition type, through many and multiple readout channels.

In an inelastic hadronic collision a significant fraction f_{em} of the energy is removed from further hadronic interaction by the production of secondary π^0/η's, whose decay photons generate high-energy electromagnetic showers. Charged secondaries ($\pi^{\pm}$, p, ...) deposit energy via ionization and excitation, but also interact with nuclei, producing evaporation neutrons, spallation protons and neutrons, and heavier spallation fragments. The charged collision products produce detectable ionization, as do the showering γ-rays from the prompt de-excitation of highly excited nuclei. The recoiling nuclei generate little or no detectable signal, as mentioned previously. The neutrons lose kinetic energy in elastic collisions which generate ionization signals via recoiling protons, thermalize on a time scale of several μs, and are finally captured, with the production of more γ-rays—usually outside the acceptance gate of the electronics. Between endothermic spallation losses, nuclear recoils, and late neutron capture, a significant fraction of the hadronic energy (20%–40%, depending on the absorber and energy of the incident particle) is used to overcome nuclear binding energies and is therefore lost or "invisible."

In a hadron-nucleus collision a large fraction of the incident energy is carried by a "leading particle" with the same quark content as the incident hadron. If the projectile is a charged pion, the leading particle is usually a pion, which can be neutral and hence contributes to the EM sector. This is not true for incident protons. The result is an increased mean hadronic fraction for incident protons.

The complexity of hadronic showers also has a significant impact on the energy measurement. In contrast to EM showers, hadronic cascade processes are characterised by the production of relatively few high-energy particles. The number multiplicity of these particles produced in hadronic interactions increases only logarithmically with energy. The lost energy and f_{em} are highly variable from event to event, and on average increase with increasing energy [379]. Electromagnetic sub-showers typically result in a higher response than the hadronic parts of the cascade, where undetectable energy loss due to nuclear dissociation, the long time scales and the material dependence of neutron signals, as well as other effects reduce the measured signal. This difference in response is often expressed by the $\langle h/e \rangle$ ratio, a calorimeter-dependent quantity which is smaller than unity for many, but not all, HCALs. The increase of the electromagnetic fraction with energy thus introduces a non-linear contribution to the response. Combined with the significant event-by-event fluctuations between electromagnetic and hadronic fractions of the showers and between different hadronic processes the non-equality of h and e deteriorates the energy resolution of HCALs. Different strategies to address this exist, as discussed further below.

Most large HCALs are parts of complex 4π detectors at colliding beam facilities. To date, all these HCALs are sampling calorimeters. This choice is imposed by the physics of hadronic showers, both by the required depth for containment which favours high-density materials with short λ_I, and by the differences in response to electromagnetic and hadronic parts of the cascade, which are particularly severe for homogeneous calorimeters. Common absorber materials are Fe, Cu, Pb, and U, with W also used occasionally. A large variety of different active materials are used, depending on application and optimisation, from plastic scintillators (plates, tiles, bars, fibers), crystals and Cherenkov media, silicon, liquid argon (LAr), to gaseous detectors. The energy loss of particles in the active medium is either detected directly by collecting charge, or via scintillation or Cherenkov light observed with conventional photomultipliers (PMTs), photodiodes or silicon photomultipliers (SiPMs). The choice of both active and passive materials is driven by different, sometimes conflicting, constraints, including performance requirements, space and other mechanical boundary conditions, radiation tolerance, and cost considerations.

A wide range of different geometries of absorbers and sensors is used, with design choices depending on the chosen priorities of addressing these constraints, also considering the need to bring the signals to the outside of the detector while achieving a hermetic coverage and other constraints. In this context it is important to note that a classic sandwich structure with absorber plates and

Downloaded from https://academic.oup.com/ptep/article/2022/8/083C01/6651666 by KIT Library user on 27 September 2022

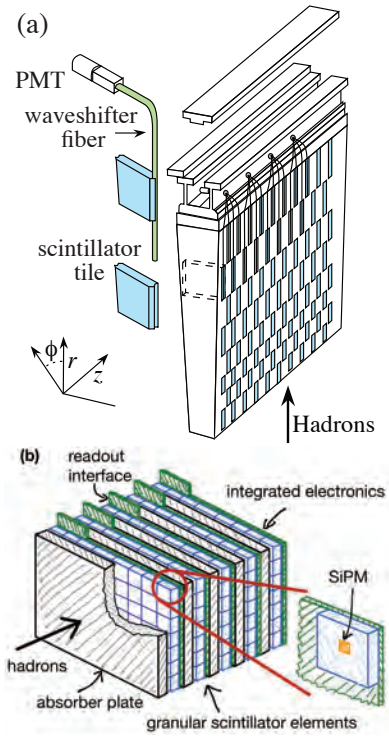

Figure 35.32: Two examples of geometrical structures of scintillator-based HCALs. (a) A wedge of the ATLAS central tile calorimeter consisting of scintillator tiles in iron, read out via wavelength-shifting fibers and PMTs [380]. The coordinate system is that of the ATLAS calorimeter within the experiment, with the z axis along the beam direction, r pointing radially outward, and ϕ being the azimuthal angle. (b) An illustration of the "SiPM-on-tile" structure used in the CALICE analogue HCAL prototype, and in the CMS High-Granularity Calorimeter (HGCAL), highly granular calorimeters with steel absorbers and small scintillator tiles directly read out via SiPMs with embedded electronics [377, 381, 385].

active elements approximately perpendicular to the particle incidence is not required, and arbitrary orientations are viable for good calorimetric measurements, as long as channelling, meaning the extended passage of primary particles through low-density active regions, is excluded. Figure 35.32 shows two examples of plastic scintillator-based calorimeters to illustrate differences in design between coarsely-segmented and highly-granular calorimeters. The ATLAS tile calorimeter [380] uses scintillator tiles coupled to wavelength-shifting fibers which collect the light from the tiles and guide them to PMTs outside of the active region of the calorimeter. The calorimeter is segmented in ϕ (azimuthal angle) and η (pseudorapidity, defined as $\eta = -\ln\tan(\theta/2)$, where θ is the angle relative to the beam axis), with coarse longitudinal segmentation. The technological prototype of the CALICE analog HCAL, a highly granular SiPM-on-tile calorimeter is based on scintillator tiles directly coupled to SiPMs, which, together with the front-end electronics, are embedded inside of the the active volume of the calorimeter. The CMS HGCAL [381] uses the same concept in part of the detector, and in addition embeds elements for digital data concentration and power distribution in the active volume. Other detector solutions include scintillating fibres threading an absorber [382], liquid-argon-filled tubes [383] and the "accordion" LAr detector [384]. The latter has zig-zag absorber plates to minimize channeling effects; the calorimeter is hermetic (no cracks), and plates are oriented so that cascades cross the same plate repeatedly.

In particular, but not exclusively, the combination of heavy absorber materials (Pb, U) with plastic scintillators allows the construction of HCALs that have a near-equal response to electromagnetic and hadronic parts of the cascade, so-called compensating calorimeters [386]. In this first study, it was recognized that nuclear fission can amplify the hadronic signal when using uranium absorbers. However, the key drivers of compensation are the reduction of the electromagnetic response with high-Z absorbers and an increased sensitivity to neutrons, which are strongly correlated to otherwise invisible energy loss due to nuclear dissociation, with a hydrogeneous active medium [387–391]. Since the electromagnetic cross section increases, and the critical energy decreases with Z, and since most of the energy of an electromagnetic shower is deposited by low-energy, short-range electrons, a disproportionate fraction of the total electromagnetic energy is deposited in the absorber in the high-Z case. Hydrogenous active media, such as organic scintillators, have a high sensitivity to spallation neutrons via elastic $n-p$ scattering. The number of produced neutrons is highly correlated with the invisible energy of the hadronic cascade. Increasing the sensitivity to these particles can thus boost the visible hadronic signal. Achieving compensation requires carefully-chosen sampling fractions and frequencies, with the response to the hadronic parts of the shower also sensitive to the integration time of the electronics due to the time structure of the neutron component of the signal.

Since Cherenkov light, for example in quartz plates or fibers, or in crystals, is produced only by relativistic particles in the cascade and thus predominantly by the electromagnetic component of the shower, such media are less common in hadronic than in ECALs. Notable exceptions are applications that require high radiation tolerance, and dual-readout calorimeters which specifically exploit this feature, as discussed below.

Silicon offers high compactness, high granularity, high radiation tolerance, long-term stability and fast charge collection, and is thus an interesting active material for sampling calorimeters. A thorough overview of the development and of the features of this technology can be found in a recent review paper [392]. The first silicon-based calorimeter in a collider experiment was a HCAL, the H1 PLUG calorimeter [393] covering the very forward region of the H1 experiment at HERA. The SICAPO collaboration has demonstrated the conceptual possibility of constructing compensating HCALs using silicon sensors [394]. Silicon is currently the technology of choice for several ECALs for future Higgs factories [395–397]. It is also being used extensively in the CMS HGCAL [381] in both electromagnetic and hadronic sections, complemented by scintillator tiles with on-tile SiPM readout where the radiation levels allow.

More generally, high-granularity calorimeters play an increasingly important role, in particular motivated by the use of particle-flow algorithms for global event reconstruction (see Section 35.10.1). The associated technologies for both electromagnetic and HCALs have been pioneered by the CALICE collaboration, which has built and tested an increasingly sophisticated series of "imaging" calorimeters with a highly granular readout [398]. In the area of HCALs, this includes the scintillator-based analog HCAL [399] with the latest SiPM-on-tile technological prototype with fully-integrated electronics having approximately 22,000 channels [385], as well as digital [400] and semidigital [401] calorimeters using gas detectors, such as RPCs (Sec. 35.6.7) and micropattern gas detectors (Sec. 35.6.4), with channel counts of up to 500,000. The large numbers of channels of high-granularity calorimeters presents a significant integration challenge for full detector systems, and requires the full integration of the front-end electronics inside of the active volume of the detector, as well as very compact data concentration and interface units. The first such detector in construction for a collider experiment is the CMS HGCAL [381]. The total silicon area of this detector amounts to about 600 m^2, and about 240,000 SiPMs are foreseen. The calibration of such calorimeters requires the monitoring of a large number of cells, which is achieved in-situ using reconstructed track segments within hadronic showers [381, 402] or externally identified muons. For this method, the capability to detect the most probable energy loss of a minimum-ionizing particle in a single cell is essential. This is required over the full lifetime of the detector, also after the active elements have received significant radiation damage, resulting in increased noise and reduced charge or signal collection efficiency. Due to the large number of cells contribut-

Downloaded from https://academic.oup.com/ptep/article/2022/8/083C01/6651666 by KIT Library user on 27 September 2022

ing to the measurement of one shower, the requirements on the precision of the calibration of individual cells is relaxed relative to the global energy calibration of the calorimeter.

The energy resolution of HCALs is severely affected by fluctuations between different components of the cascade, exacerbated by differences in response to purely hadronic and to electromagnetic sub-showers. In many detectors, fluctuations in the electromagnetic energy fraction, $f_{\rm em}$, and the related, consequential variations in nuclear energy dissociation losses, represent the biggest single contribution to the hadron energy resolution. One strategy to address this problem is the construction of intrinsically-compensating calorimeters, which imposes stringent constraints on materials and geometries as discussed above. Compensating calorimeters are not used in current large collider experiments, and are at the moment not considered for future collider detectors. Two different strategies are presently followed to improve the energy resolution in non-compensating calorimeters: Offline weighting or software compensation in longitudinally-segmented or in highly-granular calorimeters; and dual-readout calorimetry.

Software compensation techniques exploit the fact that electromagnetic sub-showers typically have a higher spatial density than the purely hadronic parts of the cascade. Amplitude (or energy-density) dependent weights are applied in the reconstruction to reduce the effects of shower-to-shower fluctuations. These techniques were pioneered by the CDHS collaboration for a longitudinally segmented steel-plastic scintillator calorimeter [403], where an improvement of the energy resolution of 10% (at 10 GeV) to 30% (at 140 GeV) for charged pion showers was achieved. Similar techniques were successfully applied in the H1 [404] liquid argon calorimeter system resulting in a stochastic term of $51\%/\sqrt{E}$, and in the ATLAS [405] endcap calorimeters, also based on liquid argon, with an energy resolution of $84\%/\sqrt{E}$. Inspired by these approaches, a software compensation technique using the detailed spatial information provided by highly-granular calorimeters of the CALICE collaboration has been developed, achieving up to 25% improvement of the energy resolution compared to the resolution without software compensation, resulting in a stochastic term of $45\%/\sqrt{E}$ [406] in a scintillator tile calorimeter with steel absorbers. This technique has also been successfully transferred to particle-flow reconstruction [407], resulting in an improvement of the jet-energy resolution in simulated events by 8% - 15%, depending on jet energy. Highly-granular calorimeters with software compensation and particle-flow reconstruction are currently studied as the baseline configuration for several Higgs-factory detectors.

The *dual-readout method*, originally proposed by Mockett in 1983 [408], measures $f_{\rm em}$ event by event in parallel to the total deposited energy. It uses the fact that most of the relativistic particles in the shower originate from the electromagnetic part, and that only those produce Cherenkov light, while the signal of the hadronic part is mostly due to non-relativistic protons. In practice either two different active media, e.g. scintillator and quartz, are used to register scintillation and Cherenkov light, respectively, or the optical signals from the two processes occurring in heavy crystals are disentangled, using their different spectral, directional or timing properties.

The Cherenkov and scintillation signals, normalised to the response for electrons, are given by

$$C = [f_{\rm em} + (h/e)_C(1 - f_{\rm em})]E\,, \tag{35.43}$$

$$S = [f_{\rm em} + (h/e)_S(1 - f_{\rm em})]E\,, \tag{35.44}$$

respectively, which can be solved for the fraction $f_{\rm em}$ and the energy

$$E = (\xi S - C)/(\xi - 1)\,, \tag{35.45}$$

where $\xi = [1 - (h/e)_C]/[1 - (h/e)_S]$ and $(h/e)_{C,S}$ denote the average ratios of hadronic to electromagnetic response in the Cherenkov and scintillator parts, respectively. This is illustrated in Figure 35.33, which shows their correlation for a set of simulated negative pion events [409] using FLUKA [361].

It was noted that the method demands a steep slope ξ, which implies that the scintillator read-out should be as compensating as possible, which however reduces the room for improvement by adding Cherenkov information.

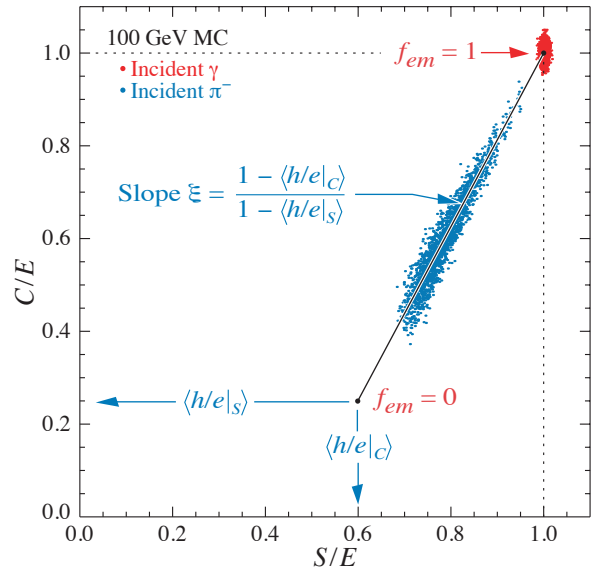

Figure 35.33: Scatter plot of Monte Carlo C/E (Cherenkov) vs S/E (scintillator) signals for individual events in a dual-readout calorimeter for 100 GeV negative pions and photons. Hadronic events are shown in blue, and scatter about the indicated event locus. Electromagnetic events cluster about $(C/E, S/E) = (1,1)$. In this case worse resolution (fewer p.e.'s) was assumed for the Cherenkov events, leading to the "elliptical" distribution.

The method was tested by the DREAM/RD52 collaboration [410,411], using a 1 ton copper matrix with embedded quartz and scintillating fibers. The value of ξ was about 3 in this detector. With this detector, a resolution of $70\%/\sqrt{E(\mathrm{GeV})}$ was obtained for single hadrons [412]. Due to the small size of the module, this includes contributions from transverse leakage which prevent the full exploitation of key features of dual readout, and thus underestimates the potential of the method.

The separate Cherenkov read-out evidently provides excellent pion-electron separation for particle identification. In another RD52 prototype, each fiber is read out individually by SiPMs, giving also a superior transverse granularity. A fiber-based calorimeter with full solid-angle coverage requires a pointing geometry due to the limited or missing longitudinal segmentation. The resulting challenges for a mechanical design are studied in the framework of the IDEA detector concept [413].

Table 35.12 shows selected examples of the energy resolution of HCALs for single charged pions achieved in beam tests. The examples are selected to illustrate the performance achieved with different designs ranging from intrinsic compensation to software compensation and dual readout, with a focus on results by R&D projects. It should be noted that the exact values of the different resolution terms depend on the functional form used in the fit, here the addition in quadrature is used for the cases where more than just the stochastic term is quoted. The results shown in the table illustrate that (close to) compensating calorimeters with optimized sampling fraction and frequency, such as HELIOS (U-plastic scintillator) and SPACAL (Pb-plastic scintillator), achieve a very good energy resolution. The comparison with Bernardi *et al.*, which has the same Pb/scintillator ratio by volume as SPACAL, but coarser sampling in a sandwich structure, illustrates the importance of the geometrical details. Beyond the examples shown in the table, liquid argon has also been explored as an active medium, for example in the context of the SLD detector with different absorber options [418]. Due to the reduced sensitivity to neutrons in the shower, not the same resolution as for plastic-scintillator-based systems is achieved. This technology has also been used in the D0 experiment, as discussed below. The dual-readout method has the potential to reach or surpass this

Downloaded from https://academic.oup.com/ptep/article/2022/8/083C01/6651666 by KIT Library user on 27 September 2022

Table 35.12: Energy resolution of selected hadron calorimeters for single charged hadrons obtained in beam tests.

Calorimeter	Passive	Active	Resolution	Ref.
Bernardi *et al.*	Pb	Scintillator layers	$44.2\%/\sqrt{E}$ §	[414]
CALICE AHCAL	Fe	Scintillator tiles	$44.3\%/\sqrt{E} \oplus 1.8\%$ †	[406]
CALICE W-AHCAL	W	Scintillator tiles	$57.9\%/\sqrt{E} \oplus 4.6\% \oplus 0.065/E$ §	[415]
CDHS	Fe	Scintillator layers	$58\%/\sqrt{E}$ ♯	[403]
DREAM/RD52	Pb	Scint.+ Quartz fibers	$70\%/\sqrt{E}$ *	[412]
HELIOS	U	Scintillator layers	$34\%/\sqrt{E}$ §	[416]
SPACAL	Pb	Scintillating fibers	$33.3\%/\sqrt{E} \oplus 2.2\%$ §	[417]

§ Bernardi *et al.*, CALICE W-AHCAL, HELIOS, SPACAL: (near-)compensating calorimeters.
† CALICE AHCAL: Local software compensation exploiting the high granularity of the calorimeter.
♯ CDHS: Offline weighting using longitudinal information.
* DREAM/RD52: Due to the relatively small transverse size of the detector lateral leakage was significant, deteriorating the energy resolution with respect to the full potential of the dual readout method.

performance, but would require a prototype sufficiently large for full longitudinal and transverse shower containment for an experimental demonstration. The two CALICE calorimeters shown, which use the same active elements (5 mm thick scintillator tiles) but different absorbers (21.4 mm Fe vs 10 mm W + 4 mm Fe) per layer, illustrate the impact of the absorber choice on energy resolution and reconstruction possibilities. While the tungsten-based W-AHCAL setup is very close to compensating, the steel-based AHCAL achieves a better energy resolution when software compensation is applied, profiting from the finer sampling of the electromagnetic parts of the cascade and the correction for shower-to-shower fluctuations of the electromagnetic fraction in the reconstruction. In the case of tungsten, software compensation does not significantly improve the energy resolution, as expected. The comparison of the CALICE AHCAL performance with the one of CDHS illustrates the benefits of higher granularity for software compensation techniques, but it should be noted that the absorber thickness of the latter is 25 mm, with the same scintillator thickness as in the case of CALICE.

As explained in the introduction, in most high-energy physics experiments, the HCAL follows after an ECAL, making the response of the latter to hadronic cascades highly relevant for the overall performance of the combined ECAL HCAL system. For scenarios where the electromagnetic and the HCAL have very different $\langle h/e \rangle$, as is typically the case for crystal-based ECALs, the fluctuations of the fraction of the hadronic shower contained within the ECAL result in a significant deterioration of the energy resolution for hadrons. A deterioration of the hadronic performance also results from larger amounts of not-instrumented material, e.g. supports and services, between electromagnetic and hadronic sections. In particle-flow calorimeters, a large value of the λ_I/X_0 ratio of the absorber material, like in tungsten, maximises the longitudinal separation of electromagnetic and hadronic showers. This is reflected in the design of particle-flow-based detector concepts for future Higgs Factories.

Table 35.13 summarizes the single hadron energy resolution obtained from test beams of the combined ECAL and HCAL systems of the large multi-purpose experiments at HERA, the Tevatron and at the LHC. These systems are examples of different optimization strategies. D0 and ZEUS are near-compensating systems with the same technology in ECAL and HCAL emphasizing hadronic performance. ATLAS and H1 use sampling ECALs with good electromagnetic resolution and weighting techniques exploiting longitudinal and transverse shower information for hadronic energy reconstruction. CMS, with a crystal ECAL and a scintillator-brass HCAL, prioritizes electromagnetic performance, with very different $\langle h/e \rangle$ in the electromagnetic and hadronic system. Of the detectors shown in the table, CMS has the best electromagnetic resolution by a comfortable margin, but consequently the weakest hadronic resolution. The best hadronic performance is achieved with the compensating calorimeter of ZEUS, which however has a weaker electromagnetic performance than the other calorimeter systems shown here. It should be noted that an excellent single-hadron resolution in general does not fully propagate into the jet-energy performance. Inactive material in front of the calorimeter can significantly worsen the energy resolution for jets, with an impact in particular on lower-energy particles. For example, the core of the invariant mass distribution of hadronically-decaying Z^0 bosons measured in ZEUS, which had a superconducting coil in front of the calorimeter, is well described by a Gaussian with a σ of 6 GeV [425], approximately 40% wider than would be expected for a jet-energy resolution that is identical to the single-hadron performance.

35.10.4 *Free electron drift velocities in liquid ionization chambers*

Revised August 2009 by W. Walkowiak (Siegen U.).

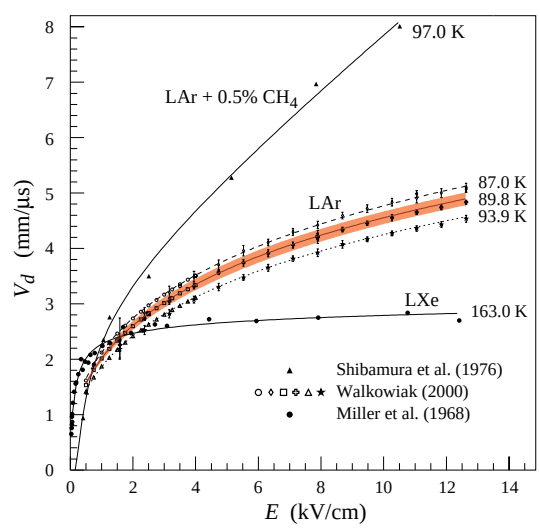

Figure 35.34: Drift velocity of free electrons as a function of electric field strength for LAr [284], LAr + 0.5% CH_4 [426] and LXe [427]. The average temperatures of the liquids are indicated. Results of a fit to an empirical function [428] are superimposed. In case of LAr at 91 K the error band for the global fit [284] including statistical and systematic errors as well as correlations of the data points is given. Only statistical errors are shown for the individual LAr data points.

Drift velocities of free electrons in LAr [284] are given as a function of electric field strength for different temperatures of the medium in Fig. 35.34. The drift velocites in LAr have been measured using a double-gridded drift chamber with electrons produced by a laser pulse on a gold-plated cathode. The average temperature gradient of the drift velocity of the free electrons in LAr is described [284] by

$$\frac{\Delta v_d}{\Delta T\, v_d} = (-1.72 \pm 0.08)\ \%/\mathrm{K}. \qquad (35.46)$$

Downloaded from https://academic.oup.com/ptep/article/2022/8/083C01/6651666 by KIT Library user on 27 September 2022

Table 35.13: Energy resolution of selected combined electromagnetic and hadronic calorimeter systems in past and present high-energy collider experiments for single hadrons. The results are taken from beam tests of prototypes with the electromagnetic calorimeter upstream of the hadronic calorimeter.

Experiment	technology (ECAL, HCAL)	Combined hadronic resolution	Reference
H1	Pb/LAr, Steel / LAr	$46\%/\sqrt{E} \oplus 2.6\% \oplus 0.73/E$	[419]
ZEUS	depleted U / plastic scintillator	$35\%/\sqrt{E}$	[420]
CDF	Pb/plastic scint., Steel/plastic scint.	$68\%/\sqrt{E} \oplus 4.1\%$	[421]
D0	depleted U / LAr	$44.6\%/\sqrt{E} \oplus 3.9\%$	[422]
ATLAS	Pb/LAr, Steel/plastic scintillator	$52\%/\sqrt{E} \oplus 3.0\% \oplus 1.6/E$	[423]
CMS	$PbWO_4$, brass/plastic scintillator	$84.7\%/\sqrt{E} \oplus 7.4\%$	[424]

Previous measurements [426, 427, 429, 430] range from 13% higher [427] to 18% lower [429] than these measurements. They used different techniques and show drift velocities for free electrons which cannot be explained by the temperature dependence mentioned above.

Drift velocities of free electrons in LXe [426] as a function of electric field strength are also displayed in Fig. 35.34. The drift velocity saturates for $|E| > 3$ kV/cm, and decreases with increasing temperature for LXe as well as measured e.g. by [431].

The addition of small concentrations of other molecules like N_2, H_2 and CH_4 in solution to the liquid typically increases the drift velocities of free electrons above the saturation value [426, 429], see example for CH_4 admixture to LAr in Fig. 35.34. Therefore, actual drift velocities are critically dependent on even small additions or contaminations.

35.11 Accelerator-based neutrino detectors

Written by M.O. Wascko (Imperial Coll. London). Minor revision in October 2021 by F. Pietropaolo (CERN; INFN, Padua) and S.H. Pordes (FNAL).

.

35.11.1 *Introduction*

Accelerator-based neutrino experiments span many orders of magnitude in neutrino energy, from a few MeV to hundreds of GeV. This wide range of neutrino energy is driven by the many physics applications of accelerator-based neutrino beams. Foremost among them is neutrino oscillation, which varies as the ratio L/E_ν, where L is the neutrino baseline (distance traveled), and E_ν is the neutrino energy. But accelerator-based neutrino beams have also been used to study the nature of the weak interaction, to probe nucleon form factors and structure functions, and to study nuclear structure.

The first accelerator-based neutrino experiment used neutrinos from the decays of high energy pions in flight to show that the neutrinos emitted from pion decay are different from the neutrinos emitted by beta decay [432]. The field of accelerator-based neutrino experiments would likely not have expanded beyond this without Simon van der Meer's invention of the magnetic focusing horn [433], which significantly increased the flux of neutrinos aimed toward the detector. In this mini-review, we focus on experiments employing decay-in-flight beams—pions, kaons, charmed mesons, and taus—producing fluxes of neutrinos and antineutrinos from $\sim$ 10 MeV to $\sim$ 100 GeV.

Neutrino interactions with matter proceed only through the weak interaction, making the cross section extremely small and requiring high fluxes of neutrinos and large detector masses in order to achieve satisfactory event rates. Therefore, neutrino detector design is a balancing act taking into account sufficient numbers of nuclear targets (often achieved with inactive detector materials), adequate sampling/segmentation to ensure accurate reconstruction of the tracks and showers produced by neutrino-interaction secondary particles, and practical readout systems to allow timely analysis of data.

35.11.2 *Signals and Backgrounds*

The neutrino interaction processes available increase with increasing neutrino energy as interaction thresholds are crossed; in general neutrino-interaction cross sections grow with energy; for a detailed discussion of neutrino interactions see [434]. The multiplicity of secondary particles from each interaction process grows in complexity with neutrino energy, while the forward-boost due to increasing E_ν compresses the occupied phase space in the lab frame, impacting detector designs. Because decay-in-fight beams produce neutrinos at well-defined times, leading to very small duty factors, the predominant backgrounds usually stem from unwanted beam-induced neutrino interactions, i.e. neutrinos interacting via other processes than the one being studied. A noteworthy exception is time projection chambers, wherein the long drift times can admit substantially more cosmic backgrounds than most other detection methods. Cosmic backgrounds are more rare at higher energies because the secondary particles produced by neutrino interactions yield detector signals that resemble cosmic backgrounds less and less.

Below, we describe a few of the dominant neutrino interaction processes, with a focus on the final state particle content and topologies.

35.11.2.1 *Charged-Current Quasi-Elastic Scattering and Pion Production*

Below $\sim$ 2 GeV neutrino energy, the dominant neutrino-nucleus interaction process is quasi-elastic (QE) scattering. In the charged current (CC) mode, the CCQE base neutrino reaction is $\nu_\ell\, n \to \ell^-\, p$, where $\ell = e, \mu, \tau$, and similarly for antineutrinos, $\overline{\nu}_\ell\, p \to \ell^+\, n$. The final state particles are a charged lepton, and perhaps a recoiling nucleon if it is given enough energy to escape the nucleus. Detectors designed to observe this process should have good single-particle track resolution for muon neutrino interactions, but should have good μ/e separation for electron neutrino interactions. Because the interaction cross section falls sharply with Q^2, the lepton typically carries away more of the neutrino's kinetic energy than the recoiling nucleon. The fraction of backward-scattered leptons is large, however, so detectors with 4π coverage are desirable. The dominant backgrounds in this channel tend to come from single pion production events in which the pion is not detected.

Near 1 GeV, the quasi-elastic cross section is eclipsed by pion production processes. A typical single pion production (CC1π) reaction is $\nu_\ell\, n \to \ell^-\, \pi^+\, n$, but many more final state particle combinations are possible. Single pion production proceeds through the coherent channel and many incoherent processes, dominated by resonance production. With increasing neutrino energy, higher-order resonances can be excited, leading to multiple pions in the final state. Separating these processes from quasi-elastic scattering, and indeed from each other, requires tagging, and ideally reconstructing, the pions. Since these processes can produce neutral pions, electromagnetic (EM) shower reconstruction is more important here than it is for the quasi-elastic channel. The predominant backgrounds for pion production change with increasing neutrino energy. Detection of pion processes is also complicated because near threshold the quasi-elastic channel creates pion backgrounds through final state interactions of the recoiling nucleon, and at higher energies backgrounds come from

Downloaded from https://academic.oup.com/ptep/article/2022/8/083C01/6651666 by KIT Library user on 27 September 2022

migration of multiple pion events in which one or more pions is not detected.

35.11.2.2 *Deep Inelastic Scattering*

Beyond a few GeV, the neutrino has enough energy to probe the nucleon at the parton scale, leading to deep inelastic scattering (DIS). In the charged-current channel, the DIS neutrino reaction is $\nu_\ell N \to \ell^- X$, where N is a nucleon and X encompasses the entire recoiling hadronic system. The final state particle reconstruction revolves around accurate reconstruction of the lepton momentum and containment and reconstruction of the hadronic shower energy. Because of the high neutrino energies involved, DIS events are very forward boosted, and can have extremely long particle tracks. For this reason, detectors measuring DIS interactions must be large to contain the hadronic showers in the detector volume.

35.11.2.3 *Neutral Currents*

Neutrino interactions proceeding through the neutral current (NC) channel are identified by the lack of a charged lepton in the final state. For example, the NC elastic reaction is $\nu_l N \to \nu_l N$, and the NC DIS reaction is $\nu_l N \to \nu_l X$. NC interactions are suppressed relative to CC interactions by a factor involving the weak mixing angle; the primary backgrounds for NC interactions come from CC interactions in which the charged lepton is misidentified.

35.11.3 *Instances of Neutrino Detector Technology*

Below we describe many of the actual detectors that have been built and operated for use in accelerator-based neutrino beams.

35.11.3.1 *Spark Chambers*

In the first accelerator-based neutrino beam experiment, Lederman, Schwartz, and Steinberger [432] used an internally-triggered spark chamber detector, filled with 10 tons of Al planes and surrounded by external scintillator veto planes, to distinguish muon tracks from electron showers, and hence muon neutrinos from electron neutrinos. The inactive Al planes served as the neutrino interaction target and as radiators for EM shower development. The detector successfully showed the presence of muon tracks from neutrino interactions. It was also sensitive to the hadronic showers induced by NC interactions, which were unknown at the time. In 1963, CERN also built and ran a large (20 ton) Al plane spark chamber in a wideband beam based on the PS accelerator [435]. More than a decade later, the Aachen-Padova [436] experiment at CERN employed a 40 ton Al spark chamber in the PS-WBB.

35.11.3.2 *Bubble Chambers*

Several large bubble chamber detectors were employed as accelerator neutrino detectors in the 1970s and 80s, performing many of the first studies of the properties of the weak interaction. Bubble chambers provide exquisite granularity in the reconstruction of secondary particles, allowing very accurate separation of interaction processes. However, the extremely slow and labor-intensive acquisition and analysis of the data from photographic film led to them being phased out in favor of electronically read out detectors.

The Gargamelle [437] detector at CERN used Freon and propane gas targets to make the first observation of neutrino-induced NC interactions and more. The BEBC [438] detector at CERN was a bubble chamber that was alternately filled with liquid hydrogen, deuterium, and a neon-hydrogen mixture; BEBC was also outfitted with a track-sensitive detector to improve event tagging, and sometimes used with a small emulsion chamber. The SKAT [439] Freon bubble chamber was exposed to wideband neutrino and antineutrino beams at the Serpukhov laboratory in the former Soviet Union. A series of American bubble chambers in the 1970's and 1980's made measurements on free nucleons that are still crucial inputs for neutrino-nucleus scattering predictions. The 12-foot bubble chamber at ANL [440] in the USA used both deuterium and hydrogen targets, as did the 7-foot bubble chamber at BNL [441]. Fermilab's 15 foot bubble chamber [442] used deuterium and neon targets.

35.11.3.3 *Iron Tracking Calorimeters*

Because of the forward boost of high energy interactions, long detectors made of magnetized iron interspersed with active detector layers have been very successfully employed. The long magnetized detectors allow measurements of the momentum of penetrating muons. The iron planes also act as shower-inducing layers, allowing separation of EM and hadronic showers; the large number of iron planes provide enough mass for high statistics and/or shower containment. Magnetized iron spectrometers have been used for studies of the weak interaction, measurements of structure functions, and searches for neutrino oscillation. Non-magnetized iron detectors have also been successfully employed as neutrino monitors for oscillation experiments and also for neutrino-nucleus interaction studies.

The Caltech-Fermilab counter (CITF) [440] combined a 92 ton iron-scintillator target-calorimeter detector with a downstream toroidal magnet to perform early studies of weak interactions—including observations of neutral currents. The CDHS [443] detector used layers of magnetized iron modules interspersed with wire drift chambers, with a fiducial mass of 1250 t, to detector neutrinos in the range 10–200 GeV. Within each iron module, 5 cm (or 15 cm) iron plates were interspersed with scintillation counters. The MINOS [444] detectors, a near detector of 980 t at FNAL and a far detector of 5500 t in the Soudan Underground Laboratory (SUL), were functionally identical magnetized iron calorimeters, comprised of iron plates interleaved with layers of 4 cm wide plastic scintillator strips in alternating orientations. The T2K [445] on-axis detector, INGRID, consists of 16 non-magnetized iron scintillator sandwich detectors, each with nine 6.5 cm iron plane (7.1 t total) interspersed between layers of 5 cm wide plastic scintillator strips readout out by multi-pixel photon counters (MPPCs) coupled to WLS fibers. Fourteen of the INGRID modules are arranged in a cross-hair configuration centered on the neutrino beam axis.

35.11.3.4 *Cherenkov Detectors*

Open volume water Cherenkov detectors were originally built to search for proton decay. Large volumes of ultra-pure water were lined with photomultipliers to collect Cherenkov light emitted by the passage of relativistic charged particles. See Sec. 36.3.1 for a detailed discussion of deep liquid detectors for rare processes. The Cherenkov light, which has significant production in the visible range, appears on the walls of the detectors in distinctive ring patterns, and topological characteristics of the rings are employed to separate muon-induced rings from electron-induced with very high accuracy. As neutrino detectors, Cherenkov detectors optimize the design balance since the entire neutrino target is also active detector medium.

When used to detect $\sim$ GeV neutrinos, the detector medium acts as a natural filter for final state particles below the Cherenkov threshold; this feature has been exploited successfully by the K2K, MiniBooNE (using mineral oil instead of water), and T2K neutrino oscillation experiments. This makes event reconstruction simple and robust since electrons and muons have very different signatures, but does require making assumptions when inferring neutrino energy since not all final state particles are observed. At higher energies Cherenkov detectors become less accurate because the overlapping rings from many final state particles become increasingly difficult to resolve.

The second-generation Cherenkov detector in Japan, Super-Kamiokande [84] (Super-K), comprises 22.5 kt of water viewed by 50 cm photomultiplier tubes with 40% photocathode coverage; it is surrounded by an outer detector region viewed by 20 cm photomultipliers. Super-K is the far detector for K2K and T2K, and is described in greater detail elsewhere in this review. The K2K experiment also employed a 1 kt water Cherenkov detector in the suite of near detectors [446], with 40% photocathode coverage. The MiniBooNE detector at FNAL was a 0.8 kt [447] mineral oil Cherenkov detector, with 20 cm photomultipliers giving 10% photocathode coverage, surrounded by a veto detector also with 20 cm photomultipliers.

Downloaded from https://academic.oup.com/ptep/article/2022/8/083C01/6651666 by KIT Library user on 27 September 2022

Table 35.14: Properties of detectors for accelerator-based neutrino beams. Revised in October 2021 by F. Pietropaolo (CERN; INFN, Padua) and S.H. Pordes (FNAL).

Name	Type	Target	Total Mass (fiducial) [t]	$\langle E_\nu \rangle$ [GeV]	Location	Dates
Lederman et al.	Spark	Al	10	[0.2-3]	BNL	1962
CERN-spark.	Spark	Al	20	1.5	CERN	1963
Serpukhov	Spark	Al	20	[3-30]	IHEP	1974-82
Aachen-Padova	Spark	Al	40(20)	1.4	CERN	1976-77
Gargamelle	Bubble	Freon	12	[1-10]	CERN	1970-79
BEBC	Bubble	H,D,Ne-H	2-42	[50-150] & 20	CERN	1977-84
SKAT	Bubble	Freon	8	7	IHEP	1976-1987
ANL-12ft	Bubble	H,D	1-2	0.5	ANL	1970
BNL-7ft	Bubble	HD	0.4-0.9	1.3,3	BNL	1976-82
Fermilab-15ft	Bubble	D, Ne	1,20	[50-180] & [25-100]	FNAL	1973-92
CITF	Iron	Fe	92	[50-180]	FNAL	1974-83
CDHS	Iron	Fe	1250(520)	10-200	CERN	1976-84
MINOS	Iron	Fe	980(23.7), 5.5k (4.2k)	3	FNAL, SUL	2005-2012
MINOS+	Iron	Fe	980, 5.5k	4-10	FNAL, SUL	2013-2016
INGRID	Iron	Fe	160	0.6-3	J-PARC	2010-
Super-Kamiokande	Cherenkov	H_2O	50k (22.5k)	0.6	Kamioka	1996-
HyperK	Cherenkov	H_2O	260k(190k)	0.6	Kamioka	2027-
K2K-1kt	Cherenkov	H_2O	25	0.8	KEK	1998-2004
MiniBooNE	Cherenkov	CH_2	818(440)	0.5	FNAL	2002-19
HWPF	Scintillation	CH_2, Fe	160	[50-180]	FNAL	1974-78
LSND	Scintillation	CH_2	167	0.003-0.06	LANL	1993-1998
NOvA	Scintillation	CH_2	300, 14k	2	FNAL,Ash River	2014-
SciBar	Scintillation	CH	15(9.5)	0.6	KEK	2003-2004
SciBooNE,	Scintillation	CH	15(9.5)	0.8	FNAL	2007-08
ICARUS	LArTPC	Ar	760(476)	17	LNGS	2006-12
ICARUS	LArTPC	Ar	760(476)	0.8	FNAL	2020-
Argoneut	LArTPC	Ar	0.025	3	FNAL	2009-10
MicroBooNE	LArTPC	Ar	170(85)	0.8	FNAL	2014-
DUNE	LArTPC	Ar	70(40)	3	FNAL	2026-
FNAL-E-531	Emulsion	Ag, Br	0.009	22	FNAL	1984
CHORUS	Emulsion	Ag, Br	0.8	27	CERN	1994-97
DONuT	Emulsion	Fe	0.26	53	FNAL	1997
OPERA	Emulsion	Pb	1.25k	17	LNGS	2008-12
NINJA	Emulsion	Fe	0.002(0.001)	0.6	J-PARC	2015-
CHARM	Hybrid	$CaCO_3$	(27),156(122)	20	CERN	1978-84
CHARM-II	Hybrid	glass	692	20	CERN	1984-91
BNL-E-734	Hybrid	CH_2	172	1.3	BNL	1981-86
BNL-E-776	Hybrid	concrete	240	1.4	BNL	1986
NOMAD	Hybrid	CH	2.9(2.7)	27	CERN	1995-98
CCFR	Hybrid	Fe	690	[30-260]	FNAL	1985-88
NuTeV	Hybrid	Fe	690	[70-180]	FNAL	1996-97
MINERvA	Hybrid	CH,H_2O,Fe,Pb,C,He	8	3.8	FNAL	2010-19
T2K-ND280	Hybrid	CH,H_2O	2	0.6	J-PARC	2010-

35.11.3.5 *Scintillation Detectors*

Liquid and solid scintillator detectors also employ fully (or nearly fully) active detector media. Typically organic scintillators, which emit into the ultraviolet range, are dissolved in mineral oil or plastic and read out by photomultipliers coupled to wavelength shifters (WLS). Open volume scintillation detectors lined with photomultipliers are conceptually similar to Cherenkov detectors, although energy reconstruction is calorimetric in nature as opposed to kinematic (see also Sec. 36.3.1). For higher energies and higher particle multiplicities, it becomes beneficial to use segmented detectors to help distinguish particle tracks and showers from each other.

The HWPF collaboration [448] employed a 2 t liquid scintillator total-absorption hadron calorimeter followed by a magnetic spectrometer to observe neutral current events in the early days of Fermilab. The LSND [449] detector at LANL was a 130 t open volume liquid scintillator detector employed to detect relatively low energy (<300 MeV) neutrinos. The NOvA [450] detectors use segmented volumes of liquid scintillator in which the scintillation light is collected by WLS fibers in the segments that are coupled to avalanche photodiodes (APDs) at the ends of the volumes. The NOvA far detector, located in Ash River, MN, is comprised of 896 layers of 15.6 m long extruded PVC scintillator cells for a total mass of 14 kt; the NOνA near detector is comprised of 214 layers of 4.1 m scintillator volumes for a total mass of of 300 t. Both are placed in the NuMI beamline at 0.8° off-axis. The SciBar (Scintillation Bar) detector was originally built for K2K at KEK in Japan and then re-used for SciBooNE [451] at FNAL. SciBar used plastic scintillator strips with 1.5 cm×2.5 cm rectangular cross section, read out by multianode photomultipliers (MAPMTs) coupled to WLS fibers, arranged in alternating horizontal and vertical layers. Both SciBooNE and K2K employed an EM calorimeter downstream of SciBar and a muon range detector (MRD) downstream of that.

35.11.3.6 *Liquid Argon Time Projection Chambers*

Liquid argon time projection chambers (LAr-TPCs) were conceived in the 1970s as a way to achieve a fully active detector with sub-centimeter track reconstruction [452]. A massive volume of purified liquid argon is put under a strong electric field (hundreds of V/cm), so that the liberated electrons from the paths of ionizing particles can be drifted to the edge of the volume and read out, directly by collecting charge from wire planes or non-destructively

Downloaded from https://academic.oup.com/ptep/article/2022/8/083C01/6651666 by KIT Library user on 27 September 2022

through charge induction in the wire planes. Dual-phase readout methods have also been developed, in which the charge is drifted vertically and then passed through an amplification region inside a gas volume above the liquid volume; the bottom of the liquid volume is equipped with a PMT array for detecting scintillation photons form the liquid argon. The first large scale LAr-TPC was the ICARUS T-600 module [453], comprising 760 t of liquid argon with a charge drift length of 1.5 m read out by wires with 3 mm pitch, which operated in LNGS, both standalone and also exposed to the CNGS high energy neutrino beam. The ICARUS detector has been transported to Fermilab and is being installed in an on-axis position in the Booster Neutrino Beamline, where it will also be exposed to off-axis neutrinos from the NuMI beamline. The ArgoNeuT [454] detector at FNAL, with fiducial mass 25 kg of argon read out with 4 mm pitch wires, was exposed to the NuMI neutrino and antineutrino beams. The MicroBooNE [455] detector at FNAL comprises 170 t (85t active) of liquid Ar, read out with 3 mm wire pitch, which began collecting data in the Booster Neutrino Beam Oct 2015. A LAr-TPC has also been chosen as the multi-kton detector design for the future DUNE neutrino oscillation experiment, from FNAL to Sanford Underground Research Facility .

35.11.3.7 *Emulsion Detectors*

Photographic film emulsions have been employed in particle physics experiments since the 1940s [456]. Thanks to advances in scanning technology and automation [457], they have been successfully employed as neutrino detectors. Emulsions are used for experiments observing CC tau neutrino interactions, where the short lifetime of the tau, $\tau_\tau = 2.90 \times 10^{-13}$s, leading to the short mean path length, $c \times \tau = 87\mu$m, requires extremely precise track resolution. They are employed in hybrid detectors in which the emulsion bricks are embedded inside fine-grained tracker detectors. In the data analysis, the tracker data are used to select events with characteristics typical of a tau decay in the final state, such as missing energy and unbalanced transverse momentum. The reconstructed tracks are projected back into an emulsion brick and used as the search seed for a neutrino interaction vertex.

E531 [458] at Fermilab tested many of the emulsion-tracker hybrid techniques employed by later neutrino experiments, in a detector with approximately 9 kg of emulsion target. The CHORUS [457] experiment at CERN used 1,600 kg of emulsion, in a hybrid detector with a fiber tracker, high resolution calorimeter, and muon spectrometer, to search for $\nu_\mu \to \nu_\tau$ oscillation. The DONuT [459] experiment at FNAL used a hybrid detector, with 260 kg of emulsion bricks interspersed with fiber trackers, followed by a magnetic spectrometer, and calorimeter, to make the first direct observation of tau neutrino CC interactions. The OPERA [460] [461] [462] experiment used an automated hybrid emulsion detector, with 1,25x0 t of emulsion, to make the first direct observation of the appearance of ν_τ in a ν_μ beam. Recently, the NINJA collaboration has developed an emulsion cloud chamber detector to observe neutrinos in the J-PARC neutrino beam [463].

35.11.3.8 *Hybrid Detectors*

In the previous neutrino detector examples, one can point to a specific detection technology or configuration that defines a category of detectors. In this section we look at detectors that combine multiple elements or techniques, without one facet being specifically dominant or crucial; we call these detectors hybrids.

The CHARM detector [464] at CERN was built to study neutral-current interactions and search for muon neutrino oscillation. It was a fine-grained ionization calorimeter tracker with approximately 150 t of marble as neutrino target, surrounded by a magnetized iron muon system for tagging high angle muons, and followed downstream by a muon spectrometer. The CHARM II detector [465] at CERN comprised a target calorimeter followed by a downstream muon spectrometer. Each target calorimeter module consists of a 4.8 cm thick glass plate followed by a layer of plastic streamer tubes, with spacing 1 cm, instrumented with 2 cm wide pickup strips. Every fifth module is followed by a 3 cm thick scintillator layer. The total mass of the target calorimeter was 692 t.

The Brookhaven E-734 [466] detector was a tracking calorimeter made up of 172 t liquid scintillator modules interspersed with proportional drift tubes, followed by a dense EM calorimeter and a muon spectrometer downstream of that. The detector was exposed to a wideband horn-focused beam with peak neutrino energy near 1 GeV. The Brookhaven E-776 [467] experiment comprised a finely segmented EM calorimeter, with 2.54 cm concrete absorbers interspersed with planes of drift tubes and acrylic scintillation counters, with total mass 240 t, followed by a muon spectrometer.

The FNAL Lab-E neutrino detector was used by the CCFR [468] and NuTeV [469] collaborations to perform a series of experiments in the Fermilab high energy neutrino beam (50 GeV$<$ E_ν $<$ 300 GeV). The detector was comprised of six iron target calorimeter modules, with 690 t total target mass, followed by three muon spectrometer modules, followed by two drift chambers. Each iron target calorimeter module comprised 5.2 cm thick steel plates interspersed with liquid scintillation counters and drift chambers.

The NOMAD [470] detector at CERN consisted of central tracker detector inside a 0.4 T dipole magnet (the magnet was originally used by the UA1 experiment at CERN) followed by a hadronic calorimeter and muon detectors downstream of the magnet. The main neutrino target is 3 t of drift chambers followed downstream by transition radiation detectors which are followed by an EM calorimeter. NOMAD was exposed to the same wideband neutrino beam as was CHORUS.

MINERvA [471] is a hybrid detector based around a central plastic scintillator tracker: 8.3 t of plastic scintillator strips with triangular cross section read out by MAPMTs coupled to WLS fibers. The scintillator tracker is surrounded by electromagnetic and hadronic calorimetry, which is achieved by interleaving thin lead (steel) layers between the scintillator layers for the ECAL (HCAL). MINERvA is situated upstream of the MINOS near detector which acts as a muon spectrometer. Upstream of the scintillator tracker is a nuclear target region containing inactive layers of C (graphite), Pb, Fe (steel), and O (water). MINERvA's physics goals span a wide range of neutrino-nucleus interaction studies, from form factors to nuclear effects.

T2K [445] in Japan employs two near detectors at 280 m from the neutrino beam target, one centered on the axis of the horn-focused J-PARC neutrino beam and one placed 2.5° off-axis. The on-axis detector, INGRID, is described above. The 2.5° off-axis detector, ND280, employs the UA1 magnet (at 0.2 T) previously used by NOMAD. Inside the magnet volume are three separate detector systems: the trackers, the Pi0 Detector (P0D), and several ECal modules. The tracker detectors comprise two fine-grained scintillator detectors (FGDs), read out by MPPCs coupled to WLS fibers, interleaved between three gas TPCs read out by micromegas planes. The downstream FGD contains inactive water layers in addition to the scintillators. Upstream of the tracker is the P0D, a sampling tracker calorimeter with active detector materials comprising plastic scintillator read out by MPPCs and WLS fibers, and inactive sheets of brass radiators and refillable water modules. Surrounding the tracker and P0D, but still inside the magnet, are lead-scintillator EM sampling calorimeters.

35.11.4 *Outlook*

Detectors for accelerator-based neutrino beams have been in use, and constantly evolving, for six decades now. The rich program of neutrino oscillation physics and attendant need for newer and better neutrino-nucleus scattering measurements means that more neutrino detectors with broader capabilities will be needed in the coming decades.

One of the most intriguing prospects is a large volume, high pressure gas time projection chamber (HPTPC). With the prospect of megawatt power accelerator-based neutrino beams, it is entirely feasible to collect high statistics data sets with a gas target. The low momentum thresholds for particle detection, and excellent momentum resolution and particle identification capabilities, of an HPTPC would open a new window into the physics of neutrino-nucleus scattering. Moreover, the ability to change the gas mixtures in the HPTPC would allow measurements in the same detector on multiple nuclear targets, which would, in

Downloaded from https://academic.oup.com/ptep/article/2022/8/083C01/6651666 by KIT Library user on 27 September 2022

turn, allow unprecedentedly accurate constraints and tuning of neutrino-nucleus interaction models.

35.12 Superconducting magnets for collider detectors

Revised August 2019 by Y. Makida (KEK).

35.12.1 *Solenoid Magnets*

In all cases SI unit are assumed, so that the magnetic field, B, is in Tesla, the stored energy, E, is in joules, the dimensions are in meters, and vacuum permeability of $\mu_0 = 4\pi \times 10^{-7}$.

The magnetic field (B) in an simple solenoid with a flux return iron yoke, in which the magnetic field is lower than magnetic saturation of < 2 T, is given by

$$B = \frac{\mu_0\, n\, I}{L} \tag{35.47}$$

where n is the number of turns, I is the current and L is the coil length.

In an air-core solenoid case, the central field is given by

$$B(0,0) = \mu_0\, n\, I \frac{1}{\sqrt{L^2 + 4R^2}}\ , \tag{35.48}$$

where R is the coil radius.

In most cases, momentum analysis is made by measuring the circular trajectory of the passing particles according to $p = mv = qrB$, where p is the momentum, m the mass, q the charge, r the bending radius. The sagitta, s, of the trajectory is given by

$$s = q\, B\, \ell^2/8p\ , \tag{35.49}$$

where ℓ is the path length in the magnetic field. In a practical momentum measurement in colliding beam detectors, it is more effective to increase the magnetic volume than the field strength, since

$$dp/p \propto p/B\,\ell^2\ , \tag{35.50}$$

where ℓ corresponds to the solenoid coil radius R. The energy stored in the magnetic field of any magnet is calculated by integrating B^2 over all space:

$$E = \frac{1}{2\mu_0}\int B^2 dV \tag{35.51}$$

If the coil thin and inside an iron return yoke , (which is the case if it is to superconducting coil), then

$$E \approx (B^2/2\mu_0)\pi R^2 L\ . \tag{35.52}$$

For a detector in which the calorimetry is outside the aperture of the solenoid, the coil must be transparent in terms of radiation and absorption lengths. This usually means that the superconducting solenoid and its cryostat is of minimum real thickness and is made of a material with long radiation length. There are two major contributors to the thickness of a thin solenoid:

1. The conductor consisting of the current-carrying superconducting material (usually Nb-Ti/Cu) and the quench protecting stabilizer (usually aluminum) are wound on the inside of a structural support cylinder (usually aluminum alloy). The coil thickness scales as B^2R, so the thickness in radiation lengths (X_0) is

$$t_{\rm coil}/X_0 = (R/\sigma_h X_0)(B^2/2\mu_0)\ , \tag{35.53}$$

where $t_{\rm coil}$ is the physical thickness of the coil, X_0 the average radiation length of the coil/stabilizer material, and σ_h is the hoop stress in the coil [472]. $B^2/2\mu_0$ is the magnetic pressure. In large detector solenoids, the aluminum stabilizer and support cylinders dominate the thickness; the superconductor (Nb-TI/Cu) contributes a smaller fraction. The main coil and support cylinder components typically contribute about 2/3 of the total thickness in radiation lengths.

2. Another contribution to the material comes from the outer cylindrical shell of the vacuum vessel. Since this shell is susceptible to buckling collapse, its thickness is determined by the diameter, length and the modulus of the material of which it is fabricated. The outer vacuum shell represents about 1/3 of the total thickness in radiation length.

35.12.2 *Properties of collider detector magnets*

The physical dimensions, central field stored energy and thickness in radiation lengths normal to the beam line of the superconducting solenoids associated with the major collider are given in Table 35.15 [473]. Fig. 35.35 shows thickness in radiation lengths as a function of B^2R in various collider detector solenoids.

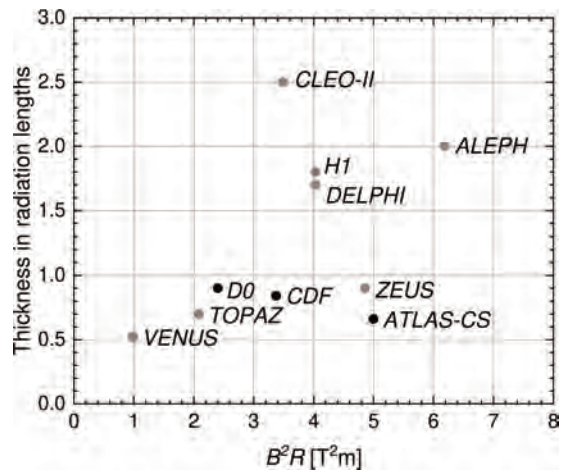

Figure 35.35: Magnet wall thickness in radiation length as a function of B^2R for various detector solenoids. Gray entries are for magnets no longer in use.

The ratio of stored energy to cold mass (E/M) is a useful performance measure. It can also be expressed as the ratio of the stress, σ_h, to twice the equivalent density, ρ, in the coil [472]:

$$\frac{E}{M} = \frac{E}{\rho\, 2\pi t_{\rm coil} RL} \approx \frac{\sigma_h}{2\rho} \tag{35.54}$$

The E/M ratio in the coil is approximately equivalent to H,[‖] the enthalpy of the coil, and it determines the average coil temperature rise after energy absorption in a quench:

$$E/M = H(T_2) - H(T_1) \approx H(T_2) \tag{35.55}$$

where T_2 is the average coil temperature after the full energy absorption in a quench, and T_1 is the initial temperature. E/M ratios of 5, 10, and 20 kJ/kg correspond to ∼65, ∼80, and ∼100 K, respectively. The E/M ratios of various detector magnets are shown in Fig. 35.36 as a function of total stored energy. One would like the cold mass to be as small as possible to minimize the thickness, but temperature rise during a quench must also be minimized. An E/M ratio as large as 12 kJ/kg is designed into the CMS solenoid, with the possibility that about half of the stored energy can go to an external dump resistor. Thus the coil temperature can be kept below 80 K if the energy extraction system works well. The limit is set by the maximum temperature that the coil design can tolerate during a quench. This maximum local temperature should be <130 K (50 K + 80 K), so that thermal expansion effects, which are remarkable beyond 80 K, in the coil are manageable less than 50 K.

35.12.3 *Toroidal magnets*

Toroidal coils uniquely provide a closed magnetic field without the necessity of an iron flux-return yoke. Because no field exists at the collision point and along the beam line, there is, in

‖ The enthalpy, or heat content, is called H in the thermodynamics literature. It is not to be confused with the magnetic field intensity B/μ.

Downloaded from https://academic.oup.com/ptep/article/2022/8/083C01/6651666 by KIT Library user on 27 September 2022

Table 35.15: Progress of superconducting magnets for particle physics detectors.

Experiment	Laboratory	B [T]	Radius [m]	Length [m]	Energy [MJ]	X/X_0	E/M [kJ/kg]
TOPAZ*	KEK	1.2	1.45	5.4	20	0.70	4.3
CDF*	Tsukuba/Fermi	1.5	1.5	5.07	30	0.84	5.4
VENUS*	KEK	0.75	1.75	5.64	12	0.52	2.8
AMY*	KEK	3	1.29	3	40	†	
CLEO-II*	Cornell	1.5	1.55	3.8	25	2.5	3.7
ALEPH*	Saclay/CERN	1.5	2.75	7.0	130	2.0	5.5
DELPHI*	RAL/CERN	1.2	2.8	7.4	109	1.7	4.2
ZEUS*	INFN/DESY	1.8	1.5	2.85	11	0.9	5.5
H1*	RAL/DESY	1.2	2.8	5.75	120	1.8	4.8
BaBar*	INFN/SLAC	1.5	1.5	3.46	27	†	3.6
D0*	Fermi	2.0	0.6	2.73	5.6	0.9	3.7
BELLE*	KEK	1.5	1.8	4	42	†	5.3
BES-III	IHEP	1.0	1.475	3.5	9.5	†	2.6
ATLAS-CS	ATLAS/CERN	2.0	1.25	5.3	38	0.66	7.0
ATLAS-BT	ATLAS/CERN	1	4.7–9.75	26	1080	(Toroid)†	
ATLAS-ET	ATLAS/CERN	1	0.825–5.35	5	2×250	(Toroid)†	
CMS	CMS/CERN	4	6	12.5	2600	†	12
SiD**	ILC	5	2.9	5.6	1560	†	12
ILD**	ILC	4	3.8	7.5	2300	†	13
SiD**	CLIC	5	2.8	6.2	2300	†	14
ILD**	CLIC	4	3.8	7.9	2300	†	13
FCC**		6	6	23	54000	†	12

* No longer in service
** Conceptual design in future
† EM calorimeter is inside solenoid, so small X/X_0 is not a goal

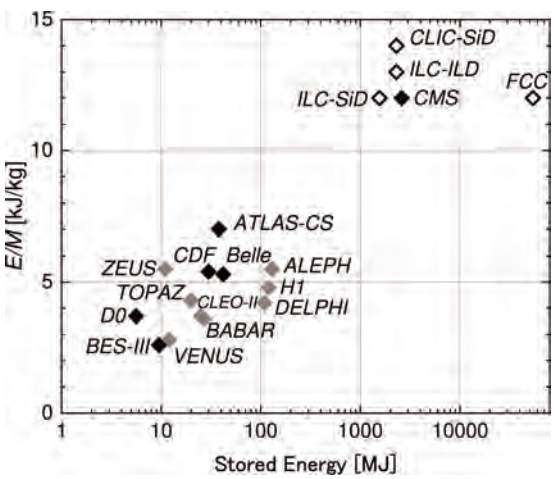

Figure 35.36: Ratio of stored energy to cold mass for major detector solenoids. Gray indicates magnets no longer in operation.

principle, no effect on the beam. On the other hand, the field profile generally has $1/r$ dependence. The particle momentum may be determined by measurements of the deflection angle combined with the sagitta. The deflection (bending) power BL is

$$BL \approx \int_{R_i}^{R_0} \frac{B_i R_i \, dR}{R \sin\theta} = \frac{B_i \, R_i}{\sin\theta} \ln(R_0/R_i) \ , \tag{35.56}$$

where R_i is the inner coil radius, R_0 is the outer coil radius, and θ is the angle between the particle trajectory and the beam line axis . The momentum resolution given by the deflection may be expressed as

$$\frac{\Delta p}{p} \propto \frac{p}{BL} \approx \frac{p \sin\theta}{B_i R_i \ \ln(R_0/R_i)} \ . \tag{35.57}$$

The momentum resolution is better in the forward/backward (smaller θ) direction. The geometry has been found to be optimal when $R_0/R_i \approx 3$–4. In practical designs, the coil is divided into 6–12 lumped coils in order to have reasonable acceptance and accessibility. This causes the coil design to be much more complex. The mechanical structure needs to sustain the decentering force between adjacent coils, and the peak field in the coil is 3–5 times higher than the useful magnetic field for the momentum analysis [474].

35.13 Measurement of particle momenta in a uniform magnetic field

The trajectory of a particle with momentum p (in GeV/c) and charge ze in a constant magnetic field $\vec{B}$ is a helix, with radius of curvature R and pitch angle λ. The radius of curvature and momentum component perpendicular to $\vec{B}$ are related by

$$p \cos\lambda = 0.3 \, z \, B \, R \ , \tag{35.58}$$

where B is in tesla and R is in meters.

The distribution of measurements of the curvature $k \equiv 1/R$ is approximately Gaussian. The curvature error for a large number of uniformly spaced measurements on the trajectory of a charged particle in a uniform magnetic field can be approximated by

$$(\delta k)^2 = (\delta k_{\rm res})^2 + (\delta k_{\rm ms})^2, \tag{35.59}$$

where δk = curvature error
$\delta k_{\rm res}$ = curvature error due to finite measurement resolution
$\delta k_{\rm ms}$ = curvature error due to multiple scattering.

If many (≥ 10) uniformly spaced position measurements are made along a trajectory in a uniform medium,

$$\delta k_{\rm res} = \frac{\epsilon}{L'^2} \sqrt{\frac{720}{N+4}}, \tag{35.60}$$

where N = number of points measured along track
L' = the projected length of the track onto the bending plane
ϵ = measurement error for each point, perpendicular to the trajectory.

If a vertex constraint is applied at the origin of the track, the coefficient under the radical becomes 320.

For arbitrary spacing of coordinates s_i measured along the projected trajectory and with variable measurement errors ϵ_i the curvature error $\delta k_{\rm res}$ is calculated from:

$$(\delta k_{\rm res})^2 = \frac{4}{w} \ \frac{V_{ss}}{V_{ss} V_{s^2 s^2} - (V_{ss^2})^2}, \tag{35.61}$$

Downloaded from https://academic.oup.com/ptep/article/2022/8/083C01/6651666 by KIT Library user on 27 September 2022

where V are covariances defined as $V_{s^m s^n} = \langle s^m s^n - \rangle s^m \langle s^n$ with $\rangle s^m = w^{-1} \sum ({s_i}^m / {\epsilon_i}^2)$ and $w = \sum {\epsilon_i}^{-2}$.

The contribution due to multiple Coulomb scattering is approximately

$$\delta k_{\rm ms} \approx \frac{(0.016)({\rm GeV}/c)z}{Lp\beta\cos^2\lambda}\sqrt{\frac{L}{X_0}}, \qquad (35.62)$$

where p = momentum (GeV/c)
z = charge of incident particle in units of e
L = the total track length
X_0 = radiation length of the scattering medium (in units of length; the X_0 defined elsewhere must be multiplied by density)
β = the kinematic variable v/c.

More accurate approximations for multiple scattering may be found in the section on Passage of Particles Through Matter (Sec. 34 of this *Review*). The contribution to the curvature error is given approximately by $\delta k_{\rm ms} \approx 8 s^{\rm rms}_{\rm plane}/L^2$, where $s^{\rm rms}_{\rm plane}$ is defined there.

References

[1] H. Kolanoski and N. Wermes, *Particle Detectors - Fundamentals and Applications*, Oxford University Press (2020), ISBN 978-0-19-885836-2.

[2] T. Ferbel, *Experimental techniques in high energy physics; 1st ed.*, Frontiers in physics, Addison-Wesley, Menlo Park, CA (1987), URL https://cds.cern.ch/record/110951.

[3] K. Kleinknecht, *Detectors for particle radiation* (1998), ISBN 978-0-521-64854-7.

[4] G. Knoll, *Radiation Detection and Measurement (4th ed.)*, John Wiley, Hoboken, NJ (2010), ISBN 978-0-470-13148-0.

[5] D. Green, *The physics of particle detectors*, Cambridge University Press, Cambridge, UK (2000), ISBN 9780521675680.

[6] C. Leroy and P.-G. Rancoita, *Principles of radiation interaction in matter and detection*, World Scientific, Singapore (2011), ISBN 978-981-238-909-1.

[7] C. Grupen and B. Schwartz, *Particle detectors*, Cambridge University Press, Cambridge, UK (2008), ISBN 9780521187954.

[8] H. Spieler, *Semiconductor Detector Systems*, Oxford University Press, Oxford (2005), ISBN 978-0-19-852784-8.

[9] K. Arisaka, Nucl. Instrum. Meth. **A442**, 80 (2000).

[10] N. Matsunaga (ed.), *Photomultiplier Tubes: Basics and Applications*, 4th edition, Hamamatsu Photonics K.K., Hamamatsu (2017), https://www.hamamatsu.com/resources/pdf/etd/PMT_handbook_v4E.pdf.

[11] M. Böhm *et al.*, JINST **15**, 11, C11015 (2020).

[12] M. J. Minot *et al.*, Nuovo Cim. C **43**, 1, 11 (2020).

[13] A. Braem *et al.*, Nucl. Instrum. Meth. **A518**, 574 (2004).

[14] S. Korpar *et al.*, Nucl. Instrum. Meth. A **766**, 145 (2014).

[15] R. Arnold *et al.*, Nucl. Instrum. Meth. **A314**, 465 (1992).

[16] P. Mangeot *et al.*, Nucl. Instrum. Methods **A216**, 79 (1983).

[17] R. Apsimon *et al.*, IEEE Trans. **NS33**, 112 (1986).

[18] R. Arnold *et al.*, Nucl. Instrum. Meth. **A270**, 255 (1988).

[19] D. Aston *et al.*, Nucl. Instrum. Meth. **A283**, 582 (1989).

[20] R. Haitz *et al.*, J. Appl. Phys. **36**, 3123 (1965).

[21] R. McIntyre, IEEE Trans. Electron Devices **13**, 164 (1966).

[22] H. Dautet *et al.*, Applied Optics, **32**, 3894 (1993).

[23] Perkin-Elmer Optoelectronics, *Avalanche Photodiodes: A User's Guide*, (2003).

[24] P. Buzhan *et al.*, Nucl. Instrum. Meth. **A504**, 48 (2003).

[25] Z. Sadygov *et al.*, Nucl. Instrum. Methods **A504**, 301 (2003).

[26] V. Golovin and V. Savelev, Nucl. Instrum. Meth. **A518**, 560 (2004).

[27] F. Simon, Nuclear Instruments and Methods in Physics Research Section A: Accelerators, Spectrometers, Detectors and Associated Equipment **926**, 85–100 (2019), ISSN 0168-9002, URL http://dx.doi.org/10.1016/j.nima.2018.11.042.

[28] S. Korpar *et al.*, Nucl. Instrum. Meth. **A766**, 107 (2014).

[29] R. H. Pots *et al.*, Nucl. Instrum. Meth. **A940**, 254 (2019).

[30] D. R. Schaart *et al.*, Nuclear Instruments and Methods in Physics Research Section A: Accelerators, Spectrometers, Detectors and Associated Equipment **809**, 31 (2016).

[31] M. Petrov, M. Stapelbroek, and W. Kleinhans, Appl. Phys. Lett. **51**, 406 (1987).

[32] M. Atac and M. Petrov, IEEE Trans. **NS36**, 163 (1989).

[33] M. Atac *et al.*, Nucl. Instrum. Meth. **A314**, 56 (1992).

[34] B. Korzh *et al.*, Nature Photonics **14**, 250 (2020).

[35] J. S. Carlson *et al.*, J. Am. Chem. Soc. **139**, 28, 9621 (2017).

[36] J.B. Birks, *The Theory and Practice of Scintillation Counting*, Pergamon, London (1964).

[37] D. Clark, Nucl. Instru. Meth. **117**, 1, 295 (1974).

[38] Y. Kharzheev, Ann. Rev. Nucl. Part. **4**, 1 (2017).

[39] S. Moser *et al.*, Rad. Phys. and Chem. **41**, 1, 31 (1993), ISSN 0969-806X.

[40] M. Moszyński and B. Bengtson, Nucl. Instrum. Methods **158**, 1 (1979).

[41] J. B. Birks, Proc. Phys. Soc. **A64**, 874 (1951).

[42] D. Dexter, J. Chem. Phys. **21**, 836 (1953).

[43] M. Hamel, *Plastic scintillators: chemistry and applications*, Springer (2021), ISBN 978-3-030-73487-9.

[44] J. Son, D. Lee and et al., J. Korean Phys. Soc **73**, 887 (2018).

[45] S. Lee, M. Livan and R. Wigmans, Rev. Mod. Phys. **90**, 025002 (2018).

[46] R. C. Ruchti, Ann. Rev. Nucl. Part. **46**, 281 (1996).

[47] C. Joram, G. Haefeli and B. Leverington, JINST **10**, 08, C08005 (2015).

[48] D. Horstmann and U. Holm, Radiat. Phys. Chem. **41**, 1, 395 (1993), ISSN 0969-806X.

[49] Y. Kharzheev, Phys. Part. Nucl. **50**, 1, 42 (2019).

[50] C. Zorn, in F. Sauli, editor, "Instrumentation in high-energy physics, Advanced Series on Directions in High Energy Physics," volume 9, 218, World Scientific (1992).

[51] CMS Collaboration, J. Instrum. **15**, 06, P06009 (2020).

[52] K. Gillen and R. Clough, Polymer **38**, 1929 (1992).

[53] T. Seguchi *et al.*, Radiat. Phys. Chem. **17**, 195 (1981), ISSN 0146-5724.

[54] S.E. Derenzo, W.-S. Choong and W.W. Moses, Phys. Med. Biol. **59**, 3261 (2014).

[55] C. Melcher and J. Schweitzer, Nucl. Instrum. Methods **A314**, 212 (1992).

[56] D.W. Cooke *et al.*, J. Appl. Phys. **88**, 7360 (2000).

[57] J.M. Chen *et al.*, IEEE Trans. **NS54**, 718 (2007).

[58] J.M. Chen *et al.*, IEEE Trans. **NS54**, 1319 (2007).

[59] E.V.D. van Loef *et al.*, Nucl. Instrum. Methods **A486**, 254 (2002).

[60] W. Drozdowski *et al.*, IEEE Trans. **NS55**, 1391 (2008).

[61] M.S. Alekhin *et al.*, Appl. Phys. Lett. **102**, 161915 (2013).

[62] C. Kuntner *et al.* (Crystal Clear), Nucl. Instrum. Meth. **A493**, 131 (2002).

[63] N. Akchurin *et al.*, Nucl. Instrum. Meth. **A595**, 359 (2008).

[64] H. Wenzel, Journal of Physics: Conference Series **404**, 012049 (2012).

[65] A. Benaglia *et al.*, IEEE Transactions on Nuclear Science **63**, 2, 574 (2016).

Downloaded from https://academic.oup.com/ptep/article/2022/8/083C01/6651666 by KIT Library user on 27 September 2022

[66] R.H. Mao, L.Y. Zhang and R.Y. Zhu, IEEE Trans. **NS59**, 2229 (2012).

[67] R. Y. Zhu, TIPP 2017, SPPHY 213, 70 (2018).

[68] C. Hu *et al.*, IEEE Transactions on Nuclear Science **66**, 7, 1854 (2019).

[69] W.W. Moses, W.-S. Choong and S.E. Derenzo, Acta Physica Polonica **B7**, 725 (2014).

[70] R.H. Mao, L.Y. Zhang and R.Y. Zhu, IEEE Trans. **NS55**, 2425 (2008).

[71] B.D. Rooney and J.D. Valentine, IEEE Trans. **NS44**, 509 (1997).

[72] W.W. Moses *et al.*, IEEE Trans. **NS55**, 1049 (2008).

[73] G. Gratta, H. Newman and R. Y. Zhu, Ann. Rev. Nucl. Part. Sci. **44**, 453 (1994).

[74] R.-Y. Zhu, in "Handbook of Particle Detection and Imaging," 1–25, Springer International Publishing (2020).

[75] F. Yang *et al.*, IEEE Trans. **NS63**, 612 (2016).

[76] F. Yang *et al.*, IEEE Trans. **NS64**, 665 (2017).

[77] C. Hu *et al.*, IEEE Transactions on Nuclear Science **67**, 6, 1086 (2020).

[78] G. Dissertori *et al.*, Nucl. Instrum. Methods **745**, 1 (2014), and references therein.

[79] S. Ecklund, C. Field and G. Mazaheri, Nucl. Instr. and Meth. Res. Sect. **A463**, 68 (2001).

[80] M. G. Albrow *et al.*, JINST **7**, P10027 (2012), [arXiv:1207.7248].

[81] B. Aubert *et al.* (BaBar), Nucl. Instr. and Meth. Res. Sect. **A479**, 1 (2002), [hep-ex/0105044].

[82] E. Torassa (Belle-II PID Group), Nucl. Instr. and Meth. Res. Sect. **A824**, 152 (2016).

[83] G. Bayatian *et al.* (CMS), Eur. Phys. J. **C53**, 139 (2008).

[84] Y. Fukuda *et al.* (Super-Kamiokande), Nucl. Instrum. Meth. **A501**, 418 (2003).

[85] Proceedings of the International Workshops on Ring Imaging Cherenkov Detectors, Nucl. Instr. and Meth. Res. Sect. **A343**, 1 (1993); Nucl. Instr. and Meth. Res. Sect. **A371**, 1 (1996); Nucl. Instr. and Meth. Res. Sect. **A433**, 1 (1999); Nucl. Instr. and Meth. Res. Sect. **A502**, 1 (2003); Nucl. Instr. and Meth. Res. Sect. **A553**, 1 (2005); Nucl. Instr. and Meth. Res. Sect. **A595**, 1 (2008); Nucl. Instr. and Meth. Res. Sect. **A639**, 1 (2011); Nucl. Instr. and Meth. Res. Sect. **A766**, 1 (2014); Nucl. Instr. and Meth. Res. Sect. **A876**, 1 (2017); Nucl. Instr. and Meth. Res. Sect. **A 952**, 1 (2019).

[86] J. Litt and R. Meunier, Ann. Rev. Nucl. Part. Sci. **23**, 1 (1973).

[87] D. Bartlett *et al.*, Nucl. Instr. and Meth. Res. Sect. **A260**, 55 (1987).

[88] A. Abashian *et al.*, Nucl. Instr. and Meth. Res. Sect. **A479**, 117 (2002).

[89] B. N. Ratcliff, Nucl. Instr. and Meth. Res. Sect. **A502**, 211 (2003).

[90] T. Iijima *et al.*, Nucl. Instr. and Meth. Res. Sect. **A548**, 383 (2005), [arXiv:physics/0504220].

[91] B. Ratcliff and J. Va'vra, Nucl. Instrum. Meth. **A**, 163442 (2020).

[92] W. Blum, W. Riegler, and L. Rolandi, *Particle Detection with Drift Chambers*, Springer-Verlag, Berlin (2008).

[93] R. M. Sternheimer and R. F. Peierls, Phys. Rev. B **3**, 3681 (1971); L. Landau, J. Phys. (USSR) **8**, 201 (1944); W. W. M. Allison and J. H. Cobb, Ann. Rev. Nucl. Part. Sci. **30**, 253 (1980).

[94] I. Smirnov, Nucl. Instrum. Meth. **A554**, 474 (2005); I. Smirnov, HEED - High Energy Electro Dynamics, http://ismirnov.web.cern.ch/ismirnov/heed.

[95] L.G. Christophorou, *Atomic and Molecular Radiation Physics*, John Wiley & Sons, Hoboken (1971); J. Berkowitz, *Atomic and Molecular Photoabsorption*, Academic Press, Cambridge (2015).

[96] F. Sauli, *Gaseous Radiation Detectors: Fundamentals and Applications*, Cambridge University Press (2014).

[97] H. Bichsel, Nucl. Instrum. Meth. **A562**, 154 (2006).

[98] R. Veenhof, Garfield - Simulation of Gaseous Detectors, http://garfield.web.cern.ch/garfield/.

[99] Degrad - cluster size distribution and primary cluster distribution in gas mixtures for minimum ionising particles and X-rays, http://magboltz.web.cern.ch/magboltz/.

[100] S. F. Biagi, Nucl. Instrum. Meth. **A421**, 1-2, 234 (1999).

[101] S. Biagi, R. Veenhof, Magboltz - Boltzmann transport equations for electrons in gas mixtures under the influence of electric and magnetic fields, http://magboltz.web.cern.ch/magboltz/.

[102] S. Mukhopadhyay and N. Majumdar, in "17th DAE-BRNS High Energy Physics Symposium," (2007), [arXiv:physics/0703009].

[103] H. Fischle, J. Heintze and B. Schmidt, Nucl. Instrum. Meth. **A301**, 202 (1991).

[104] M. M. F. R. Fraga *et al.*, Nucl. Instrum. Meth. A **504**, 88 (2003).

[105] A. Peisert and F. Sauli, "Drift and diffusion of electrons in gases: A compilation (with an introduction to the use of computing program)," CERN-84-08, CERN-YELLOW-84-08 (1984).

[106] https://fr.lxcat.net/instructions/categories.php.

[107] O. Şahin, T. Z. Kowalski and R. Veenhof, Nucl. Instrum. Meth. A **768**, 104 (2014).

[108] O. Şahin *et al.*, JINST **5**, 05, P05002 (2010); O. Şahin, JINST **16**, 03, P03026 (2021).

[109] E. McDaniel and E. Mason, *The Mobility and Diffusion of Ions in Gases*, John Wiley & Sons, Hoboken (1973); G. Schultz, G. Charpak and F. Sauli, Rev. Phys. Appl. **12**, 1, 67 (1977).

[110] Y. Kalkan *et al.*, JINST **10**, 07, P07004 (2015).

[111] T. Ikeda *et al.*, JINST **15**, 07, P07015 (2020), [arXiv:2004.09706].

[112] G.F. Knoll, *Radiation Detection and Measurement*, 3nd edition, John Wiley & Sons, New York (1999).

[113] G. Charpak *et al.*, Nucl. Instrum. Methods **A62**, 262 (1968).

[114] G. Charpak and F. Sauli, Ann. Rev. Nucl. Sci. **34**, 285 (1984).

[115] G. Charpak *et al.*, Nucl. Instrum. Methods **A97**, 377 (1971).

[116] W. Blum, W. Riegler, and L. Rolandi, *Particle Detection with Drift Chambers*, Springer-Verlag, Berlin (2008).

[117] T. Ferbel (ed.), *Experimental Techniques in High Energy Physics*, Addison-Wesley, Menlo Park, CA (1987), see "Principles of Operation of Multiwire Proportional and Drift Chambers".

[118] R. Veenhof, Nucl. Instrum. Meth. A **419**, 726 (1998).

[119] G. Charpak *et al.*, Nucl. Instrum. Methods **A167**, 455 (1979).

[120] A.H. Walenta *et al.*, Nucl. Instrum. Methods **A92**, 373 (1971).

[121] A. Breskin *et al.*, Nucl. Instrum. Methods **A124**, 189 (1975).

[122] A. Breskin *et al.*, Nucl. Instrum. Methods **A156**, 147 (1978).

[123] R. Bouclier *et al.*, Nucl. Instrum. Meth. **A265**, 78 (1988), [,556(1987)].

Downloaded from https://academic.oup.com/ptep/article/2022/8/083C01/6651666 by KIT Library user on 27 September 2022

[124] H. Drumm *et al.*, Nucl. Instrum. Methods **A176**, 333 (1980).

[125] D.R. Nygren and J.N. Marx, Phys. Today **31N10**, 46 (1978).

[126] C. Grupen, *Particle Detectors*, Cambridge Monographs on Particle Physics, Nuclear Physics and Cosmology, Cambridge University Press (2008).

[127] G. F. Tassielli *et al.*, JINST **15**, 09, C09051 (2020), [arXiv:2006.02378].

[128] M. Titov, ICFA Instrum. Bull. **26**, 002 (2004), [arXiv:physics/0403055]; M. Titov *et al.*, ICFA Instrum. Bull. **24**, 22 (2002), [hep-ex/0204005].

[129] P. S. Baringer *et al.*, Nucl. Instrum. Meth. **A254**, 542 (1987).

[130] J. Virdee, Phys. Reports **403**, 401 (2004).

[131] A. Sergi, Phys. Procedia **37**, 530 (2012).

[132] A. H. Walenta, Phys. Scripta **23**, 354 (1981).

[133] https://indico.cern.ch/event/1022051/ .

[134] J. A. Kadyk, Nucl. Instrum. Meth. A **300**, 436 (1991); J. Va'vra, ICFA Instrum. Bull. **24**, 1 (2002).

[135] M. Aleksa *et al.*, Nucl. Instrum. Meth. **A446**, 435 (2000).

[136] A. Oed, Nucl. Instrum. Meth. **A263**, 351 (1988).

[137] F. Sauli, Nucl. Instrum. Meth. **A386**, 531 (1997).

[138] Y. Giomataris *et al.*, Nucl. Instrum. Meth. **A376**, 29 (1996).

[139] Input to the European Particle Physics Strategy no. 87 (2019), S. Dalla Torre, E. Oliveri, L. Ropelewski, M. Titov, Development of the Micro-Pattern Gaseous Detector Technologies: an overview of the CERN-RD51 Collaboration, https://indico.cern.ch/event/765096/contributions/3295721.

[140] F. Sauli, *Micro-pattern gaseous detectors principles of operation and applications*, World Scientific, Singapore (2020).

[141] R. Bouclier *et al.*, Nucl. Instrum. Meth. A **381**, 289 (1996); Y. Bagaturia *et al.*, Nucl. Instrum. Meth. A **490**, 223 (2002).

[142] A. Bressan *et al.*, Nucl. Instrum. Meth. **A425**, 262 (1999).

[143] S. Bachmann *et al.*, Nucl. Instrum. Meth. **A479**, 294 (2002); A. Bressan *et al.*, Nucl. Instrum. Meth. **A424**, 321 (1999).

[144] M. Alfonsi *et al.*, Nucl. Instrum. Meth. A **671**, 6 (2012).

[145] J. Derre *et al.*, Nucl. Instrum. Meth. A **459**, 523 (2001).

[146] I. Giomataris *et al.*, Nucl. Instrum. Meth. A **560**, 405 (2006); S. Andriamonje *et al.*, JINST **5**, P02001 (2010).

[147] A. Breskin *et al.*, Nucl. Instrum. Meth. **124**, 189 (1975).

[148] J. Benlloch *et al.*, IEEE Trans. Nucl. Sci. **45**, 234 (1998).

[149] Y. Giomataris, Nucl. Instrum. Meth. **A419**, 239 (1998).

[150] M. Chefdeville *et al.*, Nucl. Instrum. Meth. A **556**, 490 (2006).

[151] M. Lupberger *et al.*, IEEE Trans. Nucl. Sci. **64**, 5, 1159 (2017).

[152] J. Leidner, F. Murtas and M. Silari, Applied Sciences **11**, 1 (2021).

[153] A. Curioni *et al.*, Nucl. Instrum. Meth. A **849**, 60 (2017).

[154] R. Chechik *et al.*, Nucl. Instrum. Meth. A **535**, 303 (2004); M. Alexeev *et al.*, JINST **8**, C12005 (2013).

[155] S. Dalla Torre, Nucl. Instrum. Meth. A **639**, 111 (2011).

[156] L. Moleri *et al.*, JINST **12**, 10, P10017 (2017), [arXiv:1707.00125].

[157] G. Bencivenni *et al.*, JINST **10**, 02, P02008 (2015), [arXiv:1411.2466].

[158] G. Bencivenni *et al.*, JINST **15**, 09, C09034 (2020).

[159] F. Yamane *et al.*, Nucl. Instrum. Meth. A **951**, 162938 (2020), [arXiv:1901.03836].

[160] T. Alexopoulos *et al.*, Nucl. Instrum. Meth. A **640**, 110 (2011).

[161] D. Abbaneo *et al.*, Nucl. Instrum. Meth. A **718**, 383 (2013).

[162] T. Alexopoulos *et al.*, Nucl. Instrum. Meth. A **617**, 161 (2010); L. Lavezzi *et al.*, in "2017 IEEE Nuclear Science Symposium and Medical Imaging Conference," (2017), [arXiv:1803.07266].

[163] A. Balla *et al.*, Nucl. Instrum. Meth. A **732**, 221 (2013).

[164] J. Bortfeldt *et al.*, Nucl. Instrum. Meth. A **903**, 317 (2018), [arXiv:1712.05256].

[165] RD51 DLC Workshop Report, RD51-NOTE-2021-002 (2021) .

[166] RD51 Collaboration: https://rd51-public.web.cern.ch/ ; S. Dalla Torre *et al.* (2018), [arXiv:1806.09955].

[167] D.R. Nygren and J.N. Marx, Phys. Today **31N10**, 46 (1978).

[168] J. Alme *et al.*, Nucl. Instrum. Meth. **A622**, 316 (2010), [arXiv:1001.1950].

[169] J. Adolfsson *et al.*, Journal of Instrumentation **16**, 03, P03022 (2021), URL https://doi.org/10.1088/1748-0221/16/03/p03022.

[170] N. Abgrall *et al.* (T2K ND280 TPC), Nucl. Instrum. Meth. A **637**, 25 (2011), [arXiv:1012.0865].

[171] A. H. Walenta *et al.*, Nucl. Instrum. Meth. **161**, 45 (1979).

[172] H. Aihara *et al.*, IEEE Trans. **NS30**, 63 (1983).

[173] K. Dehmelt (sPHENIX), PoS **MPGD2017**, 044 (2019).

[174] P. Colas, I. Giomataris and V. Lepeltier, Nucl. Instrum. Meth. **A535**, 226 (2004).

[175] X. Artru, G. B. Yodh and G. Mennessier, Phys. Rev. **D12**, 1289 (1975).

[176] J. Alozy *et al.*, Nucl. Instrum. Meth. **A961**, 163681 (2020).

[177] M. L. Cherry *et al.*, Phys. Rev. **D10**, 3594 (1974).

[178] B. Dolgoshein, Nucl. Instrum. Meth. **A326**, 434 (1993).

[179] A. Andronic and J. P. Wessels, Nucl. Instrum. Meth. **A666**, 130 (2012).

[180] S. Acharya *et al.* (ALICE), Nucl. Instrum. Meth. **A881**, 88 (2018), [arXiv:1709.02743].

[181] M. Petris *et al.*, Nucl. Instrum. Meth. **A714**, 17 (2013).

[182] T. Akesson *et al.* (ATLAS TRT), Nucl. Instrum. Meth. **A522**, 131 (2004).

[183] M. Ambriola *et al.*, Nucl. Instrum. Meth. **A522**, 77 (2004).

[184] J. Adelman (ATLAS), Nucl. Instrum. Meth. **A706**, 33 (2013).

[185] T. Kirn (AMS 02 TRD), Nucl. Instrum. Meth. **A706**, 43 (2013).

[186] G. M. Garibian, L. A. Gevorgian and C. Yang, Nucl. Instrum. Meth. **125**, 133 (1975).

[187] P. Nevski, Nucl. Instrum. Meth. **A522**, 116 (2004).

[188] J. Alozy *et al.*, Nucl. Instrum. Meth. **A927**, 1 (2019), [arXiv:1901.11265].

[189] V. M. Grishin and S. S. Sadilov, Nucl. Instrum. Meth. **A522**, 122 (2004).

[190] B. Beischer *et al.*, Nucl. Instrum. Meth. **A583**, 485 (2007).

[191] A. A. Savchenko *et al.*, JINST **15**, 06, C06024 (2020).

[192] T. Akesson *et al.* (ATLAS TRT), Nucl. Instrum. Meth. **A412**, 200 (1998).

[193] M. Ave *et al.*, Nucl. Instrum. Meth. **A654**, 140 (2011).

[194] M. L. Cherry, Nucl. Instrum. Meth. **A706**, 39 (2013).

[195] J. Alozy *et al.*, J. Phys. Conf. Ser. **1690**, 1, 012041 (2020).

[196] M. Brigida *et al.*, Nucl. Instrum. Meth. **A706**, 69 (2013).

[197] F. Hartjes *et al.*, Nucl. Instrum. Meth. **A706**, 59 (2013).

[198] V. V. Berdnikov *et al.*, Nucl. Instrum. Meth. **A706**, 65 (2013).

Downloaded from https://academic.oup.com/ptep/article/2022/8/083C01/6651666 by KIT Library user on 27 September 2022

[199] R. Santonico and R. Cardarelli, Nucl. Instrum. Meth. **187**, 377 (1981).

[200] V. Parkhomchuck, Y. Pestov and N. Petrovykh, Nuclear Instruments and Methods **93**, 2, 269 (1971).

[201] G. V. Fedotovich, Y. N. Pestov and K. N. Putilin, in "International Conference on Instrumentation for Colliding Beam Physics," 127–131 (1982).

[202] E. Cerron Zeballos *et al.*, Nucl. Instrum. Meth. **A374**, 132 (1996).

[203] J. Juita *et al.*, Fire Science Reviews **1** (2012).

[204] G. Aielli *et al.*, Nucl. Instrum. Meth. **A508**, 6 (2003).

[205] R. Cardarelli, R. Santonico and V. Makeev, Nucl. Instrum. Meth. **A382**, 470 (1996).

[206] R. Cardarelli, A. Di Ciaccio and R. Santonico, Nucl. Instrum. Meth. **A333**, 399 (1993).

[207] R. Cardarelli, Sci Acta **8**, 159 (1993).

[208] P. Camarri *et al.*, Nucl. Instrum. Meth. **A414**, 317 (1998).

[209] L. Pontecorvo, ATLAS Muon Internal note **20** (1993).

[210] W. Riegler, JINST **11**, 11, P11002 (2016).

[211] R. Santonico, Nucl. Instrum. Meth. **A456**, 1 (2000).

[212] R. Cardarelli *et al.*, JINST **8**, P01003 (2013).

[213] G. Aielli *et al.*, JINST **9**, 09, C09030 (2014).

[214] R. Santonico, JINST **9**, 11, C11007 (2014).

[215] G. Aad *et al.* (ATLAS), JINST **3**, S08003 (2008).

[216] S. Chatrchyan *et al.* (CMS), JINST **3**, S08004 (2008).

[217] G. Aielli *et al.*, Nucl. Instrum. Meth. A **562**, 92 (2006).

[218] A. Bertolin *et al.*, Nucl. Instrum. Meth. A **602**, 631 (2009).

[219] Aielli, Giulio *et al.*, Eur. Phys. J. C **80**, 12, 1177 (2020).

[220] M. Bauer *et al.*, "Anubis: Proposal to search for long-lived neutral particles in cern service shafts," (2019), [arXiv:1909.13022].

[221] M. Bedjidian *et al.*, JINST **6**, P02001 (2011), [arXiv:1011.5969].

[222] P. Fonte, A. Smirnitsky and M. C. S. Williams (ALICE), Nucl. Instrum. Meth. **A443**, 201 (2000).

[223] M. Abbrescia, V. Peskov and P. Fonte, *Resistive Gaseous Detectors: Designs, Performance, and Perspectives*, Wiley (2018), ISBN 9783527340767.

[224] W. Riegler and C. Lippmann, Nucl. Instrum. Meth **A508**, 14 (2003).

[225] P. Fonte (AIDA2020), "Validation of new resistive materials for RPCs ," .

[226] A. Akindinov *et al.*, Eur. Phys. J. Plus **128**, 44 (2013).

[227] D. Belver *et al.*, Nucl. Instrum. Meth. A **602**, 687 (2009).

[228] A. Schuttauf (FOPI), Nucl. Instrum. Meth. A **533**, 65 (2004).

[229] M. Ablikim *et al.*, Nucl. Instrum. Meth. A **614**, 3, 345 (2010), ISSN 0168-9002.

[230] A. Blanco *et al.*, IEEE Symposium Conference Record Nuclear Science 2004. **4**, 2356 (2004).

[231] I. Deppner and N. Herrmann, JINST **15**, 10, C10030 (2020).

[232] J. P. Chen *et al.*, "A white paper on solid (solenoidal large intensity device)," (2014), [arXiv:1409.7741].

[233] M. Benoit *et al.*, Journal of Instrumentation **11** (2015).

[234] S. An *et al.*, Nucl. Instrum. Meth. **A594**, 39 (2008).

[235] A. Blanco *et al.*, JINST **7**, P11012 (2012).

[236] C. Iacobaeus *et al.*, Nucl. Instrum. Meth. **A513**, 244 (2003), [arXiv:physics/0210006].

[237] G. Aielli *et al.*, Nucl. Instrum. Meth. **A456**, 82 (2000).

[238] G. Aielli *et al.*, Nucl. Instrum. Meth. **533**, 1, 86 (2004), ISSN 0168-9002, proceedings of the Seventh International Workshop on Resistive Plate Chambers and Related Detectors.

[239] H. Sakai *et al.*, Nucl. Instrum. Meth. **A484**, 153 (2002).

[240] R. Santonico, JINST **8**, P04023 (2013).

[241] L. Lopes *et al.*, Nucl. Instrum. Meth. **A533**, 69 (2004).

[242] R. Cardarelli, JINST **16**, 05, C05004 (2021).

[243] C. Rubbia, "The liquid-argon time projection chamber: a new concept for neutrino detectors: CERN-EP-INT-77-8," (1977), URL https://cds.cern.ch/record/117852.

[244] H. H. Chen and J. F. Lathrop, Nucl. Instrum. Meth. **150**, 585 (1978).

[245] A. Marchionni, Ann. Rev. Nucl. Part. Sci. **63**, 269 (2013), [arXiv:1307.6918].

[246] K. Majumdar and K. Mavrokoridis, Appl. Sciences **11**, 6, 2455 (2021), [arXiv:2103.06395].

[247] F. Arneodo *et al.* (The ICARUS-Milano Collaboration), Phys. Rev. D **74**, 112001 (2006).

[248] S. Amerio *et al.* (ICARUS), Nucl. Instrum. Meth. A **527**, 329 (2004).

[249] C. Anderson *et al.* (ArgoNeuT), JINST **7**, P10019 (2012), [arXiv:1205.6747].

[250] R. Acciarri *et al.* (MicroBooNE), JINST **12**, 02, P02017 (2017), [arXiv:1612.05824].

[251] R. Acciarri *et al.* (LArIAT), JINST **15**, 04, P04026 (2020), [arXiv:1911.10379].

[252] C. E. Taylor *et al.* (CAPTAIN), Nucl. Instrum. Meth. A **1001**, 165131 (2021), [arXiv:2008.11422].

[253] A. A. Abud *et al.* (DUNE (protoDUNE-SP)) (2021), [arXiv:2108.01902].

[254] P. Abratenko *et al.* (MicroBooNE), JINST **16**, 06, P06043 (2021), [arXiv:2011.01375].

[255] M. Wang *et al.* (2020), [arXiv:2009.04509].

[256] B. Abi *et al.* (DUNE), Phys. Rev. D **102**, 9, 092003 (2020), [arXiv:2006.15052].

[257] G. Carugno *et al.* (ICARUS), Nucl. Instrum. Meth. A **292**, 580 (1990).

[258] M. Adamowski *et al.*, JINST **9**, P07005 (2014), [arXiv:1403.7236].

[259] C. Adams *et al.* (MicroBooNE), JINST **15**, 07, P07010 (2020), [arXiv:1910.01430].

[260] H. Loosli, Earth and Planetary Science Letters **63**, 1, 51 (1983), ISSN 0012-821X.

[261] P. Benetti *et al.* (WARP), Nucl. Instrum. Meth. A **574**, 83 (2007), [arXiv:astro-ph/0603131].

[262] "Summary of Liquid Argon Properties," Accessed August 2021, URL https://lar.bnl.gov/properties/.

[263] E. W. Lemmon *et al.*, "NIST Standard Reference Database 23: Reference Fluid Thermodynamic and Transport Properties-REFPROP, Version 10.0, National Institute of Standards and Technology," (2018), URL https://www.nist.gov/srd/refprop.

[264] G. Bakale, U. Sowada and W. F. Schmidt, The Journal of Physical Chemistry **80**, 23, 2556 (1976).

[265] A. Bettini *et al.* (ICARUS), Nucl. Instrum. Meth. A **305**, 177 (1991).

[266] R. Andrews *et al.*, Nucl. Instrum. Meth. A **608**, 251 (2009).

[267] R. Acciarri *et al.* (WArP), JINST **5**, P06003 (2010), [arXiv:0804.1217].

[268] B. J. P. Jones *et al.*, JINST **8**, P07011 (2013), [Erratum: JINST 8, E09001 (2013)], [arXiv:1306.4605].

[269] R. Acciarri *et al.* (WArP), JINST **5**, P05003 (2010), [arXiv:0804.1222].

Downloaded from https://academic.oup.com/ptep/article/2022/8/083C01/6651666 by KIT Library user on 27 September 2022

[270] W. Jaskierny *et al.* (Fermilab-TM-2384-E), Technical report (2006), URL https://lss.fnal.gov/archive/test-tm/2000/fermilab-tm-2384-e.pdf.

[271] Sigma-Aldrich 4A, BASF Copper Getter CU-0226S.

[272] P. Cennini *et al.*, Nucl. Instrum. Meth. A **333**, 567 (1993).

[273] M. Miyajima *et al.*, Phys. Rev. A **9**, 1438 (1974).

[274] R. T. Scalettar *et al.*, Phys. Rev. A **25**, 2419 (1982).

[275] E. Aprile *et al.*, Nucl. Instrum. Meth. A **261**, 519 (1987).

[276] P. Cennini *et al.* (ICARUS), Nucl. Instrum. Meth. A **345**, 230 (1994).

[277] S. Amoruso *et al.* (ICARUS), Nucl. Instrum. Meth. A **523**, 275 (2004).

[278] R. Acciarri *et al.* (ArgoNeuT), JINST **8**, P08005 (2013), [arXiv:1306.1712].

[279] G. Jaffe, Annalen der Physik **42**, 12, 303 (1913).

[280] L. Onsager, Phys. Rev. **54**, 554 (1938).

[281] J. Thomas and D. A. Imel, Phys. Rev. A **36**, 614 (1987).

[282] T. Yang, Instruments **5**, 1, 2 (2020), [arXiv:2012.01319].

[283] S. Amoruso *et al.* (ICARUS), Nucl. Instrum. Meth. A **516**, 68 (2004).

[284] W. Walkowiak, Nucl. Instrum. Meth. A **449**, 288 (2000).

[285] M. Antonello *et al.* (ICARUS), JINST **9**, 12, P12006 (2014), [arXiv:1409.5592].

[286] V. Meddage (MicroBooNE), in "Meeting of the APS Division of Particles and Fields," (2017), [arXiv:1710.00396].

[287] B. Abi *et al.* (DUNE), JINST **15**, 12, P12004 (2020), [arXiv:2007.06722].

[288] Y. Li *et al.*, Nucl. Instrum. Meth. A **816**, 160 (2016), [arXiv:1508.07059].

[289] P. Agnes *et al.* (DarkSide), Nucl. Instrum. Meth. A **904**, 23 (2018), [arXiv:1802.01427].

[290] P. Abratenko *et al.* (MicroBooNE), JINST **16**, 09, P09025 (2021), [arXiv:2104.06551].

[291] M. Miyajima *et al.*, Phys. Rev. A **10**, 1452 (1974).

[292] N. Gee *et al.*, Journal of Applied Physics **57**, 4, 1097 (1985).

[293] T. Doke *et al.*, Nucl. Instrum. Meth. A **269**, 291 (1988).

[294] T. Doke, K. Masuda and E. Shibamura, Nucl. Instrum. Meth. A **291**, 617 (1990).

[295] T. Heindl *et al.*, EPL **91**, 6, 62002 (2010), [arXiv:1511.07718].

[296] M. Babicz *et al.*, JINST **15**, 09, P09009 (2020), [arXiv:2002.09346].

[297] G. M. Seidel, R. E. Lanou and W. Yao, Nucl. Instrum. Meth. A **489**, 189 (2002), [hep-ex/0111054].

[298] E. Grace and J. A. Nikkel, Nucl. Instrum. Meth. A **867**, 204 (2017), [arXiv:1502.04213].

[299] A. Hitachi *et al.*, Phys. Rev. B **27**, 5279 (1983).

[300] P. Adhikari *et al.* (DEAP), Eur. Phys. J. C **80**, 4, 303 (2020), [arXiv:2001.09855].

[301] B. Abi *et al.* (DUNE), JINST **15**, 08, T08010 (2020), [arXiv:2002.03010].

[302] M. Auger *et al.*, JINST **11**, 03, P03017 (2016), [arXiv:1512.05968].

[303] S. Kubota *et al.*, Phys. Rev. B **20**, 8, 3486 (1979).

[304] M. Kuźniak and A. M. Szelc, Instruments **5**, 1, 4 (2020), [arXiv:2012.15626].

[305] F. Spiegelmann and J.-P. Malrieu, Chemical Physics Letters **57**, 2, 214 (1978), ISSN 0009-2614.

[306] B. Jones *et al.*, JINST **8**, P12015 (2013), [arXiv:1308.3658].

[307] A. Buzulutskov, EPL **117**, 3, 39002 (2017), [arXiv:1702.03612].

[308] J. Soto-Oton (DUNE), in "International Conference on Technology and Instrumentation in Particle Physics," (2021), [arXiv:2109.05858].

[309] B. A. Dolgoshein, V. N. Lebedenko and B. U. Rodionv, JETP Letters (1970), URL http://jetpletters.ru/ps/1724/article_26181.pdf.

[310] J. Lekner, Phys. Rev. **158**, 130 (1967).

[311] E. Shibamura *et al.*, Phys. Rev. A **20**, 6, 2547 (1979).

[312] A. Badertscher *et al.*, JINST **8**, P04012 (2013), [arXiv:1301.4817].

[313] B. Aimard *et al.* (WA105), JINST **16**, 08, P08063 (2021), [arXiv:2104.08227].

[314] A. Abed Abud *et al.* (DUNE) (2021), [arXiv:2103.13910].

[315] P. Abratenko *et al.* (MicroBooNE), JINST **15**, 12, P12037 (2020), [arXiv:2008.09765].

[316] M. Antonello *et al.* (ICARUS), JINST **15**, 07, P07001 (2020), [arXiv:2001.08934].

[317] S. Palestini, Instruments **5**, 1, 9 (2021), [arXiv:2102.06082].

[318] C. Cantini *et al.*, JINST **12**, 03, P03021 (2017), [arXiv:1611.02085].

[319] J. Asaadi *et al.*, JINST **9**, P09002 (2014), [arXiv:1406.5216].

[320] O. Bunemann, T. E. Cranshaw and J. A. Harvey, Canadian Journal of Research **27a**, 5, 191 (1949).

[321] V. Radeka *et al.*, J. Phys. Conf. Ser. **308**, 012021 (2011).

[322] H. Chen *et al.*, Phys. Procedia **37**, 1287 (2012).

[323] S. Li *et al.*, IEEE Transactions on Nuclear Science **60**, 6, 4737 (2013).

[324] H. Chen *et al.*, Nucl. Instrum. Meth. A **936**, 271 (2019).

[325] R. Acciarri *et al.* (MicroBooNE), JINST **12**, 08, P08003 (2017), [arXiv:1705.07341].

[326] P. Cennini *et al.* (ICARUS), Nucl. Instrum. Meth. A **432**, 240 (1999).

[327] D. Caratelli (MicroBooNE), JINST **15**, 03, C03023 (2020).

[328] B. Ali-Mohammadzadeh *et al.* (ICARUS), JINST **15**, 10, T10007 (2020), [arXiv:2006.05261].

[329] A. Ankowski *et al.* (ICARUS), Nucl. Instrum. Meth. A **556**, 146 (2006).

[330] N. Anfimov *et al.*, JINST **15**, 07, C07022 (2020).

[331] E. Segreto *et al.*, JINST **15**, 05, C05045 (2020).

[332] C. Rubbia *et al.* (ICARUS), JINST **6**, P07011 (2011), [arXiv:1106.0975].

[333] D. A. Dwyer *et al.*, JINST **13**, 10, P10007 (2018), [arXiv:1808.02969].

[334] B. Baibussinov *et al.* (ICARUS), JINST **13**, 03, T03001 (2018), [arXiv:1711.06781].

[335] A. Lowe *et al.*, Instruments **4**, 4, 35 (2020), [arXiv:2011.02292].

[336] E. Segreto, Phys. Rev. D **103**, 4, 043001 (2021), [arXiv:2012.06527].

[337] "Lidine 2021," Accessed October 2021, URL https://indico.physics.ucsd.edu/event/1/book-of-abstracts.pdf.

[338] A. Rogalski, Adv. Opt. Photon. **11**, 2, 314 (2019).

[339] V. Saraswat, R. Jacobberger and M. Arnold, ACS Nano 15:3, 3674–3708 (2021).

[340] F. Hartmann, *Evolution of Silicon Sensor Technology in Particle Physics*, volume 275 of *Springer Tracts in Modern Physics*, Springer (2017), ISBN 978-3-319-64434-9, 978-3-319-64436-3.

[341] G. Lutz and R. Klanner, *Particle Physics Reference Library (Vol. 2, Ch. 5., Solid State Detectors)*, Springer Nature (2020), ISBN 978-3-030-35317-9, 978-3-030-35318-6.

[342] Landolt-Börnstein, Springer (Berlin), 2002, https://doi.org/10.1007/10832182_456 and https://doi.org/10.1007/10832182_458.

Downloaded from https://academic.oup.com/ptep/article/2022/8/083C01/6651666 by KIT Library user on 27 September 2022

[343] C. Da Via *et al.*, Nucl. Instrum. Meth. **587**, 243 (2008).

[344] L. Rossi *et al.*, *Pixel Detectors – From Fundamentals to Applications*, Springer, Berlin (2006), ISBN 978-3-540-28332-4, 978-3-540-28333-1.

[345] M. Garcia-Sciveres and N. Wermes, Rept. Prog. Phys. **81**, 6, 066101 (2018), [arXiv:1705.10150].

[346] Y. Arai *et al.*, Nucl. Instrum. Meth. A **623**, 186 (2010).

[347] H.-G. Moser *et al.*, PoS **VERTEX2007**, 022 (2007).

[348] W. Riegler and G. Aglieri Rinella, JINST **12**, 11, P11017 (2017), [arXiv:1706.04883].

[349] H. F. W. Sadrozinski, A. Seiden and N. Cartiglia, Rept. Prog. Phys. **81**, 2, 026101 (2018), [arXiv:1704.08666].

[350] G. Kramberger, *Particle Physics Reference Library (Vol. 2, Ch. 21., Solid State Detectors for High Radiation Environments)*, Springer Nature (2020), ISBN 978-3-030-35317-9, 978-3-030-35318-6.

[351] M. Moll, IEEE Trans. Nucl. Sci. **65**, 8, 1561 (2018).

[352] W. Blum, L. Rolandi and W. Riegler, *Particle detection with drift chambers*, Particle Acceleration and Detection, Springer (2008), ISBN 978-3-540-76683-4, 978-3-540-76684-1.

[353] F. S. Goulding, Nucl. Instrum. Meth. **100**, 493 (1972).

[354] V. Radeka, Ann. Rev. Nucl. Part. Sci. **38**, 217 (1988).

[355] C. Agapopoulou *et al.*, JINST **15**, 07, P07007 (2020).

[356] R. Wigmans, *Calorimetry*, International Series of Monographs on Physics, Oxford University Press (2017).

[357] S. Agostinelli *et al.* (GEANT4), Nucl. Instrum. Meth. A **506**, 250 (2003).

[358] J. Allison *et al.*, IEEE Trans. Nucl. Sci. **53**, 270 (2006).

[359] T. Gabriel and L. Charlton (1997).

[360] T. T. Böhlen *et al.*, Nucl. Data Sheets **120**, 211 (2014).

[361] A. Ferrari *et al.* (2005).

[362] J. Allison *et al.*, Nucl. Instrum. Meth. A **835**, 186 (2016).

[363] D. Buskulic *et al.* (ALEPH), Nucl. Instrum. Meth. A **360**, 481 (1995).

[364] A. M. Sirunyan *et al.* (CMS), JINST **12**, 10, P10003 (2017), [arXiv:1706.04965].

[365] M. A. Thomson, Nucl. Instrum. Meth. A **611**, 25 (2009), [arXiv:0907.3577].

[366] L. Linssen *et al.* (2012), [arXiv:1202.5940].

[367] H. L. Tran *et al.*, Eur. Phys. J. C **77**, 10, 698 (2017), [arXiv:1705.10363].

[368] W.R. Nelson, H. Hirayama, and D.W.O. Rogers, SLAC-265 (1985) .

[369] ATLAS Collab., CERN/LHCC 96-41 (1996).

[370] D. Hitlin *et al.*, Nucl. Instrum. Meth. **137**, 225 (1976).

[371] W. J. Willis and V. Radeka, Nucl. Instrum. Meth. **120**, 221 (1974).

[372] R. Wigmans, *Calorimetry: Energy Measurement in Particle Physics*, Inter. Series of Monographs on Phys. **107**, Second Edition, Oxford Schlarship Online (2017).

[373] R. Y. Zhu, Nucl. Instrum. Meth. **A413**, 297 (1998).

[374] R.Y. Zhu, Journal of Physics: Conference Series **587**, 012055 (2015).

[375] CMS Collab., CERN/LHCC 97-33 (1997).

[376] C. Leroy and P. Rancoita, Rept. Prog. Phys. **63**, 505 (2000).

[377] F. Sefkow and F. Simon, *Calorimeters*, in Fleck I., Titov M., Grupen C., Buvat I. (eds) Handbook of Particle Detection and Imaging, Springer (2021), ISBN 978-3-319-47999-6.

[378] C. Adloff *et al.* (CALICE), JINST **8**, 07005 (2013).

[379] T. A. Gabriel *et al.*, Nucl. Instrum. Meth. **A338**, 336 (1994).

[380] F. Ariztizabal *et al.* (RD-34), Nucl. Instrum. Meth. **A349**, 384 (1994).

[381] CMS, CERN-LHCC-2017-023, CMS-TDR-019 (2017).

[382] N. Akchurin *et al.*, Nucl. Instrum. Meth. **A399**, 202 (1997).

[383] A. Artamonov *et al.*, JINST **3**, P02010 (2008).

[384] B. Aubert *et al.*, Nucl. Instrum. Meth. **A321**, 467 (1992).

[385] F. Sefkow and F. Simon (CALICE), J. Phys. Conf. Ser. **1162**, 1, 012012 (2019), [arXiv:1808.09281].

[386] C. W. Fabjan *et al.*, Nucl. Instrum. Meth. **141**, 61 (1977).

[387] J. Brau *et al.*, Nucl. Instrum. Meth. **A238**, 489 (1985).

[388] H. Brückmann and H. Kowalski, ZEUS Int. Note 86/026 DESY, Hamburg (1986).

[389] R. Wigmans, Nucl. Instrum. Meth. **A259**, 389 (1987).

[390] R. Wigmans, Nucl. Instrum. Meth. **A265**, 273 (1988).

[391] J. E. Brau and T. A. Gabriel, Nucl. Instrum. Meth. A **275**, 190 (1989).

[392] J. C. Brient, R. Rusack and F. Sefkow, Ann. Rev. Nucl. Part. Sci. **68**, 271 (2018).

[393] E. Fretwurst *et al.* (1989), URL http://cds.cern.ch/record/368113.

[394] E. Borchi *et al.* (SICAPO), Nucl. Instrum. Meth. **A279**, 57 (1989).

[395] H. Abramowicz *et al.* (2013), [arXiv:1306.6329].

[396] N. Alipour Tehrani *et al.* (CLICdp) (2017), CLICdp-Note-2017-001.

[397] N. Bacchetta *et al.* (2019), [arXiv:1911.12230].

[398] https://twiki.cern.ch/twiki/bin/view/CALICE/CaliceDetectors.

[399] C. Adloff *et al.* (CALICE), JINST **5**, P05004 (2010), [arXiv:1003.2662].

[400] M. Chefdeville *et al.* (CALICE), Nucl. Instrum. Meth. A **939**, 89 (2019), [arXiv:1901.08818].

[401] G. Baulieu *et al.*, JINST **10**, 10, P10039 (2015), [arXiv:1506.05316].

[402] C. Adloff *et al.* (CALICE), JINST **8**, P09001 (2013), [arXiv:1305.7027].

[403] H. Abramowicz *et al.*, Nucl. Instrum. Meth. **180**, 429 (1981).

[404] B. Andrieu *et al.* (H1 Calorimeter Group), Nucl. Instrum. Meth. A **336**, 499 (1993).

[405] C. Cojocaru *et al.* (ATLAS Liquid Argon EMEC/HEC), Nucl. Instrum. Meth. A **531**, 481 (2004), [arXiv:physics/0407009].

[406] C. Adloff *et al.* (CALICE), J. Instr. **7**, 09, P09017 (2012).

[407] H. L. Tran *et al.*, The European Physical Journal C **77**, 10, 698 (2017).

[408] P. Mockett, SLAC-267, 335 (1983).

[409] D. E. Groom, Nucl. Instrum. Meth. **A572**, 633 (2007), erratum: Nucl. Instrum. Meth. **A593**, 628 (2008).

[410] R. Wigmans, *Proc. 7th Inter. Conf. on Calorimetry in High Energy Physics*, 182 World Scientific, River Edge, NJ, (1998);.

[411] S. Lee, M. Livan and R. Wigmans, Rev. Mod. Phys. **90**, 2, 025002 (2018).

[412] S. Lee *et al.*, Nucl. Instrum. Meth. A **866**, 76 (2017), [arXiv:1703.09120].

[413] M. Antonello *et al.*, JINST **15**, 06, C06015 (2020).

[414] E. Bernardi *et al.*, Nucl. Instrum. Meth. **A262**, 229 (1987).

[415] M. Chefdeville *et al.* (CALICE), JINST **10**, 12, P12006 (2015), [arXiv:1509.00617].

[416] T. Akesson *et al.*, Nucl. Instrum. Meth. **A262**, 243 (1987).

[417] D. Acosta *et al.*, Nucl. Instrum. Meth. **A308**, 481 (1991).

[418] R. Dubois *et al.*, IEEE Trans. Nucl. Sci. **33**, 194 (1986).

[419] B. Andrieu *et al.* (H1 Calorimeter Group), Nucl. Instrum. Meth. A **336**, 460 (1993).

Downloaded from https://academic.oup.com/ptep/article/2022/8/083C01/6651666 by KIT Library user on 27 September 2022

[420] A. Bernstein *et al.* (ZEUS Barrel Calorimeter Group), Nucl. Instrum. Meth. A **336**, 23 (1993).

[421] J.-b. Liu (CDF), in "7th International Conference on Calorimetry in High-Energy Physics (ICCHEP 97)," 237–240 (1997).

[422] S. Abachi *et al.* (D0), Nucl. Instrum. Meth. A **324**, 53 (1993).

[423] G. Aad *et al.* (ATLAS), JINST **3**, S08003 (2008).

[424] S. Abdullin *et al.* (USCMS, ECAL/HCAL), Eur. Phys. J. C **60**, 359 (2009), [Erratum: Eur.Phys.J.C 61, 353–356 (2009)].

[425] H. Abramowicz *et al.* (ZEUS), Phys. Lett. B **718**, 915 (2013), [arXiv:1210.5511].

[426] E. Shibamura *et al.*, Nucl. Instrum. Methods **A316**, 184 (1975).

[427] L. S. Miller, S. Howe and W. E. Spear, Phys. Rev. **166**, 871 (1968).

[428] A.M. Kalinin *et al.*, ATLAS-LARG-NO-058 (1996).

[429] K. Yoshino, U. Sowada and W. F. Schmidt, Phys. Rev. **A14**, 438 (1976).

[430] A.O. Allen *et al.*, NSRDS-NBS-58 (1976).

[431] P. Benetti *et al.*, Nucl. Instrum. Methods **A32**, 361 (1993).

[432] G. Danby *et al.*, Phys. Rev. Lett. **9**, 36 (1962).

[433] S. van der Meer (1961).

[434] J. A. Formaggio and G. P. Zeller, Rev. Mod. Phys. **84**, 1307 (2012), [arXiv:1305.7513].

[435] H. Faissner, "CERN Spark Chamber Neutrino Experiment", INSPIRE-1377455.

[436] H. Faissner *et al.*, Phys. Lett. **68B**, 377 (1977).

[437] F. J. Hasert *et al.* (Gargamelle Neutrino), Nucl. Phys. **B73**, 1 (1974).

[438] N. Armenise *et al.* (BEBC TST Neutrino), Phys. Lett. **81B**, 385 (1979).

[439] A.E. Asratien *et al.*, Phys. Lett. **79**, 497 (1978).

[440] S. J. Barish *et al.*, Phys. Rev. **D16**, 3103 (1977).

[441] N. J. Baker *et al.*, Phys. Rev. **D23**, 2499 (1981).

[442] J. W. Chapman *et al.*, Phys. Rev. **D14**, 5 (1976).

[443] M. Holder *et al.*, Nucl. Instrum. Meth. **148**, 235 (1978).

[444] I. Ambats *et al.* (MINOS) (1998).

[445] K. Abe *et al.* (T2K), Nucl. Instrum. Meth. **A659**, 106 (2011), [arXiv:1106.1238].

[446] M. H. Ahn *et al.* (K2K), Phys. Rev. **D74**, 072003 (2006), [hep-ex/0606032].

[447] A. A. Aguilar-Arevalo *et al.* (MiniBooNE), Nucl. Instrum. Meth. **A599**, 28 (2009), [arXiv:0806.4201].

[448] A. C. Benvenuti *et al.*, Nucl. Instrum. Meth. **125**, 447 (1975).

[449] C. Athanassopoulos *et al.* (LSND), Nucl. Instrum. Meth. **A388**, 149 (1997), [arXiv:nucl-ex/9605002].

[450] D. S. Ayres *et al.* (NOvA) (2007).

[451] K. Hiraide *et al.* (SciBooNE), Phys. Rev. **D78**, 112004 (2008), [arXiv:0811.0369].

[452] C. Rubbia, CERN-EP-INT-77-08 (1977).

[453] S. Amerio *et al.* (ICARUS), Nucl. Instrum. Meth. **A527**, 329 (2004).

[454] C. Anderson *et al.*, JINST **7**, 10020 (2012).

[455] H. Chen *et al.*, FERMILAB-PROPOSAL-0974 (2007).

[456] D. H. Perkins, Nature **159**, 126 (1947).

[457] S. Aoki *et al.*, Nucl. Instrum. Meth. **A447**, 361 (2000).

[458] N. Uhida *et al.*, Nucl. Instrum. Methods **224**, 50 (1984).

[459] K. Kodama *et al.*, Nucl. Instrum. Meth. **B93**, 340 (1994).

[460] T. Adam *et al.*, Nucl. Instrum. Meth. **A577**, 523 (2007), [arXiv:physics/0701153].

[461] D. Di Ferdinando (OPERA), Radiat. Meas. **44**, 840 (2009), [arXiv:0812.0451].

[462] R. Acquafredda *et al.* (OPERA), New J. Phys. **8**, 303 (2006), [hep-ex/0611023].

[463] T. Fukuda *et al.*, PTEP **2017**, no. 6, 063C02 (2017).

[464] A. N. Diddens *et al.* (CERN-Hamburg-Amsterdam-Rome-Moscow), Nucl. Instrum. Meth. **178**, 27 (1980).

[465] D. Geiregat *et al.* (CHARM-II), Nucl. Instrum. Meth. **A325**, 92 (1993).

[466] L. A. Ahrens *et al.*, Nucl. Instrum. Meth. **A254**, 515 (1987).

[467] G. Gidal, LBL-91 Suppl., Rev. (1985).

[468] W. K. Sakumoto *et al.*, Nucl. Instrum. Meth. **A294**, 179 (1990).

[469] D. A. Harris *et al.* (NuTeV), Nucl. Instrum. Meth. **A447**, 377 (2000), [hep-ex/9908056].

[470] J. Altegoer *et al.* (NOMAD), Nucl. Instrum. Meth. **A404**, 96 (1998).

[471] L. Aliaga *et al.* (MINERvA), Nucl. Instrum. Meth. **A743**, 130 (2014), [arXiv:1305.5199].

[472] A. Yamamoto, Nucl. Instrum. Meth. **A453**, 445 (2000).

[473] A. Yamamoto and Y. Makida, Nucl. Instrum. Meth. **A494**, 255 (2002).

[474] T. M. Taylor, Phys. Scripta **23**, 459 (1981).

[475] R. L. Gluckstern, Nucl. Instrum. Meth. **24**, 381 (1963).

[476] V. Karimaki, Nucl. Instrum. Meth. **A410**, 284 (1998).

Downloaded from https://academic.oup.com/ptep/article/2022/8/083C01/6651666 by KIT Library user on 27 September 2022

36. Particle Detectors for Non-Accelerator Physics

Revised 2021. See the various sections for authors.

36.1 Introduction . . . 618
36.2 High-energy cosmic-ray hadron and gamma-ray detectors . . . 618
36.2.1 Atmospheric fluorescence detectors . . . 618
36.2.2 Atmospheric Cherenkov telescopes for high-energy gamma ray astronomy . . . 620
36.3 Large neutrino detectors . . . 621
36.3.1 Deep liquid detectors for rare processes . . . 621
36.3.2 Neutrino telescopes . . . 623
36.3.3 Radio emission from (ultra-)high energy particle showers . . . 627
36.4 Large time-projection chambers for rare event detection . . . 630
36.4.1 Dark matter and other low energy signals . . . 631
36.4.2 $0\nu\beta\beta$ Decay . . . 632
36.5 Sub-kelvin detectors . . . 633
36.5.1 Motivation for Sub-kelvin Detectors . . . 633
36.5.2 Detector Types . . . 633
36.5.3 Experimental Applications . . . 636
36.6 Low-radioactivity background techniques . . . 638
36.6.1 Introduction . . . 638
36.6.2 Radio-purity assay . . . 638
36.6.3 Radon and its progeny . . . 639
36.6.4 Surface backgrounds . . . 639
36.6.5 Mitigation of backgrounds and active background discrimination . . . 640

36.1 Introduction

Non-accelerator experiments have become increasingly important in particle physics and astrophysics. From them comes the evidence of physics beyond the SM, with the discovery of neutrino oscillations and adiabatic flavor conversion. Explored energies range from the meV scale to above the EeV, some 24 orders of magnitude. The physics and the design of the detectors vary as a consequence. Some experiments look at astrophysical high-energy phenomena using the atmosphere as a detector in the fluorescence and Cherenkov observatories or the polar ice and the ocean water in neutrino telescopes. Experiments on extremely rare events, such as neutrino-less double beta decay, solar neutrinos and dark matter induced scattering, need dedicated fully equipped deep underground laboratories, existing in different countries. Critical is the research to push back the ultra-low radioactive background frontier, with dedicated facilities in these laboratories. Detectors range from hyper-pure liquid scintillators, both organic and not, to thermalized and ballistic phonon detectors at the sub-Kelvin temperature, to dual phase noble fluid TPCs, etc. Space-based detectors also use some unique instrumentation, but these are beyond the present scope of this review. Gravitational wave detectors are not included as well.

36.2 High-energy cosmic-ray hadron and gamma-ray detectors

36.2.1 *Atmospheric fluorescence detectors*

Revised March 2022 by L.R. Wiencke (Colorado School of Mines).

Cosmic-ray fluorescence detectors (FDs) use the atmosphere as a giant calorimeter to measure isotropic scintillation light that traces the development profiles of extensive air showers. An extensive air shower (EAS) is produced by the interactions of ultra high-energy ($E > 10^{17}$ eV) subatomic particles in the stratosphere and upper troposphere. The amount of scintillation light generated by an EAS is proportional to the energy deposited in the atmosphere and nearly independent of the primary species. With energies extending beyond 10^{20} eV these are the highest energy subatomic particles known to exist. In addition to particle arrival directions, energy spectra and primary composition, the astroparticle science investigated with FDs also includes multi-messenger studies, searches for high energy photons, neutrinos, monopoles and deeply penetrating forms of dark matter. The Pierre Auger Observatory FD also measures UV scintillation that traces the development of ring-shaped atmospheric transient luminous events, called Elves, in the ionosphere that are initiated by strong lightning [1].

Previous experiments with FDs included the pioneering Fly's Eye [2, 3], and the High Resolution Fly's Eye (HiRes and HiRes prototype) [4]. A history of the fluorescence technique includes earlier studies in the 1950's and 1960's [5]. The current generation of experiments include the Telescope Array (TA) [6] in the northern hemisphere, and the much larger Pierre Auger Observatory (Auger) [7] in the southern hemisphere. Both are hybrid observatories. Their FD telescopes overlook sparse arrays of particle detectors on the ground. Select parameters are listed in Table 36.1. TA and Auger have each one FD site populated with additional telescopes that view up to 60° in elevation to measure lower EASs using a combination of scintillation and direct Cherenkov light. As part of a fourfold coverage upgrade of TA (TAx4), 12 HiRes refurbished telescopes have been installed at the north and south-east sites of TA. A set of prototype FD telescopes, dubbed FAST [8], have observed EASs at the TA site using design that features wide field of view PMTs, fast timing and economical optics for a next-generation ground-based observatory.

The fluorescence light is emitted primarily between 290 and 430 nm (Figure 36.1) with major lines at 337, 357, and 391 nm, when relativistic charged particles, primarily electrons and positrons, excite nitrogen molecules in air, resulting in transitions of the 1P and 2P systems. Reviews and references for the pioneering and recent laboratory measurements of fluorescence yield, $Y(\lambda, P, T, u)$, including dependence on wavelength (λ), temperature (T), pressure (p), and humidity (u) may be found in Refs. [9–11]. The results of various laboratory experiments have been combined (Figure 36.2) to obtain an absolute average and uncertainty for Y(337 nm, 800 hPa, 293 K, dry air) of 7.04 ± 0.24 ph/ MeV after corrections for different electron beam energies and other factors. The units of ph/ MeV correspond to the number of fluorescence photons produced per MeV of energy deposited in the atmosphere by the electromagnetic component of an EAS.

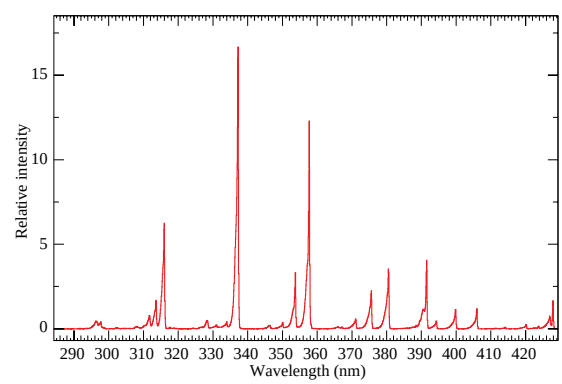

Figure 36.1: Measured fluorescence spectrum excited by 3 MeV electrons in dry air at 800 hPa and 293 K. Airfly experiment. Figure from Ref [12].

An FD element (telescope) consists of a non-tracking spherical mirror of less than astronomical quality, a"camera" of photomultiplier tubes (PMTs) near the focal plane, and a flash ADC readout system with a pulse and track-finding trigger scheme [7, 14]. The major experiments listed in Table 36.1 all use conventional PMTs (for example, Hamamatsu R9508 or Photonis XP3062) with grounded cathodes and AC coupled readout. Segmented mirrors have been fabricated from slumped or slumped/polished glass with an anodized aluminum coating or fabricated using shaped aluminum that was then chemically anodized with $AlMgSiO_5$. A broadband UV filter (custom fabricated, BG-3, or Schott MUG-6) reduces background light such as starlight, airglow, man-made light pollution, and airplane strobe-lights.

Downloaded from https://academic.oup.com/ptep/article/2022/8/083C01/6651666 by KIT Library user on 27 September 2022

Table 36.1: Parameters of major fluorescence detectors. Note 1: Year when all FD sites were operational. Note 2: At TA 1 of the 3 FD sites features 24 telescopes from the HiRes experiment. Note 3: A-C for one telescope where A is the full area and C the area obscured by the camera and support structures. Thus A-C is the effective light collecting area. For the modified Schmidt design at Auger, the area of the entrance pupil, A, is listed because the pupil is smaller than the mirror and thus defines the entrance aperture. For the other experiments, the area of the mirror, A, is listed

Observatory	Fly's Eye	HiRes	Telescope Array	Pierre Auger
Location	Dugway UT US	Dugway UT US	Delta UT US	Malargüe AR
Start-End	1981-1992	1996-2006	2008-present	2005-present
Sites (note 1)	2 (1986)	2 (1999)	3 (2008)	4 (2008)
Separation	3.3 km	12.6 km	31-40 km	39-62 km
Telescopes/site	67,18	21,42	12+8,12,14+10+4	6, 6, 6, 6+3
Pixel FOV	5.5°	1°	1°	1.5°
Telescope FOV Azi×Elv	≈18°×≈18°	16°×13.5°	18°×15° (note 2)	30°×28.1°
Light collection area (note 3)	1.95 m^2 - 0.25 m^2	3.72 m^2 - 0.5 m^2	6.8 m^2 - 0.85 m^2 (for 2 sites)	3.80 m^2 - 0.80 m^2 (modified schmidt)
Energy Scale Uncertainty	≤40%	≈20%	≈20%	14%

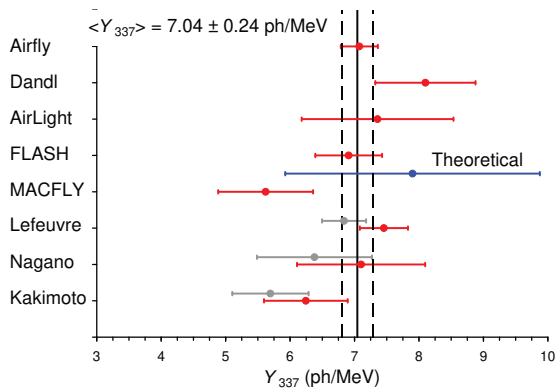

Figure 36.2: Fluorescence yield values and associated uncertainties at 337 nm (Y_{337}) in dry air at 800 hPa and 293 K The methodology and corrections that were applied to obtain the average and the uncertainty are discussed extensively in this reference. The vertical axis denotes different laboratory experiments that measured FY. The gray bars show three of the original measurements to illustrate the scale of the corrections applied. Figure from Ref [13].

At 10^{20} eV, where the flux drops below 1 EAS/km^{2}century, the aperture for an eye of adjacent FD telescopes that span the horizon can reach 10^4 km^2 sr. FD operation requires (nearly) moonless nights and clear atmospheric conditions, which typically imposes a duty cycle of about 10%. Arrangements of LEDs, calibrated diffuse sources [15], pulsed UV lasers [16], LIDARs [1] and IR detectors that are sensitive to clouds are used for photometric calibration, atmospheric calibration [17], and determination of exposure [18]. For purposes of optical transmission, the atmosphere is treated as having a dominant molecular component and a secondary aerosol component. The latter is well described [19] by molecular scattering theory and models derived from radiosonde measurements. The aerosol component can include dust, haze and pollution and the aerosol optical depth profile must be measured on site in the UV during FD data taking.

The EAS generates a track consistent with a light source moving at $v = c$ across the FOV. The number of photons (N_γ) as a function of atmospheric depth (X) can be expressed as [10]

$$\frac{\mathrm{d}N_\gamma}{\mathrm{d}X} = \frac{dE^{\mathrm{tot}}_{\mathrm{dep}}}{dX} \int Y(\lambda, P, T, u) \cdot \tau_{\mathrm{atm}}(\lambda, X) \cdot \varepsilon_{\mathrm{FD}}(\lambda)\mathrm{d}\lambda, \quad (36.1)$$

where $\tau_{atm}(\lambda, X)$ is the atmospheric transmission, including wavelength (λ) dependence, and $\varepsilon_{\mathrm{FD}}(\lambda)$ is the FD efficiency. $\varepsilon_{\mathrm{FD}}(\lambda)$ includes geometric factors and collection efficiency of the optics, quantum efficiency of the PMTs, and other throughput factors. The typical systematic uncertainties, τ_{atm} (10%) and $\varepsilon_{\mathrm{FD}}$ (photometric calibration 10%), currently dominate the systematic uncertainty the absolute EAS energy scale. FD energy resolution, defined as event-to-event statistical uncertainty, is typically less than 10% for final data samples used for science analysis.

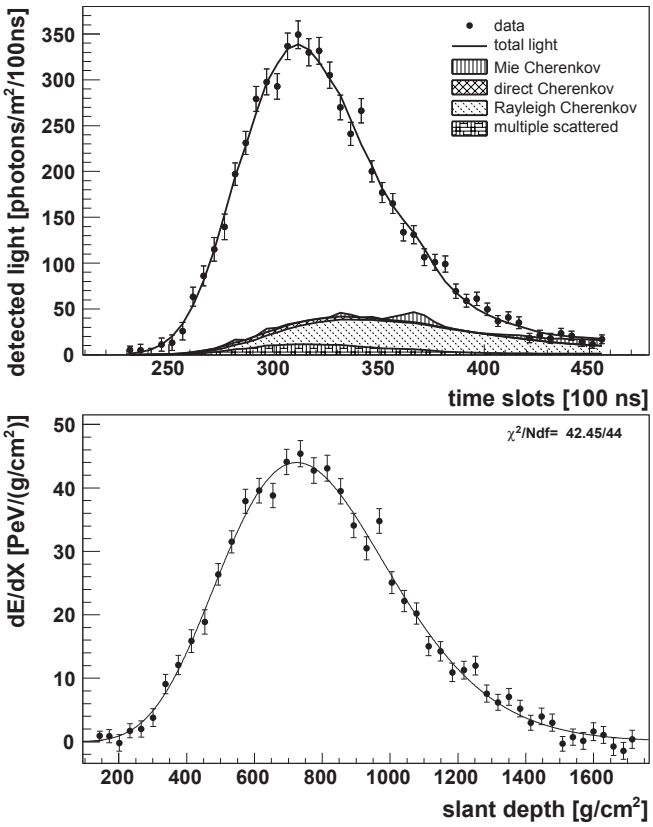

Figure 36.3: Example light profile (left) of one EAS recorded by the Pierre Auger FD and the corresponding profile (right) of energy deposited in the atmosphere vs atmospheric slant depth. The light profiles include the estimated components of Cherenkov light that have been scattered out of the forward beam by the molecular and aerosol (Mie) components of the atmosphere. The reconstructed energy of this EAS was $3.0 \pm 0.2 \times 10^{19}$ eV. Figure from Ref [20].

Analysis methods to reconstruct the EAS profile and deconvolve

[1] LIDAR stands for "Light Detection and Ranging" and refers here to systems that measure atmospheric properties from the light scattered backwards from laser pulses directed into the sky.

Downloaded from https://academic.oup.com/ptep/article/2022/8/083C01/6651666 by KIT Library user on 27 September 2022

the contributions of re-scattered scintillation light, and direct and scattered Cherenkov light are described in [2] and more recently in [21]. The EAS energy is typically obtained by integrating over the Gaisser-Hillas function [22]

$$E_{\rm cal} = \int_0^\infty [w_{\rm max} \left(\frac{X - X_0}{X_{\rm max} - X_0}\right)^{(X_{\rm max}-X_0)/\lambda} e^{(X{\rm max}-X)/\lambda}] {\rm d}X, \tag{36.2}$$

where $E_{\rm cal}$ is the energy of electromagnetic energy component of the EAS and $X_{\rm max}$ is the atmospheric slant depth at which the shower reaches its maximum energy deposit rate. This maximum dE/dX is denoted as $w_{\rm max}$. X_0 and λ are two shape parameters. The energy of the primary cosmic ray is obtained by correcting $E_{\rm cal}$ upward by about 10% to account for the invisible energy carried by particles that do not interact in the atmosphere. Auger recently reported a data-driven method to estimate the invisible energy from the muon number at ground level and Xmax to reduce systematic uncertainties [23]. Energy resolution, $\Delta E/E$, of 15-20% is achievable, provided the geometric fit of the EAS axis is constrained, typically by multi-eye stereo projection or hybrid observations, and the profile fit of EAS development along the track is constrained by the observed rise and fall about $X_{\rm max}$. An example of a recorded EAS light profile and its corresponding dE/dX development profile are shown in Fig. 36.3. The EAS generates a track consistent with a light source moving at $v = c$ across the FOV. The number of photons (N_γ) as a function of atmospheric depth (X) can be expressed as [10]

An FD that would look down on the earth's atmosphere from space orbit to view a much larger area than ground based instruments is an active area of R&D. Prototypes that have been built and flown in orbit include the pioneering TUS instrument [24], [25] operated 2016-2018 onboard the Lomonosov satellite. The JEM-EUSO collabration has flown prototype FD telescopes on two stratospheric balloon flights [26] and [27] with a third in preparation. The Mini-EUSO [28] FD is recording terrestial UV emission by looking down through a 25 cm diameter UV window from inside the International Space Station. The Probe of Extreme Multimessenger Astrophysics (POEMMA) project has completed a detailed conceptual design study for a twin-satellite mission [29] that would observe UHECRs and PeV scale cosmogenic tau neutrinos.

36.2.2 *Atmospheric Cherenkov telescopes for high-energy gamma ray astronomy*

Revised August 2019 by J. Holder (Delaware U.; Delaware U., Bartol Inst.).

A wide variety of astrophysical objects are now known to produce high-energy γ-ray photons. Leptonic or hadronic particles, accelerated to relativistic energies in the source, produce γ-rays typically through inverse Compton boosting of ambient photons or through the decay of neutral pions produced in hadronic interactions. At energies below ∼30 GeV, γ-ray emission can be efficiently detected using satellite or balloon-borne instrumentation, with an effective area approximately equal to the size of the detector (typically < 1 m^2). At higher energies, a technique with much larger effective collection area is desirable to measure astrophysical γ-ray fluxes, which decrease rapidly with increasing energy. Atmospheric Cherenkov detectors achieve effective collection areas of $>10^5$ m^2 by employing the Earth's atmosphere as an intrinsic part of the detection technique.

As described in Chapter 30, a hadronic cosmic ray or high energy γ-ray incident on the Earth's atmosphere triggers a particle cascade, or air shower. Relativistic charged particles in the cascade generate Cherenkov radiation, which is emitted along the shower direction, resulting in a light pool on the ground with a radius of ∼130 m. Cherenkov light is produced throughout the cascade development, with the maximum emission occurring when the number of particles in the cascade is largest, at an altitude of ∼10 km for primary energies of 100 GeV–1 TeV. Following absorption and scattering in the atmosphere, the Cherenkov light at ground level peaks at a wavelength, $\lambda \approx 300$–350 nm. The photon density is typically ∼100 photons/m^2 for a 1 TeV primary, arriving in a brief flash of a few nanoseconds duration. This Cherenkov pulse can be detected from any point within the light pool radius by using large reflecting surfaces to focus the Cherenkov light on to fast photon detectors (Fig. 36.4).

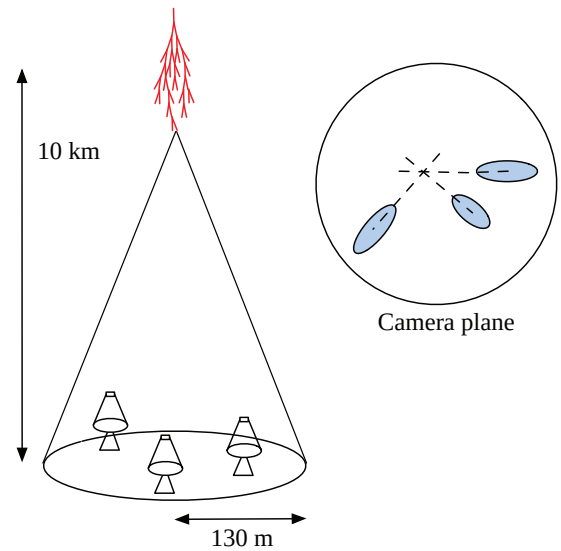

Figure 36.4: A schematic illustration of an imaging atmospheric Cherenkov telescope array. The primary particle initiates an air shower, resulting in a cone of Cherenkov radiation. Telescopes within the Cherenkov light pool record elliptical images; the intersection of the long axes of these images indicates the arrival direction of the primary, and hence the location of a γ-ray source in the sky

Modern atmospheric Cherenkov telescopes, such as those built and operated by the VERITAS [30], H.E.S.S. [31] and MAGIC [32] collaborations, consist of large ($> 100\,$m^2) segmented mirrors on steerable altitude-azimuth mounts. A camera made from an array of photosensors is placed at the focus of each mirror and used to record a Cherenkov image of each air shower. In these imaging atmospheric Cherenkov telescopes, single-anode photomultipliers tubes (PMTs) have traditionally been used (2048, in the case of H.E.S.S. II), but silicon devices now feature in more modern designs. The telescope cameras typically cover a field-of-view of $3 - 10°$ in diameter. Images are recorded at kHz rates, the vast majority of which are due to showers with hadronic cosmic-ray primaries. The shape and orientation of the Cherenkov images are used to discriminate γ-ray photon events from this cosmic-ray background, and to reconstruct the photon energy and arrival direction. γ-ray images result from purely electromagnetic cascades and appear as narrow, elongated ellipses in the camera plane. The long axis of the ellipse corresponds to the vertical extension of the air shower, and points back towards the source position in the field-of-view. If multiple telescopes are used to view the same shower ("stereoscopy"), the source position is simply the intersection point of the various image axes. Cosmic-ray primaries produce secondaries with large transverse momenta, which initiate sub-showers. Their images are consequently wider and less regular than those with γ-ray primaries and, since the original charged particle has been deflected by Galactic magnetic fields before reaching the Earth, the images have no preferred orientation.

The measurable differences in Cherenkov image orientation and morphology provide the background discrimination which makes ground-based γ-ray astronomy possible. For point-like sources, such as distant active galactic nuclei, modern instruments can reject over 99.999% of the triggered cosmic-ray events, while retaining up to 50% of the γ-ray population. In the case of spatially extended sources, such as Galactic supernova remnants, the background rejection is less efficient, but the technique can be used to produce γ-ray maps of the emission from the source. The angular resolution depends upon the number of telescopes which view the

Downloaded from https://academic.oup.com/ptep/article/2022/8/083C01/6651666 by KIT Library user on 27 September 2022

image and the energy of the primary γ-ray, but is typically less than 0.1° per event (68% containment radius) at energies above a few hundred GeV.

The total Cherenkov yield from the air shower is proportional to the energy of the primary particle. The image intensity, combined with the reconstructed distance of the shower core from each telescope, can therefore be used to estimate the primary energy. The energy resolution of this technique, also energy-dependent, is typically 15–20% at energies above a few hundred GeV. Energy spectra of γ-ray sources can be measured over a wide range, depending upon the instrument characteristics, source properties (flux, spectral slope, elevation angle, *etc.*), and exposure time. The effective energy range is typically from 30 GeV to 100 TeV and peak sensitivity lies in the range from 100 GeV to a few TeV.

The first astrophysical source to be convincingly detected using the imaging atmospheric Cherenkov technique was the Crab Nebula [33], with an integral flux of 2.1×10^{-11} photons cm^{-2} s^{-1} above 1 TeV [34]. Modern imaging atmospheric Cherenkov telescopes have sensitivity sufficient to detect sources with less than 1% of the Crab Nebula flux in a few tens of hours. The TeV source catalog now consists of over 200 sources (see e.g. Ref. [35]). A large fraction of these were detected by scanning the Galactic plane from the southern hemisphere with the H.E.S.S. telescope array [36]. Recent reviews of the field include [37] and [38], and a historical overview can be found in [39].

Major upgrades of the existing telescope arrays have recently been completed, including the addition of a 28 m diameter central telescope to H.E.S.S. (H.E.S.S. II). Development is also underway for the next generation instrument, the Cherenkov Telescope Array (CTA), which will consist of a northern and a southern hemisphere observatory, with a combined total of more than 100 telescopes [40]. Telescopes of three different sizes are planned, spread over an area of > 1 km^2, providing wider energy coverage, improved angular and energy resolutions, and an order of magnitude improvement in sensitivity relative to existing imaging atmospheric Cherenkov telescopes. Baseline telescope designs are similar to existing devices, but exploit technological developments such as dual mirror optics and silicon photo-detectors.

36.3 Large neutrino detectors

36.3.1 *Deep liquid detectors for rare processes*

Revised August 2021 by K. Scholberg (Duke U.) and C.W. Walter (Duke U.).

Deep, large detectors for rare processes tend to be multipurpose with physics reach that includes not only solar, reactor, supernova and atmospheric neutrinos, but also searches for baryon number violation and lepton number violation, searches for exotic particles and beyond-the-standard-model physics, and neutrino and cosmic-ray astrophysics in different energy regimes. The detectors may also serve as targets for long-baseline neutrino beams for neutrino oscillation physics studies. In general, detector design considerations can be divided into high- and low-energy regimes, for which background and event reconstruction issues differ. The high-energy regime, from about 100 MeV to a few hundred GeV, is relevant for proton decay searches, atmospheric neutrinos and high-energy astrophysical neutrinos. The low-energy regime (a few tens of MeV or less) is relevant for supernova, solar, reactor and geological neutrinos.

Large water Cherenkov and scintillator detectors (see Table 36.2) usually consist of a volume of transparent liquid viewed by photomultiplier tubes (PMTs) (see Sec 35.2); the liquid serves as active target. PMT hit charges and times are recorded and digitized, and triggering is usually based on coincidence of PMT hits within a time window comparable to the detector's light-crossing time. Because photosensors lining an inner surface represent a driving cost that scales as surface area, very large volumes can be used for comparatively reasonable cost. Some detectors are segmented into subvolumes individually viewed by PMTs, and may include other detector elements (*e.g.*, tracking detectors). Devices to increase light collection, *e.g.*, reflectors or waveshifter plates, may be employed. A common configuration is to have at least one concentric outer layer of liquid material separated from the inner part of the detector to serve as shielding against ambient background. If optically separated and instrumented with PMTs, an outer layer may also serve as an active veto against entering cosmic rays and other background events. The PMTs for large detectors typically range in size from 20 cm to 51 cm diameter, and typical quantum efficiencies are in the 20–25% range for scintillation and water-Cherenkov photons. PMTs with higher quantum efficiencies, 35% or higher, have recently become available. The active liquid volume requires purification and there may be continuous recirculation of liquid. For large homogeneous detectors, the event interaction vertex is determined using relative timing of PMT hits, and energy deposition is determined from the number of recorded photoelectrons. A "fiducial volume" is usually defined within the full detector volume, some distance away from the PMT array. Inside the fiducial volume, enough PMTs are illuminated per event that reconstruction is considered reliable, and furthermore, entering background from the enclosing walls is suppressed by a buffer of self-shielding. PMT and detector optical parameters are calibrated using laser, LED, or other light sources. Quality of event reconstruction typically depends on photoelectron yield, pixelization and timing.

Because in most cases one is searching for rare events, large detectors are usually sited underground to reduce cosmic-ray-related background (see Chapter 30). The minimum depth required varies according to the physics goals [41].

36.3.1.1 *Liquid scintillator detectors*

Past and current large underground detectors based on hydrocarbon scintillators include LVD, MACRO, Baksan, Borexino, KamLAND and SNO+; JUNO is a future detector. Experiments at nuclear reactors include CHOOZ, Double CHOOZ, Daya Bay, and RENO. Organic liquid scintillators (see Section 35.3) for large detectors are chosen for high light yield and attenuation length, good stability, compatibility with other detector materials, high flash point, low toxicity, appropriate density for mechanical stability, and low cost. They may be doped with waveshifters and stabilizing agents. Popular choices are pseudocumene (1,2,4-trimethylbenzene) with a few g/L of the PPO (2,5-diphenyloxazole) fluor, and linear alkylbenzene (LAB), with light yield $\sim 10^4$ photons/MeV. In a typical detector configuration there will be active or passive regions of undoped scintillator, non-scintillating mineral oil or water surrounding the inner neutrino target volume. A thin vessel or balloon made of nylon, acrylic or other material transparent to scintillation light may contain the inner target; if the scintillator is buoyant with respect to its buffer, ropes may hold the balloon in place. For phototube surface coverages in the 20–40% range, yields in the few hundreds of photoelectrons per MeV of energy deposition can be obtained. Typical energy resolution is about $5-7\%/\sqrt{E(\mathrm{MeV})}$ [42,43], and typical position reconstruction resolution is a few tens of cm at $\sim$ 1 MeV, scaling as $\sim N^{-1/2}$, where N is the number of photoelectrons detected.

Shallow detectors for reactor neutrino oscillation experiments require excellent muon veto capabilities. For $\bar{\nu}_e$ detection via inverse beta decay on free protons, $\bar{\nu}_e + p \to n + e^+$, the neutron is captured by a proton on a $\sim$180 μs timescale, resulting in a 2.2 MeV γ ray, observable by Compton scattering and which can be used as a tag in coincidence with the positron signal. The positron annihilation γ rays may also contribute. Inverse beta decay tagging may be improved by addition of Gd at $\sim$0.1% by mass, which for natural isotope abundance has a $\sim$49,000 barn cross-section for neutron capture (in contrast to the 0.3 barn cross-section for capture on free protons). Gd capture takes $\sim$30 μs, and is followed by a cascade of γ rays adding up to about 8 MeV. Gadolinium doping of scintillator requires specialized formulation to ensure adequate attenuation length and stability.

Scintillation detectors have an advantage over water Cherenkov detectors in the lack of Cherenkov threshold and the high light yield. However, scintillation light emission is nearly isotropic, and therefore directional capabilities are relatively weak. Liquid scintillator is especially suitable for detection of low-energy events. Radioactive backgrounds are a serious issue, and include long-lived cosmogenics such as ^{14}C. To go below a few MeV, very

Downloaded from https://academic.oup.com/ptep/article/2022/8/083C01/6651666 by KIT Library user on 27 September 2022

Table 36.2: Properties of large detectors for rare processes. If total target mass is divided into large submodules, the number of subdetectors is indicated in parentheses. Projects with first data expected in 2023 or later are indicated in italics.

Detector	Mass, kton (modules)	PMTs (diameter, cm)	ξ	p.e./MeV	Dates
Baksan	0.33, scint (3150)	1/module (15)	segmented	40	1980–
MACRO	0.56, scint (476)	2-4/module (20)	segmented	18	1989–2000
LVD	1, scint. (840)	3/module (15)	segmented	15	1992–
KamLAND	0.41*, scint	1325(43)+554(51)†	34%	460	2002–
Borexino	0.1*, scint	2212 (20)	30%	500	2007–
SNO+	0.78, scint‡	9394 (20)	47%	400–600	2021–
CHOOZ	0.005, scint (Gd)	192 (20)	15%	130	1997–1998
Double Chooz	0.017, scint (Gd)(2)	534/module (20)	13%	180	2011–2017
Daya Bay	0.160, scint (Gd)(8)	192/module (20)	5.6%§	100	2011–2020
RENO	0.032, scint (Gd)(2)	342/module (25)	12.6%	100	2011–
JUNO	20.0*, scint	17613 (51)/25600 (8)	77.9%	1200	2023 (exp.)
IMB-1	3.3*, H_2O	2048 (12.5)	1%	0.25	1982–1985
IMB-2	3.3*, H_2O	2048 (20)	4.5%	1.1	1987–1990
Kam I	0.88/0.78*, H_2O	1000/948 (51)	20%	3.4	1983–1985
Kam II	1.04*, H_2O	948 (51)	20%	3.4	1986–1990
Kam III	1.04*, H_2O	948 (51)	20%¶	4.3	1990–1995
SK I	22.5*, H_2O	11146 (51)	40%	6	1996–2001
SK II	22.5*, H_2O	5182 (51)	19%	3	2002–2005
SK III-V	22.5*, H_2O	11129 (51)	40%	6	2006–2020
SK-Gd	22.5*, H_2O (Gd)	11129 (51)	40%	6	2020–
Hyper-K	187*, H_2O‖	>20000 (51)**	>20%	>6	2027 (exp.)
SNO	1, D_2O/1.7, H_2O	9438 (20)	31%††	9	1999–2006
DUNE	40*, Ar (4)	TBD‡‡	TBD‡‡	TBD‡‡	2029 (exp.)

*Indicates typical fiducial mass used for data analysis; this may vary by physics topic.
†Measurements made before 2003 only considered data from the 43 cm PMTs.
‡SNO+ ran with water fill from May 2017 to July 2019.
§The effective Daya Bay coverage is 12% with top and bottom reflectors.
¶The effective Kamiokande III coverage was 25% with light collectors.
‖A second staged module is being investigated.
**Additional photosensor modules and PMTs are planned.
††The effective SNO coverage was 54% with light collectors.
‡‡Photodetector technology and coverage varies according to TPC type and is not yet fully determined.

careful selection of materials and purification of the scintillator is required (see Section 36.6). Fiducialization and tagging can reduce background. One can also dissolve neutrinoless double beta decay ($0\nu\beta\beta$) isotopes in scintillator. This has been realized by KamLAND-Zen, which deployed a 1.5 m-radius balloon containing enriched Xe dissolved in scintillator inside KamLAND, and ^{130}Te is planned for SNO+.

36.3.1.2 *Water Cherenkov detectors*

Very large imaging water detectors reconstruct ten-meter-scale Cherenkov rings produced by charged particles (see Section 35.5). The first such large detectors were IMB and Kamiokande. The only currently existing instance of this class of detector, with fiducial mass of 22.5 kton and total mass of 50 kton, is Super-Kamiokande (Super-K, SK). Hyper-Kamiokande (Hyper-K) plans at least one, and possibly two, detectors with 187-kton fiducial mass. For volumes of this scale, absorption and scattering of Cherenkov light are non-negligible, and a wavelength-dependent factor $\exp(-d/L(\lambda))$ (where d is the distance from emission to the sensor and $L(\lambda)$ is the attenuation length of the medium) must be included in the integral of Eq. (35.6) for the photoelectron yield. Attenuation lengths on the order of 100 meters have been achieved.

Cherenkov detectors are excellent electromagnetic calorimeters, and the number of Cherenkov photons produced by an e/γ is nearly proportional to its kinetic energy. For massive particles, the number of photons produced is also related to the energy, but not linearly. For any type of particle, the *visible energy* $E_{\rm vis}$ is defined as the energy of an electron which would produce the same number of Cherenkov photons. The number of collected photoelectrons depends on the scattering and attenuation in the water along with the photo-cathode coverage, quantum efficiency and the optical parameters of any external light collection systems or protective material surrounding them. Event-by-event corrections are made for geometry and attenuation. For a typical case, in water $N_{\rm p.e.} \sim 15\,\xi\,E_{\rm vis}({\rm MeV})$, where ξ is the effective fractional photosensor coverage. Cherenkov photoelectron yield per MeV of energy is relatively small compared to that for scintillator, *e.g.*, $\sim$ 6 pe/MeV for Super-K with a PMT surface coverage of $\sim$ 40%. In spite of light yield and Cherenkov threshold issues, the intrinsic directionality of Cherenkov light allows individual particle tracks to be reconstructed. Vertex and direction fits are performed using PMT hit charges and times, requiring that the hit pattern be consistent with a Cherenkov ring.

High-energy ($\sim$100 MeV or more) neutrinos from the atmosphere or beams interact with nucleons; for the nucleons bound inside the ^{16}O nucleus, nuclear effects must be considered both at the interaction and as the particles leave the nucleus. Various event topologies, with final-state particles contained, exiting, or entering the detector, can be distinguished by their timing and fit patterns, and by presence or absence of light in a veto. At high energies, multi-photoelectron hits are likely and the charge collected by each PMT (rather than the number of PMTs firing) must be used; the energy resolution in this case is approximately $2\%/\sqrt{\xi\,E_{\rm vis}({\rm GeV})}$. The absolute energy scale in this regime can be known to $\sim$2–3% using cosmic-ray muon energy deposition, Michel electrons and π^0 from atmospheric neutrino interactions. Typical vertex resolutions for GeV energies are a few tens of cm [44]. Angular resolution for determination of the direction of a charged particle track is a few degrees. For a neutrino interaction, because some final-state particles are usually below Cherenkov threshold, knowledge of direction of the incoming neutrino direction itself is generally worse than that of the lepton direction, and dependent on neutrino energy.

Multiple particles in an interaction (so long as they are above Cherenkov threshold) may be reconstructed, allowing for the exclusive reconstruction of final states. In searches for proton decay,

Downloaded from https://academic.oup.com/ptep/article/2022/8/083C01/6651666 by KIT Library user on 27 September 2022

multiple particles can be kinematically reconstructed to form a decaying nucleon. High-quality particle identification is also possible: γ rays and electrons shower, and electrons scatter, which results in fuzzy rings, whereas muons, pions and protons make sharp rings. These patterns can be quantitatively separated with high reliability using maximum likelihood methods [45]. Sources of background for high energy interactions include misidentified cosmic muons and anomalous light patterns when the PMTs sometimes "flash" and emit photons themselves. The latter class of events can be removed using its distinctive PMT signal patterns, which may be repeated. More information about high energy event selection and reconstruction may be found in reference [46].

In spite of the fairly low light yield, large water Cherenkov detectors may be employed for reconstructing low-energy events, down to *e.g.* $\sim$ 4-5 MeV for Super-K [47]. Low-energy neutrino interactions of solar neutrinos in water are predominantly elastic scattering off atomic electrons; single electron events are then reconstructed. At solar neutrino energies, the visible energy resolution ($\sim 30\%/\sqrt{\xi\, E_{\rm vis}(\rm MeV)}$) is about 20% worse than photoelectron counting statistics would imply. Using an electron LINAC and/or nuclear sources, approximately 0.5% determination of the absolute energy scale has been achieved at solar neutrino energies. Angular resolution is limited by multiple scattering in this energy regime (25–30°). At these energies, radioactive backgrounds become a dominant issue. These backgrounds include radon in the water itself or emanated from detector materials, and γ rays from the rock and detector materials. In the few to few tens of MeV range, radioactive products of cosmic-ray-muon-induced spallation are troublesome, and are removed by proximity in time and space to preceding muons, at some cost in dead time. Gadolinium doping using 0.2% $Gd_2(SO_4)_3$ has now been initiated for Super-K to improve selection of low-energy $\bar{\nu}_e$ and other events with accompanying neutrons [48].

The Sudbury Neutrino Observatory (SNO) detector [49] is the only instance of a large heavy water detector. In addition to an outer 1.7 kton of light water, SNO contained 1 kton of D_2O, giving it unique sensitivity to neutrino neutral current ($\nu_x + d \to \nu_x + p + n$), and charged current ($\nu_e + d \to p + p + e^-$) deuteron breakup reactions. The neutrons were detected in three ways: via capture on deuterons, via capture on dissolved ^{35}Cl, and via specialized ^{3}He counters.

36.3.1.3 *Noble liquid detectors*

Noble liquids scintillate and can be used as the active medium for particle detection. Detectors employing argon and xenon are also used as time-projection chambers (TPCs), either as dual-phase low-energy recoil detectors, or as track-imaging detectors. Noble-liquid detectors with low energy (few to few tens of keV) capability for detecting electronic and nuclear recoils are employed for dark matter and other rare event searches and are described in Sec. 36.4. These detectors can also be employed for some of the same physics (baryon number violation, astrophysical neutrino transient searches, etc.) as for the other large detectors described here, especially as they approach tens of ton scale and higher (e.g., DARWIN, DarkSide-20, ARGO). Track-imaging time-projection chambers, which are described in detail Section 36.4, have a dynamic range reaching down to the few to few tens of MeV scale, enabling sensitivity to e.g., solar and supernova burst neutrinos. Surface LArTPCs have significant cosmic backgrounds, but may still have sensitivity to astrophysical transients such as supernova burst neutrinos. DUNE will be sufficiently deep to have sensitivity to steady-state low-energy neutrino sources such as solar neutrinos.

36.3.2 *Neutrino telescopes*

Revised November 2021 by U.F. Katz (Erlangen U.) and C. Spiering (DESY, Zeuthen).

The primary goal of neutrino telescopes (NTs) is the detection of astrophysical neutrinos, in particular those which are expected to accompany the production of high-energy cosmic rays in astrophysical accelerators. NTs in addition address a variety of other fundamental physics issues like the indirect search for dark matter, studies of neutrino oscillations, searches for exotic particles like magnetic monopoles or study of cosmic rays and their interactions [50–52]. Electromagnetic radio frequency detectors for high energy neutrinos are discussed in "Radio emission from (ultra-) high energy particle showers" section 36.3.3.

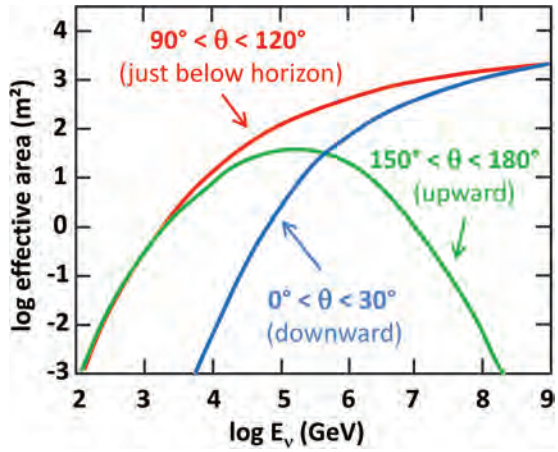

Figure 36.5: Average over the effective ν_μ and $\bar{\nu}_\mu$ areas for IceCube as an example of a cubic-kilometre NT, as a function of neutrino energy for three intervals of the zenith angle θ. The values shown here correspond to a specific event selection for point source searches.

NTs are large-volume arrays of "optical modules" (OMs) installed in open transparent media like water or ice, at depths that completely block the daylight. The OMs are sensitive to individual photons of the Cherenkov light induced by charged secondary particles produced in reactions of high-energy neutrinos in or around the instrumented volume. The time of photon-induced signals ("hits") is registered with a precision of a few nanoseconds. The neutrino energy, E_ν, and direction can be reconstructed from the hit pattern recorded. NTs typically target an energy range $E_\nu \gtrsim 100\,$GeV; sensitivity to lower energies is achieved in dedicated setups with denser instrumentation.

In detecting cosmic neutrinos, three sources of backgrounds have to be considered: (i) *atmospheric neutrinos* from cosmic-ray interactions in the atmosphere, which can be separated from cosmic neutrinos on a statistical basis, or, for down-going neutrinos, by vetoing accompanying muons; (ii) down-going punch-through *atmospheric muons* from cosmic-ray interactions, which are suppressed by several orders of magnitude with respect to the ground level due to the large detector depths and can be further reduced by selecting upward-going or high-energy neutrinos or by self-veto methods; (iii) random backgrounds due to photomultiplier (PMT) dark counts, ^{40}K decays (mainly in sea water) or bioluminescence (only water). Note that atmospheric neutrinos and muons allow for investigating neutrino oscillations and cosmic ray anisotropies, respectively.

In the last decade, it has become obvious that a precise measurement of the energy-zenith-distribution of atmospheric neutrinos in the energy range from a few to about 100 GeV may allow for determining the neutrino mass hierarchy by exploiting matter-induced oscillation effects in the Earth [53, 54].

Neutrinos can interact with target nucleons N through charged current ($\overset{(-)}{\nu}_\ell N \to \ell^\mp X$, CC) or neutral current ($\overset{(-)}{\nu}_\ell N \to \overset{(-)}{\nu}_\ell X$, NC) processes. A CC reaction of a $\overset{(-)}{\nu}_\mu$ produces a muon track and a hadronic particle cascade, whereas all NC reactions and CC reactions of $\overset{(-)}{\nu}_e$ produce particle cascades only. CC interactions of $\overset{(-)}{\nu}_\tau$ can have either signature, depending on the τ decay mode. Of particular interest is the so-called double-bang signature, where the τ decays sufficiently far away from the primary interaction to create a second, distinguishable cascade (typically at PeV energies and above). In most astrophysical models, neutrinos are expected to be produced through the $\pi/K \to \mu \to e$ decay chain, *i.e.*, with a flavour ratio $\nu_e : \nu_\mu : \nu_\tau \approx 1 : 2 : 0$. For sources outside the solar system, neutrino oscillations turn this ratio to $\nu_e : \nu_\mu : \nu_\tau \approx 1 : 1 : 1$ upon arrival on Earth.

Downloaded from https://academic.oup.com/ptep/article/2022/8/083C01/6651666 by KIT Library user on 27 September 2022

The total neutrino-nucleon cross section is about $10^{-34}\,\mathrm{cm}^2$ at $E_\nu = 20\,\mathrm{TeV}$ and rises roughly linearly with E_ν below this energy and as $E_\nu^{0.3-0.5}$ above, flattening out towards high energies. The CC:NC cross-section ratio is about 2:1. At energies above several TeV, neutrino absorption in the Earth becomes noticeable; for vertically upward-moving neutrinos (zenith angle $\theta = 180°$), the survival probability is $74\,(27, < 2)\%$ for $10\,(100, 1000)$ TeV. The energy transferred to the final-state lepton varies between 0 and 100% of E_ν, with a mean of 50% (65%) for neutrinos (antineutrinos) at 100 GeV and 75% for both neutrinos and antineutrinos at 10 PeV.

The final-state lepton follows the initial (anti)neutrino direction with an average mismatch angle of about $\langle\phi_{\nu\ell}\rangle \approx 1°/(E_\nu/\mathrm{TeV})^{0.55}$, with a steeper decrease beyond 10 TeV, reaching 0.005° at 1 PeV [55]. These values indicate the intrinsic kinematic limit to the angular resolution of NTs. For CC $\overset{(-)}{\nu}_\mu$ reactions at energies above about 10 TeV, the angular resolution is dominated by the muon reconstruction accuracy of a few times 0.1° at most. For muon energies $E_\mu \gtrsim 1\,\mathrm{TeV}$, the increasing light emission due to radiative processes allows for reconstructing E_μ from the measured Cherenkov light intensity with an accuracy of $\sigma(\log E_\mu) \approx 0.3$; at lower energies, E_μ can be estimated from the length of the muon track if it is contained in the detector. These properties make CC $\overset{(-)}{\nu}_\mu$ reactions the prime channel for the identification of individual astrophysical neutrino sources.

Hadronic and electromagnetic particle cascades at the relevant energies are 5–20 m long, *i.e.*, short compared to typical OM spacings. The total amount of Cherenkov light provides a direct measurement of the cascade energy with an accuracy of about 20% at energies above 10 TeV and 10% beyond 100 TeV for events contained in the instrumented volume. Except for double-bang events, the neutrino flavour and reaction mechanism can, however, be determined on a statistical basis at best, and neutrinos from NC reactions or τ decays may carry away significant "invisible" energy. Above 100 TeV, the average directional reconstruction accuracy of cascades is better than 10 (2) degrees in polar ice (sea water), the difference being due to the inhomogeneity of the ice and stronger light scattering in ice. These features, together with the small background of atmospheric $\overset{(-)}{\nu}_e$ and $\overset{(-)}{\nu}_\tau$ events, makes the cascade channel particularly interesting for searches for a diffuse, high-energy excess of extraterrestrial over atmospheric neutrinos. Cascade events can also be used to complement the muon channel in searches for point sources or transient signals, albeit with inferior angular accuracy compared to muon tracks.

The detection efficiency of a NT is quantified by its effective area, *e.g.*, the fictitious area for which the full incoming neutrino flux would be recorded (see Figure 36.5). The increase with E_ν is due to the rise of neutrino cross section and muon range, while neutrino absorption in the Earth causes the decrease at large θ for large E_ν. Identification of downward-going neutrinos requires strong cuts against atmospheric muons, hence the cut-off towards low E_ν at low θ. Due to the small cross section, the effective area is many orders of magnitude smaller than the geometrical dimension of the detector; a $\overset{(-)}{\nu}_\mu$ with 1 TeV can, *e.g.*, be detected with a probability of the order 10^{-6} if the NT is on its path.

Due to the long muon range, CC interactions of up-going $\overset{(-)}{\nu}_\mu$ can be detected from far outside the instrumented volume. This method also works for horizontal neutrinos up to about 10° above the horizon (depth dependent), where the background from atmospheric muons become prohibitive. Alternatively, one can select events that start inside the instrumented volume and thus remove incoming muons that generate early hits in the outer layers of the detector. Such a veto-based event selection is sensitive to neutrinos of all flavours from all directions, albeit with a reduced efficiency since a part of the instrumented volume is sacrificed for the veto. Such a muon veto, or vetoing events with a coincident signal in the surface array, also rejects down-going atmospheric neutrinos that are accompanied by muons from the same air shower and thus reduces the atmospheric-neutrino background. Actually, the breakthrough in detecting high-energy cosmic neutrinos was first achieved with this technique.

Note that the fields of view of NTs at the South Pole and in the Northern hemisphere are complementary for each reaction channel and neutrino energy.

36.3.2.1 *The Projects*

Table 36.3 lists past, present and future neutrino telescope projects and their main parameters.

36.3.2.2 *Properties of media*

The efficiency and quality of event reconstruction depend strongly on the optical properties (absorption and scattering length, intrinsic optical activity) of the medium in the spectral range of bialkali photocathodes (300–550 nm). Large absorption lengths result in a better light collection, large scattering lengths in superior angular resolution. Deep-sea sites typically have effective scattering lengths of > 100 m and, at their peak transparency around 450 nm, absorption lengths of 50–65 m. The absorption length for Lake Baikal is 22–24 m. The properties of South Polar ice vary strongly with depth; at the peak transparency wave length (400 nm), the scattering length is between 5 and 75 m and the absorption length between 15 and 250 m, with the best values in the depth region 2200–2450 m and the worst ones in the layer 1950–2100 m.

Noise rates measured by PMTs with a diameter of 25 cm in deep polar ice are about 0.5 kHz per PMT and almost entirely due to radioactivity in the OM components. The corresponding rates in sea water are typically 60 kHz, mostly due to ^{40}K decays. Bioluminescence activity can locally cause rates on the MHz scale for seconds; the frequency and intensity of such "bursts" depends strongly on the sea current, the season, the geographic location, and the geometry of the detector elements. Experience from ANTARES shows that these backgrounds are manageable without a major loss of efficiency or experimental resolution.

36.3.2.3 *Technical realisation*

Optical modules (OMs) and PMTs: An OM is a pressure-tight glass sphere housing one or several PMTs with a time resolution in the nanosecond range, and in most cases also electronics for control, HV generation, operation of calibration LEDs, time synchronisation and signal digitisation.

Hybrid PMTs with 37 cm diameter have been used for NT-200, conventional hemispheric PMTs with 20 cm diameter for AMANDA and with 25 cm diameter for ANTARES, IceCube and Baikal-GVD. A novel concept has been chosen for KM3NeT. Each OM (43 cm) is equipped with 31 PMTs (7.5 cm), plus control, calibration and digitisation electronics. Advantages are that (i) the overall photocathode area exceeds that of a 25 cm PMT by more than a factor of 3; (ii) the individual readout of the PMTs results in a very good separation between one- and two-photoelectron signals which is essential for online data filtering and random background suppression; (iii) the hit pattern on an OM provides directional information; (iv) no mu-metal shielding against the Earth magnetic field is required. Figure 36.6 shows the OM designs of IceCube and KM3NeT.

Readout and data filtering: In current NTs the PMT data are digitised in situ: for ANTARES and Baikal-GVD in special electronics containers close to the OMs, for IceCube and KM3NeT inside the OMs. For IceCube, data are transmitted via electrical cables of up to 3.3 km length, depending on the location of the strings and the depth of the OMs; for ANTARES, KM3NeT and Baikal-GVD optical fibre connections have been chosen (several 10 km for the first two and 4 km for GVD).

The full digitised waveforms of the IceCube OMs are transmitted to the surface for pulses appearing in local coincidences on a string; for other pulses, only time and charge information is provided. For ANTARES (time and charge) and KM3NeT (time and time over threshold), all PMT signals above an adjustable threshold are sent to shore.

The raw data are subsequently processed on online computer farms, where multiplicity- and topology-driven filter algorithms are applied to select event candidates. The filter output data rate is about 10 GByte/day for ANTARES and of the order 1 TByte/day for IceCube (100 GByte/day transferred via satellite) and KM3NeT.

Downloaded from https://academic.oup.com/ptep/article/2022/8/083C01/6651666 by KIT Library user on 27 September 2022

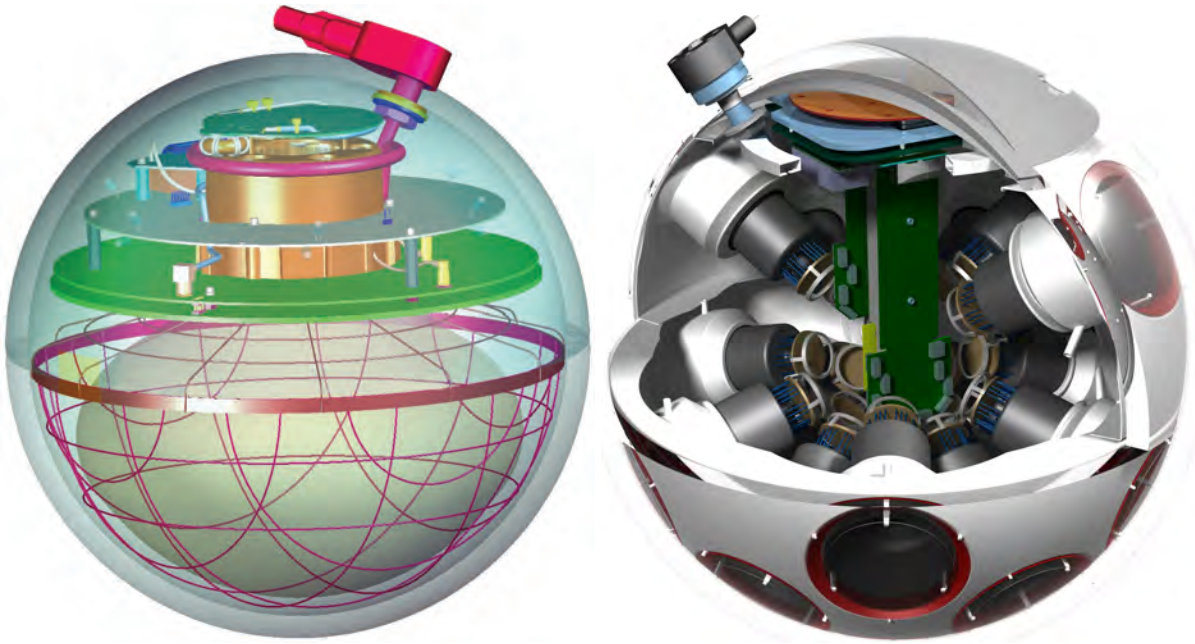

Figure 36.6: Schematic views of the digital OMs of IceCube (left) and KM3NeT (right).

Table 36.3: Past, present and future NT projects and their main parameters. The milestone years give the times of project start, of first data taking with partial configurations, of detector completion, and of project termination. Projects with first data expected past 2022 are indicated in italics. The size refers to the largest instrumented volume reached during the project development. See [52] for references to the different projects where unspecified.

Experiment	Milestones	Location	Size (km^3)	Remarks
DUMAND	1978/–/–/1995	Pacific Ocean		Terminated due to technical/funding problems
NT-200	1980/1993/1998/2015	Lake Baikal	10^{-4}	First proof of principle
GVD [56]	2012/2015/–/–	Lake Baikal	0.5–1.5	High-energy ν astronomy first 8 clusters installed
NESTOR	1991/–/–/–	Med. Sea		2004 data taking with prototype
NEMO	1998/–/–/–	Med. Sea		R&D project, prototype tests
AMANDA	1990/1996/2000/2009	South Pole	0.015	First deep-ice NT
ANTARES	1997/2006/2008/–	Med. Sea	0.010	First deep-sea NT
IceCube [57]	2001/2005/2010/–	South Pole	1.0	First km^3-sized detector
IceCube-Gen2 [58, 59]	2014/–/–/–	South Pole	5–10	Planned extension of IceCube covering low and high energies, a surface array and radio detection
KM3NeT/ARCA [54]	2013/2021/–/–	Med. Sea	ca. 1	High-energy configuration for neutrino astronomy. Under construction, data taking with 8 strings
KM3NeT/ORCA [54]	2014/2020/–/–	Med. Sea	0.007	Low-energy configuration for neutrino mass hierarchy. Under construction, data taking with 10 strings
KM3NeT Phase 3	2013/–/–/–	Med. Sea	ca. 3	6 ARCA blocks + ORCA
P-ONE [60]	2018/–/–/–	Pacific Ocean	$\mathcal{O}(1)$	Possible future NT, R&D phase

Calibration: For efficient event recognition and reconstruction, the OM timing must be synchronised at the few-nanosecond level and the OM positions and orientations must be known to a few 10 cm and a few degrees, respectively. Time calibration is achieved by sending time synchronisation signals to the OM electronics and also by light calibration signals emitted in situ at known times by LED or laser flashers (ANTARES, KM3NeT). Precise position calibration is achieved by measuring the travel time of light calibration signals sent from OM to OM (IceCube) or acoustic signals sent from transducers at the sea floor to receivers on the detector strings (ANTARES, KM3NeT, Baikal-GVD). Absolute pointing and angular resolution can be determined by measuring the "shadow of the moon" (*i.e.*, the directional depletion of muons generated in cosmic-ray interactions). IceCube and ANTARES have both shown that they have angular resolution below 1°, confirming MC calculations which indicate a precision of $\approx 0.5°$ for energies above 10 TeV. For KM3NeT, simulations indicate that sub-degree precision in the absolute pointing can be

Downloaded from https://academic.oup.com/ptep/article/2022/8/083C01/6651666 by KIT Library user on 27 September 2022

reached within a few weeks of operation.

Detector configurations: IceCube [57] (see Figure 36.7) consists of 5160 Digital OMs (DOMs) installed on 86 strings at depths of 1450 to 2450 m in the Antarctic ice; except for the DeepCore region, string distances are 125 m and vertical distances between OMs 17 m. 324 further DOMs are installed in IceTop, an array of detector stations on the ice surface above the strings. DeepCore is a high-density sub-array at large depths (*i.e.*, in the best ice layer) at the centre of IceCube.

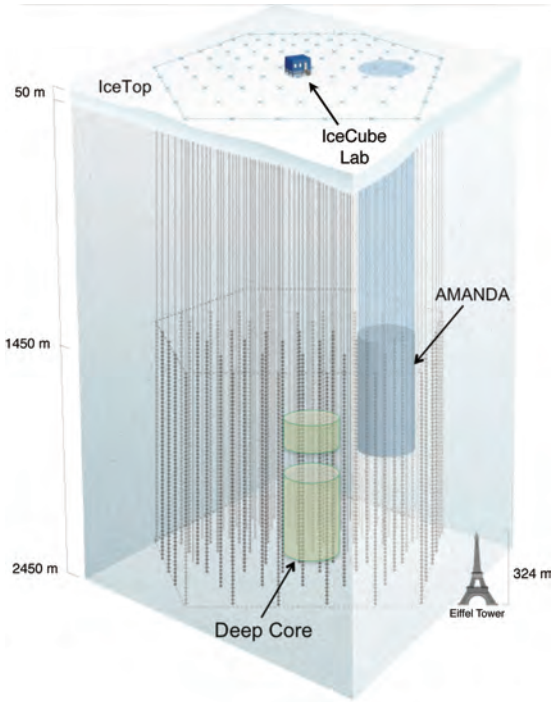

Figure 36.7: Schematic view of the IceCube neutrino observatory comprising the deep-ice detector including its nested dense part DeepCore, and the surface air shower array IceTop. The IceCube Lab houses data acquisition electronics and the computer farm for online processing. Operation of AMANDA was terminated in 2009.

The NT200 detector in Lake Baikal at a depth of 1100 m consisted of 8 strings attached to an umbrella-like frame, with 12 pairs of OMs per string. The diameter of the instrumented volume was 42 m, its height 70 m. Meanwhile (2021), the Baikal collaboration has installed the first eight clusters of a future cubic-kilometre array, GVD [56]. A first phase, covering a volume of about 0.7 km^3, will consist of 14 clusters, each with 288 OMs at 8 strings; its completion is scheduled for 2024. A next stage could cover up to 1.5 km^3.

ANTARES (see [52] and references therein) comprises 12 strings with lateral distances of 60–70 m, each carrying 25 triplets of OMs at vertical distances of 14.5 m. The OMs are located at depths of 2.1–2.4 km, starting 100 m above the sea floor. An additional string holds devices for calibration and environmental monitoring. A system to investigate the feasibility of acoustic neutrino detection has also been implemented.

KM3NeT will consist of building blocks of 115 strings each, with 18 OMs per string. Operation of prototypes and the first strings deployed have successfully verified the KM3NeT technology [61]. In the upcoming phase 2.0 of its staged implementation, KM3NeT aims at two building blocks for neutrino astronomy, with vertical distances between OMs of 36 m and a lateral distance between adjacent strings of 90 m (ARCA, for *Astroparticle Research with Cosmics in the Abyss*) and at one block for the measurement of the neutrino mass hierarchy, with vertical distances between OMs of 9 m and a lateral distance between adjacent strings of about 20 m (ORCA, for *Oscillation Research with Cosmics in the Abyss*) [54]. The installation of ARCA near Capo Passero, East of Sicily (depth 3440 m) and of ORCA near Toulon (depth 2450 m) is ongoing and as of now (August 2021) for each of both six strings have been deployed and are continuously operated. Completion of the full ARCA (ORCA) arrays is planned for 2026 (2025). The possibility of directing a neutrino beam from the Protvino accelerator to ORCA (P2O) is also under study [62].

P-ONE (*Pacific Ocean Neutrino Experiment*) [60] is a new initiative in an early R&D phase, envisaging a large NT in the Pacific Ocean off the Canadian coast. It is intended to use an existing deep-sea cable infrastructure and to optimise the sensitivity for horizontal neutrinos with energies of about 100 TeV and beyond.

36.3.2.4 *Results*

Atmospheric neutrino fluxes have been precisely measured with AMANDA ($\overset{(-)}{\nu}_\mu$), with IceCube and ANTARES ($\overset{(-)}{\nu}_\mu$, $\overset{(-)}{\nu}_e$) and have recently also been detected with KM3NeT ($\overset{(-)}{\nu}_\mu$); the results are in agreement with predicted spectra.

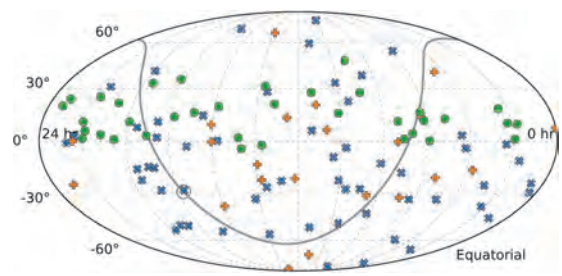

Figure 36.8: Arrival directions of IceCube candidate events for cosmic neutrinos in equatorial coordinates. The plot contains 82 HESE events, with shower-like events marked as blue × and muon tracks as orange +, and in addition 36 through-going muons tracks with an energy deposit exceeding 200 TeV (green circles). Approximately 40% of the events are expected to originate from atmospheric backgrounds. The grey curve denotes the Galactic Plane and the grey circle the Galactic Centre (from [63]).

In 2013, an excess of track and cascade events between 30 TeV and 1 PeV above background expectations was reported by IceCube; this analysis used the data taken in 2010 and 2011 and for the first time employed containment conditions and an atmospheric muon veto for suppression of down-going atmospheric neutrinos (High-Energy Starting Event analysis, HESE). The observed excess reached a significance of 5.7σ in a subsequent analysis of 3 years of data [64] and increased in significance since then. The excess is therefore interpreted to be due to an astrophysical neutrino flux. A consistent observation has also been made by ANTARES [65], albeit with much lower significance. The skymap of HESE and high-energy through-going muon events (see Figure 36.8) does not indicate statistically significant event clusters, nor deviations from an isotropic cosmic neutrino flux. Meanwhile the energy range of IceCube analyses has been extended down to about 10 TeV and the high-energy excess confirmed; also, events with through-going muons showed a corresponding excess of cosmic origin. In [66], the various analyses have been combined. Assuming the cosmic neutrino flux to be isotropic, flavour-symmetric and ν-$\overline{\nu}$-symmetric at Earth, the all-flavour spectrum is well described by a power law with normalisation $6.7^{+1.1}_{-1.2} \times 10^{-18}\,\mathrm{GeV^{-1}s^{-1}sr^{-1}cm^{-2}}$ at 100 TeV and a spectral index -2.50 ± 0.09 for energies between 25 TeV and 2.8 PeV. A spectral index of -2, an often quoted benchmark value, is disfavoured with a significance of 3.8σ.

Multi-messenger observations triggered by a high-energy IceCube neutrino event in 2017 (see Figure 36.9 for an event display), together with a neutrino excess from the same celestial direction in the 2014/15 archival IceCube data, yielded evidence for a first neutrino signal related to a known astronomical object, the blasar[2] TXS 0506+056 [67, 68]. Multi-messenger investigations in conjunction with gravitational waves, ultra-high-energy cosmic rays or gamma-ray observations have not revealed further,

[2] An Active Galactic Nucleus with a relativistic jet outflow pointing to the observer.

Downloaded from https://academic.oup.com/ptep/article/2022/8/083C01/6651666 by KIT Library user on 27 September 2022

similarly significant neutrino signals to date. Also, no further astrophysical neutrino sources were found in a recent combined IceCube/ANTARES search for steady sources [69].

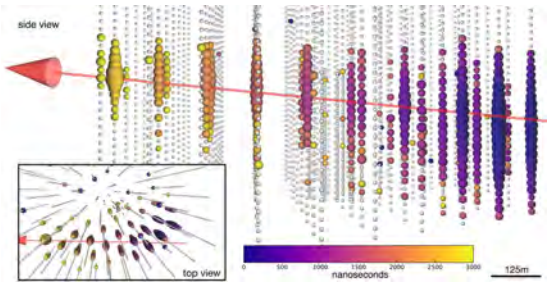

Figure 36.9: Display of the event IceCube-170922A, consistent with a neutrino from the blasar TXS 0506+056. The deposited energy is 24 TeV, the most probable neutrino energy is 290 TeV. The colour code indicates the signal timing (blue: early; yellow: late), the size of the coloured circles is a logarithmic measure of the light intensity registered per DOM. The arrow indicates the reconstructed neutrino direction, corresponding to a zenith angle of $5.7^{+0.5}_{-0.3}$ degrees below horizon. Figure from [67].

IceCube has reported an energy-dependent anisotropy of cosmic-ray induced muons, a measurement of the neutrino-nucleon cross section using neutrino absorption in Earth, and the observation of a cascade event consistent with the process $\overline{\nu}_e + e^- \to W^- \to$ hadrons (Glashow resonance).

No indications for neutrino fluxes from dark matter annihilations or for other exotic phenomena have been found.

At lower energies, down to 10 GeV, IceCube/DeepCore, ANTARES and meanwhile also KM3NeT have identified clear signals of oscillations of atmospheric neutrinos. The closely spaced OMs of DeepCore allow for selecting a very pure sample of low-energy $\overset{(-)}{\nu}_\mu$ (6–56 GeV) that produce upward moving muons inside the detector. The neutrino energy is determined from the energy of the hadronic shower at the vertex and the muon range. Fits to the energy/zenith-dependent deficit of muon neutrinos provide constraints on the oscillation parameters $\sin^2\theta_{23}$ and Δm^2_{23}. The analysis of the same dependence for cascade-like events provides a $\sim 3\sigma$ evidence for ν_τ appearance – an important measurement to test the unitarity of the PMNS matrix [70].

See [71–73] for summaries of status, recent results and future plans of IceCube, ANTARES, KM3NeT, and GVD.

36.3.2.5 *Plans beyond 2021*

Within the future IceCube-Gen2 project, it is planned to extend the sensitivity of IceCube towards both higher and lower energies. To increase the detector sensitivity at high energies, a large-volume extension is envisaged, combined with a radio array for highest-energy neutrinos and a surface array providing also a powerful veto against atmospheric events [58, 59]. A substantially denser instrumentation of a sub-volume of DeepCore will be achieved with 7 closely spaced strings to be deployed in 2024/25 (the IceCube Upgrade), aiming to cover a low-energy program, to better calibrate the existing IceCube detector and the archival data, and to test new technologies. More information on the future extensions of GVD and KM3NeT and on P-ONE are given above, in Table 36.3 and in [54, 72].

36.3.3 *Radio emission from (ultra-)high energy particle showers*

Revised October 2021 by S.R. Klein (NSD LBNL; UC Berkeley) and A. Nelles (DESY, Zeuthen; Erlangen U.).

Coherent radio-frequency (RF) electromagnetic radiation is an attractive signature to search for particle cascades produced by interactions of high-energy particles. RF signatures have been used to study both cosmic-ray air showers and to search for neutrino-induced showers. This article will discuss the radio signal generation, the relevant energy regime and the application in detectors. Air showers are discussed in more detail in two recent reviews [74, 75]. At lower energies, incoherent optical Cherenkov radiation is frequently used, as discussed in "Neutrino telescopes" section 36.3.2. This article uses the general definitions and properties of neutrino telescopes as described in 36.3.2.

36.3.3.1 *Signal generation and its characteristics*

As discussed in the "Passage of Particles Through Matter" review Sec. 34 the electromagnetic component of a high energy shower gives rise to radio emission. For the signal generation itself the type of primary particle is irrelevant. However, the signal medium is important. It must be non-conducting (and non-absorptive at RF frequencies). The different shower length scales (radiation length, X_0) between air and the solid materials used for neutrino searches leads to surprisingly large differences in shower development. Due to the interaction with the medium the shower contains more electrons than positrons, which results in a net charge excess and leads to coherent Cherenkov emission, also known as Askaryan effect [76–78]. In air, during propagation through the geomagnetic field, the relative motion of electrons and positrons is affected, which leads to a varying transverse current, usually referred to as the geomagnetic effect [74]. Both effects may be described more generally as being due to radiation from a time-varying net charge [79]. Their relative importance is governed by the density of the medium, as the electric field scales as the net charge excess, and a lower density allows the geomagnetic effect to gain importance. Thus, in solid materials the emission from the Askaryan effect dominates, but it is a $< 20\%$ correction in air showers.

Coherent radiation is possible at wavelengths longer than the instantaneous thickness of the shower along an observer's line of sight. Since air showers have a larger extent than showers in solid media, their coherent radiation appears at lower frequencies.

High-frequency radiation is concentrated around the Cherenkov angle θ_C. Viewed directly on the Cherenkov cone, the electric field strength, $\epsilon_{\rm Ch}$ at a frequency f from an electromagnetic shower from a ν_e with energy E_ν in ice may be roughly parameterized as [80, 81]

$$\epsilon_{\rm Ch}(V/{\rm mMHz}) = 2.53\times 10^{-7}\,\frac{E_\nu}{1{\rm TeV}}\,\frac{f}{f_c}\left[\frac{1}{1+(f/f_c)^{1.44}}\right]. \quad (36.3)$$

The electric field strength increases linearly with frequency, up to a cut-off frequency f_c, which is set by the transverse size of the shower [82, 83]. The maximum wavelength c/f_c is roughly the Moliere radius divided by $\cos(\theta_C)$ where θ_C is the Cherenkov angle. The cutoff frequencies depend on the density (which affects the Moliere radius). They are about 1 GHz in ice, about 3 GHz in the lunar regolith, and below 100 MHz in air.

Near f_c, radiation is narrowly concentrated around θ_C [82, 83]. At lower frequencies, the limited length of the emitting region leads to a broadening in emission angle around the Cherenkov cone. Away from θ_C, the electric field from Eq. (36.3) is reduced by [80],

$$\frac{\epsilon}{\epsilon_{\rm Ch}} = \exp\left(-\frac{1}{2}\,\frac{(\theta-\theta_C)^2}{(2.2^\circ\times[1{\rm GHz}/f])^2}\right). \quad (36.4)$$

The angular distribution of the signal around θ_C can be parameterized by a Gaussian peak modulated by a $\sin\theta$. In both ice and the lunar regolith, θ_C is about 56°, in air only 1°. Close to θ_C, the 1 GHz maximum frequency in ice/regolith leads to a generated pulse width of ≈ 1 nsec.

These equations are appropriate for ice. More general parameterizations can be found in [81, 84].

More accurate calculations of the predicted radio signal, in particular air showers are not easily parameterized, but require detailed Monte Carlo simulations. For air showers, these are built on microscopic air shower simulations, calculate the emission from all individual particles in the shower development and add them for different observer positions [74]. For neutrinos, most approaches calculate (directly or from a parameterization) the Askaryan signal from a shower profile. The signal is then propagated through the medium and into an antenna model [81].

At energies above 10^{16} eV in ice, the Landau-Pomeranchuk-Migdal effect lengthens electromagnetic showers, by reducing the

Downloaded from https://academic.oup.com/ptep/article/2022/8/083C01/6651666 by KIT Library user on 27 September 2022

cross-sections for bremsstrahlung and pair production [85]. The lengthening of the shower leads to a narrowing of the radio emission around the Cherenkov cone, and a reduction in high-frequency emission away from the cone [81]. At higher energies, this leads to two separate components of the Askaryan radiation from a neutrino interaction: an un-altered component from the hadronic portion of the shower and an angularly narrowed component from the LPM-lengthened electromagnetic shower. The width of the narrowed component scales as $E_\nu^{1/3}$. If these two components can be observed separately, they could, in principle, be combined to determine the inelasticity of the neutrino interaction [86], allowing for improved measurements of low$-x$ parton distributions and searches for beyond-standard-model interactions.

Similarly, energetic outgoing $\mu^\pm$ and $\tau^\pm$ from neutrino interactions will dominantly lose energy via stochastic pair production and photonuclear interactions. These secondary particles will produce electromagnetic showers that can be detected by radio detectors, if they are above threshold energy. This will enable multiple detections of the same particle track and thus present interesting reconstruction opportunities [87].

At still higher energies, above 10^{20} eV, the LPM effect strengthens, and the electromagnetic shower splits into multiple subshowers with significant separation. When these separations become large enough, the subshowers will effectively become independent radiators, with the total emission showing substantial event-by-event variation, depending on the division into subshowers [85]. Because of this, many experiments that study higher energy (well above 10^{20} eV) neutrinos focus on the hadronic shower from the struck nucleus. This contains an average of only about 20% of the energy, but with fewer large fluctuations.

36.3.3.2 *Energy regime of radio detectors*

The electric field amplitude is linearly proportional to the shower energy. Since the signal is a radio wave, the field amplitude decreases as $1/R$, plus potential absorption in the intervening medium, while the energy fluence decreases as $1/R^2$, again, plus potential absorption. The detection threshold depends on the distance to the antenna and the bandwidth and noise characteristics of the antenna and detector. For an antenna located in the detection medium, at a distance of 1 km the typical threshold is around 10^{17} eV. For stand-off (remote sensing) detectors, the threshold rises roughly linearly with the distance. These thresholds can be reduced by using directional antennas and/or combining the signals from multiple antennas using beam-forming techniques.

RF detectors are used to search for energetic neutrinos from three types of sources: astrophysical objects (*i.e.* extending measurements of the neutrino energy spectrum observed at TeV to PeV energies upward in energy), cosmogenic neutrinos associated with cosmic-ray-cosmic microwave background radiation (CMBR) interactions, and neutrinos from beyond-standard-model physics. These types are very roughly associated with energies below 10^{18} eV, the energy range 10^{18} to 10^{20} eV, and above 10^{20} eV.

Cosmogenic neutrinos are produced when ultra-high energy (UHE) protons with energy $E > 5\times10^{19}$ eV interact with photons from the CMBR, infrared light from old stars, and other extragalactic background light. These protons are excited to a Δ^+ resonance which may decay via $\Delta^+ \to n\pi^+$, leading to neutrinos with energies above 10^{18} eV [88, 89]. The cosmogenic neutrino signal depends heavily on the fraction of UHE cosmic-rays that are protons. For a 100% proton composition (disfavored by most data [90]), observing a cosmogenic neutrino signal of at least a few events per year requires a solid or liquid detector with an active volume of about 100 km^3.

To reach the effective volumes necessary to observe the expected low fluxes of UHE neutrinos, common, naturally occurring, non-conducting solid (or potentially liquid) media, with a long absorption length for radio waves are needed. Optical Cherenkov and acoustical detectors are limited by short ($<$ 100 m) attenuation lengths [91] so would require a prohibitively expensive number of sensors. The radio detection technique has been used to detect air showers, targeting neutrinos as well as cosmic rays, and to search for neutrino showers in ice, salt domes and the lunar regolith.

36.3.3.3 *Reconstruction of particle energy and direction and background suppression*

Since radio detectors view the interaction from afar, the reconstruction techniques differ from optical neutrino telescopes.

Radio detection is a calorimetric measurement, thus provides good energy estimates of the shower energy. The energy fluence (integrated pulse power) of the signal scales quadratically with shower energy. It also depends on the distance to the shower, through potential attenuation losses and the usual $1/R$ loss in electric field amplitude. The arrival times in antennas and a spherical wave approximation can be used to determine the interaction vertex, although some uncertainty due to the viewing angle with respect to the Cherenkov angle may remain, if not corrected for by using the frequency information. If the radio signal travels through media where the index of refraction varies (like the firn of glacial ice), then ray-tracing techniques may be required to follow the signal back to the interaction point. For buried antennas, the bending of the signal trajectories due to the index of refraction creates an opportunity. For some geometries, there may be two paths to the detector: a 'direct' path, with minor bending, and a second where the signal is bent beyond horizontal, bouncing off the surface before reaching the antenna. By measuring the time difference between the two paths, the distance to the interaction vertex may be determined; this greatly simplifies the energy determination [92,93]. For most neutrino interactions (except for ν_e charged-current interactions), the shower energy is less than the neutrino energy. The uncertainty on the interaction inelasticity is a major contributor to the uncertainty in the neutrino energy, along with uncertainties on the distance between the antenna(s) and the interaction vertex [94].

Reconstruction of the neutrino arrival direction depends on several aspects of the signal. First, the direction from the antenna to the interaction site must be determined. This can be done by using the relative timing from separated antennas, or using beam-forming techniques with multi-element arrays. For air showers, the signal arrival direction is (almost) equal to the particle arrival direction, with corrections being obtainable by fitting a hyperbolic wavefront [74, 75].

For showers in solid/liquid media, the arrival direction with respect to the interaction point - antenna vector is determined from two additional angles. The frequency spectrum can be used to determine the angle between signal arrival direction and Cherenkov cone according to Eq. (36.4) [95]. The second angle can be determined from the polarization of the signal. The radio signal is produced with a linear polarization in the plane containing both the particle direction and the radio wave direction. These two angles can be combined to determine the direction, subject to a (usually) four-fold ambiguity, due to uncertainty as to whether the antenna is inside or outside the Cherenkov cone, and because the particle direction can be flipped 180° without affecting the observed signal. Often, some of these solutions can be rejected because they correspond to long path lengths through the Moon or the Earth, where the neutrino would be absorbed.

Spectral information is crucial for the reconstruction and background rejection. However, large bandwidth antennas typically disperse (i.e. broaden) the pulses. As long as the dispersion can be compensated for and backgrounds controlled, a large bandwidth detector is the most sensitive.

All radio experiments must contend with background. Common sources are anthropogenic noise, antenna/preamp noise, charge generated by blowing snow, lightning, and, at low frequencies, radiation from the Milky Way. While narrowband noise impacts triggering and contaminates signal quality, impulsive backgrounds could mimic a signal. One of the major issues for radio-detection experiments is anthropogenic noise. Most anthropogenic noise has distinctive characteristics (such as being narrow-band, and coming from near the horizon) which makes it relatively easy to reject during data analysis, via narrow-band filters and other techniques [74]. However, these factors complicate triggering and reduce data purity. This is even an issue in Antarctica, where communication radios and passing satellites can mimic showers, at least at the trigger level. The need to limit anthropogenic noise has led most experimental groups to select remote locations for

Downloaded from https://academic.oup.com/ptep/article/2022/8/083C01/6651666 by KIT Library user on 27 September 2022

their detectors. Still, experiments have used approaches to reduce trigger-level noise, and/or to reject background at the analysis level. For example, for multi-element arrays, the threshold drops as the square root of number of antennas, since the signal adds in-phase while the backgrounds add with random phases [96].

Most dedicated air shower experiments have used radio antennas in combination with at least one other detector technology, such as scintillation counters, if the site quality is not sufficient and/or computing power on autonomous stations is limited. One exception is ARIANNA, which is located in an uninhabited part of Antarctica, enabling them to efficiently self-trigger on air showers [97].

Lunar experiments (discussed below) use different techniques to reduce the anthropogenic background. Some experiments use multiple antennas, separated by at least hundreds of meters; by requiring a coincidence within a small time window, anthropogenic noise can be rejected. With good enough timing, beam-forming techniques can be used to further reduce the background. An alternative approach is to use beam forming with multiple feed antennas viewing a single reflector, to ensure that the signal points back to the moon.

Due to the similarity in the radio emission of air showers and neutrino showers, the more abundant cosmic rays can act as background to neutrino searches. In-ice detectors need to suppress in-air emission that is refracted into the ice, emission that is created from developing air showers continuing in the ice, as well as from stochastic energy-losses of atmospheric muons. Lunar experiments may faces challenges in separating neutrino interactions from cosmic ray interactions.

36.3.3.4 *Recent experiments*

Figure 36.10 shows some current limits from neutrino searches, including from prototype arrays. Except for LOFAR, which is fully operational, projected limits from future experiments are not shown in the figure.

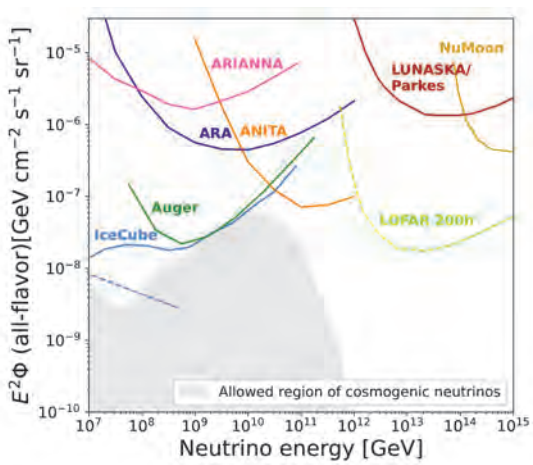

Figure 36.10: Representative 3-flavor (summed, assuming equal fluxes of each flavor) differential (over one decade in energy) limits from different experiments and prototype experiments. Shown are limits from the IceCube ultra-high energy ν search [98], the Auger search for earth-skimming ν_τ [99], the LUNASKA/Parkes [100] and NuMoon lunar searches [101], the ANITA balloon experiment [102], ARA [103] and ARIANNA prototypes [104], along with projections for the LOFAR array [105]. The dashed blue line is the extrapolation of the IceCube through-going ν_μ flux measured at lower energies (few 10s of TeV to 10 PeV), with spectral index $\alpha = -2.28$ [106]. Because of the long extrapolation, this should only be treated as a rough reference. The ARA and ARIANNA limits are from prototype arrays, and indicate the energy range that might be covered, with far higher sensitivity by larger arrays. The shaded area is the allowed region for cosmogenic neutrinos, from a recent global analysis that included the measured cosmic-ray spectrum and composition [107].

i. *Ice*

The most common dense medium transparent to radio waves is ice. Natural ice is an attractive medium for neutrino detection with radio attenuation lengths from over 300 m to 1 km [108]. The attenuation length varies with frequency and ice temperature, with higher attenuation in warmer ice. Although glacial ice is mostly uniform, the top $\approx$ 100 m of ice, the 'firn,' exhibits a gradual transition from packed snow at the surface (typically $\rho = 0.35$ g/cm^3) to solid ice ($\rho = 0.92$ g/cm^3) below [109]. The thickness of the firn varies with location; it is thicker in central Antarctica than in the coastal ice sheets or in Greenland. The varying density has several implications.

The index of refraction depends linearly on the density, so radio waves curve downward in the firn. This bending reduces the effective volume of surface or aerial antennas. A surface antenna cannot see near-surface interactions at large horizontal distances. There are also indications that the increase in firn density is non-monotonic [110, 111]. This leads to non-monotonic changes in index of refraction which may create waveguides that trap a small fraction of the radio energy and propagate it horizontally.

In one type of experiment, antennas mounted on high-altitude balloons observe the ice from above. Radio signals from in-ice neutrino interactions propagate to the surface, traverse the ice-air interface, and then travel to the balloon. The surface roughness of the ice can affect signals as they transition from the ice to the atmosphere. The best known example, ANITA, has made four flights around Antarctica, floating at an altitude around 35 km [112]. Its 32/40/48 (depending on the flight) dual-polarization horn antennas scanned the surrounding ice, out to the horizon (650 km away). Because of the small angle of incidence, ANITA could use polarization information to separate signals from background; ν signals should be vertically polarized, while most background from cosmic-ray air showers should be horizontally polarized.

As with all radio-detection experiments, ANITA had to contend with anthropogenic backgrounds. The ANITA collaboration uses their multiple antennas as a phased array to achieve good pointing accuracy, with a resolution of 0.2-0.4° in elevation, and 0.5-1.1° in azimuth. They rejected all events that pointed toward known or suspected areas of human activity. ANITA has set the most stringent flux limits yet on neutrinos with energies above 10^{20} eV [102]. The ANITA experiment has also reported several anomalous events, matching cosmic ray signals, but with unexpected polarization signature, which the collaboration has indicated might be from Earth-skimming ν_τ [113, 114]. However, this interpretation is controversial.

Because of the significant source-detector separation, ANITA is most sensitive at energies above 10^{19} eV. A lower energy threshold requires a smaller antenna-target separation.

Other ice based experiments use antennas located within the active volume, allowing them to reach thresholds around 10^{17} eV, or lower with phased array antennas. This approach was pioneered by the RICE experiment [115] which buried 18 half-wave dipole antennas in holes drilled for AMANDA at the South Pole, at depths from 100 to 300 m. The hardware was sensitive from 200 MHz to 1 GHz. Each antenna fed an in-situ preamplifier which transmitted the signals to surface digitizing electronics.

More recently, two groups have deployed prototype arrays which have explored different detector concepts. The Askaryan Radio Array (ARA) deployed surface and buried antennas at the South Pole [116], while the Antarctic Ross Iceshelf Antenna Neutrino Array (ARIANNA) installed surface antennas on the Ross Ice Shelf [104], about 110 km north of McMurdo station. ARIANNA offered the possibility of detecting downward-going ν, from the radio waves reflected off the ice-sea water interface on the bottom of the Ross Ice Shelf, while ARA took advantage of the colder, deeper ice at the South Pole, with its longer radio attenuation length. ARA buried antennas up to 200 m deep to be able to observe a larger portion of ice, due to the refraction of the signal in the firn. In contrast, ARIANNA deployed antennas just below the surface, allowing them to use high-gain, but large log periodic dipole antennas. Recently, phased-array trigger techniques have been demonstrated that can reduce the energy threshold by a

Downloaded from https://academic.oup.com/ptep/article/2022/8/083C01/6651666 by KIT Library user on 27 September 2022

factor of several [96, 117].

Both experiments use stations which operate independently, spaced far enough to maximize sensitivity, but where only a small fraction of neutrino events will be visible in multiple stations. Each station includes multiple antennas, which will be sensitive to both horizontal and vertical polarization. The expected angular resolution is a few degrees [95].

In 2021, the Radio Neutrino Observatory Greenland (RNO-G) started deploying stations at Summit Station. RNO-G is planned to consist of 35 stations, which employ ARIANNA-style surface antennas, an ARA-style phased array and deep antennas, and draw heavily on ANITA's electronics heritage [118].

ii. *The Moon*

Because of its large size and non-conducting regolith, and the availability of large radio-telescopes, the Moon is an attractive target [119]. Conventional radio-telescopes are quite well suited to lunar neutrino searches, with natural beam widths not too dissimilar from the size of the Moon. Still, there are experimental challenges. The attenuation length is typically estimated to be 9m/f(GHz) [120], so only near-surface interactions can be studied. The composition of the lunar regolith is not well known, and there are significant uncertainties due to this uncertainty. One big limitation of lunar experiments is that the 385,000 km target-antenna separation leads to energy thresholds above 10^{20} eV.

The effective volume probed by experiments depends on the geometry, which itself depends on the frequency range used. At high frequencies f, the electric field strength is high, leading to a lower energy threshold, but the sensitive volume is limited because the Cherenkov cone only points toward the Earth for a narrow range of geometries. Lower frequency radiation is more isotropic, so the effective volume is larger, but, because the electric field is weaker, the energy threshold is higher. The $1/f$ dependence of the attenuation length in the lunar regolith further increases the effective volume at low frequencies. The frequency range affects the energy dependence of the sensitivity. As can be seen in Fig. 36.10, a low-frequency experiment like NuMoon (which covered 115-180 MHz) has good sensitivity, but only above about 10^{14} GeV, while Lunaska/Parkes, which observed in the range 1200-1500 MHz, has a higher flux limit, but is sensitive above about $10^{12.5}$ GeV.

Current limits and projected sensitivities are sensitive to many details. A recent review [121] compared different radio-detection experiments using a common framework, and found some significant shifts in sensitivities due to, e.g. different assumptions about lunar composition and inelasticities.

With modern technology, it is increasingly viable to search over very broad frequency ranges [122]. One technical challenge is due to dispersion (frequency dependent time delays) in the ionosphere. Dispersion can be largely removed with a de-dispersion filter, using either analog circuitry or post-collection digital processing.

iii. *Air*

Radio detection in air is sensitive to all particles inducing air showers. Radio-detection can be used to determine the energy of cosmic rays, as done by e.g. the Auger and Tunka-Rex experiments [123, 124]. Radio signals can also be used to infer the altitude for shower-maximum, where the shower contains the most particles, as done by e.g. the LOFAR and Tunka-Rex collaborations [124, 125]. This altitude is sensitive to the cosmic-ray composition. Reconstructing the particle arrival direction is much easier in air since the Cherenkov angle, and thus the radio wavefront, aligns with the axis to 1°. Radio-detection is also useful for energy cross-calibrations between different experiments and may be able to provide an independent energy scale calibration for air shower arrays [126].

One variation on the radio-detection approach is to look for radio emission from Earth-skimming ν_τ. Although ν_τ are much less commonly produced than ν_μ and ν_e, over astrophysical distances, oscillations lead to a $\nu_e : \nu_\mu : \nu_\tau$ ratio near $1 : 1 : 1$, for almost all non-exotic acceleration and propagation mechanisms [127].

If the ν_τ traverse the Earth and interact while traveling upward, near the surface, the resulting $\tau^\pm$ may exit the Earth before decaying. 83% of the time, the decay produces a hadronic or electromagnetic shower in the atmosphere [128]. Experiments have searched for these upgoing showers, and for the resulting optical Cherenkov and coherent RF radiation. The threshold energy dependence for these searches depends on several factors, notably including the average $\tau^\pm$ decay length, which increases linearly with energy; the Pierre Auger observatory sets stringent limits on the neutrino flux at energies above 10^{17} eV [99].

36.3.3.5 *Future experiments*

Looking ahead, RNO-G [118] will continue deployment until 2024 and reach the largest yearly sensitivity of any radio array thus far. Further out, the proposed IceCube Gen2 expansion includes a substantial radio array component [59], which will be sensitive to both neutrinos from the ice and air showers from cosmic rays. PUEO, a successor of ANITA has been funded and is scheduled for its first flight in 2024 [129].

In the near future, several large radio detector arrays should reach significantly lower energies for lunar neutrino detection. The LOFAR array is taking data with 36 detector clusters spread over Northern Europe [105]. In the longer term, the Square Kilometer Array (SKA) with its 1 km^2 effective area will push thresholds down to near 10^{20} eV [122]. The SKA will also study air showers.

A number of dedicated prototype ν_τ radio-detection experiments exist. The GRAND Collaboration recently proposed to deploy a 10,000 antenna array, eventually growing to 200,000 antennas spread over 200,000 km^2. Its stations are simple autonomous units that sample the 30-100 MHz range using antennas optimized for near-horizontal signals [130]. The first phase GRAND-proto 300 is scheduled for deployment in 2021. The Pierre Auger Collaboration is currently upgrading their surface array to include radio antennas at all water Cherenkov detectors. This array will improve the sensitivity of the instrument to horizontal showers, both for composition sensitivity for cosmic rays and for the detection of Earth skimming neutrinos [131].

36.4 Large time-projection chambers for rare event detection

Revised October 2019 by T. Shutt (SLAC).

Rare event searches require detectors that combine large target masses and low levels of radioactivity, and that are located deep underground to eliminate cosmic-ray related backgrounds. Past and present efforts include searches for the scattering of particle dark matter, neutrinoless double beta decay, and the measurement of solar neutrinos, while next generation experiments will also probe coherent scattering of solar, atmospheric and diffuse supernova background neutrinos. Large time project chambers (TPCs) [132], adapted from particle collider experiments, have emerged as a leading technology for these efforts. Events are measured in a central region confined by a field cage and usually filled with a liquid noble element target. Ionization electrons are drifted (in the z direction) to an anode region by use of electrode grids and field shaping rings, where their magnitude and $x - y$ location is measured. In rare event searches (with no external trigger available) scintillation generated at the initial event site is also measured, and the time difference between this prompt signal and the later-arriving charge signal gives the event location in z for a known electron drift speed. Thus, 3D imaging is a achieved in a monolithic central volume. The relatively slow readout due to the drift of charges ($\sim 1/2$ ms/m at 1 kV/cm) [133] is not a major pile-up concern in low background experiments. Noble elements have relatively high light yields (comparable to or exceeding the best inorganic scintillators), and the charge signal can be amplified by multiplication or electroluminescence. Radioactive backgrounds are distinguished by event imaging, the separate measurements of charge and light, and scintillation pulse shape. For recent reviews of noble element detectors, see [134–137].

Methods for achieving very low radioactive backgrounds are discussed in general in section 35.6. The basic architecture of large TPCs is very favorable for this application because gas or liquid targets can be relatively easily purified, while the gener-

Downloaded from https://academic.oup.com/ptep/article/2022/8/083C01/6651666 by KIT Library user on 27 September 2022

ally more radioactive readout and support materials are confined to the periphery. The 3D imaging of the TPC then allows self shielding in the target material, which is quite powerful when the target is large compared to mean scattering lengths of order $\sim$ 10 cm for $\sim$ MeV neutrons and gammas from radioactivity. Most recent experiments have immersed the TPCs in hermetic water shields to eliminate external radioactive backgrounds, and several are also using an active scintillator inner layer to further veto backgrounds from detector materials. While other target fluids are possible, almost all recent efforts have used Xe and Ar. In LHe and LNe the mobility of electrons is $\sim 10^3$ times lower than in the heaver noble elements due to the formation "bubbles" around electrons. [138, 139] It is worth noting that scintillation and electron drift are possible in a number of organic fluids, possibly providing a route to economical large detectors, but with much reduced performance compared to noble elements.

In noble element targets, all non-noble impurities are readily removed (e.g., by chemical reaction in a commercial getter) so that only radioactive noble isotopes are a significant background concern. Xe, Ne and He have have no long lived radioactive isotopes (apart from the ^{136}Xe, discussed below, and the very long-lived ^{124}Xe [140]). Kr has $\sim$ 0.3 MBq/kg of the beta emitter ^{85}Kr created by nuclear fuel reprocessing [141], making it unusable as a target, while the $\sim$ 1 Bq/kg level of the beta emitter ^{39}Ar [142] is a nuisance for Ar-based experiments. Both of these can be backgrounds in other target materials, as can Rn emanating from detector components. Relatively low background materials are available for most of the structures surrounding the central target, with the exception of radioactive glasses and ceramics usually present in PMTs, feedthroughs and electrical components. Very low background PMTs with synthetic quartz windows, available over the last 15 years (see, e.g., [143]), have been a key enabling technology for dark matter searches. Radio-clean SiPMs and related Si-based photon detectors are increasingly being used in cases where their dark rates (which are significantly higher than PMTs) can be tolerated.

An important technical challenge in liquid detectors is achieving the high voltages needed for electron drift and measurement. In general, quench gases which stabilize charge gain and speed electron transport in wire chambers cannot be used, since these absorb and/or quench scintillation light and can trap electrons. It is also important to suppress low-level emission of electrons and associated photons which can otherwise swamp low energy signals. Drift of electrons over meter scales with minimal loss from attachment on trace levels of dissolved impurities (e.g., O_2) has so far required continuous circulating purification.

36.4.1 *Dark matter and other low energy signals*

A major goal of low background experiments is detection of WIMP (Weakly Interacting Massive Particle) dark matter through scattering on nuclei in a terrestrial detector (for a recent review, see [144]). Energy transfers are generally small, a few tens of keV at most. Liquid noble TPCs distinguish single nuclear recoils (NR) from dark matter from the dominant background of electron recoils (ER) from gamma rays and beta decays by rejecting multiple scatters, and, as described below, based on both the ratio of charge to light and the scintillation pulse shape. Neutrons are a NR background, but are present at much lower rates than gammas and betas, and also undergo significant multiply scattering. To detect small charge signals, a dual phase technique is used wherein electrons from interactions in the liquid target are drifted to the liquid surface and extracted with high field ($\sim$ 5 kV/cm) into the gas phase where they create an amplified electroluminescence signal which is usually measured by an array of PMTs located just above the liquid. (While both charge multiplication and electroluminescence are possible in liquid, they require very high fields created by very small electron structures and thus have not seen widespread adoption. For recent progress see [145]) This technique readily measures single electrons with $\sim$ cm $x - y$ resolution.

The measurement of the initial scintillation signal, by contrast, suffers from loss upon reflection from the TPC walls, and inefficiency in the readout, and usually limits the energy threshold. In LXe, the $\sim$ 178 nm wavelength is just long enough to be transmitted through high purity synthetic quartz PMTs windows, and, remarkably, PTFE immersed in LXe has $\sim$ 97% reflectivity. [146] The $\sim$ 128 nm scintillation light of LAr requires waveshifting (usually using TPB) both for reflectivity (usually on PTFE) and for efficient measurement. With both liquids, a second sensor array at the bottom of the TPC is used to maximize light collection, and total photon efficiencies have been in the 10-15% range. Typical raw yields for ER are several tens of electrons and photons per keV, and, in LXe, a NR threshold of $\sim 5\ keV$ has been achieved [147].

The microscopic processes leading to signals in liquid nobles are complex. Energy deposited by an event generates pairs of free electron and ions, and also atoms in their lowest excited state. The latter rapidly form excimers which de-excite by emitting light. Excimers arise in both triplet and singlet states which have the same energy but different decay times. In an event track, some fraction of electrons recombine with ions, while the rest escape and are measured. Each recombined ion creates an additional excimer, and hence another photon. Finally, some part of the energy is lost as heat - a small fraction for ER but a dominant and energy dependent fraction for NR. The branching into these various modes depends on drift field, energy, and particle type, requiring extensive calibrations. These have largely been carried out for LXe (see, e.g., [148]), and have been incorporated into the NEST Monte Carlo framework. [149]

This complexity also gives rise to discrimination between ER and NR: for the same visible energy, the slower NR create short, denser tracks and generate a higher fraction of initial excitons, leading to a smaller ratio of measured charge to light. NR also generate a higher ratio of short-lived singlet state to long-lived triplet states than ER, so that the scintillation signal itself gives pulse shape discrimination (PSD). Charge/light discrimination has been well mapped in LXe, and, remarkably, is very high (>99.9%) below $\sim$10 keV for NR. [147] It has only recently been measured in LAr [150], and has not yet played an important role in LAr based experiments. Qualitatively, PSD is similar in LXe and LAr - strong at high energy and weak at low energy. However it is well mapped only in LAr where it is very high above $\sim$ 50 keV, achieving values above $\sim 10^8$. [151]

This extremely powerful PSD in LAr is sufficient to overcome the ER background from ^{39}Ar, which is roughly 10^7 times higher than the fundamental low energy ER background from p-p solar neutrinos. In a multi-ton detector the event rate from ^{39}Ar poses a significant pile-up challenge, and the DarkSide collaboration is pursuing ^{39}Ar reduction through two methods. One, for which a factor 1400 reduction in $\sim$ 50 kg Ar has been demonstrated, is extracting "aged" Ar from underground (cosmic ray shielded) gas deposits in which the 269 yr half-life ^{39}Ar has decayed. [152] The other method is removal by distillation. The need for ^{39}Ar depleted Ar negates the much lower raw material cost of Ar compared to Xe. Kr must also be removed from both Xe and Ar experiments (and Ar must be from Xe experiments), comparatively easy tasks compared to isotopic separation. This is done through distillation or a chromatographic technique. In current LXe experiments the remaining dominant ER backgrounds is the beta decay of a daughter of ^{222}Rn in the active LXe, where the Rn has emanated from detector materials or external plumbing. Rn will be even more important as experiments scale up in size, but can in principle be reduced by better materials screening and online Rn separation, again by either distillation or chromatography. Neutrons are in general some six orders of magnitude less abundant than gamma rays and betas in U and Th decay chains, but they naturally scatter in the WIMP energy range, and their single scatters cannot be discriminated against. Self shielding is less powerful for neutrons than gamma rays, so that they are an increasingly important background at the current ton scale and future larger experiments, both in Ar and Xe. Active outer shielding layers which tag and veto neutrons are being included in most next generation experiments.

The WIMP sensitivity is a combination of backgrounds, discrimination, and WIMP scattering rates. The scattering rates are model dependent, but are in general dominated by spin-independent coherent scattering on the full nucleus. This has an

Downloaded from https://academic.oup.com/ptep/article/2022/8/083C01/6651666 by KIT Library user on 27 September 2022

A^2 dependence, favoring high mass targets. The energy spectrum is close to a falling exponential, so that the lowest possible energy threshold maximizes sensitivity. Experiments using LXe TPCs have had the leading sensitivity for standard WIMP dark matter for well over a decade, for all but the lowest WIMP masses. The ton-scale XENON1T [153] achieved a WIMP-nucleon sensitivity of $4.1 \times 10^{-47}\ cm^2$ at 30 GeV mass, closely followed by PANDAX-II [154] and LUX [155]. The next generation $\sim$ 7 tonne experiments LZ [156] and XENONnT [157], and $\sim$ 4 tonne PandaX-4T [158] are currently in late stages of construction. The DarkSide program is carrying out WIMP searches with LAr TPCs. The 50 kg DarkSide-50 achieved a sensitivity $\gtrsim$ 40 times poorer than XENON1T. A 50 ton scale-up, DarkSide-20 is being pursued which features SiPMs instead of PMTs. [159]. (The best current limit using LAr is not from a TPC, but instead the scintillation-only DEAP-3600 experiment. [151])

LZ and XENONnT project sensitivity to WIMPs about a decade above the"floor" of coherent scattering of astrophysical neutrinos, which, absent a directional measurement (see below), are essentially indistinguishable from WIMPs. DARWIN, a proposed a 50 ton LXe TPC would approach the practical limit set by this floor for WIMP masses above $\sim$ 5 GeV [160], while ARGO a $\sim$ 200 ton LAr detector would achieve similar sensitivity for WIMPs masses well above $\sim$ 50 GeV. [159]

There has been recent interest in models featuring low mass dark matter. These give rise to low energy recoils, and also strongly favor low mass target nuclei (despite the A^2 rate penalty). This has led to renewed focus on events below the scintillation threshold, where the charge signal alone achieves very low threshold due to the gain of the electroluminescence readout. This preserves $x - y$ spatial information, but only very weak depth information based on electron diffusion. Thus it is subject to the high backgrounds at the top and bottom of the active region, and decays of Rn daughters on grids. While the first such results came from XENON10, a recent result in LAr from DarkSide-50 extends to much lower dark matter mass because of the lower mass of Ar. To maximize the sensitivity of such searches in the future, studies have begun to understand and minimize the sources of electron backgrounds from both radioactivity and spurious sources such as field emission from grids. There is also an effort to develop a superfluid He TPC [161] read out with superconducting sensors (similar to the proposed HERON solar neutrino experiment). The rich set of signals in this case - scintillation, rotons, and ionization - potentially offer significant background rejection.

Measurement of NR recoil track direction would provide proof of the galactic origin of a dark matter signal since the prevailing WIMP direction varies on a daily basis as the earth spins. This cannot be achieved for the sub-micron tracks in any existing solid or liquid technology, but the mm-scale tracks in a low pressure gas (typically, P $\sim$ 50 Torr) could be imaged with sufficiently dense instrumentation. Directionality can be established with $O(10^2)$ events by measuring just the track direction, while, with finer resolution that distinguishes the diffuse (dense) tail and dense (diffuse) head of NR (ER) tracks, only $O(10)$ events are required. Such imaging requires a high energy threshold, decreasing WIMP sensitivity, but also powerfully rejecting less dense ER background tracks.

A variety of TPC configurations are being pursued to accomplish this, most with a CF_4 target. The longest established effort, DRIFT, avoids diffusion washing out tracks for electron drift distances greater than $\sim$ 20 cm by attaching electrons to CS_2, which drifts with vastly reduced diffusion. Other efforts drift electrons directly and use a variety of techniques for their measurement: DMTPC (electroluminescence + CCDs), MIMAC (MicroMegas), NEWAGE (GEMs), and D^3 (Si pixels). A related suggestion is that the amount of recombination in a high pressure Xe gas with an electron-cooling additive could be sensitive to the angle between the track and electric field [162], eliminating the need for track imaging. Directional measurements appear to be the only possibility to push beyond the floor of coherent neutrino scatters [163], though at the cost of enormous target mass and channel count.

36.4.2 $0\nu\beta\beta$ *Decay*

Another major class of rare event search is neutrinoless double beta decay ($0\nu\beta\beta$). A limited set of nuclei are unstable against simultaneous beta decay of two neutrons. Fortuitously, this includes the Xe isotope ^{136}Xe (Q-value 2458 keV), which can be used as the active material in a detector, and which, as an inert gas, can also be more readily enriched from its natural 8.9% abundance than any other $\beta\beta$ isotope. Observation of the lepton-number violating neutrinoless version of this decay would establish that neutrinos are Majorana particles and provide a direct measure of neutrino mass. For a recent review, see [137, 164]. The signal in $0\nu\beta\beta$ decay is distinctive: the full Q-value energy of the nuclear decay appears as equal energy back-to-back recoil electrons. A large TPC is advantageous for observing this low rate decay for all the reasons described above. The first detector to observe the standard model process two neutrino double beta decay was a gaseous TPC which imaged the two electrons tracks from ^{82}Se embedded in a foil. [165] Modern TPCs use Xe as the detector medium.

The dominant background is gamma rays originating outside the active volume. Most of these undergo multiple Compton-scatters which are efficiently recognized and rejected through sub-cm position resolution, though the few percent of gammas at this energy that photoabsorb are not. Self shielding of gamma rays in the double beta decay energy window is less powerful than in the low energy dark matter window, since in the former case there is some small probability of penetrating to some depth followed by the modestly small probability of photo-absorption. The latter case consists of three small probability processes: penetration to some depth, a very low-energy scatter, and the gamma exiting without a second interaction. Because of this and the fact that background and the signal are both electron recoils (i.e., NR/ER discrimination is of no value), the requirements on radioactivity in all the surrounding materials of a $\beta\beta$ TPC are much more stringent than an otherwise similar dark matter detector, unless other background rejection tools are available. However $\beta\beta$ searches are insensitive to low energy backgrounds (e.g., ^{85}Kr and ^{39}Ar) important for dark matter.

Very good energy resolution is crucial to avoid background from $2\nu\beta\beta$ decays and gammas including the prominent 2615 keV line from ^{208}Tl in the Th chain. Here a combined charge and light measurement largely eliminates the otherwise dominant fluctuations in recombination which lead to anti-correlated fluctuations in charge and light. Because of the high energy of the $\beta\beta$ signal, charge can be read out directly, and the scintillation measurement is easily tolerant of the dark rates of SiPMs. These goals have led $\beta\beta$ detectors to have somewhat different optimization than dark matter detectors, although the next generation large Xe dark matter experiments (LZ, XENONnT, DARWIN) have significant $\beta\beta$ reach.

The recently completed EXO-200 experiment used a single-phase LXe TPC with roughly 110 active kg of Xe enriched to 80.7 % ^{136}Xe to achieve one of the best $\beta\beta$ search limits [166]. The energy resolution obtained is (FWHM) of 2.71% (at 2458 keV), and lower values in LXe appear possible. A multi-ton successor experiment, nEXO, has been proposed which would fully cover the inverted neutrino mass hierarchy. [167] EXO-200 featured LAAPDs for light readout, and direct charge readout, while nEXO will use SiPMs.

A related but different approach is to use high pressure gaseous Xe TPC. [168] The lower density requires a large apparatus for given target mass, but has two significant advantages. The larger track size allows the two-electron topology of $0\nu\beta\beta$ events to be distinguished from single electrons from photoabsorption of background gammas. In addition, the low recombination fraction in the gas phase suppresses recombination fluctuations, allowing higher energy resolution. Recent progress with a 5 kg prototype by the NEXT collaboration has demonstrated the topology based discrimination, and, notably, 1% (FWHM) energy resolution. A $\sim$ 100 kg detector is now under construction, and ton-scale designs being studied. Finally, a long-standing idea that would provide definitive identification of a $0\nu\beta\beta$ signal is to extract and tag the ionized Ba daughter via atomic physics techniques [169], either

Downloaded from https://academic.oup.com/ptep/article/2022/8/083C01/6651666 by KIT Library user on 27 September 2022

in gas or liquid and gas phases. Significant recent progress by both the EXO and NEXT collaborations has now achieved the key milestone of demonstrating single Ba ion sensitivity in test setups. [170–172]

36.5 Sub-kelvin detectors

Written October 2021 by O. Cremonesi (INFN, Milano-Bicocca), L. Hsu (FNAL) and G. Signorelli (INFN, Pisa).

36.5.1 *Motivation for Sub-kelvin Detectors*

Detectors operating below 1 K are referred to as low-temperature detectors (LTDs). The advantage of using LTDs over conventional detectors resides in their better energy resolutions, lower noise, and improved energy thresholds, which can all be achieved with a versatile choice in materials. In certain applications, these advantages outweigh the potential drawbacks of cooling and reading out a detector payload at sub-kelvin temperatures, and thus enable exploration of new frontiers in fundamental physics, astrophysics and cosmology. Among the endeavors enabled by LTDs are direct searches for dark matter over a wide mass range, precision experiments to measure the electron neutrino mass, searches for neutrinoless double-beta decay, and X-ray observation of the Universe. Large arrays of LTDs are also employed to measure the properties of the cosmic microwave background (CMB) spectrum whose parameters are determined by fundamental physics. These include dark matter and dark energy densities, the sum of neutrino masses and the number of light relativistic species, as well as probing the physics of inflation at energy scales of $\sim 10^{16}$ GeV. This article presents a brief overview of LTDs, their features, and several applications. More detailed treatment of this subject is available in the literature [173–176].

The advantages of LTDs are enabled by the detection of very low energy excitations (e.g. phonons and quasiparticles). In a typical interaction, energy from an incident particle is dissipated through excitation of secondary particles such as electrons, ions, holes, photons, phonons etc. These particles will in turn produce their own secondaries. Thus there is a cascade down in energy until the original energy deposit is converted entirely into heat and the detector reaches thermal equilibrium. Prior to the equilibrium phase, the energy at any given moment is partitioned among multiple excitation modes. Conventional particle detectors work by sensing the higher energy excitation modes, such as ionization and scintillation, which require an average minimum energy of few eV to 10's of eV to produce. For such detectors, a large fraction of the deposited energy remains undetected in the form of heat. Furthermore, the measurements are subject to the fluctuations inherent in the partition of energy across different excitation modes. Secondaries that don't eventually escape the detector, will de-excite or recombine to dissipate their energy in the form of phonons and quasiparticles, which are characterized by energies in the range of meV down to μeV. These can be detected by LTDs at various stages of their final degradation towards thermal equilibrium. Thus LTDs allow for energy resolutions and operational thresholds much lower than detectors that only sense scintillation and ionization. Furthermore, LTDs provide a precise energy measurement owing to the relatively large number of excitation quanta that can be detected. In fact, LTDs designed to measure thermal phonons achieve the highest possible energy resolutions with optimal noise performance.

At thermal equilibrium, energy E deposited in an LTD causes a temperature rise $\Delta T = E/C$ where C is the heat capacity. Thermal equilibrium is characterized by the condition where the average heat flowing to an LTD equals the average heat flowing from the LTD (into a proper heat sink or bath). In this state, the ideal intrinsic energy resolution is determined by the statistical fluctuations in the phonon system. Fluctuations in the total number of phonons in the LTD absorber have variance C/k_B, which yields a minimum resolution of $\Delta E^2 = k_B T^2 C$ to the device energy resolution, where k_B is Boltzmann's constant. Thus, the smaller the heat capacity, the more sensitive the response of the calorimeter and the better the energy resolution. The most relevant feature of this result is that the latter is independent of the energy deposition. The heat capacity itself is the product of the detector volume (V) and the specific heat (c_p). Optimization of LTD response can be achieved by using small detector volumes and materials with low specific heat. Noise contributions from additional sources will increase the variance and are generally parameterized as a multiplicative factor ($\xi \gtrsim 1$) to the variance expression above.

Similarly, the power P from incident particles or radiation can be measured through a temperature rise given by $\Delta T = P/G$, where G is the thermal conductance to a weakly linked bath held at constant temperature. Power fluctuations are limited by G and have a spectral density of $S_P = NEP^2 = 4k_{\rm B}T^2G$, where NEP is the noise equivalent power, defined as the power in a 1 Hz bandwidth that gives a response signal with an equal amplitude to the noise. Hence lower conductance yields better sensitivities. To minimize thermal conductance in precise power measurements, weak thermal links can be realized by using thin membranes or by decoupling the electron and phonon systems. However, a compromise must be made. While lower G yields better noise metrics, conversely, larger G is needed to dissipate all incident power (which can be large in the case of CMB detectors) or to have a faster detector response (the characteristic response time being $\tau = C/G$).

LTDs that measure power are sometimes referred to as *bolometers* in literature, as opposed to *calorimeters* that measure energy, generating some confusion. In principle, there is no clear distinction between a calorimeter and a bolometer. The operation mode is generally determined by the ratio of the characteristic time constant and the average time between the arrival of incident particles or quanta [177].Yet another convention is to refer to *non-equilibrium* LTDs as those detectors that measure incident energy or power by counting excitations that have energy $\gg k_B T$. In such detectors, energy resolution is determined by the statistical fluctuations of the energy partition, similar to conventional ionization detectors but with a much lower average excitation energy and hence a larger number of excitation quanta.

Table 36.4: Low temperature dependence on temperature (T) for specific heat, based on different material classes. In the table below Θ_D is the Debye temperature and T_C is the transition temperature of the superconductor.

Heat Capacity	Material
$\left(\frac{T}{\Theta_D}\right)^3$	Dielectric and diamagnetic
T	Conductor
$\exp\left(-\frac{2T_C}{T}\right)$	Superconductor
$\left(\frac{\mu_B B}{k_B T}\right)^2 \operatorname{sech}^2\left(\frac{\mu_B B}{k_B T}\right)$	Paramagnet (in magnetic field **B**)

A variety of possible detector materials and sensor technologies makes LTDs very versatile and highly customizable. Dielectric, superconducting and paramagnetic materials are often used owing to the fact that at very low temperatures, the specific heat decreases strongly as a function of T (see table 36.4). Superconductors offer additional advantages: the abrupt change in resistance when a material transitions from its normal to superconducting state enables highly sensitive measures of temperature changes. Additionally, the existence of a small (less than a meV) but distinct energy gap that is required to break a Cooper pair, provides a means to measure energy deposits by counting the resulting quasiparticles (QP). QP relaxation processes are typically faster than thermal processes making these detectors suitable for high-rate photo-counting. In summary, both the sensitivity and energy resolution of an LTD benefit greatly from low temperature operation.

36.5.2 *Detector Types*

A generalized LTD calorimeter consists of an absorber in thermal contact with a phonon or quasiparticle sensor, and a thermal link to a heat bath at a constant temperature (see figure

Downloaded from https://academic.oup.com/ptep/article/2022/8/083C01/6651666 by KIT Library user on 27 September 2022

36.11). The absorber provides the mass necessary for the interaction of the particle and a fast and complete thermalization of the deposited energy. The sensor accomplishes the task of translating the particle interaction into measurable parameters. It is generally sensitive to equilibrium phonons (e.g. thermistors and MMCs) and thus provides a precise measurement of the temperature. However, non-equilibrium (e.g. STJ's) and mixed (e.g. TES) phonon sensors have been devised and implemented in many applications as well. The goal of the thermal link is to cool the absorber down to its equilibrium temperature after the absorption of a particle. In monolithic detectors the thermometer and absorber are identical, while in composite detectors the thermometer is attached to a separate absorber. This basic design applies to single-event particle detection as well as for continuous radiation measurement devices. In the case of the latter, a suitable absorber whose mass is irrelevant, *e.g.* an antenna at the end of a waveguide, collects the incident power and dissipates it onto a resistive (*e.g.* Au) film, which is put in contact with a sensor capable of detecting tiny temperature changes (e.g. semiconductor thermistors, transition-edge sensors, and kinetic inductance detectors, to name a few).

Superconducting Tunnel Junctions (STJs) and Kinetic Inductance Detectors (KIDs) are examples of non-equilibrium detectors. STJs exploit Josephson tunnelling of particles and QPs between two superconductors. The superconductors act as radiation absorbers, and are separated by a thin insulating layer. When such a junction is DC biased at a voltage just below the gap voltage, the excess quasiparticles generated by the incoming radiation are detected as a tunneling-current proportional to the incoming energy. Statistical fluctuations in the tunnelling process limit the energy resolution which is given by:

$$\sigma_E = \sqrt{\varepsilon(F+G)E_0}, \tag{36.5}$$

where $\varepsilon \sim \Delta$, the band-gap, while $F \sim 0.2$ and $G > 1$ are the Fano factor and tunnelling fluctuation respectively. STJs have been proven to be excellent single photon and UV-VIS spectroscopic detectors with near theoretical energy resolutions, high detection efficiencies and excellent time resolution. In astrophysics they are used as mixers to detect radiation in the 100 GHz to 1 THz range by exploiting the non-linear behaviour of its current versus voltage characteristic curve. STJs share similar design elements to charge qubits, which are being used for the development of quantum computers. Such qubits have also recently been used in dark matter searches as single photon detectors to evade the standard quantum limit in measurement noise [178]. Despite their extremely good energy resolutions, STJs cannot be scaled-up to produce sensors with large observing volumes due to readout complexity and the difficulty in uniformly suppressing the superconducting Josephson current, which is superimposed on the QP current.

KIDs exploit the variation of the kinetic energy T stored in a superconductor by Cooper pairs whose inertia acts as an effective inductance, given by:

$$T = \frac{1}{2}nm^*v^2 = \frac{1}{2}LI^2 \tag{36.6}$$

where n is the number density of Cooper pairs, $m^* = 2m_e$ is the Cooper pair mass and $I = 2nev$ is the Cooper pair current. $L = m_e/2ne$ is defined as Kinetic Inductance and is inversely proportional to the number of Cooper pairs [179]. When a KID is placed in series with a superconducting capacitor, the resonance frequency of the circuit will be temporarily shifted by incident radiation, which converts Cooper pairs to QPs, thus changing the effective inductance. The presence and amount of radiation is observed as a change in amplitude or phase of a tuned sinusoidal signal that is sent through the circuit. In practice the change in L is small, and very high Q microwave resonance circuits are needed to sense this variation (hence the name MKIDs, for Microwave-KIDs). Furthermore, only areas of the film where large currents are flowing will be sensitive to pair breaking, thus making the response of a distributed KID position dependent. To overcome this issue, QP trapping (by coupling two superconductors with different band-gaps) is used for absorbing optical photons and X-rays. To detect lower frequencies (*e.g.* in the 100-1000 GHz range for CMB) a lumped element resonator (LEKID), with little current variation across the device, is used. The device itself, based on a series LC circuit inductively coupled to a microstrip feed line, can act as the absorber as well as the sensing element in a detector system. Macroscopic devices (few mm^2) can be fabricated by shaping the inductor in the form of a meander coupled to an inter-digitated capacitor [180]. The theoretical noise limit of these devices is governed by generation-recombination noise and takes the form:

$$NEP_{QP} = 2\Delta\sqrt{\frac{n_{QP}}{\tau_{QP}}}, \tag{36.7}$$

where n_{QP} and τ_{QP} are the QP number and lifetime respectively. KIDs are easy to fabricate, very sensitive, broad band and easily multiplexable: they can be coupled with a single microstrip that simultaneously reads 1000s of detectors resonating at different frequencies. They provide therefore a promising solution for deploying large arrays of detectors with applications to high-energy physics, astronomy or CMB measurements, although there are still some challenges, especially at frequencies below 100 GHz, related to their worse noise performance when compared to other LTDs, and to the choice of materials with a sufficiently small energy-gap.

Semiconductor thermistors are resistive elements characterised by a strong dependence of the resistance on the temperature. Usually, they consist of small crystals of germanium or silicon with a dopant concentration slightly below the metal-to-insulator transition. However, they can also be realized in the form of amorphous films such as NbSi. At low temperatures, their resistivity (ρ) is governed by variable range hopping (VRH) conduction and is described by the expression $\rho(T) = \rho_0\ \exp\left((T_0/T)^\gamma\right)$, where T_0 and ρ_0 are parameters controlled by the doping level, while γ depends on the compensation level K (ratio of acceptor to donor concentrations). For low values of K it is well approximated by 1/4 while it converges to 1/2 as K increases.

Semiconductor thermistors are high impedance devices (1–100 MΩ) whose performance is usually parameterized in terms of the logarithmic sensitivity $\alpha = \mathrm{d}\log R/\mathrm{d}\log T$, typically in the range of 1–10. Silicon thermistors are fabricated using a multiple ion implantation process in high purity silicon wafers to produce a thin and uniformly doped box-like volume. The best germanium thermistors are fabricated starting from bulk, high-purity germanium crystals doped by means of neutron irradiation in the core of a nuclear reactor, referred to as nuclear transmutation doping (NTD). Individual sensors are then produced by dicing the irradiated samples and finishing them by hand. The great advantage of NTDs is the highly uniform doping level over large volumes which results in a better signal to noise ratio with respect to other doping techniques. The doping level depends on the isotopic composition of the starting material and the irradiation time.

The weak coupling to the heat sink can be provided by the electrical leads used for the read-out. However, nowadays microelectronic planar technologies and silicon micromachining are more commonly preferred, and sensors are suspended on thin silicon nitride membranes or thin silicon beams. Thermistors are read-out in an approximately constant current biasing configuration obtained by inserting large load resistors in the bias circuit, which allows for direct conversion of the thermal signal (ΔT) into a voltage signal (ΔV).

Semiconductor thermistors are very practical to use with some drawbacks. One of these is related to their high impedance which requires a JFET front-end placed as close as possible to the device in order to minimize the signal integration on parasitic electrical capacitances. This can represent a technical challenge, because JFETs must be maintained at significantly higher temperatures ($\gtrsim$100 K). Furthermore, deviations from the exponential behaviour of the conductivity have been observed at low temperatures. They are usually described in terms of a finite thermal coupling between electrons and phonons which results in an intrinsic limit to the signal rise times, which is of the order of hundreds of milliseconds at temperatures below 100 mK. Nevertheless, semiconductor thermistors are an established and robust technology, and arrays of detectors based on these devices have been widely

Downloaded from https://academic.oup.com/ptep/article/2022/8/083C01/6651666 by KIT Library user on 27 September 2022

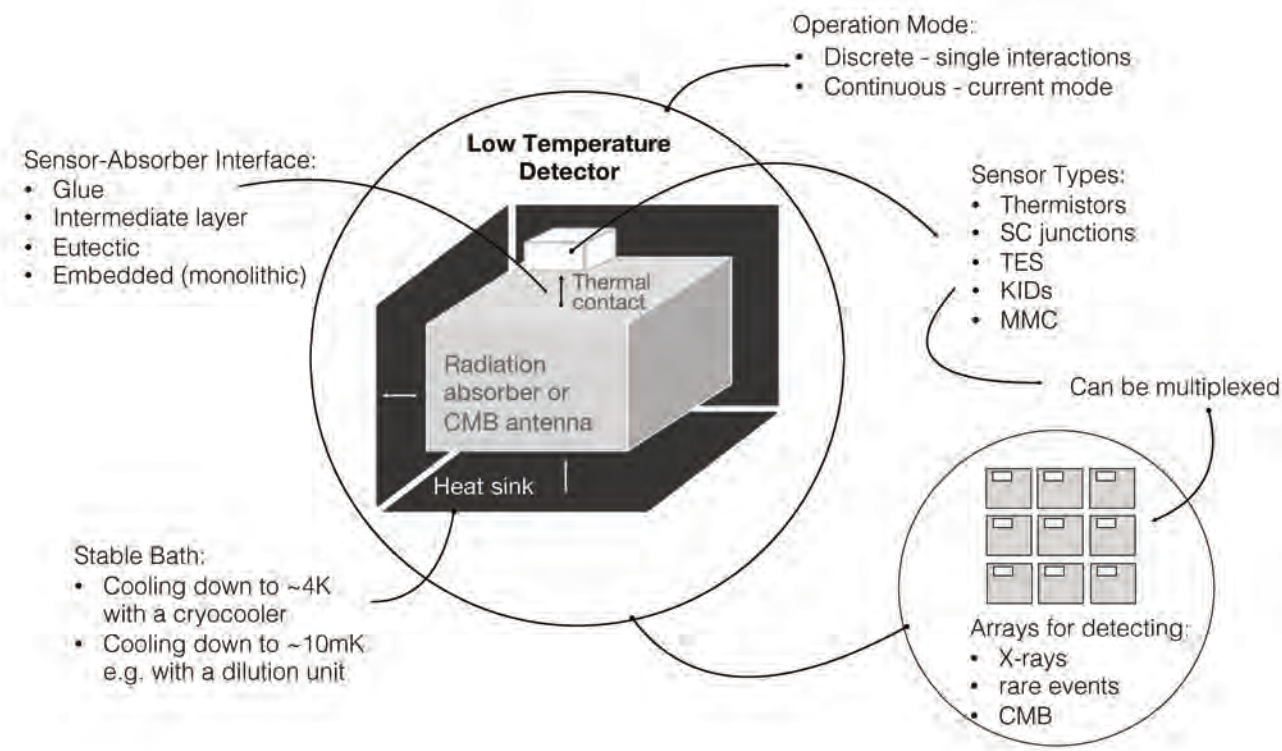

Figure 36.11: A generalized LTD consists of an absorber, a sensor and a thermal link to a stable-temperature bath. Biasing schemes and readout is described in detail in the text for individual sensor types.

used for neutrinoless double beta decay searches, neutrino mass measurements and X-ray spectroscopy. Energy resolutions lower than 5 eV have been achieved with Sn or HgTe absorbers.

Superconducting Transition Edge Sensors (TESs) exploit the sharp transition between superconducting and normal conducting phases, yielding a high sensitivity to temperature variations. Temperature perturbations, and hence resistance changes, are sensed as modulations in the current through the TES. TESs are operated in a constant voltage biasing configuration where Joule heating, arising from the current flowing in the TES, decreases with a rise in resistance, which then brings the TES back to its nominal operating temperature. This electrothermal feedback (EFT) is achieved by providing a TES with a voltage bias whose power, $P_J = V_{\rm bias}^2/R(T)$, heats the TES to its nominal operation point, the superconducting transition temperature. Operation in ETF mode improves linearity, speeds up response (to faster than $\tau = C/G$), and in some cases it provides tolerance for $T_{\rm C}$ (critical temperature) variation between multiple TESs in a large array. The low impedance in this configuration makes them well-suited for readout by SQUID (Superconducting QUantum Interference Device) based amplifiers. Logarithmic sensitivities $\alpha = {\rm d}\log R/{\rm d}\log T$ of the order of several hundreds can be achieved. By using different superconductors, or superconductor-metal pairs patterned in suitable shapes, a wide range of resistances, transition temperatures and time constants are obtainable to meet the requirements of the desired application [181].

Nano-TESs are fabricated by lithographic techniques in the form of long (few μm) and narrow (nm) wires that exhibit extremely small NEPs due to their reduced C and G, enabling single-photon sensing. Superconducting Nanonwire Single-Photon Detectors (SNSPDs) are similarly patterned superconductors or superconducting bilayers maintained at a temperature well below their $T_{\rm C}$. When a DC current just below the critical current is driven through the nanowire, the absorption of a single photon causes the formation of a hot spot that drives the superconductor to a normal conducting state, resulting in a very fast (tens of picoseconds) current pulse through a shunt resistor. For this reason, nano-TESs and SNSPDs are used as single photon detectors for light dark matter and axion searches in applications where large detecting mass is not critical [182].

Magnetic Metallic Calorimeters (MMC) exploit paramagnetic sensors exposed to a weak magnetic field with a weak thermal link to a heat bath. A temperature rise causes a change in the sensor magnetization, which is sensed by a SQUID magnetometer. A common material is an Au:Er mixture, with the addition of a few hundred ppm of enriched ^{166}Er, which is needed to reduce the unwanted contribution of nuclear magnetic moments of other Er isotopes. The read-out is non-dissipative and avoids the noise sources common to the dissipative devices. The use of a metallic host ensures relatively fast time response, since the typical spin-electron relaxation times are of the order of 0.1 microseconds at ~50 mK [183]. For an optimized MMC, the energy resolution is given by $\Delta_E = \sqrt{2k_B T^2 C}\,(\tau_0/\tau_1)^{1/4}$, where τ_0 (order of micro second) and τ_1 (order of milli second) denote the signal rising and decay times respectively [173]. In order to obtain a fast and efficient energy thermalization, MMC are typically fabricated from gold. The intrinsically large heat capacity of the paramagnet does not spoil the temperature sensitivity and allows the use of relatively large gold absorbers without degrading the device performance. Furthermore, thermal isolation from the heat sink is not generally an issue. Owing to the simple concept of these devices, MMC can be precisely customized and fabricated by employing standard microtechnology. Planar MMC arrays characterized by an excellent energy resolution, large dynamic range and good linearity have been successfully used for the detection of soft X-rays.

Performance and technological constraints limit the maximum size of LTDs. To improve overall experimental sensitivities, a large number of sensors must be deployed, typically at temperatures of a few tens of mK, where cooling power is limited to a few μW. To reduce the readout complexity and the heat load at the colder stages, multiplexing (MUX) techniques are often employed. Multiplexing consists of reading multiple detectors out

Downloaded from https://academic.oup.com/ptep/article/2022/8/083C01/6651666 by KIT Library user on 27 September 2022

through a limited number of lines that traverse room temperature to cryogenic temperatures [184]. In frequency-domain multiplexing (FDM), a tuned superconducting LC circuit is placed in series with each sensor, and a frequency comb of AC biases (usually in the MHz range) is sent to a group of sensors in parallel. A synchronous demodulation of the amplified current signal allows the recovery of the resistance variation of each detector. Microwave-multiplexing (μMUX) represents a variation of this concept, based on the usage of rf-SQUIDs, where the frequency comb is in the GHz range. Alternatively, the signal from a single detector can be recovered by readout of one detector at a time (time-domain multiplexing, TDM). KIDs have been gaining popularity owing to the fact that they naturally form resonant circuits, hence multiplexing in the frequency domain is readily achieved by adjusting their capacitance.

36.5.3 *Experimental Applications*

LTDs are sensitive over a wide range of energy, from centimetre wavelength ($\sim$ meV) through the visible spectrum ($\sim$ eV) up to the X-ray domain ($\sim$ keV) and beyond. Several broad categories of LTD applications towards measurements of fundamental physics are described in more detail in the text below and summarized in tables 36.5 and 36.6.

Bolometric detectors are favored as microwave detectors owing to their nearly constant response over frequency, playing an important role in far-infrared astronomy and in the survey of the cosmic background radiation. The high-frequency instrument of the Planck satellite (HFI) used spiderweb bolometers read by NTD-Ge thermistors, but current experiments use mainly TESs or, more recently, KIDs. Depending on the objective of the experiment, antenna coupling or absorber coupling is used. In the former case, the bolometer detects one polarization and one (or a few) modes of the radiation, while absorber-coupled bolometers do not distinguish between polarizations. In order to avoid the absorption or emission from Earth's atmosphere, many (CMB) instruments are operated by observatories located at high altitude, dry places (such as the Atacama desert or Antarctica), balloon-borne platforms, or from space. In Table 36.5, we list a subset of the ongoing or planned CMB experiments (see Section 29 of this Review for the details on present challenges). In the Atacama desert in Chile, CLASS is taking data, POLARBEAR is being upgraded to Simons Array and ACTPol is being upgraded to AdvancedACT-Pol, the next big step being the deployment of the Simons Observatory. At the South Pole, SPTPol has been upgraded to SPT-3G, while BICEP3 and BICEP array will constitute the South Pole Observatory. The most powerful upgrade in terms of both size and sensitivity will be CMB-S4, a consortium of telescopes both at the Pole and in Chile. In the Canary islands, QUIJOTE and GroundBIRD are operating and LSPE/STRIP is in preparation. QUBIC will soon start operations in Argentina and AliCPT is in preparation in Tibet. Regarding balloon projects, SPIDER and EBEX were already launched while LSPE/SWIPE and PIPER will be in the near future. Finally from space, after the success of Planck, LiteBIRD has been selected by the Japan Aerospace Exploration Agency (JAXA) as the next strategic large mission to be launched in the 2020s.

The incoming radiation couples directly to the antenna probes (as in BICEP/Keck) or through micro-machined horn waveguides (AdvancedACT-Pol, CLASS) or lenslets (Simons Array, SPT-3G), depending on the frequency range. All of these experiments have focal planes with hundreds to hundreds of thousands of sensors. To optimize focal plane occupancy, multi-mode or multi-chroic, dual polarization sensitive detectors are used. In the former case, the sensitivity is enhanced by collecting power from a larger number of modes at the expense of angular resolution. In the latter, one single mode of the radiation is focused on a broad band antenna, and on-chip polarization separation and band-pass filters split the signal in different frequency bands directing the power to different absorbers and sensors.

Experimental design is driven by a trade-off between the sensitivity and the complexity of the production processes and readout. On the one front, single-sensor NEP at the level of 10^{-21} W/$\sqrt{\text{Hz}}$ has been achieved in laboratories and research centers. Meanwhile, efforts are in place for the industrialization of the fabrication processes, which is essential for scaling up production for the large number of detectors needed for future experiments.

Massive cryogenic calorimeters have been proposed since the 1980's as particle detectors for the search of rare processes (e.g. dark matter, neutrinoless double beta decay) [185]. Almost simultaneously, the use of arrays of small mass calorimeters was suggested for X-ray astrophysics [186] and precision measurements of the neutrino mass [187, 188]. Although essential to understanding the nature of neutrinos, neutrinoless double beta decay (NDBD) has eluded discovery (or definitive exclusion) for over 50 years. Calorimeteric techniques provide the best sensitivities to NDBD. However, before the advent of low temperature calorimeters (LTC), only a few isotopes (^{48}Ca, ^{136}Xe and ^{76}Ge) could be utilized for NDBD studies with the calorimetric approach. This limitation was removed by the advancement of LTC's, and in particular by CUORE, which takes advantage of the naturally high abundance of ^{130}Te in TeO_2 crystals. Additionally, the operation of CUORE at LNGS [189] has demonstrated that the technical challenges of operating ton-sized LTD detectors in a deep, underground location are surmountable. Currently, the most promising future approach is based on the hybrid approach of scintillating LTCs, which unfortunately cannot be used for ^{130}Te. Now, new projects are being proposed based on different scintillating compounds. In particular ^{100}Mo is the choice of CUPID [190] (NTD thermistors glued to $Li_2{}^{100}MoO_4$ crystals), which will use the same infrastructure of CUORE and follows from the successful operation of several demonstrators (CUPID-0 [191] and CUPID-Mo [192]), and AMORE (MMC sensors on $Ca^{100}MoO_4$ or $Li_2{}^{100}MoO_4$ crystals) [193]. With an energy resolution comparable to germanium diodes and a mass of the order of a ton, these experiments aim to probe the inverted hierarchy of neutrino masses. The slow response of these detectors is still a dominant limitation because pile-up may prove to be a serious background. Extremely pure materials, careful assembly procedures, and deep underground laboratories are therefore necessary.

In the 1980's, the calorimetric technique was recognized as a feasible approach to make a direct measurement of the neutrino mass from the end-point of a beta spectrum. Thus, LTCs were proposed as a possible alternative to the standard spectrometric measurements [194]. Calorimetric measurements offer a number of advantages: i) a weak dependence on the final excited states, ii) no source effects (e.g. self-absorption), and iii) lack of backscattering from the detector. Therefore LTCs provide a faithful reconstruction of the beta spectral shape over a broad energy range below the end-point. However, the difficulty in resolving a small fraction of the spectrum near the end-point is a serious limitation that strongly constrains the source strength and the statistics that need to be accumulated. Such an inconvenience can be mitigated by selecting beta emitters with a small Q value, owing to the fact that the fraction of counts in an interval, δ close to Q, scales as $(\delta/Q)^3$. However, this is generally at the cost of choosing decays with more complex nuclear transitions. In addition, LTCs may be affected by specific systematics (e.g. solid state effects). Ultimately it is recognized that spectrometers and calorimeters have complicated but different systematic effects. It is therefore critical to develop complementary experiments exploiting both techniques.

LTCs were initially proposed as perfect calorimeters to measure the energy spectrum of a low Q beta emitter embedded in an absorber. However, the requirements of excellent energy resolution and a low rate (to avoid pileup) requires a very large number, $O(10^4 - 10^6)$, of small mass devices (micro-calorimeters). Early experiments used ^{187}Re, which is a long-lived beta emitter that is naturally abundant in rhenium samples and is characterised by a very low Q value (2.4709 keV [199]). A large number of ^{187}Re based experiments have been developed over the years (MANU [200], MIBETA [201], MARE [202]). Nowadays a different approach is preferred and is based on the measurement of the atomic radiation following electron capture, typically in ^{163}Ho which is also characterized by a very low Q (2.837 keV [203]). Different experiments have been proposed to face the challenge: ECHo in Germany [195] (using MMC sensors), HOLMES in Italy [196] and NUMECS [197] in the US (using TESs). The very large number

Downloaded from https://academic.oup.com/ptep/article/2022/8/083C01/6651666 by KIT Library user on 27 September 2022

Table 36.5: Some selected experiments using LTDs to measure the CMB. These experiments constrain the physics of inflation and the absolute mass, hierarchy, and number of neutrino species. The experiment location determines the part of the sky that is observed. The size of the aperture determines the angular resolution. The table also indicates the type of sensor used, the number of sensors, the frequency range, and the number of frequency bands. Data for planned upgrades or future experiments are provided in parentheses.

Sub-K CMB Experiment	Location	Aperture	Sensor type	# Sensors (planned)	Frequency (planned)	Bands (planned)
Ground-based						
Atacama Cosmology Telescope (2007–)	Chile	6 m	TES	5,614	30–230 GHz	5
BICEP/Keck (2006–)	South Pole	26/68 cm	TES	2,500	95–270 GHz	6
CLASS (2015–)	Chile	60 cm	TES	3,488	40–220 GHz	4
GroundBIRD (2021-)	Canary Island	30 cm	MKID	322	145–220 GHz	2
POLARBEAR / Simons Array (2012–)	Chile	3.5 m	TES	1,274 (22,764)	150 GHz (90–280 GHz)	1 (4)
South Pole Telescope (2007–)	South Pole	10 m	TES	16,260	90–220 GHz	3
Simons Observatory (2022–)	Chile	6 m/0.5 m	TES	(60,000)	(27–280 GHz)	(6)
CMB-S4 (2024–)	Chile + South Pole	21 telescopes	TES	(500,000)	(20–280 GHz)	(11)
Balloon						
EBEX (2013–)	McMurdo	1.5 m	TES	∼1,000	150–410 GHz	3
PIPER (2016–)	New Mexico	2 m	TES	5,120	200–600 GHz	4
SPIDER (2014–)	McMurdo	30 cm	TES	1,959	90–280 GHz	3
LSPE (2022–)	Longyearbyen	60 cm	TES	(326)	(140–270 GHz)	(3)
Satellite						
Planck HFI (2003-2013)	L2	1.5 m	NTD	52	100-857 GHz	9
LiteBIRD (2028–)	L2	20–40 cm	TES	(4,508)	(34–448 GHz)	(15)

Table 36.6: Selected experiments using low temperature calorimeters. The table shows currently or soon-to-be operating experiments that will search for dark matter or neutrino properties. The dates refer to the start of the program.

Sub-K Experiment	Location	Detection mode	Absorber (Total mass)	Sensor type	# Sensor # Crystal
WIMPs					
CRESST III (2016)	LNGS Italy	Athermal phonon and scint.	$CaWO_4/Al_2O_3$	TES	10
EDELWEISS † (_SubGeV)	LSM Modane France	Thermal phonon and ion.	Ge	NTD Ge	-
SuperCDMS (2023)	SNOLAB Canada	Athermal phonon and ion.	Ge/Si	TES	24
Neutrino mass					
ECHo [195] (2012)	Heidelberg Germany	Thermal phonon	Au:^{163}Ho (0.2μg)	MMC	16
HOLMES [196] (2015)	Milan Italy	Thermal phonon	implanted ^{163}Ho (18 μg)	TES	1000
NUMECS† [197] (2015)	LANL USA	Thermal phonon	implanted ^{163}Ho	TES	4096
$0\nu\beta\beta$ decay					
CUORE [189,198] (2015)	LNGS Italy	Thermal phonon	$^{nat}TeO_2$ (741 kg)	NTD Ge	988
CUPID [190] (2015)	LNGS Italy	Phonon and scint.	$Li_2^{100}MoO_4$ (450 kg)	NTD Ge	1596
AMoRe-I [193] (2018)	Y2L South Korea	Phonon and scint.	$Ca^{100}MoO_4/Li_2{}^{100}MoO_4$ (6 kg)	MMC	13/5

†No payload size quoted for experiments that are primarily in R&D phase.

of microcalorimeters needed to obtain sensitivities comparable to spectrometric measurements is a serious challenge, both for the readout and the thermal heat load. An alternative readout based on the use of KIDs, for their multiplexing capability, has been proposed and is presently under development.

Traditional searches for WIMP-like dark matter aim to measure the scatter of a massive dark matter particle off of a target nucleus. Similar to detectors employed for neutrinoless double beta decay, these searches benefit from large-mass absorbers for the target because the dark matter interaction rate scales directly with the number of nuclei in the target and hence its mass. Among the most successful experiments to date, are those that combine the detection of phonons with another channel such as ionization energy (EDELWEISS and SuperCDMS) or scintilation light (CRESST). This simultaneous, dual measurement takes advantage of the fact that the energy deposited in the absorber is partitioned into these channels differently depending on whether the initial particle interaction produces electron or nuclear recoils (or

Downloaded from https://academic.oup.com/ptep/article/2022/8/083C01/6651666 by KIT Library user on 27 September 2022

both). This particle identification allows for the rejection of background from natural sources of radiation, which most commonly manifest themselves as electron recoils in the detector.

In recent years, multi-ton liquid noble detectors have outclassed LTD-based technologies in searches for heavy (>10 GeV/c^2) dark matter owing to their ability to more easily and cheaply scale to large target masses. However, the lower thresholds achieved by LTDs continue to make them the technology of choice for low-mass dark matter searches. New advances have enabled these detectors to reach much lower energy thresholds than previously obtained, albeit sometimes at the cost of being able to detect energy in more than one channel as described above. For example, the use of an electric field to generate Neganov-Trofimov-Luke [204, 205] phonons in proportion to the applied voltage, has enabled the detection of single electron hole pairs in Si detectors with thresholds as low as a few eV (SuperCDMS HVeV). This and similar advances in Ge LTDs (EDELWEISS_SubGeV) have enabled sensitive searches for dark photons and dark matter that scatters off electrons [206, 207]. Next generation experiments such as SPICE/HERALD aim to further optimize the intrinsic energy resolution of TES detectors, coupled with a strategic choice of target materials (superfluid He and polar crystals) to enable sensitivites to dark matter with masses below an MeV/c^2 [208]. Current state-of-the-art axion searches use SQUID based quantum amplifies such as Josephson Parametric Amplifiers along with resonant cavities operating below 100 mK to look for a signal above fluctuations in the thermal noise [209]. Future axion experiments are also working to close the sensitivity gap between particle and wave-like dark matter with the help of LTDs. Broad-band axion searches in the THz range are being proposed, which will make use of TES, SNSPDs or KIDs for single photon detection [210]. Finally, LTD-based dark matter detectors are also actively employed to study coherent neutrino scattering, owing to the fact that the hypothesized signal from dark matter-nucleus scattering is nearly identical to that from neutrino-nucleus scattering, with both inducing nuclear recoils in a similar energy range [211, 212].

36.6 Low-radioactivity background techniques

Revised October 2021 by Al. Ianni (INFN, LNGS) and S. Schönert (Munich Tech. U.).

36.6.1 *Introduction*

The study of rare phenomena in fundamental physics, such as proton decay, neutrinoless double beta decay, dark matter, and MeV-scale neutrino interactions, requires extremely low levels of background radiation. Experiments searching for these rare events record electron recoils or nuclear recoils in the energy scale from a few eV to several MeV. The detector technologies used are multiple from organic and cryogenic liquid scintillators, to bolometers, solide state calorimeters, gaseous detectors, and crystal scintillators. As far as the background contamination is concerned at some extent the application defines the requirements, although the common denominator is that an extreme reduction of all background sources is essential. Leading experiments in rare events search have achieved trace contaminations that generate background events in the region of interest (ROI) as low as order of 50 pBq/kg. As a first and crucial step, a dedicated radiopurity assay of the detector set-up components has to be carried out. Over the last fifty years, special screening and cleaning techniques have been developed to measure and mitigate ultra-low levels of background. In order to characterize the background sources we refer to Heusser [213] and identify the following five main categories:

- environmental radioactivity in the location where the detector is installed;
- radioimpurities in the detector and shielding;
- radon and its progenies;
- cosmic rays and induced radioactivity;
- neutrons from natural fission, (α,n) reactions, and from cosmic-ray muons interactions.

The energy range affected by these background sources is mainly <10 MeV. All materials contain traces of long-lived primordial radioimpurities, such as ^{238}U, ^{232}Th, ^{235}U (^{238}U/^{235}U ~ 138), and ^{40}K (^{40}K/K$^{nat} \sim 1.17 \times 10^{-4}$). We recall that 1 *ppt* of ^{238}U and ^{232}Th corresponds to 12.36 and 4.06 μBq/kg, respectively; 1 *ppb* of K^{nat} corresponds to 30.25 μBq/kg. In the Earth's crust the abundance of uranium and thorium is of the order of $1-10$ ppm which corresponds to about $10-100$ Bq/kg. Taking into account these contamination levels and the low background requirements, a fundamental background reduction and mitigation is essential to carry out rare phenomena research.

Besides primordial radionuclides other radioactive elements are produced through interactions with matter of secondary cosmic ray particles. Among these so-called cosmogenic radionuclides we recall, in particular, ^{3}H, ^{14}C, ^{7}Be, ^{39}Ar, ^{42}Ar , and, in copper, steel and iron often used as shielding materials, ^{57,60}Co.

A third category of background source in our environment consists of anthropogenic radionuclides. These are artificially produced mainly through nuclear reactions in nuclear power plants, nuclear fuel reprocessing plants, and nuclear weapons testing. Anthropogenic background elements of concern for rare phenomena are ^{85}Kr, ^{137}Cs, ^{241}Am, ^{60}Co, and ^{90}Sr. The concentration of ^{85}Kr ($T_{1/2}$=10.76 y, Q_β=687 keV) in air has been slowly increasing since World War Two with a present activity of order 1 Bq/m^3. As a consequence ^{85}Kr is a crucial background in experiments making use of nitrogen, xenon, and argon from air.

Once detectors components radioactive backgrounds have been assayed and reduced by a careful selection campaign, which can last several years, a further step to push the background level beyond the screening possibilities is needed to reach the required sensitivity. For this purpose special active vetos, purification methods, and offline analyses have been developed. A meticulous background understanding and mitigation is crucial to explain any possible signal excess which may be detected. Background mitigation techniques are based on:

- use of radio-pure materials that absorb ionizing radiation;
- identify radio-pure material for detector construction;
- perform advanced surface and sub-surface cleaning treatment;
- reduce muon flux with underground detector deployment and using active vetos;
- exploit advanced detection and tagging techniques to discriminate signal from background.

In the following we describe radio-assay and background mitigation techniques developed and exploited in the framework of rare phenomena searches in deep underground laboratories.

36.6.2 *Radio-purity assay*

The radio-purity assay of detector components is a basic prerequisite to be carried out in low counting experiments. Several techniques are exploited for radio-purity assay. They are complementary to characterise the radio-purity of materials for shielding or core detector components. Next generation experiments radioassay campaign requires a considerable effort and organization for several years [214–216].

Gamma spectroscopy (GS) via high purity germanium (HPGe) detectors is a powerful and crucial technique [213]. It is nondestructive and thanks to the energy resolution allows to distinguish various radionuclides elements. Radiation from ^{238}U and ^{232}Th comes with all decay products in the radioactive chains. However, if secular equilibrium is broken, this crucial information can be addressed by separating different gamma-ray lines characterizing elements in the decay chains. In the ^{238}U chain one can have three sub-chains out of equilibrium. The first sub-chain can be assessed through ^{234}Th direct progeny of ^{238}U. The second sub-chain, which originates from ^{226}Ra, can be probed by ^{214}Pb and ^{214}Bi. A third sub-chain, which starts from ^{210}Pb, cannot be efficiently probed by GS, yet is of crucial importance and alternative methods must be used. In the ^{232}Th chain again one can probe two sub-chains which can be out of secular equilibrium: the first one through ^{228}Ac from ^{228}Ra; the second from ^{228}Th can be measured through ^{212}Pb, ^{212}Bi and ^{208}Tl. The technology for HPGe operated in deep underground counting facilities [217, 218] or in shallow laboratories with an efficient active

Downloaded from https://academic.oup.com/ptep/article/2022/8/083C01/6651666 by KIT Library user on 27 September 2022

veto shielding [219] has been boosted to sensitivities of the order of 10-100 μBq/kg by carefully selecting detector components, electronics and sample handling systems. The HPGe screening method requires order of ≥ 100 g of material, and weeks of acquisition to produce a reliable measurement.

A second crucial technique is based on inductively coupled plasma mass spectrometry (ICP-MS) [220]. This technique can probe primordial parents activity at the level of 1 μBq/kg. It is a destructive method and often needs special sample preparation on a small quantity of material. The ICP-MS does not measure the radioactive decay of isotopes but determines their concentration. At present, it is the most sensitive and rapid screening technique which allows to select materials at sub-ppt level of impurities. The drawback is that ICP-MS cannot assess whether the uranium and thorium chains are out of equilibrium and to reach ultra-high sensitivities one needs to carefully prepare and handle the samples in a cleanroom environment. ICP-MS screening must be coupled with other methods to properly assess the radio-purity of materials in the context of rare events searches. The Glow Discharge Mass Spectroscopy (GDMS) is a trace element analysis technique somehow alternative to ICP-MS. An advantage of GDMS is the possibility to determine the bulk composition of the sample, assuming homogeneity. Sensitivities of the order of 10 ppt can be achieved.

A third screening technique is based on neutron activation analysis (NAA) [221]. A sample exposed to a neutrons flux can be activated to form radioactive isotopes which can be detected using HPGe detectors or ICP-MS. Considering the difficulties to irradiate samples, this method is not often used. NAA can probe sensitivities at the level of 0.01 μBq/kg. This method is not destructive and the irradiated sample can be used if the activated products are not long-lived.

In case out of secular equilibrium conditions are measured for uranium and thorium from GS screening, a rigorous assessment cannot avoid radon emanation measurements. This matter is discussed in Section 36.6.3.

Complementarity between radio-purity assay techniques is a crucial parameter to design detectors for rare phenomena searches. As it has been pointed out above, requirements can be more stringent than the best sensitivity which can be obtained with the current radioassay techniques. In these cases, a number of prototype detectors have been built and operated to prove the feasibility to reach ultra-low backgrounds.

36.6.3 *Radon and its progeny*

Radon is considered to be rare in nature because most of its isotopes are short-lived. However, ^{222}Rn ($T_{1/2}$=3.82 d) is of particular concern in our context. ^{222}Rn is produced by ^{226}Ra and is a radioactive noble gas which can move within active detector components. ^{222}Rn daughters are heavy metals which can deposit on surfaces. If diffusive ^{222}Rn is supported by ^{226}Ra this can deposit on surfaces the long-lived ^{210}Pb, which is a major concern for low counting experiments. In addition, due to $\sim$100 keV nuclear recoil energies from alpha decays in the ^{226}Ra sub-chain, eventually ^{210}Pb can be implanted into a sub-surface layer of a material exposed to radon. This sub-surface contamination can remain even after surface cleaning. Surface contamination of ^{210}Pb is a serious background for direct dark matter experiments through alpha decay of ^{210}Po, which can generate neutrons by (α,n) reactions. Low energy beta/gamma emissions from ^{210}Pb are also a concern. Therefore, radon-free cleanrooms are essential for the assembly of the detector components. Effective radon abatement systems are available for this purpose.

In assembling and commissioning rare events experiments, special care must be dedicated to the estimate of radon emanation of the materials and continuous radon monitoring. For this purpose different methods for radon assay have been developed and exploited since the beginning of solar neutrino observations. ^{222}Rn atoms are collected inside an exhalation chamber for several half-lives before adsorption and counting. Detection limits of the order of 100 μBq (about 50 ^{222}Rn atoms) can be obtained with $\sim$50 l stainless steel electro-polished chambers [222]. This limit can be pushed down to 30 μBq for 1-liter scale chamber. Emanation of large vessels (cryostats, storage tanks, purification columns) can be determined by collecting exhaled radon into transportable charcoal traps [223]. The same method can be used for liquid samples. In this case instead of evacuating the exhalation chamber into a charcoal trap, He is flushed through a sparger tube for about 10 times the volume of the liquid used. Sensitivities of the order of 10 μBq/kg have been reached.

Nitrogen or synthetic air is often used in rare events experiments for purging, stripping, and assembling the experimental apparatus. These gases might contain radon. In gases ^{222}Rn can also be detected using electrostatic collection of ^{218}Po and ^{214}Po [224, 225]. Sensitivities of the order of mBq/m^3 can be obtained. In Borexino three grades of nitrogen purity were used: regular purity, high purity, and low argon and krypton purity. The regular purity is obtained from boil-off gas and has radon, measured with the method reported above, at the level of $< 100\mu$Bq/m^3. For stripping the purified liquid scintillator a higher purity is needed. To remove radon from regular purity nitrogen a dedicated absorber plant has been built. This system can reduce radon by a factor of 100. Finally, we mention that not only radon is found in nitrogen. For specific applications the long-lived ^{39}Ar and ^{85}Kr in nitrogen are an important source of background.

36.6.4 *Surface backgrounds*

Surface contamination of long-lived ^{222}Rn daughters can be challenging in low-counting experiments. Considering required sensitivities of the next generation experiments, this source of background has to be properly quantified and mitigated. Therefore, exposure to ^{222}Rn should be monitored and limited to reduce build-up of ^{210}Pb on surfaces. In addition, ^{222}Rn exposure could also produce sub-surface contamination as discussed in Section 36.6.3. For one cannot avoid radon contamination in many circumstances during production of detectors components, it is crucial to quantify the effectiveness of cleaning aiming at removing surface contamination of ^{210}Pb, ^{210}Bi, and ^{210}Po. A simple cleaning procedure, which implies degreasing, wiping, and rinsing the material surfaces is not effective in removing these surface contaminants. Studies of cleaning procedures have been carried out exposing stainless steel, copper and other materials to a strong radon source. Etching and electropolishing with subsequential passivation and rinsing have been investigated in great details. Several recipes for etching and electropolishing have been proposed [226]. Electropolishing has been shown to be very effective in reducing ^{210}Pb, ^{210}Bi, and ^{210}Po from both copper and stainless steel by a factor greater than 100. Etching, which is easier to perform than electropolishing, followed by passivation and rinsing with deionized water is effective in reducing ^{210}Pb and ^{210}Bi by a factor between 50 and 100. However, it is less effective for ^{210}Po, which in copper is very poorly reduced. Removing ^{210}Po from surfaces is crucial, therefore, naturally ^{210}Po contaminated copper and stainless steel surfaces have been deeply investigated with a high sensitivity (1 mBq/m^2) alpha spectrometer [227]. After multi-etching steps (≥ 3), followed by a passivation, a reduction of order 100 has been obtained. On the contrary, static etching (single step) is poorly effective. Electropolishing, or multi-etching are recommended in case copper is in direct contact with the active core of the detector and ultra-high radio-purity is essential or when copper electroforming cannot be used. Electroplating of a thin layer of high radio-pure copper onto the surface of less radio-pure copper has also been investigate to mitigate surface background [227]. This technique is shown to be near-perfect in reducing surface activity of ^{210}Po when electroformed copper is used [227].

Besides copper and steel other materials often used, such as polyethylene and teflon, have been investigated to understand how to reduce radon plate-out contaminations [228].

As far as surface contamination is concerned particulate fallout in cleanrooms environment could be of concern. In general, chemical composition of dust reflects local composition of soil and dust. This is not necessarily true in cleanroom spaces, where the composition of dust depends on ongoing activities and handled materials [229]. The rate of fallout is an important information in the framework of rare events experiments, where assembling is performed in cleanrooms. The ^{210}Pb contamination, inferred from stable lead measured by ICP-MS, due to dust fallout has been

Downloaded from https://academic.oup.com/ptep/article/2022/8/083C01/6651666 by KIT Library user on 27 September 2022

investigated [229]. This contamination has a different origin with respect to ^{210}Pb from radon progeny implantation. Ultimately, one can conclude that radon exposure is more crucial than dust fallout. Therefore, the best practice for rare events experiments to face surface background contamination is to perform cleaning and assembling in a radon-free cleanroom environment.

36.6.5 *Mitigation of backgrounds and active background discrimination*

In this Section we discuss a selection of different background mitigation techniques used in experiments to search for rare events in deep underground laboratories. This includes both the avoidance or reduction of specific radioactive contamination, as well as active background suppression techniques based on specific event features and topologies.

- *Mitigation of ^{222}Rn daughters deposition.* In dark matter direct search radiogenic (α,n) reactions due to radioactive decays are of great concern. The emitted neutron can mimic a nuclear recoil induced by a dark matter particle interaction. In the DarkSide-50 and LUX-ZEPLIN (LZ) experiments to mitigate this background, cleaning of parts and assembling of the dual-phase Time Projection Chamber have been carried out in a radon-free cleanroom with ^{222}Rn activity of the order of $\lesssim 50\,\mathrm{mBq/m^3}$.
- *Underground argon.* Liquid argon is an excellent scintillator to search for dark matter interactions due to the high electron-recoils rejection power through pulse shape discrimination. Events from $\beta-\gamma$ background can be rejected at the level of 10^7 or better with respect to nuclear-recoils. Moreover, liquid argon is used as an active shield in GERDA and the upcoming LEGEND experiment searching for neutrinoless double beta decay. However, a major drawback for dark matter search is due to the fact that atmospheric argon contains about 1 Bq/kg of cosmogenic ^{39}Ar ($T_{1/2}$=269 y, Q_β=565 keV) [230]. For neutrinoless double beta decay search with GERDA and LEGEND, ^{42}Ar ($T_{1/2}$=32.9 y, Q_β=599 keV) with its short lived progeny ^{42}K ($T_{1/2}$=12 h, Q_β=3525 keV) is a major source of background. This limits significantly the dark matter and neutrinoless double beta decay sensitivity search. Therefore, a source of argon with reduced ^{39}Ar and ^{42}Ar is crucial. Centrifugation or differential thermal diffusion are established methods to separate $^{39/42}$Ar and ^{40}Ar. However, this is an expensive method for a large fiducial mass. Argon from underground natural gas reservoirs is shown to contain low ^{39}Ar [231], and it is expected that ^{42}Ar is similar or even better reduced. Therefore, the use of underground argon mitigates the $^{39/42}$Ar backgrounds. DarkSide-50, with a mass of 150 kg of underground argon, has shown that this source of argon contains ^{39}Ar at a level reduced by a factor of $(1.4 \pm 0.3) \times 10^3$ with respect to atmospheric argon.
- *Electro-formed copper.* High radio-purity copper is often used as shielding and as core detectors components. The radioimpurities in the copper can be a dominant source of external background. Copper electro-forming is a technique used to reduce this background component in rare events experiments. Copper electro-forming is a well known process to obtain ultra-high radio-purity copper. This technique has been used in the framework of the Majorana Demonstrator experiment to search for neutrinoless double beta decay and in ANAIS to search for dark matter annual modulation. Sub-ppt levels in uranium and thorium have been achieved with electro-formed copper.
- *Background suppression using topological event information.* In addition to rigorous selection of high-purity target and shielding materials from external radiation, additional active suppression techniques must usually be employed in low background experiments to achieve the appropriate experimental sensitivities. While signal and background events may be indistinguishable if only their energy deposition is measured, their event features may differ significantly in time and space. Liquid scintillators use the characteristic photon emission time distributions to distinguish between electron- and alpha-like signals [232] and nuclear recoils [233], respectively. High-purity germanium detectors use the time evolution of the induced charges to separate point-like signal candidates for neutrinoless double-beta decay events from background signals induced, for example, by gamma interactions with multiple interactions within a crystal, or from β or α events on the n+ or p+ electrodes [234]. The operation of bare high-purity germanium detectors in an instrumented liquid argon shield enabled the GERDA experiment to identify backgrounds with signal-like event topology within the HPGe detectors, but with random energy deposition in the surrounding liquid argon. These synergistic background suppression techniques enabled for a first time ever a quasi background-free search for neutrinoless double beta decays with GERDA.

  The NEXT experiment for neutrinoless double beta decay in ^{136}Xe exploits differences in the spatial ionization patterns of double beta decay and single electron events to reject the background [235]. The former is characterized by two Bragg peaks at opposite ends of the tracks, the latter on the contrary displays only one peak. The combination of topology information and good energy resolution offer a powerful tool for background rejection.

  In addition, the 3D location of detected events in a multivariate fit, which accounts for spacial surface and bulk distributions of signal and background together with other properties, such as pulse shape and topological features, is a powerful tool for background mitigation.
- *Signal detection in rare events searches.* In direct dark matter experiments electron recoil events have to be mitigated with respect to nuclear recoil events. In semiconductor bolometers, operating at a few tens of mK under a bias electric field and used as calorimeters, drifting charges produce a large phonon signal proportional to the ionization, which allows to discriminate electron recoils by the combination of charge and phonon signals [236]. In scintillating bolometers the phonon and light signals are used for the same purpose [237]. Cryogenic scintillators, such as xenon and argon, in time projection chambers offer a strong electron recoils background mitigation through the detection of a primary scintillation signal in liquid and a secondary signal in gas from the drift and extraction of ionization electrons. This background mitigation technique is also being used for neutrinoless double beta decay with ^{136}Xe. The accurate fiducialization and good rejection of multiple-scattering events allow dark matter optimized experiments to attempt a search for this very rare phenomenon.
- *Neutron tagging in dark matter searches.* Present and next generation experiments need large neutron tagging detectors. In DarkSide-50 a dedicated active veto has been developed to both suppress and measure *in situ* the rate of neutron-induced background events [238]. The detector consists of a boron-loaded liquid scintillator, which serves both as shielding against γ-rays and as a tag for neutrons. Neutrons are thermalised and captured on ^{10}B. Experimental data has shown a neutron rejection power greater than 99.1% with 5% concentration of TMB in 30 tonnes pseudocumene-based liquid scintillator. The LZ direct dark matter detector with a central TPC of 7 tonnes of liquid xenon makes use of an outer Gd-loaded liquid scintillator neutron tagging veto, which works similarly to the DarkSide-50 veto, replacing boron with gadolinium. The 22 tonnes liquid scintillator is based on linear alkyl benzene (LAB) as solvent. This detector has been designed to operate with a neutron tagging efficiency greater than 95%. The nuclear-recoil background is reduced by a factor of 10. The XENONnT detector makes use of a cylindrical stainless steel tank filled with Gd-loaded water, which surrounds the cryostat with a TPC of 5.9 tonnes of active liquid xenon. The Gd concentration in water is 0.2% in mass. Neutrons leaving the TPC volume will be moderated and captured by the Gd with a probability of 91%. The gamma-rays emitted after the capture are detected from

Downloaded from https://academic.oup.com/ptep/article/2022/8/083C01/6651666 by KIT Library user on 27 September 2022

Cherenkov photons, providing a neutron tagging.

- *Mitigation of cosmogenic background.* In recent years the required sensitivity to search for dark matter and neutrinoless double beta decay asks for a strong reduction of cosmogenic background. We have emphasized that muons can produce neutrons that can enter the active volume of the detector from the surrounding rock or from external detector components. The yield of these so-called *cosmogenic neutrons* depend on the muon energies and the material properties of the medium the muon passes through. In addition, muons can produce by spallation radioisotopes inside the detector active volume. Cosmogenic backgrounds are a function of depth and experimental design, and can limit the sensitivity to search for rare events. Most of these radioisotopes are short-lived and their effect can be easily removed by an active veto based on the time correlation with a crossing muon. However, a number of cosmogenic radioisotopes are long-lived and they require an important consideration. Mitigation of these cosmogenic backgrounds produced in-situ deep underground are a major challenge for upcoming and future experiments. Optimizing the detector design and analysis strategies at a given depth equals an effective muon flux reduction. In particular, we mention two discrimination techniques for muon-induced isotopes: 1) ^{11}C tagging by a three-fold coincidence between the crossing muon, the capture of the ejected neutron from ^{12}C, and the ^{11}C decay [239]; 2) similar delayed coincidence tagging can be exploited to mitigate the background due to ^{77}Ge and its metastable state ^{77m}Ge, which have been identified as dominant cosmogenic background in the search for neutrinoless double beta decay of ^{76}Ge.
- *Purification.* A number of high efficiency specific purification methods have been developed for different detectors in order to remove long-lived radio-isotopes, ^{39}Ar, ^{85}Kr, and ^{210}Pb progeny. For organic liquid scintillators, distillation and water extraction have been shown to be very effective to reach radiopurity levels of the order of $10^{-5}\mu$Bq/kg or better in uranium and thorium, and $10^{-3}\mu$Bq/kg in ^{210}Pb [240]. Distillation has been used to reduce ^{85}Kr in xenon by a factor of 10^3 [241]. Cryogenic distillation will be used to reduce the isotopic abundance of ^{39}Ar in argon extracted from underground with a 350 m column in the ARIA project [242]. For semiconductors [243] and scintillating crystals [244] zone-refining has been exploited to remove impurities at the cost of a small fraction of material kept after the purification.
- *Direct isotope tagging.* In neutrinoless double beta decay in order to explore half-lives greater than 10^{28} y one needs an almost background-free detector. A robust method to reject backgrounds from radioactive decays would be the identification of the daughter atom of the double beta decaying nucleus: for example, for ^{136}Xe, the $^{136}Ba^{2+}$. Important step forwards to establish a valid and promising method for this tagging have been recently made [245, 246].

References

[1] A. Aab *et al.* (Pierre Auger), Earth and Space Science **7**, 4, e2019EA000582 (2020), URL `https://agupubs.onlinelibrary.wiley.com/doi/abs/10.1029/2019EA000582`.

[2] R. M. Baltrusaitis *et al.*, Nucl. Instrum. Meth. **A240**, 410 (1985).

[3] D. J. Bird *et al.* (HiRes), Astrophys. J. **424**, 491 (1994).

[4] T. Abu-Zayyad *et al.*, Nucl. Instrum. Meth. **A450**, 253 (2000).

[5] A. Watson **210**, 00001 (2019), [arXiv:1901.06676].

[6] H. Tokuno *et al.*, Nucl. Instrum. Meth. **A676**, 54 (2012), [arXiv:1201.0002].

[7] J. Abraham *et al.* (Pierre Auger), Nucl. Instrum. Meth. **A620**, 227 (2010), [arXiv:0907.4282].

[8] M. M. Malacari *et al.* (FAST), Astroparticle Physics **119**, 102430 (2020), ISSN 0927-6505, URL `https://www.sciencedirect.com/science/article/pii/S0927650520300037`.

[9] F. Arqueros, J. R. Hoerandel and B. Keilhauer, Nucl. Instrum. Meth. **A597**, 23 (2008), [arXiv:0807.3844].

[10] F. Arqueros, J. R. Hoerandel and B. Keilhauer, Nucl. Instrum. Meth. **A597**, 1 (2008), [arXiv:0807.3760].

[11] J. Rosado, F. Blanco and F. Arqueros, Astropart. Phys. **34**, 164 (2010), [arXiv:1004.3971].

[12] M. Ave *et al.* (AIRFLY), Astropart. Phys. **28**, 41 (2007), [arXiv:astro-ph/0703132].

[13] J. Rosado, F. Blanco and F. Arqueros, Astropart. Phys. **55**, 51 (2014), [arXiv:1401.4310].

[14] J. H. Boyer *et al.*, Nucl. Instrum. Meth. **A482**, 457 (2002).

[15] J. T. Brack *et al.*, Astropart. Phys. **20**, 653 (2004).

[16] B. Fick *et al.*, JINST **1**, 11, P11003 (2006).

[17] J. Abraham *et al.* (Pierre Auger), Astropart. Phys. **33**, 108 (2010), [arXiv:1002.0366].

[18] P. Abreu *et al.* (Pierre Auger), Astropart. Phys. **34**, 368 (2011), [arXiv:1010.6162].

[19] R. Thalman *et al.* Journal of Quantitative Spectroscopy and Radiative Transfer , **147**, 171 (2014), Erratum-ibid. **189**, 281 (2017).

[20] J.Abraham *et al.* [Pierre Auger Collab.], Nucl. Instrum. Methods **A789**, 172 (2015).

[21] M. Unger *et al.*, Nucl. Instrum. Meth. **A588**, 433 (2008), [arXiv:0801.4309].

[22] T.K. Gaisser and A.M. Hillas, *Proc. 15th Int. Cosmic Ray Conf.* Bulgarska Akademiia na Naukite, Conf. Papers **8**, 353 (1978), (archived at http://adsabs.harvard.edu/abs/1977ICRC....8..353G).

[23] A. e. a. T. P. A. C. Aab (The Pierre Auger Collaboration), Phys. Rev. D **100**, 082003 (2019), URL `https://link.aps.org/doi/10.1103/PhysRevD.100.082003`.

[24] P. A. Klimov *et al.*, Space Sci. Rev. **212**, 3-4, 1687 (2017), [arXiv:1706.04976].

[25] B. A. e. a. Khrenov, Cosmic Research **58**, 5, 317 (2020).

[26] G. Abdellaoui *et al.* (JEM-EUSO), Journal of Instrumentation **13**, 5 (2018), ISSN 17480221.

[27] J. e. a. Adams, Experimental Astronomy (2021).

[28] F. Capel *et al.*, Advances in Space Research **62**, 2954 (2018).

[29] A. O. et al., Journal of Cosmology and Astroparticle Physics **2021**, 06, 007 (2021), URL `https://doi.org/10.1088/1475-7516/2021/06/007`.

[30] J. Holder *et al.*, AIP Conf. Proc. **1085**, 657 (2009), [arXiv:0810.0474].

[31] F. Aharonian *et al.* (H.E.S.S.), Astron. Astrophys. **457**, 899 (2006), [arXiv:astro-ph/0607333].

[32] J. Albert *et al.* (MAGIC), Astrophys. J. **674**, 1037 (2008), [arXiv:0705.3244].

[33] T. C. Weekes *et al.*, Astrophys. J. **342**, 379 (1989).

[34] A. M. Hillas *et al.*, Astrophys. J. **503**, 744 (1998).

[35] `http://tevcat.uchicago.edu/`.

[36] F. Aharonian *et al.* (H.E.S.S.), Astrophys. J. **636**, 777 (2006), [arXiv:astro-ph/0510397].

[37] M. de Naurois and D. Mazin, Comptes Rendus Physique **16**, 610 (2015), [arXiv:1511.00463].

[38] N. Park, PoS **ICRC2017**, arXiv:1808.10495 (2018), [arXiv:1808.10495].

[39] A. M. Hillas, Astropart. Phys. **43**, 19 (2013).

[40] B. S. Acharya *et al.* (CTA Consortium), Astropart. Phys. **43**, 3 (2013).

[41] A. Bernstein *et al.*, *Report on the Depth Requirements for a Massive Detector at Homestake* (2009), [arXiv:0907.4183].

[42] K. Eguchi *et al.* (KamLAND), Phys. Rev. Lett. **90**, 021802 (2003), [hep-ex/0212021].

Downloaded from https://academic.oup.com/ptep/article/2022/8/083C01/6651666 by KIT Library user on 27 September 2022

[43] G. Alimonti *et al.* (Borexino), Nucl. Instrum. Meth. A **600**, 568 (2009), [arXiv:0806.2400].

[44] Y. Ashie *et al.* (Super-Kamiokande), Phys. Rev. **D71**, 112005 (2005), [hep-ex/0501064].

[45] S. Kasuga *et al.*, Phys. Lett. **B374**, 238 (1996).

[46] M. Shiozawa (Super-Kamiokande), Nucl. Instrum. Meth. **A433**, 240 (1999).

[47] K. Abe *et al.* (Super-Kamiokande), Phys. Rev. **D83**, 052010 (2011), [arXiv:1010.0118].

[48] J. F. Beacom and M. R. Vagins, Phys. Rev. Lett. **93**, 171101 (2004), [hep-ph/0309300].

[49] J. Boger *et al.* (SNO), Nucl. Instrum. Meth. **A449**, 172 (2000), [arXiv:nucl-ex/9910016].

[50] T. K. Gaisser, F. Halzen and T. Stanev, Phys. Rept. **258**, 173 (1995), [Erratum: Phys. Rept.271,355(1996)], [hep-ph/9410384].

[51] J.G. Learned and K. Mannheim, Ann. Rev. Nucl. and Part. Sci. **50**, 679 (2000).

[52] U. F. Katz and C. Spiering, Prog. Part. Nucl. Phys. **67**, 651 (2012), [arXiv:1111.0507].

[53] M. G. Aartsen *et al.* (IceCube), J. Phys. **G44**, 5, 054006 (2017), [arXiv:1607.02671].

[54] S. Adrián-Martínez *et al.* (KM3NeT), J. Phys. **G43**, 8, 084001 (2016), [arXiv:1601.07459].

[55] A. Gazizov and M. P. Kowalski, Comput. Phys. Commun. **172**, 203 (2005), [arXiv:astro-ph/0406439].

[56] A. D. Avrorin *et al.*, Phys. Part. Nucl. **46**, 2, 211 (2015).

[57] M. G. Aartsen *et al.* (IceCube), JINST **12**, 03, P03012 (2017), [arXiv:1612.05093].

[58] M. G. Aartsen *et al.* (IceCube) (2014), [arXiv:1412.5106].

[59] M. G. Aartsen *et al.* (IceCube-Gen2), J. Phys. G **48**, 6, 060501 (2021), [arXiv:2008.04323].

[60] M. Agostini *et al.* (P-ONE), Nature Astron. **4**, 10, 913 (2020), [arXiv:2005.09493].

[61] S. Adrián-Martínez *et al.* (KM3NeT), Eur. Phys. J. **C74**, 9, 3056 (2014), [arXiv:1405.0839].

[62] A. V. Akindinov *et al.*, Eur. Phys. J. **C79**, 9, 758 (2019), [arXiv:1902.06083].

[63] C. Kopper (for the IceCube Collab.), contribution to ICRC2017.

[64] M. G. Aartsen *et al.* (IceCube), Phys. Rev. Lett. **113**, 101101 (2014), [arXiv:1405.5303].

[65] A. Albert *et al.* (ANTARES), Astrophys. J. **853**, 1, L7 (2018), [arXiv:1711.07212].

[66] M. G. Aartsen *et al.* (IceCube), Astrophys. J. **809**, 1, 98 (2015), [arXiv:1507.03991].

[67] M. G. Aartsen *et al.* (IceCube, Fermi-LAT, MAGIC, AGILE, ASAS-SN, HAWC, H.E.S.S., INTEGRAL, Kanata, Kiso, Kapteyn, Liverpool Telescope, Subaru, Swift NuSTAR, VERITAS, VLA/17B-403), Science **361**, 6398, eaat1378 (2018), [arXiv:1807.08816].

[68] M. G. Aartsen *et al.* (IceCube), Science **361**, 6398, 147 (2018), [arXiv:1807.08794].

[69] A. Albert *et al.* (ANTARES, IceCube), Astrophys. J. **892**, 92 (2020), [arXiv:2001.04412].

[70] M. G. Aartsen *et al.* (IceCube), Phys. Rev. **D99**, 3, 032007 (2019), [arXiv:1901.05366].

[71] M. Kowalski (for the IceCube and IceCube-Gen2 Collabs.), contribution to ICRC2021.

[72] P. Coyle, contribution to ICRC2021.

[73] G. Dzhilkibaev (for the Bailkal Collab.), contribution to ICRC2021.

[74] T. Huege, Phys. Rept. **620**, 1 (2016), [arXiv:1601.07426].

[75] F. G. Schroder, Prog. Part. Nucl. Phys. **93**, 1 (2017), [arXiv:1607.08781].

[76] G. A. Askar'yan, Sov. Phys. JETP **14**, 2, 441 (1962), [Zh. Eksp. Teor. Fiz.41,616(1961)].

[77] G.A. Askaryan, Sov. Phys. JETP **21**, 658 (1965).

[78] E. Zas, F. Halzen and T. Stanev, Phys. Rev. D **45**, 362 (1992).

[79] C. W. James *et al.*, Phys. Rev. **E84**, 056602 (2011), [arXiv:1007.4146].

[80] J. Alvarez-Muniz, R. A. Vazquez and E. Zas, Phys. Rev. **D62**, 063001 (2000), [arXiv:astro-ph/0003315].

[81] C. Glaser *et al.*, Eur. Phys. J. C **80**, 77 (2020), [arXiv:1906.01670].

[82] D. Saltzberg *et al.*, Phys. Rev. Lett. **86**, 2802 (2001), [hep-ex/0011001].

[83] O. Scholten *et al.*, J. Phys. Conf. Ser. **81**, 012004 (2007).

[84] J. Alvarez-Muñiz *et al.*, Phys. Rev. D **74**, 023007 (2006), URL `https://link.aps.org/doi/10.1103/PhysRevD.74.023007`.

[85] L. Gerhardt and S. R. Klein, Phys. Rev. **D82**, 074017 (2010), [arXiv:1007.0039].

[86] J. Alvarez-Muniz, R. A. Vazquez and E. Zas, Phys. Rev. **D61**, 023001 (2000), [arXiv:astro-ph/9901278].

[87] D. García-Fernández, A. Nelles and C. Glaser, Phys. Rev. D **102**, 8, 083011 (2020), [arXiv:2003.13442].

[88] K. Greisen, Phys. Rev. Lett. **16**, 748 (1966).

[89] G. T. Zatsepin and V. A. Kuzmin, JETP Lett. **4**, 78 (1966), [Pisma Zh. Eksp. Teor. Fiz.4,114(1966)].

[90] V. de Souza (Pierre Auger, Telescope Array), PoS **ICRC2017**, 522 (2018).

[91] R. Abbasi *et al.* (IceCube), Astropart. Phys. **34**, 382 (2011), [arXiv:1004.1694].

[92] P. Allison *et al.* (ARA), Astropart. Phys. **108**, 63 (2019), [arXiv:1712.03301].

[93] A. Anker *et al.* (ARIANNA), JCAP **1911**, 030 (2019), [arXiv:1909.02677].

[94] J. A. Aguilar *et al.* (RNO-G) (2021), [arXiv:2107.02604].

[95] I. Plaisier *et al.* (RNO-G), PoS **395**, 1026 (2021).

[96] A. G. Vieregg, K. Bechtol and A. Romero-Wolf, JCAP **1602**, 02, 005 (2016), [arXiv:1504.08006].

[97] S. W. Barwick *et al.* (ARIANNA), Astropart. Phys. **90**, 50 (2017), [arXiv:1612.04473].

[98] M. G. Aartsen *et al.* (IceCube), Phys. Rev. **D98**, 6, 062003 (2018), [arXiv:1807.01820].

[99] A. Aab *et al.* (Pierre Auger), JCAP **1910**, 10, 022 (2019), [arXiv:1906.07422].

[100] J. D. Bray *et al.*, Phys. Rev. **D91**, 6, 063002 (2015), [arXiv:1502.03313].

[101] O. Scholten *et al.*, Phys. Rev. Lett. **103**, 191301 (2009), [arXiv:0910.4745].

[102] P. W. Gorham *et al.* (ANITA), Phys. Rev. **D99**, 12, 122001 (2019), [arXiv:1902.04005].

[103] P. Allison *et al.* (ARA), Phys. Rev. D **102**, 4, 043021 (2020), [arXiv:1912.00987].

[104] A. Anker *et al.* (ARIANNA), JCAP **03**, 053 (2020), [arXiv:1909.00840].

[105] T. Winchen *et al.*, J. Phys. Conf. Ser. **1181**, 1, 012077 (2019), [arXiv:1903.08472].

[106] J. Stettner (IceCube), PoS **ICRC2019**, 1017 (2019), [arXiv:1908.09551].

[107] A. van Vliet, R. Alves Batista and J. R. Hörandel, Phys. Rev. D **100**, 2, 021302 (2019), [arXiv:1901.01899].

[108] S. Barwick *et al.*, Journal of Glaciology **51**, 173, 231–238 (2005).

Downloaded from https://academic.oup.com/ptep/article/2022/8/083C01/6651666 by KIT Library user on 27 September 2022

[109] J.A. Dowdeswell and S. Evans, Rept. on Prog. in Phys. **67**, 1821 (2004).

[110] S. W. Barwick *et al.*, JCAP **1807**, 07, 055 (2018), [arXiv:1804.10430].

[111] C. Deaconu *et al.*, Phys. Rev. **D98**, 4, 043010 (2018), [arXiv:1805.12576].

[112] P. W. Gorham *et al.* (ANITA), Phys. Rev. Lett. **103**, 051103 (2009), [arXiv:0812.2715].

[113] P. W. Gorham *et al.* (ANITA), Phys. Rev. Lett. **121**, 16, 161102 (2018), [arXiv:1803.05088].

[114] P. W. Gorham *et al.* (ANITA), Phys. Rev. Lett. **126**, 7, 071103 (2021), [arXiv:2008.05690].

[115] I. Kravchenko *et al.* (RICE), Phys. Rev. **D73**, 082002 (2006), [arXiv:astro-ph/0601148].

[116] P. Allison *et al.* (ARA), Phys. Rev. **D93**, 8, 082003 (2016), [arXiv:1507.08991].

[117] J. Avva *et al.*, Nucl. Instrum. Meth. **A869**, 46 (2017), [arXiv:1605.03525].

[118] J. A. Aguilar *et al.* (RNO-G), JINST **16**, 03, P03025 (2021), [arXiv:2010.12279].

[119] R.D. Dagkesamanskii and I.M. Zheleznykh, Sov. Phys. JETP Lett. **50**, 233 (1989).

[120] G. R. Olhoeft and D. W. Strangway, Earth and Planetary Science Letters **24**, 3, 394 (1975).

[121] J. D. Bray, Astropart. Phys. **77**, 1 (2016), [arXiv:1601.02980].

[122] C. W. James *et al.*, EPJ Web Conf. **135**, 04001 (2017), [arXiv:1704.05336].

[123] A. Aab *et al.* (Pierre Auger), Phys. Rev. Lett. **116**, 24, 241101 (2016), [arXiv:1605.02564].

[124] P. A. Bezyazeekov *et al.* (Tunka-Rex), Phys. Rev. **D97**, 12, 122004 (2018), [arXiv:1803.06862].

[125] S. Buitink *et al.* (LOFAR), Phys. Rev. **D90**, 8, 082003 (2014), [arXiv:1408.7001].

[126] K. Mulrey *et al.* (LOFAR), JCAP **11**, 017 (2020), [arXiv:2005.13441].

[127] J. G. Learned and S. Pakvasa, Astropart. Phys. **3**, 267 (1995), [hep-ph/9405296].

[128] J. L. Feng *et al.*, Phys. Rev. Lett. **88**, 161102 (2002), [hep-ph/0105067].

[129] A. G. Vieregg (PUEO), PoS **ICRC2021**, 1029 (2021).

[130] J. Álvarez Muñiz *et al.* (GRAND), Sci. China Phys. Mech. Astron. **63**, 1, 219501 (2020), [arXiv:1810.09994].

[131] P. Abreu *et al.* (Pierre Auger), PoS **ICRC2021**, 262 (2021).

[132] D. R. Nygren, in "Proceedings, 1975 PEP Summer Study, Berkeley, July 28-August 20, 1975," 126–133 (1975).

[133] L. S. Miller, S. Howe and W. E. Spear, Phys. Rev. **166**, 871 (1968), URL `https://link.aps.org/doi/10.1103/PhysRev.166.871`.

[134] E. Aprile and T. Doke, Rev. Mod. Phys. **82**, 2053 (2010), [arXiv:0910.4956].

[135] V. Chepel and H. Araujo, JINST **8**, R04001 (2013), [arXiv:1207.2292].

[136] D. Gonzalez-Diaz, F. Monrabal and S. Murphy, Nucl. Instrum. Meth. **A878**, 200 (2018), [arXiv:1710.01018].

[137] J. J. Gomez-Cadenas, F. Monrabal Capilla and P. Ferrario, Front.in Phys. **7**, 51 (2019), [arXiv:1903.02435].

[138] H. J. Maris, Journal of the Physical Society of Japan **77**, 11, 111008 (2008), URL `https://doi.org/10.1143/JPSJ.77.111008`.

[139] L. Bruschi, G. Mazzi and M. Santini, Phys. Rev. Lett. **28**, 1504 (1972), URL `https://link.aps.org/doi/10.1103/PhysRevLett.28.1504`.

[140] E. Aprile *et al.*, Nature **568**, 7753, 532 (2019), URL `https://doi.org/10.1038/s41586-019-1124-4`.

[141] K. Winger *et al.*, Journal of Environmental Radioactivity **80**, 2, 183 (2005), ISSN 0265-931X, URL `http://www.sciencedirect.com/science/article/pii/S0265931X04002887`.

[142] H. Loosli, Earth and Planetary Science Letters **63**, 1, 51 (1983), ISSN 0012-821X, URL `http://www.sciencedirect.com/science/article/pii/0012821X83900213`.

[143] E. Aprile *et al.* (XENON), Eur. Phys. J. **C75**, 11, 546 (2015), [arXiv:1503.07698].

[144] M. Schumann, J. Phys. **G46**, 10, 103003 (2019), [arXiv:1903.03026].

[145] E. Aprile *et al.*, JINST **9**, 11, P11012 (2014), [arXiv:1408.6206].

[146] F. Neves *et al.*, JINST **12**, 01, P01017 (2017), [arXiv:1612.07965].

[147] D. S. Akerib *et al.* (LUX Collaboration), Phys. Rev. D **97**, 102008 (2018), URL `https://link.aps.org/doi/10.1103/PhysRevD.97.102008`.

[148] D. S. Akerib *et al.* (LUX), Phys. Rev. **D95**, 1, 012008 (2017), [arXiv:1610.02076].

[149] M. Szydagis *et al.*, Journal of Instrumentation **6**, 10, P10002 (2011), URL `https://doi.org/10.1088%2F1748-0221%2F6%2F10%2Fp10002`.

[150] M. Kimura *et al.*, Phys. Rev. **D100**, 3, 032002 (2019), [arXiv:1902.01501].

[151] R. Ajaj *et al.* (DEAP), Phys. Rev. **D100**, 2, 022004 (2019), [arXiv:1902.04048].

[152] P. Agnes *et al.* (DarkSide), Phys. Rev. **D93**, 8, 081101 (2016), [Addendum: Phys. Rev.D95,no.6,069901(2017)], [arXiv:1510.00702].

[153] E. Aprile *et al.* (XENON), Phys. Rev. Lett. **119**, 18, 181301 (2017), [arXiv:1705.06655].

[154] X. Cui *et al.* (PandaX-II), Phys. Rev. Lett. **119**, 18, 181302 (2017), [arXiv:1708.06917].

[155] D. S. Akerib *et al.*, Phys. Rev. Lett. **118**, 25, 251302 (2017).

[156] D. S. Akerib *et al.* (LUX-ZEPLIN) (2018), [arXiv:1802.06039].

[157] E. Aprile *et al.* (XENON), JCAP **1604**, 04, 027 (2016), [arXiv:1512.07501].

[158] H. Zhang *et al.* (PandaX), Sci. China Phys. Mech. Astron. **62**, 3, 31011 (2019), [arXiv:1806.02229].

[159] C. E. Aalseth *et al.*, Eur. Phys. J. Plus **133**, 131 (2018), [arXiv:1707.08145].

[160] J. Aalbers *et al.*, Journal of Cosmology and Astroparticle Physics **2016**, 11, 017 (2016), URL `https://doi.org/10.1088%2F1475-7516%2F2016%2F11%2F017`.

[161] W. Guo and D. N. McKinsey, Phys. Rev. **D87**, 11, 115001 (2013), [arXiv:1302.0534].

[162] D. R. Nygren, J. Phys. Conf. Ser. **460**, 012006 (2013).

[163] C. A. J. O'Hare *et al.*, Phys. Rev. **D92**, 6, 063518 (2015), [arXiv:1505.08061].

[164] S. M. Bilenky and C. Giunti, Mod. Phys. Lett. **A27**, 1230015 (2012), [arXiv:1203.5250].

[165] S. R. Elliott, A. A. Hahn and M. K. Moe, Phys. Rev. Lett. **59**, 2020 (1987), URL `http://link.aps.org/doi/10.1103/PhysRevLett.59.2020`.

[166] G. Anton *et al.* (EXO-200), Phys. Rev. Lett. **123**, 16, 161802 (2019), [arXiv:1906.02723].

[167] S. A. Kharusi *et al.* (nEXO) (2018), [arXiv:1805.11142].

[168] D. Nygren, Nucl. Instrum. Meth. **A603**, 337 (2009).

[169] M. K. Moe, Phys. Rev. **C44**, 931 (1991), [,1019(1991)].

[170] A. D. McDonald *et al.*, Phys. Rev. Lett. **120**, 13, 132504 (2018), [arXiv:1711.04782].

Downloaded from https://academic.oup.com/ptep/article/2022/8/083C01/6651666 by KIT Library user on 27 September 2022

[171] C. Chambers *et al.* (nEXO), Nature **569**, 7755, 203 (2019), [arXiv:1806.10694].

[172] P. Thapa *et al.* (2019), [arXiv:1904.05901].

[173] C. Enss, editor, *Cryogenic particle detection*, volume 99 of *Topics in applied physics*, Springer, Berlin, Germany (2005).

[174] K. Pretzl, *Cryogenic Detectors* (2020).

[175] *Proc. of the Low Temperature Detectors for Neutrinos and Dark Matter*, Low Temperature Detectors for Neutrinos and Dark Matter (start 1987).

[176] G. H. Rieke, *Detection of Light*, Cambridge University Press, 3rd edition (2021).

[177] H. Kraus, Superconductor Science and Technology **9**, 10, 827 (1996), URL https://doi.org/10.1088/0953-2048/9/10/001.

[178] A. V. Dixit *et al.*, Phys. Rev. Lett. **126**, 14, 141302 (2021), [arXiv:2008.12231].

[179] J. Zmuidzinas, Annual Review of Condensed Matter Physics **3**, 1, 169 (2012), URL https://doi.org/10.1146/annurev-conmatphys-020911-125022.

[180] S. Doyle *et al.*, Journal of Low Temperature Physics **151**, 1, 530 (2008), URL https://doi.org/10.1007/s10909-007-9685-2.

[181] K. Irwin and G. Hilton, *Transition-Edge Sensors*, 63–150, Springer Berlin Heidelberg, Berlin, Heidelberg (2005), ISBN 978-3-540-31478-3, URL https://doi.org/10.1007/10933596_3.

[182] F. Paolucci and F. Giazotto, Instruments **5**, 2 (2021), ISSN 2410-390X, URL https://www.mdpi.com/2410-390X/5/2/14.

[183] S. B. Bandler *et al.*, J. Low Temp. Phys. **93**, 709 (1993).

[184] D. Prele, Journal of Instrumentation **10**, 08, C08015 (2015), URL https://doi.org/10.1088/1748-0221/10/08/c08015.

[185] E. Fiorini and T. Niinikoski, Nucl. Instrum. Meth. A **224**, 83 (1984).

[186] S. H. Moseley, J. C. Mather and D. McCammon, "Thermal detectors as x-ray spectrometers," (1984).

[187] V. Barger and D. Cline (1985), telemark, 1984.

[188] A. Blasi *et al.* (1985), I.N.F.N./BE-85/2, internal report.

[189] D. Q. Adams *et al.* (CUORE) (2021), [arXiv:2104.06906].

[190] W. R. Armstrong *et al.* (CUPID) (2019), [arXiv:1907.09376].

[191] O. Azzolini *et al.* (CUPID), Phys. Rev. Lett. **123**, 3, 032501 (2019), [arXiv:1906.05001].

[192] E. Armengaud *et al.* (CUPID), Phys. Rev. Lett. **126**, 18, 181802 (2021), [arXiv:2011.13243].

[193] V. Alenkov *et al.*, Eur. Phys. J. C **79**, 9, 791 (2019), [arXiv:1903.09483].

[194] D. Mccammon *et al.* (1984).

[195] L. Gastaldo *et al.*, Eur. Phys. J. ST **226**, 8, 1623 (2017).

[196] B. Alpert *et al.*, Eur. Phys. J. C **75**, 3, 112 (2015), [arXiv:1412.5060].

[197] M. P. Croce *et al.*, J. Low Temp. Phys. **184**, 3-4, 958 (2016), [arXiv:1510.03874].

[198] R. Ardito *et al.* (2005), [hep-ex/0501010].

[199] P. Filianin *et al.*, Phys. Rev. Lett. **127**, 7, 072502 (2021), [arXiv:2108.07039].

[200] D. Pergolesi *et al.*, Nucl. Instrum. Meth. A **559**, 349 (2006).

[201] M. Sisti *et al.*, Nuclear Instruments and Methods in Physics Research Section A: Accelerators, Spectrometers, Detectors and Associated Equipment **520**, 1, 125 (2004), ISSN 0168-9002, proceedings of the 10th International Workshop on Low Temperature Detectors, URL https://www.sciencedirect.com/science/article/pii/S0168900203031814.

[202] E. Ferri *et al.*, Phys. Procedia **61**, 227 (2015).

[203] C. Velte, *Measurement of a high energy resolution and high-statistics 163Ho electron capture spectrum for theECHo experiment.*, Ph.D. thesis, U. Heidelberg (main) (2020).

[204] P. Luke *et al.*, Nucl. Instrum. Meth. A **289**, 406 (1990).

[205] B. Neganov *et al.*, J Low Temp Phys **93**, 417–422 (1993), URL https://doi.org/10.1007/BF00693454.

[206] I. Alkhatib *et al.* (SuperCDMS), Phys. Rev. Lett. **127**, 8, 081802 (2021), [arXiv:2011.09183].

[207] Q. Arnaud *et al.* (EDELWEISS), Phys. Rev. Lett. **125**, 14, 141301 (2020), [arXiv:2003.01046].

[208] *Snowmass2021-Letter of Interest The TESSERACT Dark Matter Project* (2020).

[209] T. Braine *et al.* (ADMX), Phys. Rev. Lett. **124**, 10, 101303 (2020), [arXiv:1910.08638].

[210] *Snowmass2021-Letter of Interest Opening the Terahertz Axion Window* (2020).

[211] C. Bellenghi *et al.*, Eur. Phys. J. C **79**, 9, 727 (2019), [arXiv:1905.10611].

[212] I. Colantoni *et al.*, J. Low Temp. Phys. **199**, 3-4, 593 (2020).

[213] G. Heusser, Ann. Rev. Nucl. Part. Sci. **45**, 543 (1995).

[214] D. S. Akerib *et al.*, The European Physical Journal C **80**, 11 (2020), URL https://doi.org/10.1140%2Fepjc%2Fs10052-020-8420-x.

[215] D. S. Leonard *et al.*, Nucl. Instrum. Meth. A **871**, 169 (2017), [arXiv:1703.10799].

[216] N. Abgrall *et al.* (Majorana), Nucl. Instrum. Meth. A **823**, 83 (2016), [arXiv:1603.08483].

[217] M. Laubenstein, International Journal of Modern Physics A **32**, 30, 1743002 (2017), URL https://doi.org/10.1142/s0217751x17430023.

[218] P. Scovell *et al.*, Astroparticle Physics **97**, 160 (2018), URL https://doi.org/10.1016/j.astropartphys.2017.11.006.

[219] G. Heusser *et al.*, The European Physical Journal C **75**, 11 (2015), URL https://doi.org/10.1140%2Fepjc%2Fs10052-015-3704-2.

[220] N. Jakubowski, Analytical and Bioanalytical Chemistry **392**, 5, 775 (2008), URL https://doi.org/10.1007%2Fs00216-008-2374-4.

[221] M. Clemenza, J. Radioanal. Nucl. Chem. **318**, 3, 1765 (2018).

[222] G. Heusser *et al.*, Applied Radiation and Isotopes **52**, 3, 691 (2000), URL https://doi.org/10.1016%2Fs0969-8043%2899%2900231-6.

[223] M. Wojcik, G. Zuzel and H. Simgen, International Journal of Modern Physics A **32**, 30, 1743004 (2017), URL https://doi.org/10.1142%2Fs0217751x17430047.

[224] Y. Takeuchi *et al.*, Nuclear Instruments and Methods in Physics Research Section A: Accelerators, Spectrometers, Detectors and Associated Equipment **421**, 1-2, 334 (1999), URL https://doi.org/10.1016%2Fs0168-9002%2898%2901204-2.

[225] J. Kiko, Nuclear Instruments and Methods in Physics Research Section A: Accelerators, Spectrometers, Detectors and Associated Equipment **460**, 2-3, 272 (2001), URL https://doi.org/10.1016%2Fs0168-9002%2800%2901082-2.

[226] E. Hoppe *et al.*, Nuclear Instruments and Methods in Physics Research Section A: Accelerators, Spectrometers, Detectors and Associated Equipment **579**, 1, 486 (2007), URL https://doi.org/10.1016%2Fj.nima.2007.04.101.

[227] R. Bunker *et al.*, Nuclear Instruments and Methods in Physics Research Section A: Accelerators, Spectrometers, Detectors and Associated Equipment **967**, 163870 (2020), URL https://doi.org/10.1016/j.nima.2020.163870.

Downloaded from https://academic.oup.com/ptep/article/2022/8/083C01/6651666 by KIT Library user on 27 September 2022

[228] S. Bruenner *et al.*, The European Physical Journal C **81**, 4 (2021), URL https://doi.org/10.1140/epjc/s10052-021-09047-2.

[229] M. L. di Vacri *et al.*, Nucl. Instrum. Meth. A **994**, 165051 (2021), [arXiv:2006.12746].

[230] H. Loosli, Earth and Planetary Science Letters **63**, 1, 51 (1983), URL https://doi.org/10.1016%2F0012-821x%2883%2990021-3.

[231] D. Acosta-Kane *et al.*, Nuclear Instruments and Methods in Physics Research Section A: Accelerators, Spectrometers, Detectors and Associated Equipment **587**, 1, 46 (2008), URL https://doi.org/10.1016%2Fj.nima.2007.12.032.

[232] G. Ranucci, in "IEEE Symposium Conference Record Nuclear Science 2004.", volume 2, 804–809 Vol. 2 (2004).

[233] P. Adhikari *et al.*, The European Physical Journal C **80**, 4 (2020), URL https://doi.org/10.1140%2Fepjc%2Fs10052-020-7789-x.

[234] D. Budjáš *et al.*, Journal of Instrumentation **4**, 10, P10007 (2009), URL https://doi.org/10.1088/1748-0221/4/10/p10007.

[235] A. Simón *et al.* (NEXT), JHEP **21**, 146 (2020), [arXiv:2102.11931].

[236] R. Agnese *et al.* (SuperCDMS Collaboration), Phys. Rev. Lett. **120**, 061802 (2018), URL https://link.aps.org/doi/10.1103/PhysRevLett.120.061802.

[237] W. Westphal *et al.*, Nucl. Instrum. Meth. A **559**, 372 (2006).

[238] S. Westerdale, E. Shields and F. Calaprice, Astroparticle Physics **79**, 10 (2016), URL https://doi.org/10.1016%2Fj.astropartphys.2016.01.005.

[239] H. Back *et al.* (Borexino Collaboration), Phys. Rev. C **74**, 045805 (2006), URL https://link.aps.org/doi/10.1103/PhysRevC.74.045805.

[240] J. Benziger *et al.*, Nuclear Instruments and Methods in Physics Research Section A: Accelerators, Spectrometers, Detectors and Associated Equipment **587**, 2-3, 277 (2008), URL https://doi.org/10.1016/j.nima.2007.12.043.

[241] K. Abe *et al.*, Nucl. Instrum. Meth. A **716**, 78 (2013), [arXiv:1301.2815].

[242] P. Agnes *et al.*, The European Physical Journal C **81**, 4 (2021), URL https://doi.org/10.1140/epjc/s10052-021-09121-9.

[243] K.-P. Gradwohl *et al.*, Journal of Instrumentation **15**, 12, P12010 (2020), URL https://doi.org/10.1088/1748-0221/15/12/p12010.

[244] B. Suerfu, F. Calaprice and M. Souza, Physical Review Applied **16**, 1 (2021), URL https://doi.org/10.1103/physrevapplied.16.014060.

[245] I. Rivilla *et al.*, Nature **583**, 7814, 48 (2020), URL https://doi.org/10.1038/s41586-020-2431-5.

[246] A. McDonald *et al.*, Physical Review Letters **120**, 13 (2018), URL https://doi.org/10.1103/physrevlett.120.132504.

Downloaded from https://academic.oup.com/ptep/article/2022/8/083C01/6651666 by KIT Library user on 27 September 2022

37. Radioactivity and Radiation Protection

Revised August 2021 by S. Roesler (CERN) and M. Silari (CERN).

37.1 Definitions [1–3]

It would be desirable if legal protection limits could be expressed in directly measurable *physical quantities*. However, this does not allow quantifying biological effects of the exposure of the human body and its detriment to ionizing radiation.

For this reason, dose limits are expressed in terms of so-called *protection quantities* which, although calculable, are not measurable. Protection quantities are used to quantify the extent of exposure of the human body to ionizing radiation from both whole and partial body external irradiation and from intakes of radionuclides.

In order to demonstrate compliance with dose limits, so-called *operational quantities* are typically used, which aim at providing conservative estimates of protection quantities. Often radiation protection detectors used for individual and area monitoring are calibrated in terms of operational quantities and, thus, these quantities become "measurable".

37.1.1 *Physical quantities*

• **Fluence,** Φ (unit: $1/\mathrm{m}^2$): The fluence is the quotient of the sum of the particle track lengths dl in the volume dV

$$\Phi = dl/dV \ .$$

It can also be expressed in terms of number of particles dN incident upon a small sphere of cross-sectional area da

$$\Phi = dN/da \ .$$

• **Absorbed dose,** D (unit: gray, 1 Gy=1 J/kg=100 rad): The absorbed dose is the energy imparted by ionizing radiation in a volume element of a specified material divided by the mass of this volume element.

• **Kerma,** K (unit: gray): Kerma is the sum of the initial kinetic energies of all charged particles set in motion by indirectly ionizing radiation in a volume element of the specified material divided by the mass of this volume element.

• **Linear energy transfer,** L **or** LET (unit: J/m, often given in keV/μm, 1 keV/μm $\approx 1.602 \times 10^{-10}$ J/m): The linear energy transfer is the mean energy, dE, lost by a charged particle owing to collisions with electrons in traversing a distance dl in matter. *Low-LET radiation:* X rays and gamma rays (accompanied by charged particles due to interactions with the surrounding medium) or light charged particles such as electrons that produce sparse ionizing events far apart at a molecular scale ($L < 10$ keV/μm). *High-LET radiation:* neutrons and heavy charged particles that produce ionizing events densely spaced at a molecular scale ($L > 10$ keV/μm). While the above LET definition refers to electronic stopping power only, at low energy nuclear stopping power could be a significant fraction of the total stopping power.

• **Activity,** A (unit: Becquerel, 1 Bq=1/s=27 pCi): Activity is the expectation value of the number of nuclear decays occurring in a given quantity of material per unit time.

37.1.2 *Protection quantities*

• **Organ absorbed dose,** D_T (unit: gray): The mean absorbed dose in an organ or tissue T of mass m_T is defined as

$$D_T = \frac{1}{m_T} \int_{m_T} D dm \ .$$

• **Equivalent dose,** H_T (unit: sievert, 1 Sv=1 J/kg=100 rem):

The equivalent dose H_T in an organ or tissue T is equal to the sum of the absorbed doses $D_{T,R}$ in the organ or tissue caused by different radiation types R weighted with so-called radiation weighting factors w_R:

$$H_T = \sum_R w_R \times D_{T,R} \ .$$

It expresses long-term risks (primarily cancer and leukemia) from low-level chronic exposure. The values for w_R recommended by ICRP [2] are given in Table 37.1.

Table 37.1: Radiation weighting factors, w_R.

Radiation type	w_R
Photons, electrons and muons	1
Neutrons, $E_n < 1$ MeV	$2.5 + 18.2 \times \exp[-(\ln E_n)^2/6]$
1 MeV $\leq E_n \leq$ 50 MeV	$5.0 + 17.0 \times \exp[-(\ln(2E_n))^2/6]$
$E_n > 50$ MeV	$2.5 + 3.25 \times \exp[-(\ln(0.04E_n))^2/6]$
Protons and charged pions	2
Alpha particles, fission fragments, heavy ions	20

• **Effective dose,** E (unit: sievert): The sum of the equivalent doses, weighted by the tissue weighting factors w_T ($\sum_T w_T = 1$) of several organs and tissues T of the body that are considered to be most sensitive [2], is called "effective dose":

$$E = \sum_T w_T \times H_T \ . \tag{37.1}$$

37.1.3 *Operational quantities*

• **Dose equivalent,** H (unit: sievert): The dose equivalent at a point in tissue is given by:

$$H = D \times Q \tag{37.2}$$

where D is the absorbed dose and Q is the quality factor at that point. The quality factor at a point in tissue, is given by:

$$Q = \frac{1}{D} \int_{L=0}^{\infty} Q(L) D_L dL$$

where D_L is the distribution of D in unrestricted linear energy transfer L at the point of interest, and $Q(L)$ is the quality factor as a function of L. The integration is to be performed over D_L, due to all charged particles, excluding their secondary electrons.

• **Ambient dose equivalent,** $H^*(10)$ (unit: sievert): The dose equivalent at a point in a radiation field that would be produced by the corresponding expanded and aligned field in a 30 cm diameter sphere of unit density tissue (so-called ICRU sphere/tissue with a mass composition of 76.2% oxygen, 11.1% carbon, 10.1% hydrogen and 2.6% nitrogen) at a depth of 10 mm on the radius vector opposing the direction of the aligned field. Ambient dose equivalent is the operational quantity for *area monitoring*.

• **Personal dose equivalent,** $H_p(d)$ (unit: sievert): The dose equivalent in ICRU tissue at an appropriate depth, d, below a specified point on the human body. The specified point is normally taken to be where the individual dosimeter is worn. For the assessment of effective dose, $H_p(10)$ with a depth $d = 10$ mm is chosen, and for the assessment of the dose to the skin and to the hands and feet the personal dose equivalent, $H_p(0.07)$, with a depth $d = 0.07$ mm, is used. Personal dose equivalent is the operational quantity for *individual monitoring*.

37.1.4 *Dose conversion coefficients*

Dose conversion coefficients allow direct calculation of protection or operational quantities from particle fluence and are functions of particle type, energy and irradiation configuration. The most common coefficients are those for effective dose and ambient dose equivalent. The former are based on simulations in which the dose to organs of anthropomorphic phantoms is calculated for approximate actual conditions of exposure, such as irradiation of the front of the body (antero-posterior irradiation) or isotropic irradiation.

Conversion coefficients from fluence to effective dose are given for anterior-posterior irradiation and various particle types in Fig. 37.1 [4]. For example, the effective dose from an anterior-posterior irradiation in a field of 1-MeV neutrons with a fluence of 1 neutron per cm^2 is about 290 pSv. In Monte Carlo simulations such coefficients allow multiplication with fluence at scoring

Downloaded from https://academic.oup.com/ptep/article/2022/8/083C01/6651666 by KIT Library user on 27 September 2022

time such that effective dose to a human body at the considered location is directly obtained.

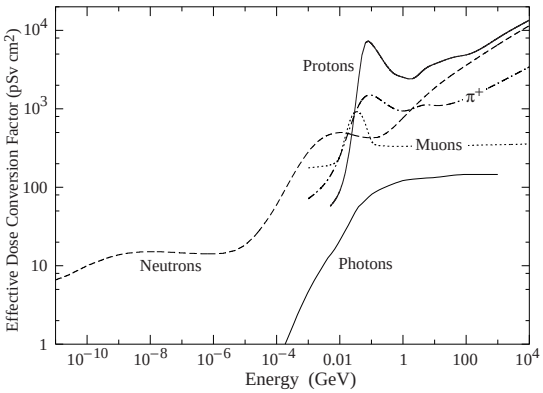

Figure 37.1: Fluence to effective dose conversion coefficients for anterior-posterior irradiation and various particle types [4].

37.2 Radiation levels [5]

• **Natural background radiation**:

On a worldwide average, the annual whole-body dose equivalent due to all sources of natural background radiation ranges from 1.0 to 13 mSv (0.1–1.3 rem) with an annual average of 2.4 mSv [6]. In certain areas values up to 50 mSv (5 rem) have been measured. A large fraction (typically more than 50%) originates from inhaled natural radioactivity, mostly radon and radon daughters [7]. The latter can vary by more than one order of magnitude: it is 0.1–0.2 mSv in open areas, 2 mSv on average in a house and more than 20 mSv in poorly ventilated mines.

• **Cosmic ray background radiation**: At sea level, the whole-body dose equivalent due to cosmic ray background radiation is dominated by muons; at higher altitudes also nucleons contribute. Dose equivalent rates range from less than 0.1 μSv/h at sea level to a few μSv/h at aircraft altitudes. Details on cosmic ray fluence levels are given in the Cosmic Rays section (Sec. 30 of this *Review*).

37.3 Health effects of ionizing radiation

Radiation can cause two types of health effects, deterministic and stochastic:

• **Deterministic effects** are tissue reactions which cause injury to a population of cells if a given threshold of absorbed dose is exceeded. The severity of the reaction increases with dose. The quantity in use for tissue reactions is the absorbed dose, D. When particles other than photons and electrons (low-LET radiation) are involved, a Relative Biological Effectiveness (RBE)-weighted dose may be used. The RBE of a given radiation is the reciprocal of the ratio of the absorbed dose of that radiation to the absorbed dose of a reference radiation (usually X rays) required to produce the same degree of biological effect. It is a complex quantity that depends on many factors such as cell type, dose rate, fractionation, etc.

• **Stochastic effects** are malignant diseases and heritable effects for which the probability of an effect occurring, but not its severity, is a function of dose without threshold.

• **Lethal dose**: The whole-body dose from penetrating ionizing radiation resulting in 50% mortality in 30 days (assuming no medical treatment) is 2.5–4.5 Gy (250–450 rad)[1], as measured internally on the body longitudinal center line. The surface dose varies due to variable body attenuation and may be a strong function of energy.

• **Cancer induction**:

The cancer induction probability is about 5% per Sv on average for the entire population [3].

• **Recommended effective dose limits**: The International Commission on Radiological Protection (ICRP) recommends a limit for radiation workers of 20 mSv effective dose per year averaged over 5 years, with the provision that the dose should not exceed 50 mSv in any single year [3]. The limit in the EU-countries and Switzerland is 20 mSv per year, in the U.S. it is 50 mSv per year (5 rem per year). Many physics laboratories in the U.S. and elsewhere set lower limits. The effective dose limit for the general public is typically 1 mSv per year.

[1] RBE-weighted when necessary

37.4 Prompt neutrons at accelerators

Neutrons dominate the radiation environment outside thick shielding (*e.g.*, > 1 m of concrete) for high energy (> a few hundred MeV) electron and hadron accelerators. In addition, for accelerators with energies above about 10 GeV, muons contribute significantly at small angles with regard to the beam, even behind several meters of shielding. Another special case are synchrotron light sources where particular care has to be taken to shield the very intense low-energy photons extracted from the electron synchrotron into the experimental areas. Due to its importance at high energy accelerators this section focuses on prompt neutrons.

37.4.1 *Electron accelerators*

At electron accelerators, neutrons are generated via photonuclear reactions from bremsstrahlung photons. Neutron production takes place above a threshold value which varies from 10 to 19 MeV for light nuclei (with important exceptions, such as 2.23 MeV for deuterium and 1.67 MeV for beryllium) and from 4 to 6 MeV for heavy nuclei. It is commonly described by different mechanisms depending on the photon energy: the giant dipole resonance interactions (from threshold up to about 30 MeV, often the dominant process), the quasi-deuteron effect (between 30 MeV and a few hundred MeV), the delta resonance mechanism (between 200 MeV and a few GeV) and the vector meson dominance model at higher energies.

The giant dipole resonance reaction consists in a collective excitation of the nucleus, in which neutrons and protons oscillate in the direction of the photon electric field. The oscillation is damped by friction in a few cycles, with the photon energy being transferred to the nucleus in a process similar to evaporation. Nucleons emitted in the dipolar interaction have an anisotropic angular distribution, with a maximum at 90°, while those leaving the nucleus as a result of evaporation are emitted isotropically with a Maxwellian energy distribution described as [8]:

$$\frac{dN}{dE_n} = \frac{E_n}{T^2} e^{-E_n/T} , \tag{37.3}$$

where T is a nuclear 'temperature' (in units of MeV) characteristic of the particular target nucleus and its excitation energy. For heavy nuclei the 'temperature' generally lies in the range of $T =$ 0.5–1.0 MeV. Neutron yields from semi-infinite targets per kW of electron beam power are plotted in Fig. 37.2 as a function of the electron beam energy [8].

While for thick targets neutron production is mainly due to photonuclear interactions, for thin targets (thickness of fractions of the radiation length) electronuclear interactions are the dominating process.

Typical neutron energy spectra outside of concrete (80 cm thick, 2.35 g/cm^3) and iron (40 cm thick) shields are shown in Fig. 37.3. In order to compare these spectra to those caused by proton beams (see below) the spectra are scaled by a factor of 100, which roughly corresponds to the difference in the high energy hadronic cross sections for photons and hadrons (*e.g.*, the fine structure constant). The shape of these spectra are generally characterized by a low-energy peak at around 1 MeV (evaporation neutrons) and a high-energy shoulder at around 70–80 MeV. In case of concrete shielding, the spectrum also shows a pronounced peak at thermal neutron energies.

37.4.2 *Proton accelerators*

At proton accelerators, neutron yields emitted per incident proton by different target materials are roughly independent of proton energy between 20 MeV and 1 GeV, and are given by the ratio C : Al : Cu-Fe : Sn : Ta-Pb = 0.3 : 0.6 : 1.0 : 1.5 : 1.7 [12]. Above about 1 GeV, the neutron yield is proportional to E^m, where $0.80 \leq m \leq 0.85$ [13].

Downloaded from https://academic.oup.com/ptep/article/2022/8/083C01/6651666 by KIT Library user on 27 September 2022

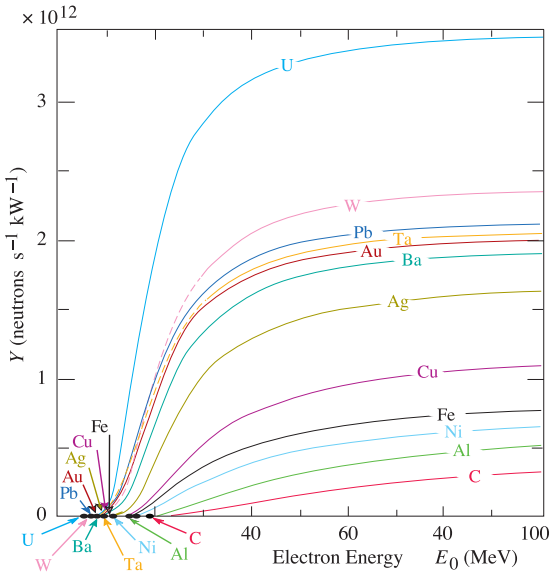

Figure 37.2: Neutron yields from semi-infinite targets per kW of electron beam power, as a function of the electron beam energy, disregarding target self-shielding [8].

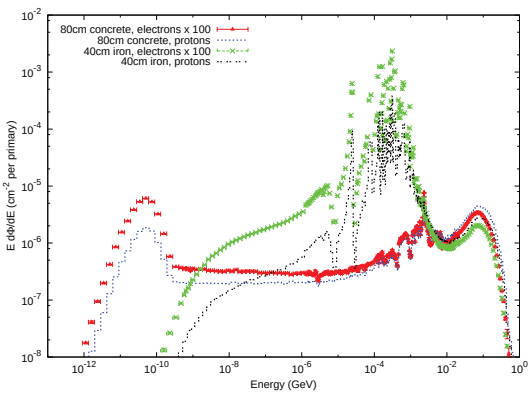

Figure 37.3: Neutron energy spectra calculated with the FLUKA code [9–11] from 25 GeV proton and electron beams on a thick copper target. Spectra are evaluated at 90° to the beam direction behind 80 cm of concrete or 40 cm of iron. All spectra are normalized per beam particle. For better visualization, spectra for electron beam are multiplied by a factor of 100.

Typical neutron energy spectra outside of concrete and iron shielding are shown in Fig. 37.3. Here, the radiation fields are caused by a 25 GeV proton beam interacting with a thick copper target. The comparison of these spectra with those for an electron beam of the same energy reflects the difference in the hadronic cross sections between photons and hadrons above a few 100 MeV. Differences are increasing towards lower energies because of different interaction mechanisms. Furthermore, the slight shift in energy above about 100 MeV follows from the fact that the energies of the interacting photons are lower than 25 GeV. Apart from this the shapes of the two spectra are similar.

The neutron-attenuation length is shown in Fig. 37.4 for concrete and mono-energetic broad-beam conditions. It reaches an asymptotic value of about 117 g/cm^2 above 200 MeV. As the cascade through thick shielding is carried by particles with energies between about 100 MeV and 300 MeV (in this energy range non-elastic cross sections are at minimum and are dominated by quasi-elastic processes leading to low attenuation) this value is equal to the equilibrium attenuation length for particles emitted at 90° in concrete.

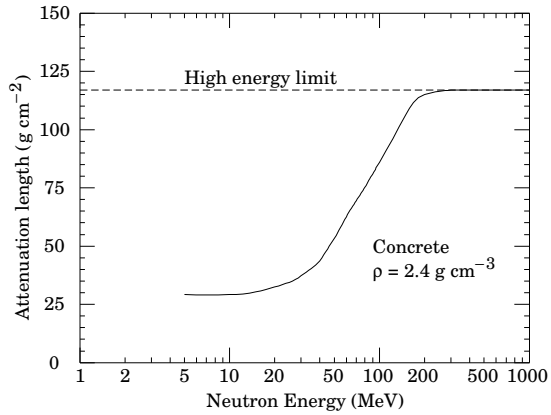

Figure 37.4: The variation of the attenuation length for mono-energetic neutrons in concrete as a function of neutron energy [12].

37.5 Photon sources

The dose equivalent rate in tissue (in mSv/h) from a gamma point source emitting one photon of energy E (in MeV) per second at a distance of 1 m is $4.6\times10^{-9}\,\mu_{en}/\rho\,E$, where μ_{en}/ρ is the mass energy absorption coefficient. The latter has a value of 0.029 ± 0.004 cm^2/g for photons in tissue over an energy range between 60 keV and 2 MeV (see Ref. [14] for tabulated values).

Similarly, the dose equivalent rate in tissue (in mSv/h) at the surface of a semi-infinite slab of uniformly activated material containing 1 Bq/g of a gamma emitter of energy E (in MeV) is $2.9 \times 10^{-4}\,R_\mu\,E$, where R_μ is the ratio of the mass energy absorption coefficients of the photons in tissue and in the material.

37.6 Accelerator-induced radioactivity

Typical medium- and long-lived activation products in metallic components of accelerators are ^{22}Na, ^{46}Sc, ^{48}V, ^{51}Cr, ^{54}Mn, ^{55}Fe, ^{59}Fe, ^{56}Co, ^{57}Co, ^{58}Co, ^{60}Co, ^{63}Ni and ^{65}Zn. Gamma-emitting nuclides dominate doses from external irradiation at longer decay times (more than one day) while at short decay times β^+ emitters are also important (through photons produced by β^+ annihilation). Due to their short range, β^- emitters are relevant, for example, only for dose to the skin and eyes or for doses due to inhalation or ingestion. Fig. 37.5 and Fig. 37.6 illustrate the contributions of gamma and β^+ emitters to the total dose rate at 12.4 cm distance to a copper sample [15]. The sample was activated by the stray radiation field created by a 120 GeV mixed hadron beam dumped in a copper target during about 8 hours at intensities between $10^7 - 10^8$ hadrons per second. Here, the contributions by individual nuclides were calculated analytically assuming exponential decay of the nuclide inventory present at 20 minute cooling time. The total dose rate, however, also includes decay chains and as such also contributions from daughter nuclides.

Typically, dose rates at a certain decay time are mainly determined by radionuclides having a half-life of the order of the decay time. Extended irradiation periods might be an exception to this general rule as in this case the activity of long-lived nuclides can build up sufficiently so that it dominates that one of short-lived even at short cooling times.

Activation in concrete is dominated by ^{24}Na (short decay time) and ^{22}Na (long decay time). Both nuclides can be produced either by low-energy neutron reactions on the sodium-component in the concrete or by spallation reactions on silicon, calcium and other constituents such as aluminum. At long decay times nuclides of radiological interest in activated concrete can also be ^{60}Co, ^{152}Eu, ^{154}Eu and ^{134}Cs, all of which produced by (n,γ)-reactions with traces of natural cobalt, europium and cesium, Thus, such trace elements might be important even if their content in concrete is only a few parts per million or less by weight.

The explicit simulation of radionuclide production with general-purpose Monte Carlo codes has become the most commonly applied method to calculate induced radioactivity and its radiologi-

Downloaded from https://academic.oup.com/ptep/article/2022/8/083C01/6651666 by KIT Library user on 27 September 2022

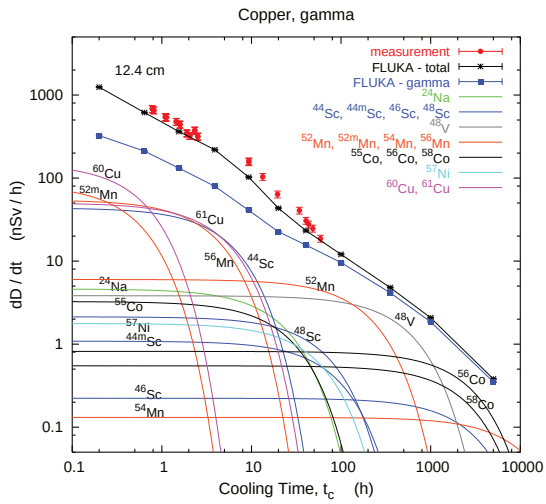

Figure 37.5: Contribution of individual gamma-emitting nuclides to the total dose rate at 12.4 cm distance to an activated copper sample [15].

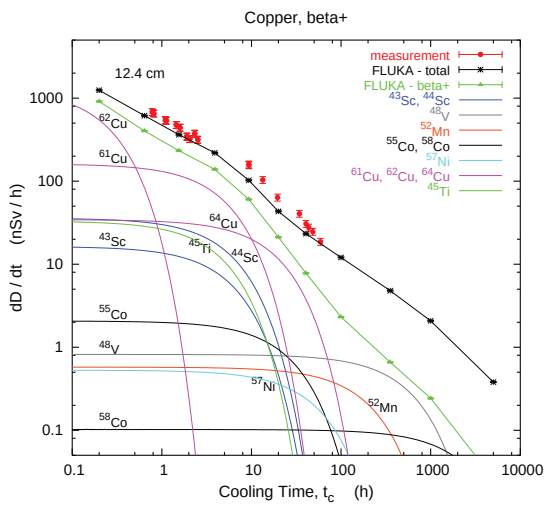

Figure 37.6: Contribution of individual positron-emitting nuclides to the total dose rate at 12.4 cm distance to an activated copper sample [15].

cal consequences [15] (see also Sec. 37.8). They are complemented by analytical codes based on folding particle fluence spectra with nuclide production cross sections. ActiWiz [16, 17] is an example of such a code targeting the domain of radiological characterization and material optimization. It allows for calculating nuclide inventories by convolution of fluence spectra with nuclide production data for 85 chemical elements and arbitrary compounds from threshold to an energy of 100 TeV.

37.7 Radiation protection instrumentation

The capacity to distinguish and measure the high-LET (mostly neutrons) and the low-LET components (photons, electrons, muons) of the radiation field at workplaces is of primary importance to evaluate the exposure of personnel. At proton accelerators the prompt dose equivalent outside a shield is mainly due to neutrons, with some contribution from photons and, to a minor extent, charged particles. At high-energy electron accelerators the dominant stray radiation during operation consists also of neutrons, because the shielding is normally thick enough to absorb most of the bremsstrahlung photons. Most of the personnel exposure at accelerator facilities is often received during maintenance interventions, and is due to gamma/beta radiation coming from residual radioactivity in accelerator components.

Radiation detectors used both for radiation surveys and area monitoring are normally calibrated in ambient dose equivalent $H^*(10)$.

37.7.1 *Neutron detectors*

• **Rem counters:** A rem counter [18] is a portable detector consisting of a thermal neutron counter embedded in a polyethylene moderator, with a response function that approximately follows the curve of the conversion coefficients from neutron fluence to $H^*(10)$ over a wide energy range. Conventional rem counters provide a response to neutrons up to approximately 10-15 MeV, extended-range units are heavier as they include a converter consisting of a material with high mass number to correctly measure $H^*(10)$ up to several hundred MeV [19].

• **Bonner Sphere Spectrometer (BSS):** A BSS [20] consists of a thermal neutron detector at the centre of moderating spheres of different diameters made of polyethylene (PE) or a combination of PE and a high-A material to enhance its response to high energy neutrons (similar to rem counters). Each sphere has a different response function versus neutron energy, and the neutron energy, at which the sensitivity peaks, increases with sphere diameter. The energy resolution of the system is rather low but satisfactory for radiation protection purposes. The neutron spectrum is obtained by unfolding the experimental counts of the BSS with its response matrix by a computer code that is often based on an iterative algorithm such as GRAVEL [21] and MAXED [22]. BSS exist in active (using ^{3}He or BF_3 proportional counters or ^{6}LiI scintillators) and passive versions (using CR-39 track detectors or LiF), for use *e.g.* in strongly pulsed fields. With ^{3}He counters the discrimination with respect to gamma rays and noise is excellent.

• **Bubble detectors:** A bubble detector [23] is a dosimeter based on a super-heated emulsion (super-heated droplets suspended in a gel) contained in a vial and acting as a continuously sensitive, miniature bubble chamber. The total number of bubbles evolved from the radiation-induced nucleation of drops gives an integrated measure of the total neutron exposure. Various techniques exist to record and count the bubbles, *e.g.*, visual inspection, automated reading with video cameras or acoustic counting. Bubble detectors are insensitive to low-LET radiation. Super-heated emulsions are used as personal, area and environmental dosimeters, as well as neutron spectrometers.

• **Track etched detectors:** Track etched detectors (TEDs) [24] are based on the preferential dissolution of suitable, mostly insulator, materials along the damage trails of charged particles of sufficiently high-energy deposition density. The detectors are effectively not sensitive to radiation which deposits the energy through the interactions of particles with low LET. These dosimeters are generally able to determine neutron ambient dose equivalent down to around 100 μSv. They are used both as personal dosimeters and for area monitoring, *e.g.*, in BSS.

37.7.2 *Photon detectors* [25]

• **Geiger Müller (GM) counters:** GM counters are low cost devices simple to operate. They work in pulse mode and since they only count radiation-induced events, any spectrometric information is lost. In general they are calibrated in terms of air kerma, for instance in a ^{60}Co field. The response of GM counters to photons is constant within 15% for energies up to 2 MeV and shows considerable energy dependence above.

• **Ionization chambers:** Ionization chambers are gas-filled detectors used both as hand-held instruments (*e.g.*, for radiation surveys) and environmental monitors. They are normally operated in current mode although pulse-mode operation is also possible. They possess a relatively flat response to a wide range of X- and gamma ray energies (typically from 10 keV to several MeV), can measure radiation over a wide intensity range and are capable of discriminating between the beta and gamma components of a radiation field (by use of, *e.g.*, a beta window). Pressurized ion chambers (filled, *e.g.*, with Ar or H gas to several tens of bars) are used for environmental and stray radiation monitoring applications. They have good sensitivity to neutrons and charged hadrons in addition to low LET radiation (gammas and muons),

Downloaded from https://academic.oup.com/ptep/article/2022/8/083C01/6651666 by KIT Library user on 27 September 2022

with the response function to the former being strongly non-linear with energy.

• **Proportional counters:** Proportional counters are another type of gas-filled detector, operated in pulse mode. They are normally of cylindrical geometry, with a thin central wire (the anode) on the axis of a hollow tube (the cathode). The initial electron charge created by the interaction of the radiation with the gas is amplified by the multiplication process (Townsend avalanche) produced by the strong electric field in a narrow volume around the anode. The generated pulses are still proportional to the original number of ion pairs but are much larger than in an ionization chamber, yielding a much improved signal-to-noise ratio. Proportional counters are also used for neutron detection: the rem counter and BSS discussed in the previous sections typically employ ^{3}He or BF_3 filled tubes with a large sensitivity to thermal neutrons.

• **Scintillators:** Scintillation-based detectors are used in radiation protection as hand-held probes and in fixed installations, *e.g.*, portal monitors. A scintillation detector or counter is obtained coupling a scintillator to an electronic light sensor such as a photomultiplier tube (PMT), a photodiode or a silicon photomultiplier (SiPM). There is a wide range of scintillating materials, inorganic (such as CsI and BGO), organic or plastic; they find application in both photon dosimetry and spectrometry.

37.7.3 *Operation in pulsed radiation fields*

There are many practical situations with particle accelerators used for scientific, industrial and medical applications where the time structure of the stray radiation limits the use of active monitors or requires specifically designed electronics. Pulsed neutron and gamma fields may be present because of beam losses at, *e.g.*, targets, collimators and beam dumps. The time duration of a single burst can range from a few ns to about 1 ms with a typical repetition rate in the range 0.1–100 Hz. Conventional detectors generally suffer from dead time effects and have strong limitations in the measurements of pulsed fields. Severe under response has been observed, *e.g.*, in commercial rem counters, with tremendous underestimation of the ambient dose equivalent, $H^*(10)$, up to three orders of magnitude [26]. The common techniques used to correct the response of radiation detectors which include dead-time corrections operate properly in a steady-state radiation field, whereas it is much more difficult to cope with dead time losses in a pulsed radiation field of unknown time structure and burst dose. Generally speaking the monitoring instrumentation must be chosen on the basis of the knowledge of the radiation field. Detectors with specifically designed electronics must be employed in pulsed field conditions in place of conventional rem counters for neutrons, such as the LUPIN detector [27]. If real-time monitoring is not required, passive detectors or dosimeters such as TEDs mentioned in Sec. 37.7.1 or LiF mentioned in Sec. 37.7.5 can be employed, as they are insensitive to the time structure of the radiation.

37.7.4 *Operation in presence of magnetic fields*

There may be circumstances in which a radiation survey needs to be performed in the presence of a magnetic field. This may be the case for example for measurements on activated detector components in the underground experimental areas of CERN LHC experiments without switching off the intense magnetic field ofthe detectors; or measurements of the residual radioactivity of permanent magnets sometimes used in particle accelerators. In hospitals, one of most advanced diagnostic modalities is PET-MRI, in which PET imaging uses radioactive substances (radiopharmaceuticals) in proximity of the strong magnetic field of the MRI scanner. Most of the commercial survey meters do not operate correctly or do not function at all in the presence of even comparatively weak magnetic fields below 0.3 T, and often already at 0.1 T. This is either because of the presence of components in their electronics sensitive to magnetic field (e.g. inductive elements), ferromagnetic materials in general (such as shells, screws and frames), battery drain/heating or LCD screen failure. An instrument called B-RAD has recently been developed [28] that overcomes the above limitations and is now commercially available. It is a hand-held instrument for gamma dose rate and gamma spectrometry measurements, consisting of a central unit (housing a microcontroller, magnetic field insensitive electronic circuitry, the battery and two displays) and a probe connected through a cable, certified to operate up to 3 T fields. The probe uses a $LaBr_3$(Ce) crystal coupled to an array of silicon photomultipliers. The excellent scintillation properties and the high photon resolution of the scintillator (3.3% FWHM at 662 keV) make the device capable of operating in the energy range from 30 keV to 2 MeV photons with a very fast response.

37.7.5 *Personal dosimeters*

Personal dosimeters, calibrated in $H_p(10)$, are worn by persons exposed to ionizing radiation for professional reasons to record the dose received. They are typically passive detectors, either film, track etched detectors, ^{6}Li/^{7}Li-based dosimeters (*e.g.* LiF), optically stimulated luminescence (OSL) or radiophotoluminescence detectors (RPL) but semi-active dosimeters using miniaturized ion-chambers also exist, like the Direct Ion Storage (DIS) dosimeters in use at CERN.

Electronic personal dosimeters are small active units for on-line monitoring of individual exposure, designed to be worn on the body. They can give an alarm on both the integral dose received or dose rate once a pre-set threshold is exceeded.

37.8 Monte Carlo codes for radiation protection studies

The use of general-purpose particle interaction and transport Monte Carlo codes is often the most accurate and efficient choice for assessing radiation protection quantities at accelerators. Due to the vast spread of such codes to all areas of particle physics and the associated extensive benchmarking with experimental data, the modeling has reached an unprecedented accuracy. Furthermore, most codes allow the user to simulate all aspects of a high energy particle cascade in one and the same run: from the first interaction of a TeV nucleus over the transport and re-interactions (hadronic and electromagnetic) of the produced secondaries, to detailed nuclear fragmentation, the calculation of radioactive decays and even of the electromagnetic shower caused by the radiation from such decays. A brief account of the codes most widely used for radiation protection studies at high energy accelerators is given in the following.

• **FLUKA [9–11]:** FLUKA is a general-purpose particle interaction and transport code. It comprises all features needed for radiation protection, such as detailed hadronic and nuclear interaction models up to 10 PeV, full coupling between hadronic and electromagnetic processes and numerous variance reduction options. The latter include weight windows, region importance biasing, and leading particle, interaction, and decay length biasing (among others). The capabilities of FLUKA are unique for studies of induced radioactivity, especially with regard to nuclide production, decay, and transport of residual radiation. In particular, particle cascades by prompt and residual radiation are simulated in parallel based on the microscopic models for nuclide production and a solution of the Bateman equations for activity build-up and decay.

• **GEANT4 [29–31]:** GEANT4 is an object-oriented toolkit consisting of a kernel that provides the framework for particle transport, including tracking, geometry description, material specifications, management of events and interfaces to external graphics systems. The kernel also provides interfaces to physics processes. It allows the user to freely select the physics models that best serve the particular application needs. Implementations of interaction models exist over an extended range of energies, from optical photons and thermal neutrons to high-energy interactions required for the simulation of accelerator and cosmic ray experiments. To facilitate the use of variance reduction techniques, general-purpose biasing methods such as importance biasing, weight windows, and a weight cut-off method have been introduced directly into the toolkit. Other variance reduction methods, such as leading particle biasing for hadronic processes, come with the respective physics packages.

• **MARS15 [32,33]:** The MARS15 code system is a set of Monte Carlo programs for the simulation of hadronic and electromagnetic cascades. It covers a wide energy range: 1 keV to 100 TeV for muons, charged hadrons, heavy ions and electromagnetic showers;

Downloaded from https://academic.oup.com/ptep/article/2022/8/083C01/6651666 by KIT Library user on 27 September 2022

and 0.00215 eV to 100 TeV for neutrons. Hadron-nucleus interactions as well as practically all other strong, weak and electromagnetic interactions in the entire energy range can be simulated either inclusively or exclusively. MARS15 uses ENDFB-VII nuclear data to handle interactions of neutrons with energies below 14 MeV. Several variance reduction techniques, such as weight windows, particle splitting, and Russian roulette, are available. A tagging module allows tagging the origin of a given signal for source term or sensitivity analyses. The geometry module allows either a basic solid body representation option or a ROOT-based powerful engine. Further features of MARS15 include a MAD-MARS merge for a convenient creation of accelerator models and multi-turn tracking and cascade simulation in accelerator and beamline lattices.

• **MCNP6 [34, 35]:** MCNP6 is the latest version of the Monte Carlo N-Particle transport (MCNP) family of neutron interaction and transport codes and, therefore, features one of the most comprehensive and detailed descriptions of the related physical processes. It transports 37 different particle types, including ions and electromagnetic particles. The neutron interaction and transport modules use standard evaluated data libraries mixed with physics models where such libraries are not available. The transport is continuous in energy. MCNP6 contains one of the most powerful implementations of variance reduction techniques. Spherical mesh weight windows can be created by a generator in order to focus the simulation time on certain spatial regions of interest. In addition, a more generalized phase space biasing is also possible through energy- and time-dependent weight windows. Other biasing options include pulse-height tallies with variance reduction and criticality source convergence acceleration.

• **PHITS [36, 37]:** The Particle and Heavy-Ion Transport code System PHITS was among the first general-purpose codes to simulate the transport and interactions of heavy ions in a wide energy range, from 10 MeV/nucleon to 100 GeV/nucleon. It is based on the high-energy hadron transport code NMTC/JAM that was extended to heavy ions. The transport of low-energy neutrons employs cross sections from evaluated nuclear data libraries such as ENDF and JENDL below 20 MeV. Electromagnetic interactions are simulated based on the ITS code in the energy range between 1 keV and 100 MeV for electrons and positrons and between 1 keV and 100 GeV for photons. Several variance reduction techniques, including weight windows and region importance biasing, are available.

References

[1] International Commission on Radiation Units and Measurements, *Fundamental Quantities and Units for Ionizing Radiation*, ICRU Report 60 (1998).

[2] ICRP, 2010. *Conversion Coefficients for Radiological Protection Quantities for External Radiation Exposures*, ICRP Publication 116, Annals of the ICRP 40(2-5).

[3] ICRP Publication 103, *The 2007 Recommendations of the International Commission on Radiological Protection*, Annals of the ICRP, Elsevier (2007).

[4] M. Pelliccioni, Radiation Protection Dosimetry **88**, 279 (2000).

[5] E. Pochin, *Nuclear Radiation: Risks and Benefits*, Clarendon Press, Oxford, 1983.

[6] United Nations, *Report of the United Nations Scientific Committee on the Effect of Atomic Radiation*, General Assembly, Official Records A/63/46 (2008).

[7] G. Cinelli *et al.*, *European Atlas of Natural Radiation*, G. Cinelli, M. De Cort, and T. Tollefsen, editor(s), Publications Office of the European Union, Luxembourg, 2019, ISBN 978-92-76-08259-0, JRC116795.

[8] W. P. Swanson, *Radiological Safety Aspects of the Operation of Electron Linear Accelerators,* IAEA Technical Reports Series No. 188 (1979) (1979).

[9] A. Ferrari, *et al.*, FLUKA:, A Multi-particle Transport Code, CERN-2005-010 (2005), SLAC-R-773, INFN-TC-05-11,`http://www.fluka.org, http://fluka.cern` .

[10] T. T. Böhlen *et al.*, Nucl. Data Sheets **120**, 211 (2014).

[11] G. Battistoni *et al.*, Annals of Nuclear Energy **82**, 10 (2015).

[12] R.H. Thomas and G.R. Stevenson, *Radiological Safety Aspects of the Operation of Proton Accelerators,* SSC-N-354 (1986), IAEA Technical Report Series No. 283 (1988).

[13] T. Gabriel *et al.*, Nucl. Instrum. Meth. A **338**, 336 (1994).

[14] `http://physics.nist.gov/PhysRefData/XrayMassCoef/cover.html`.

[15] S. Roesler, *et al.*, "Simulation of Remanent Dose Rates and Benchmark Measurements at the CERN-EU High Energy Reference Field Facility," in *Proceedings of the Sixth International Meeting on Nuclear Applications of Accelerator Technology,* San Diego, CA, 1-5 June 2003, 655–662 (2003).

[16] C. Theis and H. Vincke, "The use of ActiWiz in operational radiation protection," in *Proceedings of the Twelfth Meeting of Task-Force on Shielding Aspects of Accelerators, Targets and Irradiation Facilities of Accelerator Technology, SATIF12* FNAL, 28-30 April 2014, Nuclear Science Report NEA/NSC/R 3, (2015).

[17] C. Theis and H. Vincke, "ActiWiz3 an overview of the concepts, architecture and new features," CERN Technical Note CERN-RP-2016-117-REPORTS-TN (2016), `http://actiwiz.web.cern.ch` .

[18] I.O. Andersson and J. Braun, "A neutron rem counter with uniform sensitivity from 0.025 eV to 10 MeV" in *Proceedings of the IAEA Symposium on Neutron dosimetry,* IAEA, Vienna, Vol. II, 87–95, (1963).

[19] C. Birattari, *et al.*, Radiation Protection Dosimetry **76**, 135 (1998).

[20] R.L. Bramblett, R.I. Ewing and T.W. Bonner, Nucl. Instrum. Methods **9**, 1 (1960).

[21] M. Matzke, PTB, Braunschweig PTBN-19, (1994).

[22] M. Reginatto and P. Goldhagen, Health Physics **77**, 579 (1999).

[23] F. d'Errico, Nucl. Instrum. Methods **B184**, 229 (2001).

[24] K. Becker, Dosimetric applications of track etching, in *Topics in Radiation Dosimetry* Ed. F.H. Attix, Academic Press, London, 79–143, (1972).

[25] G.F. Knoll, *Radiation detection and measurements,* Wiley (2010).

[26] M. Caresana *et al.*, Nucl. Instrum. Meth. A **737**, 203 (2014).

[27] M. Caresana, *et al.*, A new version of the LUPIN detector: Improvements and latest experimental verification, Review of Scientific Instruments **85**, 065102 (2014).

[28] D. Celeste, A. Curioni, A. Fazzi, M. Silari and V. Varoli, B-RAD: a radiation survey meter for operation in intense magnetic fields Journal of Instrumentation **14**, T05007 (2019).

[29] S. Agostinelli *et al.* (GEANT4), Nucl. Instrum. Meth. A **506**, 250 (2003).

[30] J. Allison *et al.*, IEEE Trans. Nucl. Sci. **53**, 270 (2006).

[31] J. Allison *et al.*, Nucl. Instrum. Meth. A **835**, 186 (2016), `http://geant4.cern.ch`.

[32] N.V. Mokhov and C.C. James, The MARS Code System User's Guide, Fermilab-FN-1058-APC (2018), `https://mars.fnal.gov`.

[33] N. Mokhov *et al.*, Prog. Nucl. Sci. Tech. **4**, 496 (2014), [arXiv:1409.0033].

[34] J.T. Goorley, *et al.*, Nuclear Technology **180**, 298 (2012).

[35] C.J. Werner (editor), MCNP Users Manual - Code Version 6.2, Los Alamos National Laboratory report, LA-UR-17-29981 (2017), `https://mcnp.lanl.gov`.

[36] T. Sato, *et al.*, Journal of Nuclear Science and Technology **55**, 684 (2018).

[37] T. Sato, *et al.*, PHITS Particle and Heavy Ion Transport code System, Version 3.10 (2019), `https://phits.jaea.go.jp`.

Downloaded from https://academic.oup.com/ptep/article/2022/8/083C01/6651666 by KIT Library user on 27 September 2022

38. Commonly Used Radioactive Sources

Revised April 2021 by D.E. Groom (LBNL).

Table 38.1: Radioactive sources

Nuclide	Half-life	Type of Decay	Particle Energy (MeV)	Particle Emission prob.	Photon Energy (MeV)	Photon Emission prob.
$^{22}_{11}$Na	2.603 y	β^+,	0.546	90%	0.511	Annih.
		EC			1.275	100%
$^{51}_{24}$Cr	27.70 d	EC			0.320	10%
					V K x rays	100%
Neutrino calibration source						
$^{54}_{25}$Mn	0.855 y	EC			0.835	100%
					Cr K x rays	26%
$^{55}_{26}$Fe	2.747 y	EC			Mn K x rays:	
					0.00590	24.4%
					0.00649	2.86%
$^{57}_{27}$Co	271.8 d	EC			0.014	9%
					0.122	86%
					0.136	11%
					Fe K x rays	58%
$^{60}_{27}$Co	5.271 y	β^-	0.317	99.9%	1.173	99.9%
					1.333	99.9%
$^{68}_{32}$Ge	271.0 d	EC			Ga K x rays	42%
$\rightarrow {}^{68}_{31}$Ga						
	67.8 m	β^+,	1.899	90%	0.511	Annih.
		EC			1.077	3%
$^{90}_{38}$Sr	28.8 y	β^-	0.546	100%		
$\rightarrow {}^{90}_{39}$Y	2.67 d	β^-	2.279	100%		
$^{106}_{44}$Ru	371.5 d	β^-	0.039	100%		
$\rightarrow {}^{106}_{45}$Rh						
	30.1 s	β^-	3.546	79%	0.512	21%
					0.622	10%
$^{109}_{48}$Cd	1.265 y	EC	0.063 e^-	42%	0.088	3.7%
			0.084 e^-	44%	Ag K x rays	100%
$^{113}_{50}$Sn	115.1 d	EC	0.364 e^-	28%	0.392	65%
			0.388 e^-	6%	In K x rays	97
$^{137}_{55}$Cs	30.0 y	β^-	0.514	94%	0.662	85%
			1.176	6%		
$^{133}_{56}$Ba	10.55 y	EC	0.045 e^-	50%	0.081	33%
			0.075 e^-	6%	0.356	62%
					Cs K x rays	121%
$^{152}_{63}$Eu	13.537 y	EC		72.1%	Many γ's	
		β^-		27.9%	0.1218–1.408 MeV	
$^{207}_{83}$Bi	32.9 y	EC	0.481 e^-	2%	0.569	98%
			0.975 e^-	7%	1.063	75%
			1.047 e^-	2%	1.770	7%
					Pb K x rays	78%
$^{228}_{90}$Th	1.912 y	6α:	5.341 – 8.785		0.239	44%
		$3\beta^-$:	0.334 – 2.246		0.583	31%
					2.614	36%
$\left(\rightarrow {}^{224}_{88}\text{Ra}\ 361\text{ d} \rightarrow {}^{220}_{86}\text{Rn}\ 55.8\text{ s} \rightarrow {}^{216}_{84}\text{Po}\ 0.148\text{ s} \rightarrow {}^{212}_{82}\text{Pb}\ 10.64\text{ h} \rightarrow {}^{212}_{83}\text{Bi}\ 60.54\text{ m} \rightarrow {}^{212}_{84}\text{Po}\ 300\text{ ns}\right)$						
$^{241}_{95}$Am	432.6 y	α	5.443	13%	0.060	36%
			5.486	84%	Np L x rays	38%
$^{241}_{95}$Am/Be	432.6 y	neutrons ($\langle E\rangle = 4$ MeV) and γ's (4.43 MeV from ${}^{9}_{4}$Be(α, n))				
$^{244}_{96}$Cm	18.11 y	α	5.763	24%	Pu L x rays	$\sim 9\%$
			5.805	76%		
$^{252}_{98}$Cf	2.645 y	α	6.076	15%		
		(97%)	6.118	82%		
Fission (3.1%): Average 7.8 γ's/fission; $\langle E_\gamma\rangle = 0.88$ MeV ≈ 4 neutrons/fission; $\langle E_n\rangle = 2.14$ MeV						

"Emission probability" is the probability per decay of a given emission; because of cascades these may total more than 100%. Only principal emissions are listed. EC means electron capture, and e^- means monoenergetic internal conversion (Auger) electron. The intensity of 0.511 MeV e^+e^- annihilation photons depends upon the number of stopped positrons. Endpoint $\beta^\pm$ energies are listed. In some cases when energies are closely spaced, the γ-ray values are approximate weighted averages. Radiation from short-lived daughter isotopes is included where relevant.

Isotopic data may be found at `https://physics.nist.gov/cgi-bin/Compositions/stand_alone.pl`.

Neutron sources: See *e.g.* J. Liu *et al.*, "Neutron Calibration Sources in the Daya Bay Experiment" [1]. ${}^{51}_{24}$Cr calibration of neutrino detectors is discussed in *e.g.* J.N. Abdurashitov *et al.*, "Measurement of the response of a gallium metal solar neutrino experiment to neutrinos from a ^{51}Cr source" [2]. The use of ${}^{75}_{34}$Se and other isotopes has also been proposed.

References

[1] J. Liu *et al.*, Nucl. Instrum. Meth. A **797**, 260 (2015), [arXiv:1504.07911].

[2] J. N. Abdurashitov *et al.* (SAGE), Phys. Rev. C **59**, 2246 (1999), [hep-ph/9803418].

Downloaded from https://academic.oup.com/ptep/article/2022/8/083C01/6651666 by KIT Library user on 27 September 2022

Mathematical Tools or Statistics, Monte Carlo, Group Theory

39. Probability (rev.) 655
40. Statistics (rev.) 660
41. Machine Learning (new) 676
42. Monte Carlo techniques (rev.) 713
43. Monte Carlo event generators (rev.) 717
44. Monte Carlo neutrino event generators (rev.) 729
45. Monte Carlo particle numbering scheme (rev.) 733
46. Clebsch-Gordan coefficients, spherical harmonics, and d functions 737
47. SU(3) isoscalar factors and representation matrices 738
48. SU(n) multiplets and Young diagrams 739

Downloaded from https://academic.oup.com/ptep/article/2022/8/083C01/6651666 by KIT Library user on 27 September 2022

Downloaded from https://academic.oup.com/ptep/article/2022/8/083C01/6651666 by KIT Library user on 27 September 2022

39. Probability

Revised August 2021 by G. Cowan (RHUL).

39.1 General

Further discussion of probability can be found, *e.g.*, in Refs. [1–8].

An abstract definition of probability can be given by considering a set S, called the sample space, and possible subsets $A, B, \ldots$, the interpretation of which is left open. The probability P is a real-valued function defined by the following axioms due to Kolmogorov [9]:

1. For every subset A in S, $P(A) \geq 0$;
2. For disjoint subsets (*i.e.*, $A \cap B = \emptyset$), $P(A \cup B) = P(A) + P(B)$;
3. $P(S) = 1$.

In addition, one defines the conditional probability $P(A|B)$ (read as P of A given B) as

$$P(A|B) = \frac{P(A \cap B)}{P(B)} \ . \tag{39.1}$$

From this definition and using the fact that $A \cap B$ and $B \cap A$ are the same, one obtains *Bayes' theorem*,

$$P(A|B) = \frac{P(B|A)P(A)}{P(B)} \ . \tag{39.2}$$

From the three axioms of probability and the definition of conditional probability, one obtains the *law of total probability*,

$$P(B) = \sum_i P(B|A_i)P(A_i) \ , \tag{39.3}$$

for any subset B and for disjoint A_i with $\cup_i A_i = S$. This can be combined with Bayes' theorem (Eq. (39.2)) to give

$$P(A|B) = \frac{P(B|A)P(A)}{\sum_i P(B|A_i)P(A_i)} \ , \tag{39.4}$$

where the subset A could, for example, be one of the A_i.

The most commonly used interpretation of the elements of the sample space are outcomes of a repeatable experiment. The probability $P(A)$ is assigned a value equal to the limiting frequency of occurrence of A. This interpretation forms the basis of *frequentist statistics*.

The elements of the sample space might also be interpreted as *hypotheses*, *i.e.*, statements that are either true or false, such as 'The mass of the W boson lies between 80.3 and 80.5 GeV.' Upon repetition of a measurement, however, such statements are either always true or always false, *i.e.*, the corresponding probabilities in the frequentist interpretation are either 0 or 1. Using *subjective probability*, however, $P(A)$ is interpreted as the degree of belief that the hypothesis A is true. Subjective probability is used in *Bayesian* (as opposed to frequentist) statistics. Bayes' theorem can be written

$$P(\text{theory}|\text{data}) \propto P(\text{data}|\text{theory})P(\text{theory}) \ , \tag{39.5}$$

where 'theory' represents some hypothesis and 'data' is the outcome of the experiment. Here $P(\text{theory})$ is the *prior* probability for the theory, which reflects the experimenter's degree of belief before carrying out the measurement, and $P(\text{data}|\text{theory})$ is the probability to have gotten the data actually obtained, given the theory, which is also called the *likelihood*.

Bayesian statistics provides no fundamental rule for obtaining the prior probability, which may depend on previous measurements, theoretical prejudices, *etc.* Once this has been specified, however, Eq. (39.5) tells how the probability for the theory must be modified in the light of the new data to give the *posterior* probability, $P(\text{theory}|\text{data})$. As Eq. (39.5) is stated as a proportionality, the probability must be normalized by summing (or integrating) over all possible hypotheses.

39.2 Random variables

A *random variable* is a numerical characteristic assigned to an element of the sample space. In the frequency interpretation of probability, it corresponds to an outcome of a repeatable experiment. Let x be a possible outcome of an observation. If x can take on any value from a continuous range, we write $f(x;\theta)dx$ as the probability that the measurement's outcome lies between x and $x + dx$. The function $f(x;\theta)$ is called the *probability density function* (p.d.f.), which may depend on one or more parameters θ. If x can take on only discrete values (*e.g.*, the non-negative integers), then we use $f(x;\theta)$ to denote the probability to find the value x. In the following the term p.d.f. is often taken to cover both the continuous and discrete cases, although technically the term density should only be used in the continuous case.

The p.d.f. is always normalized to unity. Both x and θ may have multiple components and are then often written as vectors. If θ is unknown, we may wish to estimate its value from a given set of measurements of x; this is a central topic of *statistics* (see Sec. 40).

The *cumulative distribution function* $F(a)$ is the probability that $x \leq a$:

$$F(a) = \int_{-\infty}^{a} f(x)\, dx \ . \tag{39.6}$$

Here and below, if x is discrete-valued, the integral is replaced by a sum. The endpoint a is expressly included in the integral or sum. Then $0 \leq F(x) \leq 1$, $F(x)$ is nondecreasing, and $P(a < x \leq b) = F(b) - F(a)$. If x is discrete, $F(x)$ is flat except at allowed values of x, where it has discontinuous jumps equal to $f(x)$.

Any function of random variables is itself a random variable, with (in general) a different p.d.f. The *expectation value* of any function $u(x)$ is

$$E[u(x)] = \int_{-\infty}^{\infty} u(x)\, f(x)\, dx \ , \tag{39.7}$$

assuming the integral is finite. The expectation value is linear, *i.e.*, for any two functions u and v of x and constants c_1 and c_2, $E[c_1 u + c_2 v] = c_1 E[u] + c_2 E[v]$.

The nth moment of a random variable x is

$$\alpha_n \equiv E[x^n] = \int_{-\infty}^{\infty} x^n f(x)\, dx \ , \tag{39.8a}$$

and the nth central moment of x (or moment about the mean, α_1) is

$$m_n \equiv E[(x - \alpha_1)^n] = \int_{-\infty}^{\infty} (x - \alpha_1)^n f(x)\, dx \ . \tag{39.8b}$$

The most commonly used moments are the mean μ and variance σ^2:

$$\mu \equiv \alpha_1 \ , \tag{39.9a}$$

$$\sigma^2 \equiv V[x] \equiv m_2 = \alpha_2 - \mu^2 \ . \tag{39.9b}$$

The mean is the location of the "center of mass" of the p.d.f., and the variance is a measure of the square of its width. Note that $V[cx + k] = c^2 V[x]$. It is often convenient to use the *standard deviation* of x, σ, defined as the square root of the variance.

Any odd moment about the mean is a measure of the skewness of the p.d.f. The simplest of these is the dimensionless coefficient of skewness $\gamma_1 = m_3/\sigma^3$.

The fourth central moment m_4 provides a convenient measure of the tails of a distribution. For the Gaussian distribution (see Sec. 39.4), one has $m_4 = 3\sigma^4$. The *kurtosis* is defined as $\gamma_2 = m_4/\sigma^4 - 3$, *i.e.*, it is zero for a Gaussian, positive for a *leptokurtic* distribution with longer tails, and negative for a *platykurtic* distribution with tails that die off more quickly than those of a Gaussian.

The *quantile* x_α is the value of the random variable x at which the cumulative distribution is equal to α. That is, the quantile

Downloaded from https://academic.oup.com/ptep/article/2022/8/083C01/6651666 by KIT Library user on 27 September 2022

is the inverse of the cumulative distribution function, *i.e.*, $x_\alpha = F^{-1}(\alpha)$. An important special case is the *median*, $x_{\rm med}$, defined by $F(x_{\rm med}) = 1/2$, *i.e.*, half the probability lies above and half lies below $x_{\rm med}$. (More rigorously, $x_{\rm med}$ is a median if $P(x \geq x_{\rm med}) \geq 1/2$ and $P(x \leq x_{\rm med}) \geq 1/2$. If only one value exists, it is called '*the* median.')

Under a monotonic change of variable $x \to y(x)$, the quantiles of a distribution (and hence also the median) obey $y_\alpha = y(x_\alpha)$. In general the expectation value and *mode* (most probable value) of a distribution do not, however, transform in this way.

Let x and y be two random variables with a *joint* p.d.f. $f(x,y)$. The *marginal* p.d.f. of x (the distribution of x with y unobserved) is

$$f_1(x) = \int_{-\infty}^{\infty} f(x,y)\,dy\ , \tag{39.10}$$

and similarly for the marginal p.d.f. $f_2(y)$. The *conditional* p.d.f. of y given fixed x (with $f_1(x) \neq 0$) is defined by $f_3(y|x) = f(x,y)/f_1(x)$, and similarly $f_4(x|y) = f(x,y)/f_2(y)$. From these, we immediately obtain Bayes' theorem (see Eqs. (39.2) and (39.4)),

$$f_4(x|y) = \frac{f_3(y|x)f_1(x)}{f_2(y)} = \frac{f_3(y|x)f_1(x)}{\int f_3(y|x')f_1(x')\,dx'}\ . \tag{39.11}$$

The mean of x is

$$\mu_x = \int_{-\infty}^{\infty}\int_{-\infty}^{\infty} x\,f(x,y)\,dx\,dy = \int_{-\infty}^{\infty} x\,f_1(x)\,dx\ , \tag{39.12}$$

and similarly for y. The *covariance* of x and y is

$$\mathrm{cov}[x,y] = E[(x-\mu_x)(y-\mu_y)] = E[xy] - \mu_x\mu_y\ . \tag{39.13}$$

A dimensionless measure of the covariance of x and y is given by the *correlation coefficient*,

$$\rho_{xy} = \mathrm{cov}[x,y]/\sigma_x\sigma_y\ , \tag{39.14}$$

where σ_x and σ_y are the standard deviations of x and y. It can be shown that $-1 \leq \rho_{xy} \leq 1$.

Two random variables x and y are *independent* if and only if

$$f(x,y) = f_1(x)f_2(y)\ . \tag{39.15}$$

If x and y are independent, then $\rho_{xy} = 0$; the converse is not necessarily true. If x and y are independent, $E[u(x)v(y)] = E[u(x)]E[v(y)]$, and $V[x+y] = V[x]+V[y]$; otherwise, $V[x+y] = V[x]+V[y]+2\mathrm{cov}[x,y]$, and $E[uv]$ does not necessarily factorize.

Consider a set of n continuous random variables $\boldsymbol{x} = (x_1,\ldots,x_n)$ with joint p.d.f. $f(\boldsymbol{x})$, and a set of n new variables $\boldsymbol{y} = (y_1,\ldots,y_n)$, related to $\boldsymbol{x}$ by means of a function $\boldsymbol{y}(\boldsymbol{x})$ that is one-to-one, *i.e.*, the inverse $\boldsymbol{x}(\boldsymbol{y})$ exists. The joint p.d.f. for $\boldsymbol{y}$ is given by

$$g(\boldsymbol{y}) = f(\boldsymbol{x}(\boldsymbol{y}))|J|\ , \tag{39.16}$$

where $|J|$ is the absolute value of the determinant of the square matrix $J_{ij} = \partial x_i/\partial y_j$ (the Jacobian determinant). If the transformation from $\boldsymbol{x}$ to $\boldsymbol{y}$ is not one-to-one, the $\boldsymbol{x}$-space must be broken into regions where the function $\boldsymbol{y}(\boldsymbol{x})$ can be inverted, and the contributions to $g(\boldsymbol{y})$ from each region summed.

Given a set of functions $\boldsymbol{y} = (y_1,\ldots,y_m)$ with $m < n$, one can construct $n-m$ additional independent functions, apply the procedure above, then integrate the resulting $g(\boldsymbol{y})$ over the unwanted y_i to find the marginal distribution of those of interest.

For a one-to-one transformation of discrete random variables, the probability is obtained by simple substitution; no Jacobian is necessary because in this case f is a probability rather than a probability density. If the transformation is not one-to-one, then one must sum the probabilities for all values of the original variable that contribute to a given value of the transformed variable. If f depends on a set of parameters $\boldsymbol{\theta}$, a change to a different parameter set $\boldsymbol{\eta}(\boldsymbol{\theta})$ is made by simple substitution; no Jacobian is used.

39.2.1 *Propagation of errors*

Consider n random variables $\boldsymbol{x} = (x_1,\ldots,x_n)$ and m functions $\boldsymbol{y}(\boldsymbol{x}) = (y_1(\boldsymbol{x}),\ldots,y_m(\boldsymbol{x}))$. Suppose here that the mean values $\boldsymbol{\mu} = (\mu_1,\ldots,\mu_n) = E[\boldsymbol{x}]$ are known, although in practice they will only be estimated, and suppose we also know or have estimated the covariance matrix $V_{ij} = \mathrm{cov}[x_i,x_j]$. The goal of *error propagation* is to determine the covariance matrix for the functions, $U_{ij} = \mathrm{cov}[y_i,y_j]$. In particular, the diagonal elements $U_{ii} = V[y_i]$ give the variances. The new covariance matrix can be found by expanding the functions $\boldsymbol{y}(\boldsymbol{x})$ about the means $\boldsymbol{\mu}$ to first order in a Taylor series. Using this one finds

$$U_{ij} \approx \sum_{k,l} \frac{\partial y_i}{\partial x_k}\frac{\partial y_j}{\partial x_l}\bigg|_{\boldsymbol{\mu}} V_{kl}\ . \tag{39.17}$$

This can be written in matrix notation as $U \approx AVA^T$ where the matrix of derivatives A is

$$A_{ij} = \frac{\partial y_i}{\partial x_j}\bigg|_{\boldsymbol{\mu}}\ , \tag{39.18}$$

and A^T is its transpose. The approximation is exact if $\boldsymbol{y}(\boldsymbol{x})$ is linear. If this is not the case, the approximation can break down if, for example, $\boldsymbol{y}(\boldsymbol{x})$ is significantly nonlinear close to $\boldsymbol{\mu}$ in a region of a size comparable to the standard deviations of $\boldsymbol{x}$.

39.3 Characteristic functions

The characteristic function $\phi(u)$ associated with the p.d.f. $f(x)$ is essentially its Fourier transform, or the expectation value of e^{iux}:

$$\phi(u) = E\left[e^{iux}\right] = \int_{-\infty}^{\infty} e^{iux} f(x)\,dx\ . \tag{39.19}$$

Once $\phi(u)$ is specified, the p.d.f. $f(x)$ is uniquely determined and vice versa; knowing one is equivalent to the other. Characteristic functions are useful in deriving a number of important results about moments and sums of random variables.

It follows from Eqs. (39.8) and (39.19) that the nth moment of a random variable x that follows $f(x)$ is given by

$$i^{-n}\ \frac{d^n\phi}{du^n}\bigg|_{u=0} = \int_{-\infty}^{\infty} x^n f(x)\,dx = \alpha_n\ . \tag{39.20}$$

Thus it is often easy to calculate all the moments of a distribution defined by $\phi(u)$, even when $f(x)$ cannot be written down explicitly.

If the p.d.f.s $f_1(x)$ and $f_2(y)$ for independent random variables x and y have characteristic functions $\phi_1(u)$ and $\phi_2(u)$, then the characteristic function of the weighted sum $ax+by$ is $\phi_1(au)\phi_2(bu)$. The rules of addition for several important distributions (*e.g.*, that the sum of two Gaussian distributed variables also follows a Gaussian distribution) easily follow from this observation.

Let the (partial) characteristic function corresponding to the conditional p.d.f. $f_2(x|z)$ be $\phi_2(u|z)$, and the p.d.f. of z be $f_1(z)$. The characteristic function after integration over the conditional value is

$$\phi(u) = \int \phi_2(u|z)f_1(z)\,dz\ . \tag{39.21}$$

Suppose we can write ϕ_2 in the form

$$\phi_2(u|z) = A(u)e^{ig(u)z}\ . \tag{39.22}$$

Then

$$\phi(u) = A(u)\phi_1(g(u))\ . \tag{39.23}$$

The cumulants (semi-invariants) κ_n of a distribution with characteristic function $\phi(u)$ are defined by the relation

$$\phi(u) = \exp\left[\sum_{n=1}^{\infty}\frac{\kappa_n}{n!}(iu)^n\right] = \exp\left(i\kappa_1 u - \frac{1}{2}\kappa_2 u^2 + \ldots\right)\ . \tag{39.24}$$

Downloaded from https://academic.oup.com/ptep/article/2022/8/083C01/6651666 by KIT Library user on 27 September 2022

The values κ_n are related to the moments α_n and m_n. The first few relations are

$$\begin{aligned}\kappa_1 &= \alpha_1 \ (= \mu, \text{ the mean})\\ \kappa_2 &= m_2 \ = \alpha_2 - \alpha_1^2 \ (= \sigma^2, \text{ the variance})\\ \kappa_3 &= m_3 = \alpha_3 - 3\alpha_1\alpha_2 + 2\alpha_1^3.\end{aligned} \tag{39.25}$$

39.4 Commonly used probability distributions

Table 39.1 gives a number of common probability density functions and corresponding characteristic functions, means, and variances. Further information may be found in Refs. [1–8] [10], and [11], which has particularly detailed tables. Monte Carlo techniques for generating each of them may be found in our Sec. 42.4 and in Ref. [10]. We comment below on all except the trivial uniform distribution.

39.4.1 *Binomial and multinomial distributions*

A random process with exactly two possible outcomes which occur with fixed probabilities is called a *Bernoulli* process. If the probability of obtaining a certain outcome (a "success") in an individual trial is p, then the probability of obtaining exactly r successes ($r = 0, 1, 2, \ldots, N$) in N independent trials, without regard to the order of the successes and failures, is given by the binomial distribution $f(r; N, p)$ in Table 39.1. If r and s are binomially distributed with parameters (N_r, p) and (N_s, p), then $t = r + s$ follows a binomial distribution with parameters $(N_r + N_s, p)$. If there are are m possible outcomes for each trial having probabilities $p_1, p_2, \ldots, p_m$, then the joint probability to find $r_1, r_2, \ldots, r_m$ of each outcome after a total of N independent trials is given by the multinomial distribution as shown in Table 39.1. We can regard outcome i as "success" and all the rest as "failure", so individually, any of the r_i follow a binomial distribution for N trials and a success probability p_i.

39.4.2 *Poisson distribution*

The Poisson distribution $f(n; \nu)$ gives the probability of finding exactly n events in a given interval of x (*e.g.*, space or time) when the events occur independently of one another and of x at an average rate of ν per the given interval. The variance σ^2 equals ν. It is the limiting case $p \to 0$, $N \to \infty$, $Np = \nu$ of the binomial distribution. The Poisson distribution approaches the Gaussian distribution for large ν.

For example, a large number of radioactive nuclei of a given type will result in a certain number of decays in a fixed time interval. If this interval is small compared to the mean lifetime, then the probability for a given nucleus to decay is small, and thus the number of decays in the time interval is well modeled as a Poisson variable.

39.4.3 *Normal or Gaussian distribution*

The normal (or Gaussian) probability density function $f(x; \mu, \sigma^2)$ given in Table 39.1 has mean $E[x] = \mu$ and variance $V[x] = \sigma^2$. Comparison of the characteristic function $\phi(u)$ given in Table 39.1 with Eq. (39.24) shows that all cumulants κ_n beyond κ_2 vanish; this is a unique property of the Gaussian distribution. Some other properties are:

$$\begin{aligned}&P(x \text{ in range } \mu \pm \sigma) = 0.6827,\\ &P(x \text{ in range } \mu \pm 0.6745\sigma) = 0.5,\\ &E[|x - \mu|] = \sqrt{2/\pi}\,\sigma = 0.7979\sigma,\\ &\text{half-width at half maximum} = \sqrt{2\ln 2}\,\sigma = 1.177\sigma.\end{aligned}$$

For a Gaussian with $\mu = 0$ and $\sigma^2 = 1$ (the *standard normal*) the cumulative distribution, often written $\Phi(x)$, is related to the error function erf by

$$F(x; 0, 1) \equiv \Phi(x) = \frac{1}{2}\left[1 + \mathrm{erf}(x/\sqrt{2})\right] \ . \tag{39.26}$$

The error function and standard Gaussian are tabulated in many references (*e.g.*, Ref. [11, 12]) and are available in software packages such as ROOT [13]. For a mean μ and variance σ^2, replace x by $(x - \mu)/\sigma$. The probability of x in a given range can be calculated with Eq. (40.71).

For x and y independent and normally distributed, $z = ax + by$ follows a normal p.d.f. $f(z; a\mu_x + b\mu_y, a^2\sigma_x^2 + b^2\sigma_y^2)$; that is, the weighted means and variances add.

The Gaussian derives its importance in large part from the *central limit theorem*:

If independent random variables $x_1, \ldots, x_n$ are distributed according to *any* p.d.f. with finite mean and variance, then the sum $y = \sum_{i=1}^n x_i$ will have a p.d.f. that approaches a Gaussian for large n. If the p.d.f.s of the x_i are not identical, the theorem still holds under somewhat more restrictive conditions. The mean and variance are given by the sums of corresponding terms from the individual x_i. Therefore, the sum of a large number of fluctuations x_i will be distributed as a Gaussian, even if the x_i themselves are not.

For a set of n Gaussian random variables $\boldsymbol{x}$ with means $\boldsymbol{\mu}$ and covariances $V_{ij} = \mathrm{cov}[x_i, x_j]$, the p.d.f. for the one-dimensional Gaussian is generalized to

$$f(\boldsymbol{x}; \boldsymbol{\mu}, V) = \frac{1}{(2\pi)^{n/2}\sqrt{|V|}} \exp\left[-\frac{1}{2}(\boldsymbol{x} - \boldsymbol{\mu})^T V^{-1} (\boldsymbol{x} - \boldsymbol{\mu})\right] \ , \tag{39.27}$$

where the determinant $|V|$ must be greater than 0. For diagonal V (independent variables), $f(\boldsymbol{x}; \boldsymbol{\mu}, V)$ is the product of the p.d.f.s of n Gaussian distributions.

For $n = 2$, $f(\boldsymbol{x}; \boldsymbol{\mu}, V)$ is

$$\begin{aligned}f(x_1, x_2;\ \mu_1, \mu_2, \sigma_1, \sigma_2, \rho) &= \frac{1}{2\pi\sigma_1\sigma_2\sqrt{1-\rho^2}}\\ &\times \ \exp\left\{\frac{-1}{2(1-\rho^2)}\left[\frac{(x_1-\mu_1)^2}{\sigma_1^2} - \frac{2\rho(x_1-\mu_1)(x_2-\mu_2)}{\sigma_1\sigma_2}\right.\right.\\ &\left.\left. + \frac{(x_2-\mu_2)^2}{\sigma_2^2}\right]\right\}.\end{aligned} \tag{39.28}$$

The characteristic function for the multivariate Gaussian is

$$\phi(\boldsymbol{u}; \boldsymbol{\mu}, V) = \exp\left[i\boldsymbol{\mu}\cdot\boldsymbol{u} - \frac{1}{2}\boldsymbol{u}^T V \boldsymbol{u}\right] \ . \tag{39.29}$$

If the components of $\boldsymbol{x}$ are independent, then Eq. (39.29) is the product of the characteristic functions of n Gaussians.

For an n-dimensional Gaussian distribution for $\boldsymbol{x}$ with mean $\boldsymbol{\mu}$ and covariance matrix V, the marginal distribution for any single x_i is is a one-dimensional Gaussian with mean μ_i and variance V_{ii}. The equation $(\boldsymbol{x} - \boldsymbol{a})^T V^{-1} (\boldsymbol{x} - \boldsymbol{a}) = C$, where C is any positive number, defines an n-dimensional ellipse centered about $\boldsymbol{a}$. If $\boldsymbol{a}$ is equal to the mean $\boldsymbol{\mu}$, then C is a random variable obeying the χ^2 distribution for n degrees of freedom, which is discussed in the following section. The probability that $\boldsymbol{x}$ lies outside the ellipsoid for a given value of C is given by $1 - F_{\chi^2}(C; n)$, where F_{χ^2} is the cumulative χ^2 distribution. This may be read from Fig. 40.1. For example, the "s-standard-deviation ellipsoid" occurs at $C = s^2$. For the two-variable case ($n = 2$), the point $\boldsymbol{x}$ lies outside the one-standard-deviation ellipsoid with 61% probability. The use of these ellipsoids as indicators of probable error is described in Sec. 40.4.2.2; the validity of those indicators assumes that $\boldsymbol{\mu}$ and V are correct.

39.4.4 *Log-normal distribution*

If a random variable y follows a Gaussian distribution with mean μ and variance σ^2, then $x = e^y$ follows a log-normal distribution, as given in Table 39.1. As a consequence of the central limit theorem described in Sec. 39.4.3, the distribution of the product of a large number of positive random variables approaches a log-normal. It is bounded below by zero and is thus well suited for modeling quantities that are intrinsically non-negative such as an efficiency. One can implement a log-normal model for a random variable x by defining $y = \ln x$ so that y follows a Gaussian distribution.

39.4.5 χ^2 *distribution*

If $x_1, \ldots, x_n$ are independent Gaussian random variables, the sum $z = \sum_{i=1}^n (x_i - \mu_i)^2/\sigma_i^2$ follows the χ^2 p.d.f. with n *degrees*

Downloaded from https://academic.oup.com/ptep/article/2022/8/083C01/6651666 by KIT Library user on 27 September 2022

Table 39.1: Some common probability density functions, with corresponding characteristic functions and means and variances. In the Table, $\Gamma(k)$ is the gamma function, equal to $(k-1)!$ when k is an integer; ${}_1F_1$ is the confluent hypergeometric function of the 1st kind [11].

Distribution	Probability density function f (variable; parameters)	Characteristic function $\phi(u)$	Mean	Variance
Uniform	$f(x;a,b) = \begin{cases} 1/(b-a) & a \le x \le b \\ 0 & \text{otherwise} \end{cases}$	$\frac{e^{ibu}-e^{iau}}{(b-a)iu}$	$\frac{a+b}{2}$	$\frac{(b-a)^2}{12}$
Binomial	$f(r;N,p) = \frac{N!}{r!(N-r)!}\, p^r q^{N-r}$ $r = 0,1,2,\ldots,N;\quad 0 \le p \le 1;\quad q = 1-p$	$(q+pe^{iu})^N$	Np	Npq
Multinomial	$f(r_1,\ldots,r_m;N,p_1,\ldots,p_m) = \frac{N!}{r_1!\cdots r_m!} p_1^{r_1}\cdots p_m^{r_m}$	$\left(\sum_{k=1}^m p_k e^{iu_k}\right)^N$	$E[r_i] = Np_i$	$\mathrm{cov}[r_i,r_j] = Np_i(\delta_{ij}-p_j)$
Poisson	$f(n;\nu) = \frac{\nu^n e^{-\nu}}{n!};\ n = 0,1,2,\ldots;\ \nu > 0$	$\exp[\nu(e^{iu}-1)]$	ν	ν
Normal (Gaussian)	$f(x;\mu,\sigma^2) = \frac{1}{\sigma\sqrt{2\pi}}\ \exp(-(x-\mu)^2/2\sigma^2)$	$\exp(i\mu u - \frac{1}{2}\sigma^2 u^2)$	μ	σ^2
Multivariate Gaussian	$f(\boldsymbol{x};\boldsymbol{\mu},\boldsymbol{V}) = \frac{1}{(2\pi)^{n/2}\sqrt{\lvert V\rvert}}$ $\times \exp\left[-\frac{1}{2}(\boldsymbol{x}-\boldsymbol{\mu})^T V^{-1}(\boldsymbol{x}-\boldsymbol{\mu})\right]$ $-\infty < x_j < \infty;\quad -\infty < \mu_j < \infty;\quad \lvert V\rvert > 0$	$\exp\left[i\boldsymbol{\mu}\cdot\boldsymbol{u} - \frac{1}{2}\boldsymbol{u}^T V \boldsymbol{u}\right]$	$\boldsymbol{u}$	V_{jk}
Log-normal	$f(x;\mu,\sigma^2) = \frac{1}{\sigma\sqrt{2\pi}}\frac{1}{x}\ \exp(-(\ln x-\mu)^2/2\sigma^2)$ $0 < x < \infty;\quad -\infty < \mu < \infty;\quad \sigma > 0$	—	$\exp(\mu+\sigma^2/2)$	$\exp(2\mu+\sigma^2)$ $\times[\exp(\sigma^2)-1]$
χ^2	$f(z;n) = \frac{z^{n/2-1}e^{-z/2}}{2^{n/2}\Gamma(n/2)};\quad z \ge 0$	$(1-2iu)^{-n/2}$	n	$2n$
Student's t	$f(t;n) = \frac{1}{\sqrt{n\pi}}\ \frac{\Gamma[(n+1)/2]}{\Gamma(n/2)}\left(1+\frac{t^2}{n}\right)^{-(n+1)/2}$ $-\infty < t < \infty;\quad$ n not required to be integer	—	0 for $n > 1$	$n/(n-2)$ for $n > 2$
Gamma	$f(x;\lambda,k) = \frac{x^{k-1}\lambda^k e^{-\lambda x}}{\Gamma(k)};\quad 0 \le x < \infty$; k not required to be integer	$(1-iu/\lambda)^{-k}$	k/λ	k/λ^2
Beta	$f(x;\alpha,\beta) = \frac{\Gamma(\alpha+\beta)}{\Gamma(\alpha)\Gamma(\beta)} x^{\alpha-1}(1-x)^{\beta-1}$ $0 \le x \le 1$	${}_1F_1(\alpha;\alpha+\beta;iu)$	$\frac{\alpha}{\alpha+\beta}$	$\frac{\alpha\beta}{(\alpha+\beta)^2(\alpha+\beta+1)}$

of freedom, which we denote by $\chi^2(n)$. More generally, for n correlated Gaussian variables as components of a vector $\boldsymbol{X}$ with covariance matrix V, $z = \boldsymbol{X}^T V^{-1}\boldsymbol{X}$ follows $\chi^2(n)$ as in the previous section. For a set of z_i, each of which follows $\chi^2(n_i)$, $\sum z_i$ follows $\chi^2(\sum n_i)$. For large n, the χ^2 p.d.f. approaches a Gaussian with a mean and variance given by $\mu = n$ and $\sigma^2 = 2n$, respectively (here the formulae for μ and σ^2 are valid for all n).

The χ^2 p.d.f. is often used in evaluating the level of compatibility between observed data and a hypothesis for the p.d.f. that the data might follow. This is discussed further in Sec. 40.3.2 on significance tests.

39.4.6 *Student's t distribution*

Suppose that y and $x_1,\ldots,x_n$ are independent and Gaussian distributed with mean 0 and variance 1. We then define

$$z = \sum_{i=1}^n x_i^2 \quad \text{and} \quad t = \frac{y}{\sqrt{z/n}}\,. \tag{39.30}$$

The variable z thus follows a $\chi^2(n)$ distribution. Then t is distributed according to Student's t distribution with n degrees of freedom, $f(t;n)$, given in Table 39.1.

If defined through gamma functions as in Table 39.1, the parameter n is not required to be an integer. As $n \to \infty$, the distribution approaches a Gaussian, and for $n = 1$ it is a *Cauchy* or *Breit–Wigner* distribution.

As an example, consider the *sample mean* $\overline{x} = \sum x_i/n$ and the *sample variance* $s^2 = \sum(x_i-\overline{x})^2/(n-1)$ for normally distributed x_i with unknown mean μ and variance σ^2. The sample mean has a Gaussian distribution with a variance σ^2/n, so the variable $(\overline{x}-\mu)/\sqrt{\sigma^2/n}$ is normal with mean 0 and variance 1. The quantity $(n-1)s^2/\sigma^2$ is independent of this and follows $\chi^2(n-1)$. The ratio

$$t = \frac{(\overline{x}-\mu)/\sqrt{\sigma^2/n}}{\sqrt{(n-1)s^2/\sigma^2(n-1)}} = \frac{\overline{x}-\mu}{\sqrt{s^2/n}} \tag{39.31}$$

is distributed as $f(t;n-1)$. The unknown variance σ^2 cancels, and t can be used to test the hypothesis that the true mean is some particular value μ.

39.4.7 *Gamma distribution*

For a process that generates events as a function of x (*e.g.*, space or time) according to a Poisson distribution, the distance in x from an arbitrary starting point (which may be some particular event) to the kth event follows a *gamma* distribution, $f(x;\lambda,k)$. The Poisson parameter μ is λ per unit x. The special case $k = 1$ (*i.e.*, $f(x;\lambda,1) = \lambda e^{-\lambda x}$) is called the *exponential* distribution. A sum of k' exponential random variables x_i is distributed as $f(\sum x_i;\lambda,k')$.

The parameter k is not required to be an integer. For $\lambda = 1/2$ and $k = n/2$, the gamma distribution reduces to the $\chi^2(n)$ distribution.

39.4.8 *Beta distribution*

The beta distribution describes a continuous random variable x in the interval $[0,1]$. By scaling and translation one can easily generalize it to have arbitrary endpoints. In Bayesian inference about the parameter p of a binomial process, if the prior p.d.f. is a beta distribution $f(p;\alpha,\beta)$ then the observation of r successes out of N trials gives a posterior beta distribution $f(p;r+\alpha,N-r+\beta)$ (Bayesian methods are discussed further in Sec. 40). The uniform distribution is a beta distribution with $\alpha = \beta = 1$.

References

[1] H. Cramér, *Mathematical Methods of Statistics,* (Princeton Univ. Press, New Jersey, 1958).

Downloaded from https://academic.oup.com/ptep/article/2022/8/083C01/6651666 by KIT Library user on 27 September 2022

[2] A. Stuart and J.K. Ord, *Kendall's Advanced Theory of Statistics*, Vol. 1 *Distribution Theory* 6th Ed., (Halsted Press, New York, 1994), and earlier editions by Kendall and Stuart.

[3] F.E. James, *Statistical Methods in Experimental Physics*, 2nd Ed., (World Scientific, Singapore, 2006).

[4] L. Lyons, *Statistics for Nuclear and Particle Physicists*, (Cambridge University Press, New York, 1986).

[5] B.R. Roe, *Probability and Statistics in Experimental Physics,* 2nd Ed., (Springer, New York, 2001).

[6] R.J. Barlow, *Statistics: A Guide to the Use of Statistical Methods in the Physical Sciences*, (John Wiley, New York, 1989).

[7] S. Brandt, *Data Analysis*, 3rd Ed., (Springer, New York, 1999).

[8] G. Cowan, *Statistical Data Analysis*, (Oxford University Press, Oxford, 1998).

[9] A.N. Kolmogorov, *Grundbegriffe der Wahrscheinlichkeitsrechnung*, (Springer, Berlin, 1933); *Foundations of the Theory of Probability*, 2nd Ed., (Chelsea, New York 1956).

[10] Ch. Walck, *Hand-book on Statistical Distributions for Experimentalists*, University of Stockholm Internal Report SUF-PFY/96-01, available from `www.physto.se~walck`.

[11] M. Abramowitz and I. Stegun, eds., *Handbook of Mathematical Functions*, (Dover, New York, 1972).

[12] F.W.J. Olver *et al.*, eds., NIST Handbook of Mathematical Functions, (Cambridge University Press, 2010); A companion Digital Library of Mathematical Functions is available at `dlmf.nist.gov`.

[13] R. Brun and F. Rademakers, Nucl. Instrum. Meth. **A389**, 81 (1997); See also `root.cern.ch`.

Downloaded from https://academic.oup.com/ptep/article/2022/8/083C01/6651666 by KIT Library user on 27 September 2022

40. Statistics

Revised August 2021 by G. Cowan (RHUL).

This chapter gives an overview of statistical methods used in high-energy physics. In statistics, we are interested in using a given sample of data to make inferences about a probabilistic model, *e.g.*, to assess the model's validity or to determine the values of its parameters. There are two main approaches to statistical inference, which we may call frequentist and Bayesian.

In frequentist statistics, probability is interpreted as the limiting frequency of the outcome of a repeatable experiment. The most important tools in this framework are parameter estimation, covered in Section 40.2, statistical tests, discussed in Section 40.3, and confidence intervals, which are constructed so as to cover the true value of a parameter with a specified probability, as described in Section 40.4.2. Note that in frequentist statistics one does not define a probability for a hypothesis or for the value of a parameter.

In Bayesian statistics, the subjective interpretation of probability is used to quantify one's *degree of belief* in a hypothesis. This allows one to define a probability density function (p.d.f.) for a parameter, which reflects one's knowledge about where its true value lies.

Bayesian methods provide a natural means to include additional information, which in general may be subjective; in fact they *require* prior probabilities for the hypotheses (or parameters) in question, *i.e.*, the degree of belief about the parameters' values, before carrying out the measurement. Using Bayes' theorem (Eq. (39.4)), the prior degree of belief is updated by the data from the experiment. Bayesian methods for interval estimation are discussed in Sections 40.4.1 and 40.4.2.4.

For many inference problems, the frequentist and Bayesian approaches give similar numerical values, even though they answer different questions and are based on fundamentally different interpretations of probability. In some important cases, however, the two approaches may yield very different results. For a discussion of Bayesian vs. non-Bayesian methods, see references written by a statistician [1], by a physicist [2], or the detailed comparison in Ref. [3].

40.1 Fundamental concepts

Consider an experiment whose outcome is characterized by one or more data values, which we can write as a vector $\boldsymbol{x}$. A *hypothesis* H is a statement about the probability for the data, often written $P(\boldsymbol{x}|H)$. (We will usually use a capital letter for a probability and lower case for a probability density. Often the term p.d.f. is used loosely to refer to either a probability or a probability density.) This could, for example, define completely the p.d.f. for the data (a *simple* hypothesis), or it could specify only the functional form of the p.d.f., with the values of one or more parameters not determined (a *composite* hypothesis).

If the probability $P(\boldsymbol{x}|H)$ for data $\boldsymbol{x}$ is regarded as a function of the hypothesis H, then it is called the *likelihood* of H, usually written $L(H)$. Often the hypothesis is characterized by one or more parameters $\boldsymbol{\theta}$, in which case $L(\boldsymbol{\theta}) = P(\boldsymbol{x}|\boldsymbol{\theta})$ is called the likelihood function.

In some cases one can obtain at least approximate frequentist results using the likelihood evaluated only with the data obtained, for example, when determining confidence regions with Eq. (40.74). In general, however, the frequentist approach requires a full specification of the probability model $P(\boldsymbol{x}|H)$ both as a function of the data $\boldsymbol{x}$ and hypothesis H.

In the Bayesian approach, inference is based on the posterior probability for H given the data $\boldsymbol{x}$, which represents one's degree of belief that H is true given the data. This is obtained from Bayes' theorem (39.4), which can be written

$$P(H|\boldsymbol{x}) = \frac{P(\boldsymbol{x}|H)\pi(H)}{\int P(\boldsymbol{x}|H')\pi(H')\,dH'} \ . \tag{40.1}$$

Here $P(\boldsymbol{x}|H)$ is the likelihood for H, which depends only on the data actually obtained. The quantity $\pi(H)$ is the prior probability for H, which represents one's degree of belief for H before carrying out the measurement. The integral in the denominator (or sum, for discrete hypotheses) serves as a normalization factor. If H is characterized by a continuous parameter θ then the posterior probability is a p.d.f. $p(\theta|\boldsymbol{x})$. Note that the likelihood function itself is not a p.d.f. for θ.

40.2 Parameter estimation

Here we review *point estimation* of parameters, first with an overview of the frequentist approach and its two most important methods, maximum likelihood and least squares, treated in Sections 40.2.2 and 40.2.3. The Bayesian approach is outlined in Sec. 40.2.6.

An *estimator* $\widehat{\theta}$ (written with a hat) is a function of the data used to estimate the value of the parameter θ. Sometimes the word 'estimate' is used to denote the value of the estimator when evaluated with given data. There is no fundamental rule dictating how an estimator must be constructed. One tries, therefore, to choose that estimator which has the best properties. The most important of these are (a) *consistency*, (b) *bias*, (c) *efficiency*, and (d) *robustness*.

(a) An estimator is said to be *consistent* if the estimate $\widehat{\theta}$ converges in probability (see Ref. [3]) to the true value θ as the amount of data increases. This property is so important that it is possessed by all commonly used estimators.

(b) The *bias*, $b = E[\widehat{\theta}] - \theta$, is the difference between the expectation value of the estimator and the true value of the parameter. The expectation value is taken over a hypothetical set of similar experiments in which $\widehat{\theta}$ is constructed in the same way. When $b = 0$, the estimator is said to be unbiased. The bias depends on the chosen metric, *i.e.*, if $\widehat{\theta}$ is an unbiased estimator of θ, then $\widehat{\theta}^2$ is not in general an unbiased estimator for θ^2.

(c) *Efficiency* is the ratio of the minimum possible variance for any estimator of θ to the variance $V[\widehat{\theta}]$ of the estimator $\widehat{\theta}$. For the case of a single parameter, under rather general conditions the minimum variance is given by the Rao-Cramér-Fréchet bound,

$$\sigma^2_{\rm min} = \left(1 + \frac{\partial b}{\partial \theta}\right)^2 / I(\theta) \ , \tag{40.2}$$

where

$$I(\theta) = E\left[\left(\frac{\partial \ln L}{\partial \theta}\right)^2\right] = -E\left[\frac{\partial^2 \ln L}{\partial \theta^2}\right] \tag{40.3}$$

is the *Fisher information*, L is the likelihood, and the operator $E[]$ in (40.3) is the expectation value with respect to the data. For the final equality to hold, the range of allowed data values must not depend on θ.

The *mean-squared error*,

$$\text{MSE} = E[(\widehat{\theta} - \theta)^2] = V[\widehat{\theta}] + b^2 \ , \tag{40.4}$$

is a measure of an estimator's quality which combines bias and variance.

(d) *Robustness* is the property of being insensitive to departures from assumptions about the p.d.f., *e.g.*, owing to uncertainties in the distribution's tails.

It is not in general possible to optimize simultaneously for all the measures of estimator quality described above. For some common estimators, the properties above are known exactly. More generally, it is possible to evaluate them by Monte Carlo simulation. Note that they will in general depend on the unknown θ.

40.2.1 *Estimators for mean, variance, and median*

Suppose we have a set of n independent measurements, $x_1, \ldots, x_n$, each assumed to follow a p.d.f. with unknown mean μ and unknown variance σ^2 (the measurements do not necessarily have to follow a Gaussian distribution). Then

$$\widehat{\mu} = \frac{1}{n}\sum_{i=1}^{n} x_i \tag{40.5}$$

$$\widehat{\sigma^2} = \frac{1}{n-1}\sum_{i=1}^{n}(x_i - \widehat{\mu})^2 \tag{40.6}$$

Downloaded from https://academic.oup.com/ptep/article/2022/8/083C01/6651666 by KIT Library user on 27 September 2022

are unbiased estimators of μ and σ^2. The variance of $\widehat{\mu}$ is σ^2/n and the variance of $\widehat{\sigma^2}$ is

$$V\left[\widehat{\sigma^2}\right] = \frac{1}{n}\left(m_4 - \frac{n-3}{n-1}\sigma^4\right) , \tag{40.7}$$

where m_4 is the 4th central moment of x (see Eq. (39.8)). For Gaussian distributed x_i, this becomes $2\sigma^4/(n-1)$ for any $n \geq 2$, and for large n the standard deviation of $\widehat{\sigma}$ is $\sigma/\sqrt{2n}$. For any n and Gaussian x_i, $\widehat{\mu}$ is an efficient estimator for μ, and the estimators $\widehat{\mu}$ and $\widehat{\sigma^2}$ are uncorrelated. Otherwise the arithmetic mean (40.5) is not necessarily the most efficient estimator; this is discussed further in Sec. 8.7 of Ref. [4].

If σ^2 is known, it does not improve the estimate $\widehat{\mu}$, as can be seen from Eq. (40.5); however, if μ is known, one can substitute it for $\widehat{\mu}$ in Eq. (40.6) and replace $n-1$ by n to obtain an estimator of σ^2 still with zero bias but smaller variance. If the x_i have different, known variances σ_i^2, then the weighted average

$$\widehat{\mu} = \frac{1}{w}\sum_{i=1}^{n} w_i x_i , \tag{40.8}$$

where $w_i = 1/\sigma_i^2$ and $w = \sum_i w_i$, is an unbiased estimator for μ with a smaller variance than an unweighted average. The standard deviation of $\widehat{\mu}$ is $1/\sqrt{w}$.

As an estimator for the median x_{med}, one can use the value $\widehat{x}_{\text{med}}$ such that half the x_i are below and half above (the sample median). If there are an even number of observations and the sample median lies between two observed values, the estimator is set by convention to their arithmetic average. If the p.d.f. of x has the form $f(x-\mu)$ and μ is both mean and median, then for large n the variance of the sample median approaches $1/[4nf^2(0)]$, provided $f(0) > 0$. Although estimating the median can often be more difficult computationally than the mean, the resulting estimator is generally more robust, as it is insensitive to the exact shape of the tails of a distribution.

40.2.2 *The method of maximum likelihood*

Suppose we have a set of measured quantities $\boldsymbol{x}$ and the likelihood $L(\boldsymbol{\theta}) = P(\boldsymbol{x}|\boldsymbol{\theta})$ for a set of parameters $\boldsymbol{\theta} = (\theta_1, \ldots, \theta_M)$. The *maximum likelihood* (ML) estimators for $\boldsymbol{\theta}$ are defined as the values that give the maximum of L. Because of the properties of the logarithm, it is usually easier to work with $\ln L$, and since both are maximized for the same parameter values $\boldsymbol{\theta}$, the ML estimators can be found by solving the *likelihood equations*,

$$\frac{\partial \ln L}{\partial \theta_i} = 0 , \qquad i = 1, \ldots, M . \tag{40.9}$$

Often the solution must be found numerically. Maximum likelihood estimators are important because they are asymptotically (*i.e.*, for large data samples) unbiased, efficient and have a Gaussian sampling distribution under quite general conditions, and the method has a wide range of applicability.

In general the likelihood function is obtained from the probability of the data under assumption of the parameters. An important special case is when the data consist of *i.i.d.* (independent and identically distributed) values. Here one has a set of n statistically independent quantities $\boldsymbol{x} = (x_1, \ldots, x_n)$, where each component follows the same p.d.f. $f(x;\boldsymbol{\theta})$. In this case the joint p.d.f. of the data sample factorizes and the likelihood function is

$$L(\boldsymbol{\theta}) = \prod_{i=1}^{n} f(x_i;\boldsymbol{\theta}) . \tag{40.10}$$

In this case the number n of observations (usually individual "events" in particle physics) is regarded as fixed. If, however, the probability to observe n events itself depends on the parameters $\boldsymbol{\theta}$, then this dependence should be included in the likelihood. For example, if n follows a Poisson distribution with mean μ and the independent x values all follow $f(x;\boldsymbol{\theta})$, then the likelihood becomes

$$L(\boldsymbol{\theta}) = \frac{\mu^n}{n!}e^{-\mu}\prod_{i=1}^{n} f(x_i;\boldsymbol{\theta}) . \tag{40.11}$$

Equation (40.11) is often called the *extended likelihood* (see, *e.g.*, Refs. [5–7]). If μ is given as a function of $\boldsymbol{\theta}$, then including the probability for n given $\boldsymbol{\theta}$ in the likelihood provides additional information about the parameters. This therefore leads to a reduction in their statistical uncertainties and in general changes their estimated values.

In evaluating the likelihood function, it is important that any normalization factors in the p.d.f. that involve $\boldsymbol{\theta}$ be included. However, we will only be interested in the maximum of L and in ratios of L at different values of the parameters; hence any multiplicative factors that do not involve the parameters that we want to estimate may be dropped, including factors that depend on the data but not on $\boldsymbol{\theta}$.

Under a one-to-one change of parameters from $\boldsymbol{\theta}$ to $\boldsymbol{\eta}$, the ML estimators $\widehat{\boldsymbol{\theta}}$ transform to $\boldsymbol{\eta}(\widehat{\boldsymbol{\theta}})$. That is, the ML solution is invariant under change of parameter. However, other properties of ML estimators, in particular the bias, are not invariant under change of parameter.

The inverse V^{-1} of the covariance matrix $V_{ij} = \text{cov}[\widehat{\theta}_i, \widehat{\theta}_j]$ for a set of ML estimators can be estimated by using

$$(\widehat{V}^{-1})_{ij} = -\left.\frac{\partial^2 \ln L}{\partial\theta_i \partial\theta_j}\right|_{\widehat{\boldsymbol{\theta}}} . \tag{40.12}$$

Equation (40.12) holds for a sufficiently large data sample (or for a small sample only in special cases, e.g., where the means of Gaussian distributed data are linear functions of the parameters); otherwise it can result in a misestimation of the variances. Under the conditions where the equation is valid, L has a Gaussian form and $\ln L$ is (hyper)parabolic. In this case, s times the standard deviations σ_i of the estimators for the parameters can be obtained from the hypersurface defined by the $\boldsymbol{\theta}$ such that

$$\ln L(\boldsymbol{\theta}) = \ln L_{\max} - s^2/2 , \tag{40.13}$$

where $\ln L_{\max}$ is the value of $\ln L$ at the solution point (compare with Eq. (40.74)). The minimum and maximum values of θ_i on the hypersurface then give an approximate s-standard deviation confidence interval for θ_i (see Section 40.4.2.2).

40.2.2.1 *ML with binned data*

If the total number of data values x_i, $(i = 1, \ldots, n_{\text{tot}})$, is small, the unbinned maximum likelihood method, *i.e.*, use of Equation (40.10) (or (40.11) for extended ML), is preferred since binning can only result in a loss of information, and hence larger statistical errors for the parameter estimates. If the sample is large, it can be convenient to bin the values in a histogram with N bins, so that one obtains a vector of data $\boldsymbol{n} = (n_1, \ldots, n_N)$ with expectation values $\boldsymbol{\mu} = E[\boldsymbol{n}]$ and probabilities $f(\boldsymbol{n};\boldsymbol{\mu})$. Suppose the mean values $\boldsymbol{\mu}$ can be determined as a function of a set of parameters $\boldsymbol{\theta}$. Then one may maximize the likelihood function based on the contents of the bins.

As mentioned in Sec. 40.2.2, the total number of events $n_{\text{tot}} = \sum_i n_i$ can be regarded either as fixed or as a random variable. If it is fixed, the histogram follows a multinomial distribution,

$$f_{\text{M}}(\boldsymbol{n};\boldsymbol{\theta}) = \frac{n_{\text{tot}}!}{n_1! \cdots n_N!} p_1^{n_1} \cdots p_N^{n_N} , \tag{40.14}$$

where we assume the probabilities p_i are given functions of the parameters $\boldsymbol{\theta}$. The distribution can be written equivalently in terms of the expected number of events in each bin, $\mu_i = n_{\text{tot}} p_i$. If the n_i are regarded as independent and Poisson distributed, then the data are instead described by a product of Poisson probabilities,

$$f_{\text{P}}(\boldsymbol{n};\boldsymbol{\theta}) = \prod_{i=1}^{N} \frac{\mu_i^{n_i}}{n_i!} e^{-\mu_i} , \tag{40.15}$$

where the mean values μ_i are given functions of $\boldsymbol{\theta}$. The total number of events n_{tot} thus follows a Poisson distribution with mean $\mu_{\text{tot}} = \sum_i \mu_i$.

When using maximum likelihood with binned data, one can find the ML estimators and at the same time obtain a statistic

Downloaded from https://academic.oup.com/ptep/article/2022/8/083C01/6651666 by KIT Library user on 27 September 2022

usable for a test of goodness-of-fit (see Sec. 40.3.2). Maximizing the likelihood $L(\boldsymbol{\theta}) = f_{\mathrm{M/P}}(\boldsymbol{n};\boldsymbol{\theta})$ is equivalent to maximizing the likelihood ratio $\lambda(\boldsymbol{\theta}) = f_{\mathrm{M/P}}(\boldsymbol{n};\boldsymbol{\theta})/f(\boldsymbol{n};\hat{\boldsymbol{\mu}})$, where in the denominator $f(\boldsymbol{n};\boldsymbol{\mu})$ is a model with an adjustable parameter for each bin, $\boldsymbol{\mu} = (\mu_1,\ldots,\mu_N)$, and the corresponding estimators are $\hat{\boldsymbol{\mu}} = (n_1,\ldots,n_N)$ (called the "saturated model"). Equivalently one often minimizes the quantity $-2\ln\lambda(\boldsymbol{\theta})$. For independent Poisson distributed n_i this is [8]

$$-2\ln\lambda(\boldsymbol{\theta}) = 2\sum_{i=1}^{N}\left[\mu_i(\boldsymbol{\theta}) - n_i + n_i\ln\frac{n_i}{\mu_i(\boldsymbol{\theta})}\right] , \qquad (40.16)$$

where for bins with $n_i = 0$, the last term in (40.16) is zero. The expression (40.16) without the terms $\mu_i - n_i$ also gives $-2\ln\lambda(\boldsymbol{\theta})$ for multinomially distributed n_i, *i.e.*, when the total number of entries is regarded as fixed. In the limit of zero bin width, minimizing (40.16) is equivalent to maximizing the unbinned extended likelihood function (40.11); in the corresponding multinomial case without the $\mu_i - n_i$ terms one obtains Eq. (40.10).

A smaller value of $-2\ln\lambda(\widehat{\boldsymbol{\theta}})$ corresponds to better agreement between the data and the hypothesized form of $\boldsymbol{\mu}(\boldsymbol{\theta})$. The value of $-2\ln\lambda(\widehat{\boldsymbol{\theta}})$ can thus be translated into a p-value as a measure of goodness-of-fit, as described in Sec. 40.3.2. Assuming the model is correct, then according to Wilks' theorem [9], for sufficiently large μ_i and provided certain regularity conditions are met, the minimum of $-2\ln\lambda$ as defined by Eq. (40.16) follows a χ^2 distribution (see, *e.g.*, Ref. [8]). If there are N bins and M fitted parameters, then the number of degrees of freedom for the χ^2 distribution is $N - M$ if the data are treated as Poisson-distributed, and $N - M - 1$ if the n_i are multinomially distributed.

Suppose the n_i are Poisson-distributed and the overall normalization $\mu_{\mathrm{tot}} = \sum_i \mu_i$ is taken as an adjustable parameter, so that $\mu_i = \mu_{\mathrm{tot}} p_i(\boldsymbol{\theta})$, where the probability to be in the ith bin, $p_i(\boldsymbol{\theta})$, does not depend on μ_{tot}. Then by minimizing Eq. (40.16), one obtains that the area under the fitted function is equal to the sum of the histogram contents, *i.e.*, $\sum_i \hat{\mu}_i = \sum_i n_i$. This is a property not possessed by the estimators from the method of least squares (see, *e.g.*, Sec. 40.2.3 and Ref. [7]).

40.2.2.2 *Frequentist treatment of nuisance parameters*

Suppose we want to determine the values of parameters $\boldsymbol{\theta}$ using a set of measurements $\boldsymbol{x}$ described by a probability model $P(\boldsymbol{x}|\boldsymbol{\theta})$. In general the model is not perfect, which is to say it cannot provide an accurate description of the data even at the most optimal point of its parameter space. As a result, the estimated parameters can have a systematic bias.

One can improve the model by including in it additional parameters. That is, $P(\boldsymbol{x}|\boldsymbol{\theta})$ is replaced by a more general model $P(\boldsymbol{x}|\boldsymbol{\theta},\boldsymbol{\nu})$, which depends on parameters of interest $\boldsymbol{\theta}$ and *nuisance parameters* $\boldsymbol{\nu}$. The additional parameters are not of intrinsic interest but must be included for the model to be sufficiently accurate for some point in the enlarged parameter space.

Although including additional parameters may eliminate or at least reduce the effect of systematic uncertainties, their presence will result in increased statistical uncertainties for the parameters of interest. This occurs because the estimators for the nuisance parameters and those of interest will in general be correlated, which results in an enlargement of the contour defined by Eq. (40.13).

To reduce the impact of the nuisance parameters one often tries to constrain their values by means of control or calibration measurements, say, having data $\boldsymbol{y}$. For example, some components of $\boldsymbol{y}$ could represent estimates of the nuisance parameters, often from separate experiments. Suppose the measurements $\boldsymbol{y}$ are statistically independent from $\boldsymbol{x}$ and are described by a model $P(\boldsymbol{y}|\boldsymbol{\nu})$. The joint model for both $\boldsymbol{x}$ and $\boldsymbol{y}$ is in this case therefore the product of the probabilities for $\boldsymbol{x}$ and $\boldsymbol{y}$, and thus the likelihood function for the full set of parameters is

$$L(\boldsymbol{\theta},\boldsymbol{\nu}) = P(\boldsymbol{x}|\boldsymbol{\theta},\boldsymbol{\nu})P(\boldsymbol{y}|\boldsymbol{\nu}) . \qquad (40.17)$$

Note that in this case if one wants to simulate the experiment by means of Monte Carlo, both the primary and control measurements, $\boldsymbol{x}$ and $\boldsymbol{y}$, must be generated for each repetition under assumption of fixed values for the parameters $\boldsymbol{\theta}$ and $\boldsymbol{\nu}$.

Using all of the parameters $(\boldsymbol{\theta},\boldsymbol{\nu})$ in Eq. (40.13) to find the statistical errors in the parameters of interest $\boldsymbol{\theta}$ is equivalent to using the *profile likelihood*, which depends only on $\boldsymbol{\theta}$. It is defined as

$$L_{\mathrm{p}}(\boldsymbol{\theta}) = L(\boldsymbol{\theta},\widehat{\widehat{\boldsymbol{\nu}}}(\boldsymbol{\theta})), \qquad (40.18)$$

where the double-hat notation indicates the profiled values of the parameters $\boldsymbol{\nu}$, defined as the values that maximize L for the specified $\boldsymbol{\theta}$. The profile likelihood is discussed further in Section 40.3.2.1 in connection with hypothesis tests.

40.2.3 *The method of least squares*

The *method of least squares* (LS) coincides with the method of maximum likelihood in the following special case. Consider a set of N independent measurements y_i at known points x_i. The measurement y_i is assumed to be Gaussian distributed with mean $\mu(x_i;\boldsymbol{\theta})$ and known variance σ_i^2. The goal is to construct estimators for the unknown parameters $\boldsymbol{\theta}$. The log-likelihood function contains the sum of squares

$$\chi^2(\boldsymbol{\theta}) = -2\ln L(\boldsymbol{\theta}) + \text{ constant } = \sum_{i=1}^{N}\frac{(y_i - \mu(x_i;\boldsymbol{\theta}))^2}{\sigma_i^2} . \qquad (40.19)$$

The parameter values that maximize L are the same as those which minimize χ^2.

The minimum of the chi-square function in Equation (40.19) defines the least-squares estimators $\widehat{\boldsymbol{\theta}}$ for the more general case where the y_i are not Gaussian distributed as long as they are independent. If they are not independent but rather have a covariance matrix $V_{ij} = \mathrm{cov}[y_i, y_j]$, then the LS estimators are determined by the minimum of

$$\chi^2(\boldsymbol{\theta}) = (\boldsymbol{y} - \boldsymbol{\mu}(\boldsymbol{\theta}))^T V^{-1}(\boldsymbol{y} - \boldsymbol{\mu}(\boldsymbol{\theta})) , \qquad (40.20)$$

where $\boldsymbol{y} = (y_1,\ldots,y_N)$ is the (column) vector of measurements, $\boldsymbol{\mu}(\boldsymbol{\theta})$ is the corresponding vector of predicted values, and the superscript T denotes the transpose. If the y_i are not Gaussian distributed, then the LS and ML estimators will not in general coincide.

Often one further restricts the problem to the case where $\mu(x_i;\boldsymbol{\theta})$ is a linear function of the parameters, *i.e.*,

$$\mu(x_i;\boldsymbol{\theta}) = \sum_{j=1}^{m}\theta_j h_j(x_i) . \qquad (40.21)$$

Here the $h_j(x)$ are m linearly independent functions, *e.g.*, $1, x, x^2, \ldots, x^{m-1}$ or Legendre polynomials. We require $m < N$ and at least m of the x_i must be distinct.

Minimizing χ^2 in this case with m parameters reduces to solving a system of m linear equations. Defining $H_{ij} = h_j(x_i)$ and minimizing χ^2 by setting its derivatives with respect to the θ_i equal to zero gives the LS estimators,

$$\widehat{\boldsymbol{\theta}} = (H^T V^{-1} H)^{-1} H^T V^{-1}\boldsymbol{y} \equiv D\boldsymbol{y} . \qquad (40.22)$$

The covariance matrix for the estimators $U_{ij} = \mathrm{cov}[\widehat{\theta}_i, \widehat{\theta}_j]$ is given by

$$U = DVD^T = (H^T V^{-1} H)^{-1} , \qquad (40.23)$$

or equivalently, its inverse U^{-1} can be found from

$$(U^{-1})_{ij} = \frac{1}{2}\frac{\partial^2\chi^2}{\partial\theta_i\partial\theta_j}\bigg|_{\boldsymbol{\theta}=\widehat{\boldsymbol{\theta}}} = \sum_{k,l=1}^{N} h_i(x_k)(V^{-1})_{kl}h_j(x_l) . \qquad (40.24)$$

The LS estimators can also be found from the expression

$$\widehat{\boldsymbol{\theta}} = U\boldsymbol{g} , \qquad (40.25)$$

where the vector $\boldsymbol{g}$ is defined by

$$g_i = \sum_{j,k=1}^{N} y_j h_i(x_k)(V^{-1})_{jk} . \qquad (40.26)$$

Downloaded from https://academic.oup.com/ptep/article/2022/8/083C01/6651666 by KIT Library user on 27 September 2022

For the case of uncorrelated y_i, for example, one can use (40.25) with

$$(U^{-1})_{ij} = \sum_{k=1}^{N} \frac{h_i(x_k)h_j(x_k)}{\sigma_k^2} \ , \tag{40.27}$$

$$g_i = \sum_{k=1}^{N} \frac{y_k h_i(x_k)}{\sigma_k^2} \ . \tag{40.28}$$

Expanding $\chi^2(\boldsymbol{\theta})$ about $\widehat{\boldsymbol{\theta}}$, one finds that the contour in parameter space defined by

$$\chi^2(\boldsymbol{\theta}) = \chi^2(\widehat{\boldsymbol{\theta}}) + 1 = \chi^2_{\min} + 1 \tag{40.29}$$

has tangent planes located at plus-or-minus-one standard deviation $\sigma_{\widehat{\boldsymbol{\theta}}}$ from the LS estimates $\widehat{\boldsymbol{\theta}}$ (the relation is approximate if the fit function $\mu(x;\boldsymbol{\theta})$ is nonlinear in the parameters).

In constructing the quantity $\chi^2(\boldsymbol{\theta})$ one requires the variances or, in the case of correlated measurements, the covariance matrix. Often these quantities are not known *a priori* and must be estimated from the data. In this case the least-squares and maximum-likelihood methods are no longer exactly equivalent even for Gaussian distributed measurements. An important example is where the measured value y_i represents the event count in a histogram bin. If, for example, y_i represents a Poisson variable, for which the variance is equal to the mean, then one can either estimate the variance from the predicted value, $\mu(x_i;\boldsymbol{\theta})$, or from the observed number itself, y_i. In the first option, the variances become functions of the parameters, and as a result the estimators may need to be found numerically. The second option can be undefined if y_i is zero, and for small y_i, the variance will be poorly estimated. In either case, one should constrain the normalization of the fitted curve to the correct value, *i.e.*, one should determine the area under the fitted curve directly from the number of entries in the histogram (see Ref. [7], Section 7.4). As noted in Sec. 40.2.2.1, this issue is avoided when using the method of extended maximum likelihood with binned data by minimizing Eq. (40.16). In that case if the expected number of events $\mu_{\rm tot}$ does not depend on the other fitted parameters $\boldsymbol{\theta}$, then its extended ML estimator is equal to the observed total number of events.

As the minimum value of the χ^2 represents the level of agreement between the measurements and the fitted function, it can be used for assessing the goodness-of-fit; this is discussed further in Section 40.3.2.

40.2.4 *Parameter estimation with constraints*

In some applications one is interested in using a set of measured quantities $\boldsymbol{y} = (y_1, \ldots, y_N)$ to estimate a set of parameters $\boldsymbol{\theta} = (\theta_1, \ldots, \theta_M)$ subject to a number of constraints. For example, one may have measured coordinates from two tracks, and one wishes to estimate their momentum vectors subject to the constraint that the tracks have a common vertex. The parameters can also include momenta of undetected particles such as neutrinos, as long as the constraints from conservation of energy and momentum and from known masses of particles involved in the reaction chain provide enough information for these quantities to be inferred.

A set of K constraints can be given in the form of equations

$$c_k(\boldsymbol{\theta}) = 0 \ , \quad k = 1, \ldots, K \ . \tag{40.30}$$

In some problems it may be possible to define a new set of parameters $\boldsymbol{\eta} = (\eta_1, \ldots, \eta_L)$ with $L = M - K$ such that every point in $\boldsymbol{\eta}$-space automatically satisfies the constraints. If this is possible then the problem reduces to one of estimating $\boldsymbol{\eta}$ with, *e.g.*, maximum likelihood or least squares and then transforming the estimators back into $\boldsymbol{\theta}$-space.

In many cases it may be difficult or impossible to find an appropriate transformation $\boldsymbol{\eta}(\boldsymbol{\theta})$. Suppose that the parameters are determined through minimizing an objective function such as $\chi^2(\boldsymbol{\theta})$ in the method of least squares. Here one may enforce the constraints by finding the stationary points of the *Lagrange function*

$$\mathcal{L}(\boldsymbol{\theta}, \boldsymbol{\lambda}, \boldsymbol{y}) = \chi^2(\boldsymbol{\theta}, \boldsymbol{y}) + \sum_{k=1}^{K} \lambda_k c_k(\boldsymbol{\theta}) \tag{40.31}$$

with respect to both the parameters $\boldsymbol{\theta}$ and a set of *Lagrange multipliers* $\boldsymbol{\lambda} = (\lambda_1, \ldots, \lambda_K)$. Combining the parameters and Lagrange multipliers into an $(M + K)$-component vector $\boldsymbol{\gamma} = (\theta_1, \ldots, \theta_M, \lambda_1, \ldots, \lambda_K)$, the solutions for $\boldsymbol{\gamma}$, *i.e.*, the estimators $\hat{\boldsymbol{\gamma}}$, are found (*e.g.*, numerically) from the system of equations

$$F_i(\boldsymbol{\gamma}, \boldsymbol{y}) \equiv \frac{\partial \mathcal{L}}{\partial \gamma_i} = 0 \ , \quad i = 1, \ldots, M + K \ . \tag{40.32}$$

To obtain the covariance matrix of the estimated parameters one can find solutions $\tilde{\boldsymbol{\gamma}}$ corresponding to the expectation values of the data $\langle \boldsymbol{y} \rangle$ and expand $F_i(\hat{\boldsymbol{\gamma}}, \boldsymbol{y})$ to first order about these values. This gives (see, e.g., Sec. 11.6 of Ref. [7]) linearized approximations for the estimators, $\hat{\boldsymbol{\gamma}}(\boldsymbol{y}) \approx \tilde{\boldsymbol{\gamma}} + C(\boldsymbol{y} - \langle \boldsymbol{y} \rangle)$, where the matrix $C = -A^{-1}B$, and A and B are given by

$$A_{ij} = \left[\frac{\partial F_i}{\partial \gamma_j} \right]_{\tilde{\boldsymbol{\gamma}}, \langle \boldsymbol{y} \rangle} \quad \text{and} \quad B_{ij} = \left[\frac{\partial F_i}{\partial y_j} \right]_{\tilde{\boldsymbol{\gamma}}, \langle \boldsymbol{y} \rangle} \ . \tag{40.33}$$

In practice the values $\langle \boldsymbol{y} \rangle$ and corresponding solutions $\tilde{\boldsymbol{\gamma}}$ are estimated using the data from the actual measurement. Using this approximation for $\hat{\boldsymbol{\gamma}}(\boldsymbol{y})$, one can find the covariance matrix $U_{ij} = \mathrm{cov}[\hat{\gamma}_i, \hat{\gamma}_j]$ of the estimators for the γ_i in terms of that of the data $V_{ij} = \mathrm{cov}[y_i, y_j]$ using error propagation (cf. Eqs. (39.17) and (39.18)),

$$U = CVC^T \ . \tag{40.34}$$

The upper-left $M \times M$ block of the matrix U gives the covariance matrix for the estimated parameters $\mathrm{cov}[\hat{\theta}_i, \hat{\theta}_j]$. One can show for linear constraints that $\mathrm{cov}[\hat{\theta}_i, \hat{\theta}_j]$ is also given by the upper-left $M \times M$ block of $2A^{-1}$. If the parameters are estimated using the method of least squares, then the number of degrees of freedom for the distribution of the minimized χ^2 is increased by the number of constraints, *i.e.*, it becomes $N - M + K$. Further details can be found in, *e.g.*, Ch. 8 of Ref. [4] and Ch. 7 of Ref. [10].

40.2.5 *Unfolding*

An important class of parameter estimation problem involves measurement of the differential distribution of a kinematic variable in the form of a histogram with N bins. The data thus consist of the vector of measured data values $\boldsymbol{n} = (n_1, \ldots n_N)$, with expectation values $\nu_i = E[n_i]$. The n_i are usually independent and often modeled as Poisson distributed, from which it follows that the maximum-likelihood estimators are $\hat{\nu}_i = n_i$ for all i.

Because of the limited acceptance and resolution of the experiment, however, the measured values of the kinematic variable in question differ in general from their true values, and as a consequence the form of the data histogram is distorted relative to what would be obtained with perfect resolution. The desired parameters are not, therefore, the ν_i but rather one wants to estimate the expected number of entries in a given bin that would be found with a perfect detector. We call this the "true histogram" and denote it with $\boldsymbol{\mu} = (\mu_1, \ldots, \mu_M)$, where the number of bins M is not required to equal that of the observed histogram. The μ_i are related to the expected numbers of events in the observed histogram by

$$\nu_i = \sum_{j=1}^{M} R_{ij}\mu_j + \beta_i \ , \tag{40.35}$$

where β_i here represents the expected number of events in bin i due to background processes and the $N \times M$ *response matrix* R_{ij} gives the probability for an event to be observed in bin i of $\boldsymbol{\nu}$ given that the true value of the variable was in bin j of $\boldsymbol{\mu}$. For purposes of this discussion let us suppose that the response matrix and expected background values are known. There are two main approaches to this type of problem, which we can call *unfolding* and *folding*.

Downloaded from https://academic.oup.com/ptep/article/2022/8/083C01/6651666 by KIT Library user on 27 September 2022

In unfolding, one treats the true histogram $\boldsymbol{\mu}$ as the parameters of interest. The result is thus given by estimators $\hat{\boldsymbol{\mu}}$ and the corresponding covariance matrix $U_{ij} = \mathrm{cov}[\hat{\mu}_i, \hat{\mu}_j]$. Provided the response matrix can be inverted, the maximum-likelihood solution is easily found as $\hat{\boldsymbol{\mu}} = R^{-1}(\boldsymbol{n} - \boldsymbol{\beta})$. If the response matrix allows for significant migration of events between bins, then the variances of these estimators can be very large, sometimes to the point where the $\hat{\boldsymbol{\mu}}$ bear essentially no resemblance to the true $\boldsymbol{\mu}$. In such cases the estimators can be found by maximizing a linear combination of the log-likelihood and a regularization function that imposes some degree of smoothness on the unfolded distribution. In achieving a reduction in variance one inevitably introduces some bias into the estimators.

In the approach of folding, by contrast, to test a given model prediction for the true histogram $\boldsymbol{\mu}$ it is first "folded" with the response matrix and corrected for expected background to give the corresponding $\boldsymbol{\nu}$ according to Eq. (40.35), and these are compared to the corresponding $\boldsymbol{n}$ using, e.g., a likelihood ratio as shown in Sec. 40.2.2.1. In this way, one avoids any bias due to regularization.

To account for systematic uncertainties, the response matrix and background values may not be expressed as constants but rather as functions of nuisance parameters $\boldsymbol{\theta}$. These may be constrained by auxiliary measurements $\boldsymbol{u}$ with pdf $p(\boldsymbol{u}|\boldsymbol{\theta})$ so that the full likelihood becomes (as in Eq. (40.17) but with different notation)

$$L(\boldsymbol{\mu}, \boldsymbol{\theta}) = P(\boldsymbol{n}|\boldsymbol{\nu}(\boldsymbol{\mu}, \boldsymbol{\theta}))p(\boldsymbol{u}|\boldsymbol{\theta}) \ . \tag{40.36}$$

Here the mean values $\boldsymbol{\nu} = R(\boldsymbol{\theta})\boldsymbol{\mu} + \boldsymbol{\beta}(\boldsymbol{\theta})$ now depend on both the true histogram parameters $\boldsymbol{\mu}$ as well as the nuisance parameters $\boldsymbol{\theta}$. Thus to record enough information for a future analysis using folding one must provide all of the ingredients used above: the primary data $\boldsymbol{n}$, the auxiliary measurements $\boldsymbol{u}$, and also the response matrix $R(\boldsymbol{\theta})$ and expected backgrounds $\boldsymbol{\beta}(\boldsymbol{\theta})$ as functions of the nuisance parameters. If unfolding is used, then future model tests or comparisons with other experiments can be carried out directly using the estimators $\hat{\boldsymbol{\mu}}$ and their covariance matrix.

If several distributions are unfolded, then to combine these in a test of a given model one should know how estimators for bins of different distributions are correlated, as can arise, e.g., through common systematic effects. If only the unfolded distributions and their separate covariance matrices are reported, however, then information on such correlations is not retained. In folding, one can include information on correlated systematic effects if the ingredients (R and $\boldsymbol{\beta}$) are known in terms of nuisance parameters that are common to different distributions.

In unfolding, the estimators for $\boldsymbol{\mu}$ can be constructed either by maximizing the log-likelihood using Eq. (40.36) or in the case where regularization is required one can maximize $\varphi(\boldsymbol{\mu}, \boldsymbol{\theta}) = \ln L(\boldsymbol{\mu}, \boldsymbol{\theta}) + \tau S(\boldsymbol{\mu})$, where the *regularization function* $S(\boldsymbol{\mu})$ reflects the smoothness of the true histogram and serves to reduce the variances of the estimators. Possible functions are based on the mean squared second derivative (a commonly used type of Tikhonov regularization) or the entropy of the true histogram. The parameter τ fixes the relative weighting of the log-likelihood and the regularization function and thus determines the balance between the bias and variance of the resulting estimators. Further discussion of the unfolding problem including methods for choosing the regularization function and parameter, as well as techniques that employ other types of regularization such as the iterative Bayes (Richardson-Lucy) method, can be found in Refs. [7, 10–12] and references therein.

40.2.6 *The Bayesian approach*

In the frequentist methods discussed above, probability is associated only with data, not with the value of a parameter. This is no longer the case in Bayesian statistics, however, which we introduce in this section. For general introductions to Bayesian statistics see, *e.g.*, Refs. [13–16].

Suppose the outcome of an experiment is characterized by a vector of data $\boldsymbol{x}$, whose probability distribution depends on an unknown parameter (or parameters) $\boldsymbol{\theta}$ that we wish to determine. In Bayesian statistics, all knowledge about $\boldsymbol{\theta}$ is summarized by the posterior p.d.f. $p(\boldsymbol{\theta}|\boldsymbol{x})$, whose integral over any given region gives the degree of belief for $\boldsymbol{\theta}$ to take on values in that region, given the data $\boldsymbol{x}$. It is obtained by using Bayes' theorem,

$$p(\boldsymbol{\theta}|\boldsymbol{x}) = \frac{P(\boldsymbol{x}|\boldsymbol{\theta})\pi(\boldsymbol{\theta})}{\int P(\boldsymbol{x}|\boldsymbol{\theta}')\pi(\boldsymbol{\theta}')\, d\boldsymbol{\theta}'} \ , \tag{40.37}$$

where $P(\boldsymbol{x}|\boldsymbol{\theta})$ is the likelihood function, *i.e.*, the joint p.d.f. for the data viewed as a function of $\boldsymbol{\theta}$, evaluated with the data actually obtained in the experiment, and $\pi(\boldsymbol{\theta})$ is the prior p.d.f. for $\boldsymbol{\theta}$. Note that the denominator in Eq. (40.37) serves to normalize the posterior p.d.f. to unity.

As it can be difficult to report the full posterior p.d.f. $p(\boldsymbol{\theta}|\boldsymbol{x})$, one would usually summarize it with statistics such as the mean (or median) value, and covariance matrix. In addition one may construct intervals with a given probability content, as is discussed in Sec. 40.4.1 on Bayesian interval estimation.

40.2.6.1 *Priors*

Bayesian statistics supplies no unique rule for determining the prior $\pi(\boldsymbol{\theta})$; this reflects the analyst's subjective degree of belief (or state of knowledge) about $\boldsymbol{\theta}$ before the measurement was carried out. For the result to be of value to the broader community, whose members may not share these beliefs, it is important to carry out a *sensitivity analysis*, that is, to show how the result changes under a reasonable variation of the prior probabilities.

One might like to construct $\pi(\boldsymbol{\theta})$ to represent complete ignorance about the parameters by setting it equal to a constant. A problem here is that if the prior p.d.f. is flat in $\boldsymbol{\theta}$, then it is not flat for a nonlinear function of $\boldsymbol{\theta}$, and so a different parametrization of the problem would lead in general to a non-equivalent posterior p.d.f.

For the special case of a constant prior, one can see from Bayes' theorem (40.37) that the posterior is proportional to the likelihood, and therefore the mode (peak position) of the posterior is equal to the ML estimator. The posterior mode, however, will change in general upon a transformation of parameter. One may use as the Bayesian estimator a summary statistic other than the mode, such as the median, which is invariant under parameter transformation. But this will not in general coincide with the ML estimator.

The difficult and subjective nature of encoding personal knowledge into priors has led to what is called *objective Bayesian statistics*, where prior probabilities are based not on an actual degree of belief but rather derived from formal rules. These give, for example, priors which are invariant under a transformation of parameters, or ones which result in a maximum gain in information for a given set of measurements. For an extensive review see, *e.g.*, Ref. [17].

Objective priors do not in general reflect degree of belief, but they could in some cases be taken as possible, although perhaps extreme, subjective priors. The posterior probabilities as well therefore do not necessarily reflect a degree of belief. However one may regard investigating a variety of objective priors to be an important part of the sensitivity analysis. Furthermore, use of objective priors with Bayes' theorem can be viewed as a recipe for producing estimators or intervals which have desirable frequentist properties.

An important procedure for deriving objective priors is due to Jeffreys. According to *Jeffreys' rule* one takes the prior as

$$\pi(\boldsymbol{\theta}) \propto \sqrt{\det(I(\boldsymbol{\theta}))} \ , \tag{40.38}$$

where

$$I_{ij}(\boldsymbol{\theta}) = -E\left[\frac{\partial^2 \ln P(\boldsymbol{x}|\boldsymbol{\theta})}{\partial\theta_i \partial\theta_j}\right] \tag{40.39}$$

is the *Fisher information matrix*. One can show that the Jeffreys prior leads to inference that is invariant under a transformation of parameters. One should note that the Jeffreys prior does not in general correspond to one's degree of belief about the value of a parameter. As examples, the Jeffreys prior for the mean μ of a Gaussian distribution is a constant, and for the mean of a Poisson distribution one finds $\pi(\mu) \propto 1/\sqrt{\mu}$.

Downloaded from https://academic.oup.com/ptep/article/2022/8/083C01/6651666 by KIT Library user on 27 September 2022

Neither the constant nor $1/\sqrt{\mu}$ priors can be normalized to unit area and are therefore said to be *improper*. This can be allowed because the prior always appears multiplied by the likelihood function, and if the likelihood falls to zero sufficiently quickly then one may have a normalizable posterior density.

An important type of objective prior is the reference prior due to Bernardo and Berger [18]. To find the reference prior for a given problem one considers the Kullback-Leibler divergence $D_n[\pi, p]$ of the posterior $p(\boldsymbol{\theta}|\boldsymbol{x})$ relative to a prior $\pi(\boldsymbol{\theta})$, obtained from a set of i.i.d. data $\boldsymbol{x} = (x_1, \ldots, x_n)$:

$$D_n[\pi, p] = \int p(\boldsymbol{\theta}|\boldsymbol{x}) \ln \frac{p(\boldsymbol{\theta}|\boldsymbol{x})}{\pi(\boldsymbol{\theta})} \, d\boldsymbol{\theta} \; . \tag{40.40}$$

This is effectively a measure of the gain in information provided by the data. The reference prior is chosen so that the expectation value of this information gain is maximized for the limiting case of $n \to \infty$, where the expectation is computed with respect to the marginal distribution of the data,

$$p(\boldsymbol{x}) = \int p(\boldsymbol{x}|\boldsymbol{\theta}) \pi(\boldsymbol{\theta}) \, d\boldsymbol{\theta} \; . \tag{40.41}$$

For a single, continuous parameter the reference prior is usually identical to the Jeffreys prior. In the multiparameter case an iterative algorithm exists, which requires sorting the parameters by order of inferential importance. Often the result does not depend on this order, but when it does, this can be part of a sensitivity analysis. Further discussion and applications to particle physics problems can be found in Ref. [19].

40.2.6.2 *Bayesian treatment of nuisance parameters*

As discussed in Sec. 40.2.2, a model may depend on parameters of interest $\boldsymbol{\theta}$ as well as on nuisance parameters $\boldsymbol{\nu}$, which must be included for an accurate description of the data. Knowledge about the values of $\boldsymbol{\nu}$ may be supplied by control measurements, theoretical insights, physical constraints, etc. Suppose, for example, one has data $\boldsymbol{y}$ from a control measurement which is characterized by a probability $P(\boldsymbol{y}|\boldsymbol{\nu})$. Suppose further that before carrying out the control measurement one's state of knowledge about $\boldsymbol{\nu}$ is described by an initial prior $\pi_0(\boldsymbol{\nu})$, which in practice is often taken to be a constant or in any case very broad. By using Bayes' theorem (40.1) one obtains the updated prior $\pi(\boldsymbol{\nu})$ (*i.e.*, now $\pi(\boldsymbol{\nu}) = \pi(\boldsymbol{\nu}|\boldsymbol{y})$, the probability for $\boldsymbol{\nu}$ given $\boldsymbol{y}$),

$$\pi(\boldsymbol{\nu}|\boldsymbol{y}) \propto P(\boldsymbol{y}|\boldsymbol{\nu}) \pi_0(\boldsymbol{\nu}) \; . \tag{40.42}$$

In the absence of a model for $P(\boldsymbol{y}|\boldsymbol{\nu})$ one may make some reasonable but *ad hoc* choices in order to approximate $\pi(\boldsymbol{\nu})$. For a single nuisance parameter ν, for example, one might characterize the uncertainty by a p.d.f. $\pi(\nu)$ centered about its nominal value with a certain standard deviation σ_ν. Often a Gaussian p.d.f. provides a reasonable model for one's degree of belief about a nuisance parameter; in other cases, more complicated shapes may be appropriate. If, for example, the parameter represents a non-negative quantity then a log-normal or gamma p.d.f. can be a more natural choice than a Gaussian truncated at zero. Note also that truncation of the prior of a nuisance parameter ν at zero will in general make $\pi(\nu)$ nonzero at $\nu = 0$, which can lead to an unnormalizable posterior for a parameter of interest that appears multiplied by ν.

The likelihood function, prior, and posterior p.d.f.s all depend on both $\boldsymbol{\theta}$ and $\boldsymbol{\nu}$, and are related by Bayes' theorem, as usual. Note that the likelihood here only refers to the primary measurement $\boldsymbol{x}$. Once any control measurements $\boldsymbol{y}$ are used to find the updated prior $\pi(\boldsymbol{\nu})$ for the nuisance parameters, this information is fully encapsulated in $\pi(\boldsymbol{\nu})$ and the control measurements do not appear further.

One can obtain the posterior p.d.f. for $\boldsymbol{\theta}$ alone by integrating over the nuisance parameters, *i.e.*,

$$p(\boldsymbol{\theta}|\boldsymbol{x}) = \int p(\boldsymbol{\theta}, \boldsymbol{\nu}|\boldsymbol{x}) \, d\boldsymbol{\nu} \; . \tag{40.43}$$

Such integrals can often not be carried out in closed form, and if the number of nuisance parameters is large, then they can be difficult to compute with standard Monte Carlo methods. *Markov Chain Monte Carlo* (MCMC) techniques are often used for computing integrals of this type (see Sec. 42.6).

40.3 Statistical tests

In addition to estimating parameters, one often wants to assess the validity of certain statements concerning the data's underlying distribution. Frequentist *hypothesis tests*, described in Sec. 40.3.1, provide a rule for accepting or rejecting hypotheses depending on the outcome of a measurement. In *significance tests*, covered in Sec. 40.3.2, one gives the probability to obtain a level of incompatibility with a certain hypothesis that is greater than or equal to the level observed with the actual data. In the Bayesian approach, the corresponding procedure is based fundamentally on the posterior probabilities of the competing hypotheses. In Sec. 40.3.3 we describe a related construct called the Bayes factor, which can be used to quantify the degree to which the data prefer one or another hypothesis.

40.3.1 *Hypothesis tests*

A frequentist *test* of a hypothesis (often called the null hypothesis, H_0) is a rule that states for which data values $\boldsymbol{x}$ the hypothesis is rejected. A region of $\boldsymbol{x}$-space called the critical region, w, is specified such that there is no more than a given probability under H_0, α, called the *size* or *significance level* of the test, to find $\boldsymbol{x} \in w$. If the data are discrete, it may not be possible to find a critical region with exact probability content α, and thus we require $P(\boldsymbol{x} \in w|H_0) \leq \alpha$. If the data are observed in the critical region, H_0 is rejected.

The data $\boldsymbol{x}$ used to construct a test could be, for example, a set of values that characterizes an individual event. In this case the test corresponds to classification as, *e.g.*, signal or background. Alternatively the data could represent a set of values from a collection of events. Often one is interested in knowing whether all of the events are of a certain type (background), or whether the sample contains at least some events of a new type (signal). Here the background-only hypothesis plays the role of H_0, and in the alternative H_1 both signal and background are present. Rejecting H_0 is, from the standpoint of frequentist statistics, the required step to establish discovery of the signal process.

The critical region is not unique. Its choice should take into account the probabilities for the data predicted by some alternative hypothesis (or set of alternatives) H_1. Rejecting H_0 if it is true is called a *type-I error*, and occurs by construction with probability no greater than α. Not rejecting H_0 if an alternative H_1 is true is called a *type-II error*, and for a given test this will have a certain probability $\beta = P(\boldsymbol{x} \notin w|H_1)$. The quantity $1 - \beta$ is called the *power* of the test of H_0 with respect to the alternative H_1. A strategy for defining the critical region can therefore be to maximize the power with respect to some alternative (or alternatives) given a fixed size α.

To maximize the power of a test of H_0 with respect to the alternative H_1, the *Neyman–Pearson lemma* states that the critical region w should be chosen such that for all data values $\boldsymbol{x}$ inside w, the likelihood ratio

$$\lambda(\boldsymbol{x}) = \frac{f(\boldsymbol{x}|H_1)}{f(\boldsymbol{x}|H_0)} \tag{40.44}$$

is greater than or equal to a given constant c_α, and everywhere outside the critical region one has $\lambda(\boldsymbol{x}) < c_\alpha$, where the value of c_α is determined by the size of the test α. Here H_0 and H_1 must be simple hypotheses, *i.e.*, they should not contain undetermined parameters.

It is convenient to define the test using a scalar function of the data $\boldsymbol{x}$ called a *test statistic*, $t(\boldsymbol{x})$, such that the boundary of the critical region is given by a surface of constant $t(\boldsymbol{x})$. The Neyman–Pearson lemma is equivalent to the statement that the likelihood ratio (40.44) represents the optimal test statistic. It can be difficult in practice, however, to determine $\lambda(\boldsymbol{x})$, since this requires knowledge of the joint p.d.f.s $f(\boldsymbol{x}|H_0)$ and $f(\boldsymbol{x}|H_1)$. Often one does not have explicit formulae for these, but rather

Downloaded from https://academic.oup.com/ptep/article/2022/8/083C01/6651666 by KIT Library user on 27 September 2022

Monte Carlo models that allow one to generate instances of $\boldsymbol{x}$ that follow the p.d.f.s.

In the case where the likelihood ratio (40.44) cannot be used explicitly, there exist a variety of other multivariate methods for constructing a test statistic that may approach its performance. These are based on machine-learning algorithms that use samples of *training data* corresponding to the hypotheses in question, often generated from Monte Carlo models. Further information on Machine Learning can be found in Sec. 41 of this Review.

The multivariate algorithms designed to classify events into signal and background types also form the basis of tests of the hypothesis that a sample of events consists of background only. Such a test can be constructed using the distributions of the test statistic $t(\boldsymbol{x})$ for event classification obtained from a multivariate algorithm such as a Neural Network output. The distributions $p(t|s)$ and $p(t|b)$ for signal and background events, respectively, are used to construct the likelihood ratio of the signal-plus-background hypothesis relative to that of background only. To the extent that the test statistic $t(\boldsymbol{x})$ approximates the likelihood ratio (or a monotonic function thereof) for individual events given by (40.44), the resulting test of the background-only hypothesis for the event sample will have maximum power with respect to the signal-plus-background alternative (see Ref. [20]).

40.3.2 *Tests of significance (goodness-of-fit)*

Often one wants to quantify the level of agreement between the data and a hypothesis without explicit reference to alternative hypotheses. This can be done by defining a statistic t whose value reflects in some way the level of agreement between the data and the hypothesis. The analyst must decide what values of the statistic correspond to better or worse levels of agreement with the hypothesis in question; the choice will in general depend on the relevant alternative hypotheses.

The hypothesis in question, H_0, will determine the p.d.f. $f(t|H_0)$ for the statistic. The significance of a discrepancy between the data and what one expects under the assumption of H_0 is quantified by giving the p-value, defined as the probability to find t in the region of equal or lesser compatibility with H_0 than the level of compatibility observed with the actual data. For example, if t is defined such that large values correspond to poor agreement with the hypothesis, then the p-value would be

$$p = \int_{t_{\rm obs}}^{\infty} f(t|H_0)\, dt \ , \tag{40.45}$$

where $t_{\rm obs}$ is the value of the statistic obtained in the actual experiment.

The p-value is a function of the data, and is therefore itself a random variable. If the hypothesis used to compute the p-value is true, then for continuous data p will be uniformly distributed between zero and one. Note that the p-value is not the probability for the hypothesis; in frequentist statistics, this is not defined.

The p-value should not be confused with the size (significance level) of a test, or the confidence level of a confidence interval (Section 40.4), both of which are pre-specified constants. We may formulate a hypothesis test, however, by defining the critical region to correspond to the data outcomes that give the lowest p-values, so that finding $p \leq \alpha$ implies that the data outcome was in the critical region. When constructing a p-value, one generally chooses the region of data space deemed to have lower compatibility with the model being tested as one having higher compatibility with a given alternative, such that the corresponding test will have a high power with respect to this alternative. For data generated according to the alternative, the distribution of the p-value of H_0 will be concentrated at low values.

When searching for a new phenomenon, one tries to reject the hypothesis H_0 that the data are consistent with known (*e.g.*, Standard Model) processes. If the p-value of H_0 is sufficiently low, then one is willing to accept that some alternative hypothesis is true. Often one converts the p-value into an effective significance Z, defined as an equivalent number of standard deviations of a Gaussian distributed random variable. In a search for an intrinsically positive signal, *i.e.*, where only upward fluctuations of the estimated rate appear signal like, this is defined as

$$Z = \Phi^{-1}(1-p) \ . \tag{40.46}$$

Here Φ is the cumulative distribution of the standard Gaussian, and Φ^{-1} is its inverse (quantile) function. In this way, a p-value of $1/2$ gives $Z = 0$, *i.e.*, having an estimated signal rate of zero corresponds to zero significance. If either positive or negative data fluctuations would indicate evidence of the signal, then one defines

$$Z = \Phi^{-1}(1-p/2) \ . \tag{40.47}$$

In this case an estimated signal rate of zero gives $p = 1$ and $Z = 0$.

Often in particle physics the level of significance where an effect is said to qualify as a discovery is $Z = 5$, *i.e.*, a 5σ effect, corresponding to a p-value of 2.87×10^{-7}. One's actual degree of belief that a new process is present, however, will depend in general on other factors as well, such as the plausibility of the new signal hypothesis and the degree to which it can describe the data, one's confidence in the model that led to the observed p-value, and possible corrections for multiple observations out of which one focuses on the smallest p-value obtained (the "look-elsewhere effect", discussed in Section 40.3.2.2).

40.3.2.1 *Treatment of nuisance parameters for frequentist tests*

Suppose one wants to test hypothetical values of parameters $\boldsymbol{\theta}$, but the model also contains nuisance parameters $\boldsymbol{\nu}$. To find a p-value for $\boldsymbol{\theta}$ we can construct a test statistic $q_{\boldsymbol{\theta}}$ such that larger values constitute increasing incompatibility between the data and the hypothesis. Then for an observed value of the statistic $q_{\boldsymbol{\theta},\rm obs}$, the p-value of $\boldsymbol{\theta}$ is

$$p_{\boldsymbol{\theta}}(\boldsymbol{\nu}) = \int_{q_{\boldsymbol{\theta},\rm obs}}^{\infty} f(q_{\boldsymbol{\theta}}|\boldsymbol{\theta},\boldsymbol{\nu})\, dq_{\boldsymbol{\theta}} \ , \tag{40.48}$$

which depends in general on the nuisance parameters $\boldsymbol{\nu}$. In the strict frequentist approach, $\boldsymbol{\theta}$ is rejected only if the p-value is less than α for all possible values of the nuisance parameters.

The difficulty described above is effectively solved if we can define the test statistic $q_{\boldsymbol{\theta}}$ in such a way that its distribution $f(q_{\boldsymbol{\theta}}|\boldsymbol{\theta})$ is independent of the nuisance parameters. Although exact independence is only found in special cases, it can be achieved approximately by use of the *profile likelihood ratio*. This is given by the profile likelihood from Eq.(40.18) divided by the value of the likelihood at its maximum, *i.e.*, when evaluated with the ML estimators $\widehat{\boldsymbol{\theta}}$ and $\widehat{\boldsymbol{\nu}}$:

$$\lambda_p(\boldsymbol{\theta}) = \frac{L(\boldsymbol{\theta}, \widehat{\widehat{\boldsymbol{\nu}}}(\boldsymbol{\theta}))}{L(\widehat{\boldsymbol{\theta}}, \widehat{\boldsymbol{\nu}})} \ . \tag{40.49}$$

Wilks' theorem [9] states that, providing certain general conditions are satisfied, the distribution of $-2\ln\lambda_{\rm p}(\boldsymbol{\theta})$, under assumption of $\boldsymbol{\theta}$, approaches a χ^2 distribution in the limit where the data sample is very large, independent of the values of the nuisance parameters $\boldsymbol{\nu}$. Here the number of degrees of freedom is equal to the number of components of $\boldsymbol{\theta}$. More details on use of the profile likelihood are given in Refs. [21, 22] and in contributions to the PHYSTAT conferences [23]; explicit formulae for special cases can be found in Ref. [24]. Further discussion on how to incorporate systematic uncertainties into p-values can be found in Ref. [25].

Even with use of the profile likelihood ratio, for a finite data sample the p-value of hypothesized parameters $\boldsymbol{\theta}$ will retain in general some dependence on the nuisance parameters $\boldsymbol{\nu}$. Ideally one would find the the maximum of $p_\theta(\boldsymbol{\nu})$ from Eq. (40.48) explicitly, but that is often impractical. An approximate and computationally feasible technique is to use $p_\theta(\widehat{\widehat{\boldsymbol{\nu}}}(\theta))$, where $\widehat{\widehat{\boldsymbol{\nu}}}(\theta)$ are the profiled values of the nuisance parameters as defined in Section 40.2.2.2. The resulting p-value is correct if the true values of the nuisance parameters are equal to the profiled values used; otherwise it could be either too high or too low. This is discussed further in Section 40.4.2 on confidence intervals.

One may also treat model uncertainties in a Bayesian manner but then use the resulting model in a frequentist test. Suppose the uncertainty in a set of nuisance parameters $\boldsymbol{\nu}$ is characterized

Downloaded from https://academic.oup.com/ptep/article/2022/8/083C01/6651666 by KIT Library user on 27 September 2022

by a Bayesian prior p.d.f. $\pi(\boldsymbol{\nu})$. This can be used to construct the marginal (also called the prior predictive) model for the data $\boldsymbol{x}$ and parameters of interest $\boldsymbol{\theta}$,

$$P_{\rm m}(\boldsymbol{x}|\boldsymbol{\theta}) = \int P(\boldsymbol{x}|\boldsymbol{\theta},\boldsymbol{\nu})\pi(\boldsymbol{\nu})\,d\boldsymbol{\nu}\ . \tag{40.50}$$

The marginal model does not represent the probability of data that would be generated if one were really to repeat the experiment, as in that case one would assume that the nuisance parameters do not vary. Rather, the marginal model represents a situation in which every repetition of the experiment is carried out with new values of $\boldsymbol{\nu}$, randomly sampled from $\pi(\boldsymbol{\nu})$. It is in effect an average of models each with a given $\boldsymbol{\nu}$, where the average is carried out with respect to the prior p.d.f. $\pi(\boldsymbol{\nu})$.

The marginal model for the data $\boldsymbol{x}$ can be used to determine the distribution of a test statistic Q, which can be written

$$P_{\rm m}(Q|\boldsymbol{\theta}) = \int P(Q|\boldsymbol{\theta},\boldsymbol{\nu})\pi(\boldsymbol{\nu})\,d\boldsymbol{\nu}\ . \tag{40.51}$$

In a search for a new signal process, the test statistic can be based on the ratio of likelihoods corresponding to the experiments where signal and background events are both present, L_{s+b}, to that of background only, L_b. Often the likelihoods are evaluated with the profiled values of the nuisance parameters, which may give improved performance. It is important to note, however, that it is through use of the marginal model for the distribution of Q that the uncertainties related to the nuisance parameters are incorporated into the result of the test. Different choices for the test statistic itself only result in variations of the power of the test with respect to different alternatives.

40.3.2.2 *The look-elsewhere effect*

The "look-elsewhere effect" relates to multiple measurements used to test a single hypothesis. The classic example is when one searches in a distribution for a peak whose position is not predicted in advance. Here the no-peak hypothesis is tested using data in a given range of the distribution. In the frequentist approach the correct p-value of the no-peak hypothesis is the probability, assuming background only, to find a signal as significant as the one found or more so anywhere in the search region. This can be substantially higher than the probability to find a peak of equal or greater significance in the particular place where it appeared. There is in general some ambiguity as to what constitutes the relevant search region or even the broader set of relevant measurements. Although the desired p-value is well defined once the search region has been fixed, an exact treatment can require extensive computation.

The "brute-force" solution to this problem by Monte Carlo involves generating data under the background-only hypothesis and for each data set, fitting a peak of unknown position and recording a measure of its significance. To establish a discovery one often requires a p-value smaller than 2.87×10^{-7}, corresponding to a 5σ or larger effect. Determining this with Monte Carlo thus requires generating and fitting a very large number of experiments, perhaps several times 10^7. In contrast, if the position of the peak is fixed, then the fit to the distribution is much easier, and furthermore one can in many cases use formulae valid for sufficiently large samples that bypass completely the need for Monte Carlo (see, *e.g.*, [24]). However, this fixed-position or "local" p-value would not be correct in general, as it assumes the position of the peak was known in advance.

A method that allows one to modify the local p-value computed under assumption of a fixed position to obtain an approximation to the correct "global" value using a relatively simple calculation is described in Ref. [26]. Suppose a test statistic q_0, defined so that larger values indicate increasing disagreement with the data, is observed to have a value u. Furthermore suppose the model contains a nuisance parameter such as the peak position that is only defined under the signal model (there is no peak in the background-only model). An approximation for the global p-value is found to be

$$p_{\rm global} \approx p_{\rm local} + \langle N_u \rangle\ , \tag{40.52}$$

where $\langle N_u \rangle$, which is much smaller than one in cases of interest, is the mean number of "upcrossings" (as defined in [26]) of the statistic q_0 above the level u in the range of the nuisance parameter considered (*e.g.*, the mass range).

The value of $\langle N_u \rangle$ can be estimated from the number of upcrossings $\langle N_{u_0} \rangle$ above some much lower value, u_0, by using a relation due to Davis [27],

$$\langle N_u \rangle \approx \langle N_{u_0} \rangle e^{-(u-u_0)/2}\ . \tag{40.53}$$

By choosing u_0 sufficiently low, the value of $\langle N_u \rangle$ can be estimated by simulating only a very small number of experiments, or even from the observed data, rather than of the order 10^7 needed if one is dealing with a 5σ effect.

40.3.2.3 *Goodness-of-fit with the method of least squares*

When estimating parameters using the method of least squares, one obtains the minimum value of the quantity χ^2 (40.19). This statistic can be used to test the *goodness-of-fit*, *i.e.*, the test provides a measure of the significance of a discrepancy between the data and the hypothesized functional form used in the fit. It may also happen that no parameters are estimated from the data, but that one simply wants to compare a histogram, *e.g.*, a vector of Poisson distributed numbers $\boldsymbol{n} = (n_1, \ldots, n_N)$, with a hypothesis for their expectation values $\mu_i = E[n_i]$. As the distribution is Poisson with variances $\sigma_i^2 = \mu_i$, the χ^2 (40.19) becomes *Pearson's* χ^2 *statistic*,

$$\chi^2 = \sum_{i=1}^{N} \frac{(n_i - \mu_i)^2}{\mu_i}\ . \tag{40.54}$$

If the hypothesis $\boldsymbol{\mu} = (\mu_1, \ldots, \mu_N)$ is correct, and if the expected values μ_i in (40.54) are sufficiently large (or equivalently, if the measurements n_i can be treated as following a Gaussian distribution), then the χ^2 statistic will follow the χ^2 p.d.f. with the number of degrees of freedom equal to the number of measurements N minus the number of fitted parameters.

Alternatively, one may fit parameters and evaluate goodness-of-fit by minimizing $-2\ln\lambda$ from Eq. (40.16). One finds that the distribution of this statistic approaches the asymptotic limit faster than does Pearson's χ^2. Therefore if one uses the asymptotic χ^2 p.d.f. as the statistic's approximate sampling distribution to compute a p-value, one obtains in general a more accurate result from $-2\ln\lambda$ than from Pearson's χ^2 (see Ref. [8] and references therein).

Assuming the goodness-of-fit statistic follows a χ^2 p.d.f., the p-value for the hypothesis is then

$$p = \int_{\chi^2}^{\infty} f(z; n_{\rm d})\,dz\ , \tag{40.55}$$

where $f(z; n_{\rm d})$ is the χ^2 p.d.f. and $n_{\rm d}$ is the appropriate number of degrees of freedom. Values are shown in Fig. 40.1 or obtained, e.g., from the ROOT function `TMath::Prob`. If the asymptotic conditions for using the χ^2 p.d.f. do not hold, the statistic can still be defined as before, but its p.d.f. must be determined by other means in order to obtain the p-value, *e.g.*, using a Monte Carlo calculation.

Since the mean of the χ^2 distribution is equal to $n_{\rm d}$, one expects in a "reasonable" experiment to obtain $\chi^2 \approx n_{\rm d}$. Hence the quantity $\chi^2/n_{\rm d}$ is sometimes reported. Since the p.d.f. of $\chi^2/n_{\rm d}$ depends on $n_{\rm d}$, however, one must report $n_{\rm d}$ as well if one wishes to determine the p-value. The p-values obtained for different values of $\chi^2/n_{\rm d}$ are shown in Fig. 40.2.

If the minimized χ^2 value indicates a low level of agreement between data and hypothesis, one may be tempted to expect a high degree of uncertainty for any fitted parameters. Poor goodness-of-fit, however, does not mean that one will have large statistical errors for parameter estimates. If, for example, the error bars (or covariance matrix) used in constructing the χ^2 are underestimated, then this will lead to underestimated statistical errors for the fitted parameters and an increased value of the minimized χ^2. The standard deviations of estimators that one finds from, say, Eq. (40.13) reflect how widely the estimates would be distributed

Downloaded from https://academic.oup.com/ptep/article/2022/8/083C01/6651666 by KIT Library user on 27 September 2022

if one were to repeat the measurement many times, assuming that the hypothesis and measurement errors used in the χ^2 are also correct. They do not include the systematic error which may result from an incorrect hypothesis or incorrectly estimated measurement errors in the χ^2.

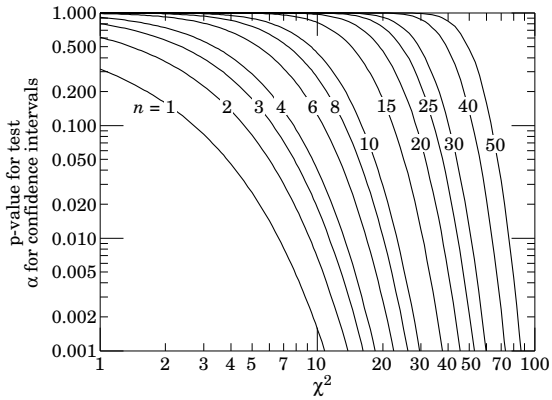

Figure 40.1: One minus the χ^2 cumulative distribution, $1 - F(\chi^2; n)$, for n degrees of freedom. This gives the p-value for the χ^2 goodness-of-fit test as well as one minus the coverage probability for confidence regions (see Sec. 40.4.2.2).

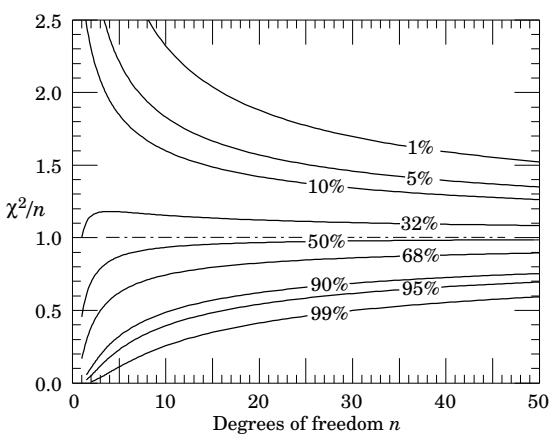

Figure 40.2: The 'reduced' χ^2, equal to χ^2/n, for n degrees of freedom. The curves show as a function of n the χ^2/n that corresponds to a given p-value.

40.3.3 *Bayes factors*

In Bayesian statistics, all of one's knowledge about a model is contained in its posterior probability, which one obtains using Bayes' theorem (Eq. (40.37)). Thus one could reject a hypothesis H if its posterior probability $P(H|\boldsymbol{x})$ is sufficiently small. The difficulty here is that $P(H|\boldsymbol{x})$ is proportional to the prior probability $P(H)$, and there will not be a consensus about the prior probabilities for the existence of new phenomena. Nevertheless one can construct a quantity called the Bayes factor (described below), which can be used to quantify the degree to which the data prefer one hypothesis over another, and is independent of their prior probabilities.

Consider two models (hypotheses), H_i and H_j, described by vectors of parameters $\boldsymbol{\theta}_i$ and $\boldsymbol{\theta}_j$, respectively. Some of the components will be common to both models and others may be distinct. The full prior probability for each model can be written in the form

$$\pi(H_i, \boldsymbol{\theta}_i) = P(H_i)\pi(\boldsymbol{\theta}_i|H_i) \ . \tag{40.56}$$

Here $P(H_i)$ is the overall prior probability for H_i, and $\pi(\boldsymbol{\theta}_i|H_i)$ is the normalized p.d.f. of its parameters. For each model, the posterior probability is found using Bayes' theorem,

$$P(H_i|\boldsymbol{x}) = \frac{\int P(\boldsymbol{x}|\boldsymbol{\theta}_i, H_i)P(H_i)\pi(\boldsymbol{\theta}_i|H_i)\, d\boldsymbol{\theta}_i}{P(\boldsymbol{x})} \ , \tag{40.57}$$

where the integration is carried out over the internal parameters $\boldsymbol{\theta}_i$ of the model. The ratio of posterior probabilities for the models is therefore

$$\frac{P(H_i|\boldsymbol{x})}{P(H_j|\boldsymbol{x})} = \frac{\int P(\boldsymbol{x}|\boldsymbol{\theta}_i, H_i)\pi(\boldsymbol{\theta}_i|H_i)\, d\boldsymbol{\theta}_i}{\int P(\boldsymbol{x}|\boldsymbol{\theta}_j, H_j)\pi(\boldsymbol{\theta}_j|H_j)\, d\boldsymbol{\theta}_j} \frac{P(H_i)}{P(H_j)} \ . \tag{40.58}$$

The *Bayes factor* is defined as

$$B_{ij} = \frac{\int P(\boldsymbol{x}|\boldsymbol{\theta}_i, H_i)\pi(\boldsymbol{\theta}_i|H_i)\, d\boldsymbol{\theta}_i}{\int P(\boldsymbol{x}|\boldsymbol{\theta}_j, H_j)\pi(\boldsymbol{\theta}_j|H_j)\, d\boldsymbol{\theta}_j} \ . \tag{40.59}$$

This gives what the ratio of posterior probabilities for models i and j would be if the overall prior probabilities for the two models were equal. If the models have no nuisance parameters, *i.e.*, no internal parameters described by priors, then the Bayes factor is simply the likelihood ratio. The Bayes factor therefore shows by how much the probability ratio of model i to model j changes in the light of the data, and thus can be viewed as a numerical measure of evidence supplied by the data in favor of one hypothesis over the other.

Although the Bayes factor is by construction independent of the overall prior probabilities $P(H_i)$ and $P(H_j)$, it does require priors for all internal parameters of a model, *i.e.*, one needs the functions $\pi(\boldsymbol{\theta}_i|H_i)$ and $\pi(\boldsymbol{\theta}_j|H_j)$. In a Bayesian analysis where one is only interested in the posterior p.d.f. of a parameter, it may be acceptable to take an unnormalizable function for the prior (an improper prior) as long as the product of likelihood and prior can be normalized. Improper priors are, however, only defined up to an arbitrary multiplicative constant, and so the Bayes factor would depend on this constant. Furthermore, although the range of a constant normalized prior is unimportant for parameter determination (provided it is wider than the likelihood), this is not so for the Bayes factor when such a prior is used for only one of the hypotheses. So to compute a Bayes factor, all internal parameters must be described by normalized priors that represent meaningful probabilities over the entire range where they are defined.

An exception to this rule may be considered when the identical parameter appears in the models for both numerator and denominator of the Bayes factor. In this case one can argue that the arbitrary constants would cancel. One must exercise some caution, however, as parameters with the same name and physical meaning may still play different roles in the two models.

Both integrals in Equation (40.59) are of the form

$$m = \int P(\boldsymbol{x}|\boldsymbol{\theta})\pi(\boldsymbol{\theta})\, d\boldsymbol{\theta} \ , \tag{40.60}$$

which is similar to the marginal likelihood seen previously in Eq. (40.50) (in some fields this quantity is called the *evidence*). Computing marginal likelihoods can be difficult; in many cases it can be done with the nested sampling algorithm [28] as implemented, *e.g.*, in the program `MultiNest` [29]. A review of Bayes factors can be found in Ref. [30].

40.4 Intervals and limits

When the goal of an experiment is to determine a parameter θ, the result is usually expressed by quoting, in addition to the point estimate, some sort of interval which reflects the statistical precision of the measurement. In the simplest case, this can be given by the parameter's estimated value $\widehat{\theta}$ plus or minus an estimate of the standard deviation of $\widehat{\theta}$, $\widehat{\sigma}_{\widehat{\theta}}$. If, however, the p.d.f. of the estimator is not Gaussian or if there are physical boundaries on the possible values of the parameter, then one usually quotes instead an interval according to one of the procedures described below.

In reporting an interval or limit, the experimenter may wish to

Downloaded from https://academic.oup.com/ptep/article/2022/8/083C01/6651666 by KIT Library user on 27 September 2022

- communicate as objectively as possible the result of the experiment;
- provide an interval that is constructed to cover on average the true value of the parameter with a specified probability;
- provide the information needed by the consumer of the result to draw conclusions about the parameter or to make a particular decision;
- draw conclusions about the parameter that incorporate stated prior beliefs.

With a sufficiently large data sample, the point estimate and standard deviation (or for the multiparameter case, the parameter estimates and covariance matrix) satisfy essentially all of these goals. For small data samples, no single method for quoting an interval will achieve all of them.

In addition to the goals listed above, the choice of method may be influenced by practical considerations such as ease of producing an interval from the results of several measurements. Of course the experimenter is not restricted to quoting a single interval or limit; one may choose, for example, first to communicate the result with a confidence interval having certain frequentist properties, and then in addition to draw conclusions about a parameter using a judiciously chosen subjective Bayesian prior. It is recommended, however, that there be a clear separation between these two aspects of reporting a result. In the remainder of this section, we assess the extent to which various types of intervals achieve the goals stated here.

40.4.1 *Bayesian intervals*

As described in Sec. 40.2.6, a Bayesian posterior probability may be used to determine regions that will have a given probability of containing the true value of a parameter. In the single parameter case, for example, an interval (called a Bayesian or credible interval) $[\theta_{\rm lo}, \theta_{\rm up}]$ can be determined which contains a given fraction $1-\alpha$ of the posterior probability, *i.e.*,

$$1-\alpha = \int_{\theta_{\rm lo}}^{\theta_{\rm up}} p(\theta|\boldsymbol{x})\, d\theta \ . \tag{40.61}$$

Sometimes an upper or lower limit is desired, *i.e.*, $\theta_{\rm lo}$ or $\theta_{\rm up}$ can be set to a physical boundary or to plus or minus infinity. In other cases, one might be interested in the set of θ values for which $p(\theta|\boldsymbol{x})$ is higher than for any θ not belonging to the set, which may constitute a single interval or a set of disjoint regions; these are called highest posterior density (HPD) intervals. Note that HPD intervals are not invariant under a nonlinear transformation of the parameter.

If a parameter is constrained to be non-negative, then the prior p.d.f. can simply be set to zero for negative values. An important example is the case of a Poisson variable n, which counts signal events with unknown mean s, as well as background with mean b, assumed known. For the signal mean s, one often uses the prior

$$\pi(s) = \begin{cases} 0 & s < 0 \\ 1 & s \geq 0 \end{cases} \ . \tag{40.62}$$

This prior may be regarded as providing an interval whose frequentist properties can be studied, rather than as representing a degree of belief. For example, to obtain an upper limit on s, one may proceed as follows. The likelihood for s is given by the Poisson distribution for n with mean $s+b$,

$$P(n|s) = \frac{(s+b)^n}{n!} e^{-(s+b)} \ , \tag{40.63}$$

along with the prior (40.62) in (40.37) gives the posterior density for s. An upper limit $s_{\rm up}$ at confidence level (or here, rather, *credibility* level) $1-\alpha$ can be obtained by requiring

$$1-\alpha = \int_{-\infty}^{s_{\rm up}} p(s|n) ds = \frac{\int_{-\infty}^{s_{\rm up}} P(n|s)\, \pi(s)\, ds}{\int_{-\infty}^{\infty} P(n|s)\, \pi(s)\, ds} \ , \tag{40.64}$$

where the lower limit of integration is effectively zero because of the cut-off in $\pi(s)$. By relating the integrals in Eq. (40.64) to incomplete gamma functions, the solution for the upper limit is found to be

$$s_{\rm up} = \frac{1}{2} F_{\chi^2}^{-1}\left[p, 2(n+1)\right] - b \ , \tag{40.65}$$

where $F_{\chi^2}^{-1}$ is the quantile of the χ^2 distribution (inverse of the cumulative distribution). Here the quantity p is

$$p = 1 - \alpha \left(1 - F_{\chi^2}\left[2b, 2(n+1)\right]\right) \ , \tag{40.66}$$

where F_{χ^2} is the cumulative χ^2 distribution. For both F_{χ^2} and $F_{\chi^2}^{-1}$ above, the argument $2(n+1)$ gives the number of degrees of freedom. For the special case of $b=0$, the limit reduces to

$$s_{\rm up} = \frac{1}{2} F_{\chi^2}^{-1}(1-\alpha; 2(n+1)) \ . \tag{40.67}$$

It happens that for the case of $b=0$, the upper limit from Eq. (40.67) coincides numerically with the frequentist upper limit discussed in Section 40.4.2.3. Values for $1-\alpha = 0.9$ and 0.95 are given by the values $\mu_{\rm up}$ in Table 40.3. The frequentist properties of confidence intervals for the Poisson mean found in this way are discussed in Refs. [2] and [31].

As in any Bayesian analysis, it is important to show how the result changes under assumption of different prior probabilities. For example, one could consider the Jeffreys prior as described in Sec. 40.2.6. For this problem one finds the Jeffreys prior $\pi(s) \propto 1/\sqrt{s+b}$ for $s \geq 0$ and zero otherwise. As with the constant prior, one would not regard this as representing one's prior beliefs about s, both because it is improper and also as it depends on b. Rather it is used with Bayes' theorem to produce an interval whose frequentist properties can be studied.

If the model contains nuisance parameters then these are eliminated by marginalizing, as in Eq. (40.43), to obtain the p.d.f. for the parameters of interest. For example, if the parameter b in the Poisson counting problem above were to be characterized by a prior p.d.f. $\pi(b)$, then one would first use Bayes' theorem to find $p(s,b|n)$. This is then marginalized to find $p(s|n) = \int p(s,b|n)\pi(b)\, db$, from which one may determine an interval for s. One may not be certain whether to extend a model by including more nuisance parameters. In this case, a Bayes factor may be used to determine to what extent the data prefer a model with additional parameters, as described in Section 40.3.3.

40.4.2 *Frequentist confidence intervals*

The unqualified phrase "confidence intervals" refers to frequentist intervals obtained with a procedure due to Neyman [32], described below. The boundary of the interval (or in the multiparameter case, region) is given by a specific function of the data, which would fluctuate if one were to repeat the experiment many times. The *coverage probability* refers to the fraction of intervals in such an ensemble that contain the true parameter value. Confidence intervals are constructed so as to have a coverage probability greater than or equal to a given *confidence level*, regardless of the true parameter's value. It is important to note that in the frequentist approach, such a probability is not meaningful for a fixed interval. In this section we discuss several techniques for producing intervals that have, at least approximately, this property of coverage.

40.4.2.1 *The Neyman construction for confidence intervals*

Consider a p.d.f. $f(x;\theta)$ where x represents the outcome of the experiment and θ is the unknown parameter for which we want to construct a confidence interval. The variable x could (and often does) represent an estimator for θ. Using $f(x;\theta)$, we can find using a pre-defined rule and probability $1-\alpha$ for every value of θ, a set of values $x_1(\theta,\alpha)$ and $x_2(\theta,\alpha)$ such that

$$P(x_1 < x < x_2; \theta) = \int_{x_1}^{x_2} f(x;\theta)\, dx \geq 1-\alpha \ . \tag{40.68}$$

If x is discrete, the integral is replaced by the corresponding sum. In that case there may not exist a range of x values whose summed probability is exactly equal to a given value of $1-\alpha$, and one requires by convention $P(x_1 < x < x_2; \theta) \geq 1-\alpha$.

Downloaded from https://academic.oup.com/ptep/article/2022/8/083C01/6651666 by KIT Library user on 27 September 2022

This is illustrated for continuous x in Fig. 40.3: a horizontal line segment $[x_1(\theta,\alpha), x_2(\theta,\alpha)]$ is drawn for representative values of θ. The union of such intervals for all values of θ, designated in the figure as $D(\alpha)$, is known as a *confidence belt*. Typically the curves $x_1(\theta,\alpha)$ and $x_2(\theta,\alpha)$ are monotonic functions of θ, which we assume for this discussion.

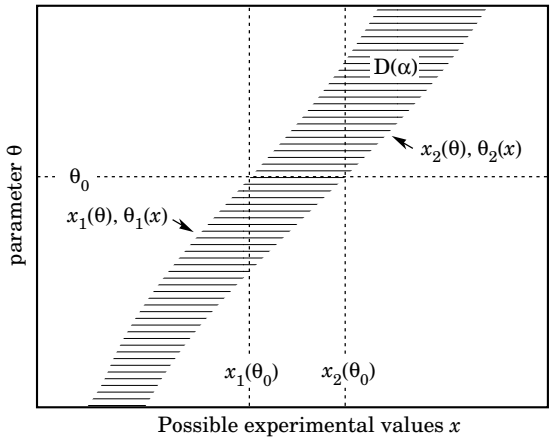

Figure 40.3: Construction of the confidence belt (see text).

Upon performing an experiment to measure x and obtaining a value x_0, one draws a vertical line through x_0. The confidence interval for θ is the set of all values of θ for which the corresponding line segment $[x_1(\theta,\alpha), x_2(\theta,\alpha)]$ is intercepted by this vertical line. Such confidence intervals are said to have a *confidence level* (CL) equal to $1-\alpha$.

Now suppose that the true value of θ is θ_0, indicated in the figure. We see from the figure that θ_0 lies between $\theta_1(x)$ and $\theta_2(x)$ if and only if x lies between $x_1(\theta_0)$ and $x_2(\theta_0)$. The two events thus have the same probability, and since this is true for any value θ_0, we can drop the subscript 0 and obtain

$$1-\alpha = P(x_1(\theta) < x < x_2(\theta)) = P(\theta_2(x) < \theta < \theta_1(x)) \ . \quad (40.69)$$

In this probability statement, $\theta_1(x)$ and $\theta_2(x)$, *i.e.*, the endpoints of the interval, are the random variables and θ is an unknown constant. If the experiment were to be repeated a large number of times, the interval $[\theta_1, \theta_2]$ would vary, covering the fixed value θ in a fraction $1-\alpha$ of the experiments.

The condition of coverage in Eq. (40.68) does not determine x_1 and x_2 uniquely, and additional criteria are needed. One possibility is to choose *central intervals* such that the probabilities to find x below x_1 and above x_2 are each $\alpha/2$. In other cases, one may want to report only an upper or lower limit, in which case one of $P(x \le x_1)$ or $P(x \ge x_2)$ can be set to α and the other to zero. Another principle based on *likelihood ratio ordering* for determining which values of x should be included in the confidence belt is discussed below.

When the observed random variable x is continuous, the coverage probability obtained with the Neyman construction is $1-\alpha$, regardless of the true value of the parameter. Because of the requirement $P(x_1 < x < x_2) \ge 1-\alpha$ when x is discrete, one obtains in that case confidence intervals that include the true parameter with a probability greater than or equal to $1-\alpha$.

An equivalent method of constructing confidence intervals is to consider a test (see Sec. 40.3) of the hypothesis that the parameter's true value is θ (assume one constructs a test for all physical values of θ). One then excludes all values of θ where the hypothesis would be rejected in a test of size α or less. The remaining values constitute the confidence interval at confidence level $1-\alpha$. If the critical region of the test is characterized by having a p-value $p_\theta \le \alpha$, then the endpoints of the confidence interval are found in practice by solving $p_\theta = \alpha$ for θ.

In the procedure outlined above, one is still free to choose the test to be used; this corresponds to the freedom in the Neyman construction as to which values of the data are included in the confidence belt. One possibility is to use a test statistic based on the *likelihood ratio*,

$$\lambda(\theta) = \frac{f(x;\theta)}{f(x;\widehat{\theta}\,)} \ , \quad (40.70)$$

where $\widehat{\theta}$ is the value of the parameter which, out of all allowed values, maximizes $f(x;\theta)$. The confidence belt is taken to contain the values of x that give the greatest values of $\lambda(\theta)$. This results in the intervals described in Ref. [33] by Feldman and Cousins.

If the model contains nuisance parameters $\boldsymbol{\nu}$, then these can be incorporated into the test (or the p-values) used to determine the limit by profiling as discussed in Section 40.3.2.1. As mentioned there, the strict frequentist approach is to regard the parameter of interest θ as excluded only if it is rejected for all possible values of $\boldsymbol{\nu}$. The resulting interval for θ will then cover the true value with a probability greater than or equal to the nominal confidence level for all points in $\boldsymbol{\nu}$-space.

If the p-value is based on the profiled values of the nuisance parameters, *i.e.*, with $\boldsymbol{\nu} = \widehat{\widehat{\boldsymbol{\nu}}}(\theta)$ used in Eq. (40.48), then the resulting interval for the parameter of interest will have the correct coverage if the true values of $\boldsymbol{\nu}$ are equal to the profiled values. Otherwise the coverage probability may be too high or too low. This procedure has been called *profile construction* in particle physics [34] (see also [25]).

40.4.2.2 *Gaussian distributed measurements*

An important example of constructing a confidence interval is when the data consists of a single random variable x that follows a Gaussian distribution; this is often the case when x represents an estimator for a parameter and one has a sufficiently large data sample. If there is more than one parameter being estimated, the multivariate Gaussian is used. For the univariate case with known σ, the probability that the measured value x will fall within $\pm\delta$ of the true value μ is

$$\begin{aligned} 1-\alpha &= \frac{1}{\sqrt{2\pi}\sigma}\int_{\mu-\delta}^{\mu+\delta} e^{-(x-\mu)^2/2\sigma^2}\,dx \\ &= \mathrm{erf}\left(\frac{\delta}{\sqrt{2}\,\sigma}\right) = 2\Phi\left(\frac{\delta}{\sigma}\right) - 1 \ , \end{aligned} \quad (40.71)$$

where erf is the Gaussian error function, which is rewritten in the final equality using Φ, the Gaussian cumulative distribution. Fig. 40.4 shows a $\delta = 1.64\sigma$ confidence interval unshaded. The choice $\delta = \sigma$ gives an interval called the *standard error* which has $1-\alpha = 68.27\%$ if σ is known. Values of α for other frequently used choices of δ are given in Table 40.1.

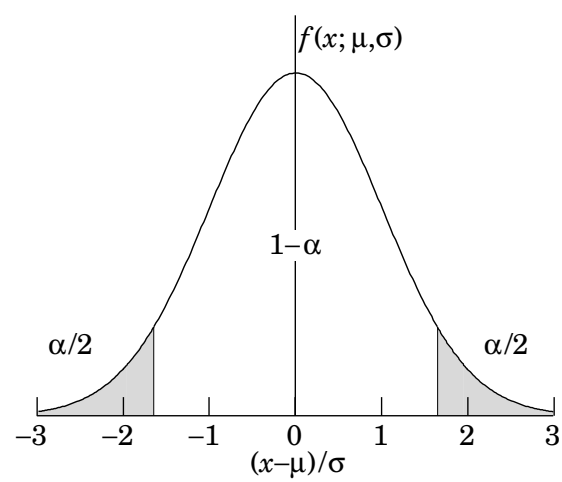

Figure 40.4: Illustration of a symmetric 90% confidence interval (unshaded) for a Gaussian-distributed measurement of a single quantity. Integrated probabilities, defined by $\alpha = 0.1$, are as shown.

Downloaded from https://academic.oup.com/ptep/article/2022/8/083C01/6651666 by KIT Library user on 27 September 2022

Table 40.1: Area of the tails α outside $\pm\delta$ from the mean of a Gaussian distribution.

α	δ	α	δ
0.3173	1σ	0.2	1.28σ
4.55×10^{-2}	2σ	0.1	1.64σ
2.7×10^{-3}	3σ	0.05	1.96σ
6.3×10^{-5}	4σ	0.01	2.58σ
5.7×10^{-7}	5σ	0.001	3.29σ
2.0×10^{-9}	6σ	10^{-4}	3.89σ

We can set a one-sided (upper or lower) limit by excluding above $x+\delta$ (or below $x-\delta$). The values of α for such limits are half the values in Table 40.1.

The relation (40.71) can be re-expressed using the cumulative distribution function for the χ^2 distribution as

$$\alpha = 1 - F(\chi^2; n) \ , \tag{40.72}$$

for $\chi^2 = (\delta/\sigma)^2$ and $n = 1$ degree of freedom. This can be seen as the $n = 1$ curve in Fig. 40.1 or obtained by using, e.g., the ROOT function `TMath::Prob`. For multivariate measurements of, say, M parameter estimates $\widehat{\boldsymbol{\theta}} = (\widehat{\theta}_1, \ldots, \widehat{\theta}_M)$, construction of the confidence region requires the full covariance matrix $V_{ij} = \mathrm{cov}[\widehat{\theta}_i, \widehat{\theta}_j]$, which can be estimated as described in Sections 40.2.2 and 40.2.3. Under fairly general conditions with the methods of maximum-likelihood or least-squares in the large sample limit, the estimators will be distributed according to a multivariate Gaussian centered about the true (unknown) values $\boldsymbol{\theta}$, and furthermore, the likelihood function itself will take on a Gaussian shape.

The standard error ellipse for the pair $(\widehat{\theta}_i, \widehat{\theta}_j)$ is shown in Fig. 40.5, corresponding to a contour $\chi^2 = \chi^2_{\min} + 1$ or $\ln L = \ln L_{\max} - 1/2$. The ellipse is centered about the estimated values $\widehat{\boldsymbol{\theta}}$, and the tangents to the ellipse give the standard deviations of the estimators, σ_i and σ_j. The angle of the major axis of the ellipse is given by

$$\tan 2\phi = \frac{2\rho_{ij}\sigma_i\sigma_j}{\sigma_j^2 - \sigma_i^2} \ , \tag{40.73}$$

where $\rho_{ij} = \mathrm{cov}[\widehat{\theta}_i, \widehat{\theta}_j]/\sigma_i\sigma_j$ is the correlation coefficient.

The correlation coefficient can be visualized as the fraction of the distance σ_i from the ellipse's horizontal center-line at which the ellipse becomes tangent to vertical, *i.e.*, at the distance $\rho_{ij}\sigma_i$ below the center-line as shown. As ρ_{ij} goes to $+1$ or -1, the ellipse thins to a diagonal line.

It could happen that one of the parameters, say, θ_j, is known from previous measurements to a precision much better than σ_j, so that the current measurement contributes almost nothing to the knowledge of θ_j. However, the current measurement of θ_i and its dependence on θ_j may still be important. In this case, instead of quoting both parameter estimates and their correlation, one sometimes reports the value of θ_i, which minimizes χ^2 at a fixed value of θ_j, such as the PDG best value. This θ_i value lies along the dotted line between the points where the ellipse becomes tangent to vertical, and has statistical error σ_{inner} as shown on the figure, where $\sigma_{\mathrm{inner}} = (1-\rho_{ij}^2)^{1/2}\sigma_i$. Instead of the correlation ρ_{ij}, one reports the dependency $d\widehat{\theta}_i/d\theta_j$, which is the slope of the dotted line. This slope is related to the correlation coefficient by $d\widehat{\theta}_i/d\theta_j = \rho_{ij} \times \frac{\sigma_i}{\sigma_j}$.

As in the single-variable case, because of the symmetry of the Gaussian function between $\boldsymbol{\theta}$ and $\widehat{\boldsymbol{\theta}}$, one finds that contours of constant $\ln L$ or χ^2 cover the true values with a certain, fixed probability. That is, the confidence region is determined by

$$\ln L(\boldsymbol{\theta}) \geq \ln L_{\max} - \Delta \ln L \ , \tag{40.74}$$

or where a χ^2 has been defined for use with the method of least-squares,

$$\chi^2(\boldsymbol{\theta}) \leq \chi^2_{\min} + \Delta\chi^2 \ . \tag{40.75}$$

Values of $\Delta\chi^2$ or $2\Delta\ln L$ are given in Table 40.2 for several values of the coverage probability $1-\alpha$ and number of fitted parameters

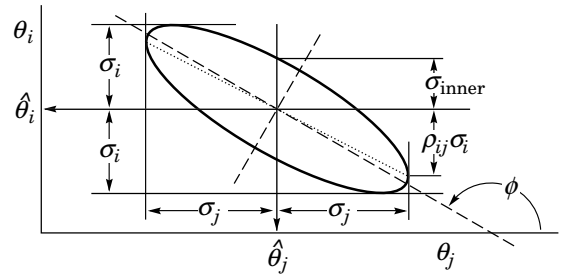

Figure 40.5: Standard error ellipse for the estimators $\widehat{\theta}_i$ and $\widehat{\theta}_j$. In the case shown the correlation is negative.

M. For Gaussian distributed data, these are related by $\Delta\chi^2 = 2\Delta\ln L = F^{-1}_{\chi^2_M}(1-\alpha)$, where $F^{-1}_{\chi^2_M}$ is the chi-square quantile (inverse of the cumulative distribution) for M degrees of freedom.

Table 40.2: Values of $\Delta\chi^2$ or $2\Delta\ln L$ corresponding to a coverage probability $1-\alpha$ in the large data sample limit, for joint estimation of M parameters.

$(1-\alpha)$ (%)	$M=1$	$M=2$	$M=3$
68.27	1.00	2.30	3.53
90.	2.71	4.61	6.25
95.	3.84	5.99	7.82
95.45	4.00	6.18	8.03
99.	6.63	9.21	11.34
99.73	9.00	11.83	14.16

For non-Gaussian data samples, the probability for the regions determined by Equations (40.74) or (40.75) to cover the true value of $\boldsymbol{\theta}$ becomes independent of $\boldsymbol{\theta}$ only in the large-sample limit. So for a finite data sample these are not exact confidence regions according to our previous definition. Nevertheless, they can still have a coverage probability only weakly dependent on the true parameter, and approximately as given in Table 40.2. In any case, the coverage probability of the intervals or regions obtained according to this procedure can in principle be determined as a function of the true parameter(s), for example, using a Monte Carlo calculation.

One of the practical advantages of intervals that can be constructed from the log-likelihood function or χ^2 is that it is relatively simple to produce the interval for the combination of several experiments. If N independent measurements result in log-likelihood functions $\ln L_i(\boldsymbol{\theta})$, then the combined log-likelihood function is simply the sum,

$$\ln L(\boldsymbol{\theta}) = \sum_{i=1}^{N} \ln L_i(\boldsymbol{\theta}) \ . \tag{40.76}$$

This can then be used to determine an approximate confidence interval or region with Eq. (40.74), just as with a single experiment.

40.4.2.3 *Poisson or binomial data*

Another important class of measurements consists of counting a certain number of events, n. In this section, we will assume these are all events of the desired type, *i.e.*, there is no background. If n represents the number of events produced in a reaction with cross section σ, say, in a fixed integrated luminosity $\mathcal{L}$, then it follows a Poisson distribution with mean $\mu = \sigma\mathcal{L}$. If, on the other hand, one has selected a larger sample of N events and found n of them to have a particular property, then n follows a binomial distribution where the parameter p gives the probability for the event to possess the property in question. This is appropriate, *e.g.*, for estimates of branching ratios or selection efficiencies based on a given total number of events.

For the case of Poisson distributed n, limits on the mean value μ can be found from the Neyman procedure as discussed in Sec-

Downloaded from https://academic.oup.com/ptep/article/2022/8/083C01/6651666 by KIT Library user on 27 September 2022

tion 40.4.2.1 with n used directly as the statistic x . The upper and lower limits are found to be

$$\mu_{\rm lo} = \frac{1}{2} F^{-1}_{\chi^2}(\alpha_{\rm lo}; 2n) \ , \tag{40.77a}$$

$$\mu_{\rm up} = \frac{1}{2} F^{-1}_{\chi^2}(1-\alpha_{\rm up}; 2(n+1)) \ , \tag{40.77b}$$

where confidence levels of $1-\alpha_{\rm lo}$ and $1-\alpha_{\rm up}$ refer separately to the corresponding intervals $\mu \geq \mu_{\rm lo}$ and $\mu \leq \mu_{\rm up}$, and $F^{-1}_{\chi^2}$ is the quantile of the χ^2 distribution (inverse of the cumulative distribution). For central confidence intervals at confidence level $1-\alpha$, set $\alpha_{\rm lo} = \alpha_{\rm up} = \alpha/2$.

Table 40.3: Lower and upper (one-sided) limits for the mean μ of a Poisson variable given n observed events in the absence of background, for confidence levels of 90% and 95%.

	$1-\alpha$ =90%		$1-\alpha$ =95%	
n	$\mu_{\rm lo}$	$\mu_{\rm up}$	$\mu_{\rm lo}$	$\mu_{\rm up}$
0	–	2.30	–	3.00
1	0.105	3.89	0.051	4.74
2	0.532	5.32	0.355	6.30
3	1.10	6.68	0.818	7.75
4	1.74	7.99	1.37	9.15
5	2.43	9.27	1.97	10.51
6	3.15	10.53	2.61	11.84
7	3.89	11.77	3.29	13.15
8	4.66	12.99	3.98	14.43
9	5.43	14.21	4.70	15.71
10	6.22	15.41	5.43	16.96

It happens that the upper limit from Eq. (40.77b) coincides numerically with the Bayesian upper limit for a Poisson parameter, using a uniform prior p.d.f. for μ. Values for confidence levels of 90% and 95% are shown in Table 40.3. For the case of binomially distributed n successes out of N trials with probability of success p, the upper and lower limits on p are found to be

$$p_{\rm lo} = \frac{nF^{-1}_F[\alpha_{\rm lo}; 2n, 2(N-n+1)]}{N-n+1 \ + \ nF^{-1}_F[\alpha_{\rm lo}; 2n, 2(N-n+1)]} \ , \tag{40.78a}$$

$$p_{\rm up} = \frac{(n+1)F^{-1}_F[1-\alpha_{\rm up}; 2(n+1), 2(N-n)]}{(N-n) \ + \ (n+1)F^{-1}_F[1-\alpha_{\rm up}; 2(n+1), 2(N-n)]} \ . \tag{40.78b}$$

Here F^{-1}_F is the quantile of the F distribution (also called the Fisher–Snedecor distribution; see Ref. [4]).

40.4.2.4 *Parameter exclusion in cases of low sensitivity*

An important example of a statistical test arises in the search for a new signal process. Suppose the parameter μ is defined such that it is proportional to the signal cross section. A statistical test may be carried out for hypothesized values of μ, which may be done by computing a p-value, p_μ, for all μ. Those values not rejected in a test of size α, *i.e.*, for which one does not find $p_\mu \leq \alpha$, constitute a confidence interval with confidence level $1-\alpha$.

In general one will find that for some regions in the parameter space of the signal model, the predictions for data are almost indistinguishable from those of the background-only model. This corresponds to the case where μ is very small, as would occur, *e.g.*, in a search for a new particle with a mass so high that its production rate in a given experiment is negligible. That is, one has essentially no experimental sensitivity to such a model.

One would prefer that if the sensitivity to a model (or a point in a model's parameter space) is very low, then it should not be excluded. Even if the outcomes predicted with or without signal are identical, however, the probability to reject the signal model will equal α, the type-I error rate. As one often takes α to be 5%, this would mean that in a large number of searches covering a broad range of a signal model's parameter space, there would inevitably be excluded regions in which the experimental sensitivity is very small, and thus one may question whether it is justified to regard such parameter values as disfavored.

Exclusion of models to which one has little or no sensitivity occurs, for example, if the data fluctuate very low relative to the expectation of the background-only hypothesis. In this case the resulting upper limit on μ may be anomalously low. As a means of controlling this effect one often determines the mean or median limit under assumption of the background-only hypothesis, as discussed in Sec. 40.5.

One way to mitigate the problem of excluding models to which one is not sensitive is the $\mathrm{CL_s}$ method, where the measure used to test a parameter is increased for decreasing sensitivity [35, 36]. The procedure is based on a statistic called $\mathrm{CL_s}$, which is defined as

$$\mathrm{CL_s} = \frac{p_\mu}{1-p_{\rm b}} \ , \tag{40.79}$$

where $p_{\rm b}$ is the p-value of the background-only hypothesis. In the usual formulation of the method, both p_μ and $p_{\rm b}$ are defined using a single test statistic, and the definition of $\mathrm{CL_s}$ above assumes this statistic is continuous; more details can be found in Refs. [35, 36].

A point in a model's parameter space is regarded as excluded if one finds $\mathrm{CL_s} \leq \alpha$. As the denominator in Eq. (40.79) is always less than or equal to unity, the exclusion criterion based on $\mathrm{CL_s}$ is more stringent than the usual requirement $p_\mu \leq \alpha$. In this sense the $\mathrm{CL_s}$ procedure is conservative, and the coverage probability of the corresponding intervals will exceed the nominal confidence level $1-\alpha$. If the experimental sensitivity to a given value of μ is very low, then one finds that as p_μ decreases, so does the denominator $1-p_{\rm b}$, and thus the condition $\mathrm{CL_s} \leq \alpha$ is effectively prevented from being satisfied. In this way the exclusion of parameters in the case of low sensitivity is suppressed.

The $\mathrm{CL_s}$ procedure has the attractive feature that the resulting intervals coincide with those obtained from the Bayesian method in two important cases: the mean value of a Poisson or Gaussian distributed measurement with a constant prior. The $\mathrm{CL_s}$ intervals overcover for all values of the parameter μ, however, by an amount that depends on μ.

The problem of excluding parameter values to which one has little sensitivity is particularly acute when one wants to set a one-sided limit, *e.g.*, an upper limit on a cross section. Here one tests a value of a rate parameter μ against the alternative of a lower rate, and therefore the critical region of the test is taken to correspond to data outcomes with a low event yield. If the number of events found in the search region fluctuates low enough, however, it can happen that all physically meaningful signal parameter values, including those to which one has very little sensitivity, are rejected by the test.

Another solution to this problem, therefore, is to replace the one-sided test by one based on the likelihood ratio, where the critical region is not restricted to low rates. This is the approach followed in the Feldman-Cousins procedure described in Section 40.4.2.1. The critical region for the test of a given value of μ contains data values characteristic of both higher and lower rates. As a result, for a given observed rate one can in general obtain a two-sided interval. If, however, the parameter estimate $\hat{\mu}$ is sufficiently close to the lower limit of zero, then only high values of μ are rejected, and the lower edge of the confidence interval is at zero. Note, however, that the coverage property of $1-\alpha$ pertains to the entire interval, not to the probability for the upper edge $\mu_{\rm up}$ to be greater than the true value μ. For parameter estimates increasingly far away from the boundary, *i.e.*, for increasing signal significance, the point $\mu = 0$ is excluded and the interval has nonzero upper and lower edges.

An additional difficulty arises when a parameter estimate is not significantly far away from the boundary, in which case it is natural to report a one-sided confidence interval (often an upper limit). It is straightforward to force the Neyman prescription to produce only an upper limit by setting $x_2 = \infty$ in Eq. (40.68). Then x_1 is uniquely determined and the upper limit can be obtained. If, however, the data come out such that the parameter estimate is not so close to the boundary, one might wish to report a central confidence interval (*i.e.*, an interval based on a two-sided test with equal upper and lower tail areas). As pointed out by Feldman and

Downloaded from https://academic.oup.com/ptep/article/2022/8/083C01/6651666 by KIT Library user on 27 September 2022

Cousins [33], if the decision to report an upper limit or two-sided interval is made by looking at the data ("flip-flopping"), then in general there will be parameter values for which the resulting intervals have a coverage probability less than $1-\alpha$. With the confidence intervals suggested in [33], the prescription determines whether the interval is one- or two-sided in a way which preserves the coverage probability (and are thus said to be *unified*).

The intervals according to this method for the mean of Poisson variable in the absence of background are given in Table 40.4. (Note that α in Ref. [33] is defined following Neyman [32] as the coverage probability; this is opposite the modern convention used here in which the coverage probability is $1-\alpha$.) The values of $1-\alpha$ given here refer to the coverage of the true parameter by the whole interval $[\mu_1, \mu_2]$. In Table 40.3 for the one-sided upper limit, however, $1-\alpha$ refers to the probability to have $\mu_{\rm up} \geq \mu$ (or $\mu_{\rm lo} \leq \mu$ for lower limits).

Table 40.4: Unified confidence intervals $[\mu_1, \mu_2]$ for a the mean of a Poisson variable given n observed events in the absence of background, for confidence levels of 90% and 95%.

	$1-\alpha$ =90%		$1-\alpha$ =95%	
n	μ_1	μ_2	μ_1	μ_2
0	0.00	2.44	0.00	3.09
1	0.11	4.36	0.05	5.14
2	0.53	5.91	0.36	6.72
3	1.10	7.42	0.82	8.25
4	1.47	8.60	1.37	9.76
5	1.84	9.99	1.84	11.26
6	2.21	11.47	2.21	12.75
7	3.56	12.53	2.58	13.81
8	3.96	13.99	2.94	15.29
9	4.36	15.30	4.36	16.77
10	5.50	16.50	4.75	17.82

A potential difficulty with unified intervals arises if, for example, one constructs such an interval for a Poisson parameter s of some yet to be discovered signal process with, say, $1-\alpha = 0.9$. If the true signal parameter is zero, or in any case much less than the expected background, one will usually obtain a one-sided upper limit on s. In a certain fraction of the experiments, however, a two-sided interval for s will result. Since, however, one typically chooses $1-\alpha$ to be only 0.9 or 0.95 when setting limits, the value $s = 0$ may be found below the lower edge of the interval before the existence of the effect is well established. It must then be communicated carefully that in excluding $s = 0$ at, say, 90% or 95% confidence level from the interval, one is not necessarily claiming to have discovered the effect, for which one would usually require a higher level of significance (*e.g.*, 5 σ).

Another possibility is to construct a Bayesian interval as described in Section 40.4.1. The presence of the boundary can be incorporated simply by setting the prior density to zero in the unphysical region. More specifically, the prior may be chosen using formal rules such as the reference prior or Jeffreys prior mentioned in Sec. 40.2.6.

In particle physics a widely used prior for the mean μ of a Poisson distributed measurement has been the uniform distribution for $\mu \geq 0$. This prior does not follow from any fundamental rule nor can it be regarded as reflecting a reasonable degree of belief, since the prior probability for μ to lie between any two finite values is zero. The procedure above can be more appropriately regarded as a way for obtaining intervals with frequentist properties that can be investigated. The resulting upper limits have a coverage probability that depends on the true value of the Poisson parameter, and is nowhere smaller than the stated probability content. Lower limits and two-sided intervals for the Poisson mean based on uniform priors undercover, however, for some values of the parameter, although to an extent that in practical cases may not be too severe [2, 31].

In any case, it is important to always report sufficient information so that the result can be combined with other measurements. Often this means giving an unbiased estimator and its standard deviation, even if the estimated value is in the unphysical region.

It can also be useful with a frequentist interval to calculate its subjective probability content using the posterior p.d.f. based on one or several reasonable guesses for the prior p.d.f. If it turns out to be significantly less than the stated confidence level, this warns that it would be particularly misleading to draw conclusions about the parameter's value from the interval alone.

40.5 Experimental sensitivity

In this section we describe methods for characterizing the sensitivity of a search for a new physics signal. As discussed in Sec. 40.3, an experimental analysis can often be formulated as a test of hypothetical model parameters. Therefore we may quantify the sensitivity by giving the results that we expect from such a test under specific assumptions about the signal process.

Here to be concrete we will consider a parameter μ proportional to the rate of a signal process, although the concepts described in this section may be easily generalized to other parameters. One may wish to establish discovery of the signal process by testing and rejecting the hypothesis that $\mu = 0$, and in addition one often wants to test nonzero values of μ to construct a confidence interval (*e.g.*, limits) as described in Sec. 40.4. In the frequentist framework, the result of each tested value of μ is the p-value p_μ or equivalently the significance $Z_\mu = \Phi^{-1}(1-p_\mu)$, where as usual Φ is the standard Gaussian cumulative distribution and its inverse Φ^{-1} is the standard Gaussian quantile.

Prior to carrying out the experiment, one generally wants to quantify what significance Z_μ is expected under given assumptions for the presence or absence of the signal process. Specifically, for the significance of a test of $\mu = 0$ (the discovery significance) one usually quotes the Z_0 one would expect if the signal is present at a given nominal rate, which we can define in general to correspond to $\mu = 1$. For limits, one often gives the expected limit under assumption of the background-only ($\mu = 0$) model. These quantities are used to optimize the analysis and to quantify the experimental sensitivity, that is, to characterize how likely it is to make a discovery if the signal is present, and to say what values of μ one may be able to exclude if the signal is in fact absent.

First we clarify the notion of *expected significance*. Because the significance Z_μ is a function of the data, it is itself a random quantity characterized by a certain sampling distribution. This distribution depends on the assumed value of μ, which is not necessarily the same as the hypothesized value of μ being tested. We may therefore consider the distribution $f(Z_\mu|\mu')$, *i.e.*, the distribution of Z_μ that would be obtained by considering data samples generated under assumption of μ'. In a similar way one can talk about the sampling distribution of an upper limit for μ, $f(\mu_{\rm up}|\mu')$.

One can identify the expected significance or limit with either the mean or median of these distributions, but the median may be preferred since it is invariant under monotonic transformations. For example, the monotonic relation between p-value and significance, $p = 1-\Phi(Z)$, then gives $\mathrm{med}[p_\mu|\mu'] = 1-\Phi(\mathrm{med}[Z_\mu|\mu'])$, whereas the corresponding relation does not hold in general for the mean.

In some cases one may be able to write down approximate formulae for the distributions of Z_μ and for limits, but more generally they must be determined from Monte Carlo calculations. In many cases of interest, the significance Z_μ and the limits on μ will have approximate Gaussian distributions.

As an example, consider a Poisson counting experiment, where the result consists of an observed number n of events, modeled as a Poisson distributed variable with a mean of $\mu s + b$. Here s and b, the expected numbers of events from signal and background processes, are taken to be known. If we are interested in discovering the signal process we test and try to reject the hypothesis $\mu = 0$. To characterize the experimental sensitivity, we want to give the discovery significance expected under the assumption of $\mu = 1$.

In the limit where its mean value is large, the Poisson variable n can be approximated as an almost continuous Gaussian variable with mean $\mu s + b$ and standard deviation $\sigma = \sqrt{\mu s + b}$. In the usual case where a physical signal model corresponds to $\mu > 0$,

Downloaded from https://academic.oup.com/ptep/article/2022/8/083C01/6651666 by KIT Library user on 27 September 2022

the p-value of $\mu = 0$ is the probability to find n greater than or equal to the value observed,

$$p_0 = \Phi\left(\frac{n-b}{\sqrt{b}}\right) , \tag{40.80}$$

and the corresponding significance is $Z_0 = \Phi^{-1}(1-p_0) = (n-b)/\sqrt{b}$. The median (here equal to the mean) of n assuming $\mu = 1$ is $s+b$, and therefore the median discovery significance is

$$\mathrm{med}[Z_0|\mu=1] = \frac{s}{\sqrt{b}} . \tag{40.81}$$

The figure of merit "$s/\sqrt{b}$" has been widely used in particle physics as a measure of expected discovery significance. A better approximation for the Poisson counting experiment, however, may be obtained by testing $\mu = 0$ using the likelihood ratio (40.49) $\lambda(0) = L(0)/L(\hat{\mu})$, where

$$L(\mu) = \frac{(\mu s + b)^n}{n!} e^{-(\mu s + b)} \tag{40.82}$$

is the likelihood function, and $\hat{\mu} = (n-b)/s$ is the ML estimator. In this example there are no nuisance parameters, as s and b are taken to be known. For the case where the relevant signal models correspond to positive μ, one may test the $\mu = 0$ hypothesis with the statistic $q_0 = -2\ln\lambda(0)$ when $\hat{\mu} > 0$, *i.e.*, an excess is observed, and $q_0 = 0$ otherwise. One can show (see, *e.g.*, [24]) that in the large-sample limit, the discovery significance is then $Z_0 = \sqrt{q_0}$, for which one finds

$$Z_0 = \sqrt{2\left(n\ln\frac{n}{b} + b - n\right)} \tag{40.83}$$

for $n > b$ and $Z_0 = 0$ otherwise. To approximate the expected discovery significance assuming $\mu = 1$, one may simply replace n with the expected value $E[n|\mu=1] = s+b$ (the so-called "Asimov data set"), giving

$$\mathrm{med}[Z_0|\mu=1] = \sqrt{2\left((s+b)\ln\left(1+\frac{s}{b}\right) - s\right)} . \tag{40.84}$$

This has been shown in Ref. [24] to provide a good approximation to the median discovery significance for values of s of several and for b well below unity. The right-hand side of Eq. (40.84) reduces to $s/\sqrt{b}$ in the limit $s \ll b$.

Beyond the simple Poisson counting experiment, in general one may test values of a parameter μ with more complicated functions of the measured data to obtain a p-value p_μ, and from this one can quote the equivalent significance Z_μ or find, *e.g.*, an upper limit μ_{up}. In this case as well one may quantify the experimental sensitivity by giving the significance Z_μ expected if the data are generated with a different value of the parameter μ'. In some problems, finding the sampling distribution of the significance or limits may be possible using large-sample formulae as described, *e.g.*, in Ref. [24]. In other cases a Monte Carlo study may be needed. Using whatever method of calculation is most appropriate, one usually quotes the expected (mean or, preferably, median) significance or limit as the primary measures of experimental sensitivity.

Even if the true signal is present at its nominal rate, the actual discovery significance Z_0 obtained from the real data is subject to statistical fluctuations and will not in general be equal to its expected value. In an analogous way, the observed limit will differ from the expected limit even if the signal is absent. Upon observing such a difference one would like to know how large this is compared to expected statistical fluctuations. Therefore, in addition to the observed significance and limits it is useful to communicate not only their expected values but also a measure of the width of their distributions.

As the distributions of significance and limits are often well approximated by a Gaussian, one may indicate the intervals corresponding to plus-or-minus one and/or two standard deviations. If the distributions are significantly non-Gaussian, one may use instead the quantiles that give the same probability content, *i.e.*, $[0.1587, 0.8413]$ for $\pm 1\sigma$, $[0.02275, 0.97725]$ for $\pm 2\sigma$. An upper limit found significantly below the background-only expectation may indicate a strong downward fluctuation of the data, or perhaps as well an incorrect estimate of the background rate.

The procedures described above pertain to frequentist hypothesis tests and limits. Bayesian limits, just like those found from a frequentist procedure, are functions of the data and one may therefore find, usually with approximations or Monte Carlo studies, their sampling distribution and corresponding mean (or, preferably, median) and standard deviation.

When trying to establish discovery of a signal process, the Bayesian approach may employ a Bayes factor as described in Sec. 40.3.3. In the case of the Poisson counting experiment with the likelihood from Eq. (40.82), the log of the Bayes factor that compares $\mu = 1$ to $\mu = 0$ is $\ln B_{10} = \ln(L(1)/L(0)) = n\ln(1+s/b) - s$. That is, the expectation value, assuming $\mu = 1$, of $\ln B_{10}$ for this problem is

$$E[\ln B_{10}|\mu=1] = (s+b)\ln\left(1+\frac{s}{b}\right) - s . \tag{40.85}$$

Comparing this to Eq. (40.84), one finds $\mathrm{med}[Z_0|1] = \sqrt{2E[\ln B_{10}|1]}$. Thus for this particular problem the frequentist median discovery significance can be related to the corresponding Bayes factor in a simple way.

In some analyses, the goal may not be to establish discovery of a signal process but rather to measure, as accurately as possible, the signal rate. If we consider again the Poisson counting experiment described by the likelihood function of Eq. (40.82), the ML estimator $\hat{\mu} = (n-b)/s$ has a variance, assuming $\mu = 1$, of

$$V[\hat{\mu}] = V\left[\frac{n-b}{s}\right] = \frac{1}{s^2}V[n] = \frac{s+b}{s^2} , \tag{40.86}$$

so that the standard deviation of $\hat{\mu}$ is $\sigma_{\hat{\mu}} = \sqrt{s+b}/s$. One may therefore use $s/\sqrt{s+b}$ as a figure of merit to be maximized in order to obtain the best measurement accuracy of a rate parameter. The quantity $s/\sqrt{s+b}$ is also the expected significance with which one rejects s assuming the signal is absent, and thus can be used to optimize the expected upper limit on s.

References

[1] B. Efron, Am. Stat. **40**, 11 (1986).

[2] R. D. Cousins, Am. J. Phys. **63**, 398 (1995).

[3] A. Stuart, J.K. Ord, and S. Arnold, *Kendall's Advanced Theory of Statistics*, Vol. 2A: *Classical Inference and the Linear Model*, 6th ed., Oxford Univ. Press (1999), and earlier editions by Kendall and Stuart. The likelihood-ratio ordering principle is described at the beginning of Ch. 23. Chapter 26 compares different schools of statistical inference.

[4] F. James, *Statistical methods in experimental physics* (2006), ISBN 9789812567956.

[5] L. Lyons, *Statistics for Nuclear and Particle Physicists* (1986), ISBN 9780521379342, URL `http://www.cambridge.org/uk/catalogue/catalogue.asp?isbn=0521255406`.

[6] R. J. Barlow, Nucl. Instrum. Meth. **A297**, 496 (1990).

[7] G. Cowan, *Statistical data analysis* (1998), ISBN 9780198501565.

[8] S. Baker and R. D. Cousins, Nucl. Instrum. Meth. **221**, 437 (1984).

[9] S. S. Wilks, Annals Math. Statist. **9**, 1, 60 (1938).

[10] O. Behnke *et al.*, editors, *Data analysis in high energy physics*, Wiley-VCH, Weinheim, Germany (2013), ISBN 9783527410583, 9783527653447, 9783527653430, URL `http://www.wiley-vch.de/publish/dt/books/ISBN3-527-41058-9`.

[11] S. Schmitt, EPJ Web of Conferences **137**, 11008 (2017), ISSN 2100-014X, URL `http://dx.doi.org/10.1051/epjconf/201713711008`.

Downloaded from https://academic.oup.com/ptep/article/2022/8/083C01/6651666 by KIT Library user on 27 September 2022

[12] L. Brenner *et al.*, Int. J. Mod. Phys. A **35**, 24, 2050145 (2020), [arXiv:1910.14654].

[13] A. O'Hagan and J.J. Forster, *Bayesian Inference*, (2nd edition, volume 2B of *Kendall's Advanced Theory of Statistics*, Arnold, London, 2004).

[14] D. Sivia and J. Skilling, *Data Analysis: A Bayesian Tutorial*, (Oxford University Press, 2006).

[15] P.C. Gregory, *Bayesian Logical Data Analysis for the Physical Sciences*, (Cambridge University Press, 2005).

[16] J.M. Bernardo and A.F.M. Smith, *Bayesian Theory*, (Wiley, 2000).

[17] Robert E. Kass and Larry Wasserman, J. Am. Stat. Assoc. **91**, 1343 (1996).

[18] J.M. Bernardo, J. R. Statist. Soc. **B41**, 113 (1979); J.M. Bernardo and J.O. Berger, J. Am. Stat. Assoc. **84**, 200 (1989). See also J.M. Bernardo, *Reference Analysis*, in *Handbook of Statistics*, 25 (D.K. Dey and C.R. Rao, eds.), 17-90, Elsevier (2005) and references therein.

[19] L. Demortier, S. Jain and H. B. Prosper, Phys. Rev. **D82**, 034002 (2010), [arXiv:1002.1111].

[20] K. Cranmer, J. Pavez and G. Louppe (2015), [arXiv:1506.02169].

[21] N. Reid, *Likelihood Inference in the Presence of Nuisance Parameters*, *Proceedings of PHYSTAT2003*, L. Lyons, R. Mount, and R. Reitmeyer, eds., eConf C030908, Stanford, 2003.

[22] W. A. Rolke, A. M. Lopez and J. Conrad, Nucl. Instrum. Meth. **A551**, 493 (2005), [arXiv:physics/0403059].

[23] Links to the *Proceedings of the PHYSTAT* conference series (Durham 2002, Stanford 2003, Oxford 2005, and Geneva 2007, 2011) can be found at `phystat.org`.

[24] G. Cowan *et al.*, Eur. Phys. J. **C71**, 1554 (2011), [Erratum: Eur. Phys. J.C73,2501(2013)], [arXiv:1007.1727].

[25] L. Demortier, *P-Values and Nuisance Parameters, Proceedings of PHYSTAT 2007*, CERN-2008-001, p. 23.

[26] E. Gross and O. Vitells, Eur. Phys. J. **C70**, 525 (2010), [arXiv:1005.1891].

[27] R. B. Davies, Biometrika **74**, 33 (1987).

[28] J. Skilling, *Nested Sampling*, *AIP Conference Proceedings*, **735**, 395–405 (2004).

[29] F. Feroz, M. P. Hobson and M. Bridges, Mon. Not. Roy. Astron. Soc. **398**, 1601 (2009), [arXiv:0809.3437].

[30] R. E. Kass and A. E. Raftery, J. Am. Statist. Assoc. **90**, 430, 773 (1995).

[31] B. P. Roe and M. B. Woodroofe, Phys. Rev. **D63**, 013009 (2001), [hep-ex/0007048].

[32] J. Neyman, Phil. Trans. Roy. Soc. Lond. **A236**, 767, 333 (1937); Reprinted in *A Selection of Early Statistical Papers on J. Neyman*, (University of California Press, Berkeley, 1967).

[33] G. J. Feldman and R. D. Cousins, Phys. Rev. **D57**, 3873 (1998), [arXiv:physics/9711021]; This paper does not specify what to do if the ordering principle gives equal rank to some values of x. Eq. 21.6 of Ref. [3] gives the rule: all such points are included in the acceptance region (the domain $D(\alpha)$). Some authors have assumed the contrary, and shown that one can then obtain null intervals.

[34] K. Cranmer, in "Statistical Problems in Particle Physics, Astrophysics and Cosmology (PHYSTAT 05): Proceedings, Oxford, UK, September 12-15, 2005," 112–123 (2005), [arXiv:physics/0511028], URL `http://www.physics.ox.ac.uk/phystat05/proceedings/files//Cranmer_LHCStatisticalChallenges.ps`.

[35] A. L. Read, in "Workshop on confidence limits, CERN, Geneva, Switzerland, 17-18 Jan 2000: Proceedings," 81–101 (2000), URL `http://weblib.cern.ch/abstract?CERN-OPEN-2000-205`.

[36] T. Junk, Nucl. Instrum. Meth. **A434**, 435 (1999), [hep-ex/9902006].

Downloaded from https://academic.oup.com/ptep/article/2022/8/083C01/6651666 by KIT Library user on 27 September 2022

41. Machine Learning

Written November 2021 by K. Cranmer (NYU), U. Seljak (UC Berkeley; LBNL) and K. Terao (SLAC; Stanford U.).

41.1 Introduction . . . 676
41.1.1 A gentle introduction with a representative example . . . 677
41.2 Fundamental concepts . . . 677
41.2.1 Loss, risk, empirical risk . . . 677
41.2.2 Generalization . . . 678
41.3 Common tasks and their associated loss functions 678
41.3.1 Supervised learning . . . 678
41.3.1.1 Regression . . . 678
41.3.1.2 A note on regularization . . . 679
41.3.1.3 Classification . . . 679
41.3.2 Unsupervised learning . . . 680
41.3.2.1 Density estimation . . . 680
41.3.2.2 Representation learning, compression, and auto-encoders . . . 681
41.3.2.3 Clustering . . . 681
41.3.3 Optimal control, reinforcement learning, and active learning . . . 682
Reinforcement learning . 682
Multi-arm bandits . . . 682
Bayesian optimization . . 682
Connection to experimental design . . . 683
Active learning . . . 683
41.3.4 Anomaly detection and out-of-distribution detection . . . 683
41.3.5 Simulation-based inference . . . 684
41.3.5.1 Differentiable simulations . . . 684
41.3.5.2 Unfolding as an inverse problem . 684
41.4 Data representations, inductive bias, and example applications . . . 685
41.5 Flavors of ML models . . . 686
41.5.1 Support vector machines and kernel machines 686
Maximum-margin classifiers . . . 686
Soft margins and slack variables . . . 686
The dual problem . . . 686
The kernel trick . . . 686
Support vector regression 687
Kernel ridge regression . 687
Gaussian Process Regression (krigging) . . . 687
41.5.2 Decision trees . . . 687
Tree-based models . . . 687
Ensemble methods . . . 688
Bagging . . . 688
Random forests . . . 688
AdaBoost . . . 689
Gradient boosting . . . 689
41.5.3 Neural networks . . . 689
41.5.3.1 Feed-forward multi-layer perceptron 689
41.5.3.2 Activation functions . . . 689
41.5.3.3 Softmax . . . 690
41.5.3.4 The rise of deep learning . . . 690
41.5.3.5 Convolutional neural networks . . 690
41.5.3.6 Pooling . . . 690
41.5.3.7 CNN architectures for image analysis . . . 691
Region Convolutional Neural Network . . . 691
U-Net . . . 691
41.5.3.8 Residual networks and skip connections . . . 692
41.5.3.9 Recurrent neural networks . . . 692
41.5.3.10 LSTM and GRU . . . 694
41.5.3.11 Attention . . . 694
41.5.3.12 Scaled dot-product attention . . . 695
41.5.3.13 Transformer and multi-head attention . . . 696
41.5.3.14 Graph networks and geometric deep learning . . . 696
41.5.4 Deep generative models . . . 697
41.5.4.1 Variational auto-encoders . . . 698
41.5.4.2 Generative adversarial networks . 698
41.5.4.3 Normalizing flows, autoregressive models, and score based models . 699
41.6 Learning algorithms . . . 700
41.6.1 Gradient-based optimization . . . 700
41.6.2 Stochastic gradient descent . . . 700
41.6.3 Optimization algorithms . . . 700
41.6.4 Automatic differentiation and back propagation . . . 700
41.6.5 The vanishing and exploding gradient problems . . . 701
41.6.6 Early stopping . . . 701
41.6.7 Initialization of model parameters . . . 701
41.6.8 Input normalization . . . 701
41.6.9 Batch normalization . . . 701
41.6.10 Transfer learning: pre-training and fine-tuning . . . 702
41.6.11 Zero, one, and a few shot learning . . . 702
41.7 Incorporating uncertainty . . . 702
41.7.1 Propagation of errors . . . 703
41.7.2 Domain adaptation . . . 703
41.7.3 Parameterized models . . . 704
41.7.4 Data augmentation . . . 704
41.7.5 Aleatoric and epistemic uncertainty . . . 704
41.7.6 Model averaging and Bayesian machine learning . . . 705
41.7.7 Connection to probabilistic machine learning 705
41.8 Infrastructure for deployment in experiments . . 706

41.1 Introduction

This chapter gives an overview of the core concepts of machine learning that are relevant to particle physics with some examples of applications to the energy, intensity, cosmic, and accelerator frontiers. Machine learning (ML) is an enormous field that has grown substantially in the last decade, propelled largely by the emergence of so-called deep learning (DL) [1, 2]. ML has a long history in particle physics going back to the late 1980s and early 1990s, see Refs. [3–5] for recent reviews.

Physicists are exploring and contributing to machine learning at an unprecedented rate, which poses a challenge for those that wish to have an up-to-date view of the field. This motivated an effort to create *A Living Review of Machine Learning for Particle and Nuclear Physics* [6], which can be downloaded here: `https://github.com/iml-wg/HEPML-LivingReview`. As of the time of this writing, the Living Review includes over 500 references organized hierarchically by topic. While we make references to some of these papers, this chapter focuses on the methodology and does not attempt to give a comprehensive review of the applications.

Despite the connotations of machine learning and artificial intelligence as a mysterious and radical departure from traditional approaches, we stress that machine learning has a mathematical formulation that is closely tied to statistics, the calculus of variations, approximation theory, and optimal control theory.

The topic can be organized along a few axes, which we use to organize this section. First, there are different learning paradigms, for example supervised learning, unsupervised learning, and reinforcement learning. We focus on the first two in this review, since reinforcement learning is less commonly used in particle physics. Within these paradigms there are various tasks; for example, classification and regression – which have been the primary use of ML in particle physics – are examples of supervised learning. In addition to the learning paradigm and tasks, there are various types of machine learning models that generically process some input and produce some output. The types of models vary based on what it is they are modelling (*e.g.* so-called discriminative vs. generative

Downloaded from https://academic.oup.com/ptep/article/2022/8/083C01/6651666 by KIT Library user on 27 September 2022

models), as well as the way that they are implemented (*e.g.* neural networks, decision trees, and kernel machines). Next, there are the issues around training or learning within the context of a given task and model class, which connects to optimization and regularization. We will briefly discuss the various considerations that emerge in the application of machine learning methods to physics, such as the treatment of systematic uncertainty, the interpretability of the models, the incorporation of symmetry, *etc.*.

41.1.1 *A gentle introduction with a representative example*

We will use a specific, familiar example to introduce the various ingredients in context before factorizing and abstracting them. Consider the task of *classifying* energy deposits in a particle detector as electrons or protons. For this example, let the detector data consist of energy deposits in d sensors so that the data can be represented as *feature vector* $x \in \mathbb{R}^d$. Different components of x may have different units (e.g. units of energy, momentum, position etc.). Due to the complex interactions of particles in the detector, we do not have an explicit probability model for the high-dimensional data for the electron and proton scenarios, but we do have a simulator that allows us to generate Monte Carlo samples for each. This allows us to assemble a *training dataset* $\{x_i, y_i\}_{i=1,\ldots,n}$, where y is used as a *label* to identify how the example was generated (*e.g.* $y = 0$ for electrons and $y = 1$ for protons). We would like to find a function $f : x \to y$ that is able to accurately *predict* the label on new data. Because we have feature-label pairs, this is considered a *supervised learning* problem. We can use a *neural network* to provide a flexible family of functions $f_\phi : \mathbb{R}^d \to \mathbb{R}$, where ϕ denotes the internal parameters of the neural network (*i.e.* the weights and biases that we will discuss in Sec.41.5.3). The goal of the *training procedure* is to find the value of the parameters ϕ that provide the 'best' predictions, but since no model is perfect, we must be explicit about the tradeoffs. This is made concrete through a *loss function* $\mathcal{L}(f_\phi(x), y)$. For this example, instead of the obvious zero-one loss (which is 0 if $f_\phi(x)$ equals y and 1 if they are not), we choose to use the squared-loss $\mathcal{L}_{\text{sq}}(f_\phi(x), y) = (y - f_\phi(x))^2$ (which may seem *ad hoc* now, but will be motivated in Sec. 41.3.1.3). We can evaluate the average of the loss on the training set of size n, which is referred to as the *emprical risk* $\mathcal{R}_{\text{emp}}(f_\phi) = \sum_{i=1}^n \mathcal{L}(f_\phi(x), y)/n$. *Training* refers to numerically minimizing the empirical risk (often referred to as the *training loss* through some abuse of terminology). We can numerically optimize the model through *gradient descent*, which iteratively adjusts the parameters of the network according to $\phi^{t+1} = \phi^t - \lambda \nabla_\phi \mathcal{R}_{\text{emp}}(f_\phi)$, where λ is referred to as the *learning rate*. Once the optimization is complete and we obtain the solution $\hat{\phi}$, it is natural to assess the quality of the trained model $f_{\hat{\phi}}$ on an independent *testing dataset*. The empirical risk evaluated on the testing set is often larger than on the training set, and large differences indicate *overfitting*, which indicates that the model does not generalize well to the unseen data. The ability to accurately predict on unseen data is referred to as *generalization* and the empirical risk on the test data provides a measure of the *generalization error*. In order to reduce the *generalization error* one might explore different model choices (*e.g.* neural network architectures), additional regularization terms in the loss function, different learning rates, optimization algorithms, or early stopping criterion in the optimization. Once trained, the model can be applied to data. In order to produce a binary electron vs. proton decision from the continuous ouptut of the neural network, we must threshold (*i.e.* classify as proton if $f_{\hat{\phi}}(x) > k$). The choice of the threshold k is often referred to as a working point and it sets the tradeoff between electron and proton efficiency, fake-rates, purity, etc. These familiar concepts in particle physics are usually referred to in different terms in machine learning and a *receiver operating characteristic curve*, or ROC curve, is used to summarize the tradeoff between true positive rate (TPR) and false positive rate (FPR). Importantly, the characterization of the efficiency / rejection (or equivalently the ROC curve) requires labeled data. In a particle physics context, it is recognized that the simulation is not perfect and the mismodelling is associated to the presence of systematic uncertainty. In machine learning, the discrepancy between the distribution of the training dataset and the distribution of the data that the model will be applied to in practice is referred to as *domain shift* or *distribution shift*. While mismodelling in the training dataset might lead to a less-than-optimal classifier in practice, the real source of systematic uncertainty comes from mismatch between the data used to characterize the performance of the classifier and the unlabeled data that the classifier is applied to. This motivates the use of data-driven methods to calibrate the resulting model.

This example provides a vertical slice through the various aspects of supervised machine learning in particle physics. Now we factorize and abstract the various ingredients in order to provide a more general treatment with a broader scope.

41.2 Fundamental concepts

41.2.1 *Loss, risk, empirical risk*

The term *learning* in machine learning generally refers to optimization of some objective, which can be thought of as maximizing utility or minimizing *risk*. The risk brings together three main ingredients. The first is the *model family* $\mathcal{F}$ (where $f \in \mathcal{F}$ is the quantity that we vary during optimization), the second is the *loss function* $\mathcal{L}$, and the third is a data distribution $p(u)$. The *risk* for a model $f \in \mathcal{F}$ is defined as its expected loss

$$\mathcal{R}[f] \coloneqq \mathbb{E}_{p(u)}[\mathcal{L}(u, f(u))] \equiv \int \mathcal{L}(u, f(u)), p(u)\, \mathrm{d}u \,, \tag{41.1}$$

where $\mathbb{E}_p[\cdot]$ refers to the expectation with respect to the distribution p. In the context of supervised learning, the distribution $p(u)$ describes a joint distribution over the features x and the labels y (*i.e.* $p(u) = p(x, y)$), the model only depends on the features $f(u) = f(x)$, and the loss function takes on the special form $\mathcal{L}(u, f(u)) = \mathcal{L}(y, f(x))$. In the context of unsupervised learning there are no labels, and $u = x$. Written this way, the risk is a functional, and the idealized goal for machine learning is to solve the optimization problem

$$f^* = \arg\min_{f \in \mathcal{F}} \mathcal{R}[f] \,, \tag{41.2}$$

where $\mathcal{F}$ would include all possible functions.

One of the defining characteristics of machine learning in practice is that one does not know the data distribution $p(u)$, but does have access to samples from that distribution, *i.e.* $\{u_i\}_{i=1,\ldots,n}$ with $u_i \overset{i.i.d.}{\sim} p(u)$. This leads to the corresponding *empirical risk*

$$\mathcal{R}_{\text{emp}}[f] \coloneqq \mathbb{E}_{\hat{p}(u)}[\mathcal{L}(u, f(u))] \equiv \frac{1}{n} \sum_{i=1}^{n} \mathcal{L}(u_i, f(u_i)) \,, \tag{41.3}$$

where $\hat{p}(u) = \frac{1}{n} \sum_{i=1}^n \delta(u - u_i)$ is referred to as the empirical distribution of the dataset $\{u_i\}_{i=1,\ldots,n}$. The *empirical risk minimization* principle is a core idea in statistical learning theory [7], which approximates f^* with its empirical analogue

$$\hat{f} = \arg\min_{f \in \hat{\mathcal{F}}} \mathcal{R}_{\text{emp}}[f] \,, \tag{41.4}$$

where $\hat{\mathcal{F}}$ are all possible functions parametrized by the model parameters ϕ. In an idealized infinite parameter limit machine learning functions, such as neural networks, are universal approximators, such that they cover all functions and $\mathcal{F} = \hat{\mathcal{F}}$. For finite size networks this may or may not be a valid assumption. Expressivity of the network characterizes this universality property and is a function of the network architecture and its parameters such as width and depth of neural network layers. If the expressivity is too small it leads to underfitting. However, an equally important consideration is the risk of overfitting if we optimize equation 41.4 for too long.

While the loss function may quantify some well-motivated notion of (negative) utility, it is also common to design loss functions so that f^* has some desired property. While in practice one does not know the data distribution $p(u)$, it is constructive to imagine that one does and analyze Eq. 41.2 with the calculus of variations. In Secs. 41.3 we will consider several such loss functions where one can show that the corresponding f^* has the desired property even

Downloaded from https://academic.oup.com/ptep/article/2022/8/083C01/6651666 by KIT Library user on 27 September 2022

if the form of the loss is not obvious from the point of view of utility. Furthermore, there are often multiple loss functions that can lead to the same f^*. Then one can think of machine learning as applied calculus of variations where one solves Eq. 41.4 with a sufficiently flexible model, powerful optimization algorithms, and practical considerations to break the degeneracy between different loss functions that lead to the same f^*.

41.2.2 *Generalization*

With a sufficiently flexible model, it is possible to fit the training dataset very well, though the model might not *generalize* well to unseen data due to overfitting. More concretely, for a non-negative loss function one might have $\mathcal{R}_{\text{emp}}[\hat{f}] \to 0$, while the true risk might be large ($\mathcal{R}[\hat{f}] \gg 0$). The gap between the $\mathcal{R}[\hat{f}] - \mathcal{R}_{\text{emp}}[\hat{f}]$ is typically referred to as the *excess risk*[1]. While it is generally not possible to evaluate $\mathcal{R}[\hat{f}]$ exactly because we do not know $p(u)$, we can use an independent testing dataset (also called validation dataset) to obtain an unbiased estimate of it. This *cross-validation* method motivates the test – train split of the data.

Intuitively, a model with many parameters has more flexibility and is more prone to overfitting. A common and intuitive heuristic is that one should not fit a model with more parameters than there are data points. However, a more careful treatment reveals that this heuristic can be both pessimistic and optimistic. For example, the single-parameter model $f_\phi(x) = \text{sign}(\sin(\phi x))$ can perfectly classify any assignment of labels on data (x_i, y_i) with $x \in \mathbb{R}$ and $y \in \{-1, 1\}$ and generalize poorly. Conversely, sometimes highly over-parameterized models (that have large subspaces of their parameters where $\mathcal{R}_{\text{emp}}[\hat{f}_\phi] \to 0$) might generalize well [8,9]. Often this is achieved through *regularization*, both explicit and implicit (section 41.3.1.2).

Structural risk minimization is a modification to the empirical risk minimization principle that was introduced by Vapnik and Chervonenkis to account for the potential for overfitting [7]. However, the bounds are based on a worst-case type analysis and are often very weak. Recall that while one cannot calculate the true risk, one can obtain an unbiased estimate of it with a held-out, independent testing sample. Thus one can empirically compare the generalization error of two models and find that one generalizes better than the other even if the bounds might suggest the opposite. One of the major conceptual shifts that happened with the rise of deep learning was to more fully appreciate that these bounds and structural risk minimization were not a good learning principle in practice and that more theoretical work is needed to close the gap between formal bounds and empirical estimates of generalization error.

41.3 Common tasks and their associated loss functions

We now move to common tasks encountered in machine learning and their associated loss functions.

41.3.1 *Supervised learning*

Supervised learning generally refers to the class of problems where the training dataset are presented as input-output pairs $\{x_i, y_i\}_{i=1,\ldots,n}$, where $x_i \in \mathcal{X}$ are the input features and $y_i \in \mathcal{Y}$ are the corresponding target labels. Furthermore, it is typically assumed that $(x_i, y_i) \overset{i.i.d.}{\sim} p(x, y)$, though $p(x, y)$ is usually not known explicitly. Finally, the loss function in supervised learning takes on the special form $\mathcal{L}(y, f(x))$. The resulting trained model is then used to predict the labels for dataset where labels are not available.

In what follows we will make use of the equalities $p(x, y) = p(x|y)p(y) = p(y|x)p(x)$ and Bayes theorem, which is discussed in Sec. 39.1. We will also use the notation $x \sim p(x)$ to indicate that the random variable x is being drawn, sampled, or generated from the distribution $p(x)$.

[1]Similarly, the gap between the true risk of the learned model and the true risk of the optimal model (*i.e.* $\mathcal{R}[\hat{f}] - \mathcal{R}[f^*]$) is referred to as the *regret*. This quantity is mainly of interest for theoretical analysis of machine learning algorithms, and not of practical concern since usually neither term is tractable.

41.3.1.1 *Regression*

The goal of regression is to predict a label $y \in \mathcal{Y}$ given an input feature vector $x \in \mathcal{X}$. Typically, the label is a real-valued scalar, but $\mathcal{X}$ can be $\mathbb{R}^d$ or some more structured target (*e.g.* an image, sequence, graph, quantile, or distribution). When $\mathcal{Y}$ is discrete, the task is usually referred to as classification; however, the two are closely related and *logistic regression* is an example where the model predicts a continuous probability associated to the possible label values. In elementary statistical language, the target label y is often called a dependent variable, while the feature x is called the independent variable. In classical statistics, one often assumes a model for the data such as

$$y_i = f_\phi(x_i) + e_i \ , \tag{41.5}$$

where e_i is an additive error term that is often assumed to be independent of x and often assumed to be normally distributed. This leads to classic approaches like least-squares (see Sec. 40.2.3), and when the model f_ϕ is linear in ϕ (not in x!) one has linear regression that has a closed-form solution. However, we can relax these assumptions and consider the general case of an arbitrary joint distribution $p(x, y)$, which can be written as $p(y|x)p(x)$ without loss of generality. Consider the *squared error* as a loss function, which leads to the mean-squared error (MSE) for the empirical risk:

$$\mathcal{L}_{\text{MSE}}(y, f(x)) = (y - f(x))^2 \ . \tag{41.6}$$

One might expect that the squared error would only be appropriate in the case that the conditional distribution $p(y|x)$ is normally distributed, but one can use the calculus of variations to show that in general

$$f^*_{\text{MSE}}(x) = \mathbb{E}_{p(y|x)}[y] \ , \tag{41.7}$$

that is the optimal regressor for the MSE is the conditional expectation of y given x.

One issue with the squared-error as a loss function is that it is sensitive to outliers. Alternatively, one can use the absolute error $|y - f(x)|$ as a loss function[2]. However, the discontinuous derivative of the absolute (L1) error leads to challenges in optimization. As a result there are various other loss functions, such as the Huber loss, that aim to be both robust and more amenable to optimization that we do not discuss here.

Note that these this framing of regression yields a function $f(x)$ that only provides a point estimate for y. An alternative approach to regression is to model the full conditional distribution $p(y|x)$. One such example is Gaussian Process regression, which is discussed in Sec. 41.5.1. In that probabilistic approach, one can still obtain a point estimator, such as the conditional expectation or the maximum a posteriori (MAP) estimator

$$f^*(x) = \arg\max_y p(y|x) \ , \tag{41.8}$$

and one can also derive uncertainty estimates on the predicted value y. In this setting, the prior distribution on the model family is closely related to the concept of regularization, which we touch on in Sec. in Sec. 41.3.1.2 and in Sec. 41.5.1.

When one directly models $p(y|x)$, or goes further to model the joint distribution $p(x, y) = p(y|x)p(x)$, then one can use maximum likelihood for the loss function. In that approach, the problem is really one of density estimation, which is a type of unsupervised learning that we discuss in Sec. 41.3.2.1. These two approaches are a classic examples of two different approaches to modelling. Regression with $f^*_{\text{MSE}}(x)$ is the prototypical example of *descriminative* modelling, while modelling the joint distribution is a prototypical example of *generative* modelling. Generally, discriminative approaches with supervised learning out perform generative approaches when there is sufficient data, but generative approaches can be beneficial in data-starved settings [10].

[2]The absolute error and squared error are often denoted as L1 and L2 errors, respectively, in reference to the corresponding norms.

Downloaded from https://academic.oup.com/ptep/article/2022/8/083C01/6651666 by KIT Library user on 27 September 2022

41.3.1.2 *A note on regularization*

The trained model $\hat{f}$, or equivalently, the parameters of the trained model $\hat{\phi}$ can be thought of as point estimates of f^*, and there is a correspondence to the issues of bias and variance discussed in Sec. 40.2 on parameter estimation. Generically, there is a bias–variance tradeoff, and when the number of parameters is large and the number of data points is not much larger, introducing a small bias can often lead to a significant reduction in variance. This motivates the explicit addition of a *regularization* term to the loss function, which will introduce some bias $f^*_{\text{reg}} \neq f^*$. A common form for of regularization is to penalize by the L2 norm of the parameters (*i.e.* $\|\phi\|^2$), which is referred to as *Tikhonov regularization*. This appears in the form of penalized maximum likelihood, and it is also commonly used in unfolding [11]. One can also interpret the regularization term as an explicit prior on the parameters, and the resulting model as the Bayesian maximum a posteriori (MAP) estimator. When paired with linear regression this is known as *ridge regression*, and when paired with kernel machines (see Sec. 41.5.1) this gives rise to kernel ridge regression or Gaussian process regression.

Another form of regularization is to restrict the model class $\hat{\mathcal{F}}$. For example, a neural network and a sequence of narrow step functions (delta functions) can both be shown to be universal approximators in infinite parameter size limit, but on real world examples the former generalizes much better than the latter. Within the class of neural network models, convolutional neural networks are a subset of generic feedforward neural networks that enforce translational symmetry (see Sec. 41.5.3.5 for more discussion). Similarly, one might restrict to Lipschitz continuous functions. These types of choices are often encoded in the architecture of a neural network and are broadly referred to as *inductive bias* in the model.

In addition to explicit regularization terms in the loss function or through restrictions to the model class, it is also possible to regularize implicitly. One implicit regularization is through early stopping [11, 12], where we monitor the loss on training dataset and the loss on test dataset. While the training dataset loss continues to decrease with more gradient descent cycles, the test loss may not, and early stopping stops the training when test loss flattens out or begins to increase. Another powerful form of regularization used in deep learning models is known as *dropout* [13], which randomly removes some some parts of the model during training and can be thought of as implementing a type of model averaging [14]. What is more surprising is that in the case of highly over-parameterized models where there is a large degenerate parameter space that achieves zero loss, $\Phi_0 = \{\phi | \mathcal{R}_{\text{emp}}[f_\phi]\} = 0$, that the dynamics of the optimization algorithm that is used will break the degeneracy and favor some particular $\hat{\phi} \in \Phi_0$ as if an additional regularization term was secretly included. Despite zero loss and over-parametrization, the corresponding generalization error may be small, a phenomenon called *benign overfitting* [15]. Importantly, the dynamics of different optimization algorithms will have different implicit regularization effects, and thus favor different parameter points in Φ_0 that will have different generalization error [16]. Understanding this interaction is a topic of contemporary research in machine learning [17].

41.3.1.3 *Classification*

The goal of classification is to predict one of a finite number of class labels $y \in \mathcal{Y}$ given an input feature vector $x \in \mathbb{X}$. It is similar to regression in this way, but the focus is on discrete target space $\mathcal{Y}$. An important special case is when the label can only take on one of two values (*e.g.* "signal" or "background"), which is referred to as binary classification and is equivalent to simple hypothesis testing in statistics. It is common for a classifier to be the composition of a model $g : \mathcal{X} \to \mathbb{R}^{|\mathcal{Y}|}$ that predicts continuous probabilities for each class (*i.e.* $g(x) \approx p(y|x)$) followed by an operation that then chooses the discrete label $y \in \mathcal{Y}$, such as a fixed threshold or $f(x) = \arg\max g(x) \approx \arg\max_y p(y|x)$. This is the case for both classical methods like logistic regression and modern, deep learning approaches to classification; therefore, we will use the term probabilistic classifier for $g(x)$ or just classifier when it is clear in context.

An intuitive loss function for classification is the zero-one loss, which simply counts the number of mis-classifications:

$$\mathcal{L}_{0/1}(y, f(x)) = \begin{cases} 0, & \text{if } f(x) = y \\ 1, & \text{otherwise} \,. \end{cases} \tag{41.9}$$

The zero-one loss can also be written as $\mathcal{L}_{0/1}(y, f(x)) = \mathbf{1}(y \neq f(x))$, where $\mathbf{1}(\cdot)$ is the indicator function. The zero-one loss is non-differentiable, so it does not pair well with gradient-based optimization.

For binary classification, one can use $y = \{0, 1\}$ as numerical values for the class labels and the mean-squared error $\mathcal{L}_{\text{MSE}}(y, f(x))$ in Eq. 41.6 for the loss function. The resulting model will approximate f^*_{MSE}, the conditional expectation of Eq. 41.7 takes on the form

$$\begin{aligned} f^*_{\text{MSE}}(x) &= \mathbb{E}_{p(y|x)}[y] \to p(y = 1|x) \\ &= \frac{p(x|y = 1)p(y = 1)}{p(x|y = 0)p(y = 0) + p(x|y = 1)p(y = 1)} \,. \end{aligned} \tag{41.10}$$

That is the MSE loss for binary classification leads to the Bayesian posterior probability that the label $y = 1$ given the feature vector x.

Equation 41.10 highlights an important general feature of supervised learning relevant for particle physics, which is that the joint distribution $p(x, y)$ of the training dataset implies a prior distribution $p(y)$ on the labels or classes. This prior distribution need not reflect a degree of belief or the frequency in real data, it represents the frequency in the training dataset. However, it is important to keep in mind that when applying the resulting model to a different dataset with the same conditional distribution (data likelihood) $p(x|y)$ for the features and a different prior $p'(y)$ for the labels that the probabilistic interpretation of the result will not be properly calibrated. A common choice for binary classification is to use a balanced training dataset with $p(y = 0) = p(y = 1) = \frac{1}{2}$, while in many cases the true $p'(y = 1)$ in the experimental data might be very small (*i.e.* low signal-to-background), unknown, or zero (*i.e.* a hypothetical particle that does not exist).

If $p'(y)$ and $p(y)$ are known then the Bayes theorem can be used to re-calibrate the posterior $p(y|x)$ from one prior to another. One example of such re-calibration is the correspondence of binary classification to simple hypothesis tests in frequentist statistics discussed in Sec. 40.3.1 of the Statistics chapter. In that setting, the Neyman-Pearson lemma states that the optimal classifier is given by the likelihood-ratio. Adapting to the notation of this chapter, we have

$$f^*_{\text{N.P.}}(x) = \frac{p(x|y = 1)}{p(x|y = 0)} \,, \tag{41.11}$$

which does not depend on the prior probabilities $p'(y = 0)$ or $p'(y = 1)$ as in Eq. 41.10, or, equivalently, assumes equal priors $p'(y = 0) = p'(y = 1)$. From Bayes theorem, we have the identity $p(y = 1|x)/p(y = 0|x) = [p(x|y = 1)p(y = 1)]/[p(x|y = 0)p(y = 0)]$, which can be used to show that the two functions are related by a one-to-one, monotonic transformation

$$f^*_{\text{N.P.}}(x) = \frac{p(y = 0)}{p(y = 1)} \frac{f^*_{\text{MSE}}(x)}{1 - f^*_{\text{MSE}}(x)} \,, \tag{41.12}$$

which is referred to as the *likelihood-ratio trick*, which plays an important role in simulation-based inference (see Sec. 41.3.5). Importantly, the monotonic transformation does not impact the tradeoff of type-I and type-II error (or, equivalently, the FPR and TPR), therefore the ROC curve for $f_{\text{N.P.}}(x)$ and $f_{\text{MSE}}(x)$ are identical and do not depend on the prior probabilities $p(y)$. This property has been leveraged in the context of *weakly supervised* approaches [18] and enables one to train a classifier on data without access to labels as long as one has two datasets with different ratios $p(y = 1)/p(y = 0)$ and the same conditional distribution $p(x|y)$ of the features given the labels.

Downloaded from https://academic.oup.com/ptep/article/2022/8/083C01/6651666 by KIT Library user on 27 September 2022

A generalization of the binary loss function for classification of Eq. 41.10, which applies to multiple classes, is the *cross-entropy* loss

$$\mathcal{L}_{\rm xe}(y, f(x)) = -\sum_{c\in|\mathcal{Y}|} \mathbf{1}(y=c)\log(f_c(x)) \ , \tag{41.13}$$

where $f : \mathcal{X} \to \mathbb{R}^{|\mathcal{Y}|}$ and the indicator function picks out the term in the sum for the corresponding class label y. This loss can be derived from maximizing the posterior of Eq. 41.57 using a discrete set of class labels y, which identifies $f_c(x) = \tilde{f}(y=c|x) = p(y=c|x)$ and thus enforces the constraint $\sum_c f_c(x) = 1$ and $f_c(x) \geq 0$ (for all $x \in \mathcal{X}$, *e.g.* by using the *softmax* function). The notation is aligned with the interpretation of $\tilde{f}(y|x)$ as a conditional distribution, i.e. an approximation to the true posterior $p(y|x)$. The risk associated to the cross entropy loss function is

$$\begin{aligned}\mathcal{R}_{\rm xe}[f] &= \mathbb{E}_{p(x,y)}\left[-\sum_{c\in|\mathcal{Y}|}\mathbf{1}(y=c)\log f_c(x)\right] \\ &= -\sum_{c\in|\mathcal{Y}|} p(y=c)\mathbb{E}_{p(x|y)}[\log\tilde{f}(y=c|x)] \ .\end{aligned} \tag{41.14}$$

This is equivalent to $\mathcal{R}_{\rm xe}[f] = \mathbb{E}_{p(x)}[H[p(y|x), \tilde{f}(y|x)]]$, where $H[p,f] = \mathbb{E}_p[-\log f]$ is the cross-entropy between the two distributions. One can use a Lagrange multiplier λ to enforce the normalization constraint (e.g. equation 41.10) and the calculus of variations to show that

$$f^*_{\rm x.e.,c}(x) = \lambda p(x, y=c) = \lambda p(y=c|x)p(x) = p(y=c|x) \ . \tag{41.15}$$

This approach is closely related to the loss functions that are used for density estimation, the forward Kullback–Leibler (KL) divergence, and the maximum likelihood estimation. Minimizing cross entropy $H[p, f_\phi]$ with respect to ϕ is equivalent to minimizing the forward KL divergence

$$KL(p||f_\phi) \coloneqq \mathbb{E}_p[\log p(x)) - \log f_\phi] = H[p, f_\phi] - H[p] \ , \tag{41.16}$$

where $H[p] \coloneqq \int p(x)\log p(x)dx$ is the entropy and independent of f_ϕ. The KL divergence $KL[p||f] \geq 0$, and equal if and only if $p = f$.

One can also consider the reverse KL divergence $KL[f_\phi||p]$, which is also minimized by $f_\phi = p$; however, this requires one to be able to generate samples $x_i \sim f_\phi(x)$ and be able to evaluate the probability density $p(x_i)$. Often this is not the case for real world data, but this approach is useful in the context of variational inference, where $f_\phi(x)$ is an approximation to the posterior of x, and $p(x)$ is the likelihood times the prior, which can be evaluated on samples x_i drawn from f_ϕ. Because likelihood times prior is not normalized this KL divergence optimizes the lower bound to the normalization (Evidence Lower Bound Objective or ELBO).

The forward KL is also closely related to the variational free energy principle in statistical mechanics where $H[f_\phi]$ represents the entropy of the variational distribution, $p(x) \propto \exp(-E(x)/kT)$ is the Boltzman factor for the state x with energy $E(x)$, and $H[f_\phi, p] = \mathbb{E}_{f_\phi}[E(x)]$ represents the expected energy for the variational distribution. As is well known to physicists, minimizing the free energy involves a balance between minimizing the energy and maximizing the entropy.

In some cases it is possible to augment the training dataset with an unbiased, stochastic estimate of $p(y=c|x)$ that we denote $s_c(x,z)$. For example, when the simulation involves latent variables z (*i.e.* Monte Carlo truth quantities), then the simulation encodes $p(x,z|y)$, the joint distribution over the observed features x and the latent variables z conditioned on the class y. In many cases the simulation evolves through a Markov process (*e.g.* the detector response only depends on the momenta of the incoming particles z, not the details of the hard scattering y). In that case, it is often possible to calculate $s_c(x,z) = p(y=c|x,z)$ for each training sample [19]. Using the identity, $\mathbb{E}_{p(z|x)}[p(y|x,z)] = p(y|x)$, we see that $s_c(x,z)$ is an unbiased estimator of $p(y=c|x)$. In this case, one can use $s_c(x,z)$ in place of the indicator function in Eq. 41.13 to construct an improved (lower-variance) loss function that reproduces the same cross-entropy risk function[3,4]

$$\begin{aligned}\mathcal{R}'_{\rm xe}[f] &= \mathbb{E}_{p(x,y,z)}\left[-\sum_{c\in|\mathcal{Y}|} s_c(x,z)\log f_c(x)\right] \\ &= -\sum_{c\in|\mathcal{Y}|}\mathbb{E}_{p(x)}[p(y=c|x)\log f_c(x)] \ ,\end{aligned} \tag{41.17}$$

which yields the same optimal classifier $f^*_{\rm x.e.,c}(x) = p(y=c|x)$ [20, 21].

We note that unlike in the binary classification case, the multi-class classifier is sensitive to the priors $p(y)$ used in training. This leads to complications as often the class proportions are unknown. For example, one might be interested in classifying a signal when multiple backgrounds are present and the relative proportion of those different background components is uncertain. Ideally one would like the class proportions for the background components used in training to match those in the data, which presents an additional training challenge if those proportions are heavily unbalanced.

41.3.2 *Unsupervised learning*

Unsupervised learning generally refers to the class of problems that use unlabeled training dataset $\{x_i\}_{i=1,\ldots,n}$, where $x_i \in \mathcal{X}$ are the input features. Furthermore, it is typically assumed that $(x_i) \overset{i.i.d.}{\sim} p(x)$, though $p(x)$ is usually not known explicitly. Finally, the loss function in supervised learning takes on the special form $\mathcal{L}(x, f(x))$.

A related concept is that of self-supervised learning, which also aims to distill useful features in the data without requiring supervision labels for every sample in the input data. Self-supervised methods can make use of large unsupervised datasets and build meaningful representations by performing data augmentation, and learning the latent space mapping that is insensitive to it. For example, in the case of galaxy images one may augment the data by performing image rotations, adding noise, size scaling, adding point spread function smoothing etc., all of which are realistic transformations expected in a real galaxy image survey [22]. Self-supervised learning then learns the latent space representation where all of these augmentations of the same training sample result in the same latent space position. This training is augmented with contrastive learning, which ensures that different training samples do not all collapse to the same latent space position. When this latent space representation is used for downstream tasks such as classification it outperforms other forms of supervised learning [23].

41.3.2.1 *Density estimation*

The goal of density estimation is to estimate a distribution $p(x)$ based on samples $\{x_i\}_{i=1,\ldots,n}$ with $x_i \overset{i.i.d.}{\sim} p(x)$. Conceptually, this is the same goal as when fitting a parameterized distribution $f(x;\theta)$ to data using the method of maximum likelihood as described in Sec. 40.2.2 of the chapter on statistics. In practice, the difference in the machine learning context has to do with the flexibility of the model and the dimensionality of the data. A highly-flexible model, which can effectively approximate any distribution, is referred to as a non-parametric model (though, ironically, usually this means the model has many parameters). In contrast, typical maximum likelihood fits in particle physics are based on restricted families of distributions with relatively few parameters and the data is typically one- or two-dimensional, though occasionally five- or six-dimensional.

Maximizing the likelihood function in Eq. 40.10 $\mathcal{L}(\theta) =$

[3] A similar approach can also be used for the squared-error, see Ref. [20].

[4] The right hand side of Eqs. 41.14 and 41.17 are written in a different form, but are equivalent.

Downloaded from https://academic.oup.com/ptep/article/2022/8/083C01/6651666 by KIT Library user on 27 September 2022

$\prod_{i=1}^{n} f(x_i;\theta)$ is equivalent to minimizing the empirical risk:

$$\mathcal{R}_{\text{emp,xe}}[f_\phi] = -\frac{1}{n}\sum_{i=1}^{n} \log f_\phi(x) \ , \tag{41.18}$$

where we adopt the notion used in this chapter. The loss is simply $\mathcal{L}(x, f_\phi(x)) = -\log f_\phi(x)$, and the corresponding risk is

$$\mathcal{R}_{\text{xe}}[f_\phi] = \mathbb{E}_{p(x)}[-\log f_\phi(x)] \ , \tag{41.19}$$

which is the cross entropy $H[p, f_\phi]$. For density estimation, the model is usually constructed to enforce $\int f_\phi(x)dx = 1$ and $f_\phi(x) \geq 0$ so that it can be interpreted as a distribution. With this constraint, one can show that $f^*_{\text{xe}}(x) = p(x)$.

The concepts of generalization and overfitting are particularly acute in unsupervised learning, where the likelihood maximization of equation 41.18, combined with universal approximator assumption, must converge onto $\hat{p}(x) = \frac{1}{n}\sum_{i=1}^{n} \delta(x - x_i)$, the empirical distribution of the dataset $\{x_i\}_{i=1,\ldots,n}$. This distribution has the highest likelihood on the training dataset and the lowest likelihood on the test data where it gives $\hat{p}(x) = 0$. as long as the test dataset are not identical to the training dataset. So the empirical distribution of the training dataset has the worst possible generalization property, yet it is the solution we converge to for sufficiently expressive architectures in the absence of any regularization. In contrast, in supervised learning we often observe the phenomenon of benign overfitting, where even zero loss can generalize well.

In addition to approaches to density estimation that involve learning in the sense of minimizing a loss or risk function, we note that there are also classical density estimation techniques such as histogramming and kernel density estimation [24–26].

41.3.2.2 *Representation learning, compression, and auto-encoders*

A recurring topic in machine learning and statistics is how to represent the data. Much of classical statistics involves constructing a low-dimensional summary statistic that extracts the relevant information from the data for a particular task (a sufficient statistic in language of classical statistics). There is a spectrum of representations with trade-offs. At one end of this spectrum is lossless compression that allows you to encode the data into a smaller, intermediate representation that carries all the information since it can be decoded back into the original data. At the other end of the spectrum is something like the likelihood-ratio, which is a single scalar that carries the relevant information needed for hypothesis testing for a single hypothesis, but it discards all the other information that might be needed for other tasks (such as testing other hypotheses). An intermediate point in this spectrum is the process of feature engineering, which refers to the creation of new features $\mathcal{X}'$ from the original features $\mathcal{X}$ in hopes that the down-stream task will be easier with the new features. For example, instead of working directly with the energy and momentum of particles, one might compute invariant masses, angles between particles, etc. This type of feature engineering generally improved performance for shallow neural networks, decision trees, *etc.*; however, with the rise of deep learning this is often no longer necessary and often limits performance compared to working with the original features. One can think of the intermediate layers of a neural network between the input and the output a representation of the data that is good for the task at hand, and by training all the layers of the network simultaneously (or "end-to-end") one can see the intermediate layers as a learned representations. For a review see Ref. [27].

An example of a linear dimensionality reduction representation and data compression is principal component analysis (PCA) of data $x \in \mathbb{R}^d$ at fixed latent space dimensionality k ($k<d$), which finds the orthogonal linear transformation, O,

$$O : \mathbb{R}^k \to \mathbb{R}^d, z \mapsto Oz, \ OO^T = I_d \tag{41.20}$$

that maximizes the data variance in the latent space. Maximizing the variance of the transformed data is equivalent to minimizing the average reconstruction error (the residual variance in data space),

$$\mathcal{L}_{a.e.}(x, f(x)) = \|x - f(x)\|^2 \ . \tag{41.21}$$

A PCA can thus be interpreted as a linear, orthogonal model that is trained to minimize the L_2-distance between the input data and the reconstructed data given the fixed dimensionality k. In practice, the PCA problem can be solved analytically without the use of optimization algorithms or the loss function: the principal components are given by the eigenvectors of the data covariance matrix.

A suitable latent space dimensionality, k, is chosen by ordering the eigenvalues, λ_i, of the data covariance in descending order, and keeping only the first few eigenvectors that correspond to the largest eigenvalues. The cut is often made at dimensionalities that capture around 90% of the data variance. For many data sets this results in $k \ll d$. The average reconstruction error that originates from the discarded eigenvalues is $\sigma^2_{\text{recon}} = \sum_{i=k+1}^{d} \lambda_i$.

Another common type of representation learning and nonlinear dimensionality reduction is based on the *auto-encoder* $f = g \circ e : \mathcal{X} \to \mathcal{X}$, where $e : \mathcal{X} \to \mathcal{Z}$ is referred to as the *encoder* and $g : \mathcal{Z} \to \mathcal{X}$ is referred to as the *generator* or *decoder*. Typically the dimensionality of $\mathcal{Z}$ is much less than $\mathcal{X}$, and $z = e(x)$ can be thought of as a compressed representation of the input. The intermediate space $\mathcal{Z}$ is sometimes referred to as the bottleneck or the latent space of the auto-encoder. If the bottleneck is sufficiently large and the encoder and decoder are sufficiently flexible, then the function f could just be the identity (*i.e.* lossless compression). However, if the encoder and decoder are not sufficiently flexible or the dimensionality of the latent space is not large enough there will be some reconstruction error. Therefore the reconstruction error of Eq. 41.21 serves as a natural loss function of an auto-encoder.

Once trained, the encoder $e(x)$ can be used independently of the decoder to provide a generic low-dimensional representation of the data. The flexibility of this approach is attractive; however, there are no guarantees that this representation will be optimal for the other task. Indeed, the transition from pre-trained auto-encoders to end-to-end learning is one of the important trends that characterized the onset of the deep learning era.

While achieving zero reconstruction error may seem good as it would imply lossless compression, it often performs poorly in practice. First, the encoder may be overfit to the training dataset and not generalize well to held out data. Secondly, it may not be robust to domain shift (see Sec. 41.7.2). One approach to address these issues is the *denoising auto-encoder*, which uses a form of regularization that corrupts the input with noise $x' \sim q(x'|x)$ while still targeting reconstruction of the uncorrupted input x.

$$\mathcal{L}_{d.a.e.}(x, f(x)) = \|x - f(x')\|^2 \qquad \text{with} \qquad x' \sim q(x'|x) \ , \tag{41.22}$$

where $q(x'|x)$ is some probability distribution such as a multivariate normal.

41.3.2.3 *Clustering*

The goal of clustering is to group the data $\{x_i\}_{i=1,\ldots,n}$ into k groups, or *clusters*, usually with $k \ll n$. Intuitively, if two data points belong to the same cluster, then they should be similar in some sense. Conversely, if two data points are very different, then they should be assigned to different clusters. The notion of similarity usually is based on some heuristic, and there are a variety of algorithmic and probabilistic clustering algorithms. In some cases k is specified, while in others it is determined by the clustering algorithm. There is also a distinction between flat clustering that directly partitions the data into k clusters and hierarchical clustering where clusters are nested hierarchically as the name suggests. In many cases clustering uses some notion of distance $d(x_i, x_j)$, which may be the L_p norm $\|x_i - x_j\|_p$.

One of the most common clustering algorithms is known as k-means, where k is specified by the user and results in sets $S = \{S_1, \ldots, S_k\}$ that minimize the variance of each cluster. Thus,

Downloaded from https://academic.oup.com/ptep/article/2022/8/083C01/6651666 by KIT Library user on 27 September 2022

the objective is

$$\begin{aligned}\arg\min_{\mathbf{S}} \sum_{i=1}^{k} \sum_{\mathbf{x}\in S_i} \|\mathbf{x}-\boldsymbol{\mu}_i\|^2 &= \arg\min_{\mathbf{S}} \sum_{i=1}^{k} |S_i| \operatorname{Var} S_i \\ &= \arg\min_{\mathbf{S}} \sum_{i=1}^{k} \frac{1}{2|S_i|} \sum_{\mathbf{x},\mathbf{y}\in S_i} \|\mathbf{x}-\mathbf{y}\|^2\end{aligned} \tag{41.23}$$

where μ_i is the mean of points in S_i.

While k-means and many other clustering algorithms are defined in terms of an optimization problem, the optimization objective is often not representative of the actual notions of performance in a given context. As a result, there are a number of quantities used for the evaluation and assessment of the resulting clustering. These include Davies–Bouldin index, Dunn index, Rand index, Jaccard index, purity, F-measure, Hopkins statistic, *etc.* [28].

41.3.3 *Optimal control, reinforcement learning, and active learning*

Many problems in science and engineering can be cast as a control problem, which comprises a cost functional that is a function of state and some control variables that specify some underlying dynamical system. This is relevant for the control of accelerators where the dynamical system is physical. This formalism can also be used to describe the design of experiments, planning of an observational survey, and other decision making processes relevant to the scientific method. There is a tremendous amount of literature on the subject, and it is closely connected to planning, dynamic programming, and reinforcement learning. Optimal control can be seen as an extension of the calculus of variations, and thus generalizes the framing of learning presented in Sec. 41.2.

Optimal control theory deals with finding a control for a dynamical system over a period of time such that the objective function is optimized. The underlying system can be discrete or continuous and may be deterministic or stochastic. The commonalities and differences between optimal control and reinforcement learning can be best understood through the formalism of a Markov decision process (MDP), which is a discrete-time stochastic control process. We follow common notation, such as that found in Wikipedia.

A Markov decision process comprises four components often organized as a 4-tuple (S, A, P_a, R_a), where: S is a set of states called the state space, A is a set of actions called the action space, $P_a(s,s') = \Pr(s_{t+1} = s' \mid s_t = s, a_t = a)$ is the probability that action a in state s at time t will lead to state s' at time $t+1$, $R_a(s,s')$ is the immediate reward (or expected immediate reward) received after transitioning from state s to state s', due to action a.

The policy function π is a mapping from state space to action space that can be either deterministic or probabilistic. For examples, the policy that drives a computer chess playing system, decides which move to make given the current state of the board. Similarly, policies dictate which experiment should be built next, which field of the sky should be observed, or how to adjust the operational parameters of an accelerator. The dynamics of the resulting system are then fixed by combining the policy with the underlying MDP. The evolution of the resulting dynamical system behaves like a Markov chain since the action chosen in state s is completely determined by $\pi(s)$ and $\Pr(s_{t+1} = s' \mid s_t = s, a_t = a)$ implies the Markov transition matrix $\Pr(s_{t+1} = s' \mid s_t = s)$.

The objective optimal control is to choose a policy π that will maximize a cumulative function of the instantaneous rewards R_a. A common choice is the expected discounted sum:

$$\mathbb{E}\left[\sum_{t=0}^{\infty} \gamma^t R_{a_t}(s_t, s_{t+1})\right], \tag{41.24}$$

where $a_t \sim \pi(s_t)$ are the actions given by the policy, the expectation computed with respect to the distribution $s_{t+1} \sim P_{a_t}(s_t, s_{t+1})$, and γ is the discount factor satisfying $0 \leq \gamma \leq 1$. The discount factor is usually close to 1 and sometimes reparameterized as $\gamma = 1/(1+r)$, where r is called the discount rate. A lower discount factor motivates the decision maker to favor taking actions early, rather than postpone them indefinitely.

A policy that maximizes the objective function is called an optimal policy and denoted π^*, though the optimal policy need not be unique. Importantly, the Markov property implies that the optimal policy is only a function of the current state. Dynamic programming can be used to find the optimal policy for MDPs with finite state and action spaces. For instance, in value iteration (a.k.a. backward induction) can be used to solve the "Bellman equation" [29]. For continuous-time systems, the optimal policy is defined by the Hamilton–Jacobi–Bellman equation [30].

In many settings, it is assumed that the state s is fully known when action is to be taken and there are no latent variables. When this assumption is not true, the problem is called a partially observable MDP. These problems are generally more difficult and the dynamic programming algorithms do not directly apply [31].

Reinforcement learning The main difference between the classical dynamic programming methods and reinforcement learning (RL) algorithms is that the latter do not assume knowledge of an exact mathematical model of the MDP and they target large MDPs where exact methods become infeasible. For example, RL was used in the context of jet physics to search for the most likely jet clustering when the number of constituents was too large for the exact dynamic programming algorithm to be used [32]. In addition, RL can be used when the probabilities or rewards are unknown. Instead, the transition probabilities are often accessed indirectly through interaction with a real or simulated environment. For example, in Q-learning one uses experience to estimate the array $Q(s,a)$ defined as

$$Q(s,a) = \sum_{s'} P_a(s,s')(R_a(s,s') + \gamma V(s')). \tag{41.25}$$

While this function is also unknown, it can be estimated during learning based on (s,a) pairs together with the outcome s'.

Numerous variations to RL exist, which include so-called model-based and model-free approaches (referring to models of the instantaneous rewards and the state transitions) and on-policy and off-policy (which describes how the actions taken during learning are related to the current policy). See Ref. [33] for an introduction and Ref. [34] for a recent review.

Multi-arm bandits Multi-arm bandit problems are a classic reinforcement learning problem where one tries to maximize the expected gain by allocating a limited set of resources to various alternatives. The name is a reference to a gambler with a fixed amount of money that must choose between multiple slot machines (or "one-armed" bandits) when the payoff for the individual machines is unknown. A hallmark of multi-arm bandit problems is that they involve a trade-off between exploration (playing machines to estimate their payoff) and exploitation (playing machines with the highest estimated payoff). Multi-armed bandits are used to manage large projects, organizations, and scheduling problems. The theory has a long history going back to Robbins in 1952 that used it to study the sequential design of experiments [35] and Gittins who derived an optimal policy under some conditions [36].

Bayesian optimization A closely related set of techniques involve optimizing some expensive black box function $f(x)$. For instance, the function may be computationally expensive to evaluate or low-latency, *e.g.* it may involve manually re-configuring a system. This is particularly relevant for analysis optimization in particle physics where evaluating $f(x)$ involves processing large numbers of simulated collisions. Another common use case involves optimizing the hyperparameters of a learning algorithm.

Without any assumptions about the function $f(x)$ this is hopeless; however, if one assumes something about the functions (*e.g.*

Downloaded from https://academic.oup.com/ptep/article/2022/8/083C01/6651666 by KIT Library user on 27 September 2022

some notion of smoothness) then one can leverage function evaluations evaluations $\{f(x_t)\}_{t=1,\ldots,T}$ to say something about what value the function might take on at other values of x. This is usually cast in Bayesian terms, and Gaussian processes (Section 41.5.1) are often used to model the distribution over $f(x)$. The optimization techniques that use this framing are generically referred to as Bayesian Optimization [37].

Optimization in this context is usually characterized by an *exploration-exploitation* trade-off, similar to what is found in multi-arm bandits. Here, exploration refers to function evaluations that characterize the function in regions that haven't been evaluated, while exploitation refers to evaluations near what is predicted to be its maximum. This setting is similar to reinforcement learning in that it involves sequential decisions (*i.e.* where to evaluate the function next), but usually the target function $f(x)$ is assumed to be static. In that sense, the state referred to in the language of an MDP is the state of knowledge about the function after sequential evaluations $\{f(x_t)\}_{t=1,\ldots,T}$. The reward at time t is not the value of the function $f(x_t)$, but some quantity that characterizes what was learned about the function's maximum. In this literature, one often refers to the *acquisition function*, which plays a similar role as the expected value of the reward in RL. Common acquisition functions include the probability of improvement, the expected improvement, and an upper-confidence bound [38].

Connection to experimental design In the context of physics experiments we often want to build the next generation experiment which can reach certain target precision on parameters of interest that the experiment can measure. To achieve this precision we may deploy the concept of *experimental design*, where we the objective is to optimize some objective that quantifies the expected performance of an experiment. Moreover, we would like to achieve this within some constraints such as a minimal cost. Such problems are often solved using the Fisher matrix optimization, where Fisher matrix can be viewed as the expectation of the inverse covariance matrix. We can define

$$t(x|\theta_0) \coloneqq \nabla_\theta \log p(x|\theta)|_{\theta_0} \ , \tag{41.26}$$

where $t(x|\theta_0)$ is referred to by statisticians as the score [20]. The score plays an important role in the classical statistics as it is a sufficient statistic when $p(x|\theta)$ is in the exponential family, and through the Rao-Cramér-Fréchet bound on the variance of an estimator for θ, and is used to define the Fisher information matrix $I_{ij}(\theta) \coloneqq \mathbb{E}_{p(x|\theta)}[t_i(x|\theta)t_j(x|\theta)]$. The Fisher information, in turn is an important object in experimental design. In particle physics, the score is closely related to the concept of optimal observables. The corresponding diagonal element of the inverse of the Fisher matrix thus provides expected uncertainty estimation of a given parameter, and is a lower bound to the error of an unbiased estimator (Cramér-Rao bound). In experimental design we vary the experiment parameters within the constraints such as the total cost to minimize this uncertainty. This framework has been widely used in cosmology, where Fisher analysis is the foundation of any experiment proposal.

Active learning Active learning is closely related to Bayesian optimization, described above. In Bayesian optimization one estimates the function $f(x)$ from some set of evaluations $\{y_t = f(x_t)\}_{t=1,\ldots,T}$; however, the goal is to find the maximum $x^* = \arg\max_x f(x)$. In active learning, the goal is not to find the maximum of $f(x)$, but to approximate the function as one does in supervised learning. The main difference compared to vanilla supervised learning is that the labeled training dataset isn't provided a priori in a passive way, but the learning algorithm actively decides where to generate $(x_t, y_t = f(x_t))$ pairs. The function $f(x)$ is sometimes referred to as an *oracle*. Active learning is particularly attractive when obtaining labelled data is a costly process.

More broadly, a challenge of many machine learning applications is obtaining labeled data, which can be a costly process. If a system could learn from small amounts of data, and choose by itself what data it would like the user to label via an external process called oracle, it would make machine learning more powerful. Such frameworks are also called Experiment Design or Active Learning. In Active Learning, a model is trained on a small amount of data (the initial training dataset), and an acquisition function (often based on the model's uncertainty) decides on which data points to ask for a label. The acquisition function selects one or more points from a pool of unlabelled data points, with the pool points lying outside of the training dataset. Once we label the selected data points, these are added to the training dataset, and a new model is trained on the updated training dataset. This process is then repeated, with the training dataset increasing in size over time. The advantage of such systems is that they often result in dramatic reductions in the amount of labelling required to train an ML system (and therefore cost and time).

41.3.4 *Anomaly detection and out-of-distribution detection*

Unsupervised anomaly detection techniques detect anomalies in an unlabeled test data set under the assumption that the majority of the in-distribution data are normal under some measure, while out-of-distribution (OOD) data are not. In the context of auto-encoders a popular technique is to use the reconstruction error of Eq. 41.21 to identify an outlier as one with a large reconstruction error [39, 40]. One issue with this method is that for higher dimensional latent space and flexible neural network architectures the encoder-decoder map become identity for any input data, $f(x) = x$, regardless of whether input x is from the in-distribution training dataset or from the out-of-distribution data. The choice of auto-encoder latent space dimensionality is thus an important hyperparameter that must be tuned.

Another set of anomaly detection techniques construct a model representing normal behavior from a given In Distribution training dataset, and then test the likelihood of a test instance to be generated by the utilized model. For instance, one can use density estimation methods such as normalizing flows (section 41.5.4.3) to learn the density (likelihood) of the In Distribution training dataset $p(x)$, and apply it to the test data. The expectation is that out-of-distribution data will have a lower density (likelihood) under the in-distribution density model. This expectation is however not always met in high dimensions and the method suffers because likelihood based training is sensitive to the smallest variance directions [41]: for example, a zero variance pixels leads to an infinite $p(x)$, and noise must be added to regularize it. But low variance directions may contain little or no information on the global structure of the image, so there is a mismatch between the training objective and outlier detection objective. A related issue is that of typicality: an in-distribution likelihood will typically be lower than the maximum value. For a Gaussian likelihood the typical set is on average be $n/2$ in log likelihood below the peak value, where n is the dimensionality of the data. So an out-of-distribution dataset that is closer to the peak would be preferred in terms of likelihood even though its distribution does not match the in-distribution data. If this happens by chance on low variance directions which dominate the likelihood, normalizing flows can assign higher likelihoods to out-of-distribution data than to in-distribution training dataset [42]. A number of techniques have been proposed to circumvent these limitations, such as likelihood regret [43], likelihood-ratio [41], likelihood in auto-encoder latent space [44], and Wasserstein distance training of the likelihood $p(x)$ [45]. These methods can achieve better anomaly detection performance than the auto-encoder reconstruction error [44, 46].

Supervised anomaly detection techniques require a data set that has been labeled as in-distribution and out-of-distribution and involves training a classifier (the key difference to many other statistical classification problems is the inherent unbalanced nature of outlier detection). These methods assume some form for what out-of-distribution data may look like, and their success relies on whether the assumed form is a realistic representation of actual out-of-distribution data. When this assumption is valid these methods can be more powerful than unsupervised methods, but the reverse is also true. A hybrid between the two approaches is to train a classifier without labels [47]. All these approaches are largely complementary to each other [48]. An example of different anomaly detection methods applied to HEP is LHC Olympics

Downloaded from https://academic.oup.com/ptep/article/2022/8/083C01/6651666 by KIT Library user on 27 September 2022

2020 and Dark Machines challenges [49, 50].

41.3.5 *Simulation-based inference*

The goal of simulation-based inference (related to, but distinct from, likelihood-free inference) is to extend the statistical procedures described in the Chapter on Statistics (*e.g.* parameter estimation, hypothesis tests, confidence intervals, and Bayesian posterior distributions) to the situation where one does not know the explicit likelihood $p(x|\theta)$, the probability of the data given the parameters θ, but has access to a simulator that defines the likelihood $p(x|\theta)$ implicitly [51, 52]. In a typical setup we would like to solve the so called inverse problem of getting the posterior of the parameters given the data, $p(\theta|x)$, but we cannot use Bayes theorem directly because we do not have explicit $p(x|\theta)$.

In particle physics, the simulators usually use Monte Carlo event generators (see Sec. 43) to sample unobserved latent variables z, such as the z_p phase space of the hard scattering (see Sec. 49.4), z_s associated to showering and hadronization, and z_d associated to the interaction of particles with the detector (see Sec. 34). As such, the full simulation chain can be expressed symbolically as

$$\begin{aligned} p(x|\theta) &= \int dz p(x,z|\theta) \\ &= \int \mathrm{d}z_d \int \mathrm{d}z_s \int \mathrm{d}z_p \, p(x|z_d)p(z_d|z_s)p(z_s|z_p)p(z_p|\theta) \ , \end{aligned} \tag{41.27}$$

where θ are the Lagrangian parameters that dictate the hard scattering. Evaluating the likelihood is intractable as it would require evaluating the integral above for each event.

While the likelihood is intractable, simulators provide the ability to generate synthetic data $x_i \overset{i.i.d.}{\sim} p(x|\theta)$ for any value of the parameters θ. One can use a suitable proposal distribution $\tilde{p}(\theta)$, sample $\theta_i \overset{i.i.d.}{\sim} \tilde{p}(\theta)$, generate synthetic data $x_i \sim p(x|\theta_i)$, and then assemble a training dataset $\{x_i, \theta_i\}_{i=1,\ldots,n}$ that can be used to train various machine learning models.

There is thus a close analogy between Simulation-based Inference and data driven machine learning tasks discussed so far, replacing θ with y. One difference is that in simulation-based inference we can always generate new samples by running additional simulations, while we typically view training dataset in machine learning as fixed. This property of Simulation-based Inference enables Active Learning, where the additional simulations are chosen such as to minimize the error on the desired statistical inference task. Another difference is that we often have access to the joint likelihood $p(x, z|\theta)$, where z are unobserved latent variables[5].

Typically in particle physics, one uses histograms or kernel density estimation to model the distribution of observables (low-dimensional summary statistics such as the invariant mass) of simulated data [53]. Alternatively, one can use an explicit parametric family (such as a falling exponential, a Gaussian distribution, *etc.*) to model $\hat{f}(x|\theta) \approx p(x|\theta)$. That model is then used as as a surrogate for the unknown density implicitly defined by the simulator. A related approach is known as Approximate Bayesian Computation (ABC), which approximates the likelihood through an acceptance probability that synthetic data is sufficiently close to the observed data [54, 55]. In practice, these techniques are limited to low-dimensional representations of the data. Thus the potential of recent machine learning approaches to simulation-based inference is to extend this approach to higher-dimensional data, while maintaining the already well-established statistical procedures.

For instance, one can use normalizing flows (see Sec. 41.5.4.3) and the loss functions for density estimation (see Sec. 41.3.2.1) to learn a surrogate model for the likelihood $\hat{f}(x|\theta) \approx p(x|\theta)$ [56]. Similarly, one can use conditional density estimation to learn a surrogate model for the posterior $\hat{f}(\theta|x) \approx p(\theta|x)$, which may involve including the prior-to-proposal ratio $\tilde{p}(\theta)/p(\theta)$ [57]. In addition to the unsupervised learning techniques, one can also use supervised learning to learn the likelihood-ratio $r(x|\theta_0, \theta_1) = p(x|\theta_0)/p(x|\theta_1)$ by leveraging the *likelihood-ratio trick* of Eq. 41.12 [20, 58].

In some cases one can also augment the training dataset to include the joint likelihood-ratio

$$r(x_i, z_i|\theta_0, \theta_1) := p(x_i, z_i|\theta_0)/p(x_i, z_i|\theta_1) \ , \tag{41.28}$$

which can be used to reduce the variance for the squared-error loss or the improved cross-entropy estimator of Eq. 41.17 [20, 21]. While the marginal likelihood $p(x|\theta)$ is intractable due to the high-dimensional integral over the latent space, the joint likelihood is often tractable since no integration is necessary. In addition, one can often augment the training dataset with the joint score

$$t(x_i, z_i|\theta_0) := \nabla_\theta \log p(x_i, z_i|\theta)|_{\theta_0} \ . \tag{41.29}$$

Regressing on the joint score with the squared loss function $\mathcal{L}(t(x, z|\theta_0), f(x)) = (t(x, z|\theta_0) - f(x))^2$ corresponds to risk functional

$$\mathcal{R}_{\text{score}}[f] :- \mathbb{E}_{p(x,z|\theta_0)}[(\nabla_\theta \log p(x_i, z_i|\theta)|_{\theta_0} - f(x))^2] \ . \tag{41.30}$$

One can show with the calculus of variations that the risk is minimized by the score of equation 41.26.

41.3.5.1 *Differentiable simulations*

One of the approaches to make inference feasible in high dimensional latent space is to make simulations differentiable with respect to all of its parameters, global variables θ and latent variables z. Latent variable models are known in Machine Learning as generative models and are discussed below, but latent variable models are also common in scientific applications. As an example, in cosmology one can view the initial conditions of the large scale structure or cosmic microwave background as Gaussian distributed latent variables.

While differentiable simulations have traditionally not been developed for scientific applications, the success of Machine Learning, where backpropagation algorithm combined with gradient descent optimization (see Sec. 41.6.1) is the basis of its recent advances, has inspired a new look at this. One recent example is FlowPM cosmological N-body simulation, which takes advantage of Mesh-Tensorflow to achieve a GPU-accelerated, distributed, and differentiable simulation [59].

One broad class of inference problems where gradients make the problem simpler are the so called inverse problems. As a simple example let's assume the data x are observed with some Gaussian noise with known variance σ^2, equal for all data points. The likelihood of the data can be written as

$$\log p(x|z,\theta) = -\frac{N}{2}\log[2\pi\sigma^2] - \frac{||x - g(z,\theta)||^2}{2\sigma^2}. \tag{41.31}$$

Here $g(z, \theta)$ is the forward model (generator or decoder), i.e. the simulation output in the absence of noise. The joint distribution is $p(x, z|\theta) = p(x|z, \theta)p(z|\theta)$, where $p(z|\theta)$ is the prior of latent space variables, assumed to be known, with a known gradient with respect to θ and z. In this case the gradients $\nabla_\theta \log p(x, z|\theta)$ and $\nabla_z \log p(x, z|\theta)$ are available when the simulation forward model gradients $\nabla_\theta g(z, \theta)$ and $\nabla_z g(z, \theta)$ are available.

Availability of simulation gradients in turn enables gradient based optimization or sampling. In sampling approach one can use Monte Carlo Markov Chains to obtain the posterior samples of latent space z and parameter space θ [60]. In optimization approach one can find the best-fit point $\hat{z}$, which is the MAP estimate of the latent space variables z given x and fixed θ [61]. Another optimization approach is Variational Inference, which attempts to model the posterior probability distribution using optimization. This is discussed further in Section 41.5.4.

41.3.5.2 *Unfolding as an inverse problem*

While much of the work on simulation-based inference described above is aimed at inferring the parameters θ of the simulator, there is also work that aims to to infer the latent variables z. Here it is useful to think of the parameters θ as parameters of a theory, such as masses, coupling constants, or Lagrangian parameters, while z

[5] For this reason we prefer to use simulation-based inference instead of likelihood-free inference: joint likelihood $p(x, z|\theta)$ is often available, it is the marginal integral over latent space z that is assumed to be intractable.

Downloaded from https://academic.oup.com/ptep/article/2022/8/083C01/6651666 by KIT Library user on 27 September 2022

might describe the kinematics of a collision before the detector response.

Inferring the distribution $p(z|\{x_1, \ldots, x_n\})$ from a dataset of multiple observations is commonly referred to as unfolding in particle physics, and deconvolution in other contexts. Unfolding is a classic inverse problem, and the collection of ideas being used for machine-learning based simulation-based inference are also being applied in this setting. Examples of recent work exploring these approaches are Refs. [62–73]. In addition, there has been work to infer the posterior distribution for an individual event $p(z|x_i)$ using probabilistic programming techniques [74–76].

41.4 Data representations, inductive bias, and example applications

In Sec. 41.3 we describe the input data as living in an abstract space $x_i \in \mathcal{X}$. In this section, we briefly describe some of the common types of structured data that are encountered in physics and refer to the corresponding models classes that have been developed to work with them. We will describe the model classes in more detail in the following section.

The most basic and common type of data structure is when $\mathcal{X} = \mathbb{R}^d$. This is often referred to as *tabular data* since the entire data set $\{x_i\}_{i=1,\ldots,n}$ can be thought of as a table with n rows and d columns. It is common to think of an individual entry x_i as a vector in d-dimensional Euclidean space, where the coordinates correspond to the columns of this table. In some cases individual components of x_i might be integers or take on only discrete values, in which case describing the space of the data as real-valued is a slight abuse of notation and representation. For many years this was the dominant type of data in high energy physics as it is a natural input type for shallow neural networks, multi-layer perceptrons, support vector machines, and tree-based methods found in popular tools such as `TMVA` [77].

For categorical data, one typically uses a numerical representation such as *integer encoding* where different categories are mapped to integers with a corresponding dictionary. Another common representation of categorical data is based on the so-called *one-hot encoding* (aka 'one-of-K' or 'dummy'), in which case the category is mapped to a k-dimensional binary vector where k is the number of categories and each component of this vector corresponds to a particular category. In the one-hot encoding, only one of the components is non-zero. Finally, there are approaches in one learns an *embedding* that maps discrete categories into $\mathbb{R}^d$; an example of this is `Word2Vec` [78]. Interestingly, such embeddings can preserve various types of semantics; for instance, the vector `walking-walk` is similar to the vector`swimming-swam` as are the vectors connecting countries and their capital cities. This allows for a loose sense of algebra on the word embedings such as `walking-swimming+swam = walk`. Similar types of embeddings have also been used in a number of scientific use-cases including biological sequences (e.g. DNA, RNA, and Proteins) for bioinformatics applications [79].

Particle physics data often is represented with an extension of the simple tabular data structure where the number of columns is not fixed. For instance, if the rows correspond to data for individual collisions, the number of electrons (and positrons) reconstructed in the event is variable. Thus the number of columns needed to represent the energy, momentum, and charge of these particles is also variable. A common solution to this problem is to fix a maximum number of particles and then *truncate* and *zero-pad* to fit the data into a fixed tabular representation, though this is not the natural representation of the data and it leads to a loss of information.

Sequential data is also commonly encountered in physics (*e.g.* in time series). Here an individual entry $x_i = (x_i^1, \ldots, x_i^t, \ldots x_i^{T_i})$ where t is index for the ordered sequence, T_i is the length of the sequence (which might be variable), and the data associated to each "time" $x_i^t \in \mathbb{R}^d$. This is similar to the previous example where the energy, momentum, and charge of the t-th electron in the i-the event would be x_i^t and the electrons might be sorted according to their energy or transverse momentum. Sequential data is also encountered in natural language processing, where x_i^t correspond to individual words in a sentence. Recurrent neural networks (see Sec. 41.5.3.9) are particularly well suited to sequential data. Examples applications from the Living Review include [80–85].

Image-like data is one of the most dominant forms of data in industrial applications of deep learning, is very relevant for astronomy and cosmology, and also appears in particle physics in various forms. Image-like data typically involves d-dimensional features associated to a regular grid or lattice that does not vary across the individual instances x_i. The canonical example is a standard image from a camera with $W \times H$ pixels where the p-th pixel has data $x_i^p \in \mathbb{R}^3$ corresponding to the three *channels* in the RGB color model. It is important to recognize that the data corresponding to the 2-dimensional image is not 2-dimensional; instead, it is $(W \times H \times c)$-dimensional, where c is the number of channels. In astronomy, an image may be grey scale ($c = 1$) or there may be more *channels* ($c > 3$) corresponding to different color filters. In other applications, the grid or lattice might be 3- or 4-dimensional. For example, the data associated to a regularly segmented calorimeter can be thought of as a 3-dimensional image and the data associated to a lattice simulation of a classical or quantum system can be thought of as a 4-dimensional image. Convolutional neural networks, described in Sec. 41.5.3.5, are particularly well suited to image-like data. Example applications from the Living Review include [81, 86–108].

It is also possible that the the data (or features) associated to one "pixel" or lattice site may itself be structured. For example, the single read-out plane of a Liquid Argon time projection chamber (LArTPC) may involve a 1-dimensional or 2-dimensional grid, but the data associated to each "pixel" is itself a sequence or waveform. Example applications in Neutrino Physics from the Living Review include [109–139]. Similarly, in lattice quantum chromodynamics, the data associate to a particular site (or link) would be group valued (*e.g.* $x_i^p \in SU(3)$ as in Refs. [140, 141]).

Both sequential and image-like data have a notion of temporal or spatial structure. While it is possible to unroll an image into a $(W \times H \times c)$-dimensional vector, that would erase the spatial structure and obfuscate the fact that nearby pixels are highly correlated. Similarly, one could permute the time index for sequential data, but that would destroy the temporal structure of the data. The complementary point of view is that the model class should also be aware of the structure of the data. Recurrent neural networks and convolutional neural networks are good examples of what is called *inductive bias* as the models do incorporate something about the structure of the data that they are expected to be used with. In some cases this can be formalized in terms of symmetry. For example, if we train model to classify images of cats and dogs, we would like it's prediction to be invariant to where in the image the cat is. This type of translational invariance can be enforced in the design of the model class.

While permuting the elements of a sequence destroys the temporal structure of a time series, attaching a temporal index t to a set of objects with features x_i^t can also be problematic. If the data corresponding to x_i really are a set $\{x_i^1, \ldots, x_i^{T_i}\}$ (*e.g.* a point cloud), then we would like the output of the model to be *permutation invariance*. A standard sequential or convolutional model will not generally be permutation invariant, but recently models such as Deep Sets, various types of graph neural networks, and transformers can be made to enforce permutation symmetry. Example applications from the Living Review include [100, 142–152]

The temporal and spatial structure of sequences and image like data can also be generalized. For instance, a 1-dimensional sequence can be generalized to a tree structured data like one finds in the hierarchical clustering of jets or as in a directed-acyclic graph (DAG). Generalizations of recurrent neural networks have been constructed that can operate over these more complex data structures [153, 154]. More generally, one can considered graph-structured data composed of nodes and edges or multi-graphs that group together three nodes into faces or k nodes into k-edges. Graph neural networks are a class of models that work with this type of data. The emerging subfield of geometric deep learning aims to unify the notation, terminology, and theory that connect these considerations of the structure of the data and the corresponding model architecture. Example applications in the Living Review include [121, 128, 131, 132, 134, 155–181].

Downloaded from https://academic.oup.com/ptep/article/2022/8/083C01/6651666 by KIT Library user on 27 September 2022

If the data are expected to have a symmetry associated to them but one is working with a model class that does not enforce this symmetry, then *data augmentation* is a common procedure used to improve generalization performance. Here one starts with an initial dataset $\{x_i\}_{i=1,\ldots,n}$ and produces an augmented dataset $\{x'_i\}_{i'=1,\ldots,n'}$ through some data augmentation strategy. For example, one might apply a random rotation $R_{i'}$ to an image to produce $x'_i = R_{i'}(x_i)$ if one assumes rotational invariance in the underlying problem.

In some cases some of the individual features (components) of x are functions of other features. For instance, one may include components of a four-vector (E, p_x, p_y, p_z) as well as redundant information such as transverse momentum, azimuthal angles, rapidity, etc. In this case, the data is restricted to a lower-dimensional surface embeded in $\mathcal{X}$. Even if the features aren't redundant, statistically the data are often effectively restricted to a small subspace of statistically likely samples and those that are exceedingly unlikely. For instance, the space of natural images is a small and highly structured subspace of all possible images, which are dominated by what we would perceive visually as noise. The term *data manifold* is used to describe this restricted subspace where the data are to be found, even though it does not necessarily satisfy the formal requirements of a manifold in the mathematical sense.

These considerations on the structure of the data not only apply not to the input data $x_i \in \mathcal{X}$, but also to the output data $y_i \in \mathcal{Y}$. For instance, one might want a sequence-to-sequence model as in machine translation of written text [182] or to learn a function that takes sets as input and produces graphs as output as in the Set2Graph mode [183]. One might also want the input and output of the model to be different in representations of an underlying symmetry group and for the model to enforce group-equivariance [140, 141]. The development of the necessary modelling components to enable practitioners to compose and train these types of models is a significant development for the field of physics.

41.5 Flavors of ML models

41.5.1 *Support vector machines and kernel machines*

Support Vector Machines (SVM) are a class of supervised learning models used for classification and regression. The learning algorithm involves a convex optimization problem that has a unique solution and can be solved with quadratic programming techniques. In this sense, they are robust and easier to characterize than neural networks that involve non-convex optimization. While their history goes back to Vapnik and Chervonenkis in the 1960s, they gained popularity after Bernhard Boser, Isabelle Guyon and Vladimir Vapnik suggested a way to create nonlinear classifiers by applying the kernel trick in 1992 [184]. Originally they were developed for binary classification and only supported therestricted case where the training dataset can be separated without errors, but in 1995 Cortes and Vapnik extended the technique to non-separable training dataset [185]. A variant targeting regression, known as support vector regression (SVR), was developed in 1997 [186]. The theory around support vector machines was well developed, and they dominated machine learning research for roughly a decade before the rise of deep learning (see Sec. 41.5.3.4).

Maximum-margin classifiers Linear support vector machines are used for binary classification, where $\mathcal{X} = \mathbb{R}^d$ and the target labels are conventionally defined as $\mathcal{Y} = \{-1, 1\}$. The classification is simply based on which side of a hyperplane the data lie. Any hyperplane can be written as the set of points x satisfying $w^T x - b = 0$, where $w, b \in \mathbb{R}^d$ are the parameters of the model. The vector w is normal to the hyperplane, but not necessarily normalized. The quantity $\frac{b}{\|w\|}$ quantifies the offset of the hyperplane from the origin along the normal vector w.

If the training dataset is linearly separable, then there is a region bounded by two parallel hyperplanes, called the *margin*, that separate the two classes of data. The maximum margin classifier is uniquely defined by making the distance between these two hyperplanes as large as possible. The boundaries of the margin can be defined by $w^T x_i - b = \pm 1$, and the width of the margin is given by $\frac{2}{\|w\|}$. Figure 41.1 illustrates this for $x \in \mathbb{R}^2$.

Since the width of the margin is maximized when $\|w\|$ is minimized, we can state the goal of the (hard) maximum-margin classifier in the linear separable case as the following constrained optimization problem: Minimize $\|w\|^2$ subject to the constraint $y_i(w^T x_i - b) \geq 1$ for $i = 1, \ldots, n$. The w and b that solve this problem uniquely determine the resulting classifier, $\hat{y}(x) = \mathrm{sgn}(w^T x - b)$.

This geometric description makes it clear that the maximum-margin hyperplane is completely determined by those x_i that lie nearest to it: the eponymous *support vectors*.

Soft margins and slack variables Often the data will not be linearly separable and thus the hard-margin optimization problem described above has no solution. Such a non-separable case can be accommodated with the use of so-called *slack variables*. One slack variable $\xi_i > 0$ is introduced for each data point. As shown in Figure 41.1 (right), if a data point x_i is outside the margin and correctly classified as in the separable case, then $\xi_i = 0$. If it within the margin but still correctly classified, then $0 < \xi_i < 1$. If it is misclassified, then $\xi_i > 1$. The new constrained optimization problem is to minimize

$$\sum_i \xi_i + \lambda \|w\|^2 \tag{41.32}$$

subject to the constraints $y_i(w^T x_i - b) \geq 1 - \xi_i$ and $\xi_i > 0$ for $i = 1, \ldots, n$. Effectively, this corresponds to minimizing $\sum_i \max(0, 1 - y_i(w^T x_i - b)) + \lambda \|w\|^2$, where the first term is called the *hinge loss*.

The dual problem In the language of convex optimization, linear programming, and quadratic programming the optimization problems stated above for the hard and soft maximum-margin classifiers define the *primal* objective to be minimized. There is a *Lagrange dual* problem where the solution corresponds to maximization with $\min_\phi L(\phi) = \sup_{\alpha > 0} \bar{L}(\phi, \alpha)$, where α are Lagrange multipliers. While it is not apparent in the primal formulation of the constrained optimization problems, the solution to the dual problem takes on the form

$$\hat{y}(x) = \mathrm{sgn}(\sum_i y_i \alpha_i x_i^T x - b) \ , \tag{41.33}$$

where the $\alpha_i > 0$ for the support vectors and otherwise zero. This reformulation is plausible since the orientation of the maximum-margin hyperplanes defined by w is completely specified by the support vectors. The crucial observation for the kernel trick described below is that the final model is defined in terms of coefficients and the inner product $\langle x_i, x \rangle_{\mathcal{X}} = x_i^T x$.

The kernel trick One approach to obtain non-linear decision boundaries is introduce a non-linear mapping $\varphi \colon \mathcal{X} \to \mathcal{V}$ that embeds the data in some higher-dimensional space $\mathcal{V}$. One can then use the linear SVM described above in the space $\mathcal{V}$. This is not unlike the many neural network models where the first layers use a non-linear activation function while the last layer is linear.

The *kernel trick* avoids the explicit mapping φ that is needed to get linear learning algorithms to learn a nonlinear function or decision boundary. This is possible because the solution to the dual problem in Eq. 41.33 is represented in terms of inner products $\langle \varphi(x_i), \varphi(x) \rangle_{\mathcal{V}} = \varphi(x_i)^T \varphi(x)$ corresponding to the candidate point x and the support vectors x_i. Thus all that is needed is a way to evaluate the inner products. A *kernel* or a kernel function $k \colon \mathcal{X} \times \mathcal{X} \to \mathbb{R}$ is a function that can be expressed as an inner product in another space $\mathcal{V}$ via $k(x, x') = \langle \varphi(x), \varphi(x') \rangle_{\mathcal{V}}$. Critically, one does not need to ever evaluate the map $\varphi(x')$, which is implicitly defined by the kernel. In some cases the kernel is straight forward to evaluate, even though the target space $\mathcal{V}$ implicitly defined by the kernel would be infinite dimensional.

The choice of the kernel is roughly the analog of the architecture of a neural network. It dictates the types of non-linearities the

Downloaded from https://academic.oup.com/ptep/article/2022/8/083C01/6651666 by KIT Library user on 27 September 2022

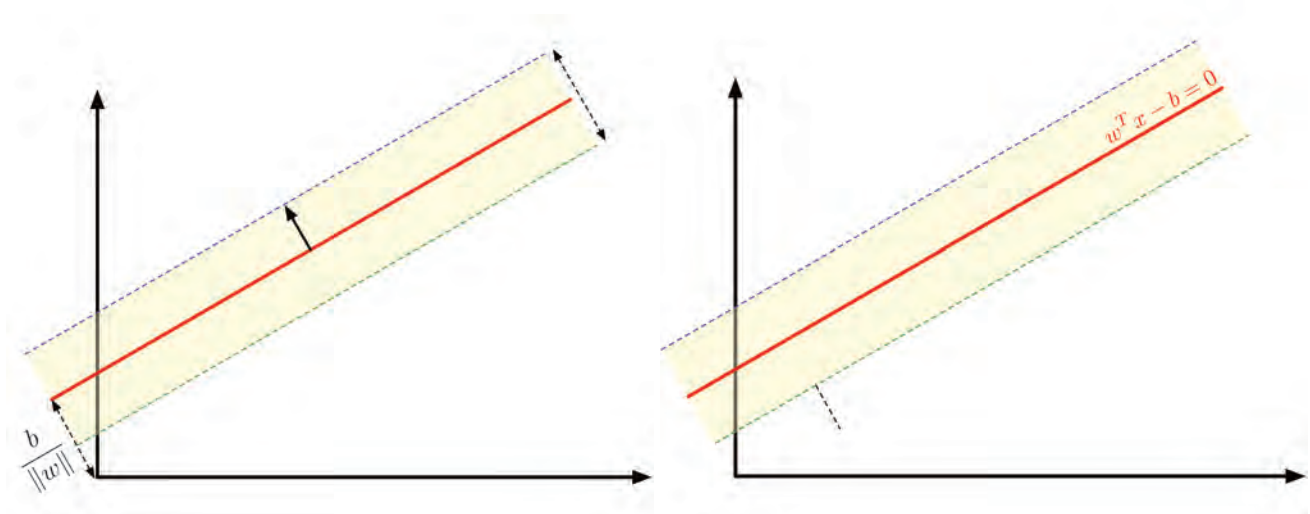

Figure 41.1: Illustration of a maximum margin classifier for a linear support vector machine in the separable case (left) and with the soft-margin and slack variables ξ (right).

SVM can implement in the input space. It also provides an opportunity to encode prior knowledge from physics such as symmetries, length scales, *etc.* There are also connections between very wide neural networks with random weights and biases and the kernel of a Gaussian process [187–189], which, when applied to deep networks, lead to the concept of neural tangent kernel [190]. While it is beyond the scope of this chapter, the interested reader may also be curious to understand the connections as formalized in the language of Reproducing kernel Hilbert spaces (RKHS) [191].

Support vector regression There are a few flavors of SVR. In Vapnik's ϵ-SVR formulation is similar to the picture for classification, but the boundary hyperplane serves as the prediction and the width of the margin for which there is no penalty is ϵ. Again, one can introduce a non-linear map $\phi(x)$ explicitly or implicitly via the corresponding kernel $k(x, x')$. One can view the predictive model as $\hat{y}(x) = w^T\phi(x) - b$ and the goal of the optimization problem is to minimize

$$\|w\|^2 + C\sum_i(\xi_i + \xi_i^*) \tag{41.34}$$

where ξ_i and ξ_i^* are slack variables associated to the model over or under-estimating $y_i \in \mathbb{R}$. The constrained optimization is subject to $w^T x_i - b - y_i \leq \epsilon + \xi_i$, $y_i - w^T x_i + b \leq \epsilon + \xi_i^*$, $\xi_i, \xi_i^* \geq 0$ for $i = 1 \ldots, n$. The solution to the dual problem leads to a kernelized representation of the solution

$$\hat{y}(x) = \sum_i(\alpha^* - \alpha)K(x, x_i) - b\ , \tag{41.35}$$

where the α_i, α_i^* are the parameters of the dual problem. In libraries like `LibSVM` the output of the algorithm is just $\alpha_i^* - \alpha_i$ for $i = 1 \ldots, n$.

Kernel ridge regression Kernel Ridge Regression (KRR) uses the same model as in SVR; however, it uses a different loss function. KRR uses the squared error loss while support vector regression uses the ϵ-insensitive loss function (*i.e.* no penalty is encured if the prediction is within ϵ). Both are combined with l2 regularization (the $\|w\|^2$ term). While SVR leads to a sparse solution that only depends on the support vectors, it can be slow to solve the constrained convex optimization problem. In contrast, KRR can be done in closed-form and is typically faster to train for medium-sized datasets. The consequence is that the learned model is non-sparse and thus slower than SVR to evaluate at prediction-time.

Gaussian Process Regression (krigging) Another variation on kernel-based regression is Gaussian process regression (GPR), also referred to as *krigging*. Again the model is based on the kernel trick. While KRR aims to minimize the mean-squared error loss $(y_i - \hat{y}(x_i))^2$ along with an l2 regularization term proportional to $\|w\|^2$, GPR elevates these terms to a probabilistic interpretation where the first is proportional to a log-likelihood for Gaussian $N(y_i|\hat{y}(x_i)), \sigma)$ likelihood and the second corresponds to the log of a Gaussian prior on w_i. This is related to the discussion on Tikhonov regularization found in Sec. 41.3.1.2. GPR goes further and uses a mean function $m(x)$ and kernel $k(x, x')$ to define a probabilistic model for $y(x)$ and $y(x')$ that includes correlations. For any finite number of points $\{x_j\}_{j=1,\ldots,m}$, the Gaussian process defines the joint distribution for the values that $f(x_i)$ might take. Typically, one specifies the prior mean $m(x)$ and prior covariance function $k(x, x')$ and then conditions on the training dataset $\{x_i, y_i\}_{i=1,\ldots,n}$. The posterior can then be evaluated for an independent set of points $\{x_j\}_{j=1,\ldots,m}$. The posterior mean is typically used as the prediction equivalent to SVR and KRR, but GPR also gives a meaningful notion of uncertainty in the predictions, and can be viewed as a realization of kernel Bayesian regression [192].

One advantage of GPR is that one can work with a family of kernel functions parameterized by some hyperparameters η. One can then optimize the hyperparameters via gradient-ascent on the marginal likelihood function. In contrast, hyperparameter tuning in SVR and KRR typically requires a grid search or some other black-box optimization procedure evaluated on held out data or some form of cross-validation.

Rasmussen and Williams provides an excellent review of Gaussian processes [193]. Numerically, Gaussian Process libraries are confronted with computing the log determinant of the covariance kernel, which naively scales like $\mathcal{O}(n^3)$ in computational complexity. However, recently there have been a number of numerical advances that make these methods fast and scalable to large datasets [194, 195]. While Gaussian Processes are used more widely in cosmology, they are not widely used in particle physics or astro-particle physics. Recent works explore the design of physics-inspired kernels and use Gaussian Processes to model the intensity for a Poisson point process like those found in experimental particle physics and γ-ray and X-ray astronomy [196–198]. Gaussian Processes are also extensively used in Bayesian Optimization (Section 41.3.3).

41.5.2 *Decision trees*

Tree-based models Classification and Regression Trees (CART) typically partition the input space into J disjoint regions $\mathcal{X} = \mathcal{X}^1 \cup \cdots \cup \mathcal{X}^J$ through a sequence of $J-1$ binary splits based

Downloaded from https://academic.oup.com/ptep/article/2022/8/083C01/6651666 by KIT Library user on 27 September 2022

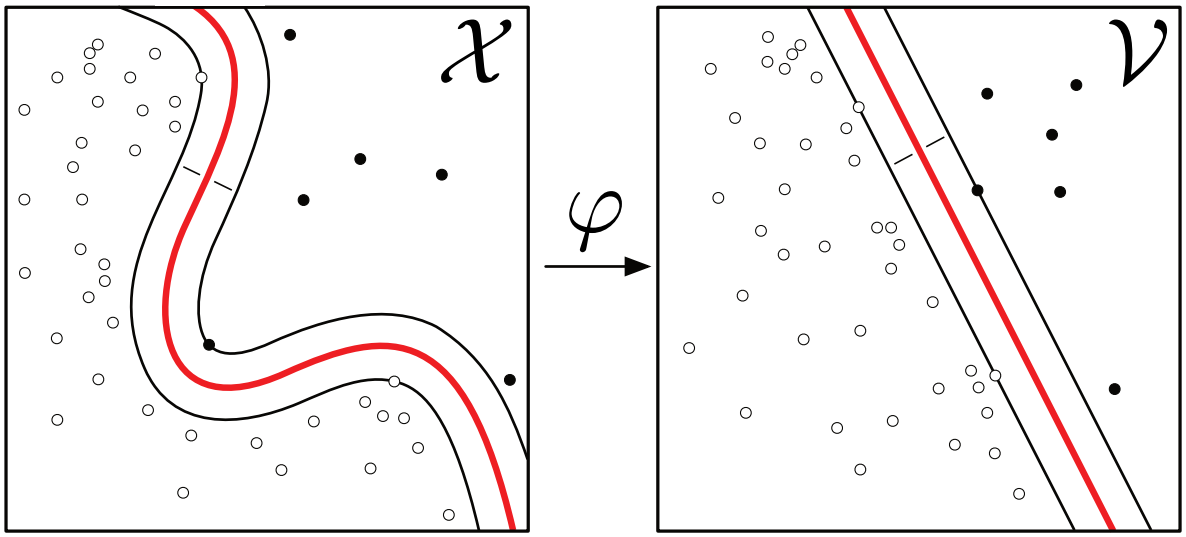

Figure 41.2: Figure depicting the nonlinear SVM decision boundary in $\mathcal{X}$ (left) and the corresponding linear maximum margin classifier in $\mathcal{V}$ (right). Figure adapted from Kernel_Macine.svg Wikimedia Commons (CC BY-SA 4.0) by Cranmer.

on an individual components of $x \in \mathcal{X}$ (*e.g.* $x_4 < 0.7$) [199]. The model is piecewise constant and assigns the value $b_j \in \mathcal{Y}$ to the j-th terminal region $\mathcal{X}^j$. The model can be written

$$\hat{y}(x) = f_\phi(x) = \sum_j b_j \mathbf{1}(x \in \mathcal{X}^j) \; . \tag{41.36}$$

The parameters ϕ of the model comprise the components index and thresholds for the successive splittings and the coefficients b_j.

Tree learning refers to the algorithm used to choosing the tree structure and determining the predictions at leaf nodes. Optimization of the tree structure involves a difficult discrete optimization since the change in the loss with respect to the tree structure is non-differentiable and it is intractable to explore the combinatorially large space of possible trees with brute force. Therefore, the discrete optimization component of tree learning typically involves some approximate algorithm based on heuristics. In contrast, optimization of the b_j for a given tree structure can exploit gradient-based optimization algorithms.

Common approaches to building the decision tree start with a root node and grow with splits based on individual attributes (components of x). These are referred to as top-down induction strategies. There are various impurity heuristics used for choosing the best attribute to split on such as the Gini index, cross-entropy and mis-classification error. Generally they aim to find a split that will refine the the terminal nodes such that they have higher purity than the parent node.

Because most tree learning algorithms consider splits aligned with individual feature components, there are some failure modes for tree-based models. However, tree-based models work well with tabular data that is composed of a mix of continuous and discrete features. Tools such as `XGBoost` [200] are widely used in data science competitions such as Kaggle and the boosted decision trees (BDTs) implemented in `StatPatternRecognition` [201] and `TMVA` [77] have been one of the most used techniques in particle physics [3].

Individual trees are often referred to as weak-learners and they can be combined in various ways described below. Regularization is also an important consideration with tree-based models as one can always learn a tree that assigns exactly one training dataset point per terminal node and memorize the training dataset exactly. One approach to this is called *pre-pruning*, which simply terminates the growing of the trees if the number of training samples reaching the terminal node drops below some threshold, the purity of a terminal nodes is below some threshold, or if the improvement in purity due to a proposed split is not above a threshold. Another regularization approach is called *post-pruning*, which uses a validation data set that is disjoint from the training dataset to probe generalization performance. In this approach, after initially growing a tree with the training dataset, one considers a sequences of pruned trees where splits are removed based on some heuristic. One finds the tree in this sequence of pruned trees that minimizes the generalization error on the validation set. Alternatively, in tools such as *XGBoost* there is an explicit regularization term included in the loss function (see Eq. 41.43).

Ensemble methods The idea of ensemble methods is to combine multiple models into a more performant one by exploiting the bias-variance tradeoff [202]. This is most commonly achieved through averaging (*e.g.* bagging and random forests), which primarily reduces variance, or boosting (*e.g.* AdaBoost and gradient boosting), which primarily reduces bias. Here bias refers to the difference between the Bayes optimal model and the average model produced by the learning procedure with different training sets and variance quantifies how much the learned model varies from one training set to another.

The motivation of boosting is to combine the outputs of many "weak" models to produce a more expressive model. Compared to averagaing techniques like bagging and random forests, the model is built sequentially on modified versions of the data and the final predictions are combined through a weighted sum

$$\hat{y}(x) = \sum_{t=1}^{T} \beta_t \hat{y}_t(x) \; , \tag{41.37}$$

where β_t expand the parameters of the model ϕ.

Bagging The idea behind bagging (bootstrap aggregating) is to create T bootstrap training datasets $B_1, \ldots, B_T$ drawn from the training dataset $\{x_i, y_i\}_{i=1,\ldots,n}$, then learn a model $\hat{y}_t$ for each, and finally construct an average model $\hat{y}(x) = (1/T)\sum_t \hat{y}_t(x)$. If one had T independent training datasets each of size n, then the bias of the average model would be the same as the original model, but the variance would be reduced by a factor of T. By using bootstrap resampling, the bias may increase but the reduction in variance often dominates, which leads to improved performance.

Random forests Random forests refers to a type of "perturb and combine algorithm" that combines bagging and random attribute subset selection. Again one builds trees $\hat{y}_t(x)$ from bootstrap training datasets B_t, but instead of choosing the best split

Downloaded from https://academic.oup.com/ptep/article/2022/8/083C01/6651666 by KIT Library user on 27 September 2022

among all attributes, one select the best split among a random subset of k attributes. If k includes all attributes, then it is equivalent to bagging.

AdaBoost In AdaBoost (adaptive boost) the sequence of trees $\hat{y}_1, \ldots, \hat{y}_T$ are trained with reweighted versions of the original training dataset such that the weight of individual training sample is based on the prediction error in the previous iteration [203]. This requires working with a loss function that and learning procedure for the individual iterations that is amenable to weighted training dataset $\{x_i, y_i, w_i\}_{i=1,\ldots,n}$. Incorporating the weights w_i is straight forward when the risk is expressed as an expectation, since the emperical risk of Eq. 41.3 is just replaced with the weighted average. Similarly, the heuristic for many of the tree-based learning algorithms (*e.g.* the Gini index) also have natural generalizations with weighted events.

In the context of classification, the weighted error of the model $\hat{y}_t(x)$ is

$$\mathrm{err}_t = \frac{\sum_i w_i^{(t)} \mathbf{1}[y_i \neq \hat{y}_t(x_i)]}{\sum_i w_i^{(t)}} \ . \tag{41.38}$$

Based on this weighted error, the coefficient β_t of the component $\hat{y}_t(x)$ in Eq. 41.37 is given by

$$\beta_t = \log\left(\frac{1-\mathrm{err}_t}{\mathrm{err}_t}\right) \ . \tag{41.39}$$

Then for the next iteration the weights of the misclassified events are updated as $w^{(t+1)} = w^{(t)} \exp(\beta_t)$ and then renormalized so that the sum of all weights is 1. This reweighted dataset is then used to train the next model $\hat{y}_{t+1}(x)$ and the entire procedure is initialized with uniform weights $w_i^{t=0} = 1/n$.

There is an analogous procedure for regression with the squared loss function based on the residuals $r_i = y_i - \hat{y}_t(x_i)$ (see for example Ref. [77] for details).

Gradient boosting One of the most powerful forms of tree based models, which is implemented in the tool `XGBoost` is referred to as *gradient boosting* [204]. In this setup, the model is purely additive as in the case of random forests, so the model is Eq. 41.37 with all $\beta_t = 1$. Note this is without loss of generality since the β_t can be absorbed into the b_j of Eq. 41.36. As with AdaBoost, the model is built sequentially through the sequence $\hat{y}_1, \ldots, \hat{y}_T$.

At each iteration, a new term f_t will be added to the sum in Eq. 41.37. For a given decision tree defined by splits on attributes, one can approximate the objective function (the loss function $\mathcal{L}$ plus a regularization term Ω) as a function of b_j in a second order Taylor series:

$$\mathrm{obj}^{(t)} = \sum_{i=1}^{n} [\mathcal{L}(y_i, \hat{y}_i^{(t-1)}) + g_i f_t(x_i) + \frac{1}{2} h_i f_t^2(x_i)] + \Omega(f_t) + \\ + \mathrm{constant} \ , \tag{41.40}$$

where

$$g_i = \partial_{\hat{y}_i^{(t-1)}} \mathcal{L}(y_i, \hat{y}_i^{(t-1)}) \tag{41.41}$$

and

$$h_i = \partial^2_{\hat{y}_i^{(t-1)}} \mathcal{L}(y_i, \hat{y}_i^{(t-1)}) \tag{41.42}$$

In `XGBoost`, the regularization term is taken to be

$$\Omega(f) = \gamma J + \frac{1}{2}\lambda \sum_{j=1}^{J} b_j^2 \ , \tag{41.43}$$

where J is the number of terminal nodes in the tree. With the second-order approximation of the objective, one can directly solve for the optimal b_j for the next tree and the corresponding value of the optimized objective function. The improvement in the objective function can then be used as a heuristic for choosing the best split. Specifically, define $G_j = \sum_{i \in I_j} g_i$ and $H_j = \sum_{i \in I_j} h_i$, where I_j is the set of indices of data points assigned to the j-th leaf. The heuristic used in `XGBoost` for splitting a node is

$$\mathrm{Gain} = \frac{1}{2}\left[\frac{G_L^2}{H_L+\lambda} + \frac{G_R^2}{H_R+\lambda} - \frac{(G_L+G_R)^2}{H_L+H_R+\lambda}\right] - \gamma \ . \tag{41.44}$$

This formula can be interpreted as the score on the new left leaf plus the score on the new right leaf minus the score on the original leaf minus a regularization penalty on the additional leaf. If the gain from splitting a leaf is smaller than γ, then the total Gain is negative and the split will not be added, which can be seen as implementing a form of pruning.

41.5.3 *Neural networks*

In this section we focus on the different types of components used in modern neural network architectures. Gradient-based optimization techniques are most commonly used for training neural networks, and they are described in Sec. 41.6.1. Similarly, other important aspects to effectively training neural network models such as parameter initialization, early stopping, *etc.* are discussed in Sec. 41.6.

The vanishing and exploding gradient problem is a common challenge for gradient-based optimization of neural networks and is described in Sec. 41.6.5. That problem is referred to repeatedly in this section because it has motivated the development of numerous architectural components described below.

41.5.3.1 *Feed-forward multi-layer perceptron*

One of the core components in neural networks is the fully-connected, feedforward network or*multi-layer perceptron* (MLP), which is composed of L *layers*: $f = f^{(L)} \circ \cdots \circ f^{(1)}$. The lth layer defines a function that maps a d_{l-1}-dimensional input vector, called *features*, to an d_l-dimensional output $f^{(l)} : \mathbb{R}^{d_{l-1}} \to \mathbb{R}^{d_l}$. A unit responsible for producing an individual output in d_l-dimesional output is called a *neuron* or a *filter* interchangeably. For $l < L$, the functions f_l are called hidden layers, and the number of neurons (d_l) is referred to as the width of the hidden layers. The layers in an MLP take on the form:

$$f^{(l)}(u) = \sigma^{(l)}(W^{(l)}u + b^{(l)}) \ , \tag{41.45}$$

where $W^{(l)} \in \mathbb{R}^{d_l \times d_{l-1}}$ is called the *weight matrix*, the components of the vector $b^{(l)} \in \mathbb{R}^{d_l}$ are referred to as the *biases*, $u \in \mathbb{R}^{d_{l-1}}$ is the input from the previous layer, $W^{(l)}u$ denotes a matrix-vector product, and $\sigma^{(l)}$ is a non-linear *activation function* that is usually applied element-wise. The parameters of the network comprise the full collection of weights and biases, $\phi = (W^{(1)}, \ldots, W^{(L)}, b^{(1)}, \ldots, b^{(L)})$.

41.5.3.2 *Activation functions*

The activation functions σ in neural networks are nonlinear functions and key to the expressiveness of the resulting family of functions. Two traditionally used functions are *logistic* and *hyperbolic tangent* functions. These functions are bounded to be $(0,1)$ and $(-1,1)$ respectively, and are symmetric about the input value of zero. On the other hand, away from the zero input value, a gradient of both functions quickly vanishes and this poses a challenge in using gradient-based optimization method (see Sec. 41.6.1). This can be avoided, to some extent, by normalizing the input values and carefully initializing the values of $W^{(l)}$ and $b^{(l)}$. These are discussed in Sec. 41.6.7, 41.6.8 and 41.6.9. Yet, it becomes difficult to maintain a null input value for a *deep* neural network, a model with many layers. Instead, a popular choice for a deep neural network is *Rectified Linear Unit* (ReLU):

$$\sigma(x) = \begin{cases} x & \text{if } x > 0 \\ 0 & \text{otherwise} \end{cases} \tag{41.46}$$

which computational cost is small and provides the gradient does not vanish for $x \in (0, +\mathrm{inf})$ [205,206]. An alternative to preserve a non-zero gradient in negative input values are called *Leaky ReLU* and modifies the output to $0.01x$ for $x \in (-inf, 0)$ [207]. Another variant, called *Parametric ReLU* (PReLU), turns the coefficient

Downloaded from https://academic.oup.com/ptep/article/2022/8/083C01/6651666 by KIT Library user on 27 September 2022

0.01 into a variable that is optimized as a part of the model during optimization [208].

The choice of activation functions depends on the model architecture and applications. As described, while the use of ReLU types are a typical choice for a deep neural network, a logistic function is a popular choice at the final layer for classification tasks. Recently, in the area of neural scene representation, sinusoidal activation functions have been found to be surprisingly effective [209].

41.5.3.3 *Softmax*

A softmax function is often used to normalize elements of a discrete vector u, or to interpret the output as a probability over a set of n discrete categories. Given a real-valued input vector $u \in \mathbb{R}^n$, the softmax function computes the output vector $v \in \mathbb{R}^n$ the i-th component is given by:

$$v_i = \frac{\exp(u_i)}{\sum_{j=1}^{n} \exp(u_j)} \ . \tag{41.47}$$

The result has the property that $v_i \in (0,1)$ and $\sum v_i = 1$. The components of the input vector u are often referred to as *logits* in reference to their connection to the logistic function used in logistic regression. The softmax function is commonly used as the last layer in multi-class classifier. The softmax is also used in the context of attention (see Sec. 41.5.3.11).

41.5.3.4 *The rise of deep learning*

There are a number of universal approximation theorems in the theory of neural networks. One of the first was that even with one hidden layer ($L = 2$), an MLP can approximate any continuous function if the non-linear activation function σ not a polynomial and the width d_1 is large enough [210]. However, it is often more efficient (in terms of the number of parameters) to increase the *depth* of the network L [211].

Training a deep network (*i.e.* $L > 2$) that generalizes well can be more difficult, requiring large training datasets, many gradient updates, and suitable regularization. The introduction of large labeled training sets, advances in computing (*e.g.* graphic processing units or GPUs which enabled orders of magnitude acceleration in parallel computation including matrix multiplies [212]), development of ReLU, research progress in initialization and optimization algorithms for model parameters, and regularization techniques like *dropout* [13] all played an important role in the rise of *deep learning* [2, 213]. Though the name deep learning was originally a reference to the depth L of such networks, modern deep learning is characterized more by the composition of various types of modules that are trained through gradient-based optimization. Below we introduce some other common network architectures.

41.5.3.5 *Convolutional neural networks*

Convolutional Neural Networks (CNNs) are widely used for image-like data. They implement the convolution of the input image u and a *filter* W (also referred to as a kernel). The parameters of the filter are learnable and the convolution involves traversing over input and calculating the inner product of the filter W with the part of the input in the *receptive field*, which has the same spatial shape as the filter and is centered at the target pixel. At each location – indexed by i and j below – there is a pixel that may have a vector of features associated with it. In the context of CNNs, these components of these features – indexed by c and c' below – are often referred to as *channels* in reference to the red, green, and blue color channels in a traditional image. The convolution operation is often denoted with a $*$, and the result can be expressed as

$$v_c(j) = (W * u_c)(j) = \sum_{c'} \sum_{i} W_{c,c'}(i) u_{c'}(\text{“}j - i\text{”}) \ , \tag{41.48}$$

where “$j - i$” is shorthand for the pixel index corresponding to the translation from pixel j to i. By repeating the operation over all pixels, the result of a kernel convolution is also an image as illustrated in Figure 41.3. Note that the the number of channels in the output v does not need to be the same as in the input, and the collection of filters $W_{c,c'}$ is often referred to as a filter bank. The entire image for a fixed channel index is often referred to as a *feature map*.

A key feature of the CNN architecture is that it is *equivariant* to translations, meaning that if the input image is shifted (*e.g.* $u(i) \to u'(i) = u(i-k)$), then the output is also shifted by the same amount (*e.g.* $v(j) \to v'(j) = v(j-k)$). This equivariance property is a natural consequence of using convolutions. A fully connected MLP would not generally have this symmetry; however, it is enlightening to imagine transferring the computation performed by a CNN to the weights and biases of a fully connected MLP, which would result in duplicating the weights of the filters multiple times. In this view, the CNN can be interpreted as a fully connected MLP with *shared weights*, which would maintain the equivariance property. This view is helpful for gaining intuition about the inductive bias of models and makes clear that a CNN is a subset of the fully connected MLPs that satisfy the translation equivariance property.

The discussion above makes it clear that CNNs will have fewer parameters than the corresponding fully connected MLP, which can alleviate the optimization challenge. In addition, the convolutional structure allows for data to be reused effectively as patterns in one part of an image in the training dataset effectively contribute to learning that pattern anywhere in the image. Larger kernel sizes allow for the filters to learn more complicated patterns, but at the expense of having more parameters and needing more data to train (the extreme case being a kernel size that is the the size of the entire image, which would be equivalent to a fully connected MLP). In practice, kernel sizes of 3 are popular, 5 is sometimes used, and larger kernels are rarely used.

A kernel convolution involves three hyperparameters, the size of kernel (typically an odd number so that the filter has an unambiguous center), *stride*, and *padding*. The stride is the number of pixels between each target pixel (*i.e.* the center of the filter). The stride size of 1 implies the target pixels are adjacent, and a stride of 2 implies skipping 1 pixel in between (along each spatial axis). Padding is an operation to expand the input image by a specified number of pixels (i.e. “padding size") for when the target pixel is near the edge and the filter would extend beyond the input image. In Figure 41.3, the input image is 4×4 pixels, the kernel is of size 3, and no (zero) padding is applied. The result is a smaller image. Alternatively, With the padding of size 1, the output would retain the 4×4 shape of the input image.

A kernel size of 1 is also frequently used and is referred to as a *1×1 convolution*. While it cannot capture a geometrical features, it can perform linear operations on the input features, including increasing or decreasing the number of features. When combined with a non-linearity and stacked repeatedly this can be seen as a small MLP attached to an individual pixel, and for this reason the 1×1 convolution is sometimes referred to as a *network-in-network* [214]. This is often used to extract more powerful features to be used by the latter layers, and also to compress features when the next layers may be computationally demanding such as a block of many convolution layers with a large kernel size [215, 216].

One may wonder how CNNs identify features with a spatial size larger than a typical kernel size. One mechanism for this is by stacking multiple convolutional layers – *e.g.* the composition of two 3×3 kernels will lead to an effective 4×4 kernel. In addition, a typical CNN architecture uses pooling (described below), which effectively down-samples the image so that it can be processed at different resolutions. The effective receptive field in the input image may be much larger than the kernel size in this case. An alternative approach is to use an *inception module* which is designed to extract features simultaneously using kernels of different size [215].

41.5.3.6 *Pooling*

Pooling plays an important role in convolutional neural networks both practically and in terms of their mathematical properties. A pooling operation is a type of aggregation or downsampling that takes many pixels as input and produce one pixel for output. Typically, the pooling operation is applied indepen-

Downloaded from https://academic.oup.com/ptep/article/2022/8/083C01/6651666 by KIT Library user on 27 September 2022

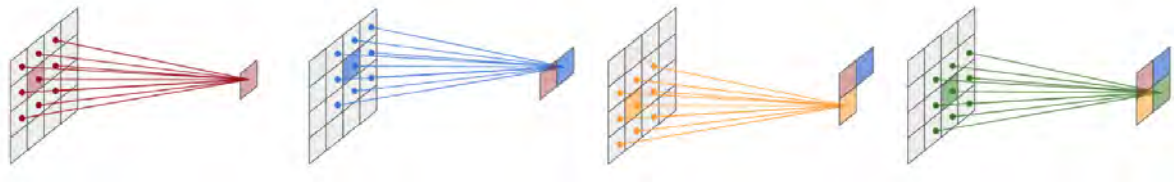

Figure 41.3: A pictorial description of a kernel convolution over four input pixels. It takes a product of the weight matrix (kernel) and the local input matrix centered at a target pixel. The operation is repeated over the input image using the same kernel. The size of the output image depends on the size of the kernel, stride, and padding. In this figure, the kernel size of 3, stride of 1, and padding of 0 is used.

dently for each channel or feature component. The most popular pooling operations are *max* and *average* pooling. Max-pooling picks the highest activation pixel value within the specified receptive field, while the average pooling computes the average pixel value in the receptive field. The idea of pooling generalizes to other architectures, including graph neural networks where the receptive field includes the neighbors of a particular node in the graph (see Sec. 41.5.3.14). The pooling operation gives rise to robustness of the model to small, local deformations in the input, a property called *geometric stability* [217–219]. This type of local deformation is important and distinct from the equivariance to rigid translations provided by the convolutional structure. Repeated pooling operations that eventually lead to a single feature vector with no spatial index is what gives rise to the invariance of common CNN architectures to translations (*i.e.* an image with a dog will be labeled 'dog' even independent of where the dog is in the image).

On the practical side, it is also beneficial to reduce the dimensionality of the input to a smaller hidden state representation. This can be done either a convolution operation with the stride size larger than 1, or employing a *pooling*.

A typical CNN for extracting a 1-dimensional array of features is designed with repeating blocks of convolution layers and pooling operations [220]. Figure 41.4 shows an example evolution of a data tensor through the succession of a convolution and pooling operations in order to extract a 1-dimensional array of features, which then can be fed into a block of MLP for an image classification (or a regression) task. This type of an architecture is referred to as an *encoder* or *feature extractor*.

The reduction in the spatial size of an image is performed *slowly*, typically by a factor of 2, which is the minimum possible reduction factor. After the reduction of the spatial extent, the number of channels is typically increased (also by a factor of 2 in most cases), converging one set of feature maps into a larger number of down-sampled feature maps. There may be more than one convolution layer within each spatial resolution (*i.e.* in between pooling operations). Following these design principles, CNN encoders typically become *deep*, consisting of dozens or sometimes hundreds of convolution layers, and face challenges of vanishing gradients problem (see Sec. 41.6.5). A standard practice to mitigate this issue is explicitly *normalize* the input tensor input at each convolution layer using algorithms like *Batch Normalization*. This will be discussed in Sec. 41.6.9.

41.5.3.7 *CNN architectures for image analysis*

There are three major categories of computer vision tasks where CNNs are often used:

- *Image classification or regression* requires a prediction of single value for the whole image (*i.e.* a category or target value)
- *Object detection* produces a list location information for arbitrary number of objects in the input image
- *Semantic segmentation* outputs an image of the same spatial dimension as the input, in which every pixel is segmented by a predicted value for a target task (classification or regression).

As discussed previously, a CNN feature extractor followed by MLP is often used for image classification and regression tasks in wide range of applications including particle physics. Many successful CNN architectures for object detection and semantic segmentation applications share key designs which we briefly discuss below.

Region Convolutional Neural Network (R-CNN) is one of the most successful design for object detection [221]. R-CNN is explored in HEP experiments where the number and location of signal (e.g. neutrino interactions) are not known apriori in large image data such as neutrino detectors [3, 116, 222].

R-CNN consists of multiple CNNs. The first is a feature extractor which produces a spatially compressed feature tensor. The second CNN applies 1×1 convolution to predict two information: an *object score* which indicates whether there is an object in this (spatially compressed) pixel or not, and prediction of the location and size of a rectangular, axis-aligned bounding box that contains the object (if exists). This second CNN is called *Region Proposal Network* (RPN), and the bounding box is called *Region of Interest* (ROI). The the size of a bounding box is not directly solved by a regression. Instead, the model requires a set of pre-defined *anchor* boxes, which sizes and aspect ratios are hyperparameters, and predict the object score, location, and size (as a multiplicative factor to the defined anchor box) for each anchor box. This allows RPN to detect multiple objects with different aspect ratios even if they are within the same receptive field in the original input image. For each ROI with an object score above threshold (hyperparameter), the third CNN operates in the corresponding sub-field of an already-compressed tensor (*i.e.* by the first CNN) to perform a classification for an object inside the ROI.

This approach can produce multiple ROIs for the same object with a high overlap. Those predictions are reduced using Non-Maximum Suppression (NMS) algorithm. Given a list of bounding boxes with confidence scores, NMS takes the box with the highest score, and computes the Intersection-over-Union (IoU) of this box and all the rest of boxes. Boxes with the IoU higher than a threshold (hyperparameter) are eliminated as they are likely to represent the same object. Then NMS repeats the same operation for the box with the second highest score among the remaining boxes. This is repeated till the list is exhausted.

U-Net is one of the of most successful models used for semantic segmentation [223]. As the output of U-Net is also an image, it gives some interpretability compared to models for an image-level classification or regression tasks. The model is used widely in HEP experiments in both 2D and 3D image data [112, 113, 118, 125, 127].

The architecture of U-Net consists of a CNN encoder and *decoder*. A decoder consists of convolution and *convolution-transpose* layer (also called strided transpose-convolution, or rarely deconvolution). The operation of a convolution transpose can be seen an opposite of a convolution: for every pixel in an input image, its value is multiplied to the kernel and copied to the output. $3x3$ kernel in transpose-convolution layer fills $3x3$ pixels in the output tensor. The concept of padding and the stride are also applied to the output tensor. For instance, the stride 2 transpose-convolution fills $3x3$ fields centered at every other pixel (*i.e.* stride 2) for every input pixel. The spatial size of an output tensor is therefore determined by the spatial size of an input tensor, stride, and padding. In the decoder of U-Net, convolution-transpose layers are used to up-sample spatially compressed feature tensors back to the original image resolution. The

Downloaded from https://academic.oup.com/ptep/article/2022/8/083C01/6651666 by KIT Library user on 27 September 2022

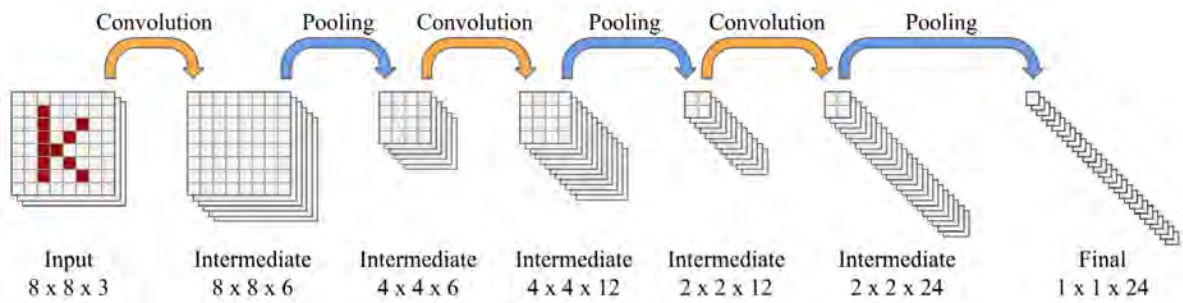

Figure 41.4: An example CNN architecture to extract a 1-dimensional array of features from an image via succession of convolution layers and pooling operations. The (square) kernel, stride, and padding size of a convolution operation are 3, 1, and 1 in respective order. The pooling operation uses a square kernel size of 2. The number of filters at the first convolution layer is 6, and is increased by a factor of 2 at subsequent convolution layers.

stride size of a convolution-transpose layer is almost always 2 in order to *slowly* transform the spatial size, and standard convolution layers (with stride 1) are placed in-between up-sampling operations. Because the output of the decoder has the same size as the input image, features for every pixel can be used for either a classification or a regression task at the pixel-level.

The idea behind encoder-decoder architecture is to extract features in the encoder, and the decoder interpolates those features back to the original spatial resolution. The down-sampling operation (*e.g.* max-pooling) in the encoder is, however, a lossy process where spatial information is permanently lost. This prevents a simple encoder-decoder architecture to perform a semantic segmentation task at the level of precision required for science research and industrial use. Interesting observation made by the U-Net authors is a symmetry in the encoder-decoder architecture in which there are tensors of corresponding (*i.e.* the same) spatial size between two parts of the model. This observation inspired them to concatenate the intermediate tensors in the encoder block to the intermediate tensors of the corresponding size in the decoder block before convolution layers are applied in the decoder, which dramatically improved the performance of semantic segmentation. This is a type of a *skip connection* discussed below.

41.5.3.8 *Residual networks and skip connections*

The representation power of a neural network increases as more hidden layers are added, but gradient-based optimization of deep models can be notoriously difficult due to vanishing gradients (see Sec. 41.6.5). One of powerful techniques to address this challenge is a *residual network* (ResNet), which is a modular architecture design that can be applied to neural network models [216]. Suppose a $f^*(x)$ as the target transformation to be learned by a few stacked layers where x is the input to the first layer. The authors of ResNet hypothesized that it may be easier for a model to learn a residual transformation $\tilde{f}x) := f^*(x) - x$, thus the objective to learn is $\tilde{f}(x) + x$ where $\tilde{f}(x)$ denotes the output of stacked layers. This form assumes $\tilde{f}(x)$ and x share the same tensor dimension and size. If they differ in the feature dimension, equivalently the count of channels in an image tensor, one could use 1×1 convolutions to transform and match the dimension. The design is modular as it can be applied per a stack of convolution layers (e.g. U-ResNet introduced for LArTPC detectors uses ResNet modules within a U-Net architecture [112, 113]) widely in the present applications.

The authors of ResNet successfully demonstrated an improved performance of some models at the depth exceeding 1000 layers where the non-residual counter part could not improve the accuracy beyond a few dozens of layers. This remarkable success was due to the *skip connections* in ResNet, namely the element-wise addition of the input to the output at each block of convolution layers as shown in Figure 41.5. Without the presence of the skip connections, the gradients from the loss function is forced to go through all convolution layers (i.e. the reverse direction of orange allows in Figure 41.5), which results in the gradient being altered at every convolution layer. The layers closer to the input receive altered gradients by the continuously updated weights of deeper layers, making conversion difficult and slow. The skip connections provides the path for the gradient to flow directly to the preceding layers. As a result, the gradient can flow more directly to preceding layers and allows simultaneous optimization across layers. It is possible, however, that some convolution layers in ResNet may learn an identity mapping, thus contributing no effect to solving a given task despite consuming computing power.

Another type of skip connections is a concatenation of feature maps, in which case the input and the output of a block of convolution layers do not necessarily have to have the same number of features. This is shown to be very powerful in number of popular model architectures including U-Net [223] and DenseNet [224]. In this case, the input features are re-used: the next block of hidden layers can learn an optimal way to combine the input and the output of the preceding block (i.e. it could learn a simple addition operation, which makes it identical to ResNet). In DenseNet, input to a convolution layer is concatenated with the output of all preceding convolution layers of the same spatial dimension, thus $x_l = f_l([x_1, x_2, \cdots, x_{l-1}])$ where x_l is the output of l-th layer f_l and $[x_1, \cdots, x_{l-1}]$ denotes a concatenation of the inputs. In U-Net, tensors from the encoder block are concatenated with the tensors in the decoder block where they have the same size in spatial dimensions. This was critical for achieving a high spatial resolution for *semantic segmentation*, a class of tasks in Computer Vision to classify every pixel in an image among the predefined set of types (semantics), because the geometrical features at each spatial resolution is otherwise lost via pooling operation in the encoder block [223].

41.5.3.9 *Recurrent neural networks*

Recurrent Neural Networks (RNNs) [225] are a family of neural networks designed for sequential data (*e.g.* time series). Consider sequential data where x_t represents each step in a sequence with $t \in [1, n]$. A typical RNN takes the following form:

$$h_t = g_h(h_{t-1}, x_t, \theta) \tag{41.49}$$

where h_t and θ denote the *hidden state* of the system and parameters of g_h, the RNN model. The term *recurrent* refers the nature of the model operating on the previous state of the system (and hence the whole history). RNNs operate on three types of tasks:

- *One-to-many* takes a single input and generates a sequence (e.g. generates a sequence data, such as a sentence or waveform, given a category).
- *Many-to-one* takes a sequence and generates an output (e.g. sequence-labeling).
- *Many-to-many* takes a sequence and generates a sequence where the length of input and output sequence may be same (e.g. classification of individual element in a sequence) or different (e.g. sequence to sequence mapping).

Figure 41.6 shows an example for a many-to-many task, where $\{x_t\}_{t=1:n}$, $\{y_t\}_{t=1:n}$, and $\{h_t\}_{t=0:n}$ denote the inputs, outputs,

Downloaded from https://academic.oup.com/ptep/article/2022/8/083C01/6651666 by KIT Library user on 27 September 2022

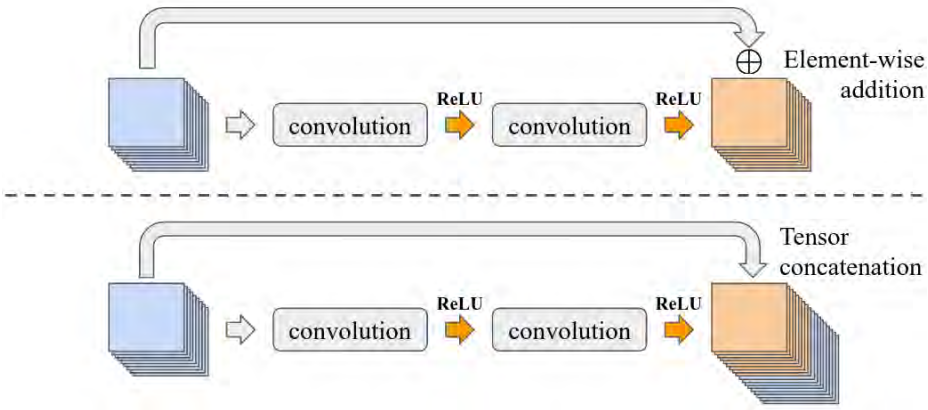

Figure 41.5: Two types of skip connections: the top is from ResNet where the input is element-wise added to the output tensor of a block of convolution layers while the bottom shows a concatenation of the input to the output tensor as employed in other models including U-Net and DenseNet.

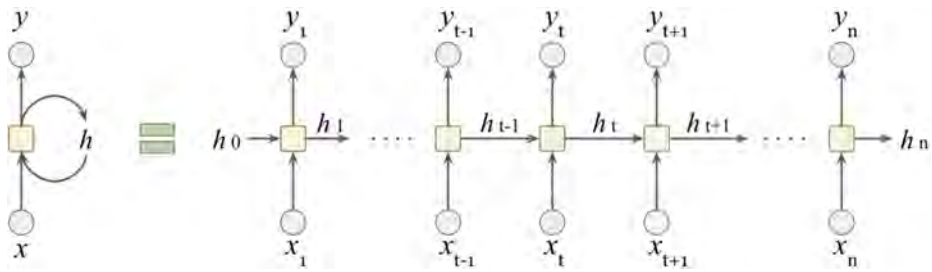

Figure 41.6: Pictorial description of a RNN (on the left) which takes an input and produces an output at every step with a hidden-to-hidden connection. The right diagram is unrolled over discrete steps. The yellow box represents a cell: a set of operations unique to each architecture.

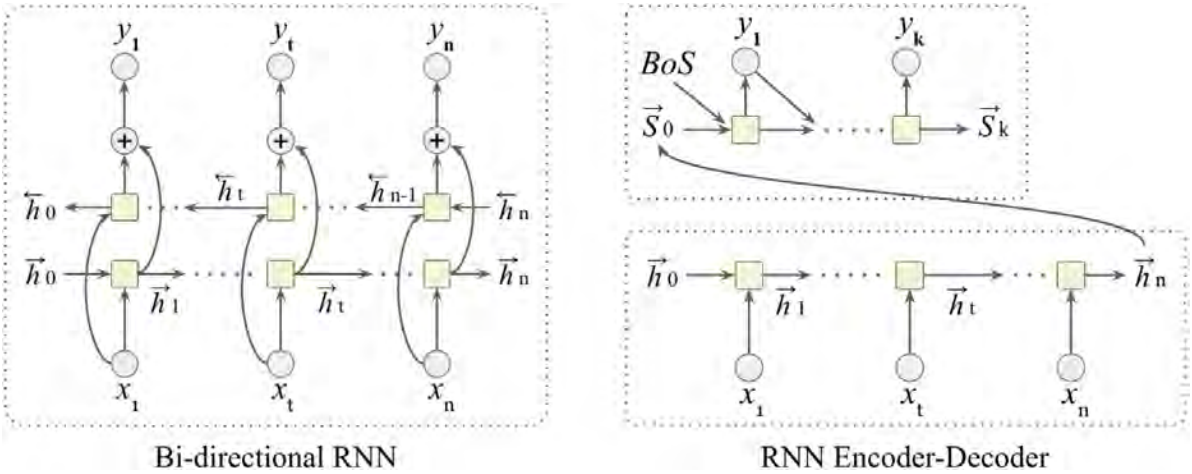

Figure 41.7: Bi-directional RNN (left) provides contexts in the preceding and subsequent parts of the input sequence. RNN encoder-decoder (right) can generate an output with a different sequence length from an input. Each cell in the decoder may take a previously generated element, starting from a special marker that signals the beginning of the sequence (BoS) and ending when the end of sequence is generated.

Downloaded from https://academic.oup.com/ptep/article/2022/8/083C01/6651666 by KIT Library user on 27 September 2022

and hidden states respectively. A set of operations at each time step is called a *cell*. A simple RNN cell may look like:

$$\begin{aligned} h_t &= g_h(Wx_t + Vh_{t-1} + b) \\ y_t &= g_o(Uh_t) \end{aligned} \tag{41.50}$$

where $W \in \mathbb{R}^{d_h \times d_i}$, $V \in \mathbb{R}^{d_h \times d_h}$, $U \in \mathbb{R}^{d_o \times d_h}$ are matrices g_h and g_o represent functions. d_i, d_h, and d_o are the dimension of input, hidden state, and output. $b \in \mathbb{R}^{d_h}$ is a bias term. An example application is sequence-labeling where the goal is for y_t to classify each input x_t in the sequence. In that case, one might use $g_h = \tanh$ and $g_o = \text{softmax}$ and use a loss function that averages clasification accuracy over the sequence.

Variations in RNN architectures result from the design of cells (described below) and flow of information across the cells. For instance, a bi-directional RNN (Figure 41.7 left) employs two set of RNNs, one processing the sequence in the forward direction and the other in the backward direction, and the hidden states from both directions are then combined to capture the context from both parts of the sequence. An RNN encoder-decoder (Figure 41.7 right) use one RNN to generate a context vector that encodes the whole input sequence, and use a separate RNN to generate another sequence from the encoded context. This can be used for machine translation.

41.5.3.10 *LSTM and GRU*

An RNN applies the same functions g_h and g_o in Eq. 41.50 repeatedly for each element of the sequence. This repeated component is similar to the shared weights for a convolutional filter in a CNN.

A hyperbolic tangent (tanh) is traditionally a popular choice for g_h as it regulates the magnitude of the hidden states and prevents it from diverging. Yet, this simple model is challenging to train for a long sequence of data [226, 227]. This is partially due to the fact that tanh contributes to the vanishing gradient problem and because repeated multiplication of the same weight matrices (i.e. V and W in Eq. 41.50) can lead to gradients that can either explode or vanish (see Sec. 41.6.5). Additionally, the way the signal accumulates means that changes early in the sequence have different impact from changes late in the sequence.

Long Short-Term Memory (LSTM) [228] is a model designed to address the issue of vanishing gradient for RNNs. In this model, a *context* is introduced as a way to enable the model to hold long-term memory while the hidden states remain to hold short-term memory. The context c_t and hidden state h_t at step t are computed as follows:

$$\begin{aligned} c_t &= f_t \odot c_{t-1} + i_t \odot \tilde{c}_t \\ h_t &= o_t \odot c_t \end{aligned} \quad \text{where} \quad \begin{aligned} f_t &= \sigma\left(W^f x_t + V^f h_{t-1} + b^f\right) \\ i_t &= \sigma\left(W^i x_t + V^i h_{t-1} + b^i\right) \\ o_t &= \sigma\left(W^o x_t + V^o h_{t-1} + b^o\right) \\ \tilde{c}_t &= \tanh\left(W^c x_t + V^c h_{t-1} + b^c\right) \end{aligned} \tag{41.51}$$

where σ and $\odot$ denote logistic function and an element-wise (i.e. Hadamard) product and f_t, i_t, and o_t are referred to as *gates*. Each gate outputs a value between 0 and 1, and is associated with unique weights, W and V, and a bias b. One can see c_t is a combination of the previous context vector c_{t-1} and a new context vector $\tilde{c}_t$. The *forget* gate f_t controls which and how much of the past context should be kept or forgotten. The *input* gate i_t controls how much of the present context $\tilde{c}_t$ should propagate to the current state c_t. The output gate o_t controls which and how much of the context vector should represent the present hidden state h_t. From Figure 41.8, one can see that the context vector c_t evolves with a gated addition operation. As such, it can be seen as an uninterrupted path for gradients to flow. This is similar to a residual connection (see ResNet in Sec. 41.5.3.8), which enabled training of CNNs with thousands of layers.

Another gated model to solve a vanishing gradient problem is the *Gated Recurrent Unit* (GRU) [182]. The GRU is similar to the LSTM with a few simplifications: the GRU merges the context vector and the hidden states and combines three gates into two. As a result, it requires less computational resources while retaining a similar level of performance for long sequences. The GRU operations are defined as follows:

$$h_t = z_t \odot h_{t-1} + (1 - z_t)\tilde{h}_t \quad \text{where} \quad \begin{aligned} r_t &= \sigma\left(W^r x_t + V^r h_{t-1} + b^r\right) \\ z_t &= \sigma\left(W^z x_t + V^z h_{t-1} + b^z\right) \\ \tilde{h}_t &= \tanh\left(W^h x_t + V^h \left(r_t \odot h_{t-1}\right) + b^h\right) \end{aligned} \tag{41.52}$$

where r_t and z_t are referred to as *reset* and *update* gate. As one can see in Figure 41.6, the reset gate in GRU performs the same task as the forget gate in LSTM by removing or reducing the elements of its memory (*i.e.* the hidden state). The update gate z_t determines the relative proportion of the previous hidden state h_{t-1} and the new context $\tilde{h}_t$ to be mixed in producing the new hidden state.

In addition to sequential data, the LSTM and GRU units can be used for data that has a tree-like structure. In this setting, the networks are often referred to as recursive neural networks or TreeRNN and they have found applications in natural language processing and jet physics [153, 154, 229–231].

41.5.3.11 *Attention*

Many tasks encountered in machine learning can be divided into subtasks. For example, classifying each pixel of an image or element of a sequence, predicting a target for each node in a graph, *etc.*. For each subtask the model may need to draw upon information from the entire input, but some parts of the input will be more relevant than others. At some point, the model will need to form a representation for the input as context for the subtask at hand. A fixed length vector c as a global context for this subtask is possible, but this approach scales poorly as the size of the input and number of subtasks grow. Either the size of the global context must grow or it will not have the capacity to represent all the relevant information, which would lead to a degredation in performance.

The idea behind *attention* is intuitive: one still forms a representation for the entire input, but different parts of the input are weighted differently according to the task at hand. By making the weights a learnable component, the network can learn to attend to the relevant parts of the input. A softmax function is a natural way to represent attention as it assigns a positive value to each component of the input and sums to one. Then for the i-th task, one can simply form a task-specific context c_i by computing the weighted average of the hidden state representations h_j for each component of the input. Let α_{ij} be the weights assigned to the j-th input for the i-th task, such that $\sum_j \alpha_{ij} = 1$. We can satisfy this naturally if for each i the α_{ij} are computed from the logits β_{ij} using a softmax function that normalizes by summing over j.

Downloaded from https://academic.oup.com/ptep/article/2022/8/083C01/6651666 by KIT Library user on 27 September 2022

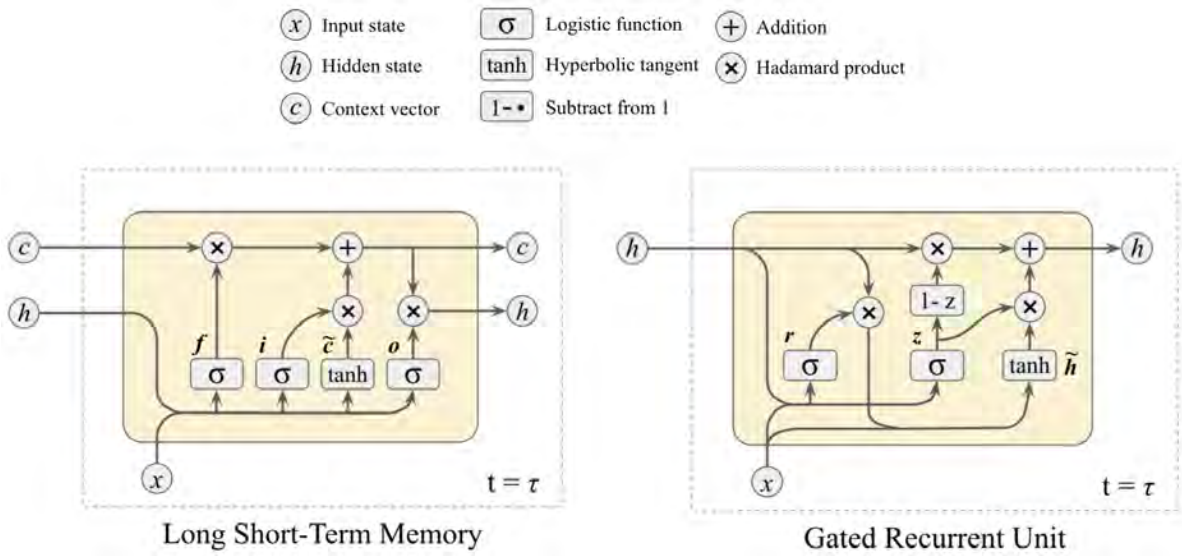

Figure 41.8: LSTM (left) and GRU (right) are both gated neural network designed to address a vanishing gradient problem for RNNs.

Putting these ingredients together, we have the *additive attention mechanism*

$$c_i = \sum_{j=1}^{n} \alpha_{ij} h_j \qquad \text{where} \qquad \alpha_{ij} = \text{softmax}\left(\beta_{ij}\right)_{\text{ over } j} \ . \tag{41.53}$$

As in the case of a multi-class classifier, the logits β_{ij} can be computed from a network component with learnable parameters. For instance, in the case of a cell of an RNN encoder-decoder network (see Fig. 41.7) that is decoding element i with an incoming input state s_{i-1}, the logits for the attention mechanism could be computed as follows

$$\beta_{ij} = U \tanh\left(W s_{i-1} + \tilde{W} h_j + b_i\right) \ , \tag{41.54}$$

where U, W, $\tilde{W}$ are the weights and b is the bias term of the model. Fig. 41.9 from Ref. [232] illustrates the full attention mechanism. The idea was implemented by a model called *RNNSearch* which made a breakthrough in machine translation by combining a bi-directional RNN with an additive attention mechanism [233].

We end this section by noting that the softmax α_{ij} can be used to visualize the influence of the j-th input element on the i-th output eleement, which improves interpretability of the model. An example of this from Ref. [232] is shown in Fig. 41.10.

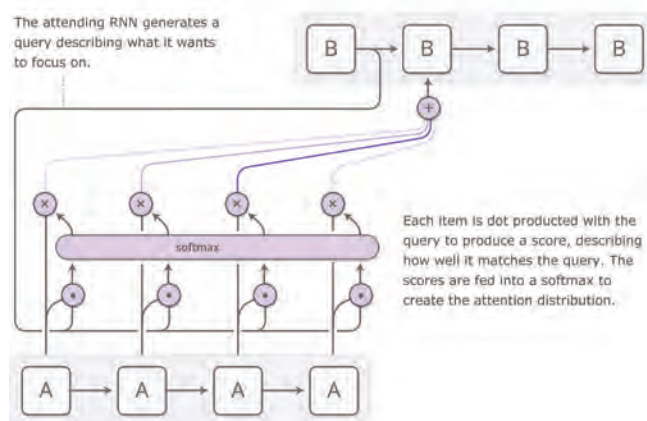

Figure 41.9: An illustration of the attention mechanism From Olah and Carter, "Attention and Augmented Recurrent Neural Networks". Lower boxes labeled `A` represent input elements in the sequence and upper boxes labeled `B` indicate output elements. The left-most line originating from the first `B` corresponds to the state s_{i-1} in the text.

41.5.3.12 *Scaled dot-product attention*

Shortly after the introduction of RNNSearch, the attention mechanism has been recognized as a powerful tool. One such variant is *scaled dot-product attention*, which is most widely recognized as the foundation of the *Transformer* architecture [234], which is described in more detail below.

In additive attention (Eq. 41.53) the hidden representations h_j were combined through a weighted average based on the coefficients α_{ij}, resulting in a task-specific context vector c_i. In the literature around scaled dot-product attention, multi-head attention, and transformers, the hidden states that will be combined are referred to as *values*, and they are often arranged in a matrix labeled $V \in \mathbb{R}^{m \times d_v}$, where the m rows of the matrix correspond to individual hidden state vectors of length d_v. The α_{ij} can also be represented as a $n \times m$ matrix α resulting from applying the softmax function to the $n \times m$ matrix β, normalized independently for each row. With this notation, Eq. 41.53 could be rewritten as $c = \text{softmax}(\beta)V$, where the softmax is normalized per row.

In scaled dot-product attention, the basic structure will be different, but instead of using an non-linear network component to compute the logits β as in Eq. 41.54, the logits will be computed by forming a dot product between a in incoming *query* and a *key*. The set of n query vectors can be arranged into the matrix $Q \in \mathbb{R}^{n \times d}$ and the set of d key vectors can be arranged into the matrix (transpose) $K^T \in \mathbb{R}^{d \times m}$. When the dot product between a particular query vector $q_i \in \mathbb{R}^d$ and key vector $k_j \in \mathbb{R}^d$ is large, then the resulting logit β_{ij} and attention weight α_{ij} will be large. One can interpret the keys as trying to detect certain types of queries and routing the attention to the relevant value. Typically, the dot-product is scalled by a factor of $1/\sqrt{d}$. The resulting task-dependent context is $c_i = \text{softmax}_j(q_i \cdot k_j/\sqrt{d})v_j$, where softmax_j indicates that normalizing sum runs over the index j. A common, though sometimes confusing, notation is simply

$$c = \text{Attention}\left(Q, K, V\right) = \text{softmax}\left(\frac{QK^T}{\sqrt{d}}\right) V \ , \tag{41.55}$$

where c is a $n \times d_v$ matrix organizing the n context vectors of length d_v that are taylored summaries of the input vector for each of the n tasks.

Downloaded from https://academic.oup.com/ptep/article/2022/8/083C01/6651666 by KIT Library user on 27 September 2022

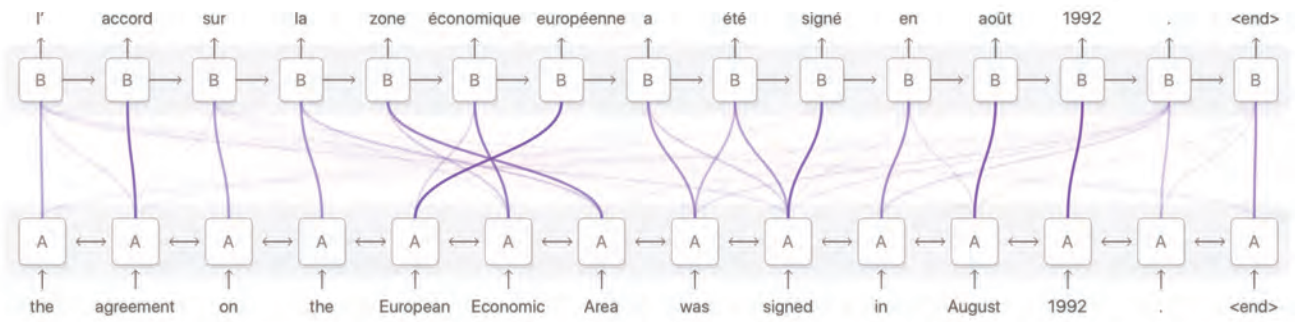

Figure 41.10: Visualization of the attention weights in a sequence-to-sequence problem taken from Olah & Carter, "Attention and Augmented Recurrent Neural Networks" The thickness of the lines is proportional to the attention weights α_{ij}..

41.5.3.13 *Transformer and multi-head attention*

The Transformer architecture is a powerful encoder-decoder model based on the scaled-dot product attention mechanism. It was originally designed for sequential data like RNNSearch, and subsequently used in other areas of research including computer vision. One advantage of scaled-dot product attention compared to the approach used in *RNNSearch* (Eq. 41.54) is that computing the logits β_{ij} (and thus the attention weights) does not involve any sequential processing. This allows the models to better leverage parallelism of the hardware to train much more expressive models than before. In place of the gated unites of an RNN that are key to avoiding the vanishing gradient problem, the Transformer architecture employs a residual connections at every attention module (*i.e.* the input tensor is added to the output as in Fig 41.5).

The second major ingredient in the Transformer architecture is the *multi-head attention* mechanism. A multi-head attention module executes multiple scaled dot-product attention in parallel. The query Q, key K, and value V matrices in each scaled dot-product attention module is obtained by applying a linear transformation (with learnable weights) to the common Q, K, and V input matrices. Each of them can be considered as a different (albeit rotated) *perspective* to derive attention.

For a sequence-to-sequence mapping task, the output of encoder is used to derive key K and value V matrices for the multi-head attention module in the decoder. The decoder is then responsible for mapping between the key-value features derived from the input (the encoder) and the queries from the decoder (which is still executed sequentially) in order to produce the final decoded output.

Finally, we note that the Transformer architecture does not just employ an attention mechanism in the decoder. By employing attention in the encoder as well the model has more capacity to "interpret" the input – a concept referred to as *self-attention*.

Models such as these have made breakthroughs in many areas of scientific and industrial research [235].

41.5.3.14 *Graph networks and geometric deep learning*

Graphs are a powerful data structure for representing structure data. A graph consists of *nodes* as elements and *edges* between between them. Graphs are sufficiently flexible to describe many types of structured data including images and sequences. Graph-based neural networks can also be seen as a generalization of many common types of machine learning models such as recurrent networks, convolutional neural networks, *etc.* [219]. The term *geometric deep learning* refers to this recent formulation that focuses largely on the symmetries of the data.

An earlier attempt to organize the variations on different flavors of graph-based neural networks can be found in Ref. [236]. In their formalism a Graph Network may be represented as $G(\mathbf{u}, V, E)$ where $\mathbf{u}$ represents an array of global features, $V = \{\mathbf{v}_i\}_{i=1:N^v}$ represents a set of N^v nodes with $\mathbf{v}_i$ as features for the i-th node (e.g. such as RGB channels if a node represents a pixel in image data), and $E = \{(\mathbf{e}_k, r_k, s_k)\}_{k=1:N^e}$ represents a set of N^e edges with $\mathbf{e}_k$ as features for the k-th edge. An edge may be (bi-)directional where r_k and s_k denotes the destination and origin nodes respectively. The features of a graph may evolve with three *update* functions ϕ and and three *aggregate* functions ρ:

$$\begin{aligned}
\mathbf{e}'_k &= \phi^e(\mathbf{e}_k, \mathbf{v}_{r_k}, \mathbf{v}_{s_k}, \mathbf{u}) & \mathbf{e}'_i &= \rho^{e\to v}(E'_i) & &\text{where} \quad E'_i = \{(\mathbf{e}'_k, r_k, s_k)\}_{r_k=i, k=1:N^e} \\
\mathbf{v}'_i &= \phi^v(\bar{\mathbf{e}}_i, \mathbf{v}_i, \mathbf{u}) & \bar{\mathbf{e}}' &= \rho^{e\to u}(E') & &\text{where} \quad E' = \cup_i E'_i = \{(\mathbf{e}'_k, r_k, s_k)\}_{k=1:N^e} \\
\mathbf{u}' &= \phi^u(\bar{\mathbf{e}}', \bar{\mathbf{v}}', \mathbf{u}) & \bar{\mathbf{v}}' &= \rho^{v\to u}(V') & &\text{where} \quad V' = \{\mathbf{v}'_i\}_{i=1:N^v}
\end{aligned} \tag{41.56}$$

where $\mathbf{e}'$, $\mathbf{v}'$, and $\mathbf{u}'$ denote the updated node, edge, and graph features. In Graph Networks, three types of information are updated in the following order. The first step is ϕ^e to update every edge. The second step updates every node: for i-th node, compute $\rho^{e\to v}$ to aggregate updated attributes from the edges with $r_k = i$ then compute ϕ^v to update the node attributes. The third step updates the graph attributes through ϕ^u which takes the original state $\mathbf{u}$, aggregated node and edge attributes by $\rho^{v\to u}$ and $\rho^{e\to u}$ respectively.

Graph Neural Networks [237] (GNNs) are the class of neural networks that work on graph-structured data. A direct analog in Computer Vision and physics is the *point cloud* data type, which is an unordered set of points. Operations on point cloud need to be permutation invariant (e.g. *min, max*, $+$, $\cdot$), and analysis of 3-dimensional physical object represented by point cloud need to be rotation and translation invariant as in the case for an image. PointNet [238, 239], a GNN that performs an object classification on point cloud of 3-dimensional positions, treats each point as a node, applies MLPs as ϕ^v to update node features, and global max-pooling operation as $\rho^{v\to u}$. There is no explicit edge definition in PointNet (though the model applies affine transformation to all points using Spatial Transformer Network [240], which could be considered as a separate graph operation, to introduce rotation and translation invariance and to capture topological features). Deep Sets [241] follows the same manner except ϕ^v takes the global entities $\mathbf{u}$. This is same for PointNet when performing point cloud segmentation: ϕ^v takes a step of simply concatenating $\mathbf{u}$ to node entities to combine a local and global features. Dynamic Graph CNN [242] is a variant that (re)define edges dynamically using attention mechanism: $\rho^{e\to v}$ aggregates k neighbor nodes where the inter-node distance is defined as a Cartesian distance in the feature space. ϕ^v remains a MLP and, while edges are defined, there is no associated entity. A similar technique is used in Non-Local Neural Network [243] to efficiently propagate local

Downloaded from https://academic.oup.com/ptep/article/2022/8/083C01/6651666 by KIT Library user on 27 September 2022

feature information to points that may be far in the 3D cartesian coordinate. Message Passing Neural Network [244] (MPNN) explicitly defines a feature vector as edge entities. In MPNN, $\rho^{e\to v}$ performs element-wise sum of features and feed into ϕ^e, explicitly passing features across nodes as the name suggests. While these are representative models that are frequently used in particle physics applications [117, 121, 132, 142, 156, 183, 245, 246], it is only a tiny fraction of GNN models developed over the past decade.

Graph-based models are particularly interesting for science applications because they often offer a natural way to organize the entities in the data and encode how those components should interact each other. This particular type of inductive bias is referred to as *relational inductive bias* in Ref. [237]. The structure of the graph is both an opportunity and a responsibility as one needs to define the graph structure including the edges to define the mode. A naive approach may be defining a fully-connected graph. However, for applications on hundreds of thousands of nodes (e.g. high resolution 3D point cloud), this may require a prohibitive amount of memory and computation. On the other hand, if the graph is too sparse, it may negatively impact the performance. One may need to compare the model performance among differently constructed graphs and balance against computational burden. Ideally the graph would be based on some knowledge of the interactions, but in the absence of such knowledge, popular graph construction methods include fully-connected, $k-$Nearest Neighbors, a Delaunay graph, and Minimum Spanning Tree.

Classification and regression tasks for graphs can be formulated such that the prediction is made for the entire graph or its individual nodes or edges. Graph-level prediction is like classifying an entire image, while node-level prediction is like semantic segmentation where individual pixels are classified. For clustering of points, GNNs can approximate a transformation function for nodes into the latent space where an optimal clustering of points can be performed. Alternatively, one can formulate clustering as an edge classification task. A comprehensive review on particle physics applications have been made available recently [247].

41.5.4 *Deep generative models*

Deep generative models are powerful machine learning models that can learn complex, high-dimensional distributions and generate samples from them. Because of their inherently probabilistic formulation, generative models are rapidly becoming an indispensable tool for scientific data analysis in a range of domains. Generative models can be contrasted against discriminative models that are primarily used for supervised learning tasks. Roughly, discriminative models are used for prediction and $f(x)$ provides a point estimate of the target y, and they are more closely connected to function approximation. In contrast, generative models describe the data distribution $p(x)$ (or the joint data distribuiton $p(x, y)$ in a supervised setting). An enlightening discussion of these two approaches can be found in Ref. [10].

There are a number of different types of deep generative models that have various pros and cons as they do not all have the same capabilities. We will focus on Variational Auto-Encoders (VAEs) [248,249] , Generative Adversarial Networks (GANs) [250, 251], and Normalizing Flows (NFs) [252–256], though there other approaches have been explored in this quickly developing area of research. Consider these three distinct types of functionality:

- **generation:** ability to sample or "generate" a data point $x_i \sim p(x)$.
- **likelihood for generated data:** ability to evaluate the probability density (likelihood) $p(x_i)$ for a data point x_i sampled from the model $x_i \sim p(x)$.
- **likelihood for arbitrary data:** ability to evaluate the probability density $p(x_i)$ for an arbitrary data point $x_i \in \mathcal{X}$.

Each of the models above can be used for generation; however, only normalizing flows provide all three capabilities. For reasons that we will describe below, GANs and VAEs do not provide a tractable likelihood function, and they are sometimes referred to as *implicit models*. This establishes a connection to simulation-based inference where most scientific simulators are also implicit models with an intractable likelihood. Because normalizing flows have a tractable likelihood, they can be trained via maximum likelihood (Eq. 41.18) as described in Sec. 41.3.2.1. GANs and VAEs, on the other hand, need to employ some other loss function to be trained. In the case of VAEs, training is based on the ELBO used in variational inference (see Sec. 41.3.1.3 and the discussion around the reverse KL divergence below Eq. 41.16). While GANs are also implicit models they data they can generate is typically restricted to a lower-dimensional manifold $\mathcal{M} \subset \mathcal{X}$, meaning that almost all real training dataset doesn't "live on" the subspace of possibilities that the model can produce. In this case, the liklelihood is for almost all data is zero, and so even ELBO-based training will not work. The breakthrough idea introduced in Ref. [250] was to use adversarial training where a classifier would be used to quantify how different the data generated from the model is from the data from the target distribution.

VAEs, GANs, and normalizing flows introduce a mapping $g(z, \theta)$ from a base random variable z to the space of the data $\mathcal{X}$. The map $g(z, \theta)$ is typically implemented with a neural network. The random variable z is sampled from some known base distribution $p(z)$ that is both easy to sample and has a density that is easy to evaluate. Typically, the base distribution is a multivariate normal.

In the literature on GANs and normalizing flows, this base random variable is often referred to as a latent variable and $p(z)$ is often referred to as a prior distribution, but this may cause confusion as the relationship between z and the observed x is deterministic. Typically, one would reserve the term latent variable for situations where one must marginalize (integrate) over z to obtain the marginal likelihood as in $p(x) = \int p(x, z)dz$. In this integral would involve a delta function imposing the deterministic relationship $x = g(z, \theta)$. A more natural interpretation of the relationship between x and z is through the change of variables formula, which is the essence of normalizing flows.

In the case of VAEs, the one additionally adds some normally-distributed (Gaussian) random noise ϵ to the output so that $x = g(z, \theta) + \epsilon$. In this case, x and z are not deterministically related and z is a legitimate latent variable in the model and $p(z)$ can be interpreted as the prior on that latent variable. In this case, the model can populate the full space of the data. Unfortunately, the marginal likelihood $p(x) = \int p(x, z)dz$ involves an intractable integral, thus maximum likelihood training is infeasible. However, the likelihood term $p(x|z)$ is tractable (*i.e.* the Gaussian noise), so training with the ELBO is possible.

Note that the dimensionality of of z need not be the same as that of x. If $z \in \mathbb{R}^q$ and $\mathcal{X} = \mathbb{R}^d$ with $q < d$, then all points $g(z, \theta)$ will lie on a d-dimensional surface in $\mathbb{R}^d$. In the case of a VAE, the Gaussian noise ϵ means that the generted data x will be distributed in a thin region around the surface defined by $g(z, \theta)$. The presence of a bottleneck (*i.e.* $q < d$) leads to advantages and disadvantages. The disadvantages for GANs is that the likelihood assigned to almost all real world data (*i.e.* data not generated by the model) will be zero, so training is more difficult and many tasks in probabilistic inference won't be applicable. However, often real world data is also effectively described by a low-dimensional subspace in the full space of the data – random images look like noise, while natural images are in some sense special. For this reason, images produced by GANs for instance often have better visual quality than those produced by other techniques. This points to the ambiguity encountered in quantifying how close two distributions are, and also motivates the use of distance measures such as the Earth Movers distance or Wasserstein distance [257, 258]. Conversely, the lack of a bottleneck (*i.e.* $q = d$) leads to very large models and scalability issues when the data is high dimensional.

Recent work has also focused on combining ideas from VAEs, GANs, and normalizing flows so that the generative model does involve a bottleneck but can still provide tractable likelihoods for density estimation restricted to that manifold [44,46,252,259,260]. Some of these models can also be used in the context of anomaly detection and out of distribution detection by identifying data that is off the manifold.

The parametrization of the mapping (the architecture of the neural network) should match the structure of the data and be

Downloaded from https://academic.oup.com/ptep/article/2022/8/083C01/6651666 by KIT Library user on 27 September 2022

expressive enough. For problems with explicit symmetries it is beneficial to include them into the architecture of the network explicitly, which restricts the allowed space of the models and matches their inductive bias (implicit regularization inherently built into the choice of architecture of the network) to the data. Different architectures have been proposed [255, 261–263], and to achieve the best performance on a new dataset one needs extensive hyperparameter explorations [264].

41.5.4.1 *Variational auto-encoders*

The auto-encoder was described in Sec. 41.3.2.2 as model for compression and representation learning. The model is $f = g \circ e : \mathcal{X} \to \mathcal{X}$, where $e : \mathcal{X} \to \mathcal{Z}$ is referred to as the *encoder* and $g : \mathcal{Z} \to \mathcal{X}$ is referred to as the *generator* or *decoder*. The standard auto-encoder is not a probabilistic model, but additional probabilitic structure can be added.

One approach is VAE mentioned above [248, 249]. By equipping the latent space with a prior distribution $p(z)$, the decoder of the auto-encoder $g(z, \theta)$ implies a distribution on a manifold in the output space $\mathcal{X}$. VAEs additionally add some normally-distributed (Gaussian) random noise ϵ to the output so that $x = g(z, \theta) + \epsilon$. This implies that $p_\theta(x|z)$ is a tractable quantity, and it is interpreted as the likelihood in this context.

In a VAE one also elevates the encoder to have a probabilistic form. Instead of encoding $z = e(x)$ in a deterministic way, one seeks a distribution over z given x. A natural target for the probabilistic encoder would be to probabilistically invert the decoder. This inverse problem is solved by the posterior distribution $p(z|x)$ via Bayes theorem

$$p(z|x) = \frac{p(x|z)p(z)}{p(x)} \ . \tag{41.57}$$

While the likleihood and the prior may both be tractable, the normalizing constant $p(x) = \int p(x, z)dz$ involves an intractable integral (the same intractable integral that makes maximum likelihood training of the VAE infeasible).

One approach to Bayesian inference in these settings is variational inference (VI). In VI one approximates the posterior with some parametric family $q_\phi(z|x)$ in a parametric form, and then uses optimization to optimize the ELBO with respect to its parameters ϕ.

$$\begin{aligned} \text{ELBO} &= \mathbb{E}_{q(z)} \log p(x|z) - D_{KL}[q(z)||p(z)] \\ &\leq \log \mathbb{E}_{q(z)} \left[\frac{p(x, z)}{q(z)} \right] = \log p(x) \ , \end{aligned} \tag{41.58}$$

where we used Jensen's inequality for concave functions (log) and the reverse Kullback-Leibler (KL) divergence term is

$$D_{KL}[q(z)||p(z)] = \mathbb{E}_{q(z)}[\log q(z) - \log p(z)] \geq 0. \tag{41.59}$$

In a VAE, the variational model for the posterior $q_\phi(z|x)$ is often assumed to be an uncorrelated Gaussian (this is often called mean field approximation) defined by the mean μ and variance Σ. Instead of optimizing the mean and variance independently for each x, VAEs use neural networks to predict the mean $\mu_\phi(x)$ and the variance $\Sigma_\phi(x)$. This is called *amortized inference*, since after an up-front training cost the approximate posterior $q_\phi(z|x)$ can be evaluated effeciently with a single forward pass of the neural network. Note the standard auto-enocder is recovered if one only used the mean $\mu_\phi(x)$ for the encoder and did not add noise ϵ to the decoder.

Both the probabilistic encoder $q_\phi(z|x)$ and the probabilistic decoder $p_\theta(x|z)$ are trained jointly by optimizing the ELBO. Unlike the standard auto-encoder, which only minimizes the reconstruction error, ELBO optimization of Eq. 41.58 has a trade-off between minimizing the reconstruction error in the first term (averaged over the approximate posterior $q(z)$), which encourages high quality reconstructions, and minimizing the KL divergence term, which forces the posterior $q(z)$ to be as close to the chosen prior $p(z)$, and thus controls the sample quality by matching the aggregate posterior with a chosen prior distribution [265]. This term regularizes the VAE latent space, such that every sample drawn from the prior $p(z)$ correspond to a valid sample. Successful VAE training requires to find a delicate balance between the two contributing terms to the ELBO. Whether the VAE training process succeeds in striking this balance depends on a number of factors, including the network architectures, the chosen prior and the class of allowed posterior distributions. Once trained, the VAE can be used as a generative model by sampling from the prior $z_i \sim p(z)$ and then decoding according to $p_\theta(x|z) = g(z, \theta) + \epsilon$.

VAEs allow for expressive architectures, enjoy the benefits of regularization through data compression and have a firm theoretical foundation. Compared to GANs [250], VAEs are of particular interest to the scientific community as they provide a lower bound to the marginal likelihood (albeit potentially with a large gap) and a posterior distribution for the latent variables.

It is also interesting to consider a special case of the auto-encoder and VAE where the encoder and decoder are restricted to be linear transformations, which is effectively PCA. In PCA the (linear) decoder can be written $g(z) = Oz$, where O is a matrix. As in the case of the auto-encoder, PCA is not a probabilitic model, but probabilistic structure can be added. Probabilistic PCA [266] assumes that the latent variables follow a Gaussian distribution with mean zero and covariance Λ, where Λ is a diagonal matrix with the rank-ordered eigenvalues λ_i along its diagonal. The true distribution of the PCA components may be non-Gaussian, but a Gaussian is the maximum entropy approximation given their first two moments. Note that in Probabilistic PCA these moments are measured on training dataset (when finding the principal components).

One can generalize Probabilistic PCA to use non-linear encoder and decoder as in an auto-encoder. A Gaussian prior is a poor ansatz for the latent space distribution of data proceed by an auto-encoder. Instead one can learn the density of the training samples in latent space using a normalizing flow. This model was introduced in $\mathcal{M}$-flows [46] and in Probabilistic Auto-Encoder (PAE) [44], which achieves similar performance to a VAE in terms of sample quality without explicit ELBO optimization. In all these cases the dimensionality of the latent space is a hyperparameter to be chosen or optimized by the user. Unlike a standard VAE, these models do not add noise to the decoded output, thus the data is strictly restricted to the manifold defined by the decoder $g(z, \theta)$. However, unlike a GAN there is a well defined way to take an arbitrary data point x, project it onto the manifold, and calculate the density of the data point projected onto the manifold. Thus these models can also be used in the context of anomaly detection and out of distribution detection by identifying data that is off the manifold.

41.5.4.2 *Generative adversarial networks*

GANs [250] also typically choose a low dimensional latent space z with a known prior distribution $p(z)$, typically a normal (Gaussian) distribution with zero mean and unit variance. GANs do not add noise to the output $g(z, \theta)$, so the likelihood $p(x|z)$ (and marginal likleihood $p(x)$) for almost all of the data space is 0, which precludes training by maximum likelihood and the ELBO. Instead of training on ELBO, GANs train on a dissimilarity measure defined implicitly by a discriminator $D(x)$ (also referred to as the critic). Calculating the dissimilarity often involves it's own learning problem (*i.e.* adversarial training of the discriminator).

The training is usually framed as a mini-max game

$$\begin{aligned} &\min_g \max_D \mathcal{L}_{\text{GAN}} = \\ &\min_g \max_D \{\mathbb{E}_{x\sim p(x)} \log D(x) + \mathbb{E}_{z\sim p(z)} \log[1 - D[g(z)]]\}. \end{aligned} \tag{41.60}$$

The goal of the discriminator is to distinguish between true and generated data, hence we want to maximize this loss with respect to D, assigning 1 to true data and 0 to generated data. The goal of generator is to fool the discriminator such that it cannot distinguish between true and generated data, hence we want to minimize this loss with respect to g at fixed D. This can be viewed as a game theoretical setup in a zero sum game between generator and distriminator.

Instead of this game theory interpretation we can view the internal objective $\max_D \mathcal{L}_{\text{GAN}}$ as an implicit loss function that mea-

Downloaded from https://academic.oup.com/ptep/article/2022/8/083C01/6651666 by KIT Library user on 27 September 2022

sures the dissimilarity between the target and generated distributions. The loss of Eq. 41.60 corresponds to the Jensen-Shannon (JS) divergence, which is a symmetrized form of KL divergence. However, JS divergence is hard to directly work with, and the adversarial training could bring many problems such as vanishing gradient, mode collapse (tendency of generator to cluster the samples around the training samples, with holes between them) and non-convergence [257, 258]. One of the core issues is that the distribution generated by the GAN is restricted to a manifold and the KL divergence isn't well defined in this case (because p is not absolutely continuous with respect to q). To address these issues Wasserstein GANs train on

$$\min_g \max_D \mathcal{L}_{WGAN} = \min_g \max_D \{\mathbb{E}_{x\sim p(x)} D(x) - \mathbb{E}_{z\sim p(z)} D[g(z)]\}. \tag{41.61}$$

Here again the goal of discriminator is to make the loss as large as possible between the true data and the generated data, while the goal of generator is to make it as small as possible, so that the discriminator cannot distinguish between the two. There is no requirement for $D(x)$ to be between 0 and 1, which helps with the above mentioned problems of JS divergence. Instead, this is replaced with a requirement that $D(x)$ is 1-Lipshitz, i.e. the absolute value of the norm of the gradient of the discriminator output with respect to the input has to be less or equal to 1.

Eq. 41.61 can be interpreted as the dual form of the 1-Wasserstein distance between the true and generated distribution [267]. Wasserstein distances are a measure of dissimilarity between two distributions used in the context of Optimal Transport, mathematical theory of how to optimally transport one distribution to another. Since the transport distance increases with the separation between the two distributions when they are non-overlapping, there is no gradient collapse that plagues other measures. In its primal form p-Wasserstein distance, $p \in [1, \infty)$, between two probability distributions p_1 and p_2, is defined as $W_p(p_1, p_2) = \inf_{\gamma\in\Pi(p_1,p_2)} \left(\mathbb{E}_{(x,y)\sim\gamma} [|x - y|^p]\right)^{\frac{1}{p}}$, where $\Pi(p_1, p_2)$ is the set of all possible joint distributions $\gamma(x, y)$ with marginalized distributions p_1 and p_2. In 1D the Wasserstein distance has a closed form solution via Cumulative Distribution Functions (CDFs), but this evaluation is intractable in high dimensions.

In the dual form of 1-Wasserstein distance, one instead maximizes Eq. 41.61 over all possible functions $D(x)$ that are 1-Lipschitz. One way to implement this is through weight clipping of the parameters of discriminator network, but a simpler solution is to add a gradient norm penalty term explicitly to the loss function [268].

Because of the discriminative nature of the dissimilarity measure defined in data space, GANs often generate more realistic samples than VAE or normalizing flows in high dimensions such as natural images. However, GANs do not provide an encoder from data to latent space, do not provide a tractable likelihood $p(x)$.

41.5.4.3 *Normalizing flows, autoregressive models, and score based models*

Normalizing Flows (NF) provide a powerful framework for density estimation and sampling [252–256, 269]. These models map the data x to latent variables z through a sequence of invertible transformations $f = f_1 \circ f_2 \circ \cdots \circ f_n$, such that $z = f(x)$ or $x = g(z) = f^{-1}(x)$. As in the VAE and GAN, z is modelled as a random number with a simple base distribution $p_Z(z)$, which is typically chosen to be a standard normal (Gaussian) distribution. The probability density of the model be evaluated using the change of variables formula:

$$p_X(x) = p_Z(f(x)) \left|\det\left(\frac{\partial f(x)}{\partial x}\right)\right| = p_Z(f(x)) \prod_{l=1}^{n} \left|\det\left(\frac{\partial f_l(x)}{\partial x}\right)\right|, \tag{41.62}$$

where we have added subscripts to $p_X(x)$ and $p_Z(z)$ for clarity. The Jacobian determinant $\det(\frac{\partial f_l(x)}{\partial x})$ must be efficient to compute for density estimation to be practical, and the transformation f_l should be easy to invert for sampling. In contrast to VAE and GANs, standard normalizing flows preserve the dimensionality of the data space as they are invertible (though there are normalizing flows that are defined on lower dimensional manifolds embeded in the data space [44,46,252,259,260]). As such, they do not have the problems of GANs and VAEs they can be trained via maximum likelihood (Eq. 41.18) as described in Sec. 41.3.2.1.

There are several popular architectures of NFs. A method used by NICE, RealNVP and Glow [253–255] is to split the space into two disjoint sets z_1 and z_2, and then use an identity forward map $z \to x$ for x_1, $x_1 = z_1$, and an affine transformation for x_2 of the form

$$x_2 = \exp(s(z_1)) \odot z_2 + m(z_1), \tag{41.63}$$

where $\odot$ is elementwise product and $m(z_1)$, $s(z_1)$ are neural networks. The Jacobian of this map is lower triangular, and its determinant is simply the product of elements along the diagonal, which is tractable, as is the inverse of the transformation. At the next layer one then performs a different split of dimensions into z_1 and z_2. The affine transformation can be further generalized to a nonlinear form using rational splines [270].

One can interpret the sequence of invertible transformations $f_1 \circ f_2 \circ \cdots \circ f_n$ as n discrete time steps in a continuous flow. In particular, one can think of a continuous-time flow described by an ordinary differential equation (ODE) and then interpret the discrete time steps as the result of a numerical integration of that ODE. This is the approach taken by the Ffjord algorithm [271] and other variants.

A different approach creating a deep generative model with a tractable likelihood is to model $p(x)$ autoregressively as

$$p(x) = \prod_{i=1}^{n} p(x_i|x_1, x_2, \ldots, x_{i-1}) \,. \tag{41.64}$$

This form describes each new dimension conditionally on all previous dimensions. It can model a general likelihood $p(x)$ as a sequence of conditional 1d distributions, whose conditional dependence on the parameters $x_1, x_2, \ldots, x_{i-1}$ can be modeled with neural networks. If x is a time series this form imposes a causal structure where x_i depends on all previous times x_j, $j < i$. WaveNet [272] and PixelCNN [273]) are two well known examples. Sampling from an autoregressive model is sequential, and can be slow in high dimensions. Inverse autoregressive flow reverses this process and makes sampling fast, but the likelihood evaluation is slow. Some normalizing flows have autoregressive coupling layers, such as Masked Autoregressive Flow (MAF) [269].

All of the methods above use maximum likelihood training of likelihood $p(x)$ against network parameters, so the training is to minimize KL divergence between the data distribution and a Gaussian in latent space. This can be overly sensitive to small variance directions that dominate the likelihood, without being sensitive to the global structure of the data. An alternative is to use Optimal Transport Wasserstein distance between the density of the generated samples and the data, which can be evaluated either in data space or in latent space. As Wasserstein distance is difficult to evaluate in high dimensions, one can instead use slices, 1d projections of the data along different directions in high dimensional space, to build the flow [45]. Along each slice direction one obtains the 1d marginal distribution that can be mapped to a Normal distribution using a cumulative distribution function method. In 1d the Jacobian and the inverse transformation are tractable. The projection directions are chosen to maximize the sliced 1d Wasserstein distance between the data and the distribution generated by the samples, or between the inverse flow from the data to the latent space and the target distribution (typically chosen as the Normal distribution). Because this training is less sensitive to small variance directions than maximum likelihood training it achieves better results on anomaly detection tasks [45].

One can reduce the architectural restrictions imposed by normalizing flows or autoregressive models by modeling the "score" $\nabla_x \log p(x)$ instead of $p(x)$. Note this usage of the term "score" is non-standard and goes back to Ref. [274]; the standard use of the term score is theta of Eq. 41.26. Score-based training avoids the normalization requirement. Score based models learn gradients of log probability density functions on a large number of

Downloaded from https://academic.oup.com/ptep/article/2022/8/083C01/6651666 by KIT Library user on 27 September 2022

noise-perturbed data distributions, and then generate samples by Langevin-type sampling. The resulting generative models, called score-based generative models [275] or diffusion probabilistic models [276], have several advantages over existing model families. They achieve GAN-level sample quality without adversarial training, and enable exact log-likelihood computation through their connection to continuous-time flows, which can be represented as a probability flow ordinary differential equation [276]. The main advantage is that the distribution $p(x)$ can be specified solely by its gradient, which can subsequently be sampled from using Langevin dynamics. This is similar to the gradient based Monte Carlo Markov Chain methods (such as Langevin or Hamiltonian Monte Carlo) that sample from Bayesian posteriors without directly estimating the normalizing constant. This in turn enables more flexible model architectures than what can be used in normalizing flows or autoregressive models.

We end by noting that normalizing flows, autoregressive models, and other deep generative models that provide a tractable likelihood are incredibly powerful tools for simulation-based inference. They can provide surrogate models trained from large simulated datasets when the simulators have intractable likelihood functions, which is usually the case. As described in Sec. 41.3.5, one would like to work with models that can provide conditional density estimation in order to model either the likelihood $p(x|\theta)$ or the posterior $p(\theta|x)$ [56, 57]. These techniques are being actively explored and applied to a number of scientific problems.

41.6 Learning algorithms

41.6.1 *Gradient-based optimization*

Given a parameterized model $f(x,\theta)$ and a loss function $\mathcal{L}(x,\theta)$, where x and θ denotes data and model parameters, one way to optimize θ is to first apply an appropriate initialization, $\theta_{t=0}$ (e.g. Sec. 41.6.7 for neural networks), and perform an iterative update:

$$\theta_t = \theta_{t-1} - \lambda \nabla_\theta \mathcal{L}(x,\theta), \tag{41.65}$$

where λ is a small, real valued hyperparameter called *learning rate*. To see how this works, define $\delta\theta \equiv \theta_t - \theta_{t-1}$ and consider $\delta(\nabla_\theta \mathcal{L}(x,\theta))$:

$$\delta\left(\nabla_\theta \mathcal{L}(x,\theta)\right) \approx \delta\theta \cdot \nabla_\theta \mathcal{L}(x,\theta) = -\lambda |\nabla_\theta \mathcal{L}(x,\theta)|^2 \tag{41.66}$$

which would monotonically decrease the loss function, and locally move the parameter values in the desired direction of loss function minimization. This algorithm is called *Gradient Descent* . We note that λ needs to be sufficiently small for the approximation to hold. When λ is too large, this can be a cause of a gradient explosion discussed in Sec. 41.6.7.

41.6.2 *Stochastic gradient descent*

Stochastic Gradient Descent (SGD) follows GD but replaces the exact gradient term $\nabla_\theta \mathcal{L}(x,\theta)$ with a stochastic approximation, where we subsample the data in the loss function using N samples, where $N < n$,

$$\nabla_\theta \mathbb{E}_{\hat{p}(x)} \mathcal{L} \approx \frac{1}{N} \sum_i^N \nabla_\theta \mathcal{L}_i, \tag{41.67}$$

where $\mathcal{L}_i$ is the loss function for data sample i. It should be noted that N needs to be randomly and independently sampled for the approximation to hold. Implementation of SGD follows three steps: take new samples of size N, approximate the gradient, then update the parameters θ.

In the case of optimizing the loss using a static database (*i.e.* one cannot take new N samples for every update), *mini-batch learning* is often employed. This replaces the first step with a randomly sampled *batch* of data, which is a subset of all the samples in the database. In this case, however, since a batch of data used for each parameter update is not entirely independent, a model may overfit. In practice, a part of the whole dataset is reserved as a *validation* sample, and the model performance is carefully monitored during the optimization process to avoid overfitting via an early stopping criterion (see Sec. 41.6.6 and Fig. 41.11).

SGD with slowly decreasing learning rate can be shown to converge to a local minimum almost surely under mild conditions, and to a global minimum for unimodal loss functions. SGD may also prevent getting stuck in shallow local minima of the loss function, thereby reaching a better local minimum for multi-modal loss functions. The noise in SGD with a constant learning rate can be viewed as a form of Langevin dynamics, which under proper conditions on the learning rate and mini-batch size converges to the stationary posterior distribution of the weights [277]. Thus SGD at a constant learning rate can be viewed as a sampler bouncing around and exploring the posterior surface for better solutions, descending onto the best found solution as the learning rate is decreased, a process related to temperature annealing in global optimization.

Another advantage of SGD is simply the computational cost: rather than evaluating the loss over all the data samples at each update, we use a small subset of data instead at each update. Furthermore, mini-batching can take advantage of vectorization libraries and GPU architectures. Large batch training requires specialized methods of training, such as Layer-wise Adaptivee Rate Scaling (LARS).

41.6.3 *Optimization algorithms*

GD and SGD are the basic building blocks for more advanced optimization algorithms. One can improve the convergence rate of gradient based optimization by considering the learning rate λ to depend on individual θ_i. Second order algorithms such as Newton's method take into account second order derivatives (Hessian) to find the minimum, and give an exact solution in a single update when the loss is quadratic around the peak. However, this requires a matrix inversion of the Hessian, which is exceedingly expensive in ML applications, where the number of network parameters is very large. As a consequence, second order optimization is rarely used in ML.

There are several improvements to the basic SGD even in the absence of Hessian information. Momentum based optimization takes a physics perspective of a viscous fluid in an external potential, where one updates current velocity with the potential gradient (force), followed by an update in position based on velocity. This approach therefore uses previous gradients in addition to the current one to compute a running average of the gradient, with a forgetting factor that controls how far back the averaging goes. This helps move faster towards the minimum in ravines, where gradient descent is usually inefficient due to the high condition number of the Hessian.

One way to make the learning rate dependent on θ_i is to consider the gradient norm squared $(\nabla_{\theta_i}\mathcal{L})^2$. RMSprop learns its running average and then reduces the learning rate in directions with a large average gradient norm squared, thereby reducing the oscillations along that direction. ADAM (Adaptive Moment Estimation) combines the momentum and gradient norm ideas, computing running averages of both the gradient and the gradient norm squared, each with its own forgetting factor [278].

41.6.4 *Automatic differentiation and back propagation*

In practice, $f(x,\theta)$ might take a complex form and may include a large set of parameters. The term $\nabla_\theta \mathcal{L} = \nabla_\theta \mathcal{L}(f(x,\theta))$ requires computing partial derivatives with respect to individual parameter θ_i. If f is a composite model (i.e. $f = f_n(f_{n-1}(\cdots, \theta_{n-1}), \theta_n)$), and if all of $f_{i:1,n}$ are differentiable, a chain rule can be applied:

$$\nabla_{\theta_i}\mathcal{L} = \frac{\partial \mathcal{L}(f(x,\theta))}{\partial \theta_i} = \frac{\partial \mathcal{L}}{\partial x_n} \cdot \frac{\partial x_n}{\partial x_{n-1}} \cdots \frac{\partial x_i}{\partial \theta_i} \tag{41.68}$$

where x_n denotes the output of n-th composite function f_n. In order to compute $\nabla_{\theta_i}\mathcal{L}$ for f_i, it needs computation of a gradient at all preceeding (or subsequent if seen in the forward context) functions. As the gradients accumulate across differentiable functions in the reverse order of the model composition, this technique is called *back propagation* [225]. An example of f that satisfies conditions to apply back propagation is a neural network, which consists of repeating blocks of a (differentiable) activation function and an affine transformation.

When the model $f(x,\theta)$ is implemented as a computer program in practice, *automatic differentiation* (AD), also called *algorithmic differentiation*, is used to compute the derivatives. AD ex-

Downloaded from https://academic.oup.com/ptep/article/2022/8/083C01/6651666 by KIT Library user on 27 September 2022

ploits the fact that any computer program consists of a sequence of elementary arithmetic operations (i.e. addition, subtraction, multiplication, division) and functions (e.g. log, exp, sin, cos) and apply chain rules to compute the target derivative. AD has advantages over traditional approaches including symbolic and numerical differentiation. The symbolic differentiation faces a serious difficulty of converting a program into a single expression, and the numerical differentiation suffers from round-off errors. Finally, both methods scale poorly in speed of computation for calculating partial derivatives with a large number of inputs. AD delivers much faster speed and does not suffer from increasing errors for calculating higher derivatives.

There are two modes of AD: the *forward* and *backward* mode. Consider a composite function $f(x,\theta) = f_n(f_{n-1}(\cdots f_1(x,\theta_1)\cdots),\theta_{n-1}),\theta_n)$. The forward mode applies the chain rule in the same order of the forward evaluation of f by computing $\partial f_1/\partial x$ first, then $\partial f_2/\partial f_1$, and continue to $\partial f_n/\partial f_{n-1}$. The backward mode traverses the reverse direction: starting from the last (outer-most) function $\partial f_n/\partial f_{n-1}$, next $\partial f_{n-1}/\partial f_{n-2}$, and continue to $\partial f_1/\partial x$. Therefore, the back propagation of gradients can be implemented using the backward AD, in which the target variable to be differentiated is fixed and the derivative is computed with respect to each sub-expression recursively as shown in Eq. 41.68. The forward mode is simpler to implement as the order of gradient calculation follows the order of composite functions to be executed. The reverse mode typically requires less amount of computation than the forward mode, but more memory is required to store intermediate function output values to calculate derivatives efficiently. Another consideration is the mapping of dimensionality $f : \mathbb{R}^k \to \mathbb{R}^\ell$ as it concerns the number of variables to sweep from each end. The forward mode is efficient when $k << \ell$ while the reverse mode takes an advantage if $\ell << k$. For instance, in the case of an image classification where $(k,\ell) = (\text{pixel count}, 1)$, the reverse AD is more efficient.

41.6.5 *The vanishing and exploding gradient problems*

Gradient based optimization crucially depends on the size of gradient with respect to each model parameter. If the magnitude of gradient is too large with respect to the distance to an optimal parameter value, it may repeatedly overshoot the target and cause an oscillation preventing convergence. If the gradient is too small, it may take an impractically long time to converge. As shown in Eq. 41.68, the gradient of i-th function f_i is a product of gradients from the subsequent functions. If those gradients are too large or too small, the magnitude can can either increase or decrease exponentially in the number of layers. These are called *exploding* and *vanishing* gradient problem respectively.

Modern deep neural networks consist with many composite functions (i.e. layers) and are particularly prone to this effect. Let us consider a simple RNN. From Eq. 41.50, we can write the back-propagating gradient:

$$\frac{\partial h_t}{\partial h_{t-1}} = \text{diagonal}\left(f'\left(Wx_t + Vh_{t-1} + b1\right)\right)W \tag{41.69}$$

where f' denotes the derivative of an activation function. The gradient of the contribution to the loss $\mathcal{L}_i$ from the i-th element in the sequence with respect to the j-th hidden state h_j is therefore:

$$\frac{\partial \mathcal{L}_i}{\partial h_j} = \frac{\partial \mathcal{L}_i}{\partial h_i} V^{i-j} \prod_{j<t\leq i} \text{diagonal}\left(f'\left(Wx_t + Vh_{t-1} + b1\right)\right) \tag{41.70}$$

where we can see that V contributes multiplicatively with $i-j$ powers when $i-j>1$. This example is explored in depth for recurrent models [226, 227] but is common for all types of deep neural networks.

In practice, one may explicitly inspect the magnitude of gradients propagating across layers to ensure an effective optimization. One way to mitigate an exploding gradient is to set the maximum gradient value $\delta_{\max}$ as a model hyperparameter and *clip* any larger gradients δ where it appears in the back propagation:

$$\delta = \frac{\delta_{\max}}{\|\delta\|}\delta \text{if} \|\delta\| > \delta_{\max}. \tag{41.71}$$

This is called *gradient clipping* [227].

Alternatively, there are many architecture designs that are motivated by the vanishing and exploding gradient problem or which aim to help propagate gradients across many layers. These considerations drove the design of gated models like the LSTM and GRU for sequential data and also motivated the ReLU non-linearity. Other example architectural designs or components motivated by these considerations include identity mapping and skip connections used in ResNet, U-Net, and DenseNet, which allow gradients to flow across many layers.

Other factors contributing to vanishing and exploding gradient include initialization of model parameters and normalization of input data. These factors contribute in keeping the magnitude of activation, which also concerns the magnitude of gradient, within a reasonable range. A recommended practice for a gradient-based optimization of a neural network is to maintain the input values centered around zero and a similar level of covariance across the inputs (and the outputs that are the inputs to the next layer) [279]. These factors are discussed in the following.

41.6.6 *Early stopping*

Early stopping is a form of regularization used to avoid overfitting when an iterative method, such as gradient descent, is used as a learning algorithm. Imagine a plot of the training loss and test loss as a function of iterations (*i.e.* parameter updates). As learning proceeds, the training loss will generally decrease. However, the test loss will often decrease initially and then start to increase, which is the classic sign of overfitting as shown in Fig. 41.11. The basic idea of early stopping is simply to stop training before overfitting takes place. In some approaches to early stopping theoretical analysis of the learning problem provides a prescription for when to stop the training [280]; however, the most straight forward approaches use a held-out validation dataset to monitor the generalization performance [281].

41.6.7 *Initialization of model parameters*

An improper initialization can slow down the optimization process or even result in a loss of convergence. While $b^{(l)}$ is typically initialized to zero, $W^{(l)}$ values need to be stochastic to avoid identical updates during optimization. One way is to sample $W^{(l)}$ from a zero-centered Gaussian distribution with a small variance (e.g. 0.01) [282]. However, this method does not guarantee the same variance in the input to each layer, which depends on the size of the input layer, and makes it difficult to train a deep neural network [220]. The *Xavier* initialization takes this into account and sets the variance of a Gaussian distribution to be $\sigma^2 = 1/d^{(l-1)}$ assuming a symmetric activation function around zero, such as a logistic function or hyperbolic tangent [283]. The *He* initialization uses the variance $\sigma^2 = 0.5/d^{(l-1)}$, and is a simple extension of Xavier initialization for leaky, parametric, and standard ReLU activation [208].

41.6.8 *Input normalization*

Input data to a neural network is often pre-processed for the same goals discussed previously: values are shift to have the mean of zero and scaled to keep a similar covariance across features. Furthermore, a data may be transformed using techniques including PCA and whitening (sphering) to keep input features independent and uncorrelated from each other [279].

41.6.9 *Batch normalization*

Even with careful normalization of the input data and initialization of model parameters, the mean and covariance of the data representations in hidden layers will evolve during training and may pose challenges for learning for downstream layers. This is called an *internal covariate shift* [284] and may cause negative effects to an optimization process. Accordingly, techniques to explicitly normalize features in between hidden layers are often employed for a deep neural network. One of them is *Batch Normalization*, which shifts and scales the input to a hidden layer:

$$\tilde{u}^{(l)} = \gamma \frac{u^{(l)} - \mu_B}{\sqrt{\sigma_B^2 + \epsilon}} + \beta \tag{41.72}$$

Downloaded from https://academic.oup.com/ptep/article/2022/8/083C01/6651666 by KIT Library user on 27 September 2022

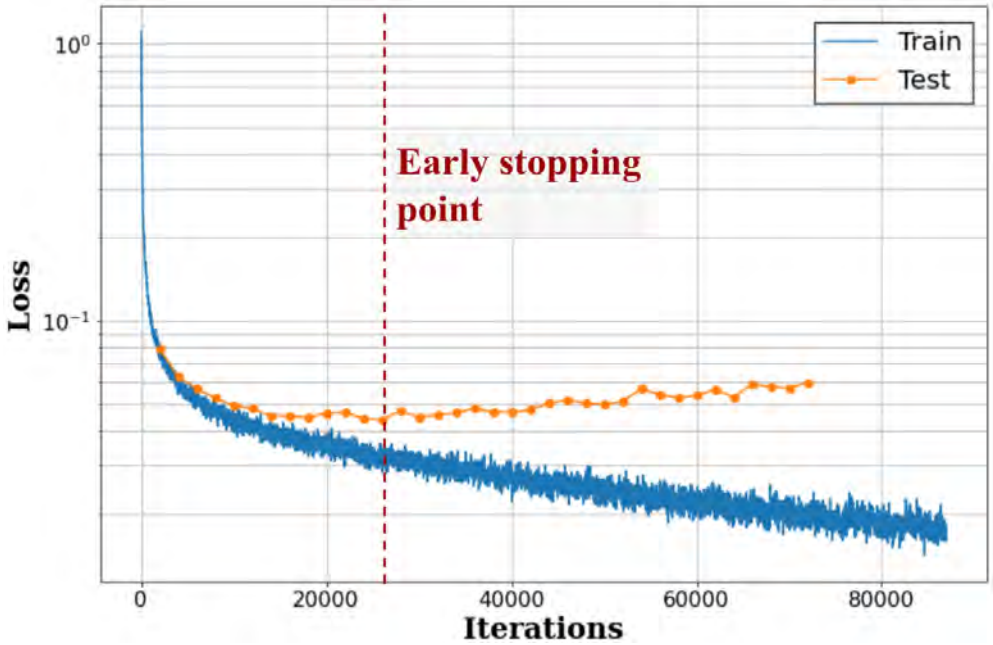

Figure 41.11: An example instance of overfitting. The training loss (vertical axis) shown in blue decreasing over iterations (horizontal axis) while the loss values evaluated on test samples shown in orange start to increase at around 26,000 iterations as indicated by the vertical line.

where $u^{(l)}$ and $\tilde{u}^{(l)}$ refer to the raw and normalized input to the l-th layer, μ_B and σ_B represent the mean and mean-squared-error of $u^{(l)}$ calculated using a *batch* of input data used to update the network parameters. γ and β are part of model parameters that are updated during the optimization. After optimization is complete, these parameters are fixed for model evaluation during production. ϵ is a small, fixed constant value to ensure numerical stability. While it is popular (especially in Computer Vision), a downside of BN is its dependency on the batch size. In situations where the batch size is limited to be a small number (e.g. memory limitation for a large data or a model), the performance using BN could degrade since β and γ values may not be generalized for the dataset during training.

There are several variants to batch normalization with considerations on how to group a subset of values in u^l. For instance, an image naturally has three groupings: a set of pixels across spatial axis, features within one pixel (i.e. image *channels*), alongside with a grouping across multiple images (i.e. batch). Different groupings have been studied and found and some are found effective to particular type of applications: Layer Normalization groups values along the channel and spatial dimensions [285], Instance Normalization groups along the spatial dimension but not along the batch nor channel [286], and Group Normalization is similar to Layer Normalization but forms multiple sub-groups of channels [287]. These variants does not apply normalization across samples within a batch, and thus agnostic to the batch size.

41.6.10 *Transfer learning: pre-training and fine-tuning*

Transfer learning is a technique to improve performance and accelerate optimization process by reusing a pre-trained machine learning model for a new task. Two tasks and data sets for each task may be different: the idea is that fundamental features may be reusable across different data and tasks. Transfer learning typically takes two steps: the first is to alter the model or data if necessary, then train (*fine-tuning*) the model. The first step is required, for example, when solving a different task that requires a different architecture (e.g. regression v.s. classification), or when input data format requires a change (e.g. original model trained on three channel image, such as RGB images, while new data has a single channel). Transfer learning has been widely practiced in the field of Computer Vision where large, labeled data sets are available [288–291]: a CNN trained for classifying images of an animal can be largely reused for object detection, or even for analyzing image data in science (e.g. particle trajectories recorded by an imaging detector). It is a critical aspect for the development of generic AI as well as interdisciplinary sharing of models across research fields.

For sequential models, transfer learning had been challenging before the appearance of Transformer. While Transformer was initially introduced for machine translation, Generative Pre-trained Transformer (GPT-1) showed that the model can be generalized to multiple NLP tasks by achieving the state-of-the-art in several seemingly different tasks including a sentence classification, semantic similarity, question answering and commonsense reasoning [292].

41.6.11 *Zero, one, and a few shot learning*

Fine-tuning (and thus transfer learning) may not be necessary if model is well generalized: humans can picture an imaginary animal in mind just from descriptions, or perform a task that he or she has never done before. One-shot learning is an extreme case of transfer learning where only one example is presented at the fine-tuning stage [293]. A similar variant is called a few-shot learning (fine-tuning using a few examples). This is possible only if the model has already learned the solution during the pre-training and the example is used to map the solution to the task. Zero-shot [294–296] learning is even more extreme where the model is given a new task without any example. This is only possible if the task is already learned during the pre-training in an implicit or unsupervised manner since zero-shot training implies that the model was never trained for the task.

41.7 Incorporating uncertainty

A fundamental aspect of data analysis is the quantification of uncertainty. This broad topic includes the traditional distinction between statistical and systematic uncertainty, procedures for propagation of errors, and the incorporation of uncertainty in to the statistical models (*e.g.* with nuisance parameters) that are used in Bayesian or frequentist statistical procedures (see Sec. 40). Accounting for systematic uncertainty can be seen as a requirement, but ideally systematic uncertainties are also taken into account in the design of the analysis so as to mitigate their effect. The introduction of machine learning into the analysis pipeline

Downloaded from https://academic.oup.com/ptep/article/2022/8/083C01/6651666 by KIT Library user on 27 September 2022

requires revisiting the techniques used for uncertainty quantification and exposes many fundamental issues that have nothing to do with the use of machine learning per se. See Ref. [297] for a recent review on this topic.

In machine learning research and industrial settings, the mismatch between the data distribution $p_{\rm train}(x,y)$ used for training and the data distribution $p_{\rm prod}(x,y)$ that the model will be applied to in production is referred to as *covariate shift* or *domain shift*. For example, one might train a classifier to identify cats and dogs with images from a well lit studio and then apply the classifier on images taken in doors with poor lighting conditions and a scratched lens. Not surprisingly, the mis-classification rate of the classifier will be different between the two settings.

Physicists are keenly aware that the simulations that we use to describe the data are not perfect, and this mismodelling corresponds to a large fraction of the of systematic uncertainties accounted for in published works. Since simulated data is often used to train machine learning models (*i.e.* $p_{\rm train}(x,y)$), it is important to understand and account for how this mismodelling will influence results when applied to real data (*i.e.* $p_{\rm prod}(x,y)$).

One of the primary approaches to incorporating this type uncertainty is to introduce nuisance parameters ν corresponding to the uncertain inputs to the simulation and to parameterize various types of perturbations (*e.g.* corrections to efficiencies, energy scales, *etc.*) in hopes that the resulting family of distributions $p(x|y,\nu)$ is flexible enough to encompass the true data distribution for class y. In this approach one does not have just two "domains" for the data (*i.e.* $p_{\rm train}$ and $p_{\rm prod}$), but a continuous family of domains parameterized by the nuisance parameters ν.

With this framing in mind, there are several approaches to incorporating uncertainty into an analysis that includes ML-based components:

- **propagation of errors:** one works with a model $f(x)$ and simply characterizes how uncertainty in the data distribution propagate through the function to the down-stream task irrespective of how it was trained.
- **domain adaptation:** one incorporates knowledge of the distribution for domains (or the parameterized family of distributions $p(x|y,\nu)$) into the training procedure so that the performance of $f(x)$ for the down-stream task is robust or insensitive to the uncertainty in ν.
- **parameterized models:** instead of learning a single function of the data $f(x)$, one learns a family of functions $f(x;\nu)$ that is explicitly parameterized in terms of nuisance parameters and then accounts for the dependence on the nuisance parameters in the down-stream task.
- **data augmentation:** one trains a model $f(x)$ in the usual way using training dataset from multiple domains by sampling from some distribution over ν.

In this setting it is best to consider the trained model $f(x)$ or $f(x;\nu)$ to be a fixed function and decouple the variability associated to training or the choice of architecture. The fact that one could have chosen a different architecture or learning algorithm should be treated in the same way as other choices that are made in the data analysis pipeline. While it is reasonable to want downstream inference and decisions to be robust to these choices, they are of a different nature than the uncertainty in the modelling of the data distribution. We return to this point in Sections 41.7.5 and 41.7.6.

41.7.1 *Propagation of errors*

In this Section we consider the common scenario in which one has used some machine learning technique to train a model $f(x)$ for classification or regression and wants to assess the sensitivity of the output of $f(x)$ to uncertainty in the input x. We regard the function $f(x)$ as fixed and we are not concerned with how the model was trained.

Propagating uncertainty through a ML-based model $f(x)$ is not fundamentally different than for any other function, and one can use the standard propagation of errors formula of Sec. 39.2.1. As always, it is important to recognize the limitations of the propagation of errors formula, which is accurate when the uncertainty on x is Gaussian and the function $f(x)$ is approximately linear within the region set by the uncertainty on x.

Similarly, classifiers are often used for particle identification or event selection. In that case, one is primarily interested in the efficiency ϵ to satisfy a cut on the classifier output. The efficiency depends on the distribution $p(x|y)$ through the equation $\epsilon_y = P(f(x) > f_{\rm cut}|y) = \int H(f(x) - f_{\rm cut})p(x|y)dx$, where H is the Heaviside step function and y is an index or label for the category of data that is being considered (*e.g.* signal or background, electron or jet, *etc.*). Thus, the question in this context is what is the uncertainty on the efficiency ϵ_y due to uncertainty in the distribution $p(x|y)$. In practice, the quantification of the uncertainty in the efficiency ϵ_y is usually based on either a calibration measurement on real data or estimated with simulated data. These procedures typically treat the classifier as a black-box, and thus nothing precludes using those procedures on a ML-based classifier. An early example of this approach for b-tagging can be found in Ref. [298].

In the case where simulation is used to estimate the efficiency ϵ_y and its uncertainty, one usually varies nuisance parameters ν associated to the simulation. One then uses simulated samples to approximate $\epsilon_y(\nu) = P(f(x) > f_{\rm cut}|y,\nu) = \int H(f(x) - f_{\rm cut})p(x|y,\nu)dx$. Again, the procedure for incorporating uncertainty isn't fundamentally different if the classifier $f(x)$ is based on machine learning or a hand-crafted observable.

41.7.2 *Domain adaptation*

While estimating the uncertainty for a ML-based model is not fundamentally different than any other hand-crafted observable used for regression or classification, the worry of many physicists is that by working with a high-dimensional set of features x that one is more susceptible to mismodelling of subtle correlations. This is a valid concern, and it should be appreciated that a great deal of prior knowledge and physical insight goes into the construction of hand-crafted observables so that they will be robust to the most uncertain aspects of data. However, much of this craft is based on heuristics that are difficult to systematize. Furthermore, one can only validate that such an observable is robust if one can explicitly evaluate the performance for a perturbed distribution. Thus in the settings where one can validate the robustness to a perturbed scenario ν_0, one must have access to $p(x|y,\nu_0)$.

One approach to formalize this type of robustness is to consider the dependence on the distribution of the output of the model $f(x)$ to the nuisance parameters. In statistics, if the distribution of f is independent of the nuisance parameters, then f is referred to as a *pivotal quantity*. This is a property that we can incorporate directly into the training procedure to target a particular notion of robustness. The authors of Ref. [299] introduced an adversarial approach (similar to what is used in the generative adversarial network of Sec. 41.5.4.2) to penalize a model during training if the distribution of the output varies with the nuisance parameters. To construct the training dataset $\{x_i, y_i, \nu_i\}_{i=1,\ldots,n}$, one must sample y and ν according to some proposal distribution (similar to a prior, but only used for the creation of training dataset, not necessarily for statistical inference), corresponding to a joint distribution $p(x,y,\nu)$. Instead of minimizing the target loss $\mathcal{L}_f$ (*e.g.* cross-entropy, squared-error, *etc.*) with respect to the parameters ϕ_f that parameterize the model f, one trains with a minimax strategy that also includes an adversary q with parameters ϕ_r. The trained model is characterized by the saddle point

$$\hat{\phi}_f, \hat{\phi}_r = \arg\min_{\phi_f} \arg\max_{\phi_r} E_\lambda(\phi_f, \phi_r) \ , \tag{41.73}$$

where the value function E_λ includes the target loss as well as a regularization term associated to the adversary

$$E_\lambda(\phi_f, \phi_r) = \mathcal{L}_f(\phi_f) - \lambda \mathcal{L}_r(\phi_f, \phi_r) \ . \tag{41.74}$$

The constant λ is a hyperparameter, since generally there is a tradeoff between the two terms and only in special cases can the model that minimizes $\mathcal{L}_f$ also be a pivotal quantity. The regularization term

$$\mathcal{L}_r(\phi_f, \phi_r) = \mathbb{E}_{p(x,y,\nu)}[-\log q_{\phi_r}(\nu|f_{\phi_f}(x))] \tag{41.75}$$

Downloaded from https://academic.oup.com/ptep/article/2022/8/083C01/6651666 by KIT Library user on 27 September 2022

is an example of conditional density estimation (see Sec. 41.3.2.1), where the model $q_{\phi_r}(\nu|f)$ is trying to predict the distribution of the nuisance parameter ν given the output of the model $f(x)$. This term is maximized when f is independent of ν. Earlier work had also used an adversarial technique for domain adaptation, but was limited to just two domains [300–302], while here ν parameterizes a continuous family of distributions and can have multiple components corresponding to different sources of uncertainty. Furthermore, the previous work aimed to make the distribution for a high-dimensional, intermediate representation of the data be invariant to the domain shift as opposed to just the final output $f(x)$.

One way of interpreting Eq. 41.73 is that the goal is to minimize a regularized loss function $\hat{\mathcal{L}}(\phi_f) = \arg\max_{\phi_r} E_\lambda(\phi_f, \phi_r)$, where the optimization with respect to ϕ_r is not exposed. This motivates another approach in which the regularization is not achieved through a learned adversary, but by a measure of discrepancy between distributions that can be computed directly from samples. In particular, the authors of Ref. [303] proposed the use of *distance correlation* to avoid what can be a challenging min-max optimization problem.

In either case, the optimization of the hyperparameter λ is based on the downstream task. For example, in Ref. [299] considered the case where f was a signal vs. background binary classifier where the nuisance parameter ν was associated to uncertainty in the background model. The hyperparameter λ was then optimized to maximize the approximate median significance (AMS). Similarly, the authors of Refs. [304] and [303] considered new physics searches in the context of boosted jet tagging, where the hyperparameter controls the sculpting of the side-bands used for background estimation.

While these strategies modify the training procedure so that the sensitivity to the nuisance parameters is reduced, it does not typically eliminate it. As a result, one still needs to propagate the uncertainty in the data distribution through the learned model as described in the preceding section.

Note, this adversarial technique has also been employed in other settings where one would like to decorrelate the output of the classifier with an observed quantity so that it can be used for background estimation [304]. Widely used alternative approaches to decorrelation include uboost [305] and DDT [306]. Other examples of the domain adaptation and decorrelation use cases from the Living Review include [299, 303–318].

41.7.3 *Parameterized models*

An alternative to learning a model $f(x)$ that is pivotal — *i.e.* whose distribution is independent of the nuisance parameter ν — is to learn a family of models $f(x;\nu)$ that is parameterized in terms of the nuisance parameters. In general, there is a tradeoff between the two terms of Eq. 41.74 for a single model $f(x)$. In a parameterized model, $f(x;\nu)$ optimizes the performance of the model for every value of ν. Parameterized classifiers were first advocated in Ref. [58] in the context of simulation-based inference (see Sec. 41.7.7) and in Ref. [319] for new physics searches. It has also been applied to simulation-based inference for effective field theory parameters in Ref. [19] and Ref. [320] provides additional pedagogical examples.

The training of a parameterized model is similar to the standard procedure. For example, if one originally wanted to minimize the squared loss function $\mathcal{L}(y, f(x)) = (y - f(x))^2$ with training dataset $\{x_i, y_i\}_{i=1,\ldots,n}$, then the corresponding training procedure for the parameterized model would be as follows. One would need to construct a training set $\{x_i, y_i, \nu_i\}_{i=1,\ldots,n}$ as described in the preceeding section, construct a parameterized model $f(x;\nu)$ that takes as input the original feature vector x as well as the nuisance parameters ν, and then train using the same loss $\mathcal{L}(y, f(x;\nu)) = (y - f(x;\nu))^2$.

One complication of the parameterized approach is that it is no longer possible to evaluate the model on a dataset $\{x_i\}$ and pass on only $\{f_i\}$ for downstream analysis tasks since $f(x_i;\nu)$ still depends on ν. Instead, one delay evaluating the model to some down-stream stage when the dependence on ν would accounted for. For example, in the context of a likelihood based analysis where one is testing a hypothesis where the nuisance parameters take on a particular value ν_{test}, then one will consider the data distribution $p(x|\nu_{\text{test}})$, and at that point one would evaluate the model at the corresponding nuisance parameter value, *i.e.* $f(x;\nu_{\text{test}})$. Explicit examples are given in Refs. [19, 58, 297, 320]. While this may seem complicated, it actually corresponds to what is done in a typical likelihood-based fit when the statistical model has nuisance parameters; *i.e.* the likelihood-ratio corresponds to the model $f(x;\nu)$ as in Eq. 41.12.

41.7.4 *Data augmentation*

An intuitive approach to building in robustness to systematic effects that can lead to domain shift, is simply to augment the training dataset so that it includes examples corresponding to several values of the nuisance parameter or systematic variations. As before one can construct a dataset $\{x_i, y_i, \nu_i\}_{i=1,\ldots,n}$, but instead of leveraging the information about ν_i, one simply discards this information. This corresponds to sampling from the marginal distribution $x_i, y_i \sim p(x,y) = \int d\nu p(x,y|\nu)p(\nu)$, and is often referred to as *smearing*. One can then use this smeared dataset for supervised learning in the traditional way. While it is possible that this approach will lead to improved robustness to systematic variations (*i.e.* generalization for ν other than the nominal value) than if systematic uncertainty weren't considered at all), this intuitive approach has several shortcomings. The approach does not yield a pivotal quantity as in the adversarial approach, so propagation of uncertainty through the network is still required. Moreover, there is no direct way to control the trade-off between independence from the nuisance parameter and the original target loss as in the adversarial approach. Finally, it can lead to significant performance loss compared to what is possible with the parameterized approach. These trade-offs were studied in Refs. [319, 320] with both pedagogical and physically-motivated examples.

41.7.5 *Aleatoric and epistemic uncertainty*

In the machine learning and risk assessment literature, uncertainty is often characterized in terms of *aleatoric* and *epistemic* uncertainty [321–324]. Familiarity with these terms is useful, but the distinction between the two can be ambiguous, the terms are not always consistently used, and they do not clearly map onto the concepts used physics.

For example, Ref. [323], states that "roughly speaking, aleatoric (aka statistical) uncertainty refers to the notion of randomness, that is, the variability in the outcome of an experiment which is due to inherently random effects", while "epistemic (aka systematic) uncertainty refers to uncertainty caused by a lack of knowledge (about the best model)". This seems clear enough, but in that same reference (and in Ref. [325]) the aleatoric uncertainty is considered irreducible, while the epistemic uncertainty could be reduced with additional information. This may seem backwards for many physicists since often in particle physics, we think of how uncertainties scale as we collect more data but keep the experimental design fixed. In that case, the statistical uncertainty will be reduced with time while the systematic uncertainty will remain constant[6]. There is no paradox here, it is simply a different point of view. The emphasis of the risk assessment community is not on collecting more data with the same experimental design, but collecting different types of data that will inform the models themselves. Clearly even for physicists, data from new experiments or calibration measurements could also reduce our systematic uncertainties. While there are exceptions in the literature, the bulk of it associates aleatoric uncertainty with the randomness of classical probability (*i.e.* the statistical uncertainty associated to repeating the same experiment many times) and epistemic uncertainty with our state of knowledge.

Perhaps a more important distinction between the perspective of physicists and machine learning researchers has to do with the use of the term "model" and what exactly is uncertain. In physics, the systematic and epistemic uncertainty is typically associated to our understanding of the underlying physics and "the model" usually refers to the physics model, detector model encapsulated

[6] Further complicating the relationship between the terms is that many experimental uncertainties that are characterized as systematic are actually statistical in nature as auxiliary measurements and control regions are used to constrain the corresponding nuisance parameters.

Downloaded from https://academic.oup.com/ptep/article/2022/8/083C01/6651666 by KIT Library user on 27 September 2022

in a simulation. In contrast, for machine learning research, "the model" usually refers to the trained model $\hat{f} \in \mathcal{F}$ used as described in Section 41.2.1 (or the class of functions $\mathcal{F}$ itself). This makes sense if we recall that in the bulk of machine learning research, one has little insight into the process that generated the data (*e.g.* images of cats and dogs, natural language, *etc.*). In that sense, the epistemic uncertainty in machine learning is usually associated to uncertainty in the model parameters ϕ after training, which would be reduced if one could collect more training dataset (see Ref. [324] for this point of view).

In the literature on Uncertainty Quantification (UQ), which is more closely connected to physics given the role of computer simulations, the terminology is more fine grained and less ambiguous. That community uses the terms parameter uncertainty (*i.e.* nuisance parameters), structural uncertainty (*i.e.* mismodelling), algorithmic uncertainty (*i.e.* numerical uncertainty), experimental uncertainty (*i.e.* uncertainty from experimental resolution and statistical fluctuations), and interpolation uncertainty (*i.e.* uncertainty due to interpolating between different parameter values due to lack of computational resources).

41.7.6 *Model averaging and Bayesian machine learning*

The core of Bayesian machine learning is the model averaging view. Here one often takes a more ambitious view of learning than described in Sec. 41.2.1, which is framed mainly as function approximation. While in Sec. 41.2.1, the goal is to find a function that minimizes the risk, in Bayesian machine learning one explicitly builds a probability model $q_\phi(x, y)$ for the training dataset $\mathcal{D} = \{x_i, y_i\}_{i=1,\ldots,n}$. It is the same change in perspective that one has when one views the squared error loss function $\mathcal{L}_{MSE} = (y - f_\phi(x))^2$ as the log-likelihood for a probability model $y \sim N(f(x), \sigma)$. In addition, one assumes some prior on the model parameters $p(\phi)$, which is often a Gaussian distribution, and is analogous to Tikhonov regularization (see Sec. 41.3.1.2). With this view in mind, a single trained model $\hat{f} = f_{\hat{\phi}}$ is the MAP point estimate and the more complete Bayesian solution is the entire posterior distribution over the model parameters $p(\phi|\mathcal{D})$. With this view, it is clear how increasing the number of training examples n will lead to a reduction in uncertainty on ϕ. However, this notion of epistemic uncertainty has little to do with the notion of systematic uncertainty as the term is used by particle physicists.

Bayesian methods can be applied to non-probabilistic regression problems, in which case they can provide uncertainty quantification. Consider the case of regression in traditional (non-Bayesian) machine learning. The trained model $f_{\hat{\phi}}(x)$ is used to predict the target label y. For a fixed x, the model does not provide any notion of uncertainty on the prediction. One could propagate uncertainty on x through $f(x)$, but that is also not the desired quantity to characterize the intrinsic spread $p(y|x)$ in the data, which may exist even if x has negligible uncertainty. In contrast, Gaussian process regression (a Bayesian method) does provide a natural way to communicate the uncertainty on the prediction, which is possible because one first had to specify a prior on the mean and covariance of the Gaussian process.

In the context of Bayesian deep learning and Bayesian Neural Networks, one would place a prior on the weights and biases of the neural network $p(\phi)$ and then use one of the many emerging techniques to calculate the approximate posterior $p(\phi|\mathcal{D})$. However, we should recognize that we have little-to-no insight into the parameters of a deep neural network, so the prior on ϕ is hardly well-justified. Furthermore, just as in all Bayesian approaches, the prior is not invariant to reparametrizing the model: $\phi \to \eta(\phi)$. While it is difficult to justify the choice of the prior on the parameters (and, thus, the resulting posterior), the resulting model may perform well empirically. In such high-dimensional parameter spaces, the bias-variance tradeoff can be dramatic.

Bayesian model averaging (BMA) performs Bayesian average over the posterior $p(\phi|\mathcal{D})$. This can be applied to any quantity f_ϕ, such as a regression or classification prediction y. Suppose we can draw from the posterior $\phi \sim p(\phi|\mathcal{D})$. For each draw we can evaluate the predicted regression variable $y = f_\phi(x) + \epsilon$, where ϵ is some noise to account for uncertainty in the predictions. We can denote this process as a draw from $p(y|x, \phi)$, $y \sim p(y|x, \phi) = N(f_\phi(x), \sigma_\epsilon^2)$, where σ_ϵ^2 is the noise variance. The BMA then performs

$$p(y|x, \mathcal{D}) = \int d\phi p(\phi|\mathcal{D}) p(y|x, \phi). \tag{41.76}$$

In practice $p(y|x, \phi)$ is evaluated by drawing samples of y and ϕ, so the posterior is defined implicitly by the samples. For example, the mean prediction is obtained by averaging $f_\phi(x)$ over the samples of ϕ, and the covariance matrix is similarly evaluated by averaging the second moments over the samples of ϕ.

Ref. [326] provides a different perspective on BMA analyzed in what are referred to as the $\mathcal{M}$-open and $\mathcal{M}$-closed settings [326]. The $\mathcal{M}$-closed setting refers to the situation where the true data generating process is in the space of models, even if it is unknown to us. In contrast, the $\mathcal{M}$-open setting refers to when the true data generating process is not in model space (*i.e.* the model is mis-specified). Interestingly, in the $\mathcal{M}$-open case one can potentially do better than any one model in the model class by considering an average over the models, since averaging can create a new model that is not in the model class. BMA provides one such averaging, but other averages, which are not weighted by $p(\phi|\mathcal{D})$, can be a better choice. When the weights of each model are optimized against appropriate loss the resulting procedure is called stacking, which has been shown to be superior to BMA in the $\mathcal{M}$-open setting [326]. Ref. [327] performed experiments indicating that in some cases model averaging can also improve predictive uncertainty estimates under domain shifts.

Neural network model averaging beyond BMA comes in several different flavors. Two successful model averaging procedures are Monte Carlo dropout [328], which uses dropout ensembling, and deep ensembles [329], which use random initialization ensembling. These methods may not only be superior to BMA, they are also often significantly faster than BMA. Whether these model averages are an approximation to BMA, or an alternative to it, remains a debated topic, and both views have been advocated. BMA itself can be accelerated using approximate methods, such as stochastic Variational Inference with reparametrization trick [330].

41.7.7 *Connection to probabilistic machine learning*

We end this Section by reinforcing the connection between uncertainty quantification in traditional machine learning and the more probabilistic approaches to machine learning exemplified by simulation-based inference (see Sec 41.3.5) and deep generative models (see Sec. 41.5.4). In the standard approach to supervised learning (*e.g.* classification and regression) the model $f(x)$ provides a point estimate for y. Estimating an uncertainty on y goes a step further, but the complete picture would be to model the posterior distribution $p(y|x)$. Gaussian processes (see Sec. 41.5.1) are an example, but the form of the models is limited to Gaussian posteriors. In Sec 41.3.5 we discussed approaches to model $p(y|x)$ using conditional density estimation [51, 56, 57]. If we extend this task to include a family of distributions parameterized by some nuisance parameters ν, then the task is to model $p(y|x, \nu)$, which is structurally similar.

In the context of classification, the output is already probabilistic, and the interpretation of the resulting classifier is $\hat{f}_{MSE}(x) \approx p(y = 1|x)$ (see Eq. 41.10). Incorporating the dependence on the nuisance parameter, then connects to the likelihood-ratio trick (see Eq. 41.12), approaches to simulation-based inference that involve learning the likelihood-ratio, and the parameterized approaches described in Sec. 41.7.3.

If one pairs the training procedure for classification, regression, or density estimation used in the approaches above with model averaging techniques such as BMA, then it would be possible to incorporate both uncertainty associated to finite training dataset and the uncertainty associated to systematic uncertainties. However, as described in Sec. 41.7.5 and Sec. 41.7.1, it is not clear that in physics applications it is desirable to account for the variability associated to training when the more common practice is to regard the trained model $\hat{f}(x)$ as fixed.

While these probabilistic approaches to machine learning are attractive conceptually, it is known in the machine learning community that classifiers often are poorly calibrated and often overly

Downloaded from https://academic.oup.com/ptep/article/2022/8/083C01/6651666 by KIT Library user on 27 September 2022

confident in their predictions. This is a problem even if one regards the trained model $\hat{f}(x)$ as fixed. Various approaches, including model averaging, are being pursued to improve the calibration of trained models, but the problem is unlikely to be eliminated entirely. Miscalibration can be verified by evaluating the true positive and false positive rates on held out data. This is common practice in experimental particle physics, where the output of a binary classifier is rarely taken at face value. Instead, the true and false positive rates are estimated with simulated data or control samples as described in Sec. 41.7.1. Furthermore, the true and false positives can be characterized as a function of the nuisance parameters. These procedures can be used to help calibrate parameterized models based on the likelihood-ratio trick (see Refs. [58, 320]). Unfortunately, calibration in the context of density estimation is more challenging. This connects to topics and challenges in anomaly detection (see Sec. 41.3.4).

41.8 Infrastructure for deployment in experiments

The software and computing needs of training a machine learning model are different than those encountered when it deployed for use. In machine learning jargon, the two stages are often referred to as *training* and *inference*, where inference might refer to making a prediction for y given x in a classification or regression problem. Sometimes this transition also involves using different programming languages for implementing the trained model from the ones used for training them. Modern machine learning frameworks support various serialization formats to exchange trained models. For instance, `ONNX` provides an open source format for many types of models and is is widely supported and can be found in many frameworks, tools, and hardware. This is important when integrating a trained model into the large software frameworks used by the large experiments.

While hardware acceleration with GPUs is important for efficiently training modern machine learning techniques, there are also advantages of hardware acceleration at inference time. This may include GPUs or Field Programmable Gate Arrays (FPGAs), and the Living Review includes many example works focusing on efficient inference for a given hardware architecture [81, 108, 331–340]. For applications where latency is a key concern (eg triggering at collider experiments), various accelerators have been investigated [167, 171, 341–355]. In addition, some solutions for deployment of ML models involve deployment in the cloud [356, 357].

References

[1] Y. Lecun, Y. Bengio and G. Hinton, Nature **521**, 7553, 436 (2015), ISSN 14764687.

[2] J. Schmidhuber, Neural Networks **61**, 85 (2015).

[3] A. Radovic *et al.*, Nature **560**, 7716, 41 (2018).

[4] D. Guest, K. Cranmer and D. Whiteson, Ann. Rev. Nucl. Part. Sci. **68**, 161 (2018), [arXiv:1806.11484].

[5] G. Carleo *et al.*, Rev. Mod. Phys. **91**, 4, 045002 (2019), [arXiv:1903.10563].

[6] M. Feickert and B. Nachman (2021), [arXiv:2102.02770].

[7] V. Vapnik, *The nature of statistical learning theory*, Springer science & business media (2013).

[8] C. Zhang *et al.*, Communications of the ACM **64**, 3, 107 (2021).

[9] P. Nakkiran *et al.*, arXiv preprint arXiv:1912.02292 (2019).

[10] A. Y. Ng and M. I. Jordan, in T. G. Dietterich, S. Becker and Z. Ghahramani, editors, "Advances in Neural Information Processing Systems 14 [Neural Information Processing Systems: Natural and Synthetic, NIPS 2001, December 3-8, 2001, Vancouver, British Columbia, Canada]," 841–848, MIT Press (2001), URL `https://proceedings.neurips.cc/paper/2001/hash/7b7a53e239400a13bd6be6c91c4f6c4e-Abstract.html`.

[11] M. Kuusela and V. M. Panaretos, Ann. Appl. Stat. **9**, 1671 (2015), [arXiv:1505.04768].

[12] L. Rosasco, A. Tacchetti and S. Villa, CoRR **abs/1405.0042** (2014), URL `http://arxiv.org/abs/1405.0042`.

[13] G. E. Hinton *et al.*, CoRR **abs/1207.0580** (2012), [arXiv:1207.0580], URL `http://arxiv.org/abs/1207.0580`.

[14] P. Baldi and P. J. Sadowski, Advances in neural information processing systems **26**, 2814 (2013).

[15] M. Belkin, S. Ma and S. Mandal, in J. G. Dy and A. Krause, editors, "Proceedings of the 35th International Conference on Machine Learning, ICML 2018, Stockholmsmässan, Stockholm, Sweden, July 10-15, 2018," volume 80 of *Proceedings of Machine Learning Research*, 540–548, PMLR (2018), URL `http://proceedings.mlr.press/v80/belkin18a.html`.

[16] S. Gunasekar *et al.*, in J. Dy and A. Krause, editors, "Proceedings of the 35th International Conference on Machine Learning," volume 80 of *Proceedings of Machine Learning Research*, 1832–1841, PMLR (2018), URL `http://proceedings.mlr.press/v80/gunasekar18a.html`.

[17] L. Zdeborová, Nature Physics **16**, 6, 602 (2020).

[18] E. M. Metodiev, B. Nachman and J. Thaler, JHEP **10**, 174 (2017), [arXiv:1708.02949].

[19] J. Brehmer *et al.*, Phys. Rev. **D98**, 5, 052004 (2018), [arXiv:1805.00020].

[20] J. Brehmer *et al.*, Proc. Nat. Acad. Sci. 201915980 (2020), [arXiv:1805.12244].

[21] M. Stoye *et al.* (2018), [arXiv:1808.00973].

[22] M. A. Hayat *et al.*, ApJ Letters **911**, 2, L33 (2021).

[23] T. Chen *et al.*, in "Proceedings of the 37th International Conference on Machine Learning, ICML 2020, 13-18 July 2020, Virtual Event," volume 119 of *Proceedings of Machine Learning Research*, 1597–1607, PMLR (2020), URL `http://proceedings.mlr.press/v119/chen20j.html`.

[24] E. Parzen, The annals of mathematical statistics **33**, 3, 1065 (1962).

[25] R. A. Davis, K.-S. Lii and D. N. Politis, in "Selected Works of Murray Rosenblatt," 95–100, Springer (2011).

[26] K. S. Cranmer, Comput. Phys. Commun. **136**, 198 (2001), [hep-ex/0011057].

[27] Y. Bengio, A. Courville and P. Vincent, IEEE transactions on pattern analysis and machine intelligence **35**, 8, 1798 (2013).

[28] `https://en.wikipedia.org/wiki/Cluster_analysis`.

[29] R. E. Bellman, *Dynamic Programming*, Princeton University Press, USA (1957), ISBN 069107951X.

[30] D. E. Kirk, *Optimal control theory: an introduction*, Courier Corporation (2004).

[31] K. J. Åström, Journal of Mathematical Analysis and Applications **10**, 174 (1965).

[32] J. Brehmer *et al.*, in "34th Conference on Neural Information Processing Systems," (2020), [arXiv:2011.08191].

[33] R. S. Sutton and A. G. Barto, Cambridge, MA **22447** (1998).

[34] K. Arulkumaran *et al.*, IEEE Signal Processing Magazine **34**, 6, 26 (2017).

[35] H. Robbins, Bulletin of the American Mathematical Society **58**, 5, 527 (1952).

[36] J. C. Gittins, Journal of the Royal Statistical Society: Series B (Methodological) **41**, 2, 148 (1979).

[37] J. Mockus, *Bayesian approach to global optimization: theory and applications*, volume 37, Springer Science & Business Media (2012).

[38] E. Brochu, V. M. Cora and N. De Freitas, arXiv preprint arXiv:1012.2599 (2010).

Downloaded from https://academic.oup.com/ptep/article/2022/8/083C01/6651666 by KIT Library user on 27 September 2022

[39] M. Farina, Y. Nakai and D. Shih, Physical Review D **101**, 7 (2020), ISSN 2470-0029, URL http://dx.doi.org/10.1103/PhysRevD.101.075021.

[40] T. Heimel *et al.*, SciPost Physics **6**, 3 (2019), ISSN 2542-4653, URL http://dx.doi.org/10.21468/SciPostPhys.6.3.030.

[41] J. Ren *et al.*, in H. M. Wallach *et al.*, editors, "Advances in Neural Information Processing Systems 32: Annual Conference on Neural Information Processing Systems 2019, NeurIPS 2019, December 8-14, 2019, Vancouver, BC, Canada," 14680–14691 (2019).

[42] E. T. Nalisnick *et al.*, in "7th International Conference on Learning Representations, ICLR 2019, New Orleans, LA, USA, May 6-9, 2019," OpenReview.net (2019), URL https://openreview.net/forum?id=H1xwNhCcYm.

[43] Z. Xiao, Q. Yan and Y. Amit, arXiv preprint arXiv:2003.02977 (2020).

[44] V. Böhm and U. Seljak, arXiv preprint arXiv:2006.05479 (2020).

[45] B. Dai and U. Seljak, in M. Meila and T. Zhang, editors, "Proceedings of the 38th International Conference on Machine Learning, ICML 2021, 18-24 July 2021, Virtual Event," volume 139 of *Proceedings of Machine Learning Research*, 2352–2364, PMLR (2021), URL http://proceedings.mlr.press/v139/dai21a.html.

[46] J. Brehmer and K. Cranmer (2020), [arXiv:2003.13913].

[47] E. M. Metodiev, B. Nachman and J. Thaler, Journal of High Energy Physics **2017**, 10 (2017), ISSN 1029-8479, URL http://dx.doi.org/10.1007/JHEP10(2017)174.

[48] J. H. Collins *et al.*, The European Physical Journal C **81**, 7 (2021), ISSN 1434-6052, URL http://dx.doi.org/10.1140/epjc/s10052-021-09389-x.

[49] G. Kasieczka *et al.* (2021), [arXiv:2101.08320].

[50] T. Aarrestad *et al.* (2021), [arXiv:2105.14027].

[51] K. Cranmer, J. Brehmer and G. Louppe, Proc. Nat. Acad. Sci. **117**, 48, 30055 (2020), [arXiv:1911.01429].

[52] J. Brehmer and K. Cranmer, *Artificial Intelligence for Particle Physics*, chapter Simulation-based inference methods for particle physics, World Scientific Publishing Co (2021).

[53] P. J. Diggle and R. J. Gratton, in "Journal of the Royal Statistical Society: Series B (Methodological)," volume 46, 193–212 (1984), ISSN 0035-9246.

[54] D. B. Rubin, The Annals of Statistics **12**, 4, 1151 (1984), ISSN 0090-5364, URL https://doi.org/10.1214/aos/1176346785.

[55] M. A. Beaumont, W. Zhang and D. J. Balding, Genetics **162**, 4, 2025 (2002), ISSN 00166731.

[56] K. Cranmer and G. Louppe, J. Brief Ideas (2016), 10.5281/zenodo.198541.

[57] G. Papamakarios and I. Murray, in "Advances in Neural Information Processing Systems," 1036–1044 (2016), ISSN 10495258, [arXiv:1605.06376].

[58] K. Cranmer, J. Pavez and G. Louppe, arXiv:1506.02169 (2015), [arXiv:1506.02169], URL http://arxiv.org/abs/1506.02169.

[59] C. Modi, F. Lanusse and U. Seljak, "Flowpm: Distributed tensorflow implementation of the fastpm cosmological n-body solver," (2020), [arXiv:2010.11847].

[60] J. Jasche and B. D. Wandelt, Mon. Not. Roy. Astron. Soc. **432**, 894 (2013), [arXiv:1203.3639].

[61] U. Seljak *et al.*, JCAP **12**, 009 (2017), [arXiv:1706.06645].

[62] A. Andreassen *et al.*, Phys. Rev. Lett. **124**, 18, 182001 (2020), [arXiv:1911.09107].

[63] K. Datta, D. Kar and D. Roy (2018), [arXiv:1806.00433].

[64] M. Bellagente *et al.* (2019), [arXiv:1912.00477].

[65] N. D. Gagunashvili (2010), [arXiv:1004.2006].

[66] A. Glazov (2017), [arXiv:1712.01814].

[67] M. Bellagente *et al.* (2020), [arXiv:2006.06685].

[68] M. Vandegar *et al.*, in A. Banerjee and K. Fukumizu, editors, "Proceedings of The 24th International Conference on Artificial Intelligence and Statistics," volume 130 of *Proceedings of Machine Learning Research*, 2107–2115, PMLR (2021), [arXiv:2011.05836], URL https://proceedings.mlr.press/v130/vandegar21a.html.

[69] P. Baroň (2021), [arXiv:2104.03036].

[70] A. Andreassen *et al.* (2021), [arXiv:2105.04448].

[71] P. Komiske, W. P. McCormack and B. Nachman (2021), [arXiv:2105.09923].

[72] V. Andreev *et al.* (H1) (2021), [arXiv:2108.12376].

[73] M. Arratia *et al.* (2021), [arXiv:2109.13243].

[74] T. A. Le, A. G. Baydin and F. Wood, in "Proceedings of the 20th International Conference on Artificial Intelligence and Statistics, AISTATS 2017," volume 54 of *Proceedings of Machine Learning Research*, 1338–1348, PMLR, Fort Lauderdale, FL, USA (2017), [arXiv:1610.09900].

[75] A. G. Baydin *et al.* (2018), [arXiv:1807.07706].

[76] A. G. Baydin *et al.*, International Conference for High Performance Computing, Networking, Storage and Analysis, SC arXiv:1907.03382 (2019), ISSN 21674337, [arXiv:1907.03382].

[77] A. Hocker *et al.*, PoS **ACAT**, 040 (2007), [arXiv:physics/0703039].

[78] T. Mikolov *et al.*, arXiv preprint arXiv:1301.3781 (2013).

[79] E. Asgari and M. R. Mofrad, PloS one **10**, 11, e0141287 (2015).

[80] D. Guest *et al.*, Phys. Rev. **D94**, 11, 112002 (2016), [arXiv:1607.08633].

[81] T. Q. Nguyen *et al.*, Comput. Softw. Big Sci. **3**, 1, 12 (2019), [arXiv:1807.00083].

[82] E. Bols *et al.* (2020), [arXiv:2008.10519].

[83] K. Goto *et al.*, "Development of a Vertex Finding Algorithm using Recurrent Neural Network," (2021), [arXiv:2101.11906].

[84] R. T. de Lima (2021), [arXiv:2102.06128].

[85] Technical Report ATL-PHYS-PUB-2017-003, CERN, Geneva (2017), URL http://cdsweb.cern.ch/record/2255226.

[86] J. Pumplin, Phys. Rev. D **44**, 2025 (1991).

[87] J. Cogan *et al.*, JHEP **02**, 118 (2015), [arXiv:1407.5675].

[88] L. G. Almeida *et al.*, JHEP **07**, 086 (2015), [arXiv:1501.05968].

[89] L. de Oliveira *et al.*, JHEP **07**, 069 (2016), [arXiv:1511.05190].

[90] Technical Report ATL-PHYS-PUB-2017-017, CERN, Geneva (2017), URL http://cds.cern.ch/record/2275641.

[91] J. Lin *et al.*, JHEP **10**, 101 (2018), [arXiv:1807.10768].

[92] P. T. Komiske *et al.*, Phys. Rev. **D98**, 1, 011502 (2018), [arXiv:1801.10158].

[93] J. Barnard *et al.*, Phys. Rev. **D95**, 1, 014018 (2017), [arXiv:1609.00607].

[94] P. T. Komiske, E. M. Metodiev and M. D. Schwartz, JHEP **01**, 110 (2017), [arXiv:1612.01551].

[95] G. Kasieczka *et al.*, JHEP **05**, 006 (2017), [arXiv:1701.08784].

[96] S. Macaluso and D. Shih, JHEP **10**, 121 (2018), [arXiv:1803.00107].

[97] J. Li, T. Li and F.-Z. Xu (2020), [arXiv:2008.13529].

[98] J. Li and H. Sun (2020), [arXiv:2009.00170].

[99] J. S. H. Lee *et al.*, J. Korean Phys. Soc. **74**, 3, 219 (2019), [arXiv:2012.02531].

Downloaded from https://academic.oup.com/ptep/article/2022/8/083C01/6651666 by KIT Library user on 27 September 2022

[100] J. Collado *et al.*, "Learning to Isolate Muons," (2021), [arXiv:2102.02278].

[101] Y.-L. Du, D. Pablos and K. Tywoniuk (2020), [arXiv:2012.07797].

[102] J. Filipek *et al.* (2021), [arXiv:2105.04582].

[103] Technical Report ATL-PHYS-PUB-2019-028, CERN, Geneva (2019), URL `http://cds.cern.ch/record/2684070`.

[104] M. Andrews *et al.* (2018), [arXiv:1807.11916].

[105] Y.-L. Chung, S.-C. Hsu and B. Nachman (2020), [arXiv:2009.05930].

[106] Y.-L. Du *et al.*, Eur. Phys. J. C **80**, 6, 516 (2020), [arXiv:1910.11530].

[107] M. Andrews *et al.* (2021), [arXiv:2104.14659].

[108] A. A. Pol *et al.* (2021), [arXiv:2105.05785].

[109] A. Aurisano *et al.*, JINST **11**, 09, P09001 (2016), [arXiv:1604.01444].

[110] R. Acciarri *et al.* (MicroBooNE), JINST **12**, 03, P03011 (2017), [arXiv:1611.05531].

[111] L. Hertel *et al.* (2017), URL `https://dl4physicalsciences.github.io/files/nips_dlps_2017_7.pdf`.

[112] C. Adams *et al.* (MicroBooNE), Phys. Rev. **D99**, 9, 092001 (2019), [arXiv:1808.07269].

[113] L. Dominé and K. Terao (DeepLearnPhysics), Phys. Rev. D **102**, 1, 012005 (2020), [arXiv:1903.05663].

[114] S. Aiello *et al.* (KM3NeT) (2020), [arXiv:2004.08254].

[115] C. Adams, K. Terao and T. Wongjirad (2020), [arXiv:2006.01993].

[116] L. Dominé *et al.* (DeepLearnPhysics), Phys. Rev. D **104**, 3, 032004 (2021), [arXiv:2006.14745].

[117] F. Drielsma *et al.* (DeepLearnPhysics), Phys. Rev. D **104**, 7, 072004 (2021), [arXiv:2007.01335].

[118] D. H. Koh *et al.* (DeepLearnPhysics) (2020), [arXiv:2007.03083].

[119] H. Yu *et al.*, JINST **16**, 01, P01036 (2021), [arXiv:2007.12743].

[120] F. Psihas *et al.* (2020), [arXiv:2008.01242].

[121] S. Alonso-Monsalve *et al.*, Phys. Rev. D **103**, 3, 032005 (2021), [arXiv:2009.00688].

[122] P. Abratenko *et al.* (MicroBooNE) (2020), [arXiv:2010.08653].

[123] B. Clerbaux *et al.* (2020), [arXiv:2011.08847].

[124] J. Liu *et al.* (2020), [arXiv:2012.06181].

[125] P. Abratenko *et al.* (MicroBooNE) (2020), [arXiv:2012.08513].

[126] S. Y.-C. Chen *et al.* (2020), [arXiv:2012.12177].

[127] R. Acciarri *et al.* (SBND) (2020), [arXiv:2012.01301].

[128] Z. Qian *et al.* (2021), [arXiv:2101.04839].

[129] R. Abbasi *et al.* (IceCube), "A Convolutional Neural Network based Cascade Reconstruction for the IceCube Neutrino Observatory," (2021), [arXiv:2101.11589].

[130] F. Drielsma *et al.*, in "34th Conference on Neural Information Processing Systems," (2021), [arXiv:2102.01033].

[131] M. Rossi and S. Vallecorsa, in "25th International Conference on Computing in High-Energy and Nuclear Physics," (2021), [arXiv:2103.01596].

[132] J. Hewes *et al.* (2021), [arXiv:2103.06233].

[133] R. Acciarri *et al.* (ArgoNeuT) (2021), [arXiv:2103.06391].

[134] V. Belavin, E. Trofimova and A. Ustyuzhanin (2021), [arXiv:2104.02040].

[135] D. Maksimović, M. Nieslony and M. Wurm (2021), [arXiv:2104.13426].

[136] A. Gavrikov and F. Ratnikov, in "25th International Conference on Computing in High-Energy and Nuclear Physics," (2021), [arXiv:2106.02907].

[137] J. García-Méndez *et al.* (2021), [arXiv:2107.13654].

[138] K. Carloni *et al.* (2021), [arXiv:2110.10766].

[139] P. Abratenko *et al.* (MicroBooNE) (2021), [arXiv:2110.11874].

[140] D. Boyda *et al.*, Phys. Rev. D **103**, 7, 074504 (2021), [arXiv:2008.05456].

[141] G. Kanwar *et al.*, Phys. Rev. Lett. **125**, 12, 121601 (2020), [arXiv:2003.06413].

[142] P. T. Komiske, E. M. Metodiev and J. Thaler, JHEP **01**, 121 (2019), [arXiv:1810.05165].

[143] H. Qu and L. Gouskos, Phys. Rev. D **101**, 5, 056019 (2020), [arXiv:1902.08570].

[144] V. Mikuni and F. Canelli, Eur. Phys. J. Plus **135**, 6, 463 (2020), [arXiv:2001.05311].

[145] J. Shlomi *et al.* (2020), [arXiv:2008.02831].

[146] M. J. Dolan and A. Ore (2020), [arXiv:2012.00964].

[147] M. J. Fenton *et al.* (2020), [arXiv:2010.09206].

[148] J. S. H. Lee *et al.* (2020), [arXiv:2012.03542].

[149] V. Mikuni and F. Canelli (2021), [arXiv:2102.05073].

[150] A. Shmakov *et al.* (2021), [arXiv:2106.03898].

[151] C. Shimmin (2021), [arXiv:2107.02908].

[152] Technical Report ATL-PHYS-PUB-2020-014, CERN, Geneva (2020), URL `https://cds.cern.ch/record/2718948`.

[153] G. Louppe *et al.*, Journal of High Energy Physics **2019**, 1, 57 (2019), ISSN 10298479, [arXiv:1702.00748].

[154] T. Cheng (2017), [arXiv:1711.02633].

[155] I. Henrion *et al.* (2017), URL `https://dl4physicalsciences.github.io/files/nips_dlps_2017_29.pdf`.

[156] X. Ju *et al.*, 33rd Annual Conference on Neural Information Processing Systems (2020), [arXiv:2003.11603].

[157] M. Abdughani *et al.*, JHEP **08**, 055 (2019), [arXiv:1807.09088].

[158] J. Arjona Martínez *et al.*, Eur. Phys. J. Plus **134**, 7, 333 (2019), [arXiv:1810.07988].

[159] J. Ren, L. Wu and J. M. Yang, Phys. Lett. B **802**, 135198 (2020), [arXiv:1901.05627].

[160] E. A. Moreno *et al.*, Eur. Phys. J. C **80**, 1, 58 (2020), [arXiv:1908.05318].

[161] S. R. Qasim *et al.*, Eur. Phys. J. C **79**, 7, 608 (2019), [arXiv:1902.07987].

[162] A. Chakraborty, S. H. Lim and M. M. Nojiri, JHEP **19**, 135 (2020), [arXiv:1904.02092].

[163] A. Chakraborty *et al.* (2020), [arXiv:2003.11787].

[164] M. Abdughani *et al.* (2020), [arXiv:2005.11086].

[165] E. Bernreuther *et al.* (2020), [arXiv:2006.08639].

[166] J. Shlomi, P. Battaglia and J.-R. Vlimant, Machine Learning: Science and Technology **2**, 2, 021001 (2021), ISSN 2632-2153, URL `http://dx.doi.org/10.1088/2632-2153/abbf9a`.

[167] Y. Iiyama *et al.*, Front. Big Data **3**, 598927 (2020), [arXiv:2008.03601].

[168] X. Ju and B. Nachman, Phys. Rev. D **102**, 075014 (2020), [arXiv:2008.06064].

[169] N. Choma *et al.* (2020), [arXiv:2007.00149].

[170] Jun Guo and Jinmian Li and Tianjun Li (2020), [arXiv:2010.05464].

[171] A. Heintz *et al.*, 34th Conference on Neural Information Processing Systems (2020), [arXiv:2012.01563].

Downloaded from https://academic.oup.com/ptep/article/2022/8/083C01/6651666 by KIT Library user on 27 September 2022

[172] Y. Verma and S. Jena (2020), [arXiv:2012.08515].

[173] F. A. Dreyer and H. Qu (2020), [arXiv:2012.08526].

[174] J. Pata *et al.* (2021), [arXiv:2101.08578].

[175] C. Biscarat *et al.*, in "25th International Conference on Computing in High-Energy and Nuclear Physics," (2021), [arXiv:2103.00916].

[176] S. Thais and G. DeZoort (2021), [arXiv:2103.06509].

[177] G. Dezoort *et al.* (2021), [arXiv:2103.16701].

[178] Y. Verma and S. Jena (2021), [arXiv:2103.14906].

[179] A. Hariri, D. Dyachkova and S. Gleyzer (2021), [arXiv:2104.01725].

[180] O. Atkinson *et al.* (2021), [arXiv:2105.07988].

[181] P. Konar, V. S. Ngairangbam and M. Spannowsky (2021), [arXiv:2109.14636].

[182] K. Cho *et al.*, in "Conference on Empirical Methods in Natural Language Processing (EMNLP 2014)," (2014).

[183] H. Serviansky *et al.*, in H. Larochelle *et al.*, editors, "Advances in Neural Information Processing Systems," volume 33, 22080–22091, Curran Associates, Inc. (2020), URL `https://proceedings.neurips.cc/paper/2020/file/fb4ab556bc42d6f0ee0f9e24ec4d1af0-Paper.pdf`.

[184] B. E. Boser, I. M. Guyon and V. N. Vapnik, in "Proceedings of the fifth annual workshop on Computational learning theory," 144–152 (1992).

[185] C. Cortes and V. Vapnik, Machine learning **20**, 3, 273 (1995).

[186] H. Drucker *et al.*, Advances in neural information processing systems **9**, 155 (1997).

[187] R. M. Neal, University of Toronto (1994).

[188] C. K. Williams, Advances in neural information processing systems 295–301 (1997).

[189] J. Lee *et al.*, in "6th International Conference on Learning Representations, ICLR 2018, Vancouver, BC, Canada, April 30 - May 3, 2018, Conference Track Proceedings," OpenReview.net (2018), URL `https://openreview.net/forum?id=B1EA-M-0Z`.

[190] A. Jacot, C. Hongler and F. Gabriel, in S. Bengio *et al.*, editors, "Advances in Neural Information Processing Systems 31: Annual Conference on Neural Information Processing Systems 2018, NeurIPS 2018, December 3-8, 2018, Montréal, Canada," 8580–8589 (2018), URL `https://proceedings.neurips.cc/paper/2018/hash/5a4be1fa34e62bb8a6ec6b91d2462f5a-Abstract.html`.

[191] T. Hofmann, B. Schölkopf and A. J. Smola, The Annals of Statistics 1171–1220 (2008).

[192] C. M. Bishop, *Pattern recognition and machine learning*, springer (2006).

[193] C. K. Williams and C. E. Rasmussen, *Gaussian processes for machine learning*, volume 2, MIT press Cambridge, MA (2006).

[194] S. Ambikasaran *et al.*, IEEE transactions on pattern analysis and machine intelligence **38**, 2, 252 (2015).

[195] J. R. Gardner *et al.*, arXiv preprint arXiv:1809.11165 (2018).

[196] M. Frate *et al.* (2017), [arXiv:1709.05681].

[197] S. Mishra-Sharma and K. Cranmer, in "34th Conference on Neural Information Processing Systems," (2020), [arXiv:2010.10450].

[198] J. W. Foster *et al.*, Phys. Rev. Lett. **127**, 5, 051101 (2021), [arXiv:2102.02207].

[199] L. Breiman *et al.* (1984).

[200] "Xgboost," `https://xgboost.readthedocs.io/`.

[201] I. Narsky (2005), [arXiv:physics/0507143].

[202] G. Louppe, arXiv preprint arXiv:1407.7502 (2014).

[203] Y. Freund and R. E. Schapire, Journal of computer and system sciences **55**, 1, 119 (1997).

[204] J. H. Friedman, Annals of statistics 1189–1232 (2001).

[205] K. Fukushima, Biological Cybernetics **36**, 193 (1980).

[206] V. Nair and G. E. Hinton, in "ICML," (2010).

[207] A. L. Maas, A. Y. Hannun and A. Y. Ng, in "in ICML Workshop on Deep Learning for Audio, Speech and Language Processing," (2013).

[208] K. He *et al.*, IEEE International Conference on Computer Vision (ICCV 2015) **1502** (2015).

[209] V. Sitzmann *et al.*, in "Proc. NeurIPS," (2020).

[210] G. Cybenko, Mathematics of control, signals and systems **2**, 4, 303 (1989).

[211] O. Delalleau and Y. Bengio, in J. Shawe-Taylor *et al.*, editors, "Advances in Neural Information Processing Systems," volume 24, Curran Associates, Inc. (2011), URL `https://proceedings.neurips.cc/paper/2011/file/8e6b42f1644ecb1327dc03ab345e618b-Paper.pdf`.

[212] R. Raina, A. Madhavan and A. Y. Ng, in "Proceedings of the 26th Annual International Conference on Machine Learning," ICML '09, 873–880, Association for Computing Machinery, New York, NY, USA (2009), ISBN 9781605585161, URL `https://doi.org/10.1145/1553374.1553486`.

[213] Y. LeCun, "Deep Learning est mort. Vive Differentiable Programming!" `https://www.facebook.com/yann.lecun/posts/10155003011462143` (2018), `https://www.facebook.com/yann.lecun/posts/10155003011462143`, https://techburst.io/deep-learning-est-mort-vive-differentiable-programming-5060d3c55074.

[214] M. Lin, Q. Chen and S. Yan, arXiv preprint arXiv:1312.4400 (2013).

[215] C. Szegedy *et al.*, in "2015 IEEE Conference on Computer Vision and Pattern Recognition (CVPR)," 1–9 (2015).

[216] K. He *et al.*, in "2016 IEEE Conference on Computer Vision and Pattern Recognition (CVPR)," 770–778 (2016).

[217] N. Cohen and A. Shashua, CoRR **abs/1605.06743** (2016), URL `http://arxiv.org/abs/1605.06743`.

[218] A. Bietti, L. Venturi and J. Bruna, arXiv preprint arXiv:2106.07148 (2021).

[219] M. M. Bronstein *et al.*, arXiv preprint arXiv:2104.13478 (2021).

[220] K. Simonyan and A. Zisserman, CoRR **abs/1409.1556** (2015).

[221] S. Ren *et al.*, in C. Cortes *et al.*, editors, "Advances in Neural Information Processing Systems," volume 28, Curran Associates, Inc. (2015), URL `https://proceedings.neurips.cc/paper/2015/file/14bfa6bb14875e45bba028a21ed38046-Paper.pdf`.

[222] M. collaboration, Journal of Instrumentation **12**, 03, P03011 (2017), URL `https://doi.org/10.1088/1748-0221/12/03/p03011`.

[223] O. Ronneberger, P. Fischer and T. Brox, in N. Navab *et al.*, editors, "Medical Image Computing and Computer-Assisted Intervention – MICCAI 2015," 234–241, Springer International Publishing, Cham (2015), ISBN 978-3-319-24574-4.

[224] G. Huang *et al.*, in "2017 IEEE Conference on Computer Vision and Pattern Recognition (CVPR)," 2261–2269 (2017).

[225] D. Rumelhart, G. Hinton and R. Williams .

[226] Y. Bengio, P. Simard and P. Frasconi, Neural Networks, IEEE Transactions on **5**, 2, 157 (1994).

[227] R. Pascanu, T. Mikolov and Y. Bengio, in S. Dasgupta and D. McAllester, editors, "Proceedings of the 30th International Conference on Machine Learning," volume 28 of *Proceedings of Machine Learning Research*, 1310–1318, PMLR, Atlanta, Georgia, USA (2013), URL `https://proceedings.mlr.press/v28/pascanu13.html`.

Downloaded from https://academic.oup.com/ptep/article/2022/8/083C01/6651666 by KIT Library user on 27 September 2022

[228] S. Hochreiter and J. Schmidhuber, Neural Computation **9**, 8, 1735 (1997).

[229] R. Socher *et al.*, in "ICML," (2011).

[230] R. Socher *et al.*, in "Proceedings of the 2011 conference on empirical methods in natural language processing," 151–161 (2011).

[231] X. Chen *et al.*, in "Proceedings of the 2015 conference on empirical methods in natural language processing," 793–798 (2015).

[232] C. Olah and S. Carter, Distill (2016), URL `http://distill.pub/2016/augmented-rnns`.

[233] D. Bahdanau, K. Cho and Y. Bengio (2015), 3rd International Conference on Learning Representations, ICLR 2015 ; Conference date: 07-05-2015 Through 09-05-2015.

[234] A. Vaswani *et al.*, in I. Guyon *et al.*, editors, "Advances in Neural Information Processing Systems," volume 30, Curran Associates, Inc. (2017), URL `https://proceedings.neurips.cc/paper/2017/file/3f5ee243547dee91fbd053c1c4a845aa-Paper.pdf`.

[235] R. Bommasani *et al.*, arXiv preprint arXiv:2108.07258 (2021).

[236] P. Battaglia *et al.*, arXiv (2018), URL `https://arxiv.org/pdf/1806.01261.pdf`.

[237] M. Gori, G. Monfardini and F. Scarselli, in "Proceedings. 2005 IEEE International Joint Conference on Neural Networks, 2005.", volume 2, 729–734 vol. 2 (2005).

[238] C. R. Qi *et al.*, in "Proceedings of the IEEE Conference on Computer Vision and Pattern Recognition (CVPR)," (2017).

[239] C. Qi *et al.*, in "NIPS," (2017).

[240] M. Jaderberg *et al.*, in C. Cortes *et al.*, editors, "Advances in Neural Information Processing Systems," volume 28, Curran Associates, Inc. (2015), URL `https://proceedings.neurips.cc/paper/2015/file/33ceb07bf4eeb3da587e268d663aba1a-Paper.pdf`.

[241] M. Zaheer *et al.*, in I. Guyon *et al.*, editors, "Advances in Neural Information Processing Systems," volume 30, Curran Associates, Inc. (2017), URL `https://proceedings.neurips.cc/paper/2017/file/f22e4747da1aa27e363d86d40ff442fe-Paper.pdf`.

[242] Y. Wang *et al.*, ACM Transactions on Graphics **38** (2018).

[243] X. Wang *et al.*, in "2018 IEEE/CVF Conference on Computer Vision and Pattern Recognition (CVPR)," 7794–7803, IEEE Computer Society, Los Alamitos, CA, USA (2018), URL `https://doi.ieeecomputersociety.org/10.1109/CVPR.2018.00813`.

[244] J. Gilmer *et al.*, in D. Precup and Y. W. Teh, editors, "Proceedings of the 34th International Conference on Machine Learning," volume 70 of *Proceedings of Machine Learning Research*, 1263–1272, PMLR (2017), URL `https://proceedings.mlr.press/v70/gilmer17a.html`.

[245] N. Choma *et al.* (IceCube) (2018), [arXiv:1809.06166].

[246] S. R. Qasim *et al.*, The European Physical Journal C **79**, 7 (2019), ISSN 1434-6052, URL `http://dx.doi.org/10.1140/epjc/s10052-019-7113-9`.

[247] J. Shlomi, P. Battaglia and J.-R. Vlimant, Machine Learning: Science and Technology **2**, 2, 021001 (2021), URL `https://doi.org/10.1088/2632-2153/abbf9a`.

[248] D. P. Kingma and M. Welling, arXiv preprint arXiv:1312.6114 (2013).

[249] D. J. Rezende, S. Mohamed and D. Wierstra, in "Proceedings of the 31th International Conference on Machine Learning, ICML 2014, Beijing, China, 21-26 June 2014," volume 32 of *JMLR Workshop and Conference Proceedings*, 1278–1286, JMLR.org (2014), URL `http://proceedings.mlr.press/v32/rezende14.html`.

[250] I. J. Goodfellow *et al.*, in Z. Ghahramani *et al.*, editors, "Advances in Neural Information Processing Systems 27: Annual Conference on Neural Information Processing Systems 2014, December 8-13 2014, Montreal, Quebec, Canada," 2672–2680 (2014), URL `http://papers.nips.cc/paper/5423-generative-adversarial-nets`.

[251] A. Radford, L. Metz and S. Chintala, in Y. Bengio and Y. LeCun, editors, "4th International Conference on Learning Representations, ICLR 2016, San Juan, Puerto Rico, May 2-4, 2016, Conference Track Proceedings," (2016), URL `http://arxiv.org/abs/1511.06434`.

[252] D. Rezende and S. Mohamed, Proceedings of the 32nd International Conference on Machine Learning **37**, 1530 (2015), URL `http://proceedings.mlr.press/v37/rezende15.html`.

[253] L. Dinh, D. Krueger and Y. Bengio, 3rd International Conference on Learning Representations, ICLR 2015 - Workshop Track Proceedings (2015), [arXiv:1410.8516].

[254] L. Dinh, J. Sohl-Dickstein and S. Bengio, in "5th International Conference on Learning Representations, ICLR 2017, Toulon, France, April 24-26, 2017, Conference Track Proceedings," OpenReview.net (2017), URL `https://openreview.net/forum?id=HkpbnH9lx`.

[255] D. P. Kingma and P. Dhariwal, in S. Bengio *et al.*, editors, "Advances in Neural Information Processing Systems 31: Annual Conference on Neural Information Processing Systems 2018, NeurIPS 2018, December 3-8, 2018, Montréal, Canada," 10236–10245 (2018).

[256] I. Kobyzev, S. Prince and M. Brubaker, IEEE Transactions on Pattern Analysis and Machine Intelligence (2020).

[257] M. Arjovsky and L. Bottou, in "5th International Conference on Learning Representations, ICLR 2017, Toulon, France, April 24-26, 2017, Conference Track Proceedings," OpenReview.net (2017), URL `https://openreview.net/forum?id=Hk4_qw5xe`.

[258] M. Wiatrak and S. V. Albrecht, arXiv preprint arXiv:1910.00927 (2019).

[259] D. J. Rezende *et al.*, in "International Conference on Machine Learning," 8083–8092, PMLR (2020).

[260] M. C. Gemici, D. Rezende and S. Mohamed, arXiv preprint arXiv:1611.02304 (2016).

[261] A. van den Oord, O. Vinyals and K. Kavukcuoglu, in I. Guyon *et al.*, editors, "Advances in Neural Information Processing Systems 30: Annual Conference on Neural Information Processing Systems 2017, December 4-9, 2017, Long Beach, CA, USA," 6306–6315 (2017).

[262] T. Karras *et al.*, in "6th International Conference on Learning Representations, ICLR 2018, Vancouver, BC, Canada, April 30 - May 3, 2018, Conference Track Proceedings," OpenReview.net (2018), URL `https://openreview.net/forum?id=Hk99zCeAb`.

[263] T. Karras, S. Laine and T. Aila, in "IEEE Conference on Computer Vision and Pattern Recognition, CVPR 2019, Long Beach, CA, USA, June 16-20, 2019," 4401–4410, Computer Vision Foundation / IEEE (2019), URL `http://openaccess.thecvf.com/content_CVPR_2019/html/Karras_A_Style-Based_Generator_Architecture_for_Generative_Adversarial_Networks_CVPR_2019_paper.html`.

[264] M. Lucic *et al.*, in S. Bengio *et al.*, editors, "Advances in Neural Information Processing Systems 31: Annual Conference on Neural Information Processing Systems 2018, NeurIPS 2018, December 3-8, 2018, Montréal, Canada," 698–707 (2018).

[265] A. A. Alemi *et al.*, in J. G. Dy and A. Krause, editors, "Proceedings of the 35th International Conference on Machine Learning, ICML 2018, Stockholmsmässan, Stockholm, Sweden, July 10-15, 2018," volume 80 of *Proceedings of Machine Learning Research*, 159–168, PMLR (2018), URL `http://proceedings.mlr.press/v80/alemi18a.html`.

Downloaded from https://academic.oup.com/ptep/article/2022/8/083C01/6651666 by KIT Library user on 27 September 2022

[266] M. E. Tipping and C. M. Bishop, Journal of the Royal Statistical Society: Series B (Statistical Methodology) **61**, 3, 611 (1999), URL https://rss.onlinelibrary.wiley.com/doi/abs/10.1111/1467-9868.00196.

[267] M. Arjovsky, S. Chintala and L. Bottou, arXiv preprint arXiv:1701.07875 (2017).

[268] L. Mescheder, S. Nowozin and A. Geiger, in I. Guyon *et al.*, editors, "Advances in Neural Information Processing Systems," volume 30, Curran Associates, Inc. (2017), URL https://proceedings.neurips.cc/paper/2017/file/4588e674d3f0faf985047d4c3f13ed0d-Paper.pdf.

[269] G. Papamakarios, I. Murray and T. Pavlakou, in "Advances in Neural Information Processing Systems," 2335–2344 (2017).

[270] C. Durkan *et al.*, in H. M. Wallach *et al.*, editors, "Advances in Neural Information Processing Systems 32: Annual Conference on Neural Information Processing Systems 2019, NeurIPS 2019, December 8-14, 2019, Vancouver, BC, Canada," 7509–7520 (2019).

[271] W. Grathwohl *et al.*, in "7th International Conference on Learning Representations, ICLR 2019, New Orleans, LA, USA, May 6-9, 2019," OpenReview.net (2019), URL https://openreview.net/forum?id=rJxgknCcK7.

[272] A. van den Oord *et al.*, arXiv:1609.03499 (2016), [arXiv:1609.03499], URL http://arxiv.org/abs/1609.03499.

[273] A. van den Oord *et al.*, in D. D. Lee *et al.*, editors, "Advances in Neural Information Processing Systems 29: Annual Conference on Neural Information Processing Systems 2016, December 5-10, 2016, Barcelona, Spain," 4790–4798 (2016), URL https://proceedings.neurips.cc/paper/2016/hash/b1301141feffabac455e1f90a7de2054-Abstract.html.

[274] A. Hyvärinen and P. Dayan, Journal of Machine Learning Research **6**, 4 (2005).

[275] Y. Song and S. Ermon, in Wallach *et al.* [358], 11895–11907, URL https://proceedings.neurips.cc/paper/2019/hash/3001ef257407d5a371a96dcd947c7d93-Abstract.html.

[276] Y. Song *et al.*, CoRR **abs/2011.13456** (2020), [arXiv:2011.13456], URL https://arxiv.org/abs/2011.13456.

[277] S. Mandt, M. D. Hoffman and D. M. Blei, J. Mach. Learn. Res. **18**, 134:1 (2017), URL http://jmlr.org/papers/v18/17-214.html.

[278] D. P. Kingma and J. Ba, arXiv e-prints arXiv:1412.6980 (2014), [arXiv:1412.6980].

[279] Y. LeCun *et al.*, *Efficient backprop*, 9–48, Lecture Notes in Computer Science (including subseries Lecture Notes in Artificial Intelligence and Lecture Notes in Bioinformatics), Springer Verlag (2012), ISBN 9783642352881, copyright: Copyright 2021 Elsevier B.V., All rights reserved.

[280] Y. Yao, L. Rosasco and A. Caponnetto, Constructive Approximation **26**, 2, 289 (2007).

[281] L. Prechelt, in "Neural Networks: Tricks of the trade," 55–69, Springer (1998).

[282] A. Krizhevsky, I. Sutskever and G. Hinton, Neural Information Processing Systems **25** (2012).

[283] X. Glorot and Y. Bengio, in Y. W. Teh and M. Titterington, editors, "Proceedings of the Thirteenth International Conference on Artificial Intelligence and Statistics," volume 9 of *Proceedings of Machine Learning Research*, 249–256, PMLR, Chia Laguna Resort, Sardinia, Italy (2010), URL http://proceedings.mlr.press/v9/glorot10a.html.

[284] S. Ioffe and C. Szegedy, CoRR **abs/1502.03167** (2015), [arXiv:1502.03167], URL http://arxiv.org/abs/1502.03167.

[285] J. L. Ba, J. R. Kiros and G. E. Hinton, "Layer normalization," (2016), [arXiv:1607.06450].

[286] D. Ulyanov, A. Vedaldi and V. Lempitsky, "Instance normalization: The missing ingredient for fast stylization," (2017), [arXiv:1607.08022].

[287] Y. Wu and K. He, "Group normalization," (2018), [arXiv:1803.08494].

[288] T.-Y. Lin *et al.*, in D. Fleet *et al.*, editors, "Computer Vision – ECCV 2014," 740–755, Springer International Publishing, Cham (2014), ISBN 978-3-319-10602-1.

[289] O. Russakovsky *et al.*, International Journal of Computer Vision (IJCV) **115**, 3, 211 (2015).

[290] M. Cordts *et al.*, in "Proc. of the IEEE Conference on Computer Vision and Pattern Recognition (CVPR)," (2016).

[291] L. Yi *et al.*, SIGGRAPH Asia (2016).

[292] A. Radford *et al.* (2018), URL https://s3-us-west-2.amazonaws.com/openai-assets/research-covers/language-unsupervised/language_understanding_paper.pdf.

[293] L. Fei-Fei, R. Fergus and P. Perona, IEEE Transactions on Pattern Analysis and Machine Intelligence **28**, 4, 594 (2006).

[294] H. Larochelle, D. Erhan and Y. Bengio, in "Proceedings of the 23rd National Conference on Artificial Intelligence - Volume 2," AAAI'08, 646–651, AAAI Press (2008), ISBN 9781577353683.

[295] M. Palatucci *et al.*, in Y. Bengio *et al.*, editors, "Advances in Neural Information Processing Systems," volume 22, Curran Associates, Inc. (2009), URL https://proceedings.neurips.cc/paper/2009/file/1543843a4723ed2ab08e18053ae6dc5b-Paper.pdf.

[296] R. Socher *et al.*, in "Proceedings of the 26th International Conference on Neural Information Processing Systems - Volume 1," NIPS'13, 935–943, Curran Associates Inc., Red Hook, NY, USA (2013).

[297] T. Dorigo and P. De Castro Manzano (2020), [arXiv:2007.09121].

[298] R. Barate *et al.* (ALEPH), Phys. Lett. B **412**, 173 (1997).

[299] G. Louppe, M. Kagan and K. Cranmer, in I. Guyon *et al.*, editors, "Advances in Neural Information Processing Systems," volume 30, Curran Associates, Inc. (2017), [arXiv:1611.01046], URL https://papers.nips.cc/paper/2017/hash/48ab2f9b45957ab574cf005eb8a76760-Abstract.html.

[300] H. Edwards and A. Storkey, arXiv preprint arXiv:1511.05897 (2015).

[301] Y. Ganin and V. Lempitsky, in "International conference on machine learning," 1180–1189, PMLR (2015).

[302] H. Ajakan *et al.*, ArXiv e-prints (2014), [arXiv:1412.4446].

[303] G. Kasieczka and D. Shih, Phys. Rev. Lett. **125**, 12, 122001 (2020), [arXiv:2001.05310].

[304] C. Shimmin *et al.*, Phys. Rev. **D96**, 7, 074034 (2017), [arXiv:1703.03507].

[305] J. Stevens and M. Williams, JINST **8**, P12013 (2013), [arXiv:1305.7248].

[306] J. Dolen *et al.*, JHEP **05**, 156 (2016), [arXiv:1603.00027].

[307] I. Moult, B. Nachman and D. Neill, JHEP **05**, 002 (2018), [arXiv:1710.06859].

[308] L. Bradshaw *et al.* (2019), [arXiv:1908.08959].

[309] ATL-PHYS-PUB-2018-014 (2018), URL http://cds.cern.ch/record/2630973.

[310] L.-G. Xia, Nucl. Instrum. Meth. **A930**, 15 (2019), [arXiv:1810.08387].

[311] C. Englert *et al.*, Eur. Phys. J. **C79**, 1, 4 (2019), [arXiv:1807.08763].

[312] S. Wunsch *et al.* (2019), [arXiv:1907.11674].

[313] A. Rogozhnikov *et al.*, JINST **10**, 03, T03002 (2015), [arXiv:1410.4140].

Downloaded from https://academic.oup.com/ptep/article/2022/8/083C01/6651666 by KIT Library user on 27 September 2022

[314] C. Collaboration, Machine Learning: Science and Technology (2020).

[315] J. M. Clavijo, P. Glaysher and J. M. Katzy (2020), [arXiv:2005.00568].

[316] G. Kasieczka *et al.* (2020), [arXiv:2007.14400].

[317] O. Kitouni *et al.* (2020), [arXiv:2010.09745].

[318] A. Ghosh and B. Nachman (2021), [arXiv:2109.08159].

[319] P. Baldi *et al.*, Eur. Phys. J. **C76**, 5, 235 (2016), [arXiv:1601.07913].

[320] A. Ghosh, B. Nachman and D. Whiteson (2021), [arXiv:2105.08742].

[321] W. L. Oberkampf *et al.*, Reliability Engineering & System Safety **85**, 1, 11 (2004), ISSN 0951-8320, alternative Representations of Epistemic Uncertainty, URL `https://www.sciencedirect.com/science/article/pii/S0951832004000493`.

[322] A. O'Hagan and J. E. Oakley, Reliability Engineering & System Safety **85**, 1, 239 (2004), ISSN 0951-8320, alternative Representations of Epistemic Uncertainty, URL `https://www.sciencedirect.com/science/article/pii/S0951832004000638`.

[323] E. Hüllermeier and W. Waegeman, CoRR **abs/1910.09457** (2019), URL `http://arxiv.org/abs/1910.09457`.

[324] A. Kendall and Y. Gal, in I. Guyon *et al.*, editors, "Advances in Neural Information Processing Systems," volume 30, Curran Associates, Inc. (2017), URL `https://proceedings.neurips.cc/paper/2017/file/2650d6089a6d640c5e85b2b88265dc2b-Paper.pdf`.

[325] A. D. Kiureghian and O. Ditlevsen, Structural Safety **31**, 2, 105 (2009), ISSN 0167-4730, risk Acceptance and Risk Communication, URL `https://www.sciencedirect.com/science/article/pii/S0167473008000556`.

[326] Y. Yao *et al.*, Bayesian Analysis **13**, 3 (2018), ISSN 1936-0975, URL `http://dx.doi.org/10.1214/17-BA1091`.

[327] J. Snoek *et al.*, in Wallach *et al.* [358], 13969–13980, URL `https://proceedings.neurips.cc/paper/2019/hash/8558cb408c1d76621371888657d2eb1d-Abstract.html`.

[328] Y. Gal and Z. Ghahramani, in M. Balcan and K. Q. Weinberger, editors, "Proceedings of the 33nd International Conference on Machine Learning, ICML 2016, New York City, NY, USA, June 19-24, 2016," volume 48 of *JMLR Workshop and Conference Proceedings*, 1050–1059, JMLR.org (2016), URL `http://proceedings.mlr.press/v48/gal16.html`.

[329] B. Lakshminarayanan, A. Pritzel and C. Blundell, in I. Guyon *et al.*, editors, "Advances in Neural Information Processing Systems 30: Annual Conference on Neural Information Processing Systems 2017, December 4-9, 2017, Long Beach, CA, USA," 6402–6413 (2017), URL `https://proceedings.neurips.cc/paper/2017/hash/9ef2ed4b7fd2c810847ffa5fa85bce38-Abstract.html`.

[330] D. P. Kingma, T. Salimans and M. Welling, CoRR **abs/1506.02557** (2015), URL `http://arxiv.org/abs/1506.02557`.

[331] G. C. Strong (2020), [arXiv:2002.01427].

[332] V. V. Gligorov and M. Williams, JINST **8**, P02013 (2013), [arXiv:1210.6861].

[333] D. W. III *et al.* (2017), URL `https://dl4physicalsciences.github.io/files/nips_dlps_2017_3.pdf`.

[334] D. Bourgeois, C. Fitzpatrick and S. Stahl (2018), [arXiv:1808.00711].

[335] J. Alimena, Y. Iiyama and J. Kieseler (2020), [arXiv:2004.10744].

[336] C. Balázs *et al.* (DarkMachines High Dimensional Sampling Group) (2021), [arXiv:2101.04525].

[337] F. Rehm *et al.* (2021), [arXiv:2103.10142].

[338] C. Mahesh *et al.*, in "34th Conference on Neural Information Processing Systems," (2021), [arXiv:2104.06622].

[339] S. Amrouche *et al.* (2021), [arXiv:2105.01160].

[340] P. Goncharov *et al.*, in "24th International Scientific Conference of Young Scientists and Specialists," (2021), [arXiv:2109.08982].

[341] J. Duarte *et al.*, JINST **13**, 07, P07027 (2018), [arXiv:1804.06913].

[342] J. Ngadiuba *et al.*, Mach. Learn.: Sci. Tech. **2**, 1, 015001 (2020), [arXiv:2003.06308].

[343] S. Summers *et al.*, JINST **15**, 05, P05026 (2020), [arXiv:2002.02534].

[344] J. Krupa *et al.* (2020), [arXiv:2007.10359].

[345] L. R. M. Mohan *et al.* (2020), [arXiv:2008.09210].

[346] S. Carrazza, J. M. Cruz-Martinez and M. Rossi (2020), [arXiv:2009.06635].

[347] D. S. Rankin *et al.*, 2020 IEEE/ACM International Workshop on Heterogeneous High-performance Reconfigurable Computing (H2RC) 38 (2020), [arXiv:2010.08556].

[348] M. Rossi, S. Carrazza and J. M. Cruz-Martinez (2020), [arXiv:2012.08221].

[349] T. Aarrestad *et al.* (2021), [arXiv:2101.05108].

[350] B. Hawks *et al.* (2021), [arXiv:2102.11289].

[351] T. Teixeira, L. Andrade and J. M. de Seixas (2021), [arXiv:2103.12467].

[352] T. M. Hong *et al.* (2021), [arXiv:2104.03408].

[353] G. Di Guglielmo *et al.* (2021), [arXiv:2105.01683].

[354] M. Migliorini *et al.* (2021), [arXiv:2105.04428].

[355] E. Govorkova *et al.* (2021), [arXiv:2108.03986].

[356] V. Kuznetsov, L. Giommi and D. Bonacorsi (2020), [arXiv:2007.14781].

[357] O. Sunneborn Gudnadottir *et al.*, EPJ Web Conf. **251**, 02054 (2021), [arXiv:2109.00264].

[358] H. M. Wallach *et al.*, editors, *Advances in Neural Information Processing Systems 32: Annual Conference on Neural Information Processing Systems 2019, NeurIPS 2019, December 8-14, 2019, Vancouver, BC, Canada* (2019), URL `https://proceedings.neurips.cc/paper/2019`.

Downloaded from https://academic.oup.com/ptep/article/2022/8/083C01/6651666 by KIT Library user on 27 September 2022

42. Monte Carlo Techniques

Revised September 2021 by G. Cowan (RHUL).

Monte Carlo techniques are often the only practical way to evaluate difficult integrals or to sample random variables governed by complicated probability density functions. Here we describe an assortment of methods for sampling some commonly occurring probability density functions.

42.1 Sampling the uniform distribution

Most Monte Carlo sampling or integration techniques assume a "random number generator," which generates uniform statistically independent values on the half open interval $[0, 1)$; for reviews see, *e.g.*, Refs. [1, 2].

Uniform random number generators are available in software libraries such as CLHEP [3], and ROOT [4]. For example, in addition to a basic congruential generator `TRandom` (see below), ROOT provides three more sophisticated routines: `TRandom1` implements the RANLUX generator [5] based on the method by Lüscher, and allows the user to select different quality levels, trading off quality with speed; `TRandom2` is based on the maximally equidistributed combined Tausworthe generator by L'Ecuyer [6]; the `TRandom3` generator implements the Mersenne twister algorithm of Matsumoto and Nishimura [7]. All of the algorithms produce a periodic sequence of numbers, and to obtain effectively random values, one must not use more than a small subset of a single period. The Mersenne twister algorithm has an extremely long period of $2^{19937} - 1$. A recent review of high-quality random number generators can be found in Ref. [8].

The performance of the generators can be investigated with tests such as DIEHARD [9] or TestU01 [10]. Many commonly available congruential generators fail these tests and often have sequences (typically with periods less than 2^{32}), which can be easily exhausted on modern computers. A short period is a problem for the `TRandom` generator in ROOT, which, however, has the advantage that its state is stored in a single 32-bit word. The generators `TRandom1`, `TRandom2`, or `TRandom3` have much longer periods, with `TRandom3` being recommended by the ROOT authors as providing the best combination of speed and good random properties. For further information see, *e.g.*, Ref. [11].

42.2 Inverse transform method

If the desired probability density function is $f(x)$ on the range $-\infty < x < \infty$, its cumulative distribution function (expressing the probability that $x \leq a$) is given by Eq. (39.6). If a is chosen with probability density $f(a)$, then the integrated probability up to point a, $F(a)$, is itself a random variable which will occur with uniform probability density on $[0, 1]$. Suppose u is generated according to a uniformly distributed in $(0, 1)$. If x can take on any value, and ignoring the endpoints, we can then find a unique x chosen from the p.d.f. $f(x)$ for a given u if we set

$$u = F(x) \ , \tag{42.1}$$

provided we can find an inverse of F, defined by

$$x = F^{-1}(u) \ . \tag{42.2}$$

This method is shown in Fig. 42.1a. It is most convenient when one can calculate by hand the inverse function of the indefinite integral of f. This is the case for some common functions $f(x)$ such as $\exp(x)$, $(1 - x)^n$, and $1/(1 + x^2)$ (Cauchy or Breit-Wigner), although it does not necessarily produce the fastest generator. Standard libraries contain software to implement this method numerically, working from functions or histograms in one or more dimensions, *e.g.*, the UNU.RAN package [12], available in ROOT. For a discrete distribution, $F(x)$ will have a discontinuous jump of size $f(x_k)$ at each allowed $x_k, k = 1, 2, \cdots$. Choose u from a uniform distribution on (0,1) as before. Find x_k such that

$$F(x_{k-1}) < u \leq F(x_k) \equiv \text{Prob}\ (x \leq x_k) = \sum_{i=1}^{k} f(x_i) \ ; \tag{42.3}$$

then x_k is the value we seek (note: $F(x_0) \equiv 0$). This algorithm is illustrated in Fig. 42.1b.

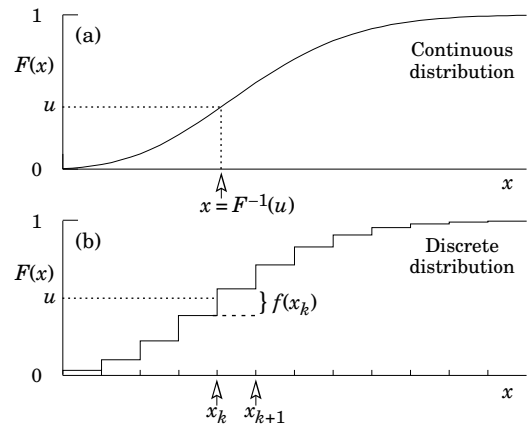

Figure 42.1: Use of a random number u chosen from a uniform distribution (0,1) to find a random number x from a distribution with cumulative distribution function $F(x)$.

42.3 Acceptance-rejection method (Von Neumann)

Very commonly an analytic form for $F(x)$ is unknown or too complex to work with, so that obtaining an inverse as in Eq. (42.2) is impractical. We suppose that for any given value of x, the probability density function $f(x)$ can be computed, and further that enough is known about $f(x)$ that we can enclose it entirely inside a shape which is C times an easily generated distribution $h(x)$, as illustrated in Fig. 42.2. That is, $Ch(x) \geq f(x)$ must hold for all x. Frequently $h(x)$ is uniform or is a normalized

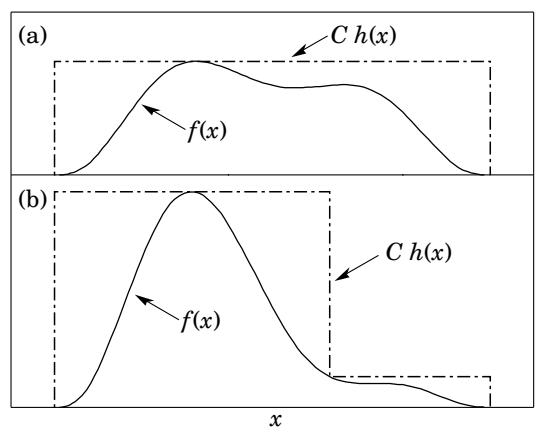

Figure 42.2: Illustration of the acceptance-rejection method. Random points are chosen inside the upper bounding figure, and rejected if the ordinate exceeds $f(x)$. The lower figure illustrates a method to increase the efficiency (see text).

sum of uniform distributions. Note that both $f(x)$ and $h(x)$ must be normalized to unit area, and therefore, the proportionality constant $C > 1$. To generate $f(x)$, first generate a candidate x according to $h(x)$. Calculate $f(x)$ and the height of the envelope $C\,h(x)$; generate u and test if $uC\,h(x) \leq f(x)$. If so, accept x; if not reject x and try again. If we regard x and $uC\,h(x)$ as the abscissa and ordinate of a point in a two-dimensional plot, these points will populate the entire area $C\,h(x)$ in a smooth manner; then we accept those which fall under $f(x)$. The efficiency is the ratio of areas, which must equal $1/C$; therefore we must keep C as close as possible to 1.0. Therefore, we try to choose $C\,h(x)$ to be as close to $f(x)$ as convenience dictates, as in the lower part of Fig. 42.2.

Downloaded from https://academic.oup.com/ptep/article/2022/8/083C01/6651666 by KIT Library user on 27 September 2022

42.4 Algorithms

Algorithms for generating random numbers belonging to many different distributions are given for example by Press [13], Ahrens and Dieter [14], Rubinstein [15], Devroye [16], Walck [17] and Gentle [18]. For many distributions, alternative algorithms exist, varying in complexity, speed, and accuracy. For time-critical applications, these algorithms may be coded in-line to remove the significant overhead often encountered in making function calls.

In the examples given below, we use the notation for the variables and parameters given in Table 39.1. Variables named "u" are assumed to be independent and uniform on [0,1). Denominators must be verified to be non-zero where relevant.

42.4.1 *Exponential decay*

This is a common application of the inverse transform method, and uses the fact that if u is uniformly distributed in $[0,1]$, then $(1-u)$ is as well. Consider an exponential p.d.f. $f(t) = (1/\tau)\exp(-t/\tau)$ that is truncated so as to lie between two values, a and b, and renormalized to unit area. To generate decay times t according to this p.d.f., first let $\alpha = \exp(-a/\tau)$ and $\beta = \exp(-b/\tau)$; then generate u and let

$$t = -\tau \ln(\beta + u(\alpha - \beta)). \tag{42.4}$$

For $(a,b) = (0,\infty)$, we have simply $t = -\tau \ln u$. (See also Sec. 42.4.6.)

42.4.2 *Isotropic direction in 3D*

Isotropy means the density is proportional to solid angle, the differential element of which is $d\Omega = d(\cos\theta)d\phi$. Hence $\cos\theta$ is uniform $(2u_1 - 1)$ and ϕ is uniform $(2\pi u_2)$. For alternative generation of $\sin\phi$ and $\cos\phi$, see the next subsection.

42.4.3 *Sine and cosine of random angle in 2D*

Generate u_1 and u_2. Then $v_1 = 2u_1 - 1$ is uniform on (−1,1), and $v_2 = u_2$ is uniform on (0,1). Calculate $r^2 = v_1^2 + v_2^2$. If $r^2 > 1$, start over. Otherwise, the sine (S) and cosine (C) of a random angle (*i.e.*, uniformly distributed between zero and 2π) are given by

$$S = 2v_1v_2/r^2 \quad \text{and} \quad C = (v_1^2 - v_2^2)/r^2 \ . \tag{42.5}$$

42.4.4 *Gaussian distribution*

If u_1 and u_2 are uniform on (0,1), then

$$z_1 = \sin(2\pi u_1)\sqrt{-2\ln u_2} \quad \text{and} \quad z_2 = \cos(2\pi u_1)\sqrt{-2\ln u_2} \tag{42.6}$$

are independent and Gaussian distributed with mean 0 and $\sigma = 1$.

There are many variants of this basic algorithm, which may be faster. For example, construct $v_1 = 2u_1 - 1$ and $v_2 = 2u_2 - 1$, which are uniform on (−1,1). Calculate $r^2 = v_1^2 + v_2^2$, and if $r^2 > 1$ start over. If $r^2 < 1$, it is uniform on (0,1). Then

$$z_1 = v_1\sqrt{\frac{-2\ln r^2}{r^2}} \quad \text{and} \quad z_2 = v_2\sqrt{\frac{-2\ln r^2}{r^2}} \tag{42.7}$$

are independent numbers chosen from a normal distribution with mean 0 and variance 1. $z_i' = \mu + \sigma z_i$ distributes with mean μ and variance σ^2.

For a multivariate Gaussian with an $n \times n$ covariance matrix V, one can start by generating n independent Gaussian variables, $\{\eta_j\}$, with mean 0 and variance 1 as above. Then the new set $\{x_i\}$ is obtained as $x_i = \mu_i + \sum_j L_{ij}\eta_j$, where μ_i is the mean of x_i, and L_{ij} are the components of L, the unique lower triangular matrix that fulfils $V = LL^T$. The matrix L can be easily computed by the following recursive relation (Cholesky's method):

$$L_{jj} = \left(V_{jj} - \sum_{k=1}^{j-1} L_{jk}^2\right)^{1/2} , \tag{42.8a}$$

$$L_{ij} = \frac{V_{ij} - \sum_{k=1}^{j-1} L_{ik}L_{jk}}{L_{jj}} \ , \ j = 1, ..., n \ ; \ i = j+1, ..., n, \tag{42.8b}$$

where $V_{ij} = \rho_{ij}\sigma_i\sigma_j$ are the components of V. For $n = 2$ one has

$$L = \begin{pmatrix} \sigma_1 & 0 \\ \rho\sigma_2 & \sqrt{1-\rho^2}\,\sigma_2 \end{pmatrix} , \tag{42.9}$$

and therefore the correlated Gaussian variables are generated as $x_1 = \mu_1 + \sigma_1\eta_1$, $x_2 = \mu_2 + \rho\sigma_2\eta_1 + \sqrt{1-\rho^2}\,\sigma_2\eta_2$.

42.4.5 $\chi^2(n)$ distribution

To generate a variable following the χ^2 distribution for n degrees of freedom, use the Gamma distribution with $k = n/2$ and $\lambda = 1/2$ using the method of Sec. 42.4.6.

42.4.6 *Gamma distribution*

All of the following algorithms are given for $\lambda = 1$. For $\lambda \neq 1$, divide the resulting random number x by λ.

- If $k = 1$ (the *exponential* distribution), accept $x = -\ln u$. (See also Sec. 42.4.1.)

- If $0 < k < 1$, initialize with $v_1 = (e+k)/e$ (with $e = 2.71828...$ being the natural log base). Generate u_1, u_2. Define $v_2 = v_1u_1$.

  Case 1: $v_2 \leq 1$. Define $x = v_2^{1/k}$. If $u_2 \leq e^{-x}$, accept x and stop, else restart by generating new u_1, u_2.

  Case 2: $v_2 > 1$. Define $x = -\ln([v_1 - v_2]/k)$. If $u_2 \leq x^{k-1}$, accept x and stop, else restart by generating new u_1, u_2. Note that, for $k < 1$, the probability density has a pole at $x = 0$, so that return values of zero due to underflow must be accepted or otherwise dealt with.

- Otherwise, if $k > 1$, initialize with $c = 3k - 0.75$. Generate u_1 and compute $v_1 = u_1(1-u_1)$ and $v_2 = (u_1 - 0.5)\sqrt{c/v_1}$. If $x = k + v_2 - 1 \leq 0$, go back and generate new u_1; otherwise generate u_2 and compute $v_3 = 64v_1^3u_2^2$. If $v_3 \leq 1 - 2v_2^2/x$ **or** if $\ln v_3 \leq 2\{[k-1]\ln[x/(k-1)] - v_2\}$, accept x and stop; otherwise go back and generate new u_1.

42.4.7 *Binomial distribution*

Begin with $k = 0$ and generate u uniform in $[0,1)$. Compute $P_k = (1-p)^n$ and store P_k into B. If $u \leq B$ accept $r_k = k$ and stop. Otherwise, increment k by one; compute the next P_k as $P_k \cdot (p/(1-p)) \cdot (n-k)/(k+1)$; add this to B. Again, if $u \leq B$, accept $r_k = k$ and stop, otherwise iterate until a value is accepted. If $p > 1/2$, it will be more efficient to generate r from $f(r; n, q)$, *i.e.*, with p and q interchanged, and then set $r_k = n - r$.

42.4.8 *Poisson distribution*

Iterate until a successful choice is made: Begin with $k = 1$ and set $A = 1$ to start. Generate u. Replace A with uA; if now $A < \exp(-\mu)$, where μ is the Poisson parameter, accept $n_k = k - 1$ and stop. Otherwise increment k by 1, generate a new u and repeat, always starting with the value of A left from the previous try.

Note that the Poisson generator used in ROOT's `TRandom` classes before version 5.12 (including the derived classes `TRandom1, TRandom2, TRandom3`) uses a Gaussian approximation when μ exceeds a given threshold. This may be satisfactory (and much faster) for some applications. To do this, generate z from a Gaussian with zero mean and unit standard deviation; then use $x = \max(0, [\mu + z\sqrt{\mu} + 0.5])$ where [ ] signifies the greatest integer $\leq$ the expression. The routines from Numerical Recipes [13] and CLHEP's routine `RandPoisson` do not make this approximation (see, *e.g.*, Ref. [11]).

42.4.9 *Student's t distribution*

Generate u_1 and u_2 uniform in $(0,1)$; then $t = \sin(2\pi u_1)[n(u_2^{-2/n} - 1)]^{1/2}$ follows the Student's t distribution for $n > 0$ degrees of freedom (n not necessarily an integer).

Alternatively, generate x from a Gaussian with mean 0 and $\sigma^2 = 1$ according to the method of 42.4.4. Next generate y,

Downloaded from https://academic.oup.com/ptep/article/2022/8/083C01/6651666 by KIT Library user on 27 September 2022

an independent gamma random variate, according to 42.4.6 with $\lambda = 1/2$ and $k = n/2$. Then $z = x/\sqrt{y/n}$ is distributed as a t with n degrees of freedom.

For the special case $n = 1$, the Breit-Wigner distribution, generate u_1 and u_2; set $v_1 = 2u_1 - 1$ and $v_2 = 2u_2 - 1$. If $v_1^2 + v_2^2 \leq 1$ accept $z = v_1/v_2$ as a Breit-Wigner distribution with unit area, center at 0.0, and FWHM 2.0. Otherwise start over. For center M_0 and FWHM Γ, use $W = z\Gamma/2 + M_0$.

42.4.10 *Beta distribution*

The choice of an appropriate algorithm for generation of beta distributed random numbers depends on the values of the parameters α and β. For, *e.g.*, $\alpha = 1$, one can use the transformation method to find $x = 1 - u^{1/\beta}$, and similarly if $\beta = 1$ one has $x = u^{1/\alpha}$. For more general cases see, *e.g.*, Refs. [17, 18] and references therein.

42.5 Importance sampling and weighted Monte Carlo

Often the goal of a Monte Carlo calculation is to determine an expectation value of a function $h(x)$, where x is a (single or vector) random variable that follows a pdf $f(x)$,

$$E_f[h(x)] = \int h(x) f(x)\, dx \equiv \mu \; . \tag{42.10}$$

A Monte-Carlo estimator $\hat{\mu}_{\rm MC}$ for μ is the average of N values of $h(x)$ where x is sampled (generated) from $f(x)$, i.e., $\hat{\mu}_{\rm MC} = \frac{1}{N}\sum_{i=1}^{N} h(x_i)$. This has a variance

$$V[\hat{\mu}_{\rm MC}] = \frac{1}{N} V_f[h(x)] = \frac{1}{N}\left(E_f[h^2(x)] - \mu^2\right) \; . \tag{42.11}$$

By using the method of *importance sampling*, one can achieve a reduction in this variance and thus a more accurate determination of the expectation value for a given number of random values generated. The key idea is to rewrite the expectation value in Eq. (42.10) as

$$\mu = \int h(x) f(x)\, dx = \int \frac{h(x) f(x)}{g(x)}\, g(x)\, dx = E_g\left[\frac{h(x) f(x)}{g(x)}\right] \; , \tag{42.12}$$

where $g(x)$ is any other pdf of x with the same support as $f(x)$ (i.e., nonzero for the same region of x). Thus the desired quantity μ is the expectation value with respect to g of $h(x)f(x)/g(x)$. It can be estimated by generating N values of x sampled from g and computing

$$\hat{\mu}_{\rm IS} = \frac{1}{N}\sum_{i=1}^{N} \frac{h(x_i) f(x_i)}{g(x_i)} \; . \tag{42.13}$$

The variance of $\hat{\mu}_{\rm IS}$ is given by

$$V[\hat{\mu}_{\rm IS}] = \frac{1}{N} V_g\left[\frac{h(x) f(x)}{g(x)}\right] = \frac{1}{N}\left(E_g\left[\frac{h^2(x) f^2(x)}{g^2(x)}\right] - \mu^2\right) \; , \tag{42.14}$$

By choosing $g(x)$ such that $h(x)f(x)/g(x)$ is as constant as possible, the variance of $\hat{\mu}_{\rm IS}$ can be substantially reduced. One can show (see, e.g., Refs. [19,20]) that the variance is minimized when $g(x) \propto |h(x)| f(x)$.

An alternative importance sampling estimator can be constructed by replacing the number of generated values N in Eq. (42.13) by the sum $\sum_{i=1}^{N} f(x_i)/g(x_i)$. This can given an even smaller variance at the price of a small bias. It can be of further advantage in problems where the pdf $f(x)$ is known only up to a normalization constant, which then cancels (see Refs. [19, 20]).

A closely related application of importance sampling is the use of weighted Monte Carlo to compute the probability $P_f(x \in A)$ for x to be in a specified region A:

$$P_f(x \in A) = \int_A f(x)\, dx \; . \tag{42.15}$$

It may be, however, that one does not have an MC model capable of generating $x \sim f(x)$, but rather one can generate x according to a different density $g(x)$. The probability $P_f(x \in A)$ can be written

$$\begin{aligned} P_f(x \in A) &= \frac{\int_A \frac{f(x)}{g(x)}\, g(x)\, dx}{\int_A g(x)\, dx} \int_A g(x)\, dx \\ &= E_g[w(x) | x \in A]\, P_g(x \in A) \; , \end{aligned} \tag{42.16}$$

where $w(x) = f(x)/g(x)$ is the *weight function* and $P_g(x \in A) = \int_A g(x)\, dx$ is the probability to find $x \in A$ assuming $x \sim g(x)$. That is, $P_f(x \in A)$ is the conditional expectation value of $w(x)$ with respect to $g(x)$ given $x \in A$ multiplied by the probability to find $x \in A$ under assumption of $g(x)$.

Suppose N values of x are generated according to $g(x)$ and m of them are found in the region A. Then the probability to be in A for $x \sim g(x)$ can be estimated by m/N, and the expectation value above can be obtained from the average of the weights in A. Therefore the desired probability $P_f(x \in A)$ can be estimated using

$$\hat{P}_f(x \in A) = \frac{1}{m}\sum_{i=1}^{m} w_i \times \frac{m}{N} = \frac{1}{N}\sum_{i=1}^{m} w_i \; , \tag{42.17}$$

where $w_i = w(x_i)$ and the sum includes only the m values of x found in A. That is, when generating the x values according to $g(x)$ instead of $f(x)$, the number of events m found in A is replaced by the corresponding sum of weights. The variance of $\hat{P}_f(x \in A)$ can be found from

$$\widehat{V}[\hat{P}_f(x \in A)] = \frac{1}{N^2}\sum_{i=1}^{m} w_i^2 \; . \tag{42.18}$$

By choosing $g(x)$ so that a larger fraction of x values are sampled in the "important" region A, one can reduce the variance of the estimated probability for a given total number of generated values.

42.6 Markov Chain Monte Carlo

In applications involving generation of random numbers following a multivariate distribution with a high number of dimensions, the transformation method may not be possible and the acceptance-rejection technique may have too low of an efficiency to be practical. If it is not required to have independent random values, but only that they follow a certain distribution, then Markov Chain Monte Carlo (MCMC) methods can be used. In depth treatments of MCMC can be found, *e.g.*, in the texts by Robert and Casella [19], Liu [20], and the review by Neal [21]. HEP-oriented software for MCMC is available from the Bayesian Analysis Toolkit (BAT) [22, 23].

MCMC is particularly useful in connection with Bayesian statistics, where a p.d.f. $p(\boldsymbol{\theta})$ for an n-dimensional vector of parameters $\boldsymbol{\theta} = (\theta_1, \ldots, \theta_n)$ is obtained, and one needs the marginal distribution of a subset of the components. Here one samples $\boldsymbol{\theta}$ from $p(\boldsymbol{\theta})$ and simply records the marginal distribution for the components of interest.

A simple and broadly applicable MCMC method is the Metropolis-Hastings algorithm, which allows one to generate multidimensional points $\boldsymbol{\theta}$ distributed according to a target p.d.f. that is proportional to a given function $p(\boldsymbol{\theta})$. It is not necessary to have

Downloaded from https://academic.oup.com/ptep/article/2022/8/083C01/6651666 by KIT Library user on 27 September 2022

$p(\boldsymbol{\theta})$ normalized to unit area, which is useful in Bayesian statistics, as posterior probability densities are often determined only up to an unknown normalization constant.

To generate points that follow $p(\boldsymbol{\theta})$, one first needs a proposal p.d.f. $q(\boldsymbol{\theta};\boldsymbol{\theta}_0)$, which can be (almost) any p.d.f. from which independent random values $\boldsymbol{\theta}$ can be generated, and which contains as a parameter another point in the same space $\boldsymbol{\theta}_0$. For example, a multivariate Gaussian centered about $\boldsymbol{\theta}_0$ can be used. Beginning at an arbitrary starting point $\boldsymbol{\theta}_0$, the Hastings algorithm iterates the following steps:

1. Generate a value $\boldsymbol{\theta}$ using the proposal density $q(\boldsymbol{\theta};\boldsymbol{\theta}_0)$;
2. Form the Hastings test ratio, $\alpha = \min\left[1, \frac{p(\boldsymbol{\theta})q(\boldsymbol{\theta}_0;\boldsymbol{\theta})}{p(\boldsymbol{\theta}_0)q(\boldsymbol{\theta};\boldsymbol{\theta}_0)}\right]$;
3. Generate a value u uniformly distributed in $[0,1]$;
4. If $u \leq \alpha$, take $\boldsymbol{\theta}_1 = \boldsymbol{\theta}$. Otherwise, repeat the old point, *i.e.*, $\boldsymbol{\theta}_1 = \boldsymbol{\theta}_0$.
5. Set $\boldsymbol{\theta}_0 = \boldsymbol{\theta}_1$ and return to step 1.

If one takes the proposal density to be symmetric in $\boldsymbol{\theta}$ and $\boldsymbol{\theta}_0$, then this is the *Metropolis*-Hastings algorithm, and the test ratio becomes $\alpha = \min[1, p(\boldsymbol{\theta})/p(\boldsymbol{\theta}_0)]$. That is, if the proposed $\boldsymbol{\theta}$ is at a value of probability higher than $\boldsymbol{\theta}_0$, the step is taken. If the proposed step is rejected, the old point is repeated.

Methods for assessing and optimizing the performance of the algorithm are discussed in, *e.g.*, Refs. [19–21]. One can, for example, examine the autocorrelation as a function of the lag k, *i.e.*, the correlation of a sampled point with that k steps removed. This should decrease as quickly as possible for increasing k.

Generally one chooses the proposal density so as to optimize some quality measure such as the autocorrelation. For certain problems it has been shown that one achieves optimal performance when the acceptance fraction, that is, the fraction of points with $u \leq \alpha$, is around 40%. This can be adjusted by varying the width of the proposal density. For example, one can use for the proposal p.d.f. a multivariate Gaussian with the same covariance matrix as that of the target p.d.f., but scaled by a constant.

References

[1] F. James, Comput. Phys. Commun. **60**, 329 (1990).

[2] P. L'Ecuyer, *Proc. 1997 Winter Simulation Conference*, IEEE Press, Dec. 1997, 127–134.

[3] L. Lonnblad, Comput. Phys. Commun. **84**, 307 (1994).

[4] R. Brun and F. Rademakers, Nucl. Instrum. Meth. **A389**, 81 (1997); See also `root.cern.ch`.

[5] F. James, Comput. Phys. Commun. **79**, 111 (1994), [Erratum: Comput. Phys. Commun.97,357(1996)]; M. Luscher, Comput. Phys. Commun. **79**, 100 (1994), [hep-lat/9309020].

[6] P. L'Ecuyer, Mathematics of Computation, **65**, 213 (1996) and **65**, 225 (1999).

[7] M. Matsumoto and T. Nishimura, *ACM Transactions on Modeling and Computer Simulation*, Vol. 8, No. 1, January 1998, 3–30.

[8] F. James and L. Moneta, Comput. Softw. Big Sci. **4**, 2. 12 p (2019), 4 figures, [arXiv:1903.01247], URL `http://cds.cern.ch/record/2678858`.

[9] Much of DIEHARD is described in: G. Marsaglia, *A Current View of Random Number Generators*, keynote address, *Computer Science and Statistics: 16th Symposium on the Interface*, Elsevier (1985).

[10] P. L'Ecuyer and R. Simard, *ACM Transactions on Mathematical Software* 33, 4, Article 1, December 2007.

[11] J. Heinrich, CDF Note CDF/MEMO/STATISTICS/PUBLIC /8032, 2006.

[12] UNU.RAN is described at `statmath.wu.ac.at/software/unuran`; See also W. Hörmann, J. Leydold, and G. Derflinger, *Automatic Nonuniform Random Variate Generation*, (Springer, New York, 2004).

[13] W.H. Press *et al.*, *Numerical Recipes*, 3rd edition, (Cambridge University Press, New York, 2007).

[14] J.H. Ahrens and U. Dieter, Computing **12**, 223 (1974).

[15] R.Y. Rubinstein, *Simulation and the Monte Carlo Method*, (John Wiley and Sons, Inc., New York, 1981).

[16] L. Devroye, *Non-Uniform Random Variate Generation*, (Springer-Verlag, New York, 1986); Available online at `luc.devroye.org/rnbookindex.html`.

[17] C. Walck, *Handbook on Statistical Distributions for Experimentalists*, University of Stockholm Report SUF-PFY/96-01, available from `www.fysik.su.se/~walck`.

[18] J.E. Gentle, *Random Number Generation and Monte Carlo Methods*, 2nd ed., (Springer, New York, 2003).

[19] C.P. Robert and G. Casella, *Monte Carlo Statistical Methods*, 2nd ed., (Springer, New York, 2004).

[20] J.S. Liu, *Monte Carlo Strategies in Scientific Computing*, (Springer, New York, 2001).

[21] R.M. Neal, *Probabilistic Inference Using Markov Chain Monte Carlo Methods*, Technical Report CRG-TR-93-1, Dept. of Computer Science, University of Toronto, available from `www.cs.toronto.edu/~radford/res-mcmc.html` .

[22] A. Caldwell, D. Kollar, K. Kröninger, Comput. Phys. Commun. 180 (2009) pages 2197-2209.

[23] Schulz, O., Beaujean, F., Caldwell, A. et al., SN Computer Science 2, 210 (2021).

Downloaded from https://academic.oup.com/ptep/article/2022/8/083C01/6651666 by KIT Library user on 27 September 2022

43. Monte Carlo Event Generators

Revised July 2021 by P. Nason (INFN, Milano-Bicocca; Milano-Bicocca U.) and P. Skands (Monash U.).

General-purpose Monte Carlo (GPMC) generators like HERWIG [1–3], PYTHIA [4,5], and SHERPA [6], provide detailed simulations of high-energy collisions. They play an essential role in QCD modeling (in particular for aspects beyond fixed-order perturbative QCD) and in data analysis and the planning of new experiments, where they are used together with detector simulation to estimate signals and backgrounds in high-energy processes. They are built from several components, that describe the physics starting from very short distance scales, up to the typical scale of hadron formation and decay. Since QCD is weakly interacting at short distances (below a femtometer), the components of the GPMC dealing with short-distance physics are based upon perturbation theory. At larger distances, all soft hadronic phenomena, like hadronization and the formation of the underlying event in hadron collisions, cannot be computed from first principles at present, and one must rely upon QCD-inspired models.

The purpose of this review is to illustrate the main components of these generators. It is divided into four sections. The first one deals with short-distance, perturbative phenomena. The basic concepts leading to the simulations of the dominant QCD processes are illustrated here. In the second section, the nonperturbative transition from partons to hadrons ("hadronization") is treated. The two most popular hadronization models, the string and cluster models, are illustrated. The basics of the implementation of decay chains of unstable "primary" hadrons into stable "secondaries" is also illustrated here. In the third section, models for soft hadron physics are discussed. These include models for the underlying event and for low-$p_\perp$ ("minimum-bias") interactions. Issues of collective effects, such as Bose-Einstein and color-reconnection effects, are also discussed here. The fourth section briefly introduces the challenges of MC uncertainty estimates and tuning.

We use natural units throughout, such that $c = 1$ and $\hbar = 1$, with energies, momenta and masses measured in GeV, and times and distances measured in GeV^{-1}.

43.1 Short-distance physics in GPMC generators

The short-distance components of a GPMC generator deal with the computation of the primary process at hand, with decays of short-lived particles, and with the generation of QCD and QED radiation. QCD radiation is computable in perturbation theory as long as the time scales involved are well below $1/\Lambda$, where Λ is a typical hadronic scale of few hundred MeV. Because of the presence of logarithmic enhancements due to both collinear and soft emissions, this description involves an indefinite number of final-state particles that are emitted at time scales below $1/\Lambda$. In e^+e^- annihilation into hadrons, for example, the time scale of the primary process is of the order of the inverse of the annihilation energy Q. Collinear and soft emissions take place at all time scales between $1/Q$ and $1/\Lambda$, Technically, the computation of the dominant collinear and soft radiation is carried out by the so called shower algorithms. Historically, "Parton Shower" algorithms were first developed for resummation of collinear singularities. We will briefly describe this approach in this section. We stress, however, that many modern generators adopt approaches that focus initially upon soft singularities, leading to "Dipole Showers", discussed in Sec. 43.1.3.

Collinear singularities arise when the angle between two emitted light partons becomes small. For example, in a process in which a quark and a gluon are emitted, if the angle θ among them is very small (and is smaller than the angles among all other pairs of light partons in the process) the squared amplitude factorizes as follows

$$|M_{qg}|^2 \mathrm{d}\Phi_{qg} \approx |M_q|^2\, \mathrm{d}\Phi_q \frac{\alpha_s}{2\pi} P_{q,qg}(z) \mathrm{d}z \frac{\mathrm{d}\phi}{2\pi} \frac{\mathrm{d}\theta^2}{\theta^2} \tag{43.1}$$

where M_{qg}, $\mathrm{d}\Phi_{qg}$ are the amplitude and phase space when both the gluon and the quark are emitted; M_q, $\mathrm{d}\Phi_q$ are the amplitude and phase space when only the quark is emitted; $z = E_q/(E_q+E_g)$ is the fraction of energy carried by the quark; ϕ is the azimuth of the splitting plane, and $P_{q,qg}(z) = C_F(1+z^2)/(1-z)$ is the Altarelli-Parisi splitting kernel for gluon emission from a quark line, with color factor $C_F = 4/3$. The factorized form of Eq. (43.1) is due to the fact that for small angle the process is dominated by a single amplitude in which the splitting quark is almost on shell and hence propagates for long distances. We define the energy scale corresponding to the inverse of this distance as the *hardness* of the splitting process, so that larger hardness corresponds to shorter distance. We can define the hardness t as the product $E^2\theta^2$, or as the virtuality of the splitting parton p^2, or as a measure of the relative transverse momentum in the splitting such as the k_t of an emitted parton relative to its parent, defined by

$$\begin{aligned} p^2 &= 2E^2 z(1-z)(1-\cos\theta) \approx z(1-z)E^2\theta^2\,, \\ k_t^2 &= z^2(1-z)^2 E^2\theta^2\,. \end{aligned} \tag{43.2}$$

If the region of small values of z and $1-z$ was not important, these definitions would be equivalent. In QCD we also have soft divergences, arising when soft gluons are emitted. In Eq. (43.1) they appear as $z \to 1$, because of the $1/(1-z)$ singularity of $P_{q,qg}(z)$. Thus, we expect that the choice of the appropriate ordering variable will be relevant when dealing with soft divergences (see Sec. 43.3). The $\mathrm{d}\theta^2/\theta^2$ factor in Eq. (43.1) can be equivalently written in terms of the hardness $\mathrm{d}t/t$. After integration, it gives rise to a logarithmic factor $\log(Q^2/\Lambda^2)$. We can have many subsequent splittings, that we can describe by applying Eq. (43.1) recursively, as long as the splittings are strongly ordered in decreasing hardness. This means that, from a typical final-state configuration, by clustering together final-state parton pairs with the smallest hardness recursively, we can reconstruct a branching tree, that may be viewed as the splitting history of the event. We stress that all hardness values between the hardness of the primary process and the cutoff scale Λ are equally involved here. The collinear approximation is applied recursively to splitting processes that have much smaller hardness with respect to all previous ones.

By integrating over the phase space, a process with n collinear splittings will be of order $(\alpha_S(Q^2)\log(Q^2/\Lambda^2))^n$ with respect to the primary process. Since $\alpha_S(Q^2) \propto 1/\log(Q^2/\Lambda^2)$ [7], these corrections are not small. The so-called KLN theorem [8,9] guarantees that large logarithmic enhancements arising from final-state collinear splitting cancel against the virtual corrections in inclusive cross sections, order by order in perturbation theory. Furthermore, the factorization theorem guarantees that initial-state collinear singularities can be factorized into the parton density functions (PDFs) [7]. Therefore, the cross section for the basic process remains accurate up to corrections of higher orders in $\alpha_S(Q)$, provided it is interpreted as an inclusive cross section, rather than as a bare partonic cross section. For example, the leading order (LO) cross section for $e^+e^- \to q\bar{q}$ is a good LO estimate of the e^+e^- cross section for the production of a pair of quarks accompanied by an arbitrary number of collinear and soft gluons, but is not a good estimate of the cross section for the production of a $q\bar{q}$ pair with no extra radiation. In summary, perturbation theory at fixed order can yield increasingly accurate predictions for inclusive observables, but cannot be used to describe the indefinite sequence of collinear and soft radiations that accompany the hard partons.

Parton-Shower algorithms are used to compute the cross section for generic hard processes including all dominant collinear radiation. These algorithms begin with the generation of the kinematics of the basic process, performed with a probability proportional to its LO partonic cross section. This is interpreted physically as the inclusive cross section for the basic process, followed by an arbitrary sequence of shower splittings. The algorithm then assigns a probability to each splitting sequence, so that the initial LO cross section is partitioned into the cross sections for a multitude of final states of arbitrary multiplicity, with their sum equal to the cross section of the primary process. This property of the GPMCs reflects the KLN cancellation mentioned earlier, and it is often called "unitarity of the shower process", a name that reminds us that the KLN cancellation itself is a consequence

Downloaded from https://academic.oup.com/ptep/article/2022/8/083C01/6651666 by KIT Library user on 27 September 2022

of unitarity. The fact that a quantum mechanical process can be described in terms of composition of probabilities, rather than amplitudes, follows from the collinear approximation. In fact, because of strong ordering, a radiated parton cannot be collinear to more than one parton in the amplitude, and this suppresses interference effects.

We now illustrate the basic parton-shower algorithm, as first introduced in Ref. [10]. (For more pedagogical introductions see Ref. [11] and references therein.) For simplicity, we consider the example of e^+e^- annihilation into $q\bar{q}$ pairs, where we only have to deal with final state radiation (FSR). We consider all final states that can be built by dressing the q and $\bar{q}$ partons with an indefinite number of splitting processes. By recursively clustering together final state parton pairs with the smallest relative hardness, from each final state configuration we can construct two trees rooted at the q and $\bar{q}$ partons. The momenta of all intermediate lines of the tree diagrams are then uniquely determined from the final-state momenta. Hardnesses in the trees are ordered. One assigns to each splitting vertex the hardness t, the energy fractions z and $1-z$ of the two generated partons, and the azimuth ϕ of the splitting process with respect to the momentum of the incoming parton. For definiteness, we assume that z and ϕ are defined in the center-of-mass (CM) frame of the e^+e^- collision. The differential cross section for a given final state is given by the product of the differential cross section for the initial $e^+e^- \to q\bar{q}$ process, multiplied by a factor

$$\Delta_i(t_m, t_n)\frac{\alpha_{\rm S}(t)}{2\pi}P_{i,jk}(z)\frac{dt_m}{t_m}dz\frac{d\phi}{2\pi} \tag{43.3}$$

for each intermediate line arising from the $n^{\rm th}$ and ending in the $m^{\rm th}$ splitting vertex. $\Delta(t_m, t_n)$ is the so-called Sudakov form factor

$$\Delta_i(t_m, t_n) = \exp\left[-\int_{t_m}^{t_n}\frac{dq^2}{q^2}\,\frac{\alpha_{\rm S}(q^2)}{2\pi}\sum_{jk}P_{i,jk}(z)dz\frac{d\phi}{2\pi}\right]. \tag{43.4}$$

The suffixes i and jk represent the parton species of the incoming and final partons, respectively, and $P_{i,jk}(z)$ are the Altarelli-Parisi [12] splitting kernels. Notice that the endpoints on the z integration depend upon the definition of hardness. For example, in case of virtuality or transverse momentum ordering, the z integration is automatically cut-off near the extremes, see eq. (1.2). When this is not the case (as, for example, for angular ordering) an explicit cut-off on z must be introduced, corresponding to the requirement that an emission must have some minimum energy to be distinguishable from no emission. For lines originating at the primary vertex, the scale t_n is replaced by the typical scale of the primary process and for lines ending without any further splitting the scale t_m is replaced by t_0, an infrared cutoff defined by the shower hadronization scale (at which the charges are screened by hadronization) or, for an unstable particle, its width (a source cannot emit radiation with a period exceeding its lifetime).

Eq. (43.3) can be obtained by iterating formula Eq. (43.1) recursively, with two important corrections: a) the strong coupling is evaluated at a scale corresponding to the hardness of the splitting process; b) the presence of the Sudakov form factor. Both these modifications arise from the inclusion of all collinear-dominant virtual corrections.

Notice that the Sudakov form factor for a small hardness interval $\Delta_i(t, t+\delta t)$ is equal to one minus the integrated emission probability of Eq. (43.3), i.e. it can be interpreted as the probability of no emission in the interval $t, t+\delta t$. From this, it immediately follows that $\Delta_i(t_m, t_n)$ can be interpreted as the no-emission probability in the full t_m, t_n interval. This interpretation allows to formulate the shower process as a probabilistic algorithm. We first notice that $0 < \Delta_i(t_m, t_n) \leq 1$, where the upper extreme is reached for $t_m = t_n$, and the lower extreme is approached for $t_m = t_0$. Starting from each of the partons in the primary process (e.g., $e^+e^- \to q\bar{q}$), event generation then proceeds recursively as follows. Given a parton exiting a vertex with hardness t_n, (taken to be of order the annihilation scale Q^2 for the first branching) one seeks a solution of the equation $r = \Delta_i(t_m, t_n)$, with $r \in [0, 1]$ a uniform random number, and solves it for the hardness of the next branching t_m. If $t_m \leq t_0$, no splitting is generated and the line is interpreted as a final parton. If $t_m > t_0$, a branching is generated at the scale t_m. Its z value and the final parton species jk are generated with a probability proportional to $P_{i,jk}(z)$. The azimuth is generated uniformly, neglecting angular correlations (see Sec. 43.1.1). This procedure is started with each of the primary process partons, and is applied recursively to all generated partons. It may generate an arbitrary number of partons, and it stops when no final-state partons undergo further splitting.

The four-momenta of the final-state partons are reconstructed from the momenta of the initial ones, and from the whole sequence of splitting variables, subject to overall momentum conservation. Different algorithms employ different strategies to treat recoil effects due to momentum conservation, which may be applied either locally for each splitting, or globally for the entire set of partons (a procedure called *momentum reshuffling*.) This has a subleading effect with respect to the collinear approximation.

We emphasize that the shower cross sections described above can be derived from perturbative QCD by keeping only the collinear-dominant real and virtual contributions to the cross section. As such it is unpredictive for large-angle radiation. It is thus unsafe to rely upon Parton Shower Monte Carlo alone to compute backgrounds to new physics signals that are characterized by several widely separated jets.

A Shower Monte Carlo builds its final state as if it developed from an iterative process, often with each intermediate stage made available to the user. It should be remarked that the meaning of these intermediate stages is only relevant within the approximation adopted by the generator, and could also differ in different implementations.

43.1.1 *Angular correlations*

In gluon-splitting processes ($g \to q\bar{q},\ g \to gg$) in the collinear approximation, the distribution of the split pair is not uniform in azimuth, and the Altarelli-Parisi splitting functions are recovered only after azimuthal averaging. This dependence is due to the interference of positive and negative helicity states for the gluon that undergoes splitting. Spin correlations propagate through the splitting process, and determine acausal correlations of the EPR kind [13]. A method to partially account for these effects was introduced in Ref. [14], in which the azimuthal correlation between two successive splittings is computed by averaging over polarizations. This can then be applied at each branching step. Acausal correlations are argued to be small, and are discarded with this method, that is still used in `PYTHIA` [4]. A method that fully includes spin correlation effects was later proposed [15], and has been implemented in `HERWIG` [3, 16].

43.1.2 *Initial-state radiation*

Initial-state radiation (ISR) arises because incoming particles may undergo collinear radiation before entering the hard-scattering process. In doing so, they acquire a non-vanishing transverse momentum, and their virtuality becomes negative (spacelike). It turns out to be convenient to develop the ISR shower starting with the highest hardness (i.e. with the hard process) and ending with the smallest (i.e. with the incoming parton in the hadron). Unlike the case of FSR, however, hardness ordering is opposite to time ordering in the ISR case. A corresponding backwards-evolution algorithm was formulated by Sjöstrand [17], and was basically adopted in all shower models. It can be illustrated by considering a primary interaction initiated by a quark where no collinear emission of hardness $\geq t$ have taken place, and the same process where the quark also emits a collinear gluon of hardness t. The respective cross sections are proportional to

$$\begin{aligned} &|M_q(x)|^2 \mathrm{d}x f_q(x,t), \quad \text{and} \\ &|M_q(x)|^2\,\mathrm{d}x\frac{\alpha_s(t)}{2\pi}f_q(x/z,t)P_{q,qg}(z)\mathrm{d}z\frac{\mathrm{d}\text{Œ}}{2\pi}\frac{\mathrm{d}t}{t}\,. \end{aligned} \tag{43.5}$$

Here f_q is the quark PDF in the incoming hadron, x is the fraction of momentum of the incoming quark that enters the basic process, while x/z is the fraction of momentum of the incoming quark *before* it emits the collinear gluon. The elementary *emission probability* is the ratio of the second over the first expression

Downloaded from https://academic.oup.com/ptep/article/2022/8/083C01/6651666 by KIT Library user on 27 September 2022

in Eq. (43.5). In analogy with the final state radiation case, this ratio will appear in the exponent of the Sudakov form factor, that (after the inclusion of all splitting subprocesses) is given by

$$\Delta_i^{\rm ISR}(t,t') = \exp\left[-\int_{t'}^{t}\frac{dt''}{t''}\frac{\alpha_{\rm S}(t'')}{2\pi}\int_x^1\frac{dz}{z}\sum_{jk}P_{j,ik}(z)\frac{f_j(t'',x/z)}{f_i(t'',x)}\right]. \tag{43.6}$$

Notice that there are two uses of the PDFs: they are used to compute the cross section for the basic hard process, and they control ISR via backward evolution. Since the evolution is generated with leading-logarithmic accuracy, it is acceptable to use two different PDF sets for these two tasks, provided they agree at the LO level.

In the context of GPMC evolution, each ISR emission generates a finite amount of transverse momentum. Details on how the recoils generated by these transverse "kicks" are distributed among other partons in the event, in particular the ones involved in the hard process, constitute one of the main areas of difference between existing algorithms, see Ref. [11]. An additional $\mathcal{O}(1\,\mathrm{GeV})$ of "primordial k_T" is typically added, to represent the sum of unresolved and/or non-perturbative motion below the shower cutoff scale.

43.1.3 *Soft emissions and QCD coherence*

Soft singularities arise in QCD due to the real or virtual emission of soft gluons. For example, the cross section for the emission of a soft gluon in e^+e^- annihilation into hadrons is given by

$$\begin{aligned}\mathrm{d}\sigma_{q\bar{q}g} &\approx \mathrm{d}\sigma_{q\bar{q}}\frac{4}{3}(4\pi\alpha_s)\left[\frac{2\,p_q\cdot p_{\bar{q}}}{p_q\cdot l\,p_{\bar{q}}\cdot l}\right]\frac{\mathrm{d}^3 l}{2l^0(2\pi)^3}\\ &= \mathrm{d}\sigma_{q\bar{q}}\frac{\alpha_s}{2\pi}\frac{4}{3}\frac{\mathrm{d}l^0}{l^0}\frac{\mathrm{d}\phi}{2\pi}\frac{\mathrm{d}\cos\theta}{1-\cos^2\theta},\end{aligned} \tag{43.7}$$

where p_q, $p_{\bar{q}}$ and l are the quark, antiquark and gluon momentum, and θ and ϕ are the polar and azimuthal angle of the gluon momentum with respect to the quark direction. Since the gluon is soft, we may assume that p_q and $p_{\bar{q}}$ are unaffected by the gluon emission. The soft singularity is manifest in the $\mathrm{d}l^0/l^0$ factor. Notice that also collinear singularities are present at the same time when $\theta\to 0$ and $\theta\to\pi$, corresponding to the gluon becoming collinear to either the quark or the antiquark. It is easy to check that in the collinear limits Eq. (43.7) becomes equivalent to Eq. (43.1) with $P_{q,qg}(z) = (4/3)2/(1-z)$, i.e. the limiting form of $P_{q,qg}(z)$ when z approaches 1. Thus, soft singularities coexist with collinear ones, so that two potentially large logarithms can arise simultaneously due to gluon emission.

Unlike the case of collinear emission, soft emission is not tied to a single emitting particle. The amplitude for the emission of a soft gluon from an external (incoming or outgoing) line with momentum p is proportional to $p\cdot\epsilon/p\cdot l$. When squaring the amplitude, products like the one appearing in the square bracket of Eq. (43.1) arise for all pairs of external particles, with the product of a single emission amplitude with itself appearing only if $p^2>0$, i.e. for massive colored particles. Thus, interference plays here a crucial role. This is unlike the case of collinear singularities, where because of strong ordering a radiated parton cannot be collinear to more than one other parton.

It was shown in a set of publications (see Ref. [18]) that, within the conventional parton-shower formalism based on collinear factorization, the region of collinear and soft emissions can be correctly described by using the angle of the emissions as the ordering variable, rather than the virtuality, and by setting the argument of $\alpha_{\rm S}$ at the splitting vertex equal to the relative parton transverse momentum after the splitting. Physically, the ordering in angle approximates the coherent interference arising from large-angle soft emission from a bunch of collinear partons. Without this effect, the particle multiplicity would grow too rapidly with energy, in conflict with e^+e^- data. For this reason, angular ordering is used as the default evolution variable in all versions of `HERWIG` (see Ref. [19]). To partially account for soft interference effects, an angular veto is imposed on the virtuality-ordered evolution in `PYTHIA` 6 [20].

A radical alternative formulation of QCD cascades first proposed in Ref. [21] focuses upon soft emission, rather than collinear emission, as the basic splitting mechanism. It then becomes natural to consider a branching process where it is a parton pair (i.e. a dipole) rather than a single parton, that emits a soft parton. Adding a suitable correction for non-soft, collinear partons, one can simultaneously achieve the correct logarithmic structure for both the collinear and soft emissions in the so called leading color approximation, i.e. when terms suppressed by a power of the number of colors are neglected. The `ARIADNE` [22] and `VINCIA` [23] programs are based on this approach. Dipole-type showers [24] are also used by default in `SHERPA` [25] and exist as an option in `HERWIG` [26]. An alternative dipole-based model is available in `PYTHIA` and `SHERPA` via the `DIRE` [27] plugin. The $p_\perp$-ordered showers in `PYTHIA` 6 and 8 represent a hybrid, combining collinear splitting kernels with dipole kinematics [28].

43.1.4 *Resummation*

Shower Monte Carlo generators perform resummation of all-order collinear- and/or soft-enhanced perturbative contributions, and it is thus natural to compare them to QCD resummation calculations [7]. The latter start from the definition of specific infrared-safe observables, that develop towers of large logarithms in certain regions of phase space, typically organized as

$$A(\alpha_{\rm S})\exp[Lg_0(\alpha_{\rm S}L)+g_1(\alpha_{\rm S}L)+g_2(\alpha_{\rm S}L)+\ldots] \tag{43.8}$$

where L is the large logarithm, $\alpha_{\rm S}$ is the strong coupling constant evaluated at some hard scale, and the functions A and g_i have an all-order expansion in their arguments. We talk about N^{n}LL accuracy if all g_i functions for $i\le n$ have been computed correctly in the resummation formula. In particular we talk about LL accuracy if the function g_0 is given correctly, NLL accuracy if g_2 is correct, and so on.

In general, a dedicated resummation calculation must be performed for each new observable. The predictions of shower MCs, on the other hand, are cast in terms of complete sets of final-state momenta, on which one can evaluate any observable; i.e., the shower algorithm itself is normally independent of the specific observable(s) under study. Because of this, it is not easy to qualifying the accuracy of a shower MC using the same criteria adopted in resummation calculation. In spite of this fact, shower MCs perform generally quite well in the description of observables that require resummation. This is related to their inclusion of several universal but formally subleading aspects. There is no guarantee, however, that the shower MC should perform to a certain level of accuracy for all distributions that require resummation. Thus, a more systematic treatment of subleading effects is quite desirable.

Several studies have appeared in the literature, aiming at either improving the current shower algorithms or formulate totally new ones, in such a way that the theoretical accuracy can be discussed in more precise terms [29–34]. In particular, in refs [29–31] (the PanScales collaboration), it was shown that criteria for defining the accuracy of Shower Generators can indeed be given on a quite general ground. They identified two such criteria: the first one regards the multi-parton real matrix-elements generated by the shower algorithm, that are required to be accurate in the region of phase space that are relevant for N^{n}LL accuracy. The second one regards the implementation of the virtual corrections, and it requires that for a large class of shape variables the shower MC must agree with the resummed calculation at the N^{n}LL level. The PanScale collaboration has also constructed shower algorithms that, at least in the leading color approximation, are NLL accurate according to these criteria.

43.1.5 *Massive quarks*

Quark masses act as a cut-off on collinear singularities. If the mass of a quark is below, or of the order of Λ, its effect in the shower is small. For larger quark masses, like in c, b, or t production, it is the mass, rather than the typical hadronic scale, that cuts off collinear radiation. For a quark with energy E and mass m_Q, the divergent behavior $d\theta/\theta$ of the collinear splitting process

Downloaded from https://academic.oup.com/ptep/article/2022/8/083C01/6651666 by KIT Library user on 27 September 2022

is regulated for $\theta \leq \theta_0 = m_Q/E$. We thus expect less collinear activity for heavy quarks than for light ones, which in turn is the reason why heavy quarks carry a larger fraction of the momentum acquired in the hard production process.

This feature can be implemented with different levels of sophistication. Using the fact that soft emission exhibits a zero at zero emission angle, older parton shower algorithms simply limited the shower emission to be not smaller than the angle θ_0. More modern approaches are used in both `PYTHIA`, where mass effects are included using a kind of matrix-element correction method [35], and in `HERWIG++` and `SHERPA`, where a generalization of the Altarelli-Parisi splitting kernel is used for massive quarks [36].

43.1.6 *Color information*

In event generators, quarks and antiquarks are represented by color lines, with arrows indicating the direction of color flow. In the limit of infinitely many colors (called the leading color approximation), each such line can be associated with a unique label; the probability for two quarks (or antiquarks) to have the same color (anticolor) vanishes. Moreover, in the same limit gluons can be represented by a pair of color lines with opposite arrows, as can be realized e.g. from the SU(3) group relation $8 = 3 \otimes \bar{3} \ominus 1$. The rules for color propagation are:

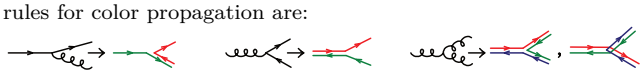

During the shower development, partons are connected by color lines. We can have a quark directly connected by a color line to an antiquark, or via an arbitrary number of intermediate gluons, as shown in Fig. 43.1. It is also possible for a set of gluons to be connected cyclically in color, as e.g. in the decay $\Upsilon \to ggg$. The

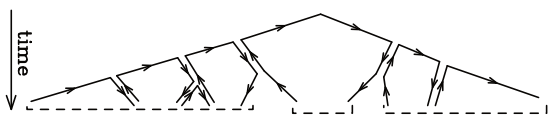

Figure 43.1: Color development of a shower in e^+e^- annihilation. Color-neutral clusters of partons are indicated by the dashed under-brackets.

color information is used in angular-ordered showers, where the angle of color-connected partons (i.e. partons connected by the same color line) determines the initial angle for the shower development, and in dipole showers, where dipoles are always color-connected partons. It is also used in hadronization models, where the initial strings or clusters used for hadronization are formed by color-neutral clusters of partons.

43.1.7 *Electromagnetic (and weak) corrections*

The physics of photon emission from charged particles, and of photon splittings to pairs of charged fermions, can also be treated with a shower MC algorithm. High-energy electrons and quarks, for example, are accompanied by bremsstrahlung photons. Also here, similarly to the QCD case, electromagnetic corrections are of order $\alpha_{\rm em} \ln(Q/m)$, where m is the mass of the radiating particle, or even of order $\alpha_{\rm em} \ln(Q/m) \ln(E_\gamma/E)$ for soft γ emissions, so that, especially for the case of electrons, their inclusion in the simulation process is mandatory. This is done in most GPMCs (for a comparative study see [37]), which typically agree in collinear (DGLAP) limits but differ in whether and how soft (multipole) QED interference effects are handled. The specialized generator PHOTOS [38] is sometimes used as an afterburner for an improved treatment of QED radiation in non-hadronic resonance decays.

For photon emissions off leptons, the shower can be continued down to virtualities arbitrarily close to the lepton mass shell (unlike the case in QCD). In practice, an infrared cutoff is still required for the shower algorithm to terminate. Therefore, there is always an energy cut-off for emitted photons that depends upon the implementations [37]. In the case of electrons, this energy is typically of the order of its mass. Electromagnetic radiation below this scale is not enhanced by collinear singularities, and is thus bound to be soft, so that the electron momentum is not affected by it.

For photons emitted from quarks, we have instead the obvious limitation that the photon wavelength cannot exceed the typical hadronic size. Longer-wavelength photons are in fact emitted by hadrons, rather than quarks. This last effect is in practice never modeled by existing shower MC implementations. Thus, electromagnetic radiation from quarks is cut off at a typical hadronic scale. Finally, hadron (and τ) decays involving charged particles can produce additional soft bremsstrahlung. This is implemented in a general way in `HERWIG++`/`HERWIG 7` [39] and `SHERPA` [40].

At energies significantly above the electroweak (EW) scale, showers involving emissions (and splittings) of weak gauge and Higgs bosons can also be relevant, with recent implementations based on collinear limits ranging from weak-boson emissions from fermions in `PYTHIA 8` [41], to triple-boson couplings in `HERWIG 7` [42], to the full set of EW branching processes in `VINCIA` [43].

43.1.8 *Beyond-the-Standard-Model Physics*

The inclusion of processes for physics beyond the Standard Model (BSM) in event generators is to some extent only a matter of implementing the relevant hard processes and (chains of) decays, with the level of difficulty depending on the complexity of the model and the degree of automation [44, 45]. Notable exceptions are long-lived colored particles [46], particles in exotic color representations, and particles showering under new gauge symmetries, with a growing set of implementations documented in the individual GPMC manuals. Further complications that may be relevant are finite-width effects (discussed in Sec. 43.1.9) and the assumed threshold behavior.

In addition to code-specific implementations [11], there are a few commonly adopted standards that are useful for transferring information and events between codes. Currently, the most important of these is the Les Houches Event File (LHEF) standard [47], normally used to transfer parton-level events from a hard-process generator to a shower generator. Another important standard is the Supersymmetry Les Houches Accord (SLHA) format [48], originally used to transfer information on supersymmetric particle spectra and couplings, but by now extended to apply also to more general BSM frameworks and incorporated within the LHEF standard [49].

43.1.9 *Decay Chains and Particle Widths*

In most BSM processes and some SM ones, an important aspect of the event simulation is how decays of short-lived particles, such as top quarks, EW and Higgs bosons, and new BSM resonances, are handled. We here briefly summarize the spectrum of possibilities, but emphasize that there is no universal standard. Users are advised to check whether the treatment of a given code is adequate for the physics study at hand.

The appearance of an unstable resonance as a physical particle at an intermediate stage of the event generation implies that its production and decay processes are treated as being factorized. This is valid up to corrections of order Γ/m_0, with Γ the width and m_0 the pole mass. States whose widths are a substantial fraction of their mass should instead be treated as intrinsically off-shell internal propagator lines.

For states treated as physical particles, two aspects are relevant: the mass distribution of the decaying particle itself and the distributions of its decay products. For the former, matrix-element generators often use a simple δ function at m_0. The next level up, typically used in GPMCs, is to use a Breit-Wigner distribution, which formally resums higher-order virtual corrections to the mass distribution. Note, however, that this still only generates an improved picture for *moderate* fluctuations away from m_0. Similarly to above, particles that are significantly off-shell (in units of Γ) should not be treated as resonant, but rather as internal off-shell propagator lines. In most GPMCs, further refinements are included, for instance by letting Γ be a function of m ("running widths") and by limiting the magnitude of the allowed fluctuations away from m_0. We finally point out that NLO+PS generators have appeared that can deal with resonances including off-shell effects, non-resonance contributions and interference of radiation generated in resonance decay and production, see [50] and references therein. A new "interleaved" shower treatment also allows for interference between production and decay in the Vincia model [43].

Downloaded from https://academic.oup.com/ptep/article/2022/8/083C01/6651666 by KIT Library user on 27 September 2022

For the distributions of the decay products, the simplest treatment is again to assign them their respective m_0 values, with a uniform phase-space distribution. A more sophisticated treatment distributes the decay products according to the differential decay matrix elements, capturing at least the internal dynamics and helicity structure of the decay process, including EPR-like correlations. Further refinements include polarizations of the external states [51] and assigning the decay products their own Breit-Wigner distributions, the latter of which opens the possibility to include also intrinsically off-shell decay channels, like $H \to WW^*$.

GPMC manuals often give instructions on how to include new decay modes, at varying levels of sophistications ranging from simple uniform phase-space sampling (which the user can reweight a posteriori) and step-function thresholds, to fully matrix-element weighted decay implementations including potential off-shell / threshold effects.

During subsequent showering of the decay products, most parton-shower models will preserve the total invariant mass of the decayed resonance, so as not to skew the original resonance shape. In the context of passing externally generated LHEF files [47] to a GPMC for showering, note that this is only possible if the intermediate resonances are present (with status code 2) in the LHEF event record [52].

43.1.10 *Matching and Merging with Fixed-Order Matrix Elements*

Shower algorithms are based upon a combination of the collinear (small-angle) and soft (small-energy) approximations and are thus normally inaccurate for hard, wide-angle emissions (i.e., additional well-resolved jets). They also contain only the leading singular pieces of next-to-leading order (NLO) and higher corrections to the basic process.

Traditional GPMCs, like `HERWIG` and `PYTHIA`, have included for a long time the so called Matrix Element Corrections (MEC), first formulated in Ref. [53] with later developments summarized in Ref. [11]. They are typically available for $2 \to 1$ or $1 \to 2$ processes, like DIS, vector boson and Higgs production and decays, and top decays. The MEC corrects the emission of the hardest jet at large angles, so that it becomes exact at LO. A generalization of the method to multiple emissions was formulated in [54].

Aside from MECs implemented directly in the GPMCs, the improvements on the parton-shower description of hard collisions have been made in two main directions: the so called Matrix Elements and Parton Shower matching (ME+PS from now on), and the matching of NLO calculations and Parton Showers (NLO+PS). We now discuss each of these, and then briefly summarize techniques becoming available for combining them.

The ME+PS method allows one to use tree-level matrix elements for hard, large-angle emissions. It was first formulated in the so-called CKKW paper [55], and several variants have appeared, including the CKKW-L, MLM, pseudoshower and MESS methods, see Refs. [11, 56, 57] and references therein. So called "Truncated Showers" are required [58] to maintain color coherence when interfacing to angular-ordered parton showers, and care must be taken to use consistent α_S choices for the real (ME-driven) and virtual (PS-driven) corrections [59].

In the ME+PS method one typically starts by generating LO matrix elements for the production of the basic process plus a certain number $\leq n$ of other partons. A minimum separation is imposed on the produced partons, requiring, for example, that the relative transverse momentum in any pair of partons is above a given cut $Q_{\rm cut}$. One then reweights these amplitudes in such a way that, in the strongly ordered region, the virtual effects that are included in the shower algorithm (i.e. running couplings and Sudakov form factors) are also accounted for. At this stage, before parton showers are added, the generated configurations are tree-level accurate at large angle, and at small angle they match the results of the shower algorithm, except that there are no emissions below the scale $Q_{\rm cut}$, and no final states with more than n partons. These kinematic configurations are thus fed into a GPMC, that must generate all splittings with relative transverse momentum below the scale $Q_{\rm cut}$, for initial events with less than n partons, or below the scale of the smallest pair transverse momentum, for events with n partons. The matching parameter $Q_{\rm cut}$ must be chosen to be large enough for fixed-order perturbation theory to hold, but small enough so that the shower is accurate for emissions below it. Notice that the accuracy achieved with MEC is equivalent to that of ME+PS with $n = 1$, where MEC has the advantage of not having a matching parameter $Q_{\rm cut}$.

The popularity of the ME+PS method is due to the fact that processes with many jets often appear as backgrounds to new-physics searches. These jets are typically required to be well separated, and to have large transverse momenta. These kinematic configurations are exactly those for which pure shower algorithms are unreliable, hence it is mandatory to describe them using at least LO matrix elements.

Several ME+PS implementations use existing LO generators, like `ALPGEN` [60], `MADGRAPH` [61], and others summarized in Ref. [56], for the calculation of the matrix elements, and feed the partonic events to a GPMC like `PYTHIA` or `HERWIG` using the Les Houches Interface for User Processes (LHI/LHEF) [47, 52]. `SHERPA` and `HERWIG 7` also include their own matrix-element generators.

The NLO+PS methods promote the accuracy of the generation of the basic process from LO to NLO in QCD. They must thus include the radiation of one extra parton with tree-level accuracy, since this radiation constitutes a NLO correction to the basic process. They must also include NLO virtual corrections. They can be viewed as an extension of the MEC methods with the inclusion of NLO virtual corrections. They are however more general, since they are applicable to processes of arbitrary complexity. Two of these methods are now widely used: MC@NLO [62] and Powheg [58, 63], with several alternative methods now also being pursued, see Ref. [11] and references therein.

NLO+PS generators produce NLO accurate distributions for inclusive quantities, and generate the hardest jet with tree-level accuracy. It should be recalled, though, that in $2 \to 1$ processes like Z/W production, GPMCs including MEC and weighted by a constant K factor may perform nearly as well, and, if suitably tuned, may even yield a better description of data. In this context, note also that the optimal tuning of an NLO+PS generator may well be different from that of the pure PS.

Several NLO+PS processes are implemented in the MC@NLO program [62], together with the `AMC@NLO` development [64], and in the Powheg-Box framework [63]. `HERWIG 7` supports its own variants of Powheg and MC@NLO for several processes. `SHERPA` instead implements a variant of the MC@NLO method.

For applications that require an accurate description of more than one hard, large-angle jet associated with the primary process, ME+PS schemes are still superior to NLO+PS ones. Ideally, one would like to improve NLO generators in such a way that also the production of associated jets achieves NLO accuracy. The FXFX [65], UNLOPS [66], MiNLO [67] and `MEPS@NLO` [68] methods address this problem. The solution of this problem is also a prerequisite for the construction of NNLO+PS generators, i.e. generators that, besides being NLO accurate for the production of an associated jet, are also NNLO accurate for fully inclusive observables. Three different approaches have appeared in the literature for dealing with this problem: the UN^{2}NLOPS, based upon UNLOPS method [69]; methods extending the MiNLO approach by reweigthting [70] and by the so called MiNNLO$_{\rm PS}$ technique [71]; and the GENEVA method [72]. Several processes have been implemented with the MiNLO related and GENEVA methods, mostly for the production of color singlet systems, with the exception of the recent MiNNLO$_{\rm PS}$ implementation of $t\bar{t}$ production (see refs. [73, 74] for an extensive list of references).

43.2 Hadronization Models

In the context of GPMCs, *hadronization* denotes the process by which a set of colored partons (*after* showering) is transformed into a set of "primary hadrons", which may then subsequently decay further (to "secondary hadrons"). This non-perturbative transition takes place at the *hadronization scale* $Q_{\rm had}$, which by construction is equal to the infrared cutoff of the parton shower. In the absence of a first-principles solution to the relevant dynamics, GPMCs use QCD-inspired phenomenological models to describe this transition.

An important result in "quenched" lattice QCD (see Chap. 17

Downloaded from https://academic.oup.com/ptep/article/2022/8/083C01/6651666 by KIT Library user on 27 September 2022

of PDG book) is that the potential energy between two partons with opposite color charges grows linearly with their separation, at distances greater than about a femtometer. This is known as "linear confinement", and it forms the starting point for the *string model of hadronization*, discussed below in Sec. 43.2.1. Alternatively, a property of perturbative QCD called "preconfinement" is the basis of the *cluster model of hadronization*, discussed in Sec. 43.2.2.

A key difference between MC hadronization models and the fragmentation-function (FF) formalism used to describe inclusive hadron spectra in perturbative QCD (see Chap. 9 and Chap. 19 of PDG book) is that FFs can be defined at an arbitrary perturbative scale Q while MC hadronization models are intrinsically defined at the scale $Q_{\rm had}$. Direct comparisons are therefore only meaningful if the perturbative evolution between Q and $Q_{\rm had}$ is taken into account. FFs are calculable in pQCD, given a non-perturbative initial condition obtained by fits to hadron spectra. In the MC context, one can prove that the correct QCD evolution of the FFs arises from the shower formalism, with the hadronization model providing an explicit parameterization of the non-perturbative component. However, the MC modeling of shower and hadronization includes much more information on the final state since it is fully exclusive (i.e., it addresses all particles in the final state explicitly), while FFs only describe inclusive spectra. This exclusivity also enables MC models to make use of the color-flow information coming from the perturbative shower evolution (see Sec. 43.1.6) to determine between which partons confining potentials should arise. E.g., in the string picture, the nonperturbative limit of a QCD dipole is a string piece [75].

Given an exact hadronization model, its dependence on the scale $Q_{\rm had}$ should in principle be compensated by the corresponding scale dependence of the shower algorithm, which stops generating branchings at the scale $Q_{\rm had}$. However, due to their complicated and fully exclusive nature, it is generally not possible to enforce this compensation automatically in MC models. One must therefore be aware that the nonperturbative model parameters must be "retuned" by hand if the infrared cutoff is modified. Any other changes to the perturbative part of the calculation, such as matching to further (fixed-order or resummed) coefficients, may also necessitate a retuning. Tuning is discussed briefly in Sec. 43.4.

Finally, it should be emphasized that the so-called "parton level" that can be obtained by switching off hadronization in a GPMC, is not a universal concept, since each model defines $Q_{\rm had}$ differently (e.g. via a cutoff in $p_\perp$, invariant mass, etc., with different tunes using different values for the cutoff). Comparisons to distributions at this level may therefore be used to provide an idea of the overall impact of hadronization corrections within a given model, but should be avoided in the context of physical observables.

43.2.1 *The String Model*

Starting from early concepts [76], several hadronization models based on strings have been proposed [11]. Of these, the most widely used today is the so-called Lund model [77, 78], implemented in `PYTHIA` [4, 5]. We concentrate on that particular model here, though many of the overall concepts would be shared by any string-inspired method.

Consider a quark and an antiquark that have a large relative momentum and which are in an overall color-singlet state, such as the $\bar{q}q$ pair produced at the end of the shower in the center of Fig. 43.1). As the charges move apart, linear confinement implies that a potential $V(r) = \kappa\, r$ is reached for large distances r. (At short distances, there is a Coulomb term $\propto 1/r$ as well, but this is neglected in the Lund string.) This potential describes a string with tension $\kappa \sim 1\,\mathrm{GeV/fm} \sim 0.2\,\mathrm{GeV}^2$. The physical picture is that of a color flux tube being stretched between the q and the $\bar{q}$. As the string grows, the nonperturbative creation of quark-antiquark pairs can break the string, via the process illustrated in Fig. 43.2. If either of the resulting string pieces after the break still has a large invariant mass, new breaks will then continue to occur until every piece has a mass of order a typical hadron. In nature, quantum mechanics ensures that these masses are (Breit-Wigner-distributed around) those of the physical hadron states in QCD, while in an algorithmic implementation, this is less trivial

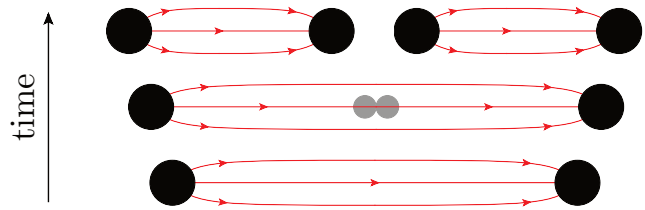

Figure 43.2: Illustration of string breaking by quark pair-creation in the string field.

to impose. Within the Lund model, the constraint that each final string piece must have a mass consistent with that of physical hadron is addressed by first noting that each breakup vertex is spacelike separated from all others (the string cannot break again in the forward lightcone of a point where it has already broken); since the breakups are therefore causally disconnected, they do not have to be considered in any particular order. The Lund model exploits this to perform the fragmentation in an outwards-in manner [78], splitting off one physical hadron at a time from either the left or right endpoint (chosen randomly in each step).

The first hadron to be generated (starting either from the left or right) is thus the "outermost" one (sometimes called the "first-rank" hadron), formed by combining the original hadronizing endpoint quark (or antiquark) q_0 with an antiquark (or quark) $\bar{q}_1$ produced by the first breakup. The new leftover quark (or antiquark) q_1 becomes the string endpoint for the next iteration, in a Markov chain which continues, alternating randomly between the left and right ends of the string, until finally a small last bit of string is decayed directly to two hadrons, with no energy left over.

Not only does this allow for the hadron that is split off in each step to be assigned a physical mass, the fact that the fragmentation spectrum should be independent of whether one performs the fragmentation from left to right or vice versa places a strong constraint on the form of the nonperturbative *fragmentation function*, $f(z)$, which governs the probability for the hadron produced in a given step to take a fraction $z \in [0, 1]$ of the remaining energy. Thus, in the Lund model, causality dictates that the fragmentation function should be of the form,

$$f(z) \propto \frac{1}{z}(1-z)^a \exp\left(-\frac{b\,(m_h^2 + p_{\rm T} h^2)}{z}\right) . \qquad (43.9)$$

This is known as the Lund symmetric fragmentation function (normalized to unit integral). The dimensionless parameter a dampens the hard tail of the fragmentation function, towards $z \to 1$, and may in principle be flavor-dependent, while b, with dimension GeV^{-2}, is a universal constant related to the string tension [78] which determines the behavior in the soft limit, $z \to 0$. Note that the dependence on the hadron mass, m_h, in $f(z)$ implies that heavier hadrons have higher $\langle z \rangle$. We return to the transverse momentum $p_{\rm T} h$ below.

The model is Lorentz invariant, so considerations involving boosted string systems are straightforward, involving the usual Lorentz effects.

As a by-product, the probability distribution in invariant time τ of $q'\bar{q}$ breakup vertices, or equivalently $\Gamma = (\kappa\tau)^2$, is also obtained, with $dP/d\Gamma \propto \Gamma^a \exp(-b\Gamma)$ implying an area law for the color flux, and the average breakup time lying along a hyperbola of constant invariant time $\tau_0 \sim 10^{-23}$s [78].

For massive endpoints (e.g. c and b quarks), which do not move along straight lightcone sections, the exponential suppression with string area leads to modifications of the form $f(z) \to f(z)/z^{b\,m_Q^2}$, with m_Q the mass of the heavy quark [79]. Although different forms, such as the Peterson formula [80], can also be used to describe inclusive heavy-meson spectra (see Sec 19.8 of PDG book), such choices are not strictly consistent with causality in the string framework.

Downloaded from https://academic.oup.com/ptep/article/2022/8/083C01/6651666 by KIT Library user on 27 September 2022

43.2.1.1 *Strings with Gluons*

In the string model, energetic gluons lead to transverse "kinks" on strings, illustrated in Fig. 43.3. The order of these kinks follows from the color ordering produced by the parton shower, cf. the $\bar{q}gggq$ and $\bar{q}gq$ systems on the left and right part of Fig. 43.1. (Modifications to this order, by possible color reconnection/rearrangement effects, are discussed in Sec. 43.3.2.) Thus gluons

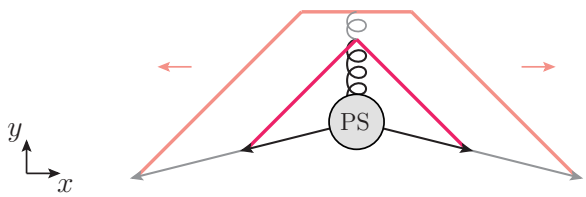

Figure 43.3: Schematic illustration of an $e^+e^- \to qg\bar{q}$ configuration emerging from the parton shower (PS). Snapshots of string positions are shown at two different times (full and shaded lines respectively). The gluon forms a transverse kink which grows in the y direction until all the gluon's kinetic energy has been used up.

effectively build up a transverse structure in the originally one-dimensional object, with infinitely soft ones smoothly absorbed into the string. Note: cyclic topologies made entirely of gluons (closed strings) are also possible, e.g. in decays such as $H \to gg$ or $\Upsilon \to ggg$. The space-time evolution is more involved when kinks are taken into account [78], but no additional free parameters need to be introduced. The main difference between quark and gluon hadronization stems from the fact that gluons are connected to two string pieces (one on either side), while quarks are only connected to a single string piece. Hence, the relative rate of energy loss per unit invariant time — and consequently also the rate of hadron production — is larger by a factor of 2 for gluons (analogously to the ratio of gluon to quark color charges $C_A/C_F = 2.25$).

43.2.1.2 *Transverse Momentum and Flavors*

For each breakup vertex, quantum mechanical tunneling is assumed to control the masses and p_T kicks (transverse to the string axis, in a frame in which the string itself has no transverse motion) that can be produced, leading to a Gaussian suppression

$$\mathrm{Prob}(m_q^2, p_\mathrm{T}q^2) \;\propto\; \exp\left(\frac{-\pi m_q^2}{\kappa}\right)\exp\left(\frac{-\pi p_\mathrm{T}q^2}{\kappa}\right) \;, \quad (43.10)$$

where m_q is the mass of the produced quark flavor and p_T is the nonperturbative transverse momentum imparted to it by the breakup process, with a universal average value of $\left\langle p_\mathrm{T}q^2\right\rangle = \kappa/\pi \sim (250\,\mathrm{MeV})^2$. The antiquark has the same mass and opposite p_T.

In an MC model with a fixed shower cutoff t_0, the effective amount of p_T in string breaks may be larger than the purely nonperturbative κ/π above, to account for effects of additional (unresolved) radiation below t_0.

From the mass term in Eq. (43.10), one concludes that charm and bottom quarks are too heavy to be produced in string breaks, while strange quarks will be suppressed relative to up and down ones. Lacking unambiguous and precise mass definitions for light quarks, however, the effective amount of strangeness suppression is normally extracted from experimental data, using observables such as K/π, K^*/ρ, and ϕ/K^* ratios.

Baryon production can also be incorporated, at various levels of sophistication. The simplest option is to allow string breaks to produce pairs of *diquarks*, loosely bound states of two quarks in an overall $\bar{3}$ representation. Again, the relative rate of such pairs is extracted from data, e.g. using p/π or Λ/K ratios. Since the perturbative shower splittings do not produce diquarks, the optimal value for this parameter is mildly correlated with the amount of $g \to q\bar{q}$ splittings in the shower. More sophisticated options, including the so-called "popcorn" mechanism, are discussed in Ref. [78]. Finally, the PYTHIA framework also allows for baryon string junctions [81]. These represent epsilon tensors in color space (analogously to how color dipoles represent Kronecker deltas), and are used, e.g., to model the fragmentation of baryon beam remnants. They can also be created (in pairs of junctions and antijunctions) in some color-reconnection scenarios [82], making the effective baryon-to-meson ratios in such models dependent on the amount and type of color reconnections that occur in each event.

The next step of the algorithm is the assignment of the produced quarks within hadron multiplets. Using a nonrelativistic classification of spin states, the hadronizing q may combine with the $\bar{q}'$ from a newly created breakup to produce a hadron of a given spin S and angular momentum L. The lowest-lying pseudoscalar and vector meson multiplets, and spin-1/2 and -3/2 baryons, are assumed to dominate in a string framework[1], but individual rates are not predicted by the model, and hence the ratios of spin-1 to spin-0 mesons and diquarks are free parameters (modulo a factor 3 from spin counting) which must be constrained by data. In that context, it is often advisable to begin with the heaviest states, since so-called feed-down from the decays of higher-lying hadron states complicates the extraction for lighter particles, see Sec. 43.2.3.

43.2.2 *The Cluster Model*

The cluster hadronization model is based on *preconfinement*, i.e., on the observation [83, 84] that the color structure of a perturbative QCD shower evolution at any scale Q_0 is such that color-singlet subsystems of partons (labeled "clusters") occur with a universal invariant mass distribution which is power suppressed at large masses. For any starting scale $Q \gg Q_0 \gg \Lambda_\mathrm{QCD}$, only the number of such clusters depends on Q, while the shape of their mass distribution only depends on Q_0 and on Λ_QCD.

Following early models based on this universality [10, 85], the cluster model developed by Webber [86] has for many years been a hallmark of the HERWIG generators, with an alternative implementation [87] now available in the SHERPA generator. The key idea, in addition to preconfinement, is to force "by hand" all gluons to split into quark-antiquark pairs at the end of the parton shower. Compared with the string description, this effectively amounts to viewing gluons as "seeds" for string breaks, rather than as kinks in a continuous object. After the splittings, a new set of low-mass color-singlet clusters is obtained, formed only by quark-antiquark pairs. These can be decayed to on-shell hadrons in a simple manner, with the relative yields of different hadron species mainly governed by their masses and the size of the phase space.

The algorithm starts by generating the forced $g \to q\bar{q}$ breakups, and by assigning flavors and momenta to the produced quark pairs. For a typical shower cutoff corresponding to a gluon virtuality of $Q_\mathrm{had} \sim 1\,\mathrm{GeV}$, the p_T generated by the splittings can be neglected. The constituent light-quark masses, $m_{u,d} \sim 300\,\mathrm{MeV}$ and $m_s \sim 450\,\mathrm{MeV}$, imply a suppression (typically even an absence) of strangeness production. In principle, the model also allows for diquarks to be produced at this stage, but due to the larger constituent masses this would only become relevant for shower cutoffs larger than 1 GeV.

If a cluster formed in this way has an invariant mass above some cutoff value, typically 3–4 GeV, it is forced to undergo sequential $1 \to 2$ cluster breakups, along an axis defined by the constituent partons of the original cluster, until all sub-cluster masses fall below the cutoff value. Due to the preservation of the original axis in these breakups, this treatment has some resemblance to the string-like picture, though the nonperturbative $p_\perp$ kicks generated in this way are generally larger, up to half the allowed cluster mass.

Next, on the low-mass side of the spectrum, some clusters are allowed to decay directly to a single hadron, with nearby clusters absorbing any excess momentum. This improves the description of the high-z part of the spectrum — where the hadron carries almost

[1] In PYTHIA, the four $L = 1$ meson multiplets (scalar, tensor, and 2 pseudovectors) are also available but are disabled by default, since many states (and their decays) are poorly known.

Downloaded from https://academic.oup.com/ptep/article/2022/8/083C01/6651666 by KIT Library user on 27 September 2022

all the momentum of its parent jet — at the cost of introducing one additional parameter, controlling the probability for single-hadron cluster decay.

Having obtained a final distribution of small-mass clusters, now with a strict cutoff at 3–4 GeV and with the component destined to decay to single hadrons already removed, the remaining clusters are interpreted as a smoothed-out spectrum of excited mesons, each of which decays isotropically to two hadrons, with relative probabilities proportional to the available phase space for each possible two-hadron combination that is consistent with the cluster's internal flavors, including spin degeneracy. It is important that all the light members (containing only uds) of each hadron multiplet be included, as the absence of members can lead to unphysical isospin or SU(3) flavor violation. Typically, the lightest pseudoscalar, vector, scalar, even and odd charge conjugation pseudovector, and tensor multiplets of light mesons are included. In addition, some excited vector multiplets of light mesons may be available. For baryons, usually only the lightest flavor-octet, -decuplet and -singlet baryons are present, although both the HERWIG++ and SHERPA implementations now include some heavier baryon multiplets as well.

Differently from the string model, the mechanism of phase-space suppression employed here leads to a natural enhancement of the lighter pseudoscalars, and no parameters beyond the spectrum of hadron masses need to be introduced at this point. The phase space also limits the transverse momenta of the produced hadrons relative to the jet axis.

Note that, since the masses and decays of excited heavy-flavor hadrons in particular are not well known, there is some freedom in the model to adjust these, which in turn will affect their relative phase-space populations.

43.2.3 *Hadron and τ Decays*

Of the so-called primary hadrons, originating directly from string breaks and/or cluster decays (see above), many are unstable and so decay further, until a set of particles is obtained that can be considered stable on time scales relevant to the given measurement. (A typical hadron-collider definition of a "stable particle" $c\tau \geq 10\,\mathrm{mm}$ includes weakly-decaying strange hadrons K, Λ, $\Sigma^{\pm}$, $\bar{\Sigma}^{\pm}$, Ξ, Ω.) The decay modeling can therefore have a significant impact on final particle yields and spectra, especially for the lowest-lying hadronic states, which receive the largest relative contributions from decays (feed-down). This interplay also implies that hadronization parameters may need to be retuned if significant changes to the decay treatment are made.

Particle summary tables, such as those given elsewhere in this *Review*, represent a condensed summary of the available experimental measurements and hence may be incomplete and/or exhibit inconsistencies within the experimental precision. In an MC decay package, on the other hand, all information must be quantified and consistent, with all branching ratios summing to unity. When adapting particle summary information for use in a decay package, a number of choices must therefore be made. The amount of ambiguity increases as more excited hadron multiplets are added to the simulation, about which less and less is known from experiment, with each GPMC making its own choices.

A related choice is how to distribute the decay products differentially in phase space, in particular which matrix elements to use. Historically, MC generators contained matrix elements only for selected (generator-specific) classes of hadron and τ decays, coupled with a Breit-Wigner smearing of the masses, truncated at the edges of the physical decay phase space (the treatment of decay thresholds can be important for certain modes [11]). A more sophisticated treatment can then be obtained by reweighting the generated events using the obtained particle four-momenta and/or by using specialized external packages such as EVTGEN [88] for hadron decays and TAUOLA [89] for τ decays.

More recently, HERWIG++ and SHERPA include helicity-dependence in τ decays [6, 90], with a more limited treatment available in PYTHIA 8 [5]. The HERWIG++ and SHERPA generators have also included significantly improved internal simulations of hadronic decays, which include spin correlations between those decays for which matrix elements are used. Photon-bremsstrahlung effects are discussed in Sec. 43.1.7.

HERWIG++ and PYTHIA include the probability for B mesons to oscillate into $\bar{B}$ ones before decay. SHERPA and EVTGEN also include CP-violating effects and, for common decay modes of the neutral meson and its antiparticle, the interference between the direct decay and oscillation followed by decay.

We end on a note of warning on double counting. This may occur if a particle can decay via an intermediate on-shell resonance. An example is $a_1 \to \pi\pi\pi$ which may proceed via $a_1 \to \rho\pi$, $\rho \to \pi\pi$. If these decay channels of the a_1 are both included, each with their full partial width, a double counting of the on-shell $a_1 \to \rho\pi$ contribution would result. Such cases are normally dealt with consistently in the default MC generator packages, so this warning is mostly for users that wish to edit decay tables on their own.

43.3 Models for Soft Hadron-Hadron Physics

43.3.1 *Underlying Event*

In the GPMC context, "underlying event" (UE) denotes any additional activity *beyond* the basic process and its associated ISR and FSR activity. The UE is thus only defined in the context of events selected with a "hard" (i.e., high-$p_\perp$) trigger which defines the basic process at hand. The dominant contribution to the UE is believed to come from additional color exchanges between the colliding hadronic states. These multiple exchanges can be modeled either as additional perturbative (mainly t-channel gluon) exchanges, called multiple parton-parton interactions (MPI), or nonperturbatively using so-called cut pomerons (roughly equivalent to exchange of gluons with $p_\perp \to 0$). The experimental observation that events with a hard trigger are accompanied by a higher-than-average level of associated activity is called the "jet pedestal" effect.

The most clearly identifiable consequence of MPI is arguably the possibility of observing several hard parton-parton interactions in one and the same hadron-hadron event. Typically, these are QCD $2 \to 2$ interactions, which produce additional back-to-back jet pairs, with each pair having a small value of sum($\vec{p}_\perp$). The fraction of MPI that give rise to additional reconstructible jets is, however, small. Soft interactions, that exchange color and a small amount of momentum without giving rise to observable jets, are much more plentiful, and can give significant corrections to the color flow and total scattered energy of the event. This affects the final-state activity in a more global way, increasing hadron-multiplicity and summed E_T distributions, and contributing to the break-up of the beam remnants in the forward direction.

The first detailed Monte Carlo model for perturbative MPI was proposed in Ref. [91], and with some variation this still forms the basis for most modern implementations. Some useful additional references can be found in Ref. [11]. The first crucial observation is that the t-channel propagators appearing in perturbative QCD $2 \to 2$ scattering almost go on shell at low p_T, causing the differential cross sections to behave roughly as

$$d\sigma_{2\to 2} \propto \frac{dt}{t^2} \sim \frac{dp_\mathrm{T}{}^2}{p_\mathrm{T}{}^4} \ . \tag{43.11}$$

This cross section represents the inclusive scattering of partons against partons in perturbative QCD, summed over all partons. Thus, if a single hadron-hadron scattering contains *two* parton-parton interactions, that event will contribute twice to the parton-parton cross section $\sigma_{2\to 2}$ but only once to the hadron-hadron one σ_tot, and so on. In the limit that all the parton-parton interactions are independent and equivalent, one has

$$\sigma_{2\to 2} = \langle n \rangle \ \sigma_\mathrm{tot} \ , \tag{43.12}$$

with $\langle n \rangle$ the average number of parton-parton interactions, typically defined with some minimal $p_\mathrm{T} > p_{\perp\mathrm{min}}$ to render the parton-parton cross section finite. The probability for n parton-parton scatterings then follows a Poisson distribution,

$$\mathcal{P}_n = \langle n \rangle^n \frac{\exp\left(-\langle n \rangle\right)}{n!} \ . \tag{43.13}$$

This simple argument expresses unitarity; instead of the total hadron-hadron interaction cross section diverging as the parton-parton $p_\mathrm{T} \to 0$ (which would violate unitarity), we have restated

Downloaded from https://academic.oup.com/ptep/article/2022/8/083C01/6651666 by KIT Library user on 27 September 2022

the problem so that it is now the *number of parton-parton interactions per hadron-hadron collision* that diverges, with the total hadron-hadron cross section remaining finite. At LHC energies, the parton-parton scattering cross sections computed using the LO QCD cross section folded with modern PDFs become larger than the total pp one for $p_{\perp\min}$ values of order 4–5 GeV (see e.g. [92, 93]). One therefore expects the average number of perturbative MPI to exceed unity at around that scale.

Two ingredients remain to fully regulate the remaining divergence. Firstly, the interactions cannot use up more momentum than is available in the parent hadron. This suppresses the large-n tail of the estimate above. In PYTHIA-based models, the MPI are ordered in p_{T}, and the parton densities for each successive interaction are explicitly constructed so that the sum of x fractions can never be greater than unity. In the HERWIG models, the Poisson estimate of $\langle n\rangle$ above is used as an initial guess, but the generation of actual MPI is stopped once the energy-momentum conservation limit is reached. Both of these approaches generate momentum (conservation) correlations among the MPI.

The second ingredient invoked to suppress the number of interactions, at low p_{T} and x, is color screening; if the wavelength $\sim 1/p_{\mathrm{T}}$ of an exchanged colored parton becomes larger than a typical color-anticolor separation distance, it will only see an *average* color charge that vanishes in the limit $p_{\mathrm{T}} \to 0$. This provides an infrared cutoff for MPI similar to that provided by the hadronization scale for parton showers. A first estimate of the color-screening cutoff would be the proton size, $p_{\perp\min} \approx \hbar/r_p \approx 0.3\,\mathrm{GeV} \approx \Lambda_{\mathrm{QCD}}$, but empirically this appears to be far too low. In current models, one replaces the proton radius r_p in the above formula by a "typical color screening distance," i.e., an average size of a region within which the net compensation of a given color charge occurs. This number is not known from first principles [94] and is perceived of simply as an effective cutoff parameter. The simplest choice is to introduce a step function $\Theta(p_{\mathrm{T}} - p_{\perp\min})$. Alternatively, one may note that the jet cross section is divergent like $\alpha_{\mathrm{S}}^2({p_{\mathrm{T}}}^2)/{p_{\mathrm{T}}}^4$, cf. Eq. (43.11), and that therefore a factor

$$\frac{\alpha_{\mathrm{S}}^2({p_{\mathrm{T}}}0^2 + {p_{\mathrm{T}}}^2)}{\alpha_{\mathrm{S}}^2({p_{\mathrm{T}}}^2)}\,\frac{{p_{\mathrm{T}}}^4}{({p_{\mathrm{T}}}0^2 + {p_{\mathrm{T}}}^2)^2} \tag{43.14}$$

would smoothly regulate the divergences, now with ${p_{\mathrm{T}}}0$ as the free parameter. Regardless of whether it is imposed as a smooth (PYTHIA and SHERPA) or steep (HERWIG++) function, this is effectively the main "tuning" parameter in such models.

Note that the numerical value obtained for the cross section depends upon the PDF set used, and therefore the optimal value to use for the cutoff will also depend on this choice. Note also that the cutoff does not have to be energy-independent. Higher energies imply that parton densities can be probed at smaller x values, where the number of partons rapidly increases. Partons then become closer packed and the color screening distance d decreases. The uncertainty on the energy and/or x scaling of the cutoff is a major concern when extrapolating between different collider energies [95].

We now turn to the origin of the observational fact that hard jets appear to sit on top of a higher "pedestal" of underlying activity than events with no hard jets. This is interpreted as a consequence of impact-parameter-dependence: in peripheral collisions, only a small fraction of events contain any high-p_{T} activity, whereas central collisions are more likely to contain at least one hard scattering; a high-p_{T} triggered sample will therefore be biased towards small impact parameters, b. The ability of a model to describe both the UE in events with a hard trigger as well as the activity in inclusive "minimum-bias" (MB) samples (see below) therefore depends upon its modeling of the b-dependence, and correspondingly the impact-parameter shape constitutes another main tuning parameter.

For each impact parameter b, the number of interactions $\tilde{n}(b)$ can still be assumed to be distributed according to Eq. (43.13), again modulo momentum conservation, but now with the mean value of the Poisson distribution depending on impact parameter, $\langle\tilde{n}(b)\rangle$. This causes the final n-distribution (integrated over b) to be wider than a Poissonian.

Finally, there are two perturbative modeling aspects which go beyond the introduction of MPI themselves: 1) parton showers off the MPI, and 2) perturbative parton-rescattering effects. Without showers, MPI models would generate very sharp peaks for back-to-back MPI jets, caused by unshowered partons passed directly to the hadronization model. However, with the exception of the oldest PYTHIA6 model, all GPMC models do include such showers [11], and hence should exhibit more realistic (i.e., broader and more decorrelated) MPI jets. On the initial-state side, the main questions are whether and how correlated multi-parton densities are taken into account and, as discussed previously, how the showers are regulated at low p_{T} and/or low x. Although none of the MC models currently impose a rigorous correlated multi-parton evolution, all of them include some elementary aspects. The most significant for parton-level results is arguably momentum conservation, which is enforced explicitly in all the models. The so-called "interleaved" models [28] attempt to go a step further, generating an explicitly correlated multi-parton evolution in which flavor sum rules are imposed to conserve, e.g. the total numbers of valence and sea quarks [81].

Perturbative rescattering in the final state can occur if partons are allowed to undergo several distinct interactions, with showering activity possibly taking place in-between. This has so far not been studied extensively, but a first exploratory model is available [96]. In the initial state, parton rescattering/recombination effects have so far not been included in any of the GPMC models.

43.3.2 *Bose-Einstein and Color-Reconnection Effects*

In the context of e^+e^- collisions, Bose-Einstein (BE) correlations have mostly been discussed as a source of uncertainty on high-precision W mass determinations at LEP [97]. In hadron-hadron (and nucleus-nucleus) collisions, however, BE correlations are used extensively to study the space-time structure of hadronizing matter ("femtoscopy").

In MC models of hadronization, each string break or particle/-cluster decay is normally factorized from all other ones. This reduces the number of variables that must be considered in each step, but also makes it intrinsically difficult to introduce correlations among particles from different breaks/decays. In GPMCs, a few semi-classical models are available within the PYTHIA 6 and 8 generators [98], in which the BE effect is mimicked by an attractive interaction between pairs of identical particles in the final state, with no higher correlations included. Variants of this model differ mainly by the assumed shape of the correlation function and how overall momentum conservation is handled.

As discussed in Sec. 43.2, leading-color ("planar") color flows are used to set up the hadronizing systems (clusters or strings) at the hadronization stage. If the systems do not overlap significantly in space and time, subleading-color ambiguities and/or nonperturbative reconnections are expected to be small. However, if the density of displaced color charges is sufficiently high that several systems can overlap significantly, full-color and/or reconnection effects should become progressively larger.

In the specific context of MPI, a crucial question is how color is neutralized *between* different MPI systems, including the remnants. The large rapidity differences involved imply large invariant masses (though normally low p_{T}), and hence large amounts of (soft) particle production. Indeed, in the context of soft-inclusive physics, it is these "inter-system" strings/clusters that furnish the dominant particle-production mechanism, and hence their modeling is an essential part of the soft-physics description, affecting topics such as MB/UE multiplicity and p_{T} distributions, rapidity gaps, and precision mass measurements. Reviews of color-reconnection effects can be found in [11, 82].

43.3.3 *Minimum-Bias Events and Diffraction*

The term "minimum bias" (MB) originates from the experimental requirement of a minimal number of tracks (or hits) in a given instrumented region. In order to make MC predictions for such observables, all possible contributions to the relevant phase-space region must be accounted for. There are essentially four types of physics processes, which together make up the total hadron-

Downloaded from https://academic.oup.com/ptep/article/2022/8/083C01/6651666 by KIT Library user on 27 September 2022

hadron (hh) cross section: 1) elastic scattering[2]: $hh \to hh$, 2) single diffractive dissociation: $hh \to h + \text{gap} + X$, with X denoting anything that is not the original beam particle, and "gap" denoting a rapidity region devoid of observed activity; 3) double diffractive dissociation: $hh \to X + \text{gap} + X$, and 4) inelastic non-diffractive scattering: everything else. A fifth class may also be defined, called central diffraction ($hh \to h + \text{gap} + X + \text{gap} + h$). Note that different terminologies exist [99]: in experimental settings, diffraction is typically defined by an observable gap, of some minimal size in rapidity, while in the MC context, each diffractive physics process produces a whole spectrum of gaps, with small ones suppressed but not excluded.

The inelastic non-diffractive part of the cross section is typically modeled either by smoothly regulating and extending the perturbative QCD scattering cross sections all the way to zero $p_\perp$ [91] (`PYTHIA` and `SHERPA`), or by regulating the QCD cross sections with a sharp cutoff [100] and adding a separate class of nonperturbative scatterings below that scale [101] (`HERWIG`). See also Sec. 43.3.1. In all cases, the most important ingredients are: 1) the IR regularization of the perturbative scattering cross sections, including their PDF dependence, 2) the assumed matter distribution of the colliding hadrons, possibly including multi-parton correlations [81] and/or x dependence [102], and 3) additional soft-QCD effects such as color reconnections, discussed in Sec. 43.3.2.

Currently, there are essentially three methods for simulating diffraction in the main MC models: 1) in `PYTHIA` 6, one picks a diffractive mass according to parameterized cross sections $\propto \mathrm{d}M^2/M^2$ [103]. This mass is represented as a string, which is hadronized as described in Sec. 43.2.1, though differences in the effective scale of the hadronization may necessitate a (re)tuning of the hadronization parameters for diffraction; 2) in `PYTHIA` 8, the high-mass tail beyond $M \sim 10\,\text{GeV}$ is augmented by a partonic description in terms of pomeron PDFs [104], allowing diffractive jet production including showers and underlying event [105]; 3) the `PHOJET` and `DPMJET` programs also include central diffraction and rely directly on a formulation in terms of pomerons (color-singlet multi-gluon states) [106–108]. Cut pomerons correspond to exchanges of soft gluons while uncut ones give elastic and diffractive topologies as well as virtual corrections that help preserve unitarity. So-called "hard pomerons" provide a transition to the perturbative regime. Hadronization is still handled using the Lund string model, so there is some overlap with the above models at the hadronization stage. In addition, a pomeron-based package exists for `HERWIG` [109], and an effort is underway to construct an MC implementation of the "KMR" model [94] within the `SHERPA` generator. Color reconnections (Sec. 43.3.2) may also play a role in creating rapidity gaps and the underlying event (Sec. 43.3.1) in filling them.

43.4 Uncertainties and Tuning

The accuracy that can be achieved by a GPMC model depends on the sophistication of the theory models it incorporates, on the available constraints on its free parameters, and on the nature of the observable(s) under study. Using existing data (or more accurate theory calculations) to constrain the model parameters is referred to as generator tuning. Although tuned models do tend to yield improved results also for observables that they have not been tuned to, the question of evaluating the remaining uncertainties reliably is still far from solved. It is worth noting, however, that all of the GPMCs now provide options for automatic evaluation of perturbative shower uncertainties (e.g., via renormalization-scale variations), in the form of vectors of alternative event weights [110–112]. One must be aware that these variations are not necessarily exhaustive and significant weight fluctuations can be a problem for processes with large shower phase spaces. Nonperturbative uncertainties must normally still be evaluated by varying salient model parameters by hand. A general method called eigentunes [113] is also available, based on global fits to data.

Typically, the overall event properties are determined by only a few, very important parameters, such as the value of α_S, for perturbative corrections, and the shape of the fragmentation functions, for nonperturbative ones. More parameters may then be introduced to describe successively more detailed aspects (e.g., the rates and decays of individual hadron species), but these should have progressively less impact on the overall modeling. One may therefore take a factorized approach, first constraining the perturbative parameters and thereafter the nonperturbative ones, in order of decreasing significance to the overall modeling. Furthermore, by identifying which measurements are most sensitive to each parameter, this ordering can be reflected in the way that data is selected and applied to constrain the models. Thus, measurements sensitive to global event properties would typically be applied first, to constrain the most inclusive parameters, and so on for progressively more exclusive aspects.

At LO×LL, perturbation theory is doing well if it agrees with an IR safe measurement within $\sim 10\%$. It would therefore not make much sense to tune a GPMC beyond roughly 5% (it might even be dangerous, due to overfitting). The advent of NLO Monte Carlos may reduce this number slightly, but only for quantities for which one expects NLO precision. For quantities governed by nonperturbative physics, uncertainties are larger. For some quantities, e.g. ones for which the underlying modeling is known to be poor, an order-of-magnitude agreement or worse may have to be accepted. Note further that the unitarity of shower and hadronization models implies that the Born-level cross-section normalization is not tunable, hence in tuning contexts one tends to focus on the shapes of distributions rather than their normalizations.

In the context of LO×LL GPMC tuning, subleading aspects of coupling-constant and PDF choices are relevant. In particular, one should be aware that the choice of QCD Λ parameter $\Lambda_\mathrm{MC} = 1.569\Lambda_{\overline{\mathrm{MS}}}$ (for 5 active flavors) improves the predictions of coherent shower algorithms at the NLL level for a class of relevant observables [114], and hence this scheme is often considered the baseline for shower tuning. The question of LO vs. NLO PDFs is more involved [11], but it should be emphasized that the gluon PDF at (very) low x is important for determining the level of the underlying event in MPI models (Sec. 43.3.1), and hence the MB/UE tuning (and energy scaling [95]) is linked to the choice of PDF in such models. Further issues and an example of a specific recipe that could be followed in a realistic set-up can be found in Ref. [92]. A useful online resource can be found at the mcplots.cern.ch website [115], based on the RIVET tool [116].

Recent years have seen the emergence of automated tools to reduce the amount of both computer and manpower required for tuning [113]. Automating the human expert input is more difficult. In the tools currently on the market, this is addressed by a combination of input solicited from the GPMC authors (e.g., which parameters and ranges to consider, which observables constitute a complete set, etc) and a set of weights determining the relative priority given to each bin in each distribution. The final result is therefore still subjective but at least reproducible. When backed by careful demonstrations of sensitivities, correlations, and uncertainties, the quality of the resulting tunes is by now competitive. The field is still burgeoning, with future sophistications to be expected.

[2]The QED elastic cross section diverges and is normally a non-default option.

References

[1] G. Corcella *et al.*, JHEP **01**, 010 (2001), [hep-ph/0011363].

[2] M. Bahr *et al.*, Eur. Phys. J. C **58**, 639 (2008), [arXiv:0803.0883].

[3] J. Bellm *et al.*, Eur. Phys. J. C **76**, 4, 196 (2016), [arXiv:1512.01178].

[4] T. Sjostrand, S. Mrenna and P. Z. Skands, JHEP **05**, 026 (2006), [hep-ph/0603175].

[5] T. Sjöstrand *et al.*, Comput. Phys. Commun. **191**, 159 (2015), [arXiv:1410.3012].

[6] T. Gleisberg *et al.*, JHEP **02**, 007 (2009), [arXiv:0811.4622].

[7] QCD summary, PDG.

[8] T. Kinoshita, J. Math. Phys. **3**, 650 (1962).

[9] T. Lee and M. Nauenberg, Phys. Rev. **133**, B1549 (1964).

[10] G. C. Fox and S. Wolfram, Nucl. Phys. B **168**, 285 (1980).

Downloaded from https://academic.oup.com/ptep/article/2022/8/083C01/6651666 by KIT Library user on 27 September 2022

[11] A. Buckley *et al.*, Phys. Rept. **504**, 145 (2011), [arXiv:1101.2599].

[12] G. Altarelli and G. Parisi, Nucl. Phys. B **126**, 298 (1977).

[13] A. Einstein, B. Podolsky and N. Rosen, Phys. Rev. **47**, 777 (1935).

[14] B. Webber, Phys. Lett. B **193**, 91 (1987).

[15] J. C. Collins, Nucl. Phys. B **304**, 794 (1988).

[16] I. Knowles, Comput. Phys. Commun. **58**, 271 (1990).

[17] T. Sjostrand, Phys. Lett. B **157**, 321 (1985).

[18] G. Marchesini and B. Webber, Nucl. Phys. B **310**, 461 (1988).

[19] S. Gieseke, P. Stephens and B. Webber, JHEP **12**, 045 (2003), [hep-ph/0310083].

[20] M. Bengtsson and T. Sjostrand, Nucl. Phys. B **289**, 810 (1987).

[21] G. Gustafson and U. Pettersson, Nucl. Phys. B **306**, 746 (1988).

[22] L. Lonnblad, Comput. Phys. Commun. **71**, 15 (1992).

[23] W. T. Giele, D. A. Kosower and P. Z. Skands, Phys. Rev. D **78**, 014026 (2008), [arXiv:0707.3652].

[24] Z. Nagy and D. E. Soper, JHEP **10**, 024 (2005), [hep-ph/0503053].

[25] S. Schumann and F. Krauss, JHEP **03**, 038 (2008), [arXiv:0709.1027].

[26] S. Platzer and S. Gieseke, Eur. Phys. J. C **72**, 2187 (2012), [arXiv:1109.6256].

[27] S. Höche and S. Prestel, Eur. Phys. J. C **75**, 9, 461 (2015), [arXiv:1506.05057].

[28] T. Sjostrand and P. Z. Skands, Eur. Phys. J. C **39**, 129 (2005), [hep-ph/0408302].

[29] M. Dasgupta *et al.*, JHEP **09**, 033 (2018), [Erratum: JHEP 03, 083 (2020)], [arXiv:1805.09327].

[30] M. Dasgupta *et al.*, Phys. Rev. Lett. **125**, 5, 052002 (2020), [arXiv:2002.11114].

[31] A. Karlberg *et al.*, Eur. Phys. J. C **81**, 8, 681 (2021), [arXiv:2103.16526].

[32] J. R. Forshaw, J. Holguin and S. Plätzer, JHEP **09**, 014 (2020), [arXiv:2003.06400].

[33] J. R. Forshaw, J. Holguin and S. Plätzer, JHEP **08**, 145 (2019), [arXiv:1905.08686].

[34] Z. Nagy and D. E. Soper, Phys. Rev. D **99**, 5, 054009 (2019), [arXiv:1902.02105].

[35] E. Norrbin and T. Sjostrand, Nucl. Phys. B **603**, 297 (2001), [hep-ph/0010012].

[36] S. Catani *et al.*, Nucl. Phys. B **627**, 189 (2002), [hep-ph/0201036].

[37] J. Cembranos *et al.*, JHEP **09**, 077 (2013), [arXiv:1305.2124].

[38] N. Davidson, T. Przedzinski and Z. Was, Comput. Phys. Commun. **199**, 86 (2016), [arXiv:1011.0937].

[39] K. Hamilton and P. Richardson, JHEP **07**, 010 (2006), [hep-ph/0603034].

[40] M. Schonherr and F. Krauss, JHEP **12**, 018 (2008), [arXiv:0810.5071].

[41] J. R. Christiansen and T. Sjöstrand, JHEP **04**, 115 (2014), [arXiv:1401.5238].

[42] M. R. Masouminia and P. Richardson (2021), [arXiv:2108.10817].

[43] H. Brooks, P. Skands and R. Verheyen (2021), [arXiv:2108.10786].

[44] A. Semenov, Comput. Phys. Commun. **180**, 431 (2009), [arXiv:0805.0555].

[45] N. D. Christensen and C. Duhr, Comput. Phys. Commun. **180**, 1614 (2009), [arXiv:0806.4194].

[46] M. Fairbairn *et al.*, Phys. Rept. **438**, 1 (2007), [hep-ph/0611040].

[47] J. Alwall *et al.*, Comput. Phys. Commun. **176**, 300 (2007), [hep-ph/0609017].

[48] P. Z. Skands *et al.*, JHEP **07**, 036 (2004), [hep-ph/0311123].

[49] J. Alwall *et al.* (2007), [arXiv:0712.3311].

[50] T. Ježo *et al.*, Eur. Phys. J. C **76**, 12, 691 (2016), [arXiv:1607.04538].

[51] P. Richardson, JHEP **11**, 029 (2001), [hep-ph/0110108].

[52] E. Boos *et al.*, in "2nd Les Houches Workshop on Physics at TeV Colliders," (2001), [hep-ph/0109068].

[53] M. Bengtsson and T. Sjostrand, Phys. Lett. B **185**, 435 (1987).

[54] W. Giele, D. Kosower and P. Skands, Phys. Rev. D **84**, 054003 (2011), [arXiv:1102.2126].

[55] S. Catani *et al.*, JHEP **11**, 063 (2001), [hep-ph/0109231].

[56] J. Alwall *et al.*, Eur. Phys. J. C **53**, 473 (2008), [arXiv:0706.2569].

[57] H. Brooks and C. T. Preuss, Comput. Phys. Commun. **264**, 107985 (2021), [arXiv:2008.09468].

[58] P. Nason, JHEP **11**, 040 (2004), [hep-ph/0409146].

[59] B. Cooper *et al.*, Eur. Phys. J. C **72**, 2078 (2012), [arXiv:1109.5295].

[60] M. L. Mangano *et al.*, JHEP **07**, 001 (2003), [hep-ph/0206293].

[61] J. Alwall *et al.*, JHEP **06**, 128 (2011), [arXiv:1106.0522].

[62] S. Frixione and B. R. Webber, JHEP **06**, 029 (2002), [hep-ph/0204244].

[63] S. Alioli *et al.*, JHEP **06**, 043 (2010), [arXiv:1002.2581].

[64] J. Alwall *et al.*, JHEP **07**, 079 (2014), [arXiv:1405.0301].

[65] R. Frederix and S. Frixione, JHEP **12**, 061 (2012), [arXiv:1209.6215].

[66] L. Lönnblad and S. Prestel, JHEP **03**, 166 (2013), [arXiv:1211.7278].

[67] K. Hamilton, P. Nason and G. Zanderighi, JHEP **10**, 155 (2012), [arXiv:1206.3572].

[68] S. Hoeche *et al.*, JHEP **04**, 027 (2013), [arXiv:1207.5030].

[69] S. Höche, Y. Li and S. Prestel, Phys. Rev. D **91**, 7, 074015 (2015), [arXiv:1405.3607].

[70] K. Hamilton *et al.*, JHEP **05**, 082 (2013), [arXiv:1212.4504].

[71] P. F. Monni *et al.*, JHEP **05**, 143 (2020), [arXiv:1908.06987].

[72] S. Alioli *et al.*, JHEP **06**, 089 (2014), [arXiv:1311.0286].

[73] J. Mazzitelli *et al.*, Phys. Rev. Lett. **127**, 6, 062001 (2021), [arXiv:2012.14267].

[74] S. Alioli *et al.*, Phys. Lett. B **818**, 136380 (2021), [arXiv:2103.01214].

[75] G. Gustafson 193–198 (1986).

[76] X. Artru and G. Mennessier, Nucl. Phys. B **70**, 93 (1974).

[77] B. Andersson *et al.*, Phys. Rept. **97**, 31 (1983).

[78] B. Andersson, *The Lund model*, volume 7, Cambridge University Press (2005), ISBN 978-0-521-01734-3, 978-0-521-42094-5, 978-0-511-88149-7.

[79] M. Bowler, Z. Phys. C **11**, 169 (1981).

[80] C. Peterson *et al.*, Phys. Rev. D **27**, 105 (1983).

[81] T. Sjostrand and P. Z. Skands, JHEP **03**, 053 (2004), [hep-ph/0402078].

[82] J. R. Christiansen and P. Z. Skands, JHEP **08**, 003 (2015), [arXiv:1505.01681].

[83] D. Amati and G. Veneziano, Phys. Lett. B **83**, 87 (1979).

Downloaded from https://academic.oup.com/ptep/article/2022/8/083C01/6651666 by KIT Library user on 27 September 2022

[84] A. Bassetto, M. Ciafaloni and G. Marchesini, Phys. Lett. B **83**, 207 (1979).

[85] R. D. Field and S. Wolfram, Nucl. Phys. B **213**, 65 (1983).

[86] B. Webber, Nucl. Phys. B **238**, 492 (1984).

[87] J.-C. Winter, F. Krauss and G. Soff, Eur. Phys. J. C **36**, 381 (2004), [hep-ph/0311085].

[88] D. Lange, Nucl. Instrum. Meth. A **462**, 152 (2001).

[89] S. Jadach *et al.*, Comput. Phys. Commun. **76**, 361 (1993).

[90] D. Grellscheid and P. Richardson (2007), [arXiv:0710.1951].

[91] T. Sjostrand and M. van Zijl, Phys. Rev. D **36**, 2019 (1987).

[92] P. Skands, S. Carrazza and J. Rojo, Eur. Phys. J. C **74**, 8, 3024 (2014), [arXiv:1404.5630].

[93] M. Bahr, J. M. Butterworth and M. H. Seymour, JHEP **01**, 065 (2009), [arXiv:0806.2949].

[94] M. Ryskin, A. Martin and V. Khoze, Eur. Phys. J. C **71**, 1617 (2011), [arXiv:1102.2844].

[95] H. Schulz and P. Skands, Eur. Phys. J. C **71**, 1644 (2011), [arXiv:1103.3649].

[96] R. Casalbuoni *et al.*, JHEP **01**, 035 (2009), [arXiv:0812.1982].

[97] (2005), [hep-ex/0511027].

[98] L. Lonnblad and T. Sjostrand, Eur. Phys. J. C **2**, 165 (1998), [hep-ph/9711460].

[99] V. Khoze *et al.*, Eur. Phys. J. C **69**, 85 (2010), [arXiv:1005.4839].

[100] J. Butterworth, J. R. Forshaw and M. Seymour, Z. Phys. C **72**, 637 (1996), [hep-ph/9601371].

[101] M. Bahr *et al.*, in "1st International Workshop on Multiple Partonic Interactions at the LHC," 239–248 (2009), [arXiv:0905.4671].

[102] R. Corke and T. Sjostrand, JHEP **05**, 009 (2011), [arXiv:1101.5953].

[103] G. A. Schuler and T. Sjostrand, Phys. Rev. D **49**, 2257 (1994).

[104] G. Ingelman and P. Schlein, Phys. Lett. B **152**, 256 (1985).

[105] S. Navin (2010), [arXiv:1005.3894].

[106] P. Aurenche *et al.*, Comput. Phys. Commun. **83**, 107 (1994), [hep-ph/9402351].

[107] F. W. Bopp, R. Engel and J. Ranft, in "LAFEX International School on High-Energy Physics (LISHEP 98) Session A: Particle Physics for High School Teachers - Session B: Advanced School in HEP - Session C: Workshop on Diffractive Physics," 729–741 (1998), [hep-ph/9803437].

[108] S. Roesler, R. Engel and J. Ranft, in "International Conference on Advanced Monte Carlo for Radiation Physics, Particle Transport Simulation and Applications (MC 2000)," 1033–1038 (2000), [hep-ph/0012252].

[109] B. E. Cox and J. R. Forshaw, Comput. Phys. Commun. **144**, 104 (2002), [hep-ph/0010303].

[110] J. Bellm *et al.*, Phys. Rev. D **94**, 3, 034028 (2016), [arXiv:1605.08256].

[111] S. Mrenna and P. Skands, Phys. Rev. D **94**, 7, 074005 (2016), [arXiv:1605.08352].

[112] E. Bothmann, M. Schönherr and S. Schumann, Eur. Phys. J. C **76**, 11, 590 (2016), [arXiv:1606.08753].

[113] A. Buckley *et al.*, Eur. Phys. J. C **65**, 331 (2010), [arXiv:0907.2973].

[114] S. Catani, B. Webber and G. Marchesini, Nucl. Phys. B **349**, 635 (1991).

[115] A. Karneyeu *et al.*, Eur. Phys. J. C **74**, 2714 (2014), [arXiv:1306.3436].

[116] A. Buckley *et al.*, Comput. Phys. Commun. **184**, 2803 (2013), [arXiv:1003.0694].

Downloaded from https://academic.oup.com/ptep/article/2022/8/083C01/6651666 by KIT Library user on 27 September 2022

44. Monte Carlo Neutrino Generators

Revised September 2021 by H. Gallagher (Tufts U.) and Y. Hayato (Kamioka Observatory, ICRR, UTokyo; Kavli IPMU (WPI), UTokyo).

Monte Carlo neutrino generators are programs or libraries which simulate neutrino interactions with electrons, nucleons and nuclei. In this capacity their usual task is to take an input neutrino and nucleus and produce a set of 4-vectors for particles emerging from the interaction, which are then input to full detector simulations. Since these generators have to simulate not only the initial interaction of neutrinos with target particles, but reinteractions of the generated particles in the nucleus, they contain a wide range of elementary particle and nuclear physics. Viewed more broadly, they are the access point for neutrino experimentalists to the theory inputs needed for analysis. Examples include cross section libraries for event rate calculations and parameter uncertainties and reweighting tools for systematic error evaluation.

Neutrino experiments typically operate in neutrino beams that are neither completely pure nor mono-energetic. Generators are a crucial component in the convolution of beam flux, neutrino interaction physics, and detector response that is necessary to make predictions about observable quantities. Generated events are used to define experimental analyses, like event selection criteria, for efficiency determination and background subtraction. Similarly they are used to relate reconstructed quantities back to true quantities. In these various capacities they are used from the detector design stage through the extraction of physics measurements from reconstructed observable. Monte Carlo neutrino generators play unique and important roles in the experimental study of neutrino interactions and oscillations.

There are several neutrino event generators available, such as ANIS [1], GENIE [2, 3], GiBUU [4, 5], MARLEY [6], NEGN [7], NEUT [8], NUANCE [9], the FLUKA routines NUNDIS/-NUNRES [10, 11], and NuWro [12], as well as tools to facilitate cross-generator comparisons, such as NUISANCE [13]. Historically, experiments would develop their own generators. This was often because they were focused on a particular measurement, energy range, or target, and wanted to ensure that the best physics was included for them. These 'home-grown' generators were often tuned primarily or exclusively to the neutrino data most similar to the data that the experiment would be collecting. A major advance in the field was the introduction of conference series devoted to the topic of neutrino interaction physics, NuINT (https://indico.cern.ch/event/703880/) and NuFACT (https://indico.cern.ch/event/855372/) in particular. Event generator comparisons have been a regular staple of the NuINT conference series from its inception, and a great deal of information on this topic can be found in the Proceedings of these meetings. These meetings have facilitated experiment-theory discussions leading to the first generator developed by a theory group (NuWro) [12], the extension of established nuclear interaction codes (FLUKA and GiBUU) to include neutrino-nuclear processes [4,5,10,11], and inclusion of theorists in existing generator development teams.

These activities have led to more careful scrutiny of the crucial hadron and nuclear theory inputs to these generators, which is evaluated in particular through comparisons to electron-scattering data. At this point in time all simulation codes face challenges in describing the full extent of the lepton scattering data, and the tension between incorporating the best available theory versus obtaining the best agreement with the data plays out in a variety of ways within the field. For the field to make progress, inclusion of state of the art theory needs to be coupled to global analyses that correctly incorporate correlations between measurements. Given the rapid pace of new data and the complexity of analyses, this is a significant challenge for the field in the coming years.

There are many neutrino experiments which use various sources of neutrinos, from reactors, accelerators, the atmosphere, and astrophysical sources, thereby covering a range of energies from MeV to TeV. Much of the emphasis has been on the few-GeV region in the generators, as this is the relevant energy range for short- and long-baseline neutrino oscillation experiments. These generators use the impulse approximation, which treats the nucleus as a collection of independent nucleons and the primary interaction occurs between the probe and a single nucleon, for most of the initial interaction, and subsequently simulates the interactions of secondary particles in the nucleus in semi-classical ways. Semi-classical hadron transport approaches are commonly used as they are able simulate a variety of nuclei in a single model, fully describe complex multi-particle final states, and for practical considerations as these approaches are fast. However, there are several challenges facing these simulations coming mainly from the complexity of the nuclear physics, and the need to avoid double counting in combining perturbative and non-perturbative models for the neutrino-nucleon scattering processes. The overall validity of this impulse approximation-based scheme, and in particular the importance of scattering channels that involve more than one nucleon, is a crucial question that is the topic of much current work. While generators share many common ingredients, differences in implementation, parameter values, and approaches to avoid double counting can yield dramatically different predictions [14]. In the following sections, interaction models and their implementations, including final-state interactions of hadrons produced in the nuclei, are described.

In order to assure their validity, neutrino event generators are tuned and validated against a wide variety of data. This means that the quality of the outputs from generators is limited by the quality of experimental data. The existing neutrino-nucleon and neutrino-nucleus scattering data sets are not restrictive enough to eliminate many approaches. On the other hand, there are various precise data sets, which use photon, charged lepton, and hadron probes. These data sets are extensively used to validate the generators. The results from these external data tuning exercises are important for experiments as they quantify the uncertainty on model parameters, needed by experiments in the evaluation of generator-related systematic errors. Electron scattering data plays an important role in determining the vector contribution to the form-factors and structure functions, as well as in evaluating specific aspects of the nuclear model [15, 16]. Hadron scattering data is used in validating the nuclear model, in particular of interactions between hadrons produced in the primary interaction and the residual target nucleus (final state interactions). As mentioned, tuning of neutrino-nucleon scattering and hadronization models relies heavily on the previous generation of high energy neutrino scattering and hydrogen and deuterium bubble chamber experiments. More recent data from the K2K, MiniBooNE, NOMAD, SciBooNE, MINOS, T2K, ArgoNEUT, MINERvA, NOvA, MicroBooNE, ICARUS, SBND and Ninja experiments has been, or will be, used for this purpose, although caution is advisable due to possible biases that mismodeled nuclear effects might introduce. In practice, there are often choices to be made about which models to include in an overall simulation, and which data sets to use for tuning. The process of developing a comprehensive tune in GENIE is discussed in Ref. [3].

However, all the recent experiments use nuclear targets and it is challenging to disentangle the neutrino-nucleon interaction from the effects of the nuclear environment. For example, it is difficult to separate charged current quasi-elastic scattering from the multi-nucleon quasi-elastic like scattering or single pion production, in which a pion is absorbed in the nucleus. Sometimes, there are tensions between the data sets from different experiments. Data on multi-pion and meson production are limited, but are anticipated to be measured in the near future experiments. Next generation experiments are expected to provide better detection capabilities with higher statistics and these data will help in evaluating and validating the models implemented in the generators.

44.1 Neutrino-Nucleon Scattering

Event generators typically begin with free-nucleon cross sections which are then embedded into a nuclear physics model. The most important processes are quasi-elastic (elastic for neutral current (NC)) scattering, resonance production, and non-resonant inelastic scattering, which make comparable contributions for few-GeV interactions. The neutrino cross sections in this energy range can be seen in Figure 52.1 of this *Review*.

Downloaded from https://academic.oup.com/ptep/article/2022/8/083C01/6651666 by KIT Library user on 27 September 2022

44.1.1 *Quasi-Elastic Scattering*

The cross section for the neutrino nucleon charged current quasi-elastic scattering is described in terms of the leptonic and hadronic weak currents, where dominant contributions to the hadronic current come from the vector (V) and axial-vector (A) form factors. Contributions from the pseudo-scalar form factor (P) are typically small for muon and electron neutrinos and are related to the axial form factor (A) assuming partially conserved axial currents (PCAC). Owing to isospin symmetry, the vector form factors are related to those measured by precise electron scattering experiments [17]. Therefore, most of the generators use parametrizations of these form factors taken directly from the data. For the axial form factor there is no such precise experiment, and most of the generators use a dipole form [18]. Generally, the value of axial form factor at $q^2 = 0$ (q is the four-momentum transfer) is extracted from the polarized nucleon beta decay experiment. However, the selection of the axial vector mass parameter depends on each generator, with values typically around 1.00 GeV/c^2. Recently, there are several attempts to use the other functions for the axial form factors [19, 20] and some generators have already implemented these form factors [8, 21].

44.1.2 *Inelastic Production*

Most generators use the prescriptions of Rein-Sehgal [22] to simulate neutrino-induced single pion production, or updated versions that incorporate lepton mass terms and pion pole contributions [23, 24]. To obtain the cross section for a particular channel, they calculate the amplitude for the production of each resonance multiplied by the probability for the decay of that resonance into that particular channel. Implementation differences include the number of resonances included, whether the amplitudes are added coherently or incoherently, the invariant mass range over which the model is used, how non-resonant backgrounds are included, inclusion of lepton mass terms, and the model parameter values (in particular the axial mass). In this model it is also possible to calculate the cross-sections of single photon, and η production by changing the decay probability of the resonances, which are included in some of the programs. However, it is known that discrepancies exist between the recent pion electro/photo-production data and the results from the simulation data with the same framework, i.e. vector part of this model. There are several attempts to overcome this issue [25] and some of the generators started using more appropriate form factors. Recently, there are approaches that improve the theoretical description of non-resonant contributions in the resonance region, [26–28], and which account for interference between resonant and non-resonant amplitudes. This work is expected to be implemented in the generators soon. GiBUU and NuWro generators do not use the Rein-Sehgal model, and instead rely directly on electro-production data for the vector contribution and fit bubble chamber data to determine the remaining parameters for the axial contribution [29–32]. The dynamical coupled-channel model, which has been developed to simulate various electro- and photo-meson productions, was extended to simulate the neutrino single pion production [33]. In this approach pion-nucleon scattering is used to fix the form of the axial current at $q^2 = 0$. This model is also being implemented and expected to be available in some of the generators in future.

44.1.3 *Deep and Shallow Inelastic Scattering*

For this process the fundamental target shifts from the nucleon to its quark constituents. Therefore, the generators construct the nucleon structure functions F_2 and xF_3 from parton distributions for high Q^2 (the DIS regime: W$\gtrsim$ 2 GeV/c^2 and Q$^2 \gtrsim$ 1 GeV^2) to calculate the direction and momentum of the lepton. The first challenge is in extending this picture to the lower values of Q^2 and W that dominate the available phase space for few-GeV interactions (the so-called 'shallow inelastic scattering', or SIS regime). GRV98LO parton distribution functions [34] with the corrections proposed in [35, 36] are widely used, while others [10] implement their own modifications to the parton distributions at low Q^2. Both DIS and SIS generate hadrons but their production depends on each generator's implementation of a hadronization model as described in the next section. There are various difficulties not only in the actual hadronization but the relation with the single meson production. It is necessary to avoid double counting between the resonance and SIS/DIS models, and all generators are different in this regard. The scheme chosen can have a significant impact on the results of simulations at a few-GeV neutrino energies. For simulating ultra-high energy interactions currently being studied with neutrino telescopes, fully partonic descriptions, which utilize beyond-leading-order pQCD calculations [37, 38] are the norm [39].

44.2 Hadronization Models

For hadrons produced via baryonic resonances, the underlying model amplitudes and resonance branching fractions can be used to fully characterize the hadronic system. For shallow- and deep-inelastic scattering, a hadronization model is required. Most generators use PYTHIA [40] for this purpose, although some with modified parameters. In addition some implement their own models to handle invariant masses that are too low for PYTHIA, typically somewhere around 2.0 GeV/c^2. Such models rely heavily on measurements of neutrino hadro-production in high-resolution devices, such as bubble chambers and the CHORUS [41] and NOMAD experiments [42], to construct empirical parametrizations that reproduce the key features of the data [43, 44]. The basic ingredients are the empirical observations that average charged particle multiplicities increase logarithmically with the invariant mass of the hadronic system, and that the distribution of charged particle multiplicities about this average are described by a single function (an observation known as KNO scaling [45]). The multiplicity of the neutral particles are usually obtained by scaling the charged particle multiplicity. Simple parametrizations to more accurately reproduce differences observed in the forward/backward hemispheres of hadronic systems are included in GENIE, NEUT, and NuWro.

44.3 Nuclear Physics

The nuclear physics relevant to neutrino-nucleus scattering at few-GeV energies is complicated, involving Fermi motion, nuclear binding, Pauli blocking, in-medium modifications of form factors and hadronization, intranuclear rescattering of hadrons, and many-body scattering mechanisms including long- and short-range nucleon-nucleon correlations.

44.3.1 *Treatment of nuclear effects*

In order to obtain the cross-section off nucleons in the nucleus, it is necessary to take into account various in-medium effects. Most of the models used for neutrino-nuclear scattering kinematics were developed in the context of few-GeV inclusive electron scattering, by experiments going back nearly 50 years. The basic models employed in event generators rely on impulse approximation schemes, the most simple of which is the Relativistic Fermi Gas Model. The most common implementations have been the Smith-Moniz [46] and Bodek-Ritchie [47] models. However, the results from neutrino-nucleus scattering experiments in 2000 and afterwards, beginning with K2K, MiniBooNE have shown large discrepancies from the naive expectation from the models. Most striking differences are a suppression of forward going muons (low Q^2), a high Q^2 enhancement in the event rate, and an overall larger than expected number of observed events. In order to reproduce the data, the quasi-elastic axial mass was used as the effective parameter and increased by roughly 20% from the nominal values obtained by an earlier generation of bubble chamber experiments using hydrogen or deuterium [18]. This inconsistency between nucleon and nucleus targets suggests that the simple nuclear model is not appropriate in describing the data. Moreover, these simple Fermi-Gas models are not expected to describe the kinematical distributions of final state nucleons. Therefore, several generators have to implement better models, such as local Fermi-Gas model or more sophisticated models. Within the electron scattering community, the analogous calculations have for decades relied on spectral functions, which incorporate information about nucleon momenta and binding energies in the impulse approximation scheme [15]. Therefore, most of the generators have implemented the realistic spectral functions in their latest releases.

Actually, the discrepancies in small q^2 could not be solved alone

Downloaded from https://academic.oup.com/ptep/article/2022/8/083C01/6651666 by KIT Library user on 27 September 2022

by just introducing the local Fermi-gas model nor spectral function models. This implies that the additional medium correction effects are needed to be taken into account. One of the implemented solutions is the local Fermi-Gas model with medium correction calculated using the random phase approximation, which is known to give large suppression in small q^2 [48, 49]. Although, the fundamental parts of the models are same, actual implementations are quite different between the generators. Especially, the constructions of the final state hadron kinematics are quite different. Especially for the quasi-elastic scattering case, treatment of the nucleon masses in the nucleus, the binding and the separation energies are sometimes quite different [50]. Recently, Super-Scaling model with relativistic mean field theory effects (SuSAv2) [51, 52] is implemented in some of the generators. Indications of the suppression in small q^2 in the single pion productions were also observed in K2K and MiniBooNE and it is clearly observed at the MINERνA and NOνA experiments. However, the models to explain the suppression have not been implemented, other than the phenomenological ones. Also, q^2 dependence of the cross-section is largely model and parameter dependent. Further studies of newly implemented single pion models may give new insights. The cause of the discrepancy of small q^2 seems to be identified but the issue of the observed interaction rates are not solved. This implies that there must be some interaction channels which are missing and not considered in the generators.

These led to a revisitation of the role played by excitation of multiple particle-hole states in the nucleus, and the experimental study of these scattering channels is an area of intense experimental interest [53]. The contribution of these scattering processes is an extremely active area of theoretical research as well, with significant implications for generators and analyses [54]. Several approaches, ranging from strictly phenomenological descriptions to full theoretical calculations, have recently been incorporated into generators [55–57]. One example of a phenomenological approach utilizes an Effective Spectral Function [58] and a Transverse Enhancement Model [59], which together encapsulate information derived from electron scattering experiments at relevant kinematics. The microscopic model of Nieves and collaborators is now available in GENIE and NEUT [60, 61]. SuSAv2 model [52] also has capability to simulate this multi-nucleon quasi-elastic like interaction and is also implemented in GENIE.

One of the challenges in incorporating full theoretical models of these processes is that they are typically slow, so generators have developed new approaches whereby much of the computation is done offline, and the generators simply read in the hadronic tensor components. This allows for a full prediction of the lepton kinematics, however the ability to simulate the hadronic component of these multinucleon states then relies on separate models. The other challenge is that the theoretical models are not designed to describe exclusive final states. These approaches, while making simulations computationally tractable, neglect correlations between the lepton and hadron kinematics. Also, there are limitations of the model itself to describe some of the kinematic regions. However, the generators need to simulate final all the state particles and thus, several assumptions are made by authors of the generators from time to time.

Also, it is known from photo and electro-nuclear scattering that the Delta width is affected by Pauli blocking and collisional broadening. These effects are included in some, but not all generators.

The remnant nucleus after the scattering is usually in an excited state. Therefore, the remnant may emit gamma-rays, additional nucleons or an alpha particle during the de-excitation process. This de-excitation gamma-ray is used in searching for proton decay in water Cherenkov detectors. Some generators have implemented this process. NEUT implemented the de-excitation process but only for Oxygen. Recently, GENIE has de-excitation processes for various nuclei.

When scattering from a nucleus, coherent scattering of various kinds is possible. Most simulations incorporate, at least, coherent neutral and charged single pion production. While the interaction rate for these interactions is typically around a percent of the total yield, the unique kinematic features of these events can make them potential backgrounds for oscillation searches. Implemented in Monte Carlo are several PCAC-based methods [62, 63]. Microscopic models, valid at lower neutrino energies [64–67], have also been implemented in several generators. One commonly used model by Rein and Sehgal [62] predicts a cross section for charged-current coherent pion production that is much larger than what is observed by K2K, MINERvA and T2K. However, the cross-section is sensitive to the pion cross-section used in the model as parameters and improved models with lepton mass correction [63] give better agreement with the recent data. This improved model is implemented in most of the generators. In addition to coherent pion production, some generators can simulate coherent single photon production [68] and coherent elastic neutrino-nucleus scattering.

44.3.2 *Hadron Production in Nuclei*

Neutrino pion production is one of the dominant neutrino scattering mechanisms in the few-GeV region and the pions produced in the nucleus have quite large interaction cross sections. Therefore, pion intranuclear scattering can have sizable effects on the results of simulations at these energies. Also, recent neutrino oscillation experiments use the observed information of protons and pions more extensively, in addition to the charged leptons. Therefore, most generators implement this physics through an intranuclear cascade simulation. In generators which utilize cascade models, a hadron, which has been formed in the nucleus, is moved step by step until it interacts with a nucleon or escapes from the nucleus. The probabilities of each interaction in nucleus are usually given as the mean free paths and used to determine whether the hadron has interacted or not. If the hadron is found to have interacted, appropriate final states are selected. Usually, absorption, elastic, charge exchange, and inelastic scatterings including particle productions are simulated as intranuclear interactions. The determination method of the kinematics for the final state particles heavily depends on the generators but most of them use experimentally validated models to simulate hadron interactions in nucleus. No two intranuclear cascade simulations implemented in neutrino event generators are the same [69]. In all cases hadrons propagate from an interaction vertex chosen based on the density distribution of the target nucleus. In determining the generated position of the hadrons in nucleus, the concept of the formation length is sometimes employed. Based on this idea, the hadronization process is not instantaneous and it takes some time before generating the hadrons [12]. The basis for formation times are measurements at relatively high energy and Q^2, and most generators that employ the concept do not apply them to resonance interactions.

GiBUU does not employ an intranuclear cascade simulation, instead, it utilizes a semi-classical transport model in coupled channels that describes the space-time evolution of a many body system in the presence of potentials and a collision term [4]. This approach assures consistency between nuclear effects in the initial state, such as Fermi motion, Pauli blocking, hadron self-energies [70], and modified cross sections, and the final state, such as particle re-interactions, since the two are derived from the same model. This model has been previously used to describe a wide variety of nuclear interaction data. Similarly, the hadronic simulation of the NUNDIS/NUNRES programs are handled by the well-established FLUKA hadronic simulation package [10]. Recently, GENIE included the interface to the external hadronic simulation package INCL++ [71].

References

[1] A. Gazizov and M. P. Kowalski, Comput. Phys. Commun. **172**, 203 (2005), [arXiv:astro-ph/0406439].

[2] C. Andreopoulos *et al.*, Nucl. Instrum. Meth. **A614**, 87 (2010), [arXiv:0905.2517].

[3] J. Tena-Vidal *et al.* (GENIE) (2021), [arXiv:2104.09179].

[4] O. Buss *et al.*, Phys. Rept. **512**, 1 (2012), [arXiv:1106.1344].

[5] K. Gallmeister, U. Mosel and J. Weil, Phys. Rev. **C94**, 3, 035502 (2016), [arXiv:1605.09391].

[6] S. Gardiner, C. Grant, E. Panic, and R. Svoboda, `http://www.marleygen.org`.

[7] D. Autiero, Nucl. Phys. Proc. Suppl. **139**, 253 (2005).

Downloaded from https://academic.oup.com/ptep/article/2022/8/083C01/6651666 by KIT Library user on 27 September 2022

[8] Y. Hayato and L. Pickering, Eur. Phys. J. Spec. Top. (2021), [arXiv:2106.15809].

[9] D. Casper, Nucl. Phys. Proc. Suppl. **112**, 161 (2002), [hep-ph/0208030].

[10] G. Battistoni *et al.*, Acta Phys. Polon. **B40**, 2491 (2009).

[11] T. T. Böhlen *et al.*, Nucl. Data Sheets **120**, 211 (2014).

[12] T. Golan, C. Juszczak and J. T. Sobczyk, Phys. Rev. **C86**, 015505 (2012), [arXiv:1202.4197].

[13] P. Stowell *et al.*, JINST **12**, 01, P01016 (2017), [arXiv:1612.07393].

[14] M. Betancourt *et al.*, Phys. Rept. **773-774**, 1 (2018), [arXiv:1805.07378].

[15] O. Benhar, D. day and I. Sick, Rev. Mod. Phys. **80**, 189 (2008), [arXiv:nucl-ex/0603029].

[16] B. Schmookler *et al.* (CLAS), Nature **566**, 7744, 354 (2019), [arXiv:2004.12065].

[17] A. Bodek *et al.*, Eur. Phys. J. **C53**, 349 (2008), [arXiv:0708.1946].

[18] H. Gallagher, G. Garvey and G. P. Zeller, Ann. Rev. Nucl. Part. Sci. **61**, 355 (2011).

[19] E. Tomasi-Gustafsson, G. I. Gakh and C. Adamuscin, Phys. Rev. **C73**, 045204 (2006), [arXiv:nucl-th/0512039].

[20] B. Bhattacharya, R. J. Hill and G. Paz, Phys. Rev. **D84**, 073006 (2011), [arXiv:1108.0423].

[21] A. S. Meyer *et al.*, Phys. Rev. **D93**, 11, 113015 (2016), [arXiv:1603.03048].

[22] D. Rein and L. M. Sehgal, Annals Phys. **133**, 79 (1981).

[23] K. S. Kuzmin, V. V. Lyubushkin and V. A. Naumov, Mod. Phys. Lett. A **19**, 2815 (2004), [hep-ph/0312107].

[24] C. Berger and L. M. Sehgal, Phys. Rev. D **76**, 113004 (2007), [arXiv:0709.4378].

[25] K. M. Graczyk and J. T. Sobczyk, Phys. Rev. **D77**, 053001 (2008), [Erratum: Phys. Rev.D79,079903(2009)], [arXiv:0707.3561].

[26] M. Kabirnezhad, Phys. Rev. **D97**, 1, 013002 (2018), [arXiv:1711.02403].

[27] M. Kabirnezhad, Phys. Rev. D **102**, 5, 053009 (2020), [arXiv:2006.13765].

[28] E. Hernandez, J. Nieves and M. Valverde, Phys. Rev. D **76**, 033005 (2007), [hep-ph/0701149].

[29] O. Lalakulich and E. A. Paschos, Phys. Rev. **D71**, 074003 (2005), [hep-ph/0501109].

[30] J. A. Nowak, Phys. Scripta **T127**, 70 (2006), [hep-ph/0607081].

[31] T. Leitner *et al.*, Phys. Rev. C **79**, 034601 (2009), [arXiv:0812.0587].

[32] L. Alvarez-Ruso, S. K. Singh and M. J. Vicente Vacas, Phys. Rev. **C57**, 2693 (1998), [arXiv:nucl-th/9712058].

[33] S. X. Nakamura, H. Kamano and T. Sato, Phys. Rev. **D92**, 7, 074024 (2015), [arXiv:1506.03403].

[34] M. Glück, E. Reya and A. Vogt, Eur. Phys. J. **C5**, 461 (1998), [hep-ph/9806404].

[35] A. Bodek and U. K. Yang, J. Phys. **G29**, 1899 (2003), [hep-ex/0210024].

[36] A. Bodek, U. K. Yang and Y. Xu (2021), [arXiv:2108.09240].

[37] A. Cooper-Sarkar, P. Mertsch and S. Sarkar, JHEP **08**, 042 (2011), [arXiv:1106.3723].

[38] V. Bertone, R. Gauld and J. Rojo, JHEP **01**, 217 (2019), [arXiv:1808.02034].

[39] A. Garcia and A. Heijboer (KM3NeT), PoS **ICRC2019**, 895 (2020), [arXiv:1908.10077].

[40] T. Sjostrand, S. Mrenna and P. Z. Skands, JHEP **05**, 026 (2006), [hep-ph/0603175].

[41] A. Kayis-Topaksu *et al.* (CHORUS), Eur. Phys. J. **C51**, 775 (2007), [arXiv:0707.1586].

[42] J. Altegoer *et al.* (NOMAD), Phys. Lett. **B445**, 439 (1999).

[43] T. Yang *et al.*, Eur. Phys. J. **C63**, 1 (2009), [arXiv:0904.4043].

[44] J. A. Nowak and J. T. Sobczyk, Acta Phys. Polon. **B37**, 2371 (2006), [hep-ph/0608108].

[45] Z. Koba, H. B. Nielsen and P. Olesen, Nucl. Phys. **B40**, 317 (1972).

[46] R. A. Smith and E. J. Moniz, Nucl. Phys. **B43**, 605 (1972), [Erratum: Nucl. Phys.B101,547(1975)].

[47] A. Bodek and J. L. Ritchie, Phys. Rev. **D24**, 1400 (1981).

[48] M. C. Martinez *et al.*, Phys. Rev. C **73**, 024607 (2006), [arXiv:nucl-th/0505008].

[49] J. Nieves, J. E. Amaro and M. Valverde, Phys. Rev. C **70**, 055503 (2004), [Erratum: Phys.Rev.C 72, 019902 (2005)], [arXiv:nucl-th/0408005].

[50] A. Bodek and T. Cai, Eur. Phys. J. C **79**, 4, 293 (2019), [arXiv:1801.07975].

[51] J. A. Caballero *et al.*, Phys. Lett. **B653**, 366 (2007), [arXiv:0705.1429].

[52] R. Gonzaléz-Jiménez *et al.*, Phys. Rev. C **90**, 3, 035501 (2014), [arXiv:1407.8346].

[53] X. G. Lu *et al.* (MINERvA) (2021), [arXiv:2107.02064].

[54] L. Alvarez-Ruso *et al.*, Prog. Part. Nucl. Phys. **100**, 1 (2018), [arXiv:1706.03621].

[55] T. Katori, AIP Conf. Proc. **1663**, 1, 030001 (2015), [arXiv:1304.6014].

[56] M. Alam *et al.* (2015), [arXiv:1512.06882].

[57] C. Wilkinson *et al.*, Phys. Rev. **D93**, 7, 072010 (2016), [arXiv:1601.05592].

[58] A. Bodek, M. E. Christy and B. Coopersmith, Eur. Phys. J. **C74**, 10, 3091 (2014), [arXiv:1405.0583].

[59] A. Bodek, H. S. Budd and M. E. Christy, Eur. Phys. J. **C71**, 1726 (2011), [arXiv:1106.0340].

[60] J. Nieves, I. Ruiz Simo and M. J. Vicente Vacas, Phys. Rev. **C83**, 045501 (2011), [arXiv:1102.2777].

[61] R. Gran *et al.*, Phys. Rev. **D88**, 11, 113007 (2013), [arXiv:1307.8105].

[62] D. Rein and L. M. Sehgal, Nucl. Phys. **B223**, 29 (1983).

[63] C. Berger and L. M. Sehgal, Phys. Rev. **D79**, 053003 (2009), [arXiv:0812.2653].

[64] L. Alvarez-Ruso *et al.*, Phys. Rev. **C75**, 055501 (2007), [Erratum: Phys. Rev.C80,019906(2009)], [arXiv:nucl-th/0701098].

[65] L. Alvarez-Ruso, L. S. Geng and M. J. Vicente Vacas, Phys. Rev. **C76**, 068501 (2007), [Erratum: Phys. Rev.C80,029904(2009)], [arXiv:0707.2172].

[66] J. E. Amaro *et al.*, Phys. Rev. D **79**, 013002 (2009), [arXiv:0811.1421].

[67] S. X. Nakamura *et al.*, Phys. Rev. C **81**, 035502 (2010), [arXiv:0910.1057].

[68] E. Wang, L. Alvarez-Ruso and J. Nieves, Phys. Rev. C **89**, 1, 015503 (2014), [arXiv:1311.2151].

[69] S. Dytman *et al.*, Phys. Rev. D **104**, 5, 053006 (2021), [arXiv:2103.07535].

[70] S. K. Singh, M. J. Vicente-Vacas and E. Oset, Phys. Lett. B **416**, 23 (1998), [Erratum: Phys.Lett.B 423, 428 (1998)].

[71] A. Boudard *et al.*, Phys. Rev. C **87**, 014606 (2013), URL `https://link.aps.org/doi/10.1103/PhysRevC.87.014606`.

Downloaded from https://academic.oup.com/ptep/article/2022/8/083C01/6651666 by KIT Library user on 27 September 2022

45. Monte Carlo Particle Numbering Scheme

Revised August 2021 by F. Krauss (Durham U.), S. Navas (Granada U.), P. Richardson (Durham U.) and T. Sjöstrand (Lund U.).

The Monte Carlo particle numbering scheme presented here is intended to facilitate interfacing between matrix-element generators, event generators, detector simulators, and analysis packages used in particle physics, and is widely accepted as the "industry standard". The numbering scheme was introduced in 1988 [1], and has since been revised and expanded in the light of new information on hadronic resonances, and expanded to encompass as yet undiscovered and hypothetical particles.

The general form is a 7–digit number:

$$\pm n\ n_r\ n_L\ n_{q_1}\ n_{q_2}\ n_{q_3}\ n_J\ .$$

This encodes information about the particle's spin, flavor content, and internal quantum numbers. A 9–digit extension is used specifically for tetra- and penta-quark states, and a distinct 10-digit scheme is used for encoding (hyper)nuclear states. The details are as follows:

1. Particles are given positive numbers, antiparticles negative numbers. The PDG convention for mesons is used, so that K^+ and B^+ are particles.
2. Quarks and leptons are numbered consecutively starting from 1 and 11 respectively; to do this they are first ordered by family and within families by weak isospin.
3. In composite quark systems (diquarks, mesons, and baryons) $n_{q_{1-3}}$ are quark numbers used to specify the quark content, while the rightmost digit $n_J = 2J+1$ gives the system's spin (except for the K^0_S and K^0_L). The scheme does not cover particles of spin $J > 4$.
4. Diquarks have 4-digit numbers with $n_{q_1} \geq n_{q_2}$ and $n_{q_3} = 0$.
5. The numbering of mesons is guided by the nonrelativistic (L–S decoupled) quark model, as listed in Tables 15.2, 15.3, and 15.4.
   (a) The numbers specifying the meson's quark content conform to the convention $n_{q_1} = 0$ and $n_{q_2} \geq n_{q_3}$. The special case K^0_L is the sole exception to this rule.
   (b) The quark numbers of flavorless, light (u, d, s) mesons are: 11 for the member of the isotriplet $(\pi^0, \rho^0, \ldots)$, 22 for the lighter isosinglet $(\eta, \omega, \ldots)$, and 33 for the heavier isosinglet $(\eta', \phi, \ldots)$. Since isosinglet mesons are often large mixtures of $u\bar{u} + d\bar{d}$ and $s\bar{s}$ states, 22 and 33 are assigned by mass and do not necessarily specify the dominant quark composition.
   (c) The special numbers 310 and 130 are given to the K^0_S and K^0_L respectively.
   (d) The fifth digit n_L is reserved to distinguish mesons of the same total (J) but different spin (S) and orbital (L) angular momentum quantum numbers. For $J > 0$ the numbers are: $(L, S) = (J-1, 1)$ $n_L = 0$, $(J, 0)$ $n_L = 1$, $(J, 1)$ $n_L = 2$ and $(J+1, 1)$ $n_L = 3$. For the exceptional case $J = 0$ the numbers are $(0, 0)$ $n_L = 0$ and $(1, 1)$ $n_L = 1$ (*i.e.* $n_L = L$). See Table 45.1.
   (e) If a set of physical mesons correspond to a (non-negligible) mixture of basis states, differing in their internal quantum numbers, then the lightest physical state gets the smallest basis state number. For example the $K_1(1270)$ is numbered 10313 (1^1P_1 K_{1B}) and the $K_1(1400)$ is numbered 20313 (1^3P_1 K_{1A}).
   (f) The sixth digit n_r is used to label mesons radially excited above the ground state.
   (g) Numbers have been assigned for complete $n_r = 0$ S- and P-wave multiplets, even where states remain to be identified.
   (h) In some instances assignments within the $q\bar{q}$ meson model are only tentative; here best guess assignments are made.

Table 45.1: Meson numbering logic. Here qq stands for $n_{q2}\, n_{q3}$.

	$L=J-1,\ S=1$			$L=J,\ S=0$			$L=J,\ S=1$			$L=J+1,\ S=1$		
J	code	J^{PC}	L	code	J^{PC}	L	code	J^{PC}	L	code	J^{PC}	L
0	—	—	—	00qq1	0^{-+}	0	—	—	—	10qq1	0^{++}	1
1	00qq3	1^{--}	0	10qq3	1^{+-}	1	20qq3	1^{++}	1	30qq3	1^{--}	2
2	00qq5	2^{++}	1	10qq5	2^{-+}	2	20qq5	2^{--}	2	30qq5	2^{++}	3
3	00qq7	3^{--}	2	10qq7	3^{+-}	3	20qq7	3^{++}	3	30qq7	3^{--}	4
4	00qq9	4^{++}	3	10qq9	4^{-+}	4	20qq9	4^{--}	4	30qq9	4^{++}	5

   (i) Many states appearing in the Meson Listings are not yet assigned within the $q\bar{q}$ model. Here $n_{q_{2-3}}$ and n_J are assigned according to the state's likely flavors and spin; all such unassigned light isoscalar states are given the flavor code 22. Within these groups $n_L = 0, 1, 2, \ldots$ is used to distinguish states of increasing mass. These states are flagged using $n = 9$. It is to be expected that these numbers will evolve as the nature of the states are elucidated. Codes are assigned to all mesons which are listed in the one-page table at the end of the Meson Summary Table as long as they have a prefered or established spin. Additional heavy meson states expected from heavy quark spectroscopy are also assigned codes.
6. The numbering of baryons is again guided by the nonrelativistic quark model, see Table 15.6. This numbering scheme is illustrated through a few examples in Table 45.2.
   (a) The numbers specifying a baryon's quark content are such that in general $n_{q_1} \geq n_{q_2} \geq n_{q_3}$.
   (b) Two states exist for $J = 1/2$ baryons containing 3 different types of quarks. In the lighter baryon $(\Lambda, \Xi, \Omega, \ldots)$ the light quarks are in an antisymmetric ($J = 0$) state while for the heavier baryon $(\Sigma^0, \Xi', \Omega', \ldots)$ they are in a symmetric ($J = 1$) state. In this situation n_{q_2} and n_{q_3} are reversed for the lighter state, so that the smaller number corresponds to the lighter baryon.
   (c) For excited baryons a scheme is adopted, where the n_r label is used to denote the excitation bands in the harmonic oscillator model, see Sec. 15.5. Using the notation employed there, n_r is given by the N-index of the D_N band identifier.
   (d) Further degeneracies of excited hadron multiplets with the same excitation number n_r and spin J are lifted by labelling such multiplets with the n_L index according to their mass, as given by its N or Δ-equivalent.
   (e) In such excited multiplets extra singlets may occur, the $\Lambda(1520)$ being a prominent example. In such cases the ordering is reversed such that the heaviest quark label is pushed to the last position: $n_{q_3} > n_{q_1} > n_{q_2}$.
7. The gluon, when considered as a gauge boson, has official number 21. In codes for glueballs, however, 9 is used to allow a notation in close analogy with that of hadrons.
8. The pomeron and odderon trajectories and a generic reggeon trajectory of states in QCD are assigned codes 990, 9990, and 110 respectively, where the final 0 indicates the indeterminate nature of the spin, and the other digits reflect the expected "valence" flavor content. We do not attempt a complete classification of all reggeon trajectories, since there is currently no need to distinguish a specific such trajectory from its lowest-lying member.
9. Two-digit numbers in the range 21–30 are provided for the Standard Model gauge and Higgs bosons.
10. Codes 81–100 are reserved for generator-specific pseudoparticles and concepts. Codes 901–930, 1901–1930, 2901–2930, and 3901–3930 are for additional components of Standard Model parton distribution functions, where the latter three ranges are intended to distinguish left/ right/ longitudinal components. Codes 998 and 999 are reserved for GEANT tracking purposes.

Downloaded from https://academic.oup.com/ptep/article/2022/8/083C01/6651666 by KIT Library user on 27 September 2022

Table 45.2: Some examples of octet (top) and decuplet (bottom) members for the numbering scheme for excited baryons. Here qqq stands for $n_{q_1}n_{q_2}n_{q_3}$. See the text for the definition of the notation. The numbers in parenthesis correspond to the mass of the baryons. The states marked as (?) are not experimentally confirmed.

J^P	(D, L_N^P)	$n_r n_L n_{q_1} n_{q_2} n_{q_3} n_J$	N	Λ_8	Σ	Ξ	Λ_1
	Octet		211,221	312	311,321,322	331,332	213
$1/2^+$	$(\mathbf{56}, \mathbf{0}_{\mathbf{0}}^+)$	$00qqq2$	(939)	(1116)	(1193)	(1318)	—
$1/2^+$	$(\mathbf{56}, \mathbf{0}_{\mathbf{2}}^+)$	$20qqq2$	(1440)	(1600)	(1660)	(1690)	—
$1/2^+$	$(\mathbf{70}, \mathbf{0}_{\mathbf{2}}^+)$	$21qqq2$	(1710)	(1810)	(1880)	(?)	(?)
$1/2^-$	$(\mathbf{70}, \mathbf{1}_{\mathbf{1}}^-)$	$10qqq2$	(1535)	(1670)	(1620)	(1750)	(1405)
J^P	(D, L_N^P)	$n_r n_L n_{q_1} n_{q_2} n_{q_3} n_J$	Δ		Σ	Ξ	Ω
	Decuplet		111,211,221,222		311,321,322	331,332	333
$3/2^+$	$(\mathbf{56}, \mathbf{0}_{\mathbf{0}}^+)$	$00qqq4$	(1232)		(1385)	(1530)	(1672)
$3/2^+$	$(\mathbf{56}, \mathbf{0}_{\mathbf{2}}^+)$	$20qqq4$	(1600)		(1690)	(?)	(?)
$1/2^-$	$(\mathbf{70}, \mathbf{1}_{\mathbf{1}}^-)$	$11qqq2$	(1620)		(1750)	(?)	(?)
$3/2^-$	$(\mathbf{70}, \mathbf{1}_{\mathbf{1}}^-)$	$12qqq4$	(1700)		(?)	(?)	(?)

11. The search for physics beyond the Standard Model is an active area, so these codes are also standardized as far as possible.

    (a) A standard fourth generation of fermions is included by analogy with the first three.

    (b) The graviton and the boson content of a two-Higgs-doublet scenario and of additional SU(2)×U(1) groups are found in the range 31–40.

    (c) "One-of-a-kind" exotic particles are assigned numbers in the range 41–80.The subrange 61-80 can be used for new heavier fermions in generic models, where partners to the SM fermions would have codes offset by 60. If required, however, other assignments could be made.

    (d) Fundamental supersymmetric particles are identified by adding a nonzero n to the particle number. The superpartner of a boson or a left-handed fermion has $n = 1$ while the superpartner of a right-handed fermion has $n = 2$. When mixing occurs, such as between the winos and charged Higgsinos to give charginos, or between left and right sfermions, the lighter physical state is given the smaller basis state number.

    (e) Technicolor states have $n = 3$, with technifermions treated like ordinary fermions. States which are ordinary color singlets have $n_r = 0$. Color octets have $n_r = 1$. If a state has non-trivial quantum numbers under the topcolor groups $\mathrm{SU}(3)_1 \times \mathrm{SU}(3)_2$, the quantum numbers are specified by tech,ij, where i and j are 1 or 2. n_L is then $2i + j$. The coloron, V_8, is a heavy gluon color octet and thus is 3100021.

    (f) Excited (composite) quarks and leptons are identified by setting $n = 4$ and $n_r = 0$.

    (g) Within several scenarios of new physics, it is possible to have colored particles sufficiently long-lived for color-singlet hadronic states to form around them. In the context of supersymmetric scenarios, these states are called R-hadrons, since they carry odd R-parity. R-hadron codes, defined here, should be viewed as templates for corresponding codes also in other scenarios, for any long-lived particle that is either an unflavored color octet or a flavored color triplet. The R-hadron code is obtained by combining the SUSY particle code with a code for the light degrees of freedom, with as many intermediate zeros removed from the former as required to make place for the latter at the end. (To exemplify, a sparticle $n00000n_{\tilde{q}}$ combined with quarks q_1 and q_2 obtains code $n00n_{\tilde{q}}n_{q_1}n_{q_2}n_J$.) Specifically, the new-particle spin decouples in the limit of large masses, so that the final n_J digit is defined by the spin state of the light-quark system alone. An appropriate number of n_q digits is used to define the ordinary-quark content. As usual, 9 rather than 21 is used to denote a gluon/gluino in composite states. The sign of the hadron agrees with that of the constituent new particle (a color triplet) where there is a distinct new antiparticle, and else is defined as for normal hadrons. Particle names are R with the flavor content as lower index.

    (h) A black hole in models with extra dimensions has code 5000040. Kaluza-Klein excitations in models with extra dimensions have $n = 5$ or $n = 6$, to distinquish excitations of left- or right-handed fermions or, in case of mixing, the lighter or heavier state (cf. 11d). The nonzero n_r digit gives the radial excitation number, in scenarios where the level spacing allow these to be distinguished. Should the model also contain supersymmetry, excited SUSY states would be denoted by an $n_r > 0$, with $n = 1$ or 2 as usual. Should some colored states be long-lived enough that hadrons would form around them, the coding strategy of 11g applies, with the initial two nn_r digits preserved in the combined code.

    (i) Magnetic monopoles and dyons are assumed to have one unit of Dirac monopole charge and a variable integer number $n_{q1}n_{q_2}n_{q_3}$ units of electric charge. Codes $411n_{q1}n_{q_2}n_{q_3}0$ are then used when the magnetic and electrical charge sign agree and $412n_{q1}n_{q_2}n_{q_3}0$ when they disagree, with the overall sign of the particle set by the magnetic charge. For now no spin information is provided.

    (j) The nature of Dark Matter (DM) is not known, and therefore a definitive classification is too early. Candidates within specific scenarios are classified therein, such as 1000022 for the lightest neutralino. Generic fundamental states can be given temporary codes in the range 51 - 60, with 51, 52 and 53 reserved for spin 0, 1/2 and 1 ones (this could also be an axion state). Generic mediators of s-channel DM pair creation of annihilation can be given codes 54 and 55 for spin 0 or 1 ones. Separate antiparticles, with negative codes, may or may not exist. More elaborate new scenarios should be constructed with $n = 5$ and $n_r = 9$.

    (k) Hidden Valley particles have $n = 4$ and $n_r = 9$, and trailing numbers in agreement with their nearest-analog standard particles, as far as possible. Thus 4900021 is the gauge boson g_v of a confining gauge field, $490000n_{q_v}$ and $490001n_{\ell_v}$ fundamental constituents charged or not under this, 4900022 is the γ_v of a non-confining field, and $4900n_{q_{v1}}n_{q_{v2}}n_J$ a Hidden Valley meson.

12. Occasionally program authors add their own states. To avoid confusion, these should be flagged by setting $nn_r = 99$.

13. Concerning the non-99 numbers, it may be noted that only quarks, excited quarks, squarks, and diquarks have $n_{q_3} = 0$; only diquarks, baryons, and the odderon have $n_{q_1} \neq 0$; and only mesons, the reggeon, and the pomeron have $n_{q_1} = 0$ and $n_{q_2} \neq 0$. Concerning mesons (not antimesons), if n_{q_1} is odd then it labels a quark and an antiquark if even.

14. The 9-digit tetra-quark codes are $\pm 1n_r n_L n_{q_1} n_{q_2} 0 n_{q_3} n_{q_4} n_J$. For the particle $q_1 q_2$ is a diquark and $\bar{q}_3 \bar{q}_4$ an antidiquark,

Downloaded from https://academic.oup.com/ptep/article/2022/8/083C01/6651666 by KIT Library user on 27 September 2022

sorted such that $n_{q_1} \geq n_{q_2}$, $n_{q_3} \geq n_{q_4}$, $n_{q_1} \geq n_{q_3}$, and $n_{q_2} \geq n_{q_4}$ if $n_{q_1} = n_{q_3}$. For the antiparticle, given with a negative sign, $\bar{q}_1\bar{q}_2$ is an antidiquark and q_3q_4 a diquark, with the same sorting except that either $n_{q_1} > n_{q_3}$ or $n_{q_2} > n_{q_4}$ (so that flavour-diagonal states are particles). The n_r, n_L, and n_J numbers have the same meaning as for ordinary hadrons.

15. The 9-digit penta-quark codes are $\pm 1 n_r n_L n_{q_1} n_{q_2} n_{q_3} n_{q_4} n_{q_5} n_J$, sorted such that $n_{q_1} \geq n_{q_2} \geq n_{q_3} \geq n_{q_4}$. In the particle the first four are quarks and the fifth an antiquark while the opposite holds in the antiparticle, which is given with a negative sign. The n_r, n_L, and n_J numbers have the same meaning as for ordinary hadrons.

16. Nuclear codes are given as 10-digit numbers $\pm 10LZZZAAAI$. For a (hyper)nucleus consisting of n_p protons, n_n neutrons and n_Λ Λ's, $A = n_p + n_n + n_\Lambda$ gives the total baryon number, $Z = n_p$ the total charge and $L = n_\Lambda$ the total number of strange quarks. I gives the isomer level, with $I = 0$ corresponding to the ground state and $I > 0$ to excitations, see [2], where states denoted m, n, p, q translate to $I = 1$–4. As examples, the deuteron is 1000010020 and ^{235}U is 1000922350. To avoid ambiguities, nuclear codes should not be applied to a single hadron, like p, n or Λ^0, where quark-contents-based codes already exist.

QUARKS	
d	1
u	2
s	3
c	4
b	5
t	6
b'	7
t'	8

LEPTONS	
e^-	11
ν_e	12
μ^-	13
ν_μ	14
τ^-	15
ν_τ	16
τ'^-	17
$\nu_{\tau'}$	18

GAUGE AND HIGGS BOSONS	
g	(9) 21
γ	22
Z^0	23
W^+	24
h^0/H_1^0	25
Z'/Z_2^0	32
Z''/Z_3^0	33
W'/W_2^+	34
H^0/H_2^0	35
A^0/H_3^0	36
H^+	37
H^{++}	38
a^0/H_4^0	40

SPECIAL PARTICLES	
G (graviton)	39
R^0	41
LQ^c	42
DM ($S=0$)	51
DM ($S=\frac{1}{2}$)	52
DM ($S=1$)	53
reggeon	110
pomeron	990
odderon	9990

for MC internal use
81–100, 901–930,
998-999, 1901–1930,
2901–2930, and
3901–3930

DIQUARKS	
$(dd)_1$	1103
$(ud)_0$	2101
$(ud)_1$	2103
$(uu)_1$	2203
$(sd)_0$	3101
$(sd)_1$	3103
$(su)_0$	3201
$(su)_1$	3203
$(ss)_1$	3303
$(cd)_0$	4101
$(cd)_1$	4103
$(cu)_0$	4201
$(cu)_1$	4203
$(cs)_0$	4301
$(cs)_1$	4303
$(cc)_1$	4403
$(bd)_0$	5101
$(bd)_1$	5103
$(bu)_0$	5201
$(bu)_1$	5203
$(bs)_0$	5301
$(bs)_1$	5303
$(bc)_0$	5401
$(bc)_1$	5403
$(bb)_1$	5503

SUSY PARTICLES	
$\tilde{d}_L$	1000001
$\tilde{u}_L$	1000002
$\tilde{s}_L$	1000003
$\tilde{c}_L$	1000004
$\tilde{b}_1$	1000005[a]
$\tilde{t}_1$	1000006[a]
$\tilde{e}_L^-$	1000011
$\tilde{\nu}_{eL}$	1000012
$\tilde{\mu}_L^-$	1000013
$\tilde{\nu}_{\mu L}$	1000014
$\tilde{\tau}_1^-$	1000015[a]
$\tilde{\nu}_{\tau L}$	1000016
$\tilde{d}_R$	2000001
$\tilde{u}_R$	2000002
$\tilde{s}_R$	2000003
$\tilde{c}_R$	2000004
$\tilde{b}_2$	2000005[a]
$\tilde{t}_2$	2000006[a]
$\tilde{e}_R^-$	2000011
$\tilde{\mu}_R^-$	2000013
$\tilde{\tau}_2^-$	2000015[a]
$\tilde{g}$	1000021
$\tilde{\chi}_1^0$	1000022[b]
$\tilde{\chi}_2^0$	1000023[b]
$\tilde{\chi}_1^+$	1000024[b]
$\tilde{\chi}_3^0$	1000025[b]
$\tilde{\chi}_4^0$	1000035[b]
$\tilde{\chi}_2^+$	1000037[b]
$\tilde{G}$	1000039

LIGHT $I = 1$ MESONS	
π^0	111
π^+	211
$a_0(980)^0$	9000111
$a_0(980)^+$	9000211
$\pi(1300)^0$	100111
$\pi(1300)^+$	100211
$a_0(1450)^0$	10111
$a_0(1450)^+$	10211
$\pi(1800)^0$	9010111
$\pi(1800)^+$	9010211
$\rho(770)^0$	113
$\rho(770)^+$	213
$b_1(1235)^0$	10113
$b_1(1235)^+$	10213
$a_1(1260)^0$	20113
$a_1(1260)^+$	20213
$\pi_1(1400)^0$	9000113
$\pi_1(1400)^+$	9000213
$\rho(1450)^0$	100113
$\rho(1450)^+$	100213
$\pi_1(1600)^0$	9010113
$\pi_1(1600)^+$	9010213
$a_1(1640)^0$	9020113
$a_1(1640)^+$	9020213
$\rho(1700)^0$	30113
$\rho(1700)^+$	30213
$\rho(1900)^0$	9030113
$\rho(1900)^+$	9030213
$\rho(2150)^0$	9040113
$\rho(2150)^+$	9040213
$a_2(1320)^0$	115
$a_2(1320)^+$	215
$\pi_2(1670)^0$	10115
$\pi_2(1670)^+$	10215
$a_2(1700)^0$	9000115
$a_2(1700)^+$	9000215
$\pi_2(2100)^0$	9010115
$\pi_2(2100)^+$	9010215
$\rho_3(1690)^0$	117
$\rho_3(1690)^+$	217
$\rho_3(1990)^0$	9000117
$\rho_3(1990)^+$	9000217
$\rho_3(2250)^0$	9010117
$\rho_3(2250)^+$	9010217
$a_4(2040)^0$	119
$a_4(2040)^+$	219

LIGHT $I = 0$ MESONS ($u\bar{u}$, $d\bar{d}$, $s\bar{s}$ admixtures)	
η	221
$\eta'(958)$	331
$f_0(500)$	9000221
$f_0(980)$	9010221
$\eta(1295)$	100221
$f_0(1370)$	10221
$\eta(1405)$	9020221
$\eta(1475)$	100331
$f_0(1500)$	9030221
$f_0(1710)$	10331
$\eta(1760)$	9040221
$f_0(2020)$	9050221
$f_0(2100)$	9060221
$f_0(2200)$	9070221
$\eta(2225)$	9080221
$\omega(782)$	223
$\phi(1020)$	333
$h_1(1170)$	10223
$f_1(1285)$	20223
$h_1(1380)$	10333
$f_1(1420)$	20333
$\omega(1420)$	100223
$f_1(1510)$	9000223
$h_1(1595)$	9010223
$\omega(1650)$	30223
$\phi(1680)$	100333
$f_2(1270)$	225
$f_2(1430)$	9000225
$f_2'(1525)$	335
$f_2(1565)$	9010225
$f_2(1640)$	9020225
$\eta_2(1645)$	10225
$f_2(1810)$	9030225
$\eta_2(1870)$	10335
$f_2(1910)$	9040225
$f_2(1950)$	9050225
$f_2(2010)$	9060225
$f_2(2150)$	9070225
$f_2(2300)$	9080225
$f_2(2340)$	9090225
$\omega_3(1670)$	227
$\phi_3(1850)$	337
$f_4(2050)$	229
$f_J(2220)$	9000229
$f_4(2300)$	9010229

STRANGE MESONS	
K_L^0	130
K_S^0	310
K^0	311
K^+	321
$K_0^*(700)^0$	9000311
$K_0^*(700)^+$	9000321
$K_0^*(1430)^0$	10311
$K_0^*(1430)^+$	10321
$K(1460)^0$	100311
$K(1460)^+$	100321
$K(1830)^0$	9010311
$K(1830)^+$	9010321
$K_0^*(1950)^0$	9020311
$K_0^*(1950)^+$	9020321
$K^*(892)^0$	313
$K^*(892)^+$	323
$K_1(1270)^0$	10313
$K_1(1270)^+$	10323
$K_1(1400)^0$	20313
$K_1(1400)^+$	20323
$K^*(1410)^0$	100313
$K^*(1410)^+$	100323
$K_1(1650)^0$	9000313
$K_1(1650)^+$	9000323
$K^*(1680)^0$	30313
$K^*(1680)^+$	30323
$K_2^*(1430)^0$	315
$K_2^*(1430)^+$	325
$K_2(1580)^0$	9000315
$K_2(1580)^+$	9000325
$K_2(1770)^0$	10315
$K_2(1770)^+$	10325
$K_2(1820)^0$	20315
$K_2(1820)^+$	20325
$K_2^*(1980)^0$	9010315
$K_2^*(1980)^+$	9010325
$K_2(2250)^0$	9020315
$K_2(2250)^+$	9020325
$K_3^*(1780)^0$	317
$K_3^*(1780)^+$	327
$K_3(2320)^0$	9010317
$K_3(2320)^+$	9010327
$K_4^*(2045)^0$	319
$K_4^*(2045)^+$	329
$K_4(2500)^0$	9000319
$K_4(2500)^+$	9000329

Downloaded from https://academic.oup.com/ptep/article/2022/8/083C01/6651666 by KIT Library user on 27 September 2022

CHARMED MESONS	
D^+	411
D^0	421
$D_0^*(2400)^+$	10411
$D_0^*(2400)^0$	10421
$D^*(2010)^+$	413
$D^*(2007)^0$	423
$D_1(2420)^+$	10413
$D_1(2420)^0$	10423
$D_1(H)^+$	20413
$D_1(2430)^0$	20423
$D_2^*(2460)^+$	415
$D_2^*(2460)^0$	425
D_s^+	431
$D_{s0}^*(2317)^+$	10431
D_s^{*+}	433
$D_{s1}(2536)^+$	10433
$D_{s1}(2460)^+$	20433
$D_{s2}^*(2573)^+$	435

BOTTOM MESONS	
B^0	511
B^+	521
B_0^{*0}	10511
B_0^{*+}	10521
B^{*0}	513
B^{*+}	523
$B_1(L)^0$	10513
$B_1(L)^+$	10523
$B_1(H)^0$	20513
$B_1(H)^+$	20523
B_2^{*0}	515
B_2^{*+}	525
B_s^0	531
B_{s0}^{*0}	10531
B_s^{*0}	533
$B_{s1}(L)^0$	10533
$B_{s1}(H)^0$	20533
B_{s2}^{*0}	535
B_c^+	541
B_{c0}^{*+}	10541
B_c^{*+}	543
$B_{c1}(L)^+$	10543
$B_{c1}(H)^+$	20543
B_{c2}^{*+}	545

$c\bar{c}$ MESONS	
$\eta_c(1S)$	441
$\chi_{c0}(1P)$	10441
$\eta_c(2S)$	100441
$J/\psi(1S)$	443
$h_c(1P)$	10443
$\chi_{c1}(1P)$	20443
$\psi(2S)$	100443
$\psi(3770)$	30443
$\psi(4040)$	9000443
$\psi(4160)$	9010443
$\psi(4415)$	9020443
$\chi_{c2}(1P)$	445
$\chi_{c2}(3930)$	100445

$b\bar{b}$ MESONS	
$\eta_b(1S)$	551
$\chi_{b0}(1P)$	10551
$\eta_b(2S)$	100551
$\chi_{b0}(2P)$	110551
$\eta_b(3S)$	200551
$\chi_{b0}(3P)$	210551
$\Upsilon(1S)$	553
$h_b(1P)$	10553
$\chi_{b1}(1P)$	20553
$\Upsilon_1(1D)$	30553
$\Upsilon(2S)$	100553
$h_b(2P)$	110553
$\chi_{b1}(2P)$	120553
$\Upsilon_1(2D)$	130553
$\Upsilon(3S)$	200553
$h_b(3P)$	210553
$\chi_{b1}(3P)$	220553
$\Upsilon(4S)$	300553
$\Upsilon(10860)$	9000553
$\Upsilon(11020)$	9010553
$\chi_{b2}(1P)$	555
$\eta_{b2}(1D)$	10555
$\Upsilon_2(1D)$	20555
$\chi_{b2}(2P)$	100555
$\eta_{b2}(2D)$	110555
$\Upsilon_2(2D)$	120555
$\chi_{b2}(3P)$	200555
$\Upsilon_3(1D)$	557
$\Upsilon_3(2D)$	100557

LIGHT BARYONS	
p	2212
n	2112
Δ^{++}	2224
Δ^+	2214
Δ^0	2114
Δ^-	1114

STRANGE BARYONS	
Λ	3122
Σ^+	3222
Σ^0	3212
Σ^-	3112
Σ^{*+}	3224[c]
Σ^{*0}	3214[c]
Σ^{*-}	3114[c]
Ξ^0	3322
Ξ^-	3312
Ξ^{*0}	3324[c]
Ξ^{*-}	3314[c]
Ω^-	3334

CHARMED BARYONS	
Λ_c^+	4122
Σ_c^{++}	4222
Σ_c^+	4212
Σ_c^0	4112
Σ_c^{*++}	4224
Σ_c^{*+}	4214
Σ_c^{*0}	4114
Ξ_c^+	4232
Ξ_c^0	4132
$\Xi_c'^+$	4322
$\Xi_c'^0$	4312
Ξ_c^{*+}	4324
Ξ_c^{*0}	4314
Ω_c^0	4332
Ω_c^{*0}	4334
Ξ_{cc}^+	4412
Ξ_{cc}^{++}	4422
Ξ_{cc}^{*+}	4414
Ξ_{cc}^{*++}	4424
Ω_{cc}^+	4432
Ω_{cc}^{*+}	4434
Ω_{ccc}^{++}	4444

BOTTOM BARYONS	
Λ_b^0	5122
Σ_b^-	5112
Σ_b^0	5212
Σ_b^+	5222
Σ_b^{*-}	5114
Σ_b^{*0}	5214
Σ_b^{*+}	5224
Ξ_b^-	5132
Ξ_b^0	5232
$\Xi_b'^-$	5312
$\Xi_b'^0$	5322
Ξ_b^{*-}	5314
Ξ_b^{*0}	5324
Ω_b^-	5332
Ω_b^{*-}	5334
Ξ_{bc}^0	5142
Ξ_{bc}^+	5242
$\Xi_{bc}'^0$	5412
$\Xi_{bc}'^+$	5422
Ξ_{bc}^{*0}	5414
Ξ_{bc}^{*+}	5424
Ω_{bc}^0	5342
$\Omega_{bc}'^0$	5432
Ω_{bc}^{*0}	5434
Ω_{bcc}^+	5442
Ω_{bcc}^{*+}	5444
Ξ_{bb}^-	5512
Ξ_{bb}^0	5522
Ξ_{bb}^{*-}	5514
Ξ_{bb}^{*0}	5524
Ω_{bb}^-	5532
Ω_{bb}^{*-}	5534
Ω_{bbc}^0	5542
Ω_{bbc}^{*0}	5544
Ω_{bbb}^-	5554

PENTAQUARKS	
$\boldsymbol{\Theta^+}$	**100221132***
$\boldsymbol{\Phi^{--}}$	**100331122***

Footnotes to the tables:

$*$) Numbers or names in bold face are new or have changed since the 2020 *Review*.

a) Particulary in the third generation, the left and right sfermion states may mix, as shown.

The lighter mixed state is given the smaller number.

b) The physical $\widetilde{\chi}$ states are admixtures of the pure $\widetilde{\gamma}$, $\widetilde{Z}^0$, $\widetilde{W}^+$, $\widetilde{H}_1^0$, $\widetilde{H}_2^0$, and $\widetilde{H}^+$ states.

c) Σ^* and Ξ^* are alternate names for $\Sigma(1385)$ and $\Xi(1530)$.

References

[1] G. P. Yost *et al.* (Particle Data Group), Phys. Lett. **B204**, 1 (1988).

[2] G. Audi *et al.*, Nucl. Phys. **A729**, 3 (2003).

Downloaded from https://academic.oup.com/ptep/article/2022/8/083C01/6651666 by KIT Library user on 27 September 2022

46. Clebsch-Gordan Coefficients, Spherical Harmonics, and *d* Functions

Note: A square-root sign is to be understood over *every* coefficient, *e.g.*, for $-8/15$ read $-\sqrt{8/15}$.

Notation:

J	J	…
M	M	…
m_1	m_2	
m_1	m_2	Coefficients
⋮	⋮	

1/2×1/2

m_1	m_2	$J=1$, $M=+1$	$J=1$, $M=0$	$J=0$, $M=0$
+1/2	+1/2	1		
+1/2	−1/2		1/2	1/2
−1/2	+1/2		1/2	−1/2
−1/2	−1/2			1

1×1/2

m_1	m_2	$J=3/2$, $M=+3/2$	$J=3/2$, $M=+1/2$	$J=1/2$, $M=+1/2$
+1	+1/2	1		
+1	−1/2		1/3	2/3
0	+1/2		2/3	−1/3
0	−1/2		2/3	1/3
−1	+1/2		1/3	−2/3
−1	−1/2			1

2×1

m_1	m_2	$J=3$, $M=+3$	$J=3$, $M=+2$	$J=2$, $M=+2$	$J=1$, $M=+1$
+2	+1	1			
+2	0		1/3	2/3	
+1	+1		2/3	−1/3	
+2	−1			1/15	1/3	3/5
+1	0			8/15	1/6	−3/10
0	+1			2/5	−1/2	1/10
+1	−1			1/5	1/2	3/10
0	0			3/5	0	−2/5
−1	+1			1/5	−1/2	3/10
0	−1				2/5	1/2	1/10
−1	0				8/15	−1/6	−3/10
−2	+1				1/15	−1/3	3/5
−1	−1					2/3	1/3
−2	0					1/3	−2/3
−2	−1						1

1×1

m_1	m_2	$J=2$, $M=+2$	$J=2$, $M=+1$	$J=1$, $M=+1$	$J=0$, $M=0$
+1	+1	1			
+1	0		1/2	1/2	
0	+1		1/2	−1/2	
+1	−1			1/6	1/2	1/3
0	0			2/3	0	−1/3
−1	+1			1/6	−1/2	1/3
0	−1				1/2	1/2
−1	0				1/2	−1/2
−1	−1					1

$$Y_1^0 = \sqrt{\frac{3}{4\pi}}\cos\theta$$

$$Y_1^1 = -\sqrt{\frac{3}{8\pi}}\sin\theta\, e^{i\phi}$$

$$Y_2^0 = \sqrt{\frac{5}{4\pi}}\Big(\frac{3}{2}\cos^2\theta - \frac{1}{2}\Big)$$

$$Y_2^1 = -\sqrt{\frac{15}{8\pi}}\sin\theta\cos\theta\, e^{i\phi}$$

$$Y_2^2 = \frac{1}{4}\sqrt{\frac{15}{2\pi}}\sin^2\theta\, e^{2i\phi}$$

$$Y_\ell^{-m} = (-1)^m Y_\ell^{m*}$$

$$d^\ell_{m,0} = \sqrt{\frac{4\pi}{2\ell+1}}\, Y_\ell^m\, e^{-im\phi}$$

2×1/2

m_1	m_2	$J=5/2$, $M=+5/2$	$J=5/2$, $M=+3/2$	$J=3/2$, $M=+3/2$
+2	+1/2	1		
+2	−1/2		1/5	4/5
+1	+1/2		4/5	−1/5
+1	−1/2			2/5	3/5
0	+1/2			3/5	−2/5
0	−1/2				3/5	2/5
−1	+1/2				2/5	−3/5
−1	−1/2					4/5	1/5
−2	+1/2					1/5	−4/5
−2	−1/2						1

3/2×1/2

m_1	m_2	$J=2$, $M=+2$	$J=2$, $M=+1$	$J=1$, $M=+1$	$J=1$, $M=0$	$J=0$, $M=0$
+3/2	+1/2	1				
+3/2	−1/2		1/4	3/4		
+1/2	+1/2		3/4	−1/4		
+1/2	−1/2			1/2	1/2	
−1/2	+1/2			1/2	−1/2	
−1/2	−1/2				3/4	1/4
−3/2	+1/2				1/4	−3/4
−3/2	−1/2					1

3/2×1

m_1	m_2	$J=5/2$, $M=+5/2$	$J=5/2$, $M=+3/2$	$J=3/2$, $M=+3/2$	$J=1/2$, $M=+1/2$
+3/2	+1	1			
+3/2	0		2/5	3/5	
+1/2	+1		3/5	−2/5	
+3/2	−1			1/10	2/5	1/2
+1/2	0			3/5	1/15	−1/3
−1/2	+1			3/10	−8/15	1/6
+1/2	−1				3/10	8/15	1/6
−1/2	0				3/5	−1/15	−1/3
−3/2	+1				1/10	−2/5	1/2
−1/2	−1					3/5	2/5
−3/2	0					2/5	−3/5
−3/2	−1						1

$$\langle j_1 j_2 m_1 m_2 | j_1 j_2 J M\rangle = (-1)^{J-j_1-j_2}\langle j_2 j_1 m_2 m_1 | j_2 j_1 J M\rangle$$

$$d^j_{m',m} = (-1)^{m-m'} d^j_{m,m'} = d^j_{-m,-m'}$$

$$d^1_{0,0} = \cos\theta \qquad d^{1/2}_{1/2,1/2} = \cos\frac{\theta}{2} \qquad d^1_{1,1} = \frac{1+\cos\theta}{2}$$

$$d^{1/2}_{1/2,-1/2} = -\sin\frac{\theta}{2} \qquad d^1_{1,0} = -\frac{\sin\theta}{\sqrt{2}}$$

$$d^1_{1,-1} = \frac{1-\cos\theta}{2}$$

3/2×3/2

m_1	m_2	$J=3$, $M=+3$	$J=3$, $M=+2$	$J=2$, $M=+2$	$J=1$, $M=+1$
+3/2	+3/2	1			
+3/2	+1/2		1/2	1/2	
+1/2	+3/2		1/2	−1/2	
+3/2	−1/2			1/5	1/2	3/10
+1/2	+1/2			3/5	0	−2/5
−1/2	+3/2			1/5	−1/2	3/10
+3/2	−3/2			1/20	1/4	9/20	1/4
+1/2	−1/2			9/20	1/4	−1/20	−1/4
−1/2	+1/2			9/20	−1/4	−1/20	1/4
−3/2	+3/2			1/20	−1/4	9/20	−1/4
+1/2	−3/2				1/5	1/2	3/10
−1/2	−1/2				3/5	0	−2/5
−3/2	+1/2				1/5	−1/2	3/10
−1/2	−3/2					1/2	1/2
−3/2	−1/2					1/2	−1/2
−3/2	−3/2						1

2×3/2

m_1	m_2	$J=7/2$, $M=+7/2$	$J=7/2$, $M=+5/2$	$J=5/2$, $M=+5/2$	$J=3/2$, $M=+3/2$
+2	+3/2	1			
+2	+1/2		3/7	4/7	
+1	+3/2		4/7	−3/7	
+2	−1/2			1/7	16/35	2/5
+1	+1/2			4/7	1/35	−2/5
0	+3/2			2/7	−18/35	1/5
+2	−3/2				1/35	6/35	2/5	2/5
+1	−1/2				12/35	5/14	0	−3/10
0	+1/2				18/35	−3/35	−1/5	1/5
−1	+3/2				4/35	−27/70	2/5	−1/10
+1	−3/2					4/35	27/70	2/5	1/10
0	−1/2					18/35	3/35	−1/5	−1/5
−1	+1/2					12/35	−5/14	0	3/10
−2	+3/2					1/35	−6/35	2/5	−2/5
0	−3/2						2/7	18/35	1/5
−1	−1/2						4/7	−1/35	−2/5
−2	+1/2						1/7	−16/35	2/5
−1	−3/2							4/7	3/7
−2	−1/2							3/7	−4/7
−2	−3/2								1

2×2

m_1	m_2	$J=4$, $M=+4$	$J=4$, $M=+3$	$J=3$, $M=+3$	$J=2$, $M=+2$	$J=1$, $M=+1$	$J=0$, $M=0$
+2	+2	1					
+2	+1		1/2	1/2			
+1	+2		1/2	−1/2			
+2	0			3/14	1/2	2/7	
+1	+1			4/7	0	−3/7	
0	+2			3/14	−1/2	2/7	
+2	−1				1/14	3/10	3/7	1/5
+1	0				3/7	1/5	−1/14	−3/10
0	+1				3/7	−1/5	−1/14	3/10
−1	+2				1/14	−3/10	3/7	−1/5
+2	−2					1/70	1/10	2/7	2/5	1/5
+1	−1					8/35	2/5	1/14	−1/10	−1/5
0	0					18/35	0	−2/7	0	1/5
−1	+1					8/35	−2/5	1/14	1/10	−1/5
−2	+2					1/70	−1/10	2/7	−2/5	1/5
+1	−2						1/14	3/10	3/7	1/5
0	−1						3/7	1/5	−1/14	−3/10
−1	0						3/7	−1/5	−1/14	3/10
−2	+1						1/14	−3/10	3/7	−1/5
0	−2							3/14	1/2	2/7
−1	−1							4/7	0	−3/7
−2	0							3/14	−1/2	2/7
−1	−2								1/2	1/2
−2	−1								1/2	−1/2
−2	−2									1

$$d^{3/2}_{3/2,3/2} = \frac{1+\cos\theta}{2}\cos\frac{\theta}{2}$$

$$d^{3/2}_{3/2,1/2} = -\sqrt{3}\frac{1+\cos\theta}{2}\sin\frac{\theta}{2}$$

$$d^{3/2}_{3/2,-1/2} = \sqrt{3}\frac{1-\cos\theta}{2}\cos\frac{\theta}{2}$$

$$d^{3/2}_{3/2,-3/2} = -\frac{1-\cos\theta}{2}\sin\frac{\theta}{2}$$

$$d^{3/2}_{1/2,1/2} = \frac{3\cos\theta-1}{2}\cos\frac{\theta}{2}$$

$$d^{3/2}_{1/2,-1/2} = -\frac{3\cos\theta+1}{2}\sin\frac{\theta}{2}$$

$$d^2_{2,2} = \Big(\frac{1+\cos\theta}{2}\Big)^2$$

$$d^2_{2,1} = -\frac{1+\cos\theta}{2}\sin\theta$$

$$d^2_{2,0} = \frac{\sqrt{6}}{4}\sin^2\theta$$

$$d^2_{2,-1} = -\frac{1-\cos\theta}{2}\sin\theta$$

$$d^2_{2,-2} = \Big(\frac{1-\cos\theta}{2}\Big)^2$$

$$d^2_{1,1} = \frac{1+\cos\theta}{2}(2\cos\theta-1)$$

$$d^2_{1,0} = -\sqrt{\frac{3}{2}}\sin\theta\cos\theta$$

$$d^2_{1,-1} = \frac{1-\cos\theta}{2}(2\cos\theta+1)$$

$$d^2_{0,0} = \Big(\frac{3}{2}\cos^2\theta - \frac{1}{2}\Big)$$

Figure 46.1: The sign convention is that of Wigner (*Group Theory*, Academic Press, New York, 1959), also used by Condon and Shortley (*The Theory of Atomic Spectra*, Cambridge Univ. Press, New York, 1953), Rose (*Elementary Theory of Angular Momentum*, Wiley, New York, 1957), and Cohen (*Tables of the Clebsch-Gordan Coefficients*, North American Rockwell Science Center, Thousand Oaks, Calif., 1974).

Downloaded from https://academic.oup.com/ptep/article/2022/8/083C01/6651666 by KIT Library user on 27 September 2022

47. SU(3) Isoscalar Factors and Representation Matrices

Revised August 2019 by R. Kelly (LBNL).

The most commonly used SU(3) isoscalar factors, corresponding to the singlet, octet, and decuplet content of $8 \otimes 8$ and $10 \otimes 8$, are shown at the right. The notation uses particle names to identify the coefficients, so that the pattern of relative couplings may be seen at a glance. We illustrate the use of the coefficients below. See J.J de Swart, Rev. Mod. Phys. **35**, 916 (1963) for detailed explanations and phase conventions.

A $\sqrt{\ }$ *is to be understood over every integer in the matrices;* the exponent 1/2 on each matrix is a reminder of this. For example, the $\Xi \to \Omega K$ element of the $10 \to 10 \otimes 8$ matrix is $-\sqrt{6}/\sqrt{24} = -1/2$.

Intramultiplet relative decay strengths may be read directly from the matrices. For example, in decuplet $\to$ octet + octet decays, the ratio of $\Omega^* \to \Xi\overline{K}$ and $\Delta \to N\pi$ partial widths is, from the $10 \to 8 \times 8$ matrix,

$$\frac{\Gamma\,(\Omega^* \to \Xi\overline{K})}{\Gamma\,(\Delta \to N\pi)} = \frac{12}{6} \times \text{ (phase space factors) .} \tag{47.1}$$

Including isospin Clebsch-Gordan coefficients, we obtain, *e.g.*,

$$\frac{\Gamma(\Omega^{*-} \to \Xi^0 K^-)}{\Gamma(\Delta^+ \to p\,\pi^0)} = \frac{1/2}{2/3} \times \frac{12}{6} \times p.s.f. = \frac{3}{2} \times p.s.f. \tag{47.2}$$

Partial widths for $8 \to 8 \otimes 8$ involve a linear superposition of 8_1 (symmetric) and 8_2 (antisymmetric) couplings. For example,

$$\Gamma(\Xi^* \to \Xi\pi) \sim \left(-\sqrt{\frac{9}{20}}\, g_1 + \sqrt{\frac{3}{12}}\, g_2\right)^2 . \tag{47.3}$$

The relations between g_1 and g_2 (with de Swart's normalization) and the standard D and F couplings that appear in the interaction Lagrangian,

$$\mathscr{L} = -\sqrt{2}\; D\; Tr\,(\{\overline{B}, B\}M) + \sqrt{2}\; F\; Tr\,([\overline{B}, B]\,M) \;, \tag{47.4}$$

where $[\overline{B}, B] \equiv \overline{B}B - B\overline{B}$ and $\{\overline{B}, B\} \equiv \overline{B}B + B\overline{B}$, are

$$D = \frac{\sqrt{30}}{40}\, g_1 \;, \qquad F = \frac{\sqrt{6}}{24}\, g_2 \;. \tag{47.5}$$

Thus, for example,

$$\Gamma(\Xi^* \to \Xi\pi) \sim (F - D)^2 \sim (1 - 2\alpha)^2 \;, \tag{47.6}$$

where $\alpha \equiv F/(D + F)$. (This definition of α is de Swart's. The alternative $D/(D + F)$, due to Gell-Mann, is also used.)

The generators of SU(3) transformations, λ_a $(a = 1, 8)$, are 3×3 matrices that obey the following commutation and anticommutation relationships:

$$[\lambda_a,\ \lambda_b] \equiv \lambda_a\lambda_b - \lambda_b\lambda_a = 2i f_{abc}\lambda_c \tag{47.7}$$

$$\{\lambda_a,\ \lambda_b\} \equiv \lambda_a\lambda_b + \lambda_b\lambda_a = \frac{4}{3}\delta_{ab} I + 2d_{abc}\lambda_c \;, \tag{47.8}$$

where I is the 3×3 identity matrix, and δ_{ab} is the Kronecker delta symbol. The f_{abc} are odd under the permutation of any pair of indices, while the d_{abc} are even. The nonzero values are:

$1 \to 8 \otimes 8$

$$\begin{pmatrix}\Lambda\end{pmatrix} \to \begin{pmatrix} N\overline{K} & \Sigma\pi & \Lambda\eta & \Xi K \end{pmatrix} = \frac{1}{\sqrt{8}}\begin{pmatrix} 2 & 3 & -1 & -2 \end{pmatrix}^{1/2}$$

$8_1 \to 8 \otimes 8$

$$\begin{pmatrix} N \\ \Sigma \\ \Lambda \\ \Xi \end{pmatrix} \to \begin{pmatrix} & N\pi & N\eta & \Sigma K & \Lambda K & \\ N\overline{K} & \Sigma\pi & \Lambda\pi & \Sigma\eta & \Xi K & \\ & N\overline{K} & \Sigma\pi & \Lambda\eta & \Xi K & \\ & \Sigma\overline{K} & \Lambda\overline{K} & \Xi\pi & \Xi\eta & \end{pmatrix} = \frac{1}{\sqrt{20}}\begin{pmatrix} 9 & -1 & -9 & -1 \\ -6 & 0 & 4 & 4 & -6 \\ 2 & -12 & -4 & -2 \\ 9 & -1 & -9 & -1 \end{pmatrix}^{1/2}$$

$8_2 \to 8 \otimes 8$

$$\begin{pmatrix} N \\ \Sigma \\ \Lambda \\ \Xi \end{pmatrix} \to \begin{pmatrix} & N\pi & N\eta & \Sigma K & \Lambda K & \\ N\overline{K} & \Sigma\pi & \Lambda\pi & \Sigma\eta & \Xi K & \\ & N\overline{K} & \Sigma\pi & \Lambda\eta & \Xi K & \\ & \Sigma\overline{K} & \Lambda\overline{K} & \Xi\pi & \Xi\eta & \end{pmatrix} = \frac{1}{\sqrt{12}}\begin{pmatrix} 3 & 3 & 3 & -3 \\ 2 & 8 & 0 & 0 & -2 \\ 6 & 0 & 0 & 6 \\ 3 & 3 & 3 & -3 \end{pmatrix}^{1/2}$$

$10 \to 8 \otimes 8$

$$\begin{pmatrix} \Delta \\ \Sigma \\ \Xi \\ \Omega \end{pmatrix} \to \begin{pmatrix} & N\pi & \Sigma K & & & \\ N\overline{K} & \Sigma\pi & \Lambda\pi & \Sigma\eta & \Xi K & \\ & \Sigma\overline{K} & \Lambda\overline{K} & \Xi\pi & \Xi\eta & \\ & & \Xi\overline{K} & & & \end{pmatrix} = \frac{1}{\sqrt{12}}\begin{pmatrix} & -6 & 6 & & \\ -2 & 2 & -3 & 3 & 2 \\ & 3 & -3 & 3 & 3 \\ & & 12 & & \end{pmatrix}^{1/2}$$

$8 \to 10 \otimes 8$

$$\begin{pmatrix} N \\ \Sigma \\ \Lambda \\ \Xi \end{pmatrix} \to \begin{pmatrix} & \Delta\pi & \Sigma K & \\ \Delta\overline{K} & \Sigma\pi & \Sigma\eta & \Xi K \\ & \Sigma\pi & \Xi K & \\ \Sigma\overline{K} & \Xi\pi & \Xi\eta & \Omega K \end{pmatrix} = \frac{1}{\sqrt{15}}\begin{pmatrix} & -12 & 3 & \\ 8 & -2 & -3 & 2 \\ & -9 & 6 & \\ 3 & -3 & -3 & 6 \end{pmatrix}^{1/2}$$

$10 \to 10 \otimes 8$

$$\begin{pmatrix} \Delta \\ \Sigma \\ \Xi \\ \Omega \end{pmatrix} \to \begin{pmatrix} & \Delta\pi & \Delta\eta & \Sigma K & \\ \Delta\overline{K} & \Sigma\pi & \Sigma\eta & \Xi K & \\ \Sigma\overline{K} & \Xi\pi & \Xi\eta & \Omega K & \\ & \Xi\overline{K} & \Omega\eta & & \end{pmatrix} = \frac{1}{\sqrt{24}}\begin{pmatrix} & 15 & 3 & -6 & \\ 8 & 8 & & 0 & -8 \\ 12 & 3 & -3 & -6 \\ & 12 & -12 & & \end{pmatrix}^{1/2}$$

abc	f_{abc}	abc	d_{abc}	abc	d_{abc}
123	1	118	$1/\sqrt{3}$	355	1/2
147	1/2	146	1/2	366	−1/2
156	−1/2	157	1/2	377	−1/2
246	1/2	228	$1/\sqrt{3}$	448	$-1/(2\sqrt{3})$
257	1/2	247	−1/2	558	$-1/(2\sqrt{3})$
345	1/2	256	1/2	668	$-1/(2\sqrt{3})$
367	−1/2	338	$1/\sqrt{3}$	778	$-1/(2\sqrt{3})$
458	$\sqrt{3}/2$	344	1/2	888	$-1/\sqrt{3}$
678	$\sqrt{3}/2$				

The λ_a's are

$$\lambda_1 = \begin{pmatrix} 0 & 1 & 0 \\ 1 & 0 & 0 \\ 0 & 0 & 0 \end{pmatrix} \quad \lambda_2 = \begin{pmatrix} 0 & -i & 0 \\ i & 0 & 0 \\ 0 & 0 & 0 \end{pmatrix} \quad \lambda_3 = \begin{pmatrix} 1 & 0 & 0 \\ 0 & -1 & 0 \\ 0 & 0 & 0 \end{pmatrix}$$

$$\lambda_4 = \begin{pmatrix} 0 & 0 & 1 \\ 0 & 0 & 0 \\ 1 & 0 & 0 \end{pmatrix} \quad \lambda_5 = \begin{pmatrix} 0 & 0 & -i \\ 0 & 0 & 0 \\ i & 0 & 0 \end{pmatrix} \quad \lambda_6 = \begin{pmatrix} 0 & 0 & 0 \\ 0 & 0 & 1 \\ 0 & 1 & 0 \end{pmatrix}$$

$$\lambda_7 = \begin{pmatrix} 0 & 0 & 0 \\ 0 & 0 & -i \\ 0 & i & 0 \end{pmatrix} \quad \lambda_8 = \frac{1}{\sqrt{3}}\begin{pmatrix} 1 & 0 & 0 \\ 0 & 1 & 0 \\ 0 & 0 & -2 \end{pmatrix}$$

Equation (47.7) defines the Lie algebra of SU(3). A general d-dimensional representation is given by a set of $d \times d$ matrices satisfying Eq. (47.7) with the f_{abc} given above. Equation (47.8) is specific to the defining 3-dimensional representation.

Downloaded from https://academic.oup.com/ptep/article/2022/8/083C01/6651666 by KIT Library user on 27 September 2022

48. SU(n) Multiplets and Young Diagrams

Revised August 2019 by C.G. Wohl (LBNL).

This note tells (1) how SU(n) particle multiplets are identified or labeled, (2) how to find the number of particles in a multiplet from its label, (3) how to draw the Young diagram for a multiplet, and (4) how to use Young diagrams to determine the overall multiplet structure of a composite system, such as a 3-quark or a meson-baryon system.

In much of the literature, the word "representation" is used where we use "multiplet," and "tableau" is used where we use "diagram."

48.1 Multiplet labels

An SU(n) multiplet is uniquely identified by a string of (n−1) nonnegative integers: $(\alpha, \beta, \gamma, \ldots)$. Any such set of integers specifies a multiplet. For an SU(2) multiplet such as an isospin multiplet, the single integer α is the number of *steps* from one end of the multiplet to the other (*i.e.*, it is one fewer than the number of particles in the multiplet). In SU(3), the two integers α and β are the numbers of steps across the top and bottom levels of the multiplet diagram. Thus the labels for the SU(3) octet and decuplet

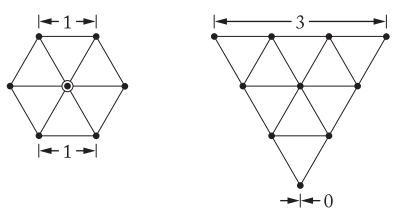

are (1,1) and (3,0). For larger n, the interpretation of the integers in terms of the geometry of the multiplets, which exist in an (n−1)-dimensional space, is not so readily apparent.

The label for the SU(n) singlet is $(0, 0, \ldots, 0)$. In a flavor SU(n), the n quarks together form a $(1, 0, \ldots, 0)$ multiplet, and the n antiquarks belong to a $(0, \ldots, 0, 1)$ multiplet. These two multiplets are *conjugate* to one another, which means their labels are related by $(\alpha, \beta, \ldots) \leftrightarrow (\ldots, \beta, \alpha)$.

48.2 Number of particles

The number of particles in a multiplet, $N = N(\alpha, \beta, \ldots)$, is given as follows (note the pattern of the equations). In SU(2), $N = N(\alpha)$ is

$$N = \frac{(\alpha + 1)}{1} \ . \tag{48.1}$$

In SU(3), $N = N(\alpha, \beta)$ is

$$N = \frac{(\alpha + 1)}{1} \cdot \frac{(\beta + 1)}{1} \cdot \frac{(\alpha + \beta + 2)}{2} \ . \tag{48.2}$$

In SU(4), $N = N(\alpha, \beta, \gamma)$ is

$$N = \frac{(\alpha+1)}{1} \cdot \frac{(\beta+1)}{1} \cdot \frac{(\gamma+1)}{1} \cdot \frac{(\alpha+\beta+2)}{2} \cdot \frac{(\beta+\gamma+2)}{2} \cdot \frac{(\alpha+\beta+\gamma+3)}{3} \ . \tag{48.3}$$

Note that in Eq. (48.3) there is no factor with $(\alpha + \gamma + 2)$: only a *consecutive* sequence of the label integers appears in any factor. One more example should make the pattern clear for any SU(n). In SU(5), $N = N(\alpha, \beta, \gamma, \delta)$ is

$$N = \frac{(\alpha+1)}{1} \cdot \frac{(\beta+1)}{1} \cdot \frac{(\gamma+1)}{1} \cdot \frac{(\delta+1)}{1} \cdot \frac{(\alpha+\beta+2)}{2} \cdot \frac{(\beta+\gamma+2)}{2} \times \frac{(\gamma+\delta+2)}{2} \cdot \frac{(\alpha+\beta+\gamma+3)}{3} \cdot \frac{(\beta+\gamma+\delta+3)}{3} \cdot \frac{(\alpha+\beta+\gamma+\delta+4)}{4} \ . \tag{48.4}$$

From the symmetry of these equations, it is clear that multiplets that are conjugate to one another have the same number of particles, but so can other multiplets. For example, the SU(4) multiplets (3,0,0) and (1,1,0) each have 20 particles. Try the equations and see.

48.3 Young diagrams

A Young diagram consists of an array of boxes (or some other symbol) arranged in one or more *left-justified* rows, with each row being *at least as long* as the row beneath. The correspondence between a diagram and a multiplet label is: The top row juts out α boxes to the right past the end of the second row, the second row juts out β boxes to the right past the end of the third row, *etc.* A diagram in SU(n) has at most n rows. There can be any number of "completed" columns of n boxes buttressing the left of a diagram; these don't affect the label. Thus in SU(3) the diagrams

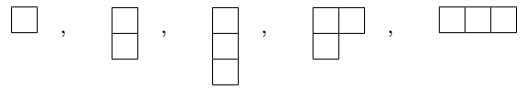

represent the multiplets (1,0), (0,1), (0,0), (1,1), and (3,0). In any SU(n), the quark multiplet is represented by a single box, the antiquark multiplet by a column of (n−1) boxes, and a singlet by a completed column of n boxes.

48.4 Coupling multiplets together

The following recipe tells how to find the multiplets that occur in coupling two multiplets together. To couple together more than two multiplets, first couple two, then couple a third with each of the multiplets obtained from the first two, *etc.*

First a definition: A sequence of the letters $a, b, c, \ldots$ is *admissible* if at any point in the sequence at least as many a's have occurred as b's, at least as many b's have occurred as c's, *etc.* Thus *abcd* and *aabcb* are admissible sequences and *abb* and *acb* are not. Now the recipe:

(a) Draw the Young diagrams for the two multiplets, but in one of the diagrams replace the boxes in the first row with a's, the boxes in the second row with b's, *etc.* Thus, to couple two SU(3) octets (such as the π-meson octet and the baryon octet), we start with and . The *unlettered* diagram forms the *upper left-hand corner* of all the enlarged diagrams constructed below.

(b) Add the a's from the lettered diagram to the right-hand ends of the rows of the unlettered diagram to form all possible legitimate Young diagrams that have no more than one a per column. In general, there will be several distinct diagrams, and all the a's appear in each diagram. At this stage, for the coupling of the two SU(3) octets, we have:

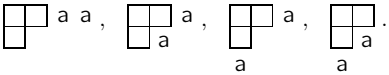

(c) Use the b's to further enlarge the diagrams already obtained, subject to the same rules. Then throw away any diagram in which the full sequence of letters formed by reading *right to left* in the first row, then the second row, *etc.*, is not admissible.

(d) Proceed as in (c) with the c's (if any), *etc.*

The final result of the coupling of the two SU(3) octets is:

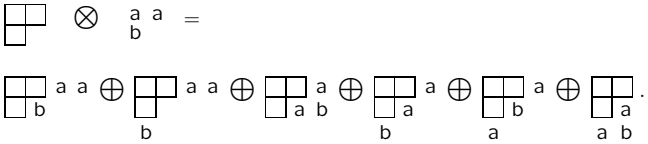

Here only the diagrams with admissible sequences of a's and b's and with fewer than four rows (since $n = 3$) have been kept. In terms of multiplet labels, the above may be written

$$(1, 1) \otimes (1, 1) = (2, 2) \oplus (3, 0) \oplus (0, 3) \oplus (1, 1) \oplus (1, 1) \oplus (0, 0) \ .$$

In terms of numbers of particles, it may be written

$$\mathbf{8} \otimes \mathbf{8} = \mathbf{27} \oplus \mathbf{10} \oplus \overline{\mathbf{10}} \oplus \mathbf{8} \oplus \mathbf{8} \oplus \mathbf{1} \ .$$

The product of the numbers on the left here is equal to the sum on the right, a useful check. (See also Sec. 15 on the Quark Model.)

Downloaded from https://academic.oup.com/ptep/article/2022/8/083C01/6651666 by KIT Library user on 27 September 2022

Downloaded from https://academic.oup.com/ptep/article/2022/8/083C01/6651666 by KIT Library user on 27 September 2022

Kinematics, Cross-Section Formulae, and Plots

49. Kinematics (rev.) 743
50. Resonances (rev.) 747
51. Cross-section formulae for specific processes (rev.) 756
52. Neutrino cross section measurements (rev.) 765
53. Plots of cross sections and related quantities (rev.) 770

Downloaded from https://academic.oup.com/ptep/article/2022/8/083C01/6651666 by KIT Library user on 27 September 2022

Downloaded from https://academic.oup.com/ptep/article/2022/8/083C01/6651666 by KIT Library user on 27 September 2022

49. Kinematics

Reviewed August 2021 by D. Miller (Glasgow), D.R. Tovey (Sheffield), written January 2000 by J.D. Jackson (LBNL).

Throughout this section units are used in which $\hbar = c = 1$. The following conversions are useful: $\hbar c = 197.3$ MeV fm, $(\hbar c)^2 = 0.3894$ (GeV)^2 mb.

49.1 Lorentz transformations

The energy E and 3-momentum $\boldsymbol{p}$ of a particle of mass m form a 4-vector $p = (E, \boldsymbol{p})$ whose square $p^2 \equiv E^2 - |\boldsymbol{p}|^2 = m^2$. The velocity of the particle is $\boldsymbol{\beta} = \boldsymbol{p}/E$. The energy and momentum $(E^*, \boldsymbol{p}^*)$ viewed from a frame moving with velocity $\boldsymbol{\beta}_f$ are given by

$$\begin{pmatrix} E^* \\ p^*_\parallel \end{pmatrix} = \begin{pmatrix} \gamma_f & -\gamma_f\beta_f \\ -\gamma_f\beta_f & \gamma_f \end{pmatrix} \begin{pmatrix} E \\ p_\parallel \end{pmatrix} , \quad p^*_T = p_T , \tag{49.1}$$

where $\gamma_f = (1-\beta_f^2)^{-1/2}$ and p_T ($p_\parallel$) are the components of $\boldsymbol{p}$ perpendicular (parallel) to $\boldsymbol{\beta}_f$. Other 4-vectors, such as the space-time coordinates of events, of course transform in the same way. The scalar product of two 4-momenta $p_1 \cdot p_2 = E_1E_2 - \boldsymbol{p}_1 \cdot \boldsymbol{p}_2$ is invariant (frame independent).

49.2 Center-of-mass energy and momentum

In the collision of two particles of masses m_1 and m_2 the total center-of-mass energy can be expressed in the Lorentz-invariant form

$$\begin{aligned} E_{\rm cm} &= \left[(E_1+E_2)^2 - (\boldsymbol{p}_1+\boldsymbol{p}_2)^2\right]^{1/2} , \\ &= \left[m_1^2 + m_2^2 + 2E_1E_2(1-\beta_1\beta_2\cos\theta)\right]^{1/2} , \end{aligned} \tag{49.2}$$

where θ is the angle between the particles. In the frame where one particle (of mass m_2) is at rest (lab frame),

$$E_{\rm cm} = (m_1^2 + m_2^2 + 2E_{1\,\rm lab}\, m_2)^{1/2} . \tag{49.3}$$

The velocity of the center-of-mass in the lab frame is

$$\boldsymbol{\beta}_{\rm cm} = \boldsymbol{p}_{\rm lab}/(E_{1\,\rm lab} + m_2) , \tag{49.4}$$

where $\boldsymbol{p}_{\rm lab} \equiv \boldsymbol{p}_{1\,\rm lab}$ and

$$\gamma_{\rm cm} = (E_{1\,\rm lab} + m_2)/E_{\rm cm} . \tag{49.5}$$

The c.m. momenta of particles 1 and 2 are of magnitude

$$p_{\rm cm} = p_{\rm lab}\frac{m_2}{E_{\rm cm}} . \tag{49.6}$$

For example, if a 0.80 GeV/c kaon beam is incident on a proton target, the center of mass energy is 1.699 GeV and the center of mass momentum of either particle is 0.442 GeV/c. It is also useful to note that

$$E_{\rm cm}\, dE_{\rm cm} = m_2\, dE_{1\,\rm lab} = m_2\, \beta_{1\,\rm lab}\, dp_{\rm lab} . \tag{49.7}$$

49.3 Lorentz-invariant amplitudes

The matrix elements for a scattering or decay process are written in terms of an invariant amplitude $-i\mathscr{M}$. As an example, the S-matrix for $2 \to 2$ scattering is related to $\mathscr{M}$ by

$$\langle p_1' p_2' \,|S-1|\, p_1 p_2\rangle = i(2\pi)^4\, \delta^4(p_1+p_2-p_1'-p_2')\mathscr{M}(p_1,\, p_2;\, p_1',\, p_2') . \tag{49.8}$$

The state normalization is such that

$$\langle p'|p\rangle = (2\pi)^3\, 2E_p\, \delta^3(\boldsymbol{p}' - \boldsymbol{p}) , \tag{49.9}$$

with $E_p = \sqrt{\boldsymbol{p}^2 + m^2}$.

For a $2 \to 2$ scattering process producing unstable particles $1'$ and $2'$ decaying via $1' \to 3'4'$ and $2' \to 5'6'$ the matrix element for the complete process can be written in the narrow width approximation as:

$$\mathscr{M}(12 \to 3'4'5'6') = \sum_{h_{1'},h_{2'}} \frac{\mathscr{M}(12 \to 1'2')\mathscr{M}(1' \to 3'4')\mathscr{M}(2' \to 5'6')}{(m^2_{3'4'} - m^2_{1'} + im_{1'}\Gamma_{1'})(m^2_{5'6'} - m^2_{2'} + im_{2'}\Gamma_{2'})} . \tag{49.10}$$

Here, m_{ij} is the invariant mass of particles i and j, m_k and Γ_k are the mass and total width of particle k, and the sum runs over the helicities of the intermediate particles. This enables the cross section for such a process to be written as the product of the cross section for the initial $2 \to 2$ scattering process with the branching ratios (relative partial decay rates) of the subsequent decays. A more sophisticated treatment, beyond the narrow width approximation, can be found in the review on "Resonances".

49.4 Particle decays

The partial decay rate of a particle of mass M into n bodies in its rest frame is given in terms of the Lorentz-invariant matrix element $\mathscr{M}$ by

$$d\Gamma = \frac{(2\pi)^4}{2M}\, |\mathscr{M}|^2\, d\Phi_n\, (P;\, p_1,\, \ldots,\, p_n), \tag{49.11}$$

where $d\Phi_n$ is an element of n-body phase space given by

$$d\Phi_n(P;\, p_1,\, \ldots,\, p_n) = \delta^4\, (P - \sum_{i=1}^n p_i)\, \prod_{i=1}^n \frac{d^3p_i}{(2\pi)^3 2E_i} . \tag{49.12}$$

This phase space is reduced by combinatoric factors whenever there are identical particles in the final state. The phase space can be generated recursively, viz.

$$\begin{aligned} d\Phi_n(P;\, p_1,\, \ldots,\, p_n) &= d\Phi_j(q;\, p_1,\, \ldots,\, p_j) \\ &\times\ d\Phi_{n-j+1}\, (P;\, q,\, p_{j+1},\, \ldots,\, p_n)(2\pi)^3 dq^2 , \end{aligned} \tag{49.13}$$

where $q^2 = (\sum_{i=1}^j E_i)^2 - \left|\sum_{i=1}^j \boldsymbol{p}_i\right|^2$. This form is particularly useful in the case where a particle decays into another particle that subsequently decays.

49.4.1 *Survival probability*

If a particle of mass M has mean proper lifetime τ $(= 1/\Gamma)$ and has momentum $(E, \boldsymbol{p})$, then the probability that it lives for a time t_0 or greater before decaying is given by

$$P(t_0) = e^{-t_0\, \Gamma/\gamma} = e^{-Mt_0\, \Gamma/E} , \tag{49.14}$$

and the probability that it travels a distance x_0 or greater is

$$P(x_0) = e^{-Mx_0\, \Gamma/|\boldsymbol{p}|} . \tag{49.15}$$

49.4.2 *Two-body decays*

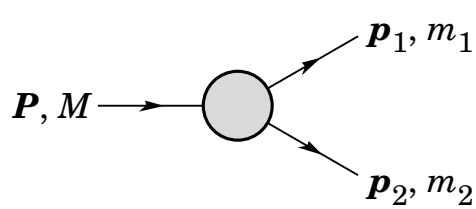

Figure 49.1: Definitions of variables for two-body decays.

In the rest frame of a particle of mass M, decaying into 2 particles labeled 1 and 2,

$$E_1 = \frac{M^2 - m_2^2 + m_1^2}{2M} , \tag{49.16}$$

$$|\boldsymbol{p}_1| = |\boldsymbol{p}_2| = \frac{1}{2M}\sqrt{\lambda(M^2, m_1^2, m_2^2)} , \tag{49.17}$$

and

$$d\Gamma = \frac{1}{32\pi^2}\, |\mathscr{M}|^2\, \frac{|\boldsymbol{p}_1|}{M^2}\, d\Omega , \tag{49.18}$$

Downloaded from https://academic.oup.com/ptep/article/2022/8/083C01/6651666 by KIT Library user on 27 September 2022

where $\lambda(\alpha,\beta,\gamma) = \alpha^2+\beta^2+\gamma^2-2\alpha\beta-2\alpha\gamma-2\beta\gamma$ is the Källén function and $d\Omega = d\phi_1 d(\cos\theta_1)$ is the solid angle of particle 1. The invariant mass M can be determined from the energies and momenta using Eq. (49.2) with $M = E_{\rm cm}$.

49.4.3 *Three-body decays*

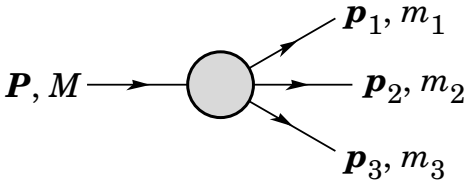

Figure 49.2: Definitions of variables for three-body decays.

Defining $p_{ij} = p_i + p_j$ and $m_{ij}^2 = p_{ij}^2$, then $m_{12}^2+m_{23}^2+m_{13}^2 = M^2+m_1^2+m_2^2+m_3^2$ and $m_{12}^2 = (P-p_3)^2 = M^2+m_3^2-2ME_3$, where E_3 is the energy of particle 3 in the rest frame of M. In that frame, the momenta of the three decay particles lie in a plane. The relative orientation of these three momenta is fixed if their energies are known. The momenta can therefore be specified in space by giving three Euler angles (α,β,γ) that specify the orientation of the final system relative to the initial particle. The direction of any one of the particles relative to the frame in which the initial particle is described can be specified in space by two angles (α,β) while a third angle, γ, can be set as the azimuthal angle of a second particle around the first [1]. Then

$$d\Gamma = \frac{1}{(2\pi)^5}\frac{1}{16M}\,|\mathscr{M}|^2\,dE_1\,dE_3\,d\alpha\,d(\cos\beta)\,d\gamma\,. \tag{49.19}$$

Alternatively

$$d\Gamma = \frac{1}{(2\pi)^5}\frac{1}{16M^2}\,|\mathscr{M}|^2\,|\boldsymbol{p}_1^*|\,|\boldsymbol{p}_3|\,dm_{12}\,d\Omega_1^*\,d\Omega_3\,, \tag{49.20}$$

where $(|\boldsymbol{p}_1^*|,\,\Omega_1^*)$ is the momentum of particle 1 in the rest frame of 1 and 2, and Ω_3 is the angle of particle 3 in the rest frame of the decaying particle. $|\boldsymbol{p}_1^*|$ and $|\boldsymbol{p}_3|$ are given by

$$|\boldsymbol{p}_1^*| = \frac{1}{2m_{12}}\sqrt{\lambda(m_{12}^2,m_1^2,m_2^2)}\,, \tag{49.21a}$$

and

$$|\boldsymbol{p}_3| = \frac{1}{2M}\sqrt{\lambda(M^2,m_{12}^2,m_3^2)}\,. \tag{49.21b}$$

[Compare with Eq. (49.17).]

If the decaying particle is a scalar, or we average over its spin states, then integration over the angles in Eq. (49.19) gives

$$\begin{aligned} d\Gamma &= \frac{1}{(2\pi)^3}\frac{1}{8M}\,\overline{|\mathscr{M}|^2}\,dE_1\,dE_3 \\ &= \frac{1}{(2\pi)^3}\frac{1}{32M^3}\,\overline{|\mathscr{M}|^2}\,dm_{12}^2\,dm_{23}^2\,. \end{aligned} \tag{49.22}$$

This is the standard form for the Dalitz plot.

49.4.3.1 *Dalitz plot*

For a given value of m_{12}^2, the range of m_{23}^2 is determined by its values when $\boldsymbol{p}_2$ is parallel or antiparallel to $\boldsymbol{p}_3$:

$$(m_{23}^2)_{\rm max} = (E_2^*+E_3^*)^2 - \left(\sqrt{E_2^{*2}-m_2^2}-\sqrt{E_3^{*2}-m_3^2}\right)^2\,, \tag{49.23a}$$

$$(m_{23}^2)_{\rm min} = (E_2^*+E_3^*)^2 - \left(\sqrt{E_2^{*2}-m_2^2}+\sqrt{E_3^{*2}-m_3^2}\right)^2\,. \tag{49.23b}$$

Here $E_2^* = (m_{12}^2-m_1^2+m_2^2)/2m_{12}$ and $E_3^* = (M^2-m_{12}^2-m_3^2)/2m_{12}$ are the energies of particles 2 and 3 in the m_{12} rest frame. The scatter plot in m_{12}^2 and m_{23}^2 is called a Dalitz plot. If $\overline{|\mathscr{M}|^2}$ is constant, the allowed region of the plot will be uniformly populated with events [see Eq. (49.22)]. A nonuniformity in the plot gives immediate information on $|\mathscr{M}|^2$. For example, in the case of $D \to K\pi\pi$, bands appear when $m_{(K\pi)} = m_{K^*(892)}$, reflecting the appearance of the decay chain $D \to K^*(892)\pi \to K\pi\pi$.

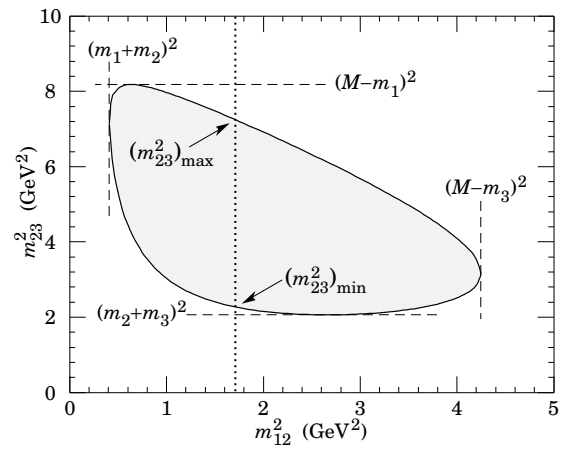

Figure 49.3: Dalitz plot for a three-body final state. In this example, the state is $\pi^+\overline{K}^0p$ at 3 GeV. Four-momentum conservation restricts events to the shaded region.

49.4.4 *Kinematic limits*

49.4.4.1 *Three-body decays*

In a three-body decay (Fig. 49.2) the maximum of $|\boldsymbol{p}_3|$, [given by Eq. (49.21)], is achieved when $m_{12} = m_1+m_2$, *i.e.*, particles 1 and 2 have the same vector velocity in the rest frame of the decaying particle. If, in addition, $m_3 > m_1, m_2$, then $|\boldsymbol{p}_3|_{\rm max} > |\boldsymbol{p}_1|_{\rm max}$, $|\boldsymbol{p}_2|_{\rm max}$. The distribution of m_{12} values possesses an end-point or maximum value at $m_{12} = M-m_3$. This can be used to constrain the mass difference of a parent particle and one invisible decay product.

49.4.4.2 *Sequential two-body decays*

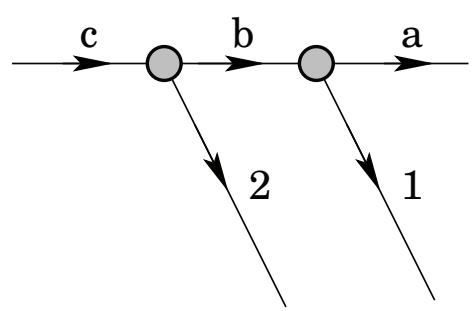

Figure 49.4: Particles participating in sequential two-body decay chain. Particles labeled 1 and 2 are visible while the particle terminating the chain (a) is invisible.

When a heavy particle initiates a sequential chain of two-body decays terminating in an invisible particle, constraints on the masses of the states participating in the chain can be obtained from end-points and thresholds in invariant mass distributions of the aggregated decay products. For the two-step decay chain depicted in Fig. 49.4 the invariant mass distribution of the two visible particles possesses an end-point given by:

$$(m_{12}^{\rm max})^2 = \frac{(m_{\rm c}^2-m_{\rm b}^2)(m_{\rm b}^2-m_{\rm a}^2)}{m_{\rm b}^2}\,, \tag{49.24}$$

provided particles 1 and 2 are massless. If visible particle 1 has

Downloaded from https://academic.oup.com/ptep/article/2022/8/083C01/6651666 by KIT Library user on 27 September 2022

non-zero mass m_1 then Eq. (49.24) is replaced by

$$(m_{12}^{\max})^2 = m_1^2 + \frac{(m_c^2 - m_b^2)}{2m_b^2} \times \left(m_1^2 + m_b^2 - m_a^2 + \sqrt{(-m_1^2 + m_b^2 - m_a^2)^2 - 4m_1^2 m_a^2}\right) . \quad (49.25)$$

See Refs. [2] and [3] for other cases.

49.4.5 *Multibody decays*

The above results may be generalized to final states containing any number of particles by combining some of the particles into "effective particles" and treating the final states as 2 or 3 "effective particle" states. Thus, if $p_{ijk\ldots} = p_i + p_j + p_k + \ldots$, then

$$m_{ijk\ldots} = \sqrt{p^2{}_{ijk\ldots}} \ , \quad (49.26)$$

and $m_{ijk\ldots}$ may be used in place of *e.g.*, m_{12} in the relations in Sec. 49.4.3 or Sec. 49.4.4 above.

49.5 Cross sections

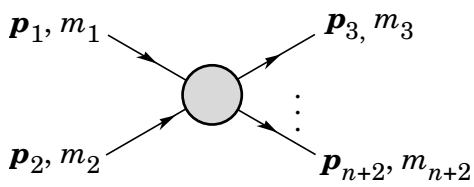

Figure 49.5: Definitions of variables for production of an n-body final state.

The differential cross section is given by

$$d\sigma = \frac{(2\pi)^4 |\mathscr{M}|^2}{4\sqrt{(p_1 \cdot p_2)^2 - m_1^2 m_2^2}} \times \ d\Phi_n(p_1 + p_2;\ p_3, \ldots, p_{n+2}) \ . \quad (49.27)$$

[See Eq. (49.12).] In the rest frame of m_2(lab),

$$\sqrt{(p_1 \cdot p_2)^2 - m_1^2 m_2^2} = m_2 p_{1\,\mathrm{lab}}; \quad (49.28a)$$

while in the center-of-mass frame

$$\sqrt{(p_1 \cdot p_2)^2 - m_1^2 m_2^2} = p_{1\mathrm{cm}} \sqrt{s} \ . \quad (49.28b)$$

49.5.1 *Two-body reactions*

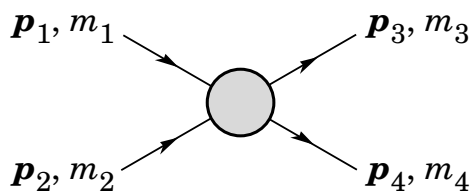

Figure 49.6: Definitions of variables for a two-body final state.

Two particles of momenta p_1 and p_2 and masses m_1 and m_2 scatter to particles of momenta p_3 and p_4 and masses m_3 and m_4; the Lorentz-invariant Mandelstam variables are defined by

$$\begin{aligned} s &= (p_1 + p_2)^2 = (p_3 + p_4)^2 \\ &= m_1^2 + 2E_1 E_2 - 2\boldsymbol{p}_1 \cdot \boldsymbol{p}_2 + m_2^2 \ , \quad (49.29) \\ t &= (p_1 - p_3)^2 = (p_2 - p_4)^2 \\ &= m_1^2 - 2E_1 E_3 + 2\boldsymbol{p}_1 \cdot \boldsymbol{p}_3 + m_3^2 \ , \quad (49.30) \\ u &= (p_1 - p_4)^2 = (p_2 - p_3)^2 \\ &= m_1^2 - 2E_1 E_4 + 2\boldsymbol{p}_1 \cdot \boldsymbol{p}_4 + m_4^2 \ , \quad (49.31) \end{aligned}$$

and they satisfy

$$s + t + u = m_1^2 + m_2^2 + m_3^2 + m_4^2 \ . \quad (49.32)$$

The two-body cross section may be written as

$$\frac{d\sigma}{dt} = \frac{1}{64\pi s} \frac{1}{|\boldsymbol{p}_{1\mathrm{cm}}|^2} |\mathscr{M}|^2 \ . \quad (49.33)$$

In the center-of-mass frame

$$\begin{aligned} t &= (E_{1\mathrm{cm}} - E_{3\mathrm{cm}})^2 - (p_{1\mathrm{cm}} - p_{3\mathrm{cm}})^2 - 4p_{1\mathrm{cm}}\, p_{3\mathrm{cm}}\, \sin^2(\theta_{\mathrm{cm}}/2) \\ &= t_0 - 4p_{1\mathrm{cm}}\, p_{3\mathrm{cm}}\, \sin^2(\theta_{\mathrm{cm}}/2) \ , \end{aligned} \quad (49.34)$$

where θ_{cm} is the angle between particle 1 and 3. The limiting values t_0 ($\theta_{\mathrm{cm}} = 0$) and t_1 ($\theta_{\mathrm{cm}} = \pi$) for $2 \to 2$ scattering are

$$t_0(t_1) = \left[\frac{m_1^2 - m_3^2 - m_2^2 + m_4^2}{2\sqrt{s}}\right]^2 - (p_{1\,\mathrm{cm}} \mp p_{3\,\mathrm{cm}})^2 \ . \quad (49.35)$$

In the literature the notation $t_{\min}$ ($t_{\max}$) for t_0 (t_1) is sometimes used, which should be discouraged since $t_0 > t_1$. The center-of-mass energies and momenta of the incoming particles are

$$E_{1\mathrm{cm}} = \frac{s + m_1^2 - m_2^2}{2\sqrt{s}} \ , \qquad E_{2\mathrm{cm}} = \frac{s + m_2^2 - m_1^2}{2\sqrt{s}} \ , \quad (49.36)$$

For $E_{3\mathrm{cm}}$ and $E_{4\mathrm{cm}}$, change m_1 to m_3 and m_2 to m_4. Then

$$p_{i\,\mathrm{cm}} = \sqrt{E_{i\,\mathrm{cm}}^2 - m_i^2} \text{ and } p_{1\mathrm{cm}} = \frac{p_{1\,\mathrm{lab}}\, m_2}{\sqrt{s}} \ . \quad (49.37)$$

Here the subscript lab refers to the frame where particle 2 is at rest. [For other relations see Eqs. (49.2)–(49.4).]

49.5.2 *Inclusive reactions*

Choose some direction (usually the beam direction) for the z-axis; then the energy and momentum of a particle can be written as

$$E = m_T \cosh y \ , \ p_x \ , \ p_y \ , \ p_z = m_T \sinh y \ , \quad (49.38)$$

where m_T, conventionally called the 'transverse mass', is given by

$$m_T^2 = m^2 + p_x^2 + p_y^2 \ . \quad (49.39)$$

and the rapidity y is defined by

$$\begin{aligned} y &= \frac{1}{2} \ln\left(\frac{E + p_z}{E - p_z}\right) \\ &= \ln\left(\frac{E + p_z}{m_T}\right) = \tanh^{-1}\left(\frac{p_z}{E}\right) \ . \end{aligned} \quad (49.40)$$

Note that the definition of the transverse mass in Eq. (49.39) differs from that used by experimentalists at hadron colliders (see Sec. 49.6.1 below). Under a boost in the z-direction to a frame with velocity β, $y \to y - \tanh^{-1}\beta$. Hence, the shape of the rapidity distribution dN/dy is invariant, as are differences in rapidity. The invariant cross section may also be rewritten

$$E\frac{d^3\sigma}{d^3p} = \frac{d^3\sigma}{d\phi\, dy\, p_T\, dp_T} \Longrightarrow \frac{d^2\sigma}{\pi\, dy\, d(p_T^2)} \ . \quad (49.41)$$

The second form is obtained using the identity $dy/dp_z = 1/E$, and the third form represents the average over ϕ.

Feynman's x variable is given by

$$x = \frac{p_z}{p_{z\,\max}} \approx \frac{E + p_z}{(E + p_z)_{\max}} \quad (p_T \ll |p_z|) \ . \quad (49.42)$$

In the c.m. frame,

$$x \approx \frac{2p_{z\,\mathrm{cm}}}{\sqrt{s}} = \frac{2m_T \sinh y_{\mathrm{cm}}}{\sqrt{s}} \quad (49.43)$$

Downloaded from https://academic.oup.com/ptep/article/2022/8/083C01/6651666 by KIT Library user on 27 September 2022

and

$$= (y_{\rm cm})_{\rm max} = \ln(\sqrt{s}/m) \ . \tag{49.44}$$

The invariant mass M of the two-particle system described in Sec. 49.4.2 can be written in terms of these variables as

$$M^2 = m_1^2 + m_2^2 + 2[E_T(1)E_T(2)\cosh\Delta y - \boldsymbol{p}_T(1)\cdot\boldsymbol{p}_T(2)] \ , \tag{49.45}$$

where

$$E_T(i) = \sqrt{|\boldsymbol{p}_T(i)|^2 + m_i^2} \ , \tag{49.46}$$

and $\boldsymbol{p}_T(i)$ denotes the transverse momentum vector of particle i.

For $p \gg m$, the rapidity [Eq. (49.40)] may be expanded to obtain

$$y = \frac{1}{2}\ln\frac{\cos^2(\theta/2) + m^2/4p^2 + \ldots}{\sin^2(\theta/2) + m^2/4p^2 + \ldots} \approx -\ln\tan(\theta/2) \equiv \eta \tag{49.47}$$

where $\cos\theta = p_z/p$. The pseudorapidity η defined by the second line is approximately equal to the rapidity y for $p \gg m$ and $\theta \gg 1/\gamma$, and in any case can be measured when the mass and momentum of the particle are unknown. From the definition one can obtain the identities

$$\sinh\eta = \cot\theta \ , \ \ \cosh\eta = 1/\sin\theta \ , \ \ \tanh\eta = \cos\theta \ . \tag{49.48}$$

49.6 Transverse variables

At hadron colliders, a significant and unknown proportion of the energy of the incoming hadrons in each event escapes down the beam-pipe. Consequently, if invisible particles are created in the final state, their net momentum can only be constrained in the plane transverse to the beam direction. Defining the z-axis as the beam direction, this net momentum is equal to the missing transverse energy vector

$$\boldsymbol{E}_T^{\rm miss} = -\sum_i \boldsymbol{p}_T(i) \ , \tag{49.49}$$

where the sum runs over the transverse momenta of all visible final state particles.

49.6.1 *Single production with semi-invisible final state*

Consider a single heavy particle of mass M produced in association with visible particles which decays as in Fig. 49.1 to two particles, of which one (labeled particle 1) is invisible. The mass of the parent particle can be constrained with the quantity M_T defined by

$$M_T^2 \equiv [E_T(1) + E_T(2)]^2 - [\boldsymbol{p}_T(1) + \boldsymbol{p}_T(2)]^2 = m_1^2 + m_2^2 + 2[E_T(1)E_T(2) - \boldsymbol{p}_T(1)\cdot\boldsymbol{p}_T(2)] \ , \tag{49.50}$$

where

$$\boldsymbol{p}_T(1) = \boldsymbol{E}_T^{\rm miss} \ . \tag{49.51}$$

This quantity is called the 'transverse mass' by hadron collider experimentalists but it should be noted that it is quite different from that used in the description of inclusive reactions [Eq. (49.39)]. The distribution of event M_T values possesses an end-point at $M_T^{\rm max} = M$. If $m_1 = m_2 = 0$ then

$$M_T^2 = 2|\boldsymbol{p}_T(1)||\boldsymbol{p}_T(2)|(1 - \cos\phi_{12}) \ , \tag{49.52}$$

where ϕ_{ij} is defined as the angle between particles i and j in the transverse plane.

49.6.2 *Pair production with semi-invisible final states*

Consider two identical heavy particles of mass M produced such that their combined center-of-mass is at rest in the transverse plane (Fig. 49.7). Each particle decays to a final state consisting of an invisible particle of fixed mass m_1 together with an additional visible particle. M and m_1 can be constrained with the variables M_{T2} and M_{CT} which are defined in Refs. [4] and [5].

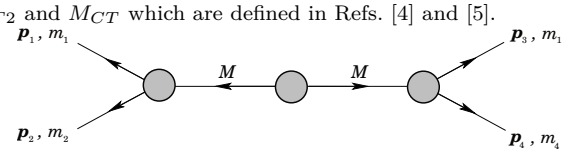

Figure 49.7: Definitions of variables for pair production of semi-invisible final states. Particles 1 and 3 are invisible while particles 2 and 4 are visible.

References

[1] J.D. Jackson in *High Energy Physics, Les Houches 1965 Summer School*, GORDON AND BREACH Science Publishers (1965), p. 348.

[2] I. Hinchliffe *et al.*, Phys. Rev. **D55**, 5520 (1997), [hep-ph/9610544].

[3] B. C. Allanach *et al.*, JHEP **09**, 004 (2000), [hep-ph/0007009].

[4] C. G. Lester and D. J. Summers, Phys. Lett. **B463**, 99 (1999), [hep-ph/9906349].

[5] D. R. Tovey, JHEP **04**, 034 (2008), [arXiv:0802.2879].

Downloaded from https://academic.oup.com/ptep/article/2022/8/083C01/6651666 by KIT Library user on 27 September 2022

50. Resonances

Revised August 2021 by D.M. Asner (BNL) and C. Hanhart (Jülich).

50.1 General Considerations

Perturbative methods can be applied to systems of quarks and gluons only for large momentum transfers (see review on 'Quantum Chromodynamics') and, under certain conditions, to some properties of systems that contain heavy quarks or very large momentum scales (see review on "Heavy-quark and soft-collinear effective theory"). Dealing with Quantum Chromodynamics (QCD) in the low momentum transfer region is a very complicated, non-perturbative problem. Accordingly, most hadrons are resonances, which means that they appear as poles of the S-matrix in the complex plane on unphysical sheets. These resonances can show up either in so-called formation experiments,

$$A + B \to \mathbf{R} \to C_1 + ... + C_n \ ,$$

where they become visible in an energy scan (for example, the R-function measured in e^+e^- annihilations — *cf.* the corresponding plots in the review on "Plots of Cross Sections and Related Quantities"), or together with a spectator particle S in production experiments of the kind

$$\begin{aligned} A + B \to \mathbf{R} + S \to [C_1 + ... + C_n] + S \ , \\ Z \to \mathbf{R} + S \to [C_1 + ... + C_n] + S \ , \end{aligned}$$

where the first reaction corresponds to an associated production, the second is a decay (see "Review of Multibody Charm Analyses"). In the latter case, the resonance properties are commonly extracted from a Dalitz-plot analysis (see review on "Kinematics") or projections thereof.

Resonance phenomena are very rich: while typical hadronic widths are of the order of 100 MeV (*e.g.*, for the meson resonances $\rho(770)$ or $\psi(4040)$ or the baryon resonance $\Delta(1232)$) corresponding to a lifetime of 10^{-23} s, the widths can also be as small as a few MeV (*e.g.* of $\phi(1020)$ or J/ψ) or as large as several hundred MeV (*e.g.* of the meson resonances $f_0(500)$ or $D_1(2430)$ or the baryon resonance $N(2190)$).

Typically, a resonance appears as a peak in the total cross section. If the structure is narrow and if there are no relevant thresholds or other resonances nearby, the resonance properties may be extracted employing a Breit–Wigner parameterization, if necessary improved by using an energy-dependent width (*cf.* Sec. 50.3.1 of this review). However, in general, unitarity and analyticity call for the use of more refined tools. When there are overlapping resonances with the same quantum numbers, the resonance terms should not simply be added but combined in a non-trivial way either in a K-matrix approach (*cf.* Sec. 50.3.2 of this review) or using other advanced methods (*cf.* Sec. 50.3.6 of this review). Additional constraints from the S-matrix allow one to build more reliable amplitudes and, in turn, to reduce the systematic uncertainties of the resonance parameters: pole locations and residues. In addition, for broad resonances there is no direct relation between pole location and the total width/lifetime — then, the pole residues need to be used in order to quantify the decay properties.

For simplicity, throughout this review the formulas are given for resonances in a system of distinguishable, scalar particles. The additional complications that appear in the presence of spins can be controlled in the helicity framework developed by Jacob and Wick [1], or in a non-covariant [2] or covariant [3] tensor-operator formalisms. Within these approaches, sequential (cascade) decays are commonly treated as a coherent sum of two-body interactions. Most of the expressions below are given for two-body kinematics.

50.1.1 *Properties of the S-matrix*

The unitary operator that connects asymptotic *in* and *out* states is called the S-matrix. The scattering amplitude is defined as the interacting part of the S matrix. For a two-particles scattering process, it reads:

$$\begin{aligned} i(2\pi)^4\delta^4(p_1 + p_2 - p_1' - p_2')\,\mathcal{M}(p_1, p_2; p_1', p_2')_{ba} = \\ = {}_{\rm out}\left\langle p_1'p_2', b\right| S - 1\,|p_1p_2, a\rangle_{\rm in} \end{aligned} \tag{50.1}$$

where $|p_1p_2, a\rangle$ and $\left|p_1'p_2', b\right\rangle$ are asymptotic states of two non-interacting particles with momentum p_1, p_2 and p_1', p_2'. The channel labels a and b are multi-indices specifying all additional properties of the channel. In general, $\mathcal{M}$ is a matrix in channel space. For a single-particle state, we employ the relativistic normalization,

$$\left\langle p'|p\right\rangle = (2\pi)^3 2E_p\,\delta^3(\vec{p}\,' - \vec{p}), \tag{50.2}$$

with $E_p = \sqrt{\vec{p}\,^2 + m^2}$. The Mandelstam variables $s = (p_1+p_2)^2$, $t = (p_1 - p_1')^2$, and $u = (p_1 - p_2')^2$ are the invariant variables describing the scattering. With these definitions the process in Eq. (50.1) is referred to as the s-channel scattering, where the total energy of the interacting system is given by $\sqrt{s}$, while the variable t is related to the scattering angle, *i.e.* the angle between the momenta of the particles 1 and $1'$ in the center-of-momentum frame. The variable u is not independent of s and t, but the relation

$$s + t + u = m_1^2 + m_2^2 + m_{1'}^2 + m_{2'}^2$$

holds, where the m_i denote the masses of the incoming and outgoing particles, $i \in 1, 1', 2, 2'$. Therefore, the reaction amplitude is a function of two variables, $\mathcal{M}(s,t)$. The function $\mathcal{M}(s,t)$ is a multi-valued function due to the complex branch points in the Mandelstam variables. Branch points appear whenever there is a channel opening. Each two-particle threshold introduces a square-root singularity and the number of Riemann sheets doubles. For resonances coupled to multi-particle states with odd number of particles the threshold branch point is logarithmic [4]. The branch points appear in the complex plane of an unphysical sheet when there is a resonance in a subsystem of the final-state particles [4]. The cuts related to the openings of the crossed channels are located on the left-hand side of the complex plane, and, therefore, are referred to as the left-hand cuts. Triangle topologies can induce logarithmic branch points on the unphysical sheets often called triangle singularities (TS) [4–6].

Poles of reaction amplitude refer either to bound states or to resonances. The former poles are located on the physical sheet, the latter are located on unphysical sheets. Naturally, those located on the unphysical sheet closest to the physical one, often called the second sheet, have usually the largest impact on observables. Moreover, as follows from analyticity, if there is a pole at some complex value of s, there must be another pole at its complex conjugate value, s^*. For a single-channel case this is illustrated in Fig. 50.1: the pole with a negative imaginary part is closer to the physical axis and thus influences the observables in the vicinity of the resonance region more strongly. However, at the threshold both poles are equally distant and accordingly equally important. Any of these singularities can lead to some structure in the observables (see also Ref. [7]). If certain kinematical constraints are met, especially the TS can mimic resonance signals, as claimed in Refs. [8–13] or cause significant changes of resonance signals [14]. In addition to not all bumps being resonances, not every resonance generates a bump in all observables. For instance, there is no clear trace of the $N(1440)1/2^+$, the so called Roper resonance, in the πN observables or phase shifts, although careful analyses reveal a pole [15].

In case of two relevant channels we are faced with four Riemann sheets. Then, the sheet that is the closest to the physical axis changes, as the energy increases. This can be seen from the illustration in Fig. 50.2: for energies higher than the first, but lower than the second threshold, the sheet that connects smoothly to the upper half plane of the physical sheet (11) is sheet (21). However, for energies above the second threshold this role is taken over by sheet (22). Accordingly, a pole on sheet (21), but above the second threshold, will show up in data only as a cusp exactly at the second threshold. Sheet (12), on the other hand, is remote for all energies.

The analyticity principle of the S-matrix forbids any singularities on the first Riemann sheet except poles and branch points on the real axis. Unitarity constrains the imaginary part of the amplitude on the real axis as further discussed in the following

Downloaded from https://academic.oup.com/ptep/article/2022/8/083C01/6651666 by KIT Library user on 27 September 2022

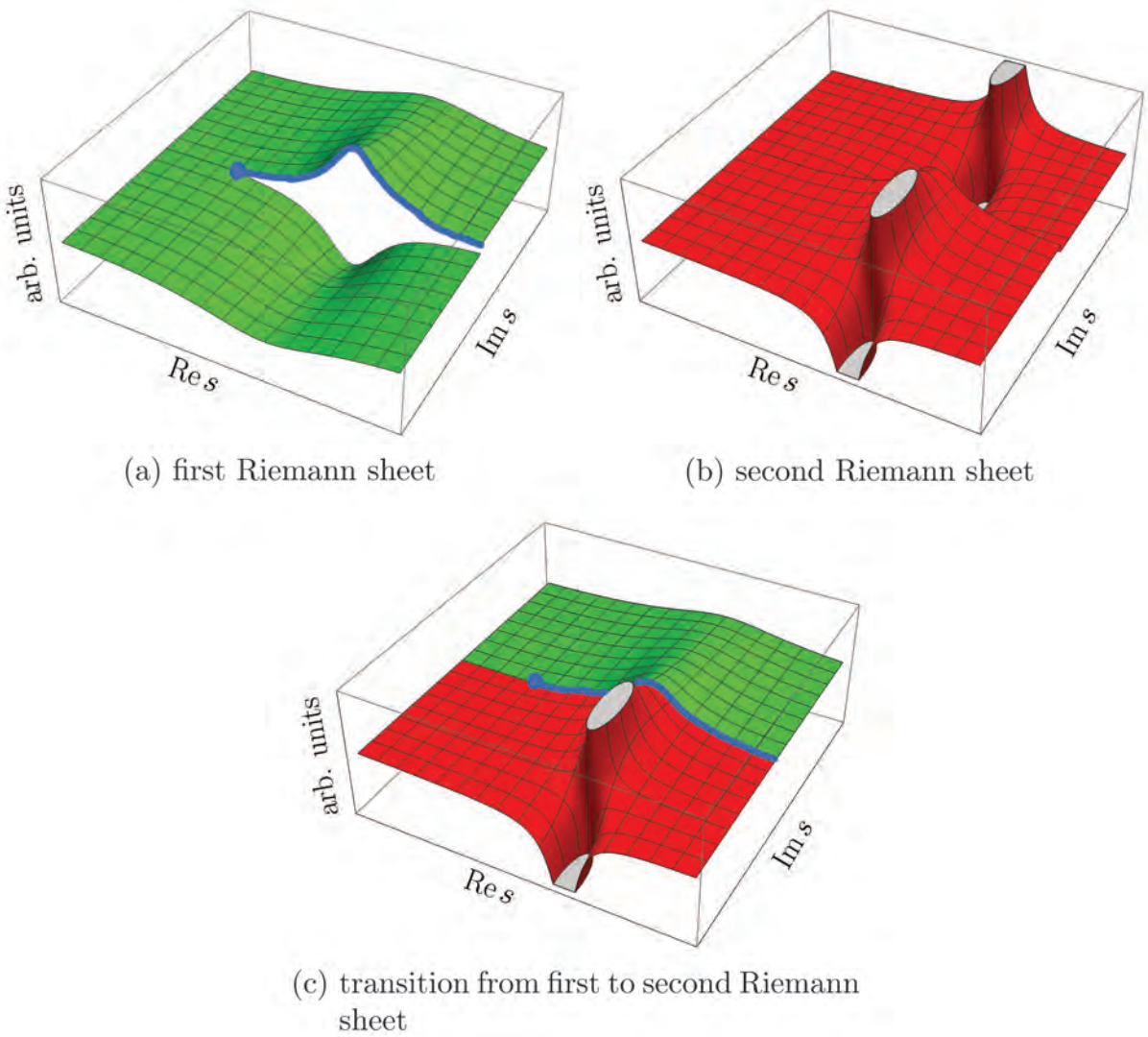

Figure 50.1: Imaginary part of a typical single-channel scattering amplitude with an isolated resonance. The blue line shows the physical range of the Mandelstam variable s: it is real and starts from the threshold shown by the blue dot. Plot (a) shows the imaginary part of the amplitude in the complex s-plane that corresponds to the first or physical sheet (green surface), plot (b) shows the related unphysical or the second sheet (red surface) which contains the resonance poles, and plot (c) shows the analytic continuation of the same amplitude from the upper half plane of the physical sheet to the lower half plane of the unphysical sheet. The two sheets are connected smoothly along the real axis above the threshold.

section. Further constraints come, *e.g.*, from crossing symmetry and duality [16]. Approaches based on analyticity and crossing symmetry, implemented via dispersion theory, like the Roy equations [17] or variants thereof, were developed and applied to $\pi\pi \to \pi\pi$ scattering [18–20], πK scattering [21], $\gamma\gamma \to \pi\pi$ [22] as well as pion-nucleon scattering [23, 24].

50.1.2 *Consequences from unitarity*

In what follows, scattering amplitudes, $\mathcal{M}$, and production amplitudes, $\mathcal{A}$, will be distinguished, since unitarity puts different constraints on these. For the scattering amplitude, all considered channels are supposed to be of comparable importance, while for the production amplitudes we require that the initial state is only weakly coupled and, therefore, the probability of the time-reversed reaction is negligibly small compared to the other coupled channels. Most of the strong-interaction processes are then described by the scattering amplitude, *e.g.* $\pi^+\pi^- \to K\bar{K}$, or $D^0\bar{D}^0 \to D^0\bar{D}^0$. Examples for production processes are $e^+e^- \to \pi^+\pi^-$, $\tau \to K^-\pi^0\nu$, $B^0 \to J/\psi\pi^+\pi^-$.

Unitarity of the S matrix, $S^\dagger S = 1$, which is equivalent to the conservation of probability, translates to a constraint for the imaginary part of the reaction amplitude. The amplitude is real below the first threshold. Above the threshold, the discontinuity across the cut related to the threshold branch point, obeys the relation [25]:

$$\mathcal{M}_{ba} - \mathcal{M}^*_{ab} = i\,(2\pi)^4 \sum_c \int d\Phi_c \mathcal{M}^*_{cb}\mathcal{M}_{ca}\ , \tag{50.3}$$

where Φ_c is the invariant phase space for channel c. The sum includes only open channels, *i.e.* those for which the production threshold is below the energy of the scattered system. Complementary, the channels with the threshold higher than the energy of the system are called closed. Using time-reversal symmetry, and $\mathrm{Disc}\,\mathcal{M}(s,t) = 2i\,\mathrm{Im}(\mathcal{M}(s+i\epsilon,t))$ for the s-channel, the optical theorem follows:

$$\mathrm{Im}\,\mathcal{M}_{aa}(s,0) = 2q_a\sqrt{s}\,\sigma_{\mathrm{tot}}(a \to \text{anything})\,. \tag{50.4}$$

Here, q_a is the momentum of particles in their center-of-

Downloaded from https://academic.oup.com/ptep/article/2022/8/083C01/6651666 by KIT Library user on 27 September 2022

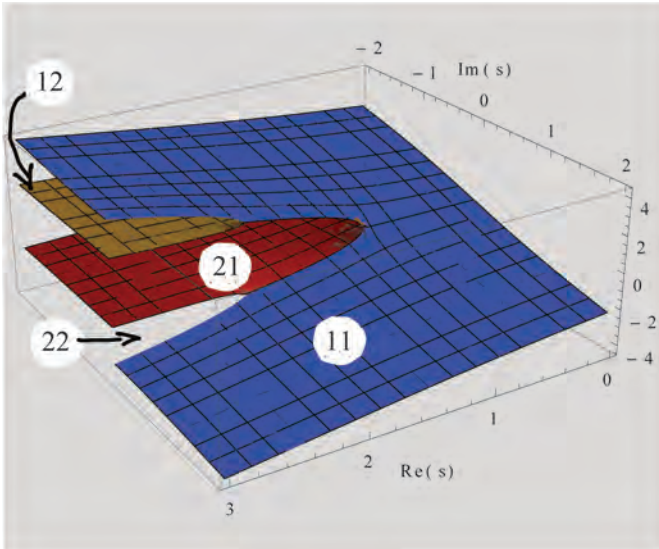

Figure 50.2: Cut structure of the S-matrix in the presence of two-channels. The four sheets are labelled as (ij) with $i = 1, 2$ and $j = 1, 2$ referring to the doubling of the sheets at the first and the second thresholds, respectively.

momentum frame,

$$q_a = \frac{\lambda^{1/2}(s, m_{1,a}^2, m_{2,a}^2)}{2\sqrt{s}} \ , \tag{50.5}$$

where $\lambda(x, y, z) = x^2 + y^2 + z^2 - 2xy - 2yz - 2yx$ is the Källén function, $m_{1,a}$ and $m_{2,b}$ are the masses of the two particles in the channel a, *cf.* Eq. (17) of the review on "Kinematics". The value $t = 0$ in Eq. (50.4) corresponds to forward scattering.

The unitarity relation for a production amplitude for a channel a is given by

$$\mathcal{A}_a - \mathcal{A}_a^* = i\,(2\pi)^4 \sum_c \int d\Phi_c \mathcal{M}_{ca}^* \mathcal{A}_c \,. \tag{50.6}$$

Note that production amplitude written as a linear combination of the scattering amplitudes satisfies Eq. (50.6) due to Eq. (50.3). This solution are often practical, especially, when the scattering matrix is well known, as for example for $\pi\pi$ system below 1.1 GeV [26, 27]. However, it should be understood that this kind of treatment is only approximate, since it imports the analytic structure of the scattering amplitude including its left-hand cuts to the production amplitude which in general has a different cut structure. A more sophisticated application of the two-body-unitarity constraints from Eq. (50.6) is the Khuri-Treiman framework often employed to study three-body decays [28]. The standard procedure here is to derive the equations for the production amplitude for small values of the mass of the decaying particle in the scattering domain and relate it to the decay kinematics by an analytic continuation in the decay mass. The method was successfully applied to various decays of light mesons, $\eta \to 3\pi$ in Refs. [29–34], $\phi/\omega \to 3\pi$ in Ref. [35, 36], $\eta' \to \eta\pi\pi$ in Ref. [37], as well as to the charm-mesons decays $D^+ \to K^{0/-}\pi^{0/+}\pi^+$ [38, 39].

50.1.3 *Partial-wave decomposition*

It is often convenient to expand the scattering amplitude in partial waves. Since resonances have a well-defined spin, they appear only in a specific partial wave of the reaction amplitude. For scalar particles the expansion reads:

$$\mathcal{M}_{ba}(s, t) = \sum_{j=0}^{\infty} (2j + 1)\mathcal{M}_{ba}^j(s) P_j(\cos(\theta)) \ , \tag{50.7}$$

where j denotes the total angular momentum and the $P_j(\cos(\theta))$ denotes the Legendre polynomials. In the presence of spins an expansion more complicated than Eq. (50.7) is necessary. In the absence of spins the parameter j coincides with the orbital angular momentum of the particle pairs in the initial and the final state. To simplify notations we will drop the label j for the single-argument function $\mathcal{M}_{ba}(s)$. The unitarity constraint for $\mathcal{M}_{ba}(s)$ reads,

$$\mathrm{Im}\,\mathcal{M}_{ba}(s) = \sum_c \mathcal{M}_{cb}(s)^*\, \rho_c(s)\, \mathcal{M}_{ca}(s) \tag{50.8}$$

with $\rho_c(s)$ being a factor that is related to the two-body phase space in Eq. (12) of the review on "Kinematics",

$$\rho_c(s) = \frac{(2\pi)^4}{2} \int \mathrm{d}\Phi_2 = \frac{1}{16\pi} \frac{2|\vec{q}_c|}{\sqrt{s}} \ , \tag{50.9}$$

with the momentum q_c being defined in Eq. (50.5). Note that in case of the two particles being identical the inclusion of symmetry factors becomes necessary. The partial-wave amplitude $f_{ba}(s)$ is introduced via

$$f_{ba}(s) = \sqrt{\rho_b}\, \mathcal{M}_{ba}(s)\, \sqrt{\rho_a} \ . \tag{50.10}$$

From the unitarity condition Eq. (50.8) it follows that $\mathrm{Im}\, f_{ba}^{-1} = -\delta_{ba}$. Moreover, $\mathbb{I} + 2if$ is a unitary matrix. Hence, the diagonal elements of f can be parameterized as,

$$f_{bb} = (\eta_b \exp(2i\delta_b) - 1)/2i \ , \tag{50.11}$$

where δ_b denotes the phase shift for the scattering from channel b to channel b, η_b is elasticity parameter — also called inelasticity. One has $0 \le \eta_b \le 1$, where $\eta_b = 1$ is referred to as a purely elastic scattering. The evolution of the partial-wave amplitude f_{bb} with energy can be displayed as a trajectory in the Argand plot, as shown in Fig. 50.3. In case of a two-channel problem, $\eta_b = \eta_a = \eta$, and the off-diagonal element is $f_{ba} = \sqrt{1 - \eta^2}/2 \exp(i(\delta_b + \delta_a))$. The unitarity condition Eq. (50.11) sets the limit to the squared amplitude f_{bb}:

$$|f_{bb}|^2 = \frac{1}{4}(\eta_b^2 - 2\eta_b \cos(2\delta_b) + 1) \le \frac{1}{4}(\eta_b + 1)^2 \ , \tag{50.12}$$

where the maximum value is achieved for $\delta_b = \pi/2$. For the partial-wave-projected scattering amplitude the unitarity bound reads:

$$|\mathcal{M}_{bb}| \ \le \ \frac{1}{2\rho_b}(\eta_b + 1) \ \le \ \frac{8\pi}{q_b}\sqrt{s}\,, \tag{50.13}$$

where the second inequality comes from $\eta_b \le 1$. For energies much larger than the masses of the scattering particles. One finds that the upper bound for $|\mathcal{M}_{bb}|$ tends to 16π for large s.

The partial-wave-projected production amplitude $\mathcal{A}(s)$ (the label j is dropped for consistency) is also constrained by unitarity. From Eq. (50.6) it follows:

$$\mathrm{Im}\,\mathcal{A}_a = \sum_b \mathcal{M}_{ba}^*\, \rho_b\, \mathcal{A}_b \ , \tag{50.14}$$

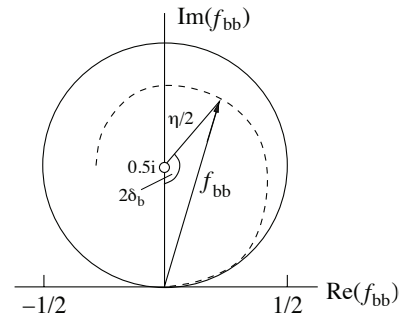

Figure 50.3: Argand plot showing a diagonal element of a partial-wave amplitude, a_{bb}, as a function of energy. The amplitude leaves the unitary circle (solid line) as soon as inelasticity sets in, $\eta < 1$ (dashed line).

Downloaded from https://academic.oup.com/ptep/article/2022/8/083C01/6651666 by KIT Library user on 27 September 2022

where the sum runs over all open channels. For elastic processes, the sum collapses to the channel a. In this case, the phase of $\mathcal{A}_a$ must agree with the phase of $\mathcal{M}_{aa}$ since the left-hand side of Eq. (50.14) is a real number. The statement is known as the Watson theorem [40].

50.2 Properties of resonances

The main characteristics of a resonance is its pole position in the complex s-plane, s_R. The pole mass $M_{\rm R}$ and pole width $\Gamma_{\rm R}$ are introduced via the pole parameters

$$\sqrt{s_{\rm R}} = M_{\rm R} - i\Gamma_{\rm R}/2 \ . \tag{50.15}$$

Note that the standard Breit–Wigner parameters $M_{\rm BW}$ and $\Gamma_{\rm BW}$, also introduced below, in general, deviate from the pole parameters, *e.g.*, due to finite width effects and the influence of thresholds. It should be stressed, however, that the pole location $s_{\rm R}$ as well as the pole residues to be introduced below, are the only resonance properties that are model- and parametrisation independent.

In addition to the pole position, a resonance is characterized by its couplings to the various channels called residues. The Baryon Particle Listings give the elastic pole residues and normalized transition residues. However, different conventions are used in the two sectors, which are shortly outlined here.

In the close vicinity of the resonance pole the scattering matrix $\mathcal{M}$ can be written as

$$\lim_{s\to s_R} (s - s_R)\mathcal{M}_{ba} = -\mathcal{R}_{ba} \ . \tag{50.16}$$

The residues are calculated via an integration along a closed contour around the pole using

$$\mathcal{R}_{ba} = -\frac{1}{2\pi i}\oint ds\mathcal{M}_{ba} \ . \tag{50.17}$$

The factorization of the residue $(\mathcal{R}_{ba})^2 = \mathcal{R}_{aa} \times \mathcal{R}_{bb}$ allows one to introduce pole couplings according to

$$\tilde{g}_a = \mathcal{R}_{ba}/\sqrt{\mathcal{R}_{bb}} \ . \tag{50.18}$$

The pole couplings characterize the transition strength of a given resonance to some channel a independently of how the particular resonance was produced. For a two-particle decays in the S-wave, one may define a partial width and a branching fraction for a resonance via

$$\Gamma_{{\rm R}\to a} = \frac{|\tilde{g}_a|^2}{M_{\rm R}}\rho_a(M_{\rm R}^2) \quad \text{and} \quad {\rm Br}_a = \Gamma_{{\rm R}\to a}/\Gamma_{\rm R} \ , \tag{50.19}$$

where $M_{\rm R}$ and $\Gamma_{\rm R}$ were introduced in Eq. (50.15). This expression was used to define a two-photon width for the broad $f_0(500)$ [41,42] as well as in the corresponding section of the Meson Particle Listings. Analogously, one should use residues to quantify the coupling of resonances to certain production channels [43]. For an application of this formalism to the coupling of the $K_0^*(1430)$ resonance to a leptonic current see Ref. [44]. Equation (50.19) defines a partial-decay width independent of the reaction used to extract the parameters. For a narrow resonances it maps smoothly onto the other common definition of the branching fraction, discussed in Eq. (50.20) more closely related to observables. For broad, overlapping resonances, however, it should be understood that Eq. (50.19) serves the purpose to convert the residues to quantities that allow for a more direct comparison of resonance transitions to different channels. In case of resonances with significant couplings to channels that are still closed at the resonance mass, Eq. (50.19) cannot be used since the phase-space factor yields zero.

In the baryon sector, it is common to define the residue of the pole of the f_{ba} amplitude defined in Eq. (50.10) in variable $\sqrt{s}$ instead of s. Accordingly, in the baryon listings the elastic pole residue, which refers to $\pi N \to \pi N$ scattering, is related to the residues introduced above via

$$r_{\pi N,\pi N} = \frac{\rho_{\pi N}(s_{\rm R})}{\sqrt{4s_{\rm R}}}\,\mathcal{R}_{\pi N,\pi N} \ , \tag{50.20}$$

where $s_{\rm R}$ is the position of the pole. For evaluation of the phase-space factor for the complex argument, analytic continuation is required.

In the literature there are alternative definitions of a branching fraction, which are more close to what is observed in experiment than what follows from Eq. (50.19). Usually those are defined from the probability of the decay of a resonance to a certain channel as provided by the corresponding amplitude on the real axis, where the measurements are performed. It should be understood that in order to isolate an individual resonance in an amplitude defined on the real axis in general some model dependence is unavoidable (*e.g.* this is possible if the amplitude is provided by a sum of Breit–Wigner functions, however, since such a sum violates unitarity the parametrisation comes with an intrinsic theoretical uncertainty difficult to quantify). Having that said one may define the partial width of a resonance alternatively via

$$\Gamma_{{\rm R}\to a} = \frac{(2\pi)^4}{2M_{\rm R}}\int |\mathcal{A}_a|^2\,{\rm d}\Phi_a \ , \tag{50.21}$$

where $\mathcal{A}_a$ is the decay amplitude of the resonance into channel a, which for multi-body final states may even contain resonances in a subchannel. For the two-body decay of a narrow, isolated resonance, $\mathcal{A}_a$ is to a good approximation just $\tilde{g}_a$ and we get back to Eq. (50.19). If the mass of the decaying resonance lies below the threshold of the final state, an integration over the resonance lineshape needs to be employed in addition. For example, for some generic three-body decay with two of the final-state particles going through a resonance one commonly defines (avoiding complications from spins or centrifugal barrier factors), for simplicity written in terms of Breit–Wigner functions (see next section)

$$\begin{aligned}{\rm Br}_{R\to cR'}{\rm Br}_{R'\to ab} &= (2\pi)^3\int_{m^2_{{\rm min}R}}^{\infty} dm^2 \left|\frac{g_{R\to R'c}}{M^2_{{\rm BW}R} - m^2 - iM_{{\rm BW}R}\Gamma_R(m^2)}\right|^2 \\ &\times(2\pi)^3\int_{m^2_{{\rm min}R'}}^{(m-m_c)^2} dm^2_{ab}\left|\frac{g_{R'\to ab}}{M^2_{{\rm BW}R'} - m^2_{ab} - iM_{{\rm BW}R'}\Gamma_{R'}(m^2_{ab})}\right|^2 \int {\rm d}\Phi_{ab}\int {\rm d}\Phi_{R'(m^2_{ab})c} \ ,\end{aligned} \tag{50.22}$$

where $\Gamma_{R^{(\prime)}}(m^2)$ denotes the energy dependent width of resonance R (R') (details are given in the next section), ${\rm d}\Phi_{R'(m^2_{ab})c}$ denotes the two-body phase space for resonance R', at a fixed mass m_{ab}, and particle c for a total energy m, and ${\rm d}\Phi_{ab}$ the two-body phase space for particles a and b for a total energy m_{ab}, respectively. Furthermore, $m^2_{{\rm min}R^{(\prime)}}$ denotes the threshold of the lightest channel resonance R (R') couples to. For example, employing the parameters of the decay of $N^*(1520)$ to ρN one observes that the equation given above only allows the tail of the ρ-meson to contribute to the partial width of the $N^*(1520)$. If in a certain experiment the kinematics do not allow for a scan of the complete line shape of the mother particle, the appropriate procedure to determine the partial width in the approximation outlined above is to determine the effective resonance parameters from a fit to data and to then evaluate Eq. (50.22) in the limits given there. As stressed above, Eq. (50.22) is correct only,

Downloaded from https://academic.oup.com/ptep/article/2022/8/083C01/6651666 by KIT Library user on 27 September 2022

if the use of Breit–Wigner functions is indeed justified for the mother and the daughter particles, which is often not the case. Then, to compare with experiment, the amplitudes need to be parametrised in a more sophisticated way and branching ratios can model independently only be defined via the residues.

In studies of decays where resonance R is very narrow, the first integral in Eq. (50.22) is obsolete and m in the boundaries of the second integral gets fixed to the mass of the mother particle. For recent use of such formulas for B-decays see, e.g., Refs. [45–48]. They were applied to study the three-pion system in Ref. [49].

50.3 Common parameterizations

In general, there is no universal, model-independent recipe to build scattering amplitudes. However, a few approaches presented in this section are practical to extract resonance properties in experimental analyses. The systematic theory uncertainties need to be assessed from a range of model variations that are permitted by general S-matrix principles and that provide a sufficient quality of description of the available data.

50.3.1 *The Breit–Wigner parametrization*

The relativistic Breit–Wigner parametrization provides a propagator for a single, isolated resonance,

$$\mathcal{A}(s) = \frac{N_a(s)}{M_{\rm BW}^2 - s - iM_{\rm BW}\Gamma(s)} \tag{50.23}$$

where $M_{\rm BW}$ is the Breit–Wigner mass, and $\Gamma_{\rm BW} = \Gamma(M_{\rm BW}^2)$ is the Breit–Wigner width. The function $\Gamma(s)$ is determined by the channels that the resonance can decay to. The numerator function $N_a(s)$ is specific to the production process. It includes kinematic factors and couplings related to the production process and the decay. Breit–Wigner functions with a s-independent width are justified only, if there is no relevant threshold in the vicinity of the resonance.

To give a concrete example, we consider a resonance observed in the channel a, that is also coupled to a set of channels labeled by index $b = 1, 2, \ldots$, with the orbital angular momentum l_b. Couplings to the channels are denoted, g_b.

$$N_a(s) = \alpha\, g_a\, n_a(s) \tag{50.24}$$

$$\Gamma(s) = \frac{1}{M_{\rm BW}} \sum_b g_b^2 \rho_b(s) n_b^2(s) \tag{50.25}$$

where the factor $n_a(s)$ includes the kinematic threshold factor q^{l_a}, and the barrier factor $F_{l_a}(q_a/q_0)$ that regularize the high–energy behaviour:

$$n_a = (q_a/q_0)^{l_a} F_{l_a}(q_a/q_0)\,, \tag{50.26}$$

with l_a being the orbital angular momentum in channel a, $q_a(s)$ is defined in Eq. (50.5), and q_0 denotes some conveniently chosen momentum scale. The factor $(q_a)^l$ guarantees the correct threshold behavior. The rapid growth of this factor for angular momenta $l > 0$ is commonly compensated at higher energies by a phenomenological form factor, here denoted by $F_{l_a}(q_a, q_0)$. Often, the Blatt-Weisskopf form factors, $F_j(q/q_0)$, are used [50–52]:

$$\begin{aligned} F_0^2(z) &= 1\,, \\ F_1^2(z) &= 1/(1+z^2)\,, \\ F_2^2(z) &= 1/(9+3z^2+z^4)\,, \end{aligned} \tag{50.27}$$

with the scale parameter $R = 1/q_0$ in the range from $1\,\mathrm{GeV}^{-1}$ to $5\,\mathrm{GeV}^{-1}$. Instead of using coupling constant in Eq. (50.25), one can define the energy-dependent partial width:

$$\Gamma_b(s) = \Gamma_{{\rm BW},b} \frac{\rho_b(s)}{\rho_b(M_{\rm BW}^2)} \left(\frac{q_b}{q_{b\,\rm R}}\right)^{2l_b} \frac{F_{l_b}^2(q_b, q_0)}{F_{l_b}^2(q_{b\,\rm R}, q_0)}\,. \tag{50.28}$$

Here $q_{a\,\rm R}$ are the values of the break-up momentum evaluated at $s = M_{\rm BW}^2$. The substitution is possible only for those channels where the threshold of the decay channel is located below the nominal resonance mass, otherwise, Eq. (50.25) should be used.

The Breit–Wigner parametrization provides an effective description of resonance phenomena. However, the parameters agree with the pole parameters only if the resonance is narrow, isolated (no nearby resonances in the same partial wave) and the background is smooth. Otherwise, the Breit–Wigner parameters deviate from the pole parameters and are reaction-dependent. If there is more than one resonance in one partial wave that significantly couples to the same channel, it is in general incorrect to use a sum of Breit–Wigner functions, for this usually leads to a violation of unitarity constraints, and hence, a non-quantifiable bias to resonance properties which are inferred from the reaction amplitude. In case of overlapping resonances in the same partial wave more refined methods should be used, like the K-matrix approach described in the next section.

50.3.2 *K-matrix approach and Flatté parameterizations*

The K-matrix method is a general construction for coupled-channel scattering amplitudes $\mathcal{M}_{ba}$ that guarantees two-particle unitarity, but does not allow for the inclusion of left-hand cuts [53]. The amplitude reads,

$$n_b\, \mathcal{M}_{ba}^{-1}\, n_a = \mathcal{K}_{ba}^{-1} - i\delta_{ba}\rho_a n_a^2, \tag{50.29}$$

where $\mathcal{K}_{ba}$ is a real function, a subject to modeling. The factor n_a, defined in Eq. (50.26), becomes important for waves with non-zero angular momentum. As there is no unique rigorous recipe to build $\mathcal{K}$, various parameterizations thereof have to be studied, in order to get access to the theoretical systematic uncertainty. One possible choice for the K-matrix is

$$\mathcal{K}_{ba}(s) = \sum_R \frac{g_b^R g_a^R}{m_R^2 - s} + \sum_{i=0}^{N_{\rm b.g.}} b_{ba}^{(i)} s^i, \tag{50.30}$$

where m_R is referred to as the bare mass of the resonance R (not to be confused with the physical mass), the g_a^R are the bare couplings of the resonance R to the channel a (not to be confused with the residues). The $b_{ba}^{(i)}$ are matrices parameterizing the non-pole parts of the K-matrix. As long as all parameters appearing in Eq. (50.30) are real the amplitude is unitary. From the ansatz given above the scattering amplitude $\mathcal{M}$ can be calculated directly using the matrix form,

$$\mathcal{M} = n[1 - \mathcal{K}\, i\rho\, n^2]^{-1}\mathcal{K}\, n\ , \tag{50.31}$$

where the diagonal matrix in the channel space $n = \mathrm{diag}(n_a, n_b, \ldots)$. As an alternative to Eq. (50.30), the same functional form as on the right side of Eq. (50.30) can be used to parameterize the inverse K-matrix, called by authors of Ref. [54] the M-matrix. Many other alternative expressions in the K-matrix framework are used for amplitude studies in lattice-QCD calculations [55–57].

Evaluation of the K-matrix amplitude for the multichannel problem requires an analytic continuation already on the real axis. For a given closed channel c, the factor $q_c(s)$ that enters ρ_c and n_c has to be calculated below the corresponding threshold, *i.e.* in the unphysical region of the particular channel c. This is done using analytic continuation as described *e.g.* in Refs. [27, 58]:

$$q_c = i\sqrt{-q_c^2} \quad \text{for} \quad q_c^2 < 0. \tag{50.32}$$

The resulting line shape above and below the threshold of channel c is called the Flatté parameterization [58]. The contiuation given above stays on the physical sheet. To reach the unphysical sheet the negative square root needs to be chosen. If the coupling of a resonance to the channel opening nearby is very strong, the Flatté parameterization shows a scaling invariance and does not allow for an extraction of individual partial decay widths, but only of ratios [59]. The position of the resonance poles can be determined by a study of the zeros of the analytic function $\det[1 - \mathcal{K}\, i\rho\, n^2]$. Due to the ρ factor, this determinant has a complicated multisheet structure, however, the closest unphysical sheet is always the one which is determined by the heaviest threshold below the studied point in s (*cf.* Fig. 50.2).

Downloaded from https://academic.oup.com/ptep/article/2022/8/083C01/6651666 by KIT Library user on 27 September 2022

50.3.3 *Scattering-length approximation*

A scattering length, a, is defined as the first term in an expansion of the scattering phase shift introduced in Eq. (50.11). For S-waves one finds,

$$q \cot \delta = 1/a + O(q^2)\,, \tag{50.33}$$

where q is the break-up momentum of the scattering system. The sign convention used in Eq. (50.33) is the one commonly employed in particle physics. In this convention a positive scattering length indicates attraction; if, however, the attraction is strong enough to generate a bound state, the scattering length changes sign and turns negative. A negative scattering length also occurs for repuslive interactions. Note that in nuclear physics the leading term in the expansion of Eq. (50.33) is usually defined as $-1/a$ such that *e.g.* a bound state would be related to a positive scattering length. Employing Eq. (50.33) the scattering amplitude reads

$$\mathcal{M}(s) = \frac{8\pi\sqrt{s}}{1/a - iq(s)}\,. \tag{50.34}$$

The scattering length is proportional to the value of the amplitude at threshold. A scattering length approximation is applicable only in a very limited energy range, however, might well be appropriate to analyse the recently discovered narrow near-threshold states [60,61] from this point of view, *e.g.*, in Refs. [62–64]. Moreover, it is possible to introduce the effect of a weakly coupled lower channel. To see this one might start from

$$\mathcal{K} = \begin{pmatrix} \gamma & \beta \\ \beta & 0 \end{pmatrix}\,, \tag{50.35}$$

with β, γ being real numbers. It leads to

$$\mathcal{M}_{\rm el.}(s) = \frac{1}{1/(\gamma + i\beta^2\rho_{\rm inel.}(s)) - i\rho(s)}\,, \tag{50.36}$$

with $\rho_{\rm inel.}(s)$ being the phase-space factor of the inelastic channel. The scattering length for the amplitude in Eq. (50.36) obtains an imaginary part due to the coupling to the lower channel,

$$a = \frac{1}{8\pi\sqrt{s_{\rm thr}}}\left(\gamma + i\beta^2\rho_{\rm inel.}(s_{\rm thr})\right)\,. \tag{50.37}$$

If the function $\beta^2\rho_{\rm inel.}(s)$ does not vary significantly in the energy range studied, the scattering-length approximation with a complex value is justified. For large values of a the amplitude of Eq. (50.36) develops a near-threshold pole located on the physical or unphysical sheet for negative or positive values of γ, respectively. While easy to use, it is important to stress, however, that the approximation in Eq. (50.35) is a specific choice of the dynamic function that produces a single pole near the physical region pointing at a hadronic molecule nature of the state studied [64–67]. Virtual states are discussed in this context in Ref. [68]. For practical analyses, various modifications of the parameterization have to be tested.

50.3.4 *Two methods to build the production amplitude*

When the unitary scattering amplitude is fixed, it can be used to build the production amplitude in a way that it is consistent with unitarity [52,69].

1. The **Q-vector** approach is discussed in Ref. [52,54,70]. It reads,

$$\mathcal{A}_a(s) = \sum_c \mathcal{M}_{ac}(s) Q_c(s)/n_c, \qquad Q_c(s) = \sum Q_c^{(i)} s^i. \tag{50.38}$$

The unitarity condition of Eq. (50.14) is satisfied when $Q_c(s)$ is a real function and in particular does not have singularities above the lowest threshold for all channels c. Besides these conditions $Q_c(s)$ is arbitrary. Note that in the Q-vector approach the left hand cuts of the scattering matrix $\mathcal{M}_{ac}(s)$ get imported to the production amplitude which might generate a wrong analytic structure. If this problem is relevant needs to be investigated on a case-by-case basis. In a study of $\gamma\gamma \to \pi\pi$, *cf.* Ref. [41,42] a low-order polynomial is claimed to be sufficient to parametrize the energy dependence of the function $Q_c(s)$. The Q-vector method is convenient, if the full matrix $\mathcal{M}$ is known, *cf.* Ref. [54].

2. The **P-vector** is a parameterization that exploits the K-matrix of the scattering amplitude [53,69]. It contains two components: the background term B_c that is coupled to the K-matrix via an intermediate loop represented by the $i\rho$ factor, and the "direct" resonance production term with couplings α_c^R:

$$\begin{aligned} \mathcal{A}_a(s) &= n_a \sum_c \left[1 - \mathcal{K}\, i\rho n^2\right]^{-1}_{ac} P_c, \\ P_c &= \sum_R \frac{\alpha^R g_c^R}{m_R^2 - s} + B_c. \end{aligned} \tag{50.39}$$

Again, unitarity requires the parameters B_c and α^R to be real.Here, the masses m_R and the couplings g_c^R need to agree with those in $\mathcal{K}$ in Eq. (50.30).

An important difference between the methods is to be noticed [69]. When the two-particle scattering amplitude goes to zero, the production amplitude in the Q–vector method vanishes for finite values of Q_c, while it stays finite in the P-vector approach. An version of the P-vector approach that exploits the analytic properties of production amplitudes [69,71,72] is widely used, *e.g.* in the dispersive Khuri-Treiman framework [28,73] for the construction of three-body-decay amplitudes.

50.3.5 *Further improvements: Chew-Mandelstam function*

The K-matrix described above usually allows one to get a proper fit of physical amplitudes and it is easy to deal with, however, it also has an important deficit: it violates constraints from analyticity — *e.g.*, ρ_a, given by Eq. (50.9), is ill-defined at $s = 0$, and for unequal masses it develops an unphysical cut (see left panel of Fig. 50.4). A method to improve the analytic properties was suggested in Refs. [74–78]. It replaces the phase-space factor $i\rho_a(s)$ in Eq. (50.29) by the analytic function $\Sigma_a(s)$ that produces the identical imaginary part on the right-hand cut. This function is called the Chew-Mandelstam function and for S-waves it reads [72,76]:

$$\begin{aligned} \Sigma_a(s) = \frac{1}{16\pi^2}\Bigg[&\frac{2q_a}{\sqrt{s}} \log \frac{m_1^2 + m_2^2 - s + 2\sqrt{s}q_a}{2m_1m_2} - \\ &- (m_1^2 - m_2^2)\left(\frac{1}{s} - \frac{1}{(m_1+m_2)^2}\right)\log\frac{m_1}{m_2}\Bigg], \end{aligned} \tag{50.40}$$

where m_1 and m_2 are masses of the final-state particles in channel a, $s_{{\rm thr}_a} = (m_1+m_2)^2$. The function along the real axis is plotted in the right panel of Fig. 50.4. For channels with $j > 0$, the threshold behavior has to be incorporated properly. This can be done, *e.g.*, by computing the dispersion integral

$$\Sigma_a(s + i0) = \frac{s - s_{{\rm thr}_a}}{\pi} \int_{s_{{\rm thr}_a}}^{\infty} \frac{\rho_a(s') n_a^2(s')}{(s' - s_{{\rm thr}_a})(s' - s - i0)}\, {\rm d}s'. \tag{50.41}$$

A further discussion of the calculation of the Chew-Mandelstam function can be found in Refs. [79,80].

If there is only a single resonance in a given channel, it is possible to feed the imaginary part of the Breit–Wigner function, Eq. (50.23) with an energy-dependent width, directly into a dispersion integral to get a resonance propagator with the correct analytic structure [81,82].

50.3.6 *Two-potential decomposition*

Another advanced technique to construct the scattering amplitude which is widely used in the literature [83–87] is based on the two-potential formalism [88]. The method is usually formulated for the full unprojected amplitude $\mathcal{M}_{ba}(s,t)$, however, in order to simplify the discussion we present the equations in the partial-wave-projected form.

Downloaded from https://academic.oup.com/ptep/article/2022/8/083C01/6651666 by KIT Library user on 27 September 2022

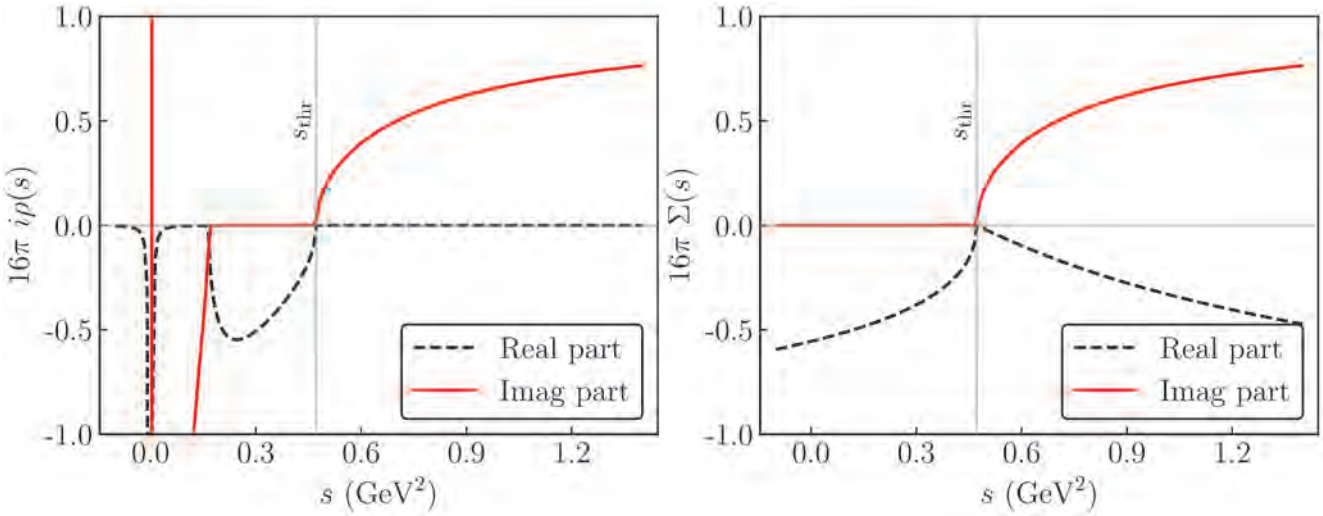

Figure 50.4: Comparison of the $i\rho$ function (left plot) to the Chew-Mandelstam function from Eq. (50.40) (right plot), evaluated for the case of S-wave $\eta\pi$ scattering. The values of s are taken slightly above the real axis, $s + i0$. The solid red line shows the imaginary part that is the same for both functions above threshold. The dashed black line presents the real part. One finds indications of the unphysical left-hand singularities of the function $i\rho$ on the left plot, while the Chew-Mandelstam function in analytic below the two-particle threshold.

The scattering amplitude $\mathcal{M}$ is decomposed into a pole part and a non-pole part, often called background (b.g.)

$$\mathcal{M}(s) = \mathcal{M}^{\rm b.g.}(s) + \mathcal{M}^{\rm pole}(s)\,. \tag{50.42}$$

The splitting given in Eq. (50.42) is not unique and model-dependent (see, *e.g.*, the discussions in Refs. [89, 90]). The background scattering matrix is assumed to be unitary by itself. One option is to parameterize it, *e.g.* at low energies directly in terms of phase shifts and inelasticities — see, *e.g.*, Refs. [44, 87, 91]. In this case the vertex functions $\Omega(s)_{ab}$ introduced below can be written in terms of an Omnes matrix [91], which reduces to the well-known Omnes function in the single-channel case [71]. Alternatively, it can be computed based on some potential, $V^{\rm b.g.}$, fed into a proper scattering equation.

The complete amplitude $\mathcal{M}$ of Eq. (50.42) is unitary, if the pole part is chosen as

$$\mathcal{M}^{\rm pole}(s) = \Omega(s)\ [1 - V^{\rm R}(s)\Sigma^u(s)]^{-1} V^{\rm R}(s)\ \Omega^T(s)\ . \tag{50.43}$$

where the resonance potential reads in channel space

$$V^{\rm R}_{ab}(s) = \sum_R \frac{g^R_a\ g^R_b}{M^2_R - s}\ , \tag{50.44}$$

Σ^u_{ab} denotes the self-energy matrix, and g^R_a and M_R denote the bare coupling of the resonance R to channel a and its bare mass, respectively. A relation analogous to Eq. (50.6) holds for the normalized vertex functions, however, with the final state interaction provided by $\mathcal{M}^{\rm b.g.}$

$$\text{Disc}\,\Omega_{ab}(s) = 2i \sum_c \mathcal{M}^{\rm b.g.\,*}_{ca}(s)\,\rho_c(s)\,\Omega_{cb}(s)\ . \tag{50.45}$$

The discontinuity of the self-energy matrix $\Sigma^u(s)$ is

$$\text{Disc}\,\Sigma^u_{ab}(s) = 2i \sum_c \Omega^*_{ca}(s)\,\rho_c(s)\,\Omega_{cb}(s)\ . \tag{50.46}$$

The real part of Σ^u can be calculated from Eq. (50.46) via a properly subtracted dispersion integral. If $\mathcal{M}^{\rm b.g.}$ is unitary, the use of Eq. (50.43) leads to a unitary full amplitude, *cf.* Eq. (50.42). However, the pole term alone is unitary only for a vanishing background amplitude. In this situation the amplitude just described reduces to the analytically improved K-matrix of Sec. 50.3.5. While the omission of non-pole terms is a bad approximation for, *e.g.*, scalar-isoscalar $\pi\pi$ interactions at low energies [92], it typically works well for higher partial waves.

The algebra of the two potential splitting presented in Eq. (50.42) is found to be very practical in various other cases, beyond the pole-background separation. It was employed in Refs. [87, 91] to treat the pion vector and scalar form factor, respectively, over a sizable energy range including inelasticities. A similar decomposition applied to the $3 \to 3$ scattering problem provided a way to isolate the non-separable one-particle exchange singularity from the short-range resonance interaction [93].

Acknowledgement

We are very grateful to Mikhail Mikhasenko, who gave vital input to improve this review and to Ulf-G. Meißner for valuable comments on the manuscript.

References

[1] M. Jacob and G. C. Wick, Annals Phys. **7**, 404 (1959), [Annals Phys.281,774(2000)].

[2] C. Zemach, Phys. Rev. **140B**, 97, 109 (1965).

[3] A. V. Anisovich *et al.*, J. Phys. **G28**, 15 (2002), [hep-ph/0105330].

[4] V. N. Gribov, Y. L. Dokshitzer and J. Nyiri, *Strong Interactions of Hadrons at High Energies – Gribov Lectures on Theoretical Physics*, Cambridge University Press, Cambridge (2009).

[5] L. Landau, Nucl. Phys. **13**, 181 (1959).

[6] R. Cutkosky, J. Math. Phys. **1**, 429 (1960).

[7] A rapid change in an amplitude is not an unambiguous signal of a singularity of the S–matrix [94], however, for realistic interactions this connection holds.

[8] S. Coleman and R. E. Norton, Nuovo Cim. **38**, 438 (1965).

[9] C. Schmid, Phys. Rev. **154**, 5, 1363 (1967).

[10] I. J. R. Aitchison and C. Kacser, Il Nuovo Cimento A (1965-1970) **40**, 2, 576 (1965), ISSN 1826-9869, URL `https://doi.org/10.1007/BF02721045`.

[11] M. Mikhasenko, B. Ketzer and A. Sarantsev, Phys. Rev. **D91**, 9, 094015 (2015), [arXiv:1501.07023].

[12] M. Bayar *et al.*, Phys. Rev. **D94**, 7, 074039 (2016), [arXiv:1609.04133].

[13] F. Aceti, L. R. Dai and E. Oset, Phys. Rev. **D94**, 9, 096015 (2016), [arXiv:1606.06893].

Downloaded from https://academic.oup.com/ptep/article/2022/8/083C01/6651666 by KIT Library user on 27 September 2022

[14] J.-J. Wu *et al.*, Phys. Rev. Lett. **108**, 081803 (2012), [arXiv:1108.3772].

[15] L. D. Roper, Phys. Rev. Lett. **12**, 340 (1964).

[16] M. Fukugita and K. Igi, Phys. Rept. **31**, 237 (1977).

[17] S. M. Roy, Phys. Lett. **36B**, 353 (1971).

[18] B. Ananthanarayan *et al.*, Phys. Rept. **353**, 207 (2001), [hep-ph/0005297].

[19] G. Colangelo, J. Gasser and H. Leutwyler, Nucl. Phys. **B603**, 125 (2001), [hep-ph/0103088].

[20] R. Garcia-Martin *et al.*, Phys. Rev. **D83**, 074004 (2011), [arXiv:1102.2183].

[21] P. Buettiker, S. Descotes-Genon and B. Moussallam, Eur. Phys. J. **C33**, 409 (2004), [hep-ph/0310283].

[22] M. Hoferichter, D. R. Phillips and C. Schat, Eur. Phys. J. **C71**, 1743 (2011), [arXiv:1106.4147].

[23] G. E. Hite and F. Steiner, Nuovo Cim. A **18**, 237 (1973).

[24] M. Hoferichter *et al.*, Phys. Rept. **625**, 1 (2016), [arXiv:1510.06039].

[25] M. P. Peskin and D. V. Schroeder, *An Introduction to Quantum Field Theory*, Westview Press, 1995.

[26] R. Garcia-Martin *et al.*, Phys. Rev. D **83**, 074004 (2011), [arXiv:1102.2183].

[27] V. V. Anisovich and A. V. Sarantsev, Eur. Phys. J. **A16**, 229 (2003), [hep-ph/0204328].

[28] N. N. Khuri and S. B. Treiman, Phys. Rev. **119**, 1115 (1960).

[29] J. Kambor, C. Wiesendanger and D. Wyler, Nucl. Phys. B **465**, 215 (1996), [hep-ph/9509374].

[30] A. V. Anisovich and H. Leutwyler, Phys. Lett. B **375**, 335 (1996), [hep-ph/9601237].

[31] P. Guo *et al.*, Phys. Lett. **B771**, 497 (2017), [arXiv:1608.01447].

[32] M. Albaladejo and B. Moussallam, Eur. Phys. J. **C77**, 8, 508 (2017), [arXiv:1702.04931].

[33] G. Colangelo *et al.*, Eur. Phys. J. **C78**, 11, 947 (2018), [arXiv:1807.11937].

[34] K. Kampf *et al.*, Phys. Rev. D **101**, 7, 074043 (2020), [arXiv:1911.11762].

[35] F. Niecknig, B. Kubis and S. P. Schneider, Eur. Phys. J. **C72**, 2014 (2012), [arXiv:1203.2501].

[36] I. V. Danilkin *et al.*, Phys. Rev. **D91**, 9, 094029 (2015), [arXiv:1409.7708].

[37] T. Isken *et al.*, Eur. Phys. J. **C77**, 7, 489 (2017), [arXiv:1705.04339].

[38] F. Niecknig and B. Kubis, JHEP **10**, 142 (2015), [arXiv:1509.03188].

[39] F. Niecknig and B. Kubis, Phys. Lett. **B780**, 471 (2018), [arXiv:1708.00446].

[40] K. M. Watson, Phys. Rev. **95**, 228 (1954).

[41] D. Morgan and M. R. Pennington, Z. Phys. **C37**, 431 (1988), [Erratum: Z. Phys.C39,590(1988)].

[42] D. Morgan and M. R. Pennington, Z. Phys. **C48**, 623 (1990).

[43] B. Moussallam, Eur. Phys. J. C **71**, 1814 (2011), [arXiv:1110.6074].

[44] L. Von Detten *et al.*, Eur. Phys. J. C **81**, 5, 420 (2021), [arXiv:2103.01966].

[45] R. Aaij *et al.* (LHCb), Phys. Rev. D **94**, 7, 072001 (2016), [arXiv:1608.01289].

[46] R. Aaij *et al.* (LHCb), Phys. Rev. D **92**, 1, 012012 (2015), [arXiv:1505.01505].

[47] R. Aaij *et al.* (LHCb), Phys. Rev. D **91**, 9, 092002 (2015), [Erratum: Phys.Rev.D 93, 119901 (2016)], [arXiv:1503.02995].

[48] R. Aaij *et al.* (LHCb), Phys. Rev. D **102**, 112003 (2020), [arXiv:2009.00026].

[49] M. Aghasyan *et al.* (COMPASS), Phys. Rev. D **98**, 9, 092003 (2018), [arXiv:1802.05913].

[50] J. M. Blatt and V. F. Weisskopf, *Theoretical nuclear physics*, Springer, New York (1952), ISBN 9780471080190.

[51] F. Von Hippel and C. Quigg, Phys. Rev. **D5**, 624 (1972).

[52] S. U. Chung *et al.*, Annalen Phys. **4**, 404 (1995).

[53] I. J. R. Aitchison, Nucl. Phys. **A189**, 417 (1972).

[54] K. L. Au, D. Morgan and M. R. Pennington, Phys. Rev. **D35**, 1633 (1987).

[55] J. J. Dudek, R. G. Edwards and D. J. Wilson (Hadron Spectrum), Phys. Rev. **D93**, 9, 094506 (2016), [arXiv:1602.05122].

[56] R. A. Briceno *et al.*, Phys. Rev. **D97**, 5, 054513 (2018), [arXiv:1708.06667].

[57] A. J. Woss *et al.* (2019), [arXiv:1904.04136].

[58] S. M. Flatte, Phys. Lett. **63B**, 224 (1976).

[59] V. Baru *et al.*, Eur. Phys. J. **A23**, 523 (2005), [arXiv:nucl-th/0410099].

[60] S. K. Choi *et al.* (Belle), Phys. Rev. Lett. **91**, 262001 (2003), [hep-ex/0309032].

[61] R. Aaij *et al.* (LHCb), Phys. Rev. Lett. **122**, 22, 222001 (2019), [arXiv:1904.03947].

[62] E. Braaten and J. Stapleton, Phys. Rev. **D81**, 014019 (2010), [arXiv:0907.3167].

[63] V. Baru *et al.*, Eur. Phys. J. **A44**, 93 (2010), [arXiv:1001.0369].

[64] C. Fernández-Ramírez *et al.* (JPAC), Phys. Rev. Lett. **123**, 9, 092001 (2019), [arXiv:1904.10021].

[65] D. Morgan, Nucl. Phys. **A543**, 632 (1992).

[66] V. Baru *et al.*, Phys. Lett. **B586**, 53 (2004), [hep-ph/0308129].

[67] F.-K. Guo *et al.*, Rev. Mod. Phys. **90**, 1, 015004 (2018), [arXiv:1705.00141].

[68] I. Matuschek *et al.*, Eur. Phys. J. A **57**, 3, 101 (2021), [arXiv:2007.05329].

[69] I. J. R. Aitchison (2015), [arXiv:1507.02697].

[70] R. N. Cahn and P. V. Landshoff, Nucl. Phys. **B266**, 451 (1986).

[71] R. Omnes, Nuovo Cim. **8**, 316 (1958).

[72] J. L. Basdevant and E. L. Berger, Phys. Rev. **D16**, 657 (1977).

[73] I. J. R. Aitchison and R. Pasquier, Phys. Rev. **152**, 4, 1274 (1966).

[74] G. J. Gounaris and J. J. Sakurai, Phys. Rev. Lett. **21**, 244 (1968).

[75] M. R. Pennington *et al.*, Eur. Phys. J. **C56**, 1 (2008), [arXiv:0803.3389].

[76] J. A. Oller and E. Oset, Phys. Rev. **D60**, 074023 (1999), [hep-ph/9809337].

[77] N. N. Achasov and A. V. Kiselev, Phys. Rev. **D83**, 054008 (2011), [arXiv:1011.4446].

[78] A. V. Anisovich *et al.*, Phys. Rev. **D84**, 076001 (2011).

[79] J. H. Reid and N. N. Trofimenkoff, J. Math. Phys. **25**, 3540 (1984).

[80] J. A. Oller and U. G. Meissner, Phys. Lett. B **500**, 263 (2001), [hep-ph/0011146].

[81] E. L. Lomon and S. Pacetti, Phys. Rev. **D85**, 113004 (2012), [Erratum: Phys. Rev.D86,039901(2012)], [arXiv:1201.6126].

[82] B. Moussallam, Eur. Phys. J. **C73**, 2539 (2013), [arXiv:1305.3143].

[83] I. R. Afnan and B. Blankleider, Phys. Rev. **C22**, 1638 (1980).

[84] A. D. Lahiff and I. R. Afnan, Phys. Rev. **C60**, 024608 (1999), [arXiv:nucl-th/9903058].

Downloaded from https://academic.oup.com/ptep/article/2022/8/083C01/6651666 by KIT Library user on 27 September 2022

[85] A. Matsuyama, T. Sato and T. S. H. Lee, Phys. Rept. **439**, 193 (2007), [arXiv:nucl-th/0608051].

[86] D. Ronchen *et al.*, Eur. Phys. J. **A49**, 44 (2013), [arXiv:1211.6998].

[87] C. Hanhart, Phys. Lett. **B715**, 170 (2012), [arXiv:1203.6839].

[88] K. Nakano, Phys. Rev. **C26**, 1123 (1982).

[89] D. Djukanovic, J. Gegelia and S. Scherer, Phys. Rev. **D76**, 037501 (2007), [arXiv:0707.2030].

[90] M. Doring *et al.*, Phys. Lett. **B681**, 26 (2009), [arXiv:0903.1781].

[91] S. Ropertz, C. Hanhart and B. Kubis, Eur. Phys. J. **C78**, 12, 1000 (2018), [arXiv:1809.06867].

[92] J. Gasser and U. G. Meissner, Nucl. Phys. **B357**, 90 (1991).

[93] M. Mikhasenko *et al.*, JHEP **08**, 080 (2019), [arXiv:1904.11894].

[94] G. Calucci, L. Fonda and G. C. Ghirardi, Phys. Rev. **166**, 1719 (1968).

Downloaded from https://academic.oup.com/ptep/article/2022/8/083C01/6651666 by KIT Library user on 27 September 2022

51. Cross-Section Formulae for Specific Processes

Revised August 2019 by H. Baer (Oklahoma U.) and R.N. Cahn (LBNL).

PART I: STANDARD MODEL PROCESSES

Setting aside leptoproduction (for which, see Sec. 16 of this *Review*), the cross sections of primary interest are those with light incident particles, e^+e^-, $\gamma\gamma$, $q\overline{q}$, gq , gg, *etc.*, where g and q represent gluons and light quarks. The produced particles include both light particles and heavy ones - t, W, Z, and the Higgs boson H. We provide the production cross sections calculated within the Standard Model for several such processes.

51.1 Resonance Formation

Resonant cross sections are generally described by the Breit-Wigner formula (Sec. 50.3 of this *Review*).

$$\sigma(E) = \frac{2J+1}{(2S_1+1)(2S_2+1)}\frac{4\pi}{k^2}\left[\frac{\Gamma^2/4}{(E-E_0)^2+\Gamma^2/4}\right]B_{in}B_{out}, \tag{51.1}$$

where E is the c.m. energy, J is the spin of the resonance, and the number of polarization states of the two incident particles are $2S_1+1$ and $2S_2+1$. The c.m. momentum in the initial state is k, E_0 is the c.m. energy at the resonance, and Γ is the full width at half maximum height of the resonance. The branching fraction for the resonance into the initial-state channel is B_{in} and into the final-state channel is B_{out}. For a narrow resonance, the factor in square brackets may be replaced by $\pi\Gamma\delta(E-E_0)/2$.

51.2 Production of light particles

The production of point-like, spin-1/2 fermions in e^+e^- annihilation through a virtual photon, $e^+e^- \to \gamma^* \to f\overline{f}$, at c.m. energy squared s is given by

$$\frac{d\sigma}{d\Omega} = N_c\frac{\alpha^2}{4s}\beta\left[1+\cos^2\theta+(1-\beta^2)\sin^2\theta\right]Q_f^2 , \tag{51.2}$$

where β is v/c for the produced fermions in the c.m., θ is the c.m. scattering angle, and Q_f is the charge of the fermion. The factor N_c is 1 for charged leptons and 3 for quarks. In the ultrarelativistic limit, $\beta \to 1$,

$$\sigma = N_cQ_f^2\frac{4\pi\alpha^2}{3s} = N_cQ_f^2\frac{86.8\text{ nb}}{s\,(\text{GeV}^2)} . \tag{51.3}$$

The cross section for the annihilation of a $q\overline{q}$ pair into a distinct pair $q'\overline{q}'$ through a gluon is completely analogous up to color factors, with the replacement $\alpha \to \alpha_s$. Treating all quarks as massless, averaging over the colors of the initial quarks and defining $t = -s\sin^2(\theta/2)$, $u = -s\cos^2(\theta/2)$, one finds [1]

$$\frac{d\sigma}{d\Omega}(q\overline{q} \to q'\overline{q}') = \frac{\alpha_s^2}{9s}\frac{t^2+u^2}{s^2} . \tag{51.4}$$

Crossing symmetry gives

$$\frac{d\sigma}{d\Omega}(qq' \to qq') = \frac{\alpha_s^2}{9s}\frac{s^2+u^2}{t^2} . \tag{51.5}$$

If the quarks q and q' are identical, we have

$$\frac{d\sigma}{d\Omega}(q\overline{q} \to q\overline{q}) = \frac{\alpha_s^2}{9s}\left[\frac{t^2+u^2}{s^2}+\frac{s^2+u^2}{t^2}-\frac{2u^2}{3st}\right] , \tag{51.6}$$

and by crossing

$$\frac{d\sigma}{d\Omega}(qq \to qq) = \frac{\alpha_s^2}{9s}\left[\frac{t^2+s^2}{u^2}+\frac{s^2+u^2}{t^2}-\frac{2s^2}{3ut}\right] . \tag{51.7}$$

Annihilation of e^+e^- into $\gamma\gamma$ has the cross section

$$\frac{d\sigma}{d\Omega}(e^+e^- \to \gamma\gamma) = \frac{\alpha^2}{2s}\frac{u^2+t^2}{tu} . \tag{51.8}$$

The related QCD process also has a triple-gluon coupling. The cross section is

$$\frac{d\sigma}{d\Omega}(q\overline{q} \to gg) = \frac{8\alpha_s^2}{27s}(t^2+u^2)\left(\frac{1}{tu}-\frac{9}{4s^2}\right) . \tag{51.9}$$

The crossed reactions are

$$\frac{d\sigma}{d\Omega}(qg \to qg) = \frac{\alpha_s^2}{9s}(s^2+u^2)(-\frac{1}{su}+\frac{9}{4t^2}) \tag{51.10}$$

and

$$\frac{d\sigma}{d\Omega}(gg \to q\overline{q}) = \frac{\alpha_s^2}{24s}(t^2+u^2)(\frac{1}{tu}-\frac{9}{4s^2}) . \tag{51.11}$$

Finally,

$$\frac{d\sigma}{d\Omega}(gg \to gg) = \frac{9\alpha_s^2}{8s}(3-\frac{ut}{s^2}-\frac{su}{t^2}-\frac{st}{u^2}) . \tag{51.12}$$

Lepton-quark scattering is analogous (neglecting Z exchange)

$$\frac{d\sigma}{d\Omega}(eq \to eq) = \frac{\alpha^2}{2s}e_q^2\frac{s^2+u^2}{t^2} . \tag{51.13}$$

where e_q is the charge of the quark. For neutrino scattering with the four-Fermi interaction

$$\frac{d\sigma}{d\Omega}(\nu d \to \ell^- u) = \frac{G_F^2 s}{4\pi^2} , \tag{51.14}$$

where the Cabibbo angle suppression is ignored. Similarly

$$\frac{d\sigma}{d\Omega}(\nu\overline{u} \to \ell^-\overline{d}) = \frac{G_F^2 s}{4\pi^2}\frac{(1+\cos\theta)^2}{4} . \tag{51.15}$$

To obtain the formulae for deep inelastic scattering (presented in more detail in Section 18) we consider quarks of type i carrying a fraction $x = Q^2/(2M\nu)$ of the nucleon's energy, where $\nu = E - E'$ is the energy lost by the lepton in the nucleon rest frame. With $y = \nu/E$ we have the correspondences

$$1+\cos\theta \to 2(1-y) ,$$

$$d\Omega_{cm} \to 4\pi f_i(x)dx\,dy , \tag{51.16}$$

where the latter incorporates the quark distribution, $f_i(x)$. In this way we find

$$\frac{d\sigma}{dx\,dy}(eN \to eX) = \frac{4\pi\alpha^2 xs}{Q^4}\frac{1}{2}\left[1+(1-y)^2\right] \times \left[\frac{4}{9}(u(x)+\overline{u}(x)+\ldots)+\frac{1}{9}(d(x)+\overline{d}(x)+\ldots)\right] \tag{51.17}$$

where now $s = 2ME$ is the cm energy squared for the electron-nucleon collision, and we have suppressed contributions from higher mass quarks.

Similarly,

$$\frac{d\sigma}{dx\,dy}(\nu N \to \ell^- X) = \frac{G_F^2 xs}{\pi}[(d(x)+\ldots)+(1-y)^2(\overline{u}(x)+\ldots)] \tag{51.18}$$

and

$$\frac{d\sigma}{dx\,dy}(\overline{\nu}N \to \ell^+ X) = \frac{G_F^2 xs}{\pi}[(\overline{d}(x)+\ldots)+(1-y)^2(u(x)+\ldots)] . \tag{51.19}$$

Quasi-elastic neutrino scattering ($\nu_\mu n \to \mu^- p$, $\overline{\nu}_\mu p \to \mu^+ n$) is directly related to the crossed reaction, neutron decay. The formula for the differential cross section is presented, for example, in N.J. Baker *et al.*, Phys. Rev. **D23**, 2499 (1981).

Downloaded from https://academic.oup.com/ptep/article/2022/8/083C01/6651666 by KIT Library user on 27 September 2022

51.3 Hadroproduction of heavy quarks

For hadroproduction of heavy quarks $Q = c,\ b,\ t$, it is important to include mass effects in the formulae. For $q\bar{q} \to Q\bar{Q}$, one has

$$\frac{d\sigma}{d\Omega}(q\bar{q} \to Q\bar{Q}) = \frac{\alpha_s^2}{9s^3}\sqrt{1-\frac{4m_Q^2}{s}} \times \left[(m_Q^2-t)^2+(m_Q^2-u)^2+2m_Q^2 s\right], \tag{51.20}$$

while for $gg \to Q\bar{Q}$ one has

$$\begin{aligned}\frac{d\sigma}{d\Omega}(gg \to Q\bar{Q}) = \frac{\alpha_s^2}{32s}\sqrt{1-\frac{4m_Q^2}{s}}\Bigg[&\frac{6}{s^2}(m_Q^2-t)(m_Q^2-u)- \\ &-\frac{m_Q^2(s-4m_Q^2)}{3(m_Q^2-t)(m_Q^2-u)}+ \\ &\frac{4}{3}\frac{(m_Q^2-t)(m_Q^2-u)-2m_Q^2(m_Q^2+t)}{(m_Q^2-t)^2} \\ &+\frac{4}{3}\frac{(m_Q^2-t)(m_Q^2-u)-2m_Q^2(m_Q^2+u)}{(m_Q^2-u)^2} \\ &-3\frac{(m_Q^2-t)(m_Q^2-u)+m_Q^2(u-t)}{s(m_Q^2-t)} \\ &-3\frac{(m_Q^2-t)(m_Q^2-u)+m_Q^2(t-u)}{s(m_Q^2-u)}\Bigg].\end{aligned} \tag{51.21}$$

51.4 Production of Weak Gauge Bosons

51.4.1 *W and Z resonant production*

Resonant production of a single W or Z is governed by the partial widths

$$\Gamma(W \to \ell_i\bar{\nu}_i) = \frac{\sqrt{2}G_F m_W^3}{12\pi} \tag{51.22}$$

$$\Gamma(W \to q_i\bar{q}_j) = 3\frac{\sqrt{2}G_F|V_{ij}|^2 m_W^3}{12\pi} \tag{51.23}$$

$$\Gamma(Z \to f\bar{f}) = N_c\frac{\sqrt{2}G_F m_Z^3}{6\pi} \times \left[(T_3 - Q_f\sin^2\theta_W)^2 + (Q_f\sin^2\theta_W)^2\right]. \tag{51.24}$$

The weak mixing angle is θ_W. The CKM matrix elements are indicated by V_{ij} and N_c is 3 for $q\bar{q}$ final states and 1 for leptonic final states.

The full differential cross section for $f_i\bar{f}_j \to (W,Z) \to f_{i'}\bar{f}_{j'}$ is given by

$$\begin{aligned}\frac{d\sigma}{d\Omega} = &\frac{N_c^f}{N_c^i}\cdot\frac{1}{256\pi^2 s}\cdot\frac{s^2}{(s-M^2)^2+s\Gamma^2} \\ &\times\Big[(L^2+R^2)(L'^2+R'^2)(1+\cos^2\theta) \\ &+(L^2-R^2)(L'^2-R'^2)2\,cos\theta\Big]\end{aligned} \tag{51.25}$$

where M is the mass of the W or Z. The couplings for the W are $L = (8G_F m_W^2/\sqrt{2})^{1/2}V_{ij}/\sqrt{2}; R = 0$ where V_{ij} is the corresponding CKM matrix element, with an analogous expression for L' and R'. For Z, the couplings are $L = (8G_F m_Z^2/\sqrt{2})^{1/2}(T_3 - \sin^2\theta_W Q); R = -(8G_F m_Z^2/\sqrt{2})^{1/2}\sin^2\theta_W Q$, where T_3 is the weak isospin of the initial left-handed fermion and Q is the initial fermion's electric charge. The expressions for L' and R' are analogous. The color factors $N_c^{i,f}$ are 3 for initial or final quarks and 1 for initial or final leptons.

51.4.2 *Production of pairs of weak gauge bosons*

The cross section for $f\bar{f} \to W^+W^-$ is given in term of the couplings of the left-handed and right-handed fermion f, $\ell = 2(T_3 - Qx_W)$, $r = -2Qx_W$, where T_3 is the third component of weak isospin for the left-handed f, Q is its electric charge (in units of the proton charge), and $x_W = \sin^2\theta_W$:

$$\begin{aligned}\frac{d\sigma}{dt} = &\frac{2\pi\alpha^2}{N_c s^2}\Bigg\{\Bigg[\left(Q+\frac{\ell+r}{4x_W}\frac{s}{s-m_Z^2}\right)^2 \\ &+\left(\frac{\ell-r}{4x_W}\frac{s}{s-m_Z^2}\right)^2\Bigg]A(s,t,u) \\ &+\frac{1}{2x_W}\left(Q+\frac{\ell}{2x_W}\frac{s}{s-m_Z^2}\right) \\ &\qquad(\Theta(-Q)I(s,t,u)-\Theta(Q)I(s,u,t)) \\ &+\frac{1}{8x_W^2}\left(\Theta(-Q)E(s,t,u)+\Theta(Q)E(s,u,t)\right)\Bigg\},\end{aligned} \tag{51.26}$$

where $\Theta(x)$ is 1 for $x > 0$ and 0 for $x < 0$, and where

$$\begin{aligned}A(s,t,u) &= \left(\frac{tu}{m_W^4}-1\right)\left(\frac{1}{4}-\frac{m_W^2}{s}+3\frac{m_W^4}{s^2}\right)+\frac{s}{m_W^2}-4, \\ I(s,t,u) &= \left(\frac{tu}{m_W^4}-1\right)\left(\frac{1}{4}-\frac{m_W^2}{2s}-\frac{m_W^4}{st}\right)+\frac{s}{m_W^2}-2+2\frac{m_W^2}{t}, \\ E(s,t,u) &= \left(\frac{tu}{m_W^4}-1\right)\left(\frac{1}{4}+\frac{m_W^4}{t^2}\right)+\frac{s}{m_W^2},\end{aligned} \tag{51.27}$$

and s,t,u are the usual Mandelstam variables with $s = (p_f + p_{\bar{f}})^2, t = (p_f - p_{W^-})^2, u = (p_f - p_{W^+})^2$. The factor N_c is 3 for quarks and 1 for leptons.

The analogous cross-section for $q_i\bar{q}_j \to W^\pm Z^0$ is

$$\begin{aligned}\frac{d\sigma}{dt} = &\frac{\pi\alpha^2|V_{ij}|^2}{6s^2x_W^2}\Bigg\{\left(\frac{1}{s-m_W^2}\right)^2\Bigg[\left(\frac{9-8x_W}{4}\right)\left(ut-m_W^2m_Z^2\right) \\ &+(8x_W-6)\,s\left(m_W^2+m_Z^2\right)\Bigg] \\ &+\left[\frac{ut-m_W^2m_Z^2-s(m_W^2+m_Z^2)}{s-m_W^2}\right]\left[\frac{\ell_j}{t}-\frac{\ell_i}{u}\right] \\ &+\frac{ut-m_W^2m_Z^2}{4(1-x_W)}\left[\frac{\ell_j^2}{t^2}+\frac{\ell_i^2}{u^2}\right]+\frac{s(m_W^2+m_Z^2)}{2(1-x_W)}\frac{\ell_i\ell_j}{tu}\Bigg\},\end{aligned} \tag{51.28}$$

where ℓ_i and ℓ_j are the couplings of the left-handed q_i and q_j as defined above. The CKM matrix element between q_i and q_j is V_{ij}.

The cross section for $q_i\bar{q}_i \to Z^0Z^0$ is

$$\frac{d\sigma}{dt} = \frac{\pi\alpha^2}{96}\frac{\ell_i^4+r_i^4}{x_W^2(1-x_W^2)^2s^2}\left[\frac{t}{u}+\frac{u}{t}+\frac{4m_Z^2s}{tu}-m_Z^4\left(\frac{1}{t^2}+\frac{1}{u^2}\right)\right]. \tag{51.29}$$

51.5 Production of Higgs Bosons

51.5.1 *Resonant Production*

The Higgs boson of the Standard Model can be produced resonantly in the collisions of quarks, leptons, W or Z bosons, gluons, or photons. The production cross section is thus controlled by the partial width of the Higgs boson into the entrance channel and its total width. The branching fractions for the Standard Model Higgs boson are shown in Fig. 1 of the "Searches for Higgs bosons"

Downloaded from https://academic.oup.com/ptep/article/2022/8/083C01/6651666 by KIT Library user on 27 September 2022

review in the Particle Listings section, as a function of the Higgs boson mass. The partial widths are given by the relations

$$\Gamma(H \to f\bar{f}) = \frac{G_F m_f^2 m_H N_c}{4\pi\sqrt{2}} \left(1 - 4m_f^2/m_H^2\right)^{3/2}, \qquad (51.30)$$

$$\Gamma(H \to W^+W^-) = \frac{G_F m_H^3 \beta_W}{32\pi\sqrt{2}} \left(4 - 4a_W + 3a_W^2\right), \qquad (51.31)$$

$$\Gamma(H \to ZZ) = \frac{G_F m_H^3 \beta_Z}{64\pi\sqrt{2}} \left(4 - 4a_Z + 3a_Z^2\right), \qquad (51.32)$$

where N_c is 3 for quarks and 1 for leptons and where $a_W = 1 - \beta_W^2 = 4m_W^2/m_H^2$ and $a_Z = 1 - \beta_Z^2 = 4m_Z^2/m_H^2$. The decay to two gluons proceeds through quark loops, with the t quark dominating [2]. Explicitly,

$$\Gamma(H \to gg) = \frac{\alpha_s^2 G_F m_H^3}{36\pi^3\sqrt{2}} \left| \sum_q I(m_q^2/m_H^2) \right|^2, \qquad (51.33)$$

where $I(z)$ is complex for $z < 1/4$. For $z < 2 \times 10^{-3}$, $|I(z)|$ is small so the light quarks contribute negligibly. For $m_H < 2m_t$, $z > 1/4$ and

$$I(z) = 3\left[2z + 2z(1-4z)\left(\sin^{-1}\frac{1}{2\sqrt{z}}\right)^2\right], \qquad (51.34)$$

which has the limit $I(z) \to 1$ as $z \to \infty$.

51.5.2 *Higgs Boson Production in W^* and Z^* decay*

The Standard Model Higgs boson can be produced in the decay of a virtual W or Z ("Higgstrahlung") [3,4]: In particular, if k is the c.m. momentum of the Higgs boson,

$$\sigma(q_i\bar{q}_j \to WH) = \frac{\pi\alpha^2|V_{ij}|^2}{36\sin^4\theta_W}\,\frac{2k}{\sqrt{s}}\,\frac{k^2+3m_W^2}{(s-m_W^2)^2} \qquad (51.35)$$

$$\sigma(f\bar{f} \to ZH) = \frac{2\pi\alpha^2(\ell_f^2 + r_f^2)}{48N_c\sin^4\theta_W\cos^4\theta_W}\,\frac{2k}{\sqrt{s}}\,\frac{k^2+3m_Z^2}{(s-m_Z^2)^2}, \qquad (51.36)$$

where ℓ and r are defined as above.

51.5.3 *W and Z Fusion*

Just as high-energy electrons can be regarded as sources of virtual photon beams, at very high energies they are sources of virtual W and Z beams. For Higgs boson production, it is the longitudinal components of the Ws and Zs that are important [5]. The distribution of longitudinal Ws carrying a fraction y of the electron's energy is [6]

$$f(y) = \frac{g^2}{16\pi^2}\,\frac{1-y}{y}, \qquad (51.37)$$

where $g = e/\sin\theta_W$. In the limit $s \gg m_H \gg m_W$, the partial decay rate is $\Gamma(H \to W_L W_L) = (g^2/64\pi)(m_H^3/m_W^2)$ and in the equivalent W approximation [7]

$$\sigma(e^+e^- \to \bar{\nu}_e\nu_e H) = \frac{1}{16m_W^2}\left(\frac{\alpha}{\sin^2\theta_W}\right)^3 \times \left[\left(1 + \frac{m_H^2}{s}\right)\log\frac{s}{m_H^2} - 2 + 2\frac{m_H^2}{s}\right]. \qquad (51.38)$$

There are significant corrections to this relation when m_H is not large compared to m_W [8]. For $m_H = 150$ GeV, the estimate is too high by 51% for $\sqrt{s} = 1000$ GeV, 32% too high at $\sqrt{s} = 2000$ GeV, and 22% too high at $\sqrt{s} = 4000$ GeV. Fusion of ZZ to make a Higgs boson can be treated similarly. Identical formulae apply for Higgs production in the collisions of quarks whose charges permit the emission of a W^+ and a W^-, except that QCD corrections and CKM matrix elements are required. Even in the absence of QCD corrections, the fine-structure constant ought to be evaluated at the scale of the collision, say m_W. All quarks contribute to the ZZ fusion process.

51.6 Inclusive hadronic reactions

One-particle inclusive cross sections $Ed^3\sigma/d^3p$ for the production of a particle of momentum p are conveniently expressed in terms of rapidity y (see above) and the momentum p_T transverse to the beam direction (in the c.m.):

$$E\frac{d^3\sigma}{d^3p} = \frac{d^3\sigma}{d\phi\,dy\,p_T\,dp_T}. \qquad (51.39)$$

In appropriate circumstances, the cross section may be decomposed as a partonic cross section multiplied by the probabilities of finding partons of the prescribed momenta:

$$\sigma_{\text{hadronic}} = \sum_{ij}\int dx_1\,dx_2\,f_i(x_1)\,f_j(x_2)\,d\widehat{\sigma}_{\text{partonic}}, \qquad (51.40)$$

The probability that a parton of type i carries a fraction of the incident particle's that lies between x_1 and $x_1 + dx_1$ is $f_i(x_1)dx_1$ and similarly for partons in the other incident particle. The partonic collision is specified by its c.m. energy squared $\hat{s} = x_1x_2s$ and the momentum transfer squared $\hat{t}$. The final hadronic state is more conveniently specified by the rapidities y_1, y_2 of the two jets resulting from the collision and the transverse momentum p_T. The connection between the differentials is

$$dx_1dx_2d\hat{t} = dy_1dy_2\frac{\hat{s}}{s}dp_T^2, \qquad (51.41)$$

so that

$$\frac{d^3\sigma}{dy_1dy_2dp_T^2} = \frac{\hat{s}}{s}\left[f_i(x_1)f_j(x_2)\frac{d\hat{\sigma}}{d\hat{t}}(\hat{s},\hat{t},\hat{u}) + f_i(x_2)f_j(x_1)\frac{d\hat{\sigma}}{d\hat{t}}(\hat{s},\hat{u},\hat{t})\right], \qquad (51.42)$$

where we have taken into account the possibility that the incident parton types might arise from either incident particle. The second term should be dropped if the types are identical: $i = j$.

51.7 Two-photon processes

In the Weizsäcker-Williams picture, a high-energy electron beam is accompanied by a spectrum of virtual photons of energies ω and invariant-mass squared $q^2 = -Q^2$, for which the photon number density is

$$dn = \frac{\alpha}{\pi}\left[1 - \frac{\omega}{E} + \frac{\omega^2}{E^2} - \frac{m_e^2\,\omega^2}{Q^2E^2}\right]\frac{d\omega}{\omega}\frac{dQ^2}{Q^2}, \qquad (51.43)$$

where E is the energy of the electron beam. The cross section for $e^+e^- \to e^+e^-X$ is then [9]

$$d\sigma_{e^+e^-\to e^+e^-X}(s) = dn_1dn_2d\sigma_{\gamma\gamma\to X}(W^2), \qquad (51.44)$$

where $W^2 = m_X^2$. Integrating from the lower limit $Q^2 = m_e^2\frac{\omega_i^2}{E_i(E_i-\omega_i)}$ to a maximum Q^2 gives

$$\sigma_{e^+e^-\to e^+e^-X}(s) = \frac{\alpha^2}{\pi^2}\int_{z_{th}}^1\frac{dz}{z} \times \left[\left(\ln\frac{Q^2_{max}}{zm_e^2} - 1\right)^2 f(z) + \frac{1}{3}(\ln z)^3\right]\sigma_{\gamma\gamma\to X}(zs), \qquad (51.45)$$

where

$$f(z) = \left(1 + \tfrac{1}{2}z\right)^2\ln(1/z) - \tfrac{1}{2}(1-z)(3+z). \qquad (51.46)$$

Downloaded from https://academic.oup.com/ptep/article/2022/8/083C01/6651666 by KIT Library user on 27 September 2022

The appropriate value of Q^2_{max} depends on the properties of the produced system X. For production of hadronic systems, $Q^2_{max} \approx m^2_\rho$, while for lepton-pair production, $Q^2 \approx W^2$. For production of a resonance with spin $J \neq 1$, we have

$$\sigma_{e^+e^-\to e^+e^-R}(s) = (2J+1)\frac{8\alpha^2\Gamma_{R\to\gamma\gamma}}{m^3_R} \times \left[f(m^2_R/s)\left(\ln\frac{m^2_V s}{m^2_e m^2_R} - 1\right)^2 - \frac{1}{3}\left(\ln\frac{s}{M^2_R}\right)^3\right], \tag{51.47}$$

where m_V is the mass that enters into the form factor for the $\gamma\gamma \to R$ transition, typically m_ρ.

PART II: PROCESSES BEYOND THE STANDARD MODEL

51.8 Production of supersymmetric particles

In supersymmetric (SUSY) theories (see Supersymmetric Particle Searches in this *Review*), every boson has a fermionic superpartner, and every fermion has a bosonic superpartner. The minimal supersymmetric Standard Model (MSSM) is a direct supersymmetrization of the Standard Model (SM), although a second Higgs doublet is needed to avoid triangle anomalies [10]. Under *soft* SUSY breaking, superpartner masses are lifted above the SM particle masses. In weak scale SUSY, the superpartners are invoked to stabilize the weak scale under radiative corrections, so the superpartners are expected to have masses of order the TeV scale.

51.8.1 *Gluino and squark production*

The superpartners of gluons are the color octet, spin$-\frac{1}{2}$ gluinos ($\tilde{g}$), while each helicity component of quark flavor has a spin-0 *squark* partner, *e.g.* $\tilde{q}_L$ and $\tilde{q}_R$. Third generation left- and right- squarks are expected to have large mixing, resulting in mass eigenstates $\tilde{q}_1$ and $\tilde{q}_2$, with $m_{\tilde{q}_1} < m_{\tilde{q}_2}$ (here, q denotes any of the SM flavors of quarks and $\tilde{q}_i$ the corresponding flavor and type ($i = L, R$ or $1, 2$) of squark). Gluino pair production ($\tilde{g}\tilde{g}$) takes place via either glue-glue or quark-antiquark annihilation [11].

The subprocess cross sections are usually presented as differential distributions in the Mandelstam variables s, t and u. Note that for a $2 \to 2$ scattering subprocess $ab \to cd$, the Mandelstam variable $s = (p_a + p_b)^2 = (p_c + p_d)^2$, where p_a is the 4-momentum of particle a, and so forth. The variable $t = (p_c - p_a)^2$, where c and a are taken conventionally to be the most similar particles in the subprocess. The variable u would then be equal to $(p_d - p_a)^2$. Note that since s, t and u are squares of 4-vectors, they are invariants in any inertial reference frame.

Gluino pair production at hadron colliders is described by:

$$\begin{aligned}\frac{d\sigma}{dt}(gg \to \tilde{g}\tilde{g}) = \frac{9\pi\alpha^2_s}{4s^2}\Bigg\{&\frac{2(m^2_{\tilde{g}}-t)(m^2_{\tilde{g}}-u)}{s^2} \\ &+ \frac{(m^2_{\tilde{g}}-t)(m^2_{\tilde{g}}-u) - 2m^2_{\tilde{g}}(m^2_{\tilde{g}}+t)}{(m^2_{\tilde{g}}-t)^2} \\ &+ \frac{(m^2_{\tilde{g}}-t)(m^2_{\tilde{g}}-u) - 2m^2_{\tilde{g}}(m^2_{\tilde{g}}+u)}{(m^2_{\tilde{g}}-u)^2} + \frac{m^2_{\tilde{g}}(s-4m^2_{\tilde{g}})}{(m^2_{\tilde{g}}-t)(m^2_{\tilde{g}}-u)} \\ &- \frac{(m^2_{\tilde{g}}-t)(m^2_{\tilde{g}}-u) + m^2_{\tilde{g}}(u-t)}{s(m^2_{\tilde{g}}-t)} \\ &- \frac{(m^2_{\tilde{g}}-t)(m^2_{\tilde{g}}-u) + m^2_{\tilde{g}}(t-u)}{s(m^2_{\tilde{g}}-u)}\Bigg\},\end{aligned} \tag{51.48}$$

where α_s is the strong fine structure constant. Also,

$$\begin{aligned}\frac{d\sigma}{dt}(q\bar{q} \to \tilde{g}\tilde{g}) = \frac{8\pi\alpha^2_s}{9s^2}\Bigg\{&\frac{4}{3}\left(\frac{m^2_{\tilde{g}}-t}{m^2_{\tilde{q}}-t}\right)^2 + \frac{4}{3}\left(\frac{m^2_{\tilde{g}}-u}{m^2_{\tilde{q}}-u}\right)^2 \\ &+ \frac{3}{s^2}\left[(m^2_{\tilde{g}}-t)^2 + (m^2_{\tilde{g}}-u)^2 + 2m^2_{\tilde{g}}s\right] \\ &- 3\frac{\left[(m^2_{\tilde{g}}-t)^2 + m^2_{\tilde{g}}s\right]}{s(m^2_{\tilde{q}}-t)} \\ &- 3\frac{\left[(m^2_{\tilde{g}}-u)^2 + m^2_{\tilde{g}}s\right]}{s(m^2_{\tilde{q}}-u)} + \frac{1}{3}\frac{m^2_{\tilde{g}}s}{(m^2_{\tilde{q}}-t)(m^2_{\tilde{q}}-u)}\Bigg\}.\end{aligned} \tag{51.49}$$

Gluinos can also be produced in association with squarks: $\tilde{g}\tilde{q}_i$ production, where $\tilde{q}_i$ represents any of the various types (left, right- or mixed) and flavors of squarks. The subprocess cross section is independent of whether the squark is the right-, left- or mixed type:

$$\begin{aligned}\frac{d\sigma}{dt}(gq \to \tilde{g}\tilde{q}_i) = \frac{\pi\alpha^2_s}{24s^2}&\frac{\left[\frac{16}{3}(s^2 + (m^2_{\tilde{q}_i}-u)^2) + \frac{4}{3}s(m^2_{\tilde{q}_i}-u)\right]}{s(m^2_{\tilde{g}}-t)(m^2_{\tilde{q}_i}-u)^2} \\ &\times\left((m^2_{\tilde{g}}-u)^2 + (m^2_{\tilde{q}_i}-m^2_{\tilde{g}})^2 + \frac{2sm^2_{\tilde{g}}(m^2_{\tilde{q}_i}-m^2_{\tilde{g}})}{(m^2_{\tilde{g}}-t)}\right).\end{aligned} \tag{51.50}$$

There are many different subprocesses for production of squark pairs. Since left- and right- squarks generally have different masses and different decay patterns, we present the differential cross section for each subprocess of $\tilde{q}_i$ ($i = L,\ R$ or $1,\ 2$) separately. (In early literature, the following formulae were often combined into a single equation which didn't differentiate the various squark types.) The result for $gg \to \tilde{q}_i\bar{\tilde{q}}_i$ is:

$$\begin{aligned}\frac{d\sigma}{dt}(gg \to \tilde{q}_i\bar{\tilde{q}}_i) = \frac{\pi\alpha^2_s}{4s^2}\Bigg\{&\frac{1}{3}\left(\frac{m^2_{\tilde{q}}+t}{m^2_{\tilde{q}}-t}\right)^2 + \frac{1}{3}\left(\frac{m^2_{\tilde{q}}+u}{m^2_{\tilde{q}}-u}\right)^2 \\ &+ \frac{3}{32s^2}\left(8s(4m^2_{\tilde{q}}-s) + 4(u-t)^2\right) + \frac{7}{12} \\ &- \frac{1}{48}\frac{(4m^2_{\tilde{q}}-s)^2}{(m^2_{\tilde{q}}-t)(m^2_{\tilde{q}}-u)} \\ &+ \frac{3}{32}\frac{\left[(t-u)(4m^2_{\tilde{q}}+4t-s) - 2(m^2_{\tilde{q}}-u)(6m^2_{\tilde{q}}+2t-s)\right]}{s(m^2_{\tilde{q}}-t)} \\ &+ \frac{3}{32}\frac{\left[(u-t)(4m^2_{\tilde{q}}+4u-s) - 2(m^2_{\tilde{q}}-t)(6m^2_{\tilde{q}}+2u-s)\right]}{s(m^2_{\tilde{q}}-u)} \\ &+ \frac{7}{96}\frac{\left[4m^2_{\tilde{q}}+4t-s\right]}{m^2_{\tilde{q}}-t} + \frac{7}{96}\frac{\left[4m^2_{\tilde{q}}+4u-s\right]}{m^2_{\tilde{q}}-u}\Bigg\},\end{aligned} \tag{51.51}$$

which has an obvious $u \leftrightarrow t$ symmetry.

For $q\bar{q} \to \tilde{q}_i\bar{\tilde{q}}_i$ with the same initial and final state flavors, we have

$$\begin{aligned}\frac{d\sigma}{dt}(q\bar{q} \to \tilde{q}_i\bar{\tilde{q}}_i) = \frac{2\pi\alpha^2_s}{9s^2}&\left\{\frac{1}{(t-m^2_{\tilde{g}})^2} + \frac{2}{s^2} - \frac{2/3}{s(t-m^2_{\tilde{g}})}\right\} \\ &\times\left[-st - (t-m^2_{\tilde{q}_i})^2\right],\end{aligned} \tag{51.52}$$

while if initial and final state flavors are different ($q\bar{q} \to \tilde{q}'_i\bar{\tilde{q}}'_i$) we

Downloaded from https://academic.oup.com/ptep/article/2022/8/083C01/6651666 by KIT Library user on 27 September 2022

instead have

$$\frac{d\sigma}{dt}(q\bar{q} \to \tilde{q}_i'\bar{\tilde{q}}_i') = \frac{4\pi\alpha_s^2}{9s^4}\left[-st - (t - m^2_{\tilde{q}_i'})^2\right]. \tag{51.53}$$

If the two initial state quarks are of different flavors, then we have

$$\frac{d\sigma}{dt}(q\bar{q}' \to \tilde{q}_i\bar{\tilde{q}}_i') = \frac{2\pi\alpha_s^2}{9s^2}\frac{-st - (t - m^2_{\tilde{q}_i})^2}{(t - m^2_{\tilde{g}})^2}. \tag{51.54}$$

If the initial quarks are of different flavor and final state squarks are of different type ($i \neq j$) then

$$\frac{d\sigma}{dt}(q\bar{q}' \to \tilde{q}_i\bar{\tilde{q}}_j') = \frac{2\pi\alpha_s^2}{9s^2}\frac{m^2_{\tilde{g}}s}{(t - m^2_{\tilde{g}})^2}. \tag{51.55}$$

For same-flavor initial state quarks, but final state unlike-type squarks, we also have

$$\frac{d\sigma}{dt}(q\bar{q} \to \tilde{q}_i\bar{\tilde{q}}_j) = \frac{2\pi\alpha_s^2}{9s^2}\frac{m^2_{\tilde{g}}s}{(t - m^2_{\tilde{g}})^2}. \tag{51.56}$$

There also exist cross sections for quark-quark annihilation to squark pairs. For same flavor quark-quark annihilation to same flavor/same type final state squarks,

$$\frac{d\sigma}{dt}(qq \to \tilde{q}_i\tilde{q}_i) =$$

$$= \frac{\pi\alpha_s^2}{9s^2}m^2_{\tilde{g}}s\left\{\frac{1}{(t - m^2_{\tilde{g}})^2} + \frac{1}{(u - m^2_{\tilde{g}})^2} - \frac{2/3}{(t - m^2_{\tilde{g}})(u - m^2_{\tilde{g}})}\right\}, \tag{51.57}$$

while if the final type squarks are different ($i \neq j$), we have

$$\frac{d\sigma}{dt}(qq \to \tilde{q}_i\tilde{q}_j) =$$

$$\frac{2\pi\alpha_s^2}{9s^2}\times$$
$$\left\{\frac{[-st - (t - m^2_{\tilde{q}_i})(t - m^2_{\tilde{q}_j})]}{(t - m^2_{\tilde{g}})} + \frac{[-su - (u - m^2_{\tilde{q}_i})(u - m^2_{\tilde{q}_j})]}{(u - m^2_{\tilde{g}})}\right\}. \tag{51.58}$$

If initial/final state flavors are different, but final state squark types are the same, then

$$\frac{d\sigma}{dt}(qq' \to \tilde{q}_i\tilde{q}_i') = \frac{2\pi\alpha_s^2}{9s^2}\frac{m^2_{\tilde{g}}s}{(t - m^2_{\tilde{g}})^2}. \tag{51.59}$$

If initial quark flavors are different and final squark types are different, then

$$\frac{d\sigma}{dt}(qq' \to \tilde{q}_i\tilde{q}_j') = \frac{2\pi\alpha_s^2}{9s^2}\frac{-st - (t - m^2_{\tilde{q}_i})(t - m^2_{\tilde{q}_j})}{(t - m^2_{\tilde{g}})^2}. \tag{51.60}$$

51.8.2 *Gluino and squark associated production*

In the MSSM, the charged spin-$\frac{1}{2}$ winos and higgsinos mix to make chargino states $\chi_1^\pm$ and $\chi_2^\pm$, with $m_{\chi_1^\pm} < m_{\chi_2^\pm}$. The spin$-\frac{1}{2}$ neutral bino, wino and higgsino fields mix to give four neutralino mass eigenstates $\chi^0_{1,2,3,4}$ ordered according to mass. We sometimes denote the charginos and neutralinos collectively as -inos for notational simplicity

For gluino and squark production in association with charginos and neutralinos [12], the quark-squark-neutralino couplings[1] are defined by the interaction Lagrangian terms

$$\mathcal{L}_{\tilde{f}f\tilde{\chi}_i^0} = \left[iA^f_{\tilde{\chi}_i^0}\tilde{f}_L^\dagger\bar{\tilde{\chi}}_i^0 P_L f + iB^f_{\tilde{\chi}_i^0}\tilde{f}_R^\dagger\bar{\tilde{\chi}}_i^0 P_R f + \text{h.c.}\right]$$

[1]The couplings $A^f_{\tilde{\chi}_i^0}$ and $B^f_{\tilde{\chi}_i^0}$ are given explicitly in Ref. [13] in Eq. (8.87). Also, the couplings $A^d_{\tilde{\chi}_i^-}$ and $A^u_{\tilde{\chi}_i^-}$ are given in Eq. (8.93). The couplings X_i^j and Y_i^j are given by Eq. (8.103), while the x_i and y_i couplings are given in Eq. (8.100). Finally, the couplings W_{ij} are given in Eq. (8.101).

, where $A^f_{\tilde{\chi}_i^0}$ and $B^f_{\tilde{\chi}_i^0}$ are coupling constants involving gauge couplings, neutralino mixing elements and in the case of third generation fermions, Yukawa couplings. Their form depends on the conventions used for setting up the MSSM Lagrangian, and can be found in various reviews [14] and textbooks [13, 15]. P_L and P_R are the usual left- and right- spinor projection operators and f denotes any of the SM fermions u, d, e, $\nu_e, \cdots$. The fermion-sfermion- chargino couplings have the form $\mathcal{L} = \left[iA^d_{\tilde{\chi}_i^-}\tilde{u}_L^\dagger\overline{\tilde{\chi}_i^-}P_L d + iA^u_{\tilde{\chi}_i^-}\tilde{d}_L^\dagger\overline{\tilde{\chi}_i^c}P_L u + \text{h.c.}\right]$ for u and d quarks, where the $A^d_{\tilde{\chi}_i^-}$ and $A^u_{\tilde{\chi}_i^-}$ couplings are again convention-dependent, and can be found in textbooks. The superscript c denotes "charge conjugate spinor", defined by $\psi^c \equiv C\bar{\psi}^T$.

The subprocess cross sections for chargino-squark associated production occur via squark exchange and are given by

$$\frac{d\sigma}{dt}(\bar{u}g \to \tilde{\chi}_i^-\bar{\tilde{d}}_L) = \frac{\alpha_s}{24s^2}|A^u_{\tilde{\chi}_i^-}|^2\psi(m_{\tilde{d}_L}, m_{\tilde{\chi}_i^-}, t), \tag{51.61}$$

$$\frac{d\sigma}{dt}(dg \to \tilde{\chi}_i^-\tilde{u}_L) = \frac{\alpha_s}{24s^2}|A^d_{\tilde{\chi}_i^-}|^2\psi(m_{\tilde{u}_L}, m_{\tilde{\chi}_i^-}, t), \tag{51.62}$$

while neutralino-squark production is given by

$$\frac{d\sigma}{dt}(qg \to \tilde{\chi}_i^0\tilde{q}) = \frac{\alpha_s}{24s^2}\left(|A^q_{\tilde{\chi}_i^0}|^2 + |B^q_{\tilde{\chi}_i^0}|^2\right)\psi(m_{\tilde{q}}, m_{\tilde{\chi}_i^0}, t), \tag{51.63}$$

where

$$\psi(m_1, m_2, t) = \frac{s + t - m_1^2}{2s} - \frac{m_1^2(m_2^2 - t)}{(m_1^2 - t)^2} + \frac{t(m_2^2 - m_1^2) + m_2^2(s - m_2^2 + m_1^2)}{s(m_1^2 - t)}. \tag{51.64}$$

Here, the variable t is given by the square of "squark-minus-quark" four-momentum. The neutralino-gluino associated production cross section also occurs via squark exchange and is given by

$$\frac{d\sigma}{dt}(q\bar{q} \to \tilde{\chi}_i^0\tilde{g}) = \frac{\alpha_s}{18s^2}\left(|A^q_{\tilde{\chi}_i^0}|^2 + |B^q_{\tilde{\chi}_i^0}|^2\right)\left[\frac{(m^2_{\tilde{\chi}_i^0} - t)(m^2_{\tilde{g}} - t)}{(m^2_{\tilde{q}} - t)^2} + \frac{(m^2_{\tilde{\chi}_i^0} - u)(m^2_{\tilde{g}} - u)}{(m^2_{\tilde{q}} - u)^2} - \frac{2\eta_i\eta_{\tilde{g}}m_{\tilde{g}}m_{\tilde{\chi}_i^0}s}{(m^2_{\tilde{q}} - t)(m^2_{\tilde{q}} - u)}\right], \tag{51.65}$$

where η_i is the sign of the neutralino mass eigenvalue and $\eta_{\tilde{g}}$ is the sign of the gluino mass eigenvalue. We also have chargino-gluino associated production:

$$\frac{d\sigma}{dt}(\bar{u}d \to \tilde{\chi}_i^-\tilde{g}) = \frac{\alpha_s}{18s^2}\left[|A^u_{\tilde{\chi}_i^-}|^2\frac{(m^2_{\tilde{\chi}_i^-} - t)(m^2_{\tilde{g}} - t)}{(m^2_{\tilde{d}_L} - t)^2} + |A^d_{\tilde{\chi}_i^-}|^2\frac{(m^2_{\tilde{\chi}_i^-} - u)(m^2_{\tilde{g}} - u)}{(m^2_{\tilde{u}_L} - u)^2} + \frac{2\eta_{\tilde{g}}Re(A^u_{\tilde{\chi}_i^-}A^d_{\tilde{\chi}_i^-})m_{\tilde{g}}m_{\tilde{\chi}_i}s}{(m^2_{\tilde{d}_L} - t)(m^2_{\tilde{u}_L} - u)}\right], \tag{51.66}$$

where $\hat{t} = (\tilde{g} - d)^2$ and in the third term one must take the real part of the in general complex coupling constant product.

51.8.3 *Slepton and sneutrino production*

The subprocess cross section for $\tilde{\ell}_L\bar{\tilde{\nu}}_{\ell_L}$ production ($\ell = e$ or μ) occurs via s-channel W exchange and is given by

$$\frac{d\sigma}{dt}(d\bar{u} \to \tilde{\ell}_L\bar{\tilde{\nu}}_{\ell_L}) = \frac{g^4|D_W(s)|^2}{192\pi s^2}\left(tu - m^2_{\tilde{\ell}_L}m^2_{\tilde{\nu}_{\ell_L}}\right), \tag{51.67}$$

where $D_W(s) = 1/(s - M_W^2 + iM_W\Gamma_W)$ is the W-boson propagator denominator. The production of $\tilde{\tau}_1\bar{\tilde{\nu}}_\tau$ is given as above, but

Downloaded from https://academic.oup.com/ptep/article/2022/8/083C01/6651666 by KIT Library user on 27 September 2022

replacing $m_{\tilde{\ell}_L} \to m_{\tilde{\tau}_1}$, $m_{\tilde{\nu}_{\ell_L}} \to m_{\tilde{\nu}_\tau}$ and multiplying by an overall factor of $\cos^2\theta_\tau$ (where θ_τ is the tau-slepton mixing angle). Similar substitutions hold for $\tilde{\tau}_2\bar{\tilde{\nu}}_\tau$ production, except the overall factor is $\sin^2\theta_\tau$.

Table 51.1: The constants α_f and β_f that appear in in the SM neutral current Lagrangian. Here $t \equiv \tan\theta_W$ and $c \equiv \cot\theta_W$.

f	q_f	α_f	β_f
ℓ	-1	$\frac{1}{4}(3t-c)$	$\frac{1}{4}(t+c)$
ν_ℓ	0	$\frac{1}{4}$(t+c)	$-\frac{1}{4}(t+c)$
u	$\frac{2}{3}$	$-\frac{5}{12}t+\frac{1}{4}c$	$-\frac{1}{4}(t+c)$
d	$-\frac{1}{3}$	$\frac{1}{12}t-\frac{1}{4}c$	$\frac{1}{4}(t+c)$

The subprocess cross section for $\tilde{\ell}_L\bar{\tilde{\ell}}_L$ production occurs via s-channel γ and Z exchange, and depends on the neutral current interaction, with fermion couplings to γ and Z^0 given by $\mathcal{L}_{\rm neutral} = -eq_f\bar{f}\gamma^\mu f A_\mu + e\bar{f}\gamma^\mu(\alpha_f+\beta_f\gamma_5)fZ_\mu$ (with values of q_f, α_f, and β_f given in Table-51.1.

The subprocess cross section is given by

$$\frac{d\sigma}{dt}(q\bar{q}\to\tilde{\ell}_L\bar{\tilde{\ell}}_L) = \frac{e^4}{24\pi s^2}\left(tu - m^4_{\tilde{\ell}_L}\right)\times$$
$$\left\{\frac{q_\ell^2 q_q^2}{s^2} + (\alpha_\ell-\beta_\ell)^2(\alpha_q^2+\beta_q^2)|D_Z(s)|^2\right.$$
$$\left. + \frac{2q_\ell q_q\alpha_q(\alpha_\ell-\beta_\ell)(s-M_Z^2)}{s}|D_Z(s)|^2\right\}, \qquad (51.68)$$

where $D_Z(s) = 1/(s-M_Z^2+iM_Z\Gamma_Z)$. The cross section for sneutrino production is given by the same formula, but with α_ℓ, β_ℓ, q_ℓ and $m_{\tilde{\ell}_L}$ replaced by α_ν, β_ν, 0 and $m_{\tilde{\nu}_L}$, respectively. The cross section for $\tilde{\tau}_1\bar{\tilde{\tau}}_1$ production is obtained by replacing $m_{\tilde{\ell}_L}\to m_{\tilde{\tau}_1}$ and $\beta_\ell\to\beta_\ell\cos 2\theta_\tau$. The cross section for $\tilde{\ell}_R\bar{\tilde{\ell}}_R$ production is given by substituting $\alpha_\ell-\beta_\ell\to\alpha_\ell+\beta_\ell$ and $m_{\tilde{\ell}_L}\to m_{\tilde{\ell}_R}$ in the equation above. The cross section for $\tilde{\tau}_2\bar{\tilde{\tau}}_2$ production is obtained from the formula for $\tilde{\ell}_R\bar{\tilde{\ell}}_R$ production by replacing $m_{\tilde{\ell}_R}\to m_{\tilde{\tau}_2}$ and $\beta_\ell\to\beta_\ell\cos 2\theta_\tau$.

Finally, the cross section for $\tilde{\tau}_1\bar{\tilde{\tau}}_2$ production occurs only via Z exchange, and is given by

$$\frac{d\sigma}{dt}(q\bar{q}\to\tilde{\tau}_1\bar{\tilde{\tau}}_2) = \frac{d\sigma}{dt}(q\bar{q}\to\bar{\tilde{\tau}}_1\tilde{\tau}_2) =$$
$$\frac{e^4}{24\pi s^2}(\alpha_q^2+\beta_q^2)\beta_\ell^2\sin^2 2\theta_\tau|D_Z(s)|^2(ut - m^2_{\tilde{\tau}_1}m^2_{\tilde{\tau}_2}). \qquad (51.69)$$

51.8.4 *Chargino and neutralino pair production*

51.8.4.1 $\tilde{\chi}_i^-\tilde{\chi}_j^0$ *production*

The subprocess cross section for $d\bar{u}\to\tilde{\chi}_i^-\tilde{\chi}_j^0$ depends on Lagrangian couplings

$$\mathcal{L}_{W\bar{u}d} = -\frac{g}{\sqrt{2}}\bar{u}\gamma_\mu P_L d W^{+\mu} \ + \text{h.c.}$$

,

$$\mathcal{L}_{W\tilde{\chi}_i^-\tilde{\chi}_j^0} = -g(-i)^{\theta_j}\overline{\tilde{\chi}^-}_i[X_i^j + Y_i^j\gamma_5]\gamma_\mu\tilde{\chi}_j^0 W^{-\mu} \ + \text{h.c.}$$

,

$$\mathcal{L}_{q\bar{q}\tilde{\chi}_i^-} = iA^d_{\tilde{\chi}_i^-}\tilde{u}_L^\dagger\overline{\tilde{\chi}_i^-}P_L d + iA^u_{\tilde{\chi}_i^-}\tilde{d}_L^\dagger\overline{\tilde{\chi}_i^c}P_L u \ + \text{h.c.}$$

and

$$\mathcal{L}_{q\bar{q}\tilde{\chi}_j^0} = iA^q_{\tilde{\chi}_j^0}\tilde{q}_L^\dagger\overline{\tilde{\chi}^0}_j P_L q \ + \text{h.c.}$$

. Contributing diagrams include W exchange and also $\tilde{d}_L$ and $\tilde{u}_L$ squark exchange. The X_i^j and Y_i^j couplings are new, and again convention-dependent: the cross section formulae works if the interaction Lagrangian is written in the above form, so that the couplings can be suitably extracted. The term $\theta_j = 0$ (1) if $m_{\tilde{\chi}_j^0} > 0$ (< 0); it comes about because the neutralino field must be re-defined by a $-i\gamma_5$ transformation if its mass eigenvalue is negative [13]. The subprocess cross section is given in terms of dot products of four momenta, where particle labels are used to denote their four-momenta; note that all mass terms in the cross section formulae are positive definite, so that the signs of mass eigenstates have been absorbed into the Lagrangian couplings, as for instance in Ref. [13]. We then have

$$\frac{d\sigma}{dt}(d\bar{u}\to\tilde{\chi}_i^-\tilde{\chi}_j^0) = \frac{1}{192\pi s^2}$$
$$\left[T_W + T_{\tilde{d}_L} + T_{\tilde{u}_L} + T_{W\tilde{d}_L} + T_{W\tilde{u}_L} + T_{\tilde{d}_L\tilde{u}_L}\right] \qquad (51.70)$$

where

$$T_W = 8g^4|D_W(s)|^2\left\{[X_i^{j2}+Y_i^{j2}](\tilde{\chi}_j^0\cdot d\tilde{\chi}_i^-\cdot\bar{u} + \tilde{\chi}_j^0\cdot\bar{u}\tilde{\chi}_i^-\cdot d)\right.$$
$$+ 2(X_i^jY_i^j)(\tilde{\chi}_j^0\cdot d\tilde{\chi}_i^-\cdot\bar{u} - \tilde{\chi}_j^0\cdot\bar{u}\tilde{\chi}_i^-\cdot d)$$
$$\left. + [X_i^{j2}-Y_i^{j2}]m_{\tilde{\chi}_i^-}m_{\tilde{\chi}_j^0}d\cdot\bar{u}\right\}, \qquad (51.71)$$

$$T_{\tilde{d}_L} = \frac{4|A^u_{\tilde{\chi}_i^-}|^2|A^d_{\tilde{\chi}_j^0}|^2}{[(\tilde{\chi}_i^- - \bar{u})^2 - m^2_{\tilde{d}_L}]^2}\ d\cdot\tilde{\chi}_j^0\tilde{\chi}_i^-\cdot\bar{u}, \qquad (51.72)$$

$$T_{\tilde{u}_L} = \frac{4|A^d_{\tilde{\chi}_i^-}|^2|A^u_{\tilde{\chi}_j^0}|^2}{[(\tilde{\chi}_j^0 - \bar{u})^2 - m^2_{\tilde{u}_L}]^2}\ \bar{u}\cdot\tilde{\chi}_j^0\tilde{\chi}_i^-\cdot d \qquad (51.73)$$

$$T_{W\tilde{d}_L} = \frac{-\sqrt{2}g^2 Re[A^{d*}_{\tilde{\chi}_j^0}A^u_{\tilde{\chi}_i^-}(-i)^{\theta_j}](s-M_W^2)|D_W(s)|^2}{(\tilde{\chi}_i^- - \bar{u})^2 - m^2_{\tilde{d}_L}}$$
$$\times\left\{8(X_i^j+Y_i^j)\tilde{\chi}_j^0\cdot d\bar{u}\cdot\tilde{\chi}_i^- + 4(X_i^j-Y_i^j)m_{\tilde{\chi}_i^-}m_{\tilde{\chi}_j^0}d\cdot\bar{u}\right\} \qquad (51.74)$$

$$T_{W\tilde{u}_L} = \frac{\sqrt{2}g^2 Re[A^{d*}_{\tilde{\chi}_i^-}A^u_{\tilde{\chi}_j^0}(-i)^{\theta_j}](s-M_W^2)|D_W(s)|^2}{(\tilde{\chi}_j^0 - \bar{u})^2 - m^2_{\tilde{u}_L}}$$
$$\times\left\{8(X_i^j-Y_i^j)\tilde{\chi}_j^0\cdot\bar{u}d\cdot\tilde{\chi}_i^- + 4(X_i^j+Y_i^j)m_{\tilde{\chi}_i^-}m_{\tilde{\chi}_j^0}d\cdot\bar{u}\right\} \qquad (51.75)$$

and

$$T_{\tilde{d}_L\tilde{u}_L} = -\frac{4Re[A^d_{\tilde{\chi}_j^0}A^{u*}_{\tilde{\chi}_i^-}A^{d*}_{\tilde{\chi}_i^-}A^u_{\tilde{\chi}_j^0}]m_{\tilde{\chi}_i^-}m_{\tilde{\chi}_j^0}d\cdot\bar{u}}{[(\tilde{\chi}_i^- - \bar{u})^2 - m^2_{\tilde{d}_L}][(\tilde{\chi}_j^0 - \bar{u})^2 - m^2_{\tilde{u}_L}]}. \qquad (51.76)$$

51.8.4.2 *Chargino pair production*

The subprocess cross section for $d\bar{d}\to\tilde{\chi}_i^-\tilde{\chi}_i^+$ $(i=1,2)$ depends on Lagrangian couplings $\mathcal{L} = e\overline{\tilde{\chi}_i^-}\gamma_\mu\tilde{\chi}_i^- A^\mu - e\cot\theta_W\overline{\tilde{\chi}_i^-}\gamma_\mu(x_i - y_i\gamma_5)\tilde{\chi}_i^- Z^\mu$ and also $\mathcal{L}\ni iA^d_{\tilde{\chi}_i^-}\tilde{u}_L^\dagger\overline{\tilde{\chi}_i^-}P_L d + iA^u_{\tilde{\chi}_i^-}\tilde{d}_L^\dagger\overline{\tilde{\chi}_i^{-c}}P_L u$+h.c.. Contributing diagrams include s-channel γ, Z^0 exchange and t-channel $\tilde{u}_L$ exchange [16, 17]. The couplings x_i and y_i are again new and as usual convention-dependent.

The subprocess cross section is given by

$$\frac{d\sigma}{dt}(d\bar{d}\to\tilde{\chi}_i^-\tilde{\chi}_i^+) =$$
$$\frac{1}{192\pi s^2}\left[T_\gamma + T_Z + T_{\tilde{u}_L} + T_{\gamma Z} + T_{\gamma\tilde{u}_L} + T_{Z\tilde{u}_L}\right] \qquad (51.77)$$

where

$$T_\gamma = \frac{32e^4q_d^2}{s^2}\left[d\cdot\tilde{\chi}_i^+\bar{d}\cdot\tilde{\chi}_i^- + d\cdot\tilde{\chi}_i^-\bar{d}\cdot\tilde{\chi}_i^+ + m^2_{\tilde{\chi}_i^-}d\cdot\bar{d}\right] \qquad (51.78)$$

Downloaded from https://academic.oup.com/ptep/article/2022/8/083C01/6651666 by KIT Library user on 27 September 2022

$$T_Z = 32e^4 \cot^2\theta_W |D_Z(s)|^2$$
$$\left\{(\alpha_d^2+\beta_d^2)(x_i^2+y_i^2)\left[d\cdot\tilde{\chi}_i^+\bar{d}\cdot\tilde{\chi}_i^- + d\cdot\tilde{\chi}_i^-\bar{d}\cdot\tilde{\chi}_i^+ + m^2_{\tilde{\chi}_i^-}d\cdot\bar{d}\right]\right.$$
$$\left.\mp 4\alpha_d\beta_d x_i y_i\left[d\cdot\tilde{\chi}_i^+\bar{d}\cdot\tilde{\chi}_i^- - d\cdot\tilde{\chi}_i^-\bar{d}\cdot\tilde{\chi}_i^+\right] - 2y_i^2(\alpha_d^2+\beta_d^2)m^2_{\tilde{\chi}_i^-}d\cdot\bar{d}\right\}, \tag{51.79}$$

$$T_{\tilde{u}_L} = \frac{4|A^d_{\tilde{\chi}_i^-}|^4}{[(d-\tilde{\chi}_i^-)^2 - m^2_{\tilde{u}_L}]^2}\, d\cdot\tilde{\chi}_i^-\bar{d}\cdot\tilde{\chi}_i^+ \tag{51.80}$$

$$T_{\gamma Z} = \frac{64e^4\cot\theta_W q_d(s-M_Z^2)|D_Z(s)|^2}{s}\times$$
$$\left\{\alpha_d x_i\left(d\cdot\tilde{\chi}_i^+\bar{d}\cdot\tilde{\chi}_i^- + d\cdot\tilde{\chi}_i^-\bar{d}\cdot\tilde{\chi}_i^+ + m^2_{\tilde{\chi}_i^-}d\cdot\bar{d}\right)\right.$$
$$\left.\pm\beta_d y_i\left(d\cdot\tilde{\chi}_i^-\bar{d}\cdot\tilde{\chi}_i^+ - d\cdot\tilde{\chi}_i^+\bar{d}\cdot\tilde{\chi}_i^-\right)\right\} \tag{51.81}$$

$$T_{\gamma\tilde{u}_L} = \mp\frac{8e^2 q_d}{s}\frac{|A^d_{\tilde{\chi}_i^-}|^2}{[(d-\tilde{\chi}_i^-)^2 - m^2_{\tilde{u}_L}]}\left\{2\bar{d}\cdot\tilde{\chi}_i^+ d\cdot\tilde{\chi}_i^- + m^2_{\tilde{\chi}_i^-}d\cdot\bar{d}\right\} \tag{51.82}$$

and

$$T_{Z\tilde{u}_L} = \mp 8e^2\cot\theta_W|D_Z(s)|^2\frac{|A^d_{\tilde{\chi}_i^-}|^2(s-M_Z^2)}{[(d-\tilde{\chi}_i^-)^2 - m^2_{\tilde{u}_L}]}(\alpha_d-\beta_d)$$
$$\times\left\{2(x_i\mp y_i)d\cdot\tilde{\chi}_i^-\bar{d}\cdot\tilde{\chi}_i^+ + m^2_{\tilde{\chi}_i^-}(x_i\pm y_i)d\cdot\bar{d}\right\} \tag{51.83}$$

using the upper of the sign choices.

The cross section for $u\bar{u}\to\tilde{\chi}_i^+\tilde{\chi}_i^-$ can be obtained from the above by replacing $\alpha_d\to\alpha_u$, $\beta_d\to\beta_u$, $q_d\to q_u$, $\tilde{u}_L\to\tilde{d}_L$, $A^d_{\tilde{\chi}_i^-}\to A^u_{\tilde{\chi}_i^-}$, $d\to\bar{u}$, $\bar{d}\to u$ and adopting the lower of the sign choices everywhere.

The cross section for $q\bar{q}\to\tilde{\chi}_1^-\tilde{\chi}_2^+$, $\tilde{\chi}_1^+\tilde{\chi}_2^-$ can occur via Z and $\tilde{q}_L$ exchange. It is usually much smaller than $\tilde{\chi}_{1,2}^-\tilde{\chi}_{1,2}^+$ production, so the cross section will not be presented here. It can be found in Appendix A of Ref. [13].

51.8.4.3 *Neutralino pair production*

Neutralino pair production via $q\bar{q}$ fusion takes place via s-channel Z exchange plus t- and u-channel left- and right- squark exchange (5 diagrams) [17, 18]. The Lagrangian couplings (see previous footnote*) needed include terms given above plus terms of the form $\mathcal{L} = W_{ij}\overline{\tilde{\chi}^0}_i\gamma_\mu(\gamma_5)^{\theta_i+\theta_j+1}\tilde{\chi}_j^0 Z^\mu$. The couplings W_{ij} depend only on the *higgsino* components of the neutralinos i and j. The subprocess cross section is given by:

$$\frac{d\sigma}{dt}(q\bar{q}\to\tilde{\chi}_i^0\tilde{\chi}_j^0) = \frac{1}{192\pi s^2}\left[T_Z + T_{\tilde{q}_L} + T_{\tilde{q}_R} + T_{Z\tilde{q}_L} + T_{Z\tilde{q}_R}\right] \tag{51.84}$$

where

$$T_Z = 128e^2|W_{ij}|^2(\alpha_q^2+\beta_q^2)|D_Z(s)|^2$$
$$\left[q\cdot\tilde{\chi}_i^0\bar{q}\cdot\tilde{\chi}_j^0 + q\cdot\tilde{\chi}_j^0\bar{q}\cdot\tilde{\chi}_i^0 - \eta_i\eta_j m_{\tilde{\chi}_i^0}m_{\tilde{\chi}_j^0}q\cdot\bar{q}\right], \tag{51.85}$$

$$T_{\tilde{q}_L} = 4|A^q_{\tilde{\chi}_i^0}|^2|A^q_{\tilde{\chi}_j^0}|^2\left\{\frac{q\cdot\tilde{\chi}_i^0\bar{q}\cdot\tilde{\chi}_j^0}{[(\tilde{\chi}_i^0-q)^2-m^2_{\tilde{q}_L}]^2} + \frac{q\cdot\tilde{\chi}_j^0\bar{q}\cdot\tilde{\chi}_i^0}{[(\tilde{\chi}_j^0-q)^2-m^2_{\tilde{q}_L}]^2}\right.$$
$$\left. - \eta_i\eta_j\frac{m_{\tilde{\chi}_i^0}m_{\tilde{\chi}_j^0}q\cdot\bar{q}}{[(\tilde{\chi}_i^0-q)^2-m^2_{\tilde{q}_L}][(\tilde{\chi}_j^0-q)^2-m^2_{\tilde{q}_L}]}\right\} \tag{51.86}$$

$$T_{\tilde{q}_R} = 4|B^q_{\tilde{\chi}_i^0}|^2|B^q_{\tilde{\chi}_j^0}|^2\left\{\frac{q\cdot\tilde{\chi}_i^0\bar{q}\cdot\tilde{\chi}_j^0}{[(\tilde{\chi}_i^0-q)^2-m^2_{\tilde{q}_R}]^2} + \frac{q\cdot\tilde{\chi}_j^0\bar{q}\cdot\tilde{\chi}_i^0}{[(\tilde{\chi}_j^0-q)^2-m^2_{\tilde{q}_R}]^2}\right.$$
$$\left. - \eta_i\eta_j\frac{m_{\tilde{\chi}_i^0}m_{\tilde{\chi}_j^0}q\cdot\bar{q}}{[(\tilde{\chi}_i^0-q)^2-m^2_{\tilde{q}_R}][(\tilde{\chi}_j^0-q)^2-m^2_{\tilde{q}_R}]}\right\} \tag{51.87}$$

$$T_{Z\tilde{q}_L} = 16e(\alpha_q-\beta_q)(s-M_Z^2)|D_Z(s)|^2$$
$$\left\{\frac{Re(W_{ij}A^{q*}_{\tilde{\chi}_i^0}A^q_{\tilde{\chi}_j^0})}{[(\tilde{\chi}_i^0-q)^2-m^2_{\tilde{q}_L}]}\left[2q\cdot\tilde{\chi}_i^0\bar{q}\cdot\tilde{\chi}_j^0 - \eta_i\eta_j m_{\tilde{\chi}_i^0}m_{\tilde{\chi}_j^0}q\cdot\bar{q}\right]\right.$$
$$\left. + \eta_i\eta_j\frac{Re(W_{ij}A^q_{\tilde{\chi}_i^0}A^{q*}_{\tilde{\chi}_j^0})}{[(\tilde{\chi}_j^0-q)^2-m^2_{\tilde{q}_L}]}\left[2q\cdot\tilde{\chi}_j^0\bar{q}\cdot\tilde{\chi}_i^0 - \eta_i\eta_j m_{\tilde{\chi}_i^0}m_{\tilde{\chi}_j^0}q\cdot\bar{q}\right]\right\} \tag{51.88}$$

$$T_{Z\tilde{q}_R} = 16e(\alpha_q+\beta_q)(s-M_Z^2)|D_Z(s)|^2$$
$$\left\{\frac{Re(W_{ij}B^{q*}_{\tilde{\chi}_i^0}B^q_{\tilde{\chi}_j^0})}{[(\tilde{\chi}_i^0-q)^2-m^2_{\tilde{q}_R}]}\left[2q\cdot\tilde{\chi}_i^0\bar{q}\cdot\tilde{\chi}_j^0 - \eta_i\eta_j m_{\tilde{\chi}_i^0}m_{\tilde{\chi}_j^0}q\cdot\bar{q}\right]\right.$$
$$\left. - \frac{Re(W_{ij}B^q_{\tilde{\chi}_i^0}B^{q*}_{\tilde{\chi}_j^0})}{[(\tilde{\chi}_j^0-q)^2-m^2_{\tilde{q}_R}]}\left[2q\cdot\tilde{\chi}_j^0\bar{q}\cdot\tilde{\chi}_i^0 - \eta_i\eta_j m_{\tilde{\chi}_i^0}m_{\tilde{\chi}_j^0}q\cdot\bar{q}\right]\right\}. \tag{51.89}$$

As before, $\eta_i = \pm 1$ corresponding to whether the neutralino mass eigenvalue is positive or negative. When $i = j$ in the above formula, one must remember to integrate over just 2π steradians of solid angle to avoid double counting in the total cross section.

51.9 Universal extra dimensions

In the Universal Extra Dimension (UED) model of Ref. [19] (see Ref. [20] for a review of models with extra spacetime dimensions), the Standard Model is embedded in a five dimensional theory, where the fifth dimension is compactified on an S_1/Z_2 orbifold. Each SM chirality state is then the zero mode of an infinite tower of Kaluza-Klein excitations labeled by $n = 0-\infty$. A KK parity is usually assumed to hold, where each state is assigned KK-parity $P = (-1)^n$. If the compactification scale is around a TeV, then the $n = 1$ (or even higher) KK modes may be accessible to collider searches.

Of interest for hadron colliders are the production of massive $n \geq 1$ quark or gluon pairs. These production cross sections have been calculated in Ref. [21, 22]. We list here results for the $n = 1$ case only with $M_1 = 1/R$ (R is the compactification radius) and s, t and u are the usual Mandelstam variables; more general formulae can be found in Ref. [22]. The superscript $*$ stands for any KK excited state, while $\bullet$ stands for left chirality states and $\circ$ stands for right chirality states.

$$\frac{d\sigma}{dt} = \frac{1}{16\pi s^2}T \tag{51.90}$$

where

$$T(q\bar{q}\to g^*g^*) = \frac{2g_s^4}{27}\left[M_1^2\left(-\frac{4s^3}{t'^2u'^2} + \frac{57s}{t'u'} - \frac{108}{s}\right)\right.$$
$$\left. + \frac{20s^2}{t'u'} - 93 + \frac{108t'u'}{s^2}\right] \tag{51.91}$$

and

$$T(gg\to g^*g^*) =$$
$$\frac{9g_s^4}{27}\left[3M_1^4\frac{s^2+t'^2+u'^2}{t'^2u'^2} - 3M_1^2\frac{s^2+t'^2+u'^2}{st'u'} + 1\right.$$
$$\left. + \frac{(s^2+t'^2+u'^2)^3}{4s^2t'^2u'^2} - \frac{t'u'}{s^2}\right] \tag{51.92}$$

where $t' = t - M_1^2$ and $u' = u - M_1^2$.

Also,

$$T(q\bar{q}\to q_1^{*\prime}\bar{q}_1^{*\prime}) = \frac{4g_s^4}{9}\left[\frac{2M_1^2}{s} + \frac{t'^2+u'^2}{s^2}\right],$$

Downloaded from https://academic.oup.com/ptep/article/2022/8/083C01/6651666 by KIT Library user on 27 September 2022

$$T(q\bar{q} \to q_1^* \bar{q}_1^*) = \frac{g_2^4}{9}\left[2M_1^2\left(\frac{4}{s} + \frac{s}{t'^2} - \frac{1}{t'}\right)\right.$$
$$\left. + \frac{23}{6} + \frac{2s^2}{t'^2} + \frac{8s}{3t'} + \frac{6t'}{s} + \frac{8t'^2}{s^2}\right],$$
$$T(qq \to q_1^* q_1^*) = \frac{g_s^4}{27}\left[M_1^2\left(6\frac{t'}{u'^2} + 6\frac{u'}{t'^2} - \frac{s}{t'u'}\right)\right.$$
$$\left. + 2\left(3\frac{t'^2}{u'^2} + 3\frac{u'^2}{t'^2} + 4\frac{s^2}{t'u'} - 5\right)\right],$$
$$T(gg \to q_1^* \bar{q}_1^*) = g_s^4\left[M_1^4 \frac{-4}{t'u'}\left(\frac{s^2}{6t'u'} - \frac{3}{8}\right)\right.$$
$$\left. + M_1^2 \frac{4}{s}\left(\frac{s^2}{6t'u'} - \frac{3}{8}\right) + \frac{s^2}{6t'u'} - \frac{17}{24} + \frac{3t'u'}{4s^2}\right],$$
$$T(gq \to g^* q_1^*) = \frac{-g_s^4}{3}\left[\frac{5s^2}{12t'^2} + \frac{s^3}{t'^2 u'} + \frac{11su'}{6t'^2} + \frac{5u'^2}{12t'^2} + \frac{u'^3}{st'^2}\right],$$
$$T(q\bar{q}' \to q_1^* \bar{q}_1^{*\prime}) = \frac{g_s^4}{18}\left[4M_1^4 \frac{s}{t'^2} + 5 + 4\frac{s^2}{t'^2} + 8\frac{s}{t'}\right],$$
$$T(qq' \to q_1^* q_1^{*\prime}) = \frac{2g_s^4}{9}\left[-M_1^2 \frac{s}{t'^2} + \frac{1}{4} + \frac{s^2}{t'^2}\right],$$
$$T(qq \to q_1^\bullet q_1^\circ) =$$
$$\frac{g_s^4}{9}\left[M_1^2\left(\frac{2s^3}{t'^2 u'^2} - \frac{4s}{t'u'}\right) + 2\frac{s^4}{t'^2 u'^2} - 8\frac{s^2}{t'u'} + 5\right],$$
$$T(q\bar{q}' \to q_1^\bullet \bar{q}_1^{\prime\circ}) = \frac{g_s^4}{9}\left[2M_1^2\left(\frac{1}{t'} + \frac{u'}{t'^2}\right) + \frac{5}{2} + \frac{4u'}{t'} + \frac{2u'^2}{t'^2}\right],$$

and

$$T(qq' \to q_1^\bullet q_1^{\prime\circ}) = \frac{g_s^4}{9}\left[-2M_1^2\left(\frac{1}{t'} + \frac{u'}{t'^2}\right) + \frac{1}{2} + \frac{2u'^2}{t'^2}\right].$$

51.10 Large extra dimensions

In the ADD theory [23] with large extra dimensions (LED), the SM particles are confined to a 3-brane, while gravity propagates in the bulk. It is assumed that the n extra dimensions are compactified on an n-dimensional torus of volume $(2\pi r)^n$, so that the fundamental $4+n$ dimensional Planck scale M_* is related to the usual 4-dimensional Planck scale M_{Pl} by $M_{Pl}^2 = M_*^{n+2}(2\pi r)^n$. If $M_* \sim 1$ TeV, then the $M_W - M_{Pl}$ hierarchy problem is just due to gravity propagating in the large extra dimensions.

In these theories, the KK-excited graviton states $G_{\mu\nu}^n$ for $n = 1-\infty$ can be produced at collider experiments. The graviton couplings to matter are suppressed by $1/M_{Pl}$, so that graviton emission cross sections $d\sigma/dt \sim 1/M_{Pl}^2$. However, the mass splittings between the excited graviton states can be tiny, so the graviton eigenstates are usually approximated by a continuum distribution. A summation (integration) over all allowed graviton emissions ends up cancelling the $1/M_{Pl}^2$ factor, so that observable cross section rates can be attained. Some fundamental production formulae for a KK graviton (denoted G) of mass m at hadron colliders include the subprocesses

$$\frac{d\sigma_m}{dt}(f\bar{f} \to \gamma G) = \frac{\alpha Q_f^2}{16N_f}\frac{1}{sM_{Pl}^2}F_1(\frac{t}{s}, \frac{m^2}{s}), \tag{51.93}$$

where Q_f is the charge of fermion f and N_f is the number of QCD colors of f. Also,

$$\frac{d\sigma_m}{dt}(q\bar{q} \to gG) = \frac{\alpha_s}{36}\frac{1}{sM_{Pl}^2}F_1(\frac{t}{s}, \frac{m^2}{s}), \tag{51.94}$$

$$\frac{d\sigma_m}{dt}(qg \to qG) = \frac{\alpha_s}{96}\frac{1}{sM_{Pl}^2}F_2(\frac{t}{s}, \frac{m^2}{s}), \tag{51.95}$$

$$\frac{d\sigma_m}{dt}(gg \to gG) = \frac{3\alpha_s}{16}\frac{1}{sM_{Pl}^2}F_3(\frac{t}{s}, \frac{m^2}{s}), \tag{51.96}$$

where

$$F_1(x,y) = \frac{1}{x(y-1-x)}\left[-4x(1+x)(1+2x+2x^2)+\right.$$
$$\left. y(1+6x+18x^2+16x^3) - 6y^2x(1+2x) + y^3(1+4x)\right] \tag{51.97}$$

$$F_2(x,y) = -(y-1-x)F_1\left(\frac{x}{y-1-x}, \frac{y}{y-1-x}\right) \tag{51.98}$$

and

$$F_3(x,y) = \frac{1}{x(y-1-x)}\left[1+2x+3x^2+2x^3+x^4\right.$$
$$\left. -2y(1+x^3) + 3y^2(1+x^2) - 2y^3(1+x) + y^4\right]. \tag{51.99}$$

These formulae must then be multiplied by the graviton density of states formula
$dN = S_{n-1}\frac{M_{Pl}^2}{M_*^{n+2}}m^{n-1}dm$ to gain the cross section

$$\frac{d^2\sigma}{dtdm} = S_{n-1}\frac{M_{Pl}^2}{M_*^{n+2}}m^{n-1}\frac{d\sigma_m}{dt} \tag{51.100}$$

where $S_n = \frac{(2\pi)^{n/2}}{\Gamma(n/2)}$ is the surface area of an n-dimensional sphere of unit radius.

Virtual graviton processes can also be searched for at colliders. For instance, in Ref. [24] the cross section for Drell-Yan production of lepton pairs via gluon fusion was calculated, where it is found that, in the center-of-mass system

$$\frac{d\sigma}{dz}(gg \to \ell^+\ell^-) = \frac{\lambda^2 s^3}{64\pi M_*^8}(1-z^2)(1+z^2) \tag{51.101}$$

where $z = \cos\theta$ and λ is a model-dependent coupling constant ~ 1. Formulae for Drell-Yan production via $q\bar{q}$ fusion can also be found in Refs. [24, 25].

51.11 Warped extra dimensions

In the Randall-Sundrum model [26] of warped extra dimensions, the arena for physics is a 5-d anti-deSitter (AdS_5) spacetime, for which a non-factorizable metric exists with a metric warp factor $e^{-2\sigma(\phi)}$. It is assumed that two opposite tension 3-branes exist within AdS_5 at the two ends of an S_1/Z_2 orbifold parameterized by co-ordinate ϕ which runs from $0-\pi$. The 4-D solution of the Einstein equations yields $\sigma(\phi) = kr_c|\phi|$, where r_c is the compactification radius of the extra dimension and $k \sim M_{Pl}$. The 4-D effective action allows one to identify $\overline{M}_{Pl}^2 = \frac{M^3}{k}(1-e^{-2kr_c\pi})$, where M is the 5-D Planck scale. Physical particles on the TeV scale (SM) brane have mass $m = e^{-kr_c\pi}m_0$, where m_0 is a fundamental mass of order the Planck scale. Thus, the weak scale-Planck scale hierarchy occurs due to the existence of the exponential warp factor if $kr_c \sim 12$.

In the simplest versions of the RS model, the TeV-scale brane contains only SM particles plus a tower of KK gravitons. The RS gravitons have mass $m_n = kx_n e^{-kr_c\pi}$, where the x_i are roots of Bessel functions $J_1(x_n) = 0$, with $x_1 \simeq 3.83$, $x_2 \simeq 7.02$ etc. While the RS zero-mode graviton couplings suppressed by $1/\overline{M}_{Pl}$ and are thus inconsequential for collider searches, the $n = 1$ and higher modes have couplings suppressed instead by $\Lambda_\pi = e^{-kr_c\pi}\overline{M}_{Pl} \sim TeV$. The $n = 1$ RS graviton should have width $\Gamma_1 = \rho m_1 x_1^2 (k/\overline{M}_{Pl})^2$, where ρ is a constant depending on how many decay modes are open. The formulae for dilepton production via virtual RS graviton exchange can be gained from the above formulae for the ADD scenario via the replacement [27]

$$\frac{\lambda}{M_*^4} \to \frac{i^2}{8\Lambda_\pi^2}\sum_{n=1}^{\infty}\frac{1}{s - m_n^2 + im_n\Gamma_n}. \tag{51.102}$$

Downloaded from https://academic.oup.com/ptep/article/2022/8/083C01/6651666 by KIT Library user on 27 September 2022

References

[1] J. F. Owens, E. Reya and M. Gluck, Phys. Rev. **D18**, 1501 (1978).

[2] F. Wilczek, Phys. Rev. Lett. **39**, 1304 (1977).

[3] B. L. Ioffe and V. A. Khoze, Sov. J. Part. Nucl. **9**, 50 (1978), [Fiz. Elem. Chast. Atom. Yadra9,118(1978)].

[4] J. R. Ellis, M. K. Gaillard and D. V. Nanopoulos, Nucl. Phys. **B106**, 292 (1976).

[5] R. N. Cahn and S. Dawson, Phys. Lett. **136B**, 196 (1984), [Erratum: Phys. Lett.138B,464(1984)].

[6] S. Dawson, Nucl. Phys. **B249**, 42 (1985).

[7] M. S. Chanowitz and M. K. Gaillard, Phys. Lett. **142B**, 85 (1984).

[8] R. N. Cahn, Nucl. Phys. **B255**, 341 (1985), [Erratum: Nucl. Phys.B262,744(1985)].

[9] V. M. Budnev *et al.*, Phys. Rept. **15**, 181 (1975), see for an exhaustive treatment.

[10] See *e.g.* H.Haber, *Supersymmetry, Part I (Theory), this Review.*

[11] P. R. Harrison and C. H. Llewellyn Smith, Nucl. Phys. **B213**, 223 (1983), [Erratum: Nucl. Phys.B223,542(1983)]; S. Dawson, E. Eichten and C. Quigg, Phys. Rev. **D31**, 1581 (1985); V. D. Barger *et al.*, Phys. Rev. **D31**, 528 (1985); H. Baer and X. Tata, Phys. Lett. **160B**, 159 (1985).

[12] H. Baer, D. D. Karatas and X. Tata, Phys. Rev. **D42**, 2259 (1990).

[13] Weak Scale Supersymmetry: From Superfields to Scattering Events, H. Baer and X. Tata (Cambridge University Press) 2006.

[14] H. E. Haber and G. L. Kane, Phys. Rept. **117**, 75 (1985).

[15] Theory and Phenomenology of Sparticles, M. Drees, R. Godbole, and P. Roy (World Scientific) 2005.

[16] A. Bartl, H. Fraas and W. Majerotto, Z. Phys. **C30**, 441 (1986).

[17] H. Baer *et al.*, Int. J. Mod. Phys. **A4**, 4111 (1989).

[18] A. Bartl, H. Fraas and W. Majerotto, Nucl. Phys. **B278**, 1 (1986).

[19] T. Appelquist, H.-C. Cheng and B. A. Dobrescu, Phys. Rev. **D64**, 035002 (2001), [hep-ph/0012100].

[20] For a review of models with extra spacetime dimensions, see G. Guidice and J. Wells, *Extra Dimensions, this Review.*

[21] J. M. Smillie and B. R. Webber, JHEP **10**, 069 (2005), [hep-ph/0507170].

[22] C. Macesanu, C. D. McMullen and S. Nandi, Phys. Rev. **D66**, 015009 (2002), [hep-ph/0201300].

[23] N. Arkani-Hamed, S. Dimopoulos and G. R. Dvali, Phys. Lett. **B429**, 263 (1998), [hep-ph/9803315]; N. Arkani-Hamed, S. Dimopoulos and G. R. Dvali, Phys. Rev. **D59**, 086004 (1999), [hep-ph/9807344].

[24] J. L. Hewett, Phys. Rev. Lett. **82**, 4765 (1999), [hep-ph/9811356].

[25] G. F. Giudice, R. Rattazzi and J. D. Wells, Nucl. Phys. **B544**, 3 (1999), [hep-ph/9811291]; E. A. Mirabelli, M. Perelstein and M. E. Peskin, Phys. Rev. Lett. **82**, 2236 (1999), [hep-ph/9811337]; T. Han, J. D. Lykken and R.-J. Zhang, Phys. Rev. **D59**, 105006 (1999), [hep-ph/9811350].

[26] L. Randall and R. Sundrum, Phys. Rev. Lett. **83**, 3370 (1999), [hep-ph/9905221].

[27] H. Davoudiasl, J. L. Hewett and T. G. Rizzo, Phys. Rev. Lett. **84**, 2080 (2000), [hep-ph/9909255].

Downloaded from https://academic.oup.com/ptep/article/2022/8/083C01/6651666 by KIT Library user on 27 September 2022

52. Neutrino Cross Section Measurements

Revised August 2021 by G.P. Zeller (FNAL).

Neutrino cross sections are an essential ingredient in all neutrino experiments. Interest in neutrino scattering has increased due to the need for such information in the interpretation of neutrino oscillation data [1] and given that uncertainties in neutrino-nucleus scattering remain a dominate source of systematic uncertainty in many neutrino oscillation measurements, for example [2]. Historically, neutrino scattering results on both charged current (CC) and neutral current (NC) channels have been collected over many decades using a variety of targets, analysis techniques, and detector technologies. With the advent of intense neutrino sources constructed for neutrino oscillation investigations, experiments are now remeasuring such interaction cross sections with a renewed appreciation for nuclear effects[1] and the need for more precise neutrino flux estimations. This work summarizes accelerator-based neutrino cross section measurements performed in the $\sim 0.1-300$ GeV range with an emphasis on inclusive, quasi-elastic (pionless), and pion production processes, areas where we have the most experimental input at present (Table 52.1). For a more comprehensive discussion of neutrino cross sections, including neutrino-electron elastic scattering and lower energy neutrino measurements, the reader is directed to a review of this subject [3]. Here, we survey existing experimental data on neutrino interactions and do not attempt to provide a census of the associated theoretical calculations [4], which are both critical and plentiful. Companion electron-nucleus scattering data are additionally playing an increased role in neutrino event generator development through such efforts as the e4ν collaboration.

Table 52.1: List of beam properties, nuclear targets, and run durations for modern accelerator-based neutrino experiments studying neutrino scattering.

Experiment	beam	$\langle E_\nu \rangle$, $\langle E_{\overline{\nu}} \rangle$ GeV	neutrino target(s)	run period
ArgoNeuT	$\nu, \overline{\nu}$	4.3, 3.6	Ar	2009 – 2010
ICARUS (at CNGS)	ν	20.0	Ar	2010 – 2012
ICARUS (at FNAL)	ν	0.8	Ar	2021 –
K2K	ν	1.3	CH, H_2O	2003 – 2004
MicroBooNE	ν	0.8	Ar	2015 – 2020
MINERvA	$\nu, \overline{\nu}$	3.5 (LE), 5.5 (ME)	He, C, CH, H_2O, Fe, Pb	2009 – 2019
MiniBooNE	$\nu, \overline{\nu}$	0.8, 0.7	CH_2	2002 – 2019
MINOS	$\nu, \overline{\nu}$	3.5, 6.1	Fe	2004 – 2016
NOMAD	$\nu, \overline{\nu}$	23.4, 19.7	C–based	1995 – 1998
NOvA	$\nu, \overline{\nu}$	2.0, 2.0	CH_2	2010 –
SciBooNE	$\nu, \overline{\nu}$	0.8, 0.7	CH	2007 – 2008
T2K	ν, $\overline{\nu}$	0.6, 0.6	CH, H_2O, Fe	2010 –

52.1 Inclusive Scattering

Over the years, many experiments have measured the total inclusive charged current cross section for neutrino ($\nu_\mu N \to \mu^- X$) and antineutrino ($\overline{\nu}_\mu N \to \mu^+ X$) scattering covering a broad range of neutrino energies. As can be seen in Fig. 52.1, the inclusive cross section approaches a linear dependence on neutrino energy. This behavior is expected for point-like scattering of neutrinos from quarks, an assumption which breaks down at lower energies. Modern measurements of such inclusive scattering cross sections and their target nuclei are summarized in Table 52.2.

To provide a more complete picture, single and double differential cross sections for such inclusive scattering processes have also been reported. These include measurements on iron from NuTeV [5] and on a variety of nuclear targets from ArgoNeuT [6,7], MicroBooNE [8], MINERvA [9–11], NINJA [12], and T2K [13,14]. More recently, MINERvA has provided measurements in terms of longitudinal and transverse muon momenta [10, 11], MicroBooNE has measured the first double differential cross sections in argon [8], and T2K has provided the first measurement of the antineutrino inclusive cross section at low energy [15] (Fig. 52.1).

At high energy, the inclusive cross section is dominated by deep inelastic scattering (DIS). Several neutrino experiments have measured DIS cross sections for specific targets and final states, for example, MINERvA has measured ratios of muon neutrino inclusive and DIS cross sections on a variety of nuclear targets including lead, iron, and carbon [16, 17]. The reader is referred to a recent review of measurements in the shallow and deep inelastic scattering regions [18]. Other experiments have measured opposite-sign dimuon production, the most recent being from CHORUS [19], NOMAD [20], and NuTeV [21].

The aforementioned measurements have all been performed using beams of muon neutrinos and antineutrinos. For the first time, measurements of inclusive electron neutrino cross sections have also been reported, most recently by MicroBooNE [22] and T2K [23–25].

Table 52.2: Published measurements of neutrino and antineutrino CC inclusive cross sections from modern accelerator-based neutrino experiments.

experiment	measurement	target
ArgoNeuT	ν_μ [6, 7], $\overline{\nu}_\mu$ [7]	Ar
MicroBooNE	ν_μ [8, 26], ν_e [22]	Ar
MINERνA	ν_μ [9–11, 16, 17, 27], $\overline{\nu}_\mu$ [27], $\overline{\nu}_\mu/\nu_\mu$ [28]	CH, C/CH, Fe/CH, Pb/CH
MINOS	ν_μ [29], $\overline{\nu}_\mu$ [29]	Fe
NINJA	ν_μ [12], $\overline{\nu}_\mu$ [12]	H_2O
NOMAD	ν_μ [30]	C
SciBooNE	ν_μ [31]	CH
T2K	ν_μ [13, 14, 32–34], ν_e [23–25], $\overline{\nu}_\mu/\nu_\mu$ [15]	CH, H_2O, Fe

At lower neutrino energies, the inclusive cross section is an additionally complex combination of quasi-elastic scattering and pion production processes, two areas we discuss next.

52.2 Quasi-elastic scattering

Quasi-elastic (QE) scattering is the dominant neutrino interaction for neutrino energies less than ~ 1 GeV and represents a large fraction of the signal samples in many neutrino oscillation experiments, which is why this process has received considerable attention in recent years. Historically, neutrino (antineutrino) quasi-elastic scattering refers to the process, $\nu_\mu n \to \mu^- p$ ($\overline{\nu}_\mu p \to \mu^+ n$), where a charged lepton and single nucleon are ejected in the elastic interaction of a neutrino (or antineutrino) with a nucleon in the target material. This is the final state one would strictly observe, for example, in scattering off of a *free* nucleon target. There were many early measurements of neutrino QE scattering that span back to the 1970's [3]. In many of these initial measurements, bubble chamber experiments employed light targets (hydrogen or deuterium) and required both the detection of the final state muon and single nucleon[2]; thus the final state was clear and elastic kinematic conditions could be verified. The situation is more complicated, of course, for heavier nuclear targets used in modern neutrino experiments. In this case, nuclear effects can impact the size and shape of the cross section as well as the final state composition, kinematics, and topology. Due to intranuclear hadron rescattering and the effects of correlations between target nucleons, additional particles may be ejected in the final state; hence, a QE interaction on a nuclear target does not necessarily imply the ejection of a lepton and a *single* nucleon. One therefore needs to take care in defining what one means by neutrino QE scattering when scattering off targets heavier than hydrogen or deuterium. Because of this, modern experiments tend to instead report cross sections for processes involving pionless (e.g., nucleon-only) final states, often referred to as CC 0π or QE-like reactions in recent literature. Such measurements are

[1] Nuclear effects refer to kinematic and final state effects which impact neutrino scattering off nuclei. Such effects can be significant and are particularly relevant given that modern neutrino experiments make use of nuclear targets to increase their event yields.

[2] In the case of deuterium, many experiments additionally observed the spectator proton.

Downloaded from https://academic.oup.com/ptep/article/2022/8/083C01/6651666 by KIT Library user on 27 September 2022

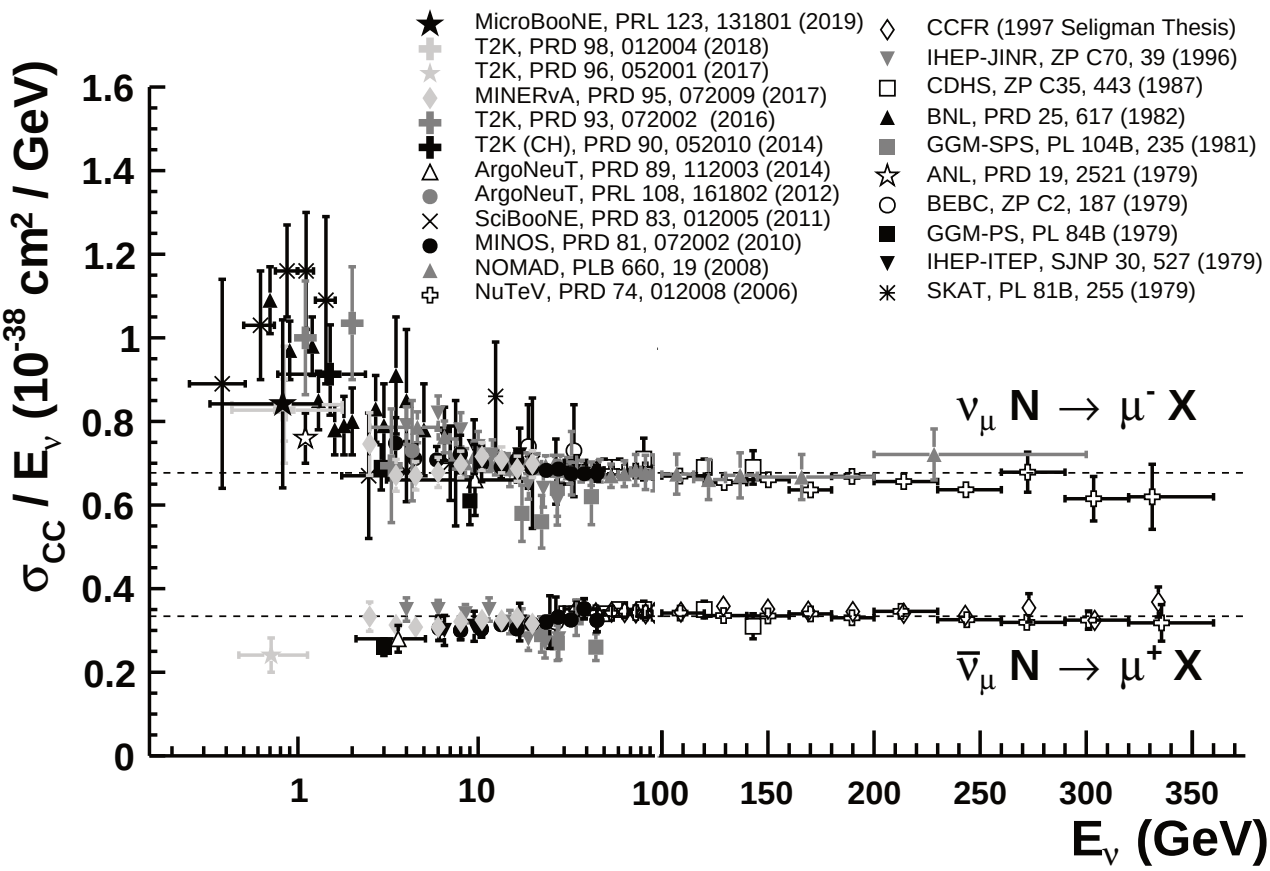

Figure 52.1: Measurements of per nucleon ν_μ and $\overline{\nu}_\mu$ CC inclusive scattering cross sections divided by neutrino energy as a function of neutrino energy. Note the transition between logarithmic and linear scales occurring at 100 GeV. Neutrino cross sections are typically twice as large as their corresponding antineutrino counterparts, although this difference can be larger at lower energies. NC cross sections (not shown) are generally smaller compared to their CC counterpart.

summarized in Table 52.3. Many modern experiments have also recently opted to report nucleon-only cross sections as a function of observed final state particle kinematics [35–48]. Such measurements can be more difficult to directly compare between experiments but have the advantage of being much less model-dependent and provide more stringent tests of the theory than historical cross sections as a function of derived quantities such as neutrino energy (E_ν) or 4-momentum transfer (Q^2). More recent work has been done to develop a means to directly compare experimental measurements produced in these less model-dependent forms [49].

The topic of neutrino QE scattering began drawing considerable attention following the first double differential cross section measurements of this process that revealed a significantly larger cross section than originally anticipated, predominantly in the backwards muon scattering region [40, 41]. Such an enhancement was observed many years prior in transverse electron-nucleus scattering [68] and was attributed to the presence of correlations between nucleons in the target nucleus. As a result, the impact of such nuclear effects on neutrino QE scattering has recently become the subject of intense experimental and theoretical scrutiny with implications on event rates, nucleon emission, neutrino energy reconstruction, and neutrino versus antineutrino cross sections. The reader is referred to reviews of the situation in [4, 69, 70]. To help drive further progress in understanding the underlying nuclear contributions, pionless (e.g., nucleon-only) cross sections have been reported for the first time in the form of double-differential distributions by MiniBooNE [40, 41], MINERvA [35–37, 55], and T2K [42–46]. Such double-differential cross sections in terms of final state particle kinematics reduce the model-dependence of the reported data, provide the most robust measurements available, and allow a more rigorous two-dimensional test of the underlying nuclear theory. MINERvA and T2K have been especially prolific in recent years in probing this interaction process (Table 52.3). Neutrino experiments have also launched dedicated studies of the hadronic side of these interactions, including ArgoNeuT [50, 71], MicroBooNE [47, 48], MINERvA [54], and T2K [67]. MINERvA has been the first modern experiment to measure neutron emission in antineutrino interactions [72]. T2K has probed ratios of oxygen to carbon [45] and asymmetries between neutrino and antineutrino scattering [46] to glean more information on the nature of the underlying nuclear effects. In addition, the exploration of transverse kinematic variables and momentum imbalances in pionless neutrino scattering is allowing better constraints on the various nuclear contributions to the cross section. Such scrutiny includes recent evaluations from MINERvA [35, 36, 38, 39] and T2K [67]. With the MiniBooNE results having first revealed these additional complexities in neutrino-nucleus QE scattering, measurements from multiple neutrino experiments, on multiple targets, and using a variety of kinematic information have been crucial in gaining a better handle on the underlying nuclear physics impacting neutrino-nucleus interactions. What we once thought was "simple" QE scattering is in fact not so simple.

In addition to such charged current investigations, measurements of the neutral current counterpart of this channel have also been performed. The most recent NC elastic scattering cross section measurements include those from BNL E734 [73], MiniBooNE [59, 60], Super-K [63], and T2K [66]. A number of measurements of the Cabibbo-suppressed antineutrino QE hyperon production cross section have additionally been reported [74, 75], although not in recent years.

Downloaded from https://academic.oup.com/ptep/article/2022/8/083C01/6651666 by KIT Library user on 27 September 2022

Table 52.3: Published modern measurements of neutrino CC and NC scattering cross sections with nucleon-only final states.

experiment	measurement	target
ArgoNeuT	2p [50]	Ar
K2K	M_A [51]	H_2O
MicroBooNE	$\frac{d\sigma}{dp_\mu}$ $\frac{d\sigma}{dp_p}$ $\frac{d\sigma}{d\cos\theta_\mu}$ $\frac{d\sigma}{d\cos\theta_p}$ [47, 48]	Ar
MINERνA	$\frac{d^2\sigma}{dp_T dp_{\|\|}}$ [35–37], $\frac{d\sigma}{d\delta p_{Tx}}$ $\frac{d\sigma}{d\delta p_{Ty}}$ [38], $\frac{d\sigma}{dp_n}$ $\frac{d\sigma}{d\delta\alpha_T}$ [39]	CH,Fe,Pb
	$\frac{d\sigma}{dQ^2}$ [52, 53], 1p [54], $\frac{d^2\sigma}{dE_{avail}dq_3}$ [55], $\frac{d\sigma}{dQ^2}$ [56], ν_e [57]	
MiniBooNE	$\frac{d^2\sigma}{dT_\mu d\theta_\mu}$ [40, 41], M_A [58], NC [59, 60]	CH_2
MINOS	M_A [61]	Fe
NOMAD	M_A, $\sigma(E_\nu)$ [62]	C
Super-K	NC [63]	H_2O
T2K	$\frac{d^2\sigma}{dT_\mu d\theta_\mu}$ [42–46], $\sigma(E_\nu)$ [64], M_A [65], NC [66], $\frac{d\sigma}{d\delta p_T}$ $\frac{d\sigma}{d\delta\alpha_T}$ [67], O/C [45]	CH,H_2O

52.3 Pion Production

In addition to such elastic scattering processes, neutrinos can also inelastically scatter producing a nucleon excited state (Δ, N^*). Such baryonic resonances quickly decay, most often to a nucleon and single-pion final state. Historically, experiments have measured various exclusive final states associated with these reactions, the majority of which have been on hydrogen and deuterium targets [3]. There have been several recent re-analyses of this data to better understand the consistency between data sets [76], nucleon form factors [77], and non-resonant contributions [78]. Also, modern measurements of neutrino-induced pion production have since been performed on a variety of nuclear targets (Table 52.4).

Table 52.4: Summary of modern measurements of NC and CC scattering cross sections involving a single pion or multiple pions in the final state.

experiment	$\pi^\pm$	π^0	target
ArgoNeuT	CC [79, 80]	NC [81]	Ar
K2K	CC[82, 83]	CC [84], NC [85]	CH, H_2O
MicroBooNE	–	CC [86]	Ar
MINERνA	CC [87–92]	CC [88, 93–95], NC [96]	CH
MiniBooNE	CC [97, 98]	CC [99], NC [100, 101]	CH_2
MINOS	–	NC [102]	Fe
NOMAD	–	NC [103]	C
NOvA	–	NC [104]	C
SciBooNE	CC [105]	NC [106, 107]	CH
T2K	CC [108–111]	–	CH, H_2O

In addition to resonance production processes, neutrinos can also coherently scatter off of the entire nucleus and produce a distinctly forward-scattered single pion final state. Both CC ($\nu_\mu\, A \to \mu^-\, A\, \pi^+$, $\overline{\nu}_\mu\, A \to \mu^+\, A\, \pi^-$) and NC ($\nu_\mu\, A \to \nu_\mu\, A\pi^0, \overline{\nu}_\mu\, A \to \overline{\nu}_\mu\, A\pi^0$) processes are possible in this case. Even though the level of coherent pion production is small compared to their resonant counterpart, observations exist across a broad energy range and on multiple nuclear targets [112]. More recently, several modern neutrino experiments have either measured or set limits on coherent pion production cross sections including ArgoNeuT [79], K2K [83], MINERvA [89, 91], MiniBooNE [101], MINOS [102], NOMAD [103], NOvA [104], SciBooNE [105, 107], and T2K [83].

As with inclusive and quasi-elastic scattering, a new appreciation for the significance of nuclear effects has also surfaced in pion production physics, again due to the use of heavy nuclear targets in modern neutrino experiments. Many experiments have been careful to report cross sections for various detected final states, thereby not correcting for large and uncertain nuclear effects (e.g., pion rescattering, charge exchange, and absorption) which can introduce significant sources of uncertainty and model dependence. Providing the most comprehensive survey of neutrino single-pion production to date, MiniBooNE has published a total of 16 single- and double-differential cross sections for both the final state muon (in the case of CC scattering) and pions in these interactions; thus, providing the first measurements of such final state kinematic distributions [97–100]. At similar neutrino energies, T2K has provided new data [108] including the first measurement of the Adler angles in neutrino-nucleus scattering [110] and the first exploration of transverse kinematic imbalances in pion production processes [111]. MINERvA has produced a similar accompaniment of measurements at higher neutrino energies [88, 90, 92, 94]. Importantly, MINERvA has been working towards an improved nuclear model [95] and one that can potentially describe all of the pion reaction channels simultaneously, an issue that many experiments have struggled with up until now [88]. ArgoNeuT [80, 81] and MicroBooNE [86] have since been adding new information on single pion production in argon. Regardless of the interaction channel or target material, differential cross section measurements in terms of observed final state particle kinematics are preferred for their reduced model dependence and for the additional kinematic information they provide. Such a new direction has been the focus of modern measurements as opposed to the reporting of more model-dependent, historical cross sections as a function of E_ν or Q^2. Together with similar results for other interaction channels, a better understanding and modeling of nuclear effects will be possible moving forward. MINERvA [113] has already taken a large step in this direction by explicitly tuning the physics in existing neutrino event generators to best fit the experimental data on pion production.

It should be noted that baryonic resonances can also decay to multi-pion, other mesonic (K, η, ρ, etc.), and even photon final states. Experimental results for these channels are typically sparse or non-existent [3]; however, photon production processes can comprise an important background for $\nu_\mu \to \nu_e$ appearance searches in some detectors and thus have become the focus of recent experimental investigations, most notably in NOMAD [114] and T2K [115, 116]. There have also been several recent measurements of kaon final states produced in neutrino NC and CC scattering in MINERvA [117–119] that are providing needed background constraints for certain nucleon decay searches.

52.4 Outlook

Neutrino experiments continue to produce critical neutrino scattering measurements on nuclei as they accumulate increased statistics and pursue new ways of reporting their measurements. Analysis of a broad energy range of data from MINERvA is providing some of the most detailed analysis of nuclear effects in neutrino interactions by examining multiple nuclei in a single experiment. Data from ArgoNeuT and MicroBooNE (and soon also ICARUS and SBND) are probing deeper into complex neutrino final states using the superior capabilities of liquid argon time projection chambers, while the T2K and NOvA near detectors continue to collect high statistics samples in intense neutrino beams. Together with dedicated discussions between experiments on how best to report neutrino cross section measurements [120] and with accompanying work being advanced by theorists to further improve nuclear model calculations [4], we are starting to significantly advance our understanding of neutrino-nucleus scattering.

52.5 Acknowledgments

The author thanks Anne Schukraft (Fermilab) for help in preparing the plots and content of this review.

Downloaded from https://academic.oup.com/ptep/article/2022/8/083C01/6651666 by KIT Library user on 27 September 2022

References

[1] O. Benhar *et al.*, Phys. Rept. **700**, 1 (2017), [arXiv:1501.06448].

[2] M. A. Acero *et al.* (NOvA, R. Group), Eur. Phys. J. C **80**, 12, 1119 (2020), [arXiv:2006.08727].

[3] J. A. Formaggio and G. P. Zeller, Rev. Mod. Phys. **84**, 1307 (2012), [arXiv:1305.7513].

[4] L. Alvarez-Ruso *et al.*, Prog. Part. Nucl. Phys. **100**, 1 (2018), [arXiv:1706.03621].

[5] M. Tzanov *et al.* (NuTeV), Phys. Rev. **D74**, 012008 (2006), [hep-ex/0509010].

[6] C. Anderson *et al.* (ArgoNeuT), Phys. Rev. Lett. **108**, 161802 (2012), [arXiv:1111.0103].

[7] R. Acciarri *et al.* (ArgoNeuT), Phys. Rev. **D89**, 11, 112003 (2014), [arXiv:1404.4809].

[8] P. Abratenko *et al.* (MicroBooNE), Phys. Rev. Lett. **123**, 13, 131801 (2019), [arXiv:1905.09694].

[9] P. A. Rodrigues *et al.* (MINERvA), Phys. Rev. Lett. **116**, 071802 (2016), [Addendum: Phys. Rev. Lett.121,no.20,209902(2018)], [arXiv:1511.05944].

[10] A. Filkins *et al.* (MINERvA), Phys. Rev. D **101**, 11, 112007 (2020), [arXiv:2002.12496].

[11] D. Ruterbories *et al.* (MINERvA) (2021), [arXiv:2106.16210].

[12] A. Hiramoto *et al.* (NINJA), Phys. Rev. D **102**, 7, 072006 (2020), [arXiv:2008.03895].

[13] K. Abe *et al.* (T2K), Phys. Rev. **D87**, 9, 092003 (2013), [arXiv:1302.4908].

[14] K. Abe *et al.* (T2K), Phys. Rev. **D98**, 012004 (2018), [arXiv:1801.05148].

[15] K. Abe *et al.* (T2K), Phys. Rev. **D96**, 5, 052001 (2017), [arXiv:1706.04257].

[16] B. G. Tice *et al.* (MINERvA), Phys. Rev. Lett. **112**, 23, 231801 (2014), [arXiv:1403.2103].

[17] J. Mousseau *et al.* (MINERvA), Phys. Rev. **D93**, 7, 071101 (2016), [arXiv:1601.06313].

[18] M. Sajjad Athar and J. G. Morfín, J. Phys. G **48**, 3, 034001 (2021), [arXiv:2006.08603].

[19] A. Kayis-Topaksu *et al.* (CHORUS), Nucl. Phys. **B798**, 1 (2008), [arXiv:0804.1869].

[20] O. Samoylov *et al.* (NOMAD), Nucl. Phys. **B876**, 339 (2013), [arXiv:1308.4750].

[21] D. Mason *et al.* (NuTeV), Phys. Rev. Lett. **99**, 192001 (2007).

[22] P. Abratenko *et al.* ((MicroBooNE Collaboration)*, MicroBooNE), Phys. Rev. D **104**, 5, 052002 (2021), [arXiv:2101.04228].

[23] K. Abe *et al.* (T2K), Phys. Rev. Lett. **113**, 24, 241803 (2014), [arXiv:1407.7389].

[24] K. Abe *et al.* (T2K), Phys. Rev. **D91**, 112010 (2015), [arXiv:1503.08815].

[25] K. Abe *et al.* (T2K), JHEP **10**, 114 (2020), [arXiv:2002.11986].

[26] C. Adams *et al.* (MicroBooNE), Eur. Phys. J. **C79**, 3, 248 (2019), [arXiv:1805.06887].

[27] J. Devan *et al.* (MINERvA), Phys. Rev. **D94**, 11, 112007 (2016), [arXiv:1610.04746].

[28] L. Ren *et al.* (MINERvA), Phys. Rev. **D95**, 7, 072009 (2017), [Addendum: Phys. Rev.D97,no.1,019902(2018)], [arXiv:1701.04857].

[29] P. Adamson *et al.* (MINOS), Phys. Rev. **D81**, 072002 (2010), [arXiv:0910.2201].

[30] Q. Wu *et al.* (NOMAD), Phys. Lett. **B660**, 19 (2008), [arXiv:0711.1183].

[31] Y. Nakajima *et al.* (SciBooNE), Phys. Rev. **D83**, 012005 (2011), [arXiv:1011.2131].

[32] K. Abe *et al.* (T2K), Phys. Rev. **D90**, 5, 052010 (2014), [arXiv:1407.4256].

[33] K. Abe *et al.* (T2K), Phys. Rev. **D93**, 7, 072002 (2016), [arXiv:1509.06940].

[34] K. Abe *et al.* (T2K), PTEP **2019**, 9, 093C02 (2019), [arXiv:1904.09611].

[35] D. Ruterbories *et al.* (MINERvA), Phys. Rev. **D99**, 1, 012004 (2019), [arXiv:1811.02774].

[36] C. E. Patrick *et al.* (MINERvA), Phys. Rev. **D97**, 5, 052002 (2018), [arXiv:1801.01197].

[37] M. F. Carneiro *et al.* (MINERvA), Phys. Rev. Lett. **124**, 12, 121801 (2020), [arXiv:1912.09890].

[38] T. Cai *et al.* (MINERvA), Phys. Rev. D **101**, 9, 092001 (2020), [arXiv:1910.08658].

[39] X. G. Lu *et al.* (MINERvA), Phys. Rev. Lett. **121**, 2, 022504 (2018), [arXiv:1805.05486].

[40] A. A. Aguilar-Arevalo *et al.* (MiniBooNE), Phys. Rev. **D81**, 092005 (2010), [arXiv:1002.2680].

[41] A. A. Aguilar-Arevalo *et al.* (MiniBooNE), Phys. Rev. **D88**, 3, 032001 (2013), [arXiv:1301.7067].

[42] K. Abe *et al.* (T2K), Phys. Rev. **D93**, 11, 112012 (2016), [arXiv:1602.03652].

[43] K. Abe *et al.* (T2K), Phys. Rev. **D97**, 1, 012001 (2018), [arXiv:1708.06771].

[44] K. Abe *et al.* (T2K), Phys. Rev. D **102**, 1, 012007 (2020), [arXiv:1908.10249].

[45] K. Abe *et al.* (T2K), Phys. Rev. D **101**, 11, 112004 (2020), [arXiv:2004.05434].

[46] K. Abe *et al.* (T2K), Phys. Rev. D **101**, 11, 112001 (2020), [arXiv:2002.09323].

[47] P. Abratenko *et al.* (MicroBooNE), Phys. Rev. D **102**, 11, 112013 (2020), [arXiv:2010.02390].

[48] P. Abratenko *et al.* (MicroBooNE), Phys. Rev. Lett. **125**, 20, 201803 (2020), [arXiv:2006.00108].

[49] K. Mahn, C. Marshall and C. Wilkinson, Ann. Rev. Nucl. Part. Sci. **68**, 105 (2018), [arXiv:1803.08848].

[50] R. Acciarri *et al.* (ArgoNeuT), Phys. Rev. **D90**, 1, 012008 (2014), [arXiv:1405.4261].

[51] R. Gran *et al.* (K2K), Phys. Rev. **D74**, 052002 (2006), [hep-ex/0603034].

[52] G. A. Fiorentini *et al.* (MINERvA), Phys. Rev. Lett. **111**, 022502 (2013), [arXiv:1305.2243].

[53] L. Fields *et al.* (MINERvA), Phys. Rev. Lett. **111**, 2, 022501 (2013), [arXiv:1305.2234].

[54] T. Walton *et al.* (MINERvA), Phys. Rev. **D91**, 7, 071301 (2015), [arXiv:1409.4497].

[55] R. Gran *et al.* (MINERvA), Phys. Rev. Lett. **120**, 22, 221805 (2018), [arXiv:1803.09377].

[56] M. Betancourt *et al.* (MINERvA), Phys. Rev. Lett. **119**, 8, 082001 (2017), [arXiv:1705.03791].

[57] J. Wolcott *et al.* (MINERvA), Phys. Rev. Lett. **116**, 8, 081802 (2016), [arXiv:1509.05729].

[58] A. A. Aguilar-Arevalo *et al.* (MiniBooNE), Phys. Rev. Lett. **100**, 032301 (2008), [arXiv:0706.0926].

[59] A. A. Aguilar-Arevalo *et al.* (MiniBooNE), Phys. Rev. **D82**, 092005 (2010), [arXiv:1007.4730].

[60] A. A. Aguilar-Arevalo *et al.* (MiniBooNE), Phys. Rev. **D91**, 1, 012004 (2015), [arXiv:1309.7257].

[61] P. Adamson *et al.* (MINOS), Phys. Rev. **D91**, 1, 012005 (2015), [arXiv:1410.8613].

[62] V. Lyubushkin *et al.* (NOMAD), Eur. Phys. J. **C63**, 355 (2009), [arXiv:0812.4543].

Downloaded from https://academic.oup.com/ptep/article/2022/8/083C01/6651666 by KIT Library user on 27 September 2022

[63] L. Wan *et al.* (Super-Kamiokande), Phys. Rev. **D99**, 3, 032005 (2019), [arXiv:1901.05281].

[64] K. Abe *et al.* (T2K), Phys. Rev. **D91**, 11, 112002 (2015), [arXiv:1503.07452].

[65] K. Abe *et al.* (T2K), Phys. Rev. **D92**, 11, 112003 (2015), [arXiv:1411.6264].

[66] K. Abe *et al.* (T2K), Phys. Rev. **D90**, 7, 072012 (2014), [arXiv:1403.3140].

[67] K. Abe *et al.* (T2K), Phys. Rev. **D98**, 3, 032003 (2018), [arXiv:1802.05078].

[68] J. Carlson *et al.*, Phys. Rev. **C65**, 024002 (2002), [arXiv:nucl-th/0106047].

[69] H. Gallagher, G. Garvey and G. P. Zeller, Ann. Rev. Nucl. Part. Sci. **61**, 355 (2011).

[70] G. T. Garvey *et al.*, Phys. Rept. **580**, 1 (2015), [arXiv:1412.4294].

[71] O. Palamara (ArgoNeuT), JPS Conf. Proc. **12**, 010017 (2016).

[72] M. Elkins *et al.* (MINERvA), Phys. Rev. **D100**, 5, 052002 (2019), [arXiv:1901.04892].

[73] L. A. Ahrens *et al.*, Phys. Rev. **D35**, 785 (1987).

[74] J. Brunner *et al.* (SKAT), Z. Phys. **C45**, 551 (1990).

[75] V. V. Ammosov *et al.*, Z. Phys. **C36**, 377 (1987); O. Erriquez *et al.*, Phys. Lett. **70B**, 383 (1977); T. Eichten *et al.*, Phys. Lett. **40B**, 593 (1972).

[76] C. Wilkinson *et al.*, Phys. Rev. **D90**, 11, 112017 (2014), [arXiv:1411.4482].

[77] A. S. Meyer *et al.*, Phys. Rev. **D93**, 11, 113015 (2016), [arXiv:1603.03048].

[78] P. Rodrigues, C. Wilkinson and K. McFarland, Eur. Phys. J. **C76**, 8, 474 (2016), [arXiv:1601.01888].

[79] R. Acciarri *et al.* (ArgoNeuT), Phys. Rev. Lett. **113**, 26, 261801 (2014), [erratum: Phys. Rev. Lett.114,no.3,039901(2015)], [arXiv:1408.0598].

[80] R. Acciarri *et al.* (ArgoNeuT), Phys. Rev. D **98**, 5, 052002 (2018), [arXiv:1804.10294].

[81] R. Acciarri *et al.* (ArgoNeuT), Phys. Rev. **D96**, 1, 012006 (2017), [arXiv:1511.00941].

[82] A. Rodriguez *et al.* (K2K), Phys. Rev. **D78**, 032003 (2008), [arXiv:0805.0186].

[83] M. Hasegawa *et al.* (K2K), Phys. Rev. Lett. **95**, 252301 (2005), [hep-ex/0506008].

[84] C. Mariani *et al.* (K2K), Phys. Rev. **D83**, 054023 (2011), [arXiv:1012.1794].

[85] S. Nakayama *et al.* (K2K), Phys. Lett. **B619**, 255 (2005), [hep-ex/0408134].

[86] C. Adams *et al.* (MicroBooNE), Phys. Rev. **D99**, 9, 091102 (2019), [arXiv:1811.02700].

[87] B. Eberly *et al.* (MINERvA), Phys. Rev. **D92**, 9, 092008 (2015), [arXiv:1406.6415].

[88] C. L. McGivern *et al.* (MINERvA), Phys. Rev. **D94**, 5, 052005 (2016), [arXiv:1606.07127].

[89] A. Higuera *et al.* (MINERvA), Phys. Rev. Lett. **113**, 26, 261802 (2014), [arXiv:1409.3835].

[90] T. Le *et al.* (MINERvA), Phys. Rev. **D100**, 5, 052008 (2019), [arXiv:1906.08300].

[91] A. Mislivec *et al.* (MINERvA), Phys. Rev. **D97**, 3, 032014 (2018), [arXiv:1711.01178].

[92] T. Le *et al.* (MINERvA), Phys. Rev. D **100**, 5, 052008 (2019), [arXiv:1906.08300].

[93] T. Le *et al.* (MINERvA), Phys. Lett. **B749**, 130 (2015), [arXiv:1503.02107].

[94] O. Altinok *et al.* (MINERvA), Phys. Rev. **D96**, 7, 072003 (2017), [arXiv:1708.03723].

[95] D. Coplowe *et al.* (MINERvA), Phys. Rev. D **102**, 7, 072007 (2020), [arXiv:2002.05812].

[96] J. Wolcott *et al.* (MINERvA), Phys. Rev. Lett. **117**, 11, 111801 (2016), [arXiv:1604.01728].

[97] A. A. Aguilar-Arevalo *et al.* (MiniBooNE), Phys. Rev. **D83**, 052007 (2011), [arXiv:1011.3572].

[98] A. A. Aguilar-Arevalo *et al.* (MiniBooNE), Phys. Rev. Lett. **103**, 081801 (2009), [arXiv:0904.3159].

[99] A. A. Aguilar-Arevalo *et al.* (MiniBooNE), Phys. Rev. **D83**, 052009 (2011), [arXiv:1010.3264].

[100] A. A. Aguilar-Arevalo *et al.* (MiniBooNE), Phys. Rev. **D81**, 013005 (2010), [arXiv:0911.2063].

[101] A. A. Aguilar-Arevalo *et al.* (MiniBooNE), Phys. Lett. **B664**, 41 (2008), [arXiv:0803.3423].

[102] P. Adamson *et al.* (MINOS), Phys. Rev. **D94**, 7, 072006 (2016), [arXiv:1608.05702].

[103] C. T. Kullenberg *et al.* (NOMAD), Phys. Lett. **B682**, 177 (2009), [arXiv:0910.0062].

[104] M. A. Acero *et al.* (NOvA), Phys. Rev. D **102**, 1, 012004 (2020), [arXiv:1902.00558].

[105] K. Hiraide *et al.* (SciBooNE), Phys. Rev. **D78**, 112004 (2008), [arXiv:0811.0369].

[106] Y. Kurimoto *et al.* (SciBooNE), Phys. Rev. **D81**, 033004 (2010), [arXiv:0910.5768].

[107] Y. Kurimoto *et al.* (SciBooNE), Phys. Rev. **D81**, 111102 (2010), [arXiv:1005.0059].

[108] K. Abe *et al.* (T2K), Phys. Rev. **D95**, 1, 012010 (2017), [arXiv:1605.07964].

[109] K. Abe *et al.* (T2K), Phys. Rev. Lett. **117**, 19, 192501 (2016), [arXiv:1604.04406].

[110] K. Abe *et al.* (T2K), Phys. Rev. D **101**, 1, 012007 (2020), [arXiv:1909.03936].

[111] K. Abe *et al.* (T2K), Phys. Rev. D **103**, 11, 112009 (2021), [arXiv:2102.03346].

[112] P. Vilain *et al.* (CHARM-II), Phys. Lett. **B313**, 267 (1993); A compilation of historical coherent pion production data.

[113] P. Stowell *et al.* (MINERvA), Phys. Rev. **D100**, 7, 072005 (2019), [arXiv:1903.01558].

[114] C. T. Kullenberg *et al.* (NOMAD), Phys. Lett. **B706**, 268 (2012), [arXiv:1111.3713].

[115] K. Abe *et al.* (T2K), J. Phys. **G46**, 8, 08LT01 (2019), [arXiv:1902.03848].

[116] K. Abe *et al.* (T2K), Phys. Rev. D **100**, 11, 112009 (2019), [arXiv:1910.09439].

[117] C. M. Marshall *et al.* (MINERvA), Phys. Rev. **D94**, 1, 012002 (2016), [arXiv:1604.03920].

[118] C. M. Marshall *et al.* (MINERvA), Phys. Rev. Lett. **119**, 1, 011802 (2017), [arXiv:1611.02224].

[119] Z. Wang *et al.* (MINERvA), Phys. Rev. Lett. **117**, 6, 061802 (2016), [arXiv:1606.08890].

[120] M. Betancourt *et al.*, Phys. Rept. **773-774**, 1 (2018), [arXiv:1805.07378].

Downloaded from https://academic.oup.com/ptep/article/2022/8/083C01/6651666 by KIT Library user on 27 September 2022

53. Plots of Cross Sections and Related Quantities

Updated in 2021. See various sections for details.

53.1 Pseudorapidity Distributions in pp and $\overline{p}p$ Interactions . . . 770
53.2 Average Hadron Multiplicities in Hadronic e^+e^- Annihilation Events . . . 771
53.3 σ and R in e^+e^- Collisions . . . 773
53.4 Annihilation Cross Section Near M_Z . . . 775
53.5 Total Hadronic Cross Sections . . . 776

53.1 Pseudorapidity Distributions in pp and $\overline{p}p$ Interactions

Revised August 2013 by D.R. Ward (Cavendish Lab.).

Pseudorapidity Distributions in pp and $\overline{p}p$ Interactions

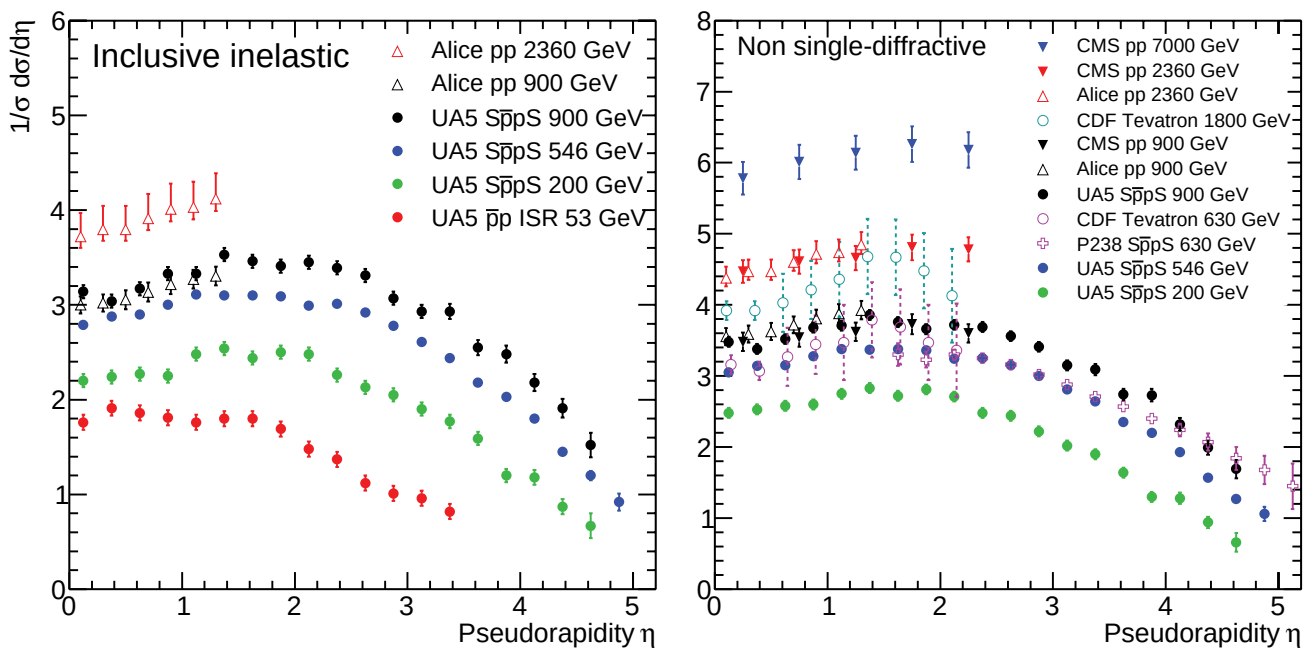

Figure 53.1: Charged particle pseudorapidity distributions in $p\overline{p}$ collisions for 53 GeV $\leq \sqrt{s} \leq$ 1800 GeV. UA5 data from the S$p\overline{p}$S are taken from [1], and from the ISR from [2]. The UA5 data are shown for both the full inelastic cross-section and with singly diffractive events excluded. Additional non single-diffractive measurements are available from CDF at the Tevatron [3] and from P238 at the S$p\overline{p}$S [4]. These may be compared with both inclusive and non single-diffractive measurements in pp collisions at the LHC from ALICE [5] and for non single-diffractive interactions from CMS [6, 7]. (Courtesy of D.R. Ward, Cambridge Univ., 2013)

Downloaded from https://academic.oup.com/ptep/article/2022/8/083C01/6651666 by KIT Library user on 27 September 2022

53.2 Average Hadron Multiplicities in Hadronic e^+e^- Annihilation Events

Revised August 2021 by O. Biebel (Ludwig-Maximilians U.).

Table 53.1: Average hadron multiplicities per hadronic e^+e^- annihilation event at $\sqrt{s} \approx 10$, 29–35, 91, and 130–200 GeV. The rates given include decay products from resonances with $c\tau < 10$ cm, and include the corresponding anti-particle state. Correlations of the systematic uncertainties were considered for the calculation of the averages. Quoted errors are not increased by scale factor S.

Particle	$\sqrt{s} \approx 10$ GeV	$\sqrt{s} = 29$–35 GeV	$\sqrt{s} = 91$ GeV	$\sqrt{s} = 130$–200 GeV	References
Pseudoscalar mesons:					
π^+	6.52 ± 0.11	0.3 ± 0.4	17.02 ± 0.19	21.24 ± 0.39	[8–17]
π^0	3.2 ± 0.3	5.83 ± 0.28	9.42 ± 0.32		[12, 18–23]
K^+	0.953 ± 0.018	1.48 ± 0.09	2.228 ± 0.059	2.82 ± 0.19	[9–17, 24, 25]
K^0	0.91 ± 0.05	1.48 ± 0.07	2.049 ± 0.026	2.10 ± 0.12	[12, 17, 20, 26–36]
η	0.20 ± 0.04	0.61 ± 0.07	1.049 ± 0.080		[12, 18, 19, 22, 23, 37–40]
$\eta\prime(958)$	0.03 ± 0.01	0.26 ± 0.10	0.152 ± 0.020		[20, 39, 41–43]
D^+	$0.194 \pm 0.019^{(a)}$	0.17 ± 0.03	0.175 ± 0.016		[12, 44–47]
D^0	$0.446 \pm 0.032^{(a)}$	0.45 ± 0.07	0.454 ± 0.030		[12, 44–47]
D_s^+	$0.063 \pm 0.014^{(a)}$	$0.45 \pm 0.20^{(b)}$	0.131 ± 0.021		[8, 39, 44, 47–49]
$B^{(c)}$	—	—	$0.134 \pm 0.016^{(d)}$		[46, 50]
B^+	—	—	$0.141 \pm 0.004^{(d)}$		[51]
B_s^0	—	—	$0.054 \pm 0.011^{(d)}$		[52, 53]
Scalar mesons:					
$f_0(980)$	0.024 ± 0.006	$0.05 \pm 0.02^{(e)}$	0.146 ± 0.012		[41, 54–56]
$a_0(980)^\pm$	—	—	$0.27 \pm 0.11^{(f)}$		[43]
Vector mesons:					
$\rho(770)^0$	0.35 ± 0.04	0.81 ± 0.08	1.231 ± 0.098		[9, 12, 55, 57, 58]
$\rho(770)^\pm$	—	—	$2.40 \pm 0.43^{(f)}$		[43]
$\omega(782)$	0.30 ± 0.08	—	1.016 ± 0.065		[40, 42, 43, 57]
$K^*(892)^+$	0.27 ± 0.03	0.64 ± 0.05	0.714 ± 0.055		[9, 12, 33, 57, 59, 60]
$K^*(892)^0$	0.29 ± 0.03	0.56 ± 0.06	0.738 ± 0.024		[9, 12, 36, 57, 58, 61, 62]
$\phi(1020)$	0.044 ± 0.003	0.085 ± 0.011	0.0963 ± 0.0032		[12, 36, 56–58, 61]
$D^*(2010)^+$	$0.177 \pm 0.022^{(a)}$	0.43 ± 0.07	$0.1937 \pm 0.0057^{(g)}$		[12, 44–46, 63, 64]
$D^*(2007)^0$	$0.168 \pm 0.019^{(a)}$	0.27 ± 0.11	—		[12, 44, 45]
$D_s^*(2112)^+$	$0.048 \pm 0.014^{(a)}$	—	$0.101 \pm 0.048^{(h)}$		[48, 65]
$B^{*\ (i)}$	—	—	0.288 ± 0.026		[66, 67]
$J/\psi(1S)$	$0.00050 \pm 0.00005^{(a)}$	—	$0.0052 \pm 0.0004^{(j)}$		[68–73]
$\psi(2S)$	—	—	$0.0023 \pm 0.0004^{(j)}$		[71, 73, 74]
$\Upsilon(1S)$	—	—	$0.00014 \pm 0.00007^{(j)}$		[75]
Pseudovector mesons:					
$f_1(1285)$	—	—	0.165 ± 0.051		[76]
$f_1(1420)$	—	—	0.056 ± 0.012		[76]
$\chi_{c1}(3510)$	—	—	$0.0041 \pm 0.0011^{(j)}$		[71, 74]
Tensor mesons:					
$f_2(1270)$	0.09 ± 0.02	0.14 ± 0.04	0.166 ± 0.020		[54–56, 77]
$f_2'(1525)$	—	—	0.012 ± 0.006		[55]
$K_2^*(1430)^+$	—	0.09 ± 0.03	—		[55, 78]
$K_2^*(1430)^0$	—	0.12 ± 0.06	0.084 ± 0.022		[54, 55, 79]
$B^{**\ (k)}$	—	—	0.118 ± 0.024		[80]
$D_{s1}^\pm$	—	—	$0.0052 \pm 0.0011^{(\ell)}$		[81]
$D_{s2}^{*\pm}$	—	—	$0.0083 \pm 0.0031^{(\ell)}$		[81]
Baryons:					
p	0.266 ± 0.008	0.640 ± 0.050	1.050 ± 0.032	1.41 ± 0.18	[10, 13–17, 24, 25, 77]
Λ	$0.093 \pm 0.006^{(a)}$	0.205 ± 0.010	0.3915 ± 0.0065	0.39 ± 0.03	[17, 20, 34, 36, 77, 82–85]
Σ^0	$0.0221 \pm 0.0018^{(a)}$	—	0.078 ± 0.010		[10, 59, 82, 86–88]
Σ^-	—	—	0.081 ± 0.010		[88, 89]
Σ^+	—	—	0.107 ± 0.011		[87, 88]
$\Sigma^\pm$	—	—	0.174 ± 0.009		[84, 88]
Ξ^-	$0.0055 \pm 0.0004^{(a)}$	0.0176 ± 0.0027	0.0262 ± 0.0009		[9, 59, 77, 82–85]
$\Delta(1232)^{++}$	0.040 ± 0.010	—	0.085 ± 0.014		[90–92]
$\Sigma(1385)^-$	0.006 ± 0.002	0.017 ± 0.004	0.0240 ± 0.0017		[59, 82, 84, 85, 93]
$\Sigma(1385)^+$	$0.0062 \pm 0.0011^{(a)}$	0.017 ± 0.004	0.0239 ± 0.0015		[59, 82–85, 93]
$\Sigma(1385)^\pm$	0.0106 ± 0.0020	0.033 ± 0.008	0.0472 ± 0.0027		[59, 82, 84, 85, 93]
$\Xi(1530)^0$	$0.00130 \pm 0.00010^{(a)}$	—	0.00694 ± 0.00049		[59, 82, 83, 85, 94]
Ω^-	$0.00060 \pm 0.00033^{(a)}$	0.014 ± 0.007	0.00124 ± 0.00018		[59, 77, 82, 83, 85, 86]
Λ_c^+	$0.0479 \pm 0.0038^{(a,m)}$	0.110 ± 0.050	0.078 ± 0.017		[47, 49, 77, 83, 95]
Λ_b^0	—	—	0.031 ± 0.016		[96]
Σ_c^0	$0.0025 \pm 0.0004^{(a)}$	—	—		[83]
$\Lambda(1520)$	$0.0046 \pm 0.0004^{(a)}$	—	0.0222 ± 0.0027		[83, 85, 89, 97]

$(a)\sigma_{\rm had} = 3.33 \pm 0.05 \pm 0.21$ nb (**CLEO**: [98]) has been used in converting the measured cross sections to average hadron multiplicities.
(b) $\mathrm{B}(D_s \to \eta\pi,\ \eta'\pi)$ was used (RPP 1994).

Downloaded from https://academic.oup.com/ptep/article/2022/8/083C01/6651666 by KIT Library user on 27 September 2022

(c) Comprises both charged and neutral B meson states.
(d) The Standard Model $\mathrm{B}(Z \to b\bar{b}) = 0.217$ was used.
(e) $x_p = p/p_{\mathrm{beam}} > 0.1$ only.
(f) Both charge states.
(g) $\mathrm{B}(D^*(2010)^+ \to D^0\pi^+) \times \mathrm{B}(D^0 \to K^-\pi^+)$ has been used (RPP 2000).
(h) $\mathrm{B}(D_s^* \to D_S^+\gamma)$, $\mathrm{B}(D_s^+ \to \phi\pi^+)$, $\mathrm{B}(\phi \to K^+K^-)$ have been used (RPP 1998).
(i) Any charge state (*i.e.*, B_d^*, B_u^*, or B_s^*).
(j) $\mathrm{B}(Z \to \mathrm{hadrons}) = 0.699$ was used (RPP 1994).
(k) Any charge state (*i.e.*, B_d^{**}, B_u^{**}, or B_s^{**}).
(ℓ) Assumes $\mathrm{B}(D_{s1}^+ \to D^{*+}K^0 + D^{*0}K^+) = 100\%$ and $\mathrm{B}(D_{s2}^+ \to D^0K^+) = 45\%$.
(m) The value was derived from the cross section of $\Lambda_c^+ \to p\pi K$ using (a) and assuming the branching fraction to be $(5.0 \pm 1.3)\%$ (RPP 2004).

References grouped by collaboration for Table-53.1:

- **RPP**: [12]
- **ALEPH**: [13, 20, 40, 58, 59, 63, 70, 81],
- **ARGUS**: [8, 24, 37, 41, 57, 82, 90, 97],
- **BaBar**: [10, 48, 68, 95],
- **Belle**: [44, 69, 83],
- **CELLO**: [19, 26],
- **CLEO**: [9, 45, 49, 98],
- **Crystal Ball**: [38],
- **DELPHI**: [14, 17, 21, 25, 33, 46, 50–52, 55, 61, 66, 71, 76, 80, 84, 86, 89, 91, 94],
- **HRS**: [27, 54, 78, 93],
- **L3**: [22, 34, 42, 67, 72, 74, 87]
- **MARK II**: [29, 39],
- **JADE**: [18, 28],
- **OPAL**: [15, 23, 35, 43, 47, 53, 56, 60, 62, 64, 65, 73, 75, 79, 85, 88, 92, 96],
- **PLUTO**: [30]
- **SLD**: [16, 36],
- **TASSO**: [31]
- **TPC**: [32].

Downloaded from https://academic.oup.com/ptep/article/2022/8/083C01/6651666 by KIT Library user on 27 September 2022

53.3 σ and R in e^+e^- Collisions

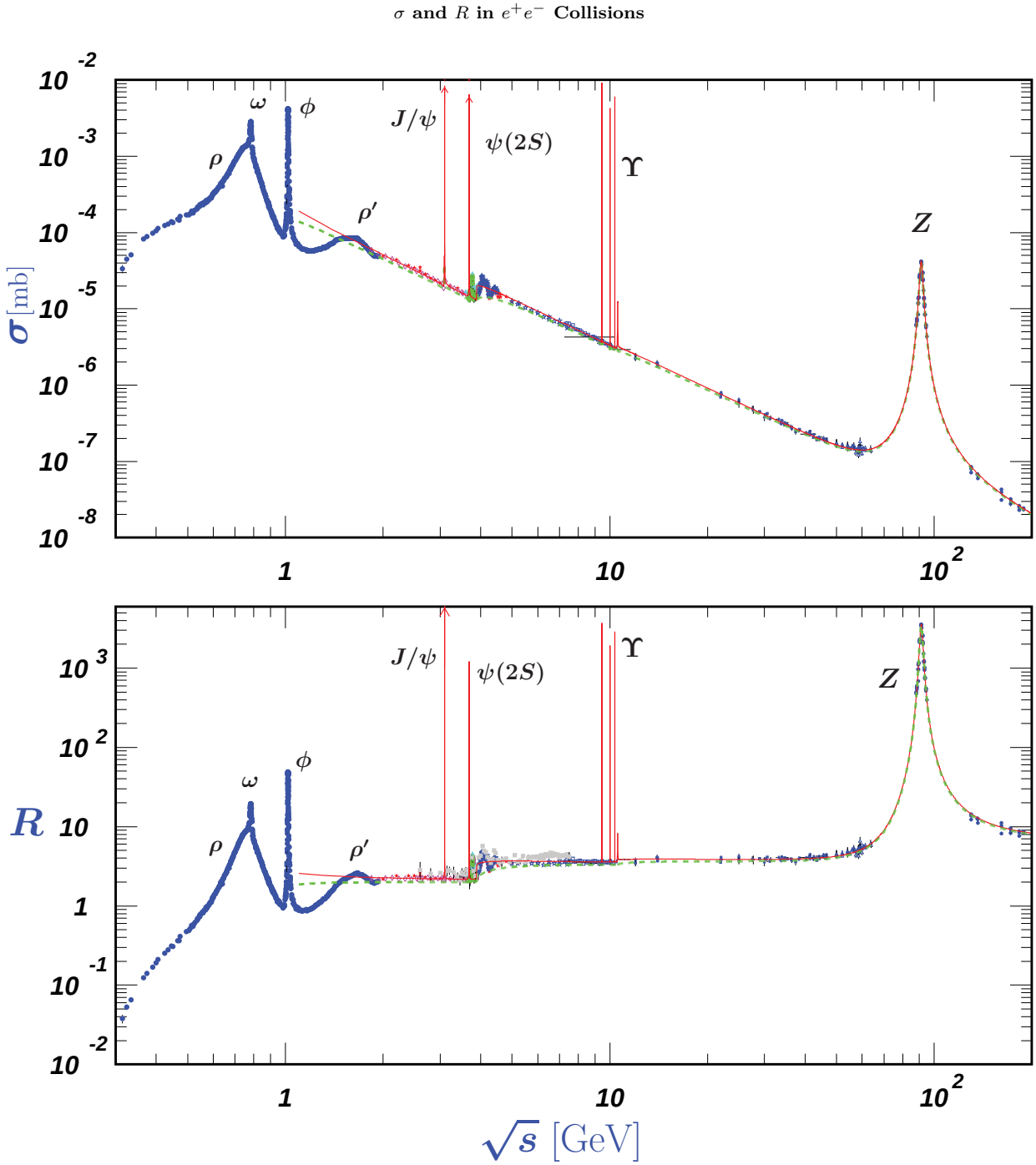

Figure 53.2: World data on the total cross section of $e^+e^- \to hadrons$ and the ratio $R(s) = \sigma(e^+e^- \to hadrons, s)/\sigma(e^+e^- \to \mu^+\mu^-, s)$. $\sigma(e^+e^- \to hadrons, s)$ is the experimental cross section corrected for initial state radiation and electron-positron vertex loops, $\sigma(e^+e^- \to \mu^+\mu^-, s) = 4\pi\alpha^2(s)/3s$. Data errors are total below 2 GeV and statistical above 2 GeV. The curves are an educative guide: the broken one (green) is a naive quark-parton model prediction, and the solid one (red) is 3-loop pQCD prediction (see "Quantum Chromodynamics" section of this *Review*, Eq. (9.7) or, for more details [99], Breit-Wigner parameterizations of J/ψ, $\psi(2S)$, and $\Upsilon(nS), n = 1, 2, 3, 4$ are also shown. The full list of references to the original data and the details of the R ratio extraction from them can be found in [100]. Corresponding computer-readable data files are available at http://pdg.lbl.gov/current/xsect/. (Courtesy of the COMPAS (Protvino) and HEPDATA (Durham) Groups, August 2021. Corrections by P. Janot (CERN) and M. Schmitt (Northwestern U.))

Downloaded from https://academic.oup.com/ptep/article/2022/8/083C01/6651666 by KIT Library user on 27 September 2022

R in Light-Flavor, Charm, and Beauty Threshold Regions

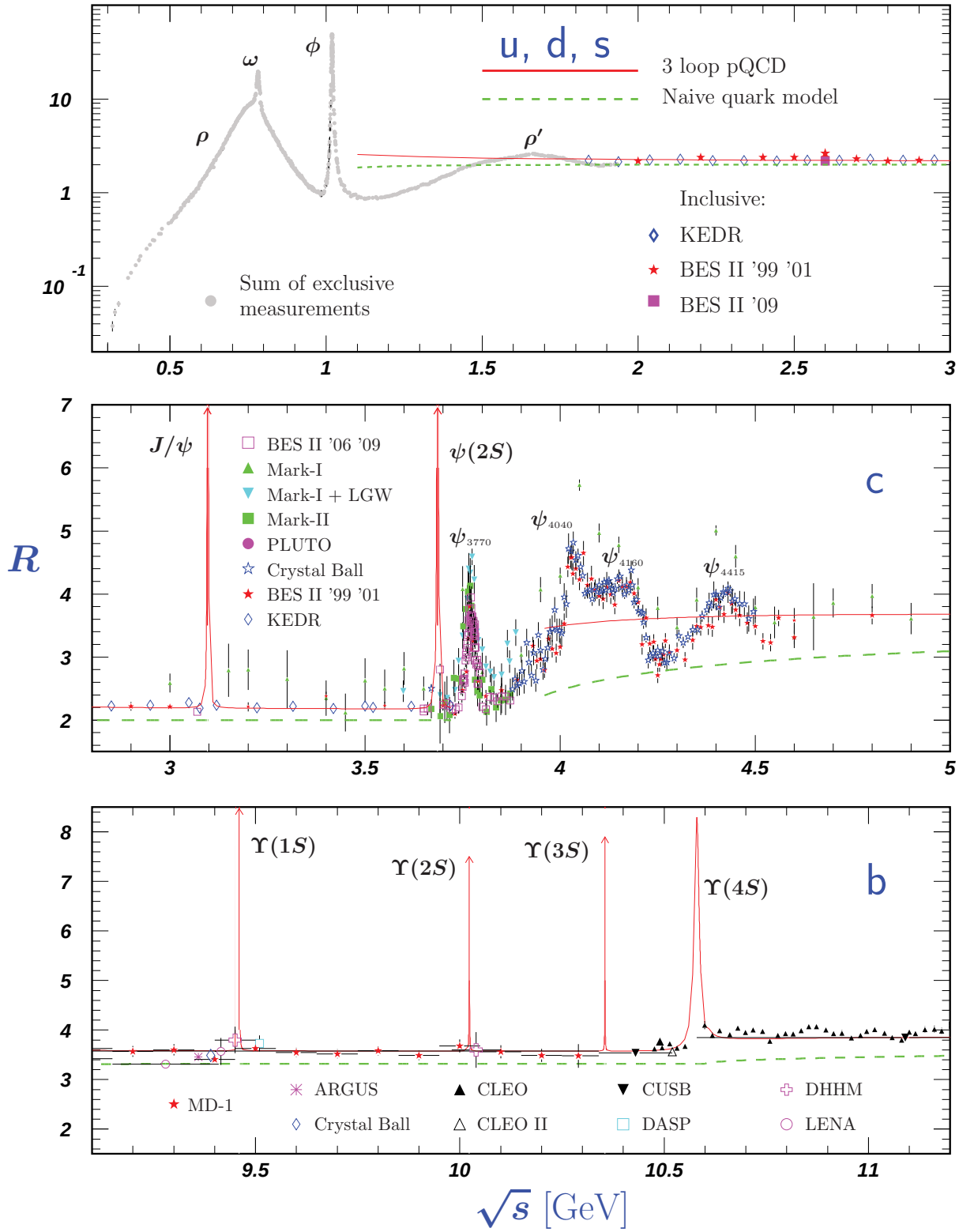

Figure 53.3: R in the light-flavor, charm, and beauty threshold regions. Data errors are total below 2 GeV and statistical above 2 GeV. The curves are the same as in Fig. 53.2. **Note:** CLEO data above $\Upsilon(4S)$ were not fully corrected for radiative effects, and we retain them on the plot only for illustrative purposes with a normalization factor of 0.8. The full list of references to the original data and the details of the R ratio extraction from them can be found in [100]. The computer-readable data are available at http://pdg.lbl.gov/current/xsect/. (Courtesy of the COMPAS (Protvino) and HEPDATA (Durham) Groups, August 2021.)

Downloaded from https://academic.oup.com/ptep/article/2022/8/083C01/6651666 by KIT Library user on 27 September 2022

53.4 Annihilation Cross Section Near M_Z

Courtesy of M. Grünewald and the LEP Electroweak Working Group, 2007.

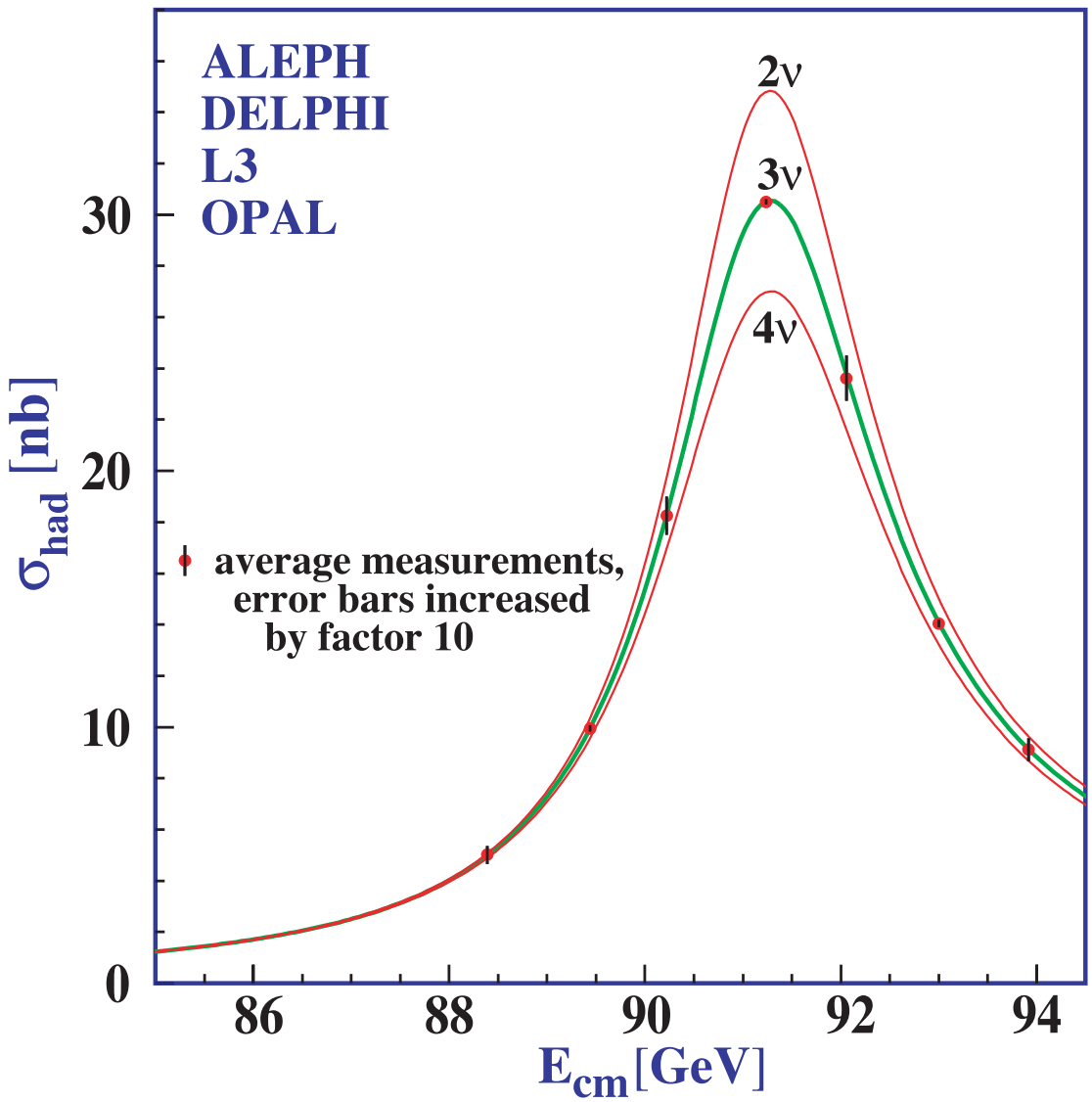

Figure 53.4: Combined data from the ALEPH, DELPHI, L3, and OPAL Collaborations for the cross section in e^+e^- annihilation into hadronic final states as a function of the center-of-mass energy near the Z pole. The curves show the predictions of the Standard Model with two, three, and four species of light neutrinos. The asymmetry of the curve is produced by initial-state radiation. Note that the error bars have been increased by a factor ten for display purposes. References: ALEPH [101], DELPHI [102], L3 [103], OPAL [104], Combination [105],

Downloaded from https://academic.oup.com/ptep/article/2022/8/083C01/6651666 by KIT Library user on 27 September 2022

53.5 Total Hadronic Cross Sections

Revised August 2021 by COMPAS Group (NRC KI – IHEP, Protvino).

There are a significant number of physical quantities extracted from experimental data that are related to the physics of hadronic interactions. Depending on the magnitude of the transverse momenta of particles in the final states, the interactions are either classified as "hard" or "soft". In hard processes, the transverse momenta are comparable in magnitude with the momenta of the initial particles, while in soft processes they are vanishingly small compared to the initial momenta. Soft processes reveal characteristic interference pattern of the scattered states, and are often referred to as diffractive processes. The set of experimentally measured quantities related to diffractive processes include total and elastic cross sections, differential cross sections of elastic scattering and diffraction dissociation processes, as well as secondary quantities such as the slopes of differential cross sections and the ratio of real parts of the scattering amplitude to its imaginary parts (ρ parameter). In this section, plots of total and elastic cross section for various processes are presented. They include the data from purely hadronic collisions such as pp and πp, as well as γp, γd, and $\gamma\gamma$[a]

One of the most important basic notions and tools in general theoretical framework related to the diffractive processes is the notion of the Regge poles, or Reggeons, generalizing a simple one-particle exchange (of Yukawa type) by virtual particles of fixed spin to exchanges by states with "running spin" dependent on the transferred momenta [106, 107]. The simplest case of the one-Reggeon exchange amplitude is given by the amplitude (at high c.m. energy $\sqrt{s}$ and fixed (small) transferred momentum squared, t): $T(s,t) = \beta(t)s^{\alpha(t)}$ which qualitatively exhibits many typical features of generic diffractive processes (e.g. the growth of the interaction radius with energy). In practice the single-pole Reggeon model is insufficient for many diffractive processes but serves as a building block for more sophisticated schemes. Up to now no firm results concerning Regge trajectories $\alpha(t)$ and Regge residues $\beta(t)$ are obtained from the first principles of QCD. Therefore one has to rely on general principles of quantum field theory as a guide. These imply, in particular, that both $\alpha(t)$ and $\beta(t)$ are analytic functions with right cuts from some $t_0 > 0$ to positive infinity.

The theoretical requisite for analyzing diffractive phenomena is therefore represented by various model approaches. The more commonly discussed models in the literatures are:

- **Regge-eikonal approach** [108–115]: this approach automatically satisfies the s-channel unitarity condition and generalizes the impact parameter approximation to the relativistic case. The main element of the model is the Born amplitude defined by one or several leading "Pomeronic" Regge trajectories with intercepts higher than 1. To take into account the difference between C-conjugated processes (such as pp and $\bar{p}p$), a term with an Odderon Reggeon is also added, as well as, if one wishes to describe low (5 to 10 GeV) energies, a secondary Reggeon with low intercepts.
- **Regge pole models with minimal corrections due to two-Reggeon exchanges** [116–118]: in this model, contribution of the leading trajectory in the scattering amplitude is supplemented by a two-Reggeon exchange with an arbitrary coefficient chosen from the fitting details.
- **U-matrix (or "resonance") approach** [119, 120]: the unitarity respecting approach with the scattering amplitude defined by a "U-matrix".
- **Direct functional modelling of the amplitudes with limited Regge trajectories** [121, 122]: this approach appeals to only very general (analytic) properties of the amplitudes leaving aside all dynamical assumptions and mostly aiming at the best phenomenological description of the data.
- **Quasi-classical approach** [123–125]: this model is based on the observation that diffractive processes deal with high quantum numbers, in particular, with large number of virtual quanta.

The ratio $\rho(s) = \mathrm{Re}T(s,0)/\mathrm{Im}T(s,0) = \cot\Phi(s,0)$, where $\Phi(s,0)$ is the phase of the forward scattering amplitude, $T(s,0) = |T(s,0)|\exp(i\Phi(s,0))$, is accessible due to Coulomb-nuclear interference (CNI). There are several different ways to deal with CNI in the literature [126–130]. The value ρ is important for measurements of the total cross-sections as well as for discrimination of different models [131, 132]. The phase $\Phi(s,0)$ starts from π at low energies, evolves further down to $\pi/2$, achieves a shallow minimum and then slowly rise up to $\pi/2$ at asymptotic energies.

The total cross-sections results shown in this review exhibit a common feature: starting from a certain energy (unique for each initial state) the cross-sections begin a slow but steady rise which continue up to several tens of TeV. The current data show the upper bound for total hadronic cross-section is well below the Froissart-Martin asymptotic bound [133, 134], more than 20000 mb at the LHC energies [135].

For readers who are interested in examples of both total and elastic cross section parametrizations and fits, see previous edition of the *Plots of Cross Sections and Related Quantities* review [136]. For the cross section plots shown in the following pages, the example fits are using parametrizations as described in [136] with the fit range starting at about $\sqrt{s} = 5$ GeV.

[a] In spite of its electromagnetic nature the photon interacts with hadron targets as an effective hadron (via transmutation of γ into virtual vector mesons $\rho^0, \omega, \phi, \ldots$).

Downloaded from https://academic.oup.com/ptep/article/2022/8/083C01/6651666 by KIT Library user on 27 September 2022

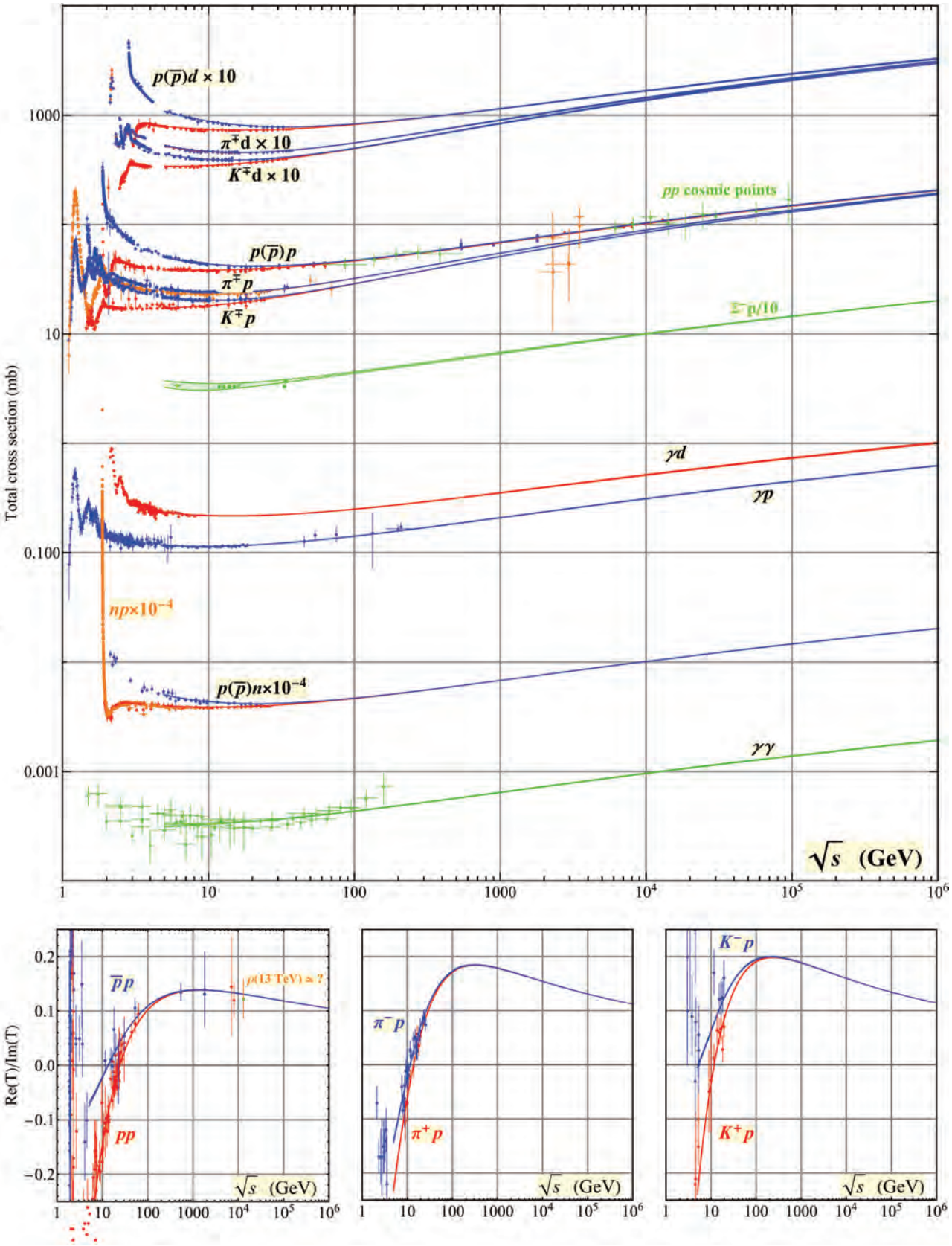

Figure 53.5: Summary of hadronic, γp, γd, and $\gamma\gamma$ total cross sections (top), and ratio of the real to imaginary parts of the forward hadronic amplitudes (bottom). Corresponding computer-readable data files can be found at https://pdg.lbl.gov/current/xsect/. (Courtesy of the COMPAS group, NRC KI – IHEP, Protvino, August 2021.)

Downloaded from https://academic.oup.com/ptep/article/2022/8/083C01/6651666 by KIT Library user on 27 September 2022

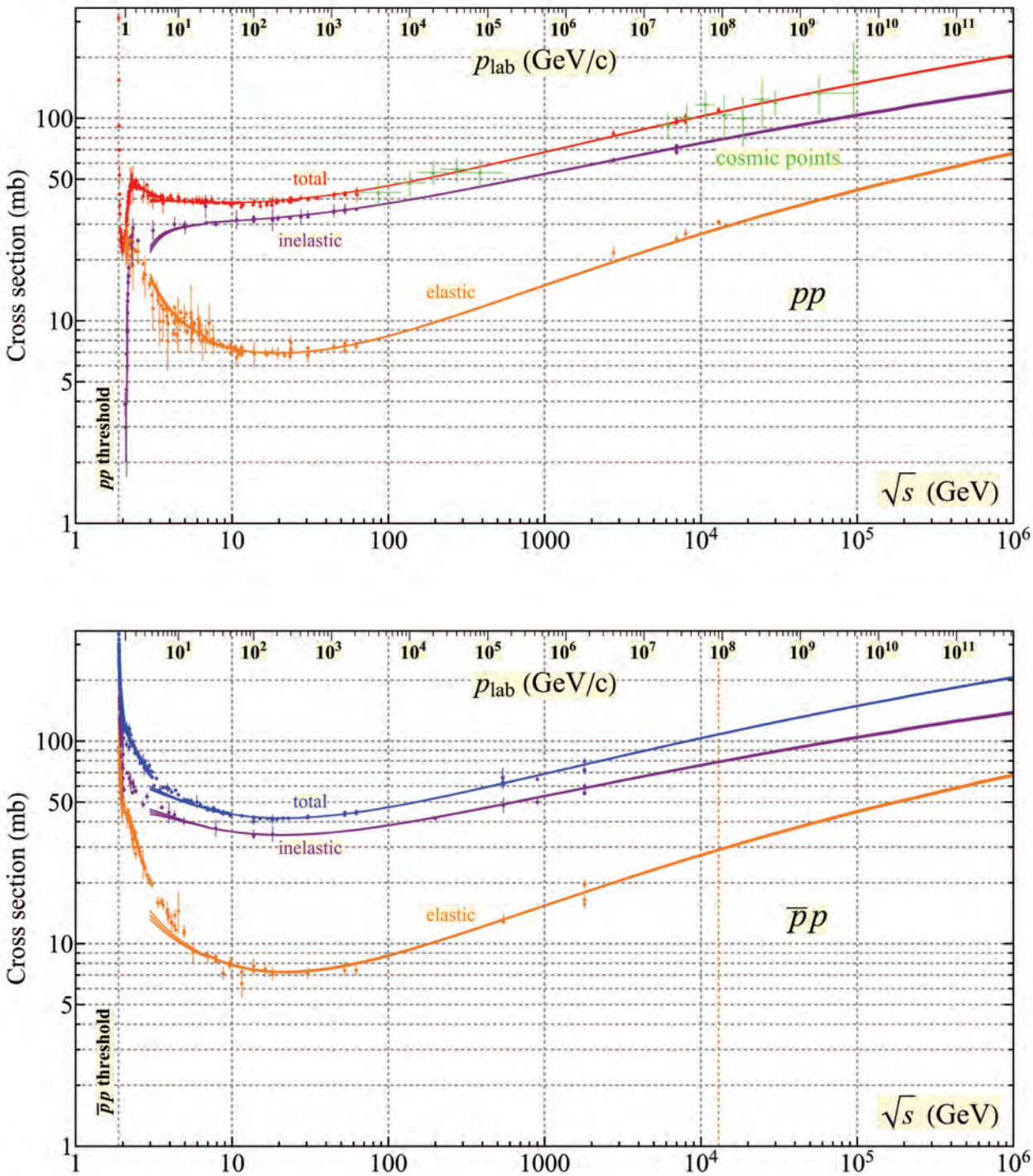

Figure 53.6: Total and elastic cross sections for pp and $\overline{p}p$ collisions as a function of laboratory beam momentum and total center-of-mass energy. $\sigma_{\rm el}$ is computed using the nuclear part of the elastic scattering amplitude [137]. Corresponding computer-readable data files may be found at https://pdg.lbl.gov/current/xsect/. (Courtesy of the COMPAS group, NRC KI – IHEP, Protvino, August 2021.)

Downloaded from https://academic.oup.com/ptep/article/2022/8/083C01/6651666 by KIT Library user on 27 September 2022

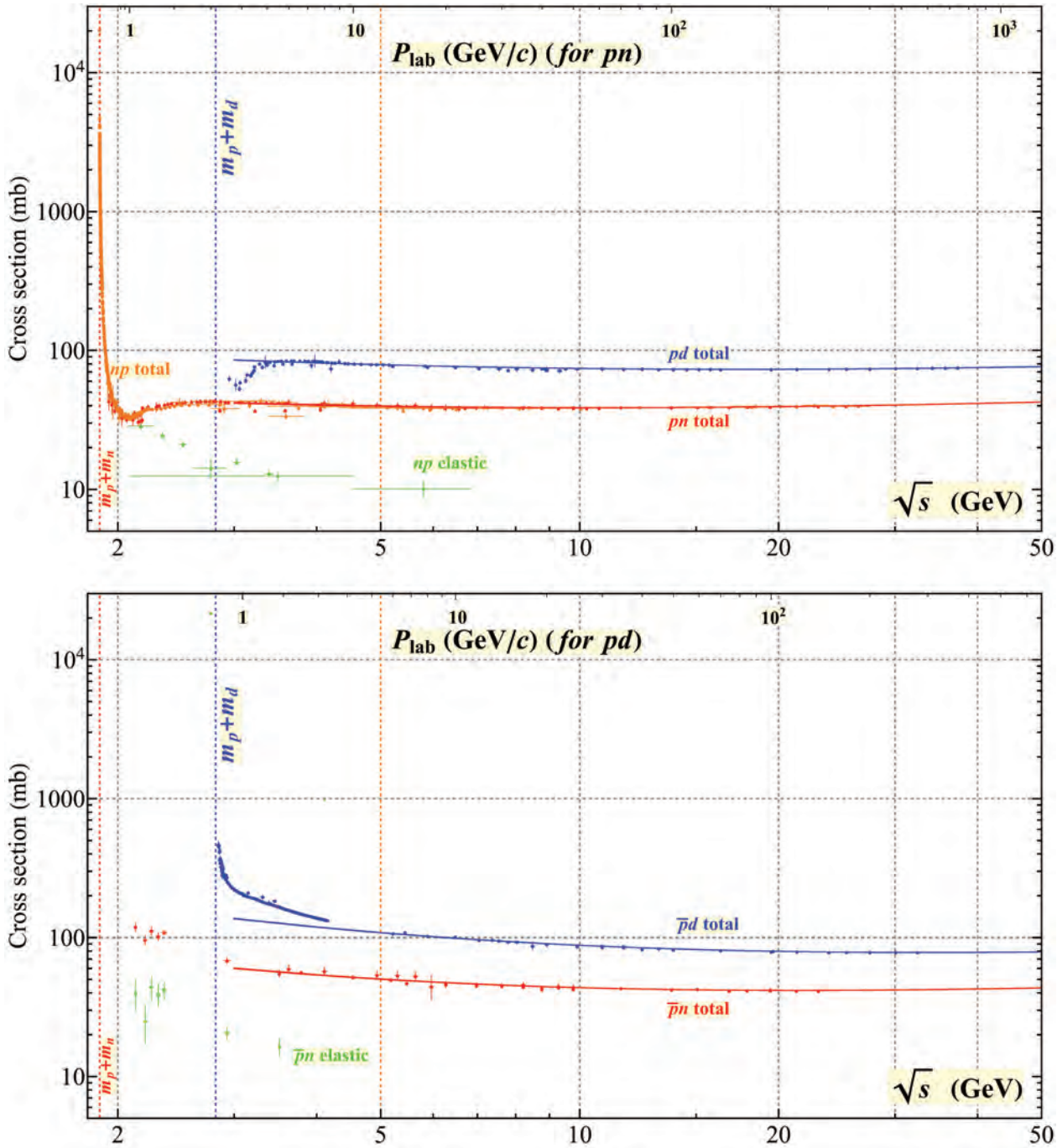

Figure 53.7: Total and elastic cross sections for pd (total only), np, $\bar{p}d$ (total only), and $\bar{p}n$ collisions as a function of laboratory beam momentum and total center-of-mass energy. Corresponding computer-readable data files may be found at https://pdg.lbl.gov/current/xsect/. (Courtesy of the COMPAS Group, NRC KI – IHEP, Protvino, August 2021. Corrections by N. Otsuka (IAEA))

Downloaded from https://academic.oup.com/ptep/article/2022/8/083C01/6651666 by KIT Library user on 27 September 2022

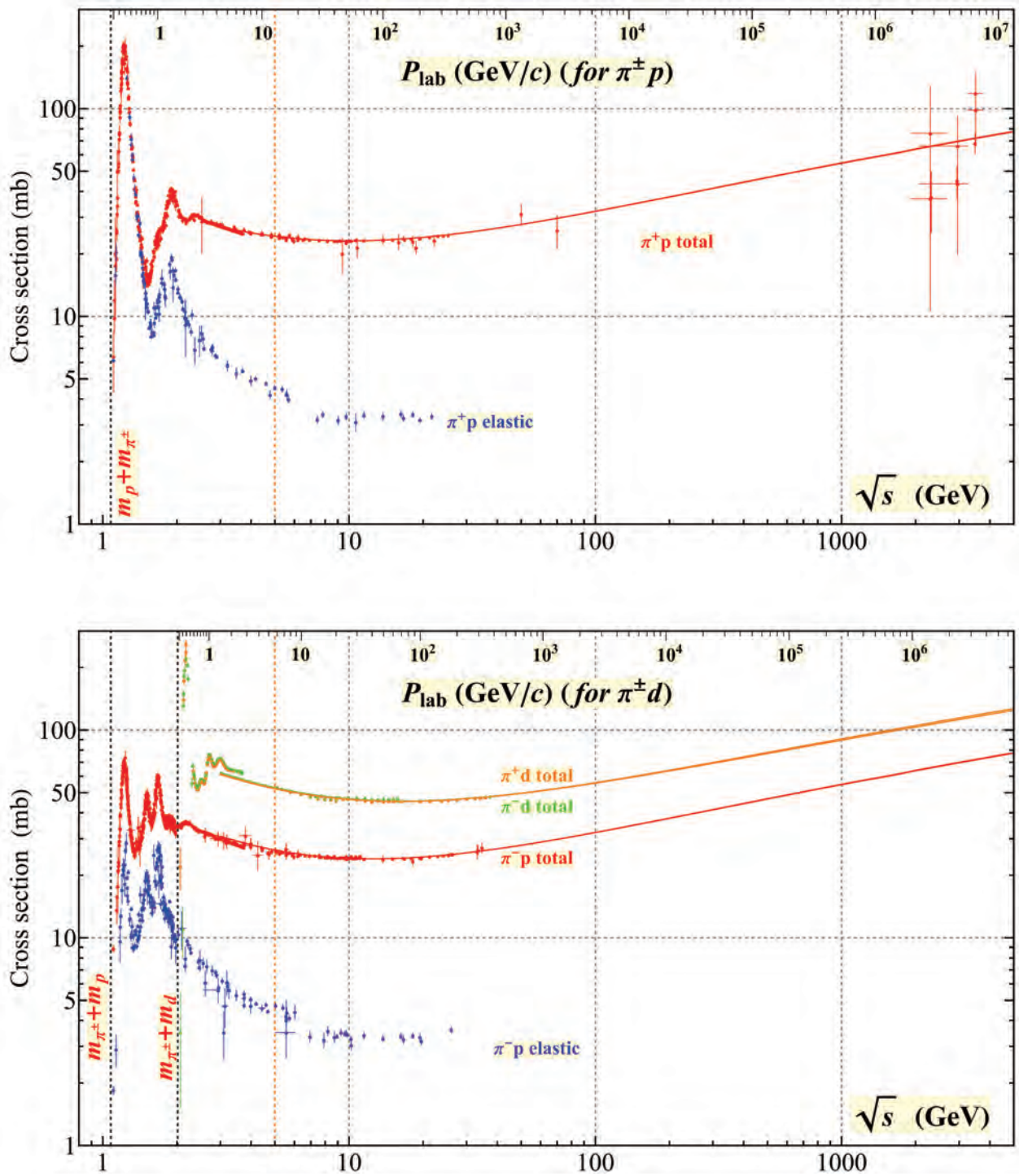

Figure 53.8: Total and elastic cross sections for $\pi^{\pm}p$ and $\pi^{\pm}d$ (total only) collisions as a function of laboratory beam momentum and total center-of-mass energy. Corresponding computer-readable data files can be found at https://pdg.lbl.gov/current/xsect/. (Courtesy of the COMPAS Group, NRC KI – IHEP, Protvino, August 2021.)

Downloaded from https://academic.oup.com/ptep/article/2022/8/083C01/6651666 by KIT Library user on 27 September 2022

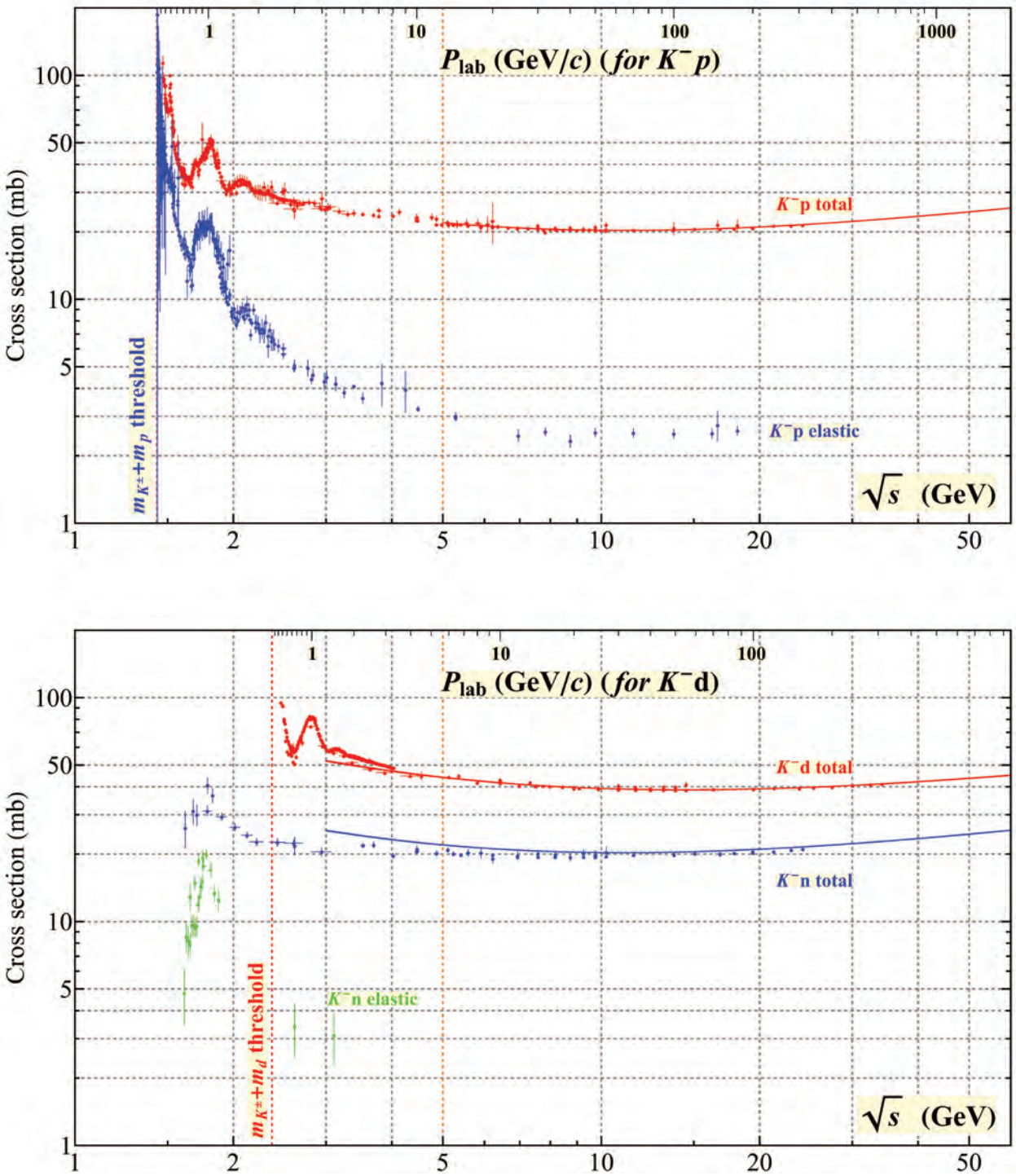

Figure 53.9: Total and elastic cross sections for K^-p and K^-d (total only), and K^-n collisions as a function of laboratory beam momentum and total center-of-mass energy. Corresponding computer-readable data files can be found at https://pdg.lbl.gov/current/xsect/. (Courtesy of the COMPAS Group, NRC KI – IHEP, Protvino, August 2021.)

Downloaded from https://academic.oup.com/ptep/article/2022/8/083C01/6651666 by KIT Library user on 27 September 2022

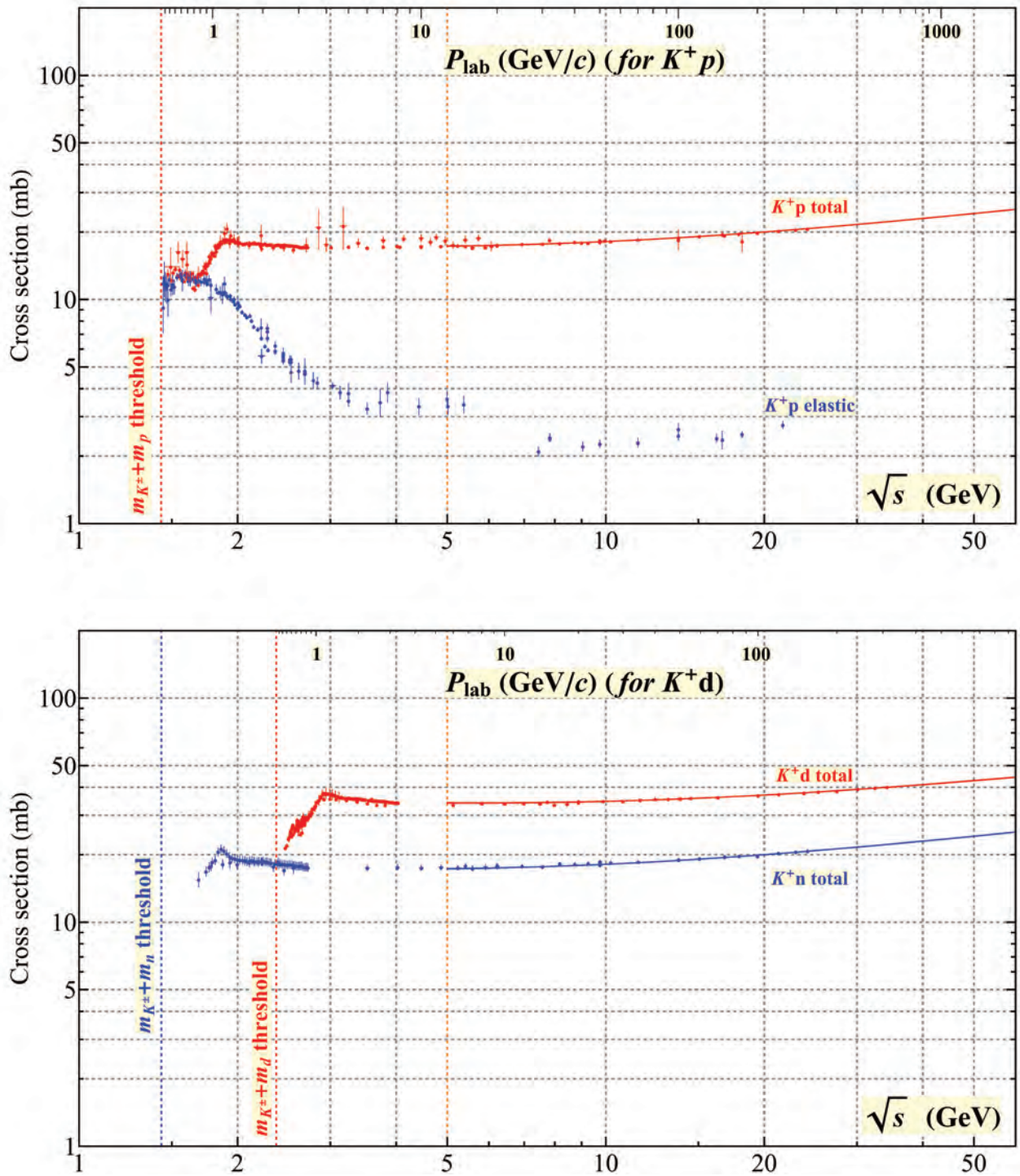

Figure 53.10: Total and elastic cross sections for K^+p and total cross sections for K^+d and K^+n collisions as a function of laboratory beam momentum and total center-of-mass energy. Corresponding computer-readable data files can be found at https://pdg.lbl.gov/current/xsect/. (Courtesy of the COMPAS Group, NRC KI – IHEP, Protvino, August 2021.)

Downloaded from https://academic.oup.com/ptep/article/2022/8/083C01/6651666 by KIT Library user on 27 September 2022

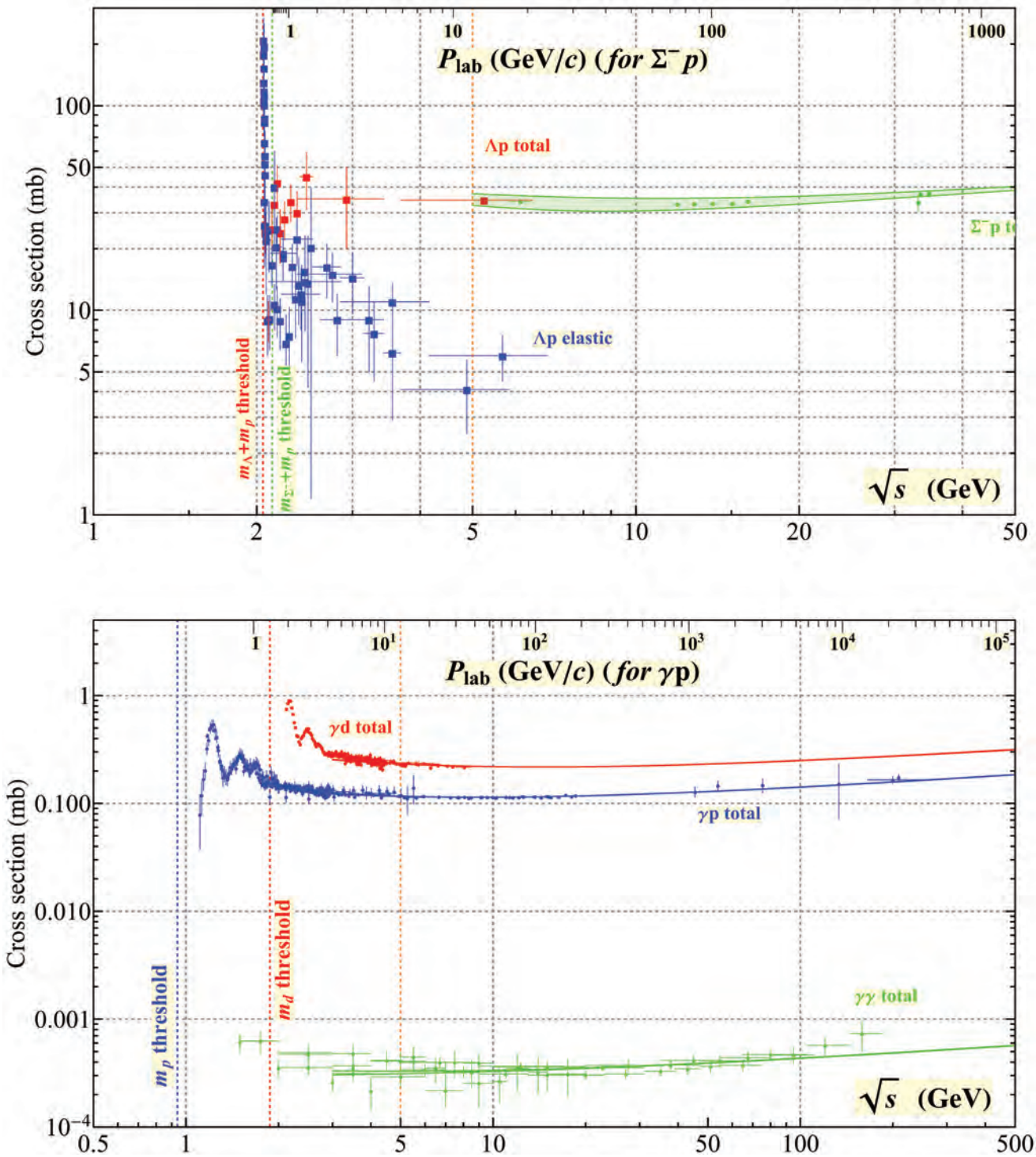

Figure 53.11: Total and elastic cross sections for Λp, total cross section for $\Sigma^- p$, and total hadronic cross sections for γd, γp, and $\gamma\gamma$ collisions as a function of laboratory beam momentum and the total center-of-mass energy. Corresponding computer-readable data files can be found at https://pdg.lbl.gov/current/xsect/. (Courtesy of the COMPAS group, NRC KI – IHEP, Protvino, August 2021.)

Downloaded from https://academic.oup.com/ptep/article/2022/8/083C01/6651666 by KIT Library user on 27 September 2022

References

[1] G. J. Alner *et al.* (UA5), Z. Phys. **C33**, 1 (1986).

[2] K. Alpgard *et al.* (UA5), Phys. Lett. **112B**, 183 (1982).

[3] F. Abe *et al.* (CDF), Phys. Rev. **D41**, 2330 (1990), [,119(1989)].

[4] R. Harr *et al.*, Phys. Lett. **B401**, 176 (1997), [hep-ex/9703002].

[5] K. Aamodt *et al.* (ALICE), Eur. Phys. J. **C68**, 89 (2010), [arXiv:1004.3034].

[6] V. Khachatryan *et al.* (CMS), JHEP **02**, 041 (2010), [arXiv:1002.0621].

[7] V. Khachatryan *et al.* (CMS), Phys. Rev. Lett. **105**, 022002 (2010), [arXiv:1005.3299].

[8] H. Albrecht *et al.* (ARGUS), Z. Phys. **C54**, 1 (1992).

[9] S. Behrends *et al.* (CLEO), Phys. Rev. **D31**, 2161 (1985).

[10] J. P. Lees *et al.* (BaBar), Phys. Rev. **D88**, 032011 (2013), [arXiv:1306.2895].

[11] H. Albrecht *et al.*, Phys. Lett. **102B**, 291 (1981).

[12] K. Hikasa *et al.* (Particle Data Group), Phys. Rev. **D45**, S1 (1992), [Erratum: Phys. Rev.D46,5210(1992)].

[13] R. Barate *et al.* (ALEPH), Eur. Phys. J. **C5**, 205 (1998).

[14] P. Abreu *et al.* (DELPHI), Eur. Phys. J. **C5**, 585 (1998).

[15] R. Akers *et al.* (OPAL), Z. Phys. **C63**, 181 (1994).

[16] K. Abe *et al.* (SLD), Phys. Rev. **D69**, 072003 (2004), [hep-ex/0310017].

[17] P. Abreu *et al.* (DELPHI), Eur. Phys. J. **C18**, 203 (2000), [Erratum: Eur. Phys. J.C25,493(2002)], [hep-ex/0103031].

[18] D. D. Pitzl *et al.* (JADE), Z. Phys. **C46**, 1 (1990), [Erratum: Z. Phys.C47,676(1990)].

[19] H. J. Behrend *et al.* (CELLO), Z. Phys. **C47**, 1 (1990).

[20] R. Barate *et al.* (ALEPH), Eur. Phys. J. **C16**, 613 (2000).

[21] W. Adam *et al.* (DELPHI), Z. Phys. **C69**, 561 (1996).

[22] M. Acciarri *et al.* (L3), Phys. Lett. **B371**, 126 (1996).

[23] G. Abbiendi *et al.* (OPAL), Eur. Phys. J. **C17**, 373 (2000), [hep-ex/0007017].

[24] H. Albrecht *et al.* (ARGUS), Z. Phys. **C44**, 547 (1989).

[25] P. Abreu *et al.* (DELPHI), Nucl. Phys. **B444**, 3 (1995).

[26] H. J. Behrend *et al.* (CELLO), Z. Phys. **C46**, 397 (1990).

[27] M. Derrick *et al.*, Phys. Rev. **D35**, 2639 (1987).

[28] W. Bartel *et al.* (JADE), Z. Phys. **C20**, 187 (1983).

[29] H. Schellman *et al.*, Phys. Rev. **D31**, 3013 (1985).

[30] C. Berger *et al.* (PLUTO), Phys. Lett. **104B**, 79 (1981).

[31] M. Althoff *et al.* (TASSO), Z. Phys. **C27**, 27 (1985).

[32] H. Aihara *et al.* (TPC/Two Gamma), Phys. Rev. Lett. **53**, 2378 (1984).

[33] P. Abreu *et al.* (DELPHI), Z. Phys. **C65**, 587 (1995).

[34] M. Acciarri *et al.* (L3), Phys. Lett. **B407**, 389 (1997), [Erratum: Phys. Lett.B427,409(1998)].

[35] R. Akers *et al.* (OPAL), Z. Phys. **C67**, 389 (1995).

[36] K. Abe *et al.* (SLD), Phys. Rev. **D59**, 052001 (1999), [hep-ex/9805029].

[37] H. Albrecht *et al.* (ARGUS), Z. Phys. **C46**, 15 (1990).

[38] C. Bieler *et al.* (Crystal Ball), Z. Phys. **C49**, 225 (1991).

[39] G. Wormser *et al.*, Phys. Rev. Lett. **61**, 1057 (1988).

[40] A. Heister *et al.* (ALEPH), Phys. Lett. **B528**, 19 (2002), [hep-ex/0201012].

[41] H. Albrecht *et al.* (ARGUS), Z. Phys. **C58**, 199 (1993).

[42] M. Acciarri *et al.* (L3), Phys. Lett. **B393**, 465 (1997).

[43] K. Ackerstaff *et al.* (OPAL), Eur. Phys. J. **C5**, 411 (1998), [hep-ex/9805011].

[44] R. Seuster *et al.* (Belle), Phys. Rev. **D73**, 032002 (2006), [hep-ex/0506068].

[45] M. Artuso *et al.* (CLEO), Phys. Rev. **D70**, 112001 (2004), [hep-ex/0402040].

[46] P. Abreu *et al.* (DELPHI), Z. Phys. **C59**, 533 (1993), [Erratum: Z. Phys.C65,709(1995)].

[47] G. Alexander *et al.* (OPAL), Z. Phys. **C72**, 1 (1996).

[48] B. Aubert *et al.* (BaBar), Phys. Rev. **D65**, 091104 (2002), [hep-ex/0201041].

[49] D. Bortoletto *et al.* (CLEO), Phys. Rev. **D37**, 1719 (1988), [Erratum: Phys. Rev.D39,1471(1989)].

[50] P. Abreu *et al.* (DELPHI), Z. Phys. **C57**, 181 (1993).

[51] J. Abdallah *et al.* (DELPHI), Phys. Lett. **B576**, 29 (2003), [hep-ex/0311005].

[52] P. Abreu *et al.* (DELPHI), Z. Phys. **C61**, 407 (1994).

[53] R. Akers *et al.* (OPAL), Z. Phys. **C66**, 555 (1995).

[54] S. Abachi *et al.*, Phys. Rev. Lett. **57**, 1990 (1986).

[55] P. Abreu *et al.* (DELPHI), Phys. Lett. **B449**, 364 (1999).

[56] K. Ackerstaff *et al.* (OPAL), Eur. Phys. J. **C4**, 19 (1998), [hep-ex/9802013].

[57] H. Albrecht *et al.* (ARGUS), Z. Phys. **C61**, 1 (1994).

[58] D. Buskulic *et al.* (ALEPH), Z. Phys. **C69**, 379 (1996).

[59] R. Barate *et al.* (ALEPH), Phys. Rept. **294**, 1 (1998).

[60] P. D. Acton *et al.* (OPAL), Phys. Lett. **B305**, 407 (1993).

[61] P. Abreu *et al.* (DELPHI), Z. Phys. **C73**, 61 (1996).

[62] K. Ackerstaff *et al.* (OPAL), Phys. Lett. **B412**, 210 (1997), [hep-ex/9708022].

[63] R. Barate *et al.* (ALEPH), Eur. Phys. J. **C16**, 597 (2000), [hep-ex/9909032].

[64] K. Ackerstaff *et al.* (OPAL), Eur. Phys. J. **C1**, 439 (1998), [hep-ex/9708021].

[65] K. Ackerstaff *et al.* (OPAL), Eur. Phys. J. **C5**, 1 (1998), [hep-ex/9802008].

[66] P. Abreu *et al.* (DELPHI), Z. Phys. **C68**, 353 (1995).

[67] M. Acciarri *et al.* (L3), Phys. Lett. **B345**, 589 (1995).

[68] B. Aubert *et al.* (BaBar), Phys. Rev. Lett. **87**, 162002 (2001), [hep-ex/0106044].

[69] K. Abe *et al.* (Belle), Phys. Rev. Lett. **88**, 052001 (2002), [hep-ex/0110012].

[70] D. Buskulic *et al.* (ALEPH), Phys. Lett. **B295**, 396 (1992).

[71] P. Abreu *et al.* (DELPHI), Phys. Lett. **B341**, 109 (1994).

[72] M. Acciarri *et al.* (L3), Phys. Lett. **B453**, 94 (1999).

[73] G. Alexander *et al.* (OPAL), Z. Phys. **C70**, 197 (1996).

[74] M. Acciarri *et al.* (L3), Phys. Lett. **B407**, 351 (1997).

[75] G. Alexander *et al.* (OPAL), Phys. Lett. **B370**, 185 (1996).

[76] J. Abdallah *et al.* (DELPHI), Phys. Lett. **B569**, 129 (2003), [hep-ex/0309057].

[77] A. De Angelis, J. Phys. **G19**, 1233 (1993).

[78] S. Abachi *et al.*, Phys. Lett. **B199**, 151 (1987).

[79] R. Akers *et al.* (OPAL), Z. Phys. **C68**, 1 (1995).

[80] P. Abreu *et al.* (DELPHI), Phys. Lett. **B345**, 598 (1995).

[81] A. Heister *et al.* (ALEPH), Phys. Lett. **B526**, 34 (2002), [hep-ex/0112010].

[82] H. Albrecht *et al.* (ARGUS), Z. Phys. **C39**, 177 (1988).

[83] M. Niiyama *et al.* (Belle), Phys. Rev. **D97**, 7, 072005 (2018), [arXiv:1706.06791].

[84] P. Abreu *et al.* (DELPHI), Z. Phys. **C67**, 543 (1995).

[85] G. Alexander *et al.* (OPAL), Z. Phys. **C73**, 569 (1997).

[86] W. Adam *et al.* (DELPHI), Z. Phys. **C70**, 371 (1996).

[87] M. Acciarri *et al.* (L3), Phys. Lett. **B479**, 79 (2000), [hep-ex/0002066].

Downloaded from https://academic.oup.com/ptep/article/2022/8/083C01/6651666 by KIT Library user on 27 September 2022

[88] G. Alexander *et al.* (OPAL), Z. Phys. **C73**, 587 (1997).

[89] P. Abreu *et al.* (DELPHI), Phys. Lett. **B475**, 429 (2000), [hep-ex/0103020].

[90] H. Albrecht *et al.* (ARGUS), Phys. Lett. **B230**, 169 (1989).

[91] P. Abreu *et al.* (DELPHI), Phys. Lett. **B361**, 207 (1995).

[92] G. Alexander *et al.* (OPAL), Phys. Lett. **B358**, 162 (1995).

[93] S. Abachi *et al.*, Phys. Rev. Lett. **58**, 2627 (1987), [Erratum: Phys. Rev. Lett.59,2388(1987)].

[94] J. Abdallah *et al.* (DELPHI), Eur. Phys. J. **C44**, 299 (2005), [hep-ex/0510023].

[95] B. Aubert *et al.* (BaBar), Phys. Rev. **D75**, 012003 (2007), [hep-ex/0609004].

[96] P. D. Acton *et al.* (OPAL), Phys. Lett. **B281**, 394 (1992).

[97] H. Albrecht *et al.* (ARGUS), Phys. Rept. **276**, 223 (1996).

[98] R. Giles *et al.* (CLEO), Phys. Rev. **D29**, 1285 (1984).

[99] K. G. Chetyrkin, R. V. Harlander and J. H. Kuhn, Nucl. Phys. **B586**, 56 (2000), [Erratum: Nucl. Phys.B634,413(2002)], [hep-ph/0005139].

[100] V. V. Ezhela, S. B. Lugovsky and O. V. Zenin (2003), [hep-ph/0312114].

[101] R. Barate *et al.* (ALEPH), Eur. Phys. J. **C14**, 1 (2000).

[102] P. Abreu *et al.* (DELPHI), Eur. Phys. J. **C16**, 371 (2000).

[103] M. Acciarri *et al.* (L3), Eur. Phys. J. **C16**, 1 (2000), [hep-ex/0002046].

[104] G. Abbiendi *et al.* (OPAL), Eur. Phys. J. **C19**, 587 (2001), [hep-ex/0012018].

[105] S. Schael *et al.* (ALEPH, DELPHI, L3, OPAL, SLD, LEP Electroweak Working Group, SLD Electroweak Group, SLD Heavy Flavour Group), Phys. Rept. **427**, 257 (2006), [hep-ex/0509008].

[106] P. Collins, *An Introduction to Regge Theory and High-Energy Physics*, Cambridge Monographs on Mathematical Physics, Cambridge Univ. Press, Cambridge, UK (2009), ISBN 9780521110358.

[107] G. Pancheri and Y. N. Srivastava, Eur. Phys. J. **C77**, 3, 150 (2017), [arXiv:1610.10038].

[108] V. A. Petrov and A. Prokudin, Phys. Rev. **D87**, 3, 036003 (2013), [arXiv:1212.1924].

[109] C. Bourrely, J. Soffer and T. T. Wu, Eur. Phys. J. **C28**, 97 (2003), [hep-ph/0210264].

[110] M. M. Block *et al.*, Phys. Rev. **D92**, 1, 014030 (2015), [arXiv:1505.04842].

[111] O. V. Selyugin, Phys. Rev. **D91**, 11, 113003 (2015), [Erratum: Phys. Rev.D92,no.9,099901(2015)], [arXiv:1505.02426].

[112] L. G. Dakhno and V. A. Nikonov, Eur. Phys. J. **A5**, 209 (1999), [hep-ph/9902320].

[113] A. A. Godizov, Phys. Lett. **B735**, 57 (2014), [arXiv:1404.2851].

[114] E. Gotsman, E. M. Levin and U. Maor, Phys. Rev. **D49**, R4321 (1994), [hep-ph/9310257].

[115] L. A. Harland-Lang, V. A. Khoze and M. G. Ryskin, Int. J. Mod. Phys. **A30**, 1542013 (2015).

[116] A. Donnachie and P. V. Landshoff, Phys. Lett. **B727**, 500 (2013), [Erratum: Phys. Lett.B750,669(2015)], [arXiv:1309.1292].

[117] E. Martynov, Phys. Rev. **D87**, 11, 114018 (2013), [arXiv:1305.3093].

[118] I. Szanyi, N. Bence and L. Jenkovszky, J. Phys. G **46**, 5, 055002 (2019), [arXiv:1808.03588].

[119] S. M. Troshin and N. E. Tyurin, Int. J. Mod. Phys. **A32**, 17, 1750103 (2017), [arXiv:1704.00443].

[120] V. V. Anisovich, Phys. Usp. **58**, 10, 963 (2015).

[121] D. A. Fagundes, M. J. Menon and P. V. R. G. Silva, Nucl. Phys. **A946**, 194 (2016), [arXiv:1509.04108].

[122] E. Martynov and B. Nicolescu, Eur. Phys. J. **C56**, 57 (2008), [arXiv:0712.1685].

[123] W. Heisenberg, Z. Phys. **133**, 65 (1952).

[124] V. V. Ezhela and O. P. Yushchenko, Submitted to: Z. Phys. C (1988).

[125] H. Nastase and J. Sonnenschein, Phys. Rev. **D92**, 105028 (2015), [arXiv:1504.01328].

[126] H. A. Bethe, Annals Phys. **3**, 190 (1958).

[127] G. B. West and D. R. Yennie, Phys. Rev. **172**, 1413 (1968).

[128] R. Cahn, Z. Phys. C **15**, 253 (1982).

[129] V. Kundrat and M. Lokajicek, Z. Phys. C **63**, 619 (1994).

[130] V. A. Petrov, Eur. Phys. J. C **78**, 3, 221 (2018), [Erratum: Eur.Phys.J.C 78, 414 (2018)], [arXiv:1801.01815].

[131] G. Antchev *et al.* (TOTEM), Eur. Phys. J. C **79**, 2, 103 (2019), [arXiv:1712.06153].

[132] V. V. Ezhela, V. A. Petrov and N. P. Tkachenko, Phys. At. Nucl. **84**, 3, 298 (2021).

[133] M. Froissart, Phys. Rev. **123**, 1053 (1961).

[134] A. Martin, Phys. Rev. **129**, 1432 (1963).

[135] V. A. Petrov and V. A. Okorokov, Int. J. Mod. Phys. A **33**, 13, 1850077 (2018), [arXiv:1802.01559].

[136] C. Patrignani *et al.* (Particle Data Group), Chin. Phys. **C40**, 10, 100001 (2016).

[137] V. I. Belousov *et al.*, Phys. Atom. Nucl. **79**, 1, 113 (2016), [Yad. Fiz.79,no.1,55(2016)].

Downloaded from https://academic.oup.com/ptep/article/2022/8/083C01/6651666 by KIT Library user on 27 September 2022

Downloaded from https://academic.oup.com/ptep/article/2022/8/083C01/6651666 by KIT Library user on 27 September 2022

Particle Properties

Gauge Bosons

54. Mass and width of the W boson (rev.) 789
55. Z boson 791

Charged Leptons

56. Muon anomalous magnetic moment (rev.) 796
57. Muon decay parameters (rev.) 800
58. τ branching fractions (rev.) 803
59. τ-lepton decay parameters (rev.) 806

Quarks

60. Quark masses (rev.) 808
61. Top quark (rev.) 817

Mesons

62. Form factors for semileptonic kaon ($K_{\ell 3}$), radiative pion ($\pi_{\ell 2\gamma}$) & kaon ($K_{\ell 2\gamma}$) decays (rev.) 842
63. Spectroscopy of light meson resonances (new) 845
64. Scalar mesons below 1 GeV (rev.) 858
65. Rare kaon decays (rev.) 865
66. CPT invariance tests in neutral kaon decay (rev.) 871
67. V_{ud}, V_{us}, Cabibbo angle, and CKM unitarity (rev.) 873
68. CP-violation in K_L decays (rev.) 877
69. Review of multibody charm analyses (rev.) 880
70. D^0–$\overline{D}^0$ mixing (rev.) 885
71. D_s^+ branching fractions (rev.) 895
72. Leptonic decays of charged pseudoscalar mesons (rev.) 897
73. Production and decay of b-flavored hadrons (rev.) 908
74. Polarization in B decays (rev.) 919
75. B^0–$\overline{B}^0$ mixing (rev.) 923
76. Semileptonic B decays, V_{cb} and V_{ub} (rev.) 930
77. CKM angles from B hadrons, determination of (rev.) 946
78. Spectroscopy of mesons containing two heavy quarks (rev.) 951
79. Heavy non-$q\overline{q}$ mesons (rev.) 959

Baryons

80. Baryon decay parameters 964
81. N and Δ resonances 965
82. Λ and Σ resonances (rev.) 970
83. Pole structure of the $\Lambda(1405)$ region (rev.) 973
84. Pentaquarks (rev.) 975

Notes in Volume 2

Triple gauge couplings (TGC's) 1146
Anomalous $ZZ\gamma$, $Z\gamma\gamma$, and ZZV couplings 1171
Anomalous W/Z quartic couplings 1173
Neutrino properties (rev.) 1273
Sum of neutrino masses (rev.) 1276
Number of light neutrino types from collider experiments 1282
Neutrinoless double-β decay 1284
Charged kaon mass 1473
Dalitz plot parameters for $K \to 3\pi$ decays 1482
CP-violation in $K_S \to 3\pi$ 1492
Heavy Flavor Averaging Group (rev.) 1609
Charmonium system (rev.) 1818
Branching ratios of $\psi(2S)$ and $\chi_{c0,1,2}$ (rev.) 1850
Bottomonium system (rev.) 1940
Width determination of the Υ states 1940
Radiative hyperon decays 2122
Ξ resonances 2126

Downloaded from https://academic.oup.com/ptep/article/2022/8/083C01/6651666 by KIT Library user on 27 September 2022

Downloaded from https://academic.oup.com/ptep/article/2022/8/083C01/6651666 by KIT Library user on 27 September 2022

54. Mass and Width of the W Boson

Revised May 2022 by M. Grünewald (University Coll. Dublin) and A. Gurtu (CERN; TIFR Mumbai).

Precision determination of the W mass is of great importance in testing the internal consistency of the Standard Model. From the time of its discovery in 1983, the W boson has been studied and its mass determined in $p\bar{p}$ and e^+e^- interactions; it is currently studied in pp interactions at the LHC. The mass and width definition used here corresponds to a Breit-Wigner with mass-dependent width.

Production of on-shell W bosons at hadron colliders is tagged by the high p_T charged lepton from its leptonic decay modes. Owing to the unknown parton-parton effective energy and missing energy in the longitudinal direction, the hadron collider experiments reconstruct the transverse mass of the W boson, and derive the W mass from comparing the transverse mass distribution with Monte Carlo predictions as a function of the mass m_W. The transverse momentum of the charged lepton itself and the transverse missing energy (arising from the neutrino in W decay) are also sensitive to the W mass and used in its determination. These analyses use the electron and muon decay modes of the W boson.

At the e^+e^- collider LEP, a precise knowledge of the beam energy enables one to determine the $e^+e^- \to W^+W^-$ cross section as a function of center of mass energy, as well as to reconstruct the W mass precisely from its decay products, even if one of them decays leptonically. Close to the W^+W^- production threshold ($\sqrt{s} = 161$ GeV), the dependence of the W-pair production cross section on m_W is large, and this was used to determine m_W. At higher centre-of-mass energies (172 to 209 GeV) this dependence is much weaker, thus W bosons were directly reconstructed and the mass determined as the invariant mass of the decay products, improving the resolution with a kinematic fit.

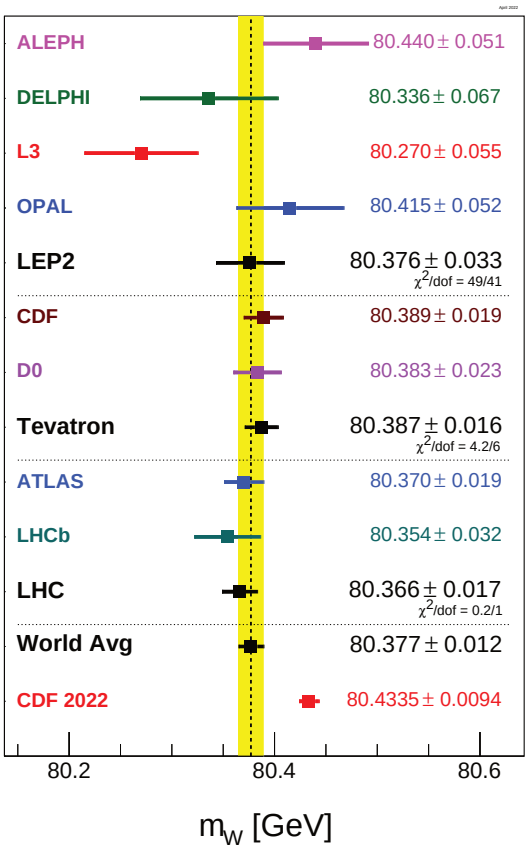

Figure 54.1: Measurements of the W boson mass by the LEP, Tevatron and LHC experiments. The pre-2022 CDF result, used in the world average, is superseded by the new CDF 2022 result.

In order to compute the LEP average W mass, each experiment provided its measured W mass for the $q\bar{q}q\bar{q}$ and $q\bar{q}\ell\nu$, $\ell = e, \mu, \tau$ channels at each center-of-mass energy, along with a detailed break-up of uncertainty contributions: statistical, uncorrelated, partially correlated and fully correlated systematics [1]. These results have been combined to obtain a LEP average W mass of $m_W = 80.376 \pm 0.033$ GeV. Errors on m_W due to uncertainties in the LEP beam energy (9 MeV), and possible effect of color reconnection (CR) and Bose-Einstein correlations (BEC) between quarks from different W bosons (8 MeV) are included. The mass difference between $q\bar{q}q\bar{q}$ and $q\bar{q}\ell\nu$ final states (due to possible CR and BEC effects) is -12 ± 45 MeV. In a similar manner, the results on the total width of the W boson obtained at LEP have been combined, resulting in an average of $\Gamma_W = 2.195 \pm 0.083$ GeV [1].

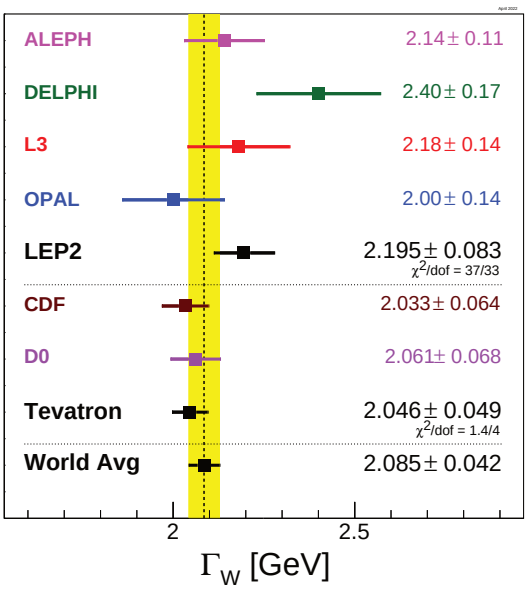

Figure 54.2: Measurements of the W-boson width by the LEP and Tevatron experiments.

The two Tevatron experiments CDF and D0 have also identified common systematic errors. Between the two experiments, uncertainties due to the parton distribution functions (PDF), radiative corrections, and choice of mass (width) in the width (mass) measurements are treated as correlated. An average W width of $\Gamma_W = 2.046 \pm 0.049$ GeV [2] is obtained. Errors of 20 MeV and 7 MeV accounting for PDF and radiative correction uncertainties in this width combination dominate the correlated uncertainties. The CDF and D0 measurements of 80.387 ± 0.019 GeV [3] and 80.375 ± 0.023 GeV [4], respectively, obtained with Run-II data, are the two single most precise determinations of the W boson mass at the Tevatron. Combining the results from Run-I and Run-II of the Tevatron using an improved treatment of correlations, following the procedure used in [5], the results are 80.389 ± 0.019 GeV for CDF and 80.383 ± 0.023 GeV for D0. A combination of all pre-2022 CDF and D0 results yields a Tevatron average of 80.387 ± 0.016 GeV [5], with common uncertainties of 10 MeV (PDF) and 4 MeV (radiative corrections).

Using pp collisions at $\sqrt{s} = 7$ TeV, the ATLAS collaboration has published the first measurement of the W boson mass at the LHC, $m_W = 80.370 \pm 0.019$ GeV [6], which is of similar precision as the best measurements of CDF and D0. The LHCb collaboration has measured the W boson mass in pp collisions at $\sqrt{s} = 13$ TeV at the LHC, $m_W = 80.354 \pm 0.032$ GeV [7]. Combining the results from ATLAS and LHCb using the BLUE procedure [8, 9] assuming a correlated uncertainty of 9 MeV (PDF), the LHC average is $m_W = 80.366 \pm 0.017$ GeV.

The results obtained by the experiments at the different accelerators are all in good agreement with each other. Assuming a correlated uncertainty of 7 MeV, a hadron collider average of the

Downloaded from https://academic.oup.com/ptep/article/2022/8/083C01/6651666 by KIT Library user on 27 September 2022

Tevatron and LHC measurements of $m_W = 80.377 \pm 0.013$ GeV is obtained, and a world average of $m_W = 80.377 \pm 0.012$ GeV, combining with the LEP result assuming no correlation, again using the BLUE procedure for these averages.

The LEP, Tevatron and LHC results on mass and width are compared in Fig. 54.1 and Fig. 54.2. The Standard Model prediction from the electroweak fit, including Z-pole data and the measured masses of the top quark and of the Higgs boson, gives a W-boson mass of $m_W = 80.356 \pm 0.006$ GeV (see Section 10, Electroweak Model and Contraints on New Physics, J.Erler and A.Freitas, 2022, this review) and a W-boson width of $\Gamma_W = 2.091 \pm 0.001$ GeV [10], which are in good agreement with the measurements.

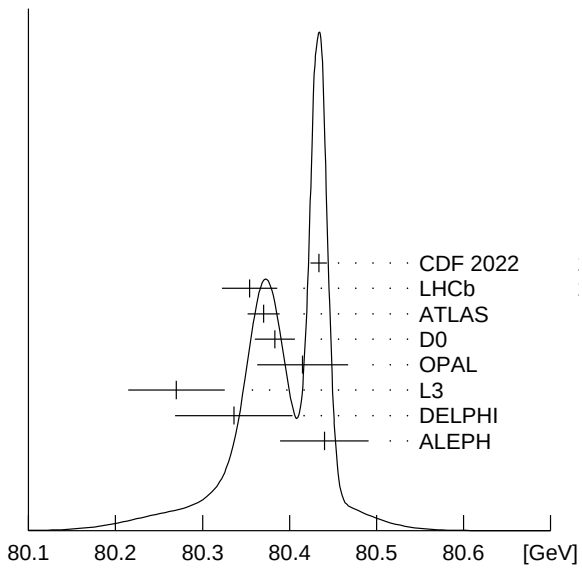

Figure 54.3: Ideogram showing the compatibility of all W-boson mass measurements, replacing the pre-2022 CDF result by the new CDF 2022 result.

In April 2022, after the cut-off of results for this review, the CDF collaboration published a measurement of the W mass based on their full Run-II dataset of 8.8 fb^{-1}, with much reduced uncertainty: $80,433.5 \pm 9.4$ MeV [11][1]. This new CDF Run-II result is of higher precision than our world average of 80.377 ± 0.012 GeV. However, the two determinations disagree significantly, as visible in Fig. 54.1. A probability ideogram comparing the results from Fig. 54.1 is shown in Fig. 54.3 (see Section 5.2 in the Introduction of this review on the construction of ideograms).

For calculating a new world average, replacing the old CDF Run-II result [3] by the new one [11], the uncertainties of all results need to be scaled by a factor of about two in order to achieve a χ^2 per degree of freedom of unity (see Section 5.2 in the Introduction of this review on the definition of the scale factor). The world average quoted above (80.377 ± 0.012 GeV) increases significantly in central value, by up to 40 MeV, while its scaled uncertainty increases by up to 6 MeV, with the exact changes depending on the assumptions made concerning correlated uncertainties. A detailed understanding of the results and their correlations is needed. Corresponding studies are currently being undertaken by the experiments.

References

[1] S. Schael *et al.* (ALEPH, DELPHI, L3, OPAL, LEP Electroweak Working Group), Phys. Rept. **532**, 119 (2013), [arXiv:1302.3415].

[2] The Tevatron Electroweak Working Group, for the CDF and D0 Collaborations, March 2010, [arXiv:1003.2826].

[3] T. Aaltonen *et al.* (CDF), Phys. Rev. Lett. **108**, 151803 (2012), [arXiv:1203.0275].

[4] V. M. Abazov *et al.* (D0), Phys. Rev. Lett. **108**, 151804 (2012), [arXiv:1203.0293].

[5] T. A. Aaltonen *et al.* (CDF, D0), Phys. Rev. D **88**, 5, 052018 (2013), [arXiv:1307.7627].

[6] M. Aaboud *et al.* (ATLAS), Eur. Phys. J. C **78**, 2, 110 (2018), [Erratum: Eur.Phys.J.C 78, 898 (2018)], [arXiv:1701.07240].

[7] R. Aaij *et al.* (LHCb), JHEP **01**, 166 (2022), [arXiv:2107.10090].

[8] L. Lyons, D. Gibaut and P. Clifford, Nucl. Instrum. Meth. A **270**, 110 (1988).

[9] A. Valassi, Nucl. Instrum. Meth. A **500**, 391 (2003).

[10] J. Haller *et al.*, Eur. Phys. J. C **78**, 8, 675 (2018), [arXiv:1803.01853].

[11] T. Aaltonen *et al.* (CDF), Science **376**, 6589, 170 (2022).

[1] The new result includes the 2.2 fb^{-1} of data used for the previous CDF Run-II result of 80.387 ± 0.019 GeV [3]. Incorporating the improved understanding of PDFs and track reconstruction, the central value of the 2.2 fb^{-1} result is increased by 13.5 MeV to 80,400.5 MeV [11].

Downloaded from https://academic.oup.com/ptep/article/2022/8/083C01/6651666 by KIT Library user on 27 September 2022

55. Z Boson

Revised August 2018 by M. Grünewald (University Coll. Dublin) and A. Gurtu (CERN; TIFR Mumbai).

Precision measurements at the Z-boson resonance using electron–positron colliding beams began in 1989 at the SLC and at LEP. During 1989–95, the four LEP experiments (ALEPH, DELPHI, L3, OPAL) made high-statistics studies of the production and decay properties of the Z. Although the SLD experiment at the SLC collected much lower statistics, it was able to match the precision of LEP experiments in determining the effective electroweak mixing angle $\sin^2\overline{\theta}_W$ and the rates of Z decay to b- and c-quarks, owing to availability of polarized electron beams, small beam size, and stable beam spot.

The Z-boson properties reported in this section may broadly be categorized as:

- The standard 'lineshape' parameters of the Z consisting of its mass, M_Z, its total width, Γ_Z, and its partial decay widths, $\Gamma(\text{hadrons})$, and $\Gamma(\ell\bar{\ell})$ where $\ell = e, \mu, \tau, \nu$;
- Z asymmetries in leptonic decays and extraction of Z couplings to charged and neutral leptons;
- The b- and c-quark-related partial widths and charge asymmetries which require special techniques;
- Determination of Z decay modes and the search for modes that violate known conservation laws;
- Average particle multiplicities in hadronic Z decay;
- Z anomalous couplings.

The effective vector and axial-vector coupling constants describing the Z-to-fermion coupling are also measured in $p\bar{p}$ and ep collisions at the Tevatron and at HERA. The corresponding cross-section formulae are given in Section 39 (Cross-section formulae for specific processes) and Section 16 (Structure Functions) in this *Review*. In this minireview, we concentrate on the measurements in e^+e^- collisions at LEP and SLC.

The standard 'lineshape' parameters of the Z are determined from an analysis of the production cross sections of these final states in e^+e^- collisions. The $Z \to \nu\overline{\nu}(\gamma)$ state is identified directly by detecting single photon production and indirectly by subtracting the visible partial widths from the total width. Inclusion in this analysis of the forward-backward asymmetry of charged leptons, $A_{FB}^{(0,\ell)}$, of the τ polarization, $P(\tau)$, and its forward-backward asymmetry, $P(\tau)^{fb}$, enables the separate determination of the effective vector ($\overline{g}_V$) and axial vector ($\overline{g}_A$) couplings of the Z to these leptons and the ratio ($\overline{g}_V/\overline{g}_A$), which is related to the effective electroweak mixing angle $\sin^2\overline{\theta}_W$ (see the "Electroweak Model and Constraints on New Physics" review).

Determination of the b- and c-quark-related partial widths and charge asymmetries involves tagging the b and c quarks for which various methods are employed: requiring the presence of a high momentum prompt lepton in the event with high transverse momentum with respect to the accompanying jet; impact parameter and lifetime tagging using precision vertex measurement with high-resolution detectors; application of neural-network techniques to classify events as b or non-b on a statistical basis using event–shape variables; and using the presence of a charmed meson (D/D^*) or a kaon as a tag.

55.1 Z-parameter determination

LEP was run at energy points on and around the Z mass (88–94 GeV) constituting an energy 'scan'. The shape of the cross-section variation around the Z peak can be described by a Breit-Wigner *ansatz* with an energy-dependent total width [1–3]. The **three** main properties of this distribution, viz., the **position** of the peak, the **width** of the distribution, and the **height** of the peak, determine respectively the values of M_Z, Γ_Z, and $\Gamma(e^+e^-) \times \Gamma(f\overline{f})$, where $\Gamma(e^+e^-)$ and $\Gamma(f\overline{f})$ are the electron and fermion partial widths of the Z. The quantitative determination of these parameters is done by writing analytic expressions for these cross sections in terms of the parameters, and fitting the calculated cross sections to the measured ones by varying these parameters, taking properly into account all the errors. Single-photon exchange (σ^0_γ) and γ-Z interference ($\sigma^0_{\gamma Z}$) are included, and the large ($\sim$25 %) initial-state radiation (ISR) effects are taken into account by convoluting the analytic expressions over a 'Radiator Function' [1–5] $H(s, s')$. Thus for the process $e^+e^- \to f\overline{f}$:

$$\sigma_f(s) = \int H(s, s')\ \sigma^0_f(s')\ ds' \tag{55.1}$$

$$\sigma^0_f(s) = \sigma^0_Z + \sigma^0_\gamma + \sigma^0_{\gamma Z} \tag{55.2}$$

$$\sigma^0_Z = \frac{12\pi}{M_Z^2}\ \frac{\Gamma(e^+e^-)\Gamma(f\overline{f})}{\Gamma_Z^2}\ \frac{s\ \Gamma_Z^2}{(s - M_Z^2)^2\ +\ s^2\Gamma_Z^2/M_Z^2} \tag{55.3}$$

$$\sigma^0_\gamma = \frac{4\pi\alpha^2(s)}{3s}\ Q_f^2 N_c^f \tag{55.4}$$

$$\sigma^0_{\gamma Z} = -\ \frac{2\sqrt{2}\alpha(s)}{3}\ (Q_f G_F N_c^f \mathcal{G}_V^e \mathcal{G}_V^f) \times \frac{(s - M_Z^2)M_Z^2}{(s - M_Z^2)^2 + s^2\Gamma_Z^2/M_Z^2} \tag{55.5}$$

where Q_f is the charge of the fermion, $N_c^f = 3$ for quarks and 1 for leptons, and $\mathcal{G}_V^f$ is the vector coupling of the Z to the fermion-antifermion pair $f\overline{f}$.

Since $\sigma^0_{\gamma Z}$ is expected to be much less than σ^0_Z, the LEP Collaborations have generally calculated the interference term in the framework of the Standard Model. This fixing of $\sigma^0_{\gamma Z}$ leads to a tighter constraint on M_Z, and consequently a smaller error on its fitted value. It is possible to relax this constraint and carry out the fit within the S-matrix framework, which is briefly described in the next section.

In the above framework, the QED radiative corrections have been explicitly taken into account by convoluting over the ISR and allowing the electromagnetic coupling constant to run [6]: $\alpha(s) = \alpha/(1-\Delta\alpha)$. On the other hand, weak radiative corrections that depend upon the assumptions of the electroweak theory and on the values of M_{top} and M_{Higgs} are accounted for by **absorbing them into the couplings**, which are then called the *effective* couplings $\mathcal{G}_V$ and $\mathcal{G}_A$ (or alternatively the effective parameters of the $\star$ scheme of Kennedy and Lynn [7].)

$\mathcal{G}_V^f$ and $\mathcal{G}_A^f$ are complex numbers with small imaginary parts. As experimental data does not allow simultaneous extraction of both real and imaginary parts of the effective couplings, the convention $g_A^f = \text{Re}(\mathcal{G}_A^f)$ and $g_V^f = \text{Re}(\mathcal{G}_V^f)$ is used and the imaginary parts are added in the fitting code [4].

Defining

$$A_f = 2\frac{g_V^f \cdot g_A^f}{(g_V^f)^2 + (g_A^f)^2} \tag{55.6}$$

the lowest-order expressions for the various lepton-related asymmetries on the Z pole are [8–10] $A_{FB}^{(0,\ell)} = (3/4)A_e A_f$, $P(\tau) = -A_\tau$, $P(\tau)^{fb} = -(3/4)A_e$, $A_{LR} = A_e$. The full analysis takes into account the energy-dependence of the asymmetries. Experimentally A_{LR} is defined as $(\sigma_L - \sigma_R)/(\sigma_L + \sigma_R)$, where $\sigma_{L(R)}$ are the $e^+e^- \to Z$ production cross sections with left- (right)-handed electrons.

The definition of the partial decay width of the Z to $f\overline{f}$ includes the effects of QED and QCD final-state corrections, as well as the contribution due to the imaginary parts of the couplings:

$$\Gamma(f\overline{f}) = \frac{G_F M_Z^3}{6\sqrt{2}\pi}\ N_c^f\,(\left|\mathcal{G}_A^f\right|^2 R_A^f + \left|\mathcal{G}_V^f\right|^2 R_V^f) + \Delta_{ew/\text{QCD}} \tag{55.7}$$

where R_V^f and R_A^f are radiator factors to account for final state QED and QCD corrections, as well as effects due to nonzero fermion masses, and $\Delta_{ew/\text{QCD}}$ represents the non-factorizable electroweak/QCD corrections.

55.2 S-matrix approach to the Z

While most experimental analyses of LEP/SLC data have followed the 'Breit-Wigner' approach, an alternative S-matrix-based

Downloaded from https://academic.oup.com/ptep/article/2022/8/083C01/6651666 by KIT Library user on 27 September 2022

analysis is also possible. The Z, like all unstable particles, is associated with a complex pole in the S matrix. The pole position is process-independent and gauge-invariant. The mass, $\overline{M}_Z$, and width, $\overline{\Gamma}_Z$, can be defined in terms of the pole in the energy plane via [11–14]

$$\overline{s} = \overline{M}_Z^2 - i\overline{M}_Z\overline{\Gamma}_Z \tag{55.8}$$

leading to the relations

$$\begin{aligned}\overline{M}_Z &= M_Z/\sqrt{1+\Gamma_Z^2/M_Z^2} \\ &\approx M_Z \ -34.1 \text{ MeV} \end{aligned} \tag{55.9}$$

$$\begin{aligned}\overline{\Gamma}_Z &= \Gamma_Z/\sqrt{1+\Gamma_Z^2/M_Z^2} \\ &\approx \Gamma_Z \ -0.9 \text{ MeV} \ . \end{aligned} \tag{55.10}$$

The LEP collaborations [15] have analyzed their data using the S–matrix approach as defined in Eq. (55.8), in addition to the conventional one. They observe a downward shift in the Z mass as expected.

55.3 Handling the large-angle e^+e^- final state

Unlike other $f\overline{f}$ decay final states of the Z, the e^+e^- final state has a contribution not only from the s-channel but also from the t-channel and s-t interference. The full amplitude is not amenable to fast calculation, which is essential if one has to carry out minimization fits within reasonable computer time. The usual procedure is to calculate the non-s channel part of the cross section separately using the Standard Model programs ALIBABA [16] or TOPAZ0 [17], with the measured value of $M_{\rm top}$, and $M_{\rm Higgs} = 150$ GeV, and add it to the s-channel cross section calculated as for other channels. This leads to two additional sources of error in the analysis: firstly, the theoretical calculation in ALIBABA itself is known to be accurate to $\sim 0.5\%$, and secondly, there is uncertainty due to the error on $M_{\rm top}$ and the unknown value of $M_{\rm Higgs}$ (100–1000 GeV). These errors are propagated into the analysis by including them in the systematic error on the e^+e^- final state. As these errors are common to the four LEP experiments, this is taken into account when performing the LEP average.

55.4 Errors due to uncertainty in LEP energy determination

The systematic errors related to the LEP energy measurement, see [18–23], can be classified as:

- The absolute energy scale error;
- Energy-point-to-energy-point errors due to the nonlinear response of the magnets to the exciting currents;
- Energy-point-to-energy-point errors due to possible higher-order effects in the relationship between the dipole field and beam energy;
- Energy reproducibility errors due to various unknown uncertainties in temperatures, tidal effects, corrector settings, RF status, *etc.*

Precise energy calibration was done outside normal data-taking using the resonant depolarization technique. Run-time energies were determined every 10 minutes by measuring the relevant machine parameters and using a model which takes into account all the known effects, including leakage currents produced by trains in the Geneva area and the tidal effects due to gravitational forces of the Sun and the Moon. The LEP Energy Working Group has provided a covariance matrix from the determination of LEP energies for the different running periods during 1993–1995 [18].

55.5 Choice of fit parameters

The LEP Collaborations have chosen the following primary set of parameters for fitting:

$$M_Z, \Gamma_Z, \sigma^0_{\rm hadron}, R(\text{lepton}), A_{FB}^{(0,\ell)},$$

where

$$\begin{aligned} R(\text{lepton}) &= \Gamma(\text{hadrons})/\Gamma(\text{lepton}), \sigma^0_{\rm hadron} \\ &= 12\pi\Gamma(e^+e^-)\Gamma(\text{hadrons})/M_Z^2\Gamma_Z^2. \end{aligned}$$

With a knowledge of these fitted parameters and their covariance matrix, any other parameter can be derived. The main advantage of these parameters is that they form a physics motivated set of parameters with much reduced correlations.

Thus, the most general fit carried out to cross section and asymmetry data determines the **nine parameters**: M_Z, Γ_Z, $\sigma^0_{\rm hadron}$, $R(e)$, $R(\mu)$, $R(\tau)$, $A_{FB}^{(0,e)}$, $A_{FB}^{(0,\mu)}$, $A_{FB}^{(0,\tau)}$. Assumption of lepton universality leads to a **five-parameter fit** determining M_Z, Γ_Z, $\sigma^0_{\rm hadron}$, $R(\text{lepton})$, $A_{FB}^{(0,\ell)}$.

55.6 Combining results from LEP and SLC experiments

With a steady increase in statistics over the years and improved understanding of the common systematic errors between LEP experiments, the procedures for combining results have evolved continuously [24]. The Line Shape Sub-group of the LEP Electroweak Working Group investigated the effects of these common errors, and devised a combination procedure for the precise determination of the Z parameters from LEP experiments. Using these procedures, this note also gives the results after combining the final parameter sets from the four experiments, and these are the results quoted as the fit results in the Z listings below. Transformation of variables leads to values of derived parameters like partial decay widths and branching ratios to hadrons and leptons. Finally, transforming the LEP combined nine parameter set to (M_Z, Γ_Z, $\sigma^\circ_{\rm hadron}$, g_A^f, g_V^f, $f = e, \mu, \tau$) using the average values of lepton asymmetry parameters (A_e, A_μ, A_τ) as constraints, leads to the best fitted values of the vector and axial-vector couplings (g_V, g_A) of the charged leptons to the Z.

Brief remarks on the handling of common errors and their magnitudes are given below. The identified common errors are those coming from

(a) LEP energy-calibration uncertainties, and

(b) the theoretical uncertainties in (i) the luminosity determination using small angle Bhabha scattering, (ii) estimating the non-s channel contribution to large angle Bhabha scattering, (iii) the calculation of QED radiative effects, and (iv) the parametrization of the cross section in terms of the parameter set used.

55.7 Common LEP energy errors

All the collaborations incorporate in their fit the full LEP energy error matrix as provided by the LEP energy group for their intersection region [18]. The effect of these errors is separated out from that of other errors by carrying out fits with energy errors scaled up and down by $\sim 10\%$ and redoing the fits. From the observed changes in the overall error matrix, the covariance matrix of the common energy errors is determined. Common LEP energy errors lead to uncertainties on M_Z, Γ_Z, and $\sigma^\circ_{\rm hadron}$ of 1.7, 1.2 MeV, and 0.011 nb, respectively.

55.8 Common luminosity errors

BHLUMI 4.04 [25] is used by all LEP collaborations for small-angle Bhabha scattering leading to a common uncertainty in their measured cross sections of 0.061% [26]. BHLUMI does not include a correction for production of light fermion pairs. OPAL explicitly corrects for this effect and reduces their luminosity uncertainty to 0.054%, which is taken fully correlated with the other experiments. The other three experiments among themselves have a common uncertainty of 0.061%.

55.9 Common non-s channel uncertainties

The same standard model programs ALIBABA [16] and TOPAZ0 [17] are used to calculate the non-s channel contribution to the large angle Bhabha scattering [27]. As this contribution is a function of the Z mass, which itself is a variable in the fit, it is parameterized as a function of M_Z by each collaboration to properly track this contribution as M_Z varies in the fit. The common errors on R_e and $A_{FB}^{(0,e)}$ are 0.024 and 0.0014 respectively, and are correlated between them.

55.10 Common theoretical uncertainties: QED

There are large initial-state photon and fermion pair radiation effects near the Z resonance, for which the best currently available evaluations include contributions up to $\mathcal{O}(\alpha^3)$. To estimate the

Downloaded from https://academic.oup.com/ptep/article/2022/8/083C01/6651666 by KIT Library user on 27 September 2022

remaining uncertainties, different schemes are incorporated in the standard model programs ZFITTER [5], TOPAZ0 [17], and MIZA [28]. Comparing the different options leads to error estimates of 0.3 and 0.2 MeV on M_Z and Γ_Z respectively, and of 0.02% on $\sigma^\circ_{\rm hadron}$.

55.11 Common theoretical uncertainties: parametrization of lineshape and asymmetries

To estimate uncertainties arising from ambiguities in the model-independent parametrization of the differential cross-section near the Z resonance, results from TOPAZ0 and ZFITTER were compared by using ZFITTER to fit the cross sections and asymmetries calculated using TOPAZ0. The resulting uncertainties on M_Z, Γ_Z, $\sigma^\circ_{\rm hadron}$, R(lepton), and $A_{FB}^{(0,\ell)}$ are 0.1 MeV, 0.1 MeV, 0.001 nb, 0.004, and 0.0001 respectively.

Thus, the overall theoretical errors on M_Z, Γ_Z, $\sigma^\circ_{\rm hadron}$ are 0.3 MeV, 0.2 MeV, and 0.008 nb respectively; on each R(lepton) is 0.004 and on each $A_{FB}^{(0,\ell)}$ is 0.0001. Within the set of three R(lepton)'s and the set of three $A_{FB}^{(0,\ell)}$'s, the respective errors are fully correlated.

All the theory-related errors mentioned above utilize Standard Model programs which need the Higgs mass and running electromagnetic coupling constant as inputs; uncertainties on these inputs will also lead to common errors. All LEP collaborations used the same set of inputs for Standard Model calculations: $M_Z = 91.187$ GeV, the Fermi constant $G_F = (1.16637 \pm 0.00001) \times 10^{-5}$ GeV^{-2} [29], $\alpha^{(5)}(M_Z) = 1/128.877 \pm 0.090$ [30], $\alpha_s(M_Z) = 0.119$ [31], $M_{\rm top} = 174.3 \pm 5.1$ GeV [31] and $M_{\rm Higgs} = 150$ GeV. The only observable effect, on M_Z, is due to the variation of $M_{\rm Higgs}$ between 100–1000 GeV (due to the variation of the γ/Z interference term which is taken from the Standard Model): M_Z changes by +0.23 MeV per unit change in $\log_{10} M_{\rm Higgs}/{\rm GeV}$, which is not an error but a correction to be applied once $M_{\rm Higgs}$ is determined. The effect is much smaller than the error on M_Z ($\pm$2.1 MeV).

55.12 Methodology of combining the LEP experimental results

The LEP experimental results actually used for combination are slightly modified from those published by the experiments (which are given in the Listings below). This has been done in order to facilitate the procedure by making the inputs more consistent. These modified results are given explicitly in [24]. The main differences compared to the published results are (a) consistent use of ZFITTER 6.23 and TOPAZ0 (the published ALEPH results used ZFITTER 6.10); (b) use of the combined energy-error matrix, which makes a difference of 0.1 MeV on the M_Z and Γ_Z for L3 only as at that intersection the RF modeling uncertainties are the largest.

Thus, nine-parameter sets from all four experiments with their covariance matrices are used together with all the common errors correlations. A grand covariance matrix, V, is constructed and a combined nine-parameter set is obtained by minimizing $\chi^2 = \Delta^T V^{-1} \Delta$, where Δ is the vector of residuals of the combined parameter set to the results of individual experiments. Imposing lepton universality in the combination results in the combined five-parameter set.

55.13 Study of $Z \to b\bar{b}$ and $Z \to c\bar{c}$

In the sector of c- and b-physics, the LEP experiments have measured the ratios of partial widths $R_b = \Gamma(Z \to b\bar{b})/\Gamma(Z \to$ hadrons), and $R_c = \Gamma(Z \to c\bar{c})/\Gamma(Z \to$ hadrons), and the forward-backward (charge) asymmetries $A_{FB}^{b\bar{b}}$ and $A_{FB}^{c\bar{c}}$. The SLD experiment at SLC has measured the ratios R_c and R_b and, utilizing the polarization of the electron beam, was able to obtain the final state coupling parameters A_b and A_c from a measurement of the left-right forward-backward asymmetry of $b-$ and $c-$quarks. The high precision measurement of R_c at SLD was made possible owing to the small beam size and very stable beam spot at SLC, coupled with a highly precise CCD pixel detector. Several of the analyses have also determined other quantities, in particular the semileptonic branching ratios, B($b \to \ell^-$), B($b \to c \to \ell^+$), and B($c \to \ell^+$), the average time-integrated $B^0\overline{B}^0$ mixing parameter $\overline{\chi}$ and the probabilities for a c–quark to fragment into a D^+, a D_s, a D^{*+} , or a charmed baryon. The latter measurements do not concern properties of the Z boson, and hence they do not appear in the Listing below. However, for completeness, we will report at the end of this minireview their values as obtained fitting the data contained in the Z section. All these quantities are correlated with the electroweak parameters, and since the mixture of b hadrons is different from the one at the $\Upsilon(4S)$, their values might differ from those measured at the $\Upsilon(4S)$.

All the above quantities are correlated to each other since:

- Several analyses (for example the lepton fits) determine more than one parameter simultaneously;
- Some of the electroweak parameters depend explicitly on the values of other parameters (for example R_b depends on R_c);
- Common tagging and analysis techniques produce common systematic uncertainties.

The LEP Electroweak Heavy Flavour Working Group has developed [32] a procedure for combining the measurements taking into account known sources of correlation. The combining procedure determines fourteen parameters: the six parameters of interest in the electroweak sector, R_b, R_c, $A_{FB}^{b\bar{b}}$, $A_{FB}^{c\bar{c}}$, A_b and A_c and, in addition, B($b \to \ell^-$), B($b \to c \to \ell^+$), B($c \to \ell^+$), $\overline{\chi}$, $f(D^+)$, $f(D_s)$, $f(c_{\rm baryon})$ and $P(c \to D^{*+}) \times$ B($D^{*+} \to \pi^+ D^0$), to take into account their correlations with the electroweak parameters. Before the fit both the peak and off-peak asymmetries are translated to the common energy $\sqrt{s} = 91.26$ GeV using the predicted energy-dependence from ZFITTER [5].

55.14 Summary of the measurements and of the various kinds of analysis

The measurements of R_b and R_c fall into two classes. In the first, named single-tag measurement, a method for selecting b and c events is applied and the number of tagged events is counted. A second technique, named double-tag measurement, has the advantage that the tagging efficiency is directly derived from the data thereby reducing the systematic error on the measurement.

The measurements in the b- and c-sector can be essentially grouped in the following categories:

- Lifetime (and lepton) double-tagging measurements of R_b. These are the most precise measurements of R_b and obviously dominate the combined result. The main sources of systematics come from the charm contamination and from estimating the hemisphere b-tagging efficiency correlation;
- Analyses with $D/D^{*\pm}$ to measure R_c. These measurements make use of several different tagging techniques (inclusive/exclusive double tag, exclusive double tag, reconstruction of all weakly decaying charmed states) and no assumptions are made on the energy-dependence of charm fragmentation;
- A measurement of R_c using single leptons and assuming B($b \to c \to \ell^+$);
- Lepton fits which use hadronic events with one or more leptons in the final state to measure the asymmetries $A_{FB}^{b\bar{b}}$ and $A_{FB}^{c\bar{c}}$. Each analysis usually gives several other electroweak parameters. The dominant sources of systematics are due to lepton identification, to other semileptonic branching ratios and to the modeling of the semileptonic decay;
- Measurements of $A_{FB}^{b\bar{b}}$ using lifetime tagged events with a hemisphere charge measurement. These measurements dominate the combined result;
- Analyses with $D/D^{*\pm}$ to measure $A_{FB}^{c\bar{c}}$ or simultaneously $A_{FB}^{b\bar{b}}$ and $A_{FB}^{c\bar{c}}$;
- Measurements of A_b and A_c from SLD, using several tagging methods (lepton, kaon, D/D^*, and vertex mass). These quantities are directly extracted from a measurement of the left–right forward–backward asymmetry in $c\bar{c}$ and $b\bar{b}$ production using a polarized electron beam.

55.15 Averaging procedure

All the measurements are provided by the LEP and SLD Collaborations in the form of tables with a detailed breakdown of

Downloaded from https://academic.oup.com/ptep/article/2022/8/083C01/6651666 by KIT Library user on 27 September 2022

the systematic errors of each measurement and its dependence on other electroweak parameters.

The averaging proceeds via the following steps:

- Define and propagate a consistent set of external inputs such as branching ratios, hadron lifetimes, fragmentation models *etc.* All the measurements are checked to ensure that all use a common set of assumptions (for instance, since the QCD corrections for the forward–backward asymmetries are strongly dependent on the experimental conditions, the data are corrected before combining);
- Form the full (statistical and systematic) covariance matrix of the measurements. The systematic correlations between different analyses are calculated from the detailed error breakdown in the measurement tables. The correlations relating several measurements made by the same analysis are also used;
- Take into account any explicit dependence of a measurement on the other electroweak parameters. As an example of this dependence, we illustrate the case of the double-tag measurement of R_b, where c-quarks constitute the main background. The normalization of the charm contribution is not usually fixed by the data and the measurement of R_b depends on the assumed value of R_c, which can be written as:

$$R_b = R_b^{\rm meas} + a(R_c)\frac{(R_c - R_c^{\rm used})}{R_c} \ , \qquad (55.11)$$

  where $R_b^{\rm meas}$ is the result of the analysis which assumed a value of $R_c = R_c^{\rm used}$ and $a(R_c)$ is the constant which gives the dependence on R_c;
- Perform a χ^2 minimization with respect to the combined electroweak parameters.

After the fit the average peak asymmetries $A_{FB}^{c\bar{c}}$ and $A_{FB}^{b\bar{b}}$ are corrected for the energy shift from 91.26 GeV to M_Z and for QED (initial state radiation), γ exchange, and γZ interference effects, to obtain the corresponding pole asymmetries $A_{FB}^{0,c}$ and $A_{FB}^{0,b}$.

This averaging procedure, using the fourteen parameters described above, and applied to the data contained in the Z particle listing below, gives the following results (where the last 8 parameters do not depend directly on the Z):

$$\begin{aligned}
R_b^0 &= 0.21629 \pm 0.00066 \\
R_c^0 &= 0.1721 \ \pm 0.0030 \\
A_{FB}^{0,b} &= 0.0992 \ \pm 0.0016 \\
A_{FB}^{0,c} &= 0.0707 \ \pm 0.0035 \\
A_b &= 0.923 \ \pm 0.020 \\
A_c &= 0.670 \ \pm 0.027
\end{aligned}$$

$$\begin{aligned}
B(b \to \ell^-) &= 0.1071 \ \pm 0.0022 \\
{\rm B}(b \to c \to \ell^+) &= 0.0801 \ \pm 0.0018 \\
B(c \to \ell^+) &= 0.0969 \ \pm 0.0031 \\
\overline{\chi} &= 0.1250 \ \pm 0.0039 \\
f(D^+) &= 0.235 \ \pm 0.016 \\
f(D_s) &= 0.126 \ \pm 0.026 \\
f(c_{\rm baryon}) &= 0.093 \ \pm 0.022 \\
P(c \to D^{*+}) \times {\rm B}(D^{*+} \to \pi^+ D^0) &= 0.1622 \ \pm 0.0048 \qquad (55.12)
\end{aligned}$$

Among the non–electroweak observables, the B semileptonic branching fraction $B(b \to \ell^-)$ is of special interest, since the dominant error source on this quantity is the dependence on the semileptonic decay model for $b \to \ell^-$, with $\Delta B(b \to \ell^-)_{b\to\ell^- -{\rm model}} = 0.0012$. Extensive studies have been made to understand the size of this error. Among the electroweak quantities, the quark asymmetries with leptons depend also on the semileptonic decay model, while the asymmetries using other methods usually do not. The fit implicitely requires that the different methods give consistent results and this effectively constrains the decay model, and thus reduces in principle the error from this source in the fit result.

To obtain a conservative estimate of the modelling error, the above fit has been repeated removing all asymmetry measurements. The results of the fit on B–decay related observables are [24]: $B(b \to \ell^-) = 0.1069 \pm 0.0022$, with $\Delta B(b \to \ell^-)_{b\to\ell^- -{\rm model}} = 0.0013$, $B(b \to c \to \ell^+) = 0.0802 \pm 0.0019$ and $\overline{\chi} = 0.1259 \pm 0.0042$.

References

[1] R. N. Cahn, Phys. Rev. D **36**, 2666 (1987), [Erratum: Phys.Rev.D 40, 922 (1989)].

[2] D. Y. Bardin *et al.*, in "LEP Physics Workshop," 89–127 (1989).

[3] A. Borrelli *et al.*, Nucl. Phys. B **333**, 357 (1990).

[4] D. Y. Bardin and G. Passarino (1998), [hep-ph/9803425]; D. Y. Bardin, M. Grunewald and G. Passarino (1999), [hep-ph/9902452].

[5] D. Bardin *et al.*, Z. Phys. C **44**, 493 (1989); D. Bardin *et al.*, Comput. Phys. Commun. **59**, 303 (1990); D. Y. Bardin *et al.*, Nucl. Phys. B **351**, 1 (1991), [hep-ph/9801208]; D. Y. Bardin *et al.*, Phys. Lett. B **255**, 290 (1991), [hep-ph/9801209]; D. Y. Bardin *et al.* (1992), [hep-ph/9412201]; D. Y. Bardin *et al.*, Comput. Phys. Commun. **133**, 229 (2001), [hep-ph/9908433].

[6] G. Burgers and F. Jegerlehner, Conf. Proc. C **8902201**, 55 (1989).

[7] D. Kennedy and B. Lynn, Nucl. Phys. B **322**, 1 (1989).

[8] M. Consoli, W. Hollik and F. Jegerlehner, in "LEP Physics Workshop," 7–54 (1989).

[9] M. Bohm *et al.*, in "LEP Physics Workshop," 203–234 (1989).

[10] P. Eberhard *et al.*, in "LEP Physics Workshop," 235–266 (1989).

[11] R. G. Stuart, Phys. Lett. B **262**, 113 (1991).

[12] A. Sirlin, Phys. Rev. Lett. **67**, 2127 (1991).

[13] A. Leike, T. Riemann and J. Rose, Phys. Lett. B **273**, 513 (1991), [hep-ph/9508390].

[14] D. Bardin *et al.*, Phys. Lett. B **206**, 539 (1988).

[15] S. Schael *et al.* (ALEPH, DELPHI, L3, OPAL, LEP Electroweak), Phys. Rept. **532**, 119 (2013), [arXiv:1302.3415].

[16] W. Beenakker, F. A. Berends and S. van der Marck, Nucl. Phys. B **349**, 323 (1991).

[17] G. Montagna *et al.*, Nucl. Phys. B **401**, 3 (1993); G. Montagna *et al.*, Comput. Phys. Commun. **76**, 328 (1993); G. Montagna *et al.*, Comput. Phys. Commun. **93**, 120 (1996), [hep-ph/9506329]; G. Montagna *et al.*, Comput. Phys. Commun. **117**, 278 (1999), [hep-ph/9804211].

[18] R. Assmann *et al.*, Eur. Phys. J. C **6**, 187 (1999).

[19] R. Assmann *et al.* (Working Group on LEP Energy), Z. Phys. C **66**, 567 (1995).

[20] L. Arnaudon *et al.* (Working Group on LEP Energy, ALEPH, DELPHI, L3, OPAL), Phys. Lett. B **307**, 187 (1993).

[21] L. Arnaudon *et al.* (Working Group on LEP energy), in "26th International Conference on High-energy Physics," (1992).

[22] L. Arnaudon *et al.* (LEP Polarization), Phys. Lett. B **284**, 431 (1992).

[23] R. Bailey *et al.*, Conf. Proc. C **900612**, 1765 (1990).

[24] S. Schael *et al.* (ALEPH, DELPHI, L3, OPAL, SLD, LEP Electroweak Working Group, SLD Electroweak Group, SLD Heavy Flavour Group), Phys. Rept. **427**, 257 (2006), [hep-ex/0509008].

[25] S. Jadach *et al.*, Comput. Phys. Commun. **102**, 229 (1997); S. Jadach and O. Nicrosini, Event generators for Bhabha scattering, in Physics at LEP2, CERN-96-01 Vol. 2, February 1996.

Downloaded from https://academic.oup.com/ptep/article/2022/8/083C01/6651666 by KIT Library user on 27 September 2022

[26] B. Ward *et al.*, Phys. Lett. B **450**, 262 (1999), [hep-ph/9811245].

[27] W. Beenakker and G. Passarino, Phys. Lett. B **425**, 199 (1998), [hep-ph/9710376].

[28] M. Martinez *et al.*, Z. Phys. C **49**, 645 (1991); M. Martinez and F. Teubert, Z. Phys. **C65**, 267 (1995), updated with results summarized in S. Jadach, B. Pietrzyk, and M. Skrzypek, Phys. Lett. **B456**, 77 (1999) and Reports of the working group on precision calculations for the Z resonance, CERN 95-03, ed. D. Bardin, W. Hollik, and G. Passarino, and references therein.

[29] T. van Ritbergen and R. G. Stuart, Phys. Lett. B **437**, 201 (1998), [hep-ph/9802341]; T. van Ritbergen and R. G. Stuart, Phys. Rev. Lett. **82**, 488 (1999), [hep-ph/9808283].

[30] S. Eidelman and F. Jegerlehner, Z. Phys. C **67**, 585 (1995), [hep-ph/9502298]; M. Steinhauser, Phys. Lett. B **429**, 158 (1998), [hep-ph/9803313].

[31] D. E. Groom *et al.* (Particle Data Group), Eur. Phys. J. C **15**, 1 (2000).

[32] Nucl. Instrum. Meth. A **378**, 101 (1996).

Downloaded from https://academic.oup.com/ptep/article/2022/8/083C01/6651666 by KIT Library user on 27 September 2022

56. Muon Anomalous Magnetic Moment

Revised August 2021 by A. Höcker (CERN) and W.J. Marciano (BNL).

The Dirac equation predicts a muon magnetic moment, $\vec{M} = g_\mu \frac{e}{2m_\mu}\vec{S}$, with gyromagnetic ratio $g_\mu = 2$. Quantum loop effects lead to a small calculable deviation from $g_\mu = 2$, parameterized by the magnetic anomaly[1]

$$a_\mu \equiv \frac{g_\mu - 2}{2} \ . \tag{56.1}$$

That quantity can be accurately measured and, within the Standard Model (SM) framework, precisely predicted. Hence, comparison of experiment and theory tests the SM at its quantum loop level. A deviation in $a_\mu^{\rm exp}$ from the SM expectation would signal effects of new physics, with current sensitivity reaching up to mass scales of $\mathcal{O}$(TeV) [1]. For recent thorough muon $g-2$ reviews, see e.g. Refs. [2–4].

The E821 experiment at Brookhaven National Lab (BNL) studied the precession of μ^+ and μ^- in a constant external magnetic field as they circulated in a confining storage ring. It found[2] [6]

$$\begin{aligned} a_{\mu^+}^{\rm exp,BNL} &= 116\,592\,040(60)(50) \times 10^{-11} \ , \\ a_{\mu^-}^{\rm exp,BNL} &= 116\,592\,150(80)(30) \times 10^{-11} \ , \end{aligned} \tag{56.2}$$

where the first errors are statistical and the second systematic. Assuming CPT invariance and taking into account correlations between systematic uncertainties, one finds for their average [5,6]

$$a_\mu^{\rm exp,BNL} = 116\,592\,089(54)(33) \times 10^{-11} \ . \tag{56.3}$$

These results represent about a factor of 14 improvement over the classic CERN experiments of the 1970's [7].

Further improvement of the measurement by a factor of four by setting up the E821 storage ring at the Fermilab National Accelerator Laboratory (FNAL), and utilizing a cleaner and more intense muon beam and improved detectors [8] is in progress. A first analysis with positive muons based on a fraction of the data found [9]

$$a_{\mu^+}^{\rm exp,FNAL} = 116\,592\,040(51)(19) \times 10^{-11} \ . \tag{56.4}$$

The FNAL result is consistent with the BNL measurement and has comparable statistical as well as improved systematic precision. Their average assuming CPT invariance reads [9]

$$a_\mu^{\rm exp} = 116\,592\,061(41) \times 10^{-11} \ , \tag{56.5}$$

providing a relative precision of 0.35 parts per million.

Another muon $g-2$ experiment with similar sensitivity but using an alternative zero-electric-field technique with a low-emittance and low-momentum muon beam is currently under construction at J-PARC in Japan [10].

The SM prediction $a_\mu^{\rm SM}$ is generally divided into three parts (see Fig. 56.1 for representative Feynman diagrams)

$$a_\mu^{\rm SM} = a_\mu^{\rm QED} + a_\mu^{\rm EW} + a_\mu^{\rm Had} \ . \tag{56.6}$$

In the following discussion we use the numerical estimates provided by the Muon $g-2$ Theory Initiative White Paper [4].

The QED part includes all photonic and leptonic (e, μ, τ) loops starting with the classic $\alpha/2\pi$ Schwinger contribution [11]. It has

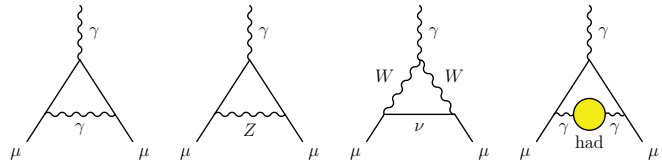

Figure 56.1: Representative diagrams contributing to $a_\mu^{\rm SM}$. From left to right: first order QED (Schwinger term), lowest-order weak, lowest-order hadronic.

been computed through five loops [4,12,13]

$$\begin{aligned} a_\mu^{\rm QED} =& \frac{\alpha}{2\pi} + 0.765\,857\,420(13)\left(\frac{\alpha}{\pi}\right)^2 + 24.050\,509\,85(23)\left(\frac{\alpha}{\pi}\right)^3 \\ &+ 130.8782(60)\left(\frac{\alpha}{\pi}\right)^4 + 751.0(9)\left(\frac{\alpha}{\pi}\right)^5 + \cdots \end{aligned} \tag{56.7}$$

with little change in the coefficients since our last update of this review. Employing $\alpha^{-1} = 137.035\,999\,046(27)$, obtained from the precise measurements of $h/m_{\rm Cs}$ [14], the Rydberg constant, and $m_{\rm Cs}/m_e$ leads to[3] [12]

$$a_\mu^{\rm QED} = 116\,584\,718.93(0.10) \times 10^{-11} \ , \tag{56.8}$$

where the small error results mainly from the uncertainties in the estimate of the six loop contribution and in α.

Loop contributions involving heavy $W^\pm, Z$ or Higgs particles are collectively labeled as $a_\mu^{\rm EW}$. They are suppressed by at least a factor of $(\alpha/\pi)\cdot(m_\mu^2/m_W^2) \simeq 4 \times 10^{-9}$. At 1-loop order [18]

$$\begin{aligned} &a_\mu^{\rm EW}[\text{1-loop}] = \\ &\frac{G_\mu m_\mu^2}{8\sqrt{2}\pi^2}\left[\frac{5}{3} + \frac{1}{3}\left(1 - 4\sin^2\theta_{\rm W}\right)^2 + \mathcal{O}\left(\frac{m_\mu^2}{M_W^2}\right) + \mathcal{O}\left(\frac{m_\mu^2}{m_H^2}\right)\right] \\ &= 194.8 \times 10^{-11} \ , \end{aligned} \tag{56.9}$$

for $\sin^2\theta_{\rm W} \equiv 1 - M_W^2/M_Z^2 \simeq 0.223$, and where $G_\mu \simeq 1.166 \times 10^{-5}$ GeV^{-2} is the Fermi coupling constant. Two-loop corrections are relatively large and negative [19]. For a Higgs boson mass of 125 GeV it amounts to $a_\mu^{\rm EW}[\text{2-loop}] = -41.2(1.0) \times 10^{-11}$ [19], where the uncertainty stems from quark triangle loops. The 3-loop leading logarithms are negligible, $\mathcal{O}(10^{-12})$ [19,20]. Overall one finds

$$a_\mu^{\rm EW} = 153.6(1.0) \times 10^{-11} \ . \tag{56.10}$$

A recent complete 2-loop numerical evaluation of the electroweak correction [21] when adjusted for appropriate light quark masses confirmed the result in Eq. (56.10).

Hadronic (quark and gluon) loop contributions to $a_\mu^{\rm SM}$ give rise to its main uncertainty. One traditionally relies on a data-driven dispersion relation approach to evaluate the lowest-order $\mathcal{O}(\alpha^2)$ hadronic vacuum polarization contribution $a_\mu^{\rm Had}[\text{LO}]$ from corresponding cross section measurements [22]

$$a_\mu^{\rm Had}[\text{LO}] = \frac{1}{3}\left(\frac{\alpha}{\pi}\right)^2 \int_{m_\pi^2}^{\infty} ds\, \frac{K(s)}{s} R^{(0)}(s) \ , \tag{56.11}$$

[1] Also referred to as *anomalous magnetic moment* despite being dimensionless.

[2] The results reported by the experiment have been updated in Eqs. (56.2) and (56.3) to the newest value for the absolute muon-to-proton magnetic ratio $\lambda = 3.183\,345\,142(71)$ [5]. The change induced in $a_\mu^{\rm exp}$ with respect to the value of $\lambda = 3.183\,345\,39(10)$ used in Ref. [6] amounts to $+10 \times 10^{-11}$.

[3] A recent measurement using Rb-87 atoms [15] resulted in $\alpha^{-1} = 137.035\,999\,206(11)$, which exhibits a larger than 5σ discrepancy with the Cs-133 based result. Using this value in Eq. (56.7) leads to a reduction of $a_\mu^{\rm QED}$ by 0.14×10^{-11}, which is larger than the quoted uncertainty in Eq. (56.8), but still negligible compared to other uncertainties affecting $a_\mu^{\rm SM}$. This discrepancy impacts, however, the SM prediction of the magnetic anomaly of the electron [13,16], which differs by respectively -2.4σ and $+1.6\sigma$ from the experimental value [17], depending on whether the Cs-133 or Rb-87 based α value is used.

Downloaded from https://academic.oup.com/ptep/article/2022/8/083C01/6651666 by KIT Library user on 27 September 2022

where $K(s)$ is a QED kernel function [23], and where $R^{(0)}(s)$ denotes the ratio of the bare[4] cross section for e^+e^- annihilation into hadrons to the pointlike muon-pair cross section at center-of-mass energy $\sqrt{s}$. The function $K(s) \sim 1/s$ in Eq. (56.11) emphasizes the low-energy part of the integral so that $a_\mu^{\rm Had}[{\rm LO}]$ is dominated by the $\rho(770) \to \pi^+\pi^-$ resonance.

The analysis of Eq. (56.11) results in the representative value [4, 24–29]

$$a_\mu^{\rm Had}[{\rm LO}] = 6\,931(40) \times 10^{-11}\,, \qquad (56.12)$$

whose error is dominated by systematic uncertainties in the $e^+e^- \to$ hadrons cross-section data, and also includes a small uncertainty due to perturbative QCD, which is used at intermediate and large energies in the dispersion integral to predict the contribution from the quark-antiquark continuum. The experimental precision is currently limited by a discrepancy between the most precise $\pi^+\pi^-$ data from the BABAR and KLOE experiments [26, 28].

Alternatively, one can use precise vector spectral functions from $\tau \to \nu_\tau +$ hadrons decays [30] that can be related to isovector $e^+e^- \to$ hadrons cross sections by isospin symmetry. Analyses replaced e^+e^- data in the two-pion and four-pion channels by the corresponding isospin- transformed τ data, and applied isospin-violating corrections [31]. Owing to the progress in the precision of the e^+e^- data, the τ data are now less precise and less reliable due to additional theoretical uncertainties, so that recent $a_\mu^{\rm Had}[{\rm LO}]$ evaluations ignored them.

Progress has been achieved on the evaluation of $a_\mu^{\rm Had}[{\rm LO}]$ using lattice QCD, which allows to directly compute the real part of the two-point correlation function without invoking the resonances occurring on the imaginary axis [32–34]. The required sub-percent precision represents a challenge requiring to master systematic and extrapolation uncertainties. A combination of recent lattice QCD evaluations [35, 36] gives [4]

$$a_\mu^{\rm Had}[{\rm LO}] = 7\,116(184) \times 10^{-11}\,, \qquad (56.13)$$

with an uncertainty that is not yet competitive with the data-driven approach. Another recent lattice QCD calculation with much reduced uncertainty found [37]

$$a_\mu^{\rm Had}[{\rm LO}] = 7\,075(55) \times 10^{-11}\,, \qquad (56.14)$$

whose error is dominated by systematic uncertainties. It exhibits a 2.1σ tension with the data-driven result, growing up to 3.7σ for the modified observable $a_{\mu,{\rm win}}$ that has favourable properties for computation on the lattice[5] [36, 37, 39]. Because of the complexity and challenges of such a calculation, it is critical that it is confronted with independent lattice results of comparable precision [36, 39, 40].

Higher order hadronic loop contributions are also obtained from dispersion relations using the same $e^+e^- \to$ hadrons data but with different integration kernels [41]. Recent evaluations found $a_\mu^{\rm Had,Disp}[{\rm NLO}] = (-98.3 \pm 0.7) \times 10^{-11}$ [4, 29] and $a_\mu^{\rm Had,Disp}[{\rm NNLO}] = (12.4 \pm 0.1) \times 10^{-11}$ [42]. In the case of hadronic light-by-light scattering contributions, which enter at NLO, recent studies [3, 4, 43, 44] based on short-distance QCD, dispersion relations and lattice QCD calculations lead to the improved prediction $a_\mu^{\rm Had,LBL}[{\rm NLO}] = 92(18) \times 10^{-11}$ [4].[6] One thus finds for the sum of the three higher order hadronic terms

$$a_\mu^{\rm Had}[{\rm N(N)LO}] = 6(18) \times 10^{-11}\,, \qquad (56.15)$$

where the error is dominated by the hadronic light-by-light scattering uncertainty.

Adding Eqs. (56.8), (56.10), (56.12) and (56.15) gives the representative SM prediction

$$a_\mu^{\rm SM} = 116\,591\,810(1)(40)(18) \times 10^{-11}\,, \qquad (56.16)$$

whose errors are due to the electroweak, lowest-order hadronic, and higher-order hadronic contributions, respectively. The difference between experiment and theory

$$\Delta a_\mu = a_\mu^{\rm exp} - a_\mu^{\rm SM} = 251(41)(43) \times 10^{-11}\,, \qquad (56.17)$$

where the errors are from experiment and theory prediction (with all errors combined in quadrature, taking into account a small anticorrelation [4] between the data-driven lowest and higher order contributions), represents an interesting but not yet conclusive discrepancy of 4.2σ.[7] The new FNAL measurement has increased the discrepancy with the SM prediction (56.16) from previously 3.7σ. Figure 56.2 represents the difference between experimental and predicted a_μ values based on the most recent data-driven and lattice QCD based evaluations of $a_\mu^{\rm Had}[{\rm LO}]$.

A leading candidate explanation for the deviation observed in Δa_μ has been supersymmetry particle loop contributions. Such a scenario is quite natural, since generically, supersymmetric models predict [1] an additional contribution to $a_\mu^{\rm SM}$

$$a_\mu^{\rm SUSY} \simeq \pm 130 \times 10^{-11} \cdot \left(\frac{100\ {\rm GeV}}{m_{\rm SUSY}}\right)^2 \tan\beta\,, \qquad (56.18)$$

where $m_{\rm SUSY}$ is a representative supersymmetric mass scale, $\tan\beta \simeq 3$–40 a potential enhancement factor, and ± 1 corresponds to the sign of the μ term in the supersymmetric Lagrangian. Supersymmetric particles in the mass range 100–500 GeV could be

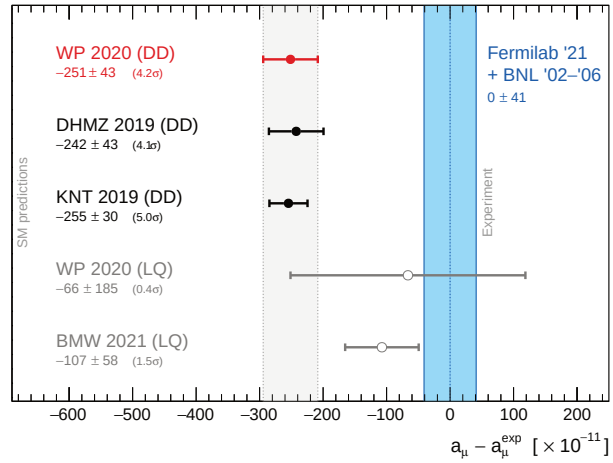

Figure 56.2: Compilation of recent results for a_μ (in units of 10^{-11}), subtracted by the central value of the experimental average (56.3). The light blue vertical band indicates the total experimental uncertainty. The SM predictions shown differ only in the value used for the $a_\mu^{\rm Had}[{\rm LO}]$ contribution. They are taken from: WP 2020 [4] (Eq. (56.16), also indicated by the light grey vertical band), DHMZ 2019 [28], KNT 2019 [29], all three based on the data-driven (DD) $a_\mu^{\rm Had}[{\rm LO}]$ evaluation, and the lattice QCD (LQ) based evaluations WP 2020 [4, 35, 36] and BMW 2021 [37]. Note that the quoted errors in the figure do not include the uncertainty on the subtracted experimental value. To obtain for each theory calculation a result equivalent to Eq. (56.17), the errors from theory and experiment must be added in quadrature.

[4] The bare cross section is defined as the measured cross section corrected for initial-state radiation, electron-vertex loop contributions and vacuum-polarization effects in the photon propagator. However, QED effects in the hadron vertex and final state, as photon radiation, are included.

[5] A dispersive approach similar to that for $a_\mu^{\rm Had}[{\rm LO}]$ is used to determine the hadronic contribution to the running of the electromagnetic fine structure constant at the Z-boson mass $\Delta\alpha_{\rm had}(m_Z)$, which is a critical ingredient of the global electroweak fit. One may therfore ask if the goodness of that fit would break down were $a_\mu^{\rm Had}[{\rm LO}]$ in Eq. (56.12) be brought in compatibility with the result (56.14). However, the difference in the relevant integration kernels (whereas 73% of the contribution to $a_\mu^{\rm Had}[{\rm LO}]$ stems from the $\pi^+\pi^-$ channel, it is only 13% in the case of $\Delta\alpha_{\rm had}(m_Z)$) allows to absorb large effects in $a_\mu^{\rm Had}[{\rm LO}]$ without creating a significant tension in the electroweak fit. Detailed discussions are available in the literature [38].

[6] A very recent lattice QCD based calculation of $a_\mu^{\rm Had,LBL}[{\rm NLO}]$ [45], not included in [4], gives a consistent result with [4, 44] using a different approach.

[7] The probabilistic interpretation of the discrepancy requires caution due to the systematic nature of the $a_\mu^{\rm SM}$ uncertainty.

Downloaded from https://academic.oup.com/ptep/article/2022/8/083C01/6651666 by KIT Library user on 27 September 2022

the source of the deviation Δa_μ. If so, those particles should be directly observable at the Large Hadron Collider at CERN. So far, there is however no direct evidence in support of the supersymmetry interpretation.

New physics effects [1] other than supersymmetry could also explain a non-vanishing Δa_μ. A popular scenario involves the "dark photon", a relatively light hypothetical vector boson from the dark matter sector that couples to our world of particle physics through mixing with the ordinary photon [46–48]. As a result, it couples to ordinary charged particles with strength $\varepsilon \cdot e$ and gives rise to an additional muon magnetic anomaly contribution

$$a_\mu^{\text{dark photon}} = \frac{\alpha}{2\pi}\varepsilon^2 F(m_V/m_\mu)\,, \tag{56.19}$$

where $F(x) = \int_0^1 2z(1-z)^2/[(1-z)^2 + x^2 z]\,dz$. For values of $\varepsilon \sim 1\text{–}2 \times 10^{-3}$ and $m_V \sim 10\text{–}100\,\text{MeV}$, the dark photon, which was originally motivated by cosmology, can provide a viable solution to the muon $g-2$ discrepancy. However, experimental constraints appear to rule out the simplest model in which the dark photon has equal couplings to electrons and muons and decays primarily to e^+e^- pairs [49] or invisible dark particles [50] that give rise to missing event energy. One can expand the dark photon scenario into a more complete theory in which several new particles contribute to the muon $g-2$. Direct searches for a dark photon, therefore, continue to be well motivated, but with primary guidance coming from astrophysics [51].

Recent popular solutions to the muon anomaly discrepancy have also focused on loop contributions induced by relatively light scalar or pseudo scalar particle appendages from physics beyond the SM [52, 53].

References

[1] A. Czarnecki and W. J. Marciano, Phys. Rev. D **64**, 013014 (2001), [hep-ph/0102122]; M. Davier and W. Marciano, Ann. Rev. Nucl. Part. Sci. **54**, 115 (2004).

[2] J. P. Miller, E. de Rafael and B. Roberts, Rept. Prog. Phys. **70**, 795 (2007), [hep-ph/0703049]; F. Jegerlehner and A. Nyffeler, Phys. Rept. **477**, 1 (2009), [arXiv:0902.3360]; J. P. Miller *et al.*, Ann. Rev. Nucl. Part. Sci. **62**, 237 (2012).

[3] F. Jegerlehner, Springer Tracts Mod. Phys. **274**, 1 (2017).

[4] T. Aoyama *et al.*, Phys. Rept. **887**, 1 (2020), [arXiv:2006.04822].

[5] P. J. Mohr, D. B. Newell and B. N. Taylor, Rev. Mod. Phys. **88**, 3, 035009 (2016), [arXiv:1507.07956].

[6] G. Bennett *et al.* (Muon g-2), Phys. Rev. Lett. **89**, 101804 (2002), [Erratum: Phys.Rev.Lett. 89, 129903 (2002)], [hep-ex/0208001]; G. Bennett *et al.* (Muon g-2), Phys. Rev. Lett. **92**, 161802 (2004), [hep-ex/0401008]; G. Bennett *et al.* (Muon g-2), Phys. Rev. D **73**, 072003 (2006), [hep-ex/0602035].

[7] J. Bailey *et al.* (CERN-Mainz-Daresbury), Nucl. Phys. B **150**, 1 (1979).

[8] J. Grange *et al.* (Muon g-2) (2015), [arXiv:1501.06858].

[9] B. Abi *et al.* (Muon g-2), Phys. Rev. Lett. **126**, 14, 141801 (2021), [arXiv:2104.03281].

[10] M. Abe *et al.*, PTEP **2019**, 5, 053C02 (2019), [arXiv:1901.03047].

[11] J. S. Schwinger, Phys. Rev. **73**, 416 (1948).

[12] T. Aoyama *et al.*, Phys. Rev. Lett. **109**, 111808 (2012), [arXiv:1205.5370]; T. Aoyama *et al.*, Phys. Rev. Lett. **109**, 111807 (2012), [arXiv:1205.5368]; T. Kinoshita and M. Nio, Phys. Rev. D **73**, 013003 (2006), [hep-ph/0507249]; T. Aoyama *et al.*, Phys. Rev. Lett. **99**, 110406 (2007), [arXiv:0706.3496]; T. Kinoshita and M. Nio, Phys. Rev. D **70**, 113001 (2004), [hep-ph/0402206]; T. Kinoshita, Nucl. Phys. B Proc. Suppl. **144**, 206 (2005); T. Kinoshita and M. Nio, Phys. Rev. D **73**, 053007 (2006), [hep-ph/0512330]; S. Laporta, Phys. Lett. B **772**, 232 (2017), [arXiv:1704.06996]; A. Kurz *et al.*, Phys. Rev. D **93**, 5, 053017 (2016), [arXiv:1602.02785]; A. Kataev, in "12th Lomonosov Conference on Elementary Particle Physics," 345–349 (2006), [hep-ph/0602098]; M. Passera, J. Phys. G **31**, R75 (2005), [hep-ph/0411168].

[13] T. Aoyama, T. Kinoshita and M. Nio, Atoms **7**, 1, 28 (2019).

[14] R. H. Parker *et al.*, Science **360**, 191 (2018), [arXiv:1812.04130].

[15] L. Morel *et al.*, Nature **588**, 7836, 61 (2020).

[16] T. Aoyama *et al.*, Phys. Rev. D **91**, 3, 033006 (2015), [Erratum: Phys.Rev.D 96, 019901 (2017)], [arXiv:1412.8284].

[17] D. Hanneke, S. Fogwell and G. Gabrielse, Phys. Rev. Lett. **100**, 120801 (2008), [arXiv:0801.1134]; D. Hanneke, S. F. Hoogerheide and G. Gabrielse, Phys. Rev. A **83**, 052122 (2011), [arXiv:1009.4831].

[18] R. Jackiw and S. Weinberg, Phys. Rev. D **5**, 2396 (1972); G. Altarelli, N. Cabibbo and L. Maiani, Phys. Lett. B **40**, 415 (1972); I. Bars and M. Yoshimura, Phys. Rev. D **6**, 374 (1972); K. Fujikawa, B. Lee and A. Sanda, Phys. Rev. D **6**, 2923 (1972).

[19] C. Gnendiger, D. Stöckinger and H. Stöckinger-Kim, Phys. Rev. D **88**, 053005 (2013), [arXiv:1306.5546]; A. Czarnecki, W. J. Marciano and A. Vainshtein, Phys. Rev. D **67**, 073006 (2003), [Erratum: Phys.Rev.D 73, 119901 (2006)], [hep-ph/0212229]; S. Heinemeyer, D. Stockinger and G. Weiglein, Nucl. Phys. B **699**, 103 (2004), [hep-ph/0405255]; T. Gribouk and A. Czarnecki, Phys. Rev. D **72**, 053016 (2005), [hep-ph/0509205]; A. Czarnecki, B. Krause and W. J. Marciano, Phys. Rev. Lett. **76**, 3267 (1996), [hep-ph/9512369]; A. Czarnecki, B. Krause and W. J. Marciano, Phys. Rev. D **52**, 2619 (1995), [hep-ph/9506256]; S. Peris, M. Perrottet and E. de Rafael, Phys. Lett. B **355**, 523 (1995), [hep-ph/9505405]; T. Kukhto *et al.*, Nucl. Phys. B **371**, 567 (1992).

[20] G. Degrassi and G. Giudice, Phys. Rev. D **58**, 053007 (1998), [hep-ph/9803384].

[21] T. Ishikawa, N. Nakazawa and Y. Yasui, Phys. Rev. D **99**, 7, 073004 (2019), [arXiv:1810.13445].

[22] C. Bouchiat and L. Michel, J. Phys. Radium **22**, 2, 121 (1961); M. Gourdin and E. De Rafael, Nucl. Phys. B **10**, 667 (1969).

[23] S. J. Brodsky and E. De Rafael, Phys. Rev. **168**, 1620 (1968).

[24] M. Davier *et al.*, Eur. Phys. J. **C77**, 12, 827 (2017), [arXiv:1706.09436].

[25] A. Keshavarzi, D. Nomura and T. Teubner, Phys. Rev. D **97**, 11, 114025 (2018), [arXiv:1802.02995].

[26] G. Colangelo, M. Hoferichter and P. Stoffer, JHEP **02**, 006 (2019), [arXiv:1810.00007].

[27] M. Hoferichter, B.-L. Hoid and B. Kubis, JHEP **08**, 137 (2019), [arXiv:1907.01556].

[28] M. Davier *et al.*, Eur. Phys. J. C **80**, 3, 241 (2020), [Erratum: Eur.Phys.J.C 80, 410 (2020)], [arXiv:1908.00921].

[29] A. Keshavarzi, D. Nomura and T. Teubner, Phys. Rev. D **101**, 1, 014029 (2020), [arXiv:1911.00367].

[30] R. Alemany, M. Davier and A. Hocker, Eur. Phys. J. C **2**, 123 (1998), [hep-ph/9703220].

[31] M. Davier *et al.*, Eur. Phys. J. C **71**, 1515 (2011), [Erratum: Eur.Phys.J.C 72, 1874 (2012)], [arXiv:1010.4180].

[32] T. Blum, Phys. Rev. Lett. **91**, 052001 (2003), [hep-lat/0212018].

[33] D. Bernecker and H. B. Meyer, Eur. Phys. J. A **47**, 148 (2011), [arXiv:1107.4388].

[34] W. A. Bardeen, R. Gastmans and B. E. Lautrup, Nucl. Phys. B **46**, 319 (1972).

[35] B. Chakraborty *et al.* (Fermilab Lattice, LATTICE-HPQCD, MILC), Phys. Rev. Lett. **120**, 15, 152001 (2018), [arXiv:1710.11212]; S. Borsanyi *et al.* (Budapest-Marseille-Wuppertal), Phys. Rev. Lett. **121**, 2, 022002 (2018),

Downloaded from https://academic.oup.com/ptep/article/2022/8/083C01/6651666 by KIT Library user on 27 September 2022

[arXiv:1711.04980]; T. Blum *et al.* (RBC, UKQCD), Phys. Rev. Lett. **121**, 2, 022003 (2018), [arXiv:1801.07224]; D. Giusti *et al.* (ETM), Phys. Rev. **D99**, 11, 114502 (2019), [arXiv:1901.10462]; E. Shintani and Y. Kuramashi, Phys. Rev. **D100**, 3, 034517 (2019), [arXiv:1902.00885]; C. T. H. Davies *et al.* (Fermilab Lattice, LATTICE-HPQCD, MILC), Phys. Rev. **D101**, 3, 034512 (2020), [arXiv:1902.04223]; A. Gérardin *et al.*, Phys. Rev. **D100**, 1, 014510 (2019), [arXiv:1904.03120].

[36] C. Aubin *et al.*, Phys. Rev. **D101**, 1, 014503 (2020), [arXiv:1905.09307]; D. Giusti and S. Simula, PoS **LATTICE2019**, 104 (2019), [arXiv:1910.03874].

[37] S. Borsanyi *et al.*, Nature **593**, 7857, 51 (2021), [arXiv:2002.12347].

[38] A. Crivellin *et al.*, Phys. Rev. Lett. **125**, 9, 091801 (2020), [arXiv:2003.04886]; A. Keshavarzi *et al.*, Phys. Rev. D **102**, 3, 033002 (2020), [arXiv:2006.12666]; E. de Rafael, Phys. Rev. D **102**, 5, 056025 (2020), [arXiv:2006.13880]; B. Malaescu and M. Schott, Eur. Phys. J. C **81**, 1, 46 (2021), [arXiv:2008.08107]; G. Colangelo, M. Hoferichter and P. Stoffer, Phys. Lett. B **814**, 136073 (2021), [arXiv:2010.07943].

[39] T. Blum *et al.* (RBC, UKQCD), Phys. Rev. Lett. **121**, 2, 022003 (2018), [arXiv:1801.07224].

[40] C. Lehner and A. S. Meyer, Phys. Rev. D **101**, 074515 (2020), [arXiv:2003.04177].

[41] B. Krause, Phys. Lett. B **390**, 392 (1997), [hep-ph/9607259].

[42] A. Kurz *et al.*, Phys. Lett. B **734**, 144 (2014), [arXiv:1403.6400].

[43] K. Melnikov and A. Vainshtein, Phys. Rev. **D70**, 113006 (2004), [hep-ph/0312226]; P. Masjuan and P. Sánchez-Puertas, Phys. Rev. **D95**, 5, 054026 (2017), [arXiv:1701.05829]; G. Colangelo *et al.*, JHEP **04**, 161 (2017), [arXiv:1702.07347]; M. Hoferichter *et al.*, JHEP **10**, 141 (2018), [arXiv:1808.04823]; A. Gérardin, H. B. Meyer and A. Nyffeler, Phys. Rev. **D100**, 3, 034520 (2019), [arXiv:1903.09471]; J. Bijnens, N. Hermansson-Truedsson and A. Rodríguez-Sánchez, Phys. Lett. **B798**, 134994 (2019), [arXiv:1908.03331]; G. Colangelo *et al.*, JHEP **03**, 101 (2020), [arXiv:1910.13432]; V. Pauk and M. Vanderhaeghen, Eur. Phys. J. **C74**, 8, 3008 (2014), [arXiv:1401.0832]; I. Danilkin and M. Vanderhaeghen, Phys. Rev. **D95**, 1, 014019 (2017), [arXiv:1611.04646]; M. Knecht *et al.*, Phys. Lett. **B787**, 111 (2018), [arXiv:1808.03848]; G. Eichmann, C. S. Fischer and R. Williams, Phys. Rev. **D101**, 5, 054015 (2020), [arXiv:1910.06795]; P. Roig and P. Sánchez-Puertas, Phys. Rev. **D101**, 7, 074019 (2020), [arXiv:1910.02881]; G. Colangelo *et al.*, Phys. Lett. **B735**, 90 (2014), [arXiv:1403.7512].

[44] T. Blum *et al.*, Phys. Rev. Lett. **124**, 13, 132002 (2020), [arXiv:1911.08123].

[45] E.-H. Chao *et al.*, Eur. Phys. J. C **81**, 7, 651 (2021), [arXiv:2104.02632].

[46] P. Fayet, Phys. Rev. D **75**, 115017 (2007), [hep-ph/0702176].

[47] M. Pospelov, Phys. Rev. D **80**, 095002 (2009), [arXiv:0811.1030].

[48] D. Tucker-Smith and I. Yavin, Phys. Rev. D **83**, 101702 (2011), [arXiv:1011.4922].

[49] J. Batley *et al.* (NA48/2), Phys. Lett. B **746**, 178 (2015), [arXiv:1504.00607].

[50] Y. M. Andreev *et al.* (NA64), Phys. Rev. Lett. **126**, 21, 211802 (2021), [arXiv:2102.01885]; J. P. Lees *et al.* (BaBar), Phys. Rev. Lett. **119**, 13, 131804 (2017), [arXiv:1702.03327].

[51] J. Alexander *et al.* (2016), [arXiv:1608.08632].

[52] K.-m. Cheung, C.-H. Chou and O. C. W. Kong, Phys. Rev. D **64**, 111301 (2001), [hep-ph/0103183].

[53] D. Chang *et al.*, Phys. Rev. D **63**, 091301 (2001), [hep-ph/0009292].

Downloaded from https://academic.oup.com/ptep/article/2022/8/083C01/6651666 by KIT Library user on 27 September 2022

57. Muon Decay Parameters

Revised August 2021 by W. Fetscher (ETH Zurich) and H.-J. Gerber (ETH Zurich).

57.1 Introduction:

All measurements in direct muon decay, $\mu^- \to e^- + 2$ neutrals, and its inverse, $\nu_\mu + e^- \to \mu^-$ + neutral, are successfully described by the "V-A interaction," which is a particular case of a local, derivative-free, lepton-number-conserving, four-fermion interaction [1]. As shown below, within this framework, the Standard Model assumptions, such as the V-A form and the nature of the neutrals (ν_μ and $\bar{\nu}_e$), and hence the doublet assignments $(\nu_e\, e^-)_L$ and $(\nu_\mu\, \mu^-)_L$, have been determined from experiments [2,3]. All considerations on muon decay are valid for the leptonic tau decays $\tau^- \to \ell^- + \nu_\tau + \bar{\nu}_\ell$ with the replacements $m_\mu \to m_\tau$, $m_e \to m_{ell}$, $\ell^- = e^-, \mu^-$.

57.2 Parameters:

The differential decay probability to obtain an $e^\pm$ with (reduced) energy between x and $x + \mathrm{d}x$, emitted in the direction $\widehat{\boldsymbol{x}}_3$ at an angle between ϑ and $\vartheta + \mathrm{d}\vartheta$ with respect to the muon polarization vector $\boldsymbol{P}_\mu$, and with its spin parallel to the arbitrary direction $\widehat{\boldsymbol{\zeta}}$, neglecting radiative corrections, is given by

$$\begin{aligned}\frac{\mathrm{d}^2\Gamma}{\mathrm{d}x\,\mathrm{d}\cos\vartheta} &= \frac{m_\mu}{4\pi^3}\, W_{e\mu}^4\, G_\mathrm{F}^2\, \sqrt{x^2 - x^{2_0}} \\ &\quad \times (F_\mathrm{IS}(x) \pm P_\mu \cos\vartheta F_\mathrm{AS}(x)) \\ &\quad \times \left[1 + \widehat{\boldsymbol{\zeta}} \cdot \boldsymbol{P}_e(x,\vartheta)\right] \ . \end{aligned} \tag{57.1}$$

Here, $W_{e\mu} = \max(E_e) = (m_\mu^2 + m_e^2)/2m_\mu$ is the maximum $e^\pm$ energy, $x = E_e/W_{e\mu}$ is the reduced energy, $x_0 = m_e/W_{e\mu} = 9.67 \times 10^{-3}$, and $P_\mu = |\boldsymbol{P}_\mu|$ is the degree of muon polarization. $\widehat{\boldsymbol{\zeta}}$ is the direction in which a perfect polarization-sensitive electron detector is most sensitive. The isotropic part of the spectrum, $F_\mathrm{IS}(x)$, the anisotropic part $F_\mathrm{AS}(x)$, and the electron polarization, $\boldsymbol{P}_e(x,\vartheta)$, may be parametrized by the Michel parameter ρ [1], by η [4], by ξ and δ [5,6], *etc.* These are bilinear combinations of the coupling constants $g^\gamma_{\varepsilon\mu}$, which occur in the matrix element (given below).

If the masses of the neutrinos as well as x_0^2 are neglected, the energy and angular distribution of the electron in the rest frame of a muon ($\mu^\pm$) measured by a polarization insensitive detector, is given by

$$\begin{aligned}\frac{\mathrm{d}^2\Gamma}{\mathrm{d}x\,\mathrm{d}\cos\vartheta} \sim x^2 \cdot \Bigg\{ & 3(1-x) + \frac{2\rho}{3}(4x-3) + 3\eta\, x_0(1-x)/x \\ & \pm P_\mu \cdot \xi \cdot \cos\vartheta \left[1 - x + \frac{2\delta}{3}(4x-3)\right]\Bigg\} \ . \end{aligned} \tag{57.2}$$

Here, ϑ is the angle between the electron momentum and the muon spin, and $x \equiv 2E_e/m_\mu$. For the Standard Model coupling, we obtain $\rho = \xi\delta = 3/4$, $\xi = 1$, $\eta = 0$ and the differential decay rate is

$$\frac{\mathrm{d}^2\Gamma}{\mathrm{d}x\,\mathrm{d}\cos\vartheta} = \frac{G_\mathrm{F}^2 m_\mu^5}{192\pi^3}\, [3 - 2x \pm P_\mu \cos\vartheta(2x-1)] \cdot x^2 \,. \tag{57.3}$$

The coefficient in front of the square bracket is the total decay rate.

If only the neutrino masses are neglected, and if the $e^\pm$ polarization is detected, then the functions in Eq. (57.1) become

$$F_\mathrm{IS}(x) = x\,(1-x) + \tfrac{2}{9}\,\rho\,(4x^2 - 3x - x_0^2) + \eta \cdot x_0\,(1-x) \tag{57.4a}$$

$$\begin{aligned}F_\mathrm{AS}(x) = \tfrac{1}{3}\,\xi\,\sqrt{x^2 - x_0^2} \\ \times \left[(1-x) + \tfrac{2}{3}\delta\left\{(4x-3) + \left(\sqrt{1-x_0^2} - 1\right)\right\}\right]\end{aligned} \tag{57.4b}$$

$$\boldsymbol{P}_e(x,\vartheta) = P_{\mathrm{T}_1} \cdot \widehat{\boldsymbol{x}}_1 + P_{\mathrm{T}_2} \cdot \widehat{\boldsymbol{x}}_2 + P_\mathrm{L} \cdot \widehat{\boldsymbol{x}}_3 \tag{57.4c}$$

Here $\widehat{\boldsymbol{x}}_1$, $\widehat{\boldsymbol{x}}_2$, and $\widehat{\boldsymbol{x}}_3$ are orthogonal unit vectors defined as follows:

$\widehat{\boldsymbol{x}}_3$	is along the e momentum $\boldsymbol{p}_e$
$\dfrac{\widehat{\boldsymbol{x}}_3 \times \boldsymbol{P}_\mu}{\lvert\widehat{\boldsymbol{x}}_3 \times \boldsymbol{P}_\mu\rvert} = \widehat{\boldsymbol{x}}_2$	is transverse to $\boldsymbol{p}_e$ and perpendicular to "the decay plane"
$\widehat{\boldsymbol{x}}_2 \times \widehat{\boldsymbol{x}}_3 = \widehat{\boldsymbol{x}}_1$	is transverse to $\boldsymbol{p}_e$ and in the decay plane

The components of $\boldsymbol{P}_e$ then are given by

$$P_{\mathrm{T}_1}(x,\vartheta) = P_\mu \sin\vartheta \cdot F_{\mathrm{T}_1}(x) / \{F_\mathrm{IS}(x) \pm P_\mu \cos\vartheta \cdot F_\mathrm{AS}(x)\} \tag{57.5a}$$

$$P_{\mathrm{T}_2}(x,\vartheta) = P_\mu \sin\vartheta \cdot F_{\mathrm{T}_2}(x) / \{F_\mathrm{IS}(x) \pm P_\mu \cos\vartheta \cdot F_\mathrm{AS}(x)\} \tag{57.5b}$$

$$P_\mathrm{L}(x,\vartheta) = \frac{\pm F_\mathrm{IP}(x) + P_\mu \cos\vartheta \cdot F_\mathrm{AP}(x)}{F_\mathrm{IS}(x) \pm P_\mu \cos\vartheta \cdot F_\mathrm{AS}(x)} \quad , \tag{57.5c}$$

where

$$\begin{aligned}F_{\mathrm{T}_1}(x) = \tfrac{1}{12}\Big\{ & -2\left[\xi'' + 12\left(\rho - \tfrac{3}{4}\right)\right](1-x)x_0 \\ & -3\,\eta\left(x^2 - x_0^2\right) + \eta''\left(-3x^2 + 4x - x_0^2\right)\Big\}\end{aligned} \tag{57.6a}$$

$$F_{\mathrm{T}_2}(x) = \tfrac{1}{3}\,\sqrt{x^2 - x_0^2} \cdot \left\{3\,\frac{\alpha'}{A}(1-x) + 2\,\frac{\beta'}{A}\sqrt{1-x_0^2}\right\} \tag{57.6b}$$

$$\begin{aligned}F_\mathrm{IP}(x) = \tfrac{1}{54}\sqrt{x^2 - x_0^2} \cdot \Big\{ & 9\,\xi'\left(-2x + 2 + \sqrt{1-x_0^2}\right) \\ & +4\,\xi\left(\delta - \tfrac{3}{4}\right)\left(4x - 4 + \sqrt{1-x_0^2}\right)\Big\}\end{aligned} \tag{57.6c}$$

$$\begin{aligned}F_\mathrm{AP}(x) = \tfrac{1}{6}\Big\{ & \xi''\left(2x^2 - x - x_0^2\right) + 4\left(\rho - \tfrac{3}{4}\right)\left(4x^2 - 3x - x_0^2\right) \\ & + 2\,\eta''(1-x)\,x_0\Big\}\,.\end{aligned} \tag{57.6d}$$

For the experimental values of the parameters ρ, ξ, ξ', ξ'', δ, η, η'', α/A, β/A, α'/A, β'/A, which are not all independent, see the Data Listings below. Experiments in the past have also been analyzed using the parameters a, b, c, a', b', c', α/A, β/A, α'/A, β'/A (and $\eta = (\alpha - 2\beta)/2A$), as defined by Kinoshita and Sirlin [5,6]. They serve as a model-independent summary of all possible measurements on the decay electron (see Listings below). The relations between the two sets of parameters are

$$\rho - \tfrac{3}{4} = \tfrac{3}{4}\,(-a + 2\,c)/A \tag{57.7a}$$

$$\eta = (\alpha - 2\beta)/A \tag{57.7b}$$

$$\eta'' = (3\,\alpha + 2\,\beta)/A \tag{57.7c}$$

$$\delta - \tfrac{3}{4} = \tfrac{9}{4} \cdot \frac{(a' - 2\,c')\,/A}{1 - [a + 3\,a' + 4\,(b + b') + 6\,c - 14\,c']\,/A} \tag{57.7d}$$

$$1 - \xi\,\frac{\delta}{\rho} = 4\,\frac{[(b + b') + 2\,(c - c')]\,/A}{1 - (a - 2\,c)/A} \tag{57.7e}$$

$$1 - \xi = \left[\left(a + a'\right) + 4\left(b + b'\right) + 6\left(c + c'\right)\right]/A \tag{57.7f}$$

$$1 - \xi'' = (-2\,a + 20\,c)/A \tag{57.7g}$$

$$\text{with} \qquad A = a + 4\,b + 6\,c \tag{57.7h}$$

The differential decay probability to obtain a *left-handed* ν_e with (reduced) energy between y and $y + dy$, neglecting radiative corrections as well as the masses of the electron and of the neutrinos, is given by [7]

$$\frac{\mathrm{d}\Gamma}{\mathrm{d}y} = \frac{m_\mu^5 G_\mathrm{F}^2}{16\,\pi^3} \cdot Q_L^{\nu_e} \cdot y^2 \left\{(1-y) - \omega_L \cdot \left(y - \tfrac{3}{4}\right)\right\} \,. \tag{57.8}$$

Downloaded from https://academic.oup.com/ptep/article/2022/8/083C01/6651666 by KIT Library user on 27 September 2022

Here, $y = 2\ E_{\nu_e}/m_\mu$. $Q_L^{\nu_e}$ and ω_L are parameters. ω_L is the neutrino analog of the spectral shape parameter ρ of Michel. Since in the Standard Model, $Q_L^{\nu_e} = 1$, $\omega_L = 0$, the measurement of $\mathrm{d}\Gamma/\mathrm{d}y$ has allowed a null-test of the Standard Model (see Listings below).

Table 57.1: Coupling constants $g^\gamma_{\varepsilon\mu}$ and some combinations of them. Ninety-percent confidence level experimental limits. The limits on $|g^S_{LL}|$ and $|g^V_{LL}|$ are from [8–10], and the others from a general analysis of muon decay measurements. Top three rows: [11], fourth row: [12], next three rows: [13], last row: [14]. The experimental uncertainty on the muon polarization in pion decay is included. Note that, by definition, $|g^S_{\varepsilon\mu}| \le 2$, $|g^V_{\varepsilon\mu}| \le 1$ and $|g^T_{\varepsilon\mu}| \le 1/\sqrt{3}$.

$\lvert g^S_{RR}\rvert < 0.035$	$\lvert g^V_{RR}\rvert < 0.017$	$\lvert g^T_{RR}\rvert \equiv 0$
$\lvert g^S_{LR}\rvert < 0.050$	$\lvert g^V_{LR}\rvert < 0.023$	$\lvert g^T_{LR}\rvert < 0.015$
$\lvert g^S_{RL}\rvert < 0.420$	$\lvert g^V_{RL}\rvert < 0.105$	$\lvert g^T_{RL}\rvert < 0.105$
$\lvert g^S_{LL}\rvert < 0.550$	$\lvert g^V_{LL}\rvert > 0.960$	$\lvert g^T_{LL}\rvert \equiv 0$
$\lvert g^S_{LR} + 6\,g^T_{LR}\rvert < 0.143$	$\lvert g^S_{RL} + 6\,g^T_{RL}\rvert < 0.418$	
$\lvert g^S_{LR} + 2\,g^T_{LR}\rvert < 0.108$	$\lvert g^S_{RL} + 2\,g^T_{RL}\rvert < 0.417$	
$\lvert g^S_{LR} - 2\,g^T_{LR}\rvert < 0.070$	$\lvert g^S_{RL} - 2\,g^T_{RL}\rvert < 0.418$	
$Q_{RR} + Q_{LR} < 8.2\times10^{-4}$		

57.3 Matrix element:

All results in direct muon decay (energy spectra of the electron and of the neutrinos, polarizations, and angular distributions), and in inverse muon decay (the reaction cross section) at energies well below $m_W c^2$, may be parametrized in terms of amplitudes $g^\gamma_{\varepsilon\mu}$ and the Fermi coupling constant G_F, using the matrix element

$$\frac{4G_\mathrm{F}}{\sqrt{2}} \sum_{\substack{\gamma=S,V,T\\ \varepsilon,\mu=R,L}} g^\gamma_{\varepsilon\mu}\, \langle \bar{e}_\varepsilon|\Gamma^\gamma|(\nu_e)_n\rangle\, \langle \bar{\nu}_\mu)_m|\Gamma_\gamma|\mu_\mu\rangle \tag{57.9}$$

We use the notation of Fetscher *et al.* [2], who in turn use the sign conventions and definitions of Scheck [15]. Here, $\gamma = S, V, T$ indicates a scalar, vector, or tensor interaction; and $\varepsilon, \mu = R, L$ indicate a right- or left-handed chirality of the electron or muon. The chiralities n and m of the ν_e and $\bar{\nu}_\mu$ are then determined by the values of γ, ε, and μ. The particles are represented by fields of definite chirality [16].

As shown by Langacker and London [17], explicit lepton-number nonconservation still leads to a matrix element equivalent to Eq. (57.9). They conclude that it is not possible, even in principle, to test lepton-number conservation in (leptonic) muon decay if the final neutrinos are massless and are not observed.

The ten complex amplitudes $g^\gamma_{\varepsilon\mu}$ (g^T_{RR} and g^T_{LL} are identically zero) and G_F constitute 19 independent (real) parameters to be determined by experiment. The Standard Model interaction corresponds to one single amplitude g^V_{LL} being unity and all the others being zero.

The (direct) muon decay experiments are compatible with an arbitrary mix of the scalar and vector amplitudes g^S_{LL} and g^V_{LL} – in the extreme even with purely scalar $g^S_{LL} = 2$, $g^V_{LL} = 0$. The decision in favour of the Standard Model comes from the quantitative observation of inverse muon decay, which would be forbidden for pure g^S_{LL} [2].

57.4 Experimental determination of V–A:

In order to determine the amplitudes $g^\gamma_{\varepsilon\mu}$ uniquely from experiment, the following set of equations, where the left-hand sides represent experimental results, has to be solved.

$$a = 16\left(|g^V_{RL}|^2 + |g^V_{LR}|^2\right) + \left|g^S_{RL} + 6\,g^T_{RL}\right|^2 + \left|g^S_{LR} + 6\,g^T_{LR}\right|^2 \tag{57.10a}$$

$$a' = 16\left(|g^V_{RL}|^2 - |g^V_{LR}|^2\right) + \left|g^S_{RL} + 6\,g^T_{RL}\right|^2 - \left|g^S_{LR} + 6\,g^T_{LR}\right|^2 \tag{57.10b}$$

$$\alpha = 8\,\mathrm{Re}\left\{g^V_{RL}\left(g^{S*}_{LR} + 6\,g^{T*}_{LR}\right) + g^V_{LR}\left(g^{S*}_{RL} + 6\,g^{T*}_{RL}\right)\right\} \tag{57.10c}$$

$$\alpha' = 8\,\mathrm{Im}\left\{-g^V_{RL}\left(g^{S*}_{LR} + 6\,g^{T*}_{LR}\right) + g^V_{LR}\left(g^{S*}_{RL} + 6\,g^{T*}_{RL}\right)\right\} \tag{57.10d}$$

$$b = 4\left(|g^V_{RR}|^2 + |g^V_{LL}|^2\right) + |g^S_{RR}|^2 + |g^S_{LL}|^2 \tag{57.10e}$$

$$b' = 4\left(|g^V_{RR}|^2 - |g^V_{LL}|^2\right) + |g^S_{RR}|^2 - |g^S_{LL}|^2 \tag{57.10f}$$

$$c = \tfrac{1}{2}\left\{|g^S_{RL} - 2\,g^T_{RL}|^2 + |g^S_{LR} - 2\,g^T_{LR}|^2\right\} \tag{57.10g}$$

$$c' = \tfrac{1}{2}\left\{|g^S_{RL} - 2\,g^T_{RL}|^2 - |g^S_{LR} - 2\,g^T_{LR}|^2\right\} \tag{57.10h}$$

and

$$Q_L^{\nu_e} = 1 - \left\{\tfrac{1}{4}|g^S_{LR}|^2 + \tfrac{1}{4}|g^S_{LL}|^2 + |g^V_{RR}|^2 + |g^V_{RL}|^2 + 3\,|g^T_{LR}|^2\right\}$$

$$\omega_L = \frac{3}{4}\,\frac{|g^S_{RR}|^2 + 4\,|g^V_{LR}|^2 + |g^S_{RL} + 2\,g^T_{LR}|^2}{|g^S_{RL}|^2 + |g^S_{RR}|^2 + 4\,|g^V_{LL}|^2 + 4\,|g^V_{LR}|^2 + 12\,|g^T_{RL}|^2}\,. \tag{57.10i}$$

It has been noted earlier by C. Jarlskog [18], that certain experiments observing the decay electron are especially informative if they yield the V-A values. The complete solution is now found as follows. Fetscher *et al.* [2] introduced four probabilities $Q_{\varepsilon\mu}(\varepsilon, \mu = R, L)$ for the decay of a μ-handed muon into an ε-handed electron, and showed that there exist upper bounds on Q_{RR}, Q_{LR}, and Q_{RL}, and a lower bound on Q_{LL}. These probabilities are given in terms of the $g^\gamma_{\varepsilon\mu}$'s by

$$Q_{\varepsilon\mu} = \tfrac{1}{4}|g^S_{\varepsilon\mu}|^2 + |g^V_{\varepsilon\mu}|^2 + 3\,(1 - \delta_{\varepsilon\mu})|g^T_{\varepsilon\mu}|^2 \tag{57.11}$$

where $\delta_{\varepsilon\mu} = 1$ for $\varepsilon = \mu$, and $\delta_{\varepsilon\mu} = 0$ for $\varepsilon \neq \mu$. They are related to the parameters a, b, c, a', b', and c' by

$$Q_{RR} = 2\,(b + b')/A \tag{57.12a}$$

$$Q_{LR} = \left[(a - a') + 6\,(c - c')\right]/2A \tag{57.12b}$$

$$Q_{RL} = \left[(a + a') + 6\,(c + c')\right]/2A \tag{57.12c}$$

$$Q_{LL} = 2\,(b - b')/A \tag{57.12d}$$

with $A = 16$. In the Standard Model, $Q_{LL} = 1$ and the others are zero.

Since the upper bounds on Q_{RR}, Q_{LR}, and Q_{RL} are found to be small, and since the helicity of the ν_μ in pion decay is known from experiment [19, 20] to very high precision to be -1 [21], the cross section S of *inverse* muon decay, normalized to the V-A value, yields [2]

$$|g^S_{LL}|^2 \le 4(1 - S) \tag{57.13a}$$

and

$$|g^V_{LL}|^2 = S\,. \tag{57.13b}$$

Thus the Standard Model assumption of a pure V-A leptonic charged weak interaction of e and μ is derived (within errors) from experiments at energies far below the mass of the $W^\pm$: Eq. (57.13 b) gives a lower limit for V-A, and Eqs. (57.12 a, b, c)

Downloaded from https://academic.oup.com/ptep/article/2022/8/083C01/6651666 by KIT Library user on 27 September 2022

and (57.13 a) give upper limits for the other four-fermion interactions. The existence of such upper limits may also be seen from $Q_{RR}+Q_{RL}=(1-\xi')/2$ (e^+ longitudinal polarization) and $Q_{RR}+Q_{LR}=\frac{1}{2}(1+\xi/3-16\,\xi\delta/9)$ (decay asymmetry). Table 57.1 gives the current experimental limits on the magnitudes of the $g^{\gamma}_{\varepsilon\mu}$'s. More stringent limits on the six coupling constants g^S_{LR}, g^V_{LR}, g^T_{LR}, g^S_{RL}, g^V_{RL}, and g^T_{RL} have been derived from upper limits on the neutrino mass [22]. Limits on the "charge retention" coordinates, as used in the older literature (*e.g.*, Ref. [23]), are given by Burkard *et al.* [24].

References

[1] L. Michel, Proc. Phys. Soc. **A63**, 514 (1950).

[2] W. Fetscher, H. J. Gerber and K. F. Johnson, Phys. Lett. **B173**, 102 (1986).

[3] P. Langacker, Comments Nucl. Part. Phys. **19**, 1, 1 (1989).

[4] C. Bouchiat and L. Michel, Phys. Rev. **106**, 170 (1957).

[5] T. Kinoshita and A. Sirlin, Phys. Rev. **107**, 593 (1957).

[6] T. Kinoshita and A. Sirlin, Phys. Rev. **108**, 844 (1957).

[7] W. Fetscher, Phys. Rev. **D49**, 5945 (1994).

[8] S. R. Mishra *et al.*, Phys. Lett. **B252**, 170 (1990).

[9] S. R. Mishra, private communication.

[10] P. Vilain *et al.* (CHARM-II), Phys. Lett. **B364**, 121 (1995).

[11] A. Hillairet *et al.* (TWIST), Phys. Rev. **D85**, 092013 (2012), [arXiv:1112.3606].

[12] R. P. MacDonald *et al.* (TWIST), Phys. Rev. **D78**, 032010 (2008), [arXiv:0807.1125].

[13] C. A. Gagliardi, R. E. Tribble and N. J. Williams, Phys. Rev. **D72**, 073002 (2005), [hep-ph/0509069].

[14] R. Bayes *et al.* (TWIST), Phys. Rev. Lett. **106**, 041804 (2011).

[15] F. Scheck, in *Electroweak and Strong Interactions* (Springer Verlag, 1996).

[16] K. Mursula and F. Scheck, Nucl. Phys. **B253**, 189 (1985).

[17] P. Langacker and D. London, Phys. Rev. **D39**, 266 (1989).

[18] C. Jarlskog, Nucl. Phys. **75**, 659 (1966).

[19] A. Jodidio *et al.*, Phys. Rev. **D34**, 1967 (1986), [Erratum: Phys. Rev.D37,237(1988)].

[20] L. P. Roesch *et al.*, Helv. Phys. Acta **55**, 74 (1982).

[21] W. Fetscher, Phys. Lett. **140B**, 117 (1984).

[22] G. Prezeau and A. Kurylov, Phys. Rev. Lett. **95**, 101802 (2005), [hep-ph/0409193].

[23] S. E. Derenzo, Phys. Rev. **181**, 1854 (1969).

[24] H. Burkard *et al.*, Phys. Lett. **160B**, 343 (1985).

Downloaded from https://academic.oup.com/ptep/article/2022/8/083C01/6651666 by KIT Library user on 27 September 2022

58. τ Branching Fractions

Revised February 2022 by Sw. Banerjee (Louisville U.) and A. Lusiani (SNS, Pisa; INFN, Pisa).

58.1 τ Branching Fractions

The τ Listings contains 244 entries that correspond to either a τ partial decay fraction into a specific decay mode (branching fraction) or a ratio of two τ partial decay fractions (branching ratio). Experimental information provides values for 147 of these quantities, upper limits for 61 branching fractions to Lepton Family number, Lepton number, or Baryon number violating modes, and 36 additional upper limits for other modes. A total of 170 measurements of τ branching fraction and branching ratio measurements is used for a global fit that determines 129 quantities.

58.2 The constrained fit to τ branching fractions

The τ branching fractions fit uses the reported values, uncertanties and statistical correlations of the τ branching fractions and branching ratios measurements. Asymmetric uncertainties are symmetrized as $\sigma^2_{\rm symm} = (\sigma^2_+ + \sigma^2_-)/2$. Additionally, the most precise experimental inputs are treated according to how they depend on external parameters on the basis of their documentation [1]. The τ measurements may depend on parameters such as the τ pair production cross-section in e^+e^- annihilations at the $\Upsilon(4S)$ peak. In some cases, measurements reported in different papers by the same collaboration may depend on common parameters like the estimate of the integrated luminosity or of particle identification efficiencies. For all the significant detected dependencies, the τ measurements and their uncertainties are updated to account for the updated values of the external parameters. The dependencies on common systematic effects are also determined in size and sign, and all the common systematic dependencies of different measurements are used together with the published statistical and systematic uncertainties and correlations in order to compute a single all-inclusive variance and covariance matrix of the experimental inputs of the fit.

The fit procedure parameters correspond to τ quantities that are fit to the experimental measurements while respecting relations described by a series of constraint equations. All the experimental inputs and all the constraint equations are reported in the τ Listings section that follows this review. With respect to the 2016, 2017 and 2018 editions, the fit uses one more experimental measurement, published by the BaBar collaboration in 2018, on $\mathcal{B}(\tau \to K^- K^0 \nu_\tau)$ [2]. If only a few measurements are correlated, the correlation coefficients are listed in the footnote for each measurement (see for example $\Gamma(\text{particle}^- \geq 0\,\text{neutrals} \geq 0\,K^0\nu_\tau$ ("1-prong"))$/\Gamma_{\rm total}$). If a large number of measurements are correlated, then the full correlation matrix is listed in the footnote to the measurement that first appears in the τ Listings. Footnotes to the other measurements refer to the first one. For example, the large correlation matrices for the branching fraction or ratio measurements contained in Refs. [3] [4] are listed in Footnotes to the $\Gamma(e^-\overline{\nu}_e\nu_\tau)/\Gamma_{\rm total}$ and $\Gamma(h^-\nu_\tau)/\Gamma_{\rm total}$ measurements respectively. The constraints between the τ branching fractions and ratios include coefficients that correspond to physical quantities, like for instance the branching fractions of the η and ω mesons. All quantities are taken from the 2018 edition of the Review of Particle Physics. Their uncertainties are neglected in the fit.

We obtain the branching fraction of $\tau \to a_1^-(\to \pi^-\gamma)\nu_\tau$ using the ALEPH estimate for $\mathcal{B}(a_1^- \to \pi^-\gamma)$ [3], which uses the measurement of $\Gamma(a_1^- \to \pi^-\gamma)$ [5]. In the fit, we assume that $\mathcal{B}(\tau^- \to a_1^-\nu_\tau)$ is equal to $\mathcal{B}(\tau \to \pi^-\pi^-\pi^+\nu_\tau$ (ex. K^0, ω)) + $\mathcal{B}(\tau \to \pi^- 2\pi^0\nu_\tau$ (ex. K^0)), neglecting the observed but negligible branching fractions to other modes, including $\mathcal{B}(a_1^- \to \pi^-\gamma)$.

In some cases, constraints describe approximate relations that nevertheless hold within the present experimental precision. For instance, the constraint $\mathcal{B}(\tau \to K^-K^-K^+\nu_\tau) = \mathcal{B}(\tau \to K^-\phi\nu_\tau) \times \mathrm{B}(\phi \to K^+K^-)$ is justified within the current experimental evidence.

In the fit, scale factors are applied to the published uncertainties of measurements only if significant inconsistency between different measurements remain after accounting for all relevant uncertainties and correlations. After examining the data and the fit pulls, it has been decided to apply just one scale factor of 5.4 on the measurements of $\mathcal{B}(\tau \to K^-K^-K^+\nu_\tau)$. The scale factor has been computed and applied according to the standard PDG procedure. Without the scale factor applied, the χ^2 probability of the fit is about 2%. On a per-measurement basis, the pull distribution in figure 58.1 indicates that just a few measurements have more than 3σ pulls. (The uncertainties to obtain the pulls are computed using the measurements variance matrix and the variance matrix of the result, accounting for the fact that the variance matrix of the result is obtained from the measurement variance with the fit.) The pull probability distribution in figure 58.2 is reasonably flat. With many measurements some entries on the tails of the normal distribution must be expected. There are 170 pulls, one per measurement. They are partially correlated, and the effective number of independent pulls is equal to the number of degrees of freedom of the fit, 125. Only the $\tau \to K^-K^-K^+\nu_\tau$ decay mode has a pull that is inconsistent at the level of more than 3σ even if considered as the largest pull in a set of 125. This confirms the choice of adopting just that one scale factor.

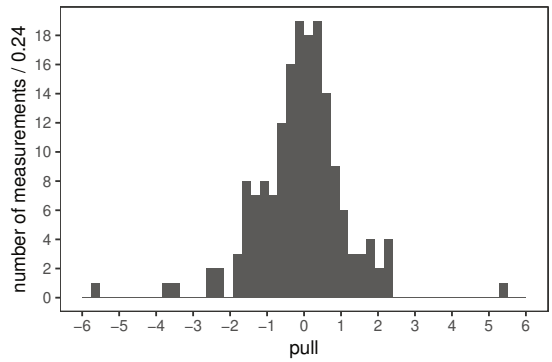

Figure 58.1: Pulls of individual measurements against the respective fitted quantity. No scale factor is used.

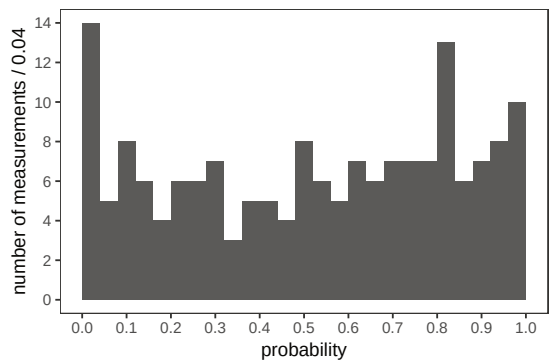

Figure 58.2: Probability of individual measurement pulls against the respective fitted quantity. No scale factor is used.

After scaling the error, the constrained fit has a χ^2 of 135 for 125 degrees of freedom, corresponding to a χ^2 probability of 26%. We use 170 measurements and 84 constraints on the branching fractions and ratios to determine 129 quantities, consisting of 112 branching fractions and 17 branching ratios. A total of 85 quantities have at least one measurement in the fit. The constraints include the unitarity constraint on the sum of all the exclusive τ decay modes, $\mathcal{B}_{\rm all} = 1$. If the unitarity constraint is released, the fit result for $\mathcal{B}_{\rm all}$ is consistent with unitarity with $1 - \mathcal{B}_{\rm all} = (0.00 \pm 0.10)\%$.

For the convenience of summarizing the fit results, we list in the following the values and uncertainties for a set of 46 "basis" decay modes, from which all remaining branching fractions and ratios can be obtained using the constraints. The basis decay modes are not intended to sum up to 1. Since some basis quantities represent multiple branching fractions that are related by constraint equations, they are properly weighted and the unitarity constraint

Downloaded from https://academic.oup.com/ptep/article/2022/8/083C01/6651666 by KIT Library user on 27 September 2022

corresponds to a linear combination whose coefficients are listed in the following. The correlation matrix between the basis modes is reported in the τ Listings.

decay mode	fit result (%)	coefficient
$\mu^-\bar{\nu}_\mu\nu_\tau$	17.3937 ± 0.0384	1.0000
$e^-\bar{\nu}_e\nu_\tau$	17.8175 ± 0.0399	1.0000
$\pi^-\nu_\tau$	10.8164 ± 0.0512	1.0000
$K^-\nu_\tau$	0.6964 ± 0.0096	1.0000
$\pi^-\pi^0\nu_\tau$	25.4941 ± 0.0893	1.0000
$K^-\pi^0\nu_\tau$	0.4328 ± 0.0148	1.0000
$\pi^-2\pi^0\nu_\tau$ (ex. K^0)	9.2595 ± 0.0964	1.0021
$K^-2\pi^0\nu_\tau$ (ex. K^0)	0.0647 ± 0.0218	1.0000
$\pi^-3\pi^0\nu_\tau$ (ex. K^0)	1.0429 ± 0.0707	1.0000
$K^-3\pi^0\nu_\tau$ (ex. K^0, η)	0.0478 ± 0.0212	1.0000
$h^-4\pi^0\nu_\tau$ (ex. K^0, η)	0.1118 ± 0.0391	1.0000
$\pi^-\bar{K}^0\nu_\tau$	0.8384 ± 0.0138	1.0000
$K^-K^0\nu_\tau$	0.1486 ± 0.0034	1.0000
$\pi^-\bar{K}^0\pi^0\nu_\tau$	0.3817 ± 0.0129	1.0000
$K^-\pi^0K^0\nu_\tau$	0.1500 ± 0.0070	1.0000
$\pi^-\bar{K}^02\pi^0\nu_\tau$ (ex. K^0)	0.0263 ± 0.0226	1.0000
$\pi^-K^0_SK^0_S\nu_\tau$	0.0235 ± 0.0006	2.0000
$\pi^-K^0_SK^0_L\nu_\tau$	0.1081 ± 0.0241	1.0000
$\pi^-\pi^0K^0_SK^0_S\nu_\tau$	0.0018 ± 0.0002	2.0000
$\pi^-\pi^0K^0_SK^0_L\nu_\tau$	0.0325 ± 0.0119	1.0000
$\bar{K}^0h^-h^-h^+\nu_\tau$	0.0247 ± 0.0199	1.0000
$\pi^-\pi^-\pi^+\nu_\tau$ (ex. K^0, ω)	8.9868 ± 0.0513	1.0021
$\pi^-\pi^-\pi^+\pi^0\nu_\tau$ (ex. K^0, ω)	2.7404 ± 0.0710	1.0000
$h^-h^-h^+2\pi^0\nu_\tau$ (ex. K^0, ω, η)	0.0981 ± 0.0356	1.0000
$\pi^-K^-K^+\nu_\tau$	0.1435 ± 0.0027	1.0000
$\pi^-K^-K^+\pi^0\nu_\tau$	0.0061 ± 0.0018	1.0000
$\pi^-\pi^0\eta\nu_\tau$	0.1389 ± 0.0072	1.0000
$K^-\eta\nu_\tau$	0.0155 ± 0.0008	1.0000
$K^-\pi^0\eta\nu_\tau$	0.0048 ± 0.0012	1.0000
$\pi^-\bar{K}^0\eta\nu_\tau$	0.0094 ± 0.0015	1.0000
$\pi^-\pi^+\pi^-\eta\nu_\tau$ (ex. K^0)	0.0220 ± 0.0013	1.0000
$K^-\omega\nu_\tau$	0.0410 ± 0.0092	1.0000
$h^-\pi^0\omega\nu_\tau$	0.4085 ± 0.0419	1.0000
$K^-\phi\nu_\tau$	0.0044 ± 0.0016	0.8320
$\pi^-\omega\nu_\tau$	1.9494 ± 0.0645	1.0000
$K^-\pi^-\pi^+\nu_\tau$ (ex. K^0, ω)	0.2927 ± 0.0068	1.0000
$K^-\pi^-\pi^+\pi^0\nu_\tau$ (ex. K^0, ω, η)	0.0394 ± 0.0142	1.0000
$\pi^-2\pi^0\omega\nu_\tau$ (ex. K^0)	0.0072 ± 0.0016	1.0000
$2\pi^-\pi^+3\pi^0\nu_\tau$ (ex. K^0, η, ω, f_1)	0.0014 ± 0.0027	1.0000
$3\pi^-2\pi^+\nu_\tau$ (ex. K^0, ω, f_1)	0.0775 ± 0.0030	1.0000
$K^-2\pi^-2\pi^+\nu_\tau$ (ex. K^0)	0.0001 ± 0.0001	1.0000
$2\pi^-\pi^+\omega\nu_\tau$ (ex. K^0)	0.0084 ± 0.0006	1.0000
$3\pi^-2\pi^+\pi^0\nu_\tau$ (ex. K^0, η, ω, f_1)	0.0038 ± 0.0009	1.0000
$K^-2\pi^-2\pi^+\pi^0\nu_\tau$ (ex. K^0)	0.0001 ± 0.0001	1.0000
$\pi^-f_1\nu_\tau$ ($f_1 \to 2\pi^-2\pi^+$)	0.0052 ± 0.0004	1.0000
$\pi^-2\pi^0\eta\nu_\tau$	0.0195 ± 0.0038	1.0000

In defining the fit constraints and in selecting the modes that sum up to one we made some assumptions and choices. We assume that some channels, like $\tau^- \to \pi^-K^+\pi^- \geq 0\pi^0\nu_\tau$ and $\tau^- \to \pi^+K^-K^- \geq 0\pi^0\nu_\tau$, have negligible branching fractions as expected from the Standard Model, even if the experimental limits for these branching fractions are not very stringent. The 95% confidence level upper limits are $\mathcal{B}(\tau^- \to \pi^-K^+\pi^- \geq 0\pi^0\nu_\tau) < 0.25\%$ and $\mathcal{B}(\tau^- \to \pi^+K^-K^- \geq 0\pi^0\nu_\tau) < 0.09\%$, values not so different from measured branching fractions for allowed 3-prong modes containing charged kaons. For decays to final states containing one neutral kaon we assume that the branching fraction with the K^0_L are the same as the corresponding one with a K^0_S. On decays with two neutral kaons we assume that the branching fractions with $K^0_LK^0_L$ are the same as the ones with $K^0_SK^0_S$.

58.3 BaBar and Belle measure on average lower branching fractions and ratios.

We compare the BaBar and Belle measurements with the results of a fit where all their measurements have been excluded. We find that that BaBar and Belle measure on average lower τ branching fractions and ratios than the other experiments. Figures 58.3 and 58.4 show histograms of the 28 normalized differences between the B-factory measurements and the respective non-B-factory fit results. The normalization is the uncertainty on the difference. The average normalized difference between the two sets of measurements is -0.8σ (-0.7σ for the 16 Belle measurements and -0.8σ for the 12 BaBar measurements).

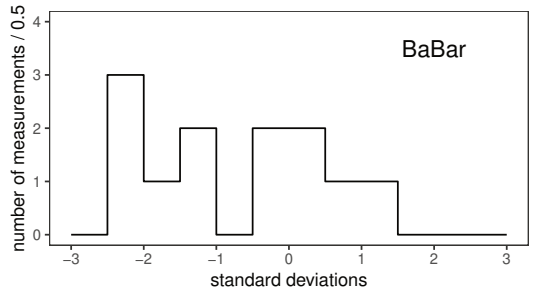

Figure 58.3: Distribution of the normalized difference between 12 measurements of branching fractions and ratios published by the BaBar collaboration and the respective averages computed using only non-B-factory measurements.

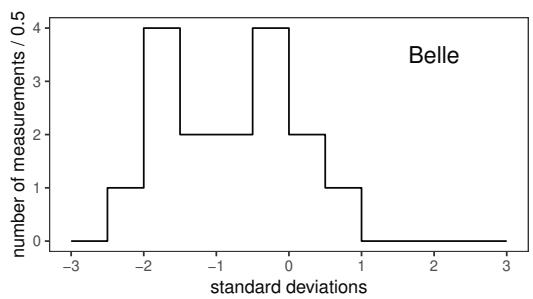

Figure 58.4: Distribution of the normalized difference between 16 measurements of branching fractions and ratios published by the Belle collaboration and the respective averages computed using only non-B-factory measurements.

58.4 Overconsistency of Leptonic Branching Fraction Measurements.

As observed in the previous editions of this review, measurements of the leptonic branching fractions are more consistent with each other than expected from the quoted errors on the individual measurements. The χ^2 is 0.34 for $\mathcal{B}_e$ and 0.08 for $\mathcal{B}_\mu$. Assuming normal errors, the probability of a smaller χ^2 is 1.3% for B_e and 0.08% for B_μ.

58.5 Technical implementation of the fit

The fit computes a set of quantities denoted with q_i by minimizing a χ^2 while respecting a series of equality constraints on the q_i. The χ^2 is computed using the measurements m_i and their covariance matrix E_{ij} as $\chi^2 = (m_i - A_{ik}q_k)^t E^{-1}_{ij}(m_j - A_{jl}q_l)$, where the model matrix A_{ij} is used to get the vector of the predicted measurements m'_i from the vector of the fit parameters q_j as $m'_i = A_{ij}q_j$. In this particular implementation the measurements are grouped by the quantity that they measure, and all quantities with at least one measurement correspond to a fit parameter. Therefore, the matrix A_{ij} has one row per measurement m_i and one column per fitted quantity q_j, with unity coefficients for the rows and column that identify a measurement m_i of the quantity q_j, respectively. The constraints are equations involving the fit parameters. The fit does not impose limitations on the functional form of the constraints. In summary, the fit requires:

$$\min\left[\chi^2(q_k)\right] = \min\left[(m_i - A_{ik}q_k)^t E^{-1}_{ij}(m_j - A_{jl}q_l)\right] \ , \quad (58.1)$$

$$\text{subjected to} \quad f_r(q_s) - c_r = 0 \ , \quad (58.2)$$

where the left term of Eq. 58.2 defines the constraint expressions. Using the method of Lagrange multipliers, a set of equations is

Downloaded from https://academic.oup.com/ptep/article/2022/8/083C01/6651666 by KIT Library user on 27 September 2022

obtained by taking the derivatives with respect to the fitted quantities q_k and the Lagrange multipliers λ_r of the sum of the χ^2 and the constraint expressions multiplied by the Lagrange multipliers λ_r, one for each constraint:

$$\min\left[(A_{ik}q_k - m_i)^t E_{ij}^{-1}(A_{jl}q_l - m_j) + 2\lambda_r(f_r(q_s) - c_r)\right] = \\ = \min\left[\tilde{\chi}^2(q_k, \lambda_r)\right] \ , \\ (\partial/\partial q_k, \partial/\partial\lambda_r)\left[\tilde{\chi}^2(q_k, \lambda_r)\right] = 0 \ . \qquad (58.3)$$

Eq. 58.3 defines a set of equations for the vector of the unknowns (q_k, λ_r), some of which may be non-linear, in case of non-linear constraints. An iterative minimization procedure approximates at each step the non-linear constraint expressions by their first order Taylor expansion around the current values of the fitted quantities, $\bar{q}_s$:

$$f_r(q_s) - c_r = f_r(\bar{q}_s) + \left.\frac{\partial f_r(q_s)}{\partial q_s}\right|_{\bar{q}_s}(q_s - \bar{q}_s) - c_r \ ,$$

which can be written as

$$B_{rs}q_s - c'_r \ ,$$

where c'_r are the resulting constant known terms, independent of q_s at first order. After linearization, the differentiation by q_k and λ_r is trivial and leads to a set of linear equations

$$A^t_{ki}E^{-1}_{ij}A_{jl}q_l + B^t_{kr}\lambda_r = A^t_{ki}E^{-1}_{ij}m_j \ , \qquad (58.4)$$

$$B_{rs}q_s = c'_r \ , \qquad (58.5)$$

which can be expressed as

$$F_{ij}u_j = v_i \ , \qquad (58.6)$$

where $u_j = (q_k, \lambda_r)$ and v_i is the vector of the known constant terms running over the index k and then r in the right terms of Eq. 58.4 and Eq. 58.5, respectively. Solving the equation set in Eq. 58.6 by matrix inversion gives the the fitted quantities and their variance and covariance matrix, using the measurements and their variance and covariance matrix. The fit procedure starts by computing the linear approximation of the non-linear constraint expressions around the quantities seed values. With an iterative procedure, the unknowns are updated at each step by solving the equations and the equations are then linearized around the updated values, until the variation of the fitted unknowns is reduced below a numerically small threshold.

References

[1] D. Asner *et al.* (Heavy Flavor Averaging Group) (2010), [arXiv:1010.1589].

[2] J. P. Lees *et al.* (BaBar), Phys. Rev. **D98**, 3, 032010 (2018), [arXiv:1806.10280].

[3] S. Schael *et al.* (ALEPH), Phys. Rept. **421**, 191 (2005), [hep-ex/0506072].

[4] J. Abdallah *et al.* (DELPHI), Eur. Phys. J. **C46**, 1 (2006), [hep-ex/0603044].

[5] M. Zielinski *et al.*, Phys. Rev. Lett. **52**, 1195 (1984).

Downloaded from https://academic.oup.com/ptep/article/2022/8/083C01/6651666 by KIT Library user on 27 September 2022

59. τ-Lepton Decay Parameters

Revised February 2022 by A. Stahl (RWTH Aachen U.).

The purpose of the measurements of the decay parameters (also known as Michel parameters) of the τ is to determine the structure (spin and chirality) of the current mediating its decays.

59.1 Leptonic Decays:

The Michel parameters are extracted from the energy spectrum of the charged daughter lepton $\ell = e, \mu$ in the decays $\tau \to \ell\nu_\ell\nu_\tau$. Ignoring radiative corrections, neglecting terms of order $(m_\ell/m_\tau)^2$ and $\left(m_\tau/\sqrt{s}\right)^2$, and setting the neutrino masses to zero, the spectrum in the laboratory frame reads

$$\frac{d\Gamma}{dx} = \frac{G^2_{\tau\ell}\, m^5_\tau}{192\,\pi^3} \times \left\{ f_0\,(x) + \rho f_1\,(x) + \eta \frac{m_\ell}{m_\tau} f_2\,(x) - P_\tau\,[\xi g_1\,(x) + \xi\delta g_2\,(x)] \right\} \tag{59.1}$$

with

$$\begin{aligned} f_0(x) &= 2 - 6\,x^2 + 4\,x^3 \\ f_1(x) &= -\tfrac{4}{9} + 4x^2 - \tfrac{32}{9}x^3 \qquad g_1(x) = -\tfrac{2}{3} + 4x - 6x^2 + \tfrac{8}{3}x^3 \\ f_2(x) &= 12\,(1-x)^2 \qquad\qquad g_2(x) = \tfrac{4}{9} - \tfrac{16}{3}x + 12x^2 - \tfrac{64}{9}\,x^3\,. \end{aligned} \tag{59.2}$$

The quantity x is the fractional energy of the daughter lepton ℓ, *i.e.*, $x = E_\ell/E_{\ell,max} \approx E_\ell/(\sqrt{s}/2)$ and P_τ is the polarization of the tau leptons. The integrated decay width is given by

$$\Gamma = \frac{G^2_{\tau\ell}\, m^5_\tau}{192\,\pi^3}\left(1 + 4\,\eta\,\frac{m_\ell}{m_\tau}\right)\,. \tag{59.3}$$

The situation is similar to muon decays $\mu \to e\nu_e\nu_\mu$. The generalized matrix element with the couplings $g^\gamma_{\varepsilon\mu}$ and their relations to the Michel parameters ρ, η, ξ, and δ have been described in the "Note on Muon Decay Parameters". The Standard Model expectations are 3/4, 0, 1, and 3/4, respectively. For more details, see Ref. [1].

Additional Michel-parameters can be defined in radiative decays $\tau \to \ell\nu_\ell\nu_\tau\gamma$, see Ref. [2]. A first measurement is presented in Ref. [3]. The experimental precision does not provide a significant impact on the knowledge about the couplings, yet.

59.2 Hadronic Decays:

In the case of hadronic decays $\tau \to h\nu_\tau$, with $h = \pi$, ρ, or a_1, the ansatz is restricted to purely vectorial currents. The matrix element is

$$\frac{G_{\tau h}}{\sqrt{2}} \sum_{\lambda=R,L} g_\lambda \;\langle\; \overline{\Psi}_\omega(\nu_\tau) \mid \gamma^\mu \mid \Psi_\lambda(\tau) \;\rangle\;\; J^h_\mu \tag{59.4}$$

with the hadronic current J^h_μ. The neutrino chirality ω is uniquely determined from λ. The spectrum depends only on a single parameter ξ_h

$$\frac{d^n\Gamma}{dx_1 dx_2 \ldots dx_n} = f\,(\vec{x}) + \xi_h P_\tau g\,(\vec{x})\;, \tag{59.5}$$

with f and g being channel-dependent functions of the n observables $\vec{x} = (x_1, x_2, \ldots, x_n)$ (see Ref. [4]). The parameter ξ_h is related to the couplings through

$$\xi_h = |g_L|^2 - |g_R|^2\;. \tag{59.6}$$

ξ_h is the negative of the chirality of the τ neutrino in these decays. In the Standard Model, $\xi_h = 1$. Also included in the Data Listings for ξ_h are measurements of the neutrino helicity which coincide with ξ_h, if the neutrino is massless (ASNER 00 [5], ACKERSTAFF 97R [6], AKERS 95P [7], ALBRECHT 93C [8], and ALBRECHT 90I [9]).

59.3 Combination of Measurements:

The individual measurements are combined, taking into account the correlations between the parameters. In a first fit, universality between the two leptonic decays, and between all hadronic decays, is assumed. A second fit is made without these assumptions. The results of the two fits are provided as OUR FIT in the Data Listings below in the tables whose title includes "(e or mu)" or "(all hadronic modes)", and "(e)", "(mu)" *etc.*, respectively. The measurements show good agreement with the Standard Model. The χ^2 values with respect to the Standard model predictions are 24.1 for 41 degrees of freedom and 26.8 for 56 degrees of freedom, respectively. The correlations are reduced through this combination to less than 20%, with the exception of ρ and η which are correlated by +23%, for the fit with universality and by +70% for $\tau \to \mu\nu_\mu\nu_\tau$.

59.4 Model-independent Analysis:

From the Michel parameters, limits can be derived on the couplings $g^\kappa_{\varepsilon\lambda}$ without further model assumptions. In the Standard model $g^V_{LL} = 1$ (leptonic decays), and $g_L = 1$ (hadronic decays) and all other couplings vanish. First, the partial decay widths have to be compared to the Standard Model predictions to derive limits on the normalization of the couplings $A_x = G^2_{\tau x}/G^2_F$ with Fermi's constant G_F:

$$\begin{aligned} A_e &= 1.0022 \pm 0.0041\;, \\ A_\mu &= 0.983 \pm 0.017\;, \\ A_\pi &= 0.9957 \pm 0.0049\;. \end{aligned} \tag{59.7}$$

Then limits on the couplings (95% CL) can be extracted (see Ref. [10] and Ref. [11]). Without the assumption of universality, the limits given in Table 59.1 are derived.

Table 59.1: Coupling constants $g^\gamma_{\varepsilon\mu}$. 95% confidence level experimental limits. The limits include the quoted values of A_e, A_μ, and A_π and assume $A_\rho = A_{a_1} = 1$.

$\tau \to e\nu_e\nu_\tau$		
$\lvert g^S_{RR}\rvert < 0.70$	$\lvert g^V_{RR}\rvert < 0.17$	$\lvert g^T_{RR}\rvert \equiv 0$
$\lvert g^S_{LR}\rvert < 0.99$	$\lvert g^V_{LR}\rvert < 0.13$	$\lvert g^T_{LR}\rvert < 0.082$
$\lvert g^S_{RL}\rvert < 2.01$	$\lvert g^V_{RL}\rvert < 0.52$	$\lvert g^T_{RL}\rvert < 0.51$
$\lvert g^S_{LL}\rvert < 2.01$	$\lvert g^V_{LL}\rvert < 1.004$	$\lvert g^T_{LL}\rvert \equiv 0$
$\tau \to \mu\nu_\mu\nu_\tau$		
$\lvert g^S_{RR}\rvert < 0.72$	$\lvert g^V_{RR}\rvert < 0.18$	$\lvert g^T_{RR}\rvert \equiv 0$
$\lvert g^S_{LR}\rvert < 0.95$	$\lvert g^V_{LR}\rvert < 0.12$	$\lvert g^T_{LR}\rvert < 0.079$
$\lvert g^S_{RL}\rvert < 2.01$	$\lvert g^V_{RL}\rvert < 0.52$	$\lvert g^T_{RL}\rvert < 0.51$
$\lvert g^S_{LL}\rvert < 2.01$	$\lvert g^V_{LL}\rvert < 1.006$	$\lvert g^T_{LL}\rvert \equiv 0$
$\tau \to \pi\nu_\tau$		
$\lvert g^V_R\rvert < 0.15$	$\lvert g^V_L\rvert > 0.984$	
$\tau \to \rho\nu_\tau$		
$\lvert g^V_R\rvert < 0.10$	$\lvert g^V_L\rvert > 0.995$	
$\tau \to a_1\nu_\tau$		
$\lvert g^V_R\rvert < 0.16$	$\lvert g^V_L\rvert > 0.987$	

59.5 Model-dependent Interpretation:

More stringent limits can be derived assuming specific models. For example, in the framework of a two Higgs doublet model, the measurements correspond to a limit of $m_{H^\pm} > 2.0$ GeV $\times \tan\beta$ on the mass of the charged Higgs boson, or a limit of 500 GeV on the mass of the second W boson in left-right symmetric models for arbitrary mixing (both 95% CL). See Ref. [11] and Ref. [12].

Downloaded from https://academic.oup.com/ptep/article/2022/8/083C01/6651666 by KIT Library user on 27 September 2022

References

[1] F. Scheck, Phys. Rept. **44**, 187 (1978); W. Fetscher and H.J. Gerber in *Precision Tests of the Standard Model*, edited by P. Langacker, World Scientific, 1993; A. Stahl, *Physics with τ Leptons*, Springer Tracts in Modern Physics, **160**, 1, (2000).

[2] A. Arbuzov and T. Kopylova, JHEP 109 (2016).

[3] N. Shimizu *et al.* (Belle), Prog. Theo. Exp. Phys. **2**, 023C01 (2018).

[4] M. Davier *et al.*, Phys. Lett. B **306**, 411 (1993).

[5] D. Asner *et al.* (CLEO), Phys. Rev. D **61**, 012002 (2000), [hep-ex/9902022].

[6] K. Ackerstaff *et al.* (OPAL), Z. Phys. C **75**, 593 (1997).

[7] R. Akers *et al.* (OPAL), Z. Phys. C **67**, 45 (1995).

[8] H. Albrecht *et al.* (ARGUS), Z. Phys. C **58**, 61 (1993).

[9] H. Albrecht *et al.* (ARGUS), Phys. Lett. B **250**, 164 (1990).

[10] K. Ackerstaff *et al.* (OPAL), Eur. Phys. J. C **8**, 3 (1999), [hep-ex/9808016].

[11] A. Stahl, Nucl. Phys. B Proc. Suppl. **76**, 173 (1999).

[12] M.-T. Dova, J. Swain and L. Taylor, Phys. Rev. D **58**, 015005 (1998), [hep-ph/9712384]; T. Hebbeker and W. Lohmann, Z. Phys. C **74**, 399 (1997); A. Pich and J. P. Silva, Phys. Rev. D **52**, 4006 (1995), [hep-ph/9505327].

Downloaded from https://academic.oup.com/ptep/article/2022/8/083C01/6651666 by KIT Library user on 27 September 2022

60. Quark Masses

Revised August 2021 by R.M. Barnett (LBNL), L.P. Lellouch (CNRS & Aix-Marseille U.) and A.V. Manohar (UC San Diego).

60.1 Introduction

This note discusses some of the theoretical issues relevant for the determination of quark masses, which are fundamental parameters of the Standard Model of particle physics. Unlike the leptons, quarks are confined inside hadrons and are not observed as physical particles. Quark masses therefore cannot be measured directly, but must be determined indirectly through their influence on hadronic properties. Although one often speaks loosely of quark masses as one would of the mass of the electron or muon, any quantitative statement about the value of a quark mass must make careful reference to the particular theoretical framework that is used to define it. It is important to keep this *scheme dependence* in mind when using the quark mass values tabulated in the data listings.

Historically, the first determinations of quark masses were performed using quark models. These are usually called constituent quark masses and are of order 350 MeV for the u and d quarks. Constituent quark masses model the effects of dynamical chiral symmetry breaking discussed below, and are not directly related to the quark mass parameters m_q of the QCD Lagrangian of Eq. (60.1). The resulting masses only make sense in the limited context of a particular quark model, and cannot be related to the quark mass parameters, m_q, of the Standard Model. In order to discuss quark masses at a fundamental level, definitions based on quantum field theory must be used, and the purpose of this note is to discuss these definitions and the corresponding determinations of the values of the masses.

60.2 Mass parameters and the QCD Lagrangian

The QCD [1] Lagrangian is

$$\mathcal{L} = \sum_{q=u,d,s,\ldots,t} \overline{q}\left(i\not{D} - m_q\right) q - \tfrac{1}{2}\mathrm{tr}\, G_{\mu\nu}G^{\mu\nu}, \tag{60.1}$$

where the sum runs over the quark flavors u, d, s, c, b and t. $\not{D} = (\partial_\mu - igA_\mu)\gamma^\mu$ is the gauge covariant derivative, A_μ is the SU(3)-valued gluon field, $G_{\mu\nu} = \frac{i}{g}[D_\mu, D_\nu]$ is the gluon field strength, m_q is the mass parameter of quark flavor q, and q is the quark Dirac field. After renormalization, the QCD Lagrangian Eq. (60.1) gives finite values for physical quantities, such as scattering amplitudes. Renormalization is a procedure that invokes a subtraction scheme to render the amplitudes finite, and requires the introduction of a dimensionful scale parameter μ. The mass parameters in the QCD Lagrangian Eq. (60.1) depend on the renormalization scheme used to define the theory, and also on the scale parameter μ. The most commonly used renormalization scheme for QCD perturbation theory is the $\overline{\mathrm{MS}}$ scheme.

The QCD Lagrangian has a chiral symmetry in the limit that the quark masses vanish. This symmetry is spontaneously broken by dynamical chiral symmetry breaking, and explicitly broken by the quark masses. The nonperturbative scale of dynamical chiral symmetry breaking, Λ_χ, is around 1 GeV [2]. It is conventional to call quarks heavy if $m_q > \Lambda_\chi$, so that explicit chiral symmetry breaking dominates (c, b, and t quarks are heavy), and light if $m_q < \Lambda_\chi$, so that spontaneous chiral symmetry breaking dominates (the u and d are light and the s is considered to be light when using $\mathrm{SU}(3)_L \times \mathrm{SU}(3)_R$ chiral perturbation theory). The determination of light- and heavy-quark masses is considered separately in Sec. 60.4 and Sec. 60.5 below.

At high energies or short distances, nonperturbative effects, such as chiral symmetry breaking, become small and one can, in principle, determine quark masses by analyzing mass-dependent effects using QCD perturbation theory. Such computations are conventionally performed using the $\overline{\mathrm{MS}}$ scheme at a scale $\mu \gg \Lambda_\chi$, and give the $\overline{\mathrm{MS}}$ "running" mass $\overline{m}(\mu)$. We use the $\overline{\mathrm{MS}}$ scheme when reporting quark masses; one can readily convert these values into other schemes using perturbation theory.

The μ dependence of $\overline{m}(\mu)$ at short distances can be calculated using the renormalization group (RG) equation,

$$\mu^2 \frac{\mathrm{d}\overline{m}\,(\mu)}{\mathrm{d}\mu^2} = -\gamma(\overline{\alpha}_s\,(\mu))\;\overline{m}\,(\mu)\,, \tag{60.2}$$

where γ is the anomalous dimension which is now known to four-loop order in perturbation theory [3] [4]. $\overline{\alpha}_s$ is the coupling constant [1] in the $\overline{\mathrm{MS}}$ scheme. Defining the expansion coefficients γ_r by

$$\gamma\left(\overline{\alpha}_s\right) \equiv \sum_{r=1}^{\infty} \gamma_r \left(\frac{\overline{\alpha}_s}{4\pi}\right)^r, \tag{60.3}$$

the first four coefficients are given by

$$\begin{aligned}
\gamma_1 &= 4,\\
\gamma_2 &= \frac{202}{3} - \frac{20N_L}{9},\\
\gamma_3 &= 1249 + \left(-\frac{2216}{27} - \frac{160}{3}\zeta\,(3)\right) N_L - \frac{140}{81}N_L^2,\\
\gamma_4 &= \frac{4603055}{162} + \frac{135680}{27}\zeta\,(3) - 8800\zeta\,(5)\\
&\quad + \left(-\frac{91723}{27} - \frac{34192}{9}\zeta\,(3) + 880\zeta\,(4) + \frac{18400}{9}\zeta\,(5)\right) N_L\\
&\quad + \left(\frac{5242}{243} + \frac{800}{9}\zeta\,(3) - \frac{160}{3}\zeta\,(4)\right) N_L^2\\
&\quad + \left(-\frac{332}{243} + \frac{64}{27}\zeta\,(3)\right) N_L^3,
\end{aligned}$$

where N_L is the number of active light quark flavors at the scale μ, i.e. flavors with masses $\leq \mu$, and ζ is the Riemann zeta function ($\zeta(3) \simeq 1.2020569$, $\zeta(4) \simeq 1.0823232$, and $\zeta(5) \simeq 1.0369278$). Eq. (60.2) must be solved in conjunction with the RG equation for $\overline{\alpha}_s\,(\mu)$ given in [1]. In addition, as the renormalization scale crosses quark mass thresholds one needs to match the scale dependence of $\overline{m}$ below and above the threshold. There are finite threshold corrections; the necessary formulae can be found in Ref. [5].

60.3 Lattice QCD

The use of lattice QCD calculations for *ab initio* determinations of the fundamental parameters of QCD, including the coupling constant and quark masses (except for the top-quark mass) is a very active area of research (see the review on Lattice Quantum Chromodynamics in this *Review*). Here we only briefly recall those features which are required for the determination of quark masses. In order to determine the lattice spacing (a, i.e. the distance between neighboring points of the lattice) and quark masses, one computes a convenient and appropriate set of physical quantities (frequently chosen to be a set of hadronic masses) for a variety of input values of the quark masses in units of the lattice spacing. These input quark masses are then tuned to their true (physical) values by requiring that the calculation correctly reproduces the set of physical quantities being used for the calibration.

The resulting values of the quark masses are bare quark masses, corresponding to a particular discretization of QCD and with the lattice spacing as the ultraviolet cut-off. In order for these results to be useful in phenomenological applications, it is necessary to relate them to renormalized masses defined in some standard renormalization scheme such as $\overline{\mathrm{MS}}$. Provided that both the ultraviolet cut-off a^{-1} and the renormalization scale μ are much greater than Λ_{QCD}, the bare and renormalized masses can be related in perturbation theory. However, in order to avoid uncertainties due to the unknown higher-order coefficients in lattice perturbation theory, most results obtained recently use *nonperturbative renormalization* to relate the bare masses to those defined in renormalization schemes which can be realized directly in lattice QCD (e.g. those obtained from quark and gluon Green functions at specified momenta in the Landau gauge [6] or those defined using finite-volume techniques and the Schrödinger functional [7], but not $\overline{\mathrm{MS}}$ that is only defined for dimensional regularization). These methods require $\mu \gg \Lambda_{\mathrm{QCD}}$ so that unwanted (nonperturbative) corrections proportional to inverse powers of μ, which appear in some

Downloaded from https://academic.oup.com/ptep/article/2022/8/083C01/6651666 by KIT Library user on 27 September 2022

approaches, remain small corrections that can be identified and removed. This condition is also necessary so that matching to other schemes can be performed reliably in perturbation theory. Moreover, these methods require $a^{-1} \gg \mu$ so that cutoff effects are small enough to be extrapolated away. Thus, the calculations are repeated for finer and finer lattice spacings and the continuum limit, $a \to 0$, of these nonperturbatively renormalized masses is taken to eliminate all cutoff effects. The conversion to the $\overline{\text{MS}}$ scheme is then performed using continuum perturbation theory, which is more readily obtained to higher orders and is usually better behaved than its lattice counterpart.

It is important to note that the final renormalized values for the quark masses must be the same in the continuum limit for any sensible choice of the physical quantities used for calibration, as long as the calculation is performed with a sufficient number of sea-quark flavors and the relevant electromagnetic and strong-isospin breaking corrections for the claimed precision. It is also worth noting that issues surrounding the renormalization of quark masses disappear when considering pairwise ratios of these masses (up to electromagnetic effects for quarks of different charge, which are still smaller than the errors bars quoted on these ratios, e.g. in the $\overline{\text{MS}}$ scheme at a scale of a few GeV). Indeed, if the same scheme and scale are implemented, QCD renormalization factors are identical for all quark flavors, and these factors therefore cancel exactly in quark-mass ratios. In particular, this means that these ratios are scheme and scale independent. Moreover, these ratios may suffer less from the uncertainties in the determination of the lattice scale, in particular in cases where the quantities used to fix the two quarks masses entering the ratio depend on these masses in a similar way, but also because these ratios are dimensionless. Thus, quark-mass ratios are often determined with significantly higher precision using lattice QCD than are the individual masses.

The determination of quark masses using lattice simulations is well established and the current emphasis is on the reduction and control of the systematic uncertainties. With improved algorithms and access to more powerful computing resources, the precision of the results has improved immensely in recent years. Vacuum polarization effects are included with $N_f = 2$, $2+1$ or $N_f = 2+1+1$ flavors of sea quarks. The number 2 here indicates that the up and down quarks are degenerate. The first $+1$ corresponds to the inclusion of strange sea-quark effects and the second $+1$ to those of the charm. Simulations with $2+1$ and $2+1+1$ flavors represent controlled approximations to physical QCD at the low energies considered for quark mass determinations, up to corrections of $O((\Lambda_{\text{QCD}}/m_c)^2/N_c)$ and $O((\Lambda_{\text{QCD}}/m_b)^2/N_c)$, respectively. This is not the case for simulations with $N_f = 2$ or in which vacuum polarization effects are completely neglected (this is the so-called *quenched* approximation) and results obtained in such frameworks will not enter the discussion here.

Particularly pleasing is the observation that different formulations of lattice QCD, with different systematic uncertainties, yield results which are largely consistent with each other. This gives us broad confidence in the estimates of the systematic errors. As the precision of the results approaches (or even exceeds in some cases) 1%, isospin breaking effects, including electromagnetic corrections need to be included and this is beginning to be done as will be discussed below. In particular, a reliable estimate of these effects is required for determining the individual u and d quark masses.

Members of the lattice QCD community have organized a Flavour Lattice Averaging Group (FLAG) which critically reviews quantities computed in lattice QCD relevant to flavor physics, including the determination of quark masses, against stated quality criteria and presents its view of the current status of the results. The latest edition reviews lattice results that have been appeared in print before April 30th 2021 [8]. Since that deadline, there have been no new lattice, quark-mass determinations.

60.4 Light quarks

In this section we review the determination of the masses of the light quarks u, d and s from lattice simulations and then discuss the consequences of the approximate chiral symmetry.

60.4.1 *Lattice QCD results*

The most reliable determinations of the strange quark mass, m_s, and of the average of the up and down quark masses, $m_{ud} = (m_u + m_d)/2$, are obtained from lattice simulations. As explained in Sec. 60.3 above, the simulations are generally performed with degenerate up and down quarks ($m_u = m_d$) and so it is the average which is obtained directly from the computations. Below we discuss the derivation of m_u and m_d separately, but we start by briefly presenting our estimate of the current status of the latest lattice results in the isospin symmetric limit. The FLAG review [8] bases its summary numbers for these quark masses on references that the review's authors consider to have the most reliable estimates of systematic uncertainties, i.e. [9–15] for $N_f = 2+1$ and [16–21] for $N_f = 2+1+1$ flavors of sea quarks. Note that the $N_f = 2+1+1$ results [22] did not make the FLAG deadline. Compared to the previous editions of the FLAG [23] and of the present reviews, this corresponds to including the new calculation [15] and to dropping [24], whose simulations do not allow for as good a control over the tuning of m_{ud} as do the other calculations. For $N_f = 2+1$ flavors, the FLAG review quotes $\overline{m}_{ud} = (3.381 \pm 0.040)\,\text{MeV}$, $\overline{m}_s = (92.2 \pm 1.0)\,\text{MeV}$ and $(\overline{m}_s/\overline{m}_{ud}) = 27.42 \pm 0.12$. These numbers are $\overline{m}_{ud} = (3.410 \pm 0.043)\,\text{MeV}$, $\overline{m}_s = (93.40 \pm 0.57)\,\text{MeV}$ and $(\overline{m}_s/\overline{m}_{ud}) = 27.23 \pm 0.10$ for $N_f = 2+1+1$ simulations. The masses are given in the $\overline{\text{MS}}$ scheme at a renormalization scale of 2 GeV. These results are not simply the combinations of all the results in quadrature, but include possible correlations between calculations. Since the different collaborations use different formulations of lattice QCD, the (relatively small) variations of the results between the groups provides important information about the reliability of the estimates.

Compared to the previous editions of the FLAG [23] and of the present reviews, the central values of these averages have changed by only a fraction of their error bars, which is not surprising given that they were obtained mostly from the same results. The most notable change is the significant increase in the error of $N_f = 2+1$ $\overline{m}_s$. This is due mainly to the inclusion of [15], whose larger value leads to a $\chi^2/\text{dof} = 1.7$ in the average, which is accounted for by increasing the uncertainties by the usual $\sqrt{\chi^2/\text{dof}}$ scale factor.

Despite being reported in the $\overline{\text{MS}}$ scheme at a renormalization scale of 2 GeV, the results for $\overline{m}_{ud}$ and $\overline{m}_s$ in the two frameworks differ in their renormalization schemes, since $N_f = 2+1$ results are renormalized with $N_L = 3$ and $N_f = 2+1+1$ ones with $N_L = 4$. Thus, for a comparison, one should convert the results to the same scheme. This is not the case for $(\overline{m}_s/\overline{m}_{ud})$, where renormalization factors cancel. The conversion of the $N_f = 2+1$ results to the $N_L = 4$ scheme can be performed, for instance, by running them down to the charm threshold in the $N_L = 3$ theory, matching the results to the $N_L = 4$ theory at that scale, and running them back up to 2 GeV with four active flavors. Such a conversion leads to an upward shift in the values of the quark masses of only around 0.3%, well within the quoted errors. There are also nonperturbative contributions to this procedure, of $O((\Lambda_{\text{QCD}}/m_c)^2/N_c) \sim 2\%$. However, lattice QCD studies of these effects have shown that they are typically an order of magnitude smaller on hadronic quantities or on Λ_{QCD} [25, 26]. Given that the total errors on the $N_f = 2+1$ results for $\overline{m}_{ud}$ and $\overline{m}_s$ are larger than 1%, we choose to neglect these matching effects and simply to average the results from the two frameworks, yielding as a final lattice QCD estimate in the $\overline{\text{MS}}$ scheme at $\mu = 2\,\text{GeV}$ in the $N_L = 4$ theory:

$$\overline{m}_{ud} = (3.39 \pm 0.04)\,\text{MeV}, \tag{60.4}$$

$$\overline{m}_s = (93.1 \pm 0.6)\,\text{MeV}, \tag{60.5}$$

and

$$r_s \equiv \frac{\overline{m}_s}{\overline{m}_{ud}} = 27.31 \pm 0.10, \tag{60.6}$$

where the error bars encompass statistical and systematic errors combined in quadrature. In performing these averages, small tensions are found in the results for $\overline{m}_s/\overline{m}_{ud}$, whose weighted av-

Downloaded from https://academic.oup.com/ptep/article/2022/8/083C01/6651666 by KIT Library user on 27 September 2022

erage comes with a $\chi^2/\text{dof} \simeq 1.5$, used to increase error bars in the usual way. As a final error we always quote the largest of the average's error and of the smaller of the erros on the individual flavor averages, to account for possible common systematics.

To obtain the individual values of $\overline{m}_u$ and $\overline{m}_d$ requires the introduction of isospin breaking effects, including electromagnetism. This is now being done completely using lattice field theory, albeit neglecting electromagnetic effects in the sea in most cases (for an exception, see [27] which includes a calculation of the QED contribution to $\Delta M_K^2 = M_{K^0}^2 - M_{K^+}^2$ that is critical for determining $\overline{m}_d - \overline{m}_u$). The effect of this neglect on the u and d quark masses has been estimated in [28], to induce a contribution to the uncertainty that ranges from about 3% in $\overline{m}_u/\overline{m}_d$ to less than 1% in $\overline{m}_d$. FLAG has also reviewed results for these masses in [8]. Again, they separate results obtained from $N_f = 2+1$ and $N_f = 2+1+1$ simulations. For the former, their number is that of [28], as in the previous review [23], and for the latter, it is the average of the results from [17, 29, 30]. Thus, for $N_f = 2+1$ they quote $\overline{m}_u = 2.27(9)\,\text{MeV}$, $\overline{m}_d = 4.67(9)\,\text{MeV}$, $(\overline{m}_u/\overline{m}_d) = 0.485(19)$ and, for $N_f = 2+1+1$, $\overline{m}_u = 2.14(8)\,\text{MeV}$, $\overline{m}_d = 4.70(5)\,\text{MeV}$, $(\overline{m}_u/\overline{m}_d) = 0.465(24)$. Compared to the previous editions of the FLAG [23] and of the present reviews, the inclusion of the $N_f = 2+1+1$ results [17, 30] changes the central values of $\overline{m}_u$ and $\overline{m}_u/\overline{m}_d$ outside error bars, indicating some tension between the results of the newer and older calculations, which is around 2 standard deviations. Here, $\overline{m}_u$ is 0.36 MeV smaller than the value given in [23] and $\overline{m}_u/\overline{m}_d$ is 0.066 units smaller. These reductions make the $N_f = 2+1+1$ results more compatible with the $N_f = 2+1$ ones.

As for the light quark masses in the isospin limit, we average the results obtained with different numbers of sea-quark flavors. Here, only the $\overline{m}_u$ average has a $\chi^2/\text{dof} = 1.2 > 1$, and its error is thus appropriately scaled. Again, we do not allow the errors to become smaller than those on the individual flavor averages because of possible common systematics. Thus, we give as a final lattice QCD estimate in the $\overline{\text{MS}}$ scheme at $\mu = 2\,\text{GeV}$ in the $N_L = 4$ theory:

$$\overline{m}_u = 2.20(8)\,\text{MeV},\ \overline{m}_d = 4.69(5)\,\text{MeV},\ r \equiv \frac{\overline{m}_u}{\overline{m}_d} = 0.477(19). \tag{60.7}$$

As a consequence of the newly included $N_f = 2+1+1$ results [17,30], the central value of $\overline{m}_u$ has been reduced by 0.12 MeV and that of $\overline{m}_u/\overline{m}_d$ by 0.016 units compared to the previous edition of this review, while the error bar on $\overline{m}_u$ is 20% smaller and that on $\overline{m}_d$ is almost 50% smaller.

It is worth noting that m_u differs from zero by more than 20 times the quoted error, making a scenario in which $m_u = 0$ very unlikely. This is important because there would be no strong CP problem if m_u were to vanish identically.

It should also be emphasized that the results for the light quark masses given in the listings are dominated by the lattice values, since most phenomenological extractions have larger uncertainties.

60.4.2 *Chiral Perturbation Theory*

For light quarks, one can use the techniques of chiral perturbation theory [31–33] to extract quark mass ratios. The mass term for light quarks in the QCD Lagrangian is

$$\overline{\Psi} M \Psi = \overline{\Psi}_L M \Psi_R + \overline{\Psi}_R M^\dagger \Psi_L, \tag{60.8}$$

where M is the light quark mass matrix,

$$M = \begin{pmatrix} m_u & 0 & 0 \\ 0 & m_d & 0 \\ 0 & 0 & m_s \end{pmatrix}, \tag{60.9}$$

$\Psi = (u, d, s)$, and L and R are the left- and right-chiral components of Ψ given by $\Psi_{L,R} = P_{L,R}\Psi$, $P_L = (1-\gamma_5)/2$, $P_R = (1+\gamma_5)/2$. The mass term is the only term in the QCD Lagrangian that mixes left- and right-handed quarks. In the limit $M \to 0$, there is an independent SU(3)×U(1) flavor symmetry for the left- and right-handed quarks. The vector U(1) symmetry is baryon number; the axial U(1) symmetry of the classical theory is broken in the quantum theory due to the anomaly. The remaining $G_\chi = \text{SU}(3)_L \times \text{SU}(3)_R$ chiral symmetry of the QCD Lagrangian is spontaneously broken to $\text{SU}(3)_V$, which, in the limit $M \to 0$, leads to eight massless Goldstone bosons, the π's, K's, and η.

The symmetry G_χ is only an approximate symmetry, since it is explicitly broken by the quark mass matrix M. The Goldstone bosons acquire masses which can be computed in a systematic expansion in M, in terms of low-energy constants, which are unknown nonperturbative parameters of the effective theory, and are not fixed by the symmetries. One treats the quark mass matrix M as a uniform, external field that transforms under G_χ as $M \to LMR^\dagger$, where $\Psi_L \to L\Psi_L$ and $\Psi_R \to R\Psi_R$ are the $\text{SU}(3)_L$ and $\text{SU}(3)_R$ transformations, and writes down the most general Lagrangian invariant under G_χ. Then one sets M to its given constant value Eq. (60.9), which implements the symmetry breaking. To first order in M one finds that [34]

$$\begin{aligned} m_{\pi^0}^2 &= B\,(m_u + m_d)\,, \\ m_{\pi^\pm}^2 &= B\,(m_u + m_d) + \Delta_{\text{em}}, \\ m_{K^0}^2 &= m_{\overline{K}^0}^2 = B\,(m_d + m_s)\,, \\ m_{K^\pm}^2 &= B\,(m_u + m_s) + \Delta_{\text{em}}, \\ m_\eta^2 &= \frac{1}{3} B\,(m_u + m_d + 4m_s)\,, \end{aligned} \tag{60.10}$$

with two unknown constants B, related to the light quark condensate, and Δ_{em}, the electromagnetic mass difference. From Eq. (60.10), one can determine the quark mass ratios [34]

$$\begin{aligned} \frac{m_u}{m_d} &= \frac{2m_{\pi^0}^2 - m_{\pi^+}^2 + m_{K^+}^2 - m_{K^0}^2}{m_{K^0}^2 - m_{K^+}^2 + m_{\pi^+}^2} = 0.56, \\ \frac{m_s}{m_d} &= \frac{m_{K^0}^2 + m_{K^+}^2 - m_{\pi^+}^2}{m_{K^0}^2 + m_{\pi^+}^2 - m_{K^+}^2} = 20.2, \end{aligned} \tag{60.11}$$

to lowest order in chiral perturbation theory, with an error which will be estimated below. Since the mass ratios extracted using chiral perturbation theory use the symmetry transformation property of M under the chiral symmetry G_χ, it is important to use a renormalization scheme for QCD that does not change this transformation law. Any mass-independent subtraction scheme such as $\overline{\text{MS}}$ is suitable. The ratios of quark masses are scale independent in such a scheme (up to electromagnetic corrections), and Eq. (60.11) can be taken to be the ratio of $\overline{\text{MS}}$ masses. Chiral perturbation theory cannot determine the overall scale of the quark masses, since it uses only the symmetry properties of M, and any multiple of M has the same G_χ transformation law as M.

Chiral perturbation theory is a systematic expansion in powers of the light quark masses. The typical expansion parameter is $m_K^2/\Lambda_\chi^2 \sim 0.25$ if one uses SU(3) chiral symmetry, and $m_\pi^2/\Lambda_\chi^2 \sim 0.02$ if instead one uses SU(2) chiral symmetry. Electromagnetic effects at the few percent level also break SU(2) and SU(3) symmetry. The mass formulæ Eq. (60.10) were derived using SU(3) chiral symmetry, and are expected to have approximately a 25% uncertainty due to second order corrections. This estimate of the uncertainty yields results consistent with the lattice results summarized in Eq. (60.5)–(60.6).

There is a subtlety which arises when one tries to determine quark mass ratios at second order in chiral perturbation theory. The second order quark mass term [35]

$$\left(M^\dagger\right)^{-1} \det M^\dagger \tag{60.12}$$

(which can be generated by instantons) transforms in the same way under G_χ as M. Chiral perturbation theory cannot distinguish between M and $(M^\dagger)^{-1} \det M^\dagger$; one can make the replacement $M \to M(\lambda) = M + \lambda M (M^\dagger M)^{-1} \det M^\dagger$ in the chiral Lagrangian,

$$\begin{aligned} M(\lambda) &= \text{diag}\,(m_u(\lambda),\ m_d(\lambda),\ m_s(\lambda)) \\ &= \text{diag}\,(m_u + \lambda m_d m_s,\ m_d + \lambda m_u m_s,\ m_s + \lambda m_u m_d)\,, \end{aligned} \tag{60.13}$$

Downloaded from https://academic.oup.com/ptep/article/2022/8/083C01/6651666 by KIT Library user on 27 September 2022

and leave all observables unchanged.

The combination

$$\left(\frac{m_u}{m_d}\right)^2 + \frac{1}{Q^2}\left(\frac{m_s}{m_d}\right)^2 = 1 \tag{60.14}$$

where

$$Q^2 = \frac{m_s^2 - m_{ud}^2}{m_d^2 - m_u^2}, \qquad m_{ud} = \frac{1}{2}\left(m_u + m_d\right),$$

is insensitive to the transformation in Eq. (60.13). Eq. (60.14) gives an ellipse in the m_u/m_d-m_s/m_d plane. The ellipse is well-determined by chiral perturbation theory, but the location on the ellipse, and the absolute normalization of the quark masses, have larger uncertainties.

A leading-order result for Q in SU(3) chiral perturbation theory can be derived using Eq. (60.10) and the values for the relevant meson masses. This result actually holds to next-to-leading order, yielding $Q^{\rm NLO} = 24.3$. Phenomenologically, the preferred way to determine Q is from $\eta \to 3\pi$ decay, giving the smaller value $Q = 22.1(7)$ [36]. Lattice QCD collaborations have also reported determinations of Q. Using $N_f = 2+1$ simulations, [28] obtains $Q = 23.4 \pm 0.6$ and [29] determines $Q = 23.8 \pm 1.1$ with $N_f = 2+1+1$ simulations, which are fully compatible. These results are also compatible with $Q = 22.9 \pm 0.4$, obtained from $Q^2 = (r_s^2 - 1)(1+r)/[4(1-r)]$ and from our lattice averages for r_s and r from Eqs. (60.6) and (60.7), respectively. On the whole, the lattice results are larger than the one from phenomenology [36]. This difference could be due to surprisingly large corrections to the NLO substitution of meson masses by Q in the phenomenological determination, as suggested by the authors of [36].

The absolute normalization of the quark masses cannot be determined using chiral perturbation theory. Other methods, such as lattice simulations discussed above, or spectral function sum rules [37,38] for hadronic correlation functions reviewed next, are necessary.

60.4.3 *Sum rules*

Sum rule methods have been used extensively to determine quark masses and for illustration we briefly discuss here their application to hadronic τ decays [39]. Other applications involve very similar techniques.

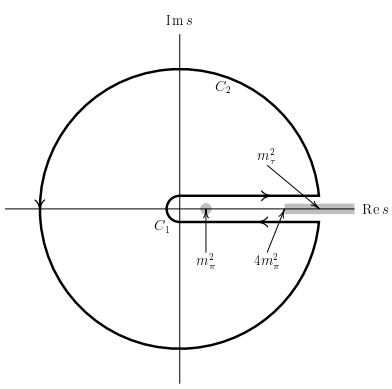

Figure 60.1: The analytic structure of $\Pi(s)$ in the complex s-plane. The contours C_1 and C_2 are the integration contours discussed in the text, and the integral over the closed contour $C_1 + C_2$ vanishes. m_τ^2 has not been drawn to scale; $m_\tau^2 \sim 40(4m_\pi^2)$.

The experimentally measured quantity is R_τ,

$$\frac{{\rm d}R_\tau}{{\rm d}s} = \frac{{\rm d}\Gamma/{\rm d}s\left(\tau^- \to {\rm hadrons} + \nu_\tau(\gamma)\right)}{\Gamma\left(\tau^- \to e^-\overline{\nu}_e\nu_\tau(\gamma)\right)} \tag{60.15}$$

the hadronic invariant mass spectrum in semihadronic τ decay, normalized to the leptonic τ decay rate. It is useful to define q as the total momentum of the hadronic final state, so $s = q^2$ is the hadronic invariant mass. The total hadronic τ decay rate R_τ is then given by integrating ${\rm d}R_\tau/{\rm d}s$ over the kinematically allowed range $0 \le s \le M_\tau^2$.

R_τ can be written as

$$R_\tau = 12\pi \int_0^{M_\tau^2} \frac{{\rm d}s}{M_\tau^2}\left(1 - \frac{s}{M_\tau^2}\right)^2 \times \left[\left(1 + 2\frac{s}{M_\tau^2}\right){\rm Im}\,\Pi^T(s) + {\rm Im}\,\Pi^L(s)\right] \tag{60.16}$$

where the hadronic spectral functions $\Pi^{L,T}$ are defined from the time-ordered correlation function of two weak currents ($j^\mu(x)$ and $j^\nu(0)$) by

$$\Pi^{\mu\nu}(q) = i\int {\rm d}^4x\; e^{iq\cdot x}\,\langle 0|\,T\left(j^\mu(x) j^\nu(0)^\dagger\right)|0\rangle\,, \tag{60.17}$$

$$\Pi^{\mu\nu}(q) = \left(-g^{\mu\nu} + q^\mu q^\nu\right)\Pi^T(s) + q^\mu q^\nu \Pi^L(s), \tag{60.18}$$

and the decomposition Eq. (60.17) is the most general possible structure consistent with Lorentz invariance.

By the optical theorem, the imaginary part of $\Pi^{\mu\nu}$ is proportional to the total cross-section for the current to produce all possible states. A detailed analysis including the phase space factors leads to Eq. (60.16). The spectral functions $\Pi^{L,T}(s)$ are analytic in the complex s plane, with singularities along the real axis. There is an isolated pole at $s = m_\pi^2$, and single- and multi-particle singularities for $s \ge 4m_\pi^2$, the two-particle threshold. The discontinuity along the real axis is $\Pi^{L,T}(s + i0^+) - \Pi^{L,T}(s - i0^+) = 2i{\rm Im}\,\Pi^{L,T}(s)$. As a result, Eq. (60.16) can be rewritten with the replacement ${\rm Im}\,\Pi^{L,T}(s) \to -i\Pi^{L,T}(s)/2$, and the integration being over the contour C_1. Finally, the contour C_1 can be deformed to $-C_2$ without crossing any singularities, and so leaving the integral unchanged, i.e. the integral over the closed contour $C_1 + C_2$ vanishes. One can derive a series of sum rules analogous to Eq. (60.16) by weighting the differential τ hadronic decay rate by different powers of the hadronic invariant mass [40],

$$R_\tau^{kl} = \int_0^{M_\tau^2} {\rm d}s\,\left(1 - \frac{s}{M_\tau^2}\right)^k \left(\frac{s}{M_\tau^2}\right)^l \frac{{\rm d}R_\tau}{{\rm d}s}\,. \tag{60.19}$$

This leads to the final form of the sum rule(s),

$$R_\tau^{kl} = -6\pi i \int_{C_2} \frac{{\rm d}s}{M_\tau^2}\left(1 - \frac{s}{M_\tau^2}\right)^{2+k}\left(\frac{s}{M_\tau^2}\right)^l \times \left[\left(1 + 2\frac{s}{M_\tau^2}\right)\Pi^T(s) + \Pi^L(s)\right]. \tag{60.20}$$

The manipulations so far are completely rigorous and exact, relying only on the general analytic structure of quantum field theory. The left-hand side of the sum rule Eq. (60.20) is obtained from experiment. The right hand-side can be computed for s far away from any physical cuts using the operator product expansion (OPE) for the time-ordered product of currents in Eq. (60.16), and QCD perturbation theory. The OPE is an expansion in a series of local operators, and is an expansion about the $q \to \infty$ limit. It gives $\Pi^{L,T}(s)$ as an expansion in powers of $\alpha_s(s)$ and $\Lambda_{\rm QCD}^2/s$, and is valid when s is far (in units of $\Lambda_{\rm QCD}^2$) from any singularities in the complex s-plane.

The OPE gives $\Pi^{L,T}(s)$ as a series in α_s, quark masses, and various nonperturbative vacuum matrix elements. By computing $\Pi^{L,T}(s)$ theoretically, and comparing with the experimental values of R_τ^{kl}, one determines various parameters such as α_s and the quark masses. The theoretical uncertainties in using Eq. (60.20) arise from neglected higher order corrections (both perturbative and nonperturbative), and because the OPE is no longer valid near the real axis, where $\Pi^{L,T}$ have singularities. The contribution of neglected higher order corrections can be estimated as for any other perturbative computation. The error due to the failure of the OPE is more difficult to estimate. In Eq. (60.20), the OPE fails on the endpoints of C_2 that touch the real axis at $s = M_\tau^2$. The weight factor $(1 - s/M_\tau^2)$ in Eq. (60.20) vanishes at

Downloaded from https://academic.oup.com/ptep/article/2022/8/083C01/6651666 by KIT Library user on 27 September 2022

this point, so the importance of the endpoint can be reduced by choosing larger values of k.

Light quark masses are often determined using QCD sum rules [38], which are similar to the τ sum rules. One takes the correlator of two light-quark-bilinear operators (e.g. an axial vector current), as in Eq. (60.16), and computes their Laplace transforms or moments

$$\mathcal{L}_n(\tau) = \int_0^\infty \mathrm{d}s\, s^n\, e^{-\tau s}\, \mathrm{Im}\,\Pi(s),$$

$$\mathcal{M}_n(Q^2) = \int_0^\infty \frac{\mathrm{d}s}{(s+Q^2)^n}\, \mathrm{Im}\,\Pi(s)$$

to get Laplace or moment sum rules, respectively. The quark masses are extracted by comparing the theoretical and experimental values of $\mathcal{L}_n(\tau)$ and $\mathcal{M}_n(Q^2)$. Considerable theoretical effort has gone into optimizing n and Q^2 to improve the precision of the resulting light quark masses.

60.5 Heavy quarks

60.5.1 *Continuum approaches and results*

For heavy quark physics one can exploit the fact that $m_Q \gg \Lambda_{\mathrm{QCD}}$ to construct effective theories (m_Q is the mass of the heavy quark Q). The masses and decay rates of hadrons containing a single heavy quark, such as the B and D mesons can be determined using the heavy quark effective theory (HQET) [41]. The theoretical calculations involve radiative corrections computed in perturbation theory with an expansion in $\alpha_s(m_Q)$ and nonperturbative corrections with an expansion in powers of $\Lambda_{\mathrm{QCD}}/m_Q$. Due to the asymptotic nature of the QCD perturbation series, the two kinds of corrections are intimately related; an example of this are renormalon effects in the perturbative expansion which are associated with nonperturbative corrections.

Systems containing two heavy quarks such as the Υ or J/Ψ are treated using non-relativistic QCD (NRQCD) [42]. The typical momentum and energy transfers in these systems are $\alpha_s m_Q$, and $\alpha_s^2 m_Q$, respectively, so these bound states are sensitive to scales much smaller than m_Q. However, smeared observables, such as the cross-section for $e^+e^- \to \bar{b}b$ averaged over some range of s that includes several bound state energy levels, are better behaved and only sensitive to scales near m_Q. For this reason, most determinations of the c, b quark masses using perturbative calculations compare smeared observables with experiment [43–45]. The method is similar to that outlined for τ decays. The current correlator in Eq. (60.16) is the electromagnetic current, and the experimental data is the value of $R(s)$ in the threshold region for $e^+e^- \to Q\overline{Q}$. The theoretical values for the moments are computed using renormalization group improved calculations in non-relativistic QCD.

There are many continuum extractions of the c and b quark masses, some with quoted errors of 10 MeV or smaller. There are systematic effects of comparable size, which are typically not included in these error estimates. Reference [46], for example, shows that even though the error estimate of m_c using the rapid convergence of the α_s perturbation series is only a few MeV, the central value of m_c can differ by a much larger amount depending on which algorithm (all of which are formally equally good) is used to determine m_c from the data. This leads to a systematic error from perturbation theory of around 20 MeV for the c quark and 25 MeV for the b quark. Electromagnetic effects, which also are important at this precision, are often not included. For this reason, we inflate the errors on the continuum extractions of m_c and m_b. The average values of m_c and m_b from continuum determinations are (see Sec. 60.6 for the 1S scheme)

$$\overline{m}_c(\overline{m}_c) = (1.280 \pm 0.025)\mathrm{GeV},$$

$$\overline{m}_b(\overline{m}_b) = (4.18 \pm 0.03)\,\mathrm{GeV}, \quad m_b^{1\mathrm{S}} = (4.65 \pm 0.03)\,\mathrm{GeV}.$$

60.5.2 *Lattice approaches and results*

Lattice QCD simulations of a heavy quark Q, described in a relativistic fermion formulation, lead to potentially large discretization errors which are powers of am_Q (modulated by logarithms); the leading power depends on the formulation of lattice QCD being used and in most cases is quadratic. Clearly those errors can be reduced by performing simulations at smaller lattice spacings a, but also by using *improved* discretizations of the theory, in which the leading discretization errors are systematically eliminated. Recently, with more powerful computing resources, better algorithms and techniques, it has become possible to perform simulations in the charm quark region and beyond, also decreasing the extrapolation which has to be performed to reach the b-quark. It is worth noting that computations using a relativistic fermion formulation for the valence charm with $N_f = 2+1$ sea-quark flavors, or with even $N_f = 2+1+1$ flavors and a relativistic b, suffer from partial-quenching effects. This is because the heavy valence quarks, in those calculations, are absent from the sea. While these effects are not expected to be large, they should be investigated when quoting results below the percent level, especially in the case of $N_f = 2+1$ sea-quark flavors. For that reason, we will omit relativistic heavy quark results obtained with $N_f = 2+1$ sea-quark flavors from our averages and, more generally focus on $N_f = 2+1+1$ results. Note that these partial-quenching effects can be and are accounted for systematically in lattice calculations in which the heavy valence quarks are described by HQET or NRQCD.

Traditionally the charm quark mass is obtained by tuning its bare, simulation input value to reproduce the physical mass of charmonium mesons or of the D, D_s mesons (requiring a more precise tuning of the light quark masses). This mass can then be renormalized and matched to the $\overline{\mathrm{MS}}$ scheme using the methods discussed for the light quarks.

An alternative approach for obtaining the $\overline{\mathrm{MS}}$ mass from the tuned bare quark mass was proposed in [47]. Euclidean-time moments of pseudoscalar, two-point functions of $c\bar{c}$ quark-bilinear operators can readily be computed on the lattice and extrapolated to the continuum limit where they can be compared to perturbative calculations of the same quantities at 4-loop order. In this way, both the strong coupling constant and the charm quark mass can be determined with remarkably small errors. As this approach uses the same perturbative expressions for two-point correlators as the continuum determinations discussed above, it suffers from similar perturbation-theory, systematic errors. FLAG [8] has reviewed lattice determinations of the charm quark mass obtained using both approaches. For their $N_f = 2+1$ average they retain the results [10, 48–50], with [51] being published after their deadline. As stated above, we focus here on $N_f = 2+1+1$ results. For these, the quoted average is

$$\overline{m}_c(\overline{m}_c) = 1.278(13)\,\mathrm{GeV},$$

based on the results of [16, 17, 19, 22, 52, 53], in good agreement with the continuum result given above, but with a smaller error. Compared to the previous editions of the FLAG [23] and of the present reviews, [53] updates [18] and [22] has appeared, but did not make the FLAG deadline.

It is worth noting that three [17, 18, 53] of the five results entering this average agree, while the two others [19, 52] are over 2 standard deviations larger, a deviation confirmed by [22]. This is taken into account by stretching errors in the usual way, but the total uncertainty on the lattice average of $\overline{m}_c$ will not significantly be reduced until this discrepancy is resolved. It should also be noted that [53] includes QED directly in the lattice calculation, albeit only for valence quarks, while some of the other computations account for these effects using phenomenology. For the moment these effects are still significantly smaller than the quoted error bars, at least when $\overline{m}_c$ is determined using the mass of the J/ψ.

Historically, the main approach to controlling the discretization errors in lattice studies of b quark physics was to perform simulations of effective theories such as HQET and NRQCD. This remains an important technique, both in its own right and in providing additional information for extrapolations from lower masses to the bottom region. Using effective theories, m_b is obtained from what is essentially a computation of the difference of $M_{H_b} - m_b$, where M_{H_b} is the mass of a hadron H_b containing a b-quark. The relative error on m_b is therefore much smaller

Downloaded from https://academic.oup.com/ptep/article/2022/8/083C01/6651666 by KIT Library user on 27 September 2022

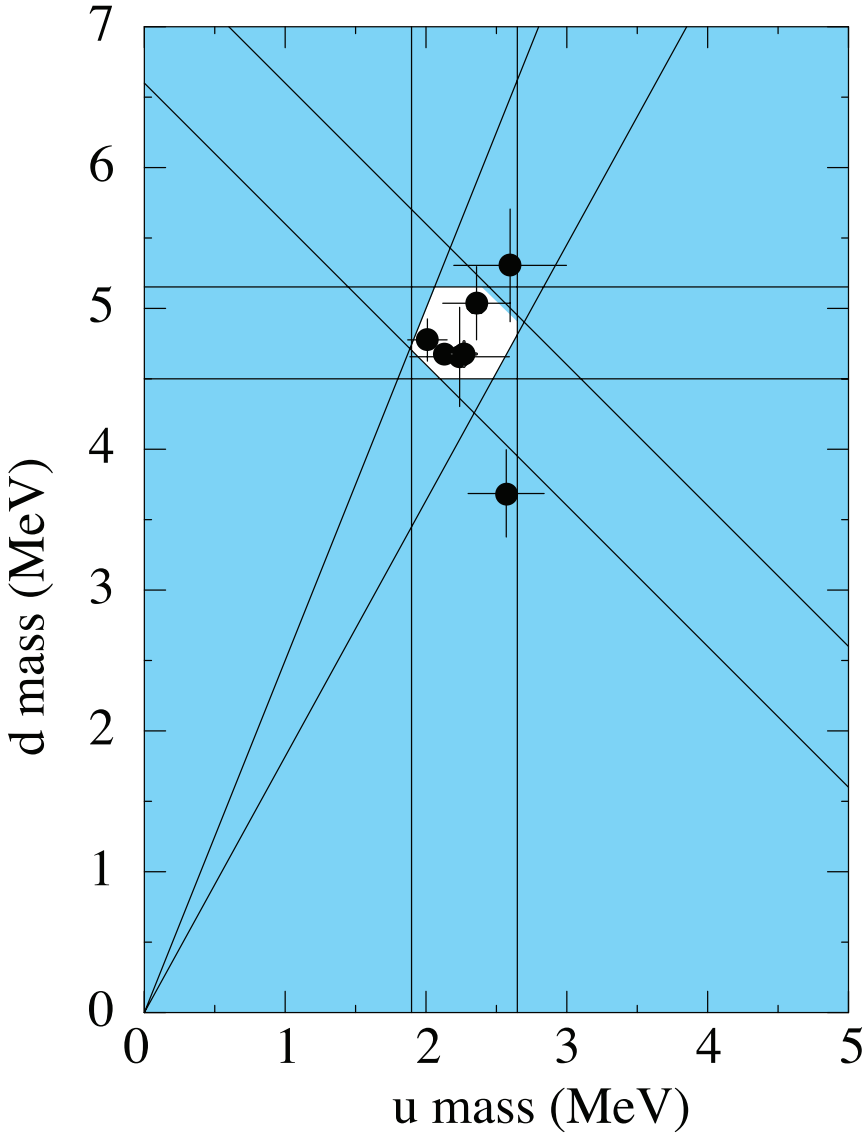

Figure 60.2: The allowed region (shown in white) for up quark and down quark masses renormalized in the $\overline{\text{MS}}$ scheme at 2 GeV. This region was determined in part from papers reporting values for m_u and m_d (data points shown) and in part from an analysis of the allowed ranges of other mass parameters (see Fig. 60.3). The parameter $(m_u + m_d)/2$ yields the two downward-sloping lines, while m_u/m_d yields the two rising lines originating at (0,0). There are two overlapping data points, so one of them is shown as a white diamond (it has very small error bars).

than that for $M_{H_b} - m_b$. The principal systematic errors are the matching of the effective theories to QCD and the presence of power divergences in a^{-1} in the $1/m_b$ corrections which have to be subtracted numerically. A procedure for performing these subtractions fully nonperturbatively was proposed and implemented for the first time in [54].

The most recent lattice QCD determinations of the b quark mass rely on a variety of approaches, including Euclidean-time moments of correlation functions with [55] or without NRQCD [56] and HQET based interpolations [57,58] or extrapolations [17] from above the charm to the b region. Compared to the previous editions of the FLAG [23] and of the present reviews, [56] updates [16] with a significantly reduced error bar. The overall agreement of the results obtained using these very different approaches, which have different systematic errors, is a confirmation that the various groups control these uncertainties. As the range of heavy-quark masses which can be used in numerical simulations increases, results obtained by extrapolating the results to the physical b mass are becoming ever more reliable (see e.g. [17]). FLAG's compilation [8] of the above $N_f = 2+1+1$ results yields

$$\overline{m}_b(\overline{m}_b) = 4.203(11)\,\text{GeV}\ ,$$

barely changed from the previous edition. Again, this result is compatible with the average value of continuum results, but with a significantly smaller uncertainty. Note that FLAG [8] also provides an average of $N_f = 2+1$ results, taken from [10, 50]. It is about 1.4 combined, standard deviations lower that the result quoted above.

As explained in Sec. 60.3, ratios of quark masses can have significantly smaller errors than the individual masses if they are determined within the same lattice QCD framework (up to small electromagnetic corrections for quarks of different charge). This led HPQCD to leverage their precise determination of m_c [47] to determine m_s and m_{ud} [59], through a precise computation of m_c/m_s [59] and of m_s/m_{ud} [60]. The $N_f = 2+1$ calculation [59] was updated using $N_f = 2+1+1$ simulations in [16]. The ratio m_s/m_c was also computed in [24,48] with $N_f = 2+1$ simulations and in [17,19] with $N_f = 2+1+1$ ones. The results of [19] should be replaced by those of [22] once the latter are published. Based

Downloaded from https://academic.oup.com/ptep/article/2022/8/083C01/6651666 by KIT Library user on 27 September 2022

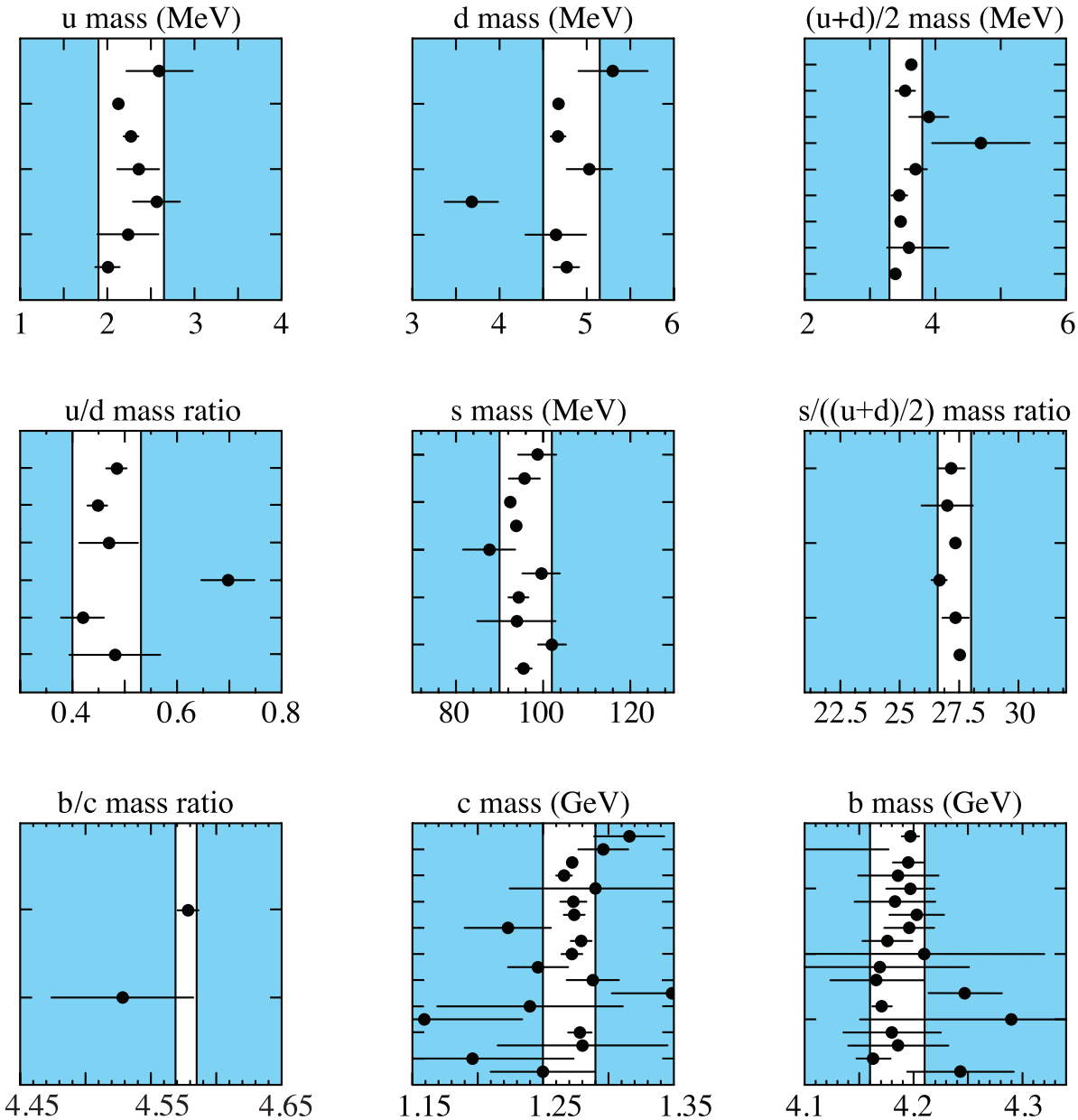

Figure 60.3: The values of each quark mass parameter taken from the Data Listings. The points are in chronological order with the more recent measurements at the top. The shaded regions indicate values excluded by our evaluations; some regions were determined in part through examination of Fig. 60.2.

on [48, 59], FLAG [8] quotes $m_c/m_s = 11.82(16)$ for $N_f = 2+1$, and $m_c/m_s = 11.769(35)$ for $N_f = 2+1+1$, based on [16, 17, 19], where a ∼50% stretch of the error bars was applied due to tensions among the results. The latter average is completely dominated by the result of [17] that has a substantially smaller error than the other results. As a final lattice number we give the $N_f = 2+1+1$ average

$$m_c/m_s = 11.769(35),$$

which is renormalization scheme and scale independent (in the absence of electromagnetic corrections) and is identical to the one given in the last edition of the present review.

The ratio m_b/m_c has also been computed on the lattice. The two $N_f = 2+1$ results which satisfy FLAG's criteria are [10, 50]. Here, as explained above, we focus on $N_f = 2+1+1$ calculations [17, 56, 57]. Amongst these, [56] updates [16], used in the previous edition of the present review, with a substantially reduced error. Averaging these results yields

$$m_b/m_c = 4.579(9),$$

where a scale factor of $\sqrt{\chi^2/\mathrm{dof}} = 1.38$ has been applied to the error bar. Indeed, [57] contributes 3.5 to the total χ^2. Note that [56] is the only calculation which accounts for QED directly in the lattice simulations, albeit only for valence quarks, and thus must specify the renormalization scheme and scale of its result, which it chooses to be $\overline{\mathrm{MS}}$ at 3 GeV.

60.5.3 *Warnings concerning the use of the pole mass*

For an observable particle such as the electron, the position of the pole in the propagator is the definition of its mass. In QCD this definition of the quark mass is known as the pole mass. It is known that the on-shell quark propagator has no infrared divergences in perturbation theory [61, 62], so this provides a perturbative definition of the quark mass. However, the pole mass cannot be used to arbitrarily high accuracy because of nonperturbative infrared effects in QCD. In fact the full quark propagator has no pole because the quarks are confined, so that the pole mass cannot be defined outside of perturbation theory. The relation between the pole mass m_Q and the $\overline{\mathrm{MS}}$ mass $\overline{m}_Q$, used throughout this

Downloaded from https://academic.oup.com/ptep/article/2022/8/083C01/6651666 by KIT Library user on 27 September 2022

review, is known to three loops [63–66]

$$m_Q = \overline{m}_Q(\overline{m}_Q)\Bigg\{1 + \frac{4\overline{\alpha}_s(\overline{m}_Q)}{3\pi} \tag{60.21}$$
$$+ \left[-1.0414\sum_q\left(1 - \frac{4}{3}\frac{\overline{m}_q}{\overline{m}_Q}\right) + 13.4434\right]\left[\frac{\overline{\alpha}_s(\overline{m}_Q)}{\pi}\right]^2$$
$$+ \left[0.6527N_L^2 - 26.655N_L + 190.595\right]\left[\frac{\overline{\alpha}_s(\overline{m}_Q)}{\pi}\right]^3\Bigg\},$$

where $\overline{\alpha}_s(\mu)$ is the strong interaction coupling constants in the $\overline{\text{MS}}$ scheme, and the sum over q extends over the N_L flavors lighter than Q. The complete mass dependence of the α_s^2 term can be found in [63]; the mass dependence of the α_s^3 term is not known. For the b-quark, Eq. (60.21) reads

$$m_b = \overline{m}_b\,(\overline{m}_b)\,[1 + 0.10 + 0.05 + 0.03]\,, \tag{60.22}$$

where the contributions from the different orders in α_s are shown explicitly. The two and three loop corrections are comparable in size and have the same sign as the one loop term. This is a signal of the asymptotic nature of the perturbation series (there is a renormalon in the pole mass [67]). Such a badly behaved perturbation expansion can be avoided by directly extracting, from data, the mass defined in the $\overline{\text{MS}}$ (used in this review) or other short-distance schemes (see below), without invoking the pole mass as an intermediate step.

60.6 Numerical values and caveats

The quark masses in the particle data listings have been obtained by using a wide variety of methods. Each method involves its own set of approximations and uncertainties. In most cases, the errors are an estimate of the size of neglected higher-order corrections or other uncertainties. The expansion parameters for some of the approximations are not very small (for example, they are $m_K^2/\Lambda_\chi^2 \sim 0.25$ for the SU(3) chiral expansion and $\Lambda_{\text{QCD}}/m_b \sim 0.1$ for the heavy-quark expansion), so an unexpectedly large coefficient in a neglected higher-order term could significantly alter the results. Thus, before using a particular result, it is important to understand the possible limitations of the approach used to obtain it. It is also important to note that the quark mass values can be significantly different in the different schemes.

We have specified all masses in the $\overline{\text{MS}}$ scheme. For light quarks, the renormalization scale has been chosen to be $\mu = 2$ GeV. Quoting these masses at smaller values of μ, where perturbative corrections become significantly larger, would introduce unnecessary uncertainties in the results. In fact, as lattice calculations, performed on finer and finer lattices, allow to determine quark masses, fully nonperturbatively, at larger and larger values of μ, it may become advantageous to quote quark mass results at renormalization scales above 2 GeV, where perturbative uncertainties are smaller.

The heavy quark masses obtained using HQET, QCD sum rules, or lattice gauge theory are consistent with each other if they are all converted into the same scheme and scale. For these quarks it is conventional to choose the renormalization scale equal to the quark mass, so we have quoted $\overline{m}_Q(\mu)$ at $\mu = \overline{m}_Q$ for the c and b quarks. Given the small size of the charm quark mass, in the future it may become advantageous to quote its value at larger values of μ so as not to introduce unnecessary perturbative uncertainties (see discussion above). Analyses of inclusive B meson decays have shown that other mass definitions lead to a better behaved perturbation series than for the $\overline{\text{MS}}$ mass, and hence to more accurate mass values [68–71]. Thus, we have chosen to also give values for one of these, the b quark mass in the 1S scheme [68, 69]. Other schemes that have been proposed are the PS-scheme [70], the kinetic scheme [72] and, most recently, the minimal renormalon-subtracted mass (MRS) [71] used in the lattice calculation [17].

If necessary, we have converted values in the original papers to our chosen scheme using two-loop formulæ. It is important to realize that our conversions introduce significant additional errors. In converting to the $\overline{\text{MS}}$ b-quark mass, for example, the three-loop conversions from the 1S and pole masses give values about 35 MeV and 135 MeV lower than the two-loop conversions. The uncertainty in $\alpha_s(M_Z) = 0.1179 \pm 0.0010$ [1] gives an uncertainty of ± 9 MeV and ± 21 MeV respectively in the same conversions. We have not added these additional errors when we do our conversions. The α_s value in the conversion is correlated with the α_s value used in determining the quark mass, so the conversion error is not a simple additional error on the quark mass.

References

[1] See the review of QCD in this volume.

[2] A. Manohar and H. Georgi, Nucl. Phys. B **234**, 189 (1984).

[3] K. Chetyrkin, Phys. Lett. B **404**, 161 (1997), [hep-ph/9703278].

[4] J. Vermaseren, S. Larin and T. van Ritbergen, Phys. Lett. B **405**, 327 (1997), [hep-ph/9703284].

[5] K. Chetyrkin, B. A. Kniehl and M. Steinhauser, Nucl. Phys. B **510**, 61 (1998), [hep-ph/9708255].

[6] G. Martinelli *et al.*, Nucl. Phys. B **445**, 81 (1995), [hep-lat/9411010].

[7] K. Jansen *et al.*, Phys. Lett. B **372**, 275 (1996), [hep-lat/9512009].

[8] Y. Aoki *et al.* (2021), [arXiv:2111.09849].

[9] A. Bazavov *et al.* (MILC), PoS **CD09**, 007 (2009), [arXiv:0910.2966].

[10] C. McNeile *et al.*, Phys. Rev. D **82**, 034512 (2010), [arXiv:1004.4285].

[11] A. Bazavov *et al.*, PoS **LATTICE2010**, 083 (2010), [arXiv:1011.1792].

[12] S. Durr *et al.*, Phys. Lett. B **701**, 265 (2011), [arXiv:1011.2403].

[13] S. Durr *et al.*, JHEP **08**, 148 (2011), [arXiv:1011.2711].

[14] T. Blum *et al.* (RBC, UKQCD), Phys. Rev. D **93**, 7, 074505 (2016), [arXiv:1411.7017].

[15] M. Bruno *et al.* (ALPHA), Eur. Phys. J. C **80**, 2, 169 (2020), [arXiv:1911.08025].

[16] B. Chakraborty *et al.*, Phys. Rev. D **91**, 5, 054508 (2015), [arXiv:1408.4169].

[17] A. Bazavov *et al.* (Fermilab Lattice, MILC, TUMQCD), Phys. Rev. D **98**, 5, 054517 (2018), [arXiv:1802.04248].

[18] A. Lytle *et al.* (HPQCD), Phys. Rev. D **98**, 1, 014513 (2018), [arXiv:1805.06225].

[19] N. Carrasco *et al.* (European Twisted Mass), Nucl. Phys. B **887**, 19 (2014), [arXiv:1403.4504].

[20] A. Bazavov *et al.* (Fermilab Lattice, MILC), Phys. Rev. D **90**, 7, 074509 (2014), [arXiv:1407.3772].

[21] A. Bazavov *et al.*, Phys. Rev. D **98**, 7, 074512 (2018), [arXiv:1712.09262].

[22] C. Alexandrou *et al.* (2021), [arXiv:2104.13408].

[23] S. Aoki *et al.* (Flavour Lattice Averaging Group), Eur. Phys. J. C **80**, 2, 113 (2020), [arXiv:1902.08191].

[24] Y. Maezawa and P. Petreczky, Phys. Rev. D **94**, 3, 034507 (2016), [arXiv:1606.08798].

[25] M. Bruno *et al.* (ALPHA), Phys. Rev. Lett. **114**, 10, 102001 (2015), [arXiv:1410.8374].

[26] A. Athenodorou *et al.* (2018), [arXiv:1809.03383].

[27] S. Borsanyi *et al.*, Science **347**, 1452 (2015), [arXiv:1406.4088].

[28] Z. Fodor *et al.*, Phys. Rev. Lett. **117**, 8, 082001 (2016), [arXiv:1604.07112].

[29] D. Giusti *et al.*, Phys. Rev. D **95**, 11, 114504 (2017), [arXiv:1704.06561].

[30] S. Basak *et al.* (MILC), Phys. Rev. D **99**, 3, 034503 (2019), [arXiv:1807.05556].

Downloaded from https://academic.oup.com/ptep/article/2022/8/083C01/6651666 by KIT Library user on 27 September 2022

[31] S. Weinberg, Physica A **96**, 1-2, 327 (1979).

[32] J. Gasser and H. Leutwyler, Annals Phys. **158**, 142 (1984).

[33] A. Pich, Rept. Prog. Phys. **58**, 563 (1995), [hep-ph/9502366].

[34] S. Weinberg, Trans. New York Acad. Sci. **38**, 185 (1977).

[35] D. B. Kaplan and A. V. Manohar, Phys. Rev. Lett. **56**, 2004 (1986).

[36] G. Colangelo *et al.*, Eur. Phys. J. C **78**, 11, 947 (2018), [arXiv:1807.11937].

[37] S. Weinberg, Phys. Rev. Lett. **18**, 507 (1967).

[38] M. A. Shifman, A. Vainshtein and V. I. Zakharov, Nucl. Phys. B **147**, 385 (1979).

[39] E. Braaten, S. Narison and A. Pich, Nucl. Phys. B **373**, 581 (1992).

[40] F. Le Diberder and A. Pich, Phys. Lett. B **286**, 147 (1992).

[41] N. Isgur and M. B. Wise, Phys. Lett. B **237**, 527 (1990).

[42] G. T. Bodwin, E. Braaten and G. Lepage, Phys. Rev. D **51**, 1125 (1995), [Erratum: Phys.Rev.D 55, 5853 (1997)], [hep-ph/9407339].

[43] A. Hoang, Phys. Rev. D **61**, 034005 (2000), [hep-ph/9905550].

[44] K. Melnikov and A. Yelkhovsky, Phys. Rev. D **59**, 114009 (1999), [hep-ph/9805270].

[45] M. Beneke and A. Signer, Phys. Lett. B **471**, 233 (1999), [hep-ph/9906475].

[46] B. Dehnadi *et al.*, JHEP **09**, 103 (2013), [arXiv:1102.2264].

[47] I. Allison *et al.* (HPQCD), Phys. Rev. D **78**, 054513 (2008), [arXiv:0805.2999].

[48] Y.-B. Yang *et al.*, Phys. Rev. D **92**, 3, 034517 (2015), [arXiv:1410.3343].

[49] K. Nakayama, B. Fahy and S. Hashimoto, Phys. Rev. D **94**, 5, 054507 (2016), [arXiv:1606.01002].

[50] P. Petreczky and J. Weber, Phys. Rev. D **100**, 3, 034519 (2019), [arXiv:1901.06424].

[51] J. Heitger, F. Joswig and S. Kuberski (ALPHA), JHEP **05**, 288 (2021), [arXiv:2101.02694].

[52] C. Alexandrou *et al.*, Phys. Rev. D **90**, 7, 074501 (2014), [arXiv:1406.4310].

[53] D. Hatton *et al.* (HPQCD), Phys. Rev. D **102**, 5, 054511 (2020), [arXiv:2005.01845].

[54] J. Heitger and R. Sommer (ALPHA), JHEP **02**, 022 (2004), [hep-lat/0310035].

[55] B. Colquhoun *et al.*, Phys. Rev. D **91**, 7, 074514 (2015), [arXiv:1408.5768].

[56] D. Hatton *et al.*, Phys. Rev. D **103**, 11, 114508 (2021), [arXiv:2102.09609].

[57] A. Bussone *et al.* (ETM), Phys. Rev. D **93**, 11, 114505 (2016), [arXiv:1603.04306].

[58] P. Gambino, A. Melis and S. Simula, Phys. Rev. D **96**, 1, 014511 (2017), [arXiv:1704.06105].

[59] C. Davies *et al.*, Phys. Rev. Lett. **104**, 132003 (2010), [arXiv:0910.3102].

[60] A. Bazavov *et al.* (MILC), Rev. Mod. Phys. **82**, 1349 (2010), [arXiv:0903.3598].

[61] R. Tarrach, Nucl. Phys. B **183**, 384 (1981).

[62] A. S. Kronfeld, Phys. Rev. D **58**, 051501 (1998), [hep-ph/9805215].

[63] N. Gray *et al.*, Z. Phys. C **48**, 673 (1990).

[64] D. J. Broadhurst, N. Gray and K. Schilcher, Z. Phys. C **52**, 111 (1991).

[65] K. Chetyrkin and M. Steinhauser, Phys. Rev. Lett. **83**, 4001 (1999), [hep-ph/9907509].

[66] K. Melnikov and T. v. Ritbergen, Phys. Lett. B **482**, 99 (2000), [hep-ph/9912391].

[67] M. Beneke and V. M. Braun, Nucl. Phys. B **426**, 301 (1994), [hep-ph/9402364].

[68] A. H. Hoang, Z. Ligeti and A. V. Manohar, Phys. Rev. Lett. **82**, 277 (1999), [hep-ph/9809423].

[69] A. H. Hoang, Z. Ligeti and A. V. Manohar, Phys. Rev. D **59**, 074017 (1999), [hep-ph/9811239].

[70] M. Beneke, Phys. Lett. B **434**, 115 (1998), [hep-ph/9804241].

[71] N. Brambilla *et al.* (TUMQCD), Phys. Rev. D **97**, 3, 034503 (2018), [arXiv:1712.04983].

[72] P. Gambino and N. Uraltsev, Eur. Phys. J. C **34**, 181 (2004), [hep-ph/0401063].

Downloaded from https://academic.oup.com/ptep/article/2022/8/083C01/6651666 by KIT Library user on 27 September 2022

61. Top Quark

Revised September 2021 by T.M. Liss (City Coll. of New York), F. Maltoni (CP3 U. catholique de Louvain; Bologna U.) and A. Quadt (Göttingen U.).

61.1 Introduction

In the Standard Model (SM), the left-handed top quark is the $Q = 2/3$, $T_3 = +1/2$ member of the weak-isospin doublet containing the bottom quark, while the right-handed top is an $SU(2)_L$ singlet (see, e.g., the review "Electroweak Model and Constraints on New Physics" here). Its phenomenology is driven by its large mass. Being heavier than a W boson, it is the only quark that decays semi-weakly, i.e., into a real W boson and a b quark. This results in a lifetime that is shorter than the hadronization time. In addition, it is the only quark whose Yukawa coupling to the Higgs boson is of order unity. For these reasons, the top quark plays a special role in the Standard Model and in many extensions thereof. Top quark physics provides a unique laboratory where our understanding of the strong, both in the perturbative and non-perturbative regimes, and electroweak interactions can be tested. An accurate knowledge of its properties (mass, couplings, production cross sections, decay branching ratios, *etc.*) can bring key information on fundamental interactions at the electroweak symmetry-breaking scale and beyond. This review provides a concise discussion of the experimental and theoretical issues involved in the determination of the top-quark properties.

61.2 Top-quark production at the Tevatron and LHC

In hadron collisions, top quarks are produced dominantly in pairs through the processes $q\bar{q} \to t\bar{t}$ and $gg \to t\bar{t}$, at leading order in QCD. At the Tevatron ($p\bar{p}$ at 1.96 TeV) approximately 85% of the production cross section is from $q\bar{q}$ annihilation, with the remainder from gluon-gluon fusion. Conversely, at the LHC about 90% (80%) of $t\bar{t}$ production is from gluon-gluon fusion at $\sqrt{s} = 13$ TeV ($\sqrt{s} = 7$ TeV).

Predictions for the top-quark production total cross sections are available at next-to-next-to leading order (NNLO) [1, 2], also including next-to-next-to-leading-log (NNLL) soft gluon resummation. Assuming a top-quark mass of 173.3 GeV/c^2, close to the Tevatron + LHC combination [3], the resulting theoretical prediction of the top-quark pair cross-section at NNLO+NNLL accuracy at the Tevatron at $\sqrt{s} = 1.96$ TeV is $\sigma_{t\bar{t}} = 7.16^{+0.11+0.17}_{-0.20-0.12}$ pb where the first uncertainty is from scale dependence and the second from parton distribution functions. At the LHC, assuming a top-quark mass of 172.5 GeV/c^2 the cross sections are: $\sigma_{t\bar{t}} = 177.3^{+4.6+9.0}_{-6.0-9.0}$ pb at $\sqrt{s} = 7$ TeV, $\sigma_{t\bar{t}} = 252.9^{+6.4+11.7}_{-8.6-11.7}$ pb at $\sqrt{s} = 8$ TeV, $\sigma_{t\bar{t}} = 831.8^{+19.8+35.1}_{-29.2-35.1}$ pb at $\sqrt{s} = 13$ TeV, and $\sigma_{t\bar{t}} = 984.5^{+23.2+41.3}_{-34.7-41.3}$ pb at $\sqrt{s} = 14$ TeV [1].

Electroweak single top-quark production mechanisms, namely from $q\bar{q}' \to t\bar{b}$ [4], $qb \to q't$ [5], mediated by virtual s-channel and t-channel W-bosons, and Wt-associated production, through $bg \to W^-t$, lead to somewhat smaller cross sections. For example, t-channel production, while suppressed by the weak coupling with respect to the strong pair production, is kinematically enhanced, resulting in a sizeable cross section both at Tevatron and LHC energies. At the Tevatron, the t- and s-channel cross sections for top quarks are identical to those for antitop quarks , while at the LHC they are not, due to the charge-asymmetric initial state. NNLO cross sections for t-channel single top-quark production ($t + \bar{t}$) are calculated for $m_t = 173.2$ GeV/c^2 to be $2.08^{+0.04+0.08}_{-0.03-0.10}$ pb in $p\bar{p}$ collisions at $\sqrt{s} = 1.96$ TeV, where the first uncertainty is from scale dependence and the second from parton distribution functions. [6]. A calculation at NNLO accuracy for the t-channel cross section at the LHC has first appeared in [7], superseded by more recent calculations [6,8] which predict ($m_t = 172.5$ GeV/c^2): $\sigma_{t+\bar{t}} = 64.0^{+0.77}_{-0.38}$ pb at $\sqrt{s} = 7$ TeV, $\sigma_{t+\bar{t}} = 84.6^{+1.0}_{-0.5}$ pb at $\sqrt{s} = 8$ TeV, $\sigma_{t+\bar{t}} = 215^{+2.1}_{-1.3}$ pb at $\sqrt{s} = 13$ TeV, and $\sigma_{t+\bar{t}} = 245^{+2.7}_{-1.3}$ pb at $\sqrt{s} = 14$ TeV, where the quoted uncertainties are from scale variation only. For the s-channel, NNLO approximated calculations yield $1.03^{+0.05}_{-0.05}$ pb for the Tevatron [9]. An NLO calculation gives $4.3^{+0.13+0.14}_{-0.10-0.14}$ pb, $5.2^{+0.15+0.16}_{-0.12-0.16}$ pb, and $10.3^{+0.29+0.27}_{-0.24-0.27}$ pb for $\sqrt{s} = 7, 8, 13$ TeV at the LHC, respectively, with 64%, 64%, 62%, of top quarks. While negligible at the Tevatron, at LHC energies the Wt-associated production becomes relevant. At $\sqrt{s} = 7, 8, 13$ TeV, an approximate NNLO calculation gives ($t + \bar{t}$), $15.7^{+0.4+1.10}_{-0.4-1.14}$ pb , $22.4^{+0.6+1.40}_{-0.6-1.40}$ pb , $71.7^{+1.8+3.40}_{-1.8-3.40}$ pb , respectively, with an equal proportion of top and anti-top quarks [10].

Assuming $|V_{tb}| \gg |V_{td}|, |V_{ts}|$ (see the review "The CKM Quark-Mixing Matrix" for more information), the cross sections for single top production are proportional to $|V_{tb}|^2$, and no extra hypothesis is needed on the number of quark families or on the unitarity of the CKM matrix in extracting $|V_{tb}|$. Separate measurements of the s- and t-channel processes provide sensitivity to physics beyond the Standard Model [11].

With a mass above the Wb threshold, and $|V_{tb}| \gg |V_{td}|$, $|V_{ts}|$, the decay width of the top quark is expected to be dominated by the two-body channel $t \to Wb$. Neglecting terms of order m_b^2/m_t^2, α_s^2, and $(\alpha_s/\pi)M_W^2/m_t^2$, the width predicted in the SM at NLO is [12]:

$$\Gamma_t = \frac{G_F m_t^3}{8\pi\sqrt{2}} \left(1 - \frac{M_W^2}{m_t^2}\right)^2 \left(1 + 2\frac{M_W^2}{m_t^2}\right) \left[1 - \frac{2\alpha_s}{3\pi}\left(\frac{2\pi^2}{3} - \frac{5}{2}\right)\right], \tag{61.1}$$

where m_t refers to the top-quark pole mass. The width for a value of $m_t = 173.3$ GeV/c^2 is 1.35 GeV/c^2 (we use $\alpha_s(M_Z) = 0.118$) and increases with mass. With its correspondingly short lifetime of about 0.5×10^{-24} s, the top quark is expected to decay before top-flavored hadrons or $t\bar{t}$-quarkonium-bound states can form [13]. In fact, since the decay time is close to the would-be-resonance binding time, a peak will be visible in e^+e^- scattering at the $t\bar{t}$ threshold [14] and it is in principle present (yet very difficult to measure) in hadron collisions too [15, 16]. The order α_s^2 QCD corrections to Γ_t are also available [17], thereby improving the overall theoretical accuracy to better than 1%.

The final states for the leading pair-production process can be divided into three classes:

A. $t\bar{t} \to W^+ b\, W^- \bar{b} \to q\bar{q}'\, bq''\, \bar{q}'''\, \bar{b}$, (45.7%)
B. $t\bar{t} \to W^+ b\, W^- \bar{b} \to q\bar{q}'\, b\ell^-\bar{\nu}_\ell\, \bar{b} + \ell^+\nu_\ell\, b\, q''\bar{q}'''\, \bar{b}$, (43.8%)
C. $t\bar{t} \to W^+ b\, W^- \bar{b} \to \ell^+\, \nu_\ell\, b\, \ell'^-\bar{\nu}_{\ell'}\, \bar{b}$. (10.5%)

The quarks in the final state evolve into jets of hadrons. A, B, and C are referred to as the all-hadronic, lepton+jets (ℓ+jets), and dilepton ($\ell\ell$) channels, respectively. Their relative contributions, including hadronic corrections, are given in parentheses assuming lepton universality. While ℓ in the above processes refers to e, μ, or τ, most of the analyses distinguish the e and μ from the τ channel, which is more difficult to reconstruct. Therefore, in what follows, we will use ℓ to refer to e or μ, unless otherwise noted. Here, typically leptonic decays of τ are included. In addition to the quarks resulting from the top-quark decays, extra QCD radiation (quarks and gluons) from the colored particles in the event can lead to extra jets.

The number of jets reconstructed in the detectors depends on the decay kinematics, as well as on the algorithm for reconstructing jets used by the analysis. Information on the transverse momenta, p_T of the neutrinos is obtained from the imbalance in transverse momentum measured in each event (missing p_T, which is here also called missing transverse energy, E_T).

The identification of top quarks in the electroweak single top channel is much more difficult than in the QCD $t\bar{t}$ channel, due to a less distinctive signature and significantly larger backgrounds, mostly due to $t\bar{t}$ and W+jets production.

Fully exclusive predictions via Monte Carlo generators for the $t\bar{t}$ and single top production processes at NLO accuracy in QCD, including top-quark decays and possibly off-shell effects are available [18,19] through the MC@NLO [20] and POWHEG [21] methods. Very recently, the first Monte Carlo implementation of the NNLO computation has become available [22].

Besides fully inclusive QCD or EW top-quark production, more exclusive final states can be accessed at hadron colliders, whose

Downloaded from https://academic.oup.com/ptep/article/2022/8/083C01/6651666 by KIT Library user on 27 September 2022

cross sections are typically much smaller, yet can provide key information on the properties of the top quark. For all relevant final states (*e.g.*, $t\bar{t}V$, $t\bar{t}VV$ with $V = \gamma, W, Z$, $t\bar{t}H, t\bar{t}$+jets, $t\bar{t}b\bar{b}, t\bar{t}t\bar{t}$) automatic or semi-automatic predictions at NLO accuracy both in QCD and EW expansions, also in the form of event generators are available (see the review "Monte Carlo event generators" for more information).

61.3 Top-quark measurements

Since the discovery of the top quark, direct measurements of $t\bar{t}$ production have been made at six center-of-mass energies in pp or $p\bar{p}$ and in pPb collisions, providing stringent tests of QCD. The first measurements were made in Run I at the Tevatron at $\sqrt{s} = 1.8$ TeV. In Run II at the Tevatron relatively precise measurements were made at $\sqrt{s} = 1.96$ TeV. Finally, beginning in 2010, measurements have been made at the LHC at $\sqrt{s} = 7$ TeV, $\sqrt{s} = 8$ TeV, and $\sqrt{s} = 13$ TeV, and recently also in dedicated low energy runs at $\sqrt{s} = 5.02$ in pp and at 8.16 TeV in pPb collisions.

Production of single top quarks through electroweak interactions has now been measured with good precision at the Tevatron at $\sqrt{s} = 1.96$ TeV, and at the LHC at $\sqrt{s} = 7$ TeV, $\sqrt{s} = 8$ TeV, and also at $\sqrt{s} = 13$ TeV. Measurements at the Tevatron have managed to separate the s- and t-channel production cross sections, and at the LHC, the tW mechanism as well, though the t-channel is measured with best precision to date. The measurements allow an extraction of the CKM matrix element V_{tb}. Also more exclusive production modes and top-quark properties have been measured in single-top production.

With approximately 10 fb^{-1} of Tevatron data, and almost 5 fb^{-1} at 7 TeV, 20 fb^{-1} at 8 TeV and 139 fb^{-1} at 13 TeV at the LHC, many properties of the top quark have been measured with high precision. These include properties related to the production mechanism, such as $t\bar{t}$ spin correlations, forward-backward or charge asymmetries, and differential production cross sections, as well as properties related to the tWb decay vertex, such as the helicity of the W-bosons from the top-quark decay. Also studies of the $t\bar{t}b\bar{b}$, $t\bar{t}t\bar{t}$, $t\bar{t}\gamma$, $t\bar{t}Z$, $t\bar{t}h$, th, tZq or $t\gamma q$ processes and the corresponding vertices as well as contact interactions have been made, some yielding first observations, others strong evidence. Those processes probe genuinely new aspects of the top-quark such as electroweak couplings to neutral gauge bosons or possibly four-top-quark interactions. In addition, many searches for physics beyond the Standard Model are being performed with increasing reach in both production and decay channels.

In the following sections we review the current status of measurements of the characteristics of the top quark.

61.3.1 *Top-quark production*

61.3.1.1 *$t\bar{t}$ production*

Fig. 61.1 summarizes the $t\bar{t}$ production cross-section measurements from both, the Tevatron and LHC. Please note that some cross section measurements at the LHC have luminosity-related uncertainties which have improved in the meantime [23]. The latest measurement from DØ [24] ($p\bar{p}$ at $\sqrt{s} = 1.96$ TeV), combining the measurements from the dilepton and lepton plus jets final states in 9.7 fb^{-1}, is 7.26 ± 0.13 (stat.)$^{+0.57}_{-0.50}$ (syst.) pb (7.5%). From CDF the most precise measurement made [25] is in 8.8 fb^{-1} in the dilepton channel requiring at least one b-tag, yielding 7.09 ± 0.84 pb. Both of these measurements assume a top-quark mass of 172.5 GeV/c^2. The dependence of the cross-section measurements on the value chosen for the mass is less than that of the theory calculations because it only affects the determination of the acceptance. In some analyses also the shape of topological variables might be modified.

Combining the recent cross section measurements with older ones in other channels yields $\sigma_{t\bar{t}} = 7.63 \pm 0.50$ pb (6.6%) for CDF, $\sigma_{t\bar{t}} = 7.56 \pm 0.59$ pb (7.8%) for DØ and $\sigma_{t\bar{t}} = 7.60 \pm 0.41$ pb (5.4%) for the Tevatron combination [26]. The contributions to the uncertainty are 0.20 pb from statistical sources, 0.29 pb from systematic sources, and 0.21 pb from the uncertainty on the integrated luminosity. The combined result is in good agreement with the SM expectation of $7.35^{+0.28}_{-0.33}$ pb at NNLO+NNLL in perturbative QCD [1] for a top mass of 172.5 GeV/c^2.

CDF has measured the $t\bar{t}$ production cross section in the dilepton channel with one hadronically decaying tau in 9.0 fb^{-1}, yielding $\sigma_{t\bar{t}} = 8.1 \pm 2.1$ pb. By separately identifying the single-tau and the ditau components, they measure the branching fraction of the top quark into the tau lepton, tau neutrino, and bottom quark to be (9.6 ± 2.8)% [27]. CDF has also performed measurements of the $t\bar{t}$ production cross section normalized to the Z production cross section in order to reduce the impact of the luminosity uncertainty [28].

DØ has performed a measurement of differential $t\bar{t}$ cross sections in 9.7 fb^{-1} of lepton+jets data as a function of the transverse momentum, and absolute value of the rapidity of the top quarks as well as of the invariant mass of the $t\bar{t}$ pair [29]. Observed differential cross sections are consistent with SM predictions.

The LHC experiments ATLAS and CMS use similar techniques to measure the $t\bar{t}$ cross section in pp collisions. The most precise measurements come from the dilepton channel, and in particular the $e\mu$ channel. In order to test consistency of the cross-section measurements with some systematic uncertainties cancelling out while testing pQCD and PDFs, cross-section ratios between measurements at 7 TeV and at 8 TeV are performed and quoted in several cases. In other cases, the cross-section ratio between $t\bar{t}$- and Z-production is determined as that is independent of luminosity uncertainties, but keeps its sensitivity to the ratio of gluon versus quark PDFs. These experimental results should be compared to the theoretical calculations at NNLO+NNLL that yield $7.16^{+0.20}_{-0.23}$ pb for top-quark mass of 173.3 GeV/c^2 [1] at $\sqrt{s} = 1.96$ TeV, $68.2 \pm 4.8^{+1.9}_{-2.3}$ pb [30] for top-quark mass of 172.5 GeV/c^2 at $\sqrt{s} = 5$ TeV, and for top-quark mass of 173.3 GeV/c^2 $\sigma_{t\bar{t}} = 173.6^{+4.5+8.9}_{-5.9-8.9}$ pb at $\sqrt{s} = 7$ TeV, $\sigma_{t\bar{t}} = 247.7^{+6.3+11.5}_{-8.5-11.5}$ pb at $\sqrt{s} = 8$ TeV, and $\sigma_{t\bar{t}} = 816.0^{+19.4+34.4}_{-28.6-34.4}$ pb at $\sqrt{s} = 13$ TeV, at the LHC [1]. In a special run, ATLAS recorded 257 pb^{-1} at $\sqrt{s} = 5.02$ TeV. Using opposite charged dilepton events and counting the number of b-jets, they perform a fit including m_{ll} information to constrain Z+jets background, yielding a result of $\sigma_{t\bar{t}} = 66.0 \pm 4.9$ pb, giving a total uncertainty of 7.5% [31]. CMS has measured the $t\bar{t}$ production cross section at $\sqrt{s} = 5.02$ TeV, accumulating 27.4 pb^{-1}. The measurement is performed by analyzing events with at least one charged lepton. The measured cross section is $\sigma_{t\bar{t}} = 69.5 \pm 8.4$ pb [32], in agreement with the expectation from the Standard Model. Recently, they performed a measurement in opposite-sign $e\mu$-dilepton events with at least two jets using 304 pb^{-1}. They obtain a Drell-Yan scale factor under the Z-boson mass to estimate the background and extract a cross section using a counting technique of $\sigma_{t\bar{t}} = 60.3 \pm 5.8$ pb. The combination of the two results yields $\sigma_{t\bar{t}} = 62.6 \pm 4.1(stat.) \pm 3.0(syst. + lumi.)$ pb with 7.9% total relative uncertainty [33]. At $\sqrt{s} = 7$ TeV, ATLAS uses 4.6 fb^{-1} of $e\mu$ events in which they select an extremely clean sample and determine the $t\bar{t}$ cross section simultaneously with the efficiency to reconstruct and tag b-jets, yielding $\sigma_{t\bar{t}} = 182.9 \pm 7.1$ pb, corresponding to 3.9% precision [34]. Other measurements by ATLAS at $\sqrt{s} = 7$ TeV, include a measurement in 0.7 fb^{-1} in the lepton+jets channel [35], in the dilepton channel [36], and in 1.02 fb^{-1} in the all-hadronic channel [37], which together yield a combined value of $\sigma_{t\bar{t}} = 177 \pm 3(stat.)^{+8}_{-7}(syst.) \pm 7(lumi.)$ pb (6.2%) assuming $m_t = 172.5$ GeV/c^2 [38]. Further analyses in the hadronic τ plus jets channel in 1.67 fb^{-1} [39] and the hadronic τ + lepton channel in 2.05 fb^{-1} [40], and the all-hadronic channel in 4.7 fb^{-1} [41] yield consistent albeit less precise results. Another simultaneous measurement of the $t\bar{t}, W^+W^-$, and $Z/\gamma^* \to \tau\tau$ cross section using the full 7 TeV dataset with 4.6 fb^{-1} yields $\sigma_{t\bar{t}} = 181 \pm 11$ pb, corresponding to a 6% precision [42]. The most precise measurement from CMS at $\sqrt{s} = 7$ TeV is also obtained in the dilepton channel, where they measure $\sigma_{t\bar{t}} = 161.9 \pm 2.5(stat.)^{+5.1}_{-5.0}(syst.) \pm 3.6(lumi.)$ pb, corresponding to a 4.2% precision [43]. Other measurements at $\sqrt{s} = 7$ TeV from CMS include measurements with 2.3 fb^{-1} in the e/μ+jets channel [44], with 3.5 fb^{-1} in the all-hadronic channel [45], with 2.2 fb^{-1} in the lepton+τ channel [46], and with 3.9 fb^{-1} in the τ+jets channel [47]. ATLAS and CMS also provide a combined cross section at $\sqrt{s} = 7$ TeV of $173.3 \pm 2.3(stat.) \pm$

Downloaded from https://academic.oup.com/ptep/article/2022/8/083C01/6651666 by KIT Library user on 27 September 2022

$7.6(syst.) \pm 6.3(lumi.)$ pb using slightly older results based on $0.7-1.1$ fb^{-1} [48]. At $\sqrt{s} = 8$ TeV, ATLAS measures the $t\bar{t}$ cross section with 20.3 fb^{-1} using $e\mu$ dilepton events, with a simultaneous measurement of the $b-$tagging efficiency, yielding $\sigma_{t\bar{t}} = 242.9 \pm 1.7(stat.) \pm 5.5(syst.) \pm 5.1(lumi.) \pm 4.2(beam\,energy)$ pb [49] assuming $m_t = 172.5$ GeV/c^2, which corresponds to a 3.6% precision. In the $\ell + jets$ channel, they measure $\sigma_{t\bar{t}} = 260 \pm 1(stat.)^{+20}_{-23}(syst.) \pm 8(lumi.) \pm 4(beam\,energy)$ pb [50] in 20.3 fb^{-1} using a likelihood discriminant fit and b-jet identification. Subsequently, ATLAS performed a new analysis in 20.2 fb^{-1} $\ell+jets$ events. They model the W+jets background using Z+jets data and employ neural networks in three jet-multiplicity and b-jet multiplicity regions for the signal and background separation, yielding $\sigma_{t\bar{t}} = 248.3 \pm 0.7(stat.) \pm 13.4(syst.) \pm 4.7(lumi.)$ pb [51]. ATLAS also performed a cross section measurement in the hadronic τ+jets channel yielding consistent, albeit less precise results [52]. CMS performs a template fit to the M_{lb} mass distribution using 19.6 fb^{-1} in the lepton+jets channel yielding $\sigma_{t\bar{t}} = 228.5 \pm 3.8(stat.) \pm 13.7(syst.) \pm 6.0(lumi.)$ pb [53, 54], which corresponds to a 6.7% precision. These 8 TeV measurements are in agreement with QCD predictions up to NLO accuracy. In the $e\mu$ channel, initially using 5.3 fb^{-1} [54] and then using 19.7 fb^{-1}, the cross sections are extracted using a binned likelihood fit to multi-differential final state distributions related to identified b quark and other jets in the event, yielding $\sigma_{t\bar{t}} = 244.9 \pm 1.4(stat.)^{+6.3}_{-5.5}(sys.) \pm 6.4(lumi.)$ pb [55]. The cross section and its ratio between 7 TeV and 8 TeV measurements are found to be consistent with pQCD calculations. The cross section is also measured in the hadronic τ+jets channel, yielding $\sigma_{t\bar{t}} = 257 \pm 3(stat.) \pm 24(syst.) \pm 7(lumi.)$ pb [56] and in the all-hadronic final state giving $\sigma_{t\bar{t}} = 275.6 \pm 6.1(stat.) \pm 37.8(syst.) \pm 7.2(lumi.)$ pb [57]. In combination of the most precise $e\mu$ measurements in $5.3-20.3$ fb^{-1}, ATLAS and CMS together yield at 8 TeV $\sigma_{t\bar{t}} = 241.5 \pm 1.4(stat.) \pm 5.7(syst.) \pm 6.2(lumi.)$ pb [58], which corresponds to a 3.5% precision, challenging the precision of the corresponding theoretical predictions. The LHCb collaboration presented the first observation of top-quark production in the forward region in pp-collisions. The $W+b$ final state with $W \to \mu\nu$ is reconstructed using muons with a transverse momentum, p_T, larger than 25 GeV in the pseudorapidity range $2.0 < \eta < 4.5$. The b-jets are required to have 50 GeV $< \mathrm{p_T} <$ 100 GeV and $2.2 < \eta < 4.2$, while the transverse component of the sum of the muon and b-jet momenta must satisfy $p_T > 20$ GeV. The results are based on data corresponding to integrated luminosities of 1.0 and 2.0 fb^{-1} collected at center-of-mass energies of 7 and 8 TeV by LHCb. The inclusive top quark production cross sections in the fiducial region are $\sigma_{t\bar{t}} = 239 \pm 53(stat.) \pm 38(syst.)$ pb at 7 TeV, and $\sigma_{t\bar{t}} = 289 \pm 43(stat.) \pm 46(syst.)$ pb at 8 TeV [59]. ATLAS and CMS have also measured the $t\bar{t}$ production cross section with Run-II data at $\sqrt{s} = 13$ TeV. In the $e\mu$ events with at least one b-tag, ATLAS uses 78 pb^{-1} and obtains $\sigma_{t\bar{t}} = 825 \pm 114$ pb [60]. This measurement is updated with lepton identification and trigger efficiencies to give $\sigma_{t\bar{t}} = 829 \pm 50(stat.) \pm 56(syst.) \pm 83(lumi)$ pb [61]. In this note, ATLAS also presents a $t\bar{t}$ cross section measurement in the ee and $\mu\mu$ dilepton channel with one and two b-tags using a counting approach, yielding $\sigma_{t\bar{t}} = 749 \pm 57(stat.) \pm 79(syst.) \pm 74(lumi.)$ pb. The cross section measurement in the $e\mu$ channel counting events with one or with two b-tags is also repeated using 3.2 pb^{-1} and yields $\sigma_{t\bar{t}} = 818 \pm 8(stat.) \pm 27(syst.) \pm 19(lumi.) \pm 12(beam)$ pb [62], consistent with theoretical QCD calculations at NNLO. In 36.1 fb^{-1} of $e\mu$ data with one or two b-tags, ATLAS measures the $t\bar{t}$ cross section to $\sigma_{t\bar{t}} = 826.4 \pm 3.6(stat.) \pm 11.5(syst.) \pm 15.7(lumi.) \pm 1.9(beam)$ pb, giving a total of 2.4%. This measurement is also used to determine the top quark pole mass and to derive ratios and double ratios of $t\bar{t}$ and Z cross-sections at different energies as well as absolute and normalised differential cross-sections as functions of single lepton and dilepton kinematic variables [63]. In the $\ell + jets$, using 85 pb^{-1}, the cross-section is extracted by counting the number of events with exactly one electron or muon and at least four jets, at least one of which is identified as originating from a b-quark, yielding $\sigma_{t\bar{t}} = 817 \pm 13(stat.) \pm 103(syst.) \pm 88(lumi.)$ pb, both assuming $m_t = 172.5$ GeV/c^2 [61]. Very recently, ATLAS measures the inclusive $t\bar{t}$ cross section in 139 fb^{-1} in the $\ell + jes$ through a profile-likelihood fit to be $\sigma_{t\bar{t}} = 830.4 \pm 0.4(stat.) \pm 36(syst.) \pm 14(lumi)$ pb, with a relative uncertainty of 4.6% [64]. The result is consistent with the theoretical calculations at NNLO order in QCD perturbation theory. CMS uses 43 pb^{-1} in the $e\mu$ channel to measure $\sigma_{t\bar{t}} = 746 \pm 58(stat.) \pm 53(syst.) \pm 36(lumi)$ pb, in agreement with the expectation from the standard model [65]. Using 2.2 fb^{-1} in the $e\mu$ channel with at least one b-jet, CMS measures $\sigma_{t\bar{t}} = 815 \pm 9(stat.) \pm 38(syst.) \pm 19(lumi.)$ pb (5.3%), in agreement with the expectation from the Standard Model [66]. Using 35.9 fb^{-1} of dilepton data, CMS measures the $t\bar{t}$ cross section using a likelihood fit $\sigma_{t\bar{t}} = 803 \pm 2(stat.) \pm 25(syst.) \pm 20(lumi.)$ pb (4.0%), in agreement with the expectation from the SM calculation at NNLO order. This result is also used to extract the top quark mass and the strong coupling constant [67]. Using the same dataset in the dilepton channel with a hadronically decaying τ, they measure $\sigma_{t\bar{t}} = 781 \pm 7(stat.) \pm 62(syst.) \pm 20(lumi.)$ pb (8.3%) [68]. A first measurement of the total inclusive and the normalized differential cross section in the $\ell + jets$ channel is made in 42 pb^{-1} yielding $\sigma_{t\bar{t}} = 836 \pm 27(stat.) \pm 88(syst.) \pm 100(lumi.)$ pb [69]. In 2.2 fb^{-1}, $\ell + jets$ events are categorized according to the accompanying jet multiplicity. From a likelihood fit to the invariant mass distribution of the isolated lepton and a b-jet, the cross section is measured to be $\sigma_{t\bar{t}} = 888 \pm 2(stat.)^{+26}_{-28}(syst.) \pm 20(lumi)$ pb, in agreement with the SM prediction [70]. This result is also used to extract the top-quark mass. Recently, CMS has used 137 pb^{-1} in four regions determined by top p_T and b-tag score to measure the cross section in the $\ell+jets$ channel. They employ a combined χ^2 fit considering the migration matrices. Most of the measured differential cross sections are well described by standard model predictions with the exception of some double-differential distributions. They obtain $\sigma_{t\bar{t}} = 791 \pm 1(stat.) \pm 21(syst.) \pm 14(lumi)$ pb (3.2%) [71]. In the all-hadronic channel, CMS uses 2.53 fb^{-1} of data, yielding a cross section of $\sigma_{t\bar{t}} = 834 \pm 25(stat.)^{+118}_{-104}(syst.) \pm 23(lumi.)$ pb [72]. Also differential cross sections as a function of the leading top quark transverse momentum are measured. As general feature across channels, it is found that the measured top quark p_T spectrum is significantly softer than the NLO+PS theory predictions considered in the corresponding publications. CMS also performed a measurement of top-quark pair production in pPb heavy ion collisions at $\sqrt{s} = 8.16$ TeV in 174 nb^{-1} of lepton+jets events. They measure a cross section of $\sigma_{t\bar{t}} = 45 \pm 8$ nb, which is consistent with pQCD calculations and with the scaled pp data [73].

In Fig. 61.1, one sees the importance of $p\bar{p}$ at Tevatron energies where the valence antiquarks in the antiprotons contribute to the dominant $q\bar{q}$ production mechanism. At LHC energies, the dominant production mode is gluon-gluon fusion and the pp-$p\bar{p}$ difference nearly disappears. The excellent agreement of these measurements with the theory calculations is a strong validation of QCD and the soft-gluon resummation techniques employed in the calculations. The measurements reach high precision and provide stringent tests of pQCD calculations at NNLO+NNLL level including their respective PDF uncertainties.

Most of these measurements assume a $t \to Wb$ branching ratio of 100%. CDF and DØ have made direct measurements of the $t \to Wb$ branching ratio [74]. Comparing the number of events with 0, 1 and 2 tagged b jets in the lepton+jets channel, and also in the dilepton channel, using the known b-tagging efficiency, the ratio $R = B(t \to Wb)/\sum_{q=d,s,b} B(t \to Wq)$ can be extracted. In 5.4 fb^{-1} of data, DØ measures $R = 0.90 \pm 0.04$, 2.5 standard deviations from unity. The currently most precise measurement was made by CMS in 19.7 fb^{-1} at $\sqrt{s} = 8$ TeV. They find $R = 1.014 \pm 0.003(stat.) \pm 0.032(syst.)$ and $R > 0.955$ at 95% C.L. [75]. A significant deviation of R from unity would imply either non-SM top-quark decay (for example a flavor-changing neutral-current decay), or a fourth generation of quarks. The latter is by other measurements.

Thanks to the large available event samples, the Tevatron and the LHC experiments also performed single-, double- or even triple-differential cross-section measurements in $t\bar{t}$ production. Such measurements are crucial, as they allow even more stringent tests of perturbative QCD as description of the production mech-

Downloaded from https://academic.oup.com/ptep/article/2022/8/083C01/6651666 by KIT Library user on 27 September 2022

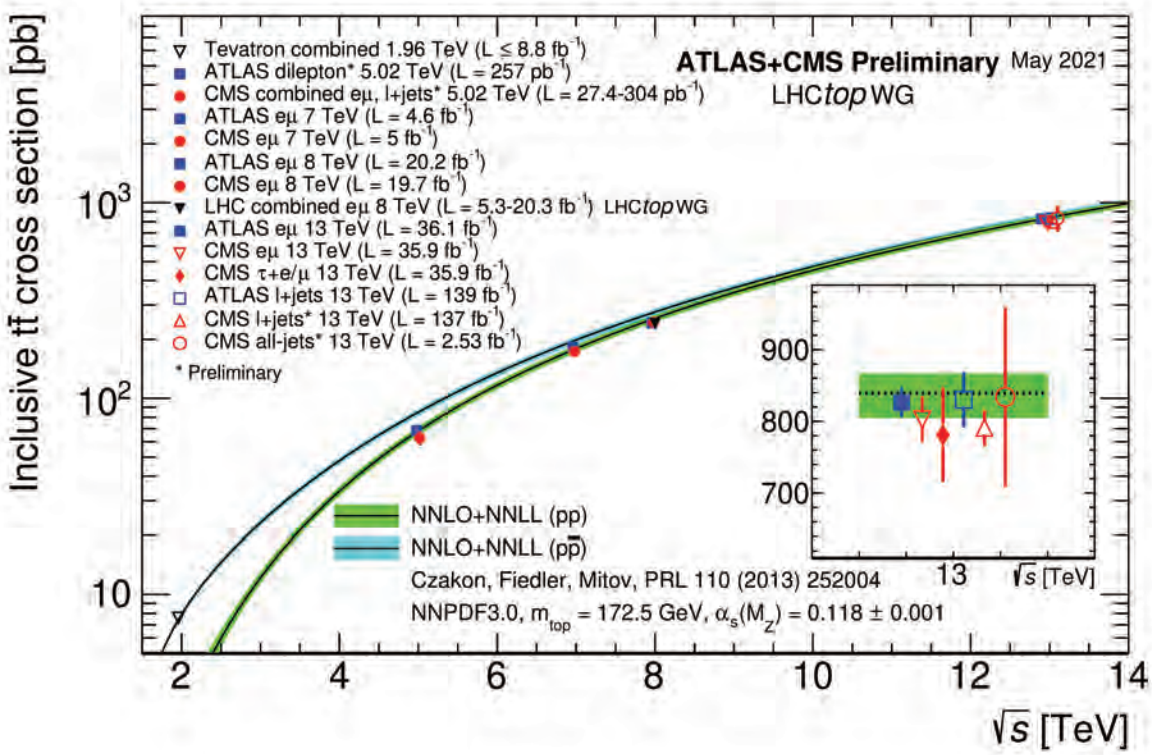

Figure 61.1: Measured and predicted $t\bar{t}$ production cross sections from Tevatron energies in $p\bar{p}$ collisions to LHC energies in pp collisions. The plot is kindly provided by the LHCtopWG working group, see `https://twiki.cern.ch/twiki/bin/view/LHCPhysics/LHCTopWGSummaryPlots`.

anism, allow along with other data the extraction of PDFs in PDF fits, and enhance the sensitivity to possible new physics contributions, especially now that NNLO predictions for the main differential observables in $t\bar{t}$ prediction have become available [76] and later confirmed [2]. Furthermore, such measurements reduce the uncertainty in the description of $t\bar{t}$ production as background in Higgs physics and searches for rare processes or beyond Standard Model physics. Differential cross sections are typically measured by a selection of candidate events, their kinematic reconstruction and subsequent unfolding of the obtained event counts in bins of kinematic distributions in order to correct for detector resolution effects, acceptance and migration effects. In some cases a bin-by-bin unfolding is used, while other analyses use more sophisticated techniques. Experiments at Tevatron and LHC measure the differential cross section with respect to the $t\bar{t}$ invariant mass, $d\sigma/dM_{t\bar{t}}$. The spectra are fully corrected for detector efficiency and resolution effects and are compared to several Monte Carlo simulations as well as selected theoretical calculations. Using 9.45 fb^{-1}, CDF measured $d\sigma/dM_{t\bar{t}}$, in the lepton+jets channel providing sensitivity to a variety of exotic particles decaying into $t\bar{t}$ pairs [77]. In 9.7 fb^{-1} of lepton+jets data, DØ measured the differential $t\bar{t}$ production cross section with respect to the transverse momentum and absolute rapidity of the top quarks as well as of the invariant mass of the $t\bar{t}$ pair [29], which are all found to be in good agreement with the SM predictions. ATLAS measured the differential $t\bar{t}$ production cross section with respect to the top-quark transverse momentum, and of the mass, transverse momentum and rapidity of the top quark, the antitop quark as well as the $t\bar{t}$ system in up to 4.6 fb^{-1} at $\sqrt{s} = 7$ TeV in the lepton+jets channel [78–80]. It is found that data is softer than all predictions for higher values of the mass of the $t\bar{t}$ system as well as in the tail of the top-quark p_T spectrum beginning at 200 GeV, particularly in the case of the `Alpgen`+`Herwig` generator. The $M_{t\bar{t}}$ spectrum is not well described by NLO+NNLL calculations and there are also disagreements between the measured rapidity of the $t\bar{t}$ system spectrum and the `MC@NLO`+`Herwig` and `POWHEG`+`Herwig` generators, both evaluated with the CT10 PDF set. All distributions show a preference for HERAPDF1.5 when used for the NLO QCD predictions. In 5.0 fb^{-1} of $\sqrt{s} = 7$ TeV data in the lepton+jets and the dilepton channels, CMS measured normalised differential $t\bar{t}$ cross sections with respect to kinematic properties of the final-state charged leptons and jets associated to b-quarks, as well as those of the top quarks and the $t\bar{t}$ system. The data are compared with several predictions from perturbative QCD calculations and found to be consistent [81]. ATLAS uses 4.6 fb^{-1} of data at 7 TeV and 20.2 fb^{-1} at 8 TeV to measure the differential $t\bar{t}$ cross section in the dilepton final state as a function of the mass, the transverse momentum and the rapidity of the $t\bar{t}$ system [82]. The results are compared with different Monte Carlo generators and theoretical calculations of $t\bar{t}$ production and found to be consistent with the majority of predictions in a wide kinematic range. Using 20.3 fb^{-1} of $t\bar{t}$ events in the lepton+jets channel, ATLAS measures the normalized differential cross sections of $t\bar{t}$ production as a function of the top-quark, $t\bar{t}$ system and event-level kinematic observables [83]. The observables have been chosen to emphasize the $t\bar{t}$ production process and to be sensitive to effects of initial- and final-state radiation, to the different parton distribution functions, and to non-resonant processes and higher-order corrections. The results are in fair agreement with the predictions over a wide kinematic range. Nevertheless, most generators predict a harder top-quark transverse momentum distribution at high values than what is observed in the data. Predictions beyond NLO accuracy improve the agreement with data at high top-quark transverse momenta. Using the current settings in the Monte Carlo programs and parton distribution functions, the rapidity distributions are not well modelled by any generator under consideration. However, the level of agreement is improved when more recent sets of parton distribution functions are used. Using 20.3 fb^{-1} of 8 TeV data, ATLAS performed a dedicated differential $t\bar{t}$ cross-section measurement of highly boosted top quarks in the lepton+jets channel, where the hadronically decaying top quark has a transverse momentum above 300 GeV [84].

Downloaded from https://academic.oup.com/ptep/article/2022/8/083C01/6651666 by KIT Library user on 27 September 2022

Jet substructure techniques are employed to identify top quarks, which are reconstructed with an anti-k_t jet with a radius parameters $R = 1.0$. The predictions of NLO and LO matrix element plus parton shower Monte Carlo generators are found to generally overestimate the measured cross sections. Using 5.0 fb^{-1} of data at 7 TeV and 19.7 fb^{-1} at 8 TeV in the lepton+jets channel, CMS reports measurements of normalized differential cross sections for $t\bar{t}$ production with respect to four kinematic event variables: the missing transverse energy; the scalar sum of the jet transverse momentum (p_T); the scalar sum of the p_T of all objects in the event; and the p_T of leptonically decaying W bosons from top quark decays [85]. No significant deviations from the predictions of several SM event generators are observed. Using the full 19.7 fb^{-1} data in the $e\mu$ channel, CMS measures normalized double-differential cross sections for $t\bar{t}$ production as a function of various pairs of observables characterizing the kinematics of the top quark and $t\bar{t}$ system [86]. The data are compared to calculations using perturbative QCD at NLO and approximate NNLO orders. They are also compared to predictions of Monte Carlo event generators that complement fixed-order computations with parton showers, hadronization, and multiple-parton interactions. Overall agreement is observed with the predictions, which is improved when the latest global sets (as determined here by CMS) of proton parton distribution functions are used. The inclusion of the measured $t\bar{t}$ cross sections in a fit of parametrized parton distribution functions is shown to have significant impact on the gluon distribution [86]. Another analysis at high transverse momentum regime for the top quarks, is performed by the CMS collaboration in 19.7 fb^{-1} at $\sqrt{s} = 8$ TeV [87]. The measurement is performed for events in $e/\mu + jets$ final states where the hadronically decaying top quark is reconstructed as a single large-radius jet and identified as a top candidate using jet substructure techniques. The integrated cross section is measured at particle-level within a fiducial region resembling the detector-level selection as well as at parton-level. At particle-level, the fiducial cross section is measured to be $\sigma_{t\bar{t}} = 0.499 \pm 0.035(stat. + syst.) \pm 0.095(theo) \pm 0.013(lumi)$ pb for $p_T > 400$ GeV. At parton-level, it translates to $\sigma_{t\bar{t}} = 1.44 \pm 0.10(stat. + syst.) \pm 0.29(theo.) \pm 0.04(lumi.)$ pb. At parton-level, interactions between incoming partons (quarks or gluons) are considered via a gauge interaction yielding final state partons. While such interactions can be well described theoretically, partons are not visible in the detector. At the particle-level, visible and measurable hadrons, i.e. bound states of quarks and antiquarks, are considered to form jets. The hadronisation process takes us from one level to the other. In 19.7 fb^{-1} at $\sqrt{s} = 8$ TeV, CMS repeated those measurements in the lepton+jets and in the dilepton channels [88]. While the overall precision is improved, no significant deviations from the Standard Model are found, yet a softer spectrum for the top quark at high p_T with respect to theoretical available predictions has been observed. This behaviour has been also observed in the all-hadronic final state [89], where a total cross section measurement is performed, yielding $\sigma_{t\bar{t}} = 275.6 \pm 6.1(stat.) \pm 37.8(syst.) \pm 7.2(lumi)$ pb. At $\sqrt{s} = 13$ TeV, in 3.2 fb^{-1}, ATLAS measured the differential $t\bar{t}$ cross section as a function of the transverse momentum and absolute rapidity of the top quark, and of the transverse momentum, absolute rapidity and invariant mass of the $t\bar{t}$ system [90]. The measured differential cross sections are compared to predictions of NLO generators matched to parton showers and the measurements are found to be consistent with all models within the experimental uncertainties with the exception of the `Powheg-Box+Herwig++` predictions, which differ significantly from the data in both the transverse momentum of the top quark and the mass of the $t\bar{t}$ system. Using 3.2 fb^{-1} of data in the lepton+jets channel, ATLAS measured the differential cross sections of $t\bar{t}$ production in fiducial phase-spaces as a function of top-quark and $t\bar{t}$ system kinematic observables [91]. Two separate selections are applied that each focus on different top-quark momentum regions, referred to as resolved and boosted topologies of the $t\bar{t}$ final state. The measured spectra are corrected for detector effects and are compared to several Monte Carlo simulations by means of calculated χ^2 and p-values.

ATLAS presents a measurement of the boosted top quark differential cross section in the all-hadronic decay mode [92]. They require two top-quark candidates, one with $p_T > 500$ GeV and a second with $p_T > 350$ GeV, with each candidate reconstructed as an anti-k_T jet with radius parameter $R = 1.0$. The top-quark candidates are separated from the multijet background using the jet substructure and the presence of a b-quark tag in each jet. The observed kinematic distributions are unfolded to recover the differential cross sections in a limited phase-space region and compared with SM predictions, showing agreement. In 36 fb^{-1}, ATLAS measures the single- and double-differential $t\bar{t}$ cross-section in the lepton + jets channel at particle and parton level. Two topologies, resolved and boosted, are considered and the results are presented as a function of several kinematic variables characterising the top and $t\bar{t}$ system and jet multiplicities. Overall, there is good agreement between the theoretical predictions and the data [93]. In 36.1 fb^{-1} of dilepton events, ATLAS measures the differential $t\bar{t}$ cross section as a function of several lepton kinematic variables [63]. The NLO+PS predictions give a good description of several observables. However, `POWHEG` predicts a harder spectrum for lepton p_T variables than observed. In 139 fb^{-1} of data in the $\ell + jets$ channel in a boosted topology with at least one large-R "top-jet" from a hadronic decay with high-p_T, ATLAS employs a parameter sensitive to the top mass to reduce the jet uncertainties and measures the differential $t\bar{t}$ cross section as a function of kinematic variables characterising the $t\bar{t}$ system and also as a function of variables that characterise the additional radiation in the events [94]. The measured distribution of the top-quark transverse momentum, which is measured to be softer than expected, is used to set limits on the Wilson coefficients describing physics beyond the standard model. The modelling of the additional radiation events show some mild disagreements to the data. In the all-hadronic channel with six separately resolved jet, using 36.1 fb^{-1}, ATLAS measures single- and double-differential cross sections at particle and parton level as a function of various kinematic variables [95]. The rapidities of t and $t\bar{t}$ are found to be well modelled while discrepancies between theoretical predictions and data are found in the p_T distributions of the three leading jets, the top and the $t\bar{t}$ system. In 42 pb^{-1}, CMS measures the differential cross section at $\sqrt{s} = 13$ TeV as a function of kinematic properties of the top quarks and the $t\bar{t}$ system, as well as of the jet multiplicity in the event. Several predictions from perturbative QCD calculations are confronted with the data and are found to describe them well [96]. In 2.1 fb^{-1} at $\sqrt{s} = 13$ TeV, CMS measures the normalized differential cross sections for $t\bar{t}$ production in the dilepton channels as a function of the kinematic properties of the leptons, jets from bottom quark hadronization, top quarks, and top quark pairs at the particle and parton levels [97]. The results are compared to several Monte Carlo generators that implement calculations up to NLO in perturbative QCD interfaced with parton showering, and also to fixed-order theoretical calculations of top quark pair production up to NNLO, showing agreement. In 2.3 fb^{-1} of events in the lepton+jets channel, CMS measures the differential and double-differential cross sections for the $t\bar{t}$ production as a function of jet multiplicity and of kinematic variables of the top quarks and the $t\bar{t}$ system [98]. The differential cross sections are presented at particle level, within a phase space close to the experimental acceptance, and at parton level in the full phase space. The results are compared to several SM predictions. Using 35.9 fb^{-1}, CMS measures the differential $t\bar{t}$ cross section in the single-lepton decay channel, as a function of a number of kinematic event variables. The data are compared to a variety of state-of-the-art LO and NLO simulations [99]. In 35.8 fb^{-1}, CMS measures the differential and double-differential $t\bar{t}$ cross sections in the $\ell + jets$ channel as a function of kinematic variables of the top quarks and the top quark-antiquark ($t\bar{t}$) system. In addition, kinematic variables and multiplicities of jets associated with the $t\bar{t}$ production are measured. The kinematic variables of the top quarks and the $t\bar{t}$ system are reasonably described in general, though none predict all the measured distributions. In particular, the transverse momentum distribution of the top quarks is more steeply falling than predicted. The kinematic distributions and multiplicities of jets are adequately modeled by certain combinations of NLO calculations and parton

Downloaded from https://academic.oup.com/ptep/article/2022/8/083C01/6651666 by KIT Library user on 27 September 2022

shower models [100]. In the dilepton channel, CMS measures differential $t\bar{t}$ cross sections in 35.9 fb^{-1} as functions of kinematic observables of the top quarks and their decay products, the $t\bar{t}$ system, and the total number of jets in the event. All results are compared with SM predictions from Monte Carlo simulations with NLO accuracy in QCD at matrix-element level interfaced to parton-shower simulations. Where possible, parton-level results are compared to calculations with beyond-NLO precision in QCD. Significant disagreement is observed between data and all predictions for several observables. The measurements are used to constrain the top quark chromomagnetic dipole moment in an effective field theory framework at NLO in QCD and to extract $t\bar{t}$ and leptonic charge asymmetries [101]. In 35.9 fb^{-1} of dilepton events, CMS measures normalised multi-differential $t\bar{t}$ cross sections as a function of the kinematic properties of the top quark and of the $t\bar{t}$ system at parton level in the full phase space. A triple-differential measurement is performed as a function of the invariant mass and rapidity of the $t\bar{t}$ system and the multiplicity of additional jets at particle level. The data are compared to predictions of Monte Carlo event generators that complement NLO QCD calculations with parton showers. The measurement is used to extract the strong coupling constant and the top-quark pole mass and parton distribution functions [102]. In 137 fb^{-1} of $\ell + jets$ data, arranged in four regions according to the top p_T, boosted vs. resolved, and the b-tagging score, CMS measures the single- and double-differential $t\bar{t}$ cross sections [71]. Here also the longitudinal momentum is measured well into the TeV range in one measurement starting in the resolved regime. Most of the measured differential cross sections are well described by standard model predictions with the exception of some double-differential distributions. The top p_T and $m_{t\bar{t}}$ is found to be softer than predicted. In 35.9 fb^{-1} of all-hadronic and $\ell + jets$ events in a boosted topology with at least two large-R jets with a b-tag inside and $p_T > 400$ GeV or one large-R jet, respectively, CMS measures the differential cross section as a function of kinematic variables of individual top quarks or of the $t\bar{t}$ system [103]. The observed absolute cross sections are significantly lower than the predictions from theory, while the normalized differential measurements are well described.

61.3.1.2 *Other $t\bar{t}$ production processes*

Further cross-section measurements are performed by ATLAS for $t\bar{t}$+heavy flavour [104] and $t\bar{t}$+jets production as well as the differential measurement of the jet multiplicity in $t\bar{t}$ events by ATLAS [105] and by CMS [106]. Here, `MC@NLO`+`Herwig` MC is found to predict too few events at higher jet multiplicities. In addition, CMS measured the cross-section ratio $\sigma_{t\bar{t}b\bar{b}}/\sigma_{t\bar{t}jj}$ using 19.6 fb^{-1} of 8 TeV data [107]. This is of high relevance for top quark production as background to searches, for example for measurements of $t\bar{t}h$ production and ongoing searches for 4-top quark production. Later, ATLAS also measured the $t\bar{t}$ production cross section along with the branching ratios into channels with leptons and quarks using 4.6 fb^{-1} of 7 TeV data [108]. They find agreement with the standard model at the level of a few percent.

Using 139 fb^{-1} of $t\bar{t} \to$ dilepton events, ATLAS distinguishes in a dedicated analysis muons originating from $W \to \mu\nu$ decays and those from $W \to \tau\nu \to \mu\nu\nu\nu$ decays via their transverse momentum spectrum and the impact parameter of the muon track, that reflects the tau lifetime, yielding high sensitivity. The measured ratio of $R(\tau/\mu) = 0.992 \pm 0.013$ is in agreement with the hypothesis of universal lepton couplings [109].

Using 36 fb^{-1} of dilepton events at 13 TeV, ATLAS also measures differential cross sections with respect to high-resolution variables, constructed to characterize the longitudinal and transverse momentum distributions of the b-hadron within the b-jets [110]. They are used to test the heavy-quark-fragmentation modelling.

Using 137 fb^{-1} of dilepton events at 13 TeV, CMS measures differential cross sections with respect to the mass of the $t\bar{t}$ system and the rapidity difference of the top-quark and antiquark [111]. Exploiting their sensitivity to the top-quark Yukawa coupling yields a best fit value of $Y_t = 1.16^{+0.24}_{-0.35}$, bounding $Y_t < 1.54$ at a 95% confidence level.

In 36.1 fb^{-1}, ATLAS measures the $t\bar{t}b\bar{b}$ cross section in the dilepton and the $\ell + jets$ channels. Results are presented at particle level in the form of inclusive cross-sections of $t\bar{t}$ final states with three and four b-jets as well as differential cross-sections as a function of global event properties and properties of b-jet pairs. The measured inclusive fiducial cross-sections generally exceed the $t\bar{t}b\bar{b}$ predictions from various NLO matrix element calculations matched to a parton shower, but are compatible within the total uncertainties [112]. In 2.3 fb^{-1}, CMS measures the $t\bar{t}b\bar{b}$ cross section in the dilepton channel [113]. They also determine the cross section ratio $\sigma_{t\bar{t}b\bar{b}}/\sigma_{t\bar{t}jj}$. In 35.9 fb^{-1}, CMS recently measured the cross section $t\bar{t}b\bar{b}$ as well as the cross section ratio $\sigma_{t\bar{t}b\bar{b}}/\sigma_{t\bar{t}jj}$ in the dilepton and the lepton+jets channel [114]. They fit the distribution of the b-tagging discriminant variable of the two jets that do not belong to the $t\bar{t}$ decay. In the same dataset, CMS measures the $t\bar{t}b\bar{b}$ cross section in the all-jet channel by selecting events containing at least eight jets, of which at least two are identified as b-jets. A combination of multivariate analysis techniques is used to reduce the large background from multijet events not containing a top quark pair, and to help discriminate between jets originating from top quark decays and other additional jets. The measured cross sections are found to be larger than theoretical predictions by a factor of 1.5-2.4, corresponding to 1-2 standard deviations [115]. Recently, CMS measured the $t\bar{t} + b\bar{b}$ cross section in 35.9 fb^{-1} of dilepton and $\ell + jets$ events [114]. The cross section is extracted from the cross section ratio $R(t\bar{t} + b\bar{b})$ in order to reduce systematic uncertainties. The assignment of jets to the top or to the additional jets is based on b-tagging scores in the dilepon channel and on a kinematic fit in the $\ell + jets$ channel. Using the same data set in the all-hadronic channel, CMS measured the $t\bar{t} + b\bar{b}$ cross section to $\approx 25\%$ precision employing a multivariate analysis technique and a 2-dimensional likelihood fit [116]. Very recently, CMS also measured the $t\bar{t} + c\bar{c}$ cross section using 41.5 fb^{-1} of events with dileptonic final states [117]. A multi-class neural network is employed to separate $t\bar{t} + b\bar{b}$, $t\bar{t} + c\bar{c}$ and $t\bar{t} + ll$. The results are compatible with the prediction within $1 - 2\,\sigma$.

The production of four top-quarks is an interesting test of QCD and at the same time sensitive to the top quark Yukawa coupling and to production mechanisms with new mediators with strong couplings to top quarks. The latest cross section calculation yields $\sigma_{t\bar{t}t\bar{t}} = 12.0$ fb $\pm 20\%$ [118]. Using the full Run-II data set of 139 fb^{-1}, ATLAS measures the four-tops cross section in the two-lepton same sign or three-lepton channel with 13% branching ratio and dominant $t\bar{t}V$ background as $\sigma_{t\bar{t}t\bar{t}} = 24^{+7}_{-6}$ fb [119]. Using the same data set in the one-lepton or two-lepton opposite-sign channel with 57% branching ratio and dominant $t\bar{t}$ + heavy flavor background, they measure $\sigma_{t\bar{t}t\bar{t}} = 26^{+17}_{-15}$ fb [120]. The combination yields $\sigma_{t\bar{t}t\bar{t}} = 24^{+7}_{-6}$ fb [120], corresponding to an observed (expected) significance of 4.7 (2.6) σ significance. CMS measures the four-top cross section in the two-lepton same sign or thee-lepton channel in 137 fb^{-1} to $\sigma_{t\bar{t}t\bar{t}} = 12.6^{+5.8}_{-5.2}$ fb [121], corresponding to an observed (expected) significance of 2.6 (2.7) σ significance. Using 35.8 fb^{-1}, they also study the one-lepton or two-lepton opposite-sign channel and obtain an upper limit of $\sigma_{t\bar{t}t\bar{t}} < 48$ fb at 95% CL [122]. The results are also interpreted in terms of the top-Yukawa coupling and various scenarios of physics beyond the standard model via effective field theory fits.

61.3.1.3 *Single-top production*

Single-top quark production was first observed in 2009 by DØ [123] and CDF [124, 125] at the Tevatron. The production cross section at the Tevatron is roughly half that of the $t\bar{t}$ cross section, but the final state with a single W-boson and typically two jets is less distinct than that for $t\bar{t}$ and much more difficult to distinguish from the background of W+jets and other sources. A comprehensive review of the first observation and the techniques used to extract the signal from the backgrounds can be found in [126].

The dominant production at the Tevatron is through s-channel and t-channel W-boson exchange. Associated production with a W-boson (tW production) has a cross section that is too small to observe at the Tevatron. The t-channel process is $qb \to q't$, while the s-channel process is $q\overline{q'} \to t\bar{b}$. The s- and t-channel

Downloaded from https://academic.oup.com/ptep/article/2022/8/083C01/6651666 by KIT Library user on 27 September 2022

productions can be separated kinematically. This is of particular interest because potential physics beyond the Standard Model, such as fourth-generation quarks, heavy W and Z bosons, flavor-changing-neutral-currents [11], or a charged Higgs boson, would affect the s- and t-channels differently. However, the separation is difficult and initial observations and measurements at the Tevatron by both experiments were of combined $s+t$-channel production. The two experiments combined their measurements for maximum precision with a resulting $s+t$-channel production cross section of $2.76^{+0.58}_{-0.47}$ pb [127]. The measured value assumes a top-quark mass of 170 GeV/c^2. The mass dependence of the result comes both from the acceptance dependence and from the $t\bar{t}$ background evaluation. Also the shape of discriminating topological variables is sensitive to m_t. The dependence on m_t is therefore not necessarily a simple linear dependence but amounts to only a few tenths of picobarns over the range $170-175$ GeV/c^2. The measured value agrees well with the theoretical calculation at $m_t = 173$ GeV/c^2 of $\sigma_{s+t} = 3.12^{+0.00}_{-0.04}(scale) \pm 0.18(pdf)$ pb (including both top and anti-top production) [9, 128].

Using the full Run-II data set of up to 9.7 fb^{-1}, CDF and DØ have measured the t-channel single-top quark production to be $\sigma_{t+\bar{t}} = 2.25^{+0.29}_{-0.31}$ pb [129, 130]. In the same publication, they also present the simultaneously measured $s-$ and $t-$channel cross sections and the $s+t$ combined cross section measurement resulting in $\sigma_{s+t} = 3.30^{+0.52}_{-0.40}$ pb, without assuming the SM ratio of σ_s/σ_t. The modulus of the CKM matrix element obtained from the $s+t$-channel measurement is $|V_{tb}| = 1.02^{+0.06}_{-0.05}$ and its value is used to set a lower limit of $|V_{tb}| > 0.92$ at 95% C.L. Those results are in good agreement with the theoretical value at the mass 172.5 GeV/c^2 of $\sigma_t = 2.08 \pm 0.13$ pb [128]. It should be noted that the theory citations here list cross sections for t or $\bar{t}$ alone, whereas the experiments measure the sum. At the Tevatron, these cross sections are equal. The theory values quoted here already include this factor of two.

Using datasets of 9.7 fb^{-1} each, CDF and DØ combine their analyses and report the first observation of single-top-quark production in the s-channel, yielding $\sigma_s = 1.29^{+0.26}_{-0.24}$ pb [131]. The probability of observing a statistical fluctuation of the background of the given size is 1.8×10^{-10}, corresponding to a significance of 6.3 standard deviations.

At the LHC, the t-channel cross section is expected to be more than three times as large as s-channel and tW production, combined. Both ATLAS and CMS have measured single top production cross sections at $\sqrt{s} = 7$ TeV in pp collisions (assuming $m_t = 172.5$ GeV/c^2 unless noted otherwise). Using 4.59 fb^{-1} of data at $\sqrt{s} = 7$ TeV, ATLAS measures the t-channel single-top quark cross section in the lepton plus 2 or 3 jets channel with one b-tag by fitting the distribution of a multivariate discriminant constructed with a neural network, yielding $\sigma_t = 46 \pm 6$ pb, $\sigma_{\bar{t}} = 23 \pm 4$ pb with a ratio $R_t = \sigma_t/\sigma_{\bar{t}} = 2.04 \pm 0.18$ and $\sigma_{t+\bar{t}} = 68 \pm 8$ pb, consistent with SM expectations [132, 133]. CMS follows two approaches in 1.6 fb^{-1} of lepton plus jets events. The first approach exploits the distributions of the pseudorapidity of the recoil jet and reconstructed top-quark mass using background estimates determined from control samples in data. The second approach is based on multivariate analysis techniques that probe the compatibility of the candidate events with the signal. They find $\sigma^{t-channel}_{t+\bar{t}} = 67.2 \pm 6.1$ pb, and $|V_{tb}| = 1.020 \pm 0.046(exp.) \pm 0.017(th.)$ [134].

At $\sqrt{s} = 8$ TeV, both experiments repeat and refine their measurements. ATLAS uses 20.2 fb^{-1} of data. Total, fiducial and differential cross-sections are measured for both top-quark and top-antiquark production [135]. An artificial neural network is employed to separate signal from background. The fiducial cross-section is measured with a precision of 5.8% (top quark) and 7.8% (top antiquark), respectively. The total cross-sections are measured to be $\sigma_t^{t-channel}(tq) = 56.7^{+4.3}_{-3.8}$ pb for top-quark production and $\sigma_{\bar{t}}^{t-channel}(\bar{t}q) = 32.9^{+3.0}_{-2.7}$ pb for top-antiquark production, in agreement with the SM prediction. In addition, the ratio of top-quark to top-antiquark production cross-sections is determined to be $R_t = 1.72 \pm 0.09$. The total cross-section is used to extract the Wtb coupling: $f_{LV} \cdot |V_{tb}| = 1.029 \pm 0.048$, which corresponds to $|V_{tb}| > 0.92$ at the 95% confidence level, when assuming $f_{LV} = 1$ and restricting the range of $|V_{tb}|$ to the interval $[0, 1]$. The differential cross-sections as a function of the transverse momentum and rapidity of both the top quark and the top antiquark are measured at both the parton and particle levels. The transverse momentum and rapidity differential cross-sections of the accompanying jet from the t-channel scattering are measured at particle level. All measurements are compared to various Monte Carlo predictions as well as to fixed-order QCD calculations where available. The SM predictions provide good descriptions of the data. Using the same dataset, ATLAS probes the Wtb vertex structure from polarization observables in t-channel single-top quark events. The polarization observables are extracted from asymmetries in angular distributions measured with respect to spin quantisation axes appropriately chosen for the top quark and the W-boson. The asymmetry measurements are performed at parton level by correcting the observed angular distributions for detector effects and hadronisation after subtracting the background contributions. The measured top-quark and W-boson polarization values are in agreement with the Standard Model predictions [136]. CMS uses 19.7 fb^{-1} in the electron or muon plus jets channel, exploiting the pseudorapidity distribution of the recoil jet. They find $\sigma_t = 53.8 \pm 1.5(stat.) \pm 4.4(syst.)$ pb and $\sigma_{\bar{t}} = 27.6 \pm 1.3(stat.) \pm 3.7(syst.)$ pb, resulting in an inclusive t-channel cross section of $\sigma_{t+\bar{t}} = 83.6 \pm 2.3(stat.) \pm 7.4(syst.)$ [137]. They measure a cross section ratio of $R_t = \sigma_t/\sigma_{\bar{t}} = 1.95 \pm 0.10(stat.) \pm 0.19(syst.)$, in agreement with the SM. The CKM matrix element V_{tb} is extracted to be $|V_{tb}| = 0.998 \pm 0.038(exp.) \pm 0.016(th.)$. Later, CMS has also provided a fiducial cross section measurement for t-channel single top at $\sqrt{s} = 8$ TeV with 19.7 fb^{-1} of data in signal events with exactly one muon or electron and two jets, one of which is associated with a b-hadron [138]. The definition of the fiducial phase space follows closely the constraints imposed by event-selection criteria and detector acceptance. The total fiducial cross section is measured using different generators at next-to-leading order plus parton-shower accuracy. Using as reference the `aMC@NLO` MC predictions in the four-flavour scheme $\sigma_t^{\rm fid} = 3.38 \pm 0.25(exp.) \pm 0.20(th.)$ pb is obtained, in good agreement with the theory predictions. At 13 TeV, ATLAS uses 3.2 fb^{-1} to measure the t-channel cross section. Using a binned maximum-likelihood fit to the discriminant distribution of a neural network, the cross-sections are determined to be $\sigma_t(tq) = 156 \pm 5(stat.) \pm 27(syst.) \pm 3(lumi.)$ pb and $\sigma(\bar{t}q) = 91 \pm 4(stat.) \pm 18(syst.) \pm 2(lumi.)$ pb [139]. The cross-section ratio is measured to be $R_t = \sigma_t/\sigma_{\bar{t}} = 1.72 \pm 0.09(stat.) \pm 0.18(syst.)$. All results are in agreement with SM predictions. A measurement of the t-channel single top-quark cross section is also available at 13 TeV with the CMS detector, corresponding to an integrated luminosity of 2.2 fb^{-1}. Fits to the transverse W-mass and the output of an artificial neural network allow the determination of the background and the signal contribution. The measured cross-section is $\sigma_t = 238 \pm 13(stat.) \pm 29(syst.)$ pb [140]. The CKM matrix element is determined to $|V_{tb}| = 1.05 \pm 0.07(exp.) \pm 0.02(th.)$. Using 35.9 fb^{-1} of data, CMS performs measurements of the t-channel cross sections of single top quarks and antiquarks in the t channel, and their ratio. Events with one muon or electron are selected, and different categories of jet and b-jet multiplicity and multivariate discriminators are applied to separate the signal from the background, resulting in $\sigma_t(tq) = 130 \pm 1(stat) \pm 19(syst)$ pb and $\sigma_t(\bar{t}q) = 77 \pm 1(stat) \pm 12(syst)$ pb, respectively, and their ratio is $1.68 \pm 0.02(stat) \pm 0.05(syst)$. The results are in agreement with the predictions from the Standard Model [141]. Recently, CMS used the same dataset to measure the CKM matrix elements from their t-channel single-top quark production cross section. In the standard model hypothesis of CKM unitarity, a lower limit of $|V_{tb}| > 0.970$ is measured at the 95% confidence level. Several theories beyond the standard model are considered, and by releasing all constraints among the involved parameters, the values $|V_{tb}| = 0.988 \pm 0.024$, and $|V_{td}|^2 + |V_{ts}|^2 = 0.06 \pm 0.06$, where the uncertainties include both statistical and systematic components, are measured [142].

The predicted cross section for the tW process at the LHC

Downloaded from https://academic.oup.com/ptep/article/2022/8/083C01/6651666 by KIT Library user on 27 September 2022

$\sqrt{s}$ = 7 TeV is 15.6 ± 1.2 pb [10]. This is of interest because it probes the Wtb vertex in a different kinematic region than s- and t-channel production, and because of its similarity to the associated production of a charged-Higgs boson and a top quark. The signal is difficult to extract because of its similarity to the $t\bar{t}$ signature. Furthermore, it is difficult to uniquely define because at NLO a subset of diagrams has the same final state as $t\bar{t}$ and the two interfere [143]. The cross section is calculated using the *diagram removal* technique [144] to define the signal process. In the diagram removal technique the interfering diagrams are removed, at the amplitude level, from the signal definition (an alternative technique, *diagram subtraction* removes these diagrams at the cross-section level and yields similar results [144]). These techniques work provided the selection cuts are defined such that the interference effects are small, which is usually the case.

Both, ATLAS and CMS, also provide evidence for the associate tW production at $\sqrt{s}$ = 7 TeV [145, 146]. ATLAS uses 2.05 fb^{-1} in the dilepton plus missing E_T plus jets channel, where a template fit to the final classifier distributions resulting from boosted decision trees as signal to background separation is performed. The result is incompatible with the background-only hypothesis at the 3.3σ (3.4σ expected) level, yielding $\sigma_{tW} = 16.8 \pm 2.9(stat.) \pm 4.9(syst.)$ pb and $|V_{tb}| = 1.03^{+0.16}_{-0.19}$ [145]. CMS uses 4.9 fb^{-1} in the dilepton plus jets channel with at least one b-tag. A multivariate analysis based on kinematic properties is utilized to separate the $t\bar{t}$ background from the signal. The observed signal has a significance of 4.0σ and corresponds to a cross section of $\sigma_{tW} = 16^{+5}_{-4}$ pb [146].

Both experiments repeated their tW-analyses at $\sqrt{s}$ = 8 TeV. ATLAS uses 20.3 fb^{-1} to select events with two leptons and one central b-jet. The tW signal is separated from the backgrounds using boosted decision trees, each of which combines a number of discriminating variables into one classifier. Production of tW events is observed with a significance of 7.7σ. The cross section is extracted in a profile likelihood fit to the classifier output distributions. The tW cross section, inclusive of decay modes, is measured to be $\sigma_{tW} = 23.0 \pm 1.3(stat.)^{+3.2}_{-3.5}(syst.) \pm 1.1(lumi.)$ pb, yielding a value for the CKM matrix element $|V_{tb}| = 1.01 \pm 0.10$ and a lower limit of 0.80 at the 95% C.L. [147]. A fiducial cross section is also measured. ATLAS and CMS also combine their early measurements and obtain $\sigma_{tW} = 16.3 \pm 4.1$ pb [148], in agreement with the NLO+NNLL expectation. Very recently, ATLAS used 20.2 fb^{-1} in the single-lepton channel with at least three jets to measure the Wt production cross section. A neural network is trained to separate the tW signal from the dominant $t\bar{t}$ background. The cross-section is extracted from a binned profile maximum-likelihood fit to a two-dimensional discriminant built from the neural-network output and the invariant mass of the hadronically decaying W boson. The measured cross section is $\sigma_{tW} = 26 \pm 7$ pb, in good agreement with the Standard Model expectation [149]. CMS uses 12.2 fb^{-1} in events with two leptons and a jet originating from a b-quark. A multivariate analysis based on kinematic properties is utilized to separate the signal and background. The tW associate production signal is observed at the level of 6.1σ, yielding $\sigma_{tW} = 23.4 \pm 5.4$ pb and $|V_{tb}| = 1.03 \pm 0.12(exp.) \pm 0.04(th.)$ [150]. ATLAS and CMS also combine their early measurements and obtain $\sigma_{tW} = 23.1 \pm 3.6$ pb [148], in agreement with the NLO+NNLL expectation. The product of a form factor with the CKM matrix element V_{tb} is determined to be $|V_{tb}| = 1.02 \pm 0.04(meas.) \pm 0.02(theo.) > 0.79$. At 13 TeV in the tW-channel, ATLAS uses 3.2 fb^{-1} of events with two opposite sign isolated leptons and at least one jet; they are separated into signal and control regions based on their jet multiplicity and the number of jets with b-tags. Signal is separated from background in two regions using boosted decision trees. The cross section is extracted by fitting templates to the data distributions, and is measured to be $\sigma_{tW} = 94 \pm 10(stat.)^{+28}_{-22}(syst.) \pm 2(lumi.)$ pb [151]. The measurement is in agreement with the SM prediction. CMS uses 36 fb^{-1} of events with two opposite sign isolated leptons, one tight and one loose jet and one b-tag. Signal and background is separated in categories depending on the number of jets and the subset of b-tagged jets using a boosted decision tree. A maximum likelihood fits yields $\sigma_{tW} = 63.1 \pm 1.8(stat.) \pm 6.4(syst.) \pm 2.1(lumi.)$ pb [152]. Very recently, CMS uses 36 fb^{-1} in the single-lepton channel, where a boosted decision tree is used to separate the tW signal from the dominant $t\bar{t}$ background, whilst the subleading W+jets and multijet backgrounds are constrained using data-based estimates. This result is the first observation of the tW process in final states containing a muon or electron and jets, with a significance exceeding 5 standard deviations. The cross section is determined to be $\sigma_{tW} = 89 \pm 4(stat) \pm 12(syst)$ pb, consistent with the Standard Model [153].

The s-channel production cross section is expected to be 4.6 ± 0.3 pb for m_t = 173 GeV/c^2 at $\sqrt{s}$ = 7 TeV [9]. At ATLAS, a search for s-channel single top quark production is performed in 0.7 fb^{-1} at 7 TeV using events containing one lepton, missing transverse energy and two b-jets. Using a cut-based analysis, an observed (expected) upper limit at 95% C.L. on the s-channel cross-section of $\sigma_s < 26.5$ (20.5) pb is obtained [154]. At 8 TeV, ATLAS uses 20.3 fb^{-1} of data with one lepton, large missing transverse momentum and exactly two b-tagged jets. They perform a maximum-likelihood fit of a discriminant based on a Matrix Element Method and optimized in order to separate single top-quark s-channel events from the main background contributions which are top-quark pair production and W boson production in association with heavy flavor jets. They find $\sigma_s = 4.8 \pm 0.8(stat.)^{+1.6}_{-1.3}(syst.)$ pb with a signal significance of 3.2 standard deviations [155], which provides first evidence for s-channel single-top production at 8 TeV. The signal is extracted through a maximum-likelihood fit to the distribution of a multivariate discriminant defined using boosted decision trees to separate the expected signal contribution from background processes. At 7 TeV and 8 TeV, CMS uses 5.1 fb^{-1} and 19.3 fb^{-1}, respectively, and analyses leptonic decay modes by performing a maximum likelihood fit to a multivariate discriminant defined using a Boosted Decision Tree, yielding cross sections of $\sigma_s = 7.1 \pm 8.1$ pb and $\sigma_s = 13.4 \pm 7.3$ pb, respectively, and a best fit value of 2.0 ± 0.9 for the combined ratio of the measured σ_s values and the ones expected in the Standard Model [156]. The signal significance is 2.5 standard deviations. ATLAS and CMS present the combinations of their single-top-quark production cross-section measurements, using Run-I data corresponding to integrated luminosities of 1.17 to 5.1 fb^{-1} at $\sqrt{s}$ = 7 TeV and 12.2 to 20.3 fb^{-1} at $\sqrt{s}$ = 8 TeV. These combinations are performed per centre-of-mass energy and for each production mode: t-channel, tW, and s-channel. The combined t-channel cross-sections are 67.5 ± 5.7 pb and 87.7 ± 5.8 pb at $\sqrt{s}$ = 7 and 8 TeV, respectively. The combined tW cross-sections are 16.3 ± 4.1 pb and 23.1 ± 3.6 pb at $\sqrt{s}$ = 7 and 8 TeV, respectively. For the s-channel cross-section, the combination yields 4.9 ± 1.4 pb at $\sqrt{s}$ = 8 TeV. The square of the magnitude of the CKM matrix element V_{tb} multiplied by a form factor f_{LV} is determined for each production mode and centre-of-mass energy, using the ratio of the measured cross-section to its theoretical prediction. All combined measurements are consistent with their corresponding SM predictions [157]. Both, ATLAS and CMS, also measured the electroweak production of single top-quarks in association with a Z-boson, see section 61.3.2.4 of this review.

Fig. 61.2 provides a summary of all single top cross-section measurements at the LHC as a function of the center-of-mass energy. All cross-section measurements are very well described by the theory calculation within their uncertainty.

Thanks to the large statistics now available at the LHC, both CMS and ATLAS experiments also performed differential cross-section measurements in single-top t-channel production [132], [158]. Such measurements are extremely useful as they test our understanding of both QCD and EW top-quark interactions. The CMS collaboration has measured differential single top quark t-channel production cross sections as functions of the transverse momentum and the absolute value of the rapidity of the top quark. The analysis is performed in the leptonic decay channels of the top quark, with either a muon or an electron in the final state, using data collected with the CMS experiment at the LHC at $\sqrt{s}$ = 8 TeV and corresponding to an integrated luminosity of 19.7 fb^{-1}. Neural networks are used to discriminate the signal process from the various background contributions. The results

Downloaded from https://academic.oup.com/ptep/article/2022/8/083C01/6651666 by KIT Library user on 27 September 2022

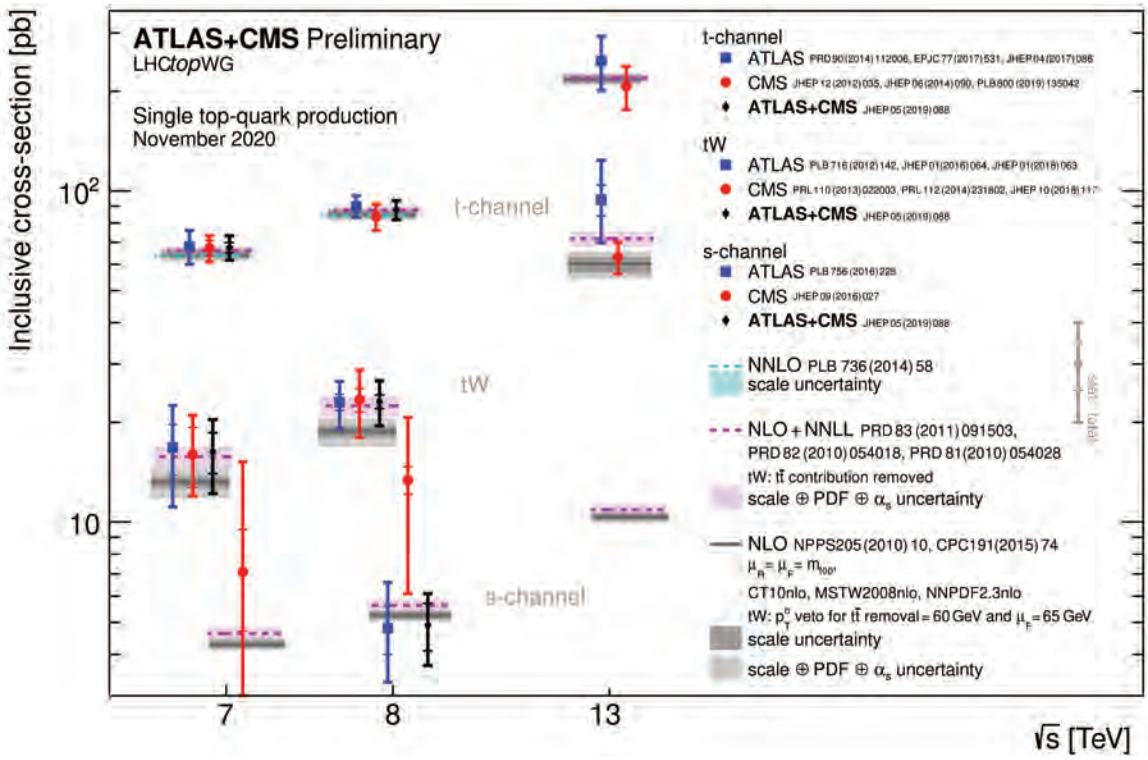

Figure 61.2: Measured and predicted single top production cross sections at LHC energies in pp collisions. The recent CMS measurement of the tW production cross section at 13 TeV in the l+jets channel is not yet shown here. The plot is kindly provided by the LHCtopWG working group, see `https://twiki.cern.ch/twiki/bin/view/LHCPhysics/LHCTopWGSummaryPlots`.

are found to agree with predictions from Monte Carlo generators [158]. Using the same data set and under the assumption that the spin analyzing power of a charged lepton is 100% as predicted in the SM, they are also able to measure the polarization of the top quark $P_t = 0.82 \pm 0.12(stat.) \pm 0.32(syst.)$ [159]. At 13 TeV, using 35.9 fb^{-1}, CMS measures the differential t-channel cross sections, for the first time in single-top production, and charge ratios for t-channel single top quark production [160]. The results are found to be in agreement with SM predictions using various NLO event generators and sets of parton distribution functions. Additionally, the spin asymmetry, sensitive to the top quark polarization, is determined from the differential distribution of the polarization angle at parton level to be 0.439 ± 0.062, in agreement with the SM prediction. This disfavours the results obtained at 8 TeV. ATLAS has measured the differential tW cross section in 36.1 fb^{-1} at 13 TeV with respect to the energy of the b-jet, the energy of the system of the two leptons and b-jet, and the transverse mass or mass of combinations of leptons, the b-jet and neutrinos [161]. Using 35.9 fb^{-1} of $e\mu$ events, CMS to measure the differential tW cross section. A fiducial region is defined according to the detector acceptance, and the requirement of exactly one b-tagged jet. The resulting distributions are unfolded to particle-level and compared with predictions calculated at next-to-leading order in perturbative QCD. Within current uncertainties, all the predictions agree with the data [162].

61.3.1.4 *Top-Quark Asymmetries*

A forward-backward asymmetry in $t\bar{t}$ production at a $p\bar{p}$ collider arises starting at order α_S^3 in QCD from the interference between the Born amplitude $q\bar{q} \to t\bar{t}$ with 1-loop box production diagrams and between diagrams with initial- and final-state gluon radiation. The asymmetry, A_{FB}, is defined by

$$A_{FB} = \frac{N(\Delta y > 0) - N(\Delta y < 0)}{N(\Delta y > 0) + N(\Delta y < 0)}, \tag{61.2}$$

where $\Delta y = y_t - y_{\bar{t}}$ is the rapidity difference between the top- and the anti-top quark. Calculations at α_S^3 predict a measurable A_{FB} at the Tevatron. The most recent calculations up to order α_S^4, including electromagnetic and electroweak corrections, yield a predicted asymmetry of $\approx(9.5 \pm 0.7)\%$ [163]. This is about 10% higher than the previous calculation at NLO [164, 165], and improves the agreement with experiment.

Both CDF and DØ measured asymmetry values in excess of the SM prediction, fueling speculation about exotic production mechanisms (see, for example, [166] and references therein). The first measurement of this asymmetry by DØ in 0.9 fb^{-1} [167] found an asymmetry at the detector level of $(12 \pm 8)\%$. The first CDF measurement in 1.9 fb^{-1} [168] yielded $(24 \pm 14)\%$ at parton level. Both values were higher, though statistically consistent with the SM expectation. With the addition of more data, the uncertainties have been reduced, and the central values, if somewhat smaller, have remained consistent with the first measurements. At the same time, the improved calculations from theory have increased the predicted asymmetry values, improving the agreement between theory and experiment.

CDF and DØ have now combined results using the full Tevatron dataset at $\sqrt{s} = 1.96$ TeV [169]. Three combined asymmetries are reported: $A_{FB}^{t\bar{t}}$ as defined in Eq. 2 for fully-reconstructed $t\bar{t}$ events, a single-lepton asymmetry, A_{FB}^{ℓ} defined as in Eq. 2 but with Δy replaced by the product of the lepton charge and pseudo-rapidity, and a dilepton asymmetry, $A_{FB}^{\ell\ell}$, defined as in Eq. 2 but with Δy replaced by $\Delta\eta$ between the two leptons. The combined results are $A_{FB}^{t\bar{t}} = 0.128 \pm 0.021 \pm 0.014$, $A_{FB}^{\ell} = 0.073 \pm 0.016 \pm 0.012$, and $A_{FB}^{\ell\ell} = 0.108 \pm 0.043 \pm 0.016$, where the first uncertainty is statistical and the second systematic. These are to be compared to SM predictions at NNLO QCD and NLO electroweak of $A_{FB}^{t\bar{t}} = 0.095 \pm 0.007$ [163], $A_{FB}^{\ell} = 0.038 \pm 0.003$, and $A_{FB}^{\ell\ell} = 0.048 \pm 0.004$ [165], respectively. Both experiments have also measured differential asymmetries, in bins of $M_{t\bar{t}}$, Δy, $q_\ell \times \eta_\ell$, and $\Delta\eta_{\ell\ell}$, with consistent results, though the growth of $A_{FB}^{t\bar{t}}$ with increasing $M_{t\bar{t}}$ and Δy appears somewhat more rapid than the SM prediction [169].

At the LHC, where the dominant $t\bar{t}$ production mechanism is the charge-symmetric gluon-gluon fusion, the measurement is

Downloaded from https://academic.oup.com/ptep/article/2022/8/083C01/6651666 by KIT Library user on 27 September 2022

more difficult. For the sub-dominant $q\bar{q}$ production mechanism, the symmetric pp collision does not define a forward and backward direction. Instead, the charge asymmetry, A_C, is defined in terms of a positive versus a negative $t-\bar{t}$ rapidity difference, Δy

$$A_C^{t\bar{t}} = \frac{N(\Delta|y|>0) - N(\Delta|y|<0)}{N(\Delta|y|>0) + N(\Delta|y|<0)}. \tag{61.3}$$

Both CMS and ATLAS have measured A_C in the LHC dataset. Using lepton+jets events in 4.7 fb^{-1} of data at $\sqrt{s}=7$ TeV, ATLAS measures $A_C^{t\bar{t}} = (0.6 \pm 1.0)\%$ [170]. ATLAS has reported on the same measurement performed at $\sqrt{s}=8$ TeV with 20.3 fb^{-1} of data, with a result of $A_C^{t\bar{t}} = (0.9 \pm 0.5)\%$ [171]. In the dilepton channel at $\sqrt{s}=8$ TeV, ATLAS measures [172] $A_C^{t\bar{t}} = (2.1 \pm 1.6)\%$, and $A_C^{\ell\ell} = (0.8 \pm 0.6)\%$ (defined in terms of the $\Delta\eta$ of the two leptons) in agreement with the SM predictions of $(1.11 \pm 0.04)\%$ and $(0.64 \pm 0.03)\%$, respectively [165]. Using lepton+jets events CMS has measured A_C at both $\sqrt{s}=7$ and 8 TeV. They measure $A_C^{t\bar{t}} = (0.4 \pm 1.5)\%$ and $A_C^{t\bar{t}} = (0.33 \pm 0.26(stat.) \pm 0.33(syst.))\%$ in 5.0 fb^{-1} at $\sqrt{s}=7$ TeV and In 19.7 fb^{-1} at $\sqrt{s}=8$ TeV, respectively [173, 174]. Both measurements are consistent with the SM expectations of $A_C^{t\bar{t}} = (1.23 \pm 0.05)\%$ at $\sqrt{s}=7$ TeV and $(1.11 \pm 0.04)\%$ at $\sqrt{s}=8$ TeV [165], although the uncertainties are still too large for a precision test. In 19.5 fb^{-1} of dilepton events at $\sqrt{s}=8$ TeV, CMS measures $A_C^{t\bar{t}} = (1.1 \pm 1.3)\%$ and $A_C^{\ell\ell} = (0.3 \pm 0.7)\%$ [175], consistent with SM expectations [176].

In their 7 and 8 TeV analyses ATLAS and CMS also provide differential measurements as a function of $M_{t\bar{t}}$ and the transverse momentum p_T and rapidity y of the $t\bar{t}$ system. To reduce model-dependence, the CMS collaboration has performed a measurement in a reduced fiducial phase space [177], with a result of $A_C = (-0.35 \pm 0.72(stat.) \pm 0.31(syst.))\%$, in agreement with SM expectations.

To specifically address the dependence of the asymmetry on $M_{t\bar{t}}$, ATLAS has performed a measurement in boosted $t\bar{t}$ events [178]. In 20.3 fb^{-1} of data at $\sqrt{s}=8$ TeV, in events with $M_{t\bar{t}} >$ 0.75 TeV, and $|(\Delta|y|)| < 2$, ATLAS measures $A_C^{t\bar{t}} = (4.2 \pm 3.2)\%$ compared to a NLO SM prediction of $(1.60 \pm 0.04)\%$. The measurement is also presented in three bins of $M_{t\bar{t}}$, each in agreement, though with large uncertainties, with the SM expectations.

Both ATLAS and CMS have measured asymmetries in the distribution of leptons from $t\bar{t}$ decays. ATLAS, in 4.6 fb^{-1} of $\sqrt{s}=7$ TeV data, has measured $A^{\ell\ell} = (2.4 \pm 1.5(\text{stat.}) \pm 0.9(\text{sys.}))\%$ in dilepton events [179]. Using a neutrino weighting technique in the same dataset to reconstruct the top quarks, ATLAS measures $A_C = (2.1 \pm 2.5\ (\text{stat.}) \pm 1.7\ (\text{sys.}))\%$. CMS, in 5.0 fb^{-1} of $\sqrt{s}=7$ TeV data, uses dilepton events to measure $A_C = (1.0 \pm 1.5\ (\text{stat.}) \pm 0.6\ (\text{sys.}))\%$, where a matrix weighting technique is used to reconstruct the top quarks, and $A^{\ell\ell} = (0.9 \pm 1.0\ (\text{stat.}) \pm 0.6\ (\text{sys.}))\%$ [180]. An earlier result using lepton+jets events from the same CMS dataset found $A_C = (0.4 \pm 1.0 \pm 1.1)\%$ [173]. Combined results from ATLAS and CMS have now been released [181]. At $\sqrt{s}=7$ TeV the combined result is $A_C = (0.5 \pm 0.7\ (\text{stat.}) \pm 0.6\ (\text{sys.}))\%$, and at $\sqrt{s}=8$ TeV it is $A_C = (0.55 \pm 0.23 \pm 0.25)\%$. These results are all consistent, within their large uncertainties, with the SM expectations of $A^{\ell\ell} = (0.70 \pm 0.03)\%$ and $A_C = (1.23 \pm 0.05)\%$ [165].

ATLAS has released a charge asymmetry measurement at $\sqrt{s} =$ 13 TeV using the full 139 fb^{-1} dataset. A Bayesian unfolding procedure is used in lepton plus jets events, combining both resolved and boosted topologies, to infer the asymmetry at parton level, correcting for detector resolution and acceptance effects. The inclusive charge asymmetry is measured as $A_C = (0.60 \pm 0.15)\%$ (stat+syst.) [182]. In addition to the inclusive measurement, the result includes differential measurements in five bins of $M_{t\bar{t}}$, and four bins of longitudinal boost. Both inclusive and differential results are found consistent with Standard Model predictions at NNLO in QCD and NLO in electroweak theory.

A model-independent comparison of the Tevatron and LHC results is made difficult by the differing $t\bar{t}$ production mechanisms at work at the two accelerators and by the symmetric nature of the pp collisions at the LHC. A recent result from the CMS Collaboration [183] in 35.9 fb^{-1} of lepton plus jets events at $\sqrt{s}=13$ TeV, uses a likelihood analysis to separate the $q\bar{q}$ process from production via gluon-gluon and gluon-quark interactions and extract $A_{FB} = (4.8^{+8.8}_{-8.4}\ (\text{stat.}) \pm 2.8\ (\text{sys.}))\%$. In addition, given a particular model of BSM physics, a comparison can be obtained through the resulting asymmetry predicted by the model at the two machines, see for example [178].

A new measurement from ATLAS explores a so-called 'energy asymmetry' in $t\bar{t}$ production in association with a high-p_T jet ($t\bar{t}j$ production). The energy asymmetry is defined as a difference between the top and anti-top quarks' energies, and is measured in ATLAS in three bins of the associated high-p_T jet angle, θ_j. Both the energies and jet angle are measured in the $t\bar{t}j$ rest frame. A Bayesian unfolding method corrects for resolution and acceptance effects. The measurement is in agreement with the Standard Model at NLO accuracy [184].

61.3.2 *Top-Quark Properties*

61.3.2.1 *Top-Quark Mass Measurements*

The most precisely studied property of the top quark is its mass. The top-quark mass has been measured in the lepton+jets, the dilepton, and the all-jets channel by all four Tevatron and LHC experiments, and now in single-top events at the LHC. The latest and/or most precise results are summarized in Table 61.1. The lepton+jets channel yields the most precise single measurements because of good signal to background ratio (in particular after b-tagging) and the presence of only a single neutrino in the final state. The momentum of a single neutrino can be reconstructed (up to a quadratic ambiguity) via the missing E_T measurement and the constraint that the lepton and neutrino momenta reconstruct to the known W boson mass. In the large data samples available at the LHC, measurements in the dilepton channel can be competitive and certainly complementary to those in the lepton+jets final state.

A large number of techniques have now been applied to measuring the top-quark mass. The original 'template method' [185], in which Monte Carlo templates of reconstructed mass distributions are fit to data, has evolved into a precision tool in the lepton+jets channel, where the systematic uncertainty due to the jet energy scale (JES) uncertainty is controlled by a simultaneous, *in situ* fit to the $W \to jj$ hypothesis [186]. All the latest measurements in the lepton+jets and the all-jets channels use this technique in one way or another. In 20.2 fb^{-1} of data at $\sqrt{s}=8$ TeV in the lepton+jets channel, ATLAS achieves a total uncertainty of 0.53% with a statistical component of 0.23% [187]. The measurement is based on a 3-dimensional template fit, determining the top-quark mass, the global jet energy scale and a b-to-light jet energy scale factor. The most precise CMS result in the lepton+jets channel uses an ideogram method and comes from a so-called 'hybrid' approach in which the prior knowledge about the jet energy scale is incorporated as a Gaussian constraint, with a width determined by the uncertainty on the jet energy corrections. In 19.7 fb^{-1} of $\sqrt{s}=8$ TeV data, CMS achieves a total uncertainty of 0.30% with a statistical component of 0.09% with the hybrid approach [188]. Using this same method, CMS has released a top-mass measurement from $\sqrt{s}=13$ TeV data. Using 35.9 fb^{-1} of lepton+jets events they measure the top mass with a precision of 0.36%, with a statistical component of 0.05% [189]. The measurements at $\sqrt{s}=13$ TeV include, for the first time, an uncertainty due to 'color reconnection' [190, 191]. In this same dataset, CMS has extracted a top mass from highly boosted top-quark decays by selecting events in which the hadronic-side top decay is reconstructed as a single jet with $P_T > 400$ GeV. The cross section as a function of jet mass is unfolded at the particle level to extract a top mass with a precision of 1.4% [192].

The template method is complemented by the 'matrix element' method. This method was first applied by the DØ Collaboration [193], and is similar to a technique originally suggested by Kondo *et al.* [194] and Dalitz and Goldstein [195] In the matrix element method a probability for each event is calculated as a function of the top-quark mass, using a LO matrix element for the production and decay of $t\bar{t}$ pairs. The *in situ* calibration of dijet pairs to the $W \to jj$ hypothesis is now also used with the matrix element

Downloaded from https://academic.oup.com/ptep/article/2022/8/083C01/6651666 by KIT Library user on 27 September 2022

technique to constrain the jet energy scale uncertainty. In the lepton+jets channel, DØ uses the full Tevatron dataset of 9.7 fb^{-1} and yields an uncertainty of about 0.43% [196].

In the dilepton channel, the signal to background is typically very good, but reconstruction of the mass is non-trivial because there are two neutrinos in the final state, yielding a kinematically unconstrained system. A variety of techniques have been developed to handle this. An analytic solution to the problem has been proposed [197], but this has not yet been used in the mass measurement. One of the most precise measurements in the dilepton channel comes from using the invariant mass of the charged lepton and b-quark system ($M_{\ell b}$), which is sensitive to the top-quark mass and avoids the kinematic difficulties of the two-neutrino final state. In 4.6 fb^{-1} of $\sqrt{s} = 7$ TeV data, ATLAS has measured the top-quark mass in the dilepton channel to a precision of 0.53% using a template fit to the $M_{\ell b}$ distribution [198]. Using 19.7 fb^{-1} of data at $\sqrt{s} = 8$ TeV, CMS has released [199] a mass measurement in the dilepton channel based on a simultaneous fit to $M_{\ell b}$ and a transverse-mass-like variable M_{T2} [200]. The most precise result in this analysis, which comes from a linear combination of fits with the jet energy scale fixed at its nominal value and one that simultaneously determines the top mass and jet energy scale, has a total uncertainty of 0.54%. At the LHC, because of their precision, these techniques have largely displaced a number of earlier techniques in the dilepton channel, though these techniques are still included, and described, in the combined results from CMS, reported in Ref. [188].

In the neutrino weighting technique, used by CDF to analyze the full Run 2 dilepton dataset of 9.1 fb^{-1}, a weight is assigned by assuming a top-quark mass value and applying energy-momentum conservation to the top-quark decay, resulting in up to four possible pairs of solutions for the neutrino and anti-neutrino momenta. The missing E_T calculated in this way is then compared to the observed missing E_T to assign a weight [205]. The CDF result achieves a precision of 1.8% using a combination of neutrino weighting and an "alternative mass", which is insensitive to the jet energy scale [206]. The alternative mass depends on the angles between the leptons and the leading jets and the lepton four-momenta.

In the all-jets channel there is no ambiguity due to neutrino momenta, but the signal to background is significantly poorer due to the severe QCD multijets background. The emphasis therefore has been on background modeling, and reduction through event selection. The most recent measurement in the all-jets channel, by CMS in 35.9 fb^{-1} of $\sqrt{s} = 13$ TeV data [201], uses an ideogram method and a 2-dimensional simultaneous fit for m_t and the jet energy scale to extract the top-quark mass and achieves a precision of 0.36%. A measurement from ATLAS [202] uses a template fit to the ratio of three-jet (m_t) to two-jet (M_W) mass in the all-hadronic channel, the two-jet denominator provides an *in situ*, fit to the $W \to jj$ hypothesis. In 20.2 fb^{-1} of data at $\sqrt{s} = 8$ TeV, the result has a precision of 0.65%. A measurement from CDF in 9.3 fb^{-1} uses a two-dimensional template fit and achieves a precision of 1.1% [207].

The CMS Collaboration extracted a top-quark mass measurement from single-top events, something not previously done because of the poor signal to background ratio. The mass is extracted from the invariant mass of the muon, bottom quark, and missing transverse energy. The first measurement with 19.7 fb^{-1} of data at $\sqrt{s} = 8$ TeV, achieved a precision of 0.71% [208]. A more recent measurement in 35.9 fb^{-1} of data at $\sqrt{s} = 13$ TeV achieves 0.44% precision [203].

A dominant systematic uncertainty in these methods is the understanding of the jet energy scale, and so several techniques have been developed that have little sensitivity to the jet energy scale uncertainty. In addition to Reference [206] mentioned above, these include the measurement of the top-quark mass using the following techniques: Fitting of the lepton p_T spectrum of candidate events [209]; fitting of the transverse decay length of the b-jet (L_{xy}) [210]; fitting the invariant mass of a lepton from the W-decay and a muon from the semileptonic b decay [211, 212], kinematic properties of secondary vertices from b-quark fragmentation [213], the invariant mass of the $J/\psi + \ell$ system in events in which a b-quark fragments to a J/ψ particle [214], fitting the b-jet energy peak [215], and dilepton kinematics in $e\mu$ events [216].

Several measurements have now been made in which the top-quark mass is extracted from the measured $t\bar{t}$ cross section using the theoretical relationship between the mass and the production cross section. These determinations make use of predictions calculated at higher orders, where the top mass enters as an input parameter defined in a given scheme. At variance with the usual methods, which involve the kinematic properties of the final states and therefore the pole mass, this approach can also directly determine a short-distance mass, such as the $\overline{\text{MS}}$ mass [217]. With an alternative method ATLAS extracted the top-quark pole mass using $t\bar{t}$ events with at least one additional jet, basing the measurement on the relationship between the differential rate of gluon radiation and the mass of the quark [218]. A similar analysis by CMS used the differential cross section as a function of the invariant mass of the $t\bar{t}$ system and the leading jet not associated with the top decays [219].

Each of the experiments has produced a measurement combining its various results. The combined measurement from CMS with up to 19.7 fb^{-1} of data achieves statistical and systematic uncertainties of 0.08% and 0.27%, respectively [188]. The combined measurement from ATLAS, with up to 20.3 fb^{-1} yields statistical and systematic uncertainties of 0.14% and 0.24%, respectively [187]. CDF has combined measurements with up to 9.3 fb^{-1} [220] and achieves a statistical precision of 0.33% and a systematic uncertainty of 0.43%. DØ achieves a 0.33% statistical+JES and a 0.28% systematic uncertainty by combining results in 9.7 fb^{-1} [221].

Combined measurements from the Tevatron experiments and from the LHC experiments take into account the correlations between different measurements from a single experiment and between measurements from different experiments. The Tevatron average [204], using up to 9.7 fb^{-1} of data, now has a precision of 0.37%. The LHC combination, using up to 4.9 fb^{-1} of data, has a precision of 0.56% [222], where more work on systematic uncertainties is required. A Tevatron-LHC combination has been released, combining the results of all four experiments, using the full Tevatron dataset and the $\sqrt{s} = 7$ TeV LHC data, with a resulting precision of 0.44% [3]

The direct measurements of the top-quark mass, such as those shown in Table 61.1, correspond to the parameter used in the Monte Carlo generators, which is closely related to the pole mass [223]. The relation between the pole mass and short-distance masses, such as $\overline{\text{MS}}$, is affected by non-perturbative effects. Recent calculations evaluate the size of this ambiguity to be below 250 MeV and therefore still smaller than the current measurement uncertainty [224, 225]. ATLAS has recently performed a 'calibration' of the top mass parameter in Powheg + Pythia 8 with respect to the so-called 'MSR' mass scheme [226]. Using simulated lepton+jets events and the mass distribution of large-radius jets containing the three quarks from the hadronically decaying top quark, they find a mass difference between the Monte Carlo mass and the MSR mass of 80 MeV with large uncertainties [227].

As a result of renormalization at higher-orders in perturbation theory, the top quark mass depends on the scale at which it is evaluated. The CMS collaboration has made the first measurement of the so-called running of the top-quark mass in the $\overline{\text{MS}}$ scheme [228]. The running mass is extracted from a measurement of the differential cross section as a function of the $t\bar{t}$ invariant mass, unfolded back to the parton level, in $e\mu$ final states. The running mass varies by about 15% from $M_{t\bar{t}} = 400$ GeV to $M_{t\bar{t}} \approx 1$ TeV, in good agreement with the renormalization group calculation at one-loop level. Compared to the hypothesis of no running, the significance of the measured running is 2.6σ. However, caveats of such an interpretation have been raised as a result of the large theoretical uncertainties [229].

With the discovery of a Higgs boson at the LHC with a mass of about 125 GeV/c^2 [230, 231], the precision measurement of the top-quark mass takes a central role in the question of the stability of the electroweak vacuum because top-quark radiative corrections tend to drive the Higgs quartic coupling, λ, negative, potentially leading to an unstable vacuum. A calculation at NNLO [232]

Downloaded from https://academic.oup.com/ptep/article/2022/8/083C01/6651666 by KIT Library user on 27 September 2022

Table 61.1: Measurements of top-quark mass from Tevatron and LHC. The results are a selection of both published and preliminary (not yet submitted for publication as of September 2021) measurements. For a complete set of published results see the Listings. Statistical uncertainties are listed first, followed by systematic uncertainties.

m_t (GeV/c^2)	Source	$\int \mathcal{L}$dt fb^{-1}	Ref.	Channel
$172.08 \pm 0.25 \pm 0.41$	ATLAS	20.2	[187]	ℓ+jets+$\ell\ell$+All jets
$172.44 \pm 0.13 \pm 0.47$	CMS	19.7	[188]	ℓ+jets+$\ell\ell$+All jets
$172.35 \pm 0.16 \pm 0.48$	CMS	19.7	[188]	ℓ+jets
$172.34 \pm 0.20 \pm 0.70$	CMS	35.9	[201]	$\ell\ell$
$173.72 \pm 0.55 \pm 1.01$	ATLAS	20.2	[202]	All jets
$172.25 \pm 0.08 \pm 0.62$	CMS	35.9	[189]	ℓ+jets
$172.6 \pm 0.4 \pm 2.4$	CMS	35.9	[192]	Boosted jets
$172.13 \pm 0.32^{+0.69}_{-0.70}$	CMS	35.9	[203]	Single top
$174.30 \pm 0.35 \pm 0.54$	CDF,DØ (I+II)	$\leq$9.7	[204]	publ. or prelim.
$173.34 \pm 0.27 \pm 0.71$	Tevatron+LHC	$\leq$8.7+$\leq$4.9	[3]	publ. or prelim.

leads to the conclusion of vacuum stability for a Higgs mass satisfying $M_H \geq 129.4 \pm 5.6$ GeV/c^2 [233]. Given the uncertainty, a Higgs mass of 125 GeV/c^2 satisfies the limit, but the central values of the Higgs and top-quark masses put the electroweak vacuum squarely in the metastable region. The uncertainty is dominated by the precision of the top-quark mass measurement and its interpretation as the pole mass. For more details, see the Higgs boson review in this volume.

As a test of the CPT-symmetry, the mass difference of top- and antitop-quarks $\Delta m_t = m_t - m_{\bar{t}}$, which is expected to be zero, can be measured. CDF measures the mass difference in 8.7 fb^{-1} of 1.96 TeV data in the lepton+jets channel using a template methode to find $\Delta m_t = -1.95 \pm 1.11(stat.) \pm 0.59(syst.)$ GeV/c^2 [234] while DØ uses 3.6 fb^{-1} of lepton+jets events and the matrix element method with at least one b-tag. They find $\Delta m_t = 0.8 \pm 1.8(stat.) \pm 0.5(syst.)$ GeV/c^2 [235]. In 4.7 fb^{-1} of 7 TeV data, ATLAS measures the mass difference in lepton+jets events with a double b-tag requirement and hence very low background to find $\Delta m_t = 0.67 \pm 0.61(stat.) \pm 0.41(syst.)$ GeV/c^2 [236]. CMS measures the top-quark mass difference in 5 fb^{-1} of 7 TeV data in the lepton+jets channel and finds $\Delta m_t = -0.44 \pm 0.46(stat.) \pm 0.27(syst.)$ GeV/c^2 [237]. They repeat this measurement with 19.6 fb^{-1} of 8 TeV data to find $\Delta m_t = -0.15 \pm 0.19(stat.) \pm 0.09(syst.)$ GeV/c^2 [238]. Now that the top mass has been measured in single-top events, the mass difference can be measured by tagging the top- or anti-top quark with the lepton charge. In 35.9 fb^{-1} of 13 TeV single-top candidate events CMS measures the mass ratio and difference to be $0.995^{+0.005}_{-0.006}$ and $0.83^{+0.77}_{-1.01}$ GeV, respectively [203]. All measurements are consistent with the SM expectation.

61.3.2.2 *Top-Quark Spin Correlations, Polarization, and Width*

One of the unique features of the top quark is that it decays before its spin can be flipped by the strong interaction. Thus the top-quark polarization is directly observable via the angular distribution of its decay products and it is possible to define and measure observables sensitive to the top-quark spin and its production mechanism. Although the top- and antitop-quarks produced by strong interactions in hadron collisions are essentially unpolarized, the spins of t and $\bar{t}$ are correlated. For QCD production at threshold, the $t\bar{t}$ system is produced in a $^3S_1$ state with parallel spins for $q\bar{q}$ annihilation or in a $^1S_0$ state with antiparallel spins for gluon-gluon fusion. The situations at the Tevatron, where the production is primarily from $q\bar{q}$ annihilation, and at the LHC, where the production is primarily from gluon-gluon fusion, are therefore somewhat complementary. However, at the LHC production of $t\bar{t}$ pairs at large invariant mass occurs primarily via fusion of gluons with opposite helicities, and the $t\bar{t}$ pairs so produced have parallel spins as in production at the Tevatron via $q\bar{q}$ annihilation. The direction of the top-quark spin is 100% correlated to the angular distributions of the down-type fermion (charged leptons or d-type quarks) in the decay. The joint angular distribution [239–241]

$$\frac{1}{\sigma}\frac{d^2\sigma}{d(\cos\theta_+)d(\cos\theta_-)} = \frac{1}{4}(1 + B_+\cos\theta_+ + B_-\cos\theta_- + \kappa\cdot\cos\theta_+\cdot\cos\theta_-), \tag{61.4}$$

where θ_+ and θ_- are the angles of the daughters in the top-quark rest frame with respect to a particular spin quantization axis (assumed here to be the same for θ_+ and θ_-), is a very sensitive observable. The maximum value for κ, 0.782 at NLO at the Tevatron [242], is found in the off-diagonal basis [239], while at the LHC the value at NLO is 0.326 in the helicity basis [242]. The coefficients B_+ and B_- are near zero in the SM because the top quarks are unpolarized in $t\bar{t}$ production. In place of κ, $A\alpha_+\alpha_-$ is often used, where α_i is the spin analyzing power, and A is the spin correlation coefficient, defined as

$$A = \frac{N(\uparrow\uparrow) + N(\downarrow\downarrow) - N(\uparrow\downarrow) - N(\downarrow\uparrow)}{N(\uparrow\uparrow) + N(\downarrow\downarrow) + N(\uparrow\downarrow) + N(\downarrow\uparrow)}, \tag{61.5}$$

where the first arrow represents the direction of the top-quark spin along a chosen quantization axis, and the second arrow represents the same for the antitop-quark. The spin analyzing power α_i is +0.998 for positively charged leptons, -0.966 for down-type quarks from W decays, and -0.393 for bottom quarks [243]. The sign of α flips for the respective antiparticles. The spin correlation could be modified by a new $t\bar{t}$ production mechanism such as through a Z' boson, Kaluza-Klein gluons, a dark-matter mediator, or a Higgs boson.

The experiments typically use a Monte Carlo to provide templates for the measured distributions, or alternatively a matrix-element technique, and fit a parameter f, representing the fraction of events with the expected Standard Model correlation, with $(1-f)$ the fraction with no correlation. The correlation coefficient is extracted via $A_{\rm meas} = f \cdot A_{\rm SM}$. A 'fraction' $f > 1$ means that the measured correlation coefficient is larger than the Standard Model expectation.

CDF used 5.1 fb^{-1} in the dilepton channel to measure the correlation coefficient in the beam axis [244]. The measurement was made using the expected distributions of $(\cos\theta_+, \cos\theta_-)$ and $(\cos\theta_b, \cos\theta_{\bar{b}})$ of the charged leptons or the b-quarks in the $t\bar{t}$ signal and background templates to calculate a likelihood of observed reconstructed distributions as a function of assumed κ. They determined the 68% confidence interval for the correlation coefficient κ as $-0.52 < \kappa < 0.61$ or $\kappa = 0.04 \pm 0.56$ assuming $m_t = 172.5$ GeV/c^2.

CDF also analyzed lepton+jets events in 5.3 fb^{-1} [245] assuming $m_t = 172.5$ GeV/c^2. They form three separate templates - the same-spin template, the opposite-spin template, and the background template for the 2-dimensional distributions in $\cos(\theta_l)\cos(\theta_d)$ vs. $\cos(\theta_l)\cos(\theta_b)$. The fit to the data in the helicity basis returns an opposite helicity fraction of $F_{OH} = 0.74 \pm 0.24(stat.) \pm 0.11(syst.)$. Converting this to the spin correlation coefficient yields $\kappa_{helicity} = 0.48 \pm 0.48(stat.) \pm 0.22(syst.)$. In the beamline basis, they find an opposite spin fraction of

Downloaded from https://academic.oup.com/ptep/article/2022/8/083C01/6651666 by KIT Library user on 27 September 2022

$F_{OS} = 0.86 \pm 0.32(stat.) \pm 0.13(syst.)$ which can be converted into a correlation coefficient of $\kappa_{beam} = 0.72 \pm 0.64(stat.) \pm 0.26(syst.)$.

DØ performed a measurement of the ratio f of events with correlated t and $\bar{t}$ spins to the total number of $t\bar{t}$ events. Combining dilepton and lepton plus jets events, and using a matrix-element technique in 9.7 fb^{-1} of Tevatron data, DØ measures $f = 1.16 \pm 0.21$, corresponding to $A_{exp.} = 0.89 \pm 0.22(stat. + syst.)$ in the off-diagonal basis [246].

In Ref. [247] DØ presents a measurement of top-quark polarization in $t\bar{t}$ production at the Tevatron. In 9.7 fb^{-1} of $p\bar{p}$ collisions, DØ uses lepton angular distributions in lepton+jets events to measure polarization in the beam, helicity, and transverse bases. The measurements are, respectively, 0.081 ± 0.048, -0.102 ± 0.061 and, 0.040 ± 0.035, where the beam-basis result is a combination with an earlier DØ result in dilepton events [248]. These results are all consistent near-zero polarization, as predicted in the SM.

Spin correlations have been conclusively measured at the LHC by both the ATLAS and CMS collaborations. In the dominant gluon fusion production mode for $t\bar{t}$ pairs at the LHC, the angular distribution between the two leptons in $t\bar{t}$ decays to dileptons is sensitive to the degree of spin correlation [249].

Measurements have been made at 7, 8, and now 13 TeV. While there is some interest in the $\sqrt{s}$ dependence of the correlations as a test of the production mechanism ($q\bar{q}$ vs gluon-gluon and possible sensitivity to new physics) the earlier measurements at 7 and 8 TeV [250–255] had relatively large uncertainties and have now been overtaken by the high-statistics 13 TeV measurements, which we review here.

The most recent result from ATLAS, in 36.1 fb^{-1} at $\sqrt{s} =$ 13 TeV, uses $\Delta\phi$, the azimuthal angle between the two charged leptons in $e\mu$ events in an analysis that also measures the differential cross sections in $\Delta\phi$ and $\Delta\eta$ between the two leptons [256]. The result, measured by comparison with NLO Monte Carlo generators, is $f = 1.249 \pm 0.024 \pm 0.061^{+0.067}_{-0.090}$, where the uncertainties are statistical, systematic, and theoretical, is again greater than 1.0. Whereas the previous results were statistically consistent with the Standard Model expectation of 1.0, this result is inconsistent at the level of 2.2σ. The NLO generators are NLO in QCD only (and only at the production level). Including electroweak couplings produces an expected Standard Model distribution consistent with the data, but results in a large scale uncertainty, giving $f = 1.03 \pm 0.13$.

In 35.9 fb^{-1} of data at $\sqrt{s} = 13$ TeV, CMS has measured spin correlations in dilepton events using $\Delta\phi$ and found $f = 1.05 \pm 0.03 \pm 0.08^{+0.09}_{-0.12}$ [257], where the uncertainties are statistical, systematic, and theoretical. The correlation is also measured using the coefficient κ in Eq. 61.4 (called $-C_{ij}$ in Reference [257]) using three orthogonal spin quantization axes defined in Ref. [258]. All results are consistent with $f = 1$. Measurements of the coefficients B_i in Eq. 61.4 in this analysis, which are expected to be nearly zero in the SM, yield $B_+ = 0.005 \pm 0.023$ and $B_- = 0.007 \pm 0.023$, consistent with the SM predictions at NLO of $0.0040^{+0.0017}_{-0.0012}$ [258]. These results are part of a complete study of the top-quark spin density matrix at $\sqrt{s} = 13$ TeV, through the measurement of the coefficients of Eq. 61.4.

In a similar ATLAS measurement at $\sqrt{s} = 8$ TeV [259], the spin-correlation coefficient κ is measured in the helicity basis to be $\kappa = 0.296 \pm 0.093$ in good agreement with the SM expectation of 0.318 (corresponding to a central value of f of 0.931). The polarization coefficients, B, in Eq. 61.4 are measured, also in the helicity basis, to be $B_+ = -0.044 \pm 0.038$ and $B_- = -0.064 \pm 0.040$, consistent with the SM predictions of 0.0030 ± 0.0010 and 0.0034 ± 0.00104, respectively.

Observation of top-quark spin correlations requires a top-quark lifetime less than the spin decorrelation timescale [260]. The top-quark width, inversely proportional to its lifetime, is expected to be of order 1 GeV/c^2 (Eq. 1). Early measurements made at CDF [261] and CMS [262] established confidence-level intervals for the width, but did not have the sensitivity to make a direct measurement.

The first direct measurement comes from an ATLAS analysis that directly fits reconstructed lepton+jets events in 20.2 fb^{-1} of data at $\sqrt{s} = 8$ TeV. They find $\Gamma_t = 1.76 \pm 0.33^{+0.79}_{-0.68}$ GeV/c^2 [263]. A more recent measurement from ATLAS with 139 fb^{-1} of data at $\sqrt{s} = 13$ TeV [264], uses a template fit to the lepton-b-quark invariant mass in dilepton final states. The result, $\Gamma_t = (1.9 \pm 0.5)$ GeV/c^2, is the most precise measurement to date.

The total width of the top-quark can also be determined from the partial decay width $\Gamma(t \to Wb)$ and the branching fraction $B(t \to Wb)$. DØ obtains $\Gamma(t \to Wb)$ from the measured t-channel cross section for single top-quark production in 5.4 fb^{-1}, and $B(t \to Wb)$ is extracted from a measurement of the ratio $R = B(t \to Wb)/B(t \to Wq)$ in $t\bar{t}$ events in lepton+jets channels with 0, 1 and 2 b-tags. Assuming $B(t \to Wq) = 1$, where q includes any kinematically accessible quark, the result is: $\Gamma_t = 2.00^{+0.47}_{-0.43}$ GeV/c^2 which translates to a top-quark lifetime of $\tau_t = (3.29^{+0.90}_{-0.63}) \times 10^{-25}$ s. Assuming a high mass fourth generation b' quark and unitarity of the four-generation quark-mixing matrix, they set the first upper limit on $|V_{tb'}| < 0.59$ at 95% C.L. [265]. A similar analysis has performed by CMS in 19.7 fb^{-1} of $\sqrt{s} = 8$ TeV data. It provides a better determination of the total width with respect to the measurement by DØ giving $\Gamma_t = 1.36 \pm 0.02(stat.)^{+0.14}_{-0.11}(syst.)$ GeV/c^2 [75].

61.3.2.3 *W-Boson Helicity in Top-Quark Decay*

The Standard Model dictates that the top quark has the same vector-minus-axial-vector ($V - A$) charged-current weak interactions $\left(-i\frac{g}{\sqrt{2}}V_{tb}\gamma^\mu \frac{1}{2}(1-\gamma_5)\right)$ as all the other fermions. In the SM, the fraction of top-quark decays to longitudinally polarized W bosons is proportional to its Yukawa coupling and hence enhanced with respect to the weak coupling. It is expected to be [266] $\mathcal{F}_0^{\rm SM} \approx x/(1+x)$, $x = m_t^2/2M_W^2$ ($\mathcal{F}_0^{\rm SM} \sim 70\%$ for $m_t = 173$ GeV/c^2). Fractions of left-handed, right-handed, or longitudinal W bosons are denoted as $\mathcal{F}_-$, $\mathcal{F}_+$, and $\mathcal{F}_0$ respectively. In the SM, $\mathcal{F}_-$ is expected to be $\approx 30\%$ and $\mathcal{F}_+ \approx 0\%$. Predictions for the W polarization fractions at NNLO in QCD are available [267].

The Tevatron and the LHC experiments use various techniques to measure the helicity of the W boson in top-quark decays, in both the lepton+jets and in dilepton channels in $t\bar{t}$ production.

The first method uses a kinematic fit, similar to that used in the lepton+jets mass analyses, but with the top-quark mass constrained to a fixed value, to improve the reconstruction of final-state observables, and render the under-constrained dilepton channel solvable. Alternatively, in the dilepton channel the final-state momenta can also be obtained through an algebraic solution of the kinematics. The distribution of the helicity angle ($\cos\theta^*$) between the lepton and the b quark in the W rest frame provides the most direct measure of the W helicity. In a simplified version of this approach, the $\cos\theta^*$ distribution is reduced to a forward-backward asymmetry.

The second method (p_T^ℓ) uses the different lepton p_T spectra from longitudinally or transversely polarized W-decays to determine the relative contributions.

A third method uses the invariant mass of the lepton and the b-quark in top-quark decays ($M_{\ell b}^2$) as an observable, which is directly related to $\cos\theta^*$.

At the LHC, top-quark pairs in the dilepton channels are reconstructed by solving a set of six independent kinematic equations in the missing transverse energy in x- and in y-direction, two W-masses, and the two top/antitop-quark masses. In addition, the two jets with the largest p_T in the event are interpreted as b-jets. The pairing of the jets to the charged leptons is based on the minimization of the sum of invariant masses M_{min}. Simulations show that this criterion gives the correct pairing in 68% of the events.

Finally, the Matrix Element Method (MEM) has also been used [194], in which a likelihood is formed from a product of event probabilities calculated from the MEM for a given set of measured kinematic variables and assumed W-helicity fractions.

The results of recent CDF, DØ, ATLAS, and CMS analyses are summarized in Table 61.2. The datasets are now large enough to allow for a simultaneous fit of $\mathcal{F}_0$, $\mathcal{F}_-$ and $\mathcal{F}_+$, which we denote by '3-param' or $\mathcal{F}_0$ and $\mathcal{F}_+$, which we denote by '2-param' in the table. Results with either $\mathcal{F}_0$ or $\mathcal{F}_+$ fixed at its SM value are denoted '1-param'. For the simultaneous fits, the correlation

Downloaded from https://academic.oup.com/ptep/article/2022/8/083C01/6651666 by KIT Library user on 27 September 2022

coefficient between the two values is about -0.8. A complete set of published results can be found in the Listings. All results are in agreement with the SM expectation.

CDF and DØ combined their results based on $2.7 - 5.4$ fb^{-1} [268] for a top-quark mass of 172.5 GeV/c^2. ATLAS presents results from 1.04 fb^{-1} of $\sqrt{s} = 7$ TeV data using a template method for the $\cos\theta^*$ distribution and angular asymmetries from the unfolded $\cos\theta^*$ distribution in the lepton+jets and the dilepton channel [269]. CMS performs a similar measurement based on template fits to the $\cos\theta^*$ distribution with 5.0 fb^{-1} of 7 TeV data in the lepton+jets final state [270]. As the polarization of the W bosons in top-quark decays is sensitive to the Wtb vertex Lorentz structure and anomalous couplings, both experiments also derive limits on anomalous contributions to the Wtb couplings. CMS and ATLAS collaborations have also combined their results from 7 TeV data to obtain values on the helicity fractions as well as limits on anomalous couplings [271].

At 8 TeV, ATLAS came out with a measurement of the W-helicity fractions in 20.2 fb^{-1} in lepton+jets events with at least one b-tag [272]. Using 19.8 fb^{-1} of 8 TeV data, CMS measured the W-helicity in lepton + 4 jet events with two b-tags [273]. In $t\bar{t}$ events with two opposite-sign leptons (electron or muon) in the final state in this dataset, CMS applied six kinematic constraints on the kinematics of the produced particles [274]. Also, using the same dataset a first measurement of the W-boson helicity in top-quark decays was made in electroweak single top production [275], yielding similarly precise and consistent results. The 8 TeV results obtained in $t\bar{t}$ and single-top events by ATLAS and CMS have also been combined recently [276]. These results are in agreement with the standard model predictions at next-to-next-to-leading order in perturbative QCD and represent an improvement in precision of 25 (29)% for F_0 (F_L) with respect to the most precise single measurement. A limit on anomalous right-handed vector (V_R), and left- and right-handed tensor (g_L, g_R) tWb couplings and on corresponding Wilson coefficients is set.

61.3.2.4 *Top-Quark Electroweak Charges and Couplings*

The top quark is the only quark whose electric charge has not been measured through production at threshold in e^+e^- collisions. Furthermore, it is the only quark whose electromagnetic coupling has not been observed and studied until recently. Since the CDF and DØ analyses on top-quark production did not associate the b, $\bar{b}$, and $W^\pm$ uniquely to the top or antitop, decays such as $t \to W^+\bar{b}, \bar{t} \to W^-b$ were not excluded. A charge 4/3 quark of this kind is consistent with current electroweak precision data. The $Z \to \ell^+\ell^-$ and $Z \to b\bar{b}$ data, in particular the discrepancy between A_{LR} from SLC at SLAC and $A_{FB}^{0,b}$ of b-quarks and $A_{FB}^{0,\ell}$ of leptons from LEP at CERN, can be fitted with a top quark of mass $m_t = 270$ GeV/c^2, provided that the right-handed b quark mixes with the isospin $+1/2$ component of an exotic doublet of charge $-1/3$ and $-4/3$ quarks, $(Q_1, Q_4)_R$ [278, 279]. Also the third component of the top quark's weak isospin has not been measured so far.

DØ studied the top-quark charge in double-tagged lepton+jets events, CDF did it in single tagged lepton+jets and dilepton events. Assuming the top- and antitop-quarks have equal but opposite electric charge, then reconstructing the charge of the b-quark through jet charge discrimination techniques, the $|Q_{top}| = 4/3$ and $|Q_{top}| = 2/3$ scenarios can be differentiated. For the exotic model of Chang *et al.* [279] with a top-quark charge $|Q_{top}| = 4/3$, CDF excluded the model at 99% C.L. [280] in 5.6 fb^{-1}, while DØ excluded the model at a significance greater than 5 standard deviations using 5.3 fb^{-1} and set an upper limit of 0.46 on the fraction of such quarks in the selected sample [281]. These results indicate that the observed particle is indeed consistent with being a SM $|Q| = 2/3$ quark.

In 2.05 fb^{-1} at $\sqrt{s} = 7$ TeV, ATLAS performed a similar analysis, reconstructing the b-quark charge either via a jet-charge technique or via the lepton charge in soft muon decays in combination with a kinematic likelihood fit. They measure the top-quark charge to be $0.64 \pm 0.02(stat.) \pm 0.08(syst.)$ from the charges of the top-quark decay products in single lepton $t\bar{t}$ events, and hence exclude the exotic scenario with charge $-4/3$ at more than 8σ [282].

In 4.6 fb^{-1} at $\sqrt{s} = 7$ TeV, CMS discriminates between the SM and the exotic top-quark charge scenario in the muon+jets final states in $t\bar{t}$ events. They exploit the charge correlation between high-p_t muons from W-boson decays and soft muons from B-hadron decays in b-jets. Using an asymmetry technique, where $A = -1$ represents the exotic $Q = -4/3$ scenario and $A = +1$ the SM $Q = +2/3$ scenario, they find $A_{meas} = 0.97 \pm 0.12(stat.) \pm 0.31(sys.)$, which agrees with the Standard Model expectation and excludes the exotic scenario at 99.9% C.L. [283].

The electromagnetic or the weak coupling of the top quark can be probed directly by investigating $t\bar{t}$ events with an additional gauge boson, such as $t\bar{t}\gamma$, $t\bar{t}W$, and $t\bar{t}Z$ events. The corresponding coupling can be extracted from the corresponding cross section or extracted from effective field theory (EFT) fits to various measured distributions and differential cross sections.

CDF performed a search for events containing a lepton, a photon, significant missing transverse momentum, and a jet identified as containing a b-quark and at least three jets and large total transverse energy in 6.0 fb^{-1}. They reported evidence for the observation of $t\bar{t}\gamma$ production with a cross section $\sigma_{t\bar{t}\gamma} = 0.18 \pm 0.08$ pb and a ratio of $\sigma_{t\bar{t}\gamma}/\sigma_{t\bar{t}} = 0.024 \pm 0.009$ [284].

ATLAS performed a first measurement of the $t\bar{t}\gamma$ cross section in pp collisions at $\sqrt{s} = 7$ TeV using 4.6 fb^{-1} of data. Events are selected that contain a large transverse momentum electron or muon and a large transverse momentum photon. The production of $t\bar{t}\gamma$ events was observed with a significance of 5.3 standard deviations. The resulting cross section times branching ratio into the single lepton channel for $t\bar{t}\gamma$ production with a photon with transverse momentum above 20 GeV is $\sigma^{fid.}(t\bar{t}\gamma) \times BR = 63 \pm 8(stat.)^{+17}_{-13}(syst.) \pm 1(lumi.)$ pb per lepton flavour [285], which is consistent with leading-order theoretical calculations.

At 8 TeV, ATLAS has used 20.2 fb^{-1} of data to measure the $t\bar{t}\gamma$ cross section with a photon above 15 GeV and $|\eta| < 2.37$. The fiducial cross section is measured to be 139 ± 18 fb [286], in good agreement with the NLO prediction [287]. Using 19.7 fb^{-1} of data at 8 TeV, CMS performed a similar measurement of the $t\bar{t}\gamma$ production cross section in the lepton+jets decay mode with a photon transverse momentum above 25 GeV and $|\eta| < 1.44$. They obtain a normalized cross section $\mathcal{R} = \sigma_{t\bar{t}+\gamma}/\sigma_{t\bar{t}} = (5.7 \pm 1.8) \times 10^{-4}$ in e+jets and $(4.7 \pm 1.3) \times 10^{-4}$ in μ+jets. The fiducial $t\bar{t}\gamma$ cross section is obtained by multiplying by the measured $t\bar{t}$ fiducial cross section of $244.9 \pm 1.4(stat.)^{+6.3}_{-5.5}(sys.) \pm 6.4(lumi.)$ pb. Extrapolating to the full phase space, the result is $\sigma_{t\bar{t}\gamma} \times$BR$=(515 \pm 108)$ fb, per lepton+jets final state [288], in good agreement with the theoretical prediction.

At $\sqrt{s} = 13$ TeV, using 36.1 fb^{-1} of single-lepton and dilepton events with exactly one photon, ATLAS measures the $t\bar{t}\gamma$ cross section. They employ neural network algorithms to separate the signal from the backgrounds. The fiducial cross-sections are measured to be $521 \pm 9(stat.) \pm 41(sys.)$ fb and $69 \pm 3(stat.) \pm 4(sys.)$ fb for the single-lepton and dilepton channels, respectively. The differential cross-sections are measured as a function of photon transverse momentum, photon absolute pseudorapidity, and angular distance between the photon and its closest lepton in both channels, as well as azimuthal opening angle and absolute pseudorapidity difference between the two leptons in the dilepton channel. All measurements are in agreement with the theoretical predictions [289]. Very recently, ATLAS uses 139 fb^{-1} of $\sqrt{s} = 13$ TeV $e\mu + \gamma$ events with at least two jets, out of which at least one is b-tagged, to measure the inclusive and differential cross-sections for the production of a top-quark pair in association with a photon. This analysis is sensitive to both processes, $t\bar{t}\gamma + tW\gamma$. The fiducial cross-section is measured to be $39.6^{+2.7}_{-2.3}$ fb in good agreement with the dedicated theoretical calculation provided by the authors of refs. [290, 291], which predicts a value of $\sigma_{fid} = 38.50^{+0.56}_{-2.18}$ (scale)$^{+1.04}_{-1.18}$ (PDF) fb for the chosen fiducial phase space. Differential cross-sections as functions of several observables are compared to state-of-the-art Monte Carlo simulations and next-to-leading order theoretical calculations. These include cross-sections as functions of the photon transverse momentum and absolute pseudorapidity and angular variables related to the photon and the leptons and between the two leptons in the event. All measurements are in agreement with the predic-

Downloaded from https://academic.oup.com/ptep/article/2022/8/083C01/6651666 by KIT Library user on 27 September 2022

Table 61.2: Measurement and 95% C.L. upper limits of the W helicity in top-quark decays. The table includes both preliminary, as of September 2021, and published results. A full set of published results is given in the Listings.

W Helicity	Source	$\int \mathcal{L}dt$ (fb^{-1})	Ref.	Method
$\mathcal{F}_0 = 0.722 \pm 0.081$	CDF+DØ Run II	2.7-5.4	[268]	$\cos\theta^*$ 2-param
$\mathcal{F}_0 = 0.682 \pm 0.057$	CDF+DØ Run II	2.7-5.4	[268]	$\cos\theta^*$ 1-param
$\mathcal{F}_0 = 0.726 \pm 0.094$	CDF Run II	8.7	[277]	ME 2-param
$\mathcal{F}_0 = 0.67 \pm 0.07$	ATLAS (7 TeV)	1.0	[269]	$\cos\theta^*$ 3-param
$\mathcal{F}_0 = 0.682 \pm 0.045$	CMS (7 TeV)	5.0	[270]	$\cos\theta^*$ 3-param
$\mathcal{F}_0 = 0.626 \pm 0.059$	ATLAS+CMS (7 TeV)	2.2	[271]	$\cos\theta^*$ 3-param
$\mathcal{F}_0 = 0.709 \pm 0.019$	ATLAS (8 TeV)	20.2	[272]	$\cos\theta^*$ 3-param
$\mathcal{F}_0 = 0.681 \pm 0.026$	CMS (8 TeV)	19.8	[273]	$\cos\theta^*$ 3-param
$\mathcal{F}_0 = 0.653 \pm 0.029$	CMS (8 TeV)	19.7	[274]	$\cos\theta^*$ 3-param
$\mathcal{F}_0 = 0.720 \pm 0.054$	CMS (8 TeV)	19.7	[275]	$\cos\theta^*$ 3-param
$\mathcal{F}_0 = 0.693 \pm 0.014$	ATLAS+CMS (8 TeV)	20	[276]	$\cos\theta^*$ 3-param
$\mathcal{F}_+ = -0.033 \pm 0.046$	CDF+DØ Run II	2.7-5.4	[268]	$\cos\theta^*$ 2-param
$\mathcal{F}_+ = -0.015 \pm 0.035$	CDF+DØ Run II	2.7-5.4	[268]	$\cos\theta^*$ 1-param
$\mathcal{F}_+ = -0.045 \pm 0.073$	CDF Run II	8.7	[277]	ME 2-param
$\mathcal{F}_+ = 0.01 \pm 0.05$	ATLAS (7 TeV)	1.0	[269]	$\cos\theta^*$ 3-param
$\mathcal{F}_+ = 0.008 \pm 0.018$	CMS (7 TeV)	5.0	[270]	$\cos\theta^*$ 3-param
$\mathcal{F}_+ = 0.015 \pm 0.034$	ATLAS+CMS (7 TeV)	2.2	[271]	$\cos\theta^*$ 3-param
$\mathcal{F}_+ = -0.008 \pm 0.014$	ATLAS (8 TeV)	20.2	[272]	$\cos\theta^*$ 3-param
$\mathcal{F}_+ = -0.004 \pm 0.015$	CMS (8 TeV)	19.8	[273]	$\cos\theta^*$ 3-param
$\mathcal{F}_+ = 0.018 \pm 0.027$	CMS (8 TeV)	19.7	[274]	$\cos\theta^*$ 3-param
$\mathcal{F}_+ = -0.018 \pm 0.022$	CMS (8 TeV)	19.7	[275]	$\cos\theta^*$ 3-param
$\mathcal{F}_+ = -0.008 \pm 0.007$	ATLAS+CMS (8 TeV)	20	[276]	$\cos\theta^*$ 3-param

tions [292]. In 35.9 fb^{-1} of lepton-plus-photon-plus-jets events, CMS manages to establish the first evidence for the associated production of a single-top quark and a photon at $\sqrt{s} = 13$ TeV. They employ a multivariate discriminant based on topological and kinematic event properties to separate signal from background processes. An excess above the background-only hypothesis is observed, with a significance of 4.4 standard deviations. A fiducial cross section is measured for isolated photons with transverse momentum greater than 25 GeV in the central region of the detector. The measured product of the cross section and branching fraction is $\sigma(pp \to t\gamma j)B(t \to \mu\gamma b) = 115 \pm 17(stat) \pm 30(syst)$ fb, which is consistent with the SM prediction [293]. Very recently, CMS used 137 fb^{-1} of data to measure the $t\bar{t}\gamma$ cross section. In the lepton-plus-jets channel, they perform measurements in a fiducial volume defined at the particle level. Events with an isolated, highly energetic lepton, at least three jets from the hadronization of quarks, among which at least one is b-tagged, and one isolated photon are selected. The inclusive fiducial $t\bar{t}\gamma$ cross section, for a photon with transverse momentum greater than 20 GeV and pseudorapidity $|\eta| < 1.4442$, is measured to be $\sigma_{t\bar{t}\gamma} = 800 \pm 7(stat) \pm 46(syst)$ fb, in good agreement with the prediction from the standard model at NLO in QCD [294]. The differential cross sections are also measured as a function of several kinematic observables and interpreted in the framework of the standard model effective field theory (EFT), leading to the most stringent direct limits to date on anomalous electromagnetic dipole moment interactions of the top quark and the photon. Using the same dataset, in the dilepton channel, an inclusive cross section of $174.4 \pm 2.5(stat) \pm 6.1(syst)$ fb is measured in a signal region with at least one b-tagged jet and exactly one photon with transverse momentum above 20 GeV [295]. In the same analysis, differential cross sections are measured as a function of several kinematic observables of the photon, leptons, and jet, and compared to standard model predictions. The measurements are also interpreted in the standard model effective field theory framework, and limits on the relevant Wilson coefficients are combined with a previous CMS measurement of the same production process using single-lepton events. Using 35.9 fb^{-1} of data with a single muon and a photon, CMS reports first evidence of events consistent with the production of a single top quark in association with a photon. A multivariate discriminant based on topological and kinematic event properties is employed to separate signal from background processes. An excess above the background-only hypothesis is observed, with a significance of 4.4 standard deviations [296]. A precision test of the vector and axial vector couplings in $t\bar{t}\gamma$ events or searches for possible tensor couplings of top-quarks to photons will only be feasible with an integrated luminosity of several hundred fb^{-1} in the future [297].

ATLAS and CMS have also studied the associate production of top-antitop quark pairs along with an electroweak gauge boson, where in the Standard Model the W-boson is expected to be produced via initial state radiation, while the Z-boson can also be radiated from a final-state top-quark and hence provides sensitivity to the top-quark neutral current weak gauge coupling, which implies a sensitivity to the third component of the top-quark's weak isospin, which has not been measured so far.

CMS performed measurements of the $t\bar{t}W$ and $t\bar{t}Z$ cross section at $\sqrt{s} = 7$ TeV with 5 fb^{-1}, yielding $\sigma_{t\bar{t}V} = 0.43^{+0.17}_{-0.15}(stat.)^{+0.09}_{-0.07}(syst.)$ pb ($V = Z, W$) and $\sigma_{t\bar{t}Z} = 0.28^{+0.14}_{-0.11}(stat.)^{+0.06}_{-0.03}(syst.)$ fb, at about 3 standard deviations significance [298] and compatible with the SM expectations of $0.306^{+0.031}_{-0.053}$ pb and $0.137^{+0.012}_{-0.016}$ pb, respectively [299, 300]. ATLAS performed a similar analysis with 4.7 fb^{-1} in the three-lepton channel and set an upper limit of 0.71 pb at 95% C.L. [301].

Using 20.3 fb^{-1} of 8 TeV data, ATLAS performs a simultaneous measurement of the $t\bar{t}W$ and $t\bar{t}Z$ cross section. They observe the $t\bar{t}W$ and $t\bar{t}Z$ production at the 5.0σ and 4.2σ level, respectively, yielding $\sigma_{t\bar{t}W} = 369^{+100}_{-91}$ fb and $\sigma_{t\bar{t}Z} = 176^{+58}_{-52}$ fb [302]. CMS performs an analysis where signal events are identified by matching reconstructed objects in the detector to specific final state particles from $t\bar{t}W$ and $t\bar{t}Z$ decays using 19.5 fb^{-1} of 8 TeV data. They obtain $\sigma_{t\bar{t}W} = 382^{+117}_{-102}$ fb and $\sigma_{t\bar{t}Z} = 242^{+65}_{-55}$ fb, yielding a significance of 4.8 and 6.4 standard deviation, respectively [303]. These measurements are used to set bounds on five anomalous dimension-six operators that would affect the $t\bar{t}W$ and $t\bar{t}Z$ cross sections.

The most recent measurements in these channels are made at 13 TeV from ATLAS and CMS in multilepton final states. ATLAS made a measurement using 36.1 fb^{-1} of events with two, three or four leptons. In multiple regions, the $t\bar{t}Z$ and $t\bar{t}W$ cross sections are simultaneously measured using a combined fit to all regions, yielding $\sigma_{t\bar{t}Z} = 0.95 \pm 0.08(stat) \pm 0.10(syst)$ pb and $\sigma_{t\bar{t}W} = 0.87 \pm 0.13(stat) \pm 0.14(syst)$ pb [304] to be compared with the NLO+NLL (QCD) and NLO (EW) SM predictions, $\sigma_{t\bar{t}W} = 579^{+14\%}_{-9\%}$ fb and $\sigma_{t\bar{t}Z} = 811^{+11\%}_{-10\%}$ fb [305]. Very recently, ATLAS uses 139 fb^{-1} in three and four lepton events to measure the inclusive and differential $t\bar{t}Z$ cross section. The inclusive cross

Downloaded from https://academic.oup.com/ptep/article/2022/8/083C01/6651666 by KIT Library user on 27 September 2022

section is measured to be $\sigma_{t\bar{t}Z} = 0.99 \pm 0.05(stat.) \pm 0.08(syst.)$ pb [306], in agreement with the most precise theoretical predictions. The differential measurements are presented as a function of a number of kinematic variables which probe the kinematics of the $t\bar{t}Z$ system. Overall, good agreement is observed between the unfolded data and the predictions. CMS uses 35.9 fb^{-1} of data to measure $\sigma_{t\bar{t}W} = 0.77^{+0.12}_{-0.11}(stat.)^{+0.13}_{-0.12}(syst.)$ pb and $\sigma_{t\bar{t}Z} = 0.99^{+0.09}_{-0.08}(stat.)^{+0.12}_{-0.10}(syst.)$ pb production cross sections, and significances over the background-only hypotheses of 5.5σ and 9.5σ, respectively [307], firmly establishing the observation of these processes. Very recently, CMS measured the inclusive $t\bar{t}Z$ cross section in 77.5 fb^{-1} of events with three or four charged leptons, and the Z boson is detected through its decay to an oppositely charged lepton pair. The production cross section is measured to be $\sigma(t\bar{t}Z) = 0.95 \pm 0.05(stat) \pm 0.06(syst)$ pb. This measurement includes differential cross sections as functions of the transverse momentum of the Z boson and the angular distribution of the negatively charged lepton from the Z boson decay as well as stringent direct limits on the anomalous tZ couplings [308].

The electroweak couplings can also be probed in single-top production in association with a Z boson. The $pp \to tZq$ process at the LHC probes both the WWZ coupling in the case where the Z emerges from the t-channel W in single-top production and, in the case where the Z is radiated from the top quark, the tZ coupling. A CMS search at 8 TeV using 19.7 fb^{-1} produced a hint of a tZq signal in tri-lepton events, with a significance compared to the background-only hypothesis of 2.4σ [309]. Very recently, CMS and ATLAS collaborations used 139 fb^{-1} in three-lepton events to measure $tZ(\to \ell^+\ell^-)q$. CMS obtains $\sigma_{tZq} = 87.9^{+7.5}_{-7.3}(stat)^{+7.3}_{-6.0}(syst)$ fb for $m(\ell\ell) > 30$ GeV [310]. The ratio between the cross sections for the top quark and the top antiquark production in association with a Z boson is measured as $2.37^{+0.56}_{-0.42}(stat)^{+0.27}_{-0.13}(syst)$. Differential measurements at parton and particle levels are performed for the first time. Additionally, the spin asymmetry, which is sensitive to the top quark polarization, is determined from the differential distribution of the polarization angle at parton level to be $0.58^{+0.15}_{-0.16}$ (stat) $\pm$ 0.06 (syst), in agreement with SM predictions at next-to-leading order. Using neural networks, ATLAS improves the background rejection and extracts the signal. The measured cross-section for $m(\ell\ell) > 30$ GeV is $97 \pm 13(stat.) \pm 7(syst.)$ fb, consistent with the Standard Model prediction [311].

Searches for and now also measurements of the associate production of a top-antitop quark pair along with a Higgs boson, $t\bar{t}h$, with various subsequent decays provide sensitivity to the top-Higgs Yukawa coupling. For further details, see the review on "Higgs".

61.3.3 *Searches for Physics Beyond the Standard Model*

The top quark plays a special role in the SM. Being the only quark with a coupling to the Higgs boson of order one, it provides the most important contributions to the quadratic radiative corrections to the Higgs mass exposing the issue of the naturalness of the SM. It is therefore very common for models where the naturalness problem is addressed to have new physics associated with the top quark. In SUSY, for instance, naturalness predicts the scalar top partners to be the lightest among the squarks and to be accessible at the LHC energies (see the review "Supersymmetry: Theory"). In models where the Higgs is a pseudo-Goldstone boson, such as Little Higgs models, naturalness predicts the existence of partners of the top quarks with the same spin and color, but with different electroweak couplings, the so-called vectorial t'. Stops and t''s are expected to have sizeable branching ratios to top quarks. Another intriguing prediction of SUSY models with universal couplings at the unification scale is that for a top-quark mass close to the measured value, the running of the Yukawa coupling down to 1 TeV naturally leads to the radiative breaking of the electroweak symmetry [312]. In fact, the top quark plays a role in the dynamics of electroweak symmetry breaking in many models [313]. One example is topcolor [314], where a large top-quark mass can be generated through the formation of a dynamic $t\bar{t}$ condensate, X, which is formed by a new strong gauge force coupling preferentially to the third generation. Another example is topcolor-assisted technicolor [315], predicting the existence of a heavy Z' boson that couples preferentially to the third generation of quarks. If light enough such a state might be directly accessible at the present hadron collider energies, or if too heavy, lead to four-top interactions possibly visible in the $t\bar{t}t\bar{t}$ final state. This final state has been recently observed by CMS [316] and by ATLAS [119].

Current strategies to search for new physics in top quark events at hadron colliders are either tailored to the discovery of specific models or model independent. They can be broadly divided in two classes. In the first class new resonant states are looked for through decay processes involving the top quarks. Current searches for bosonic resonances in $t\bar{t}$ final states, or for direct stop and t' production, or for a charged Higgs in $H^+ \to t\bar{b}$ fall in the category. On the other hand, if new states are too heavy to be directly produced, they might still give rise to deviations from the SM predictions for the strength and Lorentz form of the top-quark couplings to other SM particles. Accurate SM predictions and measurements are therefore needed and the results be interpreted in the framework of an effective field theory [317–319] as done for example in recent analyses sensitive to the strength and structure of the top quark couplings by the ATLAS [94, 184, 276, 304, 320–323] and CMS [111, 121, 324–330] collaborations. Global effective field theory interpretations based on publicly available measurements in the top quark sector have also appeared [331–337].

61.3.3.1 *New Physics in Top Quark Production*

Theoretical [338, 339] and experimental efforts have been devoted to the searches of $t\bar{t}$ resonances, both at the Tevatron and at the LHC. Most the analyses have been performed in the hypothesis that resonances are narrow, yet generalizations have been considered for specific scenarios. At the Tevatron, both the CDF and DØ collaborations have searchedfor resonant production of $t\bar{t}$ pairs in the lepton+jets channel [340, 341]. In both analyses, the data indicate no evidence of resonant production of $t\bar{t}$ pairs. They place upper limits on the production cross section times branching fraction to $t\bar{t}$ in comparison to the prediction for a narrow ($\Gamma_{Z'} = 0.012 M_{Z'}$) leptophobic topcolor Z' boson. Within this model, they exclude Z' bosons with masses below 915 (CDF-full data set) and 835 (DØ, 5 fb^{-1}) GeV/c^2 at the 95% C.L. These limits turn out to be independent of couplings of the $t\bar{t}$ resonance (pure vector, pure axial-vector, or SM-like Z'). A similar analysis has been performed by CDF in the all-hadronic channel using 2.8 fb^{-1} of data [342]. At the LHC, both the CMS and ATLAS collaborations have searched for resonant production of $t\bar{t}$ pairs, employing different techniques and final-state signatures (all-hadronic, lepton+jets, dilepton) at $\sqrt{s} = 7$, 8 and 13 TeV. In the low mass range, from the $t\bar{t}$ threshold to about one TeV/c^2, standard techniques based on the reconstruction of each of the decay objects (lepton, jets and b-jets, missing E_T) are used to identify the top quarks, while at higher invariant mass, the top quarks are boosted and the decay products more collimated and can appear as large-radius jets with substructure. Dedicated reconstruction techniques have been developed in recent years for boosted top quarks [343] that are currently employed at the LHC. Most of the analyses are model-independent (i.e., no assumption on the quantum numbers of the resonance is made) yet they assume a small width and no signal-background interference. Using lepton+jets and fully hadronic channels in a data set corresponding to an integrated luminosity of 35.9 fb^{-1} at 13 TeV, the CMS collaboration finds no significant deviations from the SM background [344]. In particular, the existence of a leptophobic topcolor particle Z' is excluded at the 95% confidence level for resonances in the mass range $0.6 < M_{Z'} < 3.8$ TeV/c^2, $0.5 < M_{Z'} < 5.25$ TeV/c^2, and $0.5 < M_{Z'} < 6.65$ TeV/c^2 for $\Gamma_{Z'} = 1\%, 10\%, 30\% M_{Z'}$, respectively [345]. Kaluza-Klein excitations of a gluon with $M_{G_{KK}} < 4.55$ TeV/c^2 (at 95% confidence level) in the Randall-Sundrum model are also excluded. A dedicated analysis [346] searching for a scalar resonance, set bounds between 400 and 750 GeV in various scenarios. The ATLAS collaboration has performed a search for resonant $t\bar{t}$ production in the lepton+jets channel using 36.1 fb^{-1} of proton-proton (pp) collision data collected at a center-of-mass energy

Downloaded from https://academic.oup.com/ptep/article/2022/8/083C01/6651666 by KIT Library user on 27 September 2022

$\sqrt{s}$ = 13 TeV [347]. A search for local excesses in the number of data events compared to the Standard Model expectation in the $t\bar{t}$ invariant mass spectrum is performed. No evidence for a $t\bar{t}$ resonance is found and 95% confidence-level limits on the production rate are determined for massive states predicted in several benchmark models. For instance, a narrow leptophobic topcolor Z' boson with a mass below 3.0 TeV/c^2 is excluded. A Kaluza-Klein excitation of the graviton is excluded for masses in the range 0.45 TeV/c^2 $< m_G <$ 0.65 TeV/c^2. A Kaluza-Klein excitation of the gluon in a Randall-Sundrum model is excluded for masses below 3.8 TeV/c^2. ATLAS has also conducted a search for resonances in the all-jet final state at 13 TeV corresponding to an integrated luminosity of 139 fb^{-1} [348]. The $t\bar{t}$ events are reconstructed by selecting two top quarks in their fully hadronic decay modes. A Z' in the topcolor-assisted-technicolor model is excluded at 95% confidence level for masses below 3.9 and 4.7 TeV for the decay widths of 1% and 3%, respectively.

Heavy charged bosons, such as W' or H^+, can also be searched for in $t\bar{b}, tj$ final states (for more information see the review "W'-boson searches" and "Higgs Bosons: theory and searches"), while heavy fermion resonances, such as vectorial or excited quarks, in final states such as tZ, tH, tW, bW. CMS has performed several searches in this context, the most stringent limits coming from those at $\sqrt{s} = 13$ TeV [349–356]. For instance, a $W' \to t\bar{b}$ has been searched for in all-hadronic final state in 137 fb^{-1}. No evidence has been found for left- and right-handed W' boson and masses below 3.4 TeV/c^2 are excluded at 95% confidence level [356]. Single production of a vector-like quark decaying to a W boson and a top quark, in fully hadronic final state also been searched in the same data set. No significant deviation from the SM background expectation is observed. The hypotheses of b* quarks with left-handed, right-handed, and vector-like chiralities are excluded at 95% confidence level for masses below 2.6, 2.8, and 3.1 TeV/c^2, respectively. These represent the most stringent exclusion limits for the single production of vector-like quarks in this channel. [357] In the same data set, searches for pair production of vector-like T or B quarks in fully hadronic final states have been performed. Lower limits are set on the mass at 95% confidence level equal to 1570 TeV/c^2 in the case where decays exclusively to a b quark and a Higgs boson, 1390 TeV/c^2 for when it decays exclusively to a b quark and a Z boson, and 1450 TeV/c^2 for when it decays equally in these two modes. [358]. ATLAS has performed searches for heavy bosons and fermions decaying to one top quark at $\sqrt{s}$ = 7, 8 and 13 TeV. A $W' \to t\bar{b}$ has been searched for at 13 TeV in lepton+jets in 36.1 fb^{-1}. No evidence has been found for a right-handed W' boson with a mass below 3.25 TeV/c^2 are excluded at 95% [359]. A $H^+ \to t\bar{b}$ has been searched for at 13 TeV in lepton+jets in 139 fb^{-1}. No significant excess above the background-only hypothesis is observed and exclusion limits are derived for the production cross-section times branching ratio as a function of its mass, ranging from 3.6 pb at 200 GeV/c^2 to 0.036 pb at 2000 GeV/c^2 at 95% confidence level. [360]. ATLAS has conducted a search for the single and pair production of a new charge +2/3 quark (T) decaying via $T \to Zt$ (and also -1/3 quark (B) decaying via $B \to Zb$) in a dataset corresponding to 139 fb^{-1} luminosity at $\sqrt{s} = 13$ TeV [361]. No significant excess of events above the SM expectation is observed, and upper limits are derived for vector-like quarks of various masses in a two-dimensional plane of branching ratios. Under branching ratio assumptions corresponding to a weak-isospin singlet scenario, a T quark with mass lower than 1.27 TeV/c^2 (1.2 TeV/c^2 for a B quark) is excluded at the 95% confidence level. Under branching ratio assumptions corresponding to a particular weak-isospin doublet scenario, a T quark with mass lower than 1.46; TeV/c^2 (1.32 TeV/c^2 for a B quark) is excluded at the 95% confidence level. In the same dataset, ATLAS combines the searches for pair-produced vector-like partners of the top and bottom quarks in various decay channels ($T \to Zt/Wb/Ht, B \to Zb/Wt/Hb$). The observed data are found to be in good agreement with the SM background prediction in all individual searches. Therefore, combined 95% confidence-level upper limits are set on the production cross-section for a range of vector-like quark scenarios, significantly improving upon the reach of the individual searches. Model-independent limits are set assuming the vector-like quarks decay to SM particles. A singlet T is excluded for masses below 1.31 TeV/c^2 and a singlet B is excluded for masses below 1.22 TeV/c^2. Assuming a weak isospin (T, B) doublet and $|V_{Tb}| << |V_{tB}|$, T and B masses below 1.37 TeV/c^2 are excluded [362].

Vector-like partners of the top and bottom quarks have been searched also in single (electroweak) production, in several decay modes: $T \to tH$ [363], $T \to Wb$ [364], $T \to t(Z \to \nu\nu)$ [365] and $B \to bH$ with $H \to b\bar{b}$ [366] and $H \to \gamma\gamma$ [367].

In many models top-quark partners preferably decay to top quarks and weakly interacting neutral stable particles, i.e., possibly dark matter candidates, that are not detected. In addition, top quarks could be coupled to states that would mostly decay to dark matter or be invisible. In both cases, an observable especially sensitive to new physics effects in $t\bar{t}$ production is therefore the missing transverse momentum. CMS has presented a differential cross section measurement of top-quark pair and single production with missing transverse energy and corresponding interpretations in the context of dark matter (effective and simplified) models at 8 and 13 TeV [368–371]. The results obtained so far are consistent with the SM expectations. In particular the search performed at 13 TeV [371] is based on 35.9 fb^{-1} of integrated luminosity. Upper limits are derived on the production cross section and interpreted in terms of a simplified model with a scalar/pseudoscalar mediator. Scalar and pseudoscalar mediator particles with masses below 290 and 300 GeV/c^2, respectively, are excluded at 95% confidence level, assuming a dark matter particle mass of 1 GeV/c^2 and mediator couplings to fermions and dark matter particles equal to unity. A generic search for new phenomena with top quark pairs in final states with one isolated electron or muon, multiple jets, and large missing transverse momentum has been performed by ATLAS in a dataset corresponding to 139 fb^{-1} luminosity at $\sqrt{s} = 13$ TeV. No significant excess above the SM background is observed, and limits at 95% confidence level are set in various models. The results exclude top squark masses up to about 1 TeV/c^2, and masses of the lightest neutralino up to about 500 GeV/c^2. Limits on dark-matter production are set for scalar (pseudoscalar) mediator masses up to about 250 (300) GeV/c^2. [372].

ATLAS has also conducted searches for missing transverse momenta in association with single top quarks [373, 374].

Flavor-changing-neutral-currents (FCNC) are hugely suppressed in the SM as non zero contributions only arise at one-loop and are proportional to the splitting between the quark masses. In the case of the top quark $B(t \to Bq)$ with $B = g, \gamma, Z, H$ and $q = u, c$ are predicted to be order of 10^{-12} $(t \to cg)$ or much smaller [375]. Several observables are accessible at colliders to test and constrain such couplings. CMS has performed several studies on the search for FCNC in top-quark production. They have considered single-top quark production in the t-channel in 5 fb^{-1} integrated luminosity at 7 TeV and 19.7 fb^{-1} integrated luminosity at 8 TeV [376]. Events with the top quark decaying into a muon, neutrino and two or three jets are selected. The upper limits on effective coupling strength can be translated to the 95% upper limits on the corresponding branching ratios $B(t \to gu) \leq 2.0 \cdot 10^{-5}$, $B(t \to gc) \leq 4.1 \cdot 10^{-4}$. They have performed a search for a single top quark produced in association with a photon in 19.1 fb^{-1} integrated luminosity at 8 TeV [377]. The event selection requires the presence of one isolated muon and jets in the final state. The upper limits on effective coupling strength can be translated to the 95% upper limits on the corresponding branching ratios $B(t \to \gamma u) \leq 0.0161\%$, $B(t \to \gamma c) \leq 0.182\%$. A search for flavor-changing neutral currents in associated production of a top quark with a Higgs boson decaying into $b\bar{b}$ has also been presented by CMS, corresponding to an integrated luminosity of 35.9 fb^{-1} at 13 TeV. Two complementary channels are considered: top quark pair production, with FCNC decay of the top quark or antiquark, and single top associated production. A final state with one isolated lepton and at least three reconstructed jets, among which at least two are identified as b quark jets, is considered. No significant deviation is observed from predicted background and upper limits at 95% confidence level are set on the branching ratios of top quark decays, $B(t \to uH) < 0.47\%$ and $B(t \to cH) < 0.47\%$ [378], which are similar to the combined limits on all decay channels ob-

Downloaded from https://academic.oup.com/ptep/article/2022/8/083C01/6651666 by KIT Library user on 27 September 2022

tained with the full data set at 8 TeV [379]. More recently, a search for the signature of flavor-changing neutral current interactions of top quarks and Higgs bosons has been performed. corresponding to an integrated luminosity of 137 fb^{-1} at 13 TeV. Multivariate machine learning techniques have been used to separate signal and standard model background processes. No significant excess above the background prediction is observed, and upper limits on the $t \to Hq$ branching fractions are derived through a binned fit to the diphoton invariant mass spectrum. The observed 95% confidence level upper limits are found to be 1.9×10^{-4} for $\Gamma(t \to Hu)$ and 7.3×10^{-4} for $\Gamma(t \to Hc)$.

ATLAS has presented results on the search for single top-quark production via FCNC's in strong interactions using data collected at $\sqrt{s}$=8 TeV and corresponding to an integrated luminosity of 20.3 fb^{-1}. Flavor-changing-neutral-current events are searched for in which a light quark (u or c) interacts with a gluon to produce a single top quark, either with or without the associated production of another light quark or gluon. Candidate events of top quarks decaying into leptons and jets are selected and classified into signal- and background-like events using a neural network. The observed 95% C.L. limit is $\sigma_{qq\to t} \times B(t \to Wb) < 3.4$ pb that can be interpreted as limits on the branching ratios, $B(t \to ug) < 4 \cdot 10^{-5}$ and $B(t \to cg) < 1.7 \cdot 10^{-4}$ [380]. ATLAS has set limits on the coupling of a top quark, a photon, and an up or charm quark using 81 fb^{-1} of data 13 TeV. Events with a photon, an electron or muon, a b-tagged jet, and missing transverse momentum are selected. The data are consistent with the background-only hypothesis, and limits are set on the strength of the $tq\gamma$ coupling in an effective field theory. These are also interpreted as 95% CL upper limits on $t \to u\gamma$ branching ratio via a left-handed (right-handed) interaction of 2.8×10^{-5} (6.1×10^{-5}) and on the $t \to c\gamma$ branching ratio for of 22×10^{-5} (18×10^{-5}) [381]. Constraints on FCNC couplings of the top quark can also be obtained from searches for anomalous single top-quark production in e^+e^- collisions, via the process $e^+e^- \to \gamma, Z^* \to t\bar{q}$ and its charge-conjugate ($q = u, c$), or in $e^{\pm}p$ collisions, via the process $e^{\pm}u \to e^{\pm}t$. For a leptonic W decay, the topology is at least a high-p_T lepton, a high-p_T jet and missing E_T, while for a hadronic W-decay, the topology is three high-p_T jets. Limits on the cross section for this reaction have been obtained by the LEP collaborations [382] in e^+e^- collisions, and by H1 [383] and ZEUS [384] in $e^{\pm}p$ collisions. When interpreted in terms of branching ratios in top decay [385, 386], the LEP limits lead to typical 95% C.L. upper bounds of $B(t \to qZ) < 0.137$. Assuming no coupling to the Z boson, the 95% C.L. limits on the anomalous FCNC coupling $\kappa_\gamma < 0.13$ and < 0.27 by ZEUS and H1, respectively, are stronger than the CDF limit of $\kappa_\gamma < 0.42$, and improve over LEP sensitivity in that domain. The H1 limit is slightly weaker than the ZEUS limit due to an observed excess of five-candidate events over an expected background of 3.2±0.4. If this excess is attributed to FCNC top-quark production, this leads to a total cross section of $\sigma(ep \to e + t + X, \sqrt{s} = 319 \text{ GeV}) < 0.25$ pb [383, 387].

61.3.3.2 *New Physics in Top-Quark decays*

The large sample of top quarks produced at the Tevatron and the LHC allows to measure or set stringent limits on the branching ratios of rare top-quark decays. For example, the existence of a light H^+ can be constrained by looking for $t \to H^+b$ decay, in particular with tau-leptons in the final state (for more information see the review "Higgs Bosons: theory and searches").

A first class of searches for new physics focuses on the structure of the Wtb vertex. Using up to 2.7 fb^{-1} of data, DØ has measured the Wtb coupling form factors by combining information from the W-boson helicity in top-quark decays in $t\bar{t}$ events and single top-quark production, allowing to place limits on the left-handed and right-handed vector and tensor couplings [388–390].

ATLAS has published the results of a search for CP-violation in the decay of single top quarks produced in the t-channel where the top quarks are predicted to be highly polarized, using the lepton+jets final state [391]. The data analyzed are from pp collisions at $\sqrt{s} = 7$ TeV and correspond to an integrated luminosity of 4.7 fb^{-1}. In the Standard Model, the couplings at the Wtb vertex are left-handed, right-handed couplings being absent. A forward-backward asymmetry with respect to the normal to the plane defined by the W-momentum and the top-quark polarization has been used to probe the complex phase of a possibly non-zero value of the right-handed coupling, signaling a source of CP-violation beyond the SM. The measured value of the asymmetry is $0.031 \pm 0.065(stat.)^{+0.029}_{-0.031}(syst.)$ in good agreement with the Standard Model.

A second class of searches focuses on FCNC's in the top-quark decays. Both, CDF and DØ, have provided the first limits for FCNC's in Run I and II. The most recent results from CDF give $B(t \to qZ) < 3.7\%$ and $B(t \to q\gamma) < 3.2\%$ at the 95% C.L. [392] while DØ [393, 394] sets $B(t \to qZ)(q = u, c$ quarks $) < 3.2\%)$ at 95% C.L., $B(t \to gu) < 2.0 \cdot 10^{-4}$, and $B(t \to gc) < 3.9 \cdot 10^{-3}$ at the 95% C.L. At the LHC, CMS has used a sample at a center-of-mass energy of 8 TeV corresponding to 19.7 fb^{-1} of integrated luminosity to perform a search for flavor changing neutral current top-quark decay $t \to Zq$. Events with a topology compatible with the decay chain $t\bar{t} \to Wb + Zq \to \ell\nu\ b + \ell\ell q$ are searched for. There is no excess seen in the observed number of events relative to the SM prediction; thus no evidence for flavor changing neutral current in top-quark decays is found. A combination with a previous search at 7 TeV excludes a $t \to Zq$ branching fraction greater than 0.05% at the 95% confidence level [395]. CMS has also performed a search for the production of a single top quark in association with a Z boson in the same data set at 8 TeV. Final states with three leptons (electrons or muons) and at least one jet are investigated. Exclusion limits at 95% confidence level on the branching fractions are found to be $B(t \to uZ) < 0.022\%$ and $B(t \to cZ) < 0.049\%$ [396].

The ATLAS collaboration has also searched for FCNC processes in 36.1 fb^{-1} of $t\bar{t}$ events at a center-of-mass energy of 13 TeV, with one top quark decaying through FCNC ($t \to qZ$) and the other through the SM dominant mode ($t \to bW$). Only the decays of the Z boson to charged leptons and leptonic W boson decays were considered as signal, leading to a final state topology characterized by the presence of three isolated leptons, at least two jets and missing transverse energy from the undetected neutrino. No evidence for an FCNC signal was found. An upper limit on the $t \to qZ$ branching ratio of $B(t \to Zu(c)) < 1.7(2.4) \times 10^{-4}$ is set at the 95% confidence level [397]. The ATLAS collaboration has also searched for a tqZ coupling, in a study that includes events where a single top quark is produced as $gq \to tZ$ (with $q = u, c$) and top-quark pair events, with one top quark decaying through the $t \to qZ$ channel, 139 fb^{-1} of data at 13 TeV. The analysis selects events with three leptons (electrons or muons), a b-tagged jet, possible additional jets and missing transverse momentum. The data are consistent with the background-only hypothesis and 95% confidence-level limits on the branching ratios are set. These are 6.2×10^{-5} (13×10^{-5}) for $t \to Zu$ ($t \to Zc$) for a left-handed coupling, and 6.6×10^{-5} (12×10^{-5}) in the case of a right-handed coupling [398].

Another search for FCNCs is the interactions of a top-quark to a Higgs boson and a light parton, tqH, $q = u, c$. The CMS collaboration has performed a search using a sample at a center-of-mass energy of 13 TeV corresponding to 35.9 fb^{-1} of integrated luminosity, [399], combining single top quark FCNC production in association with the Higgs boson ($pp \to tH$), and top quark pair production with FCNC decay of the top quark ($t \to qH$). The combined analysis sets an upper limit on the $t \to u/cH$ branching ratios of $B(t \to u/cH) < 0.47\%$ at 95% confidence level. The ATLAS collaboration considers $t \to qH$, $q = u, c$ with 36.1 fb^{-1} of $t\bar{t}$ events at $\sqrt{s} = 13$ TeV. A combined measurement including $H \to bb$ and $H \to \tau\tau$ modes yields a 95% C.L. upper limit of 0.11% and 0.12% on the branching ratios of $B(t \to cH)$ and $B(t \to uH)$, respectively [400].

61.4 Outlook

Top-quark physics at hadron colliders has developed into precision physics. Various properties of the top quark have been measured with high precision, where the LHC has by now surpassed the Tevatron precision and reach in the majority of relevant observables. Several $\sqrt{s}$-dependent physics quantities, such as the production cross-section, have been measured at several energies at the Tevatron and the LHC. Up to now, all measurements are consistent with the SM predictions and allow stringent tests of

Downloaded from https://academic.oup.com/ptep/article/2022/8/083C01/6651666 by KIT Library user on 27 September 2022

the underlying production mechanisms by strong and weak interactions. Given the very large event samples available at the LHC, top-quark properties will be further determined in $t\bar{t}$ as well as in electroweak single top-quark production. At the Tevatron, the $t-$ and $s-$channels for electroweak single top-quark production have been measured separately. At the LHC, quick progress has been achieved in the last years making all three relevant channels measured with more than 5 sigma significance. Furthermore, $t\bar{t}\gamma$, $t\bar{t}Z$, and $t\bar{t}W$ together with $t\bar{t}H$ associated production have started to provide key information on the top-quark electroweak couplings. Corresponding effective field theory (EFT) fits for the coupling extraction are being developed. At the same time various models of physics beyond the SM involving top-quark production are being constrained. While a majority of the Run-II data recorded at 13 TeV has been analysed or is in an advanced stage, the beginning of the Run-III at $\sqrt{s} = 13.6$ to 14 TeV and an expected integrated luminosity of $160 - 200$ fb^{-1}, doubling the Run-I plus Run-II data set, is immanent. With the first results to be released, top-quark physics has the potential to shed light on open questions and new aspects of physics at the TeV scale.

CDF note references can be retrieved from
`https://www-cdf.fnal.gov/physics/new/top/top.html`,
and DØ note references from
`https://www-d0.fnal.gov/Run2Physics/WWW/documents/Run2Results.htm`,
and ATLAS note references from
`https://twiki.cern.ch/twiki/bin/view/AtlasPublic/TopPublicResults`,
and CMS note references from
`https://twiki.cern.ch/twiki/bin/view/CMSPublic/PhysicsResultsTOP`,
and plots provided by the LHC Top Working Group from
`https://twiki.cern.ch/twiki/bin/view/LHCPhysics/LHCTopWGSummaryPlots`.

References

[1] M. Czakon, P. Fiedler and A. Mitov, Phys. Rev. Lett. **110**, 252004 (2013), [arXiv:1303.6254].

[2] S. Catani *et al.*, JHEP **07**, 100 (2019), [arXiv:1906.06535].

[3] ATLAS,CMS, CDF, & D0 Collab, [arXiv:1403.4427].

[4] S. Cortese and R. Petronzio, Phys. Lett. **B253**, 494 (1991).

[5] S. S. D. Willenbrock and D. A. Dicus, Phys. Rev. **D34**, 155 (1986).

[6] J. Campbell, T. Neumann and Z. Sullivan, JHEP **02**, 040 (2021), [arXiv:2012.01574].

[7] M. Brucherseifer, F. Caola and K. Melnikov, Phys. Lett. **B736**, 58 (2014), [arXiv:1404.7116].

[8] E. L. Berger, J. Gao and H. X. Zhu, JHEP **11**, 158 (2017), [arXiv:1708.09405].

[9] N. Kidonakis, Phys. Rev. **D81**, 054028 (2010), [arXiv:1001.5034].

[10] N. Kidonakis, Phys. Rev. **D82**, 054018 (2010), [arXiv:1005.4451].

[11] T. M. P. Tait and C. P. Yuan, Phys. Rev. **D63**, 014018 (2000), [hep-ph/0007298].

[12] M. Jezabek and J. H. Kuhn, Nucl. Phys. **B314**, 1 (1989).

[13] I. I. Y. Bigi *et al.*, Phys. Lett. **B181**, 157 (1986).

[14] A. H. Hoang *et al.*, Phys. Rev. **D65**, 014014 (2002), [hep-ph/0107144].

[15] K. Hagiwara, Y. Sumino and H. Yokoya, Phys. Lett. **B666**, 71 (2008), [arXiv:0804.1014].

[16] B. Fuks *et al.*, Phys. Rev. D **104**, 3, 034023 (2021), [arXiv:2102.11281].

[17] A. Czarnecki and K. Melnikov, Nucl. Phys. **B544**, 520 (1999), [hep-ph/9806244]; K. G. Chetyrkin *et al.*, Phys. Rev. **D60**, 114015 (1999), [hep-ph/9906273].

[18] S. Frixione, P. Nason and B. R. Webber, JHEP **08**, 007 (2003), [hep-ph/0305252]; W. Kim and H. Shin, JHEP **07**, 070 (2007), [arXiv:0706.3563]; S. Frixione, P. Nason and G. Ridolfi, JHEP **09**, 126 (2007), [arXiv:0707.3088]; J. M. Campbell *et al.*, JHEP **04**, 114 (2015), [arXiv:1412.1828]; T. Ježo *et al.*, Eur. Phys. J. **C76**, 12, 691 (2016), [arXiv:1607.04538].

[19] S. Frixione *et al.*, JHEP **03**, 092 (2006), [hep-ph/0512250]; V. Marotta and A. Naddeo, JHEP **08**, 029 (2008), [arXiv:0810.4759]; S. Alioli *et al.*, JHEP **09**, 111 (2009), [Erratum: JHEP02,011(2010)], [arXiv:0907.4076]; E. Re, Eur. Phys. J. **C71**, 1547 (2011), [arXiv:1009.2450]; R. Frederix, E. Re and P. Torrielli, JHEP **09**, 130 (2012), [arXiv:1207.5391]; R. Frederix *et al.*, JHEP **06**, 027 (2016), [arXiv:1603.01178].

[20] S. Frixione and B. R. Webber, JHEP **06**, 029 (2002), [hep-ph/0204244].

[21] P. Nason, JHEP **11**, 040 (2004), [hep-ph/0409146].

[22] J. Mazzitelli *et al.*, Phys. Rev. Lett. **127**, 6, 062001 (2021), [arXiv:2012.14267].

[23] E. Todesco and J. Wenninger, Phys. Rev. Accel. Beams **20**, 8, 081003 (2017).

[24] V. M. Abazov *et al.* (D0), Phys. Rev. **D94**, 092004 (2016), [arXiv:1605.06168].

[25] T. Aaltonen *et al.* (CDF), Phys. Rev. **D88**, 091103 (2013), [arXiv:1304.7961].

[26] T. A. Aaltonen *et al.* (CDF, D0), Phys. Rev. **D89**, 7, 072001 (2014), [arXiv:1309.7570].

[27] T. A. Aaltonen *et al.* (CDF), Phys. Rev. **D89**, 9, 091101 (2014), [arXiv:1402.6728].

[28] T. Aaltonen *et al.* (CDF), Phys. Rev. Lett. **105**, 012001 (2010), [arXiv:1004.3224].

[29] V. M. Abazov *et al.* (D0), Phys. Rev. **D90**, 9, 092006 (2014), [arXiv:1401.5785].

[30] M. Czakon and A. Mitov, Comput. Phys. Commun. **185**, 2930 (2014), [arXiv:1112.5675].

[31] ATLAS Collab., ATLAS-CONF-2021-003.

[32] A. M. Sirunyan *et al.* (CMS), JHEP **03**, 115 (2018), [arXiv:1711.03143].

[33] CMS Collab., CMS-PAS-TOP-20-004 (2021).

[34] G. Aad *et al.* (ATLAS), Eur. Phys. J. **C74**, 10, 3109 (2014), [Addendum: Eur. Phys. J.C76,no.11,642(2016)], [arXiv:1406.5375].

[35] ATLAS Collab., ATLAS-CONF-2011-121 (2011).

[36] G. Aad *et al.* (ATLAS), JHEP **05**, 059 (2012), [arXiv:1202.4892].

[37] ATLAS Collab., ATLAS-CONF-2011-140.

[38] ATLAS Collab., ATLAS-CONF-2012-024.

[39] G. Aad *et al.* (ATLAS), Eur. Phys. J. **C73**, 3, 2328 (2013), [arXiv:1211.7205].

[40] G. Aad *et al.* (ATLAS), Phys. Lett. **B717**, 89 (2012), [arXiv:1205.2067].

[41] ATLAS Collab., ATLAS-CONF-2012-031.

[42] G. Aad *et al.* (ATLAS), Phys. Rev. **D91**, 5, 052005 (2015), [arXiv:1407.0573].

[43] S. Chatrchyan *et al.* (CMS), JHEP **11**, 067 (2012), [arXiv:1208.2671].

[44] S. Chatrchyan *et al.* (CMS), Phys. Lett. **B720**, 83 (2013), [arXiv:1212.6682].

[45] S. Chatrchyan *et al.* (CMS), JHEP **05**, 065 (2013), [arXiv:1302.0508].

[46] S. Chatrchyan *et al.* (CMS), Phys. Rev. **D85**, 112007 (2012), [arXiv:1203.6810].

[47] S. Chatrchyan *et al.* (CMS), Eur. Phys. J. **C73**, 4, 2386 (2013), [arXiv:1301.5755].

[48] ATLAS & CMS Collab., ATLAS-CONF-2012-134, CMS-PAS-TOP-12-003.

Downloaded from https://academic.oup.com/ptep/article/2022/8/083C01/6651666 by KIT Library user on 27 September 2022

[49] G. Aad *et al.* (ATLAS), Eur. Phys. J. **C74**, 10, 3109 (2014), [Addendum: Eur. Phys. J.C76,no.11,642(2016)], [arXiv:1406.5375].

[50] G. Aad *et al.* (ATLAS), Phys. Rev. **D91**, 11, 112013 (2015), [arXiv:1504.04251].

[51] M. Aaboud *et al.* (ATLAS), Eur. Phys. J. **C78**, 487 (2018), [arXiv:1712.06857].

[52] M. Aaboud *et al.* (ATLAS), Phys. Rev. **D95**, 7, 072003 (2017), [arXiv:1702.08839].

[53] V. Khachatryan *et al.* (CMS), Eur. Phys. J. **C77**, 1, 15 (2017), [arXiv:1602.09024].

[54] S. Chatrchyan *et al.* (CMS), JHEP **02**, 024 (2014), [Erratum: JHEP02,102(2014)], [arXiv:1312.7582].

[55] V. Khachatryan *et al.* (CMS), JHEP **08**, 029 (2016), [arXiv:1603.02303].

[56] V. Khachatryan *et al.* (CMS), Phys. Lett. **B739**, 23 (2014), [arXiv:1407.6643].

[57] V. Khachatryan *et al.* (CMS), Eur. Phys. J. **C76**, 3, 128 (2016), [arXiv:1509.06076].

[58] ATLAS Collab., ATLAS-CONF-2014-054, CMS Collab., CMS-PAS-TOP-14-016.

[59] R. Aaij *et al.* (LHCb), Phys. Rev. Lett. **115**, 11, 112001 (2015), [arXiv:1506.00903].

[60] ATLAS Collab., ATLAS-CONF-2015-033.

[61] ATLAS collab., ATLAS-CONF-2015-049.

[62] M. Aaboud *et al.* (ATLAS), Phys. Lett. **B761**, 136 (2016), [Erratum: Phys. Lett.B772,879(2017)], [arXiv:1606.02699].

[63] G. Aad *et al.* (ATLAS), Eur. Phys. J. C **80**, 6, 528 (2020), [arXiv:1910.08819].

[64] G. Aad *et al.* (ATLAS), Phys. Lett. B **810**, 135797 (2020), [arXiv:2006.13076].

[65] V. Khachatryan *et al.* (CMS), Phys. Rev. Lett. **116**, 5, 052002 (2016), [arXiv:1510.05302].

[66] V. Khachatryan *et al.* (CMS), Eur. Phys. J. **C77**, 172 (2017), [arXiv:1611.04040].

[67] A. M. Sirunyan *et al.* (CMS), Eur. Phys. J. **C79**, 5, 368 (2019), [arXiv:1812.10505].

[68] A. M. Sirunyan *et al.* (CMS), JHEP **02**, 191 (2020), [arXiv:1911.13204].

[69] CMS Collab., CMS-PAS-TOP-15-005.

[70] A. M. Sirunyan *et al.* (CMS), JHEP **09**, 051 (2017), [arXiv:1701.06228].

[71] A. Tumasyan *et al.* (CMS) (2021), [arXiv:2108.02803].

[72] CMS Collab., CMS-PAS-TOP-16-013.

[73] A. M. Sirunyan *et al.* (CMS), Phys. Rev. Lett. **119**, 24, 242001 (2017), [arXiv:1709.07411].

[74] V. M. Abazov *et al.* (D0), Phys. Rev. Lett. **107**, 121802 (2011), [arXiv:1106.5436]; D. Acosta *et al.* (CDF), Phys. Rev. Lett. **95**, 102002 (2005), [hep-ex/0505091].

[75] V. Khachatryan *et al.* (CMS), Phys. Lett. **B736**, 33 (2014), [arXiv:1404.2292].

[76] M. Czakon, D. Heymes and A. Mitov, Phys. Rev. Lett. **116**, 8, 082003 (2016), [arXiv:1511.00549].

[77] T. Aaltonen *et al.* (CDF), Phys. Rev. Lett. **110**, 12, 121802 (2013), [arXiv:1211.5363].

[78] G. Aad *et al.* (ATLAS), Eur. Phys. J. **C73**, 1, 2261 (2013), [arXiv:1207.5644].

[79] G. Aad *et al.* (ATLAS), Phys. Rev. **D90**, 7, 072004 (2014), [arXiv:1407.0371].

[80] G. Aad *et al.* (ATLAS), JHEP **06**, 100 (2015), [arXiv:1502.05923].

[81] S. Chatrchyan *et al.* (CMS), Eur. Phys. J. **C73**, 3, 2339 (2013), [arXiv:1211.2220].

[82] M. Aaboud *et al.* (ATLAS), Phys. Rev. **D94**, 9, 092003 (2016), [arXiv:1607.07281].

[83] G. Aad *et al.* (ATLAS), Eur. Phys. J. **C76**, 10, 538 (2016), [arXiv:1511.04716].

[84] G. Aad *et al.* (ATLAS), Phys. Rev. **D93**, 3, 032009 (2016), [arXiv:1510.03818].

[85] V. Khachatryan *et al.* (CMS), Phys. Rev. **D94**, 5, 052006 (2016), [arXiv:1607.00837].

[86] A. M. Sirunyan *et al.* (CMS), Eur. Phys. J. **C77**, 7, 459 (2017), [arXiv:1703.01630].

[87] V. Khachatryan *et al.* (CMS), Phys. Rev. **D94**, 7, 072002 (2016), [arXiv:1605.00116].

[88] V. Khachatryan *et al.* (CMS), Eur. Phys. J. **C75**, 11, 542 (2015), [arXiv:1505.04480].

[89] V. Khachatryan *et al.* (CMS), Eur. Phys. J. **C76**, 3, 128 (2016), [arXiv:1509.06076].

[90] M. Aaboud *et al.* (ATLAS), Eur. Phys. J. **C77**, 5, 292 (2017), [arXiv:1612.05220].

[91] M. Aaboud *et al.* (ATLAS), JHEP **11**, 191 (2017), [arXiv:1708.00727].

[92] M. Aaboud *et al.* (ATLAS), Phys. Rev. **D98**, 1, 012003 (2018), [arXiv:1801.02052].

[93] G. Aad *et al.* (ATLAS), Eur. Phys. J. C **79**, 12, 1028 (2019), [Erratum: Eur.Phys.J.C 80, 1092 (2020)], [arXiv:1908.07305].

[94] ATLAS Collab., ATLAS-CONF-2021-031.

[95] G. Aad *et al.* (ATLAS), JHEP **01**, 033 (2021), [arXiv:2006.09274].

[96] CMS Collab., CMS-PAS-TOP-15-010.

[97] A. M. Sirunyan *et al.* (CMS), JHEP **04**, 060 (2018), [arXiv:1708.07638].

[98] V. Khachatryan *et al.* (CMS), Phys. Rev. **D95**, 9, 092001 (2017), [arXiv:1610.04191].

[99] A. M. Sirunyan *et al.* (CMS), JHEP **06**, 002 (2018), [arXiv:1803.03991].

[100] A. M. Sirunyan *et al.* (CMS), Phys. Rev. **D97**, 11, 112003 (2018), [arXiv:1803.08856].

[101] A. M. Sirunyan *et al.* (CMS), JHEP **02**, 149 (2019), [arXiv:1811.06625].

[102] A. M. Sirunyan *et al.* (CMS), Eur. Phys. J. C **80**, 7, 658 (2020), [arXiv:1904.05237].

[103] A. M. Sirunyan *et al.* (CMS), Phys. Rev. D **103**, 5, 052008 (2021), [arXiv:2008.07860].

[104] G. Aad *et al.* (ATLAS), Eur. Phys. J. **C76**, 1, 11 (2016), [arXiv:1508.06868].

[105] G. Aad *et al.* (ATLAS), JHEP **01**, 020 (2015), [arXiv:1407.0891].

[106] S. Chatrchyan *et al.* (CMS), Eur. Phys. J. **C74**, 3014 (2015), [Erratum: Eur. Phys. J.C75,no.5,216(2015)], [arXiv:1404.3171].

[107] V. Khachatryan *et al.* (CMS), Phys. Lett. **B746**, 132 (2015), [arXiv:1411.5621].

[108] G. Aad *et al.* (ATLAS), Phys. Rev. **D92**, 7, 072005 (2015), [arXiv:1506.05074].

[109] G. Aad *et al.* (ATLAS), Nature Phys. **17**, 7, 813 (2021).

[110] ATLAS Collab., ATLAS-CONF-2020-050.

[111] A. M. Sirunyan *et al.* (CMS), Phys. Rev. D **102**, 9, 092013 (2020), [arXiv:2009.07123].

[112] M. Aaboud *et al.* (ATLAS), JHEP **04**, 046 (2019), [arXiv:1811.12113].

[113] A. M. Sirunyan *et al.* (CMS), Phys. Lett. **B776**, 355 (2018), [arXiv:1705.10141].

[114] A. M. Sirunyan *et al.* (CMS), JHEP **07**, 125 (2020), [arXiv:2003.06467].

Downloaded from https://academic.oup.com/ptep/article/2022/8/083C01/6651666 by KIT Library user on 27 September 2022

[115] A. M. Sirunyan *et al.* (CMS) (2019), [arXiv:1909.05306].

[116] A. M. Sirunyan *et al.* (CMS), Phys. Lett. B **803**, 135285 (2020), [arXiv:1909.05306].

[117] A. M. Sirunyan *et al.* (CMS), Phys. Lett. B **820**, 136565 (2021), [arXiv:2012.09225].

[118] R. Frederix, D. Pagani and M. Zaro, JHEP **02**, 031 (2018), [arXiv:1711.02116].

[119] G. Aad *et al.* (ATLAS), Eur. Phys. J. C **80**, 11, 1085 (2020), [arXiv:2007.14858].

[120] G. Aad *et al.* (ATLAS) (2021), [arXiv:2106.11683].

[121] A. M. Sirunyan *et al.* (CMS), Eur. Phys. J. C **80**, 2, 75 (2020), [arXiv:1908.06463].

[122] A. M. Sirunyan *et al.* (CMS), JHEP **11**, 082 (2019), [arXiv:1906.02805].

[123] V. M. Abazov *et al.* (D0), Phys. Rev. Lett. **103**, 092001 (2009), [arXiv:0903.0850]; V. M. Abazov *et al.* (D0), Phys. Rev. **D78**, 012005 (2008), [arXiv:0803.0739]; V. M. Abazov *et al.* (D0), Phys. Rev. Lett. **98**, 181802 (2007), [hep-ex/0612052].

[124] T. Aaltonen *et al.* (CDF), Phys. Rev. Lett. **103**, 092002 (2009), [arXiv:0903.0885]; T. Aaltonen *et al.* (CDF), Phys. Rev. **D81**, 072003 (2010), [arXiv:1001.4577].

[125] T. Aaltonen *et al.* (CDF), Phys. Rev. **D82**, 112005 (2010), [arXiv:1004.1181].

[126] A. Heinson and T. R. Junk, Ann. Rev. Nucl. Part. Sci. **61**, 171 (2011), [arXiv:1101.1275].

[127] Tevatron Electroweak Working Group, (2009), [arXiv:0908.2171].

[128] N. Kidonakis, Phys. Rev. **D83**, 091503 (2011), [arXiv:1103.2792].

[129] CDF Collab., CDF conference note 11113 (2014), DØ Collab., DØ conference note 6448 (2014).

[130] T. A. Aaltonen *et al.* (CDF, D0), Phys. Rev. Lett. **115**, 15, 152003 (2015), [arXiv:1503.05027].

[131] T. A. Aaltonen *et al.* (CDF, D0), Phys. Rev. Lett. **112**, 231803 (2014), [arXiv:1402.5126].

[132] G. Aad *et al.* (ATLAS), Phys. Rev. **D90**, 11, 112006 (2014), [arXiv:1406.7844].

[133] G. Aad *et al.* (ATLAS), Phys. Lett. **B717**, 330 (2012), [arXiv:1205.3130].

[134] S. Chatrchyan *et al.* (CMS), JHEP **12**, 035 (2012), [arXiv:1209.4533].

[135] M. Aaboud *et al.* (ATLAS), Eur. Phys. J. **C77**, 8, 531 (2017), [arXiv:1702.02859].

[136] M. Aaboud *et al.* (ATLAS), JHEP **04**, 124 (2017), [arXiv:1702.08309].

[137] V. Khachatryan *et al.* (CMS), JHEP **06**, 090 (2014), [arXiv:1403.7366].

[138] CMS Collab., CMS-PAS-TOP-15-007.

[139] M. Aaboud *et al.* (ATLAS), JHEP **04**, 086 (2017), [arXiv:1609.03920].

[140] A. M. Sirunyan *et al.* (CMS), Phys. Lett. **B772**, 752 (2017), [arXiv:1610.00678].

[141] A. M. Sirunyan *et al.* (CMS), Phys. Lett. B **800**, 135042 (2020), [arXiv:1812.10514].

[142] A. M. Sirunyan *et al.* (CMS), Phys. Lett. B **808**, 135609 (2020), [arXiv:2004.12181].

[143] C. D. White *et al.*, JHEP **11**, 074 (2009), [arXiv:0908.0631].

[144] S. Frixione *et al.*, JHEP **07**, 029 (2008), [arXiv:0805.3067].

[145] G. Aad *et al.* (ATLAS), Phys. Lett. **B716**, 142 (2012), [arXiv:1205.5764].

[146] S. Chatrchyan *et al.* (CMS), Phys. Rev. Lett. **110**, 022003 (2013), [arXiv:1209.3489].

[147] G. Aad *et al.* (ATLAS), JHEP **01**, 064 (2016), [arXiv:1510.03752].

[148] M. Aaboud *et al.* (ATLAS, CMS), JHEP **05**, 088 (2019), [arXiv:1902.07158].

[149] G. Aad *et al.* (ATLAS), Eur. Phys. J. C **81**, 8, 720 (2021), [arXiv:2007.01554].

[150] S. Chatrchyan *et al.* (CMS), Phys. Rev. Lett. **112**, 23, 231802 (2014), [arXiv:1401.2942].

[151] M. Aaboud *et al.* (ATLAS), JHEP **01**, 063 (2018), [arXiv:1612.07231].

[152] A. M. Sirunyan *et al.* (CMS), JHEP **10**, 117 (2018), [arXiv:1805.07399].

[153] A. Tumasyan *et al.* (CMS) (2021), [arXiv:2109.01706].

[154] ATLAS Collab., ATLAS-CONF-2011-118.

[155] G. Aad *et al.* (ATLAS), Phys. Lett. **B756**, 228 (2016), [arXiv:1511.05980].

[156] V. Khachatryan *et al.* (CMS), JHEP **09**, 027 (2016), [arXiv:1603.02555].

[157] M. Aaboud *et al.* (ATLAS, CMS), JHEP **05**, 088 (2019), [arXiv:1902.07158].

[158] CMS Collab., CMS-PAS-TOP-14-004.

[159] CMS Collab., CMS-PAS-TOP-13-001.

[160] A. M. Sirunyan *et al.* (CMS), Eur. Phys. J. C **80**, 5, 370 (2020), [arXiv:1907.08330].

[161] M. Aaboud *et al.* (ATLAS), Eur. Phys. J. C **78**, 3, 186 (2018), [arXiv:1712.01602].

[162] CMS Collab., CMS-PAS-TOP-19-003.

[163] M. Czakon, P. Fiedler and A. Mitov, Phys. Rev. Lett. **115**, 5, 052001 (2015), [arXiv:1411.3007].

[164] W. Hollik and D. Pagani, Phys. Rev. **D84**, 093003 (2011), [arXiv:1107.2606].

[165] W. Bernreuther and Z.-G. Si, Phys. Rev. **D86**, 034026 (2012), [arXiv:1205.6580].

[166] S. Jung *et al.*, Phys. Rev. **D81**, 015004 (2010), [arXiv:0907.4112].

[167] V. M. Abazov *et al.* (D0), Phys. Rev. Lett. **100**, 142002 (2008), [arXiv:0712.0851].

[168] T. Aaltonen *et al.* (CDF), Phys. Rev. Lett. **101**, 202001 (2008), [arXiv:0806.2472].

[169] T. A. Aaltonen *et al.* (CDF, D0), Phys. Rev. Lett. **120**, 4, 042001 (2018), [arXiv:1709.04894].

[170] G. Aad *et al.* (ATLAS), JHEP **02**, 107 (2014), [arXiv:1311.6724].

[171] G. Aad *et al.* (ATLAS), Eur. Phys. J. **C76**, 2, 87 (2016), [Erratum: Eur. Phys. J.C77,564(2017)], [arXiv:1509.02358].

[172] G. Aad *et al.* (ATLAS), Phys. Rev. **D94**, 3, 032006 (2016), [arXiv:1604.05538].

[173] S. Chatrchyan *et al.* (CMS), Phys. Lett. **B717**, 129 (2012), [arXiv:1207.0065].

[174] V. Khachatryan *et al.* (CMS), Phys. Rev. **D93**, 3, 034014 (2016), [arXiv:1508.03862].

[175] V. Khachatryan *et al.* (CMS), Phys. Lett. **B760**, 365 (2016), [arXiv:1603.06221].

[176] M. Czakon *et al.*, Phys. Rev. **D98**, 1, 014003 (2018), [arXiv:1711.03945].

[177] V. Khachatryan *et al.* (CMS), Phys. Lett. **B757**, 154 (2016), [arXiv:1507.03119].

[178] G. Aad *et al.* (ATLAS), Phys. Lett. **B756**, 52 (2016), [arXiv:1512.06092].

[179] G. Aad *et al.* (ATLAS), JHEP **05**, 061 (2015), [arXiv:1501.07383].

[180] S. Chatrchyan *et al.* (CMS), JHEP **04**, 191 (2014), [arXiv:1402.3803].

Downloaded from https://academic.oup.com/ptep/article/2022/8/083C01/6651666 by KIT Library user on 27 September 2022

[181] M. Aaboud *et al.* (ATLAS, CMS), JHEP **04**, 033 (2018), [arXiv:1709.05327].

[182] ATLAS Collab., ATLAS-CONF-2019-026.

[183] CMS Collab., CMS-PAS-TOP-15-018.

[184] G. Aad *et al.* (ATLAS) (2021), [arXiv:2110.05453].

[185] F. Abe *et al.* (CDF), Phys. Rev. **D50**, 2966 (1994).

[186] A. Abulencia *et al.* (CDF), Phys. Rev. **D73**, 032003 (2006), [hep-ex/0510048].

[187] M. Aaboud *et al.* (ATLAS), Eur. Phys. J. **C79**, 4, 290 (2019), [arXiv:1810.01772].

[188] V. Khachatryan *et al.* (CMS), Phys. Rev. **D93**, 7, 072004 (2016), [arXiv:1509.04044].

[189] A. M. Sirunyan *et al.* (CMS), Eur. Phys. J. **C78**, 11, 891 (2018), [arXiv:1805.01428].

[190] S. Argyropoulos and T. Sjöstrand, JHEP **11**, 043 (2014), [arXiv:1407.6653].

[191] J. R. Christiansen and P. Z. Skands, JHEP **08**, 003 (2015), [arXiv:1505.01681].

[192] A. M. Sirunyan *et al.* (CMS), Phys. Rev. Lett. **124**, 20, 202001 (2020), [arXiv:1911.03800].

[193] V. M. Abazov *et al.* (D0), Nature **429**, 638 (2004), [hep-ex/0406031].

[194] K. Kondo, T. Chikamatsu and S. H. Kim, J. Phys. Soc. Jap. **62**, 1177 (1993).

[195] R. H. Dalitz and G. R. Goldstein, Phys. Rev. **D45**, 1531 (1992); R. H. Dalitz and G. R. Goldstein, Phys. Lett. **B287**, 225 (1992).

[196] V. M. Abazov *et al.* (D0), Phys. Rev. Lett. **113**, 032002 (2014), [arXiv:1405.1756].

[197] L. Sonnenschein, Phys. Rev. **D73**, 054015 (2006), [Erratum: Phys. Rev.D78,079902(2008)], [hep-ph/0603011].

[198] G. Aad *et al.* (ATLAS), Eur. Phys. J. **C75**, 7, 330 (2015), [arXiv:1503.05427].

[199] A. M. Sirunyan *et al.* (CMS), Phys. Rev. **D96**, 3, 032002 (2017), [arXiv:1704.06142].

[200] C. G. Lester and D. J. Summers, Phys. Lett. **B463**, 99 (1999), [hep-ph/9906349].

[201] A. M. Sirunyan *et al.* (CMS), Eur. Phys. J. **C79**, 4, 313 (2019), [arXiv:1812.10534].

[202] M. Aaboud *et al.* (ATLAS), JHEP **09**, 118 (2017), [arXiv:1702.07546].

[203] CMS Collab., CMS-PAS-TOP-19-009.

[204] The Tevatron Electroweak Working Group and Aaltonen, T., For the CDF and D0 Collab., arXiv:1608.01881, FERMILAB-CONF-16-298-E.

[205] B. Abbott *et al.* (D0), Phys. Rev. **D60**, 052001 (1999), [hep-ex/9808029]; F. Abe *et al.* (CDF), Phys. Rev. Lett. **82**, 271 (1999), [Erratum: Phys. Rev. Lett.82,2808(1999)], [hep-ex/9810029].

[206] T. Aaltonen *et al.* (CDF), Phys. Rev. **D92**, 3, 032003 (2015), [arXiv:1505.00500].

[207] T. A. Aaltonen *et al.* (CDF), Phys. Rev. **D90**, 9, 091101 (2014), [arXiv:1409.4906].

[208] A. M. Sirunyan *et al.* (CMS), Eur. Phys. J. **C77**, 5, 354 (2017), [arXiv:1703.02530].

[209] T. Aaltonen *et al.* (CDF), Phys. Lett. **B698**, 371 (2011), [arXiv:1101.4926].

[210] CMS Collab., CMS-PAS-TOP-12-030.

[211] T. Aaltonen *et al.* (CDF), Phys. Rev. **D80**, 051104 (2009), [arXiv:0906.5371].

[212] ATLAS Collab., ATLAS-CONF-2019-046.

[213] V. Khachatryan *et al.* (CMS), Phys. Rev. **D93**, 9, 092006 (2016), [arXiv:1603.06536].

[214] V. Khachatryan *et al.* (CMS), JHEP **12**, 123 (2016), [arXiv:1608.03560].

[215] CMS Collab., CMS-PAS-TOP-15-002.

[216] CMS Collab., CMS-PAS-TOP-16-002.

[217] V. M. Abazov *et al.* (D0), Phys. Rev. Lett. **100**, 192004 (2008), [arXiv:0803.2779]; S. Chatrchyan *et al.* (CMS), Phys. Lett. **B728**, 496 (2014), [Erratum: Phys. Lett.B738,526(2014)], [arXiv:1307.1907]; V. M. Abazov *et al.* (D0), Phys. Lett. **B703**, 422 (2011), [arXiv:1104.2887]; ATLAS Collab., ATLAS-CONF-2019-041; U. Langenfeld, S. Moch and P. Uwer, Phys. Rev. **D80**, 054009 (2009), [arXiv:0906.5273]; J. Fuster *et al.*, Eur. Phys. J. C **77**, 11, 794 (2017), [arXiv:1704.00540].

[218] G. Aad *et al.* (ATLAS) (2019), [arXiv:1905.02302].

[219] CMS Collab., CMS-PAS-TOP-13-006 (2016).

[220] CDF Collab., CDF conference note 11080 (2014).

[221] V. M. Abazov *et al.* (D0), Phys. Rev. **D91**, 11, 112003 (2015), [arXiv:1501.07912].

[222] CMS Collab., CMS-PAS-TOP-13-005.

[223] A. H. Hoang, Ann. Rev. Nucl. Part. Sci. **70**, 225 (2020), [arXiv:2004.12915].

[224] M. Beneke *et al.*, Phys. Lett. **B775**, 63 (2017), [arXiv:1605.03609].

[225] A. H. Hoang, C. Lepenik and M. Preisser, JHEP **09**, 099 (2017), [arXiv:1706.08526].

[226] A. H. Hoang *et al.*, Phys. Rev. Lett. **101**, 151602 (2008), [arXiv:0803.4214].

[227] ATLAS Collab., ATL-PHYS-PUB-2021-034.

[228] A. M. Sirunyan *et al.*, Physics Letters B **803**, 135263 (2020), [arXiv:1909.09193].

[229] S. Catani *et al.*, JHEP **08**, 08, 027 (2020), [arXiv:2005.00557].

[230] G. Aad *et al.* (ATLAS), Phys. Lett. **B716**, 1 (2012), [arXiv:1207.7214].

[231] S. Chatrchyan *et al.* (CMS), Phys. Lett. **B716**, 30 (2012), [arXiv:1207.7235].

[232] G. Degrassi *et al.*, JHEP **08**, 098 (2012), [arXiv:1205.6497].

[233] S. Alekhin, A. Djouadi and S. Moch, Phys. Lett. **B716**, 214 (2012), [arXiv:1207.0980].

[234] T. Aaltonen *et al.* (CDF), Phys. Rev. **D87**, 5, 052013 (2013), [arXiv:1210.6131].

[235] V. M. Abazov *et al.* (D0), Phys. Rev. **D84**, 052005 (2011), [arXiv:1106.2063].

[236] G. Aad *et al.* (ATLAS), Phys. Lett. **B728**, 363 (2014), [arXiv:1310.6527].

[237] S. Chatrchyan *et al.* (CMS), JHEP **06**, 109 (2012), [arXiv:1204.2807].

[238] S. Chatrchyan *et al.* (CMS), Phys. Lett. **B770**, 50 (2017), [arXiv:1610.09551].

[239] G. Mahlon and S. J. Parke, Phys. Rev. **D53**, 4886 (1996), [hep-ph/9512264]; G. Mahlon and S. J. Parke, Phys. Lett. **B411**, 173 (1997), [hep-ph/9706304].

[240] G.R. Goldstein, in *Spin 96: Proceedings of the 12th International Symposium on High Energy Spin Physics,* Amsterdam, 1996, ed. C.W. Jager (World Scientific, Singapore, 1997), p. 328.

[241] T. Stelzer and S. Willenbrock, Phys. Lett. **B374**, 169 (1996), [hep-ph/9512292].

[242] W. Bernreuther *et al.*, Nucl. Phys. **B690**, 81 (2004), [hep-ph/0403035].

[243] A. Brandenburg, Z. G. Si and P. Uwer, Phys. Lett. **B539**, 235 (2002), [hep-ph/0205023].

[244] CDF Collab., CDF conference note 10719 (2011).

[245] CDF Collab., CDF conference note 10211 (2010).

Downloaded from https://academic.oup.com/ptep/article/2022/8/083C01/6651666 by KIT Library user on 27 September 2022

[246] V. M. Abazov *et al.* (D0), Phys. Lett. **B757**, 199 (2016), [arXiv:1512.08818].

[247] V. M. Abazov *et al.* (D0), Phys. Rev. **D95**, 1, 011101 (2017), [arXiv:1607.07627].

[248] V. M. Abazov *et al.* (D0), Phys. Rev. **D92**, 052007 (2015), [arXiv:1507.05666].

[249] G. Mahlon and S. J. Parke, Phys. Rev. **D81**, 074024 (2010), [arXiv:1001.3422].

[250] G. Aad *et al.* (ATLAS), Phys. Rev. **D90**, 11, 112016 (2014), [arXiv:1407.4314].

[251] G. Aad *et al.* (ATLAS), Phys. Rev. Lett. **114**, 14, 142001 (2015), [arXiv:1412.4742].

[252] G. Aad *et al.* (ATLAS), Phys. Rev. **D93**, 1, 012002 (2016), [arXiv:1510.07478].

[253] S. Chatrchyan *et al.* (CMS), Phys. Rev. Lett. **112**, 18, 182001 (2014), [arXiv:1311.3924].

[254] V. Khachatryan *et al.* (CMS), Phys. Lett. **B758**, 321 (2016), [arXiv:1511.06170].

[255] V. Khachatryan *et al.* (CMS), Phys. Rev. **D93**, 5, 052007 (2016), [arXiv:1601.01107].

[256] M. Aaboud *et al.* (ATLAS), Eur. Phys. J. C **80**, 8, 754 (2020), [arXiv:1903.07570].

[257] A. M. Sirunyan *et al.* (CMS), Phys. Rev. **D100**, 7, 072002 (2019), [arXiv:1907.03729].

[258] W. Bernreuther, D. Heisler and Z.-G. Si, JHEP **12**, 026 (2015), [arXiv:1508.05271].

[259] M. Aaboud *et al.* (ATLAS), JHEP **03**, 113 (2017), [arXiv:1612.07004].

[260] A. F. Falk and M. E. Peskin, Phys. Rev. **D49**, 3320 (1994), [hep-ph/9308241].

[261] T. A. Aaltonen *et al.* (CDF), Phys. Rev. Lett. **111**, 20, 202001 (2013), [arXiv:1308.4050].

[262] CMS Collab., CMS-PAS-TOP-16-019.

[263] M. Aaboud *et al.* (ATLAS), Eur. Phys. J. **C78**, 2, 129 (2018), [arXiv:1709.04207].

[264] ATLAS Collab., ATLAS-CONF-2019-038.

[265] V. M. Abazov *et al.* (D0), Phys. Rev. **D85**, 091104 (2012), [arXiv:1201.4156].

[266] G. L. Kane, G. A. Ladinsky and C. P. Yuan, Phys. Rev. **D45**, 124 (1992).

[267] A. Czarnecki, J. G. Korner and J. H. Piclum, Phys. Rev. **D81**, 111503 (2010), [arXiv:1005.2625].

[268] T. Aaltonen *et al.* (CDF, D0), Phys. Rev. **D85**, 071106 (2012), [arXiv:1202.5272].

[269] G. Aad *et al.* (ATLAS), JHEP **06**, 088 (2012), [arXiv:1205.2484].

[270] S. Chatrchyan *et al.* (CMS), JHEP **10**, 167 (2013), [arXiv:1308.3879].

[271] ATLAS and CMS Collab., ATLAS-CONF-2013-033, CMS-PAS-TOP-12-025.

[272] M. Aaboud *et al.* (ATLAS), Eur. Phys. J. **C77**, 4, 264 (2017), [Erratum: Eur. Phys. J.C79,no.1,19(2019)], [arXiv:1612.02577].

[273] V. Khachatryan *et al.* (CMS), Phys. Lett. **B762**, 512 (2016), [arXiv:1605.09047].

[274] CMS Collab., CMS-PAS-TOP-14-017.

[275] V. Khachatryan *et al.* (CMS), JHEP **01**, 053 (2015), [arXiv:1410.1154].

[276] G. Aad *et al.* (CMS, ATLAS), JHEP **08**, 08, 051 (2020), [arXiv:2005.03799].

[277] T. Aaltonen *et al.* (CDF), Phys. Rev. **D87**, 3, 031104 (2013), [arXiv:1211.4523].

[278] D. Choudhury, T. M. P. Tait and C. E. M. Wagner, Phys. Rev. **D65**, 053002 (2002), [hep-ph/0109097].

[279] D. Chang, W.-F. Chang and E. Ma, Phys. Rev. **D59**, 091503 (1999), [hep-ph/9810531]; D. Chang, W.-F. Chang and E. Ma, Phys. Rev. **D61**, 037301 (2000), [hep-ph/9909537].

[280] T. Aaltonen *et al.* (CDF), Phys. Rev. **D88**, 3, 032003 (2013), [arXiv:1304.4141].

[281] V. M. Abazov *et al.* (D0), Phys. Rev. **D90**, 5, 051101 (2014), [Erratum: Phys. Rev.D90,no.7,079904(2014)], [arXiv:1407.4837].

[282] G. Aad *et al.* (ATLAS), JHEP **11**, 031 (2013), [arXiv:1307.4568].

[283] CMS Collab., CMS-PAS-TOP-11-031.

[284] T. Aaltonen *et al.* (CDF), Phys. Rev. **D84**, 031104 (2011), [arXiv:1106.3970].

[285] G. Aad *et al.* (ATLAS), Phys. Rev. **D91**, 7, 072007 (2015), [arXiv:1502.00586].

[286] M. Aaboud *et al.* (ATLAS), JHEP **11**, 086 (2017), [arXiv:1706.03046].

[287] K. Melnikov, M. Schulze and A. Scharf, Phys. Rev. **D83**, 074013 (2011), [arXiv:1102.1967].

[288] A. M. Sirunyan *et al.* (CMS), JHEP **10**, 006 (2017), [arXiv:1706.08128].

[289] M. Aaboud *et al.* (ATLAS), Eur. Phys. J. **C79**, 5, 382 (2019), [arXiv:1812.01697].

[290] G. Bevilacqua *et al.*, JHEP **10**, 158 (2018), [arXiv:1803.09916].

[291] G. Bevilacqua *et al.*, JHEP **01**, 188 (2019), [arXiv:1809.08562].

[292] G. Aad *et al.* (ATLAS), JHEP **09**, 049 (2020), [arXiv:2007.06946].

[293] A. M. Sirunyan *et al.* (CMS), Phys. Lett. **B779**, 358 (2018), [arXiv:1712.02825].

[294] A. Tumasyan *et al.* (CMS) (2021), [arXiv:2107.01508].

[295] CMS Collab., CMS-PAS-TOP-21-004.

[296] A. M. Sirunyan *et al.* (CMS), Phys. Rev. Lett. **121**, 22, 221802 (2018), [arXiv:1808.02913].

[297] M. Cepeda *et al.* (HL/HE WG2 group) (2019), [arXiv:1902.00134].

[298] S. Chatrchyan *et al.* (CMS), Phys. Rev. Lett. **110**, 172002 (2013), [arXiv:1303.3239].

[299] J. M. Campbell and R. K. Ellis, JHEP **07**, 052 (2012), [arXiv:1204.5678].

[300] M. V. Garzelli *et al.*, JHEP **11**, 056 (2012), [arXiv:1208.2665].

[301] ATLAS Collab., ATLAS-CONF-2012-126.

[302] G. Aad *et al.* (ATLAS), JHEP **11**, 172 (2015), [arXiv:1509.05276].

[303] V. Khachatryan *et al.* (CMS), JHEP **01**, 096 (2016), [arXiv:1510.01131].

[304] M. Aaboud *et al.* (ATLAS), Phys. Rev. **D99**, 7, 072009 (2019), [arXiv:1901.03584].

[305] A. Broggio *et al.*, JHEP **08**, 039 (2019), [arXiv:1907.04343].

[306] G. Aad *et al.* (ATLAS), Eur. Phys. J. C **81**, 737 (2021), [arXiv:2103.12603].

[307] A. M. Sirunyan *et al.* (CMS), JHEP **08**, 011 (2018), [arXiv:1711.02547].

[308] A. M. Sirunyan *et al.* (CMS), JHEP **03**, 056 (2020), [arXiv:1907.11270].

[309] A. M. Sirunyan *et al.* (CMS), JHEP **07**, 003 (2017), [arXiv:1702.01404].

[310] CMS Collab., CMS-PAS-TOP-20-010.

[311] G. Aad *et al.* (ATLAS), JHEP **07**, 124 (2020), [arXiv:2002.07546].

[312] S. P. Martin 1–98 (1997), [Adv. Ser. Direct. High Energy Phys.18,1(1998)], [hep-ph/9709356].

Downloaded from https://academic.oup.com/ptep/article/2022/8/083C01/6651666 by KIT Library user on 27 September 2022

[313] C. T. Hill and E. H. Simmons, Phys. Rept. **381**, 235 (2003), [Erratum: Phys. Rept.390,553(2004)], [hep-ph/0203079].

[314] C. T. Hill, Phys. Lett. **B266**, 419 (1991).

[315] C. T. Hill, Phys. Lett. **B345**, 483 (1995), [hep-ph/9411426].

[316] A. M. Sirunyan *et al.* (CMS) (2019), [arXiv:1908.06463].

[317] C. Zhang and S. Willenbrock, Phys. Rev. **D83**, 034006 (2011), [arXiv:1008.3869].

[318] J. A. Aguilar-Saavedra, Nucl. Phys. **B843**, 638 (2011), [Erratum: Nucl. Phys.B851,443(2011)], [arXiv:1008.3562].

[319] D. Barducci *et al.* (2018), [arXiv:1802.07237].

[320] M. Aaboud *et al.* (ATLAS), Phys. Rev. D **99**, 5, 052009 (2019), [arXiv:1811.02305].

[321] Technical report, CERN, Geneva (2019), all figures including auxiliary ones are available at `https://atlas.web.cern.ch/Atlas/GROUPS/PHYSICS/CONFNOTES/ATLAS-CONF-2019-026`, URL `http://cds.cern.ch/record/2682109`.

[322] Technical report, CERN, Geneva (2021), all figures including auxiliary ones are available at `https://atlas.web.cern.ch/Atlas/GROUPS/PHYSICS/CONFNOTES/ATLAS-CONF-2021-027`, URL `http://cds.cern.ch/record/2773738`.

[323] Technical report, CERN, Geneva (2021), all figures including auxiliary ones are available at `https://atlas.web.cern.ch/Atlas/GROUPS/PHYSICS/CONFNOTES/ATLAS-CONF-2021-050`, URL `http://cds.cern.ch/record/2782534`.

[324] A. M. Sirunyan *et al.* (CMS), JHEP **06**, 146 (2020), [arXiv:1912.09540].

[325] A. M. Sirunyan *et al.* (CMS), Eur. Phys. J. C **79**, 11, 886 (2019), [arXiv:1903.11144].

[326] Technical report, CERN, Geneva (2021), URL `https://cds.cern.ch/record/2776770`.

[327] A. M. Sirunyan *et al.* (CMS), JHEP **03**, 095 (2021), [arXiv:2012.04120].

[328] CMS Collab., CMS-PAS-TOP-18-007 (2020).

[329] Technical report, CERN, Geneva (2019), URL `https://cds.cern.ch/record/2668721`.

[330] A. Tumasyan *et al.* (CMS) (2021), [arXiv:2107.13896].

[331] A. Buckley *et al.*, JHEP **04**, 015 (2016), [arXiv:1512.03360].

[332] N. P. Hartland *et al.*, JHEP **04**, 100 (2019), [arXiv:1901.05965].

[333] I. Brivio *et al.* (2019), [arXiv:1910.03606].

[334] G. Durieux *et al.*, JHEP **12**, 98 (2019), [Erratum: JHEP 01, 195 (2021)], [arXiv:1907.10619].

[335] J. Ellis *et al.*, JHEP **04**, 279 (2021), [arXiv:2012.02779].

[336] J. J. Ethier *et al.* (2021), [arXiv:2105.00006].

[337] V. Miralles *et al.* (2021), [arXiv:2107.13917].

[338] V. Barger, T. Han and D. G. E. Walker, Phys. Rev. Lett. **100**, 031801 (2008), [hep-ph/0612016].

[339] R. Frederix and F. Maltoni, JHEP **01**, 047 (2009), [arXiv:0712.2355].

[340] T. Aaltonen *et al.* (CDF), Phys. Rev. Lett. **110**, 12, 121802 (2013), [arXiv:1211.5363].

[341] D. Acosta *et al.* (CDF), Phys. Rev. Lett. **94**, 211801 (2005), [hep-ex/0501050].

[342] T. Aaltonen *et al.* (CDF), Phys. Rev. **D84**, 072003 (2011), [arXiv:1108.4755].

[343] A. Altheimer *et al.*, J. Phys. **G39**, 063001 (2012), [arXiv:1201.0008].

[344] A. M. Sirunyan *et al.* (CMS), JHEP **04**, 031 (2019), [arXiv:1810.05905].

[345] A. M. Sirunyan *et al.* (CMS), JHEP **07**, 001 (2017), [arXiv:1704.03366].

[346] A. M. Sirunyan *et al.* (CMS), JHEP **04**, 171 (2020), [arXiv:1908.01115].

[347] M. Aaboud *et al.* (ATLAS), Eur. Phys. J. **C78**, 7, 565 (2018), [arXiv:1804.10823].

[348] G. Aad *et al.* (ATLAS), JHEP **10**, 061 (2020), [arXiv:2005.05138].

[349] A. M. Sirunyan *et al.* (CMS), Phys. Lett. **B777**, 39 (2018), [arXiv:1708.08539].

[350] A. M. Sirunyan *et al.* (CMS), Phys. Lett. **B781**, 574 (2018), [arXiv:1708.01062].

[351] A. M. Sirunyan *et al.* (CMS), JHEP **08**, 073 (2017), [arXiv:1705.10967].

[352] A. M. Sirunyan *et al.* (CMS), Phys. Lett. **B772**, 634 (2017), [arXiv:1701.08328].

[353] V. Khachatryan *et al.* (CMS), Phys. Lett. **B771**, 80 (2017), [arXiv:1612.00999].

[354] A. M. Sirunyan *et al.* (CMS), JHEP **04**, 136 (2017), [arXiv:1612.05336].

[355] A. M. Sirunyan *et al.* (CMS), JHEP **05**, 029 (2017), [arXiv:1701.07409].

[356] A. M. Sirunyan *et al.* (CMS), Phys. Lett. B **820**, 136535 (2021), [arXiv:2104.04831].

[357] A. M. Sirunyan *et al.* (CMS) (2021), [arXiv:2104.12853].

[358] A. M. Sirunyan *et al.* (CMS), Phys. Rev. D **102**, 112004 (2020), [arXiv:2008.09835].

[359] M. Aaboud *et al.* (ATLAS), Phys. Lett. **B788**, 347 (2019), [arXiv:1807.10473].

[360] G. Aad *et al.* (ATLAS), JHEP **06**, 145 (2021), [arXiv:2102.10076].

[361] Technical report, CERN, Geneva (2021), all figures including auxiliary ones are available at `https://atlas.web.cern.ch/Atlas/GROUPS/PHYSICS/CONFNOTES/ATLAS-CONF-2021-024`, URL `http://cds.cern.ch/record/2773300`.

[362] M. Aaboud *et al.* (ATLAS), Phys. Rev. Lett. **121**, 21, 211801 (2018), [arXiv:1808.02343].

[363] Technical report, CERN, Geneva (2021), all figures including auxiliary ones are available at `https://atlas.web.cern.ch/Atlas/GROUPS/PHYSICS/CONFNOTES/ATLAS-CONF-2021-040`, URL `http://cds.cern.ch/record/2779174`.

[364] M. Aaboud *et al.* (ATLAS), JHEP **05**, 164 (2019), [arXiv:1812.07343].

[365] M. Aaboud *et al.* (ATLAS), JHEP **05**, 041 (2019), [arXiv:1812.09743].

[366] ATLAS Collab., ATLAS-CONF-2021-018 (2021).

[367] ATLAS Collab., ATLAS-CONF-2018-024 (2018).

[368] CMS Collab. CMS-PAS-TOP-12-042 (2013).

[369] V. Khachatryan *et al.* (CMS), JHEP **06**, 121 (2015), [arXiv:1504.03198].

[370] A. M. Sirunyan *et al.* (CMS), Eur. Phys. J. **C77**, 12, 845 (2017), [arXiv:1706.02581].

[371] A. M. Sirunyan *et al.* (CMS), JHEP **03**, 141 (2019), [arXiv:1901.01553].

[372] G. Aad *et al.* (ATLAS), JHEP **04**, 165 (2021), [arXiv:2102.01444].

[373] G. Aad *et al.* (ATLAS), Eur. Phys. J. C **81**, 860 (2021), [arXiv:2011.09308].

[374] Technical report, CERN, Geneva (2021), all figures including auxiliary ones are available at `https://atlas.web.cern.ch/Atlas/GROUPS/PHYSICS/CONFNOTES/ATLAS-CONF-2021-036`, URL `http://cds.cern.ch/record/2777863`.

[375] J. A. Aguilar-Saavedra, Acta Phys. Polon. **B35**, 2695 (2004), [hep-ph/0409342].

Downloaded from https://academic.oup.com/ptep/article/2022/8/083C01/6651666 by KIT Library user on 27 September 2022

[376] V. Khachatryan *et al.* (CMS), JHEP **02**, 028 (2017), [arXiv:1610.03545].

[377] CMS Collab., CMS-PAS-TOP-14-003.

[378] CMS Collab., CMS-PAS-TOP-17-003.

[379] V. Khachatryan *et al.* (CMS), JHEP **02**, 079 (2017), [arXiv:1610.04857].

[380] G. Aad *et al.* (ATLAS), Eur. Phys. J. **C76**, 2, 55 (2016), [arXiv:1509.00294].

[381] G. Aad *et al.* (ATLAS), Phys. Lett. **B800**, 135082 (2020), [arXiv:1908.08461].

[382] A. Heister *et al.* (ALEPH), Phys. Lett. **B543**, 173 (2002), [hep-ex/0206070]; J. Abdallah *et al.* (DELPHI), Phys. Lett. **B590**, 21 (2004), [hep-ex/0404014]; P. Achard *et al.* (L3), Phys. Lett. **B549**, 290 (2002), [hep-ex/0210041]; G. Abbiendi *et al.* (OPAL), Phys. Lett. **B521**, 181 (2001), [hep-ex/0110009].

[383] F. D. Aaron *et al.* (H1), Phys. Lett. **B678**, 450 (2009), [arXiv:0904.3876].

[384] H. Abramowicz *et al.* (ZEUS), Phys. Lett. **B708**, 27 (2012), [arXiv:1111.3901].

[385] M. Beneke *et al.*, in "1999 CERN Workshop on standard model physics (and more) at the LHC, CERN, Geneva, Switzerland, 25-26 May: Proceedings," 419–529 (2000), [hep-ph/0003033], URL `http://weblib.cern.ch/abstract?CERN-TH-2000-100`.

[386] V. F. Obraztsov, S. R. Slabospitsky and O. P. Yushchenko, Phys. Lett. **B426**, 393 (1998), [hep-ph/9712394].

[387] T. Carli, D. Dannheim and L. Bellagamba, Mod. Phys. Lett. **A19**, 1881 (2004), [hep-ph/0402012].

[388] V. M. Abazov *et al.* (D0), Phys. Rev. Lett. **102**, 092002 (2009), [arXiv:0901.0151].

[389] V.M. Abazov *et al.* (DØ Collab.), DØ conference note 5838 (2009).

[390] V. M. Abazov *et al.* (D0), Phys. Lett. **B708**, 21 (2012), [arXiv:1110.4592].

[391] ATLAS Collab., ATLAS-CONF-2013-032.

[392] T. Aaltonen *et al.* (CDF), Phys. Rev. Lett. **101**, 192002 (2008), [arXiv:0805.2109].

[393] V. M. Abazov *et al.* (D0), Phys. Lett. **B701**, 313 (2011), [arXiv:1103.4574].

[394] V. M. Abazov *et al.* (D0), Phys. Lett. **B693**, 81 (2010), [arXiv:1006.3575].

[395] S. Chatrchyan *et al.* (CMS), Phys. Rev. Lett. **112**, 17, 171802 (2014), [arXiv:1312.4194].

[396] A. M. Sirunyan *et al.* (CMS), JHEP **07**, 003 (2017), [arXiv:1702.01404].

[397] M. Aaboud *et al.* (ATLAS), JHEP **07**, 176 (2018), [arXiv:1803.09923].

[398] M. Aaboud *et al.* (ATLAS), Phys. Rev. D **98**, 11, 112010 (2018), [arXiv:1806.10555].

[399] A. M. Sirunyan *et al.* (CMS), JHEP **06**, 102 (2018), [arXiv:1712.02399].

[400] M. Aaboud *et al.* (ATLAS), JHEP **05**, 123 (2019), [arXiv:1812.11568].

Downloaded from https://academic.oup.com/ptep/article/2022/8/083C01/6651666 by KIT Library user on 27 September 2022

62. Form Factors for Semileptonic Kaon ($K_{\ell 3}$), Radiative Pion ($\pi_{\ell 2\gamma}$) and Kaon ($K_{\ell 2\gamma}$) Decays

Revised August 2021 by M.A. Bychkov (Virginia U.) and G. D'Ambrosio (INFN, Napoli).

62.1 $\pi^{\pm}_{\ell 2\gamma}$ and $K^{\pm}_{\ell 2\gamma}$ Form Factors

The radiative decays, $\pi^{\pm} \to l^{\pm}\nu\gamma$ and $K^{\pm} \to l^{\pm}\nu\gamma$, with l standing for an e or a μ, and γ for a real or virtual photon (e^+e^- pair), provide a powerful tool to investigate the hadronic structure of pions and kaons. The structure-dependent part SD_i of the amplitude describes the emission of photons from virtual hadronic states, and is parametrized in terms of form factors V, A, (vector, axial vector), in the standard description [1–4]. Note that in the Listings and some literature, equivalent nomenclature F_V and F_A for the vector and axial form factors is often used. Exotic, non-standard contributions like $i = T, S$ (tensor, scalar) have also been considered. Apart from the SD terms, there is also the Inner Bremsstrahlung amplitude, IB, corresponding to photon radiation from external charged particles and described by Low theorem in terms of the physical decay $\pi^{\pm}(K^{\pm}) \to l^{\pm}\nu$. Experiments try to optimize their kinematics so as to minimize the IB part of the amplitude.

The SD amplitude in its standard form is given as

$$M(\mathrm{SD}_V) = \frac{-eG_F U_{qq'}}{\sqrt{2}m_P}\epsilon^{\mu} l^{\nu} V^P \epsilon_{\mu\nu\sigma\tau} k^{\sigma} q^{\tau} \tag{62.1}$$

$$M(\mathrm{SD}_A) = \frac{-ieG_F U_{qq'}}{\sqrt{2}m_P}\epsilon^{\mu} l^{\nu}\{A^P[(qk-k^2)g_{\mu\nu} - q_{\mu}k_{\nu}] + R^P k^2 g_{\mu\nu}\}\ , \tag{62.2}$$

which contains an additional axial form factor R^P which only can be accessed if the photon remains virtual. $U_{qq'}$ is the Cabibbo-Kobayashi-Maskawa mixing-matrix element; ϵ^{μ} is the polarization vector of the photon (or the effective vertex, $\epsilon^{\mu} = (e/k^2)\overline{u}(p_-)\gamma^{\mu}v(p_+)$, of the e^+e^- pair); $\ell^{\nu} = \overline{u}(p_{\nu})\gamma^{\nu}(1-\gamma_5)v(p_{\ell})$ is the lepton-neutrino current; q and k are the meson and photon four-momenta ($k = p_+ + p_-$ for virtual photons); and P stands for π or K.

For decay processes where the photon is real, the partial decay width can be written in analytical form as a sum of IB, SD, and IB/SD interference terms INT [1, 4]:

$$\begin{aligned}\frac{d^2\Gamma_{P\to\ell\nu\gamma}}{dxdy} &= \frac{d^2\left(\Gamma_{\mathrm{IB}} + \Gamma_{\mathrm{SD}} + \Gamma_{\mathrm{INT}}\right)}{dxdy} \\ &= \frac{\alpha}{2\pi}\Gamma_{P\to\ell\nu}\frac{1}{(1-r)^2}\Bigg\{\mathrm{IB}(x,y) \\ &+ \frac{1}{r}\left(\frac{m_P}{2f_P}\right)^2\left[(V+A)^2\mathrm{SD}^+(x,y) + (V-A)^2\mathrm{SD}^-(x,y)\right] \\ &+ \epsilon_P\frac{m_P}{f_P}\left[(V+A)\mathrm{S}^+_{\mathrm{INT}}(x,y) + (V-A)\mathrm{S}^-_{\mathrm{INT}}(x,y)\right]\Bigg\}.\end{aligned} \tag{62.3}$$

Here

$$\begin{aligned}\mathrm{IB}(x,y) &= \left[\frac{1-y+r}{x^2(x+y-1-r)}\right] \\ &\quad \left[x^2 + 2(1-x)(1-r) - \frac{2xr(1-r)}{x+y-1-r}\right] \\ \mathrm{SD}^+(x,y) &= (x+y-1-r)\Big[(x+y-1)(1-x) - r\Big] \\ \mathrm{SD}^-(x,y) &= (1-y+r)\Big[(1-x)(1-y) + r\Big] \\ \mathrm{S}^+_{\mathrm{INT}}(x,y) &= \left[\frac{1-y+r}{x(x+y-1-r)}\right]\Big[(1-x)(1-x-y) + r\Big] \\ \mathrm{S}^-_{\mathrm{INT}}(x,y) &= \left[\frac{1-y+r}{x(x+y-1-r)}\right]\Big[x^2 - (1-x)(1-x-y) - r\Big]\end{aligned} \tag{62.4}$$

where $x = 2E_{\gamma}/m_P$, $y = 2E_{\ell}/m_P$, $r = (m_{\ell}/m_P)^2$, f_P is the meson decay constant, and ϵ_P is +1 for pions and -1 for kaons. The structure dependent terms SD^+ and SD^- are shown in Fig. 1. The SD^- term is maximized in the same kinematic region where overwhelming IB term dominates (along $x + y = 1$ diagonal). Thus experimental yields with less background are dominated by SD^+ contribution and proportional to $A^P + V^P$ making simultaneous precise determination of the form factors difficult.

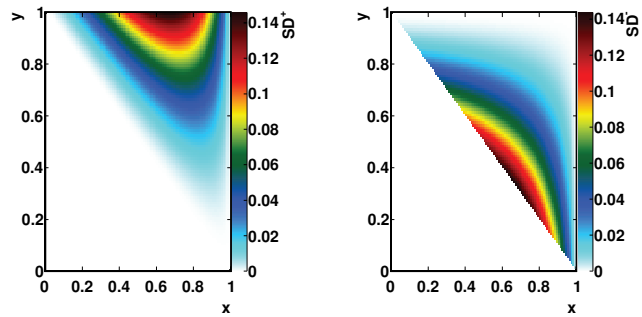

Figure 62.1: Components of the structure dependent terms of the decay width. Left: SD^+, right: SD^-

Recently, formulas 62.3 and 62.4 have been extended to describe polarized distributions in radiative meson and muon decays [5].

The "helicity" factor r is responsible for the enhancement of the SD over the IB amplitude in the decays $\pi^{\pm} \to e^{\pm}\nu\gamma$, while $\pi^{\pm} \to \mu^{\pm}\nu\gamma$ is dominated by IB. Interference terms are important for the decay $K^{\pm} \to \mu^{\pm}\nu\gamma$ [6], but contribute only a few percent correction to pion decays. However, they provide the basis for determining the signs of V and A. Radiative corrections to the decay $\pi^+ \to e^+\nu\gamma$ have to be taken into account in the analysis of the precision experiments. They make up to 4% corrections in the total decay rate [7]. In $\pi^{\pm} \to e^{\pm}\nu e^+e^-$ and $K^{\pm} \to \ell^{\pm}\nu e^+e^-$ decays, all three form factors, V^P, A^P, and R^P, can be determined [8, 9].

Theoretically, the first non-trivial χPT contributions to A^P and V^P appear at $\mathcal{O}(p^4)$ [4], respectively from Gasser-Leutwyler coefficients, L_i's, and the anomalous lagrangian:

$$A^P = \frac{4\sqrt{2}M_P}{F_{\pi}}(L^r_9 + L^r_{10}), \quad V^P = \frac{\sqrt{2}M_P}{8\pi^2 F_{\pi}}. \tag{62.5}$$

In case of the kaon $A^K = 0.042$ and $V^K = 0.096$. $\mathcal{O}(p^6)$ contributions to A^K can be predicted accurately: they are flat in the momentum dependence and shift the $\mathcal{O}(p^4)$ value to 0.034. $\mathcal{O}(p^6)$ contributions to V^K are model dependent and can be approximated by a form factor linearly dependent on momentum. For example, when looking at the spread of results obtained within two different models, the constant piece of this linear form factor is shifted to 0.078 ± 0.005 [1, 2, 4].

We give the experimental $\pi^{\pm}$ form factors V^{π}, A^{π}, and R^{π} in the Listings. In the $K^{\pm}$ Listings, we give the extracted sum $A^K + V^K$ and difference $A^K - V^K$, as well as V^K, A^K and R^K. In particular KLOE has measured for the constant piece of the form factor $A^K + V^K = 0.125 \pm 0.007 \pm 0.001$ [10] while ISTRA+, $V^K - A^K = 0.21 \pm 0.04 \pm 0.04$ [11].

The pion vector form factor, V^{π}, is related via CVC (Conserved Vector Current) to the $\pi^0 \to \gamma\gamma$ decay width. The constant term is given by $|V^{\pi}(0)| = (1/\alpha)\sqrt{2\Gamma_{\pi^0\to\gamma\gamma}/\pi m_{\pi^0}}$ [3]. The resulting value, $V^{\pi}(0) = 0.0259(9)$, has been confirmed by calculations based on chiral perturbation theory (χPT) [4], and by two experiments given in the Listings.

A recent experiment by the PIBETA collaboration [12] obtained a $V^{\pi}(0)$ that is in excellent agreement with the CVC hypothesis. It also measured the slope parameter a in $V^{\pi}(s) = V^{\pi}(0)(1+a\cdot s)$, where $s = (1-2E_{\gamma}/m_{\pi})$, and E_{γ} is the gamma energy in the pion rest frame: $a = 0.095 \pm 0.058$. A functional dependence on s is expected for all form factors. It becomes non-negligible in the

Downloaded from https://academic.oup.com/ptep/article/2022/8/083C01/6651666 by KIT Library user on 27 September 2022

case of $V^\pi(s)$ when a wide range of photon momenta is recorded; proper treatment in the analysis of K decays is mandatory.

The form factor, R^P, can be related to the electromagnetic radius, r_P, of the meson [2]: $R^P = \frac{1}{3} m_P f_P \langle r_P^2 \rangle$ using PCAC (Partial Conserved Axial vector Current).

In lowest order χPT, the ratio A^π/V^π is related to the pion electric polarizability $\alpha_E = [\alpha/(8\pi^2 m_\pi f_\pi^2)] \times A^\pi/V^\pi$ [13]. Direct experimental and theoretical status of pion polarizability studies currently is not settled. Most recent theoretical predictions from χPT at $\mathcal{O}(p^6)$ [14] and experimental results from COMPASS collaboration [15] favor a small value of pion polarizability $\alpha_\pi \sim (2 \div 3) \times 10^{-4}\,\mathrm{fm}^3$. Dispersive analysis of $\gamma\gamma \to \pi^+\pi^-$ crossection [16] and experimental results from MAMI collaboration [17] report a much larger value of $\alpha_\pi \sim 6 \times 10^{-4}\,\mathrm{fm}^3$. Precise measurement of the pion form factors by PIBETA collaboration favors smaller values of polarizability $\alpha_\pi = 2.7^{+0.6}_{-0.5} \times 10^{-4}\,\mathrm{fm}^3$.

Several searches for the exotic form factors F_T^π, F_T^K (tensor), and F_S^K (scalar) have been pursued in the past. In particular, F_T^π has been brought into focus by experimental as well as theoretical work [18]. New high-statistics data from the PIBETA collaboration have been re-analyzed together with an additional data set optimized for low backgrounds in the radiative pion decay. In particular, lower beam rates have been used in order to reduce the accidental background, thereby making the treatment of systematic uncertainties easier and more reliable. The PIBETA analysis now restricts F_T^π to the range $-5.2 \times 10^{-4} < F_T^\pi < 4.0 \times 10^{-4}$ at a 90% confidence limit [12]. This result is in excellent agreement with the most recent theoretical work [4].

Precision measurements of radiative pion and kaon decays are effective tools to study QCD in the non-perturbative region and are of interest beyond the scope of radiative decays. Meanwhile other processes such as $\pi^+ \to e^+\nu$ that seem to be better suited to search for new physics at the precision frontier are currently studied. The advantages of such process are the very accurate and reliable theoretical predictions and the more straightforward experimental analysis.

62.2 $K_{\ell 3}^\pm$ and $K_{\ell 3}^0$ Form Factors

Assuming that only the vector current contributes to $K \to \pi\ell\nu$ decays, we write the matrix element as

$$M \propto f_+(t)\left[(P_K + P_\pi)_\mu \bar{\ell}\gamma_\mu(1+\gamma_5)\nu\right] + f_-(t)\left[m_\ell \bar{\ell}(1+\gamma_5)\nu\right] , \tag{62.6}$$

where P_K and P_π are the four-momenta of the K and π mesons, m_ℓ is the lepton mass, and f_+ and f_- are dimensionless form factors which can depend only on $t = (P_K - P_\pi)^2$, the square of the four-momentum transfer to the leptons. If time-reversal invariance holds, f_+ and f_- are relatively real. $K_{\mu 3}$ experiments, discussed immediately below, measure f_+ and f_-, while K_{e3} experiments, discussed further below, are sensitive only to f_+ because the small electron mass makes the f_- term negligible.

62.2.1 $K_{\mu 3}$ *Decays*

Analyses of $K_{\mu 3}$ data frequently assume a linear dependence of f_+ and f_- on t, *i.e.*,

$$f_\pm(t) = f_\pm(0)\left[1 + \lambda_\pm (t/m_{\pi^+}^2)\right] . \tag{62.7}$$

Most $K_{\mu 3}$ data are adequately described by formula 62.7 for f_+ and a constant f_- (*i.e.*, $\lambda_- = 0$).

There are two equivalent parametrizations commonly used in these analyses: $\lambda_+, \xi(0)$ parametrization and λ_+, λ_0 parametrization.

Older analyses of $K_{\mu 3}$ data often introduce the ratio of the two form factors

$$\xi(t) = f_-(t)/f_+(t) . \tag{62.8}$$

The $K_{\mu 3}$ decay distribution is then described by the two parameters λ_+ and $\xi(0)$ (assuming time reversal invariance and $\lambda_- = 0$).

More recent $K_{\mu 3}$ analyses have parametrized in terms of the form factors f_+ and f_0, which are associated with vector and scalar exchange, respectively, to the lepton pair. f_0 is related to f_+ and f_- by

$$f_0(t) = f_+(t) + \left[t/(m_K^2 - m_\pi^2)\right] f_-(t) . \tag{62.9}$$

Here $f_0(0)$ must equal $f_+(0)$. The earlier assumption that f_+ is linear in t and f_- is constant leads to f_0 linear in t:

$$f_0(t) = f_0(0)\left[1 + \lambda_0 (t/m_{\pi^+}^2)\right] . \tag{62.10}$$

With the assumption that $f_0(0) = f_+(0)$, the two parametrizations, $(\lambda_+, \xi(0))$ and (λ_+, λ_0) are equivalent as long as correlation information is retained. (λ_+, λ_0) correlations tend to be less strong than $(\lambda_+, \xi(0))$ correlations.

Since the 2006 edition of the *Review* [19], we no longer quote results in the $(\lambda_+, \xi(0))$ parametrization. We have removed many older low statistics results from the Listings. See the 2004 version of this note [20] for these older results, and the 1982 version [21] for additional discussion of the $K_{\mu 3}^0$ parameters, correlations, and conversion between parametrizations.

More recent high-statistics experiments have included a quadratic term in the expansion of $f_+(t)$,

$$f_+(t) = f_+(0)\left[1 + \lambda_+^{'}(t/m_{\pi^+}^2) + \frac{\lambda_+^{''}}{2}(t/m_{\pi^+}^2)^2\right] . \tag{62.11}$$

If there is a non-vanishing quadratic term, then λ_+ of formula 62.7 represents the average slope, which is then different from $\lambda_+^{'}$. Our convention is to include the factor $\frac{1}{2}$ in the quadratic term, and to use m_{π^+} even for K_{e3}^+ and $K_{\mu 3}^+$ decays. We have converted other's parametrizations to match our conventions, as noted in the beginning of the "$K_{\ell 3}^\pm$ and $K_{\ell 3}^0$ Form Factors" sections of the Listings.

There are two alternatives to the Taylor parametrization: The Pole Parametrization and Dispersive Parametrization.

The pole model describes the t-dependence of $f_+(t)$ and $f_0(t)$ in terms of the exchange of the lightest vector and scalar K^* mesons with masses M_V and M_S, respectively:

$$f_+(t) = f_+(0)\left[\frac{M_V^2}{M_V^2 - t}\right] , \quad f_0(t) = f_0(0)\left[\frac{M_S^2}{M_S^2 - t}\right] . \tag{62.12}$$

The Dispersive Parametrization approach, valid in a much wider kinematic range and able to describe at the same time τ-decay data, [22] uses dispersive techniques and the known low-energy K-π phases to parametrize the vector and scalar form factors:

$$f_+(t) = f_+(0)\exp\left[\frac{t}{m_\pi^2}(\Lambda_+ + H(t))\right]; \tag{62.13}$$

$$f_0(t) = f_+(0)\exp\left[\frac{t}{(m_K^2 - m_\pi^2)}\,(ln[C] - G(t))\right], \tag{62.14}$$

where Λ_+ is the slope of the vector form factor, and $\ln C = \ln[f_0(m_K^2 - m_\pi^2)]$ is the logarithm of the scalar form factor at the Callan-Treiman point. The functions $H(t)$ and $G(t)$ are dispersive integrals.

62.2.2 K_{e3} *Decays*

Analysis of K_{e3} data is simpler than that of $K_{\mu 3}$ because the second term of the matrix element assuming a pure vector current [formula 62.6 above] can be neglected. Here f_+ can be assumed to be linear in t, in which case the linear coefficient λ_+ of formula 62.7 is determined, or quadratic, in which case the linear coefficient $\lambda_+^{'}$ and quadratic coefficient $\lambda_+^{''}$ of formula 62.11 are determined.

If we remove the assumption of a pure vector current, then the matrix element for the decay, in addition to the terms in formula 62.6, would contain

$$+2m_K\, f_S\, \bar{\ell}(1+\gamma_5)\nu + (2f_T/m_K)(P_K)_\lambda (P_\pi)_\mu\, \bar{\ell}\,\sigma_{\lambda\mu}(1+\gamma_5)\nu , \tag{62.15}$$

Downloaded from https://academic.oup.com/ptep/article/2022/8/083C01/6651666 by KIT Library user on 27 September 2022

where f_S is the scalar form factor, and f_T is the tensor form factor. In the case of the K_{e3} decays where the f_- term can be neglected, experiments have yielded limits on $|f_S/f_+|$ and $|f_T/f_+|$.

For K_{e3} data, we determine best values for the three parametrizations: linear (λ_+), quadratic ($\lambda_+^{'}$, $\lambda_+^{''}$) and pole (M_V). For $K_{\mu 3}$ data, we determine best values for the three parametrizations: linear (λ_+, λ_0), quadratic ($\lambda_+^{'}, \lambda_+^{''}$, λ_0) and pole (M_V, M_S). We then assume $\mu - e$ universality so that we can combine K_{e3} and $K_{\mu 3}$ data, and again determine best values for the three parametrizations: linear (λ_+, λ_0), quadratic ($\lambda_+^{'}, \lambda_+^{''}$, λ_0), and pole (M_V, M_S). When there is more than one parameter, fits are done including input correlations. Simple averages suffice in the two K_{e3} cases where there is only one parameter: linear (λ_+) and pole (M_V).

A comprehensive global analysis of the semileptonic kaon decay data and its effect on the CKM unitarity debate can be found in [23, 24]. An update on experimental data including NA48/2 newest results can be found in [25].

Both KTeV and KLOE see an improvement in the quality of their fits relative to linear fits when a quadratic term is introduced, as well as when the pole parametrization is used. The quadratic parametrization has the disadvantage that the quadratic parameter $\lambda_+^{''}$ is highly correlated with the linear parameter $\lambda_+^{'}$, in the neighborhood of 95%, and that neither parameter is very well determined. The pole fit has the same number of parameters as the linear fit, but yields slightly better fit probabilities, so that it would be advisable for all experiments to include the pole parametrization as one of their choices.

The "Kaon Particle Listings" show the results with and without assuming μ-e universality. The "Meson Summary Tables" show all of the results assuming μ-e universality, but most results not assuming μ-e universality are given only in the Listings.

References

[1] D. A. Bryman, P. Depommier and C. Leroy, Phys. Rept. **88**, 151 (1982), see our note on "Decay Constants of Charged Pseudoscalar Mesons" elsewhere in this *Review*; S. G. Brown and S. A. Bludman, Phys. Rev. **136**, B1160 (1964); P. DeBaenst and J. Pestieau, Nuovo Cimento **A53**, 137 (1968).

[2] W. T. Chu, T. Ebata and D. M. Scott, Phys. Rev. **166**, 1577 (1968); D. Yu. Bardin and E. A. Ivanov, Sov. J. Part. Nucl. **7**, 286 (1976), [Fiz. Elem. Chast. Atom. Yadra7,726(1976)]; A. Kersch and F. Scheck, Nucl. Phys. **B263**, 475 (1986).

[3] V.G. Vaks and B.L. Ioffe, Nuovo Cimento **10**, 342 (1958); V.F. Muller, Z. Phys. **173**, 438 (1963).

[4] C. Q. Geng, I.-L. Ho and T. H. Wu, Nucl. Phys. **B684**, 281 (2004), [hep-ph/0306165]; J. Bijnens and P. Talavera, Nucl. Phys. **B489**, 387 (1997), [hep-ph/9610269]; V. Mateu and J. Portoles, Eur. Phys. J. **C52**, 325 (2007), [arXiv:0706.1039]; R. Unterdorfer and H. Pichl, Eur. Phys. J. **C55**, 273 (2008), [arXiv:0801.2482]; V. Cirigliano *et al.*, Rev. Mod. Phys. **84**, 399 (2012), [arXiv:1107.6001].

[5] E. Gabrielli and L. Trentadue, Nucl. Phys. **B792**, 48 (2008), [hep-ph/0507191].

[6] S. Adler *et al.* (E787), Phys. Rev. Lett. **85**, 2256 (2000), [hep-ex/0003019].

[7] E. A. Kuraev, Yu. M. Bystritsky and E. P. Velicheva, Phys. Rev. **D69**, 114004 (2004), [hep-ph/0310275]; R. Unterdorfer and H. Pichl have treated radiative corrections of the structure terms to lowest order within χPT for the first time. See the reference under [4].

[8] S. Egli *et al.* (SINDRUM), Phys. Lett. **B175**, 97 (1986).

[9] A. A. Poblaguev *et al.*, Phys. Rev. Lett. **89**, 061803 (2002), [hep-ex/0204006].

[10] F. Ambrosino *et al.* (KLOE), Eur. Phys. J. **C64**, 627 (2009), [Erratum: Eur. Phys. J.65,703(2010)], [arXiv:0907.3594].

[11] V. A. Duk *et al.* (ISTRA+), Phys. Lett. **B695**, 59 (2011), [arXiv:1005.3517].

[12] D. Pocanic *et al.*, Phys. Rev. Lett. **93**, 181803 (2004), [hep-ex/0312030]; E. Frlez *et al.*, Phys. Rev. Lett. **93**, 181804 (2004), [hep-ex/0312029]; M. Bychkov *et al.*, Phys. Rev. Lett. **103**, 051802 (2009), [arXiv:0804.1815].

[13] J. F. Donoghue and B. R. Holstein, Phys. Rev. **D40**, 2378 (1989).

[14] J. Gasser, M. A. Ivanov and M. E. Sainio, Nucl. Phys. **B745**, 84 (2006), [hep-ph/0602234].

[15] C. Adolph *et al.* (COMPASS), Phys. Rev. Lett. **114**, 062002 (2015), [arXiv:1405.6377].

[16] L. V. Fil'kov and V. L. Kashevarov, Phys. Rev. **C73**, 035210 (2006), [arXiv:nucl-th/0512047].

[17] J. Ahrens *et al.*, Eur. Phys. J. **A23**, 113 (2005), [arXiv:nucl-ex/0407011].

[18] A. A. Poblaguev, Phys. Lett. **B238**, 108 (1990); V. N. Bolotov *et al.*, Phys. Lett. **B243**, 308 (1990); V. M. Belyaev and I. I. Kogan, Phys. Lett. **B280**, 238 (1992); A. V. Chernyshev *et al.*, Mod. Phys. Lett. **A12**, 1669 (1997); A. A. Poblaguev, Phys. Rev. **D68**, 054020 (2003), [hep-ph/0307166]; M. V. Chizhov, Phys. Part. Nucl. Lett. **2**, 193 (2005), [Pisma Fiz. Elem. Chast. Atom. Yadra2005,no.4,7(2005)], [hep-ph/0402105].

[19] W. Yao *et al.*, Journal of Physics G: Nuclear and Particle Physics **33**, 1 (2006), ISSN 0954-3899.

[20] S. Eidelman *et al.*, Physics Letters B **592**, 1, 1 (2004), ISSN 0370-2693, review of Particle Physics, URL `https://www.sciencedirect.com/science/article/pii/S0370269304007579`.

[21] M. Roos *et al.*, Physics Letters B **111**, i (1982), ISSN 0370-2693, URL `https://www.sciencedirect.com/science/article/pii/0370269382912862`.

[22] V. Bernard *et al.*, Physics Letters B **638**, 5, 480 (2006), ISSN 0370-2693, URL `https://www.sciencedirect.com/science/article/pii/S0370269306006812`; A. Lai *et al.*, Physics Letters B **647**, 5, 341 (2007), ISSN 0370-2693, URL `https://www.sciencedirect.com/science/article/pii/S0370269307002432`.

[23] M. Antonelli *et al.* (FlaviaNet Working Group on Kaon Decays), Eur. Phys. J. C **69**, 399 (2010), [arXiv:1005.2323].

[24] C.-Y. Seng *et al.* (2021), [arXiv:2107.14708].

[25] J. R. Batley *et al.* (NA48/2), JHEP **10**, 150 (2018), [arXiv:1808.09041].

[26] L.-M. Chounet, J.-M. Gaillard and M. Gaillard, Physics Reports **4**, 5, 199 (1972), ISSN 0370-1573, URL `https://www.sciencedirect.com/science/article/pii/037015737290018X`.

[27] H. W. Fearing, E. Fischbach and J. Smith, Phys. Rev. D **2**, 542 (1970), URL `https://link.aps.org/doi/10.1103/PhysRevD.2.542`.

[28] N. Cabibbo and A. Maksymowicz, Phys. Lett. **9**, 352 (1964).

Downloaded from https://academic.oup.com/ptep/article/2022/8/083C01/6651666 by KIT Library user on 27 September 2022

63. Spectroscopy of Light Meson Resonances

Written August 2021 by C. Amsler (Stefan Meyer Inst.), S. Eidelman (Budker Inst., Novosibirsk; Novosibirsk U.), A. Masoni (INFN, Cagliari) and G. Venanzoni (INFN, Pisa).

63.1 Introduction . . . 845
63.2 Scalar mesons . . . 845
63.3 Glueballs . . . 847
63.3.1 Scalar glueballs . . . 847
63.3.2 Tensor glueballs . . . 848
63.4 Pseudoscalar mesons . . . 848
63.5 Vector mesons . . . 849
63.5.1 The $\rho(770)$ meson . . . 849
63.5.2 The $\rho(770)$ excitations . . . 850
63.6 Axial-vector mesons . . . 850
63.7 Hybrid mesons . . . 851
63.8 Tetraquark states . . . 851
63.9 Baryonia . . . 852
63.10 Conclusions . . . 852

63.1 Introduction

According to the constituent quark model, a light meson consists of a color singlet quark-antiquark pair made of the u, d, or s quarks and the $\overline{u}$, $\overline{d}$, or $\overline{s}$ antiquarks, grouped into a flavor multiplet of SU(3). However, additional mesons made of bound gluons (glueballs) could exist in the same mass range, suggested by the self coupling of gluons in QCD. Multiquark structures are also possible, such as quark-antiquark pairs with an excited gluon (hybrid mesons). Tetraquarks are compact color singlets of diquark-antidiquark pairs ($qq\overline{q}\overline{q}$) or 'molecular' bound states of two mesons ($q\overline{q}q\overline{q}$). More complex systems such as $qqq\overline{q}\overline{q}\overline{q}$ (baryonia) are also predicted.

Fundamentals on the constituent quark model on light and heavy mesons and baryons (including hadrons with charm and bottom quarks), and on predictions from lattice gauge theories, are described in 'Quark Model' in this issue of the *Review of Particle Physics*, henceforth called the *Review*. In the present text we describe the experimental spectrum of light mesons and their classifications within the constituent quark model, with emphasis on states exhibiting properties incompatible with $q\bar{q}$ structures. The discussion is driven by the results entered in the database of the *Review*. The spectrum of kaon excitations is much less clear cut and therefore deferred to a future edition, when further data might become available. More detailed discussions on exotic mesons – including those involving the c and b quarks – can be found in Refs. [1–7] and in 'Heavy Non-$q\bar{q}$ Mesons' of the *Review*. For more information on the meson (and baryon) spectrum of light (and heavy) quarks we refer to the textbook [8].

Figure 63.1 shows the mass spectrum of $q\bar{q}$ mesons. The mass (vertical axis) increases with orbital excitations ℓ (horizontal axis) and radial excitation n. In the quark model one uses the notation nS, nP, nD... for the radial excitations ($n = 1$ for the ground states), in contrast to the usual $1s$, $2p$, $3d$... notation in atomic physics. Each box represents an SU(3) nonet containing multiplets of the isospin i, three isovectors, two strange isodoublets, and two isosinglets (one SU(3) singlet and one SU(3) octet). The spin, parity $[P = -(-1)^{\ell}]$ and C-parity $[C = (-1)^{\ell+s}]$ take the possible values $J^{PC} = 0^{++}$ (scalar), 0^{-+} (pseudoscalar), 1^{--} (vector), $1^{+\pm}$ (axial- or pseudovector), 2^{++} (tensor), etc. Therefore mesons with the *exotic* quantum numbers 0^{--}, 0^{+-}, 1^{-+}, 2^{+-}, 3^{-+}, etc. cannot be $q\bar{q}$ states. Note that the C-parity is defined only for the electrically neutral non-strange nonet members.

The two isosinglets in each nonet mix with an angle θ close to the *ideal* value of 35.3° for the 1^{--}, $1^{+\pm}$, 2^{++} and 3^{--} nonets, in which case the isosinglets decouple to $u\overline{u}+d\overline{d}$ and $s\overline{s}$. The orbital excitations $\ell \geq 1$ consist of four nonets for each value of n, since $j = \ell$ for antiparallel quark spins and $j = \ell-1, \ell$ or $\ell+1$ for parallel spins. Since the C-parity is not defined for strange mesons, the K_{1A} and K_{1B} in the axial vector 1^{++} and 1^{+-} nonets of fig. 63.1 are mathematical constructs which mix to give the observed $K_1(1270)$ and $K_1(1400)$ mesons.

As described in more detail below (section 63.2), it is hard to accommodate all the known scalar mesons in the lower $q\bar{q}$ nonets: The light scalar mesons $a_0(980)$, $K_0^*(700)$ (also known as κ), the $f_0(500)$ (also known as σ), and the $f_0(980)$, not shown in the figure, could build the lightest nonet, but could also be two-meson resonances or tetraquarks (section 63.8). Furthermore, the ground state glueball expected below 2 GeV will mix with the $q\bar{q}$ isoscalar scalar mesons (section 63.3.1). The pseudoscalar slot labeled $\eta(1440)$ may consist of two states (section 63.4). The status of vector meson excitations is described in section 63.5. The axial-vector meson $f_1(1420)$ could be replaced in the 1^{++} nonet by the $f_1(1510)$ which, however, needs confirmation (see the *Listings* and section 63.6). Mesons with exotic quantum numbers are discussed in section 63.7.

63.2 Scalar mesons

Scalar mesons decay dominantly into pairs of pseudoscalar mesons ($\pi\pi$, $K\overline{K}$, $\pi\eta$, $\eta\eta$ or $\eta\eta'$). The widths tend to be large for those decaying into $\pi\pi$, due to the absence of angular momentum barrier and the large available phase space. Identifying broad overlapping states is not straightforward. Furthermore, the onset of the $K\overline{K}$, $\eta\eta$ or $\eta\eta'$ thresholds distorts the line shapes and produces cusps. This requires high statistics data and the use of coupled channel analyses taking into account unitarity and analyticity (see 'Resonances' in the *Review*). The SU(3) classification is also not easy, because the ground state scalar glueball and multiquark states are predicted to exist below 2 GeV.

Two isovector scalars are known, the $a_0(980)$ and the $a_0(1450)$. Five isoscalar resonances are established: the very broad $f_0(500)$, the $f_0(980)$, the broad $f_0(1370)$, and the comparatively narrow $f_0(1500)$ and $f_0(1710)$. The strange partners are the $K_0^*(700)$ and the $K_0^*(1430)$. The $f_0(500)$ and $K_0^*(700)$ deserve a separate treatment and can be found in 'Scalar Mesons below 1 GeV', which contains more details on the $a_0(980)$ and $f_0(980)$, briefly reviewed in section 63.8.

The $a_0(1450)$ was first reported by the Crystal Barrel experiment in $\bar{p}p$ annihilation with stopped antiprotons [9] (see [10] for a review of Crystal Barrel results). Its mass of about 1450 MeV is not far from that of the $a_2(1320)$ meson. An isovector scalar, possibly the $a_0(1450)$ (albeit at a lower mass of 1317 MeV) is observed by Belle in $\gamma\gamma$ collisions leading to $\eta\pi^0$ [11]. The state interferes destructively with the non-resonant background. Its $\gamma\gamma$ coupling is comparable to that of the $a_2(1320)$, in accord with simple predictions (see *e.g.* [12]). A contribution from $a_0(1450) \to K\bar{K}$ is also found in the CLEO-c analysis of $D^{\pm} \to K^+K^-\pi^{\pm}$ [13] and $D^0 \to K_S^0K^{\pm}\pi^{\mp}$ from LHCb [14].

The $f_0(1370)$ and $f_0(1500)$ were observed by Crystal Barrel [15–17] and by WA102 in central production with 450 GeV protons [18,19]. They decay mostly into 2π and 4π. The $f_0(1500)$ was also observed to decay into $\eta\eta$ [20–22] and $\eta\eta'$ [23]. All data agree that the 4π decay mode represents about half of the $f_0(1500)$ decay width, but is dominant for $f_0(1370)$.

The determination of the $\pi\pi$ coupling of the very broad $f_0(1370)$ is complicated by its interference with the $f_0(500)$ and $f_0(1500)$. Its existence is questioned by COMPASS from $\pi^-p \to \pi^-\pi^-\pi^+p$ data [24]. In $\overline{B}_s^0 \to J/\psi(1S)\pi^+\pi^-$ from LHCb a strong scalar contribution from the $f_0(1370)$ was initially observed [25], although new data require the $f_0(500)$ and $f_0(1500)$, without any need for the $f_0(1370)$ [26]. In $\overline{B}^0 \to J/\psi(1S)\pi^+\pi^-$ the $\pi\pi$ mass spectrum does not show any significant scalar component above ∼1.2 GeV [27] (an analysis that is however challenged in [28]). $D^0 \to \pi^+\pi^-\pi^+\pi^-$ data from CLEO-c also require a contribution from $f_0(500)f_0(1370) \to 4\pi$ [29]. A broad 2π signal is also observed by BaBar around 1400 MeV in the decay $B^{\pm} \to \pi^{\pm}\pi^{\pm}\pi^{\mp}$ [30] which is attributed to the $f_0(1370)$, but could also be due to the $f_0(1500)$.

In Refs. [31, 32] the $f_0(1370)$ and $f_0(1710)$ (together with the $f_2(1270)$ and $f_2'(1525)$) are interpreted as bound systems of two vector mesons. This view is challenged in Ref. [33] where in a covariant formalism, e.g. the $f_2(1270)$ does not appear as a $\rho\rho$ bound state. Photoproduction data of the $f_2(1270)$ in $\gamma p \to \pi^0\pi^0p$ from CLAS [34], as a function of momentum trans-

Downloaded from https://academic.oup.com/ptep/article/2022/8/083C01/6651666 by KIT Library user on 27 September 2022

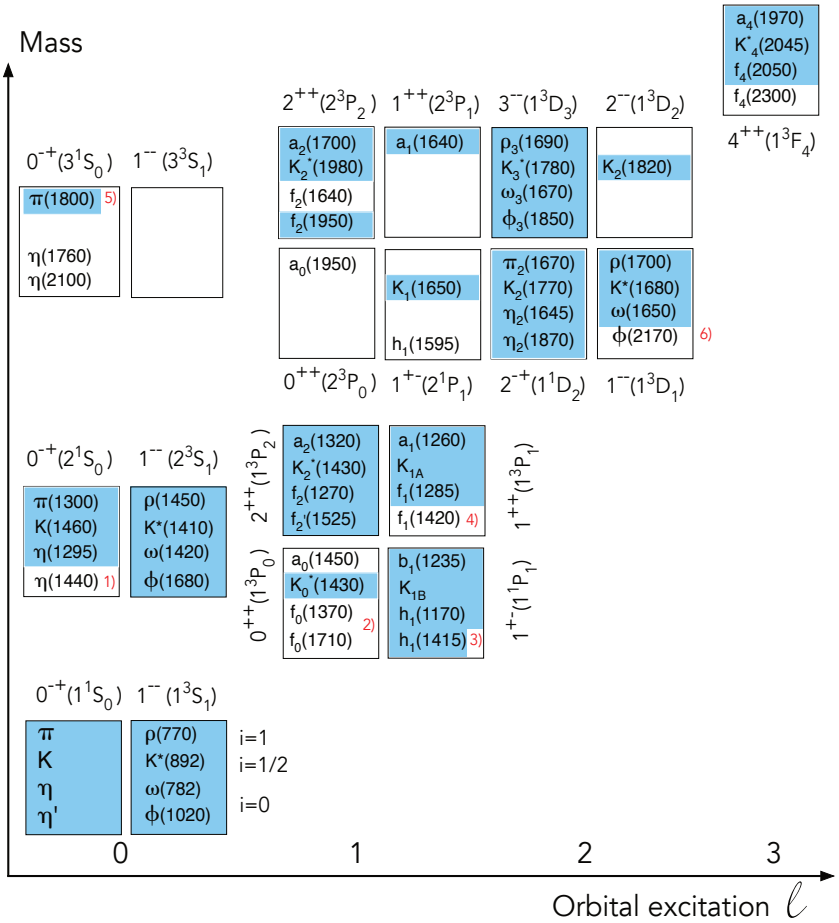

Figure 63.1: The mesons made of the u, d, and s light quarks are organised in $J^{PC}(n^{2s+1}\ell_j)$ nonets with isospin i. The established mesons (which appear in the *Summary Table* of the *Review*) are shown in the dark (blue) areas. The white areas contain those omitted in the *Summary Table* but reported in the *Listings*, or the established ones with a tentative nonet classification. States with the same J^{PC} mix, such as the 2^3S_1 and 1^3D_1 mesons. The states become broad and overlap with increasing masses, which complicates the determination of the resonance parameters *e.g.* mass, width and spin. For a complete list of mesons see the *Listings*.
[1] The $\eta(1440)$ stands for the $\eta(1405)$ and the $\eta(1475)$, section 63.4.
[2] The classification of the scalar nonet is controversial. Alternative schemes involve the $f_0(1500)$ and the light scalars below 1 GeV, section 63.2.
[3] Considered established, but more data would be desirable.
[4] An alternative to the $f_1(1420)$ is the $f_1(1510)$, section 63.6.
[5] The $\pi(1800)$ has also been proposed as a hybrid meson, section 63.7.
[6] The $\phi(2170)$ has also been proposed as a tetraquark state, section 63.8.

fer, also disagree with predictions [35] for the $f_2(1270)$ to be a $\rho\rho$ bound state.

While the $K\bar{K}$ decay branching ratio of the $f_0(1500)$ is small [18] [36], the $f_0(1710)$ decays dominantly into $K\bar{K}$. The $f_0(1710)$ is not observed in $p\bar{p}$ annihilation at rest [36] and only weakly produced in $p\bar{p}$ annihilation in flight [37], with a rate strongly suppressed compared to that of the $f_0(1500)$ ($\sim$7%). For comparison, the rate for the $(s\bar{s})$ $f_2'(1525)$ is about 9% that of the $(u\bar{u}+d\bar{d})$ $f_2(1270)$, as expected from the OZI rule [37]. On the other hand the $f_0(1370)$ does not couple strongly to $K\bar{K}$ [18]. This suggests an $n\bar{n}$ structure $(u\bar{u}+d\bar{d})$ for the $f_0(1370)$ and $s\bar{s}$ for the $f_0(1710)$. The $f_0(1500)$ would also qualify as an $n\bar{n}$ state (see 63.3.1), although it is very narrow compared to the other states. Occam's razor principle therefore suggests that the $f_0(1370)$, $a_0(1450)$, and the $f_0(1710)$ are in the same SU(3) flavor nonet, the $f_0(1370)$ and $a_0(1450)$ being the two (mostly) $n\bar{n}$ states, and the $f_0(1710)$ the (dominantly) $s\bar{s}$ one. It is important to note that the spectrum of scalar mesons above the $f_0(1710)$ is not well established: The reported ones in the *Listings* need experimental confirmation and are not included in the *Summary Table*.

According to [38] there is mounting evidence for the existence of two scalar nonets and one glueball below 2 GeV: Table 63.1 shows a proposed classification scheme. The low mass nonet is made of four-quark states which recombine at large distances to become meson-meson resonances, while the ground state 1^3P_0 $q\bar{q}$ nonet lies in the 1400 MeV region, see Ref. [1] for a review and Ref. [39] for the $f_0(500)$. The nature of the $f_0(1500)$ is discussed along this scheme in section 63.3.1.

Other schemes have been proposed, for example a tetraquark for the $f_0(1500)$ [40] or flavor octets for the $f_0(1500)$ and $f_0(1710)$ [3]. In Ref. [41] the $a_0(1450)$, $f_0(1370)$, $f_0(1500)$ and $K_0^*(1430)$ are radial excitations of the scalar nonet below 1 GeV. In Ref. [42] the light and heavy scalar nonets in Table 63.1 are interpreted as mixing of two tetraquark nonets. In the unitarized quark model with coupled $q\bar{q}$ and meson-meson channels, the scalars below 1 GeV are manifestations of bare $q\bar{q}$ confinement states, mass shifted from the 1.4 GeV region and distorted by the strong $^3P_0$ coupling to S-wave two-meson decay channels [43, 44]. Thus, in these models the light scalar nonet comprising the light and heavy scalar nonets shown in Table 63.1 are manifestations of the same bare input states (see also [45]). Surprisingly for a state decaying strongly into 2π and 4π, the $f_0(1370)$ is assumed to be an $s\bar{s}$ state in Ref. [46]. The $f_0(1500)$ is then a radial excitation and the glueball lies around 1700 MeV.

Downloaded from https://academic.oup.com/ptep/article/2022/8/083C01/6651666 by KIT Library user on 27 September 2022

Table 63.1: Tentative classification of scalar mesons (see the text). The 1^3P_0 ground state $q\bar{q}$ nonet is listed in the bottom half. The third isoscalar $f_0(1500)$ is discussed in section 63.3.1.

	Γ [MeV]	isospin i	structure
$a_0(980)$	~ 50	1	$K\bar{K}, qq\bar{q}\bar{q}$
$f_0(980)$	~ 50	0	$K\bar{K}, qq\bar{q}\bar{q}$
$f_0(500)$	~ 800	0	$\pi\pi, qq\bar{q}\bar{q}$
$K_0^*(700)$	~ 600	$\frac{1}{2}$	$K\pi, qq\bar{q}\bar{q}$
$a_0(1450)$	265	1	$u\bar{d}, d\bar{u}, d\bar{d} - u\bar{u}$
$f_0(1370)$	~ 400	0	$d\bar{d} + u\bar{u}$
$f_0(1710)$	125	0	$s\bar{s}$
$K_0^*(1430)$	294	$\frac{1}{2}$	$u\bar{s}, d\bar{s}, s\bar{u}, s\bar{d}$

63.3 Glueballs

Lattice calculations, QCD sum rules, flux tube, and constituent glue models agree that the lightest glueball has quantum numbers $J^{PC} = 0^{++}$ and the first excited state 2^{++}. Lattice calculations predict for the ground state (0^{++}) a mass around 1600 – 1700 MeV [47–50], while the 2^{++} state lies around 2300 MeV. For more information on lattice calculations see 'Quark Model' in the *Review* and fig. 15.3 therein for an example of mass spectrum. These predictions were made in the quenched approximation, neglecting $q\bar{q}$ loops. However quenched predictions and full QCD calculations lead to small mass shifts (see 'Quark Model' and fig. 15.15 therein).

Heavier glueballs with quantum numbers 0^{-+}, 2^{-+}, 1^{+-}, etc. are predicted above 2500 MeV and the lowest exotic ones (with exotic quantum numbers such as 0^{+-} and 2^{+-}) are expected above 4000 MeV [50]. In holographic QCD the 0^{-+} is predicted to be very broad [51] and the 1^{+-} is at least as broad as its width [52]. Calculations of the three lowest scalar and pseudoscalar glueballs masses in pure Yang-Mills theory are in quantitative agreement with lattice results [53]. The lightest glueballs lie in the same mass region as ordinary isoscalar $q\bar{q}$ states, in the mass range of the $1^3P_0(0^{++})$, $2^3P_2(2^{++})$, $3^3P_2(2^{++})$, and $1^3F_2(2^{++})$ $q\bar{q}$ states. Therefore, mixing of glueballs with nearby $q\bar{q}$ states of the same quantum numbers leads to supernumerary isoscalar state in the $q\bar{q}$ nonets (however, see Ref. [54] discussed in section 63.3.1).

Among the signatures naively expected for glueballs are (i) isoscalar states that do not fit into $q\bar{q}$ nonets, (ii) enhanced production in gluon-rich channels such as central production and radiative $J/\psi(1S)$ decay, (iii) decay branching fractions incompatible with SU(3) predictions for $q\bar{q}$ states, and (iv) reduced $\gamma\gamma$ couplings. However, mixing effects with isoscalar $q\bar{q}$ mesons [47, 55–63] and decay form factors [64] can obscure these simple signatures.

According to SU(3) the decay branching ratios for $q\bar{q}$ mesons and pure glueballs are different, and therefore useful to determine the internal structures of mesons. For pure glueballs with flavor symmetric couplings the decay ratios are $\pi\pi : K\bar{K} : \eta\eta : \eta\eta' = 3 : 4 : 1 : 0$, apart from phase space factors. The partial widths for the decay of a scalar (or a tensor) meson into a pair of pseudoscalar mesons are given in Fig. 63.2 (for a derivation see e.g. [8]).

The decay of a $q\bar{q}$ meson into a pair of mesons involves the creation of a $q\bar{q}$ pair, and SU(3) symmetry assumes that the matrix elements for the creation of $s\bar{s}$, $u\bar{u}$, and $d\bar{d}$ pairs are equal. (The generalization to unequal $s\bar{s}$, $u\bar{u}$, and $d\bar{d}$ couplings is given in Ref. [55].) An excellent fit to the tensor meson decay widths is obtained with $\beta \simeq 0.5$ GeV/c, $\theta_V \simeq 26\,^\circ$ and $\theta_P \simeq -17\,^\circ$ [55].

Note that the assumption of flavor symmetric couplings may not apply in models describing the scalar glueball by a dilaton field, which lead to mass dependent couplings [65, 66] (see Ref. [67] which predicts that a scalar glueball above 1 GeV would be unobservably wide).

Another way to determine the flavor contents of neutral mesons is the decay $B \to J/\psi(1S)X$ which filters out the $d\bar{d}$ content of X, while $B_s^0 \to J/\psi(1S)X$ selects its $s\bar{s}$ component [68].

63.3.1 *Scalar glueballs*

One of the three isoscalars, the $f_0(1370)$, $f_0(1500)$ or $f_0(1710)$, appears to be supernumerary. The branching ratios in Fig. 63.2 can be used to deduce the structures of these states, assuming that they are $q\bar{q}$. The comparison of decay branching ratios from Crystal Barrel annihilation and WA102 central collision data shows that the $f_0(1500)$ is compatible with an $n\bar{n}$ structure, while the $f_0(1710)$ is mostly $s\bar{s}$ [12]. However, the close vicinity of the very broad $n\bar{n}$ $f_0(1370)$, its narrow width, enhanced production at low transverse momentum transfer in central collisions [69–71] and absence in $\gamma\gamma$ collisions (see below) favor the $f_0(1500)$ to be the supernumerary non-$q\bar{q}$ state. According to [55, 60] the $f_0(1370)$ and $f_0(1710)$ would be dominantly $\bar{q}q$ states mixing with glue, while the $f_0(1500)$ would be dominantly a glueball mixing with $q\bar{q}$ states. Its suppressed $K\bar{K}$ decay would be due to interferences with the $f_0(1370)$ and $f_0(1710)$. In the analogous mixing scheme of Ref. [72], which uses central production data from WA102 and the hadronic $J/\psi(1S)$ decay data from BES [73,74], glue is shared between the $f_0(1370)$ (mainly $n\bar{n}$), $f_0(1500)$(mainly glue) and $f_0(1710)$ (dominantly $s\bar{s}$). This agrees with the analyses [55, 60]. In the mixing scheme of Ref. [75] the QCD spectral sum rule also leads to a large gluonic component in the $f_0(1500)$ (satisfying the observed strong $\pi\pi$ and $f_0(500)f_0(500) \to 4\pi$ decays).

However, not everybody agrees that the strong $K\bar{K}$ signal is indicative of an $s\bar{s}$ structure for the $f_0(1710)$. The $f_0(1710)$ could still be the glueball, since the two-gluon coupling to $n\bar{n}$ appears to be suppressed by chiral symmetry [76], thus $K\bar{K}$ would be enhanced compared to $\pi\pi$. It was argued that chiral symmetry constraints in a multichannel analysis imply that the $f_0(1710)$ is an unmixed scalar glueball [77]. However, this view is challenged in [78].

The $K\bar{K}$ decay is also naturally enhanced in the extended linear sigma model with a dilaton as glueball [65] and in the holographic model of [66, 79] which both prefer the $f_0(1710)$ as the glueball. For a scalar glueball Ref. [66] finds a strong enhancement of the decays into $K\bar{K}$ and $\eta\eta$, in fairly close agreement with the measured branching ratios of the $f_0(1710)$, while Ref. [79] predicts the (so far not measured) rate into $\eta\eta'$ to be very small.

In $\gamma\gamma$ collisions leading to K_SK_S [80] and K^+K^- [81] a spin-0 signal is observed at the $f_0(1710)$ mass (together with a dominant spin-2 component), while the $f_0(1500)$ is not observed in $\gamma\gamma \to K\bar{K}$ nor $\pi^+\pi^-$ [82]. The $f_0(1500)$ is also not observed by Belle in $\gamma\gamma \to \pi^0\pi^0$, although a shoulder is seen which could also be due to the $f_0(1370)$ [83]. The absence of $f_0(1500)$ signal in the $\pi\pi$ channel in $\gamma\gamma$ collisions does not favor an $\overline{n}n$ interpretation for the $f_0(1500)$. The upper limit for $\Gamma_{2\gamma}$ (< 1.4 keV) in $\pi^+\pi^-$ [12]) excludes a large $n\overline{n}$ content, and hence points to a mainly $s\overline{s}$ content [12], which contradicts the small $K\overline{K}$ decay branching ratio of the $f_0(1500)$ [18, 36, 84]. Belle finds that in $\gamma\gamma \to K_SK_S$ collisions the 1500 MeV region is dominated by the $f_2'(1525)$. The $f_0(1710)$ is also observed with a production rate $\times$ branching ratio compatible with an $s\bar{s}$ state [85]. Note, however, that the $\gamma\gamma$ couplings of glueballs are sensitive to glue mixing with $q\bar{q}$ [72]. Ref. [63] predicts the glueball $\gamma\gamma$ partial width in the few keV range (comparable to that of $q\bar{q}$ mesons) due to couplings of vector mesons to γ via VDM.

Alternative assignments for the scalar glueball have been proposed: In Ref. [57] the gluonic signal is distributed over $f_0(1370)$, $f_0(1500)$ and another broad isoscalar around 1530 MeV, while the gluonic contribution to the $f_0(1710)$ is small. As mentioned already, in Ref. [47, 65, 66] the $f_0(1710)$ is the glueball state, as in Ref. [61], where the $f_0(1500)$ is the $q\bar{q}$ octet state degenerate with the $a_0(1450)$. In the generalized linear sigma model [86] the $a_0(980)$ is dominantly a tetraquark and $a_0(1450)$ a $q\bar{q}$ state. The $f_0(980)$, $f_0(1370)$ and $f_0(1500)$ (or $f_0(1710)$) are dominantly tetraquark, $q\bar{q}$ and glue.

In Ref. [59] the $f_0(500)$ and $f_0(1370)$ are signals from a single broad resonance proposed as the scalar glueball. The ground state scalar nonet then consists of the $f_0(980)$, $a_0(980)$, $K_0^*(1430)$, $f_0(1500)$ and $f_0(1710)$ [62]. The $f_0(980)$ and $f_0(1500)$ mix (similarly to the η and η' in the pseudoscalar nonet), while the $f_0(1500)$ mixes with a glueball in the 500 – 1000 MeV mass range, which is identified as the $f_0(500)$. A reanalysis of the CERN-Munich

Downloaded from https://academic.oup.com/ptep/article/2022/8/083C01/6651666 by KIT Library user on 27 September 2022

Isospin	Decay channel	γ^2
0	$\pi\pi$	$3\cos^2\alpha$
	$K\overline{K}$	$(\cos\alpha - \sqrt{2}\sin\alpha)^2$
	$\eta\eta$	$(\cos\alpha\cos^2\phi - \sqrt{2}\sin\alpha\sin^2\phi)^2$
	$\eta\eta'$	$\frac{1}{2}\sin^2 2\phi\ (\cos\alpha + \sqrt{2}\sin\alpha)^2$
1	$\eta\pi$	$2\cos^2\phi$
	$\eta'\pi$	$2\sin^2\phi$
	$K\overline{K}$	1
$\frac{1}{2}$	$K\pi$	$\frac{3}{2}$
	$K\eta$	$(\sin\phi - \frac{\cos\phi}{\sqrt{2}})^2$
	$K\eta'$	$(\cos\phi + \frac{\sin\phi}{\sqrt{2}})^2$

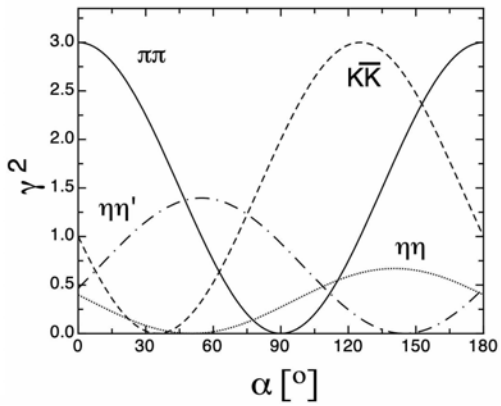

Figure 63.2: Left: SU(3) couplings γ^2 for scalar (or tensor) $q\bar{q}$ meson decays. The angles α and ϕ are defined as $\alpha = 54.7^\circ + \theta$ and $\phi = 54.7^\circ + \theta_P$, where θ is the mixing angle of the decaying isoscalars and θ_P the mixing angle in the 0^{++} (2^{++}) meson nonet. The partial decay width is given by $\Gamma = C \times \gamma^2 \times |F(q)|^2 \times q$, where C is a nonet constant, q the momentum of the decay products and $F(q)$ a form factor which may be taken as $|F(q)|^2 = q^{2\ell} \times \exp(-q^2/8\beta^2)$ with β= 0.5 GeV/c, and where ℓ is the relative angular momentum between the decay products ($\ell = 0$ for scalars and $\ell = 2$ for tensors). Right: SU(3) couplings as a function of mixing angle α for isoscalar decays for $\theta_P = -17.3^\circ$ (from [55]).

data shows no signal for the $f_0(1370)$ decaying into $\pi\pi$, in contrast to [54, 87]. However, in this scheme the $K_0^*(700)$ and the $a_0(1450)$ are also left out.

In Ref. [88], a large K^+K^- scalar signal reported by Belle in B decays into $KK\bar{K}$ [89], compatible with the $f_0(1500)$, is explained as due to constructive interference of a flavor octet with a broad glueball background. However, the Belle data are inconsistent with the BaBar measurements which show instead a broad scalar at this mass for B decays into both $K^\pm K^\pm K^\mp$ [90] and $K^+K^-\pi^0$ [91].

The $f_0(1500)$ is observed by BESII in $J/\psi(1S) \to \gamma\pi\pi$ [92] and by BESIII in $J/\psi(1S) \to \gamma\eta\eta$ [93] with a much smaller rate than for the $f_0(1710)$, which would speak against a glueball interpretation of the former, although the systematic errors are large. Also, the $f_0(1500)$ appears at a lower mass and the $f_0(1710)$ at a higher mass than the accepted values. However, the coupled channel analysis of more data on radiative $J/\psi(1S)$ decay from BESIII [54] (described in the next paragraph) finds comparable contributions from $f_0(1500)$ and $f_0(1710)$ with a preference for $\pi\pi$ decay over $K\bar{K}$ for the former and $K\bar{K}$ over $\pi\pi$ for the latter.

The authors of Ref. [54] have analyzed the high statistics data from $J/\psi(1S)$ radiative decays into $\pi^0\pi^0$, $K_S^0K_S^0$, $\eta\eta$ and $\omega\phi$ from BESIII, including data on $\pi\pi$, $\eta\eta$ and $\eta\eta'$ from the CERN SPS, BNL data on $\pi\pi \to K_S^0K_S^0$ and $\bar{p}p$ annihilation data from LEAR into various final states. The coupled channel analysis requires ten scalar mesons, the established ones in the *Review* and the four isoscalars $f_0(2020, 2100, 2200, 2330)$ so far omitted from the *Summary Table*. As a new feature, the $f_0(1710)$ splits into two states, one at about 1700 MeV, the former $f_0(1710)$, and a new one around 1770 MeV being mandatory to obtain a good fit. A broad (∼370 MeV) enhancement is observed in $J/\psi(1S)$ radiative decays around 1865 MeV, attributed to the contribution of glue distributed among the scalar mesons, with a very strong contribution from the new 1770 MeV state [94]. In this model there are no supplementary states as the glue 'fragments' between the various isoscalars.

Ref. [95] reports on a very recent re-analysis of the BESIII $J/\psi(1S)$ radiative decay data into $\pi^0\pi^0$ and $K_S^0K_S^0$. A good fit is obtained with only two scalar resonances below 2 GeV, the $f_0(1500)$ and $f_0(1710)$. The latter couples much more strongly to both channels, which points to a sizeable glueball component.

63.3.2 *Tensor glueballs*

Above the well known $f_2(1270)$ and $f_2'(1525)$ $q\bar{q}$ mesons, the $f_2(1640)$ and $f_2(1950)$ are tentatively assigned to the 2^3P_2 nonet (see Fig. 63.1). The broad $f_2(1950)$ has been observed by several experiments, *e.g.* in central production [19] and in $\bar{p}p$ annihilation in flight [96] and is often identified as the ground state of the pomeron [97, 98]. Three further isoscalar tensors are established, the $f_2(2010)$, $f_2(2300)$ and $f_2(2340)$, which are in the range of the 1^3F_2 and 3^3P_2 nonets, and in the expected region for the 2^{++} glueball. The large $\phi\phi$ cross section in $\bar{p}p$ just above threshold [99] could be due to the production of the 2^{++} glueball, in accord with earlier observations in π^-N reactions [100, 101] and in central collisions [102].

The $f_2(2010)$, $f_2(2300)$ and $f_2(2340)$ have been observed by BESIII in $J/\psi(1S) \to \gamma\phi\phi$ [103]. The production rate of a tensor glueball in $J/\psi(1S)$ radiative decay has been calculated in quenched lattice QCD to be large (around 1%) [104] and is claimed by BESIII [103] to be compatible with their rates measured in $J/\psi(1S) \to f_2(2340)$, $f_2(2340) \to \eta\eta$ [93], and $f_2(2340) \to \phi\phi$ [103]. The relatively narrow $f_2(2300)$ with a measured width of 149 MeV [101] is preferred by the holographic QCD model of Ref. [105]. However, the tensor glueball is predicted to be much broader (600-900 MeV) by the holographic model of Ref. [106].

There is no evidence for a narrow meson, $f_J(2220)$ (a tensor candidate) in $\bar{p}p$ annihilation (see the note under the $f_J(2220)$ in the 2004 issue of the *Review*). The measured partial width to $\bar{p}p$ in radiative $J/\psi(1S)$ decay [107] is too large and inconsistent with the upper limit from $\bar{p}p$ annihilation into $\pi\pi$ [108].

63.4 Pseudoscalar mesons

We now deal with the first radial excitations of the 0^{-+} nonet (Fig. 63.1). The $\pi(1300)$ is a very broad resonance (200–600 MeV) decaying into 3π. The $K(1460)$ was recently confirmed with high statistics data from LHCb in $D^0 \to K3\pi$ decays [109] and has become an established kaon excitation. The first observation of an isoscalar resonance around 1425 MeV – the E-meson – was made in $p\bar{p}$ annihilation at rest into $E\pi^+\pi^-$, $E \to K\overline{K}\pi$ [110]. This state was reported to decay into $a_0(980)\pi$ and $K^*(892)\overline{K}$ with roughly equal contributions. An isoscalar state, the ι meson, was observed in radiative $J/\psi(1S)$ decay into $K\overline{K}\pi$ [111–113] and $\gamma\rho$ [114], and was considered at that time as a glueball candidate, owing to its strong signal in radiative $J/\psi(1S)$ decay. The E and ι were later assumed to be the same state, called $\eta(1440)$.

The $\eta(1295)$ has been observed in various production mechanisms, in π^-p experiments [115–118], and in $\bar{p}p$ annihilation [84,119,120]. In $J/\psi(1S)$ radiative decay, the $\eta(1295)$ signal is also evident in the 0^{-+} $\eta\pi\pi$ wave of the DM2 data [121]. Also BaBar reports a signal around 1295 MeV in B decays into $\eta\pi\pi K$ [122]. Let us therefore assume in the following that the $\eta(1295)$ is one of the isoscalars in this nonet.

However, two isoscalars were later observed in this mass region, the $\eta(1405)$ and $\eta(1475)$. The former decays mainly into $a_0(980)\pi$ (or direct $K\overline{K}\pi$) and the latter mainly into $K^*(892)\overline{K}$. The simultaneous observation of two pseudoscalars is reported in

Downloaded from https://academic.oup.com/ptep/article/2022/8/083C01/6651666 by KIT Library user on 27 September 2022

three production mechanisms: $\pi^- p$ [115, 123], radiative $J/\psi(1S)$ decay [121, 124], and $\overline{p}p$ annihilation at rest [125–128]. All of them give values for the masses, widths, and decay modes that are in reasonable agreement. (However, Ref. [121] favors a state decaying into $K^*(892)\overline{K}$ at a lower mass than the state decaying into $a_0(980)\pi$.) In $J/\psi(1S)$ radiative decay, the $\eta(1405)$ decays into $K\overline{K}\pi$ through $a_0(980)\pi$, and hence a signal is also expected in the $\eta\pi\pi$ mass spectrum. This was indeed observed by MARK III in $\eta\pi^+\pi^-$ [129], which reported a mass of 1400 MeV, in line with the existence of the $\eta(1405)$ decaying into $a_0(980)\pi$. Two states were also reported by BES: Around 1452 MeV BESII observed a $K\bar{K}\pi$ enhancement in $J/\psi(1S) \to \omega K\bar{K}\pi$ but not in $J/\psi(1S) \to \phi K\bar{K}\pi$ [130], while BESIII reported a 52 MeV broad state in $\psi(2S) \to \omega K^* K$ [131], both left without J^{PC} determination.

The $K\overline{K}\pi$ and $\eta\pi\pi$ channels were studied in $\gamma\gamma$ collisions by L3 [132]. (For the 2γ couplings of glueballs and $q\bar{q}$ mesons see [63, 133, 134].) The analysis led to a clear $\eta(1475)$ signal in $K\overline{K}\pi$, decaying into $K^*\overline{K}$, well identified in the untagged data sample, where spin 1 resonances are not allowed. At the same time, L3 did not observe the $\eta(1405)$, neither in $K\overline{K}\pi$ nor in $\eta\pi\pi$ [132]. On the other hand, CLEO-II did not observe any pseudoscalar signal with tagged γ's in $\gamma\gamma \to \eta(1475) \to K^0_S K^\pm \pi^\mp$ [135], with an upper limit slightly smaller than the signal observed by L3. After the CLEO-II result L3 performed a further analysis with full statistics [136], confirming their previous evidence for the $\eta(1475)$. The CLEO upper limit [135] for $\Gamma_{\gamma\gamma}$, and the L3 results [136], are consistent with the world average for the $\eta(1475)$ width. BaBar [122] also reported the $\eta(1475)$ in B decays into $K\bar{K}^*$ recoiling against a K, while upper limits only were given for the $\eta(1405)$.

Hence, in radiative $J/\psi(1S)$ decay, $\pi^- p$ and $\overline{p}p$ annihilation at rest two isoscalar signals are observed in the 1400 – 1500 MeV mass region, while the $\eta(1405)$ is not seen in $\gamma\gamma$ interactions nor in B decays. The $\eta(1475)$ could be the first radial excitation of the η', with the $\eta(1295)$ being the first radial excitation of the η. Ideal mixing, suggested by the $\eta(1295)$ and $\pi(1300)$ mass degeneracy, would then imply that the second isoscalar in the nonet is mainly $s\bar{s}$, and hence couples to $K^*\overline{K}$, in agreement with properties of the $\eta(1475)$. Also, its width agrees with the expected one for the radially excited $s\bar{s}$ state [64, 69]. A study of radial excitations of pseudoscalar mesons [137] also favors the $s\bar{s}$ interpretation of the $\eta(1475)$. However, due to the strong kinematical suppression in $\eta(1405) \to K^*\overline{K}$ the data are not sufficient to exclude a sizeable $s\bar{s}$ admixture also in the $\eta(1405)$.

The supernumerary isoscalar $\eta(1405)$ would be a candidate for the 0^{-+} glueball in the fluxtube model [138], in which the 0^{++} glueball is also naturally related to a 0^{-+} glueball with mass degeneracy broken in QCD. However, this scenario is not favored by lattice gauge theories which predict the 0^{-+} state above 2 GeV [48, 139] (see 'Quark model' in this issue of the *Review*). Nevertheless, the pseudoscalar glueball could lie at a lower mass than predicted from lattice calculation [140], see also Refs. [141–143]. A detailed review of the experimental situation on the pseudoscalar glueball is available in Ref. [144].

Here also, there are alternative explanations. The mere existence of the $\eta(1295)$ is questioned in Refs. [3, 145], in which the authors also propose a single pseudoscalar meson at 1440 MeV, the first radial excitation of the η. According to Ref. [3] the splitting of the 1440 MeV state into $\eta(1405)$ and $\eta(1475)$ is due to nodes in the decay amplitudes, which differ in $\eta\pi\pi$ and $K^*(892)\overline{K}$. The splitting could also be due to a triangle singularity, hence the manifestation of one state only (Fig. 63.3) [146–148]. In Ref. [149], using the triangle singularity approach of [146], the authors conclude that the BESIII results can be reproduced either with the $\eta(1405)$ or the $\eta(1475)$, or by a mixture of these two states.

To summarise this section, the experimental data on the 1400 — 1500 MeV region span several decades, various production mechanisms and decay modes, with models for data analysis evolving with time. A comprehensive coherent picture of all available data is therefore difficult. We believe that there is sufficient evidence to consider the 0^{-+} nonet with the $\eta(1440)$ in fig. 63.1 as established. Whether one or two different states – $\eta(1405)$ and $\eta(1475)$ – exist is an open question, in which case the $\eta(1405)$ would be supernumerary. There is a wide number of experimental results indicating the presence of two separate states but, as mentioned above, data are also consistent with one state only. Theoretical interpretations of the most recent data are not able to lift the ambiguity.

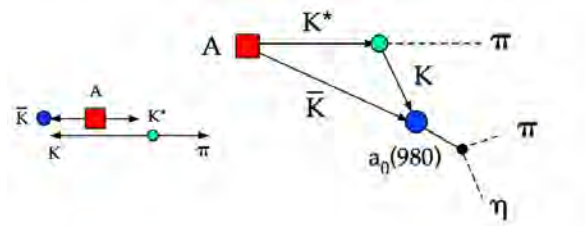

Figure 63.3: Triangle singularity: a state A decays into $K^*\overline{K}$. The K from K^* decay catches up with the $\overline{K}$ and excites the $a_0(980)$ resonance which in turn decays into $\eta\pi$. This mechanism can lead to two distinct peaks (depending on the width of A), one in $K^*\overline{K}$ and the other via rescattering in $\eta\pi\pi$. Similarly, the virtual $K^*\overline{K}$ loop can couple to $f_0(980)$ which, decaying into $\pi\pi$, leads to a peak in the 3π final state.

63.5 Vector mesons

In this section we restrict ourselves to the more interesting isovector spectrum which contains broad and overlapping states.

63.5.1 *The* $\rho(770)$ *meson*

The determination of the parameters of the $\rho(770)$ is beset with many difficulties because of its large width. The line shape depends on the production process and is not described by a relativistic Breit-Wigner function with a P-wave width, but requires some additional shape parameter. This dependence on parameterization was demonstrated long ago [150]. Bose-Einstein correlations are another source of shifts in the $\rho(770)$ line shape, particularly in multiparticle final-state systems [151].

The same model dependence afflicts any other source of resonance parameters, such as the energy dependence of the phase shift δ^1_1, or the pole position. It is, therefore, not surprising that a study of $\rho(770)$ dominance in the decays of the η and η' reveals the need for specific dynamical effects, in addition to the $\rho(770)$ pole [152, 153].

The cleanest determination of the $\rho(770)$ mass and width comes from e^+e^- annihilation and τ-lepton decays. ALEPH data [154] showed that the charged $\rho(770)$ parameters measured from τ-lepton decays are consistent with those of the neutral one determined from e^+e^- data [155]. This conclusion is qualitatively supported by the later studies of CLEO [156] and Belle [157]. However, a comparison of the two-pion mass spectrum in τ decays from OPAL [158], CLEO [156], and ALEPH [159, 160], and the $e^+e^- \to \pi^+\pi^-$ cross section from CMD-2 [161, 162], showed significant discrepancies between the two shapes which can be as high as 10% above the ρ meson mass [163, 164]. This discrepancy remains after measurements of the two-pion cross section in e^+e^- annihilation at KLOE [165–168], SND [169, 170], BaBar [171] and, more recently BESIII [172]. The effect is not accounted for by isospin breaking [173–176], but the accuracy of its calculation may be overestimated [177, 178].

This problem seems to be solved after a recent analysis in [179], which showed that after correcting the τ data for the missing ρ—γ mixing contribution, besides the other known isospin symmetry violating corrections, the $\pi\pi$ isospin 1 part of the hadronic vacuum polarization contribution to the muon $g-2$ is fully compatible between τ based and e^+e^- based evaluations. The global fit of the whole set of the ρ, ω, and ϕ decays, taking into account mixing effects in the hidden local symmetry model, also showed consistency of the data on τ decays to two pions and e^+e^- annihilation [180, 181]. However, because of the progress in e^+e^- data, the τ input is now less precise and less reliable due to additional theoretical uncertainties [182] decreasing the importance of τ decay for the determination of the $\rho(770)$ parameters.

Downloaded from https://academic.oup.com/ptep/article/2022/8/083C01/6651666 by KIT Library user on 27 September 2022

63.5.2 *The* $\rho(770)$ *excitations*

In our 1988 edition, we replaced the $\rho(1600)$ entry with two new ones, the $\rho(1450)$ and the $\rho(1700)$, because there was emerging evidence that the 1600-MeV region actually contains two ρ-like resonances. This possibility was pointed out by a theoretical analysis [183] on the consistency of the 2π and 4π electromagnetic form factors and the $\pi\pi$ scattering length. A consistent picture of $e^+e^- \to 2\pi, 4\pi$ and diffractive photoproduction is obtained with two resonances [184]. The existence of the $\rho(1450)$ was supported by the analysis of $\eta\rho^0$ mass spectra obtained in photoproduction and e^+e^- annihilation [185], as well as that of $e^+e^- \to \omega\pi$ [186].

The analysis of [184] was further extended by [187, 188] to include new data on 4π-systems produced in e^+e^- annihilation, and in τ decays ($\tau \to 4\pi$ and $e^+e^- \to 4\pi$ are related by the Conserved Vector Current hypthesis). These systems were successfully analyzed using interfering contributions from two ρ-like states, and from the tail of the $\rho(770)$ two-body decay. While specific conclusions on $\rho(1450) \to 4\pi$ were obtained, little could be said about the $\rho(1700)$. Independent evidence for two 1^- states is provided by [189] in 4π electroproduction at $\langle Q^2 \rangle = 1$ (GeV/c)^2, and by [190] in a high-statistics sample of the $\eta\pi\pi$ system in π^-p charge exchange.

This scenario with two overlapping resonances is supported by other data. DM2 [191] measured the pion form factor in the interval 1.35–2.4 GeV, and observed a deep minimum around 1.6 GeV. The best fit was obtained with the hypothesis of ρ-like resonances at 1420 and 1770 MeV, with widths of about 250 MeV. DM2 [192] found that the $e^+e^- \to \eta\pi^+\pi^-$ cross section is better fitted with two fully interfering Breit-Wigners, with parameters in fair agreement with those of [184] and [191]. These results can be considered as a confirmation of the $\rho(1450)$.

Decisive evidence for the $\pi\pi$ decay mode of both $\rho(1450)$ and $\rho(1700)$ comes from $\overline{p}p$ annihilation at rest [193]. It has been shown that these resonances possess a $K\overline{K}$ decay mode [84, 194, 195]. This decay mode has also been studied in three-body hadronic B decays [196]. High-statistics studies of the decays $\tau \to \pi\pi\nu_\tau$ [154, 156], and $\tau \to 4\pi\nu_\tau$ [197] also require the $\rho(1450)$, but are not sensitive to the $\rho(1700)$, being too close to the τ mass. A recent very-high-statistics study of the $\tau \to \pi\pi\nu_\tau$ from Belle [157] reports the first observation of both $\rho(1450)$ and $\rho(1700)$ in τ decays. A clear picture of the two $\pi^+\pi^-$ resonances interfering with the $\rho(770)$ in e^+e^- annihilation was also reported by BaBar using the ISR (Initial State Radiation) method [198].

The structure of these ρ states is not yet completely clear. The authors of Refs. [64, 199] claim that $\rho(1450)$ has a mass consistent with radial $2S$, but its decays show characteristics of hybrids, and suggest that this state may be a $2S$-hybrid mixture. Hybrid states could have a 4π decay mode dominated by the $a_1\pi$ [200]. Such behavior has been observed by [201] in $e^+e^- \to 4\pi$ in the energy range 1.05–1.38 GeV, and by [197] in $\tau \to 4\pi$ decays. CLEO [202] and Belle [203] observe the $\rho(1450) \to \omega\pi$ decay mode in B-meson decays, however, do not find $\rho(1700) \to \omega\pi^0$. A similar conclusion is made by [204, 205], who studied the process $e^+e^- \to \omega\pi^0$ and do not observe a statistically significant signal of the $\rho(1700)$. Various decay modes of the $\rho(1450)$ and $\rho(1700)$ are observed in $\overline{p}n$ and $\overline{p}p$ annihilation [206, 207], but no definite conclusions can be drawn. More data should be collected to clarify the nature of the ρ states, particularly in the energy range above 1.6 GeV.

We now list under a separate entry the $\rho(1570)$, the $\phi\pi$ state with $J^{PC} = 1^{--}$ earlier observed by [208] – referred to as $C(1480)$) – and recently confirmed by [209] and [210]. While [211] shows that it may be a threshold effect, Refs. [187] and [212] suggest two independent vector states with this decay mode. The $C(1480)$ has not been seen in the $\overline{p}p$ [213] and e^+e^- [214, 215] experiments. However, the sensitivity of the two latter is an order of magnitude lower than that of [209]. Note that [209] can not exclude that their observation is due to an OZI-suppressed decay mode of the $\rho(1700)$.

Several observations on the $\omega\pi$ system in the 1200 MeV region [216–222] may be interpreted in terms of either $J^P = 1^-$ $\rho(770) \to \omega\pi$ production [223], or $J^P = 1^+$ $b_1(1235)$ production [221, 222]. We argue that no special entry for a $\rho(1250)$ is needed. The LASS amplitude analysis [224] showing evidence for $\rho(1270)$ is preliminary and needs confirmation. However, evidence for the $\rho(1250)$ from a reanalysis of elastic scattering data is claimed in Ref. [225]. For completeness, the relevant observations are listed under the $\rho(1450)$.

Recently Ref. [226] reported a very broad 1^{--} resonance-like K^+K^- state in $J/\psi \to K^+K^-\pi^0$ decays. Its pole position corresponds to mass of 1576 MeV and width of 818 MeV. Its exotic structure (molecular or multiquark) is suggested [227–229], while in Refs. [230] and [231] this is explained by the interference between the $\rho(1450)$ and $\rho(1700)$. The latter statement is qualitatively supported by BaBar [232] and SND [233]. We quote [226] as $X(1575)$ in the section "Further States."

Evidence for ρ-like mesons decaying into 6π was first noted by [234] in the analysis of $e^+e^- \to 6\pi$ [235, 236] and diffractive photoproduction [237]. The authors of Ref. [234] argued that two states at about 2.1 and 1.8 GeV exist: while the former is a candidate for the $\rho(2150)$, the latter could be a manifestation of the $\rho(1700)$ distorted by threshold effects. BaBar reported observations of the new decay modes of the $\rho(2150)$ in the channels $\eta'(958)\pi^+\pi^-$, $f_1(1285)\pi^+\pi^-$ [238] and $\pi^+\pi^-$ [239]. The decay of the $\rho(2150)$ into K^+K^- has been observed by BESIII [240] and confirmed by BaBar [241]. The relativistic quark model [242] predicts the 2^3D_1 state with $J^{PC} = 1^{--}$ at 2.15 GeV which can be identified with the $\rho(2150)$.

Under $\rho(1900)$ we list various observations of irregular behavior of the cross sections near the $N\bar{N}$ threshold. Dips of various width around 1.9 GeV were reported by the E687 Collaboration (a narrow one in the $3\pi^+3\pi^-$ diffractive photoproduction [243, 244]), by the FENICE experiment (a narrow structure in the R value [245]), by BaBar in ISR (a narrow structure in $e^+e^- \to \phi\pi$ final state [209], but much broader in $e^+e^- \to 3\pi^+3\pi^-$ and $e^+e^- \to 2(\pi^+\pi^-\pi^0)$ [246]), by CMD-3 (also a rather broad dip in $e^+e^- \to 3\pi^+3\pi^-$ [247]). A dedicated scan of the $N\bar{N}$-threshold region by CMD-3 confirms this effect in the $e^+e^- \to 3\pi^+3\pi^-$ and $e^+e^- \to K^+K^-\pi^+\pi^-$ final states, but does not see it in the cross section of $e^+e^- \to 2\pi^+2\pi^-$ [248]. Most probably, these structures emerge as a threshold effect due to the opening of the $N\bar{N}$ channel [249–251]. A similar enhancement is observed by BESIII in $e^+e^- \to \Lambda\bar{\Lambda}$ near the $\Lambda\bar{\Lambda}$ threshold [252].

63.6 Axial-vector mesons

The $J^{PC} = 1^{++}$ nonet consists of the isovector $a_1(1260)$, the isoscalars $f_1(1285)$ and $f_1(1420)$, and the K_{1A}, which is a superposition of the physical states $K_1(1270)$ and $K_1(1400)$ with a mixing angle of about 35° [253]. The nonet mixing angle $\theta_{1^{++}}$ is around 23°. The orthogonal combination – the K_{1B} – belongs to the 1^{+-} nonet with a mixing angle $\theta_{1^{+-}}$ of about 28° [253].

The mass region above 1400 MeV is rather complex [254–256]. The $f_1(1420)$ was first reported in π^-p reactions at 4 GeV/c, decaying into $K^*\overline{K}$ [257]. The $f_1(1420) \to K\overline{K}\pi$ was also observed in a reanalysis of the MARK III data [124], and a C=+1 state seen in tagged $\gamma\gamma$ collisions [258]. Axial-vector mesons are not observed in $\overline{p}p$ annihilation at rest in liquid hydrogen, which proceeds dominantly through S-wave annihilation. However, in gaseous hydrogen, P-wave annihilation is enhanced and the $f_1(1420)$ is indeed observed, decaying into $K^*\overline{K}$ [126]. The $f_1(1420)$, decaying into $K\overline{K}\pi$, is also seen in pp central production, together with the $f_1(1285)$. The latter decays via $a_0(980)\pi$, and the former only via $K^*\overline{K}$. The $K^0_SK^0_S\pi^0$ decay mode of the $f_1(1420)$ establishes unambiguously C=+1. Neither central production [259] nor π^-p interactions at 100 GeV [117] find any evidence for a $\eta\pi\pi$ decay mode of the $f_1(1420)$.

The $f_1(1285)$ has been suggested to be a $K^*\overline{K}$ molecule [260]. However, LHCb has determined the 1^{++} nonet mixing angle to be consistent with a mostly $n\bar{n}$ structure for the $f_1(1285)$ from $\overline{B}^0/\overline{B}^0 \to J/\psi(1S)f_1(1285)$, independent of the identity of its isoscalar partner [261]. The mixing angle $\theta_{1^{++}} = 24°$ agrees with that of Ref. [253] quoted above. The ratio of $\overline{B}^0/\overline{B}^0_s$ decay rates also excludes the tetraquark interpretation of the $f_1(1285)$ [261]. This is consistent with earlier determinations assuming that the $f_1(1420)$ is the other isoscalar in the nonet [262].

A resonance candidate decaying into 3π had been reported earlier by COMPASS at 1420 MeV in $\pi^-p \to \pi^-\pi^-\pi^+p$ [263, 264].

Downloaded from https://academic.oup.com/ptep/article/2022/8/083C01/6651666 by KIT Library user on 27 September 2022

The signal appeared as a clear peak in the 1^{++} $f_0(980)\pi$ P-wave and had the expected phase motion of a new resonance, called the $a_1(1420)$. However, the signal appears to originate from a triangle singularity: the decay of the $a_1(1260)$ into $K^*(\to K\pi)\bar{K}$ is followed by rescattering into the $f_0(980)\pi$ channel, $f_0(980) \to \pi\pi$ (see the caption of fig. 63.3) [265]. Accordingly, this entry has been removed from the *Listings* in the *Review*.

A similar triangle singularity is proposed for the $f_1(1420)$, resulting from the $K^*\overline{K}$ and $a_0(980)\pi$ decay modes of the $f_1(1285)$ [266]. The $f_1(1420)$ was also suggested to be a hybrid $q\bar{q}g$ meson [267] or a $K^*\overline{K}$ molecule, due to the proximity of the $K^*\overline{K}$ threshold [268]. Indeed, the $f_1(1420)$ is not seen in K^-p [269], which argues against the $f_1(1420)$ being the $s\bar{s}$ member of the 1^{++} nonet. In this case the $s\bar{s}$ partner of the $f_1(1285)$ could be the $f_1(1510)$ which is, however, not well established [270].

The $f_1(1510)$ was seen to decay into $K\bar{K}\pi$ in K^-p interactions at 4 and 11 GeV/c, recoiling against a Λ [269,271], which points to an $s\bar{s}$ state. Evidence was also reported in π^-p interactions, based on the phase motion of the 1^{++} $K^*\overline{K}$ wave [256]. A somewhat broader 1^{++} signal is observed in $J/\psi(1S) \to \gamma\eta\pi^+\pi^-$ [272] and a small signal in $J/\psi(1S) \to \gamma\eta'\pi^+\pi^-$ [273]. However, there is no evidence for the $f_1(1510)$ in other K^-p experiments [274,275], while the $f_1(1420)$ is observed in K^-p but not in π^-p [274]. The $f_1(1510)$ is not seen in central collisions [276], nor in $\gamma\gamma$ collisions [277], although surprisingly for an assumed $s\bar{s}$ meson, a signal is reported in 4π decays [278]. Given this confusing experimental situation, the meson classification in the 1^{++} nonet is not entirely settled.

63.7 Hybrid mesons

Hybrids may be viewed as $q\bar{q}$ mesons with a vibrating gluon flux tube. In contrast to glueballs, they can have isospin 0 or 1 and be electrically charged. The mass spectrum of hybrids with exotic (non-$q\bar{q}$) quantum numbers was predicted in Ref. [279], while Ref. [280] also deals with non-exotic quantum numbers. The ground-state hybrids with quantum numbers (0^{-+}, 1^{-+}, 1^{--}, and 2^{-+}) are expected around 1.7 to 1.9 GeV. Lattice calculations predict that the hybrid with exotic quantum numbers 1^{-+} lies at a mass of 1.9 ± 0.2 GeV [281,282]. Most hybrids are expected to be rather broad, but some can be as narrow as 100 MeV [283]. They prefer to decay into a pair of S- and P-wave mesons. The lattice study in [284, 285], based on full QCD with pion masses around 400 MeV, finds that several of the high-lying states observed in their spectrum show significant overlap with gluon rich source terms interpreted as hybrid states. A very broad 1^{-+} structure is predicted by a recent lattice calculation [286]. The main decay mode is $b_1(1235)\pi$ (a pair of S- and P-wave mesons), while other modes, such as $\rho\pi$, $\eta\pi$ and $\eta'\pi$, are suppressed by at least an order of magnitude. For an experimental and theoretical review on hybrid mesons see [4, 287].

There are currently two 1^{-+} candidates, the $\pi_1(1400)$ and $\pi_1(1600)$. The ∼350–400 MeV broad $\pi_1(1400)$, was reported in $\pi^-p \to \eta\pi^-p$ [288,289] and in $\pi^-p \to \eta\pi^0 n$ [290]. It was observed as an interference between the angular momentum $L = 1$ and $L = 2$ $\eta\pi$ amplitudes, leading to a forward/backward asymmetry in the $\eta\pi$ angular distribution. This state had been reported earlier in π^-p reactions [291], but ambiguous solutions in the partial wave analysis were pointed out [292, 293]. A resonating 1^{-+} contribution to the $\eta\pi$ P-wave is also required in the Dalitz plot analysis of $\bar{p}n$ annihilation into $\pi^-\pi^0\eta$ [294], and in $\bar{p}p$ annihilation into $\pi^0\pi^0\eta$ [295]. Mass and width are consistent with the results of Ref. [288]. A coupled channel re-analysis of the $\pi^0\pi^0\eta$, $\pi^0\eta\eta$ and $K^+K^-\pi^0$ Crystal Barrel data at 900 MeV/c, supplemented with data from other collaboration in $\pi\pi \to \pi\pi, K\bar{K}, \eta\eta$ and $\eta\eta'$, leads to a single 1^{-+} ∼600 MeV broad state with a pole around 1400 MeV, decaying into $\eta\pi^0$ [296]. Ref. [297] suggested for the production in π^-p that a Deck-generated $\eta\pi$ background from final state rescattering in $\pi_1(1600)$ decay could mimic $\pi_1(1400)$, a mechanism that is, however, absent in $\bar{p}p$ annihilation.

The $\pi_1(1600)$, decaying into $\rho\pi$, was reported by COMPASS with 190 GeV pions hitting a lead target [298,299]. It had already been observed in π^-p interactions in the decay modes $\eta'\pi$ [300], $f_1(1285)\pi$ [301], and $\omega\pi\pi$ [302], $b_1(1235)\pi$, but not $\eta\pi$ [303]. A strong enhancement in the 1^{-+} $\eta'\pi$ wave, compared to $\eta\pi$, was reported at this mass in [304]. The enhancement is also observed by COMPASS in $\pi^-p \to \eta'\pi$ but in $\eta\pi$ a peak appears at 1400 MeV and in $\eta'\pi$ at 1600 MeV [305]. A coupled channel analysis of the $\eta\pi$ and $\eta'\pi$ COMPASS data leads to a single pole at 1564 ± 89 MeV, with a width of 492 ± 115 MeV [306]. Furthermore, a combined analysis of the COMPASS and Crystal Barrel data at 900 MeV/c leads to compatible results, a single pole around 1623 MeV, with a width of about 455 MeV, although a two-pole scenario cannot be completely excluded [307]. The predicted width from the lattice calculation [286] is compatible with the COMPASS result.

Hybrid candidates with the non-exotic quantum numbers 0^{-+}, 1^{--}, and 2^{-+} have also been reported: the $\pi(1800)$ is somewhat narrow if interpreted as the second radial excitation of the pion. It decays mostly into a pair of S- and P-wave mesons [308,309], in line with expectations for 0^{-+} hybrid mesons. The evidence for 1^{--} hybrids in e^+e^- annihilation and in τ decays has been discussed in [200]. The near degeneracy of the $\eta_2(1645)$ and $\pi_2(1670)$ suggests ideal mixing in the 2^{-+} $q\bar{q}$ nonet, and hence, the second isoscalar, presumably the $\eta_2(1870)$, should be mainly $s\bar{s}$. However, the $\eta_2(1870)$ is also observed in $\bar{p}p$ annihilation and decays mainly into $a_2(1320)\pi$ and $f_2(1270)\pi$ [310], with a relative rate compatible with a hybrid state [280]. Evidence for another exotic $\pi_1(2015)$ has been claimed in π^-p interactions [301,302].

Summarizing, there is evidence for a very broad 1^{-+} enhancement in the 1400–1600 MeV region which consists in one or perhaps two exotic states, the lowest one seemingly favored by $\bar{p}p$ annihilation data, the highest one by high energy π^-p data. As isovectors, $\pi_1(1400)$ and $\pi_1(1600)$ cannot be glueballs. The coupling to $\eta\pi$ of the former points to a four-quark state [311], while the $\eta'\pi$ coupling of the latter is favored for hybrid states [312,313]. The mass of $\pi_1(1600)$ is not far below the lattice and flux tube model predictions.

63.8 Tetraquark states

The existence of multiquark states was suggested a long time ago, based on duality arguments [314, 315]. The most prominent tetraquark candidates are the $a_0(980)$ and $f_0(980)$ [316–318]. A remarkable prediction for the existence of low-lying four quarks states is based on color hyperfine splitting. The lowest ground state ($L = 0$) tetraquark multiplet is predicted to be a scalar nonet. The scalar nonet lies just below 1 GeV when one assumes as mass scale the hyperfine color splitting between the ρ and the π (for a simple derivation see [8]). Assuming the classification in Table 63.1 one then gets the nonet structures

$$
\begin{aligned}
|a_0(980)\rangle &= |us\bar{d}\bar{s}\rangle, \frac{1}{\sqrt{2}}|(u\bar{u} - d\bar{d})s\bar{s}\rangle, |\bar{u}\bar{s}ds\rangle,\\
|f_0(980)\rangle &= \frac{1}{\sqrt{2}}|(u\bar{u} + d\bar{d})s\bar{s}\rangle,\\
|f_0(500)\rangle &= |\bar{u}\bar{d}ud\rangle,\\
|K_0^*(700)\rangle &= |\bar{s}\bar{d}ud\rangle, |\bar{s}\bar{u}ud\rangle \quad \text{and} \quad |\bar{u}\bar{d}us\rangle, |\bar{u}\bar{d}ds\rangle.
\end{aligned}
$$

The two isoscalars are expected to mix with the angle φ:

$$
\begin{aligned}
|f_0(980)\rangle &= \cos\varphi|s\bar{s}\rangle + \sin\varphi|n\bar{n}\rangle,\\
|f_0(500)\rangle &= -\sin\varphi|s\bar{s}\rangle + \cos\varphi|n\bar{n}\rangle.
\end{aligned} \tag{63.1}
$$

Whether these mesons are really tetraquark states or $q\bar{q}$ mesons, is still an open issue. The $f_0(980)$ is strongly produced in D_s^+ decay [320], which suggests a large $s\bar{s}$ component, due to the Cabibbo-favored $c \to s$ coupling. However, the mainly $n\bar{n}$ $f_0(1370)$ is also strongly produced in D_s^+ decay, hence additional graphs must contribute [321].

The relative branching ratios for $\bar{B}^0$ and $\bar{B}_s^0 \to J/\psi(1S)f_0(500)$ and $J/\psi(1S)f_0(980)$ can be used to probe the $q\bar{q}$ or tetraquark natures of the $f_0(500)$ and $f_0(980)$, as proposed in Refs. [319,322]. LHCb observes the $f_0(980)$ in $\bar{B}_s^0$ decays, but not the $f_0(500)$ [26], as would be expected for tetraquarks (see Table 63.2). In contrast, LHCb also observes the $f_0(500)$ in $\bar{B}^0$ decays, but not the $f_0(980)$ with an upper limit eight standard deviations below the predicted value for a tetraquark state [27]. However, these contradicting findings have been challenged by a dispersive analysis [323], using

Downloaded from https://academic.oup.com/ptep/article/2022/8/083C01/6651666 by KIT Library user on 27 September 2022

Table 63.2: Coupling amplitudes for $\bar{B}^0$ and $\bar{B}^0_s$ decays into $J/\psi(1S)f_0(500)/f_0(980)$, depending on the $q\bar{q}$ or tetraquark structures of the $f_0(500)$ and $f_0(980)$ (from [319] where illustrative decay diagrams can be found). The angle φ is defined in Eq. 63.1.

	$\bar{B}^0$		$\bar{B}^0_s$	
	$f_0(980)$	$f_0(500)$	$f_0(980)$	$f_0(500)$
$q\bar{q}$	$\sin\varphi/\sqrt{2}$	$\cos\varphi/\sqrt{2}$	$\cos\varphi$	$\sin\varphi$
$qq\bar{q}\bar{q}$	$1/\sqrt{2}$	1	$\sqrt{2}$	0

a model independent inclusion of hadronic final state interactions, in which a substantial $f_0(980)$ contribution is nevertheless found in $\bar{B}^0$-decays, thus still leaving the tetraquark structure as an open possibility.

The $f_0(980)$ and $a_0(980)$ could also be $K\overline{K}$ molecular states [324–326], being close to the $K\overline{K}$ threshold and decaying strongly into $K\overline{K}$. For $q\bar{q}$ states, the expected $\gamma\gamma$ widths [327, 328] are not significantly larger than for molecular states [327, 329] and both predictions are consistent with data. Radiative decay of the $\phi(1020)$ into $a_0(980)$ and $f_0(980)$ were proposed to disentangle compact (tetraquark) structures from hadronic molecules. Following Refs. [330, 331] the data from KLOE [332, 333], CMD-2 [334] and SND [335] seem to favor these mesons to be tetraquark states. This is also supported by a BESIII analysis of $J/\psi(1S) \to \gamma\pi^0\pi^0$ data [336] and by a measurement of $a_0(980) - f_0(980)$ mixing at BESIII [337]. In Ref. [38] these states are made of four-quark cores and virtual $K\bar{K}$ clouds at the periphery, a view that is challenged in Ref. [338] showing that radiative ϕ decay data are consistent with molecular structures of light scalars.

As mentioned already, the $f_0(1500)$ [40] and the $f_1(1285)$ [319] have been proposed as tetraquarks, the latter also as $K^*\overline{K}$ molecule [260], together with the $f_1(1420)$ [268].

Another potential candidate for a tetraquark is the $\phi(2170)$. As an excited $q\bar{q}$ state of the $\phi(1020)$, this meson should decay strongly into K^+K^- and $K^0_S K^0_L$, and also $K^*\bar{K}^*$. However, these decays are not observed. Hence, based on its observed decay into $f_0(980)\phi(1020)$ this meson could be $ss\bar{s}\bar{s}$, see Ref. [339] where relative decay rates into various channels are predicted for both $q\bar{q}$ and tetraquark structures of the $f_0(980)$. However Refs. [340, 341] claim that the $\phi(2170)$ may not be a good candidate for the $ss\bar{s}\bar{s}$ state, but could qualify as an $su\bar{s}\bar{u}$ tetraquark [341].

More information on the $a_0(980)$, $f_0(980)$, $f_0(500)$ and $K^*_0(700)$ is provided by 'Scalar Mesons below 1 GeV' in the *Review*.

63.9 Baryonia

Nucleon-antinucleon ($N\bar{N}$) bound states and resonances (baryonium) were predicted a long time ago [342, 343], based on the strongly attractive $N\bar{N}$ meson exchange potential, which is obtained from the NN one by multiplying with the G-parity of the exchanged meson. Several candidates had been reported in the seventies by experiments at CERN, BNL and KEK, some of them being indisputably statistically significant (for details on the model and on experiments, see [344, 345] and references therein). Most potential models predict a sequence of deeply bound isoscalar baryonia with quantum numbers $J^{PC} = 2^{++}$, 1^{--} and 0^{++}, the latter being the mostly bound [346, 347]. The $f_2(1565)$ which is observed in $\bar{p}p$ annihilation only [348, 349], is a good candidate for the 2^{++} $\bar{p}p$ bound state.

Enhancements close to the $\bar{p}p$ threshold have also been reported in B decays [350–352]. The strong signal in $J/\psi(1S) \to \gamma\bar{p}p$ [353–355] could be due to a 0^{-+} baryonium [356], but could also be generated by the $N\bar{N}$ final state interaction [357–360]. The strong energy dependence of the cross section in $e^+e^- \to \bar{p}p$ [361, 362] and $\bar{p}p \to e^+e^-$ [363] is attributed to the $N\bar{N}$ final state interaction [364] (see also our comments on the $\rho(1900)$ at the end of section 63.5.2). Alternative explanations to baryonia have been proposed for the signals in $B \to \bar{p}pK$, such as the dynamics of the fragmentation mechanism [351].

63.10 Conclusions

The ground states nonets 1^1S_0, 1^3S_1, 1^1P_1, 1^3P_2, 1^1D_2 and 1^3D_3 (see fig. 63.1) are complete and established (although more data are desirable for the $h_1(1415)$ in the 1^1P_1 nonet). There are uncertainties and ambiguities in all other nonets . In the pseudoscalar sector the mere existence of the $\eta(1295)$ (possibly the radial excitation of the η) has been questioned. The $\eta(1440)$ consists of two states, one at 1405 MeV, the other at 1475 MeV, which could also be the manifestation of a single state decaying into two different final states. In this case the 1475 one could be the radial excitation of the η' and the 1405 state the pseudoscalar ground state glueball predicted a long time ago by the bag model, although the lattice puts it above 2 GeV. In the 1^{++} nonet two isoscalars – the $f_1(1420)$ and $f_1(1510)$ – compete for the $s\bar{s}$ slot, the former perhaps being exotic, and the latter not being very well established. The first radial excitation 2^3S_1 is complete, but questions have been raised as to the nature of the $\rho(1450)$ and its relation to the $\rho(1700)$. The classification of scalar mesons is not settled with the ones below 1 GeV being tetraquark states or part of the ground state nonet. The nature of the scalars in the 1.5 – 1.8 GeV region is unclear, obscured by the interference with the ground state scalar glueball predicted in this mass region by most theoretical models. For example, the $f_0(1500)$ and the $f_0(1710)$ could be $q\bar{q}$ states ($n\bar{n}$ and $s\bar{s}$, respectively) or made of gluons mixed with $q\bar{q}$. The $f_0(1500)$ or alternatively the $f_0(1710)$ have been proposed as mostly gluonic. Scalar mesons above the $f_0(1710)$ need experimental confirmation. The 1.4 - 1.6 GeV mass region is populated by one or two broad isovector states with exotic (1^{-+}) quantum numbers, the $\pi_1(1400)$ and $\pi_1(1600)$. The mass of latter is not far below theoretical predictions. Above 1.8 GeV mesons are broad and overlap, which complicates the data analyses. This makes the classification difficult, in particular the identification of the 2^{++} glueball.

Acknowledgements

We thank Paolo Gauzzi, Bertram Kopf, Mikhail Mikhasenko and Anton Rebhan for carefully reading the manuscript, and for their detailed and constructive suggestions. We have also benefitted from several reviews published earlier in the *Review of Particle Physics*, jointly with Thomas Gutsche, Christoph Hanhart and Stefan Spanier, which have been merged into the current article.

References

[1] C. Amsler and N. A. Tornqvist, Phys. Rept. **389**, 61 (2004).

[2] D. V. Bugg, Phys. Rept. **397**, 257 (2004), [hep-ex/0412045].

[3] E. Klempt and A. Zaitsev, Phys. Rept. **454**, 1 (2007), [arXiv:0708.4016].

[4] C. A. Meyer and E. S. Swanson, Prog. Part. Nucl. Phys. **82**, 21 (2015), [arXiv:1502.07276].

[5] R. De Vita, EPJ Web Conf. **66**, 01004 (2014).

[6] A. Esposito, A. Pilloni and A. D. Polosa, Phys. Rept. **668**, 1 (2017), [arXiv:1611.07920].

[7] F.-K. Guo *et al.*, Rev. Mod. Phys. **90**, 015004 (2018), [arXiv:1705.00141].

[8] C. Amsler, *The Quark Structure of Hadrons: An Introduction to the Phenomenology and Spectroscopy*, volume 949 of *Lecture Notes in Physics*, Springer (2018).

[9] C. Amsler *et al.* (Crystal Barrel), Phys. Lett. **B333**, 277 (1994).

[10] C. Amsler, Rev. Mod. Phys. **70**, 1293 (1998), [hep-ex/9708025].

[11] S. Uehara *et al.* (Belle), Phys. Rev. **D80**, 032001 (2009), [arXiv:0906.1464].

[12] C. Amsler, Phys. Lett. **B541**, 22 (2002), [hep-ph/0206104].

[13] P. Rubin *et al.* (CLEO), Phys. Rev. **D78**, 072003 (2008), [arXiv:0807.4545].

[14] R. Aaij *et al.* (LHCb), Phys. Rev. **D93**, 052018 (2016), [arXiv:1509.06628].

Downloaded from https://academic.oup.com/ptep/article/2022/8/083C01/6651666 by KIT Library user on 27 September 2022

[15] C. Amsler *et al.* (Crystal Barrel), Phys. Lett. **B322**, 431 (1994).

[16] C. Amsler *et al.* (Crystal Barrel), Phys. Lett. **B342**, 433 (1995).

[17] A. Abele *et al.* (Crystal Barrel), Phys. Lett. **B380**, 453 (1996).

[18] D. Barberis *et al.* (WA102), Phys. Lett. **B462**, 462 (1999), [hep-ex/9907055].

[19] D. Barberis *et al.* (WA102), Phys. Lett. **B471**, 440 (2000), [hep-ex/9912005].

[20] C. Amsler *et al.* (Crystal Barrel), Phys. Lett. **B353**, 571 (1995).

[21] C. Amsler *et al.* (Crystal Barrel), Phys. Lett. **B355**, 425 (1995).

[22] D. Barberis *et al.* (WA102), Phys. Lett. **B479**, 59 (2000), [hep-ex/0003033].

[23] D. Barberis *et al.*, Physics Letters B **471**, 429 (2000).

[24] C. Adolph *et al.* (COMPASS), Phys. Rev. **D95**, 032004 (2017), [arXiv:1509.00992].

[25] R. Aaij *et al.* (LHCb), Phys. Rev. **D86**, 052006 (2012), [arXiv:1204.5643].

[26] R. Aaij *et al.* (LHCb), Phys. Rev. **D89**, 092006 (2014), [arXiv:1402.6248].

[27] R. Aaij *et al.* (LHCb), Phys. Rev. **D90**, 012003 (2014), [arXiv:1404.5673].

[28] F. E. Close and A. Kirk, Phys. Rev. **D91**, 114015 (2015), [arXiv:1503.06942].

[29] P. d'Argent *et al.*, JHEP **05**, 143 (2017), [arXiv:1703.08505].

[30] B. Aubert *et al.* (BaBar), Phys. Rev. **D79**, 072006 (2009), [arXiv:0902.2051].

[31] R. Molina, D. Nicmorus and E. Oset, Phys. Rev. **D78**, 114018 (2008), [arXiv:0809.2233].

[32] C. García-Recio *et al.*, Phys. Rev. **D87**, 096006 (2013), [arXiv:1304.1021].

[33] D. Gülmez, U. G. Meißner and J. A. Oller, Eur. Phys. J. **C77**, 460 (2017), [arXiv:1611.00168].

[34] M. Carver *et al.* (CLAS), Phys. Rev. Lett. **126**, 082002 (2021), [arXiv:2010.16006].

[35] J.-J. Xie and E. Oset, Eur. Phys. J. A **51**, 111 (2015), [arXiv:1412.3234].

[36] A. Abele *et al.* (Crystal Barrel), Phys. Lett. **B385**, 425 (1996).

[37] C. Amsler *et al.* (Crystal Barrel), Phys. Lett. **B639**, 165 (2006).

[38] F. E. Close and N. A. Tornqvist, J. Phys. **G28**, R249 (2002), [hep-ph/0204205].

[39] J. R. Pelaez, Phys. Rept. **658**, 1 (2016), [arXiv:1510.00653].

[40] L. Zou *et al.*, Phys. Rev. D **99**, 114024 (2019), [arXiv:1901.11205].

[41] E. Klempt, Physics Letters B **820**, 136512 (2021), [arXiv:2104.09922].

[42] H. Kim, XVIII Int. Conf. on Hadron Spectroscopy (HADRON2019), Guilin, China [arXiv:1911.09904].

[43] N. A. Tornqvist, Z. Phys. **C68**, 647 (1995), [hep-ph/9504372].

[44] E. van Beveren and G. Rupp, Eur. Phys. J. **C22**, 493 (2001), [hep-ex/0106077].

[45] M. Boglione and M. R. Pennington, Phys. Rev. **D65**, 114010 (2002), [hep-ph/0203149].

[46] L. S. Celenza *et al.*, Phys. Rev. C **61**, 035201 (2000).

[47] W.-J. Lee and D. Weingarten, Phys. Rev. **D61**, 014015 (2000), [hep-lat/9910008].

[48] G. S. Bali *et al.* (UKQCD), Phys. Lett. **B309**, 378 (1993), [hep-lat/9304012].

[49] C. J. Morningstar and M. J. Peardon, Phys. Rev. **D56**, 4043 (1997), [hep-lat/9704011].

[50] Y. Chen *et al.*, Phys. Rev. **D73**, 014516 (2006), [hep-lat/0510074].

[51] J. Leutgeb and A. Rebhan, Phys. Rev. **D101**, 014006 (2020), [arXiv:1909.12352].

[52] F. Brünner, J. Leutgeb and A. Rebhan, Physics Letters B **788**, 431 (2019).

[53] M. Q. Huber, C. S. Fischer and H. Sanchis-Alepuz, The European Physical Journal C **80**, 1077 (2020), [arXiv:2004.00415].

[54] A. Sarantsev *et al.*, Physics Letters B **816**, 136227 (2021), [arXiv:2103.09680].

[55] C. Amsler and F. E. Close, Phys. Rev. **D53**, 295 (1996), [hep-ph/9507326].

[56] N. A. Tornqvist and M. Roos, Phys. Rev. Lett. **76**, 1575 (1996), [hep-ph/9511210].

[57] A. V. Anisovich, V. V. Anisovich and A. V. Sarantsev, Phys. Lett. **B395**, 123 (1997), [hep-ph/9611333].

[58] M. Boglione and M. R. Pennington, Phys. Rev. Lett. **79**, 1998 (1997), [hep-ph/9703257].

[59] P. Minkowski and W. Ochs, Eur. Phys. J. **C9**, 283 (1999), [hep-ph/9811518].

[60] F. E. Close and A. Kirk, Eur. Phys. J. **C21**, 531 (2001), [hep-ph/0103173].

[61] H.-Y. Cheng, C.-K. Chua and K.-F. Liu, Phys. Rev. **D74**, 094005 (2006), [hep-ph/0607206].

[62] W. Ochs, J. Phys. **G40**, 043001 (2013), [arXiv:1301.5183].

[63] S. R. Cotanch and R. A. Williams, Phys. Lett. B **621**, 269 (2005), [arXiv:nucl-th/0505074].

[64] T. Barnes *et al.*, Phys. Rev. **D55**, 4157 (1997), [hep-ph/9609339].

[65] S. Janowski, F. Giacosa and D. H. Rischke, Phys. Rev. **D90**, 114005 (2014), [arXiv:1408.4921].

[66] F. Brünner and A. Rebhan, Phys. Rev. Lett. **115**, 131601 (2015), [arXiv:1504.05815].

[67] J. Ellis and J. Lánik, Physics Letters B **150**, 289 (1985).

[68] C.-D. Lu *et al.*, Eur. Phys. J. **A49**, 58 (2013), [arXiv:1301.0225].

[69] F. E. Close and A. Kirk, Phys. Lett. **B397**, 333 (1997), [hep-ph/9701222].

[70] F. E. Close, Phys. Lett. **B419**, 387 (1998), [hep-ph/9710450].

[71] A. Kirk, Phys. Lett. **B489**, 29 (2000), [hep-ph/0008053].

[72] F. E. Close and Q. Zhao, Phys. Rev. **D71**, 094022 (2005), [hep-ph/0504043].

[73] M. Ablikim *et al.* (BES), Phys. Lett. **B603**, 138 (2004), [hep-ex/0409007].

[74] M. Ablikim *et al.* (BES), Phys. Lett. **B607**, 243 (2005), [hep-ex/0411001].

[75] S. Narison, Nuclear Physics B **509**, 312 (1998).

[76] M. Chanowitz, Phys. Rev. Lett. **95**, 172001 (2005), [hep-ph/0506125].

[77] M. Albaladejo and J. A. Oller, Phys. Rev. Lett. **101**, 252002 (2008), [arXiv:0801.4929].

[78] L. S. Geng and E. Oset, Phys. Rev. **D79**, 074009 (2009), [arXiv:0812.1199].

[79] F. Brünner and A. Rebhan, Phys. Rev. D **92**, 121902 (2015), [arXiv:1510.07605].

[80] M. Acciarri *et al.* (L3), Phys. Lett. **B501**, 173 (2001), [hep-ex/0011037].

[81] K. Abe *et al.* (Belle), Eur. Phys. J. **C32**, 323 (2003), [hep-ex/0309077].

Downloaded from https://academic.oup.com/ptep/article/2022/8/083C01/6651666 by KIT Library user on 27 September 2022

[82] R. Barate *et al.* (ALEPH), Phys. Lett. **B472**, 189 (2000), [hep-ex/9911022].

[83] S. Uehara *et al.* (Belle), Phys. Rev. **D78**, 052004 (2008), [arXiv:0805.3387].

[84] A. Abele *et al.*, Phys. Rev. **D57**, 3860 (1998).

[85] S. Uehara *et al.* (Belle), PTEP **2013**, 123C01 (2013), [arXiv:1307.7457].

[86] A. H. Fariborz *et al.*, Phys. Rev. **D90**, 033009 (2014), [arXiv:1407.3870].

[87] D. V. Bugg, B. S. Zou and A. V. Sarantsev, Nucl. Phys. **B471**, 59 (1996).

[88] P. Minkowski and W. Ochs, Eur. Phys. J. **C39**, 71 (2005), [hep-ph/0404194].

[89] A. Garmash *et al.* (Belle), Phys. Rev. **D71**, 092003 (2005), [hep-ex/0412066].

[90] B. Aubert *et al.* (BaBar), Phys. Rev. **D74**, 032003 (2006), [hep-ex/0605003].

[91] B. Aubert *et al.* (BaBar), Phys. Rev. Lett. **99**, 161802 (2007), [arXiv:0706.3885].

[92] M. Ablikim *et al.*, Phys. Lett. **B642**, 441 (2006), [hep-ex/0603048].

[93] M. Ablikim *et al.* (BESIII), Phys. Rev. **D87**, 092009 (2013), [Erratum: Phys. Rev.D87, 119901(2013)], [arXiv:1301.0053].

[94] E. Klempt and A. Sarantsev, Physics Letters B **826**, 136906 (2022), [arXiv:2112.04348].

[95] A. Rodas *et al.*, Eur. Phys. J. **C82**, 80 (2022), [arXiv:2110.00027].

[96] C. Amsler *et al.* (Crystal Barrel), Eur. Phys. J. **C23**, 29 (2002).

[97] A. A. Godizov, Eur. Phys. J. C **76**, 7, 361 (2016), [arXiv:1604.01689].

[98] S. Donnachie *et al.*, *Pomeron Physics and QCD*, Cambridge Monographs on Particle Physics, Nuclear Physics and Cosmology, Cambridge University Press, p. 85 (2002).

[99] C. Evangelista *et al.* (JETSET), Phys. Rev. D **57**, 5370 (1998), [hep-ex/9802016].

[100] P. S. L. Booth *et al.*, Nucl. Phys. B **273**, 689 (1986).

[101] A. Etkin *et al.*, Phys. Lett. B **201**, 568 (1988).

[102] D. Barberis *et al.* (WA102), Phys. Lett. B **432**, 436 (1998), [hep-ex/9805018].

[103] M. Ablikim *et al.* (BESIII), Phys. Rev. D **93**, 112011 (2016), [arXiv:1602.01523].

[104] Y.-B. Yang *et al.* (CLQCD Collaboration), Phys. Rev. Lett. **111**, 091601 (2013).

[105] I. Iatrakis, A. Ramamurti and E. Shuryak, Phys. Rev. D **94**, 045005 (2016), [arXiv:1602.05014].

[106] F. Brünner, D. Parganlija and A. Rebhan, Phys. Rev. D **91**, 106002 (2015), [Erratum: Phys.Rev. D93, 109903 (2016)], [arXiv:1501.07906].

[107] J. Z. Bai *et al.* (BES), Phys. Rev. Lett. **76**, 3502 (1996).

[108] C. Amsler *et al.* (Crystal Barrel), Phys. Lett. B **520**, 175 (2001).

[109] R. Aaij *et al.* (LHCb), Eur. Phys. J. C **78**, 443 (2018), [arXiv:1712.08609].

[110] P. H. Baillon *et al.*, Nuovo Cim. **A50**, 393 (1967).

[111] D. L. Scharre *et al.*, Phys. Lett. **97B**, 329 (1980).

[112] C. Edwards *et al.*, Phys. Rev. Lett. **49**, 259 (1982), [Erratum: Phys. Rev. Lett.50,219(1983)].

[113] J. E. Augustin *et al.* (DM2), Phys. Rev. **D42**, 10 (1990).

[114] J. Z. Bai *et al.* (BES), Phys. Lett. **B594**, 47 (2004), [hep-ex/0403008].

[115] G. S. Adams *et al.* (E852), Phys. Lett. **B516**, 264 (2001), [hep-ex/0107042].

[116] S. Fukui *et al.*, Phys. Lett. **B267**, 293 (1991).

[117] D. Alde *et al.* (GAMS), Phys. Atom. Nucl. **60**, 386 (1997), [Yad. Fiz.60,458(1997)].

[118] J. J. Manak *et al.* (E852), Phys. Rev. **D62**, 012003 (2000), [hep-ex/0001051].

[119] A. V. Anisovich *et al.*, Nucl. Phys. **A690**, 567 (2001).

[120] C. Amsler *et al.*, Eur. Phys. J. **C33**, 23 (2004).

[121] J. E. Augustin *et al.* (DM2), Phys. Rev. **D46**, 1951 (1992).

[122] B. Aubert *et al.* (BaBar), Phys. Rev. Lett. **101**, 091801 (2008), [arXiv:0804.0411].

[123] M. G. Rath *et al.*, Phys. Rev. **D40**, 693 (1989).

[124] Z. Bai *et al.* (MARK-III), Phys. Rev. Lett. **65**, 2507 (1990).

[125] A. Bertin *et al.* (OBELIX), Phys. Lett. **B361**, 187 (1995).

[126] A. Bertin *et al.* (OBELIX), Phys. Lett. **B400**, 226 (1997).

[127] C. Cicalo *et al.* (OBELIX), Phys. Lett. **B462**, 453 (1999).

[128] F. Nichitiu *et al.* (OBELIX), Phys. Lett. **B545**, 261 (2002).

[129] T. Bolton *et al.*, Phys. Rev. Lett. **69**, 1328 (1992).

[130] M. Ablikim *et al.* (BES), Phys. Rev. **D77**, 032005 (2008), [arXiv:0712.1411].

[131] M. Ablikim *et al.* (BESIII), Phys. Rev. **D87**, 092006 (2013), [arXiv:1303.6360].

[132] M. Acciarri *et al.* (L3), Phys. Lett. **B501**, 1 (2001), [hep-ex/0011035].

[133] F. E. Close, G. R. Farrar and Z.-p. Li, Phys. Rev. **D55**, 5749 (1997), [hep-ph/9610280].

[134] D. M. Li, H. Yu and S. S. Fang, Eur. Phys. J. **C28**, 335 (2003).

[135] R. Ahohe *et al.* (CLEO), Phys. Rev. **D71**, 072001 (2005), [hep-ex/0501026].

[136] P. Achard *et al.* (L3), JHEP **03**, 018 (2007).

[137] T. Gutsche, V. E. Lyubovitskij and M. C. Tichy, Phys. Rev. **D79**, 014036 (2009), [arXiv:0811.0668].

[138] L. Faddeev, A. J. Niemi and U. Wiedner, Phys. Rev. **D70**, 114033 (2004), [hep-ph/0308240].

[139] C. J. Morningstar and M. J. Peardon, Phys. Rev. **D60**, 034509 (1999), [hep-lat/9901004].

[140] H.-Y. Cheng, H.-n. Li and K.-F. Liu, Phys. Rev. **D79**, 014024 (2009), [arXiv:0811.2577].

[141] G. Li, Q. Zhao and C.-H. Chang, J. Phys. **G35**, 055002 (2008), [hep-ph/0701020].

[142] T. Gutsche, V. E. Lyubovitskij and M. C. Tichy, Phys. Rev. **D80**, 014014 (2009), [arXiv:0904.3414].

[143] B. A. Li, Phys. Rev. **D81**, 114002 (2010), [arXiv:0912.2323].

[144] A. Masoni, C. Cicalo and G. L. Usai, J. Phys. **G32**, R293 (2006).

[145] E. Klempt, Int. J. Mod. Phys. **A21**, 739 (2006).

[146] J.-J. Wu *et al.*, Phys. Rev. Lett. **108**, 081803 (2012), [arXiv:1108.3772].

[147] X.-G. Wu *et al.*, Phys. Rev. **D87**, 014023 (2013), [arXiv:1211.2148].

[148] M.-C. Du and Q. Zhao, Phys. Rev. D **100**, 036005 (2019), [arXiv:1905.04207].

[149] F. Aceti *et al.*, Phys. Rev. **D86**, 114007 (2012), [arXiv:1209.6507].

[150] J. Pisut and M. Roos, Nucl. Phys. **B6**, 325 (1968).

[151] G. D. Lafferty, Z. Phys. **C60**, 659 (1993).

[152] A. Abele *et al.* (Crystal Barrel), Phys. Lett. **B402**, 195 (1997).

[153] M. Benayoun *et al.*, Eur. Phys. J. **C31**, 525 (2003), [arXiv:nucl-th/0306078].

[154] R. Barate *et al.* (ALEPH), Z. Phys. **C76**, 15 (1997).

[155] L. M. Barkov *et al.*, Nucl. Phys. **B256**, 365 (1985).

Downloaded from https://academic.oup.com/ptep/article/2022/8/083C01/6651666 by KIT Library user on 27 September 2022

[156] S. Anderson *et al.* (CLEO), Phys. Rev. **D61**, 112002 (2000), [hep-ex/9910046].

[157] M. Fujikawa *et al.* (Belle), Phys. Rev. **D78**, 072006 (2008), [arXiv:0805.3773].

[158] K. Ackerstaff *et al.* (OPAL), Eur. Phys. J. **C7**, 571 (1999), [hep-ex/9808019].

[159] M. Davier and C.-Z. Yuan, Nucl. Phys. B - Proc. Suppl. **123**, 47 (2003), [hep-ex/0211057].

[160] S. Schael *et al.* (ALEPH), Phys. Rept. **421**, 191 (2005), [hep-ex/0506072].

[161] R. R. Akhmetshin *et al.* (CMD-2), Phys. Lett. **B527**, 161 (2002), [hep-ex/0112031].

[162] R. R. Akhmetshin *et al.* (CMD-2), Phys. Lett. **B578**, 285 (2004), [hep-ex/0308008].

[163] M. Davier *et al.*, Eur. Phys. J. **C27**, 497 (2003), [hep-ph/0208177].

[164] M. Davier *et al.*, Eur. Phys. J. **C31**, 503 (2003), [hep-ph/0308213].

[165] A. Aloisio *et al.* (KLOE), Phys. Lett. **B606**, 12 (2005), [hep-ex/0407048].

[166] F. Ambrosino *et al.* (KLOE), Phys. Lett. **B670**, 285 (2009), [arXiv:0809.3950].

[167] F. Ambrosino *et al.* (KLOE), Phys. Lett. **B700**, 102 (2011), [arXiv:1006.5313].

[168] D. Babusci *et al.* (KLOE), Phys. Lett. B **720**, 336 (2013), [arXiv:1212.4524].

[169] M. N. Achasov *et al.*, J. Exp. Theor. Phys. **101**, 1053 (2005), [hep-ex/0506076].

[170] M. N. Achasov *et al.*, J. Exp. Theor. Phys. **103**, 380 (2006), [hep-ex/0605013].

[171] B. Aubert *et al.* (BaBar), Phys. Rev. Lett. **103**, 231801 (2009), [arXiv:0908.3589].

[172] M. Ablikim *et al.* (BESIII), Phys. Lett. B **753**, 629 (2016), [Erratum: Phys.Lett.B 812, 135982 (2021)], [arXiv:1507.08188].

[173] R. Alemany, M. Davier and A. Hocker, Eur. Phys. J. **C2**, 123 (1998), [hep-ph/9703220].

[174] H. Czyz and J. H. Kuhn, Eur. Phys. J. **C18**, 497 (2001), [hep-ph/0008262].

[175] V. Cirigliano, G. Ecker and H. Neufeld, Phys. Lett. **B513**, 361 (2001), [hep-ph/0104267].

[176] V. Cirigliano *et al.*, Eur. Phys. J. **C23**, 121 (2002), [hep-ph/0110153].

[177] K. Maltman and C. E. Wolfe, Phys. Rev. **D73**, 013004 (2006), [hep-ph/0509224].

[178] C. E. Wolfe and K. Maltman, Phys. Rev. **D80**, 114024 (2009), [arXiv:0908.2391].

[179] F. Jegerlehner and R. Szafron, Eur. Phys. J. **C71**, 1632 (2011), [arXiv:1101.2872].

[180] M. Benayoun *et al.*, Eur. Phys. J. **C72**, 1848 (2012), [arXiv:1106.1315].

[181] M. Benayoun *et al.*, Eur. Phys. J. C **73**, 2453 (2013), [arXiv:1210.7184].

[182] M. Davier *et al.*, Eur. Phys. J. C **77**, 827 (2017), [arXiv:1706.09436].

[183] C. Erkal and M. G. Olsson, Z. Phys. **C31**, 615 (1986).

[184] A. Donnachie and H. Mirzaie, Z. Phys. **C33**, 407 (1987).

[185] A. Donnachie and A. B. Clegg, Z. Phys. **C34**, 257 (1987).

[186] A. Donnachie and A. B. Clegg, Z. Phys. **C51**, 689 (1991).

[187] A. B. Clegg and A. Donnachie, Z. Phys. **C40**, 313 (1988).

[188] A. B. Clegg and A. Donnachie, Z. Phys. **C62**, 455 (1994).

[189] T. J. Killian *et al.*, Phys. Rev. **D21**, 3005 (1980).

[190] S. Fukui *et al.*, Phys. Lett. **B202**, 441 (1988).

[191] D. Bisello *et al.* (DM2), Phys. Lett. **B220**, 321 (1989).

[192] A. Antonelli *et al.* (DM2), Phys. Lett. **B212**, 133 (1988).

[193] A. Abele *et al.* (Crystal Barrel), Phys. Lett. **B391**, 191 (1997).

[194] A. Bertin *et al.* (OBELIX), Phys. Lett. **B434**, 180 (1998).

[195] A. Abele *et al.* (Crystal Barrel), Phys. Lett. **B468**, 178 (1999).

[196] W.-F. Wang, Phys. Rev. D **103**, 056021 (2021), [arXiv:2012.15039], URL `https://link.aps.org/doi/10.1103/PhysRevD.103.056021`.

[197] K. W. Edwards *et al.* (CLEO), Phys. Rev. **D61**, 072003 (2000), [hep-ex/9908024].

[198] J. P. Lees *et al.* (BaBar), Phys. Rev. **D86**, 032013 (2012), [arXiv:1205.2228].

[199] F. E. Close and P. R. Page, Phys. Rev. **D56**, 1584 (1997), [hep-ph/9701425].

[200] A. Donnachie and Yu. S. Kalashnikova, Phys. Rev. **D60**, 114011 (1999), [hep-ph/9901334].

[201] R. R. Akhmetshin *et al.* (CMD-2), Phys. Lett. **B466**, 392 (1999), [hep-ex/9904024].

[202] J. P. Alexander *et al.* (CLEO), Phys. Rev. **D64**, 092001 (2001), [hep-ex/0103021].

[203] D. Matvienko *et al.* (Belle), Phys. Rev. **D92**, 012013 (2015), [arXiv:1505.03362].

[204] R. R. Akhmetshin *et al.* (CMD-2), Phys. Lett. **B562**, 173 (2003), [hep-ex/0304009].

[205] M. N. Achasov *et al.*, Phys. Rev. D **94**, 112001 (2016), [arXiv:1610.00235].

[206] A. Abele *et al.* (CRYSTAL BARREL), Eur. Phys. J. **C21**, 261 (2001).

[207] M. Bargiotti *et al.* (Obelix), Phys. Lett. **B561**, 233 (2003).

[208] S. I. Bityukov *et al.*, Phys. Lett. **B188**, 383 (1987).

[209] B. Aubert *et al.* (BaBar), Phys. Rev. **D77**, 092002 (2008), [arXiv:0710.4451].

[210] M. N. Achasov *et al.*, Eur. Phys. J. C **80**, 1139 (2020).

[211] N. N. Achasov and G. N. Shestakov, Phys. Atom. Nucl. **59**, 1262 (1996), [Yad. Fiz.59N7,1319(1996)].

[212] L. G. Landsberg, Sov. J. Nucl. Phys. **55**, 1051 (1992), [Yad. Fiz.55,1896(1992)].

[213] A. Abele *et al.* (Crystal Barrel), Phys. Lett. **B415**, 280 (1997).

[214] V. M. Aulchenko *et al.*, JETP Lett. **45**, 145 (1987), [Pisma Zh. Eksp. Teor. Fiz.45,118(1987)].

[215] D. Bisello *et al.*, Z. Phys. **C52**, 227 (1991).

[216] P. Frenkiel *et al.*, Nucl. Phys. **B47**, 61 (1972).

[217] G. Cosme *et al.*, Phys. Lett. **63B**, 352 (1976).

[218] D. P. Barber *et al.* (LAMP2 Group), Z. Phys. **C4**, 169 (1980).

[219] D. Aston *et al.*, Phys. Lett. **92B**, 211 (1980), [Erratum: Phys. Lett.95B,461(1980)].

[220] M. Atkinson *et al.* (Omega Photon), Nucl. Phys. **B243**, 1 (1984).

[221] J. E. Brau *et al.* (SLAC Hybrid Facility Photon), Phys. Rev. **D37**, 2379 (1988).

[222] C. Amsler *et al.* (Crystal Barrel), Phys. Lett. **B311**, 362 (1993).

[223] J. Layssac and F. M. Renard, Nuovo Cim. **A6**, 134 (1971).

[224] D. Aston *et al.*, Nucl. Phys. Proc. Suppl. **21**, 105 (1991).

[225] N. Hammoud *et al.*, Phys. Rev. D **102**, 054029 (2020).

[226] M. Ablikim *et al.* (BES), Phys. Rev. Lett. **97**, 142002 (2006), [hep-ex/0606047].

[227] G.-J. Ding and M.-L. Yan, Phys. Lett. **B643**, 33 (2006), [hep-ph/0607253].

Downloaded from https://academic.oup.com/ptep/article/2022/8/083C01/6651666 by KIT Library user on 27 September 2022

[228] F.-K. Guo *et al.*, Nucl. Phys. **A773**, 78 (2006), [hep-ph/0509050].

[229] A. Zhang, T. Huang and T. G. Steele, Phys. Rev. **D76**, 036004 (2007), [hep-ph/0612146].

[230] B. A. Li, Phys. Rev. **D76**, 094016 (2007), [hep-ph/0701159].

[231] X. Liu *et al.*, Phys. Rev. **D75**, 074017 (2007), [hep-ph/0701022].

[232] J. P. Lees *et al.* (BaBar), Phys. Rev. D **88**, 032013 (2013), [arXiv:1306.3600].

[233] M. N. Achasov *et al.*, Phys. Rev. D **94**, 112006 (2016), [arXiv:1608.08757].

[234] A. B. Clegg and A. Donnachie, Z. Phys. **C45**, 677 (1990).

[235] D. Bisello *et al.*, Phys. Lett. **107B**, 145 (1981).

[236] A. Castro *et al.*, LAL-88-58(1988), URL `https://doi.org/10.17182/hepdata.38181`.

[237] M. Atkinson *et al.* (Omega Photon), Z. Phys. **C29**, 333 (1985).

[238] B. Aubert *et al.* (BaBar), Phys. Rev. **D76**, 092005 (2007), [Erratum: Phys. Rev.D77,119902(2008)], [arXiv:0708.2461].

[239] J. P. Lees *et al.* (BABAR Collaboration), Phys. Rev. D **86**, 032013 (2012).

[240] M. Ablikim *et al.* (BESIII Collaboration), Phys. Rev. D **99**, 032001 (2019).

[241] J. P. Lees *et al.* (BaBar Collaboration), Phys. Rev. D **101**, 012011 (2020).

[242] S. Godfrey and N. Isgur, Phys. Rev. **D32**, 189 (1985).

[243] P. L. Frabetti *et al.* (E687), Phys. Lett. **B514**, 240 (2001), [hep-ex/0106029].

[244] P. L. Frabetti *et al.*, Phys. Lett. **B578**, 290 (2004), [hep-ex/0310041].

[245] A. Antonelli *et al.* (FENICE), Phys. Lett. **B365**, 427 (1996).

[246] B. Aubert *et al.* (BaBar), Phys. Rev. **D73**, 052003 (2006), [hep-ex/0602006].

[247] R. R. Akhmetshin *et al.* (CMD-3), Phys. Lett. **B723**, 82 (2013), [arXiv:1302.0053].

[248] R. R. Akhmetshin *et al.* (CMD-3), Phys. Lett. B **794**, 64 (2019), [arXiv:1808.00145].

[249] A. E. Obrazovsky and S. I. Serednyakov, JETP Lett. **99**, 315 (2014), [arXiv:1402.5225].

[250] J. Haidenbauer *et al.*, Phys. Rev. **D92**, 054032 (2015), [arXiv:1506.08120].

[251] A. I. Milstein and S. G. Salnikov, Nucl. Phys. A **977**, 60 (2018), [arXiv:1804.01283].

[252] M. Ablikim *et al.* (BESIII Collaboration), Phys. Rev. D **97**, 032013 (2018), [arXiv:1709.10236].

[253] H.-Y. Cheng, Phys. Lett. **B707**, 116 (2012), [arXiv:1110.2249].

[254] S. U. Chung *et al.*, Phys. Rev. Lett. **55**, 779 (1985), [Erratum: Phys. Rev. Lett.55,2093(1985)].

[255] D. F. Reeves *et al.*, Phys. Rev. **D34**, 1960 (1986).

[256] A. Birman *et al.*, Phys. Rev. Lett. **61**, 1557 (1988), [Erratum: Phys. Rev. Lett.62,1577(1989)].

[257] C. Dionisi *et al.* (CERN-College de France-Madrid-Stockholm), Nucl. Phys. **B169**, 1 (1980).

[258] H. J. Behrend *et al.* (CELLO), Z. Phys. **C42**, 367 (1989).

[259] T. A. Armstrong *et al.* (WA76), Z. Phys. **C52**, 389 (1991).

[260] F. Aceti, J.-J. Xie and E. Oset, Phys. Lett. **B750**, 609 (2015), [arXiv:1505.06134].

[261] R. Aaij *et al.* (LHCb), Phys. Rev. Lett. **112**, 091802 (2014), [arXiv:1310.2145].

[262] G. Gidal *et al.*, Phys. Rev. Lett. **59**, 2012 (1987).

[263] C. Adolph *et al.* (COMPASS), Phys. Rev. Lett. **115**, 082001 (2015), [arXiv:1501.05732].

[264] M. Aghasyan *et al.* (COMPASS), Phys. Rev. **D98**, 092003 (2018), [arXiv:1802.05913].

[265] G. D. Alexeev *et al.*, Phys. Rev. Lett. **127**, 082501 (2021), [arXiv:2006.05342].

[266] V. R. Debastiani *et al.*, Phys. Rev. **D95**, 034015 (2017), [arXiv:1611.05383].

[267] S. Ishida *et al.*, Prog. Theor. Phys. **82**, 119 (1989).

[268] R. S. Longacre, Phys. Rev. **D42**, 874 (1990).

[269] D. Aston *et al.*, Phys. Lett. **B201**, 573 (1988).

[270] F. E. Close and A. Kirk, Z. Phys. **C76**, 469 (1997), [hep-ph/9706543].

[271] P. Gavillet *et al.*, Z. Phys. **C16**, 119 (1982).

[272] J. Z. Bai *et al.* (BES), Phys. Lett. **B446**, 356 (1999).

[273] M. Ablikim *et al.* (BESIII), Phys. Rev. Lett. **106**, 072002 (2011), [arXiv:1012.3510].

[274] P. F. Ermolov *et al.*, Sov. J. Nucl. Phys. **39**, 738 (1984), [Yad. Fiz.39,1170(1984)].

[275] E. King *et al.*, Nucl. Phys. Proc. Suppl. **21**, 11 (1991).

[276] D. Barberis *et al.* (WA102), Phys. Lett. **B413**, 225 (1997), [hep-ex/9707022].

[277] H. Aihara *et al.* (TPC/Two Gamma), Phys. Rev. **D38**, 1 (1988).

[278] D. A. Bauer *et al.* (TPC/Two Gamma), Phys. Rev. **D48**, 3976 (1993).

[279] N. Isgur, R. Kokoski and J. Paton, Phys. Rev. Lett. **54**, 869 (1985).

[280] F. E. Close and P. R. Page, Nucl. Phys. **B443**, 233 (1995), [hep-ph/9411301].

[281] P. Lacock *et al.* (UKQCD), Phys. Lett. **B401**, 308 (1997), [hep-lat/9611011].

[282] C. W. Bernard *et al.* (MILC), Phys. Rev. **D56**, 7039 (1997), [hep-lat/9707008].

[283] P. R. Page, E. S. Swanson and A. P. Szczepaniak, Phys. Rev. **D59**, 034016 (1999), [hep-ph/9808346].

[284] J. J. Dudek *et al.*, Phys. Rev. **D83**, 111502 (2011), [arXiv:1102.4299].

[285] J. J. Dudek *et al.*, Phys. Rev. **D88**, 094505 (2013), [arXiv:1309.2608].

[286] A. J. Woss *et al.*, Phys. Rev. D **103**, 054502 (2021), [arXiv:2009.10034].

[287] C. A. Meyer and Y. Van Haarlem, Phys. Rev. C **82**, 025208 (2010).

[288] D. R. Thompson *et al.* (E852), Phys. Rev. Lett. **79**, 1630 (1997), [hep-ex/9705011].

[289] S. U. Chung *et al.* (E852), Phys. Rev. **D60**, 092001 (1999), [hep-ex/9902003].

[290] G. S. Adams *et al.* (E862), Phys. Lett. **B657**, 27 (2007), [hep-ex/0612062].

[291] D. Alde *et al.*, Phys. Lett. **B205**, 397 (1988).

[292] Yu. D. Prokoshkin and S. A. Sadovsky, Phys. Atom. Nucl. **58**, 606 (1995), [Yad. Fiz.58N4,662(1995)].

[293] Yu. D. Prokoshkin and S. A. Sadovsky, Phys. Atom. Nucl. **58**, 853 (1995), [Yad. Fiz.58,921(1995)].

[294] A. Abele *et al.* (Crystal Barrel), Phys. Lett. **B423**, 175 (1998).

[295] A. Abele *et al.* (Crystal Barrel), Phys. Lett. **B446**, 349 (1999).

[296] M. Albrecht *et al.* (Crystal Barrel), Eur. Phys. J. **C80**, 453 (2020), [arXiv:1909.07091].

[297] A. Donnachie and P. R. Page, Phys. Rev. **D58**, 114012 (1998), [hep-ph/9808225].

[298] M. Aghasyan *et al.* (COMPASS), Phys. Rev. D **98**, 092003 (2018), [arXiv:1802.05913].

Downloaded from https://academic.oup.com/ptep/article/2022/8/083C01/6651666 by KIT Library user on 27 September 2022

[299] G. D. Alexeev *et al.*, Phys. Rev. D **105**, 012005 (2022), [arXiv:arXiv:2108.01744].

[300] E. I. Ivanov *et al.* (E852), Phys. Rev. Lett. **86**, 3977 (2001), [hep-ex/0101058].

[301] J. Kuhn *et al.* (E852), Phys. Lett. **B595**, 109 (2004), [hep-ex/0401004].

[302] M. Lu *et al.* (E852), Phys. Rev. Lett. **94**, 032002 (2005), [hep-ex/0405044].

[303] Yu.P. Gouz *et al.*, Proc. XXVI Int. Conf. on HEP, Dallas (1992).

[304] G. M. Beladidze *et al.* (VES), Phys. Lett. **B313**, 276 (1993).

[305] C. Adolph *et al.* (COMPASS), Phys. Lett. B **740**, 303 (2015), [Erratum: Phys.Lett.B 811, 135913 (2020)], [arXiv:1408.4286].

[306] A. Rodas *et al.* (JPAC), Phys. Rev. Lett. **122**, 042002 (2019), [arXiv:1810.04171].

[307] B. Kopf *et al.*, Eur. Phys. J. C **81**, 12, 1056 (2021), [arXiv:2008.11566].

[308] M. Alekseev *et al.* (COMPASS), Phys. Rev. Lett. **104**, 241803 (2010), [arXiv:0910.5842].

[309] D. V. Amelin *et al.* (VES), Phys. Lett. **B356**, 595 (1995).

[310] J. Adomeit *et al.* (Crystal Barrel), Z. Phys. **C71**, 227 (1996).

[311] S. U. Chung, E. Klempt and J. G. Korner, Eur. Phys. J. **A15**, 539 (2002), [hep-ph/0211100].

[312] F. E. Close and H. J. Lipkin, Phys. Lett. **B196**, 245 (1987).

[313] F. Iddir and A. S. Safir, Phys. Lett. **B507**, 183 (2001), [hep-ph/0010121].

[314] G. C. Rossi and G. Veneziano, Nucl. Phys. **B123**, 507 (1977).

[315] J. L. Rosner, Phys. Rev. Lett. **21**, 950 (1968).

[316] R. L. Jaffe, Phys. Rev. **D15**, 281 (1977).

[317] M. G. Alford and R. L. Jaffe, Nucl. Phys. **B578**, 367 (2000), [hep-lat/0001023].

[318] G. 't Hooft *et al.*, Phys. Lett. **B662**, 424 (2008), [arXiv:0801.2288].

[319] S. Stone and L. Zhang, Phys. Rev. Lett. **111**, 062001 (2013), [arXiv:1305.6554].

[320] E. M. Aitala *et al.* (E791), Phys. Rev. Lett. **86**, 765 (2001), [hep-ex/0007027].

[321] H.-Y. Cheng, Phys. Rev. **D67**, 054021 (2003), [hep-ph/0212361].

[322] R. Fleischer, R. Knegjens and G. Ricciardi, Eur. Phys. J. **C71**, 1832 (2011), [arXiv:1109.1112].

[323] J. T. Daub, C. Hanhart and B. Kubis, JHEP **02**, 009 (2016), [arXiv:1508.06841].

[324] J. D. Weinstein and N. Isgur, Phys. Rev. **D41**, 2236 (1990).

[325] G. Janssen *et al.*, Phys. Rev. **D52**, 2690 (1995), [arXiv:nucl-th/9411021].

[326] M. P. Locher, V. E. Markushin and H. Q. Zheng, Eur. Phys. J. **C4**, 317 (1998), [hep-ph/9705230].

[327] J. A. Oller and E. Oset, AIP Conf. Proc. **432**, 413 (1998), [hep-ph/9710557].

[328] R. Delbourgo, D.-s. Liu and M. D. Scadron, Phys. Lett. **B446**, 332 (1999), [hep-ph/9811474].

[329] C. Hanhart *et al.*, Phys. Rev. **D75**, 074015 (2007), [hep-ph/0701214].

[330] F. E. Close, N. Isgur and S. Kumano, Nucl. Phys. **B389**, 513 (1993), [hep-ph/9301253].

[331] N. N. Achasov, V. V. Gubin and V. I. Shevchenko, Phys. Rev. **D56**, 203 (1997), [hep-ph/9605245].

[332] F. Ambrosino *et al.*, Physics Letters B **681**, 5 (2009), [arXiv:0904.2539].

[333] F. Ambrosino *et al.*, Eur. Phys. J. C **49**, 473 (2007), [hep-ex/0609009].

[334] R. R. Akhmetshin *et al.* (CMD-2), Phys. Lett. **B462**, 371 (1999), [hep-ex/9907005].

[335] M. N. Achasov *et al.*, Phys. Lett. **B479**, 53 (2000), [hep-ex/0003031].

[336] N. N. Achasov *et al.*, Phys. Rev. D **103**, 014010 (2021), [arXiv:2009.04191].

[337] M. Ablikim *et al.* (BESIII Collaboration), Phys. Rev. Lett. **121**, 022001 (2018), [arXiv:1802.00583].

[338] Yu. S. Kalashnikova *et al.*, Eur. Phys. J. **A24**, 437 (2005), [hep-ph/0412340].

[339] H.-W. Ke and X.-Q. Li, Phys. Rev. D **99**, 036014 (2019).

[340] F.-X. Liu *et al.*, Phys. Rev. D **103**, 016016 (2021).

[341] S. S. Agaev, K. Azizi and H. Sundu, Phys. Rev. D **101**, 074012 (2020).

[342] O. D. Dalkarov, V. B. Mandelzweig and I. S. Shapiro, Nucl. Phys. B **21**, 88 (1970).

[343] G. Rossi and G. Veneziano, Physics Reports **63**, 153 (1980).

[344] C. Amsler, Adv. Nucl. Phys. **18**, 183 (1987).

[345] L. Montanet, Phys. Rept. **63**, 201 (1980).

[346] C. B. Dover and J. M. Richard, Annals Phys. **121**, 70 (1979).

[347] W. W. Buck, C. B. Dover and J. M. Richard, Annals Phys. **121**, 47 (1979).

[348] B. May *et al.* (ASTERIX), Z. Phys. **C46**, 203 (1990).

[349] A. Bertin *et al.* (OBELIX), Phys. Rev. **D57**, 55 (1998).

[350] K. Abe *et al.* (Belle), Phys. Rev. Lett. **88**, 181803 (2002), [hep-ex/0202017].

[351] M. Z. Wang *et al.* (Belle), Phys. Lett. **B617**, 141 (2005), [hep-ex/0503047].

[352] K. Abe *et al.* (Belle), Phys. Rev. Lett. **89**, 151802 (2002), [hep-ex/0205083].

[353] J. Z. Bai *et al.* (BES), Phys. Rev. Lett. **91**, 022001 (2003), [hep-ex/0303006].

[354] J. P. Alexander *et al.* (CLEO), Phys. Rev. **D82**, 092002 (2010), [arXiv:1007.2886].

[355] M. Ablikim *et al.* (BESIII), Phys. Rev. Lett. **108**, 112003 (2012), [arXiv:1112.0942].

[356] G.-J. Ding and M.-L. Yan, Phys. Rev. **C72**, 015208 (2005), [hep-ph/0502127].

[357] B. Loiseau and S. Wycech, Phys. Rev. **C72**, 011001 (2005), [hep-ph/0501112].

[358] A. Sibirtsev *et al.*, Phys. Rev. **D71**, 054010 (2005), [hep-ph/0411386].

[359] X.-W. Kang, J. Haidenbauer and U.-G. Meissner, JHEP **02**, 113 (2014), [arXiv:1311.1658].

[360] X.-W. Kang, J. Haidenbauer and U.-G. Meissner, Phys. Rev. **D91**, 074003 (2015), [arXiv:1502.00880].

[361] J. P. Lees *et al.* (BaBar), Phys. Rev. **D87**, 092005 (2013), [arXiv:1302.0055].

[362] E. P. Solodov *et al.*, EPJ Web Conf. **212**, 07002 (2019).

[363] G. Bardin *et al.*, Nucl. Phys. **B411**, 3 (1994).

[364] J. Haidenbauer, X. W. Kang and U. G. Meissner, Nucl. Phys. **A929**, 102 (2014), [arXiv:1405.1628].

Downloaded from https://academic.oup.com/ptep/article/2022/8/083C01/6651666 by KIT Library user on 27 September 2022

64. Scalar Mesons below 1 GeV

Revised August 2021 by S. Eidelman (Budker Inst., Novosibirsk; Novosibirsk U.), T. Gutsche (Tübingen U.), C. Hanhart (Jülich), R.E. Mitchell (Indiana U.) and S. Spanier (Tennessee U.).

64.1 Introduction

In contrast to the vector and tensor mesons, the identification of the scalar mesons is a long-standing puzzle. Scalar resonances are difficult to resolve because some of them have large decay widths, which cause a strong overlap between resonances and background. In addition, in some cases, several decay channels open up within a short mass interval (*e.g.* at the $K\bar{K}$ and $\eta\eta$ thresholds), producing cusps in the line shapes of the nearby resonances. Furthermore, one expects non-$q\bar{q}$ scalar objects, such as hadronic molecules and multiquark states, in the mass range of interest (for reviews see, *e.g.*, Refs. [1–5]).

Light scalars are produced, for example, in πN scattering on polarized/unpolarized targets, $p\bar{p}$ annihilation, central hadronic production, $J/\psi(1S)$, B-, D- and K-meson decays, $\gamma\gamma$ formation, and ϕ radiative decays. Especially for the lightest scalar mesons simple parameterizations like Breit-Wigner functions and variants thereof fail — this is demonstrated explicitly on the example of the $f_0(500)$ or σ, e.g., in Ref. [6]. Accordingly, more advanced theory tools are necessary to extract the resonance parameters from data. In the analyses available in the literature, fundamental properties of the amplitudes such as unitarity, analyticity, Lorentz invariance, and chiral and flavor symmetry are implemented at different levels of rigor. Especially, chiral symmetry implies the appearance of zeros, the so-called Adler zeros, close to the threshold in elastic S-wave scattering amplitudes involving soft (pseudo) Goldstone bosons [7,8], which may be shifted or removed in associated production processes [9]. Moreover, especially for the lightest non-strange and strange scalar resonance precision extractions of pole parameters get complicated by the presence of both left-hand cuts as well as circular cuts [5]. The methods employed are the K-matrix formalism, the N/D-method, the Dalitz-Tuan ansatz, unitarized quark models with coupled channels, effective chiral field theories and the linear sigma model, *etc.* Dynamics near the lowest two-body thresholds in some analyses are described by crossed channel (t, u) meson exchange or with an effective range parameterization instead of, or in addition to, resonant features in the s-channel. Dispersion theoretical approaches are applied to pin down the location of resonance poles for the low mass states [10–15].

The mass and width of a resonance are found from the position of the nearest pole in the process amplitude (T-matrix or S-matrix) at an unphysical sheet of the complex energy plane, traditionally labeled as

$$\sqrt{s_{\rm Pole}} = M - i\,\Gamma/2\ . \tag{64.1}$$

It is important to note that in general the pole of a Breit-Wigner parameterization does not agree with the S- or T-matrix pole. For a detailed discussion of this issue we refer to the review on *Resonances* in this Review of Particle Physics (RPP).

In this review we present proposed values for the mass parameters of the scalar resonances below 1 GeV. Note that those are labeled as 'our estimate' — it is not an average over the quoted analyses, but is chosen to include the bulk of the analyses. An averaging procedure is not justified, since the analyses use overlapping or sometimes even identical data sets so that they are not statistically independent.

On this note, we discuss the light scalars below 1 GeV organized in the *Listings* under the entries $K_0^*(700)$ (or κ) with isospin $I = 1/2$, $a_0(980)$ with $I = 1$, as well as $f_0(500)$ (or σ) and $f_0(980)$ both with $I = 0$. The $I = 2$ $\pi\pi$ and $I = 3/2$ $K\pi$ partial waves do not have any resonances.

64.2 The $K_0^*(700)$, also known as κ ($I = 1/2$)

The $K_0^*(700)$ shows up as a pole in the low energy πK scattering, although its presence and properties are difficult to establish, since it appears to have a very large width ($\Gamma \approx 500$ MeV) and resides close to the $K\pi$ threshold. Hadronic D- and B-meson decays provide additional data points in the vicinity of the $K\pi$ threshold and are discussed in detail in the *Review on Multibody Charm Analyses* in this RPP. With a few exceptions discussed there, the three- or more-hadron final states are usually treated as non-interacting two-body systems. Precision information from semileptonic D decays, where the strongly interacting two-particle final states could be treated without approximation, is not available. BES II [16] (re-analyzed in [17]) finds a $K_0^*(700)$-like structure in $J/\psi(1S)$ decays to $\bar{K}^{*0}(892)K^+\pi^-$ where $K_0^*(700)$ recoils against the $K^*(892)$. The decay $\tau^- \to K_S^0\pi^-\nu_\tau$ can be considered clean with respect to final-state interactions and is studied by Belle [18], with $K_0^*(700)$ parameters fixed to those of Ref. [16].

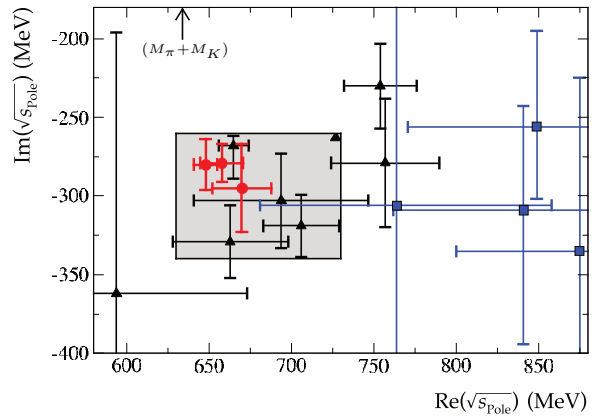

Figure 64.1: Location of the $K_0^*(700)$ (or κ) poles in the complex energy plane. Red circles denote the results of the most sophisticated analyses based on dispersion relations (see text for details), poles extracted from Breit-Wigner fits are shown as blue squares, while all other analyses quoted in the *Listings* are denoted by black triangles. The corresponding references are given in the listing. The arrow shows the location of the πK thresholds. The grey box indicates the ranges extracted as 'our estimate' of the pole locations.

Some authors find a $K_0^*(700)$ pole in their phenomenological analysis (see, *e.g.*, [19–28]), while others do not need to include it in their fits (see, *e.g.*, [29–33]). All works including constraints from chiral symmetry at low energies naturally find a light $K_0^*(700)$ below 800 MeV, see, *e.g.*, [34–39]. The analysis of Ref. [14,40] is based on the Roy-Steiner equations, which include analyticity and crossing symmetry constraints. Ref. [15] uses the Padé method to extract pole parameters after refitting scattering data constrained to satisfy forward dispersion relations. All three arrive at compatible pole positions for the $K_0^*(700)$ that are consistent with the pole parameters deduced from other theoretical methods. Due to their large uncertainties, the pole locations deduced from the Breit-Wigner fits appear to be just about consistent with the other determinations, but the real parts of all those analyses lie systematically too high. Moreover, phase shifts extracted from the Breit-Wigner functions for the $K_0^*(700)$ are very different from the known scalar πK phase shifts. The various poles are shown in in Fig. 64.1. The compilation in this figure justifies the pole parameters of the $K_0^*(700)$, which we quote as 'our estimate', namely,

$$\sqrt{s^{\kappa}_{\rm Pole}} = (630 - 730) - i(260 - 340)\ \text{MeV}\ . \tag{64.2}$$

For an extensive discussion about the πK system in general and the κ meson in particular, see Ref. [41].

64.3 The $a_0(980)$ ($I = 1$)

The $a_0(980)$ couples strongly to the channels $\pi\eta$ and $K\bar{K}$. Independent of any model, the $K\bar{K}$ component must be large in the $a_0(980)$ wave function, since the mass of the $a_0(980)$ lies very close to the opening of the $K\bar{K}$ channel, to which it strongly couples [42,43]. This generates a pronounced cusp-like behavior in the resonant amplitude and to reveal its true coupling constants the presence of the $K\bar{K}$ channel cannot be ignored. All listed $a_0(980)$

Downloaded from https://academic.oup.com/ptep/article/2022/8/083C01/6651666 by KIT Library user on 27 September 2022

measurements agree on a mass position value near 980 MeV, but the width deduced from the imaginary part of the pole location has values between 50 and 100 MeV, mostly due to the different models. For example, the analysis of the $p\bar{p}$ annihilation data [42] using a unitary K-matrix description finds a width determined from the T-matrix pole of 92 ± 8 MeV. Note that the width of the $a_0(980)$ line shape is typically smaller than what could be expected from the pole location.

The relative coupling $K\bar{K}/\pi\eta$ is determined indirectly from $f_1(1285)$ [44–46] or $\eta(1410)$ decays [47–49], from the line shape observed in the $\pi\eta$ decay mode [50–53], or from the coupled-channel analysis of the $\pi\pi\eta$ and $K\bar{K}\pi$ final states of $p\bar{p}$ annihilation at rest [42].

There are different recent extractions of the $a_0(980)$ pole location. Refs. [36, 37, 39, 54] use unitarized chiral perturbation theory. Ref. [55] used a similar formalism to extract the pole of the $a_0(980)$, employing the amplitude fixed in Ref. [56]. A dispersion theoretical approach to the isovector scalar $\pi\eta - K\bar{K}$ system is presented in Ref. [57] that may be refined further from studies of heavy meson decays [58]. Those efforts lead to a rather precise determination of the $a_0(980)$ pole location [59]. A value consistent for the mass parameter, but with a larger width, is found in a recent analysis of 1996 LEAR data for $\bar{p}p$ annihilation in flight employing a K-matrix [60]. The poles extracted in Refs. [39, 42, 53, 55, 59, 60] are shown in Fig. 64.2 together with the range of acceptable pole parameters extracted from this compilation, namely,

$$\sqrt{s_{\rm Pole}^{a_0(980)}} = (960 - 1030) - i(20 - 70)\ \text{MeV} \qquad (64.3)$$

indicated by the box.

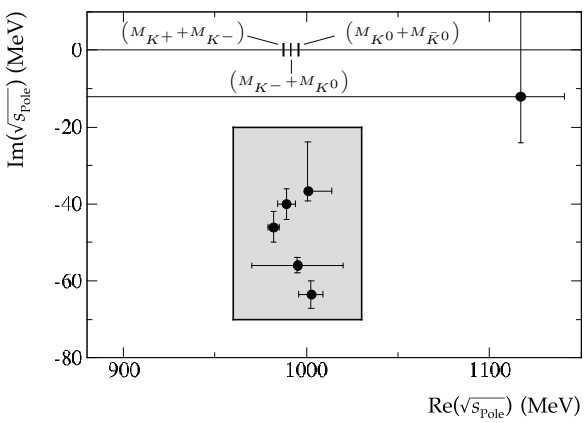

Figure 64.2: Location of the $a_0(980)$ poles from different extractions in the complex energy plane. The corresponding references are given in the *Listings*. Also shown are the thresholds for the K^+K^- and $K^0\bar{K}^0$ channels, relevant for $a_0(980)^0$, and for the K^-K^0 channel, relevant for the $a_0(980)^-$. The grey box indicates the ranges extracted as 'our estimate' of the pole locations.

64.4 The $f_0(500)$, also known as σ-meson ($I = 0$)

For discussions of the $\pi\pi$ S wave below the $K\bar{K}$ threshold and on the long history of the $f_0(500)$, which was suggested in linear sigma models more than 50 years ago, see the review [5]. Information on the $\pi\pi$ S-wave phase shift $\delta_J^I = \delta_0^0$ was already extracted many years ago from πN scattering [61–63], and near the $\pi\pi$ threshold from K_{e4} decays [64]. The kaon decays were later revisited leading to consistent data with very much improved statistics [65, 66]. The reported $\pi\pi \to K\bar{K}$ cross sections [67–70] have large uncertainties. The πN data have been analyzed in combination with high-statistics data (see entries labeled as RVUE for reanalyses of the data). The $2\pi^0$ invariant mass spectra, extracted from $p\bar{p}$ annihilation at rest into $3\pi^0$ [71, 72] and into $5\pi^0$ [73] and from central pp collision [74] do not show a distinct resonance structure below 900 MeV, but these data are consistently described with the standard solution for the $\pi\pi$ scalar isoscalar S-wave extracted from high energy $\pi N \to \pi\pi N$ data [62, 75], which allows for the existence of the broad $f_0(500)$. An enhancement is observed in the $\pi^+\pi^-$ invariant mass near threshold in the decays $D^+ \to \pi^+\pi^-\pi^+$ [76–78] and $J/\psi(1S) \to \omega\pi^+\pi^-$ [79, 80], and in $\psi(2S) \to J/\psi(1S)\pi^+\pi^-$ with very limited phase space [81, 82].

The precise $f_0(500)$ (or σ) pole is difficult to establish because of its large width. The $\pi\pi$ scattering amplitude shows an unusual energy dependence due to the presence of the Adler zero in the unphysical regime close to the threshold [7, 8], required by chiral symmetry. However, most of the analyses listed under $f_0(500)$ agree on a pole position near $(500 - i\,250$ MeV). In particular, analyses of $\pi\pi$ data that include unitarity, are consistent with the near threshold $\pi\pi$ data from K_{e4} decays, and the chiral symmetry constraints from Adler zeroes and/or scattering lengths find a light $f_0(500)$, see, *e.g.*, [83, 84].

Precise pole positions with an uncertainty of less than 20 MeV (see our table for the T-matrix pole in the *Listings*) were extracted using the Roy equations, which are twice subtracted dispersion relations derived from crossing symmetry and analyticity. In Ref. [11] the subtraction constants were fixed to the S-wave scattering lengths a_0^0 and a_0^2 derived from matching the Roy equations and two-loop chiral perturbation theory [10]. The only additional relevant input to fix the $f_0(500)$ pole turned out to be the $\pi\pi$-wave phase shifts at some higher energy point, chosen as 800 MeV. The analysis was improved further in Ref. [13]. Alternatively, in Ref. [12] Roy equations were used as constraints for a fit to the data. In that reference also once-subtracted Roy–like equations, called GKPY equations, were used, since the extrapolation into the complex plane based on the twice-subtracted equations leads to larger uncertainties, mainly due to the limited experimental information on the isospin 2 $\pi\pi$ scattering length. Ref. [85] uses Padé approximants for the analytic continuation. All these extractions find consistent results. Using analyticity and unitarity only to describe data from $K_{2\pi}$ and K_{e4} decays, Ref. [86] finds consistent values for the pole position and the scattering length a_0^0. The importance of the $\pi\pi$ scattering data for fixing the $f_0(500)$ pole is nicely illustrated by comparing analyses of $\bar{p}p \to 3\pi^0$ omitting [71, 87] or including [72, 88] information on $\pi\pi$ scattering: while the former analyses find an extremely broad structure above 1 GeV, the latter find $f_0(500)$ masses of the order of 400 MeV.

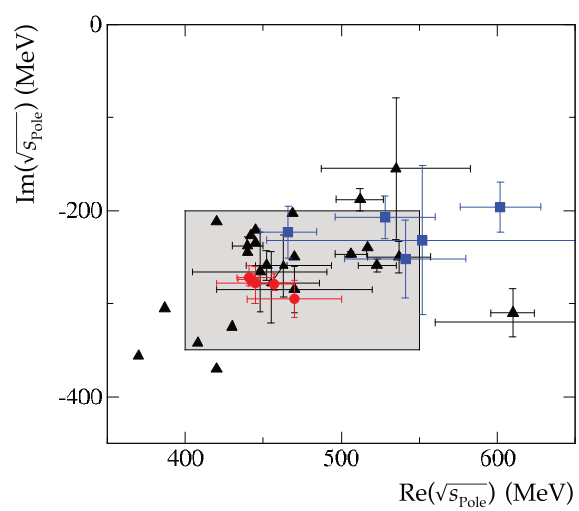

Figure 64.3: Location of the $f_0(500)$ (or σ) poles in the complex energy plane. Circles denote the recent analyses based on Roy(-like) dispersion relations, poles extracted from Breit-Wigner fits are shown as blue squares, while all other analyses are denoted by triangles. The corresponding references are given in the *Listings*. The grey box indicates the ranges extracted as 'our estimate' of the pole locations.

Downloaded from https://academic.oup.com/ptep/article/2022/8/083C01/6651666 by KIT Library user on 27 September 2022

From Fig. 64.3 we read the range of pole positions for the $f_0(500)$, namely,

$$\sqrt{s^{\sigma}_{\rm Pole}} = (400-550) - i(200-350)\ \text{MeV}\ . \qquad (64.4)$$

The plot contains the poles from Refs. [24, 35, 37, 39, 52, 54, 61, 72, 78, 81–84, 86, 88–107] as well as the advanced dispersion analyses [10–13, 85]. The extracted $f_0(500)$ pole position is very sensitive to the high accuracy low energy $\pi\pi$ scattering data [65, 66]. In fact, all analyses consistent with those data find poles within the accepted range indicated in the figure. As in case of the $K_0^*(700)$, poles extracted from Breit-Wigner analyses are shown as blue squares. Again we see that those poles have the tendency to appear at higher masses, although here the effect is not as pronounced as in case of the $K_0^*(700)$. One should not take this as an indication that using Breit-Wigners is justified in case of the $f_0(500)$, since $\pi\pi$ phase shifts extracted from Breit-Wigners are in strong discrepancy with the scattering phase shifts.

If one uses just the most advanced dispersive analyses of Refs. [10–13], shown as solid dots in Fig. 64.3 to determine the pole location of the $f_0(500)$, the range narrows down to [5]

$$\sqrt{s^{\sigma}_{\rm Pole}} = (449^{+22}_{-16}) - i(275\pm 12)\ \text{MeV}\ , \qquad (64.5)$$

which is labeled as 'conservative dispersive estimate' in this reference.

Besides $\pi\pi$, the only other decay channel of the $f_0(500)$ is two photons. Due to the large full width of the $f_0(500)$ an extraction of its two-photon width directly from data is not possible. Thus, the values for $\Gamma(\gamma\gamma)$ quoted in the literature as well as the in *Listings* are based on the expression in the narrow width approximation [108] $\Gamma(\gamma\gamma) \simeq \alpha^2|g_\gamma|^2/(4\mathrm{Re}(\sqrt{s^{\sigma}_{\rm Pole}}))$, where g_γ is derived from the residue at the $f_0(500)$ pole to two photons and α denotes the electromagnetic fine-structure constant (see also the review on *Resonances* in this issue of the RPP). The explicit form of the expression may vary between different authors due to different definitions of the coupling constant, however, the expression given for $\Gamma(\gamma\gamma)$ is free of ambiguities. According to Refs. [109–112], the data for $f_0(500) \to \gamma\gamma$ are consistent with what is expected for a two step process of $\gamma\gamma \to \pi^+\pi^-$ via pion exchange in the t- and u-channel, followed by a final state interaction $\pi^+\pi^- \to \pi^0\pi^0$. The same conclusion is drawn in Ref. [113], where the bulk part of the $f_0(500) \to \gamma\gamma$ decay width is dominated by re-scattering. Therefore, it might be difficult to learn anything new about the nature of the $f_0(500)$ from its $\gamma\gamma$ coupling. For the most recent work on $\gamma\gamma \to \pi\pi$, see Refs. [54,86–88,95–108,111–116]. There are strong indications (*e.g.*, [117–147]) that the $f_0(500)$ pole cannot be classified as a $q\bar{q}$ state.

64.5 The $f_0(980)$ $(I=0)$

The $f_0(980)$ couples predominantly to the $\pi\pi$ and $K\bar{K}$ channels and its signal overlaps strongly with the background represented mainly by the $f_0(500)$ and the $f_0(1370)$. This can lead to a dip in the $\pi\pi$ spectrum at the $K\bar{K}$ threshold. It changes from a dip into a peak structure in the $\pi^0\pi^0$ invariant mass spectrum of the reaction $\pi^-p \to \pi^0\pi^0 n$ [121], with increasing four momentum transfer to the $\pi^0\pi^0$ system, which means increasing the $a_1(1260)$ exchange contribution in the amplitude, while the π exchange decreases. Also when a $(u\bar{u}+d\bar{d})$ source is switched to a $s\bar{s}$ source, as it appears when moving from $B_d \to J/\psi(1S)\pi\pi$ to $B_s \to J/\psi(1S)\pi\pi$, the f_0 signal switches from a dip to a peak [135]. The $f_0(500)$ and the $f_0(980)$ are also observed in the data for radiative ϕ decays ($\phi \to f_0\gamma$) from SND [122,123], CMD2 [124], and KLOE [125,126].

Unitarized chiral perturbation theory was employed to extract the pole of the $f_0(980)$ in Refs. [36, 37, 39, 54, 55]. Two different dispersive analyses were used in Ref. [12] to simultaneously pin down the pole parameters of both the $f_0(500)$ and the $f_0(980)$. The poles extracted in Refs. [12, 13, 39, 55, 60, 91, 148] are shown in Fig. 64.4, together with the range of acceptable pole parameters extracted from this compilation, namely,

$$\sqrt{s^{f_0(980)}_{\rm Pole}} = (980-1010) - i(20-35)\ \text{MeV} \qquad (64.6)$$

indicated by the box. A disclaimer is important here: Both the poles of $a_0(980)$ and of $f_0(980)$ are located very close to the kaon thresholds, with the charged and neutral thresholds being 8 MeV apart — to illustrate this point the pertinent thresholds are shown explicitly in Figs. 64.2 and 64.4. This observation lead to the prediction of an enhanced a_0-f_0 mixing [149–152]. On the other hand, all analyses employed in the pole determinations quoted above are done assuming isospin symmetry. Future studies need to show the impact of isospin violation on the extraction of the $a_0(980)/f_0(980)$ pole parameters.

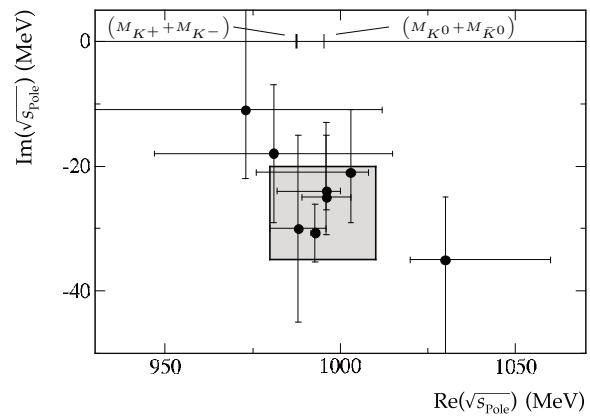

Figure 64.4: Location of the $f_0(980)$ poles from different extractions in the complex energy plane. The corresponding references are given in the *Listings*. Also shown are the thresholds for the K^+K^- and $K^0\bar{K}^0$ channels. The grey box indicates the ranges extracted as 'our estimate' of the pole locations.

Analyses of $\gamma\gamma \to \pi\pi$ data [127–129] underline the importance of the $K\bar{K}$ coupling of the $f_0(980)$, while the resulting two-photon width of the $f_0(980)$ cannot be determined precisely [130]. The prominent appearance of the $f_0(980)$ in the semileptonic D_s decays and decays of B and B_s mesons implies a dominant $(\bar{s}s)$ component: those decays occur via weak transitions that alternatively result in $\phi(1020)$ production. Ratios of decay rates of B and/or B_s mesons into $J/\psi(1S)$ plus $f_0(980)$ or $f_0(500)$ were proposed to allow for an extraction of the flavor mixing angle and to probe the tetraquark nature of those mesons within a certain model [131,132]. The resulting phenomenological fits of the LHCb collaboration [133, 134] lead the authors to conclude that their data are incompatible with a model where $f_0(500)$ and $f_0(980)$ are formed from two quarks and two antiquarks (tetraquarks). However, a dispersive analysis of the same data that allows for a model independent inclusion of the hadronic final state interactions in Ref. [135] puts into question the conclusions of Ref. [133].

64.6 Interpretation of the scalars below 1 GeV

In the literature, many structures are discussed for the light scalar mesons, such as conventional $q\bar{q}$ mesons, compact $(qq)(\bar{q}\bar{q})$ structures (tetraquarks), or meson-meson bound states (hadronic molecules). In reality, there can be superpositions of these components, and one often depends on models to determine the dominant one. Although we have seen progress in recent years, this question remains open. Here, we mention some of the present conclusions.

The $f_0(980)$ and $a_0(980)$ are often interpreted as compact tetraquark states [144–147, 153] or $K\bar{K}$ bound states [154]. The insight into their internal structure using two-photon widths [123, 155–161] is not conclusive. The $f_0(980)$ appears as a peak structure in $J/\psi(1S) \to \phi\pi^+\pi^-$ and in D_s decays without $f_0(500)$ background, while being nearly invisible in $J/\psi(1S) \to \omega\pi^+\pi^-$. Based on that observation it is suggested that $f_0(980)$ has a large $s\bar{s}$ component, which according to Ref. [162] is surrounded by a virtual $K\bar{K}$ cloud (see also Ref. [163]). Data on radiative decays ($\phi \to f_0\gamma$ and $\phi \to a_0\gamma$) from SND, CMD2, and KLOE (see above) are consistent with a prominent role of kaon loops. This

Downloaded from https://academic.oup.com/ptep/article/2022/8/083C01/6651666 by KIT Library user on 27 September 2022

observation is interpreted as evidence for a compact four-quark structure of the light scalars in Ref. [164], while it is claimed to point at a molecular nature in Ref. [165, 166]. Details of this controversy are given in the comments [167, 168]; see also Ref. [169]. There is now a rather broad consensus that the states $f_0(980)$ and $a_0(980)$, together with the $f_0(500)$ and the $K_0^*(700)$, form a nonet of predominantly four-quark states, where at larger distances the quarks recombine into a pair of pseudoscalar mesons creating a meson cloud (see, *e.g.,* Ref. [170]). Different QCD sum rule studies [171–176] do not agree on a tetraquark configuration for the same particle group.

Models that start directly from chiral Lagrangians, either in non-linear [36, 39, 83, 165] or in linear [177–183] realization, predict the existence of the $f_0(500)$ meson near 500 MeV. Here the $f_0(500)$, $a_0(980)$, $f_0(980)$, and $K_0^*(700)$ (in some models the $K_0^*(1430)$) would form a nonet (not necessarily $q\bar{q}$). In the linear sigma models the lightest pseudoscalars appear as their chiral partners.

In the non-linear approaches of Refs. [36] and [83] the above resonances together with the low mass vector states are generated starting from chiral perturbation theory predictions near the first open channel, and then by extending the predictions to the resonance regions, using unitarity and analyticity.

Ref. [177] uses a framework with explicit resonances that are unitarized and coupled to the light pseudoscalars in a chirally invariant way. Evidence for a dominant non-$\bar{q}q$ nature of the lightest scalar resonances is derived from their mixing scheme. In Ref. [178] the scheme is extended and applied to the decay $\eta' \to \eta\pi\pi$, which leads to the same conclusions. In Ref. [184] the large N_c behavior of the poles was studied to identify the nature of the resonances generated from scattering equations. This lead to the observation that, while the light vector states behave consistent with what is predicted for $\bar{q}q$ states, the light scalars behave very differently. This finding provides strong support for a dominant non-$\bar{q}q$ nature of the light scalar resonances. Note, the more refined study of Ref. [117] which found, in the case of the $f_0(500)$, indications for a subdominant $\bar{q}q$ component located around 1 GeV in addition to a dominant non-$\bar{q}q$ nature. Additional support for the dominant non-$q\bar{q}$ nature of the $f_0(500)$ is given in Ref. [185], where the connection between the pole of resonances and their Regge trajectories is analyzed. All works including constraints from chiral symmetry at low energies naturally find a light $K_0^*(700)$ below 800 MeV and a $f_0(500)$ below 600 MeV, see, *e.g.*, [34–39]. In these works the $K_0^*(700)$, $f_0(500)$, $f_0(980)$, and $a_0(980)$ appear to form a nonet [35, 38]. Additional evidence for this assignment is presented in Ref. [13], where the couplings of the nine states to $\bar{q}q$ sources are compared. The same low mass scalar nonet was also found earlier in the unitarized quark model of Ref. [94].

There are, however, alternative interpretations of the light scalars. For example Ref. [186] (for a more recent, condensed discussion of the idea see Ref. [187]), also builds on chiral symmetry, but expands around an infrared fixed point such that the $f_0(500)$ appears as a QCD dilaton with a mass driven by the QCD scale anomaly. The phenomenology studied in that work appears consistent with this proposal. In Ref. [91, 113, 188, 189] data on $\pi\pi - \bar{K}K$ scattering, as well as $\gamma\gamma \to \pi\pi$, are analysed and the authors conclude that especially the $f_0(500)$ should have a significant gluon content.

A model independent method to identify hadronic molecules goes back to a proposal by Weinberg [190] (an extension of the formalism to virtual states is provided in Ref. [191]), which was shown to be equivalent to the pole counting arguments of [149–152, 192–197] in Ref. [195]. The formalism allows one to extract the amount of molecular component in the wave function from the effective coupling constant of a physical state to a nearby continuum channel. It can be applied to near threshold states only and provides strong evidence that the $f_0(980)$ is predominantly a $\bar{K}K$ molecule, while the situation turns out to be less clear for the $a_0(980)$ (see also Refs. [159, 161]). This is in line with the findings of Ref. [55], which reports an important role of the $\pi\eta$ channel to the formation of the $a_0(980)$ in addition to the $\bar{K}K$ channel, while the $f_0(980)$ also in this work appears to be predominantly a $\bar{K}K$ molecule. The relevance of both the $\bar{K}K$ and the $\pi\eta$ channels in a dynamically generated $a_0(980)$ was also pointed out in the description of the $\chi_{c1} \to \eta\pi^+\pi^-$ and $D_s^+ \to \pi^+\pi^0\eta$ reactions [198, 199]. Further insights into $a_0(980)$ and $f_0(980)$ are expected from their mixing [149]. The corresponding signal predicted in Refs. [150, 151] was recently observed at BES III [196]. In order to get a quantitative understanding of those data, in addition to the mixing mechanism itself, some detailed understanding of the production mechanism seems necessary [152].

In the unitarized quark model with coupled $q\bar{q}$ and meson-meson channels, the light scalars are interpreted as additional manifestations of bare $q\bar{q}$ confinement states, strongly mass shifted from the 1.3 - 1.5 GeV region and very distorted due to the strong $^3P_0$ coupling to S-wave two-meson decay channels [197, 200]. Thus, in these models the light scalar nonet comprising the $f_0(500)$, $f_0(980)$, $K_0^*(700)$, and $a_0(980)$, as well as the nonet consisting of the $f_0(1370)$, $f_0(1500)$ (or $f_0(1710)$), $K_0^*(1430)$, and $a_0(1450)$, respectively, are seen as two manifestations of the same bare input states (see also Ref. [201]). It should not remain unmentioned, however, that the heavier nonet lies rather close to the input nonet and that the light scalar one emerges only, once the coupling to the two-meson channels is switched on, again highlighting that the meson-meson interaction is indispensable for the light scalars.

Acknowledgement

The authors would like to thank Claude Amsler, Eberhard Klempt, Mikhail Mikhasenko, and Jose Ramon Pelaez for helpful input and discussions in the preparation of the review.

References

[1] F. E. Close and N. A. Tornqvist, J. Phys. **G28**, R249 (2002), [hep-ph/0204205].

[2] C. Amsler and N. A. Tornqvist, Phys. Rept. **389**, 61 (2004).

[3] D. V. Bugg, Phys. Rept. **397**, 257 (2004), [hep-ex/0412045].

[4] E. Klempt and A. Zaitsev, Phys. Rept. **454**, 1 (2007), [arXiv:0708.4016].

[5] J. R. Pelaez, Phys. Rept. **658**, 1 (2016), [arXiv:1510.00653].

[6] S. Gardner and U.-G. Meissner, Phys. Rev. D **65**, 094004 (2002), [hep-ph/0112281].

[7] S. L. Adler, Phys. Rev. **137**, B1022 (1965), [,140(1964)].

[8] S. L. Adler, Phys. Rev. **139**, B1638 (1965), [,152(1965)].

[9] J. A. Oller, Phys. Rev. **D71**, 054030 (2005), [hep-ph/0411105].

[10] G. Colangelo, J. Gasser and H. Leutwyler, Nucl. Phys. **B603**, 125 (2001), [hep-ph/0103088].

[11] I. Caprini, G. Colangelo, and H. Leutwyler, Phys. Rev. Lett. **96**, 132001 (2006).

[12] R. Garcia-Martin *et al.*, Phys. Rev. Lett. **107**, 072001 (2011), [arXiv:1107.1635].

[13] B. Moussallam, Eur. Phys. J. **C71**, 1814 (2011), [arXiv:1110.6074].

[14] S. Descotes-Genon and B. Moussallam, Eur. Phys. J. C **48**, 553 (2006), [hep-ph/0607133].

[15] J. R. Peláez and A. Rodas, Phys. Rev. Lett. **124**, 17, 172001 (2020), [arXiv:2001.08153].

[16] M. Ablikim *et al.* (BES), Phys. Lett. **B633**, 681 (2006), [hep-ex/0506055].

[17] F.-K. Guo *et al.*, Nucl. Phys. **A773**, 78 (2006), [hep-ph/0509050].

[18] D. Epifanov *et al.* (Belle), Phys. Lett. **B654**, 65 (2007), [arXiv:0706.2231].

[19] C. Cawlfield *et al.* (CLEO), Phys. Rev. **D74**, 031108 (2006), [hep-ex/0606045].

[20] A. V. Anisovich and A. V. Sarantsev, Phys. Lett. **B413**, 137 (1997), [hep-ph/9705401].

[21] R. Delbourgo and M. D. Scadron, Int. J. Mod. Phys. **A13**, 657 (1998), [hep-ph/9807504].

[22] C. M. Shakin and H. Wang, Phys. Rev. **D63**, 014019 (2001).

Downloaded from https://academic.oup.com/ptep/article/2022/8/083C01/6651666 by KIT Library user on 27 September 2022

[23] M. D. Scadron *et al.*, Nucl. Phys. **A724**, 391 (2003), [hep-ph/0211275].

[24] D. V. Bugg, Phys. Lett. **B572**, 1 (2003), [Erratum: Phys. Lett.B595,556(2004)].

[25] M. Ishida, Prog. Theor. Phys. Suppl. **149**, 190 (2003), [hep-ph/0212383].

[26] H. Q. Zheng *et al.*, Nucl. Phys. **A733**, 235 (2004), [hep-ph/0310293].

[27] Z. Y. Zhou and H. Q. Zheng, Nucl. Phys. **A775**, 212 (2006), [hep-ph/0603062].

[28] J. M. Link *et al.* (FOCUS), Phys. Lett. **B653**, 1 (2007), [arXiv:0705.2248].

[29] S. N. Cherry and M. R. Pennington, Nucl. Phys. **A688**, 823 (2001), [hep-ph/0005208].

[30] B. Aubert *et al.* (BaBar), Phys. Rev. **D76**, 011102 (2007), [arXiv:0704.3593].

[31] S. Kopp *et al.* (CLEO), Phys. Rev. **D63**, 092001 (2001), [hep-ex/0011065].

[32] J. M. Link *et al.* (FOCUS), Phys. Lett. **B535**, 43 (2002), [hep-ex/0203031].

[33] J. M. Link *et al.* (FOCUS), Phys. Lett. **B621**, 72 (2005), [hep-ex/0503043].

[34] M. Jamin, J. A. Oller and A. Pich, Nucl. Phys. **B587**, 331 (2000), [hep-ph/0006045].

[35] D. Black *et al.*, Phys. Rev. **D64**, 014031 (2001), [hep-ph/0012278].

[36] J. A. Oller, E. Oset and J. R. Pelaez, Phys. Rev. **D59**, 074001 (1999), [Erratum: Phys. Rev.D75,099903(2007)], [hep-ph/9804209].

[37] J. A. Oller and E. Oset, Phys. Rev. **D60**, 074023 (1999), [hep-ph/9809337].

[38] J. A. Oller, Nucl. Phys. **A727**, 353 (2003), [hep-ph/0306031].

[39] J. R. Pelaez, Mod. Phys. Lett. **A19**, 2879 (2004), [hep-ph/0411107].

[40] J. R. Peláez, A. Rodas and J. Ruiz de Elvira, Eur. Phys. J. **C77**, 2, 91 (2017), [arXiv:1612.07966].

[41] J. R. Peláez and A. Rodas (2020), [arXiv:2010.11222].

[42] A. Abele *et al.*, Phys. Rev. **D57**, 3860 (1998).

[43] M. Bargiotti *et al.* (OBELIX), Eur. Phys. J. **C26**, 371 (2003).

[44] D. Barberis *et al.* (WA102), Phys. Lett. **B440**, 225 (1998), [hep-ex/9810003].

[45] M. J. Corden *et al.*, Nucl. Phys. **B144**, 253 (1978).

[46] C. Defoix *et al.*, Nucl. Phys. **B44**, 125 (1972).

[47] Z. Bai *et al.* (MARK-III), Phys. Rev. Lett. **65**, 2507 (1990).

[48] T. Bolton *et al.*, Phys. Rev. Lett. **69**, 1328 (1992).

[49] C. Amsler *et al.* (Crystal Barrel), Phys. Lett. **B353**, 571 (1995).

[50] S. M. Flatte, Phys. Lett. **63B**, 224 (1976).

[51] C. Amsler *et al.* (Crystal Barrel), Phys. Lett. **B333**, 277 (1994).

[52] G. Janssen *et al.*, Phys. Rev. **D52**, 2690 (1995), [arXiv:nucl-th/9411021].

[53] D. V. Bugg, Phys. Rev. **D78**, 074023 (2008), [arXiv:0808.2706].

[54] J. A. Oller and E. Oset, Nucl. Phys. **A620**, 438 (1997), [Erratum: Nucl. Phys.A652,407(1999)], [hep-ph/9702314].

[55] H. A. Ahmed and C. W. Xiao, Phys. Rev. D **101**, 9, 094034 (2020), [arXiv:2001.08141].

[56] C. W. Xiao, U. G. Meißner and J. A. Oller, Eur. Phys. J. A **56**, 1, 23 (2020), [arXiv:1907.09072].

[57] M. Albaladejo and B. Moussallam, Eur. Phys. J. C **75**, 10, 488 (2015), [arXiv:1507.04526].

[58] M. Albaladejo *et al.*, JHEP **04**, 010 (2017), [arXiv:1611.03502].

[59] J. Lu and B. Moussallam, Eur. Phys. J. C **80**, 5, 436 (2020), [arXiv:2002.04441].

[60] M. Albrecht *et al.* (Crystal Barrel), Eur. Phys. J. C **80**, 5, 453 (2020), [arXiv:1909.07091].

[61] S. D. Protopopescu *et al.*, Phys. Rev. **D7**, 1279 (1973).

[62] G. Grayer *et al.*, Nucl. Phys. **B75**, 189 (1974).

[63] H. Becker *et al.* (CERN-Cracow-Munich), Nucl. Phys. **B151**, 46 (1979).

[64] L. Rosselet *et al.*, Phys. Rev. **D15**, 574 (1977).

[65] S. Pislak *et al.* (BNL-E865), Phys. Rev. Lett. **87**, 221801 (2001), [Erratum: Phys. Rev. Lett.105,019901(2010)], [hep-ex/0106071].

[66] J. R. Batley *et al.* (NA48-2), Eur. Phys. J. **C70**, 635 (2010).

[67] W. Wetzel *et al.*, Nucl. Phys. **B115**, 208 (1976).

[68] V. A. Polychronakos *et al.*, Phys. Rev. **D19**, 1317 (1979).

[69] D. H. Cohen *et al.*, Phys. Rev. **D22**, 2595 (1980).

[70] A. Etkin *et al.*, Phys. Rev. **D25**, 1786 (1982).

[71] C. Amsler *et al.*, Phys. Lett. **B342**, 433 (1995).

[72] C. Amsler *et al.* (Crystal Barrel), Phys. Lett. **B355**, 425 (1995).

[73] A. Abele *et al.* (Crystal Barrel), Phys. Lett. **B380**, 453 (1996).

[74] D.M. Alde *et al.*, Phys. Lett. **B397**, 350 (1997).

[75] R. Kaminski, L. Lesniak and K. Rybicki, Z. Phys. **C74**, 79 (1997), [hep-ph/9606362].

[76] E. M. Aitala *et al.* (E791), Phys. Rev. Lett. **86**, 770 (2001), [hep-ex/0007028].

[77] J. M. Link *et al.* (FOCUS), Phys. Lett. **B585**, 200 (2004), [hep-ex/0312040].

[78] G. Bonvicini *et al.* (CLEO), Phys. Rev. **D76**, 012001 (2007), [arXiv:0704.3954].

[79] J. E. Augustin *et al.* (DM2), Nucl. Phys. **B320**, 1 (1989).

[80] M. Ablikim *et al.* (BES), Phys. Lett. **B598**, 149 (2004), [hep-ex/0406038].

[81] A. Gallegos, J. L. Lucio M. and J. Pestieau, Phys. Rev. **D69**, 074033 (2004), [hep-ph/0311133].

[82] M. Ablikim *et al.* (BES), Phys. Lett. **B645**, 19 (2007), [hep-ex/0610023].

[83] A. Dobado and J. R. Pelaez, Phys. Rev. **D56**, 3057 (1997), [hep-ph/9604416].

[84] I. Caprini, Phys. Rev. **D77**, 114019 (2008), [arXiv:0804.3504].

[85] P. Masjuan, J. Ruiz de Elvira, J.J. Sanz-Cillero, Phys. Rev. **D90**, 097901 (2014).

[86] R. Garcia-Martin, J. R. Pelaez and F. J. Yndurain, Phys. Rev. **D76**, 074034 (2007), [hep-ph/0701025].

[87] V.V. Anisovich *et al.*, Sov. Phys. Usp. **41**, 419 (1998).

[88] V. V. Anisovich, Int. J. Mod. Phys. **A21**, 3615 (2006), [hep-ph/0510409].

[89] M. Ablikim *et al.* (BESIII), Phys. Rev. Lett. **118**, 1, 012001 (2017), [arXiv:1606.03847].

[90] M. Albaladejo and J. A. Oller, Phys. Rev. D **86**, 034003 (2012), [arXiv:1205.6606].

[91] G. Mennessier, S. Narison and X. G. Wang, Phys. Lett. B **688**, 59 (2010), [arXiv:1002.1402].

[92] M. Ablikim *et al.* (BES), Phys. Lett. B **598**, 149 (2004), [hep-ex/0406038].

[93] P. Estabrooks, Phys. Rev. D **19**, 2678 (1979).

Downloaded from https://academic.oup.com/ptep/article/2022/8/083C01/6651666 by KIT Library user on 27 September 2022

[94] E. van Beveren *et al.*, Z. Phys. **C30**, 615 (1986), [arXiv:0710.4067].

[95] B. S. Zou and D. V. Bugg, Phys. Rev. **D48**, R3948 (1993).

[96] N. A. Tornqvist and M. Roos, Phys. Rev. Lett. **76**, 1575 (1996), [hep-ph/9511210].

[97] R. Kaminski, L. Lesniak and J. P. Maillet, Phys. Rev. **D50**, 3145 (1994), [hep-ph/9403264].

[98] N. N. Achasov and G. N. Shestakov, Phys. Rev. **D49**, 5779 (1994).

[99] M. P. Locher, V. E. Markushin and H. Q. Zheng, Eur. Phys. J. **C4**, 317 (1998), [hep-ph/9705230].

[100] T. Hannah, Phys. Rev. **D60**, 017502 (1999), [hep-ph/9905236].

[101] R. Kaminski, L. Lesniak and B. Loiseau, Phys. Lett. **B413**, 130 (1997), [hep-ph/9707377].

[102] R. Kaminski, L. Lesniak and B. Loiseau, Eur. Phys. J. **C9**, 141 (1999), [hep-ph/9810386].

[103] M. Ishida *et al.*, Prog. Theor. Phys. **104**, 203 (2000), [hep-ph/0005251].

[104] Y.S. Surovtsev *et al.*, Phys. Rev. **D61**, 054024 (2001).

[105] M. Ishida *et al.*, Phys. Lett. **B518**, 47 (2001).

[106] Z. Y. Zhou *et al.*, JHEP **02**, 043 (2005), [hep-ph/0406271].

[107] D. V. Bugg, J. Phys. **G34**, 151 (2007), [hep-ph/0608081].

[108] D. Morgan and M. R. Pennington, Z. Phys. **C48**, 623 (1990).

[109] J. F. Donoghue, B. R. Holstein and Y. C. Lin, Phys. Rev. D **37**, 2423 (1988).

[110] A. Dobado and J. R. Pelaez, Z. Phys. C **57**, 501 (1993).

[111] M. R. Pennington, Phys. Rev. Lett. **97**, 011601 (2006).

[112] M. R. Pennington, Mod. Phys. Lett. **A22**, 1439 (2007), [arXiv:0705.3314].

[113] G. Mennessier, S. Narison and W. Ochs, Phys. Lett. **B665**, 205 (2008), [arXiv:0804.4452].

[114] R. Garcia-Martin and B. Moussallam, Eur. Phys. J. **C70**, 155 (2010), [arXiv:1006.5373].

[115] M. Hoferichter, D. R. Phillips and C. Schat, Eur. Phys. J. **C71**, 1743 (2011), [arXiv:1106.4147].

[116] L.-Y. Dai and M. R. Pennington, Phys. Rev. **D90**, 3, 036004 (2014), [arXiv:1404.7524].

[117] J. R. Pelaez and G. Rios, Phys. Rev. Lett. **97**, 242002 (2006), [hep-ph/0610397].

[118] H.-X. Chen, A. Hosaka and S.-L. Zhu, Phys. Lett. **B650**, 369 (2007), [hep-ph/0609163].

[119] F. Giacosa, Phys. Rev. **D75**, 054007 (2007), [hep-ph/0611388].

[120] L. Maiani *et al.*, Eur. Phys. J. **C50**, 609 (2007), [hep-ph/0604018].

[121] N. N. Achasov and G. N. Shestakov, Phys. Rev. **D58**, 054011 (1998), [hep-ph/9802286].

[122] M. N. Achasov *et al.*, Phys. Lett. **B479**, 53 (2000), [hep-ex/0003031].

[123] M. N. Achasov *et al.*, Phys. Lett. **B485**, 349 (2000), [hep-ex/0005017].

[124] R. R. Akhmetshin *et al.* (CMD-2), Phys. Lett. **B462**, 371 (1999), [hep-ex/9907005].

[125] A. Aloisio *et al.* (KLOE), Phys. Lett. **B536**, 209 (2002), [hep-ex/0204012].

[126] F. Ambrosino *et al.* (KLOE), Eur. Phys. J. **C49**, 473 (2007), [hep-ex/0609009].

[127] M. Boglione and M. R. Pennington, Eur. Phys. J. **C9**, 11 (1999), [hep-ph/9812258].

[128] T. Mori *et al.* (Belle), Phys. Rev. **D75**, 051101 (2007), [hep-ex/0610038].

[129] N. N. Achasov and G. N. Shestakov, Phys. Rev. **D77**, 074020 (2008), [arXiv:0712.0885].

[130] M. R. Pennington *et al.*, Eur. Phys. J. **C56**, 1 (2008), [arXiv:0803.3389].

[131] R. Fleischer, R. Knegjens and G. Ricciardi, Eur. Phys. J. **C71**, 1832 (2011), [arXiv:1109.1112].

[132] S. Stone and L. Zhang, Phys. Rev. Lett. **111**, 6, 062001 (2013), [arXiv:1305.6554].

[133] R. Aaij *et al.* (LHCb), Phys. Rev. **D90**, 1, 012003 (2014), [arXiv:1404.5673].

[134] R. Aaij *et al.* (LHCb), Phys. Rev. **D89**, 9, 092006 (2014), [arXiv:1402.6248].

[135] J. T. Daub, C. Hanhart and B. Kubis, JHEP **02**, 009 (2016), [arXiv:1508.06841].

[136] D. Barberis *et al.* (WA102), Phys. Lett. **B462**, 462 (1999), [hep-ex/9907055].

[137] D. Barberis *et al.* (WA102), Phys. Lett. **B479**, 59 (2000), [hep-ex/0003033].

[138] M. Gaspero, Nucl. Phys. **A562**, 407 (1993).

[139] A. Adamo *et al.*, Nucl. Phys. **A558**, 13C (1993).

[140] C. Amsler *et al.* (Crystal Barrel), Phys. Lett. **B322**, 431 (1994).

[141] A. Abele *et al.* (Crystal Barrel), Eur. Phys. J. **C19**, 667 (2001).

[142] A. Abele *et al.* (CRYSTAL BARREL), Eur. Phys. J. **C21**, 261 (2001).

[143] D. Barberis *et al.* (WA102), Phys. Lett. **B471**, 440 (2000), [hep-ex/9912005].

[144] R. L. Jaffe, Phys. Rev. **D15**, 267 (1977).

[145] M. G. Alford and R. L. Jaffe, Nucl. Phys. **B578**, 367 (2000), [hep-lat/0001023].

[146] L. Maiani *et al.*, Phys. Rev. Lett. **93**, 212002 (2004), [hep-ph/0407017].

[147] L. Maiani, A. D. Polosa and V. Riquer, Phys. Lett. **B651**, 129 (2007), [hep-ph/0703272].

[148] V. V. Anisovich and A. V. Sarantsev, Int. J. Mod. Phys. A **24**, 2481 (2009).

[149] N. N. Achasov, S. A. Devyanin and G. N. Shestakov, Phys. Lett. **88B**, 367 (1979).

[150] J.-J. Wu, Q. Zhao and B. S. Zou, Phys. Rev. **D75**, 114012 (2007), [arXiv:0704.3652].

[151] C. Hanhart, B. Kubis and J. R. Pelaez, Phys. Rev. **D76**, 074028 (2007), [arXiv:0707.0262].

[152] L. Roca, Phys. Rev. **D88**, 014045 (2013), [arXiv:1210.4742].

[153] G. 't Hooft *et al.*, Phys. Lett. **B662**, 424 (2008), [arXiv:0801.2288].

[154] J. D. Weinstein and N. Isgur, Phys. Rev. **D41**, 2236 (1990).

[155] T. Barnes, Phys. Lett. **165B**, 434 (1985).

[156] Z. P. Li, F. E. Close and T. Barnes, Phys. Rev. **D43**, 2161 (1991).

[157] R. Delbourgo, D.-s. Liu and M. D. Scadron, Phys. Lett. **B446**, 332 (1999), [hep-ph/9811474].

[158] J. L. Lucio Martinez and M. Napsuciale, Phys. Lett. **B454**, 365 (1999), [hep-ph/9903234].

[159] C. Hanhart *et al.*, Phys. Rev. **D75**, 074015 (2007), [hep-ph/0701214].

[160] R. H. Lemmer, Phys. Lett. **B650**, 152 (2007), [hep-ph/0701027].

[161] T. Branz, T. Gutsche and V. E. Lyubovitskij, Eur. Phys. J. **A37**, 303 (2008), [arXiv:0712.0354].

[162] A. Deandrea *et al.*, Phys. Lett. **B502**, 79 (2001), [hep-ph/0012120].

Downloaded from https://academic.oup.com/ptep/article/2022/8/083C01/6651666 by KIT Library user on 27 September 2022

[163] K. M. Ecklund *et al.* (CLEO), Phys. Rev. **D80**, 052009 (2009), [arXiv:0907.3201].

[164] N. N. Achasov and V. N. Ivanchenko, Nucl. Phys. **B315**, 465 (1989).

[165] J. A. Oller, Nucl. Phys. **A714**, 161 (2003), [hep-ph/0205121].

[166] Yu. S. Kalashnikova *et al.*, Eur. Phys. J. **A24**, 437 (2005), [hep-ph/0412340].

[167] Yu. S. Kalashnikova *et al.*, Phys. Rev. **D78**, 058501 (2008), [arXiv:0711.2902].

[168] N. N. Achasov and A. V. Kiselev, Phys. Rev. **D78**, 058502 (2008), [arXiv:0806.2993].

[169] M. Boglione and M. R. Pennington, Eur. Phys. J. **C30**, 503 (2003), [hep-ph/0303200].

[170] F. Giacosa and G. Pagliara, Phys. Rev. **C76**, 065204 (2007), [arXiv:0707.3594].

[171] S. Narison, Nucl. Phys. B Proc. Suppl. **96**, 244 (2001).

[172] H.-J. Lee, Eur. Phys. J. **A30**, 423 (2006), [hep-ph/0512212].

[173] H.-X. Chen, A. Hosaka and S.-L. Zhu, Phys. Rev. **D76**, 094025 (2007), [arXiv:0707.4586].

[174] J. Sugiyama *et al.*, Phys. Rev. **D76**, 114010 (2007), [arXiv:0707.2533].

[175] T. Kojo and D. Jido, Phys. Rev. **D78**, 114005 (2008), [arXiv:0802.2372].

[176] H.-J. Lee, K. S. Kim and H. Kim, Phys. Rev. D **100**, 3, 034021 (2019), [arXiv:1904.12311].

[177] D. Black *et al.*, Phys. Rev. **D59**, 074026 (1999), [hep-ph/9808415].

[178] A. H. Fariborz *et al.*, Phys. Rev. **D90**, 3, 033009 (2014), [arXiv:1407.3870].

[179] M. D. Scadron, Eur. Phys. J. **C6**, 141 (1999), [hep-ph/9710317].

[180] M. Ishida, Prog. Theor. Phys. **101**, 661 (1999), [hep-ph/9902260].

[181] N. A. Tornqvist, Eur. Phys. J. **C11**, 359 (1999), [hep-ph/9905282].

[182] M. Napsuciale and S. Rodriguez, Phys. Lett. **B603**, 195 (2004), [hep-ph/0403072].

[183] M. Napsuciale and S. Rodriguez, Phys. Rev. **D70**, 094043 (2004), [hep-ph/0407037].

[184] J. R. Pelaez, Phys. Rev. Lett. **92**, 102001 (2004), [hep-ph/0309292].

[185] J. T. Londergan *et al.*, Phys. Lett. **B729**, 9 (2014), [arXiv:1311.7552].

[186] R. J. Crewther and L. C. Tunstall, Phys. Rev. D **91**, 3, 034016 (2015), [arXiv:1312.3319].

[187] R. J. Crewther, Universe **6**, 7, 96 (2020), [arXiv:2003.11259].

[188] R. Kaminski, G. Mennessier and S. Narison, Phys. Lett. B **680**, 148 (2009), [arXiv:0904.2555].

[189] G. Mennessier, S. Narison and X. G. Wang, Phys. Lett. B **696**, 40 (2011), [arXiv:1009.2773].

[190] S. Weinberg, Phys. Rev. **130**, 776 (1963).

[191] I. Matuschek *et al.*, Eur. Phys. J. A **57**, 3, 101 (2021), [arXiv:2007.05329].

[192] D. Morgan and M. R. Pennington, Phys. Lett. **B258**, 444 (1991), [Erratum: Phys. Lett.B269,477(1991)].

[193] D. Morgan, Nucl. Phys. **A543**, 632 (1992).

[194] N. A. Tornqvist, Phys. Rev. **D51**, 5312 (1995), [hep-ph/9403234].

[195] V. Baru *et al.*, Phys. Lett. **B586**, 53 (2004), [hep-ph/0308129].

[196] M. Ablikim *et al.* (BESIII), Phys. Rev. **D83**, 032003 (2011), [arXiv:1012.5131].

[197] N. A. Tornqvist, Z. Phys. **C68**, 647 (1995), [hep-ph/9504372].

[198] W.-H. Liang, J.-J. Xie and E. Oset, Eur. Phys. J. C **76**, 12, 700 (2016), [arXiv:1609.03864].

[199] R. Molina *et al.*, Phys. Lett. B **803**, 135279 (2020), [arXiv:1908.11557].

[200] E. van Beveren and G. Rupp, Eur. Phys. J. **C22**, 493 (2001), [hep-ex/0106077].

[201] M. Boglione and M. R. Pennington, Phys. Rev. **D65**, 114010 (2002), [hep-ph/0203149].

Downloaded from https://academic.oup.com/ptep/article/2022/8/083C01/6651666 by KIT Library user on 27 September 2022

65. Rare Kaon Decays

Revised August 2021 by L. Littenberg (BNL) and G. Valencia (Monash U.).

65.1 Introduction

There are several useful reviews on rare kaon decays and related topics [1–13]. Activity in rare kaon decays can be divided roughly into four categories:

1. Searches for explicit violations of the Standard Model (SM)
2. The golden modes: $K \to \pi\nu\bar{\nu}$
3. Other constraints on SM parameters
4. Studies of strong interactions at low energy.

The paradigm of Category 1 is the lepton flavor violating decay $K_L \to \mu e$. Category 2 includes the two modes that can be calculated with negligible theoretical uncertainty, $K^+ \to \pi^+\nu\bar{\nu}$ and $K_L \to \pi^0\nu\bar{\nu}$. These modes can lead to precision determinations of CKM parameters or, in combination with other measurements of these parameters, they can constrain new interactions. They constitute the main focus of the current experimental kaon program. The search for new light particles through the reaction $K \to \pi X^0$ is a byproduct of these measurements. Category 3 is focused on decays with charged leptons, such as $K_L \to \pi^0\ell^+\ell^-$ or $K_L \to \ell^+\ell^-$ where $\ell \equiv e, \mu$. These modes are sensitive to CKM parameters, but they suffer from multiple hadronic uncertainties that can be addressed, at least in part, through a systematic study of the peripheral modes indicated in Fig. 65.1.

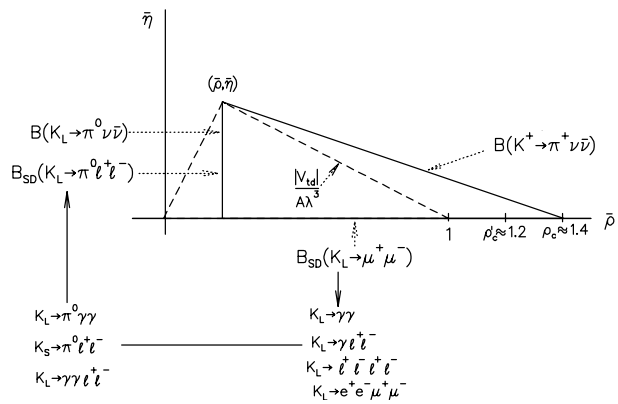

Figure 65.1: Role of rare kaon decays in determining the unitarity triangle. The solid arrows point to auxiliary modes needed to interpret the main results, or potential backgrounds to them.

The interplay between Categories 3-4 and their complementarity to Category 2 is illustrated in the figure. Category 4 includes reactions like $K^+ \to \pi^+\ell^+\ell^-$ where long distance contributions are dominant and which constitute a testing ground for the ideas of chiral perturbation theory. Other decays in this category are $K_L \to \pi^0\gamma\gamma$ and $K_L \to \ell^+\ell^-\gamma$. The former is important in understanding a CP-conserving contribution to $K_L \to \pi^0\ell^+\ell^-$, whereas the latter could shed light on long distance contributions to $K_L \to \mu^+\mu^-$.

65.2 Explicit violations of the Standard Model

Much activity has focussed on searches for lepton flavor violation (LFV). This is motivated by the fact that many extensions of the minimal Standard Model violate lepton flavor and by the potential to access very high energy scales. For example, the tree-level exchange of a LFV vector boson of mass M_X that couples to left-handed fermions with electroweak strength and without mixing angles yields $\mathrm{B}(K_L \to \mu e) = 4.7 \times 10^{-12}(148\ \mathrm{TeV}/M_X)^4$ [2]. This simple dimensional analysis may be used to read from Table 65.1 that the reaction $K_L \to \mu e$ is already probing scales of over 100 TeV. Table 65.1 summarizes the present experimental situation vis-à-vis LFV. The decays $K_L \to \mu^\pm e^\mp$ and $K^+ \to \pi^+ e^\mp \mu^\pm$ (or $K_L \to \pi^0 e^\mp \mu^\pm$) provide complementary information on potential family number violating interactions, since the former is sensitive to parity-odd couplings and the latter is sensitive to parity-even couplings.

Limits on certain lepton-number violating (LNV) kaon decays also have been obtained, with special interest arising from their role in constraining possible extensions of the neutrino sector [14, 15], and we list those in the table as well. Related searches in μ and τ processes are discussed in our section "Tests of Conservation Laws."

Table 65.1: Searches for lepton flavor and lepton number violation in K decay

LFV mode	90% CL upper limit	Experiment	Yr./Ref.	Type
$K^+ \to \pi^+ e^- \mu^+$	1.3×10^{-11}	BNL-865	2005/ [16]	LFV
$K^+ \to \pi^+ e^+ \mu^-$	6.6×10^{-11}	NA62	2021/ [17]	LFV
$K_L \to \mu e$	4.7×10^{-12}	BNL-871	1998/ [18]	LFV
$K_L \to \pi^0 e \mu$	7.6×10^{-11}	KTeV	2008/ [19]	LFV
$K_L \to \pi^0\pi^0 e \mu$	1.7×10^{-10}	KTeV	2008/ [19]	LFV
$K^+ \to \pi^- e^+ e^+$	5.3×10^{-11}	NA62	2022/ [20]	LNV
$K^+ \to \pi^-\pi^0 e^+ e^+$	8.5×10^{-10}	NA62	2022/ [20]	LNV
$K^+ \to \pi^- \mu^+ \mu^+$	4.2×10^{-11}	NA62	2019/ [21]	LNV
$K_L \to e^\pm e^\pm \mu^\mp \mu^\mp$	4.12×10^{-11}	KTeV	2003/ [22]	LNV
$K^+ \to \pi^- \mu^+ e^+$	4.2×10^{-11}	NA62	2021/ [17]	LNFV

65.3 The golden modes: $K \to \pi\nu\bar{\nu}$

In the SM, the decay $K^+ \to \pi^+\nu\bar{\nu}$ is dominated by one-loop diagrams with top-quark intermediate states while long-distance contributions are known to be quite small [23–25]. This permits a precise calculation of this rate in terms of SM parameters. Studies of this process are thus motivated by the possibility of detecting non-SM physics when comparing with the results of global fits [26, 27].

The branching ratio can be written in a compact form that exhibits the different ingredients that go into the calculation [28],

$$\mathrm{B}\left(K^+ \to \pi^+\nu\bar{\nu}(\gamma)\right) = \kappa_+(1+\Delta_{\mathrm{EM}})\left[\left(\frac{\mathrm{Im}(V_{ts}^\star V_{td})}{\lambda^5}X_t\right)^2 + \left(\frac{\mathrm{Re}(V_{cs}^\star V_{cd})}{\lambda}P_c + \frac{\mathrm{Re}(V_{ts}^\star V_{td})}{\lambda^5}X_t\right)^2\right]. \tag{65.1}$$

The parameters in Eq. 65.1 incorporate the *a priori* unknown hadronic matrix element in terms of the very well-measured K_{e3} rate [23] in κ_+; long distance QED corrections in Δ_{EM} [29]; the Inami-Lim function for the short distance top-quark contribution [30] including NLO QCD corrections [31, 32] and the two-loop electroweak correction [28], all in X_t; and the charm-quark contributions due to short distance effects including NNLO QCD corrections [33, 34] and NLO electroweak corrections via P_c [35], which also includes certain long distance dubbed $\delta P_{c,u}$ [25, 36].

An interesting approximate way to cast this result in terms of the CKM parameters λ, V_{cb}, $\bar{\rho}$ and $\bar{\eta}$ (see our Section on "The Cabibbo-Kobayashi-Maskawa mixing matrix") [9] is:

$$\mathrm{B}(K^+ \to \pi^+\nu\bar{\nu}) \approx 1.6 \times 10^{-5}|V_{cb}|^4[(\sigma\bar{\eta})^2 + (\rho_c - \bar{\rho})^2] \tag{65.2}$$

where $\rho_c \approx 1.45$ and $\sigma \equiv \frac{1}{(1-\frac{1}{2}\lambda^2)^2}$. Thus, $\mathrm{B}(K^+ \to \pi^+\nu\bar{\nu})$ determines an ellipse in the $\bar{\rho}$, $\bar{\eta}$ plane with center $(\rho_c, 0)$ and semiaxes $\approx \frac{1}{|V_{cb}|^2}\sqrt{\frac{\mathrm{B}(K^+\to\pi^+\nu\bar{\nu})}{1.6\times10^{-5}}}$ and $\frac{1}{\sigma|V_{cb}|^2}\sqrt{\frac{\mathrm{B}(K^+\to\pi^+\nu\bar{\nu})}{1.6\times10^{-5}}}$.

Downloaded from https://academic.oup.com/ptep/article/2022/8/083C01/6651666 by KIT Library user on 27 September 2022

BNL-787 observed two candidate events [37, 38] in the clean high π^+ momentum and one event [39] in the low-momentum region. The successor experiment BNL-949 observed one more in the high-momentum region [40] and three more in the low-momentum region [41], yielding a branching ratio of $(1.73^{+1.15}_{-1.05}) \times 10^{-10}$ [42].

The NA62 experiment, performed with in-flight decays at CERN, aims to reach a sensitivity of $\sim 10^{-12}$ per event. NA62 was commissioned in 2015 and has taken data in 2016, 2017 and 2018. They recently published results from the 2016-18 runs [43]. Twenty candidate events were observed, including an estimated background of 7.03, yielding $\mathrm{B}(\mathrm{K}^+ \to \pi^+\nu\overline{\nu}) = (10.6^{+4.0}_{-3.4}|_{\mathrm{stat}} \pm 0.9_{\mathrm{sys}}) \times 10^{-11}$. NA62 will continue taking data in 2021 with improvements to the detector.

Using the latest CKMfitter input (Dec. 2019) [26], we estimate $\mathrm{B}(K^+ \to \pi^+\nu\overline{\nu})_{SM} = (8.1 \pm 0.4) \times 10^{-11}$, near the lower end of the measurements of BNL-787/949 and NA62. Current parametric uncertainty in the CKM angles can result in numbers with central values differing from this one by up to 10% [44].

The second golden mode is the neutral counterpart to our preceeding discussion: $K_L \to \pi^0\nu\overline{\nu}$. It is dominantly CP-violating and free of hadronic uncertainties [23, 45, 46]. In the Standard Model, this mode is dominated by an intermediate top-quark state and does not suffer from the small uncertainty associated with the charm-quark intermediate state that affects $K^+ \to \pi^+\nu\overline{\nu}$. The branching ratio is given by Ref. [9]:

$$\mathrm{B}(K_L \to \pi^0\nu\overline{\nu}) = \kappa_L \left(\frac{\mathrm{Im}(V_{ts}^\star V_{td})}{\lambda^5} X_t\right)^2 \approx 7.6 \times 10^{-5} |V_{cb}|^4 \overline{\eta}^2 \ . \tag{65.3}$$

As with the charged mode, the hadronic matrix element can be related to that measured in $K_{\ell 3}$ decay and is parameterized in κ_L.

Our estimate for the branching ratio within the SM, using the latest CKMfitter input (Dec. 2019) [26], is $(2.8 \pm 0.2) \times 10^{-11}$. Similarly to the charged kaon case, parametric uncertainty in the CKM angles can result in a central value that differs from this one by up to almost 20% [44].

Grossman and Nir (GN) [47] pointed out that, in a nearly model-independent manner, the two golden modes satisfy the relation $\mathrm{B}(K_L \to \pi^0\nu\overline{\nu}) \lesssim 4.3\ \mathrm{B}(K^+ \to \pi^+\nu\overline{\nu})$. Using the BNL 787/949 90% CL bound on $K^+ \to \pi^+\nu\overline{\nu}$, GN then predict $B(K_L \to \pi^0\nu\overline{\nu}) < 1.46 \times 10^{-9}$. Using instead the latest NA62 result, the GN upper bound becomes $B(K_L \to \pi^0\nu\overline{\nu}) < 8.14 \times 10^{-10}$ [13].

The KOTO experiment at J-PARC, whose initial goal is to observe this decay, has been running since 2013 and in 2018 published a 90% CL upper limit of 3.0×10^{-9} [48], based on their 2015 data. They have run every year since, making incremental improvements to the experimental configuration between runs. In 2021 they published a result on the data taken between 2016 and 2018 in which three events were observed in the signal region [49]. Studies revealed two backgrounds previously unanticipated at the current level of sensitvity (7.2×10^{-10}/event), one from halo $K_L \to \gamma\gamma$ and a larger one from charged kaons produced by K_L interactions in the downstream collimator, followed by $K^\pm \to \pi^0 e^\pm \nu_e$ where the $e^\pm$ goes backwards and is not observed. These constituted more than 90 % of the expected background of 1.22 events. Conservatively assuming the three events were due to background, they extracted a 90% CL upper limit of 4.9×10^{-9}. Subsequent hardware and analysis improvements are expected to greatly reduce these backgrounds in future data collection. An increase of 3-5 in sensitivity is anticipated from runs planned in the next three years.

The current theoretical and experimental situation for the golden modes is summarized in Fig. 65.2. The red area corresponds to the 1σ SM prediction we obtain with the latest input available from CKMfitter (December 2019) [26]. The yellow region shows the result established by the combined BNL-787 and BNL-949 results, whereas the green region marks the new NA62 result for $K^+ \to \pi^+\nu\overline{\nu}$. The black shaded region marks the GN exclusion, which lies significantly above the SM expectation leaving a large window for discovery of new physics contributions by experiments seeking to measure $\mathrm{B}(K_L \to \pi^0\nu\overline{\nu})$. The 90% CL upper bound on this mode from the KOTO result published in 2018 [48] is shown as a dashed orange line, and is seen to still lie in the GN excluded zone.

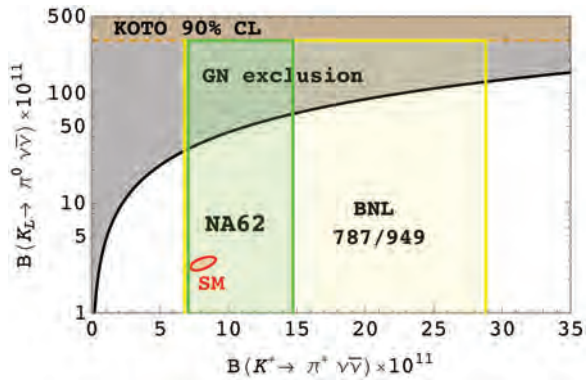

Figure 65.2: Summary of current situation for the golden modes $K \to \pi\nu\overline{\nu}$. The red ellipse shows the 1σ SM prediction with input from CKMfitter; the green (yellow) region corresponds to the NA62 (BNL787/949) 1σ measurement; and the dashed orange line marks the 90% CL KOTO upper bound. The black shaded region shows the GN exclusion.

Much theoretical work has explored beyond the SM scenarios that can populate this window as well as their correlations with other rare processes outside kaon physics. Although it would be relatively straightforward to establish the existence of new physics by observing deviations from their SM values in the $K \to \pi\nu\overline{\nu}$ modes, it would take much more extensive global fits to pinpoint the origin of any such deviation. Partial summaries with references focusing on quark flavor physics can be found in Refs. [9, 50–54]. Different possibilities emphasizing an interpretation of these modes as $K \to \pi + E_{\mathrm{miss}}$ can be found in Refs. [55–57].

There is a subtlety in converting the GN bound extracted from measurements of $K^+ \to \pi^+\nu\overline{\nu}$ into an upper bound for $K_L \to \pi^0\nu\overline{\nu}$ as applied to KOTO [58]. This is due to a lack of sensitivity of the charged kaon experiments to a kinematic window near the pion mass. New physics appearing through a two body mode $K^+ \to \pi^+ X^0$, for an invisible X^0 with mass near the pion mass, has a much weaker constraint. The situation is illustrated in Fig. 65.3 which shows the BNL787/949 [42] and NA62 [59] 90% c.l. limits on $K^+ \to \pi^+ X^0$ as a function of m_{X^0} assuming X^0 is stable. The implied GN bound for $K_L \to \pi^0 X^0$, $B(K_L \to \pi^0 X^0) \lesssim 4.3 B(K^+ \to \pi^+ X^0)$ is shown as a blue line and can be compared with the actual KOTO [48] constraint on $K_L \to \pi^0 X^0$ in red. Notice that the upper bound derived from NA62 is lower than that derived from BNL787/949 except for a small mass window. For $120 \lesssim m_{X^0} \lesssim 150$ MeV, KOTO already has better sensitivity than that implied by the GN bound in this case. The possibility of new physics in this scenario has generated much theoretical speculation [60–70].

The search for a new light particle X^0 in $K^+ \to \pi^+ X^0$ has a long tradition covering both long-lived particles (*e.g.*, hyperphoton, axion, familon, *etc.*), and short-lived ones that decay to muon, electron, photon or neutrino pairs. The longstanding 90% CL upper limit on $K^+ \to \pi^+ X^0$ from BNL787/949 7.3×10^{-11} [40] for the case of massless X^0 has been slightly improved by NA62 to 5×10^{-11} as can be read from Fig. 65.3. These limits can also be reinterpreted in connection with a dark photon [71] or dark Z [72], and in this context NA48/2 also constrained the mode $B(K^\pm \to \pi^\pm A' \to \pi^\pm e^+ e^-)$ [73]. Complementary searches for new light particles in kaon experiments use modes with two pions and include the KTeV bound $B(K_L \to \pi^0\pi^0 X^0 \to \pi^0\pi^0\mu^+\mu^-) < 1 \times 10^{-10}$ [74] and the E391a bound $B(K_L \to \pi^0\pi^0 X^0 \to \pi^0\pi^0\gamma\gamma) < 2.4 \times 10^{-7}$ [75].

Neutrino pair modes with one extra pion, $K \to \pi\pi\nu\overline{\nu}$, are similarly dominated by short distance contributions in the SM [76–78]. Even though they are theoretically clean, they occur with very

Downloaded from https://academic.oup.com/ptep/article/2022/8/083C01/6651666 by KIT Library user on 27 September 2022

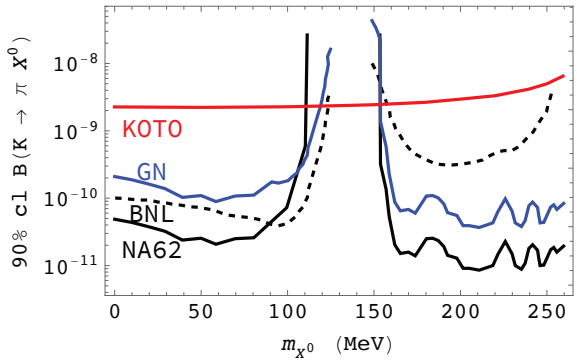

Figure 65.3: Summary of current situation for $K \to \pi X^0$. The solid (dashed) black line shows the exclusion limit for $K^+ \to \pi^+ X^0$ from NA62 (BNL787/949) assuming X^0 is stable. The blue line marks the constraint implied for $K_L \to \pi^0 X^0$ by the Grossman-Nir relation and the red line marks the current KOTO limit on $K^+ \to \pi^+ X^0$.

low rates with branching ratios of order 10^{-13}. The current best bound comes from KEK-391a, $B(K_L \to \pi^0\pi^0\nu\bar{\nu}) < 8.1 \times 10^{-7}$ at 90% CL [79]. There is also a bound for the charged kaon mode $B(K^+ \to \pi^+\pi^0\nu\bar{\nu}) < 4.3 \times 10^{-5}$ at 90% CL [80] from BNL-787. New physics contributions to these modes are discussed in [81].

65.4 Other constraints on Standard Model parameters

The decay $K_L \to \mu^+\mu^-$ has a short distance contribution sensitive to the CKM parameter $\bar{\rho}$, given by [5]:

$$\mathrm{B}_{\mathrm{SD}}(K_L \to \mu^+\mu^-) \approx 2.7 \times 10^{-4} |V_{cb}|^4 (\rho_c' - \bar{\rho})^2 \qquad (65.4)$$

where ρ_c' depends on the charm quark mass and is approximately 1.2. This decay, however, is dominated by a long-distance contribution from a two-photon intermediate state. The absorptive (imaginary) part of the long-distance component is determined by the measured rate for $K_L \to \gamma\gamma$ to be $\mathrm{B}_{\mathrm{abs}}(K_L \to \mu^+\mu^-) = (6.64 \pm 0.07) \times 10^{-9}$; and it almost completely saturates the observed rate $\mathrm{B}(K_L \to \mu^+\mu^-) = (6.84 \pm 0.11) \times 10^{-9}$ [82]. The difference between the observed rate and the absorptive component can be attributed to the (coherent) sum of the short-distance amplitude and the real part of the long-distance amplitude. The latter cannot be derived directly from experiment [83], but can be estimated with certain assumptions [84, 85].

By contrast, the decay $K_L \to e^+e^-$ is completely dominated by long distance physics and is easier to estimate. The result, $B(K_L \to e^+e^-) \sim 9 \times 10^{-12}$ [83, 86], is in good agreement with the BNL-871 measurement, $(8.7\,^{+5.7}_{-4.1}) \times 10^{-12}$ [87].

The mode $K_S \to \mu^+\mu^-$ has a short distance contribution proportional to the square of the CKM parameter $\bar{\eta}$ entering at the 10^{-13} level [10]. It also has long distance contributions arising from the two photon intermediate state which result in a rate $B(K_S \to \mu^+\mu^-)_{LD} = 5.1 \times 10^{-12}$ [10]. There is a 90% CL limit $B(K_S \to \mu^+\mu^-) < 2.1 \times 10^{-10}$ from LHCb [88, 89]. The interplay between $K_L \to \mu^+\mu^-$ and $K_S \to \mu^+\mu^-$ has been the subject of [90,91], and it has been pointed out that a measurement of time-dependent interference effects could be used to extract information on CKM angles from $K \to \mu^+\mu^-$ measurements [92].

The decay $K_L \to \pi^0 e^+e^-$ is sensitive to the CKM parameter η through its CP-violating component. There are both direct and indirect CP-violating amplitudes that can interfere. The direct CP-violating amplitude is short distance dominated and has been calculated in detail within the SM [5]. The indirect CP-violating amplitude can be inferred from a measurement of $K_S \to \pi^0 e^+e^-$. The complete CP-violating contribution to the rate can be written as [93–95]:

$$\mathrm{B}_{\mathrm{CPV}} \approx \left[15.7|a_S|^2 \pm 1.4 \left(\frac{|V_{cb}|^2\bar{\eta}}{10^{-4}} \right) |a_S| + 0.12 \left(\frac{|V_{cb}|^2\bar{\eta}}{10^{-4}} \right)^2 \right] \times 10^{-12} \qquad (65.5)$$

where the three terms correspond to the indirect CP violation, the interference, and the direct CP violation, respectively. The parameter a_S has been extracted by NA48/1 from a measurement of $K_S \to \pi^0 e^+e^-$ with the result $|a_S| = 1.06^{+0.26}_{-0.21} \pm 0.07$ [96], as well as from a measurement of $K_S \to \pi^0\mu^+\mu^-$ with the result $|a_S| = 1.54^{+0.40}_{-0.32} \pm 0.06$ [97]. With current constraints on the CKM parameters, and assuming a positive sign for the interference term [95, 98], this implies that $\mathrm{B}_{\mathrm{CPV}}(K_L \to \pi^0 e^+e^-) \approx (3.1 \pm 0.9) \times 10^{-11}$, where the three contributions to the central value from indirect, interference and direct CP violation are $(1.76, 0.9, 0.45) \times 10^{-11}$ respectively. It should be noted that more recent studies suggest a much larger uncertainty in the value of a_S [99].

$K_L \to \pi^0 e^+e^-$ also has a CP-conserving component dominated by a two-photon intermediate state. This component can be decomposed into an absorptive and a dispersive part. The absorptive part can be extracted from the measurement of the low $m_{\gamma\gamma}$ region of the $K_L \to \pi^0\gamma\gamma$ spectrum. The rate and the shape of the distribution $d\Gamma/dm_{\gamma\gamma}$ in $K_L \to \pi^0\gamma\gamma$ are well described in chiral perturbation theory in terms of three (*a priori*) unknown parameters [100–103].

Both KTeV and NA48 have studied the mode $K_L \to \pi^0\gamma\gamma$, reporting similar results. KTeV finds $B(K_L \to \pi^0\gamma\gamma) = (1.29 \pm 0.03_{\mathrm{stat}} \pm 0.05_{\mathrm{sys}}) \times 10^{-6}$ [104], while NA48 finds $B(K_L \to \pi^0\gamma\gamma) = (1.36 \pm 0.03_{\mathrm{stat}} \pm 0.03_{\mathrm{sys}} \pm 0.03_{\mathrm{norm}}) \times 10^{-6}$ [105]. Both experiments are consistent with a negligible rate in the low $m_{\gamma\gamma}$ region, suggesting a very small CP-conserving component $B_{\mathrm{CP}}(K_L \to \pi^0 e^+e^-) \sim \mathcal{O}(10^{-13})$ [95, 103, 105]. There remains some model dependence in the estimate of the dispersive part of the CP-conserving $K_L \to \pi^0 e^+e^-$ [95].

The related process, $K_L \to \pi^0\gamma e^+e^-$, is potentially an additional background to $K_L \to \pi^0 e^+e^-$ in some region of phase space [106]. This process has been observed with a branching ratio of $(1.62 \pm 0.14_{\mathrm{stat}} \pm 0.09_{\mathrm{sys}}) \times 10^{-8}$ [107].

The decay $K_L \to \gamma\gamma e^+e^-$ constitutes the dominant background to $K_L \to \pi^0 e^+e^-$. It was first observed by BNL-845 [108], and subsequently confirmed with a much larger sample by KTeV [109]. It has been estimated that this background will enter at about the 10^{-10} level [110, 111], comparable to or larger than the signal level. Because of this, the observation of $K_L \to \pi^0 e^+e^-$ at the SM level will depend on background subtraction with good statistics. Possible alternative strategies are discussed in Ref. [95] and references cited therein.

The 90% CL upper bound for the process $K_L \to \pi^0 e^+e^-$ is 2.8×10^{-10} [111]. For the closely related muonic process, the published upper bound is $\mathrm{B}(K_L \to \pi^0\mu^+\mu^-) \leq 3.8 \times 10^{-10}$ [112], compared with the SM prediction of $(1.9 \pm 0.5) \times 10^{-11}$. The latter assumes positive interference between the direct- and indirect-CP violating components and includes a CP-conserving component which contributes about 30% of the total [10, 113].

A study of $K_L \to \pi^0\mu^+\mu^-$ has indicated that it might be possible to extract the direct CP-violating contribution by a joint study of the Dalitz plot variables and the components of the μ^+ polarization [114]. The latter tends to be quite substantial so that large statistics may not be necessary.

Combined information from $K_L \to \pi^0\ell^+\ell^-$ as well as $K_L \to \mu^+\mu^-$ complements the $K \to \pi\nu\bar{\nu}$ measurements in constraining physics beyond the SM [115].

65.5 Other long distance dominated modes

The decays $K^+ \to \pi^+\ell^+\ell^-$ ($\ell = e$ or μ) have received considerable attention. The rate and spectrum have been measured for

Downloaded from https://academic.oup.com/ptep/article/2022/8/083C01/6651666 by KIT Library user on 27 September 2022

both the electron and muon modes [116–121]. A review of the theoretical status of these modes can be found in [99, 122].

Ref. [93, 94] has proposed a parameterization inspired by chiral perturbation theory, which provides a successful description of data but indicates the presence of large corrections beyond leading order. More work is needed to fully understand the origin of these large corrections. The mode $K^+ \to \pi^+\pi^0 e^+ e^-$, analyzed by NA48/2 [123], is also dominated by long distance physics but it has been argued that measuring asymmetries can provide information on the short distance components [124]. The current status of these modes is discussed in [125].

The decay $K^+ \to \pi^+\gamma\gamma$ can be predicted in terms of one unknown parameter to leading order in χPT resulting in a correlation between the rate and the diphoton mass spectrum [126]. Certain important corrections at the next order are also known [127]. The rate was first measured by E787 [128], and NA48/2 [129] has obtained a more precise result with a 6% error, as well as the corresponding spectrum fits. The most recent, and precise, result is from NA62 based on a sample of 232 events [130] but is still insufficient to distinguish between the leading order and next order χPT parameterizations. The NA48 and NA62 results have been combined in [131].

Much information has been recorded by KTeV and NA48 on the rates and spectrum for the Dalitz pair conversion modes $K_L \to \ell^+\ell^-\gamma$ [132, 133], and $K_L \to \ell^+\ell^-\ell'^+\ell'^-$ for $\ell, \ell' = e$ or μ [22, 134]. All these results are used to test hadronic models and should eventually help unravel the underlying physics in $K_L \to \mu^+\mu^-$ [85, 90, 135].

References

[1] L. Littenberg and G. Valencia, Ann. Rev. Nucl. Part. Sci. **43**, 729 (1993), [hep-ph/9303225].

[2] J. L. Ritchie and S. G. Wojcicki, Rev. Mod. Phys. **65**, 1149 (1993).

[3] B. Winstein and L. Wolfenstein, Rev. Mod. Phys. **65**, 1113 (1993).

[4] A. Pich, Rept. Prog. Phys. **58**, 563 (1995), [hep-ph/9502366].

[5] G. Buchalla, A. J. Buras and M. E. Lautenbacher, Rev. Mod. Phys. **68**, 1125 (1996), [hep-ph/9512380].

[6] G. D'Ambrosio and G. Isidori, Int. J. Mod. Phys. **A13**, 1 (1998), [hep-ph/9611284].

[7] P. Buchholz and B. Renk, Prog. Part. Nucl. Phys. **39**, 253 (1997).

[8] A. R. Barker and S. H. Kettell, Ann. Rev. Nucl. Part. Sci. **50**, 249 (2000), [hep-ex/0009024].

[9] A. J. Buras, F. Schwab and S. Uhlig, Rev. Mod. Phys. **80**, 965 (2008), [hep-ph/0405132].

[10] V. Cirigliano *et al.*, Rev. Mod. Phys. **84**, 399 (2012), [arXiv:1107.6001].

[11] D. Bryman *et al.*, Ann. Rev. Nucl. Part. Sci. **61**, 331 (2011).

[12] T. K. Komatsubara, Prog. Part. Nucl. Phys. **67**, 995 (2012), [arXiv:1203.6437].

[13] A. Ceccucci, Annual Review of Nuclear and Particle Science **71**, 1 (2021), URL `https://doi.org/10.1146/annurev-nucl-102419-054905`.

[14] A. Atre *et al.*, JHEP **05**, 030 (2009), [arXiv:0901.3589].

[15] L. S. Littenberg and R. Shrock, Phys. Lett. **B491**, 285 (2000), [hep-ph/0005285].

[16] A. Sher *et al.*, Phys. Rev. **D72**, 012005 (2005), [hep-ex/0502020].

[17] E. Cortina Gil *et al.* (NA62), Phys. Rev. Lett. **127**, 13, 131802 (2021), [arXiv:2105.06759].

[18] D. Ambrose *et al.* (BNL), Phys. Rev. Lett. **81**, 5734 (1998), [hep-ex/9811038].

[19] E. Abouzaid *et al.* (KTeV), Phys. Rev. Lett. **100**, 131803 (2008), [arXiv:0711.3472].

[20] E. Cortina Gil *et al.* (NA62) (2022), [arXiv:2202.00331].

[21] E. Cortina Gil *et al.* (NA62), Phys. Lett. **B797**, 134794 (2019), [arXiv:1905.07770].

[22] A. Alavi-Harati *et al.* (KTeV), Phys. Rev. Lett. **90**, 141801 (2003), [hep-ex/0212002].

[23] J. S. Hagelin and L. S. Littenberg, Prog. Part. Nucl. Phys. **23**, 1 (1989).

[24] M. Lu and M. B. Wise, Phys. Lett. **B324**, 461 (1994), [hep-ph/9401204].

[25] A. F. Falk, A. Lewandowski and A. A. Petrov, Phys. Lett. **B505**, 107 (2001), [hep-ph/0012099].

[26] J. Charles *et al.*, Phys. Rev. **D84**, 033005 (2011), [arXiv:1106.4041].

[27] M. Bona *et al.* (UTfit), JHEP **03**, 049 (2008), [arXiv:0707.0636].

[28] J. Brod, M. Gorbahn and E. Stamou, Phys. Rev. **D83**, 034030 (2011), [arXiv:1009.0947].

[29] F. Mescia and C. Smith, Phys. Rev. **D76**, 034017 (2007), [arXiv:0705.2025].

[30] T. Inami and C. S. Lim, Prog. Theor. Phys. **65**, 297 (1981), [Erratum: Prog. Theor. Phys. **65**, 1772 (1981)].

[31] G. Buchalla and A. J. Buras, Nucl. Phys. **B548**, 309 (1999), [hep-ph/9901288].

[32] M. Misiak and J. Urban, Phys. Lett. **B451**, 161 (1999), [hep-ph/9901278].

[33] A. J. Buras *et al.*, Phys. Rev. Lett. **95**, 261805 (2005), [hep-ph/0508165].

[34] A. J. Buras *et al.*, JHEP **11**, 002 (2006), [Erratum: JHEP **11**, 167 (2012)], [hep-ph/0603079].

[35] J. Brod and M. Gorbahn, Phys. Rev. **D78**, 034006 (2008), [arXiv:0805.4119].

[36] G. Isidori, F. Mescia and C. Smith, Nucl. Phys. **B718**, 319 (2005), [hep-ph/0503107].

[37] S. Adler *et al.* (E787), Phys. Rev. Lett. **88**, 041803 (2002), [hep-ex/0111091].

[38] S. Adler *et al.* (E787), Phys. Rev. Lett. **84**, 3768 (2000), [hep-ex/0002015].

[39] S. S. Adler *et al.* (E787), Phys. Lett. **B537**, 211 (2002), [hep-ex/0201037].

[40] V. V. Anisimovsky *et al.* (E949), Phys. Rev. Lett. **93**, 031801 (2004), [hep-ex/0403036].

[41] A. V. Artamonov *et al.* (E949), Phys. Rev. Lett. **101**, 191802 (2008), [arXiv:0808.2459].

[42] A. V. Artamonov *et al.* (BNL-E949), Phys. Rev. **D79**, 092004 (2009), [arXiv:0903.0030].

[43] E. Cortina Gil *et al.* (NA62), JHEP **06**, 093 (2021), [arXiv:2103.15389].

[44] A. J. Buras *et al.*, JHEP **11**, 033 (2015), [arXiv:1503.02693].

[45] L. S. Littenberg, Phys. Rev. **D39**, 3322 (1989).

[46] G. Buchalla and G. Isidori, Phys. Lett. **B440**, 170 (1998), [hep-ph/9806501].

[47] Y. Grossman and Y. Nir, Phys. Lett. **B398**, 163 (1997), [hep-ph/9701313].

[48] J. K. Ahn *et al.* (KOTO), Phys. Rev. Lett. **122**, 021802 (2019), [arXiv:1810.09655].

[49] J. K. Ahn *et al.* (KOTO), Phys. Rev. Lett. **126**, 121801 (2021), [arXiv:2012.07571].

[50] G. D'Ambrosio and G. Isidori, Phys. Lett. **B530**, 108 (2002), [hep-ph/0112135].

[51] D. Bryman *et al.*, Int. J. Mod. Phys. **A21**, 487 (2006), [hep-ph/0505171].

[52] A. J. Buras, D. Buttazzo and R. Knegjens, JHEP **11**, 166 (2015), [arXiv:1507.08672].

[53] X.-G. He, G. Valencia and K. Wong, Eur. Phys. J. **C78**, 472 (2018), [arXiv:1804.07449].

Downloaded from https://academic.oup.com/ptep/article/2022/8/083C01/6651666 by KIT Library user on 27 September 2022

[54] J. Aebischer, A. J. Buras and J. Kumar, JHEP **12**, 097 (2020), [arXiv:2006.01138].

[55] M. Bordone *et al.*, Eur. Phys. J. **C77**, 618 (2017), [arXiv:1705.10729].

[56] X.-G. He, J. Tandean and G. Valencia, Phys. Lett. **B797**, 134842 (2019), [arXiv:1904.04043].

[57] F. F. Deppisch, K. Fridell and J. Harz, JHEP **12**, 186 (2020), [arXiv:2009.04494].

[58] K. Fuyuto, W.-S. Hou and M. Kohda, Phys. Rev. Lett. **114**, 171802 (2015), [arXiv:1412.4397].

[59] E. Cortina Gil *et al.* (NA62), JHEP **03**, 058 (2021), [arXiv:2011.11329].

[60] T. Kitahara *et al.*, Phys. Rev. Lett. **124**, 071801 (2020), [arXiv:1909.11111].

[61] D. Egana-Ugrinovic, S. Homiller and P. Meade, Phys. Rev. Lett. **124**, 191801 (2020), [arXiv:1911.10203].

[62] P. S. B. Dev, R. N. Mohapatra and Y. Zhang, Phys. Rev. D **101**, 075014 (2020), [arXiv:1911.12334].

[63] M. Fabbrichesi and E. Gabrielli, Eur. Phys. J. C **80**, 532 (2020), [arXiv:1911.03755].

[64] Y. Liao *et al.*, Phys. Rev. D **102**, 055005 (2020), [arXiv:2005.00753].

[65] R. Ziegler, J. Zupan and R. Zwicky, JHEP **07**, 229 (2020), [arXiv:2005.00451].

[66] T. Li, X.-D. Ma and M. A. Schmidt, Phys. Rev. D **101**, 055019 (2020), [arXiv:1912.10433].

[67] X.-G. He *et al.*, JHEP **08**, 034 (2020), [arXiv:2005.02942].

[68] M. Hostert, K. Kaneta and M. Pospelov, Phys. Rev. D **102**, 055016 (2020), [arXiv:2005.07102].

[69] S. Gori, G. Perez and K. Tobioka, JHEP **08**, 110 (2020), [arXiv:2005.05170].

[70] T. B. de Melo *et al.*, Phys. Rev. D **103**, 115001 (2021), [arXiv:2102.06262].

[71] M. Pospelov, Phys. Rev. **D80**, 095002 (2009), [arXiv:0811.1030].

[72] H. Davoudiasl, H.-S. Lee and W. J. Marciano, Phys. Rev. **D89**, 095006 (2014), [arXiv:1402.3620].

[73] J. R. Batley *et al.* (NA48/2), Phys. Lett. **B746**, 178 (2015), [arXiv:1504.00607].

[74] E. Abouzaid *et al.* (KTeV), Phys. Rev. Lett. **107**, 201803 (2011), [arXiv:1105.4800].

[75] Y. C. Tung *et al.* (E391a), Phys. Rev. Lett. **102**, 051802 (2009), [arXiv:0810.4222].

[76] L. S. Littenberg and G. Valencia, Phys. Lett. **B385**, 379 (1996), [hep-ph/9512413].

[77] C.-W. Chiang and F. J. Gilman, Phys. Rev. **D62**, 094026 (2000), [hep-ph/0007063].

[78] C. Q. Geng, I. J. Hsu and Y. C. Lin, Phys. Rev. **D50**, 5744 (1994), [hep-ph/9406313].

[79] R. Ogata *et al.* (E391a), Phys. Rev. **D84**, 052009 (2011), [arXiv:1106.3404].

[80] S. Adler *et al.* (E787), Phys. Rev. **D63**, 032004 (2001), [hep-ex/0009055].

[81] C.-Q. Geng and J. Tandean, Phys. Rev. D **102**, 115021 (2020), [arXiv:2009.00608].

[82] D. Ambrose *et al.* (E871), Phys. Rev. Lett. **84**, 1389 (2000).

[83] G. Valencia, Nucl. Phys. **B517**, 339 (1998), [hep-ph/9711377].

[84] G. D'Ambrosio, G. Isidori and J. Portoles, Phys. Lett. **B423**, 385 (1998), [hep-ph/9708326].

[85] G. Isidori and R. Unterdorfer, JHEP **01**, 009 (2004), [hep-ph/0311084].

[86] D. Gomez Dumm and A. Pich, Phys. Rev. Lett. **80**, 4633 (1998), [hep-ph/9801298].

[87] D. Ambrose *et al.* (BNL E871), Phys. Rev. Lett. **81**, 4309 (1998), [hep-ex/9810007].

[88] R. Aaij *et al.* (LHCb), Eur. Phys. J. **C77**, 678 (2017), [arXiv:1706.00758].

[89] R. Aaij *et al.* (LHCb), Phys. Rev. Lett. **125**, 231801 (2020), [arXiv:2001.10354].

[90] G. D'Ambrosio and T. Kitahara, Phys. Rev. Lett. **119**, 201802 (2017), [arXiv:1707.06999].

[91] V. Chobanova *et al.*, JHEP **05**, 024 (2018), [arXiv:1711.11030].

[92] A. Dery *et al.*, JHEP **07**, 103 (2021), [arXiv:2104.06427].

[93] G. D'Ambrosio *et al.*, JHEP **08**, 004 (1998), [hep-ph/9808289].

[94] C. Dib, I. Dunietz and F. J. Gilman, Phys. Rev. **D39**, 2639 (1989).

[95] G. Buchalla, G. D'Ambrosio and G. Isidori, Nucl. Phys. **B672**, 387 (2003), [hep-ph/0308008].

[96] J. R. Batley *et al.* (NA48/1), Phys. Lett. **B576**, 43 (2003), [hep-ex/0309075].

[97] J. R. Batley *et al.* (NA48/1), Phys. Lett. **B599**, 197 (2004), [hep-ex/0409011].

[98] S. Friot, D. Greynat and E. De Rafael, Phys. Lett. **B595**, 301 (2004), [hep-ph/0404136].

[99] G. D'Ambrosio, D. Greynat and M. Knecht, JHEP **02**, 049 (2019), [arXiv:1812.00735].

[100] G. Ecker, A. Pich and E. de Rafael, Phys. Lett. **B237**, 481 (1990).

[101] L. Cappiello, G. D'Ambrosio and M. Miragliuolo, Phys. Lett. **B298**, 423 (1993).

[102] A. G. Cohen, G. Ecker and A. Pich, Phys. Lett. **B304**, 347 (1993).

[103] F. Gabbiani and G. Valencia, Phys. Rev. **D66**, 074006 (2002), [hep-ph/0207189].

[104] E. Abouzaid *et al.* (KTeV), Phys. Rev. **D77**, 112004 (2008), [arXiv:0805.0031].

[105] A. Lai *et al.* (NA48), Phys. Lett. **B536**, 229 (2002), [hep-ex/0205010].

[106] J. F. Donoghue and F. Gabbiani, Phys. Rev. **D56**, 1605 (1997), [hep-ph/9702278].

[107] E. Abouzaid *et al.* (KTeV), Phys. Rev. **D76**, 052001 (2007), [arXiv:0706.4074].

[108] W. M. Morse *et al.*, Phys. Rev. **D45**, 36 (1992).

[109] A. Alavi-Harati *et al.* (KTeV), Phys. Rev. **D64**, 012003 (2001), [hep-ex/0010059].

[110] H. B. Greenlee, Phys. Rev. **D42**, 3724 (1990).

[111] A. Alavi-Harati *et al.* (KTeV), Phys. Rev. Lett. **93**, 021805 (2004), [hep-ex/0309072].

[112] A. Alavi-Harati *et al.* (KTEV), Phys. Rev. Lett. **84**, 5279 (2000), [hep-ex/0001006].

[113] G. Isidori, C. Smith and R. Unterdorfer, Eur. Phys. J. **C36**, 57 (2004), [hep-ph/0404127].

[114] M. V. Diwan, H. Ma and T. L. Trueman, Phys. Rev. **D65**, 054020 (2002), [hep-ph/0112350].

[115] F. Mescia, C. Smith and S. Trine, JHEP **08**, 088 (2006), [hep-ph/0606081].

[116] R. Appel *et al.* (E865), Phys. Rev. Lett. **83**, 4482 (1999), [hep-ex/9907045].

[117] J. R. Batley *et al.* (NA48/2), Phys. Lett. **B677**, 246 (2009), [arXiv:0903.3130].

[118] S. Adler *et al.* (E787), Phys. Rev. Lett. **79**, 4756 (1997), [hep-ex/9708012].

[119] H. Ma *et al.* (e865), Phys. Rev. Lett. **84**, 2580 (2000), [hep-ex/9910047].

Downloaded from https://academic.oup.com/ptep/article/2022/8/083C01/6651666 by KIT Library user on 27 September 2022

[120] H. K. Park *et al.* (HyperCP), Phys. Rev. Lett. **88**, 111801 (2002), [hep-ex/0110033].

[121] J. R. Batley *et al.* (NA48/2), Phys. Lett. **B697**, 107 (2011), [arXiv:1011.4817].

[122] G. D'Ambrosio, D. Greynat and M. Knecht, Phys. Lett. B **797**, 134891 (2019), [arXiv:1906.03046].

[123] J. R. Batley *et al.* (NA48/2), Phys. Lett. **B788**, 552 (2019), [arXiv:1809.02873].

[124] L. Cappiello *et al.*, Eur. Phys. J. **C72**, 1872 (2012), [Erratum: Eur. Phys. J. **C72**, 2208 (2012)], [arXiv:1112.5184].

[125] L. Cappiello, O. Catà and G. D'Ambrosio, Eur. Phys. J. **C78**, 265 (2018), [arXiv:1712.10270].

[126] G. Ecker, A. Pich and E. de Rafael, Nucl. Phys. **B303**, 665 (1988).

[127] G. D'Ambrosio and J. Portoles, Phys. Lett. **B386**, 403 (1996), [Erratum: Phys. Lett. **B395**, 389 (1997)], [hep-ph/9606213].

[128] P. Kitching *et al.* (E787), Phys. Rev. Lett. **79**, 4079 (1997), [hep-ex/9708011].

[129] J. R. Batley *et al.* (NA48/2), Phys. Lett. **B730**, 141 (2014), [arXiv:1310.5499].

[130] C. Lazzeroni *et al.* (NA62), Phys. Lett. **B732**, 65 (2014), [arXiv:1402.4334].

[131] B. Velghe (NA62-RK, NA48/2), Nucl. Part. Phys. Proc. **273-275**, 2720 (2016).

[132] A. Alavi-Harati *et al.* (KTeV), Phys. Rev. Lett. **87**, 071801 (2001).

[133] E. Abouzaid *et al.* (KTeV), Phys. Rev. Lett. **99**, 051804 (2007), [hep-ex/0702039].

[134] V. Fanti *et al.* (NA48), Phys. Lett. **B458**, 553 (1999).

[135] G. D'Ambrosio, D. Greynat and G. Vulvert, Eur. Phys. J. **C73**, 2678 (2013), [arXiv:1309.5736].

Downloaded from https://academic.oup.com/ptep/article/2022/8/083C01/6651666 by KIT Library user on 27 September 2022

66. *CPT* Invariance Tests in Neutral Kaon Decay

Revised August 2021 by M. Antonelli (INFN, Frascati), G. D'Ambrosio (INFN, Napoli) and M.S. Sozzi (Pisa U.).

CPT theorem is based on three assumptions: quantum field theory, locality, and Lorentz invariance, and thus it is a fundamental probe of our basic understanding of particle physics. Strangeness oscillation in $K^0-\overline{K}^0$ system, described by the equation

$$i\frac{d}{dt}\begin{bmatrix}K^0\\ \overline{K}^0\end{bmatrix} = [M - i\Gamma/2]\begin{bmatrix}K^0\\ \overline{K}^0\end{bmatrix} ,$$

where M and Γ are hermitian matrices (see PDG review [1], references [2,3], and KLOE paper [4] for notations and previous literature), allows a very accurate test of CPT symmetry; indeed since CPT requires $M_{11} = M_{22}$ and $\Gamma_{11} = \Gamma_{22}$, the mass and width eigenstates, $K_{S,L}$, have a CPT-violating piece, δ, in addition to the usual CPT-conserving parameter ϵ:

$$K_{S,L} = \frac{1}{\sqrt{2\left(1+|\epsilon_{S,L}|^2\right)}}\left[\left(1+\epsilon_{S,L}\right)K^0 \pm \left(1-\epsilon_{S,L}\right)\overline{K}^0\right]$$

$$\epsilon_{S,L} = \frac{-i\Im\left(M_{12}\right) - \frac{1}{2}\Im\left(\Gamma_{12}\right) \mp \frac{1}{2}\left[M_{11} - M_{22} - \frac{i}{2}\left(\Gamma_{11}-\Gamma_{22}\right)\right]}{m_L - m_S + i(\Gamma_S - \Gamma_L)/2}$$

$$\equiv \epsilon \pm \delta. \tag{66.1}$$

Using the phase convention $\Im(\Gamma_{12}) = 0$, we determine the phase of ϵ to be $\varphi_{SW} \equiv \arctan\frac{2(m_L-m_S)}{\Gamma_S-\Gamma_L}$. Imposing unitarity to an arbitrary combination of K^0 and $\overline{K}^0$ wave functions, we obtain the Bell-Steinberger relation [5] connecting CP and CPT violation in the mass matrix to CP and CPT violation in the decay; in fact, neglecting $\mathcal{O}(\epsilon)$ corrections to the coefficient of the CPT-violating parameter, δ, we can write [4]

$$\left[\frac{\Gamma_S+\Gamma_L}{\Gamma_S-\Gamma_L} + i\tan\phi_{\rm SW}\right]\left[\frac{\Re(\epsilon)}{1+|\epsilon|^2} - i\Im(\delta)\right] = \frac{1}{\Gamma_S-\Gamma_L}\sum_f A_L(f)A_S^*(f), \tag{66.2}$$

where $A_{L,S}(f) \equiv A(K_{L,S} \to f)$. We stress that this relation is phase-convention-independent. The advantage of the neutral kaon system is that only a few decay modes give significant contributions to the r.h.s. in Eq. (66.2); in fact, defining for the hadronic modes

$$\alpha_i \equiv \frac{1}{\Gamma_S}\langle\mathcal{A}_L(i)\mathcal{A}_S^*(i)\rangle = \eta_i\ \mathcal{B}(K_S \to i),$$
$$i = \pi^0\pi^0, \pi^+\pi^-(\gamma), 3\pi^0, \pi^0\pi^+\pi^-(\gamma), \tag{66.3}$$

the recent data from CPLEAR, KLOE, KTeV, and NA48 have led to the following determinations (the analysis described in Ref. [4] has been updated by using the recent measurements of K_L branching ratios from KTeV [6, 7], NA48 [8, 9], the results described in the CP violation in K_L decays minireview, and the KLOE result [10])

$$\begin{aligned}\alpha_{\pi^+\pi^-} &= ((1.121\pm0.010) + i(1.061\pm0.010))\times10^{-3} ,\\ \alpha_{\pi^0\pi^0} &= ((0.493\pm0.005) + i(0.471\pm0.005))\times10^{-3} ,\\ \alpha_{\pi^+\pi^-\pi^0} &= ((0\pm2) + i(0\pm2))\times10^{-6},\\ |\alpha_{\pi^0\pi^0\pi^0}| &< 1.5\times10^{-6} \quad \text{at 95\% CL} .\end{aligned} \tag{66.4}$$

The semileptonic contribution to the right-handed side of Eq. (66.2) requires the determination of several observables: we define [2, 3]

$$\begin{aligned}\mathcal{A}(K^0 \to \pi^- l^+\nu) &= \mathcal{A}_0(1-y) ,\\ \mathcal{A}(K^0 \to \pi^+ l^-\nu) &= \mathcal{A}_0^*(1+y^*)(x_+ - x_-)^* ,\\ \mathcal{A}(\overline{K}^0 \to \pi^+ l^-\nu) &= \mathcal{A}_0^*(1+y^*) ,\\ \mathcal{A}(\overline{K}^0 \to \pi^- l^+\nu) &= \mathcal{A}_0(1-y)(x_+ + x_-) ,\end{aligned} \tag{66.5}$$

where x_+ (x_-) describes the violation of the $\Delta S = \Delta Q$ rule in CPT-conserving (violating) decay amplitudes, and y parameterizes CPT violation for $\Delta S = \Delta Q$ transitions. Taking advantage of their tagged $K^0(\overline{K}^0)$ beams, CPLEAR has measured $\Im(x_+)$, $\Re(x_-)$, $\Im(\delta)$, and $\Re(\delta)$ [11]. These determinations have been improved in Ref. [4] by including the information $A_S - A_L = 4[\Re(\delta) + \Re(x_-)]$ (valid at first order in the small parameters), where $A_{L,S}$ are the K_L and K_S semileptonic charge asymmetries, respectively, from the PDG [12] and the new KLOE semileptonic measurement [13]. Here we are also including the T-violating asymmetry measurement from CPLEAR [14] with a finer binning than appearing in the published article.

Table 66.1: Values, errors, and correlation coefficients for $\Re(\delta)$, $\Im(\delta)$, $\Re(x_-)$, $\Im(x_+)$, and $A_S + A_L$ obtained from a combined fit, including KLOE [4, 13] and CPLEAR [14].

	value	Correlations coefficients				
$\Re(\delta)$	$(4.3\pm2.7)\ \times10^{-4}$	1				
$\Im(\delta)$	$(-0.9\pm0.6)\times10^{-2}$	−0.40	1			
$\Re(x_-)$	$(-0.22\pm0.10)\times10^{-2}$	−0.14	−0.30	1		
$\Im(x_+)$	$(0.06\pm0.19)\times10^{-2}$	−0.12	−0.02	0.34	1	
$A_S + A_L$	$(-0.23\pm0.38)\times10^{-2}$	−0.12	−0.29	0.94	0.18	1

The value $A_S + A_L$ in Table 66.1 can be directely included in the semileptonic contributions to the Bell Steinberger relations in Eq. (66.2)

$$\begin{aligned}&\sum_{\pi\ell\nu}\langle\mathcal{A}_L(\pi\ell\nu)\mathcal{A}_S^*(\pi\ell\nu)\rangle\\ &\quad= 2\Gamma(K_L \to \pi\ell\nu)(\Re(\epsilon) - \Re(y) - i(\Im(x_+) + \Im(\delta)))\\ &\quad= 2\Gamma(K_L \to \pi\ell\nu)((A_S + A_L)/4 - i(\Im(x_+) + \Im(\delta)))\end{aligned} \tag{66.6}$$

Defining

$$\alpha_{\pi\ell\nu} \equiv \frac{1}{\Gamma_S}\sum_{\pi\ell\nu}\langle\mathcal{A}_L(\pi\ell\nu)\mathcal{A}_S^*(\pi\ell\nu)\rangle + 2i\frac{\tau_{K_S}}{\tau_{K_L}}\mathcal{B}(K_L \to \pi\ell\nu)\Im(\delta) , \tag{66.7}$$

we find:

$$\alpha_{\pi\ell\nu} = ((-0.1\pm0.2) + i(-0.1\pm0.5))\times10^{-5} . \tag{66.8}$$

Table 66.2: Summary of results: values, errors, and correlation coefficients for $\Re(\epsilon)$, $\Im(\delta)$, $\Re(\delta)$, and $\Re(x_-)$.

	value	Correlations coefficients			
$\Re(\epsilon)$	$(161.2\pm0.5)\times10^{-5}$	+1			
$\Im(\delta)$	$(-0.3\pm1.4)\times10^{-5}$	+0.08	1		
$\Re(\delta)$	$(2.6\pm2.5)\times10^{-4}$	+0.00	−0.05	1	
$\Re(x_-)$	$(-2.7\pm1.0)\times10^{-3}$	+0.05	0.13	−0.30	1

The analysis of semileptonic decay asymmetries implicitly assumes Lepton Flavour Universality (LFU) of any effect violating CPT or $\Delta S = \Delta Q$, through the use of a single set of x, y parameters, consistently with the availability of experimental information on A_S for the electron mode only. The explicit LFU assumption in the input BR measurements has been lifted exploiting the measurement of $BR(K_S \to \pi\mu\nu)$ Ref. [15], with no effect on the numerical results.

Downloaded from https://academic.oup.com/ptep/article/2022/8/083C01/6651666 by KIT Library user on 27 September 2022

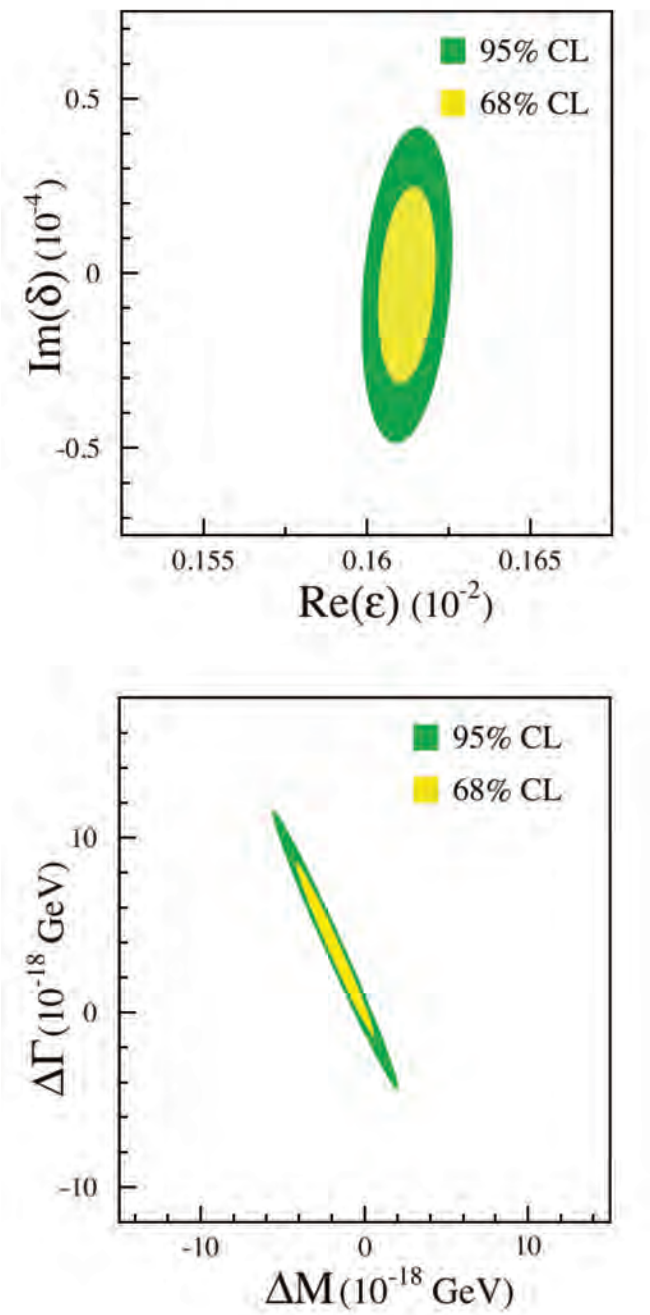

Figure 66.1: Top: allowed region at 68% and 95% C.L. in the $\Re(\epsilon)$, $\Im(\delta)$ plane. Bottom: allowed region at 68% and 95% C.L. in the $\Delta M, \Delta\Gamma$ plane.

Inserting the values of the α parameters into Eq. (66.2), we find

$$\Re(\epsilon) = (161.2 \pm 0.5) \times 10^{-5},$$
$$\Im(\delta) = (-0.3 \pm 1.4) \times 10^{-5}\,. \qquad (66.9)$$

The complete information on Eq. (66.9) is given in Table 66.2.

Now the agreement with CPT conservation, $\Im(\delta) = \Re(\delta) = \Re(x_-) = 0$, is at 18% C.L.

The allowed region in the $\Re(\epsilon) - \Im(\delta)$ plane at 68% CL and 95% C.L. is shown in the top panel of Fig. 66.1.

The process giving the largest contribution to the size of the allowed region is $K_L \to \pi^+\pi^-$, through the uncertainty on ϕ_{+-}.

The limits on $\Im(\delta)$ and $\Re(\delta)$ can be used to constrain the $K^0 - \overline{K}^0$ mass and width difference

$$\delta = \frac{i(m_{K^0} - m_{\overline{K}^0}) + \frac{1}{2}(\Gamma_{K^0} - \Gamma_{\overline{K}^0})}{\Gamma_S - \Gamma_L} \cos\phi_{SW} e^{i\phi_{SW}} [1 + \mathcal{O}(\epsilon)]\,.$$

The allowed region in the $\Delta M = (m_{K^0} - m_{\overline{K}^0}), \Delta\Gamma = (\Gamma_{K^0} - \Gamma_{\overline{K}^0})$ plane is shown in the bottom panel of Fig. 66.1. As a result, we improve on the previous limits (see for instance, P. Bloch in Ref. [12]) and in the limit $\Gamma_{K^0} - \Gamma_{\overline{K}^0} = 0$ we obtain

$$-4.0\times10^{-19}\ \text{GeV} < m_{K^0} - m_{\overline{K}^0} < 4.0\times10^{-19}\ \text{GeV} \quad \text{at 95 \% C.L}\,.$$

References

[1] See the "CP Violation in Meson Decays," in this *Review.*

[2] L. Maiani, "CP And CPT Violation in Neutral Kaon Decays," L. Maiani, G. Pancheri, and N. Paver, *The Second DAΦNE Physics Handbook,* Vol. 1,2.

[3] G. D'Ambrosio, G. Isidori and A. Pugliese, in "2nd DAΦNE Physics Handbook:63-96," 63–96 (1994), [hep-ph/9411389], URL `http://preprints.cern.ch/cgi-bin/setlink?base=preprint&categ=cern&id=th-7504-94`.

[4] G. D'Ambrosio and G. Isidori (KLOE), JHEP **12**, 011 (2006), [hep-ex/0610034].

[5] J. S. Bell and J. Steinberger, in "Wolfenstein, L. (eq.): CP violation, 42-57. (In Oxford International Symposium Conference on Elementary Particles) ," 195–208, 221–222 (1966), (See Book Index).

[6] T. Alexopoulos *et al.* (KTeV), Phys. Rev. **D70**, 092006 (2004), [hep-ex/0406002].

[7] E. Abouzaid *et al.* (KTeV), Phys. Rev. **D83**, 092001 (2011), [arXiv:1011.0127].

[8] A. Lai *et al.* (NA48), Phys. Lett. **B645**, 26 (2007), [hep-ex/0611052]; A. Lai *et al.* (NA48), Phys. Lett. **B602**, 41 (2004), [hep-ex/0410059].

[9] We thanks G. Isidori and M. Palutan for their contribution to the original analysis [4] performed with KLOE data.

[10] D. Babusci *et al.* (KLOE), Phys. Lett. **B723**, 54 (2013), [arXiv:1301.7623].

[11] A. Angelopoulos *et al.* (CPLEAR), Phys. Lett. **B444**, 52 (1998).

[12] W. M. Yao *et al.* (Particle Data Group), J. Phys. **G33**, 1 (2006).

[13] A. Anastasi *et al.* (KLOE-2), JHEP **09**, 021 (2018), [arXiv:1806.08654].

[14] P. Bloch, M. Fidecaro, private communication of the data in a finer binning format; A. Angelopoulos *et al.* (CPLEAR), Phys. Lett. **B444**, 43 (1998).

[15] D. Babusci *et al.* (KLOE-2), Phys. Lett. B **804**, 135378 (2020), [arXiv:1912.05990].

Downloaded from https://academic.oup.com/ptep/article/2022/8/083C01/6651666 by KIT Library user on 27 September 2022

67. V_{ud}, V_{us} the Cabibbo Angle, and CKM Unitarity

Revised August 2021 by E. Blucher (Chicago U.) and W.J. Marciano (BNL).

The Cabibbo-Kobayashi-Maskawa (CKM) [1, 2] three-generation quark mixing matrix written in terms of the Wolfenstein parameters (λ, A, ρ, η) [3] nicely illustrates the orthonormality constraint of unitarity, as well as the central role played by λ.

$$V_{\rm CKM} = \begin{pmatrix} V_{ud} & V_{us} & V_{ub} \\ V_{cd} & V_{cs} & V_{cb} \\ V_{td} & V_{ts} & V_{tb} \end{pmatrix} = \begin{pmatrix} 1-\lambda^2/2 & \lambda & A\lambda^3(\rho - i\eta) \\ -\lambda & 1-\lambda^2/2 & A\lambda^2 \\ A\lambda^3(1-\rho-i\eta) & -A\lambda^2 & 1 \end{pmatrix} + \mathcal{O}(\lambda^4)\,. \tag{67.1}$$

That cornerstone parameter is a carryover from the two-generation Cabibbo angle, $\lambda = \sin(\theta_{\rm Cabibbo}) = V_{us}$. Its value is an important component in tests of CKM unitarity.

Up until 2003, the precise value of λ was controversial, with kaon decays (specifically $K \to \pi e \nu$) branching fractions suggesting [4] $\lambda \simeq 0.220$, while indirect determinations via V_{ud} obtained from nuclear β-decays combined with unitarity preferred a somewhat larger $\lambda \simeq 0.225 - 0.230$. This difference implied a 2 - 2.5 sigma deviation from the first row unitarity requirement

$$|V_{ud}|^2 + |V_{us}|^2 + |V_{ub}|^2 = 1, \tag{67.2}$$

a possible hint [5, 6] of new physics effects. Below, we describe the current status of V_{ud} and V_{us}, and their implication for the unitarity test in Eq. (67.2). (Since $|V_{ub}|^2 \simeq 1.7\times10^{-5}$ is negligibly small, it is ignored in this discussion.) Eq. (67.2) is currently the most stringent test of unitarity in the CKM matrix. As we shall see, it is again showing signs of a possible 2 to 3 sigma inconsistency.

67.1 V_{ud}

Precise values of V_{ud} have been obtained from superallowed nuclear, neutron, and pion beta decays. Currently, the best determination of V_{ud} comes from analysis of a set of 15 precisely measured superallowed nuclear beta-decays [5,6] ($0^+ \to 0^+$ transitions). Measuring their half-lives, t, and Q values gives the decay rate factors, f, which lead to a precise determination of V_{ud} via [7–12]. Based on several decades of dedicated studies, Hardy and Towner recently updated the average [6]

$$|V_{ud}|^2 = 0.97154(22)(54)_{\rm NS}/(1+\Delta_{\rm R}^{\rm V}), \tag{67.3}$$

where Δ_R^V denotes the so-called inner or universal electroweak radiative corrections (RC) to superallowed nuclear beta decays. Note that an additional uncertainty $(54)_{\rm NS}$ from nuclear structure (NS) [13] has been recently included [6] in that master formula. A dispersion relation (DR) calculational approach [14] to quantum loop corrections, specifically the gamma-W box diagram, gives $\Delta_R^V = 0.02467(22)$. Because of its small uncertainty and more rigorous theoretical footing, we use that value below. A somewhat different approach [15] found $\Delta_R^V = 0.02426(32)$. These recent values are roughly consistent. Both are larger than the 2018 PDG value of 0.02361(38). Implications and possible nuclear physics modifications of those studies are still under scrutiny [13,16]. Nevertheless, currently the 15 most precisely measured superallowed transitions [12] lead to the DR based weighted average of

$$V_{ud} = 0.97373(11)_{\rm exp.,nucl.}(9)_{\rm RC}(27)_{\rm NS}\ \text{(superallowed)}\ , \tag{67.4}$$

which, assuming unitarity, corresponds to the relatively large $\lambda = 0.2277(13)$. This recent determination of V_{ud} has shifted significantly down compared to the 2018 PDG value of 0.97420(21). In addition, NS uncertainties are now the dominant contribution to the overall uncertainty. Taken at face value, along with current V_{us} determinations (see subsection 67.2), the reduced V_{ud} would seem to violate the first row unitarity requirement and thus suggest the presence of "new physics".

Measurements of the neutron lifetime, τ_n, and the ratio of axial-vector/vector couplings, $g_A \equiv G_A/G_V$, via neutron decay asymmetries combined with the inner radiative corrections can also be used to determine V_{ud} via the precise formula:

$$|V_{ud}|^2 = \frac{5024.7\ \text{s}}{\tau_n(1+3g_A^2)(1+\Delta_R^V)}, \tag{67.5}$$

where Δ_R^V represents the same inner electroweak radiative corrections [8, 9] as discussed above.

Using the current published world averages [17],

$$\begin{aligned} \tau_n^{\rm ave} &= 879.4(6)\ \text{s}\ \ \text{(1.6 PDG scale factor)} \\ g_A^{\rm ave} &= 1.2756(13),\ \text{(2.6 PDG scale factor)} \end{aligned} \tag{67.6}$$

leads to

$$|V_{ud}| = 0.9737(3)_{\tau_n}(8)_{g_A}(1)_{\rm RC}, \tag{67.7}$$

for an inner radiative correction of 0.02467(22), while for 0.02426(32) it increases to 0.9739(9). Both central values are similar to the superallowed nuclear beta decay result reported above. Reconciliation with CKM unitarity suggests a shorter neutron lifetime near 878.5 s or a smaller g_A. We note that the most precise recent neutron lifetime update reported [18], $\tau_n = 877.75(34)$ s, has an uncertainty about half as big as the average given in Eq. 67.6. It corresponds to $|V_{ud}| = 0.9746(8)$, a value more in keeping with unitarity expectations; but too large an uncertainty from g_A to be meaningful. Future neutron studies [19] are expected to resolve any current inconsistencies and further reduce the uncertainties in g_A and τ_n making them a potentially better way to determine V_{ud} without the nuclear physics uncertainties.

The PIBETA experiment at PSI measured the very small ($\mathcal{O}(10^{-8})$) branching ratio for $\pi^+ \to \pi^o e^+ \nu_e$ with about $\pm 0.6\%$ precision. Its result gives [20]

$$|V_{ud}| = 0.9739(27)\left[\frac{BR(\pi^+ \to e^+\nu_e(\gamma))}{1.2325\times10^{-4}}\right]^{\frac{1}{2}}, \tag{67.8}$$

which is normalized using the very precisely measured $BR(\pi^+ \to e^+\nu_e(\gamma)) = 1.2325(23)\times10^{-4}$ [7], rather than the theoretical branching ratio of $1.2350(2)\times10^{-4}$, which if used, would increase $|V_{ud}|$ to 0.9749(27). Theoretical uncertainties in pion beta decay are very small [21], leaving open more than an order of magnitude improvement of its experimental branching ratio before theory uncertainties become a problem. Although challenging, improved measurements of pion beta decay currently under discussion would allow this decay mode to compete with superallowed beta decays and future neutron decay efforts for the most precise direct $|V_{ud}|$ determination.

67.2 V_{us}

$|V_{us}|$ may be directly obtained from kaon decays, hyperon decays, and tau decays. Early determinations most often used $K\ell3$ decays:

$$\Gamma_{K\ell3} = \frac{G_F^2 M_K^5}{192\pi^3} S_{EW}(1+\delta_K^\ell+\delta_{SU2})C^2\,|V_{us}|^2\, f_+^2(0) I_K^\ell. \tag{67.9}$$

Here, ℓ refers to either e or μ, G_F is the Fermi constant, M_K is the kaon mass, S_{EW} is the short-distance radiative correction, δ_K^ℓ is the mode-dependent long-distance radiative correction, $f_+(0)$ is the calculated form factor at zero momentum transfer for the $\ell\nu$ system, and I_K^ℓ is the phase-space integral, which depends on measured semileptonic form factors. For charged kaon decays, δ_{SU2} is the deviation from one of the ratio of $f_+(0)$ for the charged to neutral kaon decay; it is zero for the neutral kaon. C^2 is 1 (1/2) for neutral (charged) kaon decays. Most early determinations of $|V_{us}|$ were based solely on $K \to \pi e \nu$ decays; $K \to \pi\mu\nu$ decays were not used because of large uncertainties in I_K^μ. The experimental measurements are the semileptonic decay widths (based on the semileptonic branching fractions and lifetime) and form factors (allowing calculation of the phase space integrals). Theory is needed for S_{EW}, δ_K^ℓ, δ_{SU2}, and $f_+(0)$.

Downloaded from https://academic.oup.com/ptep/article/2022/8/083C01/6651666 by KIT Library user on 27 September 2022

Many measurements during the last 20 years have resulted in a shift in $|V_{us}|$. Most importantly, the $K \to \pi e \nu$ branching fractions are significantly different than much earlier PDG averages, probably as a result of inadequate treatment of radiation in older experiments. This effect was first observed by BNL E865 [22] in the charged kaon system and then by KTeV [23,24] in the neutral kaon system; subsequent measurements were made by KLOE [25–28], NA48 [29–31], and ISTRA+ [32]. Current averages (*e.g.*, by the PDG [33] or Flavianet [34]) of the semileptonic branching fractions are based only on recent, high-statistics experiments where the treatment of radiation is clear. In addition to measurements of branching fractions, new measurements of lifetimes [35] and form factors [36–40], have resulted in improved precision for all of the experimental inputs to $|V_{us}|$. Precise measurements of form factors for $K_{\mu 3}$ decay make it possible to use both semileptonic decay modes to extract V_{us}.

Following the analysis of Moulson [41] and the Flavianet group [34, 42], along with recent improvements in the QED radiative corrections [43], one finds [44], after including the isospin violating effect, δ_{SU2} , the values of $|V_{us}|f_+(0)$ in Table 67.1. The average of these measurements, including correlation effects [44] gives

$$f_+(0)|V_{us}| = 0.21635(38)(3) \tag{67.10}$$

where the errors correspond to Kaon experimental parameters and radiative corrections respectively.

Lattice QCD calculations of $f_+(0)$ have been carried out for 2, 2+1, and 2+1+1 quark flavors and range from about 0.96 to 0.97. Here, we illustrate recent FLAG (2020) updated averages [45] for 2+1 and 2+1+1 flavors:

$$\begin{aligned} f_+(0) &= 0.9677(27) \quad N_f = 2+1 \\ f_+(0) &= 0.9698(17) \quad N_f = 2+1+1 \end{aligned} \tag{67.11}$$

One finds from Eq. (67.10) and Eq. (67.11),

$$\begin{aligned} |V_{us}| &= 0.2236(4)_{\rm exp+RC}(6)_{\rm lattice} \ (N_f = 2+1,\ K_{\ell 3} \text{ decays}) \\ &= 0.2231(4)_{\rm exp+RC}(4)_{\rm lattice} \ (N_f = 2+1+1,\ K_{\ell 3} \text{ decays}) \end{aligned} \tag{67.12}$$

Table 67.1: $|V_{us}|f_+(0)$ from $K\ell 3$, based on ref. [44]

Decay Mode	$\lvert V_{us}\rvert f_+(0)$
$K^\pm e3$	0.21714 ± 0.00091
$K^\pm \mu 3$	0.21703 ± 0.00114
$K_L e3$	0.21617 ± 0.00047
$K_L \mu 3$	0.21664 ± 0.00058
$K_S e3$	0.21530 ± 0.00122
$K_S \mu 3$	0.21265 ± 0.00467
Average (including correlation effects [44])	0.21635 ± 0.00038

A value of V_{us} can also be obtained from a comparison of the radiative inclusive decay rates for $K \to \mu\nu(\gamma)$ and $\pi \to \mu\nu(\gamma)$ combined with a lattice gauge theory calculation of f_{K^+}/f_{π^+} via

$$\frac{|V_{us}|f_{K^+}}{|V_{ud}|f_{\pi^+}} = 0.23871(20) \left[\frac{\Gamma(K \to \mu\nu(\gamma))}{\Gamma(\pi \to \mu\nu(\gamma))}\right]^{\frac{1}{2}} \tag{67.13}$$

with the small error coming from electroweak radiative corrections [46–48]; these corrections were confirmed by direct lattice calculation of the kaon and pion leptonic decay rates [47,48]. Employing

$$\frac{\Gamma(K \to \mu\nu(\gamma))}{\Gamma(\pi \to \mu\nu(\gamma))} = 1.3367(28), \tag{67.14}$$

which includes $\Gamma(K \to \mu\nu(\gamma)) = 5.134(11) \times 10^7 s^{-1}$ [41,49], leads to

$$\frac{|V_{us}|f_{K^+}}{|V_{ud}|f_{\pi^+}} = 0.27600(37). \tag{67.15}$$

Employing the FLAG [45] lattice QCD averages for the isospin broken decay constants

$$\begin{aligned} \frac{f_{K^+}}{f_{\pi^+}} &= 1.1917(37) \qquad N_f = 2+1 \\ &= 1.1932(21) \quad N_f = 2+1+1. \end{aligned} \tag{67.16}$$

along with the value of $|V_{ud}|$ in Eq. (67.4) leads to

$$\begin{aligned} |V_{us}| &= 0.2255(8) \ (N_f = 2+1,\ K_{\mu 2} \text{ decays}) \\ &= 0.2252(5) \ (N_f = 2+1+1,\ K_{\mu 2} \text{ decays}). \end{aligned} \tag{67.17}$$

Together, weighted averages of the $K\ell 3$ (Eq. (67.12)) and $K\mu 2$ (Eq. (67.17)) values give similar results for $N_f = 2{+}1$ and 2+1+1 flavors:

$$\begin{aligned} |V_{us}| &= 0.2244(5) \quad N_f = 2+1 \\ |V_{us}| &= 0.2243(4) \quad N_f = 2+1+1. \end{aligned} \tag{67.18}$$

Note that the differences between $K\ell 3$ and $K\mu 2$ values for V_{us} differ by 2 and 3 sigma, respectively, for $N_f = 2{+}1$ and $2+1+1$ flavors. One should therefore scale the uncertainties in Eq. (67.18) accordingly. For that reason, we allow for a scale factor of 2.7 for both 2+1 and 2+1+1 flavors and average the two values. That approximate procedure leads to $|V_{us}| = 0.2243(8)$ which we use when we consider the first row test of CKM unitarity.

It should be mentioned that hyperon decay fits suggest [50]

$$|V_{us}| = 0.2250(27) \text{ (Hyperon Decays)} \tag{67.19}$$

modulo SU(3) breaking effects that could shift that value up or down. We note that a representative effort [51] that incorporates SU(3) breaking found $V_{us} = 0.226(5)$. Strangeness changing tau decays, averaging both inclusive and exclusive measurements, give [52]

$$|V_{us}| = 0.2221(13) \text{ (Tau Decays)} , \tag{67.20}$$

which differs by about 2 sigma from the kaon determination discussed above, and would, if combined with V_{ud} from super-allowed beta decays, lead to a 4 sigma deviation from unitarity. This discrepancy results mainly from the inclusive tau decay results that rely on Finite Energy Sum Rule techniques and assumptions, as well as experimental uncertainties. Recent investigation of that approach suggests a larger value for V_{us}, which is more in accord with other determinations [53].

Employing the values of V_{ud} and V_{us} with an error scale factor of 2 from Eq. (67.4) and the average obtained after rescaling the errors from Eq. (67.18), respectively, leads to the unitarity consistency check

$$|V_{ud}|^2 + |V_{us}|^2 + |V_{ub}|^2 = 0.9985(6)(4). \tag{67.21}$$

where the first error is the uncertainty from $|V_{ud}|^2$ and the second error is the uncertainty from the average $|V_{us}|^2$ from $N_f = 2{+}1{+}1$. and $N_f = 2+1$. One finds about an overall 2 sigma deviation from unitarity. (The deviation increases to 3 sigma if nuclear structure uncertainties are ignored.) That deviation could be due a problem with $|V_{ud}|$ theory (RC or NS), the lattice determination of $f_+(0)$ or new physics.

67.3 CKM Unitarity Constraints

The current 2 sigma experimental disagreement with unitarity, $|V_{ud}|^2 + |V_{us}|^2 + |V_{ub}|^2 = 0.9985(7)$, still provides strong confirmation of Standard Model radiative corrections (which range between 3-4% depending on the nucleus used) at a high significance level [54]. In addition, it implies constraints on "New Physics" effects at both the tree and quantum loop levels. Those effects could be in the form of contributions to nuclear beta decays, K decays and/or muon decays, with the last of these providing normalization via the muon lifetime [55], which is used to obtain the Fermi constant, $G_\mu = 1.1663787(6) \times 10^{-5}\text{GeV}^{-2}$.

In the following examples, we illustrate the implications of CKM unitarity for (1) exotic muon decays [56] (beyond ordinary muon decay $\mu^+ \to e^+\nu_e\bar{\nu}_\mu$) and (2) new heavy quark mixing V_{uD} [57]. Other examples in the literature [58, 59] include Z_χ boson quantum loop effects, supersymmetry, leptoquarks, compositeness etc.

Downloaded from https://academic.oup.com/ptep/article/2022/8/083C01/6651666 by KIT Library user on 27 September 2022

67.3.1 *Exotic Muon Decays*

If additional lepton flavor violating decays such as $\mu^+ \to e^+\bar{\nu}_e\nu_\mu$ (wrong neutrinos) occur, they would cause confusion in searches for neutrino oscillations at, for example, muon storage rings/neutrino factories or other neutrino sources from muon decays. Calling the rate for all such decays Γ(exotic μ decays), they should be subtracted before the extraction of G_μ and normalization of the CKM matrix. Since that is not done and unitarity works, one has (at one-sided 95% CL)

$$|V_{ud}|^2 + |V_{us}|^2 + |V_{ub}|^2 = 1 - BR(\text{exotic } \mu \text{ decays}) \geq 0.9975 \tag{67.22}$$

or

$$BR(\text{exotic } \mu \text{ decays}) \leq 0.0025 \ . \tag{67.23}$$

This bound is a factor of 10 better than the direct experimental bound on $\mu^+ \to e^+\bar{\nu}_e\nu_\mu$.

67.3.2 *New Heavy Quark Mixing*

Heavy D quarks naturally occur in fourth quark generation models and some heavy quark "new physics" scenarios such as E_6 grand unification. Their mixing with ordinary quarks gives rise to V_{uD}, which is constrained by unitarity (one sided 95% CL)

$$|V_{ud}|^2 + |V_{us}|^2 + |V_{ub}|^2 = 1 - |V_{uD}|^2 \geq 0.9975$$
$$|V_{uD}| \leq 0.05 \ . \tag{67.24}$$

A similar constraint applies to heavy neutrino mixing and the couplings $V_{\mu N}$ and V_{eN}.

References

[1] N. Cabibbo, Phys. Rev. Lett. **10**, 531 (1963).

[2] M. Kobayashi and T. Maskawa, Prog. Theor. Phys. **49**, 652 (1973).

[3] L. Wolfenstein, Phys. Rev. Lett. **51**, 1945 (1983).

[4] S. Eidelman *et al.* (Particle Data Group), Phys. Lett. B **592**, 1-4, 1 (2004).

[5] I. Towner and J. Hardy, Rept. Prog. Phys. **73**, 046301 (2010).

[6] J. C. Hardy and I. S. Towner, Phys. Rev. C **102**, 4, 045501 (2020).

[7] W. J. Marciano and A. Sirlin, Phys. Rev. Lett. **71**, 3629 (1993).

[8] A. Czarnecki, W. J. Marciano and A. Sirlin, Phys. Rev. D **70**, 093006 (2004), [hep-ph/0406324].

[9] W. J. Marciano and A. Sirlin, Phys. Rev. Lett. **96**, 032002 (2006), [hep-ph/0510099].

[10] I. Towner and J. Hardy, Phys. Rev. C **77**, 025501 (2008), [arXiv:0710.3181].

[11] J. Hardy and I. Towner, Phys. Rev. C **79**, 055502 (2009), [arXiv:0812.1202].

[12] J. Hardy and I. Towner, Phys. Rev. C **91**, 2, 025501 (2015), [arXiv:1411.5987].

[13] M. Gorchtein, Phys. Rev. Lett. **123**, 4, 042503 (2019), [arXiv:1812.04229].

[14] C.-Y. Seng *et al.*, Phys. Rev. Lett. **121**, 24, 241804 (2018), [arXiv:1807.10197].

[15] A. Czarnecki, W. J. Marciano and A. Sirlin, Phys. Rev. D **100**, 7, 073008 (2019), [arXiv:1907.06737].

[16] C. Y. Seng, M. Gorchtein and M. J. Ramsey-Musolf, Phys. Rev. D **100**, 1, 013001 (2019), [arXiv:1812.03352].

[17] P. A. Zyla *et al.* (Particle Data Group), PTEP **2020**, 8, 083C01 (2020).

[18] F. M. Gonzalez *et al.* (UCNτ) (2021), [arXiv:2106.10375].

[19] H. Abele, Prog. Part. Nucl. Phys. **60**, 1 (2008).

[20] D. Pocanic *et al.*, Phys. Rev. Lett. **93**, 181803 (2004), [hep-ex/0312030]; A. Czarnecki, W. J. Marciano and A. Sirlin, Phys. Rev. D **101**, 9, 091301 (2020), [arXiv:1911.04685].

[21] X. Feng *et al.*, Phys. Rev. Lett. **124**, 19, 192002 (2020), [arXiv:2003.09798].

[22] A. Sher *et al.*, Phys. Rev. Lett. **91**, 261802 (2003), [hep-ex/0305042].

[23] T. Alexopoulos *et al.* (KTeV), Phys. Rev. Lett. **93**, 181802 (2004), [hep-ex/0406001].

[24] T. Alexopoulos *et al.* (KTeV), Phys. Rev. D **70**, 092006 (2004), [hep-ex/0406002].

[25] F. Ambrosino *et al.* (KLOE), Phys. Lett. B **632**, 43 (2006), [hep-ex/0508027].

[26] F. Ambrosino *et al.* (KLOE), Phys. Lett. B **638**, 140 (2006), [hep-ex/0603041].

[27] F. Ambrosino *et al.* (KLOE), Phys. Lett. B **636**, 173 (2006), [hep-ex/0601026].

[28] B. Sciascia (KLOE), PoS **HEP2005**, 287 (2006), [hep-ex/0510028].

[29] A. Lai *et al.* (NA48), Phys. Lett. B **602**, 41 (2004), [hep-ex/0410059].

[30] A. Lai *et al.* (NA48), Phys. Lett. B **645**, 26 (2007), [hep-ex/0611052].

[31] J. Batley *et al.* (NA48/2), Eur. Phys. J. C **50**, 329 (2007), [Erratum: Eur.Phys.J.C 52, 1021–1023 (2007)], [hep-ex/0702015].

[32] V. Romanovsky *et al.* (2007), [arXiv:0704.2052].

[33] K. Olive *et al.* (Particle Data Group), Chin. Phys. C **38**, 090001 (2014).

[34] M. Antonelli *et al.* (FlaviaNet Working Group on Kaon Decays), Eur. Phys. J. C **69**, 399 (2010), [arXiv:1005.2323]; For a detailed review, see; M. Antonelli *et al.*, Phys. Rept. **494**, 197 (2010), [arXiv:0907.5386].

[35] F. Ambrosino *et al.* (KLOE), Phys. Lett. B **626**, 15 (2005), [hep-ex/0507088].

[36] T. Alexopoulos *et al.* (KTeV), Phys. Rev. D **70**, 092007 (2004), [hep-ex/0406003].

[37] E. Abouzaid *et al.* (KTeV), Phys. Rev. D **74**, 097101 (2006), [hep-ex/0608058].

[38] F. Ambrosino *et al.* (KLOE), Phys. Lett. B **636**, 166 (2006), [hep-ex/0601038].

[39] A. Lai *et al.* (NA48), Phys. Lett. B **604**, 1 (2004), [hep-ex/0410065].

[40] O. Yushchenko *et al.*, Phys. Lett. B **589**, 111 (2004), [hep-ex/0404030].

[41] M. Moulson, PoS **CKM2016**, 033 (2017), [arXiv:1704.04104].

[42] E. Passemar, talk at CKM2018, `https://zenodo.org/record/2565480`.

[43] C.-Y. Seng *et al.* (2021), [arXiv:2103.04843].

[44] C.-Y. Seng *et al.* (2021), [arXiv:2107.14708].

[45] S. Aoki *et al.* (Flavour Lattice Averaging Group), Eur. Phys. J. C **80**, 2, 113 (2020), [arXiv:1902.08191]; A. Bazavov *et al.*, Phys. Rev. Lett. **112**, 11, 112001 (2014), [arXiv:1312.1228]; N. Carrasco *et al.*, Phys. Rev. D **93**, 11, 114512 (2016), [arXiv:1602.04113]; A. Bazavov *et al.*, Phys. Rev. D **87**, 073012 (2013), [arXiv:1212.4993]; P. A. Boyle *et al.* (RBC/UKQCD), JHEP **06**, 164 (2015), [arXiv:1504.01692]; A. Bazavov *et al.*, Phys. Rev. D **98**, 7, 074512 (2018), [arXiv:1712.09262]; T. Blum *et al.* (RBC, UKQCD), Phys. Rev. D **93**, 7, 074505 (2016), [arXiv:1411.7017]; R. Dowdall *et al.*, Phys. Rev. D **88**, 074504 (2013), [arXiv:1303.1670]; N. Carrasco *et al.*, Phys. Rev. D **91**, 5, 054507 (2015), [arXiv:1411.7908]; E. Follana *et al.* (HPQCD, UKQCD), Phys. Rev. Lett. **100**, 062002 (2008), [arXiv:0706.1726]; A. Bazavov *et al.* (MILC), PoS **LATTICE2010**, 074 (2010), [arXiv:1012.0868]; S. Durr *et al.*, Phys. Rev. D **81**, 054507 (2010), [arXiv:1001.4692]; S. Dürr *et al.*, Phys. Rev. D **95**, 5, 054513 (2017), [arXiv:1601.05998]; V. Bornyakov *et al.* (QCDSF), Phys. Lett. B **767**, 366 (2017), [arXiv:1612.04798].

Downloaded from https://academic.oup.com/ptep/article/2022/8/083C01/6651666 by KIT Library user on 27 September 2022

[46] V. Cirigliano and H. Neufeld, Phys. Lett. B **700**, 7 (2011), [arXiv:1102.0563]; W. J. Marciano, Phys. Rev. Lett. **93**, 231803 (2004), [hep-ph/0402299].

[47] D. Giusti *et al.*, Phys. Rev. Lett. **120**, 7, 072001 (2018), [arXiv:1711.06537].

[48] M. Di Carlo *et al.*, Phys. Rev. D **100**, 3, 034514 (2019), [arXiv:1904.08731].

[49] D. Babusci *et al.* (KLOE KLOE-2), Phys. Lett. B **738**, 128 (2014), [arXiv:1407.2028].

[50] N. Cabibbo, E. C. Swallow and R. Winston, Phys. Rev. Lett. **92**, 251803 (2004), [hep-ph/0307214].

[51] V. Mateu and A. Pich, JHEP **10**, 041 (2005), [hep-ph/0509045].

[52] Y. S. Amhis *et al.* (HFLAV) (2019), [arXiv:1909.12524].

[53] R. J. Hudspith *et al.*, Phys. Lett. B **781**, 206 (2018), [arXiv:1702.01767]; P. Boyle *et al.* (RBC, UKQCD), Phys. Rev. Lett. **121**, 20, 202003 (2018), [arXiv:1803.07228].

[54] A. Sirlin, Rev. Mod. Phys. **50**, 573 (1978), [Erratum: Rev.Mod.Phys. 50, 905 (1978)].

[55] D. Webber *et al.* (MuLan), Phys. Rev. Lett. **106**, 041803 (2011), [arXiv:1010.0991].

[56] K. Babu and S. Pakvasa (2002), [hep-ph/0204236].

[57] W. Marciano and A. Sirlin, Phys. Rev. Lett. **56**, 22 (1986); P. Langacker and D. London, Phys. Rev. D **38**, 886 (1988).

[58] W. Marciano and A. Sirlin, Phys. Rev. D **35**, 1672 (1987).

[59] R. Barbieri *et al.*, Phys. Lett. B **156**, 348 (1985); K. Hagiwara, S. Matsumoto and Y. Yamada, Phys. Rev. Lett. **75**, 3605 (1995), [hep-ph/9507419]; A. Kurylov and M. Ramsey-Musolf, Phys. Rev. Lett. **88**, 071804 (2002), [hep-ph/0109222]; S. Bauman, J. Erler and M. Ramsey-Musolf, Phys. Rev. D **87**, 3, 035012 (2013), [arXiv:1204.0035].

Downloaded from https://academic.oup.com/ptep/article/2022/8/083C01/6651666 by KIT Library user on 27 September 2022

68. CP Violation in K_L^0 Decays

Revised August 2021 by C.-J. Lin (LBNL).

The symmetries C (particle-antiparticle interchange) and P (space inversion) hold for strong and electromagnetic interactions. After the discovery of large C and P violation in the weak interactions, it appeared that the product CP was a good symmetry. In 1964 CP violation was observed in K^0 decays at a level given by the parameter $\epsilon \approx 2.3 \times 10^{-3}$.

A unified treatment of CP violation in K, D, B, and B_s mesons is given in "CP Violation in Meson Decays" by D. Kirkby and Y. Nir in this *Review*. A more detailed review including a thorough discussion of the experimental techniques used to determine CP violation parameters is given in a book by K. Kleinknecht [1]. Here we give a concise summary of the formalism needed to define the parameters of CP violation in K_L decays, and a description of our fits for the best values of these parameters.

68.1 Formalism for CP violation in Kaon decay

CP violation has been observed in the semi-leptonic decays $K_L^0 \to \pi^\mp \ell^\pm \nu$, and in the nonleptonic decay $K_L^0 \to 2\pi$. The experimental numbers that have been measured are

$$A_L = \frac{\Gamma(K_L^0 \to \pi^- \ell^+ \nu) - \Gamma(K_L^0 \to \pi^+ \ell^- \nu)}{\Gamma(K_L^0 \to \pi^- \ell^+ \nu) + \Gamma(K_L^0 \to \pi^+ \ell^- \nu)} \tag{68.1a}$$

$$\eta_{+-} = A(K_L^0 \to \pi^+\pi^-)/A(K_S^0 \to \pi^+\pi^-) = |\eta_{+-}|\, e^{i\phi_{+-}} \tag{68.1b}$$

$$\eta_{00} = A(K_L^0 \to \pi^0\pi^0)/A(K_S^0 \to \pi^0\pi^0) = |\eta_{00}|\, e^{i\phi_{00}} \ . \tag{68.1c}$$

CP violation can occur either in the $K^0 - \overline{K}^0$ mixing or in the decay amplitudes. Assuming CPT invariance, the mass eigenstates of the K^0–$\overline{K}^0$ system can be written

$$|K_S\rangle = p|K^0\rangle + q|\overline{K}^0\rangle \ , \quad |K_L\rangle = p|K^0\rangle - q|\overline{K}^0\rangle \ . \tag{68.2}$$

If CP invariance held, we would have $q = p$ so that K_S would be CP-even and K_L CP-odd. (We define $|\overline{K}^0\rangle$ as $CP\ |K^0\rangle$). CP violation in K^0–$\overline{K}^0$ mixing is then given by the parameter $\widetilde{\epsilon}$ where

$$\frac{p}{q} = \frac{(1+\widetilde{\epsilon})}{(1-\widetilde{\epsilon})} \ . \tag{68.3}$$

CP violation can also occur in the decay amplitudes

$$A\Big(K^0 \to \pi\pi(I)\Big) = A_I e^{i\delta_I} \ , \quad A\Big(\overline{K}^0 \to \pi\pi(I)\Big) = A_I^* e^{i\delta_I} \ , \tag{68.4}$$

where I is the isospin of $\pi\pi$, δ_I is the final-state phase shift, and A_I would be real if CP invariance held. The CP-violating observables are usually expressed in terms of ϵ and ϵ' defined by

$$\eta_{+-} = \epsilon + \epsilon' \ , \quad \eta_{00} = \epsilon - 2\epsilon' \ . \tag{68.5a}$$

One can then show [2]

$$\epsilon = \widetilde{\epsilon} + i\ \Big(\mathrm{Im}\ A_0/\mathrm{Re}\ A_0\Big) \ , \tag{68.5b}$$

$$\sqrt{2}\epsilon' = ie^{i(\delta_2-\delta_0)}(\mathrm{Re}\,A_2/\mathrm{Re}\,A_0)\ \Big(\mathrm{Im}\,A_2/\mathrm{Re}\,A_2 - \mathrm{Im}\,A_0/\mathrm{Re}\,A_0\Big) \ , \tag{68.5c}$$

$$A_L = 2\mathrm{Re}\ \epsilon/(1+|\epsilon|^2) \approx 2\mathrm{Re}\ \epsilon \ . \tag{68.5d}$$

In Eq. (68.5a), small corrections [3] of order $\epsilon' \times \mathrm{Re}\ (A_2/A_0)$ are neglected, and Eq. (68.5d) assumes the $\Delta S = \Delta Q$ rule.

The quantities Im A_0, Im A_2, and Im $\widetilde{\epsilon}$ depend on the choice of phase convention, since one can change the phases of K^0 and $\overline{K}^0$ by a transformation of the strange quark state $|s\rangle \to |s\rangle\ e^{i\alpha}$; of course, observables are unchanged. It is possible by a choice of phase convention to set Im A_0 or Im A_2 or Im $\widetilde{\epsilon}$ to zero, but none of these is zero with the usual phase conventions in the Standard Model. The choice Im $A_0 = 0$ is called the Wu-Yang phase convention [4], in which case $\epsilon = \widetilde{\epsilon}$. The value of ϵ' is independent of phase convention, and a nonzero value demonstrates CP violation in the decay amplitudes, referred to as direct CP violation. The possibility that direct CP violation is essentially zero, and that CP violation occurs only in the mixing matrix, was referred to as the superweak theory [5].

By applying CPT invariance and unitarity the phase of ϵ is given approximately by

$$\phi_\epsilon \ \approx\ \tan^{-1}\frac{2(m_{K_L} - m_{K_S})}{\Gamma_{K_S} - \Gamma_{K_L}} \approx 43.52 \pm 0.05^\circ \ , \tag{68.6a}$$

while Eq. (68.5c) gives the phase of ϵ' to be

$$\phi_{\epsilon'} = \delta_2 - \delta_0 + \frac{\pi}{2} \approx 42.3 \pm 1.5^\circ \ , \tag{68.6b}$$

where the numerical value is based on an analysis of π–π scattering using chiral perturbation theory [6]. The approximation in Eq. (68.6a) depends on the assumption that direct CP violation is very small in all K^0 decays. This is expected to be good to a few tenths of a degree, as indicated by the small value of ϵ' and of η_{+-0} and η_{000}, the CP-violation parameters in the decays $K_S \to \pi^+\pi^-\pi^0$ [7], and $K_S \to \pi^0\pi^0\pi^0$ [8]. The relation in Eq. (68.6a) is exact in the superweak theory, so this is sometimes called the superweak-phase ϕ_{SW}. An important point for the analysis is that $\cos(\phi_{\epsilon'} - \phi_\epsilon) \simeq 1$. The consequence is that only two real quantities need be measured, the magnitude of ϵ and the value of (ϵ'/ϵ), including its sign. The measured quantity $|\eta_{00}/\eta_{+-}|^2$ is very close to unity so that we can write

$$|\eta_{00}/\eta_{+-}|^2 \approx 1 - 6\mathrm{Re}\ (\epsilon'/\epsilon) \approx 1 - 6\epsilon'/\epsilon \ , \tag{68.7a}$$

$$\mathrm{Re}(\epsilon'/\epsilon) \approx \frac{1}{3}(1 - |\eta_{00}/\eta_{+-}|) \ . \tag{68.7b}$$

From the experimental measurements in this edition of the *Review*, and the fits discussed in the next section, one finds

$$|\epsilon| = (2.228 \pm 0.011) \times 10^{-3}, \tag{68.8a}$$

$$\phi_\epsilon = (43.5 \pm 0.5)^\circ, \tag{68.8b}$$

$$\mathrm{Re}(\epsilon'/\epsilon) \approx \epsilon'/\epsilon = (1.66 \pm 0.23) \times 10^{-3}, \tag{68.8c}$$

$$\phi_{+-} = (43.4 \pm 0.5)^\circ, \tag{68.8d}$$

$$\phi_{00} - \phi_{+-} = (0.34 \pm 0.32)^\circ, \tag{68.8e}$$

$$A_L = (3.32 \pm 0.06) \times 10^{-3}. \tag{68.8f}$$

Direct CP violation, as indicated by ϵ'/ϵ, is expected in the Standard Model. However, the numerical value cannot be reliably predicted because of theoretical uncertainties [9]. The value of A_L agrees with Eq. (68.5d). The values of ϕ_{+-} and $\phi_{00} - \phi_{+-}$ are used to set limits on CPT violation [see "Tests of Conservation Laws"].

68.2 Fits for K_L^0 CP-violation parameters

In recent years, K_L^0 CP-violation experiments have improved our knowledge of CP-violation parameters,

and their consistency with the expectations of CPT invariance and unitarity. To determine the best values of the CP-violation parameters in $K_L^0 \to \pi^+\pi^-$ and $\pi^0\pi^0$ decay, we make two types of fits, one for the phases ϕ_{+-} and ϕ_{00} jointly with Δm and τ_S, and the other for the amplitudes $|\eta_{+-}|$ and $|\eta_{00}|$ jointly with the $K_L^0 \to \pi\pi$ branching fractions.

68.2.1 *Fits to ϕ_{+-}, ϕ_{00}, $\Delta\phi$, Δm, and τ_S data*

These are joint fits to the data on ϕ_{+-}, ϕ_{00}, the phase difference $\Delta\phi = \phi_{00} - \phi_{+-}$, the $K_L^0 - K_S^0$ mass difference Δm, and the K_S^0 mean life τ_S, including the effects of correlations.

Measurements of ϕ_{+-} and ϕ_{00} are highly correlated with Δm and τ_S. Some measurements of τ_S are correlated with Δm. The correlations are given in the footnotes of the ϕ_{+-} and ϕ_{00} sections of the K_L^0 Listings, and the τ_S section of the K_S^0 Listings.

In most cases, the correlations are quoted as 100%, with the value and error of ϕ_{+-} or ϕ_{00} given at a fixed value of Δm and τ_S, with additional terms specifying the dependence of the value on Δm and τ_S. These cases lead to diagonal bands in Figs. 68.1

Downloaded from https://academic.oup.com/ptep/article/2022/8/083C01/6651666 by KIT Library user on 27 September 2022

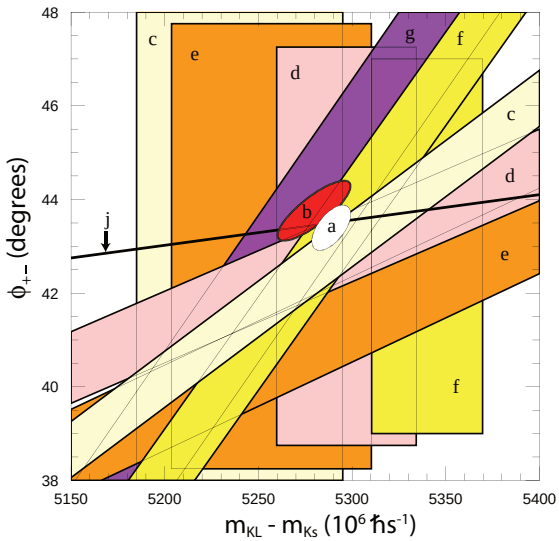

Figure 68.1: ϕ_{+-} vs Δm for experiments which do not assume CPT invariance. Δm measurements appear as vertical bands spanning $\Delta m \pm 1\sigma$, cut near the top and bottom to aid the eye. Most ϕ_{+-} measurements appear as diagonal bands spanning $\phi_{+-} \pm \sigma_\phi$. Data are labeled by letters: "b"–FNAL KTeV, "c"–CERN CPLEAR, "d"–FNAL E773, "e"–FNAL E731, "f"–CERN, "g"–CERN NA31, and are cited in Table 68.1. The narrow band "j" shows ϕ_{SW}. The ellipse "a" shows the $\chi^2 = 1$ contour of the fit result.

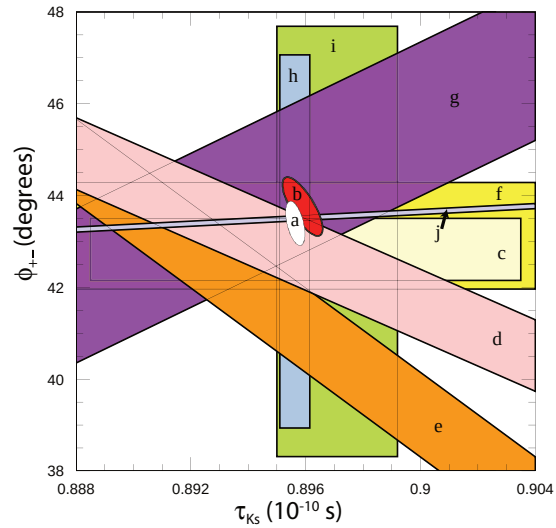

Figure 68.2: ϕ_{+-} vs τ_S. τ_S measurements appear as vertical bands spanning $\tau_S \pm 1\sigma$, some of which are cut near the top and bottom to aid the eye. Most ϕ_{+-} measurements appear as diagonal or horizontal bands spanning $\phi_{+-} \pm \sigma_\phi$. Data are labeled by letters: "b"–FNAL KTeV, "c"–CERN CPLEAR, "d"–FNAL E773, "e"–FNAL E731, "f"–CERN, "g"–CERN NA31, "h"–CERN NA48, "i"–CERN NA31, and are cited in Table 68.1. The narrow band "j" shows ϕ_{SW}. The ellipse "a" shows the fit result's $\chi^2 = 1$ contour.

and 68.2. The KTeV experiment [10] quotes its results as values of Δm, τ_S, ϕ_ϵ, $\mathrm{Re}(\epsilon'/\epsilon)$, and $\mathrm{Im}(\epsilon'/\epsilon)$ with correlations, leading to the ellipses labeled "b." The correlations for the KTeV measurements are given in the $\mathrm{Im}(\epsilon'/\epsilon)$ section of the K_L^0 Listings. For small $|\epsilon'/\epsilon|$, $\phi_{+-} \approx \phi_\epsilon + \mathrm{Im}(\epsilon'/\epsilon)$.

Table 68.1: References, Document ID's, and sources corresponding to the letter labels in the figures. The data are given in the ϕ_{+-} and Δm sections of the K_L Listings, and the τ_S section of the K_S Listings.

Label	Source	PDG Document ID	Ref.
a	This *Review*	OUR FIT	
b	FNAL KTeV	ABOUZAID 11	[10]
c	CERN CPLEAR	APOSTOLAKIS 99C	[11]
d	FNAL E773	SCHWINGENHEUER 95	[12]
e	FNAL E731	GIBBONS 93,93C	[13], [14]
f	CERN	GEWENIGER 74B,74C	[15], [16]
g	CERN NA31	CAROSI 90	[17]
h	CERN NA48	LAI 02C	[18]
i	CERN NA31	BERTANZA 97	[19]
j	This *Review*	SUPERWEAK 16	

The data on τ_S, Δm, and ϕ_{+-} shown in Figs. 68.1 and 68.2 are combined with data on ϕ_{00} and $\phi_{00} - \phi_{+-}$ in two fits, one without assuming CPT, and the other with this assumption. The results without assuming CPT are shown as ellipses labeled "a." These ellipses are seen to be in good agreement with the superweak phase

$$\phi_{SW} = \tan^{-1}\left(\frac{2\Delta m}{\Delta\Gamma}\right) = \tan^{-1}\left(\frac{2\Delta m \tau_S \tau_L}{\hbar(\tau_L - \tau_S)}\right) . \qquad (68.9)$$

In Figs. 68.1 and 68.2, ϕ_{SW} is shown as narrow bands labeled "j."

Table 68.2 column 2, "Fit w/o CPT," gives the resulting fitted parameters, while Table 68.3 gives the correlation matrix for this fit. The white ellipses labeled "a" in Figure 68.1 and 68.2 are the $\chi^2 = 1$ contours for this fit.

For experiments which have dependencies on unseen fit parameters, that is, parameters other than those shown on the x or y axis of the figure, their band positions are evaluated using the fit results and their band widths include the fitted uncertainty in the unseen parameters. This is also true for the ϕ_{SW} bands.

If CPT invariance and unitarity are assumed, then by Eq. (68.6a), the phase of ϵ is constrained to be approximately equal to

$$\begin{aligned}\phi_{SW} &= (43.50258 \pm 0.00021)^\circ + 54.1(\Delta m - 0.5289)^\circ \\ &\quad + 32.0(\tau_S - 0.89564)\end{aligned} \qquad (68.10)$$

where we have linearized the Δm and τ_S dependence of Eq. (68.9). The error ± 0.00021 is due to the uncertainty in τ_L. Here Δm has units $10^{10}\,\hbar\,\mathrm{s}^{-1}$ and τ_S has units 10^{-10} s.

If in addition we use the observation that $Re(\epsilon'/\epsilon) \ll 1$ and $cos(\phi_{\epsilon'} - \phi_\epsilon) \simeq 1$, as well as the numerical value of $\phi_{\epsilon'}$ given in Eq. (68.6b), then Eqs. 68.5a, which are sketched in Fig 68.3, lead to the constraint

$$\begin{aligned}\phi_{00} - \phi_{+-} &\approx -3\ \mathrm{Im}\left(\frac{\epsilon'}{\epsilon}\right) \\ &\approx -3\ \mathrm{Re}\left(\frac{\epsilon'}{\epsilon}\right)\tan(\phi_{\epsilon'} - \phi_\epsilon) \\ &\approx 0.006^\circ \pm 0.008^\circ\ ,\end{aligned} \qquad (68.11)$$

so that $\phi_{+-} \approx \phi_{00} \approx \phi_\epsilon \approx \phi_{SW}$.

In the fit assuming CPT, we constrain $\phi_\epsilon = \phi_{SW}$ using the linear expression in Eq. (68.10), and constrain $\phi_{00} - \phi_{+-}$ using Eq. (68.11). These constraints are inserted into the Listings with the Document ID of SUPERWEAK 16. Some additional data for which the authors assumed CPT are added to this fit or substitute for other less precise data for which the authors did not make this assumption. See the Listings for details.

The results of this fit are shown in Table 68.2, column 3, "Fit w/CPT," and the correlation matrix is shown in Table 68.4. The Δm precision is improved by the CPT assumption.

68.2.2 *Fits for ϵ'/ϵ, $|\eta_{+-}|$, $|\eta_{00}|$, and $B(K_L \to \pi\pi)$*

We list measurements of $|\eta_{+-}|$, $|\eta_{00}|$, $|\eta_{00}/\eta_{+-}|$, and ϵ'/ϵ. Independent information on $|\eta_{+-}|$ and $|\eta_{00}|$ can be obtained from

Downloaded from https://academic.oup.com/ptep/article/2022/8/083C01/6651666 by KIT Library user on 27 September 2022

Table 68.2: Fit results for ϕ_{+-}, Δm, τ_S, ϕ_{00}, $\Delta\phi = \phi_{00} - \phi_{+-}$, and ϕ_ϵ without and with the CPT assumption

Quantity(units)	Fit w/o CPT	Fit w/ CPT
$\phi_{+-}(^\circ)$	43.4 ± 0.5 (S=1.2)	43.51 ± 0.05 (S=1.2)
$\Delta m(10^{10}\hbar\,\mathrm{s}^{-1})$	0.5289 ± 0.0010	0.5293 ± 0.0009 (S=1.3)
$\tau_S\,(10^{-10}\mathrm{s})$	0.89564 ± 0.00033	0.8954 ± 0.0004 (S=1.1)
$\phi_{00}(^\circ)$	43.7 ± 0.6 (S=1.2)	43.52 ± 0.05 (S=1.3)
$\Delta\phi(^\circ)$	0.34 ± 0.32	0.006 ± 0.014 (S=1.7)
$\phi_\epsilon(^\circ)$	43.5 ± 0.5 (S=1.3)	43.52 ± 0.05 (S=1.2)
χ^2	16.4	20.0
# Deg. Free.	14	16

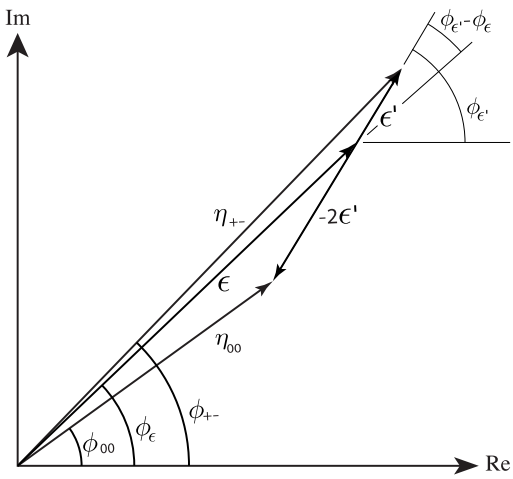

Figure 68.3: Sketch of Eqs. 68.5a. Not to scale

Table 68.3: Correlation matrix for the results of the fit without the CPT assumption

	ϕ_{+-}	Δm	τ_S	ϕ_{00}	$\Delta\phi$	ϕ_ϵ
ϕ_{+-}	1.000	0.596	-0.488	0.827	-0.040	0.976
Δm	0.596	1.000	-0.572	0.487	-0.035	0.580
τ_S	-0.488	-0.572	1.000	-0.423	-0.014	-0.484
ϕ_{00}	0.827	0.487	-0.423	1.000	0.529	0.929
$\Delta\phi$	-0.040	-0.035	-0.014	0.529	1.000	0.178
ϕ_ϵ	0.976	0.580	-0.484	0.929	0.178	1.000

Table 68.4: Correlation matrix for the results of the fit with the CPT assumption

	ϕ_{+-}	Δm	τ_S	ϕ_{00}	$\Delta\phi$	ϕ_ϵ
ϕ_{+-}	1.000	0.972	-0.311	0.957	-0.105	0.995
Δm	0.972	1.000	-0.509	0.958	-0.007	0.977
τ_S	-0.311	-0.509	1.000	-0.306	0.004	-0.312
ϕ_{00}	0.957	0.958	-0.306	1.000	0.189	0.981
$\Delta\phi$	-0.105	-0.007	0.004	0.189	1.000	-0.006
ϕ_ϵ	0.995	0.977	-0.312	0.981	-0.006	1.000

measurements of the K_L^0 and K_S^0 lifetimes (τ_L, τ_S), and branching ratios (B) to $\pi\pi$, using the relations

$$|\eta_{+-}| = \left[\frac{\mathrm{B}(K_L^0 \to \pi^+\pi^-)}{\tau_L}\,\frac{\tau_S}{\mathrm{B}(K_S^0 \to \pi^+\pi^-)}\right]^{1/2}, \quad (68.12a)$$

$$|\eta_{00}| = \left[\frac{\mathrm{B}(K_L^0 \to \pi^0\pi^0)}{\tau_L}\,\frac{\tau_S}{\mathrm{B}(K_S^0 \to \pi^0\pi^0)}\right]^{1/2}. \quad (68.12b)$$

For historical reasons, the branching ratio fits and the CP-violation fits are done separately, but we want to include the influence of $|\eta_{+-}|$, $|\eta_{00}|$, $|\eta_{00}/\eta_{+-}|$, and ϵ'/ϵ measurements on $\mathrm{B}(K_L^0 \to \pi^+\pi^-)$ and $\mathrm{B}(K_L^0 \to \pi^0\pi^0)$ and vice versa. We approximate a global fit to all of these measurements by first performing two independent fits: 1) BRFIT, a fit to the K_L^0 branching ratios, rates, and mean life, and 2) ETAFIT, a fit to the $|\eta_{+-}|$, $|\eta_{00}|$, $|\eta_{+-}/\eta_{00}|$, and ϵ'/ϵ measurements. The results from fit 1, along with the K_S^0 values from this edition, are used to compute values of $|\eta_{+-}|$ and $|\eta_{00}|$, which are included as measurements in the $|\eta_{00}|$ and $|\eta_{+-}|$ sections with a document ID of BRFIT 16. Thus, the fit values of $|\eta_{+-}|$ and $|\eta_{00}|$ given in this edition include both the direct measurements and the results from the branching ratio fit.

The process is reversed in order to include the direct $|\eta|$ measurements in the branching ratio fit. The results from fit 2 above (before including BRFIT 16 values) are used along with the K_L^0 and K_S^0 mean lives and the $K_S^0 \to \pi\pi$ branching fractions to compute the K_L^0 branching ratio $\Gamma(K_L^0 \to \pi^0\pi^0)/\Gamma(K_L^0 \to \pi^+\pi^-)$. This branching ratio value is included as a measurement in the branching ratio section with a document ID of ETAFIT 16. Thus, the K_L^0 branching ratio fit values in this edition include the results of the direct measurement of $|\eta_{00}/\eta_{+-}|$ and ϵ'/ϵ. Most individual measurements of $|\eta_{+-}|$ and $|\eta_{00}|$ enter our fits directly via the corresponding measurements of $\Gamma(K_L^0 \to \pi^+\pi^-)/\Gamma(\mathrm{total})$ and $\Gamma(K_L^0 \to \pi^0\pi^0)/\Gamma(\mathrm{total})$, and those that do not have too large errors to have any influence on the fitted values of these branching ratios. A more detailed discussion of these fits is given in the 1990 edition of this *Review* [20].

References

[1] K. Kleinknecht, *Uncovering CP violation: Experimental clarification in the neutral K meson and B meson*, volume 195, Spriger Verlag (2003).

[2] B. Winstein and L. Wolfenstein, Rev. Mod. Phys. **65**, 1113 (1993).

[3] M. S. Sozzi, Eur. Phys. J. **C36**, 37 (2004), [hep-ph/0401176].

[4] T. T. Wu and C.-N. Yang, Phys. Rev. Lett. **13**, 380 (1964).

[5] L. Wolfenstein, Phys. Rev. Lett. **13**, 562 (1964); L. Wolfenstein, Comments Nucl. Part. Phys. **21**, 5, 275 (1994).

[6] G. Colangelo, J. Gasser and H. Leutwyler, Nucl. Phys. **B603**, 125 (2001), [hep-ph/0103088].

[7] R. Adler *et al.* (CPLEAR), Phys. Lett. **B407**, 193 (1997); P. Bloch, *Proceedings of Workshop on K Physics* (Orsay 1996), ed. L. Iconomidou-Fayard, Edition Frontieres, Gif-sur-Yvette, France (1997) p. 307.

[8] A. Lai *et al.* (NA48), Phys. Lett. **B610**, 165 (2005), [hep-ex/0408053].

[9] G. Buchalla, A. J. Buras and M. E. Lautenbacher, Rev. Mod. Phys. **68**, 1125 (1996), [hep-ph/9512380]; S. Bosch *et al.*, Nucl. Phys. **B565**, 3 (2000), [hep-ph/9904408]; S. Bertolini, M. Fabbrichesi and J. O. Eeg, Rev. Mod. Phys. **72**, 65 (2000), [hep-ph/9802405].

[10] E. Abouzaid *et al.* (KTeV), Phys. Rev. **D83**, 092001 (2011), [arXiv:1011.0127].

[11] A. Apostolakis *et al.* (CPLEAR), Phys. Lett. **B458**, 545 (1999).

[12] B. Schwingenheuer *et al.*, Phys. Rev. Lett. **74**, 4376 (1995).

[13] L. K. Gibbons *et al.*, Phys. Rev. Lett. **70**, 1199 (1993).

[14] L.K. Gibbons, Thesis, RX-1487, Univ. of Chicago, 1993.

[15] C. Geweniger *et al.*, Phys. Lett. **48B**, 487 (1974).

[16] C. Geweniger *et al.*, Phys. Lett. **52B**, 108 (1974).

[17] R. Carosi *et al.* (NA31), Phys. Lett. **B237**, 303 (1990).

[18] A. Lai *et al.* (NA48), Phys. Lett. **B537**, 28 (2002), [hep-ex/0205008].

[19] L. Bertanza *et al.*, Z. Phys. **C73**, 629 (1997).

[20] J. J. Hernandez *et al.* (Particle Data Group), Phys. Lett. **B239**, 1 (1990), [Erratum: Phys. Lett.B253,524(1991)].

Downloaded from https://academic.oup.com/ptep/article/2022/8/083C01/6651666 by KIT Library user on 27 September 2022

69. Review of Multibody Charm Analyses

Revised August 2021 by D.M. Asner (BNL) and J. Rademacker (Bristol U.).

69.1 Overview

The study of multibody charm decays is a vibrant field, with many new experimental results with implications reaching beyond charm, vast and fast-increasing datasets, and new developments in theory and experimental technique. This review is structured as follows. Sec. 69.2 summarises key elements of the theory of multibody charm decays. Sec. 69.3 describes model-independent approaches for precision measurements of mixing and *CP* violation and the critical role of charm threshold data in this context. Sec. 69.4 reviews applications of the techniques described, and their results. In Sec. 69.5, we conclude.

69.2 Kinematics & Models

The differential decay rate to a point $\mathbf{s} = (s_1, \ldots, s_n)$ in n dimensional phase space can be expressed as

$$d\Gamma = |\mathcal{M}(\mathbf{s})|^2 \left| \frac{\partial^n \phi}{\partial(s_1 \ldots s_n)} \right| d^n s \tag{69.1}$$

where $|\partial^n \phi/\partial(s_1 \ldots s_n)|$ represents the density of states at $\mathbf{s}$, and $\mathcal{M}$ the matrix element for the decay at that point in phase space, which is $2, 5, 8, \ldots$ dimensional for D decays to $3, 4, 5, \ldots$ spinless particles. Additional parameters are required to fully describe decays involving particles with non-zero spin in the initial or final state.

For the important case of D decays to three pseudoscalars, the decay kinematics can be represented in a two-dimensional Dalitz plot [1]. This is usually parametrized in terms of $s_{12} \equiv (p_1 + p_2)^2$ and $s_{23} \equiv (p_2 + p_3)^2$, where p_1, p_2, and p_3 are the four-momenta of the final state particles. In terms of these variables, phase-space density is constant across the kinematically allowed region, so that any structure seen in the Dalitz plot is a direct consequence of the dynamics encoded in $|\mathcal{M}|^2$. Note that here, because the three-momenta of the decay products are confined to a plane, no parity violating kinematic observables can be constructed (unless they also violate rotational invariance). This is not the case for decays to four or more particles. These can therefore not be unambiguously described in terms of analogously-defined variables s_{ij}, s_{ijk}, which are parity-even. The use of parity-odd observables in four body decays is discussed below.

In the widely-used isobar approach, the matrix element $\mathcal{M}$ is modeled as a sum of interfering decay amplitudes, each proceeding through resonant two-body decays [2–6]. See Refs. [2,7,8] for a review of resonance phenomenology. In most analyses, each resonance is described by a relativistic Breit-Wigner [9] or Flatté [10] lineshape, and the model includes a non-resonant term with a constant phase and magnitude. This approach has well-known theoretical limitations, such as the violation of unitarity and analyticity, which can break the relationship between magnitude and phase across phase space. This motivates the use of more sophisticated descriptions, especially for broad, overlapping resonances (frequently found in S-wave components) where these limitations are particularly problematic. In charm analyses, these approaches have included the K-matrix approach [11] which respects two-body unitarity; the use of LASS scattering data [12]; dispersive methods [13–16]; multi-meson models using chiral Lagrangians [17–20] and methods based on chiral unitarity [21, 22]; QCD factorisation [23–26]; and quasi model-independent parametrizations which use generic lineshapes, with minimal theory input and many free parameters, for a subset of resonances [27–32]. An important example, with a rich resonance structure, is $D^0 \to K_S\pi^+\pi^-$, which is a key channel in Charge-Parity (*CP*) violation and charm-mixing analyses. The first analysis by CLEO [33] described the Dalitz plot with approximately 5000 signal events with 10 resonant components. This and analyses by Belle [34] and CDF [35] model the Dalitz plot as a sum of Breit Wigner and Flatté line shapes, and a non-resonant component. BaBar [36] and a more recent Belle analysis [37] on the other hand use a K-matrix description for the $\pi\pi$ S-wave based on [38] and input from LASS scattering data for the $K\pi$ S-wave, with no need to add a non-resonant component to describe the data. This approach is also followed in the latest analysis of this channel, published jointly by BaBar and Belle [39]. In total 18 resonant components, including four doubly Cabibbo suppressed ones, are required to describe the Dalitz plot with 1.1M $D^0 \to K_S\pi^+\pi^-$ events. Belle's and BaBar's data have been re-analyzed by [23] in a QCD factorization framework, using line-shape parametrizations for the S [40, 41] and P wave [14] contributions that preserve two-body unitarity and analyticity. The measurements give compatible results for the components they share.

The field of charm amplitude analyses remains very active. Publications since the last update of this review two years ago include Dalitz plot analyses of $D_s^+ \to K^+K^-\pi^+$, $K^+K_S\pi^0$, $K_S^0\pi^+\pi^0$, $\pi^+\pi^-\pi^+$, $D^0 \to K_S^0K^+K^-$ by BES III [31, 32, 42–44]; $D^0 \to K^-\pi^+\eta$ by Belle [45]; a re-analysis of BaBar's $D^0 \to K_SK^+K^-$ data in a factorisation approach [26] and of LHCb's $D^+ \to K^+K^-K^+$ data [46] in a chiral unitarity approach [22]; four-body amplitude analyses of $D_s^+ \to \pi^+\pi^+\pi^-\eta$, $K^-K^+\pi^+\pi^0$, $K_S^0K^-\pi^+\pi^+$ by BES III [31, 47–49] and of $D^0 \to K^+K^-\pi^+\pi^-$ by LHCb [50]; and the amplitude analysis of the charm baryon decay $\Xi_c^0 \to \Xi^0K^+K^-$ by Belle [51]. Noteworthy is the increasing sophistication of recent amplitude analyses, most of which go substantially beyond the isobar model with Breit Wigner and Flatté lineshapes. However, with the notable exceptions of [15, 16, 22, 46, 52], they remain within the isobar framework which describes the decay as a series of two-body processes, and ignores long-range hadronic effects such as re-scattering and does not respect three (or four)-body unitarity and analyticity.

Several groups work on improved models. Dispersive techniques, which respect three-body unitarity and analyticity, have been applied to regions of the $D^+ \to K^-\pi^+\pi^+$ and $D^+ \to K_S\pi^0\pi^+$ Dalitz plots below the $\eta' K$ threshold [15,16], where they provide a good description of the data with fewer fit parameters than the isobar approach. Ref. [52] uses a unitary coupled channel approach to describe $D^+ \to K^-\pi^+\pi^+$, which has no restrictions on the kinematic range, but requires additional parameters to describe the Dalitz plot above the $\eta' K$ threshold. Using an effective chiral Lagrangian, the authors of Ref. [19] provide a description of the annihilation contribution to the decay amplitude which respects three-body unitarity. The approach provides a good description of LHCb $D^+ \to K^+K^-K^+$ data, with fewer parameters than an equivalent isobar model [46]. The same channel has more recently been re-analysed by the authors of [22], who argue that the internal emission diagram should dominate and use a chiral unitarity-based approach to achieve a reasonable description of the data with two free parameters.

Limitations in the theoretical description of interfering resonances are the leading source of systematic uncertainty in many analyses. This is set to become increasingly problematic given the statistical precision achievable with the vast, clean charm samples available at the B factories, LHCb, and their upgrades, and BES III. In some cases, the model uncertainty can be removed through model-independent methods, often relying on input from the charm threshold, as discussed below. The authors of [53] expand the scope and applicability of the quasi model-independent approach in amplitude fits. At the same time, increasingly sophisticated models are being developed, and applied to data. The authors of [20] and [54] provide valuable frameworks for sophisticated amplitude analyses.

69.3 Model Independent Methods and the Charm Threshold

The precision measurement of mixing or *CP* violation parameters such γ/ϕ_3 from multibody charm decays requires as input the phase-differences between the D^0 and $\overline{D}^0$ amplitudes across phase space, as well as their magnitudes, for each final state of interest. While the magnitudes are fairly easily measured, the phase information requires either amplitude models with reliable phase motion, or model-independent approaches.

Model-independent measurements of the relevant phase differences rely on interference effects in the decays of well-defined coherent superpositions of D^0 and $\overline{D}^0$. These are accessible at the charm threshold, where CLEO–c and BES III operate [55–63]. Charm mixing also results in a (time-dependent) $D^0 - \overline{D}^0$ su-

Downloaded from https://academic.oup.com/ptep/article/2022/8/083C01/6651666 by KIT Library user on 27 September 2022

perposition, that can be used to measure the relevant phase information as input to γ/ϕ_3 measurements. This method is particularly powerful in doubly Cabibbo-suppressed decays such as $D^0 \to K^+\pi^-\pi^+\pi^-$, and when used in combination with threshold data [64,65]. Under some circumstances, with large data sets, the relevant strong phases and γ/ϕ_3 can be extracted simultaneously without external input, for example in simultaneous analysis of the $B^0 \to DK^+\pi^-$ Dalitz plot and that of the subsequent $D \to K^0_S\pi^+\pi^-$ decay [66]. However, the global effort to achieve a measurement of γ/ϕ_3 to sub-degree precision will continue to rely critically on input from the charm threshold and BES III's increasing datasets [67]. A particularly noteworthy recent development is the substantial improvement not only in the precision on γ but also on charm mixing parameters achieved through a combined fit of charm mixing, charm threshold, $B \to DK$ and related data [68].

The model-independent phase information of the charm decay is provided either integrated over the entire phase space of the decay, or in sub-regions/bins. The results can be expressed in terms of one complex parameter $\mathcal{Z} = Re^{-i\delta} = c + is$ per pair of CP-conjugate bins, with magnitude $R \leq 1$. Larger R values lead to higher sensitivity to γ/ϕ_3. Amplitude models can be used to optimise the binning for sensitivity to γ/ϕ_3, without introducing a model-dependent bias in the result; novel unbinned approaches are expected to increase the precision on γ in future analyses [69].

CLEO–c data have been analyzed to provide binned $\mathcal{Z}$ for the self-conjugate decays $D^0 \to K_S\pi^+\pi^-$, $K_SK^+K^-$, $\pi^+\pi^-\pi^+\pi^-$, and $K_S\pi^-\pi^+\pi^0$ and phase space-integrated values for $D^0, \overline{D}^0 \to K_SK^+\pi^-$, $K^+\pi^-\pi^0$ and $K^+\pi^-\pi^+\pi^+$ [70–75]. BES III significantly improved the precision for the $K_S\pi^+\pi^-$, $K_SK^+K^-$, $K^+\pi^-\pi^0$ and $K^+\pi^-\pi^+\pi^-$ final states [76–79]. Critically, BES III was able to perform this measurement in four separate bins of $K^+\pi^-\pi^+\pi^-$ phase space. Studies based on recent $D^0 \to K^\pm\pi^\mp\pi^\pm\pi^\mp$ amplitude models [30] indicate that such a binned analysis could lead to the most precise individual γ measurement [80], especially when combined with LHCb charm mixing data [65,75,81]. For self-conjugate decays such as $D^0 \to \pi^+\pi^-\pi^0$, analysed with a single pair of bins, $\mathcal{Z}$ is real-valued, and usually expressed in terms of the CP-even fraction $F_+ \equiv \frac{1}{2}(\mathrm{Re}(\mathcal{Z}) + 1)$, defined such that a CP-even eigenstate has $F_+ = 1$, while a CP-odd eigenstate has $F_+ = 0$ [61]. Recent analyses of CLEO–c data reveal that $D^0 \to \pi^+\pi^-\pi^0$ is compatible with being completely CP-even with $F_+ = 0.973 \pm 0.017$, while $D^0 \to K^+K^-\pi^0$ has $F_+ = 0.732 \pm 0.055$, $D^0 \to \pi^+\pi^-\pi^+\pi^-$ has $F_+ = 0.769 \pm 0.023$ and $D^0 \to K_S\pi^+\pi^-\pi^0$ has 0.238 ± 0.020 [62,72,73].

It is interesting to compare these values with those obtained from amplitude models as a cross-check of the models' phase-motion. $F_+^{4\pi\ \mathrm{model}} = 0.729 \pm 0.020$ calculated from Ref. [29]'s $D^0 \to \pi^+\pi^-\pi^+\pi^-$ model compares well to the measured value given above, as does $\left|\mathcal{Z}^{K3\pi\ \mathrm{model}}\right| = 0.459 \pm 0.025$ [30] to $\mathcal{Z}^{K3\pi\ \mathrm{meas}} = 0.44^{+0.10}_{-0.09}\ \exp(-i(161^{\circ}{}^{+28^\circ}_{-18^\circ}))$ [75, 81]. Only for self-conjugate decays or multiple bins does the model provide relevant phase information. The latest bin wise comparisons between model and data for $D^0 \to K_S\pi^+\pi^-$, $K_SK^+K^-$, $\pi^+\pi^-\pi^+\pi^-$, and $K^\pm\pi^\mp\pi^\pm\pi^\mp$ can be found in [72,76–79] and generally show good agreement, which is a welcome surprise given the preceding discussion on the theoretical shortcomings of such amplitude models.

69.4 Applications of multibody charm analyses

Amplitude analyses provide sensitivity to both relative magnitudes and phases of the interfering decay amplitudes. It is especially this sensitivity to phases that makes amplitude analyses such a uniquely powerful tool for studying a wide range of phenomena. Here we concentrate on their use for CP violation and mixing measurements in charm, and charm inputs to CP violation analyses in B meson decays (properties of light-meson resonances determined in D amplitude analyses are reported in the light-unflavored-meson section of this *Review*).

69.4.1 *Time-integrated searches for CP violation in charm*

Comparing the results of amplitude fits for CP-conjugate decay modes provides a measure of CP violation. Recent CP violation searches using this method include amplitude analyses of $D^0 \to K^0_SK^\pm\pi^\mp$ and $D^0 \to K^+K^-\pi^+\pi^-$ by LHCb [82,83], and $D^0 \to K^+K^-\pi^+\pi^-$, $D^0 \to \pi^+\pi^-\pi^+\pi^-$ [29,84] using CLEO data.

A widely-used amplitude model-independent technique to search for local CP violation is based on performing a χ^2 comparison of CP-conjugate phase-space distributions. This method was pioneered by BaBar [85] and developed further in [86–88], with results reported by BaBar [85, 89] and LHCb in $D^\pm \to K^+K^-\pi^\pm$ [90, 91], CDF in $D^0 \to K_S\pi^+\pi^-$ [35], and LHCb in $D^+ \to \pi^-\pi^+\pi^+$, $D^0 \to K^+K^-\pi^+\pi^-$, $D^0 \to \pi^+\pi^-\pi^+\pi^-$, and $\Xi_c^+ \to pK^-\pi^+$ [88, 92, 93]. Unbinned methods can increase sensitivity [94] and have been applied by LHCb to $D^+ \to \pi^-\pi^+\pi^+$, $D^0 \to \pi^+\pi^-\pi^0$, $D^0 \to \pi^+\pi^-\pi^+\pi$, and $\Xi_c^+ \to pK^-\pi^+$ [92,93,95,96].

An alternative model-independent approach is based on observables in four body decays that are odd under motion reversal ("naïve T") [97–105], which is equivalent to P for scalar particles [105]. One such observable is $C_T = \vec{p}_2 \cdot (\vec{p}_3 \times \vec{p}_4) = (1/m_D)\epsilon_{\alpha\beta\gamma\delta}\, p_1^\alpha p_2^\beta p_3^\gamma p_4^\delta$, where $\vec{p}_i$ are the decay products' three momenta in the decay's rest frame, and p_i are their four-momenta. Identical particles (as in $D^0 \to K^+\underline{\pi}^-\pi^+\underline{\pi}^-$) are ordered by momentum magnitude. Comparing the P violating asymmetry $A_T \equiv \frac{\Gamma(C_T>0)-\Gamma(C_T<0)}{\Gamma(C_T>0)+\Gamma(C_T<0)}$ with its C-conjugate provides sensitivity to CP violation. Searches for CP violation in this manner have been carried out by BaBar, Belle, FOCUS and LHCb in $D^0 \to K^+K^-\pi^+\pi^-$ [106–109], $D^+ \to K^+K_S\pi^+\pi^-$, $D_s^+ \to K^+K_S\pi^+\pi^-$ [110], $D^0 \to K_S\pi^+\pi^-\pi^0$ [111], and $D^0 \to \pi^+\pi^-\pi^+\pi^-$ [96]. The authors of [109] use additional P-odd variables and [108,111]/[96] increase sensitivity by resolving four-body phase space in a binned/unbinned approach.

The results of all measurements described in this section are compatible with CP conservation in charm. Given the discovery of CP violation in $D^0 \to K^+K^-$, $D^0 \to \pi^+\pi^-$ decays [112], and the vast data samples about to be collected, one might expect this to change in the foreseeable future.

69.4.2 *CP violation in decays of Beauty to Charm*

Neutral D mesons originating from $B^- \to DK^-$ (here denoted as D_{B^-}) are a superposition of D^0 and $\overline{D}^0$ with a relative phase that depends on the CKM unitarity triangle parameter γ/ϕ_3,

$$D_{B^-} \propto D^0 + r_B e^{i(\delta_B - \gamma)}\overline{D}^0,$$

where δ_B is a CP conserving strong phase, and $r_B \sim 0.1$. In the corresponding CP-conjugate expression, γ/ϕ_3 changes sign. An amplitude analysis of the subsequent decay of the $D_{B^\pm}$ to a state accessible to both D^0 and $\overline{D}^0$ allows the measurement of γ/ϕ_3 [56,113–116]. The method generalizes to similar B hadron decays, such as $B^0 \to DK^{*0}$. Measurements based on this technique have been reported by BaBar [117,118], Belle [34,119] and LHCb [120–129]. The most precise individual result with an uncertainty of $\sim 5^\circ$ comes from an amplitude model-independent study of $D_{B^-} \to K_S\pi^+\pi^-$ and $D_{B^-} \to K_SK^+K^-$ [130], using input from the charm threshold [70,77] as described above. Combining measurements in multiple decay modes from LHCb, CLEO–c and BES III in an amplitude-model independent approach leads to a current uncertainty on γ/ϕ_3 of 4° [68,131].

The interference between mixing and decay in $B^0 \to D^0h^0$ with $h^0 = \pi^0, \eta, \omega$ provides sensitivity to β, which can be extracted from the Dalitz plot of the subsequent $D^0 \to K_S\pi^+\pi^-$ decay [39,132–135]. The combined BaBar/Belle analysis based on this technique resolved the ambiguity in β present in other measurements, such as $B^0 \to J/\psi K_S$, in favour of the solution compatible with other unitarity triangle constraints [39].

Further details on CP violation in beauty and charm can be found in [55,136].

69.4.3 *Charm Mixing and CP violation*

Time-dependent amplitude analyses in decays to final states that are accessible to both D^0 and $\overline{D}^0$ have unique sensitivity to mixing parameters. A Dalitz plot analysis of a self-conjugate

Downloaded from https://academic.oup.com/ptep/article/2022/8/083C01/6651666 by KIT Library user on 27 September 2022

final state, such as $K_S\pi^+\pi^-$ and $K_SK^+K^-$, allows the measurement of the phase difference between the relevant D^0 and $\overline{D}^0$ decay amplitudes, and thus a direct measurement of x and y, the normalized mass and width difference of the $D^0 - \overline{D}^0$ system's mass eigenstates. This is in contrast to decays like $D^0 \to K\pi$ [137] which only provide access to the decay-specific parameters x'^2, y'. The phase differences between D^0 and $\overline{D}^0$ amplitudes across the Dalitz plot affect these measurements in the same way as measurements of γ/ϕ_3 in $B^+ \to DK^+$, and can be taken into account in an amplitude model-independent way using the same charm threshold results [70,77]. This approach recently resulted the first observation of the mass difference of the neutral charm mass eigenstates by LHCb [138], using a model-independent analysis of $D^0 \to K_S\pi^+\pi^-$. The "bin flip" technique applied in this measurements exploits that CP-conjugate regions of the $D^0 \to K_S\pi^+\pi^-$ Dalitz plot have near-identical experimental efficiencies [139]. This measurement is also sensitive to CP violation in mixing and in the interference between mixing and decay, which is discussed further in [55,136]. The most precise values for charm mixing parameters result from a combination of charm data from LHCb and the charm threshold with input from γ-sensitive decays of the type $B^+ \to D^0K^+$ [68]. The substantial impact of the latter is noteworthy, as it improves the precision on y by a factor of two compared to the previous world average.

69.5 Summary

Multibody charm decays offer a rich phenomenology, including unique sensitivity to CP violation and charm mixing. This is a highly dynamic field with many new results (some of which we presented here) and rapidly increasing, high quality datasets. These datasets constitute a huge opportunity, but also a challenge to improve the theoretical descriptions of soft hadronic effects in multibody decays. For some measurements, model-independent methods, many relying on input from the charm threshold, provide a way of removing model-induced uncertainties. At the same time, substantial progress in the theoretical description of multibody decays is being made.

References

[1] R. Dalitz, Phil. Mag. Ser. 7 **44**, 1068 (1953).

[2] M. Bauer, B. Stech and M. Wirbel, Z. Phys. C **34**, 103 (1987).

[3] L.-L. Chau and H.-Y. Cheng, Phys. Rev. D **36**, 137 (1987), [Addendum: Phys.Rev.D 39, 2788–2791 (1989)].

[4] P. F. Bedaque, A. K. Das and V. Mathur, Phys. Rev. D **49**, 269 (1994), [hep-ph/9307296].

[5] K. Terasaki, Int. J. Mod. Phys. A **10**, 3207 (1995).

[6] F. Buccella, M. Lusignoli and A. Pugliese, Phys. Lett. B **379**, 249 (1996), [hep-ph/9601343].

[7] J. D. Jackson, Nuovo Cim. **34**, 1644 (1964).

[8] See the note on Resonances in this *Review*.

[9] E. P. Wigner, Phys. Rev. **70**, 15 (1946).

[10] S. M. Flatte, Phys. Lett. B **63**, 224 (1976).

[11] I. Aitchison, Nucl. Phys. A **189**, 417 (1972).

[12] D. Aston *et al.*, Nucl. Phys. B **296**, 493 (1988).

[13] R. Omnes, Nuovo Cim. **8**, 316 (1958).

[14] C. Hanhart, Phys. Lett. B **715**, 170 (2012), [arXiv:1203.6839].

[15] F. Niecknig and B. Kubis, JHEP **10**, 142 (2015), [arXiv:1509.03188].

[16] F. Niecknig and B. Kubis, Phys. Lett. B **780**, 471 (2018), [arXiv:1708.00446].

[17] P. Magalhães and M. Robilotta, Phys. Rev. D **92**, 9, 094005 (2015), [arXiv:1504.06346].

[18] P. Magalhaes *et al.*, Phys. Rev. D **84**, 094001 (2011), [arXiv:1105.5120].

[19] R. Aoude *et al.*, Phys. Rev. D **98**, 5, 056021 (2018), [arXiv:1805.11764].

[20] P. C. Magalhães, A. C. dos Reis and M. R. Robilotta, Phys. Rev. D **102**, 7, 076012 (2020), [arXiv:2007.12304].

[21] J. A. Oller, Phys. Rev. D **71**, 054030 (2005), [hep-ph/0411105].

[22] L. Roca and E. Oset, Phys. Rev. D **103**, 3, 034020 (2021), [arXiv:2011.05185].

[23] J.-P. Dedonder *et al.*, Phys. Rev. D **89**, 9, 094018 (2014), [arXiv:1403.2971].

[24] D. Boito *et al.*, Phys. Rev. D **96**, 11, 113003 (2017), [arXiv:1709.09739].

[25] R. Klein *et al.*, JHEP **10**, 117 (2017), [arXiv:1708.02047].

[26] J. P. Dedonder *et al.*, Phys. Rev. D **103**, 11, 114028 (2021), [arXiv:2105.03355].

[27] E. Aitala *et al.* (E791), Phys. Rev. D **73**, 032004 (2006), [Erratum: Phys. Rev.D 74, 059901 (2006)], [hep-ex/0507099].

[28] G. Bonvicini *et al.* (CLEO), Phys. Rev. D **78**, 052001 (2008), [arXiv:0802.4214].

[29] P. d'Argent *et al.*, JHEP **05**, 143 (2017), [arXiv:1703.08505].

[30] R. Aaij *et al.* (LHCb), Eur. Phys. J. C **78**, 6, 443 (2018), [arXiv:1712.08609].

[31] M. Ablikim *et al.* (BESIII), Phys. Rev. D **104**, 1, 012016 (2021), [arXiv:2011.08041].

[32] M. Ablikim *et al.* (BESIII) (2021), [arXiv:2108.10050].

[33] H. Muramatsu *et al.* (CLEO), Phys. Rev. Lett. **89**, 251802 (2002), [Erratum: Phys. Rev. Lett. 90, 059901 (2003)], [hep-ex/0207067].

[34] A. Poluektov *et al.* (Belle), Phys. Rev. D **81**, 112002 (2010), [arXiv:1003.3360].

[35] T. Aaltonen *et al.* (CDF), Phys. Rev. D **86**, 032007 (2012), [arXiv:1207.0825].

[36] P. del Amo Sanchez *et al.* (BaBar), Phys. Rev. Lett. **105**, 081803 (2010), [arXiv:1004.5053].

[37] T. Peng *et al.* (Belle), Phys. Rev. D **89**, 9, 091103 (2014), [arXiv:1404.2412].

[38] V. Anisovich and A. Sarantsev, Eur. Phys. J. A **16**, 229 (2003), [hep-ph/0204328].

[39] I. Adachi *et al.* (BaBar, Belle), Phys. Rev. Lett. **121**, 26, 261801 (2018), [arXiv:1804.06152]; I. Adachi *et al.* (BaBar, Belle), Phys. Rev. D **98**, 11, 112012 (2018), [arXiv:1804.06153].

[40] B. El-Bennich *et al.*, Phys. Rev. D **79**, 094005 (2009), [Erratum: Phys. Rev. D 83, 039903 (2011)], [arXiv:0902.3645].

[41] J.-P. Dedonder *et al.*, Acta Phys. Polon. B **42**, 2013 (2011), [arXiv:1011.0960].

[42] M. Ablikim *et al.* (BESIII), JHEP **2021**, 6, 181 (2021), [arXiv:2103.15098].

[43] M. Ablikim *et al.* (BESIII) (2020), [arXiv:2006.02800].

[44] M. Ablikim *et al.* (BESIII), Phys. Rev. D **104**, 012006 (2021), [arXiv:2104.09131].

[45] Y. Q. Chen *et al.* (Belle), Phys. Rev. D **102**, 1, 012002 (2020), [arXiv:2003.07759].

[46] R. Aaij *et al.* (LHCb), JHEP **04**, 063 (2019), [arXiv:1902.05884].

[47] M. Ablikim *et al.* (BESIII) (2021), [arXiv:2106.13536].

[48] M. Ablikim *et al.* (BESIII), Phys. Rev. D **104**, 3, 032011 (2021), [arXiv:2103.02482].

[49] M. Ablikim *et al.* (BESIII), Phys. Rev. D **103**, 9, 092006 (2021), [arXiv:2102.03808].

[50] R. Aaij *et al.* (LHCb), JHEP **02**, 126 (2019), [arXiv:1811.08304].

[51] J. T. McNeil *et al.* (Belle), Phys. Rev. D **103**, 11, 112002 (2021), [arXiv:2012.05607].

[52] S. X. Nakamura, Phys. Rev. D **93**, 1, 014005 (2016), [arXiv:1504.02557].

Downloaded from https://academic.oup.com/ptep/article/2022/8/083C01/6651666 by KIT Library user on 27 September 2022

[53] F. Krinner *et al.*, Phys. Rev. D **97**, 11, 114008 (2018), [arXiv:1710.09849].

[54] M. Mikhasenko *et al.* (JPAC), Phys. Rev. D **101**, 3, 034033 (2020), [arXiv:1910.04566].

[55] See the note on D^0–$\overline{D}^0$ Mixing in this *Review*.

[56] A. Giri *et al.*, Phys. Rev. D **68**, 054018 (2003), [hep-ph/0303187].

[57] D. Atwood and A. Soni, Phys. Rev. D **68**, 033003 (2003), [hep-ph/0304085].

[58] S. Malde and G. Wilkinson, Phys. Lett. B **701**, 353 (2011), [arXiv:1104.2731].

[59] A. Bondar, A. Poluektov and V. Vorobiev, Phys. Rev. D **82**, 034033 (2010), [arXiv:1004.2350].

[60] J. Kallen *et al.*, JHEP **10**, 184 (2012), [arXiv:1207.3763].

[61] M. Nayak *et al.*, Phys. Lett. B **740**, 1 (2015), [arXiv:1410.3964].

[62] S. Malde *et al.*, Phys. Lett. B **747**, 9 (2015), [arXiv:1504.05878].

[63] S. Malde, C. Thomas and G. Wilkinson, Phys. Rev. D **91**, 9, 094032 (2015), [arXiv:1502.04560].

[64] S. Harnew and J. Rademacker, Phys. Lett. B **728**, 296 (2014), [arXiv:1309.0134].

[65] S. Harnew and J. Rademacker, JHEP **03**, 169 (2015), [arXiv:1412.7254].

[66] D. Craik, T. Gershon and A. Poluektov, Phys. Rev. D **97**, 5, 056002 (2018), [arXiv:1712.07853].

[67] M. Ablikim *et al.* (BESIII), Chin. Phys. C **44**, 4, 040001 (2020), [arXiv:1912.05983].

[68] R. Aaij *et al.* (LHCb) (2021), [arXiv:2110.02350].

[69] A. Poluektov, Eur. Phys. J. C **78**, 2, 121 (2018), [arXiv:1712.08326].

[70] J. Libby *et al.* (CLEO), Phys. Rev. D **82**, 112006 (2010), [arXiv:1010.2817].

[71] R. A. Briere *et al.* (CLEO), Phys. Rev. D **80**, 032002 (2009), [arXiv:0903.1681].

[72] S. Harnew *et al.*, JHEP **01**, 144 (2018), [arXiv:1709.03467].

[73] P. Resmi *et al.*, JHEP **01**, 082 (2018), [arXiv:1710.10086].

[74] J. Insler *et al.* (CLEO), Phys. Rev. D **85**, 092016 (2012), [Erratum: Phys. Rev. D 94, 099905 (2016)], [arXiv:1203.3804].

[75] T. Evans *et al.*, Phys. Lett. B **757**, 520 (2016), [Erratum: Phys. Lett. B 765, 402–403 (2017)], [arXiv:1602.07430].

[76] M. Ablikim *et al.* (BESIII), Phys. Rev. Lett. **124**, 24, 241802 (2020), [arXiv:2002.12791].

[77] M. Ablikim *et al.* (BESIII), Phys. Rev. D **101**, 11, 112002 (2020), [arXiv:2003.00091].

[78] M. Ablikim *et al.* (BESIII), Phys. Rev. D **102**, 5, 052008 (2020), [arXiv:2007.07959].

[79] M. Ablikim *et al.* (BESIII), JHEP **05**, 164 (2021), [arXiv:2103.05988].

[80] T. Evans *et al.*, Phys. Lett. B **802**, 135188 (2020), [arXiv:1909.10196].

[81] R. Aaij *et al.* (LHCb), Phys. Rev. Lett. **116**, 24, 241801 (2016), [arXiv:1602.07224].

[82] R. Aaij *et al.* (LHCb), Phys. Rev. D **93**, 5, 052018 (2016), [arXiv:1509.06628].

[83] R. Aaij *et al.* (LHCb), JHEP **02**, 126 (2019), [arXiv:1811.08304].

[84] M. Artuso *et al.* (CLEO), Phys. Rev. D **85**, 122002 (2012), [arXiv:1201.5716].

[85] B. Aubert *et al.* (BaBar), Phys. Rev. D **78**, 051102 (2008), [arXiv:0802.4035].

[86] I. Bediaga *et al.*, Phys. Rev. D **80**, 096006 (2009), [arXiv:0905.4233].

[87] I. Bediaga *et al.*, Phys. Rev. D **86**, 036005 (2012), [arXiv:1205.3036].

[88] R. Aaij *et al.* (LHCb), Phys. Lett. B **726**, 623 (2013), [arXiv:1308.3189].

[89] J. Lees *et al.* (BaBar), Phys. Rev. D **87**, 5, 052010 (2013), [arXiv:1212.1856].

[90] R. Aaij *et al.* (LHCb), Phys. Rev. D **84**, 112008 (2011), [arXiv:1110.3970].

[91] R. Aaij *et al.* (LHCb), JHEP **06**, 112 (2013), [arXiv:1303.4906].

[92] R. Aaij *et al.* (LHCb), Phys. Lett. B **728**, 585 (2014), [arXiv:1310.7953].

[93] R. Aaij *et al.* (LHCb), Eur. Phys. J. C **80**, 10, 986 (2020), [arXiv:2006.03145].

[94] M. Williams, Phys. Rev. D **84**, 054015 (2011), [arXiv:1105.5338].

[95] R. Aaij *et al.* (LHCb), Phys. Lett. B **740**, 158 (2015), [arXiv:1410.4170].

[96] R. Aaij *et al.* (LHCb), Phys. Lett. B **769**, 345 (2017), [arXiv:1612.03207].

[97] E. Golowich and G. Valencia, Phys. Rev. D **40**, 112 (1989).

[98] G. Valencia, Phys. Rev. D **39**, 3339 (1989).

[99] W. Bensalem and D. London, Phys. Rev. D **64**, 116003 (2001), [hep-ph/0005018].

[100] I. I. Bigi, in "KAON2001: International Conference on CP Violation," (2001), [hep-ph/0107102].

[101] W. Bensalem, A. Datta and D. London, Phys. Rev. D **66**, 094004 (2002), [hep-ph/0208054].

[102] W. Bensalem, A. Datta and D. London, Phys. Lett. B **538**, 309 (2002), [hep-ph/0205009].

[103] A. Datta and D. London, Int. J. Mod. Phys. A **19**, 2505 (2004), [hep-ph/0303159].

[104] M. Gronau and J. L. Rosner, Phys. Rev. D **84**, 096013 (2011), [arXiv:1107.1232].

[105] G. Durieux and Y. Grossman, Phys. Rev. D **92**, 7, 076013 (2015), [arXiv:1508.03054].

[106] J. Link *et al.* (FOCUS), Phys. Lett. B **622**, 239 (2005), [hep-ex/0506012].

[107] P. del Amo Sanchez *et al.* (BaBar), Phys. Rev. D **81**, 111103 (2010), [arXiv:1003.3397].

[108] R. Aaij *et al.* (LHCb), JHEP **10**, 005 (2014), [arXiv:1408.1299].

[109] J. Kim *et al.* (Belle), Phys. Rev. D **99**, 1, 011104 (2019), [arXiv:1810.06457].

[110] J. Lees *et al.* (BaBar), Phys. Rev. D **84**, 031103 (2011), [arXiv:1105.4410].

[111] K. Prasanth *et al.* (Belle), Phys. Rev. D **95**, 9, 091101 (2017), [arXiv:1703.05721].

[112] R. Aaij *et al.* (LHCb), Phys. Rev. Lett. **122**, 21, 211803 (2019), [arXiv:1903.08726].

[113] M. Gronau and D. Wyler, Phys. Lett. B **265**, 172 (1991).

[114] M. Gronau and D. London, Phys. Lett. B **253**, 483 (1991).

[115] A. Poluektov *et al.* (Belle), Phys. Rev. D **70**, 072003 (2004), [hep-ex/0406067].

[116] J. Rademacker and G. Wilkinson, Phys. Lett. B **647**, 400 (2007), [hep-ph/0611272].

[117] P. del Amo Sanchez *et al.* (BaBar), Phys. Rev. Lett. **105**, 121801 (2010), [arXiv:1005.1096].

[118] J. Lees *et al.* (BaBar), Phys. Rev. D **84**, 012002 (2011), [arXiv:1104.4472].

[119] H. Aihara *et al.* (Belle), Phys. Rev. D **85**, 112014 (2012), [arXiv:1204.6561].

[120] R. Aaij *et al.* (LHCb), Phys. Lett. B **726**, 151 (2013), [arXiv:1305.2050].

Downloaded from https://academic.oup.com/ptep/article/2022/8/083C01/6651666 by KIT Library user on 27 September 2022

[121] R. Aaij *et al.* (LHCb), Phys. Lett. B **723**, 44 (2013), [arXiv:1303.4646].

[122] R. Aaij *et al.* (LHCb), Phys. Lett. B **718**, 43 (2012), [arXiv:1209.5869].

[123] R. Aaij *et al.* (LHCb), JHEP **10**, 097 (2014), [arXiv:1408.2748].

[124] R. Aaij *et al.* (LHCb), Phys. Lett. B **733**, 36 (2014), [arXiv:1402.2982].

[125] R. Aaij *et al.* (LHCb), Nucl. Phys. B **888**, 169 (2014), [arXiv:1407.6211].

[126] R. Aaij *et al.* (LHCb), Phys. Rev. D **91**, 11, 112014 (2015), [arXiv:1504.05442].

[127] R. Aaij *et al.* (LHCb), JHEP **06**, 131 (2016), [arXiv:1604.01525].

[128] R. Aaij *et al.* (LHCb), JHEP **12**, 087 (2016), [arXiv:1611.03076].

[129] R. Aaij *et al.* (LHCb), JHEP **08**, 176 (2018), [Erratum: JHEP 10, 107 (2018)], [arXiv:1806.01202].

[130] R. Aaij *et al.* (LHCb), JHEP **02**, 169 (2021), [arXiv:2010.08483].

[131] Y. S. Amhis *et al.* (HFLAV), Eur. Phys. J. **C81**, 226 (2021), updated results and plots available at `https://hflav.web.cern.ch/`, [arXiv:1909.12524].

[132] A. Bondar, T. Gershon and P. Krokovny, Phys. Lett. B **624**, 1 (2005), [hep-ph/0503174].

[133] P. Krokovny *et al.* (Belle), Phys. Rev. Lett. **97**, 081801 (2006), [hep-ex/0605023].

[134] B. Aubert *et al.* (BaBar), Phys. Rev. Lett. **99**, 231802 (2007), [arXiv:0708.1544].

[135] V. Vorobyev *et al.* (Belle), Phys. Rev. D **94**, 5, 052004 (2016), [arXiv:1607.05813].

[136] See the note CP violation in the quark sector in this *Review*.

[137] D. Asner *et al.* (CLEO), Phys. Rev. D **72**, 012001 (2005), [hep-ex/0503045].

[138] R. Aaij *et al.* (LHCb) (2021), [arXiv:2106.03744].

[139] A. Di Canto *et al.*, Phys. Rev. D **99**, 1, 012007 (2019), [arXiv:1811.01032].

Downloaded from https://academic.oup.com/ptep/article/2022/8/083C01/6651666 by KIT Library user on 27 September 2022

70. D^0-$\overline{D}^0$ Mixing

Revised September 2021 by D.M. Asner (BNL) and A.J. Schwartz (U. of Cincinnati).

The formalism for D^0-$\overline{D}^0$ mixing is closely related to that for CP violation; for further details on the latter, see the note "CP Violation in the Quark Sector" in this *Review*. The time evolution of the D^0–$\overline{D}^0$ system is described by the Schrödinger equation

$$i\frac{\partial}{\partial t}\begin{pmatrix}D^0(t)\\ \overline{D}^0(t)\end{pmatrix} = \left(\mathbf{M} - \frac{i}{2}\mathbf{\Gamma}\right)\begin{pmatrix}D^0(t)\\ \overline{D}^0(t)\end{pmatrix}, \tag{70.1}$$

where the $\mathbf{M}$ and $\mathbf{\Gamma}$ matrices are Hermitian, and CPT invariance requires that $M_{11} = M_{22} \equiv M$ and $\Gamma_{11} = \Gamma_{22} \equiv \Gamma$. The off-diagonal elements of $\mathbf{M}$ and $\mathbf{\Gamma}$ are referred to as the dispersive and absorptive parts, respectively, of the mixing. The mass eigenstates D_1 and D_2 of the Hamiltonian $\mathbf{M}$ - $i\mathbf{\Gamma}/2$ are defined as

$$|D_{1,2}\rangle \;\equiv\; p|D^0\rangle \pm q|\overline{D}^0\rangle\,, \tag{70.2}$$

where normalization imposes $|p|^2 + |q|^2 = 1$. If $p = \pm q$, then the mass eigenstates are CP eigenstates and CP is conserved. Our phase convention is $CP|D^0\rangle = -|\overline{D}^0\rangle$, which implies that, in the absence of CP violation, D_2 is CP-even and D_1 is CP-odd.

The eigenvalues of $\mathbf{M}$ - $i\mathbf{\Gamma}/2$ are

$$\omega_{1,2} \;=\; \left(M - \frac{i}{2}\Gamma\right) \pm \frac{q}{p}\left(M_{12} - \frac{i}{2}\Gamma_{12}\right) \;\equiv\; m_{1,2} - \frac{i}{2}\Gamma_{1,2}\,, \tag{70.3}$$

where $m_{1,2}$ and $\Gamma_{1,2}$ are real and correspond to the masses and decay widths, respectively, of the $D_{1,2}$ mass eigenstates. As the trace $\Gamma_{11} + \Gamma_{22} = 2\Gamma$ is unchanged by diagonalizing $\mathbf{\Gamma}$, Γ must equal $(\Gamma_1 + \Gamma_2)/2$, the mean decay width. Solving for the eigenstates of the eigenvalues yields

$$\left(\frac{q}{p}\right)^2 = \frac{M_{12}^* - \frac{i}{2}\Gamma_{12}^*}{M_{12} - \frac{i}{2}\Gamma_{12}}\,. \tag{70.4}$$

If CP is conserved, then $(q/p)^2 = 1$ and M_{12} and Γ_{12} must be real. In this case, the difference in eigenvalues is $\Delta m \equiv m_2 - m_1 = 2M_{12}$ and $\Delta\Gamma \equiv \Gamma_2 - \Gamma_1 = 2\Gamma_{12}$. The signs of Δm and $\Delta\Gamma$ are difficult to predict from theory and thus must be determined experimentally.

We define dimensionless mixing parameters x and y as

$$x \equiv \frac{\Delta m}{\Gamma} \tag{70.5}$$

$$y \equiv \frac{\Delta\Gamma}{2\Gamma}\,. \tag{70.6}$$

These parameters are measured in several ways. The most precise values are obtained by measuring the time dependence of D^0 decays. For all methods, the initial flavor of the D^0 or $\overline{D}^0$ when produced must be determined. The most common method used for this is to reconstruct $D^{*+} \to D^0\pi^+$ or $D^{*-} \to \overline{D}^0\pi^-$ decays; the charge of the accompanying pion (which has low momentum in the lab frame and is often referred to as the "soft" pion) determines the flavor of the neutral D. BaBar and LHCb have also identified the flavor of the neutral D by reconstructing the semileptonic decays $B^+ \to \overline{D}^0\ell^+\nu$, $B^0 \to D^{*-}\ell^+\nu$, $B^- \to D^0\ell^-\nu$, and $\overline{B}^0 \to D^{*+}\ell^-\nu$; in this case the charge of the accompanying lepton determines the D flavor. Both experiments have used both tags together to select "double-tagged" $B \to D^{*\pm}\ell^\mp\nu$, $D^{*\pm} \to (D^0, \overline{D}^0)\pi^\pm$ decays, which have especially high purity. At e^+e^- collider experiments such as Belle, BaBar, and BESIII, the D flavor can also be determined by fully reconstructing a flavor-specific D decay on the "opposite side" of an event, i.e., recoiling against the signal-side D decay.

At BESIII, where $D\overline{D}$ pairs are produced near their threshold via $e^+e^- \to \psi(3770) \to D^0\overline{D}^0$, there is relatively little background and the purity of opposite-side tagging is equivalent to that achieved using $D^{*\pm}$ decays. However, BESIII operates at a symmetric e^+e^- collider, and the $D\overline{D}$ pairs are produced almost at rest in the lab frame. As a consequence, the D's do not travel any appreciable distance before decaying, and time-dependent analyses are not possible. To overcome this, measurements of mixing at BESIII utilize the quantum coherence of the initial $\psi(3770) \to D^0\overline{D}^0$ state and time-integrated measurements [1–5].

70.1 Time-Dependent Analyses

Our notation is as follows: Cabibbo-favored (CF) decay amplitudes are denoted $\overline{A}_f \equiv \langle f|H|\overline{D}^0\rangle$ and $A_{\overline{f}} \equiv \langle \overline{f}|H|D^0\rangle$; i.e, the final state is $f = K^+\ell^-\nu$, $K^+\pi^-$, $K^+\pi^-\pi^0$, etc. Doubly-Cabibbo-suppressed (DCS) decay amplitudes are denoted $A_f \equiv \langle f|H|D^0\rangle$ and $\overline{A}_{\overline{f}} \equiv \langle \overline{f}|H|\overline{D}^0\rangle$.

Starting from a pure $|D^0\rangle$ or $|\overline{D}^0\rangle$ state at $t = 0$, the time-dependent decay rates to "wrong-sign" final states can be written

$$r(t) \equiv \left|\langle f|H|D^0(t)\rangle\right|^2 = \left|\overline{A}_f\right|^2\left|\frac{q}{p}\right|^2\left|g_+(t)\,\lambda_f^{-1} + g_-(t)\right|^2 \tag{70.7}$$

$$\overline{r}(t) \;\equiv\; \left|\langle \overline{f}|H|\overline{D}^0(t)\rangle\right|^2 = \left|A_{\overline{f}}\right|^2\left|\frac{p}{q}\right|^2\left|g_+(t)\,\lambda_{\overline{f}} \;+\; g_-(t)\right|^2, \tag{70.8}$$

where

$$\lambda_f \;\equiv\; \frac{q}{p}\frac{\overline{A}_f}{A_f}\,, \quad \lambda_{\overline{f}} \;\equiv\; \frac{q}{p}\frac{\overline{A}_{\overline{f}}}{A_{\overline{f}}}\,, \tag{70.9}$$

and

$$g_\pm(t) \;=\; \frac{1}{2}\left(e^{-i\omega_1 t} \pm e^{-i\omega_2 t}\right)\,. \tag{70.10}$$

A change in convention for the relative phase of D^0 and $\overline{D}^0$ would cancel between q/p and $\overline{A}_f/A_f$ or $\overline{A}_{\overline{f}}/A_{\overline{f}}$, leaving λ_f and $\lambda_{\overline{f}}$ unchanged. For multibody final states, these equations apply separately to each point in phase-space. Integrating over regions of phase-space can lead to enhanced sensitivity to CP violation; see the discussion below on multibody decays and the note "Review of Multibody Charm Analyses" in this *Review*. As the mixing parameters x and y are very small, $r(t)$ and $\overline{r}(t)$ are usually expanded to second order in x and y.

70.2 Semileptonic decays

Consider the final state $f = K^+\ell^-\overline{\nu}_\ell$, where $A_f = \overline{A}_{\overline{f}} = 0$ is an excellent approximation in the Standard Model. The final state f is accessible from a D^0 only via mixing,[1] and the decay rate is

$$r(t) = \left|\overline{A}_f\right|^2\left|\frac{q}{p}\right|^2|g_-(t)|^2 \;\approx\; \left|\overline{A}_f\right|^2\left|\frac{q}{p}\right|^2\left(\frac{x^2+y^2}{4}\right)(\Gamma t)^2\,e^{-\Gamma t}\,. \tag{70.11}$$

For $\overline{r}(t)$, q/p is replaced by p/q. In the Standard Model, CP violation in charm mixing is small and $|q/p| \approx 1$. In the limit of CP conservation, $r(t) = \overline{r}(t)$, and the time-integrated mixed decay rate relative to the time-integrated unmixed decay rate for semileptonic decays is

$$\frac{\displaystyle\int_0^\infty r(t)\,dt}{\displaystyle\int_0^\infty \left|\overline{A}_f\right|^2 e^{-\Gamma t}\,dt} \;=\; \frac{x^2+y^2}{2} \;\equiv\; R_M\,. \tag{70.12}$$

Table 70.1 summarizes results for R_M from semileptonic decays. The world average from the Heavy Flavor Averaging Group (HFLAV) [6] is $R_M = (1.30 \pm 2.69) \times 10^{-4}$.

[1] There exists a doubly Cabibbo-suppressed amplitude in which the c and $\bar{u}$ quarks exchange a W, and then the resulting d quark (from c) decays semileptonically. We neglect this second-order process.

Downloaded from https://academic.oup.com/ptep/article/2022/8/083C01/6651666 by KIT Library user on 27 September 2022

Table 70.1: Results for $R_M = (x^2+y^2)/2$ in D^0 semileptonic decays. The HFLAV average assumes statistical and systematic uncertainties are uncorrelated. When a single uncertainty is listed, that corresponds to statistical and systematic uncertainties combined. The measurements with an asterisk (*) have been superseded and thus are not included in the HFLAV average.

Year	Experiment	Final state(s)	R_M ($\times 10^{-3}$)	90% C.L. ($\times 10^{-3}$)
2008	Belle (492 fb^{-1}) [7]	$K^{(*)+}e^-\overline{\nu}_e$	$0.13\pm0.22\pm0.20$	< 0.61
2007	BaBar (344 fb^{-1}) [8]	$K^{(*)+}e^-\overline{\nu}_e$	$0.04\,^{+0.70}_{-0.60}$	$(-1.3, 1.2)$
2005	CLEO (9.0 fb^{-1}) [9]	$K^{(*)+}e^-\overline{\nu}_e$	$1.6\pm2.9\pm2.9$	< 7.8
1996	E791 (2×10^{10} evts) [10]	$K^+\ell^-\overline{\nu}_\ell$	$1.1\,^{+3.0}_{-2.7}\,^{+0.0}_{-0.1}$	< 5.0
	HFLAV Average [6]		$\mathbf{0.130 \pm 0.269}$	
2005*	Belle (253 fb^{-1}) [11]	$K^{(*)+}e^-\overline{\nu}_e$	$0.02\pm0.47\pm0.14$	< 1.0
2004*	BaBar (87 fb^{-1}) [12]	$K^{(*)+}e^-\overline{\nu}_e$	$2.3\pm1.2\pm0.4$	< 4.2

Table 70.2: Results for R, R_D, and A_D as measured using $D^0 \to K^\pm\pi^\mp$ decays. When a single uncertainty is listed, that corresponds to statistical and systematic uncertainties combined. The measurements with an asterisk (*) have been superseded and thus are not included in the HFLAV global fit (Section 70.7). The measurements with a dagger (†) are not included in the HFLAV global fit due to much poorer precision.

Year	Experiment	R ($\times 10^{-3}$)	R_D ($\times 10^{-3}$)	A_D (%)
2018	LHCb (5.0 fb^{-1} D^* tag) [13]	—	3.454 ± 0.031	-0.01 ± 0.91
2017	LHCb (3.0 fb^{-1} $B+D^*$ double tag) [14]	—	3.48 ± 0.10	-3.15 ± 3.31
2014	Belle (976 fb^{-1}) [15]	3.86 ± 0.06	3.53 ± 0.13	—
2013	CDF (9.6 fb^{-1}) [16]	4.30 ± 0.05	3.51 ± 0.35	—
2007	BaBar (384 fb^{-1}) [17]	$3.53\pm0.08\pm0.04$	$3.03\pm0.16\pm0.10$	$-2.1\pm5.2\pm1.5$
	HFLAV Fit Result [18]		$\mathbf{3.434 \pm 0.019}$	$\mathbf{-0.70 \pm 0.36}$
2013b*	LHCb (3.0 fb^{-1} D^* tag) [19]	—	3.568 ± 0.066	-0.7 ± 1.9
2013a*	LHCb (1.0 fb^{-1}) [20]	4.25 ± 0.04	3.52 ± 0.15	—
2008*	CDF (1.5 fb^{-1}) [21]	4.15 ± 0.10	3.04 ± 0.55	—
2006*	Belle (400 fb^{-1}) [22]	$3.77\pm0.08\pm0.05$	3.64 ± 0.18	2.3 ± 4.7
2005†	FOCUS (234 evts) [23]	$4.29\,^{+0.63}_{-0.61}\pm0.27$	$5.17\,^{+1.47}_{-1.58}\pm0.76$	$13\,^{+33}_{-25}\pm10$
2000†	CLEO (9.0 fb^{-1}) [24]	$3.32\,^{+0.63}_{-0.65}\pm0.40$	$4.8\pm1.2\pm0.4$	$-1\,^{+16}_{-17}\pm1$
1998†	E791 (5643 evts) [25]	$6.8\,^{+3.4}_{-3.3}\pm0.7$	—	—

70.3 Wrong-sign decays to hadronic non-CP eigenstates

Consider the final state $f = K^+\pi^-$, i.e., $A_{\overline{f}}$ and $\overline{A}_f$ are CF, A_f and $\overline{A}_{\overline{f}}$ are DCS. Because CF and DCS decays proceed via tree-level amplitudes, and such amplitudes involve only the first two quark generations, direct CP violation is negligible[2]. The ratios of decay amplitudes can be written

$$\frac{A_f}{\overline{A}_f} = -\sqrt{R_D^+}\,e^{-i\delta_f} \qquad \frac{\overline{A}_{\overline{f}}}{A_{\overline{f}}} = -\sqrt{R_D^-}\,e^{-i\delta_f}\,, \tag{70.13}$$

where δ_f is the strong phase difference between the DCS and CF amplitudes. The minus sign originates from the weak phase difference between the amplitudes, specifically, the relative minus sign between V_{us} and V_{cd} (which produces a relative minus sign between $V_{cs}^*V_{ud}$ and $V_{us}^*V_{cd}$). The parameters R_D^+ and R_D^- are the ratios of the DCS decay rate to the CF decay rate. From the relevant CKM matrix elements, one estimates R_D^+, $R_D^- \sim \tan^4\theta_c$, where θ_c is the Cabibbo angle.

With the parameterization of Eq. (70.13), Eq. (70.9) becomes

$$\lambda_f^{-1} = \frac{p}{q}\frac{A_f}{\overline{A}_f} = -\sqrt{R_D^+}\left|\frac{p}{q}\right| e^{-i(\delta_f+\phi)} \tag{70.14}$$

$$\lambda_{\overline{f}} = \frac{q}{p}\frac{\overline{A}_{\overline{f}}}{A_{\overline{f}}} = -\sqrt{R_D^-}\left|\frac{q}{p}\right| e^{-i(\delta_f-\phi)}\,, \tag{70.15}$$

where $\phi = \mathrm{Arg}(q/p)$. The weak phase ϕ is independent of the final state f and is often referred to as "universal." For convenience, we define the mean decay rate $R_D \equiv (R_D^+ + R_D^-)/2$, and the decay rate asymmetry $A_D \equiv (R_D^+ - R_D^-)/(R_D^+ + R_D^-)$.

[2] For two quark generations, the weak phases can be defined to eliminate all weak-phase differences.

With these definitions, we expand the decay rates in Eqs. (70.7) and (70.8) to second order in the small mixing parameters x and y to obtain [26, 27]:

$$r(t) = \left|\overline{A}_f\right|^2 e^{-\Gamma t}\,\Big[\,R_D(1+A_D) + \sqrt{R_D(1+A_D)}\,\left|\frac{q}{p}\right| y'_+(\Gamma t) + \left|\frac{q}{p}\right|^2 \frac{(x'^2_+ + y'^2_+)}{4}(\Gamma t)^2\Big] \tag{70.16}$$

and

$$\overline{r}(t) = \left|A_{\overline{f}}\right|^2 e^{-\Gamma t}\,\Big[\,R_D(1-A_D) + \sqrt{R_D(1-A_D)}\,\left|\frac{p}{q}\right| y'_-(\Gamma t) + \left|\frac{p}{q}\right|^2 \frac{(x'^2_- + y'^2_-)}{4}(\Gamma t)^2\Big]\,, \tag{70.17}$$

where

$$x'_\pm = x\cos(\delta_f \pm \phi) + y\sin(\delta_f \pm \phi) \tag{70.18}$$

$$y'_\pm = y\cos(\delta_f \pm \phi) - x\sin(\delta_f \pm \phi)\,. \tag{70.19}$$

Defining the "strong-phase-rotated" mixing parameters

$$x' \equiv x\cos\delta_f + y\sin\delta_f \tag{70.20}$$

$$y' \equiv y\cos\delta_f - x\sin\delta_f \tag{70.21}$$

gives

$$x'_\pm = x'\cos\phi \pm y'\sin\phi \tag{70.22}$$

$$y'_\pm = y'\cos\phi \mp x'\sin\phi\,, \tag{70.23}$$

i.e., $x'_\pm$ and $y'_\pm$ are obtained from x', y' via an additional "weak-phase rotation." To summarize, parameters (x', y') are the mixing parameters (x, y) rotated by the strong phase δ_f, and parameters

Downloaded from https://academic.oup.com/ptep/article/2022/8/083C01/6651666 by KIT Library user on 27 September 2022

$(x'_\pm, y'_\pm)$ are the parameters (x', y') rotated by the weak phase $+\phi$ for D^0 decays and $-\phi$ for $\overline{D}^0$ decays. Note that $x'^2_+ + y'^2_+ = x'^2_- + y'^2_- = x'^2 + y'^2 = x^2 + y^2$. In Eqs. (70.16) and (70.17), a fourth term $R_D(1 \pm A_D)(x^2_\pm - y^2_\pm)(\Gamma t)^2/4$ has been dropped, as it is negligible relative to the other terms for the range of decay times measured by experiments.

Comparing Eqs. (70.16) and (70.17), one sees that $r(t) \neq \bar{r}(t)$ and CP is violated if either $A_D \neq 0$, $|q/p| \neq 1$, or $\phi \neq 0$. These three inequalities correspond, respectively, to the three types of CP violation: in the decay amplitudes ($R^+_D \neq R^-_D$); in the mixing; and due to interference between a mixed decay amplitude (i.e., mixing is followed by decay) and an unmixed decay amplitude. Whereas CP violation in the decay amplitudes is parameterized by A_D, CP violation in mixing is parameterized by $A_M \equiv (|q/p| - |p/q|)/(|q/p| + |p/q|)$.

In the limit of CP conservation, $A_D = 0$, $|q/p| = 1$, and $\phi = 0$. In this case

$$\begin{aligned} r(t) &= \bar{r}(t) \\ &= \left|A_{\overline{f}}\right|^2 e^{-\Gamma t}\left[R_D + \sqrt{R_D}\, y'(\Gamma t) + \frac{x'^2 + y'^2}{4}(\Gamma t)^2\right], \end{aligned} \tag{70.24}$$

and the total number of $D^0 \to f$ decays divided by the total number of $D^0 \to \bar{f}$ decays is

$$R = \frac{\displaystyle\int_0^\infty r(t)\, dt}{\displaystyle\int_0^\infty \left|A_{\overline{f}}\right|^2 e^{-\Gamma t}\, dt} = R_D + \sqrt{R_D}\, y' + \frac{x'^2 + y'^2}{2}. \tag{70.25}$$

The ratio R is more straightforward to measure than $r(t)$ or $\bar{r}(t)$, as there is no decay-time dependence. In Table 70.2 we report measurements of R, R_D, and A_D in $D^0 \to K^+\pi^-$ decays normalized to $D^0 \to K^-\pi^+$ decays, and results from HFLAV [18] obtained from a global fit to all relevant data that allows for both mixing and CP violation (see Section 70.7). The experiments typically perform a single fit for parameters R_D, x'^2, and y'; results for x'^2 and y' are listed in Table 70.3. Allowing for CP violation, the experiments measure parameters (R^+_D, x'^2_+, y'_+) and (R^-_D, x'^2_-, y'_-) [or equivalently (R_D, A_D) instead of (R^+_D, R^-_D)] by separately fitting the $D^0 \to K^+\pi^-$ and $\overline{D}^0 \to K^-\pi^+$ event samples.

Extraction of the mixing parameters x and y from measurements of x' and y' requires knowledge of the strong phase difference $\delta_{K\pi}$. This can be determined from the decay rates of $D_\pm \to K^+\pi^-$, where D_+ (D_-) denotes the CP-even (CP-odd) eigenstate. Since $|D_\pm\rangle = (|D^0\rangle \mp |\overline{D}^0\rangle)/\sqrt{2}$,

$$\sqrt{2}\, A(D_\pm \to K^+\pi^-) = A(D^0 \to K^+\pi^-) \mp A\left(\overline{D}^0 \to K^+\pi^-\right). \tag{70.26}$$

Squaring this amplitude and using Eq. (70.13) yields the relation

$$\cos\delta_{K\pi} = \frac{|A(D_+ \to K^+\pi^-)|^2 - |A(D_- \to K^+\pi^-)|^2}{2\,|A(D^0 \to K^+\pi^-)|\,|A(\overline{D}^0 \to K^+\pi^-)|}. \tag{70.27}$$

Measuring the right-hand side is possible if one can identify pure D_+, D_-, D^0, and $\overline{D}^0$ initial states. This is accomplished at CLEOc and BESIII utilizing the processes $e^+e^- \to \psi(3770) \to \overline{D}^0 D^0 \to (f_{CP})(K^+\pi^-)$, or $\psi(3770) \to \overline{D}^0 D^0 \to (f_{\overline{D}^0})(K^+\pi^-)$, where f_{CP} denotes a CP-specific final state, and $f_{\overline{D}^0}$ denotes a $\overline{D}^0$-flavor-specific final state. In the first case, quantum coherence and CP symmetry ensures that the $K^+\pi^-$ state originates from a neutral D with CP opposite that of f_{CP}. In the second case, at the time when the $\overline{D}^0$ decays, the opposite side is D^0. However, it can potentially mix to $\overline{D}^0$ before decaying to $K^+\pi^-$, and this introduces some dependence on the mixing parameters x and y. This dependence is seen explicitly in the observable

$$A^{CP}_{K\pi} \equiv \frac{|A(D_- \to K^-\pi^+)|^2 - |A(D_+ \to K^-\pi^+)|^2}{|A(D_- \to K^-\pi^+)|^2 + |A(D_+ \to K^-\pi^+)|^2}. \tag{70.28}$$

To lowest order in the mixing parameters [28],

$$A^{CP}_{K\pi} = \frac{2\sqrt{R_D}\cos\delta_{K\pi} + y}{1 + R}, \tag{70.29}$$

where R is defined in Eq. (70.25). Such measurements are discussed in Section 70.5.

70.3.1 *Wrong-sign decays to multibody final states*

For multibody final states, Eqs. (70.13)-(70.25) apply to each point in phase-space. Although x and y do not vary across phase-space, knowledge of the resonant substructure is needed to determine the strong phase difference δ from point to point to extract x and y. Alternatively, experimental knowledge of the strong phase difference between D^0 and $\overline{D}^0$ decay amplitudes across phase space [39] allow one to determine x and y independent of a decay model of resonant substructure. This phase information can be measured at the charm threshold, where CLEO-c and BESIII took data.

A time-dependent analysis at BaBar [40,41] of $D^0 \to K^+\pi^-\pi^0$ decays, relative to CF $\overline{D}^0 \to K^+\pi^-\pi^0$ decays, determined the strong phase variation across the Dalitz plot and reported $x'' = (2.61\,^{+0.57}_{-0.68} \pm 0.39)\%$ and $y'' = (-0.06\,^{+0.55}_{-0.64} \pm 0.34)\%$. These mixing parameters are defined as

$$x'' = x\cos\delta_{K\pi\pi^0} + y\sin\delta_{K\pi\pi^0} \tag{70.30}$$

$$y'' = y\cos\delta_{K\pi\pi^0} - x\sin\delta_{K\pi\pi^0}, \tag{70.31}$$

in analogy with x', y', and $\delta_{K\pi}$ of Eqs. (70.20) and (70.21). Here, $\delta_{K\pi\pi^0}$ is the strong phase difference between the amplitudes $A(D^0 \to K^+\pi^-\pi^0)$ and $A(\overline{D}^0 \to K^+\pi^-\pi^0)$ at a "reference point" of the Dalitz plot. For this analysis, the reference point chosen is $m_{\pi^-\pi^0} = m_{\rho^-}$. The strong phase difference $\delta_{K\pi\pi^0}$ can be determined in a manner similar to that for $\delta_{K\pi}$: by using Eq. (70.27) and quantum-correlated measurements of the branching fractions $B(D_+ \to K^+\rho^-)$, $B(D_- \to K^+\rho^-)$, $B(D^0 \to K^+\rho^-)$, and $B(\overline{D}^0 \to K^+\rho^-)$ in $e^+e^- \to \psi(3770)$ events.

For the decay modes D^0 and $\overline{D}^0 \to K^+\pi^-\pi^+\pi^-$, Belle measured $R = (0.324 \pm 0.008 \pm 0.007)\%$ [42]. Subsequently, a phase-space-integrated analysis from LHCb [43] measured the product of a "coherence factor" $R^{K3\pi}_D$ and the strong-phase-rotated mixing parameter $y''_{K3\pi}$. This measurement resulted in an observation of charm mixing with 8.2σ significance.

Both the sign and magnitude of x and y without strong phases entering or sign ambiguity can be determined by measuring the time-dependent resonant substructure of multibody D^0 decays to self-conjugate final states [37, 38]. For such decays, e.g., $D^0 \to K^0_S\pi^+\pi^-$, the DCS and CF decay amplitudes populate the same Dalitz plot, which allows for direct measurement of the strong phase difference. Belle [35, 37], BaBar [36], and CLEO [44] have measured the overall phase difference between $D^0 \to K^*(892)^-\pi^+$ and $D^0 \to K^*(892)^+\pi^-$ to be $[173.9 \pm 0.7$ (stat. only)$]^\circ$, $[177.6 \pm 1.1$ (stat. only)$]^\circ$, and $[189 \pm 10 \pm 3\,^{+15}_{-5}]^\circ$, respectively. These results are close to the 180° expected from Cabibbo factors, i.e., the relative minus sign between $V^*_{cs}V_{ud}$ and $V^*_{us}V_{cd}$; thus they indicate a small strong phase. Three LHCb measurements [31–33] of x, y using $D^0 \to K^0_S\pi^+\pi^-$ decays are decay-model independent, as the model of resonances in the intermediate state is replaced by strong-phase measurements from CLEO-c [29] and BESIII [45]. Table 70.4 summarizes results from time-dependent analyses of self-conjugate multibody final states. World average values for the measurements listed are given later, as a result of the HFLAV global fit.

With regard to resonant substructure in $D^0 \to K^0_S\pi^+\pi^-$ decays, Belle [35, 37] measured the relative strong phase (statistical errors only) and the ratio R (central values only) of the DCS fit fraction relative to the CF fit fraction for five excited K states: $K^*(892)^+\pi^-$, $K^*_0(1430)^+\pi^-$, $K^*_2(1430)^+\pi^-$, $K^*(1410)^+\pi^-$, and $K^*(1680)^+\pi^-$. Similarly, BaBar [36, 46, 47] reported central values of R for $K^*(892)^+\pi^-$, $K^*_0(1430)^+\pi^-$, and $K^*_2(1430)^+\pi^-$.

Downloaded from https://academic.oup.com/ptep/article/2022/8/083C01/6651666 by KIT Library user on 27 September 2022

Table 70.3: Results for x'^2 and y', as measured using $D^0 \to K^\pm\pi^\mp$ decays. When a single uncertainty is listed, that corresponds to statistical and systematic uncertainties combined. The measurements with an asterisk (*) have been superseded and thus are not included in the HFLAV global fit. The measurements with a dagger (†) are not included in the HFLAV global fit due to much poorer precision. All confidence limits and intervals correspond to 95% C.L. The Belle 2006 results restrict x'^2 to the physical region. The BaBar confidence intervals are obtained from the fit, whereas Belle uses a Feldman-Cousins method, and CDF uses a Bayesian method.

Year	Experiment	No CP violation		Allowing for CP violation	
		x'^2 ($\times 10^{-3}$)	y' (%)	x'^2 ($\times 10^{-3}$)	y' (%)
2018	LHCb $\begin{pmatrix} 5.0\ \text{fb}^{-1} \\ D^*\ \text{tag} \end{pmatrix}$ [13]	0.039±0.027	0.528±0.052	D^0: 0.061±0.037 $\overline{D}^0$: 0.016±0.039	0.501±0.074 0.554±0.074
2017	LHCb $\begin{pmatrix} 3.0\ \text{fb}^{-1} \\ B{+}D^* \\ \text{double tag} \end{pmatrix}$ [14]	0.028±0.310	0.46±0.37	D^0: −0.019±0.447 $\overline{D}^0$: 0.079±0.433	0.581±0.526 0.332±0.523
2014	Belle (976 fb^{-1}) [15]	0.09±0.22	0.46±0.34	—	—
2013	CDF (9.6 fb^{-1}) [16]	0.08±0.18	0.43±0.43	—	—
2007	BaBar (384 fb^{-1}) [17]	−0.22±0.37	0.97±0.54	D^0: −0.24±0.52 $\overline{D}^0$: −0.20±0.50	0.98±0.78 0.96±0.75
2006	Belle (400 fb^{-1}) [22]	$\left(0.18\,^{+0.21}_{-0.23}\right)^*$	$\left(0.06\,^{+0.40}_{-0.39}\right)^*$	< 0.72	$-2.8 < y' < 2.1$
2013b*	LHCb $\begin{pmatrix} 3.0\ \text{fb}^{-1} \\ D^*\ \text{tag} \end{pmatrix}$ [19]	0.055±0.049	0.48±0.10	D^0: 0.049±0.070 $\overline{D}^0$: 0.060±0.068	0.51±0.14 0.45±0.14
2013a*	LHCb (1.0 fb^{-1}) [20]	−0.09±0.13	0.72±0.24	—	—
2008*	CDF (1.5 fb^{-1}) [21]	−0.12±0.35	0.85±0.76	—	—
2005†	FOCUS (234 evts) [23]	< 8.3	$-7.2 < y' < 4.1$	< 8.0	$-11.2 < y' < 6.7$
2000†	CLEO (9.0 fb^{-1}) [24]	0.00±0.23	$-2.3\,^{+1.3}_{-1.4}$	0.00±0.23	$-2.5\,^{+1.4}_{-1.6}$
1998†	E791 (5643 evts) [25]	< 17	< 13	—	—

Table 70.4: Results from time-dependent multibody analyses. The errors are statistical, systematic, and, when a third error is listed, due to the decay-model, respectively. The measurement with an asterisk (*) has been superseded and thus is not included in the HFLAV global fit. The measurement with a dagger (†) is not included in the HFLAV global fit due to poorer precision. The 2019 LHCb result utilizes strong-phase measurements from CLEO-c [29] and thus is decay-model independent. This fit determines CP-violating parameters Δx and Δy; the translation of these parameters to $|q/p|$ and ϕ is given in Ref. [30].

No CP Violation

Year	Experiment	Final state(s)	x ($\times 10^{-3}$)	y ($\times 10^{-3}$)
2021	LHCb (5.4 fb^{-1} D^* tag) [31]	$K^0_S\,\pi^+\pi^-$	$3.97 \pm 0.46 \pm 0.29$	$4.59 \pm 1.20 \pm 0.85$
2019	LHCb (3.0 fb^{-1} B, D^* tags) [32]	$K^0_S\,\pi^+\pi^-$	$2.7 \pm 1.6 \pm 0.4$	$7.4 \pm 3.6 \pm 1.1$
2016	LHCb (1.0 fb^{-1} D^* tag) [33]	$K^0_S\,\pi^+\pi^-$	$-8.6 \pm 5.3 \pm 1.7$	$0.3 \pm 4.6 \pm 1.3$
2016	BaBar (468 fb^{-1}) [34]	$\pi^+\pi^-\pi^0$	$15 \pm 12 \pm 6$	$2 \pm 9 \pm 5$
2014	Belle (921 fb^{-1}) [35]	$K^0_S\,\pi^+\pi^-$	$5.6 \pm 1.9\,^{+0.3}_{-0.9}\,^{+0.6}_{-0.9}$	$3.0 \pm 1.5\,^{+0.4}_{-0.5}\,^{+0.3}_{-0.6}$
2010	BaBar (469 fb^{-1}) [36]	$K^0_S\,\pi^+\pi^-$ $K^0_S\,K^+K^-$	1.6±2.3±1.2±0.8	5.7±2.0±1.3±0.7
2007*	Belle (540 fb^{-1}) [37]	$K^0_S\,\pi^+\pi^-$	$8.0 \pm 2.9\,^{+0.9}_{-0.7}\,^{+1.0}_{-1.4}$	$3.3 \pm 2.4\,^{+0.8}_{-1.2}\,^{+0.6}_{-0.8}$
2005†	CLEO (9.0 fb^{-1}) [38]	$K^0_S\,\pi^+\pi^-$	$19\,^{+32}_{-33} \pm 4 \pm 4$	$-14 \pm 24 \pm 8 \pm 4$

With CP Violation

Year	Experiment	Final state(s)	$\lvert q/p\rvert$	ϕ
2021	LHCb (5.4 fb^{-1}) [31]	$K^0_S\,\pi^+\pi^-$	0.996 ± 0.052 $\Delta x \times 10^3 =$ $-0.27 \pm 0.18 \pm 0.01$	$(3.2\,^{+2.7}_{-2.9})^\circ$ $\Delta y \times 10^3 =$ $0.20 \pm 0.36 \pm 0.13$
2019	LHCb (3.0 fb^{-1}) [32]	$K^0_S\,\pi^+\pi^-$	$1.05\,^{+0.22}_{-0.17}$ $\Delta x \times 10^3 =$ $-0.53 \pm 0.70 \pm 0.22$	$(-5.2\,^{+6.3}_{-9.2})^\circ$ $\Delta y \times 10^3 =$ $0.6 \pm 1.6 \pm 0.3$
2014	Belle (921 fb^{-1}) [35]	$K^0_S\pi^+\pi^-$	$0.90\,^{+0.16}_{-0.15}\,^{+0.05}_{-0.04}\,^{+0.06}_{-0.05}$	$(-6 \pm 11 \pm 3\,^{+3}_{-4})^\circ$
2007*‡	Belle (540 fb^{-1}) [37]	$K^0_S\,\pi^+\pi^-$	$0.86\,^{+0.30}_{-0.29}\,^{+0.06}_{-0.03} \pm 0.08$	$(-14\,^{+16}_{-18}\,^{+5}_{-3}\,^{+2}_{-4})^\circ$

‡This result allows for all types of CP violation and is superseded by Ref. [35], which assumes no direct CP violation in CF or DCS decays.

The systematic uncertainties on R are not evaluated. Large differences in R are observed among these final states, which indicates significant hadronic effects.

70.4 Decays to CP Eigenstates

When the final state f is a CP eigenstate, there is no distinction between f and $\overline{f}$. Thus $A_f = A_{\overline{f}}$ and $\overline{A}_{\overline{f}} = \overline{A}_f$. We denote final states with CP eigenvalues ± 1 by $f_\pm$. Decays to CP eigenstates proceed mainly via singly Cabibbo-suppressed amplitudes. Such amplitudes can contain internal loops and thus involve the third quark generation; in this manner a weak phase would appear in the decay amplitude, leading to direct CP violation. However, such internal loop amplitudes are suppressed, and the presence of a weak phase is often neglected.

The mixing parameter y may be measured by comparing the rate for D^0 decays to CP eigenstates such as K^+K^- with the rate to flavor eigenstates such as $K^-\pi^+$ [27]. If decays to K^+K^- have a shorter effective lifetime than those to $K^-\pi^+$, then $\Gamma_+ > \Gamma_-$, or, since CP violation is very small, $\Gamma_2 > \Gamma_1$ and y is positive. For small mixing ($x, y \ll 1$), the decay rates for $D^0 \to f_\pm$ and

Downloaded from https://academic.oup.com/ptep/article/2022/8/083C01/6651666 by KIT Library user on 27 September 2022

Table 70.5: Results for y_{CP} and A_Γ from D^0 decays to CP eigenstates. When a single uncertainty is listed, that corresponds to statistical and systematic uncertainties combined. The measurements with an asterisk (*) have been superseded.

Year	Experiment	Final state(s)	y_{CP} (%)	A_Γ ($\times 10^{-3}$)
2021	LHCb (8.4 fb^{-1} B, D^* tags) [48]	$K^+K^- + \pi^+\pi^-$	—	$0.10 \pm 0.11 \pm 0.03$
2021	LHCb (6 fb^{-1} D^* tag) [48]	$K^+K^- + \pi^+\pi^-$	—	$0.27 \pm 0.13 \pm 0.03$
2021	LHCb (6 fb^{-1} D^* tag) [48]	K^+K^-	—	$0.23 \pm 0.15 \pm 0.03$
2021	LHCb (6 fb^{-1} D^* tag) [48]	$\pi^+\pi^-$	—	$0.40 \pm 0.28 \pm 0.04$
2020	Belle (976 fb^{-1}) [49]	$K^0_S\,\omega$	$0.96 \pm 0.91^{+0.64}_{-0.62}$	—
2020	LHCb (5.4 fb^{-1} B tag) [50]	K^+K^-	—	$-0.43 \pm 0.36 \pm 0.05$
2020	LHCb (5.4 fb^{-1} B tag) [50]	$\pi^+\pi^-$	—	$0.22 \pm 0.70 \pm 0.08$
2019	LHCb (3 fb^{-1} B tag) [51]	$K^+K^- + \pi^+\pi^-$	$0.57 \pm 0.13 \pm 0.09$	—
2017	LHCb (3 fb^{-1} D^* tag) [52]	$K^+K^- + \pi^+\pi^-$	—	$-0.13 \pm 0.28 \pm 0.10$
2017	LHCb (3 fb^{-1} D^* tag) [52]	K^+K^-	—	$-0.30 \pm 0.32 \pm 0.10$
2017	LHCb (3 fb^{-1} D^* tag) [52]	$\pi^+\pi^-$	—	$0.46 \pm 0.58 \pm 0.12$
2016	Belle (976 fb^{-1}) [53]	$K^+K^- + \pi^+\pi^-$	$1.11 \pm 0.22 \pm 0.09$	$-0.3 \pm 2.0 \pm 0.7$
2015	LHCb (3 fb^{-1} B tag) [54]	$K^+K^- + \pi^+\pi^-$	—	-1.25 ± 0.73
2015	LHCb (3 fb^{-1} B tag) [54]	K^+K^-	—	$-1.34 \pm 0.77^{+0.26}_{-0.34}$
2015	LHCb (3 fb^{-1} B tag) [54]	$\pi^+\pi^-$	—	$-0.92 \pm 1.45^{+0.25}_{-0.33}$
2015	BES III (2.9 fb^{-1}) [55]	$\begin{cases} K^+K^-,\ \pi^+\pi^- \\ K^0_S\,\pi^0,\ K^0_S\,\pi^0\pi^0 \\ K^0_S\,\eta,\ K^0_S\,\omega \end{cases}$	$-2.0 \pm 1.3 \pm 0.7$	—
2014	CDF (9.7 fb^{-1}) [56]	$K^+K^- + \pi^+\pi^-$	—	-1.2 ± 1.2
2014	CDF (9.7 fb^{-1}) [56]	K^+K^-	—	$-1.9 \pm 1.5 \pm 0.4$
2014	CDF (9.7 fb^{-1}) [56]	$\pi^+\pi^-$	—	$-0.1 \pm 1.8 \pm 0.3$
2012	BaBar (468 fb^{-1}) [57]	$K^+K^- + \pi^+\pi^-$	$0.72 \pm 0.18 \pm 0.12$	$0.9 \pm 2.6 \pm 0.6$
2009	Belle (673 fb^{-1}) [58]	$K^0_S\,K^+K^-$	$0.11 \pm 0.61 \pm 0.52$	—
2002	CLEO (9.0 fb^{-1}) [59]	$K^+K^- + \pi^+\pi^-$	$-1.2 \pm 2.5 \pm 1.4$	—
2000	FOCUS (1×10^6 evts) [60]	K^+K^-	$3.42 \pm 1.39 \pm 0.74$	—
1999	E791 (2×10^{10} evts) [61]	K^+K^-	$0.73 \pm 2.89 \pm 1.03$	—
	HFLAV Average [62]		$\mathbf{0.719 \pm 0.113}$	$\mathbf{0.089 \pm 0.113}$
2020*	LHCb (5.4 fb^{-1} B tag) [50]	K^+K^-	—	$-0.43 \pm 0.36 \pm 0.05$
2020*	LHCb (5.4 fb^{-1} B tag) [50]	$\pi^+\pi^-$	—	$0.22 \pm 0.70 \pm 0.08$
2013*	LHCb (1.0 fb^{-1} D^* tag) [63]	K^+K^-	—	$-0.35 \pm 0.62 \pm 0.12$
2013*	LHCb (1.0 fb^{-1} D^* tag) [63]	$\pi^+\pi^-$	—	$0.33 \pm 1.06 \pm 0.14$
2011*‡	LHCb (29 pb^{-1} D^* tag) [64]	K^+K^-	$0.55 \pm 0.63 \pm 0.41$	$-5.9 \pm 5.9 \pm 2.1$
2009*	BaBar (384 fb^{-1}) [65]	K^+K^-	$1.16 \pm 0.22 \pm 0.18$	—
2008*	BaBar (384 fb^{-1}) [66]	$K^+K^- + \pi^+\pi^-$	$1.03 \pm 0.33 \pm 0.19$	$2.6 \pm 3.6 \pm 0.8$
2007*	Belle (540 fb^{-1}) [67]	$K^+K^- + \pi^+\pi^-$	$1.31 \pm 0.32 \pm 0.25$	$0.1 \pm 3.0 \pm 1.5$
2003*	BaBar (91 fb^{-1}) [68]	$K^+K^- + \pi^+\pi^-$	$0.8 \pm 0.4^{+0.5}_{-0.4}$	—
2001*	Belle (23.4 fb^{-1}) [69]	K^+K^-	$-0.5 \pm 1.0^{+0.7}_{-0.8}$	—

‡This result for y_{CP} is not superseded, but it is not included in the HFLAV average due to having some correlations with the result of Ref. [51] but much worse precision.

$\overline{D}^0 \to f_\pm$ have an approximately exponential time dependence:

$$r_\pm(t) \propto \exp(-\Gamma_\pm\, t) \tag{70.32}$$

$$\overline{r}_\pm(t) \propto \exp(-\overline{\Gamma}_\pm\, t)\,, \tag{70.33}$$

where the effective decay widths are given by

$$\Gamma_\pm = \Gamma\left(1 \pm \left|\frac{q}{p}\right| (y\cos\phi - x\sin\phi)\right) \tag{70.34}$$

$$\overline{\Gamma}_\pm = \Gamma\left(1 \pm \left|\frac{p}{q}\right| (y\cos\phi + x\sin\phi)\right)\,. \tag{70.35}$$

Thus, the effective decay rate to a CP eigenstate combining equal numbers of D^0 and $\overline{D}^0$ decays (e.g., an untagged sample with no production asymmetry) is

$$r_\pm(t) \;+\; \overline{r}_\pm(t) \;\propto\; e^{-(1\pm y_{CP})\Gamma t}\,, \tag{70.36}$$

where

$$y_{CP} = \frac{1}{2}\left(\left|\frac{q}{p}\right| + \left|\frac{p}{q}\right|\right) y\cos\phi - \frac{1}{2}\left(\left|\frac{q}{p}\right| - \left|\frac{p}{q}\right|\right) x\sin\phi \tag{70.37}$$

$$\approx y\cos\phi - A_M\, x\sin\phi\,. \tag{70.38}$$

If CP is conserved, $y_{CP} = y$. Most measurements of y_{CP} have used $D^0 \to K^+K^-$ and $D^0 \to \pi^+\pi^-$ decays, which are CP-even, measured relative to $D^0 \to K^-\pi^+$. Belle measured y_{CP} also using $D^0 \to K^0_S\,\omega$ decays [49], which are CP-odd, and $D^0 \to K^0_S\,K^+K^-$ decays [58], which are dominated by the CP-odd final state $K^0_S\,\phi$. Table 70.5 summarizes the current status of measurements.

In addition to y_{CP}, Belle [53], BaBar [57], CDF [56], and LHCb [48,64] have reported measurements of the decay-rate asymmetry for CP-even final states:

$$A_\Gamma \equiv \frac{\Gamma_+ - \overline{\Gamma}_+}{\Gamma_+ + \overline{\Gamma}_+} \;=\; \frac{(1/\tau_+) - (1/\overline{\tau}_+)}{(1/\tau_+) + (1/\overline{\tau}_+)} \;=\; \frac{\overline{\tau}_+ - \tau_+}{\overline{\tau}_+ + \tau_+} \tag{70.39}$$

$$\approx \frac{1}{2}\left(\left|\frac{q}{p}\right| - \left|\frac{p}{q}\right|\right) y\cos\phi - \frac{1}{2}\left(\left|\frac{q}{p}\right| + \left|\frac{p}{q}\right|\right) x\sin\phi \tag{70.40}$$

$$\approx A_M\, y\cos\phi - x\sin\phi\,. \tag{70.41}$$

If CP is conserved, $A_\Gamma = 0$.

There is a contribution to Eq. (70.41) from direct CP violation, i.e., $|\overline{A}_f/A_f| \neq 1$ [79,80]. For $f = K^+K^-$ and $\pi^+\pi^-$, this contribution can be estimated from measurements of $A_{CP}(K^+K^-)$ and $A_{CP}(\pi^+\pi^-)$ (see below) and is much smaller than the current uncertainty on A_M; thus we neglect it here. We note that, when averaging A_Γ measurements over K^+K^- and $\pi^+\pi^-$ final states, the contribution from direct CP violation cancels, as it has the same magnitude but opposite signs for K^+K^- and $\pi^+\pi^-$ due to U-spin symmetry [80].

Downloaded from https://academic.oup.com/ptep/article/2022/8/083C01/6651666 by KIT Library user on 27 September 2022

Table 70.6: Results for the difference in time-integrated CP asymmetries ΔA_{CP} between $D^0 \to K^+K^-$ and $D^0 \to \pi^+\pi^-$ decays. When a single uncertainty is listed, that corresponds to statistical and systematic uncertainties combined. The measurements with an asterisk (*) have been either superseded or combined with subsequent results and thus are not included in the HFLAV global fit.

Year	Experiment	ΔA_{CP} ($\times 10^{-3}$)
2019	LHCb (8.9 fb^{-1} B, D^* tags) [70]	-1.54 ± 0.29
2013	CDF (9.7 fb^{-1} D^* tag) [71]	$-6.2 \pm 2.1 \pm 1.0$
2008	BaBar (386 fb^{-1}) [72]	$2.4 \pm 6.2 \pm 2.6$
2008	Belle (540 fb^{-1}) [73]	$-8.6 \pm 6.0 \pm 0.7$
2016*	LHCb (3.0 fb^{-1} D^* tag) [74]	$-1.0 \pm 0.8 \pm 0.3$
2014*	LHCb (3.0 fb^{-1} B tag) [75]	$1.4 \pm 1.6 \pm 0.8$
2013*	LHCb (1.0 fb^{-1} B tag) [76]	$4.9 \pm 3.0 \pm 1.4$
2012*	LHCb (0.62 fb^{-1} D^* tag) [77]	$-8.2 \pm 2.1 \pm 1.1$
2012‡	Belle (976 fb^{-1}) [78]	$-8.7 \pm 4.1 \pm 0.6$

‡This preliminary result was not published and thus is not included in the HFLAV global fit.

Table 70.7: HFLAV global fit results (see text) [18].

Parameter	No CP Violation	No CP Violation in DCS Decays	All CP Violation Allowed	95% C.L. Interval (CPV Allowed)
x (%)	$0.44^{+0.13}_{-0.15}$	0.409 ± 0.048	$0.409^{+0.048}_{-0.049}$	[0.313, 0.503]
y (%)	0.63 ± 0.07	$0.603^{+0.057}_{-0.056}$	$0.615^{+0.056}_{-0.055}$	[0.509, 0.725]
$\delta_{K\pi}$ (°)	$8.9^{+8.9}_{-9.8}$	$5.5^{+8.3}_{-9.9}$	$7.2^{+7.9}_{-9.2}$	[−12.6, 21.8]
R_D (%)	0.344 ± 0.002	0.343 ± 0.002	0.343 ± 0.002	[0.340, 0.347]
A_D (%)	–	–	-0.70 ± 0.36	[−1.40, 0.00]
$\lvert q/p \rvert$	–	1.005 ± 0.007	0.995 ± 0.016	[0.96, 1.03]
ϕ (°)	–	$-0.18^{+0.28}_{-0.29}$	-2.5 ± 1.2	[−4.91, −0.19]
$\delta_{K\pi\pi}$ (°)	$21.8^{+23.5}_{-23.9}$	$22.3^{+21.9}_{-23.0}$	$23.0^{+21.8}_{-22.9}$	[−22.6, 64.9]
$A_{CP}^{\pi\pi}$(%)	–	0.027 ± 0.137	0.045 ± 0.137	[−0.22, 0.31]
A_{CP}^{KK}(%)	–	-0.133 ± 0.136	-0.113 ± 0.137	[−0.38, 0.15]
x_{12} (%)	–	0.409 ± 0.048		[0.314, 0.503]
y_{12} (%)	–	$0.603^{+0.057}_{-0.056}$		[0.495, 0.715]
ϕ_{12}(°)	–	$0.58^{+0.91}_{-0.90}$		[−1.20, 2.42]
χ^2/d.o.f.	$98.68/52 = 1.90$	$66.27/53 = 1.25$	$63.64/51 = 1.25$	

The asymmetry A_Γ is an asymmetry in the full decay widths. An asymmetry in partial widths is referred to as A_{CP} and is final-state dependent:

$$A_{CP} \equiv \frac{\Gamma(D^0 \to f) - \Gamma(\overline{D}^0 \to \overline{f})}{\Gamma(D^0 \to f) + \Gamma(\overline{D}^0 \to \overline{f})} . \tag{70.42}$$

Unlike A_Γ, which is measured by fitting decay time distributions, A_{CP} is measured by fitting for signal yields and (aside from acceptance effects) does not require measuring decay times. For neutral D decays, A_{CP} receives contributions from both direct (in the decay amplitudes) and indirect (due to mixing) processes: $A_{CP}(D^0 \to f) = A_{CP}^f + A_{CP}^{\rm indirect}$. The latter indirect contribution depends on the mixing parameters x and y:

$$\begin{aligned} A_{CP}^{\rm indirect} &= \frac{1}{2}\left(\left|\frac{q}{p}\right| + \left|\frac{p}{q}\right|\right) x \sin\phi - \frac{1}{2}\left(\left|\frac{q}{p}\right| - \left|\frac{p}{q}\right|\right) y \cos\phi \\ &= -A_\Gamma . \end{aligned} \tag{70.43}$$

Numerous measurements of A_{CP} for decays to CP eigenstates are listed in this *Review* [81]. Table 70.6 summarizes the current status of measurements of the *difference* in A_{CP} for $D^0 \to K^+K^-$ and $D^0 \to \pi^+\pi^-$ decays: $\Delta A_{CP} \equiv A_{CP}(K^+K^-) - A_{CP}(\pi^+\pi^-)$. Within the Standard Model, $A_{CP}^{KK} \approx -A_{CP}^{\pi\pi}$ [82], and ΔA_{CP} essentially doubles any direct CP violation present. The difference is also advantageous experimentally, as several systematic uncertainties cancel. As $A_{CP}^{\rm indirect}$ is independent of final state, it subtracts out of ΔA_{CP}. However, at hadron experiments such as LHCb, there are differences in efficiencies between K^+K^- and $\pi^+\pi^-$ such that $\langle t \rangle_{KK} \neq \langle t \rangle_{\pi\pi}$, i.e., the mean decay times slightly differ. This difference retains a small contribution to ΔA_{CP} from $A_{CP}^{\rm indirect}$ [79]. The most recent ΔA_{CP} result from LHCb [70], based on 8.9 fb^{-1} of data, differs from zero with a statistical significance of 5.3σ. Thus, this measurement constitutes the first observation of CP violation in charm decays. These CP asymmetries are included in HFLAV's global fit for charm mixing parameters discussed below; the fit shows that the CP violation observed is due to the direct contributions A_{CP}^{KK} and $A_{CP}^{\pi\pi}$.

70.5 Quantum-correlated $D^0\overline{D}^0$ Analyses

Measurements of R_D, $\cos\delta_{K\pi}$, $\sin\delta_{K\pi}$, x, and y can be obtained from a combined fit to time-integrated yields of single-tagged (ST) and double-tagged (DT) $D^0\overline{D}^0$ events produced at the $\psi(3770)$ resonance [83, 84]. Single-tagged events are those in which either the D^0 or $\overline{D}^0$ decay is reconstructed (identified), and the other neutral D decays generically. Double-tagged events are those in which both the D^0 and $\overline{D}^0$ decay are identified. Due to quantum correlations, the decay of a D^0, $\overline{D}^0$, D_+, or D_- projects the other neutral D into a state $\overline{D}^0$, D^0, D_-, and D_+, respectively. The CP-specific D_- and D_+ decays (or, neglecting CP violation, D_1 and D_2 decays) include interference between D^0 and $\overline{D}^0$ amplitudes, and this provides sensitivity to R_D and $\cos\delta_{K\pi}$. The flavor-specific D^0 and $\overline{D}^0$ decays include interference between D_1 and D_2 amplitudes, and this provides sensitivity to x and y. For details of this method, see Refs. [1–5].

BESIII has reported results using 2.92 fb^{-1} of $e^+e^- \to \psi(3770)$ data, where the quantum-correlated $D^0\overline{D}^0$ pairs are produced in a $C = -1$ state. They measure $y_{CP} = (-2.0 \pm 1.3 \pm 0.7)\%$ [55] from DT yields using a CP-eigenstate tag for one D and a semileptonic tag for the other; and they measure $A_{K\pi}^{CP} = (12.7 \pm 1.3 \pm 0.7)\%$ [28] from DT yields using a CP tag for one D and a $K^\pm\pi^\mp$ tag for the other. For y_{CP}, the CP eigenstates used are K^-K^+ (f_+), $\pi^+\pi^-$ (f_+), $K_S^0\pi^0\pi^0$ (f_+), $K_S^0\pi^0$ (f_-), $K_S^0\eta$ (f_-), and $K_S^0\omega$ (f_-). For $A_{K\pi}^{CP}$, additional CP eigenstates included are $\pi^0\pi^0$ (f_+) and $\rho^0\pi^0$ (f_+). Using external inputs for R_D and y from HFLAV [85], and R from the PDG [86], BESIII uses Eq. (70.29)

Downloaded from https://academic.oup.com/ptep/article/2022/8/083C01/6651666 by KIT Library user on 27 September 2022

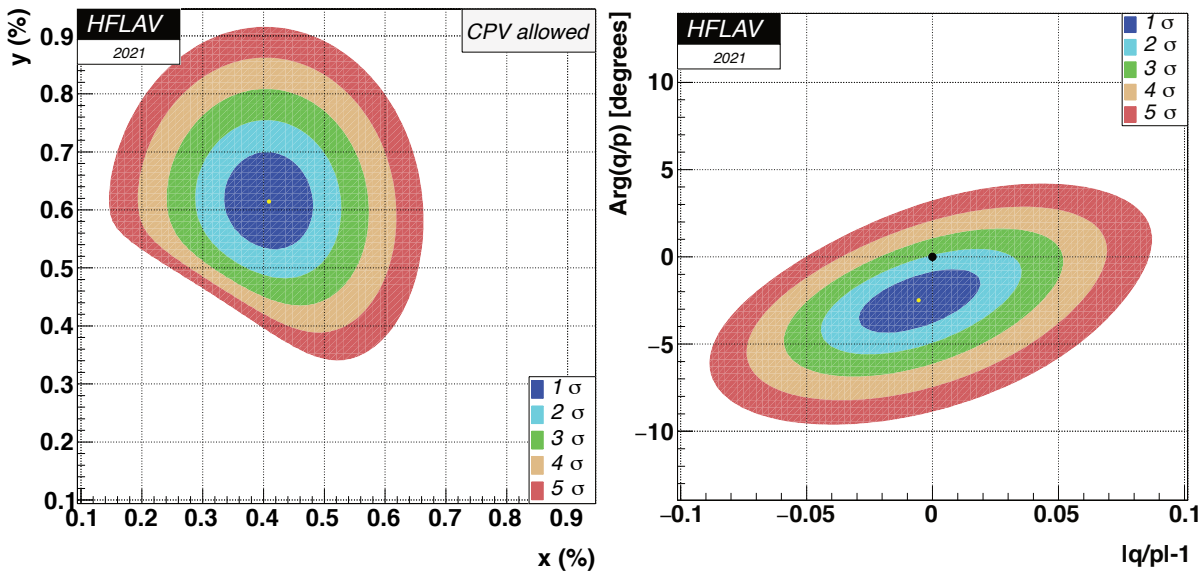

Figure 70.1: Two-dimensional 1σ-5σ contours for (x, y) (left) and for $(|q/p|,\mathrm{Arg}(q/p))$ (right) as obtained by HFLAV [18], from measurements of $D^0 \to K^{(*)+}\ell\nu$, h^+h^-, $K^+\pi^-$, $K^+\pi^-\pi^0$, $K^+\pi^-\pi^+\pi^-$, $K^0_S\pi^+\pi^-$, $K^0_S K^+K^-$, and $\pi^+\pi^-\pi^0$ decays, and double-tagged branching fractions measured at the $\psi(3770)$ resonance. In the right plot, the black dot denotes the no-CPV point $(0, 0)$.

to determine $\cos\delta_{K\pi} = 1.02 \pm 0.11 \pm 0.06 \pm 0.01$ [28], where the third uncertainty is due to the external inputs.

CLEO-c has reported results using 0.82 fb^{-1} of $e^+e^- \to \psi(3770)$ data [87–89]. The values for y, R_M, $\cos\delta_{K\pi}$, and $\sin\delta_{K\pi}$ are obtained from a combined fit to the ST (hadronic only) and DT yields. The DT yields include events in which one D is reconstructed in a hadronic mode and the other D is partially reconstructed in either $D \to K^\mp e^\pm\nu$ or $D \to K^\mp\mu^\pm\nu$. The CLEO-c analysis obtains $\cos\delta_{K\pi} = 0.81^{+0.22}_{-0.18}{}^{+0.07}_{-0.05}$ and $\sin\delta_{K\pi} = -0.01 \pm 0.41 \pm 0.04$. These fits allow $\cos\delta_{K\pi}$ and $\sin\delta_{K\pi}$ (and also x^2) to be unphysical. Constraining $\cos\delta_{K\pi}$ and $\sin\delta_{K\pi}$ to the physical range $[-1, +1]$ (i.e., interpreting $\delta_{K\pi}$ as an angle) and also using external inputs for x, y and y_{CP} from HFLAV [90], CLEO-c obtains $\delta_{K\pi} = (18^{+11}_{-17})^\circ$ [89].

70.6 Summary of Experimental Results

The first evidence for D^0-$\overline{D}^0$ mixing was obtained in 2007 by Belle [67] and BaBar [17]. These results were confirmed by CDF [91] and, much later, by LHCb [20]. There are now numerous measurements of D^0-$\overline{D}^0$ mixing with various levels of sensitivity. For $D^0 \to K^+\pi^-$ decays, LHCb [19, 20], CDF [16], and Belle [15] each exclude the no-mixing hypothesis by more than five standard deviations. LHCb [43] reported the observation of charm mixing in $D^0 \to K^+\pi^-\pi^+\pi^-$ decays with 8.2σ significance. However, the strong phase difference for this decay is not known, and thus the mixing parameters x and y cannot be extracted. The most precise measurements of x and y are obtained from a time-dependent Dalitz plot analysis of $D^0 \to K^0_S\pi^+\pi^-$ decays. This method was originally used at CLEO [92] and subsequently exploited at Belle [35, 37] and BaBar [36] with much higher statistics. BaBar has applied this method also to $D^0 \to K^0_S K^+K^-$ decays [36]. It has recently been used by LHCb with very high statistics [31] to obtain the most precise values of x and y to date. This measurement resulted in the first observation ($> 5\sigma$ significance) of dispersive mixing, i.e., $x \neq 0$.

The experimental data demonstrate that D^0 and $\overline{D}^0$ mesons mix. This mixing is presumably dominated by long-distance amplitudes, which are difficult to calculate. Under the assumption that the observed mixing is due entirely to non-Standard Model processes, significant constraints on New Physics models can be obtained [93]. A significant limitation to interpreting charm mixing in terms of New Physics is the theoretical uncertainty on Standard Model predictions [94, 95]. We note that the HFLAV global fit results for x and y (see below) indicate that charm mixing is at the upper end of the range of Standard Model predictions.

The current situation would benefit from better knowledge of the strong phase difference $\delta_{K\pi}$ than that currently available from CLEO-c [89] and BESIII [28]. Such knowledge would allow one to extract x and y directly from $D^0 \to K^+\pi^-$ measurements of x'^2 and y'. Similarly, knowledge of the strong phase difference $\delta_{K\pi\pi\pi}$ would allow one to extract x and y from measurements of x''^2 and y'' obtained using $D^0 \to K^+\pi^-\pi^+\pi^-$ decays.

With regard to CP violation, by combining four separate measurements from two data sets totalling 8.9 fb^{-1} of data, LHCb observed CP violation in D decays for the first time [70]. The amount of CP violation measured is small, only $\sim$0.15%. A theory calculation indicates that this value is consistent with Standard Model expectations [96]; however, new physics contributions cannot be excluded.

70.7 HFLAV Global Fit for Charm Mixing Parameters

The Heavy Flavor Averaging Group (HFLAV) performs a global fit to all relevant mixing measurements to obtain world average values for 10 fitted parameters: x, y, $\delta_{K\pi}$, $\delta_{K\pi\pi^0}$, $R_D(K^+\pi^-)$, $A_D(K^+\pi^-)$, $|q/p|$, $\mathrm{Arg}(q/p) \equiv \phi$, and the direct CP-violating asymmetries A^{KK}_{CP} and $A^{\pi\pi}_{CP}$. Correlations among observables are taken into account by using the error matrices provided by the experiments. Measurements of $D^0 \to K^{(*)+}\ell^-\overline{\nu}$, K^+K^-, $\pi^+\pi^-$, $K^+\pi^-$, $K^+\pi^-\pi^0$, $K^+\pi^-\pi^+\pi^-$, $K^0_S\pi^+\pi^-$, $K^0_S K^+K^-$, and $\pi^+\pi^-\pi^0$ decays are used, as well as CLEO-c fitted values of R_D, x^2, y, $\cos\delta$, and $\sin\delta$ obtained from quantum-correlated branching fractions measured in $e^+e^- \to \psi(3770) \to D^0\overline{D}^0$ reactions. There are three observables input to the fit that are

Downloaded from https://academic.oup.com/ptep/article/2022/8/083C01/6651666 by KIT Library user on 27 September 2022

themselves world average values calculated by HFLAV: R_M from $D^0 \to K^{(*)+}\ell^-\overline{\nu}$ decays (Table 70.1), and y_{CP} and A_Γ from $D^0 \to f_{CP}$ decays (Table 70.5). A measurement by LHCb of R_M using $D^0 \to K^+\pi^-\pi^+\pi^-$ decays is input separately. Details of the fitting procedure are given in Ref. [6].

The results of the fit as of July, 2021 are listed in Table 70.7. Three separate fits are performed: *(a)* assuming no CP violation; *(b)* assuming no CP violation in doubly Cabibbo-suppressed decays; and *(c)* allowing for all CP violation. The second fit *(b)* corresponds to the theory expectation [97, 98]; in this case four fitted parameters are reduced to three using the relationship $\tan\phi = (x/y)\cdot(1-|q/p|^2)/(1+|q/p|^2)$ [97–99]. Alternatively, one can fit for the three parameters $x_{12} \equiv 2|M_{12}|/\Gamma$, $y_{12} \equiv |\Gamma_{12}|/\Gamma$, and $\phi_{12} \equiv \mathrm{Arg}(M_{12}/\Gamma_{12})$, from which x, y, $|q/p|$, and ϕ can be derived.

Confidence contours in the two dimensions (x, y) and $(|q/p|, \phi)$ resulting from the fit are plotted in Fig. 70.1. These contours are obtained by allowing, for any point in the two-dimensional plane, all other fitted parameters to take their preferred values. The 1σ–5σ boundaries drawn are the loci of points in which the χ^2 has risen above the minimum by 2.30, 6.18, 11.83, 19.33, and 28.67 units. The fit excludes the no-mixing point $x=y=0$ at more than 11.5σ. The fit is consistent with CP conservation ($|q/p| = 1$, $\phi = 0$) at the 1.6σ level. The χ^2 of the fit is 63.6 for $61-10 = 51$ degrees of freedom, which is satisfactory.

One-dimensional likelihood functions for parameters are obtained by allowing, for any value of the parameter, all other fitted parameters to take their preferred values. The resulting likelihood functions give central values, 68.3% C.L. intervals, and 95% C.L. intervals as listed in Table 70.7. The parameter ranges $x \leq 0$ and $y \leq 0$ are excluded at 8.2σ and more than 11.4σ significance, respectively.

From the results of the HFLAV averaging and global fit, we conclude the following: (1) Since CP violation is small and y_{CP} is positive, the CP-even state is shorter-lived, as in the $K^0\overline{K}^0$ system. (2) Since x is positive, the CP-even state is heavier, unlike in the $K^0\overline{K}^0$ system. (3) The strong phase difference $\delta_{K\pi}$ is consistent with the $SU(3)$ expectation of zero, and large values are unlikely (the 95% C.L. interval is $-13^\circ < \delta_{K\pi} < 22^\circ$). (4) While direct CP violation has been observed in D decays, there is no evidence for indirect CP violation, i.e., $|q/p| \neq 1$ or $\phi \neq 0$. Observing such CP violation at the current level of sensitivity would indicate new physics.

70.8 Future Data

Current results are based primarily upon CLEO-c (0.82 fb^{-1} of $e^+e^- \to \psi(3770)$ data), Belle and BaBar ($\sim$1.4 ab^{-1} of $e^+e^- \to \Upsilon(4S)$ data), CDF (9.6 fb^{-1} of $p\bar{p}$ collision data at $\sqrt{s} = 1.96$ TeV), and LHCb Runs 1 and 2 (3.0 fb^{-1}+5.9 fb^{-1} of pp collision data at $\sqrt{s} = 7$, 8, 13 TeV).

BESIII has accumulated 2.9 fb^{-1} of $e^+e^- \to \psi(3770)$ data and plans to collect up to 20 fb^{-1} in the next few years. These data should provide strong phase measurements that enable improved model-independent determinations of mixing parameters from Belle II and LHCb. In 2019, Belle II began accumulating 50 ab^{-1} of $e^+e^- \to \Upsilon(4S)$ data [100], which is expected to take approximately ten years to collect. At LHCb, Run 2 was completed in 2018, Run 3 is planned for 2022-24, and Run 4 is planned for 2027-30 [101]. The goal for Runs $3+4$ is to accumulate an additional 50 fb^{-1} of pp data at $\sqrt{s} \approx 14$ TeV [102]. These data, along with the large e^+e^- dataset from Belle II, should provide more precise measurements of D^0-$\overline{D}^0$ mixing and significantly greater sensitivity to direct and indirect CP violation in D^0 decays.

References

[1] D. M. Asner and W. M. Sun, Phys. Rev. **D73**, 034024 (2006), [Erratum: Phys. Rev. **D77**, 019901 (2008)], [hep-ph/0507238].

[2] D. Atwood and A. A. Petrov, Phys. Rev. **D71**, 054032 (2005), [hep-ph/0207165].

[3] M. Gronau, Y. Grossman and J. L. Rosner, Phys. Lett. **B508**, 37 (2001), [hep-ph/0103110].

[4] Z.-z. Xing, Phys. Rev. **D55**, 196 (1997), [hep-ph/9606422].

[5] M. Goldhaber and J. L. Rosner, Phys. Rev. **D15**, 1254 (1977).

[6] Y. S. Amhis *et al.* (HFLAV), Eur. Phys. J. C **81**, 3, 226 (2021), [arXiv:1909.12524].

[7] U. Bitenc *et al.* (Belle), Phys. Rev. **D77**, 112003 (2008), [arXiv:0802.2952].

[8] B. Aubert *et al.* (BaBar), Phys. Rev. **D76**, 014018 (2007), [arXiv:0705.0704].

[9] C. Cawlfield *et al.* (CLEO), Phys. Rev. **D71**, 077101 (2005), [hep-ex/0502012].

[10] E. M. Aitala *et al.* (E791), Phys. Rev. Lett. **77**, 2384 (1996), [hep-ex/9606016].

[11] U. Bitenc *et al.* (Belle), Phys. Rev. **D72**, 071101 (2005), [hep-ex/0507020].

[12] B. Aubert *et al.* (BaBar), Phys. Rev. **D70**, 091102 (2004), [hep-ex/0408066].

[13] R. Aaij *et al.* (LHCb), Phys. Rev. **D97**, 3, 031101 (2018), [arXiv:1712.03220].

[14] R. Aaij *et al.* (LHCb), Phys. Rev. **D95**, 5, 052004 (2017), [Erratum: Phys. Rev. **D96**, 099907 (2017)], [arXiv:1611.06143].

[15] B. R. Ko *et al.* (Belle), Phys. Rev. Lett. **112**, 11, 111801 (2014), [Addendum: Phys. Rev. Lett. **112**, 139903 (2014)], [arXiv:1401.3402].

[16] T. A. Aaltonen *et al.* (CDF), Phys. Rev. Lett. **111**, 23, 231802 (2013), [arXiv:1309.4078].

[17] B. Aubert *et al.* (BaBar), Phys. Rev. Lett. **98**, 211802 (2007), [hep-ex/0703020].

[18] Heavy Flavor Averaging Group, `https://hflav-eos.web.cern.ch/hflav-eos/charm/CHARM21/results_mix_cpv.html`.

[19] R. Aaij *et al.* (LHCb), Phys. Rev. Lett. **111**, 25, 251801 (2013), [arXiv:1309.6534].

[20] R. Aaij *et al.* (LHCb), Phys. Rev. Lett. **110**, 10, 101802 (2013), [arXiv:1211.1230].

[21] T. Aaltonen *et al.* (CDF), Phys. Rev. Lett. **100**, 121802 (2008), [arXiv:0712.1567].

[22] L. M. Zhang *et al.* (Belle), Phys. Rev. Lett. **96**, 151801 (2006), [hep-ex/0601029].

[23] J. M. Link *et al.* (FOCUS), Phys. Lett. **B618**, 23 (2005), [hep-ex/0412034].

[24] R. Godang *et al.* (CLEO), Phys. Rev. Lett. **84**, 5038 (2000), [hep-ex/0001060].

[25] E. M. Aitala *et al.* (E791), Phys. Rev. **D57**, 13 (1998), [hep-ex/9608018].

[26] Y. Nir, Lectures given at 27th SLAC Summer Institute on Particle Physics: "CP Violation in and Beyond the Standard Model (SSI 99)," Stanford, California, 7-16 July 1999. Published in Trieste 1999, *Particle Physics*, pp. 165-243.

[27] S. Bergmann *et al.*, Phys. Lett. **B486**, 418 (2000), [hep-ph/0005181].

[28] M. Ablikim *et al.* (BESIII), Phys. Lett. **B734**, 227 (2014), [arXiv:1404.4691].

[29] J. Libby *et al.* (CLEO), Phys. Rev. **D82**, 112006 (2010), [arXiv:1010.2817].

[30] A. Di Canto *et al.*, Phys. Rev. **D99**, 1, 012007 (2019), [arXiv:1811.01032].

[31] R. Aaij *et al.* (LHCb), Phys. Rev. Lett. **127**, 11, 111801 (2021), [arXiv:2106.03744].

[32] R. Aaij *et al.* (LHCb), Phys. Rev. Lett. **122**, 23, 231802 (2019), [arXiv:1903.03074].

[33] R. Aaij *et al.* (LHCb), JHEP **04**, 033 (2016), [arXiv:1510.01664].

Downloaded from https://academic.oup.com/ptep/article/2022/8/083C01/6651666 by KIT Library user on 27 September 2022

[34] J. P. Lees *et al.* (BaBar), Phys. Rev. **D93**, 11, 112014 (2016), [arXiv:1604.00857].

[35] T. Peng *et al.* (Belle), Phys. Rev. **D89**, 9, 091103 (2014), [arXiv:1404.2412].

[36] P. del Amo Sanchez *et al.* (BaBar), Phys. Rev. Lett. **105**, 081803 (2010), [arXiv:1004.5053].

[37] K. Abe *et al.* (Belle), Phys. Rev. Lett. **99**, 131803 (2007), [arXiv:0704.1000].

[38] D. M. Asner *et al.* (CLEO), Phys. Rev. **D72**, 012001 (2005), [hep-ex/0503045].

[39] See "Review of Multibody Charm Analyses" in this *Review*.

[40] B. Aubert *et al.* (BaBar), Phys. Rev. Lett. **97**, 221803 (2006), [hep-ex/0608006].

[41] B. Aubert *et al.* (BaBar), Phys. Rev. Lett. **103**, 211801 (2009), [arXiv:0807.4544].

[42] E. White *et al.* (Belle), Phys. Rev. **D88**, 5, 051101 (2013), [arXiv:1307.5935].

[43] R. Aaij *et al.* (LHCb), Phys. Rev. Lett. **116**, 24, 241801 (2016), [arXiv:1602.07224].

[44] H. Muramatsu *et al.* (CLEO), Phys. Rev. Lett. **89**, 251802 (2002), [Erratum: Phys. Rev. Lett. **90**, 059901 (2003)], [hep-ex/0207067].

[45] M. Ablikim *et al.* (BESIII), Phys. Rev. D **101**, 11, 112002 (2020), [arXiv:2003.00091].

[46] B. Aubert *et al.* (BaBar), Phys. Rev. Lett. **95**, 121802 (2005), [hep-ex/0504039].

[47] B. Aubert *et al.* (BaBar), Phys. Rev. **D78**, 034023 (2008), [arXiv:0804.2089].

[48] R. Aaij *et al.* (LHCb) (2021), [arXiv:2105.09889].

[49] M. Nayak *et al.* (Belle), Phys. Rev. D **102**, 7, 071102 (2020), [arXiv:1912.10912].

[50] R. Aaij *et al.* (LHCb), Phys. Rev. **D101**, 1, 012005 (2020), [arXiv:1911.01114].

[51] R. Aaij *et al.* (LHCb), Phys. Rev. Lett. **122**, 1, 011802 (2019), [arXiv:1810.06874].

[52] R. Aaij *et al.* (LHCb), Phys. Rev. Lett. **118**, 26, 261803 (2017), [arXiv:1702.06490].

[53] M. Starič *et al.* (Belle), Phys. Lett. **B753**, 412 (2016), [arXiv:1509.08266].

[54] R. Aaij *et al.* (LHCb), JHEP **04**, 043 (2015), [arXiv:1501.06777].

[55] M. Ablikim *et al.* (BESIII), Phys. Lett. **B744**, 339 (2015), [arXiv:1501.01378].

[56] T. A. Aaltonen *et al.* (CDF), Phys. Rev. **D90**, 11, 111103 (2014), [arXiv:1410.5435].

[57] J. P. Lees *et al.* (BaBar), Phys. Rev. **D87**, 1, 012004 (2013), [arXiv:1209.3896].

[58] A. Zupanc *et al.* (Belle), Phys. Rev. **D80**, 052006 (2009), [arXiv:0905.4185].

[59] S. E. Csorna *et al.* (CLEO), Phys. Rev. **D65**, 092001 (2002), [hep-ex/0111024].

[60] J. M. Link *et al.* (FOCUS), Phys. Lett. **B485**, 62 (2000), [hep-ex/0004034].

[61] E. M. Aitala *et al.* (E791), Phys. Rev. Lett. **83**, 32 (1999), [hep-ex/9903012].

[62] Heavy Flavor Averaging Group, `https://hflav-eos.web.cern.ch/hflav-eos/charm/CHARM21/results_mixing.html`.

[63] R. Aaij *et al.* (LHCb), Phys. Rev. Lett. **112**, 4, 041801 (2014), [arXiv:1310.7201].

[64] R. Aaij *et al.* (LHCb), JHEP **04**, 129 (2012), [arXiv:1112.4698].

[65] B. Aubert *et al.* (BaBar), Phys. Rev. **D80**, 071103 (2009), [arXiv:0908.0761].

[66] B. Aubert *et al.* (BaBar), Phys. Rev. **D78**, 011105 (2008), [arXiv:0712.2249].

[67] M. Staric *et al.* (BELLE), Phys. Rev. Lett. **98**, 211803 (2007), [,65(2007)], [hep-ex/0703036].

[68] B. Aubert *et al.* (BaBar), Phys. Rev. Lett. **91**, 121801 (2003), [hep-ex/0306003].

[69] K. Abe *et al.* (Belle), Phys. Rev. Lett. **88**, 162001 (2002), [hep-ex/0111026].

[70] R. Aaij *et al.* (LHCb), Phys. Rev. Lett. **122**, 21, 211803 (2019), [arXiv:1903.08726].

[71] T. Aaltonen *et al.* (CDF), Phys. Rev. Lett. **109**, 111801 (2012), [arXiv:1207.2158].

[72] B. Aubert *et al.* (BaBar), Phys. Rev. Lett. **100**, 061803 (2008), [arXiv:0709.2715].

[73] M. Staric *et al.* (Belle), Phys. Lett. **B670**, 190 (2008), [arXiv:0807.0148].

[74] R. Aaij *et al.* (LHCb), Phys. Rev. Lett. **116**, 19, 191601 (2016), [arXiv:1602.03160].

[75] R. Aaij *et al.* (LHCb), JHEP **07**, 041 (2014), [arXiv:1405.2797].

[76] R. Aaij *et al.* (LHCb), Phys. Lett. **B723**, 33 (2013), [arXiv:1303.2614].

[77] R. Aaij *et al.* (LHCb), Phys. Rev. Lett. **108**, 111602 (2012), [arXiv:1112.0938].

[78] B. R. Ko (Belle), in "7th International Workshop on the CKM Unitarity Triangle (CKM 2012) Cincinnati, Ohio, USA, September 28-October 2, 2012," (2012), [arXiv:1212.5320].

[79] M. Gersabeck *et al.*, J. Phys. G **39**, 045005 (2012), [arXiv:1111.6515].

[80] A. L. Kagan and L. Silvestrini, Phys. Rev. D **103**, 5, 053008 (2021), [arXiv:2001.07207].

[81] See the tabulation of A_{CP} results in the D^0 and D^+ Listings in this *Review*.

[82] Y. Grossman, A. L. Kagan and Y. Nir, Phys. Rev. D **75**, 036008 (2007), [hep-ph/0609178].

[83] R.A. Briere *et al.*, (CLEO Collab.), CLNS 01-1742, (2001).

[84] D. M. Asner *et al.*, (BES-III Collab.), Int. J. Mod. Phys. **A**, 24 (2009).

[85] Heavy Flavor Averaging Group, `https://hflav-eos.web.cern.ch/hflav-eos/charm/CHARM13/results_mix_cpv.html`.

[86] J. Beringer *et al.* (Particle Data Group), Phys. Rev. **D86**, 010001 (2012).

[87] J. L. Rosner *et al.* (CLEO), Phys. Rev. Lett. **100**, 221801 (2008), [arXiv:0802.2264].

[88] D. M. Asner *et al.* (CLEO), Phys. Rev. **D78**, 012001 (2008), [arXiv:0802.2268].

[89] D. M. Asner *et al.* (CLEO), Phys. Rev. **D86**, 112001 (2012), [arXiv:1210.0939].

[90] Heavy Flavor Averaging Group, `https://hflav-eos.web.cern.ch/hflav-eos/charm/March12/results_mix_cpv.html`.

[91] T. Aaltonen *et al.* (CDF), Phys. Rev. Lett. **100**, 121802 (2008), [arXiv:0712.1567].

[92] D. M. Asner *et al.* (CLEO), Phys. Rev. D **72**, 012001 (2005), [hep-ex/0503045].

[93] E. Golowich *et al.*, Phys. Rev. **D76**, 095009 (2007), [arXiv:0705.3650].

[94] G. Isidori *et al.*, Phys. Lett. **B711**, 46 (2012), [arXiv:1111.4987].

[95] E. Franco, S. Mishima and L. Silvestrini, JHEP **05**, 140 (2012), [arXiv:1203.3131].

[96] J. Brod, A. L. Kagan and J. Zupan, Phys. Rev. D **86**, 014023 (2012), [arXiv:1111.5000].

Downloaded from https://academic.oup.com/ptep/article/2022/8/083C01/6651666 by KIT Library user on 27 September 2022

[97] Y. Grossman, Y. Nir and G. Perez, Phys. Rev. Lett. **103**, 071602 (2009), [arXiv:0904.0305].

[98] A. L. Kagan and M. D. Sokoloff, Phys. Rev. **D80**, 076008 (2009), [arXiv:0907.3917].

[99] M. Ciuchini *et al.*, Phys. Lett. **B655**, 162 (2007), [hep-ph/0703204].

[100] W. Altmannshofer *et al.* (Belle-II), PTEP **2019**, 12, 123C01 (2019), [Erratum: PTEP 2020, 029201 (2020)], [arXiv:1808.10567].

[101] CERN LHC Schedule, `https://lhc-commissioning.web.cern.ch/schedule/LHC-long-term.htm`.

[102] R. Aaij *et al.* (LHCb) (2018), [arXiv:1808.08865].

Downloaded from https://academic.oup.com/ptep/article/2022/8/083C01/6651666 by KIT Library user on 27 September 2022

71. D_s^+ Branching Fractions

Revised September 2021 by J.L. Rosner (Chicago U.) and C.G. Wohl (LBNL).

Figure 71.1 shows a partial breakdown of the D_s^+ branching fractions. The rest of this note is about how the figure was constructed. The values shown make heavy use of CLEO measurements of inclusive branching fractions [1]. For references to other data cited in the following, see the Listings. An addendum updates branching fractions to two-body final states reported by the BESIII Collaboration in 2020 [2], and the conclusion stresses modes still to be identified.

71.1 Modes with leptons

The bottom (18.0±1.0)% of Fig. 71.1 shows the fractions for the modes that include leptons. The measured $K^0e^+\nu_e$ and $K^{*0}e^+\nu_e$ fractions have been doubled to take account of the corresponding $\mu^+\nu_\mu$ fractions. The sum of the exclusive $Xe^+\nu_e$ fractions is (6.0± 0.3)%, consistent with an inclusive semileptonic measurement of (6.5 ± 0.4)%. There seems to be little missing here.

71.2 Inclusive hadronic $K\overline{K}$ fractions

The Cabibbo-favored $c \to s$ decay in D_s^+ decay produces a final state with both an s and an $\bar{s}$; and thus modes with a $K\overline{K}$ pair or with an η, ω, η', or ϕ predominate (as may already be seen in Fig. 71.1 in the semileptonic fractions). We consider the $K\overline{K}$ modes first. A complete picture of the exclusive $K\overline{K}$ charge modes is not yet possible, because branching fractions for many of those modes have not yet been measured. However, CLEO has measured the inclusive K^+, K^-, K_S^0, K^+K^-, $K^+K_S^0$, $K^-K_S^0$, and $2K_S^0$ fractions (these include modes with leptons) [1]. And each of these inclusive fractions with a K_S^0 is equal to the corresponding fraction with a K_L^0: $f(K^+K_L^0) = f(K^+K_S^0)$, $f(2K_L^0) = f(2K_S^0)$, *etc.* Therefore, of all-inclusive fractions pairing a K^+, K_S^0, or K_L^0 with a K^-, K_S^0, or K_L^0, we know all but $f(K_S^0K_L^0)$.

We can get that fraction. The total K_S^0 fraction is

$$f(K_S^0) = f(K^+K_S^0) + f(K^-K_S^0) + 2f(2K_S^0) + f(K_S^0K_L^0) + f(\text{single } K_S^0) \ ,$$

where $f(\text{single } K_S^0)$ is the sum of the branching fractions for modes such as $K_S^0\pi^+2\pi^0$ with a K_S^0 and no second K. The $K_S^0\pi^+2\pi^0$ mode is in fact the only unmeasured single-K_S^0 mode (throughout, we shall assume that fractions for modes with a K or $K\overline{K}$ and more than three pions are negligible), and we shall take its fraction to be the same as for the $K_S^0 2\pi^+\pi^-$ mode, (0.30 ± 0.11)%. Any reasonable deviation from this value would be too small to matter much in the following. Adding the several small single-K_S^0 branching fractions, including those from semileptonic modes, we get $f(\text{single } K_S^0) = (1.7 \pm 0.2)$%. Using this, we have:

$$\begin{aligned} f(K_S^0K_L^0) &= f(K_S^0) - f(K^+K_S^0) - f(K^-K_S^0) \\ &\quad - 2f(2K_S^0) - f(\text{single } K_S^0) \\ &= (19.0 \pm 1.1) - (5.8 \pm 0.5) - (1.9 \pm 0.4) \\ &\quad - 2 \times (1.7 \pm 0.3) - (1.7 \pm 0.2) \\ &= (6.2 \pm 1.4)\% \ . \end{aligned}$$

Here and below we treat the errors as uncorrelated, although often they are not. However, our main aim is to get numbers for Fig. 71.1; errors are secondary.

There is a check on our result: The ϕ inclusive branching fraction is (15.7 ± 1.0)%, of which 34%, or (5.34 ± 0.34)% of D_s^+ decays, produces a $K_S^0K_L^0$. Our $f(K_S^0K_L^0) = (6.2 \pm 1.4)$% has to be at least this large—and it is, within the sizable error.

We now have all the inclusive $K\overline{K}$ fractions. We use $f(K^+\overline{K}^0) = 2\,f(K^+K_S^0)$, and likewise for $f(K^-K^0)$. For K^+K^- and $K_S^0K_L^0$, we subtract off the contributions from $\phi\ell^+\nu$ decay to get the purely hadronic $K\overline{K}$ inclusive fractions:

$$\begin{aligned} f(K^+K^-, \text{hadronic}) &= (15.8 \pm 0.7) - (2.1 \pm 0.3) \\ &= (13.7 \pm 0.8)\% \\ f(K^+\overline{K}^0, \text{hadronic}) &= (11.6 \pm 1.0)\% \\ f(K^-K^0, \text{hadronic}) &= (3.8 \pm 0.8)\% \\ f(2K_S^0 + 2K_L^0, \text{hadronic}) &= (3.4 \pm 0.6)\% \\ f(K_S^0K_L^0, \text{hadronic}) &= (6.2 \pm 1.4) - (1.5 \pm 0.2) \\ &= (4.7 \pm 1.4)\% \ . \end{aligned}$$

The fractions are shown in Fig. 71.1. They total (37.2 ± 2.2)% of

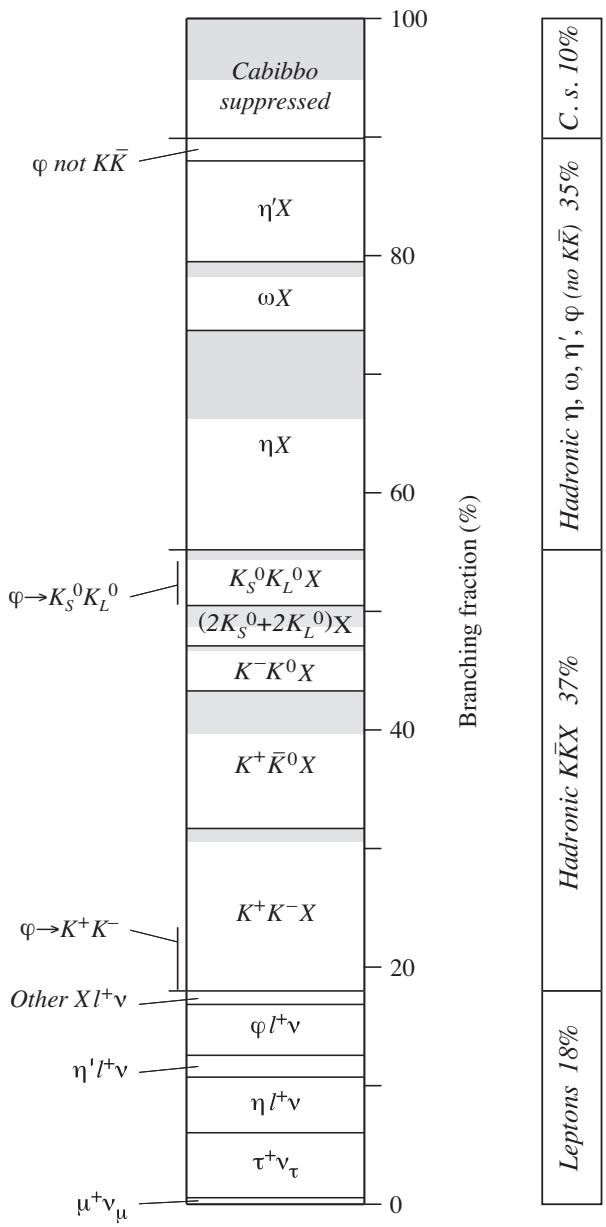

Figure 71.1: A partial breakdown of D_s^+ branching fractions. The hadronic bins in the left column show inclusive fractions. Shading within a bin shows how much of the inclusive fraction is not yet accounted for by adding up all the relevant exclusive fractions. The inclusive hadronic ϕ fraction is spread over three bins, in proportion to its decay fractions into K^+K^-, $K_S^0K_L^0$, and no-$K\bar{K}$ modes.

Downloaded from https://academic.oup.com/ptep/article/2022/8/083C01/6651666 by KIT Library user on 27 September 2022

D_s^+ decays.

We can add more information to the figure by summing up measured branching fractions for exclusive modes within each bin:

K^+K^- *modes*—The sum of measured $K^+K^-\pi^+$, $K^+K^-\pi^+\pi^0$, and $K^+K^-2\pi^+\pi^-$ branching fractions is $(12.6 \pm 0.6)\%$. That leaves $(1.1 \pm 1.0)\%$ for the $K^+K^-\pi^+2\pi^0$ mode, which is the only other K^+K^- mode with three or fewer pions. In Fig. 71.1, this unmeasured part of the K^+K^- bin is shaded.

$K^+\overline{K}^0$ *modes*—Two times the sum of the measured $K^+K^0_S$, $K^+K^0_S\pi^0$, and $K^+K^0_S\pi^+\pi^-$ branching fractions is $(8.0 \pm 0.5)\%$. This leaves $(3.6 \pm 1.1)\%$ for the unmeasured $K^+\overline{K}^0$ modes (there are three such modes with three or fewer pions). This is shaded in the figure.

K^-K^0 *modes*—Twice the $K^-K^0_S2\pi^+$ fraction is $(3.4 \pm 0.2)\%$, which leaves about $(0.4 \pm 0.8)\%$ for $K^-K^02\pi^+\pi^0$, the only other K^-K^0 mode with three or fewer pions.

$2K^0_S{+}2K^0_L$ *modes*—The $2K^0_S\pi^+$ and $2K^0_S2\pi^+\pi^-$ fractions sum to $(0.86 \pm 0.07)\%$; this times two (for the corresponding $2K^0_L$ modes) is $(1.72 \pm 0.14)\%$. This leaves about $(1.7 \pm 0.7)\%$ for other $2K^0_S + 2K^0_L$ modes.

$K^0_SK^0_L$ *modes*—Most of the $K^0_SK^0_L$ fraction is accounted for by ϕ decays (see below).

71.3 Inclusive hadronic η, ω, η', and ϕ fractions

These are easier. We start with the inclusive branching fractions, and then, to avoid double counting, subtract: (1) fractions for modes with leptons; (2) η mesons that are included in the inclusive η' fraction; and (3) K^+K^- and $K^0_SK^0_L$ from ϕ decays:

$$\begin{aligned} f(\eta \text{ hadronic}) &= f(\eta \text{ inclusive}) - 0.65\, f(\eta' \text{ inclusive}) \\ &\quad - f(\eta\ell^+\nu) = (18.5 \pm 3.0)\% \\ f(\omega \text{ hadronic}) &= f(\omega \text{ inclusive}) - 0.026\, f(\eta' \text{ inclusive}) \\ &= (5.8 \pm 1.4)\% \\ f(\eta' \text{ hadronic}) &= f(\eta' \text{ inclusive}) - f(\eta'\ell^+\nu) \\ &= (8.5 \pm 1.5)\% \\ f(\phi \text{ hadronic}, \not\to K\overline{K}) &= 0.17\, \left[f(\phi \text{ inclusive}) - f(\phi\ell^+\nu)\right] \\ &= (1.9 \pm 0.2)\% \ . \end{aligned}$$

The factors 0.65, 0.026, and 0.17 are the $\eta' \to \eta$, $\eta' \to \omega$, and $\phi \not\to K\overline{K}$ branching fractions. Figure 71.1 shows the results; the sum is $(34.7 \pm 3.6)\%$, which is about equal to the hadronic $K\overline{K}$ total.

Note that the bin marked ϕ near the top of Fig. 71.1 includes neither the $\phi\ell^+\nu$ decays nor the 83% of other ϕ decays that produce a $K\overline{K}$ pair. There is twice as much ϕ in the $K^0_SK^0_L$ bin, and nearly three times as much in the K^+K^- bin. These contributions are indicated in those bins.

Again, we can show how much of each bin is accounted for by measured exclusive branching fractions: η *modes*—The sum of $\eta\pi^+$, $\eta\pi^+\pi^0$ (nearly all $\eta\rho^+$), and ηK^+ branching fractions is $(11.1 \pm 1.2)\%$, which leaves a good part of the inclusive hadronic η fraction, $(18.5 \pm 3.0)\%$, to be accounted for. This is shaded in the figure. ω *modes*—The sum of $\omega\pi^+$, $\omega\pi^+\pi^0$, and $\omega 2\pi^+\pi^-$ fractions is $(4.6 \pm 0.9)\%$, which is nearly as large as the inclusive hadronic ω fraction, $(5.8 \pm 1.4)\%$. η' *modes*—The sum of $\eta'\pi^+$, $\eta'\rho^+$, and $\eta'K^+$ fractions is $(9.9 \pm 1.5)\%$, which is larger than but not in serious disagreement with the inclusive hadronic η' fraction, $(8.5 \pm 1.5)\%$.

71.4 Cabibbo-suppressed modes

The sum of the fractions for modes with a $K\bar{K}$, η, ω, η', or leptons is $(89.9 \pm 4.4)\%$. The remaining $(10.1 \pm 4.4)\%$ is to Cabibbo-suppressed modes, mainly single-$K+$ pions and multiple-pion modes (see below). However, it should be noted that some small parts of the modes already discussed are Cabibbo-suppressed. For example, the $(1.1 \pm 0.2)\%$ of D_s^+ decays to $K^0\ell\nu$ or $K^{*0}\ell\nu$ is already in the $X\ell\nu$ bin in Fig. 71.1. And the inclusive measurements of η, ω, and η' fractions do not distinguish between (and therefore include both) Cabibbo-allowed and -suppressed modes. We shall not try to make a separation here.

K^0 + *pions*—Above, we found that $f(\text{single } K^0_S) = (1.7 \pm 0.2)\%$. Subtracting semileptonic fractions with a K^0_S leaves $(1.3 \pm 0.2)\%$. The hadronic single-K^0 fraction is twice this, about $(2.6 \pm 0.4)\%$. The sum of measured $K^0\pi^+$, $K^0\pi^+\pi^0$, and $K^02\pi^+\pi^-$ fractions is $(1.8 \pm 0.3)\%$, about two-thirds as much.

K^+ + *pions*—The $K^+\pi^0$ and $K^+\pi^+\pi^-$ fractions sum to $(0.72 \pm 0.05)\%$. The total K^+ fraction wanted here is probably in the 1-to-2% range.

Multi-pions—The $2\pi^+\pi^-$, $\pi^+2\pi^0$, and $3\pi^+2\pi^-$ fractions total $(2.5 \pm 0.2)\%$. Modes not measured might double this.

The sum of the actually measured fractions is, including the semileptonics, $(4.9 \pm 0.3)\%$. The error on our Cabibbo-suppressed total, $(10.1 \pm 4.4)\%$ is too large to know how much we might be missing.

71.5 Addendum: Improved precision in some measurements

The Table compares measurements of branching fractions to pairs of two pseudoscalar mesons used in our 2019 update of the 2018 PDG review with values available in 2021 [2]. They have not changed much but are much better known.

Final state	2019 PDG avg or fit (%)	New BESIII entry in 2021 PDG (%)	2021 PDG avg or fit (%)
$K^+\eta'$	0.18±0.06	0.268±0.025	0.265±0.025
$K^+\eta$	0.177±0.035	0.162±0.012	0.160±0.011
$\eta\pi^+$	1.70±0.09	1.741±0.063	1.68±0.10
$K^+K^0_S$	1.50±0.05	1.502±0.055	1.46±0.04
$K^0_S\pi^+$	0.122±0.006	0.1109±0.005	0.110±0.005
$K^+\pi^0$	0.063±0.021	0.0748±0.0057	0.074±0.0057

Other recent BESIII additions include the measurements $\mathcal{B}(D_s \to \omega\pi^+, \omega K^+) = (1.77 \pm 0.32 \pm 0.13,\ 0.87 \pm 0.24 \pm 0.08) \times 10^{-3}$ [3] and $\mathcal{B}(D_s \to K_{S,L}K^+) = (1.425 \pm 0.038 \pm 0.031,\ 1.485 \pm 0.039 \pm 0.046)\%$ [4].

71.6 Concluding remarks

The shaded bands in the figure imply that about eight percent of the total D_s decay rate is into ηX, with X still to be accounted for. Unidentified Cabibbo-suppressed modes and the modes $K^+\overline{K}^0X$ and $(2K^0_S + 2K^0_L)X$ respectively correspond to $\sim (5, 3, 2)\%$ of the total. However, one can consider the vast majority of D_s decays to be represented by exclusive final states.

References

[1] S. Dobbs *et al.* (CLEO), Phys. Rev. D **79**, 112008 (2009), [arXiv:0904.2417].

[2] M. Ablikim *et al.* (BESIII), JHEP **08**, 146 (2020), [arXiv:2005.05072].

[3] M. Ablikim *et al.* (BESIII), Phys. Rev. D **99**, 9, 091101 (2019), [arXiv:1811.00392].

[4] M. Ablikim *et al.* (BESIII), Phys. Rev. D **99**, 11, 112005 (2019), [arXiv:1903.04164].

Downloaded from https://academic.oup.com/ptep/article/2022/8/083C01/6651666 by KIT Library user on 27 September 2022

72. Leptonic Decays of Charged Pseudoscalar Mesons

Revised Sept. 2021 by J.L. Rosner (Chicago U.); written with S.L. Stone (Syracuse U.) and R. Van de Water (FNAL)

72.1 Introduction

This review updates one in Ref. [1]. Extensive use is made of results of the Flavor Lattice Averaging group (FLAG 21), Ref. [2], which have not changed much since the previous compilation [3].

Charged mesons formed from a quark and antiquark can decay to a lepton-neutrino pair when these objects annihilate via a virtual W boson. Figure 72.1 illustrates this process for the purely leptonic decay of a D^+ meson.

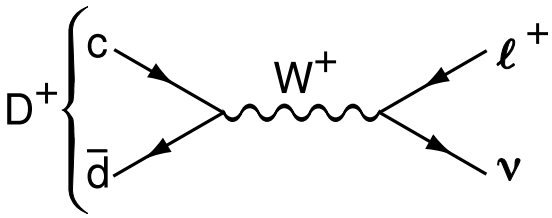

Figure 72.1: The annihilation process for pure D^+ leptonic decays in the standard model.

Similar quark-antiquark annihilations via a virtual W^+ to the $\ell^+\nu$ final states occur for the π^+, K^+, D_s^+, and B^+ mesons. (Whenever pseudoscalar-meson charges are specified in this article, use of the charge-conjugate particles and corresponding decays are also implied.) Let P be any of these pseudoscalar mesons. To lowest order, the decay width is

$$\Gamma^{(0)}(P \to \ell\nu) = \frac{G_F^2}{8\pi} f_P^2 \; m_\ell^2 M_P \left(1 - \frac{m_\ell^2}{M_P^2}\right)^2 |V_{q_1 q_2}|^2 \; . \quad (72.1)$$

Here M_P is the P mass, m_ℓ is the ℓ mass, $V_{q_1 q_2}$ is the Cabibbo-Kobayashi-Maskawa (CKM) matrix element between the quarks $q_1\bar{q}_2$ in P, and G_F is the Fermi coupling constant. The decay constant f_P is proportional to the matrix element of the axial current between the one-P-meson state and the vacuum:

$$\langle 0|\bar{q}_1\gamma_\mu\gamma_5 q_2|P(p)\rangle = ip_\mu f_P \; , \quad (72.2)$$

and can be thought of as proportional to the "wave function overlap" of the quark and antiquark. In this article, we use the convention in which $f_\pi \approx 130$ MeV. For brevity, we will often denote the purely leptonic decay width in Eq. (72.1) by $\Gamma^{(0)}$.

The decay of $P^\pm$ starts with a spin-0 meson, and ends up with a left-handed neutrino or right-handed antineutrino. By angular momentum conservation, the $\ell^\pm$ must then also be left-handed or right-handed, respectively. In the $m_\ell = 0$ limit, the decay is forbidden, and can only occur as a result of the finite ℓ mass. This helicity suppression is the origin of the m_ℓ^2 factor in the decay width.

Experimentally, it is difficult to isolate events in which there are *only* a lepton and neutrino in the final state from those with a lepton, neutrino, and soft photon. Thus, radiative contributions must be removed from the experimental measurements *a posteriori* to obtain $\Gamma^{(0)}$. The radiative contributions can be broken into three pieces: the short-distance contribution to leptonic and semileptonic decays mediated by a $W^\pm$ boson that accounts for electroweak corrections not included in the definition of G_F, the long-distance internal bremsstrahlung (IB) contribution, and the contribution from photon emission that depends upon the hadron's structure. The universal electroweak correction was calculated at $\mathcal{O}(\alpha)$ by Sirlin [4], and increases the purely leptonic decay rate by $\sim$ 1.8–2.2% depending on the decaying meson. The $\mathcal{O}(\alpha)$ IB contribution was calculated by Kinoshita [5], and again is universal for all leptonic decays at this order. Numerically, the universal long-distance contribution lowers the purely leptonic decay rate by $\sim$ 0.4–2.4%, where the correction is smallest for pions and largest for $D_{(s)}$ mesons. The structure-dependent contributions have been estimated within various effective theories to increase the purely leptonic rate by one to a few percent [6–11].

In this review, we treat the radiative corrections differently for the light, charm, and bottom meson systems for several reasons. First, the experimental uncertainties on the decay widths vary substantially Thus, while the inclusion of radiative corrections is essential for the pion, kaon, and D-meson decay widths, which have been measured to (sub)-percent precision, radiative corrections can be neglected (for now) for $B \to \tau\nu$ decay. Second, the photons are treated differently on the experimental side for the different decay processes. For pions and kaons, the experimental measurements of $\Gamma_{P\ell 2[\gamma]}$ are fully inclusive, while for D mesons, the experiments impose cuts on the energy of any neutral cluster deposited in the calorimeter, which reduce the soft-photon background substantially. Some experiments also remove the QED bremsstrahlung in the leading-logarithmic approximation using the PHOTOS Monte-Carlo generator [12]. Third, the theoretical knowledge of the structure-dependent corrections varies for each meson system.

Once radiative corrections have been accounted for, measurements of purely leptonic decay branching fractions and lifetimes allow an experimental determination of the product $|V_{q_1 q_2}|\, f_P$. If the decay constant f_P is known to sufficient precision from theory, one can obtain the corresponding CKM element within the standard model. If, on the other hand, one takes the value of $|V_{q_1 q_2}|$ assuming CKM unitarity, one can infer an "experimental measurement" of the decay constant that can then be compared with theory.

The importance of measuring $\Gamma(P \to \ell\nu)$ depends on the particle being considered. Leptonic decays of charged pseudoscalar mesons occur at tree level within the standard model. Thus one does not expect large new-physics contributions to measurements of $\Gamma(P \to \ell\nu)$ for the lighter mesons $P = \pi^+, K^+$, and these processes, in principle, provide clean standard-model determinations of $|V_{ud}|$ and $|V_{us}|$. The situation is different for leptonic decays of charm and bottom mesons. The presence of new heavy particles such as charged Higgs bosons or leptoquarks could lead to observable effects in $\Gamma(P \to \ell\nu)$ for $P = D_{(s)}^+, B^+$ [13–17]. Thus, the determination of $|V_{ub}|$ from $B^+ \to \tau\nu$ decay, in particular, should be considered a probe of new physics. More generally, the ratio of leptonic decays to $\tau\nu$ over $\mu\nu$ final states probes lepton universality [13, 18].

The determinations of CKM elements from leptonic decays of charged pseudoscalar mesons provide complementary information to those from other decay processes. The decay $P \to \ell\nu$ proceeds in the standard model via the axial-vector current $\bar{q}_1\gamma_\mu\gamma_5 q_2$, whereas semileptonic pseudoscalar meson decays $P_1 \to P_2\ell\nu$ proceed via the vector current $\bar{q}_1\gamma_\mu q_2$. Thus the comparison of determinations of $|V_{q_1 q_2}|$ from leptonic and semileptonic decays tests the $V - A$ structure of the standard-model electroweak charged-current interaction. More generally, a small right-handed admixture to the standard-model weak current would lead to discrepancies between $|V_{q_1 q_2}|$ obtained from leptonic pseudoscalar-meson decays, exclusive semileptonic pseudoscalar-meson decays, exclusive semileptonic baryon decays, and inclusive semileptonic decays [19, 20].

Both measurements of the decay rates $\Gamma(P \to \ell\nu)$ and theoretical calculations of the decay constants f_P for $P = \pi^+, K^+, D_{(s)}^+$ from numerical lattice-QCD calculations are now quite precise. As a result, the elements of the first row of the CKM matrix $|V_{ud}|$ and $|V_{us}|$ can be obtained to sub-percent precision from $\pi^+ \to \ell\nu$ and $K^+ \to \ell\nu$, where the limiting error is from continuum theory radiative ccorrections. The elements of the second row of the CKM matrix $|V_{cd(s)}|$ can be obtained from leptonic decays of charmed pseudoscalar mesons to few-percent precision, where here the limiting error is from experiment. These enable stringent tests of the unitarity of the first and second rows of the CKM matrix.

This review is organized as follows. Because the experimental and theoretical issues associated with measurements of pions and kaons, charmed mesons, and bottom mesons differ, we discuss each one separately. We begin with the pion and kaon system in Sec. 72.2. First, in Sec. 72.2.1, we review current measurements of the experimental decay rates. We provide tables of

Downloaded from https://academic.oup.com/ptep/article/2022/8/083C01/6651666 by KIT Library user on 27 September 2022

branching-ratio measurements and determinations of the product $|V_{ud(s)}|f_{\pi^+(K^+)}$, as well as average values for these quantities including correlations and other effects needed to combine results. Then, in Sec. 72.2.2, we summarize the status of theoretical calculations of the decay constants. We provide tables of recent lattice-QCD results for f_{π^+}, f_{K^+}, and their ratio from calculations including dynamical u, d, s, and (in some cases c) quarks, along with averages including correlations and strong SU(2)-isospin breaking corrections as needed. We next discuss the charmed meson system in Sec. 72.3, again reviewing current experimental rate measurements in Sec. 72.3.1 and theoretical decay-constant calculations in Sec. 72.3.2. Last, we discuss the bottom meson system in Sec. 72.4, following the same organization as the two previous sections. For almost all of the decay constants presented in Secs. 72.2.2, 72.3.2, and 72.4.2, we take as our preferred values the four-flavor averages from the FLAG 21 review [2], which incorporate all lattice-QCD results that appeared before 30 April 2021.

After having established the status of both experimental measurements and theoretical calculations of leptonic charged pseudoscalar-meson decays, we discuss some implications for phenomenology in Sec. 72.5. For each process discussed in Secs. 72.2–72.4, we combine the average $\mathcal{B}(P \to \ell\nu)$ with the decay constant f_P to infer the associated CKM matrix element. We then compare these results with determinations of the same CKM elements from other processes. We also use the CKM elements obtained from leptonic decays to test the unitarity of the first and second rows of the CKM matrix. Further, as in previous reviews, we combine the experimental $\mathcal{B}(P \to \ell\nu)$s with the associated CKM elements obtained from CKM unitarity to infer "experimental" values for the decay constants. The comparison of these values with theory provides a test of lattice and other QCD approaches, assuming that new-physics contributions to these processes are not significant.

72.2 Pions and kaons

72.2.1 *Experimental rate measurements*

Experimental rate measurements of pion and kaon leptonic decays are fully radiation inclusive. Following Refs. [21, 22], and references therein, we combine the $\mathcal{O}(\alpha)$ radiative corrections to the purely leptonic rate as follows:

$$\Gamma(P \to \ell\nu[\gamma]) = \Gamma^{(0)}(P \to \ell\nu)\left[1 + \frac{\alpha}{\pi}C_P\right], \tag{72.3}$$

where $P = \pi, K$. The full expressions for C_π and C_K are given in Eq. (114) of Ref. [8]. In addition to the universal short- [4] and long-distance [5] corrections, C_π and C_K include hadronic-structure dependent contributions [6] through $\mathcal{O}(\alpha p^4)$ in chiral perturbation theory (χPT), where p is the pion or kaon momentum. The inclusion of radiative corrections to the purely leptonic rates is numerically important given the level of precision achieved on the experimental measurements of the $\pi^\pm \to \mu^\pm\nu$ and $K^\pm \to \mu^\pm\nu$ decay widths.

We evaluate $\delta_P \equiv (\alpha/\pi)C_P$ using experimentally-measured meson and lepton masses and coupling constants from the Particle Data Group [23], and taking the low-energy constants (LECs) that parametrize the hadronic contributions from Refs. [8, 24, 25]. Because the finite non-logarithmic parts of the LECs were estimated within the large-N_C approximation assuming that contributions from the lowest-lying resonances dominate, we conservatively assign a 100% uncertainty to the LECs, which leads to a ± 0.9 error in $C_{\pi,K}$.[1] We obtain the following correction factors to the individual charged pion and kaon decay widths:

$$\delta_\pi = 0.0176(21) \quad \text{and} \quad \delta_K = 0.0107(21)\,. \tag{72.4}$$

The error on the ratio of kaon-to-pion leptonic decay widths is under better theoretical control because the hadronic contributions from low-energy constants estimated within the large-N_c framework cancel at lowest order in the chiral expansion. For the ratio, we use the correction factor

$$\delta_{K/\pi} = -0.0069(17)\,, \tag{72.5}$$

where we take the estimated error due to higher-order corrections in the chiral expansion from Ref. [27].

There have been no new measurements of the pion leptonic decay rate since the review of Ref. [28]. The sum of branching fractions for $\pi^- \to \mu^-\bar{\nu}$ and $\pi^- \to \mu^-\bar{\nu}\gamma$ is 99.98770(4)% [23]. Together with the lifetime 26.033(5) ns [23] this implies $\Gamma(\pi^- \to \mu^-\bar{\nu}[\gamma]) = 3.8408(7) \times 10^7$ s^{-1}. We then subtract the estimated radiative correction factor δ_π in Eq. (72.4) to obtain the purely leptonic rate $\Gamma^{(0)}(\pi^- \to \mu^-\bar{\nu})$. Using this rate and the masses from the 2014 PDG review [23] in Eq. (72.1) gives

$$f_{\pi^+}|V_{ud}| = (127.13 \pm 0.02 \pm 0.13)\ \text{MeV}\,, \tag{72.6}$$

where the errors are from the experimental rate measurement and the radiative correction factor, respectively.

The uncertainty on $f_{\pi^-}|V_{ud}|$ is dominated by that from theoretical estimate of the hadronic structure-dependent radiative corrections. The first direct lattice-QCD calculation of the radiative corrections to the pion and kaon leptonic decay rates was performed by the RM123-Soton Collaboration [11]. The results for both $\delta_\pi = 0.0153(19)$ and $\delta_K = 0.0088(9)$, which are given in the Gasser-Rusetsky-Scimemi scheme for separating strong and electromagnetic effects [29], are compatible with our chiral-perturbation-theory estimates above and have smaller quoted uncertainties, especially for δ_K. While independent confirmation of these results is needed, they demonstrate a promising approach for reducing the theoretical uncertainties on the pion and kaon leptonic decay rates in the future.

The world average for the $K \to \mu\nu$ decay rate is obtained from a global fit of several kaon-decay branching ratios and lifetime measurements, and was last updated by the FlaviaNet Working Group on Kaon Decays in 2014 [40]. Thus, the radiation-inclusive branching ratio $\mathcal{B}(K^+ \to \mu^+\nu[\gamma]) = 63.58(11)\%$ and lifetime $\tau_{K^\pm} = 12.384(15)$ ns are unchanged from our previous review. These measurements imply $\Gamma(K^+ \to \mu^+\nu[\gamma]) = 5.134(11) \times 10^7$ s^{-1}. As before, we subtract δ_K in Eq. (72.4) from the radiation-inclusive decay width to obtain $\Gamma^{(0)}(K^+ \to \mu^+\nu)$. We then use Eq. (72.1) to obtain

$$f_{K^+}|V_{us}| = (35.09 \pm 0.04 \pm 0.04)\ \text{MeV}\,, \tag{72.7}$$

where the errors are from the experimental rate measurement and the radiative correction factor, respectively.

Short-distance radiative corrections cancel in the ratio of pion-to-kaon decay rates [41]:

$$\frac{\Gamma_{K_{\ell 2[\gamma]}}}{\Gamma_{\pi_{\ell 2[\gamma]}}} = \frac{|V_{us}^2|f_{K^-}^2}{|V_{ud}|^2 f_{\pi^-}^2}\frac{m_K(1-m_\ell^2/m_K^2)^2}{m_\pi(1-m_\ell^2/m_\pi^2)^2}(1+\delta_{K/\pi})\,, \tag{72.8}$$

where $\delta_{K/\pi}$ is given in Eq. (72.5). The left-hand side of Eq. (72.8) is 1.3367(28), which implies

$$\frac{|V_{us}|f_{K^+}}{|V_{ud}|f_{\pi^+}} = 0.27599 \pm 0.00029 \pm 0.00024\,, \tag{72.9}$$

where the first uncertainty is from the branching fractions and the second is from $\delta_{K/\pi}$. Here, the estimated error on the hadronic structure-dependent radiative corrections is commensurate with the experimental error.

In summary, the main experimental results pertaining to charged pion and kaon leptonic decays are

$$|V_{ud}|f_{\pi^+} = (127.13 \pm 0.02 \pm 0.13)\ \text{MeV}\,, \tag{72.10}$$

$$|V_{us}|f_{K^+} = (35.09 \pm 0.04 \pm 0.04)\ \text{MeV}\,, \tag{72.11}$$

$$\frac{|V_{us}|f_{K^+}}{|V_{ud}|f_{\pi^+}} = 0.27599 \pm 0.00029 \pm 0.00024\,, \tag{72.12}$$

where the errors are from the experimental uncertainties in the branching fractions and the theoretical uncertainties in the radiative correction factors δ_P, respectively. All of these values are the same as in our earlier reviews [1, 28, 42].

[1] This uncertainty on $C_{\pi,K}$ is smaller than the error estimated by Marciano and Sirlin in Ref. [26], which predates the calculations of the hadronic-structure contributions in Refs. [6, 8, 24, 25]. The hadronic LECs incorporate the large short-distance electroweak logarithm discussed in Ref. [26], and their dependence on the chiral renormalization scale cancels the scale-dependence induced by chiral loops, thereby removing the dominant scale uncertainty of the Marciano–Sirlin analysis [26].

Downloaded from https://academic.oup.com/ptep/article/2022/8/083C01/6651666 by KIT Library user on 27 September 2022

Table 72.1: Recent published lattice-QCD results for f_{π^+}, f_{K^+}, and their ratio. The upper and lower panels show $(2+1+1)$-flavor and $(2+1)$-flavor determinations, respectively. When two errors are shown, they are statistical and systematic, respectively. Results for f_π and f_K in the isospin symmetric limit $m_u = m_d$ are noted with a ‡; they are corrected for isospin breaking via Eq. (72.13) before computing the averages. The 2+1+1 FLAG 21 averages are dominated by the Fermilab/MILC values.

Reference	N_f	f_{π^+}(MeV)	f_{K^+}(MeV)	f_{K^+}/f_{π^+}
CalLat 20 [30]	2+1+1	–	–	1.1942(32)(31)
Fermilab/MILC 17 [31] *	2+1+1	–	–	$1.1950(15)(^{+6}_{-18})$
ETM 14 [32] *	2+1+1	–	154.4(1.5)(1.3)	1.184(12)(11)
Fermilab/MILC 14 [10] * †	2+1+1	–	$155.92(13)(^{+42}_{-34})$	$1.1956(10)(^{+26}_{-18})$ † ‡
HPQCD 13 [33] *	2+1+1	–	155.37(20)(27)	1.1916(15)(16)
FLAG 21 average [2]	2+1+1	–	155.7(3)	1.1932(21)
QCDSF/UKQCD 16 [34]	2+1	–	–	1.190(10)(13)
BMW 16 [35]	2+1	–	–	1.178(10)(26)
RBC/UKQCD 14 [36]‡	2+1	130.19(89)	155.51(83)	1.1945(45)
MILC 10 [37]	2+1	129.2(0.4)(1.4)	$156.1(4)(^{+6}_{-9})$	$1.197(2)(^{+3}_{-7})$
BMW 10 [38]‡	2+1	–	–	1.192(7)(6)
HPQCD/UKQCD 07 [39]‡	2+1	132(2)	157(2)	1.189(2)(7)
FLAG 21 average [2]	2+1	130.2(8)	155.7(7)	1.1917(37)

*PDG 2014 value of $f_{\pi^+} = 130.41(21)$ MeV used to set absolute lattice scale.
†Superseded by f_{K^+}/f_{π^+} from Fermilab/MILC 17.

72.2.2 *Theoretical decay-constant calculations*

Table 72.1 presents recent published results for the charged pion and kaon decay constants and their ratio from numerical lattice-QCD calculations with three ($N_f = 2+1$) or four flavors ($N_f = 2+1+1$) of dynamical quarks. The uncertainties on both the individual decay constants and their ratio are at the sub-percent level. The SU(3)-breaking ratio f_{K^+}/f_{π^+} can be obtained with especially small errors because statistical errors associated with the Monte Carlo calculations are correlated between the numerator and denominator, as are some systematics. The results in Table 72.1 were obtained using several independent sets of gauge-field configurations, and a variety of lattice fermion actions that are sensitive to different systematic uncertainties.[2] Thus, the good agreement between them indicates that the lattice-QCD uncertainties are controlled and the associated error estimates are reliable.[3]

Table 72.1 also shows the three- and four-flavor averages for the pion and kaon decay constants and their ratio from the FLAG 21 review [2] in the lines labeled "FLAG 21 average." There is no four-flavor average for the pion decay constant in Table 72.1 because all of the four-flavor calculations use the quantity $f_{\pi^+} = 130.41(20)$ MeV [23] as an input to fix the absolute lattice scale needed to convert from lattice-spacing units to GeV [10, 32, 33].

All of the results in Table 72.1 were obtained using isospin-symmetric gauge-field configurations, *i.e.*, the dynamical up and down quarks have the same mass. Fortunately, however, the dominant effect of strong-isospin breaking is easily included in lattice-QCD calculations as follows. Because the up-down mass difference $\Delta m_{ud} \equiv (m_u - m_d) \sim -2.5$ MeV [3, 48] is much less than typical hadronic scales, the strong-isospin breaking corrections to physical observables can systematically expanded in the small parameter $\delta m_{ud} \equiv \Delta m_{ud}/\Lambda_{\rm QCD}$. The leading strong-isospin-breaking corrections to pseudoscalar-meson decay constants arise from the light *valence* quarks in the initial- and final-state hadrons. (See, *e.g.,* the discussion in Ref. [49], for a detailed discussion of isospin-breaking effects in pion and kaon observables.) Thus, to include the effect of nondegenerate up- and down-quark masses, most recent lattice-QCD calculations of f_{π^+} and f_{K^+} evaluate the masses of the valence quarks in the pion at the physical m_u and m_d, and the mass of the valence light quark in the kaon at the physical m_u. This procedure yields a correction to the kaon decay constant below 0.5%. Consequently, strong-isospin breaking corrections from the light sea-quark masses — which are suppressed by an additional power of δm_{ud} — can be neglected given present uncertainties.

Some earlier lattice-QCD calculations, however, only provide the decay constants and their ratio in the $SU(2)$ isospin-symmetric limit [36, 38, 39]. The Flavour Lattice Averaging Group corrects these results for strong-isospin breaking using chiral perturbation theory before including them in the averages. The leading strong-isospin-breaking corrections to the pion and kaon decay constants in χPT can be parametrized as [27, 50]

$$f_{\pi^+} = f_\pi\,, \qquad f_{K^+} = f_K\sqrt{1+\delta_{\rm SU(2)}}\,, \tag{72.13}$$

where f_π and f_K denote the values of the decay constants in the isospin-symmetric limit. The pion decay constant does not receive corrections linear in $m_u - m_d$ because of the G-parity symmetry of the pion triplet, so at first order the δm_{ud} expansion, strong-isospin breaking corrections are characterized by a single parameter, $\delta_{\rm SU(2)}$. Next-to-leading order χPT yields numerical values for $\delta_{\rm SU(2)}$ of approximately -0.004. Recent direct lattice-QCD calculations of $\delta_{\rm SU(2)}$ give larger values of around -0.005 to -0.008 [11, 31–33, 49, 51], but further studies are needed. Thus, to be conservative, FLAG includes an uncertainty of 100% on the χPT estimate for $\delta_{\rm SU(2)}$ when correcting those decay-constant values that are quoted in the isospin-symmetric limit.

The errors on the decay-constant results in Table 72.1 obtained from $(2+1)$-flavor lattice-QCD calculations do not include an estimate of the systematic uncertainty from the omission of charm sea quarks in the calculation. Consequently, when the uncertainty on the $(2+1+1)$-flavor FLAG average is comparable to or better than that on the $(2+1)$-flavor FLAG average, we simply use the four-flavor average as our preferred value. This is not possible, however, for the pion decay constant. To account for this, we first estimate the systematic uncertainty on pseudoscalar-meson decay constants associated with the omission of charm sea quarks. We then add this estimate in quadrature to the quoted error on the $(2+1)$-flavor FLAG average for f_{π^+} to obtain our preferred value.

The error introduced by omitting charm sea quarks can be roughly estimated by expanding the charm-quark determinant in powers of $1/m_c$ [58]; the resulting leading contribution is of order $\alpha_s\left(\Lambda_{\rm QCD}/2m_c\right)^2$ [59]. Taking the $\overline{\rm MS}$ values $\overline{m}_c(\overline{m}_c) =$

[2]See the PDG mini-review on "Lattice Quantum Chromodynamics" [43, 44] for a general review of numerical lattice-QCD calculations. Details on the different methods used in modern lattice-QCD calculations are provided in Appendix A of the FLAG "Review[s] of lattice results concerning low energy particle physics" [2, 3, 45, 46].

[3]See the review by Kronfeld [47] for a summary of the large body of evidence validating the methods employed in modern lattice-QCD calculations.

Downloaded from https://academic.oup.com/ptep/article/2022/8/083C01/6651666 by KIT Library user on 27 September 2022

Table 72.2: Experimental results for $\mathcal{B}(D^+ \to \mu^+\nu[\gamma])$, $\mathcal{B}(D^+ \to \tau^+\nu[\gamma])$, and $|V_{cd}|f_{D^+}$. The systematic errors on the inferred values of $|V_{cd}|f_{D^+}$ include those from the D^+ lifetime and mass. The error from radiative corrections is only included in the entries labeled "our average." In the second CLEO line the τ^+ decays to $\mu^+\nu_\mu\bar{\nu}_\tau$.

Experiment	Mode	$\mathcal{B}$	$\lvert V_{cd}\rvert f_{D^+}$ (MeV)
CLEO-c [52,53]	$\mu^+\nu$	$(3.93 \pm 0.35 \pm 0.09) \times 10^{-4}$	$46.70 \pm 2.10 \pm 0.55$
CLEO-c [52,53]	$\mu^+\nu{+}\tau^+\nu$	$(3.82 \pm 0.32 \pm 0.09) \times 10^{-4}$	$46.00 \pm 1.91 \pm 0.56$
BESIII [54]	$\mu^+\nu$	$(3.71 \pm 0.19 \pm 0.06) \times 10^{-4}$	$45.33 \pm 1.17 \pm 0.38$
Our average	Lines 2+3	$(3.74 \pm 0.17) \times 10^{-4}$	45.50 ± 1.22
CLEO-c [55,56]	$\tau^+\nu$ ($\pi^+\overline{\nu}$)	$< 1.2 \times 10^{-3}$	
BESIII [57]	$\tau^+\nu$ ($\pi^+\overline{\nu}$)	$(1.20 \pm 0.24 \pm 0.12) \times 10^{-3}$	49.95 ± 2.48
Our average	$\mu^+\nu + \tau^+\nu$		46.17 ± 1.16

1.275 GeV, $\overline{\Lambda}_{\rm QCD} \sim 340$ MeV from FLAG [45], and $\overline{\alpha}(\overline{m}_c) \sim 0.4$, leads to an estimate of about 0.7% for the contribution to the decay constants from charm sea quarks. We can compare this power-counting estimate of charm sea-quark contributions with the observed differences between the (2+1)- and (2+1+1)-flavor lattice-QCD averages for kaon, $D_{(s)}$-meson, and $B_{(s)}$-decay constants in Tables 72.1, 72.4, and 72.6. Looking at Table 72.1, the three- and four-flavor averages for f_{K^+} agree to much better than our simple power-counting estimate. Inspection of Tables 72.4 and 72.6 shows, however, that charm sea-quark effects of this size are still allowed for both $D_{(s)}$-meson and $B_{(s)}$-meson decay constants.

Our final preferred theoretical values for the charged pion and kaon decay constants are

$$f_{\pi^+} = 130.2(1.2)\,\text{MeV}\,, \quad f_{K^+} = 155.7(3)\,\text{MeV}\,, \quad \frac{f_{K^+}}{f_{\pi^+}} = 1.193(2)\,, \tag{72.14}$$

where f_{K^+} and f_{K^+}/f_{π^+} are simply the four-flavor FLAG 2021 averages [2], and f_{π^+} is the three-flavor flavor FLAG 2021 average with the error increased by the estimated 0.7% charm sea-quark contribution.

72.3 Charmed mesons

72.3.1 *Experimental rate measurements*

Measurements have been made of the branching fractions for D^+ and D_s^+ mesons decaying to both $\mu^+\nu$ and $\tau^+\nu$ final states. The CLEO-c and BESIII experiments have made measurements of D^+ decays using e^+e^- collisions at the $\psi(3770)$ resonant energy where D^-D^+ pairs are copiously produced. They fully reconstruct one of the D mesons; for concreteness, we will take this to be the D^-. Counting the number of these events provides the normalization for the branching fraction measurement. The experimental analyses then proceed by identifying a candidate μ^+ and forming the missing-mass squared, $MM^2 = (E_{\rm CM} - E_{D^-})^2 - \left(\vec{p}_{\rm CM} - \vec{p}_{D^-} - \vec{p}_{\mu^+}\right)^2$, where $E_{\rm CM}$ and $p_{\rm CM}$ are the center-of-mass energy (which is known) and momentum (which equals zero in e^+e^- collisions). A peak at zero MM^2 implies the existence of a missing neutrino, and hence the $\mu^+\nu$ decay of the D^+. CLEO-c does not explicitly identify the muon, so their data consists of a combination of $\mu^+\nu$ and $\tau^+\nu$, $\tau^+ \to \pi^+\nu$ events. This permits them to do two fits: in one they fit for the individual components, and in the other they fix the ratio of $\tau^+\nu/\mu^+\nu$ events to be that given by the standard-model expectation. Thus, the former measurement should be used for new-physics searches, and the latter for standard-model predictions. Our average uses the fixed-ratio value.

Table 72.2 shows the available measurements of $D^+ \to \mu^+\nu$, an upper limit on $D^+ \to \tau^+\nu$ from CLEO-c, and the first measurement of this decay from BESIII. Here there is no change since the previous review [1].

To extract the values of $|V_{cd}|f_{D^+}$ via Eq. (72.1), we use values of $m_{D^+} = 1.86961$ GeV and the well-measured D^+ lifetime of 1.040(7) ps [42], and apply radiative corrections as described below. For calculating the average $\mu^+\nu$ number, we use the CLEO-c result from $\mu^+\nu + \tau^+\nu$.

To obtain the purely leptonic rates $\Gamma^{(0)}(D^+ \to \mu^+(\tau^+)\nu)$, we subtract the radiative contributions as in Sec. 72.2.1, but use numerical values for the corrections appropriate for D mesons. First, we reduce both the $\mu^+\nu$ and $\tau^+\nu$ branching fractions in Table 72.2 by 1.8%, which is the universal short-distance electroweak contribution of Sirlin [4] evaluated using the D-meson mass for the factorization scale. We do not adjust the experimental rates by the universal long-distance correction [5]. This is because QED bremsstrahlung contributions have already been subtracted at leading-log order from the measurements in Table 72.2 using Monte-Carlo estimates computed with PHOTOS [12]. The $\mu^+\nu$ rates should also be reduced by the 1% estimate of the structure-dependent contributions from Dobrescu and Kronfeld [17]. This correction accounts for tree-level radiative processes in which the D meson decays into a real photon and an off-shell vector meson, which subsequently decays weakly to a charged lepton and neutrino. It is estimated using Eq. (12) of Burdman *et al.* [7] with the CLEO-c cut on the photon energy from Ref. [70], which is typical of all the measurements. We do not need to apply the structure-dependent correction to the $\mu^+\nu$ branching fractions in Table 72.2, however, because the experiments have already included it in their quoted results. Therefore, in summary, we reduce both the $D^+ \to \mu^+\nu$ and the $D^+ \to \tau^+\nu$ rates by 1.8% to account for radiative corrections. It is worth noting, however, that the universal long-distance electromagnetic contribution estimated for point-like charged mesons by Kinoshita [5], which we are not including because IB contributions are already subtracted from the measurements via PHOTOS, would *increase* both rates by about 2.5%.

We now discuss the D_s^+ decay process. Since our previous review [1] there have been several results from BESIII. Measurements of D_s^+ leptonic decay branching fractions by several groups are listed in Table 72.3. We exclude older values obtained by normalizing to D_s^+ decay modes that are not well-defined. Many measurements, for example, used the $\phi\pi^+$ mode. This decay is a subset of the $D_s^+ \to K^+K^-\pi^+$ channel which has interferences from other modes populating the K^+K^- mass region near the ϕ, the most prominent of which is the $f_0(980)$. Thus, the extraction of the effective $\phi\pi^+$ rate is sensitive to the mass resolution of the experiment and the cuts used to define the ϕ mass region [71].[4]

To find D_s decays in the $\mu^+\nu$ signal channels, the experiments rely on fully reconstructing all of the final state particles except for the neutrino and use a missing-mass technique to infer the existence of the neutrino. CLEO and BESIII use $e^+e^- \to D_s D_s^*$ collisions at 4170 MeV, while BaBar and Belle use $e^+e^- \to DKn\pi D_s^*$ collisions at energies near the $\Upsilon(4S)$. CLEO and BESIII do a similar analysis as was done for the D^+ above. BaBar and Belle do a similar MM^2 calculation by using the reconstructed hadrons, the photon from the D_s^{*+} decay and a detected μ^+. To get the normalization they do a MM^2 fit without the μ^+ and use the signal at the D_s^+ mass squared to determine the total D_s^+ yield.

When selecting the $\tau^+ \to \pi^+\bar{\nu}$ and $\tau^+ \to \rho^+\bar{\nu}$ decay modes, CLEO uses both the calculation of the missing-mass and the fact that there should be no extra energy in the event beyond that

[4] We have not included the BaBar result for $\mathcal{B}(D_s^+ \to \mu^+\nu)$ reported in Ref. [72] because this measurement determined the ratio of the leptonic decay rate to the hadronic decay rate $\Gamma(D_s^+ \to \ell^+\nu)/\Gamma(D_s^+ \to \phi\pi^+)$.

Downloaded from https://academic.oup.com/ptep/article/2022/8/083C01/6651666 by KIT Library user on 27 September 2022

Table 72.3: Experimental results for $\mathcal{B}(D_s^+ \to \mu^+\nu[\gamma])$, $\mathcal{B}(D_s^+ \to \tau^+\nu[\gamma])$, and $|V_{cs}|f_{D_s^+}$. The systematic errors on the inferred values of $|V_{cs}|f_{D_s^+}$ include those from the D_s^+ lifetime and mass. The entries labeled "our average" take into account correlations between systematic errors common to the experiments, and also include errors from radiative corrections.

Experiment	Mode	$\mathcal{B}(\%)$	$\lvert V_{cs}\rvert f_{D_s^+}$ (MeV)
CLEO-c [55,56]	$\mu^+\nu$	$0.565 \pm 0.045 \pm 0.017$	$247.6 \pm 9.9 \pm 4.1$
BaBar* [61]	$\mu^+\nu$	$0.602 \pm 0.038 \pm 0.034$	$254.3 \pm 8.0 \pm 7.4$
Belle [62]	$\mu^+\nu$	$0.531 \pm 0.028 \pm 0.020$	$238.8 \pm 6.3 \pm 4.8$
BESIII [63]	$\mu^+\nu$	$0.517 \pm 0.075 \pm 0.021$	$238.9 \pm 17.3 \pm 4.9$
BESIII [64]	$\mu^+\nu$	$0.535 \pm 0.013 \pm 0.016$	$240.9 \pm 2.9 \pm 4.0$
Our average	$\mu^+\nu$	0.543 ± 0.017	242.6 ± 4.0
CLEO-c [55,56]	$\tau^+\nu$ ($\pi^+\overline{\nu}$)	$6.42 \pm 0.81 \pm 0.18$	$267.3 \pm 16.9 \pm 4.2$
CLEO-c [65]	$\tau^+\nu$ ($\rho^+\overline{\nu}$)	$5.52 \pm 0.57 \pm 0.21$	$247.9 \pm 12.8 \pm 5.0$
CLEO-c [66,67]	$\tau^+\nu$ ($e^+\nu\overline{\nu}$)	$5.30 \pm 0.47 \pm 0.22$	$242.9 \pm 10.8 \pm 5.3$
BaBar [61]	$\tau^+\nu$ ($e^+(\mu^+)\nu\overline{\nu}$)	$5.00 \pm 0.35 \pm 0.49$	$236.9 \pm 8.3 \pm 11.7$
Belle [62]	$\tau^+\nu$ ($\pi^+\overline{\nu}$)	$6.04 \pm 0.43^{+0.46}_{-0.40}$	$260.3 \pm 9.3^{+10.1}_{-8.8}$
Belle [62]	$\tau^+\nu$ ($e^+\nu\overline{\nu}$)	$5.37 \pm 0.33^{+0.35}_{-0.31}$	$244.5 \pm 7.5^{+8.2}_{-7.4}$
Belle [62]	$\tau^+\nu$ ($\mu^+\nu\overline{\nu}$)	$5.86 \pm 0.37^{+0.34}_{-0.59}$	$255.4 \pm 8.0^{+7.6}_{-13.1}$
BESIII [63]	$\tau^+\nu$ ($\pi^+\overline{\nu}$)	$3.28 \pm 1.83 \pm 0.37$	$193 \pm 54 \pm 11$
BESIII [64]	$\tau^+\nu$ ($\pi^+\overline{\nu}$)	$5.21 \pm 0.25 \pm 0.17$	$240.8 \pm 5.8 \pm 4.3$
BESIII [68]	$\tau^+\nu$ ($e^+\nu_e\overline{\nu}$)	$5.27 \pm 0.10 \pm 0.12$	$242.2 \pm 2.3 \pm 3.2$
BESIII [69]	$\tau^+\nu$ ($\pi^+\pi^0\overline{\nu}$)	$5.29 \pm 0.25 \pm 0.20$	$242.7 \pm 5.7 \pm 4.0$
Our average	$\tau^+\nu$	5.33 ± 0.13	244.0 ± 3.1
Our average	$\mu^+\nu + \tau^+\nu$		243.5 ± 2.7

*We do not use a previous unpublished BaBar result from a subsample of data that uses a different technique for obtaining the branching fraction normalization [60].

deposited by the measured tagged D_s^- and the τ^+ decay products. The $\tau^+ \to e^+\nu\bar{\nu}$ mode, however, uses only extra energy. BaBar and Belle also use the extra energy to discriminate signal from background in their $\tau^+\nu$ measurements. BESIII uses $\tau^+ \to \pi^+\overline{\nu}$ decays, where they calculate the MM^2 and discriminate against μ^+ from $D_s^+ \to \mu^+\nu$ decays, and more recently $\tau^+ \to e^+\nu\overline{\nu}$ and $\tau^+ \to \pi^+\pi^0\overline{\nu}$ decays.

When extracting $|V_{cs}|f_{D_s^+}$ via Eq. (72.1), we first apply the -1.8% universal electroweak correction [4] to all of the $\mu^+\nu$ and $\tau^+\nu$ branching fractions in Table 72.3; this is the same as for D^+ mesons. We also decrease the BaBar and Belle $\mu^+\nu$ branching fractions by the 1% structure-dependent correction [17]. This correction was already included in CLEO and BESIII results for the $\mu^+\nu$ branching fractions in Table 72.3. We use the masses and lifetimes $m_{D_s^+} = 1.96834(7)$ GeV, $m_{\tau^+} = 1.77686(12)$ GeV, and $\tau_{D_s^+} = 0.504(4)$ ps [42]. The inferred values for $f_{D_s^+}|V_{cs}|$ are in good agreement for the $\mu^+\nu$ and $\tau^+\nu$ decay modes.

It is clear from the discussion of radiative corrections in this section that they are less well understood theoretically for D^+ and D_s^+ meson decays than for pions and kaons. We therefore assign a 1.4% systematic uncertainty to the purely leptonic decay rates, which is half the size of the applied radiative corrections. This translates to a 0.7% error on the products of the decay constant times CKM matrix element. Putting everything together, the main experimental results pertaining to charmed meson leptonic decays are (see the bottom lines of Tables 72.2 and 72.3):

$$|V_{cd}|f_{D^+} = 46.17 \pm 1.11 \pm 0.32 = 46.17 \pm 1.16 \text{ MeV}, \quad (72.15)$$

$$|V_{cs}|f_{D_s^+} = 243.5 \pm 2.1 \pm 1.7 = 243.5 \pm 2.7 \text{ MeV}, \quad (72.16)$$

where the errors are from the measured branching fractions and the applied radiative corrections, respectively.

72.3.2 *Theoretical decay-constant calculations*

Table 72.4 presents recent theoretical calculations of charmed heavy-light meson decay constants and their ratio in the isospin-symmetric limit $m_u = m_d$. (As in Sec. 72.2.2, we denote the physical D^+-meson decay constant by f_{D^+}, and use f_D for the isospin-symmetric value.) The upper two panels show results from lattice-QCD calculations with three ($N_f = 2+1$) or four flavors ($N_f = 2+1+1$) of dynamical quarks. Although there are fewer available results than for the pion and kaon sector, both f_D and f_{D_s} have been obtained using multiple sets of gauge-field configurations with different lattice fermion actions, providing independent confirmation. For comparison, the bottom panel of Table 72.4 shows QCD-model calculations of the D- and D_s-meson decay constants for which uncertainty estimates are provided. The lattice and non-lattice results agree, but numerical lattice-QCD calculations have now reached significantly greater precision than other approaches. There are no new results quoted from FLAG 21 [2] compared with those in our previous review [1] quoted from FLAG 19 [3].

The lattice-QCD decay-constant results in Table 72.4 were all obtained using isospin-symmetric gauge-field configurations. As discussed in Sec. 72.2.2, however, the leading strong-isospin breaking corrections to heavy-light pseudoscalar-meson decay constants can be accounted for by using the physical down (or up) quark in the D (or B) meson. Strong-isospin breaking corrections to heavy-strange meson decay constants are roughly an order-of-magnitude smaller because there are no light valence quarks involved. Recently, the Fermilab Lattice and MILC Collaborations used this approach to calculate directly the dominant strong-isospin breaking corrections to both f_D and f_B, finding [31]

$$\begin{aligned} f_{D^+} - f_D &= 0.58(1)_{\text{stat}}(7)_{\text{syst}}(1)_{\text{EM scheme}} \text{ MeV}, \\ f_{B^+} - f_B &= -0.53(5)_{\text{stat}}(7)_{\text{syst}}(0)_{\text{EM scheme}} \text{ MeV}. \end{aligned} \quad (72.17)$$

These results agree with independent estimates of the strong-isospin-breaking corrections to heavy-light meson decay constants from Borelized sum rules [85]. Combined with the determinations of f_D and f_B from the same work, Eq. (72.17) implies that the corrections to the SU(3)-flavor breaking ratios are

$$\frac{f_{D_s}}{f_{D^+}} = \frac{f_{D_s}}{f_D}\Big(1 - 0.0027(3)\Big), \qquad \frac{f_{B_s}}{f_{B^+}} = \frac{f_{B_s}}{f_B}\Big(1 + 0.0028(5)\Big). \quad (72.18)$$

These estimated strong-isospin-breaking corrections to f_D and f_{D_s}/f_D above are commensurate with the uncertainties on the

Downloaded from https://academic.oup.com/ptep/article/2022/8/083C01/6651666 by KIT Library user on 27 September 2022

Table 72.4: Recent theoretical determinations of f_D, f_{D_s}, and their ratio in the isospin-symmetric limit. The upper panels show results from lattice-QCD calculations with $(2+1+1)$ and $(2+1)$ dynamical quark flavors, respectively. Statistical and systematic errors are quoted separately. The bottom panel shows estimates from QCD sum rules (QCD SR) and the light-front quark model (LFQM). These are not used to obtain our preferred decay-constant values. The 2+1+1 averages are dominated by the Fermilab/MILC values.

Reference	Method	N_f	f_D(MeV)	f_{D_s}(MeV)	f_{D_s}/f_D
Fermilab/MILC 17 [31]	LQCD	2+1+1	212.1(0.3)(0.5)	249.9(0.3)(0.3)	1.1782(06)(15)*
ETM 14 [32]	LQCD	2+1+1	207.4(3.7)(0.9)	247.2(3.9)(1.4)	1.192(19)(11)
FLAG 21 average [2]	LQCD	2+1+1	212.0(0.7)	249.9(0.5)	1.1783(16)
χQCD 20A [73]	LQCD	2+1	213(5)	249(7)	1.16(3)
RBC/UKQCD 18A [74]†	LQCD	2+1	–	–	1.1740(51)(68)
RBC/UKQCD 17 [75]	LQCD	2+1	$208.7(2.8)(^{+2.1}_{-1.8})$	$246.4(1.3)(^{+1.3}_{-1.9})$	$1.1667(77)(^{+57}_{-43})$
χQCD 14 [76]	LQCD	2+1	–	254(2)(4)	–
HPQCD 12 [77]	LQCD	2+1	208.3(1.0)(3.3)	–	1.187(4)(12)
Fermilab/MILC 11 [78]	LQCD	2+1	218.9(9.2)(6.6)	260.1(8.9)(6.1)	1.188(14)(21)
HPQCD 10 [79]	LQCD	2+1	–	248.0(1.4)(2.1)	–
FLAG 21 average [2]	LQCD	2+1	209.0(2.4)	248.0(1.6)	1.174(7)
Pullin 21 [80]	QCD SR		190(15)	226(17)	1.19(7)
Wang 15 [81]‡	QCD SR		208(10)	240(10)	1.15(6)
Gelhausen 13 [82]	QCD SR		$201\left(^{+12}_{-13}\right)$	$238\left(^{+13}_{-23}\right)$	$1.15\left(^{+0.04}_{-0.05}\right)$
Narison 12 [83]	QCD SR		204(6)	246(6)	1.21(4)
Lucha 11 [84]	QCD SR		206.2(8.9)	245.3(16.3)	1.193(26)

*Ref. [31] provides values for f_D and f_{D_s} in the isopsin-symmetric limit, but not for their ratio. Here we infer the central value from those of the individual decay constants, and take the statistical and systematic errors to be the same as for the physical ratio f_{D_s}/f_{D^+}.

†Slight difference from preliminary value quoted in 2019 FLAG review.

‡Obtained using $m_c^{\overline{\rm MS}}$; results using $m_c^{\rm pole}$ are also given in the paper.

(2+1+1)-flavor FLAG averages in Table 72.4. Consequently, it is important to account for isospin-breaking effects before combining the theoretical decay constants with the corresponding experimental decay rates.

To obtain the charged D^+-meson decay constant, we apply the correction in Eq. (72.17) to the (2+1+1)-flavor 2021 FLAG average for the D-meson decay constant in the isospin-symmetric limit. Similarly we use Eq. (72.18) to correct the (2+1+1)-flavor 2021 FLAG average for f_{D_s}/f_D. We take the four-flavor FLAG 2021 average for f_{D_s} directly. Our final preferred theoretical values for the charmed pseudoscalar-meson decay constants are

$$\begin{aligned} f_{D^+} &= 212.0(7)\ \text{MeV}\,, \\ f_{D_s} &= 249.9(5)\ \text{MeV}\,, \\ \frac{f_{D_s}}{f_{D^+}} &= 1.1783(16)\,. \end{aligned} \tag{72.19}$$

Table 72.5: Experimental results for $\mathcal{B}(B^- \to \tau^-\overline{\nu})$ and $|V_{ub}|f_{B^+}$. To extract the values of $|V_{ub}|f_{B^+}$ via Eq. (72.1), we use the PDG 2018 value of the B^+ lifetime of 1.638±0.004 ps, and the τ^+ and B^+ masses of 1.77686 and 5.27933 GeV, respectively.

Experiment	Tag	$\mathcal{B}$ (units of 10^{-4})	$\lvert V_{ub}\rvert f_{B^+}$ (MeV)
Belle [87]	Hadronic	$0.72^{+0.27}_{-0.25} \pm 0.11$	
Belle [88]	Semileptonic	$1.25 \pm 0.28 \pm 0.27$	
Belle [88]	Average	0.91 ± 0.22	0.72 ± 0.09
BaBar [89]	Hadronic	$1.83^{+0.53}_{-0.49} \pm 0.24$	
BaBar [90]	Semileptonic	$1.7 \pm 0.8 \pm 0.2$	
BaBar [89]	Average	1.79 ± 0.48	1.01 ± 0.14
Our average		1.06 ± 0.20	0.77 ± 0.07

72.4 Bottom mesons

72.4.1 *Experimental rate measurements*

The Belle and BaBar collaborations have found evidence for $B^- \to \tau^-\overline{\nu}$ decay in $e^+e^- \to B^-B^+$ collisions at the $\Upsilon(4S)$ energy. The analysis relies on reconstructing a hadronic or semileptonic B decay tag, finding a τ candidate in the remaining track and photon candidates, and examining the extra energy in the event which should be close to zero for a real τ^- decay to $e^-\nu\bar{\nu}$ or $\mu^-\nu\bar{\nu}$ opposite a B^+ tag. While the BaBar results have remained unchanged, Belle reanalyzed both samples of their data. The branching fraction using hadronic tags changed from $1.79^{+0.56}_{-0.49}{}^{+0.46}_{-0.51} \times 10^{-4}$ (2006) [86] to $0.72^{+0.27}_{-0.25} \pm 0.11 \times 10^{-4}$ (2012) [87], while the corresponding change using semileptonic tags was from $1.54^{+0.38}_{-0.37}{}^{+0.29}_{-0.31}$ to $1.25 \pm 0.28 \pm 0.27$. These changes demonstrate the difficulty of the analysis. The results are listed in Table 72.5. These are unchanged since the previous review [1].

Because there are large backgrounds under the signals for these measurements, as well as substantial systematic errors, the significances of the individual results are still below the 5σ discovery threshold. Belle quotes 4.6σ for their combined hadronic and semileptonic tags, while BaBar quotes 3.3σ and 2.3σ, for hadronic and semileptonic tags. Greater precision is necessary to determine if any effects beyond the standard model are present.

We do not correct the measured branching ratios in Table 72.5 for radiative corrections because the experimental uncertainties are so large. The relative radiative corrections are expected to be bigger, however, for $B \to \mu\nu$ leptonic decays because the corrections are no longer helicity suppressed [9], and may be a significant fraction of the purely leptonic rate. More theoretical work is needed to understand radiative corrections to leptonic B decays in anticipation of future measurements with greater precision, and of new decay channels.

72.4.2 *Theoretical decay-constant calculations*

Table 72.6 presents recent theoretical calculations of bottom heavy-light meson decay constants and their ratio in the isospin-symmetric limit $m_u = m_d$. The upper two panels show results from lattice-QCD calculations with three $(N_f = 2+1)$ or four flavors $(N_f = 2+1+1)$ of dynamical quarks. For all decay constants, calculations using different gauge-field configurations, light-quark actions, and b-quark actions provide independent confirmation. For comparison, the bottom panel of Table 72.6 shows QCD-model calculations of the B- and B_s-meson decay constants for which uncertainty estimates are provided. These are consistent with the lattice values, but with much larger uncertainties. This table, based on the FLAG 21 averages [2], reflects the latest update of the FLAG 19 averages [3].

The lattice-QCD decay-constant results in Table 72.6 were all obtained using isospin-symmetric gauge-field configurations. Some calculations, however, account for the dominant effect of strong-isospin-breaking by using the correct value for the va-

Downloaded from https://academic.oup.com/ptep/article/2022/8/083C01/6651666 by KIT Library user on 27 September 2022

Table 72.6: Recent theoretical determinations of f_B, f_{B_s}, and their ratio in the isospin-symmetric limit. The upper panels show results from lattice-QCD calculations with $(2+1+1)$ and $(2+1)$ dynamical quark flavors, respectively. When available, statistical and systematic errors are quoted separately. The bottom panel shows estimates from the relativistic potential model (RPM), QCD sum rules, and the light-front quark model, which are not used to obtain our preferred decay-constant values. The 2+1+1 FLAG 21 averages are dominated by the Fermilab/MILC values.

Reference	Method	N_f	f_B(MeV)	f_{B_s}(MeV)	f_{B_s}/f_B
Fermilab/MILC 17 [31]	LQCD	2+1+1	189.9(1.4)	230.7(1.2)	1.2146(49)
HPQCD 17 [91]*	LQCD	2+1+1	190(4)	229(5)	1.206(5)
ETM 16 [92]	LQCD	2+1+1	193(6)	229(5)	1.184(25)
HPQCD 13 [93]	LQCD	2+1+1	186(4)	224(5)	1.205(7)
FLAG 21 average [2]	LQCD	2+1+1	190.0(1.3)	230.3(1.3)	1.209(5)
Aoki 14 [94]†	LQCD	2+1	218.8(6.5)(30.8)	263.5(4.8)(36.7)	1.193(20)(44)
RBC/UKQCD 14 [95]‡	LQCD	2+1	195.6(6.4)(13.3)	235.4(5.2)(11.1)	1.223(14)(70)
HPQCD 12 [96]	LQCD	2+1	191(1)(8)	228(3)(10)	1.188(12)(13)
HPQCD 12 [96]	LQCD	2+1	189(3)(3)*	–	–
HPQCD 11 [97]	LQCD	2+1	–	225(3)(3)	–
Fermilab/MILC 11 [78]	LQCD	2+1	196.9(5.5)(7.0)	242.0(5.1)(8.0)	1.229(13)(23)
FLAG 21 average [2]	LQCD	2+1	192.0(4.3)	228.4(3.7)	1.201(16)
Pullin 21 [80]	QCD SR		192^{+20}_{-19}	225^{+21}_{-20}	1.17(7)
Sun 16 [98]§	RPM		219(15)	266(19)	1.21(9)
Wang 15 [81]§	QCD SR		194(15)	231(16)	1.19(10)
Baker 13 [99]	QCD SR		186(14)	222 (12)	1.19(4)
Lucha 13 [100]	QCD SR		192.0(14.6)	228.0(19.8)	1.184(24)
Gelhausen 13 [82]	QCD SR		$207\binom{+17}{-9}$	$242\binom{+17}{-12}$	$1.17\binom{+3}{-4}$
Narison 12 [83]	QCD SR		206(7)	234(5)	1.14(3)

*Average of new HPQCD 17 and previous HPQCD 13 results allowing for correlations between the two sets of results.
†Obtained with static b quarks (*i.e.*, $m_b \to \infty$).
‡Ref. [95] does not provide results in the isospin-symmetric limit, so we show f_{B^+} and f_{B_s}/f_{B^+} for this work.
§Obtained using $m_b^{\overline{\rm MS}}$; results using $m_b^{\rm pole}$ are also given in the paper.

lence light-quark mass in the B meson (m_u for f_{B^+} and m_d for f_{B^0}). Early estimates of the strong-isospin-breaking correction obtained $f_{B^+} - f_B \sim -2$ MeV [93, 95], which would be significant given the present lattice-QCD uncertainties. It turns out, however, that these calculations inadvertently introduced a spurious sea-quark contribution, and therefore overestimated the size of the effect. A more recent calculation by the Fermilab/MILC Collaboration finds very little evidence for isospin violation ($f_{B^+} - f_B \sim -0.5$ MeV) [31], which is more than two times smaller than the total uncertainties on present lattice-QCD calculations. For this reason, we quote isospin averages in the current review. Our preferred theoretical values for the bottom pseudoscalar-meson decay constants are

$$\begin{aligned} f_B &= 190.0(1.3)\ \text{MeV}\,, \\ f_{B_s} &= 230.0(1.3)\ \text{MeV}\,, \\ \frac{f_{B_s}}{f_B} &= 1.209(5)\,, \end{aligned} \tag{72.20}$$

which are simply the $N_f = 2+1+1$ FLAG 2021 averages [2]. Because the uncertainties on the three-flavor results in Table 72.6 are substantially larger than those on the four-flavor results, including them in the average leaves the central values unchanged, and decreases the errors only slightly.

72.5 Phenomenological implications

72.5.1 $|V_{ud}|$, $|V_{us}|$, *and status of first-row unitarity*

Using the average values for $f_{\pi^+}|V_{ud}|$, $f_{K^+}|V_{us}|$, and their ratio from Eqs. (72.10)–(72.12) and for f_{π^+}, f_{K^+}, and their ratio from Eq. (72.14), we obtain the following determinations of the CKM matrix elements $|V_{ud}|$, $|V_{us}|$, and their ratio from leptonic decays within the standard model:

$$\begin{aligned} &|V_{ud}| = 0.9764(2)(90)(10)\,, \quad |V_{us}| = 0.2254(3)(4)(3), \\ &\frac{|V_{us}|}{|V_{ud}|} = 0.2313(2)(4)(2)\,, \end{aligned} \tag{72.21}$$

where the errors are from the experimental branching fraction(s), the pseudoscalar decay constant(s), and radiative corrections, respectively. These results enable a test of the unitarity of the first row of the CKM matrix from leptonic decays alone (the contribution from $|V_{ub}|$ is negligible). Using the values of $|V_{ud}|$ and $|V_{us}|$ from Eq. (72.21), we find

$$|V_{ud}|^2 + |V_{us}|^2 + |V_{ub}|^2 - 1 = 0.004(18)\,, \tag{72.22}$$

which is consistent with three-generation unitarity at the few-percent level.

The determinations of $|V_{ud}|$ and $|V_{us}|$ from leptonic decays in Eq. (72.21) can be compared to those obtained from other processes. The result above for $|V_{ud}|$ agrees with the determination from superallowed β-decay (a previous value of $|V_{ud}| = 0.97420(21)$ [101] has been updated to $|V_{ud}| = 0.97373(31)$ [102]) but has a considerably larger error, primarily due to the uncertainty in the theoretical determination of f_{π^+}.

The CKM element $|V_{us}|$ can be determined from semileptonic $K^+ \to \pi^0 \ell^+ \nu$ decay. Here experimental measurements provide a value for the product $f_+^{K\pi}(0)|V_{us}|$, where $f_+^{K\pi}(0)$ is the form factor at zero four-momentum transfer between the initial state kaon and the final state pion. We quote a recent analysis by Seng *et al.* [103] which finds $|V_{us}| f_+^{K\pi}(0) = 0.21635(38)(3)$, with the first error denoting experiment and the second reflecting uncertainty in higher order corrections. This is not far from the value 0.2165(4) quoted in our 2020 review [40].[5] Choosing the 2021 2+1+1-flavor FLAG average for $f_+(0)^{K\pi} = 0.9698(17)$ [2] based on the calculations of ETM [107] and Fermilab/MILC [108] gives $|V_{us}| = 0.22309(40)_{\rm exp}(39)_{\rm LQCD}(3)_{\rm HO}$ from semileptonic decay. The determinations of $|V_{us}|$ from leptonic and semileptonic kaon decays are both quite precise, with comparable errors, from but the central values differ by 2.9σ.

Finally, the combination of the ratio $|V_{us}|/|V_{ud}|$ from leptonic decays [Eq. (72.21)] with $|V_{ud}|$ from β decay implies an alternative determination of $|V_{us}| = 0.2253(5)$ which agrees with the value

[5] This was an update of the 2010 Flavianet review [41] that included new measurements of the K_S lifetime [104, 105], ${\rm Re}(\epsilon'/\epsilon)$ [105], and $\mathcal{B}(K^\pm \to \pi^\pm\pi^+\pi^-)$ [106]. The latter measurement was the primary source of the reduced error on $\mathcal{B}$(semileptonic), via the constraint that the sum of all branching ratios must equal unity.

Downloaded from https://academic.oup.com/ptep/article/2022/8/083C01/6651666 by KIT Library user on 27 September 2022

from leptonic kaon decay, but disagrees with the semileptonic-decay result at the 2.9σ level.

Given the roughly 3σ tension between $|V_{us}|$ from leptonic and semileptonic kaon decays, it is important to scrutinize the uncertainties on the theoretical and experimental inputs to $|V_{us}|$ and other elements of the first row of the CKM matrix. Seng *et al.* have introduced a new approach for calculating radiative corrections to neutron and nuclear beta decays using dispersion relations [109–112]. These calculations imply a value of $|V_{ud}| = 0.97395(23)$, consistent with the updated analysis of Ref. [102].

An independent calculation of the radiative corrections by Czarnecki and Marciano using QCD sum rules yields similar results [113]. Using this value of $|V_{ud}|$ with the determination of $|V_{us}|$ from leptonic kaon decays in Eq. (72.21), we obtain $|V_{ud}|^2 + |V_{us}|^2 + |V_{ub}|^2 - 1 = -0.0007(5)$, again consistent with first-row unitarity.

Last, we combine the experimental measurement of $f_{\pi^+}|V_{ud}|$ in Eq. (72.10) with $|V_{ud}|$ from superallowed β-decay [102] to infer an "experimental" value for the pion decay constant:

$$f_{\pi^-}^{\text{"exp"}} = 130.56(2)(3)(13)\ \text{MeV}\,, \tag{72.23}$$

where the uncertainties are from the errors on Γ, $|V_{ud}|$, and higher-order corrections, respectively. Many recent (2+1+1)-flavor lattice-QCD calculations use this quantity to set the overall physical scale in their simulations, *e.g.*, Refs. [10, 31–33]. Conversely, comparing $f_{\pi^-}^{\text{"exp"}}$ with the 2021 FLAG (2+1)-flavor average $f_{\pi^+} = 130.2(8)$ MeV, which only includes lattice-QCD results that employ other observables to set the scale [34–39], provides a test of lattice-QCD methods. The values are in good agreement within present uncertainties. We do not quote an "experimental" value for the kaon decay constant because the value of $|V_{us}|$ is less clear given the $\sim 3\sigma$ tension between the values of $|V_{us}|$ obtained from leptonic and semileptonic kaon decays.

72.5.2 $|V_{cd}|$, $|V_{cs}|$, *and status of second-row unitarity*

Using the average values for $|V_{cd}|f_{D^+}$ and $|V_{cs}|f_{D_s^+}$ from Eqs. (72.15) and (72.16), and for f_{D^+} and $f_{D_s^+}$ from Eq. (72.19), we obtain the following determinations of the CKM matrix elements $|V_{cd}|$ and $|V_{cs}|$ from leptonic decays within the standard model:

$$|V_{cd}| = 0.2178(53)(15)(7) \quad \text{and} \quad |V_{cs}| = 0.9744(84)(16)(20)\,, \tag{72.24}$$

where the errors are from the measured branching fractions, radiative corrections, and decay constants, respectively. These results enable a test of the unitarity of the second row of the CKM matrix. Taking $V_{cb} = 41.0(1.4) \times 10^{-3}$ [1], we obtain

$$|V_{cd}|^2 + |V_{cs}|^2 + |V_{cb}|^2 - 1 = -0.001(22)\,, \tag{72.25}$$

in agreement with three-generation unitarity.

The uncertainty on $|V_{cd}|$ in Eq. (72.24) is limited by the measurement error on the $D^+ \to \mu^+\nu$ decay rate. For $|V_{cs}|$, however, the experimental and radiative-correction errors are commensurate. The value of $|V_{cs}|$ from leptonic D_s decays decreased substantially from the value of 1.007(17) in an earlier version of this review [28, 114], and is now below unity as expected in the three-generation CKM framework. This change is due to our more consistent treatment of the radiative corrections, which lower the purely leptonic decay rates for $D_s^+ \to \mu^+\nu$ and $D_s^+ \to \tau^+\nu$. We emphasize, however, that we have taken a generous uncertainty on these estimates, and that more theoretical work is needed to really pin down the sizes of the radiative corrections to $D_{(s)}$-meson leptonic decays.

The CKM matrix elements $|V_{cd}|$ and $|V_{cs}|$ can also be obtained from semileptonic $D^+ \to \pi^0\ell^+\nu$ and $D_s^+ \to K^0\ell^+\nu$ decays, respectively. Here experimental measurements determine the product of the form factor times the CKM element, and theory provides the value for the form factor at zero four-momentum transfer between the initial $D_{(s)}$ meson and the final pion or kaon.

The latest experimental averages from the Heavy Flavor Averaging Group (HFLAV) are $f_+^{D\pi}(0)\ |V_{cd}| = 0.1426(19)$ and $f_+^{D_sK}(0)|V_{cs}| = 0.7226(34)$ [115]. There are not enough published lattice-QCD calculations of the zero-momentum $D_{(s)}$-meson semileptonic form factors with $N_f \geq 3$ to permit an average by the FLAG Collaboration. Taking the most precise three-flavor form-factor results $f_+^{D\pi}(0) = 0.666(29)$ and $f_+^{D_sK}(0) = 0.747(19)$ from the HPQCD Collaboration [116,117] gives for the CKM matrix elements $|V_{cd}| = 0.2141(97)$ and $|V_{cs}| = 0.967(25)$, in agreement with those from leptonic decays in Eq. (72.24). A newer, four-flavor calculation of the form factors by the ETM Collaboration [118], however, yields a smaller value of $f_+^{D\pi}(0) = 0.612(35)$ by 1.2σ and a larger $f_+^{D_sK}(0) = 0.765(31)$ by 0.5σ. These imply $|V_{cd}| = 0.233(14)$ and $|V_{cs}| = 0.945(39)$, which are about 1σ above and below the values from leptonic decays in Eq. (72.24), respectively. Independent lattice-QCD calculations of the $D^+ \to \pi^0\ell^+\nu$ and $D_s^+ \to K^0\ell^+\nu$ form factors now in progress [119,120] will help to clarify the picture. In a lattice QCD study of the decay $D \to K\ell\nu$, the HPQCD Collaboration [121] reports $|V_{cs}| = 0.9663(80)$.

We can combine the experimental measurements of $f_{D^+}|V_{cd}|$ and $f_{D_s^+}|V_{cs}|$ from Tables 72.2 and 72.3 with $|V_{cd}| = 0.2245(8)$ and $|V_{cs}| = 0.97370(14)$ from the PDG 2020 global unitarity-triangle analysis [1] to infer "experimental" values for the decay constants within the standard model. We take the CKM elements from the global fit because they are based on many input quantities, thereby reducing the sensitivity to any one outlying measurement or calculation. We obtain for the decay constants

$$\begin{aligned} f_{D^+}^{\text{"exp"}} &= 208.9(5.0)(3.8)(1.5)\ \text{MeV}\,, \\ f_{D_s^+}^{\text{"exp"}} &= 246.7(2.1)(2.8)(1.7)\ \text{MeV}\,, \\ (f_{D_s^+}/f_{D^+})^{\text{"exp"}} &= 1.181(30)(25)(12)\,. \end{aligned} \tag{72.26}$$

where the uncertainties are from the errors on $\Gamma^{(0)}$, CKM matrix elements, and radiative corrections, respectively. The "experimental" values f_{D^+} $(f_{D_s^+}/f_{D^+})$ are consistent within 1σ with the (2+1+1)-flavor lattice-QCD averages in Eq. (72.19). The CKM matrix element $|V_{cd}|$ is approximately equal to $|V_{us}|$, as first shown by Wolfenstein [122, 123]. Thus, resolving the inconsistencies between determinations of $|V_{us}|$ from leptonic and semileptonic decays discussed in Sec. 72.5.1 may benefit from the constraints observed here.

Last, we can test lepton-flavor universality in charm meson decays by checking the following relationship derived from Eq. (72.1):

$$\frac{\Gamma(D_s^+ \to \tau^+\nu)}{\Gamma(D_s^+ \to \mu^+\nu)} = \frac{m_\tau^2\left(1 - m_\tau^2/M_{D_s}^2\right)^2}{m_\mu^2\left(1 - m_\mu^2/M_{D_s}^2\right)^2} = 9.75\,, \tag{72.27}$$

where the uncertainties from the masses are negligible to the number of digits quoted. The measured ratio of $\tau^+\nu$ to $\mu^+\nu$ rates is 9.82 ± 0.40, consistent with this standard-model expectation.

72.5.3 $|V_{ub}|$ *and other applications*

Using the average value for $|V_{ub}|f_{B^+}$ from Table 72.5, and for f_{B^+} from Eq. (72.20), we obtain the following determination of the CKM matrix element $|V_{ub}|$ from leptonic decays within the standard model:

$$|V_{ub}| = 4.05(37)(3) \times 10^{-3}\,, \tag{72.28}$$

where the errors are from experiment and theory, respectively. One should bear in mind when interpreting Eq. (72.28) that none of the experimental measurements that enter the average for $|V_{ub}|f_{B^+}$ have individually reached the 5σ discovery level (see Sec. 72.4.1). Further, decays involving the third generation of quarks and leptons may be particularly sensitive to new physics associated with electroweak symmetry breaking due to their larger masses [13, 15], so Eq. (72.28) is more likely to be influenced by new physics than the determinations of the elements of the first and second rows of the CKM matrix in the previous sections.

The CKM element $|V_{ub}|$ can also be obtained from semileptonic B-meson decays. For more than a decade, there has remained a persistent 2-3σ tension between the determinations of $|V_{ub}|$ from exclusive $B \to \pi\ell\nu$ decay and from inclusive $B \to X_u\ell\nu$ decay,

Downloaded from https://academic.oup.com/ptep/article/2022/8/083C01/6651666 by KIT Library user on 27 September 2022

where X_u denotes all hadronic states populated by the $bb \to u$ weak transition [23, 115, 124–127]. The currently most precise determination of $|V_{ub}|^{\rm excl} = 3.73(14) \times 10^{-3}$ is obtained from a joint z-fit by FLAG [2] of the vector and scalar form factors $f_+^{B\pi}(q^2)$ and $f_0^{B\pi}(q^2)$ calculated in (2+1)-flavor lattice QCD [128–130] and experimental measurements of the differential decay rate from BaBar [131,132] and Belle [133,134]. On the other hand, the PDG 2018 inclusive determination obtained using the theoretical frameworks in Refs. [135–137] is $|V_{ub}|^{\rm incl} = 4.49(28) \times 10^{-3}$ [42, 138]. The value of $|V_{ub}|$ from leptonic $B \to \tau\nu$ decay in Eq. (72.28) splits the difference between the inclusive and exclusive determinations, and is compatible (within large uncertainties) with both.

Given the large uncertainties on the experimental measurements of $\mathcal{B}(B^- \to \tau^-\overline{\nu})$, and the more than 2σ disagreement between $|V_{ub}|$ obtained from inclusive and exclusive semileptonic B decays, we do not present an "experimental" value of the decay constant f_{B^+}.

72.6 Concluding remarks

The increasing precision of measurements of leptonic decays of charged pseudoscalar mesons has begun to require control over radiative corrections at a level superior to that presented here. Improvements will be called for both in theory and in experiment (for example, by BESIII and Belle II).

Unitarity of the CKM matrix is in reasonable shape. However, there is a lingering $\sim 3\sigma$ tension between the values of V_{us} determined by semileptonic and leptonic kaon decays. It will be interesting to follow experimental and theoretical developments on this quantity.

Acknowledgements

I thank R. Briere, C. Davies, S. Gottlieb, S. Hajimoto, A. Kronfeld, H.-L. Ma, W. Marciano, and S. Stone for useful discussions on this review, and S. Gottlieb for providing information on the 2021 FLAG lattice averages.

References

[1] P. A. Zyla *et al.* (Particle Data Group), PTEP **2020**, 8, 083C01 (2020).

[2] Y. Aoki *et al.* (Flavour Lattice Averaging Group) (2021).

[3] S. Aoki *et al.* (Flavour Lattice Averaging Group) (2019), [arXiv:1902.08191].

[4] A. Sirlin, Nucl. Phys. **B196**, 83 (1982).

[5] T. Kinoshita, Phys. Rev. Lett. **2**, 477 (1959).

[6] M. Knecht *et al.*, Eur. Phys. J. **C12**, 469 (2000), [hep-ph/9909284].

[7] G. Burdman, J. T. Goldman and D. Wyler, Phys. Rev. **D51**, 111 (1995), [hep-ph/9405425].

[8] V. Cirigliano and I. Rosell, JHEP **10**, 005 (2007), [arXiv:0707.4464].

[9] D. Becirevic, B. Haas and E. Kou, Phys. Lett. **B681**, 257 (2009), [arXiv:0907.1845].

[10] A. Bazavov *et al.* (Fermilab Lattice and MILC), Phys. Rev. **D90**, 074509 (2014), [arXiv:1407.3772].

[11] M. Di Carlo *et al.*, Phys. Rev. **D100**, 034514 (2019), [arXiv:1904.08731].

[12] E. Barberio and Z. Was, Comput. Phys. Commun. **79**, 291 (1994).

[13] W.-S. Hou, Phys. Rev. **D48**, 2342 (1993).

[14] A. G. Akeroyd and S. Recksiegel, Phys. Lett. **B554**, 38 (2003), [hep-ph/0210376].

[15] A. G. Akeroyd and S. Recksiegel, J. Phys. **G29**, 2311 (2003), [hep-ph/0306037].

[16] A. G. Akeroyd, Prog. Theor. Phys. **111**, 295 (2004), [hep-ph/0308260].

[17] B. A. Dobrescu and A. S. Kronfeld, Phys. Rev. Lett. **100**, 241802 (2008), [arXiv:0803.0512].

[18] J. L. Hewett, in "Heavy flavor physics. Proceedings, LISHEP 95, LAFEX International School on High-Energy Physics, session C, cbt Workshop, Rio de Janeiro, Brazil, February 21-23, 1995," 171–187 (1995), [hep-ph/9505246], URL `http://www-public.slac.stanford.edu/sciDoc/docMeta.aspx?slacPubNumber=SLAC-PUB-6821`.

[19] A. Crivellin, Phys. Rev. **D81**, 031301 (2010), [arXiv:0907.2461].

[20] F. U. Bernlochner, Z. Ligeti and S. Turczyk, Phys. Rev. **D90**, 094003 (2014), [arXiv:1408.2516].

[21] W. J. Marciano, Phys. Rev. Lett. **93**, 231803 (2004), [hep-ph/0402299].

[22] V. Cirigliano *et al.*, Rev. Mod. Phys. **84**, 399 (2012), [arXiv:1107.6001].

[23] K. A. Olive *et al.* (Particle Data Group), Chin. Phys. **C38**, 090001 (2014).

[24] B. Ananthanarayan and B. Moussallam, JHEP **06**, 047 (2004), [hep-ph/0405206].

[25] S. Descotes-Genon and B. Moussallam, Eur. Phys. J. **C42**, 403 (2005), [hep-ph/0505077].

[26] W. J. Marciano and A. Sirlin, Phys. Rev. Lett. **71**, 3629 (1993).

[27] V. Cirigliano and H. Neufeld, Phys. Lett. **B700**, 7 (2011), [arXiv:1102.0563].

[28] J. L. Rosner, S. Stone and R. S. Van de Water (2015), review prepared for PDG 2015 edition, [arXiv:1509.02220].

[29] J. Gasser, A. Rusetsky and I. Scimemi, Eur. Phys. J. **C32**, 97 (2003), [hep-ph/0305260].

[30] N. Miller *et al.*, Phys. Rev. D **102**, 3, 034507 (2020), [arXiv:2005.04795].

[31] A. Bazavov *et al.*, Phys. Rev. **D98**, 7, 074512 (2018), [arXiv:1712.09262].

[32] N. Carrasco *et al.* (ETM), Phys. Rev. **D91**, 054507 (2015), [arXiv:1411.7908].

[33] R. Dowdall *et al.* (HPQCD), Phys.Rev. **D88**, 074504 (2013), [arXiv:1303.1670].

[34] V. G. Bornyakov *et al.* (QCDSF-UKQCD), Phys. Lett. **B767**, 366 (2017), [arXiv:1612.04798].

[35] S. Durr *et al.*, Phys. Rev. **D95**, 5, 054513 (2017), [arXiv:1601.05998].

[36] T. Blum *et al.* (RBC, UKQCD), Phys. Rev. **D93**, 074505 (2016), [arXiv:1411.7017].

[37] A. Bazavov *et al.* (MILC), PoS **LATTICE2010**, 074 (2010), [arXiv:1012.0868].

[38] S. Durr *et al.* (BMW), Phys. Rev. **D81**, 054507 (2010), [arXiv:1001.4692].

[39] E. Follana *et al.* (HPQCD, UKQCD), Phys. Rev. Lett. **100**, 062002 (2008), [arXiv:0706.1726].

[40] M. Moulson, in "8th International Workshop on the CKM Unitarity Triangle (CKM2014) Vienna, Austria, September 8-12, 2014," (2014), [arXiv:1411.5252].

[41] M. Antonelli *et al.* (FlaviaNet Working Group on Kaon Decays), Eur. Phys. J. **C69**, 399 (2010), [arXiv:1005.2323].

[42] M. Tanabashi *et al.* (Particle Data Group), Phys. Rev. **D98**, 3, 030001 (2018).

[43] S. Hashimoto, J. Laiho and S. R. Sharpe, "Lattice Quantum Chromodynamics," `http://pdg.lbl.gov/2019/reviews/rpp2018-rev-lattice-qcd.pdf` (2017), review prepared for PDG 2018 edition.

[44] S. Hashimoto, J. Laiho and S. R. Sharpe, "Lattice Quantum Chromodynamics," `pdg.lbl.gov/2020/reviews/rpp2020-rev-lattice-qcd.pdf` (2020), review prepared for PDG 2020 edition.

[45] S. Aoki *et al.* (Flavour Lattice Averaging Group), Eur. Phys. J. **C74**, 2890 (2014), [arXiv:1310.8555].

Downloaded from https://academic.oup.com/ptep/article/2022/8/083C01/6651666 by KIT Library user on 27 September 2022

[46] S. Aoki *et al.*, Eur. Phys. J. **C77**, 2, 112 (2017), [arXiv:1607.00299].

[47] A. S. Kronfeld, Ann. Rev. Nucl. Part. Sci. **62**, 265 (2012), [arXiv:1203.1204].

[48] A. V. Manohar, C. T. Sachrajda and R. M. Barnett, "Quark Masses," `http://pdg.lbl.gov/2019/reviews/rpp2018-rev-quark-masses.pdf` (2018), review prepared for PDG 2018 update.

[49] G. M. de Divitiis *et al.*, JHEP **04**, 124 (2012), [arXiv:1110.6294].

[50] J. Gasser and H. Leutwyler, Nucl. Phys. **B250**, 465 (1985).

[51] G. M. de Divitiis *et al.* (RM123), Phys. Rev. **D87**, 11, 114505 (2013), [arXiv:1303.4896].

[52] M. Artuso *et al.* (CLEO), Phys. Rev. Lett. **95**, 251801 (2005), [hep-ex/0508057].

[53] B. I. Eisenstein *et al.* (CLEO), Phys. Rev. **D78**, 052003 (2008), [arXiv:0806.2112].

[54] M. Ablikim *et al.* (BESIII), Phys. Rev. **D89**, 051104 (2014), [arXiv:1312.0374].

[55] M. Artuso *et al.* (CLEO), Phys. Rev. Lett. **99**, 071802 (2007), [arXiv:0704.0629].

[56] J. P. Alexander *et al.* (CLEO), Phys. Rev. **D79**, 052001 (2009), [arXiv:0901.1216].

[57] M. Ablikim *et al.* (BESIII) (2019), [arXiv:1908.08877].

[58] M. Nobes (2005), [hep-lat/0501009].

[59] A. Bazavov *et al.* (Fermilab Lattice, MILC), Phys. Rev. **D93**, 11, 113016 (2016), [arXiv:1602.03560].

[60] J. P. Lees *et al.* (BaBar) (2010), [arXiv:1003.3063].

[61] P. del Amo Sanchez *et al.* (BaBar), Phys. Rev. **D82**, 091103 (2010), [Erratum: Phys. Rev.D91,no.1,019901(2015)], [arXiv:1008.4080].

[62] A. Zupanc *et al.* (Belle), JHEP **1309**, 139 (2013), [arXiv:1307.6240].

[63] M. Ablikim *et al.* (BESIII), Phys. Rev. D **94**, 7, 072004 (2016), [arXiv:1608.06732].

[64] M. Ablikim *et al.* (BESIII) (2021), [arXiv:2102.11734].

[65] P. Naik *et al.* (CLEO), Phys. Rev. **D80**, 112004 (2009), [arXiv:0910.3602].

[66] K. M. Ecklund *et al.* (CLEO), Phys. Rev. Lett. **100**, 161801 (2008), [arXiv:0712.1175].

[67] P. U. E. Onyisi *et al.* (CLEO), Phys. Rev. **D79**, 052002 (2009), [arXiv:0901.1147].

[68] M. Ablikim *et al.* (BESIII) (2021), [arXiv:2106.02218].

[69] M. Ablikim *et al.* (BESIII) (2021), [arXiv:2105.07178].

[70] T. K. Pedlar *et al.* (CLEO), Phys. Rev. **D76**, 072002 (2007), [arXiv:0704.0437].

[71] J. P. Alexander *et al.* (CLEO), Phys. Rev. Lett. **100**, 161804 (2008), [arXiv:0801.0680].

[72] B. Aubert *et al.* (BaBar), Phys. Rev. Lett. **98**, 141801 (2007), [hep-ex/0607094].

[73] Y. Chen *et al.* (χQCD), Chin. Phys. C **45**, 2, 023109 (2021), [arXiv:2008.05208].

[74] P. A. Boyle *et al.* (RBC/UKQCD) (2018), [arXiv:1812.08791].

[75] P. A. Boyle *et al.*, JHEP **12**, 008 (2017), [arXiv:1701.02644].

[76] Y.-B. Yang *et al.* (χQCD), Phys. Rev. **D92**, 034517 (2015), [arXiv:1410.3343].

[77] H. Na *et al.* (HPQCD), Phys. Rev. **D86**, 054510 (2012), [arXiv:1206.4936].

[78] A. Bazavov *et al.* (Fermilab Lattice and MILC), Phys. Rev. **D85**, 114506 (2012), [arXiv:1112.3051].

[79] C. T. H. Davies *et al.* (HPQCD), Phys. Rev. **D82**, 114504 (2010), [arXiv:1008.4018].

[80] B. Pullin and R. Zwicky (2021), [arXiv:2106.13617].

[81] Z.-G. Wang, Eur. Phys. J. **C75**, 427 (2015), [arXiv:1506.01993].

[82] P. Gelhausen *et al.*, Phys.Rev. **D88**, 014015 (2013), [arXiv:1305.5432].

[83] S. Narison, Phys. Lett. **B718**, 1321 (2013), [arXiv:1209.2023].

[84] W. Lucha, D. Melikhov and S. Simula, Phys. Lett. **B701**, 82 (2011), [arXiv:1101.5986].

[85] W. Lucha, D. Melikhov and S. Simula, Eur. Phys. J. **C78**, 2, 168 (2018), [Erratum: Eur. Phys. J.C78,no.11,936(2018)], [arXiv:1702.07537].

[86] K. Ikado *et al.* (Belle), Phys. Rev. Lett. **97**, 251802 (2006), [hep-ex/0604018].

[87] I. Adachi *et al.* (Belle), Phys. Rev. Lett. **110**, 131801 (2013), [arXiv:1208.4678].

[88] B. Kronenbitter *et al.* (Belle), Phys. Rev. **D92**, 051102 (2015), [arXiv:1503.05613].

[89] J. P. Lees *et al.* (BaBar), Phys. Rev. **D88**, 031102 (2013), [arXiv:1207.0698].

[90] B. Aubert *et al.* (BaBar), Phys. Rev. **D81**, 051101 (2010), [arXiv:0912.2453].

[91] C. Hughes, C. T. H. Davies and C. J. Monahan, Phys. Rev. **D97**, 5, 054509 (2018), [arXiv:1711.09981].

[92] A. Bussone *et al.* (ETM), Phys. Rev. **D93**, 11, 114505 (2016), [arXiv:1603.04306].

[93] R. Dowdall *et al.* (HPQCD), Phys. Rev. Lett. **110**, 222003 (2013), [arXiv:1302.2644].

[94] Y. Aoki *et al.*, Phys. Rev. **D91**, 114505 (2015), [arXiv:1406.6192].

[95] N. H. Christ *et al.* (RBC/UKQCD), Phys. Rev. **D91**, 054502 (2015), [arXiv:1404.4670].

[96] H. Na *et al.* (HPQCD), Phys. Rev. **D86**, 034506 (2012), [arXiv:1202.4914].

[97] C. McNeile *et al.* (HPQCD), Phys. Rev. **D85**, 031503 (2012), [arXiv:1110.4510].

[98] H.-K. Sun and M.-Z. Yang, Phys. Rev. **D95**, 11, 113001 (2017), [arXiv:1609.08958].

[99] M. J. Baker *et al.*, JHEP **07**, 032 (2014), [arXiv:1310.0941].

[100] W. Lucha, D. Melikhov and S. Simula, Phys.Rev. **D88**, 056011 (2013), [arXiv:1305.7099].

[101] J. Hardy and I. S. Towner, PoS **CKM2016**, 028 (2016).

[102] J. C. Hardy and I. S. Towner, Phys. Rev. C **102**, 4, 045501 (2020).

[103] C.-Y. Seng *et al.* (2021), [arXiv:2107.14708].

[104] F. Ambrosino *et al.* (KLOE), Eur. Phys. J. **C71**, 1604 (2011), [arXiv:1011.2668].

[105] E. Abouzaid *et al.* (KTeV), Phys. Rev. **D83**, 092001 (2011), [arXiv:1011.0127].

[106] D. Babusci *et al.* (KLOE KLOE-2), Phys. Lett. **B738**, 128 (2014), [arXiv:1407.2028].

[107] N. Carrasco *et al.*, Phys. Rev. **D93**, 11, 114512 (2016), [arXiv:1602.04113].

[108] A. Bazavov *et al.* (Fermilab Lattice and MILC), Phys. Rev. Lett. **112**, 112001 (2014), [arXiv:1312.1228].

[109] C.-Y. Seng *et al.*, Phys. Rev. Lett. **121**, 241804 (2018), [arXiv:1807.10197].

[110] C. Y. Seng, M. Gorchtein and M. J. Ramsey-Musolf, Phys. Rev. **D100**, 013001 (2019), [arXiv:1812.03352].

[111] M. Gorchtein, Phys. Rev. Lett. **123**, 042503 (2019), [arXiv:1812.04229].

[112] C.-Y. Seng and U.-G. Meissner, Phys. Rev. Lett. **122**, 211802 (2019), [arXiv:1903.07969].

Downloaded from https://academic.oup.com/ptep/article/2022/8/083C01/6651666 by KIT Library user on 27 September 2022

[113] A. Czarnecki, W. J. Marciano and A. Sirlin (2019), [arXiv:1907.06737].

[114] C. Patrignani *et al.* (Particle Data Group), Chin. Phys. **C40**, 10, 100001 (2016).

[115] Y. Amhis *et al.* (HFLAV), Eur. Phys. J. **C77**, 12, 895 (2017), [arXiv:1612.07233].

[116] H. Na *et al.* (HPQCD), Phys. Rev. **D82**, 114506 (2010), [arXiv:1008.4562].

[117] H. Na *et al.* (HPQCD), Phys. Rev. **D84**, 114505 (2011), [arXiv:1109.1501].

[118] V. Lubicz *et al.* (ETM), Phys. Rev. **D96**, 5, 054514 (2017), [erratum: Phys. Rev.D99,no.9,099902(2019)], [arXiv:1706.03017].

[119] B. Chakraborty *et al.*, EPJ Web Conf. **175**, 13027 (2018), [arXiv:1710.07334].

[120] R. Li *et al.* (Fermilab Lattice, MILC), PoS **LATTICE2018**, 269 (2019), [arXiv:1901.08989].

[121] B. Chakraborty *et al.* ((HPQCD Collaboration)), Phys. Rev. D **104**, 3, 034505 (2021), [arXiv:2104.09883].

[122] L. Wolfenstein, Phys. Rev. Lett. **51**, 1945 (1983).

[123] J. Charles *et al.* (CKMfitter Group), Eur. Phys. J. **C41**, 1 (2005), updated results and plots available at: `http://ckmfitter.in2p3.fr`, [hep-ph/0406184].

[124] M. Antonelli *et al.*, Phys. Rept. **494**, 197 (2010), [arXiv:0907.5386].

[125] J. N. Butler *et al.* (Quark Flavor Physics Working Group), in "Community Summer Study 2013: Snowmass on the Mississippi (CSS2013) Minneapolis, MN, USA, July 29-August 6, 2013," (2013), [arXiv:1311.1076], URL `http://www.slac.stanford.edu/econf/C1307292/docs/IntensityFrontier/QuarkFl-15.pdf`.

[126] Y. Amhis *et al.* (Heavy Flavor Averaging Group) (2014), [arXiv:1412.7515].

[127] A. J. Bevan *et al.* (Belle, BaBar), Eur. Phys. J. **C74**, 3026 (2014), [arXiv:1406.6311].

[128] E. Dalgic *et al.*, Phys. Rev. **D73**, 074502 (2006), [Erratum: Phys. Rev.D75,119906(2007)], [hep-lat/0601021].

[129] J. M. Flynn *et al.* (RBC/UKQCD), Phys. Rev. **D91**, 074510 (2015), [arXiv:1501.05373].

[130] J. A. Bailey *et al.* (Fermilab Lattice, MILC), Phys. Rev. **D92**, 014024 (2015), [arXiv:1503.07839].

[131] P. del Amo Sanchez *et al.* (BaBar), Phys. Rev. **D83**, 032007 (2011), [arXiv:1005.3288].

[132] J. P. Lees *et al.* (BaBar), Phys. Rev. **D86**, 092004 (2012), [arXiv:1208.1253].

[133] H. Ha *et al.* (Belle), Phys. Rev. **D83**, 071101 (2011), [arXiv:1012.0090].

[134] A. Sibidanov *et al.* (Belle), Phys.Rev. **D88**, 032005 (2013), [arXiv:1306.2781].

[135] S. W. Bosch *et al.*, Phys. Rev. Lett. **93**, 221801 (2004), [hep-ph/0403223].

[136] J. R. Andersen and E. Gardi, JHEP **01**, 097 (2006), [hep-ph/0509360].

[137] P. Gambino *et al.*, JHEP **10**, 058 (2007), [arXiv:0707.2493].

[138] R. Kowalewski and T. Mannel, "Semileptonic b-Hadron Decays, Determination of V_{cb}, V_{ub}," `http://pdg.lbl.gov/2018/reviews/rpp2018-rev-vcb-vub.pdf` (2017), review prepared for PDG 2018 update.

Downloaded from https://academic.oup.com/ptep/article/2022/8/083C01/6651666 by KIT Library user on 27 September 2022

73. Production and Decay of b-flavored Hadrons

Revised September 2021 by P. Eerola (Helsinki U.), M. Kreps (Warwick U.) and Y. Kwon (Yonsei U., Seoul).

The b quark belongs to the third generation of quarks and is the weak–doublet partner of the t quark. The existence of the third–generation quark doublet was proposed in 1973 by Kobayashi and Maskawa [1] in their model of the quark mixing matrix ("CKM" matrix), and confirmed four years later by the first observation of a $b\bar{b}$ meson [2]. In the KM model, CP violation is explained within the Standard Model (SM) by an irreducible phase of the 3×3 unitary matrix. The regular pattern of the three lepton and quark families is one of the most intriguing puzzles in particle physics. The existence of families gives rise to many of the free parameters in the SM, including the fermion masses, and the elements of the CKM matrix.

Since the b quark is the lighter element of the third–generation quark doublet, the decays of b-flavored hadrons occur via generation-changing processes through CKM matrix. Because of this, and the fact that the CKM matrix is close to a 3×3 unit matrix, many interesting features such as loop and box diagrams, flavor oscillations, as well as large CP asymmetries, can be observed in the weak decays of b-flavored hadrons.

The CKM matrix is parameterized by three real parameters and one complex phase. This complex phase is the source of CP violation in B meson decays in the Standard Model. A crucial milestone was the first observation of CP violation in the B meson system in 2001, by the BaBar [3] and Belle [4] collaborations. They measured a large value for the parameter $\sin 2\beta$ $(= \sin 2\phi_1)$ [5], almost four decades after the discovery of a small CP asymmetry in neutral kaons. A more detailed discussion of the CKM matrix and CP violation can be found elsewhere in this *Review* [6,7].

The structure of this mini-review is organized as follows. After a discussion of b-quark production and current results on spectroscopy, we discuss lifetimes of b-flavored hadrons. We then discuss some basic properties of B-meson decays, followed by summaries of dominant hadronic, rare hadronic, and electroweak penguin decays of B-mesons. There are separate mini-reviews for B^0–$\overline{B}^0$ mixing [8] and the extraction of the CKM matrix elements V_{cb} and V_{ub} from B-meson decays [9] in this *Review*.

73.1 Production and spectroscopy

The bound states of a $\bar{b}$ antiquark and a u, d, s, or c quark are referred to as the B_u (B^+), B_d (B^0), B_s (B_s^0), and B_c (B_c^+) mesons, respectively. The B_c^+ is the heaviest of the ground–state b-flavored mesons, and the most difficult to produce: it was observed for the first time in the semileptonic mode by CDF in 1998 [10], but its mass was accurately determined only in 2006, from the fully reconstructed mode $B_c^+ \to J/\psi\pi^+$ [11]. Many exclusive decay channels can now be used for the accurate mass measurements, given the large statistics available at the LHC. Currently the most precise measurement is made by LHCb and yields $m(B_c^+) = 6274.47 \pm 0.27 \pm 0.17$ MeV/c^2 [12], combining $B_c^+ \to J/\psi\pi^+$, $B_c^+ \to J/\psi\pi^+\pi^-\pi^+$, $B_c^+ \to J/\psi p\bar{p}\pi^+$, $B_c^+ \to J/\psi D_s^+$, $B_c^+ \to J/\psi D^0 K^+$ and $B_c^+ \to B_s^0\pi^+$ decay modes.

The first excited meson is called the B^* meson, while B^{**} is the generic name for the four orbitally excited $(L = 1)$ B-meson states that correspond to the P-wave mesons in the charm system, D^{**}. Excited states of the B_s^0 meson are similarly named B_s^* and B_s^{**}.

Of the possible bound $\bar{b}b$ states, the $\Upsilon(nS)$ and $\chi_{bJ}(nP)$ states are well studied. The pseudoscalar ground state η_b has been observed for the first time by BaBar [13] indirectly through the decay $\Upsilon(3S) \to \gamma\eta_b$, and then confirmed by Babar in $\Upsilon(2S)$ decays [14] and CLEO in $\Upsilon(3S)$ decays [15]. The most accurate mass and width measurements come now from Belle, using decays $\Upsilon(5S) \to h_b(1P)\pi^+\pi^-$, $h_b(1P) \to \gamma\eta_b(1S)$ [16] and $\Upsilon(4S) \to \eta h_b(1P)$, $h_b(1P) \to \gamma\eta_b(1S)$ [17]. Belle has also reported first evidence for the $\eta_b(2S)$ in the $h_b(2P) \to \eta_b(2S)\gamma$ transition [16]. In addition, Belle has observed $Z_b(10610)$ and $Z_b(10650)$ states in the processes $\Upsilon(5S) \to \Upsilon(nS)\pi^+\pi^-$ $(n = 1,2,3)$ and $\Upsilon(5S) \to h_b(mP)\pi^+\pi^-$ $(m = 1,2)$ [18]. These Z_b states are observed to decay to $\Upsilon(nS)\pi^\pm$ and $h_b(mP)\pi^\pm$, hence electrically charged and do not belong to ordinary $q\bar{q}$ mesons. For classification and naming of these and other states, see Ref. [19].

Experimental studies of b decays have been performed in e^+e^- collisions at the $\Upsilon(4S)$ (ARGUS, CLEO, Belle, BaBar) and $\Upsilon(5S)$ (CLEO, Belle) resonances. The $e^+e^- \to b\bar{b}$ production cross-section at the $\Upsilon(4S)$ $(\Upsilon(5S))$ resonance is about 1.1 nb (0.3 nb). The full data samples of BaBar and Belle are 560 fb^{-1} and 1020 fb^{-1}, respectively, of which 433 fb^{-1} and 710 fb^{-1} are at the $\Upsilon(4S)$ resonance. Since the $\Upsilon(4S)$ decays dominantly to a pair of B mesons (either B^+B^- or $B^0\overline{B}^0$), a precise knowledge of the energy-momentum of one B meson (the 'tagging B') enables deducing the properties of the other B (the 'signal B'). This property has been exploited by both BaBar and Belle, in particular, to measure inclusive decay modes as well as final states with missing neutrinos. The Belle II experiment at SuperKEKB has started recording data in 2019, and the experiment has so far collected about 210 fb^{-1} of data by summer 2021. At the Z resonance (SLC, LEP) all species of b-flavored hadrons could be studied for the first time. The $e^+e^- \to b\bar{b}$ production cross-section at the Z resonance is about 6.6 nb.

High-energy $p\bar{p}$ (Tevatron) and pp collisions (LHC) produce b-flavored hadrons of all species with large cross-sections. At the Tevatron ($\sqrt{s} = 1.96$ TeV) the visible cross section $\sigma(p\bar{p} \to bX, |\eta| < 1)$ is about 30 μb. CDF and D0 experiments at the Tevatron have accumulated by the end of their running about 10 fb^{-1} each.

At the LHC pp collider at $\sqrt{s} = 7 - 13$ TeV, the visible b-hadron cross section at the LHCb experiment with pseudorapidity acceptance $2 < \eta < 5$ has been measured to be ~ 72 μb at 7 TeV and ~ 144 μb at 13 TeV [20] (cross section at 13 TeV corrected in Erratum). LHCb has collected about 1 fb^{-1} at 7 TeV, 2 fb^{-1} at 8 TeV, and close to 5.9 fb^{-1} at 13 TeV during LHC Runs 1 and 2. CMS and ATLAS have collected each about 5 fb^{-1} of data at $\sqrt{s} = 7$, 20 fb^{-1} at 8 TeV and about 150 fb^{-1} at 13 TeV during LHC Runs 1 and 2. The LHCb experiment is undergoing currently major upgrade. The LHC operation is planned to resume in 2022.

In hadron collisions, production happens as $b\bar{b}$ pairs via leading order flavor creation or higher order processes such as gluon–splitting. Single b-quarks can be produced by flavor excitation. The total b-production cross section is an interesting test of our understanding of leading and higher order QCD processes. With a wealth of measurements at LHC and at Tevatron (see Ref. [20] and references therein), and improved calculations [21], there is a reasonable agreement between measurements and predictions.

Each quark of a $b\bar{b}$ pair produced in hadron collisions hadronizes separately and incoherently from the other, but it is still possible to obtain a statistical indication of the charge of a produced $b/\bar{b}$ quark ("flavor tag" or "charge tag") from the accompanying particles produced in the hadronization process, or from the decay products of the other quark. The momentum spectrum of produced b-quarks typically peaks near the b-quark mass, and extends to much higher momenta, dropping by about a decade for every ten GeV. Typical decay lengths are of the order of a centimeter at 13 TeV pp collisions; the resolution for the decay vertex must be more precise than this to resolve the fast oscillations of B_s^0 mesons.

In e^+e^- colliders, since the B mesons are very slow in the $\Upsilon(4S)$ rest frame, asymmetric beam energies are used to boost the decay products to allow time-dependent measurements that are crucial for the study of CP violation. At KEKB, the boost was $\beta\gamma = 0.43$, while PEP-II used a slightly larger boost, $\beta\gamma = 0.55$. The typical B-meson decay length is dilated from ≈ 20 μm to ≈ 200 μm. At SuperKEKB the boost is lower, $\beta\gamma = 0.28$, which puts more demanding requirements on the track reconstruction precision at Belle II to reach a resolution in decay time measurements similar to Belle. The two B mesons produced in $\Upsilon(4S)$ decay are in a coherent quantum state, which makes it easier than in hadron collisions to infer the charge state of one B meson from observation of the other; however, the coherence also requires determination of the decay time of both mesons, rather than just one, in order to perform time–dependent CP–violation measurements. For B_s^0, which can be produced at $\Upsilon(5S)$ the situation is less favourable,

Downloaded from https://academic.oup.com/ptep/article/2022/8/083C01/6651666 by KIT Library user on 27 September 2022

as boost is not high enough to provide sufficient time resolution to resolve the fast B_s^0 oscillations.

For the measurement of branching fractions, the initial composition of the data sample must be known. The $\Upsilon(4S)$ resonance decays predominantly to $B^0\overline{B}^0$ and B^+B^-; the current experimental upper limit for non-$B\overline{B}$ decays of the $\Upsilon(4S)$ is less than 4% at the 95% confidence level (CL) [22]. The observed modes of this category are decays to lower Υ states and a pion pair, η, or η', measured branching fractions being of order $10^{-4} - 10^{-5}$ [23], and decays to $h_b(1P)\eta$ with branching fraction of order 10^{-3} [17].

The ratio f_+/f_0 of the fractions of charged to neutral B productions from $\Upsilon(4S)$ decays has been measured by CLEO, BaBar, and Belle in various ways. They typically use pairs of isospin-related decays of B^+ and B^0, such that it can be assumed that $\Gamma(B^+ \to x^+) = \Gamma(B^0 \to x^0)$. In this way, the ratio of the number of events observed in these modes is proportional to $(f_+\tau_+)/(f_0\tau_0)$ [24,25]. BaBar has also performed an independent measurement of f_0 with a different method that does not require isospin symmetry or the value of the lifetime ratio, based on the number of events with one or two reconstructed $B^0 \to D^{*-}\ell^+\nu$ decays [26]. The combined result, from the current average of τ_+/τ_0, is $f_+/f_0 = 1.058 \pm 0.024$ [27]. The result is consistent within 2.4σ with equal production of B^+B^- and $B^0\overline{B}^0$ pairs, and we assume $f_+/f_0 = 1$ in this mini-review except where explicitly stated otherwise. This assumption is also supported by the near equality of the B^+ and B^0 masses: our fit yields $m(B^0) = 5279.65 \pm 0.12$ MeV/c^2, $m(B^+) = 5279.34 \pm 0.12$ MeV/c^2, and $m(B^0) - m(B^+) = 0.31 \pm 0.05$ MeV/c^2.

Data collected at the $\Upsilon(5S)$ resonance gave CLEO, Belle and BaBar access to B_s^0 decays. In $\Upsilon(5S)$ decays there are seven possible final states including a pair of non-strange B mesons and 0, 1 or 2 pions, and three with a pair of strange B mesons ($B_s^{*0}\overline{B}_s^{*0}$, $B_s^{*0}\overline{B}_s^0$, and $B_s^0\overline{B}_s^0$). The fraction of events with a pair of B_s^0 mesons over the total number of events with a pair of b-flavored hadrons has been measured to be $f_s[\Upsilon(5S)] = 0.199^{+0.030}_{-0.029}$ [28], of which 88% is $B_s^{*0}\bar{B}_s^{*0}$ events. However, the small boost of B_s^0 mesons produced in this way prevents resolution of their fast oscillations for time-dependent measurements; these are only accessible in hadron collisions (or at the Z peak).

In high-energy collisions, the produced b or $\bar{b}$ quarks can hadronize with different probabilities into the full spectrum of b-hadrons, either in their ground or excited states. The hadronization does not have to be identical in $p\overline{p}$ or pp collisions and in Z decay, because of the different momentum distributions of the b-quark in these processes; the sample used in the $p\overline{p}$ measurements has momenta close to the b mass, rather than $m_Z/2$ in Z decay. The available data from Tevatron and LHC show that the production fractions f_d, f_u, f_s, and $f_{\rm baryon}$ of B^0, B^+, B_s^0, and b baryons, respectively, of weakly decaying b hadrons depend on the kinematics of the produced b hadron. The production fractions of b hadrons are discussed in more detail in the $B^0 - \overline{B}^0$ mixing section in this *Review* [8].

Excited B-meson states have been thoroughly studied by CLEO, LEP, CUSB, D0 and CDF (an admixture of B mesons) and LHCb (B^{*+}-meson). The current world average of the B^*–B mass difference is 45.21 ± 0.21 MeV/c^2. Excited B_s^*-meson states have observed in $\Upsilon(5S)$ decays by CUSB, CLEO and Belle.

For orbitally excited $B_{(s)}$ meson states, with relative angular momentum L=1 of the two quarks, there exist four states $(J, j_q) = (0, 1/2), (1, 1/2), (1, 3/2), (2, 3/2)$, where j_q is the total angular momentum of the light u, d or s quark and J is the total angular momentum of the B meson. These states are collectively called as $B_{(s)}^{**}$ mesons. The $j_q = 1/2$ states are named $B_{(s)0}^*$ ($J = 0$) and $B_{(s)1}$ ($J = 1$) mesons, while the states with $j_q = 3/2$ are named $B_{(s)1}$ ($J = 1$) and $B_{(s)2}^*$ ($J = 2$) mesons. The states with $j_q = 1/2$ can decay through an S-wave transition and are expected to have a large width, but the $j_q = 3/2$ states are narrow D-wave decays. Evidence for B^{**} production has been initially obtained at LEP as a broad $B\pi$ resonance [29] or a B^+K^- enhancement [30]. Detailed results have been obtained for the narrow states $B_1(5721)^{0,+}$ and $B_2(5747)^{0,+}$ at the Tevatron and by LHCb, and clear enhancements compatible with the higher mass states $B_J(5840)^{0,+}$ and $B_J(5970)^{0,+}$ have been observed [31,32]. Also the narrow B_s^{**} states $B_{s1}(5830)^0$ and $B_{s2}(5840)^0$ have been measured at the CDF [31], LHCb [33], and CMS [34].

Excited states of B_c^+ mesons will provide important information about the strong potential. A $B_c^+\pi^+\pi^-$ resonance has been observed for the first time by ATLAS [35]. The mass of the resonance has been measured precisely by CMS and LHCb as 6871.6 ± 1.1 MeV/c^2 [36,37]. The resonance may be interpreted as the second S-wave state of the B_c^+ meson, $B_c^+(2S)$, but the quantum numbers are to be confirmed.

Baryon states containing a b quark are labeled according to the same scheme used for non-b baryons, with the addition of a b subscript [19]. The first observed b baryon was the Λ_b^0 (quark composition udb). Thanks to the large samples accumulated at the Tevatron and specially at the LHC many new b baryons have been found. The masses of all these new baryons have been measured to a precision of a few MeV/c^2, and found to be in agreement with predictions from Heavy Quark Effective Theory (HQET).

Clear signals of four strongly–decaying baryon states, Σ_b^+, Σ_b^{*+} (uub), Σ_b^-, Σ_b^{*-} (ddb) have been obtained by CDF [38] and LHCb [39]. LHCb has also observed two new mass peaks in the $\Lambda_b^0\pi^\pm$ systems, consistent with single resonances and named as $\Sigma_b^\pm(6097)$ [39]. The nature of these resonances is, however, not yet clear. The isodublet of strange b baryons Ξ_b^0 (usb) and $\Xi_b^\pm$ (dsb) has been observed by CDF and D0 [40]. Masses, lifetimes, and branching ratios have been accurately measured by LHCb [41] and CDF [42]. LHCb has also measured several parameters sensitive to P and CP violation [43]. Other observed Ξ_b baryons are spin-3/2 states $\Xi_b(5945)^0$ (Ξ_b^{*0}) [44,45] and $\Xi_b^*(5955)^-$ [46], a spin-1/2 state $\Xi_b'(5935)^-$ [46], and a resonance state $\Xi_b^-(6227)$ [47]. The doubly–strange bottom baryon Ω_b^- has been observed first by D0 and CDF [48]. Mass and mean life have been measured precisely by LHCb [49] and CDF [42].

The so-called exotic states have raised a lot of interest recently. While many exotic states were seen in the charm sector, in bottom sector there are fewer seen. The D0 Collaboration claimed a narrow state $X(5568)$ decaying into a $B_s^0\pi^\pm$ final state [50]. While this would be an interesting addition to the observed states as the first exotic state with constituent quarks with four different flavours (b, s, u, d), analysis by LHCb yields negative result [51]. Also CMS finds no such a state [52].

73.2 Lifetimes

Precise lifetimes are key in extracting the weak parameters that are important for understanding the role of the CKM matrix in CP violation, such as the determination of V_{cb} and B_s^0–$\overline{B}_s^0$ mixing parameters. In the naive spectator model, the heavy quark can decay only via the external spectator mechanism, and thus, the lifetimes of all mesons and baryons containing b quarks would be equal. Non–spectator effects, such as the interference between contributing amplitudes, modify this simple picture and give rise to a lifetime hierarchy for b-flavored hadrons similar to the one in the charm sector. However, since the lifetime differences are expected to scale as $1/m_Q^2$, where m_Q is the mass of the heavy quark, the variations in the b system are expected to be only 10% or less [53,54]. We expect:

$$\tau(B^+) \geq \tau(B^0) \approx \tau(B_s^0) > \tau(\Lambda_b^0) \gg \tau(B_c^+) \,. \qquad (73.1)$$

For the B_c^+, both quarks decay weakly, so the lifetime is much shorter.

Measurements of the lifetimes of the different b-flavored hadrons thus provide a means to determine the importance of non-spectator mechanisms in the b sector. Availability of large samples of fully–reconstructed decays of different b-hadron species has resulted in precise measurements with small statistical and systematic uncertainties (∼1%). The world averages given in Table 73.1 have been determined by the Heavy Flavor Averaging Group (HFLAV) [28].

The B_s^0 lifetime in Table 73.1 is defined as $1/\Gamma_s$, where Γ_s is the average width of the light (L) and heavy (H) mass eigenstates, $(\Gamma_L + \Gamma_H)/2$. In the absence of CP violation, the light (heavy) B_s^0

Downloaded from https://academic.oup.com/ptep/article/2022/8/083C01/6651666 by KIT Library user on 27 September 2022

Table 73.1: Summary of the world-average b-hadron lifetime measurements. For the B_s^0 lifetimes, see text below.

Particle	Lifetime [ps]
B^+	1.638 ± 0.004
B^0	1.519 ± 0.004
B_s^0	1.520 ± 0.005
B_{sL}^0	1.429 ± 0.007
B_{sH}^0	1.624 ± 0.009
B_c^+	0.510 ± 0.009
Λ_b^0	1.471 ± 0.009
Ξ_b^-	1.572 ± 0.040
Ξ_b^0	1.480 ± 0.030
Ω_b^-	$1.64^{+0.18}_{-0.17}$

mass eigenstate is the CP-even (CP-odd) eigenstate. Thus, the lifetime of the light (heavy) mass eigenstate can be measured from CP-even (odd) final states. The lifetimes can also be obtained from time-dependent angular analysis of $B_s^0 \to J/\psi\phi$ decays.

The short B_c^+ lifetime is in good agreement with predictions [55]. With large samples of B_c^+ mesons at the LHC precision on the lifetimes can still improve. The measurement using semileptonic decays gives $\tau_{B_c^+} = 0.509 \pm 0.008 \pm 0.012$ ps [56] while using decays $B_c^+ \to J/\psi\pi^+$ yields $\tau_{B_c^+} = 0.5134 \pm 0.0110 \pm 0.0057$ ps [57]. Each of these is more precise than the combination of all previous experiments.

The recent Λ_b^0 lifetime measurements from LHC experiments and CDF are precise and favour lifetime close to the lifetime of B^0 meson, in agreement with theory.

For precision comparisons with theory, lifetime ratios are more sensitive. Experimentally it is found [28]:

$$\frac{\tau_{B^+}}{\tau_{B^0}} = 1.076 \pm 0.004\,, \quad \frac{\tau_{B_s^0}}{\tau_{B^0}} = 1.001 \pm 0.004\,,$$

$$\frac{\tau_{\Lambda_b^0}}{\tau_{B^0}} = 0.969 \pm 0.006\,,$$

while recent Heavy Quark Expansion (HQE) predictions give [54]:

$$\frac{\tau_{B^+}}{\tau_{B^0}} = 1.04^{+0.05}_{-0.01} \pm 0.02 \pm 0.01\ , \quad \frac{\tau_{B_s^0}}{\tau_{B^0}} = 1.001 \pm 0.002\ ,$$

$$\frac{\tau_{\Lambda_b^0}}{\tau_{B^0}} = 0.935 \pm 0.054.$$

The ratio of B^+ to B^0 lifetimes has a precision of better than 1%, and is significantly different from 1.0, in agreement with predictions [53]. The ratio of B_s^0 to B^0 lifetimes is expected to be very close to 1.0.

For a detailed discussion on neutral B^0 and B_s^0 oscillation and relevant CP violation measurements see Ref. [8].

73.3 Features of decays

The ground states of b-flavored hadrons decay via weak interactions. In most decays of the b-flavored hadrons, where the b-quark is accompanied by lighter partner quarks (d, u, s, or c), the decay modes are well described by the decay of the b quark (spectator model) [58]. The dominant decay mode of a b quark is $b \to cW^{*-}$ (referred to as a "tree" or "spectator" decay), where the virtual W materializes either into a pair of leptons $\ell\overline{\nu}$ ("semileptonic decay"), or into a pair of quarks which then hadronizes. The transition $b \to u$ is suppressed by $|V_{ub}/V_{cb}|^2 \sim (0.1)^2$ relative to $b \to c$ transitions. The decays in which the spectator quark combines with one of the quarks from W^* to form one of the final state hadrons are suppressed by a factor $\sim (1/3)^2$, because the colors of the two quarks from different sources must match ("color–suppression").

Semileptonic B decays $B \to X_c\ell\nu$ and $B \to X_u\ell\nu$ provide an excellent way to measure the magnitude of the CKM elements $|V_{cb}|$ and $|V_{ub}|$ respectively, because the strong interaction effects are much simplified due to the two leptons in the final state. Both exclusive and inclusive decays can be used with dominant uncertainties being complementary. For exclusive decay analysis, knowledge of the form factors for the exclusive hadronic system $X_{c(u)}$ is required. For inclusive analysis, it is usually necessary to restrict the available phase-space of the decay products to suppress backgrounds; subsequently uncertainties are introduced in the extrapolation to the full phase-space. Moreover, restriction to a small corner of the phase-space may result in breakdown of the operator-product expansion scheme, thus making theoretical calculations unreliable. A more detailed discussion of B semileptonic decays and the extraction of $|V_{cb}|$ and $|V_{ub}|$ is given elsewhere in this *Review* [9]. While traditionally B^0 and B^+ decays were used, over time also other B hadron studies became available. Most notably, determination of of $|V_{ub}|$ using $\Lambda_b^0 \to p\mu^-\overline{\nu}_\mu$ decays by LHCb [59] was more precise than expected. Besides, there have been measurements of inclusive semileptonic decay rates of B_s^0 [60] and B_c^+ [61] mesons. One of the latest additions in this area is the observation of the $B_s^0 \to K^-\mu^+\nu_\mu$ decays by LHCb using only a fraction of their available data [62].

On the other hand, hadronic B decays are complicated because of strong interaction effects caused by the surrounding cloud of light quarks and gluons. While this complicates the extraction of CKM matrix elements, it also provides a great opportunity to study perturbative and non-perturbative QCD, hadronization, and Final State Interaction (FSI) effects.

Many aspects of B decays can be understood through the Heavy Quark Effective Theory (HQET) [63]. This has been particularly successful for semileptonic decays. For further discussion of HQET, see for instance Ref. [64]. For hadronic decays, one typically uses effective Hamiltonian calculations that rely on a perturbative expansion with Wilson coefficients. In addition, some form of the factorization hypothesis is commonly used, where, in analogy with semileptonic decays, two-body hadronic decays of B mesons are expressed as the product of two independent hadronic currents, one describing the formation of a charm meson (in case of the dominant $b \to cW^{*-}$ decays), and the other the hadronization of the remaining $\overline{u}d$ (or $\overline{c}s$) system from the virtual W^-. Qualitatively, for B decays with a large energy release, e.g. $b \to uW^{*-}$ transitions, the $\overline{u}d$ pair (produced as a color singlet) travels fast enough to leave the interaction region without influencing the charm meson. This is known to work well for the dominant spectator decays [65]. There are several common implementations of these ideas for hadronic B decays, the most common of which are QCD factorization (QCDF) [66–69], perturbative QCD (pQCD) [70–74], and soft collinear effective theory (SCET) [75–77].

The transitions $b \to s$ and $b \to d$ are flavor-changing neutral-current (FCNC) processes. Although they are not allowed in the SM as a tree-process, they can occur via loop diagrams (denoted "penguin" decays). The rates for $b \to s$ penguin decays are comparable to the CKM-suppressed $b \to u$ tree processes. Pure-penguin decays were first established by the observation of $B \to K^*(892)\gamma$ [78]. Penguin processes involving $b \to d$ transitions are further suppressed by CKM, and have been observed for $B \to (\rho/\omega)\gamma$ decays [79, 80]. LHCb has observed a $b \to d$ penguin transition in the $B^+ \to \pi^+\mu^+\mu^-$ mode and measured its branching fraction to be $(1.83 \pm 0.24 \pm 0.05) \times 10^{-8}$ [81].

Other decay processes discussed in this *Review* include W–exchange (a W is exchanged between initial–state quarks), penguin annihilation (the gluon from a penguin loop attaches to the spectator quark, similar to an exchange diagram), and pure–annihilation (the initial quarks annihilate to a virtual W, which then decays). Some observed decay modes such as $B^0 \to D_s^- K^+$, may be interpreted as evidence of a W-exchange process [82]. The evidence for the purely leptonic decay $B^+ \to \tau^+\nu$ from Belle [83] and BaBar [84] is the first sign of a pure annihilation decay. The average branching fraction is $(1.09 \pm 0.24) \times 10^{-4}$, which is somewhat larger than, though consistent with, the value expected in the SM. A substantial region of parameter space of charged Higgs mass vs. $\tan\beta$ is excluded by the measurements of this mode. A dedicated discussion of purely leptonic decays of charged pseudoscalar mesons is given elsewhere in this *Review* [85].

Downloaded from https://academic.oup.com/ptep/article/2022/8/083C01/6651666 by KIT Library user on 27 September 2022

73.4 Dominant hadronic decays

Most of the hadronic B decays involve $b \to c$ transition at the quark level, resulting in a charmed hadron or charmonium in the final state. Other types of hadronic decays are very rare and will be discussed separately in the next section. The experimental results on hadronic B decays have steadily improved over the years, and the measurements have reached sufficient precision to challenge our understanding of the dynamics of these decays. With good particle detection and hadron identification capabilities of B-factory detectors, a substantial fraction (roughly on the order of a few per mill) of hadronic B decay events can be fully reconstructed. In particular, good performances for detecting π^0 and other neutral particles helped Belle and BaBar to make comprehensive measurements of the decays $\overline{B}^0 \to D^{(*)0}h^0$ [86], where h^0 stands for light neutral mesons such as $\pi^0, \eta^{(\prime)}, \rho^0, \omega$. The measurements are being complemented by LHCb, in decays like $\overline{B^0} \to D^0\pi^+\pi^-$ [87], where no neutral particles reconstruction is needed. These decays proceed through color-suppressed diagrams, hence they provide useful tests on the factorization models.

Because of the kinematic constraint of $\Upsilon(4S) \to B\bar{B}$, the energy sum of the final-state particles of a B meson decay is always equal to one half of the total energy in the center of mass frame. As a result, the two variables, ΔE (energy difference) and M_B (B candidate mass with a beam-energy constraint) are very effective for reducing combinatorial background both from $\Upsilon(4S)$ and $e^+e^- \to q\bar{q}$ continuum events. In particular, the energy-constraint in M_B improves the signal resolution by almost an order of magnitude.

The kinematically clean environment of B meson decays provides an excellent opportunity to search for new states. For instance, quark-level $b \to c\bar{c}s$ decays have been used to search for new charmonium and charm-strange mesons and study their properties in detail. While narrow charm-strange states $D^*_{s0}(2317)$ [88] and $D_{s1}(2460)$ [89] were discovered by BaBar and CLEO, respectively, the properties of these new states were revealed by studying the B meson decays, $B \to DD^*_{s0}(2317)$ and $B \to DD_{s1}(2460)$ by Belle [90] and BaBar [91]. Another example is Dalitz plot analysis of decay $B^0_s \to \bar{D}^0K^-\pi^+$ in which the decay to spin-3 resonance was observed for the first time [92].

Information on B^0_s, B^+_c and Λ^0_b decays have been remarkably improved with recent studies of large samples from LHCb. Noticeable additions in B_s include decay modes to $D^{(*)+}_s D^{(*)-}_s$, $\bar{D}^0\bar{K}^0$, and $J/\psi\bar{K}^*(892)^0$. The $B^0_s \to D^{(*)+}_s D^{(*)-}_s$ decays were first observed by CDF [93], followed by Belle [94]. LHCb has improved the precision with $\mathcal{B}(B^0_s \to D^{(*)+}_s D^{(*)-}_s) = (3.07 \pm 0.22 \pm 0.33)\%$ [95], which suggests that $B^0_s \to D^{(*)+}_s D^{(*)-}_s$ decays do not saturate the CP-even modes of the B_s decays. The $B^0_s \to \bar{D}^0\bar{K}^0$ decay occurs mostly via a color-suppressed tree diagram, and has a small theoretical uncertaintiy in the SM, thus this mode can significantly improve the determination of the CP-violation angle ϕ_s. LHCb has observed this decay and the branching fraction is $(4.3 \pm 0.5 \pm 0.7) \times 10^{-4}$ [96]. The $B^0_s \to J/\psi\bar{K}^*(892)^0$ decay can be used to constrain the penguin pollution in determing ϕ_s. LHCb has updated the branching fraction and measured the CP asymmetries of this decay, thereby constraining the penguin pollution in ϕ_s [97], although a much more stringent constraint on penguin polltion can come from $B^0 \to J/\psi\rho^0$ which has been observed by BaBar [98] and LHCb [99]. The $B^+_c \to B^0_s\pi^+$ decay is unique as the only observed mode of b-flavored hadron decays where the partner quark decays (c in this case) while the b quark remains a spectator. LHCb has observed this mode and measured $[\sigma(B^+_c)/\sigma(B^0_s)] \times \mathcal{B}(B^+_c \to B^0_s\pi^+) = (2.37 \pm 0.31 \pm 0.11^{+0.17}_{-0.13}) \times 10^{-3}$ [100]. In addition, LHCb [101] and ATLAS [102] have measured $B^+_c \to J/\psi D^{(*)+}_s$, which, by comparing with $B^+_c \to B^0_s\pi^+$, provides a ratio of exclusive $b \to c$ and $c \to s$ decays of B^+_c. For $\Lambda^0_b \to \Lambda^+_c\pi^+\pi^-\pi^-$ [103], not only the total rate is measured, but also structure involving decays through excited Λ_c and Σ_c baryons.

In addition, a variety of exotic particles that do not fit the conventional meson spectroscopy have been discovered in B decays. Belle found the $X(3872)$ state by studying $B^+ \to J/\psi\pi^+\pi^-K^+$ [104], which was confirmed by CDF [105], D0 [106] and BaBar [107]. Production of $X(3872)$ has been studied by the LHC experiments, LHCb [108], CMS [109] and ATLAS [110].

A charged charmonium-like state $X(4430)^\pm$ that decays to $\psi(2S)\pi^\pm$ was observed by Belle in $B \to \psi(2S)K\pi^\pm$ [111]. Since it is charged, it could not be an ordinary charmonium state. A high-statistics study by LHCb confirmed the existence of the $X(4430)^\pm$ in decays $B \to \psi(2S)K\pi^\pm$ [112], demonstrated its resonance character by studying the phase motion, unambiguously determined its spin-parity, and saw evidence for another state. In a Dalitz plot analysis of $\bar{B}^0 \to J/\psi K^-\pi^+$ [113], Belle has found another state, labeled as $X(4200)^+$ in this *Review*, adding to the list of exotic charged charmonium-like states. In an amplitude analysis of the decay $\Lambda^0_b \to J/\psi pK^-$, LHCb observed exotic structures, labeled as $P_c(4380)^+$ and $P_c(4450)^+$ in this *Review*, in the $J/\psi p$ channel [114]. The subsequent analysis with significantly increased statistics observed additional state and resolved the peak at 4450 MeV/c^2 as being due to the two states close in the mass [115]. They are referred to as charmonium-pentaquark states. More detailed discussions of exotic meson-like states and pentaquarks are given elsewhere in this *Review* [116].

73.5 Rare hadronic decays

All B-meson decays that do not occur through the $b \to c$ transition are usually called rare B decays. These include both semileptonic and hadronic $b \to u$ decays that are suppressed at leading order by the small CKM matrix element V_{ub}, as well as higher-order $b \to s(d)$ processes such as electroweak and gluonic penguin decays. In this section, we review hadronic rare B decays, while electroweak penguin decays and others are discussed in the next.

Charmless B meson decays into two-body hadronic final states such as $B \to \pi\pi$ and $K\pi$ are experimentally clean, and provide good opportunities to probe new physics and search for indirect and direct CP violations. Since the final state particles in these decays tend to have larger momenta than average B decay products, the event environment is cleaner than for $b \to c$ decays. Branching fractions are typically around 10^{-5}. Over the past decade, many such modes have been observed not only by e^+e^- collider experiments such as BaBar and Belle, but also by hadron collider experiments such as CDF ($p\bar{p}$) and LHCb (pp). In the latter cases, huge data samples of the modes with all charged final-state particles have been reconstructed by triggering on the impact parameter of the charged tracks. This has also allowed observation of charmless decays of the B_s, in final states such as $\phi\phi$ [117, 118], K^+K^- [119, 120], and $K^-\pi^+$ [120, 121], and of charmless decays of the Λ^0_b baryon [121]. The large samples available at LHCb experiment allow to perform also time-dependent CP violation measurements [122, 123]. Charmless B_s modes are related to corresponding B^0 modes by U-spin symmetry, and are determined by similar amplitudes. Combining the observables from B^0_s and B^0 modes is a further way of eliminating hadronic uncertainties and extracting relevant CKM information [124].

Because of relatively high-momenta for final state particles, the dominant source of background in e^+e^- collisions is $q\bar{q}$ continuum events; sophisticated background suppression techniques exploiting event shape variables are essential for these analyses. In hadron collisions, the dominant background comes from QCD or partially reconstructed heavy flavors, and is similarly suppressed by a combination of kinematic and isolation requirements. The results are in general consistent among the experiments.

Most rare decay modes including $B^0 \to K^+\pi^-$ have contributions from both $b \to u$ tree and $b \to sg$ penguin processes. If the size of the two contributions are comparable, the interference between them may result in direct CP violation, seen experimentally as a charge asymmetry in the decay rate measurement. BaBar [125], Belle [126], CDF [119], and LHCb [122] have measured the direct CP violating asymmetry in $B^0 \to K^+\pi^-$ decays. Direct CP violation has been observed in this decay with a significance of more than 5σ. The world average value of the asymmetry is now rather precise, $A_{CP}(K^+\pi^-) = -0.083 \pm 0.004$. The CP asymmetry in $B^+ \to K^+\pi^0$ mode has been measured by BaBar [127], Belle [126] and LHCb [128] with the average value $A_{CP}(K^+\pi^0) = 0.017 \pm 0.016$. These two asymmetries differ signif-

Downloaded from https://academic.oup.com/ptep/article/2022/8/083C01/6651666 by KIT Library user on 27 September 2022

icantly, in constrast to a naive expectation based on simplified picture in the SM. For more detailed tests, there are sum rules [129] that relate the decay rates and decay-rate asymmetries between the four $K\pi$ charge states. A crucial ingredient of the sum rule test is $A_{CP}(K^0\pi^0)$. Currently, measured values are reported by both BaBar [130] and Belle [131]. Using the $A_{CP}(K^0\pi^0)$ value of Ref. [131], Belle reports the sum rule test result that is consistent with zero within 1.9σ [126]. With the future improvements via Belle II and upgraded LHCb, the measurements are expected to become precise enough to shape a definite conclusion. The CP asymmetry in the π^+K^- mode has also been measured in B_s^0 decays, by CDF [119] and LHCb [122]. The combined value is $A_{CP}(B_s^0 \to \pi^+K^-) = 0.221 \pm 0.015$.

In addition to $B_{(s)} \to K\pi$ modes, significant ($> 3\sigma$) non-zero CP asymmetries have been measured in several other rare decay modes: $A_{CP}(B^+ \to \rho^0K^+) = 0.37 \pm 0.10$ [132], $A_{CP}(B^+ \to \eta K^+) = -0.37 \pm 0.08$ [133], $A_{CP}(B^0 \to \eta K^{*0}) = 0.19 \pm 0.05$ [134], and $A_{CP}(B^+ \to f_2(1270)K^+) = -0.68^{+0.19}_{-0.17}$ [132]. In at least the first two cases, a large direct CP violation might be expected since the penguin amplitude is suppressed so the tree and penguin amplitudes may have comparable magnitudes. There are also measurements by LHCb of CP asymmetries in several 3-body modes: $A_{CP}(B^+ \to \pi^+\pi^-\pi^+) = 0.057 \pm 0.013$, $A_{CP}(B^+ \to K^+\pi^-\pi^+) = 0.027 \pm 0.008$, $A_{CP}(B^+ \to K^+K^-\pi^+) = -0.122 \pm 0.0021$, and $A_{CP}(B^+ \to K^+K^-K^+) = -0.033 \pm 0.008$ [135,136]. Many of these analyses now include Dalitz plot treatments with many intermediate resonances.

BaBar [137] and Belle [126, 138] have observed the decays $B^+ \to \overline{K}^0K^+$ and $B^0 \to K^0\overline{K}^0$. The world-average branching fractions are $\mathcal{B}(B^0 \to K^0\overline{K}^0) = (1.21 \pm 0.16) \times 10^{-6}$ and $\mathcal{B}(B^+ \to \overline{K}^0K^+) = (1.31 \pm 0.17) \times 10^{-6}$. These are the first observations of hadronic $b \to d$ transitions, with significance bigger than 5σ for all four measurements. CP asymmetries have been measured for these modes, but with large errors. LHCb has observed $B^0 \to K^+K^-$ mode which occurs via a weak-annihilation process and is the rarest hadronic B-meson decay thus far observed, with $\mathcal{B}(B^0 \to K^+K^-) = (7.80 \pm 1.52) \times 10^{-8}$ [139]. $B_s^0 \to K^+K^-$ decay mode, which occurs mostly via $b \to s$ penguin process, has been observed by Belle [140], CDF [141] and LHCb [120]. The average branching fraction is $\mathcal{B}(B_s^0 \to K^+K^-) = (26.6 \pm 2.2) \times 10^{-6}$. Belle has also observed $B_s^0 \to K^0\overline{K}^0$ [142] which also occurs via $b \to s$ penguin transition in the SM. This was recently confirmed by LHCb [143]. The average branching fraction is $(1.76 \pm 0.31) \times 10^{-5}$.

The decay $B^0 \to \pi^+\pi^-$ can be used to extract the CKM angle α (for details see elsewhere in this *Review* [144]). This is complicated by the presence of significant contributions from penguin diagrams. An isospin analysis [145] can be used to untangle the penguin complications. The decay $B^0 \to \pi^0\pi^0$ is crucial in this analysis. Both BaBar and Belle have observed $B^0 \to \pi^0\pi^0$, with a mild tension in the measured branching fractions: $(1.83 \pm 0.25) \times 10^{-6}$ for BaBar [125] and $(1.31 \pm 0.26) \times 10^{-6}$ for Belle [146]. It turns out that the amount of penguin pollution in the $B \to \pi\pi$ system is rather large. In the past few years, measurements in the $B^0 \to \rho\rho$ system have produced more precise values of α, since penguin amplitudes are generally smaller for decays with vector mesons. An important ingredient in the analysis is the $B^0 \to \rho^0\rho^0$ branching fraction. The average of measurements from BaBar [147] and Belle [148] yields a branching fraction of $(0.96 \pm 0.15) \times 10^{-6}$. This is only 3% of the $\rho^+\rho^-$ branching fraction, much smaller than the corresponding ratio ($\gtrsim 20\%$) in the $\pi\pi$ system.

Since $B \to \rho\rho$ has two vector mesons in the final state, the CP eigenvalue of the final state depends on the longitudinal polarization fraction f_L for the decay. Therefore, a measurement of f_L is needed to extract the CKM angle α. Both BaBar and Belle have measured f_L for the decays $\rho^+\rho^-$ [149] and $\rho^+\rho^0$ [150] and in both cases the measurements show $f_L > 0.9$, making a complete angular analysis unnecessary. In $B^0 \to \rho^0\rho^0$, f_L is measured by BaBar [147], Belle [148] and LHCb [151], with the average value being $0.71^{+0.08}_{-0.09}$.

By analyzing the angular distributions of the B decays to two vector mesons, we can learn a lot about both weak- and strong-interaction dynamics in B decays. Decays that are penguin-dominated surprisingly have values of f_L near 0.5. The list of such decays has now grown to include $B \to \phi K^*(892)$, $B \to \rho K^*(892)$, and $B \to \omega K^*(892)$. The reasons for this "polarization puzzle" are not fully understood. A detailed description of the angular analysis of B decays to two vector mesons can be found in a separate mini-review [152] in this *Review* .

73.6 Electroweak penguin decays

Electroweak decays are one-loop FCNC decays proceeding through penguin or box Feynman diagrams with final state including real photon or pair of leptons. Such decays were first observed by CLEO experiment when it observed decay $B \to K^*(892)\gamma$ [78]. Since then significant amount of experimental information was obtained. Branching fractions for these decays are 10^{-5} or less, which makes them excellent candidates for searches for new physics beyond SM. Often several observables are available, which allows for stringent tests of the SM.

Starting with radiative decays, experimentally easiest to study are exclusive decays with a fully reconstructed final state. The best studied decay in this class is $B \to K^*(892)\gamma$ seen by CLEO, Belle, BaBar experiments [153–155] with world average branching fraction $\mathcal{B}(B^0 \to K^*(892)^0\gamma) = (41.8 \pm 2.5) \times 10^{-6}$. Decays through several other kaon resonances such as $B \to K_1(1270)\gamma$, $K_2^*(1430)\gamma$, *etc.* were studied at B-factories [156–159]. It is worth to mention decay $B^+ \to K^+\pi^+\pi^-\gamma$ for which besides measurements of the branching fraction [157,160,161] one can also use the angular distribution to access photon polarization. Such a measurement was done by the LHCb experiment, which was able to clearly demonstrate that the photon in $B^+ \to K^+\pi^+\pi^-\gamma$ decay is polarized [162]. Unfortunately given non-trivial hadronic structure, more work is needed before turning this into test of the SM. The exclusive radiative decays $B_s^0 \to \phi\gamma$ was seen by the Belle and LHCb experiments [163, 164] with an average branching fraction of $(3.4 \pm 0.4) \times 10^{-5}$ and more recently also decay $\Lambda_b \to \Lambda\gamma$ was observed by LHCb [165].

Compared to $b \to s\gamma$, the $b \to d\gamma$ transitions such as $B \to \rho\gamma$, are suppressed by the CKM elements ratio $|V_{td}/V_{ts}|^2$. Both Belle and BaBar have observed these decays [79,80]. The world average $\mathcal{B}(B \to (\rho,\omega)\gamma) = (1.30 \pm 0.23) \times 10^{-6}$. This can be used to calculate $|V_{td}/V_{ts}|$ [166]; the measured values are $0.195^{+0.025}_{-0.024}$ from Belle [79] and $0.233^{+0.033}_{-0.032}$ from BaBar [80].

The observed radiative penguin branching fractions can constrain a large class of SM extensions [167]. However, due to the uncertainties in the hadronization, only the inclusive $b \to s\gamma$ rate can be reliably compared with theoretical calculations. This rate can be measured from the endpoint of the inclusive photon spectrum in B decay. By combining the measurements of $B \to X_s\gamma$ from the CLEO, BaBar, and Belle experiments [168–170], HFLAV obtains the average: $\mathcal{B}(B \to X_s\gamma) = (3.32 \pm 0.15) \times 10^{-4}$ [28] for $E_\gamma \geq 1.6$ GeV, averaging over B^+ and B^0. Consistent but less precise results have been reported by ALEPH for inclusive b–hadrons produced at the Z, which includes also contribution from B_s^0 and Λ_b^0 hadrons. Using the sum of seven exclusive final states, the BaBar experiment measured the branching fraction of inclusive $b \to d\gamma$ decays to be $(9.2 \pm 2.0 \pm 2.3) \times 10^{-6}$ [171]. The measured branching fraction can be compared to theoretical calculations. Recent calculations of $\mathcal{B}(b \to s\gamma)$ at NNLO level predict for the $E_\gamma \geq 1.6$ GeV values of $(3.36 \pm 0.23) \times 10^{-4}$ for $b \to s\gamma$ and $(1.73^{+0.12}_{-0.22}) \times 10^{-5}$ for $b \to d\gamma$ decays [172].

The CP asymmetry in $b \to s\gamma$ is extensively studied theoretically both in the SM and beyond [173]. According to the SM, the CP asymmetry in $b \to s\gamma$ is smaller than 1%, but some non-SM models allow significantly larger CP asymmetry ($\sim 10\%$) without altering the branching fraction. The current world average is $A_{CP} = 0.015 \pm 0.011$, again dominated by BaBar and Belle [174]. In addition to the CP asymmetry, BaBar and Belle also measured the isospin asymmetry $\Delta_{0-} = -0.006 \pm 0.020$ in $b \to s\gamma$ measured using sum of exclusive decays [174, 175]. An alternative measurement using full reconstruction of the companion B in the hadronic decay modes yields a consistent, but less precise result [176]. Both Belle and BaBar experiments measured the isospin asymmetry in exclusive $B \to K^*(892)\gamma$ decay with aver-

Downloaded from https://academic.oup.com/ptep/article/2022/8/083C01/6651666 by KIT Library user on 27 September 2022

age of $6.3 \pm 1.7\%$ [154, 155] and therefore providing evidence for the non-zero isospin asymmetry.

In addition, experiments have measured the inclusive photon energy spectrum for $b \to s\gamma$, and by analyzing the shape of the spectrum they obtain the first and second moments for photon energies. Belle has measured these moments covering the widest range in the photon energy ($1.7 < E_\gamma < 2.8$ GeV) [170]. The measurement by BaBar has slightly smaller range with lower limit at 1.8 GeV [177]. These results can be used to extract non-perturbative HQET parameters that are needed for precise determination of the CKM matrix element V_{ub} (see further discussion elsewhere in this *Review* [178]).

Additional information on FCNC processes can be obtained from $b \to s\ell^+\ell^-$ decays. These processes are studied as a function of dilepton invariant mass squared, q^2. Different q^2 regions are sensitive to different physics. Starting at the very low q^2 decays exhibit sensitivity to the same physics as the radiative decays. Then for the q^2 in region 1.1 to 6.0 GeV$^2/c^4$ the SM and new physics have best chance to compete. At the high q^2 above the $\psi(2S)$ mass, the interference of SM and new physics is to some extend complementary to that in lower q^2. Regions around J/ψ and $\psi(2S)$ is normally excluded from measurements as these are dominated by the $b \to c$ transitions to charmonia. For exclusive decays, theory predictions require calculations of hadronic form factors. With current theory predictions, the most useful are measurements within the q^2 regions 1.1 to 6.0 GeV$^2/c^4$ and from 16.0 GeV$^2/c^4$ up to the kinematic limit. From this reason in the listing we provide results mainly in those two regions.

Similar as for radiative decays, also for the $b \to s\ell^+\ell^-$ decays the inclusive measurements provide some benefits. Both Belle and BaBar performed such measurement without reconstructing hadronic part exclusively and measure a branching fraction of $(5.8 \pm 1.3) \times 10^{-6}$ [179]. Unfortunately this measurement is not trivially possible at hadron colliders and also does not easily allow the angular distributions of the decay products to be exploited. One alternative is to extract information on the inclusive decay as sum of exclusive decays. Such a measurement was performed by Belle [180], but in this case the difficulty lies in extrapolation for the missing hadronic states.

Turning to the exclusive decays, the initial measurements performed by B-factories typically averaged between charged and neutral B mesons as well as between e^+e^- and $\mu^+\mu^-$ finals states. The experiments CDF, LHCb, ATLAS and CMS are much better suited for the $\mu^+\mu^-$ finals states compared to the e^+e^- final states. As such most measurements at hadron colliders are done only with $\mu^+\mu^-$ pairs and by separating charged and neutral B mesons. The best studied decays are $B^+ \to K^+\ell^+\ell^-$ and $B^0 \to K^*(892)^0\ell^+\ell^-$. At hadron colliders other b hadrons are produced and as such CDF and LHCb experiments did observe also $B_s^0 \to \phi\mu^+\mu^-$ [181, 182], $\Lambda_b^0 \to \Lambda\mu^+\mu^-$ [181, 183] and $\Lambda_b^0 \to pK^-\mu^+\mu^-$ decays [184]. The averages of the total branching fractions integrated over whole q^2 regions are $(5.6\pm0.6)\times10^{-7}$ for $B^+ \to K^+e^+e^-$, $(4.53 \pm 0.35) \times 10^{-7}$ for $B^+ \to K^+\mu^+\mu^-$, $(1.03^{+0.19}_{-0.17}) \times 10^{-6}$ for $B^0 \to K^*(892)^0e^+e^-$ and $(0.94 \pm 0.05) \times 10^{-6}$ for $B^0 \to K^*(892)^0\mu^+\mu^-$ decays [185–189]. The total branching fractions for $B_s^0 \to \phi\mu^+\mu^-$ and $\Lambda_b^0 \to \Lambda\mu^+\mu^-$ decays are $(8.2\pm1.2)\times10^{-7}$ [181,182] and $(1.08\pm0.28)\times10^{-6}$ [181,183] respectively. With increased precision of $B^0 \to K^*(892)^0\ell^+\ell^-$ decay, there is a question on what fraction of the seen branching fraction is due to the $K^*(892)^0$ resonance and what fraction is due to the $K\pi$ in s-wave. This has been studied by LHCb which found that the $K\pi$ in s-wave fraction varies between 1% and about 10% depending on the q^2 region [189]. It should be noted, that for all relevant B meson decays the branching fractions so far studied are consistently below the SM expectation.

In the $b \to s\ell^+\ell^-$ decays angular distributions offer rich source of information. The full angular analysis was performed for decays $B^+ \to K^+\ell^+\ell^-$, $B^0 \to K^0\ell^+\ell^-$, $B^+ \to K^*(892)^+\ell^+\ell^-$, $B^0 \to K^*(892)^0\ell^+\ell^-$, $B_s^0 \to \phi\mu^+\mu^-$ and $\Lambda_b^0 \to \Lambda\mu^+\mu^-$ decays [190–198]. An attempt to increase sensitivity to the NP was made by constructing observables, which have reduced theory uncertainties and measurements of these are done. Most notably the observable called P_5' [199] shows a discrepancy with the SM in the q^2 region which is highly sensitive to new physics [192–194]. Measurements of the CP asymmetries [184,185,188,200,201], the isospin asymmetry [186–188, 200] were also performed. All these measurements are well consistent with the small A_{CP} and small isospin asymmetry expected in the SM [202]. With statistics available at the LHC, the measurement of phase difference between long- and short-distance contribution in $B^+ \to K^+\mu^+\mu^-$ decays became possible [203].

With the data samples available at LHC, the lepton universality in $b \to s\ell^+\ell^-$ can be tested. While in the SM decays to electron-positron and muon pairs are expected to be same up to small corrections due to the different masses of leptons, in extensions of the SM this does not have to hold. The angular analysis of $B^0 \to K^*(892)^0e^+e^-$ decays was performed by LHCb at low dilepton invariant masses [204] and Belle in several regions over whole q^2 range [194]. The LHCb measurement yields the most stringent constraint on the photon polarization. The most notable result on lepton universality test is the ratio of branching fractions between $B^+ \to K^+\mu^+\mu^-$ and $B^+ \to K^+e^+e^-$ and between $B^0 \to K^*(892)^0\mu^+\mu^-$ and $B^0 \to K^*(892)^0e^+e^-$ decays [186, 205–208]. In both cases, the measurements by LHCb show mild discrepancy from the SM, with significance of $3.1\,\sigma$ for $B^+ \to K^+\ell^+\ell^-$ and about $2.4\,\sigma$ for $B^0 \to K^*(892)^0\ell^+\ell^-$. LHCb experiment performed similar test with $\Lambda_b^0 \to pK^-\ell^+\ell^-$ decays [209].

While $b \to d\ell^+\ell^-$ decays are further suppressed, they recently became accessible. Signals were observed for $B^+ \to \pi^+\mu^+\mu^-$ [81], $B^0 \to \pi^+\pi^-\mu^+\mu^-$ [210] and $\Lambda_b^0 \to p\pi^-\mu^+\mu^-$ [211] decays. The total branching fractions are only quantities measured and these are about 2×10^{-8} for the meson decays and about 7×10^{-8} for the Λ_b^0 decay.

A closely related process is $B \to X_s\nu\overline{\nu}$. Since the neutrinos are not detected, the final state is a strange hadron system X_s plus missing energy-momentum. Depending on X_s, the SM branching fraction is $\mathcal{O}(10^{-6})$. New physics effects beyond SM, e.g. those from dark sector models can greatly enhance the yield of X_s plus missing energy. Both BaBar [212] and Belle [213] have searched for these decays and determined the upper limits in the range $\mathcal{O}(10^{-5})$.

Finally the decays $B_{(s)}^0 \to e^+e^-$ and $\mu^+\mu^-$ are interesting since they only proceed at second order in weak interactions in the SM, but may have large contributions from supersymmetric loops, proportional to $(\tan\beta)^6$. First limits were published 30 years ago and since then experiments at Tevatron, B-factories and LHC gradually improved those and effectively excluded whole models of new physics and significantly constrained allowed parameter space of others. For the decays to $\mu^+\mu^-$, Tevatron experiments pushed the limits down to roughly factor of 5-10 above the SM expectation [214, 215]. The long journey in the search for these decays culminated in 2012, when first evidence for $B_s^0 \to \mu^+\mu^-$ decay was seen [216]. Subsequently, LHC experiments ATLAS [217], CMS [218] and LHCb [219] observed statitically significant signal for $B_s^0 \to \mu^+\mu^-$ decay. The average branching fraction is found to be $(2.9\pm0.4)\times10^{-9}$. In experiments at hadron colliders searches for $B^0 \to \mu^+\mu^-$ decays are performed at the same time. The best limit on $B(B^0 \to \mu^+\mu^-) < 2.1 \times 10^{-10}$ at 95% C.L. [217]. The limits for the e^+e^- modes are: $< 9.4 \times 10^{-9}$ and $< 2.5 \times 10^{-9}$, respectively, for B_s^0 and B^0 [220]. The searches for decays to $\tau^+\tau^-$ are more challenging with current best limits of $B(B^0 \to \tau^+\tau^-) < 2.1\times10^{-3}$ and $B(B_s^0 \to \tau^+\tau^-) < 6.8\times10^{-3}$ at 95% C.L. [221]. All existing measurements of B^0 and B_s^0 decays to same flavour dilepton pair is consistent with SM expectation [222]. With $B_s^0 \to \mu^+\mu^-$ decay observed, it was suggested that the effective lifetime is useful further test of the decay [223]. Attempt was made by LHCb and CMS experiments, but its precision is not yet sufficient to provide test of the SM [218, 219]. It will take couple of years until interesting precision is reached. The searches were also performed for lepton flavour violating decays to two leptons with best limits in $e^\pm\mu^\mp$ channel, where limits are $< 1.3 \times 10^{-9}$ for B^0 and $< 6.3 \times 10^{-9}$ for B_s^0, at 95% confidence level [224].

Several theory groups performed global analysis of electroweak decays concluding that significant tension between data and SM is

Downloaded from https://academic.oup.com/ptep/article/2022/8/083C01/6651666 by KIT Library user on 27 September 2022

present [225]. The tension can be relieved by new physics beyond SM. For more detailed reviews see e.g. Ref. [226].

73.7 Summary and Outlook

The study of B mesons continues to be one of the most productive fields in particle physics. With the two asymmetric B-factory experiments Belle and BaBar, we now have a combined data sample of well over 1 ab^{-1}. CP violation has been firmly established in many decays of B mesons. Evidence for direct CP violation has been observed. Many rare decays resulting from hadronic $b \to u$ transitions and $b \to s(d)$ penguin decays have been observed, and the emerging pattern is still full of surprises. Despite the remarkable successes of the B-factory experiments, many fundamental questions in the flavor sector remain unanswered.

At Fermilab, CDF and D0 each has accumulated about 10 fb^{-1}, which is the equivalent of about 10^{12} b-hadrons produced. In spite of the low trigger efficiency of hadronic experiments, a selection of modes have been reconstructed in large quantities, giving a start to a program of studies on B_s and b-flavored baryons, in which a first major step has been the determination of the B_s oscillation frequency.

As Tevatron and B-factories finished their data taking few year ago, the experiments at the LHC have become very active. LHCb has collected about 1 fb^{-1} at 7 TeV, 2 fb^{-1} at 8 TeV, and close to 5.9 fb^{-1} at 13 TeV during LHC Runs 1 and 2. CMS and ATLAS have collected each about 5 fb^{-1} of data at $\sqrt{s} = 7$ TeV, 20 fb^{-1} at 8 TeV and about 150 fb^{-1} at 13 TeV during LHC Runs 1 and 2. LHCb, which is dedicated to the studies of b- and c-hadrons, has a data sample that is for many decays larger than the sum of all previous experiments. With it, we are entering to regime of precision physics even for many rare decays, which allows much more detailed measurements.

The Belle II experiment at the SuperKEKB has started recording data in 2019 and has so far collected about 200 fb^{-1} of data (August 2021). The aim to increase sample to $\sim$ 50 ab^{-1} will make it possible to explore the indirect evidence of new physics beyond the SM in the heavy-flavor particles (b, c, and τ), in a way that is complementary to the LHC. In the same time period, LHCb Collaboration is working on the upgrade of its detector, installation of which is ongoing. The aim of the upgrade is to increase flexibility of the trigger, which will allow about a factor of five increase in instantaneous luminosity and of about a factor of two in efficiencies on triggering on purely hadronic decays. The plan is to integrate about 50 fb^{-1} of data starting from 2022.

These experiments promise a rich spectrum of rare and precise measurements that have the potential to fundamentally affecting our understanding of the SM and CP-violating phenomena.

References

[1] M. Kobayashi and T. Maskawa, Prog. Theor. Phys. **49**, 652 (1973).

[2] S. W. Herb *et al.*, Phys. Rev. Lett. **39**, 252 (1977).

[3] B. Aubert *et al.* (BaBar), Phys. Rev. Lett. **87**, 091801 (2001), [hep-ex/0107013].

[4] K. Abe *et al.* (Belle), Phys. Rev. Lett. **87**, 091802 (2001), [hep-ex/0107061].

[5] Currently two different notations (ϕ_1, ϕ_2, ϕ_3) and (α, β, γ) are used in the literature for CKM unitarity angles. In this mini-review, we use the latter notation following the other mini-reviews in this *Review*. The two notations are related by $\phi_1 = \beta$, $\phi_2 = \alpha$ and $\phi_3 = \gamma$.

[6] See the "CP Violation in Meson Decays" by D. Kirkby and Y. Nir in this *Review*.

[7] See the "CKM Quark Mixing Matrix," by A. Cecucci, Z. Ligeti, and Y. Sakai, in this *Review*.

[8] See the note on "$B^0 - \overline{B}^0$ mixing," by O. Schneider in this *Review*.

[9] See the "Determination of $|V_{cb}|$ and $|V_{ub}|$," by R. Kowalewski and T. Mannel in this *Review*.

[10] F. Abe *et al.* (CDF), Phys. Rev. Lett. **81**, 2432 (1998), [hep-ex/9805034]; F. Abe *et al.* (CDF), Phys. Rev. **D58**, 112004 (1998), [hep-ex/9804014].

[11] A. Abulencia *et al.* (CDF), Phys. Rev. Lett. **96**, 082002 (2006), [hep-ex/0505076].

[12] R. Aaij *et al.* (LHCb), JHEP **07**, 123 (2020), [arXiv:2004.08163].

[13] B. Aubert *et al.* (BaBar), Phys. Rev. Lett. **101**, 071801 (2008), [Erratum: Phys. Rev. Lett.102,029901(2009)], [arXiv:0807.1086].

[14] B. Aubert *et al.* (BaBar), Phys. Rev. Lett. **103**, 161801 (2009), [arXiv:0903.1124].

[15] G. Bonvicini *et al.* (CLEO), Phys. Rev. **D81**, 031104 (2010), [arXiv:0909.5474].

[16] R. Mizuk *et al.* (Belle), Phys. Rev. Lett. **109**, 232002 (2012), [arXiv:1205.6351].

[17] U. Tamponi *et al.* (Belle), Phys. Rev. Lett. **115**, 14, 142001 (2015), [arXiv:1506.08914].

[18] A. Bondar *et al.* (Belle), Phys. Rev. Lett. **108**, 122001 (2012), [arXiv:1110.2251].

[19] See the note on "Naming scheme for hadrons," by M. Roos and C.G. Wohl in this *Review*.

[20] R. Aaij *et al.* (LHCb), Phys. Rev. Lett. **118**, 5, 052002 (2017), [Erratum: Phys. Rev. Lett.119,no.16,169901(2017)], [arXiv:1612.05140].

[21] M. Cacciari *et al.*, JHEP **10**, 137 (2012), [arXiv:1205.6344]; B. A. Kniehl *et al.*, Phys. Rev. **D84**, 094026 (2011), [arXiv:1109.2472]; M. Cacciari, M. L. Mangano and P. Nason, Eur. Phys. J. **C75**, 12, 610 (2015), [arXiv:1507.06197].

[22] B. Barish *et al.* (CLEO), Phys. Rev. Lett. **76**, 1570 (1996).

[23] E. Guido *et al.* (Belle), Phys. Rev. Lett. **121**, 062001 (2018), [arXiv:1803.10303]; E. Guido *et al.* (Belle), Phys. Rev. **D96**, 052005 (2017), [arXiv:1707.04973]; A. Sokolov *et al.* (Belle), Phys. Rev. **D79**, 051103 (2009), [arXiv:0901.1431]; B. Aubert *et al.* (BaBar), Phys. Rev. **D78**, 112002 (2008), [arXiv:0807.2014].

[24] J. P. Alexander *et al.* (CLEO), Phys. Rev. Lett. **86**, 2737 (2001), [hep-ex/0006002]; S. B. Athar *et al.* (CLEO), Phys. Rev. **D66**, 052003 (2002), [hep-ex/0202033].

[25] N. C. Hastings *et al.* (Belle), Phys. Rev. **D67**, 052004 (2003), [hep-ex/0212033].

[26] B. Aubert *et al.* (BaBar), Phys. Rev. Lett. **95**, 042001 (2005), [hep-ex/0504001].

[27] Y. Amhis *et al.* (HFLAV), Eur. Phys. J. **C77**, 12, 895 (2017), [arXiv:1612.07233].

[28] Y. S. Amhis *et al.* (HFLAV) (2019), and online update at https://hflav.web.cern.ch/content/lifetimes-and-oscillation-parameters, [arXiv:1909.12524].

[29] P. Abreu *et al.* (DELPHI), Phys. Lett. **B345**, 598 (1995).

[30] R. Akers *et al.* (OPAL), Z. Phys. **C66**, 19 (1995).

[31] T. A. Aaltonen *et al.* (CDF), Phys. Rev. **D90**, 1, 012013 (2014), [arXiv:1309.5961].

[32] R. Aaij *et al.* (LHCb), JHEP **04**, 024 (2015), [arXiv:1502.02638].

[33] R. Aaij *et al.* (LHCb), Phys. Rev. Lett. **110**, 15, 151803 (2013), [arXiv:1211.5994].

[34] A. M. Sirunyan *et al.* (CMS), Eur. Phys. J. **C78**, 939 (2018), [arXiv:1809.03578].

[35] G. Aad *et al.* (ATLAS), Phys. Rev. Lett. **113**, 21, 212004 (2014), [arXiv:1407.1032].

[36] A. Sirunyan *et al.* (CMS), Phys. Rev. Lett. **122**, 132001 (2019), [arXiv:1902.00571].

[37] R. Aaij *et al.* (LHCb), Phys. Rev. Lett. **122**, 232001 (2019), [arXiv:1904.00081].

[38] T. Aaltonen *et al.* (CDF), Phys. Rev. Lett. **99**, 202001 (2007), [arXiv:0706.3868]; T. Aaltonen *et al.* (CDF), Phys. Rev. **D85**, 092011 (2012), [arXiv:1112.2808].

Downloaded from https://academic.oup.com/ptep/article/2022/8/083C01/6651666 by KIT Library user on 27 September 2022

[39] R. Aaij *et al.* (LHCb), Phys. Rev. Lett. **122**, 012001 (2019), [arXiv:1809.07752].

[40] V. M. Abazov *et al.* (D0), Phys. Rev. Lett. **99**, 052001 (2007), [arXiv:0706.1690]; T. Aaltonen *et al.* (CDF), Phys. Rev. Lett. **99**, 052002 (2007), [arXiv:0707.0589].

[41] R. Aaij *et al.* (LHCb), Phys. Rev. Lett. **113**, 032001 (2014), [arXiv:1405.7223]; R. Aaij *et al.* (LHCb), Phys. Lett. **B736**, 154 (2014), [arXiv:1405.1543]; R. Aaij *et al.* (LHCb), Phys. Rev. **D89**, 3, 032001 (2014), [arXiv:1311.4823]; R. Aaij *et al.* (LHCb), Phys. Rev. Lett. **113**, 24, 242002 (2014), [arXiv:1409.8568]; R. Aaij *et al.* (LHCb), Phys. Rev. Lett. **115**, 24, 241801 (2015), [arXiv:1510.03829]; R. Aaij *et al.* (LHCb), Phys. Rev. Lett. **118**, 7, 071801 (2017), [arXiv:1612.02244]; R. Aaij *et al.* (LHCb), Phys. Lett. **B722**, 265 (2017), [arXiv:1701.05274]; R. Aaij *et al.* (LHCb), Phys. Rev. Lett. **118**, 071801 (2017), [arXiv:1612.02244]; R. Aaij *et al.* (LHCb), JHEP **02**, 98 (2018), [arXiv:1711.05490]; R. Aaij *et al.* (LHCb), Phys. Rev. **D99**, 052006 (2019), [arXiv:1901.07075].

[42] T. A. Aaltonen *et al.* (CDF), Phys. Rev. **D89**, 7, 072014 (2014), [arXiv:1403.8126].

[43] R. Aaij *et al.* (LHCb), JHEP **08**, 039 (2018), [arXiv:1805.03941].

[44] S. Chatrchyan *et al.* (CMS), Phys. Rev. Lett. **108**, 252002 (2012), [arXiv:1204.5955].

[45] R. Aaij *et al.* (LHCb), JHEP **1605**, 161 (2016), [arXiv:1604.03896].

[46] R. Aaij *et al.* (LHCb), Phys. Rev. Lett. **114**, 062004 (2015), [arXiv:1411.4849].

[47] R. Aaij *et al.* (LHCb), Phys. Rev. Lett. **121**, 072002 (2018), [arXiv:1805.09418].

[48] V. M. Abazov *et al.* (D0), Phys. Rev. Lett. **101**, 232002 (2008), [arXiv:0808.4142]; T. Aaltonen *et al.* (CDF), Phys. Rev. **D80**, 072003 (2009), [arXiv:0905.3123].

[49] R. Aaij *et al.* (LHCb), Phys. Rev. Lett. **110**, 18, 182001 (2013), [arXiv:1302.1072]; R. Aaij *et al.* (LHCb), Phys. Lett. **B736**, 154 (2014), [arXiv:1405.1543]; R. Aaij *et al.* (LHCb), Phys. Rev. **D93**, 9, 092007 (2016), [arXiv:1604.01412].

[50] V. M. Abazov *et al.* (D0), Phys. Rev. Lett. **117**, 2, 022003 (2016), [arXiv:1602.07588]; V. M. Abazov *et al.* (D0), Phys. Rev. **D97**, 092004 (2018), [arXiv:1712.10176].

[51] R. Aaij *et al.* (LHCb), Phys. Rev. Lett. **117**, 15, 152003 (2016), [Addendum: Phys. Rev. Lett.118,no.10,109904(2017)], [arXiv:1608.00435].

[52] A. Sirunyan *et al.* (CMS), Phys. Rev. Lett. **120**, 202005 (2018), [arXiv:1712.06144].

[53] C. Tarantino, Eur. Phys. J. **C33**, S895 (2004), [hep-ph/0310241]; F. Gabbiani, A. I. Onishchenko and A. A. Petrov, Phys. Rev. **D70**, 094031 (2004), [hep-ph/0407004]; F. Gabbiani, A. I. Onishchenko and A. A. Petrov, Phys. Rev. **D68**, 114006 (2003), [hep-ph/0303235].

[54] A. Lenz, Int. J. Mod. Phys. **A30**, 10, 1543005 (2015), [arXiv:1405.3601].

[55] C.-H. Chang *et al.*, Phys. Rev. **D64**, 014003 (2001), [hep-ph/0007162]; V. V. Kiselev, A. E. Kovalsky and A. K. Likhoded, Nucl. Phys. **B585**, 353 (2000), [hep-ph/0002127]; A. Yu. Anisimov *et al.*, Phys. Lett. **B452**, 129 (1999), [hep-ph/9812514]; M. Beneke and G. Buchalla, Phys. Rev. **D53**, 4991 (1996), [hep-ph/9601249].

[56] R. Aaij *et al.* (LHCb), Eur. Phys. J. **C74**, 5, 2839 (2014), [arXiv:1401.6932].

[57] R. Aaij *et al.* (LHCb), Phys. Lett. **B742**, 29 (2015), [arXiv:1411.6899].

[58] The B_c is a special case, where a weak decay of the c quark is also possible, but the spectator model still applies.

[59] R. Aaij *et al.* (LHCb), Nature Phys. **11**, 743 (2015), [arXiv:1504.01568].

[60] J. P. Lees *et al.* (BaBar), Phys. Rev. **D85**, 011101 (2012), [arXiv:1110.5600]; C. Oswald *et al.* (Belle), Phys. Rev. **D87**, 7, 072008 (2013), [Erratum: Phys. Rev.D90,no.11,119901(2014)], [arXiv:1212.6400]; C. Oswald *et al.* (Belle), Phys. Rev. **D92**, 7, 072013 (2015), [arXiv:1504.02004].

[61] T. A. Aaltonen *et al.* (CDF), Phys. Rev. **D93**, 5, 052001 (2016), [arXiv:1601.03819].

[62] R. Aaij *et al.* (LHCb), Phys. Rev. Lett. **126**, 8, 081804 (2021), [arXiv:2012.05143].

[63] B. Grinstein, Nucl. Phys. **B339**, 253 (1990); H. Georgi, Phys. Lett. **B240**, 447 (1990); A. F. Falk *et al.*, Nucl. Phys. **B343**, 1 (1990); E. Eichten and B. R. Hill, Phys. Lett. **B234**, 511 (1990).

[64] "Heavy-Quark and Soft-Collinear Effective Theory" by C.W. Bauer and M. Neubert in this *Review*.

[65] M. Neubert, "Aspects of QCD Factorization," `hep-ph/0110093`, *Proceedings of HF9*, Pasadena (2001) and references therein; Z. Ligeti, M. E. Luke and M. B. Wise, Phys. Lett. **B507**, 142 (2001), [hep-ph/0103020].

[66] M. Beneke *et al.*, Phys. Rev. Lett. **83**, 1914 (1999), [hep-ph/9905312].

[67] M. Beneke *et al.*, Nucl. Phys. **B591**, 313 (2000), [hep-ph/0006124].

[68] M. Beneke *et al.*, Nucl. Phys. **B606**, 245 (2001), [hep-ph/0104110].

[69] M. Beneke and M. Neubert, Nucl. Phys. **B675**, 333 (2003), [hep-ph/0308039].

[70] Y.-Y. Keum, H.-n. Li and A. I. Sanda, Phys. Lett. **B504**, 6 (2001), [hep-ph/0004004].

[71] Y. Y. Keum, H.-N. Li and A. I. Sanda, Phys. Rev. **D63**, 054008 (2001), [hep-ph/0004173].

[72] Y.-Y. Keum and H.-n. Li, Phys. Rev. **D63**, 074006 (2001), [hep-ph/0006001].

[73] C.-D. Lu, K. Ukai and M.-Z. Yang, Phys. Rev. **D63**, 074009 (2001), [hep-ph/0004213].

[74] C.-D. Lu and M.-Z. Yang, Eur. Phys. J. **C23**, 275 (2002), [hep-ph/0011238].

[75] C. W. Bauer, S. Fleming and M. E. Luke, Phys. Rev. **D63**, 014006 (2000), [hep-ph/0005275].

[76] C. W. Bauer *et al.*, Phys. Rev. **D63**, 114020 (2001), [hep-ph/0011336].

[77] C. W. Bauer and I. W. Stewart, Phys. Lett. **B516**, 134 (2001), [hep-ph/0107001].

[78] R. Ammar *et al.* (CLEO), Phys. Rev. Lett. **71**, 674 (1993).

[79] N. Taniguchi *et al.* (Belle), Phys. Rev. Lett. **101**, 111801 (2008), [Erratum: Phys. Rev. Lett.101,129904(2008)], [arXiv:0804.4770].

[80] B. Aubert *et al.* (BaBar), Phys. Rev. **D78**, 112001 (2008), [arXiv:0808.1379].

[81] R. Aaij *et al.* (LHCb), JHEP **10**, 034 (2015), [arXiv:1509.00414].

[82] P. Krokovny *et al.* (Belle), Phys. Rev. Lett. **89**, 231804 (2002), [hep-ex/0207077]; B. Aubert *et al.* (BaBar), Phys. Rev. Lett. **98**, 081801 (2007), [hep-ex/0604012].

[83] B. Kronenbitter *et al.* (Belle), Phys. Rev. **D92**, 5, 051102 (2015), [arXiv:1503.05613]; I. Adachi *et al.* (Belle), Phys. Rev. Lett. **110**, 13, 131801 (2013), [arXiv:1208.4678].

[84] J. P. Lees *et al.* (BaBar), Phys. Rev. **D88**, 3, 031102 (2013), [arXiv:1207.0698]; B. Aubert *et al.* (BaBar), Phys. Rev. **D81**, 051101 (2010), [arXiv:0912.2453].

[85] See the "Leptonic decays of charged pseudoscalar mesons," by J. Rosner, S. Stone, and R. Van de Water, in this *Review*.

[86] J. P. Lees *et al.* (BaBar), Phys. Rev. **D84**, 112007 (2011), [Erratum: Phys. Rev.D87,no.3,039901(2013)], [arXiv:1107.5751]; S. Blyth *et al.* (Belle), Phys. Rev. **D74**, 092002 (2006), [hep-ex/0607029].

Downloaded from https://academic.oup.com/ptep/article/2022/8/083C01/6651666 by KIT Library user on 27 September 2022

[87] R. Aaij *et al.* (LHCb), Phys. Rev. D **92**, 3, 032002 (2015), [arXiv:1505.01710].

[88] B. Aubert *et al.* (BaBar), Phys. Rev. Lett. **90**, 242001 (2003), [hep-ex/0304021].

[89] D. Besson *et al.* (CLEO), Phys. Rev. **D68**, 032002 (2003), [Erratum: Phys. Rev.D75,119908(2007)], [hep-ex/0305100].

[90] P. Krokovny *et al.* (Belle), Phys. Rev. Lett. **91**, 262002 (2003), [hep-ex/0308019]; Y. Mikami *et al.* (Belle), Phys. Rev. Lett. **92**, 012002 (2004), [hep-ex/0307052].

[91] B. Aubert *et al.* (BaBar), Phys. Rev. Lett. **93**, 181801 (2004), [hep-ex/0408041].

[92] R. Aaij *et al.* (LHCb), Phys. Rev. Lett. **113**, 162001 (2014), [arXiv:1407.7574].

[93] T. Aaltonen *et al.* (CDF), Phys. Rev. Lett. **108**, 201801 (2012), [arXiv:1204.0536].

[94] S. Esen *et al.* (Belle), Phys. Rev. **D87**, 3, 031101 (2013), [arXiv:1208.0323].

[95] R. Aaij *et al.* (LHCb), Phys. Rev. **D93**, 9, 092008 (2016), [arXiv:1602.07543].

[96] R. Aaij *et al.* (LHCb), Phys. Rev. Lett. **116**, 16, 161802 (2016), [arXiv:1603.02408].

[97] R. Aaij *et al.* (LHCb), JHEP **11**, 082 (2015), [arXiv:1509.00400].

[98] B. Aubert *et al.* (BaBar), Phys. Rev. **D76**, 031101 (2007), [arXiv:0704.1266].

[99] R. Aaij *et al.* (LHCb), Phys. Rev. **D90**, 1, 012003 (2014), [arXiv:1404.5673].

[100] R. Aaij *et al.* (LHCb), Phys. Rev. Lett. **111**, 18, 181801 (2013), [arXiv:1308.4544].

[101] R. Aaij *et al.* (LHCb), Phys. Rev. **D87**, 11, 112012 (2013), [Addendum: Phys. Rev.D89,no.1,019901(2014)], [arXiv:1304.4530].

[102] G. Aad *et al.* (ATLAS), Eur. Phys. J. **C76**, 1, 4 (2016), [arXiv:1507.07099].

[103] R. Aaij *et al.* (LHCb), Phys. Rev. **D84**, 092001 (2011), [Erratum: Phys. Rev.D85,039904(2012)], [arXiv:1109.6831]; T. Aaltonen *et al.* (CDF), Phys. Rev. **D85**, 032003 (2012), [arXiv:1112.3334].

[104] S. K. Choi *et al.* (Belle), Phys. Rev. Lett. **91**, 262001 (2003), [hep-ex/0309032].

[105] D. Acosta *et al.* (CDF), Phys. Rev. Lett. **93**, 072001 (2004), [hep-ex/0312021].

[106] V. M. Abazov *et al.* (D0), Phys. Rev. Lett. **93**, 162002 (2004), [hep-ex/0405004].

[107] B. Aubert *et al.* (BaBar), Phys. Rev. **D71**, 071103 (2005), [hep-ex/0406022].

[108] R. Aaij *et al.* (LHCb), Eur. Phys. J. **C72**, 1972 (2012), [arXiv:1112.5310].

[109] S. Chatrchyan *et al.* (CMS), JHEP **04**, 154 (2013), [arXiv:1302.3968].

[110] M. Aaboud *et al.* (ATLAS), JHEP **01**, 117 (2017), [arXiv:1610.09303].

[111] S. K. Choi *et al.* (Belle), Phys. Rev. Lett. **100**, 142001 (2008), [arXiv:0708.1790]; R. Mizuk *et al.* (Belle), Phys. Rev. **D80**, 031104 (2009), [arXiv:0905.2869].

[112] R. Aaij *et al.* (LHCb), Phys. Rev. Lett. **112**, 22, 222002 (2014), [arXiv:1404.1903]; R. Aaij *et al.* (LHCb), Phys. Rev. **D92**, 11, 112009 (2015), [arXiv:1510.01951].

[113] K. Chilikin *et al.* (Belle), Phys. Rev. **D90**, 11, 112009 (2014), [arXiv:1408.6457].

[114] R. Aaij *et al.* (LHCb), Phys. Rev. Lett. **115**, 072001 (2015), [arXiv:1507.03414].

[115] R. Aaij *et al.* (LHCb), Phys. Rev. Lett. **122**, 22, 222001 (2019), [arXiv:1904.03947].

[116] See the "Non-$q\bar{q}$ mesons," by C. Amsler and C. Hanhart, and "Pentaquarks," by M. Karliner and T. Skwarnicki, in this *Review*.

[117] T. Aaltonen *et al.* (CDF), Phys. Rev. Lett. **107**, 261802 (2011), [arXiv:1107.4999].

[118] R. Aaij *et al.* (LHCb), JHEP **10**, 053 (2015), [arXiv:1508.00788].

[119] T. A. Aaltonen *et al.* (CDF), Phys. Rev. Lett. **113**, 24, 242001 (2014), [arXiv:1403.5586].

[120] R. Aaij *et al.* (LHCb), JHEP **10**, 037 (2012), [arXiv:1206.2794].

[121] T. Aaltonen *et al.* (CDF), Phys. Rev. Lett. **103**, 031801 (2009), [arXiv:0812.4271].

[122] R. Aaij *et al.* (LHCb), Phys. Rev. D **98**, 3, 032004 (2018), [arXiv:1805.06759].

[123] R. Aaij *et al.* (LHCb), JHEP **12**, 155 (2019), [arXiv:1907.10003].

[124] R. Fleischer, Phys. Lett. **B459**, 306 (1999), [hep-ph/9903456]; D. London and J. Matias, Phys. Rev. **D70**, 031502 (2004), [hep-ph/0404009].

[125] J. P. Lees *et al.* (BaBar), Phys. Rev. **D87**, 5, 052009 (2013), [arXiv:1206.3525].

[126] Y. T. Duh *et al.* (Belle), Phys. Rev. **D87**, 3, 031103 (2013), [arXiv:1210.1348].

[127] B. Aubert *et al.* (BaBar), Phys. Rev. **D76**, 091102 (2007), [arXiv:0707.2798].

[128] R. Aaij *et al.* (LHCb), Phys. Lett. B **726**, 646 (2013), [arXiv:1308.1277].

[129] M. Gronau and J. L. Rosner, Phys. Rev. **D71**, 074019 (2005), [hep-ph/0503131]; M. Gronau, Phys. Lett. **B627**, 82 (2005), [hep-ph/0508047].

[130] B. Aubert *et al.* (BaBar), Phys. Rev. D **79**, 052003 (2009), [arXiv:0809.1174].

[131] M. Fujikawa *et al.* (Belle), Phys. Rev. D **81**, 011101 (2010), [arXiv:0809.4366].

[132] B. Aubert *et al.* (BaBar), Phys. Rev. **D78**, 012004 (2008), [arXiv:0803.4451]; A. Garmash *et al.* (Belle), Phys. Rev. Lett. **96**, 251803 (2006), [hep-ex/0512066].

[133] C. T. Hoi *et al.* (Belle), Phys. Rev. Lett. **108**, 031801 (2012), [arXiv:1110.2000]; B. Aubert *et al.* (BaBar), Phys. Rev. **D80**, 112002 (2009), [arXiv:0907.1743].

[134] B. Aubert *et al.* (BaBar), Phys. Rev. Lett. **97**, 201802 (2006), [hep-ex/0608005]; C. H. Wang *et al.* (Belle), Phys. Rev. **D75**, 092005 (2007), [hep-ex/0701057].

[135] R. Aaij *et al.* (LHCb), Phys. Rev. **D90**, 11, 112004 (2014), [arXiv:1408.5373].

[136] C.-L. Hsu *et al.* (Belle), Phys. Rev. D **96**, 3, 031101 (2017), [arXiv:1705.02640].

[137] B. Aubert *et al.* (BaBar), Phys. Rev. Lett. **97**, 171805 (2006), [hep-ex/0608036].

[138] K. Abe *et al.* (Belle), Phys. Rev. Lett. **98**, 181804 (2007), [hep-ex/0608049].

[139] R. Aaij *et al.* (LHCb), Phys. Rev. Lett. **118**, 8, 081801 (2017), [arXiv:1610.08288].

[140] C. C. Peng *et al.* (Belle), Phys. Rev. **D82**, 072007 (2010), [arXiv:1006.5115].

[141] T. Aaltonen *et al.* (CDF), Phys. Rev. Lett. **106**, 181802 (2011), [arXiv:1103.5762].

[142] B. Pal *et al.* (Belle), Phys. Rev. Lett. **116**, 16, 161801 (2016), [arXiv:1512.02145].

[143] R. Aaij *et al.* (LHCb), Phys. Rev. D **102**, 1, 012011 (2020), [arXiv:2002.08229].

[144] See the "Determination of CKM angles from B hadrons," by T. Gershon, M. Kenzie, and K. Trabelsi, in this *Review*.

Downloaded from https://academic.oup.com/ptep/article/2022/8/083C01/6651666 by KIT Library user on 27 September 2022

[145] M. Gronau and D. London, Phys. Rev. Lett. **65**, 3381 (1990).

[146] T. Julius *et al.* (Belle), Phys. Rev. **D96**, 3, 032007 (2017), [arXiv:1705.02083].

[147] B. Aubert *et al.* (BaBar), Phys. Rev. **D78**, 071104 (2008), [arXiv:0807.4977].

[148] P. Vanhoefer *et al.* (Belle), Phys. Rev. **D89**, 072008 (2014), [Addendum: Phys. Rev.D89,119903(2014)], [arXiv:1212.4015].

[149] B. Aubert *et al.* (BaBar), Phys. Rev. **D76**, 052007 (2007), [arXiv:0705.2157]; P. Vanhoefer *et al.* (Belle), Phys. Rev. D **93**, 3, 032010 (2016), [Addendum: Phys.Rev.D 94, 099903 (2016)], [arXiv:1510.01245].

[150] B. Aubert *et al.* (BaBar), Phys. Rev. Lett. **102**, 141802 (2009), [arXiv:0901.3522]; J. Zhang *et al.* (Belle), Phys. Rev. Lett. **91**, 221801 (2003), [hep-ex/0306007].

[151] R. Aaij *et al.* (LHCb), Phys. Lett. **B747**, 468 (2015), [arXiv:1503.07770].

[152] See the "Polarization in B Decays," by A. Gritsan in this *Review*.

[153] T. E. Coan *et al.* (CLEO), Phys. Rev. Lett. **84**, 5283 (2000), [hep-ex/9912057].

[154] T. Horiguchi *et al.* (Belle), Phys. Rev. Lett. **119**, 19, 191802 (2017), [arXiv:1707.00394].

[155] B. Aubert *et al.* (BaBar), Phys. Rev. Lett. **103**, 211802 (2009), [arXiv:0906.2177].

[156] B. Aubert *et al.* (BaBar), Phys. Rev. **D70**, 091105 (2004), [hep-ex/0409035].

[157] H. Yang *et al.* (Belle), Phys. Rev. Lett. **94**, 111802 (2005), [hep-ex/0412039].

[158] S. Nishida *et al.* (Belle), Phys. Lett. **B610**, 23 (2005), [hep-ex/0411065].

[159] B. Aubert *et al.* (BaBar), Phys. Rev. **D74**, 031102 (2006), [hep-ex/0603054].

[160] B. Aubert *et al.* (BaBar), Phys. Rev. Lett. **98**, 211804 (2007), [Erratum: Phys. Rev. Lett.100,199905(2008)], [hep-ex/0507031].

[161] P. del Amo Sanchez *et al.* (BaBar), Phys. Rev. **D93**, 5, 052013 (2016), [arXiv:1512.03579].

[162] R. Aaij *et al.* (LHCb), Phys. Rev. Lett. **112**, 16, 161801 (2014), [arXiv:1402.6852].

[163] J. Wicht *et al.* (Belle), Phys. Rev. Lett. **100**, 121801 (2008), [arXiv:0712.2659]; D. Dutta *et al.* (Belle), Phys. Rev. **D91**, 1, 011101 (2015), [arXiv:1411.7771].

[164] R. Aaij *et al.* (LHCb), Nucl. Phys. **B867**, 1 (2013), [arXiv:1209.0313].

[165] R. Aaij *et al.* (LHCb), Phys. Rev. Lett. **123**, 3, 031801 (2019), [arXiv:1904.06697].

[166] A. Ali, E. Lunghi and A. Ya. Parkhomenko, Phys. Lett. **B595**, 323 (2004), [hep-ph/0405075]; P. Ball, G. W. Jones and R. Zwicky, Phys. Rev. **D75**, 054004 (2007), [hep-ph/0612081].

[167] J. L. Hewett, Phys. Rev. Lett. **70**, 1045 (1993), [hep-ph/9211256].

[168] S. Chen *et al.* (CLEO), Phys. Rev. Lett. **87**, 251807 (2001), [hep-ex/0108032].

[169] J. P. Lees *et al.* (BaBar), Phys. Rev. **D86**, 112008 (2012), [arXiv:1207.5772].

[170] A. Limosani *et al.* (Belle), Phys. Rev. Lett. **103**, 241801 (2009), [arXiv:0907.1384]; T. Saito *et al.* (Belle), Phys. Rev. **D91**, 5, 052004 (2015), [arXiv:1411.7198].

[171] P. del Amo Sanchez *et al.* (BaBar), Phys. Rev. **D82**, 051101 (2010), [arXiv:1005.4087].

[172] M. Misiak *et al.*, Phys. Rev. Lett. **114**, 22, 221801 (2015), [arXiv:1503.01789]; M. Czakon *et al.*, JHEP **04**, 168 (2015), [arXiv:1503.01791].

[173] L. Wolfenstein and Y. L. Wu, Phys. Rev. Lett. **73**, 2809 (1994), [hep-ph/9410253]; G. M. Asatrian and A. Ioannisian, Phys. Rev. **D54**, 5642 (1996), [hep-ph/9603318]; M. Ciuchini, E. Gabrielli and G. F. Giudice, Phys. Lett. **B388**, 353 (1996), [Erratum: Phys. Lett.B393,489(1997)], [hep-ph/9604438]; S. Baek and P. Ko, Phys. Rev. Lett. **83**, 488 (1999), [hep-ph/9812229]; A. L. Kagan and M. Neubert, Phys. Rev. **D58**, 094012 (1998), [hep-ph/9803368]; K. Kiers, A. Soni and G.-H. Wu, Phys. Rev. **D62**, 116004 (2000), [hep-ph/0006280].

[174] S. Watanuki *et al.* (Belle), Phys. Rev. D **99**, 3, 032012 (2019), [arXiv:1807.04236]; J. P. Lees *et al.* (BaBar), Phys. Rev. **D90**, 9, 092001 (2014), [arXiv:1406.0534].

[175] B. Aubert *et al.* (BaBar), Phys. Rev. **D72**, 052004 (2005), [hep-ex/0508004].

[176] B. Aubert *et al.* (BaBar), Phys. Rev. **D77**, 051103 (2008), [arXiv:0711.4889].

[177] J. P. Lees *et al.* (BaBar), Phys. Rev. Lett. **109**, 191801 (2012), [arXiv:1207.2690].

[178] See the "Semileptonic b-Hadron Decays, Determination of V_{cb}, V_{ub}," by T. Mannel and P. Urquijo in this *Review*.

[179] M. Iwasaki *et al.* (Belle), Phys. Rev. **D72**, 092005 (2005), [hep-ex/0503044]; J. P. Lees *et al.* (BaBar), Phys. Rev. Lett. **112**, 211802 (2014), [arXiv:1312.5364].

[180] Y. Sato *et al.* (Belle), Phys. Rev. **D93**, 3, 032008 (2016), [Addendum: Phys. Rev.D93,no.5,059901(2016)], [arXiv:1402.7134].

[181] T. Aaltonen *et al.* (CDF), Phys. Rev. Lett. **107**, 201802 (2011), [arXiv:1107.3753].

[182] R. Aaij *et al.* (LHCb), JHEP **07**, 084 (2013), [arXiv:1305.2168]; R. Aaij *et al.* (LHCb), JHEP **09**, 179 (2015), [arXiv:1506.08777].

[183] R. Aaij *et al.* (LHCb), Phys. Lett. **B725**, 25 (2013), [arXiv:1306.2577].

[184] R. Aaij *et al.* (LHCb), JHEP **06**, 108 (2017), [arXiv:1703.00256].

[185] B. Aubert *et al.* (BaBar), Phys. Rev. Lett. **102**, 091803 (2009), [arXiv:0807.4119].

[186] S. Choudhury *et al.* (BELLE), JHEP **03**, 105 (2021), [arXiv:1908.01848].

[187] R. Aaij *et al.* (LHCb), JHEP **06**, 133 (2014), [arXiv:1403.8044].

[188] J. T. Wei *et al.* (Belle), Phys. Rev. Lett. **103**, 171801 (2009), [arXiv:0904.0770].

[189] R. Aaij *et al.* (LHCb), JHEP **11**, 047 (2016), [Erratum: JHEP 04, 142 (2017)], [arXiv:1606.04731].

[190] T. Aaltonen *et al.* (CDF), Phys. Rev. Lett. **108**, 081807 (2012), [arXiv:1108.0695].

[191] R. Aaij *et al.* (LHCb), JHEP **05**, 082 (2014), [arXiv:1403.8045].

[192] A. M. Sirunyan *et al.* (CMS), Phys. Lett. B **781**, 517 (2018), [arXiv:1710.02846].

[193] R. Aaij *et al.* (LHCb), Phys. Rev. Lett. **125**, 1, 011802 (2020), [arXiv:2003.04831].

[194] S. Wehle *et al.* (Belle), Phys. Rev. Lett. **118**, 11, 111801 (2017), [arXiv:1612.05014].

[195] M. Aaboud *et al.* (ATLAS), JHEP **10**, 047 (2018), [arXiv:1805.04000].

[196] R. Aaij *et al.* (LHCb), Phys. Rev. Lett. **126**, 16, 161802 (2021), [arXiv:2012.13241].

[197] R. Aaij *et al.* (LHCb) (2021), [arXiv:2107.13428].

[198] R. Aaij *et al.* (LHCb), JHEP **09**, 146 (2018), [arXiv:1808.00264].

[199] S. Descotes-Genon *et al.*, JHEP **01**, 048 (2013), [arXiv:1207.2753].

Downloaded from https://academic.oup.com/ptep/article/2022/8/083C01/6651666 by KIT Library user on 27 September 2022

[200] J. P. Lees *et al.* (BaBar), Phys. Rev. **D86**, 032012 (2012), [arXiv:1204.3933].

[201] R. Aaij *et al.* (LHCb), JHEP **09**, 177 (2014), [arXiv:1408.0978].

[202] J. Lyon and R. Zwicky, Phys. Rev. **D88**, 9, 094004 (2013), [arXiv:1305.4797].

[203] R. Aaij *et al.* (LHCb), Eur. Phys. J. **C77**, 3, 161 (2017), [arXiv:1612.06764].

[204] R. Aaij *et al.* (LHCb), JHEP **12**, 081 (2020), [arXiv:2010.06011].

[205] R. Aaij *et al.* (LHCb), Phys. Rev. Lett. **122**, 19, 191801 (2019), [arXiv:1903.09252].

[206] R. Aaij *et al.* (LHCb), JHEP **08**, 055 (2017), [arXiv:1705.05802].

[207] R. Aaij *et al.* (LHCb) (2021), [arXiv:2103.11769].

[208] A. Abdesselam *et al.* (Belle), Phys. Rev. Lett. **126**, 16, 161801 (2021), [arXiv:1904.02440].

[209] R. Aaij *et al.* (LHCb) (2019), [arXiv:1912.08139].

[210] R. Aaij *et al.* (LHCb), Phys. Lett. **B743**, 46 (2015), [arXiv:1412.6433].

[211] R. Aaij *et al.* (LHCb), JHEP **04**, 029 (2017), [arXiv:1701.08705].

[212] J. P. Lees *et al.* (BaBar), Phys. Rev. D **87**, 11, 112005 (2013), [arXiv:1303.7465].

[213] J. Grygier *et al.* (Belle), Phys. Rev. D **96**, 9, 091101 (2017), [Addendum: Phys.Rev.D 97, 099902 (2018)], [arXiv:1702.03224].

[214] T. Aaltonen *et al.* (CDF), Phys. Rev. Lett. **107**, 191801 (2011), [Addendum: Phys. Rev. Lett.107,no.23,239903(2011)], [arXiv:1107.2304].

[215] V. M. Abazov *et al.* (D0), Phys. Rev. **D87**, 7, 072006 (2013), [arXiv:1301.4507].

[216] R. Aaij *et al.* (LHCb), Phys. Rev. Lett. **110**, 2, 021801 (2013), [arXiv:1211.2674].

[217] M. Aaboud *et al.* (ATLAS), JHEP **04**, 098 (2019), [arXiv:1812.03017].

[218] A. M. Sirunyan *et al.* (CMS), JHEP **04**, 188 (2020), [arXiv:1910.12127].

[219] R. Aaij *et al.* (LHCb), Phys. Rev. Lett. **118**, 19, 191801 (2017), [arXiv:1703.05747].

[220] R. Aaij *et al.* (LHCb), Phys. Rev. Lett. **124**, 21, 211802 (2020), [arXiv:2003.03999].

[221] R. Aaij *et al.* (LHCb), Phys. Rev. Lett. **118**, 25, 251802 (2017), [arXiv:1703.02508].

[222] C. Bobeth *et al.*, Phys. Rev. Lett. **112**, 101801 (2014), [arXiv:1311.0903].

[223] K. De Bruyn *et al.*, Phys. Rev. Lett. **109**, 041801 (2012), [arXiv:1204.1737]; A. J. Buras *et al.*, JHEP **07**, 77 (2013), [arXiv:1303.3820].

[224] R. Aaij *et al.* (LHCb), JHEP **03**, 078 (2018), [arXiv:1710.04111].

[225] J. Aebischer *et al.*, Eur. Phys. J. C **80**, 3, 252 (2020), [arXiv:1903.10434]; F. Beaujean, C. Bobeth and D. van Dyk, Eur. Phys. J. **C74**, 2897 (2014), [Erratum: Eur. Phys. J.C74,3179(2014)], [arXiv:1310.2478]; M. Algueró *et al.*, JHEP **07**, 096 (2019), [arXiv:1902.04900]; A. Arbey *et al.*, Phys. Rev. D **100**, 1, 015045 (2019), [arXiv:1904.08399].

[226] T. Blake, G. Lanfranchi and D. M. Straub, Prog. Part. Nucl. Phys. **92**, 50 (2017), [arXiv:1606.00916]; J. Albrecht, S. Reichert and D. van Dyk, Int. J. Mod. Phys. A **33**, 18n19, 1830016 (2018), [arXiv:1806.05010].

Downloaded from https://academic.oup.com/ptep/article/2022/8/083C01/6651666 by KIT Library user on 27 September 2022

74. Polarization in B Decays

Revised February 2022 by A.V. Gritsan (Johns Hopkins U.).

We review the notation used in polarization measurements in particle production and decay, with a particular emphasis on the B decays and the CP-violating observables in polarization measurements. We look at several examples of vector-vector and vector-tensor B meson decays, while more details about the theory and experimental results in B decays can be found in a separate mini-review [1] in this *Review*.

Figure 74.1 illustrates angular observables in an example of the sequential process $ab \to X \to P_1 P_2 \to (p_{11}p_{12})(p_{21}p_{22})$ [2]. The angular distributions are of particular interest because they are sensitive to spin correlations and reveal properties of particles and their interactions, such as quantum numbers and couplings. In the case of a spin-zero particle X, such as B meson or a Higgs boson, there are no spin correlations in the production mechanism and the decay chain is to be analyzed. The angular distribution of decay products can be expressed as a function of three helicity angles which describe the alignment of the particles in the decay chain. The analyzer of the B-daughter polarization is normally chosen for two-body decays, as the direction of the daughters in the center-of-mass of the parent (*e.g.*, $\rho \to 2\pi$) [3], and for three-body decays as the normal to the decay plane (*e.g.*, $\omega \to 3\pi$) [4]. An equivalent set of transversity angles is sometimes used in polarization analyses [5]. The differential decay width depends on complex amplitudes $A_{\lambda_1\lambda_2}$, corresponding to the X-daughter helicity states λ_i.

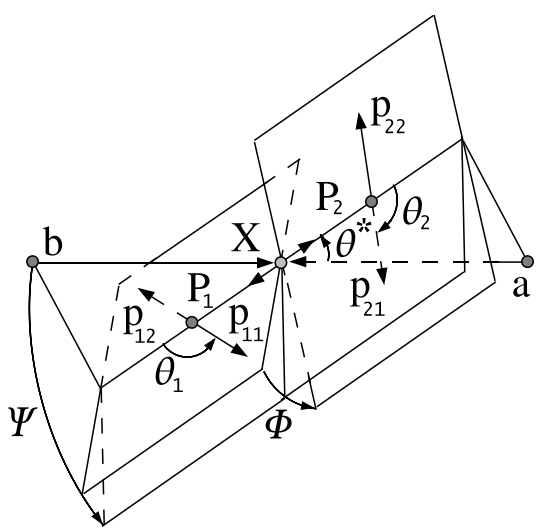

Figure 74.1: Definition of the production and helicity angles in the sequential process $ab \to X \to P_1 P_2 \to (p_{11}p_{12})(p_{21}p_{22})$. The three helicity angles include θ_1 and θ_2, defined in the rest frame of the two daughters P_1 and P_2, and Φ, defined in the X frame as the angle between the two decay planes. The two production angles θ^* and Ψ are defined in the X frame, where Ψ is the angle between the production plane and the average of the two decay planes.

In the case of a spin-zero B-meson decay, its daughter helicities are constrained to $\lambda_1 = \lambda_2 = \lambda$. Therefore we simplify amplitude notation as A_λ. Moreover, most B-decay polarization analyses are limited to the case when the spin of one of the B-meson daughters is 1. In that case, there are only three independent amplitudes corresponding to $\lambda = 0$ or ± 1 [6], where the last two can be expressed in terms of parity-even and parity-odd amplitudes $A_{\parallel,\perp} = (A_{+1} \pm A_{-1})/\sqrt{2}$. The overall decay amplitude involves three complex terms proportional to the above amplitudes and the Wigner d functions of helicity angles. The exact angular dependence would depend on the quantum numbers of the B-meson daughters and of their decay products, and can be found in the literature [6,7]. When both B-meson daughters are tensor mesons and the smaller of the two daughter spins is $J_1 > 1$, this formalism can be easily extended by introducing the parity-even and parity-odd amplitudes of higher order $A_{\parallel n,\perp n} = (A_{+n} \pm A_{-n})/\sqrt{2}$, with $1 < n \leq J_1$, while the general angular parameterization may be found in Ref. [7]. However, we limit the following discussion to $J_1 = 1$. The differential decay rate would involve six real quantities α_i, including interference terms,

$$\frac{d\Gamma}{\Gamma\, d\cos\theta_1\, d\cos\theta_2\, d\Phi} = \sum_i \alpha_i\ f_i\,(\cos\theta_1,\, \cos\theta_2,\, \Phi)\,, \qquad (74.1)$$

where each $f_i\,(\cos\theta_1,\, \cos\theta_2,\, \Phi)$ has unique angular dependence specific to particle quantum numbers, and the α_i parameters are defined as:

$$\alpha_1 = \frac{|A_0|^2}{\Sigma|A_\lambda|^2} = f_L\,, \qquad (74.2)$$

$$\alpha_2 = \frac{|A_\parallel|^2 + |A_\perp|^2}{\Sigma|A_\lambda|^2} = (1 - f_L)\,, \qquad (74.3)$$

$$\alpha_3 = \frac{|A_\parallel|^2 - |A_\perp|^2}{\Sigma|A_\lambda|^2} = (1 - f_L - 2\,f_\perp)\,, \qquad (74.4)$$

$$\alpha_4 = \frac{\Im m(A_\perp A_\parallel^*)}{\Sigma|A_\lambda|^2} = \sqrt{f_\perp(1-f_L-f_\perp)}\,\sin(\phi_\perp - \phi_\parallel)\,, \qquad (74.5)$$

$$\alpha_5 = \frac{\Re e(A_\parallel A_0^*)}{\Sigma|A_\lambda|^2} = \sqrt{f_L\,(1 - f_L - f_\perp)}\,\cos(\phi_\parallel)\,, \qquad (74.6)$$

$$\alpha_6 = \frac{\Im m(A_\perp A_0^*)}{\Sigma|A_\lambda|^2} = \sqrt{f_\perp\, f_L}\,\sin(\phi_\perp)\,, \qquad (74.7)$$

where the amplitudes have been expressed with the help of polarization parameters f_L, $f_\perp$, $\phi_\parallel$, and $\phi_\perp$ defined in Table 74.1. Note that the terms proportional to $\Re e(A_\perp A_\parallel^*)$, $\Im m(A_\parallel A_0^*)$, and $\Re e(A_\perp A_0^*)$ are absent in Eqs. (2-7). However, these terms may appear for some three-body decays of a B-meson daughter, see Ref. [7].

Table 74.1: Rate, polarization, and CP-asymmetry parameters defined for the B-meson decays to mesons with non-zero spin. Numerical examples are shown for the average of the $B^0 \to \varphi K^*(892)^0$ decay measurements obtained from BABAR [8], Belle [9], and LHCb [10]. The first six parameters are defined under the assumption of no CP violation in decay, while they are averaged between the $\overline{B}$ and B parameters in general. The last six parameters involve differences between the $\overline{B}$ and B meson decay parameters. The phase convention δ_0 is chosen with respect to a single A_{00} amplitude from a reference B decay mode, which is $B^0 \to \varphi K_0^*(1430)^0$ for numerical results.

parameter	definition	average
$\mathcal{B}$	$\Gamma/\Gamma_{\rm total}$	$(10.1^{+0.6}_{-0.5}) \times 10^{-6}$
f_L	$\lvert A_0\rvert^2/\Sigma\lvert A_\lambda\rvert^2$	0.497 ± 0.017
$f_\perp$	$\lvert A_\perp\rvert^2/\Sigma\lvert A_\lambda\rvert^2$	0.225 ± 0.015
$\phi_\parallel - \pi$	$\arg(A_\parallel/A_0) - \pi$	-0.712 ± 0.058
$\phi_\perp - \pi$	$\arg(A_\perp/A_0) - \pi$	-0.615 ± 0.056
$\delta_0 - \pi$	$\arg(A_{00}/A_0) - \pi$	-0.26 ± 0.10
A_{CP}	$(\bar{\Gamma} - \Gamma)/(\bar{\Gamma} + \Gamma)$	-0.003 ± 0.038
A_{CP}^0	$(\bar{f_L} - f_L)/(\bar{f_L} + f_L)$	-0.007 ± 0.030
$A_{CP}^\perp$	$(\bar{f_\perp} - f_\perp)/(\bar{f_\perp} + f_\perp)$	-0.014 ± 0.057
$\Delta\phi_\parallel$	$(\bar{\phi_\parallel} - \phi_\parallel)/2$	$+0.051 \pm 0.053$
$\Delta\phi_\perp$	$(\bar{\phi_\perp} - \phi_\perp - \pi)/2$	$+0.075 \pm 0.050$
$\Delta\delta_0$	$(\bar{\delta_0} - \delta_0)/2$	$+0.13 \pm 0.08$

Overall, six real parameters describe three complex amplitudes A_0, $A_\parallel$, and $A_\perp$. These could be chosen to be the four polarization

Downloaded from https://academic.oup.com/ptep/article/2022/8/083C01/6651666 by KIT Library user on 27 September 2022

parameters f_L, $f_\perp$, $\phi_\parallel$, and $\phi_\perp$, one overall size normalization, such as decay rate Γ, or branching fraction $\mathcal{B}$, and one overall phase δ_0. The phase convention is arbitrary for an isolated B decay mode. However, for several B decays, the relative phase could produce meaningful and observable effects through interference with other B decays with the same final states, such as for $B \to VK_J^*$ with $J = 0, 1, 2, 3, 4, ...$ The phase could be referenced to the single $B \to VK_0^*$ amplitude A_{00} in such a case, as shown in Table 74.1. Here V stands for any spin-one vector meson.

Moreover, *CP* violation can be tested in the angular distribution of the decay as the difference between the B and $\overline{B}$. Each of the six real parameters describing the three complex amplitudes would have a counterpart *CP*-asymmetry term, corresponding to three direct-*CP* asymmetries in three amplitudes, and three *CP*-violating phase differences, equivalent to the phase measurements from the mixing-induced *CP* asymmetries in the time evolution of B-decays [1]. In Table 74.1 and Ref. [11], these are chosen to be the direct-*CP* asymmetries in the overall decay rate $\mathcal{A}_{CP}$, in the f_L fraction $\mathcal{A}^0_{CP}$, and in the $f_\perp$ fraction $\mathcal{A}^\perp_{CP}$, and three weak phase differences:

$$\Delta\phi_\parallel = \frac{1}{2}\arg(\bar{A}_\parallel A_0/A_\parallel \bar{A}_0)\,, \tag{74.8}$$

$$\Delta\phi_\perp = \frac{1}{2}\arg(\bar{A}_\perp A_0/A_\perp \bar{A}_0) - \frac{\pi}{2}\,, \tag{74.9}$$

$$\Delta\delta_0 = \frac{1}{2}\arg(\bar{A}_{00} A_0/A_{00} \bar{A}_0)\,. \tag{74.10}$$

The $\frac{\pi}{2}$ term in Eq. (74.8) reflects the fact that $A_\perp$ and $\bar{A}_\perp$ differ in phase by π if *CP* is conserved. The two parameters $\Delta\phi_\parallel$ and $\Delta\phi_\perp$ are equivalent to triple-product asymmetries constructed from the vectors describing the decay angular distribution [12]. The *CP*-violating phase difference in the reference decay mode [11] is, in the Wolfenstein CKM quark-mixing phase convention,

$$\Delta\phi_{00} = \frac{1}{2}\arg(A_{00}/\bar{A}_{00})\,. \tag{74.11}$$

This can be measured only together with the mixing-induced phase difference for some of the neutral B-meson decays similar to other mixing-induced *CP* asymmetry measurements [1].

It may not always be possible to have a phase-reference decay mode which would define δ_0 and $\Delta\delta_0$ parameters. In that case, it may be possible to define the phase difference directly similarly to Eq. (74.11):

$$\Delta\phi_0 = \frac{1}{2}\arg(A_0/\bar{A}_0)\,. \tag{74.12}$$

One can measure the angles of the CKM unitarity triangle, assuming Standard Model contributions to the $\Delta\phi_0$ and B-mixing phases. Examples include measurements of $\beta = \phi_1$ with $B \to J/\psi K^*$ and $\alpha = \phi_2$ with $B \to \rho\rho$.

Most of the B decays that arise from tree-level $b \to c$ transitions have the amplitude hierarchy $|A_0| > |A_+| > |A_-|$ which is expected from analyses based on quark-helicity conservation [13]. The larger the mass of the vector-meson daughters, the weaker the inequality. The B meson decays to heavy vector particles with charm, such as $B \to J/\psi K^*$, $\psi(2S)K^*$, $\chi_{c1}K^*$, $D^*\rho$, D^*K^*, D^*D^*, and $D^*D_s^*$, show a substantial fraction of the amplitudes corresponding to transverse polarization of the vector mesons ($A_{\pm 1}$), in agreement with the factorization prediction. The detailed amplitude analysis of the $B \to J/\psi K^*$ decays has been performed by the BABAR [14], Belle [15], CDF [16], CLEO [17], D0 [18], and LHCb [19] collaborations. Most analyses are performed under the assumption of the absence of direct *CP* violation. The parameter values are given in the particle listing of this *Review*. The difference between the strong phases $\phi_\parallel$ and $\phi_\perp$ deviates significantly from zero. The measurements [14, 15] of *CP*-violating terms similar to those in $B \to \varphi K^*$ [8] shown in Table 74.1 are consistent with zero.

In addition, the mixing-induced *CP*-violating asymmetry is measured in the $B^0 \to J/\psi K^{*0}$ decay [1, 14, 15] where angular analysis allows one to separate *CP*-eigenstate amplitudes. This allows one to resolve the sign ambiguity of the $\cos 2\beta$ ($\cos 2\phi_1$) term that appears in the time-dependent angular distribution due to interference of parity-even and parity-odd terms. This analysis relies on the knowledge of discrete ambiguities in the strong phases $\phi_\parallel$ and $\phi_\perp$, as discussed below. The BABAR experiment used a method based on the dependence on the $K\pi$ invariant mass of the interference between the S- and P-waves to resolve the discrete ambiguity in the determination of the strong phases $(\phi_\parallel, \phi_\perp)$ in $B \to J/\psi K^*$ decays [14]. The result is in agreement with the amplitude hierarchy expectation [13]. The CDF [20], D0 [21], and LHCb [22] experiments have studied the $B_s^0 \to J/\psi(K^+K^-)$, $J/\psi(\pi^+\pi^-)$, $\psi(K^+\pi^-)$ decays and provided the lifetime, polarization, and phase measurements.

The amplitude hierarchy $|A_0| \gg |A_+| \gg |A_-|$ was expected in B decays to light vector particles in both penguin transitions [23, 24] and tree-level transitions [13]. There is confirmation by the BABAR and Belle experiments of predominantly longitudinal polarization in the tree-level $b \to u$ transition, such as $B^0 \to \rho^+\rho^-$ [25], $B^+ \to \rho^0\rho^+$ [26], and $B^+ \to \omega\rho^+$ [27]; this is consistent with the analysis of the quark helicity conservation [13]. Because the longitudinal amplitude dominates the decay, a detailed amplitude analysis is not possible with current B samples, and limits on the transverse amplitude fraction are obtained. The small branching fractions of $B^0 \to \rho^0\rho^0, \omega\rho^0, \omega\omega$ [27–30] indicate that $b \to d$ penguin pollution is small in the charmless, strangeless vector-vector B decays. There is a measurement of large longitudinal polarization in $B^0 \to \rho^0\rho^0$ [28–30] decays. The fraction of transverse polarization is large in decays to heavier mesons such as $B^0 \to a_1(1260)^+ a_1(1260)^-$ [31].

The interest in the polarization and *CP*-asymmetry measurements in penguin transition, such as $b \to s$ decays $B \to \varphi K^*$, ρK^*, ωK^*, or $B_s^0 \to \varphi\varphi$, K^*K^*, and $b \to d$ decay $B \to K^*\bar{K}^*$, is motivated by their potential sensitivity to physics beyond the Standard Model. The decay amplitudes for $B \to \varphi K^*$ have been measured by the BABAR, Belle, and LHCb experiments [9–11, 32, 33]. The fractions of longitudinal polarization are $f_L = 0.50 \pm 0.05$ for the $B^+ \to \varphi K^{*+}$ decay and $f_L = 0.497 \pm 0.017$ for the $B^0 \to \varphi K^{*0}$ decay. These indicate significant departure from the naive expectation of predominant longitudinal polarization, suggesting other contributions to the decay amplitude, previously neglected, either within the Standard Model, such as penguin annihilation [34] or QCD rescattering [35], or from physics beyond the Standard Model [36]. The complete set of twelve amplitude parameters measured in the $B^0 \to \varphi K^{*0}$ decay is given in Table 74.1. Several other parameters could be constructed from the above twelve parameters, as suggested in Ref. [37].

The discrete ambiguity in the phase $(\phi_\parallel, \phi_\perp, \Delta\phi_\parallel, \Delta\phi_\perp)$ measurements has been resolved by BABAR in favor of $|A_+| \gg |A_-|$ through interference between the S- and P-waves of $K\pi$. The search for vector-tensor and vector-axialvector $B \to \varphi K_J^{(*)}$ decays with $J = 1, 2, 3, 4$ revealed a large fraction of longitudinal polarization in the decay $B \to \varphi K_2^*(1430)$ with $f_L = 0.90^{+0.06}_{-0.07}$ [11, 38], but large contribution of transverse amplitude in $B \to \varphi K_1(1270)$ with $f_L = 0.46^{+0.13}_{-0.15}$ [39].

Like $B \to \varphi K^*$, the decays $B \to \rho K^*$ and $B \to \omega K^*$ may be sensitive to New Physics. Measurements of the longitudinal polarization fraction in $B \to \rho K^*$ [40] and in both vector-vector and vector-tensor final states of $B \to \omega K_J^*$ [27] by BABAR and Belle reveal a large fraction of transverse polarization, indicating an anomaly similar to $B \to \varphi K^*$ except for a different pattern in vector-tensor final states. An angular analysis of the $B^0 \to \rho^0 K^{*0}$ decay mode by LHCb [41] provides much higher precision and indicates remarkably small longitudinal polarization fraction and a significant direct CP asymmetry observed in angular distributions of $B \to VV$ decays for the first time. A large transverse polarization is also observed in the $B_s^0 \to \varphi\varphi$ decay by CDF [42] and LHCb [43], $B_s^0 \to K^{*0}\bar{K}^{*0}$ decays by LHCb [44], and $B_s^0 \to \varphi K^{*0}$ decays by LHCb [45]. At the same time, measurement of the polarization in the $b \to d$ penguin decays $B \to K^*\bar{K}^*$ indicates a large fraction of longitudinal polarization [44, 46]. The LHCb experiment has also provided the very first polarization results on the tensor-tensor, as well as vector-tensor, decays of the B_s^0 meson in the $(K\pi)(K\pi)$ final state [44]. The polarization pattern in penguin-dominated B-meson decays is not fully understood [34–36].

Downloaded from https://academic.oup.com/ptep/article/2022/8/083C01/6651666 by KIT Library user on 27 September 2022

The three-body semileptonic B-meson decays, such as $B \to V\ell_1\ell_2$, share many features with the two-body $B \to VV$ decays. Their differential decay width can be parameterized with the two helicity angles defined in the V and $(\ell_1\ell_2)$ frames and with the azimuthal angle, as defined in Fig. 74.1. However, since the $(\ell_1\ell_2)$ pair does not come from an on-shell particle, the angular distribution is unique to each point in the dilepton mass $m_{\ell\ell}$ spectrum. The polarization measurements as a function of $m_{\ell\ell}$ provide complementary information on physics beyond the Standard Model, as discussed for $B \to K^*\ell^+\ell^-$ and $B_s \to \phi\ell^+\ell^-$ decays in Ref. [47]. The data in these modes have been analyzed by the BABAR, Belle, CDF, CMS, and LHCb experiments [48–53].

The examples of the angular distributions and observables in $B \to K^*\ell^+\ell^-$ are discussed in Ref. [47]. Two angular observables have been measured in this decay in certain ranges of the dilepton mass $m_{\ell\ell}$. One parameter is the fraction of longitudinal polarization F_L, which is determined by the K^* angular distribution and is similar to f_L defined for exclusive two-body decays. The other parameter is the forward-backward asymmetry of the lepton pair A_{FB}, which is the asymmetry of the decay rate with positive and negative values of $\cos\theta_1$. A complete set of observables and angular terms has been adopted by the LHCb collaboration [52] following Ref. [47] with the F_L, A_{FB}, and $S_3 - S_9$ coefficients in the angular distributions. Additional set of optimized observables $P_i^{(\prime)}$ is derived from those, for example $P_2 = 2A_{FB}/(3-3F_L)$ and $P_5' = S_5/\sqrt{F_L(1-F_L)}$. These observables have the advantage that the leading form-factor uncertainties cancel. There have been hints of deviations from SM in the measurement of P_5' and lepton flavor universality [48–53].

In summary, there has been considerable interest in the polarization measurements of B-meson decays because they reveal both weak- and strong-interaction dynamics [34–36, 54]. New measurements will further elucidate the pattern of spin alignment measurements in rare B decays, and further test the Standard Model and strong interaction dynamics, including the non-factorizable contributions to the B-decay amplitudes.

References

[1] M. Kreps, Y. Kwon, and P. Eerola, "Production and Decay of b-Flavored Hadrons," mini-review in this *Review*.

[2] Y. Gao *et al.*, Phys. Rev. D **81**, 075022 (2010), [arXiv:1001.3396].

[3] M. Jacob and G. Wick, Annals Phys. **7**, 404 (1959).

[4] S. Berman and M. Jacob, Phys. Rev. **139**, B1023 (1965).

[5] I. Dunietz *et al.*, Phys. Rev. D **43**, 2193 (1991).

[6] G. Kramer and W. Palmer, Phys. Rev. D **45**, 193 (1992).

[7] A. Datta *et al.*, Phys. Rev. D **77**, 114025 (2008), [arXiv:0711.2107].

[8] B. Aubert *et al.* (BaBar), Phys. Rev. D **78**, 092008 (2008), [arXiv:0808.3586].

[9] M. Prim *et al.* (Belle), Phys. Rev. D **88**, 7, 072004 (2013), [arXiv:1308.1830].

[10] R. Aaij *et al.* (LHCb), JHEP **05**, 069 (2014), [arXiv:1403.2888].

[11] B. Aubert *et al.* (BaBar), Phys. Rev. Lett. **93**, 231804 (2004), [hep-ex/0408017]; B. Aubert *et al.* (BaBar), Phys. Rev. Lett. **98**, 051801 (2007), [hep-ex/0610073]; B. Aubert *et al.* (BaBar), Phys. Rev. D **78**, 092008 (2008), [arXiv:0808.3586].

[12] G. Valencia, Phys. Rev. D **39**, 3339 (1989); A. Datta and D. London, Int. J. Mod. Phys. A **19**, 2505 (2004), [hep-ph/0303159].

[13] A. Ali *et al.*, Z. Phys. C **1**, 269 (1979); M. Suzuki, Phys. Rev. D **64**, 117503 (2001), [hep-ph/0106354].

[14] B. Aubert *et al.* (BaBar), Phys. Rev. D **71**, 032005 (2005), [hep-ex/0411016]; B. Aubert *et al.* (BaBar), Phys. Rev. D **76**, 031102 (2007), [arXiv:0704.0522].

[15] R. Itoh *et al.* (Belle), Phys. Rev. Lett. **95**, 091601 (2005), [hep-ex/0504030]; M. Prim *et al.* (Belle), Phys. Rev. D **88**, 7, 072004 (2013), [arXiv:1308.1830].

[16] T. Affolder *et al.* (CDF), Phys. Rev. Lett. **85**, 4668 (2000), [hep-ex/0007034]; D. Acosta *et al.* (CDF), Phys. Rev. Lett. **94**, 101803 (2005), [hep-ex/0412057].

[17] C. Jessop *et al.* (CLEO), Phys. Rev. Lett. **79**, 4533 (1997), [hep-ex/9702013].

[18] V. Abazov *et al.* (D0), Phys. Rev. Lett. **102**, 032001 (2009), [arXiv:0810.0037].

[19] R. Aaij *et al.* (LHCb), Phys. Rev. D **88**, 052002 (2013), [arXiv:1307.2782].

[20] T. Aaltonen *et al.* (CDF), Phys. Rev. Lett. **100**, 121803 (2008), [arXiv:0712.2348]; T. Aaltonen *et al.* (CDF), Phys. Rev. D **85**, 072002 (2012), [arXiv:1112.1726].

[21] V. Abazov *et al.* (D0), Phys. Rev. Lett. **98**, 121801 (2007), [hep-ex/0701012]; V. M. Abazov *et al.* (D0), Phys. Rev. D **85**, 032006 (2012), [arXiv:1109.3166].

[22] R. Aaij *et al.* (LHCb), Phys. Rev. Lett. **108**, 101803 (2012), [arXiv:1112.3183]; R. Aaij *et al.* (LHCb), Phys. Rev. Lett. **114**, 4, 041801 (2015), [arXiv:1411.3104]; R. Aaij *et al.* (LHCb), Phys. Lett. B **747**, 484 (2015), [arXiv:1503.07112]; R. Aaij *et al.* (LHCb), JHEP **11**, 082 (2015), [arXiv:1509.00400]; R. Aaij *et al.* (LHCb), JHEP **08**, 037 (2017), [arXiv:1704.08217].

[23] H.-Y. Cheng and K.-C. Yang, Phys. Lett. B **511**, 40 (2001), [hep-ph/0104090]; C.-H. Chen, Y.-Y. Keum and H.-n. Li, Phys. Rev. D **66**, 054013 (2002), [hep-ph/0204166].

[24] A. L. Kagan, Phys. Lett. B **601**, 151 (2004), [hep-ph/0405134]; Y. Grossman, Int. J. Mod. Phys. A **19**, 907 (2004), [hep-ph/0310229].

[25] B. Aubert *et al.* (BaBar), Phys. Rev. D **76**, 052007 (2007), [arXiv:0705.2157]; P. Vanhoefer *et al.* (Belle), Phys. Rev. D **93**, 3, 032010 (2016), [Erratum: Phys. Rev. D **94**, 099903 (2016)], [arXiv:1510.01245].

[26] J. Zhang *et al.* (Belle), Phys. Rev. Lett. **91**, 221801 (2003), [hep-ex/0306007]; B. Aubert *et al.* (BaBar), Phys. Rev. Lett. **102**, 141802 (2009), [arXiv:0901.3522].

[27] B. Aubert *et al.* (BaBar), Phys. Rev. D **74**, 051102 (2006), [hep-ex/0605017]; B. Aubert *et al.* (BaBar), Phys. Rev. D **79**, 052005 (2009), [arXiv:0901.3703].

[28] B. Aubert *et al.* (BaBar), Phys. Rev. D **78**, 071104 (2008), [arXiv:0807.4977].

[29] I. Adachi *et al.* (Belle), Phys. Rev. D **89**, 7, 072008 (2014), [Erratum: Phys. Rev. D **89**, 119903 (2014)], [arXiv:1212.4015].

[30] R. Aaij *et al.* (LHCb), Phys. Lett. B **747**, 468 (2015), [arXiv:1503.07770].

[31] B. Aubert *et al.* (BaBar), Phys. Rev. D **80**, 092007 (2009), [arXiv:0907.1776].

[32] K.-F. Chen *et al.* (Belle), Phys. Rev. Lett. **94**, 221804 (2005), [hep-ex/0503013].

[33] B. Aubert *et al.* (BaBar), Phys. Rev. Lett. **99**, 201802 (2007), [arXiv:0705.1798].

[34] A. L. Kagan, Phys. Lett. B **601**, 151 (2004), [hep-ph/0405134]; H.-n. Li and S. Mishima, Phys. Rev. D **71**, 054025 (2005), [hep-ph/0411146]; C.-H. Chen *et al.*, Phys. Rev. D **72**, 054011 (2005), [hep-ph/0507012]; M. Beneke, J. Rohrer and D. Yang, Phys. Rev. Lett. **96**, 141801 (2006), [hep-ph/0512258]; C.-H. Chen and C.-Q. Geng, Phys. Rev. D **75**, 054010 (2007), [hep-ph/0701023]; A. Datta *et al.*, Phys. Rev. D **76**, 034015 (2007), [arXiv:0705.3915]; M. Beneke, J. Rohrer and D. Yang, Nucl. Phys. B **774**, 64 (2007), [hep-ph/0612290]; H.-Y. Cheng and K.-C. Yang, Phys. Rev. D **78**, 094001 (2008), [Erratum: Phys. Rev. D **79**, 039903 (2009)], [arXiv:0805.0329].

[35] C. W. Bauer *et al.*, Phys. Rev. D **70**, 054015 (2004), [hep-ph/0401188]; P. Colangelo, F. De Fazio and T. Pham, Phys. Lett. B **597**, 291 (2004), [hep-ph/0406162]; M. Ladisa *et al.*, Phys. Rev. D **70**, 114025 (2004), [hep-ph/0409286]; H.-Y. Cheng, C.-K. Chua and A. Soni, Phys. Rev. D **71**, 014030

Downloaded from https://academic.oup.com/ptep/article/2022/8/083C01/6651666 by KIT Library user on 27 September 2022

(2005), [hep-ph/0409317]; H.-Y. Cheng and K.-C. Yang, Phys. Rev. D **83**, 034001 (2011), [arXiv:1010.3309].

[36] Y. Grossman, Int. J. Mod. Phys. A **19**, 907 (2004), [hep-ph/0310229]; E. Alvarez *et al.*, Phys. Rev. D **70**, 115014 (2004), [hep-ph/0410096]; P. K. Das and K.-C. Yang, Phys. Rev. D **71**, 094002 (2005), [hep-ph/0412313]; C.-H. Chen and C.-Q. Geng, Phys. Rev. D **71**, 115004 (2005), [hep-ph/0504145]; Y.-D. Yang, R.-M. Wang and G.-R. Lu, Phys. Rev. D **72**, 015009 (2005), [hep-ph/0411211]; K.-C. Yang, Phys. Rev. D **72**, 034009 (2005), [Erratum: Phys. Rev. D **72**, 059901 (2005)], [hep-ph/0506040]; S. Baek *et al.*, Phys. Rev. D **72**, 094008 (2005), [hep-ph/0508149]; C.-S. Huang *et al.*, Phys. Rev. D **73**, 034026 (2006), [hep-ph/0511129]; C.-H. Chen and H. Hatanaka, Phys. Rev. D **73**, 075003 (2006), [hep-ph/0602140]; A. Faessler *et al.*, Phys. Rev. D **75**, 074029 (2007), [hep-ph/0702020].

[37] D. London, N. Sinha and R. Sinha, Phys. Rev. D **69**, 114013 (2004), [hep-ph/0402214].

[38] B. Aubert *et al.* (BaBar), Phys. Rev. D **76**, 051103 (2007), [arXiv:0705.0398].

[39] B. Aubert *et al.* (BaBar), Phys. Rev. Lett. **101**, 161801 (2008), [arXiv:0806.4419].

[40] J. Zhang *et al.* (Belle), Phys. Rev. Lett. **95**, 141801 (2005), [hep-ex/0408102]; B. Aubert *et al.* (BaBar), Phys. Rev. Lett. **97**, 201801 (2006), [hep-ex/0607057]; P. del Amo Sanchez *et al.* (BaBar), Phys. Rev. D **83**, 051101 (2011), [arXiv:1012.4044]; J. Lees *et al.* (BaBar), Phys. Rev. D **85**, 072005 (2012), [arXiv:1112.3896].

[41] R. Aaij *et al.* (LHCb), JHEP **05**, 026 (2019), [arXiv:1812.07008].

[42] T. Aaltonen *et al.* (CDF), Phys. Rev. Lett. **107**, 261802 (2011), [arXiv:1107.4999].

[43] R. Aaij *et al.* (LHCb), Phys. Lett. B **713**, 369 (2012), [arXiv:1204.2813]; R. Aaij *et al.* (LHCb), Phys. Rev. D **90**, 5, 052011 (2014), [arXiv:1407.2222]; R. Aaij *et al.* (LHCb), JHEP **12**, 155 (2019), [arXiv:1907.10003].

[44] R. Aaij *et al.* (LHCb), Phys. Lett. B **709**, 50 (2012), [arXiv:1111.4183]; R. Aaij *et al.* (LHCb), JHEP **07**, 166 (2015), [arXiv:1503.05362]; R. Aaij *et al.* (LHCb), JHEP **07**, 032 (2019), [arXiv:1905.06662].

[45] R. Aaij *et al.* (LHCb), JHEP **11**, 092 (2013), [arXiv:1306.2239].

[46] B. Aubert *et al.* (BaBar), Phys. Rev. Lett. **100**, 081801 (2008), [arXiv:0708.2248]; B. Aubert *et al.* (BaBar), Phys. Rev. D **79**, 051102 (2009), [arXiv:0901.1223].

[47] G. Burdman, Phys. Rev. D **52**, 6400 (1995), [hep-ph/9505352]; F. Kruger and J. Matias, Phys. Rev. D **71**, 094009 (2005), [hep-ph/0502060]; E. Lunghi and J. Matias, JHEP **04**, 058 (2007), [hep-ph/0612166]; W. Altmannshofer *et al.*, JHEP **01**, 019 (2009), [arXiv:0811.1214]; J. Matias *et al.*, JHEP **04**, 104 (2012), [arXiv:1202.4266]; S. Descotes-Genon *et al.*, JHEP **01**, 048 (2013), [arXiv:1207.2753].

[48] B. Aubert *et al.* (BaBar), Phys. Rev. D **79**, 031102 (2009), [arXiv:0804.4412]; J. Lees *et al.* (BaBar), Phys. Rev. D **93**, 5, 052015 (2016), [arXiv:1508.07960].

[49] J.-T. Wei *et al.* (Belle), Phys. Rev. Lett. **103**, 171801 (2009), [arXiv:0904.0770]; S. Wehle *et al.* (Belle), Phys. Rev. Lett. **118**, 11, 111801 (2017), [arXiv:1612.05014]; A. Abdesselam *et al.* (Belle), Phys. Rev. Lett. **126**, 16, 161801 (2021), [arXiv:1904.02440].

[50] T. Aaltonen *et al.* (CDF), Phys. Rev. Lett. **108**, 081807 (2012), [arXiv:1108.0695].

[51] S. Chatrchyan *et al.* (CMS), Phys. Lett. B **727**, 77 (2013), [arXiv:1308.3409]; V. Khachatryan *et al.* (CMS), Phys. Lett. B **753**, 424 (2016), [arXiv:1507.08126]; A. M. Sirunyan *et al.* (CMS), Phys. Lett. B **781**, 517 (2018), [arXiv:1710.02846]; A. M. Sirunyan *et al.* (CMS), JHEP **04**, 124 (2021), [arXiv:2010.13968].

[52] R. Aaij *et al.* (LHCb), JHEP **08**, 131 (2013), [arXiv:1304.6325]; R. Aaij *et al.* (LHCb), JHEP **04**, 064 (2015), [arXiv:1501.03038]; R. Aaij *et al.* (LHCb), JHEP **02**, 104 (2016), [arXiv:1512.04442]; R. Aaij *et al.* (LHCb), JHEP **11**, 047 (2016), [Erratum: JHEP **04**, 142 (2017)], [arXiv:1606.04731]; R. Aaij *et al.* (LHCb), JHEP **12**, 065 (2016), [arXiv:1609.04736]; R. Aaij *et al.* (LHCb), JHEP **08**, 055 (2017), [arXiv:1705.05802]; R. Aaij *et al.* (LHCb), Phys. Rev. Lett. **125**, 1, 011802 (2020), [arXiv:2003.04831]; R. Aaij *et al.* (LHCb), Phys. Rev. Lett. **126**, 16, 161802 (2021), [arXiv:2012.13241].

[53] R. Aaij *et al.* (LHCb), JHEP **09**, 179 (2015), [arXiv:1506.08777]; R. Aaij *et al.* (LHCb) (2021), [arXiv:2107.13428].

[54] C.-H. Chen and H.-N. Li, Phys. Rev. D **71**, 114008 (2005), [hep-ph/0504020].

Downloaded from https://academic.oup.com/ptep/article/2022/8/083C01/6651666 by KIT Library user on 27 September 2022

75. B^0–$\overline{B}^0$ Mixing

Revised March 2022 by O. Schneider (EPFL).

There are two neutral B^0–$\overline{B}^0$ meson systems, B^0_d–$\overline{B}^0_d$ and B^0_s–$\overline{B}^0_s$ (generically denoted B^0_q–$\overline{B}^0_q$, $q = s, d$), which exhibit particle-antiparticle mixing [1]. This mixing phenomenon is described in Ref. [2]. In the following, we adopt the notation introduced in Ref. [2], and assume CPT conservation throughout. In each system, the light (L) and heavy (H) mass eigenstates,

$$|B_{\mathrm{L,H}}\rangle = p|B^0_q\rangle \pm q|\overline{B}^0_q\rangle, \tag{75.1}$$

have a mass difference $\Delta m_q = m_{\mathrm{H}} - m_{\mathrm{L}} > 0$, a total decay width difference $\Delta\Gamma_q = \Gamma_{\mathrm{L}} - \Gamma_{\mathrm{H}}$ and an average decay width $\Gamma_q = (\Gamma_{\mathrm{L}} + \Gamma_{\mathrm{H}})/2$. In the absence of CP violation in the mixing, $|q/p| = 1$, the differences are given by $\Delta m_q = 2|M_{12}|$ and $|\Delta\Gamma_q| = 2|\Gamma_{12}|$, where M_{12} and Γ_{12} are the off-diagonal elements of the mass and decay matrices [2]. The evolution of a pure $|B^0_q\rangle$ or $|\overline{B}^0_q\rangle$ state at $t = 0$ is given by

$$|B^0_q(t)\rangle = g_+(t)\,|B^0_q\rangle + \frac{q}{p}\,g_-(t)\,|\overline{B}^0_q\rangle, \tag{75.2}$$

$$|\overline{B}^0_q(t)\rangle = g_+(t)\,|\overline{B}^0_q\rangle + \frac{p}{q}\,g_-(t)\,|B^0_q\rangle, \tag{75.3}$$

which means that the flavor states remain unchanged (+) or oscillate into each other (−) with time-dependent probabilities proportional to

$$|g_\pm(t)|^2 = \frac{e^{-\Gamma_q t}}{2}\left[\cosh\left(\frac{\Delta\Gamma_q}{2}\,t\right) \pm \cos(\Delta m_q\, t)\right]. \tag{75.4}$$

In the absence of CP violation, the time-integrated mixing probability $\int |g_-(t)|^2\,dt/(\int |g_-(t)|^2\,dt + \int |g_+(t)|^2\,dt)$ is given by

$$\chi_q = \frac{x_q^2 + y_q^2}{2(x_q^2+1)}\,, \quad \text{where} \quad x_q = \frac{\Delta m_q}{\Gamma_q}\,, \quad y_q = \frac{\Delta\Gamma_q}{2\Gamma_q}\,. \tag{75.5}$$

75.1 Standard Model predictions and phenomenology

In the Standard Model, the transitions $B^0_q \to \overline{B}^0_q$ and $\overline{B}^0_q \to B^0_q$ are due to the weak interaction. They are described, at the lowest order, by box diagrams involving two W bosons and two up-type quarks (see Fig. 75.1), as is the case for $K^0 - \overline{K}^0$ mixing. However, the long range interactions arising from intermediate virtual states are negligible for the neutral B meson systems, because the large B mass is off the region of hadronic resonances. The calculation of the dispersive and absorptive parts of the box diagrams yields the following predictions for the off-diagonal element of the mass and decay matrices [3],

$$M_{12} = -\frac{G_F^2 m_W^2 \eta_B m_{B_q} B_{B_q} f_{B_q}^2}{12\pi^2}\, S_0(m_t^2/m_W^2)\,(V^*_{tq}V_{tb})^2\,, \tag{75.6}$$

$$\Gamma_{12} = \frac{G_F^2 m_b^2 \eta'_B m_{B_q} B_{B_q} f_{B_q}^2}{8\pi} \times \left[(V^*_{tq}V_{tb})^2 + V^*_{tq}V_{tb}V^*_{cq}V_{cb}\,\mathcal{O}\left(\frac{m_c^2}{m_b^2}\right) + (V^*_{cq}V_{cb})^2\,\mathcal{O}\left(\frac{m_c^4}{m_b^4}\right)\right], \tag{75.7}$$

where G_F is the Fermi constant, m_W the W boson mass, and m_i the mass of quark i; m_{B_q}, f_{B_q} and B_{B_q} are the B^0_q mass, weak decay constant and bag parameter, respectively. The known function $S_0(x_t)$ can be approximated very well by $0.784\,x_t^{0.76}$ [4], and V_{ij} are the elements of the CKM matrix [5]. The QCD corrections η_B and η'_B are of order unity. The only non-negligible contributions to M_{12} are from box diagrams involving two top quarks. The phases of M_{12} and Γ_{12} satisfy

$$\phi_M - \phi_\Gamma = \pi + \mathcal{O}\left(\frac{m_c^2}{m_b^2}\right), \tag{75.8}$$

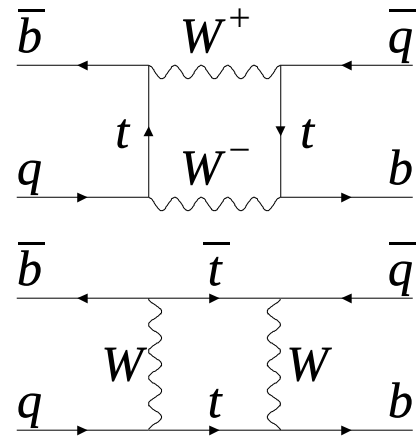

Figure 75.1: Dominant box diagrams for the $B^0_q \to \overline{B_q}^0$ transitions ($q = d$ or s). Similar diagrams exist where one or both t quarks are replaced with c or u quarks.

implying that the mass eigenstates have mass and width differences of opposite signs. This means that, like in the K^0–$\overline{K}^0$ system, the heavy state is expected to have a smaller decay width than that of the light state: $\Gamma_{\mathrm{H}} < \Gamma_{\mathrm{L}}$. Hence, $\Delta\Gamma_q = \Gamma_{\mathrm{L}} - \Gamma_{\mathrm{H}}$ is expected to be positive in the Standard Model.

Furthermore, the quantity

$$\left|\frac{\Gamma_{12}}{M_{12}}\right| \simeq \frac{3\pi}{2}\,\frac{m_b^2}{m_W^2}\,\frac{1}{S_0(m_t^2/m_W^2)} \sim \mathcal{O}\left(\frac{m_b^2}{m_t^2}\right) \tag{75.9}$$

is small, and a power expansion of $|q/p|^2$ yields

$$\left|\frac{q}{p}\right|^2 = 1 + \left|\frac{\Gamma_{12}}{M_{12}}\right| \sin(\phi_M - \phi_\Gamma) + \mathcal{O}\left(\left|\frac{\Gamma_{12}}{M_{12}}\right|^2\right). \tag{75.10}$$

Therefore, considering both Eqs. (75.8) and (75.9), the CP-violating parameter

$$1 - \left|\frac{q}{p}\right|^2 \simeq \mathrm{Im}\left(\frac{\Gamma_{12}}{M_{12}}\right) \tag{75.11}$$

is expected to be very small: $\sim \mathcal{O}(10^{-3})$ for the B^0_d–$\overline{B}^0_d$ system and $\lesssim \mathcal{O}(10^{-4})$ for the B^0_s–$\overline{B}^0_s$ system [6].

In the approximation of negligible CP violation in mixing, the ratio $\Delta\Gamma_q/\Delta m_q$ is equal to the small quantity $|\Gamma_{12}/M_{12}|$ of Eq. (75.9); it is hence independent of CKM matrix elements, *i.e.*, the same for the B^0_d–$\overline{B}^0_d$ and B^0_s–$\overline{B}^0_s$ systems. Calculations [7] yield $\sim 5 \times 10^{-3}$ with a $\sim 20\%$ uncertainty. Given the published experimental knowledge [8] on the mixing parameter x_q

$$\begin{cases} x_d = 0.769 \pm 0.004 & (B^0_d\text{–}\overline{B}^0_d \text{ system}) \\ x_s = 27.01 \pm 0.10 & (B^0_s\text{–}\overline{B}^0_s \text{ system}) \end{cases}, \tag{75.12}$$

the Standard Model thus predicts that $\Delta\Gamma_d/\Gamma_d$ is very small (below 1%), but $\Delta\Gamma_s/\Gamma_s$ considerably larger ($\sim 10\%$). These width differences are caused by the existence of final states to which both the B^0_q and $\overline{B}^0_q$ mesons can decay. Such decays involve $b \to c\overline{c}q$ quark-level transitions, which are Cabibbo-suppressed if $q = d$ and Cabibbo-allowed if $q = s$.

A complete set of Standard Model predictions for all mixing parameters in both the B^0_d–$\overline{B}^0_d$ and B^0_s–$\overline{B}^0_s$ systems can be found in Refs. [9–11].

75.2 Experimental issues and methods for oscillation analyses

Time-integrated measurements of B^0–$\overline{B}^0$ mixing were published for the first time in 1987 by UA1 [12] and ARGUS [13], and

Downloaded from https://academic.oup.com/ptep/article/2022/8/083C01/6651666 by KIT Library user on 27 September 2022

since then by many other experiments. These measurements are typically based on counting same-sign and opposite-sign lepton pairs from the semileptonic decay of the produced $b\bar{b}$ pairs. Such analyses cannot easily separate the contributions from the different b-hadron species, therefore, the clean environment of $\Upsilon(4S)$ machines (where only B_d^0 and charged B_u mesons are produced) is in principle best suited to measure χ_d.

However, better sensitivity is obtained from time-dependent analyses aiming at the direct measurement of the oscillation frequencies Δm_d and Δm_s, from the proper time distributions of B_d^0 or B_s^0 candidates identified through their decay in (mostly) flavor-specific modes, and suitably tagged as mixed or unmixed. This is particularly true for the B_s^0–$\overline{B}_s^0$ system, where the large value of x_s implies maximal mixing, *i.e.*, $\chi_s \simeq 1/2$. In such analyses, the B_d^0 or B_s^0 mesons are either fully reconstructed, partially reconstructed from a charm meson, selected from a lepton with the characteristics of a $b \to \ell^-$ decay, or selected from a reconstructed displaced vertex. At high-energy colliders (LEP, SLC, Tevatron, LHC), the proper time $t = \frac{m_B}{p} L$ is measured from the distance L between the production vertex and the B decay vertex, and from an estimate of the B momentum p. At asymmetric B factories (KEKB, PEP-II), producing $e^+e^- \to \Upsilon(4S) \to B_d^0\, \overline{B_d}^0$ events with a boost $\beta\gamma$ (= 0.425, 0.55), the proper time difference between the two B candidates is estimated as $\Delta t \simeq \frac{\Delta z}{\beta\gamma c}$, where Δz is the spatial separation between the two B decay vertices along the boost direction. In all cases, the good resolution needed on the vertex positions is obtained with silicon detectors.

The average statistical significance $\mathcal{S}$ of a B_q^0 oscillation signal can be approximated as [14]

$$\mathcal{S} \approx \sqrt{N/2}\, f_{\rm sig}\, (1-2\eta)\, e^{-(\Delta m_q\, \sigma_t)^2/2}\,, \qquad (75.13)$$

where N is the number of selected and tagged candidates, $f_{\rm sig}$ is the fraction of signal in that sample, η is the total mistag probability, and σ_t is the resolution on proper time (or proper time difference). The quantity $\mathcal{S}$ decreases very quickly as Δm_q increases; this dependence is controlled by σ_t, which is therefore a critical parameter for Δm_s analyses. At high-energy colliders, the proper time resolution $\sigma_t \sim \frac{m_B}{\langle p \rangle}\sigma_L \oplus t\frac{\sigma_p}{p}$ includes a constant contribution due to the decay length resolution σ_L (typically 0.04–0.3 ps), and a term due to the relative momentum resolution σ_p/p (typically 10–20% for partially reconstructed decays), which increases with proper time. At B factories, the boost of the B mesons is estimated from the known beam energies, and the term due to the spatial resolution dominates (typically 1–1.5 ps because of the much smaller B boost).

In order to tag a B_q^0 candidate as mixed or unmixed, it is necessary to determine its flavor both in the initial state and in the final state. The initial and final state mistag probabilities, η_i and η_f, degrade $\mathcal{S}$ by a total factor $(1-2\eta) = (1-2\eta_i)(1-2\eta_f)$. In lepton-based analyses, the final state is tagged by the charge of the lepton from $b \to \ell^-$ decays; the largest contribution to η_f is then due to $\bar{b} \to \bar{c} \to \ell^-$ decays. Alternatively, the charge of a reconstructed charm meson (D^{*-} from B_d^0 or D_s^- from B_s^0), or that of a kaon hypothesized to come from a $b \to c \to s$ decay [15], can be used. For fully-inclusive analyses based on topological vertexing, final-state tagging techniques include jet-charge [16] and charge-dipole [17, 18] methods. At high-energy colliders, the methods to tag the initial state (*i.e.*, the state at production), can be divided into two groups: the ones that tag the initial charge of the $\bar{b}$ quark contained in the B_q^0 candidate itself (same-side tag), and the ones that tag the initial charge of the other b quark produced in the event (opposite-side tag). On the same side, the sign of a charged pion, kaon or proton from the primary vertex is correlated with the production state of the B_q^0 meson if that particle is a decay product of a B^{**} state or the first in the fragmentation chain [19, 20]. Jet- and vertex-charge techniques work on both sides and on the opposite side, respectively. Finally, the charge of a lepton from $b \to \ell^-$, of a kaon from $b \to c \to s$ or of a charm hadron from $b \to c$ [21] can be used as an opposite-side tag, keeping in mind that its performance is degraded due to integrated mixing. At SLC, the beam polarization produced a sizeable forward-backward asymmetry in the $Z \to b\bar{b}$ decays, and provided another very interesting and effective initial state tag based on the polar angle of the B_q^0 candidate [17]. Initial state tags have also been combined to reach $\eta_i \sim 26\%$ at LEP [20, 22] or 22% at SLD [17] with full efficiency. In the case $\eta_f = 0$, this corresponds to an effective tagging efficiency $Q = \epsilon D^2 = \epsilon(1-2\eta)^2$, where ϵ is the tagging efficiency, in the range $23-31\%$. The equivalent figure achieved by CDF during Tevatron Run I was $\sim 3.5\%$ (see tagging summary on page 160 of Ref. [23]), reflecting the fact that tagging is more difficult at hadron colliders. The CDF and DØ analyses of Tevatron Run II data reached $\epsilon D^2 = (1.8 \pm 0.1)\%$ [24] and $(2.5 \pm 0.2)\%$ [25] for opposite-side tagging, while same-side kaon tagging (for B_s^0 analyses) contributed an additional $3.7-4.8\%$ at CDF [24], and pushed the combined performance to $(4.7 \pm 0.5)\%$ at DØ [26]. LHCb, operating in the forward region at the LHC where the environment is different in terms of track multiplicity and b-hadron production kinematics, has reported $\epsilon D^2 = (2.10 \pm 0.25)\%$ [27] for opposite-side tagging, $(1.80 \pm 0.26)\%$ [28] for same-side kaon tagging, and $(2.11 \pm 0.11)\%$ [29] for same-side pion and proton tagging: the combined figure ranges typically between $(3.73 \pm 0.15)\%$ [30] and $(5.33 \pm 0.25)\%$ [31] depending on the mode in which the tagged B_s^0 meson is reconstructed, and reaches up to $(8.1 \pm 0.6)\%$ [32] for hadronic B_d^0 modes. CMS has recently reported $\epsilon D^2 \sim 10\%$ using opposite-side muon tagging of $B_s^0 \to J/\psi\phi$ decays [33].

At B factories, the flavor of a B_d^0 meson at production cannot be determined, since the two neutral B mesons produced in a $\Upsilon(4S)$ decay evolve in a coherent P-wave state where they keep opposite flavors at any time. However, as soon as one of them decays, the other follows a time-evolution given by Eqs. (75.2) or (75.3), where t is replaced with Δt (which will take negative values half of the time). Hence, the "initial state" tag of a B can be taken as the final-state tag of the other B. Effective tagging efficiencies of 30% are achieved by BaBar and Belle [34], using different techniques including $b \to \ell^-$ and $b \to c \to s$ tags. It is worth noting that, in this case, mixing of the other B (*i.e.*, the coherent mixing occurring before the first B decay) does not contribute to the mistag probability.

Before the experimental observation of a decay-width difference, oscillation analyses typically neglected $\Delta\Gamma_q$ in Eq. (75.4), and described the time dependence with the functions $\Gamma_q e^{-\Gamma_q t}(1 \pm \cos(\Delta m_q t))/2$ (high-energy colliders) or $\Gamma_d e^{-\Gamma_d|\Delta t|}(1 \pm \cos(\Delta m_d \Delta t))/4$ (asymmetric $\Upsilon(4S)$ machines). As can be seen from Eq. (75.4), a non-zero value of $\Delta\Gamma_q$ would effectively reduce the oscillation amplitude with a small time-dependent factor that would be very difficult to distinguish from time resolution effects. Measurements of Δm_q are usually extracted from the data using a maximum likelihood fit.

75.3 Δm_d and $\Delta\Gamma_d$ measurements

Many B_d^0–$\overline{B}_d^0$ oscillations analyses have been published [35] by the ALEPH [36], DELPHI [18, 37], L3 [38], OPAL [39, 40], BaBar [41], Belle [42], CDF [19], DØ [25], and LHCb [43–46] collaborations. Although a variety of different techniques have been used, the individual Δm_d results obtained at LEP and Tevatron have remarkably similar precision. Their average is compatible with the more precise measurements at the asymmetric B factories and the LHC. The systematic uncertainties are not negligible; they are often dominated by sample composition, mistag probability, or b-hadron lifetime contributions. Before being combined, the measurements are adjusted on the basis of a common set of input values, including the b-hadron lifetimes and fractions published in this *Review*. Some measurements are statistically correlated. Systematic correlations arise both from common physics sources (fragmentation fractions, lifetimes, branching ratios of b hadrons), and from purely experimental or algorithmic effects (efficiency, resolution, tagging, background description). Combining all measurements [18, 19, 25, 36–46] and accounting for all identified correlations yields $\Delta m_d = 0.5065 \pm 0.0016(\text{stat}) \pm 0.0011(\text{syst})\ \text{ps}^{-1}$ [8], a result dominated by the latest LHCb measurement with $B^0 \to D^{(*)-}\mu^+\nu_\mu X$ decays [46].

On the other hand, ARGUS and CLEO have published time-integrated measurements [47–49], which average to $\chi_d = 0.182 \pm 0.015$. Following Ref. [49], the width difference $\Delta\Gamma_d$ could in

Downloaded from https://academic.oup.com/ptep/article/2022/8/083C01/6651666 by KIT Library user on 27 September 2022

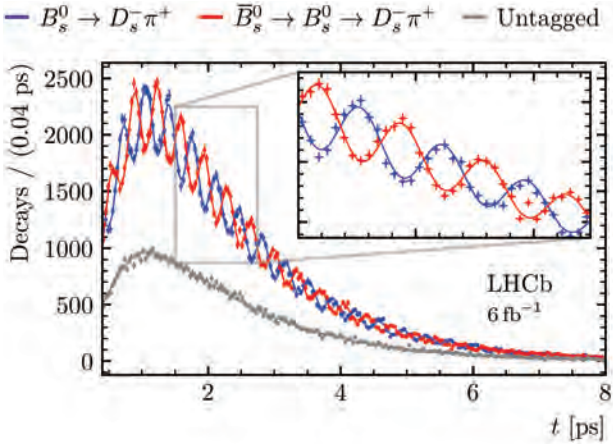

Figure 75.2: Proper time distribution of $B_s^0 \to D_s^- \pi^+$ candidates tagged as unmixed (blue), tagged as mixed (red) or untagged (grey) in the LHCb experiment, displaying B_s^0–$\overline{B}_s^0$ oscillations (from Ref. [59]).

principle be extracted from the measured value of $1/\Gamma_d$ and the above averages for Δm_d and χ_d (see Eq. (75.5)), provided that $\Delta\Gamma_d$ has a negligible impact on the Δm_d and $1/\Gamma_d$ analyses that have assumed $\Delta\Gamma_d = 0$. However, $\Delta\Gamma_d/\Gamma_d$ is too small and the knowledge of χ_d too imprecise to provide useful sensitivity on $\Delta\Gamma_d/\Gamma_d$. Direct time-dependent studies published by DELPHI [18], BaBar [50], Belle [51], LHCb [52], ATLAS [53] and CMS [54] provide stronger constraints, which can be combined to yield [8]

$$\Delta\Gamma_d/\Gamma_d = +0.001 \pm 0.010\,. \tag{75.14}$$

This determination is compatible both with zero and with the Standard Model prediction of $(3.97 \pm 0.90) \times 10^{-3}$ [11].

Assuming $\Delta\Gamma_d = 0$ and no CP violation in mixing, and using the B_d^0 lifetime average of 1.519 ± 0.004 ps [8], the Δm_d and χ_d results are combined to yield the world average

$$\Delta m_d = 0.5065 \pm 0.0019 \text{ ps}^{-1} \tag{75.15}$$

or, equivalently,

$$\chi_d = 0.1858 \pm 0.0011\,. \tag{75.16}$$

This Δm_d value provides an estimate of $2|M_{12}|$, and can be used with Eq. (75.6) to extract $|V_{td}|$ within the Standard Model [55]. The main experimental uncertainties on the result come from m_t and Δm_d, but are still completely negligible with respect to the uncertainty due to the hadronic matrix element $f_{B_d}\sqrt{B_{B_d}} = 225 \pm 9$ MeV [56] obtained from three-flavor lattice QCD calculations.

75.4 Δm_s and $\Delta\Gamma_s$ measurements

After many years of intense search at LEP and SLC, B_s^0–$\overline{B}_s^0$ oscillations were first observed in 2006 by CDF using 1 fb^{-1} of Tevatron Run II data [24]. LHCb then observed B_s^0–$\overline{B}_s^0$ oscillations independently with $B_s^0 \to D_s^- \pi^+$ [43, 57], $B_s^0 \to D_s^- \mu^+ \nu X$ [45] and $B_s^0 \to J/\psi K^+ K^-$ [30] decays, using between 1 and 4.9 fb^{-1} of data collected at the LHC until 2016. More recently measurements based on the full LHC Run 2 data have been published by CMS with $B_s^0 \to J/\psi\phi$ decays [33], and by LHCb with $B_s^0 \to D_s^- \pi^+ \pi^- \pi^+$ [58] and $B_s^0 \to D_s^- \pi^+$ [59] decays. Taking systematic correlations into account, the average [8] of all published measurements of Δm_s [24, 30, 33, 43, 45, 57–59] is

$$\Delta m_s = 17.765 \pm 0.004(\text{stat}) \pm 0.004(\text{syst}) \text{ ps}^{-1}\,, \tag{75.17}$$

with an impressive precision dominated by the most recent LHCb result (see Fig. 75.2).

The information on $|V_{ts}|$ obtained in the framework of the Standard Model is hampered by the hadronic uncertainty, as in the B_d^0 case. However, several uncertainties cancel in the frequency ratio

$$\frac{\Delta m_s}{\Delta m_d} = \frac{m_{B_s}}{m_{B_d}}\,\xi^2 \left|\frac{V_{ts}}{V_{td}}\right|^2\,, \tag{75.18}$$

where the SU(3) flavor-symmetry breaking factor $\xi = (f_{B_s}\sqrt{B_{B_s}})/(f_{B_d}\sqrt{B_{B_d}})$ is obtained as 1.206 ± 0.017 from a combination of three-flavor lattice QCD calculations [56] dominated by the results of Ref. [60], or as $1.2014^{+0.0065}_{-0.0072}$ from QCD sum rules [61]. Using the measurements of Eqs. (75.15) and (75.17), one can extract

$$\left|\frac{V_{td}}{V_{ts}}\right| = \begin{cases} 0.2053 \pm 0.0004 \pm 0.0029 \text{ (lattice QCD)} \\ 0.2045 \pm 0.0004^{+0.0011}_{-0.0012} \text{ (QCD sum rules)} \end{cases}\,, \tag{75.19}$$

in good agreement with (but much more precise than) the value obtained from the ratio of the $b \to d\gamma$ and $b \to s\gamma$ transition rates observed at the B factories [55].

The CKM matrix can be constrained using experimental results on observables such as Δm_d, Δm_s, $|V_{ub}/V_{cb}|$, ϵ_K, and $\sin(2\beta)$ together with theoretical inputs and unitarity conditions [55,62,63]. The constraint from our knowledge on the ratio $\Delta m_s/\Delta m_d$ is more effective in limiting the position of the apex of the CKM unitarity triangle than the one obtained from the Δm_d measurements alone, due to the reduced hadronic uncertainty in Eq. (75.18). We also note that the measured value of Δm_s is consistent with the Standard Model prediction obtained from CKM fits where no experimental information on Δm_s is used, *e.g.*, 17.25 ± 0.85 ps^{-1} [62] or $16.54^{+0.50}_{-0.30}$ ps^{-1} [63].

Information on $\Delta\Gamma_s$ can be obtained from the study of the proper time distribution of untagged B_s^0 samples [64]. In the case of an inclusive B_s^0 selection [65], or a flavor-specific (semileptonic or hadronic) B_s^0 decay selection [22, 66–68], both the short- and long-lived components are present, and the proper time distribution is a superposition of two exponentials with decay constants $\Gamma_{\rm L,H} = \Gamma_s \pm \Delta\Gamma_s/2$. In principle, this provides sensitivity to both Γ_s and $(\Delta\Gamma_s/\Gamma_s)^2$. Ignoring $\Delta\Gamma_s$ and fitting for a single exponential leads to an estimate of $1/\Gamma_s$ (called effective lifetime) with a relative bias proportional to $(\Delta\Gamma_s/\Gamma_s)^2$. An alternative approach, sensitive to first order in $\Delta\Gamma_s/\Gamma_s$, is to determine the effective lifetime of untagged B_s^0 decays to pure CP eigenstates; measurements exist for $B_s^0 \to D_s^+ D_s^-$ [67], $B_s^0 \to K^+K^-$ [68,69], $B_s^0 \to J/\psi\eta$ [70], $B_s^0 \to J/\psi f_0(980)$ [71], $B_s^0 \to J/\psi\pi^+\pi^-$ [54,72,73], $B_s^0 \to J/\psi K_S^0$ [74], and $B_s^0 \to \mu^+\mu^-$ [75]. The extraction of $1/\Gamma_s$ and $\Delta\Gamma_s$ from such measurements, discussed in detail in Ref. [76], requires additional information in the form of theoretical assumptions or external inputs on weak phases and hadronic parameters. In what follows, we only use the effective lifetimes of decays to CP-even ($D_s^+ D_s^-$, $J/\psi\eta$) and CP-odd ($J/\psi f_0(980)$, $J/\psi\pi^+\pi^-$) final states where CP conservation can be assumed.

The best sensitivity to $1/\Gamma_s$ and $\Delta\Gamma_s$ is achieved by the time-dependent measurements of the $B_s^0 \to J/\psi K^+K^-$ (including $B_s^0 \to J/\psi\phi$) and $B_s^0 \to \psi(2S)\phi$ decay rates performed at CDF [77], DØ [78], ATLAS [79], CMS [33, 80] and LHCb [30, 81–83], where the CP-even and CP-odd amplitudes are separated statistically through a full angular analysis. The LHCb collaboration analyzes the $B_s^0 \to J/\psi K^+K^-$ decay considering that the K^+K^- system can be in a P-wave or S-wave state, and measures the dependence of the strong phase difference between the P-wave and S-wave amplitudes as a function of the K^+K^- invariant mass [30, 84]; this allows the unambiguous determination of the sign of $\Delta\Gamma_s$, which is found to be positive. All these studies use both untagged and tagged B_s^0 candidates and are optimized for the measurement of the phase $\phi_s^{c\bar{c}s}$ that describes CP violation in the interference between B_s^0–$\overline{B}_s^0$ mixing and decay in $b \to c\bar{c}s$ transitions. The published $B_s^0 \to J/\psi K^+K^-$, $J/\psi\phi$ and $\psi(2S)\phi$ analyses [30, 33, 77–83] are combined in a multi-dimensional fit including all measured parameters and their correlations. To account for a tension in the time and angular parameters, scale factors are applied on the combined uncertainty of each parameter where a discrepancy arise. For example, the scale factors on the uncertainties of $\Delta\Gamma_s$, Γ_s and $\phi_s^{c\bar{c}s}$ are 1.72, 2.56 and 1.00, respectively. The averages are then further refined by applying

Downloaded from https://academic.oup.com/ptep/article/2022/8/083C01/6651666 by KIT Library user on 27 September 2022

Table 75.1: $\overline{\chi}$ and b-hadron fractions (see text).

	Z decays [96]	Tevatron [96]	LHC ($\sqrt{s}$) [97,98]
$\overline{\chi}$	0.1259 ± 0.0042	0.147 ± 0.011	
$f_u = f_d$	0.408 ± 0.007	0.344 ± 0.021	
f_s	0.100 ± 0.008	0.115 ± 0.013	
$f_{\rm baryon}$	0.084 ± 0.011	0.198 ± 0.046	
f_s/f_d	0.246 ± 0.023	0.333 ± 0.040	0.239 ± 0.007 (7 TeV)
			0.239 ± 0.008 (8 TeV)
			0.254 ± 0.008 (13 TeV)

constraints from the effective lifetime measurements with flavor-specific [22,66–68] and pure CP [54,67,70–73] final states, to yield

$$\Delta\Gamma_s = +0.084 \pm 0.005 \text{ ps}^{-1} \text{ and } 1/\Gamma_s = 1.520 \pm 0.005 \text{ ps}\,, \quad (75.20)$$

or, equivalently,

$$1/\Gamma_{\rm L} = 1.429 \pm 0.007 \text{ ps} \quad \text{and} \quad 1/\Gamma_{\rm H} = 1.624 \pm 0.009 \text{ ps}\,, \quad (75.21)$$

in good agreement with the Standard Model prediction $\Delta\Gamma_s = +0.091 \pm 0.013$ ps^{-1} [9].

Estimates of $\Delta\Gamma_s/\Gamma_s$ obtained from measurements of the $B_s^0 \to D_s^{(*)+} D_s^{(*)-}$ branching fractions are not included in the average, since they are based on the questionable [7] assumption that these decays account for all CP-even final states.

75.5 Average b-hadron mixing probability and b-hadron production fractions at high energy

Mixing measurements can significantly improve our knowledge on the fractions f_u, f_d, f_s, and $f_{\rm baryon}$, defined as the fractions of B_u, B_d^0, B_s^0, and b-baryons in an unbiased sample of weakly-decaying b hadrons produced in high-energy collisions. Indeed, time-integrated mixing analyses using lepton pairs from $b\overline{b}$ events at high energy measure the quantity

$$\overline{\chi} = f'_d\,\chi_d + f'_s\,\chi_s\,, \quad (75.22)$$

where f'_q ($q = s, d$) is the B_q^0 fraction in a sample of semileptonic b-hadron decays. Assuming that all b hadrons have the same semileptonic decay width implies $f'_q = f_q/(\Gamma_q \tau_b)$, where τ_b is the average b-hadron lifetime. Hence $\overline{\chi}$ measurements performed at LEP [85] and Tevatron [86,87], together with χ_d given in Eq. (75.16) and the very good approximation $\chi_s = 1/2$ (in fact $\chi_s = 0.499312 \pm 0.000004$ from Eqs. (75.5), (75.17) and (75.20)), provide constraints on f_d and f_s.

The LEP experiments have measured $\mathcal{B}(\overline{b} \to B_s^0) \times \mathcal{B}(B_s^0 \to D_s^- \ell^+ \nu_\ell X)$ [88], $\mathcal{B}(b \to \Lambda_b^0) \times \mathcal{B}(\Lambda_b^0 \to \Lambda_c^+ \ell^- \overline{\nu}_\ell X)$ [89], and $\mathcal{B}(b \to \Xi_b^-) \times \mathcal{B}(\Xi_b^- \to \Xi^- \ell^- \overline{\nu}_\ell X)$ [90] from partially reconstructed final states including a lepton, $f_{\rm baryon}$ from protons identified in b events [91], and the production rate of charged b hadrons [92]. The b-hadron fraction ratios measured at CDF are based on double semileptonic $K^*\mu\mu$ and $\phi\mu\mu$ final states [93] and lepton-charm final states [94]; in addition CDF and DØ have both measured strange b-baryon production [95]. A combination of the available information from LEP and Tevatron yields, under the constraints $f_u = f_d$, $f_u + f_d + f_s + f_{\rm baryon} = 1$ and Eq. (75.22), the averages of the first two columns of Table 75.1.

Fraction ratios have been studied by LHCb using fully reconstructed hadronic B_s^0 and B_d^0 decays as well as semileptonic decays of Λ_b^0, B_s^0, B_d^0 and B_u (see [97] and references therein). ATLAS has measured f_s/f_d using $B_s^0 \to J/\psi\phi$ and $B^0 \to J/\psi K^{*0}$ decays [98]. Both CDF and LHCb observe that the ratio $f_{\Lambda_b^0}/(f_u + f_d)$ decreases with the transverse momentum of the lepton+charm system, indicating that the b-hadron fractions are not the same in different environments. LHCb also observes that $f_s/(f_u + f_d)$ decreases with transverse momentum. The third column of Table 75.1 displays the LHC measurements of $f_s/f_u = f_s/f_d$, which increase slowly with centre-of-mass energy. The B_c^+ fraction has been measured for the first time by LHCb to be (0.26±0.06)% [99].

75.6 CP-violation studies

Evidence for CP violation in B_q^0–$\overline{B}_q^0$ mixing has been searched for, both with flavor-specific and inclusive B_q^0 decays, in samples where the initial flavor state is tagged, usually with a lepton from the other b-hadron in the event. In the case of semileptonic (or other flavor-specific) decays, where the final-state tag is also available, the following asymmetry [2]

$$\mathcal{A}^q_{\rm SL} = \frac{N(\overline{B}_q^0(t) \to \ell^+\nu_\ell X) - N(B_q^0(t) \to \ell^-\overline{\nu}_\ell X)}{N(\overline{B}_q^0(t) \to \ell^+\nu_\ell X) + N(B_q^0(t) \to \ell^-\overline{\nu}_\ell X)} \simeq 1 - |q/p|_q^2 \quad (75.23)$$

has been measured either in time-integrated analyses at CLEO [49,100], BaBar [101], CDF [102], DØ [103–105] and LHCb [106], or in time-dependent analyses at LEP [40,107], BaBar [50,108] and Belle [109]. In the inclusive case, also investigated at LEP [107,110], no final-state tag is used, and the asymmetry [111]

$$\frac{N(\overline{B}_q^0(t) \to \text{all}) - N(B_q^0(t) \to \text{all})}{N(\overline{B}_q^0(t) \to \text{all}) + N(B_q^0(t) \to \text{all})} \simeq \mathcal{A}^q_{\rm SL}\left[\sin^2\left(\frac{\Delta m_q\, t}{2}\right) - \frac{x_q}{2}\sin(\Delta m_q\, t)\right] \quad (75.24)$$

must be measured as a function of the proper time to extract information on CP violation. In addition LHCb has studied the time dependence of the charge asymmetry of $B^0 \to D^{(*)-}\mu^+\nu_\mu X$ decays without tagging the initial state [112], which would be equal to

$$\frac{N(D^{(*)-}\mu^+\nu_\mu X) - N(D^{(*)+}\mu^-\bar{\nu}_\mu X)}{N(D^{(*)-}\mu^+\nu_\mu X) + N(D^{(*)+}\mu^-\bar{\nu}_\mu X)} = \mathcal{A}^d_{\rm SL}\,\frac{1 - \cos(\Delta m_d\, t)}{2} \quad (75.25)$$

in absence of detection and production asymmetries.

The DØ collaboration measured a like-sign dimuon charge asymmetry in semileptonic b decays that deviates by $2.8\,\sigma$ from the tiny Standard Model prediction and concluded, from a more refined analysis in bins of muon impact parameters, that the overall discrepancy is at the level of $3.6\,\sigma$ [103]. In all other cases, asymmetries compatible with zero (and the Standard Model [10,11]) have been found, with a precision limited by the available statistics. Several of the analyses at high energy don't disentangle the B_d^0 and B_s^0 contributions, and either quote a mean asymmetry or a measurement of $\mathcal{A}^d_{\rm SL}$ assuming $\mathcal{A}^s_{\rm SL} = 0$: we no longer include these in the average. An exception is the dimuon DØ analysis [103], which separates the two contributions by exploiting their dependence on the muon impact parameter cut. The resulting measurements of $\mathcal{A}^d_{\rm SL}$ and $\mathcal{A}^s_{\rm SL}$ are then both compatible with the Standard Model. They are also correlated. We therefore perform a two-dimensional average of the measurements of Refs. [49,50,100,101,103–106,108,109,112] and obtain [8]

$$\mathcal{A}^d_{\rm SL} = -0.0021 \pm 0.0017 \Leftrightarrow |q/p|_d = 1.0010 \pm 0.0008\,, \quad (75.26)$$
$$\mathcal{A}^s_{\rm SL} = -0.0006 \pm 0.0028 \Leftrightarrow |q/p|_s = 1.0003 \pm 0.0014\,, \quad (75.27)$$

with a correlation coefficient of -0.054 between $\mathcal{A}^d_{\rm SL}$ and $\mathcal{A}^s_{\rm SL}$. These results show no evidence of CP violation and are compatible with the very small Standard Model predictions, $\mathcal{A}^{d,\rm SM}_{\rm SL} = -(4.73 \pm 0.42) \times 10^{-4}$ and $\mathcal{A}^{s,\rm SM}_{\rm SL} = +(2.06 \pm 0.18) \times 10^{-5}$ [9], but have insufficient precision yet to constrain the Standard Model.

CP violation induced by B_s^0–$\overline{B}_s^0$ mixing in $b \to c\bar{c}s$ decays, which is controlled by the small weak phase $\phi_s^{c\bar{c}s}$, has been a field of very active study in the past decade. In addition to the previously mentioned $B_s^0 \to J/\psi K^+K^-$ (including $B_s^0 \to J/\psi\phi$) and $B_s^0 \to \psi(2S)\phi$ studies, the decay modes $B_s^0 \to J/\psi\pi^+\pi^-$ (including $B_s^0 \to J/\psi f_0(980)$) [73,113] and $B_s^0 \to D_s^+ D_s^-$ [31] have also been analyzed by LHCb to measure $\phi_s^{c\bar{c}s}$, without the need for an angular analysis. The $J/\psi\pi^+\pi^-$ final state has been shown indeed to be (very close to) a pure CP-odd state [114]. In the $B_s^0 \to J/\psi\phi$ and $B_s^0 \to J/\psi K^+K^-$ analyses, $\phi_s^{c\bar{c}s}$ is obtained together with several other observables, including $\Delta\Gamma_s$, Γ_s, the longitudinal and perpendicular ϕ polarisation amplitudes, the S-wave amplitude, and strong phases. In order to account for all correlations, the full sets of measurements provided by the different analyses are

Downloaded from https://academic.oup.com/ptep/article/2022/8/083C01/6651666 by KIT Library user on 27 September 2022

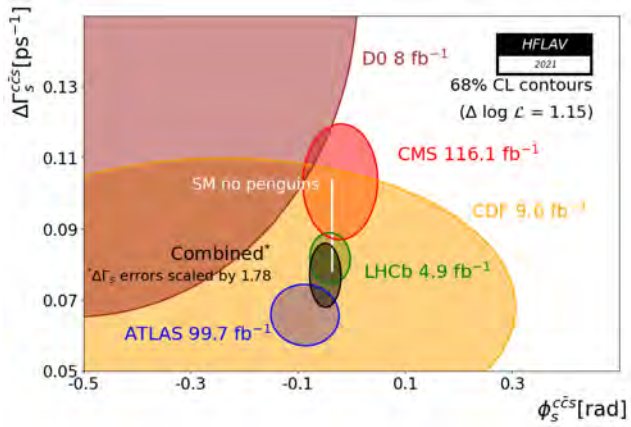

Figure 75.3: 68% CL contours in the $(\phi_s^{c\bar{c}s}, \Delta\Gamma_s)$ plane, showing all measurements from CDF [77], DØ [78], ATLAS [79], CMS [33, 80] and LHCb [30, 31, 73, 81–83, 113]. Their average [8] is represented as the black ellipse, where the combined uncertainty on $\Delta\Gamma_s$ has been multiplied by 1.78. The very thin white rectangle represents the Standard Model predictions of $\phi_s^{c\bar{c}s}$ [63] and $\Delta\Gamma_s$ [9].

combined in a multi-dimensional fit [8] of which $\phi_s^{c\bar{c}s}$ is just one of the free parameters. As already mentioned the $B_s^0 \to J/\psi\phi$ analyses of ATLAS, CMS and LHCb show a poor overall compatibility, mostly in the lifetime and angular parameters, corresponding approximately 3 standard deviations. Therefore, scale factors are applied on the combined uncertainty of each parameter where a discrepancy arises. For the parameters already in agreement, such as $\phi_s^{c\bar{c}s}$, no scale factor is applied. The combined result based on all published analyses [30, 31, 33, 73, 77–83, 113] is

$$\phi_s^{c\bar{c}s} = -0.049 \pm 0.019\,. \tag{75.28}$$

A two-dimensional projection of the overall situation in the $(\phi_s^{c\bar{c}s}, \Delta\Gamma_s)$ plane is shown in Fig. 75.3.

The experimental determination of $\phi_s^{c\bar{c}s}$ is still statistically limited. It is consistent with the Standard Model prediction, which is equal to $-2\beta_s = -2\arg(-(V_{ts}V_{tb}^*)/(V_{cs}V_{cb}^*)) = -0.0368\,^{+0.0006}_{-0.0009}$ [63] assuming negligible Penguin pollution.

75.7 Summary

B^0–$\overline{B}^0$ mixing has been and still is a field of intense study. The mass differences in the B_d^0–$\overline{B}_d^0$ and B_s^0–$\overline{B}_s^0$ systems are known to relative precisions of 0.38% and 0.03%, respectively. The non-zero decay width difference in the B_s^0–$\overline{B}_s^0$ system is well established, with a relative difference of $\Delta\Gamma_s/\Gamma_s = (12.8\pm0.7)\%$, meaning that the heavy state of the B_s^0–$\overline{B}_s^0$ system lives $\sim 14\%$ longer than the light state. In contrast, the relative decay width difference in the B_d^0–$\overline{B}_d^0$ system, $\Delta\Gamma_d/\Gamma_d = (0.1 \pm 1.0)\%$, is still consistent with zero. CP violation in B_d^0–$\overline{B}_d^0$ or B_s^0–$\overline{B}_s^0$ mixing has not been observed yet, with precisions on the semileptonic asymmetries below 0.3%. CP violation induced by B_s^0–$\overline{B}_s^0$ mixing in $b \to c\bar{c}s$ transitions has not yet been observed either, with an uncertainty on the $\phi_s^{c\bar{c}s}$ phase of 19 mrad. All observations so far remain consistent with the Standard Model expectations.

However, the measurements where New Physics might show up are still statistically limited. More results are awaited from the LHC experiments and Belle II, with promising prospects for the investigation of the CP-violating phase $\arg(-M_{12}/\Gamma_{12})$ and an improved determination of $\phi_s^{c\bar{c}s}$.

Mixing studies have clearly reached the stage of precision measurements, where much effort is needed, both on the experimental and theoretical sides, in particular to further reduce the hadronic uncertainties of lattice QCD calculations. In the long term, a stringent check of the consistency of the B_d^0 and B_s^0 mixing amplitudes (magnitudes and phases) with all other measured flavor-physics observables will be possible within the Standard Model, leading to very tight limits on (or otherwise a long-awaited surprise about) New Physics.

References

[1] T. D. Lee and C. S. Wu, Ann. Rev. Nucl. Part. Sci. **16**, 511 (1966); I. I. Bigi and A. I. Sanda, Camb. Monogr. Part. Phys. Nucl. Phys. Cosmol. **9**, 1 (2009), second edition, first published in 2000; G. C. Branco, L. Lavoura and J. P. Silva, Int. Ser. Monogr. Phys. **103**, 1 (1999).

[2] See the review on CP violation in the quark sector by T. Gershon and Y. Nir in this publication.

[3] A. J. Buras, W. Slominski and H. Steger, Nucl. Phys. **B245**, 369 (1984).

[4] T. Inami and C. S. Lim, Prog. Theor. Phys. **65**, 297 (1981), erratum *ibid.* **65**, 1772 (1981); for the power-like approximation, see A. J. Buras and R. Fleischer, page 91 in "Heavy Flavours II," eds. A. J. Buras and M. Lindner, Singapore World Scientific (1998).

[5] M. Kobayashi and T. Maskawa, Prog. Theor. Phys. **49**, 652 (1973).

[6] I. I. Bigi *et al.*, in "CP violation," ed. C. Jarlskog, Singapore World Scientific (1989).

[7] A. Lenz and U. Nierste (2011), [arXiv:1102.4274]; A. Lenz and U. Nierste, JHEP **06**, 072 (2007), [hep-ph/0612167].

[8] Y. S. Amhis *et al.* (HFLAV), Eur. Phys. J. **C81**, 226 (2021), [arXiv:1909.12524]; the combined results on b-hadron lifetimes and mixing parameters published in this *Review* have been obtained by the B lifetimes and oscillations sub-group of the Heavy Flavor Averaging (HFLAV) group in March 2022 as updates of the averages published in Chapter 4 of the above paper; for more information, see https://hflav.web.cern.ch/.

[9] A. Lenz and G. Tetlalmatzi-Xolocotzi, JHEP **07**, 177 (2020), [arXiv:1912.07621].

[10] T. Jubb *et al.*, Nucl. Phys. **B915**, 431 (2017), [arXiv:1603.07770].

[11] M. Artuso, G. Borissov and A. Lenz, Rev. Mod. Phys. **88**, 045002 (2016), [arXiv:1511.09466].

[12] C. Albajar *et al.* (UA1), Phys. Lett. **B186**, 247 (1987), erratum *ibid.* **B197**, 565 (1987).

[13] H. Albrecht *et al.* (ARGUS), Phys. Lett. **B192**, 245 (1987).

[14] H. G. Moser and A. Roussarie, Nucl. Instrum. Meth. **A384**, 491 (1997).

[15] SLD collab., SLAC-PUB-7228, SLAC-PUB-7229, and SLAC-PUB-7230, *28th Int. Conf. on High Energy Physics,* Warsaw (1996); J. L. Wittlin, *A measurement of the time dependence of B_d^0–$\overline{B}_d^0$ mixing with kaon tagging*, Ph.D. thesis, Massachusetts U., Amherst (2001), URL `http://wwwlib.umi.com/dissertations/fullcit?p3027272`.

[16] ALEPH collab., contrib. 596 to *Int. Europhysics Conf. on High Energy Physics,* Jerusalem (1997).

[17] K. Abe *et al.* (SLD), Phys. Rev. **D67**, 012006 (2003), [hep-ex/0209002].

[18] J. Abdallah *et al.* (DELPHI), Eur. Phys. J. **C28**, 155 (2003), [hep-ex/0303032].

[19] F. Abe *et al.* (CDF), Phys. Rev. Lett. **80**, 2057 (1998), [hep-ex/9712004]; F. Abe *et al.* (CDF), Phys. Rev. **D59**, 032001 (1999), [hep-ex/9806026]; F. Abe *et al.* (CDF), Phys. Rev. **D60**, 051101 (1999); F. Abe *et al.* (CDF), Phys. Rev. **D60**, 072003 (1999), [hep-ex/9903011]; T. Affolder *et al.* (CDF), Phys. Rev. **D60**, 112004 (1999), [hep-ex/9907053].

[20] R. Barate *et al.* (ALEPH), Eur. Phys. J. **C4**, 367 (1998); R. Barate *et al.* (ALEPH), Eur. Phys. J. **C7**, 553 (1999), [hep-ex/9811018].

[21] R. Aaij *et al.* (LHCb), JINST **10**, P10005 (2015), [arXiv:1507.07892].

[22] P. Abreu *et al.* (DELPHI), Eur. Phys. J. **C16**, 555 (2000), [hep-ex/0107077].

Downloaded from https://academic.oup.com/ptep/article/2022/8/083C01/6651666 by KIT Library user on 27 September 2022

[23] K. Anikeev *et al.* (2002), [hep-ph/0201071].

[24] A. Abulencia *et al.* (CDF), Phys. Rev. Lett. **97**, 242003 (2006), [hep-ex/0609040].

[25] V. M. Abazov *et al.* (DØ), Phys. Rev. **D74**, 112002 (2006), [hep-ex/0609034].

[26] V. M. Abazov *et al.* (DØ), Phys. Rev. Lett. **101**, 241801 (2008), [arXiv:0802.2255].

[27] R. Aaij *et al.* (LHCb), Eur. Phys. J. **C72**, 2022 (2012), [arXiv:1202.4979].

[28] R. Aaij *et al.* (LHCb), JINST **11**, P05010 (2016), [arXiv:1602.07252].

[29] R. Aaij *et al.* (LHCb), Eur. Phys. J. **C77**, 238 (2017), [arXiv:1610.06019].

[30] R. Aaij *et al.* (LHCb), Phys. Rev. Lett. **114**, 041801 (2015), [arXiv:1411.3104]; R. Aaij *et al.* (LHCb), Eur. Phys. J. **C79**, 706 (2019), erratum *ibid.* **C80**, 601 (2020), [arXiv:1906.08356].

[31] R. Aaij *et al.* (LHCb), Phys. Rev. Lett. **113**, 211801 (2014), [arXiv:1409.4619].

[32] R. Aaij *et al.* (LHCb), Phys. Rev. Lett. **117**, 261801 (2016), [arXiv:1608.06620].

[33] A. M. Sirunyan *et al.* (CMS), Phys. Lett. **B816**, 136188 (2021), [arXiv:2007.02434].

[34] B. Aubert *et al.* (BaBar), Phys. Rev. Lett. **94**, 161803 (2005), [hep-ex/0408127]; K. F. Chen *et al.* (Belle), Phys. Rev. **D72**, 012004 (2005), [hep-ex/0504023].

[35] Throughout this document we omit references of results that have been replaced by new published measurements.

[36] D. Buskulic *et al.* (ALEPH), Z. Phys. **C75**, 397 (1997).

[37] P. Abreu *et al.* (DELPHI), Z. Phys. **C76**, 579 (1997).

[38] M. Acciarri *et al.* (L3), Eur. Phys. J. **C5**, 195 (1998).

[39] G. Alexander *et al.* (OPAL), Z. Phys. **C72**, 377 (1996); K. Ackerstaff *et al.* (OPAL), Z. Phys. **C76**, 417 (1997), [hep-ex/9707010]; G. Abbiendi *et al.* (OPAL), Phys. Lett. **B493**, 266 (2000), [hep-ex/0010013].

[40] K. Ackerstaff *et al.* (OPAL), Z. Phys. **C76**, 401 (1997), [hep-ex/9707009].

[41] B. Aubert *et al.* (BaBar), Phys. Rev. Lett. **88**, 221802 (2002), [hep-ex/0112044]; B. Aubert *et al.* (BaBar), Phys. Rev. **D66**, 032003 (2002), [hep-ex/0201020]; B. Aubert *et al.* (BaBar), Phys. Rev. Lett. **88**, 221803 (2002), [hep-ex/0112045]; B. Aubert *et al.* (BaBar), Phys. Rev. **D67**, 072002 (2003), [hep-ex/0212017]; B. Aubert *et al.* (BaBar), Phys. Rev. **D73**, 012004 (2006), [hep-ex/0507054].

[42] N. C. Hastings *et al.* (Belle), Phys. Rev. **D67**, 052004 (2003), [hep-ex/0212033]; Y. Zheng *et al.* (Belle), Phys. Rev. **D67**, 092004 (2003), [hep-ex/0211065]; K. Abe *et al.* (Belle), Phys. Rev. **D71**, 072003 (2005), erratum *ibid.* **D71**, 079903 (2005), [hep-ex/0408111].

[43] R. Aaij *et al.* (LHCb), Phys. Lett. **B709**, 177 (2012), [arXiv:1112.4311].

[44] R. Aaij *et al.* (LHCb), Phys. Lett. **B719**, 318 (2013), [arXiv:1210.6750].

[45] R. Aaij *et al.* (LHCb), Eur. Phys. J. **C73**, 2655 (2013), [arXiv:1308.1302].

[46] R. Aaij *et al.* (LHCb), Eur. Phys. J. **C76**, 412 (2016), [arXiv:1604.03475].

[47] H. Albrecht *et al.* (ARGUS), Z. Phys. **C55**, 357 (1992); H. Albrecht *et al.* (ARGUS), Phys. Lett. **B324**, 249 (1994).

[48] J. E. Bartelt *et al.* (CLEO), Phys. Rev. Lett. **71**, 1680 (1993).

[49] B. H. Behrens *et al.* (CLEO), Phys. Lett. **B490**, 36 (2000), [hep-ex/0005013].

[50] B. Aubert *et al.* (BaBar), Phys. Rev. Lett. **92**, 181801 (2004), [hep-ex/0311037]; B. Aubert *et al.* (BaBar), Phys. Rev. **D70**, 012007 (2004), [hep-ex/0403002].

[51] T. Higuchi *et al.*, Phys. Rev. **D85**, 071105 (2012), [arXiv:1203.0930].

[52] R. Aaij *et al.* (LHCb), JHEP **04**, 114 (2014), [arXiv:1402.2554].

[53] M. Aaboud *et al.* (ATLAS), JHEP **06**, 081 (2016), [arXiv:1605.07485].

[54] A. M. Sirunyan *et al.* (CMS), Eur. Phys. J. **C78**, 457 (2018), erratum *ibid.* **C78**, 561 (2018), [arXiv:1710.08949].

[55] See the review on the CKM quark-mixing matrix by A. Ceccucci, Z. Ligeti, and Y. Sakai in this publication.

[56] S. Aoki *et al.* (Flavour Lattice Averaging Group) (2019), [arXiv:1902.08191].

[57] R. Aaij *et al.* (LHCb), New J. Phys. **15**, 053021 (2013), [arXiv:1304.4741].

[58] R. Aaij *et al.* (LHCb), JHEP **03**, 137 (2021), [arXiv:2011.12041].

[59] R. Aaij *et al.* (LHCb), Nature Phys. **18**, 1 (2022), [arXiv:2104.04421].

[60] A. Bazavov *et al.* (Fermilab Lattice and MILC), Phys. Rev. **D93**, 113016 (2016), [arXiv:1602.03560].

[61] D. King, A. Lenz and T. Rauh, JHEP **05**, 034 (2019), [arXiv:1904.00940].

[62] M. Bona *et al.* (UTfit), JHEP **10**, 081 (2006), [hep-ph/0606167]; updated results at http://www.utfit.org/.

[63] J. Charles *et al.*, Phys. Rev. **D91**, 073007 (2015), [arXiv:1501.05013]; updated results at http://ckmfitter.in2p3.fr/.

[64] K. Hartkorn and H. G. Moser, Eur. Phys. J. **C8**, 381 (1999).

[65] M. Acciarri *et al.* (L3), Phys. Lett. **B438**, 417 (1998).

[66] D. Buskulic *et al.* (ALEPH), Phys. Lett. **B377**, 205 (1996); K. Ackerstaff *et al.* (OPAL), Phys. Lett. **B426**, 161 (1998), [hep-ex/9802002]; F. Abe *et al.* (CDF), Phys. Rev. **D59**, 032004 (1999), [hep-ex/9808003]; V. M. Abazov *et al.* (DØ), Phys. Rev. Lett. **114**, 062001 (2015), [arXiv:1410.1568]; T. Aaltonen *et al.* (CDF), Phys. Rev. Lett. **107**, 272001 (2011), [arXiv:1103.1864]; R. Aaij *et al.* (LHCb), Phys. Rev. Lett. **113**, 172001 (2014), [arXiv:1407.5873]; R. Aaij *et al.* (LHCb), Phys. Rev. Lett. **119**, 101801 (2017), [arXiv:1705.03475].

[67] R. Aaij *et al.* (LHCb), Phys. Rev. Lett. **112**, 111802 (2014), [arXiv:1312.1217].

[68] R. Aaij *et al.* (LHCb), Phys. Lett. **B736**, 446 (2014), [arXiv:1406.7204].

[69] R. Aaij *et al.* (LHCb), Phys. Lett. **B707**, 349 (2012), [arXiv:1111.0521].

[70] R. Aaij *et al.* (LHCb), Phys. Lett. **B762**, 484 (2016), [arXiv:1607.06314].

[71] T. Aaltonen *et al.* (CDF), Phys. Rev. **D84**, 052012 (2011), [arXiv:1106.3682]; V. M. Abazov *et al.* (DØ), Phys. Rev. **D94**, 012001 (2016), [arXiv:1603.01302].

[72] R. Aaij *et al.* (LHCb), Phys. Rev. **D87**, 112010 (2013), [arXiv:1304.2600].

[73] R. Aaij *et al.* (LHCb), Phys. Lett. **B797**, 134789 (2019), [arXiv:1903.05530].

[74] R. Aaij *et al.* (LHCb), Nucl. Phys. **B873**, 275 (2013), [arXiv:1304.4500].

[75] R. Aaij *et al.* (LHCb), Phys. Rev. Lett. **128**, 041801 (2022), [arXiv:2108.09284]; R. Aaij *et al.* (LHCb), Phys. Rev. **D105**, 012010 (2022), [arXiv:2108.09283]; A. M. Sirunyan *et al.* (CMS), JHEP **04**, 188 (2020), [arXiv:1910.12127].

[76] R. Fleischer and R. Knegjens, Eur. Phys. J. **C71**, 1789 (2011), [arXiv:1109.5115].

[77] T. Aaltonen *et al.* (CDF), Phys. Rev. Lett. **109**, 171802 (2012), [arXiv:1208.2967].

[78] V. M. Abazov *et al.* (DØ), Phys. Rev. **D85**, 032006 (2012), [arXiv:1109.3166].

Downloaded from https://academic.oup.com/ptep/article/2022/8/083C01/6651666 by KIT Library user on 27 September 2022

[79] G. Aad *et al.* (ATLAS), Phys. Rev. **D90**, 052007 (2014), [arXiv:1407.1796]; G. Aad *et al.* (ATLAS), JHEP **08**, 147 (2016), [arXiv:1601.03297]; G. Aad *et al.* (ATLAS), Eur. Phys. J. **C81**, 342 (2021), [arXiv:2001.07115].

[80] V. Khachatryan *et al.* (CMS), Phys. Lett. **B757**, 97 (2016), [arXiv:1507.07527].

[81] R. Aaij *et al.* (LHCb), Eur. Phys. J. **C81**, 1026 (2021), [arXiv:2105.14738].

[82] R. Aaij *et al.* (LHCb), JHEP **08**, 037 (2017), [arXiv:1704.08217].

[83] R. Aaij *et al.* (LHCb), Phys. Lett. **B762**, 253 (2016), [arXiv:1608.04855].

[84] R. Aaij *et al.* (LHCb), Phys. Rev. Lett. **108**, 241801 (2012), [arXiv:1202.4717].

[85] S. Schael *et al.* (ALEPH, DELPHI, L3, OPAL, SLD, LEP Electroweak Working Group, SLD Electroweak Group, SLD Heavy Flavour Group), Phys. Rept. **427**, 257 (2006), [hep-ex/0509008]; we use the $\overline{\chi}$ average given in Eq. (5.39).

[86] D. Acosta *et al.* (CDF), Phys. Rev. **D69**, 012002 (2004), [hep-ex/0309030].

[87] V. M. Abazov *et al.* (DØ), Phys. Rev. **D74**, 092001 (2006), [hep-ex/0609014].

[88] P. Abreu *et al.* (DELPHI), Phys. Lett. **B289**, 199 (1992); P. D. Acton *et al.* (OPAL), Phys. Lett. **B295**, 357 (1992); D. Buskulic *et al.* (ALEPH), Phys. Lett. **B361**, 221 (1995).

[89] P. Abreu *et al.* (DELPHI), Z. Phys. **C68**, 375 (1995); R. Barate *et al.* (ALEPH), Eur. Phys. J. **C2**, 197 (1998).

[90] D. Buskulic *et al.* (ALEPH), Phys. Lett. **B384**, 449 (1996); J. Abdallah *et al.* (DELPHI), Eur. Phys. J. **C44**, 299 (2005), [hep-ex/0510023].

[91] R. Barate *et al.* (ALEPH), Eur. Phys. J. **C5**, 205 (1998).

[92] J. Abdallah *et al.* (DELPHI), Phys. Lett. **B576**, 29 (2003), [hep-ex/0311005].

[93] F. Abe *et al.* (CDF), Phys. Rev. **D60**, 092005 (1999).

[94] T. Aaltonen *et al.* (CDF), Phys. Rev. **D77**, 072003 (2008), [arXiv:0801.4375]; T. Affolder *et al.* (CDF), Phys. Rev. Lett. **84**, 1663 (2000), [hep-ex/9909011]; the measurement of $f_{\rm baryon}/f_d$ in the latter paper has been updated based on; T. Aaltonen *et al.* (CDF), Phys. Rev. **D79**, 032001 (2009), [arXiv:0810.3213].

[95] V. M. Abazov *et al.* (DØ), Phys. Rev. Lett. **99**, 052001 (2007), [arXiv:0706.1690]; V. M. Abazov *et al.* (DØ), Phys. Rev. Lett. **101**, 232002 (2008), [arXiv:0808.4142]; T. Aaltonen *et al.* (CDF), Phys. Rev. **D80**, 072003 (2009), [arXiv:0905.3123].

[96] Y. S. Amhis *et al.* (HFLAV), *b*-hadron fraction averages computed for the 2020 edition of this *Review*; for more information, see https://hflav.web.cern.ch/.

[97] R. Aaij *et al.* (LHCb), Phys. Rev. **D104**, 032005 (2021), [arXiv:2103.06810].

[98] G. Aad *et al.* (ATLAS), Phys. Rev. Lett. **115**, 262001 (2015), [arXiv:1507.08925].

[99] R. Aaij *et al.* (LHCb), Phys. Rev. **D100**, 112006 (2019), [arXiv:1910.13404].

[100] D. E. Jaffe *et al.* (CLEO), Phys. Rev. Lett. **86**, 5000 (2001), [hep-ex/0101006].

[101] J. P. Lees *et al.* (BaBar), Phys. Rev. Lett. **114**, 081801 (2015), [arXiv:1411.1842].

[102] F. Abe *et al.* (CDF), Phys. Rev. **D55**, 2546 (1997).

[103] V. M. Abazov *et al.* (DØ), Phys. Rev. **D89**, 012002 (2014), [arXiv:1310.0447].

[104] V. M. Abazov *et al.* (DØ), Phys. Rev. **D86**, 072009 (2012), [arXiv:1208.5813].

[105] V. M. Abazov *et al.* (DØ), Phys. Rev. Lett. **110**, 011801 (2013), [arXiv:1207.1769].

[106] R. Aaij *et al.* (LHCb), Phys. Rev. Lett. **117**, 061803 (2016), erratum *ibid.* **118**, 129903 (2017), [arXiv:1605.09768].

[107] R. Barate *et al.* (ALEPH), Eur. Phys. J. **C20**, 431 (2001).

[108] J. P. Lees *et al.* (BaBar), Phys. Rev. Lett. **111**, 101802 (2013), erratum *ibid.* **111**, 159901 (2013), [arXiv:1305.1575].

[109] E. Nakano *et al.* (Belle), Phys. Rev. **D73**, 112002 (2006), [hep-ex/0505017].

[110] G. Abbiendi *et al.* (OPAL), Eur. Phys. J. **C12**, 609 (2000), [hep-ex/9901017].

[111] M. Beneke, G. Buchalla and I. Dunietz, Phys. Lett. **B393**, 132 (1997), [hep-ph/9609357]; I. Dunietz, Eur. Phys. J. **C7**, 197 (1999), [hep-ph/9806521].

[112] R. Aaij *et al.* (LHCb), Phys. Rev. Lett. **114**, 041601 (2015), [arXiv:1409.8586].

[113] R. Aaij *et al.* (LHCb), Phys. Lett. **B736**, 186 (2014), [arXiv:1405.4140].

[114] R. Aaij *et al.* (LHCb), Phys. Rev. **D86**, 052006 (2012), [arXiv:1204.5643].

Downloaded from https://academic.oup.com/ptep/article/2022/8/083C01/6651666 by KIT Library user on 27 September 2022

76. Semileptonic b-Hadron Decays, Determination of V_{cb}, V_{ub}

Revised August 2021 by A.X. El-Khadra (Physics, Illinois U.) and P. Urquijo (School of Phys. U. of Melbourne).

76.1 Introduction

Precision determinations of $|V_{ub}|$ and $|V_{cb}|$ are central to testing the CKM sector of the Standard Model, and complement the measurements of CP asymmetries in B decays. The length of the side of the unitarity triangle opposite the well-measured angle β is proportional to the ratio $|V_{ub}|/|V_{cb}|$; its precise determination is a high priority of the heavy-flavor physics program.

The transitions $b \to c\ell\bar{\nu}_\ell$ and $b \to u\ell\bar{\nu}_\ell$ ($\ell = e, \mu$) each provide two avenues for determining these CKM matrix elements, namely through measurements of inclusive decay rates, $\bar{B} \to X\ell\bar{\nu}_\ell$ with a sum over all possible hadronic states X or of exclusive rates, where the final state hadron is a specific meson ($X = D$, D^*, π, ρ etc.).

Purely leptonic decays, such as $B_c^- \to \tau\bar{\nu}$, $B^- \to \tau\bar{\nu}$, and $B^- \to \mu\bar{\nu}$, provide a third avenue that is theoretically very simple (see the RPP mini-review [1]). However, we do not use this information at present since none of the measurements have reached a competitive level of precision. Hence the results presented here are solely obtained from exclusive and inclusive semileptonic b-hadron decays. This article and the values quoted here update the previous review [2].

The theoretical methods underlying the different determinations of $|V_{qb}|$ are quite mature. The theoretical approach for inclusive determinations uses the fact that the mass m_b of the b quark is large compared to the scale $\Lambda_{\rm QCD}$ that determines low-energy hadronic physics. Thus the basis for precise calculations is a systematic expansion in powers of Λ/m_b, where $\Lambda \sim 500 - 700$ MeV is a hadronic scale of the order of $\Lambda_{\rm QCD}$. Such an expansion can be formulated in the framework of an effective field theory which is described in a separate RPP mini-review [3]. Exclusive determinations rely on non-perturbatively calculated form factors, that encode the low-energy dynamics of the hadronic transition. Here, lattice QCD provides an, in principle, ab-initio method to calculate the non-perturbative QCD contributions to the exclusive decay amplitudes. Thanks to a combination of improved theoretical methods, better algorithms, and large increases in computational power, precise lattice QCD results are now available for the processes that are used in exclusive $|V_{ub}|$ and $|V_{cb}|$ determinations. State-of-the-art lattice QCD calculations are based on gauge-field ensembles that include realistic sea quark effects for degenerate up/down and strange quarks (aka $2+1$-flavor ensembles), and increasingly, also for charm (aka $2+1+1$-flavor ensembles). They employ ensembles generated at three (or more) lattice spacings, different spatial volumes, among other parameter variations to allow for quantification of the underlying systematic errors, and include detailed systematic error analyses. This is described in a separate RPP mini-review [4]. The lattice-QCD results discussed in this review are all state-of-the art with fully quantified uncertainties, and therefore play a central role in exclusive $|V_{qb}|$ determinations. In the case of exclusive $\bar{B} \to D^{(*)}\ell\bar{\nu}_\ell$ decays, heavy quark symmetry (HQS) and heavy quark effective theory (HQET) yield constraints on the form factors that can be used to improve exclusive $|V_{cb}|$ determinations, especially when lattice QCD form factor results are incomplete, as was the case until very recently for $\bar{B} \to D^*\ell\bar{\nu}_\ell$. Light-cone sum rules (LCSR) provide another nonperturbative approach to compute form factors. However, while the lattice-QCD results employed in this review have well-quantified uncertainties, LCSR results suffer, in general, from hard-to-quantify systematic errors. The two methods typically provide results in opposite regions of phase space. Lattice-QCD calculations work best at low hadronic recoil or high momentum transfer (q^2) to the leptons, while LCSR calculations provide estimates at high recoil, near $q^2 = 0$.

The measurements discussed in this review are of branching fractions, ratios of branching fractions, and decay kinematic distributions. The determinations of $|V_{cb}|$ and $|V_{ub}|$ also require a measurement of the total decay widths of the corresponding b hadrons, determined from lifetimes, which is the subject of a separate RPP mini-review [5]. The measurements of inclusive semileptonic decays relevant to this review come primarily from e^+e^- B factories operating at the $\Upsilon(4S)$ resonance, while the measurements of exclusive semileptonic decays come from both the e^+e^- B factories and from the LHCb experiment at CERN.

Semileptonic B-meson decay amplitudes to electrons and muons are well measured and consistent with Standard Model W-boson exchange. As they are expected to be insensitive to the effects of non-Standard-Model physics, they are used to extract $|V_{qb}|$. However, semileptonic decays to tau-lepton final states, such as $\bar{B} \to D^{(*)}\tau\bar{\nu}_\tau$, may be sensitive to effects from beyond the Standard Model particles due to the large mass of the τ lepton. The currently observed tensions between Standard Model theory and experiment for these decays indicate that semitauonic decays must be studied further.

Many of the numerical results quoted in this review have been provided by the Heavy Flavor Averaging Group (HFLAV) [6].

76.2 Determination of $|V_{cb}|$

Summary: The determination of $|V_{cb}|$ from inclusive decays has a relative uncertainty of about 2%; the limitations arise mainly from our ignorance of higher-order perturbative and non-perturbative corrections. Exclusive $\bar{B} \to D^*\ell\bar{\nu}_\ell$ decays provide a determination of $|V_{cb}|$ with a relative precision of about 2%, with comparable contributions from theory and experiment to the total uncertainty; the value determined from $\bar{B} \to D\ell\bar{\nu}_\ell$ decays is consistent and has an uncertainty of 3%. However, as discussed below, recent work has raised questions about determinations based on the CLN parameterization, and we choose to quote a result obtained from a less constraining analysis.

The values obtained from the inclusive and exclusive B decay determinations discussed below are:

$$|V_{cb}| = (42.2 \pm 0.8) \times 10^{-3} \quad \text{(inclusive)} \tag{76.1}$$

$$|V_{cb}| = (39.4 \pm 0.8) \times 10^{-3} \quad \text{(exclusive)}. \tag{76.2}$$

An average of these determinations has $p(\chi^2) = 1\%$, so we scale the error by $\sqrt{\chi^2/1} = 2.6$ to find

$$|V_{cb}| = (40.8 \pm 1.4) \times 10^{-3} \quad \text{(average)}. \tag{76.3}$$

Given the only marginal consistency, of approximately 2.4 σ, this average should be treated with caution.

76.2.1 $|V_{cb}|$ *from exclusive decays*

Exclusive determinations of $|V_{cb}|$ make use of semileptonic B decays into the ground state charmed mesons D and D^*. The corresponding hadronic matrix elements can be parameterized in terms of six independent form factors, which depend on the variable $w \equiv v \cdot v'$, where v and v' are the four velocities of the initial and final-state hadrons. In the rest frame of the decay this variable corresponds to the Lorentz factor of the final state $D^{(*)}$ meson. Determinations of $|V_{cb}|$ from experimental measurements of $\bar{B} \to D^{(*)}\ell\bar{\nu}_\ell$ decay rates require precise knowledge of these form factors. Fortunately, lattice QCD results for all relevant form factors, including their recoil dependence, are now available [7–9]. Heavy Quark Symmetry (HQS) [10, 11] predicts that in the infinite mass limit the six form factors collapse into a single one, which is normalized at the "zero recoil point" $w = 1$, the point of maximum momentum transfer to the leptons. Heavy Quark Effective Theory (HQET) provides a framework for obtaining the corrections to the HQS prediction in a systematic expansion in powers of $\Lambda_{\rm QCD}/m_c$ which is discussed in a separate RPP mini-review [3].

76.2.2 $\bar{B} \to D^*\ell\bar{\nu}_\ell$

The decay rate for $\bar{B} \to D^*\ell\bar{\nu}_\ell$, assuming massless leptons, is given by

$$\frac{d\Gamma}{dw}(\bar{B} \to D^*\ell\bar{\nu}_\ell) = \frac{G_F^2 m_B^5}{48\pi^3}|V_{cb}|^2|\eta_{\rm EW}|^2(w^2-1)^{1/2}P(w)|\mathcal{F}(w)|^2, \tag{76.4}$$

where $P(w)$ is a phase space factor,

$$P(w) = r^3(1-r)^2(w+1)^2\left(1 + \frac{4w}{w+1}\frac{1-2rw+r^2}{(1-r)^2}\right), \tag{76.5}$$

Downloaded from https://academic.oup.com/ptep/article/2022/8/083C01/6651666 by KIT Library user on 27 September 2022

with $r = m_{D^*}/m_B$. The decay amplitude $\mathcal{F}(w)$ can be expressed in terms of the form factors which parametrize the vector and axial vector current matrix elements

$$\frac{\langle D^*(v',\epsilon)|\bar{c}\gamma^\mu b|B(v)\rangle}{\sqrt{m_B m_{D^*}}} = h_V(w)\,\varepsilon^{\mu\nu\rho\sigma} v_{B,\nu} v_{D^*,\rho}\epsilon^*_\sigma\,, \tag{76.6}$$

$$\frac{\langle D^*(v',\epsilon)|\bar{c}\gamma^\mu\gamma^5 b|B(v)\rangle}{\sqrt{m_B m_{D^*}}} = i h_{A_1}(w)\,(1+w)\epsilon^{*\mu} - i\left[h_{A_2}(w)v_B^\mu + h_{A_3}(w)v_{D^*}^\mu\right]\epsilon^*\cdot v_B\,, \tag{76.7}$$

and the ratios

$$R_1(w) = \frac{h_V(w)}{h_{A_1}(w)}\,,\quad R_2(w) = \frac{h_{A_3}(w) + r\,h_{A_2}(w)}{h_{A_1}(w)}\,, \tag{76.8}$$

as

$$P(w)|\mathcal{F}(w)|^2 = |h_{A_1}(w)|^2 \times \left\{2\frac{r^2-2rw+1}{(1-r)^2}\left[1+\frac{w-1}{w+1}R_1^2(w)\right] + \left[1+\frac{w-1}{1-r}(1-R_2(w))\right]^2\right\}. \tag{76.9}$$

Note that $\mathcal{F}$ at $w=1$ is unity by HQS in the infinite-mass limit [12–15]. The effect of assuming massless leptons is typically very small, but for the muon case can be non-negligible in fits to data at high hadronic recoil.

The factor $\eta_{\rm EW} = 1.0066 \pm 0.0050$ accounts for the leading electroweak corrections to the four-fermion operator mediating the semileptonic decay [16], and includes an estimated uncertainty for missing long-distance QED radiative corrections [17]. At present it is not known if these corrections are or are not already included in the experimental analyses, so this needs to be clarified.

The determination of $|V_{cb}|$ requires knowledge of the normalization, where one commonly uses the zero recoil input, $\mathcal{F}(1)$. Theoretical knowledge of the shapes of the form factors provides crucial compatibility checks between theory and experiment, and improves the precision of the determinations. Model-independent shape parametrizations of the from factors make use of analyticity and unitarity constraints and are expressed in terms of the variable

$$z = \frac{\sqrt{w+1}-\sqrt{2}}{\sqrt{w+1}+\sqrt{2}}\,, \tag{76.10}$$

originating from a conformal transformation. In terms of this variable the form factors (generically denoted as F) may be written as [18–22]

$$F(z) = \frac{1}{P_F(z)\phi_F(z)}\sum_{n=0}^{\infty} a_n z^n \tag{76.11}$$

where the sum is bounded, $\sum |a_n|^2 < 1$. Furthermore, the function $P_F(z)$ takes into account the resonances in the $(\bar{c}b)$ system below the $\bar{D}B$ threshold, and the weighting functions $\phi_F(z)$ are derived from the unitarity constraint on the corresponding form factor. The values of z relevant to the decay are $0 \le z \le 0.06$, hence only very few terms are needed in the series in z. Eq. (76.11) will be referred to as the "BGL" expansion.

The Caprini-Lellouch-Neubert (CLN) parametrization [23] yields a simple form

$$h_{A_1}(w) = h_{A_1}(1)\left[1 - 8\rho^2 z + (53\rho^2-15)z^2 - (231\rho^2-91)z^3\right] \tag{76.12}$$

with the slope ρ and normalization $h_{A_1}(1)$ as the only parameters, albeit at the cost of introducing model dependence. Furthermore, the ratios $R_1(w)$ and $R_2(w)$ are expanded in $w-1$. However, this simple CLN parametrization does not account for higher-order corrections in the $1/m_{c/b}$ expansion, which are now relevant [22, 24–29]. Thus, this report focuses on recent analyses that employ the model-independent BGL expansion. Typical fits include up to three parameters a_n in (76.11) for the different form factors.

Results of the first complete calculation of the $\bar{B} \to D^*\ell\bar{\nu}_\ell$ form factors at non-zero recoil were recently presented by the Fermilab Lattice and MILC collaborations in Ref. [9]. Preliminary results, obtained by the JLQCD collaboration [30], are reasonably consistent. Prior lattice calculations obtained results for only the form factor at the zero-recoil point, $\mathcal{F}(1)$, [17, 31] with a total uncertainty at the (1-2)% level. The average of the two lattice predictions [32] is

$$\mathcal{F}(1) = 0.904 \pm 0.012, \tag{76.13}$$

Non-lattice estimates based on zero-recoil sum rules for the form factor tend to yield lower central values for $\mathcal{F}(1)$ [33–35]. The sum rules indicate that $\mathcal{F}(1) < 0.92$ [33, 34, 36, 37], while an explicit estimate that includes excited state contributions yields $\mathcal{F}(1) \approx 0.86$ [35, 38]. Lattice-QCD form factors at non-zero recoil provide valuable shape constraints, and hence enable more refined $|V_{cb}|$ determinations. However, since they were not available until very recently, most $|V_{cb}|$ determinations in the literature use the value for $\mathcal{F}(1)$ from Eq. (76.13) as the only quantitative lattice input. We discuss these first, before turning to results for $|V_{cb}|$ which employ the lattice-QCD form factors from Ref. [9].

While Light Cone Sum Rules (LCSR) can provide constraints on the form factors at maximum recoil, the underlying systematic errors are not fully quantified. A recent LCSR calculation [39] quotes uncertainties in the $\lesssim 20\%$ range for the $\bar{B} \to D^{(*)}\ell\bar{\nu}_\ell$ form factors at $q^2 = 0$. Dispersive methods [40] can also be used to provide additional constraints on form factors calculated in lattice QCD. Very recent work [41, 42] introduces the dispersive matrix method, which includes additional nonperturbative inputs calculable in lattice QCD from two-point correlation functions. A test of this approach for the $D \to K\ell\nu$ form factors, which can be computed in lattice-QCD over the entire kinematic range, is presented in Ref. [41], while Ref. [42] presents a first lattice-QCD calculation of the needed inputs for the $B \to D^{(*)}$ transitions. The consistency of the dispersive constraints with the form factor calculations still need to be carefully studied, and the dispersive inputs must be calculated with the same care as the form factors themselves.

Many experiments [43–53] have measured the differential decay rate as a function of w, employing a variety of methods: using either B^+ or B^0 decays, with or without B-tagging, and with or without explicit reconstruction of the transition pion from $D^* \to D$ decays. In Ref. [6] the experimental measurements were input to a four-dimensional fit for $\eta_{\rm EW}\mathcal{F}(1)|V_{cb}|$, $\rho^2_{A_1}$ and the form-factor ratios $R_1 \propto A_2/A_1$ and $R_2 \propto V/A_1$. The fit has a p-value of 0.9%, so we scale the uncertainty by a factor $\sqrt{\chi^2/23}$ to give $\eta_{\rm EW}\mathcal{F}(1)\,|V_{cb}| = (35.00 \pm 0.49) \times 10^{-3}$ (CLN).

The leading sources of uncertainty on $\eta_{\rm EW}\mathcal{F}(1)\,|V_{cb}|$ are due to detection efficiencies and $D^{(*)}$ decay branching fractions. Note that the $\bar{B} \to D^*\ell\bar{\nu}_\ell$ form factor in the fit is parameterized using the CLN form, which has the drawbacks discussed previously.

Using the value from Eq. (76.13) for $\mathcal{F}(1)$ and accounting for the electroweak correction gives

$$|V_{cb}| = (38.5 \pm 0.5 \pm 0.6) \times 10^{-3}\ (\bar{B} \to D^*\ell\bar{\nu}_\ell,\ \text{LQCD, CLN}). \tag{76.14}$$

A safer approach is to use the more general BGL form-factor parameterization [19–22, 26]. Two experiments have published analyses with BGL based parametrizations at a given order in the expansion [53, 54]. The Belle analysis [53] is based on an untagged approach in the mode $\bar{B}^0 \to D^{*+}\ell\bar{\nu}_\ell$ and measures 1-d projections in bins of the hadronic recoil w, and angular variables $\cos\theta_\ell$, $\cos\theta_V$, and χ. The BABAR analysis [54] is based on a hadronic tagged sample, and performs a full 4-d unbinned analysis of neutral and charged B decay modes. Only the BGL form factors are fit in this analysis, not the normalization, which is based on the world average $\bar{B} \to D^*\ell\bar{\nu}_\ell$ branching fraction.

At present only Ref. [53] publishes the fully-differential decay rate data and associated covariance matrix. The BGL fit results from Ref. [55], $|V_{cb}| = (38.9 \pm 1.0) \times 10^{-3}$, and Ref. [54], $|V_{cb}| = (38.4 \pm 0.9) \times 10^{-3}$, are consistent with result from the fit with the CLN parametrization, Eq. (76.14). Both studies report fit

Downloaded from https://academic.oup.com/ptep/article/2022/8/083C01/6651666 by KIT Library user on 27 September 2022

results at low order in the three BGL expansion terms, ranging from zero-order to second-order in the Belle analysis, and first order for all terms in the BABAR analysis. Studies of the impact of higher order expansions based on the Belle published decay rate data have been reported in Refs. [27, 28], where it is shown that the fit uncertainty on $|V_{cb}|$ increases by approximately 50% with respect to the results reported at lower order. This is due to larger number of degrees of freedom allowed in the higher order expansions, which are not sufficiently constrained without lattice-QCD inputs at nonzero recoil. Belle II has recently provided first preliminary branching fraction measurements of $\bar{B} \to D^* \ell \bar{\nu}_\ell$ using both tagged and untagged methods [56, 57].

In Ref. [9], BGL expansion fits to the FNAL/MILC lattice QCD form factors show that they are insensitive to truncation effects beyond quadratic order. These form factors were subsequently used in Ref. [9] to extract $|V_{cb}|$ from combined BGL fits to the Belle [53] and synthetic BABAR [54] $\bar{B} \to D^* \ell \bar{\nu}_\ell$ data, yielding $|V_{cb}| = (38.40 \pm 0.74) \times 10^{-3}$. We note that the determination of $|V_{cb}|$ in Ref. [9] applies the Coulomb factor $(1 + \alpha\pi)$ to the Belle data to account for interactions between the charged final states in the neutral B-meson decay. The p-values for the combined (experiment+lattice QCD) BGL fits reported in Ref. [9] are small, reflecting tensions between the data sets. For a fit combining only the Belle data with the lattice-QCD form factors, Ref. [9] quotes $|V_{cb}| = (38.18 \pm 0.82) \times 10^{-3}$, consistent with the result presented in Eq. (76.15), after accounting for the different values of $\eta_{\rm EW}$ used in each result. For this review, the method of Ref. [58] was employed in further fits that include the lattice-QCD inputs at non-zero recoil from FNAL/MILC [9] and from JLQCD (preliminary) [30], yielding consistent results at quadratic order. In summary, we adopt the method of Ref. [58], using the recent FNAL/MILC inputs and only the Belle data (given the lack of availability of binned data from the BABAR measurement [54]). The nominal result for $|V_{cb}|$ is therefore

$$|V_{cb}| = (38.7 \pm 1.0) \times 10^{-3} \ (\bar{B} \to D^* \ell \bar{\nu}_\ell, \ \text{LQCD, BGL}), \quad (76.15)$$

where the uncertainty contains contributions from experimental, lattice QCD, and $\eta_{\rm EW}$ sources. We note that despite the improvements in the experimental data, theoretical inputs, and $|V_{cb}|$ extraction methods, this new exclusive determination of $|V_{cb}|$ is similar in central value to earlier ones, and still in tension with the inclusive determinations discussed in Section 76.2.5 and summarized in Eq. (76.34).

76.2.3 $\bar{B} \to D \ell \bar{\nu}_\ell$

The differential rate for $\bar{B} \to D \ell \bar{\nu}_\ell$ is given by

$$\frac{d\Gamma}{dw}(\bar{B} \to D \ell \bar{\nu}_\ell) = \frac{G_F^2}{48\pi^3} |V_{cb}|^2 (m_B + m_D)^2 m_D^3 (w^2 - 1)^{3/2} (\eta_{\rm EW} \mathcal{G}(w))^2. \quad (76.16)$$

The form factor is defined in terms of

$$\frac{\langle D(v') | \bar{c} \gamma^\mu b | B(v) \rangle}{\sqrt{m_B m_D}} = h_+(w) \, (v_B + v_D)^\mu + h_-(w) \, (v_B - v_D)^\mu \quad (76.17)$$

and reads

$$\mathcal{G}(w) = h_+(w) - \frac{m_B - m_D}{m_B + m_D} h_-(w), \quad (76.18)$$

where $h_+(1)$ is normalized to unity due to HQS and $h_-(1)$ vanishes in the infinite-mass limit. Thus

$$\mathcal{G}(1) = 1 + \mathcal{O}\left(\left(\frac{m_B - m_D}{m_B + m_D} \right)^2 \frac{\Lambda_{\rm QCD}}{m_c} \right) \quad (76.19)$$

and the corrections to the HQS prediction are of order $\Lambda_{\rm QCD}/m_c$ in contrast to the case of $\mathcal{F}(1)$. The lattice-QCD result for the normalization, $\mathcal{G}(1)$, obtained in Ref. [7] is

$$\mathcal{G}(1) = 1.054 \pm 0.004 \pm 0.008 \, . \quad (76.20)$$

We first turn to $|V_{cb}|$ extractions that rely on only the normalization $\mathcal{G}(1)$ from Eq. (76.20). The most precise measurements of $\bar{B} \to D \ell \bar{\nu}_\ell$ [50, 59, 60] dominate the CLN average [6] value, $\eta_{\rm EW} \mathcal{G}(1) |V_{cb}| = (41.53 \pm 0.98) \times 10^{-3}$. Note that this average corresponds to measurements that are fit to the CLN form factor parameterization; the same concerns expressed above for $\bar{B} \to D^* \ell \bar{\nu}_\ell$ apply here. Using the value from Eq. (76.20) for $\mathcal{G}(1)$ and accounting for the electroweak correction as above gives

$$|V_{cb}| = (39.1 \pm 0.9 \pm 0.4) \times 10^{-3} \ \ (\bar{B} \to D \ell \bar{\nu}_\ell, \ \text{LQCD, CLN}), \quad (76.21)$$

where the first uncertainty is from experiment, and the second combines the lattice QCD uncertainty in Eq. (76.20) with the electroweak correction.

For the $\bar{B} \to D \ell \bar{\nu}_\ell$ modes, theoretical input on the shape of the form factor, especially near $w \sim 1$, is especially beneficial to $|V_{cb}|$ determinations, since experimental measurements of the differential decays rate near zero recoil are affected by the more severe phase space suppression, compared to the D^* case. Hence the best $|V_{cb}|$ determinations from exclusive $\bar{B} \to D \ell \bar{\nu}_\ell$ decays employ lattice-QCD form factors obtained over a range of $w \geq 1$ [7, 8], where Ref. [32] provides a lattice average of the two results. Using the BCL parametrization (z-expansion from Ref. [61]) for the form factors, they can be combined with binned measurements from Belle [60] and BABAR [59]. Only Ref. [60] published the full measurement covariance matrix, while Ref. [59] provides the statistical uncertainty covariance. Nevertheless, Ref. [60] is more precise and dominates the average [32], giving

$$|V_{cb}| = (40.1 \pm 1.0) \times 10^{-3} \ \ (\bar{B} \to D \ell \bar{\nu}_\ell, \ \text{LQCD, BCL}). \quad (76.22)$$

This result is consistent with the value reported in Ref. [62], which is based on the same experimental and lattice inputs.

The $|V_{cb}|$ averages from $\bar{B} \to D^* \ell \bar{\nu}_\ell$ and $\bar{B} \to D \ell \bar{\nu}_\ell$ decays using the BGL (Eq. (76.15)) and BCL (Eq. (76.22)) forms, respectively, are reasonably consistent. The correlations between the lattice uncertainties for $\bar{B} \to D^* \ell \bar{\nu}_\ell$ and $\bar{B} \to D \ell \bar{\nu}_\ell$ are discussed in Ref. [32], and considered to be 100% for the statistical uncertainty component. We assume an experimental uncertainty correlation of order 20% and combine the results of Eq. (76.15) and Eq. (76.22), giving

$$|V_{cb}| = (39.4 \pm 0.8) \times 10^{-3} \quad \text{(exclusive)}. \quad (76.23)$$

76.2.4 $B_s \to D_s^{(*)-} \mu^+ \nu_\mu$

Semileptonic decays of B_s mesons are being studied extensively by the LHCb experiment. On the theory side, lattice QCD calculations of the corresponding form factors can proceed using the same methods and gauge-field ensembles as for B-meson decays. In fact, the presence of a strange spectator quark in the B_s-meson decay amplitudes tends to yield smaller statistical and systematic errors in the lattice computation. Nevertheless, to-date there are still fewer lattice-QCD results for B_s-meson form factors available than for the B-meson case, but this situation is quickly changing. For the case of the $B_s \to D_s$ transition, two lattice QCD calculations of the form factors over a range of recoil momenta have been performed by the HPQCD collaboration, the first on $2+1$-flavor gauge field ensembles (generated by the MILC collaboration) using NRQCD b-quarks [63]. The second calculation uses the $2+1+1$-flavor gauge-field ensembles (also generated by MILC), employing the HISQ action for all valence quarks [64]. The all-HISQ approach avoids the need to compute renormalization factors separately, at the cost of requiring an extrapolation to the physical b-quark mass at the lattice spacings used in Ref. [64]. For the $B_s \to D_s^{*-}$ transition, Ref. [31, 65] provide lattice QCD results for the form factor at zero recoil, where Ref. [65] uses a similar set-up as Ref. [64] and reads

$$\mathcal{F}^{B_s \to D_s^*}(1) = 0.9020(96)_{\rm stat}(90)_{\rm sys} \, . \quad (76.24)$$

A first lattice QCD calculation of the $B_s \to D_s^{*-}$form factors at non-zero recoil, employing ensembles with with 4 flavors of sea quarks, was recently presented in Ref. [66].

LHCb has recently extracted $|V_{cb}|$ from semileptonic B_s^0 decays [67]. The measurement uses both $B_s^0 \to D_s^- \mu^+ \nu_\mu$ and

Downloaded from https://academic.oup.com/ptep/article/2022/8/083C01/6651666 by KIT Library user on 27 September 2022

$B_s^0 \to D_s^{*-}\mu^+\nu_\mu$ decays. The value of $|V_{cb}|$ is determined from the observed yields of B_s^0 decays normalized to those of B^0 decays after correcting for the relative reconstruction and selection efficiencies. The normalization channels are $B^0 \to D^-\mu^+\nu_\mu$ and $B^0 \to D^{*-}\mu^+\nu_\mu$ decays, where the D^- is reconstructed with the same decay mode of the D_s ($D^-_{(s)} \to [K^+K^-]_\phi\pi^-$). The shape of the form factors are extracted using $p_\perp(D_s)$, which is the component of the D_s^- momentum perpendicular to the B_s^0 flight direction. This variable is correlated with q^2 and the helicity angles in the $B_s^0 \to D_s^{*-}\mu^+\nu_\mu$ decay. For the $B_s \to D_s^-\mu^+\nu_\mu$ decay, for example, $|V_{cb}|$ is related to the measured ratio of signal yields, N_{sig}, and the normalization channel yields, N_{ref}, through the relation

$$\frac{N_{sig}}{N_{ref}} = \xi \frac{f_s}{f_d} \frac{\mathcal{B}(D_s^- \to K^+K^-\pi^-)}{\mathcal{B}(D^- \to K^+K^-\pi^-)} \frac{1}{\mathcal{B}(B^0 \to D^-\mu\nu_\mu)} \tau_s \times \int \frac{d\Gamma(B_s \to D_s\mu\nu_\mu)}{dw} dw \ ,$$

where τ_s is the B_s lifetime, and ξ is the efficiency ratio between the signal and the normalization. The analysis uses the lattice-QCD form factors obtained for $B_s \to D_s^-$ over the full kinematic range in Ref. [64] and the zero-recoil result for the $B_s \to D_s^{*-}$ form factor from Ref. [65]. Fits to both the CLN parameterization and a 5-parameter version of BGL were performed. The result for $|V_{cb}|$, updated with the most recent determination of f_s/f_d and $\mathcal{B}(D_s^- \to K^-K^+\pi^-)$ from Ref. [68], are $|V_{cb}|_{\rm CLN} = (40.8 \pm 0.6 \pm 0.9 \pm 1.1) \times 10^{-3}$, and $|V_{cb}|_{\rm BGL} = (41.7 \pm 0.8 \pm 0.9 \pm 1.1) \times 10^{-3}$, where the first uncertainty is statistical, the second systematic and the third due to the limited knowledge of the external inputs, in particular the constant $f_s/f_d \times \mathcal{B}(D_s^- \to K^+K^-\pi^-)$. The results obtained are consistent with the exclusive determinations of $|V_{cb}|$ using the B^0 and B^+ decays but are not used in the overall average in this review at this stage. These channels are important in the measurement of the ratio $|V_{ub}|/|V_{cb}|$, which cancels out the B_s normalisation uncertainties, discussed in Section 76.5.

76.2.5 $|V_{cb}|$ *from inclusive decays*

Measurements of the total semileptonic branching decay rate, along with moments of the lepton energy and hadronic invariant mass spectra in inclusive semileptonic $b \to c$ transitions, can be used for a precision determination of $|V_{cb}|$. The total semileptonic decay rate can be calculated quite reliably in terms of non-perturbative parameters that can be extracted from the information contained in the moments.

76.2.6 *Inclusive semileptonic rate*

The theoretical foundation for the calculation of the total semileptonic rate is the Operator Product Expansion (OPE) which yields the Heavy Quark Expansion (HQE) [69, 70]. Details can be found in the RPP mini-review on Effective Theories [3].

The OPE result for the total rate can be written schematically (details can be found, *e.g.*, in Ref. [71]) as

$$\begin{aligned}\Gamma =& |V_{cb}|^2 \frac{G_F^2 m_b^5(\mu)}{192\pi^3} |\eta_{\rm EW}|^2 \times \\ & \Bigg[z_0^{(0)}(r) + \frac{\alpha_s(\mu)}{\pi} z_0^{(1)}(r) + \left(\frac{\alpha_s(\mu)}{\pi}\right)^2 z_0^{(2)}(r) + \cdots \\ & + \frac{\mu_\pi^2}{m_b^2}\left(z_2^{(0)}(r) + \frac{\alpha_s(\mu)}{\pi} z_2^{(1)}(r) + \cdots \right) \\ & + \frac{\mu_G^2}{m_b^2}\left(y_2^{(0)}(r) + \frac{\alpha_s(\mu)}{\pi} y_2^{(1)}(r) + \cdots \right) \\ & + \frac{\rho_{\rm D}^3}{m_b^3}\left(z_3^{(0)}(r) + \frac{\alpha_s(\mu)}{\pi} z_3^{(1)}(r) + \cdots \right) \\ & + \frac{\rho_{\rm LS}^3}{m_b^3}\left(y_3^{(0)}(r) + \frac{\alpha_s(\mu)}{\pi} y_3^{(1)}(r) + \cdots \right) + ... \Bigg] \end{aligned} \quad (76.25)$$

where r is the ratio m_c/m_b and the y_i and z_i are perturbatively calculable Wilson coefficients functions that appear at different orders of the heavy mass expansion.

The parameters μ_π^2, μ_G^2, ρ_D^3 and ρ_{LS}^3 constitute the non-perturbative input into the heavy quark expansion; they correspond to certain matrix elements to be discussed below. In the same way the HQE can be set up for the moments of distributions of charged-lepton energy, hadronic invariant mass and hadronic energy, e.g.

$$\langle E_e^n \rangle_{E_e > E_{\rm cut}} = \int_{E_{\rm cut}}^{E_{\rm max}} \frac{d\Gamma}{dE_e} E_e^n dE_e \Bigg/ \int_{E_{\rm cut}}^{E_{\rm max}} \frac{d\Gamma}{dE_e} dE_e \ . \quad (76.26)$$

The coefficients of the HQE are known up to order $1/m_b^5$ at tree level [72–75]. The leading term $z_0^{(i)}$ is the parton model, and is known completely through order α_s^2 [76–78] and now also at α_s^3 [79]. The terms of order $\alpha_s^{n+1}\beta_0^n$ (where β_0 is the first coefficient of the QCD β function, $\beta_0 = (33 - 2n_f)/3$) have been included following the BLM procedure [71, 80–83]. Corrections of order $\alpha_s\mu_\pi^2/m_b^2$ have been computed in Ref. [84] and Ref. [85], while the $\alpha_s\mu_G^2/m_b^2$ terms have been calculated in Ref. [86] and Ref. [87], and the $\alpha_s\rho_D^3/m_b^3$ corrections in Ref. [88].

Starting at order $1/m_b^3$ contributions with an infrared sensitivity to the charm mass, m_c, appear [72, 74, 89, 90]. At order $1/m_b^3$ this "intrinsic charm" contribution manifests as a $\log(m_c)$ in the coefficient of the Darwin term ρ_D^3. At higher orders, terms such as $1/m_b^3 \times 1/m_c^2$ and $\alpha_s(m_c)1/m_b^3 \times 1/m_c$ appear, which are comparable in size to the contributions of order $1/m_b^4$.

The HQE parameters are given in terms of forward matrix elements of local operators; the parameters entering the expansion for orders up to $1/m_b^3$ are ($D_\perp^\mu = (g_{\mu\nu} - v_\mu v_\nu)D^\nu$, where $v = p_B/M_B$ is the four-velocity of the B meson)

$$\begin{aligned} \overline{\Lambda} &= M_B - m_b \ , \\ \mu_\pi^2 &= -\langle B|\bar{b}(iD_\perp)^2 b|B\rangle \ , \\ \mu_G^2 &= \langle B|\bar{b}(iD_\perp^\mu)(iD_\perp^\nu)\sigma_{\mu\nu} b|B\rangle \ , \\ \rho_{\rm D}^3 &= \langle B|\bar{b}(iD_{\perp\mu})(ivD)(iD_\perp^\mu) b|B\rangle \ , \\ \rho_{\rm LS}^3 &= \langle B|\bar{b}(iD_\perp^\mu)(ivD)(iD_\perp^\nu)\sigma_{\mu\nu} b|B\rangle . \end{aligned} \quad (76.27)$$

These parameters still depend on the heavy quark mass. Sometimes the infinite mass limits of these parameters $\overline{\Lambda} \to \overline{\Lambda}_{\rm HQET}$, $\mu_\pi^2 \to -\lambda_1$, $\mu_G^2 \to 3\lambda_2$, $\rho_D^3 \to \rho_1$ and $\rho_{LS}^3 \to 3\rho_2$, are used instead. Beyond $1/m^3$ the number of independent HQE parameters starts to proliferate [91]. In general, there are 13 parameters (at tree level) up to order $1/m^4$ and 31 (at tree level) up to order $1/m^5$, not including $\overline{\Lambda}$. The HQE parameters of the orders $1/m_b^4$ and $1/m_b^5$ have been estimated in Ref. [75, 92], their impact on the $|V_{cb}|$ determination has been studied in Ref. [93]. However, as pointed out in Ref. [94]one may reduce the number of independent parameters in the HQE by exploiting reparametrization invariance, which is a symmetry of the HQE stemming from Lorentz invariance of QCD. For a subset of observables this allows us to reduce the number of parameters to three up to order $1/m^3$ (ρ_{LS}^3 can be absorbed into μ_G^2 by a re-definition) and to 8 up to order $1/m^4$ [95].

The perturbative QCD expansion for the decay rate does not converge, in general. In addition, the expansion coefficients in the rates and spectra depend strongly on the scheme used for m_b (or equivalently on $\overline{\Lambda}$). It is well known (see eg. [96]) that using the pole mass definition for heavy quark masses leads to particularly badly behaved expansions. This motivates the use of "short-distance" mass definitions, such as the kinetic scheme [33] or the $1S$ scheme [97–99]. Both schemes are well suited for the HQE, since they allow the choice of the renormalization scale $\mu \leq m_b$. Furthermore, in both schemes, the masses can be extracted from other observables with sufficient precision, enabling a precise determination of $|V_{cb}|$, despite of the strong quark-mass dependence of the total rate.

The $1S$ scheme eliminates the b quark pole mass by relating it to the perturbative expression for the mass of the $1S$ state of the Υ system. The b quark mass in the $1S$ scheme is half of the perturbatively calculated mass of the $1S$ state of the Υ system. The best determination of the b quark mass in the $1S$ scheme is obtained

Downloaded from https://academic.oup.com/ptep/article/2022/8/083C01/6651666 by KIT Library user on 27 September 2022

from sum rules for $e^+e^- \to b\bar{b}$ [100]. A second alternative is the so-called "kinetic mass" $m_b^{\rm kin}(\mu)$, which enters the non-relativistic expression for the kinetic energy of a heavy quark, and is defined using heavy-quark sum rules [33]. The relation between $m_b^{\rm kin}$ and $m_b^{\overline{MS}}$ is known through three-loop order [101].

Finally, we note that the theoretical description of inclusive decays employed here, is based on the assumption of quark-hadron duality. While there is no evidence of violations of quark-hadron duality, the theoretical uncertainties due to such violations are not well quantified [3].

76.2.7 *Determination of HQE Parameters and $|V_{cb}|$*

Several experiments have measured moments in $\bar{B} \to X_c \ell \bar{\nu}_\ell$ decays [102–110] as a function of the minimum lepton momentum. The measurements of the moments of the electron energy spectrum ($0^{\rm th}$-$3^{\rm rd}$) and of the squared hadronic mass spectrum ($0^{\rm th}$-$2^{\rm nd}$) have statistical uncertainties that are roughly equal to their systematic uncertainties. The $3^{\rm rd}$ order hadronic mass spectrum moments have also been measured by some experiments, with relatively large statistical uncertainty. The sets of moments measured within each experiment have strong correlations; their use in a global fit requires fully specified statistical and systematic covariance matrices. Measurements of photon energy moments ($0^{\rm th}$-$2^{\rm nd}$) in $B \to X_s\gamma$ decays [111–115] as a function of the minimum accepted photon energy are also used in some fits; the dominant uncertainties on these measurements are statistical.

Global fits [110, 112, 116–121] to the full set of moments have been performed in the $1S$ and kinetic schemes. The semileptonic moments alone determine a linear combination of m_b and m_c very accurately but leave the orthogonal combination poorly determined (See e.g. [122]); additional input is required to allow a precise determination of m_b. This additional information can come from the radiative $B \to X_s\gamma$ moments (with the caveat that the OPE for $b \to s\gamma$ breaks down beyond leading order in $\Lambda_{\rm QCD}/m_b$), which provide complementary information on m_b and μ_π^2, or from precise determinations of the charm quark mass [32,123]. The values obtained in the kinetic scheme fits [6,120,121] with these two constraints are consistent. Based on the charm quark mass constraint $m_c^{\overline{\rm MS}}(3\,{\rm GeV}) = 0.986 \pm 0.013\,{\rm GeV}$ [124], a fit in the kinetic scheme [6] obtains

$$|V_{cb}| = (42.19 \pm 0.78) \times 10^{-3} \tag{76.28}$$

$$m_b^{\rm kin} = (4.554 \pm 0.018)\,{\rm GeV} \tag{76.29}$$

$$\mu_\pi^2({\rm kin}) = (0.464 \pm 0.076)\,{\rm GeV}^2, \tag{76.30}$$

where the errors include experimental and theoretical uncertainties. Theoretical uncertainties from higher orders in $1/m$ as well as in α_s are estimated and included in performing the fits. Similar values for the parameters are obtained with a variety of assumptions about the theoretical uncertainties and their correlations. The χ^2/dof is well below unity in all fits, which could suggest that the theoretical uncertainties may be overestimated. However, while one could obtain a satisfactory fit with smaller uncertainties, this would result in unrealistically small uncertainties on the extracted HQE parameters, which are used as input to other calculations (e.g. the determination of $|V_{ub}|$). The mass in the $\overline{\rm MS}$ scheme corresponding to Eq. (76.29) is $m_b^{\overline{\rm MS}} = 4.19 \pm 0.04\,{\rm GeV}$, where the uncertainty includes a contribution from the translation between mass schemes; this can be compared to the result quoted in the FLAG review [32], $m_b^{\overline{\rm MS}} = (4.198 \pm 0.012)$ GeV, which provides a non-trivial cross-check.

A fit to the measured moments in the $1S$ scheme [6, 112, 119] gives

$$|V_{cb}| = (41.98 \pm 0.45) \times 10^{-3}, \tag{76.31}$$

$$m_b^{1S} = (4.691 \pm 0.037)\,{\rm GeV}, \tag{76.32}$$

$$\lambda_1(1S) = (-0.362 \pm 0.067)\,{\rm GeV}^2. \tag{76.33}$$

This fit uses moments measurements from semileptonic and radiative decays and constrains the chromomagnetic operator using the B^*-B and D^*-D mass differences, but does not include the constraint on m_c nor all known higher order corrections.

The fits in the two renormalization schemes give consistent results for $|V_{cb}|$ and, after translation to a common renormalization scheme, for m_b and μ_π^2. We take the fit in the kinetic scheme [121], which includes higher-order corrections and results in a more conservative uncertainty, as the inclusive determination of $|V_{cb}|$:

$$|V_{cb}| = (42.2 \pm 0.8) \times 10^{-3} \text{ (inclusive)}. \tag{76.34}$$

The precision of the global fit results can be further improved by calculating higher-order perturbative corrections to the coefficients of the HQE parameters. Indeed, a very recent analysis presented in Ref. [125] includes calculations of the third-order corrections to the semi-leptonic $b \to c\ell\nu$ decay width [79] and mass relations [101, 126] to obtain a value for $|V_{cb}|$ with smaller total uncertainty than in Eq. (76.34). They obtain $|V_{cb}| = (42.16 \pm 0.51) \times 10^{-3}$, as well as an independent determination of $m_b^{\overline{\rm MS}}$, without direct constraints, $m_b^{\overline{\rm MS}} = 4.210 \pm 0.022)$GeV. Ultimately measurements of higher order moments and moments of additional variables, such as q^2, will further improve the sensitivity of the fits to higher-order terms in the HQE [95]. The Belle experiment has recently reported new measurements of q^2 moments in inclusive $b \to c\ell\nu$ decays Ref. [127], but they are not yet included in the global fit.

76.3 Determination of $|V_{ub}|$

Summary: Currently the best determinations of $|V_{ub}|$ are from $\bar{B} \to \pi\ell\bar{\nu}_\ell$ decays, where combined fits to theory and experimental data as a function of q^2 provide a precision of about 4%; the uncertainties from experiment and theory are comparable in size. Determinations based on inclusive semileptonic B decays are based on different observables and use different strategies to suppress the $b \to c$ background. Most of the determinations are consistent and provide a precision of about 7%, with comparable contributions to the uncertainty from experiment and theory.

The values obtained from inclusive and exclusive B decay determinations are

$$|V_{ub}| = (4.13 \pm 0.12\,^{+\,0.13}_{-\,0.14} \pm 0.18) \times 10^{-3} \quad \text{(inclusive)}, \tag{76.35}$$

$$|V_{ub}| = (3.70 \pm 0.10 \pm 0.12) \times 10^{-3} \quad \text{(exclusive)}, \tag{76.36}$$

where the last uncertainty on the inclusive result was added by the authors of this review and is discussed below. The exclusive and inclusive determinations are independent, and the dominant uncertainties are on multiplicative factors. The results from the two determinations are compatible to within two standard deviations.

This can be compared to the values derived from $|V_{ub}|/|V_{cb}|$ ratio measurements, described in the next section. Taking the value for this ratio from Eq. (76.56), and $|V_{cb}|$ from Eq. (76.3) we obtain.

$$|V_{ub}| = (3.43 \pm 0.32) \times 10^{-3} \qquad ({\rm B_s},\ \Lambda_{\rm b}), \tag{76.37}$$

We choose to combine only the direct determinations of $|V_{ub}|$, based on the inclusive and exclusive B measurements. In the combination they are weighted by their relative errors, where the uncertainties are treated as normally distributed. The resulting average has $p(\chi^2) = 15\%$, so we scale the error by $\sqrt{\chi^2/1} = 1.4$ to find

$$|V_{ub}| = (3.82 \pm 0.20) \times 10^{-3} \quad \text{(average)}. \tag{76.38}$$

In a future update we will consider the constraints in the $|V_{ub}|$-$|V_{cb}|$ plane from the direct determinations together with the LHCb $|V_{ub}/V_{cb}|$ results. This will require a better understanding of $|V_{ub}/V_{cb}|$ extractions across a more complete range in q^2, and with finer binning to compare between theory and experiment.

76.3.1 *$|V_{ub}|$ from inclusive decays*

The theoretical description of inclusive $\bar{B} \to X_u\ell\bar{\nu}_\ell$ decays is based on the Heavy Quark Expansion and leads to a predicted total decay rate with uncertainties below 5% [98, 128]. However, the total decay rate is hard to measure due to the large background from CKM-favored $\bar{B} \to X_c\ell\bar{\nu}_\ell$ transitions, and hence the theoretical methods differ from the $\bar{B} \to X_c\ell\bar{\nu}_\ell$ case. For a calculation of the partial decay rate in regions of phase space where

Downloaded from https://academic.oup.com/ptep/article/2022/8/083C01/6651666 by KIT Library user on 27 September 2022

$\bar{B} \to X_c \ell \bar{\nu}_\ell$ decays are suppressed one cannot use the HQE as for $b \to c$, rather one needs to introduce non-perturbative distribution functions, the "shape functions" (SF) [129, 130]. Their exact form is not known, but its moments can be related to the HQE parameters known e.g from the $b \to c$ case.

The shape functions become important when the light-cone momentum component $P_+ \equiv E_X - |P_X|$ is not large compared to Λ_{QCD}, as is the case near the endpoint of the $\bar{B} \to X_u \ell \bar{\nu}_\ell$ lepton spectrum. Partial rates for $\bar{B} \to X_u \ell \bar{\nu}_\ell$ are predicted and measured in a variety of kinematic regions that differ in their sensitivity to shape-function effects.

At leading order in $1/m_b$ only a single shape function (SF) appears, which is universal for all heavy-to-light transitions [129, 130] and can be extracted in $\bar{B} \to X_s \gamma$ decays. At subleading order in $1/m_b$, several shape functions appear [131], along with small "resolved photon contributions" specific for $\bar{B} \to X_s \gamma$ [132–134], and thus the prescriptions that relate directly the partial rates for $\bar{B} \to X_s \gamma$ and $\bar{B} \to X_u \ell \bar{\nu}_\ell$ decays [135–143] are limited to leading order in $1/m_b$.

Existing approaches use parametrizations of the leading SF that respect constraints on the normalization and on the first and second moments, which are given in terms of the HQE parameters $\bar{\Lambda} = M_B - m_b$ and μ_π^2, respectively. The relations between SF moments and the HQE parameters are known to second order in α_s [144]; as a result, measurements of HQE parameters from global fits to $\bar{B} \to X_c \ell \bar{\nu}_\ell$ and $\bar{B} \to X_s \gamma$ moments can be used to constrain the SF moments, as well as to provide accurate values of m_b and other parameters for use in determining $|V_{ub}|$. Flexible parametrizations of the SF using orthogonal basis functions [145] or artificial neural networks [146] allow global fits to inclusive B meson decay data [134] that incorporate the known short-distance contributions and renormalization properties of the SF.

HFLAV performs fits on the basis of several approaches, with varying degrees of model dependence. We will consider here the approaches documented in Ref. [147] (BLNP), Ref. [148] (GGOU) and Ref. [149] (DGE).

The triple differential rate in the variables

$$P_\ell = M_B - 2E_\ell, \quad P_- = E_X + |\vec{P}_X|, \quad P_+ = E_X - |\vec{P}_X| \quad (76.39)$$

is

$$\frac{d^3\Gamma}{dP_+\, dP_-\, dP_\ell} = \frac{G_F^2 |V_{ub}|^2}{16\pi^2}(M_B - P_+) \quad (76.40)$$
$$\Big\{(P_- - P_\ell)(M_B - P_- + P_\ell - P_+)\mathcal{F}_1 + (M_B - P_-)(P_- - P_+)\mathcal{F}_2 + (P_- - P_\ell)(P_\ell - P_+)\mathcal{F}_3\Big\}.$$

The "structure functions", $\mathcal{F}_i$, can be calculated using factorization theorems that have been proven to subleading order in the $1/m_b$ expansion [150].

The BLNP [147] calculation uses these factorization theorems to write the $\mathcal{F}_i$ terms as functions of perturbatively calculable hard coefficients and jet functions, which are convolved with the (soft) light-cone distribution functions.The calculation of $\mathcal{O}(\alpha_s^2)$ contributions [151, 152] is not yet complete and is not included in the $|V_{ub}|$ determination given below.

The leading order term in the $1/m_b$ expansion of the $\mathcal{F}_i$ terms contains a single non-perturbative function and is calculated to subleading order in α_s, while at subleading order in the $1/m_b$ expansion there are several independent non-perturbative functions that have been calculated only at tree level in the α_s expansion.

A distinct approach (GGOU) [148] uses a hard, Wilsonian cutoff that matches the definition of the kinetic mass. The non-perturbative input is similar to what is used in BLNP, but the shape functions are defined differently. In particular, they are defined at finite m_b and depend on the light-cone component k_+ of the b quark momentum and on the momentum transfer q^2 to the leptons. These functions include subleading effects to all orders; as a result they are non-universal, with one shape function corresponding to each structure function in Eq. (76.40). Their k_+ moments can be computed in the OPE.

Going to subleading order in α_s requires the definition of a renormalization scheme for the HQE parameters and for the SF. The relation between the moments of the SF and the forward matrix elements of local operators appearing the HQE is plagued by ultraviolet problems and requires additional renormalization. A scheme for improving this behavior was suggested in Ref. [147] and Ref. [153], which introduce a definition of the quark mass (the so-called shape-function scheme) based on the first moment of the measured $\bar{B} \to X_s \gamma$ photon energy spectrum. Likewise, the HQE parameters can be defined from measured moments of spectra, corresponding to moments of the SF.

There are various ideas to model the SF, but this requires additional assumptions. One approach (DGE) is the so-called "dressed gluon exponentiation" [149], where the perturbative result is continued into the infrared regime using the renormalon structure obtained in the large β_0 limit, where β_0 has been defined following Eq. (76.25). Other approaches make even stronger assumptions, such as in Ref. [154], which assumes an analytic behavior for the strong coupling in the infrared to perform an extrapolation of perturbation theory.

In order to reduce sensitivity to SF uncertainties, measurements that use a combination of cuts on the leptonic momentum transfer q^2 and the hadronic invariant mass m_X, as suggested in Ref. [155, 156], have been made. In general, experimental measurements of $\bar{B} \to X_u \ell \bar{\nu}_\ell$ into charm-dominated regions (in order to reduce SF uncertainties) are sensitive to the modeling of $\bar{B} \to X_u \ell \bar{\nu}_\ell$ and $\bar{B} \to X_c \ell \bar{\nu}_\ell$ decays. The measurements quoted below have used a variety of functional forms to parametrize the leading SF; a specific error budget for one determination is quoted in the next section. In no case is the parametrization uncertainty estimated to be more than a 2% on $|V_{ub}|$.

Weak Annihilation [148, 157, 158] (WA) can in principle contribute significantly in the high-q^2 region of $\bar{B} \to X_u \ell \bar{\nu}_\ell$ decays. Estimates based on semileptonic D_s decays [90, 155, 156, 158] lead to a $\sim 2\%$ uncertainty on the total $\bar{B} \to X_u \ell \bar{\nu}_\ell$ rate from the $\Upsilon(4S)$. The q^2 spectrum of the WA contribution is not well known, but from the OPE it is expected to contribute predominantly at high q^2. Other theoretical investigations [90, 159, 160], a direct search [161], and $\mathcal{B}(B^0 \to X_u \ell \bar{\nu})/\mathcal{B}(B^+ \to X_u \ell \bar{\nu})$ ratio measurements [162–164] indicate that WA is a small effect, but may become a significant source of uncertainty for $|V_{ub}|$ measurements that accept only a small fraction of the full $\bar{B} \to X_u \ell \bar{\nu}_\ell$ phase space.

76.3.2 *Measurements*

We summarize the measurements used in the determination of $|V_{ub}|$ below. Given the improved precision and more rigorous theoretical interpretation of more recent measurements, determinations [165–168] done with LEP data are not considered in this review.

Inclusive electron momentum measurements [169, 170] reconstruct a single charged electron to determine a partial decay rate for $\bar{B} \to X_u \ell \bar{\nu}_\ell$ near the kinematic endpoint. This results in a selection efficiency of order 50% and only modest sensitivity to the modeling of detector response. The inclusive electron momentum spectrum from $B\bar{B}$ events, after subtraction of the $e^+e^- \to q\bar{q}$ continuum background, is fitted to a model $\bar{B} \to X_u \ell \bar{\nu}_\ell$ spectrum and several components ($D\ell\bar{\nu}_\ell$, $D^*\ell\bar{\nu}_\ell$, ...) of the $\bar{B} \to X_c \ell \bar{\nu}_\ell$ background; the dominant uncertainties are related to this subtraction and modelling. The decay rate can be cleanly extracted for $E_e > 2.3\,\mathrm{GeV}$, but this is deep in the SF region, where theoretical uncertainties are large. More recent measurements have increased the accessed phase phase. The resulting $|V_{ub}|$ values for various E_e cuts are given in Table 76.1.

The most recent BABAR measurement [171] is based on the inclusive electron spectrum and determines the partial branching fraction and $|V_{ub}|$ for $E_e > 0.8\,\mathrm{GeV}$. The analysis shows that the partial branching fraction measurements can have signal model dependence when the kinematic acceptance includes regions dominated by $\bar{B} \to X_c \ell \bar{\nu}_\ell$ background. The model dependence enters primarily through the partial branching fractions, and arises because the signal yield fit has sensitivity to $\bar{B} \to X_u \ell \bar{\nu}_\ell$ decays only in regions with good signal to noise.

An untagged "neutrino reconstruction" measurement [172] from

Downloaded from https://academic.oup.com/ptep/article/2022/8/083C01/6651666 by KIT Library user on 27 September 2022

BABAR uses a combination [173] of a high-energy electron with a measurement of the missing momentum vector. This allows S/B ~ 0.7 for $E_e > 2.0$ GeV and a $\approx 5\%$ selection efficiency, but at the cost of a smaller accepted phase space for $\bar{B} \to X_u \ell \bar{\nu}_\ell$ decays and uncertainties associated with the determination of the missing momentum.

The large samples accumulated at the B factories allow studies in which one B meson is fully reconstructed and the recoiling B decays semileptonically [174–177]. The experiments can fully reconstruct a "tag" B candidate in about 0.5% (0.3%) of B^+B^- ($B^0\bar{B}^0$) events. An electron or muon with center-of-mass momentum above 1.0 GeV is required amongst the charged tracks not assigned to the tag B and the remaining particles are assigned to the X_u system. The full set of kinematic properties (E_ℓ, m_X, q^2, *etc.*) are available for studying the semileptonically decaying B, making possible selections that accept up to 90% of the full $\bar{B} \to X_u \ell \bar{\nu}_\ell$ rate; however, the sensitivity to $\bar{B} \to X_u \ell \bar{\nu}_\ell$ decays is still driven by the regions where $\bar{B} \to X_c \ell \bar{\nu}_\ell$ decays are suppressed. Despite requirements (e.g. on the square of the missing mass) aimed at rejecting events with additional missing particles, undetected or mis-measured particles from $\bar{B} \to X_c \ell \bar{\nu}_\ell$ decay (e.g., K_L^0 and additional neutrinos) remain an important source of uncertainty.

A new recoil method measurement of partial branching fractions in three phase-space regions, covering about 31% to 86% of the accessible phase space, was performed by Belle [162], where machine learning techniques were used to reduce background levels. The measurement contains substantial decay model updates and supersedes previous measurements from Belle [175,176]. The measurement of the partial branching fraction obtained in the $E_\ell^B > 1$GeV region, the most precise one, is used to obtain $|V_{ub}|$ [162]. Belle also reports preliminary measurements of the background subtracted, and unfolded differential decay spectra in bins of m_X, m_X and q^2, P_+ and E_ℓ [178] for use in global fit analyses. Earlier measurements by BABAR [174] were also performed with cuts on m_X, m_X and q^2, P_+ and E_ℓ using the recoil method. In each case the experimental systematic uncertainties have significant contributions from the modeling of $\bar{B} \to X_u \ell \bar{\nu}_\ell$ and $\bar{B} \to X_c \ell \bar{\nu}_\ell$ decays and from the detector response to charged particles, photons and neutral hadrons. The corresponding $|V_{ub}|$ values are given in Table 76.1.

76.3.3 $|V_{ub}|$ *from inclusive partial rates*

The measured partial rates and theoretical calculations from BLNP, GGOU and DGE described previously are used to determine $|V_{ub}|$ from all measured partial $\bar{B} \to X_u \ell \bar{\nu}_\ell$ rates [6]; selected values are given in Table 76.1. The correlations amongst the multiple BABAR recoil-based measurements [174] are fully accounted for in the average. The statistical correlations amongst the other measurements used in the average are small (due to small overlaps among signal events and large differences in S/B ratios) and have been ignored. Correlated systematic and theoretical errors are taken into account, both within an experiment and between experiments. As an illustration of the relative sizes of the uncertainties entering $|V_{ub}|$ we give the error breakdown for the GGOU average: statistical—1.3%; experimental—1.6%; $\bar{B} \to X_c \ell \bar{\nu}_\ell$ modeling—0.9%; $\bar{B} \to X_u \ell \bar{\nu}_\ell$ modeling—1.7%; HQE parameters (m_b) — 1.8%; higher-order corrections—1.5%; q^2 modeling—1.3%; Weak Annihilation—$^{+0.0}_{-1.1}$%; SF parametrization—0.1%.

The averages quoted here are based on the following m_b values: $m_b^{SF} = 4.582 \pm 0.023 \pm 0.018$ GeV for BLNP, $m_b^{\rm kin} = 4.554 \pm 0.018$ GeV for GGOU, and $m_b^{\overline{MS}} = 4.188 \pm 0.043$ GeV for DGE. The $m_b^{\rm kin}$ value is determined in a global fit to moments in the kinetic scheme [6]; this value is translated into m_b^{SF} and $m_b^{\overline{MS}}$ at fixed order in α_s. The second uncertainty quoted on m_b arises from the scheme translation.

Hadronization uncertainties also impact the $|V_{ub}|$ determination. The theoretical expressions are valid at the parton level and do not incorporate any resonant structure (*e.g.* $\bar{B} \to \pi \ell \bar{\nu}_\ell$); this must be added to the simulated $\bar{B} \to X_u \ell \bar{\nu}_\ell$ event samples, since the detailed final state multiplicity and structure impacts the estimates of experimental acceptance and efficiency. The experiments have adopted procedures to input resonant structure while preserving the appropriate behavior in the kinematic variables (q^2, E_ℓ, m_X) averaged over the sample, but these prescriptions are *ad hoc* and ultimately require *in situ* calibration. The resulting uncertainties have been estimated to be $\sim$ 1-2% on $|V_{ub}|$.

All calculations yield compatible $|V_{ub}|$ values and similar error estimates. The arithmetic mean of the values and errors of the HFLAV combinations listed in Table 76.1 is $|V_{ub}| = (4.13 \pm 0.12_{\rm exp}\ ^{+0.13}_{-0.14\ \rm theo}) \times 10^{-3}$, although there is a spread of approximately 10% in the evaluations with the three theoretical models. For reasons discussed below, we assign an additional uncertainty due to model dependence that is not reflected in the HFLAV averages. As highlighted in the BABAR analysis [171], model dependence entering measurement procedures can be sizeable, and is not consistently treated across analyses. Many of the analyses shown in Table 76.1 were based on partial branching fraction measurements determined in a single model (i.e. the one used by that analysis when simulating $\bar{B} \to X_u \ell \bar{\nu}_\ell$ decays), although in some cases simulated events were weighted to match the expected spectra in other models and the differences introduced as systematic uncertainties, e.g. Ref. [176]. The $|V_{ub}|$ value quoted by HFLAV for each model are, typically, derived from this unique partial branching fraction combined with another model-specific partial rate calculation. The model dependence in the partial branching fraction is sensitive to how the model predictions compare in the restricted region with good signal-to-noise, not by how they compare when integrated over the full kinematic range used in the fit. Ideally this effect needs to be accounted for by the experiments; the published information is insufficient to determine it. To account for the range in results using the different theoretical models, we take half of the spread of the averages as an additional systematic uncertainty, denoted Δmodel. With this addition, the inclusive $|V_{ub}|$ average is

$$|V_{ub}| = (4.13 \pm 0.12_{\rm exp}\ ^{+0.13}_{-0.14\ \rm theo} \pm 0.18_{\Delta \rm model}) \times 10^{-3} \quad \text{(inclusive)}. \tag{76.41}$$

76.3.4 $|V_{ub}|$ *from exclusive decays*

Exclusive charmless semileptonic decays offer a complementary means of determining $|V_{ub}|$. For the experiments, the specification of the final state provides better background rejection, but the branching fraction to a specific final state is typically only a few percent of that for inclusive decays. For theory, the calculation of the form factors for $\bar{B} \to X_u \ell \bar{\nu}_\ell$ decays is challenging, but brings in a different set of uncertainties from those encountered in inclusive decays. In this review we focus on $\bar{B} \to \pi \ell \bar{\nu}_\ell$, as it is the most promising decay mode for both experiment and theory. Measurements of other exclusive $\bar{B} \to X_u \ell \bar{\nu}_\ell$ decays can be found in Refs. [179–192].

76.3.5 $\bar{B} \to \pi \ell \bar{\nu}_\ell$ *form factor calculations*

The relevant form factors for the decay $\bar{B} \to \pi \ell \bar{\nu}_\ell$ are usually defined as

$$\langle \pi(p_\pi) | V^\mu | B(p_B) \rangle = f_+(q^2) \left[p_B^\mu + p_\pi^\mu - \frac{m_B^2 - m_\pi^2}{q^2} q^\mu \right] + f_0(q^2) \frac{m_B^2 - m_\pi^2}{q^2} q^\mu \tag{76.42}$$

in terms of which the rate becomes (in the limit $m_\ell \to 0$)

$$\frac{d\Gamma}{dq^2} = \frac{G_F^2 |V_{ub}|^2}{24\pi^3} |p_\pi|^3 |f_+(q^2)|^2, \tag{76.43}$$

where p_π is the pion momentum in the B meson rest frame.

Lattice-QCD calculations of the form factors for the $B \to \pi \ell \bar{\nu}$ and $B_s \to K \ell \bar{\nu}$ transitions are available from the Fermilab/MILC [193, 194], HPQCD [195], and RBC/UKQCD [196] collaborations. The lattice form factors are obtained in the large q^2 region, $q^2_{\rm max} > q^2 \gtrsim 15\,{\rm GeV}^2$ and the calculations differ in actions employed for the b quark. While HPQCD [195] is using lattice-nonrelativistic QCD, the results from Fermilab/MILC [193, 194]and RBC/UKQCD [196] are obtained with relativistic b quark actions based on the Fermilab approach [197]. The results agree within the quoted errors. For the $B \to \pi$

Downloaded from https://academic.oup.com/ptep/article/2022/8/083C01/6651666 by KIT Library user on 27 September 2022

Table 76.1: $|V_{ub}|$ (in units of 10^{-5}) from inclusive $\bar{B} \to X_u \ell \bar{\nu}_\ell$ measurements. The first uncertainty on $|V_{ub}|$ is experimental, while the second includes both theoretical and HQE parameter uncertainties. The values are generally listed in order of increasing kinematic acceptance, f_u (0.19 to 0.90), except for the BABAR E_e >0.8 GeV measurement; those below the horizontal bar are based on recoil methods.

Ref.	cut (GeV)	BLNP	GGOU	DGE
CLEO [169]	$E_e > 2.1$	$422 \pm 49 \,^{+29}_{-34}$	$423 \pm 49 \,^{+22}_{-31}$	$386 \pm 45 \,^{+25}_{-27}$
BABAR [172]	$E_e - q^2$	$471 \pm 32 \,^{+33}_{-38}$	not available	$435 \pm 29 \,^{+28}_{-30}$
Belle [170]	$E_e > 1.9$	$493 \pm 46 \,^{+26}_{-29}$	$495 \pm 46 \,^{+16}_{-21}$	$482 \pm 45 \,^{+23}_{-23}$
BABAR [171]	$E_e > 0.8$	$441 \pm 12 \,^{+27}_{-27}$	$396 \pm 10 \,^{+17}_{-17}$	$385 \pm 11 \,^{+8}_{-7}$
BABAR [174]	$q^2>8$, $m_X<1.7$	$432 \pm 23 \,^{+26}_{-28}$	$433 \pm 23 \,^{+24}_{-27}$	$424 \pm 22 \,^{+18}_{-21}$
BABAR [174]	$P_+ < 0.66$	$409 \pm 25 \,^{+25}_{-25}$	$425 \pm 26 \,^{+26}_{-27}$	$417 \pm 25 \,^{+28}_{-37}$
BABAR [174]	$m_X < 1.7$	$403 \pm 22 \,^{+22}_{-22}$	$410 \pm 23 \,^{+16}_{-17}$	$422 \pm 23 \,^{+21}_{-27}$
BABAR [174]	$E_\ell > 1.3$	$433 \pm 24 \,^{+19}_{-21}$	$444 \pm 24 \,^{+9}_{-10}$	$445 \pm 24 \,^{+12}_{-13}$
Belle [162]	$E_\ell > 1$	$405 \pm 23 \,^{+18}_{-20}$	$415 \pm 24 \,^{+8}_{-9}$	$416 \pm 24 \,^{+11}_{-12}$
HFLAV [6]	Combination	$428 \pm 13 \,^{+20}_{-21}$	$419 \pm 12 \,^{+11}_{-12}$	$392 \pm 10 \,^{+9}_{-10}$

form factor $f_+(q^2 = 20\,\mathrm{GeV}^2)$, Ref. [193] quotes uncertainty of 3.4%evaluated at $q^2 = 20\,\mathrm{GeV}^2$, where the leading contribution is due to the chiral-continuum extrapolation fit, which includes statistical and heavy-quark discretization errors.

The extrapolation to small values of q^2 is performed using guidance from analyticity and unitarity. Making use of the heavy-quark limit, stringent constraints on the shape of the form factor can be derived [198], and the conformal mapping of the kinematical variables onto the complex unit disc yields a rapidly converging series in the variable

$$z = \frac{\sqrt{t_+ - t_-} - \sqrt{t_+ - q^2}}{\sqrt{t_+ - t_-} + \sqrt{t_+ - q^2}} \,, \tag{76.44}$$

where $t_\pm = (M_B \pm m_\pi)^2$. The use of lattice data in combination with experimental measurements of the differential decay rate provides a stringent constraint on the shape of the form factor in addition to precise determination of $|V_{ub}|$ [199].

LCSR calculations provide estimates for the product $f_B f_+(q^2)$, valid in the region $0 < q^2 \lesssim 12$ GeV. The determination of $f_+(q^2)$ itself requires knowledge of the decay constant f_B, which is usually obtained by replacing f_B by its two-point QCD (SVZ) sum rule [200] in terms of perturbative and condensate contributions. The advantage of this procedure is the approximate cancellation of various theoretical uncertainties in the ratio $(f_B f_+)/(f_B)$. The LCSR for $f_B f_+$ is based on the light-cone OPE of the relevant vacuum-to-pion correlation function, calculated in full QCD at finite b-quark mass. The resulting expressions comprise a triple expansion: in the twist, t, of the operators near the light-cone, in α_s, and in the deviation of the pion distribution amplitudes from their asymptotic form, which is fixed from conformal symmetry. The state-of-the-art calculations include the leading twists two, three and four with full one-loop α_s corrections [201,202] and partial two-loop corrections [203]. Higher-twist contributions have been investigated in Ref. [204] and two-particle higher twist contributions are studied in Ref. [39]. Nevertheless, estimates based on LCSR generally suffer from difficult to quantify systematic uncertainties.

A detailed statistical analysis including the various correlations has been performed in Ref. [205], also including unitarity bounds on the form factor. The results obtained are numerically compatible with the lattice QCD calculations of the form factor. For a determination of V_{ub} one may use the partial rate expressed by the integral

$$\Delta\zeta(0, q^2_{max}) = \frac{G_F^2}{24\pi^3} \int_0^{q^2_{max}} dq^2\, p_\pi^3 |f_+(q^2)|^2$$
$$= \frac{1}{|V_{ub}|^2 \tau_{B_0}} \int_0^{q^2_{max}} dq^2\, \frac{d\mathcal{B}(B \to \pi\ell\nu)}{dq^2} \,, \tag{76.45}$$

for which the light-cone sum rule gives [205]

$$\Delta\zeta(0, 12\,\mathrm{GeV}^2) = \left(5.25^{+0.68}_{-0.54}\right)\ \mathrm{ps}^{-1}. \tag{76.46}$$

The uncertainty in this integral is about ten percent, which translates to a theoretical uncertainty of about five percent for the determination of V_{ub} with this method.

76.3.6 $\bar{B} \to \pi\ell\bar{\nu}_\ell$ measurements

The $\bar{B} \to \pi\ell\bar{\nu}_\ell$ measurements fall into two broad classes: untagged, in which case the reconstruction of the missing momentum of the event serves as an estimator for the unseen neutrino, and tagged, in which the second B meson in the event is fully reconstructed in either a hadronic or semileptonic decay mode. The tagged measurements have better q^2 resolution, high and uniform acceptance and S/B as high as 10, but lower statistical power. The untagged measurements have higher background (S/B < 1) and make slightly more restrictive kinematic cuts, but still provide statistical power precision on the q^2 dependence of the form factor.

CLEO has analyzed $\bar{B} \to \pi\ell\bar{\nu}_\ell$ and $\bar{B} \to \rho\ell\bar{\nu}_\ell$ using an untagged analysis [186–188]. Similar analyses have been done at BABAR [189–192] and Belle [206]. The leading systematic uncertainties in the untagged $\bar{B} \to \pi\ell\bar{\nu}_\ell$ analyses are associated with modeling the missing momentum reconstruction, with background from $\bar{B} \to X_u\ell\bar{\nu}_\ell$ decays and $e^+e^- \to q\bar{q}$ continuum events, and with varying the form factor used to model $\bar{B} \to \rho\ell\bar{\nu}_\ell$ decays.

Analyses [181,207] based on reconstructing a B in the $\bar{D}^{(*)}\ell^+\nu_\ell$ decay mode and looking for a $\bar{B} \to \pi\ell\bar{\nu}_\ell$ or $\bar{B} \to \rho\ell\bar{\nu}_\ell$ decay amongst the remaining particles in the event make use of the fact that the B and $\bar{B}$ are back-to-back in the $\Upsilon(4S)$ frame to construct a discriminant variable that provides a signal-to-noise ratio above unity for all q^2 bins. A related technique was discussed in Ref. [208]. BABAR [207] and Belle [179] have also used their samples of B mesons reconstructed in hadronic decay modes to measure exclusive charmless semileptonic decays, resulting in very clean but smaller samples. The dominant systematic uncertainties in the tagged analyses arise from tag calibration.

$|V_{ub}|$ can be obtained from the average $\bar{B} \to \pi\ell\bar{\nu}_\ell$ branching fraction and the measured q^2 spectrum. Fits to the q^2 spectrum using a theoretically motivated parametrization (e.g. "BCL" from

Downloaded from https://academic.oup.com/ptep/article/2022/8/083C01/6651666 by KIT Library user on 27 September 2022

Ref. [61]) remove most of the model dependence from theoretical uncertainties in the shape of the spectrum. The most sensitive method for determining $|V_{ub}|$ from $\bar{B} \to \pi\ell\bar{\nu}_\ell$ decays employs a simultaneous fit [6, 193, 198, 199, 209, 210] to measured experimental partial rates and lattice points versus q^2 (or z) to determine $|V_{ub}|$ and the first few coefficients of the expansion of the form factor in z. We quote the result from Ref. [6], which uses as experimental input an average of the measurements in Refs. [179, 189, 192, 206] and an average [211] of the LQCD input from Ref. [193] and Ref. [196]. The probability of the q^2 measurement average is 6%. The average for the total $B^0 \to \pi^-\ell^+\nu_\ell$ branching fraction is obtained by summing up the partial branching fractions:

$$\mathcal{B}(B^0 \to \pi^-\ell^+\nu_\ell) = (1.50 \pm 0.02_{\rm stat} \pm 0.06_{\rm syst}) \times 10^{-4} \quad (76.47)$$

The corresponding value of $|V_{ub}|$ with this approach is found to be

$$|V_{ub}| = (3.70 \pm 0.10 \pm 0.12\,) \times 10^{-3} \quad \text{(exclusive)}, \qquad (76.48)$$

where the first uncertainty is experimental and the second is from theory. A consistent result for $|V_{ub}|$ was reported in Ref. [32], which uses the same experimental and lattice-QCD inputs. Adding additional constraints using input from LCSR [203] gives [6] $|V_{ub}| = (3.67 \pm 0.09 \pm 0.12\,) \times 10^{-3}$ (exclusive, LQCD+LCSR). Other recent LCSR estimates [212, 213] have been used to obtain consistent results for $|V_{ub}|$, albeit with slightly higher central values. Ref. [213] also presents results for $|V_{ub}|$ from joint fits that exclude some of the experimental data in order to bring the exclusive values into agreement with the inclusive ones.

76.3.7 $\bar{B}_s \to K\ell\bar{\nu}_\ell$

The LHCb experiment have conducted the first observation of the decay $B_s^0 \to K^-\mu^+\nu_\mu$ and the measurements of its branching fraction normalised to the $B_s^0 \to D_s^-\mu^+\nu_\mu$ decays [214]. The measurement has been performed in two bins of q^2, derived using the B_s^0 flight direction and the known B_s^0 mass. The analysis uses a BDT classifier to suppress semileptonic b-hadron background. The results of the partial branching fractions have been translated into measurements of $|V_{ub}|/|V_{cb}|$ using form factor calculations from LCSR for $q^2 < 7$ GeV^2 [215], and a recent LQCD calculation for $q^2 > 7$ GeV^2 [194]. The results are

$$|V_{ub}|/|V_{cb}| = 0.0607 \pm 0.0021 \pm\ 0.0030,\ q^2 < 7\ \text{GeV}^2, \quad (76.49)$$
$$|V_{ub}|/|V_{cb}| = 0.0946 \pm 0.0041 \pm\ 0.0068,\ q^2 > 7\ \text{GeV}^2, \quad (76.50)$$

where the first uncertainties include also experimental and external input sources, and the latter are due to the form factor calculations. The sizeable discrepancy between the values of $|V_{ub}|/|V_{cb}|$ for the low and high q^2, requires further investigation. While the experimental measurement has higher purity in the low q^2 region, the theoretical uncertainties in the LCSR results are not fully quantified, unlike the lattice QCD results employed for the high-q^2 region.

76.4 Semileptonic *b*-baryon decays

Summary: A significant sample of Λ_b^0 baryons is available at the LHCb experiment, and methods have been developed to study their semileptonic decays. Both $\Lambda_b^0 \to p\mu\bar{\nu}$ and $\Lambda_b^0 \to \Lambda_c^+\mu\bar{\nu}$ decays have been measured at LHCb, and the ratio of branching fractions to these two decay modes is used to determine the ratio $|V_{ub}/V_{cb}|$.

76.4.1 $\Lambda_b^0 \to \Lambda_c^+\mu\bar{\nu}$ *and* $\Lambda_b^0 \to p\mu\bar{\nu}$

The $\Lambda_b^0 \to \Lambda_c^+$ and $\Lambda_b^0 \to p$ semileptonic transitions are described in terms of six form factors each. The three form factors corresponding to the vector current can be defined as [216]

$$\begin{aligned}\langle F(p',s')|\bar{q}\,\gamma_\mu\, b|\Lambda_b^0(p,s)\rangle = \bar{u}_F(p',s')\Big\{ & f_0(q^2)\,(M_{\Lambda_b^0} - m_F)\,\frac{q_\mu}{q^2} \\ & + f_+(q^2)\,\frac{M_{\Lambda_b^0} + m_F}{s_+}\left(p_\mu + p'_\mu - \frac{q_\mu}{q^2}\,(M^2_{\Lambda_b^0} - m_F^2)\right) \\ & + f_\perp(q^2)\left(\gamma_\mu - \frac{2m_F}{s_+}\,p_\mu - \frac{2M_{\Lambda_b^0}}{s_+}\,p'_\mu\right)\Big\}\,u_{\Lambda_b^0}(p,s)\,,\end{aligned} \quad (76.51)$$

where $F = p$ or Λ_c^+ and where we define $s_\pm = (M_{\Lambda_b^0} \pm m_F)^2 - q^2$. At vanishing momentum transfer, $q^2 \to 0$, the kinematic constraint $f_0(0) = f_+(0)$ holds. The form factors are defined in such a way that they correspond to time-like (scalar), longitudinal and transverse polarization with respect to the momentum-transfer q^μ for f_0, f_+ and $f_\perp$, respectively. Likewise, the expression for the axial-vector current is

$$\begin{aligned}&\langle F(p',s')|\bar{q}\,\gamma_\mu\gamma_5\, b|\Lambda_b^0(p,s)\rangle = \\ &\quad - \bar{u}_F(p',s')\gamma_5\Big\{ g_0(q^2)\,(M_{\Lambda_b^0} + m_F)\,\frac{q_\mu}{q^2} \\ &\quad + g_+(q^2)\,\frac{M_{\Lambda_b^0} - m_F}{s_-}\left(p_\mu + p'_\mu - \frac{q_\mu}{q^2}\,(M^2_{\Lambda_b^0} - m_F^2)\right) \\ &\quad + g_\perp(q^2)\left(\gamma_\mu + \frac{2m_F}{s_-}\,p_\mu - \frac{2M_{\Lambda_b^0}}{s_-}\,p'_\mu\right)\Big\}\,u_{\Lambda_b^0}(p,s)\,,\end{aligned} \quad (76.52)$$

with the kinematic constraint $g_0(0) = g_+(0)$ at $q^2 \to 0$.

In the heavy-quark limit, where both the b and c quarks are treated as heavy, all the form factors reduce to the Isgur Wise function ξ_B for baryons [216]:

$$f_0 = f_+ = f_\perp = g_0 = g_+ = g_\perp = \xi_B \qquad (76.53)$$

With a light baryon in the final state, the form factors are related through the heavy quark symmetries of the Λ_b^0, reducing the the number of independent form factors to two. It should be noted that the differential $\Lambda_b^0 \to (p/\Lambda_c^+)\mu\bar{\nu}$ decay rates peak at high q^2, so that the kinematic regions where both lattice QCD calculations and experimental measurements are precise are well matched.

The form factors for Λ_b^0 decays have been studied with lattice QCD [217]. Based on these results the differential rates for both $\Lambda_b^0 \to \Lambda_c^+\mu\bar{\nu}$ as well as for $\Lambda_b^0 \to p\mu\bar{\nu}$ can be predicted in the full phase space. In particular, for the experimentally interesting region they find the ratio of decay rates to be [217]

$$\frac{\mathcal{B}(\Lambda_b^0 \to p\mu\bar{\nu})_{q^2>15\,\text{GeV}^2}}{\mathcal{B}(\Lambda_b^0 \to \Lambda_c^+\mu\bar{\nu})_{q^2>7\,\text{GeV}^2}} = (1.471 \pm 0.095 \pm 0.109)\left|\frac{V_{ub}}{V_{cb}}\right|^2 \qquad (76.54)$$

where the first uncertainty is statistical and the second, systematic.

76.4.2 *Measurements at LHCb*

The LHCb experiment has measured the branching fractions of the semileptonic decays $\Lambda_b^0 \to \Lambda_c^+\mu\bar{\nu}$ and $\Lambda_b^0 \to p\mu\bar{\nu}$, from which they determine $|V_{ub}|/|V_{cb}|$. This is the first such determination at a hadron collider, the first to use a b baryon decay, and the first observation of $\Lambda_b^0 \to p\mu\bar{\nu}$. Excellent vertex resolution allows the $p\mu$ and production vertices to be separated, which permits the calculation of the transverse momentum $p_\perp$ of the $p\mu$ pair relative to the Λ_b^0 flight direction. The corrected mass, $m_{\rm corr} = \sqrt{p_\perp^2 + m_{p\mu}^2} + p_\perp$, peaks at the Λ_b^0 mass for signal decays and provides good discrimination against background combinations. The topologically similar decay $\Lambda_b^0 \to \Lambda_c^+\mu\bar{\nu}$ is also measured, which eliminates the need to know the production cross-section or absolute efficiencies. Using vertex and Λ_b^0 mass constraints, q^2 can be determined up to a two-fold ambiguity. The LHCb analysis requires both solutions to be in the high q^2 region to minimise contamination from the low q^2 region. Their result [218],

Downloaded from https://academic.oup.com/ptep/article/2022/8/083C01/6651666 by KIT Library user on 27 September 2022

rescaled [6] to take into account the recent branching fraction measurement [219] $\mathcal{B}(\Lambda_c^+ \to pK^-\pi^+) = (6.28 \pm 0.32)\%$, is

$$\frac{\mathcal{B}(\Lambda_b^0 \to p\mu\bar{\nu})_{q^2>15\mathrm{GeV}^2}}{\mathcal{B}(\Lambda_b^0 \to \Lambda_c^+\mu\bar{\nu})_{q^2>7\mathrm{GeV}^2}} = (0.92 \pm 0.04 \pm 0.07) \times 10^{-2} \quad . \tag{76.55}$$

The largest systematic uncertainty is from the measured $\mathcal{B}(\Lambda_c^+ \to pK^-\pi^+)$; uncertainties due to trigger, tracking and the Λ_c^+ selection efficiency are each about 3%.

A recent LHCb analysis [220] measures the normalized q^2 spectrum and finds good agreement with the shape calculated with lattice QCD [217].

The decay rate for $\Lambda_b^0 \to p\mu\bar{\nu}$ peaks at high q^2 where the calculation of the associated form factors using lattice QCD is under good control. Using the measured ratio from Eq. (76.55) along with the calculated ratio from Ref. [217] (see Eq. (76.54)) results in [6]

$$|V_{ub}|/|V_{cb}| = 0.079 \pm 0.004 \pm 0.004(\Lambda_b). \tag{76.56}$$

where the first uncertainty is experimental and the second is from the LQCD calculation.

76.5 The ratio $|V_{ub}|/|V_{cb}|$

The ratio of matrix elements, $|V_{ub}|/|V_{cb}|$, is often required when testing the compatibility of a set of measurements with theoretical predictions. It can be determined from the ratio of branching fractions measured by the LHCb experiment, quoted in the previous sections. It can also be calculated based on the $|V_{ub}|$ and $|V_{cb}|$ values quoted earlier in this review.

The average of the LHCb results extracted at high q^2 from B_s and Λ_b decays, taken to be uncorrelated, is

$$|V_{ub}|/|V_{cb}| = 0.084 \pm 0.007 \quad (\Lambda_b,\ B_s), \tag{76.57}$$

where the uncertainty has been scaled by a factor $\sqrt{\chi^2/1} = 1.6$.

Given the similarities in the theoretical frameworks used for charmed and charmless decays, we choose to quote separate ratios of $|V_{ub}|/|V_{cb}|$ for inclusive and exclusive B decays, as discussed earlier:

$$|V_{ub}|/|V_{cb}| = 0.098 \pm 0.006 \quad \text{(inclusive)}, \tag{76.58}$$

$$|V_{ub}|/|V_{cb}| = 0.094 \pm 0.005 \quad \text{(exclusive)}. \tag{76.59}$$

The respective determinations of $|V_{ub}|$ and $|V_{cb}|$ are taken to be uncorrelated in the ratio, although there could be some small cancellations of the uncertainties in both the experimental and the theoretical input. We average the B decay values, along with the B_s and baryonic result in Eq. (76.57), weighting by relative errors.The average has $p(\chi^2) = 4\%$, so we scale the uncertainty by a factor $\sqrt{\chi^2/2} = 1.8$ to find

$$|V_{ub}|/|V_{cb}| = 0.091 \pm 0.005 \quad \text{(average)}. \tag{76.60}$$

76.6 Semitauonic decays

Summary: Semileptonic decays to third-generation leptons provide sensitivity to non-Standard Model amplitudes, such as from a charged Higgs boson [221–224] and from leptoquarks [225–231]. The ratios of branching fractions of semileptonic decays involving tau leptons to those involving $\ell = e/\mu$, $R(D^{(*)}) \equiv \mathcal{B}(\bar{B} \to D^{(*)}\tau\bar{\nu}_\tau)/\mathcal{B}(\bar{B} \to D^{(*)}\ell\bar{\nu}_\ell)$, are predicted with good precision and consistency in the Standard Model [7–9, 24, 25, 27, 62], using a variety of different strategies. Because this ratio is independent of $|V_{cb}|$, it can, in principle, be computed entirely from within the Standard Model, without using experimental decay rate data. For example, in Ref. [7,9] the lattice-QCD only ratios are obtained as:

$$R(D)^{\mathrm{LQCD,FNAL-MILC}} = 0.284 \pm 0.014 \ ,$$
$$R(D^*)^{\mathrm{LQCD,FNAL-MILC}} = 0.265 \pm 0.013 \ . \tag{76.61}$$

Without constraints from experimental data at large recoil, such SM-theory only evaluations tend to be less precise than those obtained from joint fits that employ experimental data as well as Standard-Model theory inputs (lattice-QCD form factors, HQET constraints, etc.). Here we use an average of Ref. [25,62] for $R(D)$ and Ref. [9] for $R(D^*)$, where the uncertainty on $R(D^*)$ is scaled by $\sqrt{\chi^2/1} = 1.2$:

$$R(D)^{\mathrm{SM+Exp}} = 0.299 \pm 0.003 \ ,$$
$$R(D^*)^{\mathrm{LQCD+Exp}} = 0.2483 \pm 0.0016 \ . \tag{76.62}$$

Other Standard-Model predictions for $R(D^{(*)})$ [24, 25, 27, 62, 232, 233] using various combinations of experimental data, lattice-QCD form factor inputs, HQET constraints, and LCSR estimates are consistent with the values quoted above. In the case of $R(D^*)$, these predictions have larger uncertainties than the result quoted in Eq. (76.62), as non-zero lattice-QCD form factors for $B \to D^*$ were not yet available.

Measurements [234–242] of these ratios yield higher values; averaging B-tagged measurements of $R(D)$ and $R(D^*)$ at the $\Upsilon(4S)$ and the LHCb measurements of $R(D^*)$ yields [243]

$$R(D)^{\mathrm{meas}} = 0.339 \pm 0.026 \pm 0.014 \ ,$$
$$R(D^*)^{\mathrm{meas}} = 0.295 \pm 0.010 \pm 0.010 \ , \tag{76.63}$$

with a linear correlation of -0.38. These values exceed the Standard Model predictions of Eq. (76.62) by 1.4σ and 3.3σ, respectively. Not surprisingly, the tensions with respect to the lattice-QCD only prediction of Eq. (76.61) are less significant, at 1.4σ for $R(D)$ and 1.6σ for $R(D^*)$. A variety of new physics models have been proposed to explain this excess, see eg. Ref. [221–228] and recent reviews in Ref. [244–246].

Most models proposed to explain the semitauonic decay excesses tend to, but not always, have very little impact on semileptonic decays involving muons or electrons, so they do not significantly modify the $|V_{ub}|$ or $|V_{cb}|$ determinations discussed previously in this review. Lepton flavor universality in the ratio of electron and muon modes has been confirmed in direct ratio measurements from Belle: $\mathcal{B}(\bar{B} \to D^* e\bar{\nu}_e)/\mathcal{B}(\bar{B} \to D^*\mu\bar{\nu}_\mu) = 1.01 \pm 0.03$ [53] and $\Delta\mathcal{B}(B \to X_u e^-\bar{\nu}_e)/\Delta\mathcal{B}(B \to X_u\mu^-\bar{\nu}_\mu) = 0.97 \pm 0.10$ [162]. The uncertainty is dominated by lepton identification uncertainties that do not cancel in the ratio.

76.6.1 *Sensitivity of $\bar{B} \to D^{(*)}\tau\bar{\nu}_\tau$ to additional amplitudes*

In addition to the helicity amplitudes present for decays to $e\bar{\nu}_e$ and $\mu\bar{\nu}_\mu$, decays proceeding through $\tau\bar{\nu}_\tau$ include a scalar amplitude H_s. The differential decay rate is given by [247]

$$\frac{d\Gamma}{dq^2} = \frac{G_F^2\,|V_{cb}|^2\,|\mathbf{p}^*_{D^{(*)}}|q^2}{96\pi^3 m_B^2}\left(1 - \frac{m_\tau^2}{q^2}\right)^2 \left[(|H_+|^2 + |H_-|^2 + |H_0|^2)\left(1 + \frac{m_\tau^2}{2q^2}\right) + \frac{3m_\tau^2}{2q^2}|H_s|^2\right], \tag{76.64}$$

where $|\mathbf{p}^*_{D^{(*)}}|$ is the 3-momentum of the $D^{(*)}$ in the $\bar{B}$ rest frame and the helicity amplitudes H depend on the four-momentum transfer q^2. All four helicity amplitudes contribute to $\bar{B} \to D^*\tau\bar{\nu}_\tau$, while only H_0 and H_s contribute to $\bar{B} \to D\tau\bar{\nu}_\tau$; as a result, new physics contributions can produce larger effects in the latter mode. Semi-leptonic B decays into a τ lepton provide a stringent test of the two-Higgs doublet model of type II (2HDMII), i.e. where the two Higgs doublets couple separately to up- and down-type quarks. The distinct feature of the 2HDMII is that the contributions of the charged scalars scale as $m_\tau^2/m_{H^+}^2$, since the couplings to the charged Higgs particles are proportional to the mass of the lepton. As a consequence, one may expect visible effects in decays into a τ, but only small effects for decays into e and μ. The present data disfavors the 2HDMII, see below.

76.6.2 *Measurement of $R(D^{(*)})$*

$\bar{B} \to D^{(*)}\tau\bar{\nu}_\tau$ decays have been studied at the $\Upsilon(4S)$ resonance and in pp collisions. At the $\Upsilon(4S)$, the majority of experimental measurements are based on signatures that consist of a D or D^* meson, an electron or muon (denoted here by ℓ) from the decay $\tau \to \ell\nu_\tau\bar{\nu}_\ell$, a fully-reconstructed decay of the second B meson in

Downloaded from https://academic.oup.com/ptep/article/2022/8/083C01/6651666 by KIT Library user on 27 September 2022

Figure 76.1: Measurements of $R(D)$ and $R(D^*)$ and their two-dimensional average compared with the average predictions for $R(D)$ and $R(D^*)$. Contours correspond to $\Delta\chi^2 = 1$ *i.e.*, 68% CL for the bands and 39% CL for the ellipses. The average of the Lattice QCD and Experiment-Lattice QCD-HQET predictions and the experimental average deviate from each other by 2.0σ and 4.0σ respectively. The dashed ellipse corresponds to a 3σ contour of the experiment average (99.73% CL).

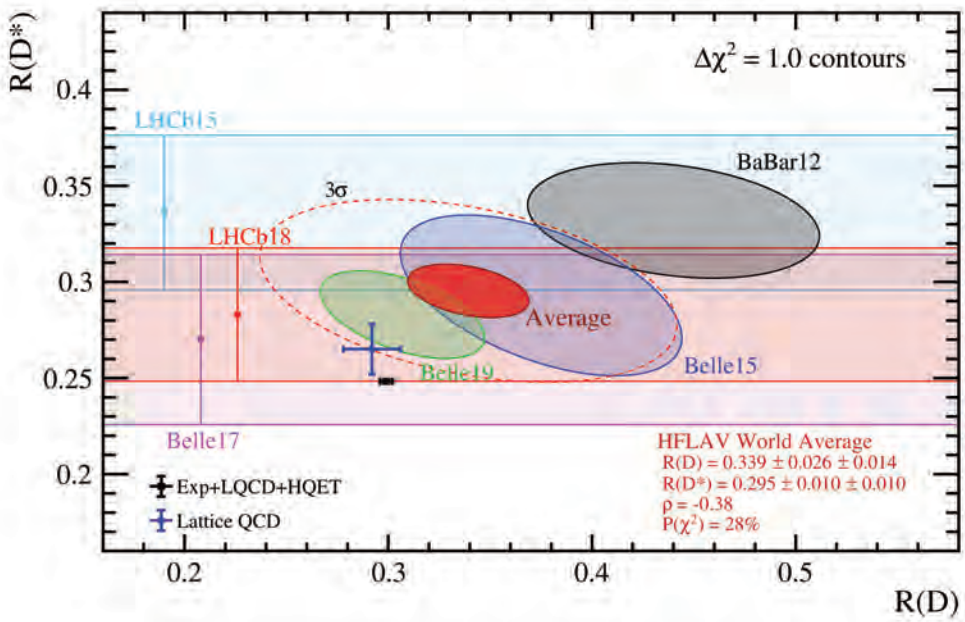

the event, and multiple missing neutrinos. One analysis reconstructs the τ in a hadronic mode. The analyses that use hadronic B tags separate signal decays from $\bar{B} \to D^{(*)}\ell\bar{\nu}_\ell$ decays using the lepton momentum and the measured missing mass squared; decays with only a single missing neutrino peak sharply at zero in this variable, while the signal is spread out to positive values. When a semileptonic B tag is used, the discrimination between signal and $\bar{B} \to D^{(*)}\ell\bar{\nu}_\ell$ decays comes from the calorimeter energy that is not associated with any particle used in the reconstruction of the B meson candidates, the measured missing mass squared and the cosine of the angle between the $D^*\ell$ system and its parent B meson, which is calculated under the assumption that only one particle (a neutrino) is missing. In both these approaches, background from $\bar{B} \to D^{**}\ell\bar{\nu}_\ell$ decays with one or more unreconstructed particles is challenging to separate from signal, as is background from $\bar{B} \to D^{(*)}H_{\bar{c}}X$ (where $H_{\bar{c}}$ is a hadron containing a $\bar{c}$ quark) decays. The leading sources of systematic uncertainty are due to the limited size of simulation samples used in constructing the PDFs, the composition of the D^{**} states, efficiency corrections, and cross-feed (swapping soft particles between the signal and tag B).

The most recent measurement from Belle [240] uses semileptonic B tags and leptonic τ decays to simultaneously measure $R(D^*)$ and $R(D)$. The measurement provides the single most precise determination of these ratios, combining results from charged and neutral B decays, and is compatible with the Standard Model expectation to approximately 1σ.

In addition to the ratio measurements, the Belle experiment has performed polarization measurements of the τ [239] and D^* [248] respectively. The τ polarization measurement uses hadronic B tags and τ^- decays to $\pi^-\nu_\tau$ or $\rho^-\nu_\tau$. The main discriminant variables are the measured missing mass squared and the unassociated calorimeter energy. This measurement provides the first determination of the τ polarization in the $\bar{B} \to D^*\tau\bar{\nu}_\tau$ decay, $\mathcal{P}_\tau(D^*) = -0.38 \pm 0.51\,^{+0.21}_{-0.16}$, compatible with the Standard Model expectation [27], $\mathcal{P}_\tau(D^*) = -0.476^{+0.037}_{-0.034}$.

The main uncertainties on the $R(D^*)$ measurement come from the composition of the hadronic B background and from modeling of semileptonic B decays and mis-reconstructed D^* mesons. The D^* polarization measurement uses an inclusive tag approach based on Refs. [249, 250], and reconstructs the τ decays in $\ell\nu_\tau\bar{\nu}_\ell$ and $\pi^+\bar{\nu}_\tau$ channels. The main discriminant variables are $X_{\rm miss}$, a quantity that approximates missing mass but does not depend on tag B reconstruction, the visible energy of the event, and the beam-energy constrained mass, $M_{\rm bc}$, of the inclusively reconstructed tag side B. This measurement provides the first determination of the D^* longitudinal polarization fraction in the $\bar{B} \to D^*\tau\bar{\nu}_\tau$ decay, $\mathcal{F}_L(D^*) = -0.38 \pm 0.60\,^{+0.08}_{-0.04}$, compatible with the Standard Model expectation [251] within 1.7σ.

The LHCb experiment has studied the decay $\bar{B} \to D^{*+}\tau\bar{\nu}_\tau$ with $D^{*+} \to D^0\pi^+$, $D^0 \to K^-\pi^+$ and $\tau \to \mu\nu_\tau\bar{\nu}_\mu$ in pp collisions. Their analysis [241] takes advantage of the measurable flight lengths of b and c hadrons and τ leptons. A multivariate discriminant is used to select decays where no additional charged particles are consistent with coming from the signal decay vertices. The separation between the primary and B decay vertices is used to calculate the momentum of the B decay products transverse to the B flight direction. The longitudinal component of the B momentum can be estimated based on the visible decay products; this allows a determination of the B rest frame, with modest resolution, and enables the calculation of the same discrimination variables available at the e^+e^- B factories. The (rest frame) muon energy, missing mass-squared and q^2 are used in a 3-d fit. The most recent LHCb result [253] on $R(D^*)$ uses three-prong τ decays that take advantage of their excellent vertex resolution to isolate the τ decay from hadronic background. A 3-d fit is performed to determine the signal yield, based on the τ-ν_τ pair q^2, the τ lifetime, as well as a boosted decision tree classifier based on isolation, invariant mass and flight distance information. The leading sources of systematic uncertainty are due to the size of the simulation sample used in constructing the fit templates, uncertainties in modelling the background from hadronic $\bar{B} \to D^{(*)}H_{\bar{c}}X$ decays, as well as reconstruction and trigger effects. The result is normalized to $B^0 \to D^{*-}\pi^+\pi^-\pi^+$ and found to be 1σ from the Standard Model expectation (using the expectation value quoted here). An analogous measurement of $B_c \to J/\psi\tau\bar{\nu}_\tau$ was performed by the LHCb measurement [254], in

Downloaded from https://academic.oup.com/ptep/article/2022/8/083C01/6651666 by KIT Library user on 27 September 2022

Table 76.2: Measurements of $R(D)$ and $R(D^*)$, their correlations, ρ, and the combined averages [6].

		$R(D) \times 10^2$	$R(D^*) \times 10^2$	ρ
BABAR [235, 236]	B^0, B^+	$44.0 \pm 5.8 \pm 4.2$	$33.2 \pm 2.4 \pm 1.8$	-0.27
Belle [237]	B^0, B^+	$37.5 \pm 6.4 \pm 2.6$	$29.3 \pm 3.8 \pm 1.5$	-0.49
Belle [239, 252]	B^0, B^+		$27.0 \pm 3.5 \,^{+\,2.8}_{-\,2.5}$	
Belle [240]	B^0, B^+	$30.7 \pm 3.7 \pm 1.6$	$28.3 \pm 1.8 \pm 1.4$	-0.51
LHCb [241]	B^0		$33.6 \pm 2.7 \pm 3.0$	
LHCb [253]	B^0		$28.3 \pm 1.9 \pm 2.9$	
Average	B^0, B^+	$33.9 \pm 2.6 \pm 1.4$	$29.5 \pm 1.0 \pm 1.0$	-0.38

leptonic τ decays. The result, $R(J/\psi) = 0.71 \pm 0.17 \pm 0.18$, while relatively high is compatible to within 2σ of a recent Standard Model evaluation [255] based on a latttice-QCD calculation [256] of the form factors. Systematic uncertainties are dominated by form factors, as B_c decays are relatively unexplored.

Measurements from BABAR [234–236], Belle [237–240] and LHCb [241, 253] result in values for $R(D)$ and $R(D^*)$ that exceed Standard Model predictions. Table 76.2 lists these values and their average. The simultaneous measurements of $R(D)$ and $R(D^*)$ have linear correlation coefficients of -0.27 (BABAR [235, 236]), -0.49 (Belle hadronic tag [237]) and -0.51 (Belle semileptonic tag [240]); the $R(D)$ and $R(D^*)$ averages have a correlation of -0.38. Two early untagged Belle measurements [249, 250] are subject to larger systematic uncertainties, with a breakdown of the respective contributions that is inconsistent with the more recent determinations, hence they cannot be reliably combined in the average. All three experiments assume the Standard Model kinematic distributions for $\bar{B} \to D^{(*)}\tau\bar{\nu}_\tau$ in their determinations of the branching fraction ratios.

The measurement combination in the $R(D) - R(D^*)$ plane is shown in Fig. 76.1, compared with the predictions in Eq. (76.61) (LQCD) and Eq. (76.62) (Experiment+LQCD+HQET). The measurement combination is based on Ref. [6]. The tension between the Standard Model prediction in Eq. (76.62) and the measurements is at the level of 1.4σ ($R(D)$) and 3.3σ ($R(D^*)$); if one considers these deviations together the significance is 4.0σ. This motivates speculation on possible new physics contributions. The measurements reported in Refs. [240, 252, 253] resulted in reduced tensions with the Standard-Model predictions in recent editions of the RPP. The main change in this edition is the availability of lattice-QCD form factors at nonzero recoil, which improves the theory uncertainty on $R(D^*)$ and brings the discrepancy to the level reported in earlier editions. There is some tension in the combination coming from the BABAR measurement, the only measurement to claim a deviation from the Standard Model of more than 3σ, although the $p-$value of the full combination is an acceptable 28%.

The current discussion of $R(D)$ and $R(D^*)$ may be embedded in the theoretical analysis of the other anomalies that have been observed in semileptonic FCNC ($b \to s\ell\ell$) transitions. More sophisticated approaches fit the data to a general effective Hamiltonian. Matching this effective Hamiltonian to simplified models, the current situation of the anomalies seems to be compatible with scenarios with an additional Z' or a leptoquark scenario, see eg. [225–231].

76.7 Conclusion

The study of semileptonic B meson decays continues to be an active area for both theory and experiment. The application of HQE calculations to inclusive decays is well established, and fits to moments of $\bar{B} \to X_c\ell\bar{\nu}_\ell$ decays provide precise values for $|V_{cb}|$ and, in conjunction with input on m_c or from $B \to X_s\gamma$ decays, provide precise and consistent values for m_b. Recent developments will make use of more types of moments and better theoretical inputs to constrain higher order effects. Further into the future, new nonperturbative methods to compute inclusive decay rates, for example, in lattice QCD [257], may provide interesting new insights.

The determination of $|V_{ub}|$ from inclusive $\bar{B} \to X_u\ell\bar{\nu}_\ell$ decays is based on multiple calculational approaches and independent measurements over a variety of kinematic regions, all of which provide consistent results. Further progress in this area is possible, but will require better theoretical control over higher-order terms, improved experimental knowledge of the $\bar{B} \to X_c\ell\bar{\nu}_\ell$ background and improvements to the modeling of the $\bar{B} \to X_u\ell\bar{\nu}_\ell$ signal distributions.

In both $b \to u$ and $b \to c$ exclusive channels there has been significant recent progress in lattice-QCD calculations, resulting in improved precision on both $|V_{ub}|$ and $|V_{cb}|$. These calculations now provide information on the form factors well away from the high q^2 region, allowing better use of experimental data. For $|V_{cb}|$ recent measurements have provided binned data enabling model-independent fits.

The values from the inclusive and exclusive determinations of $|V_{cb}|$ and $|V_{ub}|$ are only marginally consistent. This is a long-standing puzzle, which the recent improvements have, unfortunately, not yet resolved. The measurement of $|V_{ub}|/|V_{cb}|$ from LHCb based on Λ_b^0 and B_s decays also do not yet simplify the picture.

Both $|V_{cb}|$ and $|V_{ub}|$ are indispensable inputs into unitarity triangle fits. In particular, knowing $|V_{ub}|$ with good precision allows a test of CKM unitarity in a most direct way, by comparing the length of the $|V_{ub}|$ side of the unitarity triangle with the measurement of $\sin(2\beta)$. This comparison of a "tree" process ($b \to u$) with a "loop-induced" process ($B^0 - \bar{B}^0$ mixing) provides sensitivity to possible contributions from new physics.

The observation of semileptonic decays into τ leptons has opened a new window to the physics of the third generation. The measurements indicate a tension between the data and Standard-Model predictions, which could be a hint for new physics, manifesting itself as a violation of lepton universality beyond the Standard-Model couplings to the Higgs. It should be noted that none of the most recent measurements alone claim discovery of a deviation from the Standard Model. Combining the data of the semitauonic decays with the anomalies observed in the FCNC $b \to s\ell\ell$ transitions allows an interpretation in terms of additional Z' or in terms of additional leptoquarks, but the current data does not allow us to draw a definite conclusion.

The authors would like to acknowledge helpful input from D. Ferlewicz, P. Gambino, S. Hashimoto, Z. Ligeti, M. Rotondo, C. Schwanda, and A. Vaquero.

References

[1] See"Leptonic Decays of Charged Pseudoscalar Mesons" by J.L. Rosner, S.L. Stone, and R. Van de Water in this *Review*.

[2] M. Tanabashi *et al.* (Particle Data Group), Phys. Rev. D **98**, 3, 030001 (2018).

[3] See"Heavy-Quark and Soft-Collinear Effective Theory" by C.W. Bauer and M. Neubert in this *Review*.

[4] See "Lattice Quantum Chromodynamics" by S. Hashimoto, J. Laiho, and S.R. Sharpe in this *Review*.

[5] See "Production and Decay of b-Flavored Hadrons" by P. Eerola, M. Kreps and Y. Kwon in this *Review*.

[6] Y. S. Amhis *et al.* (HFLAV) (2019), [arXiv:1909.12524].

[7] J. A. Bailey *et al.* (Fermilab Lattice and MILC), Phys. Rev. **D92**, 3, 034506 (2015), [arXiv:1503.07237].

[8] H. Na *et al.* (HPQCD), Phys. Rev. **D92**, 5, 054510 (2015), [Erratum: Phys. Rev.D93,no.11,119906(2016)], [arXiv:1505.03925].

Downloaded from https://academic.oup.com/ptep/article/2022/8/083C01/6651666 by KIT Library user on 27 September 2022

[9] A. Bazavov *et al.* (Fermilab Lattice, MILC) (2021), [arXiv:2105.14019].

[10] N. Isgur and M. B. Wise, Phys. Lett. **B232**, 113 (1989); N. Isgur and M. B. Wise, Phys. Lett. **B237**, 527 (1990).

[11] M. A. Shifman and M. B. Voloshin, Sov. J. Nucl. Phys. **47**, 511 (1988), [Yad. Fiz.47,801(1988)].

[12] A. V. Manohar and M. B. Wise, Camb. Monogr. Part. Phys. Nucl. Phys. Cosmol. **10**, 1 (2000).

[13] H. Georgi, Phys. Lett. **B240**, 447 (1990).

[14] A. F. Falk *et al.*, Nucl. Phys. **B343**, 1 (1990).

[15] E. Eichten and B. R. Hill, Phys. Lett. **B234**, 511 (1990).

[16] A. Sirlin, Nucl. Phys. **B196**, 83 (1982).

[17] J. A. Bailey *et al.* (Fermilab Lattice, MILC), Phys. Rev. **D89**, 11, 114504 (2014), [arXiv:1403.0635].

[18] C. G. Boyd, B. Grinstein and R. F. Lebed, Phys. Rev. Lett. **74**, 4603 (1995), [hep-ph/9412324].

[19] C. G. Boyd, B. Grinstein and R. F. Lebed, Phys. Lett. B **353**, 306 (1995), [hep-ph/9504235].

[20] C. G. Boyd, B. Grinstein and R. F. Lebed, Nucl. Phys. B **461**, 493 (1996), [hep-ph/9508211].

[21] C. G. Boyd, B. Grinstein and R. F. Lebed, Phys. Rev. D **56**, 6895 (1997), [hep-ph/9705252].

[22] B. Grinstein and A. Kobach, Phys. Lett. **B771**, 359 (2017), [arXiv:1703.08170].

[23] I. Caprini, L. Lellouch and M. Neubert, Nucl. Phys. **B530**, 153 (1998), [hep-ph/9712417].

[24] M. Bordone, M. Jung and D. van Dyk (2019), [arXiv:1908.09398].

[25] F. U. Bernlochner *et al.*, Phys. Rev. **D95**, 11, 115008 (2017), [erratum: Phys. Rev.D97,no.5,059902(2018)], [arXiv:1703.05330].

[26] D. Bigi, P. Gambino and S. Schacht, Phys. Lett. **B769**, 441 (2017), [arXiv:1703.06124].

[27] P. Gambino, M. Jung and S. Schacht, Phys. Lett. **B795**, 386 (2019), [arXiv:1905.08209].

[28] F. U. Bernlochner, Z. Ligeti and D. J. Robinson, Phys. Rev. **D100**, 1, 013005 (2019), [arXiv:1902.09553].

[29] F. U. Bernlochner *et al.*, Phys. Rev. **D96**, 9, 091503 (2017), [arXiv:1708.07134].

[30] T. Kaneko *et al.* (JLQCD), PoS **LATTICE2019**, 139 (2019), [arXiv:1912.11770].

[31] J. Harrison, C. Davies and M. Wingate (HPQCD), Phys. Rev. **D97**, 5, 054502 (2018), [arXiv:1711.11013].

[32] S. Aoki *et al.* (Flavour Lattice Averaging Group) (2019), [arXiv:1902.08191].

[33] I. I. Y. Bigi *et al.*, Phys. Rev. **D52**, 196 (1995), [hep-ph/9405410].

[34] A. Kapustin *et al.*, Phys. Lett. **B375**, 327 (1996), [hep-ph/9602262].

[35] P. Gambino, T. Mannel and N. Uraltsev, Phys. Rev. **D81**, 113002 (2010), [arXiv:1004.2859].

[36] M. A. Shifman, N. G. Uraltsev and A. I. Vainshtein, Phys. Rev. D **51**, 2217 (1995), [Erratum: Phys.Rev.D 52, 3149 (1995)], [hep-ph/9405207].

[37] A. Czarnecki, K. Melnikov and N. Uraltsev, Phys. Rev. D **57**, 1769 (1998), [hep-ph/9706311].

[38] P. Gambino, T. Mannel and N. Uraltsev, JHEP **10**, 169 (2012), [arXiv:1206.2296].

[39] N. Gubernari, A. Kokulu and D. van Dyk, JHEP **01**, 150 (2019), [arXiv:1811.00983].

[40] L. Lellouch, Nucl. Phys. B **479**, 353 (1996), [hep-ph/9509358].

[41] M. Di Carlo *et al.*, Phys. Rev. D **104**, 5, 054502 (2021), [arXiv:2105.02497].

[42] G. Martinelli, S. Simula and L. Vittorio (2021), [arXiv:2105.07851].

[43] D. Buskulic *et al.* (ALEPH), Phys. Lett. **B395**, 373 (1997).

[44] G. Abbiendi *et al.* (OPAL), Phys. Lett. **B482**, 15 (2000), [hep-ex/0003013].

[45] P. Abreu *et al.* (DELPHI), Phys. Lett. **B510**, 55 (2001), [hep-ex/0104026].

[46] J. Abdallah *et al.* (DELPHI), Eur. Phys. J. **C33**, 213 (2004), [hep-ex/0401023].

[47] N. E. Adam *et al.* (CLEO), Phys. Rev. **D67**, 032001 (2003), [hep-ex/0210040].

[48] B. Aubert *et al.* (BaBar), Phys. Rev. **D77**, 032002 (2008), [arXiv:0705.4008].

[49] B. Aubert *et al.* (BaBar), Phys. Rev. Lett. **100**, 231803 (2008), [arXiv:0712.3493].

[50] B. Aubert *et al.* (BaBar), Phys. Rev. **D79**, 012002 (2009), [arXiv:0809.0828].

[51] W. Dungel *et al.* (Belle), Phys. Rev. **D82**, 112007 (2010), [arXiv:1010.5620].

[52] A. Abdesselam *et al.* (Belle) (2017), [arXiv:1702.01521].

[53] A. Abdesselam *et al.* (Belle) (2018), [arXiv:1809.03290].

[54] J. P. Lees *et al.* (BaBar), Phys. Rev. Lett. **123**, 091801 (2019), [arXiv:1903.10002].

[55] E. Waheed *et al.* (Belle), Phys. Rev. D **100**, 5, 052007 (2019), [Erratum: Phys.Rev.D 103, 079901 (2021)], [arXiv:1809.03290].

[56] F. Abudinén *et al.* (Belle-II) (2020), [arXiv:2008.07198].

[57] F. Abudinén *et al.* (Belle-II) (2020), [arXiv:2008.10299].

[58] D. Ferlewicz, P. Urquijo and E. Waheed, Phys. Rev. D **103**, 7, 073005 (2021), [arXiv:2008.09341].

[59] B. Aubert *et al.* (BaBar), Phys. Rev. Lett. **104**, 011802 (2010), [arXiv:0904.4063].

[60] R. Glattauer *et al.* (Belle), Phys. Rev. **D93**, 3, 032006 (2016), [arXiv:1510.03657].

[61] C. Bourrely, I. Caprini and L. Lellouch, Phys. Rev. **D79**, 013008 (2009), [Erratum: Phys. Rev.D82,099902(2010)], [arXiv:0807.2722].

[62] D. Bigi and P. Gambino, Phys. Rev. **D94**, 9, 094008 (2016), [arXiv:1606.08030].

[63] C. J. Monahan *et al.*, Phys. Rev. D **95**, 11, 114506 (2017), [arXiv:1703.09728].

[64] E. McLean *et al.*, Phys. Rev. D **101**, 7, 074513 (2020), [arXiv:1906.00701].

[65] E. McLean *et al.*, Phys. Rev. D **99**, 11, 114512 (2019), [arXiv:1904.02046].

[66] J. Harrison and C. T. H. Davies (HPQCD) (2021), [arXiv:2105.11433].

[67] R. Aaij *et al.* (LHCb), Phys. Rev. D **101**, 7, 072004 (2020), [arXiv:2001.03225].

[68] R. Aaij *et al.* (LHCb), Phys. Rev. D **104**, 3, 032005 (2021), [arXiv:2103.06810].

[69] A. V. Manohar and M. B. Wise, Phys. Rev. **D49**, 1310 (1994), [hep-ph/9308246].

[70] I. I. Y. Bigi *et al.*, Phys. Rev. Lett. **71**, 496 (1993), [,201(1993)], [hep-ph/9304225]; I. I. Y. Bigi *et al.*, Phys. Lett. **B323**, 408 (1994), [hep-ph/9311339].

[71] D. Benson *et al.*, Nucl. Phys. **B665**, 367 (2003), [hep-ph/0302262].

[72] M. Gremm and A. Kapustin, Phys. Rev. **D55**, 6924 (1997), [hep-ph/9603448].

[73] B. M. Dassinger, T. Mannel and S. Turczyk, JHEP **03**, 087 (2007), [hep-ph/0611168].

[74] I. I. Bigi, N. Uraltsev and R. Zwicky, Eur. Phys. J. **C50**, 539 (2007), [hep-ph/0511158].

Downloaded from https://academic.oup.com/ptep/article/2022/8/083C01/6651666 by KIT Library user on 27 September 2022

[75] T. Mannel, S. Turczyk and N. Uraltsev, JHEP **11**, 109 (2010), [arXiv:1009.4622].

[76] A. Pak and A. Czarnecki, Phys. Rev. **D78**, 114015 (2008), [arXiv:0808.3509].

[77] S. Biswas and K. Melnikov, JHEP **02**, 089 (2010), [arXiv:0911.4142].

[78] P. Gambino, JHEP **09**, 055 (2011), [arXiv:1107.3100].

[79] M. Fael, K. Schönwald and M. Steinhauser, Phys. Rev. D **104**, 1, 016003 (2021), [arXiv:2011.13654].

[80] P. Gambino and N. Uraltsev, Eur. Phys. J. **C34**, 181 (2004), [hep-ph/0401063].

[81] V. Aquila *et al.*, Nucl. Phys. **B719**, 77 (2005), [hep-ph/0503083].

[82] M. E. Luke, M. J. Savage and M. B. Wise, Phys. Lett. B **343**, 329 (1995), [hep-ph/9409287].

[83] M. E. Luke, M. J. Savage and M. B. Wise, Phys. Lett. B **345**, 301 (1995), [hep-ph/9410387].

[84] T. Becher, H. Boos and E. Lunghi, JHEP **12**, 062 (2007), [arXiv:0708.0855].

[85] A. Alberti *et al.*, Nucl. Phys. **B870**, 16 (2013), [arXiv:1212.5082].

[86] A. Alberti, P. Gambino and S. Nandi, JHEP **01**, 147 (2014), [arXiv:1311.7381].

[87] T. Mannel, A. A. Pivovarov and D. Rosenthal, Phys. Rev. **D92**, 5, 054025 (2015), [arXiv:1506.08167].

[88] T. Mannel and A. A. Pivovarov, Phys. Rev. D **100**, 9, 093001 (2019), [arXiv:1907.09187].

[89] C. Breidenbach *et al.*, Phys. Rev. **D78**, 014022 (2008), [arXiv:0805.0971].

[90] I. Bigi *et al.*, JHEP **04**, 073 (2010), [arXiv:0911.3322].

[91] A. Kobach and S. Pal, Phys. Lett. **B772**, 225 (2017), [arXiv:1704.00008].

[92] J. Heinonen and T. Mannel, Nucl. Phys. **B889**, 46 (2014), [arXiv:1407.4384].

[93] P. Gambino, K. J. Healey and S. Turczyk, Phys. Lett. **B763**, 60 (2016), [arXiv:1606.06174].

[94] T. Mannel and K. K. Vos, JHEP **06**, 115 (2018), [arXiv:1802.09409].

[95] M. Fael, T. Mannel and K. Keri Vos, JHEP **02**, 177 (2019), [arXiv:1812.07472].

[96] I. I. Y. Bigi *et al.*, Phys. Rev. **D50**, 2234 (1994), [hep-ph/9402360].

[97] A. H. Hoang, Z. Ligeti and A. V. Manohar, Phys. Rev. Lett. **82**, 277 (1999), [hep-ph/9809423].

[98] A. H. Hoang, Z. Ligeti and A. V. Manohar, Phys. Rev. **D59**, 074017 (1999), [hep-ph/9811239].

[99] A. H. Hoang and T. Teubner, Phys. Rev. **D60**, 114027 (1999), [hep-ph/9904468].

[100] A. Hoang, P. Ruiz-Femenia and M. Stahlhofen, JHEP **10**, 188 (2012), [arXiv:1209.0450].

[101] M. Fael, K. Schönwald and M. Steinhauser, Phys. Rev. Lett. **125**, 5, 052003 (2020), [arXiv:2005.06487].

[102] S. E. Csorna *et al.* (CLEO), Phys. Rev. **D70**, 032002 (2004), [hep-ex/0403052].

[103] A. H. Mahmood *et al.* (CLEO), Phys. Rev. **D70**, 032003 (2004), [hep-ex/0403053].

[104] B. Aubert *et al.* (BaBar), Phys. Rev. **D69**, 111103 (2004), [hep-ex/0403031].

[105] B. Aubert *et al.* (BaBar), Phys. Rev. **D69**, 111104 (2004), [hep-ex/0403030].

[106] C. Schwanda *et al.* (Belle), Phys. Rev. **D75**, 032005 (2007), [hep-ex/0611044].

[107] P. Urquijo *et al.* (Belle), Phys. Rev. **D75**, 032001 (2007), [hep-ex/0610012].

[108] J. Abdallah *et al.* (DELPHI), Eur. Phys. J. **C45**, 35 (2006), [hep-ex/0510024].

[109] D. Acosta *et al.* (CDF), Phys. Rev. **D71**, 051103 (2005), [hep-ex/0502003].

[110] B. Aubert *et al.* (BaBar), Phys. Rev. **D81**, 032003 (2010), [arXiv:0908.0415].

[111] A. Limosani *et al.* (Belle), Phys. Rev. Lett. **103**, 241801 (2009), [arXiv:0907.1384].

[112] C. Schwanda *et al.* (Belle), Phys. Rev. **D78**, 032016 (2008), [arXiv:0803.2158].

[113] B. Aubert *et al.* (BaBar), Phys. Rev. **D72**, 052004 (2005), [hep-ex/0508004].

[114] B. Aubert *et al.* (BaBar), Phys. Rev. Lett. **97**, 171803 (2006), [hep-ex/0607071].

[115] S. Chen *et al.* (CLEO), Phys. Rev. Lett. **87**, 251807 (2001), [hep-ex/0108032].

[116] M. Battaglia *et al.*, eConf **C0304052**, WG102 (2003), [Phys. Lett.B556,41(2003)], [hep-ph/0210319].

[117] B. Aubert *et al.* (BaBar), Phys. Rev. Lett. **93**, 011803 (2004), [hep-ex/0404017].

[118] O. Buchmüller and H. Flächer, `hep-ph/0507253` updated in Ref. [258].

[119] C. W. Bauer *et al.*, Phys. Rev. **D70**, 094017 (2004), updated in Ref. [258], [hep-ph/0408002].

[120] P. Gambino and C. Schwanda, Phys. Rev. **D89**, 1, 014022 (2014), [arXiv:1307.4551].

[121] A. Alberti *et al.*, Phys. Rev. Lett. **114**, 6, 061802 (2015), [arXiv:1411.6560].

[122] M. Antonelli *et al.*, Phys. Rept. **494**, 197 (2010), see section 5.4.2, [arXiv:0907.5386].

[123] See"Quark Masses" by A.V. Manohar, L.P. Lellouch , and R.M. Barnett in this *Review*.

[124] K. G. Chetyrkin *et al.*, Phys. Rev. **D80**, 074010 (2009), [arXiv:0907.2110].

[125] M. Bordone, B. Capdevila and P. Gambino, Phys. Lett. B **822**, 136679 (2021), [arXiv:2107.00604].

[126] M. Fael, K. Schönwald and M. Steinhauser, Phys. Rev. D **103**, 1, 014005 (2021), [arXiv:2011.11655].

[127] R. van Tonder *et al.* (Belle) (2021), [arXiv:2109.01685].

[128] N. Uraltsev, Int. J. Mod. Phys. **A14**, 4641 (1999), [hep-ph/9905520].

[129] M. Neubert, Phys. Rev. **D49**, 4623 (1994), [hep-ph/9312311]; M. Neubert, Phys. Rev. **D49**, 3392 (1994), [hep-ph/9311325].

[130] I. I. Y. Bigi *et al.*, Int. J. Mod. Phys. **A9**, 2467 (1994), [hep-ph/9312359].

[131] C. W. Bauer, M. E. Luke and T. Mannel, Phys. Rev. **D68**, 094001 (2003), [hep-ph/0102089].

[132] M. Benzke *et al.*, Phys. Rev. Lett. **106**, 141801 (2011), [arXiv:1012.3167].

[133] A. Gunawardana and G. Paz (2019), [arXiv:1908.02812].

[134] F. U. Bernlochner *et al.* (SIMBA), Phys. Rev. Lett. **127**, 10, 102001 (2021), [arXiv:2007.04320].

[135] M. Neubert, Phys. Lett. **B513**, 88 (2001), [hep-ph/0104280].

[136] M. Neubert, Phys. Lett. **B543**, 269 (2002), [hep-ph/0207002].

[137] A. K. Leibovich, I. Low and I. Z. Rothstein, Phys. Rev. **D61**, 053006 (2000), [hep-ph/9909404].

[138] A. K. Leibovich, I. Low and I. Z. Rothstein, Phys. Rev. **D62**, 014010 (2000), [hep-ph/0001028].

[139] A. K. Leibovich, I. Low and I. Z. Rothstein, Phys. Lett. **B486**, 86 (2000), [hep-ph/0005124].

Downloaded from https://academic.oup.com/ptep/article/2022/8/083C01/6651666 by KIT Library user on 27 September 2022

[140] A. K. Leibovich, I. Low and I. Z. Rothstein, Phys. Lett. **B513**, 83 (2001), [hep-ph/0105066].

[141] A. H. Hoang, Z. Ligeti and M. Luke, Phys. Rev. **D71**, 093007 (2005), [hep-ph/0502134].

[142] B. O. Lange, M. Neubert and G. Paz, JHEP **10**, 084 (2005), [hep-ph/0508178].

[143] B. O. Lange, JHEP **01**, 104 (2006), [hep-ph/0511098].

[144] M. Neubert, Phys. Lett. **B612**, 13 (2005), [hep-ph/0412241].

[145] Z. Ligeti, I. W. Stewart and F. J. Tackmann, Phys. Rev. **D78**, 114014 (2008), [arXiv:0807.1926].

[146] P. Gambino, K. J. Healey and C. Mondino, Phys. Rev. **D94**, 1, 014031 (2016), [arXiv:1604.07598].

[147] B. O. Lange, M. Neubert and G. Paz, Phys. Rev. **D72**, 073006 (2005), [hep-ph/0504071].

[148] P. Gambino *et al.*, JHEP **10**, 058 (2007), [arXiv:0707.2493].

[149] J. R. Andersen and E. Gardi, JHEP **01**, 097 (2006), [hep-ph/0509360].

[150] M. Beneke *et al.*, JHEP **06**, 071 (2005), [hep-ph/0411395].

[151] C. Greub, M. Neubert and B. D. Pecjak, Eur. Phys. J. **C65**, 501 (2010), [arXiv:0909.1609].

[152] M. Brucherseifer, F. Caola and K. Melnikov, Phys. Lett. **B721**, 107 (2013), [arXiv:1302.0444].

[153] T. Mannel and S. Recksiegel, Phys. Rev. **D60**, 114040 (1999), [hep-ph/9904475].

[154] U. Aglietti *et al.*, Eur. Phys. J. **C59**, 831 (2009), [arXiv:0711.0860].

[155] C. W. Bauer, Z. Ligeti and M. E. Luke, Phys. Rev. **D64**, 113004 (2001), [hep-ph/0107074].

[156] C. W. Bauer, Z. Ligeti and M. E. Luke, Phys. Lett. **B479**, 395 (2000), [hep-ph/0002161].

[157] I. I. Y. Bigi and N. G. Uraltsev, Nucl. Phys. **B423**, 33 (1994), [hep-ph/9310285].

[158] M. B. Voloshin, Phys. Lett. **B515**, 74 (2001), [hep-ph/0106040].

[159] Z. Ligeti, M. Luke and A. V. Manohar, Phys. Rev. **D82**, 033003 (2010), [arXiv:1003.1351].

[160] P. Gambino and J. F. Kamenik, Nucl. Phys. **B840**, 424 (2010), [arXiv:1004.0114].

[161] J. L. Rosner *et al.* (CLEO), Phys. Rev. Lett. **96**, 121801 (2006), [hep-ex/0601027].

[162] L. Cao *et al.* (Belle), Phys. Rev. D **104**, 1, 012008 (2021), [arXiv:2102.00020].

[163] B. Aubert *et al.* (BaBar), in "23rd International Symposium on Lepton-Photon Interactions at High Energy (LP07)," (2007), [arXiv:0708.1753].

[164] J. P. Lees *et al.* (BaBar), Phys. Rev. D **86**, 032004 (2012), [arXiv:1112.0702].

[165] R. Barate *et al.* (ALEPH), Eur. Phys. J. **C6**, 555 (1999).

[166] M. Acciarri *et al.* (L3), Phys. Lett. **B436**, 174 (1998).

[167] G. Abbiendi *et al.* (OPAL), Eur. Phys. J. **C21**, 399 (2001), [hep-ex/0107016].

[168] P. Abreu *et al.* (DELPHI), Phys. Lett. **B478**, 14 (2000), [hep-ex/0105054].

[169] A. Bornheim *et al.* (CLEO), Phys. Rev. Lett. **88**, 231803 (2002), [hep-ex/0202019].

[170] A. Limosani *et al.* (Belle), Phys. Lett. **B621**, 28 (2005), [hep-ex/0504046].

[171] J. P. Lees *et al.* (BaBar), Phys. Rev. **D95**, 7, 072001 (2017), [arXiv:1611.05624].

[172] B. Aubert *et al.* (BaBar), Phys. Rev. Lett. **95**, 111801 (2005), [Erratum: Phys. Rev. Lett.97,019903(2006)], [hep-ex/0506036].

[173] R. V. Kowalewski and S. Menke, Phys. Lett. **B541**, 29 (2002), [hep-ex/0205038].

[174] J. P. Lees *et al.* (BaBar), Phys. Rev. **D86**, 032004 (2012), [arXiv:1112.0702].

[175] I. Bizjak *et al.* (Belle), Phys. Rev. Lett. **95**, 241801 (2005), [hep-ex/0505088].

[176] P. Urquijo *et al.* (Belle), Phys. Rev. Lett. **104**, 021801 (2010), [arXiv:0907.0379].

[177] B. Aubert *et al.* (BaBar), Phys. Rev. Lett. **96**, 221801 (2006), [hep-ex/0601046].

[178] L. Cao *et al.* (Belle) (2021), [arXiv:2107.13855].

[179] A. Sibidanov *et al.* (Belle), Phys. Rev. **D88**, 3, 032005 (2013), [arXiv:1306.2781].

[180] B. Aubert *et al.* (BaBar), Phys. Rev. Lett. **90**, 181801 (2003), [eConfC0304052,WG117(2003)], [hep-ex/0301001].

[181] T. Hokuue *et al.* (Belle), Phys. Lett. **B648**, 139 (2007), [hep-ex/0604024].

[182] B. Aubert *et al.* (BaBar), Phys. Rev. **D79**, 052011 (2009), [arXiv:0808.3524].

[183] J. P. Lees *et al.* (BaBar), Phys. Rev. **D88**, 7, 072006 (2013), [arXiv:1308.2589].

[184] J. P. Lees *et al.* (BaBar), Phys. Rev. **D87**, 3, 032004 (2013), [Erratum: Phys. Rev.D87,no.9,099904(2013)], [arXiv:1205.6245].

[185] C. Schwanda *et al.* (Belle), Phys. Rev. Lett. **93**, 131803 (2004), [hep-ex/0402023].

[186] N. E. Adam *et al.* (CLEO), Phys. Rev. Lett. **99**, 041802 (2007), [hep-ex/0703041].

[187] S. B. Athar *et al.* (CLEO), Phys. Rev. **D68**, 072003 (2003), superceded by Ref. [188], [hep-ex/0304019].

[188] R. Gray *et al.* (CLEO), Phys. Rev. **D76**, 012007 (2007), [Addendum: Phys. Rev.D76,no.3,039901(2007)], [hep-ex/0703042].

[189] P. del Amo Sanchez *et al.* (BaBar), Phys. Rev. **D83**, 032007 (2011), supercedes Ref. [190], [arXiv:1005.3288].

[190] B. Aubert *et al.* (BaBar), Phys. Rev. **D72**, 051102 (2005), [hep-ex/0507003].

[191] P. del Amo Sanchez *et al.* (BaBar), Phys. Rev. **D83**, 052011 (2011), updated in Ref. [192], [arXiv:1010.0987].

[192] J. P. Lees *et al.* (BaBar), Phys. Rev. **D86**, 092004 (2012), [arXiv:1208.1253].

[193] J. A. Bailey *et al.* (Fermilab Lattice, MILC), Phys. Rev. **D92**, 1, 014024 (2015), [arXiv:1503.07839].

[194] A. Bazavov *et al.* (Fermilab Lattice, MILC), Phys. Rev. **D100**, 3, 034501 (2019), [arXiv:1901.02561].

[195] C. M. Bouchard *et al.*, Phys. Rev. **D90**, 054506 (2014), [arXiv:1406.2279].

[196] J. M. Flynn *et al.*, Phys. Rev. **D91**, 7, 074510 (2015), [arXiv:1501.05373].

[197] A. X. El-Khadra, A. S. Kronfeld and P. B. Mackenzie, Phys. Rev. D **55**, 3933 (1997), [hep-lat/9604004].

[198] T. Becher and R. J. Hill, Phys. Lett. **B633**, 61 (2006), [hep-ph/0509090].

[199] M. C. Arnesen *et al.*, Phys. Rev. Lett. **95**, 071802 (2005), [hep-ph/0504209].

[200] M. A. Shifman, A. I. Vainshtein and V. I. Zakharov, Nucl. Phys. **B147**, 385 (1979); M. A. Shifman, A. I. Vainshtein and V. I. Zakharov, Nucl. Phys. **B147**, 448 (1979).

[201] P. Ball and R. Zwicky, Phys. Rev. **D71**, 014015 (2005), [hep-ph/0406232].

[202] G. Duplancic *et al.*, JHEP **04**, 014 (2008), [arXiv:0801.1796].

[203] A. Bharucha, JHEP **05**, 092 (2012), [arXiv:1203.1359].

Downloaded from https://academic.oup.com/ptep/article/2022/8/083C01/6651666 by KIT Library user on 27 September 2022

[204] A. V. Rusov, Eur. Phys. J. **C77**, 7, 442 (2017), [arXiv:1705.01929].

[205] I. Sentitemsu Imsong *et al.*, JHEP **02**, 126 (2015), [arXiv:1409.7816].

[206] H. Ha *et al.* (Belle), Phys. Rev. **D83**, 071101 (2011), [arXiv:1012.0090].

[207] B. Aubert *et al.* (BaBar), Phys. Rev. Lett. **101**, 081801 (2008), [arXiv:0805.2408].

[208] W. S. Brower and H. P. Paar, Nucl. Instrum. Meth. **A421**, 411 (1999), [hep-ex/9710029].

[209] P. Ball, eConf **C070512**, 016 (2007), [arXiv:0705.2290].

[210] J. M. Flynn and J. Nieves, Phys. Lett. **B649**, 269 (2007), [hep-ph/0703284].

[211] S. Aoki *et al.*, Eur. Phys. J. **C77**, 2, 112 (2017), [arXiv:1607.00299].

[212] D. Leljak, B. Melić and D. van Dyk, JHEP **07**, 036 (2021), [arXiv:2102.07233].

[213] A. Biswas *et al.*, JHEP **07**, 082 (2021), [arXiv:2103.01809].

[214] R. Aaij *et al.* (LHCb), Phys. Rev. Lett. **126**, 8, 081804 (2021), [arXiv:2012.05143].

[215] A. Khodjamirian and A. V. Rusov, JHEP **08**, 112 (2017), [arXiv:1703.04765].

[216] T. Feldmann and M. W. Y. Yip, Phys. Rev. **D85**, 014035 (2012), [Erratum: Phys. Rev.D86,079901(2012)], [arXiv:1111.1844].

[217] W. Detmold, C. Lehner and S. Meinel, Phys. Rev. **D92**, 3, 034503 (2015), [arXiv:1503.01421].

[218] R. Aaij *et al.* (LHCb), Nature Phys. **11**, 743 (2015), [arXiv:1504.01568].

[219] M. Ablikim *et al.* (BESIII), Phys. Rev. Lett. **116**, 5, 052001 (2016), [arXiv:1511.08380].

[220] R. Aaij *et al.* (LHCb), Phys. Rev. **D96**, 11, 112005 (2017), [arXiv:1709.01920].

[221] M. Tanaka, Z. Phys. **C67**, 321 (1995), [hep-ph/9411405].

[222] H. Itoh, S. Komine and Y. Okada, Prog. Theor. Phys. **114**, 179 (2005), [hep-ph/0409228].

[223] U. Nierste, S. Trine and S. Westhoff, Phys. Rev. **D78**, 015006 (2008), [arXiv:0801.4938].

[224] M. Tanaka and R. Watanabe, Phys. Rev. **D82**, 034027 (2010), [arXiv:1005.4306].

[225] A. Datta, M. Duraisamy and D. Ghosh, Phys. Rev. **D86**, 034027 (2012), [arXiv:1206.3760].

[226] D. Becirevic, N. Kosnik and A. Tayduganov, Phys. Lett. **B716**, 208 (2012), [arXiv:1206.4977].

[227] S. Fajfer *et al.*, Phys. Rev. Lett. **109**, 161801 (2012), [arXiv:1206.1872].

[228] A. Crivellin, C. Greub and A. Kokulu, Phys. Rev. **D86**, 054014 (2012), [arXiv:1206.2634].

[229] M. Bauer and M. Neubert, Phys. Rev. Lett. **116**, 14, 141802 (2016), [arXiv:1511.01900].

[230] I. Doršner *et al.*, Phys. Rept. **641**, 1 (2016), [arXiv:1603.04993].

[231] A. Celis *et al.*, Phys. Lett. **B771**, 168 (2017), [arXiv:1612.07757].

[232] S. Jaiswal, S. Nandi and S. K. Patra, JHEP **12**, 060 (2017), [arXiv:1707.09977].

[233] M. Bordone *et al.*, Eur. Phys. J. C **80**, 4, 347 (2020), [arXiv:1912.09335].

[234] B. Aubert *et al.* (BaBar), Phys. Rev. Lett. **100**, 021801 (2008), [arXiv:0709.1698].

[235] J. P. Lees *et al.* (BaBar), Phys. Rev. Lett. **109**, 101802 (2012), [arXiv:1205.5442].

[236] J. P. Lees *et al.* (BaBar), Phys. Rev. **D88**, 7, 072012 (2013), [arXiv:1303.0571].

[237] M. Huschle *et al.* (Belle), Phys. Rev. **D92**, 7, 072014 (2015), [arXiv:1507.03233].

[238] Y. Sato *et al.* (Belle), Phys. Rev. **D94**, 7, 072007 (2016), [arXiv:1607.07923].

[239] S. Hirose *et al.* (Belle), Phys. Rev. Lett. **118**, 21, 211801 (2017), [arXiv:1612.00529].

[240] G. Caria *et al.* (Belle) (2019), [arXiv:1910.05864].

[241] R. Aaij *et al.* (LHCb), Phys. Rev. Lett. **115**, 11, 111803 (2015), [Erratum: Phys. Rev. Lett.115,no.15,159901(2015)], [arXiv:1506.08614].

[242] R. Aaij *et al.* (LHCb), Phys. Rev. Lett. **120**, 17, 171802 (2018), [arXiv:1708.08856].

[243] `http://www.slac.stanford.edu/xorg/hfag/semi/fpcp17/RDRDs.html`.

[244] M. Blanke, PoS **LeptonPhoton2019**, 015 (2019), [arXiv:1908.09713].

[245] S. Descotes-Genon, PoS **ALPS2019**, 016 (2020).

[246] D. London and J. Matias (2021), [arXiv:2110.13270].

[247] J. G. Korner and G. A. Schuler, Z. Phys. **C46**, 93 (1990).

[248] A. Abdesselam *et al.* (Belle), in "10th International Workshop on the CKM Unitarity Triangle (CKM 2018) Heidelberg, Germany, September 17-21, 2018," (2019), [arXiv:1903.03102].

[249] A. Matyja *et al.* (Belle), Phys. Rev. Lett. **99**, 191807 (2007), [arXiv:0706.4429].

[250] A. Bozek *et al.* (Belle), Phys. Rev. **D82**, 072005 (2010), [arXiv:1005.2302].

[251] M. Tanaka and R. Watanabe, Phys. Rev. **D87**, 3, 034028 (2013), [arXiv:1212.1878].

[252] S. Hirose *et al.* (Belle), Phys. Rev. **D97**, 1, 012004 (2018), [arXiv:1709.00129].

[253] R. Aaij *et al.* (LHCb), Phys. Rev. **D97**, 7, 072013 (2018), [arXiv:1711.02505].

[254] R. Aaij *et al.* (LHCb), Phys. Rev. Lett. **120**, 12, 121801 (2018), [arXiv:1711.05623].

[255] J. Harrison, C. T. H. Davies and A. Lytle (LATTICE-HPQCD), Phys. Rev. Lett. **125**, 22, 222003 (2020), [arXiv:2007.06956].

[256] J. Harrison, C. T. H. Davies and A. Lytle (HPQCD), Phys. Rev. D **102**, 9, 094518 (2020), [arXiv:2007.06957].

[257] P. Gambino and S. Hashimoto, Phys. Rev. Lett. **125**, 3, 032001 (2020), [arXiv:2005.13730].

[258] Y. Amhis *et al.* (HFLAV), Eur. Phys. J. **C77**, 12, 895 (2017), [arXiv:1612.07233].

Downloaded from https://academic.oup.com/ptep/article/2022/8/083C01/6651666 by KIT Library user on 27 September 2022

77. Determination of CKM angles from B hadrons

Revised February 2022 by T. Gershon (Warwick U.), M. Kenzie (Warwick U.) and K. Trabelsi (U. Paris-Saclay, IJCLab).

77.1 Introduction

The Cabibbo–Kobayashi–Maskawa (CKM) description of quark mixing [1,2] leads to a number of triangle relations between pairs of CKM matrix elements. One of these,

$$V_{ud}V_{ub}^* + V_{cd}V_{cb}^* + V_{td}V_{tb}^* = 0 \ , \tag{77.1}$$

is of particular interest since (i) all its terms are of comparable magnitude, and (ii) its properties can be measured through studies of oscillations and decays of B mesons. As the area of this unitary triangle is a measure of the amount of CP violation in the Standard Model [3], it is of particular interest to determine the values of its angles and to test the consistency of the CKM paradigm with the experimental measurements. The angles are defined as

$$\begin{aligned} \alpha &= \arg\left[-\frac{V_{td}V_{tb}^*}{V_{ud}V_{ub}^*}\right] \ , \qquad \beta = \arg\left[-\frac{V_{cd}V_{cb}^*}{V_{td}V_{tb}^*}\right] \ , \\ \gamma &= \arg\left[-\frac{V_{ud}V_{ub}^*}{V_{cd}V_{cb}^*}\right] \ , \end{aligned} \tag{77.2}$$

with an alternative notation $(\phi_2, \phi_1, \phi_3) \equiv (\alpha, \beta, \gamma)$ also widely used in the literature.

In this mini-review, the most precise methods to determine the CKM angles are described, with a particular focus on nontrivial aspects of the combination of results. More detailed discussions of these points can be found in Ref. [4]. A similar mini-review on the side of the unitarity triangle adjacent to the angle γ can be found in Ref. [5]. A detailed overview of the CKM quark-mixing matrix is given in Ref. [6] while CP violation in the quark sector is discussed in Ref. [7].

77.2 β

The relative weak (*i.e.* CP-violating) phase between the amplitude for any CKM-favoured B^0 meson decay to a CP eigenstate and that for the decay following B^0–$\overline{B}^0$ oscillation is twice the angle β. The decay-time-dependent CP asymmetry can be expressed as

$$\mathcal{A}_{f_{CP}}(t) \equiv \frac{d\Gamma/dt\left[\overline{B}^0_{\rm phys}(t) \to f_{CP}\right] - d\Gamma/dt\left[B^0_{\rm phys}(t) \to f_{CP}\right]}{d\Gamma/dt\left[\overline{B}^0_{\rm phys}(t) \to f_{CP}\right] + d\Gamma/dt\left[B^0_{\rm phys}(t) \to f_{CP}\right]} \ , \tag{77.3a}$$

$$= S_f \sin(\Delta m t) - C_f \cos(\Delta m t) \ , \tag{77.3b}$$

where the notation $B^0_{\rm phys}(t)$ ($\overline{B}^0_{\rm phys}(t)$) denotes a neutral B meson that decays at time t into the final state f_{CP}, and is known ("tagged") at time $t = 0$ to have flavour content corresponding to B^0 ($\overline{B}^0$). In Eq. (77.3b), Δm denotes the mass difference between the two physical eigenstates of the B^0–$\overline{B}^0$ system, while the corresponding decay-width difference is assumed to be negligible [8]; moreover CPT symmetry and the absence of CP violation in B^0–$\overline{B}^0$ mixing is assumed throughout this mini-review.

In the general case, one can write

$$S_f \equiv \frac{2\,\mathcal{I}m(\lambda_f)}{1+\left|\lambda_f\right|^2} \qquad \text{and} \qquad C_f \equiv \frac{1-\left|\lambda_f\right|^2}{1+\left|\lambda_f\right|^2} \ , \tag{77.4}$$

where the parameter $\lambda_f = \frac{q}{p}\frac{\overline{A}_f}{A_f}$ is defined in terms of p and q, which define the flavour content of the mass eigenstates of the B^0–$\overline{B}^0$ system [8], and the amplitudes $\overline{A}_f$ (A_f) for a $\overline{B}^0$ (B^0) decay to the final state f_{CP}. In the limit that the decay amplitude is dominated by a CKM-favoured transition, as is the case for $B^0 \to J/\psi K^0_{\rm S}$ decays, one obtains simple relations: $S_f = -\eta_{CP}\sin(2\beta)$ and $C_f = 0$, where η_{CP} is the CP eigenvalue of the final state [9,10]. This method has been pursued intensively by experiments. The current world averages, combining results for several charmonium-kaon final states but dominated by results on $B^0 \to J/\psi K^0_{\rm S}$ (CP odd) and $B^0 \to J/\psi K^0_{\rm L}$ (CP even), are [4]

$$-\eta_{CP}S_f = 0.699 \pm 0.017 \ , \qquad C_f = -0.005 \pm 0.015 \ . \tag{77.5}$$

Despite the large number of signal events in the data, the dominant uncertainties are still statistical. One important source of potential systematic correlation between results from different experiments is that due to "tag-side interference" [11], which is common to measurements exploiting production through the $e^+e^- \to \Upsilon(4S) \to B^0\overline{B}^0$ process, including the latest results from BaBar [12] and Belle [13]. It does not, however, affect the results from LHCb [14] that have comparable statistical sensitivity. Another common source of systematic uncertainty is due to knowledge of the value of Δm, but since this quantity has been measured precisely [8] the effect remains small.

The interpretation of the value of $-\eta_{CP}S_f$ from Eq. (77.5) as $\sin(2\beta)$ assumes negligible contributions from subleading amplitudes with a different weak phase to that of the tree diagram (*i.e.* to that of the CKM matrix elements $V_{cb}V_{cs}^*$). This potential additional contribution is often referred to as "penguin pollution". All existing data, including the value of C_f in Eq. (77.5), as well as several explicit calculations [15–18], are consistent with penguin pollution in B^0 meson decays to charmonium-kaon decays being negligible at the current level of precision. Therefore, the value of $-\eta_{CP}S_f$ is generally converted to $\sin(2\beta)$ without any correction or additional uncertainty being assigned due to this assumption. This gives [4]

$$\beta = (22.2 \pm 0.7)^\circ \ , \tag{77.6}$$

where only the solution consistent with the Standard Model is reported (methods to resolve the trigonometric ambiguity in the result are discussed below). It is also possible to use data-driven methods, typically based on flavour symmetries plus some additional assumptions, to constrain the effects of penguin pollution [19–21]. In this case it is necessary to consider each charmonium-kaon final state separately, since the penguin pollution to each may differ. The most common approach [19], which relies on experimental information on $B^0 \to J/\psi\pi^0$ decays, currently gives an additional uncertainty on $\sin(2\beta)$ from $B^0 \to J/\psi K^0_{\rm S}$ of around 0.01.

It is possible to avoid the issue of penguin pollution in the measurement of β by using B^0 meson decays to a charm- and light-meson final state, such as $D_{CP}\pi^0$ (where D_{CP} represents a D^0 meson decaying into a CP eigenstate), instead of the charmonium-kaon final states. These decays do have a CKM-suppressed contribution ($V_{ub}V_{cd}^*$ instead of $V_{cb}V_{ud}^*$), which can in principle bias the determination of $\sin(2\beta)$ from S_f, but this can be calculated and is known to be negligible at current precision. The requirement that the neutral D meson decays to a final state that is common to both D^0 and $\overline{D}^0$, such as the CP-even eigenstate K^+K^-, reduces the sample size that is available for analysis. Consequently, the world average [4], $\sin(2\beta) = 0.71 \pm 0.09$, with these channels is not as precise as that from the charmonium-kaon states.

Converting experimental results on $\sin(2\beta)$ into constraints on β leads to a trigonometric ambiguity in the range $[0^\circ, 180^\circ]$. This can be resolved with experimental measurements of $\cos(2\beta)$, which can be obtained from decay-time-dependent analyses of B^0 meson decays to multibody (non-CP-eigenstate) final states. Among the charmonium-kaon decays, study of $B^0 \to J/\psi K^*(892)^0$ with $K^*(892)^0 \to K^0_{\rm S}\pi^0$ is the most promising approach, but due to the limited sample size that has been analysed to date the precision is not sufficient to resolve the ambiguity conclusively. The charm- and light-meson channels such as $B^0 \to D\pi^0$ with $D \to K^0_{\rm S}\pi^+\pi^-$ have been shown to provide good statistical power for this purpose, with a joint analysis of BaBar and Belle data giving $\cos(2\beta) = 0.91 \pm 0.25$ [22,23], sufficient to rule out the alternative solution for β.

77.3 α

In the limit that only tree amplitudes contribute to B^0 meson decays to light mesons, such as $B^0 \to \pi^+\pi^-$, then the observables of the decay-time-dependent CP asymmetry of Eq. (77.3) would allow a straight-forward determination of 2α: $S_f = +\eta_{CP}\sin(2\alpha)$

Downloaded from https://academic.oup.com/ptep/article/2022/8/083C01/6651666 by KIT Library user on 27 September 2022

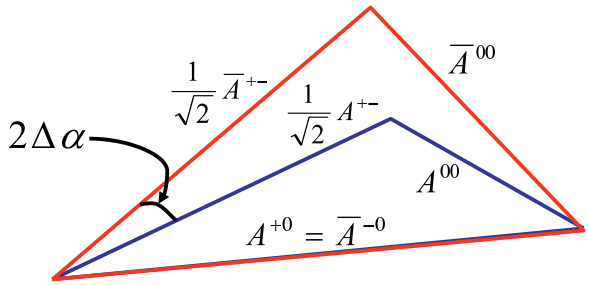

Figure 77.1: Isospin triangles for $B \to \pi\pi$ decays, reproduced from Ref. [24]. Here, the relative phase between A^{+0} and $\overline{A}^{-0}$ has been rotated away to simplify the picture. The total relative phase probed by $S_{\pi^+\pi^-}$ is $\arg\left(\frac{q}{p}\frac{\overline{A}^{+-}}{A^{+-}}\right) = 2\alpha - 2\Delta\alpha$, including contributions from B^0–$\overline{B}^0$ mixing, the tree-level amplitudes and the correction $\Delta\alpha$, and exploiting the unitarity requirement $\alpha + \beta + \gamma = 180°$.

and $C_f = 0$. In general, however, the determination of α is complicated by the presence of contributions from $b \to d(u\bar{u})$ neutral-current penguin transitions, which have a similar level of CKM-suppression as the $b \to u(\bar{u}d)$ charged-current tree amplitudes but have a different weak phase. Consequently, one obtains instead for $B^0 \to \pi^+\pi^-$

$$S_{\pi^+\pi^-} = \sqrt{1 - C^2_{\pi^+\pi^-}}\,\sin(2\alpha - 2\Delta\alpha), \qquad (77.7)$$

where $\Delta\alpha$ is the *a priori* unknown penguin contribution.

This contribution from the penguin amplitude can be accounted for in an analysis relating the amplitudes for isospin partner decays, *e.g.* A^{+-} for $B^0 \to \pi^+\pi^-$, A^{+0} for $B^+ \to \pi^+\pi^0$, A^{00} for $B^0 \to \pi^0\pi^0$ decays and $\left(\overline{A}^{+-}, \overline{A}^{-0}, \overline{A}^{00}\right)$ for their charge conjugates. The isospin analysis relies on the fact that there is no penguin contribution to A^{+0} and $\overline{A}^{-0}$, because $\pi^\pm\pi^0$ is a pure isospin-2 state, and the ($\Delta I = \frac{1}{2}$) QCD-penguin amplitudes only contribute to the isospin-0 final state. One therefore obtains the following isospin triangle relations [25]

$$A^{+0} = \frac{1}{\sqrt{2}}A^{+-} + A^{00} \quad \text{and} \quad \overline{A}^{-0} = \frac{1}{\sqrt{2}}\overline{A}^{+-} + \overline{A}^{00}\,, \qquad (77.8)$$

from which it is possible to determine $\Delta\alpha$, as shown in Fig. 77.1.

Since the determination of $\Delta\alpha$ and thus also α requires construction of amplitude-level relations, it is not appropriate to simply average results of α from different experiments. Instead, measurements of each of the observable quantities needed to determine α are input into a combination. For the $B \to \pi\pi$ system, the inputs are the branching fractions of $B^0 \to \pi^+\pi^-$, $B^+ \to \pi^+\pi^0$ and $B^0 \to \pi^0\pi^0$ decays, the lifetimes of the B^+ and B^0 mesons (which relate the branching fractions to amplitude-level quantities), and the $S_{\pi^+\pi^-}$, $C_{\pi^+\pi^-}$ and $C_{\pi^0\pi^0}$ observables. Potential sources of correlation must be taken into account, but these are predominantly systematic in origin and thus have a small effect on the combination, since the measurements are statistically limited. An exception is that the LHCb measurements of $(S_{\pi^+\pi^-}, C_{\pi^+\pi^-})$ [26,27] have a significant statistical correlation due to the fact that the time variable of Eq. (77.3) is the difference between production and decay, and hence is in the range $[0, \infty]$. This correlation is largely absent for measurements from BaBar [28] and Belle [29], where the difference between the signal and tagging B meson decay times is measured, and hence $t \in [-\infty, \infty]$. The combination itself can be performed with different statistical approaches; the procedure described in detail in Ref. [30], based on a frequentist treatment, is used here. The knowledge of $C_{\pi^0\pi^0}$ [28,31] is currently the limiting factor in the precision on α from the $B \to \pi\pi$ system, and is likely to remain so for some time due to the difficulty to reconstruct this final state.

In general, the isospin triangle construction gives a four-fold ambiguity on $2\Delta\alpha$ (each triangle can face either up or down), leading to an eight-fold ambiguity on α in the range $[0°, 180°]$. This is reduced if either or both of the triangles are flat, or if the two triangles have sides of identical length. The ambiguities can also be reduced if measurement of the $S_{\pi^0\pi^0}$ (or equivalent) observable is available, since this can be combined with the corresponding $\Delta\alpha$ parameter from the right-hand corner of the triangle in Fig. 77.1 to provide an additional constraint. None of these possibilities are realised in the $B \to \pi\pi$ system; in particular a decay-time-dependent analysis of $B^0 \to \pi^0\pi^0$ is extremely challenging experimentally due to the absence of any charged particle originating from the B decay position. Nonetheless, solutions consistent with $\alpha = 0$ can be rejected on physical grounds [24].

The isospin analysis can also be performed with the $B \to \rho\rho$ system, which contains two vector particles in the final state and so does not have a fixed CP eigenvalue. In principle the analysis can be performed separately for each $\rho\rho$ polarization state, but in practise it is found that the longitudinal polarization fraction, f_L, is close to unity, and hence the final state is approximately CP-even. Compared to $B^0 \to \pi\pi$, the $\rho\rho$ modes benefit experimentally from a higher branching fraction and smaller penguin contributions, so that the isospin triangles are flatter, reducing the ambiguities. (The value of $\Delta\alpha$ in the $B \to \rho\rho$ system, obtained from the isospin analysis, has a single solution in $[0, \pi]$ at $(3 \pm 5)°$, while for $B \to \pi\pi$ there are two solutions at 13° and 27° with $\Delta\alpha \in [7, 33]°$ at 68.3% confidence level (CL). The isospin analysis with either final state has an ambiguity under $\Delta\alpha \Leftrightarrow -\Delta\alpha$.) For the BaBar [32] and Belle [33] experiments, the high branching fraction and smaller penguin contribution compensate for the increased difficulty to reconstruct the $\rho\rho$ final state relative to $\pi\pi$. Moreover, in contrast to $S_{\pi^0\pi^0}$, measurement of $S_{\rho^0\rho^0}$ is possible due to the four charged pion final state, following $\rho^0 \to \pi^+\pi^-$ decay, as has been demonstrated by BaBar [34].

In the $B \to \rho\pi$ system there are more amplitudes to consider, so that the isospin relation corresponds to a pentagon rather than a triangle and Eq. (77.8) is modified to become

$$\begin{aligned} \sqrt{2}(A^{+0} + A^{0+}) &= A^{+-} + A^{-+} + 2A^{00} \quad \text{and} \\ \sqrt{2}(\overline{A}^{-0} + \overline{A}^{0-}) &= \overline{A}^{+-} + \overline{A}^{-+} + 2\overline{A}^{00}\,. \end{aligned} \qquad (77.9)$$

As in Eq. (77.8), the left-hand sides of these expressions correspond to a pure isospin-2 final state, and therefore the ratio of the right-hand sides gives a pure phase term that, accounting for the B^0–$\overline{B}^0$ mixing phase that also contributes to the measured quantities, is 2α. The relative amplitudes for B^0 and $\overline{B}^0$ decays to $\rho^+\pi^-$, $\rho^-\pi^+$ and $\rho^0\pi^0$ can all be determined from a decay-time-dependent analysis of the $\pi^+\pi^-\pi^0$ Dalitz plot, so that study of this channel alone allows determination of α [35]. This analysis in principle leads to a single solution for α in $[0°, 180°]$, but the precision of current measurements [36–38] is limited.

The isospin analysis used to determine α is believed to be valid to high precision, and theoretical uncertainties in the procedure are usually neglected. Nonetheless, it should be noted that the analysis assumes the absence of electroweak penguin amplitudes, which can contribute to $\Delta I = \frac{3}{2}$ transitions with a different weak phase from that of the tree amplitudes [39,40]. Moreover, isospin-breaking effects such as $\left(\pi^0, \eta, \eta'\right)$ mixing would impact on the relations of Eq. (77.8). A further complication in the $B \to \rho\rho$ system is the effect of the non-zero ρ meson width [41]. Estimates of the size of these effects on the determined value of α are typically at the 1° level or less [30]. By contrast, methods to determine α using SU(3) or other flavour symmetries are generally considered to have larger theoretical uncertainties and are not included here.

The world average obtained for the angle α from isospin analysis of $B \to \pi\pi$, $\rho\pi$ and $\rho\rho$ decays is [4]

$$\alpha = (85.2\,^{+4.8}_{-4.3})°\,, \qquad (77.10)$$

where the quoted uncertainty is at the 68.3% CL and does not include effects due to isospin-breaking. This world average, together with results split by decay mode, is shown in Fig. 77.2. The combination has a total of 51 experimental inputs from which 24 parameters are determined, and an overall χ^2 of 16.6, which corresponds to a p-value of 94%. Thus, there is excellent overall consistency between the inputs, despite the tension apparent in

Downloaded from https://academic.oup.com/ptep/article/2022/8/083C01/6651666 by KIT Library user on 27 September 2022

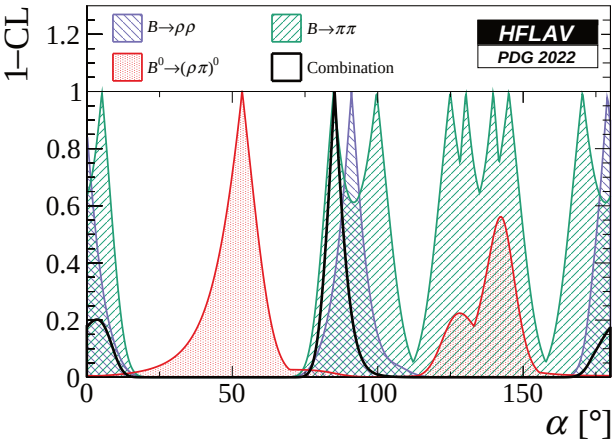

Figure 77.2: World average of α, as well as contributions from individual modes, in terms of 1−CL.

Fig. 77.2 between the results from $B^0 \to (\rho\pi)^0$ and the others. The combination gives a single best-fit for α in $[0°, 180°]$, but an ambiguous solution exists at $\alpha \Leftrightarrow \alpha{+}180°$. A secondary minimum close to zero is disfavoured [30].

77.4 γ

The angle γ is the weak phase between Cabibbo-favoured $b \to c$ and suppressed $b \to u$ quark transitions and can be determined by exploiting interference between them. Explicitly, the ratio of suppressed to favoured amplitudes is parameterized by

$$r_B e^{i(\delta_B \pm \gamma)} = \frac{A_{\rm sup}}{A_{\rm fav}} \,, \tag{77.11}$$

where r_B is the ratio of amplitude magnitudes, δ_B the strong phase difference and the + or − sign depends on whether the transition involves a $\bar{b}$ or b quark, respectively. Measurement of γ in this way has negligible theoretical uncertainty in the Standard Model [42], and therefore this approach provides a benchmark against which determinations from other methods, typically involving loop diagrams, can be compared.

Interference between these amplitudes is realised in $B^+ \to DK^+$ decays, where D represents an admixture of D^0 and $\overline{D}^0$ mesons. The simplest case is that of D decays to *CP*-eigenstates (GLW method [43, 44]), either *CP*-even such as K^+K^- (*CP*+) or *CP*-odd such as $K^0_S\pi^0$ (*CP*−). The normalized decay rate and *CP* asymmetry are given by

$$\begin{aligned} R_{CP\pm} &= \frac{\Gamma(B^- \to D_{CP\pm}K^-) + \Gamma(B^+ \to D_{CP\pm}K^+)}{\Gamma(B^- \to D^0K^-) + \Gamma(B^+ \to \overline{D}^0K^+)} \\ &= 1 + r_B^2 \pm 2r_B\cos(\delta_B)\cos(\gamma) \,, \end{aligned} \tag{77.12a}$$

$$\begin{aligned} A_{CP\pm} &= \frac{\Gamma(B^- \to D_{CP\pm}K^-) - \Gamma(B^+ \to D_{CP\pm}K^+)}{\Gamma(B^- \to D_{CP\pm}K^-) + \Gamma(B^+ \to D_{CP\pm}K^+)} \\ &= \frac{\pm 2r_B\sin(\delta_B)\sin(\gamma)}{1 + r_B^2 \pm 2r_B\cos(\delta_B)\cos(\gamma)} \,. \end{aligned} \tag{77.12b}$$

These relations assume the absence of direct *CP* violation in the charm system; experimentally allowed deviations from this assumption are too small to cause a significant bias on γ [7, 45]. It is convenient to determine the $R_{CP\pm}$ quantities through a double ratio, normalizing to $B^+ \to D\pi^+$ decays involving the same final states, since this cancels potential sources of systematic uncertainty due to the branching fractions of the D decays that are used; small possible effects of *CP* violation in $B^+ \to D\pi^+$ decays are a source of systematic uncertainty in this procedure. The GLW method can be extended to include final states that are almost *CP*-eigenstates [46], as is the case in $D \to \pi^+\pi^-\pi^0$ and $D \to K^+K^-\pi^0$ decays, via inclusion of a factor encoding the fraction of *CP*-even (or *CP*-odd) content, $F_\pm$, which dilutes the sensitivity to γ by reducing the size of the interference terms (the terms linear with r_B) in Eq. (77.12).

For other D decays, the ratio of amplitudes for the D^0 and $\overline{D}^0$ decays to the final state of interest has to be accounted for in the formalism. The ADS method [47, 48] uses D decays to final states such as $K^\mp\pi^\pm$, which involve interference between Cabibbo-favoured (CF) and doubly-Cabibbo-suppressed (DCS) transitions. The observables in this case are

$$\begin{aligned} A_{\rm ADS} &= \frac{\Gamma(B^- \to [K^+\pi^-]_D K^-) - \Gamma(B^+ \to [K^-\pi^+]_D K^+)}{\Gamma(B^- \to [K^+\pi^-]_D K^-) + \Gamma(B^+ \to [K^-\pi^+]_D K^+)} \\ &= \frac{2r_B r_D \sin(\delta_B + \delta_D)\sin(\gamma)}{r_B^2 + r_D^2 + 2r_B r_D \cos(\delta_B + \delta_D)\cos(\gamma)} \,, \end{aligned} \tag{77.13a}$$

$$\begin{aligned} R_{\rm ADS} &= \frac{\Gamma(B^- \to [K^+\pi^-]_D K^-) + \Gamma(B^+ \to [K^-\pi^+]_D K^+)}{\Gamma(B^- \to [K^-\pi^+]_D K^-) + \Gamma(B^+ \to [K^+\pi^-]_D K^+)} \\ &= r_B^2 + r_D^2 + 2r_B r_D \cos(\delta_B + \delta_D)\cos(\gamma) \,, \end{aligned} \tag{77.13b}$$

where r_D and δ_D are the amplitude magnitude ratio and strong phase difference between the CF and DCS D decay. An alternative pair of observables, (R_-, R_+), is also sometimes used, where R_- (R_+) is the ratio of decay rates between the suppressed and favoured transitions for B^- (B^+) decays. The R_- and R_+ observables are statistically independent, while $A_{\rm ADS}$ and $R_{\rm ADS}$ are not (in particular, the uncertainty on $A_{\rm ADS}$ depends on the central value of $R_{\rm ADS}$). However, the pair (R_-, R_+) has more correlated sources of systematic uncertainty compared to $(A_{\rm ADS}, R_{\rm ADS})$. The observables of Eq. (77.13) are therefore usually preferred once a significant signal is established. The ADS method can also be extended to include decays to multibody final states, such as $D \to K^\pm\pi^\mp\pi^0$ and $D \to K^\pm\pi^\mp\pi^+\pi^-$, by addition of a coherence factor [49] which appears in the interference terms of Eq. (77.13) and accounts for dilution of the sensitivity due to variation of the decay amplitude across the phase space of the final state. A similar method can be used for singly Cabibbo-suppressed D decays to non-*CP* eigenstates such as K^*K [50].

For D decays to multibody self-conjugate final states (BPGGSZ method [51,52]), such as $D \to K^0_S\pi^+\pi^-$, one can write the partial decay rate as a function of the position in the phase space in terms of the "Cartesian parameters" $x_\pm + iy_\pm = r_B e^{i(\delta_B \pm \gamma)}$:

$$\begin{aligned} d\Gamma(B^\pm \to [K^0_S\pi^+\pi^-]_D K^\pm) &= A^2_{(\mp,\pm)} + r_B^2 A^2_{(\pm,\mp)} \\ &+ 2A_{(\pm,\mp)}A_{(\mp,\pm)}[x_\pm c_{D(\pm,\mp)} + y_\pm s_{D(\pm,\mp)}], \end{aligned} \tag{77.14}$$

where the notation $(+,-)$ is shorthand for the dependence on the Dalitz-plot position — the squared invariant masses of $K^0_S\pi^+$ and $K^0_S\pi^-$ combinations, respectively. The quantities $A_{(+,-)}$ and $A_{(-,+)}$ represent the magnitudes of the D^0 and $\overline{D}^0$ decay amplitudes at the position $(+,-)$ and are interchangable with their *CP* conjugate amplitudes because *CP* conservation is assumed in the D decay (*i.e.* $A_{(-,+)} = \overline{A}_{(+,-)}$). The quantities $c_{D(\pm,\mp)}$ and $s_{D(\pm,\mp)}$ are the cosine and sine of the strong phase difference, $\delta_{D(+,-)} = \arg(\overline{A}_{(+,-)}) - \arg(A_{(+,-)})$, between the $\overline{D}^0$ and D^0 amplitudes. These quantities can be determined from an amplitude model, although this leads to a hard-to-quantify systematic uncertainty associated to the composition of the model. An alternative, "model-independent", approach involves dividing the phase space into appropriate bins. In this case, the analysis benefits from external input on the values of c_D and s_D integrated over each bin. Measurements of these external parameters have been performed for the $D \to K^0_S\pi^+\pi^-$ decay by the CLEO-c and BESIII collaborations [53–56]. The use of common input values for these parameters in model-independent determinations of γ with the BPGGSZ method by different experiments is a source of correlation between experiments that is currently negligible but will become more significant as the available B meson data samples increase in size.

The discussion above refers to $B^+ \to DK^+$ decays, but analogous measurements can be made also for additional channels such as $B^+ \to D^*K^+$ (with $D^* \to D\pi^0$, $D\gamma$) and $B^+ \to DK^{*+}$ (with $K^{*+} \to K^0_S\pi^+$, $K^+\pi^0$). In the limit that these can be treated purely as two-body decays, the expressions for $B^+ \to DK^+$ are modified only by ensuring the r_B and δ_B parameters are specific to each B decay. Moreover, for $B^+ \to D^*K^+$ decays an effective

Downloaded from https://academic.oup.com/ptep/article/2022/8/083C01/6651666 by KIT Library user on 27 September 2022

shift of the strong phase by π between $D^* \to D\pi^0$ and $D\gamma$ decays [57] has to be taken into account. In case the finite width of the decaying resonance is non-negligible, as is the case for the $K^*(892)$ state, additional amplitudes can contribute leading to a dilution of the sensitivity, which can be accounted for in the formalism through the introduction of a relevant coherence factor. For the $B^0 \to DK^{*0}$ decay, full amplitude analysis of the $B^0 \to DK^+\pi^-$ Dalitz plot provides additional sensitivity compared to the quasi-two-body approach [58, 59].

It is also possible to measure γ using decay-time-dependent analysis of the B_s^0 meson [60]. The weak phase arising in the interference between direct decay of $B_s^0 \to D_s^\mp K^\pm$ and decay via mixing is $(\gamma - 2\beta_s)$, where β_s is the angle associated with $B_s^0 \to J/\psi\phi$ decays in a similar way to the relation between β and $B^0 \to J/\psi K_S^0$ decays described in Sec. 77.2. Sufficient information can be obtained from the tagged, decay-time-dependent rates of $B_s^0 \to D_s^\mp K^\pm$ decays that this weak phase can be determined, up to an ambiguity, together with the strong phase difference between, and the ratio of the magnitudes of, the suppressed and favoured amplitudes. Since β_s is known to good precision [8], measurements of the decay-time-dependent *CP*-asymmetry observables in $B_s^0 \to D_s^\mp K^\pm$ decays can be used to infer constraints on γ. Alternatively, if effects of penguin pollution in $B_s^0 \to J/\psi\phi$ decays [17, 18] are a concern, as they will become in the future, results from the $B_s^0 \to D_s^\mp K^\pm$ mode can be combined with an independent precise measurement of γ to provide a penguin-free determination of β_s.

The average for γ requires a non-trivial combination due the complicated relations between the observables and the physics parameters of interest, such as in Eqs. (77.12), (77.13) and (77.14). Moreover, hadronic parameters such as r_B and δ_B defined in Eq. (77.11) are common to all different D decay modes (but differ for each B decay mode). Thus, it is not correct to simply average results for γ obtained by different experiments or in different channels. Instead, measurements of rate asymmetries, rate ratios and the Cartesian parameters are taken as inputs to the combination, from which results are obtained not only for γ but also for the hadronic parameters. Independent measurements of auxiliary parameters such as r_D and δ_D are also treated as inputs to the combination. In some cases the B decay data can help to reduce uncertainties on these auxiliary parameters and therefore a simultaneous fit of charm and beauty data can provide stronger constraints [61]; this approach however is not currently used for the world average.

The precision to which γ can be measured with a particular B decay is approximately inversely proportional to the value of r_B. Thus, results from channels with smaller yields but larger values of r_B, such as $B^0 \to DK^{*0}$ and $B_s^0 \to D_s^\mp K^\pm$ ($r_B \approx 0.3$–0.4), can have a significant impact on the world average and are included in the combination. By contrast the $B^+ \to D\pi^+$ mode, for which large samples are available but $r_B \approx 0.005$, has little impact and is also more sensitive to potential systematic biases; hence it is not included. The sensitivity of the world average at present is dominated by results from $B^+ \to DK^+$, where $r_B \approx 0.1$, in particular results with the GLW [62], ADS [62] and BPGGSZ [63] methods.

The world average obtained for the angle γ, obtained by combining results from $B^+ \to DK^+$, D^*K^+, DK^{*+}, $DK^+\pi^+\pi^-$, $B^0 \to DK^+\pi^-$, $B_s^0 \to D_s^\mp K^\pm$ and $B_s^0 \to D_s^\mp K^\pm\pi^+\pi^-$ decays, is [4]

$$\gamma = \left(65.9\,^{+3.3}_{-3.5}\right)^\circ \ , \qquad (77.15)$$

where the quoted uncertainty is at the 68.3% CL.

Effects related to charm and kaon mixing and *CP* violation are generally negligible at the current level of precision, in particular for modes with $r_B \gtrsim 0.1$. An exception is that a dependence of the selection efficiency on the charm decay time can induce a dependence of the observables on charm mixing parameters [64]. Such effects can be important at hadron collider experiments such as LHCb, but can be and are corrected for. Interactions of neutral kaons with detector material can also cause a bias in determination of γ from modes with low values of r_B [65], such as the BPGGSZ method applied to $B^+ \to D\pi^+$, but are negligible in modes with larger r_B values. A further subtlety is that the identification of the weak phase between suppressed and favoured amplitudes in $B \to DK$ decays with γ, as defined in Eq. (77.2), assumes that the 2×2 submatrix of the CKM matrix is real, *i.e.* that $\arg\left[V_{ud}V_{us}^*/\left(V_{cd}V_{cs}^*\right)\right] = 0$. This is true to an excellent approximation in the Standard Model, and is known experimentally from independent studies of the charm system [45] to contribute negligible bias to current measurements. Nonetheless, in future it will be possible to test directly this assumption by comparing the value of γ obtained from the $B \to DK$ and $B \to D\pi$ systems.

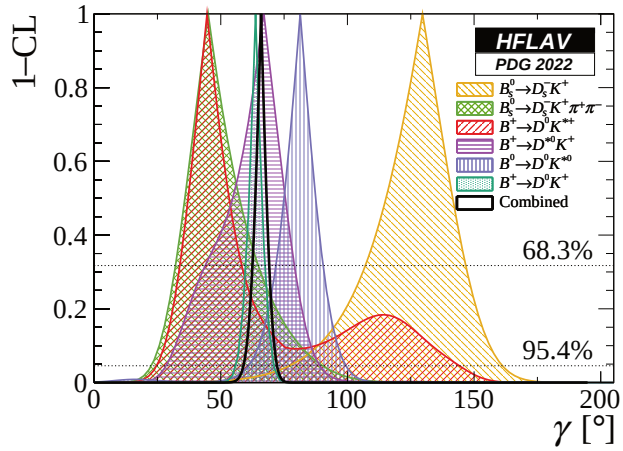

Figure 77.3: World average of $\gamma \equiv \phi_3$, as well as contributions from individual modes, in terms of 1−CL.

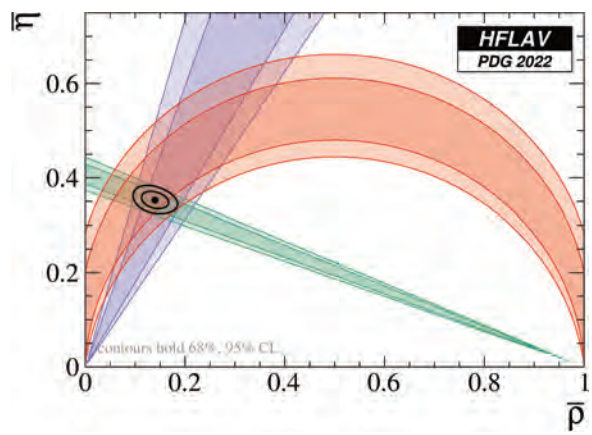

Figure 77.4: Constraints from the measurements of the angles of the CKM unitarity triangle in the $(\overline{\rho}, \overline{\eta})$ plane.

Effects from correlated uncertainties between amplitude models and strong phase differences in charm decays are negligible and are not explicitly accounted for in the combination, nor are effects related to charm and kaon mixing and *CP* violation. This world average, together with results split by decay mode, is shown in Fig. 77.3. The combination has a total of 154 experimental inputs from which 35 parameters are determined, an an overall χ^2 of 123.9, which corresponds to a p-value of 36% indicating good agreement between the inputs. The combination gives a single solution for γ in $[0°, 180°]$, but an ambiguous solution exists at $\gamma \Leftrightarrow \gamma + 180°$.

77.5 Summary

Experimental progress has resulted in all three angles of the CKM unitarity triangle being measured with good accuracy, with β known to subdegree precision and both α and γ known to better than 5°. The constraints from these three measurements in the $(\overline{\rho}, \overline{\eta})$ plane are shown in Fig. 77.4; further discussion and comparison with constraints from independent measurements can be found in Ref. [6]. The determinations of all three angles remain statistically limited, but it will be a challenge for experiments to

Downloaded from https://academic.oup.com/ptep/article/2022/8/083C01/6651666 by KIT Library user on 27 September 2022

ensure that this remains the case as the precision improves. Consequently, the correct treatment of sources of correlation between the measurements that go into the world average combinations is becoming increasingly important.

References

[1] N. Cabibbo, Phys. Rev. Lett. **10**, 531 (1963).

[2] M. Kobayashi and T. Maskawa, Prog. Theor. Phys. **49**, 652 (1973).

[3] C. Jarlskog, Phys. Rev. Lett. **55**, 1039 (1985).

[4] Y. S. Amhis *et al.* (HFLAV), Eur. Phys. J. C **81**, 3, 226 (2021), updated averages are available online at hflav.web.cern.ch, [arXiv:1909.12524].

[5] See the review on "Semileptonic *b*-Hadron Decays, Determination of V_{cb}, V_{ub}" in this *Review*.

[6] See the review on "Cabibbo-Kobayashi-Maskawa Mixing Matrix," in this *Review*.

[7] See the review on "*CP* Violation in the Quark Sector," in this *Review*.

[8] See the review on "B^0–$\overline{B}^0$ Mixing" in this *Review*.

[9] A. Carter and A. Sanda, Phys. Rev. **D23**, 1567 (1981).

[10] I. Bigi and A. Sanda, Nucl. Phys. **B193**, 85 (1981).

[11] O. Long *et al.*, Phys. Rev. **D68**, 034010 (2003), [hep-ex/0303030].

[12] B. Aubert *et al.* (BaBar), Phys. Rev. **D79**, 072009 (2009), [arXiv:0902.1708].

[13] I. Adachi *et al.*, Phys. Rev. Lett. **108**, 171802 (2012), [arXiv:1201.4643].

[14] R. Aaij *et al.* (LHCb), Phys. Rev. Lett. **115**, 031601 (2015), [arXiv:1503.07089].

[15] H.-n. Li and S. Mishima, JHEP **03**, 009 (2007), [hep-ph/0610120].

[16] M. Jung, Phys. Rev. **D86**, 053008 (2012), [arXiv:1206.2050].

[17] K. De Bruyn and R. Fleischer, JHEP **1503**, 145 (2015), [arXiv:1412.6834].

[18] P. Frings, U. Nierste and M. Wiebusch, Phys. Rev. Lett. **115**, 6, 061802 (2015), [arXiv:1503.00859].

[19] M. Ciuchini, M. Pierini and L. Silvestrini, Phys. Rev. Lett. **95**, 221804 (2005), [hep-ph/0507290].

[20] S. Faller *et al.*, Phys. Rev. **D79**, 014030 (2009), [arXiv:0809.0842].

[21] Z. Ligeti and D. Robinson, Phys. Rev. Lett. **115**, 251801 (2015), [arXiv:1507.06671].

[22] I. Adachi *et al.* (BaBar, Belle), Phys. Rev. Lett. **121**, 261801 (2018), [arXiv:1804.06152].

[23] I. Adachi *et al.* (BaBar, Belle), Phys. Rev. **D98**, 112012 (2018), [arXiv:1804.06153].

[24] M. Antonelli *et al.*, Phys. Rept. **494**, 197 (2010), [arXiv:0907.5386].

[25] M. Gronau and D. London, Phys. Rev. Lett. **65**, 3381 (1990).

[26] R. Aaij *et al.* (LHCb), Phys. Rev. **D98**, 032004 (2018), [arXiv:1805.06759].

[27] R. Aaij *et al.* (LHCb), JHEP **03**, 075 (2021), [arXiv:2012.05319].

[28] J. P. Lees *et al.* (BaBar), Phys. Rev. **D87**, 052009 (2013), [arXiv:1206.3525].

[29] I. Adachi *et al.* (Belle), Phys. Rev. **D88**, 092003 (2013), [arXiv:1302.0551].

[30] J. Charles *et al.*, Eur. Phys. J. **C77**, 574 (2017), [arXiv:1705.02981].

[31] T. Julius *et al.* (Belle), Phys. Rev. **D96**, 032007 (2017), [arXiv:1705.02083].

[32] B. Aubert *et al.* (BaBar), Phys. Rev. **D76**, 052007 (2007), [arXiv:0705.2157].

[33] P. Vanhoefer *et al.* (Belle), Phys. Rev. **D93**, 032010 (2016), [Addendum *ibid*: **D94** 099903 (2016)], [arXiv:1510.01245].

[34] B. Aubert *et al.* (BaBar), Phys. Rev. **D78**, 071104 (2008), [arXiv:0807.4977].

[35] A. E. Snyder and H. R. Quinn, Phys. Rev. **D48**, 2139 (1993).

[36] J. P. Lees *et al.* (BaBar), Phys. Rev. **D88**, 012003 (2013), [arXiv:1304.3503].

[37] A. Kusaka *et al.* (Belle), Phys. Rev. Lett. **98**, 221602 (2007), [hep-ex/0701015].

[38] A. Kusaka *et al.* (Belle), Phys. Rev. **D77**, 072001 (2008), [arXiv:0710.4974].

[39] M. Gronau and J. Zupan, Phys. Rev. **D71**, 074017 (2005), [hep-ph/0502139].

[40] S. Gardner, Phys. Rev. **D72**, 034015 (2005), [hep-ph/0505071].

[41] A. Falk *et al.*, Phys. Rev. **D69**, 011502 (2004), [hep-ph/0310242].

[42] J. Brod and J. Zupan, JHEP **01**, 051 (2014), [arXiv:1308.5663].

[43] M. Gronau and D. London, Phys. Lett. **B253**, 483 (1991).

[44] M. Gronau and D. Wyler, Phys. Lett. **B265**, 172 (1991).

[45] See the review on "D^0–$\overline{D}^0$ Mixing" in this *Review*.

[46] M. Nayak *et al.*, Phys. Lett. **B740**, 1 (2015), [arXiv:1410.3964].

[47] D. Atwood, I. Dunietz and A. Soni, Phys. Rev. Lett. **78**, 3257 (1997), [hep-ph/9612433].

[48] D. Atwood, I. Dunietz and A. Soni, Phys. Rev. **D63**, 036005 (2001), [hep-ph/0008090].

[49] D. Atwood and A. Soni, Phys. Rev. **D68**, 033003 (2003), [hep-ph/0304085].

[50] Y. Grossman, Z. Ligeti and A. Soffer, Phys. Rev. **D67**, 071301 (2003), [hep-ph/0210433].

[51] A. Giri *et al.*, Phys. Rev. **D68**, 054018 (2003), [hep-ph/0303187].

[52] A. Bondar, *Proceedings of BINP special analysis meeting on Dalitz analysis*, 24-26 Sep. 2002, unpublished.

[53] R. Briere *et al.* (CLEO), Phys. Rev. **D80**, 032002 (2009), [arXiv:0903.1681].

[54] J. Libby *et al.* (CLEO), Phys. Rev. **D82**, 112006 (2010), [arXiv:1010.2817].

[55] M. Ablikim *et al.* (BESIII), Phys. Rev. Lett. **124**, 24, 241802 (2020), [arXiv:2002.12791].

[56] M. Ablikim *et al.* (BESIII), Phys. Rev. D **101**, 11, 112002 (2020), [arXiv:2003.00091].

[57] A. Bondar and T. Gershon, Phys. Rev. **D70**, 091503 (2004), [hep-ph/0409281].

[58] T. Gershon, Phys. Rev. **D79**, 051301 (2009), [arXiv:0810.2706].

[59] T. Gershon and M. Williams, Phys. Rev. **D80**, 092002 (2009), [arXiv:0909.1495].

[60] R. Aleksan, I. Dunietz and B. Kayser, Z. Phys. **C54**, 653 (1992).

[61] R. Aaij *et al.* (LHCb), JHEP **12**, 141 (2021), [arXiv:2110.02350].

[62] R. Aaij *et al.* (LHCb), JHEP **04**, 081 (2021), [arXiv:2012.09903].

[63] R. Aaij *et al.* (LHCb), JHEP **02**, 169 (2021), [arXiv:2010.08483].

[64] M. Rama, Phys. Rev. **D89**, 014021 (2014), [arXiv:1307.4384].

[65] M. Bjørn and S. Malde, JHEP **07**, 106 (2019), [arXiv:1904.01129].

Downloaded from https://academic.oup.com/ptep/article/2022/8/083C01/6651666 by KIT Library user on 27 September 2022

78. Spectroscopy of Mesons Containing Two Heavy Quarks

Revised August 2021 by S. Eidelman (Budker Inst., Novosibirsk; Novosibirsk U.), J. J. Hernández-Rey (IFIC, Valencia), C. Lourenço (CERN), R.E. Mitchell (Indiana U.), S. Navas (Granada U.) and C. Patrignani (Bologna U.).

A golden age for heavy quarkonium physics dawned at the turn of this century, initiated by the confluence of exciting advances in quantum chromodynamics (QCD) and an explosion of related experimental activity. The subsequent broad spectrum of breakthroughs, surprises, and continuing puzzles had not been anticipated. Indeed, CLEO-c, BESIII, and the B-factories, later joined by ATLAS, CMS and LHCb, have made a series of groundbreaking observations. For an extensive presentation of the status of heavy quarkonium physics, the reader is referred to several reviews [1–7]. This note focuses on experimental developments in heavy quarkonium spectroscopy with very few theoretical comments. Possible theoretical interpretations of the states not predicted by the quark model are presented in the review "Heavy non-$q\bar{q}$ mesons." Note that in this review we follow the new naming scheme for hadrons (see the review "Naming scheme for hadrons" in the current edition).

This review covers states discovered since 2003, the year that marked the unexpected discovery of the $X(3872)$ [8]. The $X(3872)$, now called $\chi_{c1}(3872)$, was the first of the mesons containing two heavy quarks that could not be easily accommodated by the $q\bar{q}$ quark model. Its discovery was a watershed event in meson spectroscopy. In earlier versions of this write-up the particles were sorted according to an assumed *conventional* or *unconventional* nature with respect to the quark model. However, since this classification is not always unambiguous, we here follow Ref. [9] and sort the states into three groups, namely states below (*cf.* Table 78.1), above (*cf.* Table 78.2), and near (*cf.* Table 78.3) the lowest open-flavor thresholds.

78.1 States Below Open-Flavor Threshold

Table 78.1 lists properties of recently observed heavy quarkonium states located below the lowest open-flavor thresholds. Those are expected to be (at least prominently) conventional quarkonia. The majority of charmonium ($c\bar{c}$) and bottomonium ($b\bar{b}$) states were established prior to 2003.

78.1.1 *Charmonium*

The $h_c(1P)$ is the 1^1P_1 charmonium state, the singlet partner of the long-known χ_{cJ} triplet 1^3P_J. After being firmly established in 2005 through the process $\psi(2S) \to \pi^0 h_c(1P)$ [10], it has since been studied extensively by BESIII using large samples of $\psi(2S)$ decays. Exclusive hadronic decays of the $h_c(1P)$, strongly suppressed relative to the dominant radiative transition $h_c(1P) \to \gamma\eta_c(1S)$, were first observed in 2019 [11] and 2020 [12].

Belle reported an observation of the $\psi_2(1D)$ decaying to $\gamma\chi_{c1}$ with J^{PC} presumed to be 2^{--} [13]. This state is listed in Table 78.1 as $\psi_2(3823)$. Its existence was confirmed with high significance by BESIII [14]. While the negative C-parity is indeed established by its observed decay channel, the assignment of $J = 2$ was done by matching to the closest quark model state (1^3D_2) and requires experimental confirmation.

The 1^1D_2 state, or the $\eta_{c2}(1D)$, with a mass expected near 3820 MeV, has not yet been observed. Recently Belle performed a search in $B \to \eta_{c2}(1D)K(\pi)$ decays in the mass range 3795–3845 MeV and found no signal [15]. Thus, the $\eta_{c2}(1D)$ remains the only unobserved conventional charmonium state that does not have open-charm decays.

78.1.2 *Bottomonium*

The ground state of bottomonium, $\eta_b(1S)$, is well established. After the initial reports from BaBar in radiative decays of the $\Upsilon(3S)$ (observation) [16] and $\Upsilon(2S)$ (evidence) [17], Belle confirmed the existence of the $\eta_b(1S)$ with more than 5σ significance in radiative decays of the newly discovered $h_b(1P)$ [18, 19] and $h_b(2P)$ [18] (see next paragraph), as well as in $\Upsilon(2S)$ radiative decays [20]. Belle has also reported strong evidence for the $\eta_b(2S)$ [18], but it still needs confirmation at the 5σ level. Note that there are hints of tension in the $\eta_b(1S)$ mass as measured in radiative M1 and E1 transitions. In the M1 transition $\Upsilon(2S) \to \gamma\eta_b(1S)$ Belle measures a mass of $9394.8^{+2.7+4.5}_{-3.1-2.7}$ MeV/c^2 [20], while in the E1 transitions $h_b(1P, 2P) \to \gamma\eta_b(1S)$ Belle measures $9402.4 \pm 1.5 \pm 1.8$ MeV/c^2 [18]. This tension may point to an incomplete understanding of the $\eta_b(1S)$ lineshape in different production mechanisms.

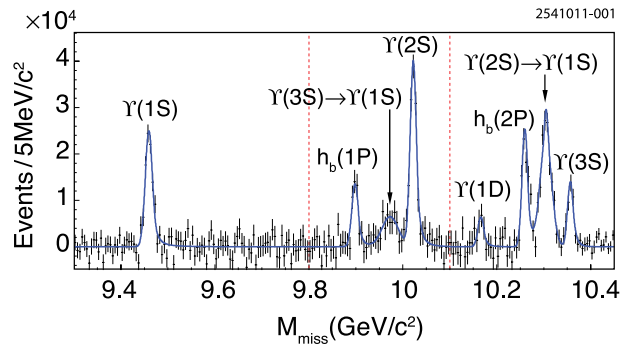

Figure 78.1: From Belle [21], the mass recoiling against $\pi^+\pi^-$ pairs, $M_{\rm miss}$, in e^+e^- collision data taken near the peak of the $\Upsilon(10860)$ (*points with error bars*). The smooth combinatorial and $K^0_S \to \pi^+\pi^-$ background contributions have been subtracted. The fit to the various labeled signal contributions is overlaid (*curve*).

The $h_b(1P)$, the bottomonium counterpart of the $h_c(1P)$, and the next excited state, the $h_b(2P)$, were simultaneously discovered by Belle using dipion transitions from the $\Upsilon(10860)$ [21] (Fig. 78.1). The same analysis also showed the $\Upsilon_J(1D)$, the lowest-lying D-wave triplet of the $b\bar{b}$ system, but did not resolve the $J = 1, 2, 3$ components. The search for the $h_b(1P)$ was directly inspired by a CLEO result [22], which found a surprisingly copious production of $e^+e^- \to \pi^+\pi^- h_c(1P)$ as well as an indication that $\psi(4230) \to \pi^+\pi^- h_c(1P)$ occurs at a comparable rate with the signature mode $\psi(4230) \to \pi^+\pi^- J/\psi(1S)$. The presence of $\Upsilon(nS)$ peaks in Fig. 78.1 at rates two orders of magnitude larger than expected, along with separate studies with exclusive decays $\Upsilon(nS) \to \mu^+\mu^-$, allow precise calibration of the $\pi^+\pi^-$ recoil mass spectrum and very accurate measurements of the $h_b(1P)$ and $h_b(2P)$ masses. Both corresponding hyperfine splittings are consistent with zero within an uncertainty of about 1.5 MeV (lowered to 1.1 MeV for the $h_b(1P)$ in Ref. [23]). Belle later observed the transition $\Upsilon(4S) \to h_b(1P)\eta$ [19] and the corresponding 1P hyperfine splitting was also found to be compatible with zero at a similar precision level.

Just before Christmas 2011, ATLAS offered the world a beautiful gift, in the form of the discovery of the $\chi_b(3P)$ quarkonium state [24], observed by combining dimuons from $\Upsilon(1S)$ or $\Upsilon(2S)$ decays with photons emitted in the radiative $\chi_b(3P)$ decays (Fig. 78.2, bottom left panel). The new resonance, with a mass of $10\,530 \pm 5(\text{stat}) \pm 9(\text{syst})$ MeV, was soon confirmed by D0 [25]. Also LHCb observed the $\chi_b(3P)$ peak, using the full Run 1 event sample, corresponding to an integrated luminosity of 3 fb^{-1} [26] (Fig. 78.2, middle left panel). Finally, CMS used 80 fb^{-1} of 13 TeV pp collisions, collected in 2016 and 2017, to show two well-resolved $\chi_{b1}(3P)$ and $\chi_{b2}(3P)$ peaks [27], separated by a mass difference of $10.60 \pm 0.64(\text{stat}) \pm 0.17(\text{syst})$ MeV (Fig. 78.2, top left panel). The remarkable precision of the individual mass measurements, with relative uncertainties as small as 50 ppm, shows that the LHC experiments can provide important results in the field of hadron spectroscopy, especially in the case of heavy particles, which require very high collision energies and large event samples.

78.1.3 B_c *System*

The $B_c^\pm$ family is quite special because these (charged) quarkonium states consist of two heavy quarks of different flavor. Among other interesting properties, this means that they cannot annihilate into gluons, the excited states only decaying to the pseudoscalar ground state, $B_c^\pm$, via electromagnetic and pionic transitions.

Downloaded from https://academic.oup.com/ptep/article/2022/8/083C01/6651666 by KIT Library user on 27 September 2022

Table 78.1: New states below the open-flavor thresholds in the $c\bar{c}$, $b\bar{c}$, and $b\bar{b}$ regions, ordered by mass. Masses m and widths Γ represent the PDG21 weighted averages with statistical and systematic uncertainties added in quadrature. In the Production column, the state is always denoted by X. Ellipses (...) indicate inclusively selected event topologies, *i.e.*, additional particles not directly detected by experiment. A question mark (?) indicates an unmeasured value. The Discovery Year column gives the date of the first measurement cited. The Summary Table column indicates whether or not the state appears in the summary tables, usually requiring at least two independent experiments with significance of $>5\sigma$. Refer to the particle listings for references and further information.

PDG Name	Former Name(s)	m (MeV)	Γ (MeV)	$I^G(J^{PC})$	Production	Decay	Discovery Year	Summary Table
$h_c(1P)$		3525.38 ± 0.11	0.7 ± 0.35	$0^-(1^{+-})$	$\psi(2S) \to \pi^0 X$ $p\bar{p} \to X$ $e^+e^- \to \pi\pi X$	$\gamma\eta_c(1S)$ hadrons (see listings)	2004	YES
$\psi_2(3823)$	$X(3823)$	3823.7 ± 0.5	< 5.2	$0^-(2^{--})$	$B \to KX$ $e^+e^- \to \pi^+\pi^- X$	$\gamma\,\chi_{c1}(1P)$ $\pi^+\pi^- J/\psi(1S)$	2013	YES
B_c^+		6274.47 ± 0.32	stable	$0(0^-)$	$\bar{p}p \to X...$ $pp \to X...$	$\pi^+ J/\psi(1S)$ (see listings)	2007	YES
$B_c^+(2S)$		6871.2 ± 1.0	?	$0(0^-)$	$pp \to X...$	$B_c^+\pi^+\pi^-$	2014	YES
$\eta_b(1S)$		9398.7 ± 2.0	10^{+5}_{-4}	$0^+(0^{-+})$	$\Upsilon(2S,3S) \to \gamma X$ $h_b(1P,2P) \to \gamma X$	hadrons (see listings)	2008	YES
$h_b(1P)$		9899.3 ± 0.8	?	$0^-(1^{+-})$	$\Upsilon(10860) \to \pi^+\pi^- X$ $\Upsilon(3S) \to \pi^0 X$ $\Upsilon(4S) \to \eta X$ $Z_b(10610)^+ \to \pi^+ X$ $Z_b(10650)^+ \to \pi^+ X$	$\gamma\eta_b(1S)$	2011	YES
$\eta_b(2S)$		$9999.0^{+4.5}_{-4.0}$	< 24	$0^+(0^{-+})$	$h_b(2P) \to \gamma X$	hadrons	2012	NO
$\Upsilon_2(1D)$		10163.7 ± 1.4	?	$0^-(2^{--})$	$\Upsilon(3S) \to \gamma\gamma X$ $\Upsilon(10860) \to \pi^+\pi^- X$	$\gamma\gamma\Upsilon(1S)$ $\pi^+\pi^-\Upsilon(1S)$	2004	YES
$h_b(2P)$		10259.8 ± 1.2	?	$0^-(1^{+-})$	$\Upsilon(10860) \to \pi^+\pi^- X$ $Z_b(10610)^+ \to \pi^+ X$ $Z_b(10650)^+ \to \pi^+ X$	$\gamma\eta_b(1S,2S)$	2011	YES
$\chi_{b1}(3P)$		10513.42 ± 0.67	?	$0^+(1^{++})$	$pp \to X...$	$\gamma\Upsilon(1S,2S,3S)$	2011	YES
$\chi_{b2}(3P)$		10524.02 ± 0.78	?	$0^+(2^{++})$	$pp \to X...$	$\gamma\Upsilon(3S)$	2011	YES

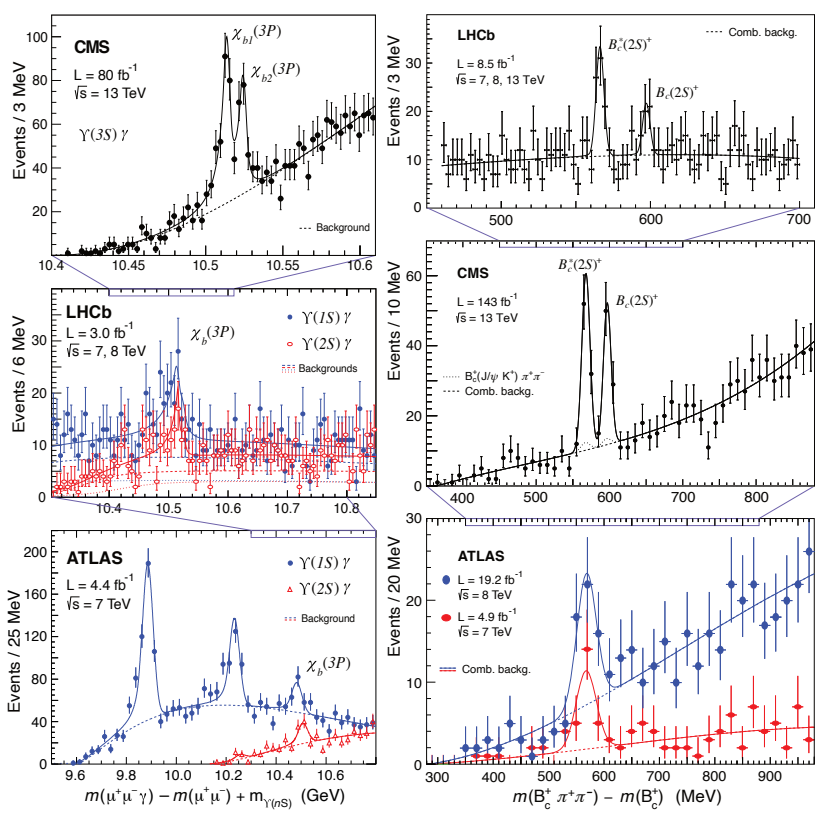

Figure 78.2: (Left Column) Invariant mass distributions measured by the ATLAS [24] (bottom), LHCb [26] (middle) and CMS [27] (top) experiments in their searches for the $\chi_b(3P)$ states through their radiative decays to one of the S-wave bottomonia. (Right Column) Invariant mass distributions measured by the ATLAS [28] (bottom), CMS [29] (middle) and LHCb [30] (top) experiments in their searches for $B_c^\pm$ excited states decaying to the $B_c^\pm$ ground state with the emission of two charged pions.

Downloaded from https://academic.oup.com/ptep/article/2022/8/083C01/6651666 by KIT Library user on 27 September 2022

On the basis of an event sample collected in the Run 1 of the LHC, corresponding to an integrated luminosity of 24 fb^{-1}, adding the 7 and 8 TeV data, the ATLAS Collaboration observed a resonance in the $B_c^+\pi^+\pi^-$ invariant mass spectrum [28] (Fig. 78.2, bottom right panel). This peak, observed with a significance of 5.2 standard deviations and a mass of $6842 \pm 4(\text{stat}) \pm 5(\text{syst})$ MeV, was immediately recognized as the $B_c(2S)^\pm$ state, the first radial excitation in the $B_c^\pm$ family. Profiting from the much larger Run 2 event sample, collected in the 2015, 2016, 2017 and 2018 running periods and corresponding to 143 fb^{-1} of 13 TeV pp collisions, as well as from a measurement resolution of around 6 MeV, the CMS Collaboration could observe *two* well-resolved peaks, separated by $29.1 \pm 1.5(\text{stat}) \pm 0.7(\text{syst})$ MeV [29] (Fig. 78.2, middle right panel). The existence of two peaks, rather than a single one, is established with a significance of 6.5 standard deviations. The "right peak" has a mass of $6871.0 \pm 1.2(\text{stat}) \pm 0.8(\text{syst}) \pm 0.8(B_c^+)$ MeV, where the last term is the uncertainty in the B_c^+ mass, and is identified as the $B_c(2S)^\pm$ state, which decays directly to the $B_c^\pm$, emitting two (easy to detect) pions. The CMS observation, reported a couple of months after the end of the LHC Run 2, was soon followed by the corresponding LHCb result [30] (Fig. 78.2, top right panel), which confirmed the existence of the two states and reported a second measurement of the $B_c(2S)^\pm$ mass, $6872.1 \pm 1.3(\text{stat}) \pm 0.1(\text{syst}) \pm 0.8(B_c^+)$ MeV.

The "left peak" is interpreted as being the $B_c^*(2S)^\pm$ signal. It is observed at a mass lower than the real value because the experiments are unable to detect the low-energy photon emitted in the decay chain, $B_c^*(2S)^\pm \to B_c^{*\pm}\pi^+\pi^-$ followed by $B_c^{*\pm} \to B_c^\pm\gamma$ (Fig. 78.3). Its energy, expected to be in the range 40–80 MeV, leads to a very small probability that the photon converts into an e^+e^- pair and the two electrons are reconstructed. The relative ordering of the two peaks is based on a generally-agreed assumption: the $M(B_c^{*\pm}) - M(B_c^\pm)$ mass difference is larger than the $M(B_c^*(2S)^\pm) - M(B_c(2S)^\pm)$ difference. Naturally, these observations provide evidence for the existence of the $B_c^*(1S)^\pm$ state. They also provide measurements of two interesting mass differences, between the masses of the pseudoscalar mesons, $M(B_c(2S)^\pm) - M(B_c(1S)^\pm) = 596.1$ MeV, and of the vector mesons, $M(B_c^*(2S)^\pm) - M(B_c^*(1S)^\pm) = 567.0$ MeV (Fig. 78.3).

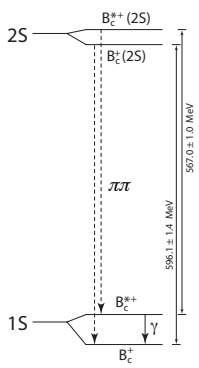

Figure 78.3: Diagram showing the decays mentioned in the text.

78.2 States Above Open-Flavor Threshold

Many states have been discovered both above and near the lowest open-flavor thresholds. They are displayed in Tables 78.2 and 78.3, respectively. With the exception of the $\psi_3(3842)$ and the tensor state located at 3930 MeV (now called $\chi_{c2}(3930)$), which have properties consistent with those expected for the $\psi_3(1^3D_3)$ and $\chi_{c2}(2^3P_2)$, respectively, none of these states can easily be assigned a place in the quark model spectrum of the charmonium or bottomonium families. At the same time, these states also have no universally accepted unconventional interpretation.

78.2.1 *Charmonium*

Using proton-proton collisions, LHCb observed a narrow state, the $\psi_3(3842)$ resonance, in the decay modes $\psi_3(3842) \to D^0\bar{D}^0$ and D^+D^- [31]. The mass and width of this state are measured to be $3842.71 \pm 0.16 \pm 0.12$ MeV and $2.79 \pm 0.51 \pm 0.35$ MeV, respectively. The observed mass and narrow width are consistent with the interpretation of the new state as the unobserved spin-3 $\psi_3(1^3D_3)$ charmonium. Accordingly, the state got the name $\psi_3(3842)$ in the listings, with the remark that the quantum numbers were fixed from the quark model and need to be confirmed.

The $\chi_{c2}(3930)$, which is a natural candidate for the $\chi_{c2}(2^3P_2)$ quark model state, was originally seen by Belle [32] and later confirmed by BaBar [33] in the $\gamma\gamma$ process $e^+e^- \to e^+e^-D\bar{D}$. This interpretation was strengthened by the more recent LHCb observation of the $\chi_{c2}(3930)$ alongside the $\psi_3(3842)$ in proton-proton collisions [31].

Unlike the $\chi_{c2}(2^3P_2)$, the identification of the $\chi_{c0}(2^3P_0)$ quark model state remains controversial. The original candidate was the $\chi_{c0}(3915)$, discovered by Belle in the $\gamma\gamma$ process $e^+e^- \to e^+e^-\omega J/\psi(1S)$ [34]. In a subsequent measurement by BaBar, its quantum numbers were determined to be $J^{PC} = 0^{++}$ [35]. However, its identification as the $\chi_{c0}(2^3P_0)$ quark model state was soon challenged [36, 37]. In addition, it was pointed out in Ref. [38] that if the assumption of helicity-2 dominance is abandoned and, instead, one allows for a sizeable helicity-0 component, a $J^{PC} = 2^{++}$ assignment is possible. This could imply that it is the same as the $\chi_{c2}(3930)$—but to explain the large helicity-0 component a sizable portion of non-$q\bar{q}$ is necessary [38]. A more recent LHCb amplitude analysis of the process $B^+ \to D^+D^-K^+$ finds distinct 0^{++} and 2^{++} components decaying to D^+D^- [39], which are currently identified in the listings as the $\chi_{c0}(3915)$ and $\chi_{c2}(3930)$, respectively.

An alternative candidate for the $\chi_{c0}(2^3P_0)$ (here referred to as the $\chi_{c0}(3860)$) was reported in Ref. [40] with properties more consistent with expectation: its mass is close to the potential model expectations, it decays to $D\bar{D}$, and the preferred quantum numbers are $J^{PC} = 0^{++}$ (this hypothesis is favored over the 2^{++} one with a 2.5σ significance).

In the excited vector charmonium spectrum, the $\psi(4040)$, $\psi(4160)$, and $\psi(4415)$ are prominent in the inclusive e^+e^- hadronic cross section and are naturally identified as the 3^3S_1, 2^3D_1, and 4^3S_1 $c\bar{c}$ quark model states, respectively. In addition to these long-established states, however, another set of mesons has been found as peaks in exclusive e^+e^- cross sections. Unlike conventional vector charmonia, they do not appear in the inclusive hadronic cross section and they apparently do not decay to $D\bar{D}$. The PDG summary table currently lists the $\psi(4230)$, $\psi(4360)$, and $\psi(4660)$ within this category. The first of these to be discovered was originally known as the $Y(4260)$ (now the $\psi(4230)$), seen by BaBar [41] and Belle [42, 43] in $e^+e^- \to \pi^+\pi^-J/\psi(1S)$ using initial state radiation. In a more recent high-statistics scan of $e^+e^- \to \pi^+\pi^-J/\psi(1S)$, BESIII demonstrated that the lineshape in this mass range is highly non-trivial [44]. The latter observation was interpreted by the authors as the presence of two states. However, this lineshape is also consistent with other possible interpretations, such as one assuming a molecular structure for the $\psi(4230)$ [45]. The data of Ref. [44] also called for a significant downward shift of the mass of what was originally called the $Y(4260)$, making it consistent with peaks in other exclusive cross sections, such as $h_c(1P)\pi\pi$ [46]. We thus merged the original $Y(4260)$ (or, more formally, the $\psi(4260)$) with the $\psi(4230)$ in the listings.

BESIII observed the $\chi_{c1}(3872)$, also known as $X(3872)$, in $e^+e^- \to \gamma\chi_{c1}(3872)$ in the $\psi(4230)$ mass range [47], which could allow for additional insight into the structure of both states (see the review on heavy non-$q\bar{q}$ mesons). BESIII also performed a recent study of the process $e^+e^- \to \pi^+\pi^-\psi(2S)$ and found evidence for a lower mass state, possibly the $\psi(4230)$, in addition to the more dominant $\psi(4360)$ [48].

Note that the data of Ref. [44] does not show any indication of the $Y(4008)$ reported by Belle; the data in this region can either be fit with a non-resonant background component or a much wider resonance at lower mass. Also the analysis of the $Y(4008)$ region in Ref. [49] indicates a wide resonance.

Downloaded from https://academic.oup.com/ptep/article/2022/8/083C01/6651666 by KIT Library user on 27 September 2022

Table 78.2: As in Table 78.1, but for new states above the first open-flavor thresholds in the $c\bar{c}$ and $b\bar{b}$ regions, ordered by mass.

PDG Name	Former Name(s)	m (MeV)	Γ (MeV)	$I^G(J^{PC})$	Production	Decay	Discovery Year	Summary Table
$\psi_3(3842)$		3842.71 ± 0.20	2.79 ± 0.62	$0^-(3^{--})^*$	$pp \to X...$	$D\bar{D}$	2019	YES
$\chi_{c0}(3860)$		3862^{+48}_{-35}	201^{+177}_{-106}	$0^+(0^{++})$	$e^+e^- \to J/\psi(1S)X$	$D\bar{D}$	2017	NO
$\chi_{c0}(3915)$	$X(3915)$, $Y(3940)$	3921.7 ± 1.8	18.8 ± 3.5	$0^+(0/2^{++})$	$B \to KX$ $e^+e^- \to e^+e^-X$	$\omega J/\psi(1S)$ $D\bar{D}$	2004	YES
$\chi_{c2}(3930)$	$\chi_{c2}(2P)$, $Z(3930)$	3922.5 ± 1.0	35.2 ± 2.2	$0^+(2^{++})$	$e^+e^- \to e^+e^-X$	$D\bar{D}$	2005	YES
$X(3940)$		3942^{+9}_{-8}	37^{+27}_{-17}	$?^?(?^{??})$	$e^+e^- \to J/\psi(1S)X$	$D\bar{D}^*$	2007	NO
$X(4050)^\pm$	$Z_1(4050)$	4051^{+24}_{-43}	82^{+51}_{-28}	$1^-(?^{?+})$	$\bar{B}^0 \to K^-X$	$\pi^+\chi_{c1}(1P)$	2008	NO
$X(4055)^\pm$	$Z_c(4055)$	4054 ± 3	45 ± 13	$1^+(?^{?-})$	$e^+e^- \to \pi^-X$	$\pi^+\psi(2S)$	2015	NO
$X(4100)^\pm$		4096^{+27}_{-30}	152^{+83}_{-68}	$1^-(?^{??})$	$\bar{B}^0 \to K^-X$	$\pi^+\eta_c(1S)$	2018	NO
$\chi_{c1}(4140)$	$Y(4140)$	4146.5 ± 3.0	19^{+7}_{-5}	$0^+(1^{++})$	$B^+ \to K^+X$	$\phi J/\psi(1S)$	2009	YES
$X(4160)$		4156^{+29}_{-25}	139^{+113}_{-65}	$?^?(?^{??})$	$e^+e^- \to J/\psi(1S)X$	$D^*\bar{D}^*$	2007	NO
$Z_c(4200)$		4196^{+35}_{-32}	370^{+99}_{-149}	$1^+(1^{+-})$	$\bar{B}^0 \to K^-X$	$J/\psi(1S)\pi^+$	2014	NO
$\psi(4230)$	$Y(4230)$ $Y(4260)$	4222.7 ± 2.6	49 ± 8	$0^-(1^{--})$	$e^+e^- \to X$	$\pi^+\pi^-J/\psi(1S)$ $\omega\chi_{c0}(1P)$ $\pi^+\pi^-h_c(1P)$ (see listings)	2015	YES
$R_{c0}(4240)$	$Z_c(4240)$	4239^{+48}_{-21}	220^{+118}_{-88}	$1^+(0^{--})$	$\bar{B}^0 \to K^-X$	$\pi^+\psi(2S)$	2014	NO
$X(4250)^\pm$	$Z_2(4250)$	4248^{+185}_{-45}	177^{+321}_{-72}	$1^-(?^{?+})$	$\bar{B}^0 \to K^-X$	$\pi^+\chi_{c1}(1P)$	2008	NO
$\chi_{c1}(4274)$	$Y(4274)$	4286^{+8}_{-9}	51 ± 7	$0^+(1^{++})$	$B^+ \to K^+X$	$\phi J/\psi(1S)$	2011	YES
$X(4350)$		$4350.6^{+4.7}_{-5.1}$	13^{+18}_{-10}	$0^+(?^{?+})$	$e^+e^- \to e^+e^-X$	$\phi J/\psi(1S)$	2009	NO
$\psi(4360)$	$Y(4360)$	4372 ± 9	115 ± 13	$0^-(1^{--})$	$e^+e^- \to X$	$\pi^+\pi^-\psi(2S)$ $\pi^+\pi^-J/\psi(1S)$	2007	YES
$Z_c(4430)$		4478^{+15}_{-18}	181 ± 31	$1^+(1^{+-})$	$\bar{B}^0 \to K^-X$	$\pi^+\psi(2S)$ $\pi^+J/\psi(1S)$	2007	YES
$\chi_{c0}(4500)$	$X(4500)$	4474 ± 4	77^{+12}_{-10}	$0^+(0^{++})$	$B^+ \to K^+X$	$\phi J/\psi(1S)$	2017	NO
$X(4630)$		4626^{+24}_{-111}	174^{+137}_{-78}	$0^+(?^{?+})$	$B^+ \to K^+X$	$\phi J/\psi(1S)$	2021	NO
$\psi(4660)$	$Y(4660)$, $X(4630)$	4630 ± 6	72^{+14}_{-12}	$0^-(1^{--})$	$e^+e^- \to X$	$\pi^+\pi^-\psi(2S)$ $\Lambda_c^+\bar{\Lambda}_c^-$ $D_s^+D_{s1}(2536)$	2007	YES
$\chi_{c1}(4685)$		4684^{+15}_{-17}	126^{+40}_{-44}	$0^+(1^{++})$	$B^+ \to K^+X$	$\phi J/\psi(1S)$	2021	NO
$\chi_{c0}(4700)$	$X(4700)$	4694^{+16}_{-5}	87^{+18}_{-10}	$0^+(0^{++})$	$B^+ \to K^+X$	$\phi J/\psi(1S)$	2017	NO
$\Upsilon(10753)$		$10752.7^{+5.9}_{-6.0}$	36^{+18}_{-12}	$?^?(1^{--})$	$e^+e^- \to X$	$\pi\pi\Upsilon(1S,2S,3S)$	2019	NO
$\Upsilon(10860)$	$\Upsilon(5S)$	$10885.2^{+2.6}_{-1.6}$	37 ± 4	$0^-(1^{--})$	$e^+e^- \to X$	$B_{(s)}^{(*)}\bar{B}_{(s)}^{(*)}(\pi)$ $\pi\pi\Upsilon(1S,2S,3S)$ $\pi^+\pi^-h_b(1P,2P)$ $\eta\Upsilon(1S,2S)$ $\pi^+\pi^-\Upsilon(1D)$ (see listings)	1985	YES
$\Upsilon(11020)$	$\Upsilon(6S)$	11000 ± 4	24^{+8}_{-6}	$0^-(1^{--})$	$e^+e^- \to X$	$B_{(s)}^{(*)}\bar{B}_{(s)}^{(*)}(\pi)$ $\pi\pi\Upsilon(1S,2S,3S)$ $\pi^+\pi^-h_b(1P,2P)$ (see listings)	1985	YES

*Quantum numbers fixed from the quark model and need confirmation.

Another interesting question is whether a heavier $\pi^+\pi^-\psi(2S)$ state, the $\psi(4660)$, discovered by Belle [50, 51] and confirmed by BaBar [52], is identical to the $\Lambda_c^+\bar{\Lambda}_c^-$ resonance observed by Belle with a nearby mass and width [53]. Most probably it is, the $\Lambda_c^+\bar{\Lambda}_c^-$ being one more decay mode of the $\psi(4660)$ (see the review on heavy non-$q\bar{q}$ mesons for more detail). Note that this is the interpretation adopted in the particle listings. In addition, Belle reported the first observation of a vector charmonium-like state decaying to $D_s^+D_{s1}(2536)$ with a significance of 5.9σ [54]. Its measured mass and width are $4625.9^{+6.2}_{-6.0} \pm 0.4$ MeV and $49.8^{+13.9}_{-11.5} \pm 4.0$ MeV, respectively, consistent with those of the $\psi(4660)$. Therefore, $D_s^+D_{s1}(2536)$ appears as an additional decay mode of the $\psi(4660)$ in the listings.

A series of isovector states containing $c\bar{c}$ have been found in B decays to $K\pi(c\bar{c})$, where the isovector state decays to $\pi(c\bar{c})$ and $(c\bar{c})$ stands for $J/\psi(1S)$, $\psi(2S)$, or χ_{c1}. They are manifestly non-$q\bar{q}$ and their discovery implied an expansion of the meson naming scheme. The $Z_c(4430)$, decaying to $\pi\psi(2S)$, is the most well established. Based on a full amplitude analysis of $B^0 \to K^+\pi^-\psi(2S)$ decays, Belle determined the spin-parity of the $Z_c(4430)$ to be $J^P = 1^+$ [55]. From their study of $B^0 \to K^+\pi^-J/\psi(1S)$ decays, Belle also found evidence for the decay mode $Z_c(4430) \to \pi J/\psi(1S)$ [56], which has an order of magnitude lower branching fraction than the discovery mode $Z_c(4430) \to \pi\psi(2S)$. In the same analysis, Belle reported evidence for one more charged state, dubbed $Z_c(4200)$, decaying to $\pi J/\psi(1S)$. The existence of the $Z_c(4430)$ in $\pi\psi(2S)$, as well as its quantum number assignments, were confirmed by LHCb [57] with a much larger data sample, leading to improved mass and

Downloaded from https://academic.oup.com/ptep/article/2022/8/083C01/6651666 by KIT Library user on 27 September 2022

width values, consistent with earlier measurements; the experiment even reports a resonant behavior of the $Z_c(4430)$ amplitude. The $Z_c(4430)$ was not confirmed (or excluded) by BaBar [58].

Belle also reported an observation of two charged states decaying to $\pi\chi_{c1}$ in an analysis of $B^0 \to K^+\pi^-\chi_{c1}$ decays [59]. These were originally called the $Z_1(4050)^\pm$ and the $Z_2(4250)^\pm$, but are referred to in Table 78.2 as $X(4050)^\pm$ and $X(4250)^\pm$. These states were not confirmed by BaBar [60]. Belle observes signals with 5.0σ significance for both the $Z_1(4050)^\pm$ and $Z_2(4250)^\pm$, whereas BABAR reports 1.1σ and 2.0σ effects, respectively, setting upper limits that are not inconsistent with Belle's measured rates. The situation remains unresolved.

The decay $B^+ \to K^+\phi J/\psi(1S)$ appears to be especially rich in resonant substructure. The $Y(4140)$ (now the $\chi_{c1}(4140)$), decaying to $\phi J/\psi(1S)$, was first observed in 2008 by CDF [61,62], and confirmed by D0 and CMS [63,64]. However, a second structure, the $Y(4274)$ (now the $\chi_{c1}(4274)$), could not be established unambiguously. Neither of the two states was seen in B decays at Belle [65], LHCb [66] and BaBar [67], or in $\gamma\gamma$ collisions at Belle [68]. The real breakthrough happened when LHCb performed a full amplitude analysis of $B^+ \to K^+\phi J/\psi(1S)$ with $J/\psi(1S) \to \mu^+\mu^-$, $\phi \to K^+K^-$ decays and showed that the data cannot be described in a model that contains only excited kaon states decaying into $K^+\phi$ [69,70]. They observe two 1^{++} states with masses close to those originally reported by CDF (the $\chi_{c1}(4140)$ and $\chi_{c1}(4274)$), but the width of the one at 4140 MeV is much larger. In addition, they find two significant 0^{++} structures at 4500 and 4700 MeV (the $\chi_{c0}(4500)$ and $\chi_{c0}(4700)$).

78.2.2 *Bottomonium*

Belle reported a new measurement of the $e^+e^- \to \Upsilon(nS)\pi^+\pi^-$ ($n = 1, 2, 3$) cross sections at energies from 10.52 to 11.02 GeV [71]. They observed, with a 5.2σ significance, a new structure in the energy dependence of the cross sections. If described by a Breit–Wigner function, its mass and width are $10752.7 \pm 5.9^{+0.7}_{-1.1}$ MeV and $35.5^{+17.6+3.9}_{-11.3-3.3}$ MeV, respectively. The new structure could have a resonant origin and correspond to the not yet observed $\Upsilon(3D)$ state, provided $S-D$ mixing is enhanced, or an exotic state, e.g., a compact tetraquark or hadrobottomonium. It could also be a non-resonant effect due to rescattering.

We no longer mention a hypothetical $Y_b(10888)$ state since a new analysis of the $\Upsilon(10860)$ energy range does not show evidence for an additional state with a mass different from that of the $\Upsilon(10860)$ [72]. After the mass of the $\eta_b(1S)$ was shifted upwards by about 10 MeV based on the Belle measurements [18,19], all of the bottomonium states mentioned above fit into their respective spectroscopies, roughly where expected. An independent experimental confirmation of the shifted masses came from the Belle observation of $\Upsilon(4S) \to \eta h_b(1P)$ decays [19]. This process turns out to be the strongest observed transition of the $\Upsilon(4S)$ to lower bottomonium states.

78.3 States Near Open-Flavor Threshold

A number of states, listed in Table 78.3, appear near open-flavor thresholds, which is likely an important factor in their theoretical interpretation [73].

78.3.1 *Charmonium*

The $\chi_{c1}(3872)$, also known as $X(3872)$, is widely studied and seen in many transitions — see Table 78.3. Yet its interpretation remains unsettled (see the heavy non-$q\bar{q}$ review). Its unique experimental features include: it has $J^{PC} = 1^{++}$ [74,75], yet it is too light to be the $\chi_{c1}(2^3P_1)$ quark model state; its mass is within 200 keV of the $D^0\bar{D}^{0*}$ threshold; it shows substantial isospin-breaking in its decays to $\rho J/\psi(1S)$ and $\pi^0\chi_{c1}$; and it is extremely narrow. Using a large sample of inclusively produced $\chi_{c1}(3872)$ decaying to $\pi^+\pi^-J/\psi(1S)$, LHCb recently determined the decay width of the $\chi_{c1}(3872)$ under two different assumptions [76]. Assuming a Flatté-inspired line shape and exploiting the strong coupling of the $\chi_{c1}(3872)$ to $D^0\bar{D}^{*0}$, LHCb performed the first exploration of the pole structure of the $\chi_{c1}(3872)$, finding a FWHM of $0.22^{+0.06+0.25}_{-0.08-0.17}$ MeV. On the other hand, assuming a Breit–Wigner line shape, its width was found to be $1.39 \pm 0.24 \pm 0.10$ MeV. While the former analysis has a more firm theoretical foundation, the LHCb detector resolution did not allow for a distinction between the different line shapes.

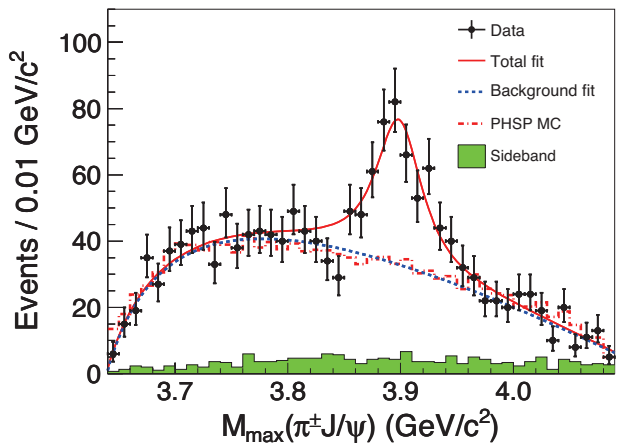

Figure 78.4: The $\pi^\pm J/\psi(1S)$ invariant mass distribution from BESIII [78] e^+e^- collision data taken at a center-of-mass energy near 4260 MeV.

In addition to the Z_c states found in B decays, discussed above, several isovector states with masses near $D\bar{D}^*$ and $D^*\bar{D}^*$ thresholds appear to be unique to e^+e^- annihilation. In 2013, a state named $Z_c(3900)$ was unearthed in the charmonium region at BESIII [78] and Belle [43] in the process $e^+e^- \to \pi^\mp Z_c(3900)^\pm$ with $Z_c(3900)^\pm \to \pi^\pm J/\psi(1S)$. The corresponding spectrum from BESIII is shown in Fig. 78.4. An analysis of CLEO data [79] confirmed this finding and also provided evidence for a neutral partner. A nearby signal was also seen in the $D\bar{D}^*$ channel [80] whose quantum numbers were fixed to 1^{+-}. BESIII reported its neutral partner in both $J/\psi(1S)\pi^0$ [81] and $D\bar{D}^*$ [82] decay modes. The masses extracted from these experiments in different decay modes have differences reaching up to 2σ. However, since the extraction of the mass and width parameters did not allow for an interference with the background and used Breit–Wigner line shapes, which is not justified near thresholds, there might be some additional systematic uncertainty in the mass values. Therefore, in the RPP listings as well as in Table 78.3 both structures appear under the name $Z_c(3900)$. BESIII also reported an observation of another charged state, the $X(4020)^\pm$ (originally called $Z_c(4020)^\pm$), in two decay modes: $h_c\pi^\pm$ [83] and $(D^*\bar{D}^*)^\pm$ [84]. The neutral partners have also been observed by BESIII in the $h_c\pi^0$ [85] and $(D^*\bar{D}^*)^0$ [86] final states. The Z_c states show some remarkable similarities to the Z_b states (discussed below), e.g. they decay dominantly to $D^{(*)}\bar{D}^*$ channels. However, current analyses suggest that the mass of the $Z_c(3900)$ might be somewhat above the $D\bar{D}^*$ threshold. If confirmed, this feature would challenge a possible $D\bar{D}^*$–molecular interpretation with S-wave interactions only — prominent D-waves can shift molecular poles above threshold (see the discussion in Sec. 78.3.2). Finally, 3.5σ evidence for one more charged charmonium-like state at 4055 MeV decaying into $\psi(2S)\pi^\pm$ was reported by Belle in their analysis of the process $e^+e^- \to \psi(2S)\pi^+\pi^-$ [51]. This state was confirmed by BESIII, although there appears to be complications in the Dalitz plot requiring further investigation [48].

78.3.2 *Bottomonium*

New results on the η_b, h_b, and Z_b mostly come from Belle [18,19, 21,23,72,87–93], all from analyses of 121.4 fb^{-1} of e^+e^- collision data collected near the peak of the $\Upsilon(10860)$ resonance, as well as from an additional 25 fb^{-1} of data collected during the scans of the c.m. energy range 10.63–11.05 GeV. The η_b, h_b, and Z_b appear in the decay chains $\Upsilon(10860) \to \pi^- Z_b^+$, $Z_b^+ \to \pi^+(b\bar{b})$, and, when the $b\bar{b}$ forms an $h_b(1P)$, frequently decaying as $h_b(1P) \to \gamma\eta_b$.

Belle soon noticed that, for events in the peaks of Fig. 78.1, there seemed to be two intermediate charged states, the $Z_b(10610)$ and the $Z_b(10650)$. For example, Fig. 78.5 shows a Dalitz plot for events restricted to the $\Upsilon(2S)$ region of $\pi^+\pi^-$ recoil mass,

Downloaded from https://academic.oup.com/ptep/article/2022/8/083C01/6651666 by KIT Library user on 27 September 2022

Table 78.3: As in Table 78.1, but for new states near the first open-flavor thresholds in the $c\bar{c}$ and $b\bar{b}$ regions, ordered by mass. Updated from Ref. [77] with kind permission, copyright (2011), Springer, and from Ref. [9] with kind permission from the authors.

PDG Name	Former Name(s)	m (MeV)	Γ (MeV)	$I^G(J^{PC})$	Production	Decay	Discovery Year	Summary Table
$\chi_{c1}(3872)$	$X(3872)$	3871.65±0.06	1.19 ± 0.21	$0^+(1^{++})$	$B \to KX$ $p\bar{p} \to X...$ $pp \to X...$ $e^+e^- \to \gamma X$	$\pi^+\pi^- J/\psi(1S)$ $3\pi J/\psi(1S)$ $D^{*0}\bar{D}^0$ $\gamma J/\psi(1S)$ $\gamma\psi(2S)$ $\pi^0\chi_{c1}(1P)$	2003	YES
$Z_c(3900)$		3887.1 ± 2.6	28.4 ± 2.6	$1^+(1^{+-})$	$\psi(4230) \to \pi^- X$ $\psi(4230) \to \pi^0 X$	$\pi^+ J/\psi(1S)$ $\pi^0 J/\psi(1S)$ $(D\bar{D}^*)^+$ $(D\bar{D}^*)^0$	2013	YES
$X(4020)$	$Z_c(4020)$	4024.1 ± 1.9	13 ± 5	$1^+(?^{?-})$	$\psi(4230, 4360) \to \pi^- X$ $\psi(4230, 4360) \to \pi^0 X$	$\pi^+ h_c$ $\pi^0 h_c$ $(D^*\bar{D}^*)^+$ $(D^*\bar{D}^*)^0$	2013	YES
$Z_b(10610)$		10607.2 ± 2.0	18.4 ± 2.4	$1^+(1^{+-})$	$\Upsilon(10860) \to \pi^- X$ $\Upsilon(10860) \to \pi^0 X$	$\pi^+\Upsilon(1S, 2S, 3S)$ $\pi^0\Upsilon(1S, 2S, 3S)$ $\pi^+ h_b(1P, 2P)$ $(B\bar{B}^*)^+$	2011	YES
$Z_b(10650)$		10652.2 ± 1.5	11.5 ± 2.2	$1^+(1^{+-})$	$\Upsilon(10860) \to \pi^- X$	$\pi^+\Upsilon(1S, 2S, 3S)$ $\pi^+ h_b(1P, 2P)$ $(B^*\bar{B}^*)^+$	2011	YES

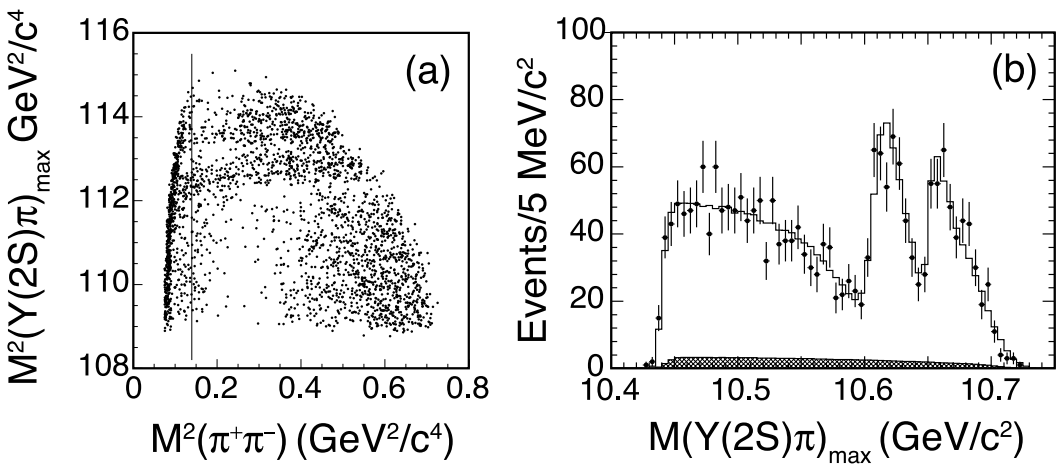

Figure 78.5: From Belle [87] e^+e^- collision data taken near the peak of the $\Upsilon(10860)$ for events with a $\pi^+\pi^-$-missing mass consistent with an $\Upsilon(2S) \to \mu^+\mu^-$, (a) the maximum of the two possible single $\pi^\pm$-missing-mass-squared combinations vs. the $\pi^+\pi^-$-mass-squared; and (b) projection of the maximum of the two possible single $\pi^\pm$-missing-mass combinations (*points with error bars*) overlaid with a fit (*curve*). Events to the left of the vertical line in (a) are excluded from the amplitude analysis. The hatched histogram in (b) corresponds to the combinatorial background. The two horizontal stripes in (a) and two peaks in (b) correspond to the two Z_b states.

with $\Upsilon(2S) \to \mu^+\mu^-$ [87]. The two bands observed in the maximum of the two $M[\pi^\pm\Upsilon(2S)]^2$ values also appear in the $\Upsilon(1S)$, $\Upsilon(3S)$, $h_b(1P)$, and $h_b(2P)$ samples. Belle fits all subsamples to resonant plus non-resonant amplitudes, allowing for interference (notably, between $\pi^- Z_b^+$ and $\pi^+ Z_b^-$), and finds consistent pairs of Z_b masses for all bottomonium transitions, and comparable strengths of the two states. A recent angular analysis assigned $J^P = 1^+$ for both Z_b states [88], which must also have negative G-parity. Transitions through Z_b to the $h_b(nP)$ saturate the observed $\pi^+\pi^- h_b(nP)$ cross sections. While the two masses of the Z_b states as extracted from Breit–Wigner fits for the various channels are just a few MeV above the $B^*\bar{B}$ and $B^*\bar{B}^*$ thresholds, more refined analyses using only S-waves find pole locations right below the corresponding thresholds either on the physical [94] or the unphysical [95] sheet. Once D-waves are included, the pole of the $Z_b(10650)$ moves above the $B^*\bar{B}^*$ threshold [96]. Regardless of their proximity to the corresponding thresholds, both states predominantly decay into these open-flavor channels [90, 97] with branching fractions that exceed 80% and 70%, respectively, at 90% CL. This feature provides strong evidence for their molecular nature.

78.4 Concluding Remarks

The discovery of the $\chi_{c1}(3872)$ (also known as the $X(3872)$) in 2003 ushered in an era of tremendous progress in experimental heavy quark meson spectroscopy. As shown in Tables 78.1 to 78.3, more than 40 new states have been reported during this period, many of which were unanticipated. While the states below open-flavor thresholds (Table 78.1) appear to be well-explained by the conventional $q\bar{q}$ quark model, a thorough understanding of the suite of states above (Table 78.2) and near (Table 78.3) open-flavor thresholds remains elusive. After nearly two decades, experimental progress remains rapid with the continuation of BESIII, the commencement of the Belle II program, and the imminent accumulation of additional data at the LHC.

Downloaded from https://academic.oup.com/ptep/article/2022/8/083C01/6651666 by KIT Library user on 27 September 2022

Acknowledgement

The authors would like to express their gratitude to Alex Bondar and Christoph Hanhart for productive discussions during the composition of this review.

References

[1] N. Brambilla *et al.*, Phys. Rept. **873**, 1 (2020), [arXiv:1907.07583].

[2] Y.-R. Liu *et al.*, Prog. Part. Nucl. Phys. **107**, 237 (2019), [arXiv:1903.11976].

[3] S. L. Olsen, T. Skwarnicki and D. Zieminska, Rev. Mod. Phys. **90**, 1, 015003 (2018), [arXiv:1708.04012].

[4] A. Ali, J. S. Lange and S. Stone, Prog. Part. Nucl. Phys. **97**, 123 (2017), [arXiv:1706.00610].

[5] F.-K. Guo *et al.*, Rev. Mod. Phys. **90**, 1, 015004 (2018), [arXiv:1705.00141].

[6] R. F. Lebed, R. E. Mitchell and E. S. Swanson, Prog. Part. Nucl. Phys. **93**, 143 (2017), [arXiv:1610.04528].

[7] A. E. Bondar, R. V. Mizuk and M. B. Voloshin, Mod. Phys. Lett. A **32**, 04, 1750025 (2017), [arXiv:1610.01102].

[8] S. K. Choi *et al.* (Belle), Phys. Rev. Lett. **91**, 262001 (2003), [hep-ex/0309032].

[9] N. Brambilla *et al.*, Eur. Phys. J. **C74**, 10, 2981 (2014), [arXiv:1404.3723].

[10] J. L. Rosner *et al.* (CLEO), Phys. Rev. Lett. **95**, 102003 (2005), [hep-ex/0505073].

[11] M. Ablikim *et al.* (BESIII), Phys. Rev. D **99**, 7, 072008 (2019), [arXiv:1810.12023].

[12] M. Ablikim *et al.* (BESIII), Phys. Rev. D **102**, 112007 (2020), [arXiv:2010.12092].

[13] V. Bhardwaj *et al.* (Belle), Phys. Rev. Lett. **111**, 3, 032001 (2013), [arXiv:1304.3975].

[14] M. Ablikim *et al.* (BESIII), Phys. Rev. Lett. **115**, 1, 011803 (2015), [arXiv:1503.08203].

[15] K. Chilikin *et al.* (Belle) (2020), [arXiv:2003.08335].

[16] B. Aubert *et al.* (BaBar), Phys. Rev. Lett. **101**, 071801 (2008), [Erratum: Phys.Rev.Lett. 102, 029901 (2009)], [arXiv:0807.1086].

[17] B. Aubert *et al.* (BaBar), Phys. Rev. Lett. **103**, 161801 (2009), [arXiv:0903.1124].

[18] R. Mizuk *et al.* (Belle), Phys. Rev. Lett. **109**, 232002 (2012), [arXiv:1205.6351].

[19] U. Tamponi *et al.* (Belle), Phys. Rev. Lett. **115**, 14, 142001 (2015), [arXiv:1506.08914].

[20] B. G. Fulsom *et al.* (Belle), Phys. Rev. Lett. **121**, 23, 232001 (2018), [arXiv:1807.01201].

[21] I. Adachi *et al.* (Belle), Phys. Rev. Lett. **108**, 032001 (2012), [arXiv:1103.3419].

[22] T. K. Pedlar *et al.* (CLEO), Phys. Rev. Lett. **107**, 041803 (2011), [arXiv:1104.2025].

[23] I. Adachi (Belle), in "8th International Workshop On Heavy Quarkonium (QWG2011) Darmstadt, Germany, October 3-7, 2011," (2011), [arXiv:1110.3934].

[24] G. Aad *et al.* (ATLAS), Phys. Rev. Lett. **108**, 152001 (2012), [arXiv:1112.5154].

[25] V. M. Abazov *et al.* (D0), Phys. Rev. D **86**, 031103 (2012), [arXiv:1203.6034].

[26] R. Aaij *et al.* (LHCb), JHEP **10**, 088 (2014), [arXiv:1409.1408].

[27] A. M. Sirunyan *et al.* (CMS), Phys. Rev. Lett. **121**, 092002 (2018), [arXiv:1805.11192].

[28] G. Aad *et al.* (ATLAS), Phys. Rev. Lett. **113**, 212004 (2014), [arXiv:1407.1032].

[29] A. M. Sirunyan *et al.* (CMS), Phys. Rev. Lett. **122**, 132001 (2019), [arXiv:1902.00571].

[30] R. Aaij *et al.* (LHCb), Phys. Rev. Lett. **122**, 232001 (2019), [arXiv:1904.00081].

[31] R. Aaij *et al.* (LHCb), JHEP **07**, 035 (2019), [arXiv:1903.12240].

[32] S. Uehara *et al.* (Belle), Phys. Rev. Lett. **96**, 082003 (2006), [hep-ex/0512035].

[33] B. Aubert *et al.* (BaBar), Phys. Rev. D **81**, 092003 (2010), [arXiv:1002.0281].

[34] K. Abe *et al.* (Belle), Phys. Rev. Lett. **94**, 182002 (2005), [hep-ex/0408126].

[35] J. P. Lees *et al.* (BaBar), Phys. Rev. **D86**, 072002 (2012), [arXiv:1207.2651].

[36] F.-K. Guo and U.-G. Meissner, Phys. Rev. **D86**, 091501 (2012), [arXiv:1208.1134].

[37] S. L. Olsen, Phys. Rev. **D91**, 5, 057501 (2015), [arXiv:1410.6534].

[38] Z.-Y. Zhou, Z. Xiao and H.-Q. Zhou, Phys. Rev. Lett. **115**, 2, 022001 (2015), [arXiv:1501.00879].

[39] R. Aaij *et al.* (LHCb), Phys. Rev. D **102**, 112003 (2020), [arXiv:2009.00026].

[40] K. Chilikin *et al.* (Belle), Phys. Rev. **D95**, 112003 (2017), [arXiv:1704.01872].

[41] B. Aubert *et al.* (BaBar), Phys. Rev. Lett. **95**, 142001 (2005), [hep-ex/0506081].

[42] C. Z. Yuan *et al.* (Belle), Phys. Rev. Lett. **99**, 182004 (2007), [arXiv:0707.2541].

[43] Z. Q. Liu *et al.* (Belle), Phys. Rev. Lett. **110**, 252002 (2013), [arXiv:1304.0121].

[44] M. Ablikim *et al.* (BESIII), Phys. Rev. Lett. **118**, 9, 092001 (2017), [arXiv:1611.01317].

[45] M. Cleven *et al.*, Phys. Rev. **D90**, 7, 074039 (2014), [arXiv:1310.2190].

[46] M. Ablikim *et al.* (BESIII), Phys. Rev. Lett. **118**, 9, 092002 (2017), [arXiv:1610.07044].

[47] M. Ablikim *et al.* (BESIII), Phys. Rev. Lett. **112**, 9, 092001 (2014), [arXiv:1310.4101].

[48] M. Ablikim *et al.* (BESIII), Phys. Rev. **D96**, 3, 032004 (2017), [erratum: Phys. Rev.D99,no.1,019903(2019)], [arXiv:1703.08787].

[49] X. Y. Gao, C. P. Shen and C. Z. Yuan, Phys. Rev. **D95**, 9, 092007 (2017), [arXiv:1703.10351].

[50] X. L. Wang *et al.* (Belle), Phys. Rev. Lett. **99**, 142002 (2007), [arXiv:0707.3699].

[51] X. L. Wang *et al.* (Belle), Phys. Rev. **D91**, 112007 (2015), [arXiv:1410.7641].

[52] J. P. Lees *et al.* (BaBar), Phys. Rev. **D89**, 11, 111103 (2014), [arXiv:1211.6271].

[53] G. Pakhlova *et al.* (Belle), Phys. Rev. Lett. **101**, 172001 (2008), [arXiv:0807.4458].

[54] S. Jia *et al.* (Belle), Phys. Rev. **D100**, 11, 111103 (2019), [arXiv:1911.00671].

[55] K. Chilikin *et al.* (Belle), Phys. Rev. **D88**, 7, 074026 (2013), [arXiv:1306.4894].

[56] K. Chilikin *et al.* (Belle), Phys. Rev. **D90**, 11, 112009 (2014), [arXiv:1408.6457].

[57] R. Aaij *et al.* (LHCb), Phys. Rev. Lett. **112**, 22, 222002 (2014), [arXiv:1404.1903].

[58] B. Aubert *et al.* (BaBar), Phys. Rev. **D79**, 112001 (2009), [arXiv:0811.0564].

[59] R. Mizuk *et al.* (Belle), Phys. Rev. **D78**, 072004 (2008), [arXiv:0806.4098].

[60] J. P. Lees *et al.* (BaBar), Phys. Rev. **D85**, 052003 (2012), [arXiv:1111.5919].

Downloaded from https://academic.oup.com/ptep/article/2022/8/083C01/6651666 by KIT Library user on 27 September 2022

[61] T. Aaltonen *et al.* (CDF), Phys. Rev. Lett. **102**, 242002 (2009), [arXiv:0903.2229].

[62] T. Aaltonen *et al.* (CDF), Mod. Phys. Lett. **A32**, 26, 1750139 (2017), [arXiv:1101.6058].

[63] V. M. Abazov *et al.* (D0), Phys. Rev. **D89**, 1, 012004 (2014), [arXiv:1309.6580].

[64] S. Chatrchyan *et al.* (CMS), Phys. Lett. **B734**, 261 (2014), [arXiv:1309.6920].

[65] J. Brodzicka, Conf. Proc. **C0908171**, 299 (2009), [,299(2009)].

[66] R. Aaij *et al.* (LHCb), Phys. Rev. **D85**, 091103 (2012), [arXiv:1202.5087].

[67] J. P. Lees *et al.* (BaBar), Phys. Rev. **D91**, 1, 012003 (2015), [arXiv:1407.7244].

[68] C. P. Shen *et al.* (Belle), Phys. Rev. Lett. **104**, 112004 (2010), [arXiv:0912.2383].

[69] R. Aaij *et al.* (LHCb), Phys. Rev. **D95**, 1, 012002 (2017), [arXiv:1606.07898].

[70] R. Aaij *et al.* (LHCb), Phys. Rev. Lett. **118**, 2, 022003 (2017), [arXiv:1606.07895].

[71] R. Mizuk *et al.* (Belle), JHEP **10**, 220 (2019), [arXiv:1905.05521].

[72] D. Santel *et al.* (Belle), Phys. Rev. **D93**, 1, 011101 (2016), [arXiv:1501.01137].

[73] F.-K. Guo, X.-H. Liu and S. Sakai, Prog. Part. Nucl. Phys. **112**, 103757 (2020), [arXiv:1912.07030].

[74] R. Aaij *et al.* (LHCb), Phys. Rev. Lett. **110**, 222001 (2013), [arXiv:1302.6269].

[75] R. Aaij *et al.* (LHCb), Phys. Rev. **D92**, 1, 011102 (2015), [arXiv:1504.06339].

[76] R. Aaij *et al.* (LHCb), Phys. Rev. D **102**, 9, 092005 (2020), [arXiv:2005.13419].

[77] N. Brambilla *et al.*, Eur. Phys. J. **C71**, 1534 (2011), [arXiv:1010.5827].

[78] M. Ablikim *et al.* (BESIII), Phys. Rev. Lett. **110**, 252001 (2013), [arXiv:1303.5949].

[79] T. Xiao *et al.*, Phys. Lett. **B727**, 366 (2013), [arXiv:1304.3036].

[80] M. Ablikim *et al.* (BESIII), Phys. Rev. Lett. **112**, 2, 022001 (2014), [arXiv:1310.1163].

[81] M. Ablikim *et al.* (BESIII), Phys. Rev. Lett. **115**, 11, 112003 (2015), [arXiv:1506.06018].

[82] M. Ablikim *et al.* (BESIII), Phys. Rev. Lett. **115**, 22, 222002 (2015), [arXiv:1509.05620].

[83] M. Ablikim *et al.* (BESIII), Phys. Rev. Lett. **111**, 24, 242001 (2013), [arXiv:1309.1896].

[84] M. Ablikim *et al.* (BESIII), Phys. Rev. Lett. **112**, 13, 132001 (2014), [arXiv:1308.2760].

[85] M. Ablikim *et al.* (BESIII), Phys. Rev. Lett. **113**, 21, 212002 (2014), [arXiv:1409.6577].

[86] M. Ablikim *et al.* (BESIII), Phys. Rev. Lett. **115**, 18, 182002 (2015), [arXiv:1507.02404].

[87] A. Bondar *et al.* (Belle), Phys. Rev. Lett. **108**, 122001 (2012), [arXiv:1110.2251].

[88] A. Garmash *et al.* (Belle), Phys. Rev. **D91**, 7, 072003 (2015), [arXiv:1403.0992].

[89] P. Krokovny *et al.* (Belle), Phys. Rev. **D88**, 5, 052016 (2013), [arXiv:1308.2646].

[90] I. Adachi *et al.* (Belle) (2012), [arXiv:1209.6450].

[91] K. F. Chen *et al.* (Belle), Phys. Rev. Lett. **100**, 112001 (2008), [arXiv:0710.2577].

[92] P. Krokovny (Belle Collab.), talk given at Les Rencontres de Physique de la Vallee d'Aoste, La Thuile, Aosta Valley, Italy, 2012.

[93] A. Abdesselam *et al.* (Belle), Phys. Rev. Lett. **117**, 14, 142001 (2016), [arXiv:1508.06562].

[94] M. Cleven *et al.*, Eur. Phys. J. **A47**, 120 (2011), [arXiv:1107.0254].

[95] F. K. Guo *et al.*, Phys. Rev. **D93**, 7, 074031 (2016), [arXiv:1602.00940].

[96] Q. Wang *et al.*, Phys. Rev. D **98**, 7, 074023 (2018), [arXiv:1805.07453].

[97] A. Garmash *et al.* (Belle), Phys. Rev. Lett. **116**, 21, 212001 (2016), [arXiv:1512.07419].

Downloaded from https://academic.oup.com/ptep/article/2022/8/083C01/6651666 by KIT Library user on 27 September 2022

79. Heavy Non-$q\bar{q}$ Mesons

Revised June 2021 by S. Eidelman (Budker Inst., Novosibirsk; Novosibirsk U.), T. Gutsche (Tübingen U.), C. Hanhart (Jülich) and R.E. Mitchell (Indiana U.).

The constituent quark model describes the observed meson spectrum as bound $q\bar{q}$ states grouped into SU(N) flavor multiplets (see the 'Quark Model' in this issue of the *Review of Particle Physics*). However, the self coupling of gluons in QCD suggests that additional mesons made of bound gluons (glueballs), or $q\bar{q}$-pairs with an excited gluon (hybrids), may exist. Furthermore, multiquark color singlet states such as $qq\overline{qq}$ (tetraquarks as compact diquark-antidiquark systems and 'molecular' bound states of two mesons) or $qqq\overline{qq}$ (six-quark, 'baryonium' or quasinuclear baryon-antibaryon bound states) have also been predicted. The focus of this review is on the current understanding of exotic states that apparently do not fit into the constituent quark model and contain at least one heavy quark (charm or bottom — the lifetime of the top quark is too short to allow it to hadronise). Light non-$q\bar{q}$ candidates (made of u, d and s quarks) are discussed in 'Spectroscopy of Light Meson Resonances' in this *Review*.

The review is split into 3 parts, discussing separately heavy–light systems, heavy–heavy systems, as well as systems with more than two heavy quarks. For a more detailed discussion of the experimental and/or theoretical status on exotic meson candidates in the doubly heavy meson sector we refer to Refs. [1–7]. Reviews with main focus on tetraquarks and molecular states are presented in Ref. [8] and in Ref. [9], respectively.

79.1 Heavy-light systems

Two very narrow states, $D_{s0}^*(2317)^\pm$ and $D_{s1}(2460)^\pm$, were observed at B factories [10, 11]. They lie far below the predicted masses for the two expected broad P-wave $c\bar{s}$ mesons. However, strong cusp effects, due to the nearby DK (DK^*) thresholds, could shift their masses downwards and quench the observed widths, still allowing for a conventional explanation of these states [12]. Such an effect was also claimed for the $a_0(980)$ and $f_0(980)$ mesons, which lie just below the $K\overline{K}$ threshold. In contrast to this picture, many authors favour exotic explanations for these lightest positive parity charmed states, such as four-quark states [13–16] or DK (DK^*) molecules [17–22]. Both states are isoscalars and thus the dominant open decay channels, $D_s^{(*)\pm}\pi^0$, lead to very small widths. For compact structures the hadronic decay is driven by $\eta - \pi^0$ mixing and one finds widths below 10 keV [12, 23]. In contrast to this a hadronic width of typically 100 keV would be the unequivocal signature for a prominent molecular nature of $D_{s0}^*(2317)^\pm$ [19, 21, 22, 24], since meson loops would then contribute significantly. The most refined analysis in the molecular scenario [24], where the parameters of the formalism are constrained by a large bulk of lattice QCD data on singly charmed systems, reports a prediction for the width in the range (104-116) keV. The currently measured upper bound for the width is 3.8 MeV.

It should be stressed that – akin to $q\bar{q}$ mesons – multiquark states also appear in multiplets. An important probe for the structure of hadrons is therefore the spectra, and in particular the SU(3) flavor multiplets within the different scenarios. For example the tetraquark model advocated in Refs. [16, 25] finds that the $D_{s0}^*(2317)^\pm$ should be degenerate with its non strange-partner state $D_0^*(2300)$ in line with the currently available experimental analyses. However, Ref. [26] showed that the recent LHCb data for $B \to D\pi\pi$ [27, 28] call for a significantly lighter lightest non-strange scalar charmed meson as soon as constraints from the chiral symmetry of QCD are employed in the analysis. This claim is in line with the recent lattice QCD study of Ref. [29]. In fact, the experimental as well as lattice data turn out to be consistent with the predictions from unitarised chiral perturbation theory pioneered for these systems in Ref. [18]. For more recent calculations see Refs. [24, 30, 31]. Moreover, all these latter calculations predict that there should be in addition a heavier flavor exotic state by about 300 MeV that indeed shows up in the above mentioned LHCb data [31]. Thus, in this picture the structure that appears as $D_0^*(2300)$ in the *Listings* originates from the interplay of two poles, similar to the $\Lambda(1405)$ in the baryon sector, see 'Pole structure of the $\Lambda(1405)$ region' in this *Review*. Two poles in the non-strange scalar sector are also generated in the tetraquark picture of Ref. [16], but in this work the real parts of the poles are located at 2308 MeV and 2666 MeV, in conflict with the data mentioned above. In the refined analysis of Ref. [25] it is shown, however, that the exact pole locations and even the ordering of the higher multiplets depend on the details of the model.

Manifestly exotic candidates around 2.9 GeV were reported in Refs. [32, 33] by LHCb in the $\bar{D}K$ system. Since the strong interactions preserve the quark flavor and the final state contains an $\bar{s}$ as well as a $\bar{c}$, color neutrality calls for a minimum quark content of $ud\bar{c}\bar{s}$. The explanation for those states include compact tetraquarks [34–36], hadronic molecules with a prominent $D^*\bar{K}^*$ component [37–39], or kinematic effects such as cusps or triangle singularities without nearby poles [40, 41]. The different pictures are contrasted and observable differences between them are discussed in Ref. [42].

79.2 Heavy-heavy systems

With the discovery of the $\chi_{c1}(3872)$[1] in $B^\pm \to K^\pm X$ ($X \to J/\psi\,\pi^+\pi^-$) by Belle [43] in 2003, soon confirmed by BaBar [44], many searches for states beyond the standard $q\bar{q}$ quark model were initiated in the charm and bottom sectors. For an updated collection of the currently available experimental information on multiquark states we refer to 'Spectroscopy of mesons containing two heavy quarks' in this *Review*, and in particular to Table 78.2. Moreover, in the decay $\Lambda_b^0 \to J/\psi\,K^-p$ the LHCb collaboration has recently reported the observation of new baryons decaying into $J/\psi(1S)\,p$, which are candidates for heavy pentaquark states [45,46]. They are discussed in some depth in 'Pentaquarks' in this *Review*.

When restricting ourselves to confirmed states we are faced with several states that do not seem to fit into the mass and quantum number schemes of basic $q\bar{q}$ quark models. This is clear for the five established charged states ($Z_c(3900)^\pm$, $Z_c(4020)^\pm$ [2], and $Z_c(4430)^\pm$ in the charmonium sector, and $Z_b(10610)^\pm$ and $Z_b(10650)^\pm$ in the bottomonium sector). The neutral states ($\chi_{c1}(3872)$, $\psi(4230)$, $\psi(4360)$, and $\psi(4660)$)[3] also challenge the quark model since their masses and decay properties are in conflict with expectations.

The quantum numbers of the $\chi_{c1}(3872)$ have been determined by LHCb to be $J^{PC} = 1^{++}$, first by assuming zero angular momentum between the $J/\psi(1S)$ and the dipion [47] and then by relaxing this constraint [48]. The $\chi_{c1}(3872)$ cannot be identified with the $\chi_{c1}(2^3P_1)$ since the latter is predicted to lie about 100 MeV higher in mass [49]. Instead, the $X(3940)$ reported by Belle in $e^+e^- \to J/\psi X$, decaying into $D^*\bar{D}$ but not into $D\bar{D}$ [50] could be the $\chi_{c1}(2^3P_1)$. The $\chi_{c2}(3930)$ 2^3P_2 tensor partner was reported by Belle at 3931 MeV in $\gamma\gamma$ interactions [51].

The $\chi_{c1}(3872)$ lies within 200 keV of the $D^0\bar{D}^{*0}$ threshold and its width is very small — recent Breit-Wigner analyses by LHCb [52, 53] result in an average value of $\Gamma = (1.19 \pm 0.21)$ MeV as indicated in the *Listings*; employing the formalism of Ref. [54] under the constraint that the $D^*\bar{D}$ decay channel dominates, results in $\Gamma = 0.22^{+0.18}_{-0.19}$ MeV, where the standard convention is applied to use twice the imaginary part of the pole location as width. In the future those values can be refined more by either a direct measurement of the width that should be possible at the planned PANDA experiment [55, 56] or by exploiting the interplay of a triangle singularity and the $\chi_{c1}(3872)$ pole [57–59]. Therefore the most natural explanation for this state is a 1^{++} $D\bar{D}^*$ molecule [60], for which strong isospin breaking is predicted [60, 61], since the distance of the pole of the $\chi_{c1}(3872)$ to the $D^0\bar{D}^{*0}$ threshold is significantly smaller than to the D^+D^{*-} threshold. Indeed, the comparable rates for $\omega J/\psi$ and $\rho^0 J/\psi$ are

[1] The $\chi_{c1}(3872)$ is also known as the $X(3872)$. According to the PDG naming scheme, which we follow in this review, the primary name for a meson expresses its quantum numbers.

[2] While the $J^P = 1^+$ quantum numbers are plausible for this state, they are not yet established experimentally. This is why this state appears as $X(4020)$ in both the *Listings* and *Summary Tables*.

[3] The $\psi(4230)$, $\psi(4360)$, and $\psi(4660)$ are also known as the $Y(4230)$, $Y(4360)$, and $Y(4660)$, respectively. Before improved mass measurements, the $\psi(4230)$ was originally called the $\psi(4260)$ or $Y(4260)$.

Downloaded from https://academic.oup.com/ptep/article/2022/8/083C01/6651666 by KIT Library user on 27 September 2022

consistent with an interpretation of $\chi_{c1}(3872)$ as an isoscalar $D\bar{D}^*$ molecule, when the different widths of the ρ and ω are taken into account [62]. Similarly, a dominant molecular $D^0\bar{D}^{*0}$ structure in the $\chi_{c1}(3872)$ with further subleading hadronic components is used to explain strong and radiative decays involving $J/\psi(1S)$ and $\psi(2S)$ in the final states [63, 64].

A four-quark state $cq\bar{c}\bar{q}'$ is another possible interpretation of the $\chi_{c1}(3872)$ [15] but a charged partner of the $\chi_{c1}(3872)$ has not been observed (e.g. not in $B^- \to \bar{K}^0 X^-$ nor in $B^0 \to K^+ X^-$, where $X^- \to J/\psi\,\pi^-\pi^0$ [65]) – see [66] for a possible explanation of this non-observation within the tetraquark approach assuming specific diquark correlations and the more recent discussion in Ref. [67]. The claim that $\chi_{c1}(3872)$ must be a compact (tetraquark) state, since it is also produced at very high p_T in $\bar{p}p$ collisions [68] and in high multiplicity final states [69], was challenged in [70] and [71], respectively, which in particular stress the importance of rescattering, see also Refs. [72, 73].

A broad structure, originally called $Y(4260)$, decaying into $J/\psi(1S)\,\pi^+\pi^-$ was reported by BaBar in initial state radiation $e^+e^- \to (\gamma_{\rm ISR})Y(4260)$ [74]. A subsequent measurement with significantly improved precision was reported by BESIII [75], and revealed that the original $Y(4260)$ cannot be described with a simple resonant lineshape. Fitting the BESIII data with two Breit-Wigner distributions leads to a narrower and lighter structure (referred to in the *Listings* as the $\psi(4230)$), but also requires a second state at 4320 MeV. However, note that the $D_1(2420)\bar{D}$ molecular model for the $\psi(4230)$ [76] can describe the same data with just one single pole [77]. How many vector states are in the mass range between 4220 MeV and 4400 MeV is not yet settled, but knowing this is crucial to allow for further progress.

There are no charmonium states expected in this mass region with quantum numbers 1^{--} from quark models using the Cornell type of interaction, although this might not be true for some screened versions thereof – for a recent discussion we refer to Ref. [78]. In addition, a charmonium state at this mass is expected to have significant couplings to one or more of the $\bar{D}^{(*)}D^{(*)}$ channels [79, 80], a feature that is not observed for the $\psi(4230)$. This state could be a hybrid charmonium with a spin-1 $\bar{c}c$ [81, 82] or a spin-0 [83, 84] core. However, provided that the observation of $\psi(4230)$ decay into $h_c(1P)\pi\pi$ by BESIII [85] is confirmed, the hybrid hypothesis would be under pressure, since the spin of the heavy quarks (coupled to zero in the $h_c(1P)$) should be conserved in leading order in the expansion in $(\Lambda_{\rm QCD}/m_c)$. (The individual conservation of the heavy quark spin and the total angular momentum of the light quark cloud is a consequence of the heavy-quark spin symmetry, see 'Heavy-Quark and Soft-Collinear Effective Theory' in this issue of the *Review*.) The same criticism applies to the hadrocharmonium interpretation of the $\psi(4230)$, which describes this state as spin-1 quarkonium surrounded by a light quark cloud [86]. To circumvent the spin-symmetry argument, Ref. [87] argues that $\psi(4230)$ and $\psi(4360)$ could be mixtures of two hadrocharmonia with spin-triplet and spin-singlet heavy quark pairs. The same kind of mixing could also be at work for hybrid structures.

A dominant $D_1(2420)\bar{D}$ component in the $\psi(4230)$ [88] explains naturally why $Z_c(3900)^\pm$ (interpreted by the authors as a $\bar{D}D^*$ bound state) is seen in $\psi(4230) \to \pi^\mp Z_c(3900)^\pm$. A similar mechanism is also found in Ref. [89] linking in addition the $J/\psi(1S)\pi^+\pi^-$ and $\psi(2S)\pi^+\pi^-$ decays of the $\psi(4230)$. Furthermore, a copious production of $\chi_{c1}(3872)$ in $\psi(4230)$ radiative decays was predicted from the prominent $D_1\bar{D}$ component of the $\psi(4230)$ [90], which was confirmed by BESIII [91]. Possible charmonia components both in $\psi(4230)$ and $\chi_{c1}(3872)$ can influence the radiative transition but they are shown to be of subleading order [92]. The $\psi(4360)$ as a $D_1\bar{D}^*$ bound state could be the spin partner of the $\psi(4230)$ [93, 94], but a detailed microscopic calculation is still lacking.

The tetraquark picture calls for four ground state vector states — once the parameters of the model are fixed from some candidate states in the negative and positive parity sector, states with other quantum numbers can be predicted. Possible scenarios are for instance discussed in Ref. [95] which builds on a tailor-made spin-spin interaction [96] to describe the $\chi_{c1}(3872)$, both $Z_c(3900)^{\pm,0}$ and $Z_c(4020)^\pm$ and even the $Z(4430)^\pm$ confirmed by Belle [97] and LHCb [98]. This model also explains the copious production of $\chi_{c1}(3872)$ in $\psi(4230)$ radiative decays mentioned above [96, 99]. However, tetraquark models (in most cases based on diquark-antidiquark configurations) tend to predict many additional charged and neutral states which have not yet been discovered. In particular, as for the conventional $\bar{q}q$ structures one should expect nearly degenerate isoscalar and isovector states in analogy to the near degeneracy of $\rho(770)$ and $\omega(782)$. The problem and possible explanations are discussed in some detail in Refs. [66, 67].

Ref. [100] found a sizeable SU(3) flavor octet contribution when analysing the $\pi\pi$ final state from $\psi(4230) \to J/\psi(1S)\pi^+\pi^-$, which is consistent with both a molecular and a tetraquark interpretation of $\psi(4230)$, but at odds with a hybrid or a $\bar{c}c$ interpretation.

In the mass range above 4600 MeV, the number of poles is also not yet settled. Experimental signals are seen in the $\psi(2S)\pi\pi$, $\Lambda_c^+\bar{\Lambda}_c^-$ and $D_s\bar{D}_{s1}$ final states. In the *Listings* the former two structures go into one node, $\psi(4660)$ due to their proximity in parameter values. Moreover, various theoretical works describe these states in a combined analysis [101–103]. The signal in the hidden strangeness mode around 4630 MeV still calls for confirmation and might be yet another realisation of the same state, but there are already speculations about its nature. While Ref. [104] argues in favor of a $D_s^{(*)}\bar{D}_{s1}(2536)$ or $D_s^{(*)}\bar{D}_{s2}(2573)$ [105] molecular nature, Ref. [106] does not confirm these claims. Ref. [107] identifies the structure as P-wave $[cs][\bar{c}\bar{s}]$ tetraquark state. Other explanations of the $\psi(4660)$ include a $\psi(2S)f_0(980)$ molecule [108] and a $\Lambda_c^+\bar{\Lambda}_c^-$ baryonium [101]. Also in this mass range studies of the partner states, driven either by spin or flavor symmetry will be very valuable — see e.g. the predictions in Ref. [109].

The isovector states $Z_c(3900)$ and $Z_c(4020)$, first observed by BESIII [110, 111], decay predominantly into $\bar{D}D^*$ and $\bar{D}^*D^*$, respectively, while the $Z_b(10610)$ and $Z_b(10650)$, first observed by Belle [112, 113], decay predominantly into $\bar{B}B^*$ and $\bar{B}^*B^*$ [114], respectively, although all four were discovered in the decay mode heavy quarkonium plus pion. This suggests that these states are close relatives and their interactions are connected via heavy quark flavor symmetry. A molecular interpretation for the bottomonium states was proposed shortly after the discovery of the two Z_b states [115] and also shortly after that of the $Z_c(3900)$ [88]. This picture is confirmed within the meson exchange model of Ref. [116]. Decay patterns of $Z_c(3900)$ and the two Z_b were also shown to be consistent with a molecular interpretation [117–119]. However, some of their properties also appear to be consistent with tetraquark structures [120]. If the molecular picture were correct for the Z_b states, spin symmetry would lead to the existence of spin partner states [121–123], which are still to be found. In Ref. [124] it was shown that the actual pole locations of these partner states would be good probes of one-pion exchange in the molecular potential, which makes the experimental search for those states even more interesting.

The heaviest confirmed charged state in the charmonium sector is the $Z(4430)^\pm$ observed by Belle [97]. It is interpreted as hadrocharmonium [86], $\bar{D}_1D^*$ molecule [125], as well as tetraquark [96]. Alternatively, in [126, 127] the $Z(4430)^\pm$ is explained as a cross-channel effect enhanced by a triangle singularity from open charm states. These works were criticised in Ref. [128] where an alternative triangle consisting of a K^*, a π, and the $\psi(4230)$, is proposed to generate the $Z_c(4430)$. The Argand diagram shows an anticlockwise circle, in line with the experimental analysis [98], while the one of Ref. [127] shows a clockwise motion. By replacing the $\psi(4230)$ by the $\psi(3770)$ and changing the K^* one can also interpret the $Z_c(4200)$ as a kinematic effect [128]. A possible interpretation of $Z_c(3900)$ and $Z_c(4020)$ as crossed channel effects is put forward in Ref. [129]. It remains to be seen, however, if this kind of explanation is also capable of explaining the observations of these lowest Z_c states, also at other total energies.

There is recent evidence for a charged charmonium-like state with strangeness, $Z_{cs}(3985)$, from BESIII [130]. The possible existence of a strange partner to the Z_c near the $D_s\bar{D}^*$ thresholds has been predicted in molecular models [131, 132], for

Downloaded from https://academic.oup.com/ptep/article/2022/8/083C01/6651666 by KIT Library user on 27 September 2022

tetraquarks [133,134], for hadrocharmonium structures [134,135], and as a coupled-channel effect [136]. Later on this state is interpreted in Refs. [137,138] as a member of the same multiquark octet and in Refs. [139,140] as a member of the same molecular one as the $Z_c(3900)$. Ref. [138] is also able to describe the recent LHCb data in the $J/\psi(1S)K^-$ system [141], although the extracted total width for their lowest Z_{cs} state is an order of magnitude larger than that found by BESIII. Refs. [142, 143] claim that both the molecular components and the compact tetraquark core are relevant to describe the $Z_c(3900)$ and $Z_{cs}(3985)$ resonances. Again, in [144] the $Z_{cs}(3985)$ can be explained as a coupled-channel effect producing the enhancement close to threshold.

It should be stressed that the various scenarios, while describing much of the available data, also make decisive predictions, *e.g.* yet unobserved quantum numbers [95,145]. The forthcoming data on heavy meson spectroscopy from various facilities should provide a much deeper understanding of how QCD forms matter out of quarks and gluons.

There is a very recent report by LHCb [146] on the observation of a narrow peak in the $D^0D^0\pi^+$ invariant mass distribution just below the $D^{*+}D^0$ threshold. This structure would possess a minimal $cc\bar{u}\bar{d}$ quark content. An assessment of this state will be discussed in the next issue of this review.

79.3 Systems containing four heavy quarks

Recently LHCb reported the observation of pronounced structures in a double-$J/\psi(1S)$ invariant mass distribution [147] thus pointing at states with $cc\bar{c}\bar{c}$ quarks contents. From quark models the possible existence of bound states like this was discussed already long ago [148,149]. There are now also many model calculations available in the literature. For discussions of those data from the compact tetraquark perspective see Refs. [150–156]. Most of these quark model calculations assign the reported structure to a $cc\bar{c}\bar{c}$ state in the $2S$ multiplet with near-degenerate $J^P = 0^+$, 1^+ and 2^+ configurations. The dominance of a compact tetraquark component in the apparently exotic structure is also supported by the coupled multichannel study of Ref. [157]. For direct analyses of the data within the tetraquark approach, see, e.g., Ref. [158]. Also QCD sum rule studies of the system were published, but do not give consistent results: For example Ref. [159] interprets the structure at 6900 MeV as a hybrid state, Ref. [160] as a tetraquark, and Ref. [161] states that both molecular and tetraquark interpretations are possible. An alternative view on the LHCb double-$J/\psi(1S)$ data is provided in Refs. [162–164] where the analyses are performed using coupled channel T-matrices. In both works the structures in the data emerge from the interplay of thresholds and resonances with the non-trivial prediction that there should exist, if this dynamical picture were correct, a state located very near the double-$J/\psi(1S)$ threshold which can be searched for experimentally.

In contrast to the works above, Ref. [165, 166] explains the double-$J/\psi(1S)$ data as cusps without nearby poles. This claim can be tested experimentally: if this explanation were correct, there should not be any narrow near threshold structure in the channel that generates the cusp, for that would call for a non-perturbative interaction in that channel as pointed out in Ref. [167].

Acknowledgement

The authors would like to thank Claude Amsler and Jean-Marc Richard for helpful input and discussions in the preparation of the review.

References

[1] N. Brambilla *et al.*, Eur. Phys. J. **C71**, 1534 (2011), [arXiv:1010.5827].

[2] H.-X. Chen *et al.*, Phys. Rept. **639**, 1 (2016), [arXiv:1601.02092].

[3] A. Ali, J. S. Lange and S. Stone, Prog. Part. Nucl. Phys. **97**, 123 (2017), [arXiv:1706.00610].

[4] R. F. Lebed, R. E. Mitchell and E. S. Swanson, Prog. Part. Nucl. Phys. **93**, 143 (2017), [arXiv:1610.04528].

[5] S. L. Olsen, T. Skwarnicki and D. Zieminska, Rev. Mod. Phys. **90**, 1, 015003 (2018), [arXiv:1708.04012].

[6] Y.-R. Liu *et al.*, Prog. Part. Nucl. Phys. **107**, 237 (2019), [arXiv:1903.11976].

[7] N. Brambilla *et al.*, Phys. Rept. **873**, 1 (2020), [arXiv:1907.07583].

[8] A. Esposito, A. Pilloni and A. D. Polosa, Phys. Rept. **668**, 1 (2017), [arXiv:1611.07920].

[9] F.-K. Guo *et al.*, Rev. Mod. Phys. **90**, 1, 015004 (2018), [arXiv:1705.00141].

[10] B. Aubert *et al.* (BaBar), Phys. Rev. Lett. **90**, 242001 (2003), [hep-ex/0304021].

[11] D. Besson *et al.* (CLEO), Phys. Rev. **D68**, 032002 (2003), [Erratum: Phys. Rev.D75,119908(2007)], [hep-ex/0305100].

[12] S. Godfrey, Phys. Lett. **B568**, 254 (2003), [hep-ph/0305122].

[13] H.-Y. Cheng and W.-S. Hou, Phys. Lett. **B566**, 193 (2003), [hep-ph/0305038].

[14] K. Terasaki, Phys. Rev. **D68**, 011501 (2003), [hep-ph/0305213].

[15] L. Maiani *et al.*, Phys. Rev. **D71**, 014028 (2005), [hep-ph/0412098].

[16] V. Dmitrasinovic, Phys. Rev. Lett. **94**, 162002 (2005).

[17] T. Barnes, F. E. Close and H. J. Lipkin, Phys. Rev. **D68**, 054006 (2003), [hep-ph/0305025].

[18] E. E. Kolomeitsev and M. F. M. Lutz, Phys. Lett. **B582**, 39 (2004), [hep-ph/0307133].

[19] A. Faessler *et al.*, Phys. Rev. **D76**, 014005 (2007), [arXiv:0705.0254].

[20] A. Faessler *et al.*, Phys. Rev. D **76**, 114008 (2007), [arXiv:0709.3946].

[21] M. F. M. Lutz and M. Soyeur, Nucl. Phys. **A813**, 14 (2008), [arXiv:0710.1545].

[22] L. Liu *et al.*, Phys. Rev. **D87**, 1, 014508 (2013), [arXiv:1208.4535].

[23] P. Colangelo and F. De Fazio, Phys. Lett. **B570**, 180 (2003), [hep-ph/0305140].

[24] X.-Y. Guo, Y. Heo and M. F. M. Lutz, Phys. Rev. **D98**, 1, 014510 (2018), [arXiv:1801.10122].

[25] V. Dmitrasinovic, Phys. Rev. D **86**, 016006 (2012).

[26] M.-L. Du *et al.*, Phys. Rev. Lett. **126**, 19, 192001 (2021), [arXiv:2012.04599].

[27] R. Aaij *et al.* (LHCb), Phys. Rev. **D94**, 7, 072001 (2016), [arXiv:1608.01289].

[28] R. Aaij *et al.* (LHCb), Phys. Rev. D **94**, 7, 072001 (2016), [arXiv:1608.01289].

[29] L. Gayer *et al.* (Hadron Spectrum), JHEP **07**, 123 (2021), [arXiv:2102.04973].

[30] M. Albaladejo *et al.*, Phys. Lett. **B767**, 465 (2017), [arXiv:1610.06727].

[31] M.-L. Du *et al.*, Phys. Rev. **D98**, 9, 094018 (2018), [arXiv:1712.07957].

[32] R. Aaij *et al.* (LHCb), Phys. Rev. D **102**, 112003 (2020), [arXiv:2009.00026].

[33] R. Aaij *et al.* (LHCb), Phys. Rev. Lett. **125**, 242001 (2020), [arXiv:2009.00025].

[34] M. Karliner and J. L. Rosner, Phys. Rev. D **102**, 9, 094016 (2020), [arXiv:2008.05993].

[35] X.-G. He, W. Wang and R. Zhu, Eur. Phys. J. C **80**, 11, 1026 (2020), [arXiv:2008.07145].

[36] Z.-G. Wang, Int. J. Mod. Phys. A **35**, 30, 2050187 (2020), [arXiv:2008.07833].

[37] R. Molina and E. Oset, Phys. Lett. B **811**, 135870 (2020), [arXiv:2008.11171].

[38] Y. Huang *et al.*, Eur. Phys. J. C **80**, 10, 973 (2020), [arXiv:2008.07959].

Downloaded from https://academic.oup.com/ptep/article/2022/8/083C01/6651666 by KIT Library user on 27 September 2022

[39] M.-Z. Liu, J.-J. Xie and L.-S. Geng, Phys. Rev. D **102**, 9, 091502 (2020), [arXiv:2008.07389].

[40] T. J. Burns and E. S. Swanson, Phys. Lett. B **813**, 136057 (2021), [arXiv:2008.12838].

[41] X.-H. Liu *et al.*, Eur. Phys. J. C **80**, 12, 1178 (2020), [arXiv:2008.07190].

[42] T. J. Burns and E. S. Swanson, Phys. Rev. D **103**, 1, 014004 (2021), [arXiv:2009.05352].

[43] S. K. Choi *et al.* (Belle), Phys. Rev. Lett. **91**, 262001 (2003), [hep-ex/0309032].

[44] B. Aubert *et al.* (BaBar), Phys. Rev. **D71**, 071103 (2005), [hep-ex/0406022].

[45] R. Aaij *et al.* (LHCb), Phys. Rev. Lett. **115**, 072001 (2015), [arXiv:1507.03414].

[46] R. Aaij *et al.* (LHCb), Phys. Rev. Lett. **122**, 22, 222001 (2019), [arXiv:1904.03947].

[47] R. Aaij *et al.* (LHCb), Phys. Rev. Lett. **110**, 222001 (2013), [arXiv:1302.6269].

[48] R. Aaij *et al.* (LHCb), Phys. Rev. **D92**, 1, 011102 (2015), [arXiv:1504.06339].

[49] T. Barnes and S. Godfrey, Phys. Rev. **D69**, 054008 (2004), [hep-ph/0311162].

[50] K. Abe *et al.* (Belle), Phys. Rev. Lett. **98**, 082001 (2007), [hep-ex/0507019].

[51] S. Uehara *et al.* (Belle), Phys. Rev. Lett. **96**, 082003 (2006), [hep-ex/0512035].

[52] R. Aaij *et al.* (LHCb), Phys. Rev. D **102**, 9, 092005 (2020), [arXiv:2005.13419].

[53] R. Aaij *et al.* (LHCb), JHEP **08**, 123 (2020), [arXiv:2005.13422].

[54] C. Hanhart *et al.*, Phys. Rev. D **76**, 034007 (2007), [arXiv:0704.0605].

[55] G. Barucca *et al.* (PANDA), Eur. Phys. J. A **55**, 3, 42 (2019), [arXiv:1812.05132].

[56] G. Barucca *et al.* (PANDA), Eur. Phys. J. A **57**, 6, 184 (2021), [arXiv:2101.11877].

[57] F.-K. Guo, Phys. Rev. Lett. **122**, 20, 202002 (2019), [arXiv:1902.11221].

[58] E. Braaten, L.-P. He and K. Ingles, Phys. Rev. D **100**, 3, 031501 (2019), [arXiv:1904.12915].

[59] S. Sakai, H.-J. Jing and F.-K. Guo, Phys. Rev. D **102**, 11, 114041 (2020), [arXiv:2008.10829].

[60] N. A. Tornqvist, Phys. Lett. **B590**, 209 (2004), [hep-ph/0402237].

[61] E. S. Swanson, Phys. Lett. **B588**, 189 (2004), [hep-ph/0311229].

[62] D. Gamermann and E. Oset, Phys. Rev. **D80**, 014003 (2009), [arXiv:0905.0402].

[63] Y.-b. Dong *et al.*, Phys. Rev. D **77**, 094013 (2008), [arXiv:0802.3610].

[64] Y. Dong *et al.*, Phys. Rev. D **79**, 094013 (2009), [arXiv:0903.5416].

[65] B. Aubert *et al.* (BaBar), Phys. Rev. **D71**, 031501 (2005), [hep-ex/0412051].

[66] L. Maiani, A. D. Polosa and V. Riquer, Phys. Lett. **B778**, 247 (2018), [arXiv:1712.05296].

[67] L. Maiani, A. D. Polosa and V. Riquer, Phys. Rev. D **102**, 3, 034017 (2020), [arXiv:2005.08764].

[68] C. Bignamini *et al.*, Phys. Rev. Lett. **103**, 162001 (2009), [arXiv:0906.0882].

[69] A. Esposito *et al.*, Eur. Phys. J. C **81**, 669 (2021), [arXiv:2006.15044].

[70] P. Artoisenet and E. Braaten, Phys. Rev. **D81**, 114018 (2010), [arXiv:0911.2016].

[71] E. Braaten *et al.*, Phys. Rev. D **103**, 7, L071901 (2021), [arXiv:2012.13499].

[72] F.-K. Guo *et al.*, JHEP **05**, 138 (2014), [arXiv:1403.4032].

[73] M. Albaladejo *et al.*, Chin. Phys. **C41**, 12, 121001 (2017), [arXiv:1709.09101].

[74] B. Aubert *et al.* (BaBar), Phys. Rev. Lett. **95**, 142001 (2005), [hep-ex/0506081].

[75] M. Ablikim *et al.* (BESIII), Phys. Rev. Lett. **118**, 9, 092001 (2017), [arXiv:1611.01317].

[76] M. Cleven *et al.*, Phys. Rev. **D90**, 7, 074039 (2014), [arXiv:1310.2190].

[77] C. Hanhart, Int. J. Mod. Phys. Conf. Ser. **46**, 1860004 (2018), [arXiv:1712.01136].

[78] C. Hanhart and E. Klempt (2019), [arXiv:1906.11971].

[79] T. Barnes, S. Godfrey and E. S. Swanson, Phys. Rev. D **72**, 054026 (2005), [hep-ph/0505002].

[80] L.-C. Gui *et al.*, Phys. Rev. D **98**, 1, 016010 (2018), [arXiv:1801.08791].

[81] F. E. Close and P. R. Page, Phys. Lett. **B628**, 215 (2005), [hep-ph/0507199].

[82] M. Berwein *et al.*, Phys. Rev. **D92**, 11, 114019 (2015), [arXiv:1510.04299].

[83] E. Kou and O. Pene, Phys. Lett. **B631**, 164 (2005), [hep-ph/0507119].

[84] Yu. S. Kalashnikova and A. V. Nefediev, Phys. Rev. **D77**, 054025 (2008), [arXiv:0801.2036].

[85] M. Ablikim *et al.* (BESIII), Phys. Rev. Lett. **111**, 24, 242001 (2013), [arXiv:1309.1896].

[86] M. B. Voloshin, Prog. Part. Nucl. Phys. **61**, 455 (2008), [arXiv:0711.4556].

[87] X. Li and M. B. Voloshin, Mod. Phys. Lett. **A29**, 12, 1450060 (2014), [arXiv:1309.1681].

[88] Q. Wang, C. Hanhart and Q. Zhao, Phys. Rev. Lett. **111**, 13, 132003 (2013), [arXiv:1303.6355].

[89] Y. Dong *et al.*, Phys. Rev. D **89**, 3, 034018 (2014), [arXiv:1310.4373].

[90] F.-K. Guo *et al.*, Phys. Lett. **B725**, 127 (2013), [arXiv:1306.3096].

[91] M. Ablikim *et al.* (BESIII), Phys. Rev. Lett. **112**, 9, 092001 (2014), [arXiv:1310.4101].

[92] Y. Dong *et al.*, Phys. Rev. D **90**, 7, 074032 (2014), [arXiv:1404.6161].

[93] Q. Wang *et al.*, Phys. Rev. **D89**, 3, 034001 (2014), [arXiv:1309.4303].

[94] V. Baru *et al.*, Phys. Rev. **D91**, 3, 034002 (2015), [arXiv:1501.02924].

[95] A. Ali *et al.*, Eur. Phys. J. **C78**, 1, 29 (2018), [arXiv:1708.04650].

[96] L. Maiani *et al.*, Phys. Rev. **D89**, 114010 (2014), [arXiv:1405.1551].

[97] K. Chilikin *et al.* (Belle), Phys. Rev. **D88**, 7, 074026 (2013), [arXiv:1306.4894].

[98] R. Aaij *et al.* (LHCb), Phys. Rev. Lett. **112**, 22, 222002 (2014), [arXiv:1404.1903].

[99] L. Maiani, A. D. Polosa and V. Riquer, Symmetry **13**, 5, 751 (2021), [arXiv:2103.14356].

[100] Y.-H. Chen *et al.*, Phys. Rev. **D99**, 7, 074016 (2019), [arXiv:1902.10957].

[101] G. Cotugno *et al.*, Phys. Rev. Lett. **104**, 132005 (2010), [arXiv:0911.2178].

[102] F.-K. Guo *et al.*, Phys. Rev. **D82**, 094008 (2010), [arXiv:1005.2055].

[103] L.-Y. Dai, J. Haidenbauer and U. G. Meissner, Phys. Rev. **D96**, 11, 116001 (2017), [arXiv:1710.03142].

Downloaded from https://academic.oup.com/ptep/article/2022/8/083C01/6651666 by KIT Library user on 27 September 2022

[104] J. He *et al.*, Eur. Phys. J. C **80**, 3, 246 (2020), [arXiv:1912.08420].

[105] F.-L. Wang and X. Liu, Phys. Rev. D **102**, 9, 094006 (2020), [arXiv:2008.13484].

[106] H.-W. Ke, X.-H. Liu and X.-Q. Li, Chin. Phys. C **44**, 9, 093104 (2020), [arXiv:2004.03167].

[107] J.-R. Zhang, Phys. Rev. D **102**, 5, 054006 (2020), [arXiv:2004.10985].

[108] F.-K. Guo, C. Hanhart and U.-G. Meissner, Phys. Lett. B **665**, 26 (2008), [arXiv:0803.1392].

[109] F.-K. Guo, C. Hanhart and U.-G. Meissner, Phys. Rev. Lett. **102**, 242004 (2009), [arXiv:0904.3338].

[110] M. Ablikim *et al.* (BESIII), Phys. Rev. Lett. **110**, 252001 (2013), [arXiv:1303.5949].

[111] M. Ablikim *et al.* (BESIII), Phys. Rev. Lett. **112**, 2, 022001 (2014), [arXiv:1310.1163].

[112] P. Krokovny *et al.* (Belle), Phys. Rev. **D88**, 5, 052016 (2013), [arXiv:1308.2646].

[113] A. Bondar *et al.* (Belle), Phys. Rev. Lett. **108**, 122001 (2012), [arXiv:1110.2251].

[114] A. Garmash *et al.* (Belle), Phys. Rev. Lett. **116**, 21, 212001 (2016), [arXiv:1512.07419].

[115] A. E. Bondar *et al.*, Phys. Rev. **D84**, 054010 (2011), [arXiv:1105.4473].

[116] Z.-M. Ding, H.-Y. Jiang and J. He, Eur. Phys. J. C **80**, 12, 1179 (2020), [arXiv:2011.04980].

[117] Y. Dong *et al.*, Phys. Rev. D **88**, 1, 014030 (2013), [arXiv:1306.0824].

[118] F. Goerke *et al.*, Phys. Rev. D **94**, 9, 094017 (2016), [arXiv:1608.04656].

[119] F. Goerke *et al.*, Phys. Rev. D **96**, 5, 054028 (2017), [arXiv:1707.00539].

[120] A. Ali *et al.*, Phys. Rev. **D91**, 1, 017502 (2015), [arXiv:1412.2049].

[121] M. B. Voloshin, Phys. Rev. **D84**, 031502 (2011), [arXiv:1105.5829].

[122] T. Mehen and J. W. Powell, Phys. Rev. **D84**, 114013 (2011), [arXiv:1109.3479].

[123] V. Baru *et al.*, JHEP **06**, 158 (2017), [arXiv:1704.07332].

[124] V. Baru *et al.*, Phys. Rev. **D99**, 9, 094013 (2019), [arXiv:1901.10319].

[125] T. Branz, T. Gutsche and V. E. Lyubovitskij, Phys. Rev. **D82**, 054025 (2010), [arXiv:1005.3168].

[126] P. Pakhlov, Phys. Lett. **B702**, 139 (2011), [arXiv:1105.2945].

[127] P. Pakhlov and T. Uglov, Phys. Lett. **B748**, 183 (2015), [arXiv:1408.5295].

[128] S. X. Nakamura and K. Tsushima, Phys. Rev. **D100**, 5, 051502 (2019), [arXiv:1901.07385].

[129] J.-Z. Wang *et al.*, Eur. Phys. J. C **80**, 11, 1040 (2020), [arXiv:2007.02263].

[130] M. Ablikim *et al.* (BESIII), Phys. Rev. Lett. **126**, 10, 102001 (2021), [arXiv:2011.07855].

[131] S. H. Lee, M. Nielsen and U. Wiedner, J. Korean Phys. Soc. **55**, 424 (2009), [arXiv:0803.1168].

[132] J. M. Dias, X. Liu and M. Nielsen, Phys. Rev. D **88**, 9, 096014 (2013), [arXiv:1307.7100].

[133] D. Ebert, R. N. Faustov and V. O. Galkin, Eur. Phys. J. C **58**, 399 (2008), [arXiv:0808.3912].

[134] J. Ferretti and E. Santopinto, JHEP **04**, 119 (2020), [arXiv:2001.01067].

[135] M. B. Voloshin, Phys. Lett. B **798**, 135022 (2019), [arXiv:1901.01936].

[136] D.-Y. Chen, X. Liu and T. Matsuki, Phys. Rev. Lett. **110**, 23, 232001 (2013), [arXiv:1303.6842].

[137] L. Meng, B. Wang and S.-L. Zhu, Phys. Rev. D **102**, 11, 111502 (2020), [arXiv:2011.08656].

[138] P. G. Ortega, D. R. Entem and F. Fernandez, Phys. Lett. B **818**, 136382 (2021), [arXiv:2103.07871].

[139] Z. Yang *et al.*, Phys. Rev. D **103**, 7, 074029 (2021), [arXiv:2011.08725].

[140] B. Wang, L. Meng and S.-L. Zhu, Phys. Rev. D **103**, 2, L021501 (2021), [arXiv:2011.10922].

[141] R. Aaij *et al.* (LHCb), Phys. Rev. Lett. **127**, 8, 082001 (2021), [arXiv:2103.01803].

[142] R. M. Albuquerque, S. Narison and D. Rabetiarivony, Phys. Rev. D **103**, 7, 074015 (2021), [arXiv:2101.07281].

[143] Z.-H. Guo and J. A. Oller, Phys. Rev. D **103**, 5, 054021 (2021), [arXiv:2012.11904].

[144] N. Ikeno, R. Molina and E. Oset, Phys. Lett. B **814**, 136120 (2021), [arXiv:2011.13425].

[145] M. Cleven *et al.*, Phys. Rev. **D92**, 1, 014005 (2015), [arXiv:1505.01771].

[146] R. Aaij *et al.* (LHCb) (2021), [arXiv:2109.01038].

[147] R. Aaij *et al.* (LHCb), Sci. Bull. **65**, 23, 1983 (2020), [arXiv:2006.16957].

[148] J. P. Ader, J. M. Richard and P. Taxil, Phys. Rev. D **25**, 2370 (1982).

[149] Y. Iwasaki, Prog. Theor. Phys. **54**, 492 (1975).

[150] L. Maiani, Sci. Bull. **65**, 1949 (2020), [arXiv:2008.01637].

[151] K.-T. Chao and S.-L. Zhu, Sci. Bull. **65**, 23, 1952 (2020), [arXiv:2008.07670].

[152] J.-M. Richard, Sci. Bull. **65**, 1954 (2020), [arXiv:2008.01962].

[153] R. N. Faustov, V. O. Galkin and E. M. Savchenko, Phys. Rev. D **102**, 11, 114030 (2020), [arXiv:2009.13237].

[154] J. F. Giron and R. F. Lebed, Phys. Rev. D **102**, 7, 074003 (2020), [arXiv:2008.01631].

[155] X. Jin *et al.*, Eur. Phys. J. C **80**, 11, 1083 (2020), [arXiv:2006.13745].

[156] Q.-F. Lü, D.-Y. Chen and Y.-B. Dong, Eur. Phys. J. C **80**, 9, 871 (2020), [arXiv:2006.14445].

[157] Z.-H. Guo and J. A. Oller, Phys. Rev. D **103**, 3, 034024 (2021), [arXiv:2011.00978].

[158] M. Karliner and J. L. Rosner, Phys. Rev. D **102**, 11, 114039 (2020), [arXiv:2009.04429].

[159] B.-D. Wan and C.-F. Qiao, Phys. Lett. B **817**, 136339 (2021), [arXiv:2012.00454].

[160] B.-C. Yang, L. Tang and C.-F. Qiao, Eur. Phys. J. C **81**, 4, 324 (2021), [arXiv:2012.04463].

[161] R. M. Albuquerque *et al.*, Phys. Rev. D **102**, 9, 094001 (2020), [arXiv:2008.01569].

[162] X.-K. Dong *et al.*, Phys. Rev. Lett. **126**, 13, 132001 (2021), [arXiv:2009.07795].

[163] C. Gong *et al.* (2020), [arXiv:2011.11374].

[164] Z.-R. Liang, X.-Y. Wu and D.-L. Yao (2021), [arXiv:2104.08589].

[165] J.-Z. Wang *et al.*, Phys. Rev. D **103**, 7, 071503 (2021), [arXiv:2008.07430].

[166] J.-Z. Wang, X. Liu and T. Matsuki, Phys. Lett. B **816**, 136209 (2021), [arXiv:2012.03281].

[167] F.-K. Guo *et al.*, Phys. Rev. D **91**, 5, 051504 (2015), [arXiv:1411.5584].

Downloaded from https://academic.oup.com/ptep/article/2022/8/083C01/6651666 by KIT Library user on 27 September 2022

80. Baryon Decay Parameters

Revised August 2019 by E.D. Commins (UC Berkeley).

80.1 Baryon semileptonic decays

The typical spin-1/2 baryon semileptonic decay is described by a matrix element, the hadronic part of which may be written as:

$$\overline{B}_f \left[f_1(q^2)\gamma_\lambda + i\, f_2(q^2)\sigma_{\lambda\mu}q^\mu + g_1(q^2)\gamma_\lambda\gamma_5 + g_3(q^2)\gamma_5 q_\lambda \right] B_i \ . \tag{80.1}$$

Here B_i and $\overline{B}_f$ are spinors describing the initial and final baryons, and $q = p_i - p_f$, while the terms in f_1, f_2, g_1, and g_3 account for vector, induced tensor ("weak magnetism"), axial vector, and induced pseudoscalar contributions [1]. Second-class current contributions are ignored here. In the limit of zero momentum transfer, f_1 reduces to the vector coupling constant g_V, and g_1 reduces to the axial-vector coupling constant g_A. The latter coefficients are related by Cabibbo's theory [2], generalized to six quarks (and three mixing angles) by Kobayashi and Maskawa [3]. The g_3 term is negligible for transitions in which an $e^\pm$ is emitted, and gives a very small correction, which can be estimated by PCAC [4], for $\mu^\pm$ modes. Recoil effects include weak magnetism, and are taken into account adequately by considering terms of first order in

$$\delta = \frac{m_i - m_f}{m_i + m_f} \ , \tag{80.2}$$

where m_i and m_f are the masses of the initial and final baryons.

The experimental quantities of interest are the total decay rate, the lepton-neutrino angular correlation, the asymmetry coefficients in the decay of a polarized initial baryon, and the polarization of the decay baryon in its own rest frame for an unpolarized initial baryon. Formulae for these quantities are derived by standard means [5] and are analogous to formulae for nuclear beta decay [6]. We use the notation of Ref. [6] in the Listings for neutron beta decay. For comparison with experiments at higher q^2, it is necessary to modify the form factors at $q^2 = 0$ by a "dipole" q^2 dependence, and for high-precision comparisons to apply appropriate radiative corrections [7].

The ratio g_A/g_V may be written as

$$g_A/g_V = |\, g_A/g_V \,|\, e^{i\phi_{AV}} \ . \tag{80.3}$$

The presence of a "triple correlation" term in the transition probability, proportional to $\mathrm{Im}(g_A/g_V)$ and of the form

$$\boldsymbol{\sigma_i} \cdot (\boldsymbol{p_\ell} \times \boldsymbol{p_\nu}) \tag{80.4}$$

for initial baryon polarization or

$$\boldsymbol{\sigma_f} \cdot (\boldsymbol{p_\ell} \times \boldsymbol{p_\nu}) \tag{80.5}$$

for final baryon polarization, would indicate failure of time-reversal invariance. The phase angle ϕ has been measured precisely only in neutron decay (and in ^{19}Ne nuclear beta decay), and the results are consistent with T invariance.

80.2 Hyperon nonleptonic decays

The amplitude for a spin-1/2 hyperon decaying into a spin-1/2 baryon and a spin-0 meson may be written in the form

$$M = G_F\, m_\pi^2 \cdot \overline{B}_f\, (A - B\gamma_5)\, B_i \ , \tag{80.6}$$

where A and B are constants [1]. The transition rate is proportional to

$$\begin{aligned} R = 1 &+ \gamma\, \widehat{\boldsymbol{\omega}}_f \cdot \widehat{\boldsymbol{\omega}}_i + (1-\gamma)(\widehat{\boldsymbol{\omega}}_f \cdot \widehat{\mathbf{n}})(\widehat{\boldsymbol{\omega}}_i \cdot \widehat{\mathbf{n}}) \\ &+ \alpha(\widehat{\boldsymbol{\omega}}_f \cdot \widehat{\mathbf{n}} + \widehat{\boldsymbol{\omega}}_i \cdot \widehat{\mathbf{n}}) + \beta\widehat{\mathbf{n}} \cdot (\widehat{\boldsymbol{\omega}}_f \times \widehat{\boldsymbol{\omega}}_i) \ , \end{aligned} \tag{80.7}$$

where $\widehat{\mathbf{n}}$ is a unit vector in the direction of the final baryon momentum, and $\widehat{\boldsymbol{\omega}}_i$ and $\widehat{\boldsymbol{\omega}}_f$ are unit vectors in the directions of the initial and final baryon spins. (The sign of the last term in the above equation was incorrect in our 1988 and 1990 editions.) The parameters α, β, and γ are defined as

$$\begin{aligned} \alpha &= 2\,\mathrm{Re}(s^*p)/(\,|\,s\,|^2 + |\,p\,|^2) \ , \\ \beta &= 2\,\mathrm{Im}(s^*p)/(\,|\,s\,|^2 + |\,p\,|^2) \ , \\ \gamma &= (\,|\,s\,|^2 - |\,p\,|^2)/(\,|\,s\,|^2 + |\,p\,|^2) \ , \end{aligned} \tag{80.8}$$

where $s = A$ and $p = |\,\mathbf{p}_f\,|\,B/(E_f + m_f)$; here E_f and $\mathbf{p}_f$ are the energy and momentum of the final baryon. The parameters α, β, and γ satisfy

$$\alpha^2 + \beta^2 + \gamma^2 = 1 \tag{80.9}$$

If the hyperon polarization is $\mathbf{P}_Y$, the polarization $\mathbf{P}_B$ of the decay baryons is

$$\mathbf{P}_B = \frac{(\alpha + \mathbf{P}_Y \cdot \widehat{\mathbf{n}})\widehat{\mathbf{n}} + \beta(\mathbf{P}_Y \times \widehat{\mathbf{n}}) + \gamma\widehat{\mathbf{n}} \times (\mathbf{P}_Y \times \widehat{\mathbf{n}})}{1 + \alpha\mathbf{P}_Y \cdot \widehat{\mathbf{n}}} \ . \tag{80.10}$$

Here $\mathbf{P}_B$ is defined in the rest system of the baryon, obtained by a Lorentz transformation along $\widehat{\mathbf{n}}$ from the hyperon rest frame, in which $\widehat{\mathbf{n}}$ and $\mathbf{P}_Y$ are defined.

An additional useful parameter ϕ is defined by

$$\beta = (1 - \alpha^2)^{1/2}\, \sin\phi \ . \tag{80.11}$$

In the Listings, we compile α and ϕ for each decay, since these quantities are most closely related to experiment and are essentially uncorrelated. When necessary, we have changed the signs of reported values to agree with our sign conventions. In the Baryon Summary Table, we give α, ϕ, and Δ (defined below) with errors, and also give the value of γ without error.

Time-reversal invariance requires, in the absence of final-state interactions, that s and p be relatively real, and therefore that $\beta = 0$. However, for the decays discussed here, the final-state interaction is strong. Thus

$$s = |\,s\,|\,e^{i\delta_s} \text{ and } p = |\,p\,|\,e^{i\delta_p} \ , \tag{80.12}$$

where δ_s and δ_p are the pion-baryon s- and p-wave strong interaction phase shifts. We then have

$$\beta = \frac{-2\,|\,s\,|\,|\,p\,|}{|\,s\,|^2 + |\,p\,|^2}\, \sin(\delta_s - \delta_p) \ . \tag{80.13}$$

One also defines $\Delta = -\tan^{-1}(\beta/\alpha)$. If T invariance holds, $\Delta = \delta_s - \delta_p$. For $\Lambda \to p\pi^-$ decay, the value of Δ may be compared with the s- and p-wave phase shifts in low-energy $\pi^- p$ scattering, and the results are consistent with T invariance.

See also the note on "Radiative Hyperon Decays" in this *Review*.

References

[1] E. Commins and P. Bucksbaum, *Weak Interactions of Leptons and Quarks* (1983), ISBN 978-0-521-27370-1, (Cambridge, USA: University Press, 473p.).

[2] N. Cabibbo, Phys. Rev. Lett. **10**, 531 (1963).

[3] M. Kobayashi and T. Maskawa, Prog. Theor. Phys. **49**, 652 (1973).

[4] M. Goldberger and S. Treiman, Phys. Rev. **111**, 354 (1958).

[5] P. Frampton and W.-K. Tung, Phys. Rev. D **3**, 1114 (1971).

[6] J. Jackson, S. Treiman and H. Wyld, Nucl. Phys. **4**, 206 (1957).

[7] Y. Yokoo, S. Suzuki and M. Morita, Prog. Theor. Phys. **50**, 1894 (1973).

Downloaded from https://academic.oup.com/ptep/article/2022/8/083C01/6651666 by KIT Library user on 27 September 2022

81. N and Δ Resonances

Revised August 2019 by V.D. Burkert (Jefferson Lab), V. Crede (Florida State U.), U. Thoma (Bonn U.), L. Tiator (KPH, JGU Mainz) and R.L. Workman (George Washington U.).

81.1 Introduction

The excited states of the nucleon have been studied in a large number of formation and production experiments. Until recently, the Breit-Wigner masses and widths, the pole positions, and the elasticities of the N and Δ resonances in the Baryon Summary Table came largely from partial-wave analyses of πN total, elastic, and charge-exchange scattering data. The most comprehensive analyses were carried out by the Karlsruhe-Helsinki (KH80) [1], Carnegie Mellon-Berkeley (CMB80) [2], and George Washington U (GWU) [3] groups. Partial-wave analyses have also been performed on much smaller πN reaction data sets to get ηN, $K\Lambda$, and $K\Sigma$ branching fractions (see the Listings for references). Other branching fractions come from analyses of $\pi N \to \pi\pi N$ data.

In recent years, a large amount of data on photoproduction of many final states has been accumulated, and these data are beginning to tell us much about the properties of baryon resonances. A survey of data on photoproduction can be found in the proceedings of recent conferences [4] and workshops [5], and in recent reviews [6, 7].

81.2 Naming scheme for baryon resonances

In the past, when nearly all resonance information came from elastic πN scattering, it was common to label resonances with the incoming partial wave $L_{2I,2J}$, as in $\Delta(1232)P_{33}$ and $N(1680)F_{15}$. However, most recent information has come from γN experiments. Therefore, we have replaced $L_{2I,2J}$ with the spin-parity J^P of the state, as in $\Delta(1232)3/2^+$ and $N(1680)5/2^+$; this name gives intrinsic properties of the resonance that are independent of the specific particles and reactions used to study them. This applies equally to all baryons, including Ξ resonances and charm baryons that are not produced in formation experiments. We do not, however, attach the mass or spin-parity to the names of the ground-state ("stable") baryons $N, \Lambda, \Sigma, \Xi, \Omega, \Lambda_c, \cdots$.

81.3 Using the N and Δ listings

Tables 81.1 and 81.2 list all the N and Δ entries in the Baryon Listings and give our evaluation of the overall status and the status channel by channel. Only the established resonances (overall status 3 or 4 stars) are promoted to the Baryon Summary Table. We long ago omitted from the Listings information from old analyses, prior to KH80 and CMB80, which can be found in earlier editions. A rather complete survey of older results was given in our 1982 edition [8].

As a rule, we award an overall status **** or *** only to those resonances which are derived from analyses of data sets that include precision differential cross sections and polarization observables, and are confirmed by independent analyses. All other signals are given ** or * status. New results that are not accompanied by proper error evaluation are less valuable for evaluating star ratings. The following criteria are guidelines for future error analysis.

1. Uncertainties in resonance parameters: The publication should have a detailed discussion on how the uncertainties of parameters were estimated. This requires that the error estimates go beyond the simple fit error as e.g. given by MINUIT, and the robustness of the results should be demonstrated.

2. Fit quality: Concrete measures for the fit quality should be provided. The reduced global χ^2 value of the fit, while useful, is insufficient. Other possibilities include quoting variations of local χ^2 values in kinematic regions where evidence for new resonances, or significantly improved information on resonance parameters, is claimed.

3. Weight factors in observables: Analyses sometimes use weight factors for certain data sets to either increase or reduce their impact on the results. This has been particularly important when polarization observables are involved, which often are sensitive to resonance amplitudes through interferences, but usually have much poorer statistics than differential cross section data. To evaluate sensitivities, the resulting resonance parameters should be checked against variations of the specific weight factors.

Table 81.1: The status of the N resonances and their decays. Sub-threshold decay modes are omitted. Only resonances with an overall status of *** or **** are included in the main Baryon Summary Table.

			Status as seen in									
Particle	J^P	overall	$N\gamma$	$N\pi$	$\Delta\pi$	$N\sigma$	$N\eta$	ΛK	ΣK	$N\rho$	$N\omega$	$N\eta'$
N	$1/2^+$	****										
$N(1440)$	$1/2^+$	****	****	****	****	***						
$N(1520)$	$3/2^-$	****	****	****	****	**	****					
$N(1535)$	$1/2^-$	****	****	****	***	*	****					
$N(1650)$	$1/2^-$	****	****	****	***	*	****	*				
$N(1675)$	$5/2^-$	****	****	****	****	***	*	*	*			
$N(1680)$	$5/2^+$	****	****	****	****	***	*	*	*			
$N(1700)$	$3/2^-$	***	**	***	***	*	*			*		
$N(1710)$	$1/2^+$	****	****	****	*		***	**	*	*	*	
$N(1720)$	$3/2^+$	****	****	****	***	*	*	****	*	*	*	
$N(1860)$	$5/2^+$	**	*	**		*	*					
$N(1875)$	$3/2^-$	***	**	**	*	**	*	*	*	*	*	
$N(1880)$	$1/2^+$	***	**	*	**	*	*	**	**		**	
$N(1895)$	$1/2^-$	****	****	*	*	*	****	**	**	*	*	****
$N(1900)$	$3/2^+$	****	****	**	**	*	*	**	**		*	**
$N(1990)$	$7/2^+$	**	**	**			*	*	*			
$N(2000)$	$5/2^+$	**	**	*	**	*	*				*	
$N(2040)$	$3/2^+$	*		*								
$N(2060)$	$5/2^-$	***	***	**	*	*	*	*	*	*	*	
$N(2100)$	$1/2^+$	***	**	***	**	**	*	*		*	*	**
$N(2120)$	$3/2^-$	***	***	**	**	**		**	*		*	*
$N(2190)$	$7/2^-$	****	****	****	****	**	*	**	*	*	*	
$N(2220)$	$9/2^+$	****	**	****			*	*	*			
$N(2250)$	$9/2^-$	****	**	****			*	*	*			
$N(2300)$	$1/2^+$	**		**								
$N(2570)$	$5/2^-$	**		**								
$N(2600)$	$11/2^-$	***		***								
$N(2700)$	$13/2^+$	**		**								

**** Existence is certain.
*** Existence is very likely.
** Evidence of existence is fair.
* Evidence of existence is poor.

Table 81.2: The status of the Δ resonances and their decays. Sub-threshold decay modes are omitted. Only resonances with an overall status of *** or **** are included in the main Baryon Summary Table.

			Status as seen in					
Particle	J^P	overall	$N\gamma$	$N\pi$	$\Delta\pi$	ΣK	$N\rho$	$\Delta\eta$
$\Delta(1232)$	$3/2^+$	****	****	****				
$\Delta(1600)$	$3/2^+$	****	****	***	****			
$\Delta(1620)$	$1/2^-$	****	****	****	****			
$\Delta(1700)$	$3/2^-$	****	****	****	****	*	*	
$\Delta(1750)$	$1/2^+$	*	*	*		*		
$\Delta(1900)$	$1/2^-$	***	***	***	*	**	*	
$\Delta(1905)$	$5/2^+$	****	****	****	**	*	*	**
$\Delta(1910)$	$1/2^+$	****	***	****	**	**		*
$\Delta(1920)$	$3/2^+$	***	***	***	***	**		**
$\Delta(1930)$	$5/2^-$	***	*	***	*	*		
$\Delta(1940)$	$3/2^-$	**	*	**	*			*
$\Delta(1950)$	$7/2^+$	****	****	****	**	***		
$\Delta(2000)$	$5/2^+$	**	*	**	*		*	
$\Delta(2150)$	$1/2^-$	*		*				
$\Delta(2200)$	$7/2^-$	***	***	**	***	**		
$\Delta(2300)$	$9/2^+$	**		**				
$\Delta(2350)$	$5/2^-$	*		*				
$\Delta(2390)$	$7/2^+$	*		*				
$\Delta(2400)$	$9/2^-$	**	**	**				
$\Delta(2420)$	$11/2^+$	****	*	****				
$\Delta(2750)$	$13/2^-$	**		**				
$\Delta(2950)$	$15/2^+$	**		**				

**** Existence is certain.
*** Existence is very likely.
** Evidence of existence is fair.
* Evidence of existence is poor.

Claims of evidence for new baryon states must be based on a sufficiently complete set of partial waves in the fit. The robustness of signals must be demonstrated, e.g. by examining the effect of

Downloaded from https://academic.oup.com/ptep/article/2022/8/083C01/6651666 by KIT Library user on 27 September 2022

higher partial waves in the fit.

81.4 Properties of resonances

Resonances are defined by poles of the S-matrix, whether in scattering, production or decay matrix elements. These are poles in the complex plane in s, as discussed in the new review on *Resonances*. As is traditional, we quote here the pole positions in the complex energy $w = \sqrt{s}$ plane. Crucially, the position of the pole of the S-matrix is independent of the process, and the production and decay properties factorize. This is the rationale for listing the pole position first for each resonance. These key properties of the S-matrix pole are in contrast to other quantities related to resonance phenomena, such as Breit-Wigner parameters or any K-matrix pole. Breit-Wigner parameters depend on the formalism used, such as angular-momentum barrier factors, or cut-off parameters, and the assumed or modeled background. However, the accurate determination of pole parameters from the analysis of data on the real energy axis is not necessarily simple, or even straightforward. It requires the implementation of the correct analytic structure of the relevant (often coupled) channels.

In principle, there are two ways to extract pole parameters from experimental data: (i) analytic continuation of theoretical single- or multi-channel models into the complex energy plane or (ii) local expansions of the partial-wave T-matrix amplitudes in the complex energy plane in the vicinity of a pole.

At present, poles are usually extracted using the first method [9–14], but considerable effort has been put into the development of alternate approaches, such as the speed plot [15], time delay [16], N/D method [17], regularization procedure [18], or Padè approximation [19].

Methods of the second type are based on the idea to use first or higher-order derivatives in energy to reduce the importance of, or totally eliminate, the background contribution. One either has to model the background contribution and introduce model dependence, or one is faced with numerical derivatives of single-energy data. In both cases, one reaches almost unsurmountable difficulties.

An alternate way to extract pole parameters from partial waves has been proposed by introducing a Laurent+Pietarinen (L+P) expansion [20–22]

$$T(W) = \sum_{i=1}^{N} \frac{Res_i}{W - W_i} + \sum_{j=1}^{M} \sum_{n=0}^{n_{max}} c_n^j \left(\frac{\alpha_j - \sqrt{x_j - W}}{\alpha_j + \sqrt{x_j - W}}\right)^n , \quad (81.1)$$

where $T(W)$ is a given partial wave amplitude, W_i and Res_i are the N complex pole positions and residues. The background is parameterized with M Pietarinen functions, where α_j are positive range parameters and x_j are real or complex branch points; c_n^j are real expansion coefficients.

The main idea of this procedure is to find the simplest analytic function, with well-defined poles and cuts, regardless of whether they are generated by a theoretical model or some energy-independent procedure. Instead of searching for the function which reproduces the input amplitudes over the complete complex energy plane, on all Riemann sheets, a representation is searched only in a limited complex energy range, near the real axis, which is defined by the radius of convergence of the Laurent decomposition, and which contains the input amplitudes. All details are found in Ref. [21]. Applications of the method can be found in [20–27].

81.5 Photoproduction

A new approach to the nucleon excitation spectrum is provided by dedicated facilities at the Universities of Bonn, Grenoble, and Mainz, and at the national laboratories Jefferson Lab in the US and SPring-8 in Japan. High-precision cross sections and polarization observables for the photoproduction of pseudoscalar mesons provide a data set that is approaching a "complete experiment," one that fully constrains the four complex amplitudes describing the spin-structure of the reaction [28]. A large number of photoproduction reactions has been studied.

In pseudoscalar meson photoproduction, the four independent helicity amplitudes can be expressed in terms of the four CGLN [29] amplitudes allowed by Lorentz and gauge invariance. These amplitudes can be expanded in a series of electric and magnetic multipoles. Except for $J = 1/2$, one electric and one magnetic multipole contributes to each J^P combination.

For a given state, these two amplitudes determine the resonance photo-decay helicity amplitudes $A_{1/2}$ and $A_{3/2}$. As described below, this resonance extraction has been carried out either assuming a Breit-Wigner resonance or at the pole.

If a Breit-Wigner parametrization is used, the $N\gamma$ partial width, Γ_γ, is given in terms of the helicity amplitudes $A_{1/2}$ and $A_{3/2}$ by

$$\Gamma_\gamma = \frac{k_{\rm BW}^2}{\pi} \frac{2m_N}{(2J+1)m_{\rm BW}} \left(|A_{1/2}|^2 + |A_{3/2}|^2 \right) . \quad (81.2)$$

Here m_N and $m_{\rm BW}$ are the nucleon and resonance masses, J is the resonance spin, and $k_{\rm BW}$ is the photon c.m. decay momentum. Most earlier analyses have provided these real quantities $A_{1/2}$ and $A_{3/2}$.

More recent studies have quoted related complex quantities, evaluated at the T-matrix pole. These complex helicity amplitudes, $\tilde{A}_{1/2}$ and $\tilde{A}_{3/2}$, can be cast onto the form

$$\tilde{A}_h = \sqrt{\frac{\pi(2J+1)w_{\rm pole}}{m_N k_{\rm pole}^2}} \frac{Res(T_h(\gamma N \to N\, b))}{\sqrt{Res(T\,(N\, b \to N\, b))}} \quad (81.3)$$

where the residues (Res) are evaluated at the pole position, $w_{\rm pole}$, and $k_{\rm pole}^2 = (w_{\rm pole}^2 - m_N^2)^2/4w_{\rm pole}^2$ [30]. For Breit-Wigner amplitudes, $w_{\rm pole} = m_{\rm BW}$ and $\tilde{A}_h = A_h$. Similar relations for the photo and electro couplings at the pole position can be found in [31,32].

The determination of eight real numbers from four complex amplitudes (with one overall phase undetermined) requires at least seven independent measurements. At least one further measurement is required to resolve discrete ambiguities that result from the fact that data are proportional to squared amplitudes. Photon beams and nucleon targets can be polarized (with linear or circular polarization $P_\perp$, $P_\odot$ and $\vec{T}$, respectively); the recoil polarization of the outgoing baryon $\vec{R}$ can be measured. The experiments can be divided into three classes: (1) the beam and target are polarized (BT); (2) the beam is polarized and the recoil baryon polarization is measured (BR); (3) the target is polarized and the recoil polarization is measured (TR). Different sign conventions are used in the literature, as summarized in [33].

One of the best studied reactions is $\gamma p \to \Lambda K^+$. Published data include differential cross sections, the beam asymmetry Σ, the target asymmetry T, the recoil polarization P, and the BR double-polarization variables $C_{x'}, C_{z'}, O_{x'}$, and $O_{z'}$. For the photoproduction of pions and etas, off proton and neutron targets, differential cross sections, single- and double-polarization asymmetries have been measured, mainly for pions.

81.6 Electroproduction

Electroproduction of mesons provides information on the internal structure of resonances. The helicity amplitudes are functions of the (squared) momentum transfer $Q^2 = -(e-e')^2$, where e and e' are the 4-momenta of the incident and scattered electron, and a third amplitude, $S_{1/2}$, measures the resonance response to the longitudinal component of the virtual photon. Most data stem from the reactions $e^-p \to e^-\, n\pi^+$ and $e^-p \to e^-\, p\pi^0$ but also the reactions $e^-p \to e^-\, p\eta$, $e^-p \to e^-\, p\pi^+\pi^-$, and $e^-p \to e^-\, \Lambda(\Sigma^0)K^+$ have been studied. The data and their interpretation are reviewed in Refs. [34,35].

The transition to the $\Delta(1232)3/2^+$ is often quantified in terms of the magnetic dipole transition moment M_{1+} (or the magnetic transition form factor $G^*_{M,Ash}(Q^2)$) [36], and the electric and scalar quadrupole transition moments E_{1+} and S_{1+}. Figure 81.1 shows the strength of the $p \to \Delta^+$ transition plotted versus the photon virtuality Q^2. At $Q^2 = 0$, M_{1+} dominates the resonance transition strength. The two amplitudes E_{1+} and S_{1+} imply a quadrupole deformation of the transition to the lowest excited state. The magnitude of $R_{EM} = E_{1+}/M_{1+}$ remains nearly constant, while the magnitude of $R_{SM} = S_{1+}/M_{1+}$ increases rapidly up to 25% at the highest Q^2 value.

Downloaded from https://academic.oup.com/ptep/article/2022/8/083C01/6651666 by KIT Library user on 27 September 2022

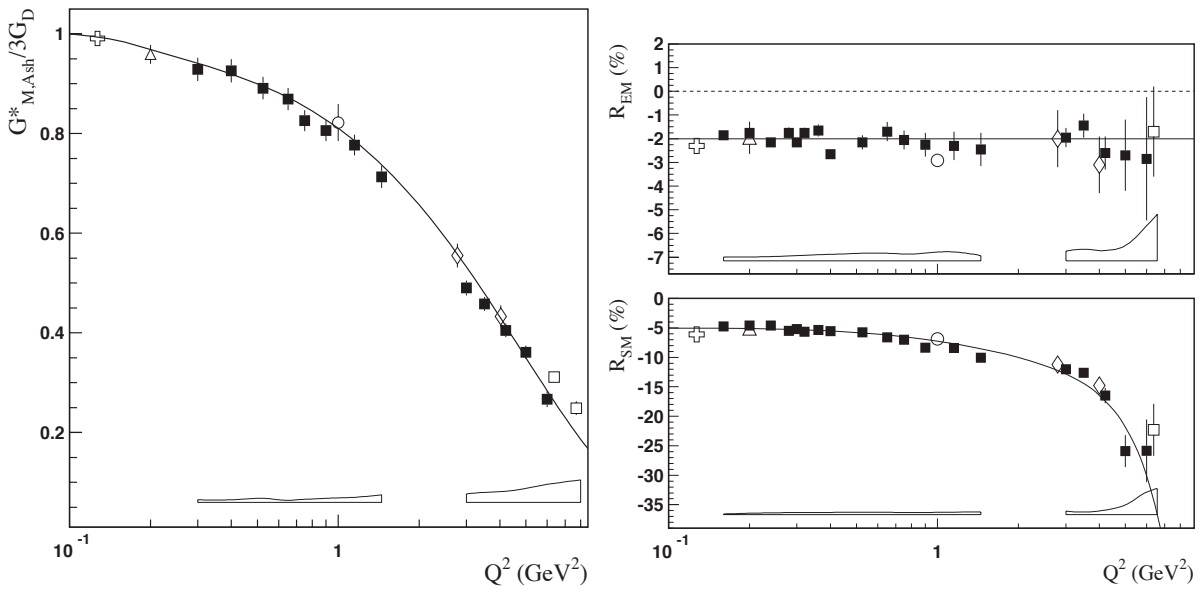

Figure 81.1: Left: The magnetic transition form factor for the $\gamma^* p \to \Delta^+(1232)$ transition versus the photon virtuality Q^2. Right: The electric and scalar quadrupole ratios R_{EM} and R_{SM}. The different symbols are results from different experiments at JLab (squares, diamonds, circle) and MAMI (triangle, cross). The boxes near the horizontal axis indicate model uncertainties of the squares. Curves to guide the eyes.

Figure 81.2 shows the transverse and scalar helicity amplitudes for the $N(1440)1/2^+$, $N(1520)3/2^-$, and $N(1535)1/2^-$ resonances from JLab [34]. Similar results have been achieved at Mainz [35]. For the states $N(1440)1/2^+$ and $N(1520)3/2^-$, helicity amplitudes and $\pi\Delta$ and ρp decays were determined at JLab in an analysis of $\pi^+\pi^- p$ electroproduction [37]. The data show distinctly different Q^2 dependencies that indicate different internal structures.

The $N(1520)3/2^-$ helicity amplitudes reveal the dominance of its three-quark nature: the $A_{3/2}$ amplitude is large at the photon point and decreases rapidly $\sim Q^{-5}$ with increasing Q^2; $A_{1/2}$ is small at the photon point, increases rapidly with Q^2 and then falls off with $\sim Q^{-3}$. Quantitative agreement with the data is, however, achieved only when meson cloud effects are included.

At high Q^2, both amplitudes for $N(1440)1/2^+$ are qualitatively described by light front quark models [38]: at short distances the resonance behaves as expected from a radial excitation of the nucleon. On the other hand, $A_{1/2}$ changes sign at about $0.6\,\mathrm{GeV}^2$. This remarkable behavior has not been observed before for any nucleon form factor or transition amplitude. Obviously, an important change in the structure occurs when the resonance is probed as a function of Q^2.

The Q^2 dependence of $A_{1/2}$ of the $N(1535)1/2^-$ resonance exhibits the expected Q^{-3} dependence, except for small Q^2 values where meson cloud effects set in.

Figure 81.3 shows the transverse and scalar amplitudes for three states in the 3rd nucleon resonance region, the $\Delta(1620)1/2^-$, the $N(1675)5/2^-$ and $N(1680)5/2^+$. The latter two states have nearly degenerate masses and are parity partners. In the quark model picture, the transverse amplitudes for $N(1675)5/2^-$ on the proton are suppressed due to the Moorhouse selection rule, allowing for a quantitative evaluation of the meson-baryon contributions. The data show significant meson-baryon strength in the $A_{1/2}$ amplitude even at quite high Q^2, while $A_{3/2}$ drops much faster with Q^2. $N(1680)5/2^+$ shows qualitatively the features predicted in constituent quark models, a dominant $A_{3/2}$ at the real photon point that drops rapidly with increasing Q^2, while $A_{1/2}$ becomes the dominant contribution at high Q^2, indicating a switch of the helicity structure in the resonance transition at short distances.

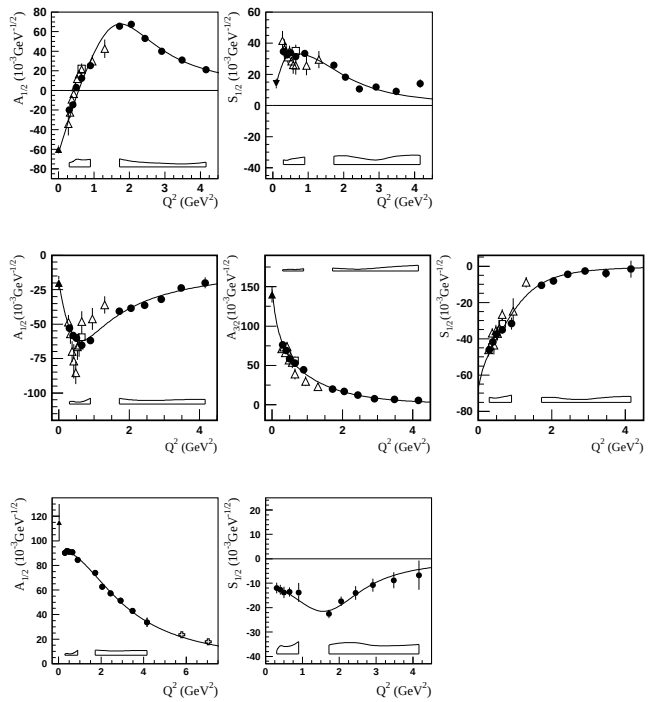

Figure 81.2: Transverse and scalar (longitudinal) helicity amplitudes for $\gamma p \to N(1440)1/2^+$ (top), $\gamma p \to N(1520)3/2^-$ (center), and $\gamma p \to N(1535)1/2^-$ (bottom) as extracted from the JLab/-CLAS data in $n\pi^+$ production (full circles), MAMI/A1 data in $p\pi^0$ production (full down triangle), in $p\pi^+\pi^-$ (open triangles), and combined single and double pion production (open squares). The solid triangle is the PDG 2014 value at $Q^2 = 0$. The open boxes are the model uncertainties of the full circles.

Downloaded from https://academic.oup.com/ptep/article/2022/8/083C01/6651666 by KIT Library user on 27 September 2022

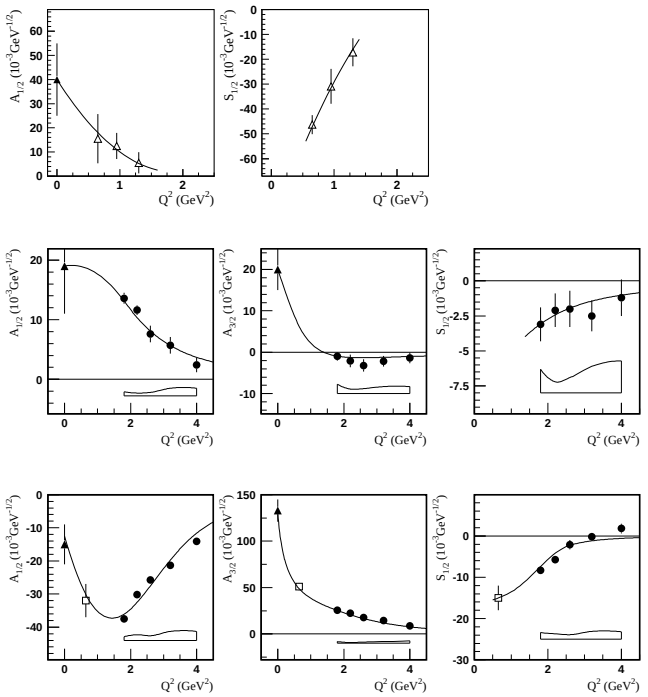

Figure 81.3: Transverse and scalar helicity amplitudes for $\gamma p \to \Delta(1620)1/2^-$ (top), $\gamma p \to N(1675)5/2^-$ (center), and $\gamma p \to N(1680)5/2^+$ (bottom) as extracted from the JLab/CLAS data in $n\pi^+$ production (full circles), $p\pi^+\pi^-$ (open triangles), combined single and double pion production (open square). The solid triangle is the 2014 PDG value at $Q^2 = 0$. The open boxes are the model uncertainties of the full circles. The curves are to guide the eye.

81.7 Partial wave analyses

Several PWA groups are now actively involved in the analysis of the new data. The GWU group maintains a nearly complete database covering reactions from πN and KN elastic scattering to $\gamma N \to N\pi$, $N\eta$, and $N\eta'$. It is presently the only group determining πN elastic amplitudes from scattering data in sliced energy bins. Given the high-precision of photoproduction data already or soon to be collected, the spectrum of N and Δ resonances will in the near future be better known.

Fits to the data are performed by various groups with the aim to understand the reaction dynamics and to identify N and Δ resonances. For practical reasons, approximations have to be made. We mention several analyses here: (1) The Mainz unitary isobar model [39] focuses on the correct treatment of the low-energy domain. Resonances are added to the unitary amplitude as a sum of Breit-Wigner amplitudes. This model also obtains resonance transition form factors and helicity amplitudes from electroproduction [35]. (2) For $N\pi$ electroproduction, the Yerevan/JLab group uses both the unitary isobar model and the dispersion relation approach developed in [38]. A phenomenological model was developed to extract resonance couplings and partial decay widths from exclusive $\pi^+\pi^-p$ electroproduction [37]. (3) Multichannel analyses using K-matrix parameterizations derive background terms from a chiral Lagrangian - providing a microscopical description of the background - (Giessen [40, 41]) or from phenomenology (KSU [42, 43], Bonn-Gatchina [44]). (4.) Several groups (EBAC-Jlab [45, 46], ANL-Osaka [47], Dubna-Mainz-Taipeh [48], Bonn-Jülich [49–51], Valencia [52]) use dynamical reaction models, driven by chiral Lagrangians, which take dispersive parts of intermediate states into account. Several other groups have made important contributions. The Giessen group pioneered multichannel analyses of large data sets on pion- and photo-induced reactions [40, 41]. The Bonn-Gatchina group included recent high-statistics data and reported systematic searches for new baryon resonances in all relevant partial waves. A summary of their results can be found in [44].

References

[1] G. Höhler, Pion-Nucleon Scattering, Landolt-Börnstein Vol. I/9b2 (1983), ed. H. Schopper, Springer Verlag.

[2] R. E. Cutkosky *et al.*, in "*VI International Conference on Baryon Resonances*," 19 (1980), Toronto, ed. N. Isgur.

[3] R. Arndt *et al.*, Phys. Rev. C **74**, 045205 (2006), [arXiv:nucl-th/0605082].

[4] "Hadron 2011: 14th International Conference on Hadron Spectroscopy", München, Germany, June, 13 - 17, 2011, published in eConf.

[5] "NSTAR 2013: 9th International Workshop on the Physics of Excited Nucleons", 27-30 May 2013, Peñíscola, Spain.

[6] E. Klempt and J.-M. Richard, Rev. Mod. Phys. **82**, 1095 (2010), [arXiv:0901.2055].

[7] V. Crede and W. Roberts, Rept. Prog. Phys. **76**, 076301 (2013), [arXiv:1302.7299].

[8] M. Roos *et al.* (Particle Data Group), Phys. Lett. B **111**, 1 (1982).

[9] M. Doring *et al.*, Nucl. Phys. A **829**, 170 (2009), [arXiv:0903.4337].

[10] N. Suzuki *et al.*, Phys. Rev. Lett. **104**, 042302 (2010), [arXiv:0909.1356].

[11] R. Cutkosky *et al.*, Phys. Rev. D **20**, 2839 (1979).

[12] R. Arndt *et al.*, Phys. Rev. C **69**, 035213 (2004), [arXiv:nucl-th/0311089].

[13] M. Batinic *et al.*, Phys. Rev. C **51**, 2310 (1995), [Erratum: Phys.Rev.C 57, 1004–1005 (1998)], [arXiv:nucl-th/9501011]; M. Batinić *et al.*, Phys. Scr. **58**, 15 (1998).

[14] A. Anisovich *et al.*, Eur. Phys. J. A **48**, 15 (2012), and references therein., [arXiv:1112.4937].

[15] G. Höhler, PiN Newslett. **1993**, 9, 1 (1993).

[16] N. Kelkar and M. Nowakowski, Phys. Rev. A **78**, 012709 (2008), and references therein., [arXiv:0805.0608].

[17] G. F. Chew and S. Mandelstam, Phys. Rev. **119**, 467 (1960).

[18] S. Ceci *et al.*, Phys. Rev. D **77**, 116007 (2008), [hep-ph/0609236].

[19] P. Masjuan and J. J. Sanz-Cillero, Eur. Phys. J. C **73**, 2594 (2013), [arXiv:1306.6308].

[20] A. Švarc *et al.*, Phys. Rev. C **88**, 3, 035206 (2013), [arXiv:1307.4613].

[21] A. Švarc *et al.*, Phys. Rev. C **89**, 4, 045205 (2014), [arXiv:1401.1947].

[22] A. Švarc *et al.*, Phys. Lett. B **755**, 452 (2016), [arXiv:1512.07403].

[23] A. Švarc *et al.*, Phys. Rev. C **89**, 6, 065208 (2014), [arXiv:1404.1544].

[24] A. Švarc *et al.*, Phys. Rev. C **91**, 1, 015207 (2015), [arXiv:1405.6474].

[25] L. Tiator *et al.*, Phys. Rev. C **94**, 6, 065204 (2016), [arXiv:1606.00371].

[26] A. Anisovich *et al.*, Eur. Phys. J. A **53**, 12, 242 (2017), [arXiv:1712.07537].

[27] A. Anisovich *et al.*, Phys. Rev. Lett. **119**, 6, 062004 (2017), [arXiv:1712.07549].

[28] C. Fasano, F. Tabakin and B. Saghai, Phys. Rev. C **46**, 2430 (1992).

[29] G. Chew *et al.*, Phys. Rev. **106**, 1345 (1957).

[30] R. Workman, L. Tiator and A. Sarantsev, Phys. Rev. C **87**, 6, 068201 (2013), [arXiv:1304.4029].

[31] N. Suzuki, T. Sato and T.-S. Lee, Phys. Rev. C **82**, 045206 (2010), [arXiv:1006.2196].

[32] H. Kamano, Phys. Rev. C **88**, 045203 (2013), [arXiv:1305.6678].

Downloaded from https://academic.oup.com/ptep/article/2022/8/083C01/6651666 by KIT Library user on 27 September 2022

[33] A. Sandorfi *et al.*, AIP Conf. Proc. **1432**, 1, 219 (2012), [arXiv:1108.5411].

[34] I. Aznauryan and V. Burkert, Prog. Part. Nucl. Phys. **67**, 1 (2012), [arXiv:1109.1720].

[35] L. Tiator *et al.*, Eur. Phys. J. ST **198**, 141 (2011), [arXiv:1109.6745]; S. Štajner *et al.*, Phys. Rev. Lett. **119**, 2, 022001 (2017).

[36] W. Ash *et al.*, Phys. Lett. B **24**, 165 (1967).

[37] V. Mokeev *et al.* (CLAS), Phys. Rev. C **86**, 035203 (2012), [arXiv:1205.3948].

[38] I. Aznauryan, Phys. Rev. C **67**, 015209 (2003), [arXiv:nucl-th/0206033].

[39] D. Drechsel, S. Kamalov and L. Tiator, Eur. Phys. J. A **34**, 69 (2007), [arXiv:0710.0306].

[40] G. Penner and U. Mosel, Phys. Rev. C **66**, 055211 (2002), [arXiv:nucl-th/0207066].

[41] G. Penner and U. Mosel, Phys. Rev. C **66**, 055212 (2002), [arXiv:nucl-th/0207069].

[42] D. Manley and E. Saleski, Phys. Rev. D **45**, 4002 (1992).

[43] M. Shrestha and D. Manley, Phys. Rev. C **86**, 055203 (2012), [arXiv:1208.2710].

[44] A. Anisovich *et al.*, Eur. Phys. J. A **48**, 15 (2012), [arXiv:1112.4937].

[45] A. Matsuyama, T. Sato and T.-S. Lee, Phys. Rept. **439**, 193 (2007), [arXiv:nucl-th/0608051].

[46] T. Sato and T.-S. Lee, J. Phys. G **36**, 073001 (2009), [arXiv:0902.3653].

[47] H. Kamano *et al.*, Phys. Rev. C **88**, 3, 035209 (2013), [arXiv:1305.4351].

[48] G. Y. Chen *et al.*, Phys. Rev. C **76**, 035206 (2007), [arXiv:nucl-th/0703096].

[49] M. Doring *et al.*, Phys. Lett. B **681**, 26 (2009), [arXiv:0903.1781].

[50] M. Doring *et al.*, Nucl. Phys. A **829**, 170 (2009), [arXiv:0903.4337].

[51] D. Ronchen *et al.*, Eur. Phys. J. A **49**, 44 (2013), [arXiv:1211.6998].

[52] S. Sarkar, E. Oset and M. Vicente Vacas, Nucl. Phys. A **750**, 294 (2005), [Erratum: Nucl.Phys.A 780, 90–90 (2006)], [arXiv:nucl-th/0407025].

Downloaded from https://academic.oup.com/ptep/article/2022/8/083C01/6651666 by KIT Library user on 27 September 2022

82. Λ and Σ Resonances

Revised August 2021 by V.D. Burkert (Jefferson Lab), V. Crede (Florida State U.), E. Klempt (Bonn U.), U. Thoma (Bonn U.), L. Tiator (KPH, JGU Mainz) and R.L. Workman (George Washington U.).

82.1 Introduction

For several decades, there has been very little new experimental data bearing on the properties of Λ and Σ resonances. An exception was the study at JLab of the reactions $\gamma p \to K^+\Sigma^\pm\pi^\mp$ and $\gamma p \to K^+\Sigma^0\pi^0$ [1], which established the spin and parity of the $\Lambda(1405)$ [2]. There was also from BNL new data on the very low energy region of K^-p scattering [3–7]. Otherwise, the field is starved for data. Recent analyses (see below) have improved what we know about the *properties* of the known Λ and Σ resonances, but the *established* resonances are the same ones that were listed in our 1984 edition [8] except for the $\Sigma(2250)$ which we consider 2-star only due to its unkown spin-parity. The 1990 Review [9] gave a full report of the status of Lambda and Sigma hyperons, and included Argand plots from the partial-wave analyses. The 2018 Review [10] has a short survey of the $\Sigma(1670)$-region.

In the last few years, four groups have re-analyzed K^-p reactions using more extensive collections of the old data. These analyses justify an update of the status of the Λ and Σ resonances. Although they have not established any new resonances, they have provided at least some evidence for new states and have given a better understanding of the old ones.

Tables 82.1 and 82.2 give our evaluation of the status, both overall and channel by channel, of each Λ and Σ resonance in the Particle Listings. In making these evaluations, we considered, in addition to the four analyses [11–14], the ratings that predated them. The ratings use a 1- to 4-star system. For more details on the evaluation of the overall star ratings, see [15]. The main Summary Table includes only established states with an overall status of 3 or 4 stars; as has already been noted, these are the same fourteen Λ resonances (including $\Lambda(1116)$) and nine Σ resonances instead of the former ten (including $\Sigma(1193)3/2^+$, and $\Sigma(1385)3/2^+$) that had long been in the Table. In addition, there are seven 1-star and two 2-star Λ's, and fourteen 1-star and three 2-star Σ's in the Particle Listings.

82.2 New analyses

The new analysis progress was pioneered by the Kent group which collected a large fraction of the available data and performed a comprehensive partial wave analysis [11,16]. K^-p scattering into a pseudoscalar meson and an octet baryon is governed by two complex amplitudes; hence four quantities need to be measured to fully construct the amplitudes (up to an arbitrary phase per energy and angular bin). Discussions of complete experiments also generally assume perfect data (no experimental uncertainties); realistic uncertainties further complicate the task of amplitude extraction. Here, the available data are limited to the differential cross section and the target or hyperon recoil polarization P; data on the polarization transfer do not exist. The authors of Ref. [16] overcame this difficulty by using start values for the partial wave amplitudes determined in [17] and/or from an energy-dependent fit and by freezing or releasing sets of amplitudes. The resulting amplitudes were fitted with a unitary multichannel parameterization [11].

The JPAC group presented a coupled-channel fit to the $\bar{K}N$ partial waves derived by the Kent group [13]. The JPAC approach was based on the K-matrix formalism. Special attention was paid to the analytical properties of the amplitudes determined by the square-root unitary branch points and the continuation to the complex angular momentum plane. The fit described the Kent partial waves reasonably well. However, when observables were calculated from their partial-wave amplitudes, significant discrepancies became apparent. The results were therefore not included in the RPP.

The ANL-Osaka group derived the energy-dependent amplitudes in fits to a large subset of the data collected in Ref. [16] and further data sets described in Ref. [18]. Their fits were based on a phenomenological SU(3) Lagrangian [18]. The two ANL-Osaka models agree on the leading contributions but differ significantly in cases with weaker candidates [12].

Table 82.1: The status of the Λ resonances. Only those with an overall status of *** or **** are included in the main Baryon Summary Table. Decay channels other than $N\overline{K}$ and $\Sigma\pi$ are only given for *** and **** resonances.

Particle	J^P	Overall status	Status as seen in — $N\overline{K}$	$\Sigma\pi$	Other channels
$\Lambda(1116)$	$1/2^+$	****			$N\pi$ (weak decay)
$\Lambda(1380)$	$1/2^-$	**	**	**	
$\Lambda(1405)$	$1/2^-$	****	****	****	
$\Lambda(1520)$	$3/2^-$	****	****	****	$\Lambda\pi\pi, \Lambda\gamma, \Sigma\pi\pi$
$\Lambda(1600)$	$1/2^+$	****	***	****	$\Lambda\pi\pi, \Sigma(1385)\pi$
$\Lambda(1670)$	$1/2^-$	****	****	****	$\Lambda\eta$
$\Lambda(1690)$	$3/2^-$	****	****	***	$\Lambda\pi\pi, \Sigma(1385)\pi$
$\Lambda(1710)$	$1/2^+$	*	*	*	
$\Lambda(1800)$	$1/2^-$	***	***	**	$\Lambda\pi\pi, N\overline{K}^*$
$\Lambda(1810)$	$1/2^+$	***	**	**	$N\overline{K}^*$
$\Lambda(1820)$	$5/2^+$	****	****	****	$\Sigma(1385)\pi$
$\Lambda(1830)$	$5/2^-$	****	****	****	$\Sigma(1385)\pi$
$\Lambda(1890)$	$3/2^+$	****	****	**	$\Sigma(1385)\pi, N\overline{K}^*$
$\Lambda(2000)$	$1/2^-$	*	*	*	
$\Lambda(2050)$	$3/2^-$	*	*	*	
$\Lambda(2070)$	$3/2^+$	*	*	*	
$\Lambda(2080)$	$5/2^-$	*	*	*	
$\Lambda(2085)$	$7/2^+$	**	**	*	
$\Lambda(2100)$	$7/2^-$	****	****	**	$N\overline{K}^*$
$\Lambda(2110)$	$5/2^+$	***	**	**	$N\overline{K}^*$
$\Lambda(2325)$	$3/2^-$	*	*		
$\Lambda(2350)$	$9/2^+$	***	***	*	
$\Lambda(2585)$		*	*		

The Bonn-Gatchina (BnGa) group added further (old) data to those analyzed in Ref. [16]. The data set was fitted in a modified K-matrix approach and the resulting amplitudes were compared with those from Refs. [16,18]. New resonances were found, other states, mostly one and two-star states could not be confirmed; all resonances were tested for their statistical significance. Additional states with any set of quantum numbers were tested and were found to produce only small improvements in the fit [14]. In Ref. [19], properties of the full set of contributing hyperons were reported.

The star ratings of Λ and Σ resonances given in our earlier editions, and the new results from the Kent, ANL-Osaka and BnGa groups were used to update the star rating of the hyperon resonances. In [19], the overall star rating is directly estimated, for [11] we estimate the star rating from the branching-ratio uncertainties. In [12], two solutions are given but no uncertainties for branching ratios. The overall star ratings are based on the evidence for the resonances in the new analyses as well as their consistency including also the results of earlier analyses given in [20]. For further details see also [15].

We decided to remove the three so-called *bumps* $\Sigma(1480)$, $\Sigma(1560)$, $\Sigma(1670)$, and $\Sigma(1690)$ as well as $\Sigma(1620)$ from production experiments. The entries from $\Sigma(1770)1/2^+$ are now listed under $\Sigma(1660)1/2^+$ and $\Sigma(1880)1/2^+$, the entries from $\Sigma(1730)3/2^+$ and $\Sigma(1840)3/2^+$ are now combined to one $\Sigma(1780)3/2^+$. The one-star $\Sigma(2000)1/2^-$ is combined with a new one-star $\Sigma(2160)1/2^-$ to a single one-star $\Sigma(2110)1/2^-$. Apart from $\Lambda(1380)1/2^-$, four further new resonances were included in the Listings: $\Lambda(2070)3/2^+$, $\Lambda(2080)5/2^-$, $\Sigma(2010)3/2^-$, and $\Sigma(2230)3/2^+$, all with one star.

Downloaded from https://academic.oup.com/ptep/article/2022/8/083C01/6651666 by KIT Library user on 27 September 2022

Table 82.2: The status of the Σ resonances. Only those with an overall status of $***$ or $****$ are included in the main Baryon Summary Table. Decay channels other than $N\overline{K}$, $\Lambda\pi$ and $\Sigma\pi$ are only given for $***$ and $****$ resonances.

Particle	J^P	Overall status	Status as seen in — $N\overline{K}$	$\Lambda\pi$	$\Sigma\pi$	Other channels
$\Sigma(1193)$	$1/2^+$	****				$N\pi$ (weak decay)
$\Sigma(1385)$	$3/2^+$	****		****	****	$\Lambda\gamma$
$\Sigma(1580)$	$3/2^-$	*	*	*	*	
$\Sigma(1620)$	$1/2^-$	*	*	*	*	
$\Sigma(1660)$	$1/2^+$	***	***	***	***	
$\Sigma(1670)$	$3/2^-$	****	****	****	****	
$\Sigma(1750)$	$1/2^-$	***	***	**	***	$\Sigma\eta$
$\Sigma(1775)$	$5/2^-$	****	****	****	**	
$\Sigma(1780)$	$3/2^+$	*	*	*	*	
$\Sigma(1880)$	$1/2^+$	**	**	*		
$\Sigma(1900)$	$1/2^-$	**	**	*	**	
$\Sigma(1910)$	$3/2^-$	***	*	*	**	
$\Sigma(1915)$	$5/2^+$	****	***	***	***	
$\Sigma(1940)$	$3/2^+$	*	*		*	
$\Sigma(2010)$	$3/2^-$	*	*	*		
$\Sigma(2030)$	$7/2^+$	****	****	****	**	$\Delta(1232)\overline{K}$, $N\overline{K}^*$, $\Sigma(1385)\pi$
$\Sigma(2070)$	$5/2^+$	*	*		*	
$\Sigma(2080)$	$3/2^+$	*		*		
$\Sigma(2100)$	$7/2^-$	*	*	*	*	
$\Sigma(2110)$	$1/2^-$	*	*	*	*	
$\Sigma(2230)$	$3/2^+$	*	*	*	*	
$\Sigma(2250)$		**	**	*	*	
$\Sigma(2455)$		*	*			
$\Sigma(2620)$		*	*			
$\Sigma(3000)$		*	*	*		
$\Sigma(3170)$		*				

82.3 Sign conventions for resonance couplings

In terms of the isospin-0 and isospin-1 elastic scattering amplitudes A_0 and A_1, the amplitude for $K^-p \to \overline{K}^0 n$ scattering is $\pm(A_1 - A_0)/2$, where the sign depends on conventions used in conjunction with the Clebsch-Gordan coefficients (such as, is the baryon or the meson the "first" particle). If this reaction is partial-wave analyzed and if the overall phase is chosen so that, say, the $\Sigma(1775)5/2^-(D_{15})$ amplitude at resonance points along the positive imaginary axis (points "up"), then any Σ at resonance will point "up" and any Λ at resonance will point "down" (along the negative imaginary axis). Thus the phase at resonance determines the isospin. The above ignores background amplitudes in the resonating partial waves.

That is the basic idea. In a similar but somewhat more complicated way, the phases of the $\overline{K}N \to \Lambda\pi$ and $\overline{K}N \to \Sigma\pi$ amplitudes for a resonating wave help determine the SU(3) multiplet to which the resonance belongs. Again, a convention has to be adopted for some overall arbitrary phases: which way is "up"? Our convention is that of Levi-Setti [21] and is shown in Fig. 82.1, which also compares experimental results with theoretical predictions for the signs of several resonances. In the Listings, a + or − sign in front of a measurement of an inelastic resonance coupling indicates the sign (the *absence* of a sign means that the sign is not determined, *not* that it is positive). Also other decay modes can be used to assign a hyperon to a SU(3) multiplet [22, 23]. Modern analyses determine properties of resonances at the pole position. In these analyses, the + or − sign is replaced by a phase. Background amplitudes can lead to significant phase shifts, and an additional phase shift due to rescattering is admitted in some analyses. In comparison to quark model predictions [19, 24], three Λ spin doublets can be identified as being mainly SU(3) singlets: the well-known ($\Lambda(1405)1/2^-$, $\Lambda(1520)3/2^-$), the ($\Lambda(2080)5/2^-$, $\Lambda(2100)7/2^-$), and ($\Lambda(2070)3/2^+$, $\Lambda(2110)5/2^+$).

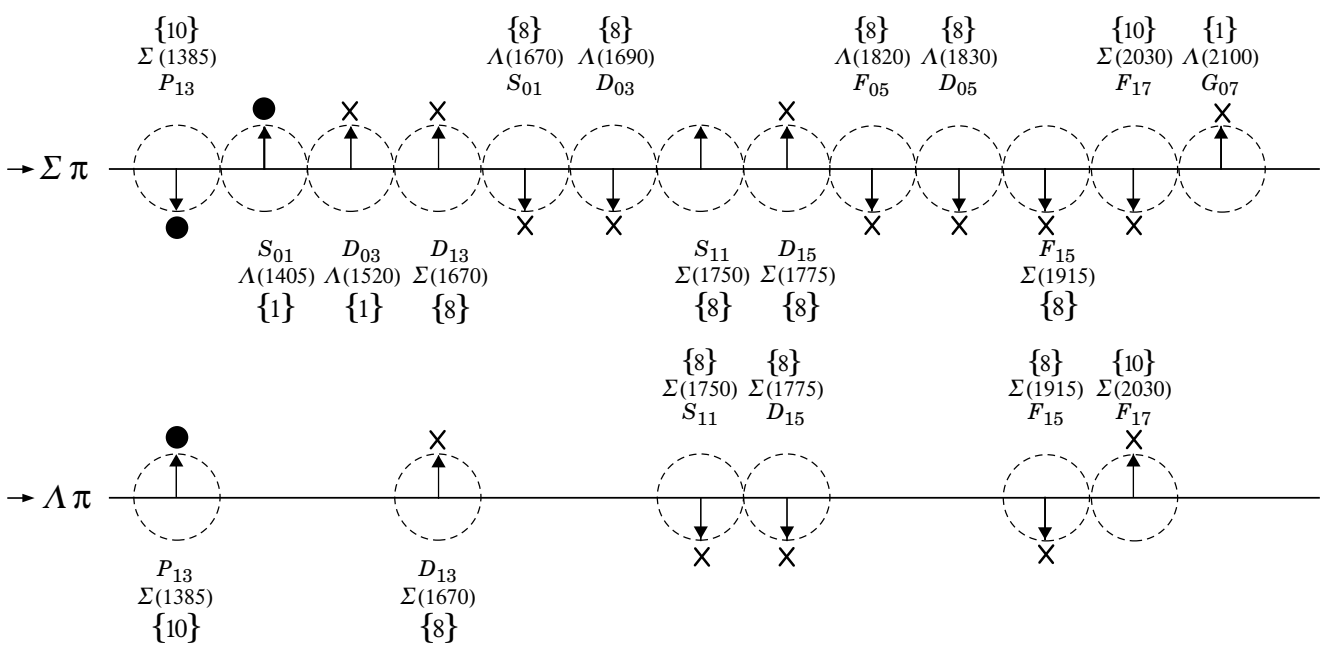

Figure 82.1: The signs of the imaginary parts of resonating amplitudes in the $\overline{K}N \to \Lambda\pi$ and $\Sigma\pi$ channels. The signs of the $\Sigma(1385)$ and $\Lambda(1405)$, marked with a •, are set by convention, and then the others are determined relative to them. The signs required by the SU(3) assignments of the resonances are shown with an arrow, and the experimentally determined signs are shown with an ×.

82.4 The $\Lambda(1405)$

In coupled-channels calculations based on the chiral SU(3) effective field theory, the strongly attractive forces between $N\overline{K}$ and $\Sigma\pi$ generate five poles, one SU(3) singlet pole, two Λ octet poles and two (or one) octet Σ poles (see Section 83). In quark models, these five states are $\Lambda(1405)$, $\Lambda(1670)$, $\Lambda(1800)$, $\Sigma(1620)$,

Downloaded from https://academic.oup.com/ptep/article/2022/8/083C01/6651666 by KIT Library user on 27 September 2022

and $\Sigma(1750)$. The octet states are found 100 to 150 MeV above the corresponding nucleon resonances. In chiral SU(3) effective field theories, at least three of these states are seen in the 1300 to 1600 MeV mass range. The appearance of two Λ poles in this mass range, a narrow SU(3) octet at ∼1420 MeV and a wider SU(3) singlet at ∼1380 MeV, was unexpected. This approach has been pursued by a number of groups; for a summary of the results see our Review 83, "Pole Structure of the $\Lambda(1405)$ Region". In the Listings, we have introduced the $\Lambda(1380)$ as a new candidate resonance (with two stars), named in accordance with its approximate pole position. The second SU(3) octet Λ state is the well-known $\Lambda(1670)$. The masses of the two associated Σ states are uncertain so far, and no new entries are introduced in the Listings.

In traditional approaches only one resonance was seen in this mass region, the narrow state at 1405 MeV. It was reported to be the SU(3) singlet state a long time ago in Ref. [25], in agreement with the quark-model expectations but in contrast to the findings based on coupled-channels calculations within chiral SU(3) effective field theories. In the Listings, the $\Lambda(1405)$ has been retained with its traditional name. In quark models, this state is identified with the SU(3) singlet state, the two Λ octet states with $\Lambda(1670)$ and $\Lambda(1800)$, and the two Σ states with $\Sigma(1620)$ and $\Sigma(1750)$.

82.5 Uncertainties on masses and widths

The uncertainties quoted on resonance parameters from partial-wave analyses are often only statistical, and the parameters can change beyond these uncertainties when a different parametrization of the waves is used. Furthermore, the different analyses use more or less the same data, so it is not really appropriate to treat the different determinations of the resonance parameters as independent or to average them. In any case, the spread of the masses, widths, and branching fractions from the different analyses is certainly a better indication of the uncertainties than are the quoted uncertainties. In the Listings, we usually give a range reflecting the spread of the values rather than a particular value with error.

82.6 Production experiments

Partial-wave analyses of course separate partial waves, whereas a peak in a cross section or an invariant mass distribution usually cannot be disentangled from background and analyzed for its quantum numbers; and more than one resonance may be contributing to the peak. The $\Sigma(1385)$ and $\Lambda(1405)$ lie below the $\overline{K}N$ threshold and nearly everything about $\Sigma(1385)$ is learned from production experiments. Our knowledge on $\Lambda(1405)$ benefits greatly from photoproduction of the three $\Sigma\pi$ charge states [1, 2] and from the precise measurement of the energy shift and width of the kaonic hydrogen atom [26].

Production and formation experiments agree quite well in the case of $\Lambda(1520)$ and results have been combined. Above this mass, no new results on peak hunting have been reported for about 40 years. For these early results, we refer the reader to our earlier editions. In photoproduction with energetic photons [27, 28] or at LHCb [29], hyperons are produced abundantly. So far, no attempt has been made to extract hyperon properties from these data. New data on hyperon spectroscopy can be expected from J-PARC [30], JLAB [31], and the forthcoming PANDA experiment [32].

References

[1] K. Moriya *et al.* (CLAS), Phys. Rev. **C87**, 3, 035206 (2013), [arXiv:1301.5000].

[2] K. Moriya *et al.* (CLAS), Phys. Rev. Lett. **112**, 8, 082004 (2014), [arXiv:1402.2296].

[3] A. Starostin *et al.* (Crystal Ball), Phys. Rev. **C64**, 055205 (2001).

[4] S. Prakhov *et al.*, Phys. Rev. **C69**, 042202 (2004).

[5] S. Prakhov *et al.* (Crystall Ball), Phys. Rev. **C70**, 034605 (2004).

[6] R. Manweiler *et al.*, Phys. Rev. **C77**, 015205 (2008).

[7] S. Prakhov *et al.*, Phys. Rev. **C80**, 025204 (2009), [arXiv:0812.1888].

[8] C. G. Wohl *et al.* (Particle Data Group), Rev. Mod. Phys. **56**, S1 (1984).

[9] J. J. Hernandez *et al.* (Particle Data Group), Phys. Lett. **B239**, 1 (1990), [Erratum: Phys. Lett.B253,524(1991)].

[10] M. Tanabashi *et al.* (Particle Data Group), Phys. Rev. **D98**, 3, 030001 (2018).

[11] H. Zhang *et al.*, Phys. Rev. **C88**, 3, 035205 (2013), [arXiv:1305.4575].

[12] H. Kamano *et al.*, Phys. Rev. **C92**, 2, 025205 (2015), [Erratum: Phys. Rev.C95,no.4,049903(2017)], [arXiv:1506.01768].

[13] C. Fernandez-Ramirez *et al.*, Phys. Rev. **D93**, 3, 034029 (2016), [arXiv:1510.07065].

[14] M. Matveev *et al.*, Eur. Phys. J. **A55**, 10, 179 (2019), [arXiv:1907.03645].

[15] E. Klempt *et al.* (Baryon@PDG Group), Eur. Phys. J. A **56**, 10, 261 (2020), [arXiv:2007.04232].

[16] H. Zhang *et al.*, Phys. Rev. **C88**, 3, 035204 (2013), [arXiv:1305.3598].

[17] J. Tulpan, PhD Disserstation, Kent State University (2007).

[18] H. Kamano *et al.*, Phys. Rev. **C90**, 6, 065204 (2014), [arXiv:1407.6839].

[19] A. V. Sarantsev *et al.*, Eur. Phys. J. **A55**, 10, 180 (2019), [arXiv:1907.13387].

[20] J. Beringer *et al.* (Particle Data Group), Phys. Rev. **D86**, 010001 (2012).

[21] R. Levi Setti, Conf. Proc. **C690625**, 339 (1969).

[22] V. Guzey and M. V. Polyakov, Annalen Phys. **13**, 673 (2004).

[23] V. Guzey and M. V. Polyakov (2005), [hep-ph/0512355].

[24] U. Loring, B. C. Metsch and H. R. Petry, Eur. Phys. J. **A10**, 447 (2001), [hep-ph/0103290].

[25] R. D. Tripp *et al.*, Phys. Rev. Lett. **21**, 1721 (1968).

[26] M. Bazzi *et al.* (SIDDHARTA), Phys. Lett. **B704**, 113 (2011), [arXiv:1105.3090].

[27] K. Moriya *et al.* (CLAS), Phys. Rev. **C88**, 045201 (2013), [Addendum: Phys. Rev.C88,no.4,049902(2013)], [arXiv:1305.6776].

[28] B. Dey *et al.* (CLAS), Phys. Rev. **C89**, 5, 055208 (2014), [Addendum: Phys. Rev.C90,no.1,019901(2014)], [arXiv:1403.2110].

[29] R. Aaij *et al.* (LHCb), Phys. Rev. Lett. **115**, 072001 (2015), [arXiv:1507.03414].

[30] K. Hicks and H. Sako, Proposal for J-PARC E45 .

[31] M. Amaryan *et al.* (KLF) (2020), [arXiv:2008.08215].

[32] F. Iazzi (PANDA), AIP Conf. Proc. **1743**, 1, 050006 (2016).

Downloaded from https://academic.oup.com/ptep/article/2022/8/083C01/6651666 by KIT Library user on 27 September 2022

83. Pole Structure of the $\Lambda(1405)$ Region

Revised June 2021 by T. Hyodo (Tokyo Metropolitan U.) and U.-G. Meißner (Bonn U.; Jülich).

The $\Lambda(1405)$ resonance emerges in the meson-baryon scattering amplitude with the strangeness $S = -1$ and isospin $I = 0$. It is the archetype of what is called a dynamically generated resonance, as pioneered by Dalitz and Tuan [1]. The most powerful and systematic approach for the low-energy regime of the strong interactions is chiral perturbation theory (ChPT), see e.g. Ref. [2]. A perturbative calculation is, however, not applicable to this sector because of the existence of the $\Lambda(1405)$ just below the $\bar{K}N$ threshold. In this case, ChPT has to be combined with a non-perturbative resummation technique, just as in the case of the nuclear forces. By solving the Lippmann-Schwinger equation with the interaction kernel determined by ChPT and using a particular regularization, in Ref. [3] a successful description of the low-energy K^-p scattering data as well as the mass distribution of the $\Lambda(1405)$ was achieved (for further developments, see Ref. [4–7] and references therein).

The study of the pole structure was initiated by Ref. [8], which finds two poles of the scattering amplitude in the complex energy plane between the $\bar{K}N$ and $\pi\Sigma$ thresholds. The spectrum in experiments exhibits one effective resonance shape, while the existence of two poles results in the reaction-dependent lineshape [9]. The origin of this two-pole structure is attributed to the two attractive channels of the leading order interaction in the SU(3) basis (singlet and octet) [9] and in the isospin basis ($\bar{K}N$ and $\pi\Sigma$) [10]. It is remarkable that the sign and the strength of the leading order interaction is determined by a low-energy theorem of chiral symmetry, i.e. the so-called Weinberg-Tomozawa term. The two-pole nature of the $\Lambda(1405)$ is qualitatively different from the case of the N(1440) resonance. Two poles of the N(1440) appear on different Riemann sheets of the complex energy plane separated by the $\pi\Delta$ branch point. These poles reflect a single state, with a nearby pole and a more distant shadow pole. In contrast, the two poles in the $\Lambda(1405)$ region on the same Riemann sheet (where $\pi\Sigma$ channels are unphysical and all other channels physical, correspondingly to the one, connected to the real axis beween the $\pi\Sigma$ and $\bar{K}N$ thresholds) are generated from two attractive forces mentioned above [9, 10].

Recently, various new experimental results on the $\Lambda(1405)$ have become available [4]. Among these, the most striking measurement is the precise determination of the energy shift and width of kaonic hydrogen by the SIDDHARTA collaboration [11,12], which provides a quantitative and stringent constraint on the K^-p amplitude at threshold through the improved Deser formula [13]. Systematic studies with error analyses based on the next-to-leading order ChPT interaction including the SIDDHARTA constraint have been performed by various groups [14–18] All these studies confirm that the new kaonic hydrogen data are compatible with the scattering data above threshold.

The results of the pole positions of $\Lambda(1405)$ in the various approaches are summarized in Table 83.1. We may regard the difference among the calculations as a systematic error, which stems from the various approximations of the Bethe-Salpeter equation, the fitting procedure, and also the inclusion of SU(3) breaking effects such as the choice of the various meson decay constants, and so on. A detailed comparison of the various approaches that enter the table is given in Ref. [19]. A recent analysis including also the $J^P = 1/2^+$ P-wave contribution (and also an explicit $\Sigma(1385)$ $3/2^+$ state) gives results consistent with the findings reported above, with the pole positions at $(1364 - i43)$ MeV and $(1430 - i15)$ MeV, respectively [20].

The main component for the $\Lambda(1405)$ is the pole 1, whose position converges within a relatively small region near the $\bar{K}N$ threshold. On the other hand, the position of the pole 2 shows a sizeable scatter. Detailed studies of the $\pi\Sigma$ spectrum in various reaction processes, together with the precise experimental lineshape (see e.g. the recent precise photoproduction data from the LEPS collaboration [21] and from the CLAS collaboration [22,23], electroproduction data from the CLAS collaboration [24], and proton-proton collision data from COSY [25] and the HADES collaboration [26]), will shed light on the position of the second pole. The $\pi\Sigma$ spectra from the CLAS data are analyzed in Ref. [27] and Ref. [18]. It was shown in Ref. [18] that several solutions, which agree with the scattering data, are ruled out if confronted with the recent CLAS data. The remaining solutions are collected as solution #2 and solution #4 in Table 83.1. The HADES data are analyzed in Ref. [28] and Ref [29]. Although the result of the pole found in Ref. [28] is not compatible with other results, the authors of Ref. [29] invoke the anomalous triangle singularity mechanism to argue that the invariant mass distribution of the $\pi\Sigma$ system is found at lower masses than in other reactions. It is thus desirable to perform more comprehensive analyses of $\pi\Sigma$ spectra together with the systematic error analysis of the scattering data.

Table 83.1: Comparison of the pole positions of $\Lambda(1405)$ in the complex energy plane from next-to-leading order chiral unitary coupled-channel approaches including the SIDDHARTA constraint. The lower two results also include the CLAS photoproduction data.

approach	pole 1 [MeV]	pole 2 [MeV]
Refs. [14, 15], NLO	$1424^{+7}_{-23} - i\ 26^{+3}_{-14}$	$1381^{+18}_{-6} - i\ 81^{+19}_{-8}$
Ref. [17], Fit II	$1421^{+3}_{-2} - i\ 19^{+8}_{-5}$	$1388^{+9}_{-9} - i\ 114^{+24}_{-25}$
Ref. [18], solution #2	$1434^{+2}_{-2} - i\ 10^{+2}_{-1}$	$1330^{+4}_{-5} - i\ 56^{+17}_{-11}$
Ref. [18], solution #4	$1429^{+8}_{-7} - i\ 12^{+2}_{-3}$	$1325^{+15}_{-15} - i\ 90^{+12}_{-18}$

References

[1] R. Dalitz and S. Tuan, Phys. Rev. Lett. **2**, 425 (1959).

[2] V. Bernard, N. Kaiser and U.-G. Meißner, Int. J. Mod. Phys. E **4**, 193 (1995), [hep-ph/9501384].

[3] N. Kaiser, P. Siegel and W. Weise, Nucl. Phys. A **594**, 325 (1995), [arXiv:nucl-th/9505043].

[4] T. Hyodo and D. Jido, Prog. Part. Nucl. Phys. **67**, 55 (2012), [arXiv:1104.4474].

[5] U.-G. Meißner, Symmetry **12**, 6, 981 (2020), [arXiv:2005.06909].

[6] M. Mai, Eur. Phys. J. ST **230**, 6, 1593 (2021), [arXiv:2010.00056].

[7] T. Hyodo and M. Niiyama, Prog. Part. Nucl. Phys. **120**, 103868 (2021), [arXiv:2010.07592].

[8] J. Oller and U.-G. Meißner, Phys. Lett. B **500**, 263 (2001), [hep-ph/0011146].

[9] D. Jido *et al.*, Nucl. Phys. A **725**, 181 (2003), [arXiv:nucl-th/0303062].

[10] T. Hyodo and W. Weise, Phys. Rev. C **77**, 035204 (2008), [arXiv:0712.1613].

[11] M. Bazzi *et al.* (SIDDHARTA), Phys. Lett. B **704**, 113 (2011), [arXiv:1105.3090].

[12] M. Bazzi *et al.* (SIDDHARTA), Nucl. Phys. A **881**, 88 (2012), [arXiv:1201.4635].

[13] U.-G. Meißner, U. Raha and A. Rusetsky, Eur. Phys. J. C **35**, 349 (2004), [hep-ph/0402261].

[14] Y. Ikeda, T. Hyodo and W. Weise, Phys. Lett. B **706**, 63 (2011), [arXiv:1109.3005].

[15] Y. Ikeda, T. Hyodo and W. Weise, Nucl. Phys. A **881**, 98 (2012), [arXiv:1201.6549].

[16] M. Mai and U.-G. Meißner, Nucl. Phys. A **900**, 51 (2013), [arXiv:1202.2030].

[17] Z.-H. Guo and J. Oller, Phys. Rev. C **87**, 3, 035202 (2013), [arXiv:1210.3485].

[18] M. Mai and U.-G. Meißner, Eur. Phys. J. A **51**, 3, 30 (2015), [arXiv:1411.7884].

[19] A. Cieplý *et al.*, Nucl. Phys. A **954**, 17 (2016), [arXiv:1603.02531].

[20] D. Sadasivan, M. Mai and M. Döring, Phys. Lett. B **789**, 329 (2019), [arXiv:1805.04534].

Downloaded from https://academic.oup.com/ptep/article/2022/8/083C01/6651666 by KIT Library user on 27 September 2022

[21] M. Niiyama *et al.*, Phys. Rev. C **78**, 035202 (2008), [arXiv:0805.4051].

[22] K. Moriya *et al.* (CLAS), Phys. Rev. C **87**, 3, 035206 (2013), [arXiv:1301.5000].

[23] K. Moriya *et al.* (CLAS), Phys. Rev. Lett. **112**, 8, 082004 (2014), [arXiv:1402.2296].

[24] H. Lu *et al.* (CLAS), Phys. Rev. C **88**, 045202 (2013), [arXiv:1307.4411].

[25] I. Zychor *et al.*, Phys. Lett. B **660**, 167 (2008), [arXiv:0705.1039].

[26] G. Agakishiev *et al.* (HADES), Phys. Rev. C **87**, 025201 (2013), [arXiv:1208.0205].

[27] L. Roca and E. Oset, Phys. Rev. C **87**, 5, 055201 (2013), [arXiv:1301.5741].

[28] M. Hassanvand *et al.*, Phys. Rev. C **87**, 5, 055202 (2013), [Addendum: Phys.Rev.C 88, 019905 (2013)], [arXiv:1210.7725].

[29] M. Bayar *et al.*, Phys. Rev. C **97**, 3, 035203 (2018), [arXiv:1710.03964].

Downloaded from https://academic.oup.com/ptep/article/2022/8/083C01/6651666 by KIT Library user on 27 September 2022

84. Pentaquarks

Revised September 2021 by M. Karliner (Tel Aviv U.) and T. Skwarnicki (Syracuse U.).

Experimental searches for pentaquark hadrons comprised of light flavors have a long and vivid history. No undisputed candidates had been found in 50 years. The first wave of claimed observations of pentaquark candidates containing a strange antiquark occurred in the early seventies, see e.g. a review in the 1976 edition of Particle Data Group listings for $Z_0(1780)$, $Z_0(1865)$ and $Z_1(1900)$ [1]. The last mention of these candidates can be found in the 1992 edition [2] with the perhaps prophetic comment "the results permit no definite conclusion - the same story for 20 years. [...] The skepticism about baryons not made of three quarks, and lack of any experimental activity in this area, make it likely that another 20 years will pass before the issue is decided." A decade later, a second wave of observations occurred, possibly motivated by specific theoretical predictions for their existence [3–5]. The evidence for pentaquarks was based on observations of peaks in the invariant mass distributions of their decay products. More data and subsequent more sensitive experiments did not confirm these claims [6]. In the last mention of the best known candidate from that period, $\Theta(1540)^+$, the 2006 Particle Data Group listing [7] included a statement: "The conclusion that pentaquarks in general, and that Θ^+, in particular, do not exist, appears compelling." which well reflected the prevailing mood in the particle physics community until a study of $\Lambda_b^0 \to J/\psi pK^-$ ($J/\psi \to \mu^+\mu^-$) decays by LHCb [8] (charge conjugate modes are implied). From an analysis of 3 fb^{-1} Run 1 data at 7 and 8 TeV at the LHC, the LHCb collaboration reported a significant $J/\psi p$ structure in $\Lambda_b^0 \to J/\psi pK^-$ decays [8]. The exotic character of this structure, with the minimal quark content of $uudc\bar{c}$, was demonstrated in a nearly model-independent way in Ref. [9], where it was shown that the $J/\psi p$ mass ($m_{J/\psi p}$) peak near 4450 MeV was too narrow to be accounted for by $\Lambda^* \to pK^-$ reflections (Λ^* denotes a generic Λ excitation), reinforcing the results from the earlier model-dependent six-dimensional amplitude analysis of invariant masses and decay angles describing the Λ_b^0 decay in the same data [8]. Even though not apparent from the $m_{J/\psi p}$ distribution, the amplitude analysis also required a second broad $J/\psi p$ state to obtain a good description of the data, which peaked at $4380 \pm 8 \pm 29$ MeV with a width of $205 \pm 18 \pm 86$ MeV and a fit fraction of $(8.4 \pm 0.7 \pm 4.2)\%$.

The LHCb 6 fb^{-1} Run 2 LHC data at 13 TeV, together with the improvements in the data selection for both runs, resulted in a nine-fold increase in the number of reconstructed $\Lambda_b^0 \to J/\psi pK^-$ decays (246,000 events) [10]. When fit with the same six-dimensional amplitude model, the enlarged data sample gives consistent results for the $P_c(4450)^+$ and $P_c(4380)^+$ parameters, corroborating the compatibility of the data samples. However, the two-state interpretation of the data is contradicted by the observation of new narrow $J/\psi p$ structures which are too faint to have been significant in the Run 1 data analysis. A second horizontal band is observed in the Dalitz plot (Fig. 84.1) near 4312 MeV in the $J/\psi p$ mass.

The 4450 MeV structure also appears to consist of two narrower peaks at 4440 and 4457 MeV. Performing a rigorous six-dimensional amplitude analysis of these faint $J/\psi p$ structures is challenging and has not been accomplished yet. Fortunately, the newly observed peaks are so narrow that it is not necessary to construct an amplitude model to prove that these states are not artifacts of interfering Λ^* resonances, as was previously demonstrated in Ref. [9]. Their masses and widths have been characterized by the LHCb (see Table 84.1) from one-dimensional fits to $J/\psi p$ mass distributions, with different levels of suppression of the Λ^* contributions, which peak at the lower pK^- masses (Fig. 84.1). Such analysis is not sensitive to any broad $J/\psi p$ contributions like $P_c(4380)^+$. The histograms analyzed by the LHCb are available in tabular form at https://www.hepdata.net/record/89271.

The fit chosen by the LHCb for the central mass and width values is displayed in Fig. 84.2. The $P_c(4312)^+$ state peaks right below the $\Sigma_c^+\bar{D}^0$ threshold and has statistical significance over 7.6σ. The $P_c(4457)^+$ state peaks right below the $\Sigma_c^+\bar{D}^{*0}$ threshold, while the $P_c(4440)^+$ state peaks about 20 MeV below it. The significance of the two-peak versus one-peak hypothesis for the

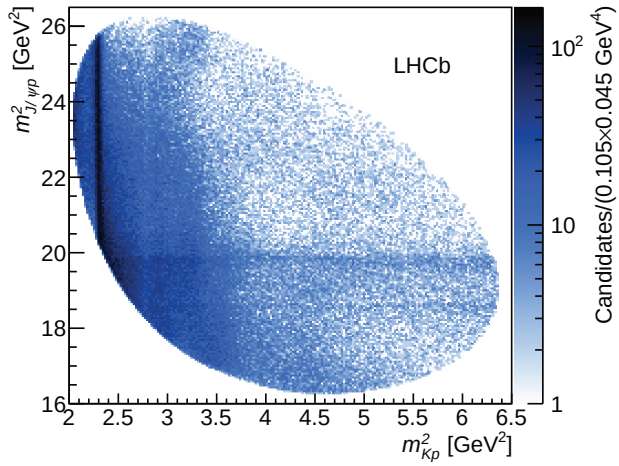

Figure 84.1: Dalitz plot distributions for $\Lambda_b^0 \to J/\psi pK^-$ decays as observed by LHCb.

4450 MeV structure is over 5.4σ, rendering the single peak interpretation of this region obsolete. The six-dimensional amplitude analysis reported in Ref. [8], which provided evidence for the $P_c(4380)^+$ state, is obsolete since it used the single $P_c(4450)^+$ state and it lacked the $P_c(4312)^+$ state. Furthermore, it used the helicity formalism in which the half-integer spin of the proton was not aligned properly between the different Λ_b decay chains [11, 12]. The newer one-dimensional analysis by LHCb [10] was not sensitive to wide P_c^+ states. The LHCb result from the six-dimensional amplitude analysis of the Cabibbo suppressed channel $\Lambda_b^0 \to J/\psi p\pi^-$ [13], which contains a statistically marginal evidence for the sum of the P_c^+ and the $Z_c(4200)^-$ contributions, took extensive input from Ref. [8] and, like the $P_c(4380)^+$ state, should be treated with caution until the both amplitude analyses are completed on the enlarged data sets with the modified helicity formalism.

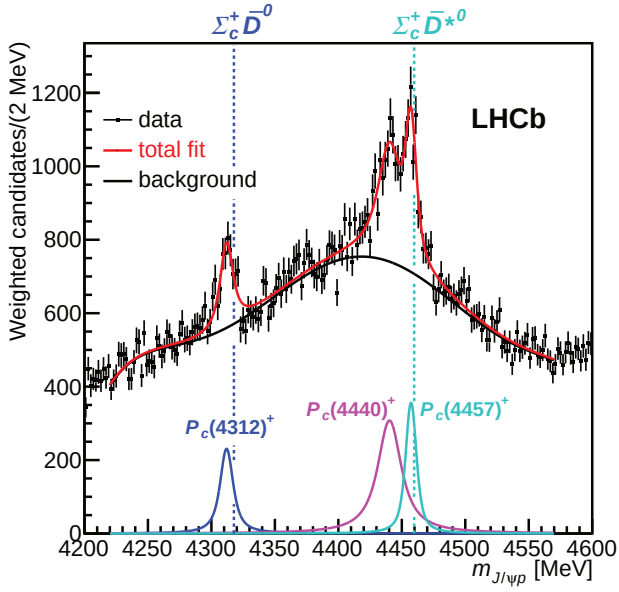

Figure 84.2: Fit to the $J/\psi p$ mass distribution, in which events were weighted to suppress $\Lambda^* \to pK^-$ backgrounds, of three Breit-Wigner functions and a sixth-order polynomial background. This fit was used to determine the central values of the masses and widths of the P_c^+ states reported by LHCb. The mass thresholds for the $\Sigma_c^+\bar{D}^0$ and $\Sigma_c^+\bar{D}^{*0}$ final states are superimposed.

While $\Sigma_c\bar{D}^{(*)}$ states had been predicted [14–17] before the first LHCb results [8], after these results became known, many theo-

Downloaded from https://academic.oup.com/ptep/article/2022/8/083C01/6651666 by KIT Library user on 27 September 2022

Table 84.1: Summary of the narrow P_c^+ properties, interpreted as Breit-Wigner resonances. The central values are based on the fit displayed in Fig. 84.2.

State	M [MeV]	Γ [MeV] (95% CL)	$\mathcal{R}$ [%]
$P_c(4312)^+$	$4311.9 \pm 0.7^{+6.8}_{-0.6}$	$9.8 \pm 2.7^{+\ 3.7}_{-\ 4.5}$ (< 27)	$0.30 \pm 0.07^{+0.34}_{-0.09}$
$P_c(4440)^+$	$4440.3 \pm 1.3^{+4.1}_{-4.7}$	$20.6 \pm 4.9^{+\ 8.7}_{-10.1}$ (< 49)	$1.11 \pm 0.33^{+0.22}_{-0.10}$
$P_c(4457)^+$	$4457.3 \pm 0.6^{+4.1}_{-1.7}$	$6.4 \pm 2.0^{+\ 5.7}_{-\ 1.9}$ (< 20)	$0.53 \pm 0.16^{+0.15}_{-0.13}$

retical groups interpreted the $P_c(4450)^+$ and $P_c(4380)^+$ states in terms of diquarks and triquarks as building blocks of a compact pentaquark [18–24]. In a different strategy, a tentative attempt has been made to treat the full 5-body dynamics, leading to states below the lowest threshold for spontaneous dissociation [25]. In the first implementation of the former approach [18], the pentaquark mass splitting was generated mostly by the change of angular momentum between the sub-components (L) from zero to one, which would also make the heavier state narrower and of opposite parity. Explicit modeling of multiquark systems [26] questions if centrifugal barrier factor provides enough width suppression via spatial separation of c and $\bar{c}$ quarks at these masses, as the phase space for $J/\psi p$ decay is very large (more than 400 MeV). Also, the observed mass splitting was too small to be only due to the mechanism proposed in Ref. [18] and required fine-tuning of such models. A variation of this model, in which the heavy (cu) diquark couples with heavy $\bar{c}$ to form colored triquark attracting the light diquark (ud), has been re-implemented for the narrow P_c^+ states [27]. In this model, the $P_c(4440)^+$ and $P_c(4457)^+$ states are accommodated via spin-orbit interactions for the $L = 1$ states, while the $P_c(4312)^+$ is one of the $L = 0$ states. However, the mass prediction for the latter is off by (-72 ± 29) MeV [27]. This work was later extended to $SU(3)_F$ [28]. The width dilemma becomes more severe in view of the narrow widths of the newly observed states (Table 84.1), especially for the $L = 0$ $P_c(4312)^+$ state, and requires a different origin of potential barrier between c and $\bar{c}$ than angular momentum [27,29], which remains a subject of theoretical controversy. Measurement of spin-parity of $P_c(4312)^+$, $P_c(4440)^+$ and $P_c(4457)^+$ will be crucial for testing these and alternative theoretical ideas discussed in the following.

More effective width suppression mechanism is offered by a loosely bound charmed baryon-anticharmed meson molecular model, in which c and $\bar{c}$ can be separated by much larger distances, resulting in a smaller probability of them getting close enough to each other in order to make a J/ψ. Since molecular binding energy cannot be large, such molecules are in S-wave, so their masses must be near the sum of the baryon and meson masses and their spin and parity are inherited from their constituent hadrons [17]. The mass coincidence of the $P_c(4312)^+$ and of $P_c(4457)^+$ states, with the two related thresholds, $\Sigma_c^+\bar{D}^0$ and $\Sigma_c^+\bar{D}^{*0}$, provides very strong experimental evidence in favor of this interpretation. Given how close $P_c(4312)^+$ is to the $\Sigma_c^+\bar{D}^0$ threshold, it might be a virtual rather than a bound state [30]. Since the spins of Σ_c^+ and of $\bar{D}^{*0}$ can be combined in two different ways, the narrow $P_c(4440)^+$ peak also finds natural explanation in this physical picture. It cannot be a virtual state since it is sufficiently below the $\Sigma_c^+\bar{D}^{*0}$ threshold.

It is worth stressing that other baryon-meson combinations, $\Lambda_c^{(*)+}\bar{D}^{(*)0}$ and $\chi_{cJ}p$ are not expected to bind [14, 31]. Before the first pentaquark observation [8] heavy quark symmetry was used to show that, in addition to the three $\Sigma_c\bar{D}^{(*)0}$ states, one expects four $\Sigma_c^*\bar{D}^{(*)0}$ states, for a total of seven [32]. Indeed, additional states at, or below, the $\Sigma_c^{*+}\bar{D}$ and $\Sigma_c^{*+}\bar{D}^*$ thresholds, are expected [33–36]. Since Σ_c^{*+} width is likely around 15 MeV [37]. more than the width of either $P_c(4312)^+$ or $P_c(4457)^+$, it is important to keep in mind that a molecule is typically as broad as the constituents[1] [38–40]. For a review on hadronic molecules, see [41, 42].

It is useful to consider the $P_c(4312)^+$, $P_c(4440)^+$ and $P_c(4457)^+$ narrow pentaquarks together with several analogous exotic states with hidden charm and bottom in the meson sector. This provides additional significant motivation for the molecular model. At least five exotic mesons are close to thresholds of two heavy-light mesons: $X(3872)$ [43–46], $Z_b(10610)$ and $Z_b(10650)$ in the bottomonium sector [47–51] and $Z_c(3900)$ [52–56] and $Z_c(4020)$ [57–59] in the charmonium sector (see Table II in Ref. [60]; for reviews of experimental information see Ref. [61,62], as well as *Spectroscopy of Mesons Containing Two Heavy Quarks* and *Heavy Non-$q\bar{q}$ Mesons* in the current Review of Particle Properties. These states share several important features: a) their masses are near thresholds and their spin and parity correspond to S-wave combination of the two mesons; b) they are very narrow, despite very large phase space for decay into quarkonium + pion(s); c) the branching fractions for "fall apart" mode into two mesons are much larger than branching fractions for decay into quarkonium and pion(s). So far, there is no experimental evidence for states at two pseudoscalar thresholds ($D\bar{D}$ and $B\bar{B}$), implying that pseudoscalar exchange is essential for binding in meson-meson systems.

The above provide a strong hint that these states are deuteron-like loosely bound states of two heavy mesons [63–71]. It is then natural to conjecture that similar bound states might exist of two heavy baryons [72, 73], or a meson and a baryon or a baryon and an antibaryon, leading to a rather accurate prediction of the $P_c(4457)^+$ mass as $3/2^-$ $\Sigma_c\bar{D}^*$ molecule (the mass threshold is 4460 MeV for $\Sigma_c^+D^{*0}$ and 4464 MeV for $\Sigma_c^{++}D^{*-}$) [17, 60], following similar predictions obtained in a wider framework of doubly heavy baryon-meson hadronic molecules, which might include mixtures of various two-hadron states [14–16,31]. However, single pion exchange is not possible in $\Sigma_c^+\bar{D}^0$ system, thus the existence of $P_c(4312)^+$ points to importance of vector or two-pion exchanges in baryon-meson molecules. Two-pion exchange in $D\bar{D}$ system is highly suppressed, because the intermediate state is $D^*\bar{D}^*$, which is 282 MeV heavier than $D\bar{D}$. On the other hand, there is little suppression in the $\Sigma_c\bar{D}$ system, because the dominant intermediate state is $\Lambda_c\bar{D}^*$ which is just 25 MeV lighter than $\Sigma_c\bar{D}$ [74]. In a generic hadronic molecule it is essential that the two hadrons are heavy, in order to minimize the repulsive kinetic energy [72,73,75].

Following the initial LHCb discovery [8], several groups carried out a detailed analysis of the P_c^+ states as hadronic molecules [76–85] followed by further analyses [35,86–110] after the updated LHCb results [10]. Partial widths of all the allowed decay channels for the P_c states have been estimated within a specific model in the molecular picture [111]. The most striking result is that $P_c(4312)$ decays are totally dominated by the $\bar{D}^*\Lambda_c$ channel. This channel is also expected to be very prominent in decays of $P_c(4440)$ and $P_c(4457)$. A recent theoretical analysis reaches an opposite conclusion, on the basis of the data available so far, expecting a rather small signal in the $\bar{D}^{(*)}\Lambda_c$ channels [112]. Obviously, experimental determination of the branching fraction of these channels is of high priority.

The P_c states have also been-interpreted as so called hadrocharmonium [113], a bound state of relatively compact charmonium states with light hadronic matter. It was proposed that $P_c(4440)^+$ and $P_c(4457)^+$ are spin-split $\psi(2S)p$ bound states with $J^P = \frac{1}{2}^-$ and $\frac{3}{2}^-$, while $P_c(4312)^+$ is a $\chi_{c0}p$ bound state with $J^P = \frac{1}{2}^+$ [114]. While very interesting from the theoretical point of view, it is not at all clear why the binding energies between charmonia and the nucleon should conspire to produce states so close to the $\Sigma_c\bar{D}$ and $\Sigma_c\bar{D}^*$ thresholds. Moreover, the predicted widths of $P_c(4440)^+$ and $P_c(4457)^+$ are too big by a factor $\sim$ 2-3. One should also keep in mind that the molecular and hadrocharmonium pictures provide opposite predictions for the parity

[1] This feature gets changed if systems are more deeply bound.

Downloaded from https://academic.oup.com/ptep/article/2022/8/083C01/6651666 by KIT Library user on 27 September 2022

of $P_c(4312)^+$. In principle LHCb can check the spin and parity through partial wave analysis, but at present it is not known if systematic uncertainties can be sufficiently reduced to make such an analysis conclusive.

Shortly after the initial experimental discovery it was conjectured that the $P_c(4450)^+$ reflects the presence of a triangle singularity near the $\chi_{c1}p$ threshold [115–118]. These explanations are no longer viable, since the $P_c(4440)^+$ mass is not at any threshold and the $P_c(4312)^+$ and $P_c(4457)^+$ peak slightly below the $\Sigma_c^+\bar{D}^0$ and $\Sigma_c^+\bar{D}^{*0}$ thresholds. The $P_c(4457)^+$ mass is exactly at $\Lambda_c^{*+}\bar{D}^0$ threshold, but LHCb has demonstrated that the observed peaking is narrower in the data than expected from the triangle-diagram when a realistic width of the excited D_s^- state exchanged in the triangle is used (Supplemental Material in Ref. [10]).

More extensive pre-2019 reviews of some of the theoretical issues can be found in Refs. [119,120]. Two recent relevant reviews are Refs. [121,122].

So far the P_c^+ states have been observed by only one experiment in only one channel. It is essential to explore other possible experimental channels, such as $P_c \to \Lambda_c\bar{D}^{(*)}$, $\eta_c p$ [112]. These channels are however much more experimentally challenging than $P_c \to J/\psi p$. Proposals have also been made to search for heavy pentaquarks in photo-production [123–130]. Ref. [131] discusses photoproduction within the string-junction physical picture of the pentaquarks. Photoproduction is also related to recent work on $J/\psi(\eta_c)N$ scattering on the lattice [132] and on computation of $J/\psi(\eta_c)N$ and $\Upsilon(\eta_b)N$ cross sections [133]. In addition, pentaquark production has been discussed in the context of antiproton-deuterium collisions [134], of heavy ion collisions at LHC [135], in pA collisions [136] and in pion-induced processes [137–139]. The GlueX Collaboration reported negative search results for the P_c^+ states in photo-production at JLAB [140]. Within the large experimental errors and considerable theoretical model dependence these results do not contradict the molecular interpretations of the narrow P_c^+ states, especially in view of the P_c decay being likely dominated by $\Lambda_c\bar{D}^{(*)}$ modes [111,141]. It has been suggested to determine the pentaquark photo-couplings and branching ratios by measuring the polarization transfer between the incident photon and the outgoing proton in the exclusive photo-production of J/ψ near threshold [142].

As noted in e.g. [17], bottom analogues of the P_c^+ might well exist, but experimental search for such states involves very significant challenges. It is therefore hardly surprising that they have not been observed so far. A detailed discussion is beyond the scope of the current review.

Recently, the LHCb collaboration has obtained a 3.1σ evidence for a $P_c^+ \to J/\psi p$ state in the four-dimensional amplitude analysis of about 800 $B_s^0 \to J/\psi p\bar{p}$ ($J/\psi \to \mu^+\mu^-$) decays [143]. The mass of the state, $4337^{+7}_{-4} \pm 2$ MeV, is not compatible with the the $P_c(4312)^+$ state at 3.1 standard deviations. The width is relatively small, $29^{+26}_{-12} \pm 14$ MeV. The present data do not provide sufficient discrimination between various J^P assignments. Its mass is about 19 MeV higher than the $\Sigma_c^+\bar{D}^0$ threshold and about 16 MeV lower than the $\chi_{c0}p$ threshold. At present, no specific explanation for this structure has been proposed, but some intriguing ideas have been raised in Ref. [144]. Since the statistical significance of this evidence is marginal, more data are required before this state is considered experimentally established.

Similarly inconclusive 3.1σ evidence for a $P_{cs}^0 \to J/\psi\Lambda$ structure was observed by the LHCb collaboration in the six-dimensional amplitude analysis of about 1750 $\Xi_b^- \to J/\psi\Lambda K^-$ ($J/\psi \to \mu^+\mu^-$, $\Lambda \to p\pi^-$ decays [12]. The strange counterparts of P_c^+ states have been predicted in both molecular and compact pentaquark models [15,98,100,145–147]. When interpreted as a single peak, its mass, $4458.8 \pm 2.9^{+4.7}_{-1.1}$ MeV, is 15 MeV above the $\Xi_c^{0\prime}\bar{D}^0$ threshold and 18 MeV below the $\Xi_c^0\bar{D}^{*0}$ threshold. Its width, $17.3 \pm 6.5^{+8.0}_{-5.7}$ MeV, is relatively narrow, thus plausibly could be interpreted as a loosely bound $\Xi_c^0\bar{D}^{*0}$ state. However, in the latter model two states are expected with J^P equal to $1/2^-$ and $3/2^-$. In fact, the LHCb data are consistent with such hypothesis, under which 4454.9 ± 2.7 MeV ($\Gamma = 7.5 \pm 9.7$ MeV) and 4467.8 ± 3.7 MeV ($\Gamma = 5.2 \pm 5.3$ MeV) mass (width) estimates are obtained (statistical errors only). It is worth noting, that the $SU(3)$ flavor structure of $\Xi_c^0\bar{D}^{*0}$ states is different from that of $\Sigma_c^+\bar{D}^{*0}$ states, since Ξ_c^0 belongs to the charmed baryon triplet, unlike Σ_c^+, which together with $\Xi_c^{0\prime}$, belong to the charmed baryon sextet. More data are required to experimentally establish this structure, clarify its composition, and determine the related quantum numbers.

If $P_{cs}(4459)^0$ indeed is a $\Xi_c^0\bar{D}^{*0}$ molecule, there likely exists another state, corresponding to $\Xi_c'\bar{D}^*$ [15,98,100,145–147], with a mass shifted upwards by approximately $\Xi_c' - \Xi_c$ mass difference [148], i.e. about 108 MeV [37]. Experimental determination whether yet additional $\Xi_c^{(*,\prime)}\bar{D}^{(*)0}$ states actually exist will provide a useful testing ground for the various theoretical approaches which have been used to predict them.

In hidden-charm exotics discussed above, the charmed and the anticharmed quarks can form a charmonium and thereby decouple from the light quarks. The molecular model provides an efficient mechanism to suppress such decays, thus making these states narrow. This type of exotic states, should not be confused with exotic hadrons containing two heavy quarks, rather than a heavy quark and a heavy antiquark. Such a decoupling is impossible in exotics which contain two heavy quarks. This has far-reaching consequences.

The first exotic hadron containing two heavy quarks has recently been reported by LHCb [149,150] and deserves a separate review. Here we briefly discuss only the essential distinction vs. hidden-charm pentaquarks. The reported T_{cc}^+ state has quark content $cc\bar{u}\bar{d}$, $I = 0$ and likely $J^P = 1^+$, and mass about 300 keV below the D^0D^{*+} threshold. Its width is a fraction of an MeV. The phase space available for decay is tiny due to absence of the decoupling mechanism. Therefore the narrow width of T_{cc}^+ is natural in both the compact tetraquark model and in those molecular models which predict the mass very close to the D^0D^{*+} threshold. On the other hand, for sufficiently heavy quarks, e.g. $bb\bar{u}\bar{d}$, such open heavy-flavor exotics are genuine compact tetraquarks which are *stable* under strong interactions; see discussion and references in Refs. [149,150].

It is quite possible that compact tetraquark states exist also for states with hidden-flavor, but such states are expected to be broader because of the decoupling mechanism. In fact, there is plenty of evidence for them in form of mass structures in $J/\psi\phi$ [151–156], $J/\psi J/\psi$ [157], $Z_c(4430)^+ \to \psi(2S)\pi^+$ [158–160] and others, although alternative explanations of these structures have been also proposed. Analogous configurations may also exist for pentaquarks, but there is no firm evidence for them yet.

References

[1] T. G. Trippe *et al.* (Particle Data Group), Rev. Mod. Phys. **48**, S1 (1976), [Erratum: Rev. Mod. Phys.48,497(1976)].

[2] K. Hikasa *et al.* (Particle Data Group), Phys. Rev. **D45**, S1 (1992), [Erratum: Phys. Rev.D46,5210(1992)].

[3] M. Praszalowicz, *Skyrmions and Anomalies, p.112, M. Jezabek Ed.*, World Scientific Publishing (1987), ISBN 9971503506.

[4] D. Diakonov, V. Petrov and M. V. Polyakov, Z. Phys. **A359**, 305 (1997), [hep-ph/9703373].

[5] H. Weigel, Eur. Phys. J. **A2**, 391 (1998), [hep-ph/9804260].

[6] K. H. Hicks, Eur.Phys.J. **H37**, 1 (2012).

[7] W. M. Yao *et al.* (Particle Data Group), J. Phys. **G33**, 1 (2006).

[8] R. Aaij *et al.* (LHCb), Phys. Rev. Lett. **115**, 072001 (2015), [arXiv:1507.03414].

[9] R. Aaij *et al.* (LHCb), Phys. Rev. Lett. **117**, 8, 082002 (2016), [arXiv:1604.05708].

[10] R. Aaij *et al.* (LHCb), Phys. Rev. Lett. **122**, 22, 222001 (2019), [arXiv:1904.03947].

[11] M. Wang *et al.*, Chin. Phys. C **45**, 6, 063103 (2021), [arXiv:2012.03699].

[12] R. Aaij *et al.* (LHCb), Sci. Bull. **66**, 1391 (2021), [arXiv:2012.10380].

Downloaded from https://academic.oup.com/ptep/article/2022/8/083C01/6651666 by KIT Library user on 27 September 2022

[13] R. Aaij *et al.* (LHCb), Phys. Rev. Lett. **117**, 8, 082003 (2016), [Addendum: Phys. Rev. Lett.118,119901(2017)], [arXiv:1606.06999].

[14] Z.-C. Yang *et al.*, Chin. Phys. **C36**, 6 (2012), [arXiv:1105.2901].

[15] J.-J. Wu *et al.*, Phys. Rev. Lett. **105**, 232001 (2010), [arXiv:1007.0573].

[16] J.-J. Wu, T. S. H. Lee and B. S. Zou, Phys. Rev. **C85**, 044002 (2012), [arXiv:1202.1036].

[17] M. Karliner and J. L. Rosner, Phys. Rev. Lett. **115**, 12, 122001 (2015), [arXiv:1506.06386].

[18] L. Maiani, A. D. Polosa and V. Riquer, Phys. Lett. **B749**, 289 (2015), [arXiv:1507.04980].

[19] R. F. Lebed, Phys. Lett. **B749**, 454 (2015), [arXiv:1507.05867].

[20] V. V. Anisovich *et al.* (2015), [arXiv:1507.07652].

[21] G.-N. Li, X.-G. He and M. He, JHEP **12**, 128 (2015), [arXiv:1507.08252].

[22] R. Ghosh, A. Bhattacharya and B. Chakrabarti, Phys. Part. Nucl. Lett. **14**, 4, 550 (2017), [arXiv:1508.00356].

[23] Z.-G. Wang, Eur. Phys. J. **C76**, 2, 70 (2016), [arXiv:1508.01468].

[24] R. Zhu and C.-F. Qiao, Phys. Lett. **B756**, 259 (2016), [arXiv:1510.08693].

[25] J. M. Richard, A. Valcarce and J. Vijande, Phys. Lett. **B774**, 710 (2017), [arXiv:1710.08239].

[26] E. Hiyama *et al.*, Phys. Rev. **C98**, 4, 045208 (2018), [arXiv:1803.11369].

[27] A. Ali and A. Y. Parkhomenko, Phys. Lett. **B793**, 365 (2019), [arXiv:1904.00446].

[28] A. Ali *et al.*, JHEP **10**, 256 (2019), [arXiv:1907.06507].

[29] L. Maiani, A. D. Polosa and V. Riquer, Phys. Lett. **B778**, 247 (2018), [arXiv:1712.05296].

[30] C. Fernandez-Ramirez *et al.* (JPAC), Phys. Rev. Lett. **123**, 9, 092001 (2019), [arXiv:1904.10021].

[31] W. L. Wang *et al.*, Phys. Rev. **C84**, 015203 (2011), [arXiv:1101.0453].

[32] J.-J. Wu *et al.*, Phys. Rev. C **84**, 015202 (2011), [arXiv:1011.2399].

[33] C. W. Xiao, J. Nieves and E. Oset, Phys. Rev. **D88**, 056012 (2013), [arXiv:1304.5368].

[34] C. W. Xiao, J. Nieves and E. Oset, Phys. Rev. **D100**, 1, 014021 (2019), [arXiv:1904.01296].

[35] M.-Z. Liu *et al.*, Phys. Rev. Lett. **122**, 24, 242001 (2019), [arXiv:1903.11560].

[36] G.-J. Wang *et al.*, Phys. Rev. D **102**, 3, 036012 (2020), [arXiv:1911.09613].

[37] P. A. Zyla *et al.* (Particle Data Group), PTEP **2020**, 8, 083C01 (2020).

[38] C. Hanhart, Yu. S. Kalashnikova and A. V. Nefediev, Phys. Rev. **D81**, 094028 (2010), [arXiv:1002.4097].

[39] A. A. Filin *et al.*, Phys. Rev. Lett. **105**, 019101 (2010), [arXiv:1004.4789].

[40] F.-K. Guo and U.-G. Meissner, Phys. Rev. **D84**, 014013 (2011), [arXiv:1102.3536].

[41] F.-K. Guo *et al.*, Rev. Mod. Phys. **90**, 1, 015004 (2018), [arXiv:1705.00141].

[42] X.-K. Dong, F.-K. Guo and B.-S. Zou (2021), [arXiv:2108.02673].

[43] S. K. Choi *et al.* (Belle), Phys. Rev. Lett. **91**, 262001 (2003), [hep-ex/0309032].

[44] D. Acosta *et al.* (CDF), Phys. Rev. Lett. **93**, 072001 (2004), [hep-ex/0312021].

[45] B. Aubert *et al.* (BaBar), Phys. Rev. **D71**, 071103 (2005), [hep-ex/0406022].

[46] V. M. Abazov *et al.* (D0), Phys. Rev. Lett. **93**, 162002 (2004), [hep-ex/0405004].

[47] M. Karliner and H. J. Lipkin (2008), [arXiv:0802.0649].

[48] K. F. Chen *et al.* (Belle), Phys. Rev. Lett. **100**, 112001 (2008), [arXiv:0710.2577].

[49] A. Bondar *et al.* (Belle), Phys. Rev. Lett. **108**, 122001 (2012), [arXiv:1110.2251].

[50] P. Krokovny *et al.* (Belle), Phys. Rev. **D88**, 5, 052016 (2013), [arXiv:1308.2646].

[51] A. Garmash *et al.* (Belle), Phys. Rev. **D91**, 7, 072003 (2015), [arXiv:1403.0992].

[52] M. Ablikim *et al.* (BESIII), Phys. Rev. Lett. **110**, 252001 (2013), [arXiv:1303.5949].

[53] Z. Q. Liu *et al.* (Belle), Phys. Rev. Lett. **110**, 252002 (2013), [arXiv:1304.0121].

[54] T. Xiao *et al.*, Phys. Lett. **B727**, 366 (2013), [arXiv:1304.3036].

[55] M. Ablikim *et al.* (BESIII), Phys. Rev. Lett. **112**, 2, 022001 (2014), [arXiv:1310.1163].

[56] M. Ablikim *et al.* (BESIII), Phys. Rev. Lett. **115**, 11, 112003 (2015), [arXiv:1506.06018].

[57] M. Ablikim *et al.* (BESIII), Phys. Rev. Lett. **111**, 24, 242001 (2013), [arXiv:1309.1896].

[58] M. Ablikim *et al.* (BESIII), Phys. Rev. Lett. **113**, 21, 212002 (2014), [arXiv:1409.6577].

[59] M. Ablikim *et al.* (BESIII), Phys. Rev. Lett. **112**, 13, 132001 (2014), [arXiv:1308.2760].

[60] M. Karliner, Acta Phys. Polon. **B47**, 117 (2016).

[61] M. Karliner, J. L. Rosner and T. Skwarnicki, Ann. Rev. Nucl. Part. Sci. **68**, 17 (2018), [arXiv:1711.10626].

[62] S. L. Olsen, T. Skwarnicki and D. Zieminska, Rev. Mod. Phys. **90**, 1, 015003 (2018), [arXiv:1708.04012].

[63] M. B. Voloshin and L. B. Okun, JETP Lett. **23**, 333 (1976), [Pisma Zh. Eksp. Teor. Fiz.23,369(1976)].

[64] A. De Rujula, H. Georgi and S. Glashow, Phys. Rev. Lett. **38**, 317 (1977).

[65] N. A. Tornqvist, Phys. Rev. Lett. **67**, 556 (1991).

[66] N. A. Tornqvist, Z. Phys. **C61**, 525 (1994), [hep-ph/9310247].

[67] N. A. Tornqvist, Phys. Lett. **B590**, 209 (2004), [hep-ph/0402237].

[68] C. E. Thomas and F. E. Close, Phys. Rev. **D78**, 034007 (2008), [arXiv:0805.3653].

[69] M. Suzuki, Phys. Rev. **D72**, 114013 (2005), [hep-ph/0508258].

[70] S. Fleming *et al.*, Phys. Rev. **D76**, 034006 (2007), [hep-ph/0703168].

[71] T. E. O. Ericson and G. Karl, Phys. Lett. **B309**, 426 (1993).

[72] M. Karliner, H. J. Lipkin and N. A. Tornqvist, in "Proceedings, 14th International Conference on Hadron spectroscopy (Hadron 2011)," (2011), [arXiv:1109.3472], URL `http://inspirehep.net/record/927616/files/arXiv:1109.3472.pdf`.

[73] M. Karliner, H. J. Lipkin and N. A. Tornqvist, Nucl. Phys. Proc. Suppl. **225-227**, 102 (2012).

[74] M. Karliner, "Hidden Charm Molecular Pentaquarks: Some Open Questions," in Proc. Bled Mini-Workshop, Slovenia, July 15-19, 2019, B. Golli et al., Eds., p. 25, `http://www-f1.ijs.si/BledPub/bled2019.pdf`.

[75] X.-Q. Li and X. Liu, Eur. Phys. J. **C74**, 12, 3198 (2014), [arXiv:1409.3332].

Downloaded from https://academic.oup.com/ptep/article/2022/8/083C01/6651666 by KIT Library user on 27 September 2022

[76] R. Chen *et al.*, Phys. Rev. Lett. **115**, 13, 132002 (2015), [arXiv:1507.03704].

[77] H.-X. Chen *et al.*, Phys. Rev. Lett. **115**, 17, 172001 (2015), [arXiv:1507.03717].

[78] L. Roca, J. Nieves and E. Oset, Phys. Rev. **D92**, 9, 094003 (2015), [arXiv:1507.04249].

[79] J. He, Phys. Lett. **B753**, 547 (2016), [arXiv:1507.05200].

[80] H. Huang *et al.*, Eur. Phys. J. **C76**, 11, 624 (2016), [arXiv:1510.04648].

[81] L. Roca and E. Oset, Eur. Phys. J. **C76**, 11, 591 (2016), [arXiv:1602.06791].

[82] Q.-F. Lü and Y.-B. Dong, Phys. Rev. **D93**, 7, 074020 (2016), [arXiv:1603.00559].

[83] Y. Shimizu, D. Suenaga and M. Harada, Phys. Rev. **D93**, 11, 114003 (2016), [arXiv:1603.02376].

[84] C.-W. Shen *et al.*, Nucl. Phys. **A954**, 393 (2016), [arXiv:1603.04672].

[85] Y. Yamaguchi *et al.*, Phys. Rev. **D96**, 11, 114031 (2017), [arXiv:1709.00819].

[86] J. F. Giron, R. F. Lebed and C. T. Peterson, JHEP **05**, 061 (2019), [arXiv:1903.04551].

[87] R. Chen *et al.*, Phys. Rev. **D100**, 1, 011502 (2019), [arXiv:1903.11013].

[88] F.-K. Guo *et al.*, Phys. Rev. **D99**, 9, 091501 (2019), [arXiv:1903.11503].

[89] J. He, Eur. Phys. J. **C79**, 5, 393 (2019), [arXiv:1903.11872].

[90] H. Huang, J. He and J. Ping (2019), [arXiv:1904.00221].

[91] Y. Shimizu, Y. Yamaguchi and M. Harada (2019), [arXiv:1904.00587].

[92] Z.-H. Guo and J. A. Oller, Phys. Lett. **B793**, 144 (2019), [arXiv:1904.00851].

[93] C.-J. Xiao *et al.*, Phys. Rev. **D100**, 1, 014022 (2019), [arXiv:1904.00872].

[94] Z.-G. Wang, Int. J. Mod. Phys. A **35**, 01, 2050003 (2020), [arXiv:1905.02892].

[95] L. Meng *et al.*, Phys. Rev. **D100**, 1, 014031 (2019), [arXiv:1905.04113].

[96] F. Giannuzzi, Phys. Rev. **D99**, 9, 094006 (2019), [arXiv:1903.04430].

[97] Q. Wu and D.-Y. Chen, Phys. Rev. D **100**, 11, 114002 (2019), [arXiv:1906.02480].

[98] C.-W. Shen, J.-J. Wu and B.-S. Zou, Phys. Rev. **D100**, 5, 056006 (2019), [arXiv:1906.03896].

[99] F. Stancu, Eur. Phys. J. C **79**, 11, 957 (2019), [arXiv:1902.07101].

[100] C. W. Xiao, J. Nieves and E. Oset, Phys. Lett. B **799**, 135051 (2019), [arXiv:1906.09010].

[101] M. B. Voloshin, Phys. Rev. **D100**, 3, 034020 (2019), [arXiv:1907.01476].

[102] S. Sakai, H.-J. Jing and F.-K. Guo, Phys. Rev. D **100**, 7, 074007 (2019), [arXiv:1907.03414].

[103] Z.-G. Wang and X. Wang, Chin. Phys. C **44**, 103102 (2020), [arXiv:1907.04582].

[104] Y. Yamaguchi *et al.*, Phys. Rev. D **101**, 9, 091502 (2020), [arXiv:1907.04684].

[105] Y.-J. Xu *et al.*, Phys. Rev. D **102**, 3, 034028 (2020), [arXiv:1907.05097].

[106] M. Pavon Valderrama, Phys. Rev. D **100**, 9, 094028 (2019), [arXiv:1907.05294].

[107] F.-Z. Peng *et al.* (2019), [arXiv:1907.05322].

[108] M.-Z. Liu *et al.*, Phys. Rev. D **103**, 5, 054004 (2021), [arXiv:1907.06093].

[109] Y.-W. Pan *et al.*, Phys. Rev. D **102**, 1, 011504 (2020), [arXiv:1907.11220].

[110] T. J. Burns and E. S. Swanson, Phys. Rev. D **100**, 11, 114033 (2019), [arXiv:1908.03528].

[111] Y.-H. Lin and B.-S. Zou, Phys. Rev. **D100**, 5, 056005 (2019), [arXiv:1908.05309].

[112] M.-L. Du *et al.* (2021), [arXiv:2102.07159].

[113] S. Dubynskiy and M. B. Voloshin, Phys. Lett. **B666**, 344 (2008), [arXiv:0803.2224].

[114] M. I. Eides, V. Y. Petrov and M. V. Polyakov, Mod. Phys. Lett. A **35**, 18, 2050151 (2020), [arXiv:1904.11616].

[115] F.-K. Guo *et al.*, Phys. Rev. **D92**, 7, 071502 (2015), [arXiv:1507.04950].

[116] U.-G. Meissner and J. A. Oller, Phys. Lett. **B751**, 59 (2015), [arXiv:1507.07478].

[117] X.-H. Liu, Q. Wang and Q. Zhao, Phys. Lett. **B757**, 231 (2016), [arXiv:1507.05359].

[118] M. Mikhasenko (2015), [arXiv:1507.06552].

[119] T. J. Burns, Eur. Phys. J. **A51**, 11, 152 (2015), [arXiv:1509.02460].

[120] H.-X. Chen *et al.*, Phys. Rept. **639**, 1 (2016), [arXiv:1601.02092].

[121] Y.-R. Liu *et al.*, Prog. Part. Nucl. Phys. **107**, 237 (2019), [arXiv:1903.11976].

[122] N. Brambilla *et al.*, Phys. Rept. **873**, 1 (2020), [arXiv:1907.07583].

[123] Y. Huang *et al.*, J. Phys. **G41**, 11, 115004 (2014), [arXiv:1305.4434].

[124] Q. Wang, X.-H. Liu and Q. Zhao, Phys. Rev. **D92**, 034022 (2015), [arXiv:1508.00339].

[125] V. Kubarovsky and M. B. Voloshin, Phys. Rev. **D92**, 3, 031502 (2015), [arXiv:1508.00888].

[126] M. Karliner and J. L. Rosner, Phys. Lett. **B752**, 329 (2016), [arXiv:1508.01496].

[127] A. N. Hiller Blin *et al.*, Phys. Rev. **D94**, 3, 034002 (2016), [arXiv:1606.08912].

[128] X. Cao and J.-p. Dai, Phys. Rev. **D100**, 5, 054033 (2019), [arXiv:1904.06015].

[129] X.-Y. Wang, X.-R. Chen and J. He, Phys. Rev. **D99**, 11, 114007 (2019), [arXiv:1904.11706].

[130] J.-J. Wu, T. S. H. Lee and B.-S. Zou, Phys. Rev. **C100**, 3, 035206 (2019), [arXiv:1906.05375].

[131] G. C. Rossi and G. Veneziano (2019), [arXiv:1909.01753].

[132] U. Skerbis and S. Prelovsek, Phys. Rev. **D99**, 9, 094505 (2019), [arXiv:1811.02285].

[133] C. W. Xiao and U. G. Meissner, Phys. Rev. **D92**, 11, 114002 (2015), [arXiv:1508.00924].

[134] M. B. Voloshin, Phys. Rev. **D99**, 9, 093003 (2019), [arXiv:1903.04422].

[135] R.-Q. Wang *et al.*, Phys. Rev. **C94**, 4, 044913 (2016), [arXiv:1601.02835].

[136] I. Schmidt and M. Siddikov, Phys. Rev. **D93**, 9, 094005 (2016), [arXiv:1601.05621].

[137] Q.-F. L"u *et al.*, Phys. Rev. **D93**, 3, 034009 (2016), [arXiv:1510.06271].

[138] X.-H. Liu and M. Oka, Nucl. Phys. **A954**, 352 (2016), [arXiv:1602.07069].

[139] X.-Y. Wang *et al.*, Phys. Lett. **B797**, 134862 (2019), [arXiv:1906.04044].

[140] A. Ali *et al.* (GlueX), Phys. Rev. Lett. **123**, 7, 072001 (2019), [arXiv:1905.10811].

[141] M.-L. Du *et al.*, Eur. Phys. J. C **80**, 11, 1053 (2020), [arXiv:2009.08345].

[142] D. Winney *et al.* (JPAC), Phys. Rev. **D100**, 3, 034019 (2019), [arXiv:1907.09393].

Downloaded from https://academic.oup.com/ptep/article/2022/8/083C01/6651666 by KIT Library user on 27 September 2022

[143] R. Aaij *et al.* (LHCb), Phys. Rev. Lett. **128**, 062001 (2021), [arXiv:2108.04720].

[144] B. Wang, L. Meng and S.-L. Zhu, JHEP **11**, 108 (2019), [arXiv:1909.13054].

[145] R. Chen, J. He and X. Liu, Chin. Phys. C **41**, 10, 103105 (2017), [arXiv:1609.03235].

[146] E. Santopinto and A. Giachino, Phys. Rev. D **96**, 1, 014014 (2017), [arXiv:1604.03769].

[147] B. Wang, L. Meng and S.-L. Zhu, Phys. Rev. D **101**, 3, 034018 (2020), [arXiv:1912.12592].

[148] M. Karliner and J. L. Rosner, Sci. Bull. **66**, 13, 1256 (2021), [arXiv:2104.15077].

[149] R. Aaij *et al.* (LHCb) (2021), [arXiv:2109.01038].

[150] R. Aaij *et al.* (LHCb) (2021), [arXiv:2109.01056].

[151] T. Aaltonen *et al.* (CDF), Phys. Rev. Lett. **102**, 242002 (2009), [arXiv:0903.2229].

[152] T. Aaltonen *et al.* (CDF), Mod. Phys. Lett. A **32**, 26, 1750139 (2017), [arXiv:1101.6058].

[153] S. Chatrchyan *et al.* (CMS), Phys. Lett. B **734**, 261 (2014), [arXiv:1309.6920].

[154] R. Aaij *et al.* (LHCb), Phys. Rev. Lett. **118**, 2, 022003 (2017), [arXiv:1606.07895].

[155] R. Aaij *et al.* (LHCb), Phys. Rev. D **95**, 1, 012002 (2017), [arXiv:1606.07898].

[156] R. Aaij *et al.* (LHCb), Phys. Rev. Lett. **127**, 8, 082001 (2021), [arXiv:2103.01803].

[157] R. Aaij *et al.* (LHCb), Sci. Bull. **65**, 23, 1983 (2020), [arXiv:2006.16957].

[158] S. K. Choi *et al.* (Belle), Phys. Rev. Lett. **100**, 142001 (2008), [arXiv:0708.1790].

[159] K. Chilikin *et al.* (Belle), Phys. Rev. D **88**, 7, 074026 (2013), [arXiv:1306.4894].

[160] R. Aaij *et al.* (LHCb), Phys. Rev. Lett. **112**, 22, 222002 (2014), [arXiv:1404.1903].

Downloaded from https://academic.oup.com/ptep/article/2022/8/083C01/6651666 by KIT Library user on 27 September 2022

Hypothetical Particles and Concepts

85. Extra dimensions (rev.) 983
86. W'-boson searches (rev.) 991
87. Z'-boson searches (rev.) 995
88. Supersymmetry: theory (rev.) 1000
89. Supersymmetry: experiment (rev.) 1019
90. Axions and other similar particles (rev.) 1038
91. Quark and lepton compositeness, searches for (rev.) . . . 1055
92. Dynamical electroweak symmetry breaking: implications of the H^0 (rev.) 1061
93. Grand unified theories 1076
94. Leptoquarks (rev.) 1090
95. Magnetic monopoles (rev.) 1093

Downloaded from https://academic.oup.com/ptep/article/2022/8/083C01/6651666 by KIT Library user on 27 September 2022

Downloaded from https://academic.oup.com/ptep/article/2022/8/083C01/6651666 by KIT Library user on 27 September 2022

85. Extra Dimensions

Revised August 2021 by Y. Gershtein (Rutgers U.) and A. Pomarol (U. Autònoma de Barcelona; IFAE).

85.1 Introduction

Proposals for a spacetime with more than three spatial dimensions date back to the 1920s, mainly through the work of Kaluza and Klein, in an attempt to unify the forces of nature [1]. Although their initial idea failed, the formalism that they and others developed is still useful nowadays. Around 1980, string theory proposed again to enlarge the number of space dimensions, this time as a requirement for describing a consistent theory of quantum gravity. The extra dimensions were supposed to be compactified at a scale close to the Planck scale, and thus not testable experimentally in the near future.

A different approach was given by Arkani-Hamed, Dimopoulos, and Dvali (ADD) in their seminal paper in 1998 [2], where they showed that the weakness of gravity could be explained by postulating two or more flat extra dimensions in which only gravity could propagate. The size of these extra dimensions should range between roughly a millimeter and ∼1/TeV, leading to possible observable consequences in current and future experiments. A year later, Randall and Sundrum (RS) [3] found a new possibility using a warped geometry, postulating a five-dimensional Anti-de Sitter (AdS) spacetime with a compactification scale of order 1/TeV. The origin of the smallness of the electroweak scale versus the Planck scale was explained by the gravitational redshift factor present in the warped AdS metric. As in the ADD model, originally only gravity was assumed to propagate in the extra dimensions, although it was soon clear that this was not necessary in warped extra dimensions and also the SM gauge fields [4, 5] and SM fermions [6, 7] could propagate in the five-dimensional spacetime.

The physics of warped extra-dimensional models has an alternative interpretation by means of the AdS/CFT correspondence [8–10]. Models with warped extra dimensions are related to four-dimensional strongly-interacting theories, allowing an understanding of the properties of five-dimensional fields as those of four-dimensional composite states [11]. This approach has opened new directions for tackling outstanding questions in particle physics, such as the flavor problem, grand unification, and the origin of electroweak symmetry breaking or supersymmetry breaking.

85.1.1 *Experimental Constraints*

Constraints on extra-dimensional models arise from astrophysical and cosmological considerations, tabletop experiments exploring gravity at sub-mm distances, and collider experiments. Collider limits on extra-dimensional models are dominated by LHC results, which can be found on the public WWW pages of ATLAS [12] and CMS [13]. This review includes the most recent limits, most of which are published results based on 140 fb^{-1}LHC data collected in 2015-18 at a center-of-mass energy of 13 TeV and legacy results from 20 $\mathrm{fb}^{-1}$of 8 TeV data collected in Run 1. For most of the models, Run 2 results surpass the sensitivity of Run 1.

85.1.2 *Kaluza-Klein Theories*

Field theories with compact extra dimensions can be written as theories in ordinary four dimensions (4D) by performing a Kaluza-Klein (KK) reduction. As an illustration, consider a simple example, namely a field theory of a complex scalar in flat five-dimensional (5D) spacetime. The action will be given by [1]

$$S_5 = -\int d^4x\, dy\, M_5 \left[|\partial_\mu \phi|^2 + |\partial_y \phi|^2 + \lambda_5 |\phi|^4\right] , \qquad (85.1)$$

where y refers to the extra (fifth) dimension. A universal scale M_5 has been extracted in front of the action in order to keep the 5D field with the same mass-dimension as in 4D. This theory is perturbative for energies $E \lesssim \ell_5 M_5/\lambda_5$ where $\ell_5 = 24\pi^3$ [14].

[1] Our convention for the metric is $\eta_{MN} = \mathrm{Diag}(-1, 1, 1, 1, 1)$.

Let us now consider that the fifth dimension is compact with the topology of a circle S^1 of radius R, which corresponds to the identification of y with $y + 2\pi R$. In such a case, the 5D complex scalar field can be expanded in a Fourier series:

$$\phi(x, y) = \frac{1}{\sqrt{2\pi R M_5}} \sum_{n=-\infty}^{\infty} e^{iny/R} \phi^{(n)}(x) , \qquad (85.2)$$

that, inserted in Eq. (85.1) and integrating over y, gives

$$S_5 = S_4^{(0)} + S_4^{(n)} , \qquad (85.3)$$

where

$$S_4^{(0)} = -\int d^4x \left[|\partial_\mu \phi^{(0)}|^2 + \lambda_4 |\phi^{(0)}|^4\right] , \qquad (85.4)$$

and,

$$S_4^{(n)} = -\int d^4x \sum_{n\neq 0} \left[|\partial_\mu \phi^{(n)}|^2 + \left(\frac{n}{R}\right)^2 |\phi^{(n)}|^2\right] + \text{quartic interactions} . \qquad (85.5)$$

The $n = 0$ mode self-coupling is given by

$$\lambda_4 = \frac{\lambda_5}{2\pi R M_5} . \qquad (85.6)$$

The above action corresponds to a 4D theory with a massless scalar $\phi^{(0)}$, referred to as the zero mode, and an infinite tower of massive modes $\phi^{(n)}$ with $n > 0$, known as KK modes. The KK reduction thus allows a treatment of 5D theories as 4D field theories with an infinite number of fields. At energies smaller than $1/R$, the KK modes can be neglected, leaving the zero-mode action of Eq. (85.4). The strength of the interaction of the zero-mode, given by Eq. (85.6), decreases as R increases. Thus, for a large extra dimension $R \gg 1/M_5$, the massless scalar is very weakly coupled.

85.2 Large Extra Dimensions for Gravity

85.2.1 *The ADD Scenario*

The ADD scenario [2, 15] (for a review see, for example, [16]) assumes a $D = 4 + \delta$ dimensional spacetime, with δ compactified spatial dimensions. The apparent weakness of gravity arises since it propagates in the higher-dimensional space. The SM is assumed to be localized in a 4D subspace, a 3-brane, as can be found in certain string theory constructions [17, 18]. Gravity is described by the Einstein-Hilbert action in $D = 4 + \delta$ spacetime dimensions

$$S_D = -\frac{\bar{M}_D^{2+\delta}}{2} \int d^4x d^\delta y \sqrt{-g}\, \mathcal{R} + \int d^4x \sqrt{-g_{\rm ind}}\, \mathcal{L}_{\rm SM} , \qquad (85.7)$$

where x labels the ordinary four coordinates, y the δ extra coordinates, g refers to the determinant of the D-dimensional metric whose Ricci scalar is defined by $\mathcal{R}$, and $\bar{M}_D$ is called the reduced Planck scale of the D-dimensional theory. In the second term of Eq. (85.7), which gives the gravitational interactions of SM fields, the D-dimensional metric reduces to the induced metric on the 3-brane where the SM fields propagate. The extra dimensions are assumed to be flat and compactified in a volume V_δ. As an example, consider a toroidal compactification of equal radii R and volume $V_\delta = (2\pi R)^\delta$. After a KK reduction, one finds that the fields that couple to the SM are the spin-2 gravitational field $G_{\mu\nu}(x, y)$ and a tower of spin-0 KK graviscalars [19]. The graviscalars, however, only couple to SM fields through the trace of the energy-momentum tensor, resulting in weaker couplings to the SM fields. The Fourier expansion of the spin-2 field is given by

$$G_{\mu\nu}(x, y) = G_{\mu\nu}^{(0)}(x) + \frac{1}{\sqrt{V_\delta}} \sum_{\vec{n}\neq 0} e^{i\vec{n}\cdot\vec{y}/R} G_{\mu\nu}^{(\vec{n})}(x) , \qquad (85.8)$$

where $\vec{y} = (y_1, y_2, ..., y_\delta)$ are the extra-dimensional coordinates and $\vec{n} = (n_1, n_2, ..., n_\delta)$. Eq. (85.8) contains a massless state,

Downloaded from https://academic.oup.com/ptep/article/2022/8/083C01/6651666 by KIT Library user on 27 September 2022

the 4D graviton $G^{(0)}_{\mu\nu}$, and its KK tower $G^{(\vec{n})}_{\mu\nu}$ with masses $m^2_{\vec{n}} = |\vec{n}|^2/R^2$. At energies below $1/R$ the action is that of the zero mode

$$S^{(0)}_4 = -\frac{\bar{M}^{2+\delta}_D}{2}\int d^4x\, V_\delta \sqrt{-g^{(0)}}\,\mathcal{R}^{(0)} + \int d^4x \sqrt{-g^{(0)}_{\rm ind}}\,\mathcal{L}_{\rm SM}\,, \tag{85.9}$$

where we can identify the 4D reduced Planck mass, $M_P \equiv 1/\sqrt{8\pi G_N} \simeq 2.4\times 10^{18}$ GeV, as a function of the D-dimensional parameters:

$$M^2_P = V^\delta \bar{M}^{2+\delta}_D \equiv R^\delta M^{2+\delta}_D\,. \tag{85.10}$$

Fixing M_D at around the electroweak scale $M_D \sim$ TeV to avoid introducing a new mass scale in the model, Eq. (85.10) gives a prediction for R:

$$\delta = 1, 2, ..., 6 \;\rightarrow\; R \sim 10^9 \text{ km}\,, 0.5 \text{ mm}\,, ...\,, 0.1 \text{ MeV}^{-1}\,. \tag{85.11}$$

The option $\delta = 1$ is clearly ruled out, as it leads to modifications of Newton's law at solar system distances. However this is not the case for $\delta \geq 2$, and possible observable consequences can be sought in present and future experiments.

Consistency of the model requires a stabilization mechanism for the radii of the extra dimensions, to the values shown in Eq. (85.11). The fact that we need $R \gg 1/M_D$ leads to a new hierarchy problem, the solution of which might require imposing supersymmetry in the extra-dimensional bulk (for the case of two extra dimensions see for example [20]).

85.2.2 *Tests of the Gravitational Force Law at Sub-mm Distances*

The KK modes of the graviton give rise to deviations from Newton's law of gravitation for distances $\lesssim R$. Such deviations are usually parameterized by a modified Newtonian potential of the form

$$V(r) = -G_N \frac{m_1 m_2}{r}\left[1 + \alpha\, e^{-r/\lambda}\right]\,. \tag{85.12}$$

For a 2-torus compactification, $\alpha = 16/3$ and $\lambda = R$. Searches for deviations from Newton's law of gravitation have been performed in several experiments [21–24]. From Ref. [23] we have the constraint $R < 30\mu$m at 95% CL for $\delta = 2$, corresponding to $M_D > 4.0$ TeV. We see then that bounds from Newton's law deviations are already pushing the scale M_D beyond the TeV for two extra dimensions.

85.2.3 *Astrophysical and Cosmological Constraints*

The light KK gravitons could be copiously produced in stars, carrying away energy. Ensuring that the graviton luminosity is low enough to preserve the agreement of stellar models with observations provides powerful bounds on the scale M_D. The most stringent bound arises from supernova SN1987A, giving $M_D > 27$ (2.4) TeV for $\delta = 2$ (3) [25]. After a supernova explosion, most of the KK gravitons stay gravitationally trapped in the remnant neutron star. The requirement that neutron stars are not excessively heated by KK decays into photons leads to $M_D > 1700$ (76) TeV for $\delta = 2$ (3) [26].

Cosmological constraints are also quite stringent [27]. To avoid overclosure of the Universe by relic gravitons one needs $M_D > 7$ TeV for $\delta = 2$. Relic KK gravitons decaying into photons contribute to the cosmic diffuse gamma radiation, from which one can derive the bound $M_D > 100$ TeV for $\delta = 2$.

We must mention however that bounds coming from the decays of KK gravitons into photons can be reduced if we assume that KK gravitons decay mainly into other non-SM states. This could happen, for example, if there were other 3-branes with hidden sectors residing on them [15].

85.2.4 *Collider Signals*

85.2.4.1 *Graviton and Other Particle Production*

Although each KK graviton has a purely gravitational coupling, suppressed by $1/M_P$, inclusive processes in which one sums over the almost continuous spectrum of available gravitons have cross sections suppressed only by powers of M_D. Processes involving gravitons are therefore detectable in collider experiments if $M_D \sim$ TeV. A number of experimental searches for evidence of large extra dimensions have been performed at colliders, and interpreted in the context of the ADD model.

One signature arises from direct graviton emission. By making a derivative expansion of Einstein gravity, one can construct an effective theory, valid for energies much lower than M_D, and use it to make predictions for graviton-emission processes at colliders [19, 28, 29]. Gravitons produced in the final state would escape detection, giving rise to missing transverse energy ($\not{E}_T$). The results quoted below are 95% CL lower limits on M_D for a range of values of δ between 2 and 6, with more stringent limits corresponding to lower δ values.

At hadron colliders, experimentally sensitive channels include the jet $(j) + \not{E}_T$ and $\gamma + \not{E}_T$ final states. ATLAS (CMS) $j + \not{E}_T$ results with 139 (137) fb^{-1} of 13 TeV data provide limits of $M_D > 5.9 - 11.2$ TeV [30] ($M_D > 5.5 - 10.7$ TeV [31]). For these analyses, both experiments are assuming leading order (LO) cross sections. Since the effective theory is only valid for energies much less than M_D, the results are quoted for the full space, and include the information that suppressing the graviton cross section by a factor $M^4_D/\hat{s}^2$ for $\sqrt{\hat{s}} > M_D$, where $\sqrt{\hat{s}}$ is the parton-level center-of-mass energy of the hard collision, weakens the limits on M_D by a negligible amount for $\delta = 2$ ($\sim$3% for $\delta = 6$). Less stringent limits are obtained by CMS [32] from analysis of 36 fb^{-1}of 13 TeV data in the $\gamma + \not{E}_T$ final state ($M_D > 2.85-2.90$ TeV for $\delta = 3-6$). The analogous ATLAS search [33] uses full Run 2 statistics but does not quote ADD interpretation of the results.

In models in which the ADD scenario is embedded in a string theory at the TeV scale [18], we expect the string scale M_s to be smaller than M_D, and therefore expect production of string resonances at the LHC [34]. A result from CMS analyzing the dijet invariant mass distribution for 137 fb^{-1}of 13 TeV data excludes string resonances that decay predominantly to $q + g$ with masses below 7.9 TeV [35]. ATLAS dijet analysis [36] provides their results in the context of model-independent limits on the cross section times acceptance for generic resonances of a variety of possible widths, from which one can deduce similar lower mass limits ~ 8 TeV for string resonances decaying to $q + g$.

85.2.4.2 *Virtual graviton effects*

One can also search for virtual graviton effects, the calculation of which however depends on the ultraviolet cut-off of the theory and is therefore very model dependent. In the literature, several different formulations exist [19,29,37] for the dimension-eight operator for gravity exchange at tree level:

$$\mathcal{L}_8 = \pm\frac{4}{M^4_{TT}}\left(T_{\mu\nu}T^{\mu\nu} - \frac{1}{\delta+2}T^\mu_\mu T^\nu_\nu\right), \tag{85.13}$$

where $T_{\mu\nu}$ is the energy-momentum tensor and M_{TT} is related to M_D by some model-dependent coefficient [38]. The relations with the parametrization of Refs. [37] and [19] are, respectively, $M_{TT} = M_S$ and $M_{TT} = (2/\pi)^{1/4}\Lambda_T$. The experimental results below are given as 95% CL lower limits on M_{TT}, including in some cases the possibility of both constructive or destructive interference, depending on the sign chosen in Eq. (9).

The most stringent limits arise from LHC analyses of the dijet angular distribution. Using 35.9 fb^{-1}of 13 TeV data, CMS [39] obtains results that correspond to an approximate limit of $M_{TT} >$ 9.1 TeV.

The next most restrictive results come from the analyses of diphoton ($M_{TT} > 6.1$ TeV from ATLAS [40] and $M_{TT} > 7.0$ TeV from CMS [41]) and dilepton mass spectra ($M_{TT} > 6.5$ TeV from CMS [42]). The complete Run 2 (139 fb^{-1}) analysis of ATLAS di-lepton data [43] does not quote the limits on ADD.

At the one-loop level, gravitons can also generate dimension-six operators with coefficients that are also model dependent. Experimental bounds on these operators can also give stringent constraints on M_D [38].

85.2.4.3 *Black Hole Production*

The physics at energies $\sqrt{s} \sim M_D$ is sensitive to the details of the unknown quantum theory of gravity. Nevertheless, in the transplanckian regime, $\sqrt{s} \gg M_D$, one can rely on a semiclassical description of gravity to obtain predictions. An interesting feature of transplanckian physics is the creation of black holes [44,45] (for

Downloaded from https://academic.oup.com/ptep/article/2022/8/083C01/6651666 by KIT Library user on 27 September 2022

a review see, for example, [46]). A black hole is expected to be formed in a collision in which the impact parameter is smaller than the Schwarzschild radius [47]:

$$R_S = \frac{1}{M_D}\left[\frac{2^\delta \pi^{(\delta-3)/2}}{\delta+2}\Gamma\left(\frac{\delta+3}{2}\right)\frac{M_{BH}}{M_D}\right]^{1/(\delta+1)}, \quad (85.14)$$

where M_{BH} is the mass of the black hole, which would roughly correspond to the total energy in the collision. The cross section for black hole production can be estimated to be of the same order as the geometric area $\sigma \sim \pi R_S^2$. For $M_D \sim$ TeV, this gives a production of $\sim 10^7$ black holes at the $\sqrt{s} = 14$ TeV LHC with an integrated luminosity of 30 fb^{-1} [44,45]. A black hole would provide a striking experimental signature since it is expected to thermally radiate with a Hawking temperature $T_H = (\delta+1)/(4\pi R_S)$, and therefore would evaporate democratically into all SM states. Nevertheless, given the present constraints on M_D, the LHC will not be able to reach energies much above M_D. This implies that predictions based on the semiclassical approximation could receive sizable modifications from model-dependent quantum-gravity effects.

The most stringent limits on microscopic black holes arise from LHC searches which observed no excesses above the SM background in high-multiplicity final states. The results are usually quoted as model-independent limits on the cross section for new physics in the final state and kinematic region analyzed. These results can then be used to provide constraints of models of low-scale gravity and weakly-coupled string theory. In addition, limits are sometimes quoted on particular implementations of models, which are used as benchmarks to illustrate the sensitivity.

A CMS analysis [48] of multi-object final states using 36 fb^{-1}of 13 TeV data, excludes semiclassical black holes below masses of up to 10.1 TeV for $M_D = 2$ TeV and $\delta = 6$. Analogous Run 2 ATLAS analysis [49], using 3.0 fb^{-1}of 13 TeV data, excludes black hole masses up to $9.0 - 9.7$ TeV, depending on M_D, for $\delta = 6$. Another ATLAS search [50] for an excess of events with multiple high transverse momentum objects, including charged leptons and jets, using 3.2 fb^{-1}of 13 TeV data, excludes semiclassical black holes below masses of ~ 8.7 TeV for $M_D = 2$ TeV and $\delta = 6$.

A complementary approach is to look for jet extinction at high transverse momenta, as we expect hard short distance scattering processes to be highly suppressed at energies above M_D [51]. The CMS analysis [52] of inclusive jet p_T spectrum in 10.7 fb^{-1}of 8 TeV data set a lower limit of 3.3 TeV on the extinction mass scale.

For black hole masses near M_D, the semi-classical approximation is not valid, and one could instead expect quantum black holes (QBH) that decay primarily into two-body final states [53]. LHC Run 2 results at 13 TeV provide lower limits on QBH masses of order $2.3 - 9.4$ TeV, depending on the details of the model. Searches that consider interpretations in terms of QBH limits include the CMS multi-object analysis (based on 2.3 fb^{-1} [54]), ATLAS dijet analysis (based on 139 fb^{-1} [36]), and different flavor di-lepton analyses at CMS ($e\mu$, 36 fb^{-1} at 13 TeV [55]) and ATLAS ($e\mu$, $e\tau$, $\mu\tau$, 36.1 fb^{-1} at 13 TeV [56]).

So [36] relies on 139 fb-1 and [54] relies on 2.3 fb-1.

In weakly-coupled string models the semiclassical description of gravity fails in the energy range between M_s and M_s/g_s^2 where stringy effects are important. In this regime one expects, instead of black holes, the formation of string balls, made of highly excited long strings, that could be copiously produced at the LHC for $M_s \sim$ TeV [57], and would evaporate thermally at the Hagedorn temperature giving rise to high-multiplicity events. The same analyses used to search for black holes can be interpreted in the context of string balls. For example, for the case of $\delta = 6$ with $M_s = M_D/1.26 = 3$ TeV, the ATLAS multiple high transverse momentum object analysis [49] excludes string balls with masses below 6.5 to 9.0 TeV for values of $0.2 < g_s < 0.8$. The CMS multi-object analysis [48] studies string ball production in two scenarios, both assuming $\delta = 6$. For the constant $g_s = 0.2$ and $1 < M_s < 3.5$ TeV the string ball masses below 7.2 to 9.4 TeV are excluded, while at constant $M_s = 3.6$ TeV and $0.2 < g_s < 0.4$ masses below 7.2 to 8.1 TeV are excluded.

85.3 TeV-Scale Extra Dimensions

85.3.1 *Warped Extra Dimensions*

The RS model [3] is the most attractive setup of warped extra dimensions at the TeV scale, since it provides an alternative solution to the hierarchy problem. The RS model is based on a 5D theory with the extra dimension compactified in an orbifold, S^1/Z_2, a circle S^1 with the extra identification of y with $-y$. This corresponds to the segment $y \in [0, \pi R]$, a manifold with boundaries at $y = 0$ and $y = \pi R$. Let us now assume that this 5D theory has a cosmological constant in the bulk Λ, and on the two boundaries Λ_0 and $\Lambda_{\pi R}$:

$$S_5 = -\int d^4x\, dy \Big\{ \sqrt{-g}\Big[\frac{1}{2}M_5^3\mathcal{R} + \Lambda\Big] + \sqrt{-g_0}\,\delta(y)\Lambda_0 + \sqrt{-g_{\pi R}}\,\delta(y-\pi R)\Lambda_{\pi R}\Big\}, \quad (85.15)$$

where g_0 and $g_{\pi R}$ are the values of the determinant of the induced metric on the two respective boundaries. Einstein's equations can be solved, giving in this case the metric

$$ds^2 = a(y)^2 dx^\mu dx^\nu \eta_{\mu\nu} + dy^2\ , \quad a(y) = e^{-ky}\,, \quad (85.16)$$

where $k = \sqrt{-\Lambda/6M_5^3}$. Consistency of the solution requires $\Lambda_0 = -\Lambda_{\pi R} = -\Lambda/k$. The metric in Eq. (85.16) corresponds to a 5D AdS space. The factor $a(y)$ is called the "warp" factor and determines how 4D scales change as a function of the position in the extra dimension. In particular, this implies that energy scales for 4D fields localized at the boundary at $y = \pi R$ are redshifted by a factor $e^{-k\pi R}$ with respect to those localized at $y = 0$. For this reason, the boundaries at $y = 0$ and $y = \pi R$ are usually referred to as the ultraviolet (UV) and infrared (IR) boundaries, respectively.

As in the ADD case, we can perform a KK reduction and obtain the low-energy effective theory of the 4D massless graviton. In this case we obtain

$$M_P^2 = \int_0^{\pi R} dy\, e^{-2ky} M_5^3 = \frac{M_5^3}{2k}\left(1 - e^{-2k\pi R}\right). \quad (85.17)$$

Taking $M_5 \sim k \sim M_P$, we can generate an IR-boundary scale of order $ke^{-k\pi R} \sim$ TeV for an extra dimension of radius $R \simeq 11/k$. Mechanisms to stabilize R to this value have been proposed [58,59] that, contrary to the ADD case, do not require introducing any new small or large parameter. Therefore a natural solution to the hierarchy problem can be achieved in this framework if the Higgs field, whose vacuum expectation value (VEV) is responsible for electroweak symmetry breaking, is localized at the IR-boundary where the effective mass scales are of order TeV. The radion field is generically heavy in models with a stabilized R. Nevertheless, it has been recently discussed that under some conditions a naturally light radion can arise [60–63]. In these cases the radion is identified with the dilaton, the Nambu-Goldstone boson associated to the spontaneous breaking of scale invariance, and its mass can be naturally below $ke^{-k\pi R} \sim$ TeV. Collider bounds on the radion mass and couplings can be found in [64–66].

In the RS model [3], all the SM fields were assumed to be localized on the IR-boundary. Nevertheless, for the hierarchy problem, only the Higgs field has to be localized there. SM gauge bosons and fermions can propagate in the 5D bulk [4–7] (for a review see, for example, [67, 68]). By performing a KK reduction from the 5D action of a gauge boson, we find [4, 5]

$$\frac{1}{g_4^2} = \int_0^{\pi R} dy\, \frac{1}{g_5^2} = \frac{\pi R}{g_5^2}\,, \quad (85.18)$$

where g_D ($D = 4, 5$) is the gauge coupling in D-dimensions. Therefore the 4D gauge couplings can be of order one, as is the case of the SM, if one demands $g_5^2 \sim \pi R$. Using $kR \sim 10$ and $g_4 \sim 0.5$, one obtains the 5D gauge coupling

$$g_5 \sim 4/\sqrt{k}\,. \quad (85.19)$$

Downloaded from https://academic.oup.com/ptep/article/2022/8/083C01/6651666 by KIT Library user on 27 September 2022

Boundary kinetic terms for the gauge bosons can modify this relation, allowing for larger values of $g_5\sqrt{k}$.

Fermions propagating in a warped extra dimension have 4D massless zero-modes with wavefunctions which vary as $f_0 \sim exp[(1/2-c_f)ky]$, where $c_f k$ is their 5D mass [7,69]. Depending on the free parameter $c_f k$, fermions can be localized either towards the UV-boundary ($c_f > 1/2$) or IR-boundary ($c_f < 1/2$). Since the Higgs boson is localized on the IR-boundary, one can generate exponentially suppressed Yukawa couplings by having the fermion zero-modes localized towards the UV-boundary, generating naturally the light SM fermion spectrum [7]. A large overlap with the wavefunction of the Higgs is needed for the top quark, in order to generate its large mass, thus requiring it to be localized towards the IR-boundary. In conclusion, the large mass hierarchies present in the SM fermion spectrum can be easily obtained in warped models via suitable choices of the order-one parameters c_f [70]. In these scenarios, deviations in flavor physics from the SM predictions are expected to arise from flavor-changing KK gluon couplings [71], putting certain constraints on the parameters of the models and predicting new physics effects to be observed in B-physics processes (see, for example, [72, 73]).

The masses of the KK states can also be calculated. One finds [7]

$$m_n \simeq \left(n + \frac{\alpha}{2} - \frac{1}{4}\right) \pi k e^{-\pi k R}\,, \qquad (85.20)$$

where $n = 1, 2, ...$ and $\alpha = \{|c_f - 1/2|, 0, 1\}$ for KK fermions, KK gauge bosons and KK gravitons, respectively. Their masses are of order $ke^{-\pi kR} \sim$ TeV (for this reason we refer to these scenarios as TeV-scale extra dimensions). The first KK state of the gauge bosons would be the lightest, while gravitons are expected to be the heaviest.

85.3.1.1 *Models of Electroweak Symmetry Breaking*

Theories in warped extra dimensions can be used to implement symmetry breaking at low energies by boundary conditions (for a review see, for example, [74]). For example, for a $U(1)$ gauge symmetry in the 5D bulk, this can be easily achieved by imposing a Dirichlet boundary condition on the IR-boundary for the gauge-boson field, $A_\mu|_{y=\pi R} = 0$. This makes the zero-mode gauge boson get a mass, given by $m_A = g_4\sqrt{2k/g_5^2}\, e^{-\pi kR}$. A very different situation occurs if the Dirichlet boundary condition is imposed on the UV-boundary, $A_\mu|_{y=0} = 0$. In this case the zero-mode gauge boson disappears from the spectrum. Finally, if a Dirichlet boundary condition is imposed on the two boundaries, one obtains a massless 4D scalar corresponding to the fifth component of the 5D gauge boson, A_5. Thus, different scenarios can be implemented by appropriately choosing the 5D bulk gauge symmetry, $\mathcal{G}_5$, and the symmetries to which it reduces on the UV and IR-boundary, $\mathcal{H}_{UV}$ and $\mathcal{H}_{IR}$, respectively. In all cases the KK spectrum comes in representations of the group $\mathcal{G}_5$.

Among the most interesting scenarios are those called gauge-Higgs unified models, where the Higgs boson appears as the fifth component of a 5D gauge boson, A_5. The Higgs mass is protected by the 5D gauge invariance and can only get a nonzero value from non-local one-loop effects [75]. To guarantee the relation $M_W^2 \simeq M_Z^2 \cos^2\theta_W$, a custodial $SU(2)_V$ symmetry is needed in the bulk and IR-boundary [76]. The simplest realization [77, 78] has

$$\mathcal{G}_5 = SU(3)_c \times SO(5) \times U(1)_X\,,$$
$$\mathcal{H}_{IR} = SU(3)_c \times SO(4) \times U(1)_X\,,$$
$$\mathcal{H}_{UV} = G_{SM}\,.$$

The Higgs boson gets a potential at the one-loop level that triggers a VEV, breaking the electroweak symmetry. In these models there is a light Higgs boson whose mass can be around 125 GeV, as required by the discovered Higgs boson [79]. This state, as will be explained in Sec. 85.3.2, behaves as a composite pseudo-Nambu-Goldstone boson with couplings that deviate from the SM Higgs [80]. The present experimental determination of the Higgs couplings at the LHC, that agrees with the SM predictions, put important constraints on these scenarios [79]. The lightest KK modes of the model are color fermions with charges $Q = -1/3, 2/3$ and $5/3$ [81].

85.3.1.2 *Constraints from Electroweak Precision Tests*

Models in which the SM gauge bosons propagate in 1/TeV-sized extra dimensions give generically large corrections to electroweak observables. When the SM fermions are confined on a boundary these corrections are universal and can be parameterized by four quantities: $\widehat{S}$, $\widehat{T}$, W and Y, as defined in Ref. [82]. For warped models, where the 5D gauge coupling of Eq. (85.19) is large, the most relevant parameter is $\widehat{T}$, which gives the bound $m_{KK} \gtrsim$ 10 TeV [67]. When a custodial symmetry is imposed [76], the main constraint comes from the $\widehat{S}$ parameter, requiring $m_{KK} \gtrsim 3$ TeV, independent of the value of g_5. Corrections to the $Zb_L\bar{b}_L$ coupling can also be important [67], especially in warped models for electroweak symmetry breaking as the ones described above.

85.3.1.3 *Kaluza-Klein Searches*

The main prediction of 1/TeV-sized extra dimensions is the presence of a discretized KK spectrum, with masses around the TeV scale, associated with the SM fields that propagate in the extra dimension.

In the RS model [3], only gravity propagates in the 5D bulk. Experimental searches have been performed for the lightest KK graviton through its decay to a variety of SM particle-antiparticle pairs. The results are usually interpreted in the plane of the dimensionless coupling k/M_P versus m_1, where M_P is the reduced Planck mass defined previously and m_1 is the mass of the lightest KK excitation of the graviton. Since the AdS curvature $\sim k$ cannot exceed the cut-off scale of the model, which is estimated to be $\ell_5^{1/3} M_5$ [38], one must demand $k \ll \sqrt{2\ell_5} M_P \simeq 40 M_P$.

The most stringent limits currently arise from LHC searches for resonances in the dilepton and diphoton final states, using 13 TeV collisions. Best sensitivities are obtained in the $\gamma\gamma$ final state, which is quite powerful since it has a branching fraction twice that of any individual lepton flavor. The CMS analysis [41] of 36 fb^{-1}of 13 TeV data excludes KK gravitons below 2.3 to 4.6 TeV, depending on the value of the coupling k/M_P, which is varied between 0.01 and 0.2, while ATLAS [83] uses the full 139 fb^{-1}and provides a lower limit on the KK graviton mass of 4.6 TeV for the coupling parameter 0.1. The CMS [42] dilepton analyses, combining results from the ee and $\mu\mu$ channels, exclude KK gravitons with masses 2.47–4.78 TeV for k/M_P values of 0.01–0.1. The ATLAS [84] analysis of 139 fb^{-1}of Run 2 data does not include a RS KK graviton interpretation of the results. Less stringent limits on the KK graviton mass can be derived from analyses of the dijet [85, 86], HH [87–90], and VV [91–94] final states, where V can represent either a W or Z boson.

In warped extra-dimensional models in which the SM fields propagate in the 5D bulk, the couplings of the KK graviton to $ee/\mu\mu/\gamma\gamma$ are suppressed [95], and the above bounds do not apply. Furthermore, the KK graviton is the heaviest KK state (see Eq. (85.20)), and therefore experimental searches for KK gauge bosons and fermions are more appropriate discovery channels in these scenarios. For the scenarios discussed above in which only the Higgs boson and the top quark are localized close to the IR-boundary, the KK gauge bosons mainly decay into top quarks, longitudinal W/Z bosons, and Higgs bosons. Couplings to light SM fermions are suppressed by a factor $g/\sqrt{g_5^2 k} \sim 0.2$ [7] for the value of Eq. (85.19) that is considered from now on. Searches have been made for evidence of the lightest KK excitation of the gluon, through its decay to $t\bar{t}$ pairs. The searches take into account the natural KK gluon width, which is typically $\sim 15\%$ of its mass. The decay of a heavy particle to $t\bar{t}$ would tend to produce highly boosted top (anti-)quarks in the final state. Products of the subsequent top decays would therefore tend to be close to each other in the detector. In the case of $t \to Wb \to jjb$ decays, the three jets could overlap with one another and not be individually reconstructed with the standard jet algorithms, while $t \to Wb \to \ell\nu b$ decays could result in the lepton failing standard isolation requirements due to its proximity to the b-jet; in both cases, the efficiency for properly reconstructing the final state would fall as the mass of the original particle increases. To avoid the loss in sensitivity which would result, a number of techniques, known generally as "top quark tagging" [96, 97], have been developed to reconstruct and identify highly boosted top quarks, for example by using a

Downloaded from https://academic.oup.com/ptep/article/2022/8/083C01/6651666 by KIT Library user on 27 September 2022

single "wide" jet to contain all the decay products of a hadronic top decay. The large backgrounds from QCD jets can then be reduced by requiring the "jet mass" be consistent with that of a top quark, and also by examining the substructure of the wide jet for indication that it resulted from the hadronic decay of a top quark. These techniques are key to extending to very high masses the range of accessible resonances decaying to $t\bar{t}$ pairs. The ATLAS search in 139 fb^{-1}of Run 2 data [98] does not provide a KK interpretation. Dedicated analysis from CMS [99] of 36 fb^{-1} of 13 TeV data combines di-lepton, lepton-plus-jet, and all-hadronic $t\bar{t}$ decays and excludes KK gluons with masses below 4.55 TeV. ATLAS uses all-hadronic [100] and lepton-plus-jet [101] final states to exclude KK gluons up to 3.4 and 3.8 TeV respectively with 36fb^{-1}of 13 TeV data. The results are not directly comparable between the two LHC experiments, since they employ in their respective analyses different implementations of the theoretical model. For masses between 3 and 5 TeV, the cross-section limits are around 20 fb for CMS analysis of 36 fb^{-1}and 30 fb (4 fb) for ATLAS analyses of 36 (139) fb^{-1}.

A gauge boson KK excitation could be also sought through its decay to longitudinal W/Z bosons. Recent analyses from ATLAS [102] (and CMS [103]) with 139 (137) fb^{-1}of 13 TeV data searching for heavy vector resonances decaying to a W or Z boson and a Higgs in the $q\bar{q}b\bar{b}$ final state have set a lower limit on the mass of these KK of 3.2 (3.7) TeV (warped models are equivalent to the Model B considered in the analyses with $g_V \sim g_5\sqrt{k}$). The decay to a pair of intermediate vector bosons has also been exploited to search for KK gravitons in models in which the SM fields propagate in the 5D bulk. The analyses typically reconstruct hadronic W/Z decays using variants of the boosted techniques mentioned previously. An ATLAS analysis [104] combines leptonic and hadronic final states from the KK graviton decay $G^* \to VV$, where V can represent either a W or Z boson, exclude KK gravitons with masses below 2.3 TeV, for a value of $k/M_P = 1$. CMS VV analysis [105] also provides cross section limits in the context of bulk gravitons; however, a maximum value of $k/M_P = 0.5$ is presented, for which no mass exclusion is possible using the 36 fb^{-1}of 13 TeV data.

The lightest KK states are, in certain models, the partners of the top quark. For example, in 5D composite Higgs models these are colored states with charges $Q = -1/3, 2/3$ and $5/3$ (arising from $SU(2)_L$ doublets with $Y = 7/6, 1/6$), and masses expected to be below the TeV [81]. They can be either singly or pair-produced, and mainly decay into a combination of W/Z with top/bottom quarks [106–109]. An exhaustive review of these searches can be found in Ref. [110]. Of particular note, the $Q = 5/3$ state decays mainly into $W^+t \to W^+W^+b$, giving a very clean signature of a pair of same-sign leptons in the final state. An analysis by ATLAS [111] searching in the lepton-plus-jets final state for evidence of pair production of the $Q = 5/3$ state provides a lower mass limit of 1.25 TeV. A CMS analysis [112] searching for pair production of the $Q = 5/3$ state using both lepton-plus-jets and same sign lepton final states excludes masses below 1.3 TeV. Both LHC experiments have searched for pair production of vector-like quarks T and B of charges $Q = 2/3$ and $-1/3$ respectively, assuming the allowable decays are $T \to Wb/Zt/Ht$ and $B \to Wt/Zb/Hb$. In each case, it is assumed the branching fractions of the three decay modes sum to unity, but the individual branching fractions, which are model-dependent, are allowed to vary within this constraint. Both ATLAS [113] and CMS [114] obtain lower limits on the mass of the T and B vector-like quarks up to 1.5 TeV.

Recent analyses from ATLAS [115] and CMS [116] also search for a single top partner production, the cross section for which is model-dependent [117] but does not carry the kinematic penalty for producing two heavy objects.

85.3.2 *Connection with Strongly Coupled Models via the AdS/CFT Correspondence*

The AdS/CFT correspondence [8] provides a connection between warped extra-dimensional models and strongly-coupled theories in ordinary 4D. Although the exact connection is only known for certain cases, the AdS/CFT techniques have been very useful to obtain, at the qualitative level, a 4D holographic description of the various phenomena in warped extra-dimensional models [11].

The connection goes as follows. The physics of the bulk AdS$_5$ models can be interpreted as that of a 4D conformal field theory (CFT) which is strongly coupled. The extra-dimensional coordinate y plays the role of the renormalization scale μ of the CFT by means of the identification $\mu \equiv ke^{-ky}$. Therefore the UV-boundary corresponds in the CFT to a UV cut-off scale at $\Lambda_{UV} = k \sim M_P$, breaking explicitly conformal invariance, while the IR-boundary can be interpreted as a spontaneous breaking of the conformal symmetry at energies $ke^{-k\pi R} \sim$ TeV. Fields localized on the UV-boundary are elementary fields external to the CFT, while fields localized on the IR-boundary and KK states corresponds to composite resonances of the CFT. Furthermore, local gauge symmetries in the 5D models, $\mathcal{G}_5$, correspond to global symmetries of the CFT, while the UV-boundary symmetry can be interpreted as a gauging of the subgroup $\mathcal{H}_{UV}$ of $\mathcal{G}_5$ in the CFT. Breaking gauge symmetries by IR-boundary conditions corresponds to the spontaneous breaking $\mathcal{G}_5 \to \mathcal{H}_{IR}$ in the CFT at energies $\sim ke^{-k\pi R}$. Using this correspondence one can easily derive the 4D massless spectrum of the compactified AdS$_5$ models. One also has the identification $k^3/M_5^3 \approx 16\pi^2/N^2$ and $g_5^2 k \approx 16\pi^2/N^r$ ($r = 1$ or 2 for CFT fields in the fundamental or adjoint representation of the gauge group), where N plays the role of the number of colors of the CFT. Therefore the weak-coupling limit in AdS$_5$ corresponds to a large-N expansion in the CFT.

Following the above AdS/CFT dictionary one can understand the RS solution to the hierarchy problem from a 4D viewpoint. The equivalent 4D model is a CFT with a TeV mass gap and a Higgs boson emerging as a composite state. In the particular case where the Higgs is the fifth-component of the gauge-boson, A_5 [118], this corresponds to models, similar to those proposed in Ref. [119,120], where the Higgs is a composite pseudo-Nambu-Goldstone boson arising from the spontaneous breaking $\mathcal{G}_5 \to \mathcal{H}_{IR}$ in the CFT. The AdS/CFT dictionary tells us that KK states must behave as composite resonances. For example, if the SM gauge bosons propagate in the 5D bulk, the lowest KK $SU(2)_L$-gauge boson must have properties similar to those of the Technirho ρ_T [110] with a coupling to longitudinal W/Z bosons given by $g_5\sqrt{k} \approx g_{\rho_T}$, while the coupling to elementary fermions is $g^2/\sqrt{g_5^2 k} \approx g^2 F_{\rho_T}/M_{\rho_T}$.

Fermions in compactified AdS$_5$ also have a simple 4D holographic interpretation. The 4D massless mode described in Sec. 85.3.1 corresponds to an external fermion ψ_i linearly coupled to a fermionic CFT operator $\mathcal{O}_i$: $\mathcal{L}_{\rm int} = \lambda_i \bar{\psi}_i \mathcal{O}_i + h.c.$. The dimension of the operator $\mathcal{O}_i$ is related to the 5D fermion mass according to $\mathrm{Dim}[\mathcal{O}_i] = |c_f + 1/2| - 1$. Therefore, by varying c_f one varies $\mathrm{Dim}[\mathcal{O}_i]$, making the coupling λ_i irrelevant ($c_f > 1/2$), marginal ($c_f = 1/2$) or relevant ($c_f < 1/2$). When irrelevant, the coupling is exponentially suppressed at low energies, and then the coupling of ψ_i to the CFT (and eventually to the composite Higgs) is very small. When relevant, the coupling grows in the IR and become as large as g_5 (in units of k), meaning that the fermion is as strongly coupled as the CFT states [77]. In this latter case ψ_i behaves as a composite fermion.

85.3.3 *Flat Extra Dimensions*

Models with quantum gravity at the TeV scale, as in the ADD scenario, can have extra (flat) dimensions of 1/TeV size, as happens in string scenarios (see, for example, [121]). All SM fields may propagate in these extra dimensions, leading to the possibility of observing their corresponding KK states.

A simple example is to assume that the SM gauge bosons propagate in a flat five-dimensional orbifold S^1/Z_2 of radius R, with the fermions localized on a 4D boundary. The KK gauge bosons behave as sequential SM gauge bosons with a coupling to fermions enhanced by a factor $\sqrt{2}$ [121]. The experimental limits on such sequential gauge bosons could therefore be recast as limits on KK gauge bosons. Such an interpretation of the ATLAS 7 TeV dilepton analysis [122] yielded the bound $1/R > 4.16$ TeV, while a CMS 8 TeV search with a lepton and missing transverse energy in the final state [123] give $1/R > 3.4$ TeV. Indirect bounds from LEP2 require however $1/R \gtrsim 6$ TeV [82, 124], a bound that can considerably improve in the future by high-energy measurements of the dilepton invariant mass spectrum from Drell-Yan processes

Downloaded from https://academic.oup.com/ptep/article/2022/8/083C01/6651666 by KIT Library user on 27 September 2022

at the LHC [125]. More recent LHC limits on leptonically decaying gauge bosons [84, 126–129] are not interpreted as bounds on $1/R$ by the collaborations, but the published results allow for independent derivation of such bounds.

An alternative scenario, known as Universal Extra Dimensions (UED) [130] (for a review see, for example, [131]), assumes that all SM fields propagate universally in a flat orbifold S^1/Z_2 with an extra Z_2 parity, called KK-parity, that interchanges the two boundaries. In this case, the lowest KK state is stable and is a Dark Matter candidate. At colliders, the KK particles would have to be created in pairs, and would then cascade decay to the lightest KK particle, which would be stable and escape detection. The UED mass-spectrum depends not only on the extra-dimensional radius R, but also on the cut-off of the 5D theory Λ, since quantum corrections sensitive to ΛR induce mass-splittings between the KK states. Experimental signatures, such as jets or leptons and $\not{E}_T$, would be similar to those of typical R-parity conserving SUSY searches. An interpretation of the recent LHC experimental SUSY searches for UED models has been presented in Refs. [132,133]. A lower bound $1/R > 1.4 - 1.5$ TeV was derived for ΛR in the range $5 - 35$ [132]. A recent analysis is given in Ref. [134] where it is shown that the minimal UED model is ruled out when LHC data is combined with Dark Matter relic density data. Extensions to the minimal UED model where boundary terms are included can however be compatible with experiments [134].

Finally, realistic models of electroweak symmetry breaking can also be constructed with flat extra spatial dimensions, similarly to those in the warped case, requiring, however, the presence of sizeable boundary kinetic terms [135]. There is also the possibility of breaking supersymmetry by boundary conditions [136]. Models of this type could explain naturally the presence of a Higgs boson lighter than $M_D \sim$ TeV (see, for example, [137–139]).

References

[1] For a comprehensive collection of the original papers see, "Modern Kaluza-Klein Theories", edited by T. Appelquist *et al.*, Addison-Wesley (1987).

[2] N. Arkani-Hamed, S. Dimopoulos and G. Dvali, Phys. Lett. **B429**, 263 (1998), [hep-ph/9803315].

[3] L. Randall and R. Sundrum, Phys. Rev. Lett. **83**, 3370 (1999), [hep-ph/9905221].

[4] H. Davoudiasl, J. L. Hewett and T. G. Rizzo, Phys. Lett. **B473**, 43 (2000), [hep-ph/9911262].

[5] A. Pomarol, Phys. Lett. **B486**, 153 (2000), [hep-ph/9911294].

[6] S. Chang *et al.*, Phys. Rev. **D62**, 084025 (2000), [hep-ph/9912498].

[7] T. Gherghetta and A. Pomarol, Nucl. Phys. **B586**, 141 (2000), [hep-ph/0003129].

[8] J. M. Maldacena, Int. J. Theor. Phys. **38**, 1113 (1999), [Adv. Theor. Math. Phys.2,231(1998)], [hep-th/9711200].

[9] E. Witten, Adv. Theor. Math. Phys. **2**, 253 (1998), [hep-th/9802150].

[10] S. S. Gubser, I. R. Klebanov and A. M. Polyakov, Phys. Lett. **B428**, 105 (1998), [hep-th/9802109].

[11] N. Arkani-Hamed, M. Porrati and L. Randall, JHEP **08**, 017 (2001), [hep-th/0012148].

[12] ATLAS public results are available on WWW at `https://twiki.cern.ch/twiki/bin/view/AtlasPublic`.

[13] CMS public results are available on WWW at `https://cms-results.web.cern.ch/cms-results/public-results/publications`.

[14] Z. Chacko, M. A. Luty and E. Ponton, JHEP **07**, 036 (2000), [hep-ph/9909248].

[15] N. Arkani-Hamed, S. Dimopoulos and G. R. Dvali, Phys. Rev. **D59**, 086004 (1999), [hep-ph/9807344].

[16] R. Rattazzi, `hep-ph/0607055 (2006)`; I. Antoniadis, Yellow report CERN-2002-002 (2002).

[17] J. D. Lykken, Phys. Rev. **D54**, R3693 (1996), [hep-th/9603133].

[18] I. Antoniadis *et al.*, Phys. Lett. **B436**, 257 (1998), [hep-ph/9804398].

[19] G. F. Giudice, R. Rattazzi and J. D. Wells, Nucl. Phys. **B544**, 3 (1999), [hep-ph/9811291].

[20] N. Arkani-Hamed *et al.*, Phys. Rev. **D62**, 105002 (2000), [hep-ph/9912453].

[21] E. G. Adelberger *et al.*, Prog. Part. Nucl. Phys. **62**, 102 (2009).

[22] J. Murata and S. Tanaka, Class. Quant. Grav. **32**, 3, 033001 (2015), [arXiv:1408.3588].

[23] W.-H. Tan *et al.*, Phys. Rev. Lett. **116**, 13, 131101 (2016).

[24] J. G. Lee *et al.*, Phys. Rev. Lett. **124**, 101101 (2020), [arXiv:2002.11761].

[25] C. Hanhart *et al.*, Phys. Lett. **B509**, 1 (2001), [arXiv:astro-ph/0102063].

[26] S. Hannestad and G. G. Raffelt, Phys. Rev. **D67**, 125008 (2003), [Erratum: Phys. Rev.D69,029901(2004)], [hep-ph/0304029].

[27] L. J. Hall and D. Tucker-Smith, Phys. Rev. **D60**, 085008 (1999), [hep-ph/9904267].

[28] E. A. Mirabelli, M. Perelstein and M. E. Peskin, Phys. Rev. Lett. **82**, 2236 (1999), [hep-ph/9811337].

[29] T. Han, J. D. Lykken and R.-J. Zhang, Phys. Rev. **D59**, 105006 (1999), [hep-ph/9811350].

[30] G. AaD *et al.* (ATLAS), Phys. Rev. D **103**, 112006 (2021), [arXiv:2102.10874].

[31] A. Tumasyan *et al.* (CMS) (2021), [arXiv:2107.13021].

[32] A. M. Sirunyan *et al.* (CMS), JHEP **02**, 074 (2019), [arXiv:1810.00196].

[33] G. Aad *et al.* (ATLAS), JHEP **02**, 226 (2021), [arXiv:2011.05259].

[34] S. Cullen, M. Perelstein and M. E. Peskin, Phys. Rev. **D62**, 055012 (2000), [hep-ph/0001166].

[35] A. M. Sirunyan *et al.* (CMS), JHEP **05**, 033 (2020), [arXiv:1911.03947].

[36] G. Aad *et al.* (ATLAS), JHEP **03**, 145 (2020), [arXiv:1910.08447].

[37] J. L. Hewett, Phys. Rev. Lett. **82**, 4765 (1999), [hep-ph/9811356].

[38] G. F. Giudice and A. Strumia, Nucl. Phys. **B663**, 377 (2003), [hep-ph/0301232].

[39] A. M. Sirunyan *et al.* (CMS), Eur. Phys. J. **C78**, 9, 789 (2018), [arXiv:1803.08030].

[40] M. Aaboud *et al.* (ATLAS), Phys. Lett. **B775**, 105 (2017), [arXiv:1707.04147].

[41] A. M. Sirunyan *et al.* (CMS), Phys. Rev. **D98**, 9, 092001 (2018), [arXiv:1809.00327].

[42] A. M. Sirunyan *et al.*, JHEP **07**, 7 (2021), [arXiv:2103.02708].

[43] G. Aad *et al.*, JHEP **11**, 005 (2020), [arXiv:2006.12946].

[44] S. B. Giddings and S. D. Thomas, Phys. Rev. **D65**, 056010 (2002), [hep-ph/0106219].

[45] S. Dimopoulos and G. L. Landsberg, Phys. Rev. Lett. **87**, 161602 (2001), [hep-ph/0106295].

[46] P. Kanti, Int. J. Mod. Phys. **A19**, 4899 (2004), [hep-ph/0402168].

[47] R. C. Myers and M. J. Perry, Annals Phys. **172**, 304 (1986).

[48] A. M. Sirunyan *et al.* (CMS), JHEP **11**, 042 (2018), [arXiv:1805.06013].

[49] G. Aad *et al.* (ATLAS), JHEP **03**, 026 (2016), [arXiv:1512.02586].

Downloaded from https://academic.oup.com/ptep/article/2022/8/083C01/6651666 by KIT Library user on 27 September 2022

[50] M. Aaboud *et al.* (ATLAS), Phys. Lett. **B760**, 520 (2016), [arXiv:1606.02265].

[51] C. Kilic *et al.*, Phys. Rev. **D89**, 1, 016003 (2014), [arXiv:1207.3525].

[52] V. Khachatryan *et al.* (CMS), Phys. Rev. **D90**, 3, 032005 (2014), [arXiv:1405.7653].

[53] P. Meade and L. Randall, JHEP **05**, 003 (2008), [arXiv:0708.3017].

[54] A. M. Sirunyan *et al.* (CMS), Phys. Lett. **B774**, 279 (2017), [arXiv:1705.01403].

[55] A. M. Sirunyan *et al.* (CMS), JHEP **04**, 073 (2018), [arXiv:1802.01122].

[56] M. Aaboud *et al.* (ATLAS), Phys. Rev. **D98**, 9, 092008 (2018), [arXiv:1807.06573].

[57] S. Dimopoulos and R. Emparan, Phys. Lett. **B526**, 393 (2002), [hep-ph/0108060].

[58] W. D. Goldberger and M. B. Wise, Phys. Rev. Lett. **83**, 4922 (1999), [hep-ph/9907447].

[59] J. Garriga and A. Pomarol, Phys. Lett. **B560**, 91 (2003), [hep-th/0212227].

[60] See talk by R. Rattazzi at Planck 2010, CERN.

[61] B. Bellazzini *et al.*, Eur. Phys. J. **C74**, 2790 (2014), [arXiv:1305.3919].

[62] F. Coradeschi *et al.*, JHEP **11**, 057 (2013), [arXiv:1306.4601].

[63] E. Megias and O. Pujolas, JHEP **08**, 081 (2014), [arXiv:1401.4998].

[64] K. Blum *et al.*, JHEP **03**, 099 (2015), [arXiv:1410.1873].

[65] A. Efrati *et al.*, Phys. Rev. **D91**, 5, 055034 (2015), [arXiv:1410.2225].

[66] F. Abu-Ajamieh, J. S. Lee and J. Terning, JHEP **10**, 050 (2018), [arXiv:1711.02697].

[67] H. Davoudiasl *et al.*, New J. Phys. **12**, 075011 (2010), [arXiv:0908.1968].

[68] T. Gherghetta, in "Physics of the large and the small, TASI 09, proceedings of the Theoretical Advanced Study Institute in Elementary Particle Physics, Boulder, Colorado, USA, 1-26 June 2009," 165–232 (2011), [arXiv:1008.2570].

[69] Y. Grossman and M. Neubert, Phys. Lett. **B474**, 361 (2000), [hep-ph/9912408].

[70] S. J. Huber and Q. Shafi, Phys. Lett. **B498**, 256 (2001), [hep-ph/0010195].

[71] A. Delgado, A. Pomarol and M. Quiros, JHEP **01**, 030 (2000), [hep-ph/9911252].

[72] K. Agashe, G. Perez and A. Soni, Phys. Rev. **D71**, 016002 (2005), [hep-ph/0408134].

[73] M. Bauer *et al.*, JHEP **09**, 017 (2010), [arXiv:0912.1625].

[74] A. Pomarol, Int. J. Mod. Phys. **A24**, 61 (2009), [In *Kane, Gordon (ed.) et al.: Perspectives on LHC physics*, 259 (2008)].

[75] Y. Hosotani, Phys. Lett. **126B**, 309 (1983).

[76] K. Agashe *et al.*, JHEP **08**, 050 (2003), [hep-ph/0308036].

[77] K. Agashe, R. Contino and A. Pomarol, Nucl. Phys. **B719**, 165 (2005), [hep-ph/0412089].

[78] For a review see, for example, R. Contino, `arXiv:1005.4269`.

[79] See, for example, PDG review of Higgs boson in this *Review*.

[80] G. F. Giudice *et al.*, JHEP **06**, 045 (2007), [hep-ph/0703164].

[81] R. Contino, L. Da Rold and A. Pomarol, Phys. Rev. **D75**, 055014 (2007), [hep-ph/0612048].

[82] R. Barbieri *et al.*, Nucl. Phys. **B703**, 127 (2004), [hep-ph/0405040].

[83] G. Aad *et al.* (ATLAS) (2021), [arXiv:2102.13405].

[84] G. Aad *et al.* (ATLAS), Phys. Lett. **B796**, 68 (2019), [arXiv:1903.06248].

[85] A. M. Sirunyan *et al.* (CMS), JHEP **08**, 130 (2018), [arXiv:1806.00843].

[86] G. Aad *et al.* (ATLAS), Phys. Rev. Lett. **125**, 13, 131801 (2020), [arXiv:2005.02983].

[87] A. M. Sirunyan *et al.* (CMS), Phys. Rev. Lett. **122**, 12, 121803 (2019), [arXiv:1811.09689].

[88] M. Aaboud *et al.* (ATLAS), JHEP **01**, 030 (2019), [arXiv:1804.06174].

[89] A. Tumasyan *et al.* (CMS) (2021), [arXiv:2106.10361].

[90] G. Aad *et al.* (ATLAS), JHEP **11**, 163 (2020), [arXiv:2007.14811].

[91] G. Aad *et al.* (ATLAS), JHEP **09**, 091 (2019), [Erratum: JHEP 06, 042 (2020)], [arXiv:1906.08589].

[92] A. M. Sirunyan *et al.* (CMS) (2019), [arXiv:1906.05977].

[93] G. Aad *et al.* (ATLAS), Eur. Phys. J. C **80**, 12, 1165 (2020), [arXiv:2004.14636].

[94] G. Aad *et al.* (ATLAS), Eur. Phys. J. C **81**, 4, 332 (2021), [arXiv:2009.14791].

[95] K. Agashe *et al.*, Phys. Rev. **D76**, 036006 (2007), [hep-ph/0701186].

[96] M. Aaboud *et al.* (ATLAS), Eur. Phys. J. C **79**, 5, 375 (2019), [arXiv:1808.07858].

[97] A. M. Sirunyan *et al.* (CMS), JINST **15**, 06, P06005 (2020), [arXiv:2004.08262].

[98] G. Aad *et al.* (ATLAS), JHEP **10**, 061 (2020), [arXiv:2005.05138].

[99] A. M. Sirunyan *et al.* (CMS), JHEP **04**, 031 (2019), [arXiv:1810.05905].

[100] M. Aaboud *et al.* (ATLAS), Phys. Rev. **D99**, 9, 092004 (2019), [arXiv:1902.10077].

[101] M. Aaboud *et al.* (ATLAS), Eur. Phys. J. **C78**, 7, 565 (2018), [arXiv:1804.10823].

[102] G. Aad *et al.* (ATLAS), Phys. Rev. D **102**, 11, 112008 (2020), [arXiv:2007.05293].

[103] A. M. Sirunyan *et al.* (CMS), Eur. Phys. J. C **81**, 8, 688 (2021), [arXiv:2102.08198].

[104] M. Aaboud *et al.* (ATLAS), Phys. Rev. **D98**, 5, 052008 (2018), [arXiv:1808.02380].

[105] A. M. Sirunyan *et al.* (CMS) (2019), [arXiv:1906.00057].

[106] R. Contino and G. Servant, JHEP **06**, 026 (2008), [arXiv:0801.1679].

[107] J. A. Aguilar-Saavedra, JHEP **11**, 030 (2009), [arXiv:0907.3155].

[108] J. Mrazek and A. Wulzer, Phys. Rev. **D81**, 075006 (2010), [arXiv:0909.3977].

[109] G. Dissertori *et al.*, JHEP **09**, 019 (2010), [arXiv:1005.4414].

[110] See, for example, PDG review of Technicolor searches in this volume.

[111] M. Aaboud *et al.* (ATLAS), JHEP **10**, 141 (2017), [arXiv:1707.03347].

[112] A. M. Sirunyan *et al.* (CMS), JHEP **03**, 082 (2019), [arXiv:1810.03188].

[113] M. Aaboud *et al.* (ATLAS), Phys. Rev. Lett. **121**, 21, 211801 (2018), [arXiv:1808.02343].

[114] A. M. Sirunyan *et al.* (CMS), Phys. Rev. D **102**, 112004 (2020), [arXiv:2008.09835].

[115] M. Aaboud *et al.* (ATLAS), JHEP **05**, 164 (2019), [arXiv:1812.07343].

[116] A. M. Sirunyan *et al.* (CMS), JHEP **01**, 036 (2020), [arXiv:1909.04721].

[117] A. De Simone *et al.*, JHEP **04**, 004 (2013), [arXiv:1211.5663].

Downloaded from https://academic.oup.com/ptep/article/2022/8/083C01/6651666 by KIT Library user on 27 September 2022

[118] R. Contino, Y. Nomura and A. Pomarol, Nucl. Phys. **B671**, 148 (2003), [hep-ph/0306259].

[119] H. Georgi, D. B. Kaplan and P. Galison, Phys. Lett. **143B**, 152 (1984).

[120] D. B. Kaplan and H. Georgi, Phys. Lett. **136B**, 183 (1984).

[121] I. Antoniadis and K. Benakli, Int. J. Mod. Phys. **A15**, 4237 (2000), [hep-ph/0007226].

[122] G. Aad *et al.* (ATLAS), JHEP **11**, 138 (2012), [arXiv:1209.2535].

[123] V. Khachatryan *et al.* (CMS), Phys. Rev. **D91**, 9, 092005 (2015), [arXiv:1408.2745].

[124] K. Cheung and G. L. Landsberg, Phys. Rev. **D65**, 076003 (2002), [hep-ph/0110346].

[125] M. Farina *et al.*, Phys. Lett. **B772**, 210 (2017), [arXiv:1609.08157].

[126] M. Aaboud *et al.* (ATLAS), Eur. Phys. J. C **78**, 5, 401 (2018), [arXiv:1706.04786].

[127] G. Aad *et al.* (ATLAS) (2019), [arXiv:1906.05609].

[128] A. M. Sirunyan *et al.* (CMS), JHEP **06**, 128 (2018), [arXiv:1803.11133].

[129] A. M. Sirunyan *et al.* (CMS), JHEP **06**, 120 (2018), [arXiv:1803.06292].

[130] T. Appelquist, H.-C. Cheng and B. A. Dobrescu, Phys. Rev. **D64**, 035002 (2001), [hep-ph/0012100].

[131] A. Datta, K. Kong and K. T. Matchev, New J. Phys. **12**, 075017 (2010), [arXiv:1002.4624].

[132] N. Deutschmann, T. Flacke and J. S. Kim, Phys. Lett. **B771**, 515 (2017), [arXiv:1702.00410].

[133] J. Beuria *et al.*, Comput. Phys. Commun. **226**, 187 (2018), [arXiv:1702.00413].

[134] Avnish *et al.*, Phys. Rev. D **103**, 115011 (2021), [arXiv:2012.15137].

[135] G. Panico, M. Safari and M. Serone, JHEP **02**, 103 (2011), [arXiv:1012.2875].

[136] J. Scherk and J. H. Schwarz, Phys. Lett. **82B**, 60 (1979).

[137] A. Pomarol and M. Quiros, Phys. Lett. **B438**, 255 (1998), [hep-ph/9806263].

[138] I. Antoniadis *et al.*, Nucl. Phys. **B544**, 503 (1999), [hep-ph/9810410].

[139] R. Barbieri, L. J. Hall and Y. Nomura, Phys. Rev. **D63**, 105007 (2001), [hep-ph/0011311].

Downloaded from https://academic.oup.com/ptep/article/2022/8/083C01/6651666 by KIT Library user on 27 September 2022

86. W'-Boson Searches

Revised October, 2021 by B.A. Dobrescu (FNAL) and S. Willocq (U. Massachusetts).

The W' boson is a massive hypothetical particle of spin 1 and electric charge ± 1, which is a color singlet and is predicted in various extensions of the Standard Model (SM).

86.1 W' couplings to quarks and leptons

The Lagrangian terms describing the couplings of a W'^+ boson to fermions are given by

$$\frac{W'^+_\mu}{\sqrt{2}}\left[\overline{u}_i\left(C^R_{q_{ij}}P_R+C^L_{q_{ij}}P_L\right)\gamma^\mu d_j+\overline{\nu}_i\left(C^R_{\ell_{ij}}P_R+C^L_{\ell_{ij}}P_L\right)\gamma^\mu e_j\right]. \tag{86.1}$$

Here, u, d, ν, and e are the SM fermions in the mass eigenstate basis, $i, j = 1, 2, 3$ label the fermion generation, and $P_{R,L} = (1 \pm \gamma_5)/2$. The coefficients $C^L_{q_{ij}}$, $C^R_{q_{ij}}$, $C^L_{\ell_{ij}}$, and $C^R_{\ell_{ij}}$ are complex dimensionless parameters. If $C^R_{\ell_{ij}} \neq 0$, then the ith generation includes a right-handed neutrino. Using this notation, the SM W couplings are $C^L_q = gV_{\rm CKM}$, $C^L_\ell = g \approx 0.63$ and $C^R_q = C^R_\ell = 0$.

Unitarity considerations imply that the W' boson is associated with a spontaneously-broken gauge symmetry. This is true even when it is a composite particle (*e.g.* $\rho^\pm$-like bound states [1]) if its mass is much smaller than the compositeness scale, or a Kaluza-Klein mode in theories where the W boson propagates in extra dimensions [2]. The simplest extension of the electroweak gauge group that includes a W' boson is $SU(2)_1 \times SU(2)_2 \times U(1)$, but larger groups are encountered in some theories. A generic property of these gauge theories is that they also include a Z' boson [3]; the W'-to-Z' mass ratio is often a free parameter.

A tree-level mass mixing may be induced between the electrically-charged gauge bosons. Upon diagonalization of their mass matrix, the W-to-Z mass ratio and the couplings of the observed W boson are shifted from the SM values. Their measurements imply that the mixing angle, θ_+, between the gauge eigenstates must be smaller than about 10^{-2} [4]. In certain theories the mixing is negligible (*e.g.*, due to a new parity [5]), even when the W' mass is near the electroweak scale. Note that $SU(2)$ gauge invariance suppresses the kinetic mixing between the W and W' bosons (in contrast to the case of a Z' boson [3]).

The W' coupling to WZ is fixed by Lorentz and gauge invariances, and to leading order in θ_+ is given by [6]

$$\frac{g\,\theta_+\,i}{\cos\theta_W}\left[W'^+_\mu\left(W^-_\nu Z^{\nu\mu}+Z_\nu W^{-\mu\nu}\right)+Z^\nu W^{-\mu}W'^+_{\nu\mu}\right]+\text{H.c.}, \tag{86.2}$$

where $W^{\mu\nu} \equiv \partial^\mu W^\nu - \partial^\nu W^\mu$, etc. The θ_W dependence shown here corrects the one given in Ref. [7], which has been referred to as the Extended Gauge Model by the experimental collaborations. The W' coupling to Wh^0, where h^0 is the SM Higgs boson, is

$$-\,\xi_h\, g_{W'}\, M_W\; W'^+_\mu\, W^{\mu-} h^0 + \text{H.c.}, \tag{86.3}$$

where $g_{W'}$ is the gauge coupling of the W' boson, and the coefficient ξ_h satisfies $\xi_h \leq 1$ in simple Higgs sectors [6].

In models based on the "left-right symmetric" gauge group [8], $SU(2)_L \times SU(2)_R \times U(1)_{B-L}$, the SM fermions that couple to the W boson transform as doublets under $SU(2)_L$ while the other fermions transform as doublets under $SU(2)_R$. Consequently, the W' boson couples primarily to right-handed fermions; its coupling to left-handed fermions arises due to the θ_+ mixing, so that C^L_q is proportional to the CKM matrix and its elements are much smaller than the diagonal elements of C^R_q. Generically, C^R_q does not need to be proportional to $V_{\rm CKM}$.

There are many other models based on the $SU(2)_1 \times SU(2)_2 \times U(1)$ gauge symmetry. In the "alternate left-right" model [9], all the couplings shown in Eq. (86.1) vanish, but there are some new fermions such that the W' boson couples to pairs involving a SM fermion and a new fermion. In the "ununified SM" [10], the left-handed quarks are doublets under one $SU(2)$, and the left-handed leptons are doublets under a different $SU(2)$, leading to a mostly leptophobic W' boson: $C^L_{\ell_{ij}} \ll C^L_{q_{ij}}$ and $C^R_{\ell_{ij}} = C^R_{q_{ij}} = 0$. Fermions of different generations may also transform as doublets under different $SU(2)$ gauge groups [11]. In particular, the couplings to third generation quarks may be enhanced [12].

It is also possible that the W' couplings to SM fermions are highly suppressed. For example, if the quarks and leptons are singlets under one $SU(2)$ [13], then the couplings are proportional to the tiny mixing angle θ_+. Similar suppressions may arise if some vectorlike fermions mix with the SM fermions [14].

Gauge groups that embed the electroweak symmetry, such as $SU(3)_W \times U(1)$ or $SU(4)_W \times U(1)$, also include one or more W' bosons [15].

86.2 Collider searches

At hadron colliders, W' bosons can be detected through resonant pair production of fermions (f and f') or electroweak bosons with a net electric charge equal to ± 1. When W' has a width much smaller than its mass ($\Gamma_{W'}/M_{W'} \lesssim 7\%$), the contribution of the s-channel W' exchange to the total rate for $pp \to f\bar{f}'X$, where X is any final state, may be approximated by the branching fraction $B(W' \to f\bar{f}')$ times the production cross section [16], which may be written as

$$\sigma\left(pp\to W'X\right) \simeq \frac{\pi}{6s}\sum_{i,j}\left[(C^L_{q_{ij}})^2+(C^R_{q_{ij}})^2\right] w_{ij}\left(M^2_{W'}/s, M_{W'}\right). \tag{86.4}$$

The functions w_{ij} include the information about proton structure, and are given to leading order in α_s by

$$w_{ij}(z,\mu) = \int_z^1 \frac{dx}{x}\left[u_i(x,\mu)\,\overline{d}_j\left(\frac{z}{x},\mu\right)+\overline{u}_i(x,\mu)\,d_j\left(\frac{z}{x},\mu\right)\right], \tag{86.5}$$

where $u_i(x,\mu)$ and $d_i(x,\mu)$ are the parton distributions inside the proton at the factorization scale μ and parton momentum fraction x for the up- and down-type quarks of the ith generation, respectively. QCD corrections to W' production are sizable (they also include quark-gluon initial states), but preserve the above factorization of couplings at next-to-leading order [17].

The most commonly studied W' signal consists of a high-momentum electron or muon and large missing transverse momentum. The signal transverse mass distribution forms a Jacobian peak with its endpoint at $M_{W'}$ (see Fig. 1 (top) of Ref. [18]). Given that the branching fractions for $W' \to e\nu$ and $W' \to \mu\nu$ could be very different, the results in these channels should be presented separately. Searches in these channels often implicitly assume that the left-handed couplings vanish (no interference between W and W'), and that the right-handed neutrino is light compared to the W' boson and escapes the detector. An example of parameter values that satisfy these assumptions is $C^R_q = gV_{\rm CKM}$, $C^R_\ell = g$, $C^L_q = C^L_\ell = 0$, which define a model that preserves lepton universality and predicts the same total cross section as the Sequential SM used in many W' searches. However, if a W' boson were discovered and the final state fermions have left-handed helicity, then the effects of $W - W'$ interference could be observed [19], providing information about the W' couplings. The effects of the W' width on interference are discussed in Ref. [20].

In the $e\nu$ channel, the ATLAS and CMS collaborations set limits on the W' production cross section times branching fraction $\sigma \times B$ (and thus indirectly on the W' couplings). These limits are set for $M_{W'}$ in the $0.15-7$ TeV range and are based on 139 fb^{-1} at $\sqrt{s} = 13$ TeV [18,21], with the most stringent limits reproduced in Fig. 86.1. ATLAS sets the strongest mass limit $M_{W'} > 6.0$ TeV in the Sequential SM (all limits in this mini-review are at the 95% CL). The coupling limits are much weaker for $M_{W'} < 150$ GeV, a range last explored with the Tevatron at $\sqrt{s} = 1.8$ TeV [22].

In the $\mu\nu$ channel, ATLAS and CMS set rate limits for $M_{W'}$ in the $0.15-7$ TeV range [18,21], with the strongest mass lower limit of 5.6 TeV in the Sequential SM set by CMS [21] using 137 fb^{-1} of $\sqrt{s} = 13$ TeV data, as shown in Fig. 86.1. When combined with the $e\nu$ channel assuming lepton universality, the upper limit on the $\sqrt{s} = 13$ TeV cross section times branching fraction to $\ell\nu$ varies between 0.05 and 2.1 fb for $M_{W'}$ values between 1 and 6 TeV [18]. Only weak limits on $W' \to \mu\nu$ exist for $M_{W'} < 150$ GeV [25]. Note that masses of the order of the electroweak

Downloaded from https://academic.oup.com/ptep/article/2022/8/083C01/6651666 by KIT Library user on 27 September 2022

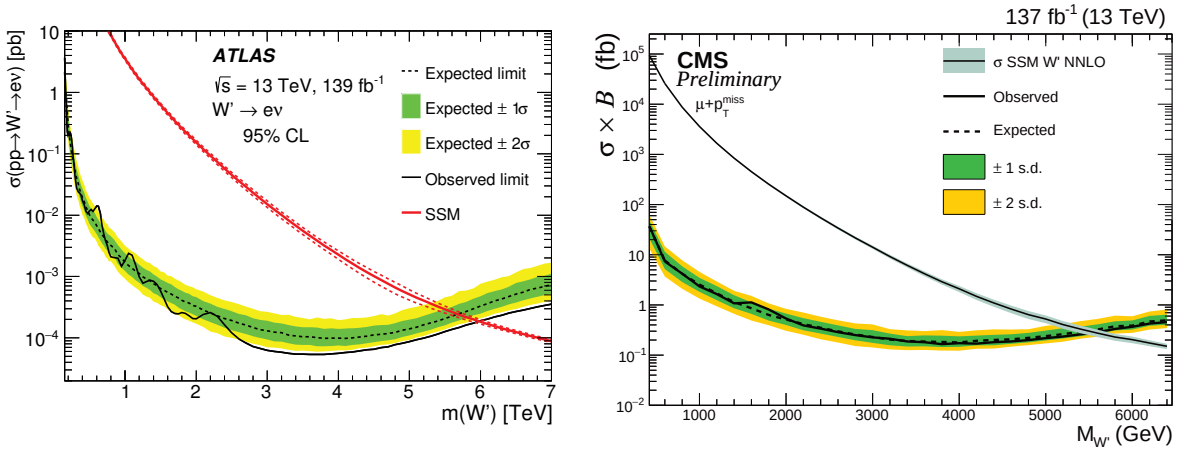

Figure 86.1: Upper limit on $\sigma(pp \to W'X) \times B(W' \to \ell\nu)$ in the $e\nu$ channel from ATLAS [18] (left) and the $\mu\nu$ channel from CMS [21] (right). The red (black) line shows the theoretical prediction in the Sequential SM in the $e\nu$ ($\mu\nu$) channel.

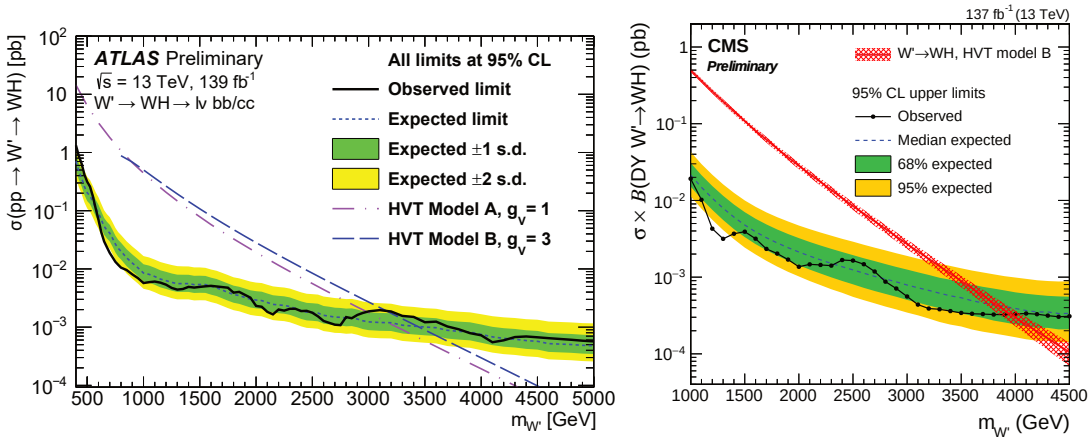

Figure 86.2: Upper limits on W' production cross section times branching fraction into a W and a SM Higgs boson decaying into heavy-flavor quarks, from ATLAS [23] (left) and CMS [24] (right).

scale are interesting from a theoretical point of view, while lepton universality does not necessarily apply to a W' boson.

Searches for $W' \to \tau\nu$ have been performed at 13 TeV by CMS with 36 fb^{-1} [26], and by ATLAS with 139 fb^{-1} [27]. Limits are set on $\sigma \times B$ for $M_{W'}$ between 0.4 and 6 TeV. A mass lower limit of 5.0 TeV is set in the Sequential SM, and the upper limit on the cross section times branching fraction to $\tau\nu$ at 13 TeV varies between 0.4 and 9 fb for $M_{W'}$ values between 1 and 5 TeV [27].

The W' decay into a charged lepton and a right-handed neutrino, ν_R, may also be followed by the ν_R decay through a virtual W' boson into a charged lepton and two quark jets. The CMS [28] and ATLAS [29] searches in the $eejj$ and $\mu\mu jj$ channels have set limits at $\sqrt{s} = 13$ TeV on the cross section times branching fractions as a function of the ν_R mass and of $M_{W'}$. No requirement is placed on the charge of the lepton pair. A related W' search in the $\tau\tau jj$ channel with hadronic τ decays was also performed by CMS [30].

The $t\bar{b}$ channel is particularly important because a W' boson that couples only to right-handed fermions cannot decay to leptons when the right-handed neutrinos are heavier than $M_{W'}$. Additional motivations are provided by a W' boson with enhanced couplings to the third generation [12], and by a leptophobic W' boson. The usual signature for $W' \to t\bar{b}$ consists of a leptonically-decaying W boson and two b-jets. Recent studies have also incorporated the fully hadronic decay channel for $M_{W'} \gg m_t$ with the use of jet substructure techniques to tag highly boosted top-jets. For a detailed discussion of this channel, see Ref. [31].

Searches for dijet resonances may be used to set limits on $W' \to q\bar{q}'$. ATLAS [32] and CMS [33] provide similar coverage in the $\sim$ 1.5−8 TeV mass range with 139 and 137 fb^{-1} of data, respectively, collected at $\sqrt{s} = 13$ TeV. Interpretation in terms of W' decays with 139 fb^{-1} of 13 TeV data yields a W' mass lower limit of 4.0 TeV in the Sequential SM [32]. For masses in the range $\sim$ 0.5 − 1.5 TeV, analyses based on jets reconstructed online provide the best sensitivity because they circumvent trigger bandwidth limitations [34, 35]. For W' masses below $\sim$ 0.5 TeV, the best limits are set in novel analyses exploiting boosted technologies and initial state radiation [36–39]. Cross-section limits for W' masses below $\sim$ 1.5 TeV can be derived from the dijet limits on Z' bosons summarized in Ref. [3].

In some theories [5] the W' couplings to SM fermions are suppressed by discrete symmetries. W' production then occurs in pairs, through a photon or Z boson. The decay modes are model-dependent and often involve other new particles. The ensuing collider signals arise from cascade decays and often include missing transverse momentum or boosted multi-jet topologies. An example is a search performed by CMS [40] for W' decays into a vector-like quark and a top or a bottom quark. The final state studied in this analysis involves a boosted SM Higgs boson or Z, as well as a $t\bar{t}$ or $b\bar{b}$ pair, with all heavy particles decaying into jets.

Searches for WZ resonances at the LHC have focused on the process $pp \to W' \to WZ$ with the production mainly from $u\bar{d} \to W'$, assuming SM-like couplings to quarks. ATLAS and CMS have set the upper limits on the $W'WZ$ coupling for $M_{W'}$ in the 0.2 − 5.0 TeV range with a combination of fully leptonic, semi-leptonic and fully hadronic channels with $\sim$ 36 fb^{-1} at 13 TeV [41, 42] (see also Ref. [31]). More recent constraints with

Downloaded from https://academic.oup.com/ptep/article/2022/8/083C01/6651666 by KIT Library user on 27 September 2022

77–139 fb^{-1} at 13 TeV were also set in individual channels by ATLAS [43, 44] and CMS [24, 45–47]. The strongest lower limit on the W' mass is set by ATLAS [44] in the semi-leptonic channel with a lower limit on $M_{W'}$ of 3.9 TeV [44] in the context of the Heavy Vector Triplet (HVT) weakly-coupled scenario A [48]. A fermiophobic W' boson that couples to WZ may be produced at hadron colliders in association with a Z boson, or via WZ fusion. This would give rise to $(WZ)Z$ and $(WZ)jj$ final states [49]. Results of the search for the latter are reported in Refs. [24,41,44,46].

W' bosons have also been searched for in final states with a W boson and a SM Higgs boson in the channels $W \to \ell\nu$ or $W \to q\bar{q}'$ and $h^0 \to b\bar{b}$ by ATLAS [23, 50] and CMS [24, 51] with 36–139 fb^{-1} at $\sqrt{s} = 13$ TeV. Cross-section limits are set for W' masses between 0.4 and 5.0 TeV. The ATLAS and CMS 13 TeV analyses with $W \to \ell\nu$ set the most stringent upper limits on the cross section at low and high $M_{W'}$, respectively, as shown in Fig. 86.2.

At lepton colliders, W' bosons may be produced in pairs via their photon coupling, which is model independent. At LEP-II, although dedicated searches for W' bosons have not been performed, the large cross section for $e^+e^- \to \gamma^* \to W'^+W'^-$ and small backgrounds suggest that any W' is ruled out up to the kinematic limit, $M_{W'} < \sqrt{s}/2 \approx 105$ GeV, for most decay modes. Sensitivity to $M_{W'}$ above $\sqrt{s}$ could be achieved [52] using the $e^+e^- \to \gamma\nu\bar{\nu}$ process via a t-channel W' exchange, if the W' coupling to $e\nu$ is large enough.

86.3 Low-energy constraints

The properties of W' bosons are also constrained by measurements of processes at energies much below $M_{W'}$. The bounds on $W - W'$ mixing [4] are mostly due to the change in W properties compared to the SM. Limits on deviations in the ZWW couplings provide a leading constraint for fermiophobic W' bosons [14].

Constraints arising from low-energy effects of W' exchange are strongly model-dependent. If the W' couplings to quarks are not suppressed, then box diagrams involving a W and a W' boson contribute to neutral meson-mixing. In the case of W' couplings to right-handed quarks as in the left-right symmetric model, the limit from $K_L - K_S$ mixing is severe: $M_{W'} > 2.9$ TeV for $C_q^R = gV_{\rm CKM}$ [53]. However, if no correlation between the W' and W couplings is assumed, then the limit on $M_{W'}$ may be significantly relaxed [54].

W' exchange also contributes at tree level to various low-energy processes. In particular, it would impact the measurement of the Fermi constant G_F in muon decay, which in turn would change the predictions of many other electroweak processes. A recent test of parity violation in polarized muon decay [55] has set limits of about 600 GeV on $M_{W'}$, assuming W' couplings to right-handed leptons as in left-right symmetric models and a light ν_R. There are also W' contributions to the neutron electric dipole moment, β decays, and other processes [4].

If right-handed neutrinos have Majorana masses, then there are tree-level contributions to neutrinoless double-beta decay, and a limit on $M_{W'}$ versus the ν_R mass may be derived [56]. For ν_R masses below a few GeV, the W' boson contributes to leptonic and semileptonic B meson decays, so that limits may be placed on various combinations of W' parameters [54]. For ν_R masses below $\sim$30 MeV, the most stringent constraints on $M_{W'}$ are due to the limits on ν_R emission from supernovae.

References

[1] M. Bando, T. Kugo and K. Yamawaki, Phys. Rept. **164**, 217 (1988).

[2] H.-C. Cheng *et al.*, Phys. Rev. **D64**, 065007 (2001), [hep-th/0104179].

[3] See the Section on "Z'-boson searches" in this *Review*.

[4] See the particle listings for W' in this *Review*.

[5] H.-C. Cheng and I. Low, JHEP **09**, 051 (2003), [hep-ph/0308199].

[6] B. A. Dobrescu and Z. Liu, JHEP **10**, 118 (2015), [arXiv:1507.01923].

[7] G. Altarelli, B. Mele and M. Ruiz-Altaba, Z. Phys. **C45**, 109 (1989), [Erratum: Z. Phys. **C47**, 676 (1990)].

[8] R. N. Mohapatra and J. C. Pati, Phys. Rev. **D11**, 566 (1975).

[9] K. S. Babu, X.-G. He and E. Ma, Phys. Rev. **D36**, 878 (1987).

[10] H. Georgi, E. E. Jenkins and E. H. Simmons, Nucl. Phys. **B331**, 541 (1990).

[11] X.-y. Li and E. Ma, J. Phys. **G19**, 1265 (1993), [hep-ph/9208210].

[12] D. J. Muller and S. Nandi, Phys. Lett. **B383**, 345 (1996), [hep-ph/9602390].

[13] A. Donini *et al.*, Nucl. Phys. **B507**, 51 (1997), [hep-ph/9705450].

[14] R. S. Chivukula *et al.*, Phys. Rev. **D74**, 075011 (2006), [hep-ph/0607124].

[15] F. Pisano and V. Pleitez, Phys. Rev. **D46**, 410 (1992), [hep-ph/9206242].

[16] V. D. Barger and R. J. N. Phillips, *Collider Physics* (1996), ISBN 978-0201149456.

[17] Z. Sullivan, Phys. Rev. **D66**, 075011 (2002), [hep-ph/0207290].

[18] G. Aad *et al.* (ATLAS), Phys. Rev. **D100**, 052013 (2019), [arXiv:1906.05609].

[19] T. G. Rizzo, JHEP **05**, 037 (2007), [arXiv:0704.0235].

[20] E. Accomando *et al.*, Phys. Rev. **D85**, 115017 (2012), [arXiv:1110.0713].

[21] CMS Collab., CMS PAS EXO-19-017, Mar. 2021.

[22] F. Abe *et al.* (CDF), Phys. Rev. Lett. **74**, 2900 (1995).

[23] ATLAS Collab., ATLAS-CONF-2021-026, Jun. 2021.

[24] A. Tumasyan *et al.* (CMS) (2021), [arXiv:2109.06055].

[25] F. Abe *et al.* (CDF), Phys. Rev. Lett. **67**, 2609 (1991).

[26] A. M. Sirunyan *et al.* (CMS), Phys. Lett. **B792**, 107 (2019), [arXiv:1807.11421].

[27] ATLAS Collab., ATLAS-CONF-2021-025, Jun. 2021.

[28] CMS Collab., CMS PAS EXO-20-002, Jul. 2021.

[29] M. Aaboud *et al.* (ATLAS), Phys. Lett. B **798**, 134942 (2019), [arXiv:1904.12679].

[30] A. M. Sirunyan *et al.* (CMS), JHEP **03**, 170 (2019), [arXiv:1811.00806].

[31] K.M. Black *et al.*, "Dynamical electroweak symmetry breaking" in this *Review*.

[32] G. Aad *et al.* (ATLAS), JHEP **03**, 145 (2020), [arXiv:1910.08447].

[33] A. M. Sirunyan *et al.* (CMS), JHEP **05**, 033 (2020), [arXiv:1911.03947].

[34] M. Aaboud *et al.* (ATLAS), Phys. Rev. Lett. **121**, 081801 (2018), [arXiv:1804.03496].

[35] A. M. Sirunyan *et al.* (CMS), JHEP **08**, 130 (2018), [arXiv:1806.00843].

[36] M. Aaboud *et al.* (ATLAS), Phys. Lett. **B788**, 316 (2019), [arXiv:1801.08769].

[37] M. Aaboud *et al.* (ATLAS), Phys. Lett. **B795**, 56 (2019), [arXiv:1901.10917].

[38] A. M. Sirunyan *et al.* (CMS), Phys. Rev. D **100**, 11, 112007 (2019), [arXiv:1909.04114].

[39] A. M. Sirunyan *et al.* (CMS), Phys. Rev. Lett. **123**, 23, 231803 (2019), [arXiv:1905.10331].

[40] CMS Collab., CMS PAS B2G-20-002, Mar. 2021.

[41] M. Aaboud *et al.* (ATLAS), Phys. Rev. **D98**, 052008 (2018), [arXiv:1808.02380].

[42] A. M. Sirunyan *et al.* (CMS), Phys. Lett. **B798**, 134952 (2019), [arXiv:1906.00057].

[43] G. Aad *et al.* (ATLAS), JHEP **09**, 091 (2019), [arXiv:1906.08589].

Downloaded from https://academic.oup.com/ptep/article/2022/8/083C01/6651666 by KIT Library user on 27 September 2022

[44] G. Aad *et al.* (ATLAS), Eur. Phys. J. C **80**, 12, 1165 (2020), [arXiv:2004.14636].

[45] A. M. Sirunyan *et al.* (CMS), Eur. Phys. J. C **80**, 3, 237 (2020), [arXiv:1906.05977].

[46] CMS Collab., CMS PAS B2G-20-008, Mar. 2021.

[47] CMS Collab., CMS PAS B2G-20-013, Jul. 2021.

[48] D. Pappadopulo *et al.*, JHEP **09**, 060 (2014), [arXiv:1402.4431].

[49] H.-J. He *et al.*, Phys. Rev. **D78**, 031701 (2008), [arXiv:0708.2588].

[50] G. Aad *et al.* (ATLAS), Phys. Rev. D **102**, 11, 112008 (2020), [arXiv:2007.05293].

[51] A. M. Sirunyan *et al.* (CMS), JHEP **11**, 172 (2018), [arXiv:1807.02826].

[52] S. Godfrey *et al.*, Phys. Rev. D **61**, 113009 (2000), [hep-ph/0001074].

[53] Y. Zhang *et al.*, Phys. Rev. **D76**, 091301 (2007), [arXiv:0704.1662].

[54] P. Langacker and S. U. Sankar, Phys. Rev. **D40**, 1569 (1989).

[55] J. F. Bueno *et al.* (TWIST), Phys. Rev. **D84**, 032005 (2011), [arXiv:1104.3632].

[56] G. Prezeau, M. Ramsey-Musolf and P. Vogel, Phys. Rev. D **68**, 034016 (2003), [hep-ph/0303205].

Downloaded from https://academic.oup.com/ptep/article/2022/8/083C01/6651666 by KIT Library user on 27 September 2022

87. Z'-Boson Searches

Revised October 2021 by B.A. Dobrescu (FNAL) and S. Willocq (U. Massachusetts).

The Z' boson is a massive, electrically-neutral and color-singlet hypothetical particle of spin 1. This particle is predicted in many extensions of the Standard Model (SM) and has been the object of extensive phenomenological studies [1].

87.1 Z' boson couplings

The couplings of a Z' boson to the first-generation fermions are given by

$$Z'_\mu \left(g_u^L\, \overline{u}_L \gamma^\mu u_L + g_d^L\, \overline{d}_L \gamma^\mu d_L + g_u^R\, \overline{u}_R \gamma^\mu u_R + g_d^R\, \overline{d}_R \gamma^\mu d_R + g_\nu^L\, \overline{\nu}_L \gamma^\mu \nu_L + g_e^L\, \overline{e}_L \gamma^\mu e_L + g_e^R\, \overline{e}_R \gamma^\mu e_R \right), \tag{87.1}$$

where u, d, ν, e are the quark and lepton fields in the mass eigenstate basis, and the coefficients g_u^L, g_d^L, g_u^R, g_d^R, g_ν^L, g_e^L, g_e^R are real dimensionless parameters. If the Z' couplings to quarks and leptons are generation-independent, then these seven parameters describe the couplings of the Z' boson to all SM fermions. More generally, however, the Z' couplings to fermions are generation-dependent, in which case Eq. (87.1) may be written with generation indices i, $j = 1, 2, 3$ labeling the quark and lepton fields, and with the seven coefficients promoted to 3×3 Hermitian matrices (*e.g.*, $g_{e\,ij}^L\, \overline{e}_L^i \gamma^\mu e_L^j$, where e_L^2 is the left-handed muon, etc.).

The parameters describing the Z' boson interactions with quarks and leptons are subject to some theoretical constraints. Quantum field theories that include a heavy spin-1 particle are well behaved at high energies only if that particle is a gauge boson associated with a spontaneously broken gauge symmetry. Quantum effects preserve the gauge symmetry only if the couplings of the gauge boson to fermions satisfy the anomaly equations [2]. Furthermore, the fermion charges under the new gauge symmetry are constrained by the requirement that the quarks and leptons get masses from gauge-invariant interactions with the Higgs fields.

The relation between the couplings displayed in Eq. (87.1) and the gauge charges z_{fi}^L and z_{fi}^R of the fermions $f = u, d, \nu, e$ involves the unitary 3×3 matrices V_f^L and V_f^R that transform the gauge eigenstate fermions f_L^i and f_R^i, respectively, into the mass eigenstates. The Z' couplings also depend on the mixings of the new gauge boson in the gauge eigenstate basis ($\tilde{Z}'_\mu$). The main mixings are a kinetic mixing $(-\chi/2) B^{\mu\nu} \tilde{Z}'_{\mu\nu}$ with the hypercharge gauge boson B^μ (χ is a dimensionless parameter), and a mass mixing $\delta M^2\, \tilde{Z}^\mu \tilde{Z}'_\mu$ with the linear combination ($\tilde{Z}_\mu$) of neutral bosons that couples as the SM Z boson [3]. Since both the kinetic and mass mixings shift the mass and couplings of the Z boson, electroweak measurements impose upper limits on χ and $\delta M^2/(M_{Z'}^2 - M_Z^2)$ of the order of 10^{-3} [4]. Keeping only linear terms in these two small quantities, the couplings of the mass-eigenstate Z' boson are given by

$$g_{f\;ij}^L = g_z V_{fii'}^L\, z_{f\;i'}^L \left(V_f^L\right)_{i'j}^\dagger + \frac{e}{c_W} \left(\frac{s_W \chi M_{Z'}^2 + \delta M^2}{2 s_W \left(M_{Z'}^2 - M_Z^2\right)} \sigma_f^3 - \epsilon\, Q_f \right), \tag{87.2}$$

$$g_{f\;ij}^R = g_z V_{fii'}^R\, z_{fi'}^R \left(V_f^R\right)_{i'j}^\dagger - \frac{e}{c_W}\, \epsilon\, Q_f, \tag{87.3}$$

where g_z is the new gauge coupling, Q_f is the electric charge of f, e is the electromagnetic gauge coupling, s_W and c_W are the sine and cosine of the weak mixing angle, $\sigma_f^3 = +1$ for $f = u, \nu$ and $\sigma_f^3 = -1$ for $f = d, e$, and

$$\epsilon = \frac{\chi \left(M_{Z'}^2 - c_W^2 M_Z^2\right) + s_W \delta M^2}{M_{Z'}^2 - M_Z^2}. \tag{87.4}$$

The interaction of the Z' boson with a pair of W bosons has the form

$$\left[i \left(W_\mu^- Z'_\nu - W_\nu^- Z'_\mu \right) \partial^\mu W^{+\nu} + \text{H.c.} \right] + i \left(W_\mu^+ W_\nu^- - W_\nu^+ W_\mu^- \right) \partial^\mu Z'^\nu \tag{87.5}$$

with a coefficient of order $M_W^2/M_{Z'}^2$ [5]. The Z' also couples to one SM Higgs boson and one Z boson, $Z'_\mu Z^\mu\, h^0$, with a coefficient of order M_Z.

87.2 Z' models

A simple origin of a Z' boson is a new $U(1)'$ gauge symmetry. In that case, the matricial equalities $z_u^L = z_d^L$ and $z_\nu^L = z_e^L$ are required by the SM $SU(2)_W$ gauge symmetry. Given that the $U(1)'$ interaction is not asymptotically free, the theory may be well-behaved at high energies (*e.g.*, by embedding $U(1)'$ in a non-Abelian gauge group) only if the charges are commensurate numbers, *i.e.* any ratio of charges is a rational number. Satisfying the anomaly equations [6] with rational numbers is highly nontrivial, and typically new fermions charged under $U(1)'$ are necessary.

If the couplings are generation-independent ($V_f^{L,R}$ are then unit matrices in Eq. (87.2)) and the mixings of $\tilde{Z}'$ are negligible, then there are five commensurate couplings: g_u^R, g_d^R, g_e^R, g_q^L ($q = u$ or d), g_l^L ($l = \nu$ or e). Four sets of charges are displayed in Table 87.1, each of them spanned by a free parameter x [6]. The first set, labeled $B - xL$, has charges proportional to the baryon number minus x times the lepton number. These charges allow all SM Yukawa couplings to the Higgs doublet which is neutral under $U(1)_{B-xL}$, so that there is no tree-level $\tilde{Z} - \tilde{Z}'$ mixing. For $x = 1$ one recovers the $U(1)_{B-L}$ group, which is non-anomalous in the presence of one "right-handed neutrino" (a chiral fermion that is a singlet under the SM gauge group) per generation. For $x \neq 1$, it is necessary to include some fermions that are vectorlike (*i.e.* their mass terms are gauge invariant) with respect to the electroweak gauge group and chiral with respect to $U(1)_{B-xL}$. In the particular cases $x = 0$ or $x \gg 1$, the Z' is leptophobic or quark-phobic, respectively.

The second set, $U(1)_{10+x\bar{5}}$, has charges that commute with the representations of the $SU(5)$ grand unified group. Here x is related to the mixing angle between the two $U(1)$ bosons encountered in the $E_6 \to SU(5) \times U(1) \times U(1)$ symmetry breaking patterns of grand unified theories [1,7]. With these charges, two Higgs doublets are typically required to generate masses for both up- and down- type fermions. This set leads to $\tilde{Z} - \tilde{Z}'$ mass mixing at tree level, such that for a Z' mass close to the electroweak scale, the measurements at the Z-pole require some fine tuning between the charges and VEVs of the two Higgs doublets. Vectorlike quarks charged under the electroweak gauge group are required (except for $x = -3$) to make this set anomaly free. The particular cases $x = -3, 1, -1/2$ are usually labeled $U(1)_\chi$, $U(1)_\psi$, and $U(1)_\eta$, respectively. Under the third set, $U(1)_{d-xu}$, the weak-doublet quarks are neutral, and the ratio of u_R and d_R charges is $-x$. For $x = 1$, this is the "right-handed" group $U(1)_R$. For $x = 0$, the charges are those of the E_6-inspired $U(1)_I$ group, which requires new quarks and leptons. Other generation-independent sets of $U(1)'$ charges are given in Ref. [8].

In the absence of new fermions charged under the SM group, the most general generation-independent charge assignment is $U(1)_{q+xu}$, which is a linear combination of hypercharge and $B-L$. Many other anomaly-free solutions exist if generation-dependent charges are allowed. An example is $B - xL_e - yL_\mu + (y-3)L_\tau$, with x, y free parameters. This allows all fermion masses to be generated by Yukawa couplings to a single Higgs doublet, without inducing tree-level flavor-changing neutral current (FCNC) processes. There are also lepton-flavor dependent charges that allow neutrino masses to arise only from operators of high dimensionality [9].

If the $SU(2)_W$-doublet quarks have generation-dependent $U(1)'$ charges, then the mass eigenstate quarks have flavor off-diagonal couplings to the Z' boson (see Eq. (87.1), and note that $V_u^L \left(V_d^L\right)^\dagger$

Downloaded from https://academic.oup.com/ptep/article/2022/8/083C01/6651666 by KIT Library user on 27 September 2022

Table 87.1: Examples of generation-independent $U(1)'$ charges for quarks and leptons. The parameter x is an arbitrary rational number. Gauge anomaly cancellation requires certain new fermions [6].

fermion	$U(1)_{B-xL}$	$U(1)_{10+x\bar{5}}$	$U(1)_{d-xu}$	$U(1)_{q+xu}$
(u_L, d_L)	$1/3$	$1/3$	0	$1/3$
u_R	$1/3$	$-1/3$	$-x/3$	$x/3$
d_R	$1/3$	$-x/3$	$1/3$	$(2-x)/3$
(ν_L, e_L)	$-x$	$x/3$	$(-1+x)/3$	-1
e_R	$-x$	$-1/3$	$x/3$	$-(2+x)/3$

is the CKM matrix). These are severely constrained by measurements of FCNC processes, which in this case are mediated at tree-level by Z' boson exchange [10]. The constraints are relaxed if the first and second generation charges are the same, although they are increasingly tightened by the measurements of B meson properties [11]. If only the $SU(2)_W$-singlet quarks have generation-dependent $U(1)'$ charges, there is more freedom in adjusting the flavor off-diagonal couplings because the $V^R_{u,d}$ matrices are not observable in the SM.

The anomaly equations for $U(1)'$ could be circumvented only if there is an axion with certain dimension-5 couplings to the gauge bosons. However, such a scenario violates unitarity unless the quantum field theory description breaks down at a scale near $M_{Z'}$ [12]. It is possible, though, that the SM fermions are not charged under the $U(1)'$, but have mass mixing with some vectorlike fermions which are charged under $U(1)'$, implying that the physical fermions have couplings to the Z' [13]. For example, if the only SM quarks that have large mixings with some vectorlike quarks are the b quarks, then the only currently known particles that couple to the Z' would be the physical b quarks.

Z' bosons may also arise from larger gauge groups. These may extend the electroweak group, as in $SU(2)\times SU(2)\times U(1)$, or may embed the electroweak group, as in $SU(3)_W \times U(1)$ [14]. If the larger group is spontaneously broken down to $SU(2)_W \times U(1)_Y \times U(1)'$ at a scale $v_\star \gg M_{Z'}/g_z$, then the above discussion applies up to corrections of order $M^2_{Z'}/(g_z v_\star)^2$. For $v_\star \sim M_{Z'}/g_z$, additional gauge bosons have masses comparable to $M_{Z'}$, including at least a W' boson [14]. If the larger gauge group breaks together with the electroweak symmetry directly to the electromagnetic $U(1)_{\rm em}$, then the left-handed fermion charges are no longer correlated ($z^L_u \neq z^L_d$, $z^L_\nu \neq z^L_e$) and a $Z'W^+W^-$ coupling is induced.

If the electroweak gauge bosons propagate in extra dimensions, then their Kaluza-Klein (KK) excitations include a series of Z' boson pairs. Each of these pairs can be associated with a different $SU(2) \times U(1)$ gauge group in four dimensions. The properties of the KK particles depend strongly on the extra dimensional theory [15]. For example, in universal extra dimensions there is a parity that forces all couplings of Eq. (87.1) to vanish in the case of the lightest KK bosons, while allowing couplings to pairs of fermions involving a SM and a heavy vectorlike fermion. There are also 4-dimensional gauge theories (*e.g.* little Higgs with T parity) with Z' bosons exhibiting similar properties. By contrast, in a warped extra dimension, the couplings of Eq. (87.1) may be sizable even when SM fields propagate along the extra dimension.

Z' bosons may also be composite particles. For example, in confining gauge theories [16], the ρ-like bound state is a spin-1 boson that may be interpreted as arising from a spontaneously broken gauge symmetry [17].

87.3 Non-resonant Z' signatures at colliders

In the presence of the couplings shown in Eq. (87.1), the Z' boson may be produced in the s-channel at colliders, and would decay to pairs of fermions. The decay width into a pair of electrons is given by

$$\Gamma\left(Z' \to e^+e^-\right) \simeq \left[\left(g^L_e\right)^2 + \left(g^R_e\right)^2\right] \frac{M_{Z'}}{24\pi}, \qquad (87.6)$$

where small corrections from electroweak loops are not included. The decay width into $q\bar{q}$ is similar, except for an additional color factor of 3, QCD radiative corrections, and fermion mass corrections. Thus, one may compute the Z' branching fractions in terms of the couplings of Eq. (87.1). However, other decay channels, such as WW or a pair of new particles, could have large widths and need to be added to the total decay width.

As mentioned above, there are theories in which the Z' couplings are controlled by a discrete symmetry that forbids decays into a pair of SM particles. Typically, such theories involve several new particles, which may be produced only in pairs and undergo cascade decays through Z' bosons, leading to signals involving missing transverse momentum. Given that the cascade decays depend on the properties of new particles other than the Z' boson (see, *e.g.* Ref. [18]), this case is not discussed further here.

The Z' contribution to the cross sections for $e^+e^- \to f\bar{f}$ proceeds through an s-channel Z' exchange (when $f = e$, there are also t- and u-channel exchanges). For $M_{Z'} < \sqrt{s}$, the Z' appears as an $f\bar{f}$ resonance in the radiative return process where photon emission tunes the effective center-of-mass energy to $M_{Z'}$. The agreement between the LEP-II measurements and the SM predictions implies that either the Z' couplings are smaller than or of order 10^{-2}, or else $M_{Z'}$ is above 209 GeV, the maximum energy of LEP-II. In the latter case, the Z' exchange may be approximated up to corrections of order $s/M^2_{Z'}$ by the contact interactions

$$\frac{g_z^2}{M^2_{Z'} - s}\left[\bar{e}\gamma_\mu\left(z^L_e P_L + z^R_e P_R\right)e\right]\left[\bar{f}\gamma^\mu\left(z^L_f P_L + z^R_f P_R\right)f\right], \qquad (87.7)$$

where $P_{L,R}$ are chirality projection operators, and the relation between Z' couplings and charges (see Eq. (87.2) in the limit where the mass and kinetic mixings are neglected) is used, assuming generation-independent charges. The four LEP collaborations have set limits on the coefficients of such operators for all possible chiral structures and for various combinations of fermions [19]. Thus, one may derive bounds on $(M_{Z'}/g_z)|z^L_e z^L_f|^{-1/2}$ and the analogous combinations of LR, RL and RR charges, which are typically on the order of a few TeV. LEP-II limits were derived [6] on the four sets of charges shown in Table 87.1.

Somewhat stronger bounds can be set on $M_{Z'}/g_z$ for specific sets of Z' couplings if the effects of several operators (87.7) are combined. Dedicated analyses by the LEP collaborations have set limits on Z' bosons for particular values of the gauge coupling (see section 3.5 of Ref. [19]). For example, $M_{Z_{\rm SSM}} > 1.76$ TeV for a "sequential" Z' of same couplings as the SM Z boson, while $M_{Z_\chi} > 0.785$ TeV for the Z' associated with $U(1)_\chi$ assuming a unification condition for the gauge coupling.

87.4 Searches at hadron colliders

Z' bosons with couplings to quarks (see Eq. (87.1)) may be produced at hadron colliders in the s-channel and would show up as resonances in the invariant mass distribution of the decay products. The cross section for producing a Z' boson at the LHC, which then decays to some $f\bar{f}$ final state, takes the form [20]

$$\sigma\left(pp \to Z'X \to f\bar{f}X\right) \simeq \frac{\pi}{6\,s}\sum_q c^f_q\, w_q\left(s, M^2_{Z'}\right) \qquad (87.8)$$

for flavor-diagonal couplings to quarks. Here, we have neglected the interference with the SM contribution to $f\bar{f}$ production, which is a good approximation for a narrow Z' resonance (deviations from the narrow width approximation are discussed in Ref. [21]). The coefficients

$$c^f_q = \left[\left(g^L_q\right)^2 + \left(g^R_q\right)^2\right] B(Z' \to f\bar{f}) \qquad (87.9)$$

contain all the dependence on the Z' couplings, while the functions w_q include all the information about parton distributions and QCD corrections [6, 8]. This factorization holds exactly to NLO and the deviations from it induced at NNLO are very small. Note that the w_u and w_d functions are substantially larger than the w_q functions for the other quarks. Eq. (87.8) also applies to

Downloaded from https://academic.oup.com/ptep/article/2022/8/083C01/6651666 by KIT Library user on 27 September 2022

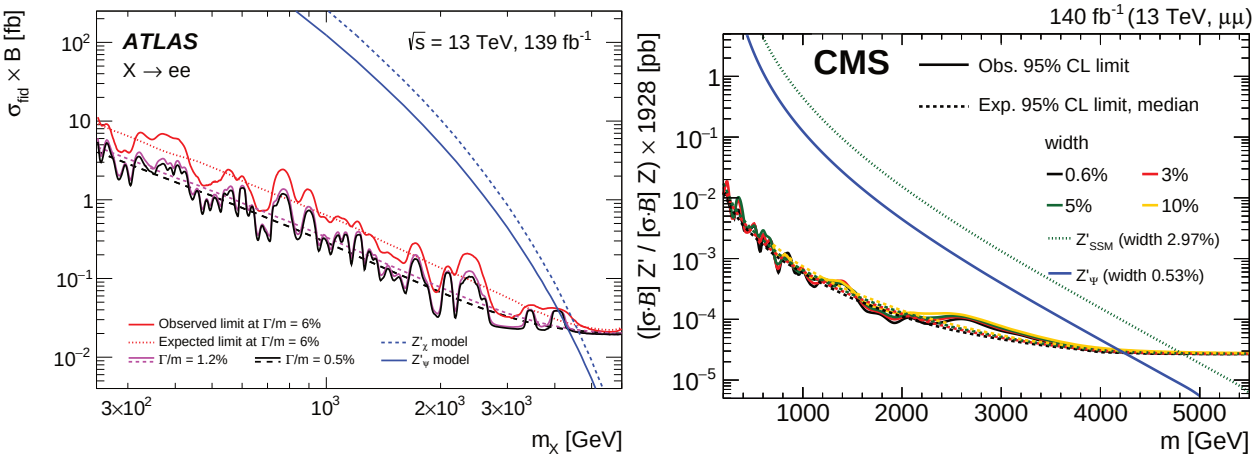

Figure 87.1: Upper limits on the cross section for Z' production times the branching fraction for $Z' \to e^+e^-$ (left panel, set by ATLAS [22]) or $Z' \to \mu^+\mu^-$ (right panel, set by CMS [23]) as a function of $M_{Z'}$. The lines labeled by Z'_ψ and Z'_χ are theoretical predictions for the $U(1)_{10+x\bar{5}}$ models in Table 87.1 with $x = -3$ and $x = +1$, respectively, for g_z fixed by an E_6 unification condition. The $Z'_{\rm SSM}$ line corresponds to Z' couplings equal to those of the Z boson.

the Tevatron, except for changing the pp initial state to $p\bar{p}$, which implies that the $w_q(s, M^2_{Z'})$ functions are replaced by some other functions $\bar{w}_q((1.96\,\text{TeV})^2, M^2_{Z'})$.

It is common to present results of Z' searches as limits on the cross section versus $M_{Z'}$ (see for example Fig. 87.1). An alternative is to plot exclusion curves for fixed $M_{Z'}$ values in the $c^f_u - c^f_d$ planes, allowing a simple derivation of the mass limit within any Z' model. CMS upper limits in the $c^\ell_u - c^\ell_d$ plane ($\ell = e$ or μ) for different $M_{Z'}$ are shown in Ref. [23] (for Tevatron limits, see Refs. [8, 24]).

The discovery of a dilepton resonance at the LHC would determine the Z' mass and width. A measurement of the total cross section would define a band in the $c^\ell_u - c^\ell_d$ plane. Angular distributions can be used to measure several combinations of Z' parameters (angular distributions were used in Ref. [25] to improve the Tevatron sensitivity). Even though the original quark direction in a pp collider is unknown, the leptonic forward-backward asymmetry $A^\ell_{\rm FB}$ can be extracted from the kinematics of the dilepton system, and is sensitive to parity-violating couplings. A fit to the Z' rapidity distribution can distinguish between the couplings to up and down quarks. These measurements, combined with off-peak observables, have the potential to differentiate among various Z' models [26]. In some cases, $A^\ell_{\rm FB}$ may provide discovery sensitivity that is competitive with the mass distribution [27]. The spin of the Z' boson may be determined from angular distributions [28].

Searches for Z' decays into e^+e^- and $\mu^+\mu^-$ by the ATLAS and CMS collaborations [22, 23] have set 95% C.L. upper cross-section limits as low as 0.02 fb (see Fig. 87.1), with the mass lower limits in specific models as high as 4.9 TeV in a single channel. Cross section limits in the dimuon channel for low mass regions, below 200 GeV but not near the Z mass, have been set at the LHC by CMS [29] and LHCb [30].

The $Z' \to \tau^+\tau^-$ decay has been searched for with 36 fb^{-1} of 13 TeV data [31], and a limit $M_{Z'} > 2.4$ TeV has been set in the case of a sequential Z'. Limits on heavy scalars in the $\tau^+\tau^-$ final state, set by ATLAS [32] with 139 fb^{-1} and CMS [33] with 36 fb^{-1} at 13 TeV, can be recast into limits on Z'. Limits in the flavor-violating leptonic final states have also been reported by ATLAS [34] and CMS [35] at 13 TeV, for resonances in the $e^\pm\mu^\mp$, $e^\pm\tau^\mp$ and $\mu^\pm\tau^\mp$ channels.

Final states with higher background, jj, $b\bar{b}$ and $t\bar{t}$, are also important as they probe various combinations of Z' couplings to quarks. Besides the improved sensitivity at masses of several TeV, the LHC searches in the dijet channel have been also extended to masses as low as 10 GeV, through the use of new techniques involving boosted topologies and initial state radiation [37]. Limits from such Z' searches in hadronic final states are summarized in Fig. 87.2.

Searches for the $Z' \to b\bar{b}$ decay have been performed for two production mechanisms. ATLAS [38] and CMS [39] searched for $b\bar{b}$ resonances in 139 fb^{-1} and 137 fb^{-1} of 13 TeV data, respectively, setting limits under the assumption that the Z' boson couples to light quarks and thus is produced in the s-channel. The CMS upper limit on the cross-section times the $Z' \to b\bar{b}$ branching fraction decreases from 40 fb at $M_{Z'} = 1.8$ TeV to 0.4 fb at $M_{Z'} = 8$ TeV. The ATLAS search covered the 1.3 TeV – 5 TeV mass range, setting a lower mass limit of 2.7 TeV for the Z'_{SSM}. Independent of any other couplings, if the Z' couples to the b quark, then it can be produced in association with a $b\bar{b}$ pair, and it decays to a second $b\bar{b}$ pair, which forms a resonance. The cross-section limit for that process, set by ATLAS [40] with 103 fb^{-1} of 13 TeV data, is between 0.1 and 0.2 pb for $M_{Z'}$ in the 1.3 – 3 TeV range. For a vector coupling g_b of Z' to b quarks, *i.e*, $g^L_{d\,33} = g^R_{d\,33} = g_b$ using the notation of Eq. (87.1), the limit is $M_{Z'} > 1.45$ TeV when $g_b = 1$. Searches for the $Z' \to t\bar{t}$ decay are discussed in Ref. [41].

Heavy resonances decaying into Zh^0 with $Z \to \ell^+\ell^-$, $\nu\bar{\nu}$ or $q\bar{q}$ and $h^0 \to b\bar{b}$ have been studied by ATLAS [42, 43] and CMS [44–46] using 13 TeV data. The most stringent constraint on Z' production in the context of the Heavy Vector Triplet (HVT) model weakly-coupled scenario A [47] is set in the semi-leptonic channel, with a mass lower limit of 3.5 TeV [46].

Searches for a Z' boson lighter than the SM Z and which couples to leptons have been performed in the 4-lepton final state. CMS [48] focused on the Z decays into a muon pair followed by the radiation of a Z' boson which decays itself into a muon pair. ATLAS [49] considered the $h^0 \to ZZ'$ and $h^0 \to Z'Z'$ processes followed by the leptonic decays of both Z and Z'.

The $pp \to Z'X \to W^+W^-X$ process has also been searched for at the LHC. The channel where the Z' boson is produced through its couplings to quarks, and the W bosons decay hadronically, has been explored using boosted techniques to analyze the 13 TeV data [50–53] with a mass lower limit of 3.5 TeV in the HVT model A [51]. The Z' boson may also be produced through its couplings to W bosons [54], which has been explored with the use of forward jets consistent with a vector boson fusion event topology [51, 53]. The latter process provides a test of fermiophobic Z' models.

At the Tevatron, the CDF and DØ collaborations have searched for Z' bosons in the e^+e^- [55], $\mu^+\mu^-$ [56], $e^\pm\mu^\mp$ [57], $\tau^+\tau^-$ [58], $t\bar{t}$ [59], jj [60] and W^+W^- [61] final states. These limits have been mostly superseded by the LHC results.

Downloaded from https://academic.oup.com/ptep/article/2022/8/083C01/6651666 by KIT Library user on 27 September 2022

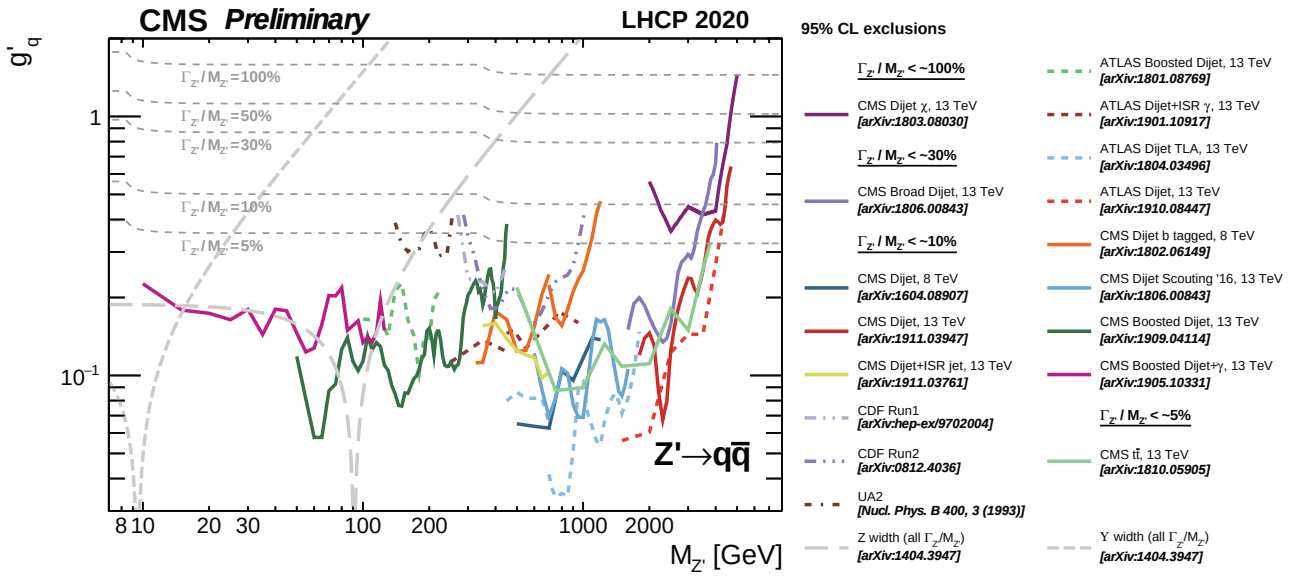

Figure 87.2: Upper limits on the Z' coupling to quarks as a function of $M_{Z'}$ based on various searches performed by the ATLAS, CMS, CDF, and UA2 experiments [36].

87.5 Low-energy constraints

Z' boson properties are also constrained by a variety of low-energy experiments [62]. Polarized electron-nucleon scattering and atomic parity violation are sensitive to electron-quark contact interactions, which get contributions from Z' exchange that can be expressed in terms of the couplings introduced in Eq. (87.1) and M'_Z. Further corrections to the electron-quark contact interactions are induced in the presence of $\tilde{Z}-\tilde{Z}'$ mixing because of the shifts in the Z couplings to quarks and leptons [3]. Deep-inelastic neutrino-nucleon scattering is similarly affected by Z' bosons. Other low-energy observables are discussed in [4]. Viable models with Z' bosons much lighter than the Z boson have been constructed, despite many additional experimental constraints [63]. Limits on the Z' coupling to leptons in the mass range 0.02–10.2 GeV have been set in e^+e^- collisions by BaBar [64], assuming a dark photon, *i.e.*, a Z' boson whose couplings arise only from the kinetic mixing with the hypercharge gauge boson.

In some models, the lower limits on $M_{Z'}$ set by low-energy data are above 1 TeV. For example, $M_{Z_\chi} > 1.1$ TeV and $M_{Z_\eta} > 0.43$ TeV assuming that the Higgs sectors consist of electroweak doublets and singlets only [4], while the gauge coupling is fixed by an $SO(10)$ unification condition for $U(1)_\chi$ and $U(1)_\eta$. For more general models, see Refs. [1, 6, 65]. The mass bounds from direct searches at the LHC [22, 23] exceed the electroweak constraints by a factor of three or more for the models mentioned here. This conclusion could change if the collider bounds are weakened by exotic decay channels [66].

Although the LHC data are most constraining for many Z' models, one should be careful in assessing the relative reach of various experiments given the freedom in Z' couplings. For example, a Z' coupled to $B-yL_\mu+(y-3)L_\tau$ has implications for the muon $g-2$, neutrino oscillations or τ decays, and would be hard to see in processes involving first-generation fermions. Moreover, the combination of LHC searches and low-energy measurements could allow a precise determination of the Z' parameters [67].

References

[1] A. Leike, Phys. Rept. **317**, 143 (1999), [hep-ph/9805494].

[2] T. P. Cheng and L. F. Li, *Gauge Theory of Elementary Particle Physics* (1984), ISBN 9780198519614.

[3] K. S. Babu, C. F. Kolda and J. March-Russell, Phys. Rev. **D57**, 6788 (1998), [hep-ph/9710441].

[4] J. Erler *et al.*, JHEP **08**, 017 (2009), [arXiv:0906.2435].

[5] B. A. Dobrescu and P. J. Fox, JHEP **05**, 047 (2016), [arXiv:1511.02148].

[6] M. Carena *et al.*, Phys. Rev. **D70**, 093009 (2004), [hep-ph/0408098].

[7] F. Del Aguila, M. Cvetic and P. Langacker, Phys. Rev. **D52**, 37 (1995), [hep-ph/9501390].

[8] E. Accomando *et al.*, Phys. Rev. **D83**, 075012 (2011), [arXiv:1010.6058].

[9] M.-C. Chen, A. de Gouvea and B. A. Dobrescu, Phys. Rev. **D75**, 055009 (2007), [hep-ph/0612017].

[10] P. Langacker and M. Plumacher, Phys. Rev. **D62**, 013006 (2000), [hep-ph/0001204].

[11] A. J. Buras, F. De Fazio and J. Girrbach, JHEP **02**, 116 (2013), [arXiv:1211.1896].

[12] L. E. Ibanez and G. G. Ross, Phys. Lett. **B332**, 100 (1994), [hep-ph/9403338].

[13] P. J. Fox *et al.*, Phys. Rev. D **84**, 115006 (2011), [arXiv:1104.4127].

[14] See the Section on "W' searches" in this *Review*.

[15] J. Parsons and A. Pomarol, "Extra dimensions" in this *Review*.

[16] K.M. Black *et al.*, "Dynamical electroweak symmetry breaking" in this *Review*.

[17] M. Bando, T. Kugo and K. Yamawaki, Phys. Rept. **164**, 217 (1988).

[18] J. Y. Araz *et al.*, JHEP **02**, 092 (2018), [arXiv:1711.06302].

[19] S. Schael *et al.* (ALEPH, DELPHI, L3, OPAL, LEP Electroweak), Phys. Rept. **532**, 119 (2013), [arXiv:1302.3415].

[20] G. Paz and J. Roy, Phys. Rev. **D97**, 075025 (2018), [arXiv:1711.02655].

[21] E. Accomando *et al.*, JHEP **10**, 153 (2013), [arXiv:1304.6700].

[22] G. Aad *et al.* (ATLAS), Phys. Lett. **B796**, 68 (2019), [arXiv:1903.06248].

[23] A. M. Sirunyan *et al.* (CMS), JHEP **07**, 208 (2021), [arXiv:2103.02708].

[24] A. Abulencia *et al.* (CDF), Phys. Rev. Lett. **95**, 252001 (2005), [hep-ex/0507104].

[25] A. Abulencia *et al.* (CDF), Phys. Rev. Lett. **96**, 211801 (2006), [hep-ex/0602045].

[26] F. Petriello and S. Quackenbush, Phys. Rev. **D77**, 115004 (2008), [arXiv:0801.4389].

Downloaded from https://academic.oup.com/ptep/article/2022/8/083C01/6651666 by KIT Library user on 27 September 2022

[27] E. Accomando *et al.*, JHEP **01**, 127 (2016), [arXiv:1503.02672].

[28] P. Osland *et al.*, Phys. Rev. **D79**, 115021 (2009), [arXiv:0904.4857].

[29] A. M. Sirunyan *et al.* (CMS), Phys. Rev. Lett. **124**, 13, 131802 (2020), [arXiv:1912.04776].

[30] R. Aaij *et al.* (LHCb), JHEP **10**, 156 (2020), [arXiv:2007.03923].

[31] M. Aaboud *et al.* (ATLAS), JHEP **01**, 055 (2018), [arXiv:1709.07242].

[32] G. Aad *et al.* (ATLAS), Phys. Rev. Lett. **125**, 5, 051801 (2020), [arXiv:2002.12223].

[33] A. M. Sirunyan *et al.* (CMS), JHEP **09**, 007 (2018), [arXiv:1803.06553].

[34] M. Aaboud *et al.* (ATLAS), Phys. Rev. **D98**, 092008 (2018), [arXiv:1807.06573].

[35] CMS Collab., PAS EXO-19-014, Aug. 2021.

[36] CMS Collab., `https://twiki.cern.ch/twiki/bin/view/CMSPublic/SummaryPlotsEXO13TeV`.

[37] A. M. Sirunyan *et al.* (CMS), Phys. Rev. Lett. **123**, 23, 231803 (2019), [arXiv:1905.10331].

[38] G. Aad *et al.* (ATLAS), JHEP **03**, 145 (2020), [arXiv:1910.08447].

[39] CMS Collab., CMS PAS EXO-20-008, July 2021.

[40] G. Aad *et al.* (ATLAS) (2021), [arXiv:2108.09059].

[41] See the Section on "Dynamical Electroweak Symmetry Breaking" in this *Review*.

[42] G. Aad *et al.* (ATLAS), Phys. Rev. D **102**, 11, 112008 (2020), [arXiv:2007.05293].

[43] ATLAS Collab., ATLAS-CONF-2020-043, Jul. 2020.

[44] A. M. Sirunyan *et al.* (CMS), Eur. Phys. J. **C77**, 636 (2017), [arXiv:1707.01303].

[45] A. M. Sirunyan *et al.* (CMS), JHEP **01**, 051 (2019), [arXiv:1808.01365].

[46] A. M. Sirunyan *et al.* (CMS), Eur. Phys. J. C **81**, 8, 688 (2021), [arXiv:2102.08198].

[47] D. Pappadopulo *et al.*, JHEP **09**, 060 (2014), [arXiv:1402.4431].

[48] A. M. Sirunyan *et al.* (CMS), Phys. Lett. **B792**, 345 (2019), [arXiv:1808.03684].

[49] ATLAS Collab., ATLAS-CONF-2021-034, Aug. 2021.

[50] G. Aad *et al.* (ATLAS), JHEP **09**, 091 (2019), [arXiv:1906.08589].

[51] G. Aad *et al.* (ATLAS), Eur. Phys. J. C **80**, 12, 1165 (2020), [arXiv:2004.14636].

[52] A. M. Sirunyan *et al.* (CMS), Eur. Phys. J. C **80**, 3, 237 (2020), [arXiv:1906.05977].

[53] A. Tumasyan *et al.* (CMS) (2021), [arXiv:2109.06055].

[54] H.-J. He *et al.*, Phys. Rev. **D78**, 031701 (2008), [arXiv:0708.2588].

[55] V. M. Abazov *et al.* (D0), Phys. Lett. **B695**, 88 (2011), [arXiv:1008.2023].

[56] T. Aaltonen *et al.* (CDF), Phys. Rev. Lett. **106**, 121801 (2011), [arXiv:1101.4578].

[57] A. Abulencia *et al.* (CDF), Phys. Rev. Lett. **96**, 211802 (2006), [hep-ex/0603006].

[58] D. Acosta *et al.* (CDF), Phys. Rev. Lett. **95**, 131801 (2005), [hep-ex/0506034].

[59] T. Aaltonen *et al.* (CDF), Phys. Rev. **D84**, 072004 (2011), [arXiv:1107.5063].

[60] T. Aaltonen *et al.* (CDF), Phys. Rev. **D79**, 112002 (2009), [arXiv:0812.4036].

[61] T. Aaltonen *et al.* (CDF), Phys. Rev. Lett. **104**, 241801 (2010), [arXiv:1004.4946].

[62] V. D. Barger *et al.*, Phys. Rev. **D57**, 391 (1998), [hep-ph/9707412].

[63] R. Harnik, J. Kopp and P. A. N. Machado, JCAP **1207**, 026 (2012), [arXiv:1202.6073].

[64] J. P. Lees *et al.* (BaBar), Phys. Rev. Lett. **113**, 201801 (2014), [arXiv:1406.2980].

[65] E. Rojas and J. Erler, JHEP **10**, 063 (2015), [arXiv:1505.03208].

[66] J. Kang and P. Langacker, Phys. Rev. **D71**, 035014 (2005), [hep-ph/0412190].

[67] Y. Li, F. Petriello and S. Quackenbush, Phys. Rev. **D80**, 055018 (2009), [arXiv:0906.4132].

Downloaded from https://academic.oup.com/ptep/article/2022/8/083C01/6651666 by KIT Library user on 27 September 2022

88. Supersymmetry, Part I (Theory)

Revised August 2021 by B.C. Allanach (DAMTP, Cambridge U.) and H.E. Haber (UC Santa Cruz).

88.1 Introduction . . . 1000
88.2 Structure of the MSSM . . . 1000
88.2.1 R-parity and the lightest supersymmetric particle . . . 1001
88.2.2 The goldstino and gravitino . . . 1001
88.2.3 Hidden sectors and the structure of SUSY breaking . . . 1002
88.2.4 SUSY and extra dimensions . . . 1002
88.2.5 Split-SUSY . . . 1002
88.3 Parameters of the MSSM . . . 1003
88.3.1 The SUSY-conserving parameters . . . 1003
88.3.2 The SUSY-breaking parameters . . . 1003
88.3.3 MSSM-124 . . . 1003
88.4 The supersymmetric-particle spectrum . . . 1004
88.4.1 The charginos and neutralinos . . . 1004
88.4.2 The squarks and sleptons . . . 1004
88.5 The supersymmetric Higgs sector . . . 1005
88.5.1 The tree-level Higgs sector . . . 1005
88.5.2 The radiatively-corrected Higgs sector . . . 1005
88.6 Restricting the MSSM parameter freedom . . . 1006
88.6.1 Gaugino mass relations . . . 1006
88.6.2 Constrained versions of the MSSM: mSUGRA, CMSSM, etc. . . . 1007
88.6.3 Gauge-mediated SUSY breaking . . . 1007
88.6.4 The phenomenological MSSM . . . 1008
88.6.5 Simplified models . . . 1008
88.7 Experimental data confronts the MSSM . . . 1008
88.7.1 Naturalness constraints and the little hierarchy . . . 1009
88.7.2 Indirect constraints on supersymmetric models . . . 1010
88.8 Massive neutrinos in weak-scale SUSY . . . 1010
88.8.1 The supersymmetric seesaw . . . 1011
88.8.2 R-parity-violating SUSY . . . 1011
88.9 Extensions beyond the MSSM . . . 1011

88.1 Introduction

Supersymmetry (SUSY) is a generalization of the space-time symmetries of quantum field theory that transforms fermions into bosons and vice versa [1]. The existence of such a non-trivial extension of the Poincaré symmetry of ordinary quantum field theory was initially surprising, and its form is highly constrained by theoretical principles [2]. SUSY also provides a framework for the unification of particle physics and gravity [3–6] at the Planck energy scale, $M_{\rm P} \sim 10^{19}$ GeV, where the gravitational interactions become comparable in strength to the gauge interactions. Moreover, supersymmetry can stabilize the hierarchy between the energy scale that characterizes electroweak symmetry breaking, $M_{\rm EW} \sim 100$ GeV, and the Planck scale [7–10] against large radiative corrections. The stability of this large gauge hierarchy with respect to radiative quantum corrections is not possible to maintain in the Standard Model (SM) without an unnatural fine-tuning of the parameters of the fundamental theory at the Planck scale. In contrast, in a supersymmetric extension of the SM, it is possible to maintain the gauge hierarchy while providing a natural framework for elementary scalar fields.

If supersymmetry were an exact symmetry of nature, then particles and their superpartners, which differ in spin by half a unit, would be degenerate in mass. Since superpartners have not (yet) been observed, supersymmetry must be a broken symmetry. Nevertheless, the stability of the gauge hierarchy can still be maintained if the SUSY breaking is soft [11,12], and the corresponding SUSY-breaking mass parameters are no larger than a few TeV. Whether this is still plausible in light of recent SUSY searches at the LHC (see Sec. 89) will be discussed in Sec. 88.7.

In particular, soft-SUSY-breaking terms of the Lagrangian involve combinations of fields with total mass dimension of three or less, with some restrictions on the dimension-three terms as elucidated in Ref. [11]. The impact of the soft terms becomes negligible at energy scales much larger than the size of the SUSY-breaking masses. Thus, a theory of weak-scale supersymmetry, where the effective scale of supersymmetry breaking is tied to the scale of electroweak symmetry breaking, provides a natural framework for the origin and the stability of the gauge hierarchy [7–10].

At present, there is no unambiguous experimental evidence for the breakdown of the SM at or below the TeV scale. The expectations for new TeV-scale physics beyond the SM are based primarily on three theoretical arguments. First, in a theory with an elementary scalar field of mass m and interaction strength λ (e.g., a quartic scalar self-coupling, the square of a gauge coupling or the square of a Yukawa coupling), the stability with respect to quantum corrections requires the existence of an energy cutoff roughly of order $(16\pi^2/\lambda)^{1/2}m$, beyond which new physics must enter [13]. A significantly larger energy cutoff would require an unnatural fine-tuning of parameters that govern the effective low-energy theory. Applying this argument to the SM leads to an expectation of new physics at the TeV scale [10].

Second, the unification of the three SM gauge couplings at a very high energy close to the Planck scale is possible if new physics beyond the SM (which modifies the running of the gauge couplings above the electroweak scale) is present. The minimal supersymmetric extension of the SM, where superpartner masses lie below a few TeV, provides an example of successful gauge coupling unification [14].

Third, the existence of dark matter that makes up approximately one quarter of the energy density of the universe, cannot be explained within the SM of particle physics [15]. Remarkably, a stable weakly-interacting massive particle (WIMP) whose mass and interaction rate are governed by new physics associated with the TeV-scale can be consistent with the observed density of dark matter (this is the so-called WIMP miracle, which is reviewed in Ref. [16]). The lightest supersymmetric particle, if stable, is a promising (although not the unique) candidate for the dark matter [17–21]. Further aspects of dark matter can be found in Sec. 27.

88.2 Structure of the MSSM

The minimal supersymmetric extension of the SM (MSSM) consists of the fields of the two-Higgs-doublet extension of the SM and the corresponding superpartners [22, 23]. A particle and its superpartner together form a supermultiplet. The corresponding field content of the supermultiplets of the MSSM and their gauge quantum numbers are shown in Table 88.1. The electric charge $Q = T_3 + \frac{1}{2}Y$ is determined in terms of the third component of the weak isospin (T_3) and the U(1) weak hypercharge (Y).

The gauge supermultiplets consist of the gluons and their gluino fermionic superpartners and the SU(2)×U(1) gauge bosons and their gaugino fermionic superpartners. The matter supermultiplets consist of three generations of left-handed quarks and leptons and their scalar superpartners (squarks and sleptons, collectively referred to as sfermions), and the corresponding antiparticles. The Higgs supermultiplets consist of two complex Higgs doublets, their higgsino fermionic superpartners, and the corresponding antiparticles. The enlarged Higgs sector of the MSSM constitutes the minimal structure needed to guarantee the cancellation of gauge anomalies [25] generated by the higgsino superpartners that can appear as internal lines in triangle diagrams with three external electroweak gauge bosons. Moreover, without a second Higgs doublet, one cannot generate mass for both "up"-type and "down"-type quarks (and charged leptons) in a way consistent with the underlying SUSY [26–28].

In the most elegant treatment of SUSY, spacetime is extended to superspace which consistsof the spacetime coordinates and new anticommuting fermionic coordinates θ and $\theta^\dagger$ [29, 30]. Each supermultiplet is represented by a superfield that is a function of the superspace coordinates. The fields of a given supermultiplet (which are functions of the spacetime coordinates) are coefficients of the θ and $\theta^\dagger$ expansion of the corresponding superfield.

Vector superfields contain the gauge-boson fields and their gaugino partners. Chiral superfields contain the spin-0 and spin-

Downloaded from https://academic.oup.com/ptep/article/2022/8/083C01/6651666 by KIT Library user on 27 September 2022

Table 88.1: The fields of the MSSM and their SU(3)×SU(2)×U(1) quantum numbers are listed. For simplicity, only one generation of quarks and leptons is exhibited. For each lepton, quark, and Higgs supermultiplet (each denoted by a hatted upper-case letter), there is a corresponding antiparticle multiplet of charge-conjugated fermions and their associated scalar partners [24].

Field Content of the MSSM						
Super-multiplets	Super-field	Bosonic fields	Fermionic partners	SU(3)	SU(2)	U(1)
gluon/gluino	$\hat{V}_8$	g	$\widetilde{g}$	8	1	0
gauge boson/	$\hat{V}$	$W^{\pm}$, W^0	$\widetilde{W}^{\pm}$, $\widetilde{W}^0$	1	3	0
gaugino	$\hat{V}'$	B	$\widetilde{B}$	1	1	0
slepton/	$\hat{L}$	$(\widetilde{\nu}_L, \widetilde{e}_L^-)$	$(\nu, e^-)_L$	1	2	−1
lepton	$\hat{E}^c$	$\tilde{e}_R^+$	e_L^c	1	1	2
squark/	$\hat{Q}$	$(\widetilde{u}_L, \widetilde{d}_L)$	$(u, d)_L$	3	2	1/3
quark	$\hat{U}^c$	$\widetilde{u}_R^*$	u_L^c	$\bar{3}$	1	−4/3
	$\hat{D}^c$	$\widetilde{d}_R^*$	d_L^c	$\bar{3}$	1	2/3
Higgs boson/	$\hat{H}_d$	(H_d^0, H_d^-)	$(\widetilde{H}_d^0, \widetilde{H}_d^-)$	1	2	−1
higgsino	$\hat{H}_u$	(H_u^+, H_u^0)	$(\widetilde{H}_u^+, \widetilde{H}_u^0)$	1	2	1

1/2 fields of the matter or Higgs supermultiplets. A general supersymmetric Lagrangian is determined by three functions of the chiral superfields [4]: the superpotential, the Kähler potential, and the gauge kinetic function (which can be appropriately generalized to accommodate higher derivative terms [31]). Minimal forms for the Kähler potential and gauge kinetic function, which generate canonical kinetic energy terms for all the fields, are required for renormalizable globally supersymmetric theories. A renormalizable superpotential, which is at most cubic in the chiral superfields, yields supersymmetric Yukawa couplings and mass terms. A combination of gauge invariance and SUSY produces couplings of gaugino fields to matter (or Higgs) fields and their corresponding superpartners. The (renormalizable) MSSM Lagrangian is then constructed by including all possible supersymmetric interaction terms (of dimension four or less) that satisfy SU(3)×SU(2)×U(1) gauge invariance and B–L conservation (where B = baryon number and L = lepton number). Finally, the most general soft-supersymmetry-breaking terms consistent with these symmetries are added [11, 12, 32].

Although the MSSM is the focus of much of this review, there is some motivation for considering non-minimal supersymmetric extensions of the SM. For example, extra structure is needed to generate non-zero neutrino masses as discussed in Sec. 88.8. In addition, in order to address some theoretical issues and tensions associated with the MSSM, it has been fruitful to introduce one additional singlet Higgs superfield. The resulting next-to-minimal supersymmetric extension of the Standard Model (NMSSM) [33] is considered further in Sec. 88.4–88.7 and 88.9. Finally, one is always free to add additional fields to the SM along with the corresponding superpartners. However, only certain choices for the new fields (*e.g.*, the addition of complete SU(5) multiplets) will preserve the successful gauge coupling unification of the MSSM. Some examples will be briefly mentioned in Sec. 88.9.

88.2.1 *R-parity and the lightest supersymmetric particle*

The (renormalizable) SM Lagrangian possesses an accidental global B–L symmetry due to the fact that B and L-violating operators composed of SM fields must have dimension $d = 5$ or larger [34]. Consequently, B and L-violating effects are suppressed by $(M_{\rm EW}/M)^{d-4}$, where M is the characteristic mass scale of the physics that generates the corresponding higher dimensional operators. Indeed, values of M of order the grand unification scale or larger may be responsible for the observed (approximate) stability of the proton and suppression of neutrino masses. Unfortunately, these results are not guaranteed in a generic supersymmetric extension of the SM. For example, it is possible to construct gauge invariant supersymmetric dimension-four B and L-violating operators made up of fields of SM particles and their superpartners. Such operators, if simultaneously present in the theory, could yield a proton decay rate many orders of magnitude larger than the current experimental bound. It is for this reason that B–L conservation is *imposed* on the supersymmetric Lagrangian when defining the MSSM, which is sufficient for eliminating all B and L-violating operators of dimension $d \leq 4$.

As a consequence of the B–L symmetry, the MSSM possesses a multiplicative R-parity invariance, where $R = (-1)^{3(B-L)+2S}$ for a particle of spin S [35]. This implies that all the particles of the SM have even R-parity, whereas the corresponding superpartners have odd R-parity. The conservation of R-parity in scattering and decay processes has a critical impact on supersymmetric phenomenology. For example, any initial state in a scattering experiment will involve ordinary (R-even) particles. Consequently, it follows that supersymmetric particles must be produced in pairs. In general, these particles are highly unstable and decay into lighter states. Moreover, R-parity invariance also implies that the lightest supersymmetric particle (LSP) is absolutely stable, and must eventually be produced at the end of a decay chain initiated by the decay of a heavy unstable supersymmetric particle. In order to be consistent with cosmological constraints, a stable LSP is almost certainly electrically and color neutral [19]. Consequently, the LSP in an R-parity-conserving (RPC) theory is weakly interacting with ordinary matter, *i.e.*, it behaves like a stable heavy neutrino and will escape collider detectors without being directly observed. Thus, the canonical signature for conventional R-parity-conserving supersymmetric theories is missing (transverse) momentum, due to the escape of the LSP. Moreover, as noted in Sec. 88.1 and reviewed in Refs. [20] and [21], the stability of the LSP in R-parity-conserving SUSY makes it a promising candidate for dark matter.

The possibility of relaxing the R-parity invariance of the MSSM (which would generate new B and/or L-violating interactions) will be addressed in Sec. 88.8.2. However, note that in R-parity violating (RPV) models, the LSP is no longer stable and thus would not be a viable candidate for the dark matter (unless its lifetime was significantly longer than the age of the universe). In such scenarios, one has to look elsewhere to explain the origin of dark matter.

88.2.2 *The goldstino and gravitino*

In the MSSM, SUSY breaking is accomplished by including the most general renormalizable soft-SUSY-breaking terms consistent with the SU(3)×SU(2)×U(1) gauge symmetry and R-parity invariance. These terms parameterize our ignorance of the fundamental mechanism of supersymmetry breaking. If supersymmetry breaking occurs spontaneously, then a massless Goldstone fermion called the goldstino ($\widetilde{G}_{1/2}$) must exist. The goldstino would then be the LSP, and could play an important role in supersymmetric phenomenology [36].

However, the goldstino degrees of freedom are physical only in models of spontaneously-broken global SUSY. If SUSY is a local symmetry, then the theory must incorporate gravity; the resulting theory is called supergravity [5, 37]. In models of spontaneously-

Downloaded from https://academic.oup.com/ptep/article/2022/8/083C01/6651666 by KIT Library user on 27 September 2022

broken supergravity, the goldstino is "absorbed" by the gravitino ($\widetilde{G}$), the spin-3/2 superpartner of the graviton, via the super-Higgs mechanism [38]. Consequently, the goldstino is removed from the physical spectrum and the gravitino acquires a mass (denoted by $m_{3/2}$). If $m_{3/2}$ is smaller than the mass of the lightest superpartner of the SM particles, then the gravitino is the LSP.

In processes with center-of-mass energy $E \gg m_{3/2}$, one can employ the goldstino–gravitino equivalence theorem [39], which implies that the interactions of the helicity $\pm\frac{1}{2}$ gravitino (whose properties approximate those of the goldstino) dominate those of the helicity $\pm\frac{3}{2}$ gravitino. The interactions of gravitinos with other light fields can be described by a low-energy effective Lagrangian that is determined by fundamental principles [40].

88.2.3 *Hidden sectors and the structure of SUSY breaking*

It is very difficult (perhaps impossible) to construct a realistic model of spontaneously-broken weak-scale supersymmetry where the supersymmetry breaking arises solely as a consequence of the interactions of the particles of the MSSM. A more successful scheme posits a theory with at least two distinct sectors: a visible sector consisting of the particles of the MSSM [32] and a sector where SUSY breaking is generated. It is often (but not always) assumed that particles of the hidden sector are neutral with respect to the SM gauge group. The effects of the hidden sector supersymmetry breaking are then transmitted to the MSSM by some mechanism (often involving the mediation by particles that comprise an additional messenger sector). Two theoretical scenarios that exhibit this structure are gravity-mediated and gauge-mediated SUSY breaking.

Supergravity models provide a natural mechanism for transmitting the SUSY breaking of the hidden sector to the particle spectrum of the MSSM. In models of gravity-mediated supersymmetry breaking, gravity is the messenger of supersymmetry breaking [41–45]. More precisely, supersymmetry breaking is mediated by effects of gravitational strength (*i.e.* suppressed by inverse powers of the Planck mass). The soft-SUSY-breaking parameters with dimensions of mass arise as model-dependent multiples of the gravitino mass $m_{3/2}$. In this scenario, $m_{3/2}$ is of order the electroweak-symmetry-breaking scale, while the gravitino couplings are roughly gravitational in strength [3,46].[1]

Under certain theoretical assumptions that govern the structure of the Kähler potential (the so-called sequestered form introduced in Ref. [48]), SUSY breaking is due entirely to the super-conformal (super-Weyl) anomaly, which is common to all supergravity models [48]. In particular, gaugino masses are radiatively generated at one-loop, and squark and slepton squared-mass matrices are flavor-diagonal. In sequestered scenarios, sfermion squared-masses arise at two-loops, which implies that gluino and sfermion masses are of the same order of magnitude. This approach is called anomaly-mediated SUSY breaking (AMSB). Indeed, anomaly mediation is more generic than originally conceived, and provides a ubiquitous source of SUSY breaking [49]. However in the simplest formulation of AMSB as applied to the MSSM, the squared-masses of the sleptons are negative (known as the tachyonic slepton problem). It may be possible to cure this otherwise fatal flaw in non-minimal extensions of the MSSM [50]. Alternatively, one can assert that anomaly mediation is not the sole source of SUSY breaking in the sfermion sector. In non-sequestered scenarios, sfermion squared-masses can arise at tree-level, in which case squark masses would be parametrically larger than the loop-suppressed gaugino masses [51].

In gauge-mediated supersymmetry breaking (GMSB), gauge forces transmit the supersymmetry breaking to the MSSM. A typical structure of such models involves a hidden sector where SUSY is broken, a messenger sector consisting of particles (messengers) with nontrivial SU(3)×SU(2)×U(1) quantum numbers, and the visible sector consisting of the fields of the MSSM [52–55]. The direct coupling of the messengers to the hidden sector generates a supersymmetry-breaking spectrum in the messenger sector. Supersymmetry breaking is then transmitted to the MSSM via the virtual exchange of the messenger fields. In models of direct gauge mediation, there is no separate hidden sector. In particular, the sector in which the SUSY breaking originates includes fields that carry nontrivial SM quantum numbers, which allows for the direct transmission of SUSY breaking to the MSSM [56].

In models of gauge-mediated SUSY breaking with a minimal Kähler potential, the gravitino is the LSP [17], as its mass can range from a few eV (in the case of low SUSY breaking scales) up to a few GeV (in the case of high SUSY breaking scales). In particular, the gravitino is a potential dark matter candidate (for a review and guide to the literature, see Ref. [21]). The couplings of the helicity $\pm\frac{1}{2}$ components of $\widetilde{G}$ to the particles of the MSSM (which approximate those of the goldstino as previously noted in Sec. 88.2.2) are significantly stronger than gravitational strength and amenable to experimental collider analyses.

The mass ranges of the gravitino in either gravity-mediated or gauge-mediated SUSY breaking are further constrained by cosmological considerations [57,58]. In particular, there is a danger of over-abundance of gravitinos if it is the dark matter or, if it decays before nucleosynthesis, modifications to the successful predictions of light element abundances. Avoiding these cosmological gravitino problems impose strong constraints on gravity-mediated and gauge-mediated SUSY breaking models.

The concept of a hidden sector is more general than SUSY. Hidden valley models [59] posit the existence of a hidden sector of new particles and interactions that are very weakly coupled to particles of the SM. The impact of a hidden valley on supersymmetric phenomenology at colliders can be significant if the LSP lies in the hidden sector [60].

88.2.4 *SUSY and extra dimensions*

Approaches to SUSY breaking have also been developed in the context of theories in which the number of spatial dimensions is greater than three. In particular, a number of SUSY-breaking mechanisms have been proposed that are inherently extra-dimensional [61]. The size of the extra dimensions can be significantly larger than $M_{\rm P}^{-1}$; in some cases of order $(\text{TeV})^{-1}$ or even larger (see, *e.g.*, Sec. 85 or Ref. [62]).

For example, in one approach the fields of the MSSM live on some brane (a lower-dimensional manifold embedded in a higher-dimensional spacetime), while the sector of the theory that breaks SUSY lives on a second spatially-separated brane. Two examples of this approach are AMSB [48] and gaugino-mediated SUSY breaking [63]. In both cases, SUSY breaking is transmitted through fields that live in the bulk (the higher-dimensional space between the two branes). This setup has some features in common with both gravity-mediated and gauge-mediated SUSY breaking (*e.g.*, hidden and visible sectors and messengers).

Since a higher dimensional theory must be compactified to four spacetime dimensions, one can also generate a source of SUSY breaking by employing boundary conditions on the compactified space that distinguish between fermions and bosons. This is the so-called Scherk-Schwarz mechanism [64]. The phenomenology of such models can be strikingly different from that of the usual MSSM [65].

88.2.5 *Split-SUSY*

If SUSY is not connected with the origin of the electroweak scale, it may still be possible that some remnant of the superparticle spectrum survives down to the TeV-scale or below. This is the idea of split-SUSY [66,67], in which scalar superpartners of the quarks and leptons are significantly heavier than 1 TeV, whereas the fermionic superpartners of the gauge and Higgs bosons have masses on the order of 1 TeV or below. With the exception of a single light neutral scalar whose properties are practically indistinguishable from those of the SM Higgs boson, all other Higgs bosons are also assumed to be very heavy. Among the supersymmetric particles, only the fermionic superpartners may be kinematically accessible at the LHC.

In models of split SUSY, the top squark masses cannot be arbitrarily large, as these parameters enter in the radiative corrections to the mass of the observed Higgs boson [68,69]. In the MSSM, a Higgs boson mass of 125 GeV (see Sec. 11) implies an upper bound on the top squark mass scale in the range of 10 to 10^8 TeV [70–72],

[1] However, such a gravitino typically plays no direct role in supersymmetric phenomenology at colliders (except perhaps indirectly in the case where the gravitino is the LSP [47]).

Downloaded from https://academic.oup.com/ptep/article/2022/8/083C01/6651666 by KIT Library user on 27 September 2022

depending on the value of the ratio of the two neutral Higgs field vacuum expectation values, although this mass range can be somewhat extended by varying other relevant MSSM parameters. In some approaches, gaugino masses are one-loop suppressed relative to the sfermion masses, corresponding to the so-called mini-split SUSY spectrum [69,73]. The higgsino mass scale may or may not be likewise suppressed depending on the details of the model [74].

The SUSY breaking required to produce such a split-SUSY spectrum would destabilize the gauge hierarchy, and thus would not provide an explanation for the scale of electroweak symmetry breaking. Nevertheless, models of split-SUSY can account for the dark matter (which is assumed to be the LSP gaugino or higgsino) and gauge coupling unification, thereby preserving two of the desirable features of weak-scale SUSY. Finally, as a consequence of the very large squark and slepton masses, neutral flavor changing and CP-violating effects, which can be problematic in models with TeV-scale SUSY-breaking masses, are sufficiently reduced to avoid conflict with experimental observations.

88.3 Parameters of the MSSM

The parameters of the MSSM are conveniently described by considering separately the supersymmetry-conserving and the supersymmetry-breaking sectors. A careful discussion of the conventions used here in defining the tree-level MSSM parameters can be found in Refs. [75,76]. For simplicity, consider first the case of one generation of quarks, leptons, and their scalar superpartners.

88.3.1 *The SUSY-conserving parameters*

The parameters of the supersymmetry-conserving sector consist of: (i) gauge couplings, g_s, g, and g', corresponding to the SM gauge group SU(3)×SU(2)×U(1) respectively; (ii) a supersymmetry-conserving higgsino mass parameter μ; and (iii) Higgs-fermion Yukawa couplings, λ_u, λ_d, and λ_e, of one generation of left- and right-handed quarks and leptons, and their superpartners to the Higgs bosons and higgsinos. Because there is no right-handed neutrino/sneutrino in the MSSM as defined here, a Yukawa coupling λ_ν is not included. The complex μ parameter and Yukawa couplings enter via the most general renormalizable R-parity-conserving superpotential,

$$W_{\rm MSSM} = \lambda_d \hat{H}_d \hat{Q} \hat{D}^c - \lambda_u \hat{H}_u \hat{Q} \hat{U}^c + \lambda_e \hat{H}_d \hat{L} \hat{E}^c + \mu \hat{H}_u \hat{H}_d \,, \quad (88.1)$$

where the superfields are defined in Table 1 and the gauge group indices are suppressed.

88.3.2 *The SUSY-breaking parameters*

The supersymmetry-breaking sector contains the following sets of parameters: (i) three complex gaugino Majorana mass parameters, M_3, M_2, and M_1, associated with the SU(3), SU(2), and U(1) subgroups of the SM; (ii) five sfermion squared-mass parameters, $M^2_{\widetilde{Q}}$, $M^2_{\widetilde{U}}$, $M^2_{\widetilde{D}}$, $M^2_{\widetilde{L}}$, and $M^2_{\widetilde{E}}$, corresponding to the five electroweak gauge multiplets, *i.e.*, superpartners of the left-handed fields $(u,d)_L$, u^c_L, d^c_L, $(\nu,\, e^-)_L$, and e^c_L, where the superscript c indicates a charge-conjugated fermion field [24]; and (iii) three Higgs-squark-squark and Higgs-slepton-slepton trilinear interaction terms, with complex coefficients $T_U \equiv \lambda_u A_U$, $T_D \equiv \lambda_d A_D$, and $T_E \equiv \lambda_e A_E$ (which define the "A-parameters"), following the notation employed in Ref. [76]. It is conventional to separate out the factors of the Yukawa couplings in defining the A-parameters (originally motivated by a simple class of gravity-mediated SUSY-breaking models [3,6]). If the A-parameters are parametrically of the same order (or smaller) relative to other SUSY-breaking mass parameters, then in most cases only the third generation A-parameters are phenomenologically relevant.

Finally, we have (iv) two real squared-mass parameters, $m^2_{H_d}$ and $m^2_{H_u}$ (also called m^2_1 and m^2_2, respectively, in the literature), and one complex squared-mass parameter, $m^2_{12} \equiv \mu B$ (the latter defines the "B-parameter"), which appear in the MSSM tree-level scalar Higgs potential [28],

$$\begin{aligned} V = {} & (m^2_{H_d} + |\mu|^2) H^\dagger_d H_d + (m^2_{H_u} + |\mu|^2) H^\dagger_u H_u \\ & + (m^2_{12} H_u H_d + \text{h.c.}) \\ & + \frac{1}{8}(g^2 + g'^2)(H^\dagger_d H_d - H^\dagger_u H_u)^2 + \frac{1}{2} g^2 |H^\dagger_d H_u|^2 \,, \end{aligned} \quad (88.2)$$

where the SU(2)-invariant combination, $H_u H_d \equiv H^+_u H^-_d - H^0_u H^0_d$. Note that the quartic Higgs couplings are related to the gauge couplings g and g' as a consequence of SUSY. The breaking of the SU(2)×U(1) electroweak symmetry group to $\mathrm{U}(1)_{\rm EM}$ is only possible after incorporating the SUSY-breaking Higgs squared-mass parameters $m^2_{H_d}$, $m^2_{H_u}$ (which can be negative) and m^2_{12}. After minimizing the Higgs scalar potential, these three squared-mass parameters can be re-expressed in terms of the two Higgs vacuum expectation values, $\langle H^0_d \rangle \equiv v_d/\sqrt{2}$ and $\langle H^0_u \rangle \equiv v_u/\sqrt{2}$, and the CP-odd Higgs mass m_A [cf. Eqs. (88.4) and (88.5) below]. One is always free to rephase the Higgs doublet fields such that v_d and v_u (also called v_1 and v_2, respectively, in the literature) are both real and positive.

The quantity, $v^2_d + v^2_u = 4m^2_W/g^2 = (2G^2_F)^{-1/2} \simeq (246\ \text{GeV})^2$, is fixed by the Fermi constant, G_F, whereas the ratio

$$\tan\beta = v_u/v_d \quad (88.3)$$

is a free parameter such that $0 < \beta < \pi/2$. By employing the tree-level conditions resulting from the minimization of the scalar potential, one can eliminate the diagonal and off-diagonal Higgs squared-masses in favor of $m^2_Z = \frac{1}{4}(g^2+g'^2)(v^2_d+v^2_u)$, the CP-odd Higgs mass m_A and the parameter $\tan\beta$,

$$\sin 2\beta = \frac{2m^2_{12}}{m^2_{H_d} + m^2_{H_u} + 2|\mu|^2} = \frac{2m^2_{12}}{m^2_A} \,, \quad (88.4)$$

$$\frac{1}{2} m^2_Z = -|\mu|^2 + \frac{m^2_{H_d} - m^2_{H_u} \tan^2\beta}{\tan^2\beta - 1} \,. \quad (88.5)$$

One must also guard against the existence of charge and/or color breaking global minima due to non-zero vacuum expectation values for the squark and charged slepton fields. This possibility can be avoided if the A-parameters are not unduly large [42,77,78]. Additional constraints must also be respected to avoid the possibility of directions in scalar field space in which the full tree-level scalar potential can become unbounded from below [78]. A computer program has been developed to calculate vacuum stability bounds in general models at the one-loop level [79], and has been applied to the MSSM in Ref. [80].

Note that SUSY-breaking mass terms for the fermionic superpartners of scalar fields and non-holomorphic trilinear scalar interactions (*i.e.*, interactions that mix scalar fields and their complex conjugates) have not been included above in the soft-SUSY-breaking sector. These terms can potentially destabilize the gauge hierarchy [11] in models with a gauge-singlet superfield. The latter is not present in the MSSM; hence as noted in Ref. [12], these so-called non-standard soft-SUSY-breaking terms are benign. The phenomenological impact of non-holomorphic soft SUSY-breaking terms has been reconsidered in Refs. [81–83]. However, in the most common approaches to constructing a fundamental theory of SUSY-breaking, the coefficients of these terms (which have dimensions of mass) are significantly suppressed compared to the TeV-scale [84]. Consequently, we follow the usual approach and omit these terms from further consideration.

88.3.3 *MSSM-124*

The total number of independent physical parameters that define the MSSM (in its most general form) is quite large, primarily due to the soft-supersymmetry-breaking sector. In particular, in the case of three generations of quarks, leptons, and their superpartners, $M^2_{\widetilde{Q}}$, $M^2_{\widetilde{U}}$, $M^2_{\widetilde{D}}$, $M^2_{\widetilde{L}}$, and $M^2_{\widetilde{E}}$ are hermitian 3×3 matrices, and A_U, A_D, and A_E are complex 3×3 matrices. In addition, M_1, M_2, M_3, B, and μ are in general complex parameters. Finally, as in the SM, the Higgs-fermion Yukawa couplings, λ_f ($f = u$, d, and e), are complex 3×3 matrices that are related to the quark and lepton mass matrices via: $M_f = \lambda_f v_f/\sqrt{2}$, where $v_e = v_d$ [with v_u and v_d as defined above Eq. (88.3)].

However, not all these parameters are physical. Some of the MSSM parameters can be eliminated by expressing interaction eigenstates in terms of the mass eigenstates, with an appropriate redefinition of the MSSM fields to remove unphysical degrees of freedom. The analysis of Ref. [85] shows that the MSSM possesses 124 independent real degrees of freedom. Of these, 18

Downloaded from https://academic.oup.com/ptep/article/2022/8/083C01/6651666 by KIT Library user on 27 September 2022

correspond to SM parameters (including the QCD vacuum angle $\theta_{\rm QCD}$), one corresponds to a Higgs sector parameter (the analogue of the SM Higgs mass), and 105 are genuinely new parameters of the model. The latter include: five real parameters and three CP-violating phases in the gaugino/higgsino sector, 21 squark and slepton (sfermion) masses, 36 real mixing angles to define the sfermion mass eigenstates, and 40 CP-violating phases that can appear in sfermion interactions. The most general parameterization of the R-parity-conserving MSSM (without additional theoretical assumptions) will be denoted henceforth as MSSM-124 [86].

88.4 The supersymmetric-particle spectrum

The supersymmetric particles (sparticles) differ in spin by half a unit from their SM partners. The superpartners of the gauge and Higgs bosons are fermions, whose names are obtained by appending "ino" to the end of the corresponding SM particle name. The gluino is the color-octet Majorana fermion partner of the gluon with mass $M_{\widetilde{g}} = |M_3|$. The superpartners of the electroweak gauge and Higgs bosons (the gauginos and higgsinos) can mix due to SU(2)×U(1) breaking effects. As a result, the physical states of definite mass are parameter dependent linear combinations of the charged or neutral gauginos and higgsinos, called charginos and neutralinos, respectively (sometimes collectively called electroweakinos). The neutralinos are Majorana fermions, which can lead to some distinctive phenomenological signatures [87,88]. The superpartners of the quarks and leptons are spin-zero bosons: the squarks, charged sleptons, and sneutrinos, respectively. A complete set of Feynman rules for the sparticles of the MSSM can be found in Ref. [89]. The MSSM Feynman rules also are implicitly contained in a number of amplitude generation and Feynman diagram software packages (see *e.g.*, Refs. [90–92]).

It should be noted that all mass formulae quoted below in this Section are tree-level results. Radiative loop corrections will modify these results and must be included in any precision study of supersymmetric phenomenology [93]. Beyond tree level, the definition of the supersymmetric parameters becomes convention-dependent. For example, one can define physical couplings or running couplings, which differ beyond the tree level. This provides a challenge to any effort that attempts to extract supersymmetric parameters from data. The SUSY Les Houches Accord (SLHA) [76,94] has been adopted, which establishes a set of conventions for specifying generic file structures for supersymmetric model specifications and input parameters, supersymmetric mass and coupling spectra, and decay tables. These provide a universal interface between spectrum calculation programs, decay packages, and high energy physics event generators.

88.4.1 *The charginos and neutralinos*

The mixing of the charged gauginos ($\widetilde{W}^\pm$) and charged higgsinos ($\widetilde{H}_u^+$ and $\widetilde{H}_d^-$) is described (at tree-level) by a 2×2 complex mass matrix [95,96],

$$M_C \equiv \begin{pmatrix} M_2 & \frac{1}{\sqrt{2}}gv_u \\ \frac{1}{\sqrt{2}}gv_d & \mu \end{pmatrix} . \tag{88.6}$$

To determine the physical chargino states and their masses, one must perform a singular value decomposition [97,98] of the complex matrix M_C:

$$U^* M_C V^{-1} = \mathrm{diag}(M_{\tilde{\chi}_1^+}\,,\, M_{\tilde{\chi}_2^+})\,, \tag{88.7}$$

where U and V are unitary matrices, and the right-hand side of Eq. (88.7) is the diagonal matrix of (real non-negative) chargino masses. Explicit formulae for the singular value decomposition of M_C can be found in Ref. [99]. The physical chargino states are denoted by $\tilde{\chi}_1^\pm$ and $\tilde{\chi}_2^\pm$. These are linear combinations of the charged gaugino and higgsino states determined by the matrix elements of U and V [95,96] The chargino masses correspond to the singular values [97] of M_C, *i.e.*, the positive square roots of the eigenvalues of $M_C^\dagger M_C$:

$$M^2_{\tilde{\chi}_1^+,\tilde{\chi}_2^+} = \frac{1}{2}\Big\{|\mu|^2 + |M_2|^2 + 2m_W^2 \mp \sqrt{\left(|\mu|^2+|M_2|^2+2m_W^2\right)^2 - 4|\mu M_2 - m_W^2\sin 2\beta|^2}\,\Big\}, \tag{88.8}$$

in a convention where v_u and v_d are real and positive, and where the states are ordered such that $M_{\tilde{\chi}_1^+} \le M_{\tilde{\chi}_2^+}$. The relative phase of μ^* and M_2 is physical and potentially observable [100].

The mixing of the neutral gauginos ($\widetilde{B}$ and $\widetilde{W}^0$) and neutral higgsinos ($\widetilde{H}_d^0$ and $\widetilde{H}_u^0$) is described (at tree-level) by a 4×4 complex symmetric mass matrix [95,96],

$$M_N \equiv \begin{pmatrix} M_1 & 0 & -\frac{1}{2}g'v_d & \frac{1}{2}g'v_u \\ 0 & M_2 & \frac{1}{2}gv_d & -\frac{1}{2}gv_u \\ -\frac{1}{2}g'v_d & \frac{1}{2}gv_d & 0 & -\mu \\ \frac{1}{2}g'v_u & -\frac{1}{2}gv_u & -\mu & 0 \end{pmatrix} . \tag{88.9}$$

To determine the physical neutralino states and their masses, one must perform an Autonne-Takagi factorization [97,101] (also called Takagi diagonalization [98,102]) of the complex symmetric matrix M_N:

$$W^T M_N W = \mathrm{diag}(M_{\tilde{\chi}_1^0}\,,\, M_{\tilde{\chi}_2^0}\,,\, M_{\tilde{\chi}_3^0}\,,\, M_{\tilde{\chi}_4^0})\,, \tag{88.10}$$

where W is a unitary matrix (which is called N^{-1} in Ref. [95]) and the right-hand side of Eq. (88.10) is the diagonal matrix of (real non-negative) neutralino masses. The physical neutralino states are denoted by $\widetilde{\chi}_i^0$ (for $i = 1,\ldots,4$), where the states are ordered such that $M_{\tilde{\chi}_1^0} \le M_{\tilde{\chi}_2^0} \le M_{\tilde{\chi}_3^0} \le M_{\tilde{\chi}_4^0}$. The $\widetilde{\chi}_i^0$ are the linear combinations of the neutral gaugino and higgsino states determined by the matrix elements of W. The neutralino masses correspond to the singular values of M_N, *i.e.*, the positive square roots of the eigenvalues of $M_N^\dagger M_N$. Exact formulae for these masses can be found in Refs. [103] and [104]. A numerical algorithm for determining the mixing matrix W has been given in Ref. [105].

If a chargino or neutralino state approximates a particular gaugino or higgsino state, it is convenient to employ the corresponding nomenclature. Specifically, if $|M_1|$ and $|M_2|$ are small compared to m_Z and $|\mu|$, then the lightest neutralino $\widetilde{\chi}_1^0$ would be nearly a pure photino, $\widetilde{\gamma}$, the superpartner of the photon. If $|M_1|$ and m_Z are small compared to $|M_2|$ and $|\mu|$, then the lightest neutralino would be nearly a pure bino, $\widetilde{B}$, the superpartner of the weak hypercharge gauge boson. If $|M_2|$ and m_Z are small compared to $|M_1|$ and $|\mu|$, then the lightest chargino pair and neutralino would constitute a triplet of roughly mass-degenerate pure winos, $\widetilde{W}^\pm$, and $\widetilde{W}_3^0$, the superpartners of the weak SU(2) gauge bosons. Finally, if $|\mu|$ and m_Z are small compared to $|M_1|$ and $|M_2|$, then the lightest chargino pair and neutralino would be nearly pure higgsino states, the superpartners of the Higgs bosons. Each of the above cases leads to a strikingly different phenomenology.

In the NMSSM, an additional Higgs singlet superfield is added to the MSSM. This superfield comprises two real Higgs scalar degrees of freedom and an associated neutral higgsino degree of freedom. Consequently, there are five neutralino mass eigenstates that are obtained by a Takagi-diagonalization of the 5×5 neutralino mass matrix. In many cases, the fifth neutralino state is dominated by its SU(2)×U(1) singlet component, and thus is very weakly coupled to the SM particles and their superpartners.

88.4.2 *The squarks and sleptons*

For a given Dirac fermion f, there are two superpartners, $\widetilde{f}_L$ and $\widetilde{f}_R$, where the L and R subscripts simply identify the scalar partners that are related by SUSY to the left-handed and right-handed fermions, $f_{L,R} \equiv \frac{1}{2}(1\mp\gamma_5)f$, respectively. (There is no $\widetilde{\nu}_R$ in the MSSM.) However, $\widetilde{f}_L$–$\widetilde{f}_R$ mixing is possible, in which case $\widetilde{f}_L$ and $\widetilde{f}_R$ are not mass eigenstates. For three generations of squarks, one must diagonalize 6×6 matrices corresponding to the basis $(\widetilde{q}_{iL}, \widetilde{q}_{iR})$, where $i = 1,2,3$ are the generation labels.

Downloaded from https://academic.oup.com/ptep/article/2022/8/083C01/6651666 by KIT Library user on 27 September 2022

For simplicity, only the one-generation case is illustrated in detail below. (The effects of second and third generation squark mixing can be significant and are treated in Ref. [106].)

Using the notation of the third family, the one-generation tree-level squark squared-mass matrix is given by [107],

$$\mathcal{M}^2 = \begin{pmatrix} M^2_{\widetilde{Q}} + m_q^2 + L_q & m_q X_q^* \\ m_q X_q & M^2_{\widetilde{R}} + m_q^2 + R_q \end{pmatrix} , \tag{88.11}$$

where

$$X_q \equiv A_q - \mu^* (\cot\beta)^{2T_{3q}} , \tag{88.12}$$

and $T_{3q} = \frac{1}{2}$ $[-\frac{1}{2}]$ for $q = t$ $[b]$. The diagonal squared-masses are governed by soft-SUSY-breaking squared-masses $M^2_{\widetilde{Q}}$ and $M^2_{\widetilde{R}} \equiv M^2_{\widetilde{U}}$ $[M^2_{\widetilde{D}}]$ for $q = t$ $[b]$, the corresponding quark masses m_t $[m_b]$ and the electroweak correction terms:

$$\begin{aligned} L_q &\equiv (T_{3q} - e_q \sin^2\theta_W) m_Z^2 \cos 2\beta , \\ R_q &\equiv e_q \sin^2\theta_W \, m_Z^2 \cos 2\beta , \end{aligned} \tag{88.13}$$

where $e_q = \frac{2}{3}$ $[-\frac{1}{3}]$ for $q = t$ $[b]$. The off-diagonal squark squared-masses are proportional to the corresponding quark masses and depend on $\tan\beta$, the soft-SUSY-breaking A-parameters and the higgsino mass parameter μ. Assuming that the A-parameters are parametrically of the same order (or smaller) relative to other SUSY-breaking mass parameters, it then follows that the first and second generation $\widetilde{q}_L$–$\widetilde{q}_R$ mixing is smaller than that of the third generation where mixing can be enhanced by factors of m_t and $m_b \tan\beta$.

In the case of third generation $\widetilde{q}_L$–$\widetilde{q}_R$ mixing, the mass eigenstates (usually denoted by $\widetilde{q}_1$ and $\widetilde{q}_2$, with $m_{\tilde{q}_1} < m_{\tilde{q}_2}$) are determined by diagonalizing the 2×2 matrix $\mathcal{M}^2$ given by Eq. (88.11). The corresponding squared-masses and mixing angle are given by [107]:

$$\begin{aligned} m^2_{\tilde{q}_{1,2}} &= \frac{1}{2}\left[\mathrm{Tr}\,\mathcal{M}^2 \mp \sqrt{(\mathrm{Tr}\mathcal{M}^2)^2 - 4\det\mathcal{M}^2} \right] , \\ \sin 2\theta_{\tilde{q}} &= \frac{2 m_q |X_q|}{m^2_{\tilde{q}_2} - m^2_{\tilde{q}_1}} . \end{aligned} \tag{88.14}$$

The one-generation results above also apply to the charged sleptons, with the obvious substitutions: $q \to \ell$ with $T_{3\ell} = -\frac{1}{2}$ and $e_\ell = -1$, and the replacement of the SUSY-breaking parameters: $M^2_{\widetilde{Q}} \to M^2_{\widetilde{L}}$, $M^2_{\widetilde{D}} \to M^2_{\widetilde{E}}$, and $A_q \to A_\tau$. For the neutral sleptons, $\widetilde{\nu}_R$ does not exist in the MSSM, so $\widetilde{\nu}_L$ is a mass eigenstate.

In the case of three generations, the SUSY-breaking scalar-squared masses [$M^2_{\widetilde{Q}}$, $M^2_{\widetilde{U}}$, $M^2_{\widetilde{D}}$, $M^2_{\widetilde{L}}$, and $M^2_{\widetilde{E}}$] and the A-parameters [A_U, A_D, and A_E] are now 3×3 matrices as noted in Sec. 88.3.3. The diagonalization of the 6×6 squark mass matrices yields $\widetilde{f}_{iL}$–$\widetilde{f}_{jR}$ mixing. In practice, since the $\widetilde{f}_L$–$\widetilde{f}_R$ mixing is appreciable only for the third generation, this additional complication can often be neglected (although see Ref. [106] for examples in which the mixing between the second and third generation squarks is relevant).

88.5 The supersymmetric Higgs sector

Consider first the MSSM Higgs sector [27, 28, 108]. Despite the large number of potential CP-violating phases among the MSSM-124 parameters, the tree-level MSSM Higgs potential given by Eq. (88.2) is automatically CP-conserving. This follows from the fact that the only potentially complex parameter (m^2_{12}) of the MSSM Higgs potential can be chosen real and positive by rephasing the Higgs fields, in which case $\tan\beta$ is a real positive parameter. Consequently, the physical neutral Higgs scalars are CP-eigenstates (at tree-level). The MSSM Higgs sector contains five physical spin-zero particles: a charged Higgs boson pair ($H^\pm$), two CP-even neutral Higgs bosons (denoted by h^0 and H^0 where $m_h < m_H$), and one CP-odd neutral Higgs boson (A^0). The discovery of a SM-like Higgs boson at the LHC with a mass of 125 GeV (see Sec. 11) strongly suggests that this state should be identified with h^0, although the possibility that the 125 GeV state should be identified with H^0 cannot yet be completely ruled out [109].

In the NMSSM [33], the scalar component of the singlet Higgs superfield adds two additional neutral states to the Higgs sector. In this model, the tree-level Higgs sector can exhibit explicit CP-violation. If CP is conserved, then the two extra neutral scalar states are CP-even and CP-odd, respectively. These states can potentially mix with the neutral Higgs states of the MSSM. If scalar states exist that are dominantly singlet, then they are weakly coupled to SM gauge bosons and fermions through their small mixing with the MSSM Higgs scalars. Consequently, it is possible that one (or both) of the singlet-dominated states is considerably lighter than the Higgs boson that was observed at the LHC.

88.5.1 *The tree-level Higgs sector*

The tree-level properties of the Higgs sector are determined by the Higgs potential given by Eq. (88.2). The quartic interaction terms are manifestly supersymmetric (although these are modified by SUSY-breaking effects at the loop level). In general, the quartic couplings arise from two sources: (i) the supersymmetric generalization of the scalar potential (the so-called "F-terms"), and (ii) interaction terms related by SUSY to the coupling of the scalar fields and the gauge fields, whose coefficients are proportional to the corresponding gauge couplings (the so-called "D-terms").

In the MSSM, F-term contributions to the quartic Higgs self-couplings are absent. As a result, the strengths of the MSSM quartic Higgs interactions are fixed in terms of the gauge couplings, as noted below Eq. (88.2). Consequently, all the tree-level MSSM Higgs-sector parameters depend only on two quantities: $\tan\beta$ [defined in Eq. (88.3)] and one Higgs mass usually taken to be m_A. From these two quantities, one can predict the values of the remaining Higgs boson masses, an angle α that measures the mixture of the hypercharge ± 1 scalar fields, H^0_u and H^0_d, in the physical CP-even neutral scalars, and the Higgs boson self-couplings. Moreover, the tree-level mass of the lighter CP-even Higgs boson is bounded, $m_h \leq m_Z |\cos 2\beta| \leq m_Z$ [27, 28]. This bound can be substantially modified when radiative corrections are included, as discussed in Sec. 88.5.2.

In the NMSSM, we set $\mu = 0$ in Eq. 88.1 and then add two additional terms to the superpotential,

$$W_{\mathrm{NMSSM}} \ni \lambda \hat{H}_u \hat{H}_d \hat{S} + \frac{1}{3}\kappa \hat{S}^3 , \tag{88.15}$$

where $\hat{S}$ is a singlet Higgs superfield. An effective μ term is generated, $\mu_{\mathrm{eff}} = \lambda\langle S\rangle$, where $\langle S\rangle$ is the vacuum expectation value of the scalar field component of $\hat{S}$. Moreover, due to the term proportional to λ in Eq. 88.15, there is now an F-term contribution to the quartic Higgs self-couplings. Consequently, the tree-level bound for the mass of the lightest CP-even MSSM Higgs boson is modified [110],

$$m_h^2 \leq m_Z^2 \cos^2 2\beta + \frac{1}{2}\lambda^2 v^2 \sin^2 2\beta , \tag{88.16}$$

where $v \equiv (v_u^2 + v_d^2)^{1/2} = 246$ GeV. By requiring that λ remain finite after renormalization-group evolution up to the Planck scale, one finds that λ is constrained to lie below about 0.7–0.8 at the electroweak scale [33] (although larger values of λ have also been considered in Ref. [111]).

The tree-level Higgs-quark and Higgs-lepton interactions of the MSSM are governed by the Yukawa couplings defined by the superpotential given in Eq. (88.1). In particular, the Higgs sector of the MSSM is a Type-II two-Higgs doublet model [112], in which one Higgs doublet (H_d) couples exclusively to the right-handed down-type quark (or lepton) fields and the second Higgs doublet (H_u) couples exclusively to the right-handed up-type quark fields. Consequently, the diagonalization of the fermion mass matrices simultaneously diagonalizes the matrix of Yukawa couplings, resulting in flavor-diagonal tree-level couplings of the neutral Higgs bosons h^0, H^0 and A^0 to quark and lepton pairs.

88.5.2 *The radiatively-corrected Higgs sector*

When radiative corrections are incorporated, additional parameters of the supersymmetric model enter via virtual supersymmetric particles that appear in loops. The impact of these corrections

Downloaded from https://academic.oup.com/ptep/article/2022/8/083C01/6651666 by KIT Library user on 27 September 2022

can be significant [113]. The qualitative behavior of these radiative corrections can be most easily seen in the large top-squark mass limit, where in addition, both the splitting of the two diagonal entries and the off-diagonal entries of the top-squark squared-mass matrix [Eq. (88.11)] are small in comparison to the geometric mean of the two top-squark squared-masses, $M_{\rm S}^2 \equiv M_{\tilde{t}_1} M_{\tilde{t}_2}$. In this case (assuming $m_A > m_Z$), the predicted upper bound for m_h is approximately given by [114]

$$m_h^2 \lesssim m_Z^2 \cos^2 2\beta + \frac{3g^2 m_t^4}{8\pi^2 m_W^2}\left[\ln\left(\frac{M_{\rm S}^2}{m_t^2}\right) + \frac{X_t^2}{M_{\rm S}^2}\left(1 - \frac{X_t^2}{12 M_{\rm S}^2}\right)\right], \tag{88.17}$$

where $X_t \equiv A_t - \mu \cot\beta$ [cf. Eq. (88.12)] is proportional to the off-diagonal entry of the top-squark squared-mass matrix (where for simplicity, A_t and μ are taken to be real). The Higgs mass upper limit specified by Eq. (88.17) is saturated when $\tan\beta$ is large (*i.e.*, $\cos^2 2\beta \sim 1$) and $X_t = \sqrt{6}\, M_S$, which defines the so-called maximal mixing scenario.

A more complete treatment of the radiative corrections shows that Eq. (88.17) somewhat overestimates the true upper bound of m_h. These more refined computations, which incorporate renormalization group improvement, the two loop and the leading three-loop contributions, yield $m_h \lesssim 135$ GeV in the region of large $\tan\beta$ (with an accuracy of a few GeV) for $m_t = 175$ GeV and $M_S \lesssim 2$ TeV [115, 116].

In addition, one-loop radiative corrections can introduce CP-violating effects in the Higgs sector that depend on some of the CP-violating phases among the MSSM-124 parameters [117]. This phenomenon is most easily understood in a scenario where $m_A \ll M_S$ (i.e., all five physical Higgs states are significantly lighter than the SUSY breaking scale). In this case, one can integrate out the heavy superpartners to obtain a low-energy effective theory with two Higgs doublets. The resulting effective two-Higgs doublet model will now contain all possible Higgs self-interaction terms (both CP-conserving and CP-violating) and Higgs-fermion interactions (beyond those of Type-II) that are consistent with electroweak gauge invariance [118].

In the NMSSM with $m_h \simeq 125$ GeV, the dominant radiative correction to Eq. (88.16) is the same as the one given in Eq. (88.17). However, in contrast to the MSSM, one does not need as large a boost from the radiative corrections to achieve a Higgs mass of 125 GeV in certain regimes of the NMSSM parameter space (*e.g.*, $\tan\beta \sim 2$ and $\lambda \sim 0.7$ [119]).

88.6 Restricting the MSSM parameter freedom

In Sections 88.4 and 88.5, we surveyed the parameters that comprise the MSSM-124. However, the MSSM in its most general form is not a phenomenologically viable theory over much of its parameter space. In particular, a generic point of the MSSM-124 parameter space exhibits: (i) no conservation of the separate lepton numbers L_e, L_μ, and L_τ; (ii) unsuppressed flavor-changing neutral currents (FCNCs); and (iii) new sources of CP violation that are inconsistent with the experimental bounds.

For example, the MSSM contains many new sources of CP violation [120]. Indeed, for TeV-scale sfermion and gaugino masses, some combinations of the complex phases of the gaugino-mass parameters, the A-parameters, and μ must be less than about 10^{-2}–10^{-3} to avoid generating electric dipole moments for the neutron, electron, and atoms [121–123] in conflict with observed data [124, 125]. The rarity of FCNCs [126–128] places additional constraints on the off-diagonal matrix elements of the squark and slepton soft-SUSY-breaking squared-masses and A-parameters (see Sec. 88.3.3).

The MSSM-124 is also theoretically incomplete as it provides no explanation for the fundamental origin of the supersymmetry-breaking parameters. The successful unification of the MSSM gauge couplings at a grand unified mass scale $M_{\rm GUT}$, close to the Planck scale [8, 67, 129–131],

$$g_s(M_{\rm GUT}) = g(M_{\rm GUT}) = \sqrt{\frac{5}{3}}\, g'(M_{\rm GUT}), \tag{88.18}$$

suggests that the high-energy structure of the theory may be considerably simpler than its low-energy realization.[2] In a top-down approach, the dynamics that governs the more fundamental theory at high energies is used to derive the effective broken-supersymmetric theory at the TeV scale. A suitable choice for the high energy dynamics is one that yields a TeV-scale theory that satisfies all relevant phenomenological constraints.

In this Section, we examine a number of theoretical frameworks that potentially yield phenomenologically viable regions of the MSSM-124 parameter space. The resulting supersymmetric particle spectrum is then a function of a relatively small number of input parameters. This is accomplished by imposing a simple structure on the soft SUSY-breaking parameters at a common high-energy scale M_X (typically chosen to be the Planck scale, M_P, the grand unified theory scale, $M_{\rm GUT}$, or the messenger scale, $M_{\rm mess}$). These serve as initial conditions for the MSSM renormalization group equations (RGEs), which are given in the two-loop approximation in Ref. [132]. Automated programs to compute RGEs for the MSSM and other supersymmetric models of new physics has been developed in Ref. [133]. Solving these equations numerically, one can then derive the low-energy MSSM parameters relevant for phenomenology. A number of software packages exist that numerically calculate the spectrum of supersymmetric particles, consistent with theoretical conditions on SUSY breaking at high energies and some experimental data at low energies [116, 134].

Examples of viable frameworks are provided by models of gravity-mediated, anomaly mediated and gauge-mediated SUSY breaking, to be discussed in more detail below. In some of these approaches, one of the diagonal Higgs squared-mass parameters is driven negative by renormalization group evolution [135]. In such models, electroweak symmetry breaking is generated radiatively, and the resulting electroweak symmetry-breaking scale is intimately tied to the scale of low-energy SUSY breaking.

88.6.1 *Gaugino mass relations*

One prediction of many supersymmetric grand unified models is the unification of the (tree-level) gaugino mass parameters[3] at some high-energy scale, M_X,

$$M_1(M_X) = M_2(M_X) = M_3(M_X) = m_{1/2}\,. \tag{88.19}$$

Due to renormalization group running, in the one-loop approximation the effective low-energy gaugino mass parameters (at the electroweak scale) are related,

$$M_3 = (g_s^2/g^2)M_2 \simeq 3.5 M_2\ , \qquad M_1 = (5g'^2/3g^2)M_2 \simeq 0.5 M_2. \tag{88.20}$$

Eq. (88.20) can arise more generally in gauge-mediated SUSY-breaking models where the gaugino masses are generated at the messenger scale $M_{\rm mess}$ (which typically lies significantly below the unification scale where the gauge couplings unify). In this case, the gaugino mass parameters are proportional to the corresponding squared gauge couplings at the messenger scale.

When Eq. (88.20) is satisfied, the chargino and neutralino masses and mixing angles depend only on three unknown parameters: the gluino mass, μ, and $\tan\beta$. It then follows that the lightest neutralino must be heavier than 46 GeV due to the non-observation of charginos at LEP [137]. If in addition $|\mu| \gg |M_1| \gtrsim m_Z$, then the lightest neutralino is nearly a pure bino, an assumption often made in supersymmetric particle searches at colliders. Although Eq. (88.20) is often assumed in many phenomenological studies, a truly model-independent approach would take the gaugino mass parameters, M_i, to be independent parameters to be determined by experiment. Indeed, an approximately massless neutralino *cannot* be ruled out at present by a model-independent analysis [138].

[2] Generically, the normalization of the U(1) hypercharges exhibited in Table 88.1 is a matter of convention. In particular, the U(1) hypercharges can be rescaled by absorbing the scaling factor into a redefinition of the hypercharge gauge coupling g'. However, the embedding of the hypercharge U(1) generator into the Lie algebra of a grand unified simple gauge group fixes the normalization of the U(1) hypercharges and results in the rescaled hypercharge gauge coupling shown in Eq. (88.18).

[3] Non-universal gaugino mass parameters can also be a viable option in grand unified models with non-minimal gauge kinetic functions [136].

Downloaded from https://academic.oup.com/ptep/article/2022/8/083C01/6651666 by KIT Library user on 27 September 2022

It is possible that the tree-level masses for the gauginos are zero. In this case, the gaugino mass parameters arise at one-loop and do not satisfy Eq. (88.20). For example, the gaugino masses in AMSB models arise entirely from a model-independent contribution derived from the super-conformal anomaly [48, 139]. In this case, Eq. (88.20) is replaced (in the one-loop approximation) by:

$$M_i \simeq \frac{b_i g_i^2}{16\pi^2} m_{3/2}\,, \tag{88.21}$$

where $m_{3/2}$ is the gravitino mass and the b_i are the coefficients of the MSSM gauge beta-functions corresponding to the corresponding U(1), SU(2), and SU(3) gauge groups, $(b_1, b_2, b_3) = (\frac{33}{5}, 1, -3)$. Eq. (88.21) yields $M_1 \simeq 2.8M_2$ and $M_3 \simeq -8.3M_2$, which implies that the lightest chargino pair and neutralino comprise a nearly mass-degenerate triplet of winos, $\widetilde{W}^{\pm}$, $\widetilde{W}^0$ (cf. Table 1), over most of the MSSM parameter space. For example, if $|\mu| \gg m_Z, |M_2|$, then Eq. (88.21) implies that $M_{\widetilde{\chi}^{\pm}} \simeq M_{\widetilde{\chi}_1^0} \simeq M_2$ [140]. Alternatively, one can construct an AMSB model where $|\mu|, m_Z \ll M_2$, which yields an LSP that is an approximate higgsino state [141]. In both cases, the corresponding supersymmetric phenomenology differs significantly from the standard phenomenology based on Eq. (88.20) [142, 143].

Finally, it should be noted that the unification of gaugino masses (and scalar masses) can be accidental. In particular, the energy scale where unification takes place may not be directly related to any physical scale. One version of this phenomenon has been called mirage unification and can occur in certain theories of fundamental SUSY breaking [144].

88.6.2 *Constrained versions of the MSSM: mSUGRA, CMSSM, etc.*

In the minimal supergravity (mSUGRA) framework [3–6, 41–43], the minimal form of the Kähler potential is employed, which yields standard kinetic energy terms for the MSSM fields [45]. As a result, the soft supersymmetry-breaking parameters at the high-energy scale M_X take a particularly simple form in which the scalar squared-masses and the A-parameters are flavor-diagonal and universal [43]:

$$\begin{aligned}
&M^2_{\widetilde{Q}}(M_X) = M^2_{\widetilde{U}}(M_X) = M^2_{\widetilde{D}}(M_X) = m_0^2\mathbf{1}\,,\\
&M^2_{\widetilde{L}}(M_X) = M^2_{\widetilde{E}}(M_X) = m_0^2\mathbf{1}\,,\\
&m_1^2(M_X) = m_2^2(M_X) = m_0^2\,,\\
&A_U(M_X) = A_D(M_X) = A_E(M_X) = A_0\mathbf{1}\,,
\end{aligned} \tag{88.22}$$

where $\mathbf{1}$ is a 3×3 identity matrix in generation space. As in the SM, this approach exhibits minimal flavor violation [145, 146], whose unique source is the nontrivial flavor structure of the Higgs-fermion Yukawa couplings. The gaugino masses are also unified according to Eq. (88.19).

Renormalization group evolution is then used to derive the values of the supersymmetric parameters at the low-energy (electroweak) scale. For example, to compute squark masses, one should use the low-energy values for $M^2_{\widetilde{Q}}$, $M^2_{\widetilde{U}}$, and $M^2_{\widetilde{D}}$ in Eq. (88.11). Through the renormalization group running with boundary conditions specified in Eq. (88.20) and Eq. (88.22), one can show that the low-energy values of $M^2_{\widetilde{Q}}$, $M^2_{\widetilde{U}}$, and $M^2_{\widetilde{D}}$ depend primarily on m_0^2 and $m_{1/2}^2$. A number of useful approximate analytic expressions for superpartner masses in terms of the mSUGRA parameters can be found in Ref. [147].

One can count the number of independent parameters in the mSUGRA framework. In addition to 18 SM parameters (excluding the Higgs mass), one must specify m_0, $m_{1/2}$, A_0, the Planck-scale values for μ and B-parameters (denoted by μ_0 and B_0), and the gravitino mass $m_{3/2}$. Without additional model assumptions, $m_{3/2}$ is independent of the parameters that govern the mass spectrum of the superpartners of the SM [43]. In principle, A_0, B_0, μ_0, and $m_{3/2}$ can be complex, although in the mSUGRA approach, these parameters are taken to be real for simplicity.

As previously noted, renormalization group evolution is used to compute the low-energy values of the mSUGRA parameters, which then fixes all the parameters of the low-energy MSSM. In particular, the two Higgs vacuum expectation values (or equivalently, m_Z and $\tan\beta$) can be expressed as a function of the Planck-scale supergravity parameters. The most common procedure is to remove μ_0 and B_0 in favor of m_Z and $\tan\beta$ [the sign of μ_0, denoted $\mathrm{sgn}(\mu_0)$ below, is not fixed in this process]. In this case, the MSSM spectrum and its interaction strengths are determined by five parameters:

$$m_0\,,\ A_0\,,\ m_{1/2}\,,\ \tan\beta\,,\ \text{and}\ \mathrm{sgn}(\mu_0)\,, \tag{88.23}$$

and an independent gravitino mass $m_{3/2}$ (in addition to the 18 parameters of the SM). In Ref. [148], this framework was dubbed the constrained minimal supersymmetric extension of the SM (CMSSM). Additional relations such as $B_0 = A_0 - m_0$ and $m_{3/2} = m_0$ comprise the original mSUGRA proposal [41, 45, 149].

One can also relax the universality of scalar masses by decoupling the squared-masses of the Higgs bosons and the squarks/sleptons. This leads to the non-universal Higgs mass models (NUHMs), thereby adding one or two new parameters to the CMSSM depending on whether the diagonal Higgs scalar squared-mass parameters ($m^2_{H_d}$ and $m^2_{H_u}$) are set equal (NUHM1 [150]) or taken to be independent (NUHM2 [151]) at the high energy scale M_X. Clearly, this modification preserves the minimal flavor violation of the mSUGRA approach. Nevertheless, the mSUGRA approach and its NUHM generalizations are probably too simplistic. Theoretical considerations suggest that the universality of Planck-scale soft SUSY-breaking parameters is not generic [152]. In particular, effective operators at the Planck scale exist that do not respect flavor universality, and it is difficult to find a theoretical principle that would forbid them.

In the framework of supergravity, if anomaly mediation is the sole source of SUSY breaking, then the gaugino mass parameters, diagonal scalar squared-mass parameters, and the SUSY-breaking trilinear scalar interaction terms (proportional to $\lambda_f A_F$) are determined in terms of the beta functions of the gauge and Yukawa couplings and the anomalous dimensions of the squark and slepton fields [48, 139, 143]. As noted in Sec. 88.2.3, this approach yields tachyonic sleptons in the MSSM unless additional sources of SUSY breaking are present. In the minimal AMSB (mAMSB) scenario, a universal squared-mass parameter, m_0^2, is added to the AMSB expressions for the diagonal scalar squared-masses [143]. Thus, the mAMSB spectrum and its interaction strengths are determined by four parameters, m_0^2, $m_{3/2}$, $\tan\beta$ and $\mathrm{sgn}(\mu_0)$.

The mAMSB scenario appears to be ruled out based on the observed value of the Higgs boson mass, assuming an upper limit on M_S of a few TeV, since the mAMSB constraint on A_F implies that the maximal mixing scenario cannot be achieved [cf. Eq. (88.17)]. Indeed, under the stated assumptions, the mAMSB Higgs mass upper bound lies below the observed Higgs mass value [153]. Thus within the AMSB scenario, either an additional SUSY-breaking contribution to $\lambda_f A_F$ and/or new ingredients beyond the MSSM are required.

88.6.3 *Gauge-mediated SUSY breaking*

In contrast to models of gravity-mediated SUSY breaking, the flavor universality of the fundamental soft SUSY-breaking squark and slepton squared-mass parameters is guaranteed in gauge-mediated SUSY breaking (GMSB) because the supersymmetry breaking is communicated to the sector of MSSM fields via gauge interactions [53, 55]. In GMSB models, the mass scale of the messenger sector (or its equivalent) is sufficiently below the Planck scale such that the additional SUSY-breaking effects mediated by supergravity can be neglected.

In the minimal GMSB approach, there is one effective mass scale, Λ, that determines all low-energy scalar and gaugino mass parameters through loop effects, while the resulting A-parameters are suppressed. In addition, the minimal form of the Kähler potential is employed. In order that the resulting superpartner masses be of order 1 TeV, one must have $\Lambda \sim \mathcal{O}(100\ \text{TeV})$. The origin of the μ and B-parameters is model-dependent, and lies somewhat outside the ansatz of gauge-mediated SUSY breaking [154].

The simplest GMSB models appear to be ruled out based on the

Downloaded from https://academic.oup.com/ptep/article/2022/8/083C01/6651666 by KIT Library user on 27 September 2022

observed value of the Higgs boson mass. Due to suppressed A parameters, it is difficult to boost the contributions of the radiative corrections in Eq. (88.17) to obtain a Higgs mass as large as 125 GeV. However, this conflict can be alleviated in more complicated GMSB models [155]. To analyze these generalized GMSB models, it has been especially fruitful to develop model-independent techniques that encompass all known GMSB models [156]. These techniques are well-suited for a comprehensive analysis [157] of the phenomenological profile of gauge-mediated SUSY breaking.

The gravitino is the LSP in minimal GMSB models, as noted in Sec. 88.2.3. As a result, the next-to-lightest supersymmetric particle (NLSP) now plays a crucial role in the phenomenology of supersymmetric particle production and decays. Note that unlike the LSP, the NLSP can be charged. In GMSB models, the most likely candidates for the NLSP are $\tilde{\chi}_1^0$ and $\widetilde{\tau}_R^{\pm}$. The NLSP will decay into its superpartner plus a gravitino (*e.g.*, $\tilde{\chi}_1^0 \to \gamma\widetilde{G}$, $\tilde{\chi}_1^0 \to Z\widetilde{G}$, $\tilde{\chi}_1^0 \to h^0\widetilde{G}$ or $\widetilde{\tau}_1^{\pm} \to \tau^{\pm}\widetilde{G}$), with lifetimes and branching ratios that depend on the model parameters. There are also GMSB scenarios in which there are several nearly degenerate co-NLSPs, any one of which can be produced at the penultimate step of a supersymmetric decay chain [158]. For example, in the slepton co-NLSP case, all three right-handed sleptons are close enough in mass and thus can each play the role of the NLSP.

Different choices for the identity of the NLSP and its decay rate lead to a variety of distinctive supersymmetric phenomenologies [55,159]. For example, a long-lived $\tilde{\chi}_1^0$-NLSP that decays outside collider detectors leads to supersymmetric decay chains with missing energy in association with leptons and/or hadronic jets (this case is indistinguishable from the standard phenomenology of the $\tilde{\chi}_1^0$-LSP). On the other hand, if $\tilde{\chi}_1^0 \to \gamma\widetilde{G}$ is the dominant decay mode, and the decay occurs inside the detector, then nearly *all* supersymmetric particle decay chains would produce a photon. In contrast, in the case of a $\widetilde{\tau}_1^{\pm}$-NLSP, the $\widetilde{\tau}_1^{\pm}$ would either be long-lived or would decay inside the detector into a τ-lepton plus missing energy.

A number of attempts have been made to address the origins of the μ and B-parameters in GMSB models based on the field content of the MSSM (see, *e.g.*, Refs. [154, 160]). An alternative approach is to consider GMSB models based on the NMSSM [161]. The vacuum expectation value of the additional singlet Higgs superfield can be used to generate effective μ and B-parameters [162]. Such models provide an alternative GMSB framework for achieving a Higgs mass of 125 GeV, while still being consistent with LHC bounds on supersymmetric particle masses.

88.6.4 *The phenomenological MSSM*

Any of the theoretical assumptions described in the previous three subsections must be tested experimentally and could turn out to be wrong. To facilitate the exploration of MSSM phenomena in a more model-independent way while respecting the constraints noted at the beginning of this Section, the phenomenological MSSM (pMSSM) has been introduced [163].

The pMSSM is governed by 19 independent real supersymmetric parameters: the three gaugino mass parameters M_1, M_2 and M_3, the Higgs sector parameters m_A and $\tan\beta$, the Higgsino mass parameter μ, five sfermion squared-mass parameters for the degenerate first and second generations ($M^2_{\widetilde{Q}}$, $M^2_{\widetilde{U}}$, $M^2_{\widetilde{D}}$, $M^2_{\widetilde{L}}$ and $M^2_{\widetilde{E}}$), the five corresponding sfermion squared-mass parameters for the third generation, and three third-generation A-parameters (A_t, A_b and A_τ). The first and second generation A-parameters are typically neglected in pMSSM studies, as their phenomenological consequences are negligible in most applications. One counterexample arises when considering the A_μ dependence of the anomalous magnetic moment of the muon, which can be as significant as other contributions due to superpartner mediated radiative corrections [164]. Since its initial proposal, the pMSSM approach has been extended to include a 20th parameter, A_μ [165]. It also has been further extended to include CP-violating SUSY-breaking parameters in Ref. [166].

The 19-parameter pMSSM is often further constrained to expedite scans over the parameter space. For example, in Ref. [167], the number of pMSSM parameters is reduced to ten by assuming one common squark squared-mass parameter for the first two generations, a second common squark squared-mass parameter for the third generation, a common (charged) slepton squared-mass parameter and a common third generation A parameter. In Ref. [168] an eleven parameter pMSSM is defined by allowing for a different stau squared-mass parameter from that of the first two generation charged sleptons. Other applications of the pMSSM approach (with a reduced pMSSM parameter space) to supersymmetric particle searches, and a discussion of the implications for past and future LHC and dark matter studies can be found in Refs. [167, 169, 170].

88.6.5 *Simplified models*

As Sec. 89 demonstrates, experiments present their searches for supersymmetric particles primarily in terms of simplified models. Simplified models for supersymmetric searches [171] are defined mostly by the empirical objects and kinematic variables involved in the search. Their interpretation by an experimental collaboration usually involves only a small number of supersymmetric particles (often two or three). Other supersymmetric particles are assumed to play no role (this may happen by virtue of them being too heavy to be produced). Experimental bounds from non-observation of a signal are usually presented in terms of the physical masses of the supersymmetric particles involved. Bounds may be presented on the relevant supersymmetric particle masses assuming certain values for the branching ratio of certain supersymmetric particle decays, or as an upper bound on the signal production cross-section as a function of the relevant supersymmetric particle masses.

For example, consider a search for hadronic jets plus missing transverse momentum. One can match such a search to the simplified model of squark pair production followed by the subsequent decay of each squark into a quark (which appears as a jet) and a neutralino LSP that produces the missing transverse momentum, *i.e.* $\tilde{q}\tilde{q} \to (q\tilde{\chi}_1^0)(q\tilde{\chi}_1^0)$. Excluded cross-sections resulting from the non-observation of a signal (which in this case could consist of some specified minimum value of missing transverse momentum and at least two hard jets) may be exhibited in the squark mass versus LSP mass plane.

Simplified models have the advantage that they have fewer free parameters than more complete supersymmetric models, whose greater number of free parameters makes it difficult to present excluded regions in any generality. If limits are quoted on supersymmetric particle masses without reference to the signal production cross-section from a simplified model analysis, then there is a potential pitfall—namely, mass limits can differ from those obtained in full models because there may be contributions to the signal coming from processes involving supersymmetric particles other than those assumed. For example, in the $\tilde{q}\tilde{q} \to q\tilde{\chi}_1^0 q\tilde{\chi}_1^0$ process mentioned above, the simplified model analysis does not account for the interference with tree-level t-channel contributions involving the gluino. Nevertheless, simplified model bounds quoted purely in terms of supersymmetric particle masses may still approximately hold over sizeable regions of parameter space of more complete models, within which the simplified model is embedded. When simplified model limits are phrased as bounds on signal cross-sections, the aforementioned pitfall is sidestepped. Simplified models thus remain an efficient tool for organizing and presenting the results of supersymmetric particle searches. A comparison between supersymmetric particle search constraints in the context of simplified models and the corresponding constraints obtained in the more complete pMSSM can be found in Ref. [172].

88.7 Experimental data confronts the MSSM

At present, there is no significant evidence for weak-scale SUSY from the data analyzed by the LHC experiments. Recent LHC data have been effectively employed in ruling out the existence of colored supersymmetric particles (primarily the gluino and the first generation of squarks) with masses below about 2 TeV (see Fig. 89.13). However, the precise mass limits are very model dependent. For example, as Fig. 89.12 demonstrates, regions of the pMSSM parameter space can be identified in which lighter squarks and gluinos below 1 TeV cannot be definitely ruled out. Under the assumption of gaugino mass unification [cf. Eq. (88.20)],

Downloaded from https://academic.oup.com/ptep/article/2022/8/083C01/6651666 by KIT Library user on 27 September 2022

LHC searches result in a lower bound on neutralino and chargino masses of roughly 200 GeV. It is difficult to place general bounds on neutralino and chargino masses, since the limit in terms of masses from direct searches tends to be particularly model dependent. Nevertheless, one must confront the tension that exists between the theoretical expectations for the magnitude of the SUSY-breaking parameters and the non-observation of supersymmetric phenomena at colliders.

88.7.1 *Naturalness constraints and the little hierarchy*

In Sec. 88.1, weak-scale SUSY was motivated as a natural solution to the hierarchy problem, which could provide an understanding of the origin of the electroweak symmetry-breaking scale without a significant fine-tuning of the fundamental parameters that govern the MSSM. In this context, the weak scale soft supersymmetry-breaking masses must be generally of the order of 1 TeV or below [173]. This requirement is most easily seen in the determination of m_Z by the scalar potential minimum condition. In light of Eq. (88.5), to avoid the fine-tuning of MSSM parameters, the soft SUSY-breaking squared-masses $m^2_{H_d}$ and $m^2_{H_u}$ and the higgsino squared-mass $|\mu|^2$ should all be roughly of $\mathcal{O}(m_Z^2)$. Many authors have proposed quantitative measures of fine-tuning [173–178]. One of the simplest measures is the one advocated by Barbieri and Giudice [173] (which was also introduced previously in Ref. [174]),

$$\Delta_i \equiv \left| \frac{\partial \ln m_Z^2}{\partial \ln p_i} \right| , \qquad \Delta \equiv \max \Delta_i , \tag{88.24}$$

where the p_i are the MSSM parameters at the high-energy scale M_X, which are set by the fundamental SUSY-breaking dynamics. The theory is more fine-tuned as Δ becomes larger. However, different measures of fine-tuning yield quantitatively different results; in particular, calculating minimal fine-tuning based on the high-scale parameters [as defined in Eq. (88.24)] yields a difference by a factor ~ 10 to fine-tuning based on TeV-scale parameters [179, 180].

One can apply the fine-tuning measure to any explicit model of SUSY breaking. For example, in the approaches discussed in Sec. 88.6, the p_i are parameters of the model at the energy scale M_X where the soft SUSY-breaking operators are generated by the dynamics of SUSY breaking. Renormalization group evolution then determines the values of the parameters appearing in Eq. (88.5) at the electroweak scale. In this way, Δ is sensitive to all the SUSY-breaking parameters of the model (see e.g. Ref. [181]). It should be noted that the computation of Δ is often based on Eq. (88.5), which is a tree-level condition. An analysis in Ref. [83], for example, shows that the fine tuning measure can be reduced by as much as a factor of two when loop corrections are included [182].

One way of taking fine-tuning into account in fits to data using Bayesian statistics is to have a prior probability distribution proportional to $1/\Delta$ [183] so that fine-tuning is balanced against the fit to empirical data. In such a Bayesian approach, it is important to choose the prior probability distribution carefully, since prior probability densities that are flat in one set of variables may not be flat in another, more fundamental set. One can in fact derive a different measure of fine-tuning resulting from a Jacobian factor when transforming to other variables.[4] By comparing the results of several Bayesian fits with different (but reasonable) prior probability distributions, one can assess the robustness of the fit with respect to their variation, mitigating for subjectivity in the interpretation of the fine-tuning measure.

As anticipated, there is a tension between the present experimental lower limits on the masses of colored supersymmetric particles [185,186] and the expectation that supersymmetry-breaking is associated with the electroweak symmetry-breaking scale. Moreover, this tension is exacerbated [187] by the observed value of the Higgs mass ($m_h \simeq 125$ GeV), which is not far from the MSSM upper bound ($m_h \lesssim 135$ GeV) [which depends on the top-squark mass and mixing as noted in Sec. 88.5.2]. If $M_{\rm SUSY}$ characterizes the scale of supersymmetric particle masses, then one would crudely expect $\Delta \sim M^2_{\rm SUSY}/m_Z^2$. For example, if $M_{\rm SUSY} \sim 1$ TeV then one expects a $\Delta^{-1} \sim 1\%$ fine-tuning of the MSSM parameters to achieve the observed value of m_Z. This separation of the electroweak symmetry-breaking and SUSY-breaking scales is an example of the little hierarchy problem [188, 189].

The fine-tuning parameter Δ can depend quite sensitively on the structure of the SUSY-breaking dynamics, such as the value of M_X and relations among SUSY-breaking parameters in the fundamental high energy theory [190]. For example, in so-called focus point SUSY models [177, 191], all squark masses can be as heavy as 5 TeV *without* significant fine-tuning. This can be attributed to a focusing behavior of the renormalization group evolution when certain relations hold among the high-energy values of the scalar squared-mass SUSY-breaking parameters. Although the focus point region of the CMSSM still yields an uncomfortably high value of Δ due to the observed Higgs mass of 125 GeV, one can achieve moderate values of Δ in models with NUHM2 boundary conditions for the scalar masses [187].

Among the colored superpartners, the third generation squarks typically have the most significant impact on the naturalness constraints [192], while their masses are the least constrained by the LHC data. Hence, in the absence of any relation between third generation squarks and those of the first two generations, the naturalness constraints due to present LHC data can be considerably weaker than those obtained in the CMSSM. Indeed, models with first and second generation squark masses in the multi-TeV range do not necessarily require significant fine tuning. Such models have the added benefit that undesirable FCNCs mediated by squark exchange are naturally suppressed [193]. Other MSSM mass spectra that are compatible with moderate fine tuning have been considered in Refs. [190] and [194].

The lower bounds on squark and gluino masses may not be as large as suggested by the experimental analyses based on the CMSSM or simplified models. For example, mass bounds for the gluino and the first and second generation squarks based on the CMSSM can often be evaded in alternative or extended MSSM models, *e.g.*, compressed SUSY [195] and stealth SUSY [196]. Moreover, the experimental upper limits for the third generation squark masses (which have a more direct impact on the fine-tuning measure) are weaker than the corresponding mass limits for other colored supersymmetric states.

Among the uncolored superpartners, the higgsinos are typically the most impacted by the naturalness constraints. Eq. (88.5) suggests that the masses of the two neutral higgsinos and charged higgsino pair (which are governed by $|\mu|$) should not be significantly larger than m_Z to avoid an unnatural fine-tuning of the supersymmetric parameters, which would imply the existence of light higgsinos (whose masses are not well constrained, as they are difficult to detect directly at the LHC due to their soft decay products). However, it may be possible to avoid the conclusion that $\mu \sim \mathcal{O}(m_Z)$ if additional correlations among the SUSY breaking mass parameters and μ are present. Such a scenario can be realized in models in which the boundary conditions for SUSY breaking are generated by approximately conformal strong dynamics. For example, in the so-called scalar-sequestering model of Ref. [197], values of $|\mu| > 1$ TeV can be achieved while naturally maintaining the observed value of m_Z.

Finally, one can also consider extensions of the MSSM in which the degree of fine-tuning is relaxed. For example, it has already been noted in Sec. 88.5 that it is possible to accommodate the observed Higgs mass more easily in the NMSSM due to contributions to m_h^2 proportional to the parameter λ^2. This means that we do not have to rely on a large contribution from the radiative corrections to boost the Higgs mass sufficiently above its tree-level bound. This allows for smaller top squark masses, which are more consistent with the demands of naturalness. The reduction of the fine-tuning in various NMSSM models was initially advocated in Ref. [198], and subsequently treated in more detail in Refs. [111, 199]. Naturalness can also be relaxed in extended supersymmetric models with vector-like quarks [200] and in gauge extensions of the MSSM [201].

[4] For example, one may consider the parameters μ and B to be more fundamental than $\tan\beta$ and M_Z. In this case, one would choose a flat prior probability distribution in μ and m_{12}^2 rather than in $\tan\beta$ and M_Z [176,184] The Jacobian factor is then obtained from Eq. (88.4) and Eq. (88.5).

Downloaded from https://academic.oup.com/ptep/article/2022/8/083C01/6651666 by KIT Library user on 27 September 2022

The experimental absence of any new physics beyond the Standard Model at the LHC suggests that the principle of naturalness is presently under significant stress [202]. Nevertheless, one must be very cautious when drawing conclusions about the viability of weak-scale SUSY to explain the origin of electroweak symmetry breaking, since different measures of fine-tuning noted above can lead to different assessments [179, 180]. Moreover, the maximal value of Δ that determines whether weak-scale SUSY is a fine-tuned model (should it be $\Delta \sim 10?$ $100?$ $1000?$) is ultimately subjective. Thus, it is premature to conclude that weak-scale SUSY is on the verge of exclusion. It might be possible to sharpen the upper bounds on superpartner masses based on naturalness arguments, which ultimately will either confirm or refute the weak scale SUSY hypothesis [203]. Of course, if evidence for supersymmetric phenomena in the multi-TeV regime were to be established at a future collider facility (with an energy reach beyond the LHC [204]), it would be viewed as a spectacularly successful explanation of the large gauge hierarchy between the (multi-)TeV scale and Planck scale. In this case, the remaining little hierarchy, characterized by the somewhat large value of the fine-tuning parameter Δ discussed above, would be regarded as a less pressing issue.

88.7.2 *Indirect constraints on supersymmetric models*

While direct empirical searches for supersymmetric particles provide various limits on their properties, indirect constraints can depend more sensitively on details of the whole model. The cold dark matter relic density inferred from cosmological fits to observational data is one such example of an indirect constraint. In supersymmetric models where the LSP is a dark matter candidate, its thermally-produced relic density depends upon the scattering of various supersymmetric particles into dark matter particles and SM particles. The resulting relic density can depend sensitively on masses of the non-LSP supersymmetric particle masses. In a typical model, an appreciable region of the parameter space is ruled out because it yields an overabundance of dark matter (see for example Ref. [205] for a fit to a seven parameter version of the pMSSM). However, subsequent model tweaks such as the introduction of R-parity violating effects can mean that the relic density constraint no longer applies to the LSP because it is unstable.

There are a number of indirect constraints based on low-energy measurements that are sensitive to the effects of new physics via supersymmetric loop effects. For example, the virtual exchange of supersymmetric particles can contribute to the muon anomalous magnetic moment, $a_\mu \equiv \frac{1}{2}(g-2)_\mu$, as reviewed in Ref. [206]. The SM prediction for a_μ, which employs dispersion relations and low energy e^+e^- scattering data to determine the hadronic corrections, exhibits a deviation of 4.2σ from the experimentally observed value [207, 208]. A recent lattice determination [209] of the leading hadronic contribution to the muon magnetic moment yields a smaller deviation from the SM prediction within 1.7σ of the experimental value, although this result has not yet been confirmed by an independent analysis. The 4.2σ deviation is difficult to accommodate in the constrained SUSY models of Sec. 88.6.2 and 88.6.3 given the present sparticle mass bounds [186]. Nevertheless, there are regions of the more general pMSSM parameter space that are consistent with the observed deviation [210].

The precision of the measured value of a_μ is not sensitive to the experimental error associated with the measured value of the fine structure constant, α. In contrast, the comparison of the SM prediction with the experimental measurement of the anomalous magnetic moment of the electron, a_e, depends critically on the value of α. Using the experimentally determined value of α given in Ref. [211] yields a SM prediction for a_e that is 2.4σ above its measured value [212]. However, this previous determination of α is in tension at the 5σ level with a more recent measurement of the fine structure constant [213]. The latter yields a SM prediction for a_e that is 1.6σ below its measured value [213].

Measurements of the fine structure constant, a_e and a_μ jointly constrain the pMSSM parameter space [214] due to shifts originating from supersymmetric loop effects. In particular, if the supersymmetric interpretation of the deviation in the measured value of a_μ from its SM prediction is combined with the experimental limits on the electron electric dipole moment [125], then the resulting upper bounds on MSSM CP-violating phases are even more constraining [215] than previously noted at the beginning of Sec. 88.6.

Flavor anomalies in radiative, leptonic and semi-leptonic b quark decays [216] provide a fertile ground for physics beyond the SM. For example, the rare inclusive decay $b \to s\gamma$ is a sensitive probe of the virtual effects of new physics beyond the SM. The experimental measurements of $B \to X_s + \gamma$ [217] are in agreement with the theoretical SM predictions of Ref. [218]. Since supersymmetric loop corrections can contribute an observable shift from the SM predictions, the absence of any significant deviation places useful constraints on the MSSM parameter space [219].

The rare decays $B_s \to \mu^+\mu^-$ and $B_d \to \mu^+\mu^-$ are especially sensitive to supersymmetric loop effects, with some loop contributions scaling as $\tan^6\beta$ when $\tan\beta \gg 1$ [220]. At present, a combination [221] of the measurements of these rare decay modes [222] are in slight tension at the 2σ level [223] with the predicted SM rates [224]. Such a tension can be resolved by the aforementioned supersymmetric loop effects [220].

Several tensions exist between SM predictions and measurements of some other experimental observables that probe the $b \to s\mu^+\mu^-$ transitions. For example, the ratio of branching ratios $R_K = BR(B \to K\mu^+\mu^-)/BR(B \to Ke^+e^-)$ exhibits a 3.1σ discrepancy in the bin of di-lepton invariant squared mass between 1 GeV^2 and 6 GeV^2 [225] and in the same invariant mass bin, R_{K^*} displays a 2.5σ discrepancy. In addition, a certain angular distribution parameter (denoted by P_5') extracted from $B^0 \to K^{*0}\mu^+\mu^-$ decays [226] deviates from SM predictions by about 4σ. Finally, a 3.6σ deviation is seen in $BR(B_s \to \phi\mu^+\mu^-)$ [227].

The decays $B^\pm \to \tau^\pm\nu_\tau$ and $B \to D^{(*)}\tau^-\overline{\nu}_\tau$ are noteworthy, since in models with extended Higgs sectors such as the MSSM, these processes possess tree-level charged Higgs exchange contributions that can compete with the dominant W-exchange. As Section 72 shows, experimental measurements of $B^\pm \to \tau^\pm\nu_\tau$ are currently consistent with SM expectations [228]. The BaBar Collaboration measured values of the rates for $\overline{B} \to D\tau^-\overline{\nu}_\tau$ and $\overline{B} \to D^*\tau^-\overline{\nu}_\tau$ [229] exhibited a combined 3.4σ discrepancy from the SM predictions, which was also not compatible with the Type-II Higgs Yukawa couplings employed by the MSSM. Subsequent measurements of the LHCb and Belle Collaborations [230] were consistent with the BaBar measurements, although more recent Belle measurements using a semi-leptonic tag are more consistent with SM expectations [231]. The combined difference between the measured and expected values of the $\overline{B} \to D\tau^-\overline{\nu}_\tau$ and $\overline{B} \to D^*\tau^-\overline{\nu}_\tau$ decay rates relative to the corresponding SM values has a significance of about three standard deviations [232]. There are a number of additional anomalies in B decay data that have recently attracted some attention, although at present the observed deviations from SM expectations are mostly at the level of about two to three standard deviations (see, *e.g.*, Ref. [223]).

In summary, although there are a few hints of possible deviations from the SM in B decays, none of the discrepancies by themselves are significant enough to conclusively imply the existence of new physics beyond the SM. Moreover, the absence of evidence for deviations in various B-physics observables from their SM predictions can place useful constraints on the MSSM parameter space [128, 185, 233, 234]. On the other hand, if these deviations were eventually confirmed, then it would be possible to accommodate them in a supersymmetric framework with R-parity violation [235]. If R-parity invariance is maintained (for example, in order to preserve the stability of a LSP dark matter candidate), then a supersymmetric explanation of the B physics anomalies would require significant modifications to the SUSY models treated in this review.

Finally, we note that the constraints from precision electroweak observables (see Sec. 10) and measurements of the ϵ'/ϵ anomaly [236], if it persists [237], in the Kaon system are easily accommodated in models of TeV-scale SUSY [168, 238, 239].

88.8 Massive neutrinos in weak-scale SUSY

In the minimal version of the SM and its supersymmetric extension, there are no right-handed neutrinos, and Majorana

Downloaded from https://academic.oup.com/ptep/article/2022/8/083C01/6651666 by KIT Library user on 27 September 2022

mass terms for the left-handed neutrinos are absent. However, given the overwhelming evidence for neutrino masses and mixing (see Sec. 14 and [240]), any viable model of the fundamental particles must provide a mechanism for generating neutrino masses [241]. In extended supersymmetric models, various mechanisms exist for producing massive neutrinos [242]. Although one can devise models for generating massive Dirac neutrinos [243], the most common approaches for incorporating neutrino masses are based on L-violating supersymmetric extensions of the MSSM, which generate massive Majorana neutrinos. Two classes of L-violating supersymmetric models will now be considered.

88.8.1 *The supersymmetric seesaw*

Neutrino masses can be incorporated into the SM by introducing SU(3)×SU(2)×U(1) singlet right-handed neutrinos (ν_R) whose mass parameters are very large, typically near the grand unification scale. In addition, one must also include a standard Yukawa couplings between the lepton doublets, the Higgs doublet, and ν_R. The Higgs vacuum expectation value then induces an off-diagonal ν_L–ν_R mass on the order of the electroweak scale. Diagonalizing the neutrino mass matrix (in the three-generation model) yields three superheavy neutrino states, and three very light neutrino states that are identified with the light neutrinos observed in nature. This is the seesaw mechanism [244].

It is straightforward to construct a supersymmetric generalization of the seesaw model of neutrino masses [245, 246] by promoting the right-handed neutrino field to a superfield $\widehat{N}^c = (\widetilde{\nu}_R\,;\,\nu_R)$. Integrating out the heavy right-handed neutrino supermultiplet yields a new term in the superpotential [cf. Eq. (88.1)] of the form

$$W_{\rm seesaw} = \frac{f}{M_R}(\widehat{H}_U\widehat{L})(\widehat{H}_U\widehat{L})\,, \tag{88.25}$$

where M_R is the mass scale of the right-handed neutrino sector and f is a dimensionless constant. Note that lepton number is broken by two units by Eq. (88.25), which implies that R-parity invariance is preserved. The supersymmetric analogue of the Majorana neutrino mass term in the sneutrino sector leads to sneutrino–antisneutrino mixing phenomena [246, 247]. The right-handed sneutrino that resides in $\widehat{L}$ also provides an intriguing dark matter candidate [248].

The SUSY Les Houches Accord [76,94], mentioned at the end of the introduction to Sec. 88.4, has been extended to the supersymmetric seesaw (and other extensions of the MSSM) in Ref. [249].

88.8.2 *R-parity-violating SUSY*

It is possible to incorporate massive neutrinos in renormalizable supersymmetric models while retaining the minimal particle content of the MSSM by relaxing the assumption of R-parity invariance. The most general R-parity-violating model involving the MSSM spectrum introduces many new parameters to both the SUSY-conserving and the SUSY-breaking sectors [76, 250]. Each new interaction term violates either B or L conservation. For example, starting from the MSSM superpotential given in Eq. (88.1) [suitably generalized to three generations of quarks, leptons and their superpartners], consider the effect of adding the following new terms:

$$\begin{aligned} W_{\rm RPV} =&(\lambda_L)_{pmn}\widehat{L}_p\widehat{L}_m\widehat{E}^c_n + (\lambda'_L)_{pmn}\widehat{L}_p\widehat{Q}_m\widehat{D}^c_n \\ &+ (\lambda_B)_{pmn}\widehat{U}^c_p\widehat{D}^c_m\widehat{D}^c_n + (\mu_L)_p\widehat{H}_u\widehat{L}_p\,, \end{aligned} \tag{88.26}$$

where p, m, and n are generation indices, and gauge group indices are suppressed. Eq. (88.26) yields new scalar-fermion Yukawa couplings consisting of all possible combinations involving two SM fermions and one scalar superpartner.

Note that the term in Eq. (88.26) proportional to λ_B violates B, while the other three terms violate L. The L-violating term in Eq. (88.26) proportional to μ_L is the RPV analog of the $\mu\widehat{H}_u\widehat{H}_d$ term of the MSSM superpotential, in which the $Y = -1$ Higgs/higgsino supermultiplet $\widehat{H}_d$ is replaced by the slepton/lepton supermultiplet $\widehat{L}_p$.

Phenomenological constraints derived from data on various low-energy B- and L-violating processes can be used to establish limits on each of the coefficients $(\lambda_L)_{pmn}$, $(\lambda'_L)_{pmn}$, and $(\lambda_B)_{pmn}$ taken one at a time [250, 251]. If more than one coefficient is simultaneously non-zero, then the limits are in general more complicated [252]. All possible RPV terms cannot be simultaneously present and unsuppressed; otherwise the proton decay rate would be many orders of magnitude larger than the present experimental bound. One way to avoid proton decay is to impose B or L invariance (either one alone would suffice). Otherwise, one must accept the requirement that certain RPV coefficients must be extremely suppressed.

One particularly interesting class of RPV models is one in which B is conserved, but L is violated. It is possible to enforce baryon number conservation (and the stability of the proton), while allowing for lepton-number-violating interactions by imposing a discrete $\mathbb{Z}_3$ baryon triality symmetry on the low-energy theory [253], in place of the standard $\mathbb{Z}_2$ R-parity. Since the distinction between the Higgs and matter supermultiplets is lost in RPV models where L is violated, the mixing of sleptons and Higgs bosons, the mixing of neutrinos and neutralinos, and the mixing of charged leptons and charginos are now possible, leading to more complicated mass matrices and mass eigenstates than in the MSSM. The treatment of neutrino masses and mixing in this framework can be found, *e.g.*, in Ref. [254].

Alternatively, one can consider imposing a lepton parity such that all lepton superfields are odd [253, 255]. In this case, only the B-violating term in Eq. (88.26) survives, and L is conserved. Models of this type have been considered in Ref. [256]. Since L is conserved in these models, the mixing of the lepton and Higgs superfields is forbidden. Moreover, neutrino masses (and mixing) are not generated if lepton parity is an exact symmetry. However, one expects that lepton parity cannot be exact due to quantum gravity effects. Remarkably, the standard $\mathbb{Z}_2$ R-parity and the $\mathbb{Z}_3$ baryon triality are stable with respect to quantum gravity effects, as they can be identified as residual discrete symmetries that arise from spontaneously broken non-anomalous gauge symmetries [253].

The symmetries employed above to either remove or suppress R-parity violating operators were flavor independent. In contrast, there exist a number of motivated scenarios based on flavor symmetries that can also yield the suppression as required by the experimental data (e.g., see Ref. [257]).

The supersymmetric phenomenology of the RPV models exhibits features that are distinct from that of the MSSM [250]. The LSP is no longer stable, which implies that not all supersymmetric decay chains must yield missing-energy events at colliders. A comprehensive examination of the phenomenology of the MSSM extended by a single R-parity violating coupling at the unification scale and its implications for LHC searches has been given in Ref. [258]. As an example, the sparticle mass bounds obtained in searches for R-parity-conserving SUSY can be considerably relaxed in certain RPV models due to the absence of large missing transverse momentum signatures [259]. This can alleviate some of the tension with naturalness (introduced in Sec. 88.7.1).

Nevertheless, the loss of the missing-energy signature is often compensated by other striking signals (which depend on which R-parity-violating parameters are dominant). For example, supersymmetric particles in RPV models can be singly produced (in contrast to R-parity-conserving models where supersymmetric particles must be produced in pairs). The phenomenology of pair-produced supersymmetric particles is also modified in RPV models due to new decay chains not present in R-parity-conserving SUSY models [250].

In RPV models with lepton number violation (these include weak-scale SUSY models with baryon triality mentioned above), both $\Delta L = 1$ and $\Delta L = 2$ phenomena are allowed, leading to neutrino masses and mixing [260], neutrinoless double-beta decay [261], sneutrino-antisneutrino mixing [262], and resonant s-channel production of sneutrinos in e^+e^- collisions [263] and in charged sleptons in $p\bar{p}$ and pp collisions [264], respectively.

88.9 Extensions beyond the MSSM

Extensions of the MSSM have been proposed to solve a variety of theoretical problems. One such problem involves the μ parameter of the MSSM. Although μ is a SUSY-*preserving* parameter, it must be of order the effective SUSY-breaking scale of the MSSM

Downloaded from https://academic.oup.com/ptep/article/2022/8/083C01/6651666 by KIT Library user on 27 September 2022

to yield a consistent supersymmetric phenomenology [265]. Any natural solution to the so-called μ-problem must incorporate a symmetry that enforces $\mu = 0$ and a small symmetry-breaking parameter that generates a value of μ that is not parametrically larger than the effective SUSY-breaking scale [266]. A number of proposed mechanisms in the literature (*e.g.*, see Refs. [265–267]) provide concrete examples of a natural solution to the μ-problem of the MSSM.

In extensions of the MSSM, new compelling solutions to the μ-problem are possible. For example, one can replace μ by the vacuum expectation value of a new SU(3)×SU(2)×U(1) singlet scalar field, as noted below Eq. 88.15. This is the NMSSM, which yields phenomena that were briefly discussed in Sections 88.4–88.7. The NMSSM superpotential consists only of trilinear terms whose coefficients are dimensionless. There are some advantages to extending the NMSSM further to the 'USSM' [102] by adding a new broken U(1) gauge symmetry [268], under which the singlet field is charged.

Alternatively, one can consider a generalized version of the NMSSM (called the GNMSSM in Ref. [199]), where all possible renormalizable terms in the superpotential are allowed, which yield new supersymmetric mass terms (analogous to the μ term of the MSSM). A discussion of the parameters of the GNMSSM can be found in Ref. [76]. Although the GNMSSM does not solve the μ-problem, it does exhibit regions of parameter space in which the degree of fine-tuning is relaxed, as discussed in Sec. 88.7.1.

The generation of the μ term may be connected with the solution to the strong CP problem [269]. Models of this type, which include new gauge singlet fields that are charged under the Peccei-Quinn (PQ) symmetry [270], were first proposed in Ref. [265]. The breaking of the PQ symmetry is thus intimately tied to SUSY breaking, while naturally yielding a value of μ that is of order the electroweak symmetry breaking scale [271].

All supersymmetric models discussed so far in this review possess self-conjugate fermions—the Majorana gluinos and neutralinos. However, it is possible to add additional chiral superfields in the adjoint representation. The spin-1/2 components of these new superfields can pair up with the gauginos to form Dirac gauginos [272, 273]. Such states appear in models of so-called supersoft SUSY breaking [274], in some generalized GMSB models [275], and in R-symmetric SUSY models [276, 277]. Such approaches often lead to improved naturalness and/or significantly relaxed flavor constraints. The implications of models of Dirac gauginos on the observed Higgs boson mass and its properties are addressed in Ref. [278].

For completeness, we briefly note other MSSM extensions considered in the literature. These include an enlarged electroweak gauge group beyond SU(2)×U(1) [279]; the addition of new Higgs supermultiplets beyond the doublets and singlets of the MSSM/NMSSM [280]; and/or the addition of new (possibly exotic) matter supermultiplets [200, 281, 282] such as vector-like fermions and their superpartners.

References

[1] *The Supersymmetric World—The Beginnings of the Theory*, World Scientific, Singapore (2000), edited by G. Kane and M. Shifman, contains an early history of supersymmetry and a guide to the original literature.

[2] R. Haag, J. T. Lopuszanski and M. Sohnius, Nucl. Phys. **B88**, 257 (1975); S. R. Coleman and J. Mandula, Phys. Rev. **159**, 1251 (1967).

[3] H. P. Nilles, Phys. Rept. **110**, 1 (1984).

[4] S. Weinberg, *The Quantum Theory of Fields, Volume III: Supersymmetry* (Cambridge University Press, Cambridge, UK, 2000).

[5] P. Nath, *Supersymmetry, Supergravity, and Unification* (Cambridge University Press, Cambridge, UK, 2017).

[6] S. P. Martin *A Supersymmetry Primer*, [hep-ph/9709356].

[7] E. Witten, Nucl. Phys. **B188**, 513 (1981).

[8] S. Dimopoulos and H. Georgi, Nucl. Phys. **B193**, 150 (1981).

[9] N. Sakai, Z. Phys. **C11**, 153 (1981).

[10] L. Susskind, Phys. Rept. **104**, 181 (1984).

[11] L. Girardello and M. T. Grisaru, Nucl. Phys. **B194**, 65 (1982).

[12] L. J. Hall and L. Randall, Phys. Rev. Lett. **65**, 2939 (1990); I. Jack and D. R. T. Jones, Phys. Lett. **B457**, 101 (1999), [hep-ph/9903365].

[13] V. F. Weisskopf, Phys. Rev. **56**, 72 (1939).

[14] See *e.g.*, N. Polonsky, *Supersymmetry: Structure and phenomena. Extensions of the standard model*, Lect. Notes Phys. **M68**, 1 (2001).

[15] G. Bertone, D. Hooper and J. Silk, Phys. Rept. **405**, 279 (2005), [hep-ph/0404175].

[16] D. Hooper, "TASI 2008 Lectures on Dark Matter," in *The Dawn of the LHC Era, Proceedings of the 2008 Theoretical and Advanced Study Institute in Elementary Particle Physics,* Boulder, Colorado, 2–27 June 2008, edited by Tao Han (World Scientific, Singapore, 2009).

[17] H. Pagels and J. R. Primack, Phys. Rev. Lett. **48**, 223 (1982).

[18] H. Goldberg, Phys. Rev. Lett. **50**, 1419 (1983).

[19] J. R. Ellis *et al.*, Nucl. Phys. **B238**, 453 (1984).

[20] G. Jungman, M. Kamionkowski, and K. Griest, Phys. Reports **267**, 195 (1996).

[21] F. D. Steffen, Eur. Phys. J. **C59**, 557 (2009), [arXiv:0811.3347].

[22] H. E. Haber and G. L. Kane, Phys. Rept. **117**, 75 (1985).

[23] M. Drees, R. Godbole, and P. Roy, *Theory and Phenomenology of Sparticles* (World Scientific, Singapore, 2005); H. Baer and X. Tata, *Weak Scale Supersymmetry: from Superfields to Scattering Events* (Cambridge University Press, Cambridge, UK, 2006); I.J.R. Aitchison, *Supersymmetry in Particle Physics: an elementary introduction* (Cambridge University Press, Cambridge, UK, 2007).

[24] Our notation for the charge-conjugated fields follows the notation of P. Langacker, *The Standard Model and Beyond*, 2nd edition (CRC Press, Boca Raton, FL, 2017).

[25] H. Georgi and S. L. Glashow, Phys. Rev. **D6**, 429 (1972).

[26] P. Fayet, Nucl. Phys. **B90**, 104 (1975).

[27] K. Inoue *et al.*, Prog. Theor. Phys. **67**, 1889 (1982).

[28] J. F. Gunion and H. E. Haber, Nucl. Phys. **B272**, 1 (1986), [Erratum: **B402**, 567 (1993)].

[29] A. Salam and J. A. Strathdee, Nucl. Phys. **B76**, 477 (1974).

[30] J. Wess and J. Bagger, *Supersymmetry and Supergravity* (Princeton University Press, Princeton, NJ, 1992).

[31] I. L. Buchbinder, S. Kuzenko and Z. Yarevskaya, Nucl. Phys. **B411**, 665 (1994); I. Antoniadis, E. Dudas and D. M. Ghilencea, JHEP **03**, 045 (2008), [arXiv:0708.0383].

[32] D. J. H. Chung *et al.*, Phys. Rept. **407**, 1 (2005), [hep-ph/0312378].

[33] J. R. Ellis *et al.*, Phys. Rev. **D39**, 844 (1989); U. Ellwanger and C. Hugonie, Eur. Phys. J. **C25**, 297 (2002), [hep-ph/9909260]; U. Ellwanger, C. Hugonie and A. M. Teixeira, Phys. Rept. **496**, 1 (2010), [arXiv:0910.1785]; M. Maniatis, Int. J. Mod. Phys. **A25**, 3505 (2010), [arXiv:0906.0777].

[34] S. Weinberg, Phys. Rev. Lett. **43**, 1566 (1979); S. Weinberg, Phys. Rev. **D22**, 1694 (1980); F. Wilczek and A. Zee, Phys. Rev. Lett. **43**, 1571 (1979); H. A. Weldon and A. Zee, Nucl. Phys. **B173**, 269 (1980).

[35] P. Fayet, Phys. Lett. **69B**, 489 (1977); G. R. Farrar and P. Fayet, Phys. Lett. **76B**, 575 (1978).

[36] P. Fayet, Phys. Lett. **84B**, 421 (1979); P. Fayet, Phys. Lett. **86B**, 272 (1979).

[37] D.Z. Freedman and A. Van Proeyen, *Supergravity* (Cambridge University Press, Cambridge, UK, 2012); M. Rausch de Traubenberg and M. Valenzuela, *A Supergravity Primer* (World Scientific, Singapore, 2020).

Downloaded from https://academic.oup.com/ptep/article/2022/8/083C01/6651666 by KIT Library user on 27 September 2022

[38] S. Deser and B. Zumino, Phys. Rev. Lett. **38**, 1433 (1977); E. Cremmer *et al.*, Phys. Lett. **79B**, 231 (1978).

[39] R. Casalbuoni *et al.*, Phys. Lett. **B215**, 313 (1988); R. Casalbuoni *et al.*, Phys. Rev. **D39**, 2281 (1989); A. L. Maroto and J. R. Pelaez, Phys. Rev. **D62**, 023518 (2000), [hep-ph/9912212].

[40] Z. Komargodski and N. Seiberg, JHEP **09**, 066 (2009), [arXiv:0907.2441]; I. Antoniadis *et al.*, Theor. Math. Phys. **170**, 26 (2012), [Teor. Mat. Fiz. **170**, 34 (2012)].

[41] A.H. Chamseddine, R. Arnowitt, and P. Nath, Phys. Rev. Lett. **49**, 970 (1982); R. Barbieri, S. Ferrara and C. A. Savoy, Phys. Lett. **119B**, 343 (1982); L. E. Ibanez, Nucl. Phys. **B218**, 514 (1983); H. P. Nilles, M. Srednicki and D. Wyler, Phys. Lett. **120B**, 346 (1983); H. P. Nilles, M. Srednicki and D. Wyler, Phys. Lett. **124B**, 337 (1983); E. Cremmer, P. Fayet and L. Girardello, Phys. Lett. **122B**, 41 (1983); N. Ohta, Prog. Theor. Phys. **70**, 542 (1983).

[42] L. Alvarez-Gaumé, J. Polchinski, and M.B. Wise, Nucl. Phys. **B221**, 495 (1983).

[43] L. J. Hall, J. D. Lykken and S. Weinberg, Phys. Rev. **D27**, 2359 (1983).

[44] S. K. Soni and H. A. Weldon, Phys. Lett. **126B**, 215 (1983); Y. Kawamura, H. Murayama and M. Yamaguchi, Phys. Rev. **D51**, 1337 (1995), [hep-ph/9406245].

[45] See, *e.g.*, A. Brignole, L.E. Ibáñez, and C. Munoz, in *Perspectives on Supersymmetry II*, edited by G.L. Kane (World Scientific, Singapore, 2010) pp. 244–268.

[46] A. B. Lahanas and D. V. Nanopoulos, Phys. Rept. **145**, 1 (1987).

[47] J. L. Feng, A. Rajaraman and F. Takayama, Phys. Rev. Lett. **91**, 011302 (2003), [hep-ph/0302215]; J. L. Feng, A. Rajaraman and F. Takayama, Phys. Rev. **D68**, 063504 (2003), [hep-ph/0306024]; J. L. Feng, A. Rajaraman and F. Takayama, Int. J. Mod. Phys. **D13**, 2355 (2004), [hep-th/0405248].

[48] L. Randall and R. Sundrum, Nucl. Phys. **B557**, 79 (1999), [hep-th/9810155].

[49] F. D'Eramo, J. Thaler and Z. Thomas, JHEP **06**, 151 (2012), [arXiv:1202.1280]; F. D'Eramo, J. Thaler and Z. Thomas, JHEP **09**, 125 (2013), [arXiv:1307.3251]; S. P. de Alwis, Phys. Rev. **D77**, 105020 (2008), [arXiv:0801.0578]; S. P. de Alwis, JHEP **01**, 006 (2013), [arXiv:1206.6775]; K. Harigaya and M. Ibe, Phys. Rev. **D90**, 085028 (2014), [arXiv:1409.5029].

[50] I. Jack, D. R. T. Jones and R. Wild, Phys. Lett. **B535**, 193 (2002), [hep-ph/0202101]; B. Murakami and J. D. Wells, Phys. Rev. **D68**, 035006 (2003), [hep-ph/0302209]; R. Kitano, G. D. Kribs and H. Murayama, Phys. Rev. **D70**, 035001 (2004), [hep-ph/0402215]; R. Hodgson *et al.*, Nucl. Phys. **B728**, 192 (2005), [hep-ph/0507193]; D. R. T. Jones and G. G. Ross, Phys. Lett. **B642**, 540 (2006), [hep-ph/0609210].

[51] S. Asai *et al.*, Phys. Lett. **B653**, 81 (2007), [arXiv:0705.3086].

[52] M. Dine, W. Fischler and M. Srednicki, Nucl. Phys. **B189**, 575 (1981); S. Dimopoulos and S. Raby, Nucl. Phys. **B192**, 353 (1981); S. Dimopoulos and S. Raby, Nucl. Phys. **B219**, 479 (1983); M. Dine and W. Fischler, Phys. Lett. **110B**, 227 (1982); C. R. Nappi and B. A. Ovrut, Phys. Lett. **113B**, 175 (1982); L. Alvarez-Gaume, M. Claudson and M. B. Wise, Nucl. Phys. **B207**, 96 (1982).

[53] M. Dine and A. E. Nelson, Phys. Rev. **D48**, 1277 (1993), [hep-ph/9303230]; M. Dine, A. E. Nelson and Y. Shirman, Phys. Rev. **D51**, 1362 (1995), [hep-ph/9408384].

[54] M. Dine *et al.*, Phys. Rev. **D53**, 2658 (1996), [hep-ph/9507378].

[55] G. F. Giudice and R. Rattazzi, Phys. Rept. **322**, 419 (1999), [hep-ph/9801271].

[56] E. Poppitz and S. P. Trivedi, Phys. Rev. **D55**, 5508 (1997), [hep-ph/9609529]; H. Murayama, Phys. Rev. Lett. **79**, 18 (1997), [hep-ph/9705271]; M. A. Luty and J. Terning, Phys. Rev. **D57**, 6799 (1998), [hep-ph/9709306]; K. Agashe, Phys. Lett. **B435**, 83 (1998), [hep-ph/9804450]; N. Arkani-Hamed, J. March-Russell and H. Murayama, Nucl. Phys. **B509**, 3 (1998), [hep-ph/9701286]; C. Csaki, Y. Shirman and J. Terning, JHEP **05**, 099 (2007), [hep-ph/0612241]; M. Ibe and R. Kitano, Phys. Rev. **D77**, 075003 (2008), [arXiv:0711.0416].

[57] S. Weinberg, Phys. Rev. Lett. **48**, 1303 (1982); M. Kawasaki, F. Takahashi and T. T. Yanagida, Phys. Rev. D **74**, 043519 (2006), [hep-ph/0605297].

[58] M. Kawasaki *et al.*, Phys. Rev. **D78**, 065011 (2008), [arXiv:0804.3745].

[59] M. J. Strassler and K. M. Zurek, Phys. Lett. **B651**, 374 (2007), [hep-ph/0604261]; T. Han *et al.*, JHEP **07**, 008 (2008), [arXiv:0712.2041].

[60] M. J. Strassler [hep-ph/0607160]; K. M. Zurek, Phys. Rev. **D79**, 115002 (2009), [arXiv:0811.4429].

[61] See *e.g.*, M. Quiros, in *Particle Physics and Cosmology: The Quest for Physics Beyond the Standard Model(s), Proceedings of the 2002 Theoretical Advanced Study Institute in Elementary Particle Physics (TASI 2002),* edited by H.E. Haber and A.E. Nelson (World Scientific, Singapore, 2004) pp. 549–601; C. Csaki, in *ibid.*, pp. 605–698.

[62] V.A. Rubakov, Sov. Phys. Usp. **44**, 871 (2001); J. L. Hewett and M. Spiropulu, Ann. Rev. Nucl. Part. Sci. **52**, 397 (2002), [hep-ph/0205106].

[63] Z. Chacko, M. A. Luty and E. Ponton, JHEP **07**, 036 (2000), [hep-ph/9909248]; D. E. Kaplan, G. D. Kribs and M. Schmaltz, Phys. Rev. **D62**, 035010 (2000), [hep-ph/9911293]; Z. Chacko *et al.*, JHEP **01**, 003 (2000), [hep-ph/9911323].

[64] J. Scherk and J. H. Schwarz, Phys. Lett. **82B**, 60 (1979); J. Scherk and J. H. Schwarz, Nucl. Phys. **B153**, 61 (1979).

[65] R. Barbieri, L. J. Hall and Y. Nomura, Phys. Rev. **D66**, 045025 (2002), [hep-ph/0106190]; R. Barbieri, L. J. Hall and Y. Nomura, Nucl. Phys. **B624**, 63 (2002), [hep-th/0107004]; I. Garcia Garcia, K. Howe and J. March-Russell, JHEP **12**, 005 (2015), [arXiv:1510.07045].

[66] J. D. Wells, in "11th International Conference on Supersymmetry and the Unification of Fundamental Interactions (SUSY 2003) Tucson, Arizona, June 5-10, 2003," (2003), [hep-ph/0306127]; J. D. Wells, Phys. Rev. **D71**, 015013 (2005), [hep-ph/0411041].

[67] N. Arkani-Hamed and S. Dimopoulos, JHEP **06**, 073 (2005), [hep-th/0405159]; G. F. Giudice and A. Romanino, Nucl. Phys. **B699**, 65 (2004), [Erratum: **B706**, 487 (2005)], [hep-ph/0406088].

[68] G. F. Giudice and A. Strumia, Nucl. Phys. **B858**, 63 (2012), [arXiv:1108.6077].

[69] A. Arvanitaki *et al.*, JHEP **02**, 126 (2013), [arXiv:1210.0555]; N. Arkani-Hamed *et al.* (2012), [arXiv:1212.6971].

[70] E. Bagnaschi *et al.*, JHEP **09**, 092 (2014), [arXiv:1407.4081].

[71] J. Pardo Vega and G. Villadoro, JHEP **07**, 159 (2015), [arXiv:1504.05200].

[72] B. C. Allanach and A. Voigt, Eur. Phys. J. **C78**, 573 (2018), [arXiv:1804.09410].

[73] Y. Kahn, M. McCullough and J. Thaler, JHEP **11**, 161 (2013), [arXiv:1308.3490].

[74] L. J. Hall and Y. Nomura, JHEP **01**, 082 (2012), [arXiv:1111.4519]; M. Ibe and T. T. Yanagida, Phys. Lett. **B709**, 374 (2012), [arXiv:1112.2462].

Downloaded from https://academic.oup.com/ptep/article/2022/8/083C01/6651666 by KIT Library user on 27 September 2022

[75] H. E. Haber and L. Stephenson Haskins (2018), *Supersymmetric Theory and Models*, in *Anticipating the Next Discoveries in Particle Physics*, Proceedings of the 2016 Theoretical Advanced Study Institute in Elementary Particle Physics, edited by Rouven Essig and Ian Low (World Scientific, Singapore, 2018) pp. 355-499, [arXiv:1712.05926].

[76] B. C. Allanach *et al.*, Comput. Phys. Commun. **180**, 8 (2009), [arXiv:0801.0045].

[77] J. M. Frere, D. R. T. Jones and S. Raby, Nucl. Phys. **B222**, 11 (1983); J. P. Derendinger and C. A. Savoy, Nucl. Phys. **B237**, 307 (1984); J. F. Gunion, H. E. Haber and M. Sher, Nucl. Phys. **B306**, 1 (1988); D. Chowdhury *et al.*, JHEP **02**, 110 (2014), [Erratum: **03**, 149 (2018)], [arXiv:1310.1932]; W. G. Hollik, JHEP **08**, 126 (2016), [arXiv:1606.08356].

[78] J. A. Casas, A. Lleyda and C. Munoz, Nucl. Phys. **B471**, 3 (1996), [hep-ph/9507294].

[79] J. E. Camargo-Molina *et al.*, Eur. Phys. J. C **73**, 10, 2588 (2013), [arXiv:1307.1477].

[80] N. Blinov and D. E. Morrissey, JHEP **03**, 106 (2014), [arXiv:1310.4174].

[81] C. S. Ün *et al.*, Phys. Rev. **D91**, 105033 (2015), [arXiv:1412.1440].

[82] G. G. Ross, K. Schmidt-Hoberg and F. Staub, Phys. Lett. **B759**, 110 (2016), [arXiv:1603.09347].

[83] G. G. Ross, K. Schmidt-Hoberg and F. Staub, JHEP **03**, 021 (2017), [arXiv:1701.03480].

[84] S. P. Martin, Phys. Rev. **D61**, 035004 (2000), [hep-ph/9907550].

[85] S. Dimopoulos and D. W. Sutter, Nucl. Phys. **B452**, 496 (1995), [hep-ph/9504415]; D.W. Sutter, Stanford Ph. D. thesis, `arXiv:hep-ph/9704390`.

[86] H.E. Haber, Nucl. Phys. B (Proc. Suppl.) **62A-C**, 469 (1998).

[87] R. M. Barnett, J. F. Gunion and H. E. Haber, Phys. Lett. **B315**, 349 (1993), [hep-ph/9306204]; H. Baer, X. Tata and J. Woodside, Phys. Rev. **D41**, 906 (1990).

[88] S. M. Bilenky, N. P. Nedelcheva and E. K. Khristova, Phys. Lett. **161B**, 397 (1985); S. M. Bilenky, E. K. Khristova and N. P. Nedelcheva, Bulg. J. Phys. **13**, 283 (1986).

[89] J. Rosiek, Phys. Rev. **D41**, 3464 (1990).

[90] J. Alwall *et al.*, JHEP **09**, 028 (2007), [arXiv:0706.2334].

[91] T. Hahn, Comput. Phys. Commun. **140**, 418 (2001), [hep-ph/0012260].

[92] A. Pukhov *et al.*, INP MSU report 98-41/542 (`arXiv:hep-ph/9908288`); E. Boos *et al.* [CompHEP Collab.], Nucl. Instrum. Methods **A534**, 50 (2004); CompHEP webpage, `https://theory.sinp.msu.ru/dokuwiki/doku.php/comphep/news`.

[93] D. M. Pierce *et al.*, Nucl. Phys. **B491**, 3 (1997), [hep-ph/9606211].

[94] P. Z. Skands *et al.*, JHEP **07**, 036 (2004), [hep-ph/0311123].

[95] For further details, see *e.g.*, Appendix C of Ref. [22] and Appendix A of Ref. [28].

[96] J. L. Kneur and G. Moultaka, Phys. Rev. **D59**, 015005 (1999), [hep-ph/9807336].

[97] R.A. Horn and C.R. Johnson, *Matrix Analysis*, 2nd Edition (Cambridge University Press, Cambridge, UK, 2003).

[98] H. K. Dreiner, H. E. Haber and S. P. Martin, Phys. Rept. **494**, 1 (2010), [arXiv:0812.1594].

[99] H. E. Haber, Int. J. Mod. Phys. A **36**, 04, 2130003 (2021), [arXiv:2009.03990].

[100] S. Pokorski, J. Rosiek and C. A. Savoy, Nucl. Phys. B **570**, 81 (2000), [hep-ph/9906206].

[101] L. Autonne, Annals de l'Université de Lyon, Nouvelle Série I, Fasc. **38**, 1 (1915); T. Takagi, Japan J. Math. **1**, 83 (1925).

[102] S. Y. Choi *et al.*, Nucl. Phys. **B778**, 85 (2007), [hep-ph/0612218].

[103] S. Y. Choi *et al.*, Eur. Phys. J. **C22**, 563 (2001), [Addendum: Eur. Phys. J. **C23**, 769 (2002)], [hep-ph/0108117].

[104] M. M. El Kheishen, A. A. Aboshousha and A. A. Shafik, Phys. Rev. **D45**, 4345 (1992).

[105] T. Hahn (2006), [arXiv:physics/0607103].

[106] K.-i. Hikasa and M. Kobayashi, Phys. Rev. **D36**, 724 (1987); F. Gabbiani and A. Masiero, Nucl. Phys. **B322**, 235 (1989); P. Brax and C. A. Savoy, Nucl. Phys. **B447**, 227 (1995), [hep-ph/9503306].

[107] J. R. Ellis and S. Rudaz, Phys. Lett. **128B**, 248 (1983); F. Browning, D. Chang and W.-Y. Keung, Phys. Rev. **D64**, 015010 (2001), [hep-ph/0012258]; A. Bartl *et al.*, Phys. Lett. **B573**, 153 (2003), [hep-ph/0307317]; A. Bartl *et al.*, Phys. Rev. **D70**, 035003 (2004), [hep-ph/0311338].

[108] J.F. Gunion *et al.*, *The Higgs Hunter's Guide* (Westview Press, Boulder, CO, 2000); M. Carena and H. E. Haber, Prog. Part. Nucl. Phys. **50**, 63 (2003), [hep-ph/0208209]; A. Djouadi, Phys. Rept. **459**, 1 (2008), [hep-ph/0503173].

[109] E. Bagnaschi *et al.*, Eur. Phys. J. **C79**, 617 (2019), [arXiv:1808.07542].

[110] H. E. Haber and M. Sher, Phys. Rev. **D35**, 2206 (1987).

[111] L. J. Hall, D. Pinner and J. T. Ruderman, JHEP **04**, 131 (2012), [arXiv:1112.2703].

[112] L. J. Hall and M. B. Wise, Nucl. Phys. **B187**, 397 (1981).

[113] H. E. Haber and R. Hempfling, Phys. Rev. Lett. **66**, 1815 (1991); Y. Okada, M. Yamaguchi and T. Yanagida, Prog. Theor. Phys. **85**, 1 (1991); J. R. Ellis, G. Ridolfi and F. Zwirner, Phys. Lett. **B257**, 83 (1991).

[114] H. E. Haber, R. Hempfling and A. H. Hoang, Z. Phys. C **75**, 539 (1997), [hep-ph/9609331].

[115] P. Draper and H. Rzehak, Phys. Rept. **619**, 1 (2016), [arXiv:1601.01890].

[116] P. Slavich *et al.*, Eur. Phys. J. C **81**, 5, 450 (2021), [arXiv:2012.15629].

[117] A. Pilaftsis and C. E. M. Wagner, Nucl. Phys. **B553**, 3 (1999), [hep-ph/9902371]; D. A. Demir, Phys. Rev. **D60**, 055006 (1999), [hep-ph/9901389]; S. Y. Choi, M. Drees and J. S. Lee, Phys. Lett. **B481**, 57 (2000), [hep-ph/0002287]; M. Carena *et al.*, Nucl. Phys. **B586**, 92 (2000), [hep-ph/0003180]; M. Carena *et al.*, Phys. Lett. **B495**, 155 (2000), [hep-ph/0009212]; M. Carena *et al.*, Nucl. Phys. **B625**, 345 (2002), [hep-ph/0111245]; M. Frank *et al.*, JHEP **02**, 047 (2007), [hep-ph/0611326]; S. Heinemeyer *et al.*, Phys. Lett. **B652**, 300 (2007), [arXiv:0705.0746].

[118] H. E. Haber and J. D. Mason, Phys. Rev. **D77**, 115011 (2008), [arXiv:0711.2890].

[119] M. Carena *et al.*, Phys. Rev. **D93**, 035013 (2016), [arXiv:1510.09137].

[120] S. Khalil, Int. J. Mod. Phys. **A18**, 1697 (2003), [hep-ph/0212050].

[121] W. Fischler, S. Paban and S. D. Thomas, Phys. Lett. **B289**, 373 (1992), [hep-ph/9205233].

[122] A. Masiero and L. Silvestrini, in *Perspectives on Supersymmetry*, edited by G.L. Kane (World Scientific, Singapore, 1998) pp. 423–441.

[123] M. Pospelov and A. Ritz, Annals Phys. **318**, 119 (2005), [hep-ph/0504231].

[124] J. M. Pendlebury *et al.*, Phys. Rev. **D92**, 092003 (2015), [arXiv:1509.04411].

[125] V. Andreev *et al.* (ACME Collaboration), Nature **562**, 355 (2018).

[126] F. Gabbiani *et al.*, Nucl. Phys. **B477**, 321 (1996), [hep-ph/9604387].

Downloaded from https://academic.oup.com/ptep/article/2022/8/083C01/6651666 by KIT Library user on 27 September 2022

[127] M. J. Ramsey-Musolf and S. Su, Phys. Rept. **456**, 1 (2008), [hep-ph/0612057].

[128] M. Carena, A. Menon and C. E. M. Wagner, Phys. Rev. **D79**, 075025 (2009), [arXiv:0812.3594].

[129] M. B. Einhorn and D. R. T. Jones, Nucl. Phys. **B196**, 475 (1982).

[130] W. J. Marciano and G. Senjanovic, Phys. Rev. **D25**, 3092 (1982).

[131] R.N. Mohapatra, *Unification and Supersymmetry*, Third Edition (Springer Science, New York, 2003).

[132] S. P. Martin and M. T. Vaughn, Phys. Rev. **D50**, 2282 (1994), [Erratum: Phys. Rev. **D78**, 039903 (2008)], [hep-ph/9311340]; R. M. Fonseca *et al.*, Nucl. Phys. **B854**, 28 (2012), [arXiv:1107.2670]; F. Staub, Comput. Phys. Commun. **182**, 808 (2011), [arXiv:1002.0840].

[133] F. Staub, Comput. Phys. Commun. **185**, 1773 (2014), [arXiv:1309.7223]; F. Staub, Adv. High Energy Phys. **2015**, 840780 (2015), [arXiv:1503.04200]; The SARAH homepage is `https://sarah.hepforge.org/`; R. M. Fonseca, Comput. Phys. Commun. **183**, 2298 (2012), [arXiv:1106.5016]; The Susyno homepage is `https://renatofonseca.net/susyno`.

[134] B. C. Allanach, Comput. Phys. Commun. **143**, 305 (2002), [hep-ph/0104145]; The SOFTSUSY homepage is `http://softsusy.hepforge.org/`; A. Djouadi, J.-L. Kneur and G. Moultaka, Comput. Phys. Commun. **176**, 426 (2007), [hep-ph/0211331]; The Suspect homepage is `http://suspect.in2p3.fr/`; F. E. Paige *et al.* (2003), [hep-ph/0312045]; Isajet may be obtained from `http://www.nhn.ou.edu/~isajet/`; W. Porod, Comput. Phys. Commun. **153**, 275 (2003), [hep-ph/0301101]; Spheno may be obtained from `https://spheno.hepforge.org/`; P. Athron *et al.*, Comput. Phys. Commun. **190**, 139 (2015), [arXiv:1406.2319]; The FlexibleSUSY homepage is `https://flexiblesusy.hepforge.org/`.

[135] L. E. Ibanez and G. G. Ross, Phys. Lett. **110B**, 215 (1982).

[136] M. Drees, Phys. Lett. B **158**, 409 (1985); J. R. Ellis *et al.*, Phys. Lett. B **155**, 381 (1985); S. P. Martin, Phys. Rev. D **79**, 095019 (2009), [arXiv:0903.3568].

[137] J. Abdallah *et al.* (DELPHI Collaboration), Eur. Phys. J. **C31**, 421 (2003), [hep-ex/0311019].

[138] H. K. Dreiner *et al.*, Eur. Phys. J. **C62**, 547 (2009), [arXiv:0901.3485].

[139] G. F. Giudice *et al.*, JHEP **12**, 027 (1998), [hep-ph/9810442]; A. Pomarol and R. Rattazzi, JHEP **05**, 013 (1999), [hep-ph/9903448]; D.-W. Jung and J. Y. Lee, JHEP **03**, 123 (2009), [arXiv:0902.0464].

[140] J. F. Gunion and H. E. Haber, Phys. Rev. **D37**, 2515 (1988); S. Y. Choi, M. Drees and B. Gaissmaier, Phys. Rev. **D70**, 014010 (2004), [hep-ph/0403054].

[141] H. Baer, V. Barger and D. Sengupta, Phys. Rev. **D98**, 015039 (2018), [arXiv:1801.09730].

[142] J. L. Feng *et al.*, Phys. Rev. Lett. **83**, 1731 (1999), [hep-ph/9904250]; J. F. Gunion and S. Mrenna, Phys. Rev. **D62**, 015002 (2000), [hep-ph/9906270].

[143] T. Gherghetta, G. F. Giudice and J. D. Wells, Nucl. Phys. **B559**, 27 (1999), [hep-ph/9904378].

[144] M. Endo, M. Yamaguchi and K. Yoshioka, Phys. Rev. **D72**, 015004 (2005), [hep-ph/0504036]; K. Choi, K. S. Jeong and K.-i. Okumura, JHEP **09**, 039 (2005), [hep-ph/0504037]; O. Loaiza-Brito *et al.*, AIP Conf. Proc. **805**, 198 (2005), [hep-th/0509158].

[145] See *e.g.*, G. D'Ambrosio *et al.*, Nucl. Phys. **B645**, 155 (2002).

[146] C. Smith, Acta Phys. Polon. Supp. **3**, 53 (2010), [arXiv:0909.4444].

[147] M. Drees and S.P. Martin, in *Electroweak Symmetry Breaking and New Physics at the TeV Scale*, edited by T. Barklow *et al.* (World Scientific, Singapore, 1996) pp. 146–215.

[148] G. L. Kane *et al.*, Phys. Rev. **D49**, 6173 (1994), [hep-ph/9312272].

[149] J. R. Ellis *et al.*, Phys. Lett. **B573**, 162 (2003), [hep-ph/0305212]; J. R. Ellis *et al.*, Phys. Rev. **D70**, 055005 (2004), [hep-ph/0405110].

[150] H. Baer *et al.*, Phys. Rev. **D71**, 095008 (2005), [hep-ph/0412059].

[151] V. Berezinsky *et al.*, Astropart. Phys. **5**, 1 (1996), [hep-ph/9508249]; J. R. Ellis *et al.*, Nucl. Phys. **B652**, 259 (2003), [hep-ph/0210205].

[152] L. E. Ibanez and D. Lust, Nucl. Phys. **B382**, 305 (1992), [hep-th/9202046]; B. de Carlos, J. A. Casas and C. Munoz, Phys. Lett. **B299**, 234 (1993), [hep-ph/9211266]; V. S. Kaplunovsky and J. Louis, Phys. Lett. **B306**, 269 (1993), [hep-th/9303040]; A. Brignole, L. E. Ibanez and C. Munoz, Nucl. Phys. **B422**, 125 (1994), [Erratum: **B436**, 747 (1995)], [hep-ph/9308271].

[153] A. Arbey *et al.*, Phys. Rev. **D87**, 115020 (2013), [arXiv:1304.0381].

[154] G. R. Dvali, G. F. Giudice and A. Pomarol, Nucl. Phys. **B478**, 31 (1996), [hep-ph/9603238].

[155] P. Draper *et al.*, Phys. Rev. **D85**, 095007 (2012), [arXiv:1112.3068].

[156] P. Meade, N. Seiberg and D. Shih, Prog. Theor. Phys. Suppl. **177**, 143 (2009), [arXiv:0801.3278]; M. Buican *et al.*, JHEP **03**, 016 (2009), [arXiv:0812.3668].

[157] A. Rajaraman *et al.*, Phys. Lett. **B678**, 367 (2009), [arXiv:0903.0668]; L. M. Carpenter *et al.*, Phys. Rev. **D79**, 035002 (2009), [arXiv:0805.2944].

[158] S. Ambrosanio, G. D. Kribs and S. P. Martin, Nucl. Phys. **B516**, 55 (1998), [hep-ph/9710217].

[159] For a review and guide to the literature, see J.F. Gunion and H.E. Haber, in *Perspectives on Supersymmetry II*, edited by G.L. Kane (World Scientific, Singapore, 2010) pp. 420–445.

[160] T. S. Roy and M. Schmaltz, Phys. Rev. **D77**, 095008 (2008), [arXiv:0708.3593].

[161] A. de Gouvea, A. Friedland and H. Murayama, Phys. Rev. **D57**, 5676 (1998), [hep-ph/9711264].

[162] T. Han, D. Marfatia and R.-J. Zhang, Phys. Rev. **D61**, 013007 (2000), [hep-ph/9906508]; Z. Chacko and E. Ponton, Phys. Rev. **D66**, 095004 (2002), [hep-ph/0112190]; A. Delgado, G. F. Giudice and P. Slavich, Phys. Lett. **B653**, 424 (2007), [arXiv:0706.3873]; T. Liu and C. E. M. Wagner, JHEP **06**, 073 (2008), [arXiv:0803.2895].

[163] A. Djouadi, J.L. Kneur, and G. Moultaka, Comp. Phys. Comm. **176**, 426 (2007); C. F. Berger *et al.*, JHEP **02**, 023 (2009), [arXiv:0812.0980]; B. Allanach *et al.*, Phys. Rev. **D92**, 015006 (2015), [arXiv:1502.05836].

[164] S. P. Martin and J. D. Wells, Phys. Rev. **D64**, 035003 (2001), [hep-ph/0103067].

[165] S. S. AbdusSalam *et al.*, Phys. Rev. D **81**, 095012 (2010), [arXiv:0904.2548].

[166] J. Berger *et al.*, Phys. Rev. **D93**, 035017 (2016), [arXiv:1510.08840].

[167] K. J. de Vries *et al.*, Eur. Phys. J. **C75**, 422 (2015), [arXiv:1504.03260].

[168] E. Bagnaschi *et al.*, Eur. Phys. J. **C78**, 256 (2018), [arXiv:1710.11091].

[169] M. Cahill-Rowley *et al.*, Phys. Rev. **D90**, 095017 (2014), [arXiv:1407.7021]; M. Cahill-Rowley *et al.*, Phys. Rev. **D91**, 055011 (2015), [arXiv:1405.6716].

[170] G. Bertone *et al.*, JCAP **1604**, 037 (2016), [arXiv:1507.07008].

[171] N. Arkani-Hamed *et al.* (2007), [hep-ph/0703088]; J. Alwall *et al.*, Phys. Rev. **D79**, 015005 (2009), [arXiv:0809.3264]; J. Alwall, P. Schuster and N. Toro, Phys. Rev. **D79**,

Downloaded from https://academic.oup.com/ptep/article/2022/8/083C01/6651666 by KIT Library user on 27 September 2022

075020 (2009), [arXiv:0810.3921]; D. S. M. Alves, E. Izaguirre and J. G. Wacker, Phys. Lett. **B702**, 64 (2011), [arXiv:1008.0407]; D. S. M. Alves, E. Izaguirre and J. G. Wacker, JHEP **10**, 012 (2011), [arXiv:1102.5338]; D. Alves (LHC New Physics Working Group), J. Phys. **G39**, 105005 (2012), [arXiv:1105.2838].

[172] F. Ambrogi *et al.*, Eur. Phys. J. **C78**, 215 (2018), [arXiv:1707.09036].

[173] R. Barbieri and G.F. Giudice, Nucl. Phys. **B305**, 63 (1988).

[174] J. R. Ellis *et al.*, Mod. Phys. Lett. **A1**, 57 (1986).

[175] G. W. Anderson and D. J. Castano, Phys. Lett. **B347**, 300 (1995), [hep-ph/9409419]; G. W. Anderson and D. J. Castano, Phys. Rev. **D52**, 1693 (1995), [hep-ph/9412322]; G. W. Anderson and D. J. Castano, Phys. Rev. **D53**, 2403 (1996), [hep-ph/9509212]; P. Athron and D. J. Miller, Phys. Rev. **D76**, 075010 (2007), [arXiv:0705.2241].

[176] M. E. Cabrera, J. A. Casas and R. Ruiz de Austri, JHEP **03**, 075 (2009), [arXiv:0812.0536]; H. Baer *et al.*, Phys. Rev. Lett. **109**, 161802 (2012), [arXiv:1207.3343].

[177] J. L. Feng, K. T. Matchev and T. Moroi, Phys. Rev. **D61**, 075005 (2000), [hep-ph/9909334].

[178] D. M. Ghilencea and G. G. Ross, Nucl. Phys. **B868**, 65 (2013), [arXiv:1208.0837].

[179] H. Baer, V. Barger and D. Mickelson, Phys. Rev. **D88**, 095013 (2013), [arXiv:1309.2984].

[180] M. van Beekveld, S. Caron and R. Ruiz de Austri, JHEP **01**, 147 (2020), [arXiv:1906.10706].

[181] G. L. Kane and S. F. King, Phys. Lett. **B451**, 113 (1999), [hep-ph/9810374]; M. Bastero-Gil, G. L. Kane and S. F. King, Phys. Lett. **B474**, 103 (2000), [hep-ph/9910506]; J. A. Casas, J. R. Espinosa and I. Hidalgo, JHEP **01**, 008 (2004), [hep-ph/0310137]; H. Abe, T. Kobayashi and Y. Omura, Phys. Rev. **D76**, 015002 (2007), [hep-ph/0703044]; R. Essig and J.-F. Fortin, JHEP **04**, 073 (2008), [arXiv:0709.0980].

[182] B. de Carlos and J. A. Casas, Phys. Lett. **B309**, 320 (1993), [hep-ph/9303291]; S. Cassel, D. M. Ghilencea and G. G. Ross, Nucl. Phys. **B825**, 203 (2010), [arXiv:0903.1115]; S. Cassel, D. M. Ghilencea and G. G. Ross, Nucl. Phys. **B835**, 110 (2010), [arXiv:1001.3884].

[183] B. C. Allanach, Phys. Lett. B **635**, 123 (2006), [hep-ph/0601089].

[184] B. C. Allanach *et al.*, JHEP **08**, 023 (2007), [arXiv:0705.0487].

[185] O. Buchmueller *et al.*, Eur. Phys. J. **C74**, 6, 2922 (2014), [arXiv:1312.5250].

[186] P. Bechtle *et al.*, Eur. Phys. J. **C76**, 96 (2016), [arXiv:1508.05951].

[187] H. Baer *et al.*, Phys. Rev. **D89**, 115019 (2014), [arXiv:1404.2277].

[188] R. Barbieri and A. Strumia, in "4th Rencontres du Vietnam: Physics at Extreme Energies (Particle Physics and Astrophysics) Hanoi, Vietnam, July 19-25, 2000," (2000), [hep-ph/0007265].

[189] L. Giusti, A. Romanino and A. Strumia, Nucl. Phys. **B550**, 3 (1999), [hep-ph/9811386]; H.-C. Cheng and I. Low, JHEP **09**, 051 (2003), [hep-ph/0308199]; H.-C. Cheng and I. Low, JHEP **08**, 061 (2004), [hep-ph/0405243]; R. Harnik *et al.*, Phys. Rev. **D70**, 015002 (2004), [hep-ph/0311349].

[190] H. Baer *et al.*, Phys. Rev. **D87**, 035017 (2013), [arXiv:1210.3019]; H. Baer *et al.*, Phys. Rev. **D87**, 115028 (2013), [arXiv:1212.2655]; J. L. Feng, Ann. Rev. Nucl. Part. Sci. **63**, 351 (2013), [arXiv:1302.6587].

[191] J. L. Feng, K. T. Matchev and T. Moroi, Phys. Rev. Lett. **84**, 2322 (2000), [hep-ph/9908309]; J. L. Feng and F. Wilczek, Phys. Lett. **B631**, 170 (2005), [hep-ph/0507032]; D. Horton and G. G. Ross, Nucl. Phys. **B830**, 221 (2010), [arXiv:0908.0857].

[192] M. Drees, Phys. Rev. **D33**, 1468 (1986); S. Dimopoulos and G. F. Giudice, Phys. Lett. **B357**, 573 (1995), [hep-ph/9507282]; A. Pomarol and D. Tommasini, Nucl. Phys. **B466**, 3 (1996), [hep-ph/9507462].

[193] M. Dine, A. Kagan and S. Samuel, Phys. Lett. **B243**, 250 (1990); A. G. Cohen, D. B. Kaplan and A. E. Nelson, Phys. Lett. **B388**, 588 (1996), [hep-ph/9607394].

[194] C. Brust *et al.*, JHEP **03**, 103 (2012), [arXiv:1110.6670].

[195] S. P. Martin, Phys. Rev. **D75**, 115005 (2007), [hep-ph/0703097]; S. P. Martin, Phys. Rev. **D78**, 055019 (2008), [arXiv:0807.2820].

[196] J. Fan, M. Reece and J. T. Ruderman, JHEP **11**, 012 (2011), [arXiv:1105.5135]; J. Fan, M. Reece and J. T. Ruderman, JHEP **07**, 196 (2012), [arXiv:1201.4875].

[197] H. Murayama, Y. Nomura and D. Poland, Phys. Rev. **D77**, 015005 (2008), [arXiv:0709.0775]; G. Perez, T. S. Roy and M. Schmaltz, Phys. Rev. **D79**, 095016 (2009), [arXiv:0811.3206].

[198] R. Dermisek and J. F. Gunion, Phys. Rev. Lett. **95**, 041801 (2005), [hep-ph/0502105]; Phys. Rev. **D75**, 095019 (2007); R. Dermisek and J. F. Gunion, Phys. Rev. **D76**, 095006 (2007), [arXiv:0705.4387].

[199] G. G. Ross and K. Schmidt-Hoberg, Nucl. Phys. **B862**, 710 (2012), [arXiv:1108.1284]; G. G. Ross, K. Schmidt-Hoberg and F. Staub, JHEP **08**, 074 (2012), [arXiv:1205.1509]; A. Kaminska, G. G. Ross and K. Schmidt-Hoberg, JHEP **11**, 209 (2013), [arXiv:1308.4168].

[200] S. P. Martin and J. D. Wells, Phys. Rev. **D86**, 035017 (2012), [arXiv:1206.2956].

[201] B. Bellazzini *et al.*, Phys. Rev. **D79**, 095003 (2009), [arXiv:0902.0015].

[202] M. Dine, Ann. Rev. Nucl. Part. Sci. **65**, 43 (2015), [arXiv:1501.01035].

[203] H. Baer, V. Barger and M. Savoy, Phys. Rev. **D93**, 035016 (2016), [arXiv:1509.02929].

[204] M.L. Mangano, editor, *Physics at the FCC-hh, a 100 TeV pp collider*, CERN Yellow Report, CERN-2017-003-M (2017).

[205] P. Athron *et al.* (GAMBIT), Eur. Phys. J. C **77**, 12, 879 (2017), [arXiv:1705.07917].

[206] D. Stockinger, J. Phys. **G34**, R45 (2007), [hep-ph/0609168]; P. Athron *et al.*, Eur. Phys. J. **C76**, 62 (2016), [arXiv:1510.08071].

[207] F. Jegerlehner, Acta Phys. Polon. **B49**, 1157 (2018), [arXiv:1804.07409]; M. Davier *et al.*, Eur. Phys. J. **C80**, 3, 241 (2020), [arXiv:1908.00921].

[208] B. Abi *et al.* (Muon $g-2$ Collboration), Phys. Rev. Lett. **126**, 141801 (2021), [arXiv:2104.03281].

[209] S. Borsanyi *et al.*, Nature **593**, 51 (2021), [arXiv:2002.12347].

[210] M. Ibe, T. T. Yanagida and N. Yokozaki, JHEP **08**, 067 (2013), [arXiv:1303.6995].

[211] D. Hanneke, S. Fogwell and G. Gabrielse, Phys. Rev. Lett. **100**, 120801 (2008), [arXiv:0801.1134].

[212] R. H. Parker *et al.*, Science **360**, 191 (2018), [arXiv:1812.04130].

[213] L. Morel *et al.*, Nature **588**, 61 (2020).

[214] B. Dutta and Y. Mimura, Phys. Lett. **B790**, 563 (2019), [arXiv:1811.10209]; M. Endo and W. Yin, JHEP **08**, 122 (2019), [arXiv:1906.08768]; M. Badziak and K. Sakurai, JHEP **10**, 024 (2019), [arXiv:1908.03607]; S. Li, Y. Xiao and J. M. Yang, Eur. Phys. J. C **82**, 3, 276 (2022), [arXiv:2107.04962].

[215] T. Ibrahim and P. Nath, Phys. Rev. D **62**, 015004 (2000), [hep-ph/9908443]; R. L. Arnowitt, B. Dutta and Y. Santoso, Phys. Rev. D **64**, 113010 (2001), [hep-ph/0106089]; C. Han (2021), [arXiv:2104.03292].

Downloaded from https://academic.oup.com/ptep/article/2022/8/083C01/6651666 by KIT Library user on 27 September 2022

[216] J. Albrecht, D. van Dyk and C. Langenbruch, Prog. Part. Nucl. Phys. **120**, 103885 (2021), [arXiv:2107.04822].

[217] A. Limosani *et al.* (Belle Collaboration), Phys. Rev. Lett. **103**, 241801 (2009), [arXiv:0907.1384]; J. P. Lees *et al.* (BaBar Collaboration), Phys. Rev. Lett. **109**, 191801 (2012), [arXiv:1207.2690]; J. P. Lees *et al.* (BaBar Collaboration), Phys. Rev. **D86**, 112008 (2012), [arXiv:1207.5772].

[218] M. Misiak *et al.*, Phys. Rev. Lett. **114**, 221801 (2015), [arXiv:1503.01789]; M. Czakon *et al.*, JHEP **04**, 168 (2015), [arXiv:1503.01791]; M. Misiak, A. Rehman and M. Steinhauser, JHEP **06**, 175 (2020), [arXiv:2002.01548].

[219] H. Baer and M. Brhlik, Phys. Rev. **D55**, 3201 (1997), [hep-ph/9610224]; M. Ciuchini *et al.*, Phys. Rev. **D67**, 075016 (2003), [Erratum: **D68**, 079901 (2003)], [hep-ph/0212397]; T. Hurth, Rev. Mod. Phys. **75**, 1159 (2003), [hep-ph/0212304]; F. Mahmoudi, JHEP **12**, 026 (2007), [arXiv:0710.3791]; K. A. Olive and L. Velasco-Sevilla, JHEP **05**, 052 (2008), [arXiv:0801.0428].

[220] S. R. Choudhury and N. Gaur, Phys. Lett. **B451**, 86 (1999), [hep-ph/9810307]; K. S. Babu and C. F. Kolda, Phys. Rev. Lett. **84**, 228 (2000), [hep-ph/9909476]; G. Isidori and A. Retico, JHEP **11**, 001 (2001), [hep-ph/0110121]; G. Isidori and A. Retico, JHEP **09**, 063 (2002), [hep-ph/0208159].

[221] W. Altmannshofer and P. Stangl, Eur. Phys. J. C **81**, 10, 952 (2021), [arXiv:2103.13370].

[222] S. Chatrchyan *et al.* (CMS Collaboration), Phys. Rev. Lett. **111**, 101804 (2013), [arXiv:1307.5025]; V. Khachatryan *et al.* (CMS and LHCb Collaborations), Nature **522**, 68 (2015), [arXiv:1411.4413]; M. Aaboud *et al.* (ATLAS Collaboration), JHEP **04**, 098 (2019), [arXiv:1812.03017]; R. Aaij *et al.* (LHCb Collaboration), Phys. Rev. Lett. **118**, 191801 (2017), [arXiv:1703.05747].

[223] J. Aebischer *et al.*, Eur. Phys. J. C **80**, 3, 252 (2020), [arXiv:1903.10434].

[224] C. Bobeth *et al.*, Phys. Rev. Lett. **112**, 101801 (2014), [arXiv:1311.0903].

[225] R. Aaij *et al.* (LHCb Collaboration), Nature Physics **18**, 3, 277 (2022), [arXiv:2103.11769].

[226] R. Aaij *et al.* (LHCb Collaboration), Phys. Rev. Lett. **125**, 1, 011802 (2020), [arXiv:2003.04831].

[227] R. Aaij *et al.* (LHCb), Phys. Rev. Lett. **127**, 15, 151801 (2021), [arXiv:2105.14007].

[228] M. Bona *et al.* (UTfit Collaboration), Phys. Lett. **B687**, 61 (2010), [arXiv:0908.3470].

[229] J. P. Lees *et al.* (BaBar Collaboration), Phys. Rev. Lett. **109**, 101802 (2012), [arXiv:1205.5442]; J. P. Lees *et al.* (BaBar Collaboration), Phys. Rev. **D88**, 072012 (2013), [arXiv:1303.0571].

[230] R. Aaij *et al.* (LHCb Collaboration), Phys. Rev. Lett. **115**, 111803 (2015), [Erratum: **115**, 159901 (2015)], [arXiv:1506.08614]; R. Aaij *et al.* (LHCb Collaboration), Phys. Rev. Lett. **120**, 171802 (2018), [arXiv:1708.08856]; M. Huschle *et al.* (Belle Collaboration), Phys. Rev. **D92**, 072014 (2015), [arXiv:1507.03233]; Y. Sato *et al.* (Belle Collaboration), Phys. Rev. **D94**, 072007 (2016), [arXiv:1607.07923]; S. Hirose *et al.* (Belle Collaboration), Phys. Rev. Lett. **118**, 211801 (2017), [arXiv:1612.00529]; S. Hirose *et al.* (Belle Collaboration), Phys. Rev. **D97**, 012004 (2018), [arXiv:1709.00129].

[231] G. Caria *et al.* (Belle Collaboration), Phys. Rev. Lett. **124**, 16, 161803 (2020), [arXiv:1910.05864].

[232] Y. S. Amhis *et al.* (HFLAV), Eur. Phys. J. C **81**, 3, 226 (2021), [arXiv:1909.12524].

[233] F. Mahmoudi, S. Neshatpour and J. Orloff, JHEP **08**, 092 (2012), [arXiv:1205.1845]; A. Arbey *et al.*, JHEP **11**, 132 (2017), [arXiv:1707.00426].

[234] H. Eberl *et al.*, Phys. Rev. D **104**, 075025 (2021), [arXiv:2106.15228].

[235] S. Trifinopoulos, Eur. Phys. J. C **78**, 10, 803 (2018), [arXiv:1807.01638]; W. Altmannshofer *et al.*, Phys. Rev. D **102**, 1, 015031 (2020), [arXiv:2002.12910]; P. S. Bhupal Dev, A. Soni and F. Xu (2021), [arXiv:2106.15647].

[236] A. J. Buras, Acta Phys. Polon. **B49**, 1043 (2018), [arXiv:1805.11096].

[237] V. Cirigliano *et al.*, JHEP **02**, 032 (2020), [arXiv:1911.01359].

[238] J. R. Ellis *et al.*, JHEP **08**, 083 (2007), [arXiv:0706.0652]; S. Heinemeyer *et al.*, JHEP **08**, 087 (2008), [arXiv:0805.2359]; G.-C. Cho *et al.*, JHEP **11**, 068 (2011), [arXiv:1104.1769].

[239] A. J. Buras *et al.*, Nucl. Phys. **B592**, 55 (2001), [hep-ph/0007313].

[240] P. F. de Salas *et al.*, JHEP **02**, 071 (2021), [arXiv:2006.11237]; I. Esteban *et al.*, JHEP **09**, 178 (2020), [arXiv:2007.14792].

[241] K. Zuber, Phys. Rept. **305**, 295 (1998), [hep-ph/9811267]; S. F. King, J. Phys. **G42**, 123001 (2015), [arXiv:1510.02091]; S. F. King, Prog. Part. Nucl. Phys. **94**, 217 (2017), [arXiv:1701.04413].

[242] For a review of neutrino masses in supersymmetry, see *e.g.*, B. Mukhopadhyaya, *Proc. Indian National Science Academy* **A70**, 239 (2004); M. Hirsch and J. W. F. Valle, New J. Phys. **6**, 76 (2004), [hep-ph/0405015].

[243] F. Borzumati and Y. Nomura, Phys. Rev. **D64**, 053005 (2001), [hep-ph/0007018].

[244] P. Minkowski, Phys. Lett. **67B**, 421 (1977); M. Gell-Mann, P. Ramond, and R. Slansky, in *Supergravity*, edited by D. Freedman and P. van Nieuwenhuizen (North Holland, Amsterdam, 1979) p. 315; T. Yanagida, Prog. Theor. Phys. **64**, 1103 (1980); R. N. Mohapatra and G. Senjanovic, Phys. Rev. Lett. **44**, 912 (1980); R. N. Mohapatra and G. Senjanovic, Phys. Rev. **D23**, 165 (1981).

[245] J. Hisano *et al.*, Phys. Lett. **B357**, 579 (1995), [hep-ph/9501407]; J. Hisano *et al.*, Phys. Rev. **D53**, 2442 (1996), [hep-ph/9510309]; J. A. Casas and A. Ibarra, Nucl. Phys. **B618**, 171 (2001), [hep-ph/0103065]; J. R. Ellis *et al.*, Phys. Rev. **D66**, 115013 (2002), [hep-ph/0206110]; A. Masiero, S. K. Vempati and O. Vives, New J. Phys. **6**, 202 (2004), [hep-ph/0407325]; E. Arganda *et al.*, Phys. Rev. **D71**, 035011 (2005), [hep-ph/0407302]; F. R. Joaquim and A. Rossi, Phys. Rev. Lett. **97**, 181801 (2006), [hep-ph/0604083]; J. R. Ellis and O. Lebedev, Phys. Lett. **B653**, 411 (2007), [arXiv:0707.3419].

[246] Y. Grossman and H. E. Haber, Phys. Rev. Lett. **78**, 3438 (1997), [hep-ph/9702421]; A. Dedes, H. E. Haber and J. Rosiek, JHEP **11**, 059 (2007), [arXiv:0707.3718].

[247] M. Hirsch, H. V. Klapdor-Kleingrothaus and S. G. Kovalenko, Phys. Lett. **B398**, 311 (1997), [hep-ph/9701253]; L. J. Hall, T. Moroi and H. Murayama, Phys. Lett. **B424**, 305 (1998), [hep-ph/9712515]; K. Choi, K. Hwang and W. Y. Song, Phys. Rev. Lett. **88**, 141801 (2002), [hep-ph/0108028]; T. Honkavaara, K. Huitu and S. Roy, Phys. Rev. **D73**, 055011 (2006), [hep-ph/0512277].

[248] T. Faber *et al.*, Phys. Rev. D **101**, 5, 055029 (2020), [arXiv:1909.11686].

[249] L. Basso *et al.*, Comput. Phys. Commun. **184**, 698 (2013), [arXiv:1206.4563].

[250] M. Chemtob, Prog. Part. Nucl. Phys. **54**, 71 (2005), [hep-ph/0406029]; R. Barbier *et al.*, Phys. Rept. **420**, 1 (2005), [hep-ph/0406039].

[251] H. Dreiner, in *Perspectives on Supersymmetry II*, edited by G.L. Kane (World Scientific, Singapore, 2010) pp. 565–583.

[252] B. C. Allanach, A. Dedes and H. K. Dreiner, Phys. Rev. **D60**, 075014 (1999), [hep-ph/9906209].

Downloaded from https://academic.oup.com/ptep/article/2022/8/083C01/6651666 by KIT Library user on 27 September 2022

[253] L. E. Ibanez and G. G. Ross, Nucl. Phys. **B368**, 3 (1992); L. E. Ibanez, Nucl. Phys. **B398**, 301 (1993), [hep-ph/9210211].

[254] A. Dedes, S. Rimmer and J. Rosiek, JHEP **08**, 005 (2006), [hep-ph/0603225]; B. C. Allanach and C. H. Kom, JHEP **04**, 081 (2008), [arXiv:0712.0852]; H. K. Dreiner *et al.*, Phys. Rev. **D84**, 113005 (2011), [arXiv:1106.4338].

[255] H. K. Dreiner, C. Luhn and M. Thormeier, Phys. Rev. **D73**, 075007 (2006), [hep-ph/0512163].

[256] K. Tamvakis, Phys. Lett. **B382**, 251 (1996), [hep-ph/9604343]; G. Eyal and Y. Nir, JHEP **06**, 024 (1999), [hep-ph/9904473]; A. Florez *et al.*, Phys. Rev. **D87**, 095010 (2013), [arXiv:1303.0278].

[257] C. Csaki, Y. Grossman and B. Heidenreich, Phys. Rev. **D85**, 095009 (2012), [arXiv:1111.1239].

[258] D. Dercks *et al.*, Eur. Phys. J. **C77**, 856 (2017), [arXiv:1706.09418].

[259] B. C. Allanach and B. Gripaios, JHEP **05**, 062 (2012), [arXiv:1202.6616]; M. Asano, K. Rolbiecki and K. Sakurai, JHEP **01**, 128 (2013), [arXiv:1209.5778]; N. Chamoun *et al.*, JHEP **08**, 142 (2014), [arXiv:1407.2248].

[260] J. C. Romao, Nucl. Phys. Proc. Suppl. **81**, 231 (2000), [hep-ph/9907466]; Y. Grossman and S. Rakshit, Phys. Rev. **D69**, 093002 (2004), [hep-ph/0311310].

[261] R. N. Mohapatra, Phys. Rev. **D34**, 3457 (1986); K. S. Babu and R. N. Mohapatra, Phys. Rev. Lett. **75**, 2276 (1995), [hep-ph/9506354]; M. Hirsch, H. V. Klapdor-Kleingrothaus and S. G. Kovalenko, Phys. Rev. Lett. **75**, 17 (1995); M. Hirsch, H. V. Klapdor-Kleingrothaus and S. G. Kovalenko, Phys. Rev. **D53**, 1329 (1996), [hep-ph/9502385].

[262] Y. Grossman and H. E. Haber, Phys. Rev. **D59**, 093008 (1999), [hep-ph/9810536].

[263] S. Dimopoulos and L. J. Hall, Phys. Lett. **B207**, 210 (1988); J. Kalinowski *et al.*, Phys. Lett. **B406**, 314 (1997), [hep-ph/9703436]; J. Erler, J. L. Feng and N. Polonsky, Phys. Rev. Lett. **78**, 3063 (1997), [hep-ph/9612397].

[264] H. K. Dreiner, P. Richardson and M. H. Seymour, Phys. Rev. **D63**, 055008 (2001), [hep-ph/0007228].

[265] J. E. Kim and H. P. Nilles, Phys. Lett. **138B**, 150 (1984).

[266] J. E. Kim and H. P. Nilles, Mod. Phys. Lett. **A9**, 3575 (1994), [hep-ph/9406296].

[267] G. F. Giudice and A. Masiero, Phys. Lett. **B206**, 480 (1988); J. A. Casas and C. Munoz, Phys. Lett. **B306**, 288 (1993), [hep-ph/9302227]; K. J. Bae *et al.*, Phys. Rev. **D99**, 115027 (2019), [arXiv:1902.10748].

[268] M. Cvetic *et al.*, Phys. Rev. **D56**, 2861 (1997), [Erratum: **D58**, 119905 (1998)], [hep-ph/9703317].

[269] R. D. Peccei, Lect. Notes Phys. **741**, 3 (2008), [hep-ph/0607268].

[270] R. D. Peccei and H. R. Quinn, Phys. Rev. Lett. **38**, 1440 (1977); R. D. Peccei and H. R. Quinn, Phys. Rev. **D16**, 1791 (1977).

[271] H. Murayama, H. Suzuki and T. Yanagida, Phys. Lett. **B291**, 418 (1992); T. Gherghetta and G. L. Kane, Phys. Lett. **B354**, 300 (1995), [hep-ph/9504420]; K. J. Bae, H. Baer and H. Serce, Phys. Rev. **D91**, 1, 015003 (2015), [arXiv:1410.7500]; H. Baer, V. Barger and D. Sengupta, Phys. Lett. **B790**, 58 (2019), [arXiv:1810.03713].

[272] P. Fayet, Phys. Lett. **78B**, 417 (1978).

[273] K. Benakli, Fortsch. Phys. **59**, 1079 (2011), [arXiv:1106.1649].

[274] P. J. Fox, A. E. Nelson and N. Weiner, JHEP **08**, 035 (2002), [hep-ph/0206096].

[275] K. Benakli and M. D. Goodsell, Nucl. Phys. **B816**, 185 (2009), [arXiv:0811.4409]; K. Benakli and M. D. Goodsell, Nucl. Phys. **B840**, 1 (2010), [arXiv:1003.4957].

[276] U. Sarkar and R. Adhikari, Phys. Rev. **D55**, 3836 (1997), [hep-ph/9608209]; R. Fok *et al.*, Phys. Rev. **D87**, 055018 (2013), [arXiv:1208.2784].

[277] G. D. Kribs, E. Poppitz and N. Weiner, Phys. Rev. **D78**, 055010 (2008), [arXiv:0712.2039].

[278] K. Benakli, M. D. Goodsell and F. Staub, JHEP **06**, 073 (2013), [arXiv:1211.0552].

[279] J. L. Hewett and T. G. Rizzo, Phys. Rept. **183**, 193 (1989).

[280] A. Delgado, G. Nardini and M. Quiros, Phys. Rev. **D86**, 115010 (2012), [arXiv:1207.6596].

[281] S. F. King, S. Moretti and R. Nevzorov, Phys. Lett. **B634**, 278 (2006), [hep-ph/0511256]; S. F. King, S. Moretti and R. Nevzorov, Phys. Rev. **D73**, 035009 (2006), [hep-ph/0510419].

[282] H. Kawase, JHEP **12**, 094 (2011), [arXiv:1110.3861]; N. Escudero, C. Munoz and A. M. Teixeira, Phys. Rev. D **73**, 055015 (2006), [hep-ph/0512046]; B. Dutta and Y. Mimura, Phys. Lett. B **790**, 589 (2019), [arXiv:1810.08413]; W. Altmannshofer *et al.*, JHEP **07**, 118 (2021), [arXiv:2104.08293].

Downloaded from https://academic.oup.com/ptep/article/2022/8/083C01/6651666 by KIT Library user on 27 September 2022

89. Supersymmetry, Part II (Experiment)

Revised September 2021 by M. D'Onofrio (Liverpool U.) and F. Moortgat (CERN; Ghent U.).

89.1 Introduction

Supersymmetry (SUSY), a transformation relating fermions to bosons and vice versa [1–9] is one of the most compelling possible extensions of the Standard Model of particle physics (SM).

On theoretical grounds SUSY is motivated as a generalization of space-time symmetries. A low-energy realization of SUSY, *i.e.*, SUSY at the TeV scale, is, however, not a necessary consequence. Instead, low-energy SUSY is motivated by the possible cancellation of quadratic divergences in radiative corrections to the Higgs boson mass [10–15]. Furthermore, it is intriguing that a weakly interacting, (meta)stable supersymmetric particle might make up some or all of the dark matter in the Universe [16–18]. In addition, SUSY predicts that gauge couplings, as measured experimentally at the electroweak scale, unify at an energy scale $\mathcal{O}(10^{16})$ GeV ("GUT scale") near the Planck scale [19–25].

In the minimal supersymmetric extension to the Standard Model, the so called MSSM [11, 26, 27], a supersymmetry transformation relates every chiral fermion and gauge boson in the SM to a supersymmetric partner with half a unit of spin difference, but otherwise with the same properties (such as mass) and quantum numbers. The MSSM Higgs sector contains two doublets, which give mass to the up-type and down-type quarks, respectively. After electroweak symmetry breaking, five Higgs bosons arise, of which two are charged. The supersymmetric partners of chiral fermions are squarks ($\tilde{q}$) and sleptons ($\tilde{\ell}$, $\tilde{\nu}$), and the "gauginos" for gauge bosons. The supersymmetric partners of the Higgs doublets are known as "higgsinos." The weak gauginos and higgsinos mix, giving rise to charged mass eigenstates called "charginos" ($\tilde{\chi}^{\pm}$), and neutral mass eigenstates called "neutralinos" ($\tilde{\chi}^{0}$). These are often collectively referred to as electroweakinos (EWkinos). The SUSY partners of the gluons are known as "gluinos" ($\tilde{g}$). The fact that such particles are not yet observed leads to the conclusion that, if supersymmetry is realized, it is a broken symmetry. A description of SUSY in the form of an effective Lagrangian with only "soft" SUSY breaking terms and SUSY particle masses of the order of TeV maintains the cancellation of quadratic divergences of soft SUSY breaking scalar mass squared parameters.

The phenomenology of SUSY is to a large extent defined by the SUSY breaking mechanism and the SUSY breaking scale. These determine the SUSY particle masses, the mass hierarchy, the field contents of physical particles, and their decay modes. In addition, phenomenology crucially depends on whether the multiplicative quantum number of R-parity [27], $R = (-1)^{3(B-L)+2S}$, where B and L are baryon and lepton numbers and S is the spin, is conserved or violated. If R-parity is conserved, SUSY particles (sparticles), which have odd R-parity, are produced in pairs and the decays of each SUSY particle must involve an odd number of lighter SUSY particles. The lightest SUSY particle (LSP) is then stable and often assumed to be a weakly interacting massive particle (WIMP). If R-parity is violated, new terms λ_{ijk}, λ'_{ijk} and λ''_{ijk} appear in the superpotential, where ijk are generation indices; λ-type couplings appear between lepton superfields only, λ''-type are between quark superfields only, and λ'-type couplings connect the two. R-parity violation implies lepton and/or baryon number violation. More details of the theoretical framework of SUSY are discussed elsewhere in this volume [28].

The discovery of a Higgs boson with a mass around 125 GeV imposes constraints on SUSY models, which are discussed elsewhere [28, 29]. Low-energy data from flavor physics experiments, high-precision electroweak observables as well as astrophysical data also impose strong constraints on the allowed SUSY parameter space. Recent examples of such data include measurements of the rare B-meson decay $B_s \to \mu^+\mu^-$ [30–32], measurements of the anomalous magnetic moment of the muon [33, 34], and accurate determinations of the cosmological dark matter relic density constraint [35, 36].

Indirect constraints can be more sensitive to higher SUSY mass scales than experiments searching for direct sparticle production at colliders, but the interpretation of these results is often strongly model dependent. In contrast, direct searches for sparticle production at collider experiments, which are the main topic of this review, are less subject to interpretation ambiguities and therefore they play a crucial role in the search for SUSY.

89.2 Overview of the experimental search programme

The electron-positron collider LEP was operational at CERN between 1989 and 2000. In the initial phase, center-of-mass energies around the Z-peak were probed, but after 1995 the LEP experiments collected a significant amount of luminosity at higher center-of-mass energies, some 235 pb^{-1} per experiment at $\sqrt{s} \geq 204$ GeV, with a maximum $\sqrt{s}$ of 209 GeV. Searches for new physics at e^+e^- colliders benefit from the clean experimental environment and the fact that momentum balance can be measured not only in the plane transverse to the beam, but also in the direction along the beam (up to the beam pipe holes), defined as the longitudinal direction. Searches at LEP are dominated by the data samples taken at the highest center-of-mass energies.

The CDF and D0 experiments at the Tevatron, a proton-antiproton collider at a center-of-mass energy of up to 1.96 TeV, had an extensive search program for supersymmetric particles. CDF and D0 collected integrated luminosities between 10 and 11 fb^{-1} each up to the end of collider operations in 2011.

The electron-proton collider HERA provided collisions to the H1 and ZEUS experiments between 1992 and 2007, at a center-of-mass energy up to 318 GeV. A total integrated luminosity of approximately 0.5 fb^{-1} was collected by each experiment. Since at HERA baryons collide with leptons, SUSY searches at HERA typically look for R-parity violating production of single SUSY particles.

The Large Hadron Collider (LHC) at CERN started proton-proton operation at a center-of-mass energy of 7 TeV in 2010. By the end of 2011 the ATLAS and CMS experiments had collected about 5 fb^{-1} of integrated luminosity each, and the LHCb experiment had collected approximately 1 fb^{-1}. In 2012, the LHC operated at a center-of-mass energy of 8 TeV, and ATLAS and CMS collected approximately 20 fb^{-1} each, whereas LHCb collected 2 fb^{-1}. In 2015, the LHC started Run 2, with a center-of-mass energy of 13 TeV. At the end of Run 2 in November 2018, ATLAS and CMS had both collected approximately 140 fb^{-1}, and LHCb had collected almost 6 fb^{-1}.

At the LHC, cross sections of QCD-mediated processes are the largest achievable at colliders, which is reflected in the higher sensitivity for SUSY particles carrying color charge, squarks and gluinos, with respect to LEP, Tevatron and HERA. In particular, proton-proton collisions at the LHC differ from proton-antiproton collisions at the Tevatron in the sense that there are no valence anti-quarks in the proton, and that gluon-initiated processes play a more dominant role. The increased center-of-mass energy of the LHC compared to the Tevatron significantly extends the kinematic reach for SUSY searches. This is reflected foremost in the sensitivity for squarks and gluinos, but also for SUSY particles produced via electroweak processes.

In this review we report results of direct searches for SUSY particles at colliders up to August 2021, mostly covering data analyses at the ATLAS and CMS experiments with reference to results from LEP, HERA and the Tevatron. For more details on LEP and Tevatron constraints, see earlier PDG reviews [37]. Results are categorized depending on the targeted SUSY particles, the nature of their production and decays, and the assumption on R-parity. Brief summaries of search techniques and approaches adopted for interpretation of the results are given in Section 89.3 and 89.4, respectively. Sections 89.5-89.9 focus on results for promptly-decaying gluinos and first and second generation squarks, top and bottom squarks, electroweakinos (charginos, neutralinos) and sleptons. Limits obtained for sparticle masses assuming R-parity violating models are also reported. Results of dedicated searches for long-lived (LL) SUSY particles are reported in Section 89.10. Finally, Section 89.11 provides examples of global reinterpretations of SUSY searches.

Downloaded from https://academic.oup.com/ptep/article/2022/8/083C01/6651666 by KIT Library user on 27 September 2022

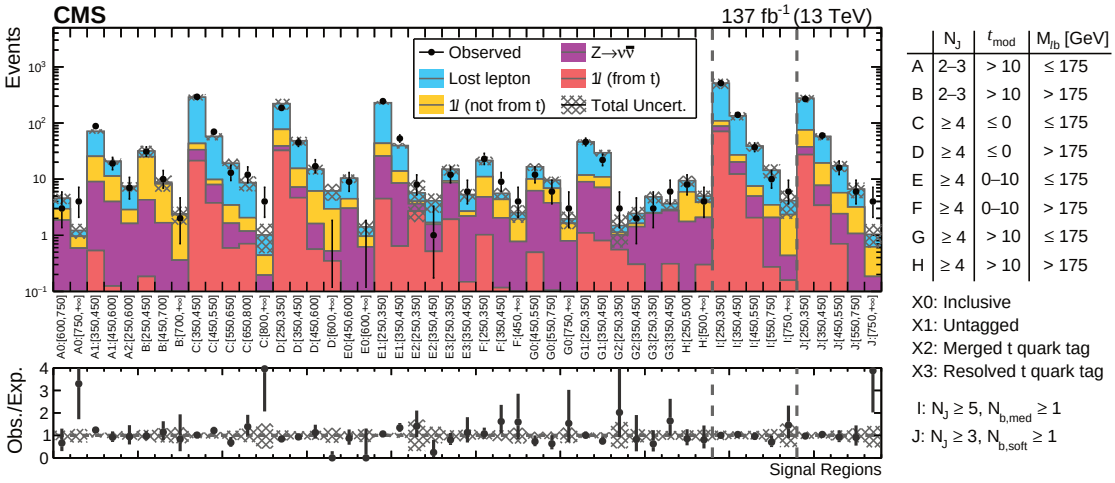

Figure 89.1: Example of multiple signal regions set for a typical SUSY search at the LHC. For definition of regions and acronyms specific for this search, see corresponding paper.

89.3 Experimental search techniques

Large background contributions from Standard Model processes pose challenges to the trigger and analysis. Such backgrounds are dominated by multijet production processes, including, particularly at the LHC, those of top quark production, as well as jet production in association with vector bosons. The proton momentum is shared between its parton constituents, and in each collision only a fraction of the total center-of-mass energy is available in the hard parton-parton scattering. Since the parton momenta in the longitudinal direction are not known on an event-by-event basis, use of momentum conservation constraints in an analysis is restricted to the transverse plane, leading to the definition of transverse variables, such as the missing transverse momentum, and the transverse mass.

Under the assumption of R-parity conservation (RPC), the typical SUSY search signature for squarks and gluinos at hadron colliders contains high-p_{T} jets, which are produced in the decay chains of heavy squarks and gluinos, and significant missing momentum originating from the two LSPs produced at the end of the decay chains, which escape experimental detection. Electroweakino decays are often characterised by the presence of leptons, for instance from W and Z bosons in the decay chain, plus missing transverse momentum. Standard Model backgrounds with missing transverse momentum include leptonic W/Z-boson decays, associated production of jets and a Z-boson decaying into neutrinos, semi-leptonic heavy-flavor decays to neutrinos, top-quark pair production with one or both W bosons decaying leptonically, and multijet events that may be affected by instrumental effects such as jet mis-measurement.

Selection variables designed to separate the SUSY signal from the Standard Model backgrounds include transverse variables such as H_{T}, $E_{\mathrm{T}}^{\mathrm{miss}}$, and m_{eff}. The quantities H_{T} and $E_{\mathrm{T}}^{\mathrm{miss}}$ refer to the measured transverse energy and the missing transverse momentum in the event, respectively. They are usually defined as the scalar sum of the transverse jet momenta or of the transverse energies of calorimeter clusters measured in the event (H_{T}), or the magnitude ($E_{\mathrm{T}}^{\mathrm{miss}}$) of the negative vector sum of transverse momenta of reconstructed objects like jets and leptons in the event ($\vec{p}_{\mathrm{T}}^{\mathrm{miss}}$). The quantity m_{eff} is referred to as the effective mass of the event and is defined as $m_{\mathrm{eff}} = H_{\mathrm{T}} + E_{\mathrm{T}}^{\mathrm{miss}}$. The peak of the m_{eff} distribution for SUSY signal events correlates with the SUSY mass scale, in particular with the mass difference between the primary produced SUSY particle and the LSP [38], whereas the Standard Model backgrounds dominate at low m_{eff}. Additional reduction of multijet backgrounds can be achieved by demanding isolated leptons or photons in the final states; in such events the lepton or photon transverse momentum may be added to H_{T} or m_{eff} for further signal-background separation. Other kinematic variables and approaches developed to increase the sensitivity to pair production of heavy sparticles with TeV-scale masses focusing on the kinematics of their decays are the α_{T} [39–43], *razor* [44], *stransverse mass* (m_{T2}) [45], and *contransverse mass* (m_{CT}) [46] variables. More recently, the topological event reconstruction methods have expanded with the *super-razor* [47] and *recursive jigsaw reconstruction* [48] techniques. Furthermore, the searches for massive SUSY particles frequently attempt to identify their decay into top quarks or vector bosons, which are themselves unstable. If these are produced with a significant boost, jets from their decay will typically overlap, and such topologies are searched for with *jet-substructure* [49] techniques.

Most analyses use simple combinations of selections on kinematic variables (often referred to as *cut-and-count* analyses) and exploit multiple signal regions defined by categorizing events on the basis of several variables and their correlations. An example is provided in Fig. 89.1 from Ref. [50]: 39 signal regions are set to search for top squarks in events with one lepton, jets and missing transverse momentum. Regions depend on jet multiplicities, reconstructed top-quark candidates and thresholds applied to the most discriminant variables used for optimisation.

In recent years, shape analyses or analyses using more sophisticated techniques, e.g. machine learning (ML), have been also developed. ML techniques often allow analyses to better capture the complexity of the events and achieve improved sensitivity with respect to counting experiments. For example, Boosted Decision Trees (BDTs) allow analyses to exploit simultaneously the discriminating power of multiple variables and that of correlations among objects in the events. Deep Neural Networks (NN) are also employed for objects reconstruction and to use directly detector-recorded energies and momenta of produced particles instead of first deriving a restricted set of physical variables. Among others, currently in use are Convolutional NN for image classification techniques, Recurrent NN and Generative Adversarial Networks.

Variables and approaches reported above are also used in searches for R-parity violating (RPV) SUSY models where signal events are often characterised by the presence of multiple leptons and/or jets, and little or no missing transverse momentum. However, if R-parity violating couplings are small, sparticles might be long-lived and may travel macroscopic distances before decaying. Similarly, long lifetimes may be due to small mass splittings, as in the case of pure higgsino/wino scenarios, or to heavy mediators, as in Split SUSY models [51, 52]. The identification of long-lived particles requires dedicated tools and their signatures can be very diverse. At the LHC, customized techniques (also based on NN) have been developed, for example, to reconstruct significantly displaced decay vertices or short track segments, and to identify tracks with atypical properties or unusual ionization, small and localized deposits of energy inside of the calorimeters without associated tracks, or stopped particles that decay out of

Downloaded from https://academic.oup.com/ptep/article/2022/8/083C01/6651666 by KIT Library user on 27 September 2022

time with collisions. For an overview, see Ref. [53].

89.4 Interpretation of search results

Since the mechanism by which SUSY is broken is unknown, a general approach to SUSY via the most general soft SUSY breaking Lagrangian adds a significant number of new free parameters. For the minimal supersymmetric standard model, MSSM, *i.e.*, the model with the minimal particle content, these comprise 105 new real degrees of freedom. A phenomenological analysis of SUSY searches leaving all these parameters free is not feasible. For the practical interpretation of SUSY searches at colliders several approaches are taken to reduce the number of free parameters.

One approach is to assume a SUSY breaking mechanism and lower the number of free parameters through the assumption of additional constraints. Before the start of the LHC, interpretations of experimental results were often performed in constrained models of gravity mediated [54, 55], gauge-mediated [56–58], and anomaly mediated [59, 60] SUSY breaking. The most popular model was the constrained MSSM (CMSSM) [54, 61, 62], which in the literature is also referred to as minimal supergravity, or MSUGRA. These constrained SUSY models are theoretically well motivated and provide a rich spectrum of experimental signatures. However, with universality relations imposed on the soft SUSY breaking parameters, they do not cover all possible kinematic signatures and mass relations of SUSY. Furthermore, LHC Run 1 results, together with other collider and non-collider measurements, limited substantially the allowed SUSY parameter space for these models. This indicates that very constrained models like the CMSSM are no longer good benchmark scenarios to solely characterize the results of SUSY searches at the LHC and efforts have been made to complement them with more flexible approaches.

A broader and more comprehensive subset of the MSSM can be studied via the so-called phenomenological-MSSM, or pMSSM [63–66]. It is derived from the MSSM, using experimental data to eliminate parameters that are free in principle but have already been highly constrained by measurements of *e.g.*, flavor mixing and CP-violation. This effective approach reduces the number of free parameters in the MSSM to typically 19 or even less, making it a practical compromise between the full MSSM and highly constrained models such as the CMSSM.

Even less dependent on fundamental assumptions are interpretations in terms of so-called simplified models [67–70]. Such models assume a limited set of SUSY particle production and decay modes and leave open the possibility to vary masses and other parameters freely. Therefore, simplified models enable comprehensive studies of individual SUSY topologies, and are useful for optimization of the experimental searches over a wide parameter space without limitations on fundamental kinematic properties such as masses, production cross sections, and decay modes.

As a consequence, ATLAS and CMS have adopted simplified models as the primary framework to provide interpretations of their searches. In addition to using simplified models that describe prompt decays of SUSY particles, the experiments are now also focusing more on the use of simplified models that allow for decays of long-lived SUSY particles as they can arise in different SUSY scenarios (see Section 89.10 for further discussion). Today, almost every individual search provides interpretations of their results in one or several simplified models that are characteristic of SUSY topologies probed by the analysis.

While simplified models are very convenient for the interpretation of individual SUSY production and decay topologies, care must be taken when applying these limits to more complex SUSY spectra. In particular, the branching ratio of SUSY particles into a specific final state is often assumed to be 100% and in many of the quoted limits the LSP is assumed to be massless. Therefore, simplified model limits should be seen as an approximation of the constraints that can be placed on sparticle masses in more complex SUSY spectra. Only on a case-by-case basis can it be determined whether the limit of a given simplified model represents a good approximation of the true underlying constraint that can be applied on a sparticle mass in a complex SUSY spectrum. In the following, we will point out explicitly the assumptions that have entered the limits when quoting interpretations from simplified models.

Since none of the searches performed so far have shown significant excess above the SM background prediction, the interpretation of the presented results are exclusion limits on SUSY parameter space. Unless stated differently, all quoted exclusion limits are at 95% confidence level. Finally, we note that many of the recent publications by ATLAS and CMS also present results in terms of model-independent limits such that their discovery potential is statistically quantified independently on a particular model.

89.5 Exclusion limits on gluino, first and second generation squark masses in RPC scenarios

Colored SUSY particles such as squarks and gluinos are produced via the strong interaction and have the highest cross sections at hadron colliders. Limits on squark masses of the order 100 GeV have been set by the LEP experiments [71], in the decay to quark plus neutralino, and for a mass difference between squark and quark plus neutralino of typically at least a few GeV. However, hadron collider experiments are able to set much more stringent mass limits.

The main production mechanisms at hadron colliders are squark-squark, squark-gluino and gluino-gluino production; when "squark" is used "antisquark" is also implied. Pair production usually involves both the s-channel and t-channel parton-parton interactions. However, since there is a negligible amount of bottom and top quark content in the proton, top and bottom squark production proceeds through s-channel diagrams only. Experimental analyses of squark and/or gluino production typically assume the first and second generation squarks to be approximately degenerate in mass. Cross section calculations shown in Fig. 89.2 (from Ref. [72]) assume mass degeneracy of left- and right-handed u, d, s, c squarks. Other sparticle masses are considered decoupled. The LHC experiments have started to also provide simplified model limits on individual first or second generation squarks. Top and bottom squarks have the same production cross section, equivalent to that of a single light squark.

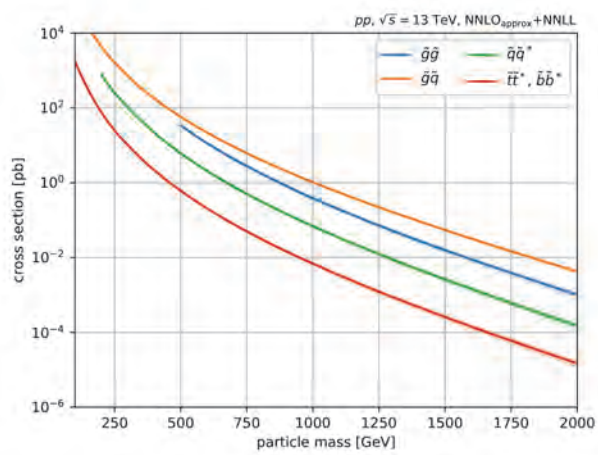

Figure 89.2: Cross sections for pair production of gluinos and squarks as a function of their mass at the LHC for a center-of-mass energy of 13 TeV. They are calculated at approximately next-to-next-to-LO (NNLO) including the resummation of soft gluon emission at the next-to-next-to-leading logarithmic accuracy (NNLO$_{\rm approx}$+NNLL).

In this section, we focus on results assuming R-parity conservation. Limits set by the Tevatron experiments on the gluino mass assume the framework of the CMSSM, with $\tan\beta = 5$ (CDF) or $\tan\beta = 3$ (D0). Furthermore, the common trilinear term A_0 is set to 0 and the higgsino mass term μ is assumed to be less than 0. The resulting lower mass limits are about 310 GeV for all squark masses, or 390 GeV for the case $m_{\tilde{q}} = m_{\tilde{g}}$ [73, 74]. These limits have been superseded by those provided by ATLAS and CMS, and the tightest constraints have been set with up to approximately

Downloaded from https://academic.oup.com/ptep/article/2022/8/083C01/6651666 by KIT Library user on 27 September 2022

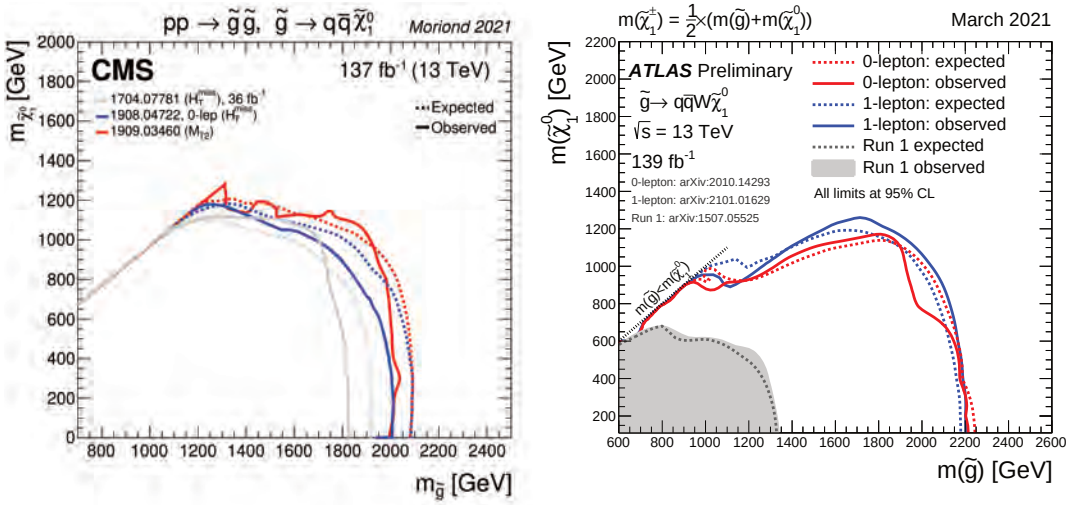

Figure 89.3: Lower mass limits, at 95% C.L., on gluino pair production for various decay chains in the framework of simplified models. Left: $\tilde{g} \to q\bar{q}\tilde{\chi}_1^0$, result of the CMS collaboration. Right: $\tilde{g} \to q\bar{q}W\tilde{\chi}_1^0$, result of the ATLAS collaboration.

140 fb^{-1} of data recorded at the LHC at a center-of-mass energy of 13 TeV.

ATLAS and CMS limits on the gluino mass have been established in the framework of simplified models. Assuming only gluino pair production, three main primary decay chains of the gluino have been considered by the LHC experiments for interpretations of their search results. The first decay chain, $\tilde{g} \to q\bar{q}\tilde{\chi}_1^0$, assumes gluino mediated production of first and second generation squarks (on-shell or off-shell) which leads to four light flavor quarks in the final state. Therefore, inclusive all-hadronic analyses searching for multijet plus $E_{\mathrm{T}}^{\mathrm{miss}}$ final states are utilized to put limits on this simplified model. These limits are derived as a function of the gluino and neutralino (LSP) mass. As shown in Fig. 89.3 (left)the CMS collaboration [75] excludes in this simplified model gluino masses below approximately 2.1 TeV for a light neutralino mass below about 600 GeV. In scenarios where neutralinos are not very light, the efficiency of the analyses is reduced by the fact that jets are less energetic, and there is less missing transverse momentum in the event. This leads to weaker limits when the mass difference $\Delta m = m_{\tilde{g}} - m_{\tilde{\chi}_1^0}$ is reduced. For example, for neutralino masses above about 1.2 TeV no limit on the gluino mass can be set for this decay chain. Therefore, limits on gluino masses are strongly affected by the assumption of the neutralino mass. Similar results for this simplified model have been obtained by ATLAS [76]. A second simplified model postulates a decay chain where $\tilde{g} \to q\bar{q}W\tilde{\chi}_1^0$, assuming that the intermediate (on-shell or off-shell) squark is left-handed and decays to a chargino and a quark, with the chargino decaying to a W boson and the LSP. This leads to two W bosons and four light flavor quarks plus $E_{\mathrm{T}}^{\mathrm{miss}}$ in the final state. Both leptonic and hadronic decays of the W can be considered. In this scenario, the ATLAS collaboration [77, 78] excludes gluino masses below approximately 2.2 TeV for a sufficiently light neutralino and assuming the chargino mass is halfway between the gluino and neutralino mass, see Fig. 89.3 (right). Again, for neutralino masses above about 1.2 TeV, there exists no limit on the gluino mass for this decay chain. Similar results have been obtained by the CMS collaboration [79].

Gluino decays are not limited to first and second generation squarks: another important decay chain of the gluino considered for interpretation in simplified models is $\tilde{g} \to b\bar{b}\tilde{\chi}_1^0$. In this case the decay is mediated via bottom squarks and thus leads to four jets from b quarks and $E_{\mathrm{T}}^{\mathrm{miss}}$ in the final state. For this topology as well, inclusive all-hadronic searches provide the highest sensitivity. However, with four b-quarks in the final state, the use of secondary vertex reconstruction for the identification of jets originating from b-quarks provides a powerful handle on the SM background. Therefore, in addition to a multijet plus $E_{\mathrm{T}}^{\mathrm{miss}}$ signature these searches also require several jets to be tagged as b-jets. As shown in Fig. 89.4 (left), for this simplified model CMS [75] excludes gluino masses below ≈ 2.3 TeV for a sufficiently light neutralino, while for neutralino masses above ≈ 1.5 TeV no limit on the gluino mass can be set. Comparable limits for this simplified model are provided by searches from ATLAS [80].

If kinematically allowed, decays of gluinos to top squarks via $\tilde{g} \to \tilde{t}t$ are also possible. This leads to a "four tops" final state, $tttt\tilde{\chi}_1^0\tilde{\chi}_1^0$, and defines the next important simplified model characterizing gluino pair production, $\tilde{g} \to t\bar{t}\tilde{\chi}_1^0$, . The topology of this decay is very rich in different experimental signatures: as many as four isolated leptons, four b-jets, several light flavor quark jets, and significant missing transverse momentum from the neutrinos in the W decay and from the two neutralinos. As shown in Fig. 89.4 (right), the ATLAS search [80] rules out gluinos with masses below ≈ 2.25 TeV for light neutralinos in this model. For neutralino masses above ≈ 1.2 TeV, no limit can be placed on the gluino mass. The CMS multiple b-jet search [81] obtains similar limits.

Assuming gluinos to be heavier than squarks, squarks will predominantly decay to a quark and a neutralino or chargino, if kinematically allowed. The decay may involve the lightest neutralino (typically the LSP) or chargino, but, depending on the masses and couplings of the gauginos and on the handedness of the squarks, may involve heavier neutralinos or charginos. For pair production of first and second generation squarks, the simplest decay modes involve two jets and missing transverse momentum, with potential extra jets stemming from initial state or final state radiation (ISR/FSR) or from decay modes with longer decay chains (cascades). In cascades, isolated photons or leptons may appear from the decays of sparticles such as neutralinos or charginos. Final states are thus characterized by significant missing transverse momentum, and at least two, and possibly many more high p_{T} jets, which can be accompanied by one or more isolated objects like photons or leptons, including τ leptons, in the final state.

Limits on first and second generation squark masses set by the Tevatron experiments assume the CMSSM, and amount to lower limits of about 380 GeV for all gluino masses, or 390 GeV for the case $m_{\tilde{q}} = m_{\tilde{g}}$ [73, 74].

At the LHC, limits on squark masses have been set using up to approximately 140 fb^{-1} of data at 13 TeV. Interpretations in simplified models typically characterize squark pair production with only one decay chain of $\tilde{q} \to q\tilde{\chi}_1^0$. Here it is assumed that the left and right-handed $\tilde{u}$, $\tilde{d}$, $\tilde{s}$ and $\tilde{c}$ squarks are degenerate in mass. Furthermore, it is assumed that the mass of the gluino is very high and thus contributions of the corresponding t-channel diagrams to squark pair production are negligible. Therefore, the total production cross section for this simplified model is eight

Downloaded from https://academic.oup.com/ptep/article/2022/8/083C01/6651666 by KIT Library user on 27 September 2022

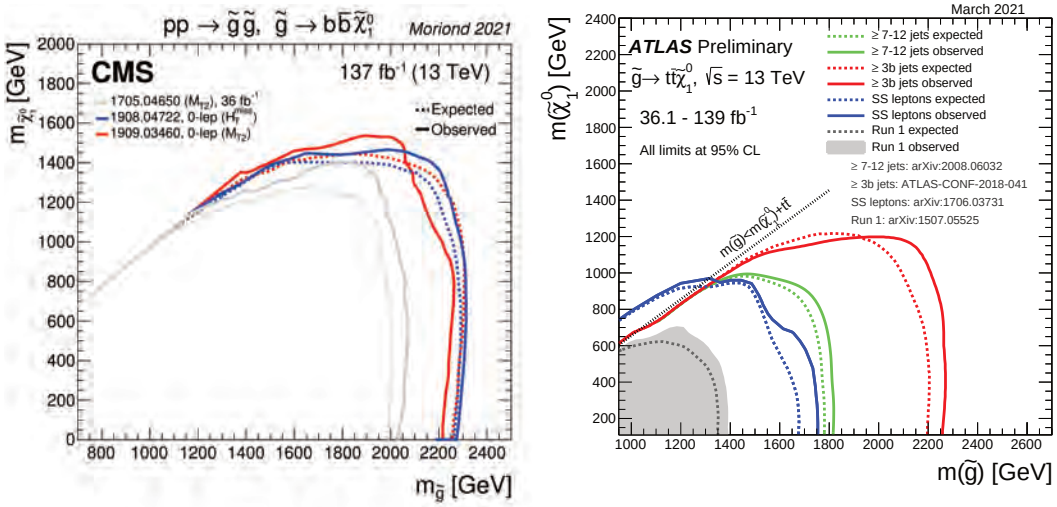

Figure 89.4: Lower mass limits, at 95% C.L., on gluino pair production for various decay chains in the framework of simplified models. Left: $\tilde{g} \to b\bar{b}\tilde{\chi}_1^0$. Right: $\tilde{g} \to t\bar{t}\tilde{\chi}_1^0$. Results from the CMS and ATLAS collaborations.

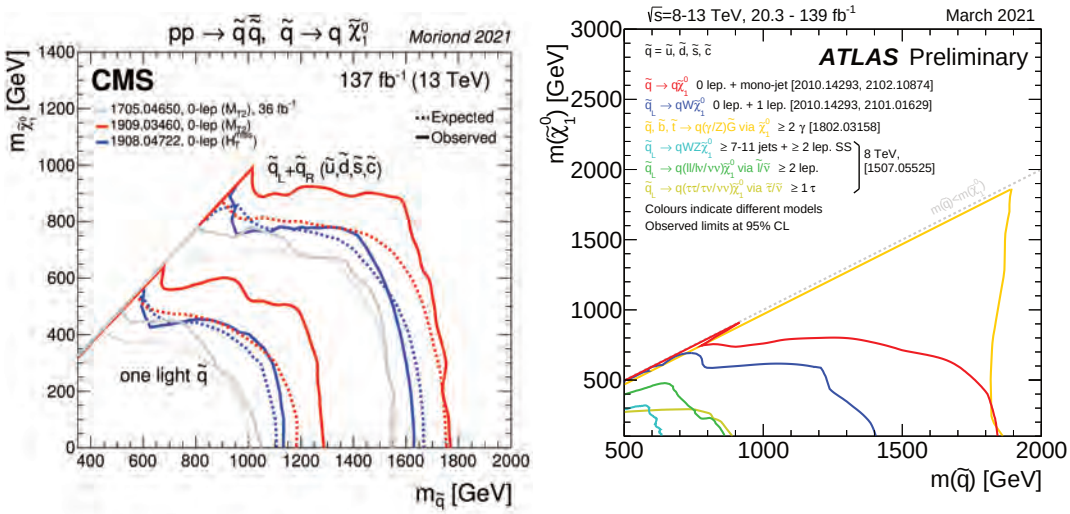

Figure 89.5: Left: 95% C.L. exclusion contours in the framework of simplified models assuming a single decay chain of $\tilde{q} \to q\tilde{\chi}_1^0$, obtained by the CMS collaboration. Right: Assuming more complicated decay chains including W or Z bosons, obtained by the ATLAS collaboration.

times the production cross section of an individual squark (e.g. $\tilde{u}_L$). Under these assumptions, CMS obtains a lower squark mass limit of ≈ 1.75 TeV for light neutralinos [81], as shown in Fig. 89.5 (left). The effects of heavy neutralinos on squark limits are similar to those discussed in the gluino case, and only for neutralino masses below ≈ 800 GeV can any squark masses be excluded. Searches for new physics in monojet channels are sensitive to very compressed scenarios, and masses up to 900 GeV are excluded for $\Delta m = m_{\tilde{q}}, m_{\tilde{\chi}_1^0} \approx 5$ GeV [82].

If the assumption of mass degenerate first and second generation squarks is dropped and only the production of a single light squark is assumed, the limits weaken significantly. For example, the CMS limit on degenerate squarks of 1750 GeV for light neutralinos drops to ≈ 1300 GeV for pair production of a single light squark, and for neutralinos heavier than ≈ 600 GeV no squark mass limit can be placed. It should be noted that this limit is not a result of a simple scaling of the above mentioned mass limits assuming eight-fold mass degeneracy but it also takes into account that for an eight times lower production cross section the analyses must probe kinematic regions of phase space that are closer to the ones of SM background production.

The results of the ATLAS searches for more complicated decay chains, where e.g. intermediate bosons are produced as well [76], can be seen in Fig. 89.5 (right). Depending on the topology, the exclusion limit can reach up to ≈ 2 TeV (this value is only reached in gaugino-mediated simplified models).

For single light squarks ATLAS also reports results of a dedicated search for pair production of scalar partners of charm quarks [83]. Assuming that the scalar-charm state exclusively decays into a charm quark and a neutralino, scalar-charm masses up to 800 GeV are excluded for neutralino masses below 260 GeV.

A summary of the most important squark and gluino mass limits for different interpretation approaches assuming R-parity conservation is shown in Table 89.1. For gluino masses rather similar limits of about 2.3 TeV are obtained from different model assumptions, indicating that the LHC is indeed probing direct gluino production at the TeV scale and beyond. However, for neutralino masses above approximately 1.2 to 1.5 TeV, even in the best case scenarios, ATLAS and CMS searches do not place any limits on the gluino mass. Limits on direct squark production, on the other hand, depend strongly on the chosen model. For neutralino masses above ≈ 600 GeV no limits on any direct squark pair production scenario are placed by the LHC.

Downloaded from https://academic.oup.com/ptep/article/2022/8/083C01/6651666 by KIT Library user on 27 September 2022

Table 89.1: Summary of squark mass and gluino mass limits using different interpretation approaches assuming R-parity conservation. Masses in this table are provided in GeV. Further details about the assumptions and analyses from which these limits are obtained are discussed in the corresponding sections of the text.

Model	Assumption	$m_{\tilde{q}}$	$m_{\tilde{g}}$
Simplified models $\tilde{g}\tilde{g}$			
$\tilde{g} \to q\bar{q}\tilde{\chi}_1^0$	$m_{\tilde{\chi}_1^0} = 0$	-	≈ 2300
	$m_{\tilde{\chi}_1^0} > \approx 1200$	-	no limit
$\tilde{g} \to b\bar{b}\tilde{\chi}_1^0$	$m_{\tilde{\chi}_1^0} = 0$	-	≈ 2300
	$m_{\tilde{\chi}_1^0} > \approx 1500$	-	no limit
$\tilde{g} \to t\bar{t}\tilde{\chi}_1^0$	$m_{\tilde{\chi}_1^0} = 0$	-	≈ 2250
	$m_{\tilde{\chi}_1^0} > \approx 1300$	-	no limit
Simplified models $\tilde{q}\tilde{q}$			
$\tilde{q} \to q\tilde{\chi}_1^0$	$m_{\tilde{\chi}_1^0} = 0$	≈ 1900	-
	$m_{\tilde{\chi}_1^0} > \approx 800$	no limit	-
$\tilde{u}_L \to q\tilde{\chi}_1^0$	$m_{\tilde{\chi}_1^0} = 0$	≈ 1300	-
	$m_{\tilde{\chi}_1^0} > \approx 600$	no limit	-

89.6 Exclusion limits on bottom and top squarks masses in RPC scenarios

Besides placing stringent limits on first and second generation squark masses, the LHC experiments also search for the production of third generation squarks. SUSY at the TeV-scale is often motivated by naturalness arguments, most notably as a solution to cancel quadratic divergences in radiative corrections to the Higgs boson mass. In this context, the most relevant terms for SUSY phenomenology arise from the interplay between the masses of the third generation squarks and the Yukawa coupling of the top quark to the Higgs boson. This motivates a potential constraint on the masses of the top squarks and the left-handed bottom squark. Due to the large top quark mass, significant mixing between $\tilde{t}_{\rm L}$ and $\tilde{t}_{\rm R}$ is expected, leading to a lighter mass state $\tilde{t}_1$ and a heavier mass state $\tilde{t}_2$. In the MSSM, the lightest top squark ($\tilde{t}_1$) can be the lightest squark.

Bottom squarks are expected to decay predominantly to $b\tilde{\chi}_1^0$ giving rise to the characteristic multi b-jet and $E_{\rm T}^{\rm miss}$ signature. Direct production of bottom squark pairs has been searched for at the Tevatron and at the LHC. Limits from the Tevatron are $m_{\tilde{b}} > 247$ GeV for a massless neutralino [84, 85]. The LHC experiments have surpassed these limits and are well above 1 TeV, and the latest results, shown in Fig. 89.6 (left), are based on up to 140 fb^{-1} of data collected at $\sqrt{s} = 13$ TeV. ATLAS has set a lower limit of $m_{\tilde{b}} > 1250$ GeV for massless neutralinos in this model [86] exploiting the two b-jets and missing transverse momentum analysis. For $m_{\tilde{\chi}_1^0} \approx 800$ GeV or higher no limit can be placed on direct bottom squark pair production in this simplified model. Limits from CMS are comparable [81]. Reinterpretations of the monojet analysis results can be used to constrain very compressed scenarios, with exclusion of masses up to 550 GeV in case of $\Delta m = m_{\tilde{b}} - m_{\tilde{\chi}_1^0} \approx 5$ GeV [82]. Further bottom squark decay modes have also been searched for by ATLAS [87–89] and CMS [75,90,91], for instance targeting more complex decay chains that include Higgs bosons in the cascade.

The top squark decay modes depend on the SUSY mass spectrum, and on the $\tilde{t}_{\rm L}$-$\tilde{t}_{\rm R}$ mixture of the top squark mass eigenstate. If kinematically allowed, the two-body decays $\tilde{t} \to t\tilde{\chi}_1^0$ (which requires $m_{\tilde{t}} - m_{\tilde{\chi}_1^0} > m_t$) and $\tilde{t} \to b\tilde{\chi}^{\pm}$ (which requires $m_{\tilde{t}} - m_{\tilde{\chi}^{\pm}} > m_b$) are expected to dominate. If not, the top squark decay may proceed either via the two-body decay $\tilde{t} \to c\tilde{\chi}_1^0$ or through $\tilde{t} \to bf\bar{f}'\tilde{\chi}_1^0$ (where f and $\bar{f}'$ denote a fermion-antifermion pair with appropriate quantum numbers). For $m_{\tilde{t}} - m_{\tilde{\chi}_1^0} > m_b$ the latter decay chain represents a four-body decay with a W boson, charged Higgs H, slepton $\tilde{\ell}$, or light flavor squark $\tilde{q}$, exchange. If the exchanged W boson and/or sleptons are kinematically allowed to be on-shell, the three-body decays $\tilde{t} \to Wb\tilde{\chi}_1^0$ and/or $\tilde{t} \to b\nu\tilde{\ell}(\tilde{\nu}\ell)$ will become dominant. For further discussion on top squark decays see for example Ref. [92].

Limits from LEP on the $\tilde{t}_1$ mass are $m_{\tilde{t}} > 96$ GeV in the charm plus neutralino final state, and > 93 GeV in the lepton, b-quark and sneutrino final state [71].

The Tevatron experiments have performed a number of searches for top squarks, often assuming direct pair production. In the $b\ell\tilde{\nu}$ decay channel, and assuming a 100% branching fraction, limits are set as $m_{\tilde{t}} > 210$ GeV for $m_{\tilde{\nu}} < 110$ GeV and $m_{\tilde{t}} - m_{\tilde{\nu}} > 30$ GeV, or $m_{\tilde{t}} > 235$ GeV for $m_{\tilde{\nu}} < 50$ GeV [93, 94]. In the $\tilde{t} \to c\tilde{\chi}_1^0$ decay mode, a top squark with a mass below 180 GeV is excluded for a neutralino lighter than 95 GeV [95, 96]. In both analyses, no limits on the top squark can be set for heavy sneutrinos or neutralinos. In the $\tilde{t} \to b\tilde{\chi}_1^{\pm}$ decay channel, searches for a relatively light top squark have been performed in the dilepton final state [97, 98]. The CDF experiment sets limits in the $\tilde{t} - \tilde{\chi}_1^0$ mass plane for various branching fractions of the chargino decay to leptons and for two values of $m_{\tilde{\chi}_1^{\pm}}$. For $m_{\tilde{\chi}_1^{\pm}} = 105.8$ GeV and $m_{\tilde{\chi}_1^0} = 47.6$ GeV, top squarks between 128 and 135 GeV are excluded for W-like leptonic branching fractions of the chargino.

The LHC experiments have improved these limits substantially. As shown in the right plot of Fig. 89.6, limits on the top squark mass assuming a simplified model with a single decay chain of $\tilde{t} \to t\tilde{\chi}_1^0$ now surpass 1 TeV. The most important searches for this top squark decay topology are dedicated searches requiring zero or one isolated lepton, modest $E_{\rm T}^{\rm miss}$, and four or more jets out of which at least one jet must be reconstructed as a b-jet [50,75,81,99–101]. For example, using an all-hadronic analysis, CMS excludes top squarks with masses below about 1300 GeV in this model for light neutralinos, while for $m_{\tilde{\chi}_1^0} > 700$ GeV no limits can be provided [101]. Similar constraints are set by the ATLAS all-hadronic search [99].

Assuming that the top squark decay exclusively proceeds via the chargino mediated decay chain $\tilde{t} \to b\tilde{\chi}_1^{\pm}$, $\tilde{\chi}_1^{\pm} \to W^{\pm(*)}\tilde{\chi}_1^0$ yields stop mass exclusion limits that vary strongly with the assumptions made on the $\tilde{t} - \tilde{\chi}_1^{\pm} - \tilde{\chi}_1^0$ mass hierarchy. For example, for $m_{\tilde{\chi}_1^{\pm}} = (m_{\tilde{t}} + m_{\tilde{\chi}_1^0})/2$, a stop mass below ≈ 1150 GeV for a light $\tilde{\chi}_1^0$ is excluded by CMS, while no limit can be placed for $m_{\tilde{\chi}_1^0} > 550$ GeV [50]. These limits, however, can weaken significantly when other assumptions about the mass hierarchy or the decay of the charginos are imposed [50, 102–104].

Other analyses with zero, one or two leptons target this kinematic region [105–111], also providing sensitivity in the case of alternative decay modes of the top squark, *i.e.* including tau sleptons [104,112,113] or Higgs and Z bosons in the decay chain [114].

If the decays $\tilde{t} \to t\tilde{\chi}_1^0$ and $\tilde{t} \to b\tilde{\chi}_1^{\pm}$, $\tilde{\chi}_1^{\pm} \to W^{\pm(*)}\tilde{\chi}_1^0$ are kinematically forbidden, the decay chains $\tilde{t} \to Wb\tilde{\chi}_1^0$ and $\tilde{t} \to c\tilde{\chi}_1^0$ can become important. The one-lepton ATLAS search provides for the kinematic region $m_{\tilde{t}} - m_{\tilde{\chi}^{\pm}} > m_b + m_W$ lower limits on the top squark mass of ≈ 700 GeV for a neutralino lighter than ≈ 570 GeV [100]. For the kinematic region in which even the production of real W bosons is not allowed, ATLAS and CMS improve the Tevatron limit on $\tilde{t} \to c\tilde{\chi}_1^0$ substantially. Based on a monojet analysis [82] ATLAS excludes top squark masses below $m_{\tilde{\chi}_1^0} \approx 550$ GeV along the kinematic boundary for the $\tilde{t} \to c\tilde{\chi}_1^0$ decay. The ATLAS monojet analysis also places similar boundaries for the other decay chain relevant in this phase region, $\tilde{t} \to bf\bar{f}'\tilde{\chi}_1^0$. Other analyses, such as the search in events with one leptons and jets, are also sensitive to this decay mode: the ATLAS one-lepton analysis excludes up to ≈ 650 GeV for $\Delta m = m_{\tilde{t}}, m_{\tilde{\chi}_1^0} \approx 50$ GeV [100]. The CMS collaboration uses the hadronic searches [101, 106, 108] to place constraints on stop decay into charm-quark and excludes $m_{\tilde{t}} \approx 630$ GeV for $\Delta m = m_{\tilde{t}}, m_{\tilde{\chi}_1^0} \approx 50$ GeV [101]. The same constraints are set in case of $\tilde{t} \to bf\bar{f}'\tilde{\chi}_1^0$, with CMS excluding $m_{\tilde{t}} \approx 640$ GeV for

Downloaded from https://academic.oup.com/ptep/article/2022/8/083C01/6651666 by KIT Library user on 27 September 2022

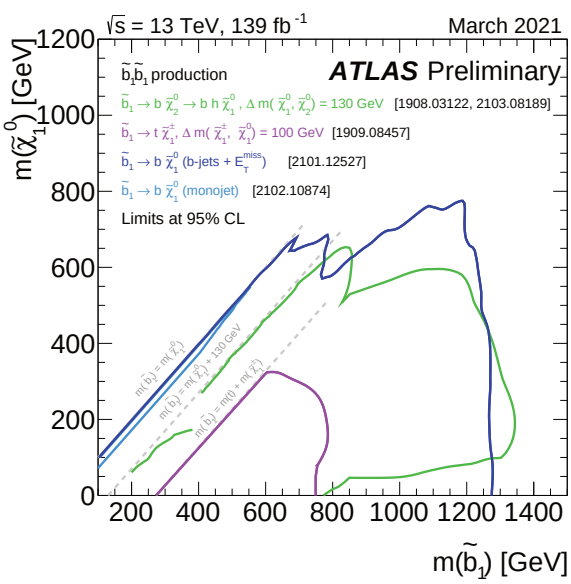

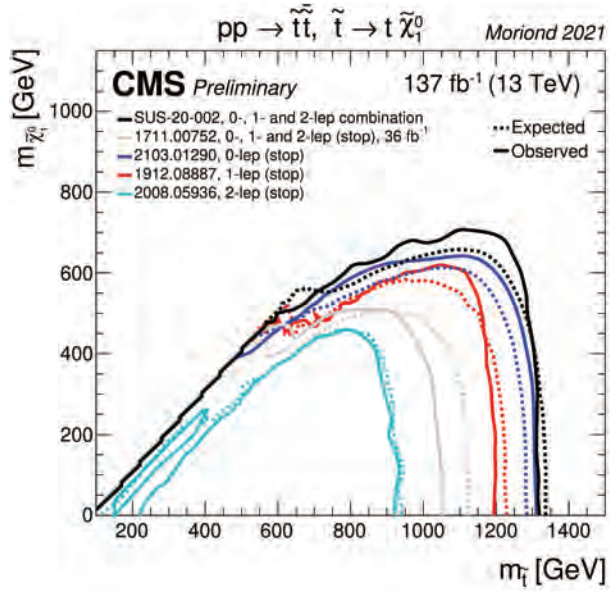

Figure 89.6: Left: A summary of the 95% C.L. exclusion contours in the sbottom-neutralino mass plane for various possible decay chains as obtained in dedicated analyses by ATLAS. Right: The 95% C.L. exclusion contours in the stop-neutralino mass plane defined in the framework of a simplified model assuming a single decay chain of $\tilde{t} \to t\tilde{\chi}_1^0$ as obtained by CMS.

$\Delta m = m_{\tilde{t}}, m_{\tilde{\chi}_1^0} \approx 50$ GeV [101].

Table 89.2: Summary of bottom and top squark mass limits using different interpretation approaches assuming R-parity conservation. Masses in this table are provided in GeV. Further details about the assumptions and analyses from which these limits are obtained are discussed in the corresponding sections of the text.

Model	Assumption	$m_{\tilde{q}}$
$\tilde{b} \to b\tilde{\chi}_1^0$	$m_{\tilde{\chi}_1^0} = 0$	≈ 1250
	$m_{\tilde{\chi}_1^0} > \approx 700$	no limit
$\tilde{t} \to t\tilde{\chi}_1^0$	$m_{\tilde{\chi}_1^0} = 0$	≈ 1300
	$m_{\tilde{\chi}_1^0} > \approx 600$	no limit
$\tilde{t} \to b\tilde{\chi}_1^\pm$	$m_{\tilde{\chi}_1^0} = 0$	≈ 1150
$(m_{\tilde{\chi}_1^\pm} = (m_{\tilde{t}} - m_{\tilde{\chi}_1^0})/2)$	$m_{\tilde{\chi}_1^0} > \approx 550$	no limit
$\tilde{t} \to Wb\tilde{\chi}_1^0$	$m_{\tilde{\chi}_1^0} < \approx 570$	≈ 700
$(m_W < m_{\tilde{t}} - m_{\tilde{\chi}^0} < m_t)$		
$\tilde{t} \to c\tilde{\chi}_1^0$	$m_{\tilde{t}} - m_{\tilde{\chi}_1^0} \approx 50$	≈ 630
	$m_{\tilde{t}} \approx m_{\tilde{\chi}_1^0}$	≈ 550
$\tilde{t} \to bff'\tilde{\chi}_1^0$	$m_{\tilde{t}} - m_{\tilde{\chi}_1^0} \approx 50$	≈ 650
	$m_{\tilde{t}} \approx m_{\tilde{\chi}_1^0}$	≈ 550
$(m_{\tilde{t}} - m_{\tilde{\chi}^0} < m_W)$		

In general, the variety of top squark decay chains in the phase space region where $\tilde{t} \to t\tilde{\chi}_1^0$ is kinematically forbidden represents a challenge for the experimental search program but more data and refined analyses in Run 2 have further improved the sensitivity in this difficult but important region of SUSY parameter space, and more is expected for future Runs of the LHC. It is also worth mentioning that precision SM measurements can provide important insights to such challenging regions. For instance, analyses of $t\bar{t}$ spin correlations can be used to set constraints on top squark masses close to the top-quark mass. ATLAS [115] excludes the mass region between 150 and 230 GeV for kinematically allowed values of the neutralino mass. CMS [116] results cover a similar mass range.

It should be noted that limits discussed in this section belong to different top and bottom squark decay channels, different sparticle mass hierarchies, and different simplified decay scenarios. Therefore, care must be taken when interpreting these limits in the context of more complete SUSY models.

89.7 Exclusion limits on squarks and gluinos in RPV scenarios

RPV gluino and squark decays are searched for in a number of final states, generally characterised by the presence of multiple leptons or jets and moderated or no missing transverse momentum. If the couplings are very small, sparticles might be long-lived and dedicated searches for non-prompt decays are reported in Section 89.10.

Searches in multilepton final states [117–121] set lower mass limits of 1 to 1.4 TeV, depending on neutralino mass and lepton flavor, on decays mediated by λ and λ' couplings, assuming prompt decays. Multijet final states have been used to search for fully hadronic gluino decays involving λ'' couplings, by CDF [122], ATLAS [88,123–126] and CMS [127–129]. Lower gluino mass limits range between 600 and 2000 GeV depending on neutralino mass and flavor content of the final state. More recently, ATLAS [130] searched in events characterised by high jet multiplicity, at least one isolated light lepton and either zero or at least three b-tagged jets, reaching as high as 2.4 TeV in gluino mass.

RPV production of single squarks via a λ'-type coupling has been studied at HERA. In such models, a lower limit on the squark mass of the order of 275 GeV has been set for electromagnetic-strength-like couplings $\lambda' = 0.3$ [131]. At the LHC, prompt [118, 121,132] R-parity violating squark decays have been searched for with mass limits are very model-dependent.

Dedicated searches for RPV top squarks (at production and/or in decays) have been carried out in the past decades. Production of single top squarks has been searched for at LEP, HERA, and the Tevatron. For example, an analysis from the ZEUS collaboration [133] makes an interpretation of its search result assuming top squarks to be produced via a λ' coupling and decay either to $b\tilde{\chi}_1^\pm$ or R-parity-violating to a lepton and a jet. Limits are set on λ'_{131} as a function of the top squark mass in an MSSM framework with gaugino mass unification at the GUT scale. The search for top squark pair production in the context of RPV supersymmetry has now also become a focus point for searches at the LHC. CMS and ATLAS have performed several searches for top squarks using a variety of multilepton and/or multijet final states and Run 2 data. The λ'-mediated top squark decay $\tilde{t} \to b\ell$ has been studied

Downloaded from https://academic.oup.com/ptep/article/2022/8/083C01/6651666 by KIT Library user on 27 September 2022

by ATLAS for prompt decays [134], and by ATLAS and CMS for non-prompt decays [135–137], setting limits up to $1.4 - 1.6$ TeV in simplified models for this mode. CMS also searched for the λ'-mediated decay $\tilde{t} \to b\ell qq$, setting lower stop mass limits of 890 GeV (e) or 1000 GeV (μ) [138]. The fully hadronic R-parity violating top squark decays $\tilde{t} \to bs$, $\tilde{t} \to ds$, and $\tilde{t} \to bd$, involving λ'', have been searched for by ATLAS [118, 124, 139–141], and CMS [142,143]. Other recent searches target top squarks decaying through cascades into several $b-$ and light-quarks, for example as in [144]. The most recent results set lower top squark mass limits up to 1.35 TeV in top-squark mass [130] if decays include top- and b-quarks [130] lower top squark mass limits are up to 1.35 TeV in top-squark mass. Constraints on masses up to 670 GeV are found if top squarks decays include top- and light-quarks [145].

RPV signatures are often similar to signatures of Stealth SUSY [146–148]. In these scenarios, squarks can decay to a quark and a chargino (neutralino), which can subsequently decay to a singlino $\tilde{S}$ and a $W^{\pm}$ (photon), with the $\tilde{S}$ decaying to two gluons and a soft gravitino $\tilde{G}$. A dedicated CMS search [149] excludes squark masses up to 1.05 TeV in the photon channel and up to 550 GeV in the charged lepton channel. Limits have also been placed on top squarks in stealth SUSY scenarios, where the top squark decays to a top quark, a gluon and a $\tilde{S}$, and the $\tilde{S}$ subsequently decays to a $\tilde{G}$ and two gluons. In such a scenario, top squark masses up to 870 GeV have been excluded [145].

89.8 Exclusion limits on the masses of charginos, neutralinos and sleptons in RPC scenarios

Charginos, neutralinos and sleptons are produced through electroweak interactions and their cross sections depend on the assumptions made for mass and mixing parameters.

Charginos and neutralinos carry no color charge and the mixing of the charged wino and higgsino states (for charginos), and the neutral bino, wino and higgsino states (for neutralinos), is determined by a limited number of parameters. For charginos these are the wino mass parameter M_2, the higgsino mass parameter μ, and $\tan\beta$, and for neutralinos these are the same parameters plus the bino mass parameter M_1. If one of the parameters M_1, M_2 or μ is substantially smaller than the others, the chargino/neutralino composition would be dominated by specific states, which are referred to as bino-like ($M_1 \ll M_2, \mu$), wino-like ($M_2 \ll M_1, \mu$), or higgsino-like ($\mu \ll M_1, M_2$). If gaugino mass unification at the GUT scale is assumed, a relation between M_1 and M_2 at the electroweak scale follows: $M_1 = 5/3 \tan^2\theta_W M_2 \approx 0.5 M_2$, with θ_W the weak mixing angle. The largest production rates at hadron machines are obtained when the LSP is bino-like and the lightest chargino and next-to-lightest neutralino are wino-like, forming an approximately mass degenerate SU(2) triplet. If the higgsino mass is much smaller than the gaugino masses, the two lightest neutralinos and the lightest chargino form an approximately mass degenerate Dirac SU(2) doublet, production rates are lower and the mass spectrum is compressed.

In models with slepton and gaugino mass unification at the GUT scale, the superpartner of the right-handed lepton, $\tilde{\ell}_{\rm R}$, is expected to be lighter than the left-handed one, $\tilde{\ell}_{\rm L}$. Cross sections depend on the L-R mixing which in turn depends on the mass of the fermion and other parameters. For tau sleptons there may be considerable mixing between the L and R states, leading to a significant mass difference between the lighter $\tilde{\tau}_1$ and the heavier $\tilde{\tau}_2$.

Fig. 89.7 [150, 151] (see also Ref. [72] for further details) shows typical production cross sections at hadron colliders for electroweakinos under various assumptions. For masses of several hundreds of GeV, they are at least two orders of magnitude smaller than for colored SUSY particles. Thanks to the large data samples collected at the LHC, the sensitivity of LEP and Tevatron searches for direct chargino/neutralino or slepton production has been surpassed in several regions of SUSY parameter space.

89.8.1 *Exclusion limits on chargino masses*

The lightest chargino $\tilde{\chi}_1^{\pm}$ is searched for either considering pair production, or through associated production of $\tilde{\chi}_1^{\pm}$ and the next-to-lightest neutralino, $\tilde{\chi}_2^0$, if they are assumed to be degenerate

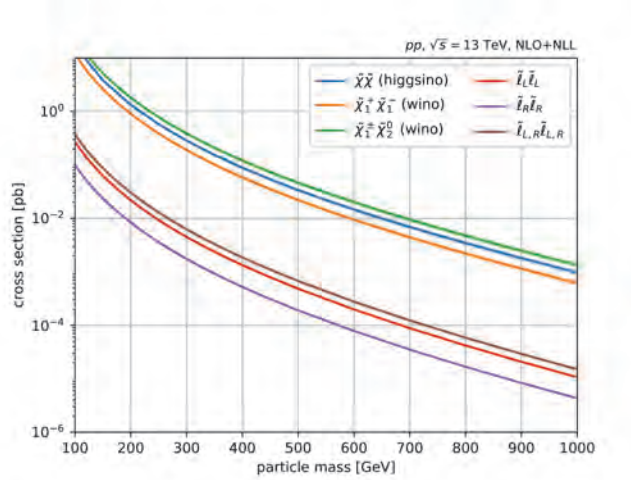

Figure 89.7: Cross sections for pair production of charginos, neutralinos and sleptons calculated for 13 TeV centre-of-mass energy at NLO plus next-to-leading-log (NLL) precision. Wino-like $\tilde{\chi}_1^{\pm}\tilde{\chi}_2^0$ and $\tilde{\chi}_1^{+}\tilde{\chi}_1^{-}$ productions are calculated in a limit of mass-degenerate $\tilde{\chi}_1^{\pm}$ and $\tilde{\chi}_2^0$, light bino $\tilde{\chi}_1^0$, and with all the other sparticles assumed to be heavy and decoupled. Higgsino-like cross sections assume mass-degenerate $\tilde{\chi}_1^{\pm}$, $\tilde{\chi}_2^0$ and $\tilde{\chi}_1^0$. For slepton pair cross sections, left(right)-handed only or 50% mixed states are considered.

in mass. If kinematically allowed, two body decay modes such as $\tilde{\chi}^{\pm} \to \tilde{f}\bar{f}'$ (including $\ell\tilde{\nu}$ and $\tilde{\ell}\nu$) are dominant. If not, three body decays $\tilde{\chi}^{\pm} \to f\bar{f}'\tilde{\chi}_1^0$, mediated through virtual W bosons or sfermions, become dominant. If sfermions are heavy, the W mediation dominates, and $f\bar{f}'$ are distributed with branching fractions similar to W decay products (barring phase space effects for small mass gaps between $\tilde{\chi}^{\pm}$ and $\tilde{\chi}^0$). If, on the other hand, sleptons are light enough to play a significant role in the decay, leptonic final states will be enhanced.

At LEP, $\tilde{\chi}_1^{+}\tilde{\chi}_1^{-}$ is the dominant production process. Charginos have been searched for in fully-hadronic, semi-leptonic and fully leptonic decay modes [152, 153]. A general lower limit on the lightest chargino mass of 103.5 GeV is derived, except in corners of phase space with low electron sneutrino mass, where destructive interference in chargino production, or two-body decay modes, play a role. The limit is also affected if the mass difference between $\tilde{\chi}_1^{\pm}$ and $\tilde{\chi}_1^0$ is small; dedicated searches for such scenarios set a lower limit of 92 GeV.

At the Tevatron, charginos have been searched for via associated production of $\tilde{\chi}_1^{\pm}\tilde{\chi}_2^0$ [154, 155]. Decay modes involving multilepton final states provide the best discrimination against the large multijet background. Analyses have looked for at least three charged isolated leptons, for two leptons with missing transverse momentum, or for two leptons with the same charge. Depending on the $(\tilde{\chi}_1^{\pm} - \tilde{\chi}_1^0)$ and/or $(\tilde{\chi}_2^0 - \tilde{\chi}_1^0)$ mass differences, leptons may have soft transverse momentum.

At the LHC, the search strategy is similar to that at the Tevatron but it also exploits the large datasets collected to target missing momentum and fully-hadronic final states and consider $\tilde{\chi}_1^{+}\tilde{\chi}_1^{-}$ production only i.e. releasing the assumption of $\tilde{\chi}_1^{\pm}, \tilde{\chi}_2^0$ mass degeneracy. Furthermore, compressed SUSY spectra are searched for considering low-momentum leptons recoiling against an ISR jet.

Chargino pair production is searched for in the dilepton plus missing momentum final state. In a simplified model interpretation of the results where only the $\tilde{\chi}_1^{+}\tilde{\chi}_1^{-}$ process is considered and assuming mediation of the chargino decay by light sleptons ($\tilde{e}$ and $\tilde{\mu}$), ATLAS [156] and CMS [157] set limits on the chargino mass up to 1 TeV for massless LSPs, but no limits on the chargino mass can be set for $\tilde{\chi}_1^0$ heavier than 480 GeV. Limits are fairly

Downloaded from https://academic.oup.com/ptep/article/2022/8/083C01/6651666 by KIT Library user on 27 September 2022

robust against variation of the slepton mass, unless the mass gap between sparticles becomes small enough that the charged lepton has a too low-momentum to be reconstructed. For decays mediated through $\tilde{\tau}$ or $\tilde{\nu}_\tau$, limits of 630 GeV are set by ATLAS [158] for LSPs not heavier than 200 GeV. The CMS experiment provides similar limits [159].

In case slepton masses are higher than the mass of the chargino, searches are performed for charginos decaying via a W boson. ATLAS sets limits on this kind of simplified models [156] for pure-wino charginos: masses below 420 GeV are excluded for massless LSPs, but no limits are set for LSPs heavier than 120 GeV. Further extension of the sensitivity in the high-mass region is achieved by ATLAS [160] and CMS [161] exploiting the large branching ratio of fully-hadronic final states and the identification of boosted W bosons through large-radius jets and jet substructure information. Considering only wino-like chargino pair production in case of a massless LSP, ATLAS excludes a region between 630 GeV and 760 GeV, while CMS excludes between 290 GeV and 670 GeV. No limits are set for LSP masses above 200 GeV.

Several final states characterised by the presence of missing transverse momentum are studied to set limits on the chargino mass through $\tilde{\chi}_1^\pm\tilde{\chi}_2^0$ associated production. Usually, wino-like $\tilde{\chi}_1^\pm$ and $\tilde{\chi}_2^0$ and bino-like $\tilde{\chi}_1^0$ are assumed with $m_{\tilde{\chi}_1^\pm} = m_{\tilde{\chi}_2^0}$, leaving $m_{\tilde{\chi}_1^\pm}$ and $m_{\tilde{\chi}_1^0}$ free. Again, the branching fraction of leptonic final states is determined by the slepton masses. If the decay is predominantly mediated by a light $\tilde{\ell}_\mathrm{L}$, i.e. $\tilde{\ell}_\mathrm{R}$ is assumed to be heavy, the three charged-lepton flavors will be produced in equal amounts, and a multi-lepton signature is favored. It is assumed that $\tilde{\ell}_\mathrm{L}$ and sneutrino masses are equal, and diagrams with sneutrinos are included. In this scenario, ATLAS [162] and CMS [163] exclude chargino masses below 1450 GeV for massless LSPs; no limits are set for LSP masses above 1 TeV. If the decay is dominated by a light $\tilde{\ell}_\mathrm{R}$, the chargino cannot be a pure wino but needs to have a large higgsino component, preferring the decays to tau leptons. Limits are set in various scenarios. If, like for $\tilde{\ell}_\mathrm{L}$, a flavor-democratic scenario is assumed (τ-enriched scenario), CMS sets limits of 1150 GeV on the chargino mass for massless LSPs, but under the assumption that both $\tilde{\chi}_1^\pm$ and $\tilde{\chi}_2^0$ decay leads to tau leptons in the final state (τ-dominated scenario), the chargino mass limit deteriorates to 970 GeV for massless LSPs [163]. ATLAS assumes a simplified model in which staus are significantly lighter than the other sleptons in order to search for a similar multi-tau final state, and sets a lower limit on the chargino mass of 760 GeV in this model [158].

If sleptons are heavy, the chargino is assumed to decay to a W boson plus LSP, and the $\tilde{\chi}_2^0$ into Z plus LSP or H plus LSP. Searches for the WZ channel exploit events with either two same-sign leptons or three leptons, or with no leptons (all-hadronic). ATLAS searches in events with three leptons and missing momentum and wino-like chargino masses below 640 GeV are excluded for massless LSPs [164]. Limits are reduced in case of higgsino-like scenarios, with exclusion down to 210 GeV. Searches exploiting all-hadronic final states where boosted, fully-hadronically decaying W, Z and Higgs boson candidates are identified using dedicated algorithm are carried out by ATLAS [160] and CMS [161]. ATLAS excludes wino-like $\tilde{\chi}_2^0$ and $\tilde{\chi}_1^\pm$ masses between 440 GeV and 960 GeV for an LSP mass below 300 GeV. Similar constraints are obtained by CMS.

Interpretations are also provided in a scenario where the $\tilde{\chi}_2^0$ does not decay exclusively into Z plus LSP. CMS [163] excludes chargino masses below 650 GeV for massless LSPs, using events with two leptons of the same sign, or with three or more leptons. No constraints are set for $\tilde{\chi}_1^0$ masses above 300 GeV. Similarly to ATLAS, limits are pushed further utilising fully-hadronic final states [161].

If $\tilde{\chi}_2^0$ decays through a Higgs boson with $m_H = 125$ GeV, searches targeting the WH channel are relevant. Assuming SM-like Higgs decay modes and branching fractions, Higgs bosons in the final state are identified by either two jets originating from bottom quarks ($h \to b\bar{b}$), two photons ($h \to \gamma\gamma$), or leptons from the WW, ZZ or $\tau\tau$ decay modes. Searches exploiting the presence of b-jets are most sensitive in the high-mass chargino region, while analyses targeting photon pair or leptonic decays of the Higgs boson provide the best sensitivity in the region of low masses. CMS [165] sets lower limits on the chargino mass up to 820 GeV for massless LSPs, but vanish for LSP masses above 350 GeV using events with at least one lepton and missing transverse momentum in the final state. Similar sensitivity is achieved by the ATLAS analyses [166–168].

Additional constraints on the chargino mass are placed exploiting all-hadronic analyses. A wino-like (higgsino-like) chargino with mass up to 1060 (900) GeV is excluded by ATLAS [160] when the LSP mass is below 400 (240) GeV and the mass splitting is larger than 400 (450) GeV. CMS [161] excludes wino-like charginos with mass up to 970 GeV for massless LSP.

In both the wino region (a characteristic of anomaly-mediated SUSY breaking models) and the higgsino region of the MSSM, the mass splitting between $\tilde{\chi}_1^\pm$ and $\tilde{\chi}_1^0$ is small. The chargino decay products are very soft and may escape detection. These compressed spectra are hard to detect, and have triggered dedicated search strategies. ATLAS [169] and CMS [170] have performed searches for charginos and neutralinos in a compressed mass spectrum using initial state radiation and two or three low-momentum (soft) leptons. For wino-like charginos, assuming degenerate $\tilde{\chi}_1^\pm$ and $\tilde{\chi}_2^0$, exclusion contours in the chargino-mass versus $\Delta m(\tilde{\chi}_1^\pm - \tilde{\chi}_1^0)$ plane are derived. As an example, such charginos are excluded by CMS (ATLAS) below 280 (240) GeV for $\Delta m(\tilde{\chi}_1^\pm - \tilde{\chi}_1^0) = 10$ GeV. Considering the higgsino model, the masses probed by CMS reach up to 215 GeV for a mass difference of 7.5 GeV and 150 GeV in the highly compressed region with a mass difference of 3 GeV. CMS has also searched for chargino-pair production through vector-boson-fusion [171], also targeting compressed mass spectra. Assuming degenerate $\tilde{\chi}_1^\pm$ and $\tilde{\chi}_2^0$, charginos with a mass below 112 GeV are excluded for $\Delta m(\tilde{\chi}_1^\pm - \tilde{\chi}_1^0) = 1$ GeV. CMS has published further searches for such compressed spectra with a soft tau lepton [172].

89.8.2 *Exclusion limits on neutralino masses*

In a considerable part of the MSSM parameter space, and in particular when demanding that the LSP carries no electric or color charge, the lightest neutralino $\tilde{\chi}_1^0$ is the LSP. If R-parity is conserved, such a $\tilde{\chi}_1^0$ is stable. Since it is weakly interacting, it will typically escape detectors unseen. Limits on the invisible width of the Z boson apply to neutralinos with a mass below 45.5 GeV, but depend on the Z-neutralino coupling. Such a coupling could be small or even absent; in such a scenario there is no general lower limit on the mass of the lightest neutralino [173]. In models with gaugino mass unification and sfermion mass unification at the GUT scale, a lower limit on the neutralino mass is derived from limits from direct searches, notably for charginos and sleptons, and amounts to 47 GeV [174]. Assuming a constrained model like the CMSSM, this limit increases to 50 GeV at LEP; however the strong constraints now set by the LHC increase such CMSSM-derived $\tilde{\chi}_1^0$ mass limits to well above a few hundred GeV (the latest reinterpretation only uses Run 1 data and indicates 200 GeV [175–177]).

In gauge-mediated SUSY breaking models (GMSB), the LSP is typically a gravitino, and the phenomenology is determined by the nature of the next-to-lightest supersymmetric particle (NLSP). A NLSP neutralino will decay to a gravitino and a SM particle whose nature is determined by the neutralino composition. Final states with two high p_T photons and missing momentum are searched for, and interpreted in gauge mediation models with bino-like neutralinos [178–183].

Assuming the production of at least two neutralinos per event, neutralinos with large non-bino components can also be searched for by their decay in final states with missing momentum plus any two bosons out of the collection γ, Z, H. A number of searches at the LHC have tried to cover the rich phenomenology predicted by the general gauge mediation model (GGM) where $\tilde{\chi}_1^0$ might decay with various BR in the Z and H decay modes [90,117,160,167,181,184–193]. As an example, strong constraints for decay modes involving Z and H bosons arise from

Downloaded from https://academic.oup.com/ptep/article/2022/8/083C01/6651666 by KIT Library user on 27 September 2022

full-hadronic searches on higgsino-like scenarios: ATLAS [160] excludes higgsino production with decays into a massless gravitino LSP in a mass range between 450 (500) GeV and 940 (850) GeV assuming BR = 1 (0.5) for the Z plus gravitino decay mode. Assuming only H plus gravitino decays, CMS [194] excludes a higgsino mass range between 175 GeV and 1025 GeV.

Heavier neutralinos, in particular $\tilde{\chi}_2^0$, have been searched for in their decays to the lightest neutralino plus a γ, a Z boson or a Higgs boson. Limits on electroweak production of $\tilde{\chi}_2^0$ plus $\tilde{\chi}_1^\pm$ from all-hadronic, same-sign dilepton and trilepton analyses have been discussed in the section on charginos; the assumption of equal mass of $\tilde{\chi}_2^0$ and $\tilde{\chi}_1^\pm$ make the limits on chargino masses apply to $\tilde{\chi}_2^0$ as well. Multilepton analyses have also been used to set limits on $\tilde{\chi}_2^0\tilde{\chi}_3^0$ production; assuming equal mass and decay through light sleptons, limits are set up to 680 GeV for massless LSPs [195]. Again, compressed spectra with small mass differences between the heavier neutralinos and the LSP form the most challenging region.

In $\tilde{\chi}_2^0$ decays to $\tilde{\chi}_1^0$ and a lepton pair, the lepton pair invariant mass distribution may show a structure that can be used to measure the $\tilde{\chi}_2^0 - \tilde{\chi}_1^0$ mass difference in case of a signal [38]. This structure, however, can also be used in the search strategy itself, as demonstrated by ATLAS [196, 197] and CMS [90, 198].

Fig. 89.8 summarizes some of the most recent results from ATLAS and CMS for chargino pair or chargino and next-to-lightest neutralino pair productions comparing results obtained with various assumptions. The limits on weak gauginos in simplified models are also summarized in Table 89.3. Only results for promptly decaying charginos and neutralinos are included: limits from searches focusing on long-lived particle scenarios are reported in Section 89.10.

Interpretations of the search results outside simplified models, such as in the phenomenological MSSM [199–204], show that the simplified model limits can translate into accurate constraints but must also be interpreted with care. Electroweak gauginos in models that are compatible with the relic density of dark matter in the Universe, for example, have particularly tuned mixing parameters and mass spectra, which are not always captured by the simplified models used.

89.8.3 *Exclusion limits on slepton masses*

The most model-independent searches for selectrons, smuons and staus originate from the LEP experiments [205]. Smuon production only takes place via s-channel γ^*/Z exchange. Search results are often quoted for $\tilde{\mu}_\mathrm{R}$, since it is typically lighter than $\tilde{\mu}_\mathrm{L}$ and has a weaker coupling to the Z boson; limits are therefore conservative. Decays are expected to be dominated by $\tilde{\mu}_\mathrm{R} \to \mu\tilde{\chi}_1^0$, leading to two non-back-to-back muons and missing momentum. Slepton mass limits are calculated in the MSSM under the assumption of gaugino mass unification at the GUT scale, and depend on the mass difference between the smuon and $\tilde{\chi}_1^0$. A $\tilde{\mu}_\mathrm{R}$ with a mass below 94 GeV is excluded for $m_{\tilde{\mu}_\mathrm{R}} - m_{\tilde{\chi}_1^0} > 10$ GeV. The selectron case is similar to the smuon case, except that an additional production mechanism is provided by t-channel neutralino exchange. The $\tilde{e}_\mathrm{R}$ lower mass limit is 100 GeV for $m_{\tilde{\chi}_1^0} < 85$ GeV. Due to the t-channel neutralino exchange, $\tilde{e}_\mathrm{R}\tilde{e}_\mathrm{L}$ pair production was possible at LEP, and a lower limit of 73 GeV was set on the selectron mass regardless of the neutralino mass by scanning over MSSM parameter space [206]. The potentially large mixing between $\tilde{\tau}_\mathrm{L}$ and $\tilde{\tau}_\mathrm{R}$ not only makes the $\tilde{\tau}_1$ light, but can also make its coupling to the Z boson small. LEP lower limits on the $\tilde{\tau}$ mass range between 87 and 93 GeV depending on the $\tilde{\chi}_1^0$ mass, for $m_{\tilde{\tau}} - m_{\tilde{\chi}_1^0} > 7$ GeV [205].

At the LHC, pair production of sleptons is not only heavily suppressed with respect to pair production of colored SUSY particles but the cross section is also almost two orders of magnitude smaller than the one of pair production of charginos and neutralinos. With the full data sets of Run 1 and Run 2, however, ATLAS and CMS have surpassed the sensitivity of the LEP analyses under certain assumptions.

Table 89.3: Summary of weak gaugino mass limits in simplified models, assuming R-parity conservation. Masses in the table are provided in GeV. Further details about assumptions and corresponding analyses are discussed in the text. Details on constraints for compressed scenarios from soft-lepton searches are not represented in the table.

Assumption	m_χ
$\tilde{\chi}_1^\pm$, all $\Delta m(\tilde{\chi}_1^\pm, \tilde{\chi}_1^0)$	> 92
$\tilde{\chi}_1^\pm$ $\Delta m > 5$, $m_{\tilde{\nu}} > 300$	> 103.5
$\tilde{\chi}_1^\pm$, $m_{(\tilde{\ell},\tilde{\nu})} = (m_{\tilde{\chi}_1^\pm} + m_{\tilde{\chi}_1^0})/2$	
$m_{\tilde{\chi}_1^0} \approx 0$	> 1000
$\tilde{\chi}_1^\pm$, $m_{\tilde{\chi}_1^0} > 480$	no LHC limit
$\tilde{\chi}_1^\pm$, $m_{\tilde{\ell}} > m_{\tilde{\chi}_1^\pm}$	
$m_{\tilde{\chi}_1^0} \approx 0$	> 420 and $290 - 760$
$\tilde{\chi}_1^\pm$, $m_{\tilde{\chi}_1^0} > 120$	no LHC limit
$m_{\tilde{\chi}_1^\pm} = m_{\tilde{\chi}_2^0}$, $m_{\tilde{\ell}_\mathrm{L}} = (m_{\tilde{\chi}_1^\pm} + m_{\tilde{\chi}_1^0})/2$	
$m_{\tilde{\chi}_1^0} \approx 0$	> 1450
$m_{\tilde{\chi}_1^0} > 1000$	no LHC limit
$m_{\tilde{\chi}_1^\pm} = m_{\tilde{\chi}_2^0}$, $m_{\tilde{\ell}_\mathrm{R}} = (m_{\tilde{\chi}_1^\pm} + m_{\tilde{\chi}_1^0})/2$	flavor-democratic
$m_{\tilde{\chi}_1^0} \approx 0$	> 1150
$m_{\tilde{\chi}_1^0} > 700$	no LHC limit
$m_{\tilde{\chi}_1^\pm} = m_{\tilde{\chi}_2^0}$, $m_{\tilde{\tau}} = (m_{\tilde{\chi}_1^\pm} + m_{\tilde{\chi}_1^0})/2$	$\tilde{\tau}$-dominated
$m_{\tilde{\chi}_1^0} \approx 0$	> 970
$m_{\tilde{\chi}_1^0} > 450$	no LHC limit
$m_{\tilde{\chi}_1^\pm} = m_{\tilde{\chi}_2^0}$, $m_{\tilde{\ell}} > m_{\tilde{\chi}_1^\pm}$, $\mathrm{BF}(WZ) = 1$	
$m_{\tilde{\chi}_1^0} \approx 0$	> 960
$m_{\tilde{\chi}_1^0} > 300$	no LHC limit
$m_{\tilde{\chi}_1^\pm} = m_{\tilde{\chi}_2^0}$, $m_{\tilde{\ell}} > m_{\tilde{\chi}_1^\pm}$, $\mathrm{BF}(WH) = 1$	
$m_{\tilde{\chi}_1^0} \approx 0$, wino-like $\tilde{\chi}_1^\pm$	> 1060
$m_{\tilde{\chi}_1^0} \approx 0$, higgsino-like $\tilde{\chi}_1^\pm$	> 900
$m_{\tilde{\chi}_1^0} > 400(240)$ no LHC limit	wino(higgsino)-like

ATLAS and CMS have searched for direct production of selectron pairs and smuon pairs at the LHC, with each slepton decaying to its corresponding SM partner lepton and the $\tilde{\chi}_1^0$ LSP. In simplified models, ATLAS [156] and CMS [198] set lower mass limits on sleptons of 700 GeV for degenerate $\tilde{\ell}_\mathrm{L}$ and $\tilde{\ell}_\mathrm{R}$, for a massless $\tilde{\chi}_1^0$ and assuming equal selectron and smuon masses, as shown in Fig. 89.9. The limits deteriorate with increasing $\tilde{\chi}_1^0$ mass due to decreasing missing momentum and lepton momentum. As a consequence, no limits are set for $\tilde{\chi}_1^0$ masses above 400 GeV. Limits are also derived without the assumption of slepton mass degeneracy [156,207]. A dedicated search for sleptons with small mass difference between $\tilde{\ell}$ and $\tilde{\chi}_1^0$ is performed by ATLAS [208] demanding the presence of ISR jets. Although no sensitivity is achieved for intermediate mass differences between the slepton and the LSP, slepton masses up to 260 GeV are excluded for slepton-LSP mass differences of 10-20 GeV.

ATLAS and CMS have also searched for $\tilde{\tau}$-pair production. In simplified models, ATLAS excludes $\tilde{\tau}$ masses between 120 and 390 GeV assuming light $\tilde{\chi}_1^0$, combining the production of degenerate left- and right-handed $\tilde{\tau}$s [209]. The CMS analysis [210] covers lower masses and closes the mass gap with LEP. A recent update from CMS [211] exclude purely left-handed $\tilde{\tau}$s with masses between 115 and 340 GeV for massless LSP.

In gauge-mediated SUSY breaking models, sleptons can be (co-)NLSPs, *i.e.*, the next-to-lightest SUSY particles and almost degenerate in mass, decaying to a lepton and a gravitino. This decay can either be prompt, or the slepton can have a non-zero lifetime. Combining several analyses, lower mass limits on $\tilde{\mu}_\mathrm{R}$ of 96.3 GeV

Downloaded from https://academic.oup.com/ptep/article/2022/8/083C01/6651666 by KIT Library user on 27 September 2022

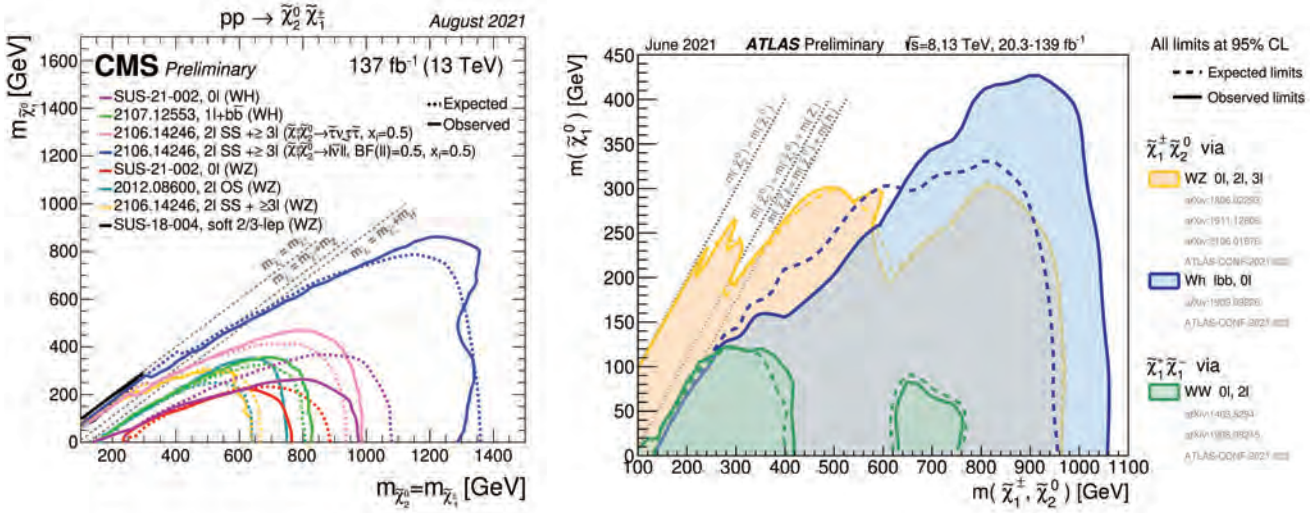

Figure 89.8: LHC exclusion limits on chargino and neutralino masses in a number of simplified models. Left: CMS limits on chargino and neutralino masses for pair production of charginos, pair production of heavier neutralinos, or pair production of chargino and neutralino, under a variety of assumptions including light sleptons mediating the decays. Right: ATLAS limits on chargino and neutralino masses for pair production of chargino and neutralino, under the assumption of decoupled sleptons, and chargino/neutralino decay through on- or off-shell W and Z or H.

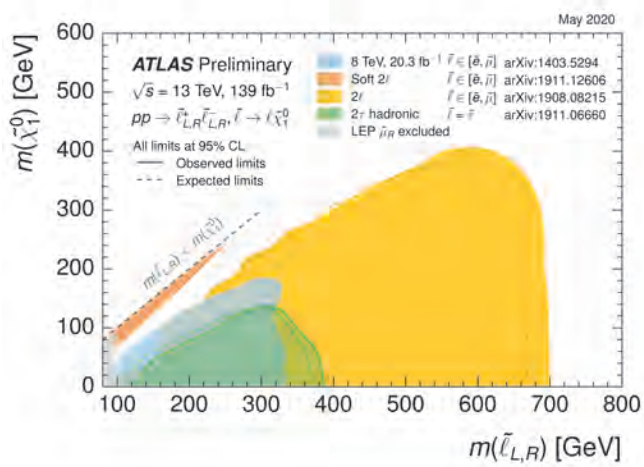

Figure 89.9: LHC exclusion limits on slepton (selectron and smuon) masses, assuming equal masses of selectrons and smuons, degeneracy of $\tilde{\ell}_{\rm L}$ and $\tilde{\ell}_{\rm R}$, and a 100% branching fraction for $\tilde{\ell} \to \ell\tilde{\chi}_1^0$.

and on $\tilde{e}_{\rm R}$ of 66 GeV are set for all slepton lifetimes at LEP [212]. In a considerable part of parameter space in these models, the $\tilde{\tau}$ is the NLSP. The LEP experiments have set lower limits on the mass of such a $\tilde{\tau}$ between 87 and 97 GeV, depending on the $\tilde{\tau}$ lifetime. ATLAS and CMS have searched for final states with τs, jets and missing transverse momentum, and have interpreted the results in GMSB models setting limits on the model parameters [213, 214]. CMS has interpreted a multilepton analysis in terms of limits on gauge mediation models with slepton NLSP [215]. CDF has put limits on gauge mediation models at high $\tan\beta$ and slepton NLSP using an analysis searching for like-charge light leptons and taus [216].

The invisible width of the Z boson puts a lower limit on the sneutrino mass of about 45 GeV. Tighter limits are derived from other searches, notably for gauginos and sleptons, under the assumption of gaugino and sfermion mass universality at the GUT scale, and amount to approximately 94 GeV in the MSSM [217].

The limits on sleptons in simplified models are summarized in Table 89.4.

Table 89.4: Summary of slepton mass limits from LEP and LHC, assuming R-parity conservation and 100% branching fraction for $\tilde{\ell} \to \ell\tilde{\chi}_1^0$. Masses in this table are provided in GeV.

Assumption	$m_{\tilde{\ell}}$
$\tilde{\mu}_{\rm R}$, $\Delta m(\tilde{\mu}_{\rm R}, \tilde{\chi}_1^0) > 10$	> 94
$\tilde{e}_{\rm R}$, $\Delta m(\tilde{e}_{\rm R}, \tilde{\chi}_1^0) > 10$	> 94
$\tilde{e}_{\rm R}$, any Δm	> 73
$\tilde{\tau}_{\rm R}$, $\Delta m(\tilde{\tau}_{\rm R}, \tilde{\chi}_1^0) > 7$	> 87
$\tilde{\nu}_e$, $\Delta m(\tilde{e}_{\rm R}, \tilde{\chi}_1^0) > 10$	> 94
$m_{\tilde{e}_{\rm L,R}} = m_{\tilde{\mu}_{\rm L,R}}$, $m_{\tilde{\chi}_1^0} \approx 0$	> 700
$m_{\tilde{\chi}_1^0} >\approx 400$	no LHC limit
$m_{\tilde{\tau}_{\rm L}} = m_{\tilde{\tau}_{\rm R}}$, $m_{\tilde{\chi}_1^0} \approx 0$	> 390
$m_{\tilde{\chi}_1^0} >\approx 130$	no LHC limit

89.9 Exclusion limits on the masses of charginos, neutralinos and sleptons in RPV scenarios

In models with R-parity violation, the lightest neutralino can decay even if it is the lightest supersymmetric particle. If the decay involves a non-zero λ coupling, the final state will be a multi-lepton one. Searches for events with four or more isolated charged leptons by ATLAS [117] and CMS [121] are interpreted in such models.

Various searches, including searches for multi-lepton and lepton plus jets events, are interpreted in a model with R-parity violating neutralino decays involving a non-zero λ' coupling [118, 126, 218, 219]. Neutralino decays involving non-zero λ'' lead to fully hadronic final states, and searches for multi-jet events and jet-pair resonances are used to set limits, typically on the production of colored particles like top squarks or gluinos, which are assumed to be the primary produced sparticles in these interpretations, as discussed earlier 89.7. For instance, the ATLAS search [130] in events with one lepton and high jet multiplicity excludes up to 320(365) GeV in higgsino (wino) masses. Recent searches [220] also set limits on the production of charginos and neutralinos for a Minimal SUSY model with an approximate $B - L$ symmetry. Charginos and neutralinos with masses between 100 GeV and 1100 GeV are excluded depending on the assumed decay BR into a lepton plus a W, Z or H boson.

Limits also exist on sleptons in R-parity violating models, both from LEP and the Tevatron experiments. From LEP, lower limits

Downloaded from https://academic.oup.com/ptep/article/2022/8/083C01/6651666 by KIT Library user on 27 September 2022

on $\tilde{\mu}_R$ and $\tilde{e}_R$ masses in such models are 97 GeV, and the limits on the stau mass are very close: 96 GeV [221]. CMS has searched for resonant smuon production in a modified CMSSM scenario [222], putting limits on λ'_{211} as a function of $m_0, m_{1/2}$.

Production of pairs of sneutrinos in R-parity violating models has been searched for at LEP [221]. Assuming fully leptonic decays via λ-type couplings, lower mass limits between 85 and 100 GeV are set. At the Tevatron [223, 224] and at the LHC [222, 225–227], searches have focused on scenarios with resonant production of a sneutrino, decaying to $e\mu$, $\mu\tau$ and $e\tau$ final states. No signal has been seen, and limits have been set on sneutrino masses as a function of the value of relevant RPV couplings. As an example, the LHC experiments exclude a resonant tau sneutrino with a mass below 2.3 TeV for $\lambda_{312} = \lambda_{321} > 0.07$ and $\lambda'_{311} > 0.11$.

89.10 Exclusion limits on long-lived sparticles

Long-lived sparticles arise in many different SUSY models. In particular in co-annihilation scenarios, where the NLSP and LSP are nearly mass-degenerate, this is rather common in order to obtain the correct Dark Matter relic density. Prominent examples are scenarios featuring stau co-annihilation, or models of SUSY breaking, e.g. minimal anomaly-mediated SUSY breaking (AMSB), in which the appropriate Dark Matter density is obtained by co-annihilation of the LSP with an almost degenerate long-lived wino. However, in general, other sparticles can also be long-lived and it is desirable to establish a comprehensive search program for these special long-lived cases, which lead to distinct experimental search signatures. Searches for events with a displaced hadronic vertex, with or without a matched lepton, are for instance interpreted in a model with R-parity violating neutralino decays involving a non-zero λ' coupling [219]. Other signatures interpreted in terms of SUSY models include disappearing tracks, identification of tracks with atypical properties or unusual ionization, small and localized deposits of energy inside of the calorimeters without associated tracks, or stopped particles that decay out of time with collisions. Some examples are reported below.

Past experiments have performed dedicated searches for long-lived SUSY signatures, but given the absence of any experimental evidence for SUSY so far, more effort and focus has gone into such searches at the LHC recently.

If the decay of gluinos is suppressed, for example if squark masses are high, gluinos may live longer than typical hadronization times. It is expected that such gluinos will hadronize to long-living strongly interacting particles known as R-hadrons. In particular, if the suppression of the gluino decay is strong, as in the case that the squark masses are much higher than the TeV scale, these R-hadrons can be (semi-)stable in collider timescales. Searches for such R-hadrons exploit the typical signature of stable charged massive particles in the detector. R-hadrons decaying in the detector are searched for using dE/dx measurements and searches for displaced vertices. As shown in the left plot of Fig. 89.10, the ATLAS experiment excludes semi-stable gluino R-hadrons with masses below $1.9 - 2.3$ TeV for all lifetimes in a simplified model where such gluinos always form R-hadrons, and decay into jets and a light neutralino, by combining a number of analyses [124, 228–230]. A combination of CMS searches for long-lived particles, as shown in Fig. 89.11, reaches similar limits [231–235].

Alternatively, since such R-hadrons are strongly interacting, they may be stopped in the calorimeter or in other material, and decay later into energetic jets. These decays are searched for by identifying the jets [236–238] or muons [238] outside the time window associated with bunch-bunch collisions. As shown in Fig. 89.11, the CMS collaboration sets limits on such stopped R-hadrons over 13 orders of magnitude in gluino lifetime, up to masses of 1390 GeV [238]. Recent results from ATLAS [239] sets constraint on the mass of gluino R-hadrons using large out-of-time energy deposits in the calorimeters. Also in this case, masses of up to 1.4 TeV are excluded for gluino lifetimes of $10^{-5} - 10^3$ s.

Top squarks can also be long-lived and hadronize to a R-hadron, for example in the scenario where the top squark is the next-to-lightest SUSY particle (NLSP), with a small mass difference to the LSP. Searches for massive stable charged particles are sensitive to such top squarks. Tevatron limits are approximately $m_{\tilde{t}} > 300$ GeV [240, 241]. ATLAS sets a limit of 1340 GeV on such top squarks [229], the CMS limits are comparable [233]. Intermediate lifetimes of top squarks decaying through RPV coupling into a quark and a lepton are also targeted by ATLAS and CMS. Limits on top squarks decaying into a quark and a muon are set by ATLAS [242] using events that pass a muon or missing-transverse-momentum trigger and contain a displaced muon track and a displaced vertex. Masses up to 1.7 TeV are excluded for a lifetime of 0.1 ns, and masses below 1.3 TeV are excluded for lifetimes between 0.01 ns and 30 ns. CMS [243] utilizes events with two leptons with transverse impact parameter values between 0.01 and 10 cm not required to form a common vertex to exclude top squarks with masses between 100 and at least 460 GeV for $0.01 < c\tau_0 < 1000$ cm, where $c\tau_0$ is the proper decay length.

In addition to colored sparticles, sparticles like charginos may also be long-lived, especially in scenarios with compressed mass spectra. Charginos decaying in the detectors away from the primary vertex could lead to signatures such as kinked-tracks, or apparently disappearing tracks, since, for example, the pion in $\tilde{\chi}_1^{\pm} \rightarrow \pi^{\pm}\tilde{\chi}_1^0$ might be too soft to be reconstructed. At the LHC, searches have been performed for such disappearing tracks, and interpreted within anomaly-mediated SUSY breaking models [244–247]. The right plot of Fig. 89.10 shows constraints for different ATLAS searches on the chargino mass-vs-lifetime plane for an AMSB model ($\tan\beta = 5$, $\mu > 0$) in which a wino-like $\tilde{\chi}^{\pm}$ decays to a soft pion and an almost mass-degenerated wino-like $\tilde{\chi}_1^0$ [229, 230, 245–247]. For a similar model, CMS excludes $c\tau$ values between 0.15 and 18 m for a chargino mass of 505 GeV [244], see Fig. 89.11. The most recent ATLAS search [247] provides constraints also for higgsino-like models. Charginos with a lifetime longer than the time needed to pass through the detector appear as charged stable massive particles. Limits have been derived by the LEP experiments [248], by D0 at the Tevatron [241], and by the LHC experiments [229, 249], and such charginos with mass below 1090 GeV are excluded.

In gauge mediation models, NLSP neutralino decays need not be prompt, and experiments have searched for late decays with photons in the final state. CDF has searched for delayed $\tilde{\chi}_1^0 \rightarrow \gamma\tilde{G}$ decays using the timing of photon signals in the calorimeter [250]. CMS has used the same technique at the LHC [251]. Results are given as exclusion contours in the neutralino mass versus lifetime plane, and for example in a GMSB model with a neutralino mass of 300 GeV, $c\tau$ values between 10 and 2000 cm are excluded [251]. D0 has looked at the direction of showers in the electromagnetic calorimeter with a similar goal [252], and ATLAS has searched for photon candidates that do not point back to the primary vertex, as well as for delayed photons [253].

Charged slepton decays may be kinematically suppressed, for example in the scenario of a NLSP slepton with a very small mass difference to the LSP. Such a slepton may appear to be a stable charged massive particle. Interpretation of searches at LEP for such signatures within GMSB models with a stau NLSP or slepton co-NLSP exclude masses up to 99 GeV [248]. Searches for stable charged particles at the Tevatron [240, 241] and at the LHC [229, 233] are also interpreted in terms of limits on stable charged sleptons. The limits obtained at the LHC exclude stable staus with masses below 430 GeV when produced directly in pairs, and below 660 GeV when staus are produced both directly and indirectly in the decay of other particles in a GMSB model. Recent results from ATLAS and CMS set constraints on long-lived charged slepton with intermediate lifetimes. ATLAS searches for charged leptons with large impact parameters and exclude selectron, smuon and stau masses up to 720 GeV, 680 GeV, and 340 GeV, respectively, in case of lifetimes of 0.1 ns. CMS [211] targets long-lived stau with $c\tau$ of about 0.1 mm excluding masses between 115 and 220 GeV for the case that the LSP is nearly massless.

Downloaded from https://academic.oup.com/ptep/article/2022/8/083C01/6651666 by KIT Library user on 27 September 2022

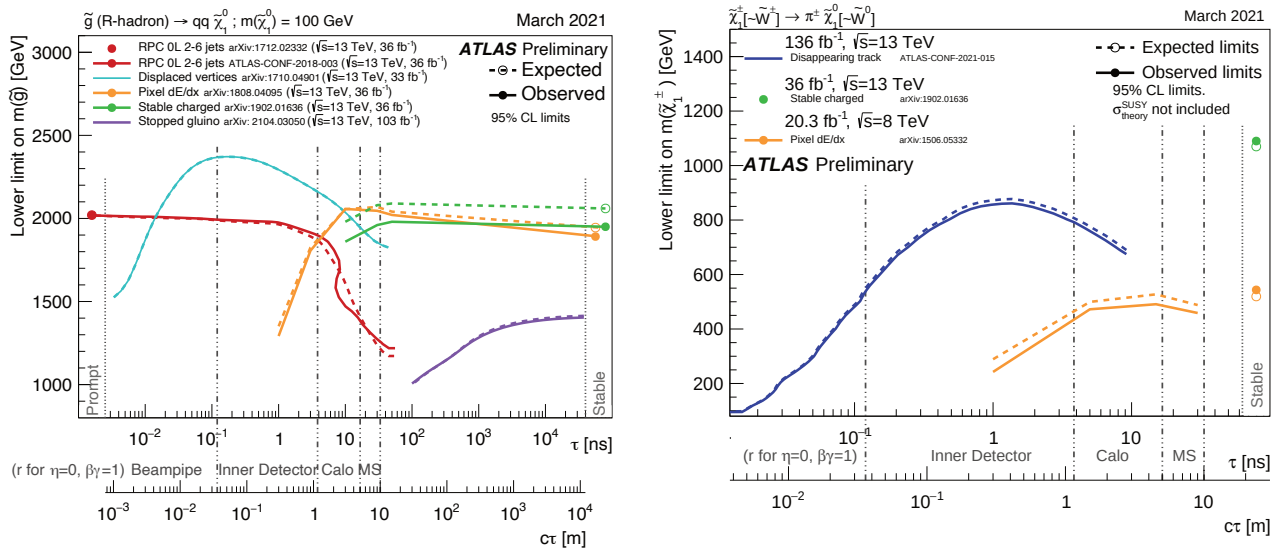

Figure 89.10: Limits at 95% C.L. on the gluino mass in R-hadron models (left), and on the chargino mass in a model where the wino-like chargino is almost degenerate with the LSP (right), as a function of gluino or chargino lifetime, as obtained by ATLAS.

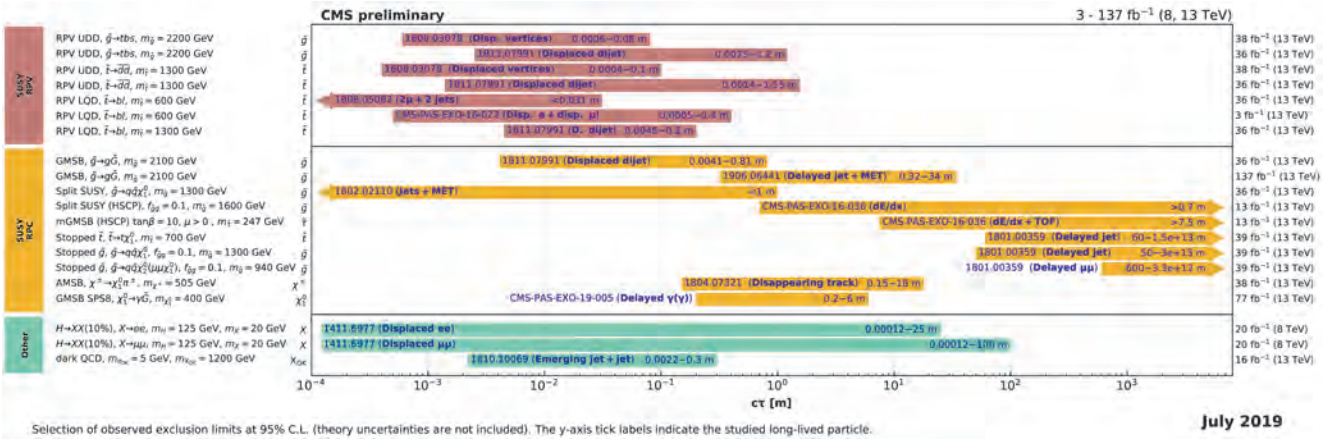

Figure 89.11: Excluded regions, at 95% C.L., in the lifetimes of long-lived particles in several models, as obtained by CMS.

89.11 Global interpretations

Apart from the interpretation of direct searches for sparticle production at colliders in terms of limits on masses of individual SUSY particles, model-dependent interpretations of allowed SUSY parameter space are derived from global SUSY fits. Typically these fits combine the results from collider experiments with indirect constraints on SUSY as obtained from low-energy experiments, flavor physics, high-precision electroweak results, and astrophysical data.

In the pre-LHC era these fits were mainly dominated by indirect constraints. Even for very constrained models like the CMSSM, the allowed parameter space, in terms of squark and gluino masses, ranged from several hundreds of GeV to a few TeV. Furthermore, these global fits indicated that squarks and gluino masses in the range of 500 to 1000 GeV were the preferred region of parameter space, although values as high as a few TeV were allowed with lower probabilities [254–261].

With ATLAS and CMS now probing mass scales around 1 TeV and beyond, the importance of the direct searches for global analyses of allowed SUSY parameter space has increased. For example, imposing the new experimental limits on constrained supergravity models pushes the most likely values of first generation squark and gluino masses significantly beyond 2 TeV, typically resulting in overall values of fit quality much worse than those in the pre-LHC era [175–177, 202, 262–269]. The measured value of m_h pushes the sparticle masses upwards. Although these constrained models are not yet ruled out, the extended experimental limits impose very tight constraints on the allowed parameter space.

For this reason, the emphasis of global SUSY fits has shifted towards less-constrained SUSY models. Interpretations in the pMSSM [200–204, 249, 262] as well as in simplified models, have been useful to generalize SUSY searches, for example to redesign experimental analyses in order to increase their sensitivity for compressed spectra, where the mass of the LSP is much closer to squark and gluino masses than predicted by the CMSSM. As shown in Table 89.1, for neutralino masses above $0.5 - 1$ TeV the current set of ATLAS and CMS searches, interpreted in simplified models, cannot exclude the existence of squarks or gluinos with masses only marginally above the neutralino mass. However, as these exclusion limits are defined in the context of simplified models, they are only valid for the assumptions in which these models are defined.

As an alternative approach, both ATLAS [200] and CMS [201] have performed an analysis of the impact of their searches on the parameter space of the pMSSM. Fig. 89.12 shows graphically the LHC exclusion power in the pMSSM based on searches performed at $\sqrt{s} = 7$ and 8 TeV. The plot on the left shows the survival probability in the gluino-neutralino mass plane, which is a measure of the parameter space that remains after inclusion of the relevant CMS search results. As can be seen, gluino masses below about 1.2 TeV are almost fully excluded. This result agrees well with the typical exclusion obtained at 8 TeV in simplified mod-

Downloaded from https://academic.oup.com/ptep/article/2022/8/083C01/6651666 by KIT Library user on 27 September 2022

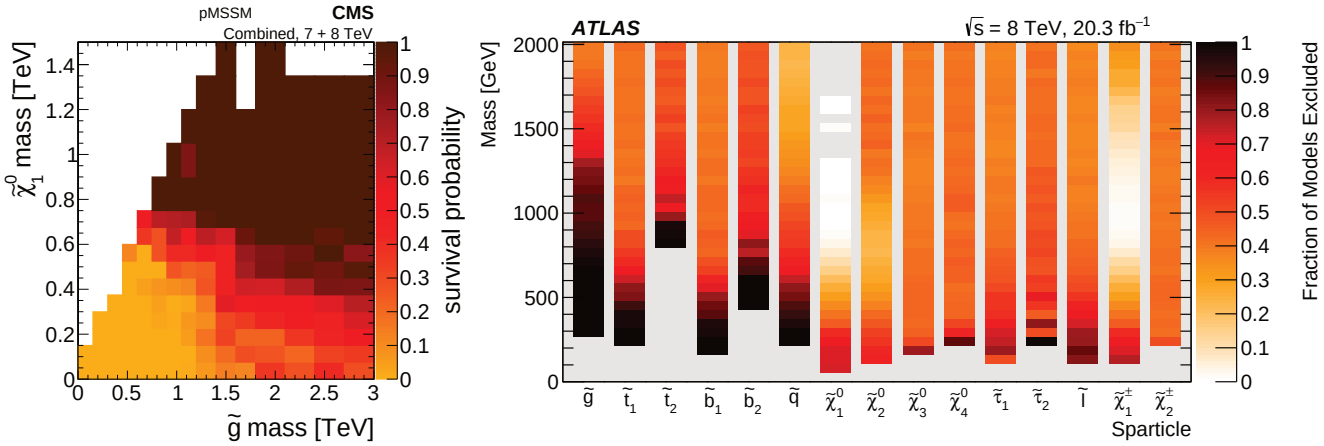

Figure 89.12: The plot on the left shows the survival probability of a pMSSM parameter space model in the gluino-neutralino mass plane after the application of the relevant CMS search results. The plot on the right shows a graphical representation of the ATLAS exclusion power in a pMSSM model. Each vertical bar is a one-dimensional projection of the fraction of models points excluded for each sparticle by ATLAS analyses. The experimental results are obtained from data taken at $\sqrt{s} = 7$ and 8 TeV.

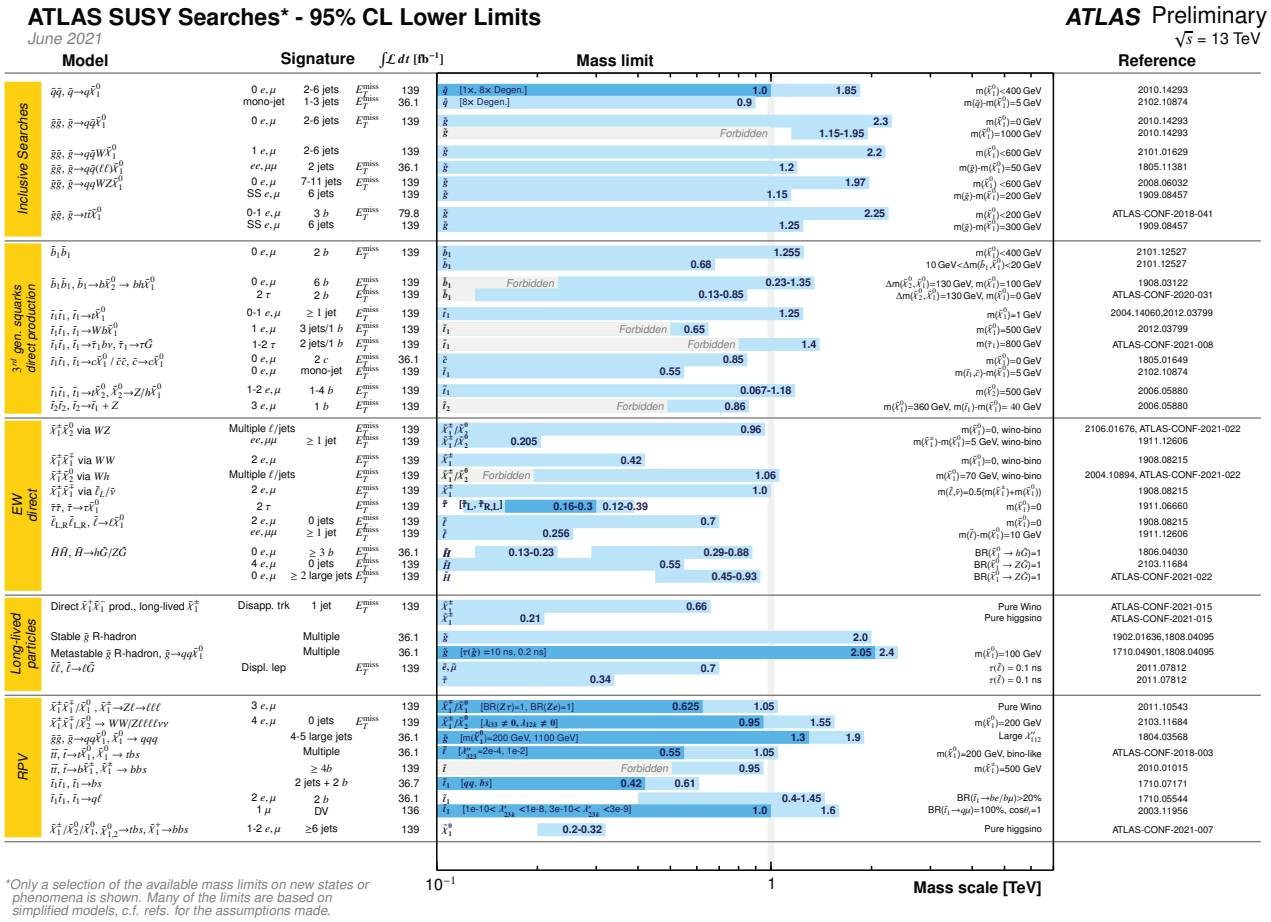

*Only a selection of the available mass limits on new states or phenomena is shown. Many of the limits are based on simplified models, c.f. refs. for the assumptions made.

Figure 89.13: Overview of the current landscape of SUSY searches at the LHC. The plot shows exclusion mass limits of ATLAS for different searches and interpretation assumptions. The corresponding results of the CMS experiment are similar.

els for gluino production. However, as shown in the right plot of Fig. 89.12, when a similar analysis for other sparticles is performed it becomes apparent that exclusions on the pMSSM parameter can be significantly less stringent than simplified model limits might suggest. This is especially apparent for the electroweak sector, where even at rather low masses several of the pMSSM test points still survive the constraint of ATLAS searches at $\sqrt{s} = 7$ and 8 TeV. This again indicates that care must be taken when interpreting results from the LHC searches and there are still several scenarios where sparticles below the 1 TeV scale are not excluded, even when considering the most recent results at $\sqrt{s} = 13$ TeV.

Furthermore, the discovery of a Higgs boson with a mass around 125 GeV has triggered many studies regarding the compatibility of SUSY parameter space with this new particle. Much of it is still work in progress and it will be interesting to see how the interplay between the results from direct SUSY searches and more precise

Downloaded from https://academic.oup.com/ptep/article/2022/8/083C01/6651666 by KIT Library user on 27 September 2022

measurements of the properties of the Higgs boson will unfold in the future.

89.12 Summary and Outlook

The absence of any observation of new phenomena at the first run of the LHC at $\sqrt{s} = 7/8$ TeV, and after the second run at $\sqrt{s} = 13$ TeV, places significant constraints on SUSY parameter space. An overview of the current landscape of SUSY searches and limits at the LHC is shown in Figure 89.13, where the ATLAS summary is reported for illustration purposes. Inclusive searches probe production of gluinos at about 2.3 TeV, first and second generation squarks in the range of about 1 to 1.9 TeV, third generation squarks at scales around 600 GeV to 1.2 TeV, electroweak gauginos at scales around $400 - 1100$ GeV, and sleptons around 700 GeV. However, depending on the assumptions made on the underlying SUSY spectrum these limits can also weaken considerably.

With the LHC having reached almost its maximum energy of about $\sqrt{s} = 14$ TeV, future sensitivity improvement will have to originate from more data, the improvement of experimental analysis techniques and the focus on special signatures like the ones arising in long-lived sparticle decays. Therefore, it is expected that the current landscape of SUSY searches and corresponding exclusion limits at the LHC, as, for example, shown in Fig. 89.13 from the ATLAS experiment [270] (CMS results are similar [271]), will not change as rapidly anymore as it did in the past, when the LHC underwent several successive increases of collision energy.

The interpretation of results at the LHC has moved away from constrained models like the CMSSM towards a large set of simplified models, or the pMSSM. On the one hand this move is because the LHC limits have put constrained models like the CMSSM under severe pressure, while on the other hand simplified models leave more freedom to vary parameters and form a better representation of the underlying sensitivity of analyses. However, these interpretations in simplified models do not come without a price: the decomposition of a potentially complicated reality in a limited set of individual decay chains can be significantly incomplete. Therefore, quoted limits in simplified models are only valid under the explicit assumptions made in these models. The recent addition of more comprehensive interpretations in the pMSSM will complement those derived from simplified models and, thus, will enable an even more refined understanding of the probed SUSY parameter space.

In this context, the limit range of $1.5 - 2.3$ TeV on generic colored SUSY particles only holds for light neutralinos, in the R-parity conserving MSSM. Limits on third generation squarks and electroweak gauginos also only hold for light neutralinos, and under specific assumptions for decay modes and slepton masses.

The next LHC runs, with $\sqrt{s}$ between 13 and 14 TeV and significantly larger integrated luminosities (notably the High-Luminosity LHC), will provide a large data sample for future SUSY searches. As mentioned above, the improvement in sensitivity will largely have to come from a larger data set, and evolution of trigger and analysis techniques, since there will be no significant energy increase at the LHC anymore. Although the sensitivity for colored sparticles will increase somewhat as well, the expanded data set will be particularly beneficial for electroweak gaugino searches, and for the more difficult final states presented by compressed particle spectra, stealth SUSY, long-lived sparticles, or R-parity violating scenarios.

References

[1] H. Miyazawa, Prog. Theor. Phys. **36**, 6, 1266 (1966).

[2] Yu. A. Golfand and E. P. Likhtman, JETP Lett. **13**, 323 (1971), [Pisma Zh. Eksp. Teor. Fiz.13,452(1971)].

[3] J.-L. Gervais and B. Sakita, Nucl. Phys. **B34**, 632 (1971).

[4] D. V. Volkov and V. P. Akulov, Phys. Lett. **46B**, 109 (1973).

[5] J. Wess and B. Zumino, Phys. Lett. **49B**, 52 (1974).

[6] J. Wess and B. Zumino, Nucl. Phys. **B70**, 39 (1974).

[7] A. Salam and J. A. Strathdee, Nucl. Phys. **B76**, 477 (1974).

[8] H. P. Nilles, Phys. Rept. **110**, 1 (1984).

[9] H. E. Haber and G. L. Kane, Phys. Rept. **117**, 75 (1985).

[10] E. Witten, Nucl. Phys. **B188**, 513 (1981).

[11] S. Dimopoulos and H. Georgi, Nucl. Phys. **B193**, 150 (1981).

[12] M. Dine, W. Fischler and M. Srednicki, Nucl. Phys. **B189**, 575 (1981).

[13] S. Dimopoulos and S. Raby, Nucl. Phys. **B192**, 353 (1981).

[14] N. Sakai, Z. Phys. **C11**, 153 (1981).

[15] R. K. Kaul and P. Majumdar, Nucl. Phys. **B199**, 36 (1982).

[16] H. Goldberg, Phys. Rev. Lett. **50**, 1419 (1983).

[17] J. R. Ellis *et al.*, Nucl. Phys. **B238**, 453 (1984).

[18] G. Jungman, M. Kamionkowski and K. Griest, Phys. Rept. **267**, 195 (1996), [hep-ph/9506380].

[19] S. Dimopoulos, S. Raby and F. Wilczek, Phys. Rev. **D24**, 1681 (1981).

[20] W. J. Marciano and G. Senjanovic, Phys. Rev. **D25**, 3092 (1982).

[21] M. B. Einhorn and D. R. T. Jones, Nucl. Phys. **B196**, 475 (1982).

[22] L. E. Ibanez and G. G. Ross, Phys. Lett. **105B**, 439 (1981).

[23] U. Amaldi, W. de Boer and H. Furstenau, Phys. Lett. **B260**, 447 (1991).

[24] P. Langacker and N. Polonsky, Phys. Rev. **D52**, 3081 (1995), [hep-ph/9503214].

[25] J. R. Ellis, S. Kelley and D. V. Nanopoulos, Phys. Lett. B **260**, 131 (1991).

[26] P. Fayet, Phys. Lett. **64B**, 159 (1976).

[27] G. R. Farrar and P. Fayet, Phys. Lett. **76B**, 575 (1978).

[28] B.C. Allanach and H.E. Haber, *Supersymmetry, Part I (Theory)*, in this *Review*.

[29] M. Carena *et al.*, *Status of Higgs Boson Physics*, in this *Review*.

[30] A. M. Sirunyan *et al.* (CMS), JHEP **04**, 188 (2020), [arXiv:1910.12127].

[31] M. Aaboud *et al.* (ATLAS), JHEP **04**, 098 (2019), [arXiv:1812.03017].

[32] R. Aaij *et al.* (LHCb), Phys. Rev. Lett. **118**, 19, 191801 (2017), [arXiv:1703.05747].

[33] A. Höcker and W.J. Marciano, *Muon Anomalous Magnetic Moment*, in this *Review*.

[34] B. Abi *et al.* (Muon g-2), Phys. Rev. Lett. **126**, 14, 141801 (2021), [arXiv:2104.03281].

[35] G. Hinshaw *et al.* (WMAP), Astrophys. J. Suppl. **208**, 19 (2013), [arXiv:1212.5226].

[36] N. Aghanim *et al.* (Planck Collaboration), A&A **641**, A1 (2020).

[37] K. Nakamura *et al.* (Particle Data Group), J. Phys. **G37**, 075021 (2010).

[38] I. Hinchliffe *et al.*, Phys. Rev. **D55**, 5520 (1997), [hep-ph/9610544].

[39] L. Randall and D. Tucker-Smith, Phys. Rev. Lett. **101**, 221803 (2008), [arXiv:0806.1049].

[40] V. Khachatryan *et al.* (CMS), Phys. Lett. **B698**, 196 (2011), [arXiv:1101.1628].

[41] S. Chatrchyan *et al.* (CMS), Phys. Rev. Lett. **107**, 221804 (2011), [arXiv:1109.2352].

[42] S. Chatrchyan *et al.* (CMS), JHEP **01**, 077 (2013), [arXiv:1210.8115].

[43] S. Chatrchyan *et al.* (CMS), Eur. Phys. J. **C73**, 9, 2568 (2013), [arXiv:1303.2985].

[44] S. Chatrchyan *et al.* (CMS), Phys. Rev. **D85**, 012004 (2012), [arXiv:1107.1279].

[45] C. G. Lester and D. J. Summers, Phys. Lett. **B463**, 99 (1999), [hep-ph/9906349].

Downloaded from https://academic.oup.com/ptep/article/2022/8/083C01/6651666 by KIT Library user on 27 September 2022

[46] D. R. Tovey, JHEP **04**, 034 (2008), [arXiv:0802.2879].

[47] M. R. Buckley *et al.*, Phys. Rev. **D89**, 5, 055020 (2014), [arXiv:1310.4827].

[48] P. Jackson, C. Rogan and M. Santoni, Phys. Rev. **D95**, 3, 035031 (2017), [arXiv:1607.08307].

[49] J. M. Butterworth *et al.*, Phys. Rev. Lett. **100**, 242001 (2008), [arXiv:0802.2470].

[50] A. M. Sirunyan *et al.* (CMS), JHEP **05**, 032 (2020), [arXiv:1912.08887].

[51] N. Arkani-Hamed and S. Dimopoulos, JHEP **06**, 073 (2005), [hep-th/0405159].

[52] G. F. Giudice and A. Romanino, Nucl. Phys. B **699**, 65 (2004), [Erratum: Nucl.Phys.B 706, 487–487 (2005)], [hep-ph/0406088].

[53] J. Alimena *et al.*, J. Phys. G **47**, 9, 090501 (2020), [arXiv:1903.04497].

[54] A.H. Chamseddine, R. Arnowitt, and P Nath, Phys. Rev. Lett. **49**, 970 (1982).

[55] E. Cremmer *et al.*, Nucl. Phys. **B212**, 413 (1983).

[56] P. Fayet, Phys. Lett. **70B**, 461 (1977).

[57] M. Dine, A. E. Nelson and Y. Shirman, Phys. Rev. **D51**, 1362 (1995), [hep-ph/9408384].

[58] P. Meade, N. Seiberg and D. Shih, Prog. Theor. Phys. Suppl. **177**, 143 (2009), [arXiv:0801.3278].

[59] G. F. Giudice *et al.*, JHEP **12**, 027 (1998), [hep-ph/9810442].

[60] L. Randall and R. Sundrum, Nucl. Phys. **B557**, 79 (1999), [hep-th/9810155].

[61] R. L. Arnowitt and P. Nath, Phys. Rev. Lett. **69**, 725 (1992).

[62] G. L. Kane *et al.*, Phys. Rev. **D49**, 6173 (1994), [hep-ph/9312272].

[63] A. Djouadi *et al.* (MSSM Working Group), in "GDR (Groupement De Recherche) - Supersymetrie," (1998), [hep-ph/9901246].

[64] A. Djouadi, J.-L. Kneur and G. Moultaka, Comput. Phys. Commun. **176**, 426 (2007), [hep-ph/0211331].

[65] C. F. Berger *et al.*, JHEP **02**, 023 (2009), [arXiv:0812.0980].

[66] H. Baer *et al.*, in "Workshop on Physics at Current Accelerators and the Supercollider Argonne, Illinois, June 2-5, 1993," 0703–720 (1993), [hep-ph/9305342], URL `http://lss.fnal.gov/cgi-bin/find_paper.pl?other/ssc/sscl-preprint-441`.

[67] R. M. Barnett, H. E. Haber and G. L. Kane, Nucl. Phys. **B267**, 625 (1986).

[68] H. Baer, D. Karatas and X. Tata, Phys. Lett. **B183**, 220 (1987).

[69] J. Alwall, P. Schuster and N. Toro, Phys. Rev. **D79**, 075020 (2009), [arXiv:0810.3921].

[70] J. Alwall *et al.*, Phys. Rev. **D79**, 015005 (2009), [arXiv:0809.3264].

[71] LEP2 SUSY Working Group, ALEPH, DELPHI, L3 and OPAL experiments, note LEPSUSYWG/04-02.1, `http://lepsusy.web.cern.ch/lepsusy`.

[72] LHC SUSY cross sections working group, `https://twiki.cern.ch/twiki/bin/view/LHCPhysics/SUSYCrossSections`.

[73] T. Aaltonen *et al.* (CDF), Phys. Rev. Lett. **102**, 121801 (2009), [arXiv:0811.2512].

[74] V. M. Abazov *et al.* (D0), Phys. Lett. **B660**, 449 (2008), [arXiv:0712.3805].

[75] A. M. Sirunyan *et al.* (CMS) (2019), [arXiv:1908.04722].

[76] ATLAS Collab., ATLAS-CONF-2019-040 (2019).

[77] G. Aad *et al.* (ATLAS), Eur. Phys. J. C **81**, 7, 600 (2021), [arXiv:2101.01629].

[78] G. Aad *et al.* (ATLAS), JHEP **02**, 143 (2021), [arXiv:2010.14293].

[79] A. M. Sirunyan *et al.* (CMS), JHEP **10**, 244 (2019), [arXiv:1908.04722].

[80] ATLAS Collab., ATLAS-CONF-2018-041 (2018).

[81] A. M. Sirunyan *et al.* (CMS) (2019), [arXiv:1909.03460].

[82] G. Aad *et al.* (ATLAS Collaboration), Phys. Rev. D **103**, 112006 (2021), URL `https://link.aps.org/doi/10.1103/PhysRevD.103.112006`.

[83] M. Aaboud *et al.* (ATLAS), JHEP **09**, 050 (2018), [arXiv:1805.01649].

[84] T. Aaltonen *et al.* (CDF), Phys. Rev. Lett. **105**, 081802 (2010), [arXiv:1005.3600].

[85] V. M. Abazov *et al.* (D0), Phys. Lett. **B693**, 95 (2010), [arXiv:1005.2222].

[86] G. Aad *et al.* (ATLAS), JHEP **05**, 093 (2021), [arXiv:2101.12527].

[87] G. Aad *et al.* (ATLAS), JHEP **12**, 060 (2019), [arXiv:1908.03122].

[88] G. Aad *et al.* (ATLAS), JHEP **06**, 046 (2020), [arXiv:1909.08457].

[89] G. Aad *et al.* (ATLAS), Phys. Rev. D **104**, 3, 032014 (2021), [arXiv:2103.08189].

[90] A. M. Sirunyan *et al.* (CMS), JHEP **03**, 076 (2018), [arXiv:1709.08908].

[91] A. M. Sirunyan *et al.* (CMS), Eur. Phys. J. C **80**, 8, 752 (2020), [arXiv:2001.10086].

[92] C. Boehm, A. Djouadi and Y. Mambrini, Phys. Rev. **D61**, 095006 (2000), [hep-ph/9907428].

[93] T. Aaltonen *et al.* (CDF), Phys. Rev. **D82**, 092001 (2010), [arXiv:1009.0266].

[94] V. M. Abazov *et al.* (D0), Phys. Lett. **B696**, 321 (2011), [arXiv:1009.5950].

[95] T. Aaltonen *et al.* (CDF), JHEP **10**, 158 (2012), [arXiv:1203.4171].

[96] V. M. Abazov *et al.* (D0), Phys. Lett. **B665**, 1 (2008), [arXiv:0803.2263].

[97] T. Aaltonen *et al.* (CDF), Phys. Rev. Lett. **104**, 251801 (2010), [arXiv:0912.1308].

[98] V. M. Abazov *et al.* (D0), Phys. Lett. **B674**, 4 (2009), [arXiv:0901.1063].

[99] G. Aad *et al.* (ATLAS), Eur. Phys. J. C **80**, 8, 737 (2020), [arXiv:2004.14060].

[100] G. Aad *et al.* (ATLAS), JHEP **04**, 174 (2021), [arXiv:2012.03799].

[101] A. M. Sirunyan *et al.* (CMS), Phys. Rev. D **104**, 5, 052001 (2021), [arXiv:2103.01290].

[102] M. Aaboud *et al.* (ATLAS), JHEP **06**, 108 (2018), [arXiv:1711.11520].

[103] M. Aaboud *et al.* (ATLAS), Phys. Rev. **D98**, 3, 032008 (2018), [arXiv:1803.10178].

[104] A. M. Sirunyan *et al.* (CMS), JHEP **02**, 015 (2020), [arXiv:1910.12932].

[105] G. Aad *et al.* (ATLAS), JHEP **04**, 165 (2021), [arXiv:2102.01444].

[106] A. M. Sirunyan *et al.* (CMS), Eur. Phys. J. **C77**, 10, 710 (2017), [arXiv:1705.04650].

[107] A. M. Sirunyan *et al.* (CMS), Phys. Rev. **D96**, 3, 032003 (2017), [arXiv:1704.07781].

[108] A. M. Sirunyan *et al.* (CMS), JHEP **10**, 005 (2017), [arXiv:1707.03316].

[109] A. M. Sirunyan *et al.* (CMS), JHEP **10**, 019 (2017), [arXiv:1706.04402].

Downloaded from https://academic.oup.com/ptep/article/2022/8/083C01/6651666 by KIT Library user on 27 September 2022

[110] A. M. Sirunyan *et al.* (CMS), Eur. Phys. J. C **81**, 1, 3 (2021), [arXiv:2008.05936].

[111] A. M. Sirunyan *et al.* (CMS), JHEP **03**, 101 (2019), [arXiv:1901.01288].

[112] M. Aaboud *et al.* (ATLAS), Phys. Rev. D **98**, 3, 032008 (2018), [arXiv:1803.10178].

[113] G. Aad *et al.* (ATLAS) (2021), [arXiv:2108.07665].

[114] G. Aad *et al.* (ATLAS), Eur. Phys. J. C **80**, 11, 1080 (2020), [arXiv:2006.05880].

[115] M. Aaboud *et al.* (ATLAS), Eur. Phys. J. C **80**, 8, 754 (2020), [arXiv:1903.07570].

[116] (2018).

[117] M. Aaboud *et al.* (ATLAS), Phys. Rev. **D98**, 3, 032009 (2018), [arXiv:1804.03602].

[118] M. Aaboud *et al.* (ATLAS), JHEP **09**, 084 (2017), [arXiv:1706.03731].

[119] CMS Collab., CMS-PAS-SUS-19-008 (2019).

[120] V. Khachatryan *et al.* (CMS), Phys. Rev. **D94**, 11, 112009 (2016), [arXiv:1606.08076].

[121] CMS Collab., CMS-PAS-SUS-13-010 (2013).

[122] T. Aaltonen *et al.* (CDF), Phys. Rev. Lett. **107**, 042001 (2011), [arXiv:1105.2815].

[123] M. Aaboud *et al.* (ATLAS), Phys. Lett. **B785**, 136 (2018), [arXiv:1804.03568].

[124] ATLAS Collab., ATLAS-CONF-2018-003 (2018).

[125] ATLAS Collab., ATLAS-CONF-2016-057 (2016).

[126] M. Aaboud *et al.* (ATLAS), JHEP **09**, 088 (2017), [arXiv:1704.08493].

[127] A. M. Sirunyan *et al.* (CMS), Phys. Lett. **B783**, 114 (2018), [arXiv:1712.08920].

[128] S. Chatrchyan *et al.* (CMS), Phys. Lett. **B730**, 193 (2014), [arXiv:1311.1799].

[129] V. Khachatryan *et al.* (CMS), Phys. Lett. **B770**, 257 (2017), [arXiv:1608.01224].

[130] G. Aad *et al.* (ATLAS) (2021), [arXiv:2106.09609].

[131] F. D. Aaron *et al.* (H1), Eur. Phys. J. **C71**, 1572 (2011), [arXiv:1011.6359].

[132] ATLAS Collab., ATLAS-CONF-2015-018 (2015).

[133] S. Chekanov *et al.* (ZEUS), Eur. Phys. J. **C50**, 269 (2007), [hep-ex/0611018].

[134] M. Aaboud *et al.* (ATLAS), Phys. Rev. **D97**, 3, 032003 (2018), [arXiv:1710.05544].

[135] ATLAS Collab., ATLAS-CONF-2019-006 (2019).

[136] A. M. Sirunyan *et al.* (CMS), Phys. Rev. **D99**, 3, 032014 (2019), [arXiv:1808.05082].

[137] CMS Collab., CMS-PAS-EXO-16-022 (2016).

[138] V. Khachatryan *et al.* (CMS), Phys. Lett. **B760**, 178 (2016), [arXiv:1602.04334].

[139] M. Aaboud *et al.* (ATLAS), Eur. Phys. J. C **78**, 3, 250 (2018), [arXiv:1710.07171].

[140] G. Aad *et al.* (ATLAS) (2019), [arXiv:1909.08457].

[141] M. Aaboud *et al.* (ATLAS), Eur. Phys. J. **C78**, 3, 250 (2018), [arXiv:1710.07171].

[142] V. Khachatryan *et al.* (CMS), Phys. Rev. **D95**, 1, 012009 (2017), [arXiv:1610.05133].

[143] V. Khachatryan *et al.* (CMS), Phys. Lett. **B747**, 98 (2015), [arXiv:1412.7706].

[144] G. Aad *et al.* (ATLAS), Eur. Phys. J. C **81**, 1, 11 (2021), [Erratum: Eur.Phys.J.C 81, 249 (2021)], [arXiv:2010.01015].

[145] A. M. Sirunyan *et al.* (CMS), Phys. Rev. D **104**, 3, 032006 (2021), [arXiv:2102.06976].

[146] J. Fan, M. Reece and J. T. Ruderman, JHEP **11**, 012 (2011), [arXiv:1105.5135].

[147] J. Fan, M. Reece and J. T. Ruderman, JHEP **07**, 196 (2012), [arXiv:1201.4875].

[148] J. Fan *et al.*, JHEP **07**, 016 (2016), [arXiv:1512.05781].

[149] V. Khachatryan *et al.* (CMS), Phys. Lett. B **743**, 503 (2015), [arXiv:1411.7255].

[150] B. Fuks *et al.*, JHEP **10**, 081 (2012), [arXiv:1207.2159].

[151] B. Fuks *et al.*, Eur. Phys. J. C **73**, 2480 (2013), [arXiv:1304.0790].

[152] LEP2 SUSY Working Group, ALEPH, DELPHI, L3 and OPAL experiments, note LEPSUSYWG/01-03.1, `http://lepsusy.web.cern.ch/lepsusy`.

[153] LEP2 SUSY Working Group, ALEPH, DELPHI, L3 and OPAL experiments, note LEPSUSYWG/02-04.1, `http://lepsusy.web.cern.ch/lepsusy`.

[154] CDF Collab., CDF Note 10636 (2011).

[155] V. M. Abazov *et al.* (D0), Phys. Lett. **B680**, 34 (2009), [arXiv:0901.0646].

[156] G. Aad *et al.* (ATLAS) (2019), [arXiv:1908.08215].

[157] A. M. Sirunyan *et al.* (CMS), JHEP **11**, 079 (2018), [arXiv:1807.07799].

[158] M. Aaboud *et al.* (ATLAS), Eur. Phys. J. **C78**, 2, 154 (2018), [arXiv:1708.07875].

[159] A. M. Sirunyan *et al.* (CMS), JHEP **11**, 151 (2018), [arXiv:1807.02048].

[160] G. Aad *et al.* (ATLAS) (2021), [arXiv:2108.07586].

[161] Technical report, CERN, Geneva (2021), URL `https://cds.cern.ch/record/2779116`.

[162] M. Aaboud *et al.* (ATLAS), Eur. Phys. J. **C78**, 12, 995 (2018), [arXiv:1803.02762].

[163] A. M. Sirunyan *et al.* (CMS) (2021), [arXiv:2106.14246].

[164] G. Aad *et al.* (ATLAS) (2021), [arXiv:2106.01676].

[165] A. Tumasyan *et al.* (CMS), JHEP **10**, 045 (2021), [arXiv:2107.12553].

[166] M. Aaboud *et al.* (ATLAS), Phys. Rev. **D100**, 1, 012006 (2019), [arXiv:1812.09432].

[167] ATLAS Collab., ATLAS-CONF-2019-019 (2019).

[168] G. Aad *et al.* (ATLAS) (2019), [arXiv:1909.09226].

[169] ATLAS Collab., ATLAS-CONF-2019-014 (2019).

[170] (2021).

[171] A. M. Sirunyan *et al.* (CMS), JHEP **08**, 150 (2019), [arXiv:1905.13059].

[172] A. M. Sirunyan *et al.* (CMS) (2019), [arXiv:1910.01185].

[173] H. K. Dreiner *et al.*, Eur. Phys. J. **C62**, 547 (2009), [arXiv:0901.3485].

[174] LEP2 SUSY Working Group, ALEPH, DELPHI, L3 and OPAL experiments, note LEPSUSYWG/04-07.1, `http://lepsusy.web.cern.ch/lepsusy`.

[175] O. Buchmueller *et al.*, Eur. Phys. J. **C74**, 6, 2922 (2014), [arXiv:1312.5250].

[176] C. Strege *et al.*, JCAP **1304**, 013 (2013), [arXiv:1212.2636].

[177] A. Fowlie *et al.*, Phys. Rev. **D86**, 075010 (2012), [arXiv:1206.0264].

[178] LEP2 SUSY Working Group, ALEPH, DELPHI, L3 and OPAL experiments, note LEPSUSYWG/04-09.1, `http://lepsusy.web.cern.ch/lepsusy`.

[179] T. Aaltonen *et al.* (CDF), Phys. Rev. Lett. **104**, 011801 (2010), [arXiv:0910.3606].

[180] V. M. Abazov *et al.* (D0), Phys. Rev. Lett. **105**, 221802 (2010), [arXiv:1008.2133].

[181] M. Aaboud *et al.* (ATLAS), Phys. Rev. **D97**, 9, 092006 (2018), [arXiv:1802.03158].

Downloaded from https://academic.oup.com/ptep/article/2022/8/083C01/6651666 by KIT Library user on 27 September 2022

[182] A. M. Sirunyan *et al.* (CMS), JHEP **06**, 143 (2019), [arXiv:1903.07070].

[183] A. M. Sirunyan *et al.* (CMS) (2019), [arXiv:1907.00857].

[184] M. Aaboud *et al.* (ATLAS), Phys. Rev. **D98**, 9, 092002 (2018), [arXiv:1806.04030].

[185] M. Aaboud *et al.* (ATLAS), Phys. Rev. **D99**, 1, 012001 (2019), [arXiv:1808.03057].

[186] G. Aad *et al.* (ATLAS), JHEP **10**, 005 (2020), [arXiv:2004.10894].

[187] A. M. Sirunyan *et al.* (CMS), JHEP **03**, 166 (2018), [arXiv:1709.05406].

[188] A. M. Sirunyan *et al.* (CMS), JHEP **03**, 160 (2018), [arXiv:1801.03957].

[189] A. M. Sirunyan *et al.* (CMS), Eur. Phys. J. **C79**, 5, 444 (2019), [arXiv:1901.06726].

[190] A. M. Sirunyan *et al.* (CMS), JHEP **01**, 154 (2019), [arXiv:1812.04066].

[191] A. M. Sirunyan *et al.* (CMS), Phys. Lett. **B780**, 118 (2018), [arXiv:1711.08008].

[192] A. M. Sirunyan *et al.* (CMS), Phys. Rev. **D97**, 3, 032007 (2018), [arXiv:1709.04896].

[193] A. M. Sirunyan *et al.* (CMS), Phys. Lett. **B779**, 166 (2018), [arXiv:1709.00384].

[194] Technical report, CERN, Geneva (2021), URL `https://cds.cern.ch/record/2777125`.

[195] G. Aad *et al.* (ATLAS), Phys. Rev. **D93**, 5, 052002 (2016), [arXiv:1509.07152].

[196] M. Aaboud *et al.* (ATLAS), Eur. Phys. J. **C78**, 8, 625 (2018), [arXiv:1805.11381].

[197] M. Aaboud *et al.* (ATLAS), Eur. Phys. J. **C77**, 3, 144 (2017), [arXiv:1611.05791].

[198] A. M. Sirunyan *et al.* (CMS), JHEP **04**, 123 (2021), [arXiv:2012.08600].

[199] A. Arbey, M. Battaglia and F. Mahmoudi, Eur. Phys. J. C **72**, 1847 (2012), [arXiv:1110.3726].

[200] G. Aad *et al.* (ATLAS), JHEP **10**, 134 (2015), [arXiv:1508.06608].

[201] V. Khachatryan *et al.* (CMS), JHEP **10**, 129 (2016), [arXiv:1606.03577].

[202] P. Athron *et al.* (GAMBIT), Eur. Phys. J. **C77**, 12, 879 (2017), [arXiv:1705.07917].

[203] K. J. de Vries *et al.*, Eur. Phys. J. **C75**, 9, 422 (2015), [arXiv:1504.03260].

[204] C. Strege *et al.*, JHEP **09**, 081 (2014), [arXiv:1405.0622].

[205] LEP2 SUSY Working Group, ALEPH, DELPHI, L3 and OPAL experiments, note LEPSUSYWG/04-01.1, `http://lepsusy.web.cern.ch/lepsusy`.

[206] A. Heister *et al.* (ALEPH), Phys. Lett. **B544**, 73 (2002), [hep-ex/0207056].

[207] A. M. Sirunyan *et al.* (CMS), Phys. Lett. **B790**, 140 (2019), [arXiv:1806.05264].

[208] G. Aad *et al.* (ATLAS), Phys. Rev. D **101**, 5, 052005 (2020), [arXiv:1911.12606].

[209] G. Aad *et al.* (ATLAS), Phys. Rev. D **101**, 3, 032009 (2020), [arXiv:1911.06660].

[210] A. M. Sirunyan *et al.* (CMS) (2019), [arXiv:1907.13179].

[211] Technical report, CERN, Geneva (2021), URL `https://cds.cern.ch/record/2777046`.

[212] LEP2 SUSY Working Group, ALEPH, DELPHI, L3 and OPAL experiments, note LEPSUSYWG/02-09.2, `http://lepsusy.web.cern.ch/lepsusy`.

[213] M. Aaboud *et al.* (ATLAS), Phys. Rev. **D99**, 1, 012009 (2019), [arXiv:1808.06358].

[214] S. Chatrchyan *et al.* (CMS), Eur. Phys. J. **C73**, 2493 (2013), [arXiv:1301.3792].

[215] S. Chatrchyan *et al.* (CMS), Phys. Rev. **D90**, 032006 (2014), [arXiv:1404.5801].

[216] T. Aaltonen *et al.* (CDF), Phys. Rev. Lett. **110**, 20, 201802 (2013), [arXiv:1302.4491].

[217] DELPHI Collab., Eur. Phys. J. **C31**, 412 (2003).

[218] G. Aad *et al.* (ATLAS), Phys. Rev. **D92**, 7, 072004 (2015), [arXiv:1504.05162].

[219] V. Khachatryan *et al.* (CMS), Phys. Rev. **D91**, 1, 012007 (2015), [arXiv:1411.6530].

[220] G. Aad *et al.* (ATLAS), Phys. Rev. D **103**, 112003 (2021), [arXiv:2011.10543].

[221] LEP2 SUSY Working Group, ALEPH, DELPHI, L3 and OPAL experiments, note LEPSUSYWG/02-10.1, `http://lepsusy.web.cern.ch/lepsusy`.

[222] A. M. Sirunyan *et al.* (CMS), Eur. Phys. J. **C79**, 4, 305 (2019), [arXiv:1811.09760].

[223] T. Aaltonen *et al.* (CDF), Phys. Rev. Lett. **105**, 191801 (2010), [arXiv:1004.3042].

[224] V. M. Abazov *et al.* (D0), Phys. Rev. Lett. **105**, 191802 (2010), [arXiv:1007.4835].

[225] G. Aad *et al.* (ATLAS), Phys. Rev. Lett. **115**, 3, 031801 (2015), [arXiv:1503.04430].

[226] M. Aaboud *et al.* (ATLAS), Eur. Phys. J. **C76**, 10, 541 (2016), [arXiv:1607.08079].

[227] V. Khachatryan *et al.* (CMS), Eur. Phys. J. **C76**, 6, 317 (2016), [arXiv:1604.05239].

[228] M. Aaboud *et al.* (ATLAS), Phys. Rev. **D97**, 5, 052012 (2018), [arXiv:1710.04901].

[229] M. Aaboud *et al.* (ATLAS), Phys. Rev. **D99**, 9, 092007 (2019), [arXiv:1902.01636].

[230] G. Aad *et al.* (ATLAS), Eur. Phys. J. **C75**, 9, 407 (2015), [arXiv:1506.05332].

[231] A. M. Sirunyan *et al.* (CMS), Phys. Lett. **B797**, 134876 (2019), [arXiv:1906.06441].

[232] A. M. Sirunyan *et al.* (CMS), JHEP **05**, 025 (2018), [arXiv:1802.02110].

[233] CMS Collab., CMS-PAS-EXO-16-036 (2016).

[234] A. M. Sirunyan *et al.* (CMS), Phys. Lett. B **806**, 135502 (2020), [arXiv:2004.05153].

[235] A. M. Sirunyan *et al.* (CMS), Phys. Rev. D **104**, 1, 012015 (2021), [arXiv:2012.01581].

[236] V. M. Abazov *et al.* (D0), Phys. Rev. Lett. **99**, 131801 (2007), [arXiv:0705.0306].

[237] G. Aad *et al.* (ATLAS), Phys. Rev. **D88**, 11, 112003 (2013), [arXiv:1310.6584].

[238] A. M. Sirunyan *et al.* (CMS), JHEP **05**, 127 (2018), [arXiv:1801.00359].

[239] G. Aad *et al.* (ATLAS), JHEP **07**, 173 (2021), [arXiv:2104.03050].

[240] T. Aaltonen *et al.* (CDF), Phys. Rev. Lett. **103**, 021802 (2009), [arXiv:0902.1266].

[241] V. M. Abazov *et al.* (D0), Phys. Rev. **D87**, 5, 052011 (2013), [arXiv:1211.2466].

[242] G. Aad *et al.* (ATLAS), Phys. Rev. D **102**, 3, 032006 (2020), [arXiv:2003.11956].

[243] A. Tumasyan *et al.* (CMS) (2021), [arXiv:2110.04809].

[244] A. M. Sirunyan *et al.* (CMS), JHEP **08**, 016 (2018), [arXiv:1804.07321].

[245] M. Aaboud *et al.* (ATLAS), JHEP **06**, 022 (2018), [arXiv:1712.02118].

[246] G. Aad *et al.* (ATLAS), Phys. Rev. **D88**, 11, 112006 (2013), [arXiv:1310.3675].

Downloaded from https://academic.oup.com/ptep/article/2022/8/083C01/6651666 by KIT Library user on 27 September 2022

[247] Technical report, CERN, Geneva (2021), all figures including auxiliary figures are available at `https://atlas.web.cern.ch/Atlas/GROUPS/PHYSICS/CONFNOTES/ATLAS-CONF-2021-015`, URL `https://cds.cern.ch/record/2759676`.

[248] LEP2 SUSY Working Group, ALEPH, DELPHI, L3 and OPAL experiments, note LEPSUSYWG/02-05.1, `http://lepsusy.web.cern.ch/lepsusy`.

[249] V. Khachatryan *et al.* (CMS), Eur. Phys. J. **C75**, 7, 325 (2015), [arXiv:1502.02522].

[250] T. Aaltonen *et al.* (CDF), Phys. Rev. **D88**, 3, 031103 (2013), [arXiv:1307.0474].

[251] A. M. Sirunyan *et al.* (CMS) (2019), [arXiv:1909.06166].

[252] V. M. Abazov *et al.* (D0), Phys. Rev. Lett. **101**, 111802 (2008), [arXiv:0806.2223].

[253] G. Aad *et al.* (ATLAS), Phys. Rev. **D90**, 11, 112005 (2014), [arXiv:1409.5542].

[254] O. Buchmueller *et al.*, Eur. Phys. J. **C71**, 1722 (2011), [arXiv:1106.2529].

[255] E. A. Baltz and P. Gondolo, JHEP **10**, 052 (2004), [hep-ph/0407039].

[256] B. C. Allanach and C. G. Lester, Phys. Rev. **D73**, 015013 (2006), [hep-ph/0507283].

[257] R. Ruiz de Austri, R. Trotta and L. Roszkowski, JHEP **05**, 002 (2006), [hep-ph/0602028].

[258] R. Lafaye *et al.*, Eur. Phys. J. **C54**, 617 (2008), [arXiv:0709.3985].

[259] M. Shaposhnikov, JHEP **08**, 008 (2008), [arXiv:0804.4542].

[260] R. Trotta *et al.*, JHEP **12**, 024 (2008), [arXiv:0809.3792].

[261] P. Bechtle *et al.*, Eur. Phys. J. **C66**, 215 (2010), [arXiv:0907.2589].

[262] E. Bagnaschi *et al.*, Eur. Phys. J. C **78**, 256, 1 (2018).

[263] J. Costa *et al.*, Eur. Phys. J. C **78**, 158, 1 (2018).

[264] E. Bagnaschi *et al.*, Eur. Phys. J. **C77**, 4, 268 (2017), [arXiv:1612.05210].

[265] E. Bagnaschi *et al.*, Eur. Phys. J. **C77**, 2, 104 (2017), [arXiv:1610.10084].

[266] L. A. Harland-Lang, V. A. Khoze and M. G. Ryskin, Eur. Phys. J. **C76**, 1, 9 (2016), [arXiv:1508.02718].

[267] E. A. Bagnaschi *et al.*, Eur. Phys. J. **C75**, 500 (2015), [arXiv:1508.01173].

[268] O. Buchmueller *et al.*, Eur. Phys. J. **C74**, 12, 3212 (2014), [arXiv:1408.4060].

[269] M. Citron *et al.*, Phys. Rev. **D87**, 3, 036012 (2013), [arXiv:1212.2886].

[270] Supersymmetry Physics Results, ATLAS experiment, `http://twiki.cern.ch/twiki/bin/view/AtlasPublic/SupersymmetryPublicResults/`.

[271] Supersymmetry Physics Results, CMS experiment, `http://cms-results.web.cern.ch/cms-results/public-results/publications/SUS/index.html`.

Downloaded from https://academic.oup.com/ptep/article/2022/8/083C01/6651666 by KIT Library user on 27 September 2022

90. Axions and Other Similar Particles

Revised October 2021 by A. Ringwald (DESY, Hamburg), L. J Rosenberg (U. Washington) and G. Rybka (U. Washington).

90.1 Introduction

In this section, we list coupling-strength and mass limits for light neutral scalar or pseudoscalar bosons that couple weakly to normal matter and radiation. Such bosons may arise from the spontaneous breaking of a global U(1) symmetry, resulting in a massless Nambu-Goldstone (NG) boson. If there is a small explicit symmetry breaking, either already in the Lagrangian or due to quantum effects such as anomalies, the boson acquires a mass and is called a pseudo-NG boson. Typical examples are axions (a) [1–4] and majorons [5,6], associated, respectively, with a spontaneously broken Peccei-Quinn and lepton-number symmetry.

A common feature of these light bosons ϕ is that their coupling to Standard-Model particles is suppressed by the energy scale that characterizes the symmetry breaking, *i.e.*, the decay constant f. The interaction Lagrangian is

$$\mathcal{L} = f^{-1} J^{\mu} \partial_{\mu} \phi \,, \tag{90.1}$$

where J^{μ} is the Noether current of the spontaneously broken global symmetry. If f is very large, these new particles interact very weakly. Detecting them would provide a window to physics far beyond what can be probed at accelerators.

Axions are of particular interest because the Peccei-Quinn (PQ) mechanism remains perhaps the most credible scheme to preserve CP-symmetry in QCD. Moreover, the cold dark matter (CDM) of the Universe may well consist of axions and they are searched for in dedicated experiments with a realistic chance of discovery.

Originally it was assumed that the PQ scale f_a was related to the electroweak symmetry-breaking scale $v_{\rm EW} = (\sqrt{2} G_{\rm F})^{-1/2} =$ 247 GeV. However, the associated "standard" and "variant" axions were quickly excluded—we refer to the Listings for detailed limits. Here we focus on "invisible axions" with $f_a \gg v_{\rm EW}$ as the main possibility.

Axions have a characteristic two-photon vertex, inherited from their mixing with π^0 and η. This coupling allows for the main search strategy based on axion-photon conversion in external magnetic fields [7], an effect that also can be of astrophysical interest. While for axions the product "$a\gamma\gamma$ interaction strength $\times$ mass" is essentially fixed by the corresponding π^0 properties, one may consider a more general class of axion-like particles (ALPs) where the two parameters (coupling and mass) are independent. A number of experiments explore this more general parameter space. ALPs populating the latter are predicted to arise generically, in addition to the axion, in low-energy effective field theories emerging from string theory [8–15]. The latter often contain also very light Abelian vector bosons under which the Standard-Model particles are not charged: so-called hidden-sector photons, dark photons or paraphotons. They share a number of phenomenological features with the axion and ALPs, notably the possibility of hidden photon to photon conversion and of hidden photon dark matter [16–18]. Their physics cases and the current constraints are compiled in Refs. [19–22].

90.2 Theory

90.2.1 *Peccei-Quinn mechanism and axions*

The QCD Lagrangian includes a CP-violating term $\mathcal{L}_{\Theta} = -\bar{\Theta}\,(\alpha_s/8\pi)\, G^{\mu\nu a} \tilde{G}^a_{\mu\nu}$, where $-\pi \le \bar{\Theta} \le +\pi$ is the effective Θ parameter after diagonalizing quark masses, $G^a_{\mu\nu}$ is the color field strength tensor, and $\tilde{G}^{a,\mu\nu} \equiv \epsilon^{\mu\nu\lambda\rho} G^a_{\lambda\rho}/2$, with $\varepsilon^{0123} = 1$, its dual. This term induces an electric dipole moment (EDM) of the neutron of size $d_n = C_{\rm EDM}\, e\, \bar{\Theta}$, where $C_{\rm EDM} = 2.4(1.0) \times 10^{-16}$ cm [23]. Experimental upper bounds on the latter, $|d_n| < 1.8 \times 10^{-26}\, e$ cm [24,25], imply $|\bar{\Theta}| \lesssim 10^{-10}$ even though $\bar{\Theta} = \mathcal{O}(1)$ is otherwise completely satisfactory. The spontaneously broken global Peccei-Quinn symmetry U(1)$_{\rm PQ}$ was introduced to solve this "strong CP problem" [1,2], the axion being the pseudo-NG boson of U(1)$_{\rm PQ}$ [3,4]. This symmetry is broken due to the axion's anomalous triangle coupling to gluons,

$$\mathcal{L} = \left(\frac{a}{f_a} - \bar{\Theta} \right) \frac{\alpha_s}{8\pi}\, G^{\mu\nu a} \tilde{G}^a_{\mu\nu} \,, \tag{90.2}$$

where a is the axion field and f_a the axion decay constant. Color anomaly factors have been absorbed in the normalization of f_a which is defined by this Lagrangian. Thus normalized, f_a is the quantity that enters all low-energy phenomena [26]. Non-perturbative topological fluctuations of the gluon fields in QCD induce a potential for a whose minimum is at $a = \bar{\Theta}\, f_a$, thereby canceling the $\bar{\Theta}$ term in the QCD Lagrangian and thus restoring CP symmetry.

The resulting axion mass, in units of the PQ scale f_a, is identical to the square root of the topological susceptibility in QCD, $m_a f_a = \sqrt{\chi}$. The latter can be evaluated further [27,28], exploiting the chiral limit (masses of up and down quarks much smaller than the scale of QCD), yielding $m_a f_a = \sqrt{\chi} \approx f_\pi m_\pi$, where $m_\pi = 135$ MeV and $f_\pi \approx 92$ MeV. In more detail one finds, by including $\mathcal{O}(\alpha)$ QED corrections and next-to-next-to-leading order (NNLO) corrections in chiral perturbation theory [29],

$$m_a = 5.691(51) \left(\frac{10^9\ \text{GeV}}{f_a} \right) \text{meV} \,. \tag{90.3}$$

A direct calculation of the topological susceptibility via QCD lattice simulations finds almost the same central value, albeit with an about five times larger error bar [30].

The axion's anomalous coupling to gluons induces, at energies below the confinement scale of QCD, a model-independent coupling of the axion to the operator giving rise to the EDM of the nucleon (N),

$$\mathcal{L}_{aN\gamma} = -\frac{i}{2} g_{aN\gamma}\, a\, \overline{\Psi}_N \sigma_{\mu\nu} \gamma_5 \Psi_N F^{\mu\nu} \,, \tag{90.4}$$

where the couplings constants of the neutron (n) and the proton (p) are given by

$$g_{an\gamma} = -g_{ap\gamma} = e\, \frac{C_{\rm EDM}}{f_a} = (3.7 \pm 1.5) \times 10^{-3} \left(\frac{1}{f_a} \right) \frac{1}{\text{GeV}} \,. \tag{90.5}$$

This coupling, as a function of the axion mass, is displayed in Fig. 90.1, where the thickness of the yellow band presents the theoretical uncertainty given in Eq. (90.5).

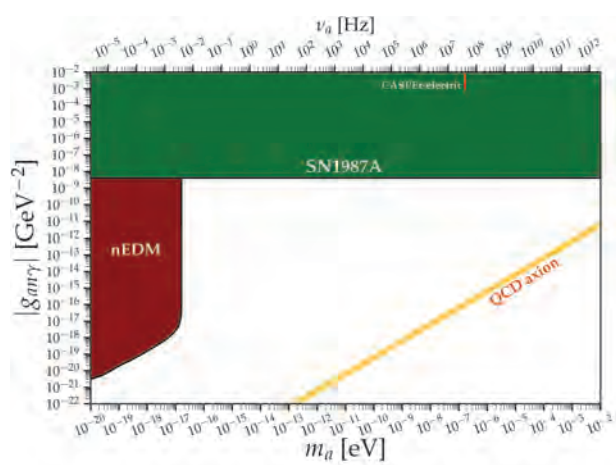

Figure 90.1: Exclusion plot for ALP-EDM coupling as described in the text. Figure courtesy of Ciaran O'Hare [31].

Axions with $f_a \gg v_{\rm EW}$ evade almost all current experimental limits. One generic class of models invokes "hadronic axions" where new heavy quarks carry U(1)$_{\rm PQ}$ charges, leaving ordinary quarks and leptons without tree-level axion couplings. The archetype is the KSVZ model [32,33], where in addition the heavy new quarks are electrically neutral. Another generic class requires at least two Higgs doublets and ordinary quarks and leptons carry PQ charges, the archetype being the DFSZ model [34,35]. All of these models contain at least one electroweak singlet scalar that acquires a vacuum expectation value and thereby breaks the PQ

Downloaded from https://academic.oup.com/ptep/article/2022/8/083C01/6651666 by KIT Library user on 27 September 2022

symmetry. The KSVZ and DFSZ models are frequently used as benchmark examples, but other models exist where both heavy quarks and Higgs doublets carry PQ charges. In supersymmetric models, the axion is part of a supermultiplet and thus inevitably accompanied by a spin-0 saxion and a spin-1/2 axino, which both also have couplings suppressed by f_a and are expected to have large masses due to supersymmetry breaking [36].

90.2.2 *Model-dependent axion couplings*

Although the generic axion interactions scale approximately with f_π/f_a from the corresponding π^0 couplings, there are non-negligible model-dependent factors and uncertainties. The axion's two-photon interaction plays a key role for many searches,

$$\mathcal{L}_{a\gamma\gamma} = -\frac{g_{a\gamma\gamma}}{4}\, a\, F_{\mu\nu}\tilde{F}^{\mu\nu} = g_{a\gamma\gamma}\, a\, \mathbf{E}\cdot\mathbf{B}\,, \tag{90.6}$$

where F is the electromagnetic field-strength tensor and $\tilde{F}^{\mu\nu} \equiv \epsilon^{\mu\nu\lambda\rho}F_{\lambda\rho}/2$, with $\varepsilon^{0123} = 1$, its dual. The coupling constant is [37]

$$g_{a\gamma\gamma} = \frac{\alpha}{2\pi f_a}\left(\frac{E}{N} - 1.92(4)\right) = \left(0.203(3)\frac{E}{N} - 0.39(1)\right)\frac{m_a}{\mathrm{GeV}^2}\,, \tag{90.7}$$

where E and N are the electromagnetic and color anomalies of the axial current associated with the axion. In grand unified models, and notably for DFSZ [34, 35], $E/N = 8/3$, whereas for KSVZ [32, 33] $E/N = 0$ if the electric charge of the new heavy quark is taken to vanish. In general, a broad range of E/N values is possible [38–41], as indicated by the diagonal yellow band in Fig. 90.2, whose width is roughly determined by the boundary values $E/N = 44/3$ and $E/N = 5/3$, respectively. However, this band still does not exhaust all the possibilities. In fact, there exist classes of QCD axion models whose photon couplings populate the entire still-allowed region outside the yellow band in Fig. 90.2 [42–46], motivating axion search efforts over a wide range of masses and couplings.

The two-photon decay width is

$$\Gamma_{a\to\gamma\gamma} = \frac{g_{a\gamma\gamma}^2 m_a^3}{64\,\pi} = 1.1\times 10^{-24}\ \mathrm{s}^{-1}\left(\frac{m_a}{\mathrm{eV}}\right)^5. \tag{90.8}$$

The second expression uses Eq. (90.7) with $E/N = 0$. Axions decay faster than the age of the Universe if $m_a \gtrsim 20$ eV.

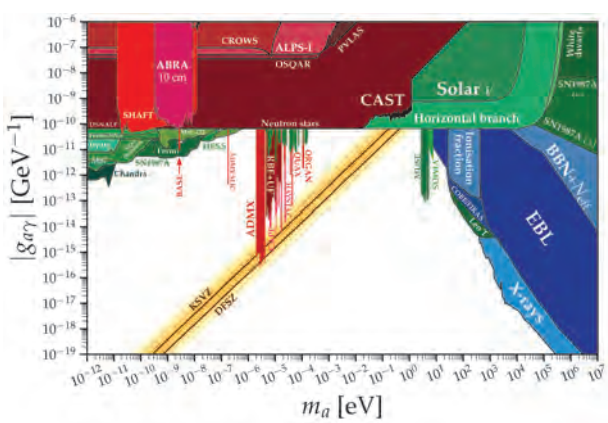

Figure 90.2: Exclusion plot for ALP-photon coupling as described in the text. Figure courtesy of Ciaran O'Hare [31].

The interaction with fermions f has derivative form and is invariant under a shift $a \to a + a_0$ as behooves a NG boson,

$$\mathcal{L}_{aff} = \frac{C_f}{2f_a}\,\partial_\mu a\,\bar{\Psi}_f\gamma^\mu\gamma_5\Psi_f\ . \tag{90.9}$$

Here, Ψ_f is the fermion field, m_f its mass, and C_f a model-dependent coefficient. The dimensionless combination $g_{aff} \equiv C_f m_f/f_a$ plays the role of a Yukawa coupling and $\alpha_{aff} \equiv g_{aff}^2/4\pi$ of a "fine-structure constant." The often-used pseudoscalar form $\mathcal{L}_{aff} = -\mathrm{i}\,(C_f m_f/f_a)\,a\,\bar{\Psi}_f\gamma_5\Psi_f$ need not be equivalent to the appropriate derivative structure, for example when two NG bosons are attached to one fermion line as in axion emission by nucleon bremsstrahlung [47–49].

In hadronic axion models, C_e vanishes at tree level, but is then generated radiatively at one loop [50, 51],

$$C_e \simeq \frac{3\alpha^2}{4\pi^2}\left[\frac{E}{N}\log\left(\frac{f_a}{m_e}\right) - 1.92\log\left(\frac{\Lambda_\chi}{m_e}\right)\right]\,, \tag{90.10}$$

where $\Lambda_\chi \simeq 1$ GeV is the chiral symmetry breaking scale. In the DFSZ model [34,35], the tree-level coupling coefficient to electrons is [50]

$$C_e = \frac{\sin^2\beta}{3}\,, \tag{90.11}$$

where $\tan\beta$ is the ratio of the vacuum expectation values of the two Higgs doublets giving masses to the up- and down-type quarks, respectively: $\tan\beta = v_u/v_d$. The resulting prediction for the axion-electron coupling, as a function of the axion mass, for the KSVZ axion ($E/N = 0$), hadronic axions, with $5/3 \le E/N \le 44/3$, and the DFSZ axion is displayed in Fig. 90.3. For the DFSZ range we have taken into account the constraint $0.28 \lesssim \tan\beta \lesssim 140$ [52] arising from the requirement of perturbative unitarity of the Yukawa couplings of Standard Model fermions.

For nucleons, $C_{p,n}$ have been determined as [37]

$$\begin{aligned} C_p &= -0.47(3) + 0.88(3)C_u - 0.39(2)C_d - 0.038(5)C_s \\ &\qquad - 0.012(5)C_c - 0.009(2)C_b - 0.0035(4)C_t\,, \\ C_n &= -0.02(3) + 0.88(3)C_d - 0.39(2)C_u - 0.038(5)C_s \\ &\qquad - 0.012(5)C_c - 0.009(2)C_b - 0.0035(4)C_t\,, \end{aligned} \tag{90.12}$$

in terms of the corresponding model-dependent quark couplings C_q, $q = u, d, s, c, b, t$. For hadronic axions, the latter vanish at tree-level, which means that C_n is expected to be much smaller than C_p. In the DFSZ model, $C_u = C_c = C_t = \frac{1}{3}\cos^2\beta$ and $C_d = C_s = C_b = \frac{1}{3}\sin^2\beta$, and C_p and C_n, as functions of β,

$$\begin{aligned} C_p &= -0.435\sin^2\beta + (-0.182 \pm 0.025)\,, \\ C_n &= 0.414\sin^2\beta + (-0.160 \pm 0.025)\,, \end{aligned} \tag{90.13}$$

The resulting prediction for the axion-neutron coupling, as a function of the axion mass, for the KSVZ axion and the DFSZ axion is displayed in Fig. 90.4.

The axion-pion interaction is given by the Lagrangian [51]

$$\mathcal{L}_{a\pi} = \frac{C_{a\pi}}{f_\pi f_a}\,\partial_\mu a\left(\pi^0\pi^+\partial_\mu\pi^- + \pi^0\pi^-\partial_\mu\pi^+ - 2\pi^+\pi^-\partial_\mu\pi^0\right)\,, \tag{90.14}$$

where $C_{a\pi} = (1-z)/[3(1+z)]$ in hadronic models and $C_{a\pi} = (1-z)/[3(1+z)] - (1/9)\cos 2\beta$ in the DFSZ model [41], with $z = m_u/m_d = 0.48(3)$ [37].

90.3 Laboratory Searches

90.3.1 *Light shining through walls*

Searching for "invisible axions" is extremely challenging due to its extraordinarily feeble coupling to normal matter and radiation. Currently, the most promising approaches rely on the axion-two-photon interaction, allowing for axion-photon conversion in external electric or magnetic fields [7]. For the Coulomb field of a charged particle, the conversion is best viewed as a scattering process, $\gamma + Ze \leftrightarrow Ze + a$, called Primakoff effect [53]. In the other extreme of a macroscopic field, usually a large-scale B-field, the momentum transfer is small, the interaction is coherent over a large distance, and the conversion is best viewed as an axion-photon oscillation phenomenon in analogy to neutrino flavor oscillations [54].

Photons propagating through a transverse magnetic field, with incident $\mathbf{E}_\gamma$ and magnetic field $\mathbf{B}$ parallel, may convert into axions. For $m_a^2 L/2\omega \ll 2\pi$, where L is the length of the B field

Downloaded from https://academic.oup.com/ptep/article/2022/8/083C01/6651666 by KIT Library user on 27 September 2022

region and ω the photon energy, the resultant axion beam is coherent with the incident photon beam and the conversion probability is $\Pi \sim (1/4)(g_{a\gamma\gamma}BL)^2$. A practical realization uses a laser beam propagating down the bore of a superconducting dipole magnet (like the bending magnets in high-energy accelerators). If another magnet is in line with the first, but shielded by an optical barrier, then photons may be regenerated from the pure axion beam [55,56]. The overall probability is $P(\gamma \to A \to \gamma) = \Pi^2$.

The first such Light-Shining-through-Walls (LSW) experiment was performed by the BFRT (Brookhaven-Fermilab-Rochester-Trieste) collaboration. It utilized two magnets of length $L = 4.4$ m and $B = 3.7$ T and found $|g_{a\gamma\gamma}| < 6.7 \times 10^{-7}$ GeV^{-1} at 95% CL for $m_a < 1$ meV [57,58]. More recently, several such experiments were performed (see Listings) [59–65]. The current best limit, $|g_{a\gamma\gamma}| < 3.5 \times 10^{-8}$ GeV^{-1} at 95% CL for $m_a \lesssim 0.3$ meV (see Fig. 90.2), has been achieved by the OSQAR (Optical Search for QED Vacuum Birefringence, Axions, and Photon Regeneration) experiment, which exploited two 9 T LHC dipole magnets and an 18.5 W continuous wave laser emitting at the wavelength of 532 nm [65]. The ALPS I (Any Light Particle Search I) experiment achieved a similar sensitivity [63], see Fig. 90.2. Some of these experiments have also reported limits for scalar bosons where the photon $\mathbf{E}_\gamma$ must be chosen perpendicular to the magnetic field $\mathbf{B}$.

The concept of resonantly enhanced photon regeneration may open unexplored regions of coupling strength [66–68]. In this scheme, both the production and detection magnets are within Fabry-Perot optical cavities and actively locked in frequency. The $\gamma \to a \to \gamma$ rate is enhanced by a factor $\mathcal{F}\mathcal{F}'/\pi^2$ relative to a single-pass experiment, where $\mathcal{F}$ and $\mathcal{F}'$ are the finesses of the two cavities. The resonant enhancement could be of order $10^{(10-12)}$, improving the $g_{a\gamma\gamma}$ sensitivity by $10^{(2.5-3)}$. The experiment ALPS II (Any Light Particle Search II) is based on this concept and aims at an improvement of the current laboratory bound on $g_{a\gamma\gamma}$ by a factor $\sim 10^3$ in the year 2022 [69].

Resonantly enhanced photon regeneration has already been exploited in experiments searching for "radiowaves shining through a shielding" [70–73]. For $m_a \lesssim 10^{-5}$ eV, the upper bound on $g_{a\gamma\gamma}$ established by the CROWS (CERN Resonant Weakly Interacting sub-eV Particle Search) experiment [74] is slightly less stringent than the one set by OSQAR, see Fig. 90.2.

90.3.2 *Photon polarization*

An alternative to regenerating the lost photons is to use the beam itself to detect conversion: the polarization of light propagating through a transverse B field suffers dichroism and birefringence [75]. Dichroism: The $E_\parallel$ component, but not $E_\perp$, is depleted by axion production, causing a small rotation of linearly polarized light. For $m_a^2 L/2\omega \ll 2\pi$, the effect is independent of m_a. For heavier axions, it oscillates and diminishes as m_a increases, and it vanishes for $m_a > \omega$. Birefringence: This effect occurs because there is mixing of virtual axions in the $E_\parallel$ state, but not for $E_\perp$. Hence, linearly polarized light will develop elliptical polarization. Higher-order QED also induces vacuum magnetic birefringence (VMB). A search for these effects was performed in the same dipole magnets of the BFRT experiment mentioned before [76]. The dichroic rotation gave a stronger limit than the ellipticity rotation: $|g_{a\gamma\gamma}| < 3.6 \times 10^{-7}$ GeV^{-1} at 95% CL, for $m_a < 5 \times 10^{-4}$ eV. The ellipticity limits are better at higher masses, as they fall off smoothly and do not terminate at m_a.

In 2006, the PVLAS collaboration reported a signature of magnetically induced vacuum dichroism that could be interpreted as the effect of a pseudoscalar with $m_a = 1$–1.5 meV and $|g_{a\gamma\gamma}| = (1.6$–$5) \times 10^{-6}$ GeV^{-1} [77]. Later, it turned out that these findings are due to instrumental artifacts [78]. This particle interpretation is also excluded by the above photon regeneration searches that were inspired by the original PVLAS result. The fourth generation setup of the PVLAS experiment has published results on searches for VMB (see Fig. 90.2) and dichroism [79]. The bounds from the non-observation of the latter on $g_{a\gamma\gamma}$ are slightly weaker than the ones from OSQAR.

90.3.3 *Long-range forces*

New bosons would mediate long-range forces, which are severely constrained by "fifth force" experiments [80]. Those looking for new mass-spin couplings provide significant constraints on pseudoscalar bosons [81–86], see for example in Fig. 90.4 the limit on the axion-neutron coupling [87] from torsion balance tests of the gravitational inverse square law [88]. Presently, the most restrictive limits are obtained from combining long-range force measurements with stellar cooling arguments [89, 90]. For the moment, any of these limits are far from realistic values expected for the QCD axion. Still, these efforts provide constraints on more general low-mass bosons.

In Ref. [91], a method was proposed that can extend the search for axion-mediated spin-dependent forces by several orders of magnitude. By combining techniques used in nuclear magnetic resonance and short-distance tests of gravity, this method appears to be sensitive to the QCD axion in the μeV – meV mass range, independent of the cosmic axion abundance, if axions have a CP-violating interaction with nuclei as large as the current experimental bound on the electric dipole moment of the neutron allows. The ARIADNE (Axion Resonant InterAction DetectioN Experiment) is under development and employs this approach to search for axion-mediated spin-dependent short-range interactions between a hyper-polarized 3-He sample and an unpolarized tungsten source mas [92]. The method relies on superconducting magnetic shielding to screen the sample from ordinary magnetic field noise. Experimental tests to demonstrate the requirements of ARIADNE, including characterization of the magnetic field backgrounds, are under way [93, 94].

90.4 Axions from Astrophysical Sources

90.4.1 *Stellar energy-loss limits*

Low-mass weakly-interacting particles (neutrinos, gravitons, axions, baryonic or leptonic gauge bosons, *etc.*) are produced in hot astrophysical plasma, and can thus transport energy out of stars. The coupling strength of these particles with normal matter and radiation is bounded by the constraint that stellar lifetimes or energy-loss rates are not in conflict with observation [95, 96].

We begin this discussion with our Sun and concentrate first on hadronic axions. They are produced predominantly by the Primakoff process $\gamma + Ze \to Ze + a$. Integrating over a standard solar model yields the axion luminosity [97]

$$L_a = g_{10}^2 \times 1.85 \times 10^{-3}\, L_\odot\,, \tag{90.15}$$

where $g_{10} = |g_{a\gamma\gamma}| \times 10^{10}$ GeV. The maximum of the spectrum is at 3.0 keV, the average at 4.2 keV, and the number flux at Earth is $g_{10}^2 \times 3.75 \times 10^{11}$ cm^{-2} s^{-1}. The solar photon luminosity is fixed, so energy losses due to the Primakoff process require enhanced nuclear energy production and thus enhanced neutrino fluxes. The all-flavor measurements by SNO (Sudbury Neutrino Observatory), together with a standard solar model, imply $L_a \lesssim 0.10\, L_\odot$, corresponding to $g_{10} \lesssim 7$ [98], mildly superseding a similar limit from helioseismology (sound speed, surface helium and convective radius) [99]. In Ref. [100], this limit was improved to $g_{10} < 4.1$ (at $3\,\sigma$), see Fig. 90.2, exploiting a new statistical analysis that combined helioseismology and solar neutrino observations, including theoretical and observational errors, and accounting for tensions between input parameters of solar models, in particular the solar element abundances. Going beyond the hadronic axion, Ref. [98] considered also a non-zero axion-electron coupling and obtained the bound on the latter displayed in Fig. 90.3.

A more restrictive limit derives from globular-cluster (GC) stars that allow for detailed tests of stellar-evolution theory. The stars on the horizontal branch (HB) in the color-magnitude diagram have reached helium burning with a core-averaged energy release of about 80 erg g^{-1} s^{-1}, compared to Primakoff axion losses of $g_{10}^2\, 30$ erg g^{-1} s^{-1}. The accelerated consumption of helium reduces the HB lifetime by about $80/(80+30\, g_{10}^2)$. Number counts of HB stars in a large sample of 39 Galactic GCs compared with the number of red giants (that are not much affected by Primakoff losses) give a weak indication of non-standard losses which may be accounted by Primakoff-like axion emission, if the photon coupling is in the range $|g_{a\gamma\gamma}| = (2.9 \pm 1.8) \times 10^{-11}$ GeV^{-1} [101,102]. Still, the upper bound found in this analysis,

$$|g_{a\gamma\gamma}| < 6.6 \times 10^{-11}\,\text{GeV}^{-1}\ (95\%\,\text{CL}), \tag{90.16}$$

Downloaded from https://academic.oup.com/ptep/article/2022/8/083C01/6651666 by KIT Library user on 27 September 2022

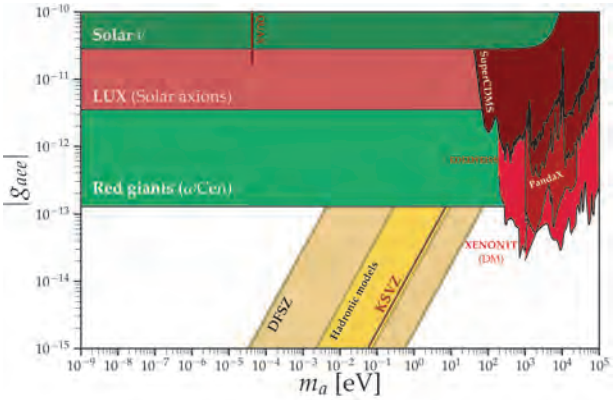

Figure 90.3: Exclusion plot for ALP-electron coupling as described in the text. Figure courtesy of Ciaran O'Hare [31].

represents the strongest limit on $g_{a\gamma\gamma}$ for a wide mass range, see Fig. 90.2. The conservative constraint, Eq. (90.16), on $g_{a\gamma\gamma}$ may be translated to $f_a > 3.4\times10^7$ GeV ($m_a < 0.2$ eV), using $E/N = 0$ as in the KSVZ model, or to $f_a > 1.3 \times 10^7$ GeV ($m_a < 0.5$ eV), for the DFSZ axion model, with $E/N = 8/3$, see Fig. 90.2.

If axions couple directly to electrons, the dominant emission processes are atomic axio-recombination and axio-deexcitation, axio-bremsstrahlung in electron-ion or electron-electron collisions, and Compton scattering [103]. Stars in the red giant (RG) branch of the color-magnitude diagram of GCs are particularly sensitive to these processes: they would lead to an extension of the latter to larger brightness. In fact, the RG branch tip – the brightest point of the RG brangh – provides the currently most sensitive method to test the axion coupling to electrons. The strongest bounds on it are derived from analyses of the RG branch tip in several globular clusters [104] and in the Galactic globular cluster ω Centauri [105]. The two analyses lead to very similar results,

$$|g_{aee}| < 1.48\times10^{-13} \text{ (95\% CL) and } |g_{aee}| < 1.3\times10^{-13} \text{ (95\% CL)}, \tag{90.17}$$

respectively, see Fig. 90.3. Reference [104] finds also a small hint for extra cooling, corresponding to $|g_{aee}| = 0.60^{+0..32}_{-0.58} \times 10^{-13}$, while Ref. [105] does not find any evidence for exotic cooling.

Bremsstrahlung is also efficient in white dwarfs (WDs), where the Primakoff and Compton processes are suppressed by the large plasma frequency. A comparison of the predicted and observed luminosity function of WDs can be used to put limits on $|g_{aee}|$ [106, 107]. An analysis based on detailed WD cooling treatment and data on the WD luminosity function (WDLF) of the Galactic disk found that electron couplings above $|g_{aee}| \gtrsim 3 \times 10^{-13}$ are disfavoured [108]. Lower couplings cannot be discarded from the current knowledge of the WDLF of the Galactic disk. On the contrary, features in some WDLFs can be interpreted as suggestions for electron couplings in the range $7.2 \times 10^{-14} \lesssim |g_{aee}| \lesssim 2.2 \times 10^{-13}$ [108–110]. This hypothesis will be further scrutinized by the Large Synoptic Survey Telescope (LSST) which is expected to increase the sample of WDs in the Galactic halo to hundreds of thousands [111]. This will allow for the determination of independent WDLFs from different Galactic populations, greatly reducing the uncertainties related to star formation histories. For pulsationally unstable WDs (ZZ Ceti stars), the period decrease $\dot{P}/P$ is a measure of the cooling speed. The corresponding observations of a handful pulsating WDs imply additional cooling that can be interpreted also in terms of similar axion losses [112–116]. In fact, the combined analysis of these observations gives a good fit for $|g_{aee}| = 2.9 \times 10^{-13}$ and favours the axion (or ALP) interpretation at slightly more than 2σ [41].

Intriguingly, a $3\,\sigma$ preference for the existence of the axion (or an ALP) is found if one combines the hints of excessive cooling of HB stars, RGs and WDs and allows for both a photon and electron coupling [117]. The best fit is obtained for $|g_{a\gamma\gamma}| \sim 1.4 \times 10^{-11}\,\text{GeV}^{-1}$ and $|g_{aee}| \sim 1.5 \times 10^{-13}$, respectively, where the photon coupling is compatible with zero at 1σ, whereas the electron coupling is non-zero at the level of 3σ [41, 117].

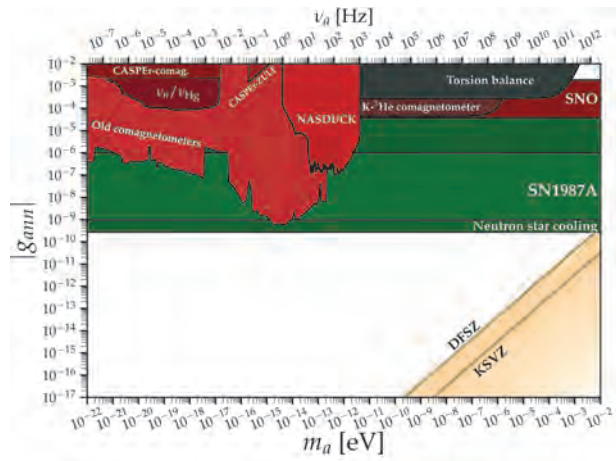

Figure 90.4: Exclusion plot for ALP-neutron coupling as described in the text. Figure courtesy of Ciaran O'Hare [31].

Analogous constraints derive from the measured duration of the neutrino signal of the supernova SN 1987A. Numerical simulations for a variety of cases, including axions and Kaluza-Klein gravitons, reveal that the energy-loss rate of a nuclear medium at the density 3×10^{14} g cm^{-3} and temperature 30 MeV should not exceed about 1×10^{19} erg g^{-1} s^{-1} [118]. The energy-loss rate from nucleon bremsstrahlung, $N + N \to N + N + a$, is $(C_N/2f_a)^2(T^4/\pi^2 m_N)\,F$. Here F is a numerical factor that represents an integral over the dynamical spin-density structure function because axions couple to the nucleon spin. For realistic conditions, even after considerable effort, one is limited to a heuristic estimate leading to $F \approx 1$ [96]. The SN 1987A limits are of particular interest for hadronic axions where the bounds on $|g_{aee}|$ are moot. Using a proton fraction of 0.3, $g_{ann} = 0$, $F = 1$, and $T = 30$ MeV, one finds $f_a > 4 \times 10^8$ GeV and $m_a < 16$ meV [96]. A more detailed numerical calculation [119] with state of the art SN models, again assuming $g_{ann} = 0$, found that a coupling larger than $|g_{app}| \gtrsim 6 \times 10^{-10}$, would shorten significantly the timescale of the neutrino emission. This result is, not surprisingly, rather close to the estimate in Ref. [96]. Improving the calculation of axion emission via nucleon-nucleon bremsstrahlung beyond the basic one-pion exchange approximation appears to loosen the bound [120, 121]. The latter analysis finds a reduction of the axion emissivity by an order of magnitude if one takes into account the non-vanishing mass of the exchanged pion, the contribution from two-pion exchange, effective in-medium nucleon masses and multiple nucleon scattering, leading to a looser bound

$$g_{ann}^2 + 0.61\, g_{app}^2 + 0.53\, g_{ann}\, g_{app} < 8.26 \times 10^{-19}\,, \tag{90.18}$$

see Fig. 90.4. This analysis, however, still neglects another very efficient mechanism for axion production in a SN: the pion production process, $\pi^- + p \to a + n$, also induced by the axion coupling to nucleons. Pion production was recognized long ago as being competitive with nucleon bremsstrahlung [122–124]. However, only recently it was shown that the pion abundance in the early stages of a SN is much larger than previously expected [125]. Although a complete study of the SN evolution which includes pions self-consistently does not exist at the moment, it was shown in Ref. [126] that pion induced processes dominate over bremsstrahlung and so strengthen the bound on the axion-nucleon coupling. In any case, with the present understanding of SNe (current lack of self-consistent 3D SN simulations) and the sparse data from SN 1987A, the constraint on the axion-nucleon couplings from SN 1987A should be considered more as indicative than as a sharp bound [119].

If axions interact sufficiently strongly they are trapped. Only about three orders of magnitude in g_{aNN}, where $N = n, p$, or m_a are excluded, see Fig. 90.4. For even larger couplings, the axion

Downloaded from https://academic.oup.com/ptep/article/2022/8/083C01/6651666 by KIT Library user on 27 September 2022

flux would have been negligible, yet it would have triggered additional events in the detectors, excluding a further range [127]. A possible gap between these two SN 1987A arguments was discussed as the "hadronic axion window" under the assumption that $g_{a\gamma\gamma}$ was anomalously small [128]. This range is now excluded by hot dark matter (HDM) bounds (see below).

Further bounds on the axion-nucleon coupling can be derived from observations of the cooling of neutron stars, in particular the neutron star (NS) in the supernova remnant Cassiopeia A (Cas A). Its surface temperature measured over 10 years reveals an unusually fast cooling rate. This rapid cooling of the Cas A NS may be explained by NS minimal cooling with neutron superfluidity and proton superconductivity [129, 130]. The rapid cooling may also arise from a phase transition of the neutron condensate into a multicomponent state [131]. Recently, Ref. [132] analyzed Cas A NS cooling in the presence of axion emission and obtained

$$g_{app}^2 + 1.6 g_{ann}^2 < 1 \times 10^{-18}, \tag{90.19}$$

which is comparable to the SN 1987A bound. Refs. [133, 134] put a less stringent bound on a KSVZ type axion, without an attempt to fit a transient behavior of Cas A,

$$f_a > (5-10) \times 10^7 \text{ GeV (or } g_{app}^2 < (1-6) \times 10^{-17}), \tag{90.20}$$

from the temperatures of Cas A and other NSs. This limit has been confirmed very recently by Ref. [135] focussing again on the CasA NS and finding $f_a > 3 \times 10^7$ GeV (KSVZ) and $f_a > 4.5 \times 10^8$ GeV (DFSZ). The Cas A NS cooling may also be interpreted as a hint for extra cooling caused by the emission of axions from the breaking and re-formation of neutron triplet Cooper pairs [136], requiring a coupling to the neutron of

$$g_{ann}^2 = (1.4 \pm 0.5) \times 10^{-19}, \tag{90.21}$$

corresponding to an axion mass

$$m_a = (2.3 \pm 0.4)\,\text{meV}/C_n. \tag{90.22}$$

However, the astrophysical versus instrumental origin of the observed cooling of the CasA NS is still being debated [137]. On the other hand, Ref. [138] considered another hot young NS in the supernova remnant HESS J1731-347. Its high temperature implies that all the neutrino emission processes except neutron-neutron bremsstrahlung must be strongly suppressed, which can be realized with a negligible neutron triplet gap and a large proton singlet gap. In this setup, the bremsstrahlung from neutrons is the dominant channel for axion emission, from which one obtains a limit

$$g_{ann}^2 < 7.7 \times 10^{-20}\,, \tag{90.23}$$

see Fig. 90.4.

The model-independent axion coupling to the nucleon EDMs, Eq. (90.5), can also be constrained by the non-observation of excess cooling from SN 1987A. Reference [139] presents a determination of the cooling rate due to the axion production process $N + \gamma \to N + a$, leading to the bound

$$|g_{aN\gamma}| < 4 \times 10^{-9}\,\text{GeV}^{-2}\,, \tag{90.24}$$

see Fig. 90.1.

Finally, let us note that if the interpretation of the various hints for additional cooling of stars, reported in this section in terms of emission of axions with $m_a \sim$meV, were correct, SNe would lose a large fraction of their energy as axions. This would lead to a diffuse SN axion background in the Universe with an energy density comparable to the extra-galactic background light [140]. However, there is no apparent way of detecting it or the axion burst from the next nearby SN. On the other hand, neutrino detectors such as IceCube, Super-Kamiokande or a future mega-ton water Cherenkov detector will probe exactly the mass region of interest by measuring the neutrino pulse duration of the next Galactic SN [119].

90.4.2 *Searches for solar axions and ALPs*

Instead of using stellar energy losses to derive axion limits, one can also search directly for these fluxes, notably from the Sun. The main focus has been on ALPs with a two-photon vertex. They are produced by the Primakoff process with a flux given by Eq. (90.15) and an average energy of 4.2 keV, and can be detected at Earth with the reverse process in a macroscopic B-field ("axion helioscope") [7]. In order to extend the sensitivity in mass towards larger values, one can endow the photon with an effective mass in a gas, $m_\gamma = \omega_{\text{plas}}$, thus matching the axion and photon dispersion relations [141].

An early implementation of these ideas used a conventional dipole magnet, with a conversion volume of variable-pressure gas with a xenon proportional chamber as x-ray detector [142]. The conversion magnet was fixed in orientation and collected data for about 1000 s/day. Axions were excluded for $|g_{a\gamma\gamma}| < 3.6 \times 10^{-9}$ GeV^{-1} for $m_a < 0.03$ eV, and $|g_{a\gamma\gamma}| < 7.7 \times 10^{-9}$ GeV^{-1} for $0.03 < m_a < 0.11$ eV at 95% CL.

Later, the Tokyo axion helioscope used a superconducting magnet on a tracking mount, viewing the Sun continuously. They reported $|g_{a\gamma\gamma}| < 6 \times 10^{-10}$ GeV^{-1} for $m_a < 0.3$ eV [143,144]. This experiment was recommissioned and a similar limit for masses around 1 eV was reported [145].

The most recent helioscope CAST (CERN Axion Solar Telescope) uses a decommissioned LHC dipole magnet on a tracking mount. The hardware includes grazing-incidence x-ray optics with solid-state x-ray detectors, as well as novel x-ray Micromegas position-sensitive gaseous detectors. Exploiting an IAXO (see below) pathfinder system, CAST has established the limit

$$|g_{a\gamma\gamma}| < 6.6 \times 10^{-11}\ \text{GeV}^{-1} \quad (95\%\ \text{CL}), \tag{90.25}$$

for $m_a < 0.02$ eV [146]. To cover larger masses, the magnet bores are filled with a gas at varying pressure. The runs with ^{4}He cover masses up to about 0.4 eV [147], providing the ^{4}He limits shown in Fig. 90.2. To cover yet larger masses, ^{3}He was used to achieve a larger pressure at cryogenic temperatures. Limits up to 1.17 eV allowed CAST to "cross the axion line" for the KSVZ model [148–150], see Fig. 90.2.

Going to yet larger masses in a helioscope search is not well motivated because of the cosmic HDM bound of $m_a \lesssim 1$ eV (see below). Sensitivity to significantly smaller values of $g_{a\gamma\gamma}$ can be achieved with a next-generation axion helioscope with a much larger magnetic-field cross section. Realistic design options for this "International Axion Observatory" (IAXO) have been studied in some detail [151] and its physics potential has been reviewed recently [152]. Such a next-generation axion helioscope may also push the sensitivity in the product of couplings to photons and to electrons, $g_{a\gamma\gamma} g_{aee}$, into a range beyond stellar energy-loss limits and test the hypothesis that WD, RG, and HB cooling is dominated by axion emission [153, 154]. As a first step towards IAXO, an intermediate experimental stage called BabyIAXO is currently under preparation at DESY [155].

Other Primakoff searches for solar axions and ALPs have been carried out using crystal detectors, exploiting the coherent conversion of axions into photons when the axion angle of incidence satisfies a Bragg condition with a crystal plane [156–160]. However, none of these limits is more restrictive than the one derived from the constraint on the solar axion luminosity ($L_a \lesssim 0.10\, L_\odot$) discussed earlier.

Direct detection experiments searching for dark matter (DM) consisting of weakly interacting massive particles have also the capability to search for solar axions and ALPs. For low masses, $m_a \lesssim 100$ eV, the LUX experiment [161] has provided the most stringent bound among those experiments on the axion-electron coupling constant,

$$|g_{aee}| < 3.5 \times 10^{-12} \quad (90\%\ \text{CL}), \tag{90.26}$$

see Fig. 90.3, by exploiting the axio-electric effect in liquid xenon. A slightly less stringent limit was set by PandaX-II [162]. However, as obvious from the same figure, this technique has not reached the sensitivity of energy-loss considerations in stars. Recently, the XENON1T collaboration has reported an excess in low

Downloaded from https://academic.oup.com/ptep/article/2022/8/083C01/6651666 by KIT Library user on 27 September 2022

energy electronic recoil data peaking around 2-3 keV [163]. A possible solar axion interpretation is, however, in stark contrast with the constraints from stellar astrophysics [164–166].

90.4.3 *Conversion of astrophysical axion fluxes*

Large-scale B fields exist in astrophysics that can induce axion-photon oscillations. In practical cases, B is much smaller than in the laboratory, whereas the conversion region L is much larger. Therefore, while the product BL can be large, realistic sensitivities are usually restricted to very low-mass particles, far away from the "axion band" in a plot like Fig. 90.2.

One example is SN 1987A, which would have emitted a burst of ALPs due to the Primakoff production in its core. They would have partially converted into γ-rays in the Galactic B-field. The lack of a gamma-ray signal in the GRS instrument of the SMM satellite in coincidence with the observation of the neutrinos emitted from SN 1987A therefore provides a strong bound on their coupling to photons [167,168]. This bound has been revisited and the underlying physics has been brought to the current state-of-the-art, as far as modeling of the supernova and the Milky-Way magnetic field are concerned, resulting in the limit [169]

$$|g_{a\gamma\gamma}| < 5.3 \times 10^{-12}\ \mathrm{GeV}^{-1},\ \text{for}\ \ m_a \lesssim 4.4 \times 10^{-10}\ \mathrm{eV}, \quad (90.27)$$

see Fig. 90.2.

Reference [170] reports no evidence of a γ-ray burst in observations of extragalactic SNe with the Fermi Large Area Telescope (LAT). Under the assumption that at least one SN was contained within the LAT field of view, the authors derive an upper bound on the axion photon coupling which is about a factor of 5 weaker than the one from SN 1987A, see Fig. 90.2.

The cumulative emission of ALPs from all past core-collapse SNe would lead to a diffuse gamma-ray flux peaked at energies $\sim 50 - 100\,\mathrm{MeV}$ which can convert in the Galactic magnetic field into photons. Using Fermi-LAT measurements of the diffuse γ-ray flux, Ref. [171] obtains a conservative bound on the photon coupling, $|g_{a\gamma\gamma}| < 5 \times 10^{-10}\ \mathrm{GeV}^{-1}$, for $m_a \lesssim 10^{-11}\,\mathrm{eV}$, see see Fig. 90.2, which can be decreased by nearly three orders of magnitude, if an ALP-nucleon coupling of maximal phenomenologically allowed strength, $|g_{aNN}| \sim 10^{-9}$, is allowed.

We use the first observation of Betelgeuse in hard x rays to perform a novel search for axionlike particles (ALPs). Betelgeuse is not expected to be a standard source of x rays, but light ALPs produced in the stellar core could be converted back into photons in the Galactic magnetic field, producing a detectable flux that peaks in the hard x-ray band ($E_\gamma > 10keV$). Using a 50 ks observation of Betelgeuse by the NuSTAR satellite telescope, we find no significant excess of events above the expected background. Using models of the regular Galactic magnetic field in the direction of Betelgeuse, we set a 95% C.L. upper limit on the ALP-photon coupling of $g_{a\gamma} < (0.5 - 1.8) \times 10^{-11} GeV^{-1}$ (depending on magnetic field model) for ALP masses $m_a < (5.5 - 3.5) \times 10^{-11} eV$.

Hot, young stars, such as Wolf-Rayet stars, are efficiently producing ALPs with energies $\sim 10 - 100\,\mathrm{keV}$ via the Primakoff effect. Large numbers of those stars are hosted by the Galactic Quintuplet and Westerlund 1 super star clusters (SSCs). The non-observation of hard x-rays originating from axion-photon conversion in the Galactic magnetic field in archival NuSTAR (Nuclear Spectroscopic Telescope Array) data from these SSCs allows to set a bound on the axion-photon coupling [172], $|g_{a\gamma\gamma}| < 3.6 \times 10^{-12}\,\mathrm{GeV}^{-1}$, for $m_a \lesssim 5 \times 10^{-11}\,\mathrm{eV}$, see Fig. 90.2. A somewhat weaker bound in the same mass range was established exploiting NuSTAR data on Betelgeuse [173].

A hard x-ray excess in data from the nearby Magnificent Seven isolated NSs [174] may be explained by ALPs produced in the core those stars and converted in the surrounding magnetic field, with $|g_{aNN} g_{a\gamma\gamma}| \in (2 \times 10^{-21}, 10^{-18})\,\mathrm{GeV}^{-1}$, for $m_a \lesssim 10^{-5}\,\mathrm{eV}$ [175]. The non-observation of an x-ray excess from the magnetic white dwarf RE J0317-853 [176] by Chandra yields the constraint $|g_{aee} g_{a\gamma\gamma}| \lesssim 1.3 \times 10^{-25}\,\mathrm{GeV}^{-1}$, for $m_a \ll 10^{-5}\,\mathrm{eV}$ [177], which provides a non-trivial constraint on the ratio g_{aee}/g_{aNN} for axion models explaining the Magnificent Seven x-ray excess.

90.4.4 *Conversion of astrophysical photon fluxes*

Magnetically induced oscillations between photons and ALPs can modify the photon fluxes from distant sources in various ways, featuring (i) frequency-dependent dimming, (ii) modified polarization, and (iii) avoiding absorption by propagation in the form of axions.

For example, dimming of SNe Ia could influence the interpretation in terms of cosmic acceleration [178], although it has become clear that photon-ALP conversion could only be a subdominant effect [179]. Searches for linearly polarized emission from magnetized white dwarfs [180] and changes of the linear polarization from radio galaxies (see, e.g., Ref. [181]) provide limits close to $g_{a\gamma\gamma} \sim 10^{-11}\ \mathrm{GeV}^{-1}$, for masses $m_a \lesssim 10^{-7}$ eV and $m_a \lesssim 10^{-15}$ eV, respectively, albeit with uncertainties related to the underlying assumptions. Even stronger limits, $g_{a\gamma\gamma} \lesssim 2 \times 10^{-13}\ \mathrm{GeV}^{-1}$, for $m_a \lesssim 10^{-14}$ eV, have been obtained by exploiting high-precision measurements of quasar polarizations [182].

Remarkably, it appears that the Universe could be too transparent to TeV γ-rays that should be absorbed by pair production on the extra-galactic background light [183–187]. The situation is not conclusive at present [188–191], but the possible role of photon-ALP oscillations in TeV γ-ray astronomy is tantalizing [192–194]. Fortunately, the region in ALP parameter space, $g_{a\gamma\gamma} \sim 10^{-12} - 10^{-10}\ \mathrm{GeV}^{-1}$ for $m_a \lesssim 10^{-7}$ eV [195], required to explain the anomalous TeV transparency of the Universe, could be conceivably probed by the next generation of laboratory experiments (ALPS II) and helioscopes (IAXO) mentioned above.

This parameter region can also be probed by searching for an irregular behavior of the gamma ray spectrum of distant active galactic nuclei (AGN), expected to arise from photon-ALP mixing in a limited energy range. In this type of studies, the uncertainty in the magnetic field around the source needs to be taken into account. This typically leads to a range of limits on the ALP-photon coupling that depend on the modeling assumptions. The H.E.S.S. collaboration has set a limit of $|g_{a\gamma\gamma}| \lesssim 2.1 \times 10^{-11}\ \mathrm{GeV}^{-1}$, for $1.5 \times 10^{-8}\ \mathrm{eV} \lesssim m_a \lesssim 6.0 \times 10^{-8}$ eV, from the non-observation of an irregular behavior of the spectrum of the AGN PKS 2155-304 [196], see Fig. 90.2. The Fermi-LAT collaboration has put an even more stringent limit on the ALP-photon coupling [197] from observations of the gamma ray spectrum of NGC 1275, the central galaxy of the Perseus cluster, see Fig. 90.2. A similar analysis has been carried out in Ref. [198], using Fermi-LAT data of PKS 2155-304, and in Ref. [199], using ARGO-YBJ and Fermi-LAT data of Mrk 421 [199], see Fig. 90.2. However, these constraints were obtained under certain theoretical assumptions about magnetic fields surrounding the sources, not confirmed yet by direct astronomical observations in these particular directions; this introduces large systematic uncertainties in the reported constraints [200].

Evidence for spectral irregularities has been reported in Galactic sources, such as pulsars and supernova remnants, and has been interpreted as hints for ALPs [201, 202] (see also discussion in Ref. [203] and references therein). However, the inferred ALP parameters, $|g_{a\gamma\gamma}| \sim 10^{-10}\,\mathrm{GeV}^{-1}$, $m_a \sim$neV, are in tension with the CAST helioscope bounds. Reference [203] updated the analysis of the pulsar signal region including astrophysical nuisance parameters and correctly deriving confidence intervals on ALP parameters by means of Monte Carlo simulations. The tension with the CAST bounds can be evaded if environmental effects in matter, which would suppress the ALP production in dense astrophysical plasmas like the solar interior, are invoked. If this explanation is correct, the claimed ALP signal would be in reach of the next-generation LSW experiment ALPS II. Other ways to make the CAST bound compatible with photon-ALP conversions in the low-density Galactic medium are invoking photon-ALP-dark photon oscillations [204] or the existence of a number of 'hidden' ALPs [205].

At smaller masses, $m_a \lesssim 10^{-12}\,\mathrm{eV}$, galaxy clusters become highly efficient at interconverting ALPs and photons at x-ray energies. Constraints on spectral irregularities in the spectra of luminous x-ray sources (Hydra A, M87, NGC 1275, NGC 3862, Seyfert galaxy 2E3140; taken by Chandra and XMM-Newton) located in or behind galaxy clusters then lead to stringent upper

Downloaded from https://academic.oup.com/ptep/article/2022/8/083C01/6651666 by KIT Library user on 27 September 2022

limits on the ALP-photon coupling [206–211], (for the limits exploiting spectra from Hydra and M87 from Refs. [206] and [208], respectively, see Fig. 90.2). Reference [211] recently performed the most sensitive x-ray searches for ALPs to date by employing Chandra's High-Energy Transmission Gratings that allow for an unsurpassed spectral resolution. New observations of the AGN NGC 1275 then led to the bound

$$|g_{a\gamma\gamma}| < 8 \times 10^{-13}\,\mathrm{GeV}^{-1} \quad (99.7\%\ \mathrm{CL}) \tag{90.28}$$

for light ALPs, see Fig. 90.2.

90.4.5 *Finite density effects*

If the QCD axion sector has a discrete, $\mathbb{Z}_{\mathcal{N}}$, shift symmetry, its potential is much shallower, and its mass, in units of its decay constant, $m_a f_a \simeq (3\pi)^{-1/4}\,\mathcal{N}^{3/4}\,2^{-\mathcal{N}/2}\,m_\pi f_\pi$, is smaller than the one of the canonical QCD axion by an exponential factor $\propto 2^{-\mathcal{N}/2}$ [44, 45]. This opens up the parameter space over which one should search for a QCD axion towards the left of the yellow canonical QCD axion band in Fig. 90.1, Fig. 90.2, Fig. 90.3, and Fig. 90.4. Novel bounds apply to this exceptionally light QCD axion due to finite density effects [212–214]. In fact, in dense stellar media, the minimum of the axion potential may be shifted to π. This has a number of phenomenological consequences that span from the modification of nuclear processes in stars due to $\theta = \mathcal{O}(\pi)$ to modifications in the orbital decay of binary systems (and subsequently in the emitted gravitational waves).

In fact, $\theta \sim 1$ in the solar core would lead to an increased proton-neutron mass difference, which would prohibit the neutrino line corresponding to the ^{7}Be-^{7}Li mass difference observed by Borexino [215].

Moreover, the fact that the position of the minimum of the axion potential depends on the nuclear density of the medium may also source a long-range force between dense stars [212]. This new long-range force sourced by the axion can be constrained by the measurement of the orbital decay of double pulsar or NS-pulsar binaries [212], Fig. 90.5. The gravitational wave signal of NS-NS mergers or black hole (BH) - NS mergers would also be modified by these axionic long-range forces [212, 213]. A corresponding bound [214] exploiting the gravitational waves observation from the binary NS inspiral GW170817 detected by LIGO (Laser Interferometer Gravitational-Wave Observatory) and Virgo [216] is also plotted in Fig. 90.5.

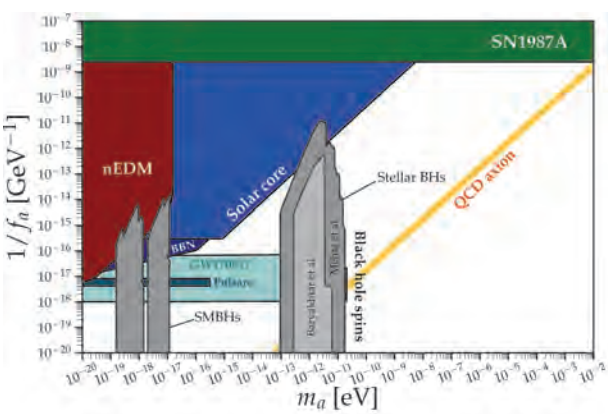

Figure 90.5: Exclusion plot for the QCD axion decay constant as described in the text. Figure courtesy of Ciaran O'Hare [31].

90.4.6 *Superradiance of black holes*

Light bosonic fields such as axions or ALPs can affect the dynamics and gravitational wave emission of rapidly rotating astrophysical BHs through the superradiance mechanism. When their Compton wavelength is of order of the size of the BH's ergoregion, they form gravitational bound states around the BH. Their occupation number grows exponentially by extracting energy and angular momentum from the black hole, forming a coherent axion or ALP bound state emitting gravitational waves. When accretion cannot replenish the spin of the BH, superradiance dominates the BH spin evolution; this is true for both supermassive and stellar mass BHs. The existence of destabilizing light bosonic fields thus leads to exclusion regions in the mass versus spin plot of rotating BHs. Stellar BH spin measurements exploiting well-studied binaries and two independent techniques exclude a mass range $6 \times 10^{-13}\,\mathrm{eV} < m_a < 2 \times 10^{-11}\,\mathrm{eV}$ at $2\,\sigma$, which for the axion excludes $3 \times 10^{17}\,\mathrm{GeV} < f_a < 1 \times 10^{19}\,\mathrm{GeV}$ [12, 217, 218]. These bounds apply when gravitational interactions dominate over the axion self-interaction, which is true for the QCD axion in this mass range. Mehta *et al.* [219, 220] considered superradiance bounds for string theory ALPs with a quartic self-coupling (of either sign) given by $\lambda = m_a^2/f_a^2$, using the bosenova model of Ref. [218]. The analysis can be recast into 95% confidence excluded regions in the plane (m_a, f_a) for ALPs, and are shown in Fig. 90.5 (also compiled in Ref. [45]). These bounds were further extended to massive vector and tensor fields in Ref. [221]. Baryakhtar *et al.* [222] used a more advanced model for the effect of self-interactions on superradiant evolution, and a different (frequentist) statistical methodology, leading to more conservative bounds from stellar mass BHs (region near 10^{-12} eV), see Fig. 90.5. Baryakhtar *et al.* [222] vetoed supermassive BHs (SMBHs) with spins measured at low significance, and thus show no bounds in the SMBH region (near 10^{-18} eV); Mehta *et al.* [219–221] included SMBHs in a (quasi-)Bayesian analysis with a flat prior on the spin.

Long lasting, monochromatic gravitational wave signals, which can be distinguished from ordinary astrophysical sources by their clustering in a narrow frequency range, are expected to be produced by axions or ALPs annihilating to gravitons. Gravitational waves could also be sourced by axions/ALPs transitioning between gravitationally bound levels. Accordingly, the gravitational wave detector Advanced LIGO should be sensitive to the axion in the $m_a \lesssim 10^{-10}\,\mathrm{eV}$ region. LIGO measurements of BH spins in binary merger events could also provide statistical evidence for the presence of an axion [223, 224]. Similar signatures could arise for supermassive and intermediate mass BHs for particles with masses $\lesssim 10^{-15}\,\mathrm{eV}$. Gravitational waves from such sources could be detected at lower-frequency observatories such as LISA (Laser Interferometer Space Antenna).

90.5 Cosmic Axions

90.5.1 *Cosmic axion populations*

There are two distinct populations of cosmic relic axion popoulations: a non-thermal one behaving as CDM, and a thermal one comprising a HDM component, in analogy to massive neutrinos. For $m_a \lesssim 0.01\,\mathrm{eV}$, thermal axions are dominantly produced by processes involving quarks and gluons [225, 226], while, for larger masses, the dominant thermalization process is $\pi + \pi \leftrightarrow \pi + a$ [51, 227, 228]. A number of evaluations exploiting cosmological precision data have found restrictive constraints on a possible HDM fraction that translate into an upper bound on the axion mass, $m_a \lesssim 1$ eV, if a LO axion-pion chiral effective field theory (EFT) analysis of the axion-pion thermalization rate is used [229–232]. Recently, it was found that the NLO contribution exceeds the LO contributions for masses below $m_a \lesssim 1.2\,(0.12/C_{a\pi})\,\mathrm{eV}$ [233]. Therefore, in order to assess the reach in sensitivity of future cosmological data sets, one has to improve the EFT description or to compute axion-pion scattering via lattice QCD techniques.

For $m_a \gtrsim 20$ eV, axions decay fast on a cosmic time scale, see Eq. (90.8), removing the axion population while injecting photons. This excess radiation provides additional limits on the axion- or ALP-photon coupling up to very large masses masses [234, 235]. In fact, photons from ALP decays could show up as peaks above known backgrounds in galactic x-ray spectra, could contribute to the extragalactic background light (EBL), could ionize primordial hydrogen and thus contribute to the optical depth after recombination, could spoil the agreement of big bang nucleosynthesis (BBN) with observations. The corresponding up-to-date bounds from Refs. [236, 237] are displayed in Fig. 90.2.

The main cosmological interest in axions derives from their possible role as CDM. In addition to thermal processes, axions are abundantly produced by the misalignment (MIS) mechanism [238–240].

Downloaded from https://academic.oup.com/ptep/article/2022/8/083C01/6651666 by KIT Library user on 27 September 2022

The axion DM abundance crucially depends on the cosmological history. Let us first consider the so called *pre-inflationary PQ symmetry breaking scenario*, in which the PQ symmetry is broken before and during inflation and not restored afterwards. After the breakdown of the PQ symmetry, the axion field relaxes somewhere in the bottom of the "wine-bottle-bottom" potential. Near the QCD epoch, topological fluctuations of the gluon fields such as instantons explicitly break the PQ symmetry. This tilting of the "wine-bottle-bottom" drives the axion field toward the CP-conserving minimum, thereby exciting coherent oscillations of the axion field that ultimately represent a condensate of CDM. The fractional cosmic mass density in this homogeneous field mode, created by the MIS mechanism, is [30, 241–243],

$$\begin{aligned}\Omega_a^{\rm MIS} h^2 &\approx 0.12 \left(\frac{f_a}{9\times 10^{11}\ {\rm GeV}}\right)^{1.165} F\,\Theta_{\rm i}^2 \\ &\approx 0.12 \left(\frac{6\ \mu{\rm eV}}{m_a}\right)^{1.165} F\,\Theta_{\rm i}^2\,,\end{aligned} \tag{90.29}$$

where h is the present-day Hubble expansion parameter in units of 100 km s^{-1} Mpc^{-1}, and $-\pi \le \Theta_{\rm i} \le \pi$ is the initial "misalignment angle" relative to the CP-conserving position attained in the causally connected region which evolved into today's observable Universe. $F = F(\Theta_{\rm i}, f_a)$ is a factor accounting for anharmonicities in the axion potential. For $F\Theta_{\rm i}^2 = \mathcal{O}(1)$, m_a should be above $\sim 6\,\mu$eV in order that the cosmic axion density does not exceed the observed CDM density, $\Omega_{\rm CDM} h^2 = 0.12$. However, much smaller axion masses (much higher PQ scales) are still possible if entropy is diluted for example by the late decay of a scalar condensate (see for example [244] and references therein) or the initial value $\Theta_{\rm i}$ just happens to be small enough in today's observable Universe ("anthropic axion window" [245]). In the latter cosmological scenario, however, quantum fluctuations of the axion field during inflation are expected to lead to isocurvature density fluctuations which get imprinted to the temperature fluctuations of the CMB [246, 247]. Their non-observation puts severe constraints on the Hubble expansion rate H_I during inflation [248–253], which read, in the simplest cosmological inflationary scenario,

$$H_I \lesssim 5.7\times 10^8\,{\rm GeV}\left(\frac{5\,{\rm neV}}{m_a}\right)^{0.4175}, \tag{90.30}$$

if axions represent all of DM. In Ref. [254] an alternative to the MIS mechanism was proposed: the so-called kinetic MIS mechanism. In this case, the axion field is assumed to have an initial velocity which may be generated e.g. by a hypothesized explicit breaking of the axion shift symmetry in the early universe. The amount of QCD axion dark matter generated by the kinetic MIS mechanism can fit the observed dark matter abundance for any $f_a \lesssim 1.5\times 10^{11}$ GeV, down to the minimum value allowed by the SN 1987A constraint.

In the *post-inflationary PQ symmetry breaking scenario*, on the other hand, $\Theta_{\rm i}$ will take on different values in different patches of the present Universe. The average contribution is [30, 241–243]

$$\Omega_a^{\rm MIS} h^2 \approx 0.12 \left(\frac{30\ \mu{\rm eV}}{m_a}\right)^{1.165}. \tag{90.31}$$

The decay of cosmic strings and domain walls gives rise to a further population of CDM axions, whose abundance suffers from significant uncertainties [242, 243, 255–267] which arise from the difficulty in understanding the energy loss process of topological defects and the generated axion spectrum in a quantitative way. In fact, in the present state-of-the-art it is still possible that the CDM contribution from the decay of topological defects is subdominant [260] or overwhelmingly large [264] in comparison to the one from the MIS mechanism. Correspondingly, the plausible range of axion masses providing all of CDM in scenarios with postinflationary PQ symmetry breaking is still rather large, namely [260, 264]

$$m_a \approx 26\ \mu{\rm eV} - 0.5\ {\rm meV}, \tag{90.32}$$

for models with short-lived (requiring unit color anomaly $N = 1$) domain walls, such as the KSVZ model. For models with long-lived ($N > 1$) domain walls, such as an accidental DFSZ model [268], where the PQ symmetry is broken by higher dimensional Planck suppressed operators, the mass is predicted to be significantly higher [152, 259, 268, 269],

$$m_a \approx (0.58 - 130)\,{\rm meV}\,. \tag{90.33}$$

However, the upper part of the predicted range is in conflict with stellar energy-loss limits on the axion.

In this post-inflationary PQ symmetry breakdown scenario, the spatial axion density variations are large at the QCD transition, and they are not erased by free streaming. Gravitationally bound "axion miniclusters" form before and around matter-radiation equality [270–272]. A significant fraction of CDM axions can reside in these bound objects [262, 273]. Remarkably, the minicluster fraction can be bounded by gravitational lensing [274–276], although more simulations are required to understand whether miniclusters are dense enough and survive in sufficient quantities for lensing bounds to apply.

In the above predictions of the fractional cosmic mass density in axions, the exponent, 1.165, arises from the non-trivial temperature dependence of the topological susceptibility $\chi(T) = m_A^2(T) f_A^2$ at temperatures slighty above the QCD quark-hadron phase transition. Lattice QCD calculations of this exponent [30, 277–281], but also Ref. [282], found it to be remarkably close to the prediction of the dilute instanton gas approximation [283] which was previously exploited. Therefore, the state-of-the-art prediction of the axion mass relevant for DM for a fixed initial misalignment angle $\Theta_{\rm i}$ differs from the previous prediction by just a factor of order one.

The non-thermal production mechanisms attributed to axions are generic to light bosonic weakly interacting particles such as ALPs [17]. The relic abundance is set by the epoch when the axion mass becomes significant, $3H(t) \approx m_a(t)$, and ALP field oscillations begin. For ALPs to contribute to the DM density this epoch must precede that of matter radiation equality. For a temperature independent ALP mass this leads to the bound:

$$m_a \gtrsim 7\times 10^{-28}\,{\rm eV}\left(\frac{\Omega_m\, h^2}{0.15}\right)^{1/2}\left(\frac{1+z_{\rm eq}}{3.4\times 10^3}\right)^{3/2}. \tag{90.34}$$

ALPs lighter than this bound are allowed if their cosmic energy density is small, but they are quite distinct from other forms of DM [284]. Ignoring anharmonicities in the ALP potential, and taking the ALP mass to be temperature independent, the relic density in DM ALPs due to the MIS mechanism is given by

$$\begin{aligned}\Omega_{\rm ALP}^{\rm MIS} h^2 =& 0.12\left(\frac{m_a}{4.7\times 10^{-19}\,{\rm eV}}\right)^{1/2}\left(\frac{f_a}{10^{16}\,{\rm GeV}}\right)^2 \times \\ &\left(\frac{\Omega_m h^2}{0.15}\right)^{3/4}\left(\frac{1+z_{\rm eq}}{3.4\times 10^3}\right)^{-3/4}\Theta_{\rm i}^2\,.\end{aligned} \tag{90.35}$$

An ALP decay constant near the GUT scale gives the correct relic abundance for *ultralight ALPs* (ULAs) with $m_{\rm ULA} \approx 10^{-19}$ eV [285, 286]. ULAs encompass the entire Earth in a single Compton wavelength, and for large occupation numbers are modelled as a coherent classical field. The coherence time is determined by the mass and virial velocity in the Milky Way, $\tau_{\rm coh} \sim 1/m_{\rm ULA} v_{\rm vir}^2$, with the detailed properties described by a stochastic model with an approximately Rayleigh Jeans distribution [287]. Natural models for ULAs can be found in string and M-theory compactifications [8–15], in field theory with accidental symmetries [288, 289], or new hidden strongly coupled sectors [290, 291].

In addition to the gravitational potential energy, the ULA field also carries gradient energy. On scales where the gradient energy is non-negligible, ULAs acquire an effective pressure and do not behave as CDM. The gradient energy opposes gravitational collapse, leading to a Jeans scale below which perturbations are stable [292]. The Jeans scale suppresses linear cosmological structure formation relative to CDM [293–295]. The Jeans scale at matter-radiation equality in the case that ULAs make up all of

Downloaded from https://academic.oup.com/ptep/article/2022/8/083C01/6651666 by KIT Library user on 27 September 2022

CDM is:

$$k_{\mathrm{J,eq}} = 8.7\,\mathrm{Mpc}^{-1}\left(\frac{1+z_{\mathrm{eq}}}{3.4\times10^3}\right)^{-1/4}\left(\frac{h^2\Omega_{\mathrm{ALP}}^{\mathrm{MIS}}}{0.12}\right)^{1/4}\times \left(\frac{m_{\mathrm{ULA}}}{10^{-22}\,\mathrm{eV}}\right)^{1/2}. \tag{90.36}$$

On non-linear scales the gradient energy leads to the existence of a class of pseudo-solitons known as oscillatons, or axion stars [296]. Axion stars are expected to form in all cosmological scenarios, and for all types of ALPs, including the QCD axion [297–299].

Cosmological and astrophysical observations are consistent with the CDM model, and departures from it are only allowed on the scales of the smallest observed DM structures with $M \sim 10^{6-8} M_\odot$. The CMB power spectrum and galaxy autocorrelation power spectrum limit the ULA mass to $m_{\mathrm{ULA}} \gtrsim \mathcal{O}(\mathrm{few}) \times 10^{-24}$ eV from linear theory of structure formation [284, 300]. Analytic models [301] and N-body simulations [302] for non-linear structures show that halo formation is suppressed in ULA models relative to CDM. This leads to constraints on the ULA mass of $m_{\mathrm{ULA}} > 10^{-22}$ eV from observations of high-z galaxies [302–304], and $m_{\mathrm{ULA}} > 2\times10^{-20}$ eV from the Lyman-alpha forest flux power spectrum [305]. Including the effects of anharmonicities on structure formation with ALPs can weaken these bounds if the misalignment angle $\Theta_{\mathrm{i}} \approx \pi$ [306]. A comprehensive study of Milky Way satellites by the DES collaboration resulted in the bound $m_{\mathrm{ULA}} > 2.9\times10^{-21}$ eV [307]. Cosmological simulations that treat gradient energy in the ULA field beyond the N-body approximation have just recently become available [297, 308–310], and show, among other things, evidence for the formation of axion stars in the centres of ULA halos (various consequences of axion stars are considered in Refs. [311]). These central axion stars have been conjectured to play a role in the apparently cored density profiles of dwarf spheroidal galaxies, and other central galactic regions [297, 312–317]. However, the relationship between the halo mass and the axion star mass [318] leads to problems with this scenario in some galaxies [319–321]. It should be emphasised that many of the conclusions about the role of ULA axion stars in galactic dynamics are based on use of simulation results that do not contain baryons and feedback could be important [322–324].

Inside DM halos the axion gradient energy causes coherence on the de Broglie wavelength and fluctuations on the coherence time [297,325]. These fluctuations can be thought of as short-lived quasiparticles and lead to relaxation processes that can be described statistically [286,326] (this relaxation processes also leads to the gravitational condensation of axion stars [298]). The typical relaxation time is:

$$t \sim 10^{10}\ \mathrm{years}\left(\frac{m_{\mathrm{ULA}}}{10^{-22}\ \mathrm{eV}}\right)^3\left(\frac{v}{100\ \mathrm{km\ s}^{-1}}\right)^2\left(\frac{r}{5\ \mathrm{kpc}}\right)^4, \tag{90.37}$$

where v and r are the velocity and radius of the orbit in the host DM halo.

Relaxation processes such as these are not observed in galaxies, though there are some circumstances where they may be desirable [286]. An absence of observed relaxation can be used to set limits on the ULA mass. An absence of Milky Way disk thickening excludes $m_{\mathrm{ULA}} > 0.6\times10^{-22}$ eV [327], while stellar streams give the stronger bound $m_{\mathrm{ULA}} > 1.5\times10^{-22}$ eV [328]. The survival of the old star cluster in Eridanus II [329] excludes the range of masses 10^{-21} eV $\lesssim m_{\mathrm{ULA}} \lesssim 10^{-19}$ eV [330]. As in the case of ULA axion stars, current constraints from heating do not fully account for the possible role of baryons.

Finally, one should note that the beyond-CDM physics of ULAs (Jeans scale, relaxation, axion star formation) of course also applies to the QCD axion on smaller length scales. This is of particular interest inside axion miniclusters [270, 271, 298, 299].

90.5.2 *Electron recoil searches*

In a DM direct detection experiment, a DM ALP featuring a coupling to the electron can be absorbed by the target material, leading to a mono-energetic electronic recoil signal peaked at m_a. This mechanism allowed the EDELWEISS [331], PandaX [332], SuperCDMS [333] and XENON1T [334] collaborations to put the bounds on the axion-electron coupling displayed in Fig. 90.3 in the keV mass range.

90.5.3 *Telescope searches*

The two-photon decay is extremely slow for axions with masses in the CDM regime, but could be detectable for eV masses. The signature would be a quasi-monochromatic emission line from galaxies and galaxy clusters. The expected optical line intensity for DFSZ axions is similar to the continuum night emission. A search for optical line emission in two Abell clusters using spectra from the VIMOS (Visible Multi-Object Spectrograph) integral field unit at the Very Large Telescope (VLT) excludes axions and ALPs with a two photon coupling bigger than $\sim 5\times10^{-12}\,\mathrm{GeV}^{-1}$ in the mass range between 4.5 and 5.5 eV, see Fig. 90.2. Spectral data on the dwarf spheroidal galaxy Leo T from the Multi Unit Spectroscopic Explorer (MUSE) at the VLT improve these constraints by more than an order of magnitude for ALP masses between 2.7 and 5.3 eV [335], see Fig. 90.2.

Very low-mass axions in halos produce a weak quasi-monochromatic radio line. Virial velocities in undisrupted dwarf galaxies are very low, and the axion decay line would therefore be extremely narrow. A search with the Haystack radio telescope on three nearby dwarf galaxies provided a limit $|g_{a\gamma\gamma}| < 1.0\times10^{-9}\,\mathrm{GeV}^{-1}$ at 96% CL for $298 < m_a < 363\ \mu$eV [336]. However, this combination of m_a and $g_{a\gamma\gamma}$ does not exclude plausible axion models.

A monochromatic signal is also produced in the conversion of DM axions in the background of slowly varying galactic B-fields [337]. The signal is, however, sensitive to magnetic field power on the scale of the axion mass [338]. Present and future radio telescopes appear to be able to probe ALP DM in the mass range $0.1 - 100\ \mu$eV for couplings $g_{a\gamma\gamma} \gtrsim 10^{-13}\ \mathrm{GeV}^{-1}$ [338] – unfortunately not reaching down to the benchmark QCD axion sensitivity.

Resonant conversion of QCD axion or ALP DM in NS magnetospheres may give a detectable signal from individual NSs for axion masses in the μeV range [339]. Recent analyses of radio data in the frequency range 1-40 GHz from several NSs have found no evidence for a narrow peak predicted from this mechanism and therefore put bounds on the axion-photon coupling around $10^{-11}\,\mathrm{GeV}^{-2}$ for $4 \lesssim m_a \lesssim 160\,\mathrm{GHz}$ [340–342], see Fig. 90.2. However, these limits may still suffer from significant uncertainties because the line intensity is difficult to predict in detail in the complicated environments of NSs [342–345]. Stimulated ALP decays in high radiation environments may be detectable, by next-generation radio telescopes such as the Square Kilometer Array, down to $g_{a\gamma\gamma} \gtrsim 10^{-11}\,\mathrm{GeV}^{-1}$, for masses between μeV and 0.1 meV [346]. Furthermore, in condensed ALP dark matter structures such as ALP stars, a parametric instability may lead to an exponential enhancement of the photon flux from ALP-photon conversion by a factor $\sim \exp\left[|g_{a\gamma\gamma}|\int ds\rho_a^{1/2}(s)\right]$, where the integral is along any photon trajectory through the ALP overdensity [347, 348].

Photon propagation on an ULA DM background can induce birefringence that can be compared with upper limits from the CMB [349–351] and may also be probed with other sources such as pulsars [352].

90.5.4 *Microwave cavity experiments*

Over a large part of the plausible m_a range for CDM, Galactic halo axions may be detected by their resonant conversion into a quasi-monochromatic microwave signal in a high-Q electromagnetic cavity permeated by a strong, static B field [7,353,354]. The cavity frequency is tunable, and the signal is maximized when the resonant frequency is the total axion energy, rest mass plus kinetic energy, of $\nu = (m_a/2\pi)\,[1+\mathcal{O}(10^{-6})]$, the width above the rest mass representing the axions' virial distribution in the galaxy near Earth. The frequency spectrum may also contain finer structure from axions more recently fallen into the galactic potential and not yet completely virialized [355, 356] or otherwise incompletely thermalized.

Downloaded from https://academic.oup.com/ptep/article/2022/8/083C01/6651666 by KIT Library user on 27 September 2022

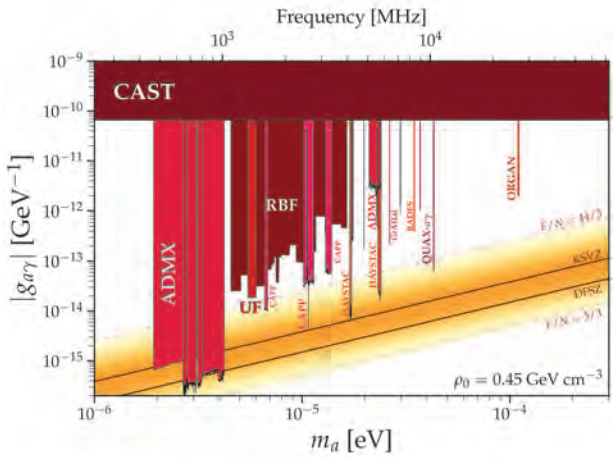

Figure 90.6: Exclusion plot for ALP-photon coupling with closeup on the parameter space of RF cavity experiments as described in the text. Figure courtesy of Ciaran O'Hare [31].

The feasibility of this technique was established in early experiments (RBF (Rochester-Brookhaven-Florida) and UF (University of Florida)) of relatively small sensitive volume, $\mathcal{O}$(1 liter), with HFET-based microwave amplifiers, setting limits in the range $4.5 < m_a < 16.3$ μeV [357–359], but lacking by 2–3 orders of magnitude the sensitivity required to detect realistic axions, see Fig. 90.6.

Later, the first generation of ADMX ($B \sim 8$ T, $V \sim 200$ liters) achieved sensitivity to KSVZ axions, assuming they saturate the local DM density and are well virialized, over the mass range 1.9–3.3 μeV [360]. Should halo axions have a significant narrow component not yet virialized, ADMX was sensitive to DFSZ axions over the entire mass range [361]. The corresponding 90% CL exclusion regions shown in Fig. 90.6 assume a local CDM density of 7.5×10^{-25} g cm^{-3} (450 MeV cm^{-3}).

Somewhat later, the ADMX experiment commissioned an upgrade [362] that replaced the microwave HFET amplifiers by near-quantum-limited low-noise dc SQUID microwave amplifiers [363] and, more recently, with Josephson parametric amplifiers (related to the earlier dc SQUID amplifiers), also with noise near-quantum-limited [364]. With its large volume and low noise, ADMX has achieved an unprecedented axion DM sensitivity in the mass range between 2.7 and 4.2 μeV [365–368], down to the DFSZ benchmark axion-photon coupling over much of the range, see Fig. 90.6. This apparatus is also sensitive to certain other hypothetical light bosons, such as hidden photons or chameleons, over a limited parameter space [17, 369, 370].

ADMX also deployed a testbed experiment to probe higher masses. This experiment – ADMX-Sidecar – sharing the magnet bore and operating in tandem with the main ADMX experiment, searches in three widely spaced frequency ranges (4202–4249 MHz, 5086–5799 MHz and 7173–7203 MHz), using both the TM_{010} and TM_{020} cavity modes, and demonstrating the use of a piezoelectric actuator for cavity tuning in the high-vacuum, high magnetic field, cryogenic environment [371].

The HAYSTAC experiment reported results from a microwave cavity search for DM axions with masses above 20 μeV. They exclude axions with two-photon coupling $|g_{a\gamma\gamma}| \gtrsim 2 \times 10^{-14}$ GeV^{-1} over the range $23.15\,\mu\text{eV} < m_a < 24.0\,\mu\text{eV}$ [372, 373], a factor of 2.7 above the KSVZ coupling benchmark, see Fig. 90.6. With a Josephson parametric amplifier, this experiment has demonstrated system noise approaching the "standard quantum limit" for the first time in an axion search. More recently, HAYSTAC explored state squeezing to reduce the system noise, where the squeezed quadrature had lower noise relative to that of the "standard quantum limit", thereby reducing the scan time by a factor of around 2 over a narrow mass range. This resulted in limits on $|g_{a\gamma\gamma}|$ about a factor of 1.4 above the KSVZ benchmark coupling over the axion-mass ranges $16.96\,\mu\text{eV} < m_a < 17.12.\,\mu\text{eV}$ and $17.14\,\mu\text{eV} < m_a < 17.28\,\mu\text{eV}$ at 90% CL [374] as shown in Fig. 90.6.

The ORGAN experiment aims to probe axions over the relatively high-mass range $60\,\mu\text{eV} < m_a < 210\,\mu\text{eV}$, which includes axion masses motivated by postinflationary PQ symmetry breaking. ORGAN is based on long, thin cavities with this early generation not being tunable and operating in the TM_{020} mode. In this pathfinding run, it set the limit $|g_{a\gamma\gamma}| < 2 \times 10^{-12}$ GeV^{-1} at 110 μeV across a narrow mass range 2.5 neV [375], see Fig. 90.6. Another non-tunable experiment is QUAX a-γ, a haloscope of otherwise conventional design sensitivity a factor of approximately 5 above the benchmark KSVZ coupling at two narrowband ranges near 10 GHz [376, 377], see Fig. 90.6. Other cavity detectors are moving into operation, including an experiment with unusual high-aspect-ratio cavities in the CAST bore (CAST-RADES [378]).

CAPP is an ambitious program to search for axions across a wide mass range at high sensitivity. Recently the CAPP-8TB detector has reported results approaching KSVZ sensitivity in the mass range 6.62–8.82 μeV [379]. A further refinement is searching the higher frequencies allowed by subdividing a cavity into smaller higher-frequency cells. Such a multi-cell cavity system has reported sensitivity around an order-of-magnitude above the KSVZ benchmark coupling in the mass range 13.0–13.9 μeV [380], see Fig. 90.6. The CAPP-PACE detector has reported limits around KSVZ benchmark sensitivity in the mass range 10.7126–10.7186 μeV and around an order-of-magnitude above benchmark KSVZ coupling in the mass range 10.16–10.37 [381], see Fig. 90.6.

90.5.5 *New concepts for axion DM direct detection*

Other new concepts for searching for axion DM are also being investigated. An alternative to the microwave cavity technique is based on a novel detector architecture consisting of an open, Fabry-Perot resonator and a series of current-carrying wire planes [382]. The Orpheus detector has demonstrated this new technique, excluding DM ALPs with masses between 68.2 and 76.5 μeV and axion-photon couplings greater than 4×10^{-7} GeV^{-1}. This technique may be able to probe DM axions in the mass range from 40 to 700 μeV. "Plasma haloscopes" are under development by the ALPHA collaboration [383]. This concept uses a metamaterial consisting of spaced out wires, inducing an effective photon mass, tunable with wire separation, and sensitive to axion masses 35–400 μeV. Another detector concept exploits the fact that a magnetized mirror would radiate photons in the background of axion DM, which could be collected like in a dish antenna [384]. The proposed MADMAX experiment will place a stack of dielectric layers in a magnetic field in order to resonantly enhance the photon signal, aiming a sensitivity to probe the mass range $40\,\mu\text{eV} \lesssim m_a \lesssim 200\,\mu\text{eV}$ [385, 386]. Optical dielectric haloscopes with single photon signal detection have been proposed to search for axions in the 50 meV – 10 eV mass range [387]. Absorption of axions on molecular transitions can be sensitive to the axion pseudoscalar coupling g_{aNN} to nucleons or the pseudoscalar coupling g_{aee} to electrons in the 0.5 – 20 eV range [388]. It has also been pointed out that the coupling induced by an axion field between photonic modes [389, 390] or atomic states [391] separated by an energy equal to the axion mass may be leveraged for axion detection, though the implementation may be challenging. Certain magnetic topological insulators are conjectured to contain axion-polaritons, quasiparticles composed of magnons and the electric field, with magnetically tunable mass in the meV to eV range [392–394]. Axion dark matter leads to resonant photon emission from such materials, which can be detected [395, 396].

In the intermediate mass region, $\text{neV} \lesssim m_a \lesssim 0.1\,\mu\text{eV}$, one may exploit a cooled LC circuit and precision magnetometry to search for the oscillating electric current induced by DM axions in a strong magnetic field [397, 398]. A number of small-scale pathfinder experiments have implemented this approach: ABRACADABRA [399, 400] used a nonresonant configuration in a toroidal magnet for a broadband search, ADMX-SLIC [401] used a resonant configuration in a solenoid magnet for a narrowband search, SHAFT [402] used a nonresonant configuration in a toroidal magnet enhanced with a ferromagnetic core, and BASE [403] used antiprotons in a Penning trap as the LC cir-

Downloaded from https://academic.oup.com/ptep/article/2022/8/083C01/6651666 by KIT Library user on 27 September 2022

cuit. The exclusion limits from these experiments are shown in Fig. 90.2; none are yet sensitive to the QCD axion. Future work in this direction is expected to have much more competitive limits [404].

The oscillating Galactic DM axion field induces oscillating nuclear electric dipole moments (EDMs) [139],

$$d_N(t) = g_{aN\gamma}\sqrt{2\rho_{\rm aDM}}\cos(m_a\,t)/m_a\,, \tag{90.38}$$

where $g_{aN\gamma}$ is the coupling of the axion to the nucleon EDM operator, defined in Eq. (90.4). An analysis of the ratio of spin-precession frequencies of stored ultracold neutrons and ^{199}Hg atoms measured by neutron EDM experiments for an axion-induced oscillating neutron EDM revealed no signal consistent with axion DM, excluding a sizeable region of parameter space in the mass region $10^{-24}\,\mathrm{eV} \le m_a \le 10^{-17}\,\mathrm{eV}$ [405], which surpass the limits on anomalous energy loss of SN 1987A by more than seven orders of magnitude, see Fig. 90.1, and are competitive with the ones from the requirement of successful BBN established in [406], see Fig. 90.5.[1] In fact, the oscillating dark matter axion field could increase the neutron-proton mass difference at neutron freeze-out and thus result in the underproduction of ^{4}He during BBN. The oscillating EDMs cause also the precession of nuclear spins in a nucleon spin polarized sample in the presence of an electric field. The resulting transverse magnetization can be searched for by exploiting magnetic-resonance (MR) techniques, which are most sensitive in the range of low oscillation frequencies corresponding to sub-neV axion masses. The aim of the corresponding Cosmic Axion Spin Precession Experiment (CASPEr) [407] is to probe axion DM in the anthropic window, $f_a \gtrsim 10^{15}\,\mathrm{GeV}$ ($m_a \lesssim$ neV), motivated from Grand Unification [408–411]. There are two interactions probed through MR: the electric dipole coupling as searched for by CASPEr-electric, whose first run has established the limits shown in Fig. 90.1 [412], and an interaction between the axion field gradient and the nuclear spin, which is aimed for by CASPEr-wind. In the meantime, the latter has been explored through comagnetometry between a variety of nuclei: H-^{12}C in CASPEr-ZULF [413,414], Xe-Rb in NASDUCK [415], and K-^{3}He [416,417]. The exclusions from these searches are shown in Fig. 90.4. Sub-μeV ALP masses can also be probed by using the storage ring EDM method proposed in Ref. [418] which exploits a combination of B and E-fields to produce a resonance between the $g-2$ spin precession frequency and the DM ALP field oscillation frequency. This method, however, does not reach the sensitivity to probe the QCD axion prediction for $g_{aN\gamma}$. An eventually non-zero axion electron coupling g_{aee} will lead to an electron spin precession about the axion DM wind [419, 420]. The QUAX a-e experiment exploits MR inside a magnetized material [421]. Because of the higher Larmor frequency of the electron, it is sensitive in the classic window. Its first run established the bound in the mass range 42.4 to 43.2 μeV [422], slightly better than the solar ν bound, shown in Fig. 90.3.

90.6 Conclusions

There is a strengthening physics case for very weakly coupled light particles beyond the Standard Model. The elegant solution of the strong CP problem proposed by Peccei and Quinn yields a particularly strong motivation for the axion. In many theoretically appealing ultraviolet completions of the Standard Model axions and ALPs occur automatically. Moreover, they are natural CDM candidates. Perhaps the first hints of their existence have already been seen in the anomalous excessive cooling of stars and the anomalous transparency of the Universe for very high energy gamma rays. Interestingly, a significant portion of previously unexplored, but phenomenologically very interesting and theoretically very well motivated axion and ALP parameter space can be tackled in the foreseeable future by a number of terrestrial experiments searching for axion/ALP DM, for solar axions/ALPs, and for light apparently shining through a wall.

[1] These limits are still to the left of the canonical QCD axion line. However, in non-minimal models where the QCD axion is a mediator between strongly interacting hidden sectors enjoying a discrete, $\mathbb{Z}_{\mathcal{N}}$, shift symmetry, the QCD axion line can be shifted to the left in discrete steps, without any fine tuning [44, 45, 291].

90.7 Acknowledgements

It is a pleasure to thank Masha Baryakhtar, Francesca Calore, Luca Di Luzio, Andrew Geraci, Maurizio Giannotti, Igor Irastorza, David J.E. Marsh, Alessandro Mirizzi, Benjamin Safdi, Ken'ichi Saikawa, Yannis Semertzidis, Guenter Sigl, and Sergey Troitsky for discussions, suggestions, and comments on this review. Particular thanks to Ciaran O'Hare for maintaining a publicly accessible collection of axion plots and providing updates to accomodate this review [31].

References

[1] R. D. Peccei and H. R. Quinn, Phys. Rev. Lett. **38**, 1440 (1977).

[2] R. D. Peccei and H. R. Quinn, Phys. Rev. **D16**, 1791 (1977).

[3] S. Weinberg, Phys. Rev. Lett. **40**, 223 (1978).

[4] F. Wilczek, Phys. Rev. Lett. **40**, 279 (1978).

[5] Y. Chikashige, R.N. Mohapatra, and R.D. Peccei, Phys. Lett. **B98**, 265 (1981).

[6] G. B. Gelmini and M. Roncadelli, Phys. Lett. **99B**, 411 (1981).

[7] P. Sikivie, Phys. Rev. Lett. **51**, 1415 (1983) and Erratum *ibid.*, **52**, 695 (1984).

[8] E. Witten, Phys. Lett. **149B**, 351 (1984).

[9] J. P. Conlon, JHEP **05**, 078 (2006), [hep-th/0602233].

[10] P. Svrcek and E. Witten, JHEP **06**, 051 (2006), [hep-th/0605206].

[11] K.-S. Choi *et al.*, Phys. Lett. **B675**, 381 (2009), [arXiv:0902.3070].

[12] A. Arvanitaki *et al.*, Phys. Rev. **D81**, 123530 (2010), [arXiv:0905.4720].

[13] B. S. Acharya, K. Bobkov and P. Kumar, JHEP **11**, 105 (2010), [arXiv:1004.5138].

[14] M. Cicoli, M. Goodsell and A. Ringwald, JHEP **10**, 146 (2012), [arXiv:1206.0819].

[15] J. Halverson, C. Long and P. Nath, Phys. Rev. **D96**, 5, 056025 (2017), [arXiv:1703.07779].

[16] A. E. Nelson and J. Scholtz, Phys. Rev. D **84**, 103501 (2011), [arXiv:1105.2812].

[17] P. Arias *et al.*, JCAP **1206**, 013 (2012), [arXiv:1201.5902].

[18] P. W. Graham, J. Mardon and S. Rajendran, Phys. Rev. D **93**, 10, 103520 (2016), [arXiv:1504.02102].

[19] J. Jaeckel and A. Ringwald, Ann. Rev. Nucl. Part. Sci. **60**, 405 (2010), [arXiv:1002.0329].

[20] A. Ringwald, Phys. Dark Univ. **1**, 116 (2012), [arXiv:1210.5081].

[21] J. Jaeckel, Frascati Phys. Ser. **56**, 172 (2012), [arXiv:1303.1821].

[22] A. Caputo *et al.* (2021), [arXiv:2105.04565].

[23] M. Pospelov and A. Ritz, Nucl. Phys. **B573**, 177 (2000), [hep-ph/9908508].

[24] C. A. Baker *et al.*, Phys. Rev. Lett. **97**, 131801 (2006), [hep-ex/0602020].

[25] C. Abel *et al.* (nEDM), Phys. Rev. Lett. **124**, 8, 081803 (2020), [arXiv:2001.11966].

[26] H. Georgi, D. B. Kaplan and L. Randall, Phys. Lett. **169B**, 73 (1986).

[27] R. J. Crewther, Phys. Lett. **70B**, 349 (1977).

[28] P. Di Vecchia and G. Veneziano, Nucl. Phys. **B171**, 253 (1980).

[29] M. Gorghetto and G. Villadoro, JHEP **03**, 033 (2019), [arXiv:1812.01008].

[30] S. Borsanyi *et al.*, Nature **539**, 7627, 69 (2016), [arXiv:1606.07494].

[31] C. O'Hare, "cajohare/axionlimits: Axionlimits," (2020), URL `https://doi.org/10.5281/zenodo.3932430`.

Downloaded from https://academic.oup.com/ptep/article/2022/8/083C01/6651666 by KIT Library user on 27 September 2022

[32] J. E. Kim, Phys. Rev. Lett. **43**, 103 (1979).

[33] M. A. Shifman, A. I. Vainshtein and V. I. Zakharov, Nucl. Phys. **B166**, 493 (1980).

[34] M. Dine, W. Fischler and M. Srednicki, Phys. Lett. **104B**, 199 (1981).

[35] A. R. Zhitnitsky, Sov. J. Nucl. Phys. **31**, 260 (1980), [Yad. Fiz.31,497(1980)].

[36] J. E. Kim and G. Carosi, Rev. Mod. Phys. **82**, 557 (2010), [arXiv:0807.3125].

[37] G. Grilli di Cortona *et al.*, JHEP **01**, 034 (2016), [arXiv:1511.02867].

[38] J. E. Kim, Phys. Rev. **D58**, 055006 (1998), [hep-ph/9802220].

[39] L. Di Luzio, F. Mescia and E. Nardi, Phys. Rev. Lett. **118**, 3, 031801 (2017), [arXiv:1610.07593].

[40] L. Di Luzio, F. Mescia and E. Nardi, Phys. Rev. D **96**, 7, 075003 (2017), [arXiv:1705.05370].

[41] L. Di Luzio *et al.*, Phys. Rept. **870**, 1 (2020), [arXiv:2003.01100].

[42] M. Farina *et al.*, JHEP **01**, 095 (2017), [arXiv:1611.09855].

[43] P. Agrawal *et al.*, JHEP **02**, 006 (2018), [arXiv:1709.06085].

[44] A. Hook, Phys. Rev. Lett. **120**, 26, 261802 (2018), [arXiv:1802.10093].

[45] L. Di Luzio *et al.*, JHEP **05**, 184 (2021), [arXiv:2102.00012].

[46] A. V. Sokolov and A. Ringwald, JHEP **06**, 123 (2021), [arXiv:2104.02574].

[47] G. Raffelt and D. Seckel, Phys. Rev. Lett. **60**, 1793 (1988).

[48] M. Carena and R. D. Peccei, Phys. Rev. **D40**, 652 (1989).

[49] K. Choi, K. Kang and J. E. Kim, Phys. Rev. Lett. **62**, 849 (1989).

[50] M. Srednicki, Nucl. Phys. **B260**, 689 (1985).

[51] S. Chang and K. Choi, Phys. Lett. **B316**, 51 (1993), [hep-ph/9306216].

[52] C.-Y. Chen and S. Dawson, Phys. Rev. **D87**, 055016 (2013), [arXiv:1301.0309].

[53] D. A. Dicus *et al.*, Phys. Rev. **D18**, 1829 (1978).

[54] G. Raffelt and L. Stodolsky, Phys. Rev. **D37**, 1237 (1988).

[55] A. A. Anselm, Yad. Fiz. **42**, 1480 (1985).

[56] K. van Bibber *et al.*, Phys. Rev. Lett. **59**, 759 (1987).

[57] G. Ruoso *et al.*, Z. Phys. **C56**, 505 (1992).

[58] R. Cameron *et al.*, Phys. Rev. **D47**, 3707 (1993).

[59] M. Fouche *et al.*, Phys. Rev. **D78**, 032013 (2008), [arXiv:0808.2800].

[60] P. Pugnat *et al.* (OSQAR), Phys. Rev. **D78**, 092003 (2008), [arXiv:0712.3362].

[61] A. S. Chou *et al.* (GammeV (T-969)), Phys. Rev. Lett. **100**, 080402 (2008), [arXiv:0710.3783].

[62] A. Afanasev *et al.*, Phys. Rev. Lett. **101**, 120401 (2008), [arXiv:0806.2631].

[63] K. Ehret *et al.* (ALPS), Phys. Lett. **B689**, 149 (2010), [arXiv:1004.1313].

[64] P. Pugnat *et al.* (OSQAR), Eur. Phys. J. **C74**, 8, 3027 (2014), [arXiv:1306.0443].

[65] R. Ballou *et al.* (OSQAR), Phys. Rev. **D92**, 9, 092002 (2015), [arXiv:1506.08082].

[66] F. Hoogeveen and T. Ziegenhagen, Nucl. Phys. **B358**, 3 (1991).

[67] P. Sikivie, D. B. Tanner and K. van Bibber, Phys. Rev. Lett. **98**, 172002 (2007), [hep-ph/0701198].

[68] G. Mueller *et al.*, Phys. Rev. **D80**, 072004 (2009), [arXiv:0907.5387].

[69] R. Bähre *et al.*, JINST **8**, T09001 (2013), [arXiv:1302.5647].

[70] F. Hoogeveen, Phys. Lett. **B288**, 195 (1992).

[71] J. Jaeckel and A. Ringwald, Phys. Lett. **B659**, 509 (2008), [arXiv:0707.2063].

[72] F. Caspers, J. Jaeckel and A. Ringwald, JINST **4**, P11013 (2009), [arXiv:0908.0759].

[73] R. Povey, J. Hartnett and M. Tobar, Phys. Rev. **D82**, 052003 (2010), [arXiv:1003.0964].

[74] M. Betz *et al.*, Phys. Rev. **D88**, 7, 075014 (2013), [arXiv:1310.8098].

[75] L. Maiani, R. Petronzio and E. Zavattini, Phys. Lett. **B175**, 359 (1986).

[76] Y. Semertzidis *et al.*, Phys. Rev. Lett. **64**, 2988 (1990).

[77] E. Zavattini *et al.* (PVLAS), Phys. Rev. Lett. **96**, 110406 (2006), [Erratum: Phys. Rev. Lett.99,129901(2007)], [hep-ex/0507107].

[78] E. Zavattini *et al.* (PVLAS), Phys. Rev. **D77**, 032006 (2008), [arXiv:0706.3419].

[79] F. Della Valle *et al.*, Eur. Phys. J. **C76**, 1, 24 (2016), [arXiv:1510.08052].

[80] E. Fischbach and C. Talmadge, Nature **356**, 207 (1992).

[81] J. E. Moody and F. Wilczek, Phys. Rev. **D30**, 130 (1984).

[82] A. N. Youdin *et al.*, Phys. Rev. Lett. **77**, 2170 (1996).

[83] W.-T. Ni *et al.*, Phys. Rev. Lett. **82**, 2439 (1999).

[84] D. F. Phillips *et al.*, Phys. Rev. **D63**, 111101 (2001), [arXiv:physics/0008230].

[85] B. R. Heckel *et al.*, Phys. Rev. Lett. **97**, 021603 (2006), [hep-ph/0606218].

[86] S. A. Hoedl *et al.*, Phys. Rev. Lett. **106**, 041801 (2011).

[87] E. G. Adelberger *et al.*, Phys. Rev. Lett. **98**, 131104 (2007), [hep-ph/0611223].

[88] D. J. Kapner *et al.*, Phys. Rev. Lett. **98**, 021101 (2007), [hep-ph/0611184].

[89] G. Raffelt, Phys. Rev. **D86**, 015001 (2012), [arXiv:1205.1776].

[90] C. A. J. O'Hare and E. Vitagliano, Phys. Rev. D **102**, 11, 115026 (2020), [arXiv:2010.03889].

[91] A. Arvanitaki and A. A. Geraci, Phys. Rev. Lett. **113**, 16, 161801 (2014), [arXiv:1403.1290].

[92] A. A. Geraci *et al.* (ARIADNE), Springer Proc. Phys. **211**, 151 (2018), [arXiv:1710.05413].

[93] H. Fosbinder-Elkins *et al.* (2017), [arXiv:1710.08102].

[94] N. Aggarwal *et al.* (ARIADNE) (2020), [arXiv:2011.12617].

[95] M. S. Turner, Phys. Rept. **197**, 67 (1990).

[96] G. G. Raffelt, Lect. Notes Phys. **741**, 51 (2008), [,51(2006)], [hep-ph/0611350].

[97] S. Andriamonje *et al.* (CAST), JCAP **0704**, 010 (2007), [hep-ex/0702006].

[98] P. Gondolo and G. G. Raffelt, Phys. Rev. **D79**, 107301 (2009), [arXiv:0807.2926].

[99] H. Schlattl, A. Weiss and G. Raffelt, Astropart. Phys. **10**, 353 (1999), [hep-ph/9807476].

[100] N. Vinyoles *et al.*, JCAP **1510**, 10, 015 (2015), [arXiv:1501.01639].

[101] A. Ayala *et al.*, Phys. Rev. Lett. **113**, 19, 191302 (2014), [arXiv:1406.6053].

[102] O. Straniero *et al.*, in "Proceedings, 11th Patras Workshop on Axions, WIMPs and WISPs (Axion-WIMP 2015): Zaragoza, Spain, June 22-26, 2015," 77–81 (2015).

[103] J. Redondo, JCAP **1312**, 008 (2013), [arXiv:1310.0823].

[104] O. Straniero *et al.*, Astron. Astrophys. **644**, A166 (2020), [arXiv:2010.03833].

[105] F. Capozzi and G. Raffelt, Phys. Rev. D **102**, 8, 083007 (2020), [arXiv:2007.03694].

Downloaded from https://academic.oup.com/ptep/article/2022/8/083C01/6651666 by KIT Library user on 27 September 2022

[106] G. G. Raffelt, Phys. Lett. **166B**, 402 (1986).

[107] S. I. Blinnikov and N. V. Dunina-Barkovskaya, Mon. Not. Roy. Astron. Soc. **266**, 289 (1994).

[108] M. M. Miller Bertolami *et al.*, JCAP **1410**, 10, 069 (2014), [arXiv:1406.7712].

[109] J. Isern *et al.*, Astrophys. J. **682**, L109 (2008), [arXiv:0806.2807].

[110] J. Isern *et al.*, J. Phys. Conf. Ser. **172**, 012005 (2009), [arXiv:0812.3043].

[111] A. Drlica-Wagner *et al.* (LSST Dark Matter Group) (2019), [arXiv:1902.01055].

[112] J. Isern *et al.*, Astron. & Astrophys. **512**, A86 (2010).

[113] A. H. Corsico *et al.*, Mon. Not. Roy. Astron. Soc. **424**, 2792 (2012), [arXiv:1205.6180].

[114] A. H. Corsico *et al.*, JCAP **1212**, 010 (2012), [arXiv:1211.3389].

[115] A. H. Córsico *et al.* (2019), [arXiv:1907.00115].

[116] M. J. Dolan, F. J. Hiskens and R. R. Volkas, Journal of Cosmology and Astroparticle Physics **2021**, 09, 010 (2021), URL `https://doi.org/10.1088/1475-7516/2021/09/010`.

[117] M. Giannotti *et al.*, JCAP **1605**, 05, 057 (2016), [arXiv:1512.08108].

[118] G.G. Raffelt, *Stars as Laboratories for Fundamental Physics*, (Univ. of Chicago Press, Chicago, 1996).

[119] T. Fischer *et al.*, Phys. Rev. **D94**, 8, 085012 (2016), [arXiv:1605.08780].

[120] J. H. Chang, R. Essig and S. D. McDermott, JHEP **09**, 051 (2018), [arXiv:1803.00993].

[121] P. Carenza *et al.*, JCAP **10**, 10, 016 (2019), [Erratum: JCAP 05, E01 (2020)], [arXiv:1906.11844].

[122] M. S. Turner, Phys. Rev. D **45**, 1066 (1992).

[123] G. Raffelt and D. Seckel, Phys. Rev. D **52**, 1780 (1995), [arXiv:astro-ph/9312019].

[124] W. Keil *et al.*, Phys. Rev. D **56**, 2419 (1997), [arXiv:astro-ph/9612222].

[125] B. Fore and S. Reddy, Phys. Rev. C **101**, 3, 035809 (2020), [arXiv:1911.02632].

[126] P. Carenza *et al.*, Phys. Rev. Lett. **126**, 7, 071102 (2021), [arXiv:2010.02943].

[127] J. Engel, D. Seckel and A. C. Hayes, Phys. Rev. Lett. **65**, 960 (1990).

[128] T. Moroi and H. Murayama, Phys. Lett. **B440**, 69 (1998), [hep-ph/9804291].

[129] D. Page *et al.*, Phys. Rev. Lett. **106**, 081101 (2011), [arXiv:1011.6142].

[130] P. S. Shternin *et al.*, Mon. Not. Roy. Astron. Soc. **412**, L108 (2011), [arXiv:1012.0045].

[131] L. B. Leinson, Phys. Lett. **B741**, 87 (2015), [arXiv:1411.6833].

[132] K. Hamaguchi *et al.*, Phys. Rev. **D98**, 10, 103015 (2018), [arXiv:1806.07151].

[133] J. Keller and A. Sedrakian, Nucl. Phys. **A897**, 62 (2013), [arXiv:1205.6940].

[134] A. Sedrakian, Phys. Rev. **D93**, 6, 065044 (2016), [arXiv:1512.07828].

[135] L. B. Leinson (2021), [arXiv:2105.14745].

[136] L. B. Leinson, JCAP **1408**, 031 (2014), [arXiv:1405.6873].

[137] B. Posselt and G. G. Pavlov, Astrophys. J. **864**, 2, 135 (2018), [arXiv:1808.00531].

[138] M. V. Beznogov *et al.*, Phys. Rev. **C98**, 3, 035802 (2018), [arXiv:1806.07991].

[139] P. W. Graham and S. Rajendran, Phys. Rev. **D88**, 035023 (2013), [arXiv:1306.6088].

[140] G. G. Raffelt, J. Redondo and N. Viaux Maira, Phys. Rev. **D84**, 103008 (2011), [arXiv:1110.6397].

[141] K. van Bibber *et al.*, Phys. Rev. **D39**, 2089 (1989).

[142] D. M. Lazarus *et al.*, Phys. Rev. Lett. **69**, 2333 (1992).

[143] S. Moriyama *et al.*, Phys. Lett. **B434**, 147 (1998), [hep-ex/9805026].

[144] Y. Inoue *et al.*, Phys. Lett. **B536**, 18 (2002), [arXiv:astro-ph/0204388].

[145] Y. Inoue *et al.*, Phys. Lett. **B668**, 93 (2008), [arXiv:0806.2230].

[146] V. Anastassopoulos *et al.* (CAST), Nature Phys. **13**, 584 (2017), [arXiv:1705.02290].

[147] E. Arik *et al.* (CAST), JCAP **0902**, 008 (2009), [arXiv:0810.4482].

[148] S. Aune *et al.* (CAST), Phys. Rev. Lett. **107**, 261302 (2011), [arXiv:1106.3919].

[149] M. Arik *et al.* (CAST), Phys. Rev. Lett. **112**, 9, 091302 (2014), [arXiv:1307.1985].

[150] M. Arik *et al.* (CAST), Phys. Rev. **D92**, 2, 021101 (2015), [arXiv:1503.00610].

[151] E. Armengaud *et al.*, JINST **9**, T05002 (2014), [arXiv:1401.3233].

[152] E. Armengaud *et al.* (IAXO), JCAP **1906**, 06, 047 (2019), [arXiv:1904.09155].

[153] M. Giannotti *et al.*, JCAP **1710**, 10, 010 (2017), [arXiv:1708.02111].

[154] K. Barth *et al.*, JCAP **1305**, 010 (2013), [arXiv:1302.6283].

[155] A. Abeln *et al.* (BabyIAXO), JCAP **2105**, 05, 137 (2021), [arXiv:2010.12076].

[156] F. T. Avignone, III *et al.* (SOLAX), Phys. Rev. Lett. **81**, 5068 (1998), [arXiv:astro-ph/9708008].

[157] S. Cebrian *et al.*, Astropart. Phys. **10**, 397 (1999), [arXiv:astro-ph/9811359].

[158] A. Morales *et al.* (COSME), Astropart. Phys. **16**, 325 (2002), [hep-ex/0101037].

[159] R. Bernabei *et al.*, Phys. Lett. **B515**, 6 (2001).

[160] Z. Ahmed *et al.* (CDMS), Phys. Rev. Lett. **103**, 141802 (2009), [arXiv:0902.4693].

[161] D. S. Akerib *et al.* (LUX), Phys. Rev. Lett. **118**, 26, 261301 (2017), [arXiv:1704.02297].

[162] X. Zhou *et al.* (PandaX-II) (2020), [arXiv:2008.06485].

[163] E. Aprile *et al.* (XENON), Phys. Rev. D **102**, 7, 072004 (2020), [arXiv:2006.09721].

[164] L. Di Luzio *et al.*, Phys. Rev. Lett. **125**, 13, 131804 (2020), [arXiv:2006.12487].

[165] C. Gao *et al.*, Phys. Rev. Lett. **125**, 13, 131806 (2020), [arXiv:2006.14598].

[166] J. B. Dent *et al.*, Phys. Rev. Lett. **125**, 13, 131805 (2020), [arXiv:2006.15118].

[167] J. W. Brockway, E. D. Carlson and G. G. Raffelt, Phys. Lett. **B383**, 439 (1996), [arXiv:astro-ph/9605197].

[168] J. A. Grifols, E. Masso and R. Toldra, Phys. Rev. Lett. **77**, 2372 (1996), [arXiv:astro-ph/9606028].

[169] A. Payez *et al.*, JCAP **1502**, 02, 006 (2015), [arXiv:1410.3747].

[170] M. Meyer and T. Petrushevska, Phys. Rev. Lett. **124**, 23, 231101 (2020), [Erratum: Phys.Rev.Lett. 125, 119901 (2020)], [arXiv:2006.06722].

[171] F. Calore *et al.*, Phys. Rev. D **102**, 12, 123005 (2020), [arXiv:2008.11741].

[172] C. Dessert, J. W. Foster and B. R. Safdi, Phys. Rev. Lett. **125**, 26, 261102 (2020), [arXiv:2008.03305].

[173] M. Xiao *et al.*, Phys. Rev. Lett. **126**, 3, 031101 (2021), [arXiv:2009.09059].

Downloaded from https://academic.oup.com/ptep/article/2022/8/083C01/6651666 by KIT Library user on 27 September 2022

[174] C. Dessert, J. W. Foster and B. R. Safdi, Astrophys. J. **904**, 1, 42 (2020), [arXiv:1910.02956].

[175] M. Buschmann *et al.*, Phys. Rev. Lett. **126**, 2, 021102 (2021), [arXiv:1910.04164].

[176] C. Dessert, A. J. Long and B. R. Safdi, Phys. Rev. Lett. **123**, 6, 061104 (2019), [arXiv:1903.05088].

[177] C. Dessert, A. J. Long and B. R. Safdi (2021), [arXiv:2104.12772].

[178] C. Csaki, N. Kaloper and J. Terning, Phys. Rev. Lett. **88**, 161302 (2002), [hep-ph/0111311].

[179] A. Mirizzi, G.G. Raffelt, and P.D. Serpico, Lect. Notes Phys. **741**, 115 (2008).

[180] R. Gill and J. S. Heyl, Phys. Rev. **D84**, 085001 (2011), [arXiv:1105.2083].

[181] D. Horns *et al.*, Phys. Rev. **D85**, 085021 (2012), [arXiv:1203.2184].

[182] A. Payez, J. R. Cudell and D. Hutsemekers, JCAP **1207**, 041 (2012), [arXiv:1204.6187].

[183] A. Dominguez, M. A. Sanchez-Conde and F. Prada, JCAP **1111**, 020 (2011), [arXiv:1106.1860].

[184] W. Essey and A. Kusenko, Astrophys. J. **751**, L11 (2012), [arXiv:1111.0815].

[185] D. Horns and M. Meyer, JCAP **1202**, 033 (2012), [arXiv:1201.4711].

[186] G. I. Rubtsov and S. V. Troitsky, JETP Lett. **100**, 6, 355 (2014), [Pisma Zh. Eksp. Teor. Fiz.100,no.6,397(2014)], [arXiv:1406.0239].

[187] K. Kohri and H. Kodama, Phys. Rev. **D96**, 5, 051701 (2017), [arXiv:1704.05189].

[188] D. A. Sanchez, S. Fegan and B. Giebels, Astron. Astrophys. **554**, A75 (2013), [arXiv:1303.5923].

[189] J. Biteau and D. A. Williams, Astrophys. J. **812**, 1, 60 (2015), [arXiv:1502.04166].

[190] A. Domínguez and M. Ajello, Astrophys. J. **813**, 2, L34 (2015), [arXiv:1510.07913].

[191] A. Korochkin, G. Rubtsov and S. Troitsky, JCAP **12**, 002 (2019), [arXiv:1810.03443].

[192] A. De Angelis, G. Galanti and M. Roncadelli, Phys. Rev. **D84**, 105030 (2011), [Erratum: Phys. Rev.D87,no.10,109903(2013)], [arXiv:1106.1132].

[193] M. Simet, D. Hooper and P. D. Serpico, Phys. Rev. **D77**, 063001 (2008), [arXiv:0712.2825].

[194] M. A. Sanchez-Conde *et al.*, Phys. Rev. **D79**, 123511 (2009), [arXiv:0905.3270].

[195] M. Meyer, D. Horns and M. Raue, Phys. Rev. **D87**, 3, 035027 (2013), [arXiv:1302.1208].

[196] A. Abramowski *et al.* (H.E.S.S.), Phys. Rev. **D88**, 10, 102003 (2013), [arXiv:1311.3148].

[197] M. Ajello *et al.* (Fermi-LAT), Phys. Rev. Lett. **116**, 16, 161101 (2016), [arXiv:1603.06978].

[198] C. Zhang *et al.*, Phys. Rev. **D97**, 6, 063009 (2018), [arXiv:1802.08420].

[199] H.-J. Li *et al.*, Phys. Rev. D **103**, 8, 083003 (2021), [arXiv:2008.09464].

[200] M. Libanov and S. Troitsky, Phys. Lett. B **802**, 135252 (2020), [arXiv:1908.03084].

[201] Z.-Q. Xia *et al.*, Phys. Rev. **D97**, 6, 063003 (2018), [arXiv:1801.01646].

[202] J. Majumdar, F. Calore and D. Horns, JCAP **1804**, 04, 048 (2018), [arXiv:1801.08813].

[203] G. A. Pallathadka *et al.* (2020), [arXiv:2008.08100].

[204] K. Choi *et al.*, Phys. Rev. D **101**, 4, 043007 (2020), [arXiv:1806.09508].

[205] F. Chadha-Day (2021), [arXiv:2107.12813].

[206] D. Wouters and P. Brun, Astrophys. J. **772**, 44 (2013), [arXiv:1304.0989].

[207] M. Berg *et al.*, Astrophys. J. **847**, 2, 101 (2017), [arXiv:1605.01043].

[208] M. C. D. Marsh *et al.*, JCAP **1712**, 12, 036 (2017), [arXiv:1703.07354].

[209] J. P. Conlon *et al.*, JCAP **1707**, 07, 005 (2017), [arXiv:1704.05256].

[210] L. Chen and J. P. Conlon, Mon. Not. Roy. Astron. Soc. **479**, 2, 2243 (2018), [arXiv:1712.08313].

[211] C. S. Reynolds *et al.*, Astrophys. J. **890**, 1, 59 (2020), [arXiv:1907.05475].

[212] A. Hook and J. Huang, JHEP **06**, 036 (2018), [arXiv:1708.08464].

[213] J. Huang *et al.*, Phys. Rev. D **99**, 6, 063013 (2019), [arXiv:1807.02133].

[214] J. Zhang *et al.* (2021), [arXiv:2105.13963].

[215] G. Bellini *et al.* (Borexino), Phys. Rev. D **89**, 11, 112007 (2014), [arXiv:1308.0443].

[216] B. P. Abbott *et al.* (LIGO Scientific, Virgo), Phys. Rev. Lett. **119**, 16, 161101 (2017), [arXiv:1710.05832].

[217] A. Arvanitaki and S. Dubovsky, Phys. Rev. **D83**, 044026 (2011), [arXiv:1004.3558].

[218] A. Arvanitaki, M. Baryakhtar and X. Huang, Phys. Rev. **D91**, 8, 084011 (2015), [arXiv:1411.2263].

[219] V. M. Mehta *et al.* (2020), [arXiv:2011.08693].

[220] V. M. Mehta *et al.*, JCAP **07**, 033 (2021), [arXiv:2103.06812].

[221] M. J. Stott (2020), [arXiv:2009.07206].

[222] M. Baryakhtar *et al.*, Phys. Rev. D **103**, 9, 095019 (2021), [arXiv:2011.11646].

[223] A. Arvanitaki *et al.*, Phys. Rev. **D95**, 4, 043001 (2017), [arXiv:1604.03958].

[224] K. K. Y. Ng *et al.*, Phys. Rev. D **103**, 6, 063010 (2021), [arXiv:1908.02312].

[225] E. Masso, F. Rota and G. Zsembinszki, Phys. Rev. D **66**, 023004 (2002), [hep-ph/0203221].

[226] P. Graf and F. D. Steffen, Phys. Rev. D **83**, 075011 (2011), [arXiv:1008.4528].

[227] Z. G. Berezhiani, A. S. Sakharov and M. Y. Khlopov, Sov. J. Nucl. Phys. **55**, 1063 (1992).

[228] S. Hannestad, A. Mirizzi and G. Raffelt, JCAP **07**, 002 (2005), [hep-ph/0504059].

[229] S. Hannestad *et al.*, JCAP **08**, 001 (2010), [arXiv:1004.0695].

[230] M. Archidiacono *et al.*, JCAP **10**, 020 (2013), [arXiv:1307.0615].

[231] E. Di Valentino *et al.*, Phys. Lett. B **752**, 182 (2016), [arXiv:1507.08665].

[232] W. Giarè *et al.*, Mon. Not. Roy. Astron. Soc. **505**, 2, 2703 (2021), [arXiv:2011.14704].

[233] L. Di Luzio, G. Martinelli and G. Piazza, Phys. Rev. Lett. **126**, 24, 241801 (2021), [arXiv:2101.10330].

[234] E. Masso and R. Toldra, Phys. Rev. D **52**, 1755 (1995), [hep-ph/9503293].

[235] E. Masso and R. Toldra, Phys. Rev. **D55**, 7967 (1997), [hep-ph/9702275].

[236] D. Cadamuro and J. Redondo, JCAP **1202**, 032 (2012), [arXiv:1110.2895].

[237] P. F. Depta, M. Hufnagel and K. Schmidt-Hoberg, JCAP **05**, 009 (2020), [arXiv:2002.08370].

[238] J. Preskill, M. B. Wise and F. Wilczek, Phys. Lett. **B120**, 127 (1983).

Downloaded from https://academic.oup.com/ptep/article/2022/8/083C01/6651666 by KIT Library user on 27 September 2022

[239] L. F. Abbott and P. Sikivie, Phys. Lett. **B120**, 133 (1983).

[240] M. Dine and W. Fischler, Phys. Lett. **B120**, 137 (1983).

[241] K. J. Bae, J.-H. Huh and J. E. Kim, JCAP **0809**, 005 (2008), [arXiv:0806.0497].

[242] O. Wantz and E. P. S. Shellard, Phys. Rev. **D82**, 123508 (2010), [arXiv:0910.1066].

[243] G. Ballesteros *et al.*, JCAP **1708**, 08, 001 (2017), [arXiv:1610.01639].

[244] R. T. Co, F. D'Eramo and L. J. Hall, Phys. Rev. D **94**, 7, 075001 (2016), [arXiv:1603.04439].

[245] M. Tegmark *et al.*, Phys. Rev. **D73**, 023505 (2006), [arXiv:astro-ph/0511774].

[246] A. D. Linde, Phys. Lett. **158B**, 375 (1985).

[247] D. Seckel and M. S. Turner, Phys. Rev. **D32**, 3178 (1985).

[248] M. Beltran, J. Garcia-Bellido and J. Lesgourgues, Phys. Rev. **D75**, 103507 (2007), [hep-ph/0606107].

[249] M. P. Hertzberg, M. Tegmark and F. Wilczek, Phys. Rev. **D78**, 083507 (2008), [arXiv:0807.1726].

[250] J. Hamann *et al.*, JCAP **0906**, 022 (2009), [arXiv:0904.0647].

[251] P. A. R. Ade *et al.* (Planck), Astron. Astrophys. **571**, A22 (2014), [arXiv:1303.5082].

[252] P. A. R. Ade *et al.* (Planck), Astron. Astrophys. **594**, A20 (2016), [arXiv:1502.02114].

[253] B. Bolliet, J. Chluba and R. Battye, Monthly Notices of the Royal Astronomical Society **507**, 3, 3148 (2021), ISSN 0035-8711, URL `https://doi.org/10.1093/mnras/stab1997`.

[254] R. T. Co, L. J. Hall and K. Harigaya, Phys. Rev. Lett. **124**, 25, 251802 (2020), [arXiv:1910.14152].

[255] S. Chang, C. Hagmann and P. Sikivie, Phys. Rev. **D59**, 023505 (1999), [hep-ph/9807374].

[256] C. Hagmann, S. Chang and P. Sikivie, Phys. Rev. **D63**, 125018 (2001), [hep-ph/0012361].

[257] T. Hiramatsu *et al.*, Phys. Rev. **D83**, 123531 (2011), [arXiv:1012.5502].

[258] T. Hiramatsu *et al.*, Phys. Rev. **D85**, 105020 (2012), [Erratum: Phys. Rev.D86,089902(2012)], [arXiv:1202.5851].

[259] M. Kawasaki, K. Saikawa and T. Sekiguchi, Phys. Rev. **D91**, 6, 065014 (2015), [arXiv:1412.0789].

[260] V. B. Klaer and G. D. Moore, JCAP **1711**, 11, 049 (2017), [arXiv:1708.07521].

[261] M. Gorghetto, E. Hardy and G. Villadoro, JHEP **07**, 151 (2018), [arXiv:1806.04677].

[262] M. Buschmann, J. W. Foster and B. R. Safdi, Phys. Rev. Lett. **124**, 16, 161103 (2020), [arXiv:1906.00967].

[263] M. Hindmarsh *et al.*, Phys. Rev. Lett. **124**, 2, 021301 (2020), [arXiv:1908.03522].

[264] M. Gorghetto, E. Hardy and G. Villadoro, SciPost Phys. **10**, 050 (2021), [arXiv:2007.04990].

[265] M. Dine *et al.* (2020), [arXiv:2012.13065].

[266] M. Hindmarsh *et al.*, Phys. Rev. D **103**, 10, 103534 (2021), [arXiv:2102.07723].

[267] M. Buschmann *et al.* (2021), [arXiv:2108.05368].

[268] A. Ringwald and K. Saikawa, Phys. Rev. **D93**, 8, 085031 (2016), [Addendum: Phys. Rev.D94,no.4,049908(2016)], [arXiv:1512.06436].

[269] T. Hiramatsu *et al.*, JCAP **1301**, 001 (2013), [arXiv:1207.3166].

[270] C. J. Hogan and M. J. Rees, Phys. Lett. **B205**, 228 (1988).

[271] E. W. Kolb and I. I. Tkachev, Phys. Rev. Lett. **71**, 3051 (1993), [hep-ph/9303313].

[272] B. Eggemeier *et al.*, Phys. Rev. Lett. **125**, 4, 041301 (2020), [arXiv:1911.09417].

[273] A. Vaquero, J. Redondo and J. Stadler (2018), [JCAP1904,no.04,012(2019)], [arXiv:1809.09241].

[274] E. W. Kolb and I. I. Tkachev, Astrophys. J. **460**, L25 (1996), [arXiv:astro-ph/9510043].

[275] M. Fairbairn, D. J. E. Marsh and J. Quevillon, Phys. Rev. Lett. **119**, 2, 021101 (2017), [arXiv:1701.04787].

[276] A. Katz *et al.*, JCAP **1812**, 005 (2018), [arXiv:1807.11495].

[277] E. Berkowitz, M. I. Buchoff and E. Rinaldi, Phys. Rev. **D92**, 3, 034507 (2015), [arXiv:1505.07455].

[278] S. Borsanyi *et al.*, Phys. Lett. **B752**, 175 (2016), [arXiv:1508.06917].

[279] R. Kitano and N. Yamada, JHEP **10**, 136 (2015), [arXiv:1506.00370].

[280] P. Petreczky, H.-P. Schadler and S. Sharma, Phys. Lett. **B762**, 498 (2016), [arXiv:1606.03145].

[281] Y. Taniguchi *et al.*, Phys. Rev. **D95**, 5, 054502 (2017), [arXiv:1611.02411].

[282] M. Dine *et al.*, Phys. Rev. **D96**, 9, 095001 (2017), [arXiv:1705.00676].

[283] R. D. Pisarski and L. G. Yaffe, Phys. Lett. **97B**, 110 (1980).

[284] R. Hlozek *et al.*, Phys. Rev. **D91**, 10, 103512 (2015), [arXiv:1410.2896].

[285] D. J. E. Marsh, Phys. Rept. **643**, 1 (2016), [arXiv:1510.07633].

[286] L. Hui *et al.*, Phys. Rev. **D95**, 4, 043541 (2017), [arXiv:1610.08297].

[287] G. P. Centers *et al.* (2019), [arXiv:1905.13650].

[288] A. G. Dias *et al.*, JHEP **06**, 037 (2014), [arXiv:1403.5760].

[289] J. E. Kim and D. J. E. Marsh, Phys. Rev. **D93**, 2, 025027 (2016), [arXiv:1510.01701].

[290] H. Davoudiasl and C. W. Murphy, Phys. Rev. Lett. **118**, 14, 141801 (2017), [arXiv:1701.01136].

[291] L. Di Luzio *et al.*, JCAP **10**, 001 (2021), [arXiv:2102.01082].

[292] M. Khlopov, B. A. Malomed and I. B. Zeldovich, Mon. Not. Roy. Astron. Soc. **215**, 575 (1985).

[293] W. Hu, R. Barkana and A. Gruzinov, Phys. Rev. Lett. **85**, 1158 (2000), [arXiv:astro-ph/0003365].

[294] L. Amendola and R. Barbieri, Phys. Lett. **B642**, 192 (2006), [hep-ph/0509257].

[295] D. J. E. Marsh and P. G. Ferreira, Phys. Rev. **D82**, 103528 (2010), [arXiv:1009.3501].

[296] E. Seidel and W. M. Suen, Phys. Rev. Lett. **66**, 1659 (1991).

[297] H.-Y. Schive, T. Chiueh and T. Broadhurst, Nature Phys. **10**, 496 (2014), [arXiv:1406.6586].

[298] D. G. Levkov, A. G. Panin and I. I. Tkachev, Phys. Rev. Lett. **121**, 15, 151301 (2018), [arXiv:1804.05857].

[299] B. Eggemeier and J. C. Niemeyer, Phys. Rev. D **100**, 6, 063528 (2019), [arXiv:1906.01348].

[300] R. Hlozek, D. J. E. Marsh and D. Grin, Mon. Not. Roy. Astron. Soc. **476**, 3, 3063 (2018), [arXiv:1708.05681].

[301] D. J. E. Marsh and J. Silk, Mon. Not. Roy. Astron. Soc. **437**, 3, 2652 (2014), [arXiv:1307.1705].

[302] H.-Y. Schive *et al.*, Astrophys. J. **818**, 1, 89 (2016), [arXiv:1508.04621].

[303] B. Bozek *et al.*, Mon. Not. Roy. Astron. Soc. **450**, 1, 209 (2015), [arXiv:1409.3544].

[304] P. S. Corasaniti *et al.*, Phys. Rev. **D95**, 8, 083512 (2017), [arXiv:1611.05892].

[305] K. K. Rogers and H. V. Peiris, Phys. Rev. Lett. **126**, 7, 071302 (2021), [arXiv:2007.12705].

[306] H.-Y. Schive and T. Chiueh, Mon. Not. Roy. Astron. Soc. **473**, 1, L36 (2018), [arXiv:1706.03723].

Downloaded from https://academic.oup.com/ptep/article/2022/8/083C01/6651666 by KIT Library user on 27 September 2022

[307] E. O. Nadler *et al.* (DES), Phys. Rev. Lett. **126**, 091101 (2021), [arXiv:2008.00022].

[308] B. Schwabe, J. C. Niemeyer and J. F. Engels, Phys. Rev. **D94**, 4, 043513 (2016), [arXiv:1606.05151].

[309] J. Veltmaat and J. C. Niemeyer, Phys. Rev. **D94**, 12, 123523 (2016), [arXiv:1608.00802].

[310] P. Mocz *et al.*, Mon. Not. Roy. Astron. Soc. **471**, 4, 4559 (2017), [arXiv:1705.05845].

[311] D. G. Levkov, A. G. Panin and I. I. Tkachev, Phys. Rev. Lett. **118**, 011301 (2017); T. Helfer *et al.*, JCAP **1703**, 03, 055 (2017), [arXiv:1609.04724].

[312] D. J. E. Marsh and A.-R. Pop, Mon. Not. Roy. Astron. Soc. **451**, 3, 2479 (2015), [arXiv:1502.03456].

[313] S.-R. Chen, H.-Y. Schive and T. Chiueh, Mon. Not. Roy. Astron. Soc. **468**, 2, 1338 (2017), [arXiv:1606.09030].

[314] A. X. González-Morales *et al.*, Mon. Not. Roy. Astron. Soc. **472**, 2, 1346 (2017), [arXiv:1609.05856].

[315] I. De Martino *et al.*, Phys. Dark Univ. **28**, 100503 (2020), [arXiv:1807.08153].

[316] T. Broadhurst *et al.*, Phys. Rev. D **101**, 8, 083012 (2020), [arXiv:1902.10488].

[317] D. Wadekar and G. R. Farrar, Phys. Rev. D **103**, 123028 (2021), URL `https://link.aps.org/doi/10.1103/PhysRevD.103.123028`.

[318] H.-Y. Schive *et al.*, Phys. Rev. Lett. **113**, 26, 261302 (2014), [arXiv:1407.7762].

[319] V. H. Robles, J. S. Bullock and M. Boylan-Kolchin, Mon. Not. Roy. Astron. Soc. **483**, 1, 289 (2019), [arXiv:1807.06018].

[320] V. Desjacques and A. Nusser (2019), [arXiv:1905.03450].

[321] M. Safarzadeh and D. N. Spergel (2019), [arXiv:1906.11848].

[322] A. Pontzen and F. Governato, Nature **506**, 171 (2014), [arXiv:1402.1764].

[323] P. Mocz *et al.*, Phys. Rev. Lett. **123**, 14, 141301 (2019), [arXiv:1910.01653].

[324] J. Veltmaat, B. Schwabe and J. C. Niemeyer, Phys. Rev. D **101**, 8, 083518 (2020), [arXiv:1911.09614].

[325] J. Veltmaat, J. C. Niemeyer and B. Schwabe, Phys. Rev. **D98**, 4, 043509 (2018), [arXiv:1804.09647].

[326] B. Bar-Or, J.-B. Fouvry and S. Tremaine, Astrophys. J. **871**, 1, 28 (2019), [arXiv:1809.07673].

[327] B. V. Church, P. Mocz and J. P. Ostriker, MNRAS **485**, 2861 (2019), [arXiv:1809.04744].

[328] N. C. Amorisco and A. Loeb (2018), [arXiv:1808.00464].

[329] T. S. Li *et al.* (DES), Astrophys. J. **838**, 1, 8 (2017), [arXiv:1611.05052].

[330] D. J. E. Marsh and J. C. Niemeyer, Phys. Rev. Lett. **123**, 5, 051103 (2019), [arXiv:1810.08543].

[331] E. Armengaud *et al.* (EDELWEISS), Phys. Rev. D **98**, 8, 082004 (2018), [arXiv:1808.02340].

[332] C. Fu *et al.* (PandaX), Phys. Rev. Lett. **119**, 18, 181806 (2017), [arXiv:1707.07921].

[333] T. Aralis *et al.* (SuperCDMS), Phys. Rev. D **101**, 5, 052008 (2020), [Erratum: Phys.Rev.D 103, 039901 (2021)], [arXiv:1911.11905].

[334] E. Aprile *et al.* (XENON), Phys. Rev. Lett. **123**, 25, 251801 (2019), [arXiv:1907.11485].

[335] M. Regis *et al.*, Phys. Lett. B **814**, 136075 (2021), [arXiv:2009.01310].

[336] B. D. Blout *et al.*, Astrophys. J. **546**, 825 (2001), [arXiv:astro-ph/0006310].

[337] K. Kelley and P. J. Quinn, Astrophys. J. **845**, 1, L4 (2017), [arXiv:1708.01399].

[338] G. Sigl, Phys. Rev. **D96**, 10, 103014 (2017), [arXiv:1708.08908].

[339] A. Hook *et al.*, Phys. Rev. Lett. **121**, 24, 241102 (2018), [arXiv:1804.03145].

[340] J. W. Foster *et al.*, Phys. Rev. Lett. **125**, 17, 171301 (2020), [arXiv:2004.00011].

[341] J. Darling, Astrophys. J. Lett. **900**, 2, L28 (2020), [arXiv:2008.11188].

[342] R. A. Battye *et al.* (2021), [arXiv:2107.01225].

[343] S. J. Witte *et al.* (2021), [arXiv:2104.07670].

[344] R. A. Battye *et al.* (2021), [arXiv:2104.08290].

[345] A. J. Millar *et al.* (2021), [arXiv:2107.07399].

[346] A. Caputo *et al.*, JCAP **1903**, 03, 027 (2019), [arXiv:1811.08436].

[347] P. Carenza, A. Mirizzi and G. Sigl, Phys. Rev. D **101**, 10, 103016 (2020), [arXiv:1911.07838].

[348] D. G. Levkov, A. G. Panin and I. I. Tkachev, Phys. Rev. D **102**, 2, 023501 (2020), [arXiv:2004.05179].

[349] M. A. Fedderke, P. W. Graham and S. Rajendran, Phys. Rev. **D100**, 1, 015040 (2019), [arXiv:1903.02666].

[350] T. Fujita *et al.*, Phys. Rev. D **103**, 4, 043509 (2021), [arXiv:2011.11894].

[351] P. A. R. Ade *et al.* (BICEP/Keck) (2021), [arXiv:2108.03316].

[352] T. Liu, G. Smoot and Y. Zhao (2019), [arXiv:1901.10981].

[353] P. Sikivie, Phys. Rev. **D32**, 2988 (1985), [Erratum: Phys. Rev.D36,974(1987)].

[354] R. Bradley *et al.*, Rev. Mod. Phys. **75**, 777 (2003).

[355] P. Sikivie and J. R. Ipser, Phys. Lett. **B291**, 288 (1992).

[356] P. Sikivie, I. I. Tkachev and Y. Wang, Phys. Rev. Lett. **75**, 2911 (1995), [arXiv:astro-ph/9504052].

[357] S. De Panfilis *et al.*, Phys. Rev. Lett. **59**, 839 (1987).

[358] W. Wuensch *et al.*, Phys. Rev. **D40**, 3153 (1989).

[359] C. Hagmann *et al.*, Phys. Rev. **D42**, 1297 (1990).

[360] S. J. Asztalos *et al.* (ADMX), Phys. Rev. **D69**, 011101 (2004), [arXiv:astro-ph/0310042].

[361] L. Duffy *et al.*, Phys. Rev. Lett. **95**, 091304 (2005), [arXiv:astro-ph/0505237]; J. Hoskins *et al.*, Phys. Rev. **D84**, 121302 (2011), [arXiv:1109.4128].

[362] S. J. Asztalos *et al.* (ADMX), Phys. Rev. Lett. **104**, 041301 (2010), [arXiv:0910.5914].

[363] S. J. Asztalos *et al.* (ADMX), Nucl. Instrum. Meth. **A656**, 39 (2011), [arXiv:1105.4203].

[364] R. Khatiwada *et al.* (ADMX) (2020), [arXiv:2010.00169].

[365] N. Du *et al.* (ADMX), Phys. Rev. Lett. **120**, 15, 151301 (2018), [arXiv:1804.05750].

[366] T. Braine *et al.* (ADMX), Phys. Rev. Lett. **124**, 10, 101303 (2020), [arXiv:1910.08638].

[367] C. Bartram *et al.* (ADMX), Phys. Rev. D **103**, 3, 032002 (2021), [arXiv:2010.06183].

[368] C. Bartram *et al.* (ADMX Collaboration), Phys. Rev. Lett. **127**, 261803 (2021), URL `https://link.aps.org/doi/10.1103/PhysRevLett.127.261803`.

[369] G. Rybka *et al.* (ADMX), Phys. Rev. Lett. **105**, 051801 (2010), [arXiv:1004.5160].

[370] A. Wagner *et al.* (ADMX), Phys. Rev. Lett. **105**, 171801 (2010), [arXiv:1007.3766].

[371] C. Boutan *et al.* (ADMX), Phys. Rev. Lett. **121**, 26, 261302 (2018), [arXiv:1901.00920].

[372] B. M. Brubaker *et al.*, Phys. Rev. Lett. **118**, 6, 061302 (2017), [arXiv:1610.02580].

[373] L. Zhong *et al.* (HAYSTAC), Phys. Rev. D **97**, 9, 092001 (2018), [arXiv:1803.03690].

Downloaded from https://academic.oup.com/ptep/article/2022/8/083C01/6651666 by KIT Library user on 27 September 2022

[374] K. M. Backes *et al.* (HAYSTAC), Nature **590**, 7845, 238 (2021), [arXiv:2008.01853].

[375] B. T. McAllister *et al.*, Phys. Dark Univ. **18**, 67 (2017), [arXiv:1706.00209].

[376] D. Alesini *et al.*, Phys. Rev. D **99**, 10, 101101 (2019), [arXiv:1903.06547].

[377] D. Alesini *et al.*, Phys. Rev. D **103**, 10, 102004 (2021), [arXiv:2012.09498].

[378] A. A. Melcón *et al.* (CAST) (2021), [arXiv:2104.13798].

[379] S. Lee *et al.*, Phys. Rev. Lett. **124**, 10, 101802 (2020), [arXiv:2001.05102].

[380] J. Jeong *et al.*, Phys. Rev. Lett. **125**, 22, 221302 (2020), [arXiv:2008.10141].

[381] O. Kwon *et al.* (CAPP), Phys. Rev. Lett. **126**, 19, 191802 (2021), [arXiv:2012.10764].

[382] G. Rybka *et al.*, Phys. Rev. **D91**, 1, 011701 (2015), [arXiv:1403.3121].

[383] M. Lawson *et al.*, Phys. Rev. Lett. **123**, 14, 141802 (2019), [arXiv:1904.11872].

[384] D. Horns *et al.*, JCAP **1304**, 016 (2013), [arXiv:1212.2970].

[385] A. Caldwell *et al.* (MADMAX Working Group), Phys. Rev. Lett. **118**, 9, 091801 (2017), [arXiv:1611.05865].

[386] P. Brun *et al.* (MADMAX), Eur. Phys. J. **C79**, 3, 186 (2019), [arXiv:1901.07401].

[387] M. Baryakhtar, J. Huang and R. Lasenby, Phys. Rev. **D98**, 3, 035006 (2018), [arXiv:1803.11455].

[388] A. Arvanitaki, S. Dimopoulos and K. Van Tilburg, Phys. Rev. **X8**, 4, 041001 (2018), [arXiv:1709.05354].

[389] C. A. Thomson *et al.*, Phys. Rev. Lett. **126**, 8, 081803 (2021), [Erratum: Phys.Rev.Lett. 127, 019901 (2021)], [arXiv:1912.07751].

[390] A. Berlin *et al.*, JHEP **07**, 07, 088 (2020), [arXiv:1912.11048].

[391] P. Sikivie, Phys. Rev. Lett. **113**, 20, 201301 (2014), [Erratum: Phys.Rev.Lett. 125, 029901 (2020)], [arXiv:1409.2806].

[392] R. Li *et al.*, Nature Phys. **6**, 284 (2010), [arXiv:0908.1537].

[393] K. Ishiwata, Phys. Rev. D **104**, 1, 016004 (2021), [arXiv:2103.02848].

[394] L. Cao *et al.*, Phys. Rev. B **104**, 054421 (2021), URL `https://link.aps.org/doi/10.1103/PhysRevB.104.054421`.

[395] D. J. E. Marsh *et al.*, Phys. Rev. Lett. **123**, 12, 121601 (2019), [arXiv:1807.08810].

[396] J. Schütte-Engel *et al.*, JCAP **08**, 066 (2021), [arXiv:2102.05366].

[397] P. Sikivie, N. Sullivan, and D. B. Tanner, Phys. Rev. Lett. **112**, 131301 (2014).

[398] Y. Kahn, B. R. Safdi and J. Thaler, Phys. Rev. Lett. **117**, 14, 141801 (2016), [arXiv:1602.01086].

[399] J. L. Ouellet *et al.* (ABRACADABRA), Phys. Rev. Lett. **122**, 12, 121802 (2019), [arXiv:1810.12257].

[400] C. P. Salemi *et al.*, Phys. Rev. Lett. **127**, 8, 081801 (2021), [arXiv:2102.06722].

[401] N. Crisosto *et al.*, Phys. Rev. Lett. **124**, 24, 241101 (2020), [arXiv:1911.05772].

[402] A. V. Gramolin *et al.*, Nature Phys. **17**, 1, 79 (2021), [arXiv:2003.03348].

[403] J. A. Devlin *et al.*, Phys. Rev. Lett. **126**, 4, 041301 (2021), [arXiv:2101.11290].

[404] M. Silva-Feaver *et al.*, IEEE Trans. Appl. Supercond. **27**, 4, 1400204 (2017), [arXiv:1610.09344].

[405] C. Abel *et al.*, Phys. Rev. **X7**, 4, 041034 (2017), [arXiv:1708.06367].

[406] K. Blum *et al.*, Phys. Lett. B **737**, 30 (2014), [arXiv:1401.6460].

[407] D. Budker *et al.*, Phys. Rev. **X4**, 2, 021030 (2014), [arXiv:1306.6089].

[408] M. B. Wise, H. Georgi and S. L. Glashow, Phys. Rev. Lett. **47**, 402 (1981).

[409] A. Ernst, A. Ringwald and C. Tamarit, JHEP **02**, 103 (2018), [arXiv:1801.04906].

[410] L. Di Luzio, A. Ringwald and C. Tamarit, Phys. Rev. **D98**, 9, 095011 (2018), [arXiv:1807.09769].

[411] P. Fileviez Perez, C. Murgui and A. D. Plascencia (2019), [arXiv:1908.01772].

[412] D. Aybas *et al.*, Phys. Rev. Lett. **126**, 14, 141802 (2021), [arXiv:2101.01241].

[413] T. Wu *et al.*, Phys. Rev. Lett. **122**, 19, 191302 (2019), [arXiv:1901.10843].

[414] A. Garcon *et al.*, Sci. Adv. **5**, 10, eaax4539 (2019), [arXiv:1902.04644].

[415] I. M. Bloch *et al.* (NASDUCK) (2021), [arXiv:2105.04603].

[416] G. Vasilakis *et al.*, Physical Review Letters **103**, 26 (2009), ISSN 1079-7114, URL `http://dx.doi.org/10.1103/PhysRevLett.103.261801`.

[417] I. M. Bloch *et al.*, JHEP **01**, 167 (2020), [arXiv:1907.03767].

[418] S. P. Chang *et al.*, Phys. Rev. **D99**, 8, 083002 (2019), [arXiv:1710.05271].

[419] L. Krauss *et al.*, Phys. Rev. Lett. **55**, 1797 (1985).

[420] R. Barbieri *et al.*, Phys. Lett. B **226**, 357 (1989).

[421] R. Barbieri *et al.*, Phys. Dark Univ. **15**, 135 (2017), [arXiv:1606.02201].

[422] N. Crescini *et al.* (QUAX), Phys. Rev. Lett. **124**, 17, 171801 (2020), [arXiv:2001.08940].

Downloaded from https://academic.oup.com/ptep/article/2022/8/083C01/6651666 by KIT Library user on 27 September 2022

91. Searches for Quark and Lepton Compositeness

Revised October 2021 by K. Hikasa (Tohoku U.), M. Tanabashi (Nagoya U.; KMI, Nagoya U.), K. Terashi (ICEPP, Tokyo U.) and N. Varelas (U. of Illinois at Chicago).

91.1 Limits on contact interactions

If quarks and leptons are made of constituents, then at the scale of constituent binding energies (compositeness scale) there should appear new interactions among them. At energies much below the compositeness scale (Λ), these interactions are suppressed by inverse powers of Λ. The dominant effect of the compositeness of fermion ψ should come from the lowest dimensional interactions with four fermions (contact terms), whose most general flavor-diagonal color-singlet chirally invariant form reads [1, 2]

$$\mathcal{L} = \mathcal{L}_{LL} + \mathcal{L}_{RR} + \mathcal{L}_{LR} + \mathcal{L}_{RL},$$

with

$$\mathcal{L}_{LL} = \frac{g^2_{\rm contact}}{2\Lambda^2} \sum_{i,j} \eta^{ij}_{LL} (\bar\psi^i_L \gamma_\mu \psi^i_L)(\bar\psi^j_L \gamma^\mu \psi^j_L),$$

$$\mathcal{L}_{RR} = \frac{g^2_{\rm contact}}{2\Lambda^2} \sum_{i,j} \eta^{ij}_{RR} (\bar\psi^i_R \gamma_\mu \psi^i_R)(\bar\psi^j_R \gamma^\mu \psi^j_R),$$

$$\mathcal{L}_{LR} = \frac{g^2_{\rm contact}}{2\Lambda^2} \sum_{i,j} \eta^{ij}_{LR} (\bar\psi^i_L \gamma_\mu \psi^i_L)(\bar\psi^j_R \gamma^\mu \psi^j_R),$$

$$\mathcal{L}_{RL} = \frac{g^2_{\rm contact}}{2\Lambda^2} \sum_{i,j} \eta^{ij}_{RL} (\bar\psi^i_R \gamma_\mu \psi^i_R)(\bar\psi^j_L \gamma^\mu \psi^j_L), \qquad (91.1)$$

where i, j are the indices of fermion species. Color and other indices are suppressed in Eq. (91.1). Chiral invariance provides a natural explanation why quark and lepton masses are much smaller than their inverse size Λ. Note $\eta^{ij}_{\alpha\beta} = \eta^{ji}_{\beta\alpha}$. Therefore, in order to specify the contact interaction among the same fermion species $i = j$, it is enough to use η_{LL}, η_{RR} and η_{LR}. We will suppress the indices of fermion species hereafter. We may determine the scale Λ unambiguously by using the above form of the effective interactions; the conventional method [1] is to fix its scale by setting $g^2_{\rm contact}/4\pi = g^2_{\rm contact}(\Lambda)/4\pi = 1$ for the new strong interaction coupling and by setting the largest magnitude of the coefficients $\eta_{\alpha\beta}$ to be unity. In the following, we denote

$$\begin{aligned}
\Lambda &= \Lambda^\pm_{LL} \quad \text{for} \quad (\eta_{LL}, \eta_{RR}, \eta_{LR}) = (\pm1,\, 0,\, 0)\ , \\
\Lambda &= \Lambda^\pm_{RR} \quad \text{for} \quad (\eta_{LL}, \eta_{RR}, \eta_{LR}) = (0,\, \pm1,\, 0)\ , \\
\Lambda &= \Lambda^\pm_{VV} \quad \text{for} \quad (\eta_{LL}, \eta_{RR}, \eta_{LR}) = (\pm1,\, \pm1,\, \pm1)\ , \\
\Lambda &= \Lambda^\pm_{AA} \quad \text{for} \quad (\eta_{LL}, \eta_{RR}, \eta_{LR}) = (\pm1,\, \pm1,\, \mp1)\ , \\
\Lambda &= \Lambda^\pm_{V-A} \quad \text{for} \quad (\eta_{LL}, \eta_{RR}, \eta_{LR}) = (0,\, 0,\, \pm1)\ . \qquad (91.2)
\end{aligned}$$

Such interactions can arise by interchanging constituents (when the fermions have common constituents), and/or by exchanging the binding quanta (whenever binding quanta couple to constituents of both particles).

Fermion scattering amplitude induced from the contact interaction in Eq. (91.1) interferes with the Standard Model (SM) amplitude destructively or constructively [2]. The sign of interference depends on the sign of $\eta_{\alpha\beta}$ ($\alpha, \beta = L, R$). For instance, in the parton level $qq \to qq$ scattering cross section in the $\Lambda^\pm_{LL}$ model, the contact interaction amplitude and the SM gluon exchange amplitude interfere destructively for $\eta_{LL} = +1$, while they interfere constructively for $\eta_{LL} = -1$. In models of quark compositeness, the quark scattering cross sections induced from the contact interactions receive sizable QCD radiative corrections. Ref. [3] provides the exact next-to-leading order (NLO) QCD corrections to the contact interaction induced quark scattering cross sections.

Over the last three decades experiments at the CERN Sp$\bar{\rm p}$S [4, 5], the Fermilab Tevatron [6, 7], and the CERN LHC [8–12] have searched for quark contact interactions, characterized by the four-fermion effective Lagrangian in Eq. (91.1), using jet final states. These searches have been performed primarily by studying the angular distribution of the two highest transverse momentum, $p_{\rm T}$, jets (dijets), and the inclusive jet $p_{\rm T}$ spectrum. The variable $\chi = \exp(|(y_1 - y_2)|)$ is used to measure the dijet angular distribution, where y_1 and y_2 are the rapidities of the two jets with the highest transverse momenta. For collinear massless parton scattering, χ is related to the polar scattering angle θ^* in the partonic center-of-mass frame by $\chi = (1+|\cos\theta^*|)/(1-|\cos\theta^*|)$. The choice of χ is motivated by the fact that the angular distribution for Rutherford scattering, which is proportional to $1/(1-\cos\theta^*)^2$, is independent of χ. In perturbative QCD the χ distributions are relatively uniform and only mildly modified by higher-order QCD or electroweak corrections. Signatures of quark contact interactions exhibit more isotropic angular distribution than QCD and can be identified as an excess at low values of χ. In the inclusive jet cross section measurement, quark contact interaction effects are searched for as deviations from the predictions of perturbative QCD in the tails of the high-$p_{\rm T}$ jet spectrum [11].

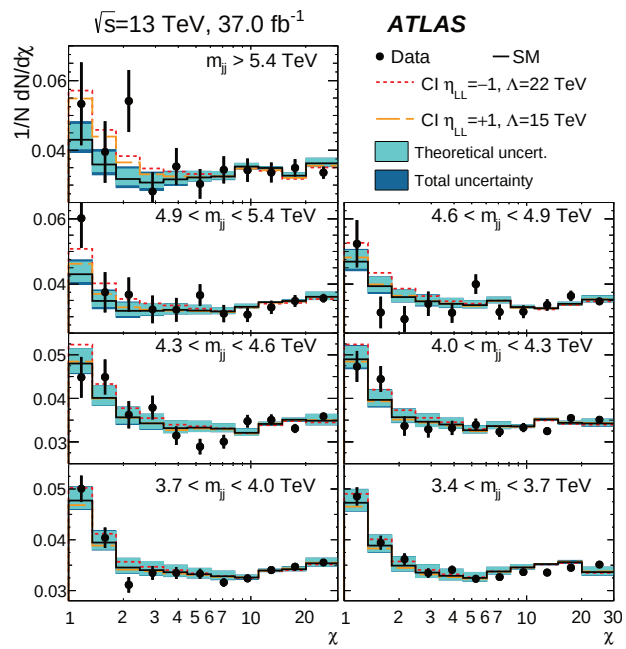

Figure 91.1: Normalized dijet angular distributions in several dijet mass (m_{jj}) ranges. The data distributions are compared to PYTHIA8 predictions with NLO and electroweak corrections applied (solid line) and with the predictions including a contact interaction (CI) term in which only left-handed quarks participate of compositeness scale $\Lambda^+_{LL} = 15$ TeV (dashed line) and $\Lambda^-_{LL} = 22$ TeV (dotted line). The theoretical uncertainties and the total theoretical and experimental uncertainties in the predictions are displayed as shaded bands around the SM prediction. Figure adopted from Ref. [9].

Recent results from the LHC, using data collected at proton-proton center-of-mass energy of $\sqrt{s} = 13$ TeV, extend previous limits on quark contact interactions. Figure 91.1 shows the normalized dijet angular distributions for several dijet mass ranges measured in ATLAS [9] at $\sqrt{s} = 13$ TeV. The data distributions are compared with SM predictions, estimated using PYTHIA8 [13] with GEANT4-based [14] ATLAS detector simulation and corrected to NLO QCD calculation provided by NLO Jet++ [15] including electroweak corrections [16], and with predictions including a contact interaction term in which only left-handed quarks participate at compositeness scale $\Lambda^+_{LL} = 15$ TeV ($\Lambda^-_{LL} = 22$ TeV) with destructive (constructive) interference. Over a wide range of χ and dijet mass the data are well described by the SM predictions. Using the dijet angular distributions measured at high dijet masses and $\sqrt{s} = 13$ TeV, the ATLAS [9] and CMS [12] Collaborations have set 95% confidence level (C.L.) lower limits on the contact interaction scale Λ, ranging

Downloaded from https://academic.oup.com/ptep/article/2022/8/083C01/6651666 by KIT Library user on 27 September 2022

from 9.2 to 29.5 TeV for different quark contact interaction models that correspond to various combinations of (η_{LL}, η_{RR}, η_{LR}), as summarized in Figure 91.2. The contact interaction scale limits extracted using the dijet angular distributions include the exact NLO QCD corrections to dijet production induced by contact interactions [3]. In proton-proton collisions, the $\Lambda^{\pm}_{LL}$ and $\Lambda^{\pm}_{RR}$ contact interaction models result in identical tree-level cross sections and NLO QCD corrections and yield the same exclusion limits. For $\Lambda^{\pm}_{VV}$ and $\Lambda^{\pm}_{AA}$, the contact interaction predictions are identical at tree level, but exhibit different NLO QCD corrections and yield different exclusion limits.

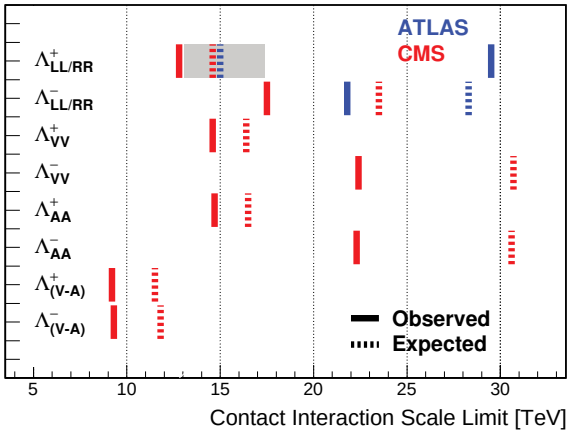

Figure 91.2: Observed (solid lines) and expected (dashed lines) 95% C.L. lower limits on the contact interaction scale Λ for different contact interaction models from ATLAS [9] and CMS [12] using the dijet angular distributions. The contact interaction models used for the dijet angular distributions include the exact NLO QCD corrections to dijet production. The shaded band for the $\Lambda^{+}_{LL/RR}$ model indicates the range of contact interaction scale that was not excluded in ATLAS [9], due to an observed excess in the data that produced a weaker limit.

If leptons (l) and quarks (q) are composite with common constituents, the interaction of these constituents will manifest itself in the form of a $llqq$-type four-fermion contact interaction Lagrangian at energies below the compositeness scale Λ. The $llqq$ terms in the contact interaction Lagrangian can be expressed as

$$\mathcal{L}_{LL} = \frac{g^2_{\rm contact}}{\Lambda^2} \sum_{i,j} \eta^{ij}_{LL} (\bar{q}^i_L \gamma_\mu q^i_L)(\bar{l}^j_L \gamma^\mu l^j_L),$$

$$\mathcal{L}_{RR} = \frac{g^2_{\rm contact}}{\Lambda^2} \sum_{i,j} \eta^{ij}_{RR} (\bar{q}^i_R \gamma_\mu q^i_R)(\bar{l}^j_R \gamma^\mu l^j_R),$$

$$\mathcal{L}_{LR} = \frac{g^2_{\rm contact}}{\Lambda^2} \sum_{i,j} \eta^{ij}_{LR} (\bar{q}^i_L \gamma_\mu q^i_L)(\bar{l}^j_R \gamma^\mu l^j_R),$$

$$\mathcal{L}_{RL} = \frac{g^2_{\rm contact}}{\Lambda^2} \sum_{i,j} \eta^{ij}_{RL} (\bar{q}^i_R \gamma_\mu q^i_R)(\bar{l}^j_L \gamma^\mu l^j_L). \qquad (91.3)$$

Searches on quark-lepton compositeness have been reported from experiments at LEP [17–20], HERA [21, 22], the Tevatron [23, 24], and recently from the ATLAS [25, 26] and CMS [27, 28] experiments at the LHC. The most stringent searches for $llqq$ contact interactions are performed by the LHC experiments using high-mass oppositely-charged lepton pairs produced through the $q\bar{q} \to l^+l^-$ Drell-Yan process. The contact interaction amplitude of the $u\bar{u} \to l^+l^-$ process ($l = e$ or μ) interferes with the corresponding SM amplitude constructively (destructively) for $\eta^{ul}_{\alpha\beta} = -1$ ($\eta^{ul}_{\alpha\beta} = +1$). The ATLAS Collaboration has extracted limits on the $llqq$ contact interaction at $\sqrt{s} = 13$ TeV for the right-right ($\eta_{RR} = \pm 1$, $\eta_{LL} = \eta_{LR} = \eta_{RL} = 0$), left-left ($\eta_{LL} = \pm 1$, $\eta_{RR} = \eta_{LR} = \eta_{RL} = 0$), and left-right ($\eta_{LR} = \eta_{RL} = \pm 1$, $\eta_{RR} = \eta_{LL} = 0$) models. In Ref. [26], ATLAS used a background estimate directly obtained from data. Combining the dielectron and dimuon channels, the 95% C.L. lower limits on the $llqq$ contact interaction scale Λ are 36 TeV (27 TeV) for the right-right model, 36 TeV (26 TeV) for the left-left model, and 33 TeV (29 TeV) for the left-right model, each with constructive (destructive) interference [26]. The CMS Collaboration, using a 140 fb^{-1} dataset at 13 TeV, has set 95% C.L. exclusion limits on the $llqq$ contact interaction scale that range from $\Lambda_{LL} > 23.9$ TeV for the destructive interference to $\Lambda_{RR} > 36.4$ TeV for the constructive interference, for the left-left and the right-right models, respectively [28].

Note that the contact interactions arising from the compositeness of quarks and leptons in Eq. (91.1) can also be regarded as a part of more general dimension six operators in the context of low energy standard model effective field theory (SMEFT). For a complete list of SM gauge invariant dimension six operators, see [29, 30]. A computation of the one loop anomalous dimension matrix for SMEFT operators are found in Refs. [31–33]. See also Refs. [34] and [35] for recent reviews. Consistent SMEFT reinterpretations of top-quark data, and high energy non-resonant dijet and dilepton data are provided, e.g., in Refs. [36–38].

Interactions of hypothetical dark matter candidate particles with SM particles through mediators can also be described as contact interactions at low energy. See *"Searches for WIMPs and Other Particles"* in this volume for limits on the interactions involving dark matter candidate particles.

91.2 Limits on excited fermions

Another typical consequence of compositeness is the appearance of excited leptons and quarks (l^* and q^*). Phenomenologically, an excited lepton is defined to be a heavy lepton which shares a leptonic quantum number with one of the existing leptons (an excited quark is defined similarly). For example, an excited electron e^* is characterized by a nonzero transition-magnetic coupling with electrons. The smallness of the lepton mass and the success of QED prediction for $g-2$ suggest chirality conservation, *i.e.,* an excited lepton should not couple to both left- and right-handed components of the corresponding lepton [39–41].

Excited leptons may be classified by $SU(2) \times U(1)$ quantum numbers. Typical examples are:

1. Sequential type

$$\begin{pmatrix} \nu^* \\ l^* \end{pmatrix}_L, \qquad [\nu^*_R], \qquad l^*_R.$$

ν^*_R is necessary if we assume ν^* has a Dirac mass.

2. Mirror type

$$[\nu^*_L], \qquad l^*_L, \qquad \begin{pmatrix} \nu^* \\ l^* \end{pmatrix}_R.$$

3. Homodoublet type

$$\begin{pmatrix} \nu^* \\ l^* \end{pmatrix}_L, \qquad \begin{pmatrix} \nu^* \\ l^* \end{pmatrix}_R.$$

Similar classification can be made for excited quarks.

Excited fermions can be pair produced via their minimal gauge couplings. The couplings of excited leptons with Z are given by

$$\frac{e}{2\sin\theta_W \cos\theta_W}(-1 + 2\sin^2\theta_W)\bar{l}^*\gamma^\mu l^* Z_\mu + \frac{e}{2\sin\theta_W\cos\theta_W}\bar{\nu}^*\gamma^\mu\nu^* Z_\mu$$

in the homodoublet model. The corresponding couplings of excited quarks can be easily obtained. Although form factor effects can be present for the gauge couplings at $q^2 \neq 0$, they are usually neglected.

Excited fermions may also be produced via the contact interactions with ordinary quarks and leptons [42]

$$\mathcal{L} = \frac{g^2_{\rm contact}}{\Lambda^2}\left[\eta'_{LL}(\bar{\psi}_L\gamma_\mu\psi_L)(\bar{\psi}^*_L\gamma^\mu\psi^*_L) + (\eta''_{LL}(\bar{\psi}_L\gamma_\mu\psi_L)(\bar{\psi}^*_L\gamma^\mu\psi_L) + \text{h.c.}) + \cdots\right]. \qquad (91.4)$$

Downloaded from https://academic.oup.com/ptep/article/2022/8/083C01/6651666 by KIT Library user on 27 September 2022

Again, the coefficient is conventionally taken $g^2_{\rm contact} = 4\pi$. It is widely assumed $\eta'_{LL} = \eta''_{LL} = 1$, $\eta'_{LR} = \eta''_{LR} = \eta'_{RL} = \eta''_{RL} = \eta'_{RR} = \eta''_{RR} = 0$ in experimental analyses for simplicity.

In addition, transition-magnetic type couplings with a gauge boson are expected. These couplings can be generally parameterized as follows:

$$\begin{aligned}\mathcal{L} =& \frac{\lambda_\gamma^{(\psi^*)} e}{2m_{\psi^*}} \bar{\psi}^* \sigma^{\mu\nu} (\eta_L \frac{1-\gamma_5}{2} + \eta_R \frac{1+\gamma_5}{2}) \psi F_{\mu\nu} \\ &+ \frac{\lambda_Z^{(\psi^*)} e}{2m_{\psi^*}} \bar{\psi}^* \sigma^{\mu\nu} (\eta_L \frac{1-\gamma_5}{2} + \eta_R \frac{1+\gamma_5}{2}) \psi Z_{\mu\nu} \\ &+ \frac{\lambda_W^{(l^*)} g}{2m_{l^*}} \bar{l}^* \sigma^{\mu\nu} \frac{1-\gamma_5}{2} \nu W_{\mu\nu} \\ &+ \frac{\lambda_W^{(\nu^*)} g}{2m_{\nu^*}} \bar{\nu}^* \sigma^{\mu\nu} (\eta_L \frac{1-\gamma_5}{2} + \eta_R \frac{1+\gamma_5}{2}) l W^\dagger_{\mu\nu} \\ &+ \text{h.c.}, \end{aligned} \tag{91.5}$$

where $g = e/\sin\theta_W$, $\psi = \nu$ or l, $F_{\mu\nu} = \partial_\mu A_\nu - \partial_\nu A_\mu$ is the photon field strength, $Z_{\mu\nu} = \partial_\mu Z_\nu - \partial_\nu Z_\mu$, *etc.*. The normalization of the coupling is chosen such that

$$\max(|\eta_L|, |\eta_R|) = 1.$$

Chirality conservation requires

$$\eta_L \eta_R = 0. \tag{91.6}$$

These couplings in Eq. (91.5) can arise from $SU(2) \times U(1)$-invariant higher-dimensional interactions. A well-studied model is the interaction of homodoublet type l^* with the Lagrangian (see [43, 44])

$$\mathcal{L} = \frac{1}{2\Lambda} \bar{L}^* \sigma^{\mu\nu} (g f \frac{\tau^a}{2} W^a_{\mu\nu} + g' f' Y B_{\mu\nu}) \frac{1-\gamma_5}{2} L + \text{h.c.}, \tag{91.7}$$

where L denotes the lepton doublet (ν, l), Λ is the compositeness scale, g, g' are $SU(2)$ and $U(1)_Y$ gauge couplings, and $W^a_{\mu\nu}$ and $B_{\mu\nu}$ are the field strengths for $SU(2)$ and $U(1)_Y$ gauge fields. These couplings satisfy the relation

$$\lambda_W = -\sqrt{2} \sin^2\theta_W (\lambda_Z \cot\theta_W + \lambda_\gamma), \tag{91.8}$$

with $\lambda_{W,Z,\gamma}$ being defined in Eq. (91.5) with $\lambda_{W,Z,\gamma} = \lambda^{(\ell^*)}_{W,Z,\gamma}$ or $\lambda_{W,Z,\gamma} = \lambda^{(\nu^*)}_{W,Z,\gamma}$. Here $(\eta_L, \eta_R) = (1, 0)$ is assumed. It should be noted that the electromagnetic radiative decay of l^* (ν^*) is forbidden if $f = -f'$ $(f = f')$.

Additional coupling with gluons is possible for excited quarks:

$$\begin{aligned}\mathcal{L} = \frac{1}{2\Lambda} \bar{Q}^* \sigma^{\mu\nu} \left(g_s f_s \frac{\lambda^a}{2} G^a_{\mu\nu} + g f \frac{\tau^a}{2} W^a_{\mu\nu} + g' f' Y B_{\mu\nu} \right) \\ \times \frac{1-\gamma_5}{2} Q + \text{h.c.}, \end{aligned} \tag{91.9}$$

where Q denotes a quark doublet, g_s is the QCD gauge coupling, and $G^a_{\mu\nu}$ the gluon field strength.

If leptons are made of color triplet and antitriplet constituents, we may expect their color-octet partners. Transitions between the octet leptons (l_8) and the ordinary lepton (l) may take place via the dimension-five interactions

$$\mathcal{L} = \frac{1}{2\Lambda} \sum_l \left\{ \bar{l}^\alpha_8 g_S F^\alpha_{\mu\nu} \sigma^{\mu\nu} (\eta_L l_L + \eta_R l_R) + \text{h.c.} \right\} \tag{91.10}$$

where the summation is over charged leptons and neutrinos. The leptonic chiral invariance implies $\eta_L \eta_R = 0$ as before.

Searches for the excited quarks and leptons have been performed over the last decades in experiments at the LEP [45–48], HERA [49, 50], Tevatron [51, 52], and LHC [53–78]. Most stringent constraints, which are described below at 95% confidence level, come from the LHC experiments.

The signature of excited quarks q^* at hadron colliders is characterized by a narrow resonant peak in the reconstructed invariant mass distribution of the q^* decay products. The decays via the transition-magnetic type operator in Eq. (91.9) are considered for excited quarks in LHC searches, and the final states to search for are dijet (qg) [53, 54, 66–69] or a jet in association with a photon $(q\gamma)$ [55, 56, 70, 71] or a weak gauge boson (qW, qZ) [72, 73]. All analyses consider only spin-1/2 excited states of first generation quarks (u^*, d^*) with degenerate masses, expected to be predominantly produced in proton-proton collisions except for the excited b quark searches described below. Only the minimal gauge interactions and the transition-magnetic couplings with the form given in Eq. (91.9) are considered in the production process, and hence the contact interactions in Eq. (91.4) are not considered. The compositeness scale Λ is taken to be the same as the excited quark mass m_{q^*}. The transition-magnetic coupling coefficients f_s, f and f' are assumed to be equal to 1 (denoted by f).

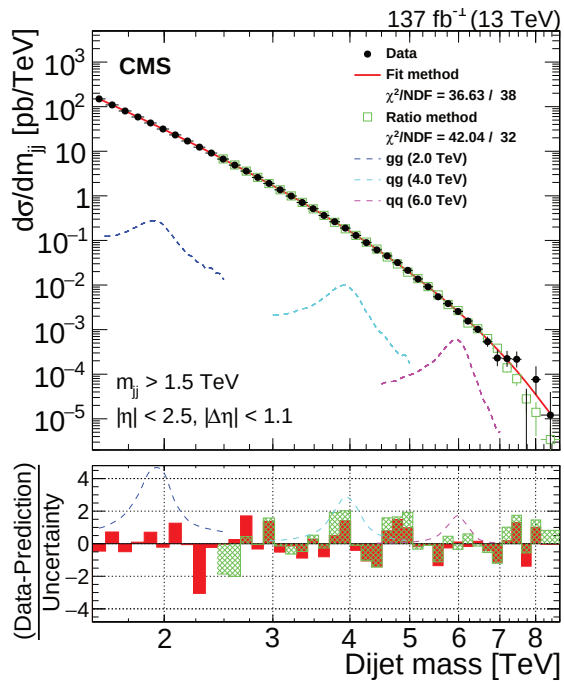

Figure 91.3: Dijet mass distribution measured by CMS using wide jets reconstructed from two highest transverse momentum jets by adding nearby jets within $\Delta R = \sqrt{\Delta\eta^2 + \Delta\phi^2} < 1.1$. The data distribution is compared to a fit representing a smooth background spectrum (solid curve) and the background prediction obtained from the $\Delta\eta_{\rm jj}$ control regions (open squares), denoted as Ratio method, at $m_{\rm jj} > 2.4$ TeV. The excited quark signal with mass of 4.0 TeV (labeled as qg) is shown together with other benchmark signals. Shown at the bottom panel is the difference between the data and the fitted parametrization from the fit method or the data and the background prediction from the Ratio method, divided by the statistical uncertainty of the data. Figure adopted from [69].

With proton-proton collision data recorded at $\sqrt{s} = 13$ TeV at the LHC, the excited quark masses are excluded in dijet resonance searches up to 6.7 TeV in ATLAS using 139 fb^{-1} [54] and 6.3 TeV in CMS using 137 fb^{-1} [69]. Figure 91.3 shows the dijet mass ($m_{\rm jj}$) distribution measured in CMS [69] by using the two highest $p_{\rm T}$ jets reconstructed with the anti-$k_{\rm T}$ algorithm [79] of a distance parameter of 0.4, and by combining nearby jets within $\Delta R = \sqrt{\Delta\eta^2 + \Delta\phi^2} < 1.1$ around the leading two jets. The measured dijet mass spectrum is compared to a fit with smoothly falling background shape (solid curve) at $m_{\rm jj} > 1.5$ TeV and the background prediction obtained from the $\Delta\eta_{\rm jj}$ control regions (open squares), denoted as Ratio method, at $m_{\rm jj} > 2.4$ TeV to look for a narrow resonance. Here $\Delta\eta_{\rm jj}$ is the pseudorapidity separation between the two jets. An excited quark signal with mass of 4.0 TeV is shown in the figure (denoted by qg) as one of the

Downloaded from https://academic.oup.com/ptep/article/2022/8/083C01/6651666 by KIT Library user on 27 September 2022

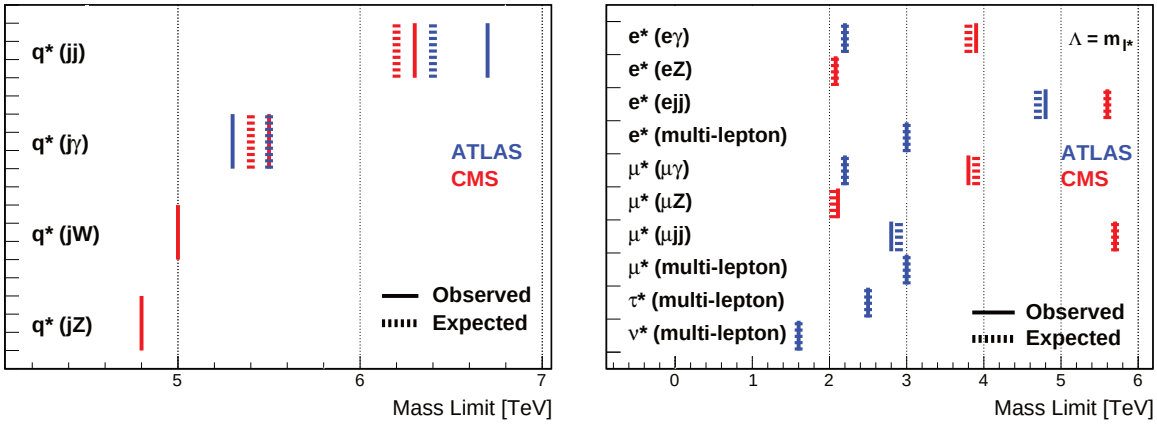

Figure 91.4: 95% C.L. lower mass limits for the excited quarks (left) and excited leptons (right) at ATLAS [54, 56, 62–64] and CMS [69, 71, 73, 76–78] experiments. Shown are the most stringent limits for each final state (denoted in parentheses) of the excited fermions from both experiments. Only first generation quarks (u, d) with transition-magnetic type interactions with $f_s = f = f' = 1$ are considered for the excited quarks. The excited lepton limits are given for the production via contact interactions with $\Lambda = m_{l^*}$.

benchmark signals considered in the analysis.

The photon + jet resonance searches, targeting excited quarks decaying into a quark and a photon ($q^* \to q + \gamma$), have excluded q^* masses up to 5.3 TeV in ATLAS [56] and 5.5 TeV in CMS [71] using collision data at $\sqrt{s} = 13$ TeV. The W/Z boson + jet final states are examined to look for the $q^* \to q + W$ and $q + Z$ signal in CMS [73], exploiting jet substructure technique designed to provide sensitivity for highly-boosted hadronically decaying W and Z bosons. The lower mass limit of 5.0 (4.8) TeV is obtained from the W + jet (Z + jet) search using dataset recorded at $\sqrt{s} = 13$ TeV.

The excited b quarks (b^*) are also considered in the present searches at the LHC. Assuming the similar production processes to the first-generation excited quarks, the b^* has been searched for in final states containing at least one jet identified as originating from a b quark (b-tagging). The searches using two jets including at least one b-tagged jet have been performed at 8 and 13 TeV [54, 57, 58, 67], resulting in b^* lower mass limits of 3.2 TeV in ATLAS using 139 fb^{-1} at $\sqrt{s} = 13$ TeV [54] and 1.6 TeV in CMS using 19.7 fb^{-1} at $\sqrt{s} = 8$ TeV [67]. The CMS Collaboration also performed a search for $b^* \to b + \gamma$ in events with a b-tagged jet in association with a photon using data at $\sqrt{s} = 13$ TeV [71], and excluded b^* masses up to 1.8 TeV. Excited b quarks with charged-current decay into a W-boson and a top quark ($b^* \to t + W$) were looked for in both ATLAS and CMS using the full 8 TeV data [59, 74]. ATLAS excluded b^* masses below 1.5 TeV for the b^* with left- and right-handed couplings [59] while CMS excluded the masses below 1.39(1.43) TeV for the left(right)-handed couplings [74].

The excited top quarks (t^*) have also been searched for at the LHC. The CMS Collaboration performed the search for pair-produced t^* quarks with the assumption of the t^* quark decay into a top quark and a gluon, in events with a charged lepton, missing transverse momentum and multiple jets including b-tagged jets at $\sqrt{s} = 8$ TeV [80] and 13 TeV [81]. With 35.9 fb^{-1} data at 13 TeV, CMS excluded the t^* masses below 1.2 TeV for spin 3/2 t^* quarks [81].

Searches for excited leptons l^* are also performed at the LHC using proton-proton collision data recorded at $\sqrt{s} = 7$ and 8 TeV [61–65, 75, 76] as well as at 13 TeV [77]. Considering single l^* production in contact interactions (Eq. (91.4)) and electromagnetic radiative decay to a SM lepton and a photon ($l^* \to l + \gamma$ where $l = e, \mu$), the excited electron and muon masses are excluded for $\Lambda = m_{l^*}$ up to 3.9 and 3.8 TeV, respectively, using 35.9 fb^{-1} at $\sqrt{s} = 13$ TeV in CMS [77] and 2.2 TeV using 13 fb^{-1} at $\sqrt{s} = 8$ TeV in ATLAS [62].

With the full 20.3 fb^{-1} data at $\sqrt{s} = 8$ TeV, the inclusive search on multi-lepton signatures with 3 or more charged leptons in ATLAS [63] further constrains the excited charged leptons and neutrinos. Considering both the transition-magnetic (Eq. (91.7)) and contact interaction (Eq. (91.4)) processes, the lower mass limits for the e^*, μ^*, τ^* and ν^* (for every excited neutrino flavor) are obtained to be 3.0, 3.0, 2.5 and 1.6 TeV, respectively, for $\Lambda = m_{e^*}$, m_{μ^*}, m_{τ^*} and m_{ν^*}. The rate of pair-produced excited leptons is independent of Λ for the minimal gauge interaction processes, and it allows to improve search sensitivity with multi-lepton signatures at high Λ, especially for excited neutrinos because the predominant $\nu_l^* \to l + W$ decays result in a higher acceptance for ≥ 3 charged lepton final states.

Both ATLAS and CMS Collaborations performed searches for singly produced excited leptons. The single excited leptons, both produced and decayed in contact interaction processes (Eq. (91.4)), were searched for in CMS using 77.4 fb^{-1} at 13 TeV [78] and in ATLAS using 20.3 fb^{-1} at 8 TeV [64] using the final states with two leptons and two jets ($q\bar{q} \to ll^* \to llq\bar{q}$). The CMS search [78] considered both excited electrons and excited muons, using the invariant mass of the combination of the two leptons and two jets as a discriminating variable to separate signal from background. The ATLAS search [64] considered only excited muons. The single excited electrons, produced in contact interactions and decayed either in contact interaction or charged-current processes, were considered in ATLAS using 36.1 fb^{-1} at 13 TeV [65] in the final states with two electrons and two jets ($q\bar{q} \to ee^* \to eeq\bar{q}$) or an electron, missing transverse momentum and a hadronically decaying W-boson candidate ($q\bar{q} \to ee^* \to e\nu W$). The excited electron (muon) mass was excluded up to 5.6 (5.7) TeV in CMS [78] at $\Lambda = m_{e^*}$ ($\Lambda = m_{\mu^*}$), which is the best limit to date on the excited electrons (muons).

The CMS Collaboration also performed an excited lepton search in the final states containing a Z boson [76], probing the excited leptons produced in contact interactions and decayed in neutral-current processes ($l^* \to l + Z$) with $f = f' = 1$ or $f = -f' = 1$. The leptonic and hadronic decays of Z bosons have been considered in the search, and the most stringent limits are obtained from the hadronic Z decay to be 2.08 (2.34) TeV and 2.11 (2.37) TeV for the e^* and μ^*, respectively, with $f = f' = 1$ ($f = -f' = 1$) at $\Lambda = m_{l^*}$.

Figure 91.4 summarizes the most stringent 95% C.L. lower mass limits for excited quarks and leptons obtained from the LHC experiments.

References

[1] E. Eichten, K. D. Lane and M. E. Peskin, Phys. Rev. Lett. **50**, 811 (1983).

[2] E. Eichten *et al.*, Rev. Mod. Phys. **56**, 579 (1984), [Addendum: Rev.Mod.Phys. 58, 1065–1073 (1986)].

Downloaded from https://academic.oup.com/ptep/article/2022/8/083C01/6651666 by KIT Library user on 27 September 2022

[3] J. Gao *et al.*, Phys. Rev. Lett. **106**, 142001 (2011), [arXiv:1101.4611].

[4] G. Arnison *et al.* (UA1), Phys. Lett. B **177**, 244 (1986).

[5] J. Appel *et al.* (UA2), Phys. Lett. B **160**, 349 (1985).

[6] F. Abe *et al.* (CDF), Phys. Rev. Lett. **62**, 613 (1989); F. Abe *et al.* (CDF), Phys. Rev. Lett. **69**, 2896 (1992); F. Abe *et al.* (CDF), Phys. Rev. Lett. **77**, 5336 (1996), [Erratum: Phys.Rev.Lett. 78, 4307 (1997)], [hep-ex/9609011].

[7] B. Abbott *et al.* (D0), Phys. Rev. Lett. **80**, 666 (1998), [hep-ex/9707016]; B. Abbott *et al.* (D0), Phys. Rev. Lett. **82**, 2457 (1999), [hep-ex/9807014]; B. Abbott *et al.* (D0), Phys. Rev. D **62**, 031101 (2000), [hep-ex/9912023]; B. Abbott *et al.* (D0), Phys. Rev. D **64**, 032003 (2001), [hep-ex/0012046]; V. Abazov *et al.* (D0), Phys. Rev. Lett. **103**, 191803 (2009), [arXiv:0906.4819].

[8] G. Aad *et al.* (ATLAS), Phys. Lett. B **694**, 327 (2011), [arXiv:1009.5069]; G. Aad *et al.* (ATLAS), New J. Phys. **13**, 053044 (2011), [arXiv:1103.3864]; G. Aad *et al.* (ATLAS), JHEP **01**, 029 (2013), [arXiv:1210.1718]; G. Aad *et al.* (ATLAS), Phys. Rev. Lett. **114**, 22, 221802 (2015), [arXiv:1504.00357]; G. Aad *et al.* (ATLAS), Phys. Lett. B **754**, 302 (2016), [arXiv:1512.01530].

[9] M. Aaboud *et al.* (ATLAS), Phys. Rev. D **96**, 5, 052004 (2017), [arXiv:1703.09127].

[10] V. Khachatryan *et al.* (CMS), Phys. Rev. Lett. **105**, 262001 (2010), [arXiv:1010.4439]; V. Khachatryan *et al.* (CMS), Phys. Rev. Lett. **106**, 201804 (2011), [arXiv:1102.2020]; S. Chatrchyan *et al.* (CMS), JHEP **05**, 055 (2012), [arXiv:1202.5535]; V. Khachatryan *et al.* (CMS), Phys. Lett. B **746**, 79 (2015), [arXiv:1411.2646]; A. M. Sirunyan *et al.* (CMS), JHEP **07**, 013 (2017), [arXiv:1703.09986].

[11] S. Chatrchyan *et al.* (CMS), Phys. Rev. D **87**, 5, 052017 (2013), [arXiv:1301.5023].

[12] A. M. Sirunyan *et al.* (CMS), Eur. Phys. J. C **78**, 9, 789 (2018), [arXiv:1803.08030].

[13] T. Sjostrand, S. Mrenna and P. Z. Skands, Comput. Phys. Commun. **178**, 852 (2008), [arXiv:0710.3820].

[14] S. Agostinelli *et al.* (GEANT4), Nucl. Instrum. Meth. A **506**, 250 (2003), :GEANT4: a simulation toolkit.

[15] Z. Nagy, Phys. Rev. Lett. **88**, 122003 (2002), [hep-ph/0110315]; Z. Nagy, Phys. Rev. D **68**, 094002 (2003), [hep-ph/0307268].

[16] S. Dittmaier, A. Huss and C. Speckner, JHEP **11**, 095 (2012), [arXiv:1210.0438].

[17] S. Schael *et al.* (ALEPH), Eur. Phys. J. C **49**, 411 (2007), [hep-ex/0609051].

[18] J. Abdallah *et al.* (DELPHI), Eur. Phys. J. C **45**, 589 (2006), [hep-ex/0512012].

[19] M. Acciarri *et al.* (L3), Phys. Lett. B **489**, 81 (2000), [hep-ex/0005028].

[20] K. Ackerstaff *et al.* (OPAL), Phys. Lett. B **391**, 221 (1997); G. Abbiendi *et al.* (OPAL), Eur. Phys. J. C **33**, 173 (2004), [hep-ex/0309053].

[21] F. Aaron *et al.* (H1), Phys. Lett. B **705**, 52 (2011), [arXiv:1107.2478].

[22] S. Chekanov *et al.* (ZEUS), Phys. Lett. B **591**, 23 (2004), [hep-ex/0401009].

[23] F. Abe *et al.* (CDF), Phys. Rev. Lett. **68**, 1463 (1992); F. Abe *et al.* (CDF), Phys. Rev. Lett. **79**, 2198 (1997); T. Affolder *et al.* (CDF), Phys. Rev. Lett. **87**, 231803 (2001), [hep-ex/0107008]; A. Abulencia *et al.* (CDF), Phys. Rev. Lett. **96**, 211801 (2006), [hep-ex/0602045].

[24] B. Abbott *et al.* (D0), Phys. Rev. Lett. **82**, 4769 (1999), [hep-ex/9812010].

[25] G. Aad *et al.* (ATLAS), Phys. Rev. D **84**, 011101 (2011), [arXiv:1104.4398]; G. Aad *et al.* (ATLAS), Phys. Lett. B **712**, 40 (2012), [arXiv:1112.4462]; G. Aad *et al.* (ATLAS), Phys. Rev. D **87**, 1, 015010 (2013), [arXiv:1211.1150]; G. Aad *et al.* (ATLAS), Eur. Phys. J. C **74**, 12, 3134 (2014), [arXiv:1407.2410]; M. Aaboud *et al.* (ATLAS), Phys. Lett. B **761**, 372 (2016), [arXiv:1607.03669]; M. Aaboud *et al.* (ATLAS), JHEP **10**, 182 (2017), [arXiv:1707.02424].

[26] G. Aad *et al.* (ATLAS), JHEP **11**, 005 (2020), [Erratum: JHEP 04, 142 (2021)], [arXiv:2006.12946].

[27] S. Chatrchyan *et al.* (CMS), Phys. Rev. D **87**, 3, 032001 (2013), [arXiv:1212.4563]; V. Khachatryan *et al.* (CMS), JHEP **04**, 025 (2015), [arXiv:1412.6302]; A. M. Sirunyan *et al.* (CMS), JHEP **04**, 114 (2019), [arXiv:1812.10443].

[28] A. M. Sirunyan *et al.* (CMS), JHEP **07**, 208 (2021), [arXiv:2103.02708].

[29] W. Buchmuller and D. Wyler, Nucl. Phys. B **268**, 621 (1986).

[30] B. Grzadkowski *et al.*, JHEP **10**, 085 (2010), [arXiv:1008.4884].

[31] E. E. Jenkins, A. V. Manohar and M. Trott, JHEP **10**, 087 (2013), [arXiv:1308.2627].

[32] E. E. Jenkins, A. V. Manohar and M. Trott, JHEP **01**, 035 (2014), [arXiv:1310.4838].

[33] R. Alonso *et al.*, JHEP **04**, 159 (2014), [arXiv:1312.2014].

[34] I. Brivio and M. Trott, Phys. Rept. **793**, 1 (2019), [arXiv:1706.08945].

[35] A. V. Manohar (2018), [arXiv:1804.05863].

[36] D. Barducci *et al.* (2018), [arXiv:1802.07237].

[37] S. Alte, M. König and W. Shepherd, JHEP **01**, 094 (2018), [arXiv:1711.07484].

[38] S. Alte, M. König and W. Shepherd, JHEP **07**, 144 (2019), [arXiv:1812.07575].

[39] F. Renard, Phys. Lett. B **116**, 264 (1982).

[40] F. del Aguila, A. Mendez and R. Pascual, Phys. Lett. B **140**, 431 (1984).

[41] M. Suzuki, Phys. Lett. B **143**, 237 (1984).

[42] U. Baur, M. Spira and P. Zerwas, Phys. Rev. D **42**, 815 (1990).

[43] K. Hagiwara, D. Zeppenfeld and S. Komamiya, Z. Phys. C **29**, 115 (1985).

[44] N. Cabibbo, L. Maiani and Y. Srivastava, Phys. Lett. B **139**, 459 (1984).

[45] D. Decamp *et al.* (ALEPH), Phys. Rept. **216**, 253 (1992); R. Barate *et al.* (ALEPH), Eur. Phys. J. C **4**, 571 (1998).

[46] P. Abreu *et al.* (DELPHI), Nucl. Phys. B **367**, 511 (1991); J. Abdallah *et al.* (DELPHI), Eur. Phys. J. C **37**, 405 (2004), [hep-ex/0409058].

[47] O. Adriani *et al.* (L3), Phys. Rept. **236**, 1 (1993); P. Achard *et al.* (L3), Phys. Lett. B **531**, 28 (2002), [hep-ex/0202025]; P. Achard *et al.* (L3), Phys. Lett. B **568**, 23 (2003), [hep-ex/0306016].

[48] G. Abbiendi *et al.* (OPAL), Phys. Lett. B **544**, 57 (2002), [hep-ex/0206061]; G. Abbiendi *et al.* (OPAL), Phys. Lett. B **602**, 167 (2004), [hep-ex/0412011].

[49] C. Adloff *et al.* (H1), Phys. Lett. B **525**, 9 (2002), [hep-ex/0110037]; F. Aaron *et al.* (H1), Phys. Lett. B **663**, 382 (2008), [arXiv:0802.1858]; F. Aaron *et al.* (H1), Phys. Lett. B **666**, 131 (2008), [arXiv:0805.4530].

[50] S. Chekanov *et al.* (ZEUS), Phys. Lett. B **549**, 32 (2002), [hep-ex/0109018].

[51] D. Acosta *et al.* (CDF), Phys. Rev. Lett. **94**, 101802 (2005), [hep-ex/0410013]; A. Abulencia *et al.* (CDF), Phys. Rev. Lett. **97**, 191802 (2006), [hep-ex/0606043]; T. Aaltonen *et al.* (CDF), Phys. Rev. D **79**, 112002 (2009), [arXiv:0812.4036].

Downloaded from https://academic.oup.com/ptep/article/2022/8/083C01/6651666 by KIT Library user on 27 September 2022

[52] V. Abazov *et al.* (D0), Phys. Rev. D **73**, 111102 (2006), [hep-ex/0604040]; V. Abazov *et al.* (D0), Phys. Rev. D **77**, 091102 (2008), [arXiv:0801.0877]; V. Abazov *et al.* (D0), Phys. Rev. Lett. **103**, 191803 (2009), [arXiv:0906.4819].

[53] G. Aad *et al.* (ATLAS), Phys. Lett. B **708**, 37 (2012), [arXiv:1108.6311]; G. Aad *et al.* (ATLAS), JHEP **01**, 029 (2013), [arXiv:1210.1718]; G. Aad *et al.* (ATLAS), Phys. Rev. D **91**, 5, 052007 (2015), [arXiv:1407.1376]; G. Aad *et al.* (ATLAS), Phys. Lett. B **754**, 302 (2016), [arXiv:1512.01530]; M. Aaboud *et al.* (ATLAS), Phys. Rev. D **96**, 5, 052004 (2017), [arXiv:1703.09127].

[54] G. Aad *et al.* (ATLAS), JHEP **03**, 145 (2020), [arXiv:1910.08447].

[55] G. Aad *et al.* (ATLAS), Phys. Rev. Lett. **108**, 211802 (2012), [arXiv:1112.3580]; G. Aad *et al.* (ATLAS), Phys. Lett. B **728**, 562 (2014), [arXiv:1309.3230]; G. Aad *et al.* (ATLAS), JHEP **03**, 041 (2016), [arXiv:1512.05910].

[56] M. Aaboud *et al.* (ATLAS), Eur. Phys. J. C **78**, 2, 102 (2018), [arXiv:1709.10440].

[57] M. Aaboud *et al.* (ATLAS), Phys. Rev. D **98**, 032016 (2018), [arXiv:1805.09299].

[58] M. Aaboud *et al.* (ATLAS), Phys. Lett. B **759**, 229 (2016), [arXiv:1603.08791].

[59] G. Aad *et al.* (ATLAS), JHEP **02**, 110 (2016), [arXiv:1510.02664].

[60] G. Aad *et al.* (ATLAS), Phys. Lett. B **721**, 171 (2013), [arXiv:1301.1583].

[61] G. Aad *et al.* (ATLAS), Phys. Rev. D **85**, 072003 (2012), [arXiv:1201.3293].

[62] G. Aad *et al.* (ATLAS), New J. Phys. **15**, 093011 (2013), [arXiv:1308.1364].

[63] G. Aad *et al.* (ATLAS), JHEP **08**, 138 (2015), [arXiv:1411.2921].

[64] G. Aad *et al.* (ATLAS), New J. Phys. **18**, 7, 073021 (2016), [Erratum: New J.Phys. 21, 109501 (2019)], [arXiv:1601.05627].

[65] M. Aaboud *et al.* (ATLAS), Eur. Phys. J. C **79**, 9, 803 (2019), [arXiv:1906.03204].

[66] S. Chatrchyan *et al.* (CMS), Phys. Lett. B **704**, 123 (2011), [arXiv:1107.4771]; S. Chatrchyan *et al.* (CMS), JHEP **01**, 013 (2013), [arXiv:1210.2387]; S. Chatrchyan *et al.* (CMS), Phys. Rev. D **87**, 11, 114015 (2013), [arXiv:1302.4794].

[67] V. Khachatryan *et al.* (CMS), Phys. Rev. D **91**, 5, 052009 (2015), [arXiv:1501.04198].

[68] V. Khachatryan *et al.* (CMS), Phys. Rev. Lett. **116**, 7, 071801 (2016), [arXiv:1512.01224]; V. Khachatryan *et al.* (CMS), Phys. Rev. Lett. **117**, 3, 031802 (2016), [arXiv:1604.08907]; A. M. Sirunyan *et al.* (CMS), Phys. Lett. B **769**, 520 (2017), [Erratum: Phys.Lett.B 772, 882–883 (2017)], [arXiv:1611.03568]; A. M. Sirunyan *et al.* (CMS), JHEP **08**, 130 (2018), [arXiv:1806.00843].

[69] A. M. Sirunyan *et al.* (CMS), JHEP **05**, 033 (2020), [arXiv:1911.03947].

[70] V. Khachatryan *et al.* (CMS), Phys. Lett. B **738**, 274 (2014), [arXiv:1406.5171].

[71] A. M. Sirunyan *et al.* (CMS), Phys. Lett. B **781**, 390 (2018), [arXiv:1711.04652].

[72] S. Chatrchyan *et al.* (CMS), Phys. Lett. B **722**, 28 (2013), [arXiv:1210.0867]; S. Chatrchyan *et al.* (CMS), Phys. Lett. B **723**, 280 (2013), [arXiv:1212.1910]; V. Khachatryan *et al.* (CMS), JHEP **08**, 173 (2014), [arXiv:1405.1994].

[73] A. M. Sirunyan *et al.* (CMS), Phys. Rev. D **97**, 7, 072006 (2018), [arXiv:1708.05379].

[74] V. Khachatryan *et al.* (CMS), JHEP **01**, 166 (2016), [arXiv:1509.08141].

[75] S. Chatrchyan *et al.* (CMS), Phys. Lett. B **704**, 143 (2011), [arXiv:1107.1773]; S. Chatrchyan *et al.* (CMS), Phys. Lett. B **720**, 309 (2013), [arXiv:1210.2422].

[76] V. Khachatryan *et al.* (CMS), JHEP **03**, 125 (2016), [arXiv:1511.01407].

[77] A. M. Sirunyan *et al.* (CMS), JHEP **04**, 015 (2019), [arXiv:1811.03052].

[78] A. M. Sirunyan *et al.* (CMS), JHEP **05**, 052 (2020), [arXiv:2001.04521].

[79] M. Cacciari, G. P. Salam and G. Soyez, JHEP **04**, 063 (2008), [arXiv:0802.1189].

[80] S. Chatrchyan *et al.* (CMS), JHEP **06**, 125 (2014), [arXiv:1311.5357].

[81] A. M. Sirunyan *et al.* (CMS), Phys. Lett. B **778**, 349 (2018), [arXiv:1711.10949].

Downloaded from https://academic.oup.com/ptep/article/2022/8/083C01/6651666 by KIT Library user on 27 September 2022

92. Dynamical Electroweak Symmetry Breaking: Implications of the H^0

Revised August 2021 by K.M. Black (Wisconsin U.), R. Sekhar Chivukula (UC San Diego) and M. Narain (Brown U.).

92.1 Introduction and Phenomenology

In theories of dynamical electroweak symmetry breaking, the electroweak interactions are broken to electromagnetism by the vacuum expectation value of a composite operator, typically a fermion bilinear. In these theories, the longitudinal components of the massive weak bosons are identified with composite Nambu-Goldstone bosons arising from dynamical symmetry breaking in a strongly-coupled extension of the standard model. Viable theories of dynamical electroweak symmetry breaking must also explain (or at least accommodate) the presence of an additional composite scalar state to be identified with the H^0 scalar boson [1,2] – a state unlike any other observed previously.

Theories of dynamical electroweak symmetry breaking can be classified by the nature of the composite singlet state to be associated with the H^0 and the corresponding dimensional scales f, the analog of the pion decay-constant in QCD, and Λ, the scale of the underlying strong dynamics.[1] Of particular importance is the ratio v/f, where $v^2 = 1/(\sqrt{2}G_F) \approx (246\,\text{GeV})^2$, since this ratio measures the expected size of the deviations of the couplings of a composite Higgs boson from those expected in the standard model. The basic possibilities, and the additional states that they predict, are described below.

92.1.1 *Technicolor, $v/f \simeq 1$, $\Lambda \simeq 1$ TeV*

Technicolor models [7–9] provided the first examples of theories of dynamical electroweak symmetry breaking. These theories incorporate a new asymptotically free gauge theory ("technicolor") and additional massless fermions ("technifermions" transforming under a vectorial representation of the gauge group). The global chiral symmetry of the fermions is spontaneously broken by the formation of a technifermion condensate, just as the approximate chiral symmetry in QCD is broken down to isospin by the formation of a quark condensate. The $\text{SU}(2)_W \times \text{U}(1)_Y$ interactions are embedded in the global technifermion chiral symmetries in such a way that the only unbroken gauge symmetry after chiral symmetry breaking is $\text{U}(1)_{em}$.[2] The theories naturally provide the Nambu-Goldstone bosons "eaten" by the W and Z boson. There would also typically be additional heavy states (e.g. vector mesons, analogous to the ρ and ω mesons in QCD) with TeV masses [13,14], and the WW and ZZ scattering amplitudes would be expected to be strong at energies of order 1 TeV.

There are various possibilities for the scalar H^0 in technicolor models. First, the H^0 could be identified as a singlet scalar resonance, analogous to the σ particle expected in pion-scattering in QCD [15, 16]. Alternatively, the H^0 could be identified as a dilaton, a (pseudo-)Goldstone boson of scale invariance in theories of "walking technicolor" [17–21].[3] Finally, the H^0 could be identified as an additional isosinglet state if the chiral symmetry breaking pattern of the technicolor theory provides for such a state.[4] In all of these cases, however, one expects large deviations in the couplings of this particle from those of the standard model Higgs boson. Since the couplings observed for the H^0 approximate those of the Higgs boson to the 10% level, models of this kind are very highly constrained.

92.1.2 *The Higgs doublet as a pseudo-Nambu-Goldstone Boson, $v/f < 1$, $\Lambda > 1$ TeV*

In technicolor models, the symmetry-breaking properties of the underlying strong dynamics necessarily breaks the electroweak gauge symmetries. An alternative possibility is that the underlying strong dynamics itself does not break the electroweak interactions, and that the entire quartet of bosons in the Higgs doublet (including the state associated with the H^0) are composite (pseudo-) Nambu-Goldstone particles [23–25]. In this case, the underlying dynamics can occur at energies exceeding 1 TeV and additional interactions with the top-quark mass generating sector (and possibly with additional weakly-coupled gauge bosons) cause the vacuum energy to be minimized when the composite Higgs doublet gains a vacuum expectation value [26, 27]. In these theories, the couplings of the remaining singlet scalar state would naturally be equal to that of the standard model Higgs boson up to corrections of order $(v/f)^2$ and, therefore, constraints on the size of deviations of the H^0 couplings from that of the standard model Higgs [28] give rise to lower bounds on the scales f and Λ.[5]

The electroweak gauge interactions, as well as the interactions responsible for the top-quark mass, explicitly break the chiral symmetries of the composite Higgs model and lead generically to sizable corrections to the mass-squared of the Higgs-doublet – the so-called "Little Hierarchy Problem" [29]. "Little Higgs" theories [30–33] are examples of composite Higgs models in which the (collective) symmetry-breaking structure is selected so as to suppress these contributions to the Higgs mass-squared.

Composite Higgs models typically require a larger global symmetry of the underlying theory, and hence additional relatively light (compared to Λ) scalar particles, extra electroweak vector bosons (e.g. an additional $\text{SU}(2)\times\text{U}(1)$ gauge group), and vector-like partners of the top-quark of charge $+2/3$ and possibly also $+5/3$ [34]. In addition to these states, one would expect the underlying dynamics to yield additional scalar and vector resonances with masses of order Λ. If the theory respects a custodial symmetry [35], the couplings of these additional states to the electroweak and Higgs boson will be related – and, for example, one might expect a charged vector resonance to have similar branching ratios to WZ and WH. Different composite Higgs models utilize different mechanisms for arranging for the hierarchy of scales $v < f$ and arranging for a scalar Higgs self-coupling small enough to produce an H^0 of mass of order 125 GeV, for a review see [36] . If the additional states in these models carry color, they can provide additional contributions to Higgs production via gluon fusion [37]. The extent to which Higgs production at the LHC conforms with standard model predictions provides additional constraints (typically lower bounds on the masses of the additional colored states of order 0.7 TeV) on these models.

In addition, if the larger symmetry of the underlying composite Higgs theory does not commute with the standard model gauge group, then the additional states found in those models – especially those related to the top-quark, which tend to have the largest couplings to the electroweak sector – may be *colorless*. For example, in twin Higgs models [38], the top-partners carry no standard model charges. The phenomenology of the additional states in twin Higgs theories is rather different, since lacking color the production of these particles at the LHC will be suppressed – and, their decays may occur only via the electroweak symmetry breaking sector, leading to their being long-lived.

92.1.3 *Top-Condensate, Top-Color, Top-Seesaw and related theories, $v/f < 1$, $\Lambda > 1$ TeV*

A final alternative is to consider a strongly interacting theory with a high (compared to a TeV) underlying dynamical scale that *would* naturally break the electroweak interactions, but whose

[1] In a strongly interacting theory "Naive Dimensional Analysis" [3, 4] implies that, in the absence of fine-tuning, $\Lambda \simeq g^* f$ where $g^* \simeq 4\pi$ is the typical size of a strong coupling in the low-energy theory [5, 6]. This estimate is modified in the presence of multiple flavors or colors [7] .

[2] For a review of technicolor models, see [10–12].

[3] If both the electroweak symmetry and the approximate scale symmetry are broken only by electroweak doublet condensate(s), then the decay-constants for scale and electroweak symmetry breaking may be approximately equal – differing only by terms formally proportional to the amount of explicit scale-symmetry breaking.

[4] In this case, however, the coupling strength of the singlet state to WW and ZZ pairs would be comparable to the couplings to gluon and photon pairs, and these would all arise from loop-level couplings in the underlying technicolor theory [22].

[5] In these models v/f is an adjustable parameter, and in the limit $v/f \to 1$ they reduce, essentially, to the technicolor models discussed in the previous subsection. Our discussion here is consistent with that given there, since we expect corrections to the SM Higgs couplings to be large for $v/f \simeq 1$. Current measurements constrain the couplings of the H^0 to equal those predicted for the Higgs in the standard model to about the 10% level [28], suggesting that f must have values of order a TeV or higher and, therefore, a dynamical scale Λ of at least several TeV.

Downloaded from https://academic.oup.com/ptep/article/2022/8/083C01/6651666 by KIT Library user on 27 September 2022

strength is adjusted ("fine-tuned") to produce electroweak symmetry breaking at 1 TeV. This alternative is possible if the electroweak (quantum) phase transition is continuous (second order) in the strength of the strong dynamics [39]. If the fine-tuning can be achieved, the underlying strong interactions will produce a light composite Higgs bound state with couplings equal to that of the standard model Higgs boson up to corrections of order $(1\ \text{TeV}/\Lambda)^2$. As in theories in which electroweak symmetry breaking occurs through vacuum alignment, therefore, constraints on the size of deviations of the H^0 couplings from that of the standard model Higgs give rise to lower bounds on the scale Λ. Formally, in the limit $\Lambda \to \infty$ (a limit which requires arbitrarily fine adjustment of the strength of the high-energy interactions), these theories are equivalent to a theory with a fundamental Higgs boson – and the fine adjustment of the coupling strength is a manifestation of the hierarchy problem of theories with a fundamental scalar particle.

In many of these theories the top-quark itself interacts strongly (at high energies), potentially through an extended color gauge sector [40, 40–44]. In these theories, top-quark condensation (or the condensation of an admixture of the top with additional vector-like quarks) is responsible for electroweak symmetry breaking, and the H^0 is identified with a bound state involving the third generation of quarks. These theories typically include an extra set of massive color-octet vector bosons (top-gluons), and an extra $U(1)$ interaction (giving rise to a top-color Z′) which couple preferentially to the third generation and whose masses define the scale Λ of the underlying physics.

92.1.4 *Flavor*

In addition to the electroweak symmetry breaking dynamics described above, which gives rise to the masses of the W and Z particles, additional interactions must be introduced to produce the masses of the standard model fermions. Two general avenues have been suggested for these new interactions. In "extended technicolor" (ETC) theories [45, 46], the gauge interactions in the underlying strongly interacting theory are extended to incorporate flavor. This extended gauge symmetry is broken down (possibly sequentially, at several different mass scales) to the residual strong interaction responsible for electroweak symmetry breaking. The massive gauge-bosons corresponding to the broken symmetries then mediate interactions between mass operators for the quarks/leptons and the corresponding bilinears of the strongly-interacting fermions, giving rise to the masses of the ordinary fermions after electroweak symmetry breaking.

In the case of "partial compositeness" [47], the additional flavor-dependent interactions arise from mixing between the ordinary quarks and leptons and massive composite fermions in the strongly-interacting underlying theory. Theories incorporating partial compositeness include additional vector-like partners of the ordinary quarks and leptons, typically with masses of order a TeV or less.

In both cases, the effects of flavor interactions on the electroweak properties of the ordinary quarks and leptons are likely to be most pronounced in the third generation of fermions.[6] The additional particles present in these theories, especially the additional scalars, often couple more strongly to heavier fermions.

Moreover, since the flavor interactions must give rise to quark mixing, we expect that a generic theory of this kind could give rise to large flavor-changing neutral-currents [46]. In ETC theories, these constraints are typically somewhat relaxed if the theory incorporates approximate generational flavor symmetries [48], the theory has a slowly running coupling constant or "walks" [17–21], or if $\Lambda > 1$ TeV [49]. In theories of partial compositeness, the masses of the ordinary fermions depend on the scaling-dimension of the operators corresponding to the composite fermions with which they mix. This leads to a new mechanism for generating the mass-hierarchy of the observed quarks and leptons that, potentially, ameliorates flavor-changing neutral current problems and can provide new contributions to the composite Higgs potential which allow for $v/f < 1$ [50–54].

Alternatively, one can assume that the underlying flavor dynamics respect flavor symmetries ("minimal" [55, 56] or "next-to-minimal" [57] flavor violation) that suppress flavor-changing neutral currents in the two light generations. Additional considerations apply when extending these arguments to potential explanation of neutrino masses (see, for example, [58, 59]).

92.1.5 *Theoretical Considerations*

Since the underlying high-energy dynamics in these theories are strongly coupled, there are no reliable calculation techniques that can be applied to analyze their properties. Instead, most phenomenological studies depend on the construction of a "low-energy" effective theory describing additional scalar, fermion, or vector boson degrees of freedom, which incorporates the relevant symmetries and, when available, dynamical principles. In some cases, motivated by the AdS/CFT correspondence [60], the strongly-interacting theories described above have been investigated by analyzing a dual compactified five-dimensional gauge theory. In these cases, the AdS/CFT "dictionary" is used to map the features of the underlying strongly coupled high-energy dynamics onto the low-energy weakly coupled dual theory [61].

More recently, progress has been made in investigating strongly-coupled models using lattice gauge theory [62–65]. These calculations offer the prospect of establishing which strongly coupled theories of electroweak symmetry breaking have a particle with properties consistent with those observed for the H^0 – and for establishing concrete predictions for these theories at the LHC [66].

92.1.6 *Summary*

The theoretical ideas and models reviewed here motivate searches for a wide variety of new states. Heavy vector bound states decaying to dibosons and additional scalar states appear naturally in both technicolor (92.1.1) and composite higgs models (92.1.2). Composite Higgs models based on collective symmetry breaking naturally include W', Z', and vector-like quark states (especially for the third-generation, and potentially including charge +5/3 custodial top-partner quarks). Vector-like states are also natural for any theory including partial compositeness in order to address the flavor problem (92.1.4). Top-condensate and related models (92.1.3) predict the existence of colorons which preferentially couple to third-generation quarks. Finally, the new states discussed here also occur in extra-dimensional models [61], which is understandable given that many strongly-coupled theories can be viewed as compactified five-dimensional gauge theories via duality (92.1.5). We turn now to a review the status of experimental searches related to dynamical electroweak symmetry breaking.

92.2 Experimental Searches

As discussed above, the extent to which the couplings of the H^0 conform to the expectations for a standard model Higgs boson constrains the viability of each of these models. Measurements of the H^0 couplings, and their interpretation in terms of effective field theory, are summarized in the H^0 review in this volume. In what follows, we will focus on searches for the additional particles that might be expected to accompany the singlet scalar: extra scalars, fermions, and vector bosons. In some cases, detailed model-specific searches have been made for the particles described above (though generally not yet taking account of the demonstrated existence of the H^0 boson).

In most cases, however, generic searches (e.g. for extra W' or Z' particles, extra scalars in the context of multi-Higgs models, or for fourth-generation quarks) are quoted that can be used – when appropriately translated – to derive bounds on a specific model of interest.

The mass scale of the new particles implied by the interpretations of the low mass of H^0 discussed above, and existing studies from the Tevatron and lower-energy colliders, suggests that only the Large Hadron Collider has any real sensitivity. A number of analyses already carried out by ATLAS and CMS use relevant final states and might have been expected to observe a deviation from standard model expectations – in no case so far has any such deviation been reported. The detailed implications of these

[6] Indeed, from this point of view, the vector-like partners of the top-quark in top-seesaw and little Higgs models can be viewed as incorporating partial compositeness to explain the origin of the top quark's large mass.

Downloaded from https://academic.oup.com/ptep/article/2022/8/083C01/6651666 by KIT Library user on 27 September 2022

searches in various model frameworks are described below.

Except where otherwise noted, all limits in this section are quoted at a confidence level of 95%. The searches at $\sqrt{s} = 8$ TeV (Run 1) are based on 20.3 fb^{-1} of data recorded by ATLAS, and an integrated luminosity of 19.7 fb^{-1} analyzed by CMS. The datasets collected at $\sqrt{s} = 13$ TeV during Run 2 of the LHC since 2015 are based on analyses with varied integrated luminosities ranging from ∼2-140 fb^{-1}.

92.2.1 *Searches for Z' or W' Bosons*

Massive vector bosons or particles with similar decay channels would be expected to arise in Little Higgs theories, in theories of Technicolor, or models involving a dilaton, adjusted to produce a light Higgs boson, consistent with the observed H^0. These particles would be expected to decay to pairs of vector bosons, or to third generation quarks, or to leptons. The generic searches for W' and Z' vector bosons listed below can, therefore, be used to constrain models incorporating a composite Higgs-like boson.

A general review of searches for Z' and W' bosons is also included in this volume [67, 68]. In the context of the dynamical electroweak symmetry breaking models, we emphasize their decays to third generation fermions by including a detailed overview, while also briefly summarizing the other searches.

$Z' \to \ell\ell$:

ATLAS [69] and CMS [70] have both searched for Z' production with $Z' \to ee$ or $\mu\mu$. No deviation from the standard model prediction was seen in the dielectron and dimuon invariant mass spectra, by either the ATLAS or the CMS analysis, and lower limits on possible Z' boson masses were set. A $Z'_{\rm SSM}$ with couplings equal to the standard model Z' (a "sequential standard model" Z') and a mass below 5.1 TeV was excluded by ATLAS, while CMS set a lower mass limit of 5.15 TeV. The experiments also place limits on the parameters of extra dimension models and in the case of ATLAS on the parameters of a minimal walking technicolor model [17–21], consistent with a 125 GeV Higgs boson [71]. For a general review of searches in these channels see the PDG review of Z prime in this volume [67].

In addition, both experiments have also searched for Z' decaying to a ditau final state [72, 73]. An excess in $\tau^+\tau^-$ could have interesting implications for models in which lepton universality is not a requirement and enhanced couplings to the third generation are allowed. This analysis led to lower limits on the mass of a $Z'_{\rm SSM}$ of 2.4 and 2.1 TeV from ATLAS and CMS respectively.

$Z' \to q\bar{q}$:

The ability to relatively cleanly select $t\bar{t}$ pairs at the LHC together with the existence of enhanced couplings to the third generation in many models makes it worthwhile to search for new particles decaying in this channel. Both ATLAS [74] and CMS [75] have carried out searches for new particles decaying into $t\bar{t}$.

Both the ATLAS and CMS collaborations searched for $t\bar{t}$ in the all hadronic mode [76] [77] in both the resolved and boosted regions. No evidence of resonance production were seen and limits were produced for various models including the Z' boson in topcolor-assisted technicolor which excludes masses less than 3.1 to 3.6 TeV (ATLAS) depending on the details of the model and 3.3, 5.25, and 6.65 TeV for widths of 1, 10 and 30 percent relative to the mass of the resonance .

ATLAS also presented results on the lepton plus jets final state, where the top quark pair decays as $t\bar{t} \to WbWb$ with one W boson decaying leptonically and the other hadronically; CMS used final states where both, one or neither W decays leptonically and then combined the results. The $t\bar{t}$ invariant mass spectrum was analyzed for any excess, and no evidence for any resonance was seen. ATLAS excluded a narrow ($\Gamma/m = 1.2\%$) leptophobic topcolor Z' boson with masses between 0.7 and 2.1 TeV and with $\Gamma/m = 3\%$ between 0.7 and 3.2 TeV. CMS set limits on leptophobic Z' bosons for three different assumed widths $\Gamma/m = 1.0\%$, $\Gamma/m = 10.0\%$, and $\Gamma/m = 30.0\%$ of 3.9 TeV to 4.0 TeV and exclude RS KK gluons up to 3.3 TeV.

Both ATLAS [78] and CMS [79] have also searched for resonances decaying into $q\bar{q}$, qg or gg using the dijet invariant mass spectrum. Excited quarks are excluded up to masses of 6.7 TeV and model-independent upper limits on cross sections with a Gaussian signal shape were set. CMS excluded string resonances with masses below 7.9 TeV, scalar diquarks below 7.5 TeV, axigluons and colorons below 6.6 TeV, excited quarks below 6.3 TeV, color-octet scalars below 3.7 TeV, W' bosons below 3.6 TeV, Z' bosons with SM-like couplings below 2.9 TeV and between 3.1 TeV and 3.3 TeV, Randall–Sundrum Gravitons below 2.6 TeV.

$W' \to \ell\nu$:

Both LHC experiments have also searched for massive charged vector bosons. In this section we include a summary of the results, with emphasis on final states with third generation fermions, while the details on other decays are discussed in the mini-review of W' [68]. ATLAS searched for a heavy W' decaying to $e\nu$ or $\mu\nu$ and found no excess over the standard model expectation. A sequential standard model (SSM) W' boson (assuming zero branching ratio to WZ) with mass less than 7 TeV was excluded [80] using the 139 fb^{-1} dataset at $\sqrt{s} = 13$ TeV. Model independent cross-section limits as a function of mass were also set. Based on a smaller dataset, the CMS experiment excluded a SSM W' boson with mass up to 4.1 TeV [81] and presented upper limits on the production of generic W' bosons decaying into this final state using a model-independent approach.

CMS [82] has carried out a complementary search in the $\tau\nu$ final state. As noted above, such searches place limits on models with enhanced couplings to the third generation. No excess was observed and limits between 2.0 and 2.7 TeV were set on the mass of a W' decaying preferentially to the third generation; a W' with universal fermion couplings was also excluded for masses less than 2.7 TeV.

$W' \to t\bar{b}$:

Heavy new gauge bosons can couple to left-handed fermions like the SM W boson or to right-handed fermions. W' bosons that couple only to right-handed fermions (W'_R) may not have leptonic decay modes, depending on the mass of the right-handed neutrino. For these W' bosons, the tb ($t\bar{b} + \bar{t}b$) decay mode is especially important because in many models the W' boson is expected to have enhanced couplings to the third generation of quarks relative to those in the first and second generations. It is also the hadronic decay mode with the best signal-to-background. ATLAS and CMS have performed searches for W' bosons via the $W' \to tb$ decay channel in the lepton+jets and all-hadronic final state.

The CMS lepton+jets search [83–86], $W' \to tb \to Wbb \to \ell\nu bb$, proceeded via selecting events with an isolated lepton (electron or muon), and at least two jets, one of which is identified to originate from a b-quark. The mass of the W' boson (M_{tb}) was reconstructed using the four-momentum vectors of the final state objects ($bb\ell\nu$). The distribution of M_{tb} is used as the search discriminant. A search [86] using 35.9 fb^{-1} of data, collected at $\sqrt{s}$ = 13 TeV, led to an exclusion of W'_R bosons with masses below 3.4 TeV (3.6 TeV) if $M_{W'_R} >> M_{\nu_R}$ ($M_{W'_R} < M_{\nu_R}$), where M_{ν_R} is the mass of the right-handed neutrino.

The CMS search for $W' \to tb$ decays using the all-hadronic final state focused on W' masses above 1 TeV [85, 87]. In this region, the top quark gets a large Lorentz boost and hence the three hadronic products from its decay merge into a single large-radius jet. Deep neural network(DNN) algorithms are used to identify the jet initiated by the bottom quark. Techniques including DNN, which rely on substructure information of the jets [88] are employed to identify boosted all hadronic W boson and top quark [87] decays. The W' candidate mass was computed from back-to-back boosted top-tagged jet and a low mass b-tagged jet. From this all-hadronic search, W' bosons were excluded for masses up to 3.4 TeV [87].

ATLAS has searched for W'_R bosons in the $t\bar{b}$ final state both for lepton+jets [89] and all-hadronic [90] decays of the top. No significant deviations from the standard model were seen in either analysis and limits were set on the $W' \to t\bar{b}$ cross section times branching ratio and W' bosons with purely right-handed couplings to fermions were excluded for masses below 3.15 TeV when the two channels are combined.

In addition, the above studies also provided upper limits on the W' effective couplings to right- and left-handed fermions.

Downloaded from https://academic.oup.com/ptep/article/2022/8/083C01/6651666 by KIT Library user on 27 September 2022

In Fig. 92.1 (bottom) the upper limits on W' couplings normalized to the SM W boson couplings derived by ATLAS [91] are shown. The top panel of Fig. 92.1 shows the upper limits for arbitrary combinations of left- and right-handed couplings of the W' boson to fermions set using a model independent approach by CMS [86].

92.2.2 *Searches for Resonances decaying to Vector Bosons and/or Higgs Bosons*

Both the ATLAS and CMS experiments have used the data collected at $\sqrt{s} = 13$ TeV to search for resonances decaying to pairs of bosons. Overall no significant excesses were seen in the full datasets that were analyzed and the results are interpreted in models with heavy vector triplets (HVT) [92], models with strong gravity and extra spatial dimensions, and model independent limits as a function of mass are set. For a full review of models including extra spatial dimensions and the interpretation of many of these results in that context please see the review of extra dimensions in this volume [61].

Utilizing data collected at $\sqrt{s} = 13$ TeV, ATLAS [93] and CMS [94], have both looked for a resonant state decaying into VV (with $V = W$ or Z) , VH (with H representing the SM Higgs boson), and HH. ATLAS searches in the $qqqq$, $\nu\nu qq$, $l\nu qq$, $llqq$, $l\nu l\nu$, $ll\nu\nu$, $l\nu ll$, $llll$, $qqbb$ $\nu\nu bb$, $l\nu bb$, and $llbb$ final states and combined the results . While CMS analyzed the $qqqq$, $\nu\nu qq$, $l\nu qq$, $llqq$, $ll\nu\nu$, $\nu\nu bb$, $l\nu bb$, $llbb$, $bbbb$, $\tau\tau bb$, and $qq\tau\tau$ final states.

The combined limits are expressed both as limits on the cross-section as a function resonance mass as well as constraints on the coupling of the heavy boson triplet to quarks, leptons, and the Higgs boson.

$X \to WZ$:

ATLAS searches for new heavy resonances decaying into WZ in the channels $WZ \to qqqq$ [95] , $l\nu qq$ [96], and $l\nu ll$ [97]. In the fully leptonic channel , the invariant mass of the W Z pair is obtained by considering all possible four lepton permutations in each event. The dominant background is Standard Model continuum WZ production, ZZ production where one lepton is not identified or falls outside the detector acceptance, and top quark plus vector boson production. No resonant production is seen in data and lower limits on the mass of a HVT decaying into WZ are set at 2260 (2460) GeV assuming a coupling constant of $g_V = 1$ ($g_V = 3$). In the $WZ \to l\nu qq$ mode, ATLAS searches in both the cases that the quarks are observed as individual jets (resolved) and where they merge into one jet in the detector (boosted) which probe the low and high p_T regime of the Z boson. No significant excess is seen in either channel and combined lower mass limits are placed at 2900 (3000) GeV for $g_V = 1$ ($g_V = 3$) in the HVT model. In the all hadronic decay mode, ATLAS searches for two high p_T hadronically decaying vector bosons looking for a resonant structure. No excess is seen and limits are placed exclude 1200-3000 (1200-3300) GeV for $g_V = 1$ ($g_V = 3$) in the HVT model.

CMS searches for new heavy resonances in the ZV final state using the semi-leptonic decay channels excluding W' masses up to 1800 GEV in HVT two models with $g_V = 1$ and 3 and in the ZZ channel excludes gravitons up to 1200 GeV. The CMS collaboration searches for $VV \to qqqq$ [98] in the large R dijet search. The W and Z boson are identified through the mass of the large R jet and substructure variables. No excess is seen and limits are set for charged HVT bosons with masses lower than 3200 (3800) GeV for $g_V = 1$ ($g_V = 3$). Cross-section limits as function of mass are reported for the charged spin-1 resonance interpretation and are placed at 44.4 fb at 1.4 TeV to 0.7 pb at 4 TeV. In the $\nu\nu qq$ final state [99], the CMS collaboration searches for a charged spin 1 resonance decaying into a VZ final state with a Z boson decaying into a pair of neutrinos and the other boson decaying into two collimated quarks reconstructed as a large R-jet. The transverse mass of the VZ candidate is reconstructed and utilized to search for evidence of resonant VZ production. No excess is seen and lower mass limits are placed on the charged resonance at 3100 (3400) GeV for $g_V = 1$ ($g_V = 3$) . In the $2l2q$ final state, the CMS collaboration searches for a heavy resonance decaying into ZV [100] looking for events with one large R-jet consistent with the hadronic decay of a vector boson and a Z boson reconstructed in the charged lepton decay channel (e or μ). Limits are set for a HVT W' with a lower mass of 2270 (2330) for $g_V = 1$ ($g_V = 3$) .

$X \to WW$:

The ATLAS collaboration searches for a new heavy resonance decaying into WW in the channels $WW \to qqqq$ [95] , $l\nu qq$ [96], and $l\nu\nu$ [101]. In the case where both Ws decay leptonically, ATLAS utilizes the transverse mass of the two lepton and two neutrino final state and searches for an excess in this distribution between 200 GeV and 5 TeV. No excess is seen and a HVT is excluded for masses below 1300 GeV. Vector boson fusion is also considered and cross-section limits as a function of mass are placed ranging from 1.3 pb to 0.006 pb at 200 GeV to 3 TeV, respectively. In the $l\nu qq$ mode , ATLAS completed a companion analysis to the $WZ \to$ analysis discussed above and places lower mass limits of 2850 (3150) GeV for $g_V = 1$ ($g_V = 3$) in the HVT model. ATLAS also interprets the all hadronic mode analysis in the hypothesis that $WW \to qqqq$ and places limits on a HVT boson decaying into WW in the all hadronic mode between 1200 and 2200 (1200 and 2800) GeV for $g_V = 1$ ($g_V = 3$).

The CMS collaboration searches for $VV \to qqqq$ [98] in the large R dijet search. The W and Z boson are identified through the mass of the large R jet and substructure variables. No excess is seen and limits are set for charged HVT bosons with masses lower than 2700 (2800) GeV for $g_V = 1$ ($g_V = 3$). Cross-section limits as function of mass are reported for the uncharged spin-1 resonance interpretation and are placed at 41.6 fb at 1.4 TeV to 0.6 pb at 4 TeV.

$X \to VH$:

The ATLAS Collaboration searches for a new heavy resonance decaying into WH and ZH in the $qqbb$ (WH and ZH) [102], $l\nu bb$ (WH), $\nu\nu bb$ (ZH), $llbb(ZH)$ [103] modes. In the all hadronic mode, ATLAS searches for boosted VH production looking for two large R jets where the larger invariant mass large R jet is interpreted as the Higgs boson decay products while the lesser invariant mass jet is taken to be the hadronically decaying vector boson requiring b-tagging on the Higgs boson subjets. The invariant mass is reconstructed and a search is done for resonant production of ZH. None is found and limits from 1100 to 2500 (1300 to 3800 GeV) are placed for $g_V = 1$ ($g_V = 3$). ATLAS also searches for XH where the W or Z boson decays into $\nu\nu$, $l\nu$, and ll . The analysis searches for both resolved and merged (boosted) b-jets from the decay of the Higgs boson and defines the signal regions based on the number of reconstructed charged leptons (0,1,or 2). In the dilepton channel the invariant mass is explicitly reconstructed of the entire diboson system, the single lepton channel reconstructs the diboson final state constraining the lepton and missing transverse momentum utilizing the known W boson mass, while the 0 charged lepton channel reconstructs the transverse mass of the diboson system. No excess is seen in any channel and limits on the production of a HVT are placed at 2800 GeV (2930) GeV for $g_V = 1$ ($g_V = 3$).

The CMS Collaboration searches for a heavy resonance decaying into VH [104] searching for a resonances decaying into a Higgs boson and a hadronically decaying W or Z boson. The search identifies events with two large-R jets using substructure variables and requires one large-R jets is tagged with a pair of b-hadrons clustered in a single jet. The invariant mass of the VH bosons is reconstructed and evidence for resonance production is sought. No excess is seen and limits are placed. With $g_V = 1$ (3) a narrow W' resonance with $m_{W'} < 2470(3150)$ GeV and $m_{Z'} < 1150(1190)$.

The CMS collaboration searches for a heavy resonance decaying into a pair of boosted Higgs boson with $HH \to b\bar{b}WW^*$ in the single and dilepton channel [105]. Events are categorized according to lepton flavor and multiplicity, along with discriminators that characterize the compatibility with having jets arising from the decay of boosted Higgs and W bosons. The reconstructed Higgs and diHiggs mass distributions are fit and used as the final discriminators. No significant deviations in the 12 sub-categories are seen and 95% confidence limits on spin-0 bosons are set from 24.5 fb at 0.8 TeV to 0.78 fb at 4.5 TeV and spin-2 bosons from

Downloaded from https://academic.oup.com/ptep/article/2022/8/083C01/6651666 by KIT Library user on 27 September 2022

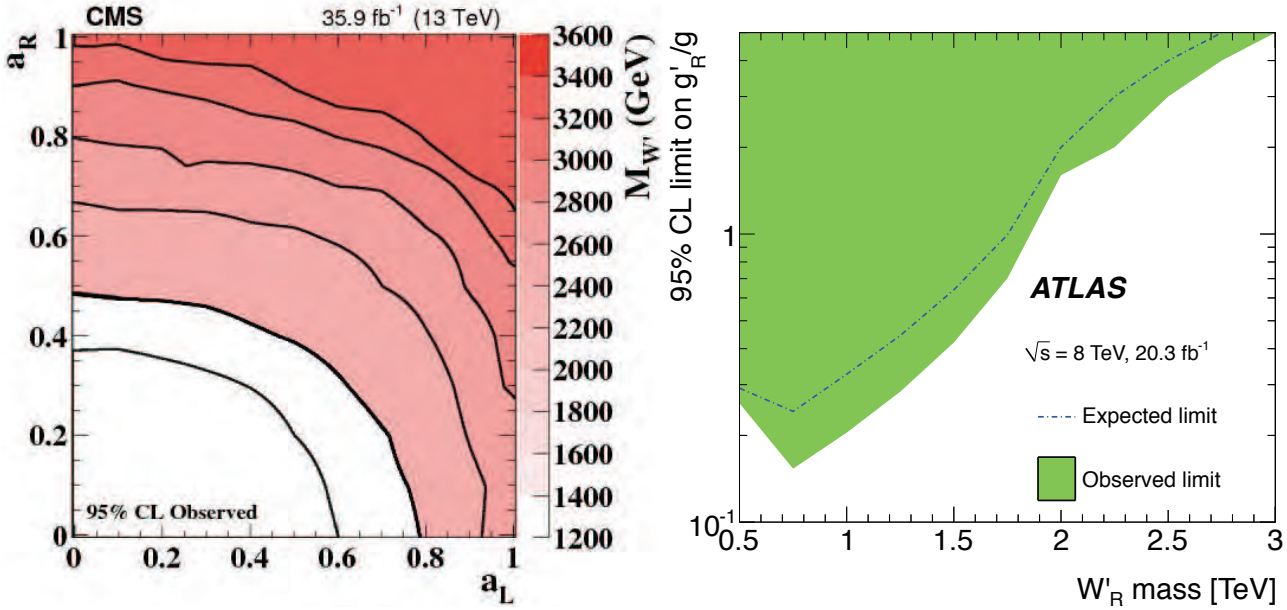

Figure 92.1: Left panel: Observed limits on the W' boson mass as function of the left-handed ($a_{\rm L}$) and right-handed ($a_{\rm R}$) couplings. Black lines represent contours of equal W' boson mass [86]. Right panel: Observed and expected regions, on the g$'$/g vs mass of the W' boson plane, that are excluded at 95% CL, for right-handed W' bosons [91] showing the exclusion of the values of a hypothetical right-handed coupling of a heavy W particle.

16.7 fb at 0.8 TeV to 0.67 fb at 4.5 TeV. A similar search in the four b-quark final state is used to set limits range 9.74 to 0.29 fb and 4.94 to 0.19 fb in the spin-0 bosons and spin-2 gravitons (respectively) interpretation with masses of 1-3 TeV [106].

$X \to H\gamma$ or $V\gamma$:

Both the CMS and ATLAS collaboration search for heavy resonances decaying into either a vector boson and a photon or a Higgs boson or a photon. These searches are motivated generically by the fact that new heavy gauge bosons are generically predicted to decay to either a Higgs boson or a vector boson and a photon by one loop decays [107]. ATLAS searches for for a heavy resonances decaying into a Higgs boson and a photon and sets limits from 0.7 to 4 TeV from 11.6 fb to 0.11 fb [108]. ATLAS searches for a heavy resonance decaying into XH where $XH \to qqbb$ [109] and sets limits from 1 to 4 TeV. CMS searches for a heavy resonance decaying into a W boson and a photon [110] setting limits for narrow resonances range between 0.17 fb at 6.0 TeV and 55 fb at 0.7 TeV.

Summary of Searches with Diboson Final States:

Both ATLAS [93] and CMS [94] provide plots summarizing the various searches results and limits combining. The results are shown in the context of HVT models and models of strong gravity with extra spatial dimensions. No excess is seen in any search and limits on the 4.3 (4.5) TeV (ATLAS) and (CMS). Inclusion of decays directly to fermions increase these limits to 5.3 (5.5) TeV and 5.0 (5.2) TeV from the ATLAS and CMS combinations, respectively. Both collaborations also place varying limits on the coupling strength as a function of HVT boson mass as well.

Searches for Triboson Resonances:

The CMS collaboration presents the first search for massive triboson resonances in both the semi-leptonic [111] and fully hadronic final state [112]. Three boson final states can be produced via the decay of Kaluza-Klein(KK) states decaying via $W_{KK} \to WR$ with $R \to WW$ where R is a scalar radion. The search utilizes novel deep neural networks to perform optimal separation between signal and background and searches for evidence of resonance structure in the triboson invariant mass-spectrum. No excesses above SM backgrounds are seen and W_{KK} and radion masses are excluded up to $M_{W_{KK}} = 3.4$ TeV and $M_R = 1$ TeV and up to $M_{W_{KK}} = 3.6$ TeV and $M_R = 0.35$ TeV . $M_{W_{KK}}$ below 3 TeV are excluded for $0.6 < \frac{M_R}{M_{W_{KK}}} < 0.7$ in the semi-leptonic final state and up to $M_{W_{KK}} = 3.0$ TeV and $M_R = 200$ GeV and up to $M_{W_{KK}} = 1.5$ TeV and $M_R = 1.5$ TeV in the fully hadronic final state.

92.2.3 *Vector-like third generation quarks*

Vector-like quarks (VLQ) have non-chiral couplings to W bosons, i.e. their left- and right-handed components couple in the same way. They therefore have vectorial couplings to W bosons. Vector-like quarks arise in Little Higgs theories, top-coloron-models, and theories of a composite Higgs boson with partial compositeness. In the following, the notation T quark refers to a vector-like quark with charge 2/3 and the notation B quark refers to a vector-like quark with charge $-1/3$, the same charges as the SM top and b quarks respectively. The exotic vector-like quarks $X_{5/3}$ and $Y_{-4/3}$ have charges 5/3, and $-4/3$ respectively. Vector-like quarks couple with SM quarks with Yukawa interactions and may exist as SU(2) singlets (T, and B), doublets $[(X_{5/3}, T)$,(T, B),$(B, Y_{-4/3})]$, or triplets $[(X_{5/3}, T, B)$, $(T, B, Y_{-4/3})]$. At the LHC, VLQs can be pair produced via the dominant gluon-gluon fusion process. VLQs can also be produced singly by their electroweak effective couplings to a weak boson and a standard model quark. The single production rate is expected to dominate over the rate of pair production at large VLQ masses. T quarks can decay to bW, tZ, or tH^0. Weak isospin singlets are expected to decay to all three final states with (asymptotic) branching fractions of 50%, 25%, 25%, respectively. Weak isospin doublets are expected to decay exclusively to tZ and to tH^0 [113] with equal branching ratios. Analogously, B quarks can decay to tW, bZ, or bH^0. The $Y_{-4/3}$ and $X_{5/3}$ quarks decay exclusively to bW and to tW. While these are taken as the benchmark scenarios, other representations and decays to exotic new particles are possible [114–116], and hence the final results are interpreted for many allowed branching fraction combinations.

Given the multiple decay modes of the VLQs, the final state signatures of both pair produced and the singly produced VLQs are fairly rich with leptons, jets, b-jets, and missing energy. Depending on the mass of the VLQ, the top quarks and $W/Z/H^0$ bosons may be Lorentz boosted and identified using jet substructure techniques. Thus the searches are performed using lepton+jets signatures, multi-lepton and all-hadronic decays. In addition, T or B quarks with their antiparticles can result in events with same-sign leptons, for example if the decay $T \to tH \to bWW^+W^-$ is present, followed by leptonic decays of two same-sign W bosons.

Downloaded from https://academic.oup.com/ptep/article/2022/8/083C01/6651666 by KIT Library user on 27 September 2022

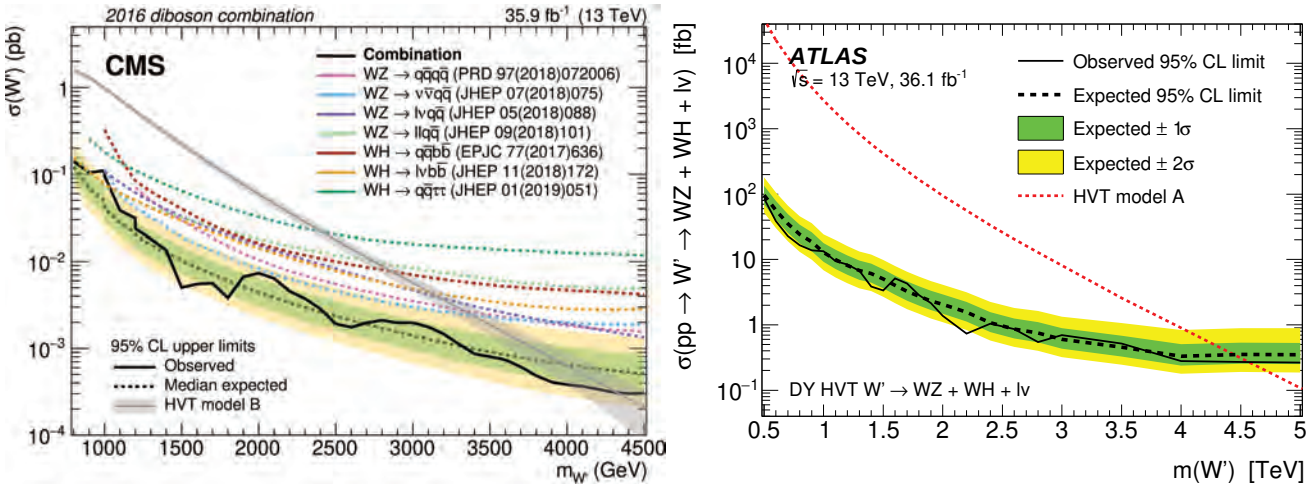

Figure 92.2: Left panel:Observed limits from W' to diboson from CMS [94]. Right panel: Observed limits from W' to diboson decays from ATLAS [93].

In the following subsections, while we describe the searches for each of the decay modes of the VLQs, the same analysis can be re-interpreted to obtain the sensitivity to a combination with varied branching fractions to the different decay modes.

In the following sections, the results obtained for T (B) quarks assuming 100% branching ratio to Wb (Wt) are also applicable to heavy vector-like $Y_{-4/3}$ ($X_{5/3}$) with charge 4/3 (5/3).

92.2.3.1 *Searches for* $\boldsymbol{T}$ *quarks that decay to* $\boldsymbol{W}$, $\boldsymbol{Z}$ *and* $\boldsymbol{H^0}$ *bosons*

$T/Y \to bW$:

CMS has searched for pair production of heavy T quarks that decay exclusively to bW [117–119]. The analysis selected events with exactly one charged lepton, assuming that the W boson from the second T quark decays hadronically. Under this hypothesis, a 2-constraint kinematic fit can be performed to reconstruct the mass of the T quark as a narrow mass peak with a mass resolution of around 7%. In Refs. [118] and [119], the two-dimensional distribution of reconstructed mass vs S_T was used to test for the signal, where S_T is the scalar sum of the missing p_T and the transverse momenta of the lepton and the leading four jets. This analysis, when combined with the search in the fully hadronic final state [120] excluded new quarks that decay 100% to bW for masses below 0.89 TeV [119]. At times the hadronically-decaying W boson is produced with a large Lorentz boost, leading to the W decay products merged into a large-radius jet. Algorithms such as jet pruning [121] were used to remove contributions from soft, wide angle radiation, from large-radius jets, leading to better discrimination between QCD jets and those arising from decays of the heavy particles. If the mass of the boosted jet was compatible with the W boson mass, then the W boson candidate jet and its subjets were used in the kinematic reconstruction of the T quark. No excess over standard model backgrounds was observed. Upper limits on the production cross section as a function of the mass of T quarks were measured. By comparing them with the predicted cross section for vector like quark pair production, the strong pair production of T quarks was excluded for masses below 1.30 TeV (1.28 TeV expected) [117].

Another "cut-based" search for pair produced T quarks in the all-hadronic final state targeting the Wb decay mode [122], relies on mass reconstruction of two highest p_T Wb combinations using boosted W boson candidates with $p_T > 200$ GeV and b-tagged jets. H_T is used as the signal discriminator, with selected events divided into nine categories based on the multiplicity of W and b-jets in the event. From this search T quarks with pure Wb decays are excluded for masses below 1.04 TeV (1.07 TeV expected).

An analogous search has been carried out by ATLAS [123,124] for the pair production of heavy T quarks. It used the lepton+jets final state with an isolated electron or muon and at least four jets, including a b-jet, and required reconstruction of the T quark mass. Given that the mass range for the T quark being explored was from a 0.4 TeV to a couple of TeV, the W boson from the T quark may fall in two categories: those with a high boost leading to merged decay products, and others where the two jets from the W boson were resolved. In addition, the selection was optimized to require large angular separation between the high p_T W bosons and the b-jets.

The $T \to Wb$ candidates were constructed from both the leptonically and hadronically decaying W bosons by pairing them with the two highest p_T b-tagged jets in the event. The pairing of b-jets with W bosons which minimizes the difference between the masses of leptonically decaying T ($m_{lep}(T)$) and the hadronic T ($m_{had}(T)$) was chosen. Finally, $m_{lep}(T)$ was used as the discriminating variable in a signal region defined by high S'_T (here S'_T is defined as the scalar sum of the missing p_T, the p_T of the lepton and jets), and the opening angle between the lepton and the neutrino ($\Delta R(e,\nu)$). With the 36.1 fb^{-1} data collected during Run 2 at $\sqrt{s} = 13$ TeV, assuming 100% branching ratio to the Wb decay, the observed lower limit on the T mass was 1.35 TeV, and in the SU(2) singlet scenario, the lower mass limit was obtained to be 1.17 TeV [123].

A targeted search for a T quark, produced singly in association with a light flavor quark and a b quark and decaying into bW, was carried out by CMS at $\sqrt{s}$=13 TeV and a dataset corresponding to 2.3 fb^{-1} [125]. The analysis used lepton+jets events, with at least one b-tagged jet with large transverse momentum, and a jet in the forward η region. Selected events were required to have $S''_T > 500$ GeV, where S''_T is defined as the scalar sum of the transverse momenta of the lepton, the leading central jet, and the missing transverse momentum. The invariant mass of the T candidate was used as the discriminating variable and was reconstructed using the four-vectors of the leptonically decaying W boson and the leading central jet. No excess over the standard model prediction was observed. As the VLQ width is proportional to the square of the coupling, upper limits were set on the production cross section assuming a narrow width VLQ with coupling greater than 0.5. For Y/T quarks with a coupling of 0.5 and a 100% branching fraction for the decay to bW the excluded masses were in the range from 0.85 to 1.40 TeV [125]. A similar search [126, 127] was performed by ATLAS for a singly produced T or $Y_{-4/3}$ quark decaying to Wb using a dataset corresponding to 36.1 fb^{-1}. The search was performed using lepton+jets events with a high p_T b-tagged jet, and at least one forward jet. The reconstructed mass of the $T/Y_{-4/3}$ quark, was used as the discriminating variable and showed no excess above the expectation from SM. Interference effects with the SM background are included in the study. This search led to 95% CL upper limits on the mixing angle $|sin(\theta_L)|$ (C_L^{Wb}) in the range of 0.18–0.35 (0.25–0.49) for singlet T quark mass between 0.8–1.2 TeV. This search

Downloaded from https://academic.oup.com/ptep/article/2022/8/083C01/6651666 by KIT Library user on 27 September 2022

also provided limits as a function of the $Y_{-4/3}$ quark mass, on the coupling of the $Y_{-4/3}$ quark to bW, and the mixing parameter $|sin\theta_R|$ (C_R^{Wb}) for a (B,$Y_{-4/3}$) doublet model [126]. For VLQ masses between 0.08–1.8 TeV, the limits on $|sin(\theta_R)|$ (C_R^{Wb}) are in the range 0.17–0.55 (0.24–0.77), and for for $Y_{-4/3}$ quark mass between 0.9–1.25 TeV, the limits on $|sin\theta_R|$ are around 0.18–0.19 and below the constraints from electroweak precision observables. For $Y_{-4/3}$ quark in the triplets (T,B,$Y_{-4/3}$), limits on $|sin(\theta_L)|$ (C_L^{Wb}) are between 0.16–0.39 (0.31–0.78) for masses between 0.8 GeV–1.6 TeV [126].

$T \to tH^0$:

ATLAS has performed a search for $T\overline{T}$ production with $T \to tH^0$ [124, 128]. Given the dominant decay mode $H^0 \to b\bar{b}$, these events are characterized by a large number of jets, many of which are b-jets. Thus the event selection required one isolated electron or muon and high jet multiplicity (including b-tagged jets). The sample is categorized by the jet multiplicity (5 and $\geq$6 jets in the 1-lepton channel; 6 and $\geq$7 jets in the 0-lepton channel), b tag multiplicity (2, 3 and $\geq$4) and mass-tagged jet multiplicity (0, 1 and $\geq$2). The distributions of $m_{\rm eff}$, defined as the scalar sum of the lepton and jet p_T and the missing p_T, for each category were used as the discriminant for the final signal and background separation. No excess of events was found. Weak isospin doublet T quarks were excluded below 1.16 TeV.

A search by ATLAS for pair produced VLQs with an all-hadronic final state signature yields an exclusion of pure decays $T \to tH^0$ upto a T quark mass of 1.01 TeV [129]. This analysis used a deep neural network technique to identify jets originating from boosted bosons and top-quarks and is described further in subsection 92.2.3.2.

The CMS search for $T\overline{T}$ production, with $T \to tH^0$ decays has been performed in lepton+jets, multilepton and all-hadronic final states. The lepton+jets analysis [130] emphasizes the presence of a large number of b-tagged jets, and combines it with other kinematic variables in a Boosted Decision Tree (BDT) to enhance signal to background discrimination. The multilepton analysis [130] was optimized for the presence of b-jets and the large hadronic activity. For $\mathcal{B}(T \to tH^0) = 1$, the combined lepton+jets and multilepton analyses led to a lower limit on T quark masses of 0.71 TeV. A search for $T \to tH^0$ in all-hadronic decays [131], optimized for a high mass T quark, and based on identifying boosted top quark jets has been carried out by CMS. This search aimed to resolve subjets within the jets arising from boosted top quark decays, including b tagging of the subjets. A likelihood discriminator was defined based on the distributions of H_T and the invariant mass of the two b-jets in the events for signal and background. No excess above background expectations was observed. Assuming 100% branching ratio for $T \to tH^0$, this analysis led to a lower limit of 0.75 TeV on the mass of the T quark.

Searches for T quarks at $\sqrt{s}$=13 TeV, based on a 2.6 fb^{-1} dataset [132] have been performed by CMS using the lepton+jets final state. This search has been optimized for high mass T quarks by exploiting techniques to identify W or Higgs bosons decaying hadronically with large transverse momenta. The boosted W channel excluded T quarks decaying only to bW with masses below 0.91 TeV, and the boosted tH channel excluded T quarks decaying only to tH for masses below 0.89 TeV.

A CMS search for $T \to tH^0$ with $H^0 \to \gamma\gamma$ decays has been performed [133] in pair production of T quarks. To identify the Higgs boson produced in the decay of the heavy T quark, and the subsequent $H^0 \to \gamma\gamma$ decay, the analysis focused on identification of two photons in events with one or more high p_T lepton+jets or events with no leptons and large hadronic activity. A search for a resonance in the invariant mass distribution of the two photons in events with large hadronic activity defined by the H_T variable showed no excess above the prediction from standard model processes. The analysis resulted in exclusion of T quark masses below 0.54 TeV.

A search for electroweak single production of T quarks decaying to tH^0 using boosted topologies in fully hadronic [134] and lepton+jets [135] in the final states has been performed by CMS. The electroweak couplings of the T quarks to the SM third generation quarks are highly model dependent, and hence these couplings determine the rates of the single T quark production. In both analyses, T quark invariant mass was reconstructed using the boosted Higgs boson jet and the top quark. Higgs boson jets were identified using jet substructure techniques and subjet b tagging. For the lepton+jets analysis, the top quark was reconstructed from the leptonically decaying W and the b jet, while in the all-hadronic analysis the top quark jet was tagged using substructure analysis. There was no excess of events observed above background. Exclusion limits on the product of the production cross section and the branching fraction ($\sigma(pp \to Tqt/b) \times \mathcal{B}(T \to tH^0)$ were derived for the T quark masses in the range 0.70-1.8 TeV. From the lepton+jets analysis, for a mass of 1.0 TeV, values of ($\sigma(pp \to Tqt/b) \times \mathcal{B}(T \to tH^0)$ greater than 0.8 and 0.7 pb were excluded assuming left- and right-handed coupling of the T quark to standard model fermions, respectively [135]. For the all-hadronic analysis, upper limits between 0.31 and 0.93 pb were obtained on ($\sigma(pp \to Tqt/b) \times \mathcal{B}(T \to tH^0)$ for T quark masses in the range 1.0-1.8 TeV [134].

$T \to tZ$:

Both ATLAS and CMS searched for T quarks that decay exclusively into tZ in pp collisions at $\sqrt{s}$ = 13 TeV. No excesses were found in either search.

ATLAS performed a search [136] optimized for pair production of vector-like top quarks decaying into tZ where the Z boson subsequently decays into neutrino pairs, utilizing 36.1 fb^{-1} of data. The search selected events with one lepton, multiple jets, and significant missing transverse momentum. No significant excesses were found and lower limits on the mass of a vector like top quark were placed, excluding masses below 0.87 TeV (weak-isopsin singlet), 1.05 TeV (weak-isospin doublet), and 1.16 TeV (pure tZ mode).

Another search by ATLAS for pair produced T decaying to tZ has been carried out by reconstructing the high transverse momentum Z boson from a pair of opposite-sign same-flavor leptons, using events with two or three charged leptons [137]. The final analysis is based on three final state signatures. In the trilepton events, at least one b-tagged jet is required and S_T is used as the discriminating variable. In events with two leptons, at least 2 b-jets are requested and events with zero or one high p_T top-tagged jet, use H_T as the discriminator. The second dilepton analysis with two top-tagged high p_T jets focuses on hadronically decaying heavy resonances and the invariant mass of the Z boson and the highest p_T b-tagged jet is found to be a good discriminating variable. No excess was observed over the background expectations. The combined analysis yields a lower limit on T quark mass of 1.03 TeV (1.21 TeV) in the singlet (doublet) model or 100% branching ratio for $T \to tZ$ a lower limit on the T quark mass of 1.34 TeV is obtained.

ATLAS has subsequently carried out a search [138] for singly produced T quarks decaying to tZ where the Z boson decays into neutrino pairs. The search is carried out using 36.1 fb^{-1} of data in events with two different final state signatures: one with jets and significant missing p_T (0L) and the other with a single lepton, jets and missing p_T (1L). Events are divided into signal and dedicated W+jets and $t\bar{t}$ background control regions. The sensitivity to the T quark signal is extracted using distributions of missing p_T for the 1L and the distribution of T quark transverse mass constructed from missing p_T and the high p_T large-radius top-tagged jet, for 0L analysis. There is no excess found over the expected background and lower limits on the production of T singlets are obtained as a function of the left- and right-handed couplings $c_{L,W}$ and $c_{R,W}$ to top quarks and W bosons, where c_W above 0.7 is excluded for T quark mass of 1.4 TeV. The limits on c_W are also recasted into expected and observed 95% CL upper limits for the mixing angle (θ_L) of a singlet T with the top quark.

CMS searched [139] for single production of T quarks decaying into tZ with the Z boson decaying to pairs of charged leptons (electrons and muons) and the top quark decaying hadronically using 35.9 fb^{-1} of data. Limits were placed on T quarks with masses between 0.7 and 1.7 TeV excluding the product of cross section and branching fraction above values of 0.27 to 0.04 pb.

Downloaded from https://academic.oup.com/ptep/article/2022/8/083C01/6651666 by KIT Library user on 27 September 2022

Additionally, limits on the product of cross section and branching fractions for a Z' boson decaying into tZ were set between 0.13 and 0.06 pb for Z' boson masses in the range from 1.5 to 2.5 TeV.

Similar searches by ATLAS for singly produced T decaying to Zt have been performed in final state signatures with two or three charged leptons [137]. The analysis relies on tagging b-jets and high p_T large-radius jets originating from top-quarks. Additional selections are devised to reduce the contributions from pair production of T quarks. For events with dilepton analysis, the discriminating variable is the mass of the T quark formed using the invariant mass of the Z boson candidate and the highest p_T top-tagged jet, while for the trilepton analysis, the variable S_T is used to search for an excess of data over the expected SM background. No excess above the SM expectations is observed. The two final states (dilepton and trileptons) are combined to obtain the final results. For the coupling parameter κ_T between 0.1–1.6, the 95% CL upper limits on the production cross section times branching fraction into Zt is between 0.16–0.18 (0.03–0.05) pb at T quark mass of 0.7 (2) TeV.

The search by the ATLAS experiment for VLQ pair production optimized to search for $T \to tZ$ decays [140] in a dataset with $139\,\mathrm{fb}^{-1}$ of luminosity has been performed in final states with either two leptons or three or more leptons. A multi-class boosted object tagger based on DNN techniques for large-radius jets is used to categorize events according to the number of high p_T boosted H^0, Z/W, and top quark jets. The discriminant in the signal to evaluate the sensitivity depends on the number of leptons in the event. For the two lepton analysis, the discriminant is the mass of the T quark which is constructed from b and Z candidates, while for the three or more lepton analysis, H_T computed using the p_T of the jets and leptons is used as the discriminant. This analysis excludes T quark masses up to 1.27 GeV (1.46 GeV), for the singlet (doublet) configuration [140].

Combination of $T \to tZ/tH^0$:

The search performed by the ATLAS experiment for electroweak single production of T quark decaying to tH^0 and tZ uses a dataset corresponding to $139\,\mathrm{fb}^{-1}$ of integrated luminosity, and events with a single lepton with multiple jets and b-jets in the final state [141]. The single production channel for VLQs probes κ, the universal coupling constant, which also controls the production cross section and the resonance width of the VLQ. The analysis uses techniques to tag boosted jets, and categorizes events by numbers of jets and b-jets. The event discriminant is the "effective mass" (meff) observable, defined as the scalar sum of the p_T of all central jets, p_T of leptons and the missing p_T in the event. No significant excess is observed. Limits on the mass of T quark and universal coupling strength (κ) are obtained. For singlet T quarks, values of κ above 0.5 are excluded for all masses below 1.8 TeV. For T quark mass of 1.6 TeV, κ above 0.41 is excluded [141].

A CMS search published in 2020 concentrates on the electroweak production of the T quark with $T \to tH^0$, and $T \to tZ$ decays, where subsequently both H^0 and Z Bosons decay hadronically, leading to fully hadronic final states [142]. The search focuses on evidence of T quarks produced in association with a b quark ($qg \to T\bar{b}q'$) or a top quark ($qg \to T\bar{t}q$). The production cross sections are model dependent, as the electroweak production depends on the strength of the T quark coupling, TbW (TtZ), for the charged-current (neutral-current) process, at the production vertex. The searches are split into two domains depending on the mass of the T quark and consider a wide range of widths of the T quark from a few percent to about 30% of the T quark mass. The event selection relies primarily on the large number of jets and on efficient identification of jets from b-quarks, in addition to double-b jet decays of the H^0 and Z bosons. The final sensitivity is derived by the search for a resonant peak in the tH^0/Z invariant mass spectrum. For low mass T quark searches, three independent regions based on the b-tagged jet requirements are examined. For T quark masses above 1 TeV, which result in highly Lorentz-boosted top quarks and H^0 or Z boson, large-area jets are used to form the T quark. This search reports upper limits at 95% confidence level on $\sigma B(T \to tH)$ and $\sigma B(T \to tZ)$ between 2 pb and 20 fb for T masses between 0.6 to 2.6 TeV in the Tbq and Ttq production channels. The analysis also reports combined results for $T \to tH$ and $T \to tZ$ associated production with a bottom quark and provides constraints on T quarks in the T singlet model for masses below 1.00 TeV. For an expected fractional width of 30%, the expected sensitivity extends to 1.28 TeV, comparable to the most stringent results.

Combination of $T \to bW/tZ/tH^0$:

Most of the analyses described above target an individual decay mode of the T quark, with 100% branching ratio to either bW, tZ or tH^0 and are optimized accordingly. However, they have varied sensitivity to all three decay modes and the results can be interpreted as a function of branching ratios to each of the three decay modes, assuming the total adds up to unity ($\mathcal{B}(tH) + \mathcal{B}(tZ) + \mathcal{B}(Wb) = 1$).

Combinations of analyses have been performed by both ATLAS and CMS. The limits set by ATLAS searches in $W(\ell\nu)b + X, H(bb)b + X, Z(\nu\bar{\nu}), Z(\ell\ell)t/b + X$, dileptons with same-sign charge, trileptons, all-hadronic final states have been combined and the results obtained for various sets of branching fractions for T quark decays to bW, tH^0 and tZ are shown in Fig. 92.3 (left). In the combined analysis, ATLAS sets lower T quarks mass limit of 1.31 TeV for all possible values of the branching fractions to the three decay modes [123, 136, 143]. In Fig. 92.3, exclusion is shown in the plane of $\mathcal{B}(T \to Ht)$ versus $\mathcal{B}(T \to Wb)$, for different values of the T quark mass. The default branching ratio values for the weak-isospin singlet and doublet cases are also shown in Fig. 92.3 as yellow circle and star symbols respectively. Assuming a weak isospin (T,B) doublet and $|V_{Tb}| << |V_{tB}|$, T quark mass below 1.37 TeV is excluded.

A CMS analysis for pair production of T combines three channels with lepton final states: single lepton, two leptons with the same sign of the electric charge (SS), or at least three leptons (trilepton) [144]. For various combinations of branching fractions for T quark decays to bW, tH^0 and tZ, the combined results exclude T quarks with masses below 1.14–1.3 TeV and are shown in Figure 92.3 (right). Single lepton events are classified into 16 signal categories and 6 background control regions based on multiplicity of b-tagged, high p_T H^0 and W-tagged jets. The discriminating variables are H_T for H^0-tagged events and the minimum invariant mass constructed from the lepton and the b jet, $\min[M_{lb}]$, for zero H^0-tagged events. For the same-sign dilepton and trilepton analyses, the non-prompt backgrounds due to misidentified jets and leptons are derived from data control regions. In the trilepton analysis the S_T variable is used as the signal discriminator binned in four categories based on the lepton flavor combinations (eee, $ee\mu$, $e\mu\mu$, $\mu\mu\mu$). The single lepton analysis is most sensitive for $tHbW$ and $WbWb$ decay modes, within the SS dilepton analysis $tHtH$ and $tHtZ$ have the best efficiency and for trileptons the $tZtZ$ and $tHtZ$ decays modes have the highest efficiency. CMS excludes singlet (doublet) T quark masses below 1.2 (1.28) TeV. Masses below 800 GeV were excluded in previous searches. For T quark masses in the range 0.8–1.8 TeV, cross sections smaller than 30.4–9.4 fb (21.2–6.1 fb) are excluded for the singlet (doublet) scenario.

Another inclusive search for pair produced T in the all-hadronic final state [122] has been performed by CMS using the boosted event shape tagger (BEST) neural network technique to classify jets in six categories W, Z, H^0, t, b, and light. This search does not focus on a given VLQ mode, but on various combinations of the boson and quark jets in the final state. Anti-k_T jets with a distance parameter of 0.8 are used. The BEST NN algorithm simultaneously classifies jets according to heavy object type. For each of the six particle hypotheses, it boosts each jet constituent into corresponding frame along the jet momentum direction, and calculates event shape and angular variables in the boosted frame, with the expectation that when boosting to the correct rest frame, jet constituents will be isotropic and show the expected N-prong structure of the decaying object in its rest frame. A neural network is trained using the event shape and angular variables in the boosted frame to classify jets according to one of those six possibilities (W, Z, H, t, b, or light). The analysis bins the events into 126 categories depending on the number of W, Z, H, t, b, or light jets in the final state with a maximum of four such objects. For

Downloaded from https://academic.oup.com/ptep/article/2022/8/083C01/6651666 by KIT Library user on 27 September 2022

each category H_T^{AK8}, the scalar sum of p_T of all AK8 jets, is used as the signal discriminator. A scan over a combination of various branching fractions is also performed. This search excludes T quark masses in the range 0.74–1.37 TeV for the tH decay mode in the NN analysis.

An inclusive search for VLQs has been carried out by CMS targeted at heavy T quarks decaying to any combination of bW, tZ, or tH^0 as described in [130]. Selected events have at least one isolated charged lepton. Events were categorized according to number and flavor of the leptons, the number of jets, and the presence of hadronic vector boson and top quark decays that are merged into a single jet. The use of jet substructure to identify hadronic decays significantly increases the acceptance for high T quark masses. No excess above standard model backgrounds was observed. Limits on the pair production cross section of the new quarks are set, combining all event categories, for all combinations of branching fractions into the three final states. For T quarks that exclusively decay to $bW/tZ/tH^0$, masses below 0.70/0.78/0.71 TeV are excluded.

92.2.3.2 *Searches for* $\boldsymbol{B}$ *quarks that decay to* $\boldsymbol{W}$, $\boldsymbol{Z}$ *and* $\boldsymbol{H^0}$ *bosons*

ATLAS and CMS have performed searches for pair production of heavy B quarks which subsequently decay to Wt, bZ or bH^0. The searches have been carried out in final states with single leptons, dileptons (with same charge or opposite charge), multileptons, as well as in fully hadronic final states.

$B \to bH^0$:

A search for B pair-produced events has been performed by the CMS experiment [123] using 137 fb^{-1} of data where the B decays into a $b/\bar{b}$ quark and either a H^0 or a Z boson. This search concentrates on final states with fully hadronic signatures, and utilizes different jet multiplicity categories to account for two resolved jets or merged single jets from H^0 or Z boson to $b\bar{b}$ decays, depending on the p_T of the H^0 or Z bosons. Nine final state categories are used, depending on the number of observed jets and the reconstructed event mode. No significant excess over expected background is observed. For the case $\mathcal{B}(B \to bH) = 100\%(50\%)$, VLQs with masses below 1.57 (1.45) TeV are ruled out.

Using 36.1 fb^{-1} of data, ATLAS has performed a search for pair produced VLQs with all-hadronic final state signature [129]. While this analysis provides exclusion limits for all third generation VLQs, it provides the strongest results for the $B \to bH^0$ decay mode and excludes decays with $\mathcal{B}(\mathcal{B} \to \lfloor\mathcal{H}') = \infty.\prime$ scenario for B masses upto 1.01 TeV. The limits are also cast in a two-dimensional plane of branching ratio values of $B \to bH^0$ vs. $B \to Wb$. This analysis required the presence of high p_T jets and multiple b tags. It used a multi-class DNN to classify jets arising from W, Z, H^0 bosons and top-quarks. In addition, the matrix element method was used to compute the likelihood for the event to arise from a particular VLQ final state and to construct the final discriminator. To increase the sensitivity of the analysis, processes with the same number of top quarks, W/Z bosons, and H^0 Higgs bosons are combined into a single hypothesis.

The ATLAS experiment has performed a search for single production of a vector-like B quark decaying to a b-quark and a H^0 boson, with $H^0 \to b\bar{b}$ decay, using a dataset corresponding to an integrated luminosity of 139 fb^{-1} [145]. The all hadronic final state signature relies on identification of at least 3 b-jets, with an additional soft forward jet from the spectator quark. Large area jets are used to identify boosted H^0 decays. This analysis results in excluding the single production of a VLQ (B, Y) doublet with relative width larger than 5% between masses of 1.0 TeV and 1.76 TeV [145].

$B \to Wt$:

A search for $B \to tW$ in B pair produced events has been performed by the ATLAS experiment [123] using lepton+jets events with one hadronically decaying W and one leptonically decaying W utilizing 36.1 fb^{-1} of data at $\sqrt{s} = 13$ TeV. The search was optimized for T production decaying into Wb. Since the analysis was optimized for $T \to Wb$ rather than Wt decays the analysis does not reconstruct the full B mass. As discussed earlier, the hadronically and leptonically decaying heavy quarks were required to have similar reconstructed masses (within 300 GeV). The interpretation of the $T \to Wb$ in the context of $B \to tW$ production led to the exclusion of heavy B like VLQs for masses less than 1.25 TeV and 1.08 TeV, assuming a 100% branching fraction to tW or SU(2) singlet B scenario, respectively.

A similar search by CMS [146], using 19.8 fb^{-1} of $\sqrt{s} = 8$ TeV data, selected events with one lepton and four or more jets, with at least one b-tagged jet, significant missing p_T, and further categorized them based on the number of jets tagged as arising from the decay of boosted W, Z or H^0 bosons. The S_T distributions of the events in different categories showed no excess of events above the expected background and yielded a lower limit on the B quark mass of 0.73 TeV for $BR(B \to Wt) = 1$.

CMS [132] also searched for pair production of both TT and BB with collisions from 2.5 fb^{-1} of $\sqrt{s} = 13$ TeV data. The analysis searches for events with one high p_T lepton , multiple jets, and highly boosted W or Higgs bosons decaying hadronically. The analysis focuses on pair production and selects events with either a boosted W or Higgs candidate and then proceeds to search for anomalous production in excess of standard model production. Seeing no significant excesses CMS then proceeded to set limits in many different interpretations. The strongest was from the $B \to Wt$ interpretation leading to excluding heavy vector-like B quarks with mass less than 0.73 TeV.

The all-hadronic inclusive analysis [122] performed by CMS using the BEST NN technique to classify $W/Z/H^0/t/b$/light jets also gives exclusion limits on B quark production for various combinations of branching fractions for decays to tW, bZ, bH^0. By considering categories based on various combinations of the boson and quark jets in the final state it excludes B quarks with masses up to 1230 GeV, for B decays to tW with a 100% branching fraction.

Electroweak production of single heavy B+b production has been studied by CMS in the decay to tW with the lepton+jets final state [147]. Single lepton events with hadronic jets, including a forward jet, and missing p_T are selected and divided into 10 different categories based on lepton flavor (e/μ), top-tagged, W-tagged, and 0/1/2 b-tagged jets. The B quark mass m_{reco} is fully reconstructed from lepton, jets, and missing p_T, where the neutrino four-momentum is computed using the missing p_T and the W mass constraint. For events within the top-tagged category, the high p_T top-tagged hadronic jet and the leptonically decaying W boson are used to compute m_{reco}. The m_{reco} distribution are used as the signal discriminator. In the absence of an excess over the expected SM background, the exclusion limits on the production cross section for B quark masses between 0.7-2 TeV varies between 0.3 to 0.03 pb. In addition, B quarks with left-handed couplings and a relative width of 10, 20, and 30% are excluded for masses below 1.49, 1.59, and 1.66 TeV respectively.

$B \to bZ$:

As mentioned above, a search for B pair produced events, with final states with fully hadronic signature, using 137 fb^{-1} of data, has been performed by the CMS experiment [123]. In this search, the B decays into a $b/\bar{b}$ quark and either a H^0 or a Z boson. For the case $\mathcal{B}(B \to bZ) = 100\%(50\%)$, VLQs with masses below 1.39 (1.45) TeV are ruled out by this analysis.

A search by CMS [148] for the pair-production of a heavy B quark and its antiparticle has been performed, where one of the heavy B quark decays to bZ. Events with a Z boson decaying to e^+e^- or $\mu^+\mu^-$ and at least one b jet are selected. The signal from $B \to bZ$ decays is expected to appear as a local enhancement in the bZ mass distribution. No such enhancement was found and B quarks that decay 100% into bZ are excluded below 0.70 TeV. This analysis also set upper limits on the branching fraction for $B \to bZ$ decays of 30-100% in the B quark mass range 0.45-0.70 TeV. A complementary search has been carried out by ATLAS for new heavy quarks decaying into a Z boson and a b-quark [149]. Selected dilepton events contain a high transverse momentum Z boson that decays leptonically, together with two b-jets. If the dilepton events have an extra lepton in addition to those from the Z boson, then only one b-jet is required. No significant excess of events above the standard model expectation

Downloaded from https://academic.oup.com/ptep/article/2022/8/083C01/6651666 by KIT Library user on 27 September 2022

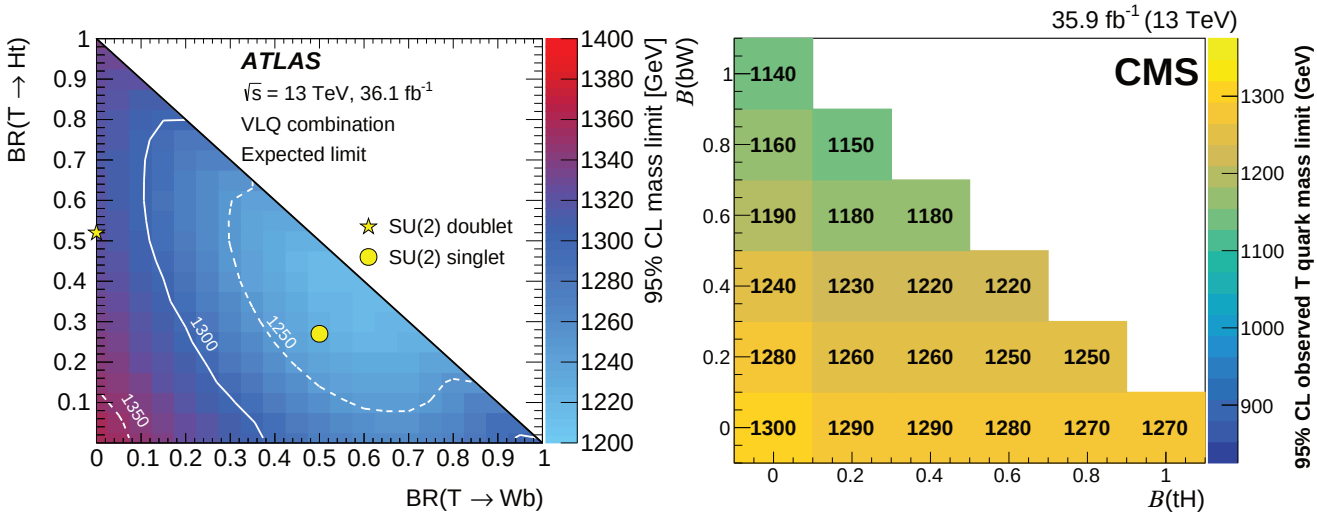

Figure 92.3: Left panel: observed limits on the mass of the T quark in the plane of $\mathcal{B}(T \to tH^0)$ versus $\mathcal{B}(T \to bW)$ from a combination [143] of all ATLAS searches for TT production. The markers indicate the default branching ratios for the SU(2) singlet and doublet scenarios. Right panel: the observed lower limits on the T quark mass (in GeV), from CMS searches after combining all lepton channels [144], for various branching fraction scenarios. $\mathcal{B}(T \to Wb) + \mathcal{B}(T \to tZ) + \mathcal{B}(T \to tH^0) = 1$ is assumed.

was observed, and mass limits were set depending on the assumed branching ratios, as shown in Fig. 92.4. In a weak-isospin singlet scenario, a B quark with mass lower than 0.65 TeV was excluded, while for a particular weak-isospin doublet scenario, a B quark with mass lower than 0.73 TeV was ruled out.

The search by the ATLAS experiment for $B \to bZ$ decays [140] in final states with either two leptons or three or more leptons using a multi-class boosted object tagger to categorize events according to the number of high p_T boosted H^0, Z/W, and top quark jets excludes B quark masses up to 1.20 GeV (1.32 GeV), for the singlet (doublet) configuration [140].

In addition to pair production, ATLAS has also searched for the electroweak production of single B quarks, which is accompanied by a b-jet and a light jet [149]. The dilepton selection for double B production was modified for the single B production study by requiring the presence of an additional energetic jet in the forward region. An upper limit of 200 fb was obtained for the process $\sigma(pp \to B\bar{b}q) \times B(B \to Zb)$ with a heavy B quark mass at 0.70 TeV. This search indicated that the electroweak mixing parameter X_{Bb} below 0.5 is neither expected nor observed to be excluded for any values of B quark mass.

Combination of $B \to tW/bZ/bH^0$:

The ATLAS experiment has combined the various analyses targeted for specific decay modes to obtain the most sensitive limit on the pair production of B quarks [123, 124, 143]. Various searches ($W(\ell\nu)t + X, Z(\ell\ell)t/b + X$, same sign charge dilepton events, trilepton events, and all-hadronic) are combined to obtain lower limit on the mass of the B quark [in the plane of $BR(B \to Wt)$ vs $BR(B \to bH)$]. The searches were optimized for 100% branching fractions and hence are most sensitive at large $BR(B \to Wt)$, and also at large $BR(B \to bH^0)$. For all possible values of branching ratios in the three decay modes tW, bZ, or bH^0, the lower limits on the B quark mass was found to be 1.03 TeV and shown in Fig. 92.4 (left) as a function of the B quark branching ratios.

CMS combined three channels with lepton final states: single lepton, two leptons with the same sign of the electric charge (SS), or at least three leptons (trilepton) [144]. For various combinations of branching fractions for B quark decays to tW, bH^0 and bZ, the combined results exclude b quarks with masses below 0.91–1.24 TeV and are shown in Figure 92.4 (right); the details are provided earlier in subsection 92.2.3.1. The single lepton analysis is most sensitive for $tHbW$ and $WbWb$ decay modes, within the SS dilepton analysis $tHtH$ and $tHtZ$ have the best efficiency and for trileptons the $tZtZ$ and $tHtZ$ decays modes have the highest efficiency. CMS excludes singlet (doublet) B quark masses below 1.17 (0.94) TeV. Masses below 800 GeV were excluded in previous searches. For B quark masses in the range 0.8–1.8 TeV, cross sections smaller than 40.6-–9.4 fb (101-–49.0 fb) are excluded for the singlet (doublet) scenario.

92.2.3.3 *Searches for top-partner quark* $\mathbf{X_{5/3}}$

Searches for a heavy top vector-like quark $X_{5/3}$, with exotic charge $\pm 5/3$, such as that proposed in Refs. [151, 152], have been performed by both ATLAS and CMS [123, 153].

The analyses assumed pair-production or single production of $X_{5/3}$ with $X_{5/3}$ decaying with 100% branching fraction to tW. Searches for $X_{5/3}$ have been performed using two final state signatures: same-sign leptons and lepton+jets.

The analysis based on searching for same-sign leptons, from the two W bosons from one of the $X_{5/3}$, has smaller backgrounds compared to the lepton+jets signature. Requiring same-sign leptons eliminates most of the standard model background processes, leaving those with smaller cross sections: $t\bar{t}W$, $t\bar{t}Z$, WWW, and same-sign WW. In addition, backgrounds from instrumental effects due to charge misidentification were considered. Assuming pair production of $X_{5/3}$, the analysis by CMS using H_T as the discriminating variable restrict the $X_{5/3}$ mass to be higher than 1.16 (1.10) TeV for a right (left) handed chirality particle [153–155]. The limits obtained by ATLAS, by classifying the signal region by number of b-jets, H_T, and missing p_T in the event, led to a lower mass limit on $X_{5/3}$ of 1.19 TeV [156, 157].

Searches for $X_{5/3}$ using leptons+jets final state signatures are based on either full or partial reconstruction of the T mass from the lepton, jets (including b-jets) and missing p_T. The CMS search [153, 158] also utilized jet substructure techniques to identify boosted $X_{5/3}$ topologies. The discriminating variable used was the mass constructed from the lepton and b-tagged jet, $M_{(\ell,b)}$, which corresponds to the visible mass of the leptonically decaying top quark. To optimize the search sensitivity, the events were further separated into categories based on lepton flavor (e, μ), the number of b-tagged jets, the number of W-tagged jets, and the number of t-tagged jets. In the absence of a signal, the CMS analysis excluded $X_{5/3}$ quark masses with right-handed (left-handed) couplings below 1.32 (1.30) TeV [158]. Combining the lepton+jets with the same-sign leptons analyses leads to a slight improvement and excludes $X_{5/3}$ quark masses with right-handed (left-handed) couplings below 1.33 (1.30) TeV.

The ATLAS lepton+jets search for $X_{5/3}$ utilized events with high p_T W bosons and b-jets. The search described earlier for T pair production, with $T \to Wb$ decays, can be reinterpreted as a search for $X \to tW$. This analysis excluded $X_{5/3}$ with masses below 1.25 TeV [123].

The single $X_{5/3}$ production cross section depends on the cou-

Downloaded from https://academic.oup.com/ptep/article/2022/8/083C01/6651666 by KIT Library user on 27 September 2022

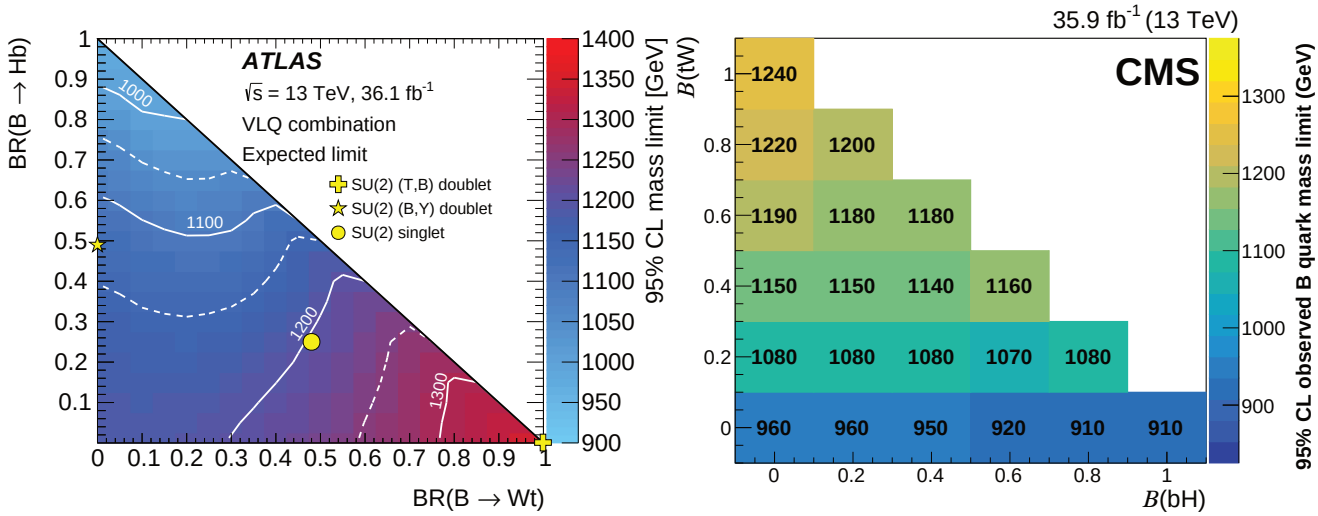

Figure 92.4: Observed limits on the mass of the B quark in the plane of $BR(B \to bH^0)$ versus $BR(B \to tW)$ from ATLAS searches [143] on the left panel, and CMS searches [144] on the right panel, for BB production. $\mathcal{B}(\mathcal{B} \to \mathcal{H}\lfloor) + \mathcal{B}(\mathcal{B} \to \lfloor\mathcal{Z}) + \mathcal{B}(\mathcal{B} \to \mathcal{W}\sqcup) = 1$ is assumed. The yellow markers indicate the branching ratios for the SU(2) singlet and doublet scenarios.

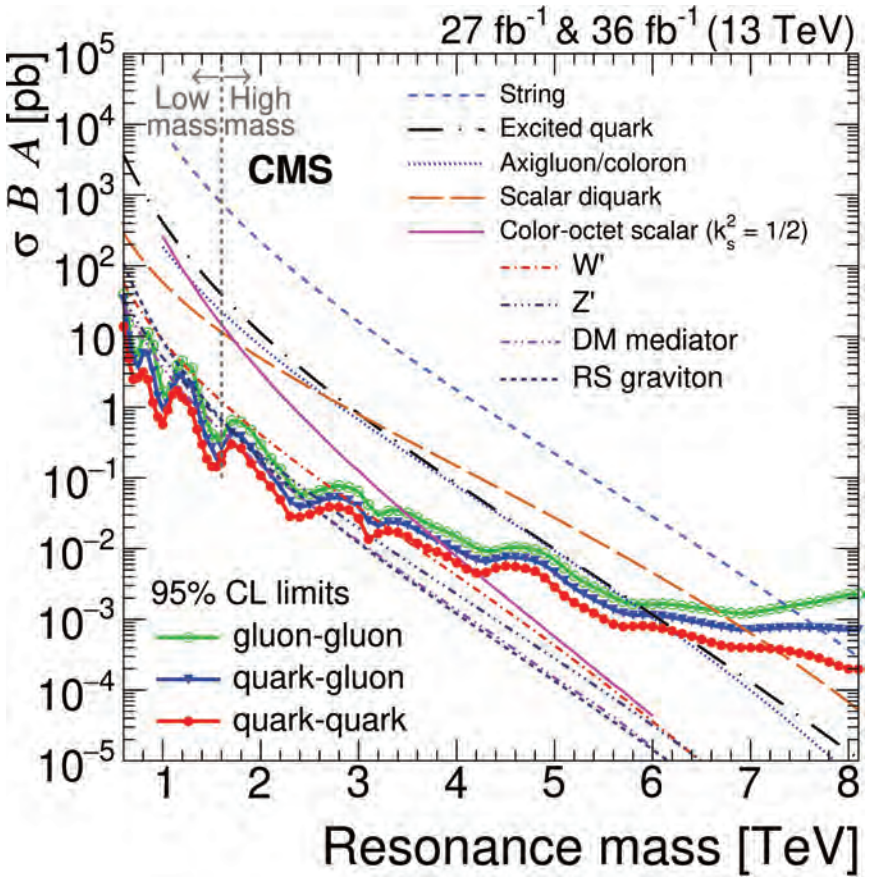

Figure 92.5: Observed 95% C.L. limits on $\sigma \times B \times A$ for string resonances, excited quarks, axigluons, colorons, E6 diquarks, s8 resonances, W' and Z' bosons, and Randall–Sundrum Gravitons g_{KK} from [150].

pling constant λ of the tWX vertex. ATLAS has performed an analysis of same-sign dileptons which includes both the single and pair production. This analysis led to a lower limit on the mass of the $X_{5/3}$ of 0.75 TeV for both values of $\lambda = 0.5$ and 1.0 [159].

Single heavy $X_{5/3}$+t production has been studied by CMS in the decay to tW with the lepton+jets final state [147]. The description of the analysis is provided earlier in the discussion of $B \to WtX$ decays, where the reconstructed mass of $X_{5/3}$, m_{reco} distribution is used as the signal discriminator. In the absence of an excess over the expected SM background, the exclusion limits on the production cross section for $X_{5/3}$ quark masses between 0.7–2 TeV varies between 0.3 to 0.03 pb, depending on the width of $X_{5/3}$ between 1–10%. In addition, $X_{5/3}$ quarks with left-handed couplings and a relative width of 10, 20, and 30% are excluded for masses below 0.92, 1.3, and 1.45 TeV respectively.

Downloaded from https://academic.oup.com/ptep/article/2022/8/083C01/6651666 by KIT Library user on 27 September 2022

92.2.4 *Heavy resonances decaying to VLQ*

CMS has performed search for VLQ production in the decay of massive resonances such as Z' and W' bosons.

$Z' \to tT$: Specifically searches are presented by CMS in Refs. [160] and [161] for massive spin-1 Z' resonances decaying to a top quark and a heavy VLQ top quark partner T. The results of this search for a heavy spin-1 resonance are interpreted in the context of two different models. In the $G^\star$ model which predicts ten VLQs (T, $B, \tilde{T}, \tilde{B}, T_{5/3}, T_{2/3}, T', B', B_{-1/3}, B_{-4/3}$) with the mass relationship $M(T_{5/3}) = M(T_{2/3}) = M(T)\cos(\phi_L)$. For the benchmark scenario [162], $\cos(\phi_L)$=0.84 and the branching fractions $T \to tH^0, tZ, Wb$ are 0.25, 0.25 and 0.5 respectively. The ρ^0 model predicts a multiplet of four new VLQs $T, B, X_{2/3}, X_{5/3}$, and in the benchmark scenario [163], the branching fractions $T \to tH^0, tZ, Wb$ are 0.5, 0.5 and 0 respectively.

Two of the three decays of the $Z' \to tT$ with $T \to tH^0, tZ, Wb$ are characterized by the presence of two top quark decays and a boson (H^0/Z). A search [161] by CMS, optimized for $T \to tH/Zt$ decays was carried out in the lepton+jets final state using a dataset corresponding to an integrated luminosity of 35.9 fb^{-1}. Jet substructure techniques are used to identify (or tag) the high p_T large-radius jets originating from H^0, Z bosons and merged top quarks. The mass of the Z' boson is used as the signal discriminator and constructed using H^0 or Z-tagged dijet, the hadronic and leptonic top quark four vectors. For the leptonic top quark reconstruction ($t \to b\ell\nu_\ell$), the neutrino four vector is obtained from the event missing p_T using the W boson mass constraint. While the high p_T hadronic top quark jets from decays of massive Z' bosons are mostly merged and identified by top tagging techniques, those from T decays maybe resolved. The reconstructed Z' candidate events are classified into six different categories requiring the presence of either a H^0-tagged jet with 2 b-tagged subjets or one b-tagged subjet or a Z-tagged boson, each with either zero or one top-tagged jet. This search does not observe any significant deviation in data over the expectation from standard model backgrounds. Within the context of the $G^\star$ model, for a T mass of 1.2 (1.5) TeV, this search excludes $G^\star$ [162] resonances with masses between 1.5–2.3 (2.0–2.4) TeV.

The search in the all-hadronic final state is based on a 2.6 fb^{-1} dataset [160], and optimized for $T \to Wb$ decays. Jet substructure techniques are deployed for tagging jets from high p_T W boson and top quarks. Events are categorized into two groups based on the presence of b-tagged subjets in the top-tagged jet. The multijet background estimation is challenging and determined using side-bands defined by inverting the b-tagging requirement. Upper limits on the cross section for $Z' \to tT$ are obtained in the range of 0.13–10 pb.

$W' \to Tb/Bt$: W' bosons are predicted to decay to VLQ third generation partners T, B quarks within composite Higgs and warped extra dimensional models [164]. In the benchmark scenarios of this framework, W' decays to Tb or Bt are equally distributed and the subsequent VLQ decays $T \to tH$ and $B \to bH^0$ each are assumed to have a branching fraction of 0.5. The search for $W' \to Tb/bH^0 \to tbH^0$ is performed using a sample of 35.9 fb^{-1} by CMS [165] in the final state with all-hadronic decays of both the Higgs boson ($H^0 \to b\bar{b}$) and the top quark. Both the H^0 boson and the top quark are expected to be boosted in the decay of a heavy W', and hence jet substructure techniques, including subjet b-tagging and double b-tagging are deployed to identify the H^0-tagged and the top-tagged jets. The three particle mass m_{tbH^0}, is used as the signal discriminant to observe the W' resonance. There is no excess observed in data above the expected SM background. This search excludes W' production cross section above 0.01–0.43 pb for masses between 1.5–4.0 TeV.

92.2.5 *Colorons and Colored Scalars*

These particles are associated with top-condensate and top-seesaw models, which involve an enlarged color gauge group. The new particles decay to dijets, $t\bar{t}$, and $b\bar{b}$.

Direct searches for colorons, color-octect scalars and other heavy objects decaying to $q\bar{q}$, qg, qq, or gg have been performed using LHC data from pp collisions at $\sqrt{s}$ =7, 8 and 13 TeV. Based on the analysis of dijet events from a data sample corresponding to a luminosity of 19.6 fb^{-1}, at $\sqrt{s} = 8$ TeV, the CMS experiment excluded pair production of colorons with mass between 1.20−3.60 and 3.90 − 4.08 TeV [166]. Analyses of inclusive 8- and 10-jet final states with low missing transverse momentum by CMS [167], set limits in several benchmark models. Colorons (axigluons) with masses between 0.6 and 0.75 (up to 1.15) TeV were excluded, and gluinos in R-parity violating supersymmetric scenarios were ruled out from 0.6 up to 1.1 TeV.

A search for pair-produced colorons based on an integrated luminosity of 5.0 fb^{-1} at $\sqrt{s} = 7$ TeV by CMS excluded colorons with masses between 0.25 TeV and 0.74 TeV, assuming colorons decay 100% into $q\bar{q}$ [168]. This analysis was based on events with at least four jets and two dijet combinations with similar dijet mass. Color-octet scalars (s8) with masses between 1.20−2.79 TeV were excluded by CMS [166], and below 2.7 TeV by ATLAS [169].

These studies have now been extended to take advantage of the increased center-of-mass energy during Run 2 of the LHC. Using 35.9 fb^{-1} of data collected at $\sqrt{s}$ =13 TeV, searches for narrow resonances have been performed by CMS. An analysis of the dijet invariant mass spectrum formed using wide jets [150, 170, 171], separated by $\Delta\eta_{jj} \leq 1.3$, led to limits on new particles decaying to parton pairs (qq, qg, gg). Specific exclusions on the masses of colorons and color-octet scalars were obtained and are shown in Fig. 92.5. Exclusions have been obtained for axigluons and colorons below 6.1 TeV, and color-octet scalars below 3.4 TeV.

Additional searches for dijet resonances have been performed by both ATLAS [172–174] and CMS [175, 176], though they have not been interpreted in the context of coloron production.

92.3 Conclusions

As the above analyses have demonstrated, there is already substantial sensitivity to possible new particles predicted to accompany the H^0 in dynamical frameworks of electroweak symmetry breaking. No significant hints of any deviations from the standard model have been observed, and limits typically at the scale of a few hundred GeV to a few TeV are set.

Given the need to better understand the H^0 and to determine in detail how it behaves, such analyses continue to be a major theme of Run 3 of the LHC, and we look forward to increased sensitivity as a result of the higher luminosity at the increased center of mass energy of collisions.

References

[1] G. Aad *et al.* (ATLAS), Phys. Lett. **B716**, 1 (2012), [arXiv:1207.7214].

[2] S. Chatrchyan *et al.* (CMS), Phys. Lett. **B716**, 30 (2012), [arXiv:1207.7235].

[3] S. Weinberg, Physica **A96**, 1-2, 327 (1979).

[4] A. Manohar and H. Georgi, Nucl. Phys. **B234**, 189 (1984).

[5] H. Georgi, Nucl. Phys. **B266**, 274 (1986).

[6] R. S. Chivukula, in "Flavor physics for the millennium. Proceedings, Theoretical Advanced Study Institute in elementary particle physics, TASI 2000, Boulder, USA, June 4-30, 2000," 731–772 (2000), [hep-ph/0011264].

[7] R. S. Chivukula, M. J. Dugan and M. Golden, Phys. Rev. **D47**, 2930 (1993), [hep-ph/9206222].

[8] S. Weinberg, Phys. Rev. **D13**, 974 (1976), [Addendum: Phys. Rev.D19,1277(1979)].

[9] L. Susskind, Phys. Rev. **D20**, 2619 (1979).

[10] K. Lane (2002), [hep-ph/0202255].

[11] C. T. Hill and E. H. Simmons, Phys. Rept. **381**, 235 (2003), [Erratum: Phys. Rept.390,553(2004)], [hep-ph/0203079].

[12] R. Shrock, in "The origin of mass and strong coupling gauge theories. Proceedings, 5th International Workshop, SCGT'06, Nagoya, Japan November 21-24, 2006," 227–241 (2007), [hep-ph/0703050].

[13] E. Eichten *et al.*, Rev. Mod. Phys. **56**, 579 (1984), [Addendum: Rev. Mod. Phys.58,1065(1986)].

[14] E. Eichten *et al.*, Phys. Rev. **D34**, 1547 (1986).

Downloaded from https://academic.oup.com/ptep/article/2022/8/083C01/6651666 by KIT Library user on 27 September 2022

[15] R. S. Chivukula and V. Koulovassilopoulos, Phys. Lett. **B309**, 371 (1993), [hep-ph/9304293].

[16] R. Foadi, M. T. Frandsen and F. Sannino, Phys. Rev. **D87**, 9, 095001 (2013), [arXiv:1211.1083].

[17] B. Holdom, Phys. Lett. **150B**, 301 (1985).

[18] K. Yamawaki, M. Bando, and K.-i. Matumoto, Phys. Rev. Lett. **56**, 1335 (1986).

[19] T. W. Appelquist, D. Karabali and L. C. R. Wijewardhana, Phys. Rev. Lett. **57**, 957 (1986).

[20] T. Appelquist and L. C. R. Wijewardhana, Phys. Rev. **D35**, 774 (1987).

[21] T. Appelquist and L. C. R. Wijewardhana, Phys. Rev. **D36**, 568 (1987).

[22] E. Eichten, K. Lane and A. Martin (2012), [arXiv:1210.5462].

[23] D. B. Kaplan and H. Georgi, Phys. Lett. **136B**, 183 (1984).

[24] D. B. Kaplan, H. Georgi and S. Dimopoulos, Phys. Lett. **136B**, 187 (1984).

[25] G. Ferretti and D. Karateev, JHEP **03**, 077 (2014), [arXiv:1312.5330].

[26] M. E. Peskin, Nucl. Phys. **B175**, 197 (1980).

[27] J. Preskill, Nucl. Phys. **B177**, 21 (1981).

[28] See "Status of Higgs Boson Physics" review in this volume.

[29] R. Barbieri and A. Strumia, in "4th Rencontres du Vietnam: Physics at Extreme Energies (Particle Physics and Astrophysics) Hanoi, Vietnam, July 19-25, 2000," (2000), [hep-ph/0007265].

[30] N. Arkani-Hamed, A. G. Cohen and H. Georgi, Phys. Lett. **B513**, 232 (2001), [hep-ph/0105239].

[31] N. Arkani-Hamed *et al.*, JHEP **08**, 020 (2002), [hep-ph/0202089].

[32] N. Arkani-Hamed *et al.*, JHEP **07**, 034 (2002), [hep-ph/0206021].

[33] M. Schmaltz and D. Tucker-Smith, Ann. Rev. Nucl. Part. Sci. **55**, 229 (2005), [hep-ph/0502182].

[34] K. Agashe *et al.*, Phys. Lett. **B641**, 62 (2006), [hep-ph/0605341].

[35] P. Sikivie *et al.*, Nucl. Phys. **B173**, 189 (1980).

[36] B. Bellazzini, C. Csáki and J. Serra, Eur. Phys. J. **C74**, 5, 2766 (2014), [arXiv:1401.2457].

[37] R. Essig *et al.*, JHEP **09**, 085 (2017), [arXiv:1707.03399].

[38] Z. Chacko, H.-S. Goh and R. Harnik, Phys. Rev. Lett. **96**, 231802 (2006), [hep-ph/0506256].

[39] R. S. Chivukula, A. G. Cohen and K. D. Lane, Nucl. Phys. **B343**, 554 (1990).

[40] V. A. Miransky, M. Tanabashi and K. Yamawaki, Mod. Phys. Lett. **A4**, 1043 (1989).

[41] W. A. Bardeen, C. T. Hill and M. Lindner, Phys. Rev. **D41**, 1647 (1990).

[42] C. T. Hill, Phys. Lett. **B266**, 419 (1991).

[43] B. A. Dobrescu and C. T. Hill, Phys. Rev. Lett. **81**, 2634 (1998), [hep-ph/9712319].

[44] R. S. Chivukula *et al.*, Phys. Rev. **D59**, 075003 (1999), [hep-ph/9809470].

[45] S. Dimopoulos and L. Susskind, Nucl. Phys. **B155**, 237 (1979), [2,930(1979)].

[46] E. Eichten and K. D. Lane, Phys. Lett. **90B**, 125 (1980).

[47] D. B. Kaplan, Nucl. Phys. **B365**, 259 (1991).

[48] T. Appelquist, M. Piai and R. Shrock, Phys. Rev. **D69**, 015002 (2004), [hep-ph/0308061].

[49] R.S. Chivukula, B.A. Dobrescu, and E.H. Simmons, Phys. Lett. **B401**, 74 (1997).

[50] Y. Grossman and M. Neubert, Phys. Lett. **B474**, 361 (2000), [hep-ph/9912408].

[51] S. J. Huber and Q. Shafi, Phys. Lett. **B498**, 256 (2001), [hep-ph/0010195].

[52] T. Gherghetta and A. Pomarol, Nucl. Phys. **B586**, 141 (2000), [hep-ph/0003129].

[53] K. Agashe, R. Contino and A. Pomarol, Nucl. Phys. **B719**, 165 (2005), [hep-ph/0412089].

[54] G. F. Giudice *et al.*, JHEP **06**, 045 (2007), [hep-ph/0703164].

[55] R. S. Chivukula and H. Georgi, Phys. Lett. **B188**, 99 (1987).

[56] G. D'Ambrosio *et al.*, Nucl. Phys. **B645**, 155 (2002), [hep-ph/0207036].

[57] K. Agashe *et al.* (2005), [hep-ph/0509117].

[58] T. Appelquist and R. Shrock, Phys. Lett. **B548**, 204 (2002), [hep-ph/0204141].

[59] K. Sakai, Nucl. Phys. **B867**, 429 (2013), [arXiv:1207.4057].

[60] J. M. Maldacena, Int. J. Theor. Phys. **38**, 1113 (1999), [Adv. Theor. Math. Phys.2,231(1998)], [hep-th/9711200].

[61] For a review, see C. Csaki, J. Hubisz, and P. Meade, `hep-ph/0510275` (2005), and "Extra Dimensions" review in this volume.

[62] C. Pica, PoS **LATTICE2016**, 015 (2016), [arXiv:1701.07782].

[63] B. Svetitsky, EPJ Web Conf. **175**, 01017 (2018), [arXiv:1708.04840].

[64] O. Witzel, PoS **LATTICE2018**, 006 (2019), [arXiv:1901.08216].

[65] V. Drach, PoS **LATTICE2019**, 242 (2020), [arXiv:2005.01002].

[66] T. Appelquist *et al.*, Phys. Rev. **D93**, 11, 114514 (2016), [arXiv:1601.04027].

[67] PDG review on "Z'-Boson Searches" in this volume.

[68] PDG review on "W'-Boson Searches" in this volume.

[69] M. Aaboud *et al.* (ATLAS), Phys. Lett. **B**, 68 (2019), [arXiv:1903.06248].

[70] CMS Collaboration, Technical Report CMS-PAS-EXO-19-019, CERN, Geneva (2019), URL `http://cds.cern.ch/record/2684757`.

[71] G. Aad *et al.* (ATLAS), Phys. Rev. **D90**, 5, 052005 (2014), [arXiv:1405.4123].

[72] M. Aaboud *et al.* (ATLAS), JHEP **01**, 055 (2018), [arXiv:1709.07242].

[73] CMS Collaboration, JHEP **0217**, 48 (2017).

[74] ATLAS Collaboration, ATLAS-CONF-2016-014 (2016).

[75] CMS Collaboration, JHEP **0717**, 001 (2016).

[76] M. Aaboud *et al.* (ATLAS), Phys. Rev. D. **99**, 092004 (2019), [arXiv:1902.10077].

[77] A. M. Sirunyan *et al.* (CMS), JHEP **04**, 031 (2019), [arXiv:1810.05905].

[78] ATLAS Collaboration, ATLAS-CONF-2019-007 (2019).

[79] CMS Collaboration, CMS-PAS-EXO-19-012 (2019).

[80] M. Aaboud *et al.* (ATLAS), Accepted by Phys. Rev. [arXiv:1906.05609].

[81] V. Khachatryan *et al.* (CMS), Phys. Lett. **B770**, 278 (2017), [arXiv:1612.09274].

[82] V. Khachatryan *et al.* (CMS), Phys. Lett. **B755**, 196 (2016), [arXiv:1508.04308].

[83] S. Chatrchyan *et al.* (CMS), JHEP **05**, 108 (2014), [arXiv:1402.2176].

[84] V. Khachatryan *et al.* (CMS), JHEP **02**, 122 (2016), [arXiv:1509.06051].

Downloaded from https://academic.oup.com/ptep/article/2022/8/083C01/6651666 by KIT Library user on 27 September 2022

[85] A. M. Sirunyan *et al.* (CMS), JHEP **08**, 029 (2017), [arXiv:1706.04260].

[86] A. M. Sirunyan *et al.* (CMS), Phys. Lett. **B777**, 39 (2018), [arXiv:1708.08539].

[87] A. M. Sirunyan *et al.* (CMS), Phys. Lett. B **820**, 136535 (2021), [arXiv:2104.04831].

[88] CMS Collaboration, Technical Report CMS-PAS-JME-15-002, CERN, Geneva (2016), URL `http://cds.cern.ch/record/2126325`.

[89] G. Aad *et al.* (ATLAS), Phys. Lett. **B788**, 347 (2019), [arXiv:1807.10473].

[90] G. Aad *et al.* (ATLAS), Eur. Phys. J. **C75**, 4, 165 (2015), [arXiv:1408.0886].

[91] G. Aad *et al.* (ATLAS), Phys. Lett. **B743**, 235 (2015), [arXiv:1410.4103].

[92] D. Pappadopulo *et al.*, JHEP **09**, 060 (2014), [arXiv:1402.4431].

[93] M. Aaboud *et al.* (ATLAS), Phys. Rev. **D98**, 5, 052008 (2018), [arXiv:1601.04027].

[94] A. M. Sirunyan *et al.* (CMS), Phys. Lett. **B798**, 134952 (2019), [arXiv:1906.00057].

[95] M. Aaboud *et al.* (ATLAS), Phys. Lett. **B**, 91 (2017), [arXiv:1708.04445].

[96] M. Aaboud *et al.* (ATLAS), JHEP **03**, 042 (2018), [arXiv:1710.07235].

[97] M. Aaboud *et al.* (ATLAS), Phys. Lett. **B**, 68 (2018), [arXiv:1806.10532].

[98] A. M. Sirunyan *et al.* (CMS), Phys. Rev. **D97**, 072006, [arXiv:1708.05379].

[99] A. M. Sirunyan *et al.* (CMS), JHEP **07**, 075, [arXiv:1802.09407].

[100] A. M. Sirunyan *et al.* (CMS), JHEP **09**, 101, [arXiv:1803.10093].

[101] M. Aaboud *et al.* (ATLAS), Eur. Phys. J. **C**, 78 (2017), [arXiv:1710.01123].

[102] M. Aaboud *et al.* (ATLAS), Phys. Lett. **B**, 774 (2017), [arXiv:1707.06858].

[103] M. Aaboud *et al.* (ATLAS), JHEP **B**, 174 (2018), [arXiv:1712.06518].

[104] A. M. Sirunyan *et al.* (CMS), Eur. Phys. J. **C**, 636, [arXiv:1707.01303.].

[105] CMS Collaboration (CMS), Technical Report CMS-PAS-B2G-20-007 (2021).

[106] CMS Collaboration (CMS), Technical Report CMS-PAS-B2G-20-004 (2021).

[107] Eur. Phys. J. C **74**, 704 (2017).

[108] A. Collaboration, PRL **125**, 251802 (2020).

[109] A. Collaboration, Physics Letters B **779**, 24 (2018).

[110] C. Collaboration (2021), [arXiv:2106.10509].

[111] CMS Collaboration (CMS), Technical Report CMS-PAS-B2G-20-001 (2021).

[112] CMS Collaboration (CMS), Technical Report CMS-PAS-B2G-20-002 (2021).

[113] F. del Aguila *et al.*, Nucl. Phys. **B334**, 1 (1990).

[114] J. Serra, Journal of High Energy Physics **2015**, 9 (2015), ISSN 1029-8479, URL `http://dx.doi.org/10.1007/JHEP09(2015)176`.

[115] A. Anandakrishnan *et al.*, Physical Review D **93**, 7 (2016), ISSN 2470-0029, URL `http://dx.doi.org/10.1103/PhysRevD.93.075009`.

[116] M. Chala, Physical Review D **96**, 1 (2017), ISSN 2470-0029, URL `http://dx.doi.org/10.1103/PhysRevD.96.015028`.

[117] A. M. Sirunyan *et al.* (CMS), Phys. Lett. **B779**, 82 (2018), [arXiv:1710.01539].

[118] CMS Collaboration, Technical Report CMS-PAS-B2G-12-017 (2014).

[119] V. Khachatryan *et al.* (CMS), Phys. Rev. **D93**, 1, 012003 (2016), [arXiv:1509.04177].

[120] CMS Collaboration, Technical Report CMS-PAS-B2G-12-013 (2012).

[121] S. D. Ellis, C. K. Vermilion and J. R. Walsh, Phys. Rev. **D80**, 051501 (2009), [arXiv:0903.5081].

[122] A. M. Sirunyan *et al.* (CMS), Phys. Rev. D **100**, 7, 072001 (2019), [arXiv:1906.11903].

[123] M. Aaboud *et al.* (ATLAS), JHEP **10**, 141 (2017), [arXiv:1707.03347].

[124] G. Aad *et al.* (ATLAS), JHEP **08**, 105 (2015), [arXiv:1505.04306].

[125] A. M. Sirunyan *et al.* (CMS), Phys. Lett. **B772**, 634 (2017), [arXiv:1701.08328].

[126] M. Aaboud *et al.* (ATLAS), JHEP **05**, 164 (2019), [arXiv:1812.07343].

[127] G. Aad *et al.* (ATLAS), Eur. Phys. J. **C76**, 8, 442 (2016), [arXiv:1602.05606].

[128] ATLAS Collaboration (ATLAS), Technical Report ATLAS-CONF-2016-104 (2016).

[129] M. Aaboud *et al.* (ATLAS), Phys. Rev. **D98**, 9, 092005 (2018), [arXiv:1808.01771].

[130] S. Chatrchyan *et al.* (CMS), Phys. Lett. **B729**, 149 (2014), [arXiv:1311.7667].

[131] V. Khachatryan *et al.* (CMS), JHEP **06**, 080 (2015), [arXiv:1503.01952].

[132] A. M. Sirunyan *et al.* (CMS), JHEP **11**, 085 (2017), [arXiv:1706.03408].

[133] CMS Collaboration, `cds.cern.ch/record/1709129` (2014).

[134] A. M. Sirunyan *et al.* (CMS), JHEP **04**, 136 (2017), [arXiv:1612.05336].

[135] V. Khachatryan *et al.* (CMS), Phys. Lett. **B771**, 80 (2017), [arXiv:1612.00999].

[136] M. Aaboud *et al.* (ATLAS), JHEP **08**, 052 (2017), [arXiv:1705.10751].

[137] M. Aaboud *et al.* (ATLAS), Phys. Rev. **D98**, 11, 112010 (2018), [arXiv:1806.10555].

[138] M. Aaboud *et al.* (ATLAS), JHEP **05**, 041 (2019), [arXiv:1812.09743].

[139] A. M. Sirunyan *et al.* (CMS), Phys. Lett. **B781**, 574 (2018), [arXiv:1708.01062].

[140] ATLAS Collaboration (ATLAS), Technical report, CERN, Geneva (2021), URL `https://cds.cern.ch/record/2773300`.

[141] ATLAS Collaboration (ATLAS), Technical report, CERN, Geneva (2021), URL `https://cds.cern.ch/record/2779174`.

[142] A. M. Sirunyan *et al.* (CMS), JHEP **01**, 036 (2020), [arXiv:1909.04721].

[143] M. Aaboud *et al.* (ATLAS), Phys. Rev. Lett. **121**, 21, 211801 (2018), [arXiv:1808.02343].

[144] A. M. Sirunyan *et al.* (CMS), JHEP **08**, 177 (2018), [arXiv:1805.04758].

[145] ATLAS Collaboration (ATLAS), Technical report, CERN, Geneva (2021), URL `https://cds.cern.ch/record/2760012`.

[146] CMS Collaboration, Technical Report CMS-PAS-B2G-12-019 (2012).

[147] A. M. Sirunyan *et al.* (CMS), Eur. Phys. J. **C79**, 90 (2019), [arXiv:1809.08597].

[148] V. Khachatryan *et al.* (CMS), Phys. Rev. **D93**, 11, 112009 (2016), [arXiv:1507.07129].

Downloaded from https://academic.oup.com/ptep/article/2022/8/083C01/6651666 by KIT Library user on 27 September 2022

[149] G. Aad *et al.* (ATLAS), JHEP **11**, 104 (2014), [arXiv:1409.5500].

[150] A. M. Sirunyan *et al.* (CMS), JHEP **08**, 130 (2018), [arXiv:1806.00843].

[151] R. Contino and G. Servant, JHEP **06**, 026 (2008), [arXiv:0801.1679].

[152] J. Mrazek and A. Wulzer, Phys. Rev. **D81**, 075006 (2010), [arXiv:0909.3977].

[153] A. M. Sirunyan *et al.* (CMS), JHEP **08**, 073 (2017), [arXiv:1705.10967].

[154] CMS Collaboration, Technical Report CMS-PAS-B2G-16-019 (2017).

[155] S. Chatrchyan *et al.* (CMS), Phys. Rev. Lett. **112**, 17, 171801 (2014), [arXiv:1312.2391].

[156] M. Aaboud *et al.* (ATLAS), JHEP **12**, 039 (2018), [arXiv:1807.11883].

[157] G. Aad *et al.* (ATLAS), Phys. Rev. **D91**, 11, 112011 (2015), [arXiv:1503.05425].

[158] A. M. Sirunyan *et al.* (CMS), JHEP **03**, 082 (2019), [arXiv:1810.03188].

[159] G. Aad *et al.* (ATLAS), JHEP **10**, 150 (2015), [arXiv:1504.04605].

[160] A. M. Sirunyan *et al.* (CMS), JHEP **09**, 053 (2017), [arXiv:1703.06352].

[161] A. M. Sirunyan *et al.* (CMS), Eur. Phys. J. **C79**, 3, 208 (2019), [arXiv:1812.06489].

[162] C. Bini, R. Contino and N. Vignaroli, JHEP **01**, 157 (2012), [arXiv:1110.6058].

[163] D. Greco and D. Liu, JHEP **12**, 126 (2014), [arXiv:1410.2883].

[164] N. Vignaroli, Phys. Rev. **D89**, 9, 095027 (2014), [arXiv:1404.5558].

[165] A. M. Sirunyan *et al.* (CMS), JHEP **03**, 127 (2019), [arXiv:1811.07010].

[166] V. Khachatryan *et al.* (CMS), Phys. Rev. **D91**, 5, 052009 (2015), [arXiv:1501.04198].

[167] V. Khachatryan *et al.* (CMS), Phys. Lett. **B770**, 257 (2017), [arXiv:1608.01224].

[168] S. Chatrchyan *et al.* (CMS), Phys. Rev. Lett. **110**, 14, 141802 (2013), [arXiv:1302.0531].

[169] G. Aad *et al.* (ATLAS), Phys. Rev. **D91**, 5, 052007 (2015), [arXiv:1407.1376].

[170] A. M. Sirunyan *et al.* (CMS), Phys. Lett. **B769**, 520 (2017), [Erratum: Phys. Lett.B772,882(2017)], [arXiv:1611.03568].

[171] CMS Collaboration, Technical Report CMS-PAS-EXO-15-001 (2015).

[172] G. Aad *et al.* (ATLAS), JHEP **06**, 151 (2020), [arXiv:2002.11325].

[173] G. Aad *et al.* (ATLAS), Phys. Rev. Lett. **125**, 13, 131801 (2020), [arXiv:2005.02983].

[174] M. Aaboud *et al.* (ATLAS), Phys. Rev. D **96**, 5, 052004 (2017), [arXiv:1703.09127].

[175] A. M. Sirunyan *et al.* (CMS), Phys. Lett. B **805**, 135448 (2020), [arXiv:1911.03761].

[176] A. M. Sirunyan *et al.* (CMS), JHEP **05**, 033 (2020), [arXiv:1911.03947].

Downloaded from https://academic.oup.com/ptep/article/2022/8/083C01/6651666 by KIT Library user on 27 September 2022

93. Grand Unified Theories

Revised August 2019 by A. Hebecker (Heidelberg U.) and J. Hisano (KMI, Nagoya U.).

93.1 The standard model

The Standard Model (SM) may be defined as the renormalizable field theory with gauge group $G_{SM} = SU(3)_C \times SU(2)_L \times U(1)_Y$, with 3 generations of fermions in the representation

$$(\mathbf{3},\mathbf{2})_{1/3} + (\bar{\mathbf{3}},\mathbf{1})_{-4/3} + (\bar{\mathbf{3}},\mathbf{1})_{2/3} + (\mathbf{1},\mathbf{2})_{-1} + (\mathbf{1},\mathbf{1})_{2}\ , \quad (93.1)$$

and a scalar Higgs doublet H transforming as $(\mathbf{1},\mathbf{2})_1$. Here and below we use boldface numbers to specify the dimension of representations of non-Abelian groups (in this case fundamental and antifundamental) and lower indices for $U(1)$ charges. The fields of Eq. (93.1) should also be familiar as $[Q, u^c, d^c, L, e^c]$, with $Q = (u, d)$ and $L = (\nu, e)$ being the quark and lepton $SU(2)$-doublets and u^c, d^c, e^c charge conjugate $SU(2)$-singlets.[1] Especially after the discovery of the Higgs, this model is remarkably complete and consistent with almost all experimental data.

A notable exception are neutrino masses, which are known to be non-zero but are absent in the SM even after the Higgs acquires its vacuum expectation value (VEV). The minimalist attitude is to allow for the dimension-five operator $(HL)^2$ [1], which induces (Majorana) neutrino masses. In the seesaw mechanism [2–4] this operator is generated by integrating out heavy singlet fermions (right-handed (r.h.) neutrinos). Alternatively, neutrinos can have Dirac masses if light singlet neutrinos are added to the SM spectrum.

Conceptual problems of the SM include the absence of a Dark Matter candidate, of a mechanism for generating the baryon asymmetry of the Universe, and of any reason for the observed smallness of the θ parameter of QCD (θ_{QCD}). In addition, the apparently rather complex group-theoretic data of Eq. (93.1) remains unexplained. Together with the abundance of seemingly arbitrary coupling constants, this disfavors the SM as a candidate fundamental theory, even before quantum gravity problems arise at energies near the Planck mass M_P.

To be precise, there are 19 SM parameters which have to be fitted to data: Three gauge couplings[2] g_3, g_2 and g_1, 13 parameters associated with the Yukawa couplings (9 charged fermion masses, three mixing angles and one CP phase in the CKM matrix.), the Higgs mass and quartic coupling, and θ_{QCD}. In addition, Majorana neutrinos introduce 3 more masses and 6 mixing angles and phases. As we will see, the paradigm of grand unification addresses mainly the group theoretic data of Eq. (93.1) and the values of the three gauge couplings. In many concrete realizations, it then impacts also the other mentioned issues of the SM, such as the family structure and fermion mass hierarchy.

More specifically, after precision measurements of the Weinberg angle θ_W in the LEP experiments, supersymmetric GUTs (SUSY GUTs) have become the leading candidates in the search for 'Physics beyond the SM'. Supersymmetry (SUSY) is a symmetry between bosons and fermions which requires the addition of superpartners to the SM spectrum. If SUSY is motivated as a solution to the gauge hierarchy problem (i.e. to the naturalness or fine-tuning problem of the electroweak scale) [5], superpartners have to be present near the weak scale. SUSY GUTs [6] then lead to the prediction of θ_W, in good agreement with subsequent observations [7]. However, the non-discovery of new particles at the LHC puts into question the presence of new physics at the TeV scale in general and in particular of low-scale supersymmetry. Still, SUSY may be present just outside the presently explored energy domain.

The measured Higgs mass (125 GeV) is in principle consistent with this picture, assuming superpartners in the region of roughly 10 TeV. Such heavy superpartners then induce radiative corrections raising the Higgs mass above the Z boson mass m_Z [8, 9]. However, from the vantage point of the hierarchy problem, heavy superpartners are problematic: They also contribute to SUSY-breaking Higgs mass parameters and thereby to the Higgs potential, tending to raise the Z mass. As a result, the incarnation of SUSY in terms of the minimal supersymmetric SM (MSSM) is becoming questionable. Turning the logic around, one may say that compared to expectations based on the MSSM with superpartner masses below about 1 TeV, the measured Higgs mass value of 125 GeV is somewhat too high [10]. Independently, the LHC has disfavored light colored superpartners (which does not imply that *all* superpartners are heavy). These facts represent new hints for future work on SUSY GUTs or on GUTs without TeV-scale supersymmetry.

93.2 Basic group theory and charge quantization

93.2.1 $SU(4)_C \times SU(2)_L \times SU(2)_R$

Historically, the first attempt at unification was the Pati-Salam model with gauge group $G_{PS} = SU(4)_C \times SU(2)_L \times SU(2)_R$ [11]. It unifies SM fermions in the sense that one generation (plus an extra SM singlet) now comes from the $(\mathbf{4},\mathbf{2},\mathbf{1}) + (\bar{\mathbf{4}},\mathbf{1},\mathbf{2})$ of G_{PS}. This is easy to verify from the breaking pattern $SU(4)_C \to SU(3)_C \times U(1)_{B-L}$ together with the identification of SM hypercharge as a linear combination between $B - L$ (baryon minus lepton number) and the T_3 generator of $SU(2)_R$. This model explains charge quantization, that is, why all electric charges are integer multiples of some smallest charge in the SM. Concretely, the $\mathbf{4}$ and $\bar{\mathbf{4}}$ of $SU(4)_C$ identify lepton number as the 4th colour and the tracelessness of the diagonal generator implies that quark charges are expressed in terms of $1/N_c$ fractions of lepton charges. However, G_{PS} is not simple (containing three simple factors), and thus it does not predict gauge coupling unification.

93.2.2 $SU(5)$

Since G_{SM} has rank four (two for $SU(3)_C$ and one for $SU(2)_L$ and $U(1)_Y$, respectively), the rank-four group $SU(5)$ is the minimal choice for unification in a simple group [12]. The three SM gauge coupling constants derive from a universal coupling α_G at the GUT scale M_G. Explicitly embedding G_{SM} in $SU(5)$ is straightforward, with $SU(3)_C$ and $SU(2)_L$ corresponding e.g. to the upper-left 3×3 and lower-right 2×2 blocks, respectively, in traceless 5×5 matrices for $SU(5)$ generators of the fundamental representation. The $U(1)_Y$ corresponds to matrices generated by $\mathrm{diag}(-2/3, -2/3, -2/3, 1, 1)$ and hence commutes with $SU(3)_C \times SU(2)_L \subset SU(5)$. It is then easy to derive how one SM generation precisely comes from the $\mathbf{10} + \bar{\mathbf{5}}$ of $SU(5)$ (where $\mathbf{10}$ is the antisymmetric rank-2 tensor):

$$\mathbf{10}: \begin{pmatrix} 0 & u_b^c & -u_g^c & u_r & d_r \\ -u_b^c & 0 & u_r^c & u_g & d_g \\ u_g^c & -u_r^c & 0 & u_b & d_b \\ -u_r & -u_g & -u_b & 0 & e^c \\ -d_r & -d_g & -d_b & -e^c & 0 \end{pmatrix} \quad \text{and} \quad \bar{\mathbf{5}}: \begin{pmatrix} d_r^c \\ d_g^c \\ d_b^c \\ e \\ -\nu_e \end{pmatrix}. \quad (93.2)$$

In addition to charge quantization this structure explains why the l.h. quark and lepton states fall in $SU(2)_L$ doublets while the r.h. states are singlets.

Since $SU(5)$ has 24 generators, $SU(5)$ GUTs have 12 new gauge bosons known as X bosons (or X/Y bosons) in addition to the SM. X bosons form an $SU(3)_C$-triplet and $SU(2)_L$-doublet. Their interaction connects quarks and leptons such that baryon and lepton numbers are not conserved and nucleon decay is predicted. Furthermore, $U(1)_Y$ hypercharge is automatically quantized since it is embedded in $SU(5)$.

In order to break the electroweak symmetry at the weak scale and give mass to quarks and leptons, Higgs doublets are needed. In the minimal $SU(5)$ model, they can sit in either a $\mathbf{5}_H$ or $\bar{\mathbf{5}}_H$. The three additional states are referred to as color-triplet Higgs scalars. Their couplings also violate baryon and lepton numbers, inducing nucleon decay. In order not to violently disagree with the non-observation of nucleon decay, the triplet mass must be greater than $\sim 10^{11}$ GeV [13]. Moreover, in SUSY GUTs [6], in order to cancel anomalies as well as give mass to both up and down quarks, both Higgs multiplets $\mathbf{5}_H$ and $\bar{\mathbf{5}}_H$ are required. As we shall discuss later, nucleon decay now constrains the Higgs triplets to have

[1] In our convention the electric charge is $Q = T_3 + Y/2$ and all our spinor fields are left-handed (l.h.).

[2] Equivalently, the $SU(2)_L$ and $U(1)_Y$ couplings are denoted as $g = g_2$ and $g' = \sqrt{3/5}\ g_1$. One also uses $\alpha_s = \alpha_3 = (g_3^2/4\pi)$, $\alpha_{\rm EM} = (e^2/4\pi)$ with $e = g\ \sin\theta_W$ and $\sin^2\theta_W = (g')^2/(g^2 + (g')^2)$.

Downloaded from https://academic.oup.com/ptep/article/2022/8/083C01/6651666 by KIT Library user on 27 September 2022

mass significantly greater than M_G in the minimal SUSY $SU(5)$ GUT since integrating out the Higgs triplets generates dimension-five baryon-number-violating operators [14]. The mass splitting between doublet and triplet in the $\mathbf{5}_H$ (and $\bar{\mathbf{5}}_H$) comes from their interaction with the $SU(5)$ breaking sector.

93.2.3 $SO(10)$

While $SU(5)$ allows for the minimal GUT models, unification is not complete: Two independent representations, **10** and $\bar{\mathbf{5}}$, are required for one SM generation. A further representation, an SU(5) singlet, has to be added to serve as r.h. neutrino in the seesaw mechanism. In this case, the r.h. neutrino masses are not necessarily related to the GUT scale. By contrast, a single **16**-dimensional spinor representation of $SO(10)$ accommodates a full SM generation together with an extra singlet, potentially providing a r.h. neutrino [15]. This is most easily understood from the breaking pattern $SO(10) \to SU(5) \times U(1)_X$ and the associated branching rule[3] $\mathbf{16} = \mathbf{10}_{-1} + \bar{\mathbf{5}}_3 + \mathbf{1}_{-4}$. Here the indices refer to charges under the $U(1)_X$ subgroup, which is orthogonal to $SU(5)$ and reflects the fact that $SO(10)$ has rank five. From the above, it is easy to see that $U(1)_X$ charges can be given as $2Y - 5(B-L)$. Intriguingly, all representations of $SO(10)$ are anomaly free in four dimensions (4d). Thus, the absence of anomalies in an $SU(5)$-GUT or a SM generation can be viewed as deriving from this feature.

We now describe in more detail how one family of quarks and leptons appears in the **16**. To understand this, recall that the Γ-matrices of the 10d Clifford algebra give rise to five independent, anticommuting 'creation-annihilation' operators $\Gamma^{a\pm} = (\Gamma^{2a-1} \pm i\Gamma^{2a})/2$ with $a = 1, ..., 5$. These correspond to five fermionic harmonic oscillators or "spin" 1/2 systems. The 32-dimensional tensor product of those is reducible since the 10d rotation generators $M_{mn} = -i[\Gamma^m, \Gamma^n]/4$ $(m, n = 1, ..., 10)$ always flip an even number of "spins". This gives rise to the **16** as displayed in Table 93.1. Next, one also recalls that the natural embedding of $SU(5)$ in $SO(10)$ relies on 'pairing up' the 10 real dimensions to produce 5 complex dimensions, $\mathbb{R}^{10} \equiv \mathbb{C}^5$, similarly to the paring up of Γ^ms used above. This makes it clear how to associate one $|\pm>$ system to each complex dimension of $SU(5)$, which explains the labeling of the "spin" columns in Table 93.1: The first three and last two "spins" correspond to $SU(3)_C$ and $SU(2)_L$, respectively. In fact, an $SU(3)_C$ rotation just raises one color index and lowers another, changing colors $\{r, g, b\}$, or changes relative phases between the three spin states. Similarly, an $SU(2)_L$ rotation raises one weak index and lowers another, thereby flipping the weak isospin from up to down or vice versa, or changes the relative phase between the two spin states. In this representation $U(1)_Y$ hypercharge is simply given by $Y = -2/3(\sum \text{ color spins}) + (\sum \text{ weak spins})$. $SU(5)$ rotations corresponding to X bosons then raise (or lower) a color index, while at the same time lowering (or raising) a weak index. It is easy to see that such rotations can mix the states $\{Q,\ u^c,\ e^c\}$ and $\{d^c, L\}$ among themselves and ν^c is a singlet. Since $SO(10)$ has 45 generators, additional 21 gauge bosons are introduced including the $U(1)_X$ above. The 20 new $SO(10)$ rotations not in $SU(5)$ are then given by either raising any two spins or lowering them. With these rotations, **1** and **5** are connected with **10**. The last $SO(10)$ rotation changes phases of states with weight $2(\sum \text{ color spins}) + 2(\sum \text{ weak spins})$, which corresponds to $U(1)_X$.

$SO(10)$ has two inequivalent maximal subgroups and hence breaking patterns, $SO(10) \to SU(5) \times U(1)_X$ and $SO(10) \to SU(4)_C \times SU(2)_L \times SU(2)_R$. In the first case, one can carry on breaking to $G_{SM} \subset SU(5)$ precisely as in the minimal $SU(5)$ case above. Alternatively, one can identify $U(1)_Y$ as an appropriate linear combination of $U(1)_X$ and the $U(1)$ factor from $SU(5)$, leading to the so-called flipped $SU(5)$ [17] as an intermediate step in breaking $SO(10)$ to G_{SM}. In the second case, we have an intermediate Pati-Salam model thanks to the branching rule $\mathbf{16} = (\mathbf{4}, \mathbf{2}, \mathbf{1}) + (\bar{\mathbf{4}}, \mathbf{1}, \mathbf{2})$. Finally, $SO(10)$ can break directly to the SM at M_G. Gauge coupling unification remains intact in the case of this 'direct' breaking and for the breaking pattern $SO(10) \to SU(5) \to G_{SM}$ (with $SU(5)$ broken at M_G). In the case of intermediate-scale Pati-Salam or flipped $SU(5)$ models, gauge coupling predictions are modified. The Higgs multiplets in the minimal $SO(10)$ come from the fundamental representation, $\mathbf{10}_H = \mathbf{5}_H + \bar{\mathbf{5}}_H$. Note, only in $SO(10)$ does the representation type distinguish SM matter from Higgs fields.

[3] Useful references on group theory in the present context include [16] and refs. therein.

Table 93.1: Quantum numbers of **16**-dimensional representation of $SO(10)$.

state	Y	Color	Weak	$SU(5)$	$SO(10)$
ν^c	0	$---$	$--$	**1**	
e^c	2	$---$	$++$		
u_r	1/3	$+--$	$-+$		
d_r	1/3	$+--$	$+-$		
u_g	1/3	$-+-$	$-+$		
d_g	1/3	$-+-$	$+-$	**10**	
u_b	1/3	$--+$	$-+$		
d_b	1/3	$--+$	$+-$		**16**
u_r^c	$-4/3$	$-++$	$--$		
u_g^c	$-4/3$	$+-+$	$--$		
u_b^c	$-4/3$	$++-$	$--$		
d_r^c	2/3	$-++$	$++$		
d_g^c	2/3	$+-+$	$++$		
d_b^c	2/3	$++-$	$++$	$\bar{\mathbf{5}}$	
ν	-1	$+++$	$-+$		
e	-1	$+++$	$+-$		

93.2.4 *Beyond* $SO(10)$

Finally, larger symmetry groups can be considered. For example, the exceptional group E_6 has maximal subgroup $SO(10) \times U(1)$ [18]. Its fundamental representation branches as $\mathbf{27} = \mathbf{16}_1 + \mathbf{10}_{-2} + \mathbf{1}_4$. Another maximal subgroup is $SU(3)_C \times SU(3)_L \times SU(3)_R \subset E_6$ with branching rule $\mathbf{27} = (\mathbf{3}, \mathbf{3}, \mathbf{1}) + (\bar{\mathbf{3}}, \mathbf{1}, \bar{\mathbf{3}}) + (\mathbf{1}, \bar{\mathbf{3}}, \mathbf{3})$. Independently of any underlying E_6, the group $[SU(3)]^3$ with additional permutation symmetry Z_3 interchanging the three factors can be considered. This is known as "trinification" [19]. The $E_6 \to [SU(3)]^3$ breaking pattern has been used in phenomenological analyses of the heterotic string [20]. However, in larger symmetry groups, such as E_6, $SU(6)$, etc., there are now many more states which have not been observed and must be removed from the effective low-energy theory.

Intriguingly, the logic by which G_{SM} is a maximal subgroup of $SU(5)$, which together with $U(1)_X$ is a maximal subgroup of $SO(10)$, continues in a very elegant and systematic way up to the largest exceptional group. The resulting famous breaking chain $E_8 \to E_7 \to E_6 \to SO(10) \to SU(5) \to G_{SM}$ together with the special role played by E_8 in group and in string theory is a tantalizing hint at deeper structures. However, since all representations of E_8 and E_7 are real and can not lead to 4d chiral fermions, this is necessarily outside the 4d GUT framework.

93.3 GUT breaking and doublet-triplet splitting

In the standard, 4d field-theoretic approach to GUTs, the unified gauge group is broken spontaneously by an appropriate GUT Higgs sector. Scalar potentials (or superpotentials in SUSY GUTs) exist whose vacua spontaneously break $SU(5)$ or $SO(10)$. While these potentials are ad hoc (just like the Higgs potential in the SM), the most naive expectation is that all their dimensionful parameters are $O(M_G)$. In the simplest case of $SU(5)$, the **24** (adjoint) GUT Higgs develops a VEV along the G_{SM}-singlet direction as $\langle\Phi\rangle \propto \text{diag}(-2/3, -2/3, -2/3, 1, 1)$. In order for $SO(10)$ to break to $SU(5)$, the **16** or **126**, which have a G_{SM}-singlet with non-zero $U(1)_X$ charge, get a VEV.

The masses of doublet and triplet in the $\mathbf{5}_H$ (and $\bar{\mathbf{5}}_H$) generically split due to their coupling to the GUT Higgs. In addition, both the doublet and the triplet masses also get an equal contribution from an $SU(5)$-invariant GUT-scale mass term. Without any further structure, an extreme fine-tuning between two large effects is then necessary to keep the doublet mass at the electroweak scale. Supersymmetry plays an important role in for-

Downloaded from https://academic.oup.com/ptep/article/2022/8/083C01/6651666 by KIT Library user on 27 September 2022

bidding large radiative correction to the doublet mass due to the non-renormalization theorem [5]. However, even in this case we have to fine tune parameters at tree level. This is the doublet-triplet splitting problem which, in the SUSY context, is clearly related the μ-term problem of the MSSM (the smallness of the coefficient of $\mu H_u\ H_d$).

Several mechanisms for natural doublet-triplet splitting have been suggested under the assumption of supersymmetry, such as the sliding singlet [21], missing partner [22], missing VEV [23], and pseudo-Nambu-Goldstone boson mechanisms [24]. Particular examples of the missing partner mechanism for $SU(5)$ [25], the missing VEV mechanism for $SO(10)$ [26, 27] and the pseudo-Nambu-Goldstone boson mechanism for $SU(6)$ [28] have been shown to be consistent with gauge coupling unification and nucleon decay. From the GUT-scale perspective, one is satisfied if the triplets are naturally heavy and the doublets are massless ($\mu \simeq 0$). There are also several mechanisms for resolving the subsequent issue of why μ is of order the SUSY breaking scale [29].[4] For a review of the μ problem and some suggested solutions in SUSY GUTs and string theory, see [30–33] and references therein.

In general, GUT-breaking sectors successfully resolving the doublet-triplet splitting problem, dynamically stabilizing all GUT-scale VEVs and allowing for realistic neutrino masses and Yukawa couplings (including the GUT-symmetry violation in the latter) require a number of ingredients. However, for validity of the effective theory, introduction of higher or many representations is limited, otherwise a Landau pole may appear below the Planck scale. In addition, GUTs are only effective theories below the Planck scale in the 4d field-theoretic approach. Since M_G is close to this scale, the effects of higher-dimension operators are not obviously negligible. In particular, operators including the GUT-breaking Higgs may affect low-energy predictions, such as quark and lepton masses.

Thus, especially in the context of GUT breaking and doublet-triplet splitting, models beyond 4d field theory appear attractive. While this is mainly the subject of the next section, some advantages can already be noted: In models with extra dimensions, in particular string constructions, GUT breaking may occur due to boundary conditions in the compactified dimensions [34–37]. No complicated GUT breaking sector is then required. Moreover, boundary conditions can give mass only to the triplet, leaving the doublet massless. This is similar to the 'missing partner mechanism' since the effective mass term does not 'pair up' the triplets from $\mathbf{5}_H$ and $\overline{\mathbf{5}}_H$ but rather each of them with further fields which are automatically present in the higher-dimensional theory. This can eliminate dimension-five nucleon decay (cf. Sec. 93.6).

93.4 String-theoretic and higher-dimensional unified models

As noted earlier, the GUT scale is dangerously close to the scale of quantum gravity. It may hence be necessary to discuss unified models of particle physics in the latter, more ambitious context. Among the models of quantum gravity, superstring or M-theory stands out as the best-studied and technically most developed proposal, possessing in particular a high level of internal, mathematical consistency. For our purposes, it is sufficient to know that five 10d and one 11d low-energy effective supergravity theories arise in this setting (cf. [38] and refs. therein).

Grand unification is realized most naturally in the context of the two 'heterotic' theories with gauge groups $\mathrm{E}_8\times\mathrm{E}_8$ and $SO(32)$, respectively [36, 39] (see [40] for some of the more recent results). Justified in part by the intriguing breaking path $\mathrm{E}_8 \to \cdots \to G_{SM}$ mentioned above, the focus has historically largely been on $\mathrm{E}_8\times\mathrm{E}_8$. To describe particle physics, solutions of the 10d theory with geometry $\mathbb{R}^{1,3} \times M_6$ are considered, where M_6 is a Calabi-Yau (CY) 3-fold (with 6 real dimensions) [36]. The background solution involves expectation values of higher-dimensional components of the $\mathrm{E}_8\times\mathrm{E}_8$ gauge fields. This includes both Wilson lines [34] and non-vanishing field-strength and leads, in general, to a reduced gauge symmetry and to chirality in the resulting 4d effective theory. The 4d fermions arise from 10d gauginos.

Given an appropriate embedding[5] of G_{SM} in $\mathrm{E}_8\times\mathrm{E}_8$, gauge coupling unification is automatic at leading order. Corrections arise mainly through (string)-loop effects and are similar to the familiar field-theory thresholds of 4d GUTs[6] [41]. Thus, one may say that coupling unification is a generic prediction in spite of the complete absence[7] of a 4d GUT at any energy scale. This absence is both an advantage and a weakness. On the up side, GUT breaking and doublet-triplet splitting [43] are more naturally realized and dimension-five nucleon decay is relatively easy to avoid. On the down side, there is no reason to expect full GUT representations in the matter sector and flavor model building is much less tied to the GUT structure than in 4d.

Let us pause to explain the beautiful idea behind the advertised solution of the doublet-triplet splitting problem: One starts with a simply connected CY X and mods out the action of a discrete group G (say $\mathbb{Z}_2$). In the absence of fixed points, X/G is smooth and has a non-contractible 1-cycle. Furthermore, let G also act on the gauge bundle, according to an embedding $G \to \mathrm{E}_8$. Now the parallel transport around the 1-cycle is tied to a gauge rotation (one says a non-trivial Wilson-line is present). Moreover, this Wilson line can not be continuously turned off since, e.g. in the case of $\mathbb{Z}_2$, its square is the unit element of the group. The induced 'Wilson-line breaking', which comes on top of the breaking by non-zero field strengths, may remove certain sub-representations (e.g. the triplet of $SU(5) \to G_{SM}$) while keeping others exactly massless. A simpler and, due to fixed points, singular version of this will appear below in the context of orbifold GUTs.

One technical problem of heterotic constructions is the dependence on the numerous size and shape parameters of M_6 (the so-called moduli), the stabilization of which is poorly understood (see [44] for recent developments). Another is the sheer mathematical complexity of the analysis, involving in particular the study of (non-Abelian) gauge-bundles on CY spaces [45] (see however [46]).

An interesting aspect of heterotic string constructions is represented by orbifold models [35]. Here the internal space is given by a six-torus, modded out by a discrete symmetry group (e.g. $T^6/\mathbb{Z}_n$). More recent progress is reported in [47, 48], including in particular the systematic exploration of the phenomenological advantages of so-called 'non-prime' (referring to n) orbifolds. The symmetry breaking to G_{SM} as well as the survival of Higgs doublets without triplet partners is ensured by the appropriate embedding of the discrete orbifold group in $\mathrm{E}_8\times\mathrm{E}_8$. String theory on such spaces, which are locally flat but include singularities, is much more calculable than in the CY case. The orbifold geometries can be viewed as singular limits of CYs.

An even simpler approach to unified models, which includes many of the advantages of full-fledged string constructions, is provided by Orbifold GUTs [37]. These are (mostly) 5d or 6d SUSY field theories with unified gauge group (e.g. $SU(5)$ or $SO(10)$), broken in the process of compactifying to 4d. To give a particularly simple example, consider $SU(5)$ on $\mathbb{R}^{1,3} \times S^1/(\mathbb{Z}_2 \times \mathbb{Z}_2')$. Here the compact space is an interval of length $\pi R/2$ and the embedding of $\mathbb{Z}_2'$ in the hypercharge direction of $SU(5)$ realizes the breaking to G_{SM}. Concretely, 5d X bosons are given Dirichlet BCs at one endpoint of the interval and thus have no Kaluza-Klein (KK) zero mode. Their lightest modes have mass $\sim 1/R$, making the KK-scale the effective GUT scale. As an implication, the boundary theory has no $SU(5)$ invariance. Nevertheless, since the $SU(5)$-symmetric 5d bulk dominates 4d gauge couplings, unification remains a prediction. Many other features but also problems

[4] The solution of [29] relies on the absence of the fundamental superpotential term $\mu H_u\ H_d$ (or $\mu\, \mathbf{5}_H \overline{\mathbf{5}}_H$). This can be ensured either by a discrete R symmetry or by a $U(1)_R$. The latter clashes with typical superpotentials for the GUT breaking sector. However, higher-dimensional or stringy GUTs, where the triplet Higgs is simply projected out, can be consistent with the $U(1)_R$ symmetry.

[5] All embeddings of G_{SM} in one E_8 factor which are consistent with a breaking-pattern $\mathrm{E}_8 \to SU(5) \to G_{SM}$ are suitable (cf. for example the natural breaking chain from E_8 to G_{SM} through maximal subgroups mentioned at the end of Sect. 93.3). Other embeddings can change the ratios between the three resulting G_{SM} couplings at the GUT scale by group-theoretic factors. Crucially, due to the single 10d gauge coupling, no continuous tuning is possible.

[6] Field-theory thresholds of 4d GUTs are discussed in 93.5.

[7] See however [42].

Downloaded from https://academic.oup.com/ptep/article/2022/8/083C01/6651666 by KIT Library user on 27 September 2022

of 4d GUTs can be circumvented, especially doublet-triplet splitting is easily realized.

With the advent of the string-theory 'flux landscape' [49], which is best understood in 10d type-IIB supergravity, the focus in string model building has shifted to this framework. While type II string theories have no gauge group in 10d, brane-stacks support gauge dynamics. A particularly appealing setting (see e.g. [50]) is provided by type IIB models with D7 branes (defining 8d submanifolds). However, in the $SO(10)$ context the **16** is not available and, for $SU(5)$, the top-Yukawa coupling vanishes at leading order [51]. As a crucial insight, this can be overcome on the non-perturbative branch of type IIB, also known as F-theory [52, 53]. This setting allows for more general branes, thus avoiding constraints of the Dp-brane framework. GUT breaking can be realized using hypercharge flux (the VEV of the $\mathrm{U}(1)_Y$ field strength), an option not available in heterotic models. The whole framework combines the advantages of the heterotic or higher-dimensional unification approach with the more recent progress in understanding moduli stabilization. It thus represents at this moment the most active and promising branch of theory-driven GUT model building (see e.g. [54] and refs. therein).

As a result of the flux-breaking, a characteristic 'type IIB' or 'F-theoretic' tree-level correction to gauge unification arises [55]. The fact that this correction can be rather significant numerically is occasionally held against the framework of F-theory GUTs. However, at a parametric level, this correction nevertheless behaves like a 4d threshold, i.e., it provides $\mathcal{O}(1)$ additive contributions to the inverse 4d gauge couplings $\alpha_i^{-1}(M_G)$.

A final important issue in string GUTs is the so-called string-scale/GUT-scale problem [56]. It arises since, in heterotic compactifications, the Planck scale and the high-scale value of the gauge coupling unambiguously fix the string-scale to about 10^{18} GeV. As the compactification radius R is raised above the string length, the GUT scale (identified with $1/R$) goes down and the string coupling goes up. Within the domain of perturbative string theory, a gap of about a factor ~ 20 remains between the lowest GUT scale achievable in this way and the phenomenological goal of 2×10^{16} GeV. The situation can be improved by venturing into the non-perturbative regime [56], by considering 'anisotropic' geometries with hierarchically different radii R [56, 57] or by including GUT scale threshold corrections [58, 59].

In F-theory GUTs, the situation is dramatically improved since the gauge theory lives only in four out of the six compact dimensions. This allows for models with a 'decoupling limit', where the GUT scale is parametrically below the Planck scale [53]. However, moduli stabilization may not be without problems in such constructions, in part due to a tension between the required large volume and the desirable low SUSY breaking scale.

93.5 Gauge coupling unification

The quantitative unification of the three SM gauge couplings at the energy scale M_G is one of the cornerstones of the GUT paradigm. It is obviously of direct phenomenological relevance. Gauge coupling unification is well understood in the framework of effective field theory (EFT) [60]. In the simplest case, the relevant EFT at energies $\mu \gg M_G$ has a unified gauge symmetry (say $SU(5)$ for definiteness) and a single running gauge coupling $\alpha_G(\mu)$. At energies $\mu \ll M_G$, states with mass $\sim M_G$ (such as X bosons, GUT Higgs, color-triplet Higgs) have to be integrated out. The EFT now has three independent couplings and SM (or SUSY SM) matter content. One-loop renormalization group equations readily allow for an extrapolation to the weak scale,

$$\alpha_i^{-1}(m_Z) = \alpha_G^{-1}(M_G) + \frac{b_i}{2\pi}\log\left(\frac{M_G}{m_Z}\right) + \delta_i\,, \tag{93.3}$$

($i = 1, 2, 3$). Here we defined δ_i to absorb all sub-leading effects, such as threshold corrections at or near the weak scale (e.g. from superpartners and the additional Higgs bosons in the case of the MSSM) and at the GUT scale, and also higher-order corrections. We will discuss them momentarily.

It is apparent from Eq. (93.3) that the three low-scale couplings can be very different. This is due to the large energy range $m_Z \ll \mu \ll M_G$ and the non-universal β-function coefficients ($b_i^{\mathrm{SM}} = \{41/10, -19/6, -7\}$ or $b_i^{\mathrm{MSSM}} = \{33/5, 1, -3\}$). Incomplete GUT multiplets, such as gauge and Higgs bosons in the SM and also their superpartners and the additional Higgs bosons in the MSSM, contribute to the differences between the β functions. Inverting the argument, one expects that extrapolating the measured couplings to the high scale, we find quantitative unification at $\mu \sim M_G$. While this fails in the SM, it works intriguingly well in the MSSM (cf. Fig. 93.1).

The three equations contained in Eq. (93.3) can be used to determine the three 'unknowns' $\alpha_3(m_Z)$, $\alpha_G(M_G)$ and M_G, assuming that all other parameters entering the equations are given. Focusing on the SUSY case and using the $\overline{\mathrm{MS}}$ coupling constants $\alpha_{\mathrm{EM}}^{-1}(m_Z)$ and $\sin^2\theta_W(m_Z)$ from [62],

$$\alpha_{\mathrm{EM}}^{-1}(m_Z) = 127.955 \pm 0.010\,, \tag{93.4}$$

$$\sin^2\theta_W(m_Z) = 0.23122 \pm 0.00003\,, \tag{93.5}$$

as input, one determines $\alpha_{1,2}^{-1}(m_Z)$, which then gives

$$\alpha_G^{-1}(M_G) \simeq 24.3 \qquad \text{and} \qquad M_G \simeq 2\times 10^{16}\ \mathrm{GeV}\,. \tag{93.6}$$

Here we have set $\delta_i = 0$ for simplicity. Crucially, one in addition obtains a prediction for the low-energy observable α_3,

$$\alpha_3^{-1}(m_Z) = -\frac{5}{7}\alpha_1^{-1}(m_Z) + \frac{12}{7}\alpha_2^{-1}(m_Z) + \Delta_3\,, \tag{93.7}$$

where

$$\Delta_3 = \frac{5}{7}\delta_1 - \frac{12}{7}\delta_2 + \delta_3\,. \tag{93.8}$$

Here we followed the elegant formulation in Ref. [63] of the classical analyses of [7]. Of course, it is a matter of convention which of the three low-energy gauge coupling parameters one 'predicts' and indeed, early works on the subject discussed the prediction of $\sin^2\theta_W$ in terms of α_{EM} and α_3 [64, 65].

Remarkably, the leading order result (i.e. Eq. (93.7) with $\delta_i = 0$) is in excellent agreement with experiments [62]:

$$\alpha_3^{\mathrm{LO}}(m_Z) = 0.117 \qquad \text{vs.} \qquad \alpha_3^{\mathrm{EXP}}(m_Z) = 0.1181 \pm 0.0011\,. \tag{93.9}$$

However, this near perfection is to some extent accidental. To see this, we now discuss the various contributions to the δ_i (and hence to Δ_3).

The two-loop running correction from the gauge sector $\Delta_3^{(2)}$ and the low-scale threshold correction $\Delta_3^{(l)}$ from superpartners can be summarized as [63]

$$\Delta_3^{(2)} \simeq -0.82 \qquad \text{and} \qquad \Delta_3^{(l)} \simeq \frac{19}{28\pi}\log\left(\frac{m_{\mathrm{SUSY}}}{m_Z}\right)\,. \tag{93.10}$$

The relevant scale m_{SUSY} can be estimated as [66]

$$m_{\mathrm{SUSY}} \quad\to\quad m_H^{3/19}\, m_{\widetilde{H}}^{12/19}\, m_{\widetilde{W}}^{4/19} \times \left(\frac{m_{\widetilde{W}}}{m_{\widetilde{g}}}\right)^{28/19} \left(\frac{m_{\widetilde{l}}}{m_{\widetilde{q}}}\right)^{3/19}\,, \tag{93.11}$$

where m_H stands for the masses of non-SM Higgs states and superpartner masses are given in self-evident notation. Detailed analyses including the above effects are best done using appropriate software packages, such as SOFTSUSY [61] (or alternatively SuSpect [67] or SPheno [68]). See also [61] for references to the underlying theoretical two-loop analyses.

To get a very rough feeling for these effects, let us assume that all superpartners are degenerate at $m_{\mathrm{SUSY}} = 1$ TeV, except for heavier gluinos: $m_{\widetilde{W}}/m_{\widetilde{g}} \simeq 1/3$. This gives $\Delta_3^{(l)} \simeq -0.35 + 0.22\ln(m_{\mathrm{SUSY}}/m_Z) \simeq 0.18$. The resulting prediction of $\alpha_3(m_Z) \simeq 0.126$ significantly upsets the perfect one-loop agreement found earlier. Before discussing this issue further, it is useful to introduce yet another important type of correction, the high or GUT scale thresholds.

To discuss high scale thresholds, let us set all other corrections to zero for the moment and write down a version of Eq. (93.3)

Downloaded from https://academic.oup.com/ptep/article/2022/8/083C01/6651666 by KIT Library user on 27 September 2022

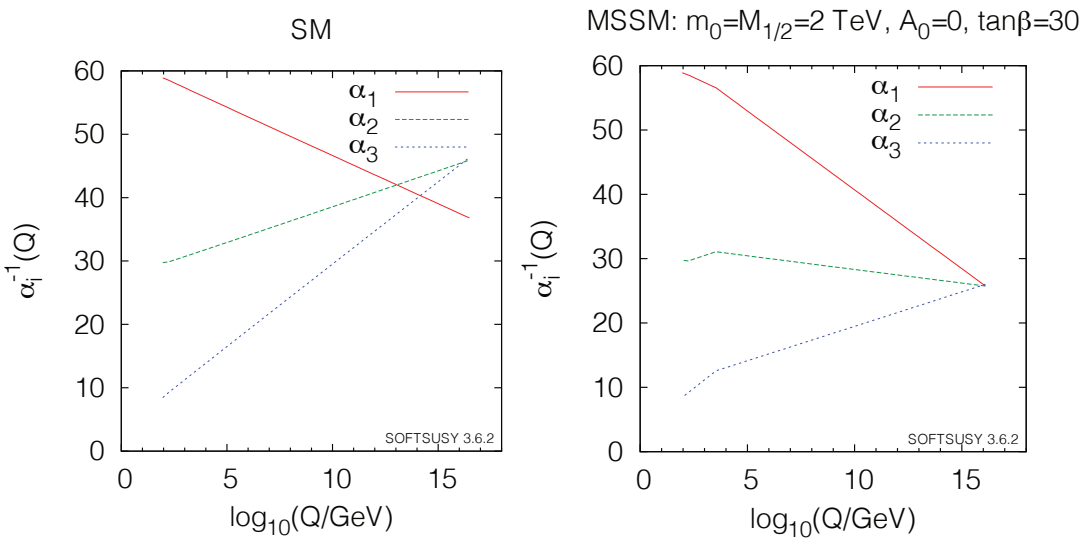

Figure 93.1: Running couplings in SM and MSSM using two-loop RG evolution. The SUSY threshold at 2 TeV is clearly visible on the MSSM side. (We thank Ben Allanach for providing the plots created using SOFTSUSY [61].)

that captures the running near and above the GUT scale more correctly. The threshold correction at one-loop level can be evaluated accurately by the simple step-function approximation for the β functions in the $\overline{\text{DR}}$ scheme[8] [72],

$$\alpha_i^{-1}(m_Z) = \alpha_G^{-1}(\mu) + \frac{1}{2\pi}\left[b_i \ln\frac{\mu}{m_Z} + b_i^C \ln\frac{\mu}{M_C} + b_i^X \ln\frac{\mu}{M_X} + b_i^\Phi \ln\frac{\mu}{M_\Phi}\right] . \tag{93.12}$$

Here we started the running at some scale $\mu \gg M_G$, including the contribution of the minimal set of states relevant for the transition from the high-scale $SU(5)$ model to the MSSM. These are the color-triplet Higgs multiplets with mass M_C, massive vector multiplets of X-bosons with mass M_X (including GUT Higgs degrees of freedom), and the remaining GUT-Higgs fields and superpartners with mass M_Φ. The coefficients $b_i^{C,X,\Phi}$ can be found in Ref. [73]. Crucially, the b_i in Eq. (93.12) conspire to make the running GUT-universal at high scales, such that the resulting prediction for α_3 does not depend on the value of μ.

To relate this to our previous discussion, we can, for example, define $M_G \equiv M_X$ and then choose $\mu = M_G$ in Eq. (93.12). This gives the high-scale threshold corrections

$$\delta_i^{(h)} = \frac{1}{2\pi}\left[b_i^C \ln\frac{M_G}{M_C} + b_i^\Phi \ln\frac{M_G}{M_\Phi}\right] , \tag{93.13}$$

and a corresponding correction $\Delta_3^{(h)}$. To get some intuition for the magnitude, one can furthermore assume $M_\Phi = M_G$, finding (with $b_i^C = \{2/5, 0, 1\}$)

$$\Delta_3^{(h)} = \frac{9}{14\pi} \ln\left(\frac{M_G}{M_C}\right) . \tag{93.14}$$

To obtain the desired effect of $-\Delta_3^{(2)} - \Delta_3^{(l)} \simeq +0.64$, the triplet Higgs would have to be by about a factor 20 lighter than the GUT scale. While this is ruled out by nucleon decay in the minimal model [74] as will be discussed Sec. 93.6, it is also clear that threshold corrections of this order of magnitude can, in general, be realized with a certain amount of GUT-scale model building, e.g. in specific $SU(5)$ [25] or $SO(10)$ [26,27] constructions. Corrections can also be much larger or of different sign if, as is required in many fully realistic 4d GUT models, many additional (and in particular higher) representations are introduced. Thus, there is considerable model building freedom. Nevertheless, a significant constraint from getting the right GUT threshold corrections while keeping the triplet Higgs heavy remains.

The above analysis implicitly assumes universal soft SUSY breaking masses at the GUT scale, which directly affect the spectrum of SUSY particles at the weak scale. In the simplest case we have a universal gaugino mass $M_{1/2}$, a universal mass for squarks and sleptons m_{16} and a universal Higgs mass m_{10}, as motivated by $SO(10)$. In some cases, threshold corrections to gauge coupling unification can be exchanged for threshold corrections to soft SUSY parameters (see [75] and refs. therein). For example, if gaugino masses were not unified at M_G and, in particular, gluinos were lighter than winos at the weak scale (cf. Eq. (93.11)), then it is possible that, due to weak scale threshold corrections, a much smaller or even slightly negative threshold correction at the GUT scale would be consistent with gauge coupling unification [76].

It is also noteworthy that perfect unification can be realized without significant GUT-scale corrections, simply by slightly raising the (universal) SUSY breaking scale. In this case the dark matter abundance produced by thermal processes in the early Universe (if the lightest neutralino is the dark matter particle) is too high. However, even if the gaugino mass in the MSSM is about 1 TeV to explain the dark matter abundance, if the Higgsino and the non-SM Higgs boson masses are about 10-100 TeV, the effective SUSY scale can be raised [77]. This setup is realized in split SUSY [78] or the pure gravity mediation model [79] based on anomaly mediation [80]. Since the squarks and sleptons are much heavier than the gaugino masses in those setups, a gauge hierarchy problem is reintroduced. The facts that no superpartners have so far been seen at the LHC and that the observed Higgs mass favors heavier stop masses than about 1 TeV force one to accept a certain amount of fine-tuning anyway.

For non-SUSY GUTs or GUTs with a very high SUSY breaking scale to fit the data, new light states in incomplete GUT multiplets or multiple GUT breaking scales are required. For example, non-SUSY models $SO(10) \to SU(4)_C \times SU(2)_L \times SU(2)_R \to$ SM, with the second breaking scale of order an intermediate scale, determined by light neutrino masses using the see-saw mechanism, can fit the low-energy data for gauge couplings [81] and at the same time survive nucleon decay bounds [82]. Alternatively, one can appeal to string-theoretic corrections discussed in Sec. 93.4 to compensate for a high SUSY breaking scale. This has, for example, been concretely analyzed in the context of F-theory GUTs in [83]. Similarly, one may even wonder whether particularly large GUT threshold corrections could be sufficient to ensure non-SUSY precision unification. Notice here that the gauge coupling unifica-

[8] The $\overline{\text{DR}}$ scheme is frequently used in a supersymmetric regularization [69]. The renormalization transformation of the gauge coupling constants from $\overline{\text{MS}}$ to $\overline{\text{DR}}$ scheme is given in Ref. [70]. For an alternative treatment using holomorphic gauge couplings and NSVZ β-functions see e.g. [71].

Downloaded from https://academic.oup.com/ptep/article/2022/8/083C01/6651666 by KIT Library user on 27 September 2022

tion predicts just one parameter. When introducing new states, typically one can fit the data by choice of their masses. This is not the case in SUSY GUTs with low-scale SUSY breaking scale where the masses are constrained by fine-tuning.

In 5d or 6d orbifold GUTs, certain "GUT scale" threshold corrections come from the Kaluza-Klein modes between the compactification scale, $M_c \sim 1/R$, and the effective cutoff scale M_*. In string theory, this cutoff scale is the string scale. Gauge coupling unification at two loops then constrains the values of M_c and M_*.[9] Often, one finds M_c to be lower than the 4d GUT scale. Since the X-bosons, responsible for nucleon decay, get mass at the compactification scale, this has significant consequences for nucleon decay.

Finally, it has been shown that non-supersymmetric GUTs in warped 5d orbifolds can be consistent with gauge coupling unification. This assumes (in 4d language) that the r.h. top quark and the Higgs doublets are composite-like objects with a compositeness scale in the TeV range [85].

93.6 Nucleon decay

Quarks and leptons are indistinguishable in any 4d GUT, and both the baryon (B) and lepton number (L) are not conserved. This leads to baryon-number-violating nucleon decay. In addition to baryon-number violation, lepton-number violation is also required for nucleon decay since, in the SM, leptons are the only free fermions which are lighter than nucleons. The lowest-dimension operators relevant for nucleon decay are (B+L) violating dimension-six four-fermion-terms in the SM, and all baryon-violating operators with dimension less than seven preserve (B–L) [1, 86].

In $SU(5)$ GUTs, the dimension-six operators are induced by X boson exchange. These operators are suppressed by $(1/M_X^2)$ (M_X is the X boson mass), and the nucleon lifetime is given by $\tau_N \propto M_X^4/(\alpha_G^2\ m_p^5)$ (m_p is proton mass). The dominant decay mode of the proton (and the baryon-violating decay mode of the neutron), via X boson exchange, is $p \to e^+\ \pi^0$ ($n \to e^+\ \pi^-$). In any simple gauge symmetry, with one universal GUT coupling α_G and scale M_X, the nucleon lifetime from gauge boson exchange is calculable. Hence, the GUT scale may be directly observed via the extremely rare decay of the nucleon. Experimental searches for nucleon decay began with the Kolar Gold Mine, Homestake, Soudan, NUSEX, Frejus, HPW, IMB, and Kamiokande detectors [64]. The present experimental bounds on the modes come from Super-Kamiokande. With 306 kton-years of data they find $\tau_p/\mathrm{Br}(p \to e^+\pi^0) > 1.67 \times 10^{34}$ years at 90% CL [87]. In addition, Hyper-Kamiokande [88] is planned to reach to $\tau_p/\mathrm{Br}(p \to e^+\pi^0) \sim 10^{35}$ years. The hadronic matrix elements for baryon-number-violating operators are evaluated with lattice QCD simulations [89]. In SUSY $SU(5)$ GUTs, the lower bound on the X boson mass from null results in nucleon decay searches is approaching 10^{16} GeV [90], which is close to the GUT scale suggested by gauge coupling unification. On the other hand, the prediction for nucleon decay in non-SUSY GUTs is hard to quantify. The reason is that gauge couplings do not unify with just the SM particle content. Once extra states or large thresholds are included to ensure precision unification, a certain range of unification scales is allowed.

In SUSY GUTs there are additional sources for baryon and/or lepton-number violation – dimension-four and five operators [14]. These arise since, in the SUSY SM, quarks and leptons have scalar partners (squarks and sleptons). Although our notation does not change, when discussing SUSY models our fields are chiral superfields and both fermionic and bosonic matter is implicitly represented by those. In this language, baryon- and/or lepton-number-violating dimension-four and five operators are given as so-called F terms of products of chiral superfields, which contain two fermionic components and the rest scalars or products of scalars. Within the context of $SU(5)$ the dimension-four and five operators have the form

$$(\mathbf{10}\ \bar{\mathbf{5}}\ \bar{\mathbf{5}}) \supset (u^c\ d^c\ d^c) + (Q\ L\ d^c) + (e^c\ L\ L),$$

$$(\mathbf{10}\ \mathbf{10}\ \mathbf{10}\ \bar{\mathbf{5}}) \supset (Q\ Q\ Q\ L) + (u^c\ u^c\ d^c\ e^c) + B\text{- and } L\text{-conserving terms},$$

respectively.

The dimension-four operators in $(\mathbf{10}\ \bar{\mathbf{5}}\ \bar{\mathbf{5}})$ violate either baryon number or lepton number. The nucleon lifetime is extremely short if both types of dimension-four operators are present in the SUSY SM since squark or slepton exchange induces the dangerous dimension-six SM operators. Even in the case that they violate baryon number or lepton number only but not both, they are constrained by various phenomena [91]. For example, the primordial baryon number in the Universe is washed out unless the dimensionless coupling constants are less than 10^{-7}. Both types of operators can be eliminated by requiring R parity, which distinguishes Higgs from ordinary matter multiplets. R parity [92] or its cousin, matter parity [6, 93], act as $F \to -F$, $H \to H$ with $F = \{\mathbf{10}, \bar{\mathbf{5}}\}$, $H = \{\bar{\mathbf{5}}_H, \mathbf{5}_H\}$ in $SU(5)$.[10] In $SU(5)$, the Higgs multiplet $\bar{\mathbf{5}}_H$ and the matter multiplets $\bar{\mathbf{5}}$ have identical gauge quantum numbers. In E_6, Higgs and matter multiplets could be unified within the fundamental **27** representation. Only in $SO(10)$ are Higgs and matter multiplets distinguished by their gauge quantum numbers. The Z_4 center of $SO(10)$ distinguishes **10**s from **16**s and can be associated with R parity [94].

The baryon-number violating dimension-five operators have a dimensionful coupling. They are generated by integrating out the color-triplet Higgs with GUT-scale mass in SUSY GUTs such that the coefficient is suppressed by $1/M_G$. Note that both triplet Higgsinos (due to their fermionic nature) and Higgs scalars (due to their mass-enhanced trilinear coupling with matter) contribute to the operators. The dimension-five operators include squarks and/or sleptons. To allow for nucleon decay, these must be converted to light quarks or leptons by exchange of a gaugino or Higgsino in the SUSY SM. The nucleon lifetime is proportional to $M_G^2\ m_{\mathrm{SUSY}}^2/m_p^5$, where m_{SUSY} is the SUSY breaking scale. Thus, dimension-five operators may predict a shorter nucleon lifetime than dimension-six operators. Unless accidental cancellations are present, the dominant decay modes from dimension-five operators include a K meson, such as $p \to K^+\ \bar{\nu}$ ($n \to K^0\ \bar{\nu}$). This is due to a simple symmetry argument: The operators are given as $(Q_i\ Q_j\ Q_k\ L_l)$ and $(u_i^c\ u_j^c\ d_k^c\ e_l^c)$, where $i, j, k, l\,(= 1, 2, 3)$ are family indices and color and weak indices are implicit. They must be invariant under $SU(3)_C$ and $SU(2)_L$ so that their color and weak doublet indices must be anti-symmetrized. Since these operators are given by bosonic superfields, they must be totally symmetric under interchange of all indices. Thus, the first operator vanishes for $i = j = k$ and the second vanishes for $i = j$. Hence a second or third generation member exists in the dominant modes of nucleon decay unless these modes are accidentally suppressed [93].

The Super-Kamiokande bounds on the proton lifetime severely constrain the dimension-five operators. With 306 kton-years of data they find $\tau_p/\mathrm{Br}(p \to K^+\bar{\nu}) > 6.61 \times 10^{33}$ years at 90% CL [87]. In the minimal SUSY $SU(5)$, $\tau_p/\mathrm{Br}(p \to K^+\bar{\nu})$ is smaller than about 10^{31} years if the triplet Higgs mass is 10^{16} GeV and $m_{\mathrm{SUSY}} = 1$ TeV [95]. The triplet Higgs mass bound from nucleon decay is then in conflict with gauge coupling unification so that this model is considered to be ruled out [74].

Since nucleon decay induced by the triplet Higgs is a severe problem in SUSY GUTs, various proposals for its suppression have been made. First, some accidental symmetry or accidental structure in non-minimal Higgs sectors in $SU(5)$ or $SO(10)$ theories may suppress the dimension-five operators [22, 26, 27, 96]. Symmetries to suppress the dimension-five operators are typically broken by the VEVs responsible for the color-triplet Higgs masses. Consequently, the dimension-five operators are generically generated via the triplet Higgs exchange in SUSY $SU(5)$ GUTs, as mentioned above. In other words, the nucleon decay is suppressed if the Higgs triplets in $\bar{\mathbf{5}}_H$ and $\mathbf{5}_H$ do not have a common mass term but, instead, their mass terms involve partners

[9] It is interesting to note that a ratio $M_*/M_c \sim 100$, needed for gauge coupling unification to work in orbifold GUTs, is typically the maximum value for this ratio consistent with perturbativity [84].

[10] This forbids the dimension-four operator $(\mathbf{10}\ \bar{\mathbf{5}}\ \bar{\mathbf{5}})$, but allows the Yukawa couplings for quark and lepton masses of the form $(\mathbf{10}\ \bar{\mathbf{5}}\ \bar{\mathbf{5}}_H)$ and $(\mathbf{10}\ \mathbf{10}\ \mathbf{5}_H)$. It also forbids the dimension-three, lepton-number-violating operator $(\bar{\mathbf{5}}\ \mathbf{5}_H) \supset (L\ H_u)$ as well as the dimension-five, baryon-number-violating operator $(\mathbf{10}\ \mathbf{10}\ \mathbf{10}\ \bar{\mathbf{5}}_H) \supset (Q\ Q\ Q\ H_d) + \cdots$.

Downloaded from https://academic.oup.com/ptep/article/2022/8/083C01/6651666 by KIT Library user on 27 September 2022

from other $SU(5)$ multiplets. Second, the SUSY breaking scale may be around $\mathcal{O}(10\text{–}100)$ TeV in order to explain the observed Higgs boson mass at the LHC. In this case, nucleon decay is automatically suppressed [78,97,98]. Third, accidental cancellations among diagrams due to a fine-tuned structure of squark and slepton flavor mixing might suppress nucleon decay [99]. Last, we have also implicitly assumed a hierarchical structure for Yukawa matrices in the analysis. It is however possible to fine-tune a hierarchical structure for quarks and leptons which baffles the family structure so that the nucleon decay is suppressed [100]. The upper bound on the proton lifetime from some of these theories is approximately a factor of 10 above the experimental bounds. Future experiments with larger neutrino detectors, such as JUNO [101], Hyper-Kamiokande [88] and DUNE [102], are planned and will have higher sensitivities to nucleon decay.

Are there ways to avoid the stringent predictions for proton decay discussed above? Orbifold GUTs and string theories, see Sec. 93.4, contain grand unified symmetries realized in higher dimensions. In the process of compactification and GUT symmetry breaking, the triplet Higgs states may be removed (projected out of the massless sector of the theory). In such models, the nucleon decay due to dimension-five operators can be severely suppressed or eliminated completely. However, nucleon decay due to dimension-six operators may be enhanced, since the gauge-bosons mediating proton decay obtain mass at the compactification scale, M_c, which is typically less than the 4d GUT scale (cf. Sec. 93.5). Alternatively, the same projections which eliminate the triplet Higgs may rearrange the quark and lepton states such that the massless states of one family come from different higher-dimensional GUT multiplets. This can suppress or completely eliminate even dimension-six proton decay. Thus, enhancement or suppression of dimension-six proton decay is model-dependent. In some complete 5d orbifold GUT models [63, 103] the lifetime for the decay $\tau_p/\mathrm{Br}(p \to e^+\pi^0)$ can be near the bound of 1×10^{34} years with, however, large model-dependence and/or theoretical uncertainties. In other cases, the modes $p \to K^+\bar{\nu}$ and $p \to K^0\mu^+$ may be dominant [63]. Thus, interestingly, the observation of nucleon decay may distinguish string or higher-dimensional GUTs from 4d ones.

In orbifold GUTs or string theory, new discrete symmetries consistent with SUSY GUTs can forbid all dimension-three and four baryon- and lepton-number-violating operators. Even the μ term and dimension-five baryon- and lepton-number-violating operators can be forbidden to all orders in perturbation theory [33]. The μ term and dimension-five baryon- and lepton-number-violating operators may then be generated, albeit sufficiently suppressed, via non-perturbative effects. The simplest example of this is a Z_4^R symmetry which is the unique discrete R symmetry consistent with $SO(10)$ [33]. Even though it forbids the dimension-five proton decay operator to the desired level, it allows the required dimension-five neutrino mass term. In this case, proton decay is dominated by dimension-six operators, leading to decays such as $p \to e^+\pi^0$.

93.7 Yukawa coupling unification

In the SM, masses and mixings for quarks and leptons come from the Yukawa couplings with the Higgs doublet, but the values of these couplings remain a mystery. GUTs provide at least a partial understanding since each generation is embedded in unified multiplet(s). Specifically, since quarks and leptons are two sides of the same coin, the GUT symmetry relates the Yukawa couplings (and hence the masses) of quarks and leptons.

In $SU(5)$, there are two types of independent renormalizable Yukawa interactions given by $\lambda_{ij}\ (\mathbf{10}_i\ \mathbf{10}_j\ \mathbf{5}_H) + \lambda'_{ij}\ (\mathbf{10}_i\ \bar{\mathbf{5}}_j\ \bar{\mathbf{5}}_H)$. These contain the SM interactions $\lambda_{ij}\ (Q_i\ u^c_j\ H_u) + \lambda'_{ij}\ (Q_i\ d^c_j\ H_d + e^c_i\ L_j\ H_d)$. Here $i, j\ (=1, 2, 3)$ are, as before, family indices. Hence, at the GUT scale we have tree-level relations between Yukawa coupling constants for charged lepton and down quark masses, such as $\lambda_b = \lambda_\tau$ in which $\lambda_{b/\tau}$ are the bottom quark $/\tau$ lepton Yukawa coupling constants [104,105]. In $SO(10)$, there is only one type of independent renormalizable Yukawa interaction given by $\lambda_{ij}\ (\mathbf{16}_i\ \mathbf{16}_j\ \mathbf{10}_H)$, leading to relations among all Yukawa coupling constants and quark and lepton masses within one generation [106,107] (such as $\lambda_t = \lambda_b = \lambda_\tau$, with λ_t the top quark Yukawa coupling constant).

In addition to gauge coupling unification, the ratio of bottom quark and τ lepton mass has been a central target in the study of GUTs since it was found that this ratio was almost consistent with observations after including the QCD correction [104]. Today the quark masses and the gauge coupling constants are known precisely such that, as discussed below, the ratio of bottom quark and τ lepton mass has become a target of precision analyses in the GUT context.

93.7.1 *The third generation, b–τ or t–b–τ unification*

Third generation Yukawa couplings are larger than those of the first two generations. Hence, the fermion mass relations predicted from renormalizable GUT interactions which we introduced above are expected to be more reliable. In order to compare them with data, we have to include the radiative correction to these relations from the RG evolution between GUT and fermion mass scale, from integrating out heavy particles at the GUT scale, and from weak scale thresholds.

Since testing Yukawa coupling unification is only possible in models with successful gauge coupling unification, we here focus on SUSY GUTs. In the MSSM, top and bottom quark and τ lepton masses are related to the Yukawa coupling constants at the scale m_Z as

$$\begin{aligned} m_t(m_Z) &= \lambda_t(m_Z)\ v_u(1 + \delta m_t/m_t), \\ m_{b/\tau}(m_Z) &= \lambda_{b/\tau}(m_Z)\ v_d(1 + \delta m_{b/\tau}/m_{b/\tau})\,, \end{aligned}$$

where $\langle H^0_u\rangle \equiv v_u = \sin\beta\ v/\sqrt{2}$, $\langle H^0_d\rangle \equiv v_d = \cos\beta\ v/\sqrt{2}$, $v_u/v_d \equiv \tan\beta$ and $v \sim 246$ GeV is fixed by the Fermi constant, G_μ. Here, $\delta m_f/m_f\ (f = t, b, \tau)$ represents the threshold correction due to integrating out SUSY partners. For the bottom quark mass, it is found [108] that the dominant corrections come from the gluino-sbottom and from the Higgsino-stop loops,

$$\begin{aligned} \left(\frac{\delta m_b}{m_b}\right)_{g3} &\sim \frac{g_3^2}{6\pi^2}\frac{m_{\tilde{g}}\mu}{m^2_{\mathrm{SUSY}}}\tan\beta \qquad \text{and} \\ \left(\frac{\delta m_b}{m_b}\right)_{\lambda_t} &\sim \frac{\lambda_t^2}{16\pi^2}\frac{A_t\mu}{m^2_{\mathrm{SUSY}}}\tan\beta\,, \end{aligned} \tag{93.16}$$

where $m_{\tilde{g}}$, μ, and A_t stand for gluino and Higgsino masses and trilinear stop coupling, respectively. Note that Eq. (93.16) only illustrates the structure of the corrections – non-trivial functional dependences on several soft parameters $\sim m_{\mathrm{SUSY}}$ have been suppressed. For the full one-loop correction to the bottom quark mass see, for example, Ref. [109].

Note also that the corrections do not go to zero as SUSY particles become much heavier than m_Z. They may change the bottom quark mass at the $\mathcal{O}(10)\%$ level for $\tan\beta = \mathcal{O}(10)$. The total effect is sensitive to the relative phase between gluino and Higgsino masses since $A_t \sim -m_{\tilde{g}}$ due to the infrared fixed point nature of the RG equation for A_t [110] in settings where SUSY breaking terms come from Planck scale dynamics, such as gravity mediation. The τ lepton mass also receives a similar correction, though only at the few % level. The top quark mass correction, not being proportional to $\tan\beta$, is at most 10% [111].

Including one loop threshold corrections at m_Z and additional RG running, one finds the top, bottom and τ pole masses. In SUSY GUTs, b–τ unification has two possible solutions with $\tan\beta \sim 1$ or $\mathcal{O}(10)$. The small $\tan\beta$ solution may be realized in the MSSM if superpartner masses are $\mathcal{O}(10)$ TeV, as suggested by the observed Higgs mass [97]. The large $\tan\beta$ limit such as $\tan\beta \sim 40$–50 overlaps the $SO(10)$ symmetry relation [111, 112]. When $\tan\beta$ is large, there are significant threshold corrections to down quark masses as mentioned above, and Yukawa unification is only consistent with low-energy data in a restricted region of SUSY parameter space, with important consequences for SUSY searches [111, 113]. More recent analyses of Yukawa unification after LHC Run-I are found in Ref. [114].

Gauge coupling unification is also successful in the scenario of split supersymmetry [78], in which squarks and sleptons have mass

Downloaded from https://academic.oup.com/ptep/article/2022/8/083C01/6651666 by KIT Library user on 27 September 2022

at a scale $\tilde{m} \gg m_Z$, while gauginos and/or Higgsinos have masses of order the weak scale. Unification of b–τ Yukawa couplings requires $\tan\beta$ to be fine-tuned close to 1 [97]. If by contrast, $\tan\beta \gtrsim 1.5$, b–τ Yukawa unification only works for $\tilde{m} \lesssim 10^4$ GeV. This is because the effective theory between the gaugino mass scale and $\tilde{m}$ includes only one Higgs doublet, as in the standard model. As a result, the large top quark Yukawa coupling tends to increase the ratio λ_b/λ_τ due to the vertex correction, which is absent in supersymmetric theories, as one runs down in energy below $\tilde{m}$. This is opposite to what happens in the MSSM where the large top quark Yukawa coupling lowers the ratio λ_b/λ_τ [105].

93.7.2 *Beyond leading order: three-family models*

Simple Yukawa unification is not possible for the first two generations. Indeed, the simplest implementation of $SU(5)$ implies $\lambda_s = \lambda_\mu$, $\lambda_d = \lambda_e$ and hence $\lambda_s/\lambda_d = \lambda_\mu/\lambda_e$. This is an RG-invariant relation which extrapolates to $m_s/m_d = m_\mu/m_e$ at the weak scale, in serious disagreement with data ($m_s/m_d \sim 20$ and $m_\mu/m_e \sim 200$). An elegant solution to this problem was given by Georgi and Jarlskog [115] (for a recent analysis in the SUSY context see [116]).

More generally, we have to recall that in all of the previous discussion of Yukawa couplings, we assumed renormalizable interactions as well as the minimal matter and Higgs content. Since the GUT scale is close to the Planck scale, higher-dimension operators involving the GUT-breaking Higgs may modify the predictions, especially for lower generations. An example is provided by the operators $\mathbf{10}\ \bar{\mathbf{5}}\ \bar{\mathbf{5}}_H\ \mathbf{24}_H$ with $\mathbf{24}_H$ the GUT-breaking Higgs of $SU(5)$. We can fit parameters to the observed fermion masses with these operators, though some fine-tuning is introduced in doing so. The SM Higgs doublet may come in part from higher representations of the GUT group. For example, the **45** of $SU(5)$ includes an $SU(2)_L$ doublet with appropriate $U(1)_Y$ charge [115]. This **45** can, in turn, come from the **120** or **126** of $SO(10)$ after its breaking to $SU(5)$ [117, 118]. These fields may also have renormalizable couplings with quarks and leptons. The relations among the Yukawa coupling constants in the SM are modified if the SM Higgs doublet is a linear combination of several such doublets from different $SU(5)$ multiplets. Finally, the SM fermions may not be embedded in GUT multiplets in the minimal way. Indeed, if all quarks and leptons are embedded in **16**s of $SO(10)$, the renormalizable interactions with $\mathbf{10}_H$ cannot explain the observed CKM mixing angles. This situation improves when extra matter multiplets, such as **10**, are introduced: After $U(1)_X$, which distinguishes the $\bar{\mathbf{5}}$s coming from the **16** and the **10** of $SO(10)$, is broken (e.g. by a VEV of $\mathbf{16}_H$ or $\mathbf{126}_H$), the r.h. down quarks and l.h. leptons in the SM can be linear combinations of components in **16**s and **10**s. As a result, $\lambda \neq \lambda'$ in $SU(5)$ [119].

To construct realistic three-family models, some or all of the above effects can be used. Even so, to achieve significant predictions for fermion masses and mixing angles grand unification alone is not sufficient. Other ingredients, for example additional global family symmetries are needed (in particular, non-Abelian symmetries can strongly reduce the number of free parameters). These family symmetries constrain the set of effective higher-dimensional fermion mass operators discussed above. In addition, sequential breaking of the family symmetry can be correlated with the hierarchy of fermion masses [120]. One simple, widely known idea in this context is to ensure that each $\mathbf{10}_i$ enters Yukawa interactions together with a suppression factor ϵ^{3-i} (ϵ being a small parameter). This way one automatically generates a stronger hierarchy in up-type quark Yukawas as compared to down-type quark and lepton Yukawas and no hierarchy for neutrinos, which agrees with observations at the $\mathcal{O}(1)$-level. Three-family models exist which fit all the data, including neutrino masses and mixing [27, 121].

Finally, a particularly ambitious variant of unification is to require that the fermions of all three generations come from a single representation of a large gauge group. A somewhat weaker assumption is that the flavor group (e.g. $SU(3)$) unifies with the SM gauge group in a simple gauge group at some energy scale $M \geq M_G$. Early work on such 'flavor-unified GUTs', see e.g. [119, 122], has been reviewed in [123, 124]. For a selection of more recent papers see [125]. In such settings, Yukawa couplings are generally determined by gauge couplings together with symmetry breaking VEVs. This is reminiscent of heterotic string GUTs, where all couplings come from the 10d gauge coupling. However, while the $E_8 \to SU(3)\times E_6$ branching rule $\mathbf{248} = (\mathbf{8},\mathbf{1}) + (\mathbf{1},\mathbf{78}) + (\mathbf{3},\mathbf{27}) + (\overline{\mathbf{3}},\overline{\mathbf{27}})$ looks very suggestive in this context, the way in which most modern heterotic models arrive at three generations is actually more complicated.

93.8 Neutrino masses

We see from atmospheric and solar neutrino oscillation observations, along with long baseline accelerator and reactor experiments, that neutrinos have finite masses. By adding three "sterile" neutrinos ν_i^c with Yukawa couplings $\lambda_{\nu,ij}\ (\nu_i^c\ L_j\ H_u)$ $(i,j = 1,2,3)$, one easily obtains three massive Dirac neutrinos with mass $m_\nu = \lambda_\nu\ v_u$, analogously to quark and charged lepton masses. However, in order to obtain a τ neutrino with mass of order 0.1 eV, one requires the exceedingly small coupling ratio $\lambda_{\nu_\tau}/\lambda_\tau \lesssim 10^{-10}$. By contrast, in GUTs the seesaw mechanism *naturally* explains such tiny neutrino masses as follows [2–4]: The sterile neutrinos have no SM gauge quantum numbers so that there is no symmetry other than global lepton number which forbids the Majorana mass term $\frac{1}{2}M_{ij}\ \nu_i^c\ \nu_j^c$. Note also that sterile neutrinos can be identified with the r.h. neutrinos necessarily contained in complete families of $SO(10)$ or Pati-Salam models. Since the Majorana mass term violates $U(1)_X$ in $SO(10)$, one might expect $M_{ij} \sim M_G$. The heavy sterile neutrinos can be integrated out, defining an effective low-energy theory with only three light active Majorana neutrinos with the effective dimension-five operator

$$-\mathcal{L}_{eff} = \frac{1}{2}c_{ij}\ (L_i\ H_u)\ (L_j\ H_u)\,, \tag{93.17}$$

where $c = \lambda_\nu^T\ M^{-1}\ \lambda_\nu$. This then leads to a 3×3 Majorana neutrino mass matrix $m = m_\nu^T\ M^{-1}\ m_\nu$.

The seesaw mechanism implemented by r.h. neutrinos is sometimes called the type-I seesaw model. There are variant models in which the dimension-five operator for neutrino masses is induced in different ways: In the type-II model, an $SU(2)_L$ triplet Higgs boson Σ is introduced to have couplings ΣL^2 and also ΣH_u^2 [117, 126]. In the type-III model, an $SU(2)_L$ triplet of fermions $\tilde{\Sigma}$ with a Yukawa coupling $\tilde{\Sigma} L H_u$ is introduced [127]. In these models, the dimension-five operator is induced by integrating out the triplet Higgs boson or fermions. Such models can also be implemented in GUTs by introducing Higgs bosons in the **15** or fermions in the **24** in $SU(5)$ GUTs or the **126** in $SO(10)$ GUTs. Notice that the gauge non-singlet fields in the type-II and III models have masses at the intermediate scale. Thus, gauge coupling unification is not automatic if these variant mechanisms are implemented in SUSY GUTs.

Atmospheric neutrino oscillations discovered by Super-Kamiokande [128] require neutrino masses with $\Delta m_\nu^2 \sim 2.5\times 10^{-3}$ eV^2 with maximal mixing [62], in the simplest scenario of two neutrino dominance. With hierarchical neutrino masses this implies $m_{\nu_\tau} = \sqrt{\Delta m_\nu^2} \sim 0.05$ eV. Next, we can try to relate the neutrino Yukawa coupling to the top quark Yukawa coupling, $\lambda_{\nu_\tau} = \lambda_t$ at the GUT scale, as in $SO(10)$ or $SU(4)\times SU(2)_L \times SU(2)_R$ models. This gives $M \sim 10^{14}$ GeV, which is remarkably close to the GUT scale.

Neutrinos pose a special problem for GUTs. The question is why the quark mixing angles in the CKM matrix are small while there are two large lepton mixing angles in the PMNS matrix. Global fits of neutrino masses and mixing angles can, for example, be found in Refs. [129] and [130]. For SUSY GUT models which fit quark and lepton masses, see Ref. [131] for reviews. Finally, for a compilation of the range of SUSY GUT predictions for neutrino mixing, see [132].

93.9 Selected topics

93.9.1 *Global symmetries*

As we discussed, global symmetries are frequently introduced to control higher-dimension operators in GUT models. This is particularly important in the context of nucleon decay but also plays a role in GUT-based flavor model building and cosmological applications, such as baryogenesis and inflation. However,

Downloaded from https://academic.oup.com/ptep/article/2022/8/083C01/6651666 by KIT Library user on 27 September 2022

we should note that appealing to global symmetries to suppress specific interactions may not be as straightforward as it naively seems. Indeed, there are two possibilities: On the one hand, the relevant symmetry might be gauged at a higher scale. Effects of the VEVs responsible for the spontaneous breaking are then in principle dangerous and need to be quantified. On the other hand, the symmetry might be truly only global. This must e.g. be the case for anomalous symmetries, which are then also violated by field-theoretic non-perturbative effects. The latter can in principle be exponentially small. It is, however, widely believed that global symmetries are always broken in quantum gravity (see e.g. [133]). One then needs to understand which power or functional form the Planck scale suppression of the relevant interaction has. For example, dimension-five baryon number violating operators suppressed by just one unit of the Planck or string scale are completely excluded.

In view of the above, it is also useful to recall that in string models 4d global symmetries generally originate in higher-dimensional gauge symmetries [38, 134]. Here 'global' implies that the gauge boson has acquired a Stückelberg-mass. This is a necessity in the anomalous case (Green-Schwarz mechanism [135]) but can also happen to non-anomalous symmetries. One expects no symmetry violation beyond the well-understood non-perturbative effects. Discrete symmetries arise as subgroups of continuous gauge symmetries, such as $\mathbb{Z}_N \subset U(1)$. In particular, non-anomalous subgroups of Stückelberg-massive $U(1)$s represent unbroken discrete gauge symmetries and as such are non-perturbatively exact (see e.g. [136]). Of course, such discrete gauge symmetries may also arise as remnants of continuous gauge symmetries after conventional 4d spontaneous breaking.

93.9.2 *Anomaly constraints vs. GUT paradigm*

As emphasized at the very beginning, the fact that the SM fermions of one generation fill out the $\mathbf{10}+\overline{\mathbf{5}}$ of $SU(5)$ appears to provide overwhelming evidence for some form of GUT embedding. However, one should be aware that a counterargument can be made which is related to the issue of 'charge quantization by anomaly cancellation' (see [137, 138] for some early papers and [139] for a more detailed reference list): Imagine we only knew that the low-energy gauge group were G_{SM} and the matter content included the $(\mathbf{3},\mathbf{2})_Y$, i.e. a 'quark doublet' with $U(1)$-charge Y. One can then ask which possibilities exist of adding further matter to ensure the cancellation of all triangle anomalies. It turns out that this problem has only three different, minimal[11] solutions [138]. One of those is precisely a single SM generation, with the apparent '$SU(5)$-ness' emerging accidentally. Thus, if one randomly picks models from the set of consistent gauge theories, preconditioning on G_{SM} and $(\mathbf{3},\mathbf{2})_Y$, one may easily end up with '$\mathbf{10}+\overline{\mathbf{5}}$' of an $SU(5)$ that is in no way dynamically present. This is precisely what happens in the context of non-GUT string model building [140].

93.9.3 *Magnetic monopoles*

In the broken phase of a GUT there are typically localized classical solutions carrying magnetic charge under an unbroken $U(1)$ symmetry [141]. These magnetic monopoles with mass of order M_G/α_G can be produced during a possible GUT phase transition in the early Universe. The flux of magnetic monopoles is experimentally found to be less than $\sim 10^{-16}$ cm^{-2} s^{-1} sr^{-1} [142]. Many more are however predicted, hence the GUT monopole problem. In fact, one of the original motivations for inflation was to solve the monopole problem by exponential expansion after the GUT phase transition [143] and hence dilution of the monopole density. Other possible solutions to the monopole problem include: sweeping them away by domain walls [144], $U(1)$ electromagnetic symmetry breaking at high temperature [145] or GUT symmetry non-restoration [146]. Parenthetically, it was also shown that GUT monopoles can catalyze nucleon decay [147]. A significantly stronger bound on the monopole flux can then be obtained by considering X-ray emission from radio pulsars due to monopole capture and the subsequent nucleon decay catalysis [148].

Note that the present upper bound on the inflationary vacuum energy density is very close to the GUT scale, $V_{inf}^{1/4} = (1.88\times 10^{16}\,\mathrm{GeV})\times(r/0.10)^{1/4}$, with the scalar-to-tensor ratio constrained to $r < 0.07$ [149]. This guarantees that reheating does not lead to temperatures above M_G and hence the monopole problem is solved by inflation (unless M_G is unexpectedly low).

93.9.4 *Flavor violation*

Yukawa interactions of GUT-scale particles with quarks and leptons may leave imprints on the flavor violation induced by SUSY breaking parameters [150]. To understand this, focus first on the MSSM with universal Planck-scale boundary conditions (as e.g. in gravity mediation). Working in a basis where up-quark and lepton Yukawas are diagonal, one finds that the large top-quark Yukawa coupling reduces the l.h. squark mass squareds in the third generation radiatively. It turns out that only the l.h. down-type squark mass matrix has sizable off-diagonal terms in the flavor basis after CKM-rotation. However, in GUTs the color-triplet Higgs has flavor violating interactions from the Yukawa coupling λ_{ij} $(\mathbf{10}_i\ \mathbf{10}_j\ \mathbf{5}_H)$, such that flavor-violating r.h. slepton mass terms are radiatively generated in addition [151]. In $SU(5)$ extension of the type-I seesaw model, where r.h. neutrinos are introduced as $SU(5)$ singlets with interactions λ''_{ij} $(\mathbf{1}_i\ \overline{\mathbf{5}}_j\ \mathbf{5}_H)$, the doublet and color-triplet Higgses acquire another type of Yukawa coupling, respectively. They then radiatively generate flavor-violating l.h. slepton [152] and r.h. down squark masses [153]. These flavor-violating SUSY breaking terms induce new contributions to FCNC processes in quark and lepton sectors, such as $\mu\to e\gamma$ and K^0–$\bar{K}^0$ and B^0–$\bar{B}^0$ mixing. Note that even if the SUSY breaking terms are generated at M_G, the r.h. neutrino Yukawa coupling may induce sizable flavor violation in l.h. slepton masses due to the running between M_G and the right-handed-neutrino mass scale.

EDMs are also induced when both l.h. and r.h. squarks/sleptons have flavor-violating mass terms with relative phases, as discussed for $SO(10)$ in [154] or for $SU(5)$ with r.h. neutrinos in [155]. Thus, such low-energy observables constrain GUT-scale interactions.

93.9.5 *From GUT baryogenesis to leptogenesis and B/L-violating transitions*

During inflation, any conserved quantum number is extremely diluted. Thus, one expects the observed baryon asymmetry of the Universe to originate at reheating or in the subsequent cosmological evolution. In detail, the situation is slightly more involved: Both baryon number B and lepton number L are global symmetries of the SM. However, $(B+L)$ is anomalous and violated by thermal fluctuations in the early Universe, via so-called sphaleron processes. Moreover, it is violated in GUT models, as is most apparent in proton decay. By contrast, $(B-L)$ is anomaly free and preserved by both the SM as well as $SU(5)$ or $SO(10)$ gauge interactions.

Now, the old idea of GUT baryogenesis [156,157] is to generate a $(B+L)$ and hence a baryon asymmetry by the out-of-equilibrium decay of the color-triplet Higgs. However such an asymmetry, generated at GUT temperatures, is washed out by sphalerons[12]. This can be overcome [159] using lepton-number violating interaction of neutrinos to create a $(B-L)$ from the $(B+L)$ asymmetry, before sphaleron processes become sufficiently fast at $T < 10^{12}$ GeV. This $(B-L)$ asymmetry can then survive the subsequent sphaleron dominated phase. Note that this does not work in the minimal SUSY GUT setting, with the triplet Higgs above the GUT scale. The reason is that a correspondingly high reheating temperature would be required which, as explained above, is ruled out by Planck data.

However, the most widely accepted simple way out of the dilemma is to directly generate a net $(B-L)$ asymmetry dynamically in the early Universe, also using r.h. neutrinos. Indeed, we have seen that neutrino oscillations suggest a new scale of physics

[11] Adding extra vector-like sets of fields, e.g. two fermions which only transform under $U(1)$ and have charges Y and $-Y$, is considered to violate minimality.

[12] To be precise, if lepton flavor numbers L_i $(i = 1\text{–}3)$ are nonzero and $(L_i - L_j) \neq 0$ $(i \neq j)$, one may obtain nonzero values for B and L even if $(B-L) = 0$ [158].

Downloaded from https://academic.oup.com/ptep/article/2022/8/083C01/6651666 by KIT Library user on 27 September 2022

of order 10^{14} GeV. This scale is associated with heavy Majorana neutrinos in the seesaw mechanism. If in the early Universe, the decay of the heavy neutrinos is out of equilibrium and violates both lepton number and CP, then a net lepton number may be generated. This lepton number will then be partially converted into baryon number via electroweak processes [160]. This mechanism is called leptogenesis.

If the three heavy Majorana neutrino masses are hierarchical, the net lepton number is produced by decay of the lightest one, and it is proportional to the CP asymmetry in the decay. The CP asymmetry is bounded from above, and the lightest neutrino mass is required to be larger than 10^9 GeV in order to explain the observed baryon asymmetry [161]. This implies that the reheating temperature after inflation should be larger than 10^9 GeV so that the heavy neutrinos are thermally produced[13]. In supersymmetric models, there is a tension between leptogenesis and Big Bang Nucleosynthesis (BBN) if gravitinos decay in the BBN era. The gravitino problem gives a constraint on the reheating temperature $\lesssim 10^{6-10}$ GeV though the precise value depends on the SUSY breaking parameters [163]. Recent reviews of leptogenesis can be found in Ref. [164].

One of the important tests of leptogenesis are searches for neutrinoless double-β ($0\nu\beta\beta$) decays[14]. In a $0\nu\beta\beta$ decay, only two electrons but no (anti-)neutrinos are emitted by the decaying nucleus. This is in contrast to ordinary double-β decay. Thus, $0\nu\beta\beta$ decays are lepton-number-violating with $\Delta L = 2$. At the nucleon level, this is described by dimension-nine effective operators for $nn \to ppee$. These operators may in turn come from SM operators of with dimension less than nine, in combination with SM weak interactions. The lowest one is the dimension-five operator generating the Majorana neutrino mass terms (Eq. (93.17)). Thus, if the lepton-number violating effective interactions come from physics at energies much above the weak scale, the $0\nu\beta\beta$ decay rates are proportional to the Majorana neutrino masses. The latest experimental results are reviewed in [62]. For recent studies of the $0\nu\beta\beta$ decay including SM operators up to mass dimension nine, see [165] and refs. therein.

In addition to L-violation, one can consider $(B-L)$ and B violating phenomena. They are interesting in their own right and may also be relevant to baryogenesis. The relevant operators have higher mass dimension than the familiar dimension-six $(B+L)$-violating operators (cf. Sec. 93.6). They may be predicted in SO(10) GUTs with an intermediate scale, at which baryogenesis is realized, such as in [166]. First, one may have nucleon decays with $\Delta(B-L) = 2$, such as $n \to e^-\pi^+$. This is induced by dimension-seven effective operators in the SM, which are suppressed by the SM Higgs VEV or derivatives. Second, there are neutron-antineutron (n–$\bar{n}$) oscillations, which are induced by $\Delta B = 2$ dimension-nine effective operators in the SM. The upper bound on the mean time for n–$\bar{n}$ transitions is directly derived using free neutrons [167]. It is also constrained from the lower limit on the lifetime for neutrons bound in ^{16}O, derived by Super-Kamiokande [168]. Their results are very similar. Super-Kamiokande also searches for dinucleon decays with $\Delta B = 2$, such as $pp \to \pi^+\pi^+$ and $nn \to \pi^\pm\pi^\mp$ [169].

93.10 Conclusion

Most conservatively, grand unification means that (some of) the SM gauge interactions of $U(1)_Y$, $SU(2)_L$ and $SU(3)_C$ become part of a larger, unifying gauge symmetry at a high energy scale. In most models, especially in the simplest and most appealing variants of $SU(5)$ and $SO(10)$ unification, the statement is much stronger: One expects the three gauge couplings to unify (up to small threshold corrections) at a unique scale, M_G, and the proton to be unstable due to exchange of gauge bosons of the larger symmetry group. Supersymmetric grand unified theories provide, by far, the most predictive and economical framework allowing for perturbative unification. Many more details than could be discussed in the present article can be found in some of the classic reviews [123,170] and the two books [171] (see also [172] for two recent overviews).

Thus, the three classical pillars of GUTs are gauge coupling unification at $M_G \sim 2 \times 10^{16}$ GeV, low-energy supersymmetry (with a large SUSY desert), and nucleon decay. The first of these may be viewed as predicting the value of the strong coupling – a prediction which has already been verified (see Fig. 93.1). Numerically, this prediction remains intact even if SUSY partner masses are somewhat above the weak scale. However, at the conceptual level a continuously increasing lower bound on the SUSY scale is nevertheless problematic for the GUT paradigm: Indeed, if the independent, gauge-hierarchy-based motivation for SUSY is completely abandoned, the SUSY scale and hence α_3 become simply free parameters and the first two pillars crumble. Thus, it is important to keep pushing bounds on proton decay which, although again not completely universal in all GUT constructions, is arguably a more generic part of the GUT paradigm than low-energy SUSY.

Whether or not Yukawa couplings unify is more model dependent. However, irrespective of possible (partial) Yukawa unification, there certainly exists a very interesting and potentially fruitful interplay between flavor model building and grand unification. Especially in the neutrino sector this is strongly influenced by the developing experimental situation.

Another phenomenological signature of grand unification is the strength of the direct coupling of the QCD axion to photons, relative to its coupling to gluons. It is quantified by the predicted anomaly ratio $E/N = 8/3$ (see [173, 174]). This arises in field-theoretic axion models consistent with GUT symmetry (such as DFSZ [175]) and in string-theoretic GUTs [174,176]. In the latter, the axion does not come from the phase of a complex scalar but is a fundamental shift-symmetric real field, coupling through a higher-dimension operator directly to the product of the GUT field-strength and its dual.

It is probably fair to say that, due to limitations of the 4d approach, including especially remaining ambiguities (free parameters or ad hoc assumptions) in models of flavor and GUT breaking, the string theoretic approach has become more important in GUT model building. In this framework, challenges include learning how to deal with the many vacua of the 'landscape' as well as, for each vacuum, developing the tools for reliably calculating detailed, phenomenological observables. Finally, due to limitations of space, the present article has barely touched on the interesting cosmological implications of GUTs. They may become more important in the future, especially in the case that a high inflationary energy scale is established observationally.

[13] This constraint may be avoided in resonant leptogenesis [162], in which the right-handed neutrinos are required to be almost degenerate in mass.

[14] Another important test of leptogenesis would be the observation of CP violation in neutrino oscillations. Strictly speaking, the CP phase in the PMNS matrix does not contribute to ϵ_1 in the seesaw model. Nevertheless, the observation of CP violation in neutrino oscillations would suggest that the seesaw mechanism is associated with a large CP violation, similarly to the quark sector.

References

[1] S. Weinberg, Phys. Rev. Lett. **43**, 1566 (1979).

[2] P. Minkowski, Phys. Lett. **67B**, 421 (1977).

[3] T. Yanagida, in *Proceedings of the Workshop on the Unified Theory and the Baryon Number of the Universe*, eds. O. Sawada and A. Sugamoto, KEK report No. 79-18, Tsukuba, Japan, 1979; S. Glashow, Quarks and leptons, published in *Proceedings of the Carg'ese Lectures*, M. Levy (ed.), Plenum Press, New York, (1980); M. Gell-Mann, P. Ramond and R. Slansky, in *Supergravity*, ed. P. van Nieuwenhuizen *et al.*, North-Holland, Amsterdam, (1979), p. 315 [arXiv:1306.4669].

[4] F. Wilczek, eConf **C790823**, 437 (1979); E. Witten, Phys. Lett. **91B**, 81 (1980); R. N. Mohapatra and G. Senjanovic, Phys. Rev. Lett. **44**, 912 (1980), [,231(1979)].

[5] G. 't Hooft, NATO Sci. Ser. B **59**, 135 (1980); M. J. G. Veltman, Acta Phys. Polon. **B12**, 437 (1981); L. Maiani, Gif-sur-Yvette Summer School on Particle Physics, 11th, Gif-sur-Yvette, France, 1979 (Inst. Nat. Phys. Nucl. Phys. Particules, Paris, 1979); E. Witten, Nucl. Phys. **B188**, 513 (1981).

[6] S. Dimopoulos, S. Raby and F. Wilczek, Phys. Rev. **D24**, 1681 (1981); S. Dimopoulos and H. Georgi, Nucl. Phys.

Downloaded from https://academic.oup.com/ptep/article/2022/8/083C01/6651666 by KIT Library user on 27 September 2022

B193, 150 (1981); L. E. Ibanez and G. G. Ross, Phys. Lett. **105B**, 439 (1981); N. Sakai, Z. Phys. **C11**, 153 (1981); M. B. Einhorn and D. R. T. Jones, Nucl. Phys. **B196**, 475 (1982); W. J. Marciano and G. Senjanovic, Phys. Rev. **D25**, 3092 (1982).

[7] U. Amaldi, W. de Boer and H. Furstenau, Phys. Lett. **B260**, 447 (1991); J. R. Ellis, S. Kelley and D. V. Nanopoulos, Phys. Lett. **B260**, 131 (1991); P. Langacker and M.-x. Luo, Phys. Rev. **D44**, 817 (1991); C. Giunti, C.W. Kim and U.W. Lee, Mod. Phys. Lett. **A6**, 1745 (1991); P. Langacker and N. Polonsky, Phys. Rev. **D47**, 4028 (1993), [hep-ph/9210235]; M. Carena, S. Pokorski and C. E. M. Wagner, Nucl. Phys. **B406**, 59 (1993), [hep-ph/9303202]; See also the review by S. Dimopoulos, S.A. Raby and F. Wilczek, Physics Today, p. 25 October (1991).

[8] Y. Okada, M. Yamaguchi and T. Yanagida, Prog. Theor. Phys. **85**, 1 (1991); J. R. Ellis, G. Ridolfi and F. Zwirner, Phys. Lett. **B257**, 83 (1991); H. E. Haber and R. Hempfling, Phys. Rev. Lett. **66**, 1815 (1991).

[9] M. Carena *et al.*, Phys. Lett. **B355**, 209 (1995), [hep-ph/9504316]; G. Degrassi *et al.*, Eur. Phys. J. **C28**, 133 (2003), [hep-ph/0212020]; P. Kant *et al.*, JHEP **08**, 104 (2010), [arXiv:1005.5709].

[10] J. L. Feng *et al.*, Phys. Rev. Lett. **111**, 131802 (2013), [arXiv:1306.2318]; S. Heinemeyer (2014), [arXiv:1405.3781]; P. Draper and H. Rzehak, Phys. Rept. **619**, 1 (2016), [arXiv:1601.01890].

[11] J. C. Pati and A. Salam, Phys. Rev. **D8**, 1240 (1973); For more discussion on the standard charge assignments in this formalism, see A. Davidson, Phys. Rev. **D20**, 776 (1979) and R.N Mohapatra and R.E. Marshak, Phys. Lett. **B91**, 222 (1980); see also J. C. Pati, Int. J. Mod. Phys. A **32**, 1741013 (2017), arXiv:1706.09531 for a recent account.

[12] H. Georgi and S. L. Glashow, Phys. Rev. Lett. **32**, 438 (1974).

[13] J. R. Ellis, M. K. Gaillard and D. V. Nanopoulos, Phys. Lett. **80B**, 360 (1979), [Erratum: Phys. Lett.82B,464(1979)]; E. Golowich, Phys. Rev. **D24**, 2899 (1981).

[14] S. Weinberg, Phys. Rev. **D26**, 287 (1982); N. Sakai and T. Yanagida, Nucl. Phys. **B197**, 533 (1982).

[15] H. Georgi, Particles and Fields, *Proceedings of the APS Div. of Particles and Fields*, ed. C. Carlson, p. 575 (1975); H. Fritzsch and P. Minkowski, Annals Phys. **93**, 193 (1975).

[16] R. Slansky, Phys. Rept. **79**, 1 (1981); H. Georgi, Front. Phys. **54**, 1 (1982); R. Feger and T. W. Kephart, Comput. Phys. Commun. **192**, 166 (2015), [arXiv:1206.6379]; N. Yamatsu, PTEP **2016**, 4, 043B02 (2016), [arXiv:1512.05559].

[17] S. M. Barr, Phys. Lett. **112B**, 219 (1982); J. P. Derendinger, J. E. Kim and D. V. Nanopoulos, Phys. Lett. **139B**, 170 (1984); I. Antoniadis *et al.*, Phys. Lett. **B194**, 231 (1987); I. Antoniadis *et al.*, Phys. Lett. **B231**, 65 (1989).

[18] F. Gursey, P. Ramond and P. Sikivie, Phys. Lett. **60B**, 177 (1976).

[19] A. de Rujula, H. Georgi and S. L. Glashow, *5th Workshop on Grand Unification*, ed. K. Kang, H. Fried and P. Frampton, World Scientific, Singapore (1984), p. 88; See also earlier paper by Y. Achiman and B. Stech, p. 303, "New Phenomena in Lepton-Hadron Physics," ed. D.E.C. Fries and J. Wess, Plenum, NY (1979).

[20] B. R. Greene *et al.*, Nucl. Phys. **B278**, 667 (1986); B. R. Greene *et al.*, Nucl. Phys. **B292**, 606 (1987); B. R. Greene, C. A. Lutken and G. G. Ross, Nucl. Phys. **B325**, 101 (1989); J. E. Kim, Phys. Lett. **B591**, 119 (2004), [hep-ph/0403196].

[21] E. Witten, Phys. Lett. **105B**, 267 (1981).

[22] A. Masiero *et al.*, Phys. Lett. **115B**, 380 (1982); B. Grinstein, Nucl. Phys. **B206**, 387 (1982).

[23] S. Dimopoulos and F. Wilczek, *Proceedings Erice Summer School*, ed. A. Zichichi (1981); M. Srednicki, Nucl. Phys. **B202**, 327 (1982).

[24] K. Inoue, A. Kakuto and H. Takano, Prog. Theor. Phys. **75**, 664 (1986).

[25] Y. Yamada, Z. Phys. **C60**, 83 (1993); J. Hisano *et al.*, Phys. Lett. **B342**, 138 (1995), [hep-ph/9406417]; G. Altarelli, F. Feruglio and I. Masina, JHEP **11**, 040 (2000), [hep-ph/0007254].

[26] K. S. Babu and S. M. Barr, Phys. Rev. **D48**, 5354 (1993), [hep-ph/9306242]; K. S. Babu and S. M. Barr, Phys. Rev. **D50**, 3529 (1994), [hep-ph/9402291]; K. S. Babu, J. C. Pati and Z. Tavartkiladze, JHEP **06**, 084 (2010), [arXiv:1003.2625].

[27] K. S. Babu and R. N. Mohapatra, Phys. Rev. Lett. **74**, 2418 (1995), [hep-ph/9410326]; V. Lucas and S. Raby, Phys. Rev. **D54**, 2261 (1996), [hep-ph/9601303]; T. Blazek *et al.*, Phys. Rev. **D56**, 6919 (1997), [hep-ph/9611217]; S. M. Barr and S. Raby, Phys. Rev. Lett. **79**, 4748 (1997), [hep-ph/9705366]; K. S. Babu, J. C. Pati and F. Wilczek, Nucl. Phys. **B566**, 33 (2000), [hep-ph/9812538]; R. Dermisek, A. Mafi and S. Raby, Phys. Rev. **D63**, 035001 (2001), [hep-ph/0007213].

[28] R. Barbieri, G. R. Dvali and A. Strumia, Nucl. Phys. **B391**, 487 (1993); Z. Berezhiani, C. Csaki and L. Randall, Nucl. Phys. **B444**, 61 (1995), [hep-ph/9501336]; Q. Shafi and Z. Tavartkiladze, Phys. Lett. **B522**, 102 (2001), [hep-ph/0105140].

[29] G. F. Giudice and A. Masiero, Phys. Lett. **B206**, 480 (1988); J. E. Kim and H. P. Nilles, Mod. Phys. Lett. **A9**, 3575 (1994), [hep-ph/9406296].

[30] L. Randall and C. Csaki, in "Supersymmetry and unification of fundamental interactions. Proceedings, International Workshop, SUSY 95, Palaiseau, France, May 15-19, 1995," 99–109 (1995), [,235(1995)], [hep-ph/9508208].

[31] E. Witten, in "Supersymmetry and unification of fundamental interactions. Proceedings, 10th International Conference, SUSY'02, Hamburg, Germany, June 17-23, 2002," 472–491 (2001), [hep-ph/0201018], URL `http://www-library.desy.de/preparch/desy/proc/proc02-02/Proceedings/susy02/special/hertz_pr.ps`; M. Dine, Y. Nir and Y. Shadmi, Phys. Rev. **D66**, 115001 (2002), [hep-ph/0206268].

[32] A. Hebecker, J. March-Russell and R. Ziegler, JHEP **08**, 064 (2009), [arXiv:0801.4101]; F. Brummer *et al.*, JHEP **08**, 011 (2009), [arXiv:0906.2957]; F. Brummer *et al.*, JHEP **04**, 006 (2010), [arXiv:1003.0084].

[33] H. M. Lee *et al.*, Phys. Lett. **B694**, 491 (2011), [arXiv:1009.0905]; R. Kappl *et al.*, Nucl. Phys. **B847**, 325 (2011), [arXiv:1012.4574]; H. M. Lee *et al.*, Nucl. Phys. **B850**, 1 (2011), [arXiv:1102.3595].

[34] Y. Hosotani, Phys. Lett. **126B**, 309 (1983).

[35] L. J. Dixon *et al.*, Nucl. Phys. **B261**, 678 (1985), [,678(1985)]; L. J. Dixon *et al.*, Nucl. Phys. **B274**, 285 (1986); L. E. Ibanez, H. P. Nilles and F. Quevedo, Phys. Lett. **B187**, 25 (1987); L. E. Ibanez *et al.*, Phys. Lett. **B191**, 282 (1987).

[36] P. Candelas *et al.*, Nucl. Phys. **B258**, 46 (1985).

[37] Y. Kawamura, Prog. Theor. Phys. **103**, 613 (2000), [hep-ph/9902423]; Y. Kawamura, Prog. Theor. Phys. **105**, 999 (2001), [hep-ph/0012125]; G. Altarelli and F. Feruglio, Phys. Lett. **B511**, 257 (2001), [hep-ph/0102301]; L. J. Hall and Y. Nomura, Phys. Rev. **D64**, 055003 (2001), [hep-ph/0103125]; A. Hebecker and J. March-Russell, Nucl. Phys. **B613**, 3 (2001), [hep-ph/0106166]; T. Asaka, W. Buchmuller and L. Covi, Phys. Lett. **B523**, 199 (2001), [hep-ph/0108021]; L. J. Hall *et al.*, Phys. Rev. **D65**, 035008 (2002), [hep-ph/0108071]; R. Dermisek and A. Mafi, Phys. Rev. **D65**, 055002 (2002), [hep-ph/0108139];

Downloaded from https://academic.oup.com/ptep/article/2022/8/083C01/6651666 by KIT Library user on 27 September 2022

H. D. Kim and S. Raby, JHEP **01**, 056 (2003), [hep-ph/0212348].

[38] L.E. Ibanez and A.M. Uranga, "String theory and particle physics: An introduction to string phenomenology," Cambridge University Press 2012; K.-S. Choi and J. E. Kim, Lect. Notes Phys. **696**, 1 (2006); R. Blumenhagen *et al.*, Phys. Rept. **445**, 1 (2007), [hep-th/0610327].

[39] D. J. Gross *et al.*, Phys. Rev. Lett. **54**, 502 (1985).

[40] V. Braun *et al.*, JHEP **05**, 043 (2006), [hep-th/0512177]; V. Bouchard and R. Donagi, Phys. Lett. **B633**, 783 (2006), [hep-th/0512149]; L. B. Anderson *et al.*, Phys. Rev. **D84**, 106005 (2011), [arXiv:1106.4804].

[41] L. J. Dixon, V. Kaplunovsky and J. Louis, Nucl. Phys. **B355**, 649 (1991).

[42] G. Aldazabal *et al.*, Nucl. Phys. **B452**, 3 (1995), [hep-th/9410206]; Z. Kakushadze *et al.*, Int. J. Mod. Phys. **A13**, 2551 (1998), [hep-th/9710149].

[43] E. Witten, Nucl. Phys. **B258**, 75 (1985).

[44] S. Gukov *et al.*, Phys. Rev. **D69**, 086008 (2004), [hep-th/0310159]; G. Curio, A. Krause and D. Lust, Fortsch. Phys. **54**, 225 (2006), [hep-th/0502168]; L. B. Anderson *et al.*, Phys. Rev. **D83**, 106011 (2011), [arXiv:1102.0011].

[45] R. Friedman, J. Morgan and E. Witten, Commun. Math. Phys. **187**, 679 (1997), [hep-th/9701162].

[46] R. Blumenhagen, G. Honecker and T. Weigand, JHEP **08**, 009 (2005), [hep-th/0507041]; L. B. Anderson *et al.*, JHEP **01**, 047 (2014), [arXiv:1307.4787].

[47] T. Kobayashi, S. Raby and R.-J. Zhang, Phys. Lett. **B593**, 262 (2004), [hep-ph/0403065].

[48] S. Forste *et al.*, Phys. Rev. **D70**, 106008 (2004), [hep-th/0406208]; T. Kobayashi, S. Raby and R.-J. Zhang, Nucl. Phys. **B704**, 3 (2005), [hep-ph/0409098]; W. Buchmuller *et al.*, Nucl. Phys. **B712**, 139 (2005), [hep-ph/0412318]; W. Buchmuller *et al.*, Phys. Rev. Lett. **96**, 121602 (2006), [hep-ph/0511035]; W. Buchmuller *et al.*, Nucl. Phys. **B785**, 149 (2007), [hep-th/0606187]; O. Lebedev *et al.*, Phys. Lett. **B645**, 88 (2007), [hep-th/0611095]; J. E. Kim, J.-H. Kim and B. Kyae, JHEP **06**, 034 (2007), [hep-ph/0702278]; O. Lebedev *et al.*, Phys. Rev. **D77**, 046013 (2008), [arXiv:0708.2691].

[49] S. B. Giddings, S. Kachru and J. Polchinski, Phys. Rev. **D66**, 106006 (2002), [hep-th/0105097]; S. Kachru *et al.*, Phys. Rev. **D68**, 046005 (2003), [hep-th/0301240].

[50] R. Blumenhagen *et al.*, Nucl. Phys. **B815**, 1 (2009), [arXiv:0811.2936].

[51] R. Blumenhagen *et al.*, Nucl. Phys. **B616**, 3 (2001), [hep-th/0107138].

[52] R. Donagi and M. Wijnholt, Adv. Theor. Math. Phys. **15**, 5, 1237 (2011), [arXiv:0802.2969].

[53] C. Beasley, J. J. Heckman and C. Vafa, JHEP **01**, 058 (2009), [arXiv:0802.3391]; C. Beasley, J. J. Heckman and C. Vafa, JHEP **01**, 059 (2009), [arXiv:0806.0102].

[54] T. Weigand, Class. Quant. Grav. **27**, 214004 (2010), [arXiv:1009.3497]; J. J. Heckman, Ann. Rev. Nucl. Part. Sci. **60**, 237 (2010), [arXiv:1001.0577]; M. Cvetic, I. Garcia-Etxebarria and J. Halverson, JHEP **01**, 073 (2011), [arXiv:1003.5337]; A. Maharana and E. Palti, Int. J. Mod. Phys. **A28**, 1330005 (2013), [arXiv:1212.0555]; S. Krippendorf, S. Schafer-Nameki and J.-M. Wong, JHEP **11**, 008 (2015), [arXiv:1507.05961].

[55] R. Donagi and M. Wijnholt, Adv. Theor. Math. Phys. **15**, 6, 1523 (2011), [arXiv:0808.2223]; R. Blumenhagen, Phys. Rev. Lett. **102**, 071601 (2009), [arXiv:0812.0248]; K.-S. Choi and J. E. Kim, Phys. Rev. **D83**, 065016 (2011), [arXiv:1012.0847]; C. Mayrhofer, E. Palti and T. Weigand, JHEP **09**, 082 (2013), [arXiv:1303.3589]; G. K. Leontaris and Q. Shafi, Phys. Rev. **D96**, 6, 066023 (2017), [arXiv:1706.08372].

[56] E. Witten, Nucl. Phys. **B471**, 135 (1996), [hep-th/9602070].

[57] A. Hebecker and M. Trapletti, Nucl. Phys. **B713**, 173 (2005), [hep-th/0411131].

[58] B. Dundee and S. Raby (2008), [arXiv:0808.0992].

[59] G. G. Ross (2004), [hep-ph/0411057].

[60] H. Georgi, H. R. Quinn and S. Weinberg, Phys. Rev. Lett. **33**, 451 (1974); S. Weinberg, Phys. Lett. **91B**, 51 (1980); L. J. Hall, Nucl. Phys. **B178**, 75 (1981).

[61] B. C. Allanach, Comput. Phys. Commun. **143**, 305 (2002), [hep-ph/0104145].

[62] M. Tanabashi *et al.* (Particle Data Group), Phys. Rev. **D98**, 3, 030001 (2018).

[63] M. L. Alciati *et al.*, JHEP **03**, 054 (2005), [hep-ph/0501086].

[64] See talks on proposed and running nucleon decay experiments, and theoretical talks by P. Langacker, p. 131, and W.J. Marciano and A. Sirlin, p. 151, in *The Second Workshop on Grand Unification*, eds. J.P. Leveille *et al.*, Birkhäuser, Boston (1981).

[65] W.J. Marciano, p. 190, *Eighth Workshop on Grand Unification*, ed. K. Wali, World Scientific Publishing Co., Singapore (1987).

[66] M.S. Carena *et al.*, in Ref. [7].

[67] A. Djouadi, J.-L. Kneur and G. Moultaka, Comput. Phys. Commun. **176**, 426 (2007), [hep-ph/0211331].

[68] W. Porod and F. Staub, Comput. Phys. Commun. **183**, 2458 (2012), [arXiv:1104.1573].

[69] W. Siegel, Phys. Lett. **94B**, 37 (1980).

[70] I. Antoniadis, C. Kounnas, and R. Lacaze, Nucl. Phys. **B221**, 377 (1983).

[71] M. A. Shifman, Int. J. Mod. Phys. **A11**, 5761 (1996), [hep-ph/9606281]; N. Arkani-Hamed and H. Murayama, JHEP **06**, 030 (2000), [hep-th/9707133]; I. Jack, D. R. T. Jones and A. Pickering, Phys. Lett. **B435**, 61 (1998), [hep-ph/9805482].

[72] M.B. Einhorn and D.R.T. Jones in Ref. [6]; I. Antoniadis, C. Kounnas and K. Tamvakis, Phys. Lett. **119B**, 377 (1982).

[73] J. Hisano, H. Murayama and T. Yanagida, Phys. Rev. Lett. **69**, 1014 (1992); J. Hisano, H. Murayama and T. Yanagida, Nucl. Phys. **B402**, 46 (1993), [hep-ph/9207279].

[74] H. Murayama and A. Pierce, Phys. Rev. **D65**, 055009 (2002), [hep-ph/0108104].

[75] G. Anderson *et al.*, eConf **C960625**, SUP107 (1996) [hep-ph/9609457].

[76] L. Roszkowski and M. A. Shifman, Phys. Rev. **D53**, 404 (1996), [hep-ph/9503358]; S. Raby, M. Ratz and K. Schmidt-Hoberg, Phys. Lett. **B687**, 342 (2010), [arXiv:0911.4249].

[77] J. Hisano, T. Kuwahara and N. Nagata, Phys. Lett. **B723**, 324 (2013), [arXiv:1304.0343].

[78] N. Arkani-Hamed, A. Delgado and G. F. Giudice, Nucl. Phys. **B741**, 108 (2006), [hep-ph/0601041].

[79] M. Ibe, T. Moroi and T. T. Yanagida, Phys. Lett. **B644**, 355 (2007), [hep-ph/0610277].

[80] G. F. Giudice *et al.*, JHEP **12**, 027 (1998), [hep-ph/9810442]; L. Randall and R. Sundrum, Nucl. Phys. **B557**, 79 (1999), [hep-th/9810155].

[81] R. N. Mohapatra and M. K. Parida, Phys. Rev. **D47**, 264 (1993), [hep-ph/9204234].

[82] D.-G. Lee *et al.*, Phys. Rev. **D51**, 229 (1995), [hep-ph/9404238].

[83] L. E. Ibanez *et al.*, JHEP **07**, 195 (2012), [arXiv:1206.2655].

[84] K. R. Dienes, E. Dudas and T. Gherghetta, Phys. Rev. Lett. **91**, 061601 (2003), [hep-th/0210294].

[85] K. Agashe, R. Contino and R. Sundrum, Phys. Rev. Lett. **95**, 171804 (2005), [hep-ph/0502222].

Downloaded from https://academic.oup.com/ptep/article/2022/8/083C01/6651666 by KIT Library user on 27 September 2022

[86] F. Wilczek and A. Zee, Phys. Rev. Lett. **43**, 1571 (1979).

[87] K. Abe *et al.* (Super-Kamiokande), Phys. Rev. **D95**, 1, 012004 (2017), [arXiv:1610.03597]; S. Mine (Super Kamiokande), J. Phys. Conf. Ser. **718**, 6, 062044 (2016).

[88] K. Abe *et al.* (Hyper-Kamiokande) (2018), [arXiv:1805.04163].

[89] Y. Aoki *et al.*, Phys. Rev. **D96**, 1, 014506 (2017), [arXiv:1705.01338].

[90] J. Hisano, T. Kuwahara and Y. Omura, Nucl. Phys. **B898**, 1 (2015), [Erratum: Nucl. Phys.B907,476(2016)], [arXiv:1503.08561].

[91] R. Barbier *et al.*, Phys. Rept. **420**, 1 (2005), [hep-ph/0406039]; F. Domingo *et al.*, JHEP **02**, 066 (2019), [arXiv:1810.08228].

[92] G. R. Farrar and P. Fayet, Phys. Lett. **76B**, 575 (1978).

[93] S. Dimopoulos, S. Raby and F. Wilczek, Phys. Lett. **112B**, 133 (1982); J. R. Ellis, D. V. Nanopoulos and S. Rudaz, Nucl. Phys. **B202**, 43 (1982).

[94] C. S. Aulakh *et al.*, Nucl. Phys. **B597**, 89 (2001), [hep-ph/0004031].

[95] T. Goto and T. Nihei, Phys. Rev. **D59**, 115009 (1999), [hep-ph/9808255].

[96] G. D. Coughlan *et al.*, Phys. Lett. **160B**, 249 (1985); J. L. Chkareuli and I. G. Gogoladze, Phys. Rev. **D58**, 055011 (1998), [hep-ph/9803335].

[97] G. F. Giudice and A. Romanino, Nucl. Phys. **B699**, 65 (2004), [Erratum: Nucl. Phys.B706,487(2005)], [hep-ph/0406088].

[98] J. Hisano *et al.*, JHEP **07**, 038 (2013), [arXiv:1304.3651].

[99] B. Bajc, P. Fileviez Perez and G. Senjanovic, Phys. Rev. **D66**, 075005 (2002), [hep-ph/0204311].

[100] K.-S. Choi, Phys. Lett. **B668**, 392 (2008), [arXiv:0807.2766].

[101] F. An *et al.* (JUNO), J. Phys. **G43**, 3, 030401 (2016), [arXiv:1507.05613].

[102] R. Acciarri *et al.* (DUNE) (2015), [arXiv:1512.06148].

[103] L. J. Hall and Y. Nomura, Phys. Rev. **D66**, 075004 (2002), [hep-ph/0205067]; H. D. Kim, S. Raby and L. Schradin, JHEP **05**, 036 (2005), [hep-ph/0411328].

[104] M.S. Chanowitz, J.R. Ellis and M.K. Gaillard, Nucl. Phys. **B128**, 506 (1977); A. J. Buras *et al.*, Nucl. Phys. **B135**, 66 (1978).

[105] K. Inoue *et al.*, Prog. Theor. Phys. **67**, 1889 (1982); L. E. Ibanez and C. Lopez, Nucl. Phys. **B233**, 511 (1984).

[106] H. Georgi and D. V. Nanopoulos, Nucl. Phys. **B159**, 16 (1979); J. A. Harvey, P. Ramond and D. B. Reiss, Phys. Lett. **92B**, 309 (1980); J. A. Harvey, D. B. Reiss and P. Ramond, Nucl. Phys. **B199**, 223 (1982).

[107] T. Banks, Nucl. Phys. **B303**, 172 (1988); M. Olechowski and S. Pokorski, Phys. Lett. **B214**, 393 (1988); S. Pokorski, Nucl. Phys. Proc. Suppl. **13**, 606 (1990); B. Ananthanarayan, G. Lazarides and Q. Shafi, Phys. Rev. **D44**, 1613 (1991); Q. Shafi and B. Ananthanarayan, ICTP Summer School lectures (1991); S. Dimopoulos, L. J. Hall and S. Raby, Phys. Rev. Lett. **68**, 1984 (1992); S. Dimopoulos, L. J. Hall and S. Raby, Phys. Rev. **D45**, 4192 (1992); G. W. Anderson *et al.*, Phys. Rev. **D47**, R3702 (1993), [hep-ph/9209250]; B. Ananthanarayan, G. Lazarides and Q. Shafi, Phys. Lett. **B300**, 245 (1993); G. Anderson *et al.*, Phys. Rev. **D49**, 3660 (1994), [hep-ph/9308333]; B. Ananthanarayan, Q. Shafi and X. M. Wang, Phys. Rev. **D50**, 5980 (1994), [hep-ph/9311225].

[108] L. J. Hall, R. Rattazzi and U. Sarid, Phys. Rev. **D50**, 7048 (1994), [hep-ph/9306309]; M. Carena *et al.*, Nucl. Phys. **B426**, 269 (1994), [hep-ph/9402253].

[109] A. Anandakrishnan, B. C. Bryant and S. Raby, JHEP **05**, 088 (2015), [arXiv:1411.7035].

[110] M. Lanzagorta and G. G. Ross, Phys. Lett. **B364**, 163 (1995), [hep-ph/9507366].

[111] K. Tobe and J. D. Wells, Nucl. Phys. **B663**, 123 (2003), [hep-ph/0301015].

[112] G. Ross and M. Serna, Phys. Lett. **B664**, 97 (2008), [arXiv:0704.1248].

[113] T. Blazek, R. Dermisek and S. Raby, Phys. Rev. Lett. **88**, 111804 (2002), [hep-ph/0107097]; T. Blazek, R. Dermisek and S. Raby, Phys. Rev. **D65**, 115004 (2002), [hep-ph/0201081]; D. Auto *et al.*, JHEP **06**, 023 (2003), [hep-ph/0302155]; R. Dermisek *et al.*, JHEP **04**, 037 (2003), [hep-ph/0304101]; R. Dermisek *et al.*, JHEP **09**, 029 (2005), [hep-ph/0507233].

[114] A. Anandakrishnan, S. Raby and A. Wingerter, Phys. Rev. **D87**, 5, 055005 (2013), [arXiv:1212.0542]; M. Adeel Ajaib *et al.*, JHEP **07**, 139 (2013), [arXiv:1303.6964]; Z. Poh and S. Raby, Phys. Rev. **D92**, 1, 015017 (2015), [arXiv:1505.00264]; M. Badziak, M. Olechowski and S. Pokorski, JHEP **10**, 088 (2013), [arXiv:1307.7999].

[115] H. Georgi and C. Jarlskog, Phys. Lett. **86B**, 297 (1979).

[116] S. Antusch and M. Spinrath, Phys. Rev. **D79**, 095004 (2009), [arXiv:0902.4644].

[117] G. Lazarides, Q. Shafi and C. Wetterich, Nucl. Phys. **B181**, 287 (1981).

[118] T. E. Clark, T.-K. Kuo and N. Nakagawa, Phys. Lett. **115B**, 26 (1982); K. S. Babu and R. N. Mohapatra, Phys. Rev. Lett. **70**, 2845 (1993), [hep-ph/9209215].

[119] R. Barbieri and D. V. Nanopoulos, Phys. Lett. **91B**, 369 (1980).

[120] C. D. Froggatt and H. B. Nielsen, Nucl. Phys. **B147**, 277 (1979).

[121] R. Barbieri *et al.*, Nucl. Phys. **B493**, 3 (1997), [hep-ph/9610449]; T. Blazek, S. Raby and K. Tobe, Phys. Rev. **D60**, 113001 (1999), [hep-ph/9903340]; T. Blazek, S. Raby and K. Tobe, Phys. Rev. **D62**, 055001 (2000), [hep-ph/9912482]; Q. Shafi and Z. Tavartkiladze, Phys. Lett. **B487**, 145 (2000), [hep-ph/9910314]; C. H. Albright and S. M. Barr, Phys. Rev. Lett. **85**, 244 (2000), [hep-ph/0002155]; Z. Berezhiani and A. Rossi, Nucl. Phys. **B594**, 113 (2001), [hep-ph/0003084]; C. H. Albright and S. M. Barr, Phys. Rev. **D64**, 073010 (2001), [hep-ph/0104294]; M.-C. Chen and K. T. Mahanthappa, Int. J. Mod. Phys. **A18**, 5819 (2003), [hep-ph/0305088]; R. Dermisek and S. Raby, Phys. Lett. **B622**, 327 (2005), [hep-ph/0507045].

[122] H. Georgi, Nucl. Phys. **B156**, 126 (1979); P. H. Frampton, Phys. Lett. **88B**, 299 (1979); P. Frampton and S. Nandi, Phys. Rev. Lett. **43**, 1460 (1979); J.E. Kim, Phys. Rev. Lett. **45**, 1916 (1980), Phys. Rev. **D23**, 2706 (1981) and Phys. Rev. **D26**, 674 (1982); Y. Fujimoto, Phys. Rev. **D26**, 3183 (1982).

[123] P. Langacker, Phys. Rept. **72**, 185 (1981).

[124] H. Georgi, Conf. Proc. C **820726**, 705 (1982).

[125] S. M. Barr, Phys. Rev. **D78**, 055008 (2008), [arXiv:0805.4808]; Y. Goto, Y. Kawamura and T. Miura, Phys. Rev. **D88**, 5, 055016 (2013), [arXiv:1307.2631]; J. E. Kim, JHEP **06**, 114 (2015), [arXiv:1503.03104]; C.H. Albright, R.P. Feger and T.W. Kephart, arXiv:1601.07523; M. Reig, J. W. F. Valle, C. A. Vaquera-Araujo and F. Wilczek, arXiv:1706.03116.

[126] M. Magg and C. Wetterich, Phys. Lett. **94B**, 61 (1980); J. Schechter and J. W. F. Valle, Phys. Rev. **D22**, 2227 (1980); R. N. Mohapatra and G. Senjanovic, Phys. Rev. **D23**, 165 (1981); G. B. Gelmini and M. Roncadelli, Phys. Lett. **99B**, 411 (1981).

[127] R. Foot *et al.*, Z. Phys. **C44**, 441 (1989).

[128] Y. Fukuda *et al.* (Super-Kamiokande), Phys. Rev. Lett. **81**, 1562 (1998), [hep-ex/9807003].

Downloaded from https://academic.oup.com/ptep/article/2022/8/083C01/6651666 by KIT Library user on 27 September 2022

[129] G. L. Fogli *et al.*, Phys. Rev. **D84**, 053007 (2011), [arXiv:1106.6028].

[130] T. Schwetz, M. Tortola and J. W. F. Valle, New J. Phys. **13**, 109401 (2011), [arXiv:1108.1376].

[131] G. Altarelli, Soryushiron Kenkyu Electron. **116**, A29 (2008), [arXiv:0711.0161]; S. F. King and C. Luhn, Rept. Prog. Phys. **76**, 056201 (2013), [arXiv:1301.1340].

[132] C. H. Albright and M.-C. Chen, Phys. Rev. **D74**, 113006 (2006), [hep-ph/0608137].

[133] R. Kallosh *et al.*, Phys. Rev. **D52**, 912 (1995), [hep-th/9502069].

[134] H. Ruegg and M. Ruiz-Altaba, Int. J. Mod. Phys. **A19**, 3265 (2004), [hep-th/0304245].

[135] M. B. Green and J. H. Schwarz, Phys. Lett. **149B**, 117 (1984).

[136] L. E. Ibanez and G. G. Ross, Nucl. Phys. **B368**, 3 (1992); M. Berasaluce-Gonzalez *et al.*, JHEP **12**, 113 (2011), [arXiv:1106.4169].

[137] N.G. Deshpande, OITS-107; C. Q. Geng and R. E. Marshak, Phys. Rev. **D39**, 693 (1989); A. Font, L. E. Ibanez and F. Quevedo, Phys. Lett. **B228**, 79 (1989); K. S. Babu and R. N. Mohapatra, Phys. Rev. Lett. **63**, 938 (1989).

[138] R. Foot *et al.*, Phys. Rev. **D39**, 3411 (1989).

[139] M. Nowakowski and A. Pilaftsis, Phys. Rev. **D48**, 259 (1993), [hep-ph/9304312].

[140] T. P. T. Dijkstra, L. R. Huiszoon and A. N. Schellekens, Phys. Lett. **B609**, 408 (2005), [hep-th/0403196]; F. Gmeiner *et al.*, JHEP **01**, 004 (2006), [hep-th/0510170]; B. Gato-Rivera and A. N. Schellekens, Nucl. Phys. **B883**, 529 (2014), [arXiv:1401.1782].

[141] G. 't Hooft, Nucl. Phys. **B79**, 276 (1974) A.M. Polyakov, Pis'ma Zh. Eksp. Teor. Fiz. **20**, 430 (1974) [Sov. Phys. JETP Lett. **20**, 194 (1974)]; For a pedagogical introduction, see S. Coleman, in *Aspects of Symmetry*, Selected Erice Lectures, Cambridge University Press, Cambridge, (1985), and P. Goddard and D. Olive, Rept. on Prog. in Phys. **41**, 1357 (1978).

[142] M. Ambrosio *et al.* (MACRO), Eur. Phys. J. **C25**, 511 (2002), [hep-ex/0207020]; S. Balestra *et al.* (2011), [arXiv:1105.5587]; L. Patrizii and M. Spurio, Ann. Rev. Nucl. Part. Sci. **65**, 279 (2015), [arXiv:1510.07125].

[143] For a review, see A.D. Linde, *Particle Physics and Inflationary Cosmology*, Harwood Academic, Switzerland (1990).

[144] G. R. Dvali, H. Liu and T. Vachaspati, Phys. Rev. Lett. **80**, 2281 (1998), [hep-ph/9710301].

[145] P. Langacker and S.-Y. Pi, Phys. Rev. Lett. **45**, 1 (1980).

[146] G. R. Dvali, A. Melfo and G. Senjanovic, Phys. Rev. Lett. **75**, 4559 (1995), [hep-ph/9507230].

[147] V. Rubakov, Nucl. Phys. **B203**, 311 (1982) and Institute of Nuclear Research Report No. P-0211, Moscow (1981), unpublished; C. G. Callan, Jr., Phys. Rev. **D26**, 2058 (1982); F. Wilczek, Phys. Rev. Lett. **48**, 1146 (1982); S. Dawson and A. N. Schellekens, Phys. Rev. **D27**, 2119 (1983).

[148] K. Freese, M. S. Turner and D. N. Schramm, Phys. Rev. Lett. **51**, 1625 (1983).

[149] P. A. R. Ade *et al.* (BICEP2, Keck Array), Phys. Rev. Lett. **116**, 031302 (2016), [arXiv:1510.09217]; N. Aghanim *et al.* (Planck) (2018), [arXiv:1807.06209].

[150] L. J. Hall, V. A. Kostelecky and S. Raby, Nucl. Phys. **B267**, 415 (1986).

[151] R. Barbieri and L. J. Hall, Phys. Lett. **B338**, 212 (1994), [hep-ph/9408406]; R. Barbieri, L. J. Hall and A. Strumia, Nucl. Phys. **B445**, 219 (1995), [hep-ph/9501334].

[152] F. Borzumati and A. Masiero, Phys. Rev. Lett. **57**, 961 (1986); J. Hisano *et al.*, Phys. Lett. **B357**, 579 (1995), [hep-ph/9501407]; J. Hisano *et al.*, Phys. Rev. **D53**, 2442 (1996), [hep-ph/9510309]; J. Hisano and D. Nomura, Phys. Rev. **D59**, 116005 (1999), [hep-ph/9810479].

[153] T. Moroi, JHEP **03**, 019 (2000), [hep-ph/0002208]; D. Chang, A. Masiero and H. Murayama, Phys. Rev. **D67**, 075013 (2003), [hep-ph/0205111].

[154] S. Dimopoulos and L. J. Hall, Phys. Lett. **B344**, 185 (1995), [hep-ph/9411273].

[155] J. Hisano *et al.*, Phys. Lett. **B604**, 216 (2004), [hep-ph/0407169].

[156] A. Yu. Ignatiev *et al.*, Phys. Lett. **76B**, 436 (1978); M. Yoshimura, Phys. Rev. Lett. **41**, 281 (1978), [Erratum: Phys. Rev. Lett.42,746(1979)].

[157] D. Toussaint *et al.*, Phys. Rev. **D19**, 1036 (1979); S. Weinberg, Phys. Rev. Lett. **42**, 850 (1979); M. Yoshimura, Phys. Lett. **88B**, 294 (1979); S. M. Barr, G. Segre and H. A. Weldon, Phys. Rev. **D20**, 2494 (1979); D. V. Nanopoulos and S. Weinberg, Phys. Rev. **D20**, 2484 (1979); A. Yildiz and P. H. Cox, Phys. Rev. **D21**, 906 (1980).

[158] H. K. Dreiner and G. G. Ross, Nucl. Phys. **B410**, 188 (1993), [hep-ph/9207221].

[159] M. Fukugita and T. Yanagida, Phys. Rev. Lett. **89**, 131602 (2002), [hep-ph/0203194].

[160] M. Fukugita and T. Yanagida, Phys. Lett. **B174**, 45 (1986).

[161] S. Davidson and A. Ibarra, Phys. Lett. **B535**, 25 (2002), [hep-ph/0202239]; K. Hamaguchi, H. Murayama and T. Yanagida, Phys. Rev. **D65**, 043512 (2002), [hep-ph/0109030].

[162] A. Pilaftsis and T. E. J. Underwood, Phys. Rev. **D72**, 113001 (2005), [hep-ph/0506107].

[163] M. Kawasaki *et al.*, Phys. Rev. **D78**, 065011 (2008), [arXiv:0804.3745].

[164] W. Buchmuller, R. D. Peccei and T. Yanagida, Ann. Rev. Nucl. Part. Sci. **55**, 311 (2005), [hep-ph/0502169]; C. S. Fong, E. Nardi and A. Riotto, Adv. High Energy Phys. **2012**, 158303 (2012), [arXiv:1301.3062].

[165] V. Cirigliano *et al.*, JHEP **12**, 097 (2018), [arXiv:1806.02780].

[166] K. S. Babu and R. N. Mohapatra, Phys. Rev. **D86**, 035018 (2012), [arXiv:1203.5544]; K. S. Babu and R. N. Mohapatra, Phys. Lett. **B715**, 328 (2012), [arXiv:1206.5701]; K. S. Babu and R. N. Mohapatra, Phys. Rev. Lett. **109**, 091803 (2012), [arXiv:1207.5771].

[167] M. Baldo-Ceolin *et al.*, Z. Phys. **C63**, 409 (1994).

[168] K. Abe *et al.* (Super-Kamiokande), Phys. Rev. **D91**, 072006 (2015), [arXiv:1109.4227].

[169] J. Gustafson *et al.* (Super-Kamiokande), Phys. Rev. **D91**, 7, 072009 (2015), [arXiv:1504.01041].

[170] K. R. Dienes, Phys. Rept. **287**, 447 (1997), [hep-th/9602045]; P. Nath and P. Fileviez Perez, Phys. Rept. **441**, 191 (2007), [hep-ph/0601023].

[171] G.G. Ross, "Grand Unified Theories", Benjamin/Cummings, 1984.; S. Raby, Lect. Notes Phys. **939**, 1 (2017).

[172] P. Nath, Int. J. Mod. Phys. **A33**, 20, 1830017 (2018), [arXiv:1807.05302]; D. Croon *et al.*, Front.in Phys. **7**, 76 (2019), [arXiv:1903.04977].

[173] A. Ringwald, L.J. Rosenberg and G. Rybka, Review of 'Axions and other Similar Particles' in Ref. [62].

[174] P. Svrcek and E. Witten, JHEP **06**, 051 (2006), [hep-th/0605206].

[175] M. Dine, W. Fischler and M. Srednicki, Phys. Lett. **104B**, 199 (1981); A. R. Zhitnitsky, Sov. J. Nucl. Phys. **31**, 260 (1980), [Yad. Fiz.31,497(1980)].

[176] J. P. Conlon, JHEP **05**, 078 (2006), [hep-th/0602233].

Downloaded from https://academic.oup.com/ptep/article/2022/8/083C01/6651666 by KIT Library user on 27 September 2022

94. Leptoquarks

Revised August 2021 by S. Rolli (DOE) and M. Tanabashi (Nagoya U.; KMI, Nagoya U.).

Leptoquarks are hypothetical particles carrying both baryon number (B) and lepton number (L). The possible quantum numbers of leptoquark states can be restricted by assuming that their direct interactions with the ordinary Standard Model (SM) fermions are dimensionless and invariant under the SM gauge group. Table 94.1 shows the list of all possible quantum numbers with this assumption [1]. The columns of $SU(3)_C$, $SU(2)_W$, and $U(1)_Y$ in Table 94.1 indicate the QCD representation, the weak isospin representation, and the weak hypercharge, respectively. The spin of a leptoquark state is taken to be 1 (vector leptoquark) or 0 (scalar leptoquark).

Table 94.1: Possible leptoquarks and their quantum numbers.

Spin	$3B+L$	$SU(3)_c$	$SU(2)_W$	$U(1)_Y$	Allowed coupling
0	-2	$\bar{3}$	1	1/3	$\bar{q}^c_L \ell_L$ or $\bar{u}^c_R e_R$
0	-2	$\bar{3}$	1	4/3	$\bar{d}^c_R e_R$
0	-2	$\bar{3}$	3	1/3	$\bar{q}^c_L \ell_L$
1	-2	$\bar{3}$	2	5/6	$\bar{q}^c_L \gamma^\mu e_R$ or $\bar{d}^c_R \gamma^\mu \ell_L$
1	-2	$\bar{3}$	2	$-1/6$	$\bar{u}^c_R \gamma^\mu \ell_L$
0	0	3	2	7/6	$\bar{q}_L e_R$ or $\bar{u}_R \ell_L$
0	0	3	2	1/6	$\bar{d}_R \ell_L$
1	0	3	1	2/3	$\bar{q}_L \gamma^\mu \ell_L$ or $\bar{d}_R \gamma^\mu e_R$
1	0	3	1	5/3	$\bar{u}_R \gamma^\mu e_R$
1	0	3	3	2/3	$\bar{q}_L \gamma^\mu \ell_L$

If we do not require leptoquark states to couple directly with SM fermions, different assignments of quantum numbers become possible [2,3].

Leptoquark states are expected to exist in various extensions of the SM. The Pati-Salam model [4] is an example predicting the existence of a leptoquark state. Leptoquark states also exist in grand unification theories based on $SU(5)$ [5], $SO(10)$ [6], which includes Pati-Salam color $SU(4)$, and larger gauge groups. Scalar quarks in supersymmetric models with R-parity violation may also have leptoquark-type Yukawa couplings. The bounds on the leptoquark states can therefore be applied to constrain R-parity-violating supersymmetric models. Scalar leptoquarks are expected to exist at the TeV scale in extended technicolor models [7,8] where leptoquark states appear as the bound states of techni-fermions. Compositeness of quarks and leptons also provides examples of models which may have light leptoquark states [9].

Bounds on leptoquark states are obtained both directly and indirectly. Direct limits are from their production cross sections at colliders, while indirect limits are calculated from bounds on leptoquark-induced four-fermion interactions, which are obtained from low-energy experiments, or from collider experiments below threshold. These four-fermion interactions often cause lepton-flavor non-universalities in heavy quark decays. Anomalies observed recently in the R_K and R_D ratios [10–12] in the semi-leptonic B decays may be explained in models with TeV scale leptoquarks.

If a leptoquark couples to quarks (leptons) belonging to more than a single generation in the mass eigenbasis, it can induce four-fermion interactions causing flavor-changing neutral currents (lepton-family-number violations). The quantum number assignment of Table 1 allows several leptoquark states to couple to both left- and right-handed quarks simultaneously. Such leptoquark states are called non-chiral and may cause four-fermion interactions affecting the $(\pi \to e\nu)/(\pi \to \mu\nu)$ ratio [13]. Non-chiral scalar leptoquarks also contribute to the muon anomalous magnetic moment [14,15]. Since indirect limits provide more stringent constraints on these types of leptoquarks, it is often assumed that a leptoquark state couples only to a single generation of quarks and a single generation of leptons in a chiral interaction, for which indirect limits become much weaker. Additionally, this assumption gives strong constraints on models of leptoquarks.

Refs. [16–18] give extensive lists of the bounds on the leptoquark-induced four-fermion interactions. For the isoscalar scalar and vector leptoquarks S_0 and V_0, for example, which couple with the first- (second-) generation left-handed quark, and the first-generation left-handed lepton, the bounds $\lambda^2 < 0.07 \times (M_{\rm LQ}/1\ {\rm TeV})^2$ for S_0, and $\lambda^2 < 0.4 \times (M_{\rm LQ}/1\ {\rm TeV})^2$ for V_0 ($\lambda^2 < 0.7 \times (M_{\rm LQ}/1\ {\rm TeV})^2$ for S_0, and $\lambda^2 < 0.5 \times (M_{\rm LQ}/1\ {\rm TeV})^2$ for V_0) with λ being the leptoquark coupling strength, can be derived from the limits listed in Ref. [19]. The e^+e^- experiments are sensitive to the indirect effects coming from t- and u-channel exchanges of leptoquarks in the $e^+e^- \to q\bar{q}$ process. The HERA experiments give bounds on the leptoquark-induced four-fermion interaction. For detailed bounds obtained in this way, see the Boson Particle Listings for "Indirect Limits for Leptoquarks" and its references.

Collider experiments provide direct limits on the leptoquark states through limits on the pair- and single-production cross sections. The leading-order cross sections of the parton processes

$$\begin{aligned} q + \bar{q} &\to {\rm LQ} + \overline{\rm LQ} \\ g + g &\to {\rm LQ} + \overline{\rm LQ} \\ e + q &\to {\rm LQ} \end{aligned} \tag{94.1}$$

may be written as [20]

$$\begin{aligned} \hat{\sigma}_{\rm LO}\left[q\bar{q} \to {\rm LQ} + \overline{\rm LQ}\right] &= \frac{2\alpha_s^2 \pi}{27\hat{s}}\beta^3, \\ \hat{\sigma}_{\rm LO}\left[gg \to {\rm LQ} + \overline{\rm LQ}\right] &= \frac{\alpha_s^2 \pi}{96\hat{s}} \\ &\quad \times \left[\beta(41 - 31\beta^2) + (18\beta^2 - \beta^4 - 17)\log\frac{1+\beta}{1-\beta}\right], \\ \hat{\sigma}_{\rm LO}\left[eq \to {\rm LQ}\right] &= \frac{\pi\lambda^2}{4}\delta(\hat{s} - M_{\rm LQ}^2) \end{aligned} \tag{94.2}$$

for a scalar leptoquark. Here $\sqrt{\hat{s}}$ is the invariant energy of the parton subprocess, and $\beta \equiv \sqrt{1 - 4M_{\rm LQ}^2/\hat{s}}$. The leptoquark Yukawa coupling is given by λ. Leptoquarks are also produced singly at hadron colliders through $g + q \to {\rm LQ} + \ell$ [21], which allows extending to higher masses the collider reach in the leptoquark search [22], depending on the leptoquark Yukawa coupling. See also Ref. [23] for a comprehensive review on the leptoquark phenomenology in precision experiments and particle colliders.

Leptoquark states which couple only to left- or right-handed quarks are called chiral leptoquarks. Leptoquark states which couple only to the first (second, third) generation are referred as the first- (second-, third-) generation leptoquarks.

The LHC, Tevatron and LEP experiments have been searching for pair production of the leptoquark states, which arises from the leptoquark gauge interaction. Due to the typical decay of the leptoquark into charged and neutral leptons and quarks, the searches are carried on in signatures including high p_T charged leptons, high E_T jets and large missing transverse energy. Additionally, searches for pair produced LQs are often organized by the decay mode of the pair of LQs, via the decay parameter β, which represents the branching fraction into a charge lepton vs a neutrino: $\beta = 1$ for both LQs decaying into a charged letpon, $\beta = 0.5$ for one LQ decaying into a charged lepton and one into a neutrino. The gauge couplings of a scalar leptoquark are determined uniquely according to its quantum numbers in Table 94.1. Since all of the leptoquark states belong to color-triplet representation, the scalar leptoquark pair-production cross section at the Tevatron and LHC can be determined solely as a function of the leptoquark mass without making further assumptions. This is in contrast to the indirect or single-production limits, which give constraints in the leptoquark mass-coupling plane.

Older results from the Tevatron run can be found here: [24–27].

Since the previous version of this review, both ATLAS and CMS have updated their results concerning searches for first, second,

Downloaded from https://academic.oup.com/ptep/article/2022/8/083C01/6651666 by KIT Library user on 27 September 2022

and third generation LQs and leptoquark states which couple only with the i-th generation quarks and the j-th generation leptons ($i \neq j$) without causing conflicts with severe indirect constraints. The datasets were almost all collected at center of mass energy of 13 TeV and corresponding to the latest integrated luminosity collected before the shutdown of the LHC occurring in 2019 and 2020.

It is worthy to note that organizing LQs by flavor quantum number first before organizing them by gauge quantum number is becoming more common and advantageous because it relates more closely to some of the experimental searches being performed. The traditional nomenclature for 1st, 2nd, and 3rd generation LQ encourages only looking for the diagonal elements in a flavor matrix of possibilities, which has been the traditional experimental search strategy.

Current results extend previous mass limits for scalar leptoquarks to > 1435 GeV (first generation, CMS, β =1, $\sqrt{s}$ = 13 TeV) and > 1270 GeV(first generation, CMS, β =0.5,$\sqrt{s}$ = 13 TeV) [28]; > 1800 GeV (first generation, ATLAS, β =1, $\sqrt{s}$ = 13 TeV) [29] and > 1290 GeV (first generation, ATLAS, β =0.5, $\sqrt{s}$ = 13 TeV) [30]; > 1530 GeV (second generation, CMS, β =1, $\sqrt{s}$ = 13 TeV) and > 1285 GeV (second generation, CMS, β =0.5, $\sqrt{s}$ = 13 TeV) [31]; and > 1700 GeV (second generation, ATLAS, β =1,$\sqrt{s}$ = 13 TeV) [29] and > 1230 GeV (second generation, ATLAS, β =0.5,$\sqrt{s}$ = 13 TeV) [30]. All limits are presented at 95% C.L.

As for third generation leptoquarks, CMS results are the following: 1) assuming that all leptoquarks decay to a top quark and a τ lepton, the existence of pair produced, third-generation leptoquark up to a mass of 900 GeV (β =1, 13 TeV) is excluded at 95% confidence level [32]; 2) assuming that all leptoquarks decay to a bottom quark and a τ lepton, the existence of pair produced, third-generation leptoquark up to a mass of 1020 GeV (β =1, 13 TeV) is excluded at 95% confidence level [33]; 3)assuming that all leptoquarks decay to a bottom quark and a τ neutrino, the existence of pair produced, third-generation leptoquark up to a mass of 450 GeV (β =0, 7 TeV)is excluded at 95% confidence level [34]. In a recent paper [35] signatures of top quark τ lepton ν bottom and top τ ν - not previously explored in dedicated searches, were analyzed in the context of searches for scalar leptoquark of charge -1/3e coupling to a top quark plus a τ lepton (tτ) or a bottom quark plus a neutrino (bν), or a vector particle of charge +2/3e, coupling to tν or bτ. These choices are motivated by models that can explain a series of anomalies observed in the measurement of B meson decays. The data are found to be in agreement with the standard model prediction. Lower limits at 95% confidence level are set on the LQ mass in the range 0.98–1.73 TeV, depending on the LQ spin and its coupling λ to a lepton and a quark, and assuming equal couplings for the two LQ decay modes considered. These are the most stringent constraints to date on the existence of leptoquarks in this scenario.

In [36], the ATLAS collaboration has limits on pair production of third generation scalar leptoquarks where all possible decays of the leptoquark into a quark (t, b) and a lepton (τ, ν) of the third generation are considered. The limits are presented as a function of the leptoquark mass and the branching ratio into charged leptons for leptoquark of up-type ($LQ_3^{up} \rightarrow \tau\nu/b\tau$) and down-type ($LQ_3^d \rightarrow b\nu/t\tau$); many results are re-interpretation of previously published ATLAS searches. The collaboration finds that masses below 800 GeV are excluded for both LQ_3^u and LQ_3^d independently of the branching ratio, with masses below about 1 TeV being excluded for the limiting cases of branching ratios equal to zero or unity. In a more recent paper [37] ATLAS present the result of searches for pair production of third-generation scalar leptoquarks decaying into a top quark and a τ-lepton, using 139 fb^{-1} of data collected at 13 TeV. Scalar leptoquarks decaying exclusively into tτ are excluded up to masses of 1.43 TeV while, for a branching fraction of 50% into tτ , the lower mass limit is 1.22 TeV.

It is also possible to consider leptoquark states which couple only with the i-th generation quarks and the j-th generation leptons ($i \neq j$) without causing conflicts with severe indirect constraints. Such couplings have received renewed attention because they may provide an explanation to anomalies in rare $B - meson$ decays and the anomalous magnetic moment of the muon. See Ref. [38, 39] and [40] and references therein for collider search strategies and limits on the pair production cross sections of this class of leptoquark states. In this framework, a novel CMS result [41] presents a non-traditional search for pair production of LQs coupled to a top quark and a muon. As no deviation from the Standard Model prediction was observed, scalar LQs decaying exclusively into $top - \mu$ are excluded up to masses of 1420 GeV. In a recent ATLAS paper [42] a search for pair production of scalar lepto- quarks, each decaying into either an electron or a muon and a top quark, is presented. This is the first leptoquark search using ATLAS data to investigate top-philic cross- generational couplings that could provide explanations for recently observed anomalies in B meson decays. In the absence of any s ignificant deviation from the background expectation, lower limits on the leptoquark masses are set at 1480 GeV and 1470 GeV for the electron and muon channel, respectively.

The magnetic-dipole-type and the electric-quadrupole-type interactions of a vector leptoquark are not determined even if we fix its gauge quantum numbers as listed in the Table 94.1 [43]. The production of vector leptoquarks depends in general on additional assumptions, where the leptoquark couplings and their pair production cross sections are enhanced relative to the scalar leptoquark contributions. The most stringent limits on vector LQ production are now from CMS [44] where previous searches for squarks and gluinos have been reinterpreted to constrain models of leptoquark production. LQ masses below 1530 GeV are excluded assuming the Yang-Mills case with coupling $\kappa = 1$, or 1115 GeV in the minimal coupling case where $\kappa = 0$, placing the most stringent constraint to date from pair production of vector LQs.

The leptoquark pair-production cross sections in e^+e^- collisions depend on the leptoquark $SU(2) \times U(1)$ quantum numbers and Yukawa coupling with electron [45].

Searches for first generation leptoquark singly produced were performed by the HERA experiments. Since the leptoquark single-production cross section depends on its Yukawa coupling, the leptoquark mass limits from HERA are usually displayed in the mass-coupling plane. For leptoquark Yukawa coupling $\lambda = 0.1$, early ZEUS Collaboration bounds on the first-generation leptoquarks range from 248 to 290 GeV, depending on the leptoquark species [46]. The ZEUS Collaboration has recently released a new paper [47] where data corresponding to a luminosity of around 1 fb^{-1} have been used in the framework of $eeqq$ contact interactions (CI) to set limits on possible high-energy contributions beyond the Standard Model to electron-quark scattering. The analysis of the ep data has been based on simultaneous fits of parton distribution functions including contributions of Contact Interaction (CI) couplings to ep scattering. Several general CI models and scenarios with heavy leptoquarks were considered. As unambiguous deviations from the SM cannot be established, limits for CI compositeness scales and LQ mass scales were set that are in the TeV range. The H1 Collaboration has a comprehensive summary of searches for first generation leptoquarks using the full data sample collected in ep collisions at HERA (446 pb^{-1}). No evidence of production of leptoquarks was observed in final states with a large transverse momentum electron or large missing transverse momentum. For a coupling strength $\lambda = 0.3$, first generation leptoquarks with masses up to 800 GeV are excluded at 95% C.L. [48].

At the LHC, the CMS collaboration performed searches for single production of first and second generation leptoquarks [49], which is complementary to the HERA searches in the high λ region (for coupling strength $\lambda = 1.0$, first generation leptoquarks are excluded for masses up to 1.73 TeV and second generation leptoquark are excluded up to masses of 530 GeV). CMS also recently searched for third generation LQ decaying into τ and *bottom* in [50]. Assuming unit Yukawa coupling (λ), a third generation scalar leptoquark is excluded for masses below 740 GeV. Limits are also set on λ of the hypothesized leptoquark as a function of its mass. Above $\lambda = 1.4$, the results provide the best upper limit on the mass of a third-generation scalar leptoquark decaying to a τ lepton and a bottom quark.

Downloaded from https://academic.oup.com/ptep/article/2022/8/083C01/6651666 by KIT Library user on 27 September 2022

Searches for LQ will continue with more LHC data, particularly in light of the renewed interest in this type of particle to explain violation of lepton flavor universality and other anomalies, which point to explanations laying outside the Standard Model.

References

[1] W. Buchmuller, R. Ruckl and D. Wyler, Phys. Lett. B **191**, 442 (1987), [Erratum: Phys.Lett.B 448, 320–320 (1999)].

[2] K. Babu, C. F. Kolda and J. March-Russell, Phys. Lett. B **408**, 261 (1997), [hep-ph/9705414].

[3] J. L. Hewett and T. G. Rizzo, Phys. Rev. D **58**, 055005 (1998), [hep-ph/9708419].

[4] J. C. Pati and A. Salam, Phys. Rev. D **10**, 275 (1974), [Erratum: Phys.Rev.D 11, 703–703 (1975)].

[5] H. Georgi and S. Glashow, Phys. Rev. Lett. **32**, 438 (1974).

[6] H. Georgi, AIP Conf. Proc. **23**, 575 (1975); H. Fritzsch and P. Minkowski, Annals Phys. **93**, 193 (1975).

[7] For a review, see, E. Farhi and L. Susskind, Phys. Rept. **74**, 277 (1981).

[8] K. D. Lane and M. Ramana, Phys. Rev. D **44**, 2678 (1991).

[9] See, for example, B. Schrempp and F. Schrempp, Phys. Lett. **153B**, 101 (1985).

[10] R. Aaij *et al.* (LHCb), Phys. Rev. Lett. **120**, 17, 171802 (2018), [arXiv:1708.08856]; R. Aaij *et al.* (LHCb), Phys. Rev. D **97**, 7, 072013 (2018), [arXiv:1711.02505].

[11] R. Aaij *et al.* (LHCb), JHEP **08**, 055 (2017), [arXiv:1705.05802]; R. Aaij *et al.* (LHCb), Phys. Rev. Lett. **122**, 19, 191801 (2019), [arXiv:1903.09252]; R. Aaij *et al.* (LHCb), Phys. Rev. Lett. **125**, 1, 011802 (2020), [arXiv:2003.04831]; R. Aaij *et al.* (LHCb) (2021), [arXiv:2103.11769].

[12] Y. S. Amhis *et al.* (HFLAV), Eur. Phys. J. C **81**, 3, 226 (2021), updated results and plots available at `https://hflav.web.cern.ch/`, [arXiv:1909.12524].

[13] O. U. Shanker, Nucl. Phys. B **204**, 375 (1982).

[14] U. Mahanta, Eur. Phys. J. C **21**, 171 (2001), [hep-ph/0102176].

[15] K.-M. Cheung, Phys. Rev. D **64**, 033001 (2001), [hep-ph/0102238].

[16] S. Davidson, D. C. Bailey and B. A. Campbell, Z. Phys. C **61**, 613 (1994), [hep-ph/9309310].

[17] M. Leurer, Phys. Rev. D **49**, 333 (1994), [hep-ph/9309266]; M. Leurer, Phys. Rev. D **50**, 536 (1994), [hep-ph/9312341].

[18] M. Carpentier and S. Davidson, Eur. Phys. J. C **70**, 1071 (2010), [arXiv:1008.0280].

[19] S. Davidson and A. Saporta, Phys. Rev. D **99**, 1, 015032 (2019), [arXiv:1807.10288].

[20] T. Plehn *et al.*, Z. Phys. C **74**, 611 (1997), [hep-ph/9703433]; M. Kramer *et al.*, Phys. Rev. Lett. **79**, 341 (1997), [hep-ph/9704322].

[21] J. Hewett and S. Pakvasa, Phys. Rev. D **37**, 3165 (1988); O. J. Eboli and A. V. Olinto, Phys. Rev. D **38**, 3461 (1988); A. Dobado, M. J. Herrero and C. Munoz, Phys. Lett. B **207**, 97 (1988); V. D. Barger *et al.*, Phys. Lett. B **220**, 464 (1989); M. De Montigny and L. Marleau, Phys. Rev. D **40**, 2869 (1989), [Erratum: Phys.Rev.D 56, 3156 (1997)].

[22] A. Belyaev *et al.*, JHEP **09**, 005 (2005), [hep-ph/0502067].

[23] I. Doršner *et al.*, Phys. Rept. **641**, 1 (2016), [arXiv:1603.04993].

[24] V. Abazov *et al.* (D0), Phys. Lett. B **681**, 224 (2009), [arXiv:0907.1048].

[25] A. Abulencia *et al.* (CDF), Phys. Rev. D **73**, 051102 (2006), [hep-ex/0512055].

[26] V. Abazov *et al.* (D0), Phys. Lett. B **671**, 224 (2009), [arXiv:0808.4023].

[27] V. M. Abazov *et al.* (D0), Phys. Lett. B **693**, 95 (2010), [arXiv:1005.2222].

[28] A. M. Sirunyan *et al.* (CMS), Phys. Rev. D **99**, 5, 052002 (2019), [arXiv:1811.01197].

[29] G. Aad *et al.* (ATLAS), JHEP **10**, 112 (2020), [arXiv:2006.05872].

[30] M. Aaboud *et al.* (ATLAS), Eur. Phys. J. C **79**, 9, 733 (2019), [arXiv:1902.00377].

[31] A. M. Sirunyan *et al.* (CMS), Phys. Rev. D **99**, 3, 032014 (2019), [arXiv:1808.05082].

[32] A. M. Sirunyan *et al.* (CMS), Eur. Phys. J. C **78**, 707 (2018), [arXiv:1803.02864].

[33] A. M. Sirunyan *et al.* (CMS), JHEP **03**, 170 (2019), [arXiv:1811.00806].

[34] S. Chatrchyan *et al.* (CMS), JHEP **12**, 055 (2012), [arXiv:1210.5627].

[35] A. M. Sirunyan *et al.* (CMS), Phys. Lett. B **819**, 136446 (2021), [arXiv:2012.04178].

[36] M. Aaboud *et al.* (ATLAS), JHEP **06**, 144 (2019), [arXiv:1902.08103].

[37] G. Aad *et al.* (ATLAS), JHEP **06**, 179 (2021), [arXiv:2101.11582].

[38] B. Diaz, M. Schmaltz and Y.-M. Zhong, JHEP **10**, 097 (2017), [arXiv:1706.05033].

[39] M. Schmaltz and Y.-M. Zhong, JHEP **01**, 132 (2019), [arXiv:1810.10017].

[40] D. Müller, EPJ Web Conf. **179**, 01015 (2018), [arXiv:1801.03380].

[41] A. M. Sirunyan *et al.* (CMS), Phys. Rev. Lett. **121**, 24, 241802 (2018), [arXiv:1809.05558].

[42] G. Aad *et al.* (ATLAS), Eur. Phys. J. C **81**, 4, 313 (2021), [arXiv:2010.02098].

[43] J. Blumlein, E. Boos and A. Kryukov, Z. Phys. C **76**, 137 (1997), [hep-ph/9610408].

[44] A. M. Sirunyan *et al.* (CMS), Phys. Rev. D **98**, 3, 032005 (2018), [arXiv:1805.10228].

[45] J. Blumlein and R. Ruckl, Phys. Lett. B **304**, 337 (1993).

[46] S. Chekanov *et al.* (ZEUS), Phys. Rev. D **68**, 052004 (2003), [hep-ex/0304008].

[47] H. Abramowicz *et al.* (ZEUS), Phys. Rev. D **99**, 9, 092006 (2019), [arXiv:1902.03048].

[48] F. Aaron *et al.* (H1), Phys. Lett. B **704**, 388 (2011), [arXiv:1107.3716].

[49] V. Khachatryan *et al.* (CMS), Phys. Rev. D **93**, 3, 032005 (2016), [Erratum: Phys.Rev.D 95, 039906 (2017)], [arXiv:1509.03750].

[50] A. Sirunyan *et al.* (CMS), JHEP **07**, 115 (2018), [arXiv:1806.03472].

Downloaded from https://academic.oup.com/ptep/article/2022/8/083C01/6651666 by KIT Library user on 27 September 2022

95. Magnetic Monopoles

Revised August 2021 by D. Milstead (Stockholm U.) and E.J. Weinberg (Columbia U.).

95.1 Theory of magnetic monopoles

The symmetry between electric and magnetic fields in the source-free Maxwell's equations naturally suggests that electric charges might have magnetic counterparts, known as magnetic monopoles. Although the greatest interest has been in the supermassive monopoles that are a firm prediction of all grand unified theories, one cannot exclude the possibility of lighter monopoles.

In either case, the magnetic charge is constrained by a quantization condition first found by Dirac [1]. Consider a monopole with magnetic charge Q_M and a Coulomb magnetic field

$$\mathbf{B} = \frac{Q_M}{4\pi}\frac{\hat{\mathbf{r}}}{r^2}\,. \tag{95.1}$$

Any vector potential $\mathbf{A}$ whose curl is equal to $\mathbf{B}$ must be singular along some line running from the origin to spatial infinity. This Dirac string singularity could potentially be detected through the extra phase that the wavefunction of a particle with electric charge Q_E would acquire if it moved along a loop encircling the string. For the string to be unobservable, this phase must be a multiple of 2π. Requiring that this be the case for any pair of electric and magnetic charges gives the condition that all charges be integer multiples of minimum charges $Q_E^{\rm min}$ and $Q_M^{\rm min}$ obeying

$$Q_E^{\rm min} Q_M^{\rm min} = 2\pi\,. \tag{95.2}$$

(For monopoles which also carry an electric charge, called dyons [2], the quantization conditions on their electric charges can be modified. However, the constraints on magnetic charges, as well as those on all purely electric particles, will be unchanged.)

Another way to understand this result is to note that the conserved orbital angular momentum of a point electric charge moving in the field of a magnetic monopole has an additional component, with

$$\mathbf{L} = m\mathbf{r}\times\mathbf{v} - 4\pi Q_E Q_M \hat{\mathbf{r}} \tag{95.3}$$

Requiring the radial component of $\mathbf{L}$ to be quantized in half-integer units yields Eq. 95.2.

If there are unbroken gauge symmetries in addition to the U(1) of electromagnetism, the above analysis must be modified [3, 4]. For example, a monopole could have both a U(1) magnetic charge and a color magnetic charge. The latter could combine with the color charge of a quark to give an additional contribution to the phase factor associated with a loop around the Dirac string, so that the U(1) charge could be the Dirac charge $Q_M^D \equiv 2\pi/e$, the result that would be obtained by substituting the electron charge into Eq. (95.2). On the other hand, for monopoles without color-magnetic charge, one would simply insert the quark electric charges into Eq. 95.2 and conclude that Q_M must be a multiple of $6\pi/e$.

The prediction of GUT monopoles arises from the work of 't Hooft [5] and Polyakov [6], who showed that certain spontaneously broken gauge theories have nonsingular classical solutions that lead to magnetic monopoles in the quantum theory. The simplest example occurs in a theory where the vacuum expectation value of a triplet Higgs field ϕ breaks an SU(2) gauge symmetry down to the U(1) of electromagnetism and gives a mass M_V to two of the gauge bosons. In order to have finite energy, ϕ must approach a vacuum value at infinity. However, there is a continuous family of possible vacua, since the scalar field potential determines only the magnitude v of $\langle\phi\rangle$, but not its orientation in the internal SU(2) space. In the monopole solution, the direction of ϕ in internal space is correlated with the position in physical space; *i.e.*, $\phi^a \sim v\hat{r}^a$. The stability of the solution follows from the fact that this twisting Higgs field cannot be smoothly deformed to a spatially uniform vacuum configuration. Reducing the energetic cost of the spatial variation of ϕ requires a nonzero gauge potential, which turns out to yield the magnetic field corresponding to a charge $Q_M = 4\pi/e$. Numerical solution of the classical field equations shows that the mass of this monopole is

$$M_{\rm mon} \sim \frac{4\pi M_V}{e^2}\,. \tag{95.4}$$

The essential ingredient here was the fact that the Higgs fields at spatial infinity could be arranged in a topologically nontrivial configuration. A discussion of the general conditions under which this is possible is beyond the scope of this review, so we restrict ourselves to the two phenomenologically most important cases.

The first is the standard electroweak theory, with SU(2) × U(1) broken to U(1). There are no topologically nontrivial configurations of the Higgs field, and hence no topologically stable monopole solutions. Although electroweak scale monopoles are thus not required, there have been claims that they might not be ruled out. For example, there have been a variety of proposals in this direction involving modifications of the Lagrangian.

The second case is when any simple Lie group is broken to a subgroup with a U(1) factor, a case that includes all grand unified theories. Here the spectrum of states must include a topologically stable monopole whose mass is determined by the mass scale of the symmetry breaking that allows nontrivial topology. For example, an SU(5) model with

$$\mathrm{SU}(5) \xrightarrow{M_X} \mathrm{SU}(3)\times\mathrm{SU}(2)\times\mathrm{U}(1) \xrightarrow{M_W} \mathrm{SU}(3)\times\mathrm{U}(1) \tag{95.5}$$

has a monopole [7] with $Q_M = 2\pi/e$ and mass

$$M_{\rm mon} \sim \frac{4\pi M_{\rm X}}{g^2}\,, \tag{95.6}$$

where g is the SU(5) gauge coupling. For a unification scale of 10^{16} GeV, these monopoles would have a mass $M_{\rm mon} \sim 10^{17}$ – 10^{18} GeV.

In theories with several stages of symmetry breaking, monopoles of different mass scales can arise. In an SO(10) theory with

$$\mathrm{SO}(10) \xrightarrow{M_1} \mathrm{SU}(4)\times\mathrm{SU}(2)\times\mathrm{SU}(2) \xrightarrow{M_2} \mathrm{SU}(3)\times\mathrm{SU}(2)\times\mathrm{U}(1) \tag{95.7}$$

there is monopole with $Q_M = 2\pi/e$ and mass $\sim 4\pi M_1/g^2$ and a much lighter monopole with $Q_M = 4\pi/e$ and mass $\sim 4\pi M_2/g^2$ [8].

The central core of a GUT monopole contains the fields of the superheavy gauge bosons that mediate baryon number violation, so one might expect that baryon number conservation could be violated in baryon–monopole scattering. The surprising feature, pointed out by Callan [9] and Rubakov [10], is that these processes are not suppressed by powers of the gauge boson mass. Instead, the cross-sections for catalysis processes such as p + monopole $\to e^+ + \pi^0$ + monopole are essentially geometric; *i.e.*, $\sigma_{\Delta B}\beta \sim 10^{-27}$ cm^2, where $\beta = v/c$. Note, however, that this catalysis is model-dependent and is not even a universal property of all GUT monopoles.

95.2 Production and Annihilation

GUT monopoles are far too massive to be produced in any foreseeable accelerator. However, they could have been produced in the early Universe as topological defects arising via the Kibble mechanism [11] in a symmetry-breaking phase transition. Estimates of the initial monopole abundance, and of the degree to which it can be reduced by monopole-antimonopole annihilation, predict a present-day monopole abundance that exceeds by many orders of magnitude the astrophysical and experimental bounds described below [12]. Cosmological inflation and other proposed solutions to this primordial monopole problem generically lead to present-day abundances exponentially smaller than could be plausibly detected, although potentially observable abundances can be obtained in scenarios with carefully tuned parameters.

If monopoles light enough to be produced at colliders exist, one would expect that these could be produced by analogs of the electromagnetic processes that produce pairs of electrically charged particles. Because of the large size of the magnetic charge, this is a strong coupling problem for which perturbation theory cannot be trusted. Indeed, the problem of obtaining reliable quantitative estimates of the production cross-sections remains an open one, on which there is no clear consensus.

Downloaded from https://academic.oup.com/ptep/article/2022/8/083C01/6651666 by KIT Library user on 27 September 2022

95.3 Astrophysical and Cosmological Bounds

If there were no galactic magnetic field, one would expect monopoles in the galaxy to have typical velocities of the order of $10^{-3}c$, comparable to the virial velocity in the galaxy (relevant if the monopoles cluster with the galaxy) and the peculiar velocity of the galaxy with respect to the CMB rest frame (relevant if the monopoles are not bound to the galaxy). This situation is modified by the existence of a galactic magnetic field $B \sim 3\mu$G. A monopole with the Dirac charge and mass M would be accelerated by this field to a velocity

$$v_{\rm mag} \sim \begin{cases} c, & M \lesssim 10^{11}\,{\rm GeV}\,, \\ 10^{-3}c\left(\frac{10^{17}\,{\rm GeV}}{M}\right)^{1/2}, & M \gtrsim 10^{11}\,{\rm GeV}\,. \end{cases} \tag{95.8}$$

Accelerating these monopoles drains energy from the magnetic field. Parker [13] obtained an upper bound on the flux of monopoles in the galaxy by requiring that the rate of this energy loss be small compared to the time scale on which the galactic field can be regenerated. With reasonable choices for the astrophysical parameters (see Ref. [14] for details), this Parker bound is

$$F < \begin{cases} 10^{-15}\,{\rm cm}^{-2}\,{\rm sr}^{-1}\,{\rm sec}^{-1}\,, & M \lesssim 10^{17}\,{\rm GeV}\,, \\ 10^{-15}\left(\frac{M}{10^{17}\,{\rm GeV}}\right){\rm cm}^{-2}\,{\rm sr}^{-1}\,{\rm sec}^{-1}\,, & M \gtrsim 10^{17}\,{\rm GeV}\,. \end{cases} \tag{95.9}$$

Applying similar arguments to an earlier seed field that was the progenitor of the current galactic field leads to a tighter bound [15],

$$F < \left[\frac{M}{10^{17}{\rm GeV}} + (3\times 10^{-6})\right] 10^{-16}\,{\rm cm}^{-2}{\rm sr}^{-1}{\rm sec}^{-1}. \tag{95.10}$$

Considering magnetic fields in galactic clusters gives a bound [16] which, although less secure, is about three orders of magnitude lower than the Parker bound.

A flux bound can also be inferred from the total mass of monopoles in the Universe. If the monopole mass density is a fraction $\Omega_{\rm M}$ of the critical density, and the monopoles were uniformly distributed throughout the Universe, there would be a monopole flux

$$F_{\rm uniform} = 1.3\times 10^{-16}\Omega_{\rm M}\left(\frac{10^{17}\,{\rm GeV}}{M}\right)\left(\frac{v}{10^{-3}c}\right){\rm cm}^{-2}{\rm sr}^{-1}{\rm sec}^{-1}. \tag{95.11}$$

If we assume that $\Omega_{\rm M} \sim 0.1$, this gives a stronger constraint than the Parker bound for $M \sim 10^{15}$ GeV. However, monopoles with masses $\sim 10^{17}$ GeV are not ejected by the galactic field and can be gravitationally bound to the galaxy. In this case their flux within the galaxy is increased by about five orders of magnitude for a given value of $\Omega_{\rm M}$, and the mass density bound only becomes stronger than the Parker bound for $M \sim 10^{18}$ GeV.

A much more stringent flux bound applies to GUT monopoles that catalyze baryon number violation. The essential idea is that compact astrophysical objects would capture monopoles at a rate proportional to the galactic flux. These monopoles would then catalyze proton decay, with the energy released in the decay leading to an observable increase in the luminosity of the object. A variety of bounds, based on neutron stars [17–21] , white dwarfs [22], and Jovian planets [23] have been obtained. These depend in the obvious manner on the catalysis cross section, but also on the details of the astrophysical scenarios; *e.g.*, on how much the accumulated density is reduced by monopole-antimonopole annihilation, and on whether monopoles accumulated in the progenitor star survive its collapse to a white dwarf or neutron star. The bounds obtained in this manner lie in the range

$$F\left(\frac{\sigma_{\Delta B}\beta}{10^{-27}{\rm cm}^2}\right) \sim (10^{-18} - 10^{-29}){\rm cm}^{-2}{\rm sr}^{-1}{\rm sec}^{-1}. \tag{95.12}$$

It is important to remember that not all GUT monopoles catalyze baryon number nonconservation. In particular, the intermediate mass monopoles that arise in some GUTs at later stages of symmetry-breaking are examples of theoretically motivated monopoles that are exempt from the bound of the above equation.

95.4 Searches for Magnetic Monopoles

To date there have been no confirmed observations of exotic particles possessing magnetic charge. Precision measurements of the properties of known particles have led to tight limits on the values of magnetic charge they may possess. Using the induction method (see below), the electron's magnetic charge has been found to be $Q_e^m < 10^{-24}Q_M^D$ [24] (where Q_M^D is the Dirac charge). Furthermore, measurements of the anomalous magnetic moment of the muon have been used to place a model dependent lower limit of 120 GeV on the monopole mass [1] [25]. Nevertheless, guided mainly by Dirac's argument and the predicted existence of monopoles from spontaneous symmetry breaking mechanisms, searches have been routinely made for monopoles produced at accelerators, in cosmic rays, and bound in matter [26]. Although the resultant limits from such searches are usually made under the assumption of a particle possessing only magnetic charge, most of the searches are also sensitive to dyons.

95.5 Search Techniques

Search strategies are determined by the expected interactions of monopoles as they pass through matter. These would give rise to a number of striking characteristic signatures. Since a complete description of monopole search techniques falls outside of the scope of this minireview, only the most common methods are described below. More comprehensive descriptions of search techniques can be found in Refs. [27, 28].

The induction method exploits the long-ranged electromagnetic interaction of the monopole with the quantum state of a superconducting ring which would lead to a monopole which passes through such a ring inducing a permanent current. The induction technique typically uses Superconducting Quantum Interference Devices (SQUID) technology for detection and is employed for searches for monopoles in cosmic rays and matter. Another approach is to exploit the electromagnetic energy loss of monopoles. Monopoles with Dirac charge would typically lose energy at a rate which is several thousand times larger than that expected from particles possessing the elementary electric charge. Consequently, scintillators, gas chambers and nuclear track detectors (NTDs) have been used in cosmic ray and collider experiments. A further approach, which has been used at colliders, is to search for particles describing a non-helical path in a uniform magnetic field.

95.5.1 *Searches for Monopoles Bound in Matter*

Monopoles have been sought in a range of bulk materials which it is assumed would have absorbed incident cosmic ray monopoles over a long exposure time of order million years. Materials which have been studied include moon rock, meteorites, manganese modules, and sea water [29, 30]. A stringent upper limit on the monopoles per nucleon ratio of $\sim 10^{-29}$ has been obtained [30].

95.5.2 *Searches in Cosmic Rays*

Direct searches for monopoles in cosmic rays refer to those experiments in which the passage of the monopole is measured by an active detector. Searches made assuming a catalysis processes in which GUT monopoles could induce nucleon decay are discussed in the next section. To interpret the results of the non-catalysis searches, the cross section for the catalysis process is typically either set to zero [31] or assigned a modest value (1mb) [32].

Although early cosmic ray searches using the induction technique [33] and NTDs [34] observed monopole candidates, none of these apparent observations have been confirmed. Recent experiments have typically employed large scale detectors. The MACRO experiment at the Gran Sasso underground laboratory comprised three different types of detector: liquid scintillator, limited stream tubes, and NTDs, which provided a total acceptance of $\sim 10000{\rm m}^2$ for an isotropic flux. As shown in Fig. 95.1, this experiment has so far provided the most extensive β-dependent flux limits for GUT monopoles with Dirac charge [32]. Also shown

[1] Where no ambiguity is likely to arise, a reference to a monopole implies a particle possessing Dirac charge.

Downloaded from https://academic.oup.com/ptep/article/2022/8/083C01/6651666 by KIT Library user on 27 September 2022

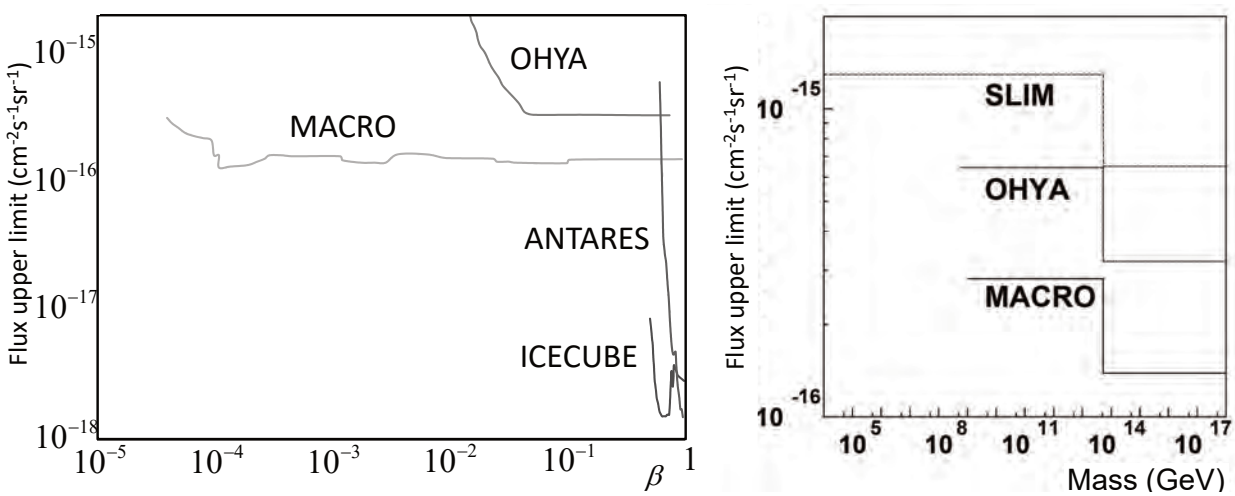

Figure 95.1: Upper flux limits for (left) GUT monopoles as a function of β (right) Monopoles as a function of mass for $\beta > 0.05$.

are limits from an experiment at the OHYA mine in Japan [31], which used a 2000m^2 array of NTDs.

In Fig. 95.1, upper flux limits are also shown as a function of mass for monopole speed $\beta > 0.05$. In addition to MACRO and OYHA flux limits, results from the SLIM [35] high-altitude experiment are shown. The SLIM experiment provided a good sensitivity to intermediate mass monopoles ($10^5 \lesssim M \lesssim 10^{12}$ GeV). In addition to the results shown in Fig. 95.1, limits as low as $\sim 1.5 \times 10^{-18}$ cm^{-2}s^{-1}sr^{-1} were obtained for monopoles with $\beta > 0.51$ and $\beta > 0.6$ by the IceCube [36] and Antares [37] experiments, respectively. Furthermore, the NoVA experiment [38] has recently set an upper limit on monopole flux of 2×10^{-14} cm^{-2}s^{-1}sr^{-1} for speeds $6 \times 10^{-4} < \beta < 10^{-3}$ for masses greater thsan 5×10^8 GeV. Stringent constraints on the flux of ultra-relativistic monopoles have been obtained at the Pierre Auger Observatory [39] which was sensitive to monopoles with γ values ranging from 10^9 to 10^{12}, leading to flux limits in the range $10^{-15} - 2.5 \times 10^{-21}$ cm^{-2}s^{-1}sr^{-1}. The RICE [40] and ANITA-II experiments [41] at the South Pole have also sought ultra-relativistic monopoles with γ values of $10^7 \lesssim \gamma \lesssim 10^{12}$ and $10^9 \lesssim \gamma \lesssim 10^{13}$, respectively, and which produced flux limits as low as 2.5×10^{-21} cm^{-2}s^{-1}sr^{-1}.

95.5.3 *Searches via the Catalysis of Nucleon-Decay*

Searches have been performed for evidence of the catalysed decay of a nucleon by a monopole, as predicted by the Callan-Rubakov mechanism. The searches are thus sensitive to the assumed value of the catalysis decay cross section. Searches have been made with the Soudan [42] and Macro [43] experiments, using tracking detectors. Searches at IMB [44], the underwater Lake Baikal experiment [45] and the The IceCube experiment [46] which exploit the Cerenkov effect have also been made. The resulting β-dependent flux limits from these experiments typically vary between $\sim 10^{-18}$ and $\sim 10^{-14}$cm^{-2}sr^{-1}s^{-1}. A recent search for low energy neutrinos (assumed to be produced from induced proton decay in the sun) was made at Super-Kamiokande [47]. A model- and β-dependent of limit of $6.3 \times 10^{-24}(\frac{\beta}{10^{-3}})^2$cm^{-2}sr^{-1}s^{-1} was obtained.

95.5.4 *Searches at Colliders*

Searches have been performed at hadron-hadron, electron-positron and lepton-hadron experiments. Collider searches can be broadly classed as being direct or indirect. In a direct search, evidence of the passage of a monopole through material, such as a charged particle track, is sought. In indirect searches, virtual monopole processes are assumed to influence the production rates of certain final states.

95.5.4.1 *Direct Searches at Colliders*

Collider experiments typically express their results in terms of upper limits on a production cross section and/or monopole mass. To calculate these limits, ansatzes are used to model the kinematics of monopole-antimonopole pair production processes since perturbative field theory cannot be used to calculate the rate and kinematic properties of produced monopoles. Limits therefore suffer from a degree of model-dependence, implying that a comparison between the results of different experiments can be problematic, in particular when this concerns excluded mass regions. A conservative approach with as little model-dependence as possible is thus to present representative values of the upper cross-section limits as a function of one half the centre-of-mass energy of the collisions, as shown in Fig. 95.2 for recent results from high energy colliders.

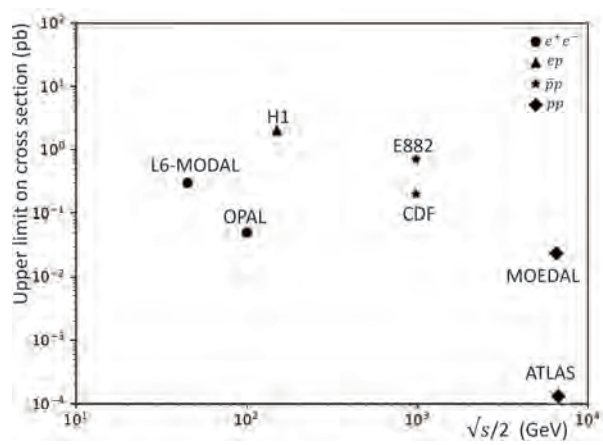

Figure 95.2: Upper limits on the production cross sections of monopoles from various collider-based experiments.

Searches for monopoles produced at the highest available energies in hadron-hadron collisions were made in pp collisions at the LHC by the ATLAS [48, 49] and MoEDAL [50, 51] experiments. The experiments looked for highly ionising particles leaving characteristic energy deposition profiles and stopped monopoles with the induction method, respectively. The charge-dependent mass limits extend up to around 4 TeV. The ATLAS work considers monopoles with $0.5Q_M^D$ and $2Q_M^D$ while MoEDAL quotes limits for monopoles with charges from Q_M^D to $5Q_M^D$. MoEDAL considered monopole-pair production via photon fusion along with, as is commonly used in hadron-hadron collisions, Drell-Yan processes [52]. Tevatron searches have also been carried out by the CDF [53] and E882 [54] experiments. The CDF experiment used a dedicated time-of-flight system whereas the E882 experiment employed the induction technique to search for stopped monopoles in discarded detector material which had been part of the CDF

Downloaded from https://academic.oup.com/ptep/article/2022/8/083C01/6651666 by KIT Library user on 27 September 2022

and D0 detectors using periods of luminosity. Earlier searches at the Tevatron, such as [55], used NTDs and were based on comparatively modest amounts of integrated luminosity. Lower energy hadron-hadron experiments have employed a variety of search techniques including plastic track detectors [56] and searches for trapped monopoles [57].

The only LEP-2 search was made by OPAL [58] which quoted cross section limits for the production of monopoles possessing masses up to around 103 GeV. At LEP-1, searches were made with NTDs deployed around an interaction region. This allowed a range of charges to be sought for masses up to ~ 45 GeV. The L6-MODAL experiment [59] gave limits for monopoles with charges in the range $0.9Q_M^D$ and $3.6Q_M^D$, whilst an earlier search by the MODAL experiment was sensitive to monopoles with charges as low as $0.1Q_M^D$ [60]. The deployment of NTDs around the beam interaction point was also used at earlier e^+e^- colliders such as KEK [61] and PETRA [62]. Searches at e^+e^- facilities have also been made for particles following non-helical trajectories [63,64].

There has so far been one search for monopole production in lepton-hadron scattering. Using the induction method, monopoles were sought which could have stopped in the aluminium beampipe which had been used by the H1 experiment at HERA [65]. Cross section limits were set for monopoles with charges in the range $Q_M^D - 6Q_M^D$ for masses up to around 140 GeV.

95.5.4.2 *Indirect Searches at Colliders*

It has been proposed that virtual monopoles can mediate processes which give rise to multi-photon final-states [66,67]. Photon-based searches were made by the D0 [68] and L3 [69] experiments. The D0 work led to spin-dependent lower mass limits of between 610 and 1580 GeV, while L3 reported a lower mass limit of 510 GeV. However, it should be stressed that uncertainties on the theoretical calculations which were used to derive these limits are difficult to estimate.

References

[1] P. A. M. Dirac, Proc. Roy. Soc. Lond. **A133**, 821, 60 (1931).

[2] J. S. Schwinger, Science **165**, 757 (1969).

[3] F. Englert and P. Windey, Phys. Rev. **D14**, 2728 (1976).

[4] P. Goddard, J. Nuyts and D. I. Olive, Nucl. Phys. **B125**, 1 (1977).

[5] G. 't Hooft, Nucl. Phys. **B79**, 276 (1974).

[6] A. M. Polyakov, JETP Lett. **20**, 194 (1974).

[7] C. P. Dokos and T. N. Tomaras, Phys. Rev. **D21**, 2940 (1980).

[8] G. Lazarides and Q. Shafi, Phys. Lett. **94B**, 149 (1980).

[9] C. G. Callan, Jr., Phys. Rev. **D26**, 2058 (1982).

[10] V. A. Rubakov, Nucl. Phys. **B203**, 311 (1982).

[11] T. W. B. Kibble, J. Phys. **A9**, 1387 (1976).

[12] J. Preskill, Phys. Rev. Lett. **43**, 1365 (1979).

[13] E. N. Parker, Astrophys. J. **160**, 383 (1970).

[14] M. S. Turner, E. N. Parker and T. J. Bogdan, Phys. Rev. **D26**, 1296 (1982).

[15] F. C. Adams *et al.*, Phys. Rev. Lett. **70**, 2511 (1993).

[16] Y. Rephaeli and M. S. Turner, Phys. Lett. **121B**, 115 (1983).

[17] E. W. Kolb, S. A. Colgate and J. A. Harvey, Phys. Rev. Lett. **49**, 1373 (1982).

[18] S. Dimopoulos, J. Preskill and F. Wilczek, Phys. Lett. **119B**, 320 (1982).

[19] K. Freese, M. S. Turner and D. N. Schramm, Phys. Rev. Lett. **51**, 1625 (1983).

[20] E. W. Kolb and M. S. Turner, Astrophys. J. **286**, 702 (1984).

[21] J. A. Harvey, Nucl. Phys. **B236**, 255 (1984).

[22] K. Freese and E. Krasteva, Phys. Rev. **D59**, 063007 (1999), [arXiv:astro-ph/9804148].

[23] J. Arafune, M. Fukugita and S. Yanagita, Phys. Rev. **D32**, 2586 (1985).

[24] L. L. Vant-Hull, Phys. Rev. **173**, 1412 (1968).

[25] S. Graf, A. Schaefer and W. Greiner, Phys. Lett. **B262**, 463 (1991).

[26] Review of Particle Physics 2020 (*this paper*), listing on *Searches for Magnetic Monopoles*.

[27] L. Patrizii and M. Spurio, Ann. Rev. Nucl. Part. Sci. **65**, 279 (2015), [arXiv:1510.07125].

[28] M. Fairbairn *et al.*, Phys. Rept. **438**, 1 (2007), [hep-ph/0611040].

[29] J. M. Kovalik and J. L. Kirschvink, Phys. Rev. **A33**, 1183 (1986).

[30] H. Jeon and M. J. Longo, Phys. Rev. Lett. **75**, 1443 (1995), [Erratum: Phys. Rev. Lett.76,159(1996)], [hep-ex/9508003].

[31] S. Orito *et al.*, Phys. Rev. Lett. **66**, 1951 (1991).

[32] M. Ambrosio *et al.* (MACRO), Eur. Phys. J. **C25**, 511 (2002), [hep-ex/0207020].

[33] B. Cabrera, Phys. Rev. Lett. **48**, 1378 (1982).

[34] P. B. Price *et al.*, Phys. Rev. Lett. **35**, 487 (1975).

[35] S. Balestra *et al.*, Eur. Phys. J. **C55**, 57 (2008), [arXiv:0801.4913].

[36] M. G. Aartsen *et al.* (IceCube), Eur. Phys. J. **C76**, 3, 133 (2016), [arXiv:1511.01350].

[37] A. Albert *et al.* (ANTARES), JHEP **07**, 054 (2017), [arXiv:1703.00424].

[38] M. A. Acero *et al.* (NOvA), Phys. Rev. D **103**, 1, 012007 (2021), [arXiv:2009.04867].

[39] A. Aab *et al.* (Pierre Auger), Phys. Rev. **D94**, 8, 082002 (2016), [arXiv:1609.04451].

[40] D. P. Hogan *et al.*, Phys. Rev. **D78**, 075031 (2008), [arXiv:0806.2129].

[41] M. Detrixhe *et al.* (ANITA-II), Phys. Rev. **D83**, 023513 (2011), [arXiv:1008.1282].

[42] J. E. Bartelt *et al.*, Phys. Rev. D **36**, 1990 (1987), [Erratum: Phys.Rev.D 40, 1701 (1989)].

[43] M. Ambrosio *et al.* (MACRO), Eur. Phys. J. **C26**, 163 (2002), [hep-ex/0207024].

[44] R. Becker-Szendy *et al.*, Phys. Rev. **D49**, 2169 (1994).

[45] V. A. Balkanov *et al.* (Baikal), Prog. Part. Nucl. Phys. **40**, 391 (1998), [arXiv:astro-ph/9801044].

[46] M. G. Aartsen *et al.* (IceCube), Eur. Phys. J. **C74**, 7, 2938 (2014), [Erratum: Eur. Phys. J.C79,no.2,124(2019)], [arXiv:1402.3460].

[47] K. Ueno *et al.* (Super-Kamiokande), Astropart. Phys. **36**, 131 (2012), [arXiv:1203.0940].

[48] G. Aad *et al.* (ATLAS), Phys. Rev. **D93**, 5, 052009 (2016), [arXiv:1509.08059].

[49] G. Aad *et al.* (ATLAS), Phys. Rev. Lett. **124**, 3, 031802 (2020), [arXiv:1905.10130].

[50] B. Acharya *et al.* (MoEDAL), Phys. Rev. Lett. **118**, 6, 061801 (2017), [arXiv:1611.06817].

[51] B. Acharya *et al.* (MoEDAL), Phys. Rev. Lett. **123**, 2, 021802 (2019), [arXiv:1903.08491].

[52] S. Baines *et al.*, Eur. Phys. J. **C78**, 11, 966 (2018), [Erratum: Eur. Phys. J.C79,no.2,166(2019)], [arXiv:1808.08942].

[53] A. Abulencia *et al.* (CDF), Phys. Rev. Lett. **96**, 201801 (2006), [hep-ex/0509015].

[54] G. R. Kalbfleisch *et al.*, Phys. Rev. **D69**, 052002 (2004), [hep-ex/0306045].

[55] P. B. Price, G.-X. Ren and K. Kinoshita, Phys. Rev. Lett. **59**, 2523 (1987).

[56] B. Aubert *et al.*, Phys. Lett. **120B**, 465 (1983).

[57] R. A. Carrigan, F. A. Nezrick and B. P. Strauss, Phys. Rev. **D8**, 3717 (1973).

Downloaded from https://academic.oup.com/ptep/article/2022/8/083C01/6651666 by KIT Library user on 27 September 2022

[58] G. Abbiendi *et al.* (OPAL), Phys. Lett. **B663**, 37 (2008), [arXiv:0707.0404].

[59] J. L. Pinfold *et al.*, Phys. Lett. **B316**, 407 (1993).

[60] K. Kinoshita *et al.*, Phys. Rev. **D46**, R881 (1992).

[61] K. Kinoshita *et al.*, Phys. Lett. **B228**, 543 (1989).

[62] P. Musset, M. Price and E. Lohrmann, Phys. Lett. **128B**, 333 (1983).

[63] T. Gentile *et al.* (CLEO), Phys. Rev. **D35**, 1081 (1987).

[64] W. Braunschweig *et al.* (TASSO), Z. Phys. **C38**, 543 (1988).

[65] A. Aktas *et al.* (H1), Eur. Phys. J. **C41**, 133 (2005), [hep-ex/0501039].

[66] A. De Rujula, Nucl. Phys. **B435**, 257 (1995), [hep-th/9405191].

[67] I. F. Ginzburg and A. Schiller, Phys. Rev. **D60**, 075016 (1999), [hep-ph/9903314].

[68] B. Abbott *et al.* (D0), Phys. Rev. Lett. **81**, 524 (1998), [hep-ex/9803023].

[69] M. Acciarri *et al.* (L3), Phys. Lett. **B345**, 609 (1995).

Downloaded from https://academic.oup.com/ptep/article/2022/8/083C01/6651666 by KIT Library user on 27 September 2022

Downloaded from https://academic.oup.com/ptep/article/2022/8/083C01/6651666 by KIT Library user on 27 September 2022

INDEX

Downloaded from https://academic.oup.com/ptep/article/2022/8/083C01/6651666 by KIT Library user on 27 September 2022

Downloaded from https://academic.oup.com/ptep/article/2022/8/083C01/6651666 by KIT Library user on 27 September 2022

Index

This index is for the complete *Review of Particle Physics* (Volume 1 and 2). Page numbers larger than 1122 refer to the Particle Listings in Volume 2 that can be found in the journal publication and online at `https://pdg.lbl.gov`.

a meson resonances
- $a_0(980)$ ... 34, 1382
- $a_0(1450)$ ... 36, 1416
- $a_0(1950)$ ... 1456
- $a_1(1260)$ ... 35, 1392
- $a_1(1640)$ ... 37, 1431
- $a_2(1320)$ ... 35, 1402
- $a_2(1700)$ ... 38, 1445
- $a_4(1970)$ [*was* $a_4(2040)$] ... 39, 1458

ABC, approximate Bayesian computation ... 684
Absolute monochromatic magnitude ... 134
Accelerating Universe evidence ... 471
Accelerator parameters ... 543
Accelerator parameters for neutrino beam lines ... 548
Accelerator-based ν detectors ... 605
Accelerator-induced radioactivity ... 648
Acceptance-rejection method (Von Neumann) ... 713
Acoustic oscillations, baryon ... 478
Activation function ... 689
Active learning ... 683, 684
Activity, unit of ... 646
AD, automatic differentiation ... 700
AdaBoost, adaptive boost ... 689
ADAM, Adaptive Momentum Estimation ... 700
AdS, anti-de Sitter spacetime ... 983
AdS/CFT
- correspondence ... 983, 1062
- dictionary ... 987, 1062

Advanced acceleration schemes ... 541
Age of the Universe ... 135, 432
Air shower extensive, EAS ... 618
Air showers (cosmic ray) ... 524
Aleatoric uncertainty ... 704
Algorithms for Monte Carlo ... 714
α, fine structure constant ... 178
α_s, QCD coupling constant ... 133
Amplitudes, Lorentz invariant ... 743
AMS, approximate median significance ... 704
AMS-02 – alpha magnetic spectrometer, ISS ... 521
AMSB, anomaly-mediated SUSY breaking ... 1002
Angular-diameter distance, d_A ... 432
Anisotropy of CBR ... 471, 509
Annihilating dark matter ... 516
Anomalous dimension quark mass ($\overline{\text{MS}}$) ... 808
Anomaly detection ... 683, 706
Anomaly-mediated SUSY breaking, AMSB ... 1002
Anthropic approach ... 435
Anthropic axion window ... 1045
Antineutrino flux from reactor ... 298
Antineutrinos, right-handed ... 897
Astronomical unit ... 134
Astrophysics ... 483
Asymmetry formulae in Standard Model ... 181
Asymptotic freedom ... 149
Asymptotics, total hadronic cross sections behaviour ... 409
ATLAS – Thoroidal LHC Apparatus, LHC ... 208
Atmospheric
- Cherenkov detectors ... 620
- cosmic rays ... 524
- fluorescence detector ... 618
  - Fly's Eye ... 618
  - HiRes (high resolution) Fly's Eye ... 618
  - Pierre Auger observatory ... 618
  - Telescope Array ... 618
- neutrino flux ... 293

Atmospheric pressure ... 133
Atomic
- and nuclear properties of materials, table ... 140
- mass unit ... 133

Atomic weights of elements ... 137
Attention ... 690, 694
Attenuation length for photons ... 557
Auger observatory ... 525, 618, 1095
Authors and consultants ... 12
Auto-encoder ... 681, 683
Averaging of data ... 16
Averaging, unconstrained ... 16
Avogadro constant ... 133
Axial vector couplings, g_V, g_A vector ... 177
Axial vector mesons $\ell = 1$; 1^{++} or 1^{+-} ... 313
Axial-vector mesons
- K_{1A}-K_{1B} mixing ... 845, 850
- $f_1(1285)$, $f_1(1420)$, $f_1(1510)$ ... 850, 851

Axion as dark matter ... 485, 1038
Axion searches ... 1038
Axion stars ... 1046
Axion-like particles (ALP) ... 1038
Axion-photon mixing ... 516
Axions (A^0) and other very light bosons searches ... 27, 1217

$B\overline{B}$ mixing ... 923
$b\bar{b}$ mesons ... 81, 1940
B decay, CP violation in ... 278, 920
B decays polarization, note ... 919
B mesons
- V_{cb} and V_{ub} CKM Matrix Elements ... 1780
- B^* ... 67, 1781
- B^0 ... 59, 1675
- $B^\pm$ ... 53, 1610
- $B^\pm/B^0$ admixture ... 65, 1750
- $B^\pm/B^0/B^0_s/B$-baryon admixture ... 66, 1772
- $B_1(5721)$ ... 68, 1782
- $B^*_2(5747)$ ... 68, 1783
- $B^*_J(5732)$ [*was* B^{**}] ... 1782
- $B_J(5840)$ ... 1783
- $B_J(5970)$ ... 68, 1784
- B^+_c ... 70, 1813
- $B_c(2S)^\pm$ ... 70, 1817
- $B_{s1}(5830)^0$ ... 70, 1811
- $B^*_{s2}(5840)^0$ ... 70, 1811
- $B^*_{sJ}(5850)$ ... 1811
- $B_{sJ}(6063)^0$ ... 1812
- $B_{sJ}(6114)^0$ ... 1812
- B^*_s ... 69, 1810
- B^0_s ... 68, 1786

b' quark (4th generation), searches for ... 829
b-baryon admixture ... 106, 2179
b-flavored Hadrons, production and decay ... 908
b-quark fragmentation ... 383, 827
$b_1(1235)$ meson ... 35, 1391
Background
- cosmic microwave, CMB ... 509
- cosmic ray radiation ... 647
- relic cosmic neutrino ... 476
- relic light gravitons ... 984

Background cosmology parameters ... 511
Backpropagation ... 684, 700
Bagging, bootstrap aggregating ... 688
Balitsky-Fadin-Kuraev-Lipatov (BFKL) limit ... 152
Barkas correcion ... 552
Baryogenesis ... 435
Baryon
- acoustic oscillations ... 447, 471, 478
- decay parameters, note on ... 964
- density of the Universe ... 134
- Hyperon nonleptonic decays ... 964
- magnetic moments ... 321, 326
- number conservation ... 116
- oscillation spectroscopic survey ... 471
- resonances, naming scheme ... 965

Downloaded from https://academic.oup.com/ptep/article/2022/8/083C01/6651666 by KIT Library user on 27 September 2022

resonances, SU(3) classification of ... 317
semileptonic decays ... 964
Baryon quick reference table ... 89
Baryon-to-photon ratio ... 134, 461
Baryonia ... 845, 852
$\rho(1900)$ ... 850
$f_2(1565)$ ... 852
Baryons in quark model ... 317
Batch ... 700, 702
Bayes' theorem ... 452, 655
Bayesian
approach ... 664
intervals ... 669
method ... 660
statistics ... 669
Bayesian machine learning ... 705
Bayesian optimization ... 682, 687
BBN, Big-Bang nucleosynthesis ... 459
Beam collimation ... 535, 540
Beam cooling ... 535
Beam dynamics ... 533
Beam momentum, c.m. energy and momentum vs ... 743
Beam-beam interaction ... 536
Beamstrahlung ... 536, 538
Becquerel, unit of radioactivity ... 646
BEPC ... 543
BEPC-II ... 543
β function of QCD ... 149
Beta distribution ... 658, 715
Beta function ... 534
β-rays, from radioactive sources ... 652
Betatron tune ... 534
Bethe equation ... 550
Beyond the general relativity physics ... 516
Beyond the SM physics, BSM ... 261, 463, 485, 720
Bhabha cross section ... 555
Bhabha scattering ... 178
Bi-directional RNN ... 694
Bias of an estimator ... 660
Big-Bang cosmology ... 443
Big-Bang cosmology, note on ... 430
Big-Bang nucleosynthesis (BBN) ... 459
Binary classification ... 679, 680, 686
Binary pulsars, strong-self-gravity ... 424
Bino ... 1004
Binomial distribution ... 658, 714
Biological damage from radiation ... 646
Birks' law ... 568
Black holes
binary ... 424
coalescing ... 421
horizon ... 419
microscopic, searches ... 985
production ... 984
strong gravitational fields ... 418
supermassive ... 424
Bloch correction ... 552
BMA, Bayesian model averaging ... 705
BN, batch normalization ... 691, 701
Bohr magneton ... 133
Bohr radius ... 133, 183
Boiling points of cryogenic gases, table ... 140
Boltzmann constant k ... 133
Booklet, Particle Physics, how to get ... 11
Boosting ... 688
Bose-Einstein correlations ... 404, 725, 789
Bosons, Nambu-Goldstone composite ... 1061
BOSS, baryon oscillation spectroscopic survey ... 471
Bottleneck ... 681, 697
Bottom baryons ... 104, 2161
Bottom mesons
experimental rate measurements ... 902
production and decay ... 908
theoretical decay-constant calculations ... 902
Bottom mesons (B, B^*) ... 53, 1610
Bottom, Charmed mesons (B_c, $B_c(2S)$) ... 70, 1813
Bottom, Strange mesons (B_s, B_s^*, X) ... 68, 1786
Bottom-changing neutral currents, tests for ... 117
Bottomonium note ... 81, 1940
Bragg additivity ... 554
Brane ... 463, 984, 1002, 1079
Breit–Wigner parametrization ... 751
Breit-Wigner distribution ... 715
Bremsstrahlung
at very high energies ... 558
by $e^{\pm}$ ... 556
by muons ... 560
B_s^0 decay, CP violation in ... 278
BSM, beyond Standard Model ... 485
Bubble chambers ... 606
Bubble Universes ... 435

$c\bar{c}$ mesons (including possibly non-$q\bar{q}$ states) ... 70, 1818
C (charge conjugation), tests of conservation ... 110
c-quark fragmentation ... 383
Cabibbo angle ... 873
Calorimeter
electromagnetic (ECAL) ... 597
hadronic (HCAL) ... 597
homogeneous ... 597
sampling ... 597
CBR – Cosmic background radiation (see CMB) ... 509
CDM, cold dark matter ... 483
Central limit theorem ... 657
CEPC ... 538
Cepheid variable stars ... 470
CESR (Cornell) ... 544
CESR-C (Cornell) ... 544
CFT, 4d conformal field theory ... 987
Chandrasekhar mass ... 134
Change of random variables ... 656
Channels ... 685, 690, 702
Characteristic functions ... 656
Charge conjugation (C) conservation ... 110
Charge conjugation of $q\bar{q}$ states ... 313
Charge conservation ... 113
Charged Higgs bosons ($H^{\pm}$ and $H^{\pm\pm}$) searches ... 26, 1196
Chargino mass limits ... 1026
Charginos ... 1004
Charm decays, CP violation in ... 276
Charm mixing and CP violation ... 881
Charm-changing neutral currents, tests for ... 117
Charmed baryons (Λ_c^+, Σ_c, Ξ_c, Ω_c^+) ... 100, 2136
Charmed baryons, note on ... 100, 2136
Charmed mesons
experimental rate measurements ... 900
theoretical decay-constant calculations ... 901
Charmed mesons (D, D^*, D_J) ... 43, 1527
Charmed, Strange mesons (D_s, D_s^*, D_{sJ}, X) ... 50, 1588
Chemical potential ... 346, 433
Chemical potential, neutrino ... 516
Cherenkov detectors ... 572
at accelerators
differential ... 573
ring imaging ... 573
threshold ... 572
tracking ... 572
electromagnetic calorimeters ... 572
fast paticle counter ... 572
nonaccelerator
atmospheric ... 620
deep underground ... 621
particle identification PID ... 572
Cherenkov radiation ... 561
χ^2 distribution ... 657, 714
χ_b and χ_c mesons

Downloaded from https://academic.oup.com/ptep/article/2022/8/083C01/6651666 by KIT Library user on 27 September 2022

$\chi_{b0}(1P)$ ... 82, 1948
$\chi_{b0}(2P)$ ... 84, 1960
$\chi_{b1}(1P)$ ... 82, 1950
$\chi_{b1}(2P)$ ... 84, 1961
$\chi_{b1}(3P)$ ... 84, 1969
$\chi_{b2}(1P)$ ... 83, 1952
$\chi_{b2}(2P)$ ... 84, 1964
$\chi_{b2}(3P)$ ... 85, 1970
$\chi_{c0}(1P)$ ... 73, 1851
$\chi_{c0}(3860)$ ... 1911
$\chi_{c0}(3915)$ [*was* $X(3915)$] ... 79, 1916
$\chi_{c0}(4500)$ [*was* $X(4500)$] ... 1936
$\chi_{c0}(4700)$ [*was* $X(4700)$] ... 1939
$\chi_{c1}(1P)$ ... 74, 1861
$\chi_{c1}(3872)$ [*aka* $X(3872)$] ... 78, 1911
$\chi_{c1}(4140)$ [*was* $X(4140)$] ... 79, 1922
$\chi_{c1}(4274)$ [*was* $X(4274)$] ... 80, 1932
$\chi_{c1}(4685)$ ... 1939
$\chi_{c2}(1P)$ ... 75, 1872
$\chi_{c2}(3930)$ ... 79, 1917
Chiral perturbation theory ... 341, 810, 859, 865
Chiral superfields ... 1000
Chromaticity ... 535
CIPT, countour improved perturbation theory ... 184
Circular Colliders ... 533
Circular Higgs factories ... 538
CKM (Cabibbo-Kobayashi-Maskawa) quark mixing matrix 946
CKM angles
α ... 946
β ... 946
γ ... 948
from B hadrons determination, note ... 946
CKM matrix elements ... 946
CKM quark-mixing matrix, note on ... 261
CKM unitarity constraints ... 874
Classical electron radius ... 133
Classification ... 676, 679, 683, 686, 687, 691, 697, 705
Clebsch-Gordan coefficients ... 737, 738
CLIC (CERN) future collider ... 544
Clustering ... 681, 697
CMB
Planck satellite ... 447, 503, 512
anisotropy ... 439, 471
anisotropy power spectrum ... 509
COBE satellite ... 468, 509
Compton distortion ... 515
concordance with baryon density ... 462
cosmic microwave background ... 509
cosmic variance ... 510
detectors ... 633
dipole ... 509
future Simons observatory ... 473
lensing ... 479
LiteBIRD satellite ... 514
Lorentz-boosted temperature pattern ... 509
mean temperature, monopole ... 509
monopole ... 509
multipoles ... 509
non-Gaussianity ... 437, 453, 468, 510
polarization ... 513
primordial perturbation ... 511
radiation density of Universe ... 134
scalar perturbations ... 511
sky map ... 509
Solar System motion ... 509
spectrum ... 509
tensor perturbations ... 511
Wilkinson Microwave Anisotropy Probe, *WMAP* ... 509
WMAP satellite ... 503
CMB–Cosmic microwave background ... 436, 471
CMS – Compact Muon Solenoid, LHC ... 208
CMSSM, Constrained MSSM ... 1007, 1021
CNN, convolutional neural network ... 679, 685, 690, 702
CNO cycle, solar neutrino ... 292
COBE – COsmic Background Explorer ... 509
Coherent radio Cherenkov radiation detectors ... 627
Cold dark matter (CDM) ... 438
Cold dark matter density ... 134
Collaboration databases ... 21
Collaborations
Planck ... 470
ALEPH ... 789
ALICE ... 397
ALPHA ... 346
ANITA ... 629
ARIANNA ... 629
ATLAS ... 397, 487, 789, 951, 991
Auger ... 525
B-factories ... 951
BaBar ... 178, 804, 902, 908, 924, 951, 1010
Belle ... 804, 902, 908, 924, 951, 1010
BERT ... 1040
BESIII ... 951
BES III ... 178
BNL E821 ... 184
CALICE ... 601
CCFR ... 608
CDF ... 789, 908
CJ ... 366
CLEO ... 178, 908
CLEO-c ... 951
CMD-3 ... 178
CMS ... 179, 487, 951, 991, 997, 1030, 1091
COHERENT ... 182
COMPASS ... 843
COMPETE ... 399, 409
CTA ... 620
D0 ... 179, 408, 789, 909, 924, 997
DarkSide ... 631
DELPHI ... 789, 924
DREAM/RD52 ... 603
DSSV ... 358
eBOSS ... 502
ETM ... 904
Event Horizon Telescope ... 425
Fermi-LAT ... 1043
FLAG ... 904
GlueX ... 977
GRAND ... 630
H.E.S.S. ... 620, 1043
H1 ... 384, 1091
HERA ... 385, 1025
HFLAV ... 904
HPQCD ... 346, 904
HWPF ... 607
Jefferson lab hall A ... 182
L3 ... 178, 789, 924
Lattice QCD ... 811
LEP ... 789, 791, 996, 1025
LHAASO ... 525
LHC ... 789, 997
LHCb ... 789, 908, 920, 951, 959, 997, 1010
LIGO-Virgo ... 421
LVC ... 421
MAGIC ... 620
MAMI ... 843
MILC ... 901
MOSCAB ... 491
MuLan ... 178
NEWS-G ... 491
NEWSdm ... 491
NEXT ... 632
NINJA ... 608
NuTeV ... 181, 608
OPAL ... 178, 789, 924
PDG, Particle Data Group ... 2

Downloaded from https://academic.oup.com/ptep/article/2022/8/083C01/6651666 by KIT Library user on 27 September 2022

PIBETA ... 842
PVLAS ... 1040
RBC/UKQCD ... 936
RD51 ... 580
RM123-Soton ... 898
RNO-G ... 630
SLD ... 186, 793
SND ... 178
Sp$\bar{\text{p}}$ ... 1055
Telescope Array ... 525
Tevatron ... 179, 789, 997, 1025
TOTEM ... 396
Tunka-Rex ... 630
UA4 ... 408
VERITAS ... 620
WMAP ... 472
ZEUS ... 187, 384, 1025, 1091
Collider parameters ... 543
Colliders ... 533
future ... 538
present ... 537
recent ... 536
Colliders based on Energy Recovery Linacs ... 539
Collinear and infrared safety ... 153, 157
Collinear factorization ... 151
Color confinement ... 1044
Color factor ... 149, 159
Color reconnection phenomenon ... 405, 725, 789
Colorons (axigluons) search ... 1072
Compact Linear Collider (CLIC) ... 539
Compactification ... 1045
Compensation
intrinsic ... 602
software ... 603
Complex ionization history ... 469
Composite Higgs boson ... 192, 235
Compton wavelength, electron ... 133
Concordance cosmology ... 468
Conditional probability density function ... 656
Confidence intervals ... 668
frequentist ... 669
Gaussian ... 16
Poisson ... 671
Confinement ... 346
-deconfinement quarks-hadrons transition ... 434
color ... 1044
harmonic ... 317
linear ... 317, 722
Conformal field theory, CFT ... 987
Conservation laws ... 110
Consistency of an estimator ... 660
Constancy of constants tests ... 423
Constrained fit ... 803
Constrained fits, procedures for ... 16
Constrained MSSM, CMSSM ... 1007, 1021
Constraints, parameter estimation with ... 663
Consultants ... 12
Contour-improved perturbation theory (CIPT) ... 163
Conversion constant ... 133
Conversion probability for photons to e^+e^- ... 557
Convolution kernel ... 690
Convolution, 1×1 ... 690
Convolution, kernel size ... 690
Convolution, padding ... 690
Convolution, stride ... 690
Convolution-transpose ... 691
Correlation coefficient, definition ... 656
Correlation matrices ... 803
Cosmic acceleration, dark energy ... 499
Cosmic background radiation temperature ... 509
Cosmic microwave background, CMB ... 436, 471, 509
Cosmic neutrino background, CνB ... 476
Cosmic ray(s) ... 520
air showers ... 524
ankle ... 525, 526
at surface of earth ... 522
background in counters ... 647
composition ... 520
fluorescence detectors FDs ... 618
fluxes ... 524
in atmosphere ... 520
instep ... 526
knee ... 525
primary spectra ... 520
radio detection of air showers ... 630
second knee ... 525
secondary neutrinos ... 523
ultra-high energy ... 526
ultra-high energy, UHE ... 628
underground ... 523
Cosmic topology ... 470
Cosmological
constant Λ ... 134, 430, 443, 499, 511
density parameter, Ω ... 431
equation of state ... 431
mass density parameter ... 430
parameters, note on ... 467
standard model ... 517
Cosmological probes
CMB ... 515
galaxy peculiar velocities ... 472
integrated Sachs-Wolfe effect ... 472
redshift ... 430
supernovae ... 470
Cosmology ... 467, 483
ΛCDM ... 483
Big-Bang ... 430, 443, 483
modern ... 483
outlook for the future ... 473
Robertson-Walker metric ... 443
scalar field ... 444
standard ... 485
standard early Universe ... 443
standard neutrino ... 476
Countour improved perturbation theory, CIPT ... 184
Coupling between matter and gravity ... 423
Coupling constant in QCD ... 133, 149
Coupling unification ... 1079
Couplings for photon, W, Z ... 177
Covariance matrix ... 662
Covariance, definition ... 656
Coverage ... 669
CP, tests of conservation ... 110
CP violation
and $D^0 - \overline{D}^0$ mixing ... 885
charm mixing ... 881
classification of effects ... 273
in $B\overline{B}$ mixing ... 926
in B and B_s^0 mixing and decay ... 278
in B decay ... 908
in K_L^0 decay ... 275
in K_L^0 decay, note on ... 877
in charm ... 276
in decays of Beauty to Charm ... 881
in the quark sector, note ... 271
interference between tree and penguin amplitudes ... 278
overview ... 110, 271
the CKM matrix ... 274
the Kobayashi-Maskawa mechanism ... 274
CPT invariance tests in neutral kaon decay ... 871
CPT tests of conservation ... 113
CRF – computer-readable files ... 770
Critical density in cosmology ... 430
Critical density of the Universe ... 134
Critical energy
for electrons ... 556

Downloaded from https://academic.oup.com/ptep/article/2022/8/083C01/6651666 by KIT Library user on 27 September 2022

for muons ... 560
Cromomagnetic dipole moment ... 822
Cross sections and related quantities, plots of ... 770
σ and R in e^+e^- Collisions ... 773
e^+e^- annihilation cross section near M_Z ... 775
pd, np, $\overline{p}d$, and $\overline{p}n$ collisions ... 779
Λp, Σp, γd, γp, and $\gamma\gamma$ collisions ... 783
$\pi^\pm p$ and $\pi^\pm d$ collisions ... 780
K^+p, K^+d and K^+n collisions ... 782
K^-p, K^-d and K^-n collisions ... 781
Pseudorapidity distribution in pp and $\overline{p}p$ interactions 770
Average hadron multiplicities
in e^+e^- annihilation events ... 771
nucleon structure functions ... 353
Cross sections, neutrino ... 765
Cross sections, relations for ... 745, 756
Cross-entropy loss ... 680
Cross-validation ... 678
Cryogenic beam vacuum system ... 539
Cryogenic gases, boiling points, table ... 140
Crystal accelerator ... 541
Cumulative distribution function, definition ... 655
Curie, unit of radioactivity ... 646
Curvature ... 135

d functions ... 737
D mesons
$D^0, \overline{D}^0$ ... 45, 1543
$D^\pm$ ... 43, 1527
$D(3000)^0$ ... 1587
$D^*(2007)^0$ ... 49, 1578
$D^*(2010)^\pm$ ... 49, 1578
$D^*(2640)^\pm$ ... 1585
$D_0^*(2300)$ [*was* $D_0^*(2400)$] ... 49, 1580
$D_0(2550)^0$ ... 1584
$D_1^*(2600)^0$ [*was* $D_J^*(2600)$] ... 1584
$D_1^*(2760)^0$ ... 1586
$D_1(2420)$ ... 49, 1580
$D_1(2430)^0$ ... 49, 1582
$D_2^*(2460)$ ... 49, 1582
$D_2(2740)^0$ [*was* $D(2740)^0$] ... 1585
$D_3^*(2750)$ ... 49, 1586
$D_{s0}^*(2317)^\pm$ ... 51, 1601
$D_{s0}(2590)^+$ ... 1605
$D_{s1}^*(2700)^\pm$ ... 52, 1606
$D_{s1}^*(2860)^\pm$ ... 1606
$D_{s1}(2460)^\pm$ ... 52, 1602
$D_{s1}(2536)^\pm$ ... 52, 1604
$D_{s2}^*(2573)$ ... 52, 1605
$D_{s3}^*(2860)^\pm$ ... 52, 1607
$D_{sJ}(3040)^\pm$ ... 1608
$D_s^{*\pm}$ ... 51, 1601
$D_s^\pm$ ... 50, 1588
D^0-$\overline{D}^0$ mixing, note on ... 885
DAΦNE ... 543
d_A, angular-diameter distance ... 471, 516
Dalitz plot, relations for ... 744
Damage, biological, from radiation ... 646
Dark energy ... 431, 469, 499
cosmic acceleration ... 499
density parameter ... 134
equation of state parameter ... 135
equation of state parameter w ... 471, 499
Euclid satellite ... 456
experiments ... 502
observational probes
baryon acoustic oscillations, BAO ... 501
CMB anisotropies ... 501
Type Ia supernovae ... 501
weak gravitational lensing ... 501
parameter, $\Omega_{\rm N}$ ... 431
quintessence ... 440
repulsive gravity ... 500
Dark energy spectroscopic instrument (DESI) ... 472, 502
Dark matter ... 438, 469
annihilating ... 516
CDM cosmology ... 483
density distribution ... 484
detectors ... 633
Gaia satellite ... 485
Galactic halo shape ... 484
genesis, cannibalization ... 484
genesis, DM anti-DM asymmetry ... 484
genesis, freeze-in ... 484
genesis, freeze-out ... 483
genesis, non-thermal production ... 484
genesis, primordial black holes ... 484
laboratory detection ... 487
missing satellites problem ... 485
non-baryonic ... 483
velocity distribution ... 485
Dark matter astrophysical detection
cosmic-ray antimatter ... 493
cosmology ... 494
gamma rays ... 492
multi-wavelength ... 494
neutrinos ... 493
PBH detection ... 494
staller physics ... 494
Dark matter candidates
axions ... 485
dark photon ... 486
gaugino ... 1003
gravitino ... 1002
higgsino ... 1003
sterile neutrinos ... 485
WIMPs ... 486
Dark matter properties
darkness ... 483
mass lower and upper limits ... 483
self-interactions ... 483
stability ... 483
Data ... 21
Data augmentation ... 686, 703, 704
Data manifold ... 686
Data, averaging and fitting procedures ... 16
Data, selecting and treatment ... 15
Databases
availability online ... 20
conferences ... 21
experiments ... 21
high-energy physics ... 20
INSPIRE ... 20
Authors ... 21
Conferences ... 21
Experiments ... 21
Jobs ... 21
Literature ... 20
Seminars ... 21
journals ... 21
literature ... 20
ADS ... 20
arXiv.org ... 20
INSPIRE ... 20
MathSciNet ... 20
ORCID ... 21
particle physics ... 20
PDGLive, PDG web browser ... 20
Review of Particle Physics (RPP) ... 20
RPP computer-readable files ... 20
Day, sidereal ... 134
dE/dx ... 549
Decay parameters, Michel ... 806
Decays, kinematics and phase space for ... 743
Deceleration parameter, q_0 ... 431

Downloaded from https://academic.oup.com/ptep/article/2022/8/083C01/6651666 by KIT Library user on 27 September 2022

Decision trees ... 677
Decoder ... 681, 691, 696, 698
Deep inelastic scattering, DIS ... 353, 398, 606
Deep learning ... 690
Deep Sets ... 685, 696
Deep-inelastic scattering (DIS) ... 151
Degree of freedom, number of ... 662
$\Delta B = 1$, weak-neutral currents, tests for ... 110
$\Delta B = 2$, tests for ... 110
$\Delta C = 1$, weak-neutral currents, tests for ... 110
$\Delta C = 2$, tests for ... 110
Δ resonances
  $\Delta(1232)$ ... 94, 2042
  $\Delta(1600)$ ... 94, 2044
  $\Delta(1620)$ ... 94, 2045
  $\Delta(1700)$ ... 94, 2047
  $\Delta(1750)$ ... 2049
  $\Delta(1900)$ ... 94, 2049
  $\Delta(1905)$ ... 94, 2051
  $\Delta(1910)$ ... 95, 2052
  $\Delta(1920)$ ... 95, 2054
  $\Delta(1930)$ ... 95, 2056
  $\Delta(1940)$ ... 2057
  $\Delta(1950)$ ... 95, 2058
  $\Delta(2000)$ ... 2059
  $\Delta(2150)$ ... 2060
  $\Delta(2200)$ ... 95, 2061
  $\Delta(2300)$ ... 2061
  $\Delta(2350)$ ... 2062
  $\Delta(2390)$ ... 2062
  $\Delta(2400)$ ... 2062
  $\Delta(2420)$ ... 95, 2063
  $\Delta(2750)$ ... 2064
  $\Delta(2950)$ ... 2064
  $\Delta(\sim 3000$ Region) Partial-Wave Analyses ... 2064
$\Delta S = 1$, weak-neutral currents, tests for ... 110
$\Delta S = \Delta Q$ tests of ... 110
$\Delta T = 1$, weak-neutral currents, tests for ... 110
δ-rays ... 553
DenseNet ... 692
Density
  of CMB photons ... 134
  of Universe, critical ... 134
  parameter of the Universe Ω_0 ... 134
Density effect in energy loss rate ... 550
Density estimation ... 680, 684, 697, 704, 705
Density of materials, table ... 140
DESI – dark energy spectroscopic instrument ... 456, 472, 502
Detectors
  bubble chambers ... 606
  calorimeters
    electromagnetic ... 599
  Cherenkov ... 572, 620
  CMB detectors ... 633
  coherent radio Cherenkov radiation ... 627
  Dark matter ... 633
  fluorescence, atmospheric ... 618
  for rare events ... 630
  gas-filled ... 574
    drift chamber ... 577, 604
    high rate effects ... 578
    micro-pattern ... 578
    micro-strip chamber ... 580
    multi-wire proportional chambers, MWPC ... 577
    resitive plate chambers, RPC ... 584
    time-projection chambers, TPC ... 581
    transition radiation, TRD ... 582
  gravitation wave observatory, Virgo ... 421
  hadronic shower ... 565
  ice-based ... 629
  inorganic scintillator ... 570
  Kinetic Inductance Detectors (KIDs) ... 634
  LAr Time projection chambers ... 586
  laser interferometer gravitation observatory, LIGO ... 421
  liquid ionization chamber ... 605
  liquid scintillator ... 621
  low noise readout ... 593
  Low Temperature Detectors (LTDs) ... 633
  low-radioactivitiy background techniques ... 638
  Magnetic Metallic Calorimeters (MMCs) ... 635
  Neutrino cryogenic detectors ... 633
  neutrino telescopes ... 623
  neutrino, calibration of ... 652
  neutrinos
    accelerator-based ... 605
    bubble chambers ... 606
    Cherenkov ... 606
    emulsion ... 608
    iron tracking calorimeters ... 606
    liquid argon TPC ... 607
    plastic scintillators ... 607
  noble liquid ... 623
  organic scintillator ... 568
  proton decay ... 621
  radio-detection of cosmic ray air showers ... 630
  rare event search
    $0\nu\beta$ decay ... 632
    WIMPs ... 631
  semiconductor ... 589
    hybrid pixels ... 591
    LGAD ... 592
    microstrip ... 591
    monolithic pixels ... 591
    radiation damage ... 592
  Semiconductor Thermistors ... 634
  showers ... 599
  superconducting solenoid magnets for ... 609
  superconducting toroidal magnets for ... 609
  Superconducting Tunnel Junctions (STJs) ... 634
  Transition Edge Sensors (TESs) ... 635
  water Cherenkov ... 622
  wire chambers ... 586
Deuterium abundance ... 459
Deuteron mass ... 133
Deuteron structure function ... 365
DIEHARD ... 713
Dielectric constant of gaseous elements, table ... 141
Dielectric laser accelerator ... 541
Dielectric suppression of bremsstrahlung ... 556
Dielectric wakefield accelerators ... 541
Differentiable simulator ... 684
Differential Cherenkov detectors ... 573
Diffraction and high energy soft QCD ... 392
Diffractive parton distribution ... 398
Diffractive processes ... 392
Dirac gauginos ... 1012
Dirac neutrinos ... 286
Direct CP asymmetry in B decays ... 920
Directories, online, people, and organizations ... 20
DIS, deep inelastic scattering ... 353, 398
Discriminative model ... 676, 678, 697
Disk density ... 134
Dispersion relation ... 408, 858, 873
Distance ladders ... 470
Distance-redshift relation ... 430, 432, 467, 470, 500
Distribution shift ... 677
Dokshitzer-Gribov-Lipatov-Altarelli-Parisi
  (DGLAP) equations ... 152
Domain adaptation ... 703
Domain shift ... 677, 703
Donnachie-Landshoff pp-scattering amplitude ... 393
Dose rate from γ ray sources ... 648
Dose, radioactivity, unit of absorbed ... 647
Double PDFs ... 358
Double-β decay ... 1284
Doubly charmed baryons ... 2160

Downloaded from https://academic.oup.com/ptep/article/2022/8/083C01/6651666 by KIT Library user on 27 September 2022

Drell-Yan process 186, 210, 334, 361
Drift chambers 577
Drift velocities of electrons 604
Dropout 679, 690
D_s^+ branching fractions, note on 895
Dual problem 686
Dual readout 603
Dynamic Graph CNN 696
Dynamical electroweak symmetry breaking 1061

e (electron) 28, 1239
e (natural log base) 133
e^- Compton wavelength 133
Early stopping 677, 679, 689, 700, 701
Early Universe 443, 459
Earth
  equatorial radius 134
  mass 134
Eddington luminosity 134
Edge 696
Education databases 21
Effective dose of radioactivity 646
Effective field theories (EFTs) 329
Effective number of neutrinos 135
Effective skin depth δ 142
Efficiency of an estimator 660
EFT – effective field theories 329
Elastic cross sections 398
Elastic scattering 392
ELBO, Evidence Lower Bound Objective 680, 697, 698
Electric charge (Q) conservation 113
Electric dipole moment, EDM 111
Electrical resistivity of elements, table 141
Electromagnetic
  calorimeters 599
  cascades 559
  effects 326
  relations 142
  showers, lateral distribution 560
  showers, longitudinal distribution 559
Electromagnetic field equations 142
Electron
  charge magnitude e 133
  critical energy 556
  cyclotron frequency/field e/m_e 133
  drift velocities 604
  mass 133
  radius, classical 133
  volt eV 133
Electron and photon interactions in matter 555
Electron configuration of element, table 138
Electron-Ion Collider (EIC) 538
Electron-positron collider rings 537
Electron-positron colliders – future 539
Electronic energy loss by heavy particles 549
Electronic structure of the elements 138
Electroweak
  dynamical symmetry breaking 1061
  interactions, Standard Model of 177
  model and constraints on new physics, review 177
  penguin decay 912, 920
Electroweak corrections 154, 162
Electroweak Symmetry Breaking (EWSB) 201
Elements
  electronic structure of 138
  ionization energies of 138
Elements, periodic table of 137
Embedding 685
Emission probability 652
Emittance 534
Empirical risk 677
Encoder 681, 691, 696, 698
Encoder-decoder 692, 694
Energy and momentum (c.m.) vs beam momentum 743
Energy density
  of CBR 134
  of dark energy 134
  of relativistic particles 134
Energy loss
  (fractional) for $e^\pm$ in lead 556
  at low energies 551
  by electrons 556
  by photons 557
  density effect 550
  higher order corrections 551
  rate for heavy charged particles 550
  rate for muons at high energies 560
  rate in compounds and mixtures 554
  rate, form factor corrections 550
  rate, most probable 553
  rate, restricted 550, 553
  scaling with mass 550
Energy Recovery Linac 539
Energy resolution (calorimeter) 597
  constant term 598
  stochastic term 598
Energy-energy correlation 158
Ensemble methods 688
Entropy density 433, 435
Entropy density / Boltzmann constant 134
e^+e^- annihilation
  cross-section formulae 756
  two-photon process 757
Epistemic uncertainty 704
ϵ_0 (permittivity of free space) 133, 142
$\widehat{\epsilon}_1, \widehat{\epsilon}_2, \widehat{\epsilon}_3$ electroweak variables 192
Equivalence principle, experimental tests of 423
Equivalence principle, GR 417
Equivalent noise charge 595
Error function 657
Error propagation 703
Errors, treatment of 16
Established nonets for the meson 314
Estimator 660
η mesons
  η 33, 1354
  $\eta(1295)$ 35, 1401
  $\eta(1405)$ 36, 1410
  $\eta(1475)$ 36, 1420
  $\eta(1760)$ 1449
  $\eta(2225)$ 1468
  $\eta'(958)$ 34, 1373
  $\eta_2(1645)$ 37, 1432
  $\eta_2(1870)$ 38, 1453
  $\eta_c(1S)$ 70, 1818
  $\eta_c(2S)$ 76, 1883
  $\eta_b(1S)$ 81, 1940
  $\eta_b(2S)$ 1954
Event pile up 540
Event shape 158
EWSB, Electroweak Symmetry Breaking 201
Excitation energy 550
Excited fermions searches 1056
Excited leptons searches 1056
Exotic baryons P_c 106, 2181
Exotic muon decays 875
Exotic quantum numbers 845
Expansion of the Universe 431
Expectation value, definition 655
Experiment databases 21
Experimental design optimization 682, 683
Experimental rate measurements
  bottom mesons 902
  charmed mesons 900
  pions and kaons 898
Experimental sensitivity 673

Downloaded from https://academic.oup.com/ptep/article/2022/8/083C01/6651666 by KIT Library user on 27 September 2022

Experimental tests of gravitational theory 417
Exploding gradient 689, 694, 701
Extensions to the cosmological standard model 468
Extensive air shower, EAS 618
Extra Dimensions 109, 1002, 2243
Extra Dimensions, note on 983

f, F mesons
- $f_0(980)$ 34, 1379
- $f_0(1370)$ 36, 1406
- $f_0(1500)$ 37, 1421
- $f_0(1710)$ 38, 1446
- $f_0(2020)$ 1459
- $f_0(2100)$ 1462
- $f_0(2200)$ 1466
- $f_0(2330)$ 1470
- $f_1(1285)$ 35, 1398
- $f_1(1420)$ 36, 1413
- $f_1(1510)$ 1424
- $f_2^{'}(1525)$ 37, 1425
- $f_2(1270)$ 35, 1395
- $f_2(1430)$ 1416
- $f_2(1565)$ 1429
- $f_2(1640)$ 1432
- $f_2(1810)$ 1451
- $f_2(1910)$ 1455
- $f_2(1950)$ 38, 1456
- $f_2(2010)$ 39, 1459
- $f_2(2150)$ 1462
- $f_2(2300)$ 39, 1469
- $f_2(2340)$ 39, 1470
- $f_4(2050)$ 39, 1460
- $f_4(2300)$ 1469
- $f_6(2510)$ 1472
- $f_J(2220)$ 1467
- $f_0(600)$ [*was* $f_0(500)$ *was* σ] 33, 1359

F_2 structure function, plots 365
Factorization scale 151
FCC-ee (Future Circular Collider) 538
FCC-hh (Future Circular Collider) 539
FCNC, flavor-changing neutral currents 833
Feature engineering 681
Feature map 690
Feature vector 677, 689
Fermi constant 178, 1003
Fermi coupling constant $G_F/(\hbar c)^3$ 133
Fermi plateau 551
Fermions
- left-handed 1063
- right-handed 1063

Feynman's x variable 745
Field equations, electromagnetic 142
Filter 689
Fine tuning 1009
Fine-structure constant, α 133, 178
Fine-structure constant, time variation 516
Fine-tuning 702
Fit to Z electroweak measurements 791
Fit, technical implementation 804
Fits to data 16
Fixed-order perturbation theory (FOPT) 163, 184
Flat extra dimension 987
Flatness of Universe 473
Flavor anomalies 1010
Flavor number scheme (FNS) 152
Flavor symmetric couplings 847
Flavor transitions (oscillations) neutrino 291
Flavor-changing neutral currents, tests for 117
Flavour Lattice Averaging Group (FLAG) 163
Fluctuation amplitude at $8\,h^{-1}$ Mpc scale 134
Fluctuations in energy loss 553
Fluorescence detector, atmospheric 618
Flux conversion 134
Fly's Eye fluorescence detector 618
FODO cell 534
FOPT, fixed-order perturbation theory 184
Forbidden states in quark model 144
Force, Lorentz 142
Form factors for radiative pion and kaon decays, note on 842
Four-quark states 317, 861
Fourth generation b' quark searches 829
Fragmentation
- functions, scaling violations in 376
- heavy-quark 383
- in e^+e^- annihilation 375
- longitudinal 378
- models 379

Fragmentation function 155
Fragmentation functions in
- e^+e^-, ep, and pp collisions, note on 375

Frequentist
- approach 660
- confidence intervals 669
- statistics 669

Friedman equation 432
Friedmann constraint equation 443
Friedmann-Lemaître equations 430
Further states mesons 1980

g (gluon) 25, 1142
g-2 muon anomalous magnetic moment 798
Galaxy clustering 456, 471
Galaxy power spectrum 471
γ (photon) 25, 1141
γ (Euler constant) 133
Gamma collider 539
Gamma distribution 658, 714
Gamma factory 541
Gamma rays, astrophysical 526
γ-rays, from radioactive sources 652
$\gamma\gamma$ collisions 847
GAN, Generative Adversarial Network 697, 698, 703
Gas electron multiplier (GEM) 579
Gas-filled detectors
- electron drift velocity 575, 604
- gas properties 574
- high rate effects 578
- mobility of ions 576
- Townsend coefficient 575

Gauge and Higgs bosons
- H^0 Higgs 26, 1175
- W 25, 1142
- Z 25, 1156
- γ (photon) 25, 1141
- g (gluon) 25, 1142
- Searches
  - graviton 25, 1142

Gauge and Higgs bosons searches
- $W^{'}$, $Z^{'}$ 27, 1200
- axion 27, 1217
- charged Higgs $H^{\pm}, H^{\pm\pm}$ 26, 1196

Gauge coupling unification 1079
Gauge hierarchy 1000
Gauge kinetic function 1001
Gauge supermultiplet 1000
Gauge symmetry principle 285
Gauge-mediated supersymmetry breaking, GMSB 1007
Gaugino 1001, 1004
Gaugino mass unification 1006
Gaussian
- n-dimensional ellipsoid 657
- (Normal) distribution 658
- confidence intervals 670
- distribution, MC algorithm 714
- distribution, Multivariate 657

General relativity predictions 417

Downloaded from https://academic.oup.com/ptep/article/2022/8/083C01/6651666 by KIT Library user on 27 September 2022

equivalence principle ... 417
gravitational waves ... 418
isotropy of space ... 423
quasi-stationary, weak-field ... 418
radiative gravity tests ... 425
strong fields, neutron stars, black holes ... 418
universality of free fall tests ... 423
General relativity, GR ... 417
General-purpose Monte Carlo generators, (GPMC) ... 717
Generalization ... 677, 678
Generalized NMSSM, GNMSSM ... 1012
Generative model ... 677, 678, 697, 705
Generator of SU(3) transformation ... 738
Geometric deep learning ... 696
GIM – Glashow-Iliopoulos-Maiani mechanism ... 214
Glashow-Iliopoulos-Maiani (GIM) mechanism ... 113, 214
Global fit in SM ... 189, 266
Glueballs ... 316, 845, 847
$\eta(1405)$ ... 849
$f_0(1500)$, $f_0(1710)$ ... 847
lattice calculations ... 847
scalar ... 847
tensor ... 848
Gluino ... 1001
Gluino mass limits ... 1021
Gluino searches ... 235
Gluon field, SU(3) valued ... 808
Gluon induced jets ... 158
GMSB, gauge-mediated supersymmetry breaking ... 1007
GNMSSM, generalized NMSSM ... 1012
GNN, graph neural network ... 685, 696
Goldstino ... 1001
GP, Gaussian Process ... 678, 683, 687
GPMC generators
General-purpose Monte Carlo generators ... 717
HERWIG ... 717
PHOTOS ... 720
PYTHIA ... 717
SHERPA ... 717
uncertainties and tuning ... 726
GR, general relativity ... 417
Gradient boosting ... 689
Gradient clipping ... 701
Gradient descent ... 677, 679, 684, 689, 700
Grand unified theories, GUTs ... 1076
Graviscalar searches ... 983
Gravitational
constant G_N ... 133
acceleration g_N ... 133
lensing ... 437, 472, 512
radiation ... 420
theory, experimental tests of ... 417
wave speed ... 421
waves in GR ... 418
Gravitino ... 1002
Graviton
disperse ... 426
mass ... 426
Randall-Sundrum ... 1063
searches ... 984
Graviton searches ... 25, 1142
Gravity
in extra dimensions ... 983
tests ... 421
Gray, unit of absorbed dose of radiation ... 646
Group normalization ... 702
GRU, Gated Recurrent Unit ... 694
GUTs
baryon-number-violating nucleon decay ... 1081
basic group theory, charge quantization ... 1076
breaking ... 1077
doublet-triplet splitting ... 1077
monopoles prediction ... 1093
neutrino masses ... 1083
Pati-Salam model ... 1076
Yukawa coupling unification ... 1082
GUTs, grand unified theories ... 1076
g_V, g_A vector, axial vector couplings ... 177

h mesons
$h_1(1170)$ ... 35, 1391
$h_1(1415)$ [*was* $h_1(1380)$] ... 36, 1412
$h_1(1595)$ ... 1430
$h_b(1P)$ ... 83, 1952
$h_b(2P)$ ... 84, 1964
$h_c(1P)$ ... 75, 1870
H^0 (Higgs boson) ... 26, 1175
Hadron colliders ... 536
Hadron colliders – future ... 540
Hadron level ... 156
Hadronic
calorimeters ... 565
shower detectors ... 565
Hadronic Molecules ... 860
Hadronization corrections ... 157
Hadronization model ... 156
Half-lives of radioactive nuclides ... 652
Harrison-Zel'dovich effect ... 467
h/e ratio ... 601
He initialization ... 701
Heavy baryons ... 320
Heavy charged lepton searches ... 30, 1272
Heavy neutral leptons searches ... 1307
Heavy Quark Expansion (HQE) ... 934
Heavy quarks masses ... 812
Heavy vector-like quark B ... 1069
Heavy vector-like quark T ... 1066
Heavy-quark
effective theory (HQET) ... 329
expansion for inclusive decays ... 330
fragmentation ... 383
spin-flavor symmetry ... 329
Heavy-quark and soft-collinear effective theory, note on ... 329
Heavy-quarkonium spectroscopy ... 951
Helium-3 abundance ... 460
Helium-4 abundance ... 460
HERA ... 536
HERA (DESY) collider parameters ... 546
Hessian ... 700
HFLAV charm mixing global fit ... 891
Hidden sector ... 1002
Hidden state ... 692
Hidden valley models ... 1002
Hierarchy problem ... 984
Higgs and electroweak factories ... 538
Higgs boson
ATLAS and CMS total inefficiency ... 208
double charged search ... 245
in MSSM ... 236
LHC runs at $\sqrt{s} = 7, 8, 13$ TeV ... 208
mass ... 203
mass in electroweak analyses ... 190
mass in Standard Model ... 177
new physics models ... 234
non-SM decay channels, searching ... 217
quantum numbers ... 203, 222
self coupling ... 215
trilinear self coupling ... 206
vector boson fusion (VBF) ... 208
width ... 226
Yukawa coupling to fermions ... 210
Higgs boson physics ... 201
Higgs production in e^+e^- annihilation ... 758
Higgsino ... 1001
High energy diffraction experiments ... 398
High energy diffraction, theoretical description ... 393

Downloaded from https://academic.oup.com/ptep/article/2022/8/083C01/6651666 by KIT Library user on 27 September 2022

High energy soft QCD and diffraction, note on 392
High intensity beams 535
High-field accelerator magnets 539
High-frequency surface impedance 142
Highlights of this edition of the RPP 6
History of measurements, discussion 18
History plots 19
HL-LHC 537
Holographic model 847, 848
Horizon scale 511
Hot Big-Bang cosmology 459
HQE parameters and V_{cb} 934
HQET – Heavy-quark effective theory 329
HST, Hubble space telescope 470
Hubble
  constant H_0 ..... 467, 511
  cosmic topology 470
  expansion 431
  expansion rate 134, 483
  flow 502
  length c/H_0 ..... 134, 432
  parameter $H(t)$ 430
  radius 511
  relativistic species 469
  scaling factor for expansion rate 134
  space telescope HST 470
  varying constants 469
Hubble's law 430
Huber loss 678
Hybrid inflation model 445
Hybrid mesons 851
  $\pi(1800)$, $\pi_1(2015)$ 851
  $\pi_1(1400)$, $\pi_1(1600)$ 851
  $\rho(1450)$ 850
Hybrid states 317
Hyperbolic tangent activation 689, 694
Hypercharge 312, 995, 1076

Ice-based detectors 629
ID particle codes for MC 733
Ideal mixing 845
Ideal mixing in quark model 315
Ideograms, criteria for presentation 16
ILC, future International Linear Collider (Japan) 544
Image data 685, 690
Imaging Cherenkov detectors 573
Impedance of free space 142
Impedance, relations for 142
Importance sampling 715
Importance sampling in Monte Carlo calculations 713
Inception 690
Inclusive hadronic reactions 758
Inclusive reactions, kinematics for 745, 758
Inconsistent data, treatment of 16
Independence of random variables 656
Inductive bias 679, 685, 697
Inelastic cross sections 398
Inference 679, 684, 703, 706
Inflation
  CMB photons 443
  de Sitter limit $\epsilon \to 0$ 446
  effective field theory of 453
  Friedman equation 443
  future probes of 456
  motivation 443
  multi-field 454
  of early Universe 435, 443, 467
  quantum fluctuations 445
  reheating 444
  slow-roll 444, 510
Inflation models
  R^2 inflation 449
  axion monodromy 449
  chaotic with power-law potentials 449
  D-brane 449
  Higgs 450
  Hilltop 449
  natural 449
  pioneering 448
  supergravity 451
  supersymmetric 450
Inflation primordial perturbations 445
  density from single-field 446
  gravitational waves 445
  metric 445
  observational bounds 447
Inflaton
  field fluctuations 446
  Higgs scalar field as candidate 451
Inflaton scalar field 419, 435, 445
Information horizon 433
Infrared and collinear safety 153, 157
Initialization 689, 700, 701
Inorganic scintillators 570
Input normalization 701
Instance normalization 702
Integer encoding 685
Integrated Sachs-Wolfe effect 440, 471, 499, 511
Inter-galactic medium clustering 472
Interaction length 597
International Linear Collider (ILC) 538
International System (SI) units 136
INTERNET address for comments 11
Interpretability 677, 691, 695
Introduction 11
Inverse problem 684
Inverse transform method in Monte Carlo 713
Invisible energy (calorimetry) 601
Ion colliders 538
Ionization
  energies of the elements 138
  energy loss at minimum, table 140
  history of the Universe 469
Ionization yields for charged particles 554
IoU, Intersection over Union 691
Isotropy of space tests 423

$J/\psi(1S)$ 71, 1826
Jansky 134
Jet algorithm
  cone 157
  sequential recombination 158
Jet definition 157
Jet shape 158
Jet substructure 158
J/ψ radiative decay 848, 849
JS, Jensen-Shannon divergence 699

K factor 156
K stable mesons
  K^0 ..... 40, 1488
  $K^\pm$ 39, 1473
  K_L^0 ..... 40, 1493
  K_L^0 decay, CP violation in 877
  K_S^0 ..... 40, 1489
K, K^* meson resonances
  $K(1460)$ 42, 1518
  $K(1630)$ 1519
  $K(1830)$ 1523
  $K(3100)$ 1526
  $K_1(1270)$ 42, 1512
  $K_1(1400)$ 42, 1513
  $K_1(1650)$ 42, 1519
  $K^*(892)$ 42, 1509
  $K_0^*(700)$ [*was* $K_0^*(800)$] 41, 1508
  $K^*(1410)$ 42, 1514

Downloaded from https://academic.oup.com/ptep/article/2022/8/083C01/6651666 by KIT Library user on 27 September 2022

$K^*(1680)$ 42, 1519
$K_0^*(1430)$ [*was* $\kappa(1350)$] 42, 1515
$K_0^*(1950)$ 1523
$K_2^*(1430)$ 42, 1516
$K_2^*(1980)$ 43, 1523
$K_2(1580)$ 1519
$K_2(1770)$ 42, 1520
$K_2(1820)$ 43, 1522
$K_2(2250)$ 1525
$K_3^*(1780)$ 42, 1521
$K_3(2320)$ 1525
$K_4^*(2045)$ 43, 1524
$K_4(2500)$ 1525
$K_5^*(2380)$ 1525
k-means clustering 681
K_L^0 decay, CP violation in 275
Kähler potential 1001
Kaluza-Klein
excitations 192, 734, 832, 996
modes 983, 991, 1081
reduction 983
searches 986
theories 421, 983
Kaon decay, CPT invariance tests in neutral 871
KEKB (KEK) collider parameters 544
Kernel machines 677
Kernel trick 686
Kinematic limits
sequential two-body decay 744
three-body decays 744
Kinematics, decays, and scattering 743
Kinetic Inductance Detectors (KIDs) 634
Kinetic Sunyaev-Zel'dovich effect 440
KL, Kullback-Leibler divergence 680, 697–699
Knock-on electrons, energetic 553
Kobayashi-Maskawa (Cabibbo-) mixing matrix 261
KRR, kernel ridge regression 687

l.h., left-handed 1076
L1 loss 678
L2 loss 678
L2 regularization 679
Label 677, 683
LAGEOS – laser geodynamics satellite 424
Lagged-Fibonacci-based random number generator 713
Lagrangian, QCD 149, 808
Lagrangian, standard electroweak 177
Λ QCD parameter 150
Λ and Σ resonances 970, 972
Λ baryons 95, 2065
Λ 95, 2065
$\Lambda(1405)$ 96, 2068
$\Lambda(1520)$ 96, 2069
$\Lambda(1600)$ 96, 2071
$\Lambda(1670)$ 96, 2072
$\Lambda(1690)$ 96, 2073
$\Lambda(1710)$ 2075
$\Lambda(1800)$ 96, 2075
$\Lambda(1810)$ 96, 2076
$\Lambda(1820)$ 96, 2077
$\Lambda(1830)$ 96, 2079
$\Lambda(1890)$ 96, 2081
$\Lambda(2000)$ 2082
$\Lambda(2050)$ 2083
$\Lambda(2070)$ 2083
$\Lambda(2085)$ 2085
$\Lambda(2100)$ 96, 2086
$\Lambda(2110)$ 97, 2087
$\Lambda(2325)$ 2088
$\Lambda(2350)$ 97, 2088
$\Lambda(2585)$ 2089
Λ_b^0 ..... 104, 2161
$\Lambda_b(5912)^0$ 105, 2169
$\Lambda_b(5920)^0$ 105, 2169
$\Lambda_b(6070)^0$ 105, 2170
$\Lambda_b(6146)^0$ 105, 2170
$\Lambda_b(6152)^0$ 105, 2170
Λ_c^+ 100, 2136
$\Lambda_c(2595)^+$ 101, 2143
$\Lambda_c(2625)^+$ 101, 2143
$\Lambda_c(2765)^+$ or $\Sigma_c(2765)$ 2144
$\Lambda_c(2860)^+$ 101, 2144
$\Lambda_c(2880)^+$ 101, 2144
$\Lambda_c(2940)^+$ 101, 2145
$\Lambda(1405)$ region, pole structure, note on 973
Λ, cosmological constant 430
ΛCDM, minimal cosmological model 476
CΛCDM, cold dark matter with dark energy 468
MΛCDM, minimal cosmological model 468
Landau distribution 553
Landau-Pomeranchuk-Migdal (LPM) effect 556
Landau-Yuang theorem 222
LAr Time projection chambers, detector 586
LARES – laser relativity satellite 424
Large extra dimensions 763, 983
Large rapidity gap 392
Large-scale structure of the Universe 438
Last scattering surface, LSS 511
Lattice calculations of spectroscopy 323
Lattice QCD 337, 808, 925, 1045
Layer normalization 702
LBL, long baseline 289
Leaky ReLU 689
Learning rate 677, 700
Least squares 662
Left-handed
fermions 1063
leptons 1076
neutrinos 897
quarks 1076
sleptons 1084
Left-handed (l.h.) 1076
Left-handedness of neutrinos 285
LEP 537
LEP (CERN) 544
Lepton
conservation, tests of 116
family number conservation 113
left-handed 1076
mixing 287
Lepton PDF 151
Lepton-flavor violation, LFV 113
Leptonic decays of charged pseudoscalar mesons,
note on 897
phenomenological implications 903
Leptons
(see individual entries for e, μ, τ and ν) 28, 1239
Leptoproduction kinematics 756
Leptoquark review 1090
Leptoquark searches 1090
Lethal dose from penetrating ionizing radiation 647
LFV – lepton-flavor violation 113
LHC 537
LHC (CERN) collider parameters 546
LHC (CERN) heavy ion collider parameters 547
LHeC 539
Light
speed in vacuum of 133
year (deprecated unit) 134
Light meson spectrum 846
Light quarks masses 809
Light unflavored mesons 33, 1349
Lightest supersymmetric particle, LSP 1001
LIGO, Laser interferometer gravitational observatory 421
Likelihood-ratio trick 679, 684, 705
Limits 668

Downloaded from https://academic.oup.com/ptep/article/2022/8/083C01/6651666 by KIT Library user on 27 September 2022

Linear colliders ... 536, 538
Linear confinement ... 317, 722
Linear Higgs factories ... 538
Linear regression ... 678
Liquid ionization chambers ... 605
Lithium-7 abundance ... 462
Little hierarchy ... 1009
Local dark matter density ... 134
Local disk density ... 134
Local Group velocity with respect to CMB ... 134
Log-normal distribution ... 658
Logistic activation ... 689
Logistic regression ... 678
Logits ... 690, 695
Lomonosov satellite. γ-ray burst,
    high-energy cosmic rays ... 618
Long baseline neutrino sources (LBL) ... 289, 1083
Long-lived sparticles masses limits ... 1030
Longitudinal fragmentation ... 378
Longitudinal structure function, plots of ... 365
Lorentz force ... 142
Lorentz invariant amplitudes ... 743
Lorentz transformations of four-vectors ... 743
Loss ... 677, 678
Low Temperature Detectors (LTDs) ... 633
Low-radioactivity background techniques ... 638
LQCD
    heavy quark masses ... 341
    heavy quarks ... 339
    light quarks masses ... 340
    Monte Carlo method ... 342
    QED ... 340
    scattering amplitudes and resonances ... 343
    status of simulations ... 344
    Wilson fermion action ... 338
    Wilson gauge action ... 337
LQCD, lattice quantum chromodynamics calculations ... 337
LSP, lightest supersymmetric particle ... 1001
LSTM, Long Short-Term Memory ... 694
Luminosity ... 533, 535
    muon collider ... 540
    circular collider ... 536
    linear collider ... 538
Luminosity conversion ... 134
Luminosity distance d_L ... 432
Lund string model ... 722
Lyα forest ... 437

M-theory ... 1045
Machine learning ... 676
MAE, mean-abssolute error ... 678
MAF, Masked Autoregressive Flow ... 699
Magnetic fields, primordial ... 516
Magnetic Metallic Calorimeters (MMCs) ... 635
Magnetic monopoles ... 1084
    GUTs prediction ... 1093
    note on ... 1093
Magnetic monopoles searches ... 108, 2185
Majorana neutrinos ... 286
mAMSB, minimal AMSB ... 1007
Mandelstam variables ... 745
MAP, maximum a posteriori ... 679, 684, 705
Marginal probability density function ... 656
Markov chain ... 715
Mass attenuation coefficient for photons ... 557
Mass matrix
    light quark ... 810
    neutrino ... 286
Masses
    heavy quarks ... 812
    light quarks ... 809
Materials, atomic and nuclear properties of, table ... 140
Matter supermultiplet ... 1000
Matter, passage of particles through ... 549
Maximal mixing scenario ... 1006
Maximum energy transfer to e^- in single collision ... 550
Maximum likelihood ... 661
Maximum-margin classifier ... 686
Maxwell equations ... 142
MC – Monte Carlo ... 733
MDP, Markov decision process ... 682
Mean energy loss rate in H_2 liquid, He gas, C, Al, Fe, Sn 550
Mean excitation energy ... 549, 550
Mean range in H_2 liquid, He gas, C, Fe, Pb ... 550
Mean siderial day ... 134
Median, definition ... 655
Meson cloud ... 861, 967
Meson electromagnetic radius ... 843
Meson multiplets in quark model ... 313
Meson nonets (established) ... 314
Meson quick reference table ... 88
Meson-meson bound states ... 860
Mesons
    Further states ... 1980
    axial vector $\ell = 1$; 1^{++} or 1^{+-} ... 313
    bottomonium ... 951
    charmonium ... 951
    conventional ... 951
    pseudoscalar $\ell = 0$, 0^{-+} ... 313
    scalar $\ell = 1$, 0^{++} ... 313, 858
    tensor $\ell = 1$, 2^{++} ... 313
    thresholds ... 951
    unconventional ... 951
    vector $\ell = 0$, 1^{--} ... 313
    XYZ ... 951
Messenger scale ... 1006
Metric prefixes, commonly used ... 136
Michel parameters ... 806
Micro-mesh gaseous structure (MicroMegas) ... 579
Micro-pattern gas detectors, MPGD ... 578
MicroMegas, micro-mesh gaseous structure ... 579
Microwave background ... 436
Mihheev-Smirnov-Wolfenstein effect for solar neutrinos .. 291
Minimal
    7-parameter model, ΛCDM+$\sum m_\nu$ ... 480
    cosmological model ΛCDM ... 476
Minimal AMSB, mAMSB ... 1007
Minimal supergravity, mSUGRA ... 1021
Minimal supergravity, mSUGRA ... 1007
Minimal supersymmetric SM, MSSM ... 1000
Minimum ionization ... 550
Minimum ionization loss, table ... 140
MIP (minimum ionizing particle) ... 550, 574
Mixing angle, weak ($\sin^2\widehat{\theta}(M_Z)$) ... 133
Mixing, D^0-$\overline{D}^0$, note on ... 885
Mixing matrix ... 288
Mixing, singlet-octet in quark model ... 323
MLP, multi-layer perceptron ... 685, 689, 696
Modified gravity ... 469
Modified minimal subtraction scheme ($\overline{\mathrm{MS}}$) ... 149
Molar volume ... 133
Molecular states ... 845, 852
Molière radius ... 560
Momenta, measurement of, in a magnetic field ... 610
Monopoles
    catalysis of nucleon decay ... 1095
    Kibble mechanism ... 1093
    Parker bound ... 1094
Monte Carlo
    acceptance-rejection method ... 713
    calculations, importance sampling in ... 713
    codes for radiation protection studies ... 650
    DIEHARD ... 713
    inverse transform method ... 713
    Lagged-Fibonacci-based generator ... 713
    LQCD ... 342

Downloaded from https://academic.oup.com/ptep/article/2022/8/083C01/6651666 by KIT Library user on 27 September 2022

neutrino event generators ... 729
particle numbering scheme ... 733
random number generators ... 713
RANLUX generator ... 713
techniques ... 713
Monte Carlo algorithm for
χ^2 distribution ... 714
beta distribution ... 715
binomial distribution ... 714
Breit-Wigner distribution ... 715
exponential decay ... 714
Gamma distribution ... 714
Gaussian distribution ... 714
Poisson distribution ... 714
sine and cosine of random angle ... 714
Student's t distribution ... 714
Monte Carlo dropout ... 705
Monte Carlo event generators ... 717
MOSCAB collaboration ... 491
MPGD, micro-pattern gas detectors ... 580
MPNN, Message Passing Neural Network ... 697
$\overline{\text{MS}}$ renormalization scheme ... 178
$\overline{\text{MS}}$ factorization scheme ... 151
$\overline{\text{MS}}$ mass ... 150
MSE, mean-squared error ... 678, 705
MSSM current experimental status ... 1008
MSSM Higgs boson phenomenology ... 237
MSSM parameters ... 1003
MSSM, minimal supersymmetric SM ... 1000
MSSM-124 ... 1003
mSUGRA, minimal supergravity ... 1007, 1021
μ (muon) ... 28, 1240
μ_0 (permeability of free space) ... 133, 142
Multi-arm bandits ... 682
Multi-class classification ... 680, 690, 695
Multi-head attention ... 696
Multi-wire proportional chamber, MWPC ... 577
Multibody charm analyses, review of ... 880
Multibody decay kinematics ... 745
Multinomial distributions ... 657
Multiple Coulomb scattering ... 554
Multiple parton-parton interactions, MPI ... 156, 397, 724
Multiplets, meson in quark model ... 313
Multiplets, SU(n) ... 739
Multiplexing ... 635
Multivariate Gaussian distribution ... 657
Multiverse ... 435, 455
Muon
anomalous magnetic moment ... 184, 798
critical energy ... 560
energy loss rate at high energies ... 560
range/energy in rock ... 523
Muon Anomalous Magnetic Moment ... 796
Muon collider ... 540
Muon collider, neutrino radiation hazard ... 540
Muon decay parameters ... 800
MWPC, Multi-wire proportional chamber
maximum wire tension ... 577
wire stability ... 577
Møller cross section ... 555

n (neutron) ... 90, 1997
N and Δ Resonances ... 91, 2003
N and Δ Resonances, note on ... 965
N baryons
$N(\sim 3000$ Region) Partial-Wave Analyses ... 2041
$N(1440)$ ... 91, 2003
$N(1520)$ ... 91, 2004
$N(1535)$ ... 91, 2007
$N(1650)$ ... 91, 2009
$N(1675)$ ... 91, 2011
$N(1680)$ ... 91, 2013
$N(1700)$ ... 92, 2015
$N(1710)$ ... 92, 2017
$N(1720)$ ... 92, 2018
$N(1860)$ ... 2021
$N(1875)$ ... 92, 2022
$N(1880)$ ... 92, 2024
$N(1895)$ ... 92, 2025
$N(1900)$ ... 93, 2027
$N(1990)$ ... 2029
$N(2000)$ ... 2030
$N(2040)$ ... 2031
$N(2060)$ ... 93, 2032
$N(2100)$ ... 93, 2033
$N(2120)$ ... 93, 2035
$N(2190)$ ... 93, 2036
$N(2220)$ ... 94, 2038
$N(2250)$ ... 94, 2039
$N(2300)$ ... 2040
$N(2570)$ ... 2040
$N(2600)$ ... 94, 2040
$N(2700)$ ... 2040
N's and Δ's note ... 91, 2003
n-body differencial cross sections ... 743
n-body phase space ... 743
Nambu-Goldstone bosons ... 985, 1038
Nambu-Goldstone composite bosons ... 1061
Names, hadrons ... 15, 144
Naming scheme for baryon resonances ... 965
Naturalness ... 1009
Network-in-network ... 690
Neural network ... 677, 679, 689, 697, 700, 701, 705
Neuron ... 689
Neutral Higgs bosons searches ... 26, 1187
Neutral-current parameters, values for ... 181, 191
Neutralinos ... 1004
Neutralinos mass limits ... 1027
Neutrino detectors (deep, large, enclosed volume) ... 621
heavy water ... 623
liquid scintillator ... 621
noble
time-projection chamber ... 623
table of detectors ... 621
water-filled ... 622
Neutrino detectors, cryogenic detectors ... 633
Neutrino telescopes
AMANDA, South Pole ... 624
ANTARES, Med. Sea ... 624
backgrounds ... 623
DUMAND, Pacific Ocean ... 624
effective area ... 624
GVD, Lake Baikal ... 624
IceCube, South Pole ... 624
KM3NeT, Med. Sea ... 624
NEMO, Med. Sea ... 624
NESTOR, Med. Sea ... 624
NT-200, Lake Baikal ... 624
P-ONE, Pacific Ocean ... 624
results ... 626
technical realisation ... 624
Neutrino(s)
astrophysical ... 526, 623
atmospheric
detectors ... 621
atmospheric flux ... 293
beam lines at high-energy proton synchrontrons ... 548
chemical potential ... 516
cosmogenic ... 526
cosmological constraints ... 476
cross section measurements ... 765
current temperature ... 476
density of the Universe ... 135
Dirac ... 286
from cosmic rays ... 520
left-handed ... 285, 897

Downloaded from https://academic.oup.com/ptep/article/2022/8/083C01/6651666 by KIT Library user on 27 September 2022

Majorana ... 286
mass density parameter, Ω_ν ... 467
mass hierarchy ... 623
mass matrix ... 286
mass, cosmological limit ... 472
masses ... 480
masses, mixing, and oscillations, note on ... 285
mixing ... 30, 1288
Monte Carlo event generators ... 729
neutrinoless double-β decay ... 307
non-standard ... 479
oscillation search ... 291
properties ... 30, 1273
reactor
detectors ... 621
relic background ... 476
right-handed ... 285, 1076
see-saw mechanism ... 286
solar flux ... 292
solar, *pp* chain ... 292
solar, CNO cycle ... 292
sterile ... 285, 287, 304
supernova burst
detectors ... 621
Neutrinoless double-β decay searches ... 307
Neutrinos in cosmology, note on ... 476
Neutron ... 90, 1997
Neutron mass ... 133
Neutrons at accelerators ... 647
Neutrons, from radioactive sources ... 652
New heavy bosons
(W', Z', leptoquarks, etc.) searches ... 27, 1200
New Physics (NP) beyond SM ... 287, 920
NEWS-G collaboration ... 491
NEWSdm collaboration ... 491
Newtonian gravitation constant G_N ... 134
Next-to-lightest supersymmetric particle, NLSP ... 1008
Next-to-minimal supersymmetric SM, NMSSM ... 1001
NF, Normalizing Flow ... 683, 684, 697, 699
NICA ... 538
NLSP, next-to-lightest supersymmetric particle ... 1008
NMS, Non-Maximum Suppression ... 691
NMSSM, next-to-minimal supersymmetric SM ... 1001
Node ... 696
Noise
equivalent noise analysis ... 594
equivalent noise charge (ENC) ... 595
in analog signal processing ... 594
in digital signal processing ... 596
in timing measurements ... 596
noise origins ... 594
Nomenclature for hadrons ... 144
Non-Gaussianity CMB ... 437, 453, 468, 510
Non-perturbative corrections ... 157
Non-standard neutrinos
interactions beyond weak force ... 479
sterile neutrinos ... 479
unstable neutrinos ... 479
Non$q\bar{q}$ candidates
$cc\bar{c}\bar{c}$ state ... 961
Double-J/*psi*(1S) invariant mass ... 961
four heavy quarks ... 961
heavy-heavy systems ... 959
heavy-light systems ... 959
Normal (Gaussian) distribution ... 658
Normal distribution ... 657
NP, new heavy quark mixing ... 875
NP, new physics beyond SM ... 287
Neutrino properties ... 30, 1273
Nuclear
and atomic properties of materials, table ... 140
interaction length, table ... 140
magneton ... 133
Nuclear PDFs ... 358
Nucleon decay ... 1081
Nucleosynthesis ... 436
Nuclides, radioactive, commonly used ... 652
Number density of baryons ... 134
Number density of CMB photons ... 134
Number of degree of freedom ... 662
Number of neutrino types
and sum of neutrino masses ... 30, 1282
Numbering scheme for particles ... 733

Object detection ... 691
Observations, the light element abundance ... 459
Occupational radiation dose, U.S. maximum permissible ... 647
Octet-singlet mixing in quark model ... 314
Odderon in soft QCD ... 407
Ω baryons
Ω^- ... 99, 2133
$\Omega(2012)^-$ ... 99, 2134
$\Omega(2250)^-$ ... 100, 2135
$\Omega(2380)^-$ ... 2135
$\Omega(2470)^-$ ... 2135
Ω_b^- ... 2179
$\Omega_b(6316)^-$ ... 2178
$\Omega_b(6330)^-$ ... 2179
$\Omega_b(6340)^-$ ... 2179
$\Omega_b(6350)^-$ ... 2179
Ω_c^0 ... 103, 2156
$\Omega_c(2770)^0$ ... 103, 2157
$\Omega_c(3000)^0$ ... 103, 2157
$\Omega_c(3050)^0$ ... 103, 2158
$\Omega_c(3065)^0$ ... 103, 2158
$\Omega_c(3090)^0$ ... 103, 2158
$\Omega_c(3120)^0$ ... 104, 2159
$\Omega_{\rm dm}$, dark matter density ... 469
ω mesons
$\omega(782)$ ... 34, 1367
$\omega(1420)$ ... 36, 1414
$\omega(1650)$ ... 37, 1433
$\omega_3(1670)$ ... 37, 1434
Ω, cosmological density parameter ... 431
$\Omega_{\rm m}$, mass density parameter ... 431
Ω_Λ, scaled cosmological constant ... 431
Ω_ν, neutrino mass density parameter ... 467
$\Omega_{\rm tot}$, total energy density of Universe ... 473
$\Omega_{\rm v}$, vacuum energy parameter ... 431
One-hot encoding ... 685
One-shot learning ... 702
OOD, out-of-distribution ... 683
Optimal control ... 682
Optimization ... 677
Organic scintillator ... 568
Other light mesons ... 1980
Other particle searches ... 2263
Overfitting ... 677–679, 681, 700, 701

p (proton) ... 90, 1987
P (parity), tests of conservation ... 110
PAE, Probabilistic Auto-Encoder ... 698
PAMELA – payload for antimatter exploration
and light nuclei ... 521
Parameter estimation ... 660
Parameter estimation with constraints ... 663
Parametrizing the Universe ... 467
Paraphotons, searches ... 1038
Pardethadcal ... 600
Parity of $q\bar{q}$ states ... 312
Parsec ... 134
Partial Conserved Axial Current, PCAC ... 730, 843
Partial wave analyses, PWA ... 968
Particle
ID numbers for MC ... 733
identification detectors, PID ... 572

Downloaded from https://academic.oup.com/ptep/article/2022/8/083C01/6651666 by KIT Library user on 27 September 2022

nomenclature ... 144
symbol style conventions ... 144
Particle flow ... 598
Particle flow confusion ... 599
Particle level ... 156
Particle nomenclature ... 15
Particle Physics Booklet, how to get ... 11
Parton
density functions ... 717
distribution function, PDF ... 398
distributions ... 356
Parton distribution function (PDF) ... 151
Parton level ... 157
Parton shower ... 156
Parton-shower formalism ... 719
Passage of particles through matter ... 549
Pati-Salam model ... 1076, 1090
$\bar{p}p$ annihilation ... 845
PBN, primordial black holes ... 494
P_c, exotic baryons
$P_c(4312)^+$ ... 106, 2181
$P_c(4380)^+$ ... 106, 2181
$P_c(4440)$ ... 107, 2181
$P_c(4457)^+$ ... 107, 2181
PCA, principle component analysis ... 681, 698
PCAC, Partial Conserved Axial Current ... 730, 843
PDF, parton distribution function ... 398
PdgLive, interactive access to RPP ... 11
PDGLive, PDG web presentation ... 20
Peccei-Quinn mechanism and axion ... 1038
Penguin decays, electroweak ... 912, 920
Penguin-dominated modes ... 265
Pentaquarks
$P_c(4312)^+$ ... 975
$P_c(4440)^+$ ... 975
$P_c(4457)^+$ ... 975
search ... 975
Pentaquarks ... 106, 2181
PEP-II (SLAC) collider parameters ... 544
Periodic table of the elements ... 137
Permeability μ_0 of free space ... 142
Permeability of free space μ_0 ... 133
Permittivity ϵ_0 of free space ... 133
Permittivity ϵ_0 of free space ... 142
Permutation invariant ... 685, 696
Perturbation of early Universe ... 467
Perturbation theory, chiral ... 859, 865
Phase space, Lorentz invariant ... 743
Phase space, relations for ... 743
Phenomenological MSSM, pMSSM ... 1008, 1021
ϕ mesons
$\phi(1020)$ ... 34, 1383
$\phi(1680)$ ... 37, 1437
$\phi(2170)$ ... 39, 1465
$\phi_3(1850)$ ... 38, 1453
Photon
attenuation length ... 557
coupling ... 177
cross section in carbon and lead, contributions to ... 557
pair production cross section ... 557
structure functions F_2^γ ... 382
to e^+e^- conversion probability ... 557
total cross sections (C and Pb) ... 557
ultra-high energy ... 559
Photon and electron interactions with matter ... 555
Photon collider ... 539
Photon detectors ... 565
Photon PDF ... 151
Photon-dark photon-paraphoton conversion ... 1038
Photoproduction ... 152
Physical constants ... 133
Physics beyond general relativity ... 516
π mesons
π^0 ... 33, 1352
$\pi^\pm$ ... 33, 1349
$\pi(1300)$ ... 35, 1402
$\pi_1(1400)$ ... 36, 1409
$\pi_1(1600)$ ... 37, 1430
$\pi_2(1670)$ ... 37, 1435
$\pi_2(1880)$ ... 38, 1454
$\pi_2(2005)$ ... 1459
$\pi_2(2100)$ ... 1461
$\pi(1800)$ ... 38, 1450
π value ... 133
PID, particle identification detectors ... 572
Pions and kaons
experimental rate measurements ... 898
theoretical decay-constant calculations ... 899
PixelCNN ... 699
Planck
constant h ... 133
constant, reduced ... 133
length ... 134
mass ... 134
Plasma acceleration ... 541
Plasma energy ... 549
pMSSM, phenomenological MSSM ... 1008
POEMMA – probe of extreme multi-mes. astrophys. ... 618
Point Net ... 696
Poisson distribution ... 658, 714
Polarization in B decays, note on ... 919
Polarization in penguin-dominated B decays ... 920
Pole mass ... 150
Pole structure of the $\Lambda(1405)$ region, note on ... 973
Pomeron effective trajectory ... 402
Pomeron in soft QCD ... 401
Pontecorvo-Maki-Nakagawa-Sakata
mixing matrix (PMNS) ... 288
Pooling ... 690
Pooling, average ... 691
Pooling, max ... 691
Potentials, electromagnetic ... 142
Power correction ... 150
pp-scattering amplitude by Donnachie-Landshoff ... 393
Precision flavor physics ... 183
Preconfinement ... 722
Prefixes, metric, commonly used ... 136
PReLU, Parametric ReLU ... 689
Present-day CMB
dipole amplitude ... 134
temperature ... 134
Pressureless matter parameter ... 134
Primary spectra, cosmic rays ... 520
Primordial element abundance ... 459
Primordial helium fraction ... 135
Primordial magnetic fields ... 516
Princeton Tritium Observatory for Light, Early universe,
Massive-neutrino Yield (PTOLEMY) ... 480
Probability ... 655
Probability density function, definition ... 655
Probability, Kolmagorovs definition ... 655
Production and Decay of b-flavored Hadrons ... 908
Propagation of errors ... 656
Properties (atomic and nuclear) of materials, table ... 140
Properties of resonances ... 750
Proton
cyclotron frequency/field e/m_p ... 133
decay ... 1081
mass ... 133
structure function ... 353
structure function, plots ... 365
Proton (see p) ... 90, 1987
Proton decay detectors ... 621
Proton structure functions ... 151
Pseudorapidity ... 392, 746
Pseudoscalar mesons ... 848

Downloaded from https://academic.oup.com/ptep/article/2022/8/083C01/6651666 by KIT Library user on 27 September 2022

$\eta(1405)$, $\eta(1475)$ 848
$\eta(1295)$ 848, 849
Pseudoscalar mesons $\ell = 0$, 0^{-+} 313
ψ mesons
$\psi_2(3823)$ [*was* $\psi(3823)$; *was* $X(3823)$] 78, 1910
$\psi_2(3842)$ 78, 1911
$\psi(2S)$ 76, 1886
$\psi(3770)$ 77, 1903
$\psi(4040)$ 79, 1919
$\psi(4160)$ 79, 1923
$\psi(4230)$ [*aka* $Y(4230)$; *was* $\psi(4260)$] 80, 1927
$\psi(4360)$ [*aka* $Y(4360)$; *was* $X(4360)$] 80, 1933
$\psi(4415)$ 81, 1934
$\psi(4660)$ [*aka* $Y(4660)$; *was* $X(4660)$] 81, 1937
PTOLEMY, neutrino background direct detection 480
Pulsars, binary 424

QCD
Λ parameter 726
$\overline{\text{MS}}$ renormalization scheme 149
β function 149
color factor 149, 159
coupling constant 149
jets 157
Lagrangian 149
lagrangian 808
Λ parameter 150
Lattice 337
lattice 808, 1045
photon structure functions 382
renormalization group equation (RGE) 149
running coupling 149, 164, 167
structure functions 355
Quality factor for biological damage due to radiation 646
Quantum
fluctuations, inflation 445
gravity theory 983
Quantum numbers in quark model 312
Quark
masses review 32, 1311
masses, note on 808
Quark induced jets 158
Quark model
baryon resonances in 317
ideal mixing in 315
meson multiplets in 313
mixing, singlet-octet in 323
quantum numbers in 312
Quark-antiquark annihilations $c\bar{d} \to W^+ \to \ell^+\nu$ 897
Quark-mixing CKM matrix 261
Quark-parton model 151
Quarks 32, 1311
and lepton compositeness searches 108, 1055, 2239
b 32, 1317
b' quark (4th generation), searches for 32, 1337
c 32, 1315
current masses of 179
d 32, 1311
fragmentation in e^+e^- annihilation, heavy 383
Free quark searches 32, 1341
left-handed 1076
model 312
model assignments 317
model, dynamical ingredients 322
properties of 312
s 32, 1311
t 32, 1319
t' quark (4th generation), searches for 32, 1339
u 32, 1311
Quasi-stationary general relativity 418

R-CNN, region convolutional neural network 691
R-parity 1001, 1019, 1090
R-parity conserving, RPC 1001
R-parity violation, RPV 1011
r.h., right-handed 1076
Rad, unit of absorbed dose of radiation 646
Radiation
-dominated epoch 434
Cherenkov 561
coherent radio Cherenkov radiation 562
gravitational 420
length 556
length of materials, table 140
length, approximate algorithm 556
protection 646
protection instrumentation 649
transition 562
weighting factor 646
Radiation damage in silicon detectors 592
Radiation length 597
Radiative
corrections in SM 180
gravity test, GR prediction 425
Radiative loss by muons 560
Radio-detection of cosmic ray air shower 630
Radioactive nuclides, half-lives of 652
Radioactive sources, commonly used 652
Radioactivity
accelerator-induced 648
accelerators prompt neutrons 647
ambient dose equivalent 646
and radiation protection 646
Becquerel, unit of 646
biological damage from chronic exposure 646
Cancer induction 647
cosmic ray background radiation 647
dose rate from γ ray sources 648
effective dose 646
effective dose limits 647
fluence, Φ 646
kerma, K 646
lethal dose from 647
long-term risk 646
natural annual background 647
personal dosimeters 650
rem, **r**oentgen **e**quivalent for **m**an 649
unit of absorbed dose, gray 646
unit of activity 646
weighting factor 646
Radion searches 985
Randall-Sundrum
model 763, 986
warped geometry 983
Randall-Sundrum graviton 1063
Random angle, MC algorithm for sine and cosine of 714
Random Forests 688
Random number generators 713
RANLUX Monte Carlo generator 713
Rapidity 745
Rare event search
$0\nu\beta$ decay 632
WIMPs 631
Rare kaon decay, constraints on CKM parameters 867
$R_{c0}(4240)$ [*was* $X(4240)^{\pm}$] 1931
Re-ionization of the Universe 471
Reactor
antineutrino flux 298
antineutrino oscillation 298
Readout, detector 593
Receptive field 690
Recombination scheme 158
Redshift 430
$z \simeq 1100$, reionization 510
age at half reionization 135
age when acceleration was zero 135

Downloaded from https://academic.oup.com/ptep/article/2022/8/083C01/6651666 by KIT Library user on 27 September 2022

age when optical depth equals unity 135
at half reionization 135
at which optical depth equals unity 135
comoving size of sound horizon at z_* 135
matter-radiation equality 135
when acceleration was zero 135
Redshift distortion 471
Refractive index of materials, table 140
Regge pole approach 392
Regge poles multiple exchange 393
Reggeon field theory 393
Regression 676, 678, 686, 687, 691, 697, 705
Regularization 677, 679, 701, 705
Reionization of the Universe 469
Reionization optical depth 134
Relativistic kinematics 743
Relativistic rise 550
Relativistic transformation of electromagnetic fields 142
ReLU, Rectified Linear Unit 689, 701
Rem, **r**oentgen **e**quivalent for **m**an 646
Renormalization group
quark mass 808
Renormalization group equation (RGE) of QCD ... 149, 1006
Renormalization in Standard Model 178
Renormalon 151, 179, 812
Representation learning 681
Representations, SU(n) 739
Repulsive gravity, dark energy 500
Resistive plate chambers 565, 584
Resistivity of metals 142
Resistivity, electrical, of elements, table 141
ResNet, Residual Network 692, 694
Resonances
K-matrix parametrization 751
Breit–Wigner parametrization 751
Chew-Mandelstam function 752
mass, M_R 750
partial-wave decomposition 749
pole position, s_R 750
properties of the S-matrix 747
scattering-length approximation 752
width, Γ_R 750
Resonances, general consideration 747
Restricted energy loss rate 550, 553
Resummation 155
Review of multibody charm analyses 880
Review of Particle Physics overview 11
RG - renormalization group 333, 338
RGE, renormalization group equation 1006
RHIC 537
RHIC (Brookhaven) collider parameters 546
RHIC (Brookhaven) heavy ion collider parameters 547
ρ mesons
$\rho(770)$ 33, 1361
$\rho(1450)$ 36, 1417
$\rho(1570)$ 1430
$\rho(1700)$ 38, 1441
$\rho(1900)$ 1455
$\rho(2150)$ 1464
$\rho_3(1690)$ 38, 1438
$\rho_3(1990)$ 1458
$\rho_3(2250)$ 1468
$\rho_5(2350)$ 1471
ρ parameter 181
Right-handed
antineutrinos 897
fermions 1063
neutrinos 285, 1076
sleptons 1084
top quark 1081
Right-handed (r.h.) 1076
Risk 677, 704
Risk minimization 677, 678
RL, reinforcement learning 676, 682
RMSprop 700
RNN, recurrent neural network 685, 692
RNNSearch 695
Robertson-Walker metric 430, 443, 467
Robustness of an estimator 660
ROC, receiver operating characteristic curve 677, 679
ROI, region of interest 691
Rotational invariance 686
Rounding errors, treatment of 17
Rounding, PDG rules 17
RPC, R-parity conserving 1001
RPC, resistive plate chambers 584
RPN, Region Proposal Network 691
RPP authors and affiliations 2
RPP criteria for measured data 16
RPV, R-parity violation 1011
Running coupling in QCD 149, 164, 167
Running spectral index, $k_0 = 0.05\,\mathrm{Mpc}^{-1}$ 135
Rydberg energy 133

S, T, U electroweak variables 192
S-matrix
approach to Z 791
for two-body scattering 743
S-matrix properties 747
Sachs-Wolfe effect 439, 511
Sachs-Wolfe effect, integrated 440, 471, 499, 511
Sampling 684
Satellite
Planck, CMB 447, 503, 509, 512
AMS-02, cosmic-rays 521
COBE, monopole 509
Euclide, dark energy 456
Gaia, density distribution 485
LAGEOS, test of gravity 424
LARES, test of gravity 424
LiteBIRD, inflation, CMB 514
Lomonosov, γ-ray bursts 618
PAMELA, cosmic rays 521
POEMMA, cosmic rays 618
SMM, sun radiation 1043
SPHEREx, inflation 456
WMAP, CMB 503
Scalar field cosmology 444
Scalar mesons 845
$a_0(1450)$ 845
$a_0(980)$, $f_0(980)$, $f_0(500)$, $K_0^*(700)$ 851
$f_0(1370)$, $f_0(1500)$, $f_0(1710)$ 845
nonets 846, 851
SU(3) couplings 847
Scalar mesons $\ell = 1$, 0^{++} 313, 858
Scalar mesons below 1 GeV, note on 858
Scalar spectral index 134
Scale dependence 150
Scale factor, definition of 16
Scaled cosmological constant, Ω_Λ 431
Scaled dot-product attention 695
Scaled Hubble constant 431
Scaling factor for Hubble expansion rate 134
Scaling for cosmological constant 134
Scaling violations in fragmentation functions 376
Scattering, relations for 756
SCET – soft-collinear effective theory 331
Scherk-Schwarz mechanism 1002
Schwarzschild
radius of a black hole 985
radius of the Earth 134
radius of the Sun 134
Scintillation neutrino detectors 607
Scintillator parameters 568
Sea-level cosmic ray fluxes 522
Searches

Downloaded from https://academic.oup.com/ptep/article/2022/8/083C01/6651666 by KIT Library user on 27 September 2022

W' bosons ... 991, 1063
Z' bosons ... 995, 1063
b' quark fourth generation ... 829
new light particles in rare K decay ... 866
axigluons ... 1063, 1072
axion like particles (ALP) ... 1042
axions (A^0) ... 486, 1038
charginos ... 237
colorons ... 1072
dark matter ... 109, 2249
dark photon ... 218
doubly charged Higgs boson ... 245
dyons ... 1094
excited fermions ... 1056
excited leptons ... 1056
extra dimensions ... 486, 983
gluinos ... 235
graviscalar ... 983
graviton ... 984
heavy charged lepton ... 30, 1272
heavy neutral leptons ... 1307
heavy non-$q\bar{q}$ mesons ... 959
leptoquark ... 1090
light Higgsinos ... 235
magnetic monopoles ... 108, 1084, 1093, 2185
neutralino ... 237
neutrino oscillation or flavor transition ... 291
neutrinoless double-β decay ... 307
paraphotons ... 1038
pentaquarks ... 975
quark and lepton compositeness ... 108, 1055, 2239
radion ... 985
rare events ... 630
sleptons ... 237
SM explicit violations ... 865, 866
solar axions ... 1042
squarks ... 235, 237
supersymmetric particle ... 108, 2187
technicolor ... 243, 486, 1061, 1090
technifermions
spontaneously broken chiral symmetry ... 1061
WIMP ... 109, 2249
Selection and treatment of data ... 15
Self-attention ... 696
Self-supervised learning ... 680
Semantic segmentation ... 691
Semiconductor
detectors ... 589
materials ... 590
Semiconductor Thermistors ... 634
Semileptonic b-hadron decays,
determination of V_{cb}, V_{ub} ... 930
Semitauonic decays ... 939
Sequential data ... 685, 692
Sequential two-body decay, kinematic limits ... 744
sfermion ... 1000
SGD, Stochastic Gradient Descent ... 700
Shape functions, SF ... 263, 331
Shared weights ... 690, 694
Shell correction ... 551
Shower detectors ... 599
Showers, electromagnetic
lateral distribution of ... 560
longitudinal distribution of ... 559
SI units, complete set ... 136
Sidereal day ... 134
Sievert, unit of radiation dose equivalent ... 646
σ ... 33, 1359
Σ baryons
Σ^+ ... 97, 2090
Σ^- ... 97, 2093
Σ^0 ... 97, 2092
Σ_b^* ... 105, 2171
$\Sigma_b(6097)^+$ ... 105, 2172
$\Sigma_b(6097)^-$ ... 105, 2172
Σ_b ... 105, 2171
$\Sigma(1385)$ ... 97, 2095
$\Sigma(1580)$ ... 2097
$\Sigma(1620)$ ... 2098
$\Sigma(1660)$ ... 97, 2099
$\Sigma(1670)$ ... 98, 2101
$\Sigma(1750)$ ... 98, 2103
$\Sigma(1775)$ ... 98, 2104
$\Sigma(1780)$ ... 2106
$\Sigma(1880)$ ... 2107
$\Sigma(1900)$ ... 2107
$\Sigma(1910)$ ... 98, 2108
$\Sigma(1915)$ ... 98, 2110
$\Sigma(2010)$ ... 2112
$\Sigma(2030)$ ... 98, 2113
$\Sigma(2070)$ ... 2115
$\Sigma(2080)$ ... 2115
$\Sigma(2100)$ ... 2116
$\Sigma(2110)$ ... 2117
$\Sigma(2250)$ ... 2118
$\Sigma(2455)$ ... 2119
$\Sigma(2620)$ ... 2119
$\Sigma(3000)$ ... 2120
$\Sigma(3170)$ ... 2120
$\Sigma_c(2455)$ ... 101, 2145
$\Sigma_c(2520)$ ... 101, 2146
$\Sigma_c(2800)$ ... 101, 2147
Σ baryons ($S = -1$, $I = 1$) ... 97, 2090
Sign conventions for resonance couplings ... 971
Silicon detector ... 589
radiation damage ... 592
timing measurement ... 592
Silk damping ... 512
Simplified models ... 1008
Simulation-based inference ... 679, 684, 697, 700, 705
$\sin^2\theta_W$, weak-mixing angle ... 190
Singlet-octet mixing in quark model ... 314
Skip connection ... 692, 694, 696, 701
Slack variable ... 686
SLC (SLAC) ... 537, 544
sleptons ... 1004
sleptons masses limits ... 1028
SLHA, SUSY Les Houches accord ... 1004
Sloan Digital Sky Survey (SDSS) ... 471
Slow-roll inflation ... 510
SMM – solar maximum mission satellite ... 1043
SN1987A
light gravitons luminosity ... 984
Sneutrino masses limits ... 1028
sneutrinos ... 1004
SNO - sudbury neutrino observatory ... 1040
Soft supersymmetry breaking ... 1000
Soft-collinear effective theory (SCET) ... 331
Softmax ... 680, 690, 694
Software ... 21
Solar
ν experiment ... 292
ν fluxes ... 292
ν problem ... 292
angular velocity around Galactic center ... 134
circular velocity ... 134
constant, nominal ... 134
distance from Galactic center ... 134
equatorial radius, nominal ... 134
escape velocity from the Galaxy ... 134
luminosity, nominal ... 134
mass ... 134
photosphere temperature, nominal ... 134
Schwarzschild radius of ... 134
standard model ... 292
velocity with respect to CMB ... 134

Downloaded from https://academic.oup.com/ptep/article/2022/8/083C01/6651666 by KIT Library user on 27 September 2022

Solid angle 134
Sparticle 1004
Specific heats of elements, table 141
Spectroscopy of mesons
containing two heavy quarks, note on 951
Speed of light in vacuum c 133
Sphaleron 1084
SPHEREx – spectro-photometer for history
of epoch reionization, satellite 456
Spherical harmonics 737
Spin polarisation 535
Spin-dependent structure functions 358
Spin-flavor symmetry 329
Split supersymmetry 1002
Splitting functions 152
Spontaneous symmetry breaking 177
SPPC 539
Squark mass limits 1021
squarks 1004
Sring theory 463
SSM, standard solar model 292
Standard
cosmological model 468
gravitational acceleration 133
neutrino cosmology 476
particle numbering for MC 733
Solar Model (SSM) 292
Standard Model of electroweak interactions 177
Standard model of particle physics
as EFT of more fundamental theory 329
Standard model, cosmological 517
Statistical procedures 16
Statistics, note on 660
Status of LQCD simulations 344
Stefan-Boltzmann constant 133
Sterile neutrinos 285, 304
Stopping power for heavy charged projectiles 549
Strangeness-changing neutral currents, tests for 110
String theory 1038
Strong coupling constant 133, 159, 162
Strong fields, neutron stars, black holes in GR 418
Structure functions 353
Student's t distribution 658, 714
SU(n) multiplets 739
SU(3)
classification of baryon resonances 317
isoscalar factors, note on 738
multiplets 317
representation matrices, note on 738
transformation, generators of 738
SU(5) 321
SU(6) multiplets 317
Sudbury
neutrino observatory, SNO 1040
Sum of neutrino masses 135
Sum rules 811
Summary tables, organization of 11
Sunyaev-Zel'dovich effect 440, 467, 471, 501, 515
Sunyaev-Zel'dovich effect, kinetic 440
Super tau-charm factories 539
Super-conformal anomaly 1002
Super-Higgs mechanism 1002
Superconducting Tunnel Junctions (STJs) 634
Supergravity 1001, 1002
SuperKEKB (KEK) collider parameters 544
Supermassive GUT monopoles 1093
Supermultiplet 1000
Supernovae
as cosmological probes 470
Type Ia 470, 480
Type II 470
Superpotential 1001
Superspace 1000
Supersymmetric particle searches 108, 2187
Supersymmetric particle spectrum 1004
Supersymmetry breaking 1002
Supersymmetry, SUSY 1000
Supervised learning 676–678, 683, 686, 697
Survival probability, relations for 743
SUSY Les Houches accord, SLHA 1004
SUSY, supersymmetry 1000
SVM, support vector machine 685, 686
SVR, support vector regression 686, 687
Symmetry breaking 1082
Synchrotron oscillations 535
Synchrotron radiation 143, 535
Synchrotron tune 535
Systematic errors, treatment of 16
SZ, Sunyaev-Zel'dovich effect 515

t (quark) 817
T (time reversal), tests of conservation 110
Tabular data 685
τ lepton 28, 1245
τ branching fractions, note on 803
τ decay parameters, note on 806
Technicolor 108, 2238
electroweak symmetry breaking 1061
Technifermion condensat formation 1061
Telescope Array (TA) 525, 618
Tensor mesons $\ell = 1$, 2^{++} 313, 847, 848
$f_J(2220)$ 848
Tensor-to-scalar field perturbations ratio, ... 135
Testing dataset 677, 679, 681
Tests of conservation laws 120
Tetraquark candidates
$K_0^*(700)$ 861
$X(3872)$ 960
$Z(4430)$ 960
$\psi(4230)$ 960
$a_0(980)$ 860
$f_0(500)$ 860
$f_0(980)$ 860
Tetraquark states 851
$\phi(2170)$ 852
$a_0(980)$, $f_0(980)$ 851
Tetraquarks 316, 845
Tevatron 536
Tevatron collider parameters 546
Theoretical decay-constant calculations
Bottom mesons 902
charmed mesons 901
pions and kaons 899
Thermal
conductivity of elements, table 141
expansion coefficients of elements, table 141
history of the Universe 433
θ_W, Weinberg angle 285
Third generation vektor-like quarks 1065
Thomson cross section σ_T 133
Three-body
decay kinematics 744
decays, kinematic limits 744
phase space 744
Threshold Cherenkov detectors 572
Thrust 158
Time variation of the fine-structure constant 516
Time-projection chambers, TPC 581, 630
Timing
silicon detectors 592
Timing measurements 596
Top quark t 817
Top quark mass 826
Top quark mass from electroweak analyses 179
Top quark, note on 817
Top-changing neutral currents, tests for 117

Downloaded from https://academic.oup.com/ptep/article/2022/8/083C01/6651666 by KIT Library user on 27 September 2022

Total cross sections ... 398
Total energy density of Universe, Ω_{tot} ... 473
Total lepton number conservation ... 116
TPC, Time-projection chambers ... 630
Training ... 677, 679, 683, 689, 706
Training dataset ... 677–681
Transfer learning ... 702
Transformation of electromagnetic fields, relativistic ... 142
Transformer ... 685, 695, 702
Transition Edge Sensors (TESs) ... 635
Transition radiation ... 562
Transition radiation detectors, TRD ... 582
Translational invariance ... 685, 690
Transverse variables ... 746
Trees ... 685, 687
Triangle singularity ... 315, 849, 851
Triangles, unitarity, note on ... 261
Trilepton events ... 1067
Trilinear coupling ... 206
Tropical year ... 134
Two-body
  decay ... 743
  differential cross sections ... 745
  partial decay rate ... 743
  reactions ... 745
  scattering kinematics ... 743
Two-Higgs-doublet models ... 240
Two-photon processes in e^+e^- annihilation ... 758
Type Ia supernovae ... 470, 480
Type II supernovae ... 470

U-Net ... 691
ULA, ultralight axion-like particles ... 1045
Ultra-high energy cosmic rays ... 526
Ultralight axion-like particles (ULAs) ... 1045
Uncertainty quantification ... 703, 705
Unconstrained averaging ... 16
Underfitting ... 677
Underground cosmic rays ... 523
Underlying event (UE) ... 156
Unified atomic mass unit ... 133
Unified theories, grand ... 1076
Uniform distribution ... 658
Units and conversion factors ... 346
Units, electromagnetic ... 142
Units, SI, complete set ... 136
Universal approximation ... 677, 679, 690
Universal Extra Dimension, UED ... 762, 988
Universality of free fall tests GR ... 423
Universe
  accelerating evidence ... 471
  age of ... 432, 473
  as a particle detector ... 480
  baryon density of ... 134, 460
  bubble ... 435
  composition ... 430, 432
  cosmological structure ... 434
  critical density of ... 134
  curvature of ... 431
  density fluctuations ... 437
  density parameter of ... 134
  entropy density ... 435
  flatness ... 473
  global description of ... 467
  Hubble expansion of ... 430, 467
  inflation ... 467
  large-scale structure of ... 432, 438
  matter-dominated ... 436
  parametrizing ... 467
  perturbation ... 467
  phase transitions ... 435
  radiation content at early times ... 434
  thermal history of ... 433, 443
  thermodynamic equilibrium ... 434
Unsupervised learning ... 676, 677, 680, 683
Υ ($b\bar{b}$) mesons
  $\Upsilon(1S)$ ... 81, 1942
  $\Upsilon(2S)$ ... 83, 1954
  $\Upsilon_2(1D)$ [*was* $\Upsilon(1D)$] ... 83, 1959
  $\Upsilon(3S)$ ... 84, 1966
  $\Upsilon(4S)$ [*was* $\Upsilon(10580)$] ... 85, 1970
  $\Upsilon(10753)$ ... 1974
  $\Upsilon(10860)$ ... 85, 1975
  $\Upsilon(11020)$ ... 86, 1978

Vacuum energy parameter $\Omega_{\rm v}$ ... 431
VAE, Variational Auto-Encoder ... 697, 698
Validation dataset ... 678
Values of particle properties, historical perspective of ... 19
Vanishing gradient ... 689, 692, 694, 701
Variance, definition ... 655
Variational inference ... 680, 684, 697, 698, 705
Varying constants
  gravitational $G_{\rm N}$, fine structure α ... 469
VBF – vector boson fusion ... 208
V_{cb} and V_{ub} determination of, note on ... 930
V_{cb} determination ... 930
Vector mesons ... 849
  ρ excitations ... 850
  $\rho(1570) - C(1480)$ ... 850
  $\rho(1900)$ ... 850
  $\rho(770)$ ... 849
Vector mesons $\ell = 0$, 1^{--} ... 313
Vector superfields ... 1000
Vector-like quarks, VLQ ... 1065
VEPP-2000 ... 543
VEPP-4M ... 543
Virgo, gravitational observatory ... 421
Virtual graviton process ... 763
VLQ, vector like quarks ... 1065
Von Neuman's acceptance-rejection method in MC ... 713
V_{ub} determination ... 934
V_{ub}/V_{cb} determination ... 938
V_{ud} determination ... 873
$V_{ud}, V_{us}, V_{ub}, V_{cd}, V_{cs}, V_{cb}, V_{td}, V_{ts}, V_{tb}$ ... 261
V_{us} determination ... 873

W and Z resonant production ... 757
W boson ... 25, 1142
  ideogram ... 790
  mass ... 789
  width ... 789
w, dark energy equation of state parameter ... 431
W-W' mixing ... 993
Warped extra dimensions ... 983
Wasserstein distance ... 683, 697, 699
Wasserstein GAN ... 699
Wavelength of 1 eV/c particle ... 133
WaveNet ... 699
Weak decay form factors ... 330
Weak gauge bosons pairs production ... 757
Weak neutral currents
  tests ($\Delta B = \Delta C = \Delta S = \Delta T = 1$) ... 110
Weak-field general relativity ... 418
Weak-mixing angle ($\sin^2\widehat{\theta}(M_Z)$) ... 133
Weakly supervised learning ... 679
Weakly-interacting massive particle, WIMP ... 1000
Weight matrix ... 689
Weinberg angle θ_W ... 285
White-dwarf, weak-self-gravity ... 424
Wien displacement law constant $b = \lambda_m axT$ ... 133
WIMP ... 485
  miracle ... 484, 1000
WIMP dark matter searches ... 109, 2249
WIMP, weakly-interacting massive particle ... 1000
Wino ... 1004

Downloaded from https://academic.oup.com/ptep/article/2022/8/083C01/6651666 by KIT Library user on 27 September 2022

WMAP, Wilkinson Microwave Anisotropy Probe 471
Wolfenstein parameters 261, 873, 904
World average of $\alpha_s(M_Z^2)$ 163, 166
W'-boson searches 991, 1072
Wraped extra dimension 763

X mesons
- $X_0(2900)$ 1607
- $X_1(2900)$ 1607
- $X(1835)$ 1452
- $X(2370)$ 1471
- $X(3872)$ [*aka* $\chi_{c1}(3872)$] 78, 1911
- $X(3940)$ 1918
- $X(4020)^{\pm}$ 79, 1918
- $X(4050)^{\pm}$ 1921
- $X(4055)^{\pm}$ 1922
- $X(4100)^{\pm}$ 1922
- $X(4160)$ 1926
- $X(4250)^{\pm}$ 1932
- $X(4350)$ 1932
- $X(4630)$ 1937
- $X(5568)^{\pm}$ 1810

x variable (of Feynman's) 745
Xavier initialization 701
xF_3 structure function, plots of 365
Ξ baryons
- Ξ^- 99, 2123
- Ξ^0 ..... 98, 2121
- Ξ_{bc}^0 2177
- $\Xi(1530)$ 99, 2126
- $\Xi(1620)$ 2127
- $\Xi(1690)$ 99, 2127
- $\Xi(1820)$ 99, 2128
- $\Xi(1950)$ 99, 2129
- $\Xi(2030)$ 99, 2130
- $\Xi(2120)$ 2131
- $\Xi(2250)$ 2131
- $\Xi(2370)$ 2131
- $\Xi(2500)$ 2132
- Ξ_{cc}^{++} 104, 2160
- Ξ_{cc}^{+} 2160
- Ξ_b^- 105, 2172
- Ξ_b^0 ..... 105, 2174
- $\Xi_b(6100)^-$ 106, 2176
- $\Xi_b(6227)^-$ 106, 2176
- $\Xi_b(6227)^0$ 106, 2177
- $\Xi_b'(5935)^-$ 106, 2175
- $\Xi_b(5945)^0$ 106, 2176
- $\Xi_b(5955)^-$ 106, 2176
- Ξ_c^+ 101, 2148
- Ξ_c^0 ..... 102, 2149
- $\Xi_c(2645)$ 102, 2152
- $\Xi_c(2790)$ 102, 2152
- $\Xi_c(2815)$ 103, 2153
- $\Xi_c(2923)$ 2153
- $\Xi_c(2930)$ 2154
- $\Xi_c(2970)$ 103, 2154
- $\Xi_c'^+$ 102, 2151
- $\Xi_c(3055)$ 103, 2155
- $\Xi_c(3080)$ 103, 2155
- $\Xi_c(3123)$ 2156
- $\Xi_c'^0$ 102, 2151

Year, sidereal 134
Year, tropical 134
Young diagrams (tableaux) 739
Young's modulus of solid elements, table 141
Yukawa coupling
- Higgs to fermions direct observation 210
- leptoquark-type 1090
- unification 1082

Z boson 25, 1156
- branching ratios 792
- coupling to fermions 179
- mass 791
- note on 791
- width 775, 791

Z'-boson searches, note on 995
Z' or W' bosons, searches for 1063
$Z_c(4200)$ [*was* $X(4200)^{\pm}$] 1926
$Z_b(10610)$ [*was* $X(10610)$] 85, 1972
$Z_b(10650)$ [*was* $X(10650)^{\pm}$] 85, 1973
$Z_c(3900)$ [*was* $X(3900)$] 79, 1915
$Z_c(4430)$ [*was* $X(4430)^{\pm}$] 81, 1936
Zeldovich-Sunyaev effect 471
Zero-shot learning 702
Z'-boson searches 1072

Downloaded from https://academic.oup.com/ptep/article/2022/8/083C01/6651666 by KIT Library user on 27 September 2022

Downloaded from https://academic.oup.com/ptep/article/2022/8/083C01/6651666 by KIT Library user on 27 September 2022

VOLUME II: TABLE OF CONTENTS

PARTICLE LISTINGS*

Illustrative key and abbreviations 1127

Gauge and Higgs bosons
(γ, gluon, graviton, W, Z, Higgs, Axions) 1141

Leptons
(e, μ, τ, Heavy-charged lepton searches, Neutrino properties, Number of neutrino types Double-β decay, Neutrino mixing, Heavy-neutral lepton searches) 1239

Quarks
(u, d, s, c, b, t, b', t' (4th gen.), Free quarks) 1311

Mesons
Light unflavored (π, ρ, a, b) (η, ω, f, ϕ, h) 1349
Strange (K, K^*) 1473
Charmed (D, D^*) 1527
Charmed, strange (D_s, D_s^*, D_{sJ}) 1588
Bottom (B, V_{cb}/V_{ub}, B^*, B_J^*) 1609
Bottom, strange (B_s, B_s^*, B_{sJ}^*) 1786
Bottom, charmed (B_c) 1813
$c\overline{c}$ (η_c, $J/\psi(1S)$, χ_c, h_c, ψ) 1818
$b\overline{b}$ (η_b, Υ, χ_b, h_b) 1940
Other mesons 1980

Baryons
N 1987
Δ 2042
Λ 2065
Σ 2090
Ξ 2121
Ω 2133
Charmed (Λ_c, Σ_c, Ξ_c, Ω_c) 2136
Doubly charmed (Ξ_{cc}) 2160
Bottom (Λ_b, Σ_b, Ξ_b, Ω_b, b-baryon admixture) 2161
Exotic baryons (P_c pentaquarks) 2181

Searches not in Other Sections
Magnetic monopole searches 2185
Supersymmetric particle searches 2187
Technicolor 2238
Searches for quark and lepton compositeness 2239
Extra dimensions 2243
WIMP and dark matter searches 2249
Other particle searches 2263

*The divider sheets give more detailed indices for each main section of the Particle Listings.

Downloaded from https://academic.oup.com/ptep/article/2022/8/083C01/6651666 by KIT Library user on 27 September 2022

Downloaded from https://academic.oup.com/ptep/article/2022/8/083C01/6651666 by KIT Library user on 27 September 2022

INTRODUCTION TO THE PARTICLE LISTINGS

Illustrative key 1127
Abbreviations 1128

Downloaded from https://academic.oup.com/ptep/article/2022/8/083C01/6651666 by KIT Library user on 27 September 2022

Downloaded from https://academic.oup.com/ptep/article/2022/8/083C01/6651666 by KIT Library user on 27 September 2022

Illustrative Key to the Particle Listings

Name of particle. "Old" name used before 1986 renaming scheme also given if different. See the section "Naming Scheme for Hadrons" for details.

$a_0(1200)$ $\quad I^G(J^{PC}) = 1^-(0^{++})$

Particle quantum numbers (where known).

OMITTED FROM SUMMARY TABLE

Indicates particle omitted from Particle Physics Summary Table, implying particle's existence is not confirmed.

Evidence not compelling, may be a kinematic effect.

General comments on particle.

Quantity tabulated below.

$a_0(1200)$ MASS

VALUE (MeV)	EVTS	DOCUMENT ID		TECN	CHG	COMMENT
1206± 7 OUR AVERAGE						
1210± 8±9	3000	FENNER	87	MMS	−	3.5 $\pi^- p$
1198±10		PIERCE	83	ASPK	+	2.1 $K^- p$
1216±11±9	1500	[1] MERRILL	81	HBC	0	3.2 $K^- p$
• • • We do not use the following data for averages, fits, limits, etc. • • •						
1192±16	200	LYNCH	81	HBC	±	2.7 $\pi^- p$

[1] Systematic error was added quadratically by us in our 1986 edition.

Top line gives our best value (and error) of quantity tabulated here, based on weighted average of measurements used. Could also be from fit, best limit, estimate, or other evaluation. See next page for details.

"Document id" for this result; full reference given below.

Footnote number linking measurement to text of footnote.

Measurement technique. (See abbreviations on next page.)

$a_0(1200)$ WIDTH

VALUE (MeV)	EVTS	DOCUMENT ID		TECN	CHG	COMMENT
41±11 OUR AVERAGE Error includes scale factor of 1.8. See the ideogram below.						
50± 8		PIERCE	83	ASPK	+	2.1 $K^- p$
70^{+30}_{-20}	200	LYNCH	81	HBC	±	2.7 $\pi^- p$
25± 5±7		MERRILL	81	HBC	0	3.2 $K^- p$
• • • We do not use the following data for averages, fits, limits, etc. • • •						
<60		FENNER	87	MMS	−	3.5 $\pi^- p$

Number of events *above background*.

Measured value used in averages, fits, limits, etc.

Scale factor > 1 indicates possibly inconsistent data.

Reaction producing particle, or general comments.

Error in measured value (often statistical only; followed by systematic if separately known; the two are combined in quadrature for averaging and fitting.)

"Change bar" indicates result added or changed since previous edition.

Charge(s) of particle(s) detected.

Measured value *not used* in averages, fits, limits, etc. See the Introductory Text for explanations.

Arrow points to weighted average.

Shaded pattern extends $\pm 1\sigma$ (scaled by "scale factor" S) from weighted average.

Ideogram to display possibly inconsistent data. Curve is sum of Gaussians, one for each experiment (area of Gaussian = 1/error; width of Gaussian = ±error). See Introductory Text for discussion.

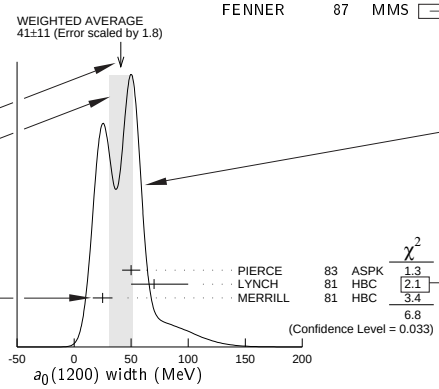

Value and error for each experiment.

Contribution of experiment to χ^2 (if no entry present, experiment not used in calculating χ^2 or scale factor because of very large error).

$a_0(1200)$ DECAY MODES

Mode	Fraction (Γ_i/Γ)	Scale factor/ Confidence level
Γ_1 3π	(65.2±1.3) %	S=1.7
Γ_2 $K\overline{K}$	(34.8±1.3) %	S=1.7
Γ_3 $\eta\pi^\pm$	< 5 $\times 10^{-4}$	CL=95%

Partial decay mode (labeled by Γ_i).

Our best value for branching fraction as determined from data averaging, fitting, evaluating, limit selection, etc. This list is basically a compact summary of results in the Branching Ratio section below.

$a_0(1200)$ BRANCHING RATIOS

Branching ratio.

$\Gamma(3\pi)/\Gamma_{total}$ $\quad \Gamma_1/\Gamma$

VALUE	DOCUMENT ID		TECN	CHG	COMMENT
0.652±0.013 OUR FIT Error includes scale factor of 1.7.					
0.643±0.010 OUR AVERAGE					
0.64 ±0.01	PIERCE	83	ASPK	+	2.1 $K^- p$
0.74 ±0.06	MERRILL	81	HBC	0	3.2 $K^- p$
• • • We do not use the following data for averages, fits, limits, etc. • • •					
0.48 ±0.15	[2] LYNCH	81	HBC	±	2.7 $\pi^- p$

[2] Data has questionable background subtraction.

Our best value (and error) of quantity tabulated, as determined from constrained fit (using *all significant* measured branching ratios for this particle).

Weighted average of measurements of this ratio only.

Footnote (referring to LYNCH 81).

$\Gamma(K\overline{K})/\Gamma_{total}$ $\quad \Gamma_2/\Gamma$

Branching ratio in terms of partial decay mode(s) Γ_i above.

VALUE	DOCUMENT ID		TECN	CHG	COMMENT
0.348±0.013 OUR FIT Error includes scale factor of 1.7.					
0.35 ±0.05	PIERCE	83	ASPK	+	2.1 $K^- p$

$\Gamma(K\overline{K})/\Gamma(3\pi)$ $\quad \Gamma_2/\Gamma_1$

VALUE	DOCUMENT ID		TECN	CHG	COMMENT
0.535±0.030 OUR FIT Error includes scale factor of 1.7.					
0.50 ±0.03	MERRILL	81	HBC	0	3.2 $K^- p$

$\Gamma(\eta(\text{neutral decay})\pi^\pm)/\Gamma_{total}$ $\quad 0.71\Gamma_3/\Gamma$

VALUE (units 10^{-4})	CL%	DOCUMENT ID		TECN	CHG	COMMENT
<3.5	95	PIERCE	83	ASPK	+	2.1 $K^- p$

Confidence level for measured upper limit.

$a_0(1200)$ REFERENCES

FENNER 87	PRL 55 14	H. Fenner *et al.*	(SLAC)	
PIERCE 83	PL 123B 230	J.H. Pierce	(FNAL)	JP
LYNCH 81	PR D24 610	G.R. Lynch *et al.*	(CLEO Collab.)	
MERRILL 81	PRL 47 143	D.W. Merrill *et al.*	(SACL, CERN)	

References, ordered inversely by year, then author.

Partial list of author(s) in addition to first author.

"Document id" used on data entries above.

Quantum number determinations in this reference.

Journal, report, preprint, etc. (See abbreviations on next page.)

Institution(s) of author(s). (See abbreviations on next page.)

Downloaded from https://academic.oup.com/ptep/article/2022/8/083C01/6651666 by KIT Library user on 27 September 2022

Abbreviations Used in the Particle Listings

Indicator of Procedure Used to Obtain Our Result

OUR AVERAGE	From a weighted average of selected data.
OUR FIT	From a constrained or overdetermined multiparameter fit of selected data.
OUR EVALUATION	Not from a direct measurement, but evaluated from measurements of other quantities.
OUR ESTIMATE	Based on the observed range of the data. Not from a formal statistical procedure.
OUR LIMIT	For special cases where the limit is evaluated by us from measured ratios or other data. Not from a direct measurement.

Measurement Techniques (i.e., Detectors and Methods of Analysis)

A1	A1 Collaboration at MAMI
A2MM	A2 spectrometer at the Mainz Microtron, MAMI
ABRA	ABRACADABRA QCD axion dark matter search
ACCM	ACCMOR Collaboration
ADMX	Axion Dark Matter Experiment
AEMS	Argonne effective mass spectrometer
ALEP	ALEPH – CERN LEP detector
ALPS	Photon regeneration experiment
AMND	AMANDA South Pole neutrino detector
AMY	AMY detector at KEK-TRISTAN
ANAI	Direct DM detection exp. with NaI at Canfranc Underground Lab, Spain
ANIC	ANTARES and IceCube combined analysis
ANIT	Antarctic Impulsive Transient Antenna balloon mission
ANTR	ANTARES underwater neutrino telescope in the Western Mediterranean Sea
APEX	FNAL APEX Collab.
ARG	ARGUS detector at DORIS
ARGD	Fit to semicircular amplitude path on Argand diagram
ASP	Anomalous single-photon detector
ASPK	Automatic spark chambers
ASTE	ASTERIX detector at LEAR
ASTR	Astronomy
ATLS	ATLAS detector at CERN LHC
AUGE	Pierre Auger Observatory
AURG	Resonant-mass gravitational wave AURIGA detector
B787	BNL experiment 787 detector
B791	BNL experiment 791 detector
B845	BNL experiment 845 detector
B852	BNL E-852
B865	BNL E865 detector
B871	BNL experiment 871 detector
B949	BNL E949 detector at AGS
BABR	BaBar Collab.
BAIK	Lake Baikal neutrino telescope
BAKS	Baksan underground scintillation telescope
BC	Bubble chamber
BDMP	Beam dump
BEAT	CERN BEATRICE Collab.
BEBC	Big European bubble chamber at CERN
BEL2	Belle II Collab.
BELL	Belle Collab.
BES	BES Beijing Spectrometer at Beijing Electron-Positron Collider
BES2	BES Beijing Spectrometer at Beijing Electron-Positron Collider
BES3	BES Beijing Spectrometer at Beijing Electron-Positron Collider
BIS2	BIS-2 spectrometer at Serpukhov
BKEI	BENKEI spectrometer system at KEK Proton Synchroton
BOLO	Bolometer, a cryogenic thermal detector
BONA	Bonanza nonmagnetic detector at DORIS
BORX	BOREXINO
BPWA	Barrelet-zero partial-wave analysis
C100	COSINE-100 experiment in South Korea
CALO	Calorimeter
CASK	CULTASK: CAPPs Ultra Low Temperature Axion Search in Korea
CASP	Cosmic Axion Spin Precession Experiments
CAST	CAST experiment at CERN
CBAL	Crystal Ball detector at SLAC-SPEAR or DORIS
CBAR	Crystal Barrel detector at CERN-LEAR
CBOX	Crystal Box at LAMPF
CBTP	CBELSA/TAPS Collaboration
CC	Cloud chamber
CCFR	Columbia-Chicago-Fermilab-Rochester detector
CDEX	China Dark Matter Experiment
CDF	Collider detector at Fermilab
CDF2	CDF-II Collab.
CDHS	CDHS neutrino detector at CERN
CDM2	CDMS II, Cryogenic Dark Matter Search at Soudan Underground Lab.
CDMS	CDMS Collaboration
CELL	CELLO detector at DESY
CGNT	CoGeNT dark matter search experiment
CHER	Cherenkov detector
CHM2	CHARM-II neutrino detector (glass) at CERN
CHOZ	Nuclear Power Station near Chooz, France
CHRM	CHARM neutrino detector (marble) at CERN
CHRS	CHORUS Collaboration – CERNS SPS
CIB	Cosmic Infrared Background
CIBS	CERN-IHEP boson spectrometer
CLAS	Jefferson CLAS Collab.
CLE2	CLEO II detector at CESR
CLE3	CLEO III detector at CESR
CLEC	CLEO-c detector at CESR
CLEO	Cornell magnetic detector at CESR
CMB	Cosmic Microwave Background
CMD	Cryogenic magnetic detector at VEPP-2M, Novosibirsk
CMD2	Cryogenic magnetic detector 2 at VEPP-2M, Novosibirsk
CMD3	Cryogenic magnetic detector 3 at VEPP-2000, Novosibirsk
CMS	CMS detector at CERN LHC
CNTR	Counters
COMB	Combined analysis of data from independent experiments.
COMP	COMPASS experiment at the CERN SPS
CONN	CONNIE: Coherent Neutrino-Nucleus Interaction Experiment
COSM	Cosmology and astrophysics
COSY	COSY-TOF Collaboration
COUP	COUPP (the Chicagoland Observatory for Underground Particle Physics) Collab.
CPLR	CPLEAR Collaboration
CRBT	Crystal Ball and TAPS detector at MAMI
CRES	CRESST cryogenic detector
CRYB	Crystal Ball at BNL
CRYM	Crystal Ball detector at Mainz Microtron MAMI
CSB2	Columbia U. - Stony Brook BGO calorimeter inserted in NaI array
CSME	COSME Collaboration
CUOR	CUORICINO experiment at Gran Sasso Laboratory.
CUSB	Columbia U. - Stony Brook segmented NaI detector at CESR
D0	D0 detector at Fermilab Tevatron Collider
DAMA	DAMA, dark matter detector at Gran Sasso National Lab.
DASP	DESY double-arm spectrometer
DAYA	Daya Bay Collaboration
DBC	Deuterium bubble chamber
DCHZ	Double Chooz Collaboration
DEAP	DEAP-3600 DM search with argon at SNOLAB
DISP	Graviton mass measurement based on dispersion measure
DLCO	DELCO detector at SLAC-SPEAR or SLAC-PEP
DLPH	DELPHI detector at LEP
DM1	Magnetic detector no. 1 at Orsay DCI collider
DM2	Magnetic detector no. 2 at Orsay DCI collider
DMIC	DAMIC Dark Matter in CCD experiment at Fermilab
DMTP	Dark Matter Time Projection Chamber (DMTPC) directional detection experiment
DONU	DONUT Collab.
DPWA	Energy-dependent partial-wave analysis
DRFT	Directional dark matter detector at Boulby Underground Science Facility
DS50	DarkSide-50 Liquid Argon TPC at Gran Sasso National Laboratory
E137	SLAC E137 beam-dump experiment
E621	Fermilab E621 detector
E653	Fermilab E653 detector
E665	Fermilab E665 detector
E687	Fermilab E687 detector
E691	Fermilab E691 detector
E705	Fermilab E705 Spectrometer-Calorimeter
E731	Fermilab E731 Spectrometer-Calorimeter
E756	Fermilab E756 detector
E760	Fermilab E760 detector
E761	Fermilab E761 detector
E771	Fermilab E771 detector
E773	Fermilab E773 Spectrometer-Calorimeter
E789	Fermilab E789 detector
E791	Fermilab E791 detector

Downloaded from https://academic.oup.com/ptep/article/2022/8/083C01/6651666 by KIT Library user on 27 September 2022

Abbreviations Used in the Particle Listings

E799	Fermilab E799 Spectrometer-Calorimeter
E835	Fermilab E835 detector
EDE2	EDELWEISS II dark matter search Collaboration
EDE3	EDELWEISS III dark matter search Collaboration
EDEL	EDELWEISS dark matter search Collaboration
EDGS	EDGES: Global EoR (Epoch of Reionization) Signature experiment
EHS	Four-pi detector at CERN
ELEC	Electronic combination
EMC	European muon collaboration detector at CERN
EMUL	Emulsions
ESR	Electron spin resonance spectroscopy
FAST	Fiber Active Scintillator Target detector at PSI
FBC	Freon bubble chamber
FENI	FENICE (at the ADONE collider of Frascati)
FIT	Fit to previously existing data
FLAT	Large Area Telescope onboard the Fermi Gamma-Ray Space Telescope (Fermi-LAT)
FMPS	Fermilab Multiparticle Spectrometer
FOCS	FNAL E831 FOCUS Collab.
FRAB	ADONE $B\overline{B}$ group detector
FRAG	ADONE $\gamma\gamma$ group detector
FRAM	ADONE MEA group detector
FREJ	FREJUS Collaboration – modular flash chamber detector (calorimeter)
FUNK	Finding U(1)'s of a Novel Kind experiment
GA24	Hodoscope Cherenkov γ calorimeter (IHEP GAMS-2000) (CERN GAMS-4000)
GALX	GALLEX solar neutrino detector in the Gran Sasso Underground Lab.
GAM2	IHEP hodoscope Cherenkov γ calorimeter GAMS-2000
GAM4	CERN hodoscope Cherenkov γ calorimeter GAMS-4000
GAMS	IHEP hodoscope Cherenkov γ calorimeter GAMS-4π
GNME	Global Network of Optical Magnetometers for Exotic searches (GNOME)
GNO	Gallium Neutrino Observatory in the Gran Sasso Underground Lab.
GOLI	CERN Goliath spectrometer
GRAL	GRAAL Collaboration
H1	H1 detector at DESY/HERA
HAWC	High Altitude Water Cherenkov Observatory experiment at Sierra Negra, Mexico
HBC	Hydrogen bubble chamber
HDBC	Hydrogen and deuterium bubble chambers
HDES	HADES Collaboration at GSI in Darmstadt
HDMO	Heidelberg-Moscow Experiment
HDMS	Heidelberg Dark Matter Search Experiment
HEBC	Helium bubble chamber
HEPT	Helium proportional tubes
HERA	H1 and ZEUS Collaborations at DESY/HERA
HERB	HERA-B detector at DESY/HERA
HERM	HERMES detector at DESY/HERA
HESS	High Energy Stereoscopic System gamma-ray instrument
HFR	HighFlow Reactor at the Institut Laue-Langevin
HFS	Hyperfine structure
HLBC	Heavy-liquid bubble chamber
HOME	Homestake underground scintillation detector
HPGE	High-purity Germanium detector
HPS	Heavy Photon Search experiment at JLAB
HPW	Harvard-Pennsylvania-Wisconsin detector
HRS	SLAC high-resolution spectrometer
HYBR	Hybrid: bubble chamber + electronics
HYCP	HyperCP Collab. (FNAL E-871)
HYST	HAYSTAC axion search experiment
IACT	Imaging Air Cherenkov Telescope
ICAR	ICARUS experiment at Gran Sasso Laboratory.
ICCB	IceCube neutrino detector at South Pole
IGEX	IGEX Collab.
IMB	Irvine-Michigan-Brookhaven underground Cherenkov detector
IMB3	Irvine-Michigan-Brookhaven underground Cherenkov detector
INDU	Magnetic induction
IPWA	Energy-independent partial-wave analysis
ISTR	IHEP ISTRA+ spectrometer-calorimeter
JADE	JADE detector at DESY
JPAC	Joint Physics Analysis Center (JPAC) Collaboration
K246	KEK E246 detector with polarimeter
K2K	KEK to Super-Kamiokande
K391	KEK E391a detector
K470	KEK-E470 Stopping K detector
KAM2	KAMIOKANDE-II underground Cherenkov detector
KAMI	KAMIOKANDE underground Cherenkov detector
KAR2	KARMEN2 calorimeter at the ISIS neutron spallation source at Rutherford
KARM	KARMEN calorimeter at the ISIS neutron spallation source at Rutherford
KEDR	detector operating at VEPP-4M collider (Novosibirsk)
KIMS	Korea Invisible Mass Search experiment at YangYang, Korea
KLND	KamLand Collab. (Japan)
KLOE	KLOE detector at DAFNE (the Frascati e+e- collider Italy)
KOLR	Kolar Gold Field underground detector
KOTO	KOTO experiment with K_L^0 beam at J-PARC
KTEV	KTeV Collaboration
L3	L3 detector at LEP
LASR	Laser
LASS	Large-angle superconducting solenoid spectrometer at SLAC
LATT	Lattice calculations
LEBC	Little European bubble chamber at CERN
LEGS	BNL LEGS Collab.
LENA	Nonmagnetic lead-glass NaI detector at DORIS
LEP	From combination of all 4 LEP experiments: ALEPH, DELPHI, L3, OPAL
LEPS	Low-Energy Pion Spectrometer at the Paul Scherrer Institute
LGW	Lead Glass Wall collaboration at SPEAR/SLAC
LHC	Combined analysis of LHC experiments
LHCB	LHCb detector at CERN LHC
L+P	Multichannel L + P model fit
LSD	Mont Blanc liquid scintillator detector
LSND	Liquid Scintillator Neutrino Detector
LSW	Light Shining through a Wall
LUX	Large Underground Xenon experiment at SURF
MAC	MAC detector at PEP/SLAC
MAJD	Majorana Demonstrator experiment at SURF
MBNE	Fermilab MiniBooNE neutrino experiment
MBR	Molecular beam resonance technique
MCBN	Fermilab MicroBooNE neutrino experiment
MCRO	MACRO detector in Gran Sasso
MD1	Magnetic detector at VEPP-4, Novosibirsk
MDRP	Millikan drop measurement
MEG	Muon to electron conversion detector at PSI
MGFL	MAGIC and Fermi-LAT Collaborations
MGIC	MAGIC Telescopes gamma-ray observatory
MICA	Underground mica deposits
MICR	MICROSCOPE satellite test of weak equivalence principle
MINS	Fermilab MINOS experiment
MIRA	MIRABELLE Liquid-hydrogen bubble chamber
MLEV	Magnetic levitation
MLS	Modified Laurent Series
MMS	Missing mass spectrometer
MOED	MoEDAL magnetic monopoles search experiment at LHC
MPS	Multiparticle spectrometer at BNL
MPS2	Multiparticle spectrometer upgrade at BNL
MPSF	Multiparticle spectrometer at Fermilab
MPWA	Model-dependent partial-wave analysis
MRK1	SLAC Mark-I detector
MRK2	SLAC Mark-II detector
MRK3	SLAC Mark-III detector
MRKJ	Mark-J detector at DESY
MRS	Magnetic resonance spectrometer
MUG2	Muon (g-2)
MWPC	Multi-Wire Proportional Chamber
NA14	CERN NA14
NA31	CERN NA31 Spectrometer-Calorimeter
NA32	CERN NA32 Spectrometer
NA48	CERN NA48 Collaboration
NA49	CERN NA49 Collaboration
NA60	CERN NA60 Collaboration
NA62	CERN NA62 Experiment
NA64	CERN SPS NA64 Experiment
NAGE	NEWAGE, New generation WIMP-search experiment with advanced gaseous tracking
NAIA	NAIAD (NaI Advanced Detector) dark matter search experiment
ND	NaI detector at VEPP-2M, Novosibirsk
NEOS	NEOS Collaboration
NEWS	NEWS-G direct dark matter search at LSM

Downloaded from https://academic.oup.com/ptep/article/2022/8/083C01/6651666 by KIT Library user on 27 September 2022

NICE Serpukhov nonmagnetic precision spectrometer
NMR Nuclear magnetic resonance
NOMD NOMAD Collaboration, CERN SPS
NOVA NOvA experiment with Fermilab's NuMI neutrino beam
NTEV NuTeV Collab. at Fermilab
nTRV neutron Time-Reversal Violation
NUSX Mont Blanc NUSEX underground detector
OBLX OBELIX detector at LEAR
OKA OKA collaboration at U70 accelerator in Protvino, Russia
OLYA Detector at VEPP-2M and VEPP-4, Novosibirsk
OMEG CERN OMEGA spectrometer
OPAL OPAL detector at LEP
OPER OPERA experiment with emulsion tracking at Gran Sasso
OSPK Optical spark chamber
PIBE The PIBETA detector at the Paul Scherrer Institute (PSI), Switzerland.
PICA PICASSO dark matter search experiment
PICO PICO bubble chamber experiment in SNOLAB underground laboratory
PIE3 πE3 beam-line of Paul Scherrer Institute
PLAS Plastic detector
PLUT DESY PLUTO detector
PMLA PAMELA space spectrometer on Resurs-DK1 satellite
PNDX PandaX dual-phase liquid xenon dark matter experiment at Jin-Ping
PPTA Parkes Pulsar Timing Array
PRMX The PRIMEX detector in Hall B at TJNAF
PWA Partial-wave analysis
QUAX QUAX axion search experiment
RADE CAST-RADES haloscope search for axions.
RDK2 NIST rare radioactive decay experiment
REDE Resonance depolarization
RENO RENO Collaboration
RICE Radio Ice Cherenkov Experiment
RVUE Review of previous data
SAGE US - Russian Gallium Experiment
SCDM SuperCDMS experiment at Soudan Underground Lab.
SELX FNAL SELEX Collab.
SENS Sub-Electron-Noise Skipper CCD Experimental Instrument (SENSEI)
SFM CERN split-field magnet
SHF SLAC Hybrid Facility Photon Collaboration
SHFT Search for Halo Axions with Ferromagnetic Toroids
SHUK SHUKET: search for U(1) dark matter with an electromagnetic telescope
SIGM Serpukhov CERN-IHEP magnetic spectrometer (SIGMA)
SILI Silicon detector
SIMP SIMPLE, dark matter detector at Laboratori Nazionali del Sud
SKAM Super-Kamiokande Collab.
SLAX Solar Axion Experiment in Canfranc Underground Laboratory
SLD SLC Large Detector for e^+e^- colliding beams at SLAC
SLIC ADMX SLIC (Superconducting LC Circuit Investigating Cold Axions)
SMPL SIMPLE, Superheated Instrument for Massive ParticLe Experiments
SND Novosibirisk Spherical neutral detector at VEPP-2M
SNDR SINDRUM spectrometer at PSI
SNO SNO Collaboration (Sudbury Neutrino Observatory)
SNO+ SNO+ Collaboration (Sudbury Neutrino Observatory)
SOU2 Soudan 2 underground detector
SOUD Soudan underground detector
SPEC Spectrometer
SPED From maximum of speed plot or resonant amplitude
SPHR Bonn SAPHIR Collab.
SPNX SPHINX spectrometer at IHEP accelerator
SPRK Spark chamber
SQID SQUID device
STRC Streamer chamber
SVD2 SVD-2 experiment at IHEP, Protvino
T2K T2K Collaboration
TASS DESY TASSO detector
TEVA Combined analysis of CDF and DØ experiments
TEXO TEXONO Collab., ultra low energy Ge detector at Kuo-Sheng Laboratory
THEO Theoretical or heavily model-dependent result
TNF TNF-IHEP facility at 70 GeV IHEP accelerator
TOF Time-of-flight
TOPZ TOPAZ detector at KEK-TRISTAN
TPC TPC detector at PEP/SLAC
TPS Tagged photon spectrometer at Fermilab
TRAP Penning trap
TWST TWIST spectrometer at TRIUMF
UA1 UA1 detector at CERN
UA2 UA2 detector at CERN
UA5 UA5 detector at CERN
UCNA UCNA collaboration using polarizeed ultracold neutrons at LANSCE
UKDM UK Dark Matter Collab.
VES Vertex Spectrometer Facility at 70 GeV IHEP accelerator
VLBI Very Long Baseline Interferometer
VNS VENUS detector at KEK-TRISTAN
VRTS Very Energetic Radiation Imaging Telescope Array System (VERITAS)
WA75 CERN WA75 experiment
WA82 CERN WA82 experiment
WA89 CERN WA89 experiment
WARP Liquid argon detector for CDM searches at Gran Sasso
WASA WASA detector at CELSIUS, Uppsala and at COSY, Juelich
WDMX WISP Dark Matter eXperiment (WISPDMX) for direct hidden photon search
WIRE Wire chamber
X100 XENON100 dark matter search experiment at Gran Sasso National Laboratory
XE10 XENON10 experiment at Gran Sasso National Laboratory
XE1T XENON1T dark matter search experiment at Gran Sasso National Laboratory
XEBC Xenon bubble chamber
XMAS XMASS, liquid xenon scintillation detector at Kamioka Observatory
YUKA Graviton mass measurement based on Yukawa potential
ZEP2 ZEPLIN-II dark matter detector
ZEP3 ZEPLIN-III dark matter detector at Palmer Underground Lab.
ZEPL ZEPLIN-I galactic dark matter detector
ZEUS ZEUS detector at DESY/HERA

Conferences

Conferences are generally referred to by the location at which they were held (e.g., HAMBURG, TORONTO, CORNELL, BRIGHTON, etc.).

Journals

AA Astronomy and Astrophysics
ADVP Advances in Physics
AFIS Anales de Fisica
AJP American Journal of Physics
AL Astronomy Letters
ANP Annals of Physics
ANPL Annals of Physics (Leipzig)
ANYAS Annals of the New York Academy of Sciences
AP Atomic Physics
APAH Acta Physica Academiae Scientiarum Hungaricae
APJ Astrophysical Journal
APJS Astrophysical Journal Suppl.
APP Acta Physica Polonica
APS Acta Physica Slovaca
ARNPS Annual Review of Nuclear and Particle Science
ARNS Annual Review of Nuclear Science
ASP Astroparticle Physics
AST American Statistician
BAPS Bulletin of the American Physical Society
BASUP Bulletin of the Academy of Science, USSR (Physics)
CJNP Chinese Journal of Nuclear Physics
CJP Canadian Journal of Physics
CNPP Comments on Nuclear and Particle Physics
CP Chinese Physics
CPC Chinese Physics C
CPL Chinese Physics Letters
CQG Classical and Quantum Gravity
CTP Communications in Theoretical Physics
CZJP Czechoslovak Journal of Physics
DANS Doklady Akademii nauk SSSR
DP Doklady Physics (Magazine)
EPJ The European Physical Journal
EPJA The European Physical Journal A
EPJC The European Physical Journal C
EPL Europhysics Letters

Downloaded from https://academic.oup.com/ptep/article/2022/8/083C01/6651666 by KIT Library user on 27 September 2022

FECAY	Fizika Elementarnykh Chastits i Atomnogo Yadra
HADJ	Hadronic Journal
IJMP	International Journal of Modern Physics
JAP	Journal of Applied Physics
JCAP	Journal of Cosmology and Astroparticle Physics
JETP	English Translation of Soviet Physics ZETF
JETPL	English Translation of Soviet Physics ZETF Letters
JHEP	Journal of High Energy Physics
JINR	Joint Inst. for Nuclear Research
JINRRC	JINR Rapid Communications
JP	Journal of Physics
JPA	Journal of Physics A
JPB	Journal of Physics B
JPCRD	Journal of Physical and Chemical Reference Data
JPCS	Journal of Physics: Conference Series
JPG	Journal of Physics G
JPSJ	Journal of the Physical Society of Japan
LHEP	Letters in High Energy Physics
LNC	Lettere Nuovo Cimento
MNRAS	Monthly Notices of the Royal Astronomical Society
MPL	Modern Physics Letters
MPLA	Modern Physics Letters A
NAST	New Astronomy
NAT	Nature
NATC	Nature Communications (NCAOBW)
NATP	Nature Physics
NC	Nuovo Cimento
NIM	Nuclear Instruments and Methods
NJP	New Journal of Physics
NP	Nuclear Physics
NPA	Nuclear Physics A
NPB	Nuclear Physics B
NPBPS	Nuclear Physics B Proceedings Supplement
NPPP	Nuclear and Particle Physics Proceedings
PAN	Physics of Atomic Nuclei (formerly SJNP)
PD	Physics Doklady (Magazine)
PDAT	Physik Daten
PL	Physics Letters
PLA	Physics Letters A
PLB	Physics Letters B
PN	Particles and Nuclei
PPCF	Plasma Physics and Controlled Fusion
PPN	Physics of Particles and Nuclei (formerly SJPN)
PPNL	Physics of Particles and Nuclei Letters
PPNP	Progress in Particles and Nuclear Physics
PPSL	Proc. of the Physical Society of London
PR	Physical Review
PRA	Physical Review A
PRAM	Pramana
PRC	Physical Review C
PRD	Physical Review D
PRL	Physical Review Letters
PRPL	Physics Reports (Physics Letters C)
PRSE	Proc. of the Royal Society of Edinburgh
PRSL	Proc. of the Royal Society of London, Section A
PS	Physica Scripta
PTEP	Progress of Theoretical and Experimental Physics
PTP	Progress of Theoretical Physics
PTPS	Progress of Theoretical Physics Supplement
PTRSL	Phil. Trans. Royal Society of London
RA	Radiochimica Acta
RMP	Reviews of Modern Physics
RNC	La Rivista del Nuovo Cimento
RPP	Reports on Progress in Physics
RRP	Revue Roumaine de Physique
SCI	Science
SCIB	Science Bulletin
SCPMA	Science China Physics, Mechanics and Astronomy
SJNP	Soviet Journal of Nuclear Physics
SJPN	Soviet Journal of Particles and Nuclei
SPD	Soviet Physics Doklady (Magazine)
SPU	Soviet Physics - Uspekhi
SYM	Symmetry
UFN	Usp. Fiz. Nauk – Russian version of SPU
YAF	Yadernaya Fizika
ZETF	Zhurnal Eksperimental'noi i Teoreticheskoi Fiziki
ZETFP	Zhurnal Eksperimental'noi i Teoreticheskoi Fiziki, Pis'ma v Redakts
ZNAT	Zeitschrift fur Naturforschung
ZPHY	Zeitschrift fur Physik

Institutions

AACH	Phys. Inst. der Techn. Hochschule **Aachen** (Historical, use for general Inst. der Techn. Hochschule)	Aachen, Germany
AACH1	I Phys. Inst. B, RWTH **Aachen**	Aachen, Germany
AACH3	III Phys. Inst. A, RWTH **Aachen** Univ.	Aachen, Germany
AACHT	Inst. für Theoretische Teilchenphysik & Kosmologie, RWTH **Aachen**	Aachen, Germany
AARH	Univ. of **Aarhus**	Aarhus C, Denmark
ABO	**Åbo** Akademi Univ.	Turku, Finland
ADEL	**Adelphi** Univ.	Garden City, NY, USA
ADLD	The Univ. of **Adelaide**	Adelaide, SA, Australia
AERE	Atomic Energy Research Estab.	Didcot, United Kingdom
AFRR	**Armed Forces** Radiobiology Res. Inst.	Bethesda, MD, USA
AHMED	Physical Research Lab.	**Ahmedabad**, Gujarat, India
AICH	**Aichi** Univ. of Education	Aichi, Japan
AKIT	**Akita** Univ.	Akita, Japan
ALAH	Univ. of **Alabama (Huntsville)**	Huntsville, AL, USA
ALAT	Univ. of **Alabama (Tuscaloosa)**	Tuscaloosa, AL, USA
ALBA	**SUNY at Albany**	Albany, NY, USA
ALBE	Univ. of **Alberta**	Edmonton, AB, Canada
AMES	**Ames Lab.**	Ames, IA, USA
AMHT	**Amherst** College	Amherst, MA, USA
AMST	Univ. van **Amsterdam**	GL Amsterdam, The Netherlands
ANIK	**NIKHEF**	**Amsterdam**, The Netherlands
ANKA	**Middle East** Technical Univ.; Dept. of Physics; Experimental HEP Lab	Ankara, Turkey
ANL	**Argonne** National Lab.; High Energy Physics Division, Bldg. 362; Physics Division, Bldg. 203	Argonne, IL, USA
ANSM	**St. Anselm** Coll.	Manchester, NH, USA
AQUI	Univ. di **LAquila**	**Aquila**, Italy
ARCBO	**Arecibo** Observatory	Arecibo, PR, USA
ARIZ	Univ. of **Arizona**	Tucson, AZ, USA
ARZS	**Arizona State** Univ.	Tempe, AZ, USA
ASCI	Russian Academy of Sciences	**Moscow**, Russian Federation
AST	**Academia Sinica**	Nankang, Taipei, Taiwan
ATEN	NCSR **"Demokritos"**	**Aghia** Paraskevi , Greece
ATHU	Univ. of **Athens**	Athens, Greece
AUCK	Univ. of **Auckland**	Auckland, New Zealand
BAKU	**Natl. Azerbaijan Academy of Sciences**, Inst. of Physics	**Baku**, Azerbaijan
BANG	Indian Inst. of Science	**Bangalore**, India
BANGB	**Bangabasi** College	Calcutta, India
BARC	Univ. Autónoma de **Barcelona**; Dept. de Fisica	Bellaterra (Barcelona), Spain
BARCE	Univ. Autónoma de **Barcelona**; Inst. de Física de Altas Energías	Bellaterra (Barcelona), Spain
BARI	Univ. e del Politecnico di **Bari**	Bari, Italy
BART	Univ. of **Delaware**; **Bartol** Research Inst.	Newark, DE, USA
BASL	Inst. für Physik der Univ. **Basel**	Basel, Switzerland
BAYR	Univ. **Bayreuth**	Bayreuth, Germany
BCEN	Centre d'Etudes Nucleaires de **Bordeaux-Gradignan**	Gradignan, France
BCIP	Natl. Inst. for Physics & Nuclear Eng. "Horia Hulubei" **(IFIN-HH)**	**Bucharest**-Magurele, Romania
BEIJ	**Beijing** Univ.	Beijing, China
BEIJT	**Inst. of Theoretical Physics**	**Beijing**, China

Downloaded from https://academic.oup.com/ptep/article/2022/8/083C01/6651666 by KIT Library user on 27 September 2022

BELG	Inter-University Inst. for High Energies (ULB-VUB)	**Brussel**, Belgium
BELL	AT & T **Bell** Labs	Murray Hill, NJ, USA
BERG	Univ. of **Bergen**	Bergen, Norway
BERL	**DESY**, Deutsches Elektronen-Synchrotron	**Zeuthen**, Germany
BERN	Univ. of **Berne**	Berne, Switzerland
BGNA	Univ. di **Bologna**, & **INFN**, Sezione di Bologna; Via Irnerio, 46, I-40126 Bologna; Viale C. Berti Pichat, n. 6/2	Bologna, Italy
BHAB	**Bhabha Atomic** Research Center	Trombay, Bombay, India
BHEP	**Inst. of High Energy Physics**	**Beijing**, China
BIEL	Univ. **Bielefeld**	Bielefeld, Germany
BING	**SUNY at Binghamton**	Binghamton, NY, USA
BIRK	**Birkbeck** College, Univ. of London	London, United Kingdom
BIRM	Univ. of **Birmingham**	Edgbaston, Birmingham, United Kingdom
BLSU	**Bloomsburg** Univ.	Bloomsburg, PA, USA
BNL	**Brookhaven National Lab.**	Upton, NY, USA
BOCH	**Ruhr** Univ. **Bochum**	Bochum, Germany
BOHR	**Niels Bohr Inst.**	Copenhagen Ø, Denmark
BOIS	**Boise** State Univ.	Boise, ID, USA
BOMB	Univ. of **Bombay**	Bombay, India
BONN	**Univ. of Bonn**	Bonn, Germany
BORD	Centre d'Etudes Nucléaires de **Bordeaux** Gradignan **(CENBG)**	Gradignan, France
BOSE	S.N. **Bose** National Centre for Basis Sciences	Calcutta, India
BOSK	**"Rudjer Bošković"** Inst.	Zagreb, Croatia
BOST	**Boston** Univ.	Boston, MA, USA
BRAN	**Brandeis** Univ.	Waltham, MA, USA
BRCO	Univ. of **British Columbia**	Vancouver, BC, Canada
BRIS	Univ. of **Bristol**	Bristol, United Kingdom
BROW	**Brown** Univ.	Providence, RI, USA
BRUN	**Brunel** Univ.	Uxbridge, Middlesex, United Kingdom
BRUX	Univ. Libre de **Bruxelles**; Physique des Particules Elémentaires	Bruxelles, Belgium
BRUXT	Univ. Libre de **Bruxelles**; Physique Théorique	Bruxelles, Belgium
BUCH	Univ. of **Bucharest**	Bucharest-Magurele, Romania
BUDA	**Wigner** Research Centre for Physics	**Budapest**, Hungary
BUFF	**SUNY at Buffalo**	Buffalo, NY, USA
BURE	Inst. des Hautes Etudes Scientifiques	**Bures-sur-Yvette**, France
CAEN	Lab. de Physique Corpusculaire, **ENSICAEN**	**Caen**, France
CAGL	Univ. degli Studi di **Cagliari**	Monserrato (CA), Italy
CAGLI	**INFN**, Sezione di **Cagliari**	Monserrato (CA), Italy
CAIR	**Cairo** University	Orman, Giza, Cairo, Egypt
CAIW	**Carnegie Inst.** of Washington	Washington, DC, USA
CALB	Univ. della **Calabria**	Cosenza, Italy
CALC	Univ. of **Calcutta**	Calcutta, India
CAMB	**DAMTP**	Cambridge, United Kingdom
CAMP	Univ. Estadual de **Campinas** (UNICAMP)	**Campinas**, SP, Brazil
CANB	**Australian National Univ.**	Canberra, ACT, Australia
CANTB	Inst. de Física de Cantabria (CSIC–Univ. **Cantabria**)	Santander, Spain
CAPE	University of **Cape Town**	Rondebosch, Cape Town, South Africa
CARA	Univ. Central de **Venezuela**	Caracas, Venezuela
CARL	**Carleton** Univ.	Ottawa, ON, Canada
CARLC	**Carleton** College	Northfield, MN, USA
CASE	**Case** Western Reserve Univ.	Cleveland, OH, USA
CAST	**China** Center of Advanced Science and Technology	Beijing, China
CATA	Univ. di **Catania**	Catania, Italy
CATH	**Catholic** Univ. of America	Washington, DC, USA
CAVE	**Cavendish** Lab.	Cambridge, United Kingdom
CBNM	CBNM	**Geel**, Belgium
CBPF	Centro Brasileiro de Pesquisas Físicas – **BIB/CDI/CBPF**	**Rio de Janeiro**, RJ, Brazil
CCAC	**Allegheny** College	Meadville, PA, USA
CDEF	**Univ. Paris VII, Denis Diderot**	Paris, France
CEA	Cambridge Electron Accelerator (Historical in *Review*)	**Cambridge, MA**, USA
CEADE	Center for Apl. Studies for Nuclear Physics	Havana, Cuba
CEBAF	**Jefferson Lab—Thomas Jefferson National Accelerator Facility**	**Newport News**, VA, USA
CENG	Centre d'Etudes Nucleaires	**Grenoble**, France
CERN	**CERN**, European Organization for Nuclear Research	Genève, Switzerland
CFPA	Univ. of **California, (Berkeley)**	Berkeley, CA, USA
CHIC	Univ. of **Chicago**	Chicago, IL, USA
CIAE	**State Nuclear Power Research Inst.**	**Beijing**, China
CINC	Univ. of **Cincinnati**	Cincinnati, OH, USA
CINV	**CINVESTAV-IPN** Centro de Investigacion y de Estudios Avanzados del IPN	**México**, DF, Mexico
CIT	**California Inst. of Tech.**	Pasadena, CA, USA
CLER	Univ. de **Clermont-Ferrand**	Aubière, France
CLEV	**Cleveland** State Univ.	Cleveland, OH, USA
CMNS	**Comenius** Univ. (FMFI UK)	**Bratislava**, Slovakia
CMU	**Carnegie Mellon** Univ.	Pittsburgh, PA, USA
CNEA	**Comisión Nacional de Energía Atómica**	Buenos Aires, Argentina
CNRC	Centre for Research in Particle Physics	Ottawa, ON, Canada
COIM	Univ. de Coimbra	**Coimbra**, Portugal
COLO	Univ. of **Colorado**	Boulder, CO, USA
COLU	**Columbia** Univ.	New York, NY, USA
CONC	**Concordia** University	Montreal, PQ, Canada
CORN	**Cornell** Univ.	Ithaca, NY, USA
COSU	**Colorado State** Univ.	Fort Collins, CO, USA
CPPM	Centre National de la Recherche Scientifique, Luminy	**Marseille**, France
CRAC	Henryk Niewodnicza'nski Inst. of Nuclear Physics	**Kraków**, Poland
CRNL	**Chalk River** Labs.	Chalk River, ON, Canada
CSOK	**Oklahoma** Central State Univ.	Edmond, OK, USA
CST	Univ. of **Science and Technology** of China	**Hefei**, Anhui 230026, China
CSULB	**California** State Univ.	Long Beach, CA, USA
CSUS	**California** State Univ.	Sacramento, CA, USA
CUNY	**City College** of **New York**	New York, NY, USA
CURCP	**Univ. Pierre et Marie Curie** (Paris VI), LCP	Paris, France
CURIN	**Univ. Pierre et Marie Curie** (Paris VI), LPNHE	Paris, France
CURIT	**Univ. Pierre et Marie Curie** (Paris VI), LPTHE	Paris, France
DALH	**Dalhousie** Univ.	Halifax, NS, Canada
DALI	**Dalian** Univ. of Tech.	Dalian, China
DARE	**Daresbury** Lab	Cheshire, United Kingdom
DARM	Tech. Hochschule **Darmstadt**	Darmstadt, Germany
DELA	Univ. of **Delaware**; Dept. of Physics & Astronomy	Newark, DE, USA
DELH	Univ. of **Delhi**	Delhi, India
DESY	**DESY**, Deutsches Elektronen-Synchrotron	**Hamburg**, Germany
DFAB	Escuela de Ingenieros	**Bilbao**, Spain
DOE	**Department of Energy**	Washington, DC, USA
DORT	Technische Univ. **Dortmund**	Dortmund, Germany
DUKE	**Duke** Univ.	Durham, NC, USA
DURH	Univ. of **Durham**	Durham , United Kingdom
DUUC	**University College** Dublin	Dublin, Ireland
ECT	Europ. Cent. for Theor. Studies in Nucl. Phys.	Trento, Italy
EDIN	Univ. of **Edinburgh**	Edinburgh, United Kingdom
EFI	Univ. of Chicago, **The Enrico Fermi Inst.**	**Chicago**, IL, USA
ELMT	**Elmhurst** College	Elmhurst, IL, USA

Downloaded from https://academic.oup.com/ptep/article/2022/8/083C01/6651666 by KIT Library user on 27 September 2022

ENSP	**l'Ecole Normale Supérieure**	**Paris**, France
EOTV	**Eötvös** University	Budapest, Hungary
EPOL	**École Polytechnique**	**Palaiseau**, France
ERLA	Univ. **Erlangen-Nurnberg**	Erlangen, Germany
ETH	Eidg. Technische Hochschule	Zürich, Switzerland
FERR	Univ. di **Ferrara**	Ferrara, Italy
FIRZ	Univ. degli Studi di **Firenze**	Sesto Fiorentino, Italy
FISK	**Fisk** Univ.	Nashville, TN, USA
FLOR	Univ. of **Florida**	Gainesville, FL, USA
FNAL	**Fermilab**	Batavia, IL, USA
FOM	**FOM**, Stichting voor Fundamenteel Onderzoek der Materie	JP **Utrecht**, The Netherlands
FRAN	**Frankfurt Inst. for Advanced Studies (FIAS)**	Frankfurt am Main, Germany
FRAS	Lab. Nazionali di **Frascati** dell'**INFN**	Frascati (Roma), Italy
FREIB	**Albert-Ludwigs** Univ.	**Freiburg**, Germany
FREIE	**Freie Univ. Berlin**	Berlin, Germany
FRIB	Univ. de **Fribourg**	Fribourg, Switzerland
FSU	**Florida State** Univ.; High Energy Physics	Tallahassee, FL, USA
FSUSC	**Florida State** Univ.; SCS (School of Computational Science)	Tallahassee, FL, USA
FUKI	**Fukui** Univ.	Fukui, Japan
FUKU	**Fukushima** Univ.	Fukushima, Japan
GENO	Univ. di **Genova**	Genova, Italy
GEOR	**E. Andronikashvili Inst. of Physics**	Tbilisi, Republic of Georgia
GESC	**General Electric** Co.	Schenectady, NY, USA
GEVA	Univ. de **Genève**	Genève, Switzerland
GIES	Univ. **Giessen**	Giessen, Germany
GIFU	**Gifu** Univ.	Gifu, Japan
GLAS	Univ. of **Glasgow**	Glasgow, United Kingdom
GMAS	**George Mason** Univ.	Fairfax, VA, USA
GOET	Univ. **Göttingen**	Göttingen, Germany
GOML	**Gomel State** Univ.	Gomel, Belarus
GRAN	Univ. de **Granada**	Granada, Spain
GRAZ	Univ. **Graz**	Graz, Austria
GRON	Univ. of **Groningen**	Groningen, The Netherlands
GSCO	**Geological Survey of Canada**	Ottawa, ON, Canada
GSI	GSI Helmholtzzentrum für Schwerionenforschung GmbH	**Darmstadt**, Germany
GUAN	Univ. de **Guanajuato**	León, Gto., Mexico
GUEL	Univ. of **Guelph**	Guelph, ON, Canada
GWU	**George Washington** Univ.	Washington, DC, USA
HAHN	**Hahn-Meitner** Inst. Berlin GmbH	Berlin, Germany
HAIF	**Technion** – Israel Inst. of Tech.	Technion, Haifa, Israel
HAMB	Univ. **Hamburg**	Hamburg, Germany
HANN	Univ. **Hannover**	Hannover, Germany
HARC	**Houston Advanced Research Ctr.**	The Woodlands, TX, USA
HARV	**Harvard** Univ.	Cambridge, MA, USA
HARV	**Harvard** Univ. (LPPC)	Cambridge, MA, USA
HAWA	Univ. of **Hawai'i**	Honolulu, HI, USA
HEBR	**Hebrew** Univ.	Jerusalem, Israel
HEID	Univ. **Heidelberg**; (unspecified division) (Historical in *Review*)	Heidelberg, Germany
HEIDH	Ruprecht-Karls Univ. **Heidelberg**	Heidelberg, Germany
HEIDP	Univ. **Heidelberg**; Physics Inst.	Heidelberg, Germany
HEIDT	Ruprecht-Karls-Univ. **Heidelberg**	Heidelberg, Germany
HELS	Univ. of **Helsinki**	University of Helsinki, Finland
HINR	Inst. of Nuclear Research (**ATOMKI**)	**Debrecen**, Hungary
HIRO	**Hiroshima** Univ.	Higashi-Hiroshima, Japan
HOUS	Univ. of **Houston**	Houston, TX, USA
HPC	**Hewlett-Packard** Corp.	Cupertino, CA, USA
HSCA	**Harvard-Smithsonian** Center for Astrophysics	Cambridge, MA, USA
HYDER	Indian Inst. of Technology	Hyderabad, India
HZDR	Helmholtz-Zentrum Dresden-Rossendorf	Dresden, Germany
IAS	**Inst. for Advanced Study**	Princeton, NJ, USA
IASD	**Dublin** Inst. for Advanced Studies	Dublin, Ireland
IBAR	**Ibaraki** Univ.	Ibaraki, Japan
IBM	**IBM** Corp.	Palo Alto, CA, USA
IBMY	**IBM**	Yorktown Heights, NY, USA
IBS	Inst. for **Boson Studies**	Pasadena, CA, USA
ICEPP	The Univ. of **Tokyo**	Tokyo, Japan
ICRR	Univ. of **Tokyo**	Chiba, Japan
ICTP	**Abdus Salam** International Centre for Theoretical Physics	**Trieste**, Italy
IFIC	**IFIC** (Instituto de Física Corpuscular)	**Paterna (Valencia)**, Spain
IFRJ	Univ. Federal do **Rio de Janeiro**	Rio de Janeiro, RJ, Brazil
IIT	**Illinois Inst. of Tech.**	Chicago, IL, USA
IITB	Indian Inst. of Tech. **IIT Bombay**	Powai, Mumbai, India
IITI	Indian Inst. of Tech. \ef IIT Indore	Simrol, Indore, India
ILL	Univ. of **Illinois at Urbana-Champaign**	Urbana, IL, USA
ILLC	Univ. of **Illinois at Chicago**	Chicago, IL, USA
ILLG	Inst. **Laue-Langevin**	Grenoble, France
IND	**Indiana** Univ.	Bloomington, IN, USA
INEL	E G and G **Idaho**, Inc.	Idaho Falls, ID, USA
INFN	Ist. Nazionale di Fisica Nuclear (Generic INFN, unknown location)	Various places, Italy
INNS	Univ. of **Innsbruck**	**Innsbruck**, Austria
INPK	Henryk Niewodniczański Inst. of Nuclear Physics	**Kraków**, Poland
INRM	**INR**, Inst. for Nucl. Research	**Moscow**, Russian Federation
INUS	**KEK**, High Energy Accelerator Research Organization	Tokyo, Japan
IOAN	Univ. of **Ioannina**	Ioannina, Greece
IOFF	A.F. **Ioffe** Phys. Tech. Inst.	St. **Petersburg**, Russian Federation
IOWA	Univ. of **Iowa**	Iowa City, IA, USA
IPN	**IPN**, Inst. de Phys. Nucl.	**Orsay**, France
IPNP	Univ. Pierre et Marie Curie (**Paris** VI)	Paris, France
IRAD	Inst. du Radium (Historical)	**Paris**, France
ISNG	Lab. de Physique Subatomique et de Cosmologie **(LPSC)**	**Grenoble**, France
ISU	**Iowa State** Univ.	Ames, IA, USA
ISUT	Isfahan University of Technology	Isfahan, Iran
ITEP	**ITEP**, Inst. of Theor. and Exp. Physics	**Moscow**, Russian Federation
ITHA	**Ithaca** College	Ithaca, NY, USA
IUPU	**Indiana** Univ., **Purdue** Univ. **Indianapolis**	Indianapolis, IN, USA
JADA	**Jadavpur** Univ.	Calcutta, India
JAGL	**Jagiellonian** Univ.	Kraków, Poland
JHU	**Johns Hopkins** Univ.	Baltimore, MD, USA
JINR	**JINR**, Joint Inst. for Nucl. Research	**Dubna**, Russian Federation
JULI	Forschungszentrum **Jülich**	Jülich, Germany
JYV	Univ. of **Jyväskylä**	Jyväskylä, Finland
KAGO	Univ. of **Kagoshima**	Kagoshima-shi, Japan
KAIST	**Korea** Advanced Inst. of Science and Technology	Yusung ku, Daejon, Republic of Korea
KANP	Indian Inst. of Tech.	**Kanpur**, UT, India
KANS	Univ. of **Kansas**	Lawrence, KS, USA
KARL	Univ. **Karlsruhe** (Historical in *Review*)	Karlsruhe, Germany
KARLE	**Karlsruhe** Inst. of Technology (KIT); Inst. for Experimental Nuclear Physics	Karlsruhe, Germany
KARLK	**Karlsruhe** Inst. of Technology (KIT)	Eggenstein-Leopoldshafen, Germany
KARLT	**Karlsruhe** Inst. of Technology (KIT); Inst. for Theoretical Physics	Karlsruhe, Germany

Downloaded from https://academic.oup.com/ptep/article/2022/8/083C01/6651666 by KIT Library user on 27 September 2022

KAZA	**Kazakh** Inst. of High Energy Physics	Alma Ata, Kazakhstan
KEK	**KEK**, High Energy Accelerator Research Organization	Ibaraki-ken, Japan
KENT	Univ. of **Kent**	Canterbury, United Kingdom
KEYN	**Open** Univ.	Milton Keynes, United Kingdom
KFTI	**Kharkov** Inst. of Physics and Tech. (NSC KIPT)	Kharkov, Ukraine
KIAE	**Kurchatov** Inst.	**Moscow**, Russian Federation
KIAM	**Keldysh** Inst. of Applied Math., Acad. Sci., Russia	Moscow, Russian Federation
KIDR	**Vinča Inst. of Nuclear Sciences**	Belgrade, Serbia
KIEV	**Institute for Nuclear Research**	**Kyiv**, Ukraine
KINK	**Kinki** Univ.	Osaka, Japan
KNTY	Univ. of **Kentucky**	Lexington, KY, USA
KOBE	**Kobe** Univ.	Kobe, Japan
KOMAB	Univ. of **Tokyo, Komaba**	Tokyo, Japan
KONAN	**Konan** Univ.	Kobe, Japan
KOSI	Inst. of Experimental Physics SAS	**Košice**, Slovakia
KYOT	**Kyoto** Univ.; Dept. of Physics, Graduate School of Science	Kyoto, Japan
KYOTU	**Kyoto** Univ.; **Yukawa** Inst. for Theor. Physics	Kyoto, Japan
KYUN	**Kyungpook** National Univ.	Daegu, Republic of Korea
KYUSH	**Kyushu** Univ.; Elementary ParticleTheory Group; Exp. Particle Physics Group; Research Center for Advanced Particle Physics	Fukuoka, Japan
LALO	**LAL**, Laboratoire de l'Accélérateur Linéaire	**Orsay**, France
LANC	**Lancaster** Univ.	Lancaster, United Kingdom
LANL	**Los Alamos National Lab.** (LANL)	Los Alamos, NM, USA
LAPL	Univ. Nacional de **La Plata**	La Plata, Argentina
LAPP	**LAPP**, Lab. d'Annecy-le-Vieux de Phys. des Particules	**Annecy-le-Vieux**, France
LASL	U.C. **Los Alamos Scientific** Lab. (Old name for LANL)	Los Alamos, NM, USA
LATV	**Latvian** State Univ.	Riga, Latvia
LAUS	EPFL **Lausanne**	Lausanne, Switzerland
LAVL	Univ. **Laval**	Quebec, QC, Canada
LBL	**Lawrence Berkeley National Lab.**	Berkeley, CA, USA
LCGT	Univ. di **Torino**	Turin, Italy
LEBD	**Lebedev** Physical Inst.	**Moscow**, Russian Federation
LECE	Univ. di **Lecce**	Lecce, Italy
LEED	Univ. of **Leeds**	Leeds, United Kingdom
LEGN	Lab. Naz. di Legnaro	**Legnaro**, Italy
LEHI	**Lehigh** Univ.	Bethlehem, PA, USA
LEHM	**Lehman** College of CUNY	Bronx, NY, USA
LEID	Univ. **Leiden**	Leiden, The Netherlands
LEMO	**Le Moyne** Coll.	Syracuse, NY, USA
LENSU	**Saint-Petersburg** State Univ.	St. **Petersburg**, Russian Federation
LEUV	Katholieke Univ. **Leuven**	Leuven, Belgium
LIEG	Univ. de **Liège**	Liège, Belgium
LINZ	Univ. **Linz**	Linz, Austria
LISB	Inst. Nacional de Investigacion Cientifica	**Lisboa** CODEX, Portugal
LISBT	Centro de Física Teórica de Partículas **(CFTP)**	**Lisboa**, Portugal
LIVP	Univ. of **Liverpool**	Liverpool, United Kingdom
LJUB	Univerza v **Ljubljani**	Ljubljana, Slovenia
LLL	**Lawrence Livermore Lab.** (Old name for LLNL)	Livermore, CA, USA
LLNL	**Lawrence Livermore National Lab.**	Livermore, CA, USA
LNUDA	Liaoning Normal Univ.	Dalian, China
LOCK	**Lockheed** Palo Alto Res. Lab	Palo Alto, CA, USA
LOIC	**Imperial** College of Science Tech. & Medicine	London, United Kingdom
LOKC	**Univ. of London**, King's College	London, United Kingdom
LOQM	Queen Mary, **Univ. of London**	London, United Kingdom
LOUC	**University College** London	London, United Kingdom
LOUV	Univ. Catholique de **Louvain**	Louvain-la-Neuve, Belgium
LOWC	**Westfield** College (Historical, see LOQM (Queen Mary and Westfield joined))	London, United Kingdom
LRL	U.C. Lawrence Radiation Lab. (Old name for LBL)	**Berkeley**, CA, USA
LSU	**Louisiana** State Univ.	Baton Rouge, LA, USA
LUND	**Fysiska Institutionen**	**Lund**, Sweden
LUND	**Lund** Univ.	Lund, Sweden
LYON	Institute de Physique Nucléaire de **Lyon** (IPN)	Villeurbanne, France
MADE	**UAM/CSIC**, Inst. de Física Teórica	**Madrid**, Cantoblanco, Spain
MADR	**C.I.E.M.A.T**	**Madrid**, Spain
MADU	Univ. Autónoma de **Madrid**	Cantoblanco, Madrid, Spain
MAINZ	**Johannes-Gutenberg-Univ.**; Inst. für Kernphysik, J.-J.-Becher-Weg 45; Inst. für Physik, Staudingerweg 7	**Mainz**, Germany
MANI	Univ. of **Manitoba**	Winnipeg, MB, Canada
MARB	Univ. **Marburg**	Marburg, Germany
MARS	Centre de Physique des Particules de **Marseille**	Marseille, France
MASA	Univ. of **Massachusetts** Amherst	**Amherst**, MA, USA
MASB	Univ. of **Massachusetts** Boston	**Boston**, MA, USA
MASD	Univ. of **Massachusetts** Dartmouth	North **Dartmouth**, MA, USA
MCGI	**McGill** Univ.	Montreal, QC, Canada
MCHS	Univ. of **Manchester**	Manchester, United Kingdom
MCMS	**McMaster** Univ.	Hamilton, ON, Canada
MDRA	Univ. of **Madras**	Madras, India
MEHTA	**Harish-Chandra** Research Inst.	Allahabad, India
MEIS	**Meisei** Univ.	Tokyo, Japan
MELB	Univ. of **Melbourne**	Victoria, Australia
MEUD	Observatoire de **Meudon**	Meudon, France
MICH	Univ. of **Michigan**	Ann Arbor, MI, USA
MILA	Univ. di **Milano**	Milano, Italy
MILAI	**INFN**, Sez. di **Milano**	Milano, Italy
MINN	Univ. of **Minnesota**	Minneapolis, MN, USA
MIPT	Moscow Institute of Physics and Technology	Moscow, Russian Federation
MISS	Univ. of **Mississippi**	University, MS, USA
MISSR	Univ. of **Missouri**	Rolla, MO, USA
MIT	**MIT Massachusetts Inst. of Technology**	Cambridge, MA, USA
MIU	**Maharishi** International Univ.	Fairfield, IA, USA
MIYA	**Miyazaki** Univ.	Miyazaki-shi, Japan
MONP	Univ. de **Montpellier** II	Montpellier, France
MONS	Univ. of **Mons**	**Mons**, Belgium
MONT	Univ. de **Montréal**; Pavillon René-J.-A.-Lévesque	Montréal, PQ, Canada
MONTC	Univ. de **Montréal**; Centre de recherches mathématiques	Montréal, PQ, Canada
MOSU	**Skobeltsyn** Inst. of Nuclear Physics, Lomonosov Moscow State Univ.; Experimental HEP Division; Theoretical HEP Division	**Moscow**, Russian Federation
MPCM	Max Planck Inst. fur Chemie	**Mainz**, Germany
MPEI	**Moscow Physical Engineering** Inst.	Moscow, Russian Federation
MPIG	**Max-Planck**-Institute für Astrophysik	Garching, Germany
MPIK	**Max-Planck-Inst.** für Kernphysik	**Heidelberg**, Germany
MPIM	**Max-Planck-Inst.** für Physik	**München**, Germany
MRION	Mirion Technologies Canberra	Meriden, CT, USA
MSST	Mississippi State University	Mississippi State, MS, USA
MSU	**Michigan State** Univ.	East Lansing, MI, USA
MTHO	**Mount Holyoke** College	South Hadley, MA, USA
MULH	Centre Univ. du **Haut-Rhin**	Mulhouse, France

Downloaded from https://academic.oup.com/ptep/article/2022/8/083C01/6651666 by KIT Library user on 27 September 2022

MUNI	**Ludwig-Maximilians-Univ. München**	Garching, Germany
MURA	**Midwestern** Univ. Research Assoc. (Historical in *Review*)	Stroughton, WI, USA
MURC	Univ. of Murcia	Murcia, Spain
NAAS	North Americal Aviation Science Center (Historical in *Review*)	Thousand Oaks, CA, USA
NAGO	**Nagoya** Univ.	Nagoya, Japan
NANJ	**Nanjing** Univ.	Nanjing, China
NAPL	Univ. di **Napoli** "Federico II"	Napoli, Italy
NASA	**NASA**	Greenbelt, MD, USA
NBS	U.S **National Bureau of Standards** (Old name for NIST)	Gaithersburg, MD, USA
NBSB	**National Inst. Standards Tech.**	Boulder, CO, USA
NCAR	**National Center for Atmospheric Research**	Boulder, CO, USA
NCSU	**North Carolina** State Univ.	**Raleigh**, NC, USA
NDAM	Univ. of **Notre Dame**	Notre Dame, IN, USA
NEAS	**Northeastern** Univ.	Boston, MA, USA
NEBR	Univ. of **Nebraska**	Lincoln, NE, USA
NEUC	Univ. de **Neuchâtel**	Neuchâtel, Switzerland
NICEA	Univ. de **Nice**	Nice, France
NICEO	Observatoire de **Nice**	Nice, France
NIHO	**Nihon** Univ.	Tokyo, Japan
NIIG	**Niigata** Univ.	Niigata, Japan
NIJM	**Radboud** Univ. Nijmegen	AJ **Nijmegen**, The Netherlands
NIRS	Nat. Inst. Radiological Sciences	**Chiba**, Japan
NIST	**National Institute of Standards & Technology**	Gaithersburg, MD, USA
NIU	**Northern Illinois** Univ.	De Kalb, IL, USA
NJU	Nanjing University	Nanjing, China
NMSU	**New Mexico** State Univ.; Dept. of Physics, MSC 3D; Part. & Nucl. Phys. Group, Box 30001/Dept.	Las Cruces, NM, USA
NORD	**Nordita**	Stockholm, Sweden
NOTT	Univ. of **Nottingham**	Nottingham, United Kingdom
NOVM	Inst. of Mathematics	**Novosibirsk**, Russian Federation
NOVO	BINP, **Budker** Inst. of Nuclear Physics	**Novosibirsk**, Russian Federation
NPOL	Polytechnic of **North London**	London, United Kingdom
NRL	**Naval Research** Lab	Washington, DC, USA
NSF	**National Science Foundation**	Arlington, VA, USA
NTHU	**National Tsing Hua** Univ.	Hsinchu, Taiwan
NTUA	**National Tech. Univ. of Athens**	Athens, Greece
NWES	**Northwestern** Univ.	Evanston, IL, USA
NYU	**New York** Univ.	New York, NY, USA
OBER	**Oberlin** College	Oberlin, OH, USA
OCH	**Ochanomizu** Univ.	Tokyo, Japan
OHIO	**Ohio** Univ.	Athens, OH, USA
OKAY	**Okayama** Univ.	Okayama, Japan
OKLA	Univ. of **Oklahoma**	Norman, OK, USA
OKSU	**Oklahoma State** Univ.	Stillwater, OK, USA
OREG	Univ. of **Oregon**; Inst. of Theoretical Science; U.O. Center for High Energy Physics	Eugene, OR, USA
ORNL	**Oak Ridge** National Laboratory	Oak Ridge, TN, USA
ORSAY	Univ. de **Paris Sud** 11	**Orsay** CEDEX, France
ORST	**Oregon State** Univ.	Corvallis, OR, USA
OSAK	**Osaka** Univ.	Osaka, Japan
OSKC	**Osaka City** Univ.	Osaka, Japan
OSLO	Univ. of **Oslo**	Oslo, Norway
OSU	**Ohio State** Univ.	Columbus, OH, USA
OTTA	Univ. of **Ottawa**	Ottawa, ON, Canada
OXF	University of **Oxford**	Oxford, United Kingdom
OXFTP	Univ. of **Oxford**	Oxford, United Kingdom
PADO	Univ. degli Studi di **Padova**	Padova, Italy
PARIN	**LPNHE**, IN^2P^3/CNRS	Paris, France
PARIS	Univ. de Paris (Historical)	**Paris**, France
PARIT	**Univ. Paris VII**, LPTHE	Paris, France
PARM	**INFN**, Gruppo Collegato di **Parma**	Parma, Italy
PAST	Institut **Pasteur**	**Paris**, France
PATR	Univ. of **Patras**	Patras, Greece
PAVI	Univ. di **Pavia**	Pavia, Italy
PAVII	INFN, Sez. di **Pavia**	**Pavia**, Italy
PENN	Univ. of **Pennsylvania**	Philadelphia, PA, USA
PGIA	**INFN**, Sezione di **Perugia**	Perugia, Italy
PISA	Univ. di **Pisa**	Pisa, Italy
PISAI	**INFN**, Sez. di **Pisa**	Pisa, Italy
PITT	Univ. of **Pittsburgh**	Pittsburgh, PA, USA
PLAT	**SUNY at Plattsburgh**	Plattsburgh, NY, USA
PLRM	Univ. di **Palermo**	Palermo, Italy
PNL	**Battelle Memorial** Inst.	Richland, WA, USA
PNPI	**Petersburg** Nuclear Physics Inst. of Russian Academy of Sciences	Gatchina, Russian Federation
PPA	Princeton-Penn. Proton Accelerator (Historical in *Review*)	Princeton, NJ, USA
PRAG	Inst. of Physics, **ASCR**	**Prague**, Czech Republic
PRIN	**Princeton** Univ.	Princeton, NJ, USA
PSI	Paul Scherrer Institute	**Villigen**, Switzerland
PSLL	**Physical Science Lab**	Las Cruces, NM, USA
PSU	**Penn State** Univ.	University Park, PA, USA
PUCB	**Pontifícia Univ. Católica do Rio de Janeiro**	Rio de Janeiro, RJ, Brazil
PUEB	Univ. Autonoma de **Puebla**	**Puebla**, Pue, Mexico
PURD	**Purdue** Univ.	West Lafayette, IN, USA
QUKI	**Queen's** Univ.	Kingston, ON, Canada
RAL	**STFC Rutherford Appleton** Lab.	Chilton, Didcot, Oxfordshire, United Kingdom
REGE	Univ. **Regensburg**	Regensburg, Germany
REHO	**Weizmann** Inst. of Science	Rehovot, Israel
REZ	Nuclear Physics Inst. **AVČR**	**Řež**, Czech Republic
RGSUL	Univ. Federal do **Rio Grande do Sul** (UFRGS)	Porto Alegre, RS, Brazil
RHBL	**Royal Holloway, Univ. of London**	Egham, Surrey, United Kingdom
RHEL	**Rutherford** High Energy Lab (Old name for RAL)	Chilton, Didcot, Oxon., United Kingdom
RICE	**Rice** Univ.	Houston, TX, USA
RIKEN	**Riken** Nishina Center for Accelerator-Based Science	Saitama, Japan
RIKK	**Rikkyo** Univ.	Tokyo, Japan
RIS	**Rowland** Inst. for Science	Cambridge, MA, USA
RISC	**Rockwell** International	Thousand Oaks, CA, USA
RISL	**Universities Research Reactor**	**Risley**, Warrington, United Kingdom
RISO	**Riso** National Laboratory	Roskilde, Denmark
RITS	Royal Inst. of Technology (**KTH**)	**Stockholm**, Sweden
RL	**Rutherford** High Energy Lab (Old name for RAL)	Chilton, Didcot, Oxon., United Kingdom
RMCS	**Royal Military** Coll. of Science	Swindon, Wilts., United Kingdom
ROCH	Univ. of **Rochester**	Rochester, NY, USA
ROCK	**Rockefeller** Univ.	New York, NY, USA
ROMA	Univ. di **Roma** (Historical)	**Roma**, Italy
ROMA2	Univ. di **Roma**, "Tor Vergata"	Roma, Italy
ROMA3	**INFN, Sez. di Roma Tre**	**Roma**, Italy
ROMAI	**INFN, Sez. di Roma**	Roma, Italy
ROSE	**Rose-Hulman** Inst. of Technology	Terre Haute, IN, USA
RPI	**Rensselaer Polytechnic** Inst.	Troy, NY, USA
RUTG	**Rutgers**, the State Univ. of New Jersey	Piscataway, NJ, USA
S0GA	**Sogang** University	Seoul, Republic of Korea
SACL	**CEA Saclay**, IRFU	Gif-sur-Yvette, France
SACL5	**CEA Saclay** – IPhT	Gif-sur-Yvette, France
SACLD	**CEA Saclay** (Essonne)	Gif-sur-Yvette, France
SAGA	**Saga** Univ.	Saga-shi, Japan
SAHA	**Saha** Inst. of Nuclear Physics	Bidhan Nagar, Calcutta, India
SANG	**Kyoto Sangyo** Univ.	Kyoto-shi, Japan
SANI	Ist. Superiore di Sanità	**Roma**, Italy

Downloaded from https://academic.oup.com/ptep/article/2022/8/083C01/6651666 by KIT Library user on 27 September 2022

SASK	Univ. of **Saskatchewan**	Saskatoon, SK, Canada
SASSO	Lab. Naz. **Gran Sasso** dell'INFN	**Assergi** (AQ), Italy
SAVO	Univ. de **Savoie**	Chambery, France
SBER	**California** State Univ.	**San Bernardino**, CA, USA
SCHAF	W.J. **Schafer** Assoc.	Livermore, DA, USA
SCIT	**Science** Univ. of **Tokyo**	Tokyo, Japan
SCOT	**Scottish** Univ. Research and Reactor Ctr.	Glasgow, United Kingdom
SCUC	Univ. of **South Carolina**	Columbia, SC, USA
SEAT	**Seattle Pacific** Coll.	Seattle, WA, USA
SEIB	Austrian Research Center, **Seibersdorf** LTD.	Seibersdorf, Austria
SEOU	**Korea** Univ.; Dept. of Physics; HEP Group	Seoul, Republic of Korea
SEOUL	**Seoul** National Univ.; Center for Theoretical Physics; Dept. of Physics & Astronomy, Coll. of Natural Sciences	Seoul, Republic of Korea
SERP	**IHEP**, Inst. for High Energy Physics	Protvino, Russian Federation
SETO	**Seton Hall** Univ.	South Orange, NJ, USA
SFLA	Univ. of **South Florida**	Tampa, FL, USA
SFRA	**Simon Fraser University**	Burnaby, BC, Canada
SFSU	**California** State Univ.	**San Francisco**, CA, USA
SHAMS	**Ain Shams** University	Abbassia, Cairo, Egypt
SHDN	**Shandong** Univ.	Jinan, Shandong, China
SHEF	Univ. of **Sheffield**	Sheffield, United Kingdom
SHMP	Univ. of **Southampton**	Southampton, United Kingdom
SHRZ	**Shiraz** Univ.	Shiraz, Iran
SIEG	Univ. **Siegen**	Siegen, Germany
SILES	Univ. of **Silesia**	Katowice, Poland
SIN	Swiss Inst. of Nuclear Research (Old name for VILL)	**Villigen**, Switzerland
SING	**National Univ.** of Singapore	Kent Ridge, Singapore
SISSA	Scuola Internazionale Superiore di Studi Avanzati	**Trieste**, Italy
SLAC	**SLAC National Accelerator Laboratory**	Menlo Park, CA, USA
SLOV	Inst. of Physics, Slovak Acad. of Sciences	**Bratislava** 45, Slovakia
SMU	**Southern Methodist** Univ.	Dallas, TX, USA
SNSP	**Scuola Normale Superiore**	**Pisa**, Italy
SOFI	Inst. for Nuclear Research and Nuclear Energy	**Sofia**, Bulgaria
SOFU	Univ. of **Sofia** "St. Kliment Ohridski"	Sofia, Bulgaria
SORB	Sorbonne Université	Paris, France
SPAUL	Univ. de **São Paulo**	São Paulo, SP, Brazil
SPIFT	Inst. de Física Teórica (**IFT**)	**São Paulo**, SP, Brazil
SSL	Univ. of **California (Berkeley)**	Berkeley, CA, USA
STAN	**Stanford** Univ.	Stanford, CA, USA
STEV	**Stevens** Inst. of Tech.	Hoboken, NJ, USA
STFN	**Jožef Stefan** Institute	**Ljubljana**, Slovenia
STLO	**St. Louis** Univ.	St. Louis, MO, USA
STOH	**Stockholm** Univ.	Stockholm, Sweden
STON	**SUNY at Stony Brook**	Stony Brook, NY, USA
STRB	Inst. Pluridisciplinaire Hubert Curien (**CNRS**)	**Strasbourg**, France
STUT	Univ. **Stuttgart**	Stuttgart, Germany
STUTM	Max-Planck-Inst.	**Stuttgart**, Germany
SUGI	**Sugiyama Jogakuen** Univ.	Aichi, Japan
SUNG	**Sungkyunkwan** Univ.	Suwon, Republic of Korea
SURR	Univ. of **Surrey**	Guildford, Surrey, United Kingdom
SUSS	Univ. of **Sussex**	Brighton, United Kingdom
SVR	**Savannah** River Labs.	Aiken, SC, USA
SYDN	Univ. of **Sydney**	Sydney, NSW, Australia
SYRA	**Syracuse** Univ.	Syracuse, NY, USA
TAJK	Acad. Sci., Tadzhik SSR	**Dushanbe**, Tadzhikstan
TAMU	**Texas A&M** Univ.	College Station, TX, USA
TATA	**Tata** Inst. of Fundamental Research	Bombay, India
TBIL	**Tbilisi State University**	Tbilisi, Republic of Georgia
TELA	**Tel-Aviv** Univ.	Tel Aviv, Israel
TELE	**Teledyne Brown** Engineering	Huntsville, AL, USA
TEMP	**Temple** Univ.	Philadelphia, PA, USA
TENN	Univ. of **Tennessee**	Knoxville, TN, USA
TEXA	Univ. of **Texas** at **Austin**	Austin, TX, USA
TGAK	**Tokyo Gakugei** Univ.	Tokyo, Japan
TGU	**Tohoku Gakuin** Univ.	Miyagi, Japan
THES	Aristotle Univ. of **Thessaloniki** (AUTh)	Thessaloniki, Greece
TINT	**Tokyo Inst. of Technology**	Tokyo, Japan
TISA	**Sagamihara** Inst. of Space & Astronautical Sci.	Kanagawa, Japan
TMSK	**Tomsk** Polytechnic Univ.	**Tomsk**, Russian Federation
TMTC	**Tokyo Metropolitan** Coll. Tech.	Tokyo, Japan
TMU	**Tokyo Metropolitan Univ.**	Tokyo, Japan
TNTO	Univ. of **Toronto**	Toronto, ON, Canada
TOHO	**Toho** Univ.	Chiba, Japan
TOHOK	**Tohoku** Univ.	Sendai, Japan
TOKA	**Tokai** Univ.	Shimizu, Japan
TOKAH	**Tokai** Univ.	Hiratsuka, Japan
TOKMS	Univ. of **Tokyo**; Meson Science Laboratory	Tokyo, Japan
TOKU	Univ. of **Tokushima**	Tokushima-shi, Japan
TOKY	Univ. of **Tokyo**; High-Energy Physics Theory Group	Tokyo, Japan
TOKYC	Univ. of **Tokyo**; Dept. of Chemistry	Tokyo, Japan
TORI	Univ. degli Studi di **Torino**	Torino, Italy
TPTI	**Uzbek** Academy of Sciences	**Tashkent**, Republic of Uzbekistan
TRIN	Trinity College **Dublin**	Dublin, Ireland
TRIU	**TRIUMF**	Vancouver, BC, Canada
TRST	Univ. di **Trieste**	Trieste, Italy
TRSTI	**INFN**, Sez. di **Trieste**	Trieste, Italy
TRSTT	Univ. degli Studi di **Trieste**	**Trieste**, Italy
TSIN	**Tsinghua Univ.**	Beijing, China
TSUK	Univ. of **Tsukuba**	Ibaraki-ken, Japan
TTAM	**Tamagawa** Univ.	Tokyo, Japan
TUAT	**Tokyo** Univ. of Agriculture Tech.	Tokyo, Japan
TUBIN	Univ. **Tübingen**	Tübingen, Germany
TUFTS	**Tufts** Univ.	Medford, MA, USA
TUM	Tech. Univ. **München**	Garching, Germany
TUW	**Technische** Univ. **Wien**	Vienna, Austria
TUZL	**Tuzla** Univ.	Tuzla, Argentina
UBA	Univ. de **Buenos Aires**	Buenos Aires, Argentina
UCB	Univ. of **California (Berkeley)**	Berkeley, CA, USA
UCD	Univ. of **California (Davis)**	Davis, CA, USA
UCI	Univ. of **California (Irvine)**	Irvine, CA, USA
UCLA	Univ. of **California (Los Angeles)**	Los Angeles, CA, USA
UCND	**Union Carbide** Corp.	Oak Ridge, TN, USA
UCR	Univ. of **California (Riverside)**	Riverside, CA, USA
UCSB	Univ. of **California (Santa Barbara)**; Physics Dept., High Energy Physics Experiment	Santa Barbara, CA, USA
UCSBT	Univ. of **California (Santa Barbara)**; Kavli Inst. for Theoretical Physics	Santa Barbara, CA, USA
UCSC	Univ. of **California (Santa Cruz)**	Santa Cruz, CA, USA
UCSD	Univ. of **California (San Diego)**	La Jolla, CA, USA
UGAZ	Univ. of **Gaziantep**	Gaziantep, Turkey
UMD	Univ. of **Maryland**	College Park, MD, USA
UNAM	Univ. Nac. Autónoma de México (**UNAM**)	**México**, DF, Mexico
UNAM	Univ. Nacional Autónoma de México (**UNAM**)	**México**, DF, Mexico
UNC	Univ. of **North Carolina**	Greensboro, NC, USA
UNCCH	Univ. of **North Carolina** at **Chapel Hill**	Chapel Hill, NC, USA
UNCS	**Union** College	Schenectady, NY, USA
UNESP	UNESP	Botucatu, Brazil
UNH	Univ. of **New Hampshire**	Durham, NH, USA
UNM	Univ. of **New Mexico**	Albuquerque, NM, USA

Downloaded from https://academic.oup.com/ptep/article/2022/8/083C01/6651666 by KIT Library user on 27 September 2022

UOEH	Univ. of Occupational and Environmental Health	**Kitakyushu**, Japan
UPNJ	**Upsala** College	East Orange, NJ, USA
UPPS	**Uppsala** Univ.	**Uppsala**, Sweden
UPR	Univ. of **Puerto Rico**	**San Juan**, PR, USA
URI	Univ. of **Rhode Island**	Kingston, RI, USA
USC	Univ. of **Southern California**	Los Angeles, CA, USA
USF	Univ. of **San Francisco**	San Francisco, CA, USA
UTAH	Univ. of **Utah**	Salt Lake City, UT, USA
UTRE	Univ. of **Utrecht**	Utrecht, The Netherlands
UTRO	**Norwegian Univ. of Science & Technology**	Trondheim, Norway
UVA	Univ. of **Virginia**	Charlottesville, VA, USA
UZINR	Acad. Sci., **Ukrainian** SSR	**Uzhgorod**, Ukraine
VALE	Univ. de **Valencia**	Burjassot, **Valencia**, Spain
VALP	**Valparaiso** Univ.	Valparaiso, IN, USA
VAND	**Vanderbilt** Univ.	Nashville, TN, USA
VASS	**Vassar** College	Poughkeepsie, NY, USA
VICT	Univ. of **Victoria**	Victoria, BC, Canada
VIEN	Inst. für Hochenergiephysik (HEPHY)	**Vienna**, Austria
VILL	Inst. for Part. Phys. and Astrophys. IPA at PSI	Villigen, Switzerland
VPI	**Virginia Tech.**	Blacksburg, VA, USA
VRIJ	**Vrije** Univ.	HV **Amsterdam**, The Netherlands
WABRN	Eidgenossisches Amt für Messwesen	**Waber**, Switzerland
WARS	Univ. of **Warsaw**	Warsaw, Poland
WASCR	**Waseda** Univ.; Cosmic Ray Division	Tokyo, Japan
WASH	Univ. of **Washington**; Elem. Particle Experiment (EPE); Particle Astrophysics (PA)	Seattle, WA, USA
WASU	**Waseda** Univ.; Dept. of Physics, High Energy Physics Group	Tokyo, Japan
WATER	Univ. of **Waterloo**	Waterloo, ON, Canada
WAUS	Univ. of **Western Australia**	Perth, WA, Australia
WAYN	**Wayne** State Univ.	Detroit, MI, USA
WESL	**Wesleyan** Univ.	Middletown, CT, USA
WIEN	Univ. **Wien**	Vienna, Austria
WILL	Coll. of **William and Mary**	Williamsburg, VA, USA
WINR	National Centre for Nuclear Research	**Warsaw**, Poland
WISC	Univ. of **Wisconsin**	Madison, WI, USA
WITW	Univ. of the **Witwatersrand**	Wits, South Africa
WMIU	**Western Michigan** Univ.	Kalamazoo, MI, USA
WONT	The Univ. of **Western Ontario**	London, ON, Canada
WOOD	**Woodstock** College (No longer in existence)	Woodstock, MD, USA
WUPP	**Bergische** Univ. Wuppertal	**Wuppertal**, Germany
WURZ	Univ. **Würzburg**	Würzburg, Germany
WUSL	**Washington** Univ.	St. Louis, MO, USA
WYOM	Univ. of **Wyoming**	Laramie, WY, USA
YALE	**Yale** Univ.	New Haven, CT, USA
YARO	**Yaroslavl** State Univ.	Yaroslavl, Russian Federation
YCC	**Yokohama** Coll. of Commerce	Yokohama, Japan
YERE	**Yerevan** Physics Inst.	Yerevan, Armenia
YOKO	**Yokohama National** Univ.	Yokohama-shi, Japan
YORKC	**York** Univ.	Toronto, Canada
ZAGR	**Zagreb** Univ.	Zagreb, Croatia
ZARA	Univ. de **Zaragoza**	Zaragoza, Spain
ZEEM	Univ. van **Amsterdam**	TV Amsterdam, The Netherlands
ZHON	**Zhongshan** (Sun Yat-Sen) Univ.	Guangzhou, China
ZHZH	**Zhengzhou** Univ.	Zhengzhou, Henan, China
ZURI	Univ. **Zürich**	Zürich, Switzerland

Downloaded from https://academic.oup.com/ptep/article/2022/8/083C01/6651666 by KIT Library user on 27 September 2022

Downloaded from https://academic.oup.com/ptep/article/2022/8/083C01/6651666 by KIT Library user on 27 September 2022

γ 1141
g (gluon) 1142
graviton 1142
W 1142
Z 1156
H^0 1175
Neutral Higgs Bosons, Searches for 1187
Charged Higgs Bosons ($H^{\pm}$ and $H^{\pm\pm}$), Searches for 1196
New Heavy Bosons 1200
Axions (A^0) and Other Very Light Bosons 1217

Notes in the Listings

Triple gauge couplings (TGC's) 1146
Anomalous $ZZ\gamma$, $Z\gamma\gamma$, and ZZV couplings 1171
Anomalous W/Z quartic couplings 1173

Related Reviews in Volume 1

54. Mass and width of the W boson (rev.) 789
55. Z boson 791

Downloaded from https://academic.oup.com/ptep/article/2022/8/083C01/6651666 by KIT Library user on 27 September 2022

Downloaded from https://academic.oup.com/ptep/article/2022/8/083C01/6651666 by KIT Library user on 27 September 2022

GAUGE AND HIGGS BOSONS

γ (photon)

$I(J^{PC}) = 0,1(1^{--})$

γ MASS

Results prior to 2008 are critiqued in GOLDHABER 10. All experimental results published prior to 2005 are summarized in detail by TU 05.

The following conversions are useful: 1 eV = 1.783×10^{-33} g = 1.957×10^{-6} m_e; $\lambda\!\!\!^{-}_C = (1.973 \times 10^{-7}$ m$)\times(1$ eV$/m_\gamma)$.

VALUE (eV)	CL%	DOCUMENT ID		COMMENT
<1 $\times 10^{-18}$		[1] RYUTOV	07	MHD of solar wind
• • • We do not use the following data for averages, fits, limits, etc. • • •				
$<2.2 \times 10^{-14}$		[2] BONETTI	17	Fast Radio Bursts, FRB 121102
$<1.8 \times 10^{-14}$		[3] BONETTI	16	Fast Radio Bursts, FRB 150418
$<1.9 \times 10^{-15}$		[4] RETINO	16	Ampere's Law in solar wind
$<2.3 \times 10^{-9}$	95	[5] EGOROV	14	Lensed quasar position
		[6] ACCIOLY	10	Anomalous magn. mom.
$<1 \times 10^{-26}$		[7] ADELBERGER	07A	Proca galactic field
no limit feasible		[7] ADELBERGER	07A	γ as Higgs particle
$<1 \times 10^{-19}$		[8] TU	06	Torque on rotating magnetized toroid
$<1.4 \times 10^{-7}$		ACCIOLY	04	Dispersion of GHz radio waves by sun
$<2 \times 10^{-16}$		[9] FULLEKRUG	04	Speed of 5-50 Hz radiation in atmosphere
$<7 \times 10^{-19}$		[10] LUO	03	Torque on rotating magnetized toroid
$<1 \times 10^{-17}$		[11] LAKES	98	Torque on toroid balance
$<6 \times 10^{-17}$		[12] RYUTOV	97	MHD of solar wind
$<8 \times 10^{-16}$	90	[13] FISCHBACH	94	Earth magnetic field
$<5 \times 10^{-13}$		[14] CHERNIKOV	92	Ampere's Law null test
$<1.5 \times 10^{-9}$	90	[15] RYAN	85	Coulomb's Law null test
$<3 \times 10^{-27}$		[16] CHIBISOV	76	Galactic magnetic field
$<6 \times 10^{-16}$	99.7	[17] DAVIS	75	Jupiter's magnetic field
$<7.3 \times 10^{-16}$		HOLLWEG	74	Alfven waves
$<6 \times 10^{-17}$		[18] FRANKEN	71	Low freq. res. circuit
$<2.4 \times 10^{-13}$		[19] KROLL	71A	Dispersion in atmosphere
$<1 \times 10^{-14}$		[20] WILLIAMS	71	Tests Coulomb's Law
$<2.3 \times 10^{-15}$		GOLDHABER	68	Satellite data

[1] RYUTOV 07 extends the method of RYUTOV 97 to the radius of Pluto's orbit.

[2] BONETTI 17 uses frequency-dependent time delays of repeating FRB with well-determined redshift, assuming the DM is caused by expected dispersion in IGM. There are several uncertainties, leading to mass limit 2.2×10^{-14} eV.

[3] BONETTI 16 uses frequency-dependent time delays of FRB, assuming the DM is caused by expected dispersion in IGM. There are several uncertainties, leading to mass limit 1.8×10^{-14} eV, if indeed the FRB is at the initially reported redshift.

[4] RETINO 16 looks for deviations from Ampere's law in the solar wind, using Cluster four spacecraft data. Authors quote a range of limits from 1.9×10^{-15} eV to 7.9×10^{-14} eV depending on the assumptions of the vector potential from the interplanetary magnetic field.

[5] EGOROV 14 studies chromatic dispersion of lensed quasar positions ("gravitational rainbows") that could be produced by any of several mechanisms, among them via photon mass. Limit not competitive but obtained on cosmological distance scales.

[6] ACCIOLY 10 limits come from possible alterations of anomalous magnetic moment of electron and gravitational deflection of electromagnetic radiation. Reported limits are not "claimed" by the authors and in any case are not competitive.

[7] When trying to measure m one must distinguish between measurements performed on large and small scales. If the photon acquires mass by the Higgs mechanism, the large-scale behavior of the photon might be effectively Maxwellian. If, on the other hand, one postulates the Proca regime for all scales, the very existence of the galactic field implies $m < 10^{-26}$ eV, as correctly calculated by YAMAGUCHI 59 and CHIBISOV 76.

[8] TU 06 continues the work of LUO 03, with extended LAKES 98 method, reporting the improved limit $\mu^2 A = (0.7 \pm 1.7) \times 10^{-13}$ T/m if $A = 0.2$ μG out to 4×10^{22} m. Reported result $\mu = (0.9 \pm 1.5) \times 10^{-52}$ g reduces to the frequentist mass limit 1.2×10^{-19} eV (FELDMAN 98).

[9] FULLEKRUG 04 adopted KROLL 71A method with newer and better Schumann resonance data. Result questionable because assumed frequency shift with photon mass is assumed to be linear. It is quadratic according to theorem by GOLDHABER 71B, KROLL 71, and PARK 71.

[10] LUO 03 extends LAKES 98 technique to set a limit on $\mu^2 A$, where μ^{-1} is the Compton wavelength $\lambda\!\!\!^{-}_C$ of the massive photon and A is the ambient vector potential. The important departure is that the apparatus rotates, removing sensitivity to the direction of A. They take $A = 10^{12}$ Tm, due to "cluster level fields." But see comment of GOLDHABER 03 and reply by LUO 03B.

[11] LAKES 98 reports limits on torque on a toroid Cavendish balance, obtaining a limit on $\mu^2 A < 2 \times 10^{-9}$ Tm/m^2 via the Maxwell-Proca equations, where μ^{-1} is the characteristic length associated with the photon mass and A is the ambient vector potential in the Lorentz gauge. Assuming $A \approx 1 \times 10^{12}$ Tm due to cluster fields he obtains $\mu^{-1} > 2 \times 10^{10}$ m, corresponding to $\mu < 1 \times 10^{-17}$ eV. A more conservative limit, using $A \approx (1$ μG$)\times(600$ pc$)$ based on the galactic field, is $\mu^{-1} > 1 \times 10^9$ m or $\mu < 2 \times 10^{-16}$ eV.

[12] RYUTOV 97 uses a magnetohydrodynamics argument concerning survival of the Sun's field to the radius of the Earth's orbit. "To reconcile observations to theory, one has to reduce [the photon mass] by approximately an order of magnitude compared with" per DAVIS 75. "Secure limit, best by this method" (per GOLDHABER 10).

[13] FISCHBACH 94 analysis is based on terrestrial magnetic fields; approach analogous to DAVIS 75. Similar result based on a much smaller planet probably follows from more precise B field mapping. "Secure limit, best by this method" (per GOLDHABER 10).

[14] CHERNIKOV 92, motivated by possibility that photon exhibits mass only below some unknown critical temperature, searches for departure from Ampere's Law at 1.24 K. See also RYAN 85.

[15] RYAN 85, motivated by possibility that photon exhibits mass only below some unknown critical temperature, sets mass limit at $< (1.5 \pm 1.4) \times 10^{-42}$ g based on Coulomb's Law departure limit at 1.36 K. We report the result as frequentist 90% CL (FELDMAN 98).

[16] CHIBISOV 76 depends in critical way on assumptions such as applicability of virial theorem. Some of the arguments given only in unpublished references.

[17] DAVIS 75 analysis of Pioneer-10 data on Jupiter's magnetic field. "Secure limit, best by this method" (per GOLDHABER 10).

[18] FRANKEN 71 method is of dubious validity (KROLL 71A, JACKSON 99, GOLDHABER 10, and references therein).

[19] KROLL 71A used low frequency Schumann resonances in cavity between the conducting earth and resistive ionosphere, overcoming objections to resonant-cavity methods (JACKSON 99, GOLDHABER 10, and references therein). "Secure limit, best by this method" (per GOLDHABER 10).

[20] WILLIAMS 71 is landmark test of Coulomb's law. "Secure limit, best by this method" (per GOLDHABER 10).

γ CHARGE

OKUN 06 has argued that schemes in which all photons are charged are inconsistent. He says that if a neutral photon is also admitted to avoid this problem, then other problems emerge, such as those connected with the emission and absorption of charged photons by charged particles. He concludes that in the absence of a self-consistent phenomenological basis, interpretation of experimental data is at best difficult.

VALUE (e)	CHARGE	DOCUMENT ID		TECN	COMMENT
<1 $\times 10^{-46}$	**mixed**	[1] ALTSCHUL	07B	VLBI	Aharonov-Bohm effect
<1 $\times 10^{-35}$	**single**	[2] CAPRINI	05	CMB	Isotropy constraint
• • • We do not use the following data for averages, fits, limits, etc. • • •					
$<1 \times 10^{-32}$	single	[1] ALTSCHUL	07B	VLBI	Aharonov-Bohm effect
$<3 \times 10^{-33}$	mixed	[3] KOBYCHEV	05	VLBI	Smear as function of B·E$_\gamma$
$<4 \times 10^{-31}$	single	[3] KOBYCHEV	05	VLBI	Deflection as function of B·E$_\gamma$
$<8.5 \times 10^{-17}$		[4] SEMERTZIDIS	03		Laser light deflection in B-field
$<3 \times 10^{-28}$	single	[5] SIVARAM	95	CMB	For $\Omega_M = 0.3$, $h^2 = 0.5$
$<5 \times 10^{-30}$		[6] RAFFELT	94	TOF	Pulsar $f_1 - f_2$
$<2 \times 10^{-28}$		[7] COCCONI	92		VLBA radio telescope resolution
$<2 \times 10^{-32}$		COCCONI	88	TOF	Pulsar $f_1 - f_2$ TOF

[1] ALTSCHUL 07B looks for Aharonov-Bohm phase shift in addition to geometric phase shift in radio interference fringes (VSOP mission).

[2] CAPRINI 05 uses isotropy of the cosmic microwave background to place stringent limits on possible charge asymmetry of the Universe. Charge limits are set on the photon, neutrino, and dark matter particles. Valid if charge asymmetries produced by different particles are not anticorrelated.

[3] KOBYCHEV 05 considers a variety of observable effects of photon charge for extragalactic compact radio sources. Best limits if source observed through a foreground cluster of galaxies.

[4] SEMERTZIDIS 03 reports the first laboratory limit on the photon charge in the last 30 years. Straightforward improvements in the apparatus could attain a sensitivity of 10^{-20} e.

[5] SIVARAM 95 requires that CMB photon charge density not overwhelm gravity. Result scales as $\Omega_M h^2$.

[6] RAFFELT 94 notes that COCCONI 88 neglects the fact that the time delay due to dispersion by free electrons in the interstellar medium has the same photon energy dependence as that due to bending of a charged photon in the magnetic field. His limit is based on the assumption that the entire observed dispersion is due to photon charge. It is a factor of 200 less stringent than the COCCONI 88 limit.

[7] See COCCONI 92 for less stringent limits in other frequency ranges. Also see RAFFELT 94 note.

γ REFERENCES

BONETTI	17	PL B768 326	L. Bonetti *et al.*	(ORLEANS, CERN)
BONETTI	16	PL B757 548	L. Bonetti *et al.*	
RETINO	16	ASP 82 49	A. Retino, A.D.A.M. Spallicci, A. Vaivads	(CURCP+)
EGOROV	14	MNRAS 437 L90	P. Egorov *et al.*	(MOSU, MIPT, INRM)
ACCIOLY	10	PR D82 065026	A. Accioly, J. Helayel-Neto, E. Scatena	(LABEX+)
GOLDHABER	10	RMP 82 939	A.S. Goldhaber, M.M. Nieto	(STON, LANL)
ADELBERGER	07A	PRL 98 010402	E. Adelberger, G. Dvali, A. Gruzinov	(WASH, NYU)
ALTSCHUL	07B	PRL 98 261801	B. Altschul	(IND)
Also		ASP 29 290	B. Altschul	(SCUC)
RYUTOV	07	PPCF 49 B429	D.D. Ryutov	(LLNL)
OKUN	06	APP B37 565	L.B. Okun	(ITEP)
TU	06	PL A352 267	L.-C. Tu *et al.*	
CAPRINI	05	JCAP 0502 006	C. Caprini, P.G. Ferreira	(GEVA, OXFTP)
KOBYCHEV	05	AL 31 147	V.V. Kobychev, S.B. Popov	(KIEV, PADO)
TU	05	RPP 68 77	L.-C. Tu, J. Luo, G.T. Gillies	
ACCIOLY	04	PR D69 107501	A. Accioly, R. Paszko	
FULLEKRUG	04	PRL 93 043901	M. Fullekrug	
GOLDHABER	03	PRL 91 149101	A.S. Goldhaber, M.M. Nieto	
LUO	03	PRL 90 081801	J. Luo *et al.*	
LUO	03B	PRL 91 149102	J. Luo *et al.*	
SEMERTZIDIS	03	PR D67 017701	Y.K. Semertzidis, G.T. Danby, D.M. Lazarus	
JACKSON	99	Classical Electrodynamics	J.D. Jackson	(3rd ed., J. Wiley and Sons (1999))
FELDMAN	98	PR D57 3873	G.J. Feldman, R.D. Cousins	
LAKES	98	PRL 80 1826	R. Lakes	(WISC)
RYUTOV	97	PPCF 39 A73	D.D. Ryutov	(LLNL)
SIVARAM	95	AJP 63 473	C. Sivaram	(BANG)
FISCHBACH	94	PRL 73 514	E. Fischbach *et al.*	(PURD, JHU+)

Downloaded from https://academic.oup.com/ptep/article/2022/8/083C01/6651666 by KIT Library user on 27 September 2022

RAFFELT	94	PR D50 7729	G. Raffelt	(MPIM)
CHERNIKOV	92	PRL 68 3383	M.A. Chernikov *et al.*	(ETH)
Also		PRL 69 2999 (erratum)	M.A. Chernikov *et al.*	(ETH)
COCCONI	92	AJP 60 750	G. Cocconi	(CERN)
COCCONI	88	PL B206 705	G. Cocconi	(CERN)
RYAN	85	PR D32 802	J.J. Ryan, F. Accetta, R.H. Austin	(PRIN)
CHIBISOV	76	SPU 19 624 Translated from UFN 119 551.	G.V. Chibisov	(LEBD)
DAVIS	75	PRL 35 1402	L. Davis, A.S. Goldhaber, M.M. Nieto	(CIT, STON+)
HOLLWEG	74	PRL 32 961	J.V. Hollweg	(NCAR)
FRANKEN	71	PRL 26 115	P.A. Franken, G.W. Ampulski	(MICH)
GOLDHABER	71B	RMP 43 277	A.S. Goldhaber, M.M. Nieto	(STON, BOHR, UCSB)
KROLL	71	PRL 26 1395	N.M. Kroll	(SLAC)
KROLL	71A	PRL 27 340	N.M. Kroll	(SLAC)
PARK	71	PRL 26 1393	D. Park, E.R. Williams	(WILC)
WILLIAMS	71	PRL 26 721	E.R. Williams, J.E. Faller, H.A. Hill	(WESL)
GOLDHABER	68	PRL 21 567	A.S. Goldhaber, M.M. Nieto	(STON)
YAMAGUCHI	59	PTPS 11 37	Y. Yamaguchi	

g or gluon

$I(J^P) = 0(1^-)$

SU(3) color octet

Mass $m = 0$. Theoretical value. A mass as large as a few MeV may not be precluded, see YNDURAIN 95.

VALUE	*DOCUMENT ID*		*TECN*	*COMMENT*
• • • We do not use the following data for averages, fits, limits, etc. • • •				
	ABREU	92E	DLPH	Spin 1, not 0
	ALEXANDER	91H	OPAL	Spin 1, not 0
	BEHREND	82D	CELL	Spin 1, not 0
	BERGER	80D	PLUT	Spin 1, not 0
	BRANDELIK	80C	TASS	Spin 1, not 0

gluon REFERENCES

YNDURAIN	95	PL B345 524	F.J. Yndurain	(MADU)
ABREU	92E	PL B274 498	P. Abreu *et al.*	(DELPHI Collab.)
ALEXANDER	91H	ZPHY C52 543	G. Alexander *et al.*	(OPAL Collab.)
BEHREND	82D	PL B110 329	H.J. Behrend *et al.*	(CELLO Collab.)
BERGER	80D	PL B97 459	C. Berger *et al.*	(PLUTO Collab.)
BRANDELIK	80C	PL B97 453	R. Brandelik *et al.*	(TASSO Collab.)

graviton

$J = 2$

graviton MASS

It is likely that the graviton is massless. More than fifty years ago Van Dam and Veltman (VANDAM 70), Iwasaki (IWASAKI 70), and Zakharov (ZAKHAROV 70) almost simultaneously showed that in the linear approximation a theory with a finite graviton mass does not approach GR as the mass approaches zero. Attempts have been made to evade this "vDVZ discontinuity" by invoking modified gravity or nonlinear theory by De Rahm (DE-RHAM 17) and others. More recently, the analysis of gravitational wave dispersion has led to bounds that are largely independent of the underlying model, even if not the strongest. We quote the best of these as our best limit.

Experimental limits have been set based on a Yukawa potential (YUKA), dispersion relation (DISP), or other modified gravity theories (MGRV).

The following conversions are useful: 1 eV $= 1.783 \times 10^{-33}$ g $= 1.957 \times 10^{-6}$ m_e; $\lambda\!\!\!^{-}_C = (1.973 \times 10^{-7}$ m$) \times (1$ eV$/m_g)$.

VALUE (eV)	*DOCUMENT ID*		*TECN*	*COMMENT*
• • • We do not use the following data for averages, fits, limits, etc. • • •				
$<1.76 \times 10^{-23}$	[1] ABBOTT	21	DISP	LIGO Virgo catalog GWTC-2
$<3.2 \times 10^{-23}$	[2] BERNUS	20	YUKA	Planetary ephemeris INPOP19a
$<2 \times 10^{-28}$	[3] SHAO	20	DISP	Binary pulsar Galileon radiation
$<4.7 \times 10^{-23}$	[4] ABBOTT	19	DISP	LIGO Virgo catalog GWTC-1
$<7 \times 10^{-23}$	[5] BERNUS	19	YUKA	Planetary ephemeris INPOP17b
$<3.1 \times 10^{-20}$	[6] MIAO	19	DISP	Binary pulsar orbital decay rate
$<1.4 \times 10^{-29}$	[7] DESAI	18	YUKA	Gal cluster Abell 1689
$<5 \times 10^{-30}$	[8] GUPTA	18	YUKA	Using SPT-SZ
$<3 \times 10^{-30}$	[8] GUPTA	18	YUKA	Using Planck all-sky SZ
$<1.3 \times 10^{-29}$	[8] GUPTA	18	YUKA	Using redMaPPer SDSS-DR8
$<6 \times 10^{-30}$	[9] RANA	18	YUKA	Weak lensing in massive clusters
$<8 \times 10^{-30}$	[10] RANA	18	YUKA	SZ effect in massive clusters
$<1.0 \times 10^{-23}$	[11] WILL	18	YUKA	Perihelion advances of planets
$<7 \times 10^{-23}$	[4] ABBOTT	17	DISP	Combined dispersion limit from three BH mergers
$<1.2 \times 10^{-22}$	[4] ABBOTT	16	DISP	Combined dispersion limit from two BH mergers
$<2.9 \times 10^{-21}$	[12] ZAKHAROV	16	YUKA	S2 star orbit
$<5 \times 10^{-23}$	[13] BRITO	13	MGRV	Spinning black holes bounds
$<6 \times 10^{-32}$	[14] GRUZINOV	05	MGRV	Solar System observations
$<6 \times 10^{-32}$	[15] CHOUDHURY	04	YUKA	Weak gravitational lensing
$<9.0 \times 10^{-34}$	[16] GERSHTEIN	04	MGRV	From Ω_{tot} value assuming RTG
$<8 \times 10^{-20}$	[17,18] FINN	02	DISP	Binary pulsar orbital period decrease
$<7 \times 10^{-23}$	TALMADGE	88	YUKA	Solar system planetary astrometric data
$<1.3 \times 10^{-29}$	[19] GOLDHABER	74	YUKA	Rich clusters
$<7 \times 10^{-28}$	HARE	73	YUKA	Galaxy
$<8 \times 10^{4}$	HARE	73	YUKA	2γ decay

[1] ABBOTT 21 assumed modified gravitational-wave dispersion to establish a limit on graviton mass, using LIGO-Virgo O1-O3a binary black hole (BBH) events.

[2] BERNUS 20 use the latest solution of the ephemeris INPOP (19a) in order to improve the constraint in BERNUS 19 on the existence of a Yukawa suppression to the Newtonian potential, generically associated to a gravitons mass.

[3] SHAO 20 sets limit, 95% CL, based on non-observation of excess gravitational radiation in 14 well-timed binary pulsars in the context of the cubic Galileon model.

[4] ABBOTT 19, ABBOTT 17, and ABBOTT 16 assumed modified gravitational waves dispersion to establish limits on graviton mass.

[5] BERNUS 19 use the planetary ephemeris INPOP 17b to constraint the existence of a Yukawa suppression to the Newtonian potential, generically associated to a gravitons mass.

[6] MIAO 19 90% CL limit is based on orbital period decay rates of 9 binary pulsars using a Bayesian prior uniform in graviton mass. Limit becomes $< 5.2 \times 10^{-21}$ eV for a prior uniform in $\ln(m_g)$.

[7] DESAI 18 limit based on dynamical mass models of galaxy cluster Abell 1689.

[8] GUPTA 18 obtains graviton mass limits using stacked clusters from 3 disparate surveys.

[9] RANA 18 limit, 68% CL, obtained using weak lensing mass profiles out to the radius at which the cluster density falls to 200 times the critical density of the Universe. Limit is based on the fractional change between Newtonian and Yukawa accelerations for the 50 most massive galaxy clusters in the Local Cluster Substructure Survey. Limits for other CL's and other density cuts are also given.

[10] RANA 18 limit, 68% CL, obtained using mass measurements via the SZ effect out to the radius at which the cluster density falls to 500 times the critical density of the Universe for 182 optically confirmed galaxy clusters in an Altacama Cosmology Telescope survey. Limits for other CL's and other density cuts are also given.

[11] WILL 18 limit from perihelion advances of the planets, notably Earth, Mars, and Saturn. Alternate analysis yields $< 6 \times 10^{-24}$.

[12] ZAKHAROV 16 constrains range of Yukawa gravity interaction from S2 star orbit about black hole at Galactic center. The limit is $< 2.9 \times 10^{-21}$ eV for $\delta = 100$.

[13] BRITO 13 explore massive graviton (spin-2) fluctuations around rotating black holes.

[14] GRUZINOV 05 uses the DGP model (DVALI 00) showing that non-perturbative effects restore continuity with Einstein's equations as the gravition mass approaches zero, then bases his limit on Solar System observations.

[15] CHOUDHURY 04 concludes from a study of weak-lensing data that masses heavier than about the inverse of 100 Mpc seem to be ruled out if the gravitation field has the Yukawa form.

[16] GERSHTEIN 04 use non-Einstein field relativistic theory of gravity (RTG), with a massive graviton, to obtain the 95% CL mass limit implied by the value of $\Omega_{tot} = 1.02 \pm 0.02$ current at the time of publication.

[17] FINN 02 analyze the orbital decay rates of PSR B1913+16 and PSR B1534+12 with a possible graviton mass as a parameter. The combined frequentist mass limit is at 90%CL.

[18] As of 2020, limits on dP/dt are now about 0.1% (see T. Damour, "Experimental tests of gravitational theory," in this *Review*).

[19] GOLDHABER 74 establish this limit considering the binding of galactic clusters, corrected to Planck $h_0 = 0.67$.

graviton REFERENCES

ABBOTT	21	PR D103 122002	R. Abbott *et al.*	(LIGO and Virgo Collabs.)
BERNUS	20	PR D102 021501	L. Bernus *et al.*	
SHAO	20	PR D102 024069	L. Shao, N. Wex, S.-Y. Zhou	
ABBOTT	19	PR D100 104036	B.P. Abbott *et al.*	(LIGO and Virgo Collabs.)
BERNUS	19	PRL 123 161103	L. Bernus *et al.*	
MIAO	19	PR D99 123015	X. Miao, L. Shao, B.-Q. Ma	
DESAI	18	PL B778 325	S. Desai	(HYDER)
GUPTA	18	ANP 399 85	S. Gupta, S. Desai	
RANA	18	PL B781 220	A. Rana *et al.*	(DELHI)
WILL	18	CQG 35 17LT01	C.M. Will	
ABBOTT	17	PRL 118 221101	B.P. Abbott *et al.*	(LIGO and Virgo Collabs.)
DE-RHAM	17	RMP 89 025004	C. de Rham *et al.*	
ABBOTT	16	PRL 116 061102	B.P. Abbott *et al.*	(LIGO and Virgo Collabs.)
ZAKHAROV	16	JCAP 1605 045	A.F. Zakharov *et al.*	
BRITO	13	PR D88 023514	R. Brito, V. Cardoso, P. Pani	(LISB, MISS, HSCA+)
GRUZINOV	05	NAST 10 311	A. Gruzinov	(NYU)
CHOUDHURY	04	ASP 21 559	S.R. Choudhury *et al.*	(DELPH, MELB)
GERSHTEIN	04	PAN 67 1596 Translated from YAF 67 1618.	S.S. Gershtein *et al.*	(SERP)
FINN	02	PR D65 044022	L.S. Finn, P.J. Sutton	
DVALI	00	PL B485 208	G.R. Dvali, G. Gabadadze, M. Porrati	(NYU)
TALMADGE	88	PRL 61 1159	C. Talmadge *et al.*	(JPL)
GOLDHABER	74	PR D9 1119	A.S. Goldhaber, M.M. Nieto	(LANL, STON)
HARE	73	CJP 51 431	M.G. Hare	(SASK)
IWASAKI	70	PR D2 2255	Y. Iwasaki	
VANDAM	70	NP B22 397	H. van Dam, M. Veltman	(UTRE)
ZAKHAROV	70	JETPL 12 312	V.I. Zakharov *et al.*	

W

$J = 1$

See the related review(s):
Mass and Width of the W Boson

W MASS

The W-mass listed here corresponds to the mass parameter in a Breit-Wigner distribution with mass-dependent width. To obtain the world average, common systematic uncertainties between experiments are properly taken into account. The LEP-2 average W mass based on published results from ALEPH, DELPHI, L3, and OPAL is 80.376 ± 0.033 GeV [SCHAEL 13A]. The combined Tevatron data from CDF and D0 yields an average W mass of 80.387 ± 0016 GeV [AALTONEN 13N]. Assuming a common systematic error of 9 MeV due to PDF uncertainty, the combined LHC data from ATLAS [AABOUD 18J] and LHCb [AAIJ 22C] yields an average W mass of 80.366 ± 0.017 GeV [J. Erler and A. Freitas, "Electroweak Model and Constraints on New Physics" review, PDG 22]. Assuming 7 MeV as the common systematic uncertainty between the LHC

Downloaded from https://academic.oup.com/ptep/article/2022/8/083C01/6651666 by KIT Library user on 27 September 2022

and Tevatron results, the average W mass from the two hadron colliders is estimated to be 80.377 ± 0.013 GeV. Combining this result with the LEP-2 value assuming no correlations, the world average W mass of 80.377 ± 0.012 GeV is obtained [Ibid]; OUR FIT quotes this value for the W mass.

In April 2022, after the cut-off of results for this review, the CDF collaboration published a determination of the W mass based on their full Run-2 dataset of 8.8 fb^{-1} [AALTONEN 22], with much reduced uncertainty: 80433.5 ± 9.4 MeV. This new CDF result, which includes the data of their previous result [AALTONEN 12E] and thus supersedes it, is of higher precision than our world average quoted above. However, the two determinations disagree significantly. More information is given in M. Grunewald and A. Gurtu, "Mass and Width of the W Boson" review [PDG 22].

VALUE (GeV)	EVTS	DOCUMENT ID		TECN	COMMENT
80.377± 0.012 OUR FIT					
80.354± 0.023±0.022	2.4M	[1] AAIJ	22C	LHCB	E^{pp}_{cm} = 13 TeV
80.370± 0.007±0.017	13.7M	[2] AABOUD	18J	ATLS	E^{pp}_{cm} = 7 TeV
80.387± 0.012±0.015	1095k	[3] AALTONEN	12E	CDF	$E^{p\overline{p}}_{cm}$ = 1.96 TeV
80.375± 0.011±0.020	2177k	[4] ABAZOV	12F	D0	$E^{p\overline{p}}_{cm}$ = 1.96 TeV
80.336± 0.055±0.039	10.3k	[5] ABDALLAH	08A	DLPH	E^{ee}_{cm} = 161–209 GeV
80.415± 0.042±0.031	11830	[6] ABBIENDI	06	OPAL	E^{ee}_{cm}= 170–209 GeV
80.270± 0.046±0.031	9909	[7] ACHARD	06	L3	E^{ee}_{cm}= 161–209 GeV
80.440± 0.043±0.027	8692	[8] SCHAEL	06	ALEP	E^{ee}_{cm}= 161–209 GeV
80.483± 0.084	49247	[9] ABAZOV	02D	D0	$E^{p\overline{p}}_{cm}$= 1.8 TeV
80.433± 0.079	53841	[10] AFFOLDER	01E	CDF	$E^{p\overline{p}}_{cm}$= 1.8 TeV
• • • We do not use the following data for averages, fits, limits, etc. • • •					
80.520± 0.070±0.092		[11] ANDREEV	18A	H1	$e^{\pm}p$
80.367± 0.013±0.022	1677k	[12] ABAZOV	12F	D0	$E^{p\overline{p}}_{cm}$ = 1.96 TeV
80.401± 0.021±0.038	500k	[13] ABAZOV	09AB	D0	$E^{p\overline{p}}_{cm}$ = 1.96 TeV
80.413± 0.034±0.034	115k	[14] AALTONEN	07F	CDF	$E^{p\overline{p}}_{cm}$ = 1.96 TeV
82.87 ± 1.82 $^{+0.30}_{-0.16}$	1500	[15] AKTAS	06	H1	$e^{\pm}p \to \overline{\nu}_e(\nu_e)X$, $\sqrt{s} \approx 300$ GeV
80.3 ± 2.1 ± 1.2 ± 1.0	645	[16] CHEKANOV	02C	ZEUS	$e^-p \to \nu_e X$, $\sqrt{s}$= 318 GeV
81.4$^{+2.7}_{-2.6}$ ± 2.0$^{+3.3}_{-3.0}$	1086	[17] BREITWEG	00D	ZEUS	$e^+p \to \overline{\nu}_e X$, $\sqrt{s} \approx$ 300 GeV
80.84 ± 0.22 ±0.83	2065	[18] ALITTI	92B	UA2	See W/Z ratio below
80.79 ± 0.31 ±0.84		[19] ALITTI	90B	UA2	$E^{p\overline{p}}_{cm}$= 546,630 GeV
80.0 ± 3.3 ±2.4	22	[20] ABE	89I	CDF	$E^{p\overline{p}}_{cm}$= 1.8 TeV
82.7 ± 1.0 ±2.7	149	[21] ALBAJAR	89	UA1	$E^{p\overline{p}}_{cm}$= 546,630 GeV
81.8 $^{+6.0}_{-5.3}$ ±2.6	46	[22] ALBAJAR	89	UA1	$E^{p\overline{p}}_{cm}$= 546,630 GeV
89 ± 3 ±6	32	[23] ALBAJAR	89	UA1	$E^{p\overline{p}}_{cm}$= 546,630 GeV
81. ± 5.	6	ARNISON	83	UA1	E^{ee}_{cm}= 546 GeV
80. $^{+10.}_{-6.}$	4	BANNER	83B	UA2	Repl. by ALITTI 90B

[1] AAIJ 22C analyse W production in the muon decay channel, with the transverse momentum of the muon required to be between 28 and 52 GeV. Analysing the distribution of the muon charge divided by the muon transverse momentum of approximately 2.4 million selected W candidates, a value of M_W = 80354 ± 23(stat.)±10(exp.)±17(theo.)±9(PDF) MeV is obtained; we combine the three systematic uncertainties in quadrature.

[2] AABOUD 18J select 4.61M $W^+ \to \mu^+\nu_\mu$, 3.40M $W^+ \to e^+\nu_e$, 3.23M $W^- \to \mu^-\overline{\nu}_\mu$ and 2.49M $W^- \to e^-\overline{\nu}_e$ events in 4.6 fb^{-1} pp data at 7 TeV. The W mass is determined using the transverse mass and transverse lepton momentum distributions, accounting for correlations. The systematic error includes 0.011 GeV experimental and 0.014 GeV modelling uncertainties.

[3] AALTONEN 12E select 470k $W \to e\nu$ decays and 625k $W \to \mu\nu$ decays in 2.2 fb^{-1} of Run-II data. The mass is determined using the transverse mass, transverse lepton momentum and transverse missing energy distributions, accounting for correlations. This result supersedes AALTONEN 07F. AALTONEN 14D gives more details on the procedures followed by the authors.

[4] Combination of results from ABAZOV 12F and ABAZOV 09AB as quoted in ABAZOV 12F.

[5] ABDALLAH 08A use direct reconstruction of the kinematics of $W^+W^- \to q\overline{q}\ell\nu$ and $W^+W^- \to q\overline{q}q\overline{q}$ events for energies 172 GeV and above. The W mass was also extracted from the dependence of the WW cross section close to the production threshold and combined appropriately to obtain the final result. The systematic error includes ±0.025 GeV due to final state interactions and ±0.009 GeV due to LEP energy uncertainty.

[6] ABBIENDI 06 use direct reconstruction of the kinematics of $W^+W^- \to q\overline{q}\ell\nu_\ell$ and $W^+W^- \to q\overline{q}q\overline{q}$ events. The result quoted here is obtained combining this mass value with the results using $W^+W^- \to \ell\nu_\ell\ell'\nu_{\ell'}$ events in the energy range 183–207 GeV (ABBIENDI 03C) and the dependence of the WW production cross-section on m_W at threshold. The systematic error includes ±0.009 GeV due to the uncertainty on the LEP beam energy.

[7] ACHARD 06 use direct reconstruction of the kinematics of $W^+W^- \to q\overline{q}\ell\nu_\ell$ and $W^+W^- \to q\overline{q}q\overline{q}$ events in the C.M. energy range 189–209 GeV. The result quoted here is obtained combining this mass value with the results obtained from a direct W mass reconstruction at 172 and 183 GeV and with those from the dependence of the WW production cross-section on m_W at 161 and 172 GeV (ACCIARRI 99).

[8] SCHAEL 06 use direct reconstruction of the kinematics of $W^+W^- \to q\overline{q}\ell\nu_\ell$ and $W^+W^- \to q\overline{q}q\overline{q}$ events in the C.M. energy range 183–209 GeV. The result quoted here is obtained combining this mass value with those obtained from the dependence of the W pair production cross-section on m_W at 161 and 172 GeV (BARATE 97 and BARATE 97S respectively). The systematic error includes ±0.009 GeV due to possible effects of final state interactions in the $q\overline{q}q\overline{q}$ channel and ±0.009 GeV due to the uncertainty on the LEP beam energy.

[9] ABAZOV 02D improve the measurement of the W-boson mass including $W \to e\nu_e$ events in which the electron is close to a boundary of a central electromagnetic calorimeter module. Properly combining the results obtained by fitting $m_T(W)$, $p_T(e)$, and $p_T(\nu)$, this sample provides a mass value of 80.574 ± 0.405 GeV. The value reported here is a combination of this measurement with all previous DØ W-boson mass measurements.

[10] AFFOLDER 01E fit the transverse mass spectrum of 30115 $W \to e\nu_e$ events (M_W= 80.473 ± 0.065 ± 0.092 GeV) and of 14740 $W \to \mu\nu_\mu$ events (M_W= 80.465 ± 0.100 ± 0.103 GeV) obtained in the run IB (1994-95). Combining the electron and muon results, accounting for correlated uncertainties, yields M_W= 80.470 ± 0.089 GeV. They combine this value with their measurement of ABE 95P reported in run IA (1992-93) to obtain the quoted value.

[11] ANDREEV 18A obtain this result in a combined electroweak and QCD analysis using all deep-inelastic e^+p and e^-p neutral current and charged current scattering cross sections published by the H1 Collaboration, including data with longitudinally polarized lepton beams.

[12] ABAZOV 12F select 1677k $W \to e\nu$ decays in 4.3 fb^{-1} of Run-II data. The mass is determined using the transverse mass and transverse lepton momentum distributions, accounting for correlations.

[13] ABAZOV 09AB study the transverse mass, transverse electron momentum, and transverse missing energy in a sample of 0.5 million $W \to e\nu$ decays selected in Run-II data. The quoted result combines all three methods, accounting for correlations.

[14] AALTONEN 07F obtain high purity $W \to e\nu_e$ and $W \to \mu\nu_\mu$ candidate samples totaling 63,964 and 51,128 events respectively. The W mass value quoted above is derived by simultaneously fitting the transverse mass and the lepton, and neutrino p_T distributions.

[15] AKTAS 06 fit the Q^2 dependence (300 < Q^2 < 30,000 GeV^2) of the charged-current differential cross section with a propagator mass. The first error is experimental and the second corresponds to uncertainties due to input parameters and model assumptions.

[16] CHEKANOV 02C fit the Q^2 dependence (200<Q^2 <60000 GeV^2) of the charged-current differential cross sections with a propagator mass fit. The last error is due to the uncertainty on the probability density functions.

[17] BREITWEG 00D fit the Q^2 dependence (200 < Q^2 < 22500 GeV^2) of the charged-current differential cross sections with a propagator mass fit. The last error is due to the uncertainty on the probability density functions.

[18] ALITTI 92B result has two contributions to the systematic error (±0.83); one (±0.81) cancels in m_W/m_Z and one (±0.17) is noncancelling. These were added in quadrature. We choose the ALITTI 92B value without using the LEP m_Z value, because we perform our own combined fit.

[19] There are two contributions to the systematic error (±0.84): one (±0.81) which cancels in m_W/m_Z and one (±0.21) which is non-cancelling. These were added in quadrature.

[20] ABE 89I systematic error dominated by the uncertainty in the absolute energy scale.

[21] ALBAJAR 89 result is from a total sample of 299 $W \to e\nu$ events.

[22] ALBAJAR 89 result is from a total sample of 67 $W \to \mu\nu$ events.

[23] ALBAJAR 89 result is from $W \to \tau\nu$ events.

W/Z MASS RATIO

VALUE	EVTS	DOCUMENT ID		TECN	COMMENT
0.88145 ± 0.00013		[1] PDG	22		
• • • We do not use the following data for averages, fits, limits, etc. • • •					
0.8821 ±0.0011 ±0.0008	28323	[2] ABBOTT	98N	D0	$E^{p\overline{p}}_{cm}$= 1.8 TeV
0.88114±0.00154±0.00252	5982	[3] ABBOTT	98P	D0	$E^{p\overline{p}}_{cm}$= 1.8 TeV
0.8813 ±0.0036 ±0.0019	156	[4] ALITTI	92B	UA2	$E^{p\overline{p}}_{cm}$= 630 GeV

[1] This value was obtained using the world average values of m_Z and m_W as listed in these listings.

[2] ABBOTT 98N obtain this from a study of 28323 $W \to e\nu_e$ and 3294 $Z \to e^+e^-$ decays. Of this latter sample, 2179 events are used to calibrate the electron energy scale.

[3] ABBOTT 98P obtain this from a study of 5982 $W \to e\nu_e$ events. The systematic error includes an uncertainty of ±0.00175 due to the electron energy scale.

[4] Scale error cancels in this ratio.

$m_Z - m_W$

VALUE (GeV)	DOCUMENT ID		TECN	COMMENT
10.811 ± 0.012	[1] PDG	22		
• • • We do not use the following data for averages, fits, limits, etc. • • •				
10.4 ±1.4 ±0.8	ALBAJAR	89	UA1	$E^{p\overline{p}}_{cm}$= 546,630 GeV
11.3 ±1.3 ±0.9	ANSARI	87	UA2	$E^{p\overline{p}}_{cm}$= 546,630 GeV

[1] This value was obtained using the world average values of m_Z and m_W as listed in these listings.

$m_{W^+} - m_{W^-}$

Test of CPT invariance.

VALUE (GeV)	EVTS	DOCUMENT ID		TECN	COMMENT
−0.029 ± 0.028 OUR AVERAGE					
−0.029±0.013±0.025	13.7M	[1] AABOUD	18J	ATLS	E^{pp}_{cm} = 7 TeV
−0.19 ±0.58	1722	ABE	90G	CDF	$E^{p\overline{p}}_{cm}$= 1.8 TeV

[1] AABOUD 18J select 4.61M $W^+ \to \mu^+\nu_\mu$, 3.40M $W^+ \to e^+\nu_e$, 3.23M $W^- \to \mu^-\overline{\nu}_\mu$ and 2.49M $W^- \to e^-\overline{\nu}_e$ events in 4.6 fb^{-1} pp data at 7 TeV. The W mass is determined using the transverse mass and transverse lepton momentum distributions,

Downloaded from https://academic.oup.com/ptep/article/2022/8/083C01/6651666 by KIT Library user on 27 September 2022

accounting for correlations. The systematic error includes 0.007 GeV experimental and 0.024 GeV modelling uncertainties.

W WIDTH

The *W* width listed here corresponds to the width parameter in a Breit-Wigner distribution with mass-dependent width. To obtain the world average, common systematic uncertainties between experiments are properly taken into account. The LEP-2 average *W* width based on published results is 2.195 ± 0.083 GeV [SCHAEL 13A]. The combined Tevatron data yields an average W width of 2.046±0.049 GeV [FERMILAB-TM-2460-E].

OUR FIT uses these average LEP and Tevatron width values and combines them assuming no correlations.

VALUE (GeV)	EVTS	DOCUMENT ID		TECN	COMMENT
2.085±0.042 OUR FIT					
2.028±0.072	5272	[1] ABAZOV	09AK	D0	$E^{p\overline{p}}_{cm}$ = 1.96 GeV
2.032±0.045±0.057	6055	[2] AALTONEN	08B	CDF	$E^{p\overline{p}}_{cm}$ = 1.96 TeV
2.404±0.140±0.101	10.3k	[3] ABDALLAH	08A	DLPH	E^{ee}_{cm}= 183–209 GeV
1.996±0.096±0.102	10729	[4] ABBIENDI	06	OPAL	E^{ee}_{cm}= 170–209 GeV
2.18 ±0.11 ±0.09	9795	[5] ACHARD	06	L3	E^{ee}_{cm}= 172–209 GeV
2.14 ±0.09 ±0.06	8717	[6] SCHAEL	06	ALEP	E^{ee}_{cm}= 183–209 GeV
$2.23\ ^{+0.15}_{-0.14}$ ±0.10	294	[7] ABAZOV	02E	D0	$E^{p\overline{p}}_{cm}$ = 1.8 TeV
2.05 ±0.10 ±0.08	662	[8] AFFOLDER	00M	CDF	$E^{p\overline{p}}_{cm}$ = 1.8 TeV
• • • We do not use the following data for averages, fits, limits, etc. • • •					
2.152±0.066	79176	[9] ABBOTT	00B	D0	Extracted value
2.064±0.060±0.059		[10] ABE	95W	CDF	Extracted value
$2.10\ ^{+0.14}_{-0.13}$ ±0.09	3559	[11] ALITTI	92	UA2	Extracted value
$2.18\ ^{+0.26}_{-0.24}$ ±0.04		[12] ALBAJAR	91	UA1	Extracted value

[1] ABAZOV 09AK obtain this result fitting the high-end tail (100-200 GeV) of the transverse mass spectrum in $W \to e\nu$ decays.

[2] AALTONEN 08B obtain this result fitting the high-end tail (90–200 GeV) of the transverse mass spectrum in semileptonic $W \to e\nu_e$ and $W \to \mu\nu_\mu$ decays.

[3] ABDALLAH 08A use direct reconstruction of the kinematics of $W^+W^- \to q\overline{q}\ell\nu$ and $W^+W^- \to q\overline{q}q\overline{q}$ events. The systematic error includes ±0.065 GeV due to final state interactions.

[4] ABBIENDI 06 use direct reconstruction of the kinematics of $W^+W^- \to q\overline{q}\ell\nu_\ell$ and $W^+W^- \to q\overline{q}q\overline{q}$ events. The systematic error includes ±0.003 GeV due to the uncertainty on the LEP beam energy.

[5] ACHARD 06 use direct reconstruction of the kinematics of $W^+W^- \to q\overline{q}\ell\nu_\ell$ and $W^+W^- \to q\overline{q}q\overline{q}$ events in the C.M. energy range 189–209 GeV. The result quoted here is obtained combining this value of the width with the result obtained from a direct *W* mass reconstruction at 172 and 183 GeV (ACCIARRI 99).

[6] SCHAEL 06 use direct reconstruction of the kinematics of $W^+W^- \to q\overline{q}\ell\nu_\ell$ and $W^+W^- \to q\overline{q}q\overline{q}$ events. The systematic error includes ±0.05 GeV due to possible effects of final state interactions in the $q\overline{q}q\overline{q}$ channel and ±0.01 GeV due to the uncertainty on the LEP beam energy.

[7] ABAZOV 02E obtain this result fitting the high-end tail (90–200 GeV) of the transverse-mass spectrum in semileptonic $W \to e\nu_e$ decays.

[8] AFFOLDER 00M fit the high transverse mass (100–200 GeV) $W \to e\nu_e$ and $W \to \mu\nu_\mu$ events to obtain Γ(*W*)= 2.04 ± 0.11(stat)±0.09(syst) GeV. This is combined with the earlier CDF measurement (ABE 95C) to obtain the quoted result.

[9] ABBOTT 00B measure R = 10.43 ± 0.27 for the $W \to e\nu_e$ decay channel. They use the SM theoretical predictions for $\sigma(W)/\sigma(Z)$ and $\Gamma(W \to e\nu_e)$ and the world average for $B(Z \to ee)$. The value quoted here is obtained combining this result (2.169 ± 0.070 GeV) with that of ABBOTT 99H.

[10] ABE 95W measured R = 10.90 ± 0.32 ± 0.29. They use m_W=80.23 ± 0.18 GeV, $\sigma(W)/\sigma(Z)$ = 3.35 ± 0.03, $\Gamma(W \to e\nu)$ = 225.9 ± 0.9 MeV, $\Gamma(Z \to e^+e^-)$ = 83.98 ± 0.18 MeV, and Γ(*Z*) = 2.4969 ± 0.0038 GeV.

[11] ALITTI 92 measured $R = 10.4\ ^{+0.7}_{-0.6}$ ± 0.3. The values of $\sigma(Z)$ and $\sigma(W)$ come from $O(\alpha_s^2)$ calculations using m_W = 80.14 ± 0.27 GeV, and m_Z = 91.175 ± 0.021 GeV along with the corresponding value of $\sin^2\theta_W$ = 0.2274. They use $\sigma(W)/\sigma(Z)$ = 3.26 ± 0.07 ± 0.05 and Γ(*Z*) = 2.487 ± 0.010 GeV.

[12] ALBAJAR 91 measured $R = 9.5\ ^{+1.1}_{-1.0}$ (stat. + syst.). $\sigma(W)/\sigma(Z)$ is calculated in QCD at the parton level using m_W = 80.18 ± 0.28 GeV and m_Z = 91.172 ± 0.031 GeV along with $\sin^2\theta_W$ = 0.2322 ± 0.0014. They use $\sigma(W)/\sigma(Z)$ = 3.23 ± 0.05 and Γ(*Z*) = 2.498 ± 0.020 GeV. This measurement is obtained combining both the electron and muon channels.

W^+ DECAY MODES

W^- modes are charge conjugates of the modes below.

	Mode		Fraction (Γ$_i$/Γ)	Confidence level
Γ_1	$\ell^+\nu$	[a]	(10.86± 0.09) %	
Γ_2	$e^+\nu$		(10.71± 0.16) %	
Γ_3	$\mu^+\nu$		(10.63± 0.15) %	
Γ_4	$\tau^+\nu$		(11.38± 0.21) %	
Γ_5	hadrons		(67.41± 0.27) %	
Γ_6	$\pi^+\gamma$		< 7 $\times 10^{-6}$	95%
Γ_7	$D_s^+\gamma$		< 1.3 $\times 10^{-3}$	95%
Γ_8	cX		(33.3 ± 2.6) %	
Γ_9	$c\overline{s}$		$(31\ ^{+13}_{-11})$ %	
Γ_{10}	invisible	[b]	(1.4 ± 2.9) %	
Γ_{11}	$\pi^+\pi^+\pi^-$		< 1.01 $\times 10^{-6}$	95%

[a] ℓ indicates each type of lepton (e, μ, and τ), not sum over them.

[b] This represents the width for the decay of the *W* boson into a charged particle with momentum below detectability, p< 200 MeV.

W PARTIAL WIDTHS

Γ(invisible) — Γ_{10}

This represents the width for the decay of the *W* boson into a charged particle with momentum below detectability, p< 200 MeV.

VALUE (MeV)	DOCUMENT ID		TECN	COMMENT
$\mathbf{30^{+52}_{-48} \pm 33}$	[1] BARATE	99I	ALEP	E^{ee}_{cm}= 161+172+183 GeV
• • • We do not use the following data for averages, fits, limits, etc. • • •				
	[2] BARATE	99L	ALEP	E^{ee}_{cm}= 161+172+183 GeV

[1] BARATE 99I measure this quantity using the dependence of the total cross section σ_{WW} upon a change in the total width. The fit is performed to the *WW* measured cross sections at 161, 172, and 183 GeV. This partial width is < 139 MeV at 95%CL.

[2] BARATE 99L use *W*-pair production to search for effectively invisible *W* decays, tagging with the decay of the other *W* boson to Standard Model particles. The partial width for effectively invisible decay is < 27 MeV at 95%CL.

W BRANCHING RATIOS

Overall fits are performed to determine the branching ratios of the *W* boson. Averages on $W \to e\nu$, $W \to \mu\nu$, and $W \to \tau\nu$, and their correlations are obtained by combining results from the four LEP experiments properly taking into account the common systematic uncertainties and their correlations [SCHAEL 13A]. A first fit determines the three individual leptonic braching ratios $B(W \to e\nu)$, $B(W \to \mu\nu)$, and $B(W \to \tau\nu)$. This fit has a χ^2 = 6.3 for 9 degrees of freedom. The correlation coefficients between the branching fractions are 0.14 ($e-\mu$), −0.20 ($e-\tau$), −0.12 ($\mu-\tau$). A second fit assumes lepton universality and determines the leptonic branching ratio $B(W \to \ell\nu)$ and the hadronic branching ratio is derived as $B(W \to \text{hadrons}) = 1 - 3\,B(W \to \ell\nu)$. This fit has a χ^2 = 15.4 for 11 degrees of freedom.

$\Gamma(\ell^+\nu)/\Gamma_{total}$ — Γ_1/Γ

ℓ indicates average over e, μ, and τ modes, not sum over modes.

VALUE (units 10^{-2})	EVTS	DOCUMENT ID		TECN	COMMENT
10.86±0.09 OUR FIT					
10.86±0.12±0.08	16438	ABBIENDI	07A	OPAL	E^{ee}_{cm}= 161–209 GeV
10.85±0.14±0.08	13600	ABDALLAH	04G	DLPH	E^{ee}_{cm}= 161–209 GeV
10.83±0.14±0.10	11246	ACHARD	04J	L3	E^{ee}_{cm}= 161–209 GeV
10.96±0.12±0.05	16116	SCHAEL	04A	ALEP	E^{ee}_{cm}= 183–209 GeV
• • • We do not use the following data for averages, fits, limits, etc. • • •					
11.02±0.52	11858	[1] ABBOTT	99H	D0	$E^{p\overline{p}}_{cm}$= 1.8 TeV
10.4 ±0.8	3642	[2] ABE	92I	CDF	$E^{p\overline{p}}_{cm}$= 1.8 TeV

[1] ABBOTT 99H measure $R \equiv [\sigma_W B(W \to \ell\nu_\ell)]/[\sigma_Z B(Z \to \ell\ell)]$ = 10.90 ± 0.52 combining electron and muon channels. They use M_W = 80.39 ± 0.06 GeV and the SM theoretical predictions for $\sigma(W)/\sigma(Z)$ and $B(Z \to \ell\ell)$.

[2] 1216 ± 38$^{+27}_{-31}$ $W \to \mu\nu$ events from ABE 92I and 2426 $W \to e\nu$ events of ABE 91C. ABE 92I give the inverse quantity as 9.6 ± 0.7 and we have inverted.

$\Gamma(e^+\nu)/\Gamma_{total}$ — Γ_2/Γ

VALUE (units 10^{-2})	EVTS	DOCUMENT ID		TECN	COMMENT
10.71±0.16 OUR FIT					
10.71±0.25±0.11	2374	ABBIENDI	07A	OPAL	E^{ee}_{cm}= 161–209 GeV
10.55±0.31±0.14	1804	ABDALLAH	04G	DLPH	E^{ee}_{cm}= 161–209 GeV
10.78±0.29±0.13	1576	ACHARD	04J	L3	E^{ee}_{cm}= 161–209 GeV
10.78±0.27±0.10	2142	SCHAEL	04A	ALEP	E^{ee}_{cm}= 183–209 GeV
• • • We do not use the following data for averages, fits, limits, etc. • • •					
10.61±0.28		[1] ABAZOV	04D	TEVA	$E^{p\overline{p}}_{cm}$= 1.8 TeV

[1] ABAZOV 04D take into account all correlations to properly combine the CDF (ABE 95W) and DØ (ABBOTT 00B) measurements of the ratio R in the electron channel. The ratio R is defined as $[\sigma_W \cdot B(W \to e\nu_e)] / [\sigma_Z \cdot B(Z \to ee)]$. The combination gives $R^{Tevatron}$ = 10.59 ± 0.23. σ_W / σ_Z is calculated at next–to–next–to–leading order (3.360 ± 0.051). The branching fraction $B(Z \to ee)$ is taken from this *Review* as (3.363 ± 0.004)%.

$\Gamma(\mu^+\nu)/\Gamma_{total}$ — Γ_3/Γ

VALUE (units 10^{-2})	EVTS	DOCUMENT ID		TECN	COMMENT
10.63±0.15 OUR FIT					
10.78±0.24±0.10	2397	ABBIENDI	07A	OPAL	E^{ee}_{cm}= 161–209 GeV
10.65±0.26±0.08	1998	ABDALLAH	04G	DLPH	E^{ee}_{cm}= 161–209 GeV
10.03±0.29±0.12	1423	ACHARD	04J	L3	E^{ee}_{cm}= 161–209 GeV
10.87±0.25±0.08	2216	SCHAEL	04A	ALEP	E^{ee}_{cm}= 183–209 GeV

Downloaded from https://academic.oup.com/ptep/article/2022/8/083C01/6651666 by KIT Library user on 27 September 2022

$\Gamma(\mu^+\nu)/\Gamma(e^+\nu)$ — Γ_3/Γ_2

VALUE	EVTS	DOCUMENT ID		TECN	COMMENT
0.996±0.008 OUR AVERAGE					
1.003±0.010		[1] AABOUD	17Q	ATLS	E^{pp}_{cm}= 7 TeV
0.980±0.018		[2] AAIJ	16AJ	LHCB	E^{pp}_{cm}= 8 TeV
0.993±0.019		SCHAEL	13A	LEP	E^{ee}_{cm}= 130–209 GeV
0.89 ±0.10	13k	[3] ABACHI	95D	D0	$E^{p\overline{p}}_{cm}$= 1.8 TeV
1.02 ±0.08	1216	[4] ABE	92I	CDF	$E^{p\overline{p}}_{cm}$= 1.8 TeV
1.00 ±0.14 ±0.08	67	ALBAJAR	89	UA1	$E^{p\overline{p}}_{cm}$= 546,630 GeV
• • • We do not use the following data for averages, fits, limits, etc. • • •					
1.24 $^{+0.6}_{-0.4}$	14	ARNISON	84D	UA1	Repl. by ALBAJAR 89

[1] AABOUD 17Q make a precise determination of $W \to e\nu$ and $W \to \mu\nu$ production in the follwoing fiducial phase space: lepton pseudo-rapidity range $|\eta| < 2.5$, lepton and neutrino transverse momenta larger than 25 GeV each, and W transverse mass larger than 25 GeV. They determine the ratio of the W branching fractions $B(W \to e\nu)/B(W \to \mu\nu) = 0.9967 \pm 0.0004 \pm 0.0101 = 0.997 \pm 0.010$.

[2] AAIJ 16AJ make precise measurements of forward $W \to e\nu$ and $W \to \mu\nu$ production in proton-proton collisions at 8 TeV and determine the ratio of the W branching fractions $B(W \to e\nu)/B(W \to \mu\nu) = 1.020 \pm 0.002 \pm 0.019$.

[3] ABACHI 95D obtain this result from the measured $\sigma_W B(W \to \mu\nu)$= 2.09 ± 0.23 ± 0.11 nb and $\sigma_W B(W \to e\nu)$= 2.36 ± 0.07 ± 0.13 nb in which the first error is the combined statistical and systematic uncertainty, the second reflects the uncertainty in the luminosity.

[4] ABE 92I obtain $\sigma_W B(W \to \mu\nu)$= 2.21 ± 0.07 ± 0.21 and combine with ABE 91C $\sigma_W B((W \to e\nu))$ to give a ratio of the couplings from which we derive this measurement.

$\Gamma(\tau^+\nu)/\Gamma_{total}$ — Γ_4/Γ

VALUE (units 10^{-2})	EVTS	DOCUMENT ID		TECN	COMMENT
11.38±0.21 OUR FIT					
11.14±0.31±0.17	2177	ABBIENDI	07A	OPAL	E^{ee}_{cm}= 161–209 GeV
11.46±0.39±0.19	2034	ABDALLAH	04G	DLPH	E^{ee}_{cm}= 161–209 GeV
11.89±0.40±0.20	1375	ACHARD	04J	L3	E^{ee}_{cm}= 161–209 GeV
11.25±0.32±0.20	2070	SCHAEL	04A	ALEP	E^{ee}_{cm}= 183–209 GeV

$\Gamma(\tau^+\nu)/\Gamma(e^+\nu)$ — Γ_4/Γ_2

VALUE	EVTS	DOCUMENT ID		TECN	COMMENT
1.004±0.020 OUR AVERAGE		Error includes scale factor of 1.7.			See the ideogram below.
0.992±0.007±0.011		[1] AAD	21AN	ATLS	E^{pp}_{cm} = 13 TeV
1.063±0.027		SCHAEL	13A	LEP	E^{ee}_{cm}= 130–209 GeV
0.961±0.061	980	[2] ABBOTT	00D	D0	$E^{p\overline{p}}_{cm}$= 1.8 TeV
0.94 ±0.14	179	[3] ABE	92E	CDF	$E^{p\overline{p}}_{cm}$= 1.8 TeV
1.04 ±0.08 ±0.08	754	[4] ALITTI	92F	UA2	$E^{p\overline{p}}_{cm}$= 630 GeV
1.02 ±0.20 ±0.12	32	ALBAJAR	89	UA1	$E^{p\overline{p}}_{cm}$= 546,630 GeV
• • • We do not use the following data for averages, fits, limits, etc. • • •					
0.995±0.112±0.083	198	ALITTI	91C	UA2	Repl. by ALITTI 92F
1.02 ±0.20 ±0.10	32	ALBAJAR	87	UA1	Repl. by ALBAJAR 89

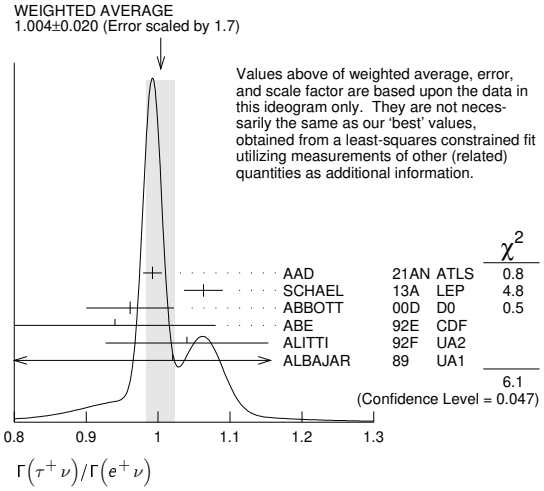

[1] AAD 21AN study $t\overline{t}$ production, with the W bosons in top-quark decay decaying to electrons or taus, with the tau decaying further into a muon. Analyzing the muon impact parameter and its transverse momentum, the contributions from prompt muons (arising from W decay) and non-prompt muons (arising from tau decay) are separated, allowing a measurement of the ratio of the W branching fractions into taus and muons, $R(\tau/\mu) = 0.992 \pm 0.007 \pm 0.011$ where the first error is statistical and the second systematic.

[2] ABBOTT 00D measure $\sigma_W \times B(W \to \tau\nu_\tau) = 2.22 \pm 0.09 \pm 0.10 \pm 0.10$ nb. Using the ABBOTT 00B result $\sigma_W \times B(W \to e\nu_e) = 2.31 \pm 0.01 \pm 0.05 \pm 0.10$ nb, they quote the ratio of the couplings from which we derive this measurement.

[3] ABE 92E use two procedures for selecting $W \to \tau\nu_\tau$ events. The missing E_T trigger leads to 132 ± 14 ± 8 events and the τ trigger to 47 ± 9 ± 4 events. Proper statistical and systematic correlations are taken into account to arrive at $\sigma B(W \to \tau\nu) = 2.05 \pm 0.27$ nb. Combined with ABE 91C result on $\sigma B(W \to e\nu)$, ABE 92E quote a ratio of the couplings from which we derive this measurement.

[4] This measurement is derived by us from the ratio of the couplings of ALITTI 92F.

$\Gamma(\tau^+\nu)/\Gamma(\mu^+\nu)$ — Γ_4/Γ_3

VALUE	DOCUMENT ID		TECN	COMMENT
1.070±0.026	SCHAEL	13A	LEP	E^{ee}_{cm}= 130–209 GeV

$\Gamma(\text{hadrons})/\Gamma_{total}$ — Γ_5/Γ

OUR FIT value is obtained by a fit to the lepton branching ratio data assuming lepton universality.

VALUE (units 10^{-2})	EVTS	DOCUMENT ID		TECN	COMMENT
67.41±0.27 OUR FIT					
67.41±0.37±0.23	16438	ABBIENDI	07A	OPAL	E^{ee}_{cm}= 161–209 GeV
67.45±0.41±0.24	13600	ABDALLAH	04G	DLPH	E^{ee}_{cm} = 161–209 GeV
67.50±0.42±0.30	11246	ACHARD	04J	L3	E^{ee}_{cm} = 161–209 GeV
67.13±0.37±0.15	16116	SCHAEL	04A	ALEP	E^{ee}_{cm} = 183–209 GeV

$\Gamma(\pi^+\gamma)/\Gamma_{total}$ — Γ_6/Γ

VALUE	CL%	DOCUMENT ID		COMMENT
$<1.50 \times 10^{-5}$	95	[1] SIRUNYAN	21I	E^{pp}_{cm} = 13 TeV

[1] SIRUNYAN 21I search for the rare decay of a W boson into a charged pion accompanied by a photon. A signal is not observed, and an upper limit on the branching fraction $B(W \to \pi\gamma) < 1.50 \times 10^{-5}$ is obtained at 95% C.L.

$\Gamma(\pi^+\gamma)/\Gamma(e^+\nu)$ — Γ_6/Γ_2

VALUE	CL%	DOCUMENT ID		TECN	COMMENT
$< 6.4 \times 10^{-5}$	95	AALTONEN	12W	CDF	$E^{p\overline{p}}_{cm}$= 1.96 Tev
$< 7 \times 10^{-4}$	95	ABE	98H	CDF	$E^{p\overline{p}}_{cm}$= 1.8 TeV
$< 4.9 \times 10^{-3}$	95	[1] ALITTI	92D	UA2	$E^{p\overline{p}}_{cm}$= 630 GeV
$<58 \times 10^{-3}$	95	[2] ALBAJAR	90	UA1	$E^{p\overline{p}}_{cm}$= 546, 630 GeV

[1] ALITTI 92D limit is 3.8×10^{-3} at 90%CL.

[2] ALBAJAR 90 obtain < 0.048 at 90%CL.

$\Gamma(D_s^+\gamma)/\Gamma(e^+\nu)$ — Γ_7/Γ_2

VALUE	CL%	DOCUMENT ID		TECN	COMMENT
$<1.2 \times 10^{-2}$	95	ABE	98P	CDF	$E^{p\overline{p}}_{cm}$= 1.8 TeV

$\Gamma(cX)/\Gamma(\text{hadrons})$ — Γ_8/Γ_5

VALUE	EVTS	DOCUMENT ID		TECN	COMMENT
0.49 ±0.04 OUR AVERAGE					
0.481±0.042±0.032	3005	[1] ABBIENDI	00V	OPAL	E^{ee}_{cm}= 183 + 189 GeV
0.51 ±0.05 ±0.03	746	[2] BARATE	99M	ALEP	E^{ee}_{cm}= 172 + 183 GeV

[1] ABBIENDI 00V tag $W \to cX$ decays using measured jet properties, lifetime information, and leptons produced in charm decays. From this result, and using the additional measurements of $\Gamma(W)$ and $B(W \to \text{hadrons})$, $|V_{cs}|$ is determined to be 0.969 ± 0.045 ± 0.036.

[2] BARATE 99M tag c jets using a neural network algorithm. From this measurement $|V_{cs}|$ is determined to be 1.00 ± 0.11 ± 0.07.

$\Gamma(\pi^+\pi^+\pi^-)/\Gamma_{total}$ — Γ_{11}/Γ

VALUE (units 10^{-6})	CL%	DOCUMENT ID		TECN	COMMENT
<1.01	95	[1] SIRUNYAN	19BG	CMS	E^{pp}_{cm} = 13 TeV

[1] SIRUNYAN 19BG search for the rare decay of a W boson into three charged pions. Three pion candidates are required in each event, with transverse momentum larger than 35 GeV, 35 GeV, 18 GeV, respectively, while the transverse momentum of the three-pion system is required to be larger than 40 GeV. Analyzing the three-pion invariant mass, no excess is observed in the W mass region, leading to the 95% C.L. upper limit on the branching fraction.

$R_{cs} = \Gamma(c\overline{s})/\Gamma(\text{hadrons})$ — Γ_9/Γ_5

VALUE	DOCUMENT ID		TECN	COMMENT
0.46 $^{+0.18}_{-0.14}$ ±0.07	[1] ABREU	98N	DLPH	E^{ee}_{cm}= 161+172 GeV

[1] ABREU 98N tag c and s jets by identifying a charged kaon as the highest momentum particle in a hadronic jet. They also use a lifetime tag to independently identify a c jet, based on the impact parameter distribution of charged particles in a jet. From this measurement $|V_{cs}|$ is determined to be 0.94 $^{+0.32}_{-0.26}$ ± 0.13.

AVERAGE PARTICLE MULTIPLICITIES IN HADRONIC *W* DECAY

Summed over particle and antiparticle, when appropriate.

$\langle N_{\pi^\pm} \rangle$

VALUE	DOCUMENT ID		TECN	COMMENT
15.70±0.35	[1] ABREU,P	00F	DLPH	E^{ee}_{cm}= 189 GeV

[1] ABREU,P 00F measure $\langle N_{\pi^\pm} \rangle$ = 31.65 ± 0.48 ± 0.76 and 15.51 ± 0.38 ± 0.40 in the fully hadronic and semileptonic final states respectively. The value quoted is a weighted average without assuming any correlations.

Downloaded from https://academic.oup.com/ptep/article/2022/8/083C01/6651666 by KIT Library user on 27 September 2022

$\langle N_{K^\pm} \rangle$

VALUE	DOCUMENT ID		TECN	COMMENT
2.20±0.19	[1] ABREU,P	00F	DLPH	E^{ee}_{cm}= 189 GeV

[1] ABREU,P 00F measure $\langle N_{K^\pm} \rangle$ = 4.38 ± 0.42 ± 0.12 and 2.23 ± 0.32 ± 0.17 in the fully hadronic and semileptonic final states respectively. The value quoted is a weighted average without assuming any correlations.

$\langle N_p \rangle$

VALUE	DOCUMENT ID		TECN	COMMENT
0.92±0.14	[1] ABREU,P	00F	DLPH	E^{ee}_{cm}= 189 GeV

[1] ABREU,P 00F measure $\langle N_p \rangle$ = 1.82 ± 0.29 ± 0.16 and 0.94 ± 0.23 ± 0.06 in the fully hadronic and semileptonic final states respectively. The value quoted is a weighted average without assuming any correlations.

$\langle N_{\rm charged} \rangle$

VALUE	DOCUMENT ID		TECN	COMMENT
19.39±0.08 OUR AVERAGE				
19.38±0.05±0.08	[1] ABBIENDI	06A	OPAL	E^{ee}_{cm}= 189–209 GeV
19.44±0.17	[2] ABREU,P	00F	DLPH	E^{ee}_{cm}= 183+189 GeV
19.3 ±0.3 ±0.3	[3] ABBIENDI	99N	OPAL	E^{ee}_{cm}= 183 GeV
19.23±0.74	[4] ABREU	98C	DLPH	E^{ee}_{cm}= 172 GeV

[1] ABBIENDI 06A measure $\langle N_{\rm charged} \rangle$ = 38.74 ± 0.12 ± 0.26 when both W bosons decay hadronically and $\langle N_{\rm charged} \rangle$ = 19.39 ± 0.11 ± 0.09 when one W boson decays semileptonically. The value quoted here is obtained under the assumption that there is no color reconnection between W bosons; the value is a weighted average taking into account correlations in the systematic uncertainties.

[2] ABREU,P 00F measure $\langle N_{\rm charged} \rangle$ = 39.12 ± 0.33 ± 0.36 and 38.11 ± 0.57 ± 0.44 in the fully hadronic final states at 189 and 183 GeV respectively, and $\langle N_{\rm charged} \rangle$ = 19.49 ± 0.31 ± 0.27 and 19.78 ± 0.49 ± 0.43 in the semileptonic final states. The value quoted is a weighted average without assuming any correlations.

[3] ABBIENDI 99N use the final states $W^+W^- \to q\overline{q}\ell\overline{\nu}_\ell$ to derive this value.

[4] ABREU 98C combine results from both the fully hadronic as well semileptonic WW final states after demonstrating that the W decay charged multiplicity is independent of the topology within errors.

TRIPLE GAUGE COUPLINGS (TGC'S)

Revised April 2017 by M.W. Grünewald (U. College Dublin) and A. Gurtu (Formerly Tata Inst.).

Fourteen independent couplings, seven each for ZWW and γWW, completely describe the VWW vertices within the most general framework of the electroweak Standard Model (SM) consistent with Lorentz invariance and U(1) gauge invariance. Of each of the seven TGCs, three conserve C and P individually, three violate CP, and one violates C and P individually while conserving CP. Assumption of C and P conservation and electromagnetic gauge invariance reduces the number of independent VWW couplings to five: one common set [1,2] is $(\kappa_\gamma, \kappa_Z, \lambda_\gamma, \lambda_Z, g_1^Z)$, where $\kappa_\gamma = \kappa_Z = g_1^Z = 1$ and $\lambda_\gamma = \lambda_Z = 0$ in the Standard Model at tree level. The parameters κ_Z and λ_Z are related to the other three due to constraints of gauge invariance as follows: $\kappa_Z = g_1^Z - (\kappa_\gamma - 1)\tan^2\theta_W$ and $\lambda_Z = \lambda_\gamma$, where θ_W is the weak mixing angle. The W magnetic dipole moment, μ_W, and the W electric quadrupole moment, q_W, are expressed as $\mu_W = e\,(1+\kappa_\gamma+\lambda_\gamma)/2M_W$ and $q_W = -e\,(\kappa_\gamma - \lambda_\gamma)/M_W^2$.

Precision measurements of suitable observables at LEP1 has already led to an exploration of much of the TGC parameter space. At LEP2, the VWW coupling arises in W-pair production via s-channel exchange, or in single W production via the radiation of a virtual photon off the incident e^+ or e^-. At the Tevatron and the LHC, hard-photon bremsstrahlung off a produced W or Z signals the presence of a triple-gauge vertex. In order to extract the value of one TGC, the others are generally kept fixed to their SM values. While most analyses use the above gauge constraints in the extraction of TGCs, one analysis of W-pair events also determines the real and imaginary parts of all 14 couplings using unconstrained single-parameter fits [3]. The results are consistent. Some experiments have determined limits on the couplings under various non-LEP scenarios and assuming different values of the form factor Λ, where the coupling parameters are scaled by $1/(1+s/\Lambda^2)^2$. For practical reasons it is not possible to quote all such determinations in the listings. For that the individual papers may be consulted. Recently, EFT-inspired sets of couplings [4,5], such as $c_{WWW}/\Lambda^2, c_W/\Lambda^2, c_B/\Lambda^2$ which are linearly related to the couplings discussed above, are also determined by the LHC experiments.

References

1. K. Hagiwara *et al.*, Nucl. Phys. **B282**, 253 (1987).
2. G. Gounaris *et al.*, CERN 96-01 p. 525.
3. S. Schael *et al.* (ALEPH Collab.), Phys. Lett. **B614**, 7 (2005).
4. K. Hagiwara *et al.*, Phys. Rev. **D48**, 2182 (1993).
5. C. Degrande *et al.*, Annals Phys. 335 (2013) 21-32.

g_1^Z

OUR FIT below is taken from [SCHAEL 13A].

VALUE	EVTS	DOCUMENT ID		TECN	COMMENT
$0.984^{+0.018}_{-0.020}$ OUR FIT					
$0.975^{+0.033}_{-0.030}$	7872	[1] ABDALLAH	10	DLPH	E^{ee}_{cm}= 189–209 GeV
1.001±0.027±0.013	9310	[2] SCHAEL	05A	ALEP	E^{ee}_{cm}= 183–209 GeV
$0.987^{+0.034}_{-0.033}$	9800	[3] ABBIENDI	04D	OPAL	E^{ee}_{cm}= 183–209 GeV
$0.966^{+0.034}_{-0.032}$±0.015	8325	[4] ACHARD	04D	L3	E^{ee}_{cm}= 161–209 GeV
• • • We do not use the following data for averages, fits, limits, etc. • • •					
		[5] SIRUNYAN	20BA	CMS	E^{pp}_{cm} = 13 TeV
		[6] SIRUNYAN	19CL	CMS	E^{pp}_{cm} = 13 TeV
		[7] SIRUNYAN	18BZ	CMS	E^{pp}_{cm} = 13 TeV
		[8] AABOUD	17S	ATLS	E^{pp}_{cm} = 7+8 TeV
		[9] AABOUD	17U	ATLS	E^{pp}_{cm} = 8 TeV
		[10] KHACHATRY...	17O	CMS	E^{pp}_{cm} = 8 TeV
		[11] SIRUNYAN	17X	CMS	E^{pp}_{cm} = 8 TeV
		[12] AAD	16AR	ATLS	E^{pp}_{cm} = 8 TeV
		[13] AAD	16P	ATLS	E^{pp}_{cm} = 8 TeV
		[14] AAD	14Y	ATLS	E^{pp}_{cm} = 8 TeV
		[15] AAD	13AL	ATLS	E^{pp}_{cm} = 7 TeV
		[16] CHATRCHYAN	13BF	CMS	E^{pp}_{cm} = 7 TeV
		[17] AAD	12CD	ATLS	E^{pp}_{cm} = 7 TeV
		[18] AALTONEN	12AC	CDF	$E^{p\overline{p}}_{cm}$ = 1.96 TeV
		[19] ABAZOV	12AG	D0	$E^{p\overline{p}}_{cm}$ = 1.96 TeV
	34	[20] ABAZOV	11	D0	$E^{p\overline{p}}_{cm}$ = 1.96 TeV
	334	[21] AALTONEN	10K	CDF	$E^{p\overline{p}}_{cm}$ = 1.96 TeV
1.04 ±0.09		[22] ABAZOV	09AD	D0	$E^{p\overline{p}}_{cm}$ = 1.96 TeV
		[23] ABAZOV	09AJ	D0	$E^{p\overline{p}}_{cm}$ = 1.96 TeV
$1.07^{+0.08}_{-0.12}$	1880	[24] ABDALLAH	08C	DLPH	Superseded by ABDALLAH 10
	13	[25] ABAZOV	07Z	D0	$E^{p\overline{p}}_{cm}$ = 1.96 TeV
	2.3	[26] ABAZOV	05S	D0	$E^{p\overline{p}}_{cm}$ = 1.96 TeV
0.98 ±0.07 ±0.01	2114	[27] ABREU	01I	DLPH	E^{ee}_{cm}= 183+189 GeV
	331	[28] ABBOTT	99I	D0	$E^{p\overline{p}}_{cm}$= 1.8 TeV

[1] ABDALLAH 10 use data on the final states $e^+e^- \to jj\ell\nu, jjjj, jjX, \ell X$, at center-of-mass energies between 189–209 GeV at LEP2, where j = jet, ℓ = lepton, and X represents missing momentum. The fit is carried out keeping all other parameters fixed at their SM values.

[2] SCHAEL 05A study single–photon, single–W, and WW–pair production from 183 to 209 GeV. The result quoted here is derived from the WW–pair production sample. Each parameter is determined from a single–parameter fit in which the other parameters assume their Standard Model values.

[3] ABBIENDI 04D combine results from W^+W^- in all decay channels. Only CP-conserving couplings are considered and each parameter is determined from a single-parameter fit in which the other parameters assume their Standard Model values. The 95% confidence interval is $0.923 < g_1^Z < 1.054$.

Downloaded from https://academic.oup.com/ptep/article/2022/8/083C01/6651666 by KIT Library user on 27 September 2022

[4] ACHARD 04D study WW–pair production, single–W production and single–photon production with missing energy from 189 to 209 GeV. The result quoted here is obtained from the WW–pair production sample including data from 161 to 183 GeV, ACCIARRI 99Q. Each parameter is determined from a single–parameter fit in which the other parameters assume their Standard Model values.

[5] SIRUNYAN 20BA study electroweak production of a W boson in association with two jets, using W decays in the electron or muon channel. The isolated muons (electrons) are required to have a transverse momentum larger than 25 (30) GeV, while the transverse momentum of the two jets has to be larger than 50 and 30 GeV. A total of 2.382 (1.051) million events are selected in the muon (electron) channel, with a Standard Model expectation of 2.39 ± 0.17 (1.054 ± 0.058) million events. Analyzing the transverse momentum distribution of the charged leptons from W decay, the following 95% C.L. limit is obtained: $0.971 < g_1^Z < 1.044$. Combining this result with that from the closely-related electroweak Z-jet-jet production SIRUNYAN 18BZ, the limit becomes: $0.979 < g_1^Z < 1.034$.

[6] SIRUNYAN 19CL study WW and WZ production in lepton + jet events, with one W boson decaying leptonically (electron or muon), and another W or Z boson decaying hadronically, reconstructed as a single massive large-radius jet. In the electron channel 2,456 (2,235) events are selected in the $WW(WZ)$ category, while in the muon channel 3,996 (3572) events are selected in the $WW(WZ)$ category. Analysing the di-boson invariant mass distribution, the following 95% C.L. limit is obtained: $0.9939 < g_1^Z < 1.0074$.

[7] SIRUNYAN 18BZ study $pp \to Z$ *jet jet* events at 13 TeV where $Z \to e^+e^-/\mu^+\mu^-$. Isolated electrons and muons are selected with p_T of the leading/sub-leading lepton > 30/20 GeV and $|\eta| < 2.4$, with the di-lepton invariant mass within 15 GeV of the Z mass. The two highest p_T jets are selected with p_T of the leading/sub-leading jet > 50/30 GeV respectively and dijet invariant mass > 200 GeV. Templates in the transverse momentum of the Z are utilized to set limits on the triple gauge couplings in the EFT and the LEP parametrizations. The following 95% C.L. limit is obtained: $0.965 < g_1^Z < 1.042$.

[8] AABOUD 17S analyze electroweak production of a W boson in association with two jets at high dijet invariant mass, with the W boson decaying to electron or muon plus neutrino. In the signal region of dijet mass larger than 1 TeV and leading-jet transverse momentum larger than 600 GeV, 30 events are observed in the data with 39 ± 4 events expected in the Standard Model, yielding the following limit at 95% CL for the form factor cut-off scale $\Lambda_{FF} \to \infty$: $0.87 < g_1^Z < 1.12$.

[9] AABOUD 17U analyze production of WW or WZ boson pairs with one W boson decaying to electron or muon plus neutrino, and the other W or Z boson decaying hadronically. The hadronic decay system is reconstructed as either a resolved two-jet system or as a single large jet. Analysing the transverse momentum distribution of the hadronic system above 100 GeV yields the following limit at 95% CL for the form factor cut-off scale $\Lambda_{FF} \to \infty$: $0.979 < g_1^Z < 1.024$.

[10] KHACHATRYAN 17O analyse WZ production where each boson decays into electrons or muons. Events are required to have a tri-lepton invariant mass larger than 100 GeV, with one of the lepton pairs having an invariant mass within 20 GeV of the Z boson mass. The Z transverse momentum spectrum is analyzed to set a 95% C.L. limit of: $0.982 < g_1^Z < 1.035$.

[11] SIRUNYAN 17X study $pp \to WW/WZ \to \ell\nu q\overline{q}$ production at 8 TeV where ℓ is an electron or muon with $p_T > 30$ or 25 GeV respectively. Suitable cuts are put on the p_T of the dijet system and the missing E_T of the event yielding a total of 285 and 204 WV events observed in the electron and muon channels. The following 95% C.L. limit is obtained: $0.9913 < g_1^Z < 1.024$.

[12] AAD 16AR study WW production in pp collisions and select 6636 WW candidates in decay modes with electrons or muons with an expected background of 1546 ± 157 events. Assuming the LEP formulation and setting the form-factor Λ to infinity, a fit to the transverse momentum distribution of the leading charged lepton, leads to a 95% C.L. range of $0.984 < g_1^Z < 1.027$.

[13] AAD 16P study WZ production in pp collisions and select 2091 WZ candidates in 4 decay modes with electrons and muons, with an expected background of 1825 ± 7 events. Analyzing the WZ transverse momentum distribution, the resulting 95% C.L. limit is: $0.981 < g_1^Z < 1.029$.

[14] AAD 14Y determine the electroweak Z-dijet cross section in 8 TeV pp collisions. $Z \to ee$ and $Z \to \mu\mu$ decays are selected with the di-lepton $p_T > 20$ GeV and mass in the 81–101 GeV range. Minimum two jets are required with $p_T > 55$ and 45 GeV and no additional jets with $p_T > 25$ GeV in the rapidity interval between them. The normalized p_T balance between the Z and the two jets is required to be < 0.15. This leads to a selection of 900 events with dijet mass > 1 TeV. The number of signal and background events expected is 261 and 592 respectively. A Poisson likelihood method is used on an event by event basis to obtain the 95% CL limit $0.5 < g_1^Z < 1.26$ for a form factor value $\Lambda = \infty$.

[15] AAD 13AL study WW production in pp collisions and select 1325 WW candidates in decay modes with electrons or muons with an expected background of 369 ± 61 events. Assuming the LEP formulation and setting the form-factor Λ = infinity, a fit to the transverse momentum distribution of the leading charged lepton, leads to a 95% C.L. range of $0.961 < g_1^Z < 1.052$. Supersedes AAD 12AC.

[16] CHATRCHYAN 13BF determine the W^+W^- production cross section using unlike sign di-lepton (e or μ) events with high $\not{p}_T$. The leptons have $p_T > 20$ GeV/c and are isolated. 1134 candidate events are observed with an expected SM background of 247 ± 34. The p_T distribution of the leading lepton is fitted to obtain 95% C.L. limits of $0.905 \leq g_1^Z \leq 1.095$.

[17] AAD 12CD study WZ production in pp collisions and select 317 WZ candidates in three $\ell\nu$ decay modes with an expected background of 68.0 ± 10.0 events. The resulting 95% C.L. range is: $0.943 < g_1^Z < 1.093$. Supersedes AAD 12V.

[18] AALTONEN 12AC study WZ production in $p\overline{p}$ collisions and select 63 WZ candidates in three $\ell\nu$ decay modes with an expected background of 7.9 ± 1.0 events. Based on the cross section and shape of the Z transverse momentum spectrum, the following 95% C.L. range is reported: $0.92 < g_1^Z < 1.20$ for a form factor of $\Lambda = 2$ TeV.

[19] ABAZOV 12AG combine new results with already published results on $W\gamma$, WW and WZ production in order to determine the couplings with increased precision, superseding ABAZOV 08R, ABAZOV 11AC, ABAZOV 09AJ, ABAZOV 09AD. The 68% C.L. result for a formfactor cutoff of $\Lambda = 2$ TeV is $g_1^Z = 1.022^{+0.032}_{-0.030}$.

[20] ABAZOV 11 study the $p\overline{p} \to 3\ell\nu$ process arising in WZ production. They observe 34 WZ candidates with an estimated background of 6 events. An analysis of the p_T spectrum of the Z boson leads to a 95% C.L. limit of $0.944 < g_1^Z < 1.154$, for a form factor $\Lambda = 2$ TeV.

[21] AALTONEN 10K study $p\overline{p} \to W^+W^-$ with $W \to e/\mu\nu$. The p_T of the leading (second) lepton is required to be > 20 (10) GeV. The final number of events selected is 654 of which 320 ± 47 are estimated to be background. The 95% C.L. interval is $0.76 < g_1^Z < 1.34$ for $\Lambda = 1.5$ TeV and $0.78 < g_1^Z < 1.30$ for $\Lambda = 2$ TeV.

[22] ABAZOV 09AD study the $p\overline{p} \to \ell\nu$ 2jet process arising in WW and WZ production. They select 12,473 (14,392) events in the electron (muon) channel with an expected di-boson signal of 436 (527) events. The results on the anomalous couplings are derived from an analysis of the p_T spectrum of the 2-jet system and quoted at 68% C.L. and for a form factor of 2 TeV. This measurement is not used for obtaining the mean as it is for a specific form factor. The 95% confidence interval is $0.88 < g_1^Z < 1.20$.

[23] ABAZOV 09AJ study the $p\overline{p} \to 2\ell 2\nu$ process arising in WW production. They select 100 events with an expected WW signal of 65 events. An analysis of the p_T spectrum of the two charged leptons leads to 95% C.L. limits of $0.86 < g_1^Z < 1.3$, for a form factor $\Lambda = 2$ TeV.

[24] ABDALLAH 08C determine this triple gauge coupling from the measurement of the spin density matrix elements in $e^+e^- \to W^+W^- \to (qq)(\ell\nu)$, where $\ell = e$ or μ. Values of all other couplings are fixed to their standard model values.

[25] ABAZOV 07Z set limits on anomalous TGCs using the measured cross section and $p_T(Z)$ distribution in WZ production with both the W and the Z decaying leptonically into electrons and muons. Setting the other couplings to their standard model values, the 95% C.L. limit for a form factor scale $\Lambda = 2$ TeV is $0.86 < g_1^Z < 1.35$.

[26] ABAZOV 05S study $\overline{p}p \to WZ$ production with a subsequent trilepton decay to $\ell\nu\ell'\overline{\ell}'$ (ℓ and $\ell' = e$ or μ). Three events (estimated background 0.71 ± 0.08 events) with WZ decay characteristics are observed from which they derive limits on the anomalous WWZ couplings. The 95% CL limit for a form factor scale $\Lambda = 1.5$ TeV is $0.51 < g_1^Z < 1.66$, fixing λ_Z and κ_Z to their Standard Model values.

[27] ABREU 01I combine results from e^+e^- interactions at 189 GeV leading to W^+W^- and $We\nu_e$ final states with results from ABREU 99L at 183 GeV. The 95% confidence interval is $0.84 < g_1^Z < 1.13$.

[28] ABBOTT 99I perform a simultaneous fit to the $W\gamma$, $WW \to$ dilepton, $WW/WZ \to e\nu jj$, $WW/WZ \to \mu\nu jj$, and $WZ \to$ trilepton data samples. For $\Lambda = 2.0$ TeV, the 95%CL limits are $0.63 < g_1^Z < 1.57$, fixing λ_Z and κ_Z to their Standard Model values, and assuming Standard Model values for the $WW\gamma$ couplings.

κ_γ

OUR FIT below is taken from [SCHAEL 13A].

VALUE	EVTS	DOCUMENT ID		TECN	COMMENT
0.982±0.042 OUR FIT					
$1.024^{+0.077}_{-0.081}$	7872	[1] ABDALLAH	10	DLPH	E_{cm}^{ee}= 189–209 GeV
$0.971 \pm 0.055 \pm 0.030$	10689	[2] SCHAEL	05A	ALEP	E_{cm}^{ee}= 183–209 GeV
$0.88^{+0.09}_{-0.08}$	9800	[3] ABBIENDI	04D	OPAL	E_{cm}^{ee}= 183–209 GeV
$1.013^{+0.067}_{-0.064} \pm 0.026$	10575	[4] ACHARD	04D	L3	E_{cm}^{ee}= 161–209 GeV
• • • We do not use the following data for averages, fits, limits, etc. • • •					
		[5] AABOUD	17U	ATLS	E_{cm}^{pp} = 8 TeV
		[6] SIRUNYAN	17X	CMS	E_{cm}^{pp} = 8 TeV
		[7] CHATRCHYAN	14AB	CMS	E_{cm}^{pp} = 7 TeV
		[8] AAD	13AN	ATLS	E_{cm}^{pp} = 7 TeV
		[9] CHATRCHYAN	13BF	CMS	E_{cm}^{pp} = 7 TeV
		[10] ABAZOV	12AG	D0	$E_{cm}^{p\overline{p}}$ = 1.96 TeV
		[11] ABAZOV	11AC	D0	$E_{cm}^{p\overline{p}}$ = 1.96 TeV
		[12] CHATRCHYAN	11M	CMS	E_{cm}^{pp} = 7 TeV
	334	[13] AALTONEN	10K	CDF	$E_{cm}^{p\overline{p}}$ = 1.96 TeV
	53	[14] AARON	09B	H1	E_{cm}^{ep} = 0.3 TeV
$1.07^{+0.26}_{-0.29}$		[15] ABAZOV	09AD	D0	$E_{cm}^{p\overline{p}}$ = 1.96 TeV
		[16] ABAZOV	09AJ	D0	$E_{cm}^{p\overline{p}}$ = 1.96 TeV
		[17] ABAZOV	08R	D0	$E_{cm}^{p\overline{p}}$ = 1.96 TeV
$0.68^{+0.17}_{-0.15}$	1880	[18] ABDALLAH	08C	DLPH	Superseded by ABDALLAH 10
	1617	[19] AALTONEN	07L	CDF	$E_{cm}^{p\overline{p}}$ = 1.96 GeV
	17	[20] ABAZOV	06H	D0	$E_{cm}^{p\overline{p}}$ = 1.96 TeV
	141	[21] ABAZOV	05J	D0	$E_{cm}^{p\overline{p}}$ = 1.96 TeV
$1.25^{+0.21}_{-0.20} \pm 0.06$	2298	[22] ABREU	01I	DLPH	E_{cm}^{ee}= 183+189 GeV
		[23] BREITWEG	00	ZEUS	$e^+p \to e^+W^\pm X$, $\sqrt{s} \approx$ 300 GeV
0.92 ± 0.34	331	[24] ABBOTT	99I	D0	$E_{cm}^{p\overline{p}}$= 1.8 TeV

[1] ABDALLAH 10 use data on the final states $e^+e^- \to jj\ell\nu$, $jjjj$, jjX, ℓX, at center-of-mass energies between 189–209 GeV at LEP2, where j = jet, ℓ = lepton, and X represents missing momentum. The fit is carried out keeping all other parameters fixed at their SM values.

[2] SCHAEL 05A study single–photon, single–W, and WW–pair production from 183 to 209 GeV. Each parameter is determined from a single–parameter fit in which the other parameters assume their Standard Model values.

[3] ABBIENDI 04D combine results from W^+W^- in all decay channels. Only *CP*-conserving couplings are considered and each parameter is determined from a single-parameter fit in which the other parameters assume their Standard Model values. The 95% confidence interval is $0.73 < \kappa_\gamma < 1.07$.

Downloaded from https://academic.oup.com/ptep/article/2022/8/083C01/6651666 by KIT Library user on 27 September 2022

[4] ACHARD 04D study WW–pair production, single–W production and single–photon production with missing energy from 189 to 209 GeV. The result quoted here is obtained including data from 161 to 183 GeV, ACCIARRI 99Q. Each parameter is determined from a single–parameter fit in which the other parameters assume their Standard Model values.

[5] AABOUD 17U analyze production of WW or WZ boson pairs with one W boson decaying to electron or muon plus neutrino, and the other W or Z boson decaying hadronically. The hadronic decay system is reconstructed as either a resolved two-jet system or as a single large jet. Analysing the transverse momentum distribution of the hadronic system above 100 GeV yields the following limit at 95% CL for the form factor cut-off scale $\Lambda_{FF} \rightarrow \infty$: $0.939 < \kappa_\gamma < 1.064$.

[6] SIRUNYAN 17X study $pp \rightarrow WW/WZ \rightarrow \ell\nu q\overline{q}$ production at 8 TeV where ℓ is an electron or muon with $p_T > 30$ or 25 GeV respectively. Suitable cuts are put on the p_T of the dijet system and the missing E_T of the event yielding a total of 285 and 204 WV events observed in the electron and muon channels. The following 95% C.L. limit is obtained: $0.956 < \kappa_\gamma < 1.063$.

[7] CHATRCHYAN 14AB measure $W\gamma$ production cross section for $p_T^\gamma > 15$ GeV and R($\ell\gamma$) > 0.7, which is the separation between the γ and the final state charged lepton (e or μ) in the azimuthal angle-pseudorapidity ($\phi - \eta$) plane. After background subtraction the number of $e\nu\gamma$ and $\mu\nu\gamma$ events is determined to be 3200 ± 325 and 4970 ± 543 respectively, compatible with expectations from the SM. This leads to a 95% CL limit of $0.62 < \kappa_\gamma < 1.29$, assuming other parameters have SM values.

[8] AAD 13AN study $W\gamma$ production in pp collisions. In events with no additional jet, 4449 (6578) W decays to electron (muon) are selected, with an expected background of 1662 ± 262 (2538 ± 362) events. Analysing the photon p_T spectrum above 100 GeV yields a 95% C.L. limit of $0.59 < \kappa_\gamma < 1.46$. Supersedes AAD 12BX.

[9] CHATRCHYAN 13BF determine the W^+W^- production cross section using unlike sign di-lepton (e or μ) events with high $\not{p}_T$. The leptons have $p_T > 20$ GeV/c and are isolated. 1134 candidate events are observed with an expected SM background of 247 ± 34. The p_T distribution of the leading lepton is fitted to obtain 95% C.L. limits of $0.79 \leq k_\gamma \leq 1.22$.

[10] ABAZOV 12AG combine new results with already published results on $W\gamma$, WW and WZ production in order to determine the couplings with increased precision, superseding ABAZOV 08R, ABAZOV 11AC, ABAZOV 09AJ, ABAZOV 09AD. The 68% C.L. result for a formfactor cutoff of $\Lambda = 2$ TeV is $\kappa_\gamma = 1.048^{+0.106}_{-0.105}$.

[11] ABAZOV 11AC study $W\gamma$ production in $p\overline{p}$ collisions at 1.96 TeV, with the W decay products containing an electron or a muon. They select 196 (363) events in the electron (muon) mode, with a SM expectation of 190 (372) events. A likelihood fit to the photon E_T spectrum above 15 GeV yields at 95% C.L. the result: $0.6 < \kappa_\gamma < 1.4$ for a formfactor $\Lambda = 2$ TeV.

[12] CHATRCHYAN 11M study $W\gamma$ production in pp collisions at $\sqrt{s} = 7$ TeV using 36 pb^{-1} pp data with the W decaying to electron and muon. The total cross section is measured for photon transverse energy $E_T^\gamma > 10$ GeV and spatial separation from charged leptons in the plane of pseudo rapidity and azimuthal angle $\Delta R(\ell,\gamma) > 0.7$. The number of candidate (background) events is 452 (228 ± 21) for the electron channel and 520 (277 ± 25) for the muon channel. Setting other couplings to their standard model value, they derive a 95% CL limit of $-0.11 < \kappa_\gamma < 2.04$.

[13] AALTONEN 10K study $p\overline{p} \rightarrow W^+W^-$ with $W \rightarrow e/\mu\nu$. The p_T of the leading (second) lepton is required to be > 20 (10) GeV. The final number of events selected is 654 of which 320 ± 47 are estimated to be background. The 95% C.L. interval is $0.37 < \kappa_\gamma < 1.72$ for $\Lambda = 1.5$ TeV and $0.43 < \kappa_\gamma < 1.65$ for $\Lambda = 2$ TeV.

[14] AARON 09B study single-W production in ep collisions at 0.3 TeV C.M. energy. They select 53 $W \rightarrow e/\mu$ events with a standard model expectation of 54.1 ± 7.4 events. Fitting the transverse momentum spectrum of the hadronic recoil system they obtain a 95% C.L. limit of $-3.7 < \kappa_\gamma < -1.5$ or $0.3 < \kappa_\gamma < 1.5$, where the ambiguity is due to the quadratic dependence of the cross section to the coupling parameter.

[15] ABAZOV 09AD study the $p\overline{p} \rightarrow \ell\nu$ 2jet process arising in WW and WZ production. They select 12,473 (14,392) events in the electron (muon) channel with an expected di-boson signal of 436 (527) events. The results on the anomalous couplings are derived from an analysis of the p_T spectrum of the 2-jet system and quoted at 68% C.L. and for a form factor of 2 TeV. This measurement is not used for obtaining the mean as it is for a specific form factor. The 95% confidence interval is $0.56 < \kappa_\gamma < 1.55$.

[16] ABAZOV 09AJ study the $p\overline{p} \rightarrow 2\ell 2\nu$ process arising in WW production. They select 100 events with an expected WW signal of 65 events. An analysis of the p_T spectrum of the two charged leptons leads to 95% C.L. limits of $0.46 < \kappa_\gamma < 1.83$, for a form factor $\Lambda = 2$ TeV.

[17] ABAZOV 08R use 0.7 fb^{-1} $p\overline{p}$ data at $\sqrt{s} = 1.96$ TeV to select 263 $W\gamma + X$ events, of which 187 constitute signal, with the W decaying into an electron or a muon, which is required to be well separated from a photon with $E_T > 9$ GeV. A likelihood fit to the photon E_T spectrum yields a 95% CL limit $0.49 < \kappa_\gamma < 1.51$ with other couplings fixed to their Standard Model values.

[18] ABDALLAH 08C determine this triple gauge coupling from the measurement of the spin density matrix elements in $e^+e^- \rightarrow W^+W^- \rightarrow (qq)(\ell\nu)$, where $\ell = e$ or μ. Values of all other couplings are fixed to their standard model values.

[19] AALTONEN 07L set limits on anomalous TGCs using the $p_T(W)$ distribution in WW and WZ production with the W decaying to an electron or muon and the Z to 2 jets. Setting other couplings to their standard model value, the 95% C.L. limits are $0.54 < \kappa_\gamma < 1.39$ for a form factor scale $\Lambda = 1.5$ TeV.

[20] ABAZOV 06H study $\overline{p}p \rightarrow WW$ production with a subsequent decay $WW \rightarrow e^+\nu_e e^-\overline{\nu}_e$, $WW \rightarrow e^\pm\nu_e\mu^\mp\nu_\mu$ or $WW \rightarrow \mu^+\nu_\mu\mu^-\overline{\nu}_\mu$. The 95% C.L. limit for a form factor scale $\Lambda = 1$ TeV is $-0.05 < \kappa_\gamma < 2.29$, fixing $\lambda_\gamma = 0$. With the assumption that the $WW\gamma$ and WWZ couplings are equal the 95% C.L. one-dimensional limit ($\Lambda = 2$ TeV) is $0.68 < \kappa < 1.45$.

[21] ABAZOV 05J perform a likelihood fit to the photon E_T spectrum of $W\gamma + X$ events, where the W decays to an electron or muon which is required to be well separated from the photon. For $\Lambda = 2.0$ TeV the 95% CL limits are $0.12 < \kappa_\gamma < 1.96$. In the fit λ_γ is kept fixed to its Standard Model value.

[22] ABREU 01I combine results from e^+e^- interactions at 189 GeV leading to W^+W^-, $We\nu_e$, and $\nu\overline{\nu}\gamma$ final states with results from ABREU 99L at 183 GeV. The 95% confidence interval is $0.87 < \kappa_\gamma < 1.68$.

[23] BREITWEG 00 search for W production in events with large hadronic p_T. For $p_T > 20$ GeV, the upper limit on the cross section gives the 95%CL limit $-3.7 < \kappa_\gamma < 2.5$ (for $\lambda_\gamma = 0$).

[24] ABBOTT 99I perform a simultaneous fit to the $W\gamma$, $WW \rightarrow$ dilepton, $WW/WZ \rightarrow e\nu jj$, $WW/WZ \rightarrow \mu\nu jj$, and $WZ \rightarrow$ trilepton data samples. For $\Lambda = 2.0$ TeV, the 95%CL limits are $0.75 < \kappa_\gamma < 1.39$.

λ_γ

OUR FIT below is taken from [SCHAEL 13A].

VALUE	EVTS	DOCUMENT ID		TECN	COMMENT
−0.022±0.019 OUR FIT					
0.002±0.035	7872	[1] ABDALLAH	10	DLPH	E_{cm}^{ee}= 189–209 GeV
−0.012±0.027±0.011	10689	[2] SCHAEL	05A	ALEP	E_{cm}^{ee}= 183–209 GeV
$-0.060^{+0.034}_{-0.033}$	9800	[3] ABBIENDI	04D	OPAL	E_{cm}^{ee}= 183–209 GeV
$-0.021^{+0.035}_{-0.034}$±0.017	10575	[4] ACHARD	04D	L3	E_{cm}^{ee}= 161–209 GeV
• • • We do not use the following data for averages, fits, limits, etc. • • •					
		[5] CHATRCHYAN	14AB	CMS	E_{cm}^{pp} = 7 TeV
		[6] AAD	13AN	ATLS	E_{cm}^{pp} = 7 TeV
		[7] ABAZOV	12AG	D0	$E_{cm}^{p\overline{p}}$ = 1.96 TeV
		[8] ABAZOV	11AC	D0	$E_{cm}^{p\overline{p}}$ = 1.96 TeV
		[9] CHATRCHYAN	11M	CMS	E_{cm}^{pp} = 7 TeV
	53	[10] AARON	09B	H1	E_{cm}^{ep} = 0.3 TeV
0.00 ±0.06		[11] ABAZOV	09AD	D0	$E_{cm}^{p\overline{p}}$ = 1.96 TeV
		[12] ABAZOV	09AJ	D0	$E_{cm}^{p\overline{p}}$ = 1.96 TeV
		[13] ABAZOV	08R	D0	$E_{cm}^{p\overline{p}}$ = 1.96 TeV
$0.16\ ^{+0.12}_{-0.13}$	1880	[14] ABDALLAH	08C	DLPH	Superseded by ABDALLAH 10
	1617	[15] AALTONEN	07L	CDF	$E_{cm}^{p\overline{p}}$ = 1.96 GeV
	17	[16] ABAZOV	06H	D0	$E_{cm}^{p\overline{p}}$ = 1.96 TeV
	141	[17] ABAZOV	05J	D0	$E_{cm}^{p\overline{p}}$ = 1.96 TeV
0.05 ±0.09 ±0.01	2298	[18] ABREU	01I	DLPH	E_{cm}^{ee}= 183+189 GeV
		[19] BREITWEG	00	ZEUS	$e^+p \rightarrow e^+W^\pm$X, $\sqrt{s} \approx$ 300 GeV
$0.00\ ^{+0.10}_{-0.09}$	331	[20] ABBOTT	99I	D0	$E_{cm}^{p\overline{p}}$ = 1.8 TeV

[1] ABDALLAH 10 use data on the final states $e^+e^- \rightarrow jj\ell\nu$, $jjjj$, jjX, ℓX, at center-of-mass energies between 189–209 GeV at LEP2, where j = jet, ℓ = lepton, and X represents missing momentum. The fit is carried out keeping all other parameters fixed at their SM values.

[2] SCHAEL 05A study single–photon, single–W, and WW–pair production from 183 to 209 GeV. Each parameter is determined from a single–parameter fit in which the other parameters assume their Standard Model values.

[3] ABBIENDI 04D combine results from W^+W^- in all decay channels. Only CP-conserving couplings are considered and each parameter is determined from a single-parameter fit in which the other parameters assume their Standard Model values. The 95% confidence interval is $-0.13 < \lambda_\gamma < 0.01$.

[4] ACHARD 04D study WW–pair production, single–W production and single–photon production with missing energy from 189 to 209 GeV. The result quoted here is obtained including data from 161 to 183 GeV, ACCIARRI 99Q. Each parameter is determined from a single–parameter fit in which the other parameters assume their Standard Model values.

[5] CHATRCHYAN 14AB measure $W\gamma$ production cross section for $p_T^\gamma > 15$ GeV and R($\ell\gamma$) > 0.7, which is the separation between the γ and the final state charged lepton (e or μ) in the azimuthal angle-pseudorapidity ($\phi - \eta$) plane. After background subtraction the number of $e\nu\gamma$ and $\mu\nu\gamma$ events is determined to be 3200 ± 325 and 4970 ± 543 respectively, compatible with expectations from the SM. This leads to a 95% CL limit of $-0.050 < \lambda_\gamma < 0.037$, assuming all other parameters have SM values.

[6] AAD 13AN study $W\gamma$ production in pp collisions. In events with no additional jet, 4449 (6578) W decays to electron (muon) are selected, with an expected background of 1662 ± 262 (2538 ± 362) events. Analysing the photon p_T spectrum above 100 GeV yields a 95% C.L. limit of $-0.065 < \lambda_\gamma < 0.061$. Supersedes AAD 12BX.

[7] ABAZOV 12AG combine new results with already published results on $W\gamma$, WW and WZ production in order to determine the couplings with increased precision, superseding ABAZOV 08R, ABAZOV 11AC, ABAZOV 09AJ, ABAZOV 09AD. The 68% C.L. result for a formfactor cutoff of $\Lambda = 2$ TeV is $\lambda_\gamma = 0.007^{+0.021}_{-0.022}$.

[8] ABAZOV 11AC study $W\gamma$ production in $p\overline{p}$ collisions at 1.96 TeV, with the W decay products containing an electron or a muon. They select 196 (363) events in the electron (muon) mode, with a SM expectation of 190 (372) events. A likelihood fit to the photon E_T spectrum above 15 GeV yields at 95% C.L. the result: $-0.08 < \lambda_\gamma < 0.07$ for a formfactor $\Lambda = 2$ TeV.

[9] CHATRCHYAN 11M study $W\gamma$ production in pp collisions at $\sqrt{s} = 7$ TeV using 36 pb^{-1} pp data with the W decaying to electron and muon. The total cross section is measured for photon transverse energy $E_T^\gamma > 10$ GeV and spatial separation from charged leptons in the plane of pseudo rapidity and azimuthal angle $\Delta R(\ell,\gamma) > 0.7$. The number of candidate (background) events is 452 (228 ± 21) for the electron channel and 520 (277 ± 25) for the muon channel. Setting other couplings to their standard model value, they derive a 95% CL limit of $-0.18 < \lambda_\gamma < 0.17$.

[10] AARON 09B study single-W production in ep collisions at 0.3 TeV C.M. energy. They select 53 $W \rightarrow e/\mu$ events with a standard model expectation of 54.1 ± 7.4 events. Fitting the transverse momentum spectrum of the hadronic recoil system they obtain a 95% C.L. limit of $-2.5 < \lambda_\gamma < 2.5$.

[11] ABAZOV 09AD study the $p\overline{p} \rightarrow \ell\nu$ 2jet process arising in WW and WZ production. They select 12,473 (14,392) events in the electron (muon) channel with an expected di-boson signal of 436 (527) events. The results on the anomalous couplings are derived from an analysis of the p_T spectrum of the 2-jet system and quoted at 68% C.L. and for a form factor of 2 TeV. This measurement is not used for obtaining the mean as it is for a specific form factor. The 95% confidence interval is $-0.10 < \lambda_\gamma < 0.11$.

Downloaded from https://academic.oup.com/ptep/article/2022/8/083C01/6651666 by KIT Library user on 27 September 2022

[12] ABAZOV 09AJ study the $p\overline{p} \rightarrow 2\ell 2\nu$ process arising in WW production. They select 100 events with an expected WW signal of 65 events. An analysis of the p_T spectrum of the two charged leptons leads to 95% C.L. limits of $-0.14 < \lambda_\gamma < 0.18$, for a form factor $\Lambda = 2$ TeV.

[13] ABAZOV 08R use 0.7 fb^{-1} $p\overline{p}$ data at $\sqrt{s} = 1.96$ TeV to select 263 $W\gamma + X$ events, of which 187 constitute signal, with the W decaying into an electron or a muon, which is required to be well separated from a photon with $E_T > 9$ GeV. A likelihood fit to the photon E_T spectrum yields a 95% CL limit $-0.12 < \lambda_\gamma < 0.13$ with other couplings fixed to their Standard Model values.

[14] ABDALLAH 08C determine this triple gauge coupling from the measurement of the spin density matrix elements in $e^+e^- \rightarrow W^+W^- \rightarrow (q\overline{q})(\ell\nu)$, where $\ell = e$ or μ. Values of all other couplings are fixed to their standard model values.

[15] AALTONEN 07L set limits on anomalous TGCs using the $p_T(W)$ distribution in WW and WZ production with the W decaying to an electron or muon and the Z to 2 jets. Setting other couplings to their standard model value, the 95% C.L. limits are $-0.18 < \lambda_\gamma < 0.17$ for a form factor scale $\Lambda = 1.5$ TeV.

[16] ABAZOV 06H study $\overline{p}p \rightarrow WW$ production with a subsequent decay $WW \rightarrow e^+\nu_e e^-\overline{\nu}_e$, $WW \rightarrow e^\pm\nu_e\mu^\mp\nu_\mu$ or $WW \rightarrow \mu^+\nu_\mu\mu^-\overline{\nu}_\mu$. The 95% C.L. limit for a form factor scale $\Lambda = 1$ TeV is $-0.97 < \lambda_\gamma < 1.04$, fixing κ_γ=1. With the assumption that the $WW\gamma$ and WWZ couplings are equal the 95% C.L. one-dimensional limit (Λ = 2 TeV) is $-0.29 < \lambda < 0.30$.

[17] ABAZOV 05J perform a likelihood fit to the photon E_T spectrum of $W\gamma$ + X events, where the W decays to an electron or muon which is required to be well separated from the photon. For $\Lambda = 2.0$ TeV the 95% CL limits are $-0.20 < \lambda_\gamma < 0.20$. In the fit κ_γ is kept fixed to its Standard Model value.

[18] ABREU 01I combine results from e^+e^- interactions at 189 GeV leading to W^+W^-, $We\nu_e$, and $\nu\overline{\nu}\gamma$ final states with results from ABREU 99L at 183 GeV. The 95% confidence interval is $-0.11 < \lambda_\gamma < 0.23$.

[19] BREITWEG 00 search for W production in events with large hadronic p_T. For p_T >20 GeV, the upper limit on the cross section gives the 95%CL limit $-3.2 < \lambda_\gamma < 3.2$ for κ_γ fixed to its Standard Model value.

[20] ABBOTT 99I perform a simultaneous fit to the $W\gamma$, $WW \rightarrow$ dilepton, $WW/WZ \rightarrow e\nu jj$, $WW/WZ \rightarrow \mu\nu jj$, and $WZ \rightarrow$ trilepton data samples. For $\Lambda = 2.0$ TeV, the 95%CL limits are $-0.18 < \lambda_\gamma < 0.19$.

κ_Z

This coupling is *CP*-conserving (*C*- and *P*- separately conserving).

VALUE	EVTS	DOCUMENT ID		TECN	COMMENT
$\mathbf{0.924^{+0.059}_{-0.056} \pm 0.024}$	7171	[1] ACHARD	04D	L3	E^{ee}_{cm} = 189–209 GeV
• • • We do not use the following data for averages, fits, limits, etc. • • •					
		[2] SIRUNYAN	20BA	CMS	E^{pp}_{cm} = 13 TeV
		[3] SIRUNYAN	19CL	CMS	E^{pp}_{cm} = 13 TeV
		[4] AABOUD	17S	ATLS	E^{pp}_{cm} = 7+8 TeV
		[5] KHACHATRY...	17O	CMS	E^{pp}_{cm} = 8 TeV
		[6] AAD	16AR	ATLS	E^{pp}_{cm} = 8 TeV
		[7] AAD	16P	ATLS	E^{pp}_{cm} = 8 TeV
		[8] AAD	13AL	ATLS	E^{pp}_{cm} = 7 TeV
		[9] AAD	12CD	ATLS	E^{pp}_{cm} = 7 TeV
		[10] AALTONEN	12AC	CDF	$E^{p\overline{p}}_{cm}$ = 1.96 TeV
	34	[11] ABAZOV	11	D0	$E^{p\overline{p}}_{cm}$ = 1.96 TeV
	17	[12] ABAZOV	06H	D0	$E^{p\overline{p}}_{cm}$ = 1.96 TeV
	2.3	[13] ABAZOV	05S	D0	$E^{p\overline{p}}_{cm}$ = 1.96 TeV

[1] ACHARD 04D study WW–pair production, single–W production and single–photon production with missing energy from 189 to 209 GeV. The result quoted here is obtained using the WW–pair production sample. Each parameter is determined from a single–parameter fit in which the other parameters assume their Standard Model values.

[2] SIRUNYAN 20BA study electroweak production of a W boson in association with two jets, using W decays in the electron or muon channel. The isolated muons (electrons) are required to have a transverse momentum larger than 25 (30) GeV, while the transverse momentum of the two jets has to be larger than 50 and 30 GeV. A total of 2.382 (1.051) million events are selected in the muon (electron) channel, with a Standard Model expectation of 2.39 ± 0.17 (1.054 ± 0.058) million events. Analysing the transverse momentum distribution of the charged leptons from W decay, the following 95% C.L. limit is obtained: $0.956 < \kappa_Z < 1.044$. Combining this result with that from the closely-related electroweak Z-jet-jet production SIRUNYAN 18BZ, the limit becomes: $0.957 < \kappa_Z < 1.042$.

[3] SIRUNYAN 19CL study WW and WZ production in lepton + jet events, with one W boson decaying leptonically (electron or muon), and another W or Z boson decaying hadronically, reconstructed as a single massive large-radius jet. In the electron channel 2,456 (2,235) events are selected in the $WW(WZ)$ category, while in the muon channel 3,996 (3572) events are selected in the $WW(WZ)$ category. Analysing the di-boson invariant mass distribution, the following 95% C.L. limit is obtained: $0.9921 < \kappa_Z < 1.0082$.

[4] AABOUD 17S analyze electroweak production of a W boson in association with two jets at high dijet invariant mass, with the W boson decaying to electron or muon plus neutrino. In the signal region of dijet mass larger than 1 TeV and leading-jet transverse momentum larger than 600 GeV, 30 events are observed in the data with 39 ± 4 events expected in the Standard Model, yielding the following limit at 95% CL for the form factor cut-off scale $\Lambda_{FF} \rightarrow \infty$: $0.85 < \kappa_Z < 1.16$.

[5] KHACHATRYAN 17O analyse WZ production where each boson decays into electrons or muons. Events are required to have a tri-lepton invariant mass larger than 100 GeV, with one of the lepton pairs having an invariant mass within 20 GeV of the Z boson mass. The Z transverse momentum spectrum is analyzed to set a 95% C.L. limit of: $0.79 < \kappa_Z < 1.25$.

[6] AAD 16AR study WW production in pp collisions and select 6636 WW candidates in decay modes with electrons or muons with an expected background of 1546 ± 157 events. Assuming the LEP formulation and setting the form-factor Λ to infinity, a fit to the transverse momentum distribution of the leading charged lepton, leads to a 95% C.L. range of $0.975 < \kappa_Z < 1.020$.

[7] AAD 16P study WZ production in pp collisions and select 2091 WZ candidates in 4 decay modes with electrons and muons, with an expected background of 1825 ± 7 events. Analyzing the WZ transverse momentum distribution, the resulting 95% C.L. limit is: $0.81 < \kappa_Z < 1.30$.

[8] AAD 13AL study WW production in pp collisions and select 1325 WW candidates in decay modes with electrons or muons with an expected background of 369 ± 61 events. Assuming the LEP formulation and setting the form-factor Λ = infinity, a fit to the transverse momentum distribution of the leading charged lepton, leads to a 95% C.L. range of $0.957 < \kappa_Z < 1.043$. Supersedes AAD 12AC.

[9] AAD 12CD study WZ production in pp collisions and select 317 WZ candidates in three $\ell\nu$ decay modes with an expected background of 68.0 ± 10.0 events. The resulting 95% C.L. range is: $0.63 < \kappa_Z < 1.57$. Supersedes AAD 12V.

[10] AALTONEN 12AC study WZ production in $p\overline{p}$ collisions and select 63 WZ candidates in three $\ell\nu$ decay modes with an expected background of 7.9 ± 1.0 events. Based on the cross section and shape of the Z transverse momentum spectrum, the following 95% C.L. range is reported: $0.61 < \kappa_Z < 1.90$ for a form factor of $\Lambda = 2$ TeV.

[11] ABAZOV 11 study the $p\overline{p} \rightarrow 3\ell\nu$ process arising in WZ production. They observe 34 WZ candidates with an estimated background of 6 events. An analysis of the p_T spectrum of the Z boson leads to a 95% C.L. limit of $0.600 < \kappa_Z < 1.675$, for a form factor $\Lambda = 2$ TeV.

[12] ABAZOV 06H study $\overline{p}p \rightarrow WW$ production with a subsequent decay $WW \rightarrow e^+\nu_e e^-\overline{\nu}_e$, $WW \rightarrow e^\pm\nu_e\mu^\mp\nu_\mu$ or $WW \rightarrow \mu^+\nu_\mu\mu^-\overline{\nu}_\mu$. The 95% C.L. limit for a form factor scale $\Lambda = 2$ TeV is $0.55 < \kappa_Z < 1.55$, fixing λ_Z=0. With the assumption that the $WW\gamma$ and WWZ couplings are equal the 95% C.L. one-dimensional limit (Λ = 2 TeV) is $0.68 < \kappa < 1.45$.

[13] ABAZOV 05S study $\overline{p}p \rightarrow WZ$ production with a subsequent trilepton decay to $\ell\nu\ell'\overline{\ell}'$ (ℓ and $\ell' = e$ or μ). Three events (estimated background 0.71 ± 0.08 events) with WZ decay characteristics are observed from which they derive limits on the anomalous WWZ couplings. The 95% CL limit for a form factor scale $\Lambda = 1$ TeV is $-1.0 < \kappa_Z < 3.4$, fixing λ_Z and g_1^Z to their Standard Model values.

λ_Z

This coupling is *CP*-conserving (*C*- and *P*- separately conserving).

VALUE	EVTS	DOCUMENT ID		TECN	COMMENT
$\mathbf{-0.088^{+0.060}_{-0.057} \pm 0.023}$	7171	[1] ACHARD	04D	L3	E^{ee}_{cm} = 189–209 GeV
• • • We do not use the following data for averages, fits, limits, etc. • • •					
		[2] SIRUNYAN	20BA	CMS	E^{pp}_{cm} = 13 TeV
		[3] SIRUNYAN	19CL	CMS	E^{pp}_{cm} = 13 TeV
		[4] SIRUNYAN	18BZ	CMS	E^{pp}_{cm} = 13 TeV
		[5] AABOUD	17S	ATLS	E^{pp}_{cm} = 7+8 TeV
		[6] AABOUD	17U	ATLS	E^{pp}_{cm} = 8 TeV
		[7] KHACHATRY...	17O	CMS	E^{pp}_{cm} = 8 TeV
		[8] SIRUNYAN	17X	CMS	E^{pp}_{cm} = 8 TeV
		[9] AAD	16AR	ATLS	E^{pp}_{cm} = 8 TeV
		[10] AAD	16P	ATLS	E^{pp}_{cm} = 8 TeV
		[11] AAD	14Y	ATLS	E^{pp}_{cm} = 8 TeV
		[12] AAD	13AL	ATLS	E^{pp}_{cm} = 7 TeV
		[13] CHATRCHYAN	13BF	CMS	E^{pp}_{cm} = 7 TeV
		[14] AAD	12CD	ATLS	E^{pp}_{cm} = 7 TeV
		[15] AALTONEN	12AC	CDF	$E^{p\overline{p}}_{cm}$ = 1.96 TeV
	34	[16] ABAZOV	11	D0	$E^{p\overline{p}}_{cm}$ = 1.96 TeV
	334	[17] AALTONEN	10K	CDF	$E^{p\overline{p}}_{cm}$ = 1.96 TeV
	13	[18] ABAZOV	07Z	D0	$E^{p\overline{p}}_{cm}$ = 1.96 TeV
	17	[19] ABAZOV	06H	D0	$E^{p\overline{p}}_{cm}$ = 1.96 TeV
	2.3	[20] ABAZOV	05S	D0	$E^{p\overline{p}}_{cm}$ = 1.96 TeV

[1] ACHARD 04D study WW–pair production, single–W production and single–photon production with missing energy from 189 to 209 GeV. The result quoted here is obtained using the WW–pair production sample. Each parameter is determined from a single–parameter fit in which the other parameters assume their Standard Model values.

[2] SIRUNYAN 20BA study electroweak production of a W boson in association with two jets, using W decays in the electron or muon channel. The isolated muons (electrons) are required to have a transverse momentum larger than 25 (30) GeV, while the transverse momentum of the two jets has to be larger than 50 and 30 GeV. A total of 2.382 (1.051) million events are selected in the muon (electron) channel, with a Standard Model expectation of 2.39 ± 0.17 (1.054 ± 0.058) million events. Analysing the transverse momentum distribution of the charged leptons from W decay, the following 95% C.L. limit is obtained: $-0.0088 < \lambda_Z < 0.0095$. Combining this result with that from the closely-related electroweak Z-jet-jet production SIRUNYAN 18BZ, the limit becomes: $-0.0071 < \lambda_Z < 0.0076$.

[3] SIRUNYAN 19CL study WW and WZ production in lepton + jet events, with one W boson decaying leptonically (electron or muon), and another W or Z boson decaying hadronically, reconstructed as a single massive large-radius jet. In the electron channel 2,456 (2,235) events are selected in the $WW(WZ)$ category, while in the muon channel 3,996 (3572) events are selected in the $WW(WZ)$ category. Analysing the di-boson invariant mass distribution, the following 95% C.L. limit is obtained: $-0.0065 < \lambda_Z < 0.0066$.

[4] SIRUNYAN 18BZ study $pp \rightarrow Z$ *jet jet* events at 13 TeV where $Z \rightarrow e^+e^-/\mu^+\mu^-$. Isolated electrons and muons are selected with p_T of the leading/sub-leading lepton > 30/20 GeV and $|\eta| < 2.4$, with the di-lepton invariant mass within 15 GeV of the Z mass. The two highest p_T jets are selected with p_T of the leading/sub-leading jet > 50/30 GeV respectively and dijet invariant mass > 200 GeV. Templates in the transverse momentum of the Z are utilized to set limits on the triple gauge couplings in the EFT and the LEP parametrizations. The following 95% C.L. limit is obtained $-0.010 < \lambda_Z < 0.010$.

Downloaded from https://academic.oup.com/ptep/article/2022/8/083C01/6651666 by KIT Library user on 27 September 2022

[5] AABOUD 17S analyze electroweak production of a W boson in association with two jets at high dijet invariant mass, with the W boson decaying to electron or muon plus neutrino. In the signal region of dijet mass larger than 1 TeV and leading-jet transverse momentum larger than 600 GeV, 30 events are observed in the data with 39 ± 4 events expected in the Standard Model, yielding the following limit at 95% CL for the form factor cut-off scale $\Lambda_{FF} \rightarrow \infty$: $-0.053 < \lambda_Z < 0.042$.

[6] AABOUD 17U analyze production of WW or WZ boson pairs with one W boson decaying to electron or muon plus neutrino, and the other W or Z boson decaying hadronically. The hadronic decay system is reconstructed as either a resolved two-jet system or as a single large jet. Analysing the transverse momentum distribution of the hadronic system above 100 GeV yields the following limit at 95% CL for the form factor cut-off scale $\Lambda_{FF} \rightarrow \infty$: $-0.013 < \lambda_Z < 0.013$.

[7] KHACHATRYAN 17O analyse WZ production where each boson decays into electrons or muons. Events are required to have a tri-lepton invariant mass larger than 100 GeV, with one of the lepton pairs having an invariant mass within 20 GeV of the Z boson mass. The Z transverse momentum spectrum is analyzed to set a 95% C.L. limit of: $-0.018 < \lambda_Z < 0.016$.

[8] SIRUNYAN 17X study $pp \rightarrow WW/WZ \rightarrow \ell\nu q\overline{q}$ production at 8 TeV where ℓ is an electron or muon with $p_T > 30$ or 25 GeV respectively. Suitable cuts are put on the p_T of the dijet system and the missing E_T of the event yielding a total of 285 and 204 WV events observed in the electron and muon channels. The following 95% C.L. limit is obtained: $-0.011 < \lambda_Z < 0.011$.

[9] AAD 16AR study WW production in pp collisions and select 6636 WW candidates in decay modes with electrons or muons with an expected background of 1546 ± 157 events. Assuming the LEP formulation and setting the form-factor Λ to infinity, a fit to the transverse momentum distribution of the leading charged lepton, leads to a 95% C.L. range of $-0.019 < \lambda_Z < 0.019$.

[10] AAD 16P study WZ production in pp collisions and select 2091 WZ candidates in 4 decay modes with electrons and muons, with an expected background of 1825 ± 7 events. Analyzing the WZ transverse momentum distribution, the resulting 95% C.L. limit is: $-0.016 < \lambda_Z < 0.016$.

[11] AAD 14Y determine the electroweak Z-dijet cross section in 8 TeV pp collisions. $Z \rightarrow ee$ and $Z \rightarrow \mu\mu$ decays are selected with the di-lepton $p_T > 20$ GeV and mass in the 81–101 GeV range. Minimum two jets are required with $p_T > 55$ and 45 GeV and no additional jets with $p_T > 25$ GeV in the rapidity interval between them. The normalized p_T balance between the Z and the two jets is required to be < 0.15. This leads to a selection of 900 events with dijet mass > 1 TeV. The number of signal and background events expected is 261 and 592 respectively. A Poisson likelihood method is used on an event by event basis to obtain the 95% CL limit $-0.15 < \lambda_Z < 0.13$ for a form factor value $\Lambda = \infty$.

[12] AAD 13AL study WW production in pp collisions and select 1325 WW candidates in decay modes with electrons or muons with an expected background of 369 ± 61 events. Assuming the LEP formulation and setting the form-factor Λ = infinity, a fit to the transverse momentum distribution of the leading charged lepton, leads to a 95% C.L. range of $-0.062 < \lambda_Z < 0.059$. Supersedes AAD 12AC.

[13] CHATRCHYAN 13BF determine the W^+W^- production cross section using unlike sign di-lepton (e or μ) events with high $\not{p}_T$. The leptons have $p_T > 20$ GeV/c and are isolated. 1134 candidate events are observed with an expected SM background of 247 ± 34. The p_T distribution of the leading lepton is fitted to obtain 95% C.L. limits of $-0.048 \leq \lambda_Z \leq 0.048$.

[14] AAD 12CD study WZ production in pp collisions and select 317 WZ candidates in three $\ell\nu$ decay modes with an expected background of 68.0 ± 10.0 events. The resulting 95% C.L. range is: $-0.046 < \lambda_Z < 0.047$. Supersedes AAD 12V.

[15] AALTONEN 12AC study WZ production in $p\overline{p}$ collisions and select 63 WZ candidates in three $\ell\nu$ decay modes with an expected background of 7.9 ± 1.0 events. Based on the cross section and shape of the Z transverse momentum spectrum, the following 95% C.L. range is reported: $-0.08 < \lambda_Z < 0.10$ for a form factor of $\Lambda = 2$ TeV.

[16] ABAZOV 11 study the $p\overline{p} \rightarrow 3\ell\nu$ process arising in WZ production. They observe 34 WZ candidates with an estimated background of 6 events. An analysis of the p_T spectrum of the Z boson leads to a 95% C.L. limit of $-0.077 < \lambda_Z < 0.093$, for a form factor $\Lambda = 2$ TeV.

[17] AALTONEN 10K study $p\overline{p} \rightarrow W^+W^-$ with $W \rightarrow e/\mu\nu$. The p_T of the leading (second) lepton is required to be > 20 (10) GeV. The final number of events selected is 654 of which 320 ± 47 are estimated to be background. The 95% C.L. interval is $-0.16 < \lambda_Z < 0.16$ for $\Lambda = 1.5$ TeV and $-0.14 < \lambda_Z < 0.15$ for $\Lambda = 2$ TeV.

[18] ABAZOV 07Z set limits on anomalous TGCs using the measured cross section and $p_T(Z)$ distribution in WZ production with both the W and the Z decaying leptonically into electrons and muons. Setting the other couplings to their standard model values, the 95% C.L. limit for a form factor scale $\Lambda = 2$ TeV is $-0.17 < \lambda_Z < 0.21$.

[19] ABAZOV 06H study $\overline{p}p \rightarrow WW$ production with a subsequent decay $WW \rightarrow e^+\nu_e e^-\overline{\nu}_e$, $WW \rightarrow e^\pm\nu_e\mu^\mp\nu_\mu$ or $WW \rightarrow \mu^+\nu_\mu\mu^-\overline{\nu}_\mu$. The 95% C.L. limit for a form factor scale $\Lambda = 2$ TeV is $-0.39 < \lambda_Z < 0.39$, fixing κ_Z=1. With the assumption that the $WW\gamma$ and WWZ couplings are equal the 95% C.L. one-dimensional limit ($\Lambda = 2$ TeV) is $-0.29 < \lambda < 0.30$.

[20] ABAZOV 05S study $\overline{p}p \rightarrow WZ$ production with a subsequent trilepton decay to $\ell\nu\ell'\overline{\ell}'$ (ℓ and $\ell' = e$ or μ). Three events (estimated background 0.71 ± 0.08 events) with WZ decay characteristics are observed from which they derive limits on the anomalous WWZ couplings. The 95% CL limit for a form factor scale $\Lambda = 1.5$ TeV is $-0.48 < \lambda_Z < 0.48$, fixing g_1^Z and κ_Z to their Standard Model values.

g_5^Z

This coupling is *CP*-conserving but *C*- and *P*-violating.

VALUE	EVTS	DOCUMENT ID		TECN	COMMENT
-0.07 ± 0.09 OUR AVERAGE		Error includes scale factor of 1.1.			
$-0.04^{+0.13}_{-0.12}$	9800	[1] ABBIENDI	04D	OPAL	E^{ee}_{cm}= 183–209 GeV
$0.00 \pm 0.13 \pm 0.05$	7171	[2] ACHARD	04D	L3	E^{ee}_{cm}= 189–209 GeV
$-0.44^{+0.23}_{-0.22} \pm 0.12$	1154	[3] ACCIARRI	99Q	L3	E^{ee}_{cm}= 161+172+ 183 GeV
• • • We do not use the following data for averages, fits, limits, etc. • • •					
-0.31 ± 0.23		[4] EBOLI	00	THEO	LEP1, SLC+ Tevatron

[1] ABBIENDI 04D combine results from W^+W^- in all decay channels. Only *CP*-conserving couplings are considered and each parameter is determined from a single-parameter fit in which the other parameters assume their Standard Model values. The 95% confidence interval is $-0.28 < g_5^Z < +0.21$.

[2] ACHARD 04D study WW–pair production, single–W production and single–photon production with missing energy from 189 to 209 GeV. The result quoted here is obtained using the WW–pair production sample. Each parameter is determined from a single–parameter fit in which the other parameters assume their Standard Model values.

[3] ACCIARRI 99Q study W-pair, single-W, and single photon events.

[4] EBOLI 00 extract this indirect value of the coupling studying the non-universal one-loop contributions to the experimental value of the $Z \rightarrow b\overline{b}$ width (Λ=1 TeV is assumed).

g_4^Z

This coupling is *CP*-violating (*C*-violating and *P*-conserving).

VALUE	EVTS	DOCUMENT ID		TECN	COMMENT
-0.30 ± 0.17 OUR AVERAGE					
$-0.39^{+0.19}_{-0.20}$	1880	[1] ABDALLAH	08C	DLPH	E^{ee}_{cm}= 189–209 GeV
$-0.02^{+0.32}_{-0.33}$	1065	[2] ABBIENDI	01H	OPAL	E^{ee}_{cm}= 189 GeV

[1] ABDALLAH 08C determine this triple gauge coupling from the measurement of the spin density matrix elements in $e^+e^- \rightarrow W^+W^- \rightarrow (qq)(\ell\nu)$, where $\ell = e$ or μ. Values of all other couplings are fixed to their standard model values.

[2] ABBIENDI 01H study W-pair events, with one leptonically and one hadronically decaying W. The coupling is extracted using information from the W production angle together with decay angles from the leptonically decaying W.

$\tilde{\kappa}_Z$

This coupling is *CP*-violating (*C*-conserving and *P*-violating).

VALUE	EVTS	DOCUMENT ID		TECN	COMMENT
$-0.12^{+0.06}_{-0.04}$ OUR AVERAGE					
$-0.09^{+0.08}_{-0.05}$	1880	[1] ABDALLAH	08C	DLPH	E^{ee}_{cm}= 189–209 GeV
$-0.20^{+0.10}_{-0.07}$	1065	[2] ABBIENDI	01H	OPAL	E^{ee}_{cm}= 189 GeV
• • • We do not use the following data for averages, fits, limits, etc. • • •					
		[3] AABOUD	17S	ATLS	E^{pp}_{cm} = 7+8 TeV
		[4] BLINOV	11	LEP	E^{ee}_{cm}= 183–207 GeV

[1] ABDALLAH 08C determine this triple gauge coupling from the measurement of the spin density matrix elements in $e^+e^- \rightarrow W^+W^- \rightarrow (qq)(\ell\nu)$, where $\ell = e$ or μ. Values of all other couplings are fixed to their standard model values.

[2] ABBIENDI 01H study W-pair events, with one leptonically and one hadronically decaying W. The coupling is extracted using information from the W production angle together with decay angles from the leptonically decaying W.

[3] AABOUD 17S analyze electroweak production of a W boson in association with two jets at high dijet invariant mass, with the W boson decaying to electron or muon plus neutrino. In the signal region of dijet mass larger than 1 TeV and leading-jet transverse momentum larger than 600 GeV, 30 events are observed in the data with 39 ± 4 events expected in the Standard Model, yielding the following limit at 95% CL for the form factor cut-off scale $\Lambda_{FF} \rightarrow \infty$: $-0.56 < \tilde{\kappa}_Z < 0.56$.

[4] BLINOV 11 use the LEP-average $e^+e^- \rightarrow W^+W^-$ cross section data for $\sqrt{s}$ = 183–207 GeV to determine an upper limit on the TGC $\tilde{\kappa}_Z$. The average values of the cross sections as well as their correlation matrix, and standard model expectations of the cross sections are taken from the LEPEWWG note hep-ex/0612034. At 95% confidence level $|\tilde{\kappa}_Z| < 0.13$.

$\tilde{\lambda}_Z$

This coupling is *CP*-violating (*C*-conserving and *P*-violating).

VALUE	EVTS	DOCUMENT ID		TECN	COMMENT
-0.09 ± 0.07 OUR AVERAGE					
-0.08 ± 0.07	1880	[1] ABDALLAH	08C	DLPH	E^{ee}_{cm}= 189–209 GeV
$-0.18^{+0.24}_{-0.16}$	1065	[2] ABBIENDI	01H	OPAL	E^{ee}_{cm}= 189 GeV
• • • We do not use the following data for averages, fits, limits, etc. • • •					
		[3] AABOUD	17S	ATLS	E^{pp}_{cm} = 7+8 TeV
		[4] BLINOV	11	LEP	E^{ee}_{cm}= 183–207 GeV

[1] ABDALLAH 08C determine this triple gauge coupling from the measurement of the spin density matrix elements in $e^+e^- \rightarrow W^+W^- \rightarrow (qq)(\ell\nu)$, where $\ell = e$ or μ. Values of all other couplings are fixed to their standard model values.

[2] ABBIENDI 01H study W-pair events, with one leptonically and one hadronically decaying W. The coupling is extracted using information from the W production angle together with decay angles from the leptonically decaying W.

[3] AABOUD 17S analyze electroweak production of a W boson in association with two jets at high dijet invariant mass, with the W boson decaying to electron or muon plus neutrino. In the signal region of dijet mass larger than 1 TeV and leading-jet transverse momentum larger than 600 GeV, 30 events are observed in the data with 39 ± 4 events expected in the Standard Model, yielding the following limit at 95% CL for the form factor cut-off scale $\Lambda_{FF} \rightarrow \infty$: $-0.047 < \tilde{\lambda}_Z < 0.046$.

[4] BLINOV 11 use the LEP-average $e^+e^- \rightarrow W^+W^-$ cross section data for $\sqrt{s}$ = 183–207 GeV to determine an upper limit on the TGC $\tilde{\lambda}_Z$. The average values of the cross sections as well as their correlation matrix, and standard model expectations of the cross sections are taken from the LEPEWWG note hep-ex/0612034. At 95% confidence level $|\tilde{\lambda}_Z| < 0.31$.

W ANOMALOUS MAGNETIC MOMENT

The full magnetic moment is given by $\mu_W = e(1+\kappa+\lambda)/2m_W$. In the Standard Model, at tree level, $\kappa = 1$ and $\lambda = 0$. Some papers have defined $\Delta\kappa = 1-\kappa$ and assume that $\lambda = 0$. Note that the electric quadrupole moment is given by $-e(\kappa-\lambda)/m_W^2$. A description of the parameterization of these moments and additional references can be found in HAGIWARA 87

Downloaded from https://academic.oup.com/ptep/article/2022/8/083C01/6651666 by KIT Library user on 27 September 2022

and BAUR 88. The parameter Λ appearing in the theoretical limits below is a regularization cutoff which roughly corresponds to the energy scale where the structure of the W boson becomes manifest.

VALUE ($e/2m_W$)	EVTS	DOCUMENT ID		TECN	COMMENT
$\mathbf{2.22^{+0.20}_{-0.19}}$	2298	[1] ABREU	01I	DLPH	E^{ee}_{cm}= 183+189 GeV
• • • We do not use the following data for averages, fits, limits, etc. • • •					
		[2] ABE	95G	CDF	
		[3] ALITTI	92C	UA2	
		[4] SAMUEL	92	THEO	
		[5] SAMUEL	91	THEO	
		[6] GRIFOLS	88	THEO	
		[7] GROTCH	87	THEO	
		[8] VANDERBIJ	87	THEO	
		[9] GRAU	85	THEO	
		[10] SUZUKI	85	THEO	
		[11] HERZOG	84	THEO	

[1] ABREU 01I combine results from e^+e^- interactions at 189 GeV leading to W^+W^-, $We\nu_e$, and $\nu\overline{\nu}\gamma$ final states with results from ABREU 99L at 183 GeV to determine Δg^Z_1, $\Delta\kappa_\gamma$, and λ_γ. $\Delta\kappa_\gamma$ and λ_γ are simultaneously floated in the fit to determine μ_W.

[2] ABE 95G report $-1.3 < \kappa < 3.2$ for λ=0 and $-0.7 < \lambda < 0.7$ for κ=1 in $p\overline{p} \rightarrow e\nu_e\gamma$X and $\mu\nu_\mu\gamma$X at $\sqrt{s} = 1.8$ TeV.

[3] ALITTI 92C measure $\kappa = 1^{+2.6}_{-2.2}$ and $\lambda = 0^{+1.7}_{-1.8}$ in $p\overline{p} \rightarrow e\nu\gamma+$ X at $\sqrt{s} = 630$ GeV. At 95%CL they report $-3.5 < \kappa < 5.9$ and $-3.6 < \lambda < 3.5$.

[4] SAMUEL 92 use preliminary CDF and UA2 data and find $-2.4 < \kappa < 3.7$ at 96%CL and $-3.1 < \kappa < 4.2$ at 95%CL respectively. They use data for $W\gamma$ production and radiative W decay.

[5] SAMUEL 91 use preliminary CDF data for $p\overline{p} \rightarrow W\gamma$X to obtain $-11.3 \leq \Delta\kappa \leq 10.9$. Note that their $\kappa = 1-\Delta\kappa$.

[6] GRIFOLS 88 uses deviation from ρ parameter to set limit $\Delta\kappa \lesssim 65\ (M^2_W/\Lambda^2)$.

[7] GROTCH 87 finds the limit $-37 < \Delta\kappa < 73.5$ (90% CL) from the experimental limits on $e^+e^- \rightarrow \nu\overline{\nu}\gamma$ assuming three neutrino generations and $-19.5 < \Delta\kappa < 56$ for four generations. Note their $\Delta\kappa$ has the opposite sign as our definition.

[8] VANDERBIJ 87 uses existing limits to the photon structure to obtain $|\Delta\kappa| < 33\ (m_W/\Lambda)$. In addition VANDERBIJ 87 discusses problems with using the ρ parameter of the Standard Model to determine $\Delta\kappa$.

[9] GRAU 85 uses the muon anomaly to derive a coupled limit on the anomalous magnetic dipole and electric quadrupole (λ) moments $1.05 > \Delta\kappa \ln(\Lambda/m_W) + \lambda/2 > -2.77$. In the Standard Model $\lambda = 0$.

[10] SUZUKI 85 uses partial-wave unitarity at high energies to obtain $|\Delta\kappa| \lesssim 190\ (m_W/\Lambda)^2$. From the anomalous magnetic moment of the muon, SUZUKI 85 obtains $|\Delta\kappa| \lesssim 2.2/\ln(\Lambda/m_W)$. Finally SUZUKI 85 uses deviations from the ρ parameter and obtains a very qualitative, order-of-magnitude limit $|\Delta\kappa| \lesssim 150\ (m_W/\Lambda)^4$ if $|\Delta\kappa| \ll 1$.

[11] HERZOG 84 consider the contribution of W-boson to muon magnetic moment including anomalous coupling of $WW\gamma$. Obtain a limit $-1 < \Delta\kappa < 3$ for $\Lambda \gtrsim 1$ TeV.

c_{WWW}/Λ^2, c_W/Λ^2, c_B/Λ^2

These couplings are used in EFT-based approaches to anomalous couplings. They are linearly related to the couplings discussed above.

VALUE	DOCUMENT ID		TECN	COMMENT
• • • We do not use the following data for averages, fits, limits, etc. • • •				
	[1] AAD	21AC	ATLS	E^{pp}_{cm} = 13 TeV
	[2] AAD	21W	ATLS	E^{pp}_{cm} = 13 TeV
	[3] SIRUNYAN	21G	CMS	E^{pp}_{cm} = 13 TeV
	[4] SIRUNYAN	20BA	CMS	E^{pp}_{cm} = 13 TeV
	[5] SIRUNYAN	20BF	CMS	E^{pp}_{cm} = 13 TeV
	[6] AABOUD	19BA	ATLS	E^{pp}_{cm} = 13 TeV
	[7] SIRUNYAN	19AD	CMS	E^{pp}_{cm} = 13 TeV
	[8] SIRUNYAN	19CL	CMS	E^{pp}_{cm} = 13 TeV
	[9] AABOUD	18Q	ATLS	E^{pp}_{cm} = 13 TeV
	[10] SIRUNYAN	18BZ	CMS	E^{pp}_{cm} = 13 TeV
	[11] AABOUD	17S	ATLS	E^{pp}_{cm} = 7+8 TeV
	[12] AABOUD	17U	ATLS	E^{pp}_{cm} = 8 TeV
	[13] KHACHATRY...	17O	CMS	E^{pp}_{cm} = 8 TeV
	[14] SIRUNYAN	17X	CMS	E^{pp}_{cm} = 8 TeV
	[15] AAD	16AR	ATLS	E^{pp}_{cm} = 8 TeV
	[16] AAD	16P	ATLS	E^{pp}_{cm} = 8 TeV
	[17] KHACHATRY...	16BI	CMS	E^{pp}_{cm} = 8 TeV

[1] AAD 21AC study the differential cross-section for the electroweak production of dijets in association with a Z boson, where the Z boson decays to electrons or muons. The number of events selected in the data is 10,870 (12,125) in the electron (muon) channel. Analyzing the distribution of the azimuthal separation of the two jets, the following 95% C.L. limits are derived in units of TeV^{-2}: $-2.7 < c_{WWW}/\Lambda^2 < 5.8$, $-1.6 < \tilde{c}_{WWW}/\Lambda^2 < 2.0$, $-0.19 < c_W/\Lambda^2 < 0.41$, $-0.11 < \tilde{c}_W/\Lambda^2 < 0.14$, $-6.31 < c_{HWB}/\Lambda^2 < 1.01$, $0.23 < \tilde{c}_{HWB}/\Lambda^2 < 2.35$.

[2] AAD 21W analyze W^+W^- production in association with at least one jet. Events with exactly one oppositely-charged electron-muon pair and at least one hadronic jet of transverse momentum larger than 30 GeV (120 GeV) are selected. In the data, 89,239 (5,825) events are found, with a total Standard-Model expectation of 91600 ± 2500 (5980 ± 150). Analyzing the electron-muon invariant mass distribution, the following limit at 95% C.L. is obtained: $-0.33 < c_W/\Lambda^2 < 0.33$ ($-0.60 < c_W/\Lambda^2 < 0.58$), for a fixed choice of $\Lambda = 1$ TeV.

[3] SIRUNYAN 21G measure $W\gamma$ production where the W decays into electrons or muons. In the data, 385,224 (395,818) events are selected in the electron (muon) channel, with a total Standard-Model expectation of 396913±54686 (396257±22837) events. Analysing the photon transverse momentum distribution, the following 95% C.L. limits are derived in units of TeV^{-2}: $-0.90 < c_{WWW}/\Lambda^2 < 0.91$, $-40 < c_B/\Lambda^2 < 41$, $-0.45 < c_{\overline{W}WW}/\Lambda^2 < 0.45$, $-20 < c_{\overline{W}}/\Lambda^2 < 20$.

[4] SIRUNYAN 20BA study electroweak production of a W boson in association with two jets, using W decays in the electron or muon channel. The isolated muons (electrons) are required to have a transverse momentum larger than 25 (30) GeV, while the transverse momentum of the two jets has to be larger than 50 and 30 GeV. A total of 2.382 (1.051) million events are selected in the muon (electron) channel, with a Standard Model expectation of 2.39±0.17 (1.054±0.058) million events. Analysing the transverse momentum distribution of the charged leptons from W decay, the following 95% C.L. limits are obtained in units of TeV^{-2}: $-2.3 < c_{WWW}/\Lambda^2 < 2.5$, $-8.8 < c_W/\Lambda^2 < 16$, $-45 < c_B/\Lambda^2 < 46$. Combining these results with those from the closely-related electroweak Z-jet-jet production SIRUNYAN 18BZ, the limits become: $-1.8 < c_{WWW}/\Lambda^2 < 2.0$, $-5.8 < c_W/\Lambda^2 < 10$, $-43 < c_B/\Lambda^2 < 45$.

[5] SIRUNYAN 20BF study W^+W^- production with the W bosons decaying to electrons or muons. The leading (subleading) lepton is required to have a transverse momentum larger than 25 (20) GeV. Events with a same-flavor di-lepton invariant mass within 15 GeV of the Z mass are rejected, as are event with a third lepton of transverse momentum larger than 10 GeV. In the same- (different-) flavor category a total of 9,604 (20,270) events are selected while the number of expected events is 9640 ± 490 (20280 ± 430). Analyzing the different-flavor di-lepton invariant mass distribution, the following 95% C.L. limits are obtained in units of TeV^{-2}: $-1.8 < c_{WWW}/\Lambda^2 < 1.8$, $-3.6 < c_W/\Lambda^2 < 2.8$, $-9.4 < c_B/\Lambda^2 < 8.5$.

[6] AABOUD 19BA study WW production in decay modes with an electron and a muon. The charged leptons are each required to have a transverse momentum larger than 27 GeV and rapidity less than 2.5. The electron-muon system is required to have a mass larger than 55 GeV and a transverse momentum larger than 30 GeV. The missing transverse energy must be larger than 20 GeV. Events containing a jet with transverse momentum exceeding 35 GeV and rapidity smaller than 4.5 are rejected. A total of 12,659 events are selected in the data, with an expected background of 4240 ± 477 events. Analysing the transverse momentum spectrum of the leading charged lepton, the following 95% C.L. limits are derived in units of TeV^{-2}: $-3.4 < c_{WWW}/\Lambda^2 < 3.3$, $-7.4 < c_W/\Lambda^2 < 4.1$, $-21 < c_B/\Lambda^2 < 18$, $-1.6 < c_{\overline{W}WW}/\Lambda^2 < 1.6$, $-76 < c_{\overline{W}}/\Lambda^2 < 76$.

[7] SIRUNYAN 19AD study inclusive WZ production, with W and Z decaying to electrons or muons. The leading (subleading) charged lepton candidate from the Z boson decay is required to have a transverse momentum larger than 25 GeV (10 GeV). The charged lepton candidate from the W boson decay is required to have a transverse momentum larger than 25 GeV. The invariant mass of the two leptons from Z decay is required to be within 15 GeV of the Z mass, while the invariant mass of the tri-lepton system is required to exceed 100 GeV. A total of 3,831 tri-lepton events are observed, with a fitted SM WZ signal of 3166 ± 62 events and a fitted background of 666 ± 45 events. The approximated WZ invariant mass distribution is analyzed to set 95% C.L. limits as follows: $-4.1 < c_W/\Lambda^2 < 1.1$, $-2.0 < c_{WWW}/\Lambda^2 < 2.1$, $-100 < c_B/\Lambda^2 < 160$, in units of TeV^{-2}.

[8] SIRUNYAN 19CL study WW and WZ production in lepton + jet events, with one W boson decaying leptonically (electron or muon), and another W or Z boson decaying hadronically, reconstructed as a single massive large-radius jet. In the electron channel 2,456 (2,235) events are selected in the WW(WZ) category, while in the muon channel 3,996 (3572) events are selected in the WW(WZ) category. Analysing the di-boson invariant mass distribution, the following 95% C.L. limits are obtained in units of TeV^{-2}: $-1.58 < c_{WWW}/\Lambda^2 < 1.59$, $-2.00 < c_W/\Lambda^2 < 2.65$, $-8.78 < c_B/\Lambda^2 < 8.54$.

[9] AABOUD 18Q study $pp \rightarrow ZZ$ events at $\sqrt{s} = 13$ TeV with $Z \rightarrow e^+e^-$ or $Z \rightarrow \mu^+\mu^-$. The number of events observed in the 4e, 2e 2μ, and 4μ channels is 249, 465, and 303 respectively. Analysing the p_T spectrum of the leading Z boson, the following the following 95% C.L. limits are derived in units of TeV^{-4}: $-5.9 < c_{\widetilde{B}W}/\Lambda^4 < 5.9$, $-3.0 < c_{WW}/\Lambda^4 < 3.0$, $-3.3 < c_{BW}/\Lambda^4 < 3.3$, $-2.7 < c_{BB}/\Lambda^4 < 2.8$.

[10] SIRUNYAN 18BZ study $pp \rightarrow Z$ *jet jet* events at 13 TeV where $Z \rightarrow e^+e^-/\mu^+\mu^-$. Isolated electrons and muons are selected with p_T of the leading/sub-leading lepton > 30/20 GeV and $|\eta| < 2.4$, with the di-lepton invariant mass within 15 GeV of the Z mass. The two highest p_T jets are selected with p_T of the leading/sub-leading jet > 50/30 GeV respectively and dijet invariant mass > 200 GeV. Templates in the transverse momentum of the Z are utilized to set limits on the triple gauge couplings in the EFT and the LEP parametrizations. The following 95% C.L. limits are obtained in units of TeV^{-2}: $-2.6 < c_{WWW}/\Lambda^2 < 2.6$ and $-8.4 < c_W/\Lambda^2 < 10.1$.

[11] AABOUD 17S analyze electroweak production of a W boson in association with two jets at high dijet invariant mass, with the W boson decaying to electron or muon plus neutrino. In the signal region of dijet mass larger than 1 TeV and leading-jet transverse momentum larger than 600 GeV, 30 events are observed in the data with 39 ± 4 events expected in the Standard Model, yielding the following limits at 95% CL for the form factor cut-off scale $\Lambda_{FF} \rightarrow \infty$: $-33 < c_W/\Lambda^2 < 30$, $-170 < c_B/\Lambda^2 < 160$, $-13 < c_{WWW}/\Lambda^2 < 9$, $-580 < c_{\widetilde{W}}/\Lambda^2 < 580$, $-11 < c_{\widetilde{W}WW}/\Lambda^2 < 11$, in units of TeV^{-2}.

[12] AABOUD 17U analyze production of WW or WZ boson pairs with one W boson decaying to electron or muon plus neutrino, and the other W or Z boson decaying hadronically. The hadronic decay system is reconstructed as either a resolved two-jet system or as a single large jet. Analysing the transverse momentum distribution of the hadronic system above 100 GeV yields the following limits at 95% CL for the form factor cut-off scale $\Lambda_{FF} \rightarrow \infty$: $-3.1 < c_{WWW}/\Lambda^2 < 3.1$, $-19 < c_B/\Lambda^2 < 20$, $-5.1 < c_W/\Lambda^2 < 5.8$, in units of TeV^{-2}.

[13] KHACHATRYAN 17O analyse WZ production where each boson decays into electrons or muons. Events are required to have a tri-lepton invariant mass larger than 100 GeV,

Downloaded from https://academic.oup.com/ptep/article/2022/8/083C01/6651666 by KIT Library user on 27 September 2022

with one of the lepton pairs having an invariant mass within 20 GeV of the Z boson mass. The Z transverse momentum spectrum is analyzed to set 95% C.L. limits of: $-260 < c_B/\Lambda^2 < 210$, $-4.2 < c_W/\Lambda^2 < 8.0$, $-4.6 < c_{WWW}/\Lambda^2 < 4.2$, in units of TeV^{-2}.

[14] SIRUNYAN 17X study $pp \to WW/WZ \to \ell\nu q\overline{q}$ production at 8 TeV where ℓ is an electron or muon with $p_T > 30$ or 25 GeV respectively. Suitable cuts are put on the p_T of the dijet system and the missing E_T of the event yielding a total of 285 and 204 WV events observed in the electron and muon channels. The following 95% C.L. limits in units of TeV^{-2} are obtained: $-2.7 < c_{WWW}/\Lambda^2 < 2.7$, $-14 < c_B/\Lambda^2 < 17$, $-2.0 < c_W/\Lambda^2 < 5.7$.

[15] AAD 16AR study WW production in pp collisions and select 6636 WW candidates in decay modes with electrons or muons with an expected background of 1546 ± 157 events. Assuming an EFT formulation, a fit to the transverse momentum distribution of the leading charged lepton, leads to 95% C.L. ranges of: $-4.61 < c_{WWW}/\Lambda^2 < 4.60$, $-5.87 < c_W/\Lambda^2 < 10.54$ and $-20.9 < c_B/\Lambda^2 < 26.3$,in units of TeV^{-2}.

[16] AAD 16P study WZ production in pp collisions and select 2091 WZ candidates in 4 decay modes with electrons and muons, with an expected background of 1825 ± 7 events. Analyzing the WZ transverse momentum distribution, the resulting 95% C.L. limits are: $-3.9 < c_{WWW}/\Lambda^2 < 4.0$, $-4.3 < c_W/\Lambda^2 < 6.8$, and $-320 < c_B/\Lambda^2 < 210$, in units of TeV^{-2}.

[17] KHACHATRYAN 16BI determine the W^+W^- production cross section using unlike sign di-lepton (e or μ) events with high p_T. The leptons have $p_T > 20$ GeV/c and are isolated. Events are required to have no jets above p_T of 30 GeV/c. 4847 (2233) events are selected with different (same) flavor leptons, with an expected total background of 1179 ± 123 (643 ± 73) events. Analysing the di-lepton invariant mass spectrum, the following values are obtained: $c_{WWW}/\Lambda^2 = 0.1 \pm 3.2$, $c_W/\Lambda^2 = -3.6^{+5.0}_{-4.5}$ and $c_B/\Lambda^2 = -3.2^{+15.0}_{-14.5}$, in units of TeV^{-2}. The limits at 95% C.L. are: $-5.7 < c_{WWW}/\Lambda^2 < 5.9$, $-11.4 < c_W/\Lambda^2 < 5.4$ and $-29.2 < c_B/\Lambda^2 < 23.9$, in units of TeV^{-2}.

ANOMALOUS *W/Z* QUARTIC COUPLINGS

Revised November 2015 by M.W. Grünewald (U. College Dublin) and A. Gurtu (Formerly Tata Inst.).

Quartic couplings, $WWZZ$, $WWZ\gamma$, $WW\gamma\gamma$, and $ZZ\gamma\gamma$, were studied at LEP and Tevatron at energies at which the Standard Model predicts negligible contributions to multiboson production. Thus, to parametrize limits on these couplings, an effective theory approach is adopted which supplements the Standard Model Lagrangian with higher dimensional operators which include quartic couplings. The LEP collaborations chose the lowest dimensional representation of operators (dimension 6) which presumes the SU(2)×U(1) gauge symmetry is broken by means other than the conventional Higgs scalar doublet [1–3]. In this representation possible quartic couplings, a_0, a_c, a_n, are expressed in terms of the following dimension-6 operators [1,2];

$$L_6^0 = -\frac{e^2}{16\Lambda^2}\, a_0\, F^{\mu\nu}\, F_{\mu\nu}\vec{W}^{\alpha}\cdot\vec{W}_{\alpha}$$
$$L_6^c = -\frac{e^2}{16\Lambda^2}\, a_c\, F^{\mu\alpha}\, F_{\mu\beta}\vec{W}^{\beta}\cdot\vec{W}_{\alpha}$$
$$L_6^n = -i\frac{e^2}{16\Lambda^2}\, a_n\epsilon_{ijk}\, W^{(i)}_{\mu\alpha}\, W^{(j)}_{\nu}\, W^{(k)\alpha}F^{\mu\nu}$$
$$\widetilde{L}_6^0 = -\frac{e^2}{16\Lambda^2}\, \widetilde{a}_0\, F^{\mu\nu}\, \widetilde{F}_{\mu\nu}\vec{W}^{\alpha}\cdot\vec{W}_{\alpha}$$
$$\widetilde{L}_6^n = -i\frac{e^2}{16\Lambda^2}\, \widetilde{a}_n\epsilon_{ijk}\, W^{(i)}_{\mu\alpha}\, W^{(j)}_{\nu}\, W^{(k)\alpha}\widetilde{F}^{\mu\nu}$$

where F, W are photon and W fields, L_6^0 and L_6^c conserve C, P separately ($\widetilde{L}_6^0$ conserves only C) and generate anomalous $W^+W^-\gamma\gamma$ and $ZZ\gamma\gamma$ couplings, L_6^n violates CP ($\widetilde{L}_6^n$ violates both C and P) and generates an anomalous $W^+W^-Z\gamma$ coupling, and Λ is an energy scale for new physics. For the $ZZ\gamma\gamma$ coupling the CP-violating term represented by L_6^n does not contribute. These couplings are assumed to be real and to vanish at tree level in the Standard Model.

Within the same framework as above, a more recent description of the quartic couplings [3] treats the anomalous parts of the $WW\gamma\gamma$ and $ZZ\gamma\gamma$ couplings separately, leading to two sets parametrized as a_0^V/Λ^2 and a_c^V/Λ^2, where $V = W$ or Z.

With the discovery of a Higgs at the LHC in 2012, it is then useful to go to the next higher dimensional representation (dimension 8 operators) in which the gauge symmetry is broken by the conventional Higgs scalar doublet [3,4]. There are 14 operators which can contribute to the anomalous quartic coupling signal. Some of the operators have analogues in the dimension 6 scheme. The CMS collaboration, [5], have used this parametrization, in which the connections between the two schemes are also summarized:

$$\begin{aligned}\mathcal{L}_{AQGC} = &-\frac{e^2}{8}\frac{a_0^W}{\Lambda^2}F_{\mu\nu}F^{\mu\nu}W^{+a}W_a^- \\ &-\frac{e^2}{16}\frac{a_c^W}{\Lambda^2}F_{\mu\nu}F^{\mu a}(W^{+\nu}W_a^- + W^{-\nu}W_a^+) \\ &-e^2g^2\frac{\kappa_0^W}{\Lambda^2}F_{\mu\nu}Z^{\mu\nu}W^{+a}W_a^- \\ &-\frac{e^2g^2}{2}\frac{\kappa_c^W}{\Lambda^2}F_{\mu\nu}Z^{\mu a}(W^{+\nu}W_a^- + W^{-\nu}W_a^+) \\ &+\frac{f_{T,0}}{\Lambda^4}Tr[\widehat{W}_{\mu\nu}\widehat{W}^{\mu\nu}]\times Tr[\widehat{W}_{\alpha\beta}\widehat{W}^{\alpha\beta}]\end{aligned}$$

The energy scale of possible new physics is Λ, and $g = e/sin(\theta_W)$, e being the unit electric charge and θ_W the Weinberg angle. The field tensors are described in [3,4].

The two dimension 6 operators a_0^W/Λ^2 and a_c^W/Λ^2 are associated with the $WW\gamma\gamma$ vertex. Among dimension 8 operators, κ_0^W/Λ^2 and κ_c^W/Λ^2 are associated with the $WWZ\gamma$ vertex, whereas the parameter $f_{T,0}/\Lambda^4$ contributes to both vertices. There is a relationship between these two dimension 6 parameters and the dimension 8 parameters $f_{M,i}/\Lambda^4$ as follows [3]:

$$\frac{a_0^W}{\Lambda^2} = -\frac{4M_W^2}{g^2}\frac{f_{M,0}}{\Lambda^4} - \frac{8M_W^2}{g'^2}\frac{f_{M,2}}{\Lambda^4}$$

$$\frac{a_c^W}{\Lambda^2} = -\frac{4M_W^2}{g^2}\frac{f_{M,1}}{\Lambda^4} - \frac{8M_W^2}{g'^2}\frac{f_{M,3}}{\Lambda^4}$$

where $g' = e/cos(\theta_W)$ and M_W is the invariant mass of the W boson. This relation provides a translation between limits on dimension 6 operators $a_{0,c}^W$ and $f_{M,j}/\Lambda^4$. It is further required [4] that $f_{M,0} = 2f_{M,2}$ and $f_{M,1} = 2f_{M,3}$ which suppresses contributions to the $WWZ\gamma$ vertex. The complete set of Lagrangian contributions as presented in [4] corresponds to 19 anomalous couplings in total – $f_{S,i}$, $i = 1, 2$, $f_{M,i}$, $i = 0, \ldots, 8$ and $f_{T,i}, i = 0, \ldots, 9$ – each scaled by $1/\Lambda^4$.

The ATLAS collaboration [6], on the other hand, follows a K-matrix driven approach of Ref. 7 in which the anomalous couplings can be expressed in terms of two parameters α_4 and α_5, which account for all BSM effects.

It is the early stages in the determination of quartic couplings by the LHC experiments. It is hoped that the two collaborations, ATLAS and CMS, will agree to use at least one common set of parameters to express these limits to enable the reader to make a comparison and allow for a possible LHC combination.

References

1. G. Belanger and F. Boudjema, Phys. Lett. **B288**, 201 (1992).
2. J.W. Stirling and A. Werthenbach, Eur. Phys. J. **C14**, 103 (2000);

Downloaded from https://academic.oup.com/ptep/article/2022/8/083C01/6651666 by KIT Library user on 27 September 2022

J.W. Stirling and A. Werthenbach, Phys. Lett. **B466**, 369 (1999);
A. Denner *et al.*, Eur. Phys. J. **C20**, 201 (2001);
G. Montagna *et al.*, Phys. Lett. **B515**, 197 (2001).

3. G. Belanger *et al.*, Eur. Phys. J. **C13**, 283 (2000).
4. O.J.P. Éboli, M.C. Gonzalez-Garcia, and S.M. Lietti, Phys. Rev. **D69**, 095005 (2004);
O.J.P. Éboli, M.C. Gonzalez-Garcia, and J.K. Mizukoshi, Phys. Rev. **D77**, 073005 (2006).
5. S. Chatrchyan *et al.*, Phys. Rev. **D90**, 032008 (2014);
S. Chatrchyan *et al.*, Phys. Rev. Lett. **114**, 051801 (2015).
6. G. Aad *et al.*, Phys. Rev. Lett. **113**, 141803 (2014).
7. A. Albateanu, W. Killian, and J. Reuter, JHEP **0811**, 010 (2008).

a_0/Λ^2, a_c/Λ^2, a_n/Λ^2, κ_0^W/Λ^2, κ_c^W/Λ^2, $f_{T,0}/\Lambda^4$, $f_{M,i}/\Lambda^4$, α_4, α_5, $F_{S,i}/\Lambda^4$, $F_{M,i}/\Lambda^4$, $F_{T,i}/\Lambda^4$

Anomalous W quartic couplings are measured by the experiments at LEP, the Tevatron, and the LHC. Some of the recent results from the Tevatron and LHC experiments individually surpass the combined LEP-2 results in precision (see below). As discussed in the review on the "Anomalous W/Z quartic couplings (QGCS)," the measurements are typically done using different operator expansions which then do not allow the results to be compared and averaged. At least one common framework should be agreed upon for the use in the future publications by the experiments.

Some publications from LHC experiments derive limits for various assumed values of the form-factor cutoff Λ_{FF}. The values quoted below are for $\Lambda_{FF} \rightarrow \infty$.

VALUE	DOCUMENT ID		TECN	COMMENT
• • • We do not use the following data for averages, fits, limits, etc. • • •				
	[1] SIRUNYAN	21	CMS	E_{cm}^{pp} = 13 TeV
	[2] TUMASYAN	21A	CMS	E_{cm}^{pp} = 13 TeV
	[3] TUMASYAN	21B	CMS	E_{cm}^{pp} = 13 TeV
	[4] SIRUNAYN	20	CMS	E_{cm}^{pp} = 13 TeV
	[5] SIRUNYAN	20AL	CMS	E_{cm}^{pp} = 13 TeV
	[6] SIRUNYAN	20BD	CMS	E_{cm}^{pp} = 13 TeV
	[7] SIRUNYAN	19BM	CMS	E_{cm}^{pp} = 13 TeV
	[8] SIRUNYAN	19BP	CMS	E_{cm}^{pp} = 13 TeV
	[9] SIRUNYAN	19CQ	CMS	E_{cm}^{pp} = 13 TeV
	[10] SIRUNYAN	18CC	CMS	E_{cm}^{pp} = 13 TeV
	[11] AABOUD	17AA	ATLS	E_{cm}^{pp} = 8 TeV
	[12] AABOUD	17AG	ATLS	E_{cm}^{pp} = 8 TeV
	[13] AABOUD	17D	ATLS	E_{cm}^{pp} = 8 TeV
	[14] AABOUD	17J	ATLS	E_{cm}^{pp} = 8 TeV
	[15] AABOUD	17M	ATLS	E_{cm}^{pp} = 8 TeV
	[16] KHACHATRY...	17AA	CMS	E_{cm}^{pp} = 8 TeV
	[17] KHACHATRY...	17M	CMS	E_{cm}^{pp} = 8 TeV
	[18] SIRUNYAN	17AD	CMS	E_{cm}^{pp} = 13 TeV
	[19] SIRUNYAN	17AR	CMS	E_{cm}^{pp} = 8 TeV
	[20] AABOUD	16E	ATLS	E_{cm}^{pp} = 8 TeV
	[21] AAD	16Q	ATLS	E_{cm}^{pp} = 8 TeV
	[22] KHACHATRY...	16AX	CMS	E_{cm}^{pp} = 8 TeV
	[23] AAD	15N	ATLS	E_{cm}^{pp} = 8 TeV
	[24] KHACHATRY...	15D	CMS	E_{cm}^{pp} = 8 TeV
	[25] AAD	14AM	ATLS	
	[26] CHATRCHYAN	14Q	CMS	
	[27] ABAZOV	13D	D0	
	[28] CHATRCHYAN	13AA	CMS	
	[29] ABBIENDI	04B	OPAL	
	[30] ABBIENDI	04L	OPAL	
	[31] HEISTER	04A	ALEP	
	[32] ABDALLAH	03I	DLPH	
	[33] ACHARD	02F	L3	

[1] SIRUNYAN 21 study electroweak Z-pair production in association with two jets, with the Z bosons decaying to oppositely-charged electron or muon pairs. Leptons with high transverse momentum are selected, with the di-lepton invariant mass of the two Z boson candidates between 60 GeV and 120 GeV, and the four-lepton invariant mass larger than 180 GeV. A total of 365 events are selected in the data, while the number of expected events is 370 $\pm$ 48. Analyzing the four-lepton invariant mass distribution, the following 95% C.L. limits are derived: $-0.24 < f_{T,0}/\Lambda^4 < 0.22$, $-0.31 < f_{T,1}/\Lambda^4 < 0.31$, $-0.63 < f_{T,2}/\Lambda^4 < 0.59$, $-0.43 < f_{T,8}/\Lambda^4 < 0.43$, $-0.92 < f_{T,9}/\Lambda^4 < 0.92$, in units of TeV^{-4}.

[2] TUMASYAN 21A study electroweak $Z\gamma$ production in association with two jets, where the Z boson decays to electron or muon pairs and the pair of two jets has high invariant mass, superseeding SIRUNYAN 20AL. The number of observed (expected) electron events in the barrel and endcap regions are 375 (349 $\pm$ 9) and 174 (166 $\pm$ 6) events, respectively, while for muon events the respective numbers are 584 (612 $\pm$ 13) and 320 (303 $\pm$ 8). Analysing the $Z\gamma$ invariant mass distribution, the following 95% C.L. limits are derived: $-15.8 < f_{M,0}/\Lambda^4 < 16.0$, $-35.0 < f_{M,1}/\Lambda^4 < 34.7$, $-6.55 < f_{M,2}/\Lambda^4 < 6.49$, $-13.0 < f_{M,3}/\Lambda^4 < 13.0$, $-13.0 < f_{M,4}/\Lambda^4 < 12.7$, $-22.2 < f_{M,5}/\Lambda^4 < 21.3$, $-56.6 < f_{M,7}/\Lambda^4 < 55.9$, $-0.64 < f_{T,0}/\Lambda^4 < 0.57$, $-0.81 < f_{T,1}/\Lambda^4 < 0.90$, $-1.68 < f_{T,2}/\Lambda^4 < 1.54$, $-0.58 < f_{T,5}/\Lambda^4 < 0.64$, $-1.30 < f_{T,6}/\Lambda^4 < 1.33$, $-2.15 < f_{T,7}/\Lambda^4 < 2.43$, $-0.47 < f_{T,8}/\Lambda^4 < 0.47$, $-0.91 < f_{T,9}/\Lambda^4 < 0.91$, in units of TeV^{-4}.

[3] TUMASYAN 21B measure W or Z boson production in association with two photons, using the leptonic decays modes of W and Z with electrons or muons. The number of selected $W \rightarrow e(\mu)\nu$ events is 1987 (2384) and the number of selected $Z \rightarrow ee(\mu\mu)$ events is 110 (272) respectively. Analyzing the transverse momentum of the di-photon system, the following 95 % C.L. limits are derived in units of TeV^{-4}: In the W production channel, the observed limits are: $-39.9 < f_{M,2}/\Lambda^4 < 39.5$, $-63.8 < f_{M,3}/\Lambda^4 < 65.0$, $-1.30 < f_{T,0}/\Lambda^4 < 1.30$, $-1.70 < f_{T,1}/\Lambda^4 < 1.66$, $-3.64 < f_{T,2}/\Lambda^4 < 3.64$, $-0.52 < f_{T,5}/\Lambda^4 < 0.60$, $-0.60 < f_{T,6}/\Lambda^4 < 0.68$, $-1.16 < f_{T,7}/\Lambda^4 < 1.16$. In the Z production channel, the observed limits are: $-5.70 < f_{T,0}/\Lambda^4 < 5.46$, $-5.70 < f_{T,1}/\Lambda^4 < 5.46$, $-11.4 < f_{T,2}/\Lambda^4 < 10.9$, $-2.92 < f_{T,5}/\Lambda^4 < 2.92$, $-3.80 < f_{T,6}/\Lambda^4 < 3.88$, $-7.88 < f_{T,7}/\Lambda^4 < 7.72$, $-1.06 < f_{T,8}/\Lambda^4 < 1.10$, $-1.82 < f_{T,9}/\Lambda^4 < 1.82$, in units of TeV^{-4}.

[4] SIRUNAYN 20 study WZ and same-sign WW production in association with two jets, using the leptonic decays modes of the W and Z bosons with electrons or muons. Overall, 524 WW events and 229 WZ events are selected, with a Standard Model expectation of 535 $\pm$ 52 and 216 $\pm$ 21 events, respectively. Analyzing the transverse mass spectrum of the di-boson system and the di-jet invariant mass, the following 95% C.L. limits are derived, not using any unitarization procedure: $-0.25 < f_{T,0}/\Lambda^4 < 0.28$, $-0.12 < f_{T,1}/\Lambda^4 < 0.14$, $-0.35 < f_{T,2}/\Lambda^4 < 0.48$, $-2.7 < f_{M,0}/\Lambda^4 < 2.9$, $-4.1 < f_{M,1}/\Lambda^4 < 4.2$, $-5.4 < f_{M,6}/\Lambda^4 < 5.8$, $-5.7 < f_{M,7}/\Lambda^4 < 6.0$, $-5.7 < f_{S,0}/\Lambda^4 < 6.1$, $-16 < f_{S,1}/\Lambda^4 < 17$, in units of TeV^{-4}. The article also reports limits on these couplings by cutting the EFT expansion at the unitarity limit.

[5] SIRUNYAN 20AL study electroweak production of a Z boson and a photon in association with two jets in the electron and muon decay modes of the Z. A signal with a significance of 3.9 standard deviations is observed, compared to a Standard Model expectation of 5.2 standard deviations. Combining with KHACHATRYAN 17AA data at 8 TeV the final observed and expected signal significance is 4.7 and 5.5 standard deviations. Analyzing the Z-photon invariant mass distribution, the following 95% C.L. limits are derived: $-19.5 < f_{M,0}/\Lambda^4 < 20.3$, $-40.5 < f_{M,1}/\Lambda^4 < 39.5$, $-8.22 < f_{M,2}/\Lambda^4 < 8.10$, $-17.7 < f_{M,3}/\Lambda^4 < 17.9$, $-15.3 < f_{M,4}/\Lambda^4 < 15.8$, $-25.1 < f_{M,5}/\Lambda^4 < 24.5$, $-38.9 < f_{M,6}/\Lambda^4 < 40.6$, $-60.3 < f_{M,7}/\Lambda^4 < 62.5$, $-0.74 < f_{T,0}/\Lambda^4 < 0.69$, $-0.98 < f_{T,1}/\Lambda^4 < 0.96$, $-1.97 < f_{T,2}/\Lambda^4 < 1.86$, $-0.70 < f_{T,5}/\Lambda^4 < 0.75$, $-1.64 < f_{T,6}/\Lambda^4 < 1.68$, $-2.59 < f_{T,7}/\Lambda^4 < 2.82$, $-0.47 < f_{T,8}/\Lambda^4 < 0.47$, $-1.27 < f_{T,9}/\Lambda^4 < 1.27$, in units of TeV^{-4}.

[6] SIRUNYAN 20BD study electroweak $W\gamma$ production in association with two jets, where the W boson decays to electron or muon and the two jets have high invariant mass. The number of observed (expected) electron events with the photon in the barrel and endcap regions are 393 (397.1 $\pm$ 18.5) and 159 (145.2 $\pm$ 10.0) respectively, while for muon events the respective numbers are 565 (537.9 $\pm$ 21.4) and 201 (188.2 $\pm$ 10.5). Analyzing the $W\gamma$ invariant mass distribution, the following 95% C.L. limits are derived: $-8.1 < f_{M,0}/\Lambda^4 < 8.0$, $-12 < f_{M,1}/\Lambda^4 < 12$, $-2.8 < f_{M,2}/\Lambda^4 < 2.8$, $-4.4 < f_{M,3}/\Lambda^4 < 4.4$, $-5.0 < f_{M,4}/\Lambda^4 < 5.0$, $-8.3 < f_{M,5}/\Lambda^4 < 8.3$, $-16 < f_{M,6}/\Lambda^4 < 16$, $-21 < f_{M,7}/\Lambda^4 < 20$, $-0.6 < f_{T,0}/\Lambda^4 < 0.6$, $-0.4 < f_{T,1}/\Lambda^4 < 0.4$, $-1.0 < f_{T,2}/\Lambda^4 < 1.2$, $-0.5 < f_{T,5}/\Lambda^4 < 0.5$, $-0.4 < f_{T,6}/\Lambda^4 < 0.4$, $-0.9 < f_{T,7}/\Lambda^4 < 0.9$, in units of TeV^{-4}.

[7] SIRUNYAN 19BM search for the final state $W^+W^-W^\pm$ using W decays to electrons or muons. Two event samples are considered, events with three leptons, or events with two oppositely charged leptons accompanied by two jets. In a kinematic region selected to enhance the effect of anomalous couplings, no events are selected in the data, and 95% C.L. upper limits are obtained as follows: $-1.2 < f_{T,0}/\Lambda^4 < 1.2$, $-3.3 < f_{T,1}/\Lambda^4 < 3.3$, $-2.7 < f_{T,2}/\Lambda^4 < 2.6$, in units of TeV^{-4} and without application of a form factor.

[8] SIRUNYAN 19BP study WZ plus 2 jets production, using W and Z decay channels with electrons or muons. In the data, 75 events are selected, with a fitted SM signal of 15.1 $\pm$ 1.6 events and a fitted background of 62.4 $\pm$ 2.8 events. The transverse mass distribution of the WZ system is analyzed to set the following limits at 95% C.L., in units of TeV^{-4}: $-9.15 < f_{M,0}/\Lambda^4 < 9.15$, $-9.15 < f_{M,1}/\Lambda^4 < 9.45$, $-26.5 < f_{S,0}/\Lambda^4 < 27.5$, $-41.2 < f_{S,1}/\Lambda^4 < 42.8$, $-0.75 < f_{T,0}/\Lambda^4 < 0.81$, $-0.49 < f_{T,1}/\Lambda^4 < 0.55$, $-1.49 < f_{T,2}/\Lambda^4 < 1.85$.

[9] SIRUNYAN 19CQ search for anomalous electroweak production of vector boson pairs in association with two jets. Events are selected by requiring two jets with a large invariant mass and rapidity separation, one or two leptons (electrons or muons), and a W or Z boson decaying hadronically. In the WV (ZV) channel, 347 (47) events are selected in the data, with a total expected background of 352 $\pm$ 19 (50.3 $\pm$ 5.8) events. Analysing the mass distribution of the WV or ZV system, the following 95% C.L. limits are obtained: $-2.7 < f_{S,0}/\Lambda^4 < 2.7$, $-3.4 < f_{S,1}/\Lambda^4 < 3.4$, $-0.69 < f_{M,0}/\Lambda^4 < 0.70$, $-2.0 < f_{M,1}/\Lambda^4 < 2.1$, $-1.3 < f_{M,6}/\Lambda^4 < 1.3$, $-3.4 < f_{M,7}/\Lambda^4 < 3.4$, $-0.12 < f_{T,0}/\Lambda^4 < 0.11$, $-0.12 < f_{T,1}/\Lambda^4 < 0.13$, $-0.28 < f_{T,2}/\Lambda^4 < 0.28$, in units of TeV^{-4}.

[10] SIRUNYAN 18CC study pp collisions at $\sqrt{s}$ = 13 TeV leading to a pair of same-sign W pairs decaying leptonically (e or μ) associated with a pair of jets. Isolated leptons

Downloaded from https://academic.oup.com/ptep/article/2022/8/083C01/6651666 by KIT Library user on 27 September 2022

with $p_T > 25$ (20) GeV for the leading (trailing) lepton, with $|\eta| < 2.5$ (2.4) for e (μ) and jets with $p_T > 30$ GeV, $|\eta| < 5.0$, $|\Delta\eta_{jj}| > 2.5$ and $m_{jj} > 500$ GeV is required. Further cuts are applied to minimize $Z \to e\,e$ events, non-prompt leptons and hadronically decaying taus. The number of selected events is 201, with an expected SM signal of 66.9 ± 2.4 and background of 138 ± 13 events. Analysing the dilepton invariant mass spectrum the following 95% C.L. limits are derived: $-7.7 < f_{S,0}/\Lambda^4 < 7.7$, $-21.6 < f_{S,1}/\Lambda^4 < 21.8$, $-6.0 < f_{M,0}/\Lambda^4 < 5.9$, $-8.7 < f_{M,1}/\Lambda^4 < 9.1$, $-11.9 < f_{M,6}/\Lambda^4 < 11.8$, $-13.3 < f_{M,7}/\Lambda^4 < 12.9$, $-0.62 < f_{T,0}/\Lambda^4 < 0.65$, $-0.28 < f_{T,1}/\Lambda^4 < 0.31$, $-0.89 < f_{T,2}/\Lambda^4 < 1.02$.

[11] AABOUD 17AA analyze $W^\pm W^\pm$ production in association with two jets and W decay modes with electrons or muons. In the kinematic region of VBS the effect of anomalous QGCs is enhanced by requiring the transverse mass of the WW system to be larger than 400 GeV. In the data, 8 events are selected with a total background expected from SM processes of 3.8 ± 0.6 events. Assuming the other QGC coupling to have the SM value of zero, the observed event yield is used to determine 95% CL limits on the QGCs: $-0.14 < \alpha_4 < 0.15$ and $-0.22 < \alpha_5 < 0.22$. Supersedes AAD 14AM.

[12] AABOUD 17AG determine the $WW\gamma$ and $WZ\gamma$ cross sections in 8 TeV pp interactions by studying the final states $e\nu\mu\nu\gamma$ and $e\nu jj\gamma$ or $\mu\nu jj\gamma$. Upper limits on the production cross sections are derived in a fiducial region optimized for BSM physics. These are used to derive the following 95% C.L. upper limits for quartic couplings assuming the form scale factor, $\Lambda_{FF} = \infty$ (all in units of 10^3 TeV^{-4}): $-0.3 < f_{M,0}/\Lambda^4 < 0.3$, $-0.5 < f_{M,1}/\Lambda^4 < 0.5$, $-1.8 < f_{M,2}/\Lambda^4 < 1.8$, $-1.1 < f_{M,4}/\Lambda^4 < 1.1$, $-1.7 < f_{M,5}/\Lambda^4 < 1.7$, $-0.6 < f_{M,6}/\Lambda^4 < 0.6$, $-1.1 < f_{M,7}/\Lambda^4 < 1.1$, $-0.1 < f_{T,0}/\Lambda^4 < 0.1$, $-0.2 < f_{T,1}/\Lambda^4 < 0.2$, $-0.4 < f_{T,4}/\Lambda^4 < 0.4$, $-1.5 < f_{T,5}/\Lambda^4 < 1.6$, $-1.9 < f_{T,6}/\Lambda^4 < 1.9$, $-4.3 < f_{T,7}/\Lambda^4 < 4.3$.

[13] AABOUD 17D analyze electroweak diboson (WV, $V = W, Z$) production in association with a high-mass dijet system. In the data, 32 events are selected with an expected total background of 32 ± 12 events. Analysing the transverse mass distribution of the WV system, the following limits are set at 95% C.L.: $-0.024 < \alpha_4 < 0.030$ and $-0.028 < \alpha_5 < 0.033$.

[14] AABOUD 17J analyze the $Z\gamma$ production in association with a high-mass dijet system, with the Z boson decaying into a pair of electrons, muons, or neutrinos. In the charged lepton (neutrino) channel, events are selected with a dijet mass larger than 500 (600) GeV and a transverse photon energy larger than 250 (150) GeV, with 2 (4) events selected in the data and 0.30 ± 0.08 (1.6 ± 0.5) expected background events. The observed event yield is used to determine 95% CL limits as follows: $-4.1 \times 10^3 < f_{T,9}/\Lambda^4 < 4.2 \times 10^3$, $-1.9 \times 10^3 < f_{T,8}/\Lambda^4 < 2.1 \times 10^3$, $-1.9 \times 10^1 < f_{T,0}/\Lambda^4 < 1.6 \times 10^1$, $-1.6 \times 10^2 < f_{M,0}/\Lambda^4 < 1.8 \times 10^2$, $-3.5 \times 10^2 < f_{M,1}/\Lambda^4 < 3.4 \times 10^2$, $-8.9 \times 10^2 < f_{M,2}/\Lambda^4 < 8.9 \times 10^2$, $-1.7 \times 10^3 < f_{M,3}/\Lambda^4 < 1.7 \times 10^3$, in units of TeV^{-4} and without application of a form factor.

[15] AABOUD 17M analyze tri-boson $W^\pm W^\pm W^\mp$ production in decay channels with three charged leptons or two like-sign charged leptons with two jets, where the lepton can be an electron or muon. In the data, 24 tri-lepton events and 21 di-lepton plus jets events are selected, compared to a total event yield expected in the SM of 30.8 ± 3.0 and 21.9 ± 2.0, respectively. Analysing the tri-lepton transverse mass or the transverse momentum sum of the two leptons, two jets and the missing transverse energy, the following limits at 95% CL are derived for the form factor cut-off scale $\Lambda_{FF} \to \infty$: $-0.13 < f_{S,0}/\Lambda^4 < 0.18$, $-0.21 < f_{S,1}/\Lambda^4 < 0.27$, in units of 10^4 TeV^{-4}, which are converted into the following limits: $-0.49 < \alpha_4 < 0.75$ and $-0.48 < \alpha_5 < 0.62$.

[16] KHACHATRYAN 17AA analyse electroweak production of $Z\gamma$ in association with two hadronic jets, with the Z boson decaying to electron or muon pairs. Events with photon transverse momentum larger than 60 GeV and di-jet invariant mass larger than 400 GeV are selected. The $Z\gamma$ inavariant mass spectrum is analysed to set 95% C.L. limits as follows: $-71 < f_{M,0}/\Lambda^4 < 75$, $-190 < f_{M,1}/\Lambda^4 < 182$, $-32 < f_{M,2}/\Lambda^4 < 31$, $-58 < f_{M,3}/\Lambda^4 < 59$, $-3.8 < f_{T,0}/\Lambda^4 < 3.4$, $-4.4 < f_{T,1}/\Lambda^4 < 4.4$, $-9.9 < f_{T,2}/\Lambda^4 < 9.0$, $-1.8 < f_{T,8}/\Lambda^4 < 1.8$, $-4.0 < f_{T,9}/\Lambda^4 < 4.0$, in units of TeV^{-4} and without application of a form factor.

[17] KHACHATRYAN 17M analyse electroweak production of $W\gamma$ in association with two hadronic jets, with the W boson decaying to electrons or muons. Events with photon transverse momentum larger than 200 GeV and di-jet invariant mass larger than 200 GeV are selected. The W transverse momentum spectrum is analysed to set 95% C.L. limits as follows: $-77 < f_{M,0}/\Lambda^4 < 74$, $-125 < f_{M,1}/\Lambda^4 < 129$, $-26 < f_{M,2}/\Lambda^4 < 26$, $-43 < f_{M,3}/\Lambda^4 < 44$, $-40 < f_{M,4}/\Lambda^4 < 40$, $-65 < f_{M,5}/\Lambda^4 < 65$, $-129 < f_{M,6}/\Lambda^4 < 129$, $-164 < f_{M,7}/\Lambda^4 < 162$, $-5.4 < f_{T,0}/\Lambda^4 < 5.6$, $-3.7 < f_{T,1}/\Lambda^4 < 4.0$, $-11 < f_{T,2}/\Lambda^4 < 12$, $-3.8 < f_{T,5}/\Lambda^4 < 3.8$, $-2.8 < f_{T,6}/\Lambda^4 < 3.0$, $-7.3 < f_{T,7}/\Lambda^4 < 7.7$, in units of TeV^{-4} and without application of a form factor.

[18] SIRUNYAN 17AD study pp collisions at $\sqrt{s} = 13$ TeV to determine the cross section of $ZZjj$ with the Z decaying to $e\,e$ or $\mu\mu$. The ZZ mass distribution is used to set upper limits on the anomalous quartic couplings. The 95% upper limits for the relevant quartic couplings in units of TeV^{-4} are: $-0.46 < f_{T,0}/\Lambda^4 < 0.44$, $-0.61 < f_{T,1}/\Lambda^4 < 0.61$, $-1.2 < f_{T,2}/\Lambda^4 < 1.2$, $-0.84 < f_{T,8}/\Lambda^4 < 0.84$, $-1.8 < f_{T,9}/\Lambda^4 < 1.8$.

[19] SIRUNYAN 17AR study pp collisions at $\sqrt{s} = 8$ TeV to determine the cross section of $pp \to W\gamma\gamma$ and $pp \to Z\gamma\gamma$ where $W \to \ell\nu$ and $Z \to \ell^+\ell^-$, ℓ being an electron or a muon. The number of W events in the e and μ channels is 63 and 108 respectively, and the number of Z events in the e and μ channels is 117 and 141. To increase sensitivity, the transverse momentum of the leading photon is required to be larger than 70 GeV. The 95% C.L. upper limits in units of TeV^{-4} are $-701 < f_{M,2}/\Lambda^4 < 683$, $-1170 < f_{M,3}/\Lambda^4 < 1220$, $-33.5 < f_{T,0}/\Lambda^4 < 34.0$, $-44.3 < f_{T,1}/\Lambda^4 < 44.8$, $-93.8 < f_{T,2}/\Lambda^4 < 93.2$.

[20] AABOUD 16E study WW production in two-photon mediated pp collisions at 8 TeV where the W boson decays into an electron or muon, probing the $\gamma\gamma WW$ vertex for anomalous quartic gauge couplings. The lepton p_T is required to be larger than 30 GeV. Limits on anomalous couplings are determined from events with p_T larger than 120 GeV where the aQGC effect is enhanced and the SM background reduced; in the data corresponding to an integrated luminosity of 20.2fb^{-1}, 1 event is selected with an expected SM background of 0.37 ± 0.13 events. The 95% C.L. limits without a form-factor cutoff ($\Lambda_{\rm cutoff} \to \infty$) are as follows: $-1.7 < a_0^W/\Lambda^2 < 1.7$ and $-6.4 < a_C^W/\Lambda^2 < 6.3$ in units of 10^{-6} GeV^{-2}. In terms of another set of variables: $-6.6 < f_{M,0}/\Lambda^4 < 6.6$ and $-24 < f_{M,1}/\Lambda^4 < 25$ in units of 10^{-11} GeV^{-4}.

[21] AAD 16Q study $Z\gamma\gamma$ production in pp collisions. In events with no additional jets, 29 (22) Z decays to electron (muon) pairs are selected, with an expected background of 3.3 ± 1.1 (6.5 ± 2.0) events, as well as 19 Z decays to netrino pairs with an expected background of 8.3 ± 4.4 events. Analysing the photon transverse momentum distribution for $m_{\gamma\gamma}$ above 200 GeV (300 GeV) for lepton (neutrino) events, yields the 95% C.L. limits: $-1.6 \times 10^4 < f_{M,2}/\Lambda^4 < 1.6 \times 10^4$, $-2.9 \times 10^4 < f_{M,3}/\Lambda^4 < 2.7 \times 10^4$, $-0.86 \times 10^2 < f_{T,0}/\Lambda^4 < 1.03 \times 10^2$, $-0.69 \times 10^3 < f_{T,5}/\Lambda^4 < 0.68 \times 10^3$, $-0.74 \times 10^4 < f_{T,9}/\Lambda^4 < 0.74 \times 10^4$ in units of TeV^{-4} and without application of a form factor $\Lambda_{\rm FF}$.

[22] KHACHATRYAN 16AX searches for anomalous $WW\gamma\gamma$ quartic gauge couplings in the two-photon-mediated process $pp \to pp\,WW$, assuming the $WW\gamma$ triple gauge boson couplings to be at their Standard Model values. 13 events containing an $e^\pm\mu^\mp$ pair with $p_T(e, \mu) > 30$ GeV are selected in a total luminosity of 19.7 fb^{-1}, with an expected $\gamma\gamma \to WW$ signal of 5.3 ± 0.1 events and an expected background of 3.9 ± 0.5 events. When combining with the data collected at 7 TeV (CHATRCHYAN 13AA), and not assuming a form factor, the following 1-parameter limits at 95% C.L. are obtained from the $p_T(e, \mu)$ spectrum: $|a_0^W/\Lambda^2| < 1.1 \times 10^{-6}$ GeV^{-2} ($a_C^W = 0$), and $|a_C^W/\Lambda^2| < 4.1 \times 10^{-6}$ GeV^{-2} ($a_0^W = 0$). In terms of another set of variables: $|f_{M,0}/\Lambda^4| < 4.2 \times 10^{-12}$ GeV^{-4}, $|f_{M,1}/\Lambda^4| < 16 \times 10^{-12}$ GeV^{-4}, $|f_{M,2}/\Lambda^4| < 2.1 \times 10^{-12}$ GeV^{-4}, $|f_{M,3}/\Lambda^4| < 7.8 \times 10^{-12}$ GeV^{-4}.

[23] AAD 15N study $W\gamma\gamma$ events in 8 TeV pp interactions, where the W decays into an electron or a muon. The events are characterized by an isolated lepton, a missing transverse energy due to the decay neutrino, and two isolated photons, with the p_T of the lepton and the photons being > 20 GeV. The number of candidate events observed in the electron channel for N(jet) ≥ 0 and N(jet) $= 0$ is 47 and 15, the corresponding numbers for the muon channel being 110 and 53. The backgrounds expected are 30.2 ± 7.4, 8.7 ± 3.0, 52.1 ± 12.2, and 24.4 ± 8.3 respectively. The 95% C.L. limits on the values of the parameters $f_{T,0}/\Lambda^4$, $f_{M,2}/\Lambda^4$ and $f_{M,3}/\Lambda^4$ are -0.9–0.9×10^2, -0.8–0.8×10^4, and -1.5–1.4×10^4 respectively, without application of a form factor $\Lambda_{\rm FF}$.

[24] KHACHATRYAN 15D study vector-boson-scattering tagged by two jets, requiring two same-sign charged leptons arising from $W^\pm W^\pm$ production and decay. The two jets must have a transverse momentum larger than 30 GeV, while the leptons, electrons or muons, must have a transverse momentum > 20 GeV. The dijet mass is required to be > 500 GeV, the dilepton mass > 50 GeV, with additional requirement of differing from the Z mass by > 15 GeV. In the two categories W^+W^+ and W^-W^-, 10 and 2 data events are observed in a data sample corresponding to an integrated luminosity of 19.4 fb^{-1}, with an expected background of 3.1 ± 0.6 and 2.6 ± 0.5 events. Analysing the distribution of the dilepton invariant mass, the following limits at 95% C.L. are obtained, in units of TeV^{-4}: $-38 < F_{S,0}/\Lambda^4 < 40$, $-118 < F_{S,1}/\Lambda^4 < 120$, $-33 < F_{M,0}/\Lambda^4 < 32$, $-44 < F_{M,1}/\Lambda^4 < 47$, $-65 < F_{M,6}/\Lambda^4 < 63$, $-70 < F_{M,7}/\Lambda^4 < 66$, $-4.2 < F_{T,0}/\Lambda^4 < 4.6$, $-1.9 < F_{T,1}/\Lambda^4 < 2.2$, $-5.2 < F_{T,2}/\Lambda^4 < 6.4$.

[25] AAD 14AM analyze electroweak production of WW jet jet same-charge diboson plus two jets production, with the W bosons decaying to electron or muon, to study the quartic $WWWW$ coupling. In a kinematic region enhancing the electroweak production over the strong production, 34 events are observed in the data while 29.8 ± 2.4 events are expected with a backgound of 15.9 ± 1.9 events. Assuming the other QGC coupling to have the SM value of zero, the observed event yield is used to determine 95% CL limits on the quartic gauge couplings: $-0.14 < \alpha_4 < 0.16$ and $-0.23 < \alpha_5 < 0.24$.

[26] CHATRCHYAN 14Q study $WV\gamma$ production in 8 TeV pp collisions, in the single lepton final state, with $W \to \ell\nu$, $Z \to$ dijet or $W \to \ell\nu$, $W \to$ dijet, the dijet mass resolution precluding differentiation between the W and Z. p_T and pseudo-rapidity cuts are put on the lepton, the photon and the two jets to minimize backgrounds. The dijet mass is required to be between 70–100 GeV and $|\Delta\eta_{jj}| < 1.4$. The selected number of muon (electron) events are 183 (139), with SM expectation being 194.2 ± 11.5 (147.9 ± 10.7) including signal and background. The photon E_T distribution is used to set limits on the anomalous quartic couplings. The following 95% CL limits are deduced (all in units of TeV^{-2} or TeV^{-4}): $-21 < a_0^W/\Lambda^2 < 20$, $-34 < a_c^W/\Lambda^2 < 32$, $-12 < \kappa_0^W/\Lambda^2 < 10$ and $-18 < \kappa_c^W/\Lambda^2 < 17$; and $-25 < f_{T,0}/\Lambda^4 < 24$ TeV^{-4}.

[27] ABAZOV 13D searches for anomalous $WW\gamma\gamma$ quartic gauge couplings in the two-photon-mediated process $pp \to pp\,WW$, assuming the $WW\gamma$ triple gauge boson couplings to be at their Standard Model values. 946 events containing an e^+e^- pair with missing energy are selected in a total luminosity of 9.7 fb^{-1}, with an expectation of 983 ± 108 events from Standard-Model processes. The following 1-parameter limits at 95% CL are otained: $|a_0^W/\Lambda^2| < 4.3 \times 10^{-4}$ GeV^{-2} ($a_c^W = 0$), $|a_c^W/\Lambda^2| < 1.5 \times 10^{-3}$ GeV^{-2} ($a_0^W = 0$).

[28] CHATRCHYAN 13AA searches for anomalous $WW\gamma\gamma$ quartic gauge couplings in the two-photon-mediated process $pp \to pp\,WW$, assuming the $WW\gamma$ triple gauge boson couplings to be at their Standard Model values. 2 events containing an $e^\pm\mu^\mp$ pair with $p_T(e, \mu) > 30$ GeV are selected in a total luminosity of 5.05 fb^{-1}, with an expected $pp\,WW$ signal of 2.2 ± 0.4 events and an expected background of 0.84 ± 0.15 events. The following 1-parameter limits at 95% CL are otained from the $p_T(e, \mu)$ spectrum: $|a_0^W/\Lambda^2| < 4.0 \times 10^{-6}$ GeV^{-2} ($a_c^W = 0$), $|a_c^W/\Lambda^2| < 1.5 \times 10^{-5}$ GeV^{-2} ($a_0^W = 0$).

[29] ABBIENDI 04B select 187 $e^+e^- \to W^+W^-\gamma$ events in the C.M. energy range 180–209 GeV, where $E_\gamma > 2.5$ GeV, the photon has a polar angle $|\cos\theta_\gamma| < 0.975$ and is well isolated from the nearest jet and charged lepton, and the effective masses of both fermion-antifermion systems agree with the W mass within 3 Γ_W. The measured differential cross section as a function of the photon energy and photon polar angle is used to extract the 95% CL limits: -0.020 GeV$^{-2} < a_0/\Lambda^2 < 0.020$ GeV^{-2}, -0.053 GeV$^{-2} < a_c/\Lambda^2 < 0.037$ GeV^{-2} and -0.16 GeV$^{-2} < a_n/\Lambda^2 < 0.15$ GeV^{-2}.

[30] ABBIENDI 04L select 20 $e^+e^- \to \nu\overline{\nu}\gamma\gamma$ acoplanar events in the energy range 180–209 GeV and 176 $e^+e^- \to q\overline{q}\gamma\gamma$ events in the energy range 130–209 GeV. These samples

Downloaded from https://academic.oup.com/ptep/article/2022/8/083C01/6651666 by KIT Library user on 27 September 2022

are used to constrain possible anomalous $W^+W^-\gamma\gamma$ and $ZZ\gamma\gamma$ quartic couplings. Further combining with the $W^+W^-\gamma$ sample of ABBIENDI 04B the following one–parameter 95% CL limits are obtained: $-0.007 < a_0^Z/\Lambda^2 < 0.023$ GeV^{-2}, $-0.029 < a_C^Z/\Lambda^2 < 0.029$ GeV^{-2}, $-0.020 < a_0^W/\Lambda^2 < 0.020$ GeV^{-2}, $-0.052 < a_C^W/\Lambda^2 < 0.037$ GeV^{-2}.

[31] In the CM energy range 183 to 209 GeV HEISTER 04A select 30 $e^+e^- \to \nu\overline{\nu}\gamma\gamma$ events with two acoplanar, high energy and high transverse momentum photons. The photon–photon acoplanarity is required to be $> 5^\circ$, $E_\gamma/\sqrt{s} > 0.025$ (the more energetic photon having energy $> 0.2\sqrt{s}$), $p_{T_\gamma}/E_{\rm beam} > 0.05$ and $|\cos\theta_\gamma| < 0.94$. A likelihood fit to the photon energy and recoil missing mass yields the following one–parameter 95% CL limits: $-0.012 < a_0^Z/\Lambda^2 < 0.019$ GeV^{-2}, $-0.041 < a_C^Z/\Lambda^2 < 0.044$ GeV^{-2}, $-0.060 < a_0^W/\Lambda^2 < 0.055$ GeV^{-2}, $-0.099 < a_C^W/\Lambda^2 < 0.093$ GeV^{-2}.

[32] ABDALLAH 03I select 122 $e^+e^- \to W^+W^-\gamma$ events in the C.M. energy range 189–209 GeV, where $E_\gamma > 5$ GeV, the photon has a polar angle $|\cos\theta_\gamma| < 0.95$ and is well isolated from the nearest charged fermion. A fit to the photon energy spectra yields $a_C/\Lambda^2 = 0.000^{+0.019}_{-0.040}$ GeV^{-2}, $a_0/\Lambda^2 = -0.004^{+0.018}_{-0.010}$ GeV^{-2}, $\tilde{a}_0/\Lambda^2 = -0.007^{+0.019}_{-0.008}$ GeV^{-2}, $a_n/\Lambda^2 = -0.09^{+0.16}_{-0.05}$ GeV^{-2}, and $\tilde{a}_n/\Lambda^2 = +0.05^{+0.07}_{-0.15}$ GeV^{-2}, keeping the other parameters fixed to their Standard Model values (0). The 95% CL limits are: -0.063 GeV$^{-2} < a_C/\Lambda^2 < +0.032$ GeV^{-2}, -0.020 GeV$^{-2} < a_0/\Lambda^2 < +0.020$ GeV^{-2}, -0.020 GeV$^{-2} < \tilde{a}_0/\Lambda^2 < +0.020$ GeV^{-2}, -0.18 GeV$^{-2} < a_n/\Lambda^2 < +0.14$ GeV^{-2}, -0.16 GeV$^{-2} < \tilde{a}_n/\Lambda^2 < +0.17$ GeV^{-2}.

[33] ACHARD 02F select 86 $e^+e^- \to W^+W^-\gamma$ events at 192–207 GeV, where $E_\gamma > 5$ GeV and the photon is well isolated. They also select 43 acoplanar $e^+e^- \to \nu\overline{\nu}\gamma\gamma$ events in this energy range, where the photon energies are >5 GeV and >1 GeV and the photon polar angles are between 14° and 166°. All these 43 events are in the recoil mass region corresponding to the Z (75–110 GeV). Using the shape and normalization of the photon spectra in the $W^+W^-\gamma$ events, and combining with the 42 event sample from 189 GeV data (ACCIARRI 00T), they obtain: $a_0/\Lambda^2 = 0.000 \pm 0.010$ GeV^{-2}, $a_C/\Lambda^2 = -0.013 \pm 0.023$ GeV^{-2}, and $a_n/\Lambda^2 = -0.002 \pm 0.076$ GeV^{-2}. Further combining the analyses of $W^+W^-\gamma$ events with the low recoil mass region of $\nu\overline{\nu}\gamma\gamma$ events (including samples collected at $183 + 189$ GeV), they obtain the following one-parameter 95% CL limits: -0.015 GeV$^{-2} < a_0/\Lambda^2 < 0.015$ GeV^{-2}, -0.048 GeV$^{-2} < a_C/\Lambda^2 < 0.026$ GeV^{-2}, and -0.14 GeV$^{-2} < a_n/\Lambda^2 < 0.13$ GeV^{-2}.

W REFERENCES

AAIJ	22C	JHEP 2201 036	R. Aaij *et al.*	(LHCb Collab.)
AALTONEN	22	SCI 376 170	T. Aaltonen *et al.*	(CDF Collab.)
PDG	22	PTEP 2022 083C01	R.L. Workman *et al.*	(PDG Collab.)
AAD	21AC	EPJ C81 163	G. Aad *et al.*	(ATLAS Collab.)
AAD	21AN	NATP 17 813	G. Aad *et al.*	(ATLAS Collab.)
AAD	21W	JHEP 2106 003	G. Aad *et al.*	(ATLAS Collab.)
SIRUNYAN	21	PL B812 135992	A.M. Sirunyan *et al.*	(CMS Collab.)
SIRUNYAN	21G	PRL 126 252002	A.M. Sirunyan *et al.*	(CMS Collab.)
SIRUNYAN	21I	PL B819 136409	A.M. Sirunyan *et al.*	(CMS Collab.)
TUMASYAN	21A	PR D104 072001	A. Tumasyan *et al.*	(CMS Collab.)
TUMASYAN	21B	JHEP 2110 174	A. Tumasyan *et al.*	(CMS Collab.)
SIRUNAYN	20	PL B809 135710	A.M. Sirunyan *et al.*	(CMS Collab.)
SIRUNYAN	20AL	JHEP 2006 076	A.M. Sirunyan *et al.*	(CMS Collab.)
SIRUNYAN	20BA	EPJ C80 43	A.M. Sirunyan *et al.*	(CMS Collab.)
SIRUNYAN	20BD	PL B811 135988	A.M. Sirunyan *et al.*	(CMS Collab.)
SIRUNYAN	20BF	PR D102 092001	A.M. Sirunyan *et al.*	(CMS Collab.)
AABOUD	19BA	EPJ C79 884	M. Aaboud *et al.*	(ATLAS Collab.)
SIRUNYAN	19AD	JHEP 1904 122	A.M. Sirunyan *et al.*	(CMS Collab.)
SIRUNYAN	19BG	PRL 122 151802	A.M. Sirunyan *et al.*	(CMS Collab.)
SIRUNYAN	19BM	PR D100 012004	A.M. Sirunyan *et al.*	(CMS Collab.)
SIRUNYAN	19BP	PL B795 281	A.M. Sirunyan *et al.*	(CMS Collab.)
SIRUNYAN	19CL	JHEP 1912 062	A.M. Sirunyan *et al.*	(CMS Collab.)
SIRUNYAN	19CQ	PL B798 134985	A.M. Sirunyan *et al.*	(CMS Collab.)
AABOUD	18J	EPJ C78 110	M. Aaboud *et al.*	(ATLAS Collab.)
Also		EPJ C78 898 (errat.)	M. Aaboud *et al.*	(ATLAS Collab.)
AABOUD	18Q	PR D97 032005	M. Aaboud *et al.*	(ATLAS Collab.)
ANDREEV	18A	EPJ C78 777	V. Andreev *et al.*	(H1 Collab.)
SIRUNYAN	18BZ	EPJ C78 589	A.M. Sirunyan *et al.*	(CMS Collab.)
SIRUNYAN	18CC	PRL 120 081801	A.M. Sirunyan *et al.*	(CMS Collab.)
AABOUD	17AA	PR D96 012007	M. Aaboud *et al.*	(ATLAS Collab.)
AABOUD	17AG	EPJ C77 646	M. Aaboud *et al.*	(ATLAS Collab.)
AABOUD	17D	PR D95 032001	M. Aaboud *et al.*	(ATLAS Collab.)
AABOUD	17J	JHEP 1707 107	M. Aaboud *et al.*	(ATLAS Collab.)
AABOUD	17M	EPJ C77 141	M. Aaboud *et al.*	(ATLAS Collab.)
AABOUD	17Q	EPJ C77 367	M. Aaboud *et al.*	(ATLAS Collab.)
AABOUD	17S	EPJ C77 474	M. Aaboud *et al.*	(ATLAS Collab.)
AABOUD	17U	EPJ C77 563	M. Aaboud *et al.*	(ATLAS Collab.)
KHACHATRY...	17AA	PL B770 380	V. Khachatryan *et al.*	(CMS Collab.)
KHACHATRY...	17M	JHEP 1706 106	V. Khachatryan *et al.*	(CMS Collab.)
KHACHATRY...	17O	EPJ C77 236	V. Khachatryan *et al.*	(CMS Collab.)
SIRUNYAN	17AD	PL B774 682	A.M. Sirunyan *et al.*	(CMS Collab.)
SIRUNYAN	17AR	JHEP 1710 072	A.M. Sirunyan *et al.*	(CMS Collab.)
SIRUNYAN	17X	PL B772 21	A.M. Sirunyan *et al.*	(CMS Collab.)
AABOUD	16E	PR D94 032011	M. Aaboud *et al.*	(ATLAS Collab.)
AAD	16AR	JHEP 1609 029	G. Aad *et al.*	(ATLAS Collab.)
AAD	16P	PR D93 092004	G. Aad *et al.*	(ATLAS Collab.)
AAD	16Q	PR D93 112002	G. Aad *et al.*	(ATLAS Collab.)
AAIJ	16AJ	JHEP 1610 030	R. Aaij *et al.*	(LHCb Collab.)
KHACHATRY...	16AX	JHEP 1608 119	V. Khachatryan *et al.*	(CMS Collab.)
KHACHATRY...	16BI	EPJ C76 401	V. Khachatryan *et al.*	(CMS Collab.)
AAD	15N	PRL 115 031802	G. Aad *et al.*	(ATLAS Collab.)
KHACHATRY...	15D	PRL 114 051801	V. Khachatryan *et al.*	(CMS Collab.)
AAD	14AM	PRL 113 141803	G. Aad *et al.*	(ATLAS Collab.)
AAD	14Y	JHEP 1404 031	G. Aad *et al.*	(ATLAS Collab.)
AALTONEN	14D	PR D89 072003	T. Aaltonen *et al.*	(CDF Collab.)
CHATRCHYAN	14AB	PR D89 092005	S. Chatrchyan *et al.*	(CMS Collab.)
CHATRCHYAN	14Q	PR D90 032008	S. Chatrchyan *et al.*	(CMS Collab.)
AAD	13AL	PR D87 112001	G. Aad *et al.*	(ATLAS Collab.)
Also		PR D88 079906 (errat.)	G. Aad *et al.*	(ATLAS Collab.)
AAD	13AN	PR D87 112003	G. Aad *et al.*	(ATLAS Collab.)
Also		PR D91 119901 (errat.)	G. Aad *et al.*	(ATLAS Collab.)
AALTONEN	13N	PR D88 052018	T. Aaltonen *et al.*	(CDF and D0 Collabs.)
ABAZOV	13D	PR D88 012005	V.M. Abazov *et al.*	(D0 Collab.)
CHATRCHYAN	13AA	JHEP 1307 116	S. Chatrchyan *et al.*	(CMS Collab.)
CHATRCHYAN	13BF	EPJ C73 2610	S. Chatrchyan *et al.*	(CMS Collab.)
SCHAEL	13A	PRPL 532 119	S. Schael *et al.*	
AAD	12AC	PL B712 289	G. Aad *et al.*	(ATLAS Collab.)
AAD	12BX	PL B717 49	G. Aad *et al.*	(ATLAS Collab.)
AAD	12CD	EPJ C72 2173	G. Aad *et al.*	(ATLAS Collab.)
AAD	12V	PL B709 341	G. Aad *et al.*	(ATLAS Collab.)
AALTONEN	12AC	PR D86 031104	T. Aaltonen *et al.*	(CDF Collab.)
AALTONEN	12E	PRL 108 151803	T. Aaltonen *et al.*	(CDF Collab.)
AALTONEN	12W	PR D85 032001	T. Aaltonen *et al.*	(CDF Collab.)
ABAZOV	12AG	PL B718 451	V.M. Abazov *et al.*	(D0 Collab.)
ABAZOV	12F	PRL 108 151804	V.M. Abazov *et al.*	(D0 Collab.)
Also		PR D89 012005	V.M. Abazov *et al.*	(D0 Collab.)
ABAZOV	11	PL B695 67	V.M. Abazov *et al.*	(D0 Collab.)
ABAZOV	11AC	PRL 107 241803	V.M. Abazov *et al.*	(D0 Collab.)
BLINOV	11	PL B699 287	A.E. Blinov, A.S. Rudenko	(NOVO)
CHATRCHYAN	11M	PL B701 535	S. Chatrchyan *et al.*	(CMS Collab.)
AALTONEN	10K	PRL 104 201801	T. Aaltonen *et al.*	(CDF Collab.)
Also		PRL 105 019905(errat.)	T. Aaltonen *et al.*	(CDF Collab.)
ABDALLAH	10	EPJ C66 35	J. Abdallah *et al.*	(DELPHI Collab.)
AARON	09B	EPJ C64 251	F.D. Aaron *et al.*	(H1 Collab.)
ABAZOV	09AB	PRL 103 141801	V.M. Abazov *et al.*	(D0 Collab.)
ABAZOV	09AD	PR D80 053012	V.M. Abazov *et al.*	(D0 Collab.)
ABAZOV	09AJ	PRL 103 191801	V.M. Abazov *et al.*	(D0 Collab.)
ABAZOV	09AK	PRL 103 231802	V.M. Abazov *et al.*	(D0 Collab.)
AALTONEN	08B	PRL 100 071801	T. Aaltonen *et al.*	(CDF Collab.)
ABAZOV	08R	PRL 100 241805	V.M. Abazov *et al.*	(D0 Collab.)
ABDALLAH	08A	EPJ C55 1	J. Abdallah *et al.*	(DELPHI Collab.)
ABDALLAH	08C	EPJ C54 345	J. Abdallah *et al.*	(DELPHI Collab.)
AALTONEN	07F	PRL 99 151801	T. Aaltonen *et al.*	(CDF Collab.)
Also		PR D77 112001	T. Aaltonen *et al.*	(CDF Collab.)
AALTONEN	07L	PR D76 111103	T. Aaltonen *et al.*	(CDF Collab.)
ABAZOV	07Z	PR D76 111104	V.M. Abazov *et al.*	(D0 Collab.)
ABBIENDI	07A	EPJ C52 767	G. Abbiendi *et al.*	(OPAL Collab.)
ABAZOV	06H	PR D74 057101	V.M. Abazov *et al.*	(D0 Collab.)
Also		PR D74 059904(errat.)	V.M. Abazov *et al.*	(D0 Collab.)
ABBIENDI	06	EPJ C45 307	G. Abbiendi *et al.*	(OPAL Collab.)
ABBIENDI	06A	EPJ C45 291	G. Abbiendi *et al.*	(OPAL Collab.)
ACHARD	06	EPJ C45 569	P. Achard *et al.*	(L3 Collab.)
AKTAS	06	PL B632 35	A. Aktas *et al.*	(H1 Collab.)
SCHAEL	06	EPJ C47 309	S. Schael *et al.*	(ALEPH Collab.)
ABAZOV	05J	PR D71 091108	V.M. Abazov *et al.*	(D0 Collab.)
ABAZOV	05S	PRL 95 141802	V.M. Abazov *et al.*	(D0 Collab.)
SCHAEL	05A	PL B614 7	S. Schael *et al.*	(ALEPH Collab.)
ABAZOV	04D	PR D70 092008	V.M. Abazov *et al.*	(D0 Collab.)
ABBIENDI	04B	PL B580 17	G. Abbiendi *et al.*	(OPAL Collab.)
ABBIENDI	04D	EPJ C33 463	G. Abbiendi *et al.*	(OPAL Collab.)
ABBIENDI	04L	PR D70 032005	G. Abbiendi *et al.*	(OPAL Collab.)
ABDALLAH	04G	EPJ C34 127	J. Abdallah *et al.*	(DELPHI Collab.)
ACHARD	04D	PL B586 151	P. Achard *et al.*	(L3 Collab.)
ACHARD	04J	PL B600 22	P. Achard *et al.*	(L3 Collab.)
HEISTER	04A	PL B602 31	A. Heister *et al.*	(ALEPH Collab.)
SCHAEL	04A	EPJ C38 147	S. Schael *et al.*	(ALEPH Collab.)
ABBIENDI	03C	EPJ C26 321	G. Abbiendi *et al.*	(OPAL Collab.)
ABDALLAH	03I	EPJ C31 139	J. Abdallah *et al.*	(DELPHI Collab.)
ABAZOV	02D	PR D66 012001	V.M. Abazov *et al.*	(D0 Collab.)
ABAZOV	02E	PR D66 032008	V.M. Abazov *et al.*	(D0 Collab.)
ACHARD	02F	PL B527 29	P. Achard *et al.*	(L3 Collab.)
CHEKANOV	02C	PL B539 197	S. Chekanov *et al.*	(ZEUS Collab.)
ABBIENDI	01H	EPJ C19 229	G. Abbiendi *et al.*	(OPAL Collab.)
ABREU	01I	PL B502 9	P. Abreu *et al.*	(DELPHI Collab.)
AFFOLDER	01E	PR D64 052001	T. Affolder *et al.*	(CDF Collab.)
ABBIENDI	00V	PL B490 71	G. Abbiendi *et al.*	(OPAL Collab.)
ABBOTT	00B	PR D61 072001	B. Abbott *et al.*	(D0 Collab.)
ABBOTT	00D	PRL 84 5710	B. Abbott *et al.*	(D0 Collab.)
ABREU,P	00F	EPJ C18 203	P. Abreu *et al.*	(DELPHI Collab.)
Also		EPJ C25 493 (errat.)	P. Abreu *et al.*	(DELPHI Collab.)
ACCIARRI	00T	PL B490 187	M. Acciarri *et al.*	(L3 Collab.)
AFFOLDER	00M	PRL 85 3347	T. Affolder *et al.*	(CDF Collab.)
BREITWEG	00	PL B471 411	J. Breitweg *et al.*	(ZEUS Collab.)
BREITWEG	00D	EPJ C12 411	J. Breitweg *et al.*	(ZEUS Collab.)
EBOLI	00	MPL A15 1	O. Eboli, M. Gonzalez-Garcia, S. Novaes	
ABBIENDI	99N	PL B453 153	G. Abbiendi *et al.*	(OPAL Collab.)
ABBOTT	99H	PR D60 052003	B. Abbott *et al.*	(D0 Collab.)
ABBOTT	99I	PR D60 072002	B. Abbott *et al.*	(D0 Collab.)
ABREU	99L	PL B459 382	P. Abreu *et al.*	(DELPHI Collab.)
ACCIARRI	99	PL B454 386	M. Acciarri *et al.*	(L3 Collab.)
ACCIARRI	99Q	PL B467 171	M. Acciarri *et al.*	(L3 Collab.)
BARATE	99I	PL B453 107	R. Barate *et al.*	(ALEPH Collab.)
BARATE	99L	PL B462 389	R. Barate *et al.*	(ALEPH Collab.)
BARATE	99M	PL B465 349	R. Barate *et al.*	(ALEPH Collab.)
ABBOTT	98N	PR D58 092003	B. Abbott *et al.*	(D0 Collab.)
ABBOTT	98P	PR D58 012002	B. Abbott *et al.*	(D0 Collab.)
ABE	98H	PR D58 031101	F. Abe *et al.*	(CDF Collab.)
ABE	98P	PR D58 091101	F. Abe *et al.*	(CDF Collab.)
ABREU	98C	PL B416 233	P. Abreu *et al.*	(DELPHI Collab.)
ABREU	98N	PL B439 209	P. Abreu *et al.*	(DELPHI Collab.)
BARATE	97	PL B401 347	R. Barate *et al.*	(ALEPH Collab.)
BARATE	97S	PL B415 435	R. Barate *et al.*	(ALEPH Collab.)
ABACHI	95D	PRL 75 1456	S. Abachi *et al.*	(D0 Collab.)
ABE	95C	PRL 74 341	F. Abe *et al.*	(CDF Collab.)
ABE	95G	PRL 74 1936	F. Abe *et al.*	(CDF Collab.)
ABE	95P	PRL 75 11	F. Abe *et al.*	(CDF Collab.)
Also		PR D52 4784	F. Abe *et al.*	(CDF Collab.)
ABE	95W	PR D52 2624	F. Abe *et al.*	(CDF Collab.)
Also		PRL 73 220	F. Abe *et al.*	(CDF Collab.)
ABE	92E	PRL 68 3398	F. Abe *et al.*	(CDF Collab.)
ABE	92I	PRL 69 28	F. Abe *et al.*	(CDF Collab.)
ALITTI	92	PL B276 365	J. Alitti *et al.*	(UA2 Collab.)
ALITTI	92B	PL B276 354	J. Alitti *et al.*	(UA2 Collab.)
ALITTI	92C	PL B277 194	J. Alitti *et al.*	(UA2 Collab.)
ALITTI	92D	PL B277 203	J. Alitti *et al.*	(UA2 Collab.)
ALITTI	92F	PL B280 137	J. Alitti *et al.*	(UA2 Collab.)
SAMUEL	92	PL B280 124	M.A. Samuel *et al.*	(OKSU, CARL)
ABE	91C	PR D44 29	F. Abe *et al.*	(CDF Collab.)
ALBAJAR	91	PL B253 503	C. Albajar *et al.*	(UA1 Collab.)
ALITTI	91C	ZPHY C52 209	J. Alitti *et al.*	(UA2 Collab.)
SAMUEL	91	PRL 67 9	M.A. Samuel *et al.*	(OKSU, CARL)
Also		PRL 67 2920 (erratum)	M.A. Samuel *et al.*	
ABE	90G	PRL 65 2243	F. Abe *et al.*	(CDF Collab.)
Also		PR D43 2070	F. Abe *et al.*	(CDF Collab.)
ALBAJAR	90	PL B241 283	C. Albajar *et al.*	(UA1 Collab.)
ALITTI	90B	PL B241 150	J. Alitti *et al.*	(UA2 Collab.)
ABE	89I	PRL 62 1005	F. Abe *et al.*	(CDF Collab.)
ALBAJAR	89	ZPHY C44 15	C. Albajar *et al.*	(UA1 Collab.)
BAUR	88	NP B308 127	U. Baur, D. Zeppenfeld	(FSU, WISC)
GRIFOLS	88	IJMP A3 225	J.A. Grifols, S. Peris, J. Sola	(BARC, DESY)
Also		PL B197 437	J.A. Grifols, S. Peris, J. Sola	(BARC, DESY)
ALBAJAR	87	PL B185 233	C. Albajar *et al.*	(UA1 Collab.)
ANSARI	87	PL B186 440	R. Ansari *et al.*	(UA2 Collab.)
GROTCH	87	PR D36 2153	H. Grotch, R.W. Robinett	(PSU)
HAGIWARA	87	NP B282 253	K. Hagiwara *et al.*	(KEK, UCLA, FSU)
VANDERBIJ	87	PR D35 1088	J.J. van der Bij	(FNAL)
GRAU	85	PL 154B 283	A. Grau, J.A. Grifols	(BARC)
SUZUKI	85	PL 153B 289	M. Suzuki	(LBL)
ARNISON	84D	PL 134B 469	G.T.J. Arnison *et al.*	(UA1 Collab.)

Downloaded from https://academic.oup.com/ptep/article/2022/8/083C01/6651666 by KIT Library user on 27 September 2022

HERZOG	84	PL 148B 355	F. Herzog	(WISC)
Also		PL 155B 468 (erratum)	F. Herzog	(WISC)
ARNISON	83	PL 122B 103	G.T.J. Arnison *et al.*	(UA1 Collab.)
BANNER	83B	PL 122B 476	M. Banner *et al.*	(UA2 Collab.)

Z

$J = 1$

See the related review(s):
Z Boson

Z MASS

OUR FIT is obtained using the fit procedure and correlations as determined by the LEP Electroweak Working Group (see the note "The Z boson" and ref. LEP-SLC 06). The fit is performed using the Z mass and width, the Z hadronic pole cross section, the ratios of hadronic to leptonic partial widths, and the Z pole forward-backward lepton asymmetries. This set is believed to be most free of correlations.

The Z-boson mass listed here corresponds to the mass parameter in a Breit-Wigner distribution with mass dependent width. The value is 34 MeV greater than the real part of the position of the pole (in the energy-squared plane) in the Z-boson propagator. Also the LEP experiments have generally assumed a fixed value of the $\gamma - Z$ interferences term based on the standard model. Keeping this term as free parameter leads to a somewhat larger error on the fitted Z mass. See ACCIARRI 00Q and ABBIENDI 04G for a detailed investigation of both these issues.

VALUE (GeV)	EVTS	DOCUMENT ID		TECN	COMMENT
91.1876±0.0021 OUR FIT					
91.1852±0.0030	4.57M	[1] ABBIENDI	01A	OPAL	E^{ee}_{cm}= 88–94 GeV
91.1863±0.0028	4.08M	[2] ABREU	00F	DLPH	E^{ee}_{cm}= 88–94 GeV
91.1898±0.0031	3.96M	[3] ACCIARRI	00C	L3	E^{ee}_{cm}= 88–94 GeV
91.1885±0.0031	4.57M	[4] BARATE	00C	ALEP	E^{ee}_{cm}= 88–94 GeV
• • • We do not use the following data for averages, fits, limits, etc. • • •					
91.084 ±0.107		[5] ANDREEV	18A	H1	$e^{\pm}p$
91.1872±0.0033		[6] ABBIENDI	04G	OPAL	E^{ee}_{cm}= LEP1 + 130–209 GeV
91.272 ±0.032 ±0.033		[7] ACHARD	04C	L3	E^{ee}_{cm}= 183–209 GeV
91.1875±0.0039	3.97M	[8] ACCIARRI	00Q	L3	E^{ee}_{cm}= LEP1 + 130–189 GeV
91.151 ±0.008		[9] MIYABAYASHI	95	TOPZ	E^{ee}_{cm}= 57.8 GeV
91.74 ±0.28 ±0.93	156	[10] ALITTI	92B	UA2	$E^{p\overline{p}}_{cm}$= 630 GeV
90.9 ±0.3 ±0.2	188	[11] ABE	89C	CDF	$E^{p\overline{p}}_{cm}$= 1.8 TeV
91.14 ±0.12	480	[12] ABRAMS	89B	MRK2	E^{ee}_{cm}= 89–93 GeV
93.1 ±1.0 ±3.0	24	[13] ALBAJAR	89	UA1	$E^{p\overline{p}}_{cm}$= 546,630 GeV

[1] ABBIENDI 01A error includes approximately 2.3 MeV due to statistics and 1.8 MeV due to LEP energy uncertainty.
[2] The error includes 1.6 MeV due to LEP energy uncertainty.
[3] The error includes 1.8 MeV due to LEP energy uncertainty.
[4] BARATE 00C error includes approximately 2.4 MeV due to statistics, 0.2 MeV due to experimental systematics, and 1.7 MeV due to LEP energy uncertainty.
[5] ANDREEV 18A obtain this result in a combined electroweak and QCD analysis using all deep-inelastic e^+p and e^-p neutral current and charged current scattering cross sections published by the H1 Collaboration, including data with longitudinally polarized lepton beams.
[6] ABBIENDI 04G obtain this result using the S–matrix formalism for a combined fit to their cross section and asymmetry data at the Z peak and their data at 130–209 GeV. The authors have corrected the measurement for the 34 MeV shift with respect to the Breit–Wigner fits.
[7] ACHARD 04C select $e^+e^- \rightarrow Z\gamma$ events with hard initial–state radiation. Z decays to $q\overline{q}$ and muon pairs are considered. The fit results obtained in the two samples are found consistent to each other and combined considering the uncertainty due to ISR modelling as fully correlated.
[8] ACCIARRI 00Q interpret the s-dependence of the cross sections and lepton forward-backward asymmetries in the framework of the S-matrix formalism. They fit to their cross section and asymmetry data at high energies, using the results of S-matrix fits to Z-peak data (ACCIARRI 00C) as constraints. The 130–189 GeV data constrains the γ/Z interference term. The authors have corrected the measurement for the 34.1 MeV shift with respect to the Breit-Wigner fits. The error contains a contribution of ±2.3 MeV due to the uncertainty on the γZ interference.
[9] MIYABAYASHI 95 combine their low energy total hadronic cross-section measurement with the ACTON 93D data and perform a fit using an S-matrix formalism. As expected, this result is below the mass values obtained with the standard Breit-Wigner parametrization.
[10] Enters fit through W/Z mass ratio given in the W Particle Listings. The ALITTI 92B systematic error (±0.93) has two contributions: one (±0.92) cancels in m_W/m_Z and one (±0.12) is noncancelling. These were added in quadrature.
[11] First error of ABE 89 is combination of statistical and systematic contributions; second is mass scale uncertainty.
[12] ABRAMS 89B uncertainty includes 35 MeV due to the absolute energy measurement.
[13] ALBAJAR 89 result is from a total sample of 33 $Z \rightarrow e^+e^-$ events.

Z WIDTH

OUR FIT is obtained using the fit procedure and correlations as determined by the LEP Electroweak Working Group (see the note "The Z boson" and ref. LEP-SLC 06).

VALUE (GeV)	EVTS	DOCUMENT ID		TECN	COMMENT
2.4952±0.0023 OUR FIT					
2.4948±0.0041	4.57M	[1] ABBIENDI	01A	OPAL	E^{ee}_{cm}= 88–94 GeV
2.4876±0.0041	4.08M	[2] ABREU	00F	DLPH	E^{ee}_{cm}= 88–94 GeV
2.5024±0.0042	3.96M	[3] ACCIARRI	00C	L3	E^{ee}_{cm}= 88–94 GeV
2.4951±0.0043	4.57M	[4] BARATE	00C	ALEP	E^{ee}_{cm}= 88–94 GeV
• • • We do not use the following data for averages, fits, limits, etc. • • •					
2.4943±0.0041		[5] ABBIENDI	04G	OPAL	E^{ee}_{cm}= LEP1 + 130–209 GeV
2.5025±0.0041	3.97M	[6] ACCIARRI	00Q	L3	E^{ee}_{cm}= LEP1 + 130–189 GeV
2.50 ±0.21 ±0.06		[7] ABREU	96R	DLPH	E^{ee}_{cm}= 91.2 GeV
3.8 ±0.8 ±1.0	188	ABE	89C	CDF	$E^{p\overline{p}}_{cm}$= 1.8 TeV
2.42 $^{+0.45}_{-0.35}$	480	[8] ABRAMS	89B	MRK2	E^{ee}_{cm}= 89–93 GeV
2.7 $^{+1.2}_{-1.0}$ ±1.3	24	[9] ALBAJAR	89	UA1	$E^{p\overline{p}}_{cm}$= 546,630 GeV
2.7 ±2.0 ±1.0	25	[10] ANSARI	87	UA2	$E^{p\overline{p}}_{cm}$= 546,630 GeV

[1] ABBIENDI 01A error includes approximately 3.6 MeV due to statistics, 1 MeV due to event selection systematics, and 1.3 MeV due to LEP energy uncertainty.
[2] The error includes 1.2 MeV due to LEP energy uncertainty.
[3] The error includes 1.3 MeV due to LEP energy uncertainty.
[4] BARATE 00C error includes approximately 3.8 MeV due to statistics, 0.9 MeV due to experimental systematics, and 1.3 MeV due to LEP energy uncertainty.
[5] ABBIENDI 04G obtain this result using the S–matrix formalism for a combined fit to their cross section and asymmetry data at the Z peak and their data at 130–209 GeV. The authors have corrected the measurement for the 1 MeV shift with respect to the Breit–Wigner fits.
[6] ACCIARRI 00Q interpret the s-dependence of the cross sections and lepton forward-backward asymmetries in the framework of the S-matrix formalism. They fit to their cross section and asymmetry data at high energies, using the results of S-matrix fits to Z-peak data (ACCIARRI 00C) as constraints. The 130–189 GeV data constrains the γ/Z interference term. The authors have corrected the measurement for the 0.9 MeV shift with respect to the Breit-Wigner fits.
[7] ABREU 96R obtain this value from a study of the interference between initial and final state radiation in the process $e^+e^- \rightarrow Z \rightarrow \mu^+\mu^-$.
[8] ABRAMS 89B uncertainty includes 50 MeV due to the miniSAM background subtraction error.
[9] ALBAJAR 89 result is from a total sample of 33 $Z \rightarrow e^+e^-$ events.
[10] Quoted values of ANSARI 87 are from direct fit. Ratio of Z and W production gives either $\Gamma(Z) < (1.09 \pm 0.07) \times \Gamma(W)$, CL = 90% or $\Gamma(Z) = (0.82^{+0.19}_{-0.14} \pm 0.06) \times \Gamma(W)$. Assuming Standard-Model value $\Gamma(W) = 2.65$ GeV then gives $\Gamma(Z) < 2.89 \pm 0.19$ or $= 2.17^{+0.50}_{-0.37} \pm 0.16$.

Z DECAY MODES

	Mode		Fraction (Γ_i/Γ)	Scale factor/ Confidence level
Γ_1	e^+e^-	[a]	(3.3632±0.0042) %	
Γ_2	$\mu^+\mu^-$	[a]	(3.3662±0.0066) %	
Γ_3	$\tau^+\tau^-$	[a]	(3.3696±0.0083) %	
Γ_4	$\ell^+\ell^-$	[a,b]	(3.3658±0.0023) %	
Γ_5	$\mu^+\mu^-\mu^+\mu^-$			
Γ_6	$\ell^+\ell^-\ell^+\ell^-$	[c]	(4.55 ±0.17) $\times 10^{-6}$	
Γ_7	invisible	[a]	(20.000 ±0.055) %	
Γ_8	hadrons	[a]	(69.911 ±0.056) %	
Γ_9	$(u\overline{u}+c\overline{c})/2$		(11.6 ±0.6) %	
Γ_{10}	$(d\overline{d}+s\overline{s}+b\overline{b})/3$		(15.6 ±0.4) %	
Γ_{11}	$c\overline{c}$		(12.03 ±0.21) %	
Γ_{12}	$b\overline{b}$		(15.12 ±0.05) %	
Γ_{13}	$b\overline{b}b\overline{b}$		(3.6 ±1.3) $\times 10^{-4}$	
Γ_{14}	ggg		< 1.1 %	CL=95%
Γ_{15}	$\pi^0\gamma$		< 2.01 $\times 10^{-5}$	CL=95%
Γ_{16}	$\eta\gamma$		< 5.1 $\times 10^{-5}$	CL=95%
Γ_{17}	$\rho^0\gamma$		< 2.5 $\times 10^{-5}$	CL=95%
Γ_{18}	$\omega\gamma$		< 6.5 $\times 10^{-4}$	CL=95%
Γ_{19}	$\eta'(958)\gamma$		< 4.2 $\times 10^{-5}$	CL=95%
Γ_{20}	$\phi\gamma$		< 9 $\times 10^{-7}$	CL=95%
Γ_{21}	$\gamma\gamma$		< 1.46 $\times 10^{-5}$	CL=95%
Γ_{22}	$\pi^0\pi^0$		< 1.52 $\times 10^{-5}$	CL=95%
Γ_{23}	$\gamma\gamma\gamma$		< 2.2 $\times 10^{-6}$	CL=95%
Γ_{24}	$\pi^{\pm}W^{\mp}$	[d]	< 7 $\times 10^{-5}$	CL=95%
Γ_{25}	$\rho^{\pm}W^{\mp}$	[d]	< 8.3 $\times 10^{-5}$	CL=95%
Γ_{26}	$J/\psi(1S)X$		(3.51 $^{+0.23}_{-0.25}$) $\times 10^{-3}$	S=1.1
Γ_{27}	$J/\psi(1S)\gamma$		< 1.4 $\times 10^{-6}$	CL=95%
Γ_{28}	$\psi(2S)X$		(1.60 ±0.29) $\times 10^{-3}$	
Γ_{29}	$\psi(2S)\gamma$		< 4.5 $\times 10^{-6}$	CL=95%
Γ_{30}	$J/\psi(1S)\ell^+\ell^-$			
Γ_{31}	$J/\psi(1S)J/\psi(1S)$		< 2.2 $\times 10^{-6}$	CL=95%
Γ_{32}	$\chi_{c1}(1P)X$		(2.9 ±0.7) $\times 10^{-3}$	
Γ_{33}	$\chi_{c2}(1P)X$		< 3.2 $\times 10^{-3}$	CL=90%

Downloaded from https://academic.oup.com/ptep/article/2022/8/083C01/6651666 by KIT Library user on 27 September 2022

Γ_{34}	$\Upsilon(1S)$ X + $\Upsilon(2S)$ X + $\Upsilon(3S)$ X		(1.0 ±0.5) $\times 10^{-4}$	
Γ_{35}	$\Upsilon(1S)$X		< 4.4 $\times 10^{-5}$	CL=95%
Γ_{36}	$\Upsilon(1S)\gamma$		< 2.8 $\times 10^{-6}$	CL=95%
Γ_{37}	$\Upsilon(2S)$X		< 1.39 $\times 10^{-4}$	CL=95%
Γ_{38}	$\Upsilon(2S)\gamma$		< 1.7 $\times 10^{-6}$	CL=95%
Γ_{39}	$\Upsilon(3S)$X		< 9.4 $\times 10^{-5}$	CL=95%
Γ_{40}	$\Upsilon(3S)\gamma$		< 4.8 $\times 10^{-6}$	CL=95%
Γ_{41}	$\Upsilon(1,2,3S)\ \Upsilon(1,2,3S)$		< 1.5 $\times 10^{-6}$	CL=95%
Γ_{42}	$(D^0/\overline{D}^0)$ X		(20.7 ±2.0) %	
Γ_{43}	$D^{\pm}$X		(12.2 ±1.7) %	
Γ_{44}	$D^*(2010)^{\pm}$X	[d]	(11.4 ±1.3) %	
Γ_{45}	$D_{s1}(2536)^{\pm}$X		(3.6 ±0.8) $\times 10^{-3}$	
Γ_{46}	$D_{sJ}(2573)^{\pm}$X		(5.8 ±2.2) $\times 10^{-3}$	
Γ_{47}	$D^{*\prime}(2629)^{\pm}$X		searched for	
Γ_{48}	BX			
Γ_{49}	B^*X			
Γ_{50}	B^+X	[e]	(6.08 ±0.13) %	
Γ_{51}	B^0_sX	[e]	(1.59 ±0.13) %	
Γ_{52}	B^+_cX		searched for	
Γ_{53}	Λ^+_cX		(1.54 ±0.33) %	
Γ_{54}	Ξ^0_cX		seen	
Γ_{55}	Ξ_bX		seen	
Γ_{56}	b-baryon X	[e]	(1.38 ±0.22) %	
Γ_{57}	anomalous γ+ hadrons	[f]	< 3.2 $\times 10^{-3}$	CL=95%
Γ_{58}	$e^+e^-\gamma$	[f]	< 5.2 $\times 10^{-4}$	CL=95%
Γ_{59}	$\mu^+\mu^-\gamma$	[f]	< 5.6 $\times 10^{-4}$	CL=95%
Γ_{60}	$\tau^+\tau^-\gamma$	[f]	< 7.3 $\times 10^{-4}$	CL=95%
Γ_{61}	$\ell^+\ell^-\gamma\gamma$	[g]	< 6.8 $\times 10^{-6}$	CL=95%
Γ_{62}	$q\overline{q}\gamma\gamma$	[g]	< 5.5 $\times 10^{-6}$	CL=95%
Γ_{63}	$\nu\overline{\nu}\gamma\gamma$	[g]	< 3.1 $\times 10^{-6}$	CL=95%
Γ_{64}	$e^{\pm}\mu^{\mp}$ LF	[d]	< 7.5 $\times 10^{-7}$	CL=95%
Γ_{65}	$e^{\pm}\tau^{\mp}$ LF	[d]	< 5.0 $\times 10^{-6}$	CL=95%
Γ_{66}	$\mu^{\pm}\tau^{\mp}$ LF	[d]	< 6.5 $\times 10^{-6}$	CL=95%
Γ_{67}	pe L,B		< 1.8 $\times 10^{-6}$	CL=95%
Γ_{68}	$p\mu$ L,B		< 1.8 $\times 10^{-6}$	CL=95%

[a] This parameter is not directly used in the overall fit but is derived using the fit results; see the note "The Z boson" and ref. LEP-SLC 06 (Physics Reports (Physics Letters C) **427** 257 (2006)).

[b] ℓ indicates each type of lepton (e, μ, and τ), not sum over them.

[c] Here ℓ indicates e or μ.

[d] The value is for the sum of the charge states or particle/antiparticle states indicated.

[e] This value is updated using the product of (i) the $Z \rightarrow b\overline{b}$ fraction from this listing and (ii) the b-hadron fraction in an unbiased sample of weakly decaying b-hadrons produced in Z-decays provided by the Heavy Flavor Averaging Group (HFLAV, http://www.slac.stanford.edu/xorg/hflav/osc/PDG_2009/#FRACZ).

[f] See the Particle Listings below for the γ energy range used in this measurement.

[g] For $m_{\gamma\gamma}$ = (60 ± 5) GeV.

Z PARTIAL WIDTHS

$\Gamma(e^+e^-)$ — Γ_1

For the LEP experiments, this parameter is not directly used in the overall fit but is derived using the fit results; see the note "The Z boson" and ref. LEP-SLC 06.

VALUE (MeV)	EVTS	DOCUMENT ID		TECN	COMMENT
83.91±0.12 OUR FIT					
83.66±0.20	137.0k	ABBIENDI	01A	OPAL	E^{ee}_{cm}= 88–94 GeV
83.54±0.27	117.8k	ABREU	00F	DLPH	E^{ee}_{cm}= 88–94 GeV
84.16±0.22	124.4k	ACCIARRI	00C	L3	E^{ee}_{cm}= 88–94 GeV
83.88±0.19		BARATE	00C	ALEP	E^{ee}_{cm}= 88–94 GeV
82.89±1.20±0.89		[1] ABE	95J	SLD	E^{ee}_{cm}= 91.31 GeV

[1] ABE 95J obtain this measurement from Bhabha events in a restricted fiducial region to improve systematics. They use the values 91.187 and 2.489 GeV for the Z mass and total decay width to extract this partial width.

$\Gamma(\mu^+\mu^-)$ — Γ_2

This parameter is not directly used in the overall fit but is derived using the fit results; see the note "The Z boson" and ref. LEP-SLC 06.

VALUE (MeV)	EVTS	DOCUMENT ID		TECN	COMMENT
83.99±0.18 OUR FIT					
84.03±0.30	182.8k	ABBIENDI	01A	OPAL	E^{ee}_{cm}= 88–94 GeV
84.48±0.40	157.6k	ABREU	00F	DLPH	E^{ee}_{cm}= 88–94 GeV
83.95±0.44	113.4k	ACCIARRI	00C	L3	E^{ee}_{cm}= 88–94 GeV
84.02±0.28		BARATE	00C	ALEP	E^{ee}_{cm}= 88–94 GeV

$\Gamma(\tau^+\tau^-)$ — Γ_3

This parameter is not directly used in the overall fit but is derived using the fit results; see the note "The Z boson" and ref. LEP-SLC 06.

VALUE (MeV)	EVTS	DOCUMENT ID		TECN	COMMENT
84.08±0.22 OUR FIT					
83.94±0.41	151.5k	ABBIENDI	01A	OPAL	E^{ee}_{cm}= 88–94 GeV
83.71±0.58	104.0k	ABREU	00F	DLPH	E^{ee}_{cm}= 88–94 GeV
84.23±0.58	103.0k	ACCIARRI	00C	L3	E^{ee}_{cm}= 88–94 GeV
84.38±0.31		BARATE	00C	ALEP	E^{ee}_{cm}= 88–94 GeV

$\Gamma(\ell^+\ell^-)$ — Γ_4

ℓ indicates each type of lepton (e, μ, and τ), not sum over them.

In our fit $\Gamma(\ell^+\ell^-)$ is defined as the partial Z width for the decay into a pair of massless charged leptons. This parameter is not directly used in the 5-parameter fit assuming lepton universality but is derived using the fit results. See the note "The Z boson" and ref. LEP-SLC 06.

VALUE (MeV)	EVTS	DOCUMENT ID		TECN	COMMENT
83.984±0.086 OUR FIT					
83.82 ±0.15	471.3k	ABBIENDI	01A	OPAL	E^{ee}_{cm}= 88–94 GeV
83.85 ±0.17	379.4k	ABREU	00F	DLPH	E^{ee}_{cm}= 88–94 GeV
84.14 ±0.17	340.8k	ACCIARRI	00C	L3	E^{ee}_{cm}= 88–94 GeV
84.02 ±0.15	500k	BARATE	00C	ALEP	E^{ee}_{cm}= 88–94 GeV

Γ(invisible) — Γ_7

We use only direct measurements of the invisible partial width using the single photon channel to obtain the average value quoted below. OUR FIT value is obtained as a difference between the total and the observed partial widths assuming lepton universality.

VALUE (MeV)	EVTS	DOCUMENT ID		TECN	COMMENT
499.0± 1.5 OUR FIT					
503 ±16 OUR AVERAGE Error includes scale factor of 1.2.					
498 ±12 ±12	1791	ACCIARRI	98G	L3	E^{ee}_{cm}= 88–94 GeV
539 ±26 ±17	410	AKERS	95C	OPAL	E^{ee}_{cm}= 88–94 GeV
450 ±34 ±34	258	BUSKULIC	93L	ALEP	E^{ee}_{cm}= 88–94 GeV
540 ±80 ±40	52	ADEVA	92	L3	E^{ee}_{cm}= 88–94 GeV
• • • We do not use the following data for averages, fits, limits, etc. • • •					
498.1± 2.6		[1] ABBIENDI	01A	OPAL	E^{ee}_{cm}= 88–94 GeV
498.1± 3.2		[1] ABREU	00F	DLPH	E^{ee}_{cm}= 88–94 GeV
499.1± 2.9		[1] ACCIARRI	00C	L3	E^{ee}_{cm}= 88–94 GeV
499.1± 2.5		[1] BARATE	00C	ALEP	E^{ee}_{cm}= 88–94 GeV

[1] This is an indirect determination of Γ(invisible) from a fit to the visible Z decay modes.

Γ(hadrons) — Γ_8

This parameter is not directly used in the 5-parameter fit assuming lepton universality, but is derived using the fit results. See the note "The Z boson" and ref. LEP-SLC 06.

VALUE (MeV)	EVTS	DOCUMENT ID		TECN	COMMENT
1744.4±2.0 OUR FIT					
1745.4±3.5	4.10M	ABBIENDI	01A	OPAL	E^{ee}_{cm}= 88–94 GeV
1738.1±4.0	3.70M	ABREU	00F	DLPH	E^{ee}_{cm}= 88–94 GeV
1751.1±3.8	3.54M	ACCIARRI	00C	L3	E^{ee}_{cm}= 88–94 GeV
1744.0±3.4	4.07M	BARATE	00C	ALEP	E^{ee}_{cm}= 88–94 GeV

Z BRANCHING RATIOS

OUR FIT is obtained using the fit procedure and correlations as determined by the LEP Electroweak Working Group (see the note "The Z boson" and ref. LEP-SLC 06).

$\Gamma(\mu^+\mu^-)/\Gamma(e^+e^-)$ — Γ_2/Γ_1

VALUE	DOCUMENT ID		TECN	COMMENT
1.0001±0.0024 OUR AVERAGE				
0.9974±0.0050	[1] AABOUD	17Q	ATLS	E^{pp}_{cm} = 7 TeV
1.0009±0.0028	[2] LEP-SLC	06		E^{ee}_{cm} = 88–94 GeV

[1] AABOUD 17Q make a precise determination of $Z \rightarrow ee$ and $Z \rightarrow \mu\mu$ production in the lepton pseudo-rapidity range $|\eta| < 2.5$ and determine the ratio of the Z branching fractions $B(Z \rightarrow ee)/B(Z \rightarrow \mu\mu) = 1.0026 \pm 0.0013 \pm 0.0048 = 1.0026 \pm 0.0050$.

[2] This parameter is not directly used in the overall fit but is derived using the fit results; see the note "The Z boson" and ref. LEP-SLC 06.

$\Gamma(\tau^+\tau^-)/\Gamma(e^+e^-)$ — Γ_3/Γ_1

VALUE	DOCUMENT ID		TECN	COMMENT
1.0020±0.0032 OUR AVERAGE				
1.02 ±0.06	[1] AAIJ	18AR	LHCB	E^{pp}_{cm} = 8 TeV
1.0019±0.0032	[2] LEP-SLC	06		E^{ee}_{cm} = 88–94 GeV

[1] AAIJ 18AR obtain the result from the ratio of the measured $pp \rightarrow Z + X$ cross sections in the corresponding Z decay channels.

[2] This parameter is not directly used in the overall fit but is derived using the fit results; see the note "The Z boson" and ref. LEP-SLC 06.

Downloaded from https://academic.oup.com/ptep/article/2022/8/083C01/6651666 by KIT Library user on 27 September 2022

$\Gamma(\tau^+\tau^-)/\Gamma(\mu^+\mu^-)$ — Γ_3/Γ_2

VALUE	DOCUMENT ID		TECN	COMMENT
1.0010±0.0026 OUR AVERAGE				
1.01 ±0.05	[1] AAIJ	18AR	LHCB	E^{pp}_{cm} = 8 TeV
1.0010±0.0026	[2] LEP-SLC	06		E^{ee}_{cm} = 88–94 GeV

[1] AAIJ 18AR obtain the result from the ratio of the measured $pp \to Z + X$ cross sections in the corresponding Z decay channels.
[2] This parameter is not directly used in the overall fit but is derived using the fit results; see the note "The Z boson" and ref. LEP-SLC 06.

$\Gamma(\ell^+\ell^-\ell^+\ell^-)/\Gamma_{total}$ — Γ_6/Γ

Here ℓ indicates either e or μ. The branching fractions in this node are given within the phase-space defined by the requirements that (i) the 4-lepton invariant mass is between 80 GeV and 100 GeV, and (ii) any opposite-sign same-flavor lepton pair has a di-lepton invariant mass larger than 4 GeV.

VALUE (units 10^{-6})	EVTS	DOCUMENT ID		TECN	COMMENT
4.55±0.17 OUR AVERAGE					
4.41±0.13±0.27		[1] AAD	21AQ	ATLS	E^{pp}_{cm} = 13 TeV
4.70±0.32±0.25		[2] AABOUD	19N	ATLS	E^{pp}_{cm} = 13 TeV
$4.83^{+0.23}_{-0.22}{}^{+0.35}_{-0.32}$	509	[3] SIRUNYAN	18BT	CMS	E^{pp}_{cm} = 13 TeV
$4.9\ ^{+0.8}_{-0.7}\ ^{+0.4}_{-0.2}$	39	[4] KHACHATRY...	16CC	CMS	E^{pp}_{cm} = 13 TeV
4.31±0.34±0.17	172	AAD	14N	ATLS	E^{pp}_{cm} = 7, 8 TeV
$4.6\ ^{+1.0}_{-0.9}\ \pm0.2$	28	[5] CHATRCHYAN	12BN	CMS	E^{pp}_{cm} = 7 TeV

[1] AAD 21AQ analyze differential cross-sections in four-lepton events. Based on the measured cross section in the $Z \to 4\ell$ channel, a branching fraction of $B(Z \to 4\ell) = (4.41 \pm 0.13 \pm 0.23 \pm 0.09 \pm 0.12) \times 10^{-6}$ is obtained, where the uncertainties are statistical, systematic, theory and luminosity, respectively.
[2] AABOUD 19N reports $(4.70 \pm 0.32 \pm 0.21 \pm 0.14) \times 10^{-6}$, where the uncertainties are statistical, systematic, and luminosity. We have combined the latter two in quadrature.
[3] SIRUNYAN 18BT report the $Z \to 4\ell$ branching fraction $= (4.83^{+0.23}_{-0.22}{}^{+0.32}_{-0.29} \pm 0.08 \pm 0.12) \times 10^{-6}$, where the uncertainties are statistical, systematic, due to theory, and luminosity. The last three have been added in quadrature to obtain the total systematic error.
[4] KHACHATRYAN 16CC reports $(4.9^{+0.8}_{-0.7}{}^{+0.3}_{-0.2}{}^{+0.2}_{-0.1}{}^{+0.1}_{-0.1}) \times 10^{-6}$ value, where the uncertainties are statistical, systematic, theory, and due to luminosity. We have combined uncertainties in quadrature.
[5] CHATRCHYAN 12BN reports $(4.2^{+0.9}_{-0.8} \pm 0.2) \times 10^{-6}$ value. Their result (both central value and uncertainties) is scaled up by 10% to account for the different phase-space definition used here (see RAINBOLT 19).

$\Gamma(\text{hadrons})/\Gamma(e^+e^-)$ — Γ_8/Γ_1

VALUE	EVTS	DOCUMENT ID		TECN	COMMENT
20.804± 0.050 OUR FIT					
20.902± 0.084	137.0k	[1] ABBIENDI	01A	OPAL	E^{ee}_{cm}= 88–94 GeV
20.88 ± 0.12	117.8k	ABREU	00F	DLPH	E^{ee}_{cm}= 88–94 GeV
20.816± 0.089	124.4k	ACCIARRI	00C	L3	E^{ee}_{cm}= 88–94 GeV
20.677± 0.075		[2] BARATE	00C	ALEP	E^{ee}_{cm}= 88–94 GeV
• • • We do not use the following data for averages, fits, limits, etc. • • •					
$27.0\ ^{+11.7}_{-8.8}$	12	[3] ABRAMS	89D	MRK2	E^{ee}_{cm}= 89–93 GeV

[1] ABBIENDI 01A error includes approximately 0.067 due to statistics, 0.040 due to event selection systematics, 0.027 due to the theoretical uncertainty in t-channel prediction, and 0.014 due to LEP energy uncertainty.
[2] BARATE 00C error includes approximately 0.062 due to statistics, 0.033 due to experimental systematics, and 0.026 due to the theoretical uncertainty in t-channel prediction.
[3] ABRAMS 89D have included both statistical and systematic uncertainties in their quoted errors.

$\Gamma(\text{hadrons})/\Gamma(\mu^+\mu^-)$ — Γ_8/Γ_2

OUR FIT is obtained using the fit procedure and correlations as determined by the LEP Electroweak Working Group (see the note "The Z boson" and ref. LEP-SLC 06).

VALUE	EVTS	DOCUMENT ID		TECN	COMMENT
20.785±0.033 OUR FIT					
20.811±0.058	182.8k	[1] ABBIENDI	01A	OPAL	E^{ee}_{cm}= 88–94 GeV
20.65 ±0.08	157.6k	ABREU	00F	DLPH	E^{ee}_{cm}= 88–94 GeV
20.861±0.097	113.4k	ACCIARRI	00C	L3	E^{ee}_{cm}= 88–94 GeV
20.799±0.056		[2] BARATE	00C	ALEP	E^{ee}_{cm}= 88–94 GeV
• • • We do not use the following data for averages, fits, limits, etc. • • •					
$18.9\ ^{+7.1}_{-5.3}$	13	[3] ABRAMS	89D	MRK2	E^{ee}_{cm}= 89–93 GeV

[1] ABBIENDI 01A error includes approximately 0.050 due to statistics and 0.027 due to event selection systematics.
[2] BARATE 00C error includes approximately 0.053 due to statistics and 0.021 due to experimental systematics.
[3] ABRAMS 89D have included both statistical and systematic uncertainties in their quoted errors.

$\Gamma(\text{hadrons})/\Gamma(\tau^+\tau^-)$ — Γ_8/Γ_3

OUR FIT is obtained using the fit procedure and correlations as determined by the LEP Electroweak Working Group (see the note "The Z boson" and ref. LEP-SLC 06).

VALUE	EVTS	DOCUMENT ID		TECN	COMMENT
20.764±0.045 OUR FIT					
20.832±0.091	151.5k	[1] ABBIENDI	01A	OPAL	E^{ee}_{cm}= 88–94 GeV
20.84 ±0.13	104.0k	ABREU	00F	DLPH	E^{ee}_{cm}= 88–94 GeV
20.792±0.133	103.0k	ACCIARRI	00C	L3	E^{ee}_{cm}= 88–94 GeV
20.707±0.062		[2] BARATE	00C	ALEP	E^{ee}_{cm}= 88–94 GeV
• • • We do not use the following data for averages, fits, limits, etc. • • •					
$15.2\ ^{+4.8}_{-3.9}$	21	[3] ABRAMS	89D	MRK2	E^{ee}_{cm}= 89–93 GeV

[1] ABBIENDI 01A error includes approximately 0.055 due to statistics and 0.071 due to event selection systematics.
[2] BARATE 00C error includes approximately 0.054 due to statistics and 0.033 due to experimental systematics.
[3] ABRAMS 89D have included both statistical and systematic uncertainties in their quoted errors.

$\Gamma(\text{hadrons})/\Gamma(\ell^+\ell^-)$ — Γ_8/Γ_4

ℓ indicates each type of lepton (e, μ, and τ), not sum over them.

Our fit result is obtained requiring lepton universality.

VALUE	EVTS	DOCUMENT ID		TECN	COMMENT
20.767±0.025 OUR FIT					
20.823±0.044	471.3k	[1] ABBIENDI	01A	OPAL	E^{ee}_{cm}= 88–94 GeV
20.730±0.060	379.4k	ABREU	00F	DLPH	E^{ee}_{cm}= 88–94 GeV
20.810±0.060	340.8k	ACCIARRI	00C	L3	E^{ee}_{cm}= 88–94 GeV
20.725±0.039	500k	[2] BARATE	00C	ALEP	E^{ee}_{cm}= 88–94 GeV
• • • We do not use the following data for averages, fits, limits, etc. • • •					
$18.9\ ^{+3.6}_{-3.2}$	46	ABRAMS	89B	MRK2	E^{ee}_{cm}= 89–93 GeV

[1] ABBIENDI 01A error includes approximately 0.034 due to statistics and 0.027 due to event selection systematics.
[2] BARATE 00C error includes approximately 0.033 due to statistics, 0.020 due to experimental systematics, and 0.005 due to the theoretical uncertainty in t-channel prediction.

$\Gamma((u\overline{u}+c\overline{c})/2)/\Gamma(\text{hadrons})$ — Γ_9/Γ_8

This quantity is the branching ratio of $Z \to$ "up-type" quarks to $Z \to$ hadrons. Except ACKERSTAFF 97T the values of $Z \to$ "up-type" and $Z \to$ "down-type" branchings are extracted from measurements of $\Gamma(\text{hadrons})$, and $\Gamma(Z \to \gamma +$ jets) where γ is a high-energy (>5 or 7 GeV) isolated photon. As the experiments use different procedures and slightly different values of M_Z, $\Gamma(\text{hadrons})$ and α_s in their extraction procedures, our average has to be taken with caution.

VALUE	DOCUMENT ID		TECN	COMMENT
0.166±0.009 OUR AVERAGE				
$0.172^{+0.011}_{-0.010}$	[1] ABBIENDI	04E	OPAL	E^{ee}_{cm} = 91.2 GeV
0.160±0.019±0.019	[2] ACKERSTAFF	97T	OPAL	E^{ee}_{cm}= 88–94 GeV
$0.137^{+0.038}_{-0.054}$	[3] ABREU	95X	DLPH	E^{ee}_{cm}= 88–94 GeV
0.137±0.033	[4] ADRIANI	93	L3	E^{ee}_{cm}= 91.2 GeV

[1] ABBIENDI 04E select photons with energy > 7 GeV and use $\Gamma(\text{hadrons}) = 1744.4 \pm 2.0$ MeV and $\alpha_s = 0.1172 \pm 0.002$ to obtain $\Gamma_u = 300^{+19}_{-18}$ MeV.
[2] ACKERSTAFF 97T measure $\Gamma_{u\overline{u}}/(\Gamma_{d\overline{d}}+\Gamma_{u\overline{u}}+\Gamma_{s\overline{s}}) = 0.258 \pm 0.031 \pm 0.032$. To obtain this branching ratio authors use $R_c+R_b = 0.380 \pm 0.010$. This measurement is fully negatively correlated with the measurement of $\Gamma_{d\overline{d},s\overline{s}}/(\Gamma_{d\overline{d}}+\Gamma_{u\overline{u}}+\Gamma_{s\overline{s}})$ given in the next data block.
[3] ABREU 95X use $M_Z = 91.187 \pm 0.009$ GeV, $\Gamma(\text{hadrons}) = 1725 \pm 12$ MeV and $\alpha_s = 0.123 \pm 0.005$. To obtain this branching ratio we divide their value of $C_{2/3} = 0.91^{+0.25}_{-0.36}$ by their value of $(3C_{1/3} + 2C_{2/3}) = 6.66 \pm 0.05$.
[4] ADRIANI 93 use $M_Z = 91.181 \pm 0.022$ GeV, $\Gamma(\text{hadrons}) = 1742 \pm 19$ MeV and $\alpha_s = 0.125 \pm 0.009$. To obtain this branching ratio we divide their value of $C_{2/3} = 0.92 \pm 0.22$ by their value of $(3C_{1/3} + 2C_{2/3}) = 6.720 \pm 0.076$.

$\Gamma((d\overline{d}+s\overline{s}+b\overline{b})/3)/\Gamma(\text{hadrons})$ — Γ_{10}/Γ_8

This quantity is the branching ratio of $Z \to$ "down-type" quarks to $Z \to$ hadrons. Except ACKERSTAFF 97T the values of $Z \to$ "up-type" and $Z \to$ "down-type" branchings are extracted from measurements of $\Gamma(\text{hadrons})$, and $\Gamma(Z \to \gamma +$ jets) where γ is a high-energy (>5 or 7 GeV) isolated photon. As the experiments use different procedures and slightly different values of M_Z, $\Gamma(\text{hadrons})$ and α_s in their extraction procedures, our average has to be taken with caution.

VALUE	DOCUMENT ID		TECN	COMMENT
0.223±0.006 OUR AVERAGE				
0.218±0.007	[1] ABBIENDI	04E	OPAL	E^{ee}_{cm} = 91.2 GeV
0.230±0.010±0.010	[2] ACKERSTAFF	97T	OPAL	E^{ee}_{cm}= 88–94 GeV
$0.243^{+0.036}_{-0.026}$	[3] ABREU	95X	DLPH	E^{ee}_{cm}= 88–94 GeV
0.243±0.022	[4] ADRIANI	93	L3	E^{ee}_{cm}= 91.2 GeV

[1] ABBIENDI 04E select photons with energy > 7 GeV and use $\Gamma(\text{hadrons}) = 1744.4 \pm 2.0$ MeV and $\alpha_s = 0.1172 \pm 0.002$ to obtain $\Gamma_d = 381 \pm 12$ MeV.
[2] ACKERSTAFF 97T measure $\Gamma_{d\overline{d},s\overline{s}}/(\Gamma_{d\overline{d}}+\Gamma_{u\overline{u}}+\Gamma_{s\overline{s}}) = 0.371 \pm 0.016 \pm 0.016$. To obtain this branching ratio authors use $R_c+R_b = 0.380 \pm 0.010$. This measurement is fully negatively correlated with the measurement of $\Gamma_{u\overline{u}}/(\Gamma_{d\overline{d}}+\Gamma_{u\overline{u}}+\Gamma_{s\overline{s}})$ presented in the previous data block.
[3] ABREU 95X use $M_Z = 91.187 \pm 0.009$ GeV, $\Gamma(\text{hadrons}) = 1725 \pm 12$ MeV and $\alpha_s = 0.123 \pm 0.005$. To obtain this branching ratio we divide their value of $C_{1/3} = 1.62^{+0.24}_{-0.17}$ by their value of $(3C_{1/3} + 2C_{2/3}) = 6.66 \pm 0.05$.
[4] ADRIANI 93 use $M_Z = 91.181 \pm 0.022$ GeV, $\Gamma(\text{hadrons}) = 1742 \pm 19$ MeV and $\alpha_s = 0.125 \pm 0.009$. To obtain this branching ratio we divide their value of $C_{1/3} = 1.63 \pm 0.15$ by their value of $(3C_{1/3} + 2C_{2/3}) = 6.720 \pm 0.076$.

Downloaded from https://academic.oup.com/ptep/article/2022/8/083C01/6651666 by KIT Library user on 27 September 2022

$R_c = \Gamma(c\overline{c})/\Gamma(\text{hadrons})$ — Γ_{11}/Γ_8

OUR FIT is obtained by a simultaneous fit to several c- and b-quark measurements as explained in the note "The Z boson" and ref. LEP-SLC 06.

The Standard Model predicts $R_c = 0.1723$ for $m_t = 174.3$ GeV and $M_H = 150$ GeV.

VALUE	DOCUMENT ID		TECN	COMMENT
0.1721±0.0030 OUR FIT				
0.1744±0.0031±0.0021	[1] ABE	05F	SLD	E^{ee}_{cm}=91.28 GeV
0.1665±0.0051±0.0081	[2] ABREU	00	DLPH	E^{ee}_{cm}= 88–94 GeV
0.1698±0.0069	[3] BARATE	00B	ALEP	E^{ee}_{cm}= 88–94 GeV
0.180 ±0.011 ±0.013	[4] ACKERSTAFF	98E	OPAL	E^{ee}_{cm}= 88–94 GeV
0.167 ±0.011 ±0.012	[5] ALEXANDER	96R	OPAL	E^{ee}_{cm}= 88–94 GeV
• • • We do not use the following data for averages, fits, limits, etc. • • •				
0.1623±0.0085±0.0209	[6] ABREU	95D	DLPH	E^{ee}_{cm}= 88–94 GeV

[1] ABE 05F use hadronic Z decays collected during 1996–98 to obtain an enriched sample of $c\overline{c}$ events using a double tag method. The single c–tag is obtained with a neural network trained to perform flavor discrimination using as input several signatures (corrected secondary vertex mass, vertex decay length, multiplicity and total momentum of the hemisphere). A multitag approach is used, defining 4 regions of the output value of the neural network and R_c is extracted from a simultaneous fit to the count rates of the 4 different tags. The quoted systematic error includes an uncertainty of ±0.0006 due to the uncertainty on R_b.

[2] ABREU 00 obtain this result properly combining the measurement from the D^{*+} production rate (R_c= 0.1610 ± 0.0104 ± 0.0077 ± 0.0043 (BR)) with that from the overall charm counting (R_c= 0.1692 ± 0.0047 ± 0.0063 ± 0.0074 (BR)) in $c\overline{c}$ events. The systematic error includes an uncertainty of ±0.0054 due to the uncertainty on the charmed hadron branching fractions.

[3] BARATE 00B use exclusive decay modes to independently determine the quantities R_c×f($c \to$ X), X=D^0, D^+, D^+_s, and Λ_c. Estimating R_c×f($c \to \Xi_c/\Omega_c$)= 0.0034, they simply sum over all the charm decays to obtain R_c= 0.1738 ± 0.0047 ± 0.0088 ± 0.0075(BR). This is combined with all previous ALEPH measurements (BARATE 98T and BUSKULIC 94G, R_c= 0.1681 ± 0.0054 ± 0.0062) to obtain the quoted value.

[4] ACKERSTAFF 98E use an inclusive/exclusive double tag. In one jet $D^{*\pm}$ mesons are exclusively reconstructed in several decay channels and in the opposite jet a slow pion (opposite charge inclusive $D^{*\pm}$) tag is used. The b content of this sample is measured by the simultaneous detection of a lepton in one jet and an inclusively reconstructed $D^{*\pm}$ meson in the opposite jet. The systematic error includes an uncertainty of ±0.006 due to the external branching ratios.

[5] ALEXANDER 96R obtain this value via direct charm counting, summing the partial contributions from D^0, D^+, D^+_s, and Λ^+_c, and assuming that strange-charmed baryons account for the 15% of the Λ^+_c production. An uncertainty of ±0.005 due to the uncertainties in the charm hadron branching ratios is included in the overall systematics.

[6] ABREU 95D perform a maximum likelihood fit to the combined p and p_T distributions of single and dilepton samples. The second error includes an uncertainty of ±0.0124 due to models and branching ratios.

$R_b = \Gamma(b\overline{b})/\Gamma(\text{hadrons})$ — Γ_{12}/Γ_8

OUR FIT is obtained by a simultaneous fit to several c- and b-quark measurements as explained in the note "The Z boson" and ref. LEP-SLC 06.

The Standard Model predicts R_b=0.21581 for m_t=174.3 GeV and M_H=150 GeV.

VALUE	DOCUMENT ID		TECN	COMMENT
0.21629±0.00066 OUR FIT				
0.21594±0.00094±0.00075	[1] ABE	05F	SLD	E^{ee}_{cm}=91.28 GeV
0.2174 ±0.0015 ±0.0028	[2] ACCIARRI	00	L3	E^{ee}_{cm}= 89–93 GeV
0.2178 ±0.0011 ±0.0013	[3] ABBIENDI	99B	OPAL	E^{ee}_{cm}= 88–94 GeV
0.21634±0.00067±0.00060	[4] ABREU	99B	DLPH	E^{ee}_{cm}= 88–94 GeV
0.2159 ±0.0009 ±0.0011	[5] BARATE	97F	ALEP	E^{ee}_{cm}= 88–94 GeV
• • • We do not use the following data for averages, fits, limits, etc. • • •				
0.2145 ±0.0089 ±0.0067	[6] ABREU	95D	DLPH	E^{ee}_{cm}= 88–94 GeV
0.219 ±0.006 ±0.005	[7] BUSKULIC	94G	ALEP	E^{ee}_{cm}= 88–94 GeV
0.251 ±0.049 ±0.030	[8] JACOBSEN	91	MRK2	E^{ee}_{cm}= 91 GeV

[1] ABE 05F use hadronic Z decays collected during 1996–98 to obtain an enriched sample of $b\overline{b}$ events using a double tag method. The single b–tag is obtained with a neural network trained to perform flavor discrimination using as input several signatures (corrected secondary vertex mass, vertex decay length, multiplicity and total momentum of the hemisphere; the key tag is obtained requiring the secondary vertex corrected mass to be above the D–meson mass). ABE 05F obtain R_b =0.21604 ± 0.00098 ± 0.00074 where the systematic error includes an uncertainty of ±0.00012 due to the uncertainty on R_c. The value reported here is obtained properly combining with ABE 98D. The quoted systematic error includes an uncertainty of ±0.00012 due to the uncertainty on R_c.

[2] ACCIARRI 00 obtain this result using a double-tagging technique, with a high p_T lepton tag and an impact parameter tag in opposite hemispheres.

[3] ABBIENDI 99B tag $Z \to b\overline{b}$ decays using leptons and/or separated decay vertices. The b-tagging efficiency is measured directly from the data using a double-tagging technique.

[4] ABREU 99B obtain this result combining in a multivariate analysis several tagging methods (impact parameter and secondary vertex reconstruction, complemented by event shape variables). For R_c different from its Standard Model value of 0.172, R_b varies as −0.024×(R_c−0.172).

[5] BARATE 97F combine the lifetime-mass hemisphere tag (BARATE 97E) with event shape information and lepton tag to identify $Z \to b\overline{b}$ candidates. They further use c- and $u\,d\,s$-selection tags to identify the background. For R_c different from its Standard Model value of 0.172, R_b varies as −0.019×(R_c − 0.172).

[6] ABREU 95D perform a maximum likelihood fit to the combined p and p_T distributions of single and dilepton samples. The second error includes an uncertainty of ±0.0023 due to models and branching ratios.

[7] BUSKULIC 94G perform a simultaneous fit to the p and p_T spectra of both single and dilepton events.

[8] JACOBSEN 91 tagged $b\overline{b}$ events by requiring coincidence of ≥ 3 tracks with significant impact parameters using vertex detector. Systematic error includes lifetime and decay uncertainties (±0.014).

$\Gamma(b\overline{b}b\overline{b})/\Gamma(\text{hadrons})$ — Γ_{13}/Γ_8

VALUE (units 10^{-4})	DOCUMENT ID		TECN	COMMENT
5.2±1.9 OUR AVERAGE				
3.6±1.7±2.7	[1] ABBIENDI	01G	OPAL	E^{ee}_{cm}= 88–94 GeV
6.0±1.9±1.4	[2] ABREU	99U	DLPH	E^{ee}_{cm}= 88–94 GeV

[1] ABBIENDI 01G use a sample of four-jet events from hadronic Z decays. To enhance the $b\overline{b}b\overline{b}$ signal, at least three of the four jets are required to have a significantly detached secondary vertex.

[2] ABREU 99U force hadronic Z decays into 3 jets to use all the available phase space and require a b tag for every jet. This decay mode includes primary and secondary $4b$ production, *e.g.*, from gluon splitting to $b\overline{b}$.

$\Gamma(ggg)/\Gamma(\text{hadrons})$ — Γ_{14}/Γ_8

VALUE	CL%	DOCUMENT ID		TECN	COMMENT
<1.6 × 10^{-2}	95	[1] ABREU	96S	DLPH	E^{ee}_{cm}= 88–94 GeV

[1] This branching ratio is slightly dependent on the jet-finder algorithm. The value we quote is obtained using the JADE algorithm, while using the DURHAM algorithm ABREU 96S obtain an upper limit of 1.5 × 10^{-2}.

$\Gamma(\pi^0\gamma)/\Gamma_{total}$ — Γ_{15}/Γ

VALUE	CL%	DOCUMENT ID		TECN	COMMENT
<2.01 × 10^{-5}	95	AALTONEN	14E	CDF	$E^{p\overline{p}}_{cm}$ = 1.96 TeV
<5.2 × 10^{-5}	95	[1] ACCIARRI	95G	L3	E^{ee}_{cm}= 88–94 GeV
<5.5 × 10^{-5}	95	ABREU	94B	DLPH	E^{ee}_{cm}= 88–94 GeV
<2.1 × 10^{-4}	95	DECAMP	92	ALEP	E^{ee}_{cm}= 88–94 GeV
<1.4 × 10^{-4}	95	AKRAWY	91F	OPAL	E^{ee}_{cm}= 88–94 GeV

[1] This limit is for both decay modes $Z \to \pi^0\gamma/\gamma\gamma$ which are indistinguishable in ACCIARRI 95G.

$\Gamma(\eta\gamma)/\Gamma_{total}$ — Γ_{16}/Γ

VALUE	CL%	DOCUMENT ID		TECN	COMMENT
<7.6 × 10^{-5}	95	ACCIARRI	95G	L3	E^{ee}_{cm}= 88–94 GeV
<8.0 × 10^{-5}	95	ABREU	94B	DLPH	E^{ee}_{cm}= 88–94 GeV
<5.1 × 10^{-5}	95	DECAMP	92	ALEP	E^{ee}_{cm}= 88–94 GeV
<2.0 × 10^{-4}	95	AKRAWY	91F	OPAL	E^{ee}_{cm}= 88–94 GeV

$\Gamma(\rho^0\gamma)/\Gamma_{total}$ — Γ_{17}/Γ

VALUE	CL%	EVTS	DOCUMENT ID		TECN	COMMENT
<2.5 × 10^{-5}	95	12.5k	[1] AABOUD	18AU	ATLS	E^{pp}_{cm} = 13 TeV

[1] AABOUD 18AU search for the $Z \to \rho\gamma$ decay mode where the ρ is identified through its decay $\rho \to \pi^+\pi^-$. In the data corresponding to 32.3 fb^{-1}, 12,583 events are selected for 635 < m($\pi^+\pi^-$) < 915 MeV.

$\Gamma(\omega\gamma)/\Gamma_{total}$ — Γ_{18}/Γ

VALUE	CL%	DOCUMENT ID		TECN	COMMENT
<6.5 × 10^{-4}	95	ABREU	94B	DLPH	E^{ee}_{cm}= 88–94 GeV

$\Gamma(\eta'(958)\gamma)/\Gamma_{total}$ — Γ_{19}/Γ

VALUE	CL%	DOCUMENT ID		TECN	COMMENT
<4.2 × 10^{-5}	95	DECAMP	92	ALEP	E^{ee}_{cm}= 88–94 GeV

$\Gamma(\phi\gamma)/\Gamma_{total}$ — Γ_{20}/Γ

VALUE	CL%	EVTS	DOCUMENT ID		TECN	COMMENT
<9 × 10^{-7}	95	3.3k	[1] AABOUD	18AU	ATLS	E^{pp}_{cm} = 13 TeV
• • • We do not use the following data for averages, fits, limits, etc. • • •						
<8.3 × 10^{-6}	95	1.0k	[2] AABOUD	16K	ATLS	E^{pp}_{cm} = 13 TeV

[1] AABOUD 18AU search for the $Z \to \phi\gamma$ decay mode where the ϕ is identified through its decay $\phi \to K^+K^-$. In the data corresponding to 32.3 fb^{-1}, 3,364 events are selected for 1012 < m(K^+K^-) < 1028 MeV.

[2] AABOUD 16K search for the $Z \to \phi\gamma$ decay mode where the ϕ is identified through its decay into K^+K^-. In the data corresponding to a total luminosity of 2.7 fb^{-1}, 1065 events are selected and their $K^+K^-\gamma$ invariant mass spectrum is analyzed.

$\Gamma(\gamma\gamma)/\Gamma_{total}$ — Γ_{21}/Γ

This decay would violate the Landau-Yang theorem.

VALUE	CL%	DOCUMENT ID		TECN	COMMENT
<1.46 × 10^{-5}	95	AALTONEN	14E	CDF	$E^{p\overline{p}}_{cm}$ = 1.96 TeV
<5.2 × 10^{-5}	95	[1] ACCIARRI	95G	L3	E^{ee}_{cm}= 88–94 GeV
<5.5 × 10^{-5}	95	ABREU	94B	DLPH	E^{ee}_{cm}= 88–94 GeV
<1.4 × 10^{-4}	95	AKRAWY	91F	OPAL	E^{ee}_{cm}= 88–94 GeV

[1] This limit is for both decay modes $Z \to \pi^0\gamma/\gamma\gamma$ which are indistinguishable in ACCIARRI 95G.

$\Gamma(\pi^0\pi^0)/\Gamma_{total}$ — Γ_{22}/Γ

VALUE	CL%	DOCUMENT ID		TECN	COMMENT
<1.52 × 10^{-5}	95	AALTONEN	14E	CDF	$E^{p\overline{p}}_{cm}$ = 1.96 TeV

Downloaded from https://academic.oup.com/ptep/article/2022/8/083C01/6651666 by KIT Library user on 27 September 2022

$\Gamma(\gamma\gamma\gamma)/\Gamma_{total}$ — Γ_{23}/Γ

VALUE	CL%	DOCUMENT ID		TECN	COMMENT
$<2.2\times10^{-6}$	95	AAD	16L	ATLS	E^{pp}_{cm} = 8 TeV
• • • We do not use the following data for averages, fits, limits, etc. • • •					
$<1.0\times10^{-5}$	95	[1] ACCIARRI	95C	L3	E^{ee}_{cm}= 88–94 GeV
$<1.7\times10^{-5}$	95	[1] ABREU	94B	DLPH	E^{ee}_{cm}= 88–94 GeV
$<6.6\times10^{-5}$	95	AKRAWY	91F	OPAL	E^{ee}_{cm}= 88–94 GeV

[1] Limit derived in the context of composite Z model.

$\Gamma(\pi^\pm W^\mp)/\Gamma_{total}$ — Γ_{24}/Γ

The value is for the sum of the charge states indicated.

VALUE	CL%	DOCUMENT ID		TECN	COMMENT
$<7\times10^{-5}$	95	DECAMP	92	ALEP	E^{ee}_{cm}= 88–94 GeV

$\Gamma(\rho^\pm W^\mp)/\Gamma_{total}$ — Γ_{25}/Γ

The value is for the sum of the charge states indicated.

VALUE	CL%	DOCUMENT ID		TECN	COMMENT
$<8.3\times10^{-5}$	95	DECAMP	92	ALEP	E^{ee}_{cm}= 88–94 GeV

$\Gamma(J/\psi(1S)X)/\Gamma_{total}$ — Γ_{26}/Γ

VALUE (units 10^{-3})	EVTS	DOCUMENT ID		TECN	COMMENT
$3.51^{+0.23}_{-0.25}$ OUR AVERAGE Error includes scale factor of 1.1.					
$3.21\pm0.21^{+0.19}_{-0.28}$	553	[1] ACCIARRI	99F	L3	E^{ee}_{cm}= 88–94 GeV
$3.9\ \pm0.2\ \pm0.3$	511	[2] ALEXANDER	96B	OPAL	E^{ee}_{cm}= 88–94 GeV
$3.73\pm0.39\pm0.36$	153	[3] ABREU	94P	DLPH	E^{ee}_{cm}= 88–94 GeV

[1] ACCIARRI 99F combine $\mu^+\mu^-$ and e^+e^- $J/\psi(1S)$ decay channels. The branching ratio for prompt $J/\psi(1S)$ production is measured to be $(2.1\pm0.6\pm0.4^{+0.4}_{-0.2}(\text{theor.}))\times10^{-4}$.

[2] ALEXANDER 96B identify $J/\psi(1S)$ from the decays into lepton pairs. (4.8 ± 2.4)% of this branching ratio is due to prompt $J/\psi(1S)$ production (ALEXANDER 96N).

[3] Combining $\mu^+\mu^-$ and e^+e^- channels and taking into account the common systematic errors. $(7.7^{+6.3}_{-5.4})$% of this branching ratio is due to prompt $J/\psi(1S)$ production.

$\Gamma(J/\psi(1S)\gamma)/\Gamma_{total}$ — Γ_{27}/Γ

VALUE	CL%	DOCUMENT ID		TECN	COMMENT
$<1.4\times10^{-6}$	95	[1] SIRUNYAN	19AJ	CMS	E^{pp}_{cm} = 13 TeV
• • • We do not use the following data for averages, fits, limits, etc. • • •					
$<2.3\times10^{-6}$	95	[2] AABOUD	18BL	ATLS	E^{pp}_{cm} = 13 TeV
$<2.6\times10^{-6}$	95	[3] AAD	15I	ATLS	E^{pp}_{cm} = 8 TeV

[1] SIRUNYAN 19AJ study $Z\to J/\psi\gamma$ with $J/\psi\to\mu^+\mu^-$. Candidate events are selected by requiring a pair of oppositely charged muons and a well isolated photon. The leading (subleading) muon is require to have a transverse momentum larger than 20 GeV (4 GeV), while the photon must have a transverse energy larger than 33 GeV. Requiring the invariant mass of the $\mu\mu$ ($\mu\mu\gamma$) system in the range 3.0 to 3.2 (81 to 101) GeV, selects 183 data events which is consistent with the expected background. The 95% C.L. limit on the Z branching fraction is obtained assuming the J/ψ to be unpolarized.

[2] AABOUD 18BL study $Z\to J/\psi\gamma$ in 13 TeV pp interactions. Two triggers were used: isolated photon of $p_T>35(25)$ GeV and a muon with $p_T>18(24)$ GeV. The J/ψ is detected via its dimuon decay and it is required that the azimuthal angle between the photon and the J/ψ in the plane transverse to the beam direction is $>\pi/2$. The number of observed/expected background events is $92/89\pm6$ in the dimuon mass range 2.9–3.3 GeV leading to the quoted 95% C.L. limit.

[3] AAD 15I use events with the highest p_T muon in the pair required to have $p_T>20$ GeV, the dimuon mass required to be within 0.2 GeV of the $J/\psi(1S)$ mass and it's transverse momentum required to be >36 GeV. The photon is also required to have it's $p_T>36$ GeV.

$\Gamma(\psi(2S)X)/\Gamma_{total}$ — Γ_{28}/Γ

VALUE (units 10^{-3})	EVTS	DOCUMENT ID		TECN	COMMENT
1.60 ± 0.29 OUR AVERAGE					
$1.6\ \pm0.5\ \pm0.3$	39	[1] ACCIARRI	97J	L3	E^{ee}_{cm}= 88–94 GeV
$1.6\ \pm0.3\ \pm0.2$	46.9	[2] ALEXANDER	96B	OPAL	E^{ee}_{cm}= 88–94 GeV
$1.60\pm0.73\pm0.33$	5.4	[3] ABREU	94P	DLPH	E^{ee}_{cm}= 88–94 GeV

[1] ACCIARRI 97J measure this branching ratio via the decay channel $\psi(2S)\to\ell^+\ell^-$ ($\ell=\mu, e$).

[2] ALEXANDER 96B measure this branching ratio via the decay channel $\psi(2S)\to J/\psi\pi^+\pi^-$, with $J/\psi\to\ell^+\ell^-$.

[3] ABREU 94P measure this branching ratio via decay channel $\psi(2S)\to J/\psi\pi^+\pi^-$, with $J/\psi\to\mu^+\mu^-$.

$\Gamma(\psi(2S)\gamma)/\Gamma_{total}$ — Γ_{29}/Γ

VALUE	CL%	DOCUMENT ID		TECN	COMMENT
$<4.5\times10^{-6}$	95	[1] AABOUD	18BL	ATLS	E^{pp}_{cm} = 13 TeV

[1] AABOUD 18BL study $Z\to\psi(2S)\gamma$ in 13 TeV pp interactions. Two triggers were used: isolated photon of $p_T>35(25)$ GeV and a muon with $p_T>18(24)$ GeV. The $\psi(2S)$ is detected via its dimuon decay and it is required that the azimuthal angle between the photon and the $\psi(2S)$ in the plane transverse to the beam direction is $>\pi/2$. The number of observed/expected background events is $43/42\pm5$ in the dimuon mass range 3.5–3.9 GeV leading to the quoted 95% C.L. limit.

$\Gamma(J/\psi(1S)\ell^+\ell^-)/\Gamma(\mu^+\mu^-\mu^+\mu^-)$ — Γ_{30}/Γ_5

VALUE	DOCUMENT ID		TECN	COMMENT
$0.67\pm0.18\pm0.05$	[1] SIRUNYAN	18DZ	CMS	pp at 13 TeV

[1] SIRUNYAN 18DZ observe the decay $Z\to\Psi\ell^+\ell^-$ in pp collisions at $\sqrt{s}=13$ TeV, where Ψ includes J/ψ as well as $\psi(2S)\to J/\psi X$, and $\ell^+\ell^-$ represents an electron or muon pair while the J/ψ is detected via its $\mu^+\mu^-$ decay channel. To reduce systematic errors they determine the ratio of the branching fraction of this decay to that of $Z\to\mu^+\mu^-\mu^+\mu^-$ within phase-space cuts imposed on lepton transverse momentum and pseudo rapidity, dilepton invariant mass, and J/ψ transverse momentum. The number of selected $\Psi\mu^+\mu^-$ (Ψe^+e^-) candidate events is 29 (18). Analyzing the $\mu^+\mu^-$ and $\mu^+\mu^-\ell^+\ell^-$ invariant mass distributions, a yield of 13.0 ± 3.9 (11.2 ± 3.4) events for the $\Psi\mu^+\mu^-$ (Ψe^+e^-) mode is obtained. The ratio of the branching fractions is determined as $0.67\pm0.18\pm0.05$ within the selected phase-space cuts. Assuming extrapolation to full phase space cancels in the ratio, and using their measured value of $B(Z\to\mu^+\mu^-\mu^+\mu^-)=(1.20\pm0.08)\times10^{-6}$, they estimate $B(Z\to J/\psi\ell^+\ell^-)=8\times10^{-7}$.

$\Gamma(J/\psi(1S)J/\psi(1S))/\Gamma_{total}$ — Γ_{31}/Γ

VALUE	CL%	EVTS	DOCUMENT ID		TECN	COMMENT
$<2.2\times10^{-6}$	95	189	[1] SIRUNYAN	19BR	CMS	E^{pp}_{cm} = 13 TeV

[1] SIRUNYAN 19BR search for Z decays to a pair of J/ψ mesons in the channel $J/\psi\to\mu^+\mu^-$. The invariant masses of the higher/lower-p_T J/ψ candidates have to be within 0.1/0.15 GeV of the nominal J/ψ mass. A total of 189 events are selected in the 40–140 GeV 4-muon invariant mass range. An un-binned extended maximum likelihood fit leads to the 95% C.L. upper limit, obtained assuming the J/ψ mesons to be unpolarised.

$\Gamma(\chi_{c1}(1P)X)/\Gamma_{total}$ — Γ_{32}/Γ

VALUE (units 10^{-3})	EVTS	DOCUMENT ID		TECN	COMMENT
2.9 ± 0.7 OUR AVERAGE					
$2.7\pm0.6\pm0.5$	33	[1] ACCIARRI	97J	L3	E^{ee}_{cm}= 88–94 GeV
$5.0\pm2.1^{+1.5}_{-0.9}$	6.4	[2] ABREU	94P	DLPH	E^{ee}_{cm}= 88–94 GeV

[1] ACCIARRI 97J measure this branching ratio via the decay channel $\chi_{c1}\to J/\psi+\gamma$, with $J/\psi\to\ell^+\ell^-$ ($\ell=\mu, e$). The $M(\ell^+\ell^-\gamma)$–$M(\ell^+\ell^-)$ mass difference spectrum is fitted with two gaussian shapes for χ_{c1} and χ_{c2}.

[2] This branching ratio is measured via the decay channel $\chi_{c1}\to J/\psi+\gamma$, with $J/\psi\to\mu^+\mu^-$.

$\Gamma(\chi_{c2}(1P)X)/\Gamma_{total}$ — Γ_{33}/Γ

VALUE	CL%	DOCUMENT ID		TECN	COMMENT
$<3.2\times10^{-3}$	90	[1] ACCIARRI	97J	L3	E^{ee}_{cm}= 88–94 GeV

[1] ACCIARRI 97J derive this limit via the decay channel $\chi_{c2}\to J/\psi+\gamma$, with $J/\psi\to\ell^+\ell^-$ ($\ell=\mu, e$). The $M(\ell^+\ell^-\gamma)$–$M(\ell^+\ell^-)$ mass difference spectrum is fitted with two gaussian shapes for χ_{c1} and χ_{c2}.

$\Gamma(\Upsilon(1S)X+\Upsilon(2S)X+\Upsilon(3S)X)/\Gamma_{total}$ — $\Gamma_{34}/\Gamma=(\Gamma_{35}+\Gamma_{37}+\Gamma_{39})/\Gamma$

VALUE (units 10^{-4})	EVTS	DOCUMENT ID		TECN	COMMENT
$1.0\pm0.4\pm0.22$	6.4	[1] ALEXANDER	96F	OPAL	E^{ee}_{cm}= 88–94 GeV

[1] ALEXANDER 96F identify the Υ (which refers to any of the three lowest bound states) through its decay into e^+e^- and $\mu^+\mu^-$. The systematic error includes an uncertainty of ±0.2 due to the production mechanism.

$\Gamma(\Upsilon(1S)X)/\Gamma_{total}$ — Γ_{35}/Γ

VALUE	CL%	DOCUMENT ID		TECN	COMMENT
$<4.4\times10^{-5}$	95	[1] ACCIARRI	99F	L3	E^{ee}_{cm}= 88–94 GeV

[1] ACCIARRI 99F search for $\Upsilon(1S)$ through its decay into $\ell^+\ell^-$ ($\ell=e$ or μ).

$\Gamma(\Upsilon(1S)\gamma)/\Gamma_{total}$ — Γ_{36}/Γ

VALUE	CL%	DOCUMENT ID		TECN	COMMENT
$<2.8\times10^{-6}$	95	[1] AABOUD	18BL	ATLS	E^{pp}_{cm} = 13 TeV
• • • We do not use the following data for averages, fits, limits, etc. • • •					
$<3.4\times10^{-6}$	95	[2] AAD	15I	ATLS	E^{pp}_{cm} = 8 TeV

[1] AABOUD 18BL study $Z\to\Upsilon(1S)\gamma$ in 13 TeV pp interactions. Two triggers were used: isolated photon of $p_T>35(25)$ GeV and a muon with $p_T>18(24)$ GeV. The $\Upsilon(1S)$ is detected via its dimuon decay and it is required that the azimuthal angle between the photon and the $\Upsilon(1S)$ in the plane transverse to the beam direction is $>\pi/2$. The number of observed/expected background events is $115/126\pm8$ in the dimuon mass range 9.0–10.0 GeV leading to the quoted 95% C.L. limit.

[2] AAD 15I use events with the highest p_T muon in the pair required to have $p_T>20$ GeV, the dimuon mass required to be in the range 8–12 GeV and it's transverse momentum required to be >36 GeV. The photon is also required to have it's $p_T>36$ GeV.

$\Gamma(\Upsilon(2S)X)/\Gamma_{total}$ — Γ_{37}/Γ

VALUE	CL%	DOCUMENT ID		TECN	COMMENT
$<13.9\times10^{-5}$	95	[1] ACCIARRI	97R	L3	E^{ee}_{cm}= 88–94 GeV

[1] ACCIARRI 97R search for $\Upsilon(2S)$ through its decay into $\ell^+\ell^-$ ($\ell=e$ or μ).

$\Gamma(\Upsilon(2S)\gamma)/\Gamma_{total}$ — Γ_{38}/Γ

VALUE	CL%	DOCUMENT ID		TECN	COMMENT
$<1.7\times10^{-6}$	95	[1] AABOUD	18BL	ATLS	E^{pp}_{cm} = 13 TeV

Downloaded from https://academic.oup.com/ptep/article/2022/8/083C01/6651666 by KIT Library user on 27 September 2022

• • • We do not use the following data for averages, fits, limits, etc. • • •

$<6.5 \times 10^{-6}$	95	[2] AAD	15I	ATLS	E^{pp}_{cm} = 8 TeV

[1] AABOUD 18BL study $Z \to \Upsilon(2S)\gamma$ in 13 TeV pp interactions. Two triggers were used: isolated photon of $p_T > 35(25)$ GeV and a muon with $p_T > 18(24)$ GeV. The $\Upsilon(2S)$ is detected via its dimuon decay and it is required that the azimuthal angle between the photon and the $\Upsilon(2S)$ in the plane transverse to the beam direction is $> \pi/2$. The number of observed/expected background events is 106/121 ± 8 in the dimuon mass range 9.5–10.5 GeV leading to the quoted 95% C.L. limit.

[2] AAD 15I use events with the highest p_T muon in the pair required to have $p_T > 20$ GeV, the dimuon mass required to be in the range 8–12 GeV and it's transverse momentum required to be > 36 GeV. The photon is also required to have it's $p_T > 36$ GeV.

$\Gamma(\Upsilon(3S)X)/\Gamma_{total}$ — Γ_{39}/Γ

VALUE	CL%	DOCUMENT ID		TECN	COMMENT
$<9.4 \times 10^{-5}$	95	[1] ACCIARRI	97R	L3	E^{ee}_{cm} = 88–94 GeV

[1] ACCIARRI 97R search for $\Upsilon(3S)$ through its decay into $\ell^+\ell^-$ ($\ell = e$ or μ).

$\Gamma(\Upsilon(3S)\gamma)/\Gamma_{total}$ — Γ_{40}/Γ

VALUE	CL%	DOCUMENT ID		TECN	COMMENT
$<4.8 \times 10^{-6}$	95	[1] AABOUD	18BL	ATLS	E^{pp}_{cm} = 13 TeV

• • • We do not use the following data for averages, fits, limits, etc. • • •

$<5.4 \times 10^{-6}$	95	[2] AAD	15I	ATLS	E^{pp}_{cm} = 8 TeV

[1] AABOUD 18BL study $Z \to \Upsilon(3S)\gamma$ in 13 TeV pp interactions. Two triggers were used: isolated photon of $p_T > 35(25)$ GeV and a muon with $p_T > 18(24)$ GeV. The $\Upsilon(3S)$ is detected via its dimuon decay and it is required that the azimuthal angle between the photon and the $\Upsilon(3S)$ in the plane transverse to the beam direction is $> \pi/2$. The number of observed/expected background events is 112/113 ± 8 in the dimuon mass range 10.0–11.0 GeV leading to the quoted 95% C.L. limit.

[2] AAD 15I use events with the highest p_T muon in the pair required to have $p_T > 20$ GeV, the dimuon mass required to be in the range 8–12 GeV and it's transverse momentum required to be > 36 GeV. The photon is also required to have it's $p_T > 36$ GeV.

$\Gamma(\Upsilon(1,2,3S)\,\Upsilon(1,2,3S))/\Gamma_{total}$ — Γ_{41}/Γ

VALUE	CL%	EVTS	DOCUMENT ID		TECN	COMMENT
$<1.5 \times 10^{-6}$	95	106	[1] SIRUNYAN	19BR	CMS	E^{pp}_{cm} = 13 TeV

[1] SIRUNYAN 19BR search for Z decays to a pair of Υ mesons in the channel $\Upsilon \to \mu^+\mu^-$. The invariant mass of the Υ candidates has to be in the range of 8.5 to 11 GeV. A total of 106 events are selected in the 20–140 GeV 4-muon invariant mass range. An un-binned extended maximum likelihood fit leads to the 95% C.L. upper limit, obtained assuming the Υ mesons to be unpolarised.

$\Gamma((D^0/\overline{D}^0)X)/\Gamma(\text{hadrons})$ — Γ_{42}/Γ_8

VALUE	EVTS	DOCUMENT ID		TECN	COMMENT
0.296±0.019±0.021	369	[1] ABREU	93I	DLPH	E^{ee}_{cm} = 88–94 GeV

[1] The $(D^0/\overline{D}^0)$ states in ABREU 93I are detected by the $K\pi$ decay mode. This is a corrected result (see the erratum of ABREU 93I).

$\Gamma(D^\pm X)/\Gamma(\text{hadrons})$ — Γ_{43}/Γ_8

VALUE	EVTS	DOCUMENT ID		TECN	COMMENT
0.174±0.016±0.018	539	[1] ABREU	93I	DLPH	E^{ee}_{cm} = 88–94 GeV

[1] The $D^\pm$ states in ABREU 93I are detected by the $K\pi\pi$ decay mode. This is a corrected result (see the erratum of ABREU 93I).

$\Gamma(D^*(2010)^\pm X)/\Gamma(\text{hadrons})$ — Γ_{44}/Γ_8

The value is for the sum of the charge states indicated.

VALUE	EVTS	DOCUMENT ID		TECN	COMMENT
0.163±0.019 OUR AVERAGE		Error includes scale factor of 1.3.			
0.155±0.010±0.013	358	[1] ABREU	93I	DLPH	E^{ee}_{cm} = 88–94 GeV
0.21 ±0.04	362	[2] DECAMP	91J	ALEP	E^{ee}_{cm} = 88–94 GeV

[1] $D^*(2010)^\pm$ in ABREU 93I are reconstructed from $D^0\pi^\pm$, with $D^0 \to K^-\pi^+$. The new CLEO II measurement of $B(D^{*\pm} \to D^0\pi^\pm)$ = (68.1 ± 1.6) % is used. This is a corrected result (see the erratum of ABREU 93I).

[2] DECAMP 91J report $B(D^*(2010)^+ \to D^0\pi^+)\ B(D^0 \to K^-\pi^+)\ \Gamma(D^*(2010)^\pm X)/\Gamma(\text{hadrons})$ = (5.11 ± 0.34) × 10^{-3}. They obtained the above number assuming $B(D^0 \to K^-\pi^+)$ = (3.62±0.34±0.44)% and $B(D^*(2010)^+ \to D^0\pi^+)$ = (55±4)%. We have rescaled their original result of 0.26 ± 0.05 taking into account the new CLEO II branching ratio $B(D^*(2010)^+ \to D^0\pi^+)$ = (68.1 ± 1.6)%.

$\Gamma(D_{s1}(2536)^\pm X)/\Gamma(\text{hadrons})$ — Γ_{45}/Γ_8

$D_{s1}(2536)^\pm$ is an expected orbitally-excited state of the D_s meson.

VALUE (%)	EVTS	DOCUMENT ID		TECN	COMMENT
0.52±0.09±0.06	92	[1] HEISTER	02B	ALEP	E^{ee}_{cm} = 88–94 GeV

[1] HEISTER 02B reconstruct this meson in the decay modes $D_{s1}(2536)^\pm \to D^{*\pm}K^0$ and $D_{s1}(2536)^\pm \to D^{*0}K^\pm$. The quoted branching ratio assumes that the decay width of the $D_{s1}(2536)$ is saturated by the two measured decay modes.

$\Gamma(D_{sJ}(2573)^\pm X)/\Gamma(\text{hadrons})$ — Γ_{46}/Γ_8

$D_{sJ}(2573)^\pm$ is an expected orbitally-excited state of the D_s meson.

VALUE (%)	EVTS	DOCUMENT ID		TECN	COMMENT
$0.83\pm0.29^{+0.07}_{-0.13}$	64	[1] HEISTER	02B	ALEP	E^{ee}_{cm} = 88–94 GeV

[1] HEISTER 02B reconstruct this meson in the decay mode $D^*_{s2}(2573)^\pm \to D^0K^\pm$. The quoted branching ratio assumes that the detected decay mode represents 45% of the full decay width.

$\Gamma(D^{*\prime}(2629)^\pm X)/\Gamma(\text{hadrons})$ — Γ_{47}/Γ_8

$D^{*\prime}(2629)^\pm$ is a predicted radial excitation of the $D^*(2010)^\pm$ meson.

VALUE	DOCUMENT ID		TECN	COMMENT
searched for	[1] ABBIENDI	01N	OPAL	E^{ee}_{cm} = 88–94 GeV

[1] ABBIENDI 01N searched for the decay mode $D^{*\prime}(2629)^\pm \to D^{*\pm}\pi^+\pi^-$ with $D^{*+} \to D^0\pi^+$, and $D^0 \to K^-\pi^+$. They quote a 95% CL limit for $Z \to D^{*\prime}(2629)^\pm \times B(D^{*\prime}(2629)^+ \to D^{*+}\pi^+\pi^-) < 3.1 \times 10^{-3}$.

$\Gamma(B^*X)/[\Gamma(BX)+\Gamma(B^*X)]$ — $\Gamma_{49}/(\Gamma_{48}+\Gamma_{49})$

As the experiments assume different values of the b-baryon contribution, our average should be taken with caution.

VALUE	EVTS	DOCUMENT ID		TECN	COMMENT
0.75 ±0.04 OUR AVERAGE					
0.760±0.036±0.083		[1] ACKERSTAFF	97M	OPAL	E^{ee}_{cm} = 88–94 GeV
0.771±0.026±0.070		[2] BUSKULIC	96D	ALEP	E^{ee}_{cm} = 88–94 GeV
0.72 ±0.03 ±0.06		[3] ABREU	95R	DLPH	E^{ee}_{cm} = 88–94 GeV
0.76 ±0.08 ±0.06	1378	[4] ACCIARRI	95B	L3	E^{ee}_{cm} = 88–94 GeV

[1] ACKERSTAFF 97M use an inclusive B reconstruction method and assume a (13.2 ± 4.1)% b-baryon contribution. The value refers to a b-flavored meson mixture of B_u, B_d, and B_s.

[2] BUSKULIC 96D use an inclusive reconstruction of B hadrons and assume a (12.2 ± 4.3)% b-baryon contribution. The value refers to a b-flavored mixture of B_u, B_d, and B_s.

[3] ABREU 95R use an inclusive B-reconstruction method and assume a (10 ± 4)% b-baryon contribution. The value refers to a b-flavored meson mixture of B_u, B_d, and B_s.

[4] ACCIARRI 95B assume a 9.4% b-baryon contribution. The value refers to a b-flavored mixture of B_u, B_d, and B_s.

$\Gamma(B^+X)/\Gamma(\text{hadrons})$ — Γ_{50}/Γ_8

"OUR EVALUATION" is obtained using our current values for $f(\overline{b} \to B^+)$ and $R_b = \Gamma(b\overline{b})/\Gamma(\text{hadrons})$. We calculate $\Gamma(B^+X)/\Gamma(\text{hadrons}) = R_b \times f(\overline{b} \to B^+)$. The decay fraction $f(\overline{b} \to B^+)$ was provided by the Heavy Flavor Averaging Group (HFLAV, https://hflav.web.cern.ch/).

VALUE	DOCUMENT ID		TECN	COMMENT
0.0869±0.0019 OUR EVALUATION				
0.0887±0.0030	[1] ABDALLAH	03K	DLPH	E^{ee}_{cm} = 88–94 GeV

[1] ABDALLAH 03K measure the production fraction of B^+ mesons in hadronic Z decays $f(B^+)$ = (40.99 ± 0.82 ± 1.11)%. The value quoted here is obtained multiplying this production fraction by our value of $R_b = \Gamma(\overline{b}b)/\Gamma(\text{hadrons})$.

$\Gamma(B^0_sX)/\Gamma(\text{hadrons})$ — Γ_{51}/Γ_8

"OUR EVALUATION" is obtained using our current values for $f(\overline{b} \to B^0_s)$ and $R_b = \Gamma(b\overline{b})/\Gamma(\text{hadrons})$. We calculate $\Gamma(B^0_sX)/\Gamma(\text{hadrons}) = R_b \times f(\overline{b} \to B^0_s)$. The decay fraction $f(\overline{b} \to B^0_s)$ was provided by the Heavy Flavor Averaging Group (HFLAV, https://hflav.web.cern.ch/).

VALUE	DOCUMENT ID		TECN	COMMENT
0.0227±0.0019 OUR EVALUATION				
seen	[1] ABREU	92M	DLPH	E^{ee}_{cm} = 88–94 GeV
seen	[2] ACTON	92N	OPAL	E^{ee}_{cm} = 88–94 GeV
seen	[3] BUSKULIC	92E	ALEP	E^{ee}_{cm} = 88–94 GeV

[1] ABREU 92M reported value is $\Gamma(B^0_sX)*B(B^0_s \to D_s\mu\nu_\mu X)*B(D_s \to \phi\pi)/\Gamma(\text{hadrons})$ = (18 ± 8) × 10^{-5}.

[2] ACTON 92N find evidence for B^0_s production using D_s-ℓ correlations, with $D^+_s \to \phi\pi^+$ and $K^*(892)K^+$. Assuming R_b from the Standard Model and averaging over the e and μ channels, authors measure the product branching fraction to be $f(\overline{b} \to B^0_s) \times B(B^0_s \to D^-_s\ell^+\nu_\ell X) \times B(D^-_s \to \phi\pi^-)$ = (3.9 ± 1.1 ± 0.8) × 10^{-4}.

[3] BUSKULIC 92E find evidence for B^0_s production using D_s-ℓ correlations, with $D^+_s \to \phi\pi^+$ and $K^*(892)K^+$. Using $B(D^+_s \to \phi\pi^+)$ = (2.7 ± 0.7)% and summing up the e and μ channels, the weighted average product branching fraction is measured to be $B(\overline{b} \to B^0_s) \times B(B^0_s \to D^-_s\ell^+\nu_\ell X)$ = 0.040 ± $0.011^{+0.010}_{-0.012}$.

$\Gamma(B^+_cX)/\Gamma(\text{hadrons})$ — Γ_{52}/Γ_8

VALUE	DOCUMENT ID		TECN	COMMENT
searched for	[1] ACKERSTAFF	98O	OPAL	E^{ee}_{cm} = 88–94 GeV
searched for	[2] ABREU	97E	DLPH	E^{ee}_{cm} = 88–94 GeV
searched for	[3] BARATE	97H	ALEP	E^{ee}_{cm} = 88–94 GeV

[1] ACKERSTAFF 98O searched for the decay modes $B_c \to J/\psi\pi^+$, $J/\psi a^+_1$, and $J/\psi\ell^+\nu_\ell$, with $J/\psi \to \ell^+\ell^-$, $\ell = e,\mu$. The number of candidates (background) for the three decay modes is 2 (0.63 ± 0.2), 0 (1.10 ± 0.22), and 1 (0.82 ± 0.19) respectively. Interpreting the 2 $B_c \to J/\psi\pi^+$ candidates as signal, they report $\Gamma(B^+_cX) \times B(B_c \to J/\psi\pi^+)/\Gamma(\text{hadrons}) = (3.8^{+5.0}_{-2.4} \pm 0.5) \times 10^{-5}$. Interpreted as background, the 90% CL bounds are $\Gamma(B^+_cX)*B(B_c \to J/\psi\pi^+)/\Gamma(\text{hadrons}) < 1.06 \times 10^{-4}$, $\Gamma(B^+_cX)*B(B_c \to J/\psi a^+_1)/\Gamma(\text{hadrons}) < 5.29 \times 10^{-4}$, $\Gamma(B^+_cX)*B(B_c \to J/\psi\ell^+\nu_\ell)/\Gamma(\text{hadrons}) < 6.96 \times 10^{-5}$.

[2] ABREU 97E searched for the decay modes $B_c \to J/\psi\pi^+$, $J/\psi\ell^+\nu_\ell$, and $J/\psi(3\pi)^+$, with $J/\psi \to \ell^+\ell^-$, $\ell = e,\mu$. The number of candidates (background) for the three decay modes is 1 (1.7), 0 (0.3), and 1 (2.3) respectively. They report the following 90% CL limits: $\Gamma(B^+_cX)*B(B_c \to J/\psi\pi^+)/\Gamma(\text{hadrons}) < (1.05–0.84) \times 10^{-4}$, $\Gamma(B^+_cX)*B(B_c \to$

Downloaded from https://academic.oup.com/ptep/article/2022/8/083C01/6651666 by KIT Library user on 27 September 2022

$J/\psi\ell\nu_\ell)/\Gamma(\text{hadrons}) < (5.8\text{–}5.0) \times 10^{-5}$, $\Gamma(B_c^+ X)*B(B_c \to J/\psi(3\pi)^+)/\Gamma(\text{hadrons}) < 1.75 \times 10^{-4}$, where the ranges are due to the predicted B_c lifetime (0.4–1.4) ps.

[3] BARATE 97H searched for the decay modes $B_c \to J/\psi\pi^+$ and $J/\psi\ell^+\nu_\ell$ with $J/\psi \to \ell^+\ell^-$, $\ell = e,\mu$. The number of candidates (background) for the two decay modes is 0 (0.44) and 2 (0.81) respectively. They report the following 90% CL limits: $\Gamma(B_c^+ X)*B(B_c \to J/\psi\pi^+)/\Gamma(\text{hadrons}) < 3.6 \times 10^{-5}$ and $\Gamma(B_c^+ X)*B(B_c \to J/\psi\ell^+\nu_\ell)/\Gamma(\text{hadrons}) < 5.2 \times 10^{-5}$.

$\Gamma(\Lambda_c^+ X)/\Gamma(\text{hadrons})$ — Γ_{53}/Γ_8

VALUE	DOCUMENT ID		TECN	COMMENT
0.022±0.005 OUR AVERAGE				
0.024±0.005±0.006	[1] ALEXANDER	96R	OPAL	E_{cm}^{ee} = 88–94 GeV
0.021±0.003±0.005	[2] BUSKULIC	96Y	ALEP	E_{cm}^{ee} = 88–94 GeV

[1] ALEXANDER 96R measure $R_b \times f(b \to \Lambda_c^+ X) \times B(\Lambda_c^+ \to pK^-\pi^+) = (0.122 \pm 0.023 \pm 0.010)\%$ in hadronic Z decays; the value quoted here is obtained using our best value $B(\Lambda_c^+ \to pK^-\pi^+) = (5.0 \pm 1.3)\%$. The first error is the total experiment's error and the second error is the systematic error due to the branching fraction uncertainty.

[2] BUSKULIC 96Y obtain the production fraction of Λ_c^+ baryons in hadronic Z decays $f(b \to \Lambda_c^+ X) = 0.110 \pm 0.014 \pm 0.006$ using $B(\Lambda_c^+ \to pK^-\pi^+) = (4.4 \pm 0.6)\%$; we have rescaled using our best value $B(\Lambda_c^+ \to pK^-\pi^+) = (5.0 \pm 1.3)\%$ obtaining $f(b \to \Lambda_c^+ X) = 0.097 \pm 0.013 \pm 0.025$ where the first error is their total experiment's error and the second error is the systematic error due to the branching fraction uncertainty. The value quoted here is obtained multiplying this production fraction by our value of $R_b = \Gamma(b\overline{b})/\Gamma(\text{hadrons})$.

$\Gamma(\Xi_c^0 X)/\Gamma(\text{hadrons})$ — Γ_{54}/Γ_8

VALUE	DOCUMENT ID		TECN	COMMENT
• • • We do not use the following data for averages, fits, limits, etc. • • •				
seen	[1] ABDALLAH	05C	DLPH	E_{cm}^{ee} = 88–94 GeV

[1] ABDALLAH 05C searched for the charmed strange baryon Ξ_c^0 in the decay channel $\Xi_c^0 \to \Xi^-\pi^+$ ($\Xi^- \to \Lambda\pi^-$). The production rate is measured to be $f_{\Xi_c^0} \times B(\Xi_c^0 \to \Xi^-\pi^+) = (4.7 \pm 1.4 \pm 1.1) \times 10^{-4}$ per hadronic Z decay.

$\Gamma(\Xi_b X)/\Gamma(\text{hadrons})$ — Γ_{55}/Γ_8

Here Ξ_b is used as a notation for the strange b-baryon states Ξ_b^- and Ξ_b^0.

VALUE	DOCUMENT ID		TECN	COMMENT
• • • We do not use the following data for averages, fits, limits, etc. • • •				
seen	[1] ABDALLAH	05C	DLPH	E_{cm}^{ee} = 88–94 GeV
seen	[2] BUSKULIC	96T	ALEP	E_{cm}^{ee} = 88–94 GeV
seen	[3] ABREU	95V	DLPH	E_{cm}^{ee} = 88–94 GeV

[1] ABDALLAH 05C searched for the beauty strange baryon Ξ_b in the inclusive semileptonic decay channel $\Xi_b \to \Xi^-\ell^-\overline{\nu}_\ell X$. Evidence for the Ξ_b production is seen from the observation of $\Xi^\mp$ production accompanied by a lepton of the same sign. From the excess of "right-sign" pairs $\Xi^\mp\ell^\mp$ compared to "wrong-sign" pairs $\Xi^\mp\ell^\pm$ the production rate is measured to be $B(b \to \Xi_b) \times B(\Xi_b \to \Xi^-\ell^-X) = (3.0 \pm 1.0 \pm 0.3) \times 10^{-4}$ per lepton species, averaged over electrons and muons.

[2] BUSKULIC 96T investigate Ξ-lepton correlations and find a significant excess of "right–sign" pairs $\Xi^\mp\ell^\mp$ compared to "wrong–sign" pairs $\Xi^\mp\ell^\pm$. This excess is interpreted as evidence for Ξ_b semileptonic decay. The measured product branching ratio is $B(b \to \Xi_b) \times B(\Xi_b \to X_c X\ell^-\overline{\nu}_\ell) \times B(X_c \to \Xi^- X') = (5.4 \pm 1.1 \pm 0.8) \times 10^{-4}$ per lepton species, averaged over electrons and muons, with X_c a charmed baryon.

[3] ABREU 95V observe an excess of "right-sign" pairs $\Xi^\mp\ell^\mp$ compared to "wrong-sign" pairs $\Xi^\mp\ell^\pm$ in jets: this excess is interpreted as evidence for the beauty strange baryon Ξ_b production, with $\Xi_b \to \Xi^-\ell^-\overline{\nu}_\ell X$. They find that the probability for this signal to come from non b-baryon decays is less than 5×10^{-4} and that Λ_b decays can account for less than 10% of these events. The Ξ_b production rate is then measured to be $B(b \to \Xi_b) \times B(\Xi_b \to \Xi^-\ell^-X) = (5.9 \pm 2.1 \pm 1.0) \times 10^{-4}$ per lepton species, averaged over electrons and muons.

$\Gamma(b\text{-baryon } X)/\Gamma(\text{hadrons})$ — Γ_{56}/Γ_8

"OUR EVALUATION" is obtained using our current values for $f(b \to b\text{-baryon})$ and $R_b = \Gamma(b\overline{b})/\Gamma(\text{hadrons})$. We calculate $\Gamma(b\text{-baryon } X)/\Gamma(\text{hadrons}) = R_b \times f(b \to b\text{-baryon})$. The decay fraction $f(b \to b\text{-baryon})$ was provided by the Heavy Flavor Averaging Group (https://hflav.web.cern.ch/).

VALUE	DOCUMENT ID		TECN	COMMENT
0.0197±0.0032 OUR EVALUATION				
0.0221±0.0015±0.0058	[1] BARATE	98V	ALEP	E_{cm}^{ee} = 88–94 GeV

[1] BARATE 98V use the overall number of identified protons in b-hadron decays to measure $f(b \to b\text{-baryon}) = 0.102 \pm 0.007 \pm 0.027$. They assume $BR(b\text{-baryon} \to pX) = (58 \pm 6)\%$ and $BR(B_s^0 \to pX) = (8.0 \pm 4.0)\%$. The value quoted here is obtained multiplying this production fraction by our value of $R_b = \Gamma(b\overline{b})/\Gamma(\text{hadrons})$.

$\Gamma(\text{anomalous } \gamma + \text{hadrons})/\Gamma_{total}$ — Γ_{57}/Γ

Limits on additional sources of prompt photons beyond expectations for final-state bremsstrahlung.

VALUE	CL%	DOCUMENT ID		TECN	COMMENT
$<3.2 \times 10^{-3}$	95	[1] AKRAWY	90J	OPAL	E_{cm}^{ee} = 88–94 GeV

[1] AKRAWY 90J report $\Gamma(\gamma X) < 8.2$ MeV at 95%CL. They assume a three-body $\gamma q\overline{q}$ distribution and use $E(\gamma) > 10$ GeV.

$\Gamma(e^+e^-\gamma)/\Gamma_{total}$ — Γ_{58}/Γ

VALUE	CL%	DOCUMENT ID		TECN	COMMENT
$<5.2 \times 10^{-4}$	95	[1] ACTON	91B	OPAL	E_{cm}^{ee} = 91.2 GeV

[1] ACTON 91B looked for isolated photons with E>2% of beam energy (> 0.9 GeV).

$\Gamma(\mu^+\mu^-\gamma)/\Gamma_{total}$ — Γ_{59}/Γ

VALUE	CL%	DOCUMENT ID		TECN	COMMENT
$<5.6 \times 10^{-4}$	95	[1] ACTON	91B	OPAL	E_{cm}^{ee} = 91.2 GeV

[1] ACTON 91B looked for isolated photons with E>2% of beam energy (> 0.9 GeV).

$\Gamma(\tau^+\tau^-\gamma)/\Gamma_{total}$ — Γ_{60}/Γ

VALUE	CL%	DOCUMENT ID		TECN	COMMENT
$<7.3 \times 10^{-4}$	95	[1] ACTON	91B	OPAL	E_{cm}^{ee} = 91.2 GeV

[1] ACTON 91B looked for isolated photons with E>2% of beam energy (> 0.9 GeV).

$\Gamma(\ell^+\ell^-\gamma\gamma)/\Gamma_{total}$ — Γ_{61}/Γ

The value is the sum over $\ell = e, \mu, \tau$.

VALUE	CL%	DOCUMENT ID		TECN	COMMENT
$<6.8 \times 10^{-6}$	95	[1] ACTON	93E	OPAL	E_{cm}^{ee} = 88–94 GeV

[1] For $m_{\gamma\gamma} = 60 \pm 5$ GeV.

$\Gamma(q\overline{q}\gamma\gamma)/\Gamma_{total}$ — Γ_{62}/Γ

VALUE	CL%	DOCUMENT ID		TECN	COMMENT
$<5.5 \times 10^{-6}$	95	[1] ACTON	93E	OPAL	E_{cm}^{ee} = 88–94 GeV

[1] For $m_{\gamma\gamma} = 60 \pm 5$ GeV.

$\Gamma(\nu\overline{\nu}\gamma\gamma)/\Gamma_{total}$ — Γ_{63}/Γ

VALUE	CL%	DOCUMENT ID		TECN	COMMENT
$<3.1 \times 10^{-6}$	95	[1] ACTON	93E	OPAL	E_{cm}^{ee} = 88–94 GeV

[1] For $m_{\gamma\gamma} = 60 \pm 5$ GeV.

$\Gamma(e^\pm\mu^\mp)/\Gamma_{total}$ — Γ_{64}/Γ

Test of lepton family number conservation. The value is for the sum of the charge states indicated.

VALUE	CL%	DOCUMENT ID		TECN	COMMENT
$<7.5 \times 10^{-7}$	95	AAD	14AU	ATLS	E_{cm}^{pp} = 8 TeV
$<2.5 \times 10^{-6}$	95	ABREU	97C	DLPH	E_{cm}^{ee} = 88–94 GeV
$<1.7 \times 10^{-6}$	95	AKERS	95W	OPAL	E_{cm}^{ee} = 88–94 GeV
$<0.6 \times 10^{-5}$	95	ADRIANI	93I	L3	E_{cm}^{ee} = 88–94 GeV
$<2.6 \times 10^{-5}$	95	DECAMP	92	ALEP	E_{cm}^{ee} = 88–94 GeV

$\Gamma(e^\pm\mu^\mp)/\Gamma(e^+e^-)$ — Γ_{64}/Γ_1

Test of lepton family number conservation. The value is for the sum of the charge states indicated.

VALUE	CL%	DOCUMENT ID		TECN	COMMENT
<0.07	90	ALBAJAR	89	UA1	$E_{cm}^{p\overline{p}}$ = 546,630 GeV

$\Gamma(e^\pm\tau^\mp)/\Gamma_{total}$ — Γ_{65}/Γ

Test of lepton family number conservation. The value is for the sum of the charge states indicated.

VALUE	CL%	DOCUMENT ID		TECN	COMMENT
$<5.0 \times 10^{-6}$	95	AAD	21AV	ATLS	E_{cm}^{pp} = 13 TeV
• • • We do not use the following data for averages, fits, limits, etc. • • •					
$<8.1 \times 10^{-6}$	95	AAD	21AO	ATLS	E_{cm}^{pp} = 13 TeV
$<5.8 \times 10^{-5}$	95	AABOUD	18CN	ATLS	E_{cm}^{pp} = 13 TeV
$<2.2 \times 10^{-5}$	95	ABREU	97C	DLPH	E_{cm}^{ee} = 88–94 GeV
$<9.8 \times 10^{-6}$	95	AKERS	95W	OPAL	E_{cm}^{ee} = 88–94 GeV
$<1.3 \times 10^{-5}$	95	ADRIANI	93I	L3	E_{cm}^{ee} = 88–94 GeV
$<1.2 \times 10^{-4}$	95	DECAMP	92	ALEP	E_{cm}^{ee} = 88–94 GeV

$\Gamma(\mu^\pm\tau^\mp)/\Gamma_{total}$ — Γ_{66}/Γ

Test of lepton family number conservation. The value is for the sum of the charge states indicated.

VALUE	CL%	DOCUMENT ID		TECN	COMMENT
$<6.5 \times 10^{-6}$	95	AAD	21AV	ATLS	E_{cm}^{pp} = 13 TeV
• • • We do not use the following data for averages, fits, limits, etc. • • •					
$<9.5 \times 10^{-6}$	95	AAD	21AO	ATLS	E_{cm}^{pp} = 13 TeV
$<1.3 \times 10^{-5}$	95	AABOUD	18CN	ATLS	E_{cm}^{pp} = 8, 13 TeV
$<1.2 \times 10^{-5}$	95	ABREU	97C	DLPH	E_{cm}^{ee} = 88–94 GeV
$<1.7 \times 10^{-5}$	95	AKERS	95W	OPAL	E_{cm}^{ee} = 88–94 GeV
$<1.9 \times 10^{-5}$	95	ADRIANI	93I	L3	E_{cm}^{ee} = 88–94 GeV
$<1.0 \times 10^{-4}$	95	DECAMP	92	ALEP	E_{cm}^{ee} = 88–94 GeV

$\Gamma(pe)/\Gamma_{total}$ — Γ_{67}/Γ

Test of baryon number and lepton number conservations. Charge conjugate states are implied.

VALUE	CL%	DOCUMENT ID		TECN	COMMENT
$<1.8 \times 10^{-6}$	95	[1] ABBIENDI	99I	OPAL	E_{cm}^{ee} = 88–94 GeV

[1] ABBIENDI 99I give the 95%CL limit on the partial width $\Gamma(Z^0 \to pe) < 4.6$ KeV and we have transformed it into a branching ratio.

Downloaded from https://academic.oup.com/ptep/article/2022/8/083C01/6651666 by KIT Library user on 27 September 2022

$\Gamma(p\mu)/\Gamma_{total}$ — Γ_{68}/Γ

Test of baryon number and lepton number conservations. Charge conjugate states are implied.

VALUE	CL%	DOCUMENT ID		TECN	COMMENT
$<1.8\times10^{-6}$	95	[1] ABBIENDI	99I	OPAL	$E^{ee}_{cm}=$ 88–94 GeV

[1] ABBIENDI 99I give the 95%CL limit on the partial width $\Gamma(Z^0\to p\mu)<4.4$ KeV and we have transformed it into a branching ratio.

AVERAGE PARTICLE MULTIPLICITIES IN HADRONIC Z DECAY

Summed over particle and antiparticle, when appropriate.

$\langle N_\gamma\rangle$

VALUE	DOCUMENT ID		TECN	COMMENT
20.97±0.02±1.15	ACKERSTAFF	98A	OPAL	$E^{ee}_{cm}=$ 91.2 GeV

$\langle N_{\pi^\pm}\rangle$

VALUE	DOCUMENT ID		TECN	COMMENT
17.03 ±0.16 OUR AVERAGE				
17.007±0.209	ABE	04C	SLD	$E^{ee}_{cm}=$ 91.2 GeV
17.26 ±0.10 ±0.88	ABREU	98L	DLPH	$E^{ee}_{cm}=$ 91.2 GeV
17.04 ±0.31	BARATE	98V	ALEP	$E^{ee}_{cm}=$ 91.2 GeV
17.05 ±0.43	AKERS	94P	OPAL	$E^{ee}_{cm}=$ 91.2 GeV

$\langle N_{\pi^0}\rangle$

VALUE	DOCUMENT ID		TECN	COMMENT
9.76±0.26 OUR AVERAGE				
9.55±0.06±0.75	ACKERSTAFF	98A	OPAL	$E^{ee}_{cm}=$ 91.2 GeV
9.63±0.13±0.63	BARATE	97J	ALEP	$E^{ee}_{cm}=$ 91.2 GeV
9.90±0.02±0.33	ACCIARRI	96	L3	$E^{ee}_{cm}=$ 91.2 GeV
9.2 ±0.2 ±1.0	ADAM	96	DLPH	$E^{ee}_{cm}=$ 91.2 GeV

$\langle N_\eta\rangle$

VALUE	DOCUMENT ID		TECN	COMMENT
1.01±0.08 OUR AVERAGE Error includes scale factor of 1.3. See the ideogram below.				
1.20±0.04±0.11	HEISTER	02C	ALEP	$E^{ee}_{cm}=$ 91.2 GeV
0.97±0.03±0.11	ACKERSTAFF	98A	OPAL	$E^{ee}_{cm}=$ 91.2 GeV
0.93±0.01±0.09	ACCIARRI	96	L3	$E^{ee}_{cm}=$ 91.2 GeV

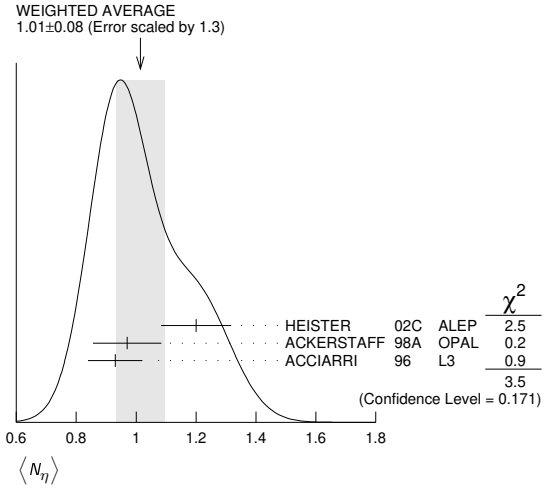

$\langle N_{\rho^\pm}\rangle$

VALUE	DOCUMENT ID		TECN	COMMENT
2.57±0.15 OUR AVERAGE				
2.59±0.03±0.16	[1] BEDDALL	09		ALEPH archive, $E^{ee}_{cm}=$ 91.2 GeV
2.40±0.06±0.43	ACKERSTAFF	98A	OPAL	$E^{ee}_{cm}=$ 91.2 GeV

[1] BEDDALL 09 analyse 3.2 million hadronic Z decays as archived by ALEPH collaboration and report a value of 2.59 ± 0.03 ± 0.15 ± 0.04. The first error is statistical, the second systematic, and the third arises from extrapolation to full phase space. We combine the systematic errors in quadrature.

$\langle N_{\rho^0}\rangle$

VALUE	DOCUMENT ID		TECN	COMMENT
1.24±0.10 OUR AVERAGE Error includes scale factor of 1.1.				
1.19±0.10	ABREU	99J	DLPH	$E^{ee}_{cm}=$ 91.2 GeV
1.45±0.06±0.20	BUSKULIC	96H	ALEP	$E^{ee}_{cm}=$ 91.2 GeV

$\langle N_\omega\rangle$

VALUE	DOCUMENT ID		TECN	COMMENT
1.02±0.06 OUR AVERAGE				
1.00±0.03±0.06	HEISTER	02C	ALEP	$E^{ee}_{cm}=$ 91.2 GeV
1.04±0.04±0.14	ACKERSTAFF	98A	OPAL	$E^{ee}_{cm}=$ 91.2 GeV
1.17±0.09±0.15	ACCIARRI	97D	L3	$E^{ee}_{cm}=$ 91.2 GeV

$\langle N_{\eta'}\rangle$

VALUE	DOCUMENT ID		TECN	COMMENT
0.17 ±0.05 OUR AVERAGE Error includes scale factor of 2.4.				
0.14 ±0.01 ±0.02	ACKERSTAFF	98A	OPAL	$E^{ee}_{cm}=$ 91.2 GeV
0.25 ±0.04	[1] ACCIARRI	97D	L3	$E^{ee}_{cm}=$ 91.2 GeV
• • • We do not use the following data for averages, fits, limits, etc. • • •				
0.068±0.018±0.016	[2] BUSKULIC	92D	ALEP	$E^{ee}_{cm}=$ 91.2 GeV

[1] ACCIARRI 97D obtain this value averaging over the two decay channels $\eta'\to\pi^+\pi^-\eta$ and $\eta'\to\rho^0\gamma$.
[2] BUSKULIC 92D obtain this value for $x>0.1$.

$\langle N_{f_0(980)}\rangle$

VALUE	DOCUMENT ID		TECN	COMMENT
0.147±0.011 OUR AVERAGE				
0.164±0.021	ABREU	99J	DLPH	$E^{ee}_{cm}=$ 91.2 GeV
0.141±0.007±0.011	ACKERSTAFF	98Q	OPAL	$E^{ee}_{cm}=$ 91.2 GeV

$\langle N_{a_0(980)^\pm}\rangle$

VALUE	DOCUMENT ID		TECN	COMMENT
0.27±0.04±0.10	ACKERSTAFF	98A	OPAL	$E^{ee}_{cm}=$ 91.2 GeV

$\langle N_\phi\rangle$

VALUE	DOCUMENT ID		TECN	COMMENT
0.098±0.006 OUR AVERAGE Error includes scale factor of 2.0. See the ideogram below.				
0.105±0.008	ABE	99E	SLD	$E^{ee}_{cm}=$ 91.2 GeV
0.091±0.002±0.003	ACKERSTAFF	98Q	OPAL	$E^{ee}_{cm}=$ 91.2 GeV
0.104±0.003±0.007	ABREU	96U	DLPH	$E^{ee}_{cm}=$ 91.2 GeV
0.122±0.004±0.008	BUSKULIC	96H	ALEP	$E^{ee}_{cm}=$ 91.2 GeV

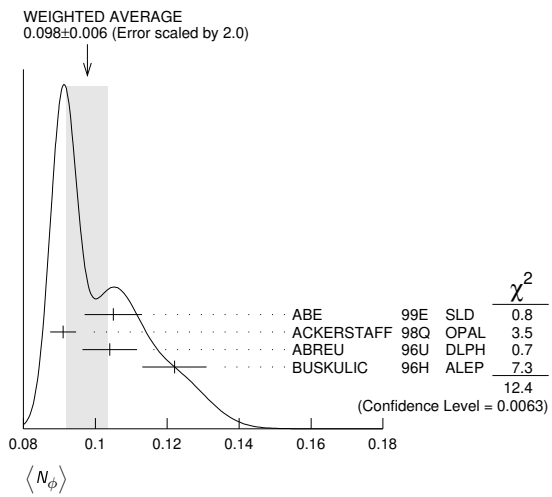

$\langle N_{f_2(1270)}\rangle$

VALUE	DOCUMENT ID		TECN	COMMENT
0.169±0.025 OUR AVERAGE Error includes scale factor of 1.4.				
0.214±0.038	ABREU	99J	DLPH	$E^{ee}_{cm}=$ 91.2 GeV
0.155±0.011±0.018	ACKERSTAFF	98Q	OPAL	$E^{ee}_{cm}=$ 91.2 GeV

$\langle N_{f_1(1285)}\rangle$

VALUE	DOCUMENT ID		TECN	COMMENT
0.165±0.051	[1] ABDALLAH	03H	DLPH	$E^{ee}_{cm}=$ 91.2 GeV

[1] ABDALLAH 03H assume a $K\overline{K}\pi$ branching ratio of (9.0 ± 0.4)%.

$\langle N_{f_1(1420)}\rangle$

VALUE	DOCUMENT ID		TECN	COMMENT
0.056±0.012	[1] ABDALLAH	03H	DLPH	$E^{ee}_{cm}=$ 91.2 GeV

[1] ABDALLAH 03H assume a $K\overline{K}\pi$ branching ratio of 100%.

$\langle N_{f'_2(1525)}\rangle$

VALUE	DOCUMENT ID		TECN	COMMENT
0.012±0.006	ABREU	99J	DLPH	$E^{ee}_{cm}=$ 91.2 GeV

$\langle N_{K^\pm}\rangle$

VALUE	DOCUMENT ID		TECN	COMMENT
2.24 ±0.04 OUR AVERAGE				
2.203±0.071	ABE	04C	SLD	$E^{ee}_{cm}=$ 91.2 GeV
2.21 ±0.05 ±0.05	ABREU	98L	DLPH	$E^{ee}_{cm}=$ 91.2 GeV
2.26 ±0.12	BARATE	98V	ALEP	$E^{ee}_{cm}=$ 91.2 GeV
2.42 ±0.13	AKERS	94P	OPAL	$E^{ee}_{cm}=$ 91.2 GeV

Downloaded from https://academic.oup.com/ptep/article/2022/8/083C01/6651666 by KIT Library user on 27 September 2022

$\langle N_{K^0} \rangle$

VALUE	DOCUMENT ID		TECN	COMMENT
2.039±0.025 OUR AVERAGE	Error includes scale factor of 1.3.			See the ideogram below.
2.093±0.004±0.029	BARATE	00O	ALEP	E^{ee}_{cm}= 91.2 GeV
2.01 ±0.08	ABE	99E	SLD	E^{ee}_{cm}= 91.2 GeV
2.024±0.006±0.042	ACCIARRI	97L	L3	E^{ee}_{cm}= 91.2 GeV
1.962±0.022±0.056	ABREU	95L	DLPH	E^{ee}_{cm}= 91.2 GeV
1.99 ±0.01 ±0.04	AKERS	95U	OPAL	E^{ee}_{cm}= 91.2 GeV

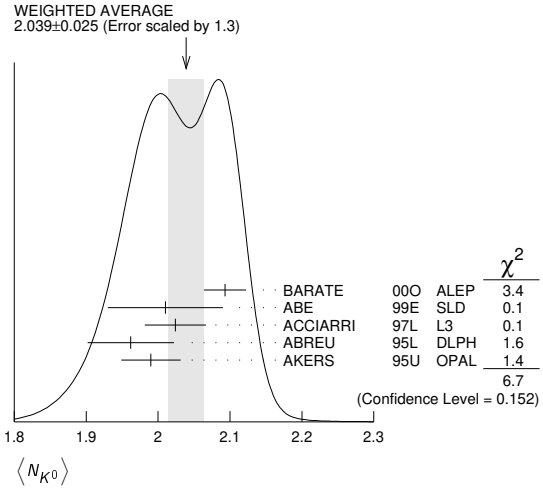

$\langle N_{K^*(892)^\pm} \rangle$

VALUE	DOCUMENT ID		TECN	COMMENT
0.72 ±0.05 OUR AVERAGE				
0.712±0.031±0.059	ABREU	95L	DLPH	E^{ee}_{cm}= 91.2 GeV
0.72 ±0.02 ±0.08	ACTON	93	OPAL	E^{ee}_{cm}= 91.2 GeV

$\langle N_{K^*(892)^0} \rangle$

VALUE	DOCUMENT ID		TECN	COMMENT
0.739±0.022 OUR AVERAGE				
0.707±0.041	ABE	99E	SLD	E^{ee}_{cm}= 91.2 GeV
0.74 ±0.02 ±0.02	ACKERSTAFF	97S	OPAL	E^{ee}_{cm}= 91.2 GeV
0.77 ±0.02 ±0.07	ABREU	96U	DLPH	E^{ee}_{cm}= 91.2 GeV
0.83 ±0.01 ±0.09	BUSKULIC	96H	ALEP	E^{ee}_{cm}= 91.2 GeV
0.97 ±0.18 ±0.31	ABREU	93	DLPH	E^{ee}_{cm}= 91.2 GeV

$\langle N_{K_2^*(1430)} \rangle$

VALUE	DOCUMENT ID		TECN	COMMENT
0.073±0.023	ABREU	99J	DLPH	E^{ee}_{cm}= 91.2 GeV
• • • We do not use the following data for averages, fits, limits, etc. • • •				
0.19 ±0.04 ±0.06	[1] AKERS	95X	OPAL	E^{ee}_{cm}= 91.2 GeV

[1] AKERS 95X obtain this value for x< 0.3.

$\langle N_{D^\pm} \rangle$

VALUE	DOCUMENT ID		TECN	COMMENT
0.187±0.020 OUR AVERAGE	Error includes scale factor of 1.5.			See the ideogram below.
0.170±0.009±0.014	ALEXANDER	96R	OPAL	E^{ee}_{cm}= 91.2 GeV
0.251±0.026±0.025	BUSKULIC	94J	ALEP	E^{ee}_{cm}= 91.2 GeV
0.199±0.019±0.024	[1] ABREU	93I	DLPH	E^{ee}_{cm}= 91.2 GeV

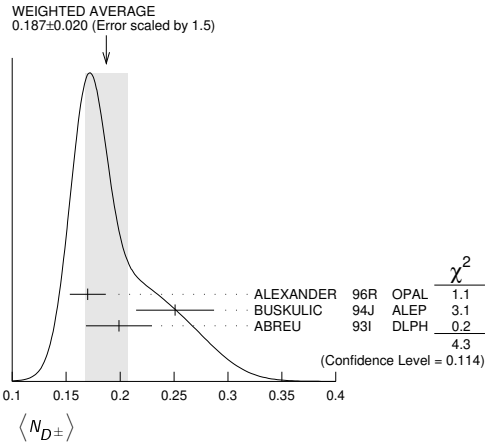

[1] See ABREU 95 (erratum).

$\langle N_{D^0} \rangle$

VALUE	DOCUMENT ID		TECN	COMMENT
0.462±0.026 OUR AVERAGE				
0.465±0.017±0.027	ALEXANDER	96R	OPAL	E^{ee}_{cm}= 91.2 GeV
0.518±0.052±0.035	BUSKULIC	94J	ALEP	E^{ee}_{cm}= 91.2 GeV
0.403±0.038±0.044	[1] ABREU	93I	DLPH	E^{ee}_{cm}= 91.2 GeV

[1] See ABREU 95 (erratum).

$\langle N_{D_s^\pm} \rangle$

VALUE	DOCUMENT ID		TECN	COMMENT
0.131±0.010±0.018	ALEXANDER	96R	OPAL	E^{ee}_{cm}= 91.2 GeV

$\langle N_{D^*(2010)^\pm} \rangle$

VALUE	DOCUMENT ID		TECN	COMMENT
0.183 ±0.008 OUR AVERAGE				
0.1854±0.0041±0.0091	[1] ACKERSTAFF	98E	OPAL	E^{ee}_{cm}= 91.2 GeV
0.187 ±0.015 ±0.013	BUSKULIC	94J	ALEP	E^{ee}_{cm}= 91.2 GeV
0.171 ±0.012 ±0.016	[2] ABREU	93I	DLPH	E^{ee}_{cm}= 91.2 GeV

[1] ACKERSTAFF 98E systematic error includes an uncertainty of ±0.0069 due to the branching ratios $B(D^{*+} \to D^0\pi^+) = 0.683 \pm 0.014$ and $B(D^0 \to K^-\pi^+) = 0.0383 \pm 0.0012$.
[2] See ABREU 95 (erratum).

$\langle N_{D_{s1}(2536)^+} \rangle$

VALUE (units 10^{-3})	DOCUMENT ID		TECN	COMMENT
• • • We do not use the following data for averages, fits, limits, etc. • • •				
$2.9^{+0.7}_{-0.6}\pm0.2$	[1] ACKERSTAFF	97W	OPAL	E^{ee}_{cm}= 91.2 GeV

[1] ACKERSTAFF 97W obtain this value for x> 0.6 and with the assumption that its decay width is saturated by the D^*K final states.

$\langle N_{B^*} \rangle$

VALUE	DOCUMENT ID		TECN	COMMENT
0.28±0.01±0.03	[1] ABREU	95R	DLPH	E^{ee}_{cm}= 91.2 GeV

[1] ABREU 95R quote this value for a flavor-averaged excited state.

$\langle N_{J/\psi(1S)} \rangle$

VALUE	DOCUMENT ID		TECN	COMMENT
0.0056±0.0003±0.0004	[1] ALEXANDER	96B	OPAL	E^{ee}_{cm}= 91.2 GeV

[1] ALEXANDER 96B identify $J/\psi(1S)$ from the decays into lepton pairs.

$\langle N_{\psi(2S)} \rangle$

VALUE	DOCUMENT ID		TECN	COMMENT
0.0023±0.0004±0.0003	ALEXANDER	96B	OPAL	E^{ee}_{cm}= 91.2 GeV

$\langle N_p \rangle$

VALUE	DOCUMENT ID		TECN	COMMENT
1.046±0.026 OUR AVERAGE				
1.054±0.035	ABE	04C	SLD	E^{ee}_{cm}= 91.2 GeV
1.08 ±0.04 ±0.03	ABREU	98L	DLPH	E^{ee}_{cm}= 91.2 GeV
1.00 ±0.07	BARATE	98V	ALEP	E^{ee}_{cm}= 91.2 GeV
0.92 ±0.11	AKERS	94P	OPAL	E^{ee}_{cm}= 91.2 GeV

$\langle N_{\Delta(1232)^{++}} \rangle$

VALUE	DOCUMENT ID		TECN	COMMENT
0.087±0.033 OUR AVERAGE	Error includes scale factor of 2.4.			
0.079±0.009±0.011	ABREU	95W	DLPH	E^{ee}_{cm}= 91.2 GeV
0.22 ±0.04 ±0.04	ALEXANDER	95D	OPAL	E^{ee}_{cm}= 91.2 GeV

$\langle N_\Lambda \rangle$

VALUE	DOCUMENT ID		TECN	COMMENT
0.388±0.009 OUR AVERAGE	Error includes scale factor of 1.7.			See the ideogram below.
0.404±0.002±0.007	BARATE	00O	ALEP	E^{ee}_{cm}= 91.2 GeV
0.395±0.022	ABE	99E	SLD	E^{ee}_{cm}= 91.2 GeV
0.364±0.004±0.017	ACCIARRI	97L	L3	E^{ee}_{cm}= 91.2 GeV
0.374±0.002±0.010	ALEXANDER	97D	OPAL	E^{ee}_{cm}= 91.2 GeV
0.357±0.003±0.017	ABREU	93L	DLPH	E^{ee}_{cm}= 91.2 GeV

Downloaded from https://academic.oup.com/ptep/article/2022/8/083C01/6651666 by KIT Library user on 27 September 2022

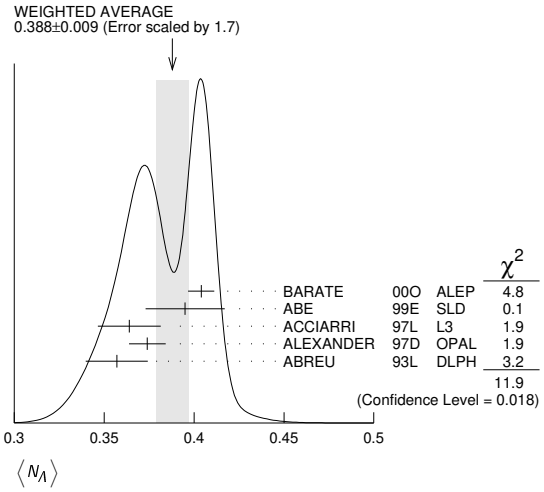

$\langle N_{\Lambda(1520)} \rangle$

VALUE	DOCUMENT ID		TECN	COMMENT
0.0224±0.0027 OUR AVERAGE				
0.029 ±0.005 ±0.005	ABREU	00P	DLPH	E^{ee}_{cm}= 91.2 GeV
0.0213±0.0021±0.0019	ALEXANDER	97D	OPAL	E^{ee}_{cm}= 91.2 GeV

$\langle N_{\Sigma^+} \rangle$

VALUE	DOCUMENT ID		TECN	COMMENT
0.107±0.010 OUR AVERAGE				
0.114±0.011±0.009	ACCIARRI	00J	L3	E^{ee}_{cm}= 91.2 GeV
0.099±0.008±0.013	ALEXANDER	97E	OPAL	E^{ee}_{cm}= 91.2 GeV

$\langle N_{\Sigma^-} \rangle$

VALUE	DOCUMENT ID		TECN	COMMENT
0.082±0.007 OUR AVERAGE				
0.081±0.002±0.010	ABREU	00P	DLPH	E^{ee}_{cm}= 91.2 GeV
0.083±0.006±0.009	ALEXANDER	97E	OPAL	E^{ee}_{cm}= 91.2 GeV

$\langle N_{\Sigma^++\Sigma^-} \rangle$

VALUE	DOCUMENT ID		TECN	COMMENT
0.181±0.018 OUR AVERAGE				
0.182±0.010±0.016	[1] ALEXANDER	97E	OPAL	E^{ee}_{cm}= 91.2 GeV
0.170±0.014±0.061	ABREU	95O	DLPH	E^{ee}_{cm}= 91.2 GeV

[1] We have combined the values of $\langle N_{\Sigma^+} \rangle$ and $\langle N_{\Sigma^-} \rangle$ from ALEXANDER 97E adding the statistical and systematic errors of the two final states separately in quadrature. If isospin symmetry is assumed this value becomes 0.174 ± 0.010 ± 0.015.

$\langle N_{\Sigma^0} \rangle$

VALUE	DOCUMENT ID		TECN	COMMENT
0.076±0.010 OUR AVERAGE				
0.095±0.015±0.013	ACCIARRI	00J	L3	E^{ee}_{cm}= 91.2 GeV
0.071±0.012±0.013	ALEXANDER	97E	OPAL	E^{ee}_{cm}= 91.2 GeV
0.070±0.010±0.010	ADAM	96B	DLPH	E^{ee}_{cm}= 91.2 GeV

$\langle N_{(\Sigma^++\Sigma^-+\Sigma^0)/3} \rangle$

VALUE	DOCUMENT ID		TECN	COMMENT
0.084±0.005±0.008	ALEXANDER	97E	OPAL	E^{ee}_{cm}= 91.2 GeV

$\langle N_{\Sigma(1385)^+} \rangle$

VALUE	DOCUMENT ID		TECN	COMMENT
0.0239±0.0009±0.0012	ALEXANDER	97D	OPAL	E^{ee}_{cm}= 91.2 GeV

$\langle N_{\Sigma(1385)^-} \rangle$

VALUE	DOCUMENT ID		TECN	COMMENT
0.0240±0.0010±0.0014	ALEXANDER	97D	OPAL	E^{ee}_{cm}= 91.2 GeV

$\langle N_{\Sigma(1385)^++\Sigma(1385)^-} \rangle$

VALUE	DOCUMENT ID		TECN	COMMENT
0.046 ±0.004 OUR AVERAGE	Error includes scale factor of 1.6.			
0.0479±0.0013±0.0026	ALEXANDER	97D	OPAL	E^{ee}_{cm}= 91.2 GeV
0.0382±0.0028±0.0045	ABREU	95O	DLPH	E^{ee}_{cm}= 91.2 GeV

$\langle N_{\Xi^-} \rangle$

VALUE	DOCUMENT ID		TECN	COMMENT
0.0258±0.0009 OUR AVERAGE				
0.0247±0.0009±0.0025	ABDALLAH	06E	DLPH	E^{ee}_{cm} = 91.2 GeV
0.0259±0.0004±0.0009	ALEXANDER	97D	OPAL	E^{ee}_{cm} = 91.2 GeV

$\langle N_{\Xi(1530)^0} \rangle$

VALUE	DOCUMENT ID		TECN	COMMENT
0.0059±0.0011 OUR AVERAGE	Error includes scale factor of 2.3.			
0.0045±0.0005±0.0006	ABDALLAH	05C	DLPH	E^{ee}_{cm}= 91.2 GeV
0.0068±0.0005±0.0004	ALEXANDER	97D	OPAL	E^{ee}_{cm}= 91.2 GeV

$\langle N_{\Omega^-} \rangle$

VALUE	DOCUMENT ID		TECN	COMMENT
0.00164±0.00028 OUR AVERAGE				
0.0018 ±0.0003 ±0.0002	ALEXANDER	97D	OPAL	E^{ee}_{cm}= 91.2 GeV
0.0014 ±0.0002 ±0.0004	ADAM	96B	DLPH	E^{ee}_{cm}= 91.2 GeV

$\langle N_{\Lambda_c^+} \rangle$

VALUE	DOCUMENT ID		TECN	COMMENT
0.078±0.012±0.012	ALEXANDER	96R	OPAL	E^{ee}_{cm}= 91.2 GeV

$\langle N_{\overline{D}} \rangle$

VALUE (units 10^{-6})	DOCUMENT ID		TECN	COMMENT
• • • We do not use the following data for averages, fits, limits, etc. • • •				
5.9±1.8±0.5	[1] SCHAEL	06A	ALEP	E^{ee}_{cm} = 91.2 GeV

[1] SCHAEL 06A obtain this anti-deuteron production rate per hadronic Z decay in the anti-deuteron momentum range from 0.62 to 1.03 GeV/c.

$\langle N_{charged} \rangle$

VALUE	DOCUMENT ID		TECN	COMMENT
20.76±0.16 OUR AVERAGE	Error includes scale factor of 2.1. See the ideogram below.			
20.46±0.01±0.11	ACHARD	03G	L3	E^{ee}_{cm}= 91.2 GeV
21.21±0.01±0.20	ABREU	99	DLPH	E^{ee}_{cm}= 91.2 GeV
21.05±0.20	AKERS	95Z	OPAL	E^{ee}_{cm}= 91.2 GeV
20.91±0.03±0.22	BUSKULIC	95R	ALEP	E^{ee}_{cm}= 91.2 GeV
21.40±0.43	ACTON	92B	OPAL	E^{ee}_{cm}= 91.2 GeV
20.71±0.04±0.77	ABREU	91H	DLPH	E^{ee}_{cm}= 91.2 GeV
20.7 ±0.7	ADEVA	91I	L3	E^{ee}_{cm}= 91.2 GeV
20.1 ±1.0 ±0.9	ABRAMS	90	MRK2	E^{ee}_{cm}= 91.1 GeV

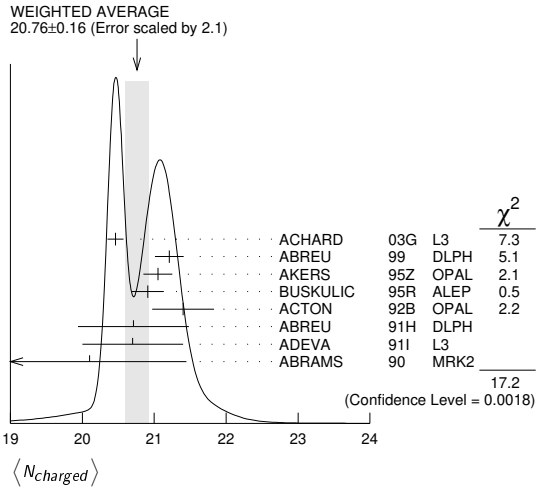

Z HADRONIC POLE CROSS SECTION

OUR FIT is obtained using the fit procedure and correlations as determined by the LEP Electroweak Working Group (see the note "The Z boson" and ref. LEP-SLC 06). This quantity is defined as

$$\sigma^0_h = \frac{12\pi}{M_Z^2} \frac{\Gamma(e^+e^-)\,\Gamma(\text{hadrons})}{\Gamma_Z^2}$$

It is one of the parameters used in the Z lineshape fit.

VALUE (nb)	EVTS	DOCUMENT ID		TECN	COMMENT
41.541±0.037 OUR FIT					
41.501±0.055	4.10M	[1] ABBIENDI	01A	OPAL	E^{ee}_{cm}= 88–94 GeV
41.578±0.069	3.70M	ABREU	00F	DLPH	E^{ee}_{cm}= 88–94 GeV
41.535±0.055	3.54M	ACCIARRI	00C	L3	E^{ee}_{cm}= 88–94 GeV
41.559±0.058	4.07M	[2] BARATE	00C	ALEP	E^{ee}_{cm}= 88–94 GeV
• • • We do not use the following data for averages, fits, limits, etc. • • •					
42 ±4	450	ABRAMS	89B	MRK2	E^{ee}_{cm}= 89.2–93.0 GeV

[1] ABBIENDI 01A error includes approximately 0.031 due to statistics, 0.033 due to event selection systematics, 0.029 due to uncertainty in luminosity measurement, and 0.011 due to LEP energy uncertainty.

[2] BARATE 00C error includes approximately 0.030 due to statistics, 0.026 due to experimental systematics, and 0.025 due to uncertainty in luminosity measurement.

Downloaded from https://academic.oup.com/ptep/article/2022/8/083C01/6651666 by KIT Library user on 27 September 2022

Z VECTOR COUPLINGS

These quantities are the effective vector couplings of the Z to charged leptons and quarks. Their magnitude is derived from a measurement of the Z lineshape and the forward-backward lepton asymmetries as a function of energy around the Z mass. The relative sign among the vector to axial-vector couplings is obtained from a measurement of the Z asymmetry parameters, A_e, A_μ, and A_τ. By convention the sign of g_A^e is fixed to be negative (and opposite to that of g^{ν_e} obtained using ν_e scattering measurements). For the light quarks, the sign of the couplings is assigned consistently with this assumption. The LEP/SLD-based fit values quoted below correspond to global nine- or five-parameter fits to lineshape, lepton forward-backward asymmetry, and A_e, A_μ, and A_τ measurements. See the note "The Z boson" and ref. LEP-SLC 06 for details. Where $p\overline{p}$ and ep data is quoted, OUR FIT value corresponds to a weighted average of this with the LEP/SLD fit result.

g_V^e

VALUE	EVTS	DOCUMENT ID		TECN	COMMENT
−0.03817±0.00047 OUR FIT					
−0.058 ±0.016 ±0.007	5026	[1] ACOSTA	05M	CDF	$E_{cm}^{p\overline{p}}$= 1.96 TeV
−0.0346 ±0.0023	137.0k	[2] ABBIENDI	01O	OPAL	E_{cm}^{ee}= 88–94 GeV
−0.0412 ±0.0027	124.4k	[3] ACCIARRI	00C	L3	E_{cm}^{ee}= 88–94 GeV
−0.0400 ±0.0037		BARATE	00C	ALEP	E_{cm}^{ee}= 88–94 GeV
−0.0414 ±0.0020		[4] ABE	95J	SLD	E_{cm}^{ee}= 91.31 GeV

[1] ACOSTA 05M determine the forward–backward asymmetry of e^+e^- pairs produced via $q\overline{q} \rightarrow Z/\gamma^* \rightarrow e^+e^-$ in 15 M(e^+e^-) effective mass bins ranging from 40 GeV to 600 GeV. These results are used to obtain the vector and axial–vector couplings of the Z to e^+e^-, assuming the quark couplings are as predicted by the standard model. Higher order radiative corrections have not been taken into account.
[2] ABBIENDI 01O use their measurement of the τ polarization in addition to the lineshape and forward-backward lepton asymmetries.
[3] ACCIARRI 00C use their measurement of the τ polarization in addition to forward-backward lepton asymmetries.
[4] ABE 95J obtain this result combining polarized Bhabha results with the A_{LR} measurement of ABE 94C. The Bhabha results alone give −0.0507 ± 0.0096 ± 0.0020.

g_V^μ

VALUE	EVTS	DOCUMENT ID		TECN	COMMENT
−0.0367±0.0023 OUR FIT					
$-0.0388^{+0.0060}_{-0.0064}$	182.8k	[1] ABBIENDI	01O	OPAL	E_{cm}^{ee}= 88–94 GeV
−0.0386±0.0073	113.4k	[2] ACCIARRI	00C	L3	E_{cm}^{ee}= 88–94 GeV
−0.0362±0.0061		BARATE	00C	ALEP	E_{cm}^{ee}= 88–94 GeV
• • • We do not use the following data for averages, fits, limits, etc. • • •					
−0.0413±0.0060	66143	[3] ABBIENDI	01K	OPAL	E_{cm}^{ee}= 89–93 GeV

[1] ABBIENDI 01O use their measurement of the τ polarization in addition to the lineshape and forward-backward lepton asymmetries.
[2] ACCIARRI 00C use their measurement of the τ polarization in addition to forward-backward lepton asymmetries.
[3] ABBIENDI 01K obtain this from an angular analysis of the muon pair asymmetry which takes into account effects of initial state radiation on an event by event basis and of initial-final state interference.

g_V^τ

VALUE	EVTS	DOCUMENT ID		TECN	COMMENT
−0.0366±0.0010 OUR FIT					
−0.0365±0.0023	151.5k	[1] ABBIENDI	01O	OPAL	E_{cm}^{ee}= 88–94 GeV
−0.0384±0.0026	103.0k	[2] ACCIARRI	00C	L3	E_{cm}^{ee}= 88–94 GeV
−0.0361±0.0068		BARATE	00C	ALEP	E_{cm}^{ee}= 88–94 GeV

[1] ABBIENDI 01O use their measurement of the τ polarization in addition to the lineshape and forward-backward lepton asymmetries.
[2] ACCIARRI 00C use their measurement of the τ polarization in addition to forward-backward lepton asymmetries.

g_V^ℓ

VALUE	EVTS	DOCUMENT ID		TECN	COMMENT
−0.03783±0.00041 OUR FIT					
−0.0358 ±0.0014	471.3k	[1] ABBIENDI	01O	OPAL	E_{cm}^{ee}= 88–94 GeV
−0.0397 ±0.0020	379.4k	[2] ABREU	00F	DLPH	E_{cm}^{ee}= 88–94 GeV
−0.0397 ±0.0017	340.8k	[3] ACCIARRI	00C	L3	E_{cm}^{ee}= 88–94 GeV
−0.0383 ±0.0018	500k	BARATE	00C	ALEP	E_{cm}^{ee}= 88–94 GeV

[1] ABBIENDI 01O use their measurement of the τ polarization in addition to the lineshape and forward-backward lepton asymmetries.
[2] Using forward-backward lepton asymmetries.
[3] ACCIARRI 00C use their measurement of the τ polarization in addition to forward-backward lepton asymmetries.

g_V^u

VALUE	EVTS	DOCUMENT ID		TECN	COMMENT
0.266±0.034 OUR AVERAGE					
0.270±0.037		[1] ANDREEV	18A	H1	$e^\pm p$
0.201±0.112	156k	[2] ABAZOV	11D	D0	$E_{cm}^{p\overline{p}}$ = 1.97 TeV
$0.24\ ^{+0.28}_{-0.11}$		[3] LEP-SLC	06		E_{cm}^{ee} = 88–94 GeV
$0.399^{+0.152}_{-0.188}$±0.066	5026	[4] ACOSTA	05M	CDF	$E_{cm}^{p\overline{p}}$= 1.96 TeV
• • • We do not use the following data for averages, fits, limits, etc. • • •					
$0.14\ ^{+0.09}_{-0.09}$		[5] ABRAMOWICZ	16A	ZEUS	
$0.144^{+0.066}_{-0.058}$		[6] ABT	16		
0.27 ±0.13	1500	[7] AKTAS	06	H1	$e^\pm p \rightarrow \overline{\nu}_e(\nu_e)X$, $\sqrt{s} \approx 300$ GeV

[1] ANDREEV 18A obtain this result in a combined electroweak and QCD analysis using all deep-inelastic e^+p and e^-p neutral current and charged current scattering cross sections published by the H1 Collaboration, including data with longitudinally polarized lepton beams.
[2] ABAZOV 11D study $p\overline{p} \rightarrow Z/\gamma^* e^+e^-$ events using 5 fb^{-1} data at $\sqrt{s}$ = 1.96 TeV. The candidate events are selected by requiring two isolated electromagnetic showers with E_T > 25 GeV, at least one electron in the central region and the di-electron mass in the range 50–1000 GeV. From the forward-backward asymmetry, determined as a function of the di-electron mass, they derive the axial and vector couplings of the u- and d- quarks and the value of $\sin^2\theta_{eff}^\ell$ = 0.2309 ± 0.0008(stat) ± 0.0006(syst).
[3] LEP-SLC 06 is a combination of the results from LEP and SLC experiments using light quark tagging. s- and d-quark couplings are assumed to be identical.
[4] ACOSTA 05M determine the forward-backward asymmetry of e^+e^- pairs produced via $q\overline{q} \rightarrow Z/\gamma^* \rightarrow e^+e^-$ in 15 M(e^+e^-) effective mass bins ranging from 40 GeV to 600 GeV. These results are used to obtain the vector and axial-vector couplings of the Z to the light quarks, assuming the electron couplings are as predicted by the Standard Model. Higher order radiative corrections have not been taken into account.
[5] ABRAMOWICZ 16A determine the Z^0 couplings to u- and d-quarks using the ZEUS polarised data from Run II together with the unpolarised data from both ZEUS and H1 Collaborations for Run I and unpolarised H1 data from Run II.
[6] ABT 16 determine the Z^0 couplings to u- and d-quarks using the same techniques and data as ABRAMOWICZ 16A but additionally use the published H1 polarised data.
[7] AKTAS 06 fit the neutral current (1.5 ≤ Q^2 ≤ 30,000 GeV^2) and charged current (1.5 ≤ Q^2 ≤ 15,000 GeV^2) differential cross sections. In the determination of the u-quark couplings the electron and d-quark couplings are fixed to their standard model values.

g_V^d

VALUE	EVTS	DOCUMENT ID		TECN	COMMENT
$-0.38\ ^{+0.04}_{-0.05}$ OUR AVERAGE					
−0.488±0.092		[1] ANDREEV	18A	H1	$e^\pm p$
−0.351±0.251	156k	[2] ABAZOV	11D	D0	$E_{cm}^{p\overline{p}}$ = 1.97 TeV
$-0.33\ ^{+0.05}_{-0.07}$		[3] LEP-SLC	06		E_{cm}^{ee} = 88–94 GeV
$-0.226^{+0.635}_{-0.290}$±0.090	5026	[4] ACOSTA	05M	CDF	$E_{cm}^{p\overline{p}}$= 1.96 TeV
• • • We do not use the following data for averages, fits, limits, etc. • • •					
$-0.41\ ^{+0.25}_{-0.20}$		[5] ABRAMOWICZ	16A	ZEUS	
$-0.503^{+0.171}_{-0.103}$		[6] ABT	16		
−0.33 ±0.33	1500	[7] AKTAS	06	H1	$e^\pm p \rightarrow \overline{\nu}_e(\nu_e)X$, $\sqrt{s} \approx 300$ GeV

[1] ANDREEV 18A obtain this result in a combined electroweak and QCD analysis using all deep-inelastic e^+p and e^-p neutral current and charged current scattering cross sections published by the H1 Collaboration, including data with longitudinally polarized lepton beams.
[2] ABAZOV 11D study $p\overline{p} \rightarrow Z/\gamma^* e^+e^-$ events using 5 fb^{-1} data at $\sqrt{s}$ = 1.96 TeV. The candidate events are selected by requiring two isolated electromagnetic showers with E_T > 25 GeV, at least one electron in the central region and the di-electron mass in the range 50–1000 GeV. From the forward-backward asymmetry, determined as a function of the di-electron mass, they derive the axial and vector couplings of the u- and d- quarks and the value of $\sin^2\theta_{eff}^\ell$ = 0.2309 ± 0.0008(stat) ± 0.0006(syst).
[3] LEP-SLC 06 is a combination of the results from LEP and SLC experiments using light quark tagging. s- and d-quark couplings are assumed to be identical.
[4] ACOSTA 05M determine the forward-backward asymmetry of e^+e^- pairs produced via $q\overline{q} \rightarrow Z/\gamma^* \rightarrow e^+e^-$ in 15 M(e^+e^-) effective mass bins ranging from 40 GeV to 600 GeV. These results are used to obtain the vector and axial-vector couplings of the Z to the light quarks, assuming the electron couplings are as predicted by the Standard Model. Higher order radiative corrections have not been taken into account.
[5] ABRAMOWICZ 16A determine the Z^0 couplings to u- and d-quarks using the ZEUS polarised data from Run II together with the unpolarised data from both ZEUS and H1 Collaborations for Run I and unpolarised H1 data from Run II.
[6] ABT 16 determine the Z^0 couplings to u- and d-quarks using the same techniques and data as ABRAMOWICZ 16A but additionally use the published H1 polarised data.
[7] AKTAS 06 fit the neutral current (1.5 ≤ Q^2 ≤ 30,000 GeV^2) and charged current (1.5 ≤ Q^2 ≤ 15,000 GeV^2) differential cross sections. In the determination of the d-quark couplings the electron and u-quark couplings are fixed to their standard model values.

Z AXIAL-VECTOR COUPLINGS

These quantities are the effective axial-vector couplings of the Z to charged leptons and quarks. Their magnitude is derived from a measurement of the Z lineshape and the forward-backward lepton asymmetries as a function of energy around the Z mass. The relative sign among the vector to axial-vector couplings is obtained from a measurement of the Z asymmetry parameters, A_e, A_μ, and A_τ. By convention the sign of g_A^e is fixed to be negative (and opposite to that of g^{ν_e} obtained using ν_e scattering measurements). For the light quarks, the sign of the couplings is assigned consistently with this assumption. The LEP/SLD-based fit values quoted below correspond to global nine- or five-parameter fits to lineshape, lepton forward-backward asymmetry, and A_e, A_μ, and A_τ measurements. See

Downloaded from https://academic.oup.com/ptep/article/2022/8/083C01/6651666 by KIT Library user on 27 September 2022

the note "The Z boson" and ref. LEP-SLC 06 for details. Where $p\overline{p}$ and ep data is quoted, OUR FIT value corresponds to a weighted average of this with the LEP/SLD fit result.

g_A^e

VALUE	EVTS	DOCUMENT ID		TECN	COMMENT
−0.50111±0.00035 OUR FIT					
−0.528 ±0.123 ±0.059	5026	[1] ACOSTA	05M	CDF	$E_{cm}^{p\overline{p}}$= 1.96 TeV
−0.50062±0.00062	137.0k	[2] ABBIENDI	01O	OPAL	E_{cm}^{ee}= 88–94 GeV
−0.5015 ±0.0007	124.4k	[3] ACCIARRI	00C	L3	E_{cm}^{ee}= 88–94 GeV
−0.50166±0.00057		BARATE	00C	ALEP	E_{cm}^{ee}= 88–94 GeV
−0.4977 ±0.0045		[4] ABE	95J	SLD	E_{cm}^{ee}= 91.31 GeV

[1] ACOSTA 05M determine the forward–backward asymmetry of e^+e^- pairs produced via $q\overline{q} \rightarrow Z/\gamma^* \rightarrow e^+e^-$ in 15 M(e^+e^-) effective mass bins ranging from 40 GeV to 600 GeV. These results are used to obtain the vector and axial–vector couplings of the Z to e^+e^-, assuming the quark couplings are as predicted by the standard model. Higher order radiative corrections have not been taken into account.

[2] ABBIENDI 01O use their measurement of the τ polarization in addition to the lineshape and forward-backward lepton asymmetries.

[3] ACCIARRI 00C use their measurement of the τ polarization in addition to forward-backward lepton asymmetries.

[4] ABE 95J obtain this result combining polarized Bhabha results with the A_{LR} measurement of ABE 94C. The Bhabha results alone give −0.4968 ± 0.0039 ± 0.0027.

g_A^μ

VALUE	EVTS	DOCUMENT ID		TECN	COMMENT
−0.50120±0.00054 OUR FIT					
−0.50117±0.00099	182.8k	[1] ABBIENDI	01O	OPAL	E_{cm}^{ee}= 88–94 GeV
−0.5009 ±0.0014	113.4k	[2] ACCIARRI	00C	L3	E_{cm}^{ee}= 88–94 GeV
−0.50046±0.00093		BARATE	00C	ALEP	E_{cm}^{ee}= 88–94 GeV
• • • We do not use the following data for averages, fits, limits, etc. • • •					
−0.520 ±0.015	66143	[3] ABBIENDI	01K	OPAL	E_{cm}^{ee}= 89–93 GeV

[1] ABBIENDI 01O use their measurement of the τ polarization in addition to the lineshape and forward-backward lepton asymmetries.

[2] ACCIARRI 00C use their measurement of the τ polarization in addition to forward-backward lepton asymmetries.

[3] ABBIENDI 01K obtain this from an angular analysis of the muon pair asymmetry which takes into account effects of initial state radiation on an event by event basis and of initial-final state interference.

g_A^τ

VALUE	EVTS	DOCUMENT ID		TECN	COMMENT
−0.50204±0.00064 OUR FIT					
−0.50165±0.00124	151.5k	[1] ABBIENDI	01O	OPAL	E_{cm}^{ee}= 88–94 GeV
−0.5023 ±0.0017	103.0k	[2] ACCIARRI	00C	L3	E_{cm}^{ee}= 88–94 GeV
−0.50216±0.00100		BARATE	00C	ALEP	E_{cm}^{ee}= 88–94 GeV

[1] ABBIENDI 01O use their measurement of the τ polarization in addition to the lineshape and forward-backward lepton asymmetries.

[2] ACCIARRI 00C use their measurement of the τ polarization in addition to forward-backward lepton asymmetries.

g_A^ℓ

VALUE	EVTS	DOCUMENT ID		TECN	COMMENT
−0.50123±0.00026 OUR FIT					
−0.50089±0.00045	471.3k	[1] ABBIENDI	01O	OPAL	E_{cm}^{ee}= 88–94 GeV
−0.5007 ±0.0005	379.4k	ABREU	00F	DLPH	E_{cm}^{ee}= 88–94 GeV
−0.50153±0.00053	340.8k	[2] ACCIARRI	00C	L3	E_{cm}^{ee}= 88–94 GeV
−0.50150±0.00046	500k	BARATE	00C	ALEP	E_{cm}^{ee}= 88–94 GeV

[1] ABBIENDI 01O use their measurement of the τ polarization in addition to the lineshape and forward-backward lepton asymmetries.

[2] ACCIARRI 00C use their measurement of the τ polarization in addition to forward-backward lepton asymmetries.

g_A^u

VALUE	EVTS	DOCUMENT ID		TECN	COMMENT
$0.519^{+0.028}_{-0.033}$ OUR AVERAGE					
0.548±0.036		[1] ANDREEV	18A	H1	$e^\pm p$
0.501±0.110	156k	[2] ABAZOV	11D	D0	$E_{cm}^{p\overline{p}}$ = 1.97 TeV
$0.47\ ^{+0.05}_{-0.33}$		[3] LEP-SLC	06		E_{cm}^{ee} = 88–94 GeV
$0.441^{+0.207}_{-0.173}$±0.067	5026	[4] ACOSTA	05M	CDF	$E_{cm}^{p\overline{p}}$= 1.96 TeV
• • • We do not use the following data for averages, fits, limits, etc. • • •					
$0.50\ ^{+0.12}_{-0.05}$		[5] ABRAMOWICZ	16A	ZEUS	
$0.532^{+0.107}_{-0.063}$		[6] ABT	16		
0.57 ±0.08	1500	[7] AKTAS	06	H1	$e^\pm p \rightarrow \overline{\nu}_e(\nu_e)X$, $\sqrt{s} \approx 300$ GeV

[1] ANDREEV 18A obtain this result in a combined electroweak and QCD analysis using all deep-inelastic e^+p and e^-p neutral current and charged current scattering cross sections published by the H1 Collaboration, including data with longitudinally polarized lepton beams.

[2] ABAZOV 11D study $p\overline{p} \rightarrow Z/\gamma^* e^+e^-$ events using 5 fb^{-1} data at $\sqrt{s}$ = 1.96 TeV. The candidate events are selected by requiring two isolated electromagnetic showers with E_T > 25 GeV, at least one electron in the central region and the di-electron mass in the range 50–1000 GeV. From the forward-backward asymmetry, determined as a function of the di-electron mass, they derive the axial and vector couplings of the u- and d- quarks and the value of $\sin^2\theta_{eff}^\ell$ = 0.2309 ± 0.0008(stat) ± 0.0006(syst).

[3] LEP-SLC 06 is a combination of the results from LEP and SLC experiments using light quark tagging. s- and d-quark couplings are assumed to be identical.

[4] ACOSTA 05M determine the forward-backward asymmetry of e^+e^- pairs produced via $q\overline{q} \rightarrow Z/\gamma^* \rightarrow e^+e^-$ in 15 M(e^+e^-) effective mass bins ranging from 40 GeV to 600 GeV. These results are used to obtain the vector and axial-vector couplings of the Z to the light quarks, assuming the electron couplings are as predicted by the Standard Model. Higher order radiative corrections have not been taken into account.

[5] ABRAMOWICZ 16A determine the Z^0 couplings to u- and d-quarks using the ZEUS polarised data from Run II together with the unpolarised data from both ZEUS and H1 Collaborations for Run I and unpolarised H1 data from Run II.

[6] ABT 16 determine the Z^0 couplings to u- and d-quarks using the same techniques and data as ABRAMOWICZ 16A but additionally use the published H1 polarised data.

[7] AKTAS 06 fit the neutral current (1.5 ≤ Q^2 ≤ 30,000 GeV^2) and charged current (1.5 ≤ Q^2 ≤ 15,000 GeV^2) differential cross sections. In the determination of the u-quark couplings the electron and d-quark couplings are fixed to their standard model values.

g_A^d

VALUE	EVTS	DOCUMENT ID		TECN	COMMENT
$-0.527^{+0.040}_{-0.028}$ OUR AVERAGE					
−0.619±0.108		[1] ANDREEV	18A	H1	$e^\pm p$
−0.497±0.165	156k	[2] ABAZOV	11D	D0	$E_{cm}^{p\overline{p}}$ = 1.97 TeV
$-0.52\ ^{+0.05}_{-0.03}$		[3] LEP-SLC	06		E_{cm}^{ee} = 88–94 GeV
$-0.016^{+0.346}_{-0.536}$±0.091	5026	[4] ACOSTA	05M	CDF	$E_{cm}^{p\overline{p}}$= 1.96 TeV
• • • We do not use the following data for averages, fits, limits, etc. • • •					
$-0.56\ ^{+0.41}_{-0.15}$		[5] ABRAMOWICZ	16A	ZEUS	
$-0.409^{+0.373}_{-0.213}$		[6] ABT	16		
−0.80 ±0.24	1500	[7] AKTAS	06	H1	$e^\pm p \rightarrow \overline{\nu}_e(\nu_e)X$, $\sqrt{s} \approx 300$ GeV

[1] ANDREEV 18A obtain this result in a combined electroweak and QCD analysis using all deep-inelastic e^+p and e^-p neutral current and charged current scattering cross sections published by the H1 Collaboration, including data with longitudinally polarized lepton beams.

[2] ABAZOV 11D study $p\overline{p} \rightarrow Z/\gamma^* e^+e^-$ events using 5 fb^{-1} data at $\sqrt{s}$ = 1.96 TeV. The candidate events are selected by requiring two isolated electromagnetic showers with E_T > 25 GeV, at least one electron in the central region and the di-electron mass in the range 50–1000 GeV. From the forward-backward asymmetry, determined as a function of the di-electron mass, they derive the axial and vector couplings of the u- and d- quarks and the value of $\sin^2\theta_{eff}^\ell$ = 0.2309 ± 0.0008(stat) ± 0.0006(syst).

[3] LEP-SLC 06 is a combination of the results from LEP and SLC experiments using light quark tagging. s- and d-quark couplings are assumed to be identical.

[4] ACOSTA 05M determine the forward-backward asymmetry of e^+e^- pairs produced via $q\overline{q} \rightarrow Z/\gamma^* \rightarrow e^+e^-$ in 15 M(e^+e^-) effective mass bins ranging from 40 GeV to 600 GeV. These results are used to obtain the vector and axial-vector couplings of the Z to the light quarks, assuming the electron couplings are as predicted by the Standard Model. Higher order radiative corrections have not been taken into account.

[5] ABRAMOWICZ 16A determine the Z^0 couplings to u- and d-quarks using the ZEUS polarised data from Run II together with the unpolarised data from both ZEUS and H1 Collaborations for Run I and unpolarised H1 data from Run II.

[6] ABT 16 determine the Z^0 couplings to u- and d-quarks using the same techniques and data as ABRAMOWICZ 16A but additionally use the published H1 polarised data.

[7] AKTAS 06 fit the neutral current (1.5 ≤ Q^2 ≤ 30,000 GeV^2) and charged current (1.5 ≤ Q^2 ≤ 15,000 GeV^2) differential cross sections. In the determination of the d-quark couplings the electron and u-quark couplings are fixed to their standard model values.

Z COUPLINGS TO NEUTRAL LEPTONS

Averaging over neutrino species, the invisible Z decay width determines the effective neutrino coupling g^{ν_ℓ}. For g^{ν_e} and g^{ν_μ}, $\nu_e e$ and $\nu_\mu e$ scattering results are combined with g_A^e and g_V^e measurements at the Z mass to obtain g^{ν_e} and g^{ν_μ} following NOVIKOV 93C.

g^{ν_ℓ}

VALUE	DOCUMENT ID		COMMENT
0.50076±0.00076	[1] LEP-SLC	06	E_{cm}^{ee} = 88–94 GeV

[1] From invisible Z-decay width.

g^{ν_e}

VALUE	DOCUMENT ID		TECN	COMMENT
0.528±0.085	[1] VILAIN	94	CHM2	From $\nu_\mu e$ and $\nu_e e$ scattering

[1] VILAIN 94 derive this value from their value of g^{ν_μ} and their ratio g^{ν_e}/g^{ν_μ} = $1.05^{+0.15}_{-0.18}$.

Downloaded from https://academic.oup.com/ptep/article/2022/8/083C01/6651666 by KIT Library user on 27 September 2022

g^{ν_μ}

VALUE	DOCUMENT ID		TECN	COMMENT
0.502±0.017	[1] VILAIN	94	CHM2	From $\nu_\mu e$ scattering

[1] VILAIN 94 derive this value from their measurement of the couplings $g_A^{e\nu_\mu} = -0.503 \pm 0.017$ and $g_V^{e\nu_\mu} = -0.035 \pm 0.017$ obtained from $\nu_\mu e$ scattering. We have re-evaluated this value using the current PDG values for g_A^e and g_V^e.

Z ASYMMETRY PARAMETERS

For each fermion-antifermion pair coupling to the Z these quantities are defined as

$$A_f = \frac{2 g_V^f g_A^f}{(g_V^f)^2 + (g_A^f)^2}$$

where g_V^f and g_A^f are the effective vector and axial-vector couplings. For their relation to the various lepton asymmetries see the note "The Z boson" and ref. LEP-SLC 06.

A_e

Using polarized beams, this quantity can also be measured as $(\sigma_L - \sigma_R)/(\sigma_L + \sigma_R)$, where σ_L and σ_R are the e^+e^- production cross sections for Z bosons produced with left-handed and right-handed electrons respectively.

VALUE	EVTS	DOCUMENT ID		TECN	COMMENT
0.1515±0.0019 OUR AVERAGE					
0.1454±0.0108±0.0036	144810	[1] ABBIENDI	01O	OPAL	E_{cm}^{ee}= 88–94 GeV
0.1516±0.0021	559000	[2] ABE	01B	SLD	E_{cm}^{ee}= 91.24 GeV
0.1504±0.0068±0.0008		[3] HEISTER	01	ALEP	E_{cm}^{ee}= 88–94 GeV
0.1382±0.0116±0.0005	105000	[4] ABREU	00E	DLPH	E_{cm}^{ee}= 88–94 GeV
0.1678±0.0127±0.0030	137092	[5] ACCIARRI	98H	L3	E_{cm}^{ee}= 88–94 GeV
0.162 ±0.041 ±0.014	89838	[6] ABE	97	SLD	E_{cm}^{ee}= 91.27 GeV
0.202 ±0.038 ±0.008		[7] ABE	95J	SLD	E_{cm}^{ee}= 91.31 GeV

[1] ABBIENDI 01O fit for A_e and A_τ from measurements of the τ polarization at varying τ production angles. The correlation between A_e and A_τ is less than 0.03.

[2] ABE 01B use the left-right production and left-right forward-backward decay asymmetries in leptonic Z decays to obtain a value of 0.1544 ± 0.0060. This is combined with left-right production asymmetry measurement using hadronic Z decays (ABE 00B) to obtain the quoted value.

[3] HEISTER 01 obtain this result fitting the τ polarization as a function of the polar production angle of the τ.

[4] ABREU 00E obtain this result fitting the τ polarization as a function of the polar τ production angle. This measurement is a combination of different analyses (exclusive τ decay modes, inclusive hadronic 1-prong reconstruction, and a neural network analysis).

[5] Derived from the measurement of forward-backward τ polarization asymmetry.

[6] ABE 97 obtain this result from a measurement of the observed left-right charge asymmetry, $A_Q^{obs} = 0.225 \pm 0.056 \pm 0.019$, in hadronic Z decays. If they combine this value of A_Q^{obs} with their earlier measurement of A_{LR}^{obs} they determine A_e to be 0.1574 ± 0.0197 ± 0.0067 independent of the beam polarization.

[7] ABE 95J obtain this result from polarized Bhabha scattering.

A_μ

This quantity is directly extracted from a measurement of the left-right forward-backward asymmetry in $\mu^+\mu^-$ production at SLC using a polarized electron beam. This double asymmetry eliminates the dependence on the Z-e-e coupling parameter A_e.

VALUE	EVTS	DOCUMENT ID		TECN	COMMENT
0.142±0.015	16844	[1] ABE	01B	SLD	E_{cm}^{ee}= 91.24 GeV
• • • We do not use the following data for averages, fits, limits, etc. • • •					
0.153±0.012	1.7M	[2] AAD	15BT	ATLS	E_{cm}^{pp} = 7 TeV

[1] ABE 01B obtain this direct measurement using the left-right production and left-right forward-backward polar angle asymmetries in $\mu^+\mu^-$ decays of the Z boson obtained with a polarized electron beam.

[2] AAD 15BT study $pp \to Z \to \ell^+\ell^-$ events where ℓ is an electron or a muon in the dilepton mass region 70–1000 GeV. The background in the Z peak region is estimated to be < 1% for the muon channel. The muon asymmetry parameter is derived from the measured forward-backward asymmetry assuming the value of the quark asymmetry parameter from the SM. For this reason it is not used in the average.

A_τ

The LEP Collaborations derive this quantity from the measurement of the τ polarization in $Z \to \tau^+\tau^-$. The SLD Collaboration directly extracts this quantity from its measured left-right forward-backward asymmetry in $Z \to \tau^+\tau^-$ produced using a polarized e^- beam. This double asymmetry eliminates the dependence on the Z-e-e coupling parameter A_e.

VALUE	EVTS	DOCUMENT ID		TECN	COMMENT
0.143 ±0.004 OUR AVERAGE					
0.1456±0.0076±0.0057	144810	[1] ABBIENDI	01O	OPAL	E_{cm}^{ee}= 88–94 GeV
0.136 ±0.015	16083	[2] ABE	01B	SLD	E_{cm}^{ee}= 91.24 GeV
0.1451±0.0052±0.0029		[3] HEISTER	01	ALEP	E_{cm}^{ee}= 88–94 GeV
0.1359±0.0079±0.0055	105000	[4] ABREU	00E	DLPH	E_{cm}^{ee}= 88–94 GeV
0.1476±0.0088±0.0062	137092	ACCIARRI	98H	L3	E_{cm}^{ee}= 88–94 GeV

[1] ABBIENDI 01O fit for A_e and A_τ from measurements of the τ polarization at varying τ production angles. The correlation between A_e and A_τ is less than 0.03.

[2] ABE 01B obtain this direct measurement using the left-right production and left-right forward-backward polar angle asymmetries in $\tau^+\tau^-$ decays of the Z boson obtained with a polarized electron beam.

[3] HEISTER 01 obtain this result fitting the τ polarization as a function of the polar production angle of the τ.

[4] ABREU 00E obtain this result fitting the τ polarization as a function of the polar τ production angle. This measurement is a combination of different analyses (exclusive τ decay modes, inclusive hadronic 1-prong reconstruction, and a neural network analysis).

A_s

The SLD Collaboration directly extracts this quantity by a simultaneous fit to four measured s-quark polar angle distributions corresponding to two states of e^- polarization (positive and negative) and to the K^+K^- and $K^\pm K_S^0$ strange particle tagging modes in the hadronic final states.

VALUE	EVTS	DOCUMENT ID		TECN	COMMENT
0.895±0.066±0.062	2870	[1] ABE	00D	SLD	E_{cm}^{ee}= 91.2 GeV

[1] ABE 00D tag $Z \to s\overline{s}$ events by an absence of B or D hadrons and the presence in each hemisphere of a high momentum $K^\pm$ or K_S^0.

A_c

This quantity is directly extracted from a measurement of the left-right forward-backward asymmetry in $c\overline{c}$ production at SLC using polarized electron beam. This double asymmetry eliminates the dependence on the Z-e-e coupling parameter A_e. OUR FIT is obtained by a simultaneous fit to several c- and b-quark measurements as explained in the note "The Z boson" and ref. LEP-SLC 06.

VALUE	DOCUMENT ID		TECN	COMMENT
0.670 ±0.027 OUR FIT				
0.6712±0.0224±0.0157	[1] ABE	05	SLD	E_{cm}^{ee}= 91.24 GeV
• • • We do not use the following data for averages, fits, limits, etc. • • •				
0.583 ±0.055 ±0.055	[2] ABE	02G	SLD	E_{cm}^{ee}= 91.24 GeV
0.688 ±0.041	[3] ABE	01C	SLD	E_{cm}^{ee}= 91.25 GeV

[1] ABE 05 use hadronic Z decays collected during 1996–98 to obtain an enriched sample of $c\overline{c}$ events tagging on the invariant mass of reconstructed secondary decay vertices. The charge of the underlying c–quark is obtained with an algorithm that takes into account the net charge of the vertex as well as the charge of tracks emanating from the vertex and identified as kaons. This yields (9970 events) $A_c = 0.6747 \pm 0.0290 \pm 0.0233$. Taking into account all correlations with earlier results reported in ABE 02G and ABE 01C, they obtain the quoted overall SLD result.

[2] ABE 02G tag b and c quarks through their semileptonic decays into electrons and muons. A maximum likelihood fit is performed to extract simultaneously A_b and A_c.

[3] ABE 01C tag $Z \to c\overline{c}$ events using two techniques: exclusive reconstruction of D^{*+}, D^+ and D^0 mesons and the soft pion tag for $D^{*+} \to D^0\pi^+$. The large background from D mesons produced in $b\overline{b}$ events is separated efficiently from the signal using precision vertex information. When combining the A_c values from these two samples, care is taken to avoid double counting of events common to the two samples, and common systematic errors are properly taken into account.

A_b

This quantity is directly extracted from a measurement of the left-right forward-backward asymmetry in $b\overline{b}$ production at SLC using polarized electron beam. This double asymmetry eliminates the dependence on the Z-e-e coupling parameter A_e. OUR FIT is obtained by a simultaneous fit to several c- and b-quark measurements as explained in the note "The Z boson" and ref. LEP-SLC 06.

VALUE	EVTS	DOCUMENT ID		TECN	COMMENT
0.923 ±0.020 OUR FIT					
0.9170±0.0147±0.0145		[1] ABE	05	SLD	E_{cm}^{ee}= 91.24 GeV
• • • We do not use the following data for averages, fits, limits, etc. • • •					
0.907 ±0.020 ±0.024	48028	[2] ABE	03F	SLD	E_{cm}^{ee}= 91.24 GeV
0.919 ±0.030 ±0.024		[3] ABE	02G	SLD	E_{cm}^{ee}= 91.24 GeV
0.855 ±0.088 ±0.102	7473	[4] ABE	99L	SLD	E_{cm}^{ee}= 91.27 GeV

[1] ABE 05 use hadronic Z decays collected during 1996–98 to obtain an enriched sample of $b\overline{b}$ events tagging on the invariant mass of reconstructed secondary decay vertices. The charge of the underlying b–quark is obtained with an algorithm that takes into account the net charge of the vertex as well as the charge of tracks emanating from the vertex and identified as kaons. This yields (25917 events) $A_b = 0.9173 \pm 0.0184 \pm 0.0173$. Taking into account all correlations with earlier results reported in ABE 03F, ABE 02G and ABE 99L, they obtain the quoted overall SLD result.

[2] ABE 03F obtain an enriched sample of $b\overline{b}$ events tagging on the invariant mass of a 3-dimensional topologically reconstructed secondary decay. The charge of the underlying b quark is obtained using a self-calibrating track-charge method. For the 1996–1998 data sample they measure $A_b = 0.906 \pm 0.022 \pm 0.023$. The value quoted here is obtained combining the above with the result of ABE 98I (1993–1995 data sample).

[3] ABE 02G tag b and c quarks through their semileptonic decays into electrons and muons. A maximum likelihood fit is performed to extract simultaneously A_b and A_c.

[4] ABE 99L obtain an enriched sample of $b\overline{b}$ events tagging with an inclusive vertex mass cut. For distinguishing b and $\overline{b}$ quarks they use the charge of identified $K^\pm$.

TRANSVERSE SPIN CORRELATIONS IN $Z \to \tau^+\tau^-$

The correlations between the transverse spin components of $\tau^+\tau^-$ produced in Z decays may be expressed in terms of the vector and axial-vector couplings:

$$C_{TT} = \frac{|g_A^\tau|^2 - |g_V^\tau|^2}{|g_A^\tau|^2 + |g_V^\tau|^2}$$

$$C_{TN} = -2\frac{|g_A^\tau||g_V^\tau|}{|g_A^\tau|^2 + |g_V^\tau|^2}\sin(\Phi_{g_V^\tau} - \Phi_{g_A^\tau})$$

Downloaded from https://academic.oup.com/ptep/article/2022/8/083C01/6651666 by KIT Library user on 27 September 2022

C_{TT} refers to the transverse-transverse (within the collision plane) spin correlation and C_{TN} refers to the transverse-normal (to the collision plane) spin correlation.

The longitudinal τ polarization P_τ ($= -A_\tau$) is given by:

$$P_\tau = -2\frac{|g_A^\tau||g_V^\tau|}{|g_A^\tau|^2+|g_V^\tau|^2}\cos(\Phi_{g_V^\tau}-\Phi_{g_A^\tau})$$

Here Φ is the phase and the phase difference $\Phi_{g_V^\tau}-\Phi_{g_A^\tau}$ can be obtained using both the measurements of C_{TN} and P_τ.

C_{TT}

VALUE	EVTS	DOCUMENT ID		TECN	COMMENT
1.01±0.12 OUR AVERAGE					
$0.87\pm0.20^{+0.10}_{-0.12}$	9.1k	ABREU	97G	DLPH	E^{ee}_{cm}= 91.2 GeV
1.06±0.13±0.05	120k	BARATE	97D	ALEP	E^{ee}_{cm}= 91.2 GeV

C_{TN}

VALUE	EVTS	DOCUMENT ID		TECN	COMMENT
0.08±0.13±0.04	120k	[1] BARATE	97D	ALEP	E^{ee}_{cm}= 91.2 GeV

[1] BARATE 97D combine their value of C_{TN} with the world average $P_\tau = -0.140 \pm 0.007$ to obtain $\tan(\Phi_{g_V^\tau}-\Phi_{g_A^\tau}) = -0.57 \pm 0.97$.

FORWARD-BACKWARD $e^+e^- \to f\bar{f}$ CHARGE ASYMMETRIES

These asymmetries are experimentally determined by tagging the respective lepton or quark flavor in e^+e^- interactions. Details of heavy flavor (c- or b-quark) tagging at LEP are described in the note on "The Z boson" and ref. LEP-SLC 06. The Standard Model predictions for LEP data have been (re)computed using the ZFITTER package (version 6.36) with input parameters M_Z=91.187 GeV, M_{top}=174.3 GeV, M_{Higgs}=150 GeV, α_s=0.119, $\alpha^{(5)}$ (M_Z)= 1/128.877 and the Fermi constant G_F= 1.16637×10^{-5} GeV^{-2} (see the note on "The Z boson" for references). For non-LEP data the Standard Model predictions are as given by the authors of the respective publications.

$A_{FB}^{(0,e)}$ CHARGE ASYMMETRY IN $e^+e^- \to e^+e^-$

OUR FIT is obtained using the fit procedure and correlations as determined by the LEP Electroweak Working Group (see the note "The Z boson" and ref. LEP-SLC 06). For the Z peak, we report the pole asymmetry defined by $(3/4)A_e^2$ as determined by the nine-parameter fit to cross-section and lepton forward-backward asymmetry data.

ASYMMETRY (%)	STD. MODEL	$\sqrt{s}$ (GeV)	DOCUMENT ID		TECN
1.45±0.25 OUR FIT					
0.89±0.44	1.57	91.2	[1] ABBIENDI	01A	OPAL
1.71±0.49	1.57	91.2	ABREU	00F	DLPH
1.06±0.58	1.57	91.2	ACCIARRI	00C	L3
1.88±0.34	1.57	91.2	[2] BARATE	00C	ALEP

[1] ABBIENDI 01A error includes approximately 0.38 due to statistics, 0.16 due to event selection systematics, and 0.18 due to the theoretical uncertainty in t-channel prediction.
[2] BARATE 00C error includes approximately 0.31 due to statistics, 0.06 due to experimental systematics, and 0.13 due to the theoretical uncertainty in t-channel prediction.

$A_{FB}^{(0,\mu)}$ CHARGE ASYMMETRY IN $e^+e^- \to \mu^+\mu^-$

OUR FIT is obtained using the fit procedure and correlations as determined by the LEP Electroweak Working Group (see the note "The Z boson" and ref. LEP-SLC 06). For the Z peak, we report the pole asymmetry defined by $(3/4)A_eA_\mu$ as determined by the nine-parameter fit to cross-section and lepton forward-backward asymmetry data.

ASYMMETRY (%)	STD. MODEL	$\sqrt{s}$ (GeV)	DOCUMENT ID		TECN
1.69± 0.13 OUR FIT					
1.59± 0.23	1.57	91.2	[1] ABBIENDI	01A	OPAL
1.65± 0.25	1.57	91.2	ABREU	00F	DLPH
1.88± 0.33	1.57	91.2	ACCIARRI	00C	L3
1.71± 0.24	1.57	91.2	[2] BARATE	00C	ALEP
• • • We do not use the following data for averages, fits, limits, etc. • • •					
9 ±30	−1.3	20	[3] ABREU	95M	DLPH
7 ±26	−8.3	40	[3] ABREU	95M	DLPH
−11 ±33	−24.1	57	[3] ABREU	95M	DLPH
−62 ±17	−44.6	69	[3] ABREU	95M	DLPH
−56 ±10	−63.5	79	[3] ABREU	95M	DLPH
−13 ± 5	−34.4	87.5	[3] ABREU	95M	DLPH
$-29.0\ ^{+5.0}_{-4.8}\ \pm0.5$	−32.1	56.9	[4] ABE	90I	VNS
− 9.9 ± 1.5 ±0.5	−9.2	35	HEGNER	90	JADE
0.05± 0.22	0.026	91.14	[5] ABRAMS	89D	MRK2
−43.4 ±17.0	−24.9	52.0	[6] BACALA	89	AMY
−11.0 ±16.5	−29.4	55.0	[6] BACALA	89	AMY
−30.0 ±12.4	−31.2	56.0	[6] BACALA	89	AMY
−46.2 ±14.9	−33.0	57.0	[6] BACALA	89	AMY
−29 ±13	−25.9	53.3	ADACHI	88C	TOPZ
+ 5.3 ± 5.0 ±0.5	−1.2	14.0	ADEVA	88	MRKJ
−10.4 ± 1.3 ±0.5	−8.6	34.8	ADEVA	88	MRKJ
−12.3 ± 5.3 ±0.5	−10.7	38.3	ADEVA	88	MRKJ
−15.6 ± 3.0 ±0.5	−14.9	43.8	ADEVA	88	MRKJ
− 1.0 ± 6.0	−1.2	13.9	BRAUNSCH...	88D	TASS
− 9.1 ± 2.3 ±0.5	−8.6	34.5	BRAUNSCH...	88D	TASS
$-10.6\ ^{+2.2}_{-2.3}\ \pm0.5$	−8.9	35.0	BRAUNSCH...	88D	TASS
$-17.6\ ^{+4.4}_{-4.3}\ \pm0.5$	−15.2	43.6	BRAUNSCH...	88D	TASS
− 4.8 ± 6.5 ±1.0	−11.5	39	BEHREND	87C	CELL
−18.8 ± 4.5 ±1.0	−15.5	44	BEHREND	87C	CELL
+ 2.7 ± 4.9	−1.2	13.9	BARTEL	86C	JADE
−11.1 ± 1.8 ±1.0	−8.6	34.4	BARTEL	86C	JADE
−17.3 ± 4.8 ±1.0	−13.7	41.5	BARTEL	86C	JADE
−22.8 ± 5.1 ±1.0	−16.6	44.8	BARTEL	86C	JADE
− 6.3 ± 0.8 ±0.2	−6.3	29	ASH	85	MAC
− 4.9 ± 1.5 ±0.5	−5.9	29	DERRICK	85	HRS
− 7.1 ± 1.7	−5.7	29	LEVI	83	MRK2
−16.1 ± 3.2	−9.2	34.2	BRANDELIK	82C	TASS

[1] ABBIENDI 01A error is almost entirely on account of statistics.
[2] BARATE 00C error is almost entirely on account of statistics.
[3] ABREU 95M perform this measurement using radiative muon-pair events associated with high-energy isolated photons.
[4] ABE 90I measurements in the range 50 $\leq \sqrt{s} \leq$ 60.8 GeV.
[5] ABRAMS 89D asymmetry includes both 9 $\mu^+\mu^-$ and 15 $\tau^+\tau^-$ events.
[6] BACALA 89 systematic error is about 5%.

$A_{FB}^{(0,\tau)}$ CHARGE ASYMMETRY IN $e^+e^- \to \tau^+\tau^-$

OUR FIT is obtained using the fit procedure and correlations as determined by the LEP Electroweak Working Group (see the note "The Z boson" and ref. LEP-SLC 06). For the Z peak, we report the pole asymmetry defined by $(3/4)A_eA_\tau$ as determined by the nine-parameter fit to cross-section and lepton forward-backward asymmetry data.

ASYMMETRY (%)	STD. MODEL	$\sqrt{s}$ (GeV)	DOCUMENT ID		TECN
1.88± 0.17 OUR FIT					
1.45± 0.30	1.57	91.2	[1] ABBIENDI	01A	OPAL
2.41± 0.37	1.57	91.2	ABREU	00F	DLPH
2.60± 0.47	1.57	91.2	ACCIARRI	00C	L3
1.70± 0.28	1.57	91.2	[2] BARATE	00C	ALEP
• • • We do not use the following data for averages, fits, limits, etc. • • •					
$-32.8\ ^{+6.4}_{-6.2}\ \pm1.5$	−32.1	56.9	[3] ABE	90I	VNS
− 8.1 ± 2.0 ±0.6	−9.2	35	HEGNER	90	JADE
−18.4 ±19.2	−24.9	52.0	[4] BACALA	89	AMY
−17.7 ±26.1	−29.4	55.0	[4] BACALA	89	AMY
−45.9 ±16.6	−31.2	56.0	[4] BACALA	89	AMY
−49.5 ±18.0	−33.0	57.0	[4] BACALA	89	AMY
−20 ±14	−25.9	53.3	ADACHI	88C	TOPZ
−10.6 ± 3.1 ±1.5	−8.5	34.7	ADEVA	88	MRKJ
− 8.5 ± 6.6 ±1.5	−15.4	43.8	ADEVA	88	MRKJ
− 6.0 ± 2.5 ±1.0	8.8	34.6	BARTEL	85F	JADE
−11.8 ± 4.6 ±1.0	14.8	43.0	BARTEL	85F	JADE
− 5.5 ± 1.2 ±0.5	−0.063	29.0	FERNANDEZ	85	MAC
− 4.2 ± 2.0	0.057	29	LEVI	83	MRK2
−10.3 ± 5.2	−9.2	34.2	BEHREND	82	CELL
− 0.4 ± 6.6	−9.1	34.2	BRANDELIK	82C	TASS

[1] ABBIENDI 01A error includes approximately 0.26 due to statistics and 0.14 due to event selection systematics.
[2] BARATE 00C error includes approximately 0.26 due to statistics and 0.11 due to experimental systematics.
[3] ABE 90I measurements in the range 50 $\leq \sqrt{s} \leq$ 60.8 GeV.
[4] BACALA 89 systematic error is about 5%.

$A_{FB}^{(0,\ell)}$ CHARGE ASYMMETRY IN $e^+e^- \to \ell^+\ell^-$

For the Z peak, we report the pole asymmetry defined by $(3/4)A_\ell^2$ as determined by the five-parameter fit to cross-section and lepton forward-backward asymmetry data assuming lepton universality. For details see the note "The Z boson" and ref. LEP-SLC 06.

ASYMMETRY (%)	STD. MODEL	$\sqrt{s}$ (GeV)	DOCUMENT ID		TECN
1.71±0.10 OUR FIT					
1.45±0.17	1.57	91.2	[1] ABBIENDI	01A	OPAL
1.87±0.19	1.57	91.2	ABREU	00F	DLPH
1.92±0.24	1.57	91.2	ACCIARRI	00C	L3
1.73±0.16	1.57	91.2	[2] BARATE	00C	ALEP

[1] ABBIENDI 01A error includes approximately 0.15 due to statistics, 0.06 due to event selection systematics, and 0.03 due to the theoretical uncertainty in t-channel prediction.
[2] BARATE 00C error includes approximately 0.15 due to statistics, 0.04 due to experimental systematics, and 0.02 due to the theoretical uncertainty in t-channel prediction.

$A_{FB}^{(0,u)}$ CHARGE ASYMMETRY IN $e^+e^- \to u\bar{u}$

ASYMMETRY (%)	STD. MODEL	$\sqrt{s}$ (GeV)	DOCUMENT ID		TECN
4.0±6.7±2.8	**7.2**	**91.2**	[1] ACKERSTAFF	97T	OPAL

Downloaded from https://academic.oup.com/ptep/article/2022/8/083C01/6651666 by KIT Library user on 27 September 2022

[1] ACKERSTAFF 97T measure the forward-backward asymmetry of various fast hadrons made of light quarks. Then using SU(2) isospin symmetry and flavor independence for down and strange quarks authors solve for the different quark types.

$A_{FB}^{(0,s)}$ CHARGE ASYMMETRY IN $e^+e^- \to s\overline{s}$

The s-quark asymmetry is derived from measurements of the forward-backward asymmetry of fast hadrons containing an s quark.

ASYMMETRY (%)	STD. MODEL	$\sqrt{s}$ (GeV)	DOCUMENT ID		TECN
9.8 ±1.1 OUR AVERAGE					
10.08±1.13±0.40	10.1	91.2	[1] ABREU	00B	DLPH
6.8 ±3.5 ±1.1	10.1	91.2	[2] ACKERSTAFF	97T	OPAL

[1] ABREU 00B tag the presence of an s quark requiring a high-momentum-identified charged kaon. The s-quark pole asymmetry is extracted from the charged-kaon asymmetry taking the expected d- and u-quark asymmetries from the Standard Model and using the measured values for the c- and b-quark asymmetries.

[2] ACKERSTAFF 97T measure the forward-backward asymmetry of various fast hadrons made of light quarks. Then using SU(2) isospin symmetry and flavor independence for down and strange quarks authors solve for the different quark types. The value reported here corresponds then to the forward-backward asymmetry for "down-type" quarks.

$A_{FB}^{(0,c)}$ CHARGE ASYMMETRY IN $e^+e^- \to c\overline{c}$

OUR FIT, which is obtained by a simultaneous fit to several c- and b-quark measurements as explained in the note "The Z boson" and ref. LEP-SLC 06, refers to the **Z pole** asymmetry. The experimental values, on the other hand, correspond to the measurements carried out at the respective energies.

ASYMMETRY (%)	STD. MODEL	$\sqrt{s}$ (GeV)	DOCUMENT ID		TECN
7.07± 0.35 OUR FIT					
6.31± 0.93±0.65	6.35	91.26	[1] ABDALLAH	04F	DLPH
5.68± 0.54±0.39	6.3	91.25	[2] ABBIENDI	03P	OPAL
6.45± 0.57±0.37	6.10	91.21	[3] HEISTER	02H	ALEP
6.59± 0.94±0.35	6.2	91.235	[4] ABREU	99Y	DLPH
6.3 ± 0.9 ±0.3	6.1	91.22	[5] BARATE	98O	ALEP
6.3 ± 1.2 ±0.6	6.1	91.22	[6] ALEXANDER	97C	OPAL
8.3 ± 3.8 ±2.7	6.2	91.24	[7] ADRIANI	92D	L3
• • • We do not use the following data for averages, fits, limits, etc. • • •					
3.1 ± 3.5 ±0.5	−3.5	89.43	[1] ABDALLAH	04F	DLPH
11.0 ± 2.8 ±0.7	12.3	92.99	[1] ABDALLAH	04F	DLPH
− 6.8 ± 2.5 ±0.9	−3.0	89.51	[2] ABBIENDI	03P	OPAL
14.6 ± 2.0 ±0.8	12.2	92.95	[2] ABBIENDI	03P	OPAL
−12.4 ±15.9 ±2.0	−9.6	88.38	[3] HEISTER	02H	ALEP
− 2.3 ± 2.6 ±0.2	−3.8	89.38	[3] HEISTER	02H	ALEP
− 0.3 ± 8.3 ±0.6	0.9	90.21	[3] HEISTER	02H	ALEP
10.6 ± 7.7 ±0.7	9.6	92.05	[3] HEISTER	02H	ALEP
11.9 ± 2.1 ±0.6	12.2	92.94	[3] HEISTER	02H	ALEP
12.1 ±11.0 ±1.0	14.2	93.90	[3] HEISTER	02H	ALEP
− 4.96± 3.68±0.53	−3.5	89.434	[4] ABREU	99Y	DLPH
11.80± 3.18±0.62	12.3	92.990	[4] ABREU	99Y	DLPH
− 1.0 ± 4.3 ±1.0	−3.9	89.37	[5] BARATE	98O	ALEP
11.0 ± 3.3 ±0.8	12.3	92.96	[5] BARATE	98O	ALEP
3.9 ± 5.1 ±0.9	−3.4	89.45	[6] ALEXANDER	97C	OPAL
15.8 ± 4.1 ±1.1	12.4	93.00	[6] ALEXANDER	97C	OPAL
−12.9 ± 7.8 ±5.5	−13.6	35	BEHREND	90D	CELL
7.7 ±13.4 ±5.0	−22.1	43	BEHREND	90D	CELL
−12.8 ± 4.4 ±4.1	−13.6	35	ELSEN	90	JADE
−10.9 ±12.9 ±4.6	−23.2	44	ELSEN	90	JADE
−14.9 ± 6.7	−13.3	35	OULD-SAADA	89	JADE

[1] ABDALLAH 04F tag b– and c–quarks using semileptonic decays combined with charge flow information from the hemisphere opposite to the lepton. Enriched samples of $c\overline{c}$ and $b\overline{b}$ events are obtained using lifetime information.

[2] ABBIENDI 03P tag heavy flavors using events with one or two identified leptons. This allows the simultaneous fitting of the b and c quark forward-backward asymmetries as well as the average B^0-$\overline{B}^0$ mixing.

[3] HEISTER 02H measure simultaneously b and c quark forward-backward asymmetries using their semileptonic decays to tag the quark charge. The flavor separation is obtained with a discriminating multivariate analysis.

[4] ABREU 99Y tag $Z \to b\overline{b}$ and $Z \to c\overline{c}$ events by an exclusive reconstruction of several D meson decay modes (D^{*+}, D^0, and D^+ with their charge-conjugate states).

[5] BARATE 98O tag $Z \to c\overline{c}$ events requiring the presence of high-momentum reconstructed D^{*+}, D^+, or D^0 mesons.

[6] ALEXANDER 97C identify the b and c events using a D/D^* tag.

[7] ADRIANI 92D use both electron and muon semileptonic decays.

$A_{FB}^{(0,b)}$ CHARGE ASYMMETRY IN $e^+e^- \to b\overline{b}$

OUR FIT, which is obtained by a simultaneous fit to several c- and b-quark measurements as explained in the note "The Z boson" and ref. LEP-SLC 06, refers to the **Z pole** asymmetry. The experimental values, on the other hand, correspond to the measurements carried out at the respective energies.

ASYMMETRY (%)	STD. MODEL	$\sqrt{s}$ (GeV)	DOCUMENT ID		TECN
9.92± 0.16 OUR FIT					
9.58± 0.32± 0.14	9.68	91.231	[1] ABDALLAH	05	DLPH
10.04± 0.56± 0.25	9.69	91.26	[2] ABDALLAH	04F	DLPH
9.72± 0.42± 0.15	9.67	91.25	[3] ABBIENDI	03P	OPAL
9.77± 0.36± 0.18	9.69	91.26	[4] ABBIENDI	02I	OPAL
9.52± 0.41± 0.17	9.59	91.21	[5] HEISTER	02H	ALEP
10.00± 0.27± 0.11	9.63	91.232	[6] HEISTER	01D	ALEP
7.62± 1.94± 0.85	9.64	91.235	[7] ABREU	99Y	DLPH
9.60± 0.66± 0.33	9.69	91.26	[8] ACCIARRI	99D	L3
9.31± 1.01± 0.55	9.65	91.24	[9] ACCIARRI	98U	L3
9.4 ± 2.7 ± 2.2	9.61	91.22	[10] ALEXANDER	97C	OPAL
• • • We do not use the following data for averages, fits, limits, etc. • • •					
6.37± 1.43± 0.17	5.8	89.449	[1] ABDALLAH	05	DLPH
10.41± 1.15± 0.24	12.1	92.990	[1] ABDALLAH	05	DLPH
6.7 ± 2.2 ± 0.2	5.7	89.43	[2] ABDALLAH	04F	DLPH
11.2 ± 1.8 ± 0.2	12.1	92.99	[2] ABDALLAH	04F	DLPH
4.7 ± 1.8 ± 0.1	5.9	89.51	[3] ABBIENDI	03P	OPAL
10.3 ± 1.5 ± 0.2	12.0	92.95	[3] ABBIENDI	03P	OPAL
5.82± 1.53± 0.12	5.9	89.50	[4] ABBIENDI	02I	OPAL
12.21± 1.23± 0.25	12.0	92.91	[4] ABBIENDI	02I	OPAL
−13.1 ±13.5 ± 1.0	3.2	88.38	[5] HEISTER	02H	ALEP
5.5 ± 1.9 ± 0.1	5.6	89.38	[5] HEISTER	02H	ALEP
− 0.4 ± 6.7 ± 0.8	7.5	90.21	[5] HEISTER	02H	ALEP
11.1 ± 6.4 ± 0.5	11.0	92.05	[5] HEISTER	02H	ALEP
10.4 ± 1.5 ± 0.3	12.0	92.94	[5] HEISTER	02H	ALEP
13.8 ± 9.3 ± 1.1	12.9	93.90	[5] HEISTER	02H	ALEP
4.36± 1.19± 0.11	5.8	89.472	[6] HEISTER	01D	ALEP
11.72± 0.97± 0.11	12.0	92.950	[6] HEISTER	01D	ALEP
5.67± 7.56± 1.17	5.7	89.434	[7] ABREU	99Y	DLPH
8.82± 6.33± 1.22	12.1	92.990	[7] ABREU	99Y	DLPH
6.11± 2.93± 0.43	5.9	89.50	[8] ACCIARRI	99D	L3
13.71± 2.40± 0.44	12.2	93.10	[8] ACCIARRI	99D	L3
4.95± 5.23± 0.40	5.8	89.45	[9] ACCIARRI	98U	L3
11.37± 3.99± 0.65	12.1	92.99	[9] ACCIARRI	98U	L3
− 8.6 ±10.8 ± 2.9	5.8	89.45	[10] ALEXANDER	97C	OPAL
− 2.1 ± 9.0 ± 2.6	12.1	93.00	[10] ALEXANDER	97C	OPAL
−71 ±34 $^{+7}_{-8}$	−58	58.3	SHIMONAKA	91	TOPZ
−22.2 ± 7.7 ± 3.5	−26.0	35	BEHREND	90D	CELL
−49.1 ±16.0 ± 5.0	−39.7	43	BEHREND	90D	CELL
−28 ±11	−23	35	BRAUNSCH...	90	TASS
−16.6 ± 7.7 ± 4.8	−24.3	35	ELSEN	90	JADE
−33.6 ±22.2 ± 5.2	−39.9	44	ELSEN	90	JADE
3.4 ± 7.0 ± 3.5	−16.0	29.0	BAND	89	MAC
−72 ±28 ±13	−56	55.2	SAGAWA	89	AMY

[1] ABDALLAH 05 obtain an enriched samples of $b\overline{b}$ events using lifetime information. The quark (or antiquark) charge is determined with a neural network using the secondary vertex charge, the jet charge and particle identification.

[2] ABDALLAH 04F tag b– and c–quarks using semileptonic decays combined with charge flow information from the hemisphere opposite to the lepton. Enriched samples of $c\overline{c}$ and $b\overline{b}$ events are obtained using lifetime information.

[3] ABBIENDI 03P tag heavy flavors using events with one or two identified leptons. This allows the simultaneous fitting of the b and c quark forward-backward asymmetries as well as the average B^0-$\overline{B}^0$ mixing.

[4] ABBIENDI 02I tag $Z^0 \to b\overline{b}$ decays using a combination of secondary vertex and lepton tags. The sign of the b-quark charge is determined using an inclusive tag based on jet, vertex, and kaon charges.

[5] HEISTER 02H measure simultaneously b and c quark forward-backward asymmetries using their semileptonic decays to tag the quark charge. The flavor separation is obtained with a discriminating multivariate analysis.

[6] HEISTER 01D tag $Z \to b\overline{b}$ events using the impact parameters of charged tracks complemented with information from displaced vertices, event shape variables, and lepton identification. The b-quark direction and charge is determined using the hemisphere charge method along with information from fast kaon tagging and charge estimators of primary and secondary vertices. The change in the quoted value due to variation of A_{FB}^c and R_b is given as $+0.103\ (A_{FB}^c - 0.0651)\ -0.440\ (R_b - 0.21585)$.

[7] ABREU 99Y tag $Z \to b\overline{b}$ and $Z \to c\overline{c}$ events by an exclusive reconstruction of several D meson decay modes (D^{*+}, D^0, and D^+ with their charge-conjugate states).

[8] ACCIARRI 99D tag $Z \to b\overline{b}$ events using high p and p_T leptons. The analysis determines simultaneously a mixing parameter $\chi_b = 0.1192 \pm 0.0068 \pm 0.0051$ which is used to correct the observed asymmetry.

[9] ACCIARRI 98U tag $Z \to b\overline{b}$ events using lifetime and measure the jet charge using the hemisphere charge.

[10] ALEXANDER 97C identify the b and c events using a D/D^* tag.

CHARGE ASYMMETRY IN $e^+e^- \to q\overline{q}$

Summed over five lighter flavors.

Experimental and Standard Model values are somewhat event-selection dependent. Standard Model expectations contain some assumptions on B^0-$\overline{B}^0$ mixing and on other electroweak parameters.

ASYMMETRY (%)	STD. MODEL	$\sqrt{s}$ (GeV)	DOCUMENT ID	TECN
• • • We do not use the following data for averages, fits, limits, etc. • • •				

Downloaded from https://academic.oup.com/ptep/article/2022/8/083C01/6651666 by KIT Library user on 27 September 2022

− 0.76 ± 0.12 ± 0.15		91.2	[1] ABREU	92I	DLPH
4.0 ± 0.4 ± 0.63	4.0	91.3	[2] ACTON	92L	OPAL
9.1 ± 1.4 ± 1.6	9.0	57.9	ADACHI	91	TOPZ
− 0.84 ± 0.15 ± 0.04		91	DECAMP	91B	ALEP
8.3 ± 2.9 ± 1.9	8.7	56.6	STUART	90	AMY
11.4 ± 2.2 ± 2.1	8.7	57.6	ABE	89L	VNS
6.0 ± 1.3	5.0	34.8	GREENSHAW	89	JADE
8.2 ± 2.9	8.5	43.6	GREENSHAW	89	JADE

[1] ABREU 92I has 0.14 systematic error due to uncertainty of quark fragmentation.

[2] ACTON 92L use the weight function method on 259k selected $Z \rightarrow$ hadrons events. The systematic error includes a contribution of 0.2 due to B^0-$\overline{B}^0$ mixing effect, 0.4 due to Monte Carlo (MC) fragmentation uncertainties and 0.3 due to MC statistics. ACTON 92L derive a value of $\sin^2\theta_W^{\rm eff}$ to be 0.2321 ± 0.0017 ± 0.0028.

CHARGE ASYMMETRY IN $p\overline{p} \rightarrow Z \rightarrow e^+e^-$

ASYMMETRY (%)	STD. MODEL	$\sqrt{s}$ (GeV)	DOCUMENT ID		TECN
• • • We do not use the following data for averages, fits, limits, etc. • • •					
5.2 ± 5.9 ± 0.4		91	ABE	91E	CDF

ANOMALOUS $ZZ\gamma$, $Z\gamma\gamma$, AND ZZV COUPLINGS

Revised September 2013 by M.W. Grünewald (U. College Dublin and U. Ghent) and A. Gurtu (Formerly Tata Inst.).

In on-shell $Z\gamma$ production, deviations from the Standard Model for the $Z\gamma\gamma^*$ and $Z\gamma Z^*$ couplings may be described in terms of eight parameters, h_i^V $(i = 1, 4;\ V = \gamma, Z)$ [1]. The parameters h_i^γ describe the $Z\gamma\gamma^*$ couplings and the parameters h_i^Z the $Z\gamma Z^*$ couplings. In this formalism h_1^V and h_2^V lead to CP-violating and h_3^V and h_4^V to CP-conserving effects. All these anomalous contributions to the cross section increase rapidly with center-of-mass energy. In order to ensure unitarity, these parameters are usually described by a form-factor representation, $h_i^V(s) = h_{i\rm o}^V/(1 + s/\Lambda^2)^n$, where Λ is the energy scale for the manifestation of a new phenomenon and n is a sufficiently large power. By convention one uses $n = 3$ for $h_{1,3}^V$ and $n = 4$ for $h_{2,4}^V$. Usually limits on h_i^V's are put assuming some value of Λ, sometimes ∞.

In on-shell ZZ production, deviations from the Standard Model for the $ZZ\gamma^*$ and ZZZ^* couplings may be described by means of four anomalous couplings f_i^V $(i = 4, 5; V = \gamma, Z)$ [2]. As above, the parameters f_i^γ describe the $ZZ\gamma^*$ couplings and the parameters f_i^Z the ZZZ^* couplings. The anomalous couplings f_5^V lead to violation of C and P symmetries while f_4^V introduces CP violation. Also here, formfactors depending on a scale Λ are used.

All these couplings h_i^V and f_i^V are zero at tree level in the Standard Model; they are measured in e^+e^-, $p\overline{p}$ and pp collisions at LEP, Tevatron and LHC.

References

1. U. Baur and E.L. Berger, Phys. Rev. **D47**, 4889 (1993).
2. K. Hagiwara *et al.*, Nucl. Phys. **B282**, 253 (1987).

h_i^V

Combining the LEP-2 results taking into account the correlations, the following 95% CL limits are derived [SCHAEL 13A]:

$$-0.12 < h_1^Z < +0.11, \qquad -0.07 < h_2^Z < +0.07,$$
$$-0.19 < h_3^Z < +0.06, \qquad -0.04 < h_4^Z < +0.13,$$
$$-0.05 < h_1^\gamma < +0.05, \qquad -0.04 < h_2^\gamma < +0.02,$$
$$-0.05 < h_3^\gamma < +0.00, \qquad +0.01 < h_4^\gamma < +0.05.$$

Some of the recent results from the Tevatron and LHC experiments individually surpass the combined LEP-2 results in precision (see below).

VALUE	DOCUMENT ID		TECN	COMMENT
• • • We do not use the following data for averages, fits, limits, etc. • • •				
	[1] AAD	16Q	ATLS	$E_{\rm cm}^{pp}$ = 8 TeV
	[2] KHACHATRY...	16AE	CMS	$E_{\rm cm}^{pp}$ = 8 TeV
	[3] KHACHATRY...	15AC	CMS	$E_{\rm cm}^{pp}$ = 8 TeV
	[4] CHATRCHYAN	14AB	CMS	$E_{\rm cm}^{pp}$ = 7 TeV
	[5] AAD	13AN	ATLS	$E_{\rm cm}^{pp}$ = 7 TeV
	[6] CHATRCHYAN	13BI	CMS	$E_{\rm cm}^{pp}$ = 7 TeV
	[7] ABAZOV	12S	D0	$E_{\rm cm}^{p\overline{p}}$ = 1.96 TeV
	[8] AALTONEN	11S	CDF	$E_{\rm cm}^{p\overline{p}}$ = 1.96 TeV
	[9] CHATRCHYAN	11M	CMS	$E_{\rm cm}^{pp}$ = 7 TeV
	[10] ABAZOV	09L	D0	$E_{\rm cm}^{p\overline{p}}$ = 1.96 TeV
	[11] ABAZOV	07M	D0	$E_{\rm cm}^{p\overline{p}}$ = 1.96 TeV
	[12] ABDALLAH	07C	DLPH	$E_{\rm cm}^{ee}$ = 183–208 GeV
	[13] ACHARD	04H	L3	$E_{\rm cm}^{ee}$ = 183–208 GeV
	[14] ABBIENDI,G	00C	OPAL	$E_{\rm cm}^{ee}$ = 189 GeV
	[15] ABBOTT	98M	D0	$E_{\rm cm}^{p\overline{p}}$ = 1.8 TeV
	[16] ABREU	98K	DLPH	$E_{\rm cm}^{ee}$ = 161, 172 GeV

[1] AAD 16Q study $Z\gamma$ production in pp collisions. In events with no additional jets, 10268 (12738) Z decays to electron (muon) pairs are selected, with an expected background of 1291 ± 340 (1537 ± 408) events, as well as 1039 Z decays to neutrino pairs with an expected background of 450 ± 96 events. Analyzing the photon transverse momentum distribution above 250 GeV (400 GeV) for lepton (neutrino) events, yields the 95% C.L. limits: $-7.8 \times 10^{-4} < h_3^Z < 8.6 \times 10^{-4}$, $-3.0 \times 10^{-6} < h_4^Z < 2.9 \times 10^{-6}$, $-9.5 \times 10^{-4} < h_3^\gamma < 9.9 \times 10^{-4}$, $-3.2 \times 10^{-6} < h_4^\gamma < 3.2 \times 10^{-6}$.

[2] KHACHATRYAN 16AE determine the $Z\gamma \rightarrow \nu\overline{\nu}\gamma$ cross section by selecting events with a photon of $E_T > 145$ GeV and $\not{E}_T > 140$ GeV. 630 candidate events are observed with an expected SM background of 269 ± 26. The E_T spectrum of the photon is used to set 95% C.L. limits as follows: $-1.5 \times 10^{-3} < h_3^Z < 1.6 \times 10^{-3}$, $-3.9 \times 10^{-6} < h_4^Z < 4.5 \times 10^{-6}$, $-1.1 \times 10^{-3} < h_3^\gamma < 0.9 \times 10^{-3}$, $-3.8 \times 10^{-6} < h_4^\gamma < 4.3 \times 10^{-6}$.

[3] KHACHATRYAN 15AC study $Z\gamma$ events in 8 TeV pp interactions, where the Z decays into 2 same-flavor, opposite sign leptons (e or μ) and a photon with $p_T > 15$ GeV. The p_T of a lepton is required to be > 20 GeV/c, their effective mass > 50 GeV, and the photon should have a separation $\Delta R > 0.7$ with each lepton. The observed p_T distribution of the photons is used to extract the 95% C.L. limits: $-3.8 \times 10^{-3} < h_3^Z < 3.7 \times 10^{-3}$, $-3.1 \times 10^{-5} < h_4^Z < 3.0 \times 10^{-5}$, $-4.6 \times 10^{-3} < h_3^\gamma < 4.6 \times 10^{-3}$, $-3.6 \times 10^{-5} < h_4^\gamma < 3.5 \times 10^{-5}$.

[4] CHATRCHYAN 14AB measure $Z\gamma$ production cross section for $p_T^\gamma > 15$ GeV and R($\ell\gamma$) > 0.7, which is the separation between the γ and the final state charged lepton (e or μ) in the azimuthal angle-pseudorapidity ($\phi - \eta$) plane. The di-lepton mass is required to be > 50 GeV. After background subtraction the number of $ee\gamma$ and $\mu\mu\gamma$ events is determined to be 3160 ± 120 and 5030 ± 233 respectively, compatible with expectations from the SM. This leads to a 95% CL limits of $-1 \times 10^{-2} < h_3^\gamma < 1 \times 10^{-2}$, $-9 \times 10^{-5} < h_4^\gamma < 9 \times 10^{-5}$, $-9 \times 10^{-3} < h_3^Z < 9 \times 10^{-3}$, $-8 \times 10^{-5} < h_4^Z < 8 \times 10^{-5}$, assuming h_1^V and h_2^V have SM values, $V = \gamma$ or Z.

[5] AAD 13AN study $Z\gamma$ production in pp collisions. In events with no additional jet, 1417 (2031) Z decays to electron (muon) pairs are selected, with an expected background of 156 ± 54 (244 ± 64) events, as well as 662 Z decays to neutrino pairs with an expected background of 302 ± 42 events. Analysing the photon p_T spectrum above 100 GeV yields the 95% C.L. limts: $-0.013 < h_3^Z < 0.014$, $-8.7 \times 10^{-5} < h_4^Z < 8.7 \times 10^{-5}$, $-0.015 < h_3^\gamma < 0.016$, $-9.4 \times 10^{-5} < h_4^\gamma < 9.2 \times 10^{-5}$. Supersedes AAD 12BX.

[6] CHATRCHYAN 13BI determine the $Z\gamma \rightarrow \nu\overline{\nu}\gamma$ cross section by selecting events with a photon of $E_T > 145$ GeV and a $\not{E}_T > 130$ GeV. 73 candidate events are observed with an expected SM background of 30.2 ± 6.5. The E_T spectrum of the photon is used to set 95% C.L. limits as follows: $|h_3^Z| < 2.7 \times 10^{-3}$, $|h_4^Z| < 1.3 \times 10^{-5}$, $|h_3^\gamma| < 2.9 \times 10^{-3}$, $|h_4^\gamma| < 1.5 \times 10^{-5}$.

[7] ABAZOV 12S study $Z\gamma$ production in $p\overline{p}$ collisions at $\sqrt{s} = 1.96$ TeV using 6.2 fb^{-1} of data where the Z decays to electron (muon) pairs and the photon has at least 10 GeV of transverse momentum. In data, 304 (308) di-electron (di-muon) events are observed with an expected background of 255 ± 16 (285 ± 24) events. Based on the photon p_T spectrum, and including also earlier data and the $Z \rightarrow \nu\overline{\nu}$ decay mode (from ABAZOV 09L), the following 95% C.L. limits are reported: $|h_{03}^Z| < 0.026$, $|h_{04}^Z| < 0.0013$, $|h_{03}^\gamma| < 0.027$, $|h_{04}^\gamma| < 0.0014$ for a form factor scale of $\Lambda = 1.5$ TeV.

[8] AALTONEN 11S study $Z\gamma$ events in $p\overline{p}$ interactions at $\sqrt{s} = 1.96$ TeV with integrated luminosity 5.1 fb^{-1} for $Z \rightarrow e^+e^-/\mu^+\mu^-$ and 4.9 fb^{-1} for $Z \rightarrow \nu\overline{\nu}$. For the charged lepton case, the two leptons must be of the same flavor with the transverse momentum/energy of one > 20 GeV and the other > 10 GeV. The isolated photon must have $E_T > 50$ GeV. They observe 91 events with 87.2 ± 7.8 events expected from standard model processes. For the $\nu\overline{\nu}$ case they require solitary photons with $E_T > 25$ GeV and missing $E_T > 25$ GeV and observe 85 events with standard model expectation of 85.9 ± 5.6 events. Taking the form factor $\Lambda = 1.5$ TeV they derive 95% C.L. limits as $|h_3^{\gamma,Z}| < 0.022$ and $|h_4^{\gamma,Z}| < 0.0009$.

[9] CHATRCHYAN 11M study $Z\gamma$ production in pp collisions at $\sqrt{s} = 7$ TeV using 36 pb^{-1} pp data, where the Z decays to e^+e^- or $\mu^+\mu^-$. The total cross sections are measured for photon transverse energy $E_T^\gamma > 10$ GeV and spatial separation from charged leptons in the plane of pseudo rapidity and azimuthal angle $\Delta R(\ell,\gamma) > 0.7$ with the dilepton invariant mass requirement of $M_{\ell\ell} > 50$ GeV. The number of $e^+e^-\gamma$ and $\mu^+\mu^-\gamma$ candidates is 81 and 90 with estimated backgrounds of 20.5 ± 2.5 and 27.3 ± 3.2

Downloaded from https://academic.oup.com/ptep/article/2022/8/083C01/6651666 by KIT Library user on 27 September 2022

events respectively. The 95% CL limits for $ZZ\gamma$ couplings are $-0.05 < h_3^Z < 0.06$ and $-0.0005 < h_4^Z < 0.0005$, and for $Z\gamma\gamma$ couplings are $-0.07 < h_3^\gamma < 0.07$ and $-0.0005 < h_4^\gamma < 0.0006$.

[10] ABAZOV 09L study $Z\gamma$, $Z \to \nu\overline{\nu}$ production in $p\overline{p}$ collisions at 1.96 TeV C.M. energy. They select 51 events with a photon of transverse energy E_T larger than 90 GeV, with an expected background of 17 events. Based on the photon E_T spectrum and including also Z decays to charged leptons (from ABAZOV 07M), the following 95% CL limits are reported: $|h_{30}^\gamma| < 0.033$, $|h_{40}^\gamma| < 0.0017$, $|h_{30}^Z| < 0.033$, $|h_{40}^Z| < 0.0017$.

[11] ABAZOV 07M use 968 $p\overline{p} \to e^+e^-/\mu^+\mu^-\gamma X$ candidates, at 1.96 TeV center of mass energy, to tag $p\overline{p} \to Z\gamma$ events by requiring $E_T(\gamma) > 7$ GeV, lepton-gamma separation $\Delta R_{\ell\gamma} > 0.7$, and di-lepton invariant mass > 30 GeV. The cross section is in agreement with the SM prediction. Using these $Z\gamma$ events they obtain 95% C.L. limits on each h_i^V, keeping all others fixed at their SM values. They report: $-0.083 < h_{30}^Z < 0.082$, $-0.0053 < h_{40}^Z < 0.0054$, $-0.085 < h_{30}^\gamma < 0.084$, $-0.0053 < h_{40}^\gamma < 0.0054$, for the form factor scale $\Lambda = 1.2$ TeV.

[12] Using data collected at $\sqrt{s} = 183$–208, ABDALLAH 07C select 1,877 $e^+e^- \to Z\gamma$ events with $Z \to q\overline{q}$ or $\nu\overline{\nu}$, 171 $e^+e^- \to ZZ$ events with $Z \to q\overline{q}$ or lepton pair (except an explicit τ pair), and 74 $e^+e^- \to Z\gamma^*$ events with a $q\overline{q}\mu^+\mu^-$ or $q\overline{q}e^+e^-$ signature, to derive 95% CL limits on h_i^V. Each limit is derived with other parameters set to zero. They report: $-0.23 < h_1^Z < 0.23$, $-0.30 < h_3^Z < 0.16$, $-0.14 < h_1^\gamma < 0.14$, $-0.049 < h_3^\gamma < 0.044$.

[13] ACHARD 04H select 3515 $e^+e^- \to Z\gamma$ events with $Z \to q\overline{q}$ or $\nu\overline{\nu}$ at $\sqrt{s} = 189$–209 GeV to derive 95% CL limits on h_i^V. For deriving each limit the other parameters are fixed at zero. They report: $-0.153 < h_1^Z < 0.141$, $-0.087 < h_2^Z < 0.079$, $-0.220 < h_3^Z < 0.112$, $-0.068 < h_4^Z < 0.148$, $-0.057 < h_1^\gamma < 0.057$, $-0.050 < h_2^\gamma < 0.023$, $-0.059 < h_3^\gamma < 0.004$, $-0.004 < h_4^\gamma < 0.042$.

[14] ABBIENDI,G 00C study $e^+e^- \to Z\gamma$ events (with $Z \to q\overline{q}$ and $Z \to \nu\overline{\nu}$) at 189 GeV to obtain the central values (and 95% CL limits) of these couplings: $h_1^Z = 0.000 \pm 0.100$ $(-0.190, 0.190)$, $h_2^Z = 0.000 \pm 0.068$ $(-0.128, 0.128)$, $h_3^Z = -0.074^{+0.102}_{-0.103}$ $(-0.269, 0.119)$, $h_4^Z = 0.046 \pm 0.068$ $(-0.084, 0.175)$, $h_1^\gamma = 0.000 \pm 0.061$ $(-0.115, 0.115)$, $h_2^\gamma = 0.000 \pm 0.041$ $(-0.077, 0.077)$, $h_3^\gamma = -0.080^{+0.039}_{-0.041}$ $(-0.164, -0.006)$, $h_4^\gamma = 0.064^{+0.033}_{-0.030}$ $(+0.007, +0.134)$. The results are derived assuming that only one coupling at a time is different from zero.

[15] ABBOTT 98M study $p\overline{p} \to Z\gamma + X$, with $Z \to e^+e^-$, $\mu^+\mu^-$, $\overline{\nu}\nu$ at 1.8 TeV, to obtain 95% CL limits at $\Lambda = 750$ GeV: $|h_{30}^Z| < 0.36$, $|h_{40}^Z| < 0.05$ (keeping $h_i^\gamma = 0$), and $|h_{30}^\gamma| < 0.37$, $|h_{40}^\gamma| < 0.05$ (keeping $h_i^Z = 0$). Limits on the *CP*-violating couplings are $|h_{10}^Z| < 0.36$, $|h_{20}^Z| < 0.05$ (keeping $h_i^\gamma = 0$), and $|h_{10}^\gamma| < 0.37$, $|h_{20}^\gamma| < 0.05$ (keeping $h_i^Z = 0$).

[16] ABREU 98K determine a 95% CL upper limit on $\sigma(e^+e^- \to \gamma +$ invisible particles$) <$ 2.5 pb using 161 and 172 GeV data. This is used to set 95% CL limits on $|h_{30}^\gamma| < 0.8$ and $|h_{30}^Z| < 1.3$, derived at a scale $\Lambda = 1$ TeV and with $n = 3$ in the form factor representation.

f_i^V

Combining the LEP-2 results taking into account the correlations, the following 95% CL limits are derived [SCHAEL 13A]:

$$-0.28 < f_4^Z < +0.32, \qquad -0.34 < f_5^Z < +0.35,$$
$$-0.17 < f_4^\gamma < +0.19, \qquad -0.35 < f_5^\gamma < +0.32.$$

Some of the recent results from the Tevatron and LHC experiments individually surpass the combined LEP-2 results in precision (see below).

VALUE	DOCUMENT ID		TECN	COMMENT
• • • We do not use the following data for averages, fits, limits, etc. • • •				
	[1] SIRUNYAN	21Q	CMS	$E_{cm}^{pp} = 13$ TeV
	[2] AABOUD	19AY	ATLS	$E_{cm}^{pp} = 13$ TeV
	[3] AABOUD	18Q	ATLS	$E_{cm}^{pp} = 13$ TeV
	[4] SIRUNYAN	18BT	CMS	$E_{cm}^{pp} = 13$ TeV
	[5] KHACHATRY...	15B	CMS	$E_{cm}^{pp} = 8$ TeV
	[6] KHACHATRY...	15BC	CMS	$E_{cm}^{pp} = 7, 8$ TeV
	[7] AAD	13Z	ATLS	$E_{cm}^{pp} = 7$ TeV
	[8] CHATRCHYAN	13B	CMS	$E_{cm}^{pp} = 7$ TeV
	[9] SCHAEL	09	ALEP	$E_{cm}^{ee} = 192$–209 GeV
	[10] ABAZOV	08K	D0	$E_{cm}^{p\overline{p}} = 1.96$ TeV
	[11] ABDALLAH	07C	DLPH	$E_{cm}^{ee} = 183$–208 GeV
	[12] ABBIENDI	04C	OPAL	
	[13] ACHARD	03D	L3	

[1] SIRUNYAN 21Q measure ZZ production where both Z bosons decay in the electron or muon channel. Analyzing the four-lepton invariant mass distribution, the following limits are derived at 95% C.L. in units of 10^{-4}: $-6.6 < f_4^Z < 6.0$, $-5.5 < f_5^Z < 7.5$, $-7.8 < f_4^\gamma < 7.1$, $-6.8 < f_5^\gamma < 7.5$. This set of parameters is linearly related to a set of EFT parameters, resulting in the following limits at 95% C.L. in units of TeV^{-4}: $-2.3 < c_{\widetilde{B}W}/\Lambda^4 < 2.5$, $-1.4 < c_{WW}/\Lambda^4 < 1.2$, $-1.4 < c_{BW}/\Lambda^4 < 1.3$, $-1.2 < c_{BB}/\Lambda^4 < 1.2$.

[2] AABOUD 19AY study ZZ production in the $\ell\ell\nu\nu$ decay channel. Events with a pair of isolated high-transverse momentum charged leptons (electron pairs or muon pairs), and with large missing energy, are selected. In the data, 371 (416) di-electron (di-muon) events are found, with a total expected background of 128 ± 8 (143 ± 8) events. Analysing the transverse momentum distribution of the charged dilepton system above 150 GeV, the following 95% C.L. limits are derived in units of 10^{-3}: $-1.2 < f_4^\gamma < 1.2$, $-1.0 < f_4^Z < 1.0$, $-1.2 < f_5^\gamma < 1.2$, $-1.0 < f_5^Z < 1.0$.

[3] AABOUD 18Q study $pp \to ZZ$ events at $\sqrt{s} = 13$ TeV with $Z \to e^+e^-$ or $Z \to \mu^+\mu^-$. The number of events observed in the $4e$, $2e\,2\mu$, and 4μ channels is 249, 465, and 303 respectively. Analysing the p_T spectrum of the leading Z boson, the following the following 95% C.L. limits are derived in units of 10^{-4}: $-1.8 < f_4^\gamma < 1.8$, $-1.5 < f_4^Z < 1.5$, $-1.8 < f_5^\gamma < 1.8$, $-1.5 < f_5^Z < 1.5$.

[4] SIRUNYAN 18BT study $ppZZ$ events at $\sqrt{s} = 13$ TeV with $Z \to e^+e^-$ or $Z \to \mu^+\mu^-$. The number of events observed in the $4e$, $2e2\mu$, and 4μ channels is 220, 543 and 335 respectively. Analysing the 4-lepton invariant mass spectrum, the following 95% C.L. limits are derived in units of 10^{-3}: $-1.2 < f_4^\gamma < 1.3$, $-1.2 < f_4^Z < 1.0$, $-1.2 < f_5^\gamma < 1.3$, $-1.0 < f_5^Z < 1.3$.

[5] KHACHATRYAN 15B study ZZ production in 8 TeV pp collisions. In the decay modes $ZZ \to 4e$, 4μ, $2e2\mu$, 54, 75, 148 events are observed, with an expected background of 2.2 ± 0.9, 1.2 ± 0.6, and 2.4 ± 1.0 events, respectively. Analysing the 4-lepton invariant mass spectrum in the range from 110 GeV to 1200 GeV, the following 95% C.L. limits are obtained: $|f_4^Z| < 0.004$, $|f_5^Z| < 0.004$, $|f_4^\gamma| < 0.005$, $|f_5^\gamma| < 0.005$.

[6] KHACHATRYAN 15BC use the cross section measurement of the final state $pp \to ZZ \to 2\ell 2\nu$, (ℓ being an electron or a muon) at 7 and 8 TeV to put limits on these triple gauge couplings. Effective mass of the charged lepton pair is required to be in the range 83.5–98.5 GeV and the dilepton $p_T > 45$ GeV. The reduced missing E_T is required to be > 65 GeV, which takes into account the fake missing E_T due to detector effects. The numbers of e^+e^- and $\mu^+\mu^-$ events selected are 35 and 40 at 7 TeV and 176 and 271 at 8 TeV respectively. The production cross sections so obtained are in agreement with SM predictions. The following 95% C.L. limits are set: $-0.0028 < f_4^Z < 0.0032$, $-0.0037 < f_4^\gamma < 0.0033$, $-0.0029 < f_5^Z < 0.0031$, $-0.0033 < f_5^\gamma < 0.0037$. Combining with previous results (KHACHATRYAN 15B and CHATRCHYAN 13B) which include 7 TeV and 8 TeV data on the final states $pp \to ZZ \to 2\ell 2\ell'$ where ℓ and ℓ' are an electron or a muon, the best limits are $-0.0022 < f_4^Z < 0.0026$, $-0.0029 < f_4^\gamma < 0.0026$, $-0.0023 < f_5^Z < 0.0023$, $-0.0026 < f_5^\gamma < 0.0027$.

[7] AAD 13Z study ZZ production in pp collisions at $\sqrt{s} = 7$ TeV. In the $ZZ \to \ell^+\ell^-\ell'^+\ell'^-$ final state they observe a total of 66 events with an expected background of 0.9 ± 1.3. In the $ZZ \to \ell^+\ell^-\nu\nu$ final state they observe a total of 87 events with an expected background of 46.9 ± 5.2. The limits on anomalous TGCs are determined using the observed and expected numbers of these ZZ events binned in p_T^Z. The 95% C.L. are as follows: for form factor scale $\Lambda = \infty$, $-0.015 < f_4^\gamma < 0.015$, $-0.013 < f_4^Z < 0.013$, $-0.016 < f_5^\gamma < 0.015$, $-0.013 < f_5^Z < 0.013$; for form factor scale $\Lambda =$ 3 TeV, $-0.022 < f_4^\gamma < 0.023$, $-0.019 < f_4^Z < 0.019$, $-0.023 < f_5^\gamma < 0.023$, $-0.020 < f_5^Z < 0.019$.

[8] CHATRCHYAN 13B study ZZ production in pp collisions and select 54 ZZ candidates in the Z decay channel with electrons or muons with an expected background of 1.4 ± 0.5 events. The resulting 95% C.L. ranges are: $-0.013 < f_4^\gamma < 0.015$, $-0.011 < f_4^Z < 0.012$, $-0.014 < f_5^\gamma < 0.014$, $-0.012 < f_5^Z < 0.012$.

[9] Using data collected in the center of mass energy range 192–209 GeV, SCHAEL 09 select 318 $e^+e^- \to ZZ$ events with 319.4 expected from the standard model. Using this data they derive the following 95% CL limits: $-0.321 < f_4^\gamma < 0.318$, $-0.534 < f_4^Z < 0.534$, $-0.724 < f_5^\gamma < 0.733$, $-1.194 < f_5^Z < 1.190$.

[10] ABAZOV 08K search for ZZ and $Z\gamma^*$ events with 1 fb^{-1} $p\overline{p}$ data at $\sqrt{s} = 1.96$ TeV in $(ee)(ee)$, $(\mu\mu)(\mu\mu)$, $(ee)(\mu\mu)$ final states requiring the lepton pair masses to be > 30 GeV. They observe 1 event, which is consistent with an expected signal of 1.71 ± 0.15 events and a background of 0.13 ± 0.03 events. From this they derive the following limits, for a form factor (Λ) value of 1.2 TeV: $-0.28 < f_{40}^Z < 0.28$, $-0.31 < f_{50}^Z < 0.29$, $-0.26 < f_{40}^\gamma < 0.26$, $-0.30 < f_{50}^\gamma < 0.28$.

[11] Using data collected at $\sqrt{s} = 183$–208 GeV, ABDALLAH 07C select 171 $e^+e^- \to ZZ$ events with $Z \to q\overline{q}$ or lepton pair (except an explicit τ pair), and 74 $e^+e^- \to Z\gamma^*$ events with a $q\overline{q}\mu^+\mu^-$ or $q\overline{q}e^+e^-$ signature, to derive 95% CL limits on f_i^V. Each limit is derived with other parameters set to zero. They report: $-0.40 < f_4^Z < 0.42$, $-0.38 < f_5^Z < 0.62$, $-0.23 < f_4^\gamma < 0.25$, $-0.52 < f_5^\gamma < 0.48$.

[12] ABBIENDI 04C study ZZ production in e^+e^- collisions in the C.M. energy range 190–209 GeV. They select 340 events with an expected background of 180 events. Including the ABBIENDI 00N data at 183 and 189 GeV (118 events with an expected background of 65 events) they report the following 95% CL limits: $-0.45 < f_4^Z < 0.58$, $-0.94 < f_5^Z < 0.25$, $-0.32 < f_4^\gamma < 0.33$, and $-0.71 < f_5^\gamma < 0.59$.

[13] ACHARD 03D study Z-boson pair production in e^+e^- collisions in the C.M. energy range 200–209 GeV. They select 549 events with an expected background of 432 events. Including the ACCIARRI 99G and ACCIARRI 99O data (183 and 189 GeV respectively, 286 events with an expected background of 241 events) and the 192–202 GeV ACCIARRI 01I results (656 events, expected background of 512 events), they report the following 95% CL limits: $-0.48 \le f_4^Z \le 0.46$, $-0.36 \le f_5^Z \le 1.03$, $-0.28 \le f_4^\gamma \le 0.28$, and $-0.40 \le f_5^\gamma \le 0.47$.

Downloaded from https://academic.oup.com/ptep/article/2022/8/083C01/6651666 by KIT Library user on 27 September 2022

ANOMALOUS W/Z QUARTIC COUPLINGS

Revised November 2015 by M.W. Grünewald (U. College Dublin) and A. Gurtu (Formerly Tata Inst.).

Quartic couplings, $WWZZ$, $WWZ\gamma$, $WW\gamma\gamma$, and $ZZ\gamma\gamma$, were studied at LEP and Tevatron at energies at which the Standard Model predicts negligible contributions to multiboson production. Thus, to parametrize limits on these couplings, an effective theory approach is adopted which supplements the Standard Model Lagrangian with higher dimensional operators which include quartic couplings. The LEP collaborations chose the lowest dimensional representation of operators (dimension 6) which presumes the SU(2)×U(1) gauge symmetry is broken by means other than the conventional Higgs scalar doublet [1–3]. In this representation possible quartic couplings, a_0, a_c, a_n, are expressed in terms of the following dimension-6 operators [1,2];

$$L_6^0 = -\frac{e^2}{16\Lambda^2}\, a_0\, F^{\mu\nu}\, F_{\mu\nu}\vec{W}^{\alpha}\cdot\vec{W}_{\alpha}$$
$$L_6^c = -\frac{e^2}{16\Lambda^2}\, a_c\, F^{\mu\alpha}\, F_{\mu\beta}\vec{W}^{\beta}\cdot\vec{W}_{\alpha}$$
$$L_6^n = -i\frac{e^2}{16\Lambda^2}\, a_n\epsilon_{ijk}\, W^{(i)}_{\mu\alpha}\, W^{(j)}_{\nu}\, W^{(k)\alpha}F^{\mu\nu}$$
$$\widetilde{L}_6^0 = -\frac{e^2}{16\Lambda^2}\, \widetilde{a}_0\, F^{\mu\nu}\, \widetilde{F}_{\mu\nu}\vec{W}^{\alpha}\cdot\vec{W}_{\alpha}$$
$$\widetilde{L}_6^n = -i\frac{e^2}{16\Lambda^2}\, \widetilde{a}_n\epsilon_{ijk}\, W^{(i)}_{\mu\alpha}\, W^{(j)}_{\nu}\, W^{(k)\alpha}\widetilde{F}^{\mu\nu}$$

where F, W are photon and W fields, L_6^0 and L_6^c conserve C, P separately ($\widetilde{L}_6^0$ conserves only C) and generate anomalous $W^+W^-\gamma\gamma$ and $ZZ\gamma\gamma$ couplings, L_6^n violates CP ($\widetilde{L}_6^n$ violates both C and P) and generates an anomalous $W^+W^-Z\gamma$ coupling, and Λ is an energy scale for new physics. For the $ZZ\gamma\gamma$ coupling the CP-violating term represented by L_6^n does not contribute. These couplings are assumed to be real and to vanish at tree level in the Standard Model.

Within the same framework as above, a more recent description of the quartic couplings [3] treats the anomalous parts of the $WW\gamma\gamma$ and $ZZ\gamma\gamma$ couplings separately, leading to two sets parametrized as a_0^V/Λ^2 and a_c^V/Λ^2, where $V = W$ or Z.

With the discovery of a Higgs at the LHC in 2012, it is then useful to go to the next higher dimensional representation (dimension 8 operators) in which the gauge symmetry is broken by the conventional Higgs scalar doublet [3,4]. There are 14 operators which can contribute to the anomalous quartic coupling signal. Some of the operators have analogues in the dimension 6 scheme. The CMS collaboration, [5], have used this parametrization, in which the connections between the two schemes are also summarized:

$$\begin{aligned}\mathcal{L}_{AQGC} = &-\frac{e^2}{8}\frac{a_0^W}{\Lambda^2}F_{\mu\nu}F^{\mu\nu}W^{+a}W_a^- \\ &-\frac{e^2}{16}\frac{a_c^W}{\Lambda^2}F_{\mu\nu}F^{\mu a}(W^{+\nu}W_a^- + W^{-\nu}W_a^+) \\ &-e^2g^2\frac{\kappa_0^W}{\Lambda^2}F_{\mu\nu}Z^{\mu\nu}W^{+a}W_a^- \\ &-\frac{e^2g^2}{2}\frac{\kappa_c^W}{\Lambda^2}F_{\mu\nu}Z^{\mu a}(W^{+\nu}W_a^- + W^{-\nu}W_a^+) \\ &+\frac{f_{T,0}}{\Lambda^4}Tr[\widehat{W}_{\mu\nu}\widehat{W}^{\mu\nu}]\times Tr[\widehat{W}_{\alpha\beta}\widehat{W}^{\alpha\beta}]\end{aligned}$$

The energy scale of possible new physics is Λ, and $g = e/sin(\theta_W)$, e being the unit electric charge and θ_W the Weinberg angle. The field tensors are described in [3,4].

The two dimension 6 operators a_0^W/Λ^2 and a_c^W/Λ^2 are associated with the $WW\gamma\gamma$ vertex. Among dimension 8 operators, κ_0^W/Λ^2 and κ_c^W/Λ^2 are associated with the $WWZ\gamma$ vertex, whereas the parameter $f_{T,0}/\Lambda^4$ contributes to both vertices. There is a relationship between these two dimension 6 parameters and the dimension 8 parameters $f_{M,i}/\Lambda^4$ as follows [3]:

$$\frac{a_0^W}{\Lambda^2} = -\frac{4M_W^2}{g^2}\frac{f_{M,0}}{\Lambda^4} - \frac{8M_W^2}{g'^2}\frac{f_{M,2}}{\Lambda^4}$$

$$\frac{a_c^W}{\Lambda^2} = -\frac{4M_W^2}{g^2}\frac{f_{M,1}}{\Lambda^4} - \frac{8M_W^2}{g'^2}\frac{f_{M,3}}{\Lambda^4}$$

where $g' = e/cos(\theta_W)$ and M_W is the invariant mass of the W boson. This relation provides a translation between limits on dimension 6 operators $a_{0,c}^W$ and $f_{M,j}/\Lambda^4$. It is further required [4] that $f_{M,0} = 2f_{M,2}$ and $f_{M,1} = 2f_{M,3}$ which suppresses contributions to the $WWZ\gamma$ vertex. The complete set of Lagrangian contributions as presented in [4] corresponds to 19 anomalous couplings in total – $f_{S,i},\ i = 1, 2,\ f_{M,i},\ i = 0, \ldots, 8$ and $f_{T,i}, i = 0, \ldots, 9$ – each scaled by $1/\Lambda^4$.

The ATLAS collaboration [6], on the other hand, follows a K-matrix driven approach of Ref. 7 in which the anomalous couplings can be expressed in terms of two parameters α_4 and α_5, which account for all BSM effects.

It is the early stages in the determination of quartic couplings by the LHC experiments. It is hoped that the two collaborations, ATLAS and CMS, will agree to use at least one common set of parameters to express these limits to enable the reader to make a comparison and allow for a possible LHC combination.

References

1. G. Belanger and F. Boudjema, Phys. Lett. **B288**, 201 (1992).
2. J.W. Stirling and A. Werthenbach, Eur. Phys. J. **C14**, 103 (2000);
   J.W. Stirling and A. Werthenbach, Phys. Lett. **B466**, 369 (1999);
   A. Denner *et al.*, Eur. Phys. J. **C20**, 201 (2001);
   G. Montagna *et al.*, Phys. Lett. **B515**, 197 (2001).
3. G. Belanger *et al.*, Eur. Phys. J. **C13**, 283 (2000).
4. O.J.P. Éboli, M.C. Gonzalez-Garcia, and S.M. Lietti, Phys. Rev. **D69**, 095005 (2004);
   O.J.P. Éboli, M.C. Gonzalez-Garcia, and J.K. Mizukoshi, Phys. Rev. **D77**, 073005 (2006).
5. S. Chatrchyan *et al.*, Phys. Rev. **D90**, 032008 (2014);
   S. Chatrchyan *et al.*, Phys. Rev. Lett. **114**, 051801 (2015).
6. G. Aad *et al.*, Phys. Rev. Lett. **113**, 141803 (2014).
7. A. Albateanu, W. Killian, and J. Reuter, JHEP **0811**, 010 (2008).

a_0/Λ^2, a_c/Λ^2

Combining published and unpublished preliminary LEP results the following 95% CL intervals for the QGCs associated with the $ZZ\gamma\gamma$ vertex are derived (CERN-PH-EP/2005-051 or hep-ex/0511027):

$$-0.008 < a_0^Z/\Lambda^2 < +0.021$$
$$-0.029 < a_c^Z/\Lambda^2 < +0.039$$

Downloaded from https://academic.oup.com/ptep/article/2022/8/083C01/6651666 by KIT Library user on 27 September 2022

Anomalous Z quartic couplings have also been measured by the Tevatron and LHC experiments. As discussed in the review on "Anomalous W/Z quartic couplings," the coupling parameters in the Anomalous QGC Lagrangian may relate to processes involving only the W or only to the Z or to both. Thus, results on all other AQGCs are reported together in the W listings.

VALUE	*DOCUMENT ID*	*TECN*
• • • We do not use the following data for averages, fits, limits, etc. • • •		
	[1] ABBIENDI 04L	OPAL
	[2] HEISTER 04A	ALEP
	[3] ACHARD 02G	L3

[1] ABBIENDI 04L select 20 $e^+e^- \to \nu\overline{\nu}\gamma\gamma$ acoplanar events in the energy range 180–209 GeV and 176 $e^+e^- \to q\overline{q}\gamma\gamma$ events in the energy range 130–209 GeV. These samples are used to constrain possible anomalous $W^+W^-\gamma\gamma$ and $ZZ\gamma\gamma$ quartic couplings. Further combining with the $W^+W^-\gamma$ sample of ABBIENDI 04B the following one–parameter 95% CL limits are obtained: $-0.007 < a_0^Z/\Lambda^2 < 0.023$ GeV^{-2}, $-0.029 < a_c^Z/\Lambda^2 < 0.029$ GeV^{-2}, $-0.020 < a_0^W/\Lambda^2 < 0.020$ GeV^{-2}, $-0.052 < a_c^W/\Lambda^2 < 0.037$ GeV^{-2}.

[2] In the CM energy range 183 to 209 GeV HEISTER 04A select 30 $e^+e^- \to \nu\overline{\nu}\gamma\gamma$ events with two acoplanar, high energy and high transverse momentum photons. The photon–photon acoplanarity is required to be $> 5^\circ$, $E_\gamma/\sqrt{s} > 0.025$ (the more energetic photon having energy $> 0.2\sqrt{s}$), $p_{T_\gamma}/E_{beam} > 0.05$ and $|\cos\theta_\gamma| < 0.94$. A likelihood fit to the photon energy and recoil missing mass yields the following one–parameter 95% CL limits: $-0.012 < a_0^Z/\Lambda^2 < 0.019$ GeV^{-2}, $-0.041 < a_c^Z/\Lambda^2 < 0.044$ GeV^{-2}, $-0.060 < a_0^W/\Lambda^2 < 0.055$ GeV^{-2}, $-0.099 < a_c^W/\Lambda^2 < 0.093$ GeV^{-2}.

[3] ACHARD 02G study $e^+e^- \to Z\gamma\gamma \to q\overline{q}\gamma\gamma$ events using data at center-of-mass energies from 200 to 209 GeV. The photons are required to be isolated, each with energy >5 GeV and $|\cos\theta| < 0.97$, and the di-jet invariant mass to be compatible with that of the Z boson (74–111 GeV). Cuts on Z velocity ($\beta < 0.73$) and on the energy of the most energetic photon reduce the backgrounds due to non-resonant production of the $q\overline{q}\gamma\gamma$ state and due to ISR respectively, yielding a total of 40 candidate events of which 8.6 are expected to be due to background. The energy spectra of the least energetic photon are fitted for all ten center-of-mass energy values from 130 GeV to 209 GeV (as obtained adding to the present analysis 130–202 GeV data of ACCIARRI 01E, for a total of 137 events with an expected background of 34.1 events) to obtain the fitted values $a_0/\Lambda^2 = 0.00^{+0.02}_{-0.01}$ GeV^{-2} and $a_c/\Lambda^2 = 0.03^{+0.01}_{-0.02}$ GeV^{-2}, where the other parameter is kept fixed to its Standard Model value (0). A simultaneous fit to both parameters yields the 95% CL limits -0.02 GeV$^{-2} < a_0/\Lambda^2 < 0.03$ GeV^{-2} and -0.07 GeV$^{-2} < a_c/\Lambda^2 < 0.05$ GeV^{-2}.

Z REFERENCES

AAD	21AO	NATP 17 819	G. Aad *et al.*	(ATLAS Collab.)
AAD	21AQ	JHEP 2107 005	G. Aad *et al.*	(ATLAS Collab.)
AAD	21AV	PRL 127 271801	G. Aad *et al.*	(ATLAS Collab.)
SIRUNYAN	21Q	EPJ C81 200	A.M. Sirunyan *et al.*	(CMS Collab.)
AABOUD	19AY	JHEP 1910 127	M. Aaboud *et al.*	(ATLAS Collab.)
AABOUD	19N	JHEP 1904 048	M. Aaboud *et al.*	(ATLAS Collab.)
RAINBOLT	19	PR D99 013004	J.L. Rainbolt, M. Schmitt	(NWES)
SIRUNYAN	19AJ	EPJ C79 94	A.M. Sirunyan *et al.*	(CMS Collab.)
SIRUNYAN	19BR	PL B797 134811	A.M. Sirunyan *et al.*	(CMS Collab.)
AABOUD	18AU	JHEP 1807 127	M. Aaboud *et al.*	(ATLAS Collab.)
AABOUD	18BL	PL B786 134	M. Aaboud *et al.*	(ATLAS Collab.)
AABOUD	18CN	PR D98 092010	M. Aaboud *et al.*	(ATLAS Collab.)
AABOUD	18Q	PR D97 032005	M. Aaboud *et al.*	(ATLAS Collab.)
AAIJ	18AR	JHEP 1809 159	R. Aaij *et al.*	(LHCb Collab.)
ANDREEV	18A	EPJ C78 777	V. Andreev *et al.*	(H1 Collab.)
SIRUNYAN	18BT	EPJ C78 165	A.M. Sirunyan *et al.*	(CMS Collab.)
SIRUNYAN	18DZ	PRL 121 141801	A.M. Sirunyan *et al.*	(CMS Collab.)
AABOUD	17Q	EPJ C77 367	M. Aaboud *et al.*	(ATLAS Collab.)
AABOUD	16K	PRL 117 111802	M. Aaboud *et al.*	(ATLAS Collab.)
AAD	16L	EPJ C76 210	G. Aad *et al.*	(ATLAS Collab.)
AAD	16Q	PR D93 112002	G. Aad *et al.*	(ATLAS Collab.)
ABRAMOWICZ	16A	PR D93 092002	H. Abramowicz *et al.*	(ZEUS Collab.)
ABT	16	PR D94 052007	I. Abt *et al.*	(MPIM, OXF, HAMB, DESY)
KHACHATRY...	16AE	PL B760 448	V. Khachatryan *et al.*	(CMS Collab.)
KHACHATRY...	16CC	PL B763 280	V. Khachatryan *et al.*	(CMS Collab.)
AAD	15BT	JHEP 1509 049	G. Aad *et al.*	(ATLAS Collab.)
AAD	15I	PRL 114 121801	G. Aad *et al.*	(ATLAS Collab.)
KHACHATRY...	15AC	JHEP 1504 164	V. Khachatryan *et al.*	(CMS Collab.)
KHACHATRY...	15B	PL B740 250	V. Khachatryan *et al.*	(CMS Collab.)
KHACHATRY...	15BC	EPJ C75 511	V. Khachatryan *et al.*	(CMS Collab.)
AAD	14AU	PR D90 072010	G. Aad *et al.*	(ATLAS Collab.)
AAD	14N	PRL 112 231806	G. Aad *et al.*	(ATLAS Collab.)
AALTONEN	14E	PRL 112 111803	T. Aaltonen *et al.*	(CDF Collab.)
CHATRCHYAN	14AB	PR D89 092005	S. Chatrchyan *et al.*	(CMS Collab.)
AAD	13AN	PR D87 112003	G. Aad *et al.*	(ATLAS Collab.)
Also		PR D91 119901 (errat.)	G. Aad *et al.*	(ATLAS Collab.)
AAD	13Z	JHEP 1303 128	G. Aad *et al.*	(ATLAS Collab.)
CHATRCHYAN	13B	JHEP 1301 063	S. Chatrchyan *et al.*	(CMS Collab.)
CHATRCHYAN	13BI	JHEP 1310 164	S. Chatrchyan *et al.*	(CMS Collab.)
SCHAEL	13A	PRPL 532 119	S. Schael *et al.*	
AAD	12BX	PL B717 49	G. Aad *et al.*	(ATLAS Collab.)
ABAZOV	12S	PR D85 052001	V.M. Abazov *et al.*	(D0 Collab.)
CHATRCHYAN	12BN	JHEP 1212 034	S. Chatrchyan *et al.*	(CMS Collab.)
AALTONEN	11S	PRL 107 051802	T. Aaltonen *et al.*	(CDF Collab.)
ABAZOV	11D	PR D84 012007	V.M. Abazov *et al.*	(D0 Collab.)
CHATRCHYAN	11M	PL B701 535	S. Chatrchyan *et al.*	(CMS Collab.)
ABAZOV	09L	PRL 102 201802	V.M. Abazov *et al.*	(D0 Collab.)
BEDDALL	09	PL B670 300	A. Beddall, A. Beddall, A. Bingul	(UGAZ)
SCHAEL	09	JHEP 0904 124	S. Schael *et al.*	(ALEPH Collab.)
ABAZOV	08K	PRL 100 131801	V.M. Abazov *et al.*	(D0 Collab.)
ABAZOV	07M	PL B653 378	V.M. Abazov *et al.*	(D0 Collab.)
ABDALLAH	07C	EPJ C51 525	J. Abdallah *et al.*	(DELPHI Collab.)
ABDALLAH	06E	PL B639 179	J. Abdallah *et al.*	(DELPHI Collab.)
AKTAS	06	PL B632 35	A. Aktas *et al.*	(H1 Collab.)
LEP-SLC	06	PRPL 427 257	ALEPH, DELPHI, L3, OPAL, SLD and working groups	
SCHAEL	06A	PL B639 192	S. Schael *et al.*	(ALEPH Collab.)
ABDALLAH	05	EPJ C40 1	J. Abdallah *et al.*	(DELPHI Collab.)
ABDALLAH	05C	EPJ C44 299	J. Abdallah *et al.*	(DELPHI Collab.)
ABE	05	PRL 94 091801	K. Abe *et al.*	(SLD Collab.)
ABE	05F	PR D71 112004	K. Abe *et al.*	(SLD Collab.)
ACOSTA	05M	PR D71 052002	D. Acosta *et al.*	(CDF Collab.)
ABBIENDI	04B	PL B580 17	G. Abbiendi *et al.*	(OPAL Collab.)
ABBIENDI	04C	EPJ C32 303	G. Abbiendi *et al.*	(OPAL Collab.)
ABBIENDI	04E	PL B586 167	G. Abbiendi *et al.*	(OPAL Collab.)
ABBIENDI	04G	EPJ C33 173	G. Abbiendi *et al.*	(OPAL Collab.)
ABBIENDI	04L	PR D70 032005	G. Abbiendi *et al.*	(OPAL Collab.)
ABDALLAH	04F	EPJ C34 109	J. Abdallah *et al.*	(DELPHI Collab.)
ABE	04C	PR D69 072003	K. Abe *et al.*	(SLD Collab.)
ACHARD	04C	PL B585 42	P. Achard *et al.*	(L3 Collab.)
ACHARD	04H	PL B597 119	P. Achard *et al.*	(L3 Collab.)
HEISTER	04A	PL B602 31	A. Heister *et al.*	(ALEPH Collab.)
ABBIENDI	03P	PL B577 18	G. Abbiendi *et al.*	(OPAL Collab.)
ABDALLAH	03H	PL B569 129	J. Abdallah *et al.*	(DELPHI Collab.)
ABDALLAH	03K	PL B576 29	J. Abdallah *et al.*	(DELPHI Collab.)
ABE	03F	PRL 90 141804	K. Abe *et al.*	(SLD Collab.)
ACHARD	03D	PL B572 133	P. Achard *et al.*	(L3 Collab.)
ACHARD	03G	PL B577 109	P. Achard *et al.*	(L3 Collab.)
ABBIENDI	02I	PL B546 29	G. Abbiendi *et al.*	(OPAL Collab.)
ABE	02G	PRL 88 151801	K. Abe *et al.*	(SLD Collab.)
ACHARD	02G	PL B540 43	P. Achard *et al.*	(L3 Collab.)
HEISTER	02B	PL B526 34	A. Heister *et al.*	(ALEPH Collab.)
HEISTER	02C	PL B528 19	A. Heister *et al.*	(ALEPH Collab.)
HEISTER	02H	EPJ C24 177	A. Heister *et al.*	(ALEPH Collab.)
ABBIENDI	01A	EPJ C19 587	G. Abbiendi *et al.*	(OPAL Collab.)
ABBIENDI	01G	EPJ C18 447	G. Abbiendi *et al.*	(OPAL Collab.)
ABBIENDI	01K	PL B516 1	G. Abbiendi *et al.*	(OPAL Collab.)
ABBIENDI	01N	EPJ C20 445	G. Abbiendi *et al.*	(OPAL Collab.)
ABBIENDI	01O	EPJ C21 1	G. Abbiendi *et al.*	(OPAL Collab.)
ABE	01B	PRL 86 1162	K. Abe *et al.*	(SLD Collab.)
ABE	01C	PR D63 032005	K. Abe *et al.*	(SLD Collab.)
ACCIARRI	01E	PL B505 47	M. Acciarri *et al.*	(L3 Collab.)
ACCIARRI	01I	PL B497 23	M. Acciarri *et al.*	(L3 Collab.)
HEISTER	01	EPJ C20 401	A. Heister *et al.*	(ALEPH Collab.)
HEISTER	01D	EPJ C22 201	A. Heister *et al.*	(ALEPH Collab.)
ABBIENDI	00N	PL B476 256	G. Abbiendi *et al.*	(OPAL Collab.)
ABBIENDI,G	00C	EPJ C17 553	G. Abbiendi *et al.*	(OPAL Collab.)
ABE	00B	PRL 84 5945	K. Abe *et al.*	(SLD Collab.)
ABE	00D	PRL 85 5059	K. Abe *et al.*	(SLD Collab.)
ABREU	00	EPJ C12 225	P. Abreu *et al.*	(DELPHI Collab.)
ABREU	00B	EPJ C14 613	P. Abreu *et al.*	(DELPHI Collab.)
ABREU	00E	EPJ C14 585	P. Abreu *et al.*	(DELPHI Collab.)
ABREU	00F	EPJ C16 371	P. Abreu *et al.*	(DELPHI Collab.)
ABREU	00P	PL B475 429	P. Abreu *et al.*	(DELPHI Collab.)
ACCIARRI	00	EPJ C13 47	M. Acciarri *et al.*	(L3 Collab.)
ACCIARRI	00C	EPJ C16 1	M. Acciarri *et al.*	(L3 Collab.)
ACCIARRI	00J	PL B479 79	M. Acciarri *et al.*	(L3 Collab.)
ACCIARRI	00Q	PL B489 93	M. Acciarri *et al.*	(L3 Collab.)
BARATE	00B	EPJ C16 597	R. Barate *et al.*	(ALEPH Collab.)
BARATE	00C	EPJ C14 1	R. Barate *et al.*	(ALEPH Collab.)
BARATE	00O	EPJ C16 613	R. Barate *et al.*	(ALEPH Collab.)
ABBIENDI	99B	EPJ C8 217	G. Abbiendi *et al.*	(OPAL Collab.)
ABBIENDI	99I	PL B447 157	G. Abbiendi *et al.*	(OPAL Collab.)
ABE	99E	PR D59 052001	K. Abe *et al.*	(SLD Collab.)
ABE	99L	PRL 83 1902	K. Abe *et al.*	(SLD Collab.)
ABREU	99	EPJ C6 19	P. Abreu *et al.*	(DELPHI Collab.)
ABREU	99B	EPJ C10 415	P. Abreu *et al.*	(DELPHI Collab.)
ABREU	99J	PL B449 364	P. Abreu *et al.*	(DELPHI Collab.)
ABREU	99U	PL B462 425	P. Abreu *et al.*	(DELPHI Collab.)
ABREU	99Y	EPJ C10 219	P. Abreu *et al.*	(DELPHI Collab.)
ACCIARRI	99D	PL B448 152	M. Acciarri *et al.*	(L3 Collab.)
ACCIARRI	99F	PL B453 94	M. Acciarri *et al.*	(L3 Collab.)
ACCIARRI	99G	PL B450 281	M. Acciarri *et al.*	(L3 Collab.)
ACCIARRI	99O	PL B465 363	M. Acciarri *et al.*	(L3 Collab.)
ABBOTT	98M	PR D57 3817	B. Abbott *et al.*	(D0 Collab.)
ABE	98D	PRL 80 660	K. Abe *et al.*	(SLD Collab.)
ABE	98I	PRL 81 942	K. Abe *et al.*	(SLD Collab.)
ABREU	98K	PL B423 194	P. Abreu *et al.*	(DELPHI Collab.)
ABREU	98L	EPJ C5 585	P. Abreu *et al.*	(DELPHI Collab.)
ACCIARRI	98G	PL B431 199	M. Acciarri *et al.*	(L3 Collab.)
ACCIARRI	98H	PL B429 387	M. Acciarri *et al.*	(L3 Collab.)
ACCIARRI	98U	PL B439 225	M. Acciarri *et al.*	(L3 Collab.)
ACKERSTAFF	98A	EPJ C5 411	K. Ackerstaff *et al.*	(OPAL Collab.)
ACKERSTAFF	98E	EPJ C1 439	K. Ackerstaff *et al.*	(OPAL Collab.)
ACKERSTAFF	98O	PL B420 157	K. Ackerstaff *et al.*	(OPAL Collab.)
ACKERSTAFF	98Q	EPJ C4 19	K. Ackerstaff *et al.*	(OPAL Collab.)
BARATE	98O	PL B434 415	R. Barate *et al.*	(ALEPH Collab.)
BARATE	98T	EPJ C4 557	R. Barate *et al.*	(ALEPH Collab.)
BARATE	98V	EPJ C5 205	R. Barate *et al.*	(ALEPH Collab.)
ABE	97	PRL 78 17	K. Abe *et al.*	(SLD Collab.)
ABREU	97C	ZPHY C73 243	P. Abreu *et al.*	(DELPHI Collab.)
ABREU	97E	PL B398 207	P. Abreu *et al.*	(DELPHI Collab.)
ABREU	97G	PL B404 194	P. Abreu *et al.*	(DELPHI Collab.)
ACCIARRI	97D	PL B393 465	M. Acciarri *et al.*	(L3 Collab.)
ACCIARRI	97J	PL B407 351	M. Acciarri *et al.*	(L3 Collab.)
ACCIARRI	97L	PL B407 389	M. Acciarri *et al.*	(L3 Collab.)
ACCIARRI	97R	PL B413 167	M. Acciarri *et al.*	(L3 Collab.)
ACKERSTAFF	97M	ZPHY C74 413	K. Ackerstaff *et al.*	(OPAL Collab.)
ACKERSTAFF	97S	PL B412 210	K. Ackerstaff *et al.*	(OPAL Collab.)
ACKERSTAFF	97T	ZPHY C76 387	K. Ackerstaff *et al.*	(OPAL Collab.)
ACKERSTAFF	97W	ZPHY C76 425	K. Ackerstaff *et al.*	(OPAL Collab.)
ALEXANDER	97C	ZPHY C73 379	G. Alexander *et al.*	(OPAL Collab.)
ALEXANDER	97D	ZPHY C73 569	G. Alexander *et al.*	(OPAL Collab.)
ALEXANDER	97E	ZPHY C73 587	G. Alexander *et al.*	(OPAL Collab.)
BARATE	97D	PL B405 191	R. Barate *et al.*	(ALEPH Collab.)
BARATE	97E	PL B401 150	R. Barate *et al.*	(ALEPH Collab.)
BARATE	97F	PL B401 163	R. Barate *et al.*	(ALEPH Collab.)
BARATE	97H	PL B402 213	R. Barate *et al.*	(ALEPH Collab.)
BARATE	97J	ZPHY C74 451	R. Barate *et al.*	(ALEPH Collab.)
ABREU	96R	ZPHY C72 31	P. Abreu *et al.*	(DELPHI Collab.)
ABREU	96S	PL B389 405	P. Abreu *et al.*	(DELPHI Collab.)
ABREU	96U	ZPHY C73 61	P. Abreu *et al.*	(DELPHI Collab.)
ACCIARRI	96	PL B371 126	M. Acciarri *et al.*	(L3 Collab.)
ADAM	96	ZPHY C69 561	W. Adam *et al.*	(DELPHI Collab.)
ADAM	96B	ZPHY C70 371	W. Adam *et al.*	(DELPHI Collab.)
ALEXANDER	96B	ZPHY C70 197	G. Alexander *et al.*	(OPAL Collab.)
ALEXANDER	96F	PL B370 185	G. Alexander *et al.*	(OPAL Collab.)
ALEXANDER	96N	PL B384 343	G. Alexander *et al.*	(OPAL Collab.)
ALEXANDER	96R	ZPHY C72 1	G. Alexander *et al.*	(OPAL Collab.)
BUSKULIC	96D	ZPHY C69 393	D. Buskulic *et al.*	(ALEPH Collab.)
BUSKULIC	96H	ZPHY C69 379	D. Buskulic *et al.*	(ALEPH Collab.)
BUSKULIC	96T	PL B384 449	D. Buskulic *et al.*	(ALEPH Collab.)
BUSKULIC	96Y	PL B388 648	D. Buskulic *et al.*	(ALEPH Collab.)
ABE	95J	PRL 74 2880	K. Abe *et al.*	(SLD Collab.)
ABREU	95	ZPHY C65 709 (erratum)	P. Abreu *et al.*	(DELPHI Collab.)
ABREU	95D	ZPHY C66 323	P. Abreu *et al.*	(DELPHI Collab.)
ABREU	95L	ZPHY C65 587	P. Abreu *et al.*	(DELPHI Collab.)
ABREU	95M	ZPHY C65 603	P. Abreu *et al.*	(DELPHI Collab.)
ABREU	95O	ZPHY C67 543	P. Abreu *et al.*	(DELPHI Collab.)
ABREU	95R	ZPHY C68 353	P. Abreu *et al.*	(DELPHI Collab.)
ABREU	95V	ZPHY C68 541	P. Abreu *et al.*	(DELPHI Collab.)
ABREU	95W	PL B361 207	P. Abreu *et al.*	(DELPHI Collab.)
ABREU	95X	ZPHY C69 1	P. Abreu *et al.*	(DELPHI Collab.)
ACCIARRI	95B	PL B345 589	M. Acciarri *et al.*	(L3 Collab.)
ACCIARRI	95C	PL B345 609	M. Acciarri *et al.*	(L3 Collab.)
ACCIARRI	95G	PL B353 136	M. Acciarri *et al.*	(L3 Collab.)

Downloaded from https://academic.oup.com/ptep/article/2022/8/083C01/6651666 by KIT Library user on 27 September 2022

AKERS	95C	ZPHY C65 47	R. Akers *et al.*	(OPAL Collab.)
AKERS	95U	ZPHY C67 389	R. Akers *et al.*	(OPAL Collab.)
AKERS	95W	ZPHY C67 555	R. Akers *et al.*	(OPAL Collab.)
AKERS	95X	ZPHY C68 1	R. Akers *et al.*	(OPAL Collab.)
AKERS	95Z	ZPHY C68 203	R. Akers *et al.*	(OPAL Collab.)
ALEXANDER	95D	PL B358 162	G. Alexander *et al.*	(OPAL Collab.)
BUSKULIC	95R	ZPHY C69 15	D. Buskulic *et al.*	(ALEPH Collab.)
MIYABAYASHI	95	PL B347 171	K. Miyabayashi *et al.*	(TOPAZ Collab.)
ABE	94C	PRL 73 25	K. Abe *et al.*	(SLD Collab.)
ABREU	94B	PL B327 386	P. Abreu *et al.*	(DELPHI Collab.)
ABREU	94P	PL B341 109	P. Abreu *et al.*	(DELPHI Collab.)
AKERS	94P	ZPHY C63 181	R. Akers *et al.*	(OPAL Collab.)
BUSKULIC	94G	ZPHY C62 179	D. Buskulic *et al.*	(ALEPH Collab.)
BUSKULIC	94J	ZPHY C62 1	D. Buskulic *et al.*	(ALEPH Collab.)
VILAIN	94	PL B320 203	P. Vilain *et al.*	(CHARM II Collab.)
ABREU	93	PL B298 236	P. Abreu *et al.*	(DELPHI Collab.)
ABREU	93I	ZPHY C59 533	P. Abreu *et al.*	(DELPHI Collab.)
Also		ZPHY C65 709 (erratum)	P. Abreu *et al.*	(DELPHI Collab.)
ABREU	93L	PL B318 249	P. Abreu *et al.*	(DELPHI Collab.)
ACTON	93	PL B305 407	P.D. Acton *et al.*	(OPAL Collab.)
ACTON	93D	ZPHY C58 219	P.D. Acton *et al.*	(OPAL Collab.)
ACTON	93E	PL B311 391	P.D. Acton *et al.*	(OPAL Collab.)
ADRIANI	93	PL B301 136	O. Adriani *et al.*	(L3 Collab.)
ADRIANI	93I	PL B316 427	O. Adriani *et al.*	(L3 Collab.)
BUSKULIC	93L	PL B313 520	D. Buskulic *et al.*	(ALEPH Collab.)
NOVIKOV	93C	PL B298 453	V.A. Novikov, L.B. Okun, M.I. Vysotsky	(ITEP)
ABREU	92I	PL B277 371	P. Abreu *et al.*	(DELPHI Collab.)
ABREU	92M	PL B289 199	P. Abreu *et al.*	(DELPHI Collab.)
ACTON	92B	ZPHY C53 539	D.P. Acton *et al.*	(OPAL Collab.)
ACTON	92L	PL B294 436	P.D. Acton *et al.*	(OPAL Collab.)
ACTON	92N	PL B295 357	P.D. Acton *et al.*	(OPAL Collab.)
ADEVA	92	PL B275 209	B. Adeva *et al.*	(L3 Collab.)
ADRIANI	92D	PL B292 454	O. Adriani *et al.*	(L3 Collab.)
ALITTI	92B	PL B276 354	J. Alitti *et al.*	(UA2 Collab.)
BUSKULIC	92D	PL B292 210	D. Buskulic *et al.*	(ALEPH Collab.)
BUSKULIC	92E	PL B294 145	D. Buskulic *et al.*	(ALEPH Collab.)
DECAMP	92	PRPL 216 253	D. Decamp *et al.*	(ALEPH Collab.)
ABE	91E	PRL 67 1502	F. Abe *et al.*	(CDF Collab.)
ABREU	91H	ZPHY C50 185	P. Abreu *et al.*	(DELPHI Collab.)
ACTON	91B	PL B273 338	D.P. Acton *et al.*	(OPAL Collab.)
ADACHI	91	PL B255 613	I. Adachi *et al.*	(TOPAZ Collab.)
ADEVA	91I	PL B259 199	B. Adeva *et al.*	(L3 Collab.)
AKRAWY	91F	PL B257 531	M.Z. Akrawy *et al.*	(OPAL Collab.)
DECAMP	91B	PL B259 377	D. Decamp *et al.*	(ALEPH Collab.)
DECAMP	91J	PL B266 218	D. Decamp *et al.*	(ALEPH Collab.)
JACOBSEN	91	PRL 67 3347	R.G. Jacobsen *et al.*	(Mark II Collab.)
SHIMONAKA	91	PL B268 457	A. Shimonaka *et al.*	(TOPAZ Collab.)
ABE	90I	ZPHY C48 13	K. Abe *et al.*	(VENUS Collab.)
ABRAMS	90	PRL 64 1334	G.S. Abrams *et al.*	(Mark II Collab.)
AKRAWY	90J	PL B246 285	M.Z. Akrawy *et al.*	(OPAL Collab.)
BEHREND	90D	ZPHY C47 333	H.J. Behrend *et al.*	(CELLO Collab.)
BRAUNSCH...	90	ZPHY C48 433	W. Braunschweig *et al.*	(TASSO Collab.)
ELSEN	90	ZPHY C46 349	E. Elsen *et al.*	(JADE Collab.)
HEGNER	90	ZPHY C46 547	S. Hegner *et al.*	(JADE Collab.)
STUART	90	PRL 64 983	D. Stuart *et al.*	(AMY Collab.)
ABE	89	PRL 62 613	F. Abe *et al.*	(CDF Collab.)
ABE	89C	PRL 63 720	F. Abe *et al.*	(CDF Collab.)
ABE	89L	PL B232 425	K. Abe *et al.*	(VENUS Collab.)
ABRAMS	89B	PRL 63 2173	G.S. Abrams *et al.*	(Mark II Collab.)
ABRAMS	89D	PRL 63 2780	G.S. Abrams *et al.*	(Mark II Collab.)
ALBAJAR	89	ZPHY C44 15	C. Albajar *et al.*	(UA1 Collab.)
BACALA	89	PL B218 112	A. Bacala *et al.*	(AMY Collab.)
BAND	89	PL B218 369	H.R. Band *et al.*	(MAC Collab.)
GREENSHAW	89	ZPHY C42 1	T. Greenshaw *et al.*	(JADE Collab.)
OULD-SAADA	89	ZPHY C44 567	F. Ould-Saada *et al.*	(JADE Collab.)
SAGAWA	89	PRL 63 2341	H. Sagawa *et al.*	(AMY Collab.)
ADACHI	88C	PL B208 319	I. Adachi *et al.*	(TOPAZ Collab.)
ADEVA	88	PR D38 2665	B. Adeva *et al.*	(Mark-J Collab.)
BRAUNSCH...	88D	ZPHY C40 163	W. Braunschweig *et al.*	(TASSO Collab.)
ANSARI	87	PL B186 440	R. Ansari *et al.*	(UA2 Collab.)
BEHREND	87C	PL B191 209	H.J. Behrend *et al.*	(CELLO Collab.)
BARTEL	86C	ZPHY C30 371	W. Bartel *et al.*	(JADE Collab.)
Also		ZPHY C26 507	W. Bartel *et al.*	(JADE Collab.)
Also		PL 108B 140	W. Bartel *et al.*	(JADE Collab.)
ASH	85	PRL 55 1831	W.W. Ash *et al.*	(MAC Collab.)
BARTEL	85F	PL 161B 188	W. Bartel *et al.*	(JADE Collab.)
DERRICK	85	PR D31 2352	M. Derrick *et al.*	(HRS Collab.)
FERNANDEZ	85	PRL 54 1624	E. Fernandez *et al.*	(MAC Collab.)
LEVI	83	PRL 51 1941	M.E. Levi *et al.*	(Mark II Collab.)
BEHREND	82	PL 114B 282	H.J. Behrend *et al.*	(CELLO Collab.)
BRANDELIK	82C	PL 110B 173	R. Brandelik *et al.*	(TASSO Collab.)

H^0

$J = 0$

In the following H^0 refers to the signal that has been discovered in the Higgs searches. Whereas the observed signal is labeled as a spin 0 particle and is called a Higgs Boson, the detailed properties of H^0 and its role in the context of electroweak symmetry breaking need to be further clarified. These issues are addressed by the measurements listed below.

Concerning mass limits and cross section limits that have been obtained in the searches for neutral and charged Higgs bosons, see the sections "Searches for Neutral Higgs Bosons" and "Searches for Charged Higgs Bosons ($H^\pm$ and $H^{\pm\pm}$)", respectively.

H^0 MASS

VALUE (GeV)	DOCUMENT ID		TECN	COMMENT
125.25±0.17 OUR AVERAGE	Error includes scale factor of 1.5. See the ideogram below.			
125.46±0.16	[1] SIRUNYAN	20L	CMS	pp, 13 TeV, $\gamma\gamma$, $ZZ^* \to 4\ell$
124.86±0.27	[2] AABOUD	18BM	ATLS	pp, 13 TeV, $\gamma\gamma$, $ZZ^* \to 4\ell$
125.09±0.21±0.11	[2,3] AAD	15B	LHC	pp, 7, 8 TeV
• • • We do not use the following data for averages, fits, limits, etc. • • •				
125.78±0.26	[4] SIRUNYAN	20L	CMS	pp, 13 TeV, $\gamma\gamma$
125.38±0.14	[5] SIRUNYAN	20L	CMS	pp, 7, 8, 13 TeV, $\gamma\gamma$, $ZZ^* \to 4\ell$
124.79±0.37	[6] AABOUD	18BM	ATLS	pp, 13 TeV, $ZZ^* \to 4\ell$
124.93±0.40	[7] AABOUD	18BM	ATLS	pp, 13 TeV, $\gamma\gamma$
124.97±0.24	[2,8] AABOUD	18BM	ATLS	pp, 7, 8, 13 TeV, $\gamma\gamma$, $ZZ^* \to 4\ell$
125.26±0.20±0.08	[9] SIRUNYAN	17AV	CMS	pp, 13 TeV, $ZZ^* \to 4\ell$
125.07±0.25±0.14	[3] AAD	15B	LHC	pp, 7, 8 TeV, $\gamma\gamma$
125.15±0.37±0.15	[3] AAD	15B	LHC	pp, 7, 8 TeV, $ZZ^* \to 4\ell$
126.02±0.43±0.27	AAD	15B	ATLS	pp, 7, 8 TeV, $\gamma\gamma$
124.51±0.52±0.04	AAD	15B	ATLS	pp, 7, 8 TeV, $ZZ^* \to 4\ell$
125.59±0.42±0.17	AAD	15B	CMS	pp, 7, 8 TeV, $ZZ^* \to 4\ell$
$125.02^{+0.26}_{-0.27}{}^{+0.14}_{-0.15}$	[10] KHACHATRY...	15AM	CMS	pp, 7, 8 TeV
125.36±0.37±0.18	[2,11] AAD	14W	ATLS	pp, 7, 8 TeV
125.98±0.42±0.28	[11] AAD	14W	ATLS	pp, 7, 8 TeV, $\gamma\gamma$
124.51±0.52±0.06	[11] AAD	14W	ATLS	pp, 7, 8 TeV, $ZZ^* \to 4\ell$
125.6 ±0.4 ±0.2	[12] CHATRCHYAN	14AA	CMS	pp, 7, 8 TeV, $ZZ^* \to 4\ell$
122 ±7	[13] CHATRCHYAN	14K	CMS	pp, 7, 8 TeV, $\tau\tau$
124.70±0.31±0.15	[14] KHACHATRY...	14P	CMS	pp, 7, 8 TeV, $\gamma\gamma$
$125.5 \pm 0.2 {}^{+0.5}_{-0.6}$	[2,15] AAD	13AK	ATLS	pp, 7, 8 TeV
126.8 ±0.2 ±0.7	[15] AAD	13AK	ATLS	pp, 7, 8 TeV, $\gamma\gamma$
$124.3 {}^{+0.6}_{-0.5} {}^{+0.5}_{-0.3}$	[15] AAD	13AK	ATLS	pp, 7, 8 TeV, $ZZ^* \to 4\ell$
125.8 ±0.4 ±0.4	[2,16] CHATRCHYAN	13J	CMS	pp, 7, 8 TeV
126.2 ±0.6 ±0.2	[16] CHATRCHYAN	13J	CMS	pp, 7, 8 TeV, $ZZ^* \to 4\ell$
126.0 ±0.4 ±0.4	[2,17] AAD	12AI	ATLS	pp, 7, 8 TeV
125.3 ±0.4 ±0.5	[2,18] CHATRCHYAN	12N	CMS	pp, 7, 8 TeV

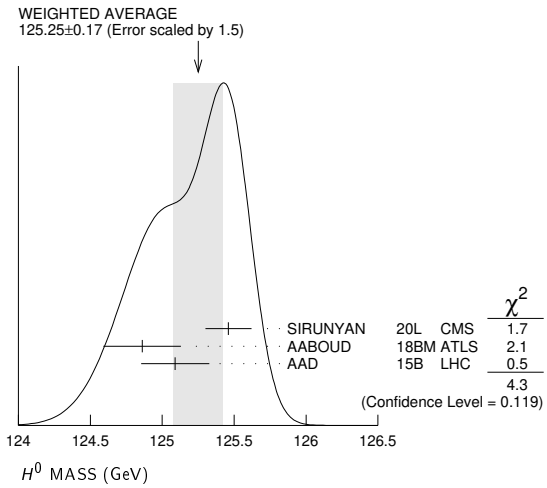

[1] SIRUNYAN 20L result of $H^0 \to \gamma\gamma$ is combined with that of $H^0 \to ZZ^* \to 4\ell$ where $\ell = e, \mu$ (SIRUNYAN 17AV).

[2] Combined value from $\gamma\gamma$ and $ZZ^* \to 4\ell$ final states.

[3] ATLAS and CMS data are fitted simultaneously.

[4] SIRUNYAN 20L use 35.9 fb^{-1} of pp collisions at E_{cm} = 13 TeV with $H^0 \to \gamma\gamma$.

[5] SIRUNYAN 20L combine 13 TeV results with 7 and 8 TeV results (KHACHATRYAN 15AM).

[6] AABOUD 18BM use 36.1 fb^{-1} of pp collisions at E_{cm} = 13 TeV with $H^0 \to ZZ^* \to 4\ell$ where $\ell = e, \mu$.

[7] AABOUD 18BM use 36.1 fb^{-1} of pp collisions at E_{cm} = 13 TeV with $H^0 \to \gamma\gamma$.

[8] AABOUD 18BM combine 13 TeV results with 7 and 8 TeV results. Other combined results are summarized in their Fig. 4.

[9] SIRUNYAN 17AV use 35.9 fb^{-1} of pp collisions at E_{cm} = 13 TeV with $H^0 \to ZZ^* \to 4\ell$ where $\ell = e, \mu$.

[10] KHACHATRYAN 15AM use up to 5.1 fb^{-1} of pp collisions at E_{cm} = 7 TeV and up to 19.7 fb^{-1} at E_{cm} = 8 TeV.

[11] AAD 14W use 4.5 fb^{-1} of pp collisions at E_{cm} = 7 TeV and 20.3 fb^{-1} at 8 TeV.

[12] CHATRCHYAN 14AA use 5.1 fb^{-1} of pp collisions at E_{cm} = 7 TeV and 19.7 fb^{-1} at E_{cm} = 8 TeV.

[13] CHATRCHYAN 14K use 4.9 fb^{-1} of pp collisions at E_{cm} = 7 TeV and 19.7 fb^{-1} at E_{cm} = 8 TeV.

[14] KHACHATRYAN 14P use 5.1 fb^{-1} of pp collisions at E_{cm} = 7 TeV and 19.7 fb^{-1} at E_{cm} = 8 TeV.

[15] AAD 13AK use 4.7 fb^{-1} of pp collisions at E_{cm}=7 TeV and 20.7 fb^{-1} at E_{cm}=8 TeV. Superseded by AAD 14W.

[16] CHATRCHYAN 13J use 5.1 fb^{-1} of pp collisions at E_{cm} = 7 TeV and 12.2 fb^{-1} at E_{cm} = 8 TeV.

[17] AAD 12AI obtain results based on 4.6–4.8 fb^{-1} of pp collisions at E_{cm} = 7 TeV and 5.8–5.9 fb^{-1} at E_{cm} = 8 TeV. An excess of events over background with a local significance of 5.9 σ is observed at m_{H^0} = 126 GeV. See also AAD 12DA.

[18] CHATRCHYAN 12N obtain results based on 4.9–5.1 fb^{-1} of pp collisions at E_{cm} = 7 TeV and 5.1–5.3 fb^{-1} at E_{cm} = 8 TeV. An excess of events over background with a local significance of 5.0 σ is observed at about m_{H^0} = 125 GeV. See also CHATRCHYAN 12BY and CHATRCHYAN 13Y.

Downloaded from https://academic.oup.com/ptep/article/2022/8/083C01/6651666 by KIT Library user on 27 September 2022

H^0 SPIN AND CP PROPERTIES

The observation of the signal in the $\gamma\gamma$ final state rules out the possibility that the discovered particle has spin 1, as a consequence of the Landau-Yang theorem. This argument relies on the assumptions that the decaying particle is an on-shell resonance and that the decay products are indeed two photons rather than two pairs of boosted photons, which each could in principle be misidentified as a single photon.

Concerning distinguishing the spin 0 hypothesis from a spin 2 hypothesis, some care has to be taken in modelling the latter in order to ensure that the discriminating power is actually based on the spin properties rather than on unphysical behavior that may affect the model of the spin 2 state.

Under the assumption that the observed signal consists of a single state rather than an overlap of more than one resonance, it is sufficient to discriminate between distinct hypotheses in the spin analyses. On the other hand, the determination of the CP properties is in general much more difficult since in principle the observed state could consist of any admixture of CP-even and CP-odd components. As a first step, the compatibility of the data with distinct hypotheses of pure CP-even and pure CP-odd states with different spin assignments has been investigated. In order to treat the case of a possible mixing of different CP states, certain cross section ratios are considered. Those cross section ratios need to be distinguished from the amount of mixing between a CP-even and a CP-odd state, as the cross section ratios depend in addition also on the coupling strengths of the CP-even and CP-odd components to the involved particles. A small relative coupling implies a small sensitivity of the corresponding cross section ratio to effects of CP mixing.

VALUE	DOCUMENT ID		TECN	COMMENT
• • • We do not use the following data for averages, fits, limits, etc. • • •				
	[1] AAD	20N	ATLS	$H^0 \to \tau\tau$, VBF, 13 TeV
	[2] AAD	20Z	ATLS	$t\overline{t}H^0$, $H^0 \to \gamma\gamma$, 13 TeV
	[3] SIRUNYAN	20AS	CMS	$t\overline{t}H^0$, $H^0 \to \gamma\gamma$, 13 TeV
	[4] SIRUNYAN	19BL	CMS	pp, 7, 8, 13 TeV, $ZZ^*/ZZ \to 4\ell$
	[5] SIRUNYAN	19BZ	CMS	$pp \to H^0$+2jets (VBF, ggF, VH), $H^0 \to \tau\tau$, 13 TeV
	[6] AABOUD	18AJ	ATLS	$H^0 \to ZZ^* \to 4\ell$ ($\ell = e, \mu$), 13TeV
	[7] SIRUNYAN	17AM	CMS	$pp \to H^0 + \geq 2j$, $H^0 \to 4\ell$ ($\ell = e, \mu$)
	[8] AAD	16	ATLS	$H^0 \to \gamma\gamma$
	[9] AAD	16BL	ATLS	$pp \to H^0 jjX$ (VBF), $H^0 \to \tau\tau$, 8 TeV
	[10] KHACHATRY...	16AB	CMS	$pp \to WH^0, ZH^0, H^0 \to b\overline{b}$, 8 TeV
	[11] AAD	15AX	ATLS	$H^0 \to WW^*$
	[12] AAD	15CI	ATLS	$H^0 \to ZZ^*, WW^*, \gamma\gamma$
	[13] AALTONEN	15	TEVA	$p\overline{p} \to WH^0, ZH^0, H^0 \to b\overline{b}$
	[14] AALTONEN	15B	CDF	$p\overline{p} \to WH^0, ZH^0, H^0 \to b\overline{b}$
	[15] KHACHATRY...	15Y	CMS	$H^0 \to 4\ell, WW^*, \gamma\gamma$
	[16] ABAZOV	14F	D0	$p\overline{p} \to WH^0, ZH^0, H^0 \to b\overline{b}$
	[17] CHATRCHYAN	14AA	CMS	$H^0 \to ZZ^*$
	[18] CHATRCHYAN	14G	CMS	$H^0 \to WW^*$
	[19] KHACHATRY...	14P	CMS	$H^0 \to \gamma\gamma$
	[20] AAD	13AJ	ATLS	$H^0 \to \gamma\gamma, ZZ^* \to 4\ell, WW^* \to \ell\nu\ell\nu$
	[21] CHATRCHYAN	13J	CMS	$H^0 \to ZZ^* \to 4\ell$

[1] AAD 20N test CP invariance in H^0 production via VBF using $H^0 \to \tau\tau$ decay channel with 36.1 fb^{-1} at E_{cm} = 13 TeV. By using the Optimal Observable method, the data constrain a parameter $\tilde{d}$, which is for the strength of CP violation in an effective field theory, to be $-0.090 \leq \tilde{d} \leq 0.035$ at 68% CL (see their Fig. 6).

[2] AAD 20Z exclude a CP-mixing angle α, $|\alpha| > 43^\circ$ at 95% CL, where $\alpha = 0$ represents the Standard Model, in 139 fb^{-1} of data at E_{cm} = 13 TeV. The pure CP-odd structure of the top Yukawa coupling ($\alpha = 90^\circ$) is excluded at 3.9 σ.

[3] SIRUNYAN 20AS exclude the pure CP-odd structure of the top Yukawa coupling at 3.2 σ using $t\overline{t}H^0$, $H^0 \to \gamma\gamma$ in 137 fb^{-1} of data at E_{cm} = 13 TeV. The fractional contribution of the CP-odd component $f_{CP}^{t\overline{t}H^0}$ is measured to be 0.00 ± 0.33.

[4] SIRUNYAN 19BL measure the anomalous HVV couplings from on-shell and off-shell production in the 4ℓ final state. Data of 80.2 fb^{-1} at 13 TeV, 19.7 fb^{-1} at 8 TeV, and 5.1 fb^{-1} at 7 TeV are used. See their Tables VI and VII for anomalous HVV couplings of CP-violating and CP-conserving parameters with on- and off-shells.

[5] SIRUNYAN 19BZ constrain anomalous HVV couplings of the Higgs boson with data of 35.9 fb^{-1} at E_{cm} = 13 TeV using Higgs boson candidates with two jets produced in VBF, ggF, and VH that decay to $\tau\tau$. See their Table 2 and Fig. 10, which show 68% CL and 95% CL intervals. Combining those with the $H^0 \to 4\ell$ (SIRUNYAN 19BL, on-shell scenario), results shown in their Tables 3, 4, and Fig. 11 are obtained. A CP-violating parameter is set to be $f_{a3}\cos(\phi_{a3}) = (0.00 \pm 0.27) \times 10^{-3}$ and CP-conserving parameters are $f_{a2}\cos(\phi_{a2}) = (0.08^{+1.04}_{-0.21}) \times 10^{-3}$, $f_{\Lambda 1}\cos(\phi_{\Lambda 1}) = (0.00^{+0.53}_{-0.09}) \times 10^{-3}$, and $f_{\Lambda 1}^{Z\gamma}\cos(\phi_{\Lambda 1}^{Z\gamma}) = (0.0^{+1.1}_{-1.3}) \times 10^{-3}$.

[6] AABOUD 18AJ study the tensor structure of the Higgs boson couplings using an effective Lagrangian using 36.1 fb^{-1} of pp collision data at E_{cm} = 13 TeV. Constraints are set on the non-Standard-Model CP-even and CP-odd couplings to Z bosons and on the CP-odd coupling to gluons. See their Figs. 9 and 10, and Tables 10 and 11.

[7] SIRUNYAN 17AM constrain anomalous couplings of the Higgs boson with 5.1 fb^{-1} of pp collisions at E_{cm} = 7 TeV, 19.7 fb^{-1} at E_{cm} = 8 TeV, and 38.6 fb^{-1} at E_{cm} = 13 TeV. See their Table 3 and Fig. 3, which show 68% CL and 95% CL intervals. A CP violation parameter f_{a3} is set to be $f_{a3}\cos(\phi_{a3}) = [-0.38, 0.46]$ at 95% CL ($\phi_{a3} = 0$ or π).

[8] AAD 16 study $H^0 \to \gamma\gamma$ with an effective Lagrangian including CP even and odd terms in 20.3 fb^{-1} of pp collisions at E_{cm} = 8 TeV. The data is consistent with the expectations for the Higgs boson of the Standard Model. Limits on anomalous couplings are also given.

[9] AAD 16BL study VBF $H^0 \to \tau\tau$ with an effective Lagrangian including a CP odd term in 20.3 fb^{-1} of pp collisions at E_{cm} = 8 TeV. The measurement is consistent with the expectation of the Standard Model. The CP-mixing parameter $\tilde{d}$ (a dimensionless coupling $\tilde{d} = -(m_W^2/\Lambda^2) f_{\widetilde{WW}}$) is constrained to the interval of (−0.11, 0.05) at 68% CL under the assumption of $d = \tilde{d}_B$.

[10] KHACHATRYAN 16AB search for anomalous pseudoscalar couplings of the Higgs boson to W and Z with 18.9 fb^{-1} of pp collisions at E_{cm} = 8 TeV. See their Table 5 and Figs 5 and 6 for limits on possible anomalous pseudoscalar coupling parameters.

[11] AAD 15AX compare the $J^{CP} = 0^+$ Standard Model assignment with other J^{CP} hypotheses in 20.3 fb^{-1} of pp collisions at E_{cm} = 8 TeV, using the process $H^0 \to WW^* \to e\nu\mu\nu$. 2^+ hypotheses are excluded at 84.5–99.4%CL, 0^- at 96.5%CL, 0^+ (field strength coupling) at 70.8%CL. See their Fig. 19 for limits on possible CP mixture parameters.

[12] AAD 15CI compare the $J^{CP} = 0^+$ Standard Model assignment with other J^{CP} hypotheses in 4.5 fb^{-1} of pp collisions at E_{cm} = 7 TeV and 20.3 fb^{-1} at E_{cm} = 8 TeV, using the processes $H^0 \to ZZ^* \to 4\ell$. $H^0 \to \gamma\gamma$ and combine with AAD 15AX data. 0^+ (field strength coupling), 0^- and several 2^+ hypotheses are excluded at more than 99.9% CL. See their Tables 7–9 for limits on possible CP mixture parameters.

[13] AALTONEN 15 combine AALTONEN 15B and ABAZOV 14F data. An upper limit of 0.36 of the Standard Model production rate at 95% CL is obtained both for a 0^- and a 2^+ state. Assuming the SM event rate, the $J^{CP} = 0^-$ (2^+) hypothesis is excluded at the 5.0σ (4.9σ) level.

[14] AALTONEN 15B compare the $J^{CP} = 0^+$ Standard Model assignment with other J^{CP} hypotheses in 9.45 fb^{-1} of $p\overline{p}$ collisions at E_{cm} = 1.96 TeV, using the processes $ZH^0 \to \ell\ell b\overline{b}$, $WH^0 \to \ell\nu b\overline{b}$, and $ZH^0 \to \nu\nu b\overline{b}$. Bounds on the production rates of 0^- and 2^+ (graviton-like) states are set, see their tables II and III.

[15] KHACHATRYAN 15Y compare the $J^{CP} = 0^+$ Standard Model assignment with other J^{CP} hypotheses in up to 5.1 fb^{-1} of pp collisions at E_{cm} = 7 TeV and up to 19.7 fb^{-1} at E_{cm} = 8 TeV, using the processes $H^0 \to 4\ell$, $H^0 \to WW^*$, and $H^0 \to \gamma\gamma$. 0^- is excluded at 99.98% CL, and several 2^+ hypotheses are excluded at more than 99% CL. Spin 1 models are excluded at more than 99.999% CL in ZZ^* and WW^* modes. Limits on anomalous couplings and several cross section fractions, treating the case of CP-mixed states, are also given.

[16] ABAZOV 14F compare the $J^{CP} = 0^+$ Standard Model assignment with $J^{CP} = 0^-$ and 2^+ (graviton-like coupling) hypotheses in up to 9.7 fb^{-1} of $p\overline{p}$ collisions at E_{cm} = 1.96 TeV. They use kinematic correlations between the decay products of the vector boson and the Higgs boson in the final states $ZH \to \ell\ell b\overline{b}$, $WH \to \ell\nu b\overline{b}$, and $ZH \to \nu\nu b\overline{b}$. The 0^- (2^+) hypothesis is excluded at 97.6% CL (99.0% CL). In order to treat the case of a possible mixture of a 0^+ state with another J^{CP} state, the cross section fractions $f_X = \sigma_X/(\sigma_{0^+} + \sigma_X)$ are considered, where $X = 0^-, 2^+$. Values for f_{0^-} (f_{2^+}) above 0.80 (0.67) are excluded at 95% CL under the assumption that the total cross section is that of the SM Higgs boson.

[17] CHATRCHYAN 14AA compare the $J^{CP} = 0^+$ Standard Model assignment with various J^{CP} hypotheses in 5.1 fb^{-1} of pp collisions at E_{cm} = 7 TeV and 19.7 fb^{-1} at E_{cm} = 8 TeV. $J^{CP} = 0^-$ and $1^\pm$ hypotheses are excluded at 99% CL, and several $J = 2$ hypotheses are excluded at 95% CL. In order to treat the case of a possible mixture of a 0^+ state with another J^{CP} state, the cross section fraction $f_{a3} = |a_3|^2 \sigma_3 / (|a_1|^2 \sigma_1 + |a_2|^2 \sigma_2 + |a_3|^2 \sigma_3)$ is considered, where the case $a_3 = 1$, $a_1 = a_2 = 0$ corresponds to a pure CP-odd state. Assuming $a_2 = 0$, a value for f_{a3} above 0.51 is excluded at 95% CL.

[18] CHATRCHYAN 14G compare the $J^{CP} = 0^+$ Standard Model assignment with $J^{CP} = 0^-$ and 2^+ (graviton-like coupling) hypotheses in 4.9 fb^{-1} of pp collisions at E_{cm} = 7 TeV and 19.4 fb^{-1} at E_{cm} = 8 TeV. Varying the fraction of the production of the 2^+ state via gg and $q\overline{q}$, 2^+ hypotheses are disfavored at CL between 83.7 and 99.8%. The 0^- hypothesis is disfavored against 0^+ at the 65.3% CL.

[19] KHACHATRYAN 14P compare the $J^{CP} = 0^+$ Standard Model assignment with a 2^+ (graviton-like coupling) hypothesis in 5.1 fb^{-1} of pp collisions at E_{cm} = 7 TeV and 19.7 fb^{-1} at E_{cm} = 8 TeV. Varying the fraction of the production of the 2^+ state via gg and $q\overline{q}$, 2^+ hypotheses are disfavored at CL between 71 and 94%.

[20] AAD 13AJ compare the spin 0, CP-even hypothesis with specific alternative hypotheses of spin 0, CP-odd, spin 1, CP-even and CP-odd, and spin 2, CP-even models using the Higgs boson decays $H \to \gamma\gamma$, $H \to ZZ^* \to 4\ell$ and $H \to WW^* \to \ell\nu\ell\nu$ and combinations thereof. The data are compatible with the spin 0, CP-even hypothesis, while all other tested hypotheses are excluded at confidence levels above 97.8%.

[21] CHATRCHYAN 13J study angular distributions of the lepton pairs in the ZZ^* channel where both Z bosons decay to e or μ pairs. Under the assumption that the observed particle has spin 0, the data are found to be consistent with the pure CP-even hypothesis, while the pure CP-odd hypothesis is disfavored.

H^0 DECAY WIDTH

The total decay width for a light Higgs boson with a mass in the observed range is not expected to be directly observable at the LHC. For the case of the Standard Model the prediction for the total width is about 4 MeV, which is three orders of magnitude smaller than the experimental mass resolution. There is no indication from the results observed so far that the natural width is broadened by new physics effects to such an extent that it could be directly observable. Furthermore, as all LHC Higgs channels rely on the identification of Higgs decay products, the total Higgs width cannot be measured indirectly without additional assumptions. The different dependence of on-peak and off-peak contributions on the total width in Higgs decays to ZZ^* and interference effects between signal and background in Higgs decays to $\gamma\gamma$ can provide additional information in this context. Constraints on the total width from the combination of on-peak and off-peak contributions in Higgs decays to ZZ^* rely on the assumption of equal on- and off-shell effective couplings. Without an experimental determination of the total width or further theoretical assumptions, only ratios of couplings can be determined at the LHC rather than absolute values of couplings.

VALUE (MeV)	CL%	DOCUMENT ID		TECN	COMMENT
$\mathbf{3.2^{+2.8}_{-2.2}}$		[1] SIRUNYAN	19BL	CMS	pp, 7, 8, 13 TeV, $ZZ^*/ZZ \to 4\ell$

Downloaded from https://academic.oup.com/ptep/article/2022/8/083C01/6651666 by KIT Library user on 27 September 2022

• • • We do not use the following data for averages, fits, limits, etc. • • •

< 14.4	95	[2] AABOUD	18BP	ATLS	pp, 13 TeV, $ZZ \to 4\ell$, $2\ell 2\nu$
<1100	95	[3] SIRUNYAN	17AV	CMS	pp, 13 TeV, $ZZ^* \to 4\ell$
< 26	95	[4] KHACHATRY...	16BA	CMS	pp, 7, 8 TeV, $WW^{(*)}$
< 13	95	[5] KHACHATRY...	16BA	CMS	pp, 7, 8 TeV, $ZZ^{(*)}$, $WW^{(*)}$
< 22.7	95	[6] AAD	15BE	ATLS	pp, 8 TeV, $ZZ^{(*)}$, $WW^{(*)}$
<1700	95	[7] KHACHATRY...	15AM	CMS	pp, 7, 8 TeV
> 3.5×10^{-9}	95	[8] KHACHATRY...	15BA	CMS	pp, 7, 8 TeV, flight distance
< 46	95	[9] KHACHATRY...	15BA	CMS	pp, 7, 8 TeV, $ZZ^{(*)} \to 4\ell$
<5000	95	[10] AAD	14W	ATLS	pp, 7, 8 TeV, $\gamma\gamma$
<2600	95	[10] AAD	14W	ATLS	pp, 7, 8 TeV, $ZZ^* \to 4\ell$
<3400	95	[11] CHATRCHYAN	14AA	CMS	pp, 7, 8 TeV, $ZZ^* \to 4\ell$
< 22	95	[12] KHACHATRY...	14D	CMS	pp, 7, 8 TeV, $ZZ^{(*)}$
<2400	95	[13] KHACHATRY...	14P	CMS	pp, 7, 8 TeV, $\gamma\gamma$

[1] SIRUNYAN 19BL measure the width and anomalous HVV couplings from on-shell and off-shell production in the 4ℓ final state. Data of 80.2 fb^{-1} at 13 TeV, 19.7 fb^{-1} at 8 TeV, and 5.1 fb^{-1} at 7 TeV are used. The total width for the SM-like couplings is measured to be also [0.08, 9.16] MeV with 95% CL, assuming SM-like couplings for on- and off-shells (see their Table VIII). Constraints on the total width for anomalous HVV interaction cases are found in their Table IX. See their Table X for the Higgs boson signal strength in the off-shell region.

[2] AABOUD 18BP use 36.1 fb^{-1} at E_{cm} = 13 TeV. An observed upper limit on the off-shell Higgs signal strength of 3.8 is obtained at 95% CL using off-shell Higgs boson production in the $ZZ \to 4\ell$ and $ZZ \to 2\ell 2\nu$ decay channels ($\ell = e, \mu$). Combining with the on-shell signal strength measurements, the quoted upper limit on the Higgs boson total width is obtained, assuming the ratios of the relevant Higgs-boson couplings to the SM predictions are constant with energy from on-shell production to the high-mass range.

[3] SIRUNYAN 17AV obtain an upper limit on the width from the $m_{4\ell}$ distribution in $ZZ^* \to 4\ell$ ($\ell = e, \mu$) decays. Data of 35.9 fb^{-1} pp collisions at E_{cm} = 13 TeV is used. The expected limit is 1.60 GeV.

[4] KHACHATRYAN 16BA derive constraints on the total width from comparing $WW^{(*)}$ production via on-shell and off-shell H^0 using 4.9 fb^{-1} of pp collisions at E_{cm} = 7 TeV and 19.4 fb^{-1} at 8 TeV.

[5] KHACHATRYAN 16BA combine the $WW^{(*)}$ result with $ZZ^{(*)}$ results of KHACHATRYAN 15BA and KHACHATRYAN 14D.

[6] AAD 15BE derive constraints on the total width from comparing $ZZ^{(*)}$ and $WW^{(*)}$ production via on-shell and off-shell H^0 using 20.3 fb^{-1} of pp collisions at E_{cm} = 8 TeV. The K factor for the background processes is assumed to be equal to that for the signal.

[7] KHACHATRYAN 15AM combine $\gamma\gamma$ and $ZZ^* \to 4\ell$ results. The expected limit is 2.3 GeV.

[8] KHACHATRYAN 15BA derive a lower limit on the total width from an upper limit on the decay flight distance $\tau < 1.9 \times 10^{-13}$ s. 5.1 fb^{-1} of pp collisions at E_{cm} = 7 TeV and 19.7 fb^{-1} at 8 TeV are used.

[9] KHACHATRYAN 15BA derive constraints on the total width from comparing $ZZ^{(*)}$ production via on-shell and off-shell H^0 with an unconstrained anomalous coupling. 4ℓ final states in 5.1 fb^{-1} of pp collisions at E_{cm} = 7 TeV and 19.7 fb^{-1} at E_{cm} = 8 TeV are used.

[10] AAD 14W use 4.5 fb^{-1} of pp collisions at E_{cm} = 7 TeV and 20.3 fb^{-1} at 8 TeV. The expected limit is 6.2 GeV.

[11] CHATRCHYAN 14AA use 5.1 fb^{-1} of pp collisions at E_{cm} = 7 TeV and 19.7 fb^{-1} at E_{cm} = 8 TeV. The expected limit is 2.8 GeV.

[12] KHACHATRYAN 14D derive constraints on the total width from comparing $ZZ^{(*)}$ production via on-shell and off-shell H^0. 4ℓ and $\ell\ell\nu\nu$ final states in 5.1 fb^{-1} of pp collisions at E_{cm} = 7 TeV and 19.7 fb^{-1} at E_{cm} = 8 TeV are used.

[13] KHACHATRYAN 14P use 5.1 fb^{-1} of pp collisions at E_{cm} = 7 TeV and 19.7 fb^{-1} at E_{cm} = 8 TeV. The expected limit is 3.1 GeV.

H^0 DECAY MODES

	Mode	Fraction (Γ_i/Γ)	Confidence level
Γ_1	WW^*		
Γ_2	ZZ^*		
Γ_3	$\gamma\gamma$		
Γ_4	$b\overline{b}$		
Γ_5	e^+e^-	$< 3.6 \times 10^{-4}$	95%
Γ_6	$\mu^+\mu^-$		
Γ_7	$\tau^+\tau^-$		
Γ_8	$Z\gamma$		
Γ_9	$Z\rho(770)$	< 1.21 %	95%
Γ_{10}	$Z\phi(1020)$	$< 3.6 \times 10^{-3}$	95%
Γ_{11}	$Z\eta_c$		
Γ_{12}	ZJ/ψ		
Γ_{13}	$\gamma^*\gamma$		
Γ_{14}	$J/\psi\gamma$	$< 3.5 \times 10^{-4}$	95%
Γ_{15}	$J/\psi J/\psi$	$< 1.8 \times 10^{-3}$	95%
Γ_{16}	$\psi(2S)\gamma$	$< 2.0 \times 10^{-3}$	95%
Γ_{17}	$\Upsilon(1S)\gamma$	$< 4.9 \times 10^{-4}$	95%
Γ_{18}	$\Upsilon(2S)\gamma$	$< 5.9 \times 10^{-4}$	95%
Γ_{19}	$\Upsilon(3S)\gamma$	$< 5.7 \times 10^{-4}$	95%
Γ_{20}	$\Upsilon(\mathrm{nS})\,\Upsilon(\mathrm{mS})$	$< 1.4 \times 10^{-3}$	95%
Γ_{21}	$\rho(770)\gamma$	$< 8.8 \times 10^{-4}$	95%
Γ_{22}	$\phi(1020)\gamma$	$< 4.8 \times 10^{-4}$	95%
Γ_{23}	$e\mu$ LF	$< 6.1 \times 10^{-5}$	95%
Γ_{24}	$e\tau$ LF	$< 2.2 \times 10^{-3}$	95%
Γ_{25}	$\mu\tau$ LF	$< 1.5 \times 10^{-3}$	95%
Γ_{26}	invisible	<19 %	95%
Γ_{27}	γ invisible		

H^0 BRANCHING RATIOS

$\Gamma(e^+e^-)/\Gamma_{total}$ — Γ_5/Γ

VALUE	CL%	DOCUMENT ID		TECN	COMMENT
<3.6 × 10^{-4}	95	[1] AAD	20F	ATLS	pp, 13 TeV
• • • We do not use the following data for averages, fits, limits, etc. • • •					
$<1.9 \times 10^{-3}$	95	[2] KHACHATRY...	15H	CMS	pp, 7, 8 TeV

[1] AAD 20F use 139 fb^{-1} of pp collisions at E_{cm} = 13 TeV. The best-fit value of the $H^0 \to ee$ branching fraction is $(0.0 \pm 1.7 \pm 0.6) \times 10^{-4}$ for m_{H^0} = 125 GeV.

[2] KHACHATRYAN 15H use 5.0 fb^{-1} of pp collisions at E_{cm} = 7 TeV and 19.7 fb^{-1} at 8 TeV.

$\Gamma(Z\rho(770))/\Gamma_{total}$ — Γ_9/Γ

VALUE	CL%	DOCUMENT ID		TECN	COMMENT
<1.21 × 10^{-2}	95	[1] SIRUNYAN	20BK	CMS	pp, 13 TeV

[1] SIRUNYAN 20BK search for $H^0 \to Z\rho$, $Z \to e^+e^-/\mu^+\mu^-$, $\rho \to \pi^+\pi^-$ with 137 fb^{-1} of pp collision data at E_{cm} = 13 TeV. The quoted branching fraction is for the unpolarized decay. See their Table 3 for different polarizations.

$\Gamma(Z\phi(1020))/\Gamma_{total}$ — Γ_{10}/Γ

VALUE	CL%	DOCUMENT ID		TECN	COMMENT
<3.6 × 10^{-3}	95	[1] SIRUNYAN	20BK	CMS	pp, 13 TeV

[1] SIRUNYAN 20BK search for $H^0 \to Z\phi$, $Z \to e^+e^-/\mu^+\mu^-$, $\phi \to K^+K^-$ with 137 fb^{-1} of pp collision data at E_{cm} = 13 TeV. The quoted branching fraction is for the unpolarized decay. See their Table 4 for different polarizations.

$\Gamma(Z\eta_c)/\Gamma_{total}$ — Γ_{11}/Γ

VALUE	CL%	DOCUMENT ID		TECN	COMMENT
• • • We do not use the following data for averages, fits, limits, etc. • • •					
		[1] AAD	20AE	ATLS	pp, 13 TeV

[1] AAD 20AE search for $H^0 \to Z\eta_c$ with two-leptons ($e^+e^-/\mu^+\mu^-$) plus jet events using 139 fb^{-1} of pp collision data at E_{cm} = 13 TeV. The upper limit of $\sigma(pp \to H^0)\cdot B(H^0 \to Z\eta_c)$ is 110 pb at 95% CL.

$\Gamma(ZJ/\psi)/\Gamma_{total}$ — Γ_{12}/Γ

VALUE	CL%	DOCUMENT ID		TECN	COMMENT
• • • We do not use the following data for averages, fits, limits, etc. • • •					
		[1] AAD	20AE	ATLS	pp, 13 TeV

[1] AAD 20AE search for $H^0 \to ZJ/\psi$ with two-leptons ($e^+e^-/\mu^+\mu^-$) plus jet events using 139 fb^{-1} of pp collision data at E_{cm} = 13 TeV. The upper limit of $\sigma(pp \to H^0)\cdot B(H^0 \to ZJ/\psi)$ is 100 pb at 95% CL.

$\Gamma(J/\psi\gamma)/\Gamma_{total}$ — Γ_{14}/Γ

VALUE	CL%	DOCUMENT ID		TECN	COMMENT
$<7.6 \times 10^{-4}$	95	[1] SIRUNYAN	19AJ	CMS	13 TeV, 35.9 fb^{-1}
<3.5 × 10^{-4}	95	[2] AABOUD	18BL	ATLS	13 TeV, 36.1 fb^{-1}
• • • We do not use the following data for averages, fits, limits, etc. • • •					
$<1.5 \times 10^{-3}$	95	[3] KHACHATRY...	16B	CMS	8 TeV
$<1.5 \times 10^{-3}$	95	[4] AAD	15I	ATLS	8 TeV

[1] SIRUNYAN 19AJ search for $H^0 \to J/\psi\gamma$, $J/\psi \to \mu^+\mu^-$ with 35.9 fb^{-1} of pp collision data at E_{cm} = 13 TeV. The upper limit corresponds to 260 times the SM prediction and by combining the KHACHATRYAN 16B, it is 220 times the SM prediction.

[2] AABOUD 18BL search for $H^0 \to J/\psi\gamma$, $J/\psi \to \mu^+\mu^-$ with 36.1 fb^{-1} of pp collision data at E_{cm} = 13 TeV.

[3] KHACHATRYAN 16B use 19.7 fb^{-1} of pp collision data at 8 TeV.

[4] AAD 15I use 19.7 fb^{-1} of pp collision data at 8 TeV.

$\Gamma(J/\psi J/\psi)/\Gamma_{total}$ — Γ_{15}/Γ

VALUE	CL%	DOCUMENT ID		TECN	COMMENT
<1.8 × 10^{-3}	95	[1] SIRUNYAN	19BR	CMS	pp at 13 TeV

[1] SIRUNYAN 19BR search for $H^0 \to J/\psi J/\psi$, $J/\psi \to \mu^+\mu^-$ with 37.5 fb^{-1} of pp collision data at E_{cm} = 13 TeV. J/ψs from the Higgs decay are assumed to be unpolarized. For fully longitudinal (transverse) polarized J/ψs, limits change by −22% (+10%).

$\Gamma(\psi(2S)\gamma)/\Gamma_{total}$ — Γ_{16}/Γ

VALUE	CL%	DOCUMENT ID		TECN	COMMENT
<2.0 × 10^{-3}	95	[1] AABOUD	18BL	ATLS	13 TeV, 36.1 fb^{-1}

[1] AABOUD 18BL search for $H^0 \to \psi(2S)\gamma$, $\psi(2S) \to \mu^+\mu^-$ with 36.1 fb^{-1} of pp collision data at E_{cm} = 13 TeV.

$\Gamma(\Upsilon(1S)\gamma)/\Gamma_{total}$ — Γ_{17}/Γ

VALUE	CL%	DOCUMENT ID		TECN	COMMENT
<4.9 × 10^{-4}	95	[1] AABOUD	18BL	ATLS	13 TeV, 36.1 fb^{-1}

Downloaded from https://academic.oup.com/ptep/article/2022/8/083C01/6651666 by KIT Library user on 27 September 2022

• • • We do not use the following data for averages, fits, limits, etc. • • •

$<1.3 \times 10^{-3}$	95	[2] AAD	15I	ATLS	8 TeV

[1] AABOUD 18BL search for $H^0 \to \Upsilon(1S)\gamma$, $\Upsilon(1S) \to \mu^+\mu^-$ with 36.1 fb^{-1} of pp collision data at E_{cm} = 13 TeV.
[2] AAD 15I use 19.7 fb^{-1} of pp collision data at 8 TeV.

$\Gamma(\Upsilon(2S)\gamma)/\Gamma_{total}$ — Γ_{18}/Γ

VALUE	CL%	DOCUMENT ID		TECN	COMMENT
$<5.9 \times 10^{-4}$	95	[1] AABOUD	18BL	ATLS	13 TeV, 36.1 fb^{-1}

• • • We do not use the following data for averages, fits, limits, etc. • • •

$<1.9 \times 10^{-3}$	95	[2] AAD	15I	ATLS	8 TeV

[1] AABOUD 18BL search for $H^0 \to \Upsilon(2S)\gamma$, $\Upsilon(2S) \to \mu^+\mu^-$ with 36.1 fb^{-1} of pp collision data at E_{cm} = 13 TeV.
[2] AAD 15I use 19.7 fb^{-1} of pp collision data at 8 TeV.

$\Gamma(\Upsilon(3S)\gamma)/\Gamma_{total}$ — Γ_{19}/Γ

VALUE	CL%	DOCUMENT ID		TECN	COMMENT
$<5.7 \times 10^{-4}$	95	[1] AABOUD	18BL	ATLS	13 TeV, 36.1 fb^{-1}

• • • We do not use the following data for averages, fits, limits, etc. • • •

$<1.3 \times 10^{-3}$	95	[2] AAD	15I	ATLS	8 TeV

[1] AABOUD 18BL search for $H^0 \to \Upsilon(3S)\gamma$, $\Upsilon(3S) \to \mu^+\mu^-$ with 36.1 fb^{-1} of pp collision data at E_{cm} = 13 TeV.
[2] AAD 15I use 19.7 fb^{-1} of pp collision data at 8 TeV.

$\Gamma(\Upsilon(nS)\,\Upsilon(mS))/\Gamma_{total}$ — Γ_{20}/Γ

VALUE	CL%	DOCUMENT ID		TECN	COMMENT
$<1.4 \times 10^{-3}$	95	[1] SIRUNYAN	19BR	CMS	pp at 13 TeV

[1] SIRUNYAN 19BR search for $H^0 \to \Upsilon(nS)\,\Upsilon(mS)$ with $\Upsilon(nS),\Upsilon(mS) \to \mu^+\mu^-$ (n, m = 1, 2, 3) for 37.5 fb^{-1} of pp collision data at E_{cm} = 13 TeV. Υs from the Higgs decay are assumed to be unpolarized. For fully longitudinal (transverse) polarized Υs, limits change by -22% ($+10\%$). The three Υ states selected in a mass range of 8.5–11 GeV are not distinguished.

$\Gamma(\rho(770)\gamma)/\Gamma_{total}$ — Γ_{21}/Γ

VALUE	CL%	DOCUMENT ID		TECN	COMMENT
$<8.8 \times 10^{-4}$	95	[1] AABOUD	18AU	ATLS	pp, 13 TeV

[1] AABOUD 18AU use 35.6 fb^{-1} of pp collision data at 13 TeV.

$\Gamma(\phi(1020)\gamma)/\Gamma_{total}$ — Γ_{22}/Γ

VALUE	CL%	DOCUMENT ID		TECN	COMMENT
$<4.8 \times 10^{-4}$	95	[1] AABOUD	18AU	ATLS	pp, 13 TeV

• • • We do not use the following data for averages, fits, limits, etc. • • •

$<1.4 \times 10^{-3}$	95	[2] AABOUD	16K	ATLS	pp, 13 TeV

[1] AABOUD 18AU use 35.6 fb^{-1} of pp collision data at 13 TeV.
[2] AABOUD 16K use 2.7 fb^{-1} of pp collision data at 13 TeV.

$\Gamma(e\mu)/\Gamma_{total}$ — Γ_{23}/Γ

VALUE	CL%	DOCUMENT ID		TECN	COMMENT
$<6.1 \times 10^{-5}$	95	[1] AAD	20F	ATLS	pp, 13 TeV

• • • We do not use the following data for averages, fits, limits, etc. • • •

$<3.5 \times 10^{-4}$	95	[2] KHACHATRY...	16CD	CMS	pp, 8 TeV

[1] AAD 20F use 139 fb^{-1} of pp collisions at E_{cm} = 13 TeV. The best-fit value of the $H^0 \to e\mu$ branching fraction is $(0.4 \pm 2.9 \pm 0.3) \times 10^{-5}$ for m_{H^0} = 125 GeV.
[2] KHACHATRYAN 16CD search for $H^0 \to e\mu$ in 19.7 fb^{-1} of pp collisions at E_{cm} = 8 TeV. The limit constrains the $Y_{e\mu}$ Yukawa coupling to $\sqrt{|Y_{e\mu}|^2 + |Y_{\mu e}|^2} < 5.4 \times 10^{-4}$ at 95% CL (see their Fig. 6).

$\Gamma(e\tau)/\Gamma_{total}$ — Γ_{24}/Γ

VALUE	CL%	DOCUMENT ID		TECN	COMMENT
$< 2.2 \times 10^{-3}$	95	[1] SIRUNYAN	21Z	CMS	pp, 13 TeV

• • • We do not use the following data for averages, fits, limits, etc. • • •

$< 4.7 \times 10^{-3}$	95	[2] AAD	20A	ATLS	pp, 13 TeV
$< 6.1 \times 10^{-3}$	95	[3] SIRUNYAN	18BH	CMS	pp, 13 TeV
$<10.4 \times 10^{-3}$	95	[4] AAD	17	ATLS	pp, 8 TeV
$< 6.9 \times 10^{-3}$	95	[5] KHACHATRY...	16CD	CMS	pp, 8 TeV

[1] SIRUNYAN 21Z search for $H^0 \to e\tau$ in 137 fb^{-1} of pp collisions at E_{cm} = 13 TeV. The limit constrains the $Y_{e\tau}$ Yukawa coupling to $\sqrt{|Y_{e\tau}|^2 + |Y_{\tau e}|^2} < 1.35 \times 10^{-3}$ at 95% CL (see their Fig. 8).
[2] AAD 20A search for $H^0 \to e\tau$ in 36.1 fb^{-1} of pp collisions at E_{cm} = 13 TeV. The limit constrains the $Y_{e\tau}$ Yukawa coupling to $\sqrt{|Y_{e\tau}|^2 + |Y_{\tau e}|^2} < 2.0 \times 10^{-3}$ at 95% CL (see their Fig. 5).
[3] SIRUNYAN 18BH search for $H^0 \to e\tau$ in 35.9 fb^{-1} of pp collisions at E_{cm} = 13 TeV. The limit constrains the $Y_{e\tau}$ Yukawa coupling to $\sqrt{|Y_{e\tau}|^2 + |Y_{\tau e}|^2} < 2.26 \times 10^{-3}$ at 95% CL (see their Fig. 10).
[4] AAD 17 search for $H^0 \to e\tau$ in 20.3 fb^{-1} of pp collisions at E_{cm} = 8 TeV.
[5] KHACHATRYAN 16CD search for $H^0 \to e\tau$ in 19.7 fb^{-1} of pp collisions at E_{cm} = 8 TeV. The limit constrains the $Y_{e\tau}$ Yukawa coupling to $\sqrt{|Y_{e\tau}|^2 + |Y_{\tau e}|^2} < 2.4 \times 10^{-3}$ at 95% CL (see their Fig. 6).

$\Gamma(\mu\tau)/\Gamma_{total}$ — Γ_{25}/Γ

VALUE	CL%	DOCUMENT ID		TECN	COMMENT
$< 1.5 \times 10^{-3}$	95	[1] SIRUNYAN	21Z	CMS	pp, 13 TeV

• • • We do not use the following data for averages, fits, limits, etc. • • •

$< 2.8 \times 10^{-3}$	95	[2] AAD	20A	ATLS	pp, 13 TeV
$<26 \times 10^{-2}$	95	[3] AAIJ	18AM	LHCB	pp, 8 TeV
$< 2.5 \times 10^{-3}$	95	[4] SIRUNYAN	18BH	CMS	pp, 13 TeV
$< 1.43 \times 10^{-2}$	95	[5] AAD	17	ATLS	pp, 8 TeV
$< 1.51 \times 10^{-2}$	95	[6] KHACHATRY...	15Q	CMS	pp, 8 TeV

[1] SIRUNYAN 21Z search for $H^0 \to \mu\tau$ in 137 fb^{-1} of pp collisions at E_{cm} = 13 TeV. The limit constrains the $Y_{\mu\tau}$ Yukawa coupling to $\sqrt{|Y_{\mu\tau}|^2 + |Y_{\tau\mu}|^2} < 1.11 \times 10^{-3}$ at 95% CL (see their Fig. 8).
[2] AAD 20A search for $H^0 \to \mu\tau$ in 36.1 fb^{-1} of pp collisions at E_{cm} = 13 TeV. The limit constrains the $Y_{\mu\tau}$ Yukawa coupling to $\sqrt{|Y_{\mu\tau}|^2 + |Y_{\tau\mu}|^2} < 1.5 \times 10^{-3}$ at 95% CL (see their Fig. 5).
[3] AAIJ 18AM search for $H^0 \to \mu\tau$ in 2.0 fb^{-1} of pp collisions at E_{cm} = 8 TeV. The limit constrains the $Y_{\mu\tau}$ Yukawa coupling to $\sqrt{|Y_{\mu\tau}|^2 + |Y_{\tau\mu}|^2} < 1.7 \times 10^{-2}$ at 95% CL assuming SM production cross sections.
[4] SIRUNYAN 18BH search for $H^0 \to \mu\tau$ in 35.9 fb^{-1} of pp collisions at E_{cm} = 13 TeV. The limit constrains the $Y_{\mu\tau}$ Yukawa coupling to $\sqrt{|Y_{\mu\tau}|^2 + |Y_{\tau\mu}|^2} < 1.43 \times 10^{-3}$ at 95% CL (see their Fig. 10).
[5] AAD 17 search for $H^0 \to \mu\tau$ in 20.3 fb^{-1} of pp collisions at E_{cm} = 8 TeV.
[6] KHACHATRYAN 15Q search for $H^0 \to \mu\tau$ with τ decaying electronically or hadronically in 19.7 fb^{-1} of pp collisions at E_{cm} = 8 TeV. The fit gives $B(H^0 \to \mu\tau) = (0.84^{+0.39}_{-0.37})\%$ with a significance of 2.4 σ.

$\Gamma(\text{invisible})/\Gamma_{total}$ — Γ_{26}/Γ

Invisible final states.

VALUE	CL%	DOCUMENT ID		TECN	COMMENT
<0.26	95	[1] AABOUD	19AL	ATLS	pp, 7, 8, 13 TeV, $H \to$ inv
<0.19	95	[2] SIRUNYAN	19BO	CMS	pp, 7, 8, 13 TeV

• • • We do not use the following data for averages, fits, limits, etc. • • •

<0.34	95	[3] AAD	21F	ATLS	pp, 13 TeV
<0.29	95	[4] SIRUNYAN	21A	CMS	$pp \to ZH^0$, $H^0 \to$ inv, 13 TeV
<0.278	95	[5] TUMASYAN	21D	CMS	pp, 13 TeV
<0.37	95	[6] AABOUD	19AI	ATLS	$pp \to qqH^0X$, $H^0 \to$ inv, 13 TeV
<0.38	95	[7] AABOUD	19AL	ATLS	pp, 13 TeV, $H \to$ inv
<0.22	95	[8] SIRUNYAN	19AT	CMS	pp, 13 TeV, $H \to$ inv
<0.33	95	[9] SIRUNYAN	19BO	CMS	$pp \to qqH^0X$, $H^0 \to$ inv, 13 TeV
<0.26	95	[10] SIRUNYAN	19BO	CMS	pp, 13 TeV
<0.67	95	[11] AABOUD	18	ATLS	$pp \to H^0ZX$, $H^0 \to$ inv., 13 TeV
<0.83	95	[12] AABOUD	18CA	ATLS	$pp \to H^0W/Z$, $W/Z \to jj$, 13 TeV
<0.40	95	[13] SIRUNYAN	18BV	CMS	$pp \to Z(\ell\ell)H^0$, $H^0 \to$ inv, 13 TeV
<0.53	95	[14] SIRUNYAN	18S	CMS	pp, 13 TeV, jet or $V(\to q\overline{q})$, $H^0 \to$ inv
<0.46	95	[15] AABOUD	17BD	ATLS	$pp \to gH^0X$, qqH^0X, $H^0 \to$ inv, 13 TeV
<0.24	95	[16] KHACHATRY...	17F	CMS	pp, 7, 8, 13 TeV
<0.28	95	[17] AAD	16AF	ATLS	$pp \to qqH^0X$, 8 TeV
<0.34	95	[18] AAD	16AN	LHC	pp, 7, 8 TeV
<0.78	95	[19] AAD	15BD	ATLS	$pp \to H^0W/ZX$, 8 TeV
<0.25	95	[20] AAD	15CX	ATLS	pp, 7, 8 TeV, $H \to$ inv
<0.75	95	[21] AAD	14O	ATLS	$pp \to H^0ZX$, 7, 8 TeV
<0.58	95	[22] CHATRCHYAN	14B	CMS	$pp \to H^0ZX$, qqH^0X
<0.81	95	[23] CHATRCHYAN	14B	CMS	$pp \to H^0ZX$, 7, 8 TeV
<0.65	95	[24] CHATRCHYAN	14B	CMS	$pp \to qqH^0X$, 8 TeV

[1] AABOUD 19AL combine results of 7, 8 (AAD 15CX), and 13 TeV for H^0 decaying to invisible final states.
[2] SIRUNYAN 19BO combine 13 TeV 35.9 fb^{-1} results with 7, 8, 13 TeV (KHACHATRYAN 17F) for H^0 decaying to invisible final states. The quoted limit on the branching ratio is given for m_{H^0} = 125.09 GeV and assumes the Standard Model production rates. The branching ratio is obtained to be 0.05 ± 0.03 (stat) ±0.07(syst).
[3] AAD 21F search for an invisibly decaying Higgs boson with an energetic jet (p_T > 150 GeV) and missing transverse momentum (> 200 GeV) in 139 fb^{-1} at E_{cm} = 13 TeV. The quoted limit on the branching ratio is given for m_{H^0} = 125 GeV.
[4] SIRUNYAN 21A search for H^0 decaying to invisible final states associated with a Z decaying $ee/\mu\mu$ using 137 fb^{-1} at 13 TeV. The limit is obtained for m_{H^0} = 125 GeV and assuming the SM ZH^0 production cross section.
[5] TUMASYAN 21D search for H^0 decaying to invisible final states associated with an energetic jet or a V, $V \to q\overline{q}$ using 101 fb^{-1} at 13 TeV and the result is combined with SIRUNYAN 18S.
[6] AABOUD 19AI search for $pp \to qqH^0X$ (VBF) with H^0 decaying to invisible final states using 36.1 fb^{-1} of data. The quoted limit on the branching ratio is given for m_{H^0} = 125 GeV and assumes the Standard Model rates for VBF and gluon-fusion production.
[7] AABOUD 19AL combine results of H^0 decaying to invisible final states with VBF(AABOUD 19AI), ZH, and WH productions (AABOUD 18, AABOUD 18CA), which use 36.1 fb^{-1} of data at 13 TeV. The quoted limit is given for m_{H^0} = 125 GeV and assumes the Standard Model rates for gluon fusion, VBF, ZH, and WH productions.

Downloaded from https://academic.oup.com/ptep/article/2022/8/083C01/6651666 by KIT Library user on 27 September 2022

[8] SIRUNYAN 19AT perform a combined fit with visible decay using 35.9 fb^{-1} of data at 13 TeV.

[9] SIRUNYAN 19BO search for $pp \rightarrow qqH^0X$ (VBF) with H^0 decaying to invisible final states using 35.9 fb^{-1} of data. The quoted limit on the branching ratio is given for $m_{H^0} = 125.09$ GeV and assumes the Standard Model production rates.

[10] SIRUNYAN 19BO combine the VBF channel with results of other 13 TeV analyses: SIRUNYAN 18BV and SIRUNYAN 18S. The quoted limit on the branching ratio is given for $m_{H^0} = 125.09$ GeV and assumes the Standard Model production rates.

[11] AABOUD 18 search for $pp \rightarrow H^0ZX$, $Z \rightarrow ee$, $\mu\mu$ with H^0 decaying to invisible final states in 36.1 fb^{-1} at $E_{cm} = 13$ TeV. The quoted limit on the branching ratio is given for $m_{H^0} = 125$ GeV and assumes the Standard Model rate for H^0Z production.

[12] AABOUD 18CA search for H^0 decaying to invisible final states using WH, and ZH productions, where W and Z hadronically decay. The data of 36.1 fb^{-1} at $E_{cm} = 13$ TeV is used. The quoted limit assumes SM production cross sections with combining the contributions from WH, ZH, ggF and VBF production modes.

[13] SIRUNYAN 18BV search for H^0 decaying to invisible final states associated with a Z, $Z \rightarrow \ell\ell$ using 35.9 fb^{-1} at 13 TeV.The limit is obtained for $m_{H^0} = 125$ GeV and assuming the SM ZH^0 production cross section.

[14] SIRUNYAN 18S search for H^0 decaying to invisible final states associated with an energetic jet or a V, $V \rightarrow q\overline{q}$ using 35.9 fb^{-1} at 13 TeV.

[15] AABOUD 17BD search for H^0 decaying to invisible final states with ≥ 1 jet and VBF events using 3.2 fb^{-1} of pp collisions at $E_{cm} = 13$ TeV. A cross-section ratio R^{miss} is used in the measurement. The quoted limit is given for $m_{H^0} = 125$ GeV.

[16] KHACHATRYAN 17F search for H^0 decaying to invisible final states with gluon fusion, VBF, ZH, and WH productions using 2.3 fb^{-1} of pp collisions at $E_{cm} = 13$ TeV, 19.7 fb^{-1} at 8 TeV, and 5.1 fb^{-1} at 7 TeV. The quoted limit is given for $m_{H^0} = 125$ GeV and assumes the Standard Model rates for gluon fusion, VBF, ZH, and WH productions.

[17] AAD 16AF search for $pp \rightarrow qqH^0X$ (VBF) with H^0 decaying to invisible final states in 20.3 fb^{-1} at $E_{cm} = 8$ TeV. The quoted limit on the branching ratio is given for $m_{H^0} = 125$ GeV and assumes the Standard Model rates for VBF and gluon-fusion production.

[18] AAD 16AN perform fits to the ATLAS and CMS data at $E_{cm} = 7$ and 8 TeV. The branching fraction of decays into BSM particles that are invisible or into undetected decay modes is measured for $m_{H^0} = 125.09$ GeV.

[19] AAD 15BD search for $pp \rightarrow H^0WX$ and $pp \rightarrow H^0ZX$ with W or Z decaying hadronically and H^0 decaying to invisible final states using data at $E_{cm} = 8$ TeV. The quoted limit is given for $m_{H^0} = 125$ GeV, assumes the Standard Model rates for the production processes and is based on a combination of the contributions from H^0W, H^0Z and the gluon-fusion process.

[20] AAD 15CX search for H^0 decaying to invisible final states with VBF, ZH, and WH productions using 20.3 fb^{-1} at 8 TeV, and 4.7 fb^{-1} at 7 TeV. The quoted limit is given for $m_{H^0} = 125.36$ GeV and assumes the Standard Model rates for gluon fusion, VBF, ZH, and WH productions. The upper limit is improved to 0.23 by adding the measured visible decay rates.

[21] AAD 14O search for $pp \rightarrow H^0ZX$, $Z \rightarrow \ell\ell$, with H^0 decaying to invisible final states in 4.5 fb^{-1} at $E_{cm} = 7$ TeV and 20.3 fb^{-1} at $E_{cm} = 8$ TeV. The quoted limit on the branching ratio is given for $m_{H^0} = 125.5$ GeV and assumes the Standard Model rate for H^0Z production.

[22] CHATRCHYAN 14B search for $pp \rightarrow H^0ZX$, $Z \rightarrow \ell\ell$ and $Z \rightarrow b\overline{b}$, and also $pp \rightarrow qqH^0X$ with H^0 decaying to invisible final states using data at $E_{cm} = 7$ and 8 TeV. The quoted limit on the branching ratio is obtained from a combination of the limits from H^0Z and qqH^0. It is given for $m_{H^0} = 125$ GeV and assumes the Standard Model rates for the two production processes.

[23] CHATRCHYAN 14B search for $pp \rightarrow H^0ZX$ with H^0 decaying to invisible final states and $Z \rightarrow \ell\ell$ in 4.9 fb^{-1} at $E_{cm} = 7$ TeV and 19.7 fb^{-1} at $E_{cm} = 8$ TeV, and also with $Z \rightarrow b\overline{b}$ in 18.9 fb^{-1} at $E_{cm} = 8$ TeV. The quoted limit on the branching ratio is given for $m_{H^0} = 125$ GeV and assumes the Standard Model rate for H^0Z production.

[24] CHATRCHYAN 14B search for $pp \rightarrow qqH^0X$ (vector boson fusion) with H^0 decaying to invisible final states in 19.5 fb^{-1} at $E_{cm} = 8$ TeV. The quoted limit on the branching ratio is given for $m_{H^0} = 125$ GeV and assumes the Standard Model rate for qqH^0 production.

$\Gamma(\gamma\text{invisible})/\Gamma_{total}$ — Γ_{27}/Γ

VALUE	CL%	DOCUMENT ID		TECN	COMMENT
<0.029	95	[1,2] SIRUNYAN	21L	CMS	VBF, H^0Z, $H^0 \rightarrow \gamma +$ invisible, 13 TeV
• • • We do not use the following data for averages, fits, limits, etc. • • •					
<0.035	95	[1] SIRUNYAN	21L	CMS	VBF, $H^0 \rightarrow \gamma +$ invisible, 13 TeV
<0.046	95	[3] SIRUNYAN	19CG	CMS	$pp \rightarrow H^0Z$, $H^0 \rightarrow \gamma +$ invisible, $Z \rightarrow \ell\ell$, 13 TeV

[1] SIRUNYAN 21L search for H^0 decaying to an invisible final state plus a γ in the VBF production using 130 fb^{-1} data at $E_{cm} = 13$ TeV. The invisible state is called a dark photon. The quoted limit on the branching ratio is given for $m_{H^0} = 125$ GeV assuming the Standard Model rates.

[2] The result of the VBF production is combined with the $pp \rightarrow H^0Z$ result (SIRUNYAN 19CG).

[3] SIRUNYAN 19CG search for $pp \rightarrow H^0Z$, $Z \rightarrow ee$, $\mu\mu$ with H^0 decaying to invisible final states plus a γ in 137 fb^{-1} at $E_{cm} = 13$ TeV. The quoted limit on the branching ratio is given for $m_{H^0} = 125$ GeV assuming the Standard Model rate for H^0Z production and is obtained in the context of a theoretical model, where the undetected (invisible) particle is massless.

H^0 SIGNAL STRENGTHS IN DIFFERENT CHANNELS

The H^0 signal strength in a particular final state xx is given by the cross section times branching ratio in this channel normalized to the Standard Model (SM) value, $\sigma \cdot B(H^0 \rightarrow xx) / (\sigma \cdot B(H^0 \rightarrow xx))_{SM}$, for the specified mass value of H^0. For the SM predictions, see DITTMAIER 11, DITTMAIER 12, and HEINEMEYER 13A. Results for fiducial and differential cross sections are also listed below.

Combined Final States

VALUE	DOCUMENT ID		TECN	COMMENT
1.13±0.06 OUR AVERAGE				
$1.11^{+0.09}_{-0.08}$	[1] AAD	20	ATLS	pp, 13 TeV
1.17 ± 0.10	[2] SIRUNYAN	19AT	CMS	pp, 13 TeV
$1.09 \pm 0.07 \pm 0.04 \pm 0.03^{+0.07}_{-0.06}$	[3,4] AAD	16AN	LHC	pp, 7, 8 TeV
$1.44^{+0.59}_{-0.56}$	[5] AALTONEN	13M	TEVA	$p\overline{p} \rightarrow H^0X$, 1.96 TeV
• • • We do not use the following data for averages, fits, limits, etc. • • •				
	[6] SIRUNYAN	19BA	CMS	pp, 13 TeV, diferential cross sections
$1.20 \pm 0.10 \pm 0.06 \pm 0.04^{+0.08}_{-0.07}$	[4] AAD	16AN	ATLS	pp, 7, 8 TeV
$0.97 \pm 0.09 \pm 0.05^{+0.04}_{-0.03}{}^{+0.07}_{-0.06}$	[4] AAD	16AN	CMS	pp, 7, 8 TeV
$1.18 \pm 0.10 \pm 0.07^{+0.08}_{-0.07}$	[7] AAD	16K	ATLS	pp, 7, 8 TeV
$0.75^{+0.28}_{-0.26}{}^{+0.13}_{-0.11}{}^{+0.08}_{-0.05}$	[7] AAD	16K	ATLS	pp, 7 TeV
$1.28 \pm 0.11^{+0.08}_{-0.07}{}^{+0.10}_{-0.08}$	[7] AAD	16K	ATLS	pp, 8 TeV
	[8] AAD	15P	ATLS	pp, 8 TeV, cross section
$1.00 \pm 0.09 \pm 0.07^{+0.08}_{-0.07}$	[9] KHACHATRY...	15AM	CMS	pp, 7, 8 TeV
$1.33^{+0.14}_{-0.10} \pm 0.15$	[10] AAD	13AK	ATLS	pp, 7 and 8 TeV
$1.54^{+0.77}_{-0.73}$	[11] AALTONEN	13L	CDF	$p\overline{p} \rightarrow H^0X$, 1.96 TeV
$1.40^{+0.92}_{-0.88}$	[12] ABAZOV	13L	D0	$p\overline{p} \rightarrow H^0X$, 1.96 TeV
1.4 ± 0.3	[13] AAD	12AI	ATLS	$pp \rightarrow H^0X$, 7, 8 TeV
1.2 ± 0.4	[13] AAD	12AI	ATLS	$pp \rightarrow H^0X$, 7 TeV
1.5 ± 0.4	[13] AAD	12AI	ATLS	$pp \rightarrow H^0X$, 8 TeV
0.87 ± 0.23	[14] CHATRCHYAN	12N	CMS	$pp \rightarrow H^0X$, 7, 8 TeV

[1] AAD 20 combine results of up to 79.8 fb^{-1} of data at $E_{cm} = 13$ TeV, assuming $m_{H^0} = 125.09$ GeV: $\gamma\gamma$, ZZ^*, WW^*, $\tau\tau$, $b\overline{b}$, $\mu\mu$, invisible, and off-shell analyses (see their Table I). The signal strengths for individual production processes are 1.04 ± 0.09 for gluon fusion, $1.21^{+0.24}_{-0.22}$ for vector boson fusion, $1.30^{+0.40}_{-0.38}$ for WH^0 production, $1.05^{+0.31}_{-0.29}$ for ZH^0 production, and $1.21^{+0.26}_{-0.24}$ for $t\overline{t}H^0 + tH^0$ production (see their Fig. 2 and Table IV). Several results with the simplified template cross section and κ-frameworks are presented: see their Figs. 9–11, Figs 20, 21 and Table VIII for stage-1 simplified template cross sections, their Figs. 12–17 and Tables X–XII for the κ-framework.

[2] SIRUNYAN 19AT combine results of 35.9 fb^{-1} of data at $E_{cm} = 13$ TeV, assuming $m_{H^0} = 125.09$ GeV. The signal strengths for individual production processes are $1.22^{+0.14}_{-0.12}$ for gluon fusion, $0.73^{+0.30}_{-0.27}$ for vector boson fusion, $2.18^{+0.58}_{-0.55}$ for WH^0 production, $0.87^{+0.44}_{-0.42}$ for ZH^0 production, and $1.18^{+0.30}_{-0.27}$ for $t\overline{t}H^0$ production. Several results with the simplified template cross section and κ-frameworks are presented: see their Fig. 8 and Table 5 for stage-0 simplified template cross sections, their Figs. 9–18 and Tables 7–11 for the κ-framework.

[3] AAD 16AN perform fits to the ATLAS and CMS data at $E_{cm} = 7$ and 8 TeV. The signal strengths for individual production processes are $1.03^{+0.16}_{-0.14}$ for gluon fusion, $1.18^{+0.25}_{-0.23}$ for vector boson fusion, $0.89^{+0.40}_{-0.38}$ for WH^0 production, $0.79^{+0.38}_{-0.36}$ for ZH^0 production, and $2.3^{+0.7}_{-0.6}$ for $t\overline{t}H^0$ production.

[4] AAD 16AN: The uncertainties represent statistics, experimental systematics, theory systematics on the background, and theory systematics on the signal. The quoted signal strengths are given for $m_{H^0} = 125.09$ GeV. In the fit, relative branching ratios and relative production cross sections are fixed to those in the Standard Model.

[5] AALTONEN 13M combine all Tevatron data from the CDF and D0 Collaborations with up to 10.0 fb^{-1} and 9.7 fb^{-1}, respectively, of $p\overline{p}$ collisions at $E_{cm} = 1.96$ TeV. The quoted signal strength is given for $m_{H^0} = 125$ GeV.

[6] SIRUNYAN 19BA measure differential cross sections for the Higgs boson transverse momentum, the number of jets, the rapidity of the Higgs boson and the transverse momentum of the leading jet using 35.9 fb^{-1} of data at $E_{cm} = 13$ TeV with $H^0 \rightarrow \gamma\gamma$, $H^0 \rightarrow ZZ^*$, and $H^0 \rightarrow b\overline{b}$. The total cross section for Higgs boson production is measured to be $61.1 \pm 6.0 \pm 3.7$ pb using $H^0 \rightarrow \gamma\gamma$ and $H^0 \rightarrow ZZ^*$ channels. Several coupling measurements in the κ-framework are performed.

[7] AAD 16K use up to 4.7 fb^{-1} of pp collisions at $E_{cm} = 7$ TeV and up to 20.3 fb^{-1} at $E_{cm} = 8$ TeV. The third uncertainty in the measurement is theory systematics. The signal strengths for individual production modes are $1.23 \pm 0.14^{+0.09}_{-0.08}{}^{+0.16}_{-0.12}$ for gluon fusion, $1.23^{+0.28}_{-0.27}{}^{+0.13}_{-0.12}{}^{+0.11}_{-0.09}$ for vector boson fusion, $0.80^{+0.31}_{-0.30} \pm 0.17^{+0.10}_{-0.05}$ for W/ZH^0 production, and $1.81^{+0.52}_{-0.50}{}^{+0.58}_{-0.55}{}^{+0.31}_{-0.12}$ for $t\overline{t}H^0$ production. The quoted signal strengths are given for $m_{H^0} = 125.36$ GeV.

[8] AAD 15P measure total and differential cross sections of the process $pp \rightarrow H^0X$ at $E_{cm} = 8$ TeV with 20.3 fb^{-1}. $\gamma\gamma$ and 4ℓ final states are used. $\sigma(pp \rightarrow H^0X) = 33.0 \pm 5.3 \pm 1.6$ pb is given. See their Figs. 2 and 3 for data on differential cross sections.

Downloaded from https://academic.oup.com/ptep/article/2022/8/083C01/6651666 by KIT Library user on 27 September 2022

[9] KHACHATRYAN 15AM use up to 5.1 fb^{-1} of pp collisions at E_{cm} = 7 TeV and up to 19.7 fb^{-1} at E_{cm} = 8 TeV. The third uncertainty in the measurement is theory systematics. Fits to each production mode give the value of $0.85^{+0.19}_{-0.16}$ for gluon fusion, $1.16^{+0.37}_{-0.34}$ for vector boson fusion, $0.92^{+0.38}_{-0.36}$ for WH^0, ZH^0 production, and $2.90^{+1.08}_{-0.94}$ for $t\overline{t}H^0$ production.

[10] AAD 13AK use 4.7 fb^{-1} of pp collisions at E_{cm} = 7 TeV and 20.7 fb^{-1} at E_{cm} = 8 TeV. The combined signal strength is based on the $\gamma\gamma$, $ZZ^* \rightarrow 4\ell$, and $WW^* \rightarrow \ell\nu\ell\nu$ channels. The quoted signal strength is given for m_{H^0} = 125.5 GeV. Reported statistical error value modified following private communication with the experiment.

[11] AALTONEN 13L combine all CDF results with 9.45–10.0 fb^{-1} of $p\overline{p}$ collisions at E_{cm} = 1.96 TeV. The quoted signal strength is given for m_{H^0} = 125 GeV.

[12] ABAZOV 13L combine all D0 results with up to 9.7 fb^{-1} of $p\overline{p}$ collisions at E_{cm} = 1.96 TeV. The quoted signal strength is given for m_{H^0} = 125 GeV.

[13] AAD 12AI obtain results based on 4.6–4.8 fb^{-1} of pp collisions at E_{cm} = 7 TeV and 5.8–5.9 fb^{-1} at E_{cm} = 8 TeV. An excess of events over background with a local significance of 5.9 σ is observed at m_{H^0} = 126 GeV. The quoted signal strengths are given for m_{H^0} = 126 GeV. See also AAD 12DA.

[14] CHATRCHYAN 12N obtain results based on 4.9–5.1 fb^{-1} of pp collisions at E_{cm} = 7 TeV and 5.1–5.3 fb^{-1} at E_{cm} = 8 TeV. An excess of events over background with a local significance of 5.0 σ is observed at about m_{H^0} = 125 GeV. The combined signal strength is based on the $\gamma\gamma$, ZZ^*, WW^*, $\tau^+\tau^-$, and $b\overline{b}$ channels. The quoted signal strength is given for m_{H^0} = 125.5 GeV. See also CHATRCHYAN 13Y.

WW^* Final State

VALUE	DOCUMENT ID		TECN	COMMENT
1.19±0.12 OUR AVERAGE				
$1.28^{+0.17}_{-0.16}$	[1] SIRUNYAN	19AT	CMS	pp, 13 TeV
$1.09^{+0.18}_{-0.16}$	[2,3] AAD	16AN	LHC	pp, 7, 8 TeV
$0.94^{+0.85}_{-0.83}$	[4] AALTONEN	13M	TEVA	$p\overline{p} \rightarrow H^0X$, 1.96 TeV
• • • We do not use the following data for averages, fits, limits, etc. • • •				
	[5] AABOUD	19F	ATLS	pp, 13 TeV, cross sections
$2.5\ ^{+0.9}_{-0.8}$	[6] AAD	19A	ATLS	$pp \rightarrow H^0W/H^0Z$, $H^0 \rightarrow WW^*$, 13 TeV
$1.28^{+0.18}_{-0.17}$	[7] SIRUNYAN	19AX	CMS	pp, 13 TeV
$1.22^{+0.23}_{-0.21}$	[3] AAD	16AN	ATLS	pp, 7, 8 TeV
$0.90^{+0.23}_{-0.21}$	[3] AAD	16AN	CMS	pp, 7, 8 TeV
	[8] AAD	16AO	ATLS	pp, 8 TeV, cross sections
$1.18\pm0.16^{+0.17}_{-0.14}$	[9] AAD	16K	ATLS	pp, 7, 8 TeV
$1.09^{+0.16}_{-0.15}{}^{+0.17}_{-0.14}$	[10] AAD	15AA	ATLS	pp, 7, 8 TeV
$3.0\ ^{+1.3}_{-1.1}\ ^{+1.0}_{-0.7}$	[11] AAD	15AQ	ATLS	$pp \rightarrow H^0W/ZX$, 7, 8 TeV
$1.16^{+0.16}_{-0.15}{}^{+0.18}_{-0.15}$	[12] AAD	15AQ	ATLS	pp, 7, 8 TeV
$0.72\pm0.12\pm0.10^{+0.12}_{-0.10}$	[13] CHATRCHYAN	14G	CMS	pp, 7, 8 TeV
$0.99^{+0.31}_{-0.28}$	[14] AAD	13AK	ATLS	pp, 7 and 8 TeV
$0.00^{+1.78}_{-0.00}$	[15] AALTONEN	13L	CDF	$p\overline{p} \rightarrow H^0X$, 1.96 TeV
$1.90^{+1.63}_{-1.52}$	[16] ABAZOV	13L	D0	$p\overline{p} \rightarrow H^0X$, 1.96 TeV
$1.3\ \pm0.5$	[17] AAD	12AI	ATLS	$pp \rightarrow H^0X$, 7, 8 TeV
$0.5\ \pm0.6$	[17] AAD	12AI	ATLS	$pp \rightarrow H^0X$, 7 TeV
$1.9\ \pm0.7$	[17] AAD	12AI	ATLS	$pp \rightarrow H^0X$, 8 TeV
$0.60^{+0.42}_{-0.37}$	[18] CHATRCHYAN	12N	CMS	$pp \rightarrow H^0X$, 7, 8 TeV

[1] SIRUNYAN 19AT perform a combine fit to 35.9 fb^{-1} of data at E_{cm} = 13 TeV.

[2] AAD 16AN perform fits to the ATLAS and CMS data at E_{cm} = 7 and 8 TeV. The signal strengths for individual production processes are 0.84 ± 0.17 for gluon fusion, 1.2 ± 0.4 for vector boson fusion, $1.6^{+1.2}_{-1.0}$ for WH^0 production, $5.9^{+2.6}_{-2.2}$ for ZH^0 production, and $5.0^{+1.8}_{-1.7}$ for $t\overline{t}H^0$ production.

[3] AAD 16AN: In the fit, relative production cross sections are fixed to those in the Standard Model. The quoted signal strength is given for m_{H^0} = 125.09 GeV.

[4] AALTONEN 13M combine all Tevatron data from the CDF and D0 Collaborations with up to 10.0 fb^{-1} and 9.7 fb^{-1}, respectively, of $p\overline{p}$ collisions at E_{cm} = 1.96 TeV. The quoted signal strength is given for m_{H^0} = 125 GeV.

[5] AABOUD 19F measure cross-sections times the $H^0 \rightarrow WW^*$ branching fraction in the $H^0 \rightarrow WW^* \rightarrow e\nu\mu\nu$ channel using 36.1 fb^{-1} of pp collisions at E_{cm} = 13 TeV: $\sigma_{ggF}\times B(H^0 \rightarrow WW^*) = 11.4^{+1.2}_{-1.1}{}^{+1.8}_{-1.7}$ pb and $\sigma_{VBF}\times B(H^0 \rightarrow WW^*) = 0.50^{+0.24}_{-0.22} \pm 0.17$ pb.

[6] AAD 19A use 36.1 fb^{-1} data at 13 TeV. The cross section times branching fraction values are measured to be $0.67^{+0.31}_{-0.27}{}^{+0.18}_{-0.14}$ pb for WH^0, $H^0 \rightarrow WW^*$ and $0.54^{+0.31}_{-0.24}{}^{+0.15}_{-0.07}$ pb for ZH^0, $H^0 \rightarrow WW^*$.

[7] SIRUNYAN 19AX measure the signal strengths, cross sections and so on using gluon fusion, VBF and VH^0 production processes with 35.9 fb^{-1} of data. The quoted signal strength is given for m_{H^0} = 125.09 GeV. Signal strengths for each production process is found in their Fig. 9. Measured cross sections and ratios to the SM predictions in the stage-0 simplified template cross section framework are shown in their Fig. 10. $\kappa_F = 1.52^{+0.48}_{-0.41}$ and κ_V = 1.10 ± 0.08 are obtained (see their Fig. 11 (right)).

[8] AAD 16AO measure fiducial total and differential cross sections of gluon fusion process at E_{cm} = 8 TeV with 20.3 fb^{-1} using $H^0 \rightarrow WW^* \rightarrow e\nu\mu\nu$. The measured fiducial total cross section is 36.0 ± 9.7 fb in their fiducial region (Table 7). See their Fig. 6 for fiducial differential cross sections. The results are given for m_{H^0} = 125 GeV.

[9] AAD 16K use up to 4.7 fb^{-1} of pp collisions at E_{cm} = 7 TeV and up to 20.3 fb^{-1} at E_{cm} = 8 TeV. The quoted signal strength is given for m_{H^0} = 125.36 GeV.

[10] AAD 15AA use 4.5 fb^{-1} of pp collisions at E_{cm} = 7 TeV and 20.3 fb^{-1} at E_{cm} = 8 TeV. The signal strength for the gluon fusion and vector boson fusion mode is $1.02 \pm 0.19^{+0.22}_{-0.18}$ and $1.27^{+0.44}_{-0.40}{}^{+0.30}_{-0.21}$, respectively. The quoted signal strengths are given for m_{H^0} = 125.36 GeV.

[11] AAD 15AQ use 4.5 fb^{-1} of pp collisions at E_{cm} = 7 TeV and 20.3 fb^{-1} at E_{cm} = 8 TeV. The quoted signal strength is given for m_{H^0} = 125.36 GeV.

[12] AAD 15AQ combine their result on W/ZH^0 production with the results of AAD 15AA (gluon fusion and vector boson fusion, slightly updated). The quoted signal strength is given for m_{H^0} = 125.36 GeV.

[13] CHATRCHYAN 14G use 4.9 fb^{-1} of pp collisions at E_{cm} = 7 TeV and 19.4 fb^{-1} at E_{cm} = 8 TeV. The last uncertainty in the measurement is theory systematics. The quoted signal strength is given for m_{H^0} = 125.6 GeV.

[14] AAD 13AK use 4.7 fb^{-1} of pp collisions at E_{cm} = 7 TeV and 20.7 fb^{-1} at E_{cm} = 8 TeV. The quoted signal strength is given for m_{H^0} = 125.5 GeV. Superseded by AAD 15AA.

[15] AALTONEN 13L combine all CDF results with 9.45–10.0 fb^{-1} of $p\overline{p}$ collisions at E_{cm} = 1.96 TeV. The quoted signal strength is given for m_{H^0} = 125 GeV.

[16] ABAZOV 13L combine all D0 results with up to 9.7 fb^{-1} of $p\overline{p}$ collisions at E_{cm} = 1.96 TeV. The quoted signal strength is given for m_{H^0} = 125 GeV.

[17] AAD 12AI obtain results based on 4.7 fb^{-1} of pp collisions at E_{cm} = 7 TeV and 5.8 fb^{-1} at E_{cm} = 8 TeV. The quoted signal strengths are given for m_{H^0} = 126 GeV. See also AAD 12DA.

[18] CHATRCHYAN 12N obtain results based on 4.9 fb^{-1} of pp collisions at E_{cm} = 7 TeV and 5.1 fb^{-1} at E_{cm} = 8 TeV. The quoted signal strength is given for m_{H^0} = 125.5 GeV. See also CHATRCHYAN 13Y.

ZZ^* Final State

VALUE	CL%	DOCUMENT ID		TECN	COMMENT
1.01±0.07 OUR AVERAGE					
$0.94\pm0.07^{+0.09}_{-0.08}$		[1] SIRUNYAN	21S	CMS	pp, 13 TeV
1.01 ± 0.11		[2,3] AAD	20AQ	ATLS	pp, 13 TeV
$1.29^{+0.26}_{-0.23}$		[4,5] AAD	16AN	LHC	pp, 7, 8 TeV
• • • We do not use the following data for averages, fits, limits, etc. • • •					
		[6] SIRUNYAN	21AE	CMS	pp, 13 TeV, couplings
		[2,7] AAD	20AQ	ATLS	pp, 13 TeV
		[8] AAD	20BA	ATLS	pp, 13 TeV cross sections
<6.5	95	[9] AABOUD	19N	ATLS	pp, 13 TeV, off-shell
$1.06^{+0.19}_{-0.17}$		[10] SIRUNYAN	19AT	CMS	pp, 13 TeV
$1.28^{+0.21}_{-0.19}$		[11] AABOUD	18AJ	ATLS	pp, 13 TeV
<3.8	95	[12] AABOUD	18BP	ATLS	pp, 13 TeV, off-shell
$1.05^{+0.15}_{-0.14}{}^{+0.11}_{-0.09}$		[13] SIRUNYAN	17AV	CMS	pp, 13 TeV
$1.52^{+0.40}_{-0.34}$		[5] AAD	16AN	ATLS	pp, 7, 8 TeV
$1.04^{+0.32}_{-0.26}$		[5] AAD	16AN	CMS	pp, 7, 8 TeV
$1.46^{+0.35}_{-0.31}{}^{+0.19}_{-0.13}$		[14] AAD	16K	ATLS	pp, 7, 8 TeV
		[15] KHACHATRY...	16AR	CMS	pp, 7, 8 TeV cross sections
$1.44^{+0.34}_{-0.31}{}^{+0.21}_{-0.11}$		[16] AAD	15F	ATLS	$pp \rightarrow H^0X$, 7, 8 TeV
		[17] AAD	14AR	ATLS	pp, 8 TeV, cross sections
$0.93^{+0.26}_{-0.23}{}^{+0.13}_{-0.09}$		[18] CHATRCHYAN	14AA	CMS	pp, 7, 8 TeV
$1.43^{+0.40}_{-0.35}$		[19] AAD	13AK	ATLS	pp, 7 and 8 TeV
$0.80^{+0.35}_{-0.28}$		[20] CHATRCHYAN	13J	CMS	$pp \rightarrow H^0X$, 7, 8 TeV
$1.2\ \pm0.6$		[21] AAD	12AI	ATLS	$pp \rightarrow H^0X$, 7, 8 TeV
$1.4\ \pm1.1$		[21] AAD	12AI	ATLS	$pp \rightarrow H^0X$, 7 TeV
$1.1\ \pm0.8$		[21] AAD	12AI	ATLS	$pp \rightarrow H^0X$, 8 TeV
$0.73^{+0.45}_{-0.33}$		[22] CHATRCHYAN	12N	CMS	$pp \rightarrow H^0X$, 7, 8 TeV

[1] SIRUNYAN 21S measure cross sections with the $H^0 \rightarrow ZZ^* \rightarrow 4\ell$ ($\ell = e, \mu$) channel using 137 fb^{-1} data at E_{cm} = 13 TeV. Results are given for m_{H^0} = 125.38 GeV. The signal strengths for individual production processes in their Table 4. Cross sections are given in their Table 6 and Fig. 14, which are based on the simplified template cross section framework (reduced stage-1.2).

[2] AAD 20AQ perform analyses using $H^0 \rightarrow ZZ^* \rightarrow 4\ell$ ($\ell = e, \mu$) with data of 139 fb^{-1} at E_{cm} = 13 TeV. Results are given for m_{H^0} = 125 GeV.

[3] AAD 20AQ measured the inclusive cross section times branching ratio for $H^0 \rightarrow ZZ^*$ decay ($|y(H^0)| < 2.5$) to be 1.34 ± 0.12 pb (with 1.33 ± 0.08 pb expected in the SM).

[4] AAD 16AN perform fits to the ATLAS and CMS data at E_{cm} = 7 and 8 TeV. The signal strengths for individual production processes are $1.13^{+0.34}_{-0.31}$ for gluon fusion and $0.1^{+1.1}_{-0.6}$ for vector boson fusion.

[5] AAD 16AN: In the fit, relative production cross sections are fixed to those in the Standard Model. The quoted signal strength is given for m_{H^0} = 125.09 GeV.

Downloaded from https://academic.oup.com/ptep/article/2022/8/083C01/6651666 by KIT Library user on 27 September 2022

[6] SIRUNYAN 21AE obtains constraints on anomalous couplings to vector bosons (W, Z, and gluon) and top quark using $H^0 \to ZZ^* \to 4\ell$ ($\ell = e, \mu$) with data of 137 fb^{-1} at E_{cm} = 13 TeV. Their Table 5 and Figs 14–17 show (effective) couplings to gluon and top with combining gluon fusion, $t\overline{t}H^0$ and tH^0 production channels and the result of $t\overline{t}H^0$, $H^0 \to \gamma\gamma$ (SIRUNYAN 20AS). Their Tables 6–9 and Figs 18–22 show couplings to W and Z for different assumptions and bases (Higgs and Warsaw).

[7] AAD 20AQ present several results for the channel $H^0 \to ZZ^* \to 4\ell$ ($\ell = e, \mu$) with the simplified template cross section with κ-frameworks and the effective field theory (EFT) approach; see their Table 8 and Fig. 10 for simplified template cross sections. κ_V = 1.02 ± 0.06 and κ_F = 0.88 ± 0.16 are obtained, see their Fig. 12 for the κ-framework. See their Tables 9 and 10 and Figs. 16–18 for the EFT-framework.

[8] AAD 20BA measure the cross section for $pp \to H^0 \to ZZ^* \to 4\ell$ ($\ell = e, \mu$) using 139 fb^{-1} at E_{cm} = 13 TeV. They give $\sigma \cdot B$ = 3.28 ± 0.30 ± 0.11 fb in their fiducial region, where 3.41 ± 0.18 fb is expected in the Standard Model for m_{H^0} = 125 GeV. Various differential cross sections are also given; see their Figs. 19-39. Constraints on Yukawa couplings for bottom and charm quarks are given in their Table 9 and Fig. 41.

[9] AABOUD 19N measure the spectrum of the four-lepton invariant mass $m_{4\ell}$ ($\ell = e$ or μ) using 36.1 fb^{-1} of data at E_{cm} = 13 TeV. The quoted signal strength upper limit is obtained from 180 GeV < $m_{4\ell}$ < 1200 GeV.

[10] SIRUNYAN 19AT perform a combine fit to 35.9 fb^{-1} of data at E_{cm} = 13 TeV.

[11] AABOUD 18AJ perform analyses using $H^0 \to ZZ^* \to 4\ell$ ($\ell = e, \mu$) with data of 36.1 fb^{-1} at E_{cm} = 13 TeV. Results are given for m_{H^0} = 125.09 GeV. The inclusive cross section times branching ratio for $H^0 \to ZZ^*$ decay ($|\eta(H^0)| < 2.5$) is measured to be $1.73^{+0.26}_{-0.24}$ pb (with $1.34^{+0.09}_{-0.09}$ pb expected in the SM).

[12] AABOUD 18BP measure an off-shell Higgs boson production using $ZZ \to 4\ell$ and $ZZ \to 2\ell 2\nu$ ($\ell = e, \mu$) decay channels with 36.1 fb^{-1} of data at E_{cm} = 13 TeV. The quoted signal strength upper limit is obtained from a combination of these two channels, where 220 GeV < $m_{4\ell}$ < 2000 GeV for $ZZ \to 4\ell$ and 250 GeV < m_T^{ZZ} < 2000 GeV for $ZZ \to 2\ell 2\nu$ (m_T^{ZZ} is defined in their Section 5). See their Table 2 for each measurement.

[13] SIRUNYAN 17AV use 35.9 fb^{-1} of pp collisions at E_{cm} = 13 TeV. The quoted signal strength, obtained from the analysis of $H^0 \to ZZ^* \to 4\ell$ ($\ell = e, \mu$) decays, is given for m_{H^0} = 125.09 GeV. The signal strengths for different production modes are given in their Table 3. The fiducial and differential cross sections are shown in their Fig. 10.

[14] AAD 16K use up to 4.7 fb^{-1} of pp collisions at E_{cm} = 7 TeV and up to 20.3 fb^{-1} at E_{cm} = 8 TeV. The quoted signal strength is given for m_{H^0} = 125.36 GeV.

[15] KHACHATRYAN 16AR use data of 5.1 fb^{-1} at E_{cm} = 7 TeV and 19.7 fb^{-1} at 8 TeV. The fiducial cross sections for the production of 4 leptons via $H^0 \to 4\ell$ decays are measured to be $0.56^{+0.67}_{-0.44}{}^{+0.21}_{-0.06}$ fb at 7 TeV and $1.11^{+0.41}_{-0.35}{}^{+0.14}_{-0.10}$ fb at 8 TeV in their fiducial region (Table 2). The differential cross sections at E_{cm} = 8 TeV are also shown in Figs. 4 and 5. The results are given for m_{H^0} = 125 GeV.

[16] AAD 15F use 4.5 fb^{-1} of pp collisions at E_{cm} = 7 TeV and 20.3 fb^{-1} at E_{cm} = 8 TeV. The quoted signal strength is given for m_{H^0} = 125.36 GeV. The signal strength for the gluon fusion production mode is $1.66^{+0.45}_{-0.41}{}^{+0.25}_{-0.15}$, while the signal strength for the vector boson fusion production mode is $0.26^{+1.60}_{-0.91}{}^{+0.36}_{-0.23}$.

[17] AAD 14AR measure the cross section for $pp \to H^0 \to ZZ^* \to 4\ell$ ($\ell = e, \mu$) using 20.3fb^{-1} at E_{cm} = 8 TeV. They give $\sigma \cdot B = 2.11^{+0.53}_{-0.47}$ ± 0.08 fbin their fiducial region, where 1.30 ± 0.13 fb is expected in the Standard Model for m_{H^0}= 125.4 GeV. Various differential cross sections are also given; see their Fig. 2.

[18] CHATRCHYAN 14AA use 5.1 fb^{-1} of pp collisions at E_{cm} = 7 TeV and 19.7 fb^{-1} at E_{cm} = 8 TeV. The quoted signal strength is given for m_{H^0} = 125.6 GeV. The signal strength for the gluon fusion and $t\overline{t}H$ production mode is $0.80^{+0.46}_{-0.36}$, while the signal strength for the vector boson fusion and WH^0, ZH^0 production mode is $1.7^{+2.2}_{-2.1}$.

[19] AAD 13AK use 4.7 fb^{-1} of pp collisions at E_{cm} = 7 TeV and 20.7 fb^{-1} at E_{cm} = 8 TeV. The quoted signal strength is given for m_{H^0} = 125.5 GeV.

[20] CHATRCHYAN 13J obtain results based on $ZZ \to 4\ell$ final states in 5.1 fb^{-1} of pp collisions at E_{cm} = 7 TeV and 12.2 fb^{-1} at E_{cm} = 8 TeV. The quoted signal strength is given for m_{H^0} = 125.8 GeV. Superseded by CHATRCHYAN 14AA.

[21] AAD 12AI obtain results based on 4.7–4.8 fb^{-1} of pp collisions at E_{cm} = 7 TeV and 5.8 fb^{-1} at E_{cm} = 8 TeV. The quoted signal strengths are given for m_{H^0} = 126 GeV. See also AAD 12DA.

[22] CHATRCHYAN 12N obtain results based on 4.9–5.1 fb^{-1} of pp collisions at E_{cm} = 7 TeV and 5.1–5.3 fb^{-1} at E_{cm} = 8 TeV. An excess of events over background with a local significance of 5.0 σ is observed at about m_{H^0} = 125 GeV. The quoted signal strengths are given for m_{H^0} = 125.5 GeV. See also CHATRCHYAN 12BY and CHATRCHYAN 13Y.

$\gamma\gamma$ Final State

VALUE	DOCUMENT ID		TECN	COMMENT
1.10±0.07 OUR AVERAGE				
1.12±0.09	[1] SIRUNYAN	21O	CMS	pp, 13 TeV
$0.99^{+0.15}_{-0.14}$	[2] AABOUD	18BO	ATLS	pp, 13 TeV, 36.1 fb^{-1}
$1.14^{+0.19}_{-0.18}$	[3,4] AAD	16AN	LHC	pp, 7, 8 TeV
$5.97^{+3.39}_{-3.12}$	[5] AALTONEN	13M	TEVA	$p\overline{p} \to H^0 X$, 1.96 TeV
• • • We do not use the following data for averages, fits, limits, etc. • • •				
$1.20^{+0.18}_{-0.14}$	[6] SIRUNYAN	19AT	CMS	pp, 13 TeV
	[7] SIRUNYAN	19L	CMS	pp, 13 TeV, diff. x-section
$1.18^{+0.17}_{-0.14}$	[8] SIRUNYAN	18DS	CMS	pp, $H^0 \to \gamma\gamma$, 13 TeV, floated m_{H^0}
$1.14^{+0.27}_{-0.25}$	[4] AAD	16AN	ATLS	pp, 7, 8 TeV
$1.11^{+0.25}_{-0.23}$	[4] AAD	16AN	CMS	pp, 7, 8 TeV
	[9] KHACHATRY...	16G	CMS	pp, 8 TeV, diff. x-section
$1.17\pm0.23^{+0.10}_{-0.08}{}^{+0.12}_{-0.08}$	[10] AAD	14BC	ATLS	$pp \to H^0 X$, 7, 8 TeV
	[11] AAD	14BJ	ATLS	pp, 8 TeV, diff. x-section
$1.14\pm0.21^{+0.09}_{-0.05}{}^{+0.13}_{-0.09}$	[12] KHACHATRY...	14P	CMS	pp, 7, 8 TeV
$1.55^{+0.33}_{-0.28}$	[13] AAD	13AK	ATLS	pp, 7 and 8 TeV
$7.81^{+4.61}_{-4.42}$	[14] AALTONEN	13L	CDF	$p\overline{p} \to H^0 X$, 1.96 TeV
$4.20^{+4.60}_{-4.20}$	[15] ABAZOV	13L	D0	$p\overline{p} \to H^0 X$, 1.96 TeV
1.8 ±0.5	[16] AAD	12AI	ATLS	$pp \to H^0 X$, 7, 8 TeV
2.2 ±0.7	[16] AAD	12AI	ATLS	$pp \to H^0 X$, 7 TeV
1.5 ±0.6	[16] AAD	12AI	ATLS	$pp \to H^0 X$, 8 TeV
$1.54^{+0.46}_{-0.42}$	[17] CHATRCHYAN	12N	CMS	$pp \to H^0 X$, 7, 8 TeV

[1] SIRUNYAN 21O measures cross sections and couplings with the $H^0 \to \gamma\gamma$ channel using 137 fb^{-1} data at E_{cm} = 13 TeV. Results are given for m_{H^0} = 125.38 GeV. The signal strengths for individual production processes are given in their Fig. 16. Cross sections are given in their Tables 12 and 13 and Figs. 18 and 20, which are based on the simplified template cross section framework (reduced stage-1.2). Results in the κ-framework are given in their Fig. 22.

[2] AABOUD 18BO use 36.1 fb^{-1} of pp collisions at E_{cm} = 13 TeV. The signal strengths for the individual production modes are: $0.81^{+0.19}_{-0.18}$ for gluon fusion, $2.0^{+0.6}_{-0.5}$ for vector boson fusion, $0.7^{+0.9}_{-0.8}$ for VH^0 production ($V = W, Z$), and 0.5 ± 0.6 for $t\overline{t}H^0$ and tH^0 production. Other measurements of cross sections and couplings are summarized in their Section 10. The quoted values are given for m_{H^0} = 125.09 GeV.

[3] AAD 16AN perform fits to the ATLAS and CMS data at E_{cm} = 7 and 8 TeV. The signal strengths for individual production processes are $1.10^{+0.23}_{-0.22}$ for gluon fusion, 1.3 ± 0.5 for vector boson fusion, $0.5^{+1.3}_{-1.2}$ for WH^0 production, $0.5^{+3.0}_{-2.5}$ for ZH^0 production, and $2.2^{+1.6}_{-1.3}$ for $t\overline{t}H^0$ production.

[4] AAD 16AN: In the fit, relative production cross sections are fixed to those in the Standard Model. The quoted signal strength is given for m_{H^0} = 125.09 GeV.

[5] AALTONEN 13M combine all Tevatron data from the CDF and D0 Collaborations with up to 10.0 fb^{-1} and 9.7 fb^{-1}, respectively, of $p\overline{p}$ collisions at E_{cm} = 1.96 TeV. The quoted signal strength is given for m_{H^0} = 125 GeV.

[6] SIRUNYAN 19AT perform a combine fit to 35.9 fb^{-1} of data at E_{cm} = 13 TeV.

[7] SIRUNYAN 19L measure fiducial and differential cross sections of the process $pp \to H^0 \to \gamma\gamma$ at E_{cm} = 13 TeV with 35.9 fb^{-1}. See their Figs. 4–11.

[8] SIRUNYAN 18DS use 35.9 fb^{-1} of $pp \to H^0$ collisions with $H^0 \to \gamma\gamma$ at E_{cm} = 13 TeV. The Higgs mass is floated in the measurement of a signal strength. The result is $1.18^{+0.12}_{-0.11}$(stat.)$^{+0.09}_{-0.07}$(syst.)$^{+0.07}_{-0.06}$(theory), which is largely insensitive to the Higgs mass around 125 GeV.

[9] KHACHATRYAN 16G measure fiducial and differential cross sections of the process $pp \to H^0 X$, $H^0 \to \gamma\gamma$ at E_{cm} = 8 TeV with 19.7 fb^{-1}. See their Figs. 4–6 and Table 1 for data.

[10] AAD 14BC use 4.5 fb^{-1} of pp collisions at E_{cm} = 7 TeV and 20.3 fb^{-1} at E_{cm} = 8 TeV. The last uncertainty in the measurement is theory systematics. The quoted signal strength is given for m_{H^0} = 125.4 GeV. The signal strengths for the individual production modes are: 1.32 ± 0.38 for gluon fusion, 0.8 ± 0.7 for vector boson fusion, 1.0 ± 1.6 for WH^0 production, $0.1^{+3.7}_{-0.1}$ for ZH^0 production, and $1.6^{+2.7}_{-1.8}$ for $t\overline{t}H^0$ production.

[11] AAD 14BJ measure fiducial and differential cross sections of the process $pp \to H^0 X$, $H^0 \to \gamma\gamma$ at E_{cm} = 8 TeV with 20.3 fb^{-1}. See their Table 3 and Figs. 3–12 for data.

[12] KHACHATRYAN 14P use 5.1 fb^{-1} of pp collisions at E_{cm} = 7 TeV and 19.7 fb^{-1} at E_{cm} = 8 TeV. The last uncertainty in the measurement is theory systematics. The quoted signal strength is given for m_{H^0} = 124.7 GeV. The signal strength for the gluon fusion and $t\overline{t}H$ production mode is $1.13^{+0.37}_{-0.31}$, while the signal strength for the vector boson fusion and WH^0, ZH^0 production mode is $1.16^{+0.63}_{-0.58}$.

[13] AAD 13AK use 4.7 fb^{-1} of pp collisions at E_{cm} = 7 TeV and 20.7 fb^{-1} at E_{cm} = 8 TeV. The quoted signal strength is given for m_{H^0} = 125.5 GeV.

[14] AALTONEN 13L combine all CDF results with 9.45–10.0 fb^{-1} of $p\overline{p}$ collisions at E_{cm} = 1.96 TeV. The quoted signal strength is given for m_{H^0} = 125 GeV.

[15] ABAZOV 13L combine all D0 results with up to 9.7 fb^{-1} of $p\overline{p}$ collisions at E_{cm} = 1.96 TeV. The quoted signal strength is given for m_{H^0} = 125 GeV.

[16] AAD 12AI obtain results based on 4.8 fb^{-1} of pp collisions at E_{cm} = 7 TeV and 5.9 fb^{-1} at E_{cm} = 8 TeV. The quoted signal strengths are given for m_{H^0} = 126 GeV. See also AAD 12DA.

[17] CHATRCHYAN 12N obtain results based on 5.1 fb^{-1} of pp collisions at E_{cm}=7 TeV and 5.3 fb^{-1} at E_{cm}=8 TeV. The quoted signal strength is given for m_{H^0}=125.5 GeV. See also CHATRCHYAN 13Y.

$c\overline{c}$ Final State

VALUE	CL%	DOCUMENT ID		TECN	COMMENT
$\mathbf{37\pm17^{+11}_{-9}}$		[1] SIRUNYAN	20AE	CMS	pp, 13 TeV
• • • We do not use the following data for averages, fits, limits, etc. • • •					
<110	95	[2] AABOUD	18M	ATLS	pp, 13 TeV

[1] SIRUNYAN 20AE use 35.9 fb^{-1} at of pp collisions at E_{cm} = 13 TeV. The measured best fit value of $\sigma(pp \to VH^0)\cdot B(H^0 \to c\overline{c})$ is $2.40^{+1.12}_{-1.11}{}^{+0.65}_{-0.61}$ pb (equivalent to < 4.5 pb at 95% CL upper limit, i.e. 70 times the standard model), where V is $W \to \ell\nu$, $Z \to \ell\ell$, or $Z \to \nu\nu$ ($\ell = e, \mu$). The quoted values are given for m_{H^0} = 125 GeV.

[2] AABOUD 18M use 36.1 fb^{-1} at of pp collisions at E_{cm} = 13 TeV. The upper limit on $\sigma(pp \to ZH^0)\cdot B(H^0 \to c\overline{c})$ is 2.7 pb at 95% CL. This corresponds to 110 times the standard model. The quoted values are given for m_{H^0} = 125 GeV.

Downloaded from https://academic.oup.com/ptep/article/2022/8/083C01/6651666 by KIT Library user on 27 September 2022

$b\overline{b}$ Final State

VALUE	DOCUMENT ID		TECN	COMMENT
0.98±0.12 OUR AVERAGE				
$1.02^{+0.12}_{-0.11}{}^{+0.14}_{-0.13}$	[1] AAD	21AB	ATLS	$pp \to H^0 W/H^0 Z$, $H^0 \to b\overline{b}$, 13 TeV, 139 fb^{-1}
$0.95 \pm 0.32^{+0.20}_{-0.17}$	[2] AAD	21AJ	ATLS	VBF, $H^0 \to b\overline{b}$, pp, 13 TeV, 126 fb^{-1}
1.06 ± 0.26	[3] SIRUNYAN	18DB	CMS	$pp \to H^0 W/H^0 Z$, $H^0 \to b\overline{b}$, 13 TeV, 77.2 fb^{-1}
$0.70^{+0.29}_{-0.27}$	[4,5] AAD	16AN	LHC	pp, 7, 8 TeV
$1.59^{+0.69}_{-0.72}$	[6] AALTONEN	13M	TEVA	$p\overline{p} \to H^0 X$, 1.96 TeV
• • • We do not use the following data for averages, fits, limits, etc. • • •				
$0.95 \pm 0.18^{+0.19}_{-0.18}$	[1] AAD	21AB	ATLS	$pp \to H^0 W$, $H^0 \to b\overline{b}$, 13 TeV, 139 fb^{-1}
$1.08 \pm 0.17^{+0.18}_{-0.15}$	[1] AAD	21AB	ATLS	$pp \to H^0 Z$, $H^0 \to b\overline{b}$, 13 TeV, 139 fb^{-1}
$0.72^{+0.29}_{-0.28}{}^{+0.26}_{-0.22}$	[7] AAD	21H	ATLS	$pp \to H^0 W/H^0 Z$, $H^0 \to b\overline{b}$, boosted W/Z, 13 TeV, 139 fb^{-1}
1.3 ± 1.0	[8] AAD	21M	ATLS	VBF+γ, $H^0 \to b\overline{b}$, pp, 13 TeV, 132 fb^{-1}
$3.7 \pm 1.2^{+0.11}_{-0.9}$	[9] SIRUNYAN	20BL	CMS	boosted $H^0 \to b\overline{b}$, pp, 13 TeV
	[10] AABOUD	19U	ATLS	$pp \to VH^0$, $H^0 \to b\overline{b}$, 13 TeV, cross sections
1.12 ± 0.29	[11] SIRUNYAN	19AT	CMS	pp, 13 TeV
$1.16^{+0.27}_{-0.25}$	[12] AABOUD	18BN	ATLS	$pp \to H^0 W/H^0 Z$, $H^0 \to b\overline{b}$, 13 TeV, 79.8 fb^{-1}
$0.98^{+0.22}_{-0.21}$	[13] AABOUD	18BN	ATLS	$pp \to H^0 W/H^0 Z$, $H^0 \to b\overline{b}$, 7, 8, 13 TeV
1.01 ± 0.20	[14] AABOUD	18BN	ATLS	$pp \to H^0 X$, ggF, VBF, VH^0, $t\overline{t}H^0$ 7, 8, 13 TeV
$2.5^{+1.4}_{-1.3}$	[15,16] AABOUD	18BQ	ATLS	$pp \to H^0 X$, VBF, ggF, VH^0, $t\overline{t}H^0$, 13 TeV
$3.0^{+1.7}_{-1.6}$	[15,17] AABOUD	18BQ	ATLS	$pp \to H^0 X$, VBF, 13 TeV
	[18] AALTONEN	18C	CDF	$p\overline{p} \to H^0 X$, 1.96 TeV
$1.19^{+0.40}_{-0.38}$	[19] SIRUNYAN	18AE	CMS	$pp \to H^0 W/H^0 Z$, $H^0 \to b\overline{b}$, 13 TeV
$1.06^{+0.31}_{-0.29}$	[20] SIRUNYAN	18AE	CMS	$pp \to H^0 W/H^0 Z$, $H^0 \to b\overline{b}$, 7, 8, 13 TeV
1.01 ± 0.22	[21] SIRUNYAN	18DB	CMS	$pp \to H^0 W/H^0 Z$, $H^0 \to b\overline{b}$, 7, 8, 13 TeV
1.04 ± 0.20	[22] SIRUNYAN	18DB	CMS	$pp \to H^0 X$, ggF, VBF, VH^0, $t\overline{t}H^0$ 7, 8, 13 TeV
$2.3^{+1.8}_{-1.6}$	[23] SIRUNYAN	18E	CMS	$pp \to H^0 X$, boosted, 13 TeV
$1.20^{+0.24}_{-0.23}{}^{+0.34}_{-0.28}$	[24] AABOUD	17BA	ATLS	$pp \to H^0 W/ZX$, $H^0 \to b\overline{b}$, 13 TeV, 36.1 fb^{-1}
$0.90 \pm 0.18^{+0.21}_{-0.19}$	[25] AABOUD	17BA	ATLS	$pp \to H^0 W/ZX$, $H^0 \to b\overline{b}$, 7, 8, 13 TeV
$-0.8 \pm 1.3^{+1.8}_{-1.9}$	[26] AABOUD	16X	ATLS	$pp \to H^0 X$, VBF, 8 TeV
0.62 ± 0.37	[5] AAD	16AN	ATLS	pp, 7, 8 TeV
$0.81^{+0.45}_{-0.43}$	[5] AAD	16AN	CMS	pp, 7, 8 TeV
$0.63^{+0.31}_{-0.30}{}^{+0.24}_{-0.23}$	[27] AAD	16K	ATLS	pp, 7, 8 TeV
$0.52 \pm 0.32 \pm 0.24$	[28] AAD	15G	ATLS	$pp \to H^0 W/ZX$, 7, 8 TeV
$2.8^{+1.6}_{-1.4}$	[29] KHACHATRY...	15Z	CMS	$pp \to H^0 X$, VBF, 8 TeV
$1.03^{+0.44}_{-0.42}$	[30] KHACHATRY...	15Z	CMS	pp, 8 TeV, combined
1.0 ± 0.5	[31] CHATRCHYAN	14AI	CMS	$pp \to H^0 W/ZX$, 7, 8 TeV
$1.72^{+0.92}_{-0.87}$	[32] AALTONEN	13L	CDF	$p\overline{p} \to H^0 X$, 1.96 TeV
$1.23^{+1.24}_{-1.17}$	[33] ABAZOV	13L	D0	$p\overline{p} \to H^0 X$, 1.96 TeV
0.5 ± 2.2	[34] AAD	12AI	ATLS	$pp \to H^0 W/ZX$, 7 TeV
	[35] AALTONEN	12T	TEVA	$p\overline{p} \to H^0 W/ZX$, 1.96 TeV
$0.48^{+0.81}_{-0.70}$	[36] CHATRCHYAN	12N	CMS	$pp \to H^0 W/ZX$, 7, 8 TeV

[1] AAD 21AB search for VH^0, $H^0 \to b\overline{b}$ ($V = W, Z$) using 139 fb^{-1} of pp collision data at E_{cm} = 13 TeV. The results are given for m_{H^0} = 125 GeV. Cross sections are given in their Table 13 and Fig. 7, which are based on the simplified template cross section framework (reduced stage-1.2). Wilson coefficients of the Warsaw-basis operators are given in their Fig. 9.

[2] AAD 21AJ present measurements of $H^0 \to b\overline{b}$ in the VBF production mode. The inclusive VBF cross sections with and without the branching ratio of $H^0 \to b\overline{b}$ are $2.07 \pm 0.70^{+0.46}_{-0.37}$ fb and $3.56 \pm 1.21^{+0.80}_{-0.64}$ fb, respectively. The latter is obtained assuming the SM value of B($H^0 \to b\overline{b}$) = 0.5809 and m_{H^0} = 125 GeV.

[3] SIRUNYAN 18DB search for VH^0, $H^0 \to b\overline{b}$ ($V = W, Z$) using 77.2 fb^{-1} of pp collision data at E_{cm} = 13 TeV. The quoted signal strength corresponds to a significance of 4.4 standard deviations and is given for m_{H^0} = 125.09 GeV.

[4] AAD 16AN perform fits to the ATLAS and CMS data at E_{cm} = 7 and 8 TeV. The signal strengths for individual production processes are 1.0 ± 0.5 for WH^0 production, 0.4 ± 0.4 for ZH^0 production, and 1.1 ± 1.0 for $t\overline{t}H^0$ production.

[5] AAD 16AN: In the fit, relative production cross sections are fixed to those in the Standard Model. The quoted signal strength is given for m_{H^0} = 125.09 GeV.

[6] AALTONEN 13M combine all Tevatron data from the CDF and D0 Collaborations with up to 10.0 fb^{-1} and 9.7 fb^{-1}, respectively, of $p\overline{p}$ collisions at E_{cm} = 1.96 TeV. The quoted signal strength is given for m_{H^0} = 125 GeV.

[7] AAD 21H present measurements of $H^0 \to b\overline{b}$ with a boosted vector boson (p_T > 250 GeV) using 139 fb^{-1} of pp collision data at E_{cm} = 13 TeV. Cross sections are given in their Table 6 and Fig. 4, which are based on the simplified template cross section framework (reduced stage-1.2). Wilson coefficients of the Warsaw-basis operators are given in their Fig. 5.

[8] AAD 21M search for VBF+γ, $H^0 \to b\overline{b}$ using 132 fb^{-1} of pp collision data at E_{cm} = 13 TeV.

[9] SIRUNYAN 20BL search for boosted $H^0 \to b\overline{b}$ ($p_T(H^0)$ > 450 GeV) using 137 fb^{-1} of pp collision data at E_{cm} = 13 TeV. The quoted signal strength corresponds to a significance of 2.5 standard deviations and is given for m_{H^0} = 125 GeV. A differential cross section as a function of Higgs boson p_T for ggF is shown in their Fig. 7, assuming the other production modes occur at the expected SM rates. The reported value is $3.7 \pm 1.2^{+0.8}_{-0.7}{}^{+0.8}_{-0.5}$ where the last uncertainty comes from theoretical modeling. We have combined the systematic uncertainties in quadrature.

[10] AABOUD 19U measure cross sections of $pp \to VH^0$, $H^0 \to b\overline{b}$ production as a function of the gauge boson transverse momentum using data of 79.8 fb^{-1}. The kinematic fiducial volumes used is based on the simplified template cross section framework (reduced stage-1). See their Table 3 and Fig. 3.

[11] SIRUNYAN 19AT perform a combine fit to 35.9 fb^{-1} of data at E_{cm} = 13 TeV.

[12] AABOUD 18BN search for VH^0, $H^0 \to b\overline{b}$ ($V = W, Z$) using 79.8 fb^{-1} of pp collision data at E_{cm} = 13 TeV. The quoted signal strength corresponds to a significance of 4.9 standard deviations and is given for m_{H^0} = 125 GeV.

[13] AABOUD 18BN combine results of 79.8 fb^{-1} at E_{cm} = 13 TeV with results of VH^0 at E_{cm} = 7 and 8 TeV.

[14] AABOUD 18BN combine results of VH^0 at E_{cm} = 7, 8 and 13 TeV with results of VBF (+gluon fusion) and $t\overline{t}H^0$ at E_{cm} = 7, 8, and 13 TeV to perform a search for the $H^0 \to b\overline{b}$ decay. The quoted signal strength assumes a SM production strength and corresponds to a significance of 5.4 standard deviations.

[15] AABOUD 18BQ search for $H^0 \to b\overline{b}$ produced through vector-boson fusion (VBF) and VBF+γ with 30.6 fb^{-1} pp collision data at E_{cm} = 13 TeV. The quoted signal strength is given for m_{H^0} = 125 GeV.

[16] The signal strength is measured including all production modes (VBF, ggF, VH^0, $t\overline{t}H^0$).

[17] The signal strength is measured for VBF-only and others (ggF, VH^0, $t\overline{t}H^0$) are constrained to Standard Model expectations with uncertainties described in their Section VIII B.

[18] AALTONEN 18C use 5.4 fb^{-1} of $p\overline{p}$ collisions at E_{cm} = 1.96 TeV. The upper limit at 95% CL on $p\overline{p} \to H^0 \to b\overline{b}$ is 33 times the SM predicion, which corresponds to a cross section of 40.6 pb.

[19] SIRUNYAN 18AE use 35.9 fb^{-1} of pp collision data at E_{cm} = 13 TeV. The quoted signal strength corresponds to 3.3 standard deviations and is given for m_{H^0} = 125.09 GeV.

[20] SIRUNYAN 18AE combine the result of 35.9 fb^{-1} at E_{cm} = 13 TeV with the results obtained from data of up to 5.1 fb^{-1} at E_{cm} = 7 TeV and up to 18.9 fb^{-1} at E_{cm} = 8 TeV (CHATRCHYAN 14AI and KHACHATRYAN 15Z). The quoted signal strength corresponds to 3.8 standard deviations and is given for m_{H^0} = 125.09 GeV.

[21] SIRUNYAN 18DB combine the result of 77.2 fb^{-1} at E_{cm} = 13 TeV with the results obtained from data of up to 5.1 fb^{-1} at E_{cm} = 7 TeV and up to 18.9 fb^{-1} at E_{cm} = 8 TeV. The quoted signal strength corresponds to a significance of 4.8 standard deviations and is given for m_{H^0} = 125.09 GeV.

[22] SIRUNYAN 18DB combine results of 77.2 fb^{-1} at E_{cm} = 13 TeV with results of gluon fusion (ggF), VBF and $t\overline{t}H^0$ at E_{cm} = 7 TeV, 8 TeV and 13 TeV to perform a search for the $H^0 \to b\overline{b}$ decay. The quoted signal strength assumes a SM production strength and corresponds to a significance of 5.6 standard deviations and is given for m_{H^0} = 125.09 GeV.

[23] SIRUNYAN 18E use 35.9 fb^{-1} at E_{cm} = 13 TeV. The quoted signal strength is given for m_{H^0} = 125 GeV. They measure $\sigma \cdot B$ for gluon fusion production of $H^0 \to b\overline{b}$ with p_T >450 GeV, $|\eta|$ <2.5 to be $74 \pm 48^{+17}_{-10}$ fb.

[24] AABOUD 17BA use 36.1 fb^{-1} at E_{cm} = 13 TeV. The quoted signal strength is given for m_{H^0} = 125 GeV. They give σ(W H)$\cdot B(H^0 \to b\overline{b}) = 1.08^{+0.54}_{-0.47}$ pb and σ(Z H)$\cdot B(H^0 \to b\overline{b}) = 0.57^{+0.26}_{-0.23}$ pb.

[25] AABOUD 17BA combine 7, 8 and 13 TeV analyses. The quoted signal strength is given for m_{H^0} = 125 GeV.

[26] AABOUD 16X search for vector-boson fusion production of H^0 decaying to $b\overline{b}$ in 20.2 fb^{-1} of pp collisions at E_{cm} = 8 TeV. The quoted signal strength is given for m_{H^0} = 125 GeV.

[27] AAD 16K use up to 4.7 fb^{-1} of pp collisions at E_{cm} = 7 TeV and up to 20.3 fb^{-1} at E_{cm} = 8 TeV. The quoted signal strength is given for m_{H^0} = 125.36 GeV.

[28] AAD 15G use 4.7 fb^{-1} of pp collisions at E_{cm} = 7 TeV and 20.3 fb^{-1} at E_{cm} = 8 TeV. The quoted signal strength is given for m_{H^0} = 125.36 GeV.

[29] KHACHATRYAN 15Z search for vector-boson fusion production of H^0 decaying to $b\overline{b}$ in up to 19.8 fb^{-1} of pp collisions at E_{cm} = 8 TeV. The quoted signal strength is given for m_{H^0} = 125 GeV.

[30] KHACHATRYAN 15Z combined vector boson fusion, WH^0, ZH^0 production, and $t\overline{t}H^0$ production results. The quoted signal strength is given for m_{H^0} = 125 GeV.

[31] CHATRCHYAN 14AI use up to 5.1 fb^{-1} of pp collisions at E_{cm} = 7 TeV and up to 18.9 fb^{-1} at E_{cm} = 8 TeV. The quoted signal strength is given for m_{H^0} = 125 GeV. See also CHATRCHYAN 14AJ.

Downloaded from https://academic.oup.com/ptep/article/2022/8/083C01/6651666 by KIT Library user on 27 September 2022

[32] AALTONEN 13L combine all CDF results with 9.45–10.0 fb^{-1} of $p\overline{p}$ collisions at E_{cm} = 1.96 TeV. The quoted signal strength is given for m_{H^0} = 125 GeV.

[33] ABAZOV 13L combine all D0 results with up to 9.7 fb^{-1} of $p\overline{p}$ collisions at E_{cm} = 1.96 TeV. The quoted signal strength is given for m_{H^0} = 125 GeV.

[34] AAD 12AI obtain results based on 4.6–4.8 fb^{-1} of pp collisions at E_{cm} = 7 TeV. The quoted signal strengths are given in their Fig. 10 for m_{H^0} = 126 GeV. See also Fig. 13 of AAD 12DA.

[35] AALTONEN 12T combine AALTONEN 12Q, AALTONEN 12R, AALTONEN 12S, ABAZOV 12O, ABAZOV 12P, and ABAZOV 12K. An excess of events over background is observed which is most significant in the region m_{H^0} = 120–135 GeV, with a local significance of up to 3.3 σ. The local significance at m_{H^0} = 125 GeV is 2.8 σ, which corresponds to $(\sigma(H^0 W) + \sigma(H^0 Z)) \cdot B(H^0 \rightarrow b\overline{b}) = (0.23^{+0.09}_{-0.08})$ pb, compared to the Standard Model expectation at m_{H^0} = 125 GeV of 0.12 ± 0.01 pb. Superseded by AALTONEN 13M.

[36] CHATRCHYAN 12N obtain results based on 5.0 fb^{-1} of pp collisions at E_{cm}=7 TeV and 5.1 fb^{-1} at E_{cm}=8 TeV. The quoted signal strength is given for m_{H^0}=125.5 GeV. See also CHATRCHYAN 13Y.

$\mu^+\mu^-$ Final State

VALUE	CL%	DOCUMENT ID		TECN	COMMENT
1.19±0.34 OUR AVERAGE					
1.2 ±0.6		[1] AAD	21	ATLAS	pp, 13 TeV
$1.19^{+0.40}_{-0.39}{}^{+0.15}_{-0.14}$		[2] SIRUNYAN	21C	CMS	pp, 13 TeV
• • • We do not use the following data for averages, fits, limits, etc. • • •					
$0.68^{+1.25}_{-1.24}$		[3] SIRUNYAN	19AT	CMS	pp, 13 TeV
$0.7 \pm 1.0\ ^{+0.2}_{-0.1}$		[4] SIRUNYAN	19E	CMS	pp, 13 TeV, 35.9 fb^{-1}
1.0 ±1.0 ±0.1		[4] SIRUNYAN	19E	CMS	pp, 7, 8, 13 TeV
−0.1 ±1.4		[5] AABOUD	17Y	ATLAS	pp, 7, 8, 13 TeV
−0.1 ±1.5		[5] AABOUD	17Y	ATLAS	pp, 13 TeV
0.1 ±2.5		[6] AAD	16AN	LHC	pp, 7, 8 TeV
−0.6 ±3.6		[6] AAD	16AN	ATLAS	pp, 7, 8 TeV
$0.9\ ^{+3.6}_{-3.5}$		[6] AAD	16AN	CMS	pp, 7, 8 TeV
< 7.4	95	[7] KHACHATRY...	15H	CMS	$pp \rightarrow H^0 X$, 7, 8 TeV
< 7.0	95	[8] AAD	14AS	ATLAS	$pp \rightarrow H^0 X$, 7, 8 TeV

[1] AAD 21 search for $H^0 \rightarrow \mu^+\mu^-$ using 139 fb^{-1} of pp collision data at E_{cm} = 13 TeV. The quoted signal strength corresponds to a significance of 2.0 standard deviations and is given for m_{H^0} = 125.09 GeV. The upper limit on the cross section times branching fraction is 2.2 times the SM prediction at 95% CL, which corresponds to the branching fraction upper limit of 4.7×10^{-4} (assuming SM production cross sections).

[2] SIRUNYAN 21 search for $H^0 \rightarrow \mu^+\mu^-$ using 137 fb^{-1} of pp collision data at E_{cm} = 13 TeV. The quoted signal strength corresponds to a significance of 3.0 standard deviations and is given for m_{H^0} = 125.38 GeV.

[3] SIRUNYAN 19AT perform a combine fit to 35.9 fb^{-1} of data at E_{cm} = 13 TeV.

[4] SIRUNYAN 19E search for $H^0 \rightarrow \mu^+\mu^-$ using 35.9 fb^{-1} of pp collisions at E_{cm} = 13 TeV and combine with results of 7 TeV (5.0 fb^{-1}) and 8 TeV (19.7 fb^{-1}). The upper limit at 95% CL on the signal strength is 2.9, which corresponds to the SM Higgs boson branching fraction to a muon pair of 6.4×10^{-4}.

[5] AABOUD 17Y use 36.1 fb^{-1} of pp collisions at E_{cm} = 13 TeV, 20.3 fb^{-1} at 8 TeV and 4.5 fb^{-1} at 7 TeV. The quoted signal strength is given for m_{H^0} = 125 GeV.

[6] AAD 16AN: In the fit, relative production cross sections are fixed to those in the Standard Model. The quoted signal strength is given for m_{H^0} = 125.09 GeV.

[7] KHACHATRYAN 15H use 5.0 fb^{-1} of pp collisions at E_{cm} = 7 TeV and 19.7 fb^{-1} at 8 TeV. The quoted signal strength is given for m_{H^0} = 125 GeV.

[8] AAD 14AS search for $H^0 \rightarrow \mu^+\mu^-$ in 4.5 fb^{-1} of pp collisions at E_{cm} = 7 TeV and 20.3 fb^{-1} at E_{cm} = 8 TeV. The quoted signal strength is given for m_{H^0} = 125.5 GeV.

$\tau^+\tau^-$ Final State

VALUE	DOCUMENT ID		TECN	COMMENT
$1.15^{+0.16}_{-0.15}$ OUR AVERAGE				
$1.09^{+0.18}_{-0.17}{}^{+0.26}_{-0.22}{}^{+0.16}_{-0.11}$	[1] AABOUD	19AQ	ATLAS	pp, 13 TeV, $H \rightarrow \tau\tau$
$1.24^{+0.29}_{-0.27}$	[2] SIRUNYAN	19AF	CMS	pp, 13 TeV
$1.11^{+0.24}_{-0.22}$	[3,4] AAD	16AN	LHC	pp, 7, 8 TeV
$1.68^{+2.28}_{-1.68}$	[5] AALTONEN	13M	TEVA	$p\overline{p} \rightarrow H^0 X$, 1.96 TeV
• • • We do not use the following data for averages, fits, limits, etc. • • •				
$2.5\ ^{+1.4}_{-1.3}$	[6] SIRUNYAN	19AF	CMS	$pp \rightarrow H^0 W/H^0 Z$, $H^0 \rightarrow \tau\tau$, 13 TeV
$1.02^{+0.26}_{-0.24}$	[7] SIRUNYAN	19AT	CMS	pp, 13 TeV
$1.09^{+0.27}_{-0.26}$	[8] SIRUNYAN	18Y	CMS	pp, 13 TeV
0.98±0.18	[9] SIRUNYAN	18Y	CMS	pp, 7, 8, 13 TeV
2.3 ±1.6	[10] AAD	16AC	ATLAS	$pp \rightarrow H^0 W/ZX$, 8 TeV
$1.41^{+0.40}_{-0.36}$	[4] AAD	16AN	ATLAS	pp, 7, 8 TeV
$0.88^{+0.30}_{-0.28}$	[4] AAD	16AN	CMS	pp, 7, 8 TeV
$1.44^{+0.30}_{-0.29}{}^{+0.29}_{-0.23}$	[11] AAD	16K	ATLAS	pp, 7, 8 TeV
$1.43^{+0.27}_{-0.26}{}^{+0.32}_{-0.25} \pm 0.09$	[12] AAD	15AH	ATLAS	$pp \rightarrow H^0 X$, 7, 8 TeV
0.78±0.27	[13] CHATRCHYAN	14K	CMS	$pp \rightarrow H^0 X$, 7, 8 TeV
$0.00^{+8.44}_{-0.00}$	[14] AALTONEN	13L	CDF	$p\overline{p} \rightarrow H^0 X$, 1.96 TeV
$3.96^{+4.11}_{-3.38}$	[15] ABAZOV	13L	D0	$p\overline{p} \rightarrow H^0 X$, 1.96 TeV
$0.4\ ^{+1.6}_{-2.0}$	[16] AAD	12AI	ATLAS	$pp \rightarrow H^0 X$, 7 TeV
$0.09^{+0.76}_{-0.74}$	[17] CHATRCHYAN	12N	CMS	$pp \rightarrow H^0 X$, 7, 8 TeV

[1] AABOUD 19AQ use 36.1 fb^{-1} of data. The first, second and third quoted errors are statistical, experimental systematic and theory systematic uncertainties, respectively. The quoted signal strength is given for m_{H^0} = 125 GeV and corresponds to 4.4 standard deviations. Combining with 7 TeV and 8 TeV results (AAD 15AH), the observed significance is 6.4 standard deviations. The cross sections in the $H^0 \rightarrow \tau\tau$ decay channel (m_{H^0} = 125 GeV) are measured to $3.77^{+0.60}_{-0.59}$ (stat) $^{+0.87}_{-0.74}$ (syst) pb for the inclusive, 0.28 ± $0.09^{+0.11}_{-0.09}$ pb for VBF, and 3.1 ± $1.0^{+1.6}_{-1.3}$ pb for gluon-fusion production. See their Table XI for the cross sections in the framework of simplified template cross sections.

[2] SIRUNYAN 19AF use 35.9 fb^{-1} of data. $H^0 W/Z$ channels are added with a few updates on gluon fusion and vector boson fusion with respect to SIRUNYAN 18Y. The quoted signal strength is given for m_{H^0} = 125 GeV and corresponds to 5.5 standard deviations. The signal strengths for the individual production modes are: $1.12^{+0.53}_{-0.50}$ for gluon fusion, $1.13^{+0.45}_{-0.42}$ for vector boson fusion, $3.39^{+1.68}_{-1.54}$ for WH^0 and $1.23^{+1.62}_{-1.35}$ for ZH^0. See their Fig. 7 for other couplings (κ_V, κ_f).

[3] AAD 16AN perform fits to the ATLAS and CMS data at E_{cm} = 7 and 8 TeV. The signal strengths for individual production processes are 1.0 ± 0.6 for gluon fusion, 1.3 ± 0.4 for vector boson fusion, −1.4 ± 1.4 for WH^0 production, $2.2^{+2.2}_{-1.8}$ for ZH^0 production, and $-1.9^{+3.7}_{-3.3}$ for $t\overline{t}H^0$ production.

[4] AAD 16AN: In the fit, relative production cross sections are fixed to those in the Standard Model. The quoted signal strength is given for m_{H^0} = 125.09 GeV.

[5] AALTONEN 13M combine all Tevatron data from the CDF and D0 Collaborations with up to 10.0 fb^{-1} and 9.7 fb^{-1}, respectively, of $p\overline{p}$ collisions at E_{cm} = 1.96 TeV. The quoted signal strength is given for m_{H^0} = 125 GeV.

[6] SIRUNYAN 19AF use 35.9 fb^{-1} of data. The quoted signal strength is given for m_{H^0} = 125 GeV and corresponds to 2.3 standard deviations.

[7] SIRUNYAN 19AT perform a combine fit to 35.9 fb^{-1} of data at E_{cm} = 13 TeV. This combination is based on SIRUNYAN 18Y.

[8] SIRUNYAN 18Y use 35.9 fb^{-1} of pp collisions at E_{cm} = 13 TeV. The quoted signal strength is given for m_{H^0} = 125.09 GeV and corresponds to 4.9 standard deviations.

[9] SIRUNYAN 18Y combine the result of 35.9 fb^{-1} at E_{cm} = 13 TeV with the results obtained from data of 4.9 fb^{-1} at E_{cm} = 7 TeV and 19.7 fb^{-1} at E_{cm} = 8 TeV (KHACHATRYAN 15AM). The quoted signal strength is given for m_{H^0} = 125.09 GeV and corresponds to 5.9 standard deviations.

[10] AAD 16AC measure the signal strength with $pp \rightarrow H^0 W/ZX$ processes using 20.3 fb^{-1} of E_{cm} = 8 TeV. The quoted signal strength is given for m_{H^0} = 125 GeV.

[11] AAD 16K use up to 4.7 fb^{-1} of pp collisions at E_{cm} = 7 TeV and up to 20.3 fb^{-1} at E_{cm} = 8 TeV. The quoted signal strength is given for m_{H^0} = 125.36 GeV.

[12] AAD 15AH use 4.5 fb^{-1} of pp collisions at E_{cm} = 7 TeV and 20.3 fb^{-1} at E_{cm} = 8 TeV. The third uncertainty in the measurement is theory systematics. The signal strength for the gluon fusion mode is 2.0 ± $0.8^{+1.2}_{-0.8}$ ± 0.3 and that for vector boson fusion and W/ZH^0 production modes is $1.24^{+0.49}_{-0.45}{}^{+0.31}_{-0.29}$ ± 0.08. The quoted signal strength is given for m_{H^0} = 125.36 GeV.

[13] CHATRCHYAN 14K use 4.9 fb^{-1} of pp collisions at E_{cm} = 7 TeV and 19.7 fb^{-1} at E_{cm} = 8 TeV. The quoted signal strength is given for m_{H^0} = 125 GeV. See also CHATRCHYAN 14AJ.

[14] AALTONEN 13L combine all CDF results with 9.45–10.0 fb^{-1} of $p\overline{p}$ collisions at E_{cm} = 1.96 TeV. The quoted signal strength is given for m_{H^0} = 125 GeV.

[15] ABAZOV 13L combine all D0 results with up to 9.7 fb^{-1} of $p\overline{p}$ collisions at E_{cm} = 1.96 TeV. The quoted signal strength is given for m_{H^0} = 125 GeV.

[16] AAD 12AI obtain results based on 4.7 fb^{-1} of pp collisions at E_{cm} = 7 TeV. The quoted signal strengths are given in their Fig. 10 for m_{H^0} = 126 GeV. See also Fig. 13 of AAD 12DA.

[17] CHATRCHYAN 12N obtain results based on 4.9 fb^{-1} of pp collisions at E_{cm}=7 TeV and 5.1 fb^{-1} at E_{cm}=8 TeV. The quoted signal strength is given for m_{H^0}=125.5 GeV. See also CHATRCHYAN 13Y .

$Z\gamma$ Final State

VALUE	CL%	DOCUMENT ID		TECN	COMMENT
< 3.6	95	[1] AAD	20AG	ATLAS	pp, 13 TeV
• • • We do not use the following data for averages, fits, limits, etc. • • •					
< 7.4	95	[2] SIRUNYAN	18DQ	CMS	pp, 13 TeV
< 6.6	95	[3] AABOUD	17AW	ATLAS	pp, 13 TeV
<11	95	[4] AAD	14J	ATLAS	pp, 7, 8 TeV
< 9.5	95	[5] CHATRCHYAN	13BK	CMS	pp, 7, 8 TeV

[1] AAD 20AG search for $H^0 \rightarrow Z\gamma$, $Z \rightarrow ee$, $\mu\mu$ in 139 fb^{-1} of pp collisions at E_{cm} = 13 TeV. The signal strength is 2.0 ± $0.9^{+0.4}_{-0.3}$ at m_{H^0} = 125.09 GeV, which corresponds to a significance of 2.2 σ. The upper limit of $\sigma(pp \rightarrow H^0) \cdot B(H^0 \rightarrow Z\gamma)$ is 305 fb at 95% CL.

[2] SIRUNYAN 18DQ search for $H^0 \rightarrow Z\gamma$, $Z \rightarrow ee$, $\mu\mu$ in 35.9 fb^{-1} of pp collisions at E_{cm} = 13 TeV. The quoted signal strength (see their Figs. 6 and 7) is given for m_{H^0} = 125 GeV.

[3] AABOUD 17AW search for $H^0 \rightarrow Z\gamma$, $Z \rightarrow ee$, $\mu\mu$ in 36.1 fb^{-1} of pp collisions at E_{cm} = 13 TeV. The quoted signal strength is given for m_{H^0} = 125.09 GeV. The upper limit on the branching ratio of $H^0 \rightarrow Z\gamma$ is 1.0% at 95% CL assuming the SM Higgs boson production.

Downloaded from https://academic.oup.com/ptep/article/2022/8/083C01/6651666 by KIT Library user on 27 September 2022

[4] AAD 14J search for $H^0 \to Z\gamma \to \ell\ell\gamma$ in 4.5 fb^{-1} of pp collisions at E_{cm} = 7 TeV and 20.3 fb^{-1} at E_{cm} = 8 TeV. The quoted signal strength is given for m_{H^0} = 125.5 GeV.

[5] CHATRCHYAN 13BK search for $H^0 \to Z\gamma \to \ell\ell\gamma$ in 5.0 fb^{-1} of pp collisions at E_{cm} = 7 TeV and 19.6 fb^{-1} at E_{cm} = 8 TeV. A limit on cross section times branching ratio which corresponds to (4–25) times the expected Standard Model cross section is given in the range m_{H^0} = 120–160 GeV at 95% CL. The quoted limit is given for m_{H^0} = 125 GeV, where 10 is expected for no signal.

$\gamma^*\gamma$ Final State

VALUE	CL%	DOCUMENT ID		TECN	COMMENT
$1.5 \pm 0.5 {}^{+0.2}_{-0.1}$		[1] AAD	21I	ATLAS	pp, 13 TeV, $H^0 \to \ell\ell\gamma$, 139 fb^{-1}
• • • We do not use the following data for averages, fits, limits, etc. • • •					
<4.0	95	[2] SIRUNYAN	18DQ	CMS	$pp \to H^0 X$, 13 TeV, $H^0 \to \gamma^*\gamma$
<6.7	95	[3] KHACHATRY...	16B	CMS	pp, 8 TeV, $ee\gamma$, $\mu\mu\gamma$

[1] AAD 21I search for $H^0 \to \ell\ell\gamma$ ($\ell = e, \mu$) in 139 fb^{-1} of pp collisions at E_{cm} = 13 TeV. The mass of dilepton $m_{\ell\ell}$ is smaller than 30 GeV. This region is dominated by the decay through γ^*. The quoted signal strength corresponds to a significance of 3.2 standard deviations and is given for m_{H^0} = 125.09 GeV. The cross section times the branching ratio of $H^0 \to \ell\ell\gamma$ for $m_{\ell\ell}$ < 30 GeV is measured to be $8.7 \pm 2.7 {}^{+0.7}_{-0.6}$ fb.

[2] SIRUNYAN 18DQ search for $H^0 \to \gamma^*\gamma$, $\gamma^* \to \mu\mu$ in 35.9 fb^{-1} of pp collisions at E_{cm} = 13 TeV. The mass of γ^* is smaller than 50 GeV except in J/ψ and Υ mass regions. The quoted signal strength (see their Figs. 6 and 7) is given for m_{H^0} = 125 GeV.

[3] KHACHATRYAN 16B search for $H^0 \to \gamma^*\gamma \to e^+e^-\gamma$ and $\mu^+\mu^-\gamma$ (with m(e^+e^-) < 3.5 GeV and m($\mu^+\mu^-$) < 20 GeV) in 19.7 fb^{-1} of pp collisions at E_{cm} = 8 TeV. See their Fig. 6 for limits on individual channels.

Higgs Yukawa couplings

top Yukawa coupling

VALUE	CL%	DOCUMENT ID		TECN	COMMENT
[−0.9, −0.7] or [0.7, 1.1]	95	[1] SIRUNYAN	21R	CMS	pp, 13 TeV
• • • We do not use the following data for averages, fits, limits, etc. • • •					
<1.7	95	[2] SIRUNYAN	20C	CMS	pp, 13 TeV
<1.67	95	[3] SIRUNYAN	19BY	CMS	pp, 13 TeV
<2.1	95	[4] SIRUNYAN	18BU	CMS	pp, 13 TeV

[1] SIRUNYAN 21R constrain the ratio of the top quark Yukawa coupling y_t to its Standard Model value from $t\overline{t}H^0$ and tH^0 production rates using 137 fb^{-1} pp collision data at E_{cm} = 13 TeV. Assuming a SM Higgs couplings to τ's, the joint interval $-0.9 < \kappa_t (= y_t/y_t^{SM}) < -0.7$ and $0.7 < \kappa_t < 1.1$ is obtained at 95% CL (see their Fig. 17).

[2] SIRUNYAN 20C search for the production of four top quarks with same-sign and multilepton final states with 137 fb^{-1} pp collision data at E_{cm} = 13 TeV. The results constraint the ratio of the top quark Yukawa coupling y_t to its Standard Model value by comparing to the central value of a theoretical prediction (see their Refs. [1-2]), yielding $|y_t/y_t^{SM}| < 1.7$ at 95% CL. See their Fig. 5.

[3] SIRUNYAN 19BY measure the top quark Yukawa coupling from $t\overline{t}$ kinematic distributions, the invariant mass of the top quark pair and the rapidity difference between t and $\overline{t}$, in the ℓ+jets final state with 35.8 fb^{-1} pp collision data at E_{cm} = 13 TeV. The results constraint the ratio of the top quark Yukawa coupling to its the Standard Model to be $1.07 {}^{+0.34}_{-0.43}$ with an upper limit of 1.67 at 95% CL (see their Table III).

[4] SIRUNYAN 18BU search for the production of four top quarks with same-sign and multilepton final states with 35.9 fb^{-1} pp collision data at E_{cm} = 13 TeV. The results constraint the ratio of the top quark Yukawa coupling y_t to its the Standard Model by comparing to the central value of a theoretical prediction (see their Ref. [16]), yielding $|y_t/y_t^{SM}| < 2.1$ at 95% CL.

OTHER H^0 PRODUCTION PROPERTIES

$t\overline{t}H^0$ Production

Signal strengh relative to the Standard Model cross section.

VALUE	DOCUMENT ID		TECN	COMMENT
1.10±0.18 OUR AVERAGE				
$0.92 \pm 0.19 {}^{+0.17}_{-0.13}$	[1] SIRUNYAN	21R	CMS	pp, 13 TeV, $H^0 \to \tau\tau$, WW^*, ZZ^*
1.2 ± 0.3	[2] AABOUD	18AC	ATLAS	pp, 13 TeV, $H^0 \to b\overline{b}$ $\tau\tau$, $\gamma\gamma$, WW^*, ZZ^*
$1.9 {}^{+0.8}_{-0.7}$	[3] AAD	16AN	ATLAS	pp, 7, 8 TeV
• • • We do not use the following data for averages, fits, limits, etc. • • •				
$1.43 {}^{+0.33}_{-0.31} {}^{+0.21}_{-0.15}$	[4] AAD	20Z	ATLAS	pp, 13 TeV, $H^0 \to \gamma\gamma$
$1.38 {}^{+0.36}_{-0.29}$	[5] SIRUNYAN	20AS	CMS	pp, 13 TeV, $H^0 \to \gamma\gamma$
$0.72 \pm 0.24 \pm 0.38$	[6] SIRUNYAN	19R	CMS	pp, 13 TeV, $H^0 \to b\overline{b}$
$1.6 {}^{+0.5}_{-0.4}$	[7] AABOUD	18AC	ATLAS	pp, 13 TeV, $H^0 \to \tau\tau$, WW^*, ZZ^*
	[8] AABOUD	18BK	ATLAS	pp, 13 TeV, $H^0 \to b\overline{b}$ $\tau\tau$, $\gamma\gamma$, WW^*, ZZ^*
$0.84 {}^{+0.64}_{-0.61}$	[9] AABOUD	18T	ATLAS	pp, 13 TeV, $H^0 \to b\overline{b}$
0.9 ± 1.5	[10] SIRUNYAN	18BD	CMS	pp, 13 TeV, $H^0 \to b\overline{b}$
$1.23 {}^{+0.45}_{-0.43}$	[11] SIRUNYAN	18BQ	CMS	pp, 13 TeV, $H^0 \to \tau\tau$, WW^*, ZZ^*
$1.26 {}^{+0.31}_{-0.26}$	[12] SIRUNYAN	18L	CMS	pp, 7, 8, 13 TeV, $H^0 \to b\overline{b}$, $\tau\tau$, $\gamma\gamma$, WW^*, ZZ^*
1.7 ± 0.8	[13] AAD	16AL	ATLAS	pp, 7, 8 TeV, $H^0 \to b\overline{b}$, $\tau\tau$, $\gamma\gamma$, WW^*, and ZZ^*
$2.3 {}^{+0.7}_{-0.6}$	[3,14] AAD	16AN	LHC	pp, 7, 8 TeV
$2.9 {}^{+1.0}_{-0.9}$	[3] AAD	16AN	CMS	pp, 7, 8 TeV
$1.81 {}^{+0.52}_{-0.50} {}^{+0.58}_{-0.55} {}^{+0.31}_{-0.12}$	[15] AAD	16K	ATLAS	pp, 7, 8 TeV
$1.4 {}^{+2.1}_{-1.4} {}^{+0.6}_{-0.3}$	[16] AAD	15	ATLAS	pp, 7, 8 TeV
1.5 ± 1.1	[17] AAD	15BC	ATLAS	pp, 8 TeV
$2.1 {}^{+1.4}_{-1.2}$	[18] AAD	15T	ATLAS	pp, 8 TeV
$1.2 {}^{+1.6}_{-1.5}$	[19] KHACHATRY...	15AN	CMS	pp, 8 TeV
$2.8 {}^{+1.0}_{-0.9}$	[20] KHACHATRY...	14H	CMS	pp, 7, 8 TeV
$9.49 {}^{+6.60}_{-6.28}$	[21] AALTONEN	13L	CDF	$p\overline{p}$, 1.96 TeV
< 5.8 at 95% CL	[22] CHATRCHYAN	13X	CMS	pp, 7, 8 TeV, $H^0 \to b\overline{b}$

[1] SIRUNYAN 21R search for $t\overline{t}H^0$ in final states with electrons, muons and hadronically decaying τ leptons ($H^0 \to WW^*$, ZZ^*, $\tau\tau$) with 137 fb^{-1} of pp collision data at E_{cm} = 13 TeV. The quoted signal strength corresponds to a significance of 4.7 standard deviations and is given for m_{H^0} = 125 GeV.

[2] AABOUD 18AC combine results of $t\overline{t}H^0$, $H^0 \to \tau\tau$, $WW^*(\to \ell\nu\ell\nu, \ell\nu q\overline{q})$, $ZZ^*(\to \ell\ell\nu\nu, \ell\ell q\overline{q})$ with results of $t\overline{t}H^0$, $H^0 \to b\overline{b}$ (AABOUD 18T), $\gamma\gamma$ (AABOUD 18BO), $ZZ^*(\to 4\ell)$ (AABOUD 18AJ) in 36.1 fb^{-1} of pp collisions at E_{cm} = 13 TeV. The quoted signal strength is given for m_{H^0} = 125 GeV. See their Table 14.

[3] AAD 16AN: In the fit, relative branching ratios are fixed to those in the Standard Model. The quoted signal strength is given for m_{H^0} = 125.09 GeV.

[4] AAD 20Z measure $\sigma_{t\overline{t}H^0} \cdot B(H^0 \to \gamma\gamma)$ to be $1.64 {}^{+0.38}_{-0.36} {}^{+0.17}_{-0.14}$ fb in 139 fb^{-1} of data at E_{cm} = 13 TeV.

[5] SIRUNYAN 20AS measure $\sigma_{t\overline{t}H^0} \cdot B(H^0 \to \gamma\gamma)$ to be $1.56 {}^{+0.34}_{-0.32}$ fb in 137 fb^{-1} of data at E_{cm} = 13 TeV.

[6] SIRUNYAN 19R search for $t\overline{t}H^0$ production with H^0 decaying to $b\overline{b}$ in 35.9 fb^{-1} of data at E_{cm} = 13 TeV. The quoted signal strength is given for m_{H^0} = 125 GeV.

[7] AABOUD 18AC search for $t\overline{t}H^0$ production with H^0 decaying to $\tau\tau$, $WW^*(\to \ell\nu\ell\nu, \ell\nu q\overline{q})$, $ZZ^*(\to \ell\ell\nu\nu, \ell\ell q\overline{q})$ in 36.1 fb^{-1} of pp collisions at E_{cm} = 13 TeV. The quoted signal strength is given for m_{H^0} = 125 GeV. See their Table 13 and Fig. 13.

[8] AABOUD 18BK use 79.8 fb^{-1} data for $t\overline{t}H^0$ production with $H^0 \to \gamma\gamma$ and $ZZ^* \to 4\ell$ ($\ell = e, \mu$) and 36.1 fb^{-1} for other decay channels at E_{cm} = 13 TeV. A significance of 5.8 standard deviations is observed for m_{H^0} = 125.09 GeV and its signal strength without the uncertainty of the $t\overline{t}H^0$ cross section is $1.32 {}^{+0.28}_{-0.26}$. Combining with results of 7 and 8 TeV (AAD 16K), the significance is 6.3 standard deviations. Assuming Standard Model branching fractions, the total $t\overline{t}H^0$ production cross section at 13 TeV is measured to be $670 \pm 90 {}^{+110}_{-100}$ fb.

[9] AABOUD 18T search for $t\overline{t}H^0$ production with H^0 decaying to $b\overline{b}$ in 36.1 fb^{-1} of pp collisions at E_{cm} = 13 TeV. The quoted signal strength is given for m_{H^0} = 125 GeV.

[10] SIRUNYAN 18BD search for $t\overline{t}H^0$, $H^0 \to b\overline{b}$ in the all-jet final state with 35.9 fb^{-1} pp collision data at E_{cm} = 13 TeV. The quoted signal strength is given for m_{H^0} = 125 GeV.

[11] SIRUNYAN 18BQ search for $t\overline{t}H^0$ in final states with electrons, muons and hadronically decaying τ leptons ($H^0 \to WW^*$, ZZ^*, $\tau\tau$) with 35.9 fb^{-1} of pp collision data at E_{cm} = 13 TeV. The quoted signal strength corresponds to a significance of 3.2 standard deviations and is given for m_{H^0} = 125 GeV.

[12] SIRUNYAN 18L use up to 5.1, 19.7 and 35.9 fb^{-1} of pp collisions at E_{cm} = 7, 8, and 13 TeV, respectively. The quoted signal strength corresponds to a significance of 5.2 standard deviations and is given for m_{H^0} = 125.09 GeV. H^0 decay channels of WW^*, ZZ^*, $\gamma\gamma$, $\tau\tau$, and $b\overline{b}$ are used. See their Table 1 and Fig. 2 for results on individual channels.

[13] AAD 16AL search for $t\overline{t}H^0$ production with H^0 decaying to $\gamma\gamma$ in 4.5 fb^{-1} of pp collisions at E_{cm} = 7 TeV and $b\overline{b}$, $\tau\tau$, $\gamma\gamma$, WW^*, and ZZ^* in 20.3 fb^{-1} at E_{cm} = 8 TeV. The quoted signal strength is given for m_{H^0} = 125 GeV. This paper combines the results of previous papers, and the new result of this paper only is: $\mu = 1.6 \pm 2.6$.

[14] AAD 16AN perform fits to the ATLAS and CMS data at E_{cm} = 7 and 8 TeV.

[15] AAD 16K use up to 4.7 fb^{-1} of pp collisions at E_{cm} = 7 TeV and up to 20.3 fb^{-1} at E_{cm} = 8 TeV. The third uncertainty in the measurement is theory systematics. The quoted signal strength is given for m_{H^0} = 125.36 GeV.

[16] AAD 15 search for $t\overline{t}H^0$ production with H^0 decaying to $\gamma\gamma$ in 4.5 fb^{-1} of pp collisions at E_{cm} = 7 TeV and 20.3 fb^{-1} at E_{cm} = 8 TeV. The quoted result on the signal strength is equivalent to an upper limit of 6.7 at 95% CL and is given for m_{H^0} = 125.4 GeV.

[17] AAD 15BC search for $t\overline{t}H^0$ production with H^0 decaying to $b\overline{b}$ in 20.3 fb^{-1} of pp collisions at E_{cm} = 8 TeV. The corresponding upper limit is 3.4 at 95% CL. The quoted signal strength is given for m_{H^0} = 125 GeV.

[18] AAD 15T search for $t\overline{t}H^0$ production with H^0 resulting in multilepton final states (mainly from WW^*, $\tau\tau$, ZZ^*) in 20.3 fb^{-1} of pp collisions at E_{cm} = 8 TeV. The quoted result on the signal strength is given for m_{H^0} = 125 GeV and corresponds to an upper limit of 4.7 at 95% CL. The data sample is independent from AAD 15 and AAD 15BC.

[19] KHACHATRYAN 15AN search for $t\overline{t}H^0$ production with H^0 decaying to $b\overline{b}$ in 19.5 fb^{-1} of pp collisions at E_{cm} = 8 TeV. The quoted result on the signal strength is equivalent to an upper limit of 4.2 at 95% CL and is given for m_{H^0} = 125 GeV.

[20] KHACHATRYAN 14H search for $t\overline{t}H^0$ production with H^0 decaying to $b\overline{b}$, $\tau\tau$, $\gamma\gamma$, WW^*, and ZZ^*, in 5.1 fb^{-1} of pp collisions at E_{cm} = 7 TeV and 19.7 fb^{-1} at E_{cm} = 8 TeV. The quoted signal strength is given for m_{H^0} = 125.6 GeV.

Downloaded from https://academic.oup.com/ptep/article/2022/8/083C01/6651666 by KIT Library user on 27 September 2022

[21] AALTONEN 13L combine all CDF results with 9.45–10.0 fb^{-1} of $p\overline{p}$ collisions at E_{cm} = 1.96 TeV. The quoted signal strength is given for m_{H^0} = 125 GeV.

[22] CHATRCHYAN 13X search for $t\overline{t}H^0$ production followed by $H^0 \to b\overline{b}$, one top decaying to $\ell\nu$ and the other to either $\ell\nu$ or $q\overline{q}$ in 5.0 fb^{-1} and 5.1 fb^{-1} of pp collisions at E_{cm} = 7 and 8 TeV. A limit on cross section times branching ratio which corresponds to (4.0–8.6) times the expected Standard Model cross section is given for m_{H^0} = 110–140 GeV at 95% CL. The quoted limit is given for m_{H^0} = 125 GeV, where 5.2 is expected for no signal.

$H^0 H^0$ Production

The 95% CL limits are for the cross section (CS) and Higgs self coupling (κ_λ) scaling factors both relative to the SM predictions.

CS	κ_λ	CL%	DOCUMENT ID		TECN	COMMENT
• • • We do not use the following data for averages, fits, limits, etc. • • •						
< 7.7	−3.3 to 8.5	95	[1] SIRUNYAN	21K	CMS	13 TeV, $\gamma\gamma b\overline{b}$
< 6.9	−5.0 to 12.0	95	[2] AAD	20C	ATLS	13 TeV, $b\overline{b}\gamma\gamma$, $b\overline{b}\tau\tau$, $b\overline{b}b\overline{b}$, $b\overline{b}WW^*$, $WW^*\gamma\gamma$, WW^*WW^*
< 40		95	[3] AAD	20E	ATLS	13 TeV, $H^0H^0 \to b\overline{b}\ell\nu\ell\nu$
<840		95	[4] AAD	20X	ATLS	13 TeV, VBF, $b\overline{b}b\overline{b}$
< 12.9		95	[5] AABOUD	19A	ATLS	13 TeV, $b\overline{b}b\overline{b}$
<300		95	[6] AABOUD	19O	ATLS	13 TeV, $b\overline{b}WW^*$
<160		95	[7] AABOUD	19T	ATLS	13 TeV, WW^*WW^*
< 24	−11 to 17	95	[8] SIRUNYAN	19	CMS	13 TeV, $\gamma\gamma b\overline{b}$
< 75		95	[9] SIRUNYAN	19AB	CMS	13 TeV, $b\overline{b}b\overline{b}$
< 22.2	−11.8 to 18.8	95	[10] SIRUNYAN	19BE	CMS	13 TeV, $b\overline{b}\gamma\gamma$, $b\overline{b}\tau\tau$, $b\overline{b}b\overline{b}$, $b\overline{b}WW^*$, $b\overline{b}ZZ^*$
<179		95	[11] SIRUNYAN	19H	CMS	13 TeV, $b\overline{b}b\overline{b}$
<230		95	[12] AABOUD	18BU	ATLS	13 TeV, $\gamma\gamma WW^*$
< 12.7		95	[13] AABOUD	18CQ	ATLS	13 TeV, $b\overline{b}\tau\tau$
< 22	−8.2 to 13.2	95	[14] AABOUD	18CW	ATLS	13 TeV, $\gamma\gamma b\overline{b}$
< 30		95	[15] SIRUNYAN	18A	CMS	13 TeV, $b\overline{b}\tau\tau$
< 79		95	[16] SIRUNYAN	18F	CMS	13 TeV, $b\overline{b}\ell\nu\ell\nu$
< 43		95	[17] SIRUNYAN	17CN	CMS	8 TeV, $b\overline{b}\tau\tau$, $\gamma\gamma b\overline{b}$, $b\overline{b}b\overline{b}$
<108		95	[18] AABOUD	16I	ATLS	13 TeV, $b\overline{b}b\overline{b}$
< 74		95	[19] KHACHATRY...	16BQ	CMS	8 TeV, $\gamma\gamma b\overline{b}$
< 70		95	[20] AAD	15CE	ATLS	8 TeV, $b\overline{b}b\overline{b}$, $b\overline{b}\tau\tau$, $\gamma\gamma b\overline{b}$, $\gamma\gamma WW$

[1] SIRUNYAN 21K search for non-resonant H^0H^0 production using $H^0H^0 \to \gamma\gamma b\overline{b}$ with data of 137 fb^{-1} at E_{cm} = 13 TeV. The upper limit on the $pp \to H^0H^0 \to \gamma\gamma b\overline{b}$ production cross section at 95% CL is measured to be 0.67 fb, which corresponds to about 7.7 times the SM prediction. The quartic coupling (VVH^0H^0, $V = W,Z$) scaling factor $\kappa_{2V}(= c_{2V})$ is measured to be $-1.3 < \kappa_{2V} < 3.5$ at 95% CL.

[2] AAD 20C combine results of up to 36.1 fb^{-1} data at E_{cm} = 13 TeV for $pp \to H^0H^0 \to b\overline{b}\gamma\gamma$, $b\overline{b}\tau\tau$, $b\overline{b}b\overline{b}$, $b\overline{b}WW^*$, $WW^*\gamma\gamma$, WW^*WW^* (AABOUD 18CW, AABOUD 18CQ, AABOUD 19A, AABOUD 19O, AABOUD 18BU, and AABOUD 19T).

[3] AAD 20E search non-resonant for H^0H^0 production using $H^0H^0 \to b\overline{b}\ell\nu\ell\nu$, where one of the Higgs bosons decays to $b\overline{b}$ and the other decays to either WW^*, ZZ^*, or $\tau\tau$, with data of 139 fb^{-1} at E_{cm} = 13 TeV. The upper limit on the $pp \to H^0H^0$ production cross section at 95% CL is measured to be 1.2 pb, which corresponds to about 40 times the SM prediction.

[4] AAD 20X search for $H^0H^0 \to b\overline{b}b\overline{b}$ process via VBF with data of 126 fb^{-1} at E_{cm} = 13 TeV. The upper limit on the SM non-resonant HH production cross section is 1460 fb at 95% CL, which corresponds to 840 times the SM prediction. The quartic coupling (VVH^0H^0, $V = W,Z$) scaling factor κ_{2V} is excluded in the region of $\kappa_{2V} < -0.43$ or $\kappa_{2V} > 2.56$ at 95% CL.

[5] AABOUD 19A search for H^0H^0 production using $H^0H^0 \to b\overline{b}b\overline{b}$ with data of 36.1 fb^{-1} at E_{cm} = 13 TeV. The upper limit on the $pp \to H^0H^0 \to b\overline{b}b\overline{b}$ production cross section at 95% is measured to be 147 fb, which corresponds to about 12.9 times the SM prediction.

[6] AABOUD 19O search for H^0H^0 production using $H^0H^0 \to b\overline{b}WW^*$ with data of 36.1 fb^{-1} at E_{cm} = 13 TeV. The upper limit on the $pp \to H^0H^0$ production cross section at 95% CL is calculated to be 10 pb from the observed upper limit on the $pp \to H^0H^0 \to b\overline{b}WW^*$ production cross section of 2.5 pb assuming the SM branching fractions. The former corresponds to about 300 times the SM prediction.

[7] AABOUD 19T search for H^0H^0 production using $H^0H^0 \to WW^*WW^*$ with data of 36.1 fb^{-1} at E_{cm} = 13 TeV. The upper limit on the $pp \to H^0H^0$ production cross section at 95% is measured to be 5.3 pb, which corresponds to about 160 times the SM prediction.

[8] SIRUNYAN 19 search for H^0H^0 production using $H^0H^0 \to \gamma\gamma b\overline{b}$ with data of 35.9 fb^{-1} at E_{cm} = 13 TeV. The upper limit on the $pp \to H^0H^0 \to \gamma\gamma b\overline{b}$ production cross section at 95% CL is measured to be 2.0 fb, which corresponds to about 24 times the SM prediction. The effective Higgs boson self-coupling κ_λ ($= \lambda_{HHH} / \lambda_{HHH}^{SM}$) is constrainted to be $-11 < \kappa_\lambda < 17$ at 95% CL assuming all other Higgs boson couplings are at their SM value.

[9] SIRUNYAN 19AB search for H^0H^0 production using $H^0H^0 \to b\overline{b}b\overline{b}$, where 4 heavy flavor jets from two Higgs bosons are resolved, with data of 35.9 fb^{-1} at E_{cm} = 13 TeV. The upper limit on the $pp \to H^0H^0 \to b\overline{b}b\overline{b}$ production cross section at 95% is measured to be 847 fb, which corresponds to about 75 times the SM prediction.

[10] SIRUNYAN 19BE combine results of 13 TeV 35.9 fb^{-1} data: SIRUNYAN 19, SIRUNYAN 18A, SIRUNYAN 19AB, SIRUNYAN 19H, and SIRUNYAN 18F.

[11] SIRUNYAN 19H search for H^0H^0 production using $H^0H^0 \to b\overline{b}b\overline{b}$, where one of $b\overline{b}$ pairs is highly boosted and the other one is resolved, with data of 35.9 fb^{-1} at E_{cm} = 13 TeV. The upper limit on the $pp \to H^0H^0 \to b\overline{b}b\overline{b}$ production cross section at 95% is measured to be 1980 fb, which corresponds to about 179 times the SM prediction.

[12] AABOUD 18BU search for H^0H^0 production using $\gamma\gamma WW^*$ with the final state of $\gamma\gamma\ell\nu jj$ using data of 36.1 fb^{-1} at E_{cm} = 13 TeV. The upper limit on the $pp \to H^0H^0$ production cross section at 95% CL is measured to be 7.7 pb, which corresponds to about 230 times the SM prediction. The upper limit on the $pp \to H^0H^0 \to \gamma\gamma WW^*$ at 95% CL is measured to be 7.5 fb (see thier Table 6).

[13] AABOUD 18CQ search for H^0H^0 production using $H^0H^0 \to b\overline{b}\tau\tau$ with data of 36.1 fb^{-1} at E_{cm} = 13 TeV. The upper limit on the $pp \to H^0H^0 \to b\overline{b}\tau\tau$ production cross section at 95% is measured to be 30.9 fb, which corresponds to about 12.7 times the SM prediction.

[14] AABOUD 18CW search for H^0H^0 production using $H^0H^0 \to \gamma\gamma b\overline{b}$ with data of 36.1 fb^{-1} at E_{cm} = 13 TeV. The upper limit on the $pp \to H^0H^0$ production cross section at 95% is measured to be 0.73 pb, which corresponds to about 22 times the SM prediction. The effective Higgs boson self-coupling κ_λ is constrained to be $-8.2 < \kappa_\lambda < 13.2$ at 95% CL assuming all other Higgs boson couplings are at their SM value.

[15] SIRUNYAN 18A search for H^0H^0 production using $H^0H^0 \to b\overline{b}\tau\tau$ with data of 35.9 fb^{-1} at E_{cm} = 13 TeV. The upper limit on the $gg \to H^0H^0 \to b\overline{b}\tau\tau$ production cross section is measured to be 75.4 fb, which corresponds to about 30 times the SM prediction. Limits on Higgs-boson trilinear coupling λ_{HHH} and top Yukawa coupling y_t are also given (see their Fig. 6).

[16] SIRUNYAN 18F search non-resonant for H^0H^0 production using $H^0H^0 \to b\overline{b}\ell\nu\ell\nu$, where $\ell\nu\ell\nu$ is either $WW \to \ell\nu\ell\nu$ or $ZZ \to \ell\ell\nu\nu$ (ℓ is e, μ or a leptonically decaying τ), with data of 35.9 fb^{-1} at E_{cm} = 13 TeV. The upper limit on the $H^0H^0 \to b\overline{b}\ell\nu\ell\nu$ production cross section at 95% CL is measured to be 72 fb, which corresponds to about 79 times the SM prediction.

[17] SIRUNYAN 17CN search for H^0H^0 production using $H^0H^0 \to b\overline{b}\tau\tau$ with data of 18.3 fb^{-1} at E_{cm} = 8 TeV. Results are then combined with the published results of the $H^0H^0 \to \gamma\gamma b\overline{b}$ and $H^0H^0 \to b\overline{b}b\overline{b}$, which use data of up to 19.7 fb^{-1} at E_{cm} = 8 TeV. The upper limit on the $gg \to H^0H^0$ production cross section is measured to be 0.59 pb from $b\overline{b}\tau\tau$, which corresponds to about 59 times the SM prediction (gluon fusion). The combined upper limit is 0.43 pb, which is about 43 times the SM prediction. The quoted values are given for m_{H^0} = 125 GeV.

[18] AABOUD 16I search for H^0H^0 production using $H^0H^0 \to b\overline{b}b\overline{b}$ with data of 3.2 fb^{-1} at E_{cm} = 13 TeV. The upper limit on the $pp \to H^0H^0 \to b\overline{b}b\overline{b}$ production cross section is measured to be 1.22 pb. This result corresponds to about 108 times the SM prediction (gluon fusion), which is $11.3^{+0.9}_{-1.0}$ fb (NNLO+NNLL) including top quark mass effects. The quoted values are given for m_{H^0} = 125 GeV .

[19] KHACHATRYAN 16BQ search for H^0H^0 production using $H^0H^0 \to \gamma\gamma b\overline{b}$ with data of 19.7 fb^{-1} at E_{cm} = 8 TeV. The upper limit on the $gg \to H^0H^0 \to \gamma\gamma b\overline{b}$ production is measured to be 1.85 fb, which corresponds to about 74 times the SM prediction and is translated into 0.71 pb for $gg \to H^0H^0$ production cross section. Limits on Higgs-boson trilinear coupling λ are also given.

[20] AAD 15CE search for H^0H^0 production using $H^0H^0 \to b\overline{b}\tau\tau$ and $H^0H^0 \to \gamma\gamma WW$ with data of 20.3 fb^{-1} at E_{cm} = 8 TeV. These results are then combined with the published results of the $H^0H^0 \to \gamma\gamma b\overline{b}$ and $H^0H^0 \to b\overline{b}b\overline{b}$, which use data of up to 20.3 fb^{-1} at E_{cm} = 8 TeV. The upper limits on the $gg \to H^0H^0$ production cross section are measured to be 1.6 pb, 11.4 pb, 2.2 pb and 0.62 pb from $b\overline{b}\tau\tau$, $\gamma\gamma WW$, $\gamma\gamma b\overline{b}$ and $b\overline{b}b\overline{b}$, respectively. The combined upper limit is 0.69 pb, which corresponds to about 70 times the SM prediction. The quoted results are given for m_{H^0} = 125.4 GeV. See their Table 4.

tH^0 production

VALUE	DOCUMENT ID		TECN	COMMENT
5.7±2.7±3.0	[1] SIRUNYAN	21R	CMS	pp, 13 TeV
• • • We do not use the following data for averages, fits, limits, etc. • • •				
	[2] AAD	20Z	ATLS	pp, 13 TeV
	[3] SIRUNYAN	19BK	CMS	pp, 13 TeV
	[4] KHACHATRY...	16AU	CMS	pp, 8 TeV

[1] SIRUNYAN 21R search for tH^0 in final states with electrons, muons and hadronically decaying τ leptons ($H^0 \to WW^*$, ZZ^*, $\tau\tau$) with 137 fb^{-1} of pp collision data at E_{cm} = 13 TeV. The quoted signal strength corresponds to a significance of 1.4 standard deviations and is given for m_{H^0} = 125 GeV.

[2] AAD 20Z search for the tH^0 associated production using $H^0 \to \gamma\gamma$ in 139 fb^{-1} of data at E_{cm} = 13 TeV. An upper limit on its rate is set to be 12 times the Standard Model at 95% CL (m_{H^0} = 125.09 GeV).

[3] SIRUNYAN 19BK search for the tH^0 associated production using multilepton signatures ($H^0 \to WW^*$, $H^0 \to \tau\tau$, $H^0 \to ZZ^*$) and signatures with a single lepton and a $b\overline{b}$ pair ($H^0 \to b\overline{b}$) using 35.9 fb^{-1} at E_{cm} = 13 TeV. Results are combined with $H^0 \to \gamma\gamma$ (SIRUNYAN 18DS). The observed 95% CL upper limit on the tH^0 production cross section times $H^0 \to WW^* + \tau\tau + ZZ^* + b\overline{b} + \gamma\gamma$ branching fraction is 1.94 pb (assuming SM $t\overline{t}H^0$ production cross section). See their Table X and Fig. 14. The values outside the ranges of [−0.9, −0.5] and [1.0, 2.1] times the standard model top quark Yukawa coupling are excluded at 95% CL.

[4] KHACHATRYAN 16AU search for the tH^0 associated production in 19.7 fb^{-1} at E_{cm} = 8 TeV. The 95% CL upper limits on the tH^0 associated production cross section is measured to be 600–1000 fb depending on the assumed $\gamma\gamma$ branching ratios of the Higgs boson. The $\gamma\gamma$ branching ratio is varied to be by a factor of 0.5–3.0 of the Standard Model Higgs boson (m_{H^0} = 125 GeV). The results of the signal strengths for a negative Higgs-boson trilinear coupling are given. The results are given for m_{H^0} = 125 GeV.

H^0 Production Cross Section in pp Collisions at $\sqrt{s}$ = 13 TeV

Assumes m_{H^0} = 125 GeV

VALUE (pb)	DOCUMENT ID		TECN	COMMENT
56 ± 4 OUR AVERAGE				
53.5± 4.9±2.1	[1] AAD	20BA	ATLS	pp, 13 TeV, $ZZ^* \to 4\ell$ ($\ell = e, \mu$)
61.1± 6.0±3.7	[2] SIRUNYAN	19BA	CMS	pp, 13 TeV, $\gamma\gamma$, $ZZ^* \to 4\ell$ ($\ell = e, \mu$)

Downloaded from https://academic.oup.com/ptep/article/2022/8/083C01/6651666 by KIT Library user on 27 September 2022

• • • We do not use the following data for averages, fits, limits, etc. • • •

$57.0^{+6.0}_{-5.9}{}^{+4.0}_{-3.3}$	[3] AABOUD	18CG	ATLS	pp, 13 TeV, $\gamma\gamma$, $ZZ^* \to 4\ell$ ($\ell = e, \mu$)
$47.9^{+9.1}_{-8.6}$	[3] AABOUD	18CG	ATLS	pp, 13 TeV, $\gamma\gamma$
$68\ ^{+11}_{-10}$	[3] AABOUD	18CG	ATLS	pp, 13 TeV, $ZZ^* \to 4\ell$ ($\ell = e, \mu$)
$69\ ^{+10}_{-9}\ \pm 5$	[4] AABOUD	17CO	ATLS	pp, 13 TeV, $ZZ^* \to 4\ell$

[1] AAD 20BA use 139 fb^{-1} of pp collisions at E_{cm} = 13 TeV with $H^0 \to ZZ^* \to 4\ell$ where $\ell = e, \mu$. The quoted value is given for m_{H^0} = 125 GeV and assumes the Standard Model branching ratio.

[2] SIRUNYAN 19BA use 35.9 fb^{-1} of pp collisions at E_{cm} = 13 TeV.

[3] AABOUD 18CG use 36.1 fb^{-1} of pp collisions at E_{cm} = 13 TeV.

[4] AABOUD 17CO use 36.1 fb^{-1} of pp collisions at E_{cm} = 13 TeV with $H^0 \to ZZ^* \to 4\ell$ where $\ell = e, \mu$ for m_{H^0} = 125 GeV. Differential cross sections for the Higgs boson transverse momentum, Higgs boson rapidity, and other related quantities are measured as shown in their Figs. 8 and 9.

H^0 REFERENCES

AAD	21	PL B812 135980	G. Aad et al.	(ATLAS Collab.)
AAD	21AB	EPJ C81 178	G. Aad et al.	(ATLAS Collab.)
AAD	21AJ	EPJ C81 537	G. Aad et al.	(ATLAS Collab.)
AAD	21F	PR D103 112006	G. Aad et al.	(ATLAS Collab.)
AAD	21H	PL B816 136204	G. Aad et al.	(ATLAS Collab.)
AAD	21I	PL B819 136412	G. Aad et al.	(ATLAS Collab.)
AAD	21M	JHEP 2103 268	G. Aad et al.	(ATLAS Collab.)
SIRUNYAN	21	PL B812 135992	A.M. Sirunyan et al.	(CMS Collab.)
SIRUNYAN	21A	EPJ C81 13	A.M. Sirunyan et al.	(CMS Collab.)
Also		EPJ C81 333 (errat.)	A.M. Sirunyan et al.	(CMS Collab.)
SIRUNYAN	21AE	PR D104 052004	A.M. Sirunyan et al.	(CMS Collab.)
SIRUNYAN	21C	JHEP 2101 148	A.M. Sirunyan et al.	(CMS Collab.)
SIRUNYAN	21K	JHEP 2103 257	A.M. Sirunyan et al.	(CMS Collab.)
SIRUNYAN	21L	JHEP 2103 011	A.M. Sirunyan et al.	(CMS Collab.)
SIRUNYAN	21O	JHEP 2107 027	A.M. Sirunyan et al.	(CMS Collab.)
SIRUNYAN	21R	EPJ C81 378	A.M. Sirunyan et al.	(CMS Collab.)
SIRUNYAN	21S	EPJ C81 488	A.M. Sirunyan et al.	(CMS Collab.)
SIRUNYAN	21Z	PR D104 032013	A.M. Sirunyan et al.	(CMS Collab.)
TUMASYAN	21D	JHEP 2111 153	A. Tumasyan et al.	(CMS Collab.)
AAD	20	PR D101 012002	G. Aad et al.	(ATLAS Collab.)
AAD	20A	PL B800 135069	G. Aad et al.	(ATLAS Collab.)
AAD	20AE	PRL 125 221802	G. Aad et al.	(ATLAS Collab.)
AAD	20AG	PL B809 135754	G. Aad et al.	(ATLAS Collab.)
AAD	20AQ	EPJ C80 957	G. Aad et al.	(ATLAS Collab.)
Also		EPJ C81 29 (errat.)	G. Aad et al.	(ATLAS Collab.)
Also		EPJ C81 398 (errat.)	G. Aad et al.	(ATLAS Collab.)
AAD	20BA	EPJ C80 942	G. Aad et al.	(ATLAS Collab.)
AAD	20C	PL B800 135103	G. Aad et al.	(ATLAS Collab.)
AAD	20E	PL B801 135145	G. Aad et al.	(ATLAS Collab.)
AAD	20F	PL B801 135148	G. Aad et al.	(ATLAS Collab.)
AAD	20N	PL B805 135426	G. Aad et al.	(ATLAS Collab.)
AAD	20X	JHEP 2007 108	G. Aad et al.	(ATLAS Collab.)
Also		JHEP 2101 145 (errat.)	G. Aad et al.	(ATLAS Collab.)
Also		JHEP 2105 207 (errat.)	G. Aad et al.	(ATLAS Collab.)
AAD	20Z	PRL 125 061802	G. Aad et al.	(ATLAS Collab.)
SIRUNYAN	20AE	JHEP 2003 131	A.M. Sirunyan et al.	(CMS Collab.)
SIRUNYAN	20AS	PRL 125 061801	A.M. Sirunyan et al.	(CMS Collab.)
SIRUNYAN	20BK	JHEP 2011 039	A.M. Sirunyan et al.	(CMS Collab.)
SIRUNYAN	20BL	JHEP 2012 085	A.M. Sirunyan et al.	(CMS Collab.)
SIRUNYAN	20C	EPJ C80 75	A.M. Sirunyan et al.	(CMS Collab.)
SIRUNYAN	20L	PL B805 135425	A.M. Sirunyan et al.	(CMS Collab.)
AABOUD	19A	JHEP 1901 030	M. Aaboud et al.	(ATLAS Collab.)
AABOUD	19AI	PL B793 499	M. Aaboud et al.	(ATLAS Collab.)
AABOUD	19AL	PRL 122 231801	M. Aaboud et al.	(ATLAS Collab.)
AABOUD	19AQ	PR D99 072001	M. Aaboud et al.	(ATLAS Collab.)
AABOUD	19F	PL B789 508	M. Aaboud et al.	(ATLAS Collab.)
AABOUD	19N	JHEP 1904 048	M. Aaboud et al.	(ATLAS Collab.)
AABOUD	19O	JHEP 1904 092	M. Aaboud et al.	(ATLAS Collab.)
AABOUD	19T	JHEP 1905 124	M. Aaboud et al.	(ATLAS Collab.)
AABOUD	19U	JHEP 1905 141	M. Aaboud et al.	(ATLAS Collab.)
AAD	19A	PL B798 134949	G. Aad et al.	(ATLAS Collab.)
SIRUNYAN	19	PL B788 7	A.M. Sirunyan et al.	(CMS Collab.)
SIRUNYAN	19AB	JHEP 1904 112	A.M. Sirunyan et al.	(CMS Collab.)
SIRUNYAN	19AF	JHEP 1906 093	A.M. Sirunyan et al.	(CMS Collab.)
SIRUNYAN	19AJ	EPJ C79 94	A.M. Sirunyan et al.	(CMS Collab.)
SIRUNYAN	19AT	EPJ C79 421	A.M. Sirunyan et al.	(CMS Collab.)
SIRUNYAN	19AX	PL B791 96	A.M. Sirunyan et al.	(CMS Collab.)
SIRUNYAN	19BA	PL B792 369	A.M. Sirunyan et al.	(CMS Collab.)
SIRUNYAN	19BE	PRL 122 121803	A.M. Sirunyan et al.	(CMS Collab.)
SIRUNYAN	19BK	PR D99 092005	A.M. Sirunyan et al.	(CMS Collab.)
SIRUNYAN	19BL	PR D99 112003	A.M. Sirunyan et al.	(CMS Collab.)
SIRUNYAN	19BO	PL B793 520	A.M. Sirunyan et al.	(CMS Collab.)
SIRUNYAN	19BR	PL B797 134811	A.M. Sirunyan et al.	(CMS Collab.)
SIRUNYAN	19BY	PR D100 072007	A.M. Sirunyan et al.	(CMS Collab.)
SIRUNYAN	19BZ	PR D100 112002	A.M. Sirunyan et al.	(CMS Collab.)
SIRUNYAN	19CG	JHEP 1910 139	A.M. Sirunyan et al.	(CMS Collab.)
SIRUNYAN	19E	PRL 122 021801	A.M. Sirunyan et al.	(CMS Collab.)
SIRUNYAN	19H	JHEP 1901 040	A.M. Sirunyan et al.	(CMS Collab.)
SIRUNYAN	19L	JHEP 1901 183	A.M. Sirunyan et al.	(CMS Collab.)
SIRUNYAN	19R	JHEP 1903 026	A.M. Sirunyan et al.	(CMS Collab.)
AABOUD	18	PL B776 318	M. Aaboud et al.	(ATLAS Collab.)
AABOUD	18AC	PR D97 072003	M. Aaboud et al.	(ATLAS Collab.)
AABOUD	18AJ	JHEP 1803 095	M. Aaboud et al.	(ATLAS Collab.)
AABOUD	18AU	JHEP 1807 127	M. Aaboud et al.	(ATLAS Collab.)
AABOUD	18BK	PL B784 173	M. Aaboud et al.	(ATLAS Collab.)
AABOUD	18BL	PL B786 134	M. Aaboud et al.	(ATLAS Collab.)
AABOUD	18BM	PL B784 345	M. Aaboud et al.	(ATLAS Collab.)
AABOUD	18BN	PL B786 59	M. Aaboud et al.	(ATLAS Collab.)
AABOUD	18BO	PR D98 052005	M. Aaboud et al.	(ATLAS Collab.)
AABOUD	18BP	PL B786 223	M. Aaboud et al.	(ATLAS Collab.)
AABOUD	18BQ	PR D98 052003	M. Aaboud et al.	(ATLAS Collab.)
AABOUD	18BU	EPJ C78 1007	M. Aaboud et al.	(ATLAS Collab.)
AABOUD	18CA	JHEP 1810 180	M. Aaboud et al.	(ATLAS Collab.)
AABOUD	18CG	PL B786 114	M. Aaboud et al.	(ATLAS Collab.)
AABOUD	18CQ	PRL 121 191801	M. Aaboud et al.	(ATLAS Collab.)
AABOUD	18CW	JHEP 1811 040	M. Aaboud et al.	(ATLAS Collab.)
AABOUD	18M	PRL 120 211802	M. Aaboud et al.	(ATLAS Collab.)
AABOUD	18T	PR D97 072016	M. Aaboud et al.	(ATLAS Collab.)
AAIJ	18AM	EPJ C78 1008	R. Aaij et al.	(LHCb Collab.)
AALTONEN	18C	PR D98 072002	T. Aaltonen et al.	(CDF Collab.)
SIRUNYAN	18A	PL B778 101	A.M. Sirunyan et al.	(CMS Collab.)
SIRUNYAN	18AE	PL B780 501	A.M. Sirunyan et al.	(CMS Collab.)
SIRUNYAN	18BD	JHEP 1806 101	A.M. Sirunyan et al.	(CMS Collab.)
SIRUNYAN	18BH	JHEP 1806 001	A.M. Sirunyan et al.	(CMS Collab.)
SIRUNYAN	18BQ	JHEP 1808 066	A.M. Sirunyan et al.	(CMS Collab.)
SIRUNYAN	18BU	EPJ C78 140	A.M. Sirunyan et al.	(CMS Collab.)
SIRUNYAN	18BV	EPJ C78 291	A.M. Sirunyan et al.	(CMS Collab.)
SIRUNYAN	18DB	PRL 121 121801	A.M. Sirunyan et al.	(CMS Collab.)
SIRUNYAN	18DQ	JHEP 1811 152	A.M. Sirunyan et al.	(CMS Collab.)
SIRUNYAN	18DS	JHEP 1811 185	A.M. Sirunyan et al.	(CMS Collab.)
SIRUNYAN	18E	PRL 120 071802	A.M. Sirunyan et al.	(CMS Collab.)
SIRUNYAN	18F	JHEP 1801 054	A.M. Sirunyan et al.	(CMS Collab.)
SIRUNYAN	18L	PRL 120 231801	A.M. Sirunyan et al.	(CMS Collab.)
SIRUNYAN	18S	PR D97 092005	A.M. Sirunyan et al.	(CMS Collab.)
SIRUNYAN	18Y	PL B779 283	A.M. Sirunyan et al.	(CMS Collab.)
AABOUD	17AW	JHEP 1710 112	M. Aaboud et al.	(ATLAS Collab.)
AABOUD	17BA	JHEP 1712 024	M. Aaboud et al.	(ATLAS Collab.)
AABOUD	17BD	EPJ C77 765	M. Aaboud et al.	(ATLAS Collab.)
AABOUD	17CO	JHEP 1710 132	M. Aaboud et al.	(ATLAS Collab.)
AABOUD	17Y	PRL 119 051802	M. Aaboud et al.	(ATLAS Collab.)
AAD	17	EPJ C77 70	G. Aad et al.	(ATLAS Collab.)
KHACHATRY...	17F	JHEP 1702 135	V. Khachatryan et al.	(CMS Collab.)
SIRUNYAN	17AM	PL B775 1	A.M. Sirunyan et al.	(CMS Collab.)
SIRUNYAN	17AV	JHEP 1711 047	A.M. Sirunyan et al.	(CMS Collab.)
SIRUNYAN	17CN	PR D96 072004	A.M. Sirunyan et al.	(CMS Collab.)
AABOUD	16I	PR D94 052002	M. Aaboud et al.	(ATLAS Collab.)
AABOUD	16K	PRL 117 111802	M. Aaboud et al.	(ATLAS Collab.)
AABOUD	16X	JHEP 1611 112	M. Aaboud et al.	(ATLAS Collab.)
AAD	16	PL B753 69	G. Aad et al.	(ATLAS Collab.)
AAD	16AC	PR D93 092005	G. Aad et al.	(ATLAS Collab.)
AAD	16AF	JHEP 1601 172	G. Aad et al.	(ATLAS Collab.)
AAD	16AL	JHEP 1605 160	G. Aad et al.	(ATLAS Collab.)
AAD	16AN	JHEP 1608 045	G. Aad et al.	(ATLAS and CMS Collabs.)
AAD	16AO	JHEP 1608 104	G. Aad et al.	(ATLAS Collab.)
AAD	16BL	EPJ C76 658	G. Aad et al.	(ATLAS Collab.)
AAD	16K	EPJ C76 6	G. Aad et al.	(ATLAS Collab.)
KHACHATRY...	16AB	PL B759 672	V. Khachatryan et al.	(CMS Collab.)
KHACHATRY...	16AR	JHEP 1604 005	V. Khachatryan et al.	(CMS Collab.)
KHACHATRY...	16AU	JHEP 1606 177	V. Khachatryan et al.	(CMS Collab.)
KHACHATRY...	16B	PL B753 341	V. Khachatryan et al.	(CMS Collab.)
KHACHATRY...	16BA	JHEP 1609 051	V. Khachatryan et al.	(CMS Collab.)
KHACHATRY...	16BQ	PR D94 052012	V. Khachatryan et al.	(CMS Collab.)
KHACHATRY...	16CD	PL B763 472	V. Khachatryan et al.	(CMS Collab.)
KHACHATRY...	16G	EPJ C76 13	V. Khachatryan et al.	(CMS Collab.)
AAD	15	PL B740 222	G. Aad et al.	(ATLAS Collab.)
AAD	15AA	PR D92 012006	G. Aad et al.	(ATLAS Collab.)
AAD	15AH	JHEP 1504 117	G. Aad et al.	(ATLAS Collab.)
AAD	15AQ	JHEP 1508 137	G. Aad et al.	(ATLAS Collab.)
AAD	15AX	EPJ C75 231	G. Aad et al.	(ATLAS Collab.)
AAD	15B	PRL 114 191803	G. Aad et al.	(ATLAS and CMS Collabs.)
AAD	15BC	EPJ C75 349	G. Aad et al.	(ATLAS Collab.)
AAD	15BD	EPJ C75 337	G. Aad et al.	(ATLAS Collab.)
AAD	15BE	EPJ C75 335	G. Aad et al.	(ATLAS Collab.)
AAD	15CE	PR D92 092004	G. Aad et al.	(ATLAS Collab.)
AAD	15CI	EPJ C75 476	G. Aad et al.	(ATLAS Collab.)
Also		EPJ C76 152 (errat.)	G. Aad et al.	(ATLAS Collab.)
AAD	15CX	JHEP 1511 206	G. Aad et al.	(ATLAS Collab.)
AAD	15F	PR D91 012006	G. Aad et al.	(ATLAS Collab.)
AAD	15G	JHEP 1501 069	G. Aad et al.	(ATLAS Collab.)
AAD	15I	PRL 114 121801	G. Aad et al.	(ATLAS Collab.)
AAD	15P	PRL 115 091801	G. Aad et al.	(ATLAS Collab.)
AAD	15T	PL B749 519	G. Aad et al.	(ATLAS Collab.)
AALTONEN	15	PRL 114 151802	T. Aaltonen et al.	(CDF and D0 Collabs.)
AALTONEN	15B	PRL 114 141802	T. Aaltonen et al.	(CDF Collab.)
KHACHATRY...	15AM	EPJ C75 212	V. Khachatryan et al.	(CMS Collab.)
KHACHATRY...	15AN	EPJ C75 251	V. Khachatryan et al.	(CMS Collab.)
KHACHATRY...	15BA	PR D92 072010	V. Khachatryan et al.	(CMS Collab.)
KHACHATRY...	15H	PL B744 184	V. Khachatryan et al.	(CMS Collab.)
KHACHATRY...	15Q	PL B749 337	V. Khachatryan et al.	(CMS Collab.)
KHACHATRY...	15Y	PR D92 012004	V. Khachatryan et al.	(CMS Collab.)
KHACHATRY...	15Z	PR D92 032008	V. Khachatryan et al.	(CMS Collab.)
AAD	14AR	PL B738 234	G. Aad et al.	(ATLAS Collab.)
AAD	14AS	PL B738 68	G. Aad et al.	(ATLAS Collab.)
AAD	14BC	PR D90 112015	G. Aad et al.	(ATLAS Collab.)
AAD	14BJ	JHEP 1409 112	G. Aad et al.	(ATLAS Collab.)
AAD	14J	PL B732 8	G. Aad et al.	(ATLAS Collab.)
AAD	14O	PRL 112 201802	G. Aad et al.	(ATLAS Collab.)
AAD	14W	PR D90 052004	G. Aad et al.	(ATLAS Collab.)
ABAZOV	14F	PRL 113 161802	V.M. Abazov et al.	(D0 Collab.)
CHATRCHYAN	14AA	PR D89 092007	S. Chatrchyan et al.	(CMS Collab.)
CHATRCHYAN	14AI	PR D89 012003	S. Chatrchyan et al.	(CMS Collab.)
CHATRCHYAN	14AJ	NATP 10 557	S. Chatrchyan et al.	(CMS Collab.)
CHATRCHYAN	14B	EPJ C74 2980	S. Chatrchyan et al.	(CMS Collab.)
CHATRCHYAN	14G	JHEP 1401 096	S. Chatrchyan et al.	(CMS Collab.)
CHATRCHYAN	14K	JHEP 1405 104	S. Chatrchyan et al.	(CMS Collab.)
KHACHATRY...	14D	PL B736 64	V. Khachatryan et al.	(CMS Collab.)
KHACHATRY...	14H	JHEP 1409 087	V. Khachartryan et al.	(CMS Collab.)
KHACHATRY...	14P	EPJ C74 3076	V. Khachatryan et al.	(CMS Collab.)
AAD	13AJ	PL B726 120	G. Aad et al.	(ATLAS Collab.)
AAD	13AK	PL B726 88	G. Aad et al.	(ATLAS Collab.)
Also		PL B734 406 (errat.)	G. Aad et al.	(ATLAS Collab.)
AALTONEN	13L	PR D88 052013	T. Aaltonen et al.	(CDF Collab.)
AALTONEN	13M	PR D88 052014	T. Aaltonen et al.	(CDF and D0 Collabs.)
ABAZOV	13L	PR D88 052011	V.M. Abazov et al.	(D0 Collab.)
CHATRCHYAN	13BK	PL B726 587	S. Chatrchyan et al.	(CMS Collab.)
CHATRCHYAN	13J	PRL 110 081803	S. Chatrchyan et al.	(CMS Collab.)
CHATRCHYAN	13X	JHEP 1305 145	S. Chatrchyan et al.	(CMS Collab.)
CHATRCHYAN	13Y	JHEP 1306 081	S. Chatrchyan et al.	(CMS Collab.)
HEINEMEYER	13A	arXiv:1307.1347	S. Heinemeyer et al.	(LHC Higgs CS Working Group)
AAD	12AI	PL B716 1	G. Aad et al.	(ATLAS Collab.)
AAD	12DA	SCI 338 1576	G. Aad et al.	(ATLAS Collab.)
AALTONEN	12Q	PRL 109 111803	T. Aaltonen et al.	(CDF Collab.)
AALTONEN	12R	PRL 109 111804	T. Aaltonen et al.	(CDF Collab.)
AALTONEN	12S	PRL 109 111805	T. Aaltonen et al.	(CDF Collab.)
AALTONEN	12T	PRL 109 071804	T. Aaltonen et al.	(CDF and D0 Collabs.)
ABAZOV	12K	PL B716 285	V.M. Abazov et al.	(D0 Collab.)
ABAZOV	12O	PRL 109 121803	V.M. Abazov et al.	(D0 Collab.)
ABAZOV	12P	PRL 109 121804	V.M. Abazov et al.	(D0 Collab.)
CHATRCHYAN	12BY	SCI 338 1569	S. Chatrchyan et al.	(CMS Collab.)
CHATRCHYAN	12N	PL B716 30	S. Chatrchyan et al.	(CMS Collab.)
DITTMAIER	12	arXiv:1201.3084	S. Dittmaier et al.	(LHC Higgs CS Working Group)
DITTMAIER	11	arXiv:1101.0593	S. Dittmaier et al.	(LHC Higgs CS Working Group)

Downloaded from https://academic.oup.com/ptep/article/2022/8/083C01/6651666 by KIT Library user on 27 September 2022

Neutral Higgs Bosons, Searches for

CONTENTS:

Mass Limits for Neutral Higgs Bosons in Supersymmetric Models
– Mass Limits for heavy neutral Higgs bosons (H^0_2, A^0) in the MSSM
– Mass Limits for H^0_1 (Higgs Boson) in Supersymmetric Models
Mass Limits for Neutral Higgs Bosons in Extended Higgs Models
– Mass Limits in General two-Higgs-doublet Models
– Mass Limits for H^0 with Vanishing Yukawa Couplings
– Mass Limits for H^0 Decaying to Invisible Final States
– Mass Limits for Light A^0
– Other Mass Limits
Searches for a Higgs Boson with Standard Model Couplings
– Direct Mass Limits for H^0
– Indirect Mass Limits for H^0 from Electroweak Analysis

MASS LIMITS FOR NEUTRAL HIGGS BOSONS IN SUPERSYMMETRIC MODELS

The minimal supersymmetric model has two complex doublets of Higgs bosons. The resulting physical states are two scalars [H^0_1 and H^0_2, where we define $m_{H^0_1} < m_{H^0_2}$], a pseudoscalar (A^0), and a charged Higgs pair ($H^\pm$). H^0_1 and H^0_2 are also called h and H in the literature. There are two free parameters in the Higgs sector which can be chosen to be m_{A^0} and $\tan\beta = v_2/v_1$, the ratio of vacuum expectation values of the two Higgs doublets. Tree-level Higgs masses are constrained by the model to be $m_{H^0_1} \leq m_Z$, $m_{H^0_2} \geq m_Z$, $m_{A^0} \geq m_{H^0_1}$, and $m_{H^\pm} \geq m_W$. However, as described in the review on "Status of Higgs Boson Physics" in this Volume these relations are violated by radiative corrections.

The observed signal at about 125 GeV, see section "H^0", can be interpreted as one of the neutral Higgs bosons of supersymmetric models. Unless otherwise noted, we identify the lighter scalar H^0_1 with the Higgs discovered at 125 GeV at the LHC (AAD 12AI, CHATRCHYAN 12N).

Unless otherwise noted, the experiments in e^+e^- collisions search for the processes $e^+e^- \rightarrow H^0_1 Z^0$ in the channels used for the Standard Model Higgs searches and $e^+e^- \rightarrow H^0_1 A^0$ in the final states $b\overline{b}b\overline{b}$ and $b\overline{b}\tau^+\tau^-$. Unless otherwise stated, the following results assume no invisible H^0_1 or A^0 decays. Unless otherwise noted, the results are given in the m_h^{max} scenario, CARENA 13.

In $p\overline{p}$ and pp collisions the experiments search for a variety of processes, as explicitly specified for each entry. Limits on the A^0 mass arise from these direct searches, as well as from the relations valid in the minimal supersymmetric model between m_{A^0} and $m_{H^0_1}$. As discussed in the review on "Status of Higgs Boson Physics" in this Volume, these relations depend, via potentially large radiative corrections, on the mass of the t quark and on the supersymmetric parameters, in particular those of the stop sector. These indirect limits are weaker for larger t and $\tilde{t}$ masses. To include the radiative corrections to the Higgs masses, unless otherwise stated, the listed papers use theoretical predictions incorporating two-loop corrections, and the results are given for the m_h^{mod+} benchmark scenario, see CARENA 13.

Mass Limits for heavy neutral Higgs bosons (H^0_2, A^0) in the MSSM

The limits rely on $pp \rightarrow H^0_2/A^0 \rightarrow \tau^+\tau^-$ and assume that H^0_2 and A^0 are (sufficiently) mass degenerate. The limits depend on $\tan\beta$.

VALUE (GeV)	CL%	DOCUMENT ID		TECN	COMMENT
> 377	95	[1] AABOUD	18G	ATLS	$\tan\beta = 10$ GeV
> 863	95	[1] AABOUD	18G	ATLS	$\tan\beta = 20$ GeV
>1157	95	[1] AABOUD	18G	ATLS	$\tan\beta = 30$ GeV
>1328	95	[1] AABOUD	18G	ATLS	$\tan\beta = 40$ GeV
>1483	95	[1] AABOUD	18G	ATLS	$\tan\beta = 50$ GeV
>1613	95	[1] AABOUD	18G	ATLS	$\tan\beta = 60$ GeV
> 389	95	[2] SIRUNYAN	18CX	CMS	$\tan\beta = 10$ GeV
> 832	95	[2] SIRUNYAN	18CX	CMS	$\tan\beta = 20$ GeV
>1148	95	[2] SIRUNYAN	18CX	CMS	$\tan\beta = 30$ GeV
>1341	95	[2] SIRUNYAN	18CX	CMS	$\tan\beta = 40$ GeV
>1496	95	[2] SIRUNYAN	18CX	CMS	$\tan\beta = 50$ GeV
>1613	95	[2] SIRUNYAN	18CX	CMS	$\tan\beta = 60$ GeV
• • • We do not use the following data for averages, fits, limits, etc. • • •					
		[3] AAD	20	ATLS	H^0 properties
		[4] AAD	20AA	ATLS	$H^0_2/A^0 \rightarrow \tau^+\tau^-$
		[5] AAD	20C	ATLS	$H^0_2 \rightarrow H^0 H^0$
		[6] AAD	20L	ATLS	$H^0_2 \rightarrow b\overline{b}$
		[7] SIRUNYAN	20AC	CMS	$A^0 \rightarrow Z H^0$
		[8] SIRUNYAN	20AF	CMS	$H^0_2/A^0 \rightarrow t\overline{t}$
		[9] SIRUNYAN	20Y	CMS	$H^0_2 \rightarrow W^+ W^-$
		[10] SIRUNYAN	19CR	CMS	$H^0_2/A^0 \rightarrow \mu^+\mu^-$
		[11] SIRUNYAN	18A	CMS	$H^0_2 \rightarrow H^0 H^0$
		[12] SIRUNYAN	18BP	CMS	$pp \rightarrow H^0_2/A^0 + b + X$, $H^0_2/A^0 \rightarrow b\overline{b}$
		[13] AABOUD	16AA	ATLS	$A^0 \rightarrow \tau^+\tau^-$
		[14] KHACHATRY...	16A	CMS	$H^0_{1,2}/A^0 \rightarrow \mu^+\mu^-$
		[15] KHACHATRY...	16P	CMS	$H^0_2 \rightarrow H^0 H^0$, $A^0 \rightarrow Z H^0$
		[16] KHACHATRY...	15AY	CMS	$pp \rightarrow H^0_{1,2}/A^0 + b + X$, $H^0_{1,2}/A^0 \rightarrow b\overline{b}$
		[17] AAD	14AW	ATLS	$pp \rightarrow H^0_{1,2}/A^0 + X$, $H^0_{1,2}/A^0 \rightarrow \tau\tau$
		[18] KHACHATRY...	14M	CMS	$pp \rightarrow H^0_{1,2}/A^0 + X$, $H^0_{1,2}/A^0 \rightarrow \tau\tau$
		[19] AAD	13O	ATLS	$pp \rightarrow H^0_{1,2}/A^0 + X$, $H^0_{1,2}/A^0 \rightarrow \tau^+\tau^-$, $\mu^+\mu^-$
		[20] AAIJ	13T	LHCB	$pp \rightarrow H^0_{1,2}/A^0 + X$, $H^0_{1,2}/A^0 \rightarrow \tau^+\tau^-$
		[21] CHATRCHYAN	13AG	CMS	$pp \rightarrow H^0_{1,2}/A^0 + b + X$, $H^0_{1,2}/A^0 \rightarrow b\overline{b}$
		[22] AALTONEN	12AQ	TEVA	$p\overline{p} \rightarrow H^0_{1,2}/A^0 + b + X$, $H^0_{1,2}/A^0 \rightarrow b\overline{b}$
		[23] AALTONEN	12X	CDF	$p\overline{p} \rightarrow H^0_{1,2}/A^0 + b + X$, $H^0_{1,2}/A^0 \rightarrow b\overline{b}$
		[24] ABAZOV	12G	D0	$p\overline{p} \rightarrow H^0_{1,2}/A^0 + X$, $H^0_{1,2}/A^0 \rightarrow \tau^+\tau^-$
		[25] CHATRCHYAN	12K	CMS	$pp \rightarrow H^0_{1,2}/A^0 + X$, $H^0_{1,2}/A^0 \rightarrow \tau^+\tau^-$
		[26] ABAZOV	11K	D0	$p\overline{p} \rightarrow H^0_{1,2}/A^0 + b + X$, $H^0_{1,2}/A^0 \rightarrow b\overline{b}$
		[27] ABAZOV	11W	D0	$p\overline{p} \rightarrow H^0_{1,2}/A^0 + b + X$, $H^0_{1,2}/A^0 \rightarrow \tau^+\tau^-$
		[28] AALTONEN	09AR	CDF	$p\overline{p} \rightarrow H^0_{1,2}/A^0 + X$, $H^0_{1,2}/A^0 \rightarrow \tau^+\tau^-$
> 90.4		[29] ABDALLAH	08B	DLPH	$E_{cm} \leq 209$ GeV
> 93.4	95	[30] SCHAEL	06B	LEP	$E_{cm} \leq 209$ GeV
		[31] ACOSTA	05Q	CDF	$p\overline{p} \rightarrow H^0_{1,2}/A^0 + X$
> 85.0	95	[32,33] ABBIENDI	04M	OPAL	$E_{cm} \leq 209$ GeV
		[34] ABBIENDI	03G	OPAL	$H^0_1 \rightarrow A^0 A^0$
> 86.5	95	[32,35] ACHARD	02H	L3	$E_{cm} \leq 209$ GeV, $\tan\beta > 0.4$
		[36] AKEROYD	02	RVUE	
> 90.1	95	[32,37] HEISTER	02	ALEP	$E_{cm} \leq 209$ GeV, $\tan\beta > 0.5$

[1] AABOUD 18G search for production of $H^0_2/A^0 \rightarrow \tau^+\tau^-$ by gluon fusion and b-associated prodution in 36.1 fb^{-1} of pp collisions at $E_{cm} = 13$ TeV. See their Fig. 10 for excluded regions in the m_{A^0}– $\tan\beta$ plane in several MSSM scenarios.

[2] SIRUNYAN 18CX search for production of $H^0_{1,2}/A^0 \rightarrow \tau^+\tau^-$ by gluon fusion and b-associated prodution in 35.9 fb^{-1} of pp collisions at $E_{cm} = 13$ TeV. See their Fig. 9 for excluded regions in the m_{A^0}– $\tan(\beta)$ plane in several MSSM scenarios.

[3] AAD 20 combine measurements on H^0 production and decay using data taken in years 2015–2017 (up to 79.8 fb^{-1}) of pp collisions at $E_{cm} = 13$ TeV. See their Fig. 19 for excluded region in the hMSSM parameter space.

[4] AAD 20AA search for $H^0_2/A^0 \rightarrow \tau^+\tau^-$ produced by gluon fusion or b-associated production using 139 fb^{-1} of pp collisions at $E_{cm} = 13$ TeV. See their Fig. 2(c) for excluded region in the M_h^{125} scenario of MSSM. Values of $\tan\beta > 8$ (21) are excluded for $m_{A^0} = 1.0$ (1.5) TeV at 95%CL.

[5] AAD 20C combine searches for a scalar resonance decaying to $H^0 H^0$ in 36.1 fb^{-1} of pp collisions at $E_{cm} = 13$ TeV from AABOUD 19A, AABOUD 19O, AABOUD 18CQ, AABOUD 19T, AABOUD 18CW, and AABOUD 18BU. See their Fig. 7(b) for the excluded region in the hMSSM parameter space.

[6] AAD 20L search for b-associated production of H^0_2 decaying to $b\overline{b}$ in 27.8 fb^{-1} of pp collisions at $E_{cm} = 13$ TeV. See their Fig. 9 for excluded regions in hMSSM, m_h^{mod+} and m_h^{mod-} scenarios of MSSM.

[7] SIRUNYAN 20AC search for gluon-fusion and b-associated production of A^0 decaying to $Z H^0$ in 35.9 fb^{-1} of pp collisions at $E_{cm} = 13$ TeV. See their Fig. 6 for excluded regions in the $M_{h\text{EFT}}^{125}$ and hMSSM scenarios of the MSSM.

[8] SIRUNYAN 20AF search for $H^0_2/A^0 \rightarrow t\overline{t}$ with one or two charged leptons in the final state using kinematic variables in 35.9 fb^{-1} of pp collisions at $E_{cm} = 13$ TeV. See their Fig. 8 for excluded region in the hMSSM scenario of MSSM. Values of $\tan\beta$ below 1.0–1.5 are excluded for $m_{A^0} = 0.4$–0.75 TeV at 95%CL.

[9] SIRUNYAN 20Y search for gluon-fusion and vector-boson-fusion production of H^0_2 decaying to $W^+ W^-$ in the final states $\ell\nu\ell\nu$ and $\ell\nu qq$ in 35.9 fb^{-1} of pp collisions at $E_{cm} = 13$ TeV. See their Figs. 8 and 9 for excluded regions in various MSSM scenarios.

[10] SIRUNYAN 19CR search for production of H^0_2/A^0 in gluon fusion and in association with a $b\overline{b}$ pair, decaying to $\mu^+\mu^-$ in 35.9 fb^{-1} of pp collisions at $E_{cm} = 13$ TeV. See their Fig. 5 for the excluded region in the MSSM parameter space in the m_h^{mod+} and hMSSM scenarios.

Downloaded from https://academic.oup.com/ptep/article/2022/8/083C01/6651666 by KIT Library user on 27 September 2022

[11] SIRUNYAN 18A search for production of a scalar resonance decaying to $H^0 H^0 \rightarrow b\overline{b}\tau^+\tau^-$ in 35.9 fb^{-1} of pp collisions at E_{cm} = 13 TeV. See their Fig. 5 (lower) for excluded regions in the $m_{A^0} - \tan\beta$ plane in the hMSSM scenario.

[12] SIRUNYAN 18BP search for production of $H^0_2/A^0 \rightarrow b\overline{b}$ by b-associated prodution in 35.7 fb^{-1} of pp collisions at E_{cm} = 13 TeV. See their Fig. 6 for the limits on cross section times branching ratio for $m_{H^0_2}$, m_{A^0} = 0.3–1.3 TeV, and Fig. 7 for excluded regions in the m_{A^0}– $\tan(\beta)$ plane in several MSSM scenarios.

[13] AABOUD 16AA search for production of a Higgs boson in gluon fusion and in association with a $b\overline{b}$ pair followed by the decay $A^0 \rightarrow \tau^+\tau^-$ in 3.2 fb^{-1} of pp collisions at E_{cm} = 13 TeV. See their Fig. 5(a, b) for limits on cross section times branching ratio for m_{A^0} = 200–1200 GeV, and Fig. 5(c, d) for the excluded region in the MSSM parameter space in the m_h^{mod+} and hMSSM scenarios.

[14] KHACHATRYAN 16A search for production of a Higgs boson in gluon fusion and in association with a $b\overline{b}$ pair followed by the decay $H^0_{1,2}/A^0 \rightarrow \mu^+\mu^-$ in 5.1 fb^{-1} of pp collisions at E_{cm} = 7 TeV and 19.3 fb^{-1} at E_{cm} = 8 TeV. See their Fig. 7 for the excluded region in the MSSM parameter space in the m_h^{mod+} benchmark scenario and Fig. 9 for limits on cross section times branching ratio.

[15] KHACHATRYAN 16P search for gluon fusion production of an H^0_2 decaying to $H^0 H^0 \rightarrow b\overline{b}\tau^+\tau^-$ and an A^0 decaying to $ZH^0 \rightarrow \ell^+\ell^-\tau^+\tau^-$ in 19.7 fb^{-1} of pp collisions at E_{cm} = 8 TeV. See their Fig. 12 for excluded region in the $\tan\beta - \cos(\beta-\alpha)$ plane for $m_{H^0_2} = m_{A^0}$ = 300 GeV.

[16] KHACHATRYAN 15AY search for production of a Higgs boson in association with a b quark in the decay $H^0_{1,2}/A^0 \rightarrow b\overline{b}$ in 19.7 fb^{-1} of pp collisions at E_{cm} = 8 TeV and combine with CHATRCHYAN 13AG 7 TeV data. See their Fig. 6 for the limits on cross section times branching ratio for m_{A^0} = 100–900 GeV and Figs. 7–9 for the excluded region in the MSSM parameter space in various benchmark scenarios.

[17] AAD 14AW search for production of a Higgs boson followed by the decay $H^0_{1,2}/A^0 \rightarrow \tau^+\tau^-$ in 19.5–20.3 fb^{-1} of pp collisions at E_{cm} = 8 TeV. See their Fig. 11 for the limits on cross section times branching ratio and their Figs. 9 and 10 for the excluded region in the MSSM parameter space. For m_{A^0} = 140 GeV, the region $\tan\beta > 5.4$ is excluded at 95% CL in the m_h^{max} scenario.

[18] KHACHATRYAN 14M search for production of a Higgs boson in gluon fusion and in association with a b quark followed by the decay $H^0_{1,2}/A^0 \rightarrow \tau^+\tau^-$ in 4.9 fb^{-1} of pp collisions at E_{cm} = 7 TeV and 19.7 fb^{-1} at E_{cm} = 8 TeV. See their Figs. 7 and 8 for one- and two-dimensional limits on cross section times branching ratio and their Figs. 5 and 6 for the excluded region in the MSSM parameter space. For m_{A^0} = 140 GeV, the region $\tan\beta > 3.8$ is excluded at 95% CL in the m_h^{max} scenario.

[19] AAD 13O search for production of a Higgs boson in the decay $H^0_{1,2}/A^0 \rightarrow \tau^+\tau^-$ and $\mu^+\mu^-$ with 4.7–4.8 fb^{-1} of pp collisions at E_{cm} = 7 TeV. See their Fig. 6 for the excluded region in the MSSM parameter space and their Fig. 7 for the limits on cross section times branching ratio. For m_{A^0} = 110–170 GeV, $\tan\beta \gtrsim 10$ is excluded, and for $\tan\beta$ = 50, m_{A^0} below 470 GeV is excluded at 95% CL in the m_h^{max} scenario.

[20] AAIJ 13T search for production of a Higgs boson in the forward region in the decay $H^0_{1,2}/A^0 \rightarrow \tau^+\tau^-$ in 1.0 fb^{-1} of pp collisions at E_{cm} = 7 TeV. See their Fig. 2 for the limits on cross section times branching ratio and the excluded region in the MSSM parameter space.

[21] CHATRCHYAN 13AG search for production of a Higgs boson in association with a b quark in the decay $H^0_{1,2}/A^0 \rightarrow b\overline{b}$ in 2.7–4.8 fb^{-1} of pp collisions at E_{cm} = 7 TeV. See their Fig. 6 for the excluded region in the MSSM parameter space and Fig. 5 for the limits on cross section times branching ratio. For m_{A^0} = 90–350 GeV, upper bounds on $\tan\beta$ of 18–42 at 95% CL are obtained in the m_h^{max} scenario with μ = +200 GeV.

[22] AALTONEN 12AQ combine AALTONEN 12X and ABAZOV 11K. See their Table I and Fig. 1 for the limit on cross section times branching ratio and Fig. 2 for the excluded region in the MSSM parameter space.

[23] AALTONEN 12X search for associated production of a Higgs boson and a b quark in the decay $H^0_{1,2}/A^0 \rightarrow b\overline{b}$, with 2.6 fb^{-1} of $p\overline{p}$ collisions at E_{cm} = 1.96 TeV. See their Table III and Fig. 15 for the limit on cross section times branching ratio and Figs. 17, 18 for the excluded region in the MSSM parameter space.

[24] ABAZOV 12G search for production of a Higgs boson in the decay $H^0_{1,2}/A^0 \rightarrow \tau^+\tau^-$ with 7.3 fb^{-1} of $p\overline{p}$ collisions at E_{cm} = 1.96 TeV and combine with ABAZOV 11W and ABAZOV 11K. See their Figs. 4, 5, and 6 for the excluded region in the MSSM parameter space. For m_{A^0} = 90–180 GeV, $\tan\beta \gtrsim 30$ is excluded at 95% CL. in the m_h^{max} scenario.

[25] CHATRCHYAN 12K search for production of a Higgs boson in the decay $H^0_{1,2}/A^0 \rightarrow \tau^+\tau^-$ with 4.6 fb^{-1} of pp collisions at E_{cm} = 7 TeV. See their Fig. 3 and Table 4 for the excluded region in the MSSM parameter space. For m_{A^0} = 160 GeV, the region $\tan\beta > 7.1$ is excluded at 95% CL in the m_h^{max} scenario. Superseded by KHACHATRYAN 14M.

[26] ABAZOV 11K search for associated production of a Higgs boson and a b quark, followed by the decay $H^0_{1,2}/A^0 \rightarrow b\overline{b}$, in 5.2 fb^{-1} of $p\overline{p}$ collisions at E_{cm} = 1.96 TeV. See their Fig. 5/Table 2 for the limit on cross section times branching ratio and Fig. 6 for the excluded region in the MSSM parameter space for μ = −200 GeV.

[27] ABAZOV 11W search for associated production of a Higgs boson and a b quark, followed by the decay $H^0_{1,2}/A^0 \rightarrow \tau\tau$, in 7.3 fb^{-1} of $p\overline{p}$ collisions at E_{cm} = 1.96 TeV. See their Fig. 2 for the limit on cross section times branching ratio and for the excluded region in the MSSM parameter space.

[28] AALTONEN 09AR search for Higgs bosons decaying to $\tau^+\tau^-$ in two doublet models in 1.8 fb^{-1} of $p\overline{p}$ collisions at E_{cm} = 1.96 TeV. See their Fig. 2 for the limit on $\sigma \cdot B(H^0_{1,2}/A^0 \rightarrow \tau^+\tau^-)$ for different Higgs masses, and see their Fig. 3 for the excluded region in the MSSM parameter space.

[29] ABDALLAH 08B give limits in eight CP-conserving benchmark scenarios and some CP-violating scenarios. See paper for excluded regions for each scenario. Supersedes ABDALLAH 04.

[30] SCHAEL 06B make a combined analysis of the LEP data. The quoted limit is for the m_h^{max} scenario with m_t = 174.3 GeV. In the CP-violating CPX scenario no lower bound on $m_{H^0_1}$ can be set at 95% CL. See paper for excluded regions in various scenarios. See Figs. 2–6 and Tabs. 14–21 for limits on $\sigma(ZH^0)\cdot B(H^0 \rightarrow b\overline{b}, \tau^+\tau^-)$ and $\sigma(H^0_1 H^0_2)\cdot B(H^0_1,H^0_2 \rightarrow b\overline{b},\tau^+\tau^-)$.

[31] ACOSTA 05Q search for $H^0_{1,2}/A^0$ production in $p\overline{p}$ collisions at E_{cm} = 1.8 TeV with $H^0_{1,2}/A^0 \rightarrow \tau^+\tau^-$. At m_{A^0} = 100 GeV, the obtained cross section upper limit is above theoretical expectation.

[32] Search for $e^+e^- \rightarrow H^0_1 A^0$ in the final states $b\overline{b}b\overline{b}$ and $b\overline{b}\tau^+\tau^-$, and $e^+e^- \rightarrow H^0_1 Z$. Universal scalar mass of 1 TeV, SU(2) gaugino mass of 200 GeV, and μ= −200 GeV are assumed, and two-loop radiative corrections incorporated. The limits hold for m_t=175 GeV, and for the m_h^{max} scenario.

[33] ABBIENDI 04M exclude $0.7 < \tan\beta < 1.9$, assuming m_t = 174.3 GeV. Limits for other MSSM benchmark scenarios, as well as for CP violating cases, are also given.

[34] ABBIENDI 03G search for $e^+e^- \rightarrow H^0_1 Z$ followed by $H^0_1 \rightarrow A^0 A^0$, $A^0 \rightarrow c\overline{c}$, gg, or $\tau^+\tau^-$. In the no-mixing scenario, the region $m_{H^0_1}$ = 45-85 GeV and m_{A^0} = 2-9.5 GeV is excluded at 95% CL.

[35] ACHARD 02H also search for the final state $H^0_1 Z \rightarrow 2A^0 q\overline{q}$, $A^0 \rightarrow q\overline{q}$. In addition, the MSSM parameter set in the "large-μ" and "no-mixing" scenarios are examined.

[36] AKEROYD 02 examine the possibility of a light A^0 with $\tan\beta$ <1. Electroweak measurements are found to be inconsistent with such a scenario.

[37] HEISTER 02 excludes the range 0.7 <$\tan\beta$ < 2.3. A wider range is excluded with different stop mixing assumptions. Updates BARATE 01C.

Mass Limits for H^0_1 (Higgs Boson) in Supersymmetric Models

VALUE (GeV)	CL%	DOCUMENT ID		TECN	COMMENT
>89.7		[1] ABDALLAH	08B	DLPH	$E_{cm} \leq$ 209 GeV
>92.8	95	[2] SCHAEL	06B	LEP	$E_{cm} \leq$ 209 GeV
>84.5	95	[3,4] ABBIENDI	04M	OPAL	$E_{cm} \leq$ 209 GeV
>86.0	95	[3,5] ACHARD	02H	L3	$E_{cm} \leq$ 209 GeV, $\tan\beta > 0.4$
>89.8	95	[3,6] HEISTER	02	ALEP	$E_{cm} \leq$ 209 GeV, $\tan\beta > 0.5$
• • • We do not use the following data for averages, fits, limits, etc. • • •					
		[7] AALTONEN	12AQ	TEVA	$p\overline{p} \rightarrow H^0_{1,2}/A^0 + b + X$, $H^0_{1,2}/A^0 \rightarrow b\overline{b}$

[1] ABDALLAH 08B give limits in eight CP-conserving benchmark scenarios and some CP-violating scenarios. See paper for excluded regions for each scenario. Supersedes ABDALLAH 04.

[2] SCHAEL 06B make a combined analysis of the LEP data. The quoted limit is for the m_h^{max} scenario with m_t = 174.3 GeV. In the CP-violating CPX scenario no lower bound on $m_{H^0_1}$ can be set at 95% CL. See paper for excluded regions in various scenarios. See Figs. 2–6 and Tabs. 14–21 for limits on $\sigma(ZH^0)\cdot B(H^0 \rightarrow b\overline{b}, \tau^+\tau^-)$ and $\sigma(H^0_1 H^0_2)\cdot B(H^0_1,H^0_2 \rightarrow b\overline{b},\tau^+\tau^-)$.

[3] Search for $e^+e^- \rightarrow H^0_1 A^0$ in the final states $b\overline{b}b\overline{b}$ and $b\overline{b}\tau^+\tau^-$, and $e^+e^- \rightarrow H^0_1 Z$. Universal scalar mass of 1 TeV, SU(2) gaugino mass of 200 GeV, and μ= −200 GeV are assumed, and two-loop radiative corrections incorporated. The limits hold for m_t=175 GeV, and for the m_h^{max} scenario.

[4] ABBIENDI 04M exclude $0.7 < \tan\beta < 1.9$, assuming m_t = 174.3 GeV. Limits for other MSSM benchmark scenarios, as well as for CP violating cases, are also given.

[5] ACHARD 02H also search for the final state $H^0_1 Z \rightarrow 2A^0 q\overline{q}$, $A^0 \rightarrow q\overline{q}$. In addition, the MSSM parameter set in the "large-μ" and "no-mixing" scenarios are examined.

[6] HEISTER 02 excludes the range 0.7 <$\tan\beta$ < 2.3. A wider range is excluded with different stop mixing assumptions. Updates BARATE 01C.

[7] AALTONEN 12AQ combine AALTONEN 12X and ABAZOV 11K. See their Table I and Fig. 1 for the limit on cross section times branching ratio and Fig. 2 for the excluded region in the MSSM parameter space.

MASS LIMITS FOR NEUTRAL HIGGS BOSONS IN EXTENDED HIGGS MODELS

This Section covers models which do not fit into either the Standard Model or its simplest minimal Supersymmetric extension (MSSM), leading to anomalous production rates, or nonstandard final states and branching ratios. In particular, this Section covers limits which may apply to generic two-Higgs-doublet models (2HDM), or to special regions of the MSSM parameter space where decays to invisible particles or to photon pairs are dominant (see the review on "Status of Higgs Boson Physics"). Concerning the mass limits for H^0 and A^0 listed below, see the footnotes or the comment lines for details on the nature of the models to which the limits apply.

The observed signal at about 125 GeV, see section "H^0", can be interpreted as one of the neutral Higgs bosons of an extended Higgs sector.

Mass Limits in General two-Higgs-doublet Models

VALUE (GeV)	CL%	DOCUMENT ID		TECN	COMMENT
• • • We do not use the following data for averages, fits, limits, etc. • • •					
		[1] AAD	21AF	ATLS	$H^0_2 \rightarrow ZZ$
		[2] AAD	21AI	ATLS	$A^0 \rightarrow ZH^0_2$
		[3] AAD	20	ATLS	H^0 properties
		[4] AAD	20L	ATLS	$H^0_2 \rightarrow b\overline{b}$

Downloaded from https://academic.oup.com/ptep/article/2022/8/083C01/6651666 by KIT Library user on 27 September 2022

		[5] SIRUNYAN	20AA CMS	$H^0_2 \to Z A^0$ or $A^0 \to Z H^0_2$
		[6] SIRUNYAN	20Y CMS	$H^0_2 \to W^+ W^-$
		[7] SIRUNYAN	19AE CMS	$A^0 \to \tau^+\tau^-$
		[8] SIRUNYAN	19AV CMS	$A^0 \to Z H^0$
		[9] AABOUD	18AH ATLS	$A^0 \to Z H^0_2$
		[10] AABOUD	18AI ATLS	$A^0 \to Z H^0$
		[11] AABOUD	18BF ATLS	$H^0_2 \to Z Z$
		[12] AABOUD	18CE ATLS	$pp \to H^0_2/A^0 t\overline{t}$, $H^0_2/A^0 \to t\overline{t}$
		[13] HALLER	18 RVUE	global fits
		[14] SIRUNYAN	18BP CMS	$pp \to H^0_2/A^0 + b + X$, $H^0_2/A^0 \to b\overline{b}$
		[15] SIRUNYAN	18ED CMS	$A^0 \to Z H^0$
		[16] AABOUD	17AN ATLS	$H^0_2, A^0 \to t\overline{t}$
		[17] SIRUNYAN	17AX CMS	$A^0 b\overline{b}$, $A^0 \to \mu^+\mu^-$
		[18] AAD	16AX ATLS	$H^0_2 \to Z Z$
		[19] KHACHATRY...	16P CMS	$H^0_2 \to H^0 H^0$, $A^0 \to Z H^0$
		[20] KHACHATRY...	16W CMS	$A^0 b\overline{b}$, $A^0 \to \tau^+\tau^-$
		[21] KHACHATRY...	16Z CMS	$H^0_2 \to Z A^0$ or $A^0 \to Z H^0_2$
		[22] AAD	15BK ATLS	$H^0_2 \to H^0 H^0$
		[23] AAD	15S ATLS	$A^0 \to Z H^0$
		[24] KHACHATRY...	15BB CMS	$H^0_2, A^0 \to \gamma\gamma$
		[25] KHACHATRY...	15N CMS	$A^0 \to Z H^0$
		[26] AAD	14M ATLS	$H^0_2 \to H^\pm W^\mp \to H^0 W^\pm W^\mp$, $H^0 \to b\overline{b}$
		[27] KHACHATRY...	14Q CMS	$H^0_2 \to H^0 H^0$, $A^0 \to Z H^0$
		[28] AALTONEN	09AR CDF	$p\overline{p} \to H^0_{1,2}/A^0 + X$, $H^0_{1,2}/A^0 \to \tau^+\tau^-$
none 1–55	95	[29] ABBIENDI	05A OPAL	H^0_1, Type II model
>110.6	95	[30] ABDALLAH	05D DLPH	$H^0 \to$ 2 jets
		[31] ABDALLAH	04O DLPH	$Z \to f\overline{f}H$
		[32] ABDALLAH	04O DLPH	$e^+e^- \to H^0 Z$, $H^0 A^0$
		[33] ABBIENDI	02D OPAL	$e^+e^- \to b\overline{b}H$
none 1–44	95	[34] ABBIENDI	01E OPAL	H^0_1, Type-II model
> 68.0	95	[35] ABBIENDI	99E OPAL	$\tan\beta > 1$
		[36] ABREU	95H DLPH	$Z \to H^0 Z^*$, $H^0 A^0$
		[37] PICH	92 RVUE	Very light Higgs

[1] AAD 21AF search for production of a heavy H^0_2 state decaying to $Z Z$ in the final states $\ell^+\ell^-\ell'^+\ell'^-$ and $\ell^+\ell^-\nu\overline{\nu}$ in 139 fb^{-1} of pp collisions at E_{cm} = 13 TeV. See their Figs. 6 and 7 for excluded parameter regions of the 2HDM Type I and II.

[2] AAD 21AI search for production of an A^0 in gluon-gluon fusion and in association with a $b\overline{b}$, decaying to $Z H^0_2 \to \ell^+\ell^- b\overline{b}$ or $\ell^+\ell^- W^+ W^-$ in 139 fb^{-1} of pp collisions at E_{cm} = 13 TeV. See their Figs. 10 and 14 for excluded regions in the parameter space of various 2HDMs.

[3] AAD 20 combine measurements on H^0 production and decay using data taken in years 2015–2017 (up to 79.8 fb^{-1}) of pp collisions at E_{cm} = 13 TeV. See their Fig. 18 for excluded regions in various 2HDMs.

[4] AAD 20L search for b-associated production of H^0_2 decaying to $b\overline{b}$ in 27.8 fb^{-1} of pp collisions at E_{cm} = 13 TeV. See their Figs. 10 and 11 for excluded regions in the flipped two Higgs doublet model.

[5] SIRUNYAN 20AA search for $H^0_2 \to Z A^0$, $A^0 \to b\overline{b}$ or $A^0 \to Z H^0_2$, $H^0_2 \to b\overline{b}$ in 35.9 fb^{-1} of pp collisions at E_{cm} = 13 TeV. See their Figs. 8 and 9 for excluded regions in the parameter space of Type-II two Higgs doublet model.

[6] SIRUNYAN 20Y search for gluon-fusion and vector-boson-fusion production of H^0_2 decaying to $W^+ W^-$ in the final states $\ell\nu\ell\nu$ and $\ell\nu qq$ in 35.9 fb^{-1} of pp collisions at E_{cm} = 13 TeV. See their Fig. 7 for excluded regions in Type I and II two Higgs doublet models.

[7] SIRUNYAN 19AE search for a pseudoscalar resonance produced in association with a $b\overline{b}$ pair, decaying to $\tau^+\tau^-$ in 35.9 fb^{-1} of pp collisions at E_{cm} = 13 TeV. See their Fig. 4 for cross section limits for m_{A^0} = 25–70 GeV and comparison with some representative 2HDMs.

[8] SIRUNYAN 19AV search for a scalar resonance produced by gluon fusion or b associated production, decaying to $Z H^0 \to \ell^+\ell^- b\overline{b}$ ($\ell = e, \mu$) or $\nu\overline{\nu} b\overline{b}$ in 35.9 fb^{-1} of pp collisions at E_{cm} = 13 TeV. See their Figs. 6 and 7 for excluded regions in the parameter space of various 2HDMs.

[9] AABOUD 18AH search for production of an A^0 in gluon-gluon fusion and in association with a $b\overline{b}$, decaying to $Z H^0_2 \to \ell^+\ell^- b\overline{b}$ in 36.1 fb^{-1} of pp collisions at E_{cm} = 13 TeV. See their Fig. 6 for excluded regions in the parameter space of various 2HDMs.

[10] AABOUD 18AI search for production of an A^0 in gluon-gluon fusion and in association with a $b\overline{b}$, decaying to $Z H^0$ in the final states $\nu\overline{\nu} b\overline{b}$ and $\ell^+\ell^- b\overline{b}$ in 36.1 fb^{-1} of pp collisions at E_{cm} = 13 TeV. See their Figs. 7 and 8 for excluded regions in the parameter space in various 2HDMs.

[11] AABOUD 18BF search for production of a heavy H^0_2 state decaying to $Z Z$ in the final states $\ell^+\ell^-\ell^+\ell^-$ and $\ell^+\ell^-\nu\overline{\nu}$ in 36.1 fb^{-1} of pp collisions at E_{cm} = 13 TeV. See their Figs. 8 and 9 for excluded parameter regions in 2HDM Type I and II.

[12] AABOUD 18CE search for the process $pp \to H^0_2/A^0 t\overline{t}$ followed by the decay $H^0_2/A^0 \to t\overline{t}$ in 36.1 fb^{-1} of pp collisions at E_{cm} = 13 TeV. See their Fig. 12 for limits on cross section times branching ratio, and for lower limits on $\tan\beta$ for $m_{H^0_2}$, m_{A^0} = 0.4–1.0 TeV in the 2HDM type II.

[13] HALLER 18 perform global fits in the framework of two-Higgs-doublet models (type I, II, lepton specific, flipped). See their Fig. 8 for allowed parameter regions from fits to LHC H^0 measurements, Fig. 9 bottom and charm decays, Fig. 10 muon anomalous magnetic moment, Fig. 11 electroweak precision data, and Fig. 12 by combination of all data.

[14] SIRUNYAN 18BP search for production of $H^0_2/A^0 \to b\overline{b}$ by b-associated prodution in 35.7 fb^{-1} of pp collisions at E_{cm} = 13 TeV. See their Fig. 6 for the limits on cross section times branching ratio for $m_{H^0_2}$, m_{A^0} = 0.3–1.3 TeV, and Figs. 8 and 9 for excluded regions in the parameter space of type-II and flipped 2HDMs.

[15] SIRUNYAN 18ED search for production of an A^0 in gluon-gluon fusion and in association with a $b\overline{b}$, decaying to $Z H^0$ in the final states $\nu\overline{\nu} b\overline{b}$ or $\ell^+\ell^- b\overline{b}$ in 35.9 fb^{-1} of pp collisions at E_{cm} = 13 TeV. See their Fig. 9 for excluded regions in the parameter space in Type I and II 2HDMs.

[16] AABOUD 17AN search for production of a heavy H^0_2 and/or A^0 decaying to $t\overline{t}$ in 20.3 fb^{-1} of pp collisions at E_{cm} = 8 TeV. See their Fig. 3 and Table III for excluded parameter regions in Type II Two-Higgs-Doublet-Models.

[17] SIRUNYAN 17AX search for $A^0 b\overline{b}$ production followed by the decay $A^0 \to \mu^+\mu^-$ in 19.7 fb^{-1} of pp collisions at E_{cm} = 8 TeV. Limits are set in the range m_{A^0} = 25–60 GeV. See their Fig. 5 for upper limits on $\sigma(A^0 b\overline{b})\cdot B(A^0 \to \mu^+\mu^-)$.

[18] AAD 16AX search for production of a heavy H^0 state decaying to $Z Z$ in the final states $\ell^+\ell^-\ell^+\ell^-$, $\ell^+\ell^-\nu\overline{\nu}$, $\ell^+\ell^- q\overline{q}$, and $\nu\overline{\nu} q\overline{q}$ in 20.3 fb^{-1} of pp collisions at E_{cm} = 8 TeV. See their Figs. 13 and 14 for excluded parameter regions in Type I and II models.

[19] KHACHATRYAN 16P search for gluon fusion production of an H^0_2 decaying to $H^0 H^0 \to b\overline{b}\tau^+\tau^-$ and an A^0 decaying to $Z H^0 \to \ell^+\ell^-\tau^+\tau^-$ in 19.7 fb^{-1} of pp collisions at E_{cm} = 8 TeV. See their Fig. 11 for limits on $\tan\beta$ for m_{A^0} = 230–350 GeV.

[20] KHACHATRYAN 16W search for $A^0 b\overline{b}$ production followed by the decay $A^0 \to \tau^+\tau^-$ in 19.7 fb^{-1} of pp collisions at E_{cm} = 8 TeV. See their Fig. 3 for upper limits on $\sigma(A^0 b\overline{b})\cdot B(A^0 \to \tau^+\tau^-)$.

[21] KHACHATRYAN 16Z search for $H^0_2 \to Z A^0$ followed by $A^0 \to b\overline{b}$ or $\tau^+\tau^-$, and $A^0 \to Z H^0_2$ followed by $H^0_2 \to b\overline{b}$ or $\tau^+\tau^-$, in 19.8 fb^{-1} of pp collisions at E_{cm} = 8 TeV. See their Fig. 4 for cross section limits and Fig. 5 for excluded region in the parameter space.

[22] AAD 15BK search for production of a heavy H^0_2 decaying to $H^0 H^0$ in the final state $b\overline{b}b\overline{b}$ in 19.5 fb^{-1} of pp collisions at E_{cm} = 8 TeV. See their Figs. 15–18 for excluded regions in the parameter space.

[23] AAD 15S search for production of A^0 decaying to $Z H^0 \to \ell^+\ell^- b\overline{b}$, $\nu\overline{\nu} b\overline{b}$ and $\ell^+\ell^-\tau^+\tau^-$ in 20.3 fb^{-1} of pp collisions at E_{cm} = 8 TeV. See their Figs. 4 and 5 for excluded regions in the parameter space.

[24] KHACHATRYAN 15BB search for H^0_2, $A^0 \to \gamma\gamma$ in 19.7 fb^{-1} of pp collisions at E_{cm} = 8 TeV. See their Fig. 10 for excluded regions in the two-Higgs-doublet model parameter space.

[25] KHACHATRYAN 15N search for production of A^0 decaying to $Z H^0 \to \ell^+\ell^- b\overline{b}$ in 19.7 fb^{-1} of pp collisions at E_{cm} = 8 TeV. See their Fig. 5 for excluded regions in the $\tan\beta - \cos(\beta-\alpha)$ plane for m_{A^0} = 300 GeV.

[26] AAD 14M search for the decay cascade $H^0_2 \to H^\pm W^\mp \to H^0 W^\pm W^\mp$, H^0 decaying to $b\overline{b}$ in 20.3 fb^{-1} of pp collisions at E_{cm} = 8 TeV. See their Table IV for limits in a two-Higgs-doublet model for $m_{H^0_2}$= 325–1025 GeV and m_{H^+}= 225–825 GeV.

[27] KHACHATRYAN 14Q search for $H^0_2 \to H^0 H^0$ and $A^0 \to Z H^0$ in 19.5 fb^{-1} of pp collisions at E_{cm} = 8 TeV. See their Figs. 4 and 5 for limits on cross section times branching ratio for m_{H_2,A^0}= 260–360 GeV and their Figs. 7–9 for limits in two-Higgs-doublet models.

[28] AALTONEN 09AR search for Higgs bosons decaying to $\tau^+\tau^-$ in two doublet models in 1.8 fb^{-1} of $p\overline{p}$ collisions at E_{cm} = 1.96 TeV. See their Fig. 2 for the limit on $\sigma \cdot B(H^0_{1,2}/A^0 \to \tau^+\tau^-)$ for different Higgs masses, and see their Fig. 3 for the excluded region in the MSSM parameter space.

[29] ABBIENDI 05A search for $e^+e^- \to H^0_1 A^0$ in general Type-II two-doublet models, with decays H^0_1, $A^0 \to q\overline{q}$, gg, $\tau^+\tau^-$, and $H^0_1 \to A^0 A^0$.

[30] ABDALLAH 05D search for $e^+e^- \to H^0 Z$ and $H^0 A^0$ with H^0, A^0 decaying to two jets of any flavor including gg. The limit is for SM $H^0 Z$ production cross section with $B(H^0 \to jj) = 1$.

[31] ABDALLAH 04O search for $Z \to b\overline{b}H^0$, $b\overline{b}A^0$, $\tau^+\tau^- H^0$ and $\tau^+\tau^- A^0$ in the final states $4b$, $b\overline{b}\tau^+\tau^-$, and 4τ. See paper for limits on Yukawa couplings.

[32] ABDALLAH 04O search for $e^+e^- \to H^0 Z$ and $H^0 A^0$, with H^0, A^0 decaying to $b\overline{b}$, $\tau^+\tau^-$, or $H^0 \to A^0 A^0$ at E_{cm} = 189–208 GeV. See paper for limits on couplings.

[33] ABBIENDI 02D search for $Z \to b\overline{b}H^0_1$ and $b\overline{b}A^0$ with $H^0_1/A^0 \to \tau^+\tau^-$, in the range $4 < m_H < 12$ GeV. See their Fig. 8 for limits on the Yukawa coupling.

[34] ABBIENDI 01E search for neutral Higgs bosons in general Type-II two-doublet models, at $E_{cm} \leq 189$ GeV. In addition to usual final states, the decays H^0_1, $A^0 \to q\overline{q}$, gg are searched for. See their Figs. 15,16 for excluded regions.

[35] ABBIENDI 99E search for $e^+e^- \to H^0 A^0$ and $H^0 Z$ at E_{cm} = 183 GeV. The limit is with m_H=m_A in general two Higgs-doublet models. See their Fig. 18 for the exclusion limit in the m_H–m_A plane. Updates the results of ACKERSTAFF 98S.

[36] See Fig. 4 of ABREU 95H for the excluded region in the $m_{H^0} - m_{A^0}$ plane for general two-doublet models. For $\tan\beta > 1$, the region $m_{H^0} + m_{A^0} \lesssim 87$ GeV, $m_{H^0} < 47$ GeV is excluded at 95% CL.

[37] PICH 92 analyse H^0 with $m_{H^0} < 2m_\mu$ in general two-doublet models. Excluded regions in the space of mass-mixing angles from LEP, beam dump, and $\pi^\pm$, η rare decays are shown in Figs. 3,4. The considered mass region is not totally excluded.

Mass Limits for H^0 with Vanishing Yukawa Couplings

These limits assume that H^0 couples to gauge bosons with the same strength as the Standard Model Higgs boson, but has no coupling to quarks and leptons (this is often referred to as "fermiophobic").

VALUE (GeV)	CL%	DOCUMENT ID	TECN	COMMENT
• • • We do not use the following data for averages, fits, limits, etc. • • •				
95		[1] AALTONEN 13K	CDF	$H^0 \to W W^{(*)}$

Downloaded from https://academic.oup.com/ptep/article/2022/8/083C01/6651666 by KIT Library user on 27 September 2022

none 100–113	95	[2] AALTONEN	13L	CDF	$H^0 \to \gamma\gamma$, WW^*, ZZ^*
none 100–116	95	[3] AALTONEN	13M	TEVA	$H^0 \to \gamma\gamma$, WW^*, ZZ^*
		[4] ABAZOV	13G	D0	$H^0 \to WW^{(*)}$
none 100–113	95	[5] ABAZOV	13H	D0	$H^0 \to \gamma\gamma$
		[6] ABAZOV	13I	D0	$H^0 \to WW^{(*)}$
		[7] ABAZOV	13J	D0	$H^0 \to WW^{(*)}$, $ZZ^{(*)}$
none 100–114	95	[8] ABAZOV	13L	D0	$H^0 \to \gamma\gamma$, WW^*, ZZ^*
none 110–147	95	[9] CHATRCHYAN	13AL	CMS	$H^0 \to \gamma\gamma$
none 110–118, 119.5–121	95	[10] AAD	12N	ATLS	$H^0 \to \gamma\gamma$
none 100–114	95	[11] AALTONEN	12AN	CDF	$H^0 \to \gamma\gamma$
none 110–194	95	[12] CHATRCHYAN	12AO	CMS	$H^0 \to \gamma\gamma$, $WW^{(*)}$, $ZZ^{(*)}$
none 70–106	95	[13] AALTONEN	09AB	CDF	$H^0 \to \gamma\gamma$
none 70–100	95	[14] ABAZOV	08U	D0	$H^0 \to \gamma\gamma$
>105.8	95	[15] SCHAEL	07	ALEP	$e^+e^- \to H^0Z$, $H^0 \to WW^*$
>104.1	95	[16,17] ABDALLAH	04L	DLPH	$e^+e^- \to H^0Z$, $H^0 \to \gamma\gamma$
>107	95	[18] ACHARD	03C	L3	$H^0 \to WW^*$,ZZ^*, $\gamma\gamma$
>105.5	95	[16,19] ABBIENDI	02F	OPAL	$H^0 \to \gamma\gamma$
>105.4	95	[20] ACHARD	02C	L3	$H^0 \to \gamma\gamma$
none 60–82	95	[21] AFFOLDER	01H	CDF	$p\overline{p} \to H^0W/Z$, $H^0 \to \gamma\gamma$
> 94.9	95	[22] ACCIARRI	00S	L3	$e^+e^- \to H^0Z$, $H^0 \to \gamma\gamma$
>100.7	95	[23] BARATE	00L	ALEP	$e^+e^- \to H^0Z$, $H^0 \to \gamma\gamma$
> 96.2	95	[24] ABBIENDI	99O	OPAL	$e^+e^- \to H^0Z$, $H^0 \to \gamma\gamma$
> 78.5	95	[25] ABBOTT	99B	D0	$p\overline{p} \to H^0W/Z$, $H^0 \to \gamma\gamma$
		[26] ABREU	99P	DLPH	$e^+e^- \to H^0\gamma$ and/or $H^0 \to \gamma\gamma$

[1] AALTONEN 13K search for $H^0 \to WW^{(*)}$ in 9.7 fb^{-1} of $p\overline{p}$ collisions at E_{cm} = 1.96 TeV. A limit on cross section times branching ratio which corresponds to (1.3–6.6) times the expected cross section is given in the range m_{H^0} = 110–200 GeV at 95% CL.

[2] AALTONEN 13L combine all CDF searches with 9.45–10.0 fb^{-1} of $p\overline{p}$ collisions at E_{cm} = 1.96 TeV.

[3] AALTONEN 13M combine all Tevatron data from the CDF and D0 Collaborations of $p\overline{p}$ collisions at E_{cm} = 1.96 TeV.

[4] ABAZOV 13G search for $H^0 \to WW^{(*)}$ in 9.7 fb^{-1} of $p\overline{p}$ collisions at E_{cm} = 1.96 TeV. A limit on cross section times branching ratio which corresponds to (2–9) times the expected cross section is given for m_{H^0} = 100–200 GeV at 95% CL.

[5] ABAZOV 13H search for $H^0 \to \gamma\gamma$ in 9.6 fb^{-1} of $p\overline{p}$ collisions at E_{cm} = 1.96 TeV.

[6] ABAZOV 13I search for H^0 production in the final state with one lepton and two or more jets plus missing E_T in 9.7 fb^{-1} of $p\overline{p}$ collisions at E_{cm} = 1.96 TeV. The search is sensitive to WH^0, ZH^0 and vector-boson fusion Higgs production with $H^0 \to WW^{(*)}$. A limit on cross section times branching ratio which corresponds to (8–30) times the expected cross section is given in the range m_{H^0} = 100–200 GeV at 95% CL.

[7] ABAZOV 13J search for H^0 production in the final states $ee\mu$, $e\mu\mu$, $\mu\tau\tau$, and $e^\pm\mu^\pm$ in 8.6–9.7 fb^{-1} of $p\overline{p}$ collisions at E_{cm} = 1.96 TeV. The search is sensitive to WH^0, ZH^0 production with $H^0 \to WW^{(*)}$, $ZZ^{(*)}$, decaying to leptonic final states. A limit on cross section times branching ratio which corresponds to (2.4–13.0) times the expected cross section is given in the range m_{H^0} = 100–200 GeV at 95% CL.

[8] ABAZOV 13L combine all D0 results with up to 9.7 fb^{-1} of $p\overline{p}$ collisions at E_{cm} = 1.96 TeV.

[9] CHATRCHYAN 13AL search for $H^0 \to \gamma\gamma$ in 5.1 fb^{-1} and 5.3 fb^{-1} of pp collisions at E_{cm} = 7 and 8 TeV.

[10] AAD 12N search for $H^0 \to \gamma\gamma$ with 4.9 fb^{-1} of pp collisions at E_{cm} = 7 TeV in the mass range m_{H^0} = 110–150 GeV.

[11] AALTONEN 12AN search for $H^0 \to \gamma\gamma$ with 10 fb^{-1} of $p\overline{p}$ collisions at E_{cm} = 1.96 TeV in the mass range m_{H^0} = 100–150 GeV.

[12] CHATRCHYAN 12AO use data from CHATRCHYAN 12G, CHATRCHYAN 12E, CHATRCHYAN 12H, CHATRCHYAN 12I, CHATRCHYAN 12D, and CHATRCHYAN 12C.

[13] AALTONEN 09AB search for $H^0 \to \gamma\gamma$ in 3.0 fb^{-1} of $p\overline{p}$ collisions at E_{cm} = 1.96 TeV in the mass range m_{H^0} = 70–150 GeV. Associated H^0W, H^0Z production and WW, ZZ fusion are considered.

[14] ABAZOV 08U search for $H^0 \to \gamma\gamma$ in $p\overline{p}$ collisions at E_{cm} = 1.96 TeV in the mass range m_{H^0} = 70–150 GeV. Associated H^0W, H^0Z production and WW, ZZ fusion are considered. See their Tab. 1 for the limit on $\sigma \cdot B(H^0 \to \gamma\gamma)$, and see their Fig. 3 for the excluded region in the m_{H^0} — $B(H^0 \to \gamma\gamma)$ plane.

[15] SCHAEL 07 search for Higgs bosons in association with a fermion pair and decaying to WW^*. The limit is from this search and HEISTER 02L for a H^0 with SM production cross section.

[16] Search for associated production of a $\gamma\gamma$ resonance with a Z boson, followed by $Z \to q\overline{q}$, $\ell^+\ell^-$, or $\nu\overline{\nu}$, at $E_{cm} \leq$ 209 GeV. The limit is for a H^0 with SM production cross section.

[17] Updates ABREU 01F.

[18] ACHARD 03C search for $e^+e^- \to ZH^0$ followed by $H^0 \to WW^*$ or ZZ^* at E_{cm}= 200-209 GeV and combine with the ACHARD 02C result. The limit is for a H^0 with SM production cross section. For $B(H^0 \to WW^*) + B(H^0 \to ZZ^*) = 1$, m_{H^0} > 108.1 GeV is obtained. See fig. 6 for the limits under different BR assumptions.

[19] For $B(H^0 \to \gamma\gamma)$=1, m_{H^0} >117 GeV is obtained.

[20] ACHARD 02C search for associated production of a $\gamma\gamma$ resonance with a Z boson, followed by $Z \to q\overline{q}$, $\ell^+\ell^-$, or $\nu\overline{\nu}$, at $E_{cm} \leq$ 209 GeV. The limit is for a H^0 with SM production cross section. For $B(H^0 \to \gamma\gamma)$=1, m_{H^0} >114 GeV is obtained.

[21] AFFOLDER 01H search for associated production of a $\gamma\gamma$ resonance and a W or Z (tagged by two jets, an isolated lepton, or missing E_T). The limit assumes Standard Model values for the production cross section and for the couplings of the H^0 to W and Z bosons. See their Fig. 11 for limits with $B(H^0 \to \gamma\gamma) < 1$.

[22] ACCIARRI 00S search for associated production of a $\gamma\gamma$ resonance with a $q\overline{q}$, $\nu\overline{\nu}$, or $\ell^+\ell^-$ pair in e^+e^- collisions at E_{cm}= 189 GeV. The limit is for a H^0 with SM production cross section. For $B(H^0 \to \gamma\gamma)$=1, m_{H^0} > 98 GeV is obtained. See their Fig. 5 for limits on $B(H \to \gamma\gamma)\cdot\sigma(e^+e^- \to Hf\overline{f})/\sigma(e^+e^- \to Hf\overline{f})$ (SM).

[23] BARATE 00L search for associated production of a $\gamma\gamma$ resonance with a $q\overline{q}$, $\nu\overline{\nu}$, or $\ell^+\ell^-$ pair in e^+e^- collisions at E_{cm}= 88–202 GeV. The limit is for a H^0 with SM production cross section. For $B(H^0 \to \gamma\gamma)$=1, m_{H^0} > 109 GeV is obtained. See their Fig. 3 for limits on $B(H \to \gamma\gamma)\cdot\sigma(e^+e^- \to Hf\overline{f})/\sigma(e^+e^- \to Hf\overline{f})$ (SM).

[24] ABBIENDI 99O search for associated production of a $\gamma\gamma$ resonance with a $q\overline{q}$, $\nu\overline{\nu}$, or $\ell^+\ell^-$ pair in e^+e^- collisions at 189 GeV. The limit is for a H^0 with SM production cross section. See their Fig. 4 for limits on $\sigma(e^+e^- \to H^0Z^0)\times B(H^0 \to \gamma\gamma)\times B(X^0 \to f\overline{f})$ for various masses. Updates the results of ACKERSTAFF 98Y.

[25] ABBOTT 99B search for associated production of a $\gamma\gamma$ resonance and a dijet pair. The limit assumes Standard Model values for the production cross section and for the couplings of the H^0 to W and Z bosons. Limits in the range of $\sigma(H^0 + Z/W)\cdot B(H^0 \to \gamma\gamma)$= 0.80–0.34 pb are obtained in the mass range m_{H^0}= 65–150 GeV.

[26] ABREU 99P search for $e^+e^- \to H^0\gamma$ with $H^0 \to b\overline{b}$ or $\gamma\gamma$, and $e^+e^- \to H^0q\overline{q}$ with $H^0 \to \gamma\gamma$. See their Fig. 4 for limits on $\sigma\times B$. Explicit limits within an effective interaction framework are also given.

Mass Limits for H^0 Decaying to Invisible Final States

These limits are for a neutral scalar H^0 which predominantly decays to invisible final states. Standard Model values are assumed for the couplings of H^0 to ordinary particles unless otherwise stated.

VALUE (GeV)	CL%	DOCUMENT ID		TECN	COMMENT
• • • We do not use the following data for averages, fits, limits, etc. • • •					
		[1] AABOUD	19AI	ATLS	WW/ZZ fusion
		[2] AAD	15BD	ATLS	$pp \to H^0WX$, H^0ZX
		[3] AAD	15BH	ATLS	jet + missing E_T
		[4] AAD	14BA	ATLS	secondary vertex
		[5] AAD	14O	ATLS	$pp \to H^0ZX$
		[6] CHATRCHYAN	14B	CMS	$pp \to H^0ZX$, qqH^0X
		[7] AAD	13AG	ATLS	secondary vertex
		[8] AAD	13AT	ATLS	electron jets
		[9] CHATRCHYAN	13BJ	CMS	
		[10] AAD	12AQ	ATLS	secondary vertex
		[11] AALTONEN	12AB	CDF	secondary vertex
		[12] AALTONEN	12U	CDF	secondary vertex
>108.2	95	[13] ABBIENDI	10	OPAL	
		[14] ABBIENDI	07	OPAL	large width
>112.3	95	[15] ACHARD	05	L3	
>112.1	95	[15] ABDALLAH	04B	DLPH	
>114.1	95	[15] HEISTER	02	ALEP	$E_{cm} \leq$ 209 GeV
>106.4	95	[15] BARATE	01C	ALEP	$E_{cm} \leq$ 202 GeV
> 89.2	95	[16] ACCIARRI	00M	L3	

[1] AABOUD 19AI search for $H^0_{1,2}$ production by vector boson fusion and decay to invisible final states in 36.1 fb^{-1} of pp collisions at E_{cm} = 13 TeV. See their Fig. 6(b) for limits on cross section times branching ratios for $m_{H^0_{1,2}}$ = 0.1–3 TeV.

[2] AAD 15BD search for $pp \to H^0WX$ and $pp \to H^0ZX$ with W or Z decaying hadronically and H^0 decaying to invisible final states in 20.3 fb^{-1} at E_{cm} = 8TeV. See their Fig. 6 for a limit on the cross section times branching ratio for m_{H^0} = 115–300 GeV.

[3] AAD 15BH search for events with a jet and missing E_T in 20.3 fb^{-1} of pp collisions at E_{cm} = 8 TeV. Limits on $\sigma(H'^0)$ $B(H'^0 \to$ invisible) < (44–10) pb (95%CL) is given for $m_{H'^0}$ = 115–300 GeV.

[4] AAD 14BA search for H^0 production in the decay mode $H^0 \to X^0X^0$, where X^0 is a long-lived particle which decays to collimated pairs of e^+e^-, $\mu^+\mu^-$, or $\pi^+\pi^-$ plus invisible particles, in 20.3 fb^{-1} of pp collisions at E_{cm} = 8 TeV. See their Figs. 15 and 16 for limits on cross section times branching ratio.

[5] AAD 14O search for $pp \to H^0ZX$, $Z \to \ell\ell$, with H^0 decaying to invisible final states in 4.5 fb^{-1} at E_{cm} = 7 TeV and 20.3 fb^{-1} at E_{cm} = 8 TeV. See their Fig. 3 for a limit on the cross section times branching ratio for m_{H^0} = 110–400 GeV.

[6] CHATRCHYAN 14B search for $pp \to H^0ZX$, $Z \to \ell\ell$ and $Z \to b\overline{b}$, and also $pp \to qqH^0X$ with H^0 decaying to invisible final states using data at E_{cm} = 7 and 8 TeV. See their Figs. 10, 11 for limits on the cross section times branching ratio for m_{H^0} = 100–400 GeV.

[7] AAD 13AG search for H^0 production in the decay mode $H^0 \to X^0X^0$, where X^0 is a long-lived particle which decays to $\mu^+\mu^-X'^0$, in 1.9 fb^{-1} of pp collisions at E_{cm} = 7 TeV. See their Fig. 7 for limits on cross section times branching ratio.

[8] AAD 13AT search for H^0 production in the decay $H^0 \to X^0X^0$, where X^0 eventually decays to clusters of collimated e^+e^- pairs, in 2.04 fb^{-1} of pp collisions at E_{cm} = 7 TeV. See their Fig. 3 for limits on cross section times branching ratio.

[9] CHATRCHYAN 13BJ search for H^0 production in the decay chain $H^0 \to X^0X^0$, $X^0 \to \mu^+\mu^-X'^0$ in 5.3 fb^{-1} of pp collisions at E_{cm} = 7 TeV. See their Fig. 2 for limits on cross section times branching ratio.

[10] AAD 12AQ search for H^0 production in the decay mode $H^0 \to X^0X^0$, where X^0 is a long-lived particle which decays mainly to $b\overline{b}$ in the muon detector, in 1.94 fb^{-1} of pp collisions at E_{cm} = 7 TeV. See their Fig. 3 for limits on cross section times branching ratio for m_{H^0} = 120, 140 GeV, m_{X^0} = 20, 40 GeV in the $c\tau$ range of 0.5–35 m.

[11] AALTONEN 12AB search for H^0 production in the decay $H^0 \to X^0X^0$, where X^0 eventually decays to clusters of collimated $\ell^+\ell^-$ pairs, in 5.1 fb^{-1} of $p\overline{p}$ collisions at E_{cm} = 1.96 TeV. Cross section limits are provided for a benchmark MSSM model incorporating the parameters given in Table VI.

[12] AALTONEN 12U search for H^0 production in the decay mode $H^0 \to X^0X^0$, where X^0 is a long-lived particle with $c\tau \approx$ 1 cm which decays mainly to $b\overline{b}$, in 3.2 fb^{-1} of $p\overline{p}$

Downloaded from https://academic.oup.com/ptep/article/2022/8/083C01/6651666 by KIT Library user on 27 September 2022

collisions at E_{cm} = 1.96 TeV. See their Figs. 9 and 10 for limits on cross section times branching ratio for m_{H^0} = (130–170) GeV, m_{χ^0} = 20, 40 GeV.

[13] ABBIENDI 10 search for $e^+e^- \to H^0 Z$ with H^0 decaying invisibly. The limit assumes SM production cross section and B($H^0 \to$ invisible) = 1.

[14] ABBIENDI 07 search for $e^+e^- \to H^0 Z$ with $Z \to q\overline{q}$ and H^0 decaying to invisible final states. The H^0 width is varied between 1 GeV and 3 TeV. A limit $\sigma \cdot$B($H^0 \to$ invisible) < (0.07–0.57) pb (95%CL) is obtained at E_{cm} = 206 GeV for m_{H^0} = 60–114 GeV.

[15] Search for $e^+e^- \to H^0 Z$ with H^0 decaying invisibly. The limit assumes SM production cross section and B($H^0 \to$ invisible) = 1.

[16] ACCIARRI 00M search for $e^+e^- \to Z H^0$ with H^0 decaying invisibly at E_{cm}=183–189 GeV. The limit assumes SM production cross section and B($H^0 \to$ invisible)=1. See their Fig. 6 for limits for smaller branching ratios.

Mass Limits for Light A^0

These limits are for a pseudoscalar A^0 in the mass range below $\mathcal{O}(10)$ GeV.

VALUE (GeV)	DOCUMENT ID		TECN	COMMENT
• • • We do not use the following data for averages, fits, limits, etc. • • •				
	[1] AAD	20AE	ATLS	$H^0 \to Z A^0$
	[2] AABOUD	18AP	ATLS	$H^0 \to A^0 A^0$
	[3] KHACHATRY...	17AZ	CMS	$H^0 \to A^0 A^0$
	[4] ABLIKIM	16E	BES3	$J/\psi \to A^0 \gamma$
	[5] KHACHATRY...	16F	CMS	$H^0 \to A^0 A^0$
	[6] LEES	15H	BABR	$\Upsilon(1S) \to A^0 \gamma$
	[7] LEES	13C	BABR	$\Upsilon(1S) \to A^0 \gamma$
	[8] LEES	13L	BABR	$\Upsilon(1S) \to A^0 \gamma$
	[9] LEES	13R	BABR	$\Upsilon(1S) \to A^0 \gamma$
	[10] ABLIKIM	12	BES3	$J/\psi \to A^0 \gamma$
	[11] CHATRCHYAN	12V	CMS	$A^0 \to \mu^+\mu^-$
	[12] AALTONEN	11P	CDF	$t \to b H^+$, $H^+ \to W^+ A^0$
	[13,14] ABOUZAID	11A	KTEV	$K_L \to \pi^0\pi^0 A^0$, $A^0 \to \mu^+\mu^-$
	[15] DEL-AMO-SA...	11J	BABR	$\Upsilon(1S) \to A^0 \gamma$
	[16] LEES	11H	BABR	$\Upsilon(2S, 3S) \to A^0 \gamma$
	[17] ANDREAS	10	RVUE	
	[14,18] HYUN	10	BELL	$B^0 \to K^{*0} A^0$, $A^0 \to \mu^+\mu^-$
	[14,19] HYUN	10	BELL	$B^0 \to \rho^0 A^0$, $A^0 \to \mu^+\mu^-$
	[20] AUBERT	09P	BABR	$\Upsilon(3S) \to A^0 \gamma$
	[21] AUBERT	09Z	BABR	$\Upsilon(2S) \to A^0 \gamma$
	[22] AUBERT	09Z	BABR	$\Upsilon(3S) \to A^0 \gamma$
	[14,23] TUNG	09	K391	$K_L \to \pi^0\pi^0 A^0$, $A^0 \to \gamma\gamma$
	[24] LOVE	08	CLEO	$\Upsilon(1S) \to A^0 \gamma$
	[25] BESSON	07	CLEO	$\Upsilon(1S) \to \eta_b \gamma$
	[26] PARK	05	HYCP	$\Sigma^+ \to p A^0$, $A^0 \to \mu^+\mu^-$
	[27] BALEST	95	CLE2	$\Upsilon(1S) \to A^0 \gamma$
	[28] ANTREASYAN	90C	CBAL	$\Upsilon(1S) \to A^0 \gamma$

[1] AAD 20AE search for the decay $H^0 \to Z A^0$, $Z \to \ell^+\ell^-$, A^0 decaying hadronically ($A^0 \to gg$ or $s\overline{s}$), in 139 fb^{-1} of pp collisions at E_{cm} = 13 TeV. Limit on the product of production cross section and the $H^0 \to Z A^0$ branching ratio in the range 17–340 pb (95% CL) is given for m_{A^0} = 0.5–4.0 GeV, see their Table I.

[2] AABOUD 18AP search for the decay $H^0 \to A^0 A^0 \to \mu^+\mu^-\mu^+\mu^-$ in 36.1 fb^{-1} of pp collisions at E_{cm} = 13 TeV. See their Fig. 10(b) for limits on B($H^0 \to A^0 A^0$) in the range m_{A^0} = 1–2.5, 4.5–8 GeV, assuming a type-II two-doublet plus singlet model with tan(β) = 5.

[3] KHACHATRYAN 17AZ search for the decay $H^0 \to A^0 A^0 \to \tau^+\tau^-\tau^+\tau^-$, $\mu^+\mu^- b\overline{b}$, and $\mu^+\mu^-\tau^+\tau^-$ in 19.7 fb^{-1} of pp collisions at E_{cm} = 8 TeV. See their Figs. 4, 5, and 6 for cross section limits in the range m_{A^0} = 5–62.5 GeV. See also their Figs. 7, 8, and 9 for interpretation of the data in terms of models with two Higgs doublets and a singlet.

[4] ABLIKIM 16E search for the process $J/\psi \to A^0 \gamma$ with A^0 decaying to $\mu^+\mu^-$ and give limits on B($J/\psi \to A^0\gamma$)·B($A^0 \to \mu^+\mu^-$) in the range 2.8×10^{-8}–5.0×10^{-6} (90% CL) for 0.212 $\leq m_{A^0} \leq$ 3.0 GeV. See their Fig. 5.

[5] KHACHATRYAN 16F search for the decay $H^0 \to A^0 A^0 \to \tau^+\tau^-\tau^+\tau^-$ in 19.7 fb^{-1} of pp collisions at E_{cm} = 8 TeV. See their Fig. 8 for cross section limits for m_{A^0} = 4–8 GeV.

[6] LEES 15H search for the process $\Upsilon(2S) \to \Upsilon(1S)\pi^+\pi^- \to A^0\gamma\pi^+\pi^-$ with A^0 decaying to $c\overline{c}$ and give limits on B($\Upsilon(1S) \to A^0\gamma$)·B($A^0 \to c\overline{c}$) in the range 7.4×10^{-5}–2.4×10^{-3} (90% CL) for 4.00 $\leq m_{A^0} \leq$ 8.95 and 9.10 $\leq m_{A^0} \leq$ 9.25 GeV. See their Fig. 6.

[7] LEES 13C search for the process $\Upsilon(2S, 3S) \to \Upsilon(1S)\pi^+\pi^- \to A^0\gamma\pi^+\pi^-$ with A^0 decaying to $\mu^+\mu^-$ and give limits on B($\Upsilon(1S) \to A^0\gamma$)·B($A^0 \to \mu^+\mu^-$) in the range (0.3–9.7) $\times 10^{-6}$ (90% CL) for 0.212 $\leq m_{A^0} \leq$ 9.20 GeV. See their Fig. 5(e) for limits on the $b-A^0$ Yukawa coupling derived by combining this result with AUBERT 09Z.

[8] LEES 13L search for the process $\Upsilon(2S) \to \Upsilon(1S)\pi^+\pi^- \to A^0\gamma\pi^+\pi^-$ with A^0 decaying to gg or $s\overline{s}$ and give limits on B($\Upsilon(1S) \to A^0\gamma$)·B($A^0 \to gg$) between 1×10^{-6} and 2×10^{-2} (90% CL) for 0.5 $\leq m_{A^0} \leq$ 9.0 GeV, and B($\Upsilon(1S) \to A^0\gamma$)·B($A^0 \to s\overline{s}$) between 4×10^{-6} and 1×10^{-3} (90%CL) for 1.5 $\leq m_{A^0} \leq$ 9.0 GeV. See their Fig. 4.

[9] LEES 13R search for the process $\Upsilon(2S) \to \Upsilon(1S)\pi^+\pi^- \to A^0\gamma\pi^+\pi^-$ with A^0 decaying to $\tau^+\tau^-$ and give limits on B($\Upsilon(1S) \to A^0\gamma$)·B($A^0 \to \tau^+\tau^-$) in the range 0.9–13 $\times 10^{-5}$ (90% CL) for 3.6 $\leq m_{A^0} \leq$ 9.2 GeV. See their Fig. 4 for limits on the $b-A^0$ Yukawa coupling derived by combining this result with AUBERT 09P.

[10] ABLIKIM 12 searches for the process $\psi(3686) \to \pi\pi J/\psi$, $J/\psi \to A^0\gamma$ with A^0 decaying to $\mu^+\mu^-$. It gives mass dependent limits on B($J/\psi \to A^0\gamma$)·B($A^0 \to \mu^+\mu^-$) in the range 4×10^{-7}–2.1×10^{-5} (90% C.L.) for 0.212 $\leq m_{A^0} \leq$ 3.0 GeV. See their Fig. 2.

[11] CHATRCHYAN 12V search for A^0 production in the decay $A^0 \to \mu^+\mu^-$ with 1.3 fb^{-1} of pp collisions at E_{cm} = 7 TeV. A limit on $\sigma(A^0)$·B($A^0 \to \mu^+\mu^-$) in the range (1.5–7.5) pb is given for m_{A^0} = (5.5–8.7) and (11.5–14) GeV at 95% CL.

[12] AALTONEN 11P search in 2.7 fb^{-1} of $p\overline{p}$ collisions at E_{cm} = 1.96 TeV for the decay chain $t \to b H^+$, $H^+ \to W^+ A^0$, $A^0 \to \tau^+\tau^-$ with m_{A^0} between 4 and 9 GeV. See their Fig. 4 for limits on B($t \to b H^+$) for 90 < m_{H^+} < 160 GeV.

[13] ABOUZAID 11A search for the decay chain $K_L \to \pi^0\pi^0 A^0$, $A^0 \to \mu^+\mu^-$ and give a limit B($K_L \to \pi^0\pi^0 A^0$) · B($A^0 \to \mu^+\mu^-$) < 1.0×10^{-10} at 90% CL for m_{A^0} = 214.3 MeV.

[14] The search was motivated by PARK 05.

[15] DEL-AMO-SANCHEZ 11J search for the process $\Upsilon(2S) \to \Upsilon(1S)\pi^+\pi^- \to A^0\gamma\pi^+\pi^-$ with A^0 decaying to invisible final states. They give limits on B($\Upsilon(1S) \to A^0\gamma$)·B($A^0 \to$ invisible) in the range (1.9–4.5) $\times 10^{-6}$ (90% CL) for 0 $\leq m_{A^0} \leq$ 8.0 GeV, and (2.7–37) $\times 10^{-6}$ for 8.0 $\leq m_{A^0} \leq$ 9.2 GeV.

[16] LEES 11H search for the process $\Upsilon(2S, 3S) \to A^0\gamma$ with A^0 decaying hadronically and give limits on B($\Upsilon(2S, 3S) \to A^0\gamma$)·B($A^0 \to$ hadrons) in the range 1×10^{-6}–8×10^{-5} (90% CL) for 0.3 < m_{A^0} < 7 GeV. The decay rates for $\Upsilon(2S)$ and $\Upsilon(3S)$ are assumed to be equal up to the phase space factor. See their Fig. 5.

[17] ANDREAS 10 analyze constraints from rare decays and other processes on a light A^0 with $m_{A^0} < 2m_\mu$ and give limits on its coupling to fermions at the level of 10^{-4} times the Standard Model value.

[18] HYUN 10 search for the decay chain $B^0 \to K^{*0} A^0$, $A^0 \to \mu^+\mu^-$ and give a limit on B($B^0 \to K^{*0} A^0$) · B($A^0 \to \mu^+\mu^-$) in the range (2.26–5.53) $\times 10^{-8}$ at 90%CL for m_{A^0} = 212–300 MeV. The limit for m_{A^0} = 214.3 MeV is 2.26×10^{-8}.

[19] HYUN 10 search for the decay chain $B^0 \to \rho^0 A^0$, $A^0 \to \mu^+\mu^-$ and give a limit on B($B^0 \to \rho^0 A^0$) · B($A^0 \to \mu^+\mu^-$) in the range (1.73–4.51) $\times 10^{-8}$ at 90%CL for m_{A^0} = 212–300 MeV. The limit for m_{A^0} = 214.3 MeV is 1.73×10^{-8}.

[20] AUBERT 09P search for the process $\Upsilon(3S) \to A^0\gamma$ with $A^0 \to \tau^+\tau^-$ for 4.03 < m_{A^0} < 9.52 and 9.61 < m_{A^0} < 10.10 GeV, and give limits on B($\Upsilon(3S) \to A^0\gamma$)·B($A^0 \to \tau^+\tau^-$) in the range (1.5–16) $\times 10^{-5}$ (90% CL).

[21] AUBERT 09Z search for the process $\Upsilon(2S) \to A^0\gamma$ with $A^0 \to \mu^+\mu^-$ for 0.212 < m_{A^0} < 9.3 GeV and give limits on B($\Upsilon(2S) \to A^0\gamma$)·B($A^0 \to \mu^+\mu^-$) in the range (0.3–8) $\times 10^{-6}$ (90% CL).

[22] AUBERT 09Z search for the process $\Upsilon(3S) \to A^0\gamma$ with $A^0 \to \mu^+\mu^-$ for 0.212 < m_{A^0} < 9.3 GeV and give limits on B($\Upsilon(3S) \to A^0\gamma$)·B($A^0 \to \mu^+\mu^-$) in the range (0.3–5) $\times 10^{-6}$ (90% CL).

[23] TUNG 09 search for the decay chain $K_L \to \pi^0\pi^0 A^0$, $A^0 \to \gamma\gamma$ and give a limit on B($K_L \to \pi^0\pi^0 A^0$) · B($A^0 \to \gamma\gamma$) in the range (2.4–10.7) $\times 10^{-7}$ at 90%CL for m_{A^0} = 194.3–219.3 MeV. The limit for m_{A^0} = 214.3 MeV is 2.4×10^{-7}.

[24] LOVE 08 search for the process $\Upsilon(1S) \to A^0\gamma$ with $A^0 \to \mu^+\mu^-$ (for $m_{A^0} < 2m_\tau$) and $A^0 \to \tau^+\tau^-$. Limits on B($\Upsilon(1S) \to A^0\gamma$) · B($A^0 \to \ell^+\ell^-$) in the range 10^{-6}–10^{-4} (90% CL) are given.

[25] BESSON 07 give a limit B($\Upsilon(1S) \to \eta_b\gamma$) · B($\eta_b \to \tau^+\tau^-$) < 0.27% (95% CL), which constrains a possible A^0 exchange contribution to the η_b decay.

[26] PARK 05 found three candidate events for $\Sigma^+ \to p\mu^+\mu^-$ in the HyperCP experiment. Due to a narrow spread in dimuon mass, they hypothesize the events as a possible signal of a new boson. It can be interpreted as a neutral particle with m_{A^0} = 214.3 ± 0.5 MeV and the branching fraction B($\Sigma^+ \to pA^0$)·B($A^0 \to \mu^+\mu^-$) = $(3.1^{+2.4}_{-1.9} \pm 1.5) \times 10^{-8}$.

[27] BALEST 95 give limits B($\Upsilon(1S) \to A^0\gamma$) ¡ 1.5×10^{-5} at 90% CL for m_{A^0} < 5 GeV. The limit becomes < 10^{-4} for m_{A^0} < 7.7 GeV.

[28] ANTREASYAN 90C give limits B($\Upsilon(1S) \to A^0\gamma$) ¡ 5.6×10^{-5} at 90% CL for m_{A^0} < 7.2 GeV. A^0 is assumed not to decay in the detector.

Other Mass Limits

We use a symbol H^0_1 if mass < 125 GeV or H^0_2 if mass > 125 GeV. The notation H^0 is reserved for the 125 GeV particle.

VALUE (GeV)	CL%	DOCUMENT ID		TECN	COMMENT
• • • We do not use the following data for averages, fits, limits, etc. • • •					
		[1] AAD	22A	ATLS	$H^0 \to A^0 A^0$
		[2] AAD	21AF	ATLS	$H^0_2 \to Z Z$
		[3] AAD	21AI	ATLS	$A^0 \to Z H^0_2$
		[4] AAD	21AY	ATLS	$H^0_2 \to \gamma\gamma$
		[5] AAD	21AZ	ATLS	$A^0_2 \to H^0 A^0_1$
		[6] AAD	21BB	ATLS	$A^0_2 \to H^0 A^0_1$
		[7] AAD	21BE	ATLS	$A^0_1 \to$ invisible
		[8] ABRATENKO	21	MCBN	$K^+ \to H^0_1 \pi^+$
		[9] SIRUNYAN	21A	CMS	$H^0_2 \to Z A^0$, $A^0 \to$ invisible
		[10] TUMASYAN	21F	CMS	$H^0_3 \to H^0 H^0_{1,2}$
		[11] AAD	20AA	ATLS	$H^0_2/A^0 \to \tau^+\tau^-$
		[12] AAD	20AI	ATLS	$H^0 \to A^0 A^0$
		[13] AAD	20AO	ATLS	$H^0_2 \to H^0 H^0$
		[14] AAD	20C	ATLS	$H^0_2 \to H^0 H^0$
		[15] AAD	20L	ATLS	$H^0_2 \to b\overline{b}$
		[16] AAD	20X	ATLS	$H^0_2 \to H^0 H^0$
		[17] AAIJ	20AL	LHCB	$A^0 \to \mu^+\mu^-$
		[18] SIRUNYAN	20	CMS	$H^0 \to A^0 A^0$
		[19] SIRUNYAN	20AA	CMS	$H^0_2 \to Z A^0$ or $A^0 \to Z H^0_2$
		[20] SIRUNYAN	20AC	CMS	$A^0 \to Z H^0$

Downloaded from https://academic.oup.com/ptep/article/2022/8/083C01/6651666 by KIT Library user on 27 September 2022

[21] SIRUNYAN	20AD	CMS	$H^0_2 \to \mu\tau,\ e\tau$	
[22] SIRUNYAN	20AF	CMS	$H^0_2/A^0 \to t\overline{t}$	
[23] SIRUNYAN	20AP	CMS	$H^0,\ H^0_2 \to A^0 A^0$	
[24] SIRUNYAN	20Y	CMS	$H^0_2 \to W^+ W^-$	
[25] SIRUNYAN	20Z	CMS	$t\overline{t}H^0_{1,2}$ or $t\overline{t}A^0$, $H^0_{1,2}/A^0 \to e^+e^-,\ \mu^+\mu^-$	
[26] AABOUD	19A	ATLS	$H^0_2 \to H^0 H^0$	
[27] AABOUD	19AG	ATLS	$H^0 \to A^0 A^0$	
[28] AABOUD	19O	ATLS	$H^0_2 \to H^0 H^0$	
[29] AABOUD	19T	ATLS	$H^0_2 \to H^0 H^0$	
[30] AABOUD	19V	ATLS	two doublet + pseudoscalar model	
[31] AABOUD	19Y	ATLS	$H^0_2 \to \mu^+\mu^-$	
[32] AALTONEN	19	CDF	$H^0_{1,2} \to b\overline{b}$	
[33] SIRUNYAN	19	CMS	$H^0_2 \to H^0 H^0$	
[34] SIRUNYAN	19AE	CMS	$A^0 \to \tau^+\tau^-$	
[35] SIRUNYAN	19AN	CMS	$A^0_2 \to H^0 A^0_1$	
[36] SIRUNYAN	19AV	CMS	$A^0 \to Z H^0$	
[37] SIRUNYAN	19B	CMS	$H^0_{1,2}/A^0 \to b\overline{b}$	
[38] SIRUNYAN	19BB	CMS	$H^0_1 \to \gamma\gamma$	
[39] SIRUNYAN	19BD	CMS	$H^0 \to A^0 A^0$	
[40] SIRUNYAN	19BE	CMS	$H^0_2 \to H^0 H^0$	
[41] SIRUNYAN	19BQ	CMS	$H^0_{1,2} \to A^0 A^0$	
[42] SIRUNYAN	19CR	CMS	$H^0_2/A^0 \to \mu^+\mu^-$	
[43] SIRUNYAN	19H	CMS	$H^0_2 \to H^0 H^0$	
[44] AABOUD	18AA	ATLS	$H^0_2 \to Z\gamma$	
[45] AABOUD	18AG	ATLS	$H^0 \to A^0 A^0$	
[46] AABOUD	18AH	ATLS	$A^0 \to Z H^0_2$	
[47] AABOUD	18AI	ATLS	$A^0 \to Z H^0$	
[48] AABOUD	18BF	ATLS	$H^0_2 \to Z Z$	
[49] AABOUD	18BU	ATLS	$H^0_2 \to H^0 H^0$	
[50] AABOUD	18BX	ATLS	$H^0 \to A^0 A^0$	
[51] AABOUD	18CQ	ATLS	$H^0_2 \to H^0 H^0$	
[52] AABOUD	18F	ATLS	$H^0_2 \to W^+ W^-,\ Z Z$	
[53] AAIJ	18AM	LHCB	$H^0_{1,2} \to \mu\tau$	
[54] AAIJ	18AQ	LHCB	$A^0 \to \mu^+\mu^-$	
[55] AAIJ	18AQ	LHCB	$H^0 \to A^0 A^0$, $A^0 \to \mu^+\mu^-$	
[56] SIRUNYAN	18AF	CMS	$H^0_2 \to H^0 H^0$	
[57] SIRUNYAN	18BA	CMS	$H^0_2 \to Z Z$	
[58] SIRUNYAN	18CW	CMS	$H^0_2 \to H^0 H^0$	
[59] SIRUNYAN	18DK	CMS	$H^0_2 \to Z\gamma$	
[60] SIRUNYAN	18DT	CMS	$H^0 \to A^0 A^0$	
[61] SIRUNYAN	18DU	CMS	$H^0_2 \to \gamma\gamma$	
[62] SIRUNYAN	18ED	CMS	$A^0 \to Z H^0$	
[63] SIRUNYAN	18EE	CMS	$H^0 \to A^0 A^0$	
[64] SIRUNYAN	18F	CMS	pp, 13 TeV, $H^0_2 \to H^0 H^0$	
[65] AABOUD	17	ATLS	$H^0_2 \to Z\gamma$	
[66] AABOUD	17AP	ATLS	$H^0_2 \to \gamma\gamma$	
[67] AABOUD	17AW	ATLS	$H^0_2 \to Z\gamma$	
[68] KHACHATRY...	17AZ	CMS	$H^0 \to A^0 A^0$	
[69] KHACHATRY...	17D	CMS	pp, 8, 13 TeV, $H^0_2 \to Z\gamma$	
[70] KHACHATRY...	17R	CMS	$H^0_2 \to \gamma\gamma$	
[71] SIRUNYAN	17CN	CMS	pp, 8 TeV, $H^0_2 \to H^0 H^0$	
[72] SIRUNYAN	17Y	CMS	pp, 8, 13 TeV, $H^0_2 \to Z\gamma$	
[73] AABOUD	16AB	ATLS	$H^0 \to A^0 A^0$	
[74] AABOUD	16AE	ATLS	$H^0_2 \to W^+ W^-,\ Z Z$	
[75] AABOUD	16H	ATLS	$H^0_2 \to \gamma\gamma$	
[76] AABOUD	16I	ATLS	$H^0_2 \to H^0 H^0$	
[77] AAD	16AX	ATLS	$H^0 \to Z Z$	
[78] AAD	16C	ATLS	$H^0 \to W^+ W^-$	
[79] AAD	16L	ATLS	$H^0 \to A^0 A^0$	
[80] AAD	16L	ATLS	$H^0_2 \to A^0 A^0$	
[81] AALTONEN	16C	CDF	$H^0_1 H^\pm \to H^0_1 H^0_1 W^*$, $H^0_1 \to \gamma\gamma$	
[82] KHACHATRY...	16BG	CMS	$H^0_2 \to H^0 H^0$	
[83] KHACHATRY...	16BQ	CMS	pp, 8 TeV, $H^0_2 \to H^0 H^0$	
[84] KHACHATRY...	16F	CMS	$H^0 \to H^0_1 H^0_1$	
[85] KHACHATRY...	16M	CMS	$H^0_2 \to \gamma\gamma$	
[86] KHACHATRY...	16P	CMS	$H^0_2 \to H^0 H^0$	
[87] KHACHATRY...	16P	CMS	$A^0 \to Z H^0$	
[88] AAD	15BK	ATLS	$H^0_2 \to H^0 H^0$	
[89] AAD	15BZ	ATLS	$H^0 \to A^0 A^0$	
[90] AAD	15BZ	ATLS	$H^0_2 \to A^0 A^0$	
[91] AAD	15CE	ATLS	$H^0_2 \to H^0 H^0$	
[92] AAD	15H	ATLS	$H^0_2 \to H^0 H^0$	
[93] AAD	15S	ATLS	$A^0 \to Z H^0$	
[94] KHACHATRY...	15AW	CMS	$H^0_2 \to W^+ W^-,\ Z Z$	
[95] KHACHATRY...	15BB	CMS	$H^0 \to \gamma\gamma$	
[96] KHACHATRY...	15N	CMS	$A^0 \to Z H^0$	
[97] KHACHATRY...	15O	CMS	$A^0 \to Z H^0$	
[98] KHACHATRY...	15R	CMS	$H^0_2 \to H^0 H^0$	
[99] AAD	14AP	ATLS	$H^0 \to \gamma\gamma$	
[100] AAD	14M	ATLS	$H^0_2 \to H^\pm W^\mp \to H^0 W^\pm W^\mp$, $H^0 \to b\overline{b}$	
[101] CHATRCHYAN	14G	CMS	$H^0 \to W W^{(*)}$	
[102] KHACHATRY...	14P	CMS	$H^0 \to \gamma\gamma$	
[103] AALTONEN	13P	CDF	$H'^0 \to H^\pm W^\mp \to H^0 W^+ W^-$	
[104] CHATRCHYAN	13BJ	CMS	$H^0 \to A^0 A^0$	
[105] AALTONEN	11P	CDF	$t \to b H^+$, $H^+ \to W^+ A^0$	
[106] ABBIENDI	10	OPAL	$H^0 \to \widetilde{\chi}^0_1 \widetilde{\chi}^0_2$	
[107] SCHAEL	10	ALEP	$H^0 \to A^0 A^0$	
[108] ABAZOV	09V	D0	$H^0 \to A^0 A^0$	
none 3–63	95	[109] ABBIENDI	05A	OPAL	A^0, Type II model
>104	95	[110] ABBIENDI	04K	OPAL	$H^0 \to$ 2 jets
		[111] ABDALLAH	04	DLPH	$H^0 V V$ couplings
>110.3	95	[112] ACHARD	04B	L3	$H^0 \to$ 2 jets
		[113] ACHARD	04F	L3	Anomalous coupling
		[114] ABBIENDI	03F	OPAL	$e^+e^- \to H^0 Z$, $H^0 \to$ any
		[115] ABBIENDI	03G	OPAL	$H^0_1 \to A^0 A^0$
>105.4	95	[116,117] HEISTER	02L	ALEP	$H^0_1 \to \gamma\gamma$
>109.1	95	[118] HEISTER	02M	ALEP	$H^0 \to$ 2 jets or $\tau^+\tau^-$
none 12–56	95	[119] ABBIENDI	01E	OPAL	A^0, Type-II model
		[120] ACCIARRI	00R	L3	$e^+e^- \to H^0\gamma$ and/or $H^0 \to \gamma\gamma$
		[121] ACCIARRI	00R	L3	$e^+e^- \to e^+e^- H^0$
		[122] GONZALEZ...	98B	RVUE	Anomalous coupling
		[123] KRAWCZYK	97	RVUE	$(g-2)_\mu$
		[124] ALEXANDER	96H	OPAL	$Z \to H^0\gamma$

[1] AAD 22A search for the decay chain $H^0 \to A^0 A^0 \to \mu^+\mu^- b\overline{b}$ in 139 fb^{-1} of pp collisions at E_{cm} = 13 TeV. See their Fig. 9 for limits on the overall branching fraction in the range m_{A^0} = 16–62 GeV. See also Fig. 11 for limits without assuming A^0 is pseudoscalar.

[2] AAD 21AF search for production of a heavy H^0_2 state decaying to $Z Z$ in the final states $\ell^+\ell^-\ell'^+\ell'^-$ and $\ell^+\ell^-\nu\overline{\nu}$ in 139 fb^{-1} of pp collisions at E_{cm} = 13 TeV. See their Fig. 4 for upper limits on cross section times branching ratio for $m_{H^0_2}$ = 0.2–2.0 TeV assuming ggF or VBF with narrow width approximation, and Fig. 5 for upper limits on cross section times branching ratio for $m_{H^0_2}$ = 0.4–2.0 TeV assuming ggF, and with several assumptions on its width.

[3] AAD 21AI search for production of an A^0 in gluon-gluon fusion and in association with a $b\overline{b}$, decaying to $Z H^0_2 \to \ell^+\ell^- b\overline{b}$ or $\ell^+\ell^- W^+ W^-$ in 139 fb^{-1} of pp collisions at E_{cm} = 13 TeV. See their Figs. 9 and 13 for cross section limits for m_{A^0} = 230–800 GeV and $m_{H^0_2}$ = 130–700 GeV.

[4] AAD 21AY search for production of a scalar resonance decaying to $\gamma\gamma$ in 139 fb^{-1} of pp collisions at E_{cm} = 13 TeV. See their Fig. 5(a) for limits on fiducial cross section times branching ratio for $m_{H^0_2}$ = 0.16–3 TeV with narrow width approximation, and Table 2 with several assumptions on the width.

[5] AAD 21AZ search for production of A^0_2 decaying to $H^0 A^0_1$ followed by $H^0 \to \gamma\gamma$, $A^0_1 \to$ invisible in 139 fb^{-1} of pp collisions at E_{cm} = 13 TeV. See their Figs. 10–12 for limits in terms of two-Higgs-doublet model plus singlet pseudoscalar and a fermionic Dark Matter particle.

[6] AAD 21BB search for production of A^0_2 by gluon fusion or associated $A^0_2 b\overline{b}$ production, decaying to $H^0 A^0_1$ followed by $H^0 \to b\overline{b}$, $A^0_1 \to$ invisible in 139 fb^{-1} of pp collisions at E_{cm} = 13 TeV. See their Fig. 8 for limits in terms of two-Higgs-doublet plus singlet pseudoscalar model.

[7] AAD 21BE search for production of A^0_1 associated with a single top quark and either a light quark or a W boson, decaying to invisible final states, in 139 fb^{-1} of pp collisions at E_{cm} = 13 TeV. See their Figs. 13–15 for limits in terms of two-Higgs-doublet model plus singlet pseudoscalar, which is assumed to decay to a pair of Dark Matter particles.

[8] ABRATENKO 21 search for a singlet scalar boson H^0_1 having a small mixing with the SM Higgs boson in the decay chain $K^+ \to H^0_1\pi^+$, $H^0_1 \to e^+e^-$ from data corresponding to 1.93×10^{20} protons on NuMI target. See their Fig. 2 for limits on the SM Higgs component of H^0_1 for $m_{H^0_1}$ = 3–210 MeV.

[9] SIRUNYAN 21A search for $H^0_2 \to Z A^0$ with $Z \to \ell^+\ell^-$, A^0 decaying invisibly, in 137 fb^{-1} of pp collisions at E_{cm} = 13 TeV. See their Fig. 8 for excluded regions in the mass parameter space of two Higgs doublet plus singlet model with a certain choice of the model parameters.

[10] TUMASYAN 21F search for gluon fusion production of H^0_3 decaying to $H^0 H^0_{1,2} \to \tau^+\tau^- b\overline{b}$ in 137 fb^{-1} of pp collisions at E_{cm} = 13 TeV. See their Figs. 5 and 6 for limits on cross section times branching ratios for $m_{H^0_{1,2}}$ = 0.06–2.8 TeV and $m_{H^0_3}$ = 0.24–3.0 TeV.

[11] AAD 20AA search for $H^0_2/A^0 \to \tau^+\tau^-$ produced by gluon fusion or b-associated production using 139 fb^{-1} of pp collisions at E_{cm} = 13 TeV. See their Fig. 2(a), 2(b) for limits on the product of cross section and branching ratio for $m_{H^0_2}$, m_{A^0} = 0.2–2.5 TeV.

Downloaded from https://academic.oup.com/ptep/article/2022/8/083C01/6651666 by KIT Library user on 27 September 2022

[12] AAD 20AI search for ZH^0 production followed by the decay $H^0 \rightarrow A^0A^0 \rightarrow b\overline{b}b\overline{b}$ in 36 fb^{-1} of pp collisions at E_{cm} = 13 TeV. The search looks for collimated $A^0 \rightarrow b\overline{b}$ decays and is complementary to AABOUD 18BX. See their Fig. 10 for limits on the product of production cross section and branching ratios in the range m_{A^0} = 15–30 GeV.

[13] AAD 20AO search for gluon fusion production of H^0_2 decaying to $H^0H^0 \rightarrow \tau^+\tau^-b\overline{b}$ (with hadronically decaying $\tau^+\tau^-$) using 139 fb^{-1} of pp collisions at E_{cm} = 13 TeV. Limit on the product of production cross section times branching ratios in the range 28–817 fb (95% CL) is given for m_{A^0} = 1.0–3.0 TeV, see their Fig. 13.

[14] AAD 20C combine searches for a scalar resonance decaying to H^0H^0 in 36.1 fb^{-1} of pp collisions at E_{cm} = 13 TeV from AABOUD 19A, AABOUD 19O, AABOUD 18CQ, AABOUD 19T, AABOUD 18CW, and AABOUD 18BU. See their Fig. 5(a) for limits on cross section times branching ratio for $m_{H^0_2}$ = 0.26–3 TeV.

[15] AAD 20L search for b-associated production of H^0_2 decaying to $b\overline{b}$ in 27.8 fb^{-1} of pp collisions at E_{cm} = 13 TeV. See their Fig. 8 for limits on the product of cross section and branching ratio for $m_{H^0_2}$ = 0.45–1.4 TeV.

[16] AAD 20X search for vector-boson-fusion production of H^0_2 decaying to H^0H^0 using 126 fb^{-1} of pp collisions at E_{cm} = 13 TeV. See their Fig. 5 for limits on the product of cross section and branching ratio for the assumptions of a narrow- and broad-width resonance.

[17] AAIJ 20AL search for dimuon resonance in the mass range 0.2–60 GeV in 5.1 fb^{-1} of pp collisions at E_{cm} = 13 TeV, in inclusive and b quark associated production. Displaced decays are searched for for masses below 3 GeV. See their Figs. 7–9 for cross section limits and Fig. 10 for limits for mixing angle in two Higgs doublet plus singlet model (at 90% CL).

[18] SIRUNYAN 20 search for the decay $H^0 \rightarrow A^0A^0 \rightarrow \tau^+\tau^-\tau^+\tau^-$ or $\tau^+\tau^-\mu^+\mu^-$ in 35.9 fb^{-1} of pp collisions at E_{cm} = 13 TeV. See their Fig. 10 for limits on the product of production cross section (normalized to the SM) and branching ratios in the range m_{A^0} = 4–15 GeV.

[19] SIRUNYAN 20AA search for $H^0_2 \rightarrow ZA^0$, $A^0 \rightarrow b\overline{b}$ or $A^0 \rightarrow ZH^0_2$, $H^0_2 \rightarrow b\overline{b}$ in 35.9 fb^{-1} of pp collisions at E_{cm} = 13 TeV. See their Fig. 7 for limits on the product of cross section and branching ratio for $m_{H^0_2}$ = 0.12–1 TeV and m_{A^0} = 0.03–1 TeV.

[20] SIRUNYAN 20AC search for gluon-fusion production of A^0 decaying to ZH^0 in 35.9 fb^{-1} of pp collisions at E_{cm} = 13 TeV. See their Fig. 5 for limits on the product of cross section and branching ratios for m_{A^0} = 220–400 GeV.

[21] SIRUNYAN 20AD search for lepton-flavor violating decays $H^0_2 \rightarrow \mu\tau$, $e\tau$ of gluon-fusion-produced H^0_2 in 35.9 fb^{-1} of pp collisions at E_{cm} = 13 TeV. See their Fig. 5 (9) and Table 5 (6) for limits on production cross section times branching ratio for $m_{H^0_2}$ = 0.2–0.9 TeV for the $\mu\tau$ ($e\tau$) final state.

[22] SIRUNYAN 20AF search for $H^0_2/A^0 \rightarrow t\overline{t}$ with one or two charged leptons in the final state using kinematic variables in 35.9 fb^{-1} of pp collisions at E_{cm} = 13 TeV. See their Figs. 5 and 6 for limits on top Yukawa coupling of H^0_2 and A^0 for $m_{H^0_2}$, m_{A^0} = 0.4–0.75 TeV for various width assumptions.

[23] SIRUNYAN 20AP search for the decay H^0 or $H^0_2 \rightarrow A^0A^0 \rightarrow \mu^+\mu^-\tau^+\tau^-$ (for $m_{H^0_2}$ = 300 GeV) with boosted final-state topology in 35.9 fb^{-1} of pp collisions at E_{cm} = 13 TeV. See their Fig. 7 for limits on the product of production cross section (normalized to the SM) and branching ratios in the range m_{A^0} = 3.6–21 GeV, and Figs. 8 and 9 for its interpretation in terms of models with two Higgs doublets plus a singlet.

[24] SIRUNYAN 20Y search for gluon-fusion and vector-boson-fusion production of H^0_2 decaying to W^+W^- in the final states $\ell\nu\ell\nu$ and $\ell\nu qq$ in 35.9 fb^{-1} of pp collisions at E_{cm} = 13 TeV. See their Fig. 6 for limits on the product of cross section and branching ratio for $m_{H^0_2}$ = 0.2–3 TeV.

[25] SIRUNYAN 20Z search for $H^0_{1,2}$ or A^0 production in association with a $t\overline{t}$ pair, decaying to e^+e^- or $\mu^+\mu^-$, in 137 fb^{-1} of pp collisions at E_{cm} = 13 TeV. See their Fig. 12 for limits on production cross section times branching ratio for $m_{H^0_{1,2}}$, m_{A^0} = 15–75 GeV and 108–340 GeV.

[26] AABOUD 19A search for a narrow scalar resonance decaying to $H^0H^0 \rightarrow b\overline{b}b\overline{b}$ in 27.5–36.1 fb^{-1} of pp collisions at E_{cm} = 13 TeV. See their Fig. 9(a) for limits on cross section times branching ratios for $m_{H^0_2}$ = 0.26–3 TeV.

[27] AABOUD 19AG search for the decay $H^0 \rightarrow A^0A^0 \rightarrow \mu^+\mu^-b\overline{b}$ in 36.7 fb^{-1} of pp collisions at E_{cm} = 13 TeV. See their Fig. 6 (a) for limits on the product of production cross section (normalized to the SM) and branching ratios in the range m_{A^0} = 20–60 GeV.

[28] AABOUD 19O search for a scalar resonance decaying to $H^0H^0 \rightarrow b\overline{b}WW^*$ in 36.1 fb^{-1} of pp collisions at E_{cm} = 13 TeV. See their Fig. 12 (left) for limits on cross section times branching ratio for $m_{H^0_2}$ = 0.5–3 TeV.

[29] AABOUD 19T search for a scalar resonance decaying to $H^0H^0 \rightarrow WW^*WW^*$ in 36.1 fb^{-1} of pp collisions at E_{cm} = 13 TeV. See their Fig. 3 for limits on cross section times branching ratio for $m_{H^0_2}$ = 260–500 GeV, assuming SM decay rates for the H^0.

[30] AABOUD 19V combine published ATLAS data to constrain two-Higgs-doublet plus singlet pseudoscalar model with A^0_1 decaying to invisible final states. See their Fig. 19 for excluded parameter regions.

[31] AABOUD 19Y search for a narrow scalar resonance produced by gluon fusion or b associated production, decaying to $\mu^+\mu^-$ in 36.1 fb^{-1} of pp collisions at E_{cm} = 13 TeV. See their Figs. 4 and 5(a) for cross section limits for $m_{H^0_2}$ = 0.2–1.0 TeV.

[32] AALTONEN 19 search for b associated production of a scalar particle decaying to $b\overline{b}$ in 5.4 fb^{-1} of $p\overline{p}$ collisions at E_{cm} = 1.96 TeV. See their Fig. 3 for limits on cross section times branching ratio for $m_{H^0_{1,2}}$ = 100–300 GeV.

[33] SIRUNYAN 19 search for a narrow scalar resonance decaying to $H^0H^0 \rightarrow \gamma\gamma b\overline{b}$ in 35.9 fb^{-1} of pp collisions at E_{cm} = 13 TeV. See their Fig. 9 (left) for limits on cross section times branching ratios for $m_{H^0_2}$ = 260–900 GeV.

[34] SIRUNYAN 19AE search for a scalar resonance produced in association with a $b\overline{b}$ pair, decaying to $\tau^+\tau^-$ in 35.9 fb^{-1} of pp collisions at E_{cm} = 13 TeV. See their Fig. 4 for cross section limits for m_{A^0} = 25–70 GeV.

[35] SIRUNYAN 19AN search for production of A^0_2 decaying to $H^0A^0_1$ followed by $H^0 \rightarrow b\overline{b}$, $A^0_1 \rightarrow$ invisible in 35.9 fb^{-1} of pp collisions at E_{cm} = 13 TeV, in the mass range $m_{A^0_2}$ = 0.2–1.6 TeV, $m_{A^0_1}$ = 0.15–0.5 TeV. See their Fig. 6 for limits in terms of two-Higgs-doublet plus singlet pseudoscalar model.

[36] SIRUNYAN 19AV search for a scalar resonance produced by gluon fusion or b-associated production, decaying to $ZH^0 \rightarrow \ell^+\ell^-b\overline{b}$ ($\ell = e, \mu$) or $\nu\overline{\nu}b\overline{b}$ in 35.9 fb^{-1} of pp collisions at E_{cm} = 13 TeV. See their Fig. 5 for cross section limits for m_{A^0} = 0.22–1.0 TeV.

[37] SIRUNYAN 19B search for gluon fusion production of narrow scalar resonance with large transverse momentum, decaying to $b\overline{b}$, in 35.9 fb^{-1} of pp collisions at E_{cm} = 13 TeV. See their Figs. 7 and 8 for limits on cross section times branching ratio for the resonance mass of 50–350 GeV.

[38] SIRUNYAN 19BB search for the decay $H^0_1 \rightarrow \gamma\gamma$ in 19.7 fb^{-1} of pp collisions at E_{cm} = 8 TeV and 35.9 fb^{-1} at E_{cm} = 13 TeV. See their Figs. 4–6 for limits on cross section times branching ratio for $m_{H^0_1}$ = 80–110 GeV (some results in Fig. 5 for $m_{H^0_1}$ = 70–110 GeV).

[39] SIRUNYAN 19BD search for the decay $H^0 \rightarrow A^0A^0 \rightarrow \mu^+\mu^-b\overline{b}$ in 35.9 fb^{-1} of pp collisions at E_{cm} = 13 TeV. See their Fig. 5 for limits on the product of cross section times branching ratios in the range m_{A^0} = 20–62.5 GeV. See also their Figs. 6 and 7 for interpretation of the data in terms of models with two Higgs doublets and a singlet.

[40] SIRUNYAN 19BE combine searches for $H^0_2 \rightarrow H^0H^0$ in 35.9 fb^{-1} of pp collisions at E_{cm} = 13 TeV in various H^0 decay modes, from SIRUNYAN 18A, SIRUNYAN 18AF, SIRUNYAN 18CW, SIRUNYAN 19, and SIRUNYAN 19H. See their Fig. 3 for limits on cross section times branching ratios for $m_{H^0_2}$ = 0.25–3 TeV.

[41] SIRUNYAN 19BQ search for production of $H^0_{1,2}$ decaying to $A^0A^0 \rightarrow \mu^+\mu^-\mu^+\mu^-$ in 35.9 fb^{-1} of pp collisions at E_{cm} = 13 TeV. See their Fig. 2 for limits on cross section times branching ratio for $m_{H^0_{1,2}}$ = 90–150 GeV, m_{A^0} = 0.25–3.55 GeV.

[42] SIRUNYAN 19CR search for production of H^0_2/A^0 in gluon fusion and in association with a $b\overline{b}$ pair, decaying to $\mu^+\mu^-$ in 35.9 fb^{-1} of pp collisions at E_{cm} = 13 TeV. See their Fig. 6 for limits on cross section times branching ratio.

[43] SIRUNYAN 19H search for a narrow scalar resonance decaying to $H^0H^0 \rightarrow b\overline{b}b\overline{b}$ in 35.9 fb^{-1} of pp collisions at E_{cm} = 13 TeV, where one $b\overline{b}$ pair is resolved and the other not. Limits on cross section times branching ratios for $m_{H^0_2}$ = 0.75–1.6 TeV are obtained and combined with data from SIRUNYAN 18AF. See their Fig. 5 (right).

[44] AABOUD 18AA search for production of a scalar resonance decaying to $Z\gamma$, with Z decaying hadronically, in 36.1 fb^{-1} of pp collisions at E_{cm} = 13 TeV. See their Fig. 8(a) for limits on cross section times branching ratio for $m_{H^0_2}$ = 1.0–6.8 TeV.

[45] AABOUD 18AG search for the decay $H^0 \rightarrow A^0A^0 \rightarrow \gamma\gamma gg$ in 36.7 fb^{-1} of pp collisions at E_{cm} = 13 TeV. See their Fig. 2 and Table 6 for cross section limits in the range m_{A^0} = 20–60 GeV.

[46] AABOUD 18AH search for production of an A^0 in gluon-gluon fusion and in association with a $b\overline{b}$, decaying to $ZH^0_2 \rightarrow \ell^+\ell^-b\overline{b}$ in 36.1 fb^{-1} of pp collisions at E_{cm} = 13 TeV. See their Fig. 5 for cross section limits for m_{A^0} = 230–800 GeV and $m_{H^0_2}$ = 130–700 GeV.

[47] AABOUD 18AI search for production of an A^0 in gluon-gluon fusion and in association with a $b\overline{b}$, decaying to ZH^0 in the final states $\nu\overline{\nu}b\overline{b}$ and $\ell^+\ell^-b\overline{b}$ in 36.1 fb^{-1} of pp collisions at E_{cm} = 13 TeV. See their Fig. 6 for cross section limits for m_{A^0} = 0.2–2 TeV. See also AABOUD 18CC.

[48] AABOUD 18BF search for production of a heavy H^0_2 state decaying to ZZ in the final states $\ell^+\ell^-\ell^+\ell^-$ and $\ell^+\ell^-\nu\overline{\nu}$ in 36.1 fb^{-1} of pp collisions at E_{cm} = 13 TeV. See their Fig. 6 for upper limits on cross section times branching ratio for $m_{H^0_2}$ = 0.2–1.2 TeV assuming ggF or VBF with the NWA. See their Fig. 7 for upper limits on cross section times branching ratio for $m_{H^0_2}$ = 0.4–1.0 TeV assuming ggF, and with several assumptions on its width.

[49] AABOUD 18BU search for a narrow scalar resonance decaying to $H^0H^0 \rightarrow \gamma\gamma WW^*$ in 36.1 fb^{-1} of pp collisions at E_{cm} = 13 TeV. See their Fig. 4 for limits on cross section times branching ratios for $m_{H^0_2}$ = 260–500 GeV.

[50] AABOUD 18BX search for associated production of WH^0 or ZH^0 followed by the decay $H^0 \rightarrow A^0A^0 \rightarrow b\overline{b}b\overline{b}$ in 36.1 fb^{-1} of pp collisions at E_{cm} = 13 TeV. See their Fig. 9 for limits on cross section times branching ratios for m_{A^0} = 20–60 GeV. See also their Fig. 10 for the dependence of the limit on A^0 lifetime.

[51] AABOUD 18CQ search for a narrow scalar resonance decaying to $H^0H^0 \rightarrow b\overline{b}\tau^+\tau^-$ in 36.1 fb^{-1} of pp collisions at E_{cm} = 13 TeV. See their Fig. 2 (above) for limits on cross section times branching ratios for $m_{H^0_2}$ = 260–1000 GeV.

[52] AABOUD 18F search for production of a narrow scalar resonance decaying to W^+W^- and ZZ, followed by hadronic decays of W and Z, in 36.7 fb^{-1} of pp collisions at E_{cm} = 13 TeV. See their Fig. 5(c) for limits on cross section times branching ratio for $m_{H^0_2}$ = 1.2–3.0 TeV.

[53] AAIJ 18AM search for gluon-fusion production of $H^0_{1,2}$ decaying to $\mu\tau$ in 2 fb^{-1} of pp collisions at E_{cm} = 8 TeV. See their Fig. 2 for limits on cross section times branching ratio for $m_{H^0_{1,2}}$ = 45–195 GeV.

[54] AAIJ 18AQ search for gluon-fusion production of a scalar particle A^0 decaying to $\mu^+\mu^-$ in 1.99 fb^{-1} of pp collisions at E_{cm} = 8 TeV and 0.98 fb^{-1} at E_{cm} = 7 TeV. See

Downloaded from https://academic.oup.com/ptep/article/2022/8/083C01/6651666 by KIT Library user on 27 September 2022

their Fig. 4 for limits on cross section times branching ratio for $m_{A^0} = 5.5$–15 GeV (using the $E_{cm} = 8$ TeV data set).

[55] AAIJ 18AQ search for the decay $H^0 \rightarrow A^0 A^0$, with one of the A^0 decaying to $\mu^+\mu^-$, in 1.99 fb^{-1} of pp collisions at $E_{cm} = 8$ TeV and 0.98 fb^{-1} at $E_{cm} = 7$ TeV. See their Fig. 5 (right) for limits on the product of branching ratios for $m_{A^0} = 5.5$–15 GeV (using the $E_{cm} = 8$ TeV data set).

[56] SIRUNYAN 18AF search for a narrow scalar resonance decaying to $H^0 H^0 \rightarrow b\overline{b}b\overline{b}$ in 35.9 fb^{-1} of pp collisions at $E_{cm} = 13$ TeV, where both $b\overline{b}$ pairs are not resolved. See their Fig. 9 for limits on cross section times branching ratios for $m_{H^0_2} = 0.75$–3 TeV.

[57] SIRUNYAN 18BA search for production of a heavy H^0_2 state decaying to ZZ in the final states $\ell^+\ell^-\ell^+\ell^-$, $\ell^+\ell^- q\overline{q}$, and $\ell^+\ell^-\nu\overline{\nu}$ in 35.9 fb^{-1} of pp collisions at $E_{cm} = 13$ TeV. See their Figs. 10 and 11 for upper limits on cross section times branching ratio for $m_{H^0_2} = 0.13$–3 TeV with several assumptions on its width and on the fraction of Vector-Boson-Fusion of the total production cross section.

[58] SIRUNYAN 18CW search for a narrow scalar resonance decaying to $H^0 H^0 \rightarrow b\overline{b}b\overline{b}$ in 35.9 fb^{-1} of pp collisions at $E_{cm} = 13$ TeV, where both $b\overline{b}$ pairs are resolved. See their Fig. 9 for limits on cross section times branching ratios for $m_{H^0_2} = 260$–1200 GeV.

[59] SIRUNYAN 18DK search for production of a scalar resonance decaying to $Z\gamma$, with Z decaying to $\ell^+\ell^-$ or hadronically, in 35.9 fb^{-1} of pp collisions at $E_{cm} = 13$ TeV. See their Fig. 7 for limits on cross section times branching ratio for $m_{H^0_2} = 0.35$–4 TeV for different assumptions on the width of the resonance.

[60] SIRUNYAN 18DT search for the decay $H^0 \rightarrow A^0 A^0 \rightarrow \tau^+\tau^- b\overline{b}$ in 35.9 fb^{-1} of pp collisions at $E_{cm} = 13$ TeV. See their Fig. 7 for limits on the product of branching ratios in the range $m_{A^0} = 15$–60 GeV. See also their Fig. 8 for interpretation of the data in terms of models with two Higgs doublets and a singlet.

[61] SIRUNYAN 18DU search for production of a narrow scalar resonance decaying to $\gamma\gamma$ in 35.9 fb^{-1} (taken in 2016) of pp collisions at $E_{cm} = 13$ TeV. See their Fig. 3 (right) for limits on cross section times branching ratio for $m_{H^0_2} = 0.5$–5 TeV for several values of its width-to-mass ratio.

[62] SIRUNYAN 18ED search for production of an A^0 in gluon-gluon fusion and in association with a $b\overline{b}$, decaying to ZH^0 in the final states $\nu\overline{\nu}b\overline{b}$ or $\ell^+\ell^- b\overline{b}$ in 35.9 fb^{-1} of pp collisions at $E_{cm} = 13$ TeV. See their Fig. 8 for cross section limits for $m_{A^0} = 0.8$–2 TeV.

[63] SIRUNYAN 18EE search for the decay $H^0 \rightarrow A^0 A^0 \rightarrow \mu^+\mu^-\tau^+\tau^-$ in 35.9 fb^{-1} of pp collisions at $E_{cm} = 13$ TeV. See their Fig. 4 for limits on the product of branching ratios in the range $m_{A^0} = 15$–62.5 GeV, normalized to the SM production cross section. See also their Fig. 5 for interpretation of the data in terms of models with two Higgs doublets and a singlet.

[64] SIRUNYAN 18F search for a narrow scalar resonance decaying to $H^0 H^0 \rightarrow WWb\overline{b}$ or $ZZb\overline{b}$ in the final state $\ell\ell\nu\nu b\overline{b}$ in 35.9 fb^{-1} of pp collisions at $E_{cm} = 13$ TeV. See their Fig. 7 for limits on cross section times branching ratios for $m_{H^0_2} = 250$–900 GeV.

[65] AABOUD 17 search for production of a scalar resonance decaying to $Z\gamma$ in 3.2 fb^{-1} of pp collisions at $E_{cm} = 13$ TeV. See their Fig. 4 for the limits on cross section times branching ratio for $m_{H^0_2} = 0.25$–3.0 TeV.

[66] AABOUD 17AP search for production of a scalar resonance decaying to $\gamma\gamma$ in 36.7 fb^{-1} of pp collisions at $E_{cm} = 13$ TeV. See their Fig. 4(a) for limits on fiducial cross section times branching ratio for $m_{H^0_2} = 0.2$–2.7 TeV with narrow width approximation.

[67] AABOUD 17AW search for production of a scalar resonance decaying to $Z\gamma$ in 36.1 fb^{-1} of pp collisions at $E_{cm} = 13$ TeV. See their Fig. 7 for limits on cross section times branching ratio for $m_{H^0_2} = 0.25$–2.4 TeV.

[68] KHACHATRYAN 17AZ search for the decay $H^0 \rightarrow A^0 A^0 \rightarrow \tau^+\tau^-\tau^+\tau^-$, $\mu^+\mu^- b\overline{b}$, and $\mu^+\mu^-\tau^+\tau^-$ in 19.7 fb^{-1} of pp collisions at $E_{cm} = 8$ TeV. See their Figs. 4, 5, and 6 for cross section limits in the range $m_{A^0} = 5$–62.5 GeV. See also their Figs. 7, 8, and 9 for interpretation of the data in terms of models with two Higgs doublets and a singlet.

[69] KHACHATRYAN 17D search for production of a scalar resonance decaying to $Z\gamma$ in 19.7 fb^{-1} of pp collisions at $E_{cm} = 8$ TeV and 2.7 fb^{-1} at $E_{cm} = 13$ TeV. See their Figs. 3 and 4 for the limits on cross section times branching ratio for $m_{H^0_2} = 0.2$–2.0 TeV.

[70] KHACHATRYAN 17R search for production of a narrow scalar resonance decaying to $\gamma\gamma$ in 12.9 fb^{-1} (taken in 2016) of pp collisions at $E_{cm} = 13$ TeV. See their Fig. 2 for limits on cross section times branching ratio for $m_{H^0_2} = 0.5$–4.5 TeV for several values of its width-to-mass ratio. Limits from combination with KHACHATRYAN 16M are shown in their Figs. 4 and 6.

[71] SIRUNYAN 17CN search for a narrow scalar resonance decaying to $H^0 H^0 \rightarrow b\overline{b}\tau^+\tau^-$ in 18.3 fb^{-1} of pp collisions at $E_{cm} = 8$ TeV. See their Fig. 5 (above) and Table II for limits on the cross section times branching ratios for $m_{H^0_2} = 0.3$–1 TeV, and Fig. 6 (above) and Table III for the corresponding limits by combining with data from KHACHATRYAN 16BQ and KHACHATRYAN 15R.

[72] SIRUNYAN 17Y search for production of a scalar resonance decaying to $Z\gamma$ in 19.7 fb^{-1} of pp collisions at $E_{cm} = 8$ TeV and 2.7 fb^{-1} at $E_{cm} = 13$ TeV. See their Figs. 3, 4 and Table 3 for limits on cross section times branching ratio for $m_{H^0_2} = 0.7$–3.0 TeV, and Fig. 5 for the corresponding limits for $m_{H^0_2} = 0.2$–3.0 TeV from combination with KHACHATRYAN 17D data.

[73] AABOUD 16AB search for associated production of WH^0 with the decay $H^0 \rightarrow A^0 A^0 \rightarrow b\overline{b}b\overline{b}$ in 3.2 fb^{-1} of pp collisions at $E_{cm} = 13$ TeV. See their Fig. 8 for limits on cross section times branching ratios for $m_{A^0} = 20$–60 GeV.

[74] AABOUD 16AE search for production of a narrow scalar resonance decaying to W^+W^- and ZZ in 3.2 fb^{-1} of pp collisions at $E_{cm} = 13$ TeV. See their Fig. 4 for limits on cross section times branching ratio for $m_{H^0_2} = 0.5$–3 TeV.

[75] AABOUD 16H search for production of a scalar resonance decaying to $\gamma\gamma$ in 3.2 fb^{-1} of pp collisions at $E_{cm} = 13$ TeV. See their Fig. 12 for limits on cross section times branching ratio for $m_{H^0_2} = 0.2$–2 TeV with different assumptions on the width.

[76] AABOUD 16I search for a narrow scalar resonance decaying to $H^0 H^0 \rightarrow b\overline{b}b\overline{b}$ in 3.2 fb^{-1} of pp collisions at $E_{cm} = 13$ TeV. See their Fig. 10(c) for limits on cross section times branching ratios for $m_{H^0_2} = 0.5$–3 TeV.

[77] AAD 16AX search for production of a heavy H^0 state decaying to ZZ in the final states $\ell^+\ell^-\ell^+\ell^-$, $\ell^+\ell^-\nu\overline{\nu}$, $\ell^+\ell^- q\overline{q}$, and $\nu\overline{\nu}q\overline{q}$ in 20.3 fb^{-1} of pp collisions at $E_{cm} = 8$ TeV. See their Fig.12 for upper limits on $\sigma(H^0)$ B$(H^0 \rightarrow ZZ)$ for m_{H^0} ranging from 140 GeV to 1000 GeV.

[78] AAD 16C search for production of a heavy H^0 state decaying to W^+W^- in the final states $\ell\nu\ell\nu$ and $\ell\nu qq$ in 20.3 fb^{-1} of pp collisions at $E_{cm} = 8$ TeV. See their Figs. 12, 13, and 16 for upper limits on $\sigma(H^0)$ B$(H^0 \rightarrow W^+W^-)$ for m_{H^0} ranging from 300 GeV to 1000 or 1500 GeV with various assumptions on the total width of H^0.

[79] AAD 16L search for the decay $H^0 \rightarrow A^0 A^0 \rightarrow \gamma\gamma\gamma\gamma$ in 20.3 fb^{-1} of pp collisions at $E_{cm} = 8$ TeV. See their Fig. 4 (upper right) for limits on cross section times branching ratios (normalized to the SM H^0 cross section) for $m_{A^0} = 10$–60 GeV.

[80] AAD 16L search for the decay $H^0_2 \rightarrow A^0 A^0 \rightarrow \gamma\gamma\gamma\gamma$ in 20.3 fb^{-1} of pp collisions at $E_{cm} = 8$ TeV. See their Fig. 4 (lower right) for limits on cross section times branching ratios for $m_{H^0_2} = 600$ GeV and $m_{A^0} = 10$–245 GeV, and Table 5 for limits for $m_{H^0_2} =$ 300 and 900 GeV.

[81] AALTONEN 16C search for electroweak associated production of $H^0_1 H^\pm$ followed by the decays $H^\pm \rightarrow H^0_1 W^*$, $H^0_1 \rightarrow \gamma\gamma$ for $m_{H^0_1} = 10$–105 GeV and $m_{H^\pm} = 30$–300 GeV. See their Fig. 3 for excluded parameter region in a two-doublet model in which H^0_1 has no direct decay to fermions.

[82] KHACHATRYAN 16BG search for a narrow scalar resonance decaying to $H^0 H^0 \rightarrow b\overline{b}b\overline{b}$ in 19.7 fb^{-1} of pp collisions at $E_{cm} = 8$ TeV. See their Fig. 6 for limits on the cross section times branching ratios for $m_{H^0_2} = 1.15$–3 TeV.

[83] KHACHATRYAN 16BQ search for a resonance decaying to $H^0 H^0 \rightarrow \gamma\gamma b\overline{b}$ in 19.7 fb^{-1} of pp collisions at $E_{cm} = 8$ TeV. See their Fig. 9 for limits on the cross section times branching ratios for $m_{H^0_2} = 0.26$–1.1 TeV.

[84] KHACHATRYAN 16F search for the decay $H^0 \rightarrow H^0_1 H^0_1 \rightarrow \tau^+\tau^-\tau^+\tau^-$ in 19.7 fb^{-1} of pp collisions at $E_{cm} = 8$ TeV. See their Fig. 8 for cross section limits for $m_{H^0_1} =$ 4–8 GeV.

[85] KHACHATRYAN 16M search for production of a narrow resonance decaying to $\gamma\gamma$ in 19.7 fb^{-1} of pp collisions at $E_{cm} = 8$ TeV and 3.3 fb^{-1} at $E_{cm} = 13$ TeV. See their Fig. 3 (top) for limits on cross section times branching ratio for $m_{H^0_2} = 0.5$–4 TeV.

[86] KHACHATRYAN 16P search for gluon fusion production of an H^0_2 decaying to $H^0 H^0 \rightarrow b\overline{b}\tau^+\tau^-$ in 19.7 fb^{-1} of pp collisions at $E_{cm} = 8$ TeV. See their Fig. 8 (lower right) for cross section limits for $m_{H^0_2} = 260$–350 GeV.

[87] KHACHATRYAN 16P search for gluon fusion production of an A^0 decaying to $ZH^0 \rightarrow \ell^+\ell^-\tau^+\tau^-$ in 19.7 fb^{-1} of pp collisions at $E_{cm} = 8$ TeV. See their Fig. 10 for cross section limits for $m_{H^0_2} = 220$–350 GeV.

[88] AAD 15BK search for production of a heavy H^0_2 decaying to $H^0 H^0$ in the final state $b\overline{b}b\overline{b}$ in 19.5 fb^{-1} of pp collisions at $E_{cm} = 8$ TeV. See their Fig. 14(c) for $\sigma(H^0_2)$ B$(H^0_2 \rightarrow H^0 H^0)$ for $m_{H^0_2} = 500$–1500 GeV with $\Gamma_{H^0_2} = 1$ GeV.

[89] AAD 15BZ search for the decay $H^0 \rightarrow A^0 A^0 \rightarrow \mu^+\mu^-\tau^+\tau^-$ ($m_{H^0} = 125$ GeV) in 20.3 fb^{-1} of pp collisions at $E_{cm} = 8$ TeV. See their Fig. 6 for limits on cross section times branching ratio for $m_{A^0} = 3.7$–50 GeV.

[90] AAD 15BZ search for a state H^0_2 via the decay $H^0_2 \rightarrow A^0 A^0 \rightarrow \mu^+\mu^-\tau^+\tau^-$ in 20.3 fb^{-1} of pp collisions at $E_{cm} = 8$ TeV. See their Fig. 6 for limits on cross section times branching ratio for $m_{H^0_2} = 100$–500 GeV and $m_{A^0} = 5$ GeV.

[91] AAD 15CE search for production of a heavy H^0_2 decaying to $H^0 H^0$ in the final states $b\overline{b}\tau^+\tau^-$ and $\gamma\gamma WW^*$ in 20.3 fb^{-1} of pp collisions at $E_{cm} = 8$ TeV and combine with data from AAD 15H and AAD 15BK. A limit $\sigma(H^0_2)$ B$(H^0_2 \rightarrow H^0 H^0) <$ 2.1–0.011 pb (95% CL) is given for $m_{H^0_2} = 260$–1000 GeV. See their Fig. 6.

[92] AAD 15H search for production of a heavy H^0_2 decaying to $H^0 H^0$ in the finalstate $\gamma\gamma b\overline{b}$ in 20.3 fb^{-1} of pp collisions at $E_{cm} = 8$ TeV.A limit of $\sigma(H^0_2)$ B$(H^0_2 \rightarrow H^0 H^0)$ $<$ 3.5–0.7 pb is given for $m_{H^0_2} = 260$–500 GeV at 95% CL. See their Fig. 3.

[93] AAD 15S search for production of A^0 decaying to $ZH^0 \rightarrow \ell^+\ell^- b\overline{b}$, $\nu\overline{\nu}b\overline{b}$ and $\ell^+\ell^-\tau^+\tau^-$ in 20.3 fb^{-1} of pp collisions at $E_{cm} = 8$ TeV. See their Fig. 3 for cross section limits for $m_{A^0} = 200$–1000 GeV.

[94] KHACHATRYAN 15AW search for production of a heavy state H^0_2 of an electroweak singlet extension of the Standard Model via the decays of H^0_2 to W^+W^- and ZZ in up to 5.1 fb^{-1} of pp collisions at $E_{cm} = 7$ TeV and up to 19.7 fb^{-1} at $E_{cm} = 8$ TeV in the range $m_{H^0_2} = 145$–1000 GeV. See their Figs. 8 and 9 for limits in the parameter space of the model.

[95] KHACHATRYAN 15BB search for production of a resonance H^0 decaying to $\gamma\gamma$ in 19.7 fb^{-1} of pp collisions at $E_{cm} = 8$ TeV. See their Fig. 7 for limits on cross section times branching ratio for $m_{H^0} = 150$–850 GeV.

[96] KHACHATRYAN 15N search for production of A^0 decaying to $ZH^0 \rightarrow \ell^+\ell^- b\overline{b}$ in 19.7 fb^{-1} of pp collisions at $E_{cm} = 8$ TeV. See their Fig. 3 for limits on cross section times branching ratios for $m_{A^0} = 225$–600 GeV.

[97] KHACHATRYAN 15O search for production of a high-mass narrow resonance A^0 decaying to $ZH^0 \rightarrow q\overline{q}\tau^+\tau^-$ in 19.7 fb^{-1} of pp collisions at $E_{cm} = 8$ TeV. See their Fig. 6 for limits on cross section times branching ratios for $m_{A^0} = 800$–2500 GeV.

[98] KHACHATRYAN 15R search for a narrow scalar resonance decaying to $H^0 H^0 \rightarrow b\overline{b}b\overline{b}$ in 17.9 fb^{-1} of pp collisions at $E_{cm} = 8$ TeV. See their Fig. 5 (top) for limits on cross section times branching ratios for $m_{H^0_2} = 0.27$–1.1 TeV.

Downloaded from https://academic.oup.com/ptep/article/2022/8/083C01/6651666 by KIT Library user on 27 September 2022

[99] AAD 14AP search for a second H^0 state decaying to $\gamma\gamma$ in addition to the state at about 125 GeV in 20.3 fb^{-1} of pp collisions at E_{cm} = 8 TeV. See their Fig. 4 for limits on cross section times branching ratio for m_{H^0} = 65–600 GeV.

[100] AAD 14M search for the decay cascade $H^0_2 \rightarrow H^\pm W^\mp \rightarrow H^0 W^\pm W^\mp$, H^0 decaying to $b\overline{b}$ in 20.3 fb^{-1} of pp collisions at E_{cm} = 8 TeV. See their Table III for limits on cross section times branching ratio for $m_{H^0_2}$= 325–1025 GeV and m_{H^+}= 225–925 GeV.

[101] CHATRCHYAN 14G search for a second H^0 state decaying to $WW^{(*)}$ in addition to the observed signal at about 125 GeV using 4.9 fb^{-1} of pp collisions at E_{cm} = 7 TeV and 19.4 fb^{-1} at E_{cm} = 8 TeV. See their Fig. 21 (right) for cross section limits in the mass range 110–600 GeV.

[102] KHACHATRYAN 14P search for a second H^0 state decaying to $\gamma\gamma$ in addition to the observed signal at about 125 GeV using 5.1 fb^{-1} of pp collisions at E_{cm} = 7 TeV and 19.7 fb^{-1} at E_{cm} = 8 TeV. See their Figs. 27 and 28 for cross section limits in the mass range 110–150 GeV.

[103] AALTONEN 13P search for production of a heavy Higgs boson H'^0 that decays into a charged Higgs boson $H^\pm$ and a lighter Higgs boson H^0 via the decay chain $H'^0 \rightarrow H^\pm W^\mp$, $H^\pm \rightarrow W^\pm H^0$, $H^0 \rightarrow b\overline{b}$ in the final state $\ell\nu$ plus 4 jets in 8.7 fb^{-1} of $p\overline{p}$ collisions at E_{cm} = 1.96 TeV. See their Fig. 4 for limits on cross section times branching ratio in the $m_{H^\pm}$–m_{H^0} plane for m_{H^0} = 126 GeV.

[104] CHATRCHYAN 13BJ search for H^0 production in the decay chain $H^0 \rightarrow A^0 A^0$, $A^0 \rightarrow \mu^+\mu^-$ in 5.3 fb^{-1} of pp collisions at E_{cm} = 7 TeV. See their Fig. 2 for limits on cross section times branching ratio.

[105] AALTONEN 11P search in 2.7 fb^{-1} of $p\overline{p}$ collisions at E_{cm} = 1.96 TeV for the decay chain $t \rightarrow bH^+$, $H^+ \rightarrow W^+A^0$, $A^0 \rightarrow \tau^+\tau^-$ with m_{A^0} between 4 and 9 GeV. See their Fig. 4 for limits on B($t \rightarrow bH^+$) for 90 < m_{H^+} < 160 GeV.

[106] ABBIENDI 10 search for $e^+e^- \rightarrow ZH^0$ with the decay chain $H^0 \rightarrow \widetilde{\chi}^0_1\widetilde{\chi}^0_2$, $\widetilde{\chi}^0_2 \rightarrow \widetilde{\chi}^0_1 + (\gamma$ or $Z^*)$, when $\widetilde{\chi}^0_1$ and $\widetilde{\chi}^0_2$ are nearly degenerate. For a mass difference of 2 (4) GeV, a lower limit on m_{H^0} of 108.4 (107.0) GeV (95% CL) is obtained for SM ZH^0 cross section and B($H^0 \rightarrow \widetilde{\chi}^0_1\widetilde{\chi}^0_2$) = 1.

[107] SCHAEL 10 search for the process $e^+e^- \rightarrow H^0Z$ followed by the decay chain $H^0 \rightarrow A^0A^0 \rightarrow \tau^+\tau^-\tau^+\tau^-$ with $Z \rightarrow \ell^+\ell^-, \nu\overline{\nu}$ at E_{cm} = 183–209 GeV. For a H^0ZZ coupling equal to the SM value, B($H^0 \rightarrow A^0A^0$) = B($A^0 \rightarrow \tau^+\tau^-$) = 1, and m_{A^0} = 4–10 GeV, m_{H^0} up to 107 GeV is excluded at 95% CL.

[108] ABAZOV 09V search for H^0 production followed by the decay chain $H^0 \rightarrow A^0A^0 \rightarrow \mu^+\mu^-\mu^+\mu^-$ or $\mu^+\mu^-\tau^+\tau^-$ in 4.2 fb^{-1} of $p\overline{p}$ collisions at E_{cm} = 1.96 TeV. See their Fig. 3 for limits on $\sigma(H^0)$·B($H^0 \rightarrow A^0A^0$) for m_{A^0} = 3.6–19 GeV.

[109] ABBIENDI 05A search for $e^+e^- \rightarrow H^0_1A^0$ in general Type-II two-doublet models, with decays H^0_1, $A^0 \rightarrow q\overline{q}, gg, \tau^+\tau^-$, and $H^0_1 \rightarrow A^0A^0$.

[110] ABBIENDI 04K search for $e^+e^- \rightarrow H^0Z$ with H^0 decaying to two jets of any flavor including gg. The limit is for SM production cross section with B($H^0 \rightarrow jj$) = 1.

[111] ABDALLAH 04 consider the full combined LEP and LEP2 datasets to set limits on the Higgs coupling to W or Z bosons, assuming SM decays of the Higgs. Results in Fig. 26.

[112] ACHARD 04B search for $e^+e^- \rightarrow H^0Z$ with H^0 decaying to $b\overline{b}$, $c\overline{c}$, or gg. The limit is for SM production cross section with B($H^0 \rightarrow jj$) = 1.

[113] ACHARD 04F search for H^0 with anomalous coupling to gauge boson pairs in the processes $e^+e^- \rightarrow H^0\gamma$, $e^+e^-H^0$, H^0Z with decays $H^0 \rightarrow f\overline{f}, \gamma\gamma, Z\gamma$, and W^*W at E_{cm} = 189–209 GeV. See paper for limits.

[114] ABBIENDI 03F search for $H^0 \rightarrow$ anything in $e^+e^- \rightarrow H^0Z$, using the recoil mass spectrum of $Z \rightarrow e^+e^-$ or $\mu^+\mu^-$. In addition, it searched for $Z \rightarrow \nu\overline{\nu}$ and $H^0 \rightarrow e^+e^-$ or photons. Scenarios with large width or continuum H^0 mass distribution are considered. See their Figs. 11–14 for the results.

[115] ABBIENDI 03G search for $e^+e^- \rightarrow H^0_1Z$ followed by $H^0_1 \rightarrow A^0A^0$, $A^0 \rightarrow c\overline{c}, gg$, or $\tau^+\tau^-$ in the region $m_{H^0_1}$ = 45-86 GeV and m_{A^0} = 2-11 GeV. See their Fig. 7 for the limits.

[116] Search for associated production of a $\gamma\gamma$ resonance with a Z boson, followed by $Z \rightarrow q\overline{q}, \ell^+\ell^-$, or $\nu\overline{\nu}$, at $E_{cm} \leq$ 209 GeV. The limit is for a H^0 with SM production cross section and B($H^0 \rightarrow f\overline{f}$)=0 for all fermions f.

[117] For B($H^0 \rightarrow \gamma\gamma$)=1, m_{H^0} > 113.1 GeV is obtained.

[118] HEISTER 02M search for $e^+e^- \rightarrow H^0Z$, assuming that H^0 decays to $q\overline{q}$, gg, or $\tau^+\tau^-$ only. The limit assumes SM production cross section.

[119] ABBIENDI 01E search for neutral Higgs bosons in general Type-II two-doublet models, at $E_{cm} \leq$ 189 GeV. In addition to usual final states, the decays H^0_1, $A^0 \rightarrow q\overline{q}, gg$ are searched for. See their Figs. 15,16 for excluded regions.

[120] ACCIARRI 00R search for $e^+e^- \rightarrow H^0\gamma$ with $H^0 \rightarrow b\overline{b}$, $Z\gamma$, or $\gamma\gamma$. See their Fig. 3 for limits on σ·B. Explicit limits within an effective interaction framework are also given, for which the Standard Model Higgs search results are used in addition.

[121] ACCIARRI 00R search for the two-photon type processes $e^+e^- \rightarrow e^+e^-H^0$ with $H^0 \rightarrow b\overline{b}$ or $\gamma\gamma$. See their Fig. 4 for limits on $\Gamma(H^0 \rightarrow \gamma\gamma)$·B($H^0 \rightarrow \gamma\gamma$or $b\overline{b}$) for m_{H^0}=70–170 GeV.

[122] GONZALEZ-GARCIA 98B use DØ limit for $\gamma\gamma$ events with missing E_T in $p\overline{p}$ collisions (ABBOTT 98) to constrain possible ZH or WH production followed by unconventional $H \rightarrow \gamma\gamma$ decay which is induced by higher-dimensional operators. See their Figs. 1 and 2 for limits on the anomalous couplings.

[123] KRAWCZYK 97 analyse the muon anomalous magnetic moment in a two-doublet Higgs model (with type II Yukawa couplings) assuming no H^0_1ZZ coupling and obtain $m_{H^0_1} \gtrsim$ 5 GeV or $m_{A^0} \gtrsim$5 GeV for tanβ > 50. Other Higgs bosons are assumed to be much heavier.

[124] ALEXANDER 96H give B($Z \rightarrow H^0\gamma$)×B($H^0 \rightarrow q\overline{q}$) < 1–4 × 10^{-5} (95%CL) and B($Z \rightarrow H^0\gamma$)×B($H^0 \rightarrow b\overline{b}$) < 0.7–2 × 10^{-5} (95%CL) in the range 20 < m_{H^0} <80 GeV.

SEARCHES FOR A HIGGS BOSON WITH STANDARD MODEL COUPLINGS

These listings are based on experimental searches for a scalar boson whose couplings to W, Z and fermions are precisely those of the Higgs boson predicted by the three-generation Standard Model with the minimal Higgs sector.

For a review and a bibliography, see the review on "Status of Higgs Boson Physics."

Indirect Mass Limits for H^0 from Electroweak Analysis

The mass limits shown below apply to a Higgs boson H^0 with Standard Model couplings whose mass is a priori unknown.

For limits obtained before the direct measurement of the top quark mass, see the 1996 (Physical Review **D54** 1 (1996)) Edition of this Review. Other studies based on data available prior to 1996 can be found in the 1998 Edition (The European Physical Journal **C3** 1 (1998)) of this Review.

VALUE (GeV)	*DOCUMENT ID*		*TECN*
90^{+21}_{-18}	[1] HALLER	18	RVUE
• • • We do not use the following data for averages, fits, limits, etc. • • •			
91^{+30}_{-23}	[2] BAAK	12	RVUE
94^{+25}_{-22}	[3] BAAK	12A	RVUE
91^{+31}_{-24}	[4] ERLER	10A	RVUE
129^{+74}_{-49}	[5] LEP-SLC	06	RVUE

[1] HALLER 18 make Standard Model fits to Z and neutral current parameters, m_t, m_W, and Γ_W measurements available in 2018. The direct mass measurement at the LHC is not used in the fit.

[2] BAAK 12 make Standard Model fits to Z and neutral current parameters, m_t, m_W, and Γ_W measurements available in 2010 (using also preliminary data). The quoted result is obtained from a fit that does not include the limit from the direct Higgs searches. The result including direct search data from LEP2, the Tevatron and the LHC is 120^{+12}_{-5} GeV.

[3] BAAK 12A make Standard Model fits to Z and neutral current parameters, m_t, m_W, and Γ_W measurements available in 2012 (using also preliminary data). The quoted result is obtained from a fit that does not include the measured mass value of the signal observed at the LHC and also no limits from direct Higgs searches.

[4] ERLER 10A makes Standard Model fits to Z and neutral current parameters, m_t, m_W measurements available in 2009 (using also preliminary data). The quoted result is obtained from a fit that does not include the limits from the direct Higgs searches. With direct search data from LEP2 and Tevatron added to the fit, the 90% CL (99% CL) interval is 115–148 (114–197) GeV.

[5] LEP-SLC 06 make Standard Model fits to Z parameters from LEP/SLC and m_t, m_W, and Γ_W measurements available in 2005 with $\Delta\alpha^{(5)}_{had}(m_Z)$ = 0.02758 ± 0.00035. The 95% CL limit is 285 GeV.

SEARCHES FOR NEUTRAL HIGGS BOSONS REFERENCES

AAD	22A	PR D105 012006	G. Aad *et al.*	(ATLAS Collab.)
AAD	21AF	EPJ C81 332	G. Aad *et al.*	(ATLAS Collab.)
AAD	21AI	EPJ C81 396	G. Aad *et al.*	(ATLAS Collab.)
AAD	21AY	PL B822 136651	G. Aad *et al.*	(ATLAS Collab.)
AAD	21AZ	JHEP 2110 013	G. Aad *et al.*	(ATLAS Collab.)
AAD	21BB	JHEP 2111 209	G. Aad *et al.*	(ATLAS Collab.)
AAD	21BE	EPJ C81 860	G. Aad *et al.*	(ATLAS Collab.)
ABRATENKO	21	PRL 127 151803	P. Abratenko *et al.*	(MicroBooNE Collab.)
SIRUNYAN	21A	EPJ C81 13	A.M. Sirunyan *et al.*	(CMS Collab.)
Also		EPJ C81 333 (errat.)	A.M. Sirunyan *et al.*	(CMS Collab.)
TUMASYAN	21F	JHEP 2111 057	A. Tumasyan *et al.*	(CMS Collab.)
AAD	20	PR D101 012002	G. Aad *et al.*	(ATLAS Collab.)
AAD	20AA	PRL 125 051801	G. Aad *et al.*	(ATLAS Collab.)
AAD	20AE	PRL 125 221802	G. Aad *et al.*	(ATLAS Collab.)
AAD	20AI	PR D102 112006	G. Aad *et al.*	(ATLAS Collab.)
AAD	20AO	JHEP 2011 163	G. Aad *et al.*	(ATLAS Collab.)
AAD	20C	PL B800 135103	G. Aad *et al.*	(ATLAS Collab.)
AAD	20L	PR D102 032004	G. Aad *et al.*	(ATLAS Collab.)
AAD	20X	JHEP 2007 108	G. Aad *et al.*	(ATLAS Collab.)
Also		JHEP 2101 145 (errat.)	G. Aad *et al.*	(ATLAS Collab.)
Also		JHEP 2105 207 (errat.)	G. Aad *et al.*	(ATLAS Collab.)
AAIJ	20AL	JHEP 2010 156	R. Aaij *et al.*	(LHCb Collab.)
SIRUNYAN	20	PL B800 135087	A.M. Sirunyan *et al.*	(CMS Collab.)
SIRUNYAN	20AA	JHEP 2003 055	A.M. Sirunyan *et al.*	(CMS Collab.)
SIRUNYAN	20AC	JHEP 2003 065	A.M. Sirunyan *et al.*	(CMS Collab.)
SIRUNYAN	20AD	JHEP 2003 103	A.M. Sirunyan *et al.*	(CMS Collab.)
SIRUNYAN	20AF	JHEP 2004 171	A.M. Sirunyan *et al.*	(CMS Collab.)
SIRUNYAN	20AP	JHEP 2008 139	A.M. Sirunyan *et al.*	(CMS Collab.)
SIRUNYAN	20Y	JHEP 2003 034	A.M. Sirunyan *et al.*	(CMS Collab.)
SIRUNYAN	20Z	JHEP 2003 051	A.M. Sirunyan *et al.*	(CMS Collab.)
AABOUD	19A	JHEP 1901 030	M. Aaboud *et al.*	(ATLAS Collab.)
AABOUD	19AG	PL B790 1	M. Aaboud *et al.*	(ATLAS Collab.)
AABOUD	19AI	PL B793 499	M. Aaboud *et al.*	(ATLAS Collab.)
AABOUD	19O	JHEP 1904 092	M. Aaboud *et al.*	(ATLAS Collab.)
AABOUD	19T	JHEP 1905 124	M. Aaboud *et al.*	(ATLAS Collab.)
AABOUD	19V	JHEP 1905 142	M. Aaboud *et al.*	(ATLAS Collab.)
AABOUD	19Y	JHEP 1907 117	M. Aaboud *et al.*	(ATLAS Collab.)
AALTONEN	19	PR D99 052001	T. Aaltonen *et al.*	(CDF Collab.)
SIRUNYAN	19	PL B788 7	A.M. Sirunyan *et al.*	(CMS Collab.)
SIRUNYAN	19AE	JHEP 1905 210	A.M. Sirunyan *et al.*	(CMS Collab.)
SIRUNYAN	19AN	EPJ C79 280	A.M. Sirunyan *et al.*	(CMS Collab.)
SIRUNYAN	19AV	EPJ C79 564	A.M. Sirunyan *et al.*	(CMS Collab.)
SIRUNYAN	19B	PR D99 012005	A.M. Sirunyan *et al.*	(CMS Collab.)
SIRUNYAN	19BB	PL B793 320	A.M. Sirunyan *et al.*	(CMS Collab.)
SIRUNYAN	19BD	PL B795 398	A.M. Sirunyan *et al.*	(CMS Collab.)
SIRUNYAN	19BE	PRL 122 121803	A.M. Sirunyan *et al.*	(CMS Collab.)
SIRUNYAN	19BQ	PL B796 131	A.M. Sirunyan *et al.*	(CMS Collab.)
SIRUNYAN	19CR	PL B798 134992	A.M. Sirunyan *et al.*	(CMS Collab.)
SIRUNYAN	19H	JHEP 1901 040	A.M. Sirunyan *et al.*	(CMS Collab.)
AABOUD	18AA	PR D98 032015	M. Aaboud *et al.*	(ATLAS Collab.)

Downloaded from https://academic.oup.com/ptep/article/2022/8/083C01/6651666 by KIT Library user on 27 September 2022

AABOUD	18AG	PL B782 750	M. Aaboud *et al.*	(ATLAS Collab.)
AABOUD	18AH	PL B783 392	M. Aaboud *et al.*	(ATLAS Collab.)
AABOUD	18AI	JHEP 1803 174	M. Aaboud *et al.*	(ATLAS Collab.)
Also		JHEP 1811 051 (errat.)	M. Aaboud *et al.*	(ATLAS Collab.)
AABOUD	18AP	JHEP 1806 166	M. Aaboud *et al.*	(ATLAS Collab.)
AABOUD	18BF	EPJ C78 293	M. Aaboud *et al.*	(ATLAS Collab.)
AABOUD	18BU	EPJ C78 1007	M. Aaboud *et al.*	(ATLAS Collab.)
AABOUD	18BX	JHEP 1810 031	M. Aaboud *et al.*	(ATLAS Collab.)
AABOUD	18CC	JHEP 1811 051 (errat.)	M. Aaboud *et al.*	(ATLAS Collab.)
AABOUD	18CE	JHEP 1812 039	M. Aaboud *et al.*	(ATLAS Collab.)
AABOUD	18CQ	PRL 121 191801	M. Aaboud *et al.*	(ATLAS Collab.)
AABOUD	18CW	JHEP 1811 040	M. Aaboud *et al.*	(ATLAS Collab.)
AABOUD	18F	PL B777 91	M. Aaboud *et al.*	(ATLAS Collab.)
AABOUD	18G	JHEP 1801 055	M. Aaboud *et al.*	(ATLAS Collab.)
AAIJ	18AM	EPJ C78 1008	R. Aaij *et al.*	(LHCb Collab.)
AAIJ	18AQ	JHEP 1809 147	R. Aaij *et al.*	(LHCb Collab.)
HALLER	18	EPJ C78 675	J. Haller *et al.*	(Gfitter Group)
SIRUNYAN	18A	PL B778 101	A.M. Sirunyan *et al.*	(CMS Collab.)
SIRUNYAN	18AF	PL B781 244	A.M. Sirunyan *et al.*	(CMS Collab.)
SIRUNYAN	18BA	JHEP 1806 127	A.M. Sirunyan *et al.*	(CMS Collab.)
Also		JHEP 1903 128 (errat.)	A.M. Sirunyan *et al.*	(CMS Collab.)
SIRUNYAN	18BP	JHEP 1808 113	A.M. Sirunyan *et al.*	(CMS Collab.)
SIRUNYAN	18CW	JHEP 1808 152	A.M. Sirunyan *et al.*	(CMS Collab.)
SIRUNYAN	18CX	JHEP 1809 007	A.M. Sirunyan *et al.*	(CMS Collab.)
SIRUNYAN	18DK	JHEP 1809 148	A.M. Sirunyan *et al.*	(CMS Collab.)
SIRUNYAN	18DT	PL B785 462	A.M. Sirunyan *et al.*	(CMS Collab.)
SIRUNYAN	18DU	PR D98 092001	A.M. Sirunyan *et al.*	(CMS Collab.)
SIRUNYAN	18ED	JHEP 1811 172	A.M. Sirunyan *et al.*	(CMS Collab.)
SIRUNYAN	18EE	JHEP 1811 018	A.M. Sirunyan *et al.*	(CMS Collab.)
SIRUNYAN	18F	JHEP 1801 054	A.M. Sirunyan *et al.*	(CMS Collab.)
AABOUD	17	PL B764 11	M. Aaboud *et al.*	(ATLAS Collab.)
AABOUD	17AN	PRL 119 191803	M. Aaboud *et al.*	(ATLAS Collab.)
AABOUD	17AP	PL B775 105	M. Aaboud *et al.*	(ATLAS Collab.)
AABOUD	17AW	JHEP 1710 112	M. Aaboud *et al.*	(ATLAS Collab.)
KHACHATRY...	17AZ	JHEP 1710 076	V. Khachatryan *et al.*	(CMS Collab.)
KHACHATRY...	17D	JHEP 1701 076	V. Khachatryan *et al.*	(CMS Collab.)
KHACHATRY...	17R	PL B767 147	V. Khachatryan *et al.*	(CMS Collab.)
SIRUNYAN	17AX	JHEP 1711 010	A.M. Sirunyan *et al.*	(CMS Collab.)
SIRUNYAN	17CN	PR D96 072004	A.M. Sirunyan *et al.*	(CMS Collab.)
SIRUNYAN	17Y	PL B772 363	A.M. Sirunyan *et al.*	(CMS Collab.)
AABOUD	16AA	EPJ C76 585	M. Aaboud *et al.*	(ATLAS Collab.)
AABOUD	16AB	EPJ C76 605	M. Aaboud *et al.*	(ATLAS Collab.)
AABOUD	16AE	JHEP 1609 173	M. Aaboud *et al.*	(ATLAS Collab.)
AABOUD	16H	JHEP 1609 001	M. Aaboud *et al.*	(ATLAS Collab.)
AABOUD	16I	PR D94 052002	M. Aaboud *et al.*	(ATLAS Collab.)
AAD	16AX	EPJ C76 45	G. Aad *et al.*	(ATLAS Collab.)
AAD	16C	JHEP 1601 032	G. Aad *et al.*	(ATLAS Collab.)
AAD	16L	EPJ C76 210	G. Aad *et al.*	(ATLAS Collab.)
AALTONEN	16C	PR D93 112010	T. Aaltonen *et al.*	(CDF Collab.)
ABLIKIM	16E	PR D93 052005	M. Ablikim *et al.*	(BESIII Collab.)
KHACHATRY...	16A	PL B752 221	V. Khachatryan *et al.*	(CMS Collab.)
KHACHATRY...	16BG	EPJ C76 371	V. Khachatryan *et al.*	(CMS Collab.)
KHACHATRY...	16BQ	PR D94 052012	V. Khachatryan *et al.*	(CMS Collab.)
KHACHATRY...	16F	JHEP 1601 079	V. Khachatryan *et al.*	(CMS Collab.)
KHACHATRY...	16M	PRL 117 051802	V. Khachatryan *et al.*	(CMS Collab.)
KHACHATRY...	16P	PL B755 217	V. Khachatryan *et al.*	(CMS Collab.)
KHACHATRY...	16W	PL B758 296	V. Khachatryan *et al.*	(CMS Collab.)
KHACHATRY...	16Z	PL B759 369	V. Khachatryan *et al.*	(CMS Collab.)
AAD	15BD	EPJ C75 337	G. Aad *et al.*	(ATLAS Collab.)
AAD	15BH	EPJ C75 299	G. Aad *et al.*	(ATLAS Collab.)
Also		EPJ C75 408 (errat.)	G. Aad *et al.*	(ATLAS Collab.)
AAD	15BK	EPJ C75 412	G. Aad *et al.*	(ATLAS Collab.)
AAD	15BZ	PR D92 052002	G. Aad *et al.*	(ATLAS Collab.)
AAD	15CE	PR D92 092004	G. Aad *et al.*	(ATLAS Collab.)
AAD	15H	PRL 114 081802	G. Aad *et al.*	(ATLAS Collab.)
AAD	15S	PL B744 163	G. Aad *et al.*	(ATLAS Collab.)
KHACHATRY...	15AW	JHEP 1510 144	V. Khachatryan *et al.*	(CMS Collab.)
KHACHATRY...	15AY	JHEP 1511 071	V. Khachatryan *et al.*	(CMS Collab.)
KHACHATRY...	15BB	PL B750 494	V. Khachatryan *et al.*	(CMS Collab.)
KHACHATRY...	15N	PL B748 221	V. Khachatryan *et al.*	(CMS Collab.)
KHACHATRY...	15O	PL B748 255	V. Khachatryan *et al.*	(CMS Collab.)
KHACHATRY...	15R	PL B749 560	V. Khachatryan *et al.*	(CMS Collab.)
LEES	15H	PR D91 071102	J.P. Lees *et al.*	(BABAR Collab.)
AAD	14AP	PRL 113 171801	G. Aad *et al.*	(ATLAS Collab.)
AAD	14AW	JHEP 1411 056	G. Aad *et al.*	(ATLAS Collab.)
AAD	14BA	JHEP 1411 088	G. Aad *et al.*	(ATLAS Collab.)
AAD	14M	PR D89 032002	G. Aad *et al.*	(ATLAS Collab.)
AAD	14O	PRL 112 201802	G. Aad *et al.*	(ATLAS Collab.)
CHATRCHYAN	14B	EPJ C74 2980	S. Chatrchyan *et al.*	(CMS Collab.)
CHATRCHYAN	14G	JHEP 1401 096	S. Chatrchyan *et al.*	(CMS Collab.)
KHACHATRY...	14M	JHEP 1410 160	V. Khachatryan *et al.*	(CMS Collab.)
KHACHATRY...	14P	EPJ C74 3076	V. Khachatryan *et al.*	(CMS Collab.)
KHACHATRY...	14Q	PR D90 112013	V. Khachatryan *et al.*	(CMS Collab.)
AAD	13AG	PL B721 32	G. Aad *et al.*	(ATLAS Collab.)
AAD	13AT	NJP 15 043009	G. Aad *et al.*	(ATLAS Collab.)
AAD	13O	JHEP 1302 095	G. Aad *et al.*	(ATLAS Collab.)
AAIJ	13T	JHEP 1305 132	R. Aaij *et al.*	(LHCb Collab.)
AALTONEN	13K	PR D88 052012	T. Aaltonen *et al.*	(CDF Collab.)
AALTONEN	13L	PR D88 052013	T. Aaltonen *et al.*	(CDF Collab.)
AALTONEN	13M	PR D88 052014	T. Aaltonen *et al.*	(CDF and D0 Collabs.)
AALTONEN	13P	PRL 110 121801	T. Aaltonen *et al.*	(CDF Collab.)
ABAZOV	13G	PR D88 052006	V.M. Abazov *et al.*	(D0 Collab.)
ABAZOV	13H	PR D88 052007	V.M. Abazov *et al.*	(D0 Collab.)
ABAZOV	13I	PR D88 052008	V.M. Abazov *et al.*	(D0 Collab.)
ABAZOV	13J	PR D88 052009	V.M. Abazov *et al.*	(D0 Collab.)
ABAZOV	13L	PR D88 052011	V.M. Abazov *et al.*	(D0 Collab.)
CARENA	13	EPJ C73 2552	M. Carena *et al.*	
CHATRCHYAN	13AG	PL B722 207	S. Chatrchyan *et al.*	(CMS Collab.)
CHATRCHYAN	13AL	PL B725 36	S. Chatrchyan *et al.*	(CMS Collab.)
CHATRCHYAN	13BJ	PL B726 564	S. Chatrchyan *et al.*	(CMS Collab.)
LEES	13C	PR D87 031102	J.P. Lees *et al.*	(BABAR Collab.)
LEES	13L	PR D88 031701	J.P. Lees *et al.*	(BABAR Collab.)
LEES	13R	PR D88 071102	J.P. Lees *et al.*	(BABAR Collab.)
AAD	12AI	PL B716 1	G. Aad *et al.*	(ATLAS Collab.)
AAD	12AQ	PRL 108 251801	G. Aad *et al.*	(ATLAS Collab.)
AAD	12N	EPJ C72 2157	G. Aad *et al.*	(ATLAS Collab.)
AALTONEN	12AB	PR D85 092001	T. Aaltonen *et al.*	(CDF Collab.)
AALTONEN	12AN	PL B717 173	T. Aaltonen *et al.*	(CDF Collab.)
AALTONEN	12AQ	PR D86 091101	T. Aaltonen *et al.*	(CDF and D0 Collabs.)
AALTONEN	12U	PR D85 012007	T. Aaltonen *et al.*	(CDF Collab.)
AALTONEN	12X	PR D85 032005	T. Aaltonen *et al.*	(CDF Collab.)
ABAZOV	12G	PL B710 569	V.M. Abazov *et al.*	(D0 Collab.)
ABLIKIM	12	PR D85 092012	M. Ablikim *et al.*	(BESIII Collab.)
BAAK	12	EPJ C72 2003	M. Baak *et al.*	(Gfitter Group)
BAAK	12A	EPJ C72 2205	M. Baak *et al.*	(Gfitter Group)
CHATRCHYAN	12AO	JHEP 1209 111	S. Chatrchyan *et al.*	(CMS Collab.)
CHATRCHYAN	12C	JHEP 1203 081	S. Chatrchyan *et al.*	(CMS Collab.)
CHATRCHYAN	12D	JHEP 1204 036	S. Chatrchyan *et al.*	(CMS Collab.)
CHATRCHYAN	12E	PL B710 91	S. Chatrchyan *et al.*	(CMS Collab.)
CHATRCHYAN	12G	PL B710 403	S. Chatrchyan *et al.*	(CMS Collab.)
CHATRCHYAN	12H	PRL 108 111804	S. Chatrchyan *et al.*	(CMS Collab.)
CHATRCHYAN	12I	JHEP 1203 040	S. Chatrchyan *et al.*	(CMS Collab.)
CHATRCHYAN	12K	PL B713 68	S. Chatrchyan *et al.*	(CMS Collab.)
CHATRCHYAN	12N	PL B716 30	S. Chatrchyan *et al.*	(CMS Collab.)
CHATRCHYAN	12V	PRL 109 121801	S. Chatrchyan *et al.*	(CMS Collab.)
AALTONEN	11P	PRL 107 031801	T. Aaltonen *et al.*	(CDF Collab.)
ABAZOV	11K	PL B698 97	V.M. Abazov *et al.*	(D0 Collab.)
ABAZOV	11W	PRL 107 121801	V.M. Abazov *et al.*	(D0 Collab.)
ABOUZAID	11A	PRL 107 201803	E. Abouzaid *et al.*	(KTeV Collab.)
DEL-AMO-SA...	11J	PRL 107 021804	P. del Amo Sanchez *et al.*	(BABAR Collab.)
LEES	11H	PRL 107 221803	J.P. Lees *et al.*	(BABAR Collab.)
ABBIENDI	10	PL B682 381	G. Abbiendi *et al.*	(OPAL Collab.)
ANDREAS	10	JHEP 1008 003	S. Andreas *et al.*	(DESY)
ERLER	10A	PR D81 051301	J. Erler	(UNAM)
HYUN	10	PRL 105 091801	H.J. Hyun *et al.*	(BELLE Collab.)
SCHAEL	10	JHEP 1005 049	S. Schael *et al.*	(ALEPH Collab.)
AALTONEN	09AB	PRL 103 061803	T. Aaltonen *et al.*	(CDF Collab.)
AALTONEN	09AR	PRL 103 201801	T. Aaltonen *et al.*	(CDF Collab.)
ABAZOV	09V	PRL 103 061801	V.M. Abazov *et al.*	(D0 Collab.)
AUBERT	09P	PRL 103 181801	B. Aubert *et al.*	(BABAR Collab.)
AUBERT	09Z	PRL 103 081803	B. Aubert *et al.*	(BABAR Collab.)
TUNG	09	PRL 102 051802	Y.C. Tung *et al.*	(KEK E391a Collab.)
ABAZOV	08U	PRL 101 051801	V.M. Abazov *et al.*	(D0 Collab.)
ABDALLAH	08B	EPJ C54 1	J. Abdallah *et al.*	(DELPHI Collab.)
Also		EPJ C56 165 (errat.)	J. Abdallah *et al.*	(DELPHI Collab.)
LOVE	08	PRL 101 151802	W. Love *et al.*	(CLEO Collab.)
ABBIENDI	07	EPJ C49 457	G. Abbiendi *et al.*	(OPAL Collab.)
BESSON	07	PRL 98 052002	D. Besson *et al.*	(CLEO Collab.)
SCHAEL	07	EPJ C49 439	S. Schael *et al.*	(ALEPH Collab.)
LEP-SLC	06	PRPL 427 257	ALEPH, DELPHI, L3, OPAL, SLD and working groups	
SCHAEL	06B	EPJ C47 547	S. Schael *et al.*	(LEP Collabs.)
ABBIENDI	05A	EPJ C40 317	G. Abbiendi *et al.*	(OPAL Collab.)
ABDALLAH	05D	EPJ C44 147	J. Abdallah *et al.*	(DELPHI Collab.)
ACHARD	05	PL B609 35	P. Achard *et al.*	(L3 Collab.)
ACOSTA	05Q	PR D72 072004	D. Acosta *et al.*	(CDF Collab.)
PARK	05	PRL 94 021801	H.K. Park *et al.*	(FNAL HyperCP Collab.)
ABBIENDI	04K	PL B597 11	G. Abbiendi *et al.*	(OPAL Collab.)
ABBIENDI	04M	EPJ C37 49	G. Abbiendi *et al.*	(OPAL Collab.)
ABDALLAH	04	EPJ C32 145	J. Abdallah *et al.*	(DELPHI Collab.)
ABDALLAH	04B	EPJ C32 475	J. Abdallah *et al.*	(DELPHI Collab.)
ABDALLAH	04L	EPJ C35 313	J. Abdallah *et al.*	(DELPHI Collab.)
ABDALLAH	04O	EPJ C38 1	J. Abdallah *et al.*	(DELPHI Collab.)
ACHARD	04B	PL B583 14	P. Achard *et al.*	(L3 Collab.)
ACHARD	04F	PL B589 89	P. Achard *et al.*	(L3 Collab.)
ABBIENDI	03F	EPJ C27 311	G. Abbiendi *et al.*	(OPAL Collab.)
ABBIENDI	03G	EPJ C27 483	G. Abbiendi *et al.*	(OPAL Collab.)
ACHARD	03C	PL B568 191	P. Achard *et al.*	(L3 Collab.)
ABBIENDI	02D	EPJ C23 397	G. Abbiendi *et al.*	(OPAL Collab.)
ABBIENDI	02F	PL B544 44	G. Abbiendi *et al.*	(OPAL Collab.)
ACHARD	02C	PL B534 28	P. Achard *et al.*	(L3 Collab.)
ACHARD	02H	PL B545 30	P. Achard *et al.*	(L3 Collab.)
AKEROYD	02	PR D66 037702	A.G. Akeroyd *et al.*	
HEISTER	02	PL B526 191	A. Heister *et al.*	(ALEPH Collab.)
HEISTER	02L	PL B544 16	A. Heister *et al.*	(ALEPH Collab.)
HEISTER	02M	PL B544 25	A. Heister *et al.*	(ALEPH Collab.)
ABBIENDI	01E	EPJ C18 425	G. Abbiendi *et al.*	(OPAL Collab.)
ABREU	01F	PL B507 89	P. Abreu *et al.*	(DELPHI Collab.)
AFFOLDER	01H	PR D64 092002	T. Affolder *et al.*	(CDF Collab.)
BARATE	01C	PL B499 53	R. Barate *et al.*	(ALEPH Collab.)
ACCIARRI	00M	PL B485 85	M. Acciarri *et al.*	(L3 Collab.)
ACCIARRI	00R	PL B489 102	M. Acciarri *et al.*	(L3 Collab.)
ACCIARRI	00S	PL B489 115	M. Acciarri *et al.*	(L3 Collab.)
BARATE	00L	PL B487 241	R. Barate *et al.*	(ALEPH Collab.)
ABBIENDI	99E	EPJ C7 407	G. Abbiendi *et al.*	(OPAL Collab.)
ABBIENDI	99O	PL B464 311	G. Abbiendi *et al.*	(OPAL Collab.)
ABBOTT	99B	PRL 82 2244	B. Abbott *et al.*	(D0 Collab.)
ABREU	99P	PL B458 431	P. Abreu *et al.*	(DELPHI Collab.)
ABBOTT	98	PRL 80 442	B. Abbott *et al.*	(D0 Collab.)
ACKERSTAFF	98S	EPJ C5 19	K. Ackerstaff *et al.*	(OPAL Collab.)
ACKERSTAFF	98Y	PL B437 218	K. Ackerstaff *et al.*	(OPAL Collab.)
GONZALEZ...	98B	PR D57 7045	M.C. Gonzalez-Garcia, S.M. Lietti, S.F. Novaes	
PDG	98	EPJ C3 1	C. Caso *et al.*	(PDG Collab.)
KRAWCZYK	97	PR D55 6968	M. Krawczyk, J. Zochowski	(WARS)
ALEXANDER	96H	ZPHY C71 1	G. Alexander *et al.*	(OPAL Collab.)
PDG	96	PR D54 1	R. M. Barnett *et al.*	(PDG Collab.)
ABREU	95H	ZPHY C67 69	P. Abreu *et al.*	(DELPHI Collab.)
BALEST	95	PR D51 2053	R. Balest *et al.*	(CLEO Collab.)
PICH	92	NP B388 31	A. Pich, J. Prades, P. Yepes	(CERN, CPPM)
ANTREASYAN	90C	PL B251 204	D. Antreasyan *et al.*	(Crystal Ball Collab.)

Charged Higgs Bosons ($H^{\pm}$ and $H^{\pm\pm}$), Searches for

CONTENTS:

$H^{\pm}$ (charged Higgs) mass limits for $m_{H^+} < m(top)$
$H^{\pm}$ (charged Higgs) mass limits for $m_{H^+} > m(top)$
$H^{\pm\pm}$ (doubly-charged Higgs boson) mass limits
– Limits for $H^{\pm\pm}$ with $T_3 = \pm 1$
– Limits for $H^{\pm\pm}$ with $T_3 = 0$

$H^{\pm}$ (charged Higgs) mass limits for $m_{H^+} < m(top)$

Unless otherwise stated, LEP limits assume $B(H^+ \to \tau^+\nu)+B(H^+ \to c\overline{s})=1$, and hold for all values of $B(H^+ \to \tau^+\nu_\tau)$, and assume H^+ weak isospin of $T_3=+1/2$. In the following, $\tan\beta$ is the ratio of the two vacuum expectation values in two-doublet models (2HDM).

The limits are also applicable to point-like technipions. For a discussion of techniparticles, see the Review of Dynamical Electroweak Symmetry Breaking in this Review.

Limits obtained at the LHC are given in the m_h^{mod-} benchmark scenario, see CARENA 13, and hold for all $\tan\beta$ values.

For limits obtained in hadronic collisions before the observation of the top quark, and based on the top mass values inconsistent with the current

Downloaded from https://academic.oup.com/ptep/article/2022/8/083C01/6651666 by KIT Library user on 27 September 2022

measurements, see the 1996 (Physical Review **D54** 1 (1996)) Edition of this Review.

Searches in e^+e^- collisions at and above the Z pole have conclusively ruled out the existence of a charged Higgs in the region $m_{H^+} \lesssim 45$ GeV, and are meanwhile superseded by the searches in higher energy e^+e^- collisions at LEP. Results that are by now obsolete are therefore not included in this compilation, and can be found in a previous Edition (The European Physical Journal **C15** 1 (2000)) of this Review.

In the following, and unless otherwise stated, results from the LEP experiments (ALEPH, DELPHI, L3, and OPAL) are assumed to derive from the study of the $e^+e^- \to H^+H^-$ process. Limits from $b \to s\gamma$ decays are usually stronger in generic 2HDM models than in Supersymmetric models.

VALUE (GeV)	CL%	DOCUMENT ID		TECN	COMMENT
none 80–140	95	[1] AAD	15AF	ATLS	$t \to bH^+$
none 90–155	95	[2] KHACHATRY...	15AX	CMS	$t \to bH^+$, $H^+ \to \tau^+\nu$
> 80	95	[3] LEP	13	LEP	$e^+e^- \to H^+H^-$, $E_{cm} \leq 209$GeV
> 76.3	95	[4] ABBIENDI	12	OPAL	$e^+e^- \to H^+H^-$, $E_{cm} \leq 209$GeV
> 74.4	95	ABDALLAH	04I	DLPH	$E_{cm} \leq 209$ GeV
> 76.5	95	ACHARD	03E	L3	$E_{cm} \leq 209$ GeV
> 79.3	95	HEISTER	02P	ALEP	$E_{cm} \leq 209$ GeV
• • • We do not use the following data for averages, fits, limits, etc. • • •					
		[5] AAD	21V	ATLS	$\overline{t}bH^+$, $H^+ \to t\overline{b}$
		[6] SIRUNYAN	21W	CMS	$H^+ \to W^+Z$
		[7] AAD	20W	ATLS	$H^+ \to t\overline{b}$
		[8] SIRUNYAN	20AO	CMS	$H^+ \to t\overline{b}$
		[9] SIRUNYAN	20AV	CMS	$H^+ \to t\overline{b}$
		[10] SIRUNYAN	20BE	CMS	$t \to bH^+$, $H^+ \to c\overline{s}$
		[11] SIRUNYAN	19AH	CMS	$H^+ \to \tau^+\nu$
		[12] SIRUNYAN	19BP	CMS	$H^+ \to W^+Z$
		[13] SIRUNYAN	19CC	CMS	$t \to bH^+$, $H^+ \to W^+A^0$, $A^0 \to \mu^+\mu^-$
		[14] SIRUNYAN	19CQ	CMS	$H^+ \to W^+Z$
		[15] AABOUD	18BW	ATLS	$\overline{t}bH^+$ or $t \to bH^+$, $H^+ \to \tau^+\nu$
		[16] AABOUD	18CD	ATLS	$\overline{t}bH^+$, $H^+ \to t\overline{b}$
		[17] AABOUD	18CH	ATLS	$H^{\pm} \to W^{\pm}Z$
		[18] HALLER	18	RVUE	$b \to s\gamma$
		[19] SIRUNYAN	18DO	CMS	$t \to bH^+$, $H^+ \to c\overline{b}$
		[20] MISIAK	17	RVUE	$b \to s(d)\gamma$
		[21] SIRUNYAN	17AE	CMS	$H^{\pm} \to W^{\pm}Z$
		[22] AABOUD	16A	ATLS	$t(b)$ H^+, $H^+ \to \tau^+\nu$
		[23] AAD	16AJ	ATLS	$t(b)$ H^+, $H^+ \to t\overline{b}$
		[24] AAD	16AJ	ATLS	$qq \to H^+$, $H^+ \to t\overline{b}$
		[25] AAD	15AF	ATLS	$tH^{\pm}$
		[26] AAD	15M	ATLS	$H^{\pm} \to W^{\pm}Z$
		[27] KHACHATRY...	15AX	CMS	tH^+, $H^+ \to t\overline{b}$
		[28] KHACHATRY...	15AX	CMS	$tH^{\pm}$, $H^{\pm} \to \tau^{\pm}\nu$
		[29] KHACHATRY...	15BF	CMS	$t \to bH^+$, $H^+ \to c\overline{s}$
		[30] AAD	14M	ATLS	$H_2^0 \to H^{\pm}W^{\mp} \to H^0W^{\pm}W^{\mp}$, $H^0 \to b\overline{b}$
		[31] AALTONEN	14A	CDF	$t \to b\tau\nu$
		[32] AAD	13AC	ATLS	$t \to bH^+$
		[33] AAD	13V	ATLS	$t \to bH^+$, lepton non-universality
		[34] AAD	12BH	ATLS	$t \to bH^+$
		[35] CHATRCHYAN	12AA	CMS	$t \to bH^+$
		[36] AALTONEN	11P	CDF	$t \to bH^+$, $H^+ \to W^+A^0$
>316	95	[37] DESCHAMPS	10	RVUE	Type II, flavor physics data
		[38] AALTONEN	09AJ	CDF	$t \to bH^+$
		[39] ABAZOV	09AC	D0	$t \to bH^+$
		[40] ABAZOV	09AG	D0	$t \to bH^+$
		[41] ABAZOV	09AI	D0	$t \to bH^+$
		[42] ABAZOV	09P	D0	$H^+ \to t\overline{b}$
		[43] ABULENCIA	06E	CDF	$t \to bH^+$
> 92.0	95	ABBIENDI	04	OPAL	$B(\tau\nu) = 1$
> 76.7	95	[44] ABDALLAH	04I	DLPH	Type I
		[45] ABBIENDI	03	OPAL	$\tau \to \mu\overline{\nu}\nu$, $e\overline{\nu}\nu$
		[46] ABAZOV	02B	D0	$t \to bH^+$, $H \to \tau\nu$
		[47] BORZUMATI	02	RVUE	
		[48] ABBIENDI	01Q	OPAL	$B \to \tau\nu_{\tau}X$
		[49] BARATE	01E	ALEP	$B \to \tau\nu_{\tau}$
>315	99	[50] GAMBINO	01	RVUE	$b \to s\gamma$
		[51] AFFOLDER	00I	CDF	$t \to bH^+$, $H \to \tau\nu$
> 59.5	95	ABBIENDI	99E	OPAL	$E_{cm} \leq 183$ GeV
		[52] ABBOTT	99E	D0	$t \to bH^+$
		[53] ACKERSTAFF	99D	OPAL	$\tau \to e\nu\nu$, $\mu\nu\nu$
		[54] ACCIARRI	97F	L3	$B \to \tau\nu_{\tau}$
		[55] AMMAR	97B	CLEO	$\tau \to \mu\nu\nu$
		[56] COARASA	97	RVUE	$B \to \tau\nu_{\tau}X$
		[57] GUCHAIT	97	RVUE	$t \to bH^+$, $H \to \tau\nu$
		[58] MANGANO	97	RVUE	$B_{u(c)} \to \tau\nu_{\tau}$
		[59] STAHL	97	RVUE	$\tau \to \mu\nu\nu$
>244	95	[60] ALAM	95	CLE2	$b \to s\gamma$
		[61] BUSKULIC	95	ALEP	$b \to \tau\nu_{\tau}X$

[1] AAD 15AF search for $t\overline{t}$ production followed by $t \to bH^+$, $H^+ \to \tau^+\nu$ in 19.5 fb^{-1} of pp collisions at $E_{cm} = 8$ TeV. Upper limits on $B(t \to bH^+)$ $B(H^+ \to \tau\nu)$ between 2.3×10^{-3} and 1.3×10^{-2} (95% CL) are given for $m_{H^+} = 80$–160 GeV. See their Fig. 8 for the excluded regions in different benchmark scenarios of the MSSM. The region $m_{H^+} < 140$ GeV is excluded for $\tan\beta > 1$ in the considered scenarios.

[2] KHACHATRYAN 15AX search for $t\overline{t}$ production followed by $t \to bH^+$, $H^+ \to \tau^+\nu$ in 19.7 fb^{-1} of pp collisions at $E_{cm} = 8$ TeV. Upper limits on $B(t \to bH^+)$ $B(H^+ \to \tau\nu)$ between 1.2×10^{-2} and 1.5×10^{-3} (95% CL) are given for $m_{H^+} = 80$–160 GeV. See their Fig. 11 for the excluded regions in different benchmark scenarios of the MSSM. The region $m_{H^+} < 155$ GeV is excluded for $\tan\beta > 1$ in the considered scenarios.

[3] LEP 13 give a limit that refers to the Type II scenario. The limit for $B(H^+ \to \tau\nu) = 1$ is 94 GeV (95% CL), and for $B(H^+ \to cs) = 1$ the region below 80.5 as well as the region 83–88 GeV is excluded (95% CL). LEP 13 also search for the decay mode $H^+ \to A^0W^*$ with $A^0 \to b\overline{b}$, which is not negligible in Type I models. The limit in Type I models is 72.5 GeV (95% CL) if $m_{A^0} > 12$ GeV.

[4] ABBIENDI 12 also search for the decay mode $H^+ \to A^0W^*$ with $A^0 \to b\overline{b}$.

[5] AAD 21V search for $\overline{t}bH^+$ associated production followed by $H^+ \to t\overline{b}$ in 139 fb^{-1} of pp collisions at $E_{cm} = 13$ TeV. See their Fig. 6 for upper limits on cross section times branching ratio for $m_{H^+} = 0.2$–2 TeV. See also their Fig. 7 for the excluded region in the parameter space of the hMSSM and the following MSSM benchmark scenarios: M_h^{125}, $M_h^{125}(\widetilde{\chi})$, $M_h^{125}(\widetilde{\tau})$, M_h^{125}(alignment), $M_{h_1}^{125}$(CPV).

[6] SIRUNYAN 21W search for vector boson fusion production of H^+ decaying to $H^+ \to W^+Z \to \ell^+\nu\ell^+\ell^-$ in 137 fb^{-1} of pp collisions at $E_{cm} = 13$ TeV. See their Fig. 8 for limits on cross section times branching ratio for $m_{H^+} = 0.2$–3.0 TeV, and also for limits on the fraction of the triplet vev contribution to the W mass in the Georgi-Machacek model.

[7] AAD 20W search for dijet resonances in events with isolated leptons using 139 fb^{-1} of pp collisions at $E_{cm} = 13$ TeV. As a byproduct, $H^+ \to t\overline{b}$ produced in association with $\overline{t}b$ is searched for. Limits on the product of cross section times branching ratio for $m_{H^+} = 0.6$–2 TeV are given in their Fig. 5(c).

[8] SIRUNYAN 20AO search for $H^+ \to t\overline{b}$ produced in association with $t(b)$ in all jet final states in 35.9 fb^{-1} of pp collisions at $E_{cm} = 13$ TeV. See their Fig. 6 for limits on the product of cross section times branching ratio for $m_{H^+} = 0.2$–3 TeV. Limits for s-channel production are also given for $m_{H^+} = 0.8$–3 TeV. See also Fig. 7 for the corresponding limits in scenarios in the minimal supersymmetric standard model. Cross section limits from combined results with SIRUNYAN 20AV are given in Fig. 8.

[9] SIRUNYAN 20AV search for $H^+ \to t\overline{b}$ produced in association with $t(b)$ in final states with one or two leptons, in 35.9 fb^{-1} of pp collisions at $E_{cm} = 13$ TeV. See their Fig. 5 for limits on the product of cross section times branching ratio for $m_{H^+} = 0.2$–3 TeV, and their Fig. 6 for the corresponding limits in scenarios in the minimal supersymmetric standard model.

[10] SIRUNYAN 20BE search for $t \to bH^+$ followed by the decay $H^+ \to c\overline{s}$ in pair produced top quark events using 35.9 fb^{-1} of pp collisions at $E_{cm} = 13$ TeV. Limits on the branching ratio in the range 1.68–0.25% (95%CL) are given for $m_{H^+} = 80$–160 GeV, see their Fig. 4.

[11] SIRUNYAN 19AH search for H^+ in the decay of a pair-produced t quark, or in associated tbH^+ or nonresonant $b\overline{b}H^+W^-$ production, followed by $H^+ \to \tau^+\nu$, in 35.9 fb^{-1} of pp collisions at $E_{cm} = 13$ TeV. Upper limits on cross section times branching ratio between 6 pb and 5 fb (95% CL) are given for $m_{H^+} = 80$–3000 GeV (including the non-resonant production near the top quark mass), see their Fig. 6 (left). See their Fig. 6 (right) for the excluded regions in the m_h^{mod-} scenario of the MSSM.

[12] SIRUNYAN 19BP search for vector boson fusion production of H^+ decaying to $H^+ \to W^+Z \to \ell^+\nu\ell^+\ell^-$ in 35.9 fb^{-1} of pp collisions at $E_{cm} = 13$ TeV. See their Fig. 7 for limits on cross section times branching ratio for $m_{H^+} = 0.3$–2.0 TeV, and also for limits on the fraction of the triplet vev contribution to the W mass in the Georgi-Machacek model.

[13] SIRUNYAN 19CC search for $t \to bH^+$ from pair produced top quarks, with the decay chain $H^+ \to W^+A^0$, $A^0 \to \mu^+\mu^-$ in 35.9 fb^{-1} of pp collisions at $E_{cm} = 13$ TeV. See their Fig. 2 for limits on the product of branching ratios for $m_{A^0} = 15$–75 GeV.

[14] SIRUNYAN 19CQ search for vector boson fusion production of H^+ decaying to $H^+ \to W^+Z \to \ell^+\nu q\overline{q}$ or $q\overline{q}\ell^+\ell^-$ in 35.9 fb^{-1} of pp collisions at $E_{cm} = 13$ TeV. See their Fig. 5 for limits on cross section times branching ratio for $m_{H^+} = 0.6$–2.0 TeV, and also for limits on the triplet vacuum expectation value fraction in the Georgi-Machacek model.

[15] AABOUD 18BW search for $\overline{t}bH^+$ associated production or the decay $t \to bH^+$, followed by $H^+ \to \tau^+\nu$, in 36.1 fb^{-1} of pp collisions at $E_{cm} = 13$ TeV. See their Fig. 8(a) for upper limits on cross section times branching ratio for $m_{H^+} = 90$–2000 GeV, and Fig. 8(b) for limits on $B(t \to bH^+)$ $B(H^+ \to \tau^+\nu)$ for $m_{H^+} = 90$–160 GeV. See also their Fig. 9 for the excluded region in the hMSSM parameter space.

[16] AABOUD 18CD search for $\overline{t}bH^+$ associated production followed by $H^+ \to t\overline{b}$ in 36.1 fb^{-1} of pp collisions at $E_{cm} = 13$ TeV. See their Fig. 8 for upper limits on cross section times branching ratio for $m_{H^+} = 0.2$–2 TeV. See also their Fig. 9 for the excluded region in the parameter space of the m_h^{mod-} and hMSSM scenarios of the MSSM. The theory predictions overlaid to the experimental limits to determine the excluded m_{H^+} range are shown without their respective uncertainty band.

[17] AABOUD 18CH search for vector boson fusion production of $H^{\pm}$ decaying to $H^{\pm} \to W^{\pm}Z \to \ell^{\pm}\nu\ell^+\ell^-$ in 36.1 fb^{-1} of pp collisions at $E_{cm} = 13$ TeV. See their Fig. 7 for limits on cross section times branching ratio for $m_{H^{\pm}} = 0.2$–0.9 TeV, and also for limits on the triplet vacuum expectation value fraction in the Georgi-Machacek model.

[18] HALLER 18 give 95% CL lower limits on m_{H^+} of 590 GeV in type II two Higgs doublet model from combined data (including an unpublished BELLE result) for $B(b \to s\gamma)$.

[19] SIRUNYAN 18DO search for $t\overline{t}$ production followed by $t \to bH^+$, $H^+ \to c\overline{b}$ in 19.7 fb^{-1} of pp collisions at $E_{cm} = 8$ TeV. See their Fig. 3 for upper limits on $B(t \to bH^+)$ for $m_{H^+} = 90$–150 GeV assuming that $B(H^+ \to c\overline{b}) = 1$ and $B(t \to bH^+) + B(t \to bW^+) = 1$.

Downloaded from https://academic.oup.com/ptep/article/2022/8/083C01/6651666 by KIT Library user on 27 September 2022

[20] MISIAK 17 give 95% CL lower limits on m_{H^+} between 570 and 800 GeV in type II two Higgs doublet model from combined data (including an unpublished BELLE result) for $B(b \to s(d)\gamma)$.

[21] SIRUNYAN 17AE search for vector boson fusion production of $H^{\pm}$ decaying to $H^{\pm} \to W^{\pm}Z \to \ell^{\pm}\nu\ell^{+}\ell^{-}$ in 15.2 fb^{-1} of pp collisions at E_{cm} = 13 TeV. See their Fig. 3 for limits on cross section times branching ratio for $m_{H^{\pm}}$ = 0.2–2.0 TeV, and also for limits on the triplet vacuum expectation value fraction in the Georgi-Machacek model.

[22] AABOUD 16A search for $t(b)$ $H^{\pm}$ associated production followed by $H^{+} \to \tau^{+}\nu$ in 3.2 fb^{-1} of pp collisions at E_{cm} = 13 TeV. Upper limits on $\sigma(t(b)\ H^{\pm})\ B(H^{+} \to \tau\nu)$ between 1.9 pb and 15 fb (95% CL) are given for m_{H^+} = 200–2000 GeV, see their Fig. 6. See their Fig. 7 for the excluded regions in the hMSSM scenario.

[23] AAD 16AJ search for $t(b)$ $H^{\pm}$ associated production followed by $H^{\pm} \to tb$ in 20.3 fb^{-1} of pp collisions at E_{cm} = 8 TeV. See their Fig. 6 for upper limits on $\sigma(t(b)\ H^{\pm})$ $B(H^{+} \to tb)$ for m_{H^+} = 200–600 GeV.

[24] AAD 16AJ search for $H^{\pm}$ production from quark-antiquark annihilation, followed by $H^{\pm} \to tb$, in 20.3 fb^{-1} of pp collisions at E_{cm} = 8 TeV. See their Fig. 10 for upper limits on $\sigma(H^{\pm})$ $B(H^{+} \to tb)$ for m_{H^+} = 400–3000 GeV.

[25] AAD 15AF search for $tH^{\pm}$ associated production followed by $H^{\pm} \to \tau^{\pm}\nu$ in 19.5 fb^{-1} of pp collisions at E_{cm} = 8 TeV. Upper limits on $\sigma(tH^{\pm})$ $B(H^{+} \to \tau\nu)$ between 760 and 4.5 fb (95% CL) are given for m_{H^+} = 180–1000 GeV. See their Fig. 8 for the excluded regions in different benchmark scenarios of the MSSM.

[26] AAD 15M search for vector boson fusion production of $H^{\pm}$ decaying to $H^{\pm} \to W^{\pm}Z \to q\overline{q}\ell^{+}\ell^{-}$ in 20.3 fb^{-1} of pp collisions at E_{cm} = 8 TeV. See their Fig. 2 for limits on cross section times branching ratio for $m_{H^{\pm}}$ = 200–1000 GeV, and Fig. 3 for limits on thetriplet vacuum expectation value fraction in the Georgi-Machacek model.

[27] KHACHATRYAN 15AX search for $tH^{\pm}$ associated production followed by $H^{\pm} \to tb$ in 19.7 fb^{-1} of pp collisions at E_{cm} = 8 TeV. Upper limits on $\sigma(tH^{\pm})$ $B(H^{+} \to t\overline{b})$ between 2.0 and 0.13 pb (95% CL) are given for m_{H^+} = 180–600 GeV. See their Fig. 11 for the excluded regions in different benchmark scenarios of the MSSM.

[28] KHACHATRYAN 15AX search for $tH^{\pm}$ associated production followed by $H^{\pm} \to \tau^{\pm}\nu$ in 19.7 fb^{-1} of pp collisions at E_{cm} = 8 TeV. Upper limits on $\sigma(tH^{\pm})$ $B(H^{+} \to \tau\nu)$ between 380 and 25 fb (95% CL) are given for m_{H^+} = 180–600 GeV. See their Fig. 11 for the excluded regions in different benchmark scenarios of the MSSM.

[29] KHACHATRYAN 15BF search for $t\overline{t}$ production followed by $t \to bH^{+}$, $H^{+} \to c\overline{s}$ in 19.7 fb^{-1} of pp collisions at E_{cm} = 8 TeV. Upper limits on $B(t \to bH^{+})$ $B(H^{+} \to c\overline{s})$ between 1.2×10^{-2} and 6.5×10^{-2} (95% CL) are given for m_{H^+} = 90–160 GeV.

[30] AAD 14M search for the decay cascade $H_2^0 \to H^{\pm}W^{\mp} \to H^0W^{\pm}W^{\mp}$, H^0 decaying to $b\overline{b}$ in 20.3 fb^{-1} of pp collisions at E_{cm} = 8 TeV. See their Table III for limits on cross section times branching ratio for $m_{H_2^0}$= 325–1025 GeV and m_{H^+}= 225–925 GeV.

[31] AALTONEN 14A measure $B(t \to b\tau\nu) = 0.096 \pm 0.028$ using 9 fb^{-1} of $p\overline{p}$ collisions at E_{cm} = 1.96 TeV. For m_{H^+}= 80–140 GeV, this measured value is translated to a limit $B(t \to bH^{+}) < 0.059$ at 95% CL assuming $B(H^{+} \to \tau^{+}\nu) = 1$.

[32] AAD 13AC search for $t\overline{t}$ production followed by $t \to bH^{+}$, $H^{+} \to c\overline{s}$ (flavor unidentified) in 4.7 fb^{-1} of pp collisions at E_{cm} = 7 TeV. Upper limits on $B(t \to bH^{+})$ between 0.05 and 0.01 (95%CL) are given for m_{H^+}=90–150 GeV and $B(H^{+} \to c\overline{s})$=1.

[33] AAD 13V search for $t\overline{t}$ production followed by $t \to bH^{+}$, $H^{+} \to \tau^{+}\nu$ through violation of lepton universality with 4.6 fb^{-1} of pp collisions at E_{cm} = 7 TeV. Upper limits on $B(t \to bH^{+})$ between 0.032 and 0.044 (95% CL) are given for m_{H^+} = 90–140 GeV and $B(H^{+} \to \tau^{+}\nu) = 1$. By combining with AAD 12BH, the limits improve to 0.008 to 0.034 for m_{H^+} = 90–160 GeV. See their Fig. 7 for the excluded region in the m_h^{max} scenario of the MSSM.

[34] AAD 12BH search for $t\overline{t}$ production followed by $t \to bH^{+}$, $H^{+} \to \tau^{+}\nu$ with 4.6 fb^{-1} of pp collisions at E_{cm} = 7 TeV. Upper limits on $B(t \to bH^{+})$ between 0.01 and 0.05 (95% CL) are given for m_{H^+} = 90–160 GeV and $B(H^{+} \to \tau^{+}\nu) = 1$. See their Fig. 8 for the excluded region in the m_h^{max} scenario of the MSSM.

[35] CHATRCHYAN 12AA search for $t\overline{t}$ production followed by $t \to bH^{+}$, $H^{+} \to \tau^{+}\nu$ with 2 fb^{-1} of pp collisions at E_{cm} = 7 TeV. Upper limits on $B(t \to bH^{+})$ between 0.019 and 0.041 (95% CL) are given for m_{H^+} = 80–160 GeV and $B(H^{+} \to \tau^{+}\nu)$=1.

[36] AALTONEN 11P search in 2.7 fb^{-1} of $p\overline{p}$ collisions at E_{cm} = 1.96 TeV for the decay chain $t \to bH^{+}$, $H^{+} \to W^{+}A^0$, $A^0 \to \tau^{+}\tau^{-}$ with m_{A^0} between 4 and 9 GeV. See their Fig. 4 for limits on $B(t \to bH^{+})$ for $90 < m_{H^+} < 160$ GeV.

[37] DESCHAMPS 10 make Type II two Higgs doublet model fits to weak leptonic and semileptonic decays, $b \to s\gamma$, B, B_s mixings, and $Z \to b\overline{b}$. The limit holds irrespective of $\tan\beta$.

[38] AALTONEN 09AJ search for $t \to bH^{+}$, $H^{+} \to c\overline{s}$ in $t\overline{t}$ events in 2.2 fb^{-1} of $p\overline{p}$ collisions at E_{cm} = 1.96 TeV. Upper limits on $B(t \to bH^{+})$ between 0.08 and 0.32 (95% CL) are given for m_{H^+} = 60–150 GeV and $B(H^{+} \to c\overline{s}) = 1$.

[39] ABAZOV 09AC search for $t \to bH^{+}$, $H^{+} \to \tau^{+}\nu$ in $t\overline{t}$ events in 0.9 fb^{-1} of $p\overline{p}$ collisions at E_{cm} = 1.96 TeV. Upper limits on $B(t \to bH^{+})$ between 0.19 and 0.25 (95% CL) are given for m_{H^+} = 80–155 GeV and $B(H^{+} \to \tau^{+}\nu) = 1$. See their Fig. 4 for an excluded region in a MSSM scenario.

[40] ABAZOV 09AG measure $t\overline{t}$ cross sections in final states with ℓ + jets ($\ell = e, \mu$), $\ell\ell$, and $\tau\ell$ in 1 fb^{-1} of $p\overline{p}$ collisions at E_{cm} = 1.96 TeV, which constrains possible $t \to bH^{+}$ branching fractions. Upper limits (95% CL) on $B(t \to bH^{+})$ between 0.15 and 0.40 (0.48 and 0.57) are given for $B(H^{+} \to \tau^{+}\nu) = 1$ ($B(H^{+} \to c\overline{s}) = 1$) for m_{H^+} = 80–155 GeV.

[41] ABAZOV 09AI search for $t \to bH^{+}$ in $t\overline{t}$ events in 1 fb^{-1} of $p\overline{p}$ collisions at E_{cm} = 1.96 TeV. Final states with ℓ + jets ($\ell = e, \mu$), $\ell\ell$, and $\tau\ell$ are examined. Upper limits on $B(t \to bH^{+})$ (95% CL) between 0.15 and 0.19 (0.19 and 0.22) are given for $B(H^{+} \to \tau^{+}\nu) = 1$ ($B(H^{+} \to c\overline{s}) = 1$) for m_{H^+} = 80–155 GeV. For $B(H^{+} \to \tau^{+}\nu) = 1$ also a simultaneous extraction of $B(t \to bH^{+})$ and the $t\overline{t}$ cross section is performed, yielding a limit on $B(t \to bH^{+})$ between 0.12 and 0.26 for m_{H^+} = 80–155 GeV. See their Figs. 5–8 for excluded regions in several MSSM scenarios.

[42] ABAZOV 09P search for H^{+} production by $q\overline{q}'$ annihilation followed by $H^{+} \to t\overline{b}$ decay in 0.9 fb^{-1} of $p\overline{p}$ collisions at E_{cm} = 1.96 TeV. Cross section limits in several two-doublet models are given for m_{H^+} = 180–300 GeV. A region with 20 $\lesssim \tan\beta \lesssim$ 70 is excluded (95% CL) for 180 GeV $\lesssim m_{H^+} \lesssim$ 184 GeV in type-I models.

[43] ABULENCIA 06E search for associated H^0W production in $p\overline{p}$ collisions at E_{cm} = 1.96 TeV. A fit is made for $t\overline{t}$ production processes in dilepton, lepton + jets, and lepton + τ final states, with the decays $t \to W^{+}b$ and $t \to H^{+}b$ followed by $H^{+} \to \tau^{+}\nu$, $c\overline{s}$, $t^*\overline{b}$, or $W^{+}H^0$. Within the MSSM the search is sensitive to the region $\tan\beta < 1$ or > 30 in the mass range m_{H^+} = 80–160 GeV. See Fig. 2 for the excluded region in a certain MSSM scenario.

[44] ABDALLAH 04I search for $e^{+}e^{-} \to H^{+}H^{-}$ with $H^{\pm}$ decaying to $\tau\nu$, cs, or W^*A^0 in Type-I two-Higgs-doublet models.

[45] ABBIENDI 03 give a limit $m_{H^+} > 1.28\tan\beta$ GeV (95%CL) in Type II two-doublet models.

[46] ABAZOV 02B search for a charged Higgs boson in top decays with $H^{+} \to \tau^{+}\nu$ at E_{cm}=1.8 TeV. For m_{H^+}=75 GeV, the region $\tan\beta > 32.0$ is excluded at 95%CL. The excluded mass region extends to over 140 GeV for $\tan\beta$ values above 100.

[47] BORZUMATI 02 point out that the decay modes such as $b\overline{b}W$, A^0W, and supersymmetric ones can have substantial branching fractions in the mass range explored at LEP II and Tevatron.

[48] ABBIENDI 01Q give a limit $\tan\beta/m_{H^+} < 0.53$ GeV^{-1} (95%CL) in Type II two-doublet models.

[49] BARATE 01E give a limit $\tan\beta/m_{H^+} < 0.40$ GeV^{-1} (90% CL) in Type II two-doublet models. An independent measurement of $B \to \tau\nu_{\tau}X$ gives $\tan\beta/m_{H^+} < 0.49$ GeV^{-1} (90% CL).

[50] GAMBINO 01 use the world average data in the summer of 2001 $B(b \to s\gamma) = (3.23 \pm 0.42) \times 10^{-4}$. The limit applies for Type-II two-doublet models.

[51] AFFOLDER 00I search for a charged Higgs boson in top decays with $H^{+} \to \tau^{+}\nu$ in $p\overline{p}$ collisions at E_{cm}=1.8 TeV. The excluded mass region extends to over 120 GeV for $\tan\beta$ values above 100 and $B(\tau\nu) = 1$. If $B(t \to bH^{+}) \gtrsim 0.6$, m_{H^+} up to 160 GeV is excluded. Updates ABE 97L.

[52] ABBOTT 99E search for a charged Higgs boson in top decays in $p\overline{p}$ collisions at E_{cm}=1.8 TeV, by comparing the observed $t\overline{t}$ cross section (extracted from the data assuming the dominant decay $t \to bW^{+}$) with theoretical expectation. The search is sensitive to regions of the domains $\tan\beta \lesssim 1$, $50 < m_{H^+}$(GeV) $\lesssim 120$ and $\tan\beta \gtrsim 40$, $50 < m_{H^+}$(GeV) $\lesssim 160$. See Fig. 3 for the details of the excluded region.

[53] ACKERSTAFF 99D measure the Michel parameters ρ, ξ, η, and $\xi\delta$ in leptonic τ decays from $Z \to \tau\tau$. Assuming e-μ universality, the limit $m_{H^+} > 0.97\tan\beta$ GeV (95%CL) is obtained for two-doublet models in which only one doublet couples to leptons.

[54] ACCIARRI 97F give a limit $m_{H^+} > 2.6\tan\beta$ GeV (90% CL) from their limit on the exclusive $B \to \tau\nu_{\tau}$ branching ratio.

[55] AMMAR 97B measure the Michel parameter ρ from $\tau \to e\nu\nu$ decays and assumes e/μ universality to extract the Michel η parameter from $\tau \to \mu\nu\nu$ decays. The measurement is translated to a lower limit on m_{H^+} in a two-doublet model $m_{H^+} > 0.97\tan\beta$ GeV (90% CL).

[56] COARASA 97 reanalyzed the constraint on the ($m_{H^{\pm}}$,$\tan\beta$) plane derived from the inclusive $B \to \tau\nu_{\tau}X$ branching ratio in GROSSMAN 95B and BUSKULIC 95. They show that the constraint is quite sensitive to supersymmetric one-loop effects.

[57] GUCHAIT 97 studies the constraints on m_{H^+} set by Tevatron data on $\ell\tau$ final states in $t\overline{t} \to (Wb)(Hb)$, $W \to \ell\nu$, $H \to \tau\nu_{\tau}$. See Fig. 2 for the excluded region.

[58] MANGANO 97 reconsiders the limit in ACCIARRI 97F including the effect of the potentially large $B_c \to \tau\nu_{\tau}$ background to $B_u \to \tau\nu_{\tau}$ decays. Stronger limits are obtained.

[59] STAHL 97 fit τ lifetime, leptonic branching ratios, and the Michel parameters and derive limit $m_{H^+} > 1.5\tan\beta$ GeV (90% CL) for a two-doublet model. See also STAHL 94.

[60] ALAM 95 measure the inclusive $b \to s\gamma$ branching ratio at $\Upsilon(4S)$ and give $B(b \to s\gamma) < 4.2 \times 10^{-4}$ (95% CL), which translates to the limit $m_{H^+} > [244 + 63/(\tan\beta)^{1.3}]$ GeV in the Type II two-doublet model. Light supersymmetric particles can invalidate this bound.

[61] BUSKULIC 95 give a limit $m_{H^+} > 1.9\tan\beta$ GeV (90% CL) for Type-II models from $b \to \tau\nu_{\tau}X$ branching ratio, as proposed in GROSSMAN 94.

$H^{\pm}$ (charged Higgs) mass limits for m_{H^+} > m(top)

Limits obtained at the LHC are given in the m_h^{mod-} benchmark scenario, see CARENA 13, and depend on the $\tan\beta$ values.

VALUE (GeV)	CL%	DOCUMENT ID		TECN	COMMENT
> 181	95	[1] AABOUD	18BW	ATLS	$\tan\beta = 10$
> 249	95	[1] AABOUD	18BW	ATLS	$\tan\beta = 20$
> 390	95	[1] AABOUD	18BW	ATLS	$\tan\beta = 30$
> 894	95	[1] AABOUD	18BW	ATLS	$\tan\beta = 40$
>1017	95	[1] AABOUD	18BW	ATLS	$\tan\beta = 50$
>1103	95	[1] AABOUD	18BW	ATLS	$\tan\beta = 60$

[1] AABOUD 18BW search for $\overline{t}bH^{+}$ associated production in 36.1 fb^{-1} of pp collisions at E_{cm} = 13 TeV. See also their Fig. 9 for the excluded region in the hMSSM parameter space.

$H^{\pm\pm}$ (doubly-charged Higgs boson) mass limits

This section covers searches for a doubly-charged Higgs boson with couplings to lepton pairs. Its weak isospin T_3 is thus restricted to two possibilities depending on lepton chiralities: $T_3(H^{\pm\pm}) = \pm 1$, with the coupling $g_{\ell\ell}$ to $\ell_L^{-}\ell_L'^{-}$ and $\ell_R^{+}\ell_R'^{+}$ ("left-handed") and $T_3(H^{\pm\pm}) = 0$, with the coupling to $\ell_R^{-}\ell_R'^{-}$ and $\ell_L^{+}\ell_L'^{+}$ ("right-handed"). These Higgs bosons appear in some left-right symmetric models based on the gauge

Downloaded from https://academic.oup.com/ptep/article/2022/8/083C01/6651666 by KIT Library user on 27 September 2022

group $SU(2)_L \times SU(2)_R \times U(1)$, the type-II seesaw model, and the Zee-Babu model. The two cases are listed separately in the following. Unless noted, one of the lepton flavor combinations is assumed to be dominant in the decay.

Limits for $H^{\pm\pm}$ with $T_3 = \pm 1$

VALUE (GeV)	CL%	DOCUMENT ID		TECN	COMMENT
>220	95	[1] AABOUD	19K	ATLS	$W^{\pm} W^{\pm}$
>768	95	[2] AABOUD	18BC	ATLS	ee
>846	95	[2] AABOUD	18BC	ATLS	$\mu\mu$
>468	95	[3] AAD	15AG	ATLS	$e\mu$
>400	95	[4] AAD	15AP	ATLS	$e\tau$
>400	95	[4] AAD	15AP	ATLS	$\mu\tau$
>169	95	[5] CHATRCHYAN	12AU	CMS	$\tau\tau$
>300	95	[5] CHATRCHYAN	12AU	CMS	$\mu\tau$
>293	95	[5] CHATRCHYAN	12AU	CMS	$e\tau$
>395	95	[5] CHATRCHYAN	12AU	CMS	$\mu\mu$
>391	95	[5] CHATRCHYAN	12AU	CMS	$e\mu$
>382	95	[5] CHATRCHYAN	12AU	CMS	ee
> 98.1	95	[6] ABDALLAH	03	DLPH	$\tau\tau$
> 99.0	95	[7] ABBIENDI	02C	OPAL	$\tau\tau$
• • • We do not use the following data for averages, fits, limits, etc. • • •					
>350	95	[8] AAD	21U	ATLS	$W^{\pm} W^{\pm}$
>230	95	[9] AAD	21U	ATLS	$H^{\pm\pm} H^{\mp}$ associated production, $H^{\pm\pm} \to W^{\pm} W^{\pm}$, $H^{\pm} \to W^{\pm} Z$
		[10] SIRUNYAN	21W	CMS	$W^{\pm} W^{\pm}$
		[11] SIRUNYAN	19CQ	CMS	$W^{\pm} W^{\pm}$
		[12] SIRUNYAN	18CC	CMS	$W^{\pm} W^{\pm}$
>551	95	[3] AAD	15AG	ATLS	ee
>516	95	[3] AAD	15AG	ATLS	$\mu\mu$
		[13] KANEMURA	15	RVUE	$W^{(*)\pm} W^{(*)\pm}$
		[14] KHACHATRY...	15D	CMS	$W^{\pm} W^{\pm}$
		[15] KANEMURA	14	RVUE	$W^{(*)\pm} W^{(*)\pm}$
>330	95	[16] AAD	13Y	ATLS	$\mu\mu$
>237	95	[16] AAD	13Y	ATLS	$\mu\tau$
>355	95	[17] AAD	12AY	ATLS	$\mu\mu$
>398	95	[18] AAD	12CQ	ATLS	$\mu\mu$
>375	95	[18] AAD	12CQ	ATLS	$e\mu$
>409	95	[18] AAD	12CQ	ATLS	ee
>128	95	[19] ABAZOV	12A	D0	$\tau\tau$
>144	95	[19] ABAZOV	12A	D0	$\mu\tau$
>245	95	[20] AALTONEN	11AF	CDF	$\mu\mu$
>210	95	[20] AALTONEN	11AF	CDF	$e\mu$
>225	95	[20] AALTONEN	11AF	CDF	ee
>114	95	[21] AALTONEN	08AA	CDF	$e\tau$
>112	95	[21] AALTONEN	08AA	CDF	$\mu\tau$
>168	95	[22] ABAZOV	08V	D0	$\mu\mu$
		[23] AKTAS	06A	H1	single $H^{\pm\pm}$
>133	95	[24] ACOSTA	05L	CDF	stable
>118.4	95	[25] ABAZOV	04E	D0	$\mu\mu$
		[26] ABBIENDI	03Q	OPAL	$E_{cm} \leq 209$ GeV, single $H^{\pm\pm}$
		[27] GORDEEV	97	SPEC	muonium conversion
		[28] ASAKA	95	THEO	
> 45.6	95	[29] ACTON	92M	OPAL	
> 30.4	95	[30] ACTON	92M	OPAL	
none 6.5–36.6	95	[31] SWARTZ	90	MRK2	

[1] AABOUD 19K search for pair production of $H^{++} H^{--}$ followed by the decay $H^{\pm\pm} \to W^{\pm} W^{\pm}$ in 36.1 fb^{-1} of pp collisions at $E_{cm} = 13$ TeV. The search is interpreted in a doublet-triplet extension of the scalar sector with a vev of 0.1 GeV, leading to $B(H^{\pm\pm} \to W^{\pm} W^{\pm}) = 1$. See their Fig. 5 for limits on the cross section for $m_{H^{++}}$ between 200 and 700 GeV.

[2] See their Figs. 11(b) and 13 for limits with smaller branching ratios.

[3] AAD 15AG search for $H^{++} H^{--}$ production in 20.3 fb^{-1} of pp collisions at $E_{cm} = 8$ TeV. The limit assumes 100% branching ratio to the specified final state. See their Fig. 5 for limits for arbitrary branching ratios.

[4] AAD 15AP search for $H^{++} H^{--}$ production in 20.3 fb^{-1} of pp collisions at $E_{cm} = 8$ TeV. The limit assumes 100% branching ratio to the specified final state.

[5] CHATRCHYAN 12AU search for $H^{++} H^{--}$ production with 4.9 fb^{-1} of pp collisions at $E_{cm} = 7$ TeV. The limit assumes 100% branching ratio to the specified final state. See their Table 6 for limits including associated $H^{++} H^{-}$ production or assuming different scenarios.

[6] ABDALLAH 03 search for $H^{++} H^{--}$ pair production either followed by $H^{++} \to \tau^{+} \tau^{+}$, or decaying outside the detector.

[7] ABBIENDI 02C searches for pair production of $H^{++} H^{--}$, with $H^{\pm\pm} \to \ell^{\pm} \ell^{\pm}$ (ℓ,ℓ' = e,μ,τ). The limit holds for ℓ=ℓ'=τ, and becomes stronger for other combinations of leptonic final states. To ensure the decay within the detector, the limit only applies for $g(H\ell\ell) \gtrsim 10^{-7}$.

[8] AAD 21U search for pair production of $H^{++} H^{--}$ followed by the decay $H^{\pm\pm} \to W^{\pm} W^{\pm}$ in 139 fb^{-1} of pp collisions at $E_{cm} = 13$ TeV. The search is interpreted in a triplet extension of the SM Higgs sector with a triplet vev of 0.1 GeV, leading to $B(H^{\pm\pm} \to W^{\pm} W^{\pm}) = 1$. See their Fig. 9(a) for limits on the cross section for $m_{H^{++}}$ between 200 and 600 GeV.

[9] AAD 21U search for associated production of $H^{\pm\pm} H^{\mp}$ followed by the decays $H^{\pm\pm} \to W^{\pm} W^{\pm}$, $H^{\pm} \to W^{\pm} Z$ in 139 fb^{-1} of pp collisions at $E_{cm} = 13$ TeV. $H^{\pm\pm}$ and $H^{\pm}$ are assumed to be degenerate in mass within 5 GeV. The search is interpreted in a triplet extension of the SM Higgs sector with a triplet vev of 0.1 GeV, leading to $B(H^{\pm\pm} \to W^{\pm} W^{\pm}) = 1$. See their Fig. 9(b) for limits on the cross section for $m_{H^{++}}$ between 200 and 600 GeV.

[10] SIRUNYAN 21W search for vector boson fusion production of $H^{\pm\pm}$ decaying to $H^{\pm\pm} \to W^{\pm} W^{\pm} \to \ell^{\pm} \nu \ell^{\pm} \nu$ in 137 fb^{-1} of pp collisions at $E_{cm} = 13$ TeV. See their Fig. 8 for limits on cross section times branching ratio for $m_{H^{++}} = 0.2$–3.0 TeV.

[11] SIRUNYAN 19CQ search for $H^{\pm\pm}$ production by vector boson fusion followed by the decay $H^{\pm\pm} \to W^{\pm} W^{\pm} \to q q \ell \nu$ in 35.9 fb^{-1} of pp collisions at $E_{cm} = 13$ TeV. See their Fig. 5 for limits on cross section times branching ratio for $m_{H^{\pm\pm}}$ between 0.6 and 2 TeV.

[12] SIRUNYAN 18CC search for $H^{\pm\pm}$ production by vector boson fusion followed by the decay $H^{\pm\pm} \to W^{\pm} W^{\pm}$ in 35.9 fb^{-1} of pp collisions at $E_{cm} = 13$ TeV. See their Fig. 3 for limits on cross section times branching ratio for $m_{H^{\pm\pm}}$ between 200 and 1000 GeV.

[13] KANEMURA 15 examine the case where H^{++} decays preferentially to $W^{(*)} W^{(*)}$ and estimate that a lower mass limit of ~ 84 GeV can be derived from the same-sign dilepton data of AAD 15AG if H^{++} decays with 100% branching ratio to $W^{(*)} W^{(*)}$.

[14] KHACHATRYAN 15D search for $H^{\pm\pm}$ production by vector boson fusion followed by the decay $H^{\pm\pm} \to W^{\pm} W^{\pm}$ in 19.4 fb^{-1} of pp collisions at $E_{cm} = 8$ TeV. See their Fig. 4 for limits on cross section times branching ratio for $m_{H^{++}}$ between 160 and 800 GeV.

[15] KANEMURA 14 examine the case where H^{++} decays preferentially to $W^{(*)} W^{(*)}$ and estimate that a lower mass limit of ~ 60 GeV can be derived from the same-sign dilepton data of AAD 12CY.

[16] AAD 13Y search for $H^{++} H^{--}$ production in a generic search of events with three charged leptons in 4.6 fb^{-1} of pp collisions at $E_{cm} = 7$ TeV. The limit assumes 100% branching ratio to the specified final state.

[17] AAD 12AY search for $H^{++} H^{--}$ production with 1.6 fb^{-1} of pp collisions at $E_{cm} = 7$ TeV. The limit assumes 100% branching ratio to the specified final state.

[18] AAD 12CQ search for $H^{++} H^{--}$ production with 4.7 fb^{-1} of pp collisions at $E_{cm} = 7$ TeV. The limit assumes 100% branching ratio to the specified final state. See their Table 1 for limits assuming smaller branching ratios.

[19] ABAZOV 12A search for $H^{++} H^{--}$ production in 7.0 fb^{-1} of $p\overline{p}$ collisions at $E_{cm} = 1.96$ TeV.

[20] AALTONEN 11AF search for $H^{++} H^{--}$ production in 6.1 fb^{-1} of $p\overline{p}$ collisions at $E_{cm} = 1.96$ TeV.

[21] AALTONEN 08AA search for $H^{++} H^{--}$ production in $p\overline{p}$ collisions at $E_{cm} = 1.96$ TeV. The limit assumes 100% branching ratio to the specified final state.

[22] ABAZOV 08V search for $H^{++} H^{--}$ production in $p\overline{p}$ collisions at $E_{cm} = 1.96$ TeV. The limit is for $B(H \to \mu\mu) = 1$. The limit is updated in ABAZOV 12A.

[23] AKTAS 06A search for single $H^{\pm\pm}$ production in ep collisions at HERA. Assuming that H^{++} only couples to $e^{+} \mu^{+}$ with $g_{e\mu} = 0.3$ (electromagnetic strength), a limit $m_{H^{++}} > 141$ GeV (95% CL) is derived. For the case where H^{++} couples to $e\tau$ only the limit is 112 GeV.

[24] ACOSTA 05L search for $H^{++} H^{--}$ pair production in $p\overline{p}$ collisions. The limit is valid for $g_{\ell\ell'} < 10^{-8}$ so that the Higgs decays outside the detector.

[25] ABAZOV 04E search for $H^{++} H^{--}$ pair production in $H^{\pm\pm} \to \mu^{\pm} \mu^{\pm}$. The limit is valid for $g_{\mu\mu} \gtrsim 10^{-7}$.

[26] ABBIENDI 03Q searches for single $H^{\pm\pm}$ via direct production in $e^{+} e^{-} \to e^{\mp} e^{\mp} H^{\pm\pm}$, and via t-channel exchange in $e^{+} e^{-} \to e^{+} e^{-}$. In the direct case, and assuming $B(H^{\pm\pm} \to \ell^{\pm} \ell^{\pm}) = 1$, a 95% CL limit on $h_{ee} < 0.071$ is set for $m_{H^{\pm\pm}} < 160$ GeV (see Fig. 6). In the second case, indirect limits on h_{ee} are set for $m_{H^{\pm\pm}} < 2$ TeV (see Fig. 8).

[27] GORDEEV 97 search for muonium-antimuonium conversion and find $G_{M\overline{M}}/G_F < 0.14$ (90% CL), where $G_{M\overline{M}}$ is the lepton-flavor violating effective four-fermion coupling. This limit may be converted to $m_{H^{++}} > 210$ GeV if the Yukawa couplings of H^{++} to ee and $\mu\mu$ are as large as the weak gauge coupling. For similar limits on muonium-antimuonium conversion, see the muon Particle Listings.

[28] ASAKA 95 point out that H^{++} decays dominantly to four fermions in a large region of parameter space where the limit of ACTON 92M from the search of dilepton modes does not apply.

[29] ACTON 92M limit assumes $H^{\pm\pm} \to \ell^{\pm} \ell^{\pm}$ or $H^{\pm\pm}$ does not decay in the detector. Thus the region $g_{\ell\ell} \approx 10^{-7}$ is not excluded.

[30] ACTON 92M from $\Delta\Gamma_Z < 40$ MeV.

[31] SWARTZ 90 assume $H^{\pm\pm} \to \ell^{\pm} \ell^{\pm}$ (any flavor). The limits are valid for the Higgs-lepton coupling $g(H\ell\ell) \gtrsim 7.4 \times 10^{-7}/[m_H/\text{GeV}]^{1/2}$. The limits improve somewhat for ee and $\mu\mu$ decay modes.

Limits for $H^{\pm\pm}$ with $T_3 = 0$

VALUE (GeV)	CL%	DOCUMENT ID		TECN	COMMENT
> 58	95	[1] AABOUD	18BC	ATLS	ee
>723	95	[1] AABOUD	18BC	ATLS	$\mu\mu$
>402	95	[2] AAD	15AG	ATLS	$e\mu$
>290	95	[3] AAD	15AP	ATLS	$e\tau$
>290	95	[3] AAD	15AP	ATLS	$\mu\tau$
> 97.3	95	[4] ABDALLAH	03	DLPH	$\tau\tau$
> 97.3	95	[5] ACHARD	03F	L3	$\tau\tau$
> 98.5	95	[6] ABBIENDI	02C	OPAL	$\tau\tau$
• • • We do not use the following data for averages, fits, limits, etc. • • •					
>374	95	[2] AAD	15AG	ATLS	ee
>438	95	[2] AAD	15AG	ATLS	$\mu\mu$
>251	95	[7] AAD	12AY	ATLS	$\mu\mu$
>306	95	[8] AAD	12CQ	ATLS	$\mu\mu$
>310	95	[8] AAD	12CQ	ATLS	$e\mu$
>322	95	[8] AAD	12CQ	ATLS	ee
>113	95	[9] ABAZOV	12A	D0	$\mu\tau$

Downloaded from https://academic.oup.com/ptep/article/2022/8/083C01/6651666 by KIT Library user on 27 September 2022

>205	95	[10] AALTONEN	11AF	CDF	$\mu\mu$
>190	95	[10] AALTONEN	11AF	CDF	$e\mu$
>205	95	[10] AALTONEN	11AF	CDF	ee
>145	95	[11] ABAZOV	08V	D0	$\mu\mu$
		[12] AKTAS	06A	H1	single $H^{\pm\pm}$
>109	95	[13] ACOSTA	05L	CDF	stable
> 98.2	95	[14] ABAZOV	04E	D0	$\mu\mu$
		[15] ABBIENDI	03Q	OPAL	$E_{cm} \leq 209$ GeV, single $H^{\pm\pm}$
		[16] GORDEEV	97	SPEC	muonium conversion
> 45.6	95	[17] ACTON	92M	OPAL	
> 25.5	95	[18] ACTON	92M	OPAL	
none 7.3–34.3	95	[19] SWARTZ	90	MRK2	

[1] See their Figs. 12(b) and 14 for limits with smaller branching ratios.

[2] AAD 15AG search for $H^{++}H^{--}$ production in 20.3 fb^{-1} of pp collisions at E_{cm} = 8 TeV. The limit assumes 100% branching ratio to the specified final state. See their Fig. 5 for limits for arbitrary branching ratios.

[3] AAD 15AP search for $H^{++}H^{--}$ production in 20.3 fb^{-1} of pp collisions at E_{cm} = 8 TeV. The limit assumes 100% branching ratio to the specified final state.

[4] ABDALLAH 03 search for $H^{++}H^{--}$ pair production either followed by $H^{++} \rightarrow \tau^+\tau^+$, or decaying outside the detector.

[5] ACHARD 03F search for $e^+e^- \rightarrow H^{++}H^{--}$ with $H^{\pm\pm} \rightarrow \ell^{\pm}\ell'^{\pm}$. The limit holds for $\ell = \ell' = \tau$, and slightly different limits apply for other flavor combinations. The limit is valid for $g_{\ell\ell'} \gtrsim 10^{-7}$.

[6] ABBIENDI 02C searches for pair production of $H^{++}H^{--}$, with $H^{\pm\pm} \rightarrow \ell^{\pm}\ell^{\pm}$ (ℓ,ℓ' = e,μ,τ). the limit holds for ℓ=ℓ'=τ, and becomes stronger for other combinations of leptonic final states. To ensure the decay within the detector, the limit only applies for $g(H\ell\ell) \gtrsim 10^{-7}$.

[7] AAD 12AY search for $H^{++}H^{--}$ production with 1.6 fb^{-1} of pp collisions at E_{cm} = 7 TeV. The limit assumes 100% branching ratio to the specified final state.

[8] AAD 12CQ search for $H^{++}H^{--}$ production with 4.7 fb^{-1} of pp collisions at E_{cm} = 7 TeV. The limit assumes 100% branching ratio to the specified final state. See their Table 1 for limits assuming smaller branching ratios.

[9] ABAZOV 12A search for $H^{++}H^{--}$ production in 7.0 fb^{-1} of $p\overline{p}$ collisions at E_{cm} = 1.96 TeV.

[10] AALTONEN 11AF search for $H^{++}H^{--}$ production in 6.1 fb^{-1} of $p\overline{p}$ collisions at E_{cm} = 1.96 TeV.

[11] ABAZOV 08V search for $H^{++}H^{--}$ production in $p\overline{p}$ collisions at E_{cm}= 1.96 TeV. The limit is for B($H \rightarrow \mu\mu$) = 1. The limit is updated in ABAZOV 12A.

[12] AKTAS 06A search for single $H^{\pm\pm}$ production in ep collisions at HERA. Assuming that H^{++} only couples to $e^+\mu^+$ with $g_{e\mu}$ = 0.3 (electromagnetic strength), a limit $m_{H^{++}}$ > 141 GeV (95% CL) is derived. For the case where H^{++} couples to $e\tau$ only the limit is 112 GeV.

[13] ACOSTA 05L search for $H^{++}H^{--}$ pair production in $p\overline{p}$ collisions. The limit is valid for $g_{\ell\ell'} < 10^{-8}$ so that the Higgs decays outside the detector.

[14] ABAZOV 04E search for $H^{++}H^{--}$ pair production in $H^{\pm\pm} \rightarrow \mu^{\pm}\mu^{\pm}$. The limit is valid for $g_{\mu\mu} \gtrsim 10^{-7}$.

[15] ABBIENDI 03Q searches for single $H^{\pm\pm}$ via direct production in $e^+e^- \rightarrow e^{\mp}e^{\mp}H^{\pm\pm}$, and via t-channel exchange in $e^+e^- \rightarrow e^+e^-$. In the direct case, and assuming B($H^{\pm\pm} \rightarrow \ell^{\pm}\ell^{\pm}$) = 1, a 95% CL limit on h_{ee} < 0.071 is set for $m_{H^{\pm\pm}}$ < 160 GeV (see Fig. 6). In the second case, indirect limits on h_{ee} are set for $m_{H^{\pm\pm}}$ < 2 TeV (see Fig. 8).

[16] GORDEEV 97 search for muonium-antimuonium conversion and find $G_{M\overline{M}}/G_F$ < 0.14 (90% CL), where $G_{M\overline{M}}$ is the lepton-flavor violating effective four-fermion coupling. This limit may be converted to $m_{H^{++}}$ > 210 GeV if the Yukawa couplings of H^{++} to ee and $\mu\mu$ are as large as the weak gauge coupling. For similar limits on muonium-antimuonium conversion, see the muon Particle Listings.

[17] ACTON 92M limit assumes $H^{\pm\pm} \rightarrow \ell^{\pm}\ell^{\pm}$ or $H^{\pm\pm}$ does not decay in the detector. Thus the region $g_{\ell\ell} \approx 10^{-7}$ is not excluded.

[18] ACTON 92M from $\Delta\Gamma_Z$ <40 MeV.

[19] SWARTZ 90 assume $H^{\pm\pm} \rightarrow \ell^{\pm}\ell^{\pm}$ (any flavor). The limits are valid for the Higgs-lepton coupling g($H\ell\ell$) $\gtrsim 7.4 \times 10^{-7}/[m_H/\text{GeV}]^{1/2}$. The limits improve somewhat for ee and $\mu\mu$ decay modes.

$H^{\pm}$ and $H^{\pm\pm}$ REFERENCES

AAD	21U	JHEP 2106 146	G. Aad *et al.*	(ATLAS Collab.)
AAD	21V	JHEP 2106 145	G. Aad *et al.*	(ATLAS Collab.)
SIRUNYAN	21W	EPJ C81 723	A.M. Sirunyan *et al.*	(CMS Collab.)
AAD	20W	JHEP 2006 151	G. Aad *et al.*	(ATLAS Collab.)
SIRUNYAN	20AO	JHEP 2007 126	A.M. Sirunyan *et al.*	(CMS Collab.)
SIRUNYAN	20AV	JHEP 2001 096	A.M. Sirunyan *et al.*	(CMS Collab.)
SIRUNYAN	20BE	PR D102 072001	A.M. Sirunyan *et al.*	(CMS Collab.)
AABOUD	19K	EPJ C79 58	M. Aaboud *et al.*	(ATLAS Collab.)
SIRUNYAN	19AH	JHEP 1907 142	A.M. Sirunyan *et al.*	(CMS Collab.)
SIRUNYAN	19BP	PL B795 281	A.M. Sirunyan *et al.*	(CMS Collab.)
SIRUNYAN	19CC	PRL 123 131802	A.M. Sirunyan *et al.*	(CMS Collab.)
SIRUNYAN	19CQ	PL B798 134985	A.M. Sirunyan *et al.*	(CMS Collab.)
AABOUD	18BC	EPJ C78 199	M. Aaboud *et al.*	(ATLAS Collab.)
AABOUD	18BW	JHEP 1809 139	M. Aaboud *et al.*	(ATLAS Collab.)
AABOUD	18CD	JHEP 1811 085	M. Aaboud *et al.*	(ATLAS Collab.)
AABOUD	18CH	PL B787 68	M. Aaboud *et al.*	(ATLAS Collab.)
HALLER	18	EPJ C78 675	J. Haller *et al.*	(Gfitter Group)
SIRUNYAN	18CC	PRL 120 081801	A.M. Sirunyan *et al.*	(CMS Collab.)
SIRUNYAN	18DO	JHEP 1811 115	A.M. Sirunyan *et al.*	(CMS Collab.)
MISIAK	17	EPJ C77 201	M. Misiak, M. Steinhauser	
SIRUNYAN	17AE	PRL 119 141802	A.M. Sirunyan *et al.*	(CMS Collab.)
AABOUD	16A	PL B759 555	M. Aaboud *et al.*	(ATLAS Collab.)
AAD	16AJ	JHEP 1603 127	G. Aad *et al.*	(ATLAS Collab.)
AAD	15AF	JHEP 1503 088	G. Aad *et al.*	(ATLAS Collab.)
AAD	15AG	JHEP 1503 041	G. Aad *et al.*	(ATLAS Collab.)
AAD	15AP	JHEP 1508 138	G. Aad *et al.*	(ATLAS Collab.)
AAD	15M	PRL 114 231801	G. Aad *et al.*	(ATLAS Collab.)
KANEMURA	15	PTEP 2015 051B02	S. Kanemura *et al.*	
KHACHATRY...	15AX	JHEP 1511 018	V. Khachatryan *et al.*	(CMS Collab.)
KHACHATRY...	15BF	JHEP 1512 178	V. Khachatryan *et al.*	(CMS Collab.)
KHACHATRY...	15D	PRL 114 051801	V. Khachatryan *et al.*	(CMS Collab.)
AAD	14M	PR D89 032002	G. Aad *et al.*	(ATLAS Collab.)
AALTONEN	14A	PR D89 091101	T. Aaltonen *et al.*	(CDF Collab.)
KANEMURA	14	PR D90 115018	S. Kanemura *et al.*	
AAD	13AC	EPJ C73 2465	G. Aad *et al.*	(ATLAS Collab.)
AAD	13V	JHEP 1303 076	G. Aad *et al.*	(ATLAS Collab.)
AAD	13Y	PR D87 052002	G. Aad *et al.*	(ATLAS Collab.)
CARENA	13	EPJ C73 2552	M. Carena *et al.*	
LEP	13	EPJ C73 2463	LEP Collabs	(ALEPH, DELPHI, L3, OPAL, LEP)
AAD	12AY	PR D85 032004	G. Aad *et al.*	(ATLAS Collab.)
AAD	12BH	JHEP 1206 039	G. Aad *et al.*	(ATLAS Collab.)
AAD	12CQ	EPJ C72 2244	G. Aad *et al.*	(ATLAS Collab.)
AAD	12CY	JHEP 1212 007	G. Aad *et al.*	(ATLAS Collab.)
ABAZOV	12A	PRL 108 021801	V.M. Abazov *et al.*	(D0 Collab.)
ABBIENDI	12	EPJ C72 2076	G. Abbiendi *et al.*	(OPAL Collab.)
CHATRCHYAN	12AA	JHEP 1207 143	S. Chatrchyan *et al.*	(CMS Collab.)
CHATRCHYAN	12AU	EPJ C72 2189	S. Chatrchyan *et al.*	(CMS Collab.)
AALTONEN	11AF	PRL 107 181801	T. Aaltonen *et al.*	(CDF Collab.)
AALTONEN	11P	PRL 107 031801	T. Aaltonen *et al.*	(CDF Collab.)
DESCHAMPS	10	PR D82 073012	O. Deschamps *et al.*	(CLER, ORSAY, LAPP)
AALTONEN	09AJ	PRL 103 101803	T. Aaltonen *et al.*	(CDF Collab.)
ABAZOV	09AC	PR D80 051107	V.M. Abazov *et al.*	(D0 Collab.)
ABAZOV	09AG	PR D80 071102	V.M. Abazov *et al.*	(D0 Collab.)
ABAZOV	09AI	PL B682 278	V.M. Abazov *et al.*	(D0 Collab.)
ABAZOV	09P	PRL 102 191802	V.M. Abazov *et al.*	(D0 Collab.)
AALTONEN	08AA	PRL 101 121801	T. Aaltonen *et al.*	(CDF Collab.)
ABAZOV	08V	PRL 101 071803	V.M. Abazov *et al.*	(D0 Collab.)
ABULENCIA	06E	PRL 96 042003	A. Abulencia *et al.*	(CDF Collab.)
AKTAS	06A	PL B638 432	A. Aktas *et al.*	(H1 Collab.)
ACOSTA	05L	PRL 95 071801	D. Acosta *et al.*	(CDF Collab.)
ABAZOV	04E	PRL 93 141801	V.M. Abazov *et al.*	(D0 Collab.)
ABBIENDI	04	EPJ C32 453	G. Abbiendi *et al.*	(OPAL Collab.)
ABDALLAH	04I	EPJ C34 399	J. Abdallah *et al.*	(DELPHI Collab.)
ABBIENDI	03	PL B551 35	G. Abbiendi *et al.*	(OPAL Collab.)
ABBIENDI	03Q	PL B577 93	G. Abbiendi *et al.*	(OPAL Collab.)
ABDALLAH	03	PL B552 127	J. Abdallah *et al.*	(DELPHI Collab.)
ACHARD	03E	PL B575 208	P. Achard *et al.*	(L3 Collab.)
ACHARD	03F	PL B576 18	P. Achard *et al.*	(L3 Collab.)
ABAZOV	02B	PRL 88 151803	V.M. Abazov *et al.*	(D0 Collab.)
ABBIENDI	02C	PL B526 221	G. Abbiendi *et al.*	(OPAL Collab.)
BORZUMATI	02	PL B549 170	F.M. Borzumati, A. Djouadi	
HEISTER	02P	PL B543 1	A. Heister *et al.*	(ALEPH Collab.)
ABBIENDI	01Q	PL B520 1	G. Abbiendi *et al.*	(OPAL Collab.)
BARATE	01E	EPJ C19 213	R. Barate *et al.*	(ALEPH Collab.)
GAMBINO	01	NP B611 338	P. Gambino, M. Misiak	
AFFOLDER	00I	PR D62 012004	T. Affolder *et al.*	(CDF Collab.)
PDG	00	EPJ C15 1	D.E. Groom *et al.*	(PDG Collab.)
ABBIENDI	99E	EPJ C7 407	G. Abbiendi *et al.*	(OPAL Collab.)
ABBOTT	99E	PRL 82 4975	B. Abbott *et al.*	(D0 Collab.)
ACKERSTAFF	99D	EPJ C8 3	K. Ackerstaff *et al.*	(OPAL Collab.)
ABE	97L	PRL 79 357	F. Abe *et al.*	(CDF Collab.)
ACCIARRI	97F	PL B396 327	M. Acciarri *et al.*	(L3 Collab.)
AMMAR	97B	PRL 78 4686	R. Ammar *et al.*	(CLEO Collab.)
COARASA	97	PL B406 337	J.A. Coarasa, R.A. Jimenez, J. Sola	
GORDEEV	97	PAN 60 1164	V.A. Gordeev *et al.*	(PNPI)
		Translated from YAF 60 1291.		
GUCHAIT	97	PR D55 7263	M. Guchait, D.P. Roy	(TATA)
MANGANO	97	PL B410 299	M. Mangano, S. Slabospitsky	
STAHL	97	ZPHY C74 73	A. Stahl, H. Voss	(BONN)
PDG	96	PR D54 1	R. M. Barnett *et al.*	(PDG Collab.)
ALAM	95	PRL 74 2885	M.S. Alam *et al.*	(CLEO Collab.)
ASAKA	95	PL B345 36	T. Asaka, K.I. Hikasa	(TOHOK)
BUSKULIC	95	PL B343 444	D. Buskulic *et al.*	(ALEPH Collab.)
GROSSMAN	95B	PL B357 630	Y. Grossman, H. Haber, Y. Nir	
GROSSMAN	94	PL B332 373	Y. Grossman, Z. Ligeti	
STAHL	94	PL B324 121	A. Stahl	(BONN)
ACTON	92M	PL B295 347	P.D. Acton *et al.*	(OPAL Collab.)
SWARTZ	90	PRL 64 2877	M.L. Swartz *et al.*	(Mark II Collab.)

New Heavy Bosons (W', Z', leptoquarks, etc.), Searches for

We list here various limits on charged and neutral heavy vector bosons (other than W's and Z's), heavy scalar bosons (other than Higgs bosons), vector or scalar leptoquarks, and axigluons. The latest unpublished results are described in "W' Searches" and "Z' Searches" reviews. For recent searches on scalar bosons which could be identified as Higgs bosons, see the listings in the Higgs boson section.

CONTENTS:

Mass Limits for W' (Heavy Charged Vector Boson Other Than W) in Hadron Collider Experiments
W_R (Right-Handed W Boson) Mass Limits
Limit on W_L-W_R Mixing Angle ζ
Mass Limits for Z' (Heavy Neutral Vector Boson Other Than Z)
– Limits for Z'_{SM}
– Limits for Z_{LR}
– Limits for Z_{χ}
– Limits for Z_{ψ}
– Limits for Z_{η}
– Limits for other Z'
– Searches for Z' with Lepton-Flavor-Violating decays
Indirect Constraints on Kaluza-Klein Gauge Bosons
Mass Limits for Leptoquarks from Pair Production
Mass Limits for Leptoquarks from Single Production
Indirect Limits for Leptoquarks
Mass Limits for Diquarks
Mass Limits for g_A (axigluon) and Other Color-Octet Gauge Bosons
Mass Limits for Color-Octet Scalar Bosons
X^0 (Heavy Boson) Searches in Z Decays

Downloaded from https://academic.oup.com/ptep/article/2022/8/083C01/6651666 by KIT Library user on 27 September 2022

Mass Limits for a Heavy Neutral Boson Coupling to e^+e^-
Search for X^0 Resonance in e^+e^- Collisions
Search for X^0 Resonance in ep Collisions
Search for X^0 Resonance in Two-Photon Process
Search for X^0 Resonance in $e^+e^- \to X^0\gamma$
Search for X^0 Resonance in $Z \to f\overline{f}X^0$
Search for X^0 Resonance in WX^0 final state
Search for X^0 Resonance in Quarkonium Decays

See the related review(s):

W'-Boson Searches

MASS LIMITS for W' (Heavy Charged Vector Boson Other Than W) in Hadron Collider Experiments

Couplings of W' to quarks and leptons are taken to be identical with those of W. The following limits are obtained from $p\overline{p}$ or $pp \to W'X$ with W' decaying to the mode indicated in the comments. New decay channels (*e.g.*, $W' \to WZ$) are assumed to be suppressed. The most recent preliminary results can be found in the "W'-boson searches" review above.

VALUE (GeV)	CL%	DOCUMENT ID		TECN	COMMENT
>6000 (CL = 95%) OUR LIMIT					
none 1000–3400	95	[1] SIRUNYAN	21Y	CMS	$W' \to tb$
>3200	95	[2] AAD	20AJ	ATLS	$W' \to WH$
>4300	95	[3] AAD	20AT	ATLS	$W' \to WZ$
none 1100–4000	95	[4] AAD	20T	ATLS	$W' \to q\overline{q}$
none 1800–3600	95	[5] SIRUNYAN	20AI	CMS	$W' \to q\overline{q}$
none 1200–3800	95	[6] SIRUNYAN	20Q	CMS	$W' \to WZ$
		[7] AABOUD	19B	ATLS	$W' \to N\ell \to \ell\ell jj$
none 500–3250	95	[8] AABOUD	19E	ATLS	$W' \to tb$
>6000	95	[9] AAD	19C	ATLS	$W' \to e\nu,\ \mu\nu$
none 1300–3600	95	[10] AAD	19D	ATLS	$W' \to WZ$
none 400–4000	95	[11] SIRUNYAN	19AY	CMS	$W' \to \tau\nu$
>4300	95	[12] SIRUNYAN	19CP	CMS	$W' \to WZ,\ WH,\ \ell\nu$
>2600	95	[13] SIRUNYAN	19I	CMS	$W' \to WH$
none 1000–3000	95	[14] AABOUD	18AF	ATLS	$W' \to tb$
none 500–2820	95	[15] AABOUD	18AI	ATLS	$W' \to WH$
none 300–3000	95	[16] AABOUD	18AK	ATLS	$W' \to WZ$
none 800–3200	95	[17] AABOUD	18AL	ATLS	$W' \to WZ$
>5100	95	[18] AABOUD	18BG	ATLS	$W' \to e\nu,\ \mu\nu$
none 250–2460	95	[19] AABOUD	18CH	ATLS	$W' \to WZ$
none 1200–3300	95	[20] AABOUD	18F	ATLS	$W' \to WZ$
none 500–3700	95	[21] AABOUD	18K	ATLS	$W' \to \tau\nu$
none 1000–3600	95	[22] SIRUNYAN	18	CMS	$W' \to tb$
none 1000–3050	95	[23] SIRUNYAN	18AX	CMS	$W' \to WZ$
none 400–5200	95	[24] SIRUNYAN	18AZ	CMS	$W' \to e\nu,\ \mu\nu$
none 1000–3400	95	[25] SIRUNYAN	18BK	CMS	$W' \to WZ$
none 600–3300	95	[26] SIRUNYAN	18BO	CMS	$W' \to q\overline{q}$
none 900–4400	95	[27] SIRUNYAN	18CV	CMS	$W' \to N\ell \to \ell\ell jj$
none 800–2330	95	[28] SIRUNYAN	18DJ	CMS	$W' \to WZ$
>2800	95	[29] SIRUNYAN	18ED	CMS	$W' \to WH$
none 1200–3200, 3300–3600	95	[30] SIRUNYAN	18P	CMS	$W' \to WZ$
>3600	95	[31] AABOUD	17AK	ATLS	$W' \to q\overline{q}$
none 1100–2500	95	[32] AABOUD	17AO	ATLS	$W' \to WH$
>2220	95	[33] AABOUD	17B	ATLS	$W' \to WH$
>2300	95	[34] KHACHATRY...	17J	CMS	$W' \to N_\tau\tau \to \tau\tau jj$
none 600–2700	95	[35] KHACHATRY...	17W	CMS	$W' \to q\overline{q}$
>4100	95	[36] KHACHATRY...	17Z	CMS	$W' \to e\nu,\ \mu\nu$
>2200	95	[37] SIRUNYAN	17A	CMS	$W' \to WZ$
>2300	95	[38] SIRUNYAN	17AK	CMS	$W' \to WZ,\ WH$
>2900	95	[39] SIRUNYAN	17H	CMS	$W' \to \tau N$
>2600	95	[40] SIRUNYAN	17I	CMS	$W' \to tb$
>2450	95	[41] SIRUNYAN	17R	CMS	$W' \to WH$
none 2780–3150	95	[41] SIRUNYAN	17R	CMS	$W' \to WH$
>2600	95	[42] AABOUD	16AE	ATLS	$W' \to WZ$
>4070	95	[43] AABOUD	16V	ATLS	$W' \to e\nu,\ \mu\nu$
>1810	95	[44] AAD	16R	ATLS	$W' \to WZ$
>2600	95	[45] AAD	16S	ATLS	$W' \to q\overline{q}$
>2150	95	[46] KHACHATRY...	16AO	CMS	$W' \to tb$
none 1000–1600	95	[47] KHACHATRY...	16AP	CMS	$W' \to WH$
none 800–1500	95	[48] KHACHATRY...	16BD	CMS	$W' \to WH \to b\overline{b}\ell\nu$
none 1500–2600	95	[49] KHACHATRY...	16K	CMS	$W' \to q\overline{q}$
none 500–1600	95	[50] KHACHATRY...	16L	CMS	$W' \to q\overline{q}$
none 300–2700	95	[51] KHACHATRY...	16O	CMS	$W' \to \tau\nu$
none 400–1590	95	[52] AAD	15AU	ATLS	$W' \to WZ$
none 1500–1760	95	[53] AAD	15AV	ATLS	$W' \to tb$
none 300–1490	95	[54] AAD	15AZ	ATLS	$W' \to WZ$
none 1300–1500	95	[55] AAD	15CP	ATLS	$W' \to WZ$
none 500–1920	95	[56] AAD	15R	ATLS	$W' \to tb$
none 800–2450	95	[57] AAD	15V	ATLS	$W' \to q\overline{q}$
>1470	95	[58] KHACHATRY...	15C	CMS	$W' \to WZ$
>3710	95	[59] KHACHATRY...	15T	CMS	$W' \to e\nu,\ \mu\nu$
none 1000–3010	95	[60] KHACHATRY...	14O	CMS	$W' \to N\ell \to \ell\ell jj$

• • • We do not use the following data for averages, fits, limits, etc. • • •

		[61] AAD	20AD	ATLS	$W' \to JJ$
		[62] AAD	20W	ATLS	$W' \to WZ' \to \ell\nu q\overline{q}$
		[63] AABOUD	19BB	ATLS	$W' \to N\ell \to j\ell\ell$
		[64] SIRUNYAN	19V	CMS	$W' \to Bt,\ Tb$
		[65] AABOUD	18AA	ATLS	$W' \to W\gamma$
		[66] AABOUD	18AD	ATLS	$W' \to HX$
>4500	95	[67] AABOUD	18CJ	ATLS	$W' \to WZ,\ WH,\ \ell\nu$
		[68] KHACHATRY...	17U	CMS	$W' \to WH$
		[69] AAD	15BB	ATLS	$W' \to WH$
none 300–880	95	[70] AALTONEN	15C	CDF	$W' \to tb$
none 1200–1900 and 2000–2200	95	[71] KHACHATRY...	15V	CMS	$W' \to q\overline{q}$
>3240	95	AAD	14AI	ATLS	$W' \to e\nu,\ \mu\nu$
		[72] AAD	14AT	ATLS	$W' \to W\gamma$
none 200–1520	95	[73] AAD	14S	ATLS	$W' \to WZ$
none 1000–1700	95	[74] KHACHATRY...	14	CMS	$W' \to WZ$
		[75] KHACHATRY...	14A	CMS	$W' \to WZ$
none 500–950	95	[76] AAD	13AO	ATLS	$W' \to WZ$
none 1100–1680	95	AAD	13D	ATLS	$W' \to q\overline{q}$
none 1000–1920	95	CHATRCHYAN	13A	CMS	$W' \to q\overline{q}$
		[77] CHATRCHYAN	13AJ	CMS	$W' \to WZ$
>2900	95	[78] CHATRCHYAN	13AQ	CMS	$W' \to e\nu,\ \mu\nu$
none 800–1510	95	[79] CHATRCHYAN	13E	CMS	$W' \to tb$
none 700–940	95	[80] CHATRCHYAN	13U	CMS	$W' \to WZ$
none 700–1130	95	[81] AAD	12AV	ATLS	$W' \to tb$
none 200–760	95	[82] AAD	12BB	ATLS	$W' \to WZ$
		[83] AAD	12CK	ATLS	$W' \to \overline{t}q$
>2550	95	[84] AAD	12CR	ATLS	$W' \to e\nu,\ \mu\nu$
		[85] AAD	12M	ATLS	$W' \to N\ell \to \ell\ell jj$
		[86] AALTONEN	12N	CDF	$W' \to \overline{t}q$
none 200–1143	95	[82] CHATRCHYAN	12AF	CMS	$W' \to WZ$
		[87] CHATRCHYAN	12AR	CMS	$W' \to \overline{t}q$
		[88] CHATRCHYAN	12BG	CMS	$W' \to N\ell \to \ell\ell jj$
>1120	95	AALTONEN	11C	CDF	$W' \to e\nu$
none 180–690	95	[89] ABAZOV	11H	D0	$W' \to WZ$
none 600–863	95	[90] ABAZOV	11L	D0	$W' \to tb$
none 285–516	95	[91] AALTONEN	10N	CDF	$W' \to WZ$
none 280–840	95	[92] AALTONEN	09AC	CDF	$W' \to q\overline{q}$
>1000	95	ABAZOV	08C	D0	$W' \to e\nu$
none 300–800	95	ABAZOV	04C	D0	$W' \to q\overline{q}$
none 225–536	95	[93] ACOSTA	03B	CDF	$W' \to tb$
none 200–480	95	[94] AFFOLDER	02C	CDF	$W' \to WZ$
> 786	95	[95] AFFOLDER	01I	CDF	$W' \to e\nu,\ \mu\nu$
none 300–420	95	[96] ABE	97G	CDF	$W' \to q\overline{q}$
> 720	95	[97] ABACHI	96C	D0	$W' \to e\nu$
> 610	95	[98] ABACHI	95E	D0	$W' \to e\nu,\ \tau\nu$
none 260–600	95	[99] RIZZO	93	RVUE	$W' \to q\overline{q}$

[1] SIRUNYAN 21Y search for resonances decaying to tb in pp collisions at $\sqrt{s} = 13$ TeV. See their Fig. 2 for limits on $\sigma \cdot$ B($W' \to tb$).

[2] AAD 20AJ search for resonances decaying to HW in pp collisions at $\sqrt{s} = 13$ TeV. The quoted limit is for heavy-vector-triplet W' with $g_V = 3$. The limit becomes $M_{W'} >$ 2900 GeV for $g_V = 1$. See their Fig. 6 for limits on $\sigma \cdot B$.

[3] AAD 20AT search for resonances decaying to WZ in pp collisions at $\sqrt{s} = 13$ TeV. The quoted limit is for heavy-vector-triplet W' with $g_V = 3$. The limit becomes $M_{W'} >$ 3900 GeV for $g_V = 1$. See their Fig. 13 for limits on $\sigma \cdot B$.

[4] AAD 20T search for W' with SM-like couplings in pp collisions at $\sqrt{s} = 13$ TeV. See their Fig. 4(c) for limits on the product of the cross section, acceptance, and branching fraction.

[5] SIRUNYAN 20AI limit is for W' with SM-like coupling using pp collisions at $\sqrt{s} = 13$ TeV.

[6] SIRUNYAN 20Q search for resonances decaying to WZ in pp collisions at $\sqrt{s} = 13$ TeV. The quoted limit is for heavy-vector-triplet W' with $g_V = 3$.

[7] AABOUD 19B search for right-handed W_R in pp collisions at $\sqrt{s} = 13$ TeV. W_R is assumed to decay into ℓ and hypothetical heavy neutrino N, with N decaying to ℓjj. See their Figs. 7 and 8 for excluded regions in $M_{W_R} - M_N$ plane.

[8] AABOUD 19E search for right-handed W' in pp collisions at $\sqrt{s} = 13$ TeV. See their Fig. 8 for limit on on $\sigma \cdot B$.

[9] AAD 19C search for W' with SM-like couplings in pp collisions at $\sqrt{s} = 13$ TeV. Bosonic decays and $W - W'$ interference are neglected. The limits on e and μ separately are 6.0 and 5.1 TeV respectively. See their Fig. 2 for limits on $\sigma \cdot B$.

[10] AAD 19D search for resonances decaying to WZ in pp collisions at $\sqrt{s} = 13$ TeV. The quoted limit is for heavy-vector-triplet W' with $g_V = 3$. The limit becomes $M_{W'} >$ 3400 GeV for $g_V = 1$. If we assume $M_{W'} = M_{Z'}$, the limit increases $M_{W'} >$ 3800 GeV and $M_{W'} >$ 3500 GeV for $g_V = 3$ and $g_V = 1$, respectively. See their Fig. 9 for limits on $\sigma \cdot B$.

[11] SIRUNYAN 19AY limits shown for W' with SM-like coupling using pp collisions at $\sqrt{s}$ = 13 TeV. $W - W'$ interference and bosonic decays of W' are not included. See their Fig. 5 for limits on $\sigma \cdot B$. Limits in the context of a nonuniversal gauge interaction are shown in Fig. 7. Model independent limits on $\sigma B A \epsilon$ can be seen in Fig. 8.

[12] SIRUNYAN 19CP present a statistical combinations of searches for W' decaying to pairs of bosons or leptons in pp collisions at $\sqrt{s} = 13$ TeV. The quoted limit is for heavy-vector-triplet W' with $g_V = 3$. If we assume $M_{W'} = M_{Z'}$, the limit becomes $M_{W'} >$ 4500 GeV for $g_V = 3$ and $M_{W'} >$ 5000 GeV for $g_V = 1$. See their Figs. 2 and 3 for limits on $\sigma \cdot B$.

Downloaded from https://academic.oup.com/ptep/article/2022/8/083C01/6651666 by KIT Library user on 27 September 2022

[13] SIRUNYAN 19I search for resonances decaying to HW in pp collisions at $\sqrt{s}$ = 13 TeV. The quoted limit is for heavy-vector-triplet W' with $g_V = 3$. The limit becomes $M_{W'} > 2800$ GeV if we assume $M_{W'} = M_{Z'}$.

[14] AABOUD 18AF give the limit above for right-handed W' using pp collisions at $\sqrt{s}$ = 13 TeV. These limits also exclude W bosons with left-handed couplings with masses below 2.9 TeV, at the 95% confidence level. $W' \to \ell\nu_R$ is assumed to be forbidden. See their Fig.5 for limits on $\sigma \cdot B$ for both cases of left- and right-handed W'.

[15] AABOUD 18AI search for resonances decaying to HW in pp collisions at $\sqrt{s}$ = 13 TeV. The quoted limit is for heavy-vector-triplet W' with $g_V = 3$. The limit becomes $M_{W'} > 2670$ GeV for $g_V = 1$. If we assume $M_{W'} = M_{Z'}$, the limit increases $M_{W'} > 2930$ GeV and $M_{W'} > 2800$ GeV for $g_V = 3$ and $g_V = 1$, respectively. See their Fig. 5 for limits on $\sigma \cdot B$.

[16] AABOUD 18AK search for resonances decaying to WZ in pp collisions at $\sqrt{s}$ = 13 TeV. The limit quoted above is for heavy-vector-triplet W' with $g_V = 3$. The limit becomes $M_{W'} > 2800$ GeV for $g_V = 1$.

[17] AABOUD 18AL search for resonances decaying to WZ in pp collisions at $\sqrt{s}$ = 13 TeV. The limit quoted above is for heavy-vector-triplet W' with $g_V = 3$. The limit becomes $M_{W'} > 2900$ GeV for $g_V = 1$.

[18] AABOUD 18BG limit is for W' with SM-like couplings using pp collisions at $\sqrt{s}$ = 13 TeV. Bosonic decays of W' and $W - W'$ interference are neglected. See Fig. 2 for limits on $\sigma \cdot B$.

[19] AABOUD 18CH search for resonances decaying to WZ in pp collisions at $\sqrt{s}$ = 13 TeV. The limit quoted above is for heavy-vector-triplet W' with $g_V = 3$. The limit becomes $M_{W'} > 2260$ GeV for $g_V = 1$.

[20] AABOUD 18F search for resonances decaying to WZ in pp collisions at $\sqrt{s}$ = 13 TeV. The quoted limit is for heavy-vector-triplet W' with $g_V = 3$. The limit becomes $M_{W'} > 3000$ GeV for $g_V = 1$. If we assume $M_{Z'} = M_{W'}$, the limit increases $M_{W'} > 3500$ GeV and $M_{W'} > 3100$ GeV for $g_V = 3$ and $g_V = 1$, respectively. See their Fig.5 for limits on $\sigma \cdot B$.

[21] AABOUD 18K limit is for W' with SM-like coupling using pp collisions at $\sqrt{s}$ = 13 TeV. $W - W'$ interference and bosonic decays of W' are not included. See their Fig. 4 for limit on $\sigma \cdot B$.

[22] SIRUNYAN 18 limit is for right-handed W' using pp collisions at $\sqrt{s}$ = 13 TeV. $W' \to \ell\nu_R$ decay is assumed to be forbidden. The limit becomes $M_{W'} > 3.4$ TeV if $M_{\nu_R} \ll M_{W'}$. See their Fig. 5 for exclusion limits on W' models having both left- and right-handed couplings.

[23] SIRUNYAN 18AX search for resonances decaying to WZ in pp collisions at $\sqrt{s}$ = 13 TeV. The quoted limit is for heavy-vector-triplet W' with $g_V = 3$. See their Fig.6 for limits on $\sigma \cdot$ B.

[24] SIRUNYAN 18AZ limit is derived for W' with SM-like coupling using pp collisions at $\sqrt{s}$ = 13 TeV. No interference with SM W process is considered. The bosonic decays are assumed to be negligible. See their Fig.6 for limits on $\sigma \cdot B$.

[25] SIRUNYAN 18BK search for resonances decaying to WZ in pp collisions at $\sqrt{s}$ = 13 TeV. The limit quoted above is for heavy-vector-triplet W' with $g_V = 3$. The limit becomes $M_{W'} > 3100$ GeV for $g_V = 1$.

[26] SIRUNYAN 18BO limit is for W' with SM-like coupling using pp collisions at $\sqrt{s}$ = 13 TeV.

[27] SIRUNYAN 18CV search for right-handed W_R in pp collisions at $\sqrt{s}$ = 13 TeV. W_R is assumed to decay into ℓ and hypothetical heavy neutrino N, with N decaying to ℓjj. The quoted limit is for $M_N = M_{W_R}/2$. See their Fig. 6 for excluded regions in the $M_{W_R} - M_N$ plane.

[28] SIRUNYAN 18DJ search for resonances decaying to WZ in pp collisions at $\sqrt{s}$ = 13 TeV. The limit quoted above is for heavy-vector-triplet W' with $g_V = 3$. The limit becomes $M_{W'} > 2270$ GeV for $g_V = 1$.

[29] SIRUNYAN 18ED search for resonances decaying to HW in pp collisions at $\sqrt{s}$ = 13 TeV. The limit above is for heavy-vector-triplet W' with $g_V = 3$. If we assume $M_{W'} = M_{Z'}$, the limit increases $M_{W'} > 2900$ GeV and $M_{W'} > 2800$ GeV for $g_V = 3$ and $g_V = 1$, respectively.

[30] SIRUNYAN 18P give this limit for a heavy-vector-triplet W' with $g_V = 3$. If they assume $M_{Z'} = M_{W'}$, the limit increases to $M_{W'} > 3800$ GeV.

[31] AABOUD 17AK search for a new resonance decaying to dijets in pp collisions at $\sqrt{s}$ = 13 TeV. The limit above is for a W' boson having axial-vector SM couplings and decaying to quarks with 75% branching fraction.

[32] AABOUD 17AO search for resonances decaying to HW in pp collisions at $\sqrt{s}$ = 13 TeV. The limit quoted above is for a W' in the heavy-vector-triplet model with $g_V = 3$. See their Fig.4 for limits on $\sigma \cdot B$.

[33] AABOUD 17B search for resonances decaying to HW ($H \to b\overline{b}$, $c\overline{c}$; $W \to \ell\nu$) in pp collisions at $\sqrt{s}$ = 13 TeV. The quoted limit is for heavy-vector-triplet W' with $g_V = 3$. The limit becomes $M_{W'} > 1750$ GeV for $g_V = 1$. If we assume $M_{W'} = M_{Z'}$, the limit increases $M_{W'} > 2310$ GeV and $M_{W'} > 1730$ GeV for $g_V = 3$ and $g_V = 1$, respectively. See their Fig.3 for limits on $\sigma \cdot B$.

[34] KHACHATRYAN 17J search for right-handed W_R in pp collisions at $\sqrt{s}$ = 13 TeV. W_R is assumed to decay into τ and hypothetical heavy neutrino N_τ, with N_τ decaying into τjj. The quoted limit is for $M_{N_\tau} = M_{W_R}/2$. The limit becomes $M_{W_R} > 2350$ GeV (1630 GeV) for $M_{W_R}/M_{N_\tau} = 0.8$ (0.2). See their Fig. 4 for excluded regions in the $M_{W_R} - M_{N_\tau}$ plane.

[35] KHACHATRYAN 17W search for resonances decaying to dijets in pp collisions at $\sqrt{s}$ = 13 TeV.

[36] KHACHATRYAN 17Z limit is for W' with SM-like coupling using pp collisions at $\sqrt{s}$ = 13 TeV. The bosonic decays of W' and the interference with SM W process are neglected.

[37] SIRUNYAN 17A search for resonances decaying to WZ with $WZ \to \ell\nu q\overline{q}$, $q\overline{q}q\overline{q}$ in pp collisions at $\sqrt{s}$ = 13 TeV. The quoted limit is for heavy-vector-triplet W' with $g_V = 3$. The limit becomes $M_{W'} > 2000$ GeV for $g_V = 1$. If we assume $M_{Z'} = M_{W'}$, the limit increases $M_{W'} > 2400$ GeV and $M_{W'} > 2300$ GeV for $g_V = 3$ and $g_V = 1$, respectively. See their Fig.6 for limits on $\sigma \cdot B$.

[38] SIRUNYAN 17AK search for resonances decaying to WZ or HW in pp collisions at $\sqrt{s}$ = 8 and 13 TeV. The quoted limit is for heavy-vector-triplet W' with $g_V = 3$. The limit becomes $M_{W'} > 2300$ GeV for $g_V = 1$. If we assume $M_{W'} = M_{Z'}$, the limit increases $M_{W'} > 2400$ GeV for both $g_V = 3$ and $g_V = 1$. See their Fig.1 and 2 for limits on $\sigma \cdot B$.

[39] SIRUNYAN 17H search for right-handed W' in pp collisions at $\sqrt{s}$ = 13 TeV. W' is assumed to decay into τ and a heavy neutrino N, with N decaying to $\tau q\overline{q}$. The limit above assumes $M_N = M_{W'}/2$.

[40] SIRUNYAN 17I limit is for a right-handed W' using pp collisions at $\sqrt{s}$ = 13 TeV. The limit becomes $M_{W'} > 2400$ GeV for $M_{\nu_R} \ll M_{W'}$.

[41] SIRUNYAN 17R search for resonances decaying to HW in pp collisions at $\sqrt{s}$ = 13 TeV. The quoted limit is for heavy-vector-triplet W' with $g_V = 3$. Mass regions $M_{W'} <$ 2370 GeV and $2870 < M_{W'} < 2970$ GeV are excluded for $g_V = 1$. If we assume $M_{Z'} = M_{W'}$, the excluded mass regions are $1000 < M_{W'} < 2500$ GeV and $2760 < M_{W'} <$ 3300 GeV for $g_V = 3$; $1000 < M_{W'} < 2430$ GeV and $2810 < M_{W'} < 3130$ GeV for $g_V = 1$. See their Fig.5 for limits on $\sigma \cdot B$.

[42] AABOUD 16AE search for resonances decaying to VV ($V = W$ or Z) in pp collisions at $\sqrt{s}$ = 13 TeV. Results from $\nu\nu qq$, $\nu\ell qq$, $\ell\ell qq$ and $qqqq$ final states are combined. The quoted limit is for a heavy-vector-triplet W' with $g_V = 3$ and $M_{W'} = M_{Z'}$.

[43] AABOUD 16V limit is for W' with SM-like coupling using pp collisions at $\sqrt{s}$ = 13 TeV. The bosonic decays of W' and the interference with SM W process are neglected.

[44] AAD 16R search for $W' \to WZ$ in pp collisions at $\sqrt{s}$ = 8 TeV. $\ell\nu\ell'\ell'$, $\ell\ell q\overline{q}$, $\ell\nu q\overline{q}$, and all hadronic channels are combined. The quoted limit assumes $g_{W'WZ}/g_{WWZ} = (M_W/M_{W'})^2$.

[45] AAD 16S search for a new resonance decaying to dijets in pp collisions at $\sqrt{s}$ = 13 TeV. The limit quoted above is for a W' having SM-like couplings to quarks.

[46] KHACHATRYAN 16AO limit is for a SM-like right-handed W' using pp collisions at $\sqrt{s}$ = 8 TeV. The quoted limit combines $t \to qqb$ and $t \to \ell\nu b$ events.

[47] KHACHATRYAN 16AP search for a resonance decaying to HW in pp collisions at $\sqrt{s}$ = 8 TeV. Both H and W are assumed to decay to fat jets. The quoted limit is for heavy-vector-triplet W' with $g_V = 3$.

[48] KHACHATRYAN 16BD search for resonance decaying to HW in pp collisions at $\sqrt{s}$ = 8 TeV. The quoted limit is for heavy-vector-triplet (HVT) W' with $g_V = 3$. The HVT model $m_{W'} = m_{Z'} > 1.8$ TeV is also obtained by combining $W'/Z' \to WH/ZH \to \ell\nu bb$, $qq\tau\tau$, $qqbb$, and $qqqqqq$ channels.

[49] KHACHATRYAN 16K search for resonances decaying to dijets in pp collisions at $\sqrt{s}$ = 13 TeV.

[50] KHACHATRYAN 16L search for resonances decaying to dijets in pp collisions at $\sqrt{s}$ = 8 TeV with the data scouting technique, increasing the sensitivity to the low mass resonances.

[51] KHACHATRYAN 16O limit is for W' having universal couplings. Interferences with the SM amplitudes are assumed to be absent.

[52] AAD 15AU search for W' decaying into the WZ final state with $W \to q\overline{q}'$, $Z \to \ell^+\ell^-$ using pp collisions at $\sqrt{s}$ = 8 TeV. The quoted limit assumes $g_{W'WZ}/g_{WWZ} = (M_W/M_{W'})^2$.

[53] AAD 15AV limit is for a SM like right-handed W' using pp collisions at $\sqrt{s}$ = 8 TeV. $W' \to \ell\nu$ decay is assumed to be forbidden.

[54] AAD 15AZ search for W' decaying into the WZ final state with $W \to \ell\nu$, $Z \to q\overline{q}$ using pp collisions at $\sqrt{s}$ = 8 TeV. The quoted limit assumes $g_{W'WZ}/g_{WWZ} = (M_W/M_{W'})^2$.

[55] AAD 15CP search for W' decaying into the WZ final state with $W \to q\overline{q}$, $Z \to q\overline{q}$ using pp collisions at $\sqrt{s}$ = 8 TeV. The quoted limit assumes $g_{W'WZ}/g_{WWZ} = (M_W/M_{W'})^2$.

[56] AAD 15R limit is for a SM like right-handed W' using pp collisions at $\sqrt{s}$ = 8 TeV. $W' \to \ell\nu$ decay is assumed to be forbidden.

[57] AAD 15V search for new resonance decaying to dijets in pp collisions at $\sqrt{s}$ = 8 TeV.

[58] KHACHATRYAN 15C search for W' decaying via WZ to fully leptonic final states using pp collisions at $\sqrt{s}$=8 TeV. The quoted limit assumes $g_{W'WZ}/g_{WWZ} = M_W M_Z/M^2_{W'}$.

[59] KHACHATRYAN 15T limit is for W' with SM-like coupling which interferes the SM W boson constructively using pp collisions at $\sqrt{s}$ = 8 TeV. For W' without interference, the limit becomes > 3280 GeV.

[60] KHACHATRYAN 14O search for right-handed W_R in pp collisions at $\sqrt{s}$ = 8 TeV. W_R is assumed to decay into ℓ and hypothetical heavy neutrino N, with N decaying into ℓjj. The quoted limit is for $M_{\nu_{eR}} = M_{\nu_{\mu R}} = M_{W_R}/2$. See their Fig. 3 and Fig. 5 for excluded regions in the $M_{W_R} - M_\nu$ plane.

[61] AAD 20AD search for a narrow resonance decaying to a pair of large-radius-jets J_1 and J_2 employing a machine-learning procedure. See their Fig. 3 for limits on $\sigma \cdot B$ depending on assumptions about invariant masses for J_1, J_2, and $J_1 J_2$.

[62] AAD 20W search for W' decaying to WZ' in pp collisions at $\sqrt{s}$ = 13 TeV. See their Fig. 5(b) for limits on $\sigma \cdot B$ as a function of $m_{Z'}$. The $W' \to WZ'$ branching fraction was chosen to be 0.5 and the mass difference between the W' and Z' was set to 250 GeV.

[63] AABOUD 19BB search for right handed W_R in pp collisions at $\sqrt{s}$ = 13 TeV. W_R is assumed to decay into ℓ and a boosted hypothetical heavy neutrino N, with N decaying to ℓ and a large radius jet $j = q\overline{q}$. See their Fig. 7 for excluded regions in $M_{W_R} - M_N$ plane.

[64] SIRUNYAN 19V search for a new resonance decaying to a top quark and a heavy vector-like bottom partner B decaying to Hb (or a bottom quark and a heavy vector-like top partner T decaying to Ht) in pp collisions at $\sqrt{s}$ = 13 TeV. See their Fig. 8 for limits on $\sigma \cdot B$.

[65] AABOUD 18AA search for a narrow charged vector boson decaying to $W\gamma$. See their Fig. 9 for the exclusion limit in $M_{W'} - \sigma$B plane.

[66] AABOUD 18AD search for resonances decaying to HX ($H \to b\overline{b}$, $X \to q\overline{q}'$) in pp collisions at $\sqrt{s}$ = 13 TeV. See their Figs. 3–5 for limits on $\sigma \cdot$ B.

Downloaded from https://academic.oup.com/ptep/article/2022/8/083C01/6651666 by KIT Library user on 27 September 2022

[67] AABOUD 18CJ search for heavy-vector-triplet W' in pp collisions at $\sqrt{s}$ = 13 TeV. The limit quoted above is for model with $g_V = 3$ assuming $M_{W'} = M_{Z'}$. The limit becomes $M_{W'} > 5500$ GeV for model with $g_V = 1$.

[68] KHACHATRYAN 17U search for resonances decaying to HW ($H \to b\overline{b}$; $W \to \ell\nu$) in pp collisions at $\sqrt{s}$ = 13 TeV. The limit on the heavy-vector-triplet model is $M_{Z'} = M_{W'} > 2$ TeV for $g_V = 3$, in which constraints from the $Z' \to HZ$ ($H \to b\overline{b}$; $Z \to \ell^+\ell^-$, $\nu\overline{\nu}$) are combined. See their Fig.3 and Fig.4 for limits on $\sigma \cdot B$.

[69] AAD 15BB search for W' decaying into WH with $W \to \ell\nu$, $H \to b\overline{b}$. See their Fig. 4 for the exclusion limits in the heavy vector triplet benchmark model parameter space.

[70] AALTONEN 15C limit is for a SM-like right-handed W' assuming $W' \to \ell\nu$ decays are forbidden, using $p\overline{p}$ collisions at $\sqrt{s}$=1.96 TeV. See their Fig. 3 for limit on $g_{W'}/g_W$.

[71] KHACHATRYAN 15V search new resonance decaying to dijets in pp collisions at $\sqrt{s}$ = 8 TeV.

[72] AAD 14AT search for a narrow charged vector boson decaying to $W\gamma$. See their Fig. 3a for the exclusion limit in $m_{W'} - \sigma B$ plane.

[73] AAD 14S search for W' decaying into the WZ final state with $W \to \ell\nu$, $Z \to \ell\ell$ using pp collisions at $\sqrt{s}$=8 TeV. The quoted limit assumes $g_{W'WZ}/g_{WWZ} = (M_W/M_{W'})^2$.

[74] KHACHATRYAN 14 search for W' decaying into WZ final state with $W \to q\overline{q}$, $Z \to q\overline{q}$ using pp collisions at $\sqrt{s}$=8 TeV. The quoted limit assumes $g_{W'WZ}/g_{WWZ} = (M_W/M_{W'})^2$.

[75] KHACHATRYAN 14A search for W' decaying into the WZ final state with $W \to \ell\nu$, $Z \to q\overline{q}$, or $W \to q\overline{q}$, $Z \to \ell\ell$. pp collisions data at $\sqrt{s}$=8 TeV are used for the search. See their Fig. 13 for the exclusion limit on the number of events in the mass−width plane.

[76] AAD 13AO search for W' decaying into the WZ final state with $W \to \ell\nu$, $Z \to 2j$ using pp collisions at $\sqrt{s}$=7 TeV. The quoted limit assumes $g_{W'WZ}/g_{WWZ} = (M_W/M_{W'})^2$.

[77] CHATRCHYAN 13AJ search for resonances decaying to WZ pair, using the hadronic decay modes of W and Z, in pp collisions at $\sqrt{s}$=7 TeV. See their Fig. 7 for the limit on the cross section.

[78] CHATRCHYAN 13AQ limit is for W' with SM-like coupling which interferes with the SM W boson using pp collisions at $\sqrt{s}$=7 TeV.

[79] CHATRCHYAN 13E limit is for W' with SM-like coupling which intereferes with the SM W boson using pp collisions at $\sqrt{s}$=7 TeV. For W' with right-handed coupling, the bound becomes >1850 GeV (>1910 GeV) if W' decays to both leptons and quarks (only to quarks). If both left- and right-handed couplings are present, the limit becomes >1640 GeV.

[80] CHATRCHYAN 13U search for W' decaying to the WZ final state, with W decaying into jets, in pp collisions at $\sqrt{s}$=7 TeV. The quoted limit assumes $g_{W'WZ}/g_{WWZ} = (M_W/M_{W'})^2$.

[81] The AAD 12AV quoted limit is for a SM-like right-handed W' using pp collisions at $\sqrt{s}$=7 TeV. $W' \to \ell\nu$ decay is assumed to be forbidden.

[82] AAD 12BB use pp collisions data at $\sqrt{s}$=7 TeV. The quoted limit assumes $g_{W'WZ}/g_{WWZ} = (M_W/M_{W'})^2$.

[83] AAD 12CK search for $pp \to tW'$, $W' \to \overline{t}q$ events in pp collisions. See their Fig. 5 for the limit on $\sigma \cdot$B.

[84] AAD 12CR use pp collisions at $\sqrt{s}$=7 TeV.

[85] AAD 12M search for right-handed W_R in pp collisions at $\sqrt{s}$ = 7 TeV. W_R is assumed to decay into ℓ and hypothetical heavy neutrino N, with N decaying into ℓjj. See their Fig. 4 for the limit in the $m_N - m_{W'}$ plane.

[86] AALTONEN 12N search for $p\overline{p} \to tW'$, $W' \to \overline{t}d$ events in $p\overline{p}$ collisions. See their Fig. 3 for the limit on $\sigma \cdot$B.

[87] CHATRCHYAN 12AR search for $pp \to tW'$, $W' \to \overline{t}d$ events in pp collisions. See their Fig. 2 for the limit on $\sigma \cdot$B.

[88] CHATRCHYAN 12BG search for right-handed W_R in pp collisions $\sqrt{s}$ = 7 TeV. W_R is assumed to decay into ℓ and hypothetical heavy neutrino N, with N decaying into ℓjj. See their Fig. 3 for the limit in the $m_N - m_{W'}$ plane.

[89] ABAZOV 11H use data from $p\overline{p}$ collisions at $\sqrt{s}$=1.96 TeV. The quoted limit is obtained assuming $W'WZ$ coupling strength is the same as the ordinary WWZ coupling strength in the Standard Model.

[90] ABAZOV 11L limit is for W' with SM-like coupling which interferes with the SM W boson, using $p\overline{p}$ collisions at $\sqrt{s}$=1.96 TeV. For W' with right-handed coupling, the bound becomes >885 GeV (>890 GeV) if W' decays to both leptons and quarks (only to quarks). If both left- and right-handed couplings present, the limit becomes >916 GeV.

[91] AALTONEN 10N use $p\overline{p}$ collision data at $\sqrt{s}$=1.96 TeV. The quoted limit assumes $g_{W'WZ}/g_{WWZ} = (M_W/M_{W'})^2$. See their Fig. 4 for limits in mass-coupling plane.

[92] AALTONEN 09AC search for new particle decaying to dijets using $p\overline{p}$ collisions at $\sqrt{s}$=1.96 TeV.

[93] The ACOSTA 03B quoted limit is for $M_{W'} \gg M_{\nu_R}$, using $p\overline{p}$ collisions at $\sqrt{s}$=1.8 TeV. For $M_{W'} < M_{\nu_R}$, $M_{W'}$ between 225 and 566 GeV is excluded.

[94] The quoted limit is obtained assuming $W'WZ$ coupling strength is the same as the ordinary WWZ coupling strength in the Standard Model, using $p\overline{p}$ collisions at $\sqrt{s}$=1.8 TeV. See their Fig. 2 for the limits on the production cross sections as a function of the W' width.

[95] AFFOLDER 01I combine a new bound on $W' \to e\nu$ of 754 GeV, using $p\overline{p}$ collisions at $\sqrt{s}$=1.8 TeV, with the bound of ABE 00 on $W' \to \mu\nu$ to obtain quoted bound.

[96] ABE 97G search for new particle decaying to dijets using $p\overline{p}$ collisions at $\sqrt{s}$=1.8 TeV.

[97] For bounds on W_R with nonzero right-handed mass, see Fig. 5 from ABACHI 96C.

[98] ABACHI 95E assume that the decay $W' \to WZ$ is suppressed and that the neutrino from W' decay is stable and has a mass significantly less $m_{W'}$.

[99] RIZZO 93 analyses CDF limit on possible two-jet resonances. The limit is sensitive to the inclusion of the assumed K factor.

W_R (Right-Handed W Boson) MASS LIMITS

Assuming a light right-handed neutrino, except for BEALL 82, LANGACKER 89B, and COLANGELO 91. $g_R = g_L$ assumed. [Limits in the section MASS LIMITS for W' below are also valid for W_R if $m_{\nu_R} \ll m_{W_R}$.] Some limits assume manifest left-right symmetry, *i.e.*, the equality of left- and right Cabibbo-Kobayashi-Maskawa matrices. For a comprehensive review, see LANGACKER 89B. Limits on the W_L-W_R mixing angle ζ are found in the next section. Values in brackets are from cosmological and astrophysical considerations and assume a light right-handed neutrino.

VALUE (GeV)	CL%	DOCUMENT ID		TECN	COMMENT
> 592	90	[1] BUENO	11	TWST	μ decay
> 715	90	[2] CZAKON	99	RVUE	Electroweak
• • • We do not use the following data for averages, fits, limits, etc. • • •					
> 235	90	[3] PRIEELS	14	PIE3	μ decay
> 245	90	[4] WAUTERS	10	CNTR	^{60}Co β decay
>2500		[5] ZHANG	08	THEO	$m_{K^0_L} - m_{K^0_S}$
> 180	90	[6] MELCONIAN	07	CNTR	^{37}K β^+ decay
> 290.7	90	[7] SCHUMANN	07	CNTR	Polarized neutron decay
[> 3300]	95	[8] CYBURT	05	COSM	Nucleosynthesis; light ν_R
> 310	90	[9] THOMAS	01	CNTR	β^+ decay
> 137	95	[10] ACKERSTAFF	99D	OPAL	τ decay
>1400	68	[11] BARENBOIM	98	RVUE	Electroweak, Z-Z' mixing
> 549	68	[12] BARENBOIM	97	RVUE	μ decay
> 220	95	[13] STAHL	97	RVUE	τ decay
> 220	90	[14] ALLET	96	CNTR	β^+ decay
> 281	90	[15] KUZNETSOV	95	CNTR	Polarized neutron decay
> 282	90	[16] KUZNETSOV	94B	CNTR	Polarized neutron decay
> 439	90	[17] BHATTACH...	93	RVUE	Z-Z' mixing
> 250	90	[18] SEVERIJNS	93	CNTR	β^+ decay
		[19] IMAZATO	92	CNTR	K^+ decay
> 475	90	[20] POLAK	92B	RVUE	μ decay
> 240	90	[21] AQUINO	91	RVUE	Neutron decay
> 496	90	[21] AQUINO	91	RVUE	Neutron and muon decay
> 700		[22] COLANGELO	91	THEO	$m_{K^0_L} - m_{K^0_S}$
> 477	90	[23] POLAK	91	RVUE	μ decay
[none 540–23000]		[24] BARBIERI	89B	ASTR	SN 1987A; light ν_R
> 300	90	[25] LANGACKER	89B	RVUE	General
> 160	90	[26] BALKE	88	CNTR	$\mu \to e\nu\overline{\nu}$
> 406	90	[27] JODIDIO	86	ELEC	Any ζ
> 482	90	[27] JODIDIO	86	ELEC	$\zeta = 0$
> 800		MOHAPATRA	86	RVUE	SU(2)$_L$×SU(2)$_R$×U(1)
> 400	95	[28] STOKER	85	ELEC	Any ζ
> 475	95	[28] STOKER	85	ELEC	ζ <0.041
		[29] BERGSMA	83	CHRM	$\nu_\mu e \to \mu\nu_e$
> 380	90	[30] CARR	83	ELEC	μ^+ decay
>1600		[31] BEALL	82	THEO	$m_{K^0_L} - m_{K^0_S}$

[1] The quoted limit is for manifest left-right symmetric model.

[2] CZAKON 99 perform a simultaneous fit to charged and neutral sectors.

[3] PRIEELS 14 limit is from $\mu^+ \to e^+\nu\overline{\nu}$ decay parameter ξ'', which is determined by the positron polarization measurement.

[4] WAUTERS 10 limit is from a measurement of the asymmetry parameter of polarized ^{60}Co β decays. The listed limit assumes no mixing.

[5] ZHANG 08 limit uses a lattice QCD calculation of the relevant hadronic matrix elements, while BEALL 82 limit used the vacuum saturation approximation.

[6] MELCONIAN 07 measure the neutrino angular asymmetry in β^+-decays of polarized ^{37}K, stored in a magneto-optical trap. Result is consistent with SM prediction and does not constrain the $W_L - W_R$ mixing angle appreciably.

[7] SCHUMANN 07 limit is from measurements of the asymmetry $\langle \vec{p}_\nu \cdot \sigma_n \rangle$ in the β decay of polarized neutrons. Zero mixing is assumed.

[8] CYBURT 05 limit follows by requiring that three light ν_R's decouple when $T_{dec} > 140$ MeV. For different T_{dec}, the bound becomes $M_{W_R} > 3.3$ TeV $(T_{dec}$ / 140 MeV$)^{3/4}$.

[9] THOMAS 01 limit is from measurement of β^+ polarization in decay of polarized ^{12}N. The listed limit assumes no mixing.

[10] ACKERSTAFF 99D limit is from τ decay parameters. Limit increase to 145 GeV for zero mixing.

[11] BARENBOIM 98 assumes minimal left-right model with Higgs of SU(2)$_R$ in SU(2)$_L$ doublet. For Higgs in SU(2)$_L$ triplet, m_{W_R} >1100 GeV. Bound calculated from effect of corresponding Z_{LR} on electroweak data through Z–Z_{LR} mixing.

[12] The quoted limit is from μ decay parameters. BARENBOIM 97 also evaluate limit from K_L-K_S mass difference.

[13] STAHL 97 limit is from fit to τ-decay parameters.

[14] ALLET 96 measured polarization-asymmetry correlation in ^{12}Nβ^+ decay. The listed limit assumes zero L-R mixing.

[15] KUZNETSOV 95 limit is from measurements of the asymmetry $\langle \vec{p}_\nu \cdot \sigma_n \rangle$ in the β decay of polarized neutrons. Zero mixing assumed. See also KUZNETSOV 94B.

[16] KUZNETSOV 94B limit is from measurements of the asymmetry $\langle \vec{p}_\nu \cdot \sigma_n \rangle$ in the β decay of polarized neutrons. Zero mixing assumed.

[17] BHATTACHARYYA 93 uses Z-Z' mixing limit from LEP '90 data, assuming a specific Higgs sector of SU(2)$_L$×SU(2)$_R$×U(1) gauge model. The limit is for m_t=200 GeV and slightly improves for smaller m_t.

[18] SEVERIJNS 93 measured polarization-asymmetry correlation in ^{107}In β^+ decay. The listed limit assumes zero L-R mixing. Value quoted here is from SEVERIJNS 94 erratum.

[19] IMAZATO 92 measure positron asymmetry in $K^+ \to \mu^+\nu_\mu$ decay and obtain $\xi P_\mu > 0.990$ (90% CL). If W_R couples to $u\overline{s}$ with full weak strength (V^R_{us}=1), the result corresponds to m_{W_R} >653 GeV. See their Fig. 4 for m_{W_R} limits for general $|V^R_{us}|^2 = 1 - |V^R_{ud}|^2$.

Downloaded from https://academic.oup.com/ptep/article/2022/8/083C01/6651666 by KIT Library user on 27 September 2022

[20] POLAK 92B limit is from fit to muon decay parameters and is essentially determined by JODIDIO 86 data assuming ζ=0. Supersedes POLAK 91.
[21] AQUINO 91 limits obtained from neutron lifetime and asymmetries together with unitarity of the CKM matrix. Manifest left-right symmetry assumed. Stronger of the two limits also includes muon decay results.
[22] COLANGELO 91 limit uses hadronic matrix elements evaluated by QCD sum rule and is less restrictive than BEALL 82 limit which uses vacuum saturation approximation. Manifest left-right symmetry assumed.
[23] POLAK 91 limit is from fit to muon decay parameters and is essentially determined by JODIDIO 86 data assuming ζ=0. Superseded by POLAK 92B.
[24] BARBIERI 89B limit holds for $m_{\nu_R} \leq 10$ MeV.
[25] LANGACKER 89B limit is for any ν_R mass (either Dirac or Majorana) and for a general class of right-handed quark mixing matrices.
[26] BALKE 88 limit is for $m_{\nu_{eR}} = 0$ and $m_{\nu_{\mu R}} \leq 50$ MeV. Limits come from precise measurements of the muon decay asymmetry as a function of the positron energy.
[27] JODIDIO 86 is the same TRIUMF experiment as STOKER 85 (and CARR 83); however, it uses a different technique. The results given here are combined results of the two techniques. The technique here involves precise measurement of the end-point e^+ spectrum in the decay of the highly polarized μ^+.
[28] STOKER 85 is same TRIUMF experiment as CARR 83. Here they measure the decay e^+ spectrum asymmetry above 46 MeV/c using a muon-spin-rotation technique. Assumed a light right-handed neutrino. Quoted limits are from combining with CARR 83.
[29] BERGSMA 83 set limit m_{W_2}/m_{W_1} >1.9 at CL = 90%.
[30] CARR 83 is TRIUMF experiment with a highly polarized μ^+ beam. Looked for deviation from $V-A$ at the high momentum end of the decay e^+ energy spectrum. Limit from previous world-average muon polarization parameter is m_{W_R} >240 GeV. Assumes a light right-handed neutrino.
[31] BEALL 82 limit is obtained assuming that W_R contribution to K^0_L-K^0_S mass difference is smaller than the standard one, neglecting the top quark contributions. Manifest left-right symmetry assumed.

Limit on W_L-W_R Mixing Angle ζ

Lighter mass eigenstate $W_1 = W_L \cos\zeta - W_R \sin\zeta$. Light ν_R assumed unless noted. Values in brackets are from cosmological and astrophysical considerations.

VALUE	CL%	DOCUMENT ID		TECN	COMMENT
• • • We do not use the following data for averages, fits, limits, etc. • • •					
−0.020 to 0.017	90	BUENO	11	TWST	$\mu \to e\nu\overline{\nu}$
< 0.022	90	MACDONALD	08	TWST	$\mu \to e\nu\overline{\nu}$
< 0.12	95	[1] ACKERSTAFF	99D	OPAL	τ decay
< 0.013	90	[2] CZAKON	99	RVUE	Electroweak
< 0.0333		[3] BARENBOIM	97	RVUE	μ decay
< 0.04	90	[4] MISHRA	92	CCFR	νN scattering
−0.0006 to 0.0028	90	[5] AQUINO	91	RVUE	
[none 0.00001–0.02]		[6] BARBIERI	89B	ASTR	SN 1987A
< 0.040	90	[7] JODIDIO	86	ELEC	μ decay
−0.056 to 0.040	90	[7] JODIDIO	86	ELEC	μ decay

[1] ACKERSTAFF 99D limit is from τ decay parameters.
[2] CZAKON 99 perform a simultaneous fit to charged and neutral sectors.
[3] The quoted limit is from μ decay parameters. BARENBOIM 97 also evaluate limit from K_L-K_S mass difference.
[4] MISHRA 92 limit is from the absence of extra large-x, large-y $\overline{\nu}_\mu N \to \overline{\nu}_\mu X$ events at Tevatron, assuming left-handed ν and right-handed $\overline{\nu}$ in the neutrino beam. The result gives $\zeta^2(1-2m^2_{W_1}/m^2_{W_2})$< 0.0015. The limit is independent of ν_R mass.
[5] AQUINO 91 limits obtained from neutron lifetime and asymmetries together with unitarity of the CKM matrix. Manifest left-right asymmetry is assumed.
[6] BARBIERI 89B limit holds for $m_{\nu_R} \leq 10$ MeV.
[7] First JODIDIO 86 result assumes $m_{W_R}=\infty$, second is for unconstrained m_{W_R}.

See the related review(s):
Z'-Boson Searches

MASS LIMITS for Z' (Heavy Neutral Vector Boson Other Than Z)

Limits for Z'_{SM}

Z'_{SM} is assumed to have couplings with quarks and leptons which are identical to those of Z, and decays only to known fermions. The most recent preliminary results can be found in the "Z'-boson searches" review above.

VALUE (GeV)	CL%	DOCUMENT ID		TECN	COMMENT
>5150 (CL = 95%) OUR LIMIT					
>5150	95	[1] SIRUNYAN	21N	CMS	pp; $Z'_{SM} \to e^+e^-$, $\mu^+\mu^-$
none 1133–2700	95	[2] AAD	20T	ATLS	pp, $Z'_{SM} \to b\overline{b}$
none 1800–2900, 3100–3300	95	[3] SIRUNYAN	20AI	CMS	pp; $Z'_{SM} \to q\overline{q}$
none 250–5100	95	[4] AAD	19L	ATLS	pp; $Z'_{SM} \to e^+e^-$, $\mu^+\mu^-$
none 600–2000	95	[5] AABOUD	18AB	ATLS	pp; $Z'_{SM} \to b\overline{b}$
>2420	95	[6] AABOUD	18G	ATLS	pp; $Z'_{SM} \to \tau^+\tau^-$
none 200–4500	95	[7] SIRUNYAN	18BB	CMS	pp; $Z'_{SM} \to e^+e^-$, $\mu^+\mu^-$
none 600–2700	95	[8] SIRUNYAN	18BO	CMS	pp; $Z'_{SM} \to q\overline{q}$
>4500	95	[9] AABOUD	17AT	ATLS	pp; $Z'_{SM} \to e^+e^-$, $\mu^+\mu^-$
>2100	95	[10] KHACHATRY...	17H	CMS	pp; $Z'_{SM} \to \tau^+\tau^-$
>3370	95	[11] KHACHATRY...	17T	CMS	pp; $Z'_{SM} \to e^+e^-$, $\mu^+\mu^-$
none 600–2100, 2300–2600	95	[12] KHACHATRY...	17W	CMS	pp; $Z'_{SM} \to q\overline{q}$
>3360	95	[13] AABOUD	16U	ATLS	pp; $Z'_{SM} \to e^+e^-$, $\mu^+\mu^-$
>2900	95	[14] KHACHATRY...	15AE	CMS	pp; $Z'_{SM} \to e^+e^-$, $\mu^+\mu^-$
none 1200–1700	95	[15] KHACHATRY...	15V	CMS	pp; $Z'_{SM} \to q\overline{q}$
>2900	95	[16] AAD	14V	ATLS	pp; $Z'_{SM} \to e^+e^-$, $\mu^+\mu^-$
• • • We do not use the following data for averages, fits, limits, etc. • • •					
		[17] BOBOVNIKOV	18	RVUE	pp, $Z'_{SM} \to W^+W^-$
>1900	95	[18] AABOUD	16AA	ATLS	pp; $Z'_{SM} \to \tau^+\tau^-$
>2020	95	[19] AAD	15AM	ATLS	pp; $Z'_{SM} \to \tau^+\tau^-$
>1400	95	[20] AAD	13S	ATLS	pp; $Z'_{SM} \to \tau^+\tau^-$
>1470	95	[21] CHATRCHYAN	13A	CMS	pp; $Z'_{SM} \to q\overline{q}$
>2590	95	[22] CHATRCHYAN	13AF	CMS	pp; $Z'_{SM} \to e^+e^-$, $\mu^+\mu^-$
>2220	95	[23] AAD	12CC	ATLS	pp; $Z'_{SM} \to e^+e^-$, $\mu^+\mu^-$
>1400	95	[24] CHATRCHYAN	12O	CMS	pp; $Z'_{SM} \to \tau^+\tau^-$
>1071	95	[25] AALTONEN	11I	CDF	$p\overline{p}$; $Z'_{SM} \to \mu^+\mu^-$
>1023	95	[26] ABAZOV	11A	D0	$p\overline{p}$, $Z'_{SM} \to e^+e^-$
none 247–544	95	[27] AALTONEN	10N	CDF	$Z' \to WW$
none 320–740	95	[28] AALTONEN	09AC	CDF	$Z' \to q\overline{q}$
> 963	95	[26] AALTONEN	09T	CDF	$p\overline{p}$, $Z'_{SM} \to e^+e^-$
>1403	95	[29] ERLER	09	RVUE	Electroweak
>1305	95	[30] ABDALLAH	06C	DLPH	e^+e^-
> 399	95	[31] ACOSTA	05R	CDF	$\overline{p}p$: $Z'_{SM} \to \tau^+\tau^-$
none 400–640	95	ABAZOV	04C	D0	$p\overline{p}$: $Z'_{SM} \to q\overline{q}$
>1018	95	[32] ABBIENDI	04G	OPAL	e^+e^-
> 670	95	[33] ABAZOV	01B	D0	$p\overline{p}$, $Z'_{SM} \to e^+e^-$
>1500	95	[34] CHEUNG	01B	RVUE	Electroweak
> 710	95	[35] ABREU	00S	DLPH	e^+e^-
> 898	95	[36] BARATE	00I	ALEP	e^+e^-
> 809	95	[37] ERLER	99	RVUE	Electroweak
> 690	95	[38] ABE	97S	CDF	$p\overline{p}$; $Z'_{SM} \to e^+e^-$, $\mu^+\mu^-$
> 398	95	[39] VILAIN	94B	CHM2	$\nu_\mu e \to \nu_\mu e$ and $\overline{\nu}_\mu e \to \overline{\nu}_\mu e$
> 237	90	[40] ALITTI	93	UA2	$p\overline{p}$; $Z'_{SM} \to q\overline{q}$
none 260–600	95	[41] RIZZO	93	RVUE	$p\overline{p}$; $Z'_{SM} \to q\overline{q}$
> 426	90	[42] ABE	90F	VNS	e^+e^-

[1] SIRUNYAN 21N search for resonance decaying to e^+e^-, $\mu^+\mu^-$ in pp collisions at $\sqrt{s}$ = 13 TeV.
[2] AAD 20T search for resonances decaying to $b\overline{b}$ in pp collisions at $\sqrt{s}$ = 13 TeV. See their Fig. 7(b) for limits on the product of the cross section, acceptance, b-tagging efficiency, and branching fraction.
[3] SIRUNYAN 20AI search for resonances decaying into dijets in pp collisions at $\sqrt{s}$ = 13 TeV.
[4] AAD 19L search for resonances decaying to $\ell^+\ell^-$ in pp collisions at $\sqrt{s}$ = 13 TeV.
[5] AABOUD 18AB search for resonances decaying to $b\overline{b}$ in pp collisions at $\sqrt{s}$ = 13 TeV.
[6] AABOUD 18G search for resonances decaying to $\tau^+\tau^-$ in pp collisions at $\sqrt{s}$ = 13 TeV.
[7] SIRUNYAN 18BB search for resonances decaying to $\ell^+\ell^-$ in pp collisions at $\sqrt{s}$ = 13 TeV. See their Fig.5 for limits on the Z' coupling strengths with light quarks.
[8] SIRUNYAN 18BO search for resonances decaying to dijets in pp collisions at $\sqrt{s}$ = 13 TeV.
[9] AABOUD 17AT search for resonances decaying to $\ell^+\ell^-$ in pp collisions at $\sqrt{s}$ = 13 TeV.
[10] KHACHATRYAN 17H search for resonances decaying to $\tau^+\tau^-$ in pp collisions at $\sqrt{s}$ = 13 TeV.
[11] KHACHATRYAN 17T search for resonances decaying to e^+e^-, $\mu^+\mu^-$ in pp collisions at $\sqrt{s}$ = 8, 13 TeV.
[12] KHACHATRYAN 17W search for resonances decaying to dijets in pp collisions at $\sqrt{s}$ = 13 TeV.
[13] AABOUD 16U search for resonances decaying to $\ell^+\ell^-$ in pp collisions at $\sqrt{s}$ = 13 TeV.
[14] KHACHATRYAN 15AE search for resonances decaying to e^+e^-, $\mu^+\mu^-$ in pp collisions at $\sqrt{s}$ = 8 TeV.
[15] KHACHATRYAN 15V search for resonances decaying to dijets in pp collisions at $\sqrt{s}$ = 8 TeV.
[16] AAD 14V search for resonances decaying to e^+e^-, $\mu^+\mu^-$ in pp collisions at $\sqrt{s}$ = 8 TeV.
[17] BOBOVNIKOV 18 use the ATLAS limits on $\sigma(pp \to Z')\cdot B(Z' \to W^+W^-)$ to constrain the Z-Z' mixing parameter ξ. See their Fig. 11 for limits in $M_{Z'} - \xi$ plane.
[18] AABOUD 16AA search for resonances decaying to $\tau^+\tau^-$ in pp collisions at $\sqrt{s}$ = 13 TeV.
[19] AAD 15AM search for resonances decaying to $\tau^+\tau^-$ in pp collisions at $\sqrt{s}$ = 8 TeV.
[20] AAD 13S search for resonances decaying to $\tau^+\tau^-$ in pp collisions at $\sqrt{s}$ = 7 TeV.
[21] CHATRCHYAN 13A use pp collisions at $\sqrt{s}$=7 TeV.
[22] CHATRCHYAN 13AF search for resonances decaying to e^+e^-, $\mu^+\mu^-$ in pp collisions at $\sqrt{s}$ = 7 TeV and 8 TeV.
[23] AAD 12CC search for resonances decaying to e^+e^-, $\mu^+\mu^-$ in pp collisions at $\sqrt{s}$ = 7 TeV.
[24] CHATRCHYAN 12O search for resonances decaying to $\tau^+\tau^-$ in pp collisions at $\sqrt{s}$ = 7 TeV.
[25] AALTONEN 11I search for resonances decaying to $\mu^+\mu^-$ in $p\overline{p}$ collisions at $\sqrt{s}$ = 1.96 TeV.
[26] ABAZOV 11A, AALTONEN 09T, AALTONEN 07H, and ABULENCIA 06L search for resonances decaying to e^+e^- in $p\overline{p}$ collisions at $\sqrt{s}$ = 1.96 TeV.
[27] The quoted limit assumes $g_{WWZ'}/g_{WWZ} = (M_W/M_{Z'})^2$. See their Fig. 4 for limits in mass-coupling plane.
[28] AALTONEN 09AC search for new particle decaying to dijets.
[29] ERLER 09 give 95% CL limit on the Z-Z' mixing $-0.0026 < \theta < 0.0006$.
[30] ABDALLAH 06C use data $\sqrt{s}$ = 130–207 GeV.

Downloaded from https://academic.oup.com/ptep/article/2022/8/083C01/6651666 by KIT Library user on 27 September 2022

[31] ACOSTA 05R search for resonances decaying to tau lepton pairs in $\overline{p}p$ collisions at $\sqrt{s}$ = 1.96 TeV.
[32] ABBIENDI 04G give 95% CL limit on Z-Z' mixing $-0.00422 < \theta < 0.00091$. $\sqrt{s}$ = 91 to 207 GeV.
[33] ABAZOV 01B search for resonances in $p\overline{p} \rightarrow e^+e^-$ at $\sqrt{s}$=1.8 TeV. They find $\sigma \cdot$ B($Z' \rightarrow ee$)< 0.06 pb for $M_{Z'} >$ 500 GeV.
[34] CHEUNG 01B limit is derived from bounds on contact interactions in a global electroweak analysis.
[35] ABREU 00S uses LEP data at $\sqrt{s}$=90 to 189 GeV.
[36] BARATE 00I search for deviations in cross section and asymmetries in $e^+e^- \rightarrow$ fermions at $\sqrt{s}$=90 to 183 GeV. Assume θ=0. Bounds in the mass-mixing plane are shown in their Figure 18.
[37] ERLER 99 give 90%CL limit on the Z-Z' mixing $-0.0041 < \theta < 0.0003$. ρ_0=1 is assumed.
[38] ABE 97S find $\sigma(Z')\times$B(e^+e^-,$\mu^+\mu^-$)< 40 fb for $m_{Z'} >$ 600 GeV at $\sqrt{s}$= 1.8 TeV.
[39] VILAIN 94B assume m_t = 150 GeV.
[40] ALITTI 93 search for resonances in the two-jet invariant mass. The limit assumes B($Z' \rightarrow q\overline{q}$)=0.7. See their Fig. 5 for limits in the $m_{Z'}$–B($q\overline{q}$) plane.
[41] RIZZO 93 analyses CDF limit on possible two-jet resonances.
[42] ABE 90F use data for R, $R_{\ell\ell}$, and $A_{\ell\ell}$. They fix m_W = 80.49 ± 0.43 ± 0.24 GeV and m_Z = 91.13 ± 0.03 GeV.

Limits for Z_{LR}

Z_{LR} is the extra neutral boson in left-right symmetric models. $g_L = g_R$ is assumed unless noted. Values in parentheses assume stronger constraint on the Higgs sector, usually motivated by specific left-right symmetric models (see the Note on the W'). Values in brackets are from cosmological and astrophysical considerations and assume a light right-handed neutrino. Direct search bounds assume decays to Standard Model fermions only, unless noted.

VALUE (GeV)	CL%	DOCUMENT ID		TECN	COMMENT
>1162	95	[1] DEL-AGUILA	10	RVUE	Electroweak
> 630	95	[2] ABE	97S	CDF	$p\overline{p}$; $Z'_{LR} \rightarrow e^+e^-, \mu^+\mu^-$
• • • We do not use the following data for averages, fits, limits, etc. • • •					
		[3] BOBOVNIKOV	18	RVUE	pp, $Z'_{LR} \rightarrow W^+W^-$
> 998	95	[4] ERLER	09	RVUE	Electroweak
> 600	95	SCHAEL	07A	ALEP	e^+e^-
> 455	95	[5] ABDALLAH	06C	DLPH	e^+e^-
> 518	95	[6] ABBIENDI	04G	OPAL	e^+e^-
> 860	95	[7] CHEUNG	01B	RVUE	Electroweak
> 380	95	[8] ABREU	00S	DLPH	e^+e^-
> 436	95	[9] BARATE	00I	ALEP	Repl. by SCHAEL 07A
> 550	95	[10] CHAY	00	RVUE	Electroweak
		[11] ERLER	00	RVUE	Cs
		[12] CASALBUONI	99	RVUE	Cs
(> 1205)	90	[13] CZAKON	99	RVUE	Electroweak
> 564	95	[14] ERLER	99	RVUE	Electroweak
(> 1673)	95	[15] ERLER	99	RVUE	Electroweak
(> 1700)	68	[16] BARENBOIM	98	RVUE	Electroweak
> 244	95	[17] CONRAD	98	RVUE	$\nu_\mu N$ scattering
> 253	95	[18] VILAIN	94B	CHM2	$\nu_\mu e \rightarrow \nu_\mu e$ and $\overline{\nu}_\mu e \rightarrow \overline{\nu}_\mu e$
none 200–600	95	[19] RIZZO	93	RVUE	$p\overline{p}$; $Z_{LR} \rightarrow q\overline{q}$
[> 2000]		WALKER	91	COSM	Nucleosynthesis; light ν_R
none 200–500		[20] GRIFOLS	90	ASTR	SN 1987A; light ν_R
none 350–2400		[21] BARBIERI	89B	ASTR	SN 1987A; light ν_R

[1] DEL-AGUILA 10 give 95% CL limit on the Z-Z' mixing $-0.0012 < \theta < 0.0004$.
[2] ABE 97S find $\sigma(Z')\times$B(e^+e^-,$\mu^+\mu^-$)< 40 fb for $m_{Z'} >$ 600 GeV at $\sqrt{s}$= 1.8 TeV.
[3] BOBOVNIKOV 18 use the ATLAS limits on $\sigma(pp \rightarrow Z')\cdot$B($Z' \rightarrow W^+W^-$) to constrain the Z-Z' mixing parameter ξ. See their Fig. 10 for limits in $M_{Z'} - \xi$ plane.
[4] ERLER 09 give 95% CL limit on the Z-Z' mixing $-0.0013 < \theta < 0.0006$.
[5] ABDALLAH 06C give 95% CL limit $|\theta| < 0.0028$. See their Fig. 14 for limit contours in the mass-mixing plane.
[6] ABBIENDI 04G give 95% CL limit on Z-Z' mixing $-0.00098 < \theta < 0.00190$. See their Fig. 20 for the limit contour in the mass-mixing plane. $\sqrt{s}$ = 91 to 207 GeV.
[7] CHEUNG 01B limit is derived from bounds on contact interactions in a global electroweak analysis.
[8] ABREU 00S give 95% CL limit on Z-Z' mixing $|\theta| < 0.0018$. See their Fig. 6 for the limit contour in the mass-mixing plane. $\sqrt{s}$=90 to 189 GeV.
[9] BARATE 00I search for deviations in cross section and asymmetries in $e^+e^- \rightarrow$ fermions at $\sqrt{s}$=90 to 183 GeV. Assume θ=0. Bounds in the mass-mixing plane are shown in their Figure 18.
[10] CHAY 00 also find $-0.0003 < \theta < 0.0019$. For g_R free, $m_{Z'} >$ 430 GeV.
[11] ERLER 00 discuss the possibility that a discrepancy between the observed and predicted values of Q_W(Cs) is due to the exchange of Z'. The data are better described in a certain class of the Z' models including Z_{LR} and Z_χ.
[12] CASALBUONI 99 discuss the discrepancy between the observed and predicted values of Q_W(Cs). It is shown that the data are better described in a class of models including the Z_{LR} model.
[13] CZAKON 99 perform a simultaneous fit to charged and neutral sectors. Assumes manifest left-right symmetric model. Finds $|\theta| < 0.0042$.
[14] ERLER 99 give 90% CL limit on the Z-Z' mixing $-0.0009 < \theta < 0.0017$.
[15] ERLER 99 assumes 2 Higgs doublets, transforming as 10 of SO(10), embedded in E_6.
[16] BARENBOIM 98 also gives 68% CL limits on the Z-Z' mixing $-0.0005 < \theta < 0.0033$. Assumes Higgs sector of minimal left-right model.
[17] CONRAD 98 limit is from measurements at CCFR, assuming no Z-Z' mixing.
[18] VILAIN 94B assume m_t = 150 GeV and θ=0. See Fig. 2 for limit contours in the mass-mixing plane.
[19] RIZZO 93 analyses CDF limit on possible two-jet resonances.
[20] GRIFOLS 90 limit holds for $m_{\nu_R} \lesssim$ 1 MeV. A specific Higgs sector is assumed. See also GRIFOLS 90D, RIZZO 91.
[21] BARBIERI 89B limit holds for $m_{\nu_R} \leq$ 10 MeV. Bounds depend on assumed supernova core temperature.

Limits for Z_χ

Z_χ is the extra neutral boson in SO(10) $\rightarrow$ SU(5) $\times$ U(1)$_\chi$. $g_\chi = e/\cos\theta_W$ is assumed unless otherwise stated. We list limits with the assumption ρ=1 but with no further constraints on the Higgs sector. Values in parentheses assume stronger constraint on the Higgs sector motivated by superstring models. Values in brackets are from cosmological and astrophysical considerations and assume a light right-handed neutrino.

VALUE (GeV)	CL%	DOCUMENT ID		TECN	COMMENT
>4800 (CL = 95%) OUR LIMIT					
none 250–4800	95	[1] AAD	19L	ATLS	pp; $Z'_\chi \rightarrow e^+e^-, \mu^+\mu^-$
>4100	95	[2] AABOUD	17AT	ATLS	pp; $Z'_\chi \rightarrow e^+e^-, \mu^+\mu^-$
• • • We do not use the following data for averages, fits, limits, etc. • • •					
		[3] BOBOVNIKOV	18	RVUE	pp, $Z'_\chi \rightarrow W^+W^-$
>3050	95	[4] AABOUD	16U	ATLS	pp; $Z'_\chi \rightarrow e^+e^-, \mu^+\mu^-$
>2620	95	[5] AAD	14V	ATLS	pp, $Z'_\chi \rightarrow e^+e^-, \mu^+\mu^-$
>1970	95	[6] AAD	12CC	ATLS	pp, $Z'_\chi \rightarrow e^+e^-, \mu^+\mu^-$
> 930	95	[7] AALTONEN	11I	CDF	$p\overline{p}$; $Z'_\chi \rightarrow \mu^+\mu^-$
> 903	95	[8] ABAZOV	11A	D0	$p\overline{p}$, $Z'_\chi \rightarrow e^+e^-$
>1022	95	[9] DEL-AGUILA	10	RVUE	Electroweak
> 862	95	[8] AALTONEN	09T	CDF	$p\overline{p}$, $Z'_\chi \rightarrow e^+e^-$
> 892	95	[10] AALTONEN	09V	CDF	Repl. by AALTONEN 11I
>1141	95	[11] ERLER	09	RVUE	Electroweak
> 822	95	[8] AALTONEN	07H	CDF	Repl. by AALTONEN 09T
> 680	95	SCHAEL	07A	ALEP	e^+e^-
> 545	95	[12] ABDALLAH	06C	DLPH	e^+e^-
> 740		[8] ABULENCIA	06L	CDF	Repl. by AALTONEN 07H
> 690	95	[13] ABULENCIA	05A	CDF	$p\overline{p}$; $Z'_\chi \rightarrow e^+e^-, \mu^+\mu^-$
> 781	95	[14] ABBIENDI	04G	OPAL	e^+e^-
>2100		[15] BARGER	03B	COSM	Nucleosynthesis; light ν_R
> 680	95	[16] CHEUNG	01B	RVUE	Electroweak
> 440	95	[17] ABREU	00S	DLPH	e^+e^-
> 533	95	[18] BARATE	00I	ALEP	Repl. by SCHAEL 07A
> 554	95	[19] CHO	00	RVUE	Electroweak
		[20] ERLER	00	RVUE	Cs
		[21] ROSNER	00	RVUE	Cs
> 545	95	[22] ERLER	99	RVUE	Electroweak
(> 1368)	95	[23] ERLER	99	RVUE	Electroweak
> 215	95	[24] CONRAD	98	RVUE	$\nu_\mu N$ scattering
> 595	95	[25] ABE	97S	CDF	$p\overline{p}$; $Z'_\chi \rightarrow e^+e^-, \mu^+\mu^-$
> 190	95	[26] ARIMA	97	VNS	Bhabha scattering
> 262	95	[27] VILAIN	94B	CHM2	$\nu_\mu e \rightarrow \nu_\mu e$; $\overline{\nu}_\mu e \rightarrow \overline{\nu}_\mu e$
[>1470]		[28] FARAGGI	91	COSM	Nucleosynthesis; light ν_R
> 231	90	[29] ABE	90F	VNS	e^+e^-
[> 1140]		[30] GONZALEZ...	90D	COSM	Nucleosynthesis; light ν_R
[> 2100]		[31] GRIFOLS	90	ASTR	SN 1987A; light ν_R

[1] AAD 19L search for resonances decaying to $\ell^+\ell^-$ in pp collisions at $\sqrt{s}$ = 13 TeV.
[2] AABOUD 17AT search for resonances decaying to $\ell^+\ell^-$ in pp collisions at $\sqrt{s}$ = 13 TeV.
[3] BOBOVNIKOV 18 use the ATLAS limits on $\sigma(pp \rightarrow Z')\cdot$B($Z' \rightarrow W^+W^-$) to constrain the Z-Z' mixing parameter ξ. See their Fig. 9 for limits in $M_{Z'} - \xi$ plane.
[4] AABOUD 16U search for resonances decaying to $\ell^+\ell^-$ in pp collisions at $\sqrt{s}$ = 13 TeV.
[5] AAD 14V search for resonances decaying to e^+e^-, $\mu^+\mu^-$ in pp collisions at $\sqrt{s}$ = 8 TeV.
[6] AAD 12CC search for resonances decaying to e^+e^-, $\mu^+\mu^-$ in pp collisions at $\sqrt{s}$ = 7 TeV.
[7] AALTONEN 11I search for resonances decaying to $\mu^+\mu^-$ in $p\overline{p}$ collisions at $\sqrt{s}$ = 1.96 TeV.
[8] ABAZOV 11A, AALTONEN 09T, AALTONEN 07H, and ABULENCIA 06L search for resonances decaying to e^+e^- in $p\overline{p}$ collisions at $\sqrt{s}$ = 1.96 TeV.
[9] DEL-AGUILA 10 give 95% CL limit on the Z-Z' mixing $-0.0011 < \theta < 0.0007$.
[10] AALTONEN 09V search for resonances decaying to $\mu^+\mu^-$ in $p\overline{p}$ collisions at $\sqrt{s}$ = 1.96 TeV.
[11] ERLER 09 give 95% CL limit on the Z-Z' mixing $-0.0016 < \theta < 0.0006$.
[12] ABDALLAH 06C give 95% CL limit $|\theta| < 0.0031$. See their Fig. 14 for limit contours in the mass-mixing plane.
[13] ABULENCIA 05A search for resonances decaying to electron or muon pairs in $p\overline{p}$ collisions at $\sqrt{s}$ = 1.96 TeV.
[14] ABBIENDI 04G give 95% CL limit on Z-Z' mixing $-0.00099 < \theta < 0.00194$. See their Fig. 20 for the limit contour in the mass-mixing plane. $\sqrt{s}$ = 91 to 207 GeV.
[15] BARGER 03B limit is from the nucleosynthesis bound on the effective number of light neutrino δN_ν <1. The quark-hadron transition temperature T_c=150 MeV is assumed. The limit with T_c=400 MeV is >4300 GeV.
[16] CHEUNG 01B limit is derived from bounds on contact interactions in a global electroweak analysis.
[17] ABREU 00S give 95% CL limit on Z-Z' mixing $|\theta| < 0.0017$. See their Fig. 6 for the limit contour in the mass-mixing plane. $\sqrt{s}$=90 to 189 GeV.
[18] BARATE 00I search for deviations in cross section and asymmetries in $e^+e^- \rightarrow$ fermions at $\sqrt{s}$=90 to 183 GeV. Assume θ=0. Bounds in the mass-mixing plane are shown in their Figure 18.

Downloaded from https://academic.oup.com/ptep/article/2022/8/083C01/6651666 by KIT Library user on 27 September 2022

[19] CHO 00 use various electroweak data to constrain Z' models assuming m_H=100 GeV. See Fig. 3 for limits in the mass-mixing plane.
[20] ERLER 00 discuss the possibility that a discrepancy between the observed and predicted values of Q_W(Cs) is due to the exchange of Z'. The data are better described in a certain class of the Z' models including Z_{LR} and Z_χ.
[21] ROSNER 00 discusses the possibility that a discrepancy between the observed and predicted values of Q_W(Cs) is due to the exchange of Z'. The data are better described in a certain class of the Z' models including Z_χ.
[22] ERLER 99 give 90% CL limit on the Z-Z' mixing $-0.0020 < \theta < 0.0015$.
[23] ERLER 99 assumes 2 Higgs doublets, transforming as 10 of SO(10), embedded in E_6.
[24] CONRAD 98 limit is from measurements at CCFR, assuming no Z-Z' mixing.
[25] ABE 97S find $\sigma(Z')\times B(e^+e^-,\mu^+\mu^-)<$ 40 fb for $m_{Z'}>$ 600 GeV at $\sqrt{s}$= 1.8 TeV.
[26] Z-Z' mixing is assumed to be zero. $\sqrt{s}$= 57.77 GeV.
[27] VILAIN 94B assume m_t = 150 GeV and θ=0. See Fig. 2 for limit contours in the mass-mixing plane.
[28] FARAGGI 91 limit assumes the nucleosynthesis bound on the effective number of neutrinos ΔN_ν < 0.5 and is valid for m_{ν_R} < 1 MeV.
[29] ABE 90F use data for R, $R_{\ell\ell}$, and $A_{\ell\ell}$. ABE 90F fix m_W = 80.49 ± 0.43 ± 0.24 GeV and m_Z = 91.13 ± 0.03 GeV.
[30] Assumes the nucleosynthesis bound on the effective number of light neutrinos (δN_ν < 1) and that ν_R is light ($\lesssim$ 1 MeV).
[31] GRIFOLS 90 limit holds for $m_{\nu_R} \lesssim$ 1 MeV. See also GRIFOLS 90D, RIZZO 91.

Limits for Z_ψ

Z_ψ is the extra neutral boson in $E_6 \to SO(10) \times U(1)_\psi$. $g_\psi = e/\cos\theta_W$ is assumed unless otherwise stated. We list limits with the assumption $\rho = 1$ but with no further constraints on the Higgs sector. Values in brackets are from cosmological and astrophysical considerations and assume a light right-handed neutrino.

VALUE (GeV)	CL%	DOCUMENT ID		TECN	COMMENT
>4560 (CL = 95%) OUR LIMIT					
>4560	95	[1] SIRUNYAN	21N	CMS	pp; $Z'_\psi \to e^+e^-$, $\mu^+\mu^-$
none 250–4500	95	[2] AAD	19L	ATLS	pp; $Z'_\psi \to e^+e^-$, $\mu^+\mu^-$
none 200–3900	95	[3] SIRUNYAN	18BB	CMS	pp; $Z'_\psi \to e^+e^-$, $\mu^+\mu^-$
>3800	95	[4] AABOUD	17AT	ATLS	pp; $Z'_\psi \to e^+e^-$, $\mu^+\mu^-$
>2820	95	[5] KHACHATRY...	17T	CMS	pp; $Z'_\psi \to e^+e^-$, $\mu^+\mu^-$
>1100	95	[6] CHATRCHYAN	12O	CMS	pp, $Z'_\psi \to \tau^+\tau^-$
• • • We do not use the following data for averages, fits, limits, etc. • • •					
		[7] BOBOVNIKOV	18	RVUE	pp, $Z'_\psi \to W^+W^-$
>2740	95	[8] AABOUD	16U	ATLS	pp; $Z'_\psi \to e^+e^-$, $\mu^+\mu^-$
>2570	95	[9] KHACHATRY...	15AE	CMS	pp; $Z'_\psi \to e^+e^-$, $\mu^+\mu^-$
>2510	95	[10] AAD	14V	ATLS	pp, $Z'_\psi \to e^+e^-$, $\mu^+\mu^-$
>2260	95	[11] CHATRCHYAN	13AF	CMS	pp, $Z'_\psi \to e^+e^-$, $\mu^+\mu^-$
>1790	95	[12] AAD	12CC	ATLS	pp, $Z'_\psi \to e^+e^-$, $\mu^+\mu^-$
>2000	95	[13] CHATRCHYAN	12M	CMS	Repl. by CHATRCHYAN 13AF
> 917	95	[14] AALTONEN	11I	CDF	$p\overline{p}$; $Z'_\psi \to \mu^+\mu^-$
> 891	95	[15] ABAZOV	11A	D0	$p\overline{p}$, $Z'_\psi \to e^+e^-$
> 476	95	[16] DEL-AGUILA	10	RVUE	Electroweak
> 851	95	[15] AALTONEN	09T	CDF	$p\overline{p}$, $Z'_\psi \to e^+e^-$
> 878	95	[17] AALTONEN	09V	CDF	Repl. by AALTONEN 11I
> 147	95	[18] ERLER	09	RVUE	Electroweak
> 822	95	[15] AALTONEN	07H	CDF	Repl. by AALTONEN 09T
> 410	95	SCHAEL	07A	ALEP	e^+e^-
> 475	95	[19] ABDALLAH	06C	DLPH	e^+e^-
> 725		[15] ABULENCIA	06L	CDF	Repl. by AALTONEN 07H
> 675	95	[20] ABULENCIA	05A	CDF	Repl. by AALTONEN 11I and AALTONEN 09T
> 366	95	[21] ABBIENDI	04G	OPAL	e^+e^-
> 600		[22] BARGER	03B	COSM	Nucleosynthesis; light ν_R
> 350	95	[23] ABREU	00S	DLPH	e^+e^-
> 294	95	[24] BARATE	00I	ALEP	Repl. by SCHAEL 07A
> 137	95	[25] CHO	00	RVUE	Electroweak
> 146	95	[26] ERLER	99	RVUE	Electroweak
> 54	95	[27] CONRAD	98	RVUE	$\nu_\mu N$ scattering
> 590	95	[28] ABE	97S	CDF	$p\overline{p}$; $Z'_\psi \to e^+e^-$, $\mu^+\mu^-$
> 135	95	[29] VILAIN	94B	CHM2	$\nu_\mu e \to \nu_\mu e$; $\overline{\nu}_\mu e \to \overline{\nu}_\mu e$
> 105	90	[30] ABE	90F	VNS	e^+e^-
[> 160]		[31] GONZALEZ...	90D	COSM	Nucleosynthesis; light ν_R
[> 2000]		[32] GRIFOLS	90D	ASTR	SN 1987A; light ν_R

[1] SIRUNYAN 21N search for resonance decaying to e^+e^-, $\mu^+\mu^-$ in pp collisions at $\sqrt{s}$ = 13 TeV.
[2] AAD 19L search for resonances decaying to $\ell^+\ell^-$ in pp collisions at $\sqrt{s}$ = 13 TeV.
[3] SIRUNYAN 18BB search for resonances decaying to $\ell^+\ell^-$ in pp collisions at $\sqrt{s}$ = 13 TeV.
[4] AABOUD 17AT search for resonances decaying to $\ell^+\ell^-$ in pp collisions at $\sqrt{s}$ = 13 TeV.
[5] KHACHATRYAN 17T search for resonances decaying to e^+e^-, $\mu^+\mu^-$ in pp collisions at $\sqrt{s}$ = 8, 13 TeV.
[6] CHATRCHYAN 12O search for resonances decaying to $\tau^+\tau^-$ in pp collisions at $\sqrt{s}$ = 7 TeV.
[7] BOBOVNIKOV 18 use the ATLAS limits on $\sigma(pp \to Z')\cdot B(Z' \to W^+W^-)$ to constrain the Z-Z' mixing parameter ξ. See their Fig. 10 for limits in $M_{Z'} - \xi$ plane.
[8] AABOUD 16U search for resonances decaying to $\ell^+\ell^-$ in pp collisions at $\sqrt{s}$ = 13 TeV.
[9] KHACHATRYAN 15AE search for resonances decaying to e^+e^-, $\mu^+\mu^-$ in pp collisions at $\sqrt{s}$ = 8 TeV.
[10] AAD 14V search for resonances decaying to e^+e^-, $\mu^+\mu^-$ in pp collisions at $\sqrt{s}$ = 8 TeV.
[11] CHATRCHYAN 13AF search for resonances decaying to e^+e^-, $\mu^+\mu^-$ in pp collisions at $\sqrt{s}$ = 7 TeV and 8 TeV.
[12] AAD 12CC search for resonances decaying to e^+e^-, $\mu^+\mu^-$ in pp collisions at $\sqrt{s}$ = 7 TeV.
[13] CHATRCHYAN 12M search for resonances decaying to e^+e^- or $\mu^+\mu^-$ in pp collisions at $\sqrt{s}$ = 7 TeV.
[14] AALTONEN 11I search for resonances decaying to $\mu^+\mu^-$ in $p\overline{p}$ collisions at $\sqrt{s}$ = 1.96 TeV.
[15] ABAZOV 11A, AALTONEN 09T, AALTONEN 07H, and ABULENCIA 06L search for resonances decaying to e^+e^- in $p\overline{p}$ collisions at $\sqrt{s}$ = 1.96 TeV.
[16] DEL-AGUILA 10 give 95% CL limit on the Z-Z' mixing $-0.0019 < \theta < 0.0007$.
[17] AALTONEN 09V search for resonances decaying to $\mu^+\mu^-$ in $p\overline{p}$ collisions at $\sqrt{s}$ = 1.96 TeV.
[18] ERLER 09 give 95% CL limit on the Z-Z' mixing $-0.0018 < \theta < 0.0009$.
[19] ABDALLAH 06C give 95% CL limit $|\theta| < 0.0027$. See their Fig. 14 for limit contours in the mass-mixing plane.
[20] ABULENCIA 05A search for resonances decaying to electron or muon pairs in $p\overline{p}$ collisions at $\sqrt{s}$ = 1.96 TeV.
[21] ABBIENDI 04G give 95% CL limit on Z-Z' mixing $-0.00129 < \theta < 0.00258$. See their Fig. 20 for the limit contour in the mass-mixing plane. $\sqrt{s}$ = 91 to 207 GeV.
[22] BARGER 03B limit is from the nucleosynthesis bound on the effective number of light neutrino δN_ν <1. The quark-hadron transition temperature T_c=150 MeV is assumed. The limit with T_c=400 MeV is >1100 GeV.
[23] ABREU 00S give 95% CL limit on Z-Z' mixing $|\theta| < 0.0018$. See their Fig. 6 for the limit contour in the mass-mixing plane. $\sqrt{s}$=90 to 189 GeV.
[24] BARATE 00I search for deviations in cross section and asymmetries in $e^+e^- \to$ fermions at $\sqrt{s}$=90 to 183 GeV. Assume θ=0. Bounds in the mass-mixing plane are shown in their Figure 18.
[25] CHO 00 use various electroweak data to constrain Z' models assuming m_H=100 GeV. See Fig. 3 for limits in the mass-mixing plane.
[26] ERLER 99 give 90% CL limit on the Z-Z' mixing $-0.0013 < \theta < 0.0024$.
[27] CONRAD 98 limit is from measurements at CCFR, assuming no Z-Z' mixing.
[28] ABE 97S find $\sigma(Z')\times B(e^+e^-,\mu^+\mu^-)<$ 40 fb for $m_{Z'}>$ 600 GeV at $\sqrt{s}$= 1.8 TeV.
[29] VILAIN 94B assume m_t = 150 GeV and θ=0. See Fig. 2 for limit contours in the mass-mixing plane.
[30] ABE 90F use data for R, $R_{\ell\ell}$, and $A_{\ell\ell}$. ABE 90F fix m_W = 80.49 ± 0.43 ± 0.24 GeV and m_Z = 91.13 ± 0.03 GeV.
[31] Assumes the nucleosynthesis bound on the effective number of light neutrinos (δN_ν < 1) and that ν_R is light ($\lesssim$ 1 MeV).
[32] GRIFOLS 90D limit holds for $m_{\nu_R} \lesssim$ 1 MeV. See also RIZZO 91.

Limits for Z_η

Z_η is the extra neutral boson in E_6 models, corresponding to $Q_\eta = \sqrt{3/8}\, Q_\chi - \sqrt{5/8}\, Q_\psi$. $g_\eta = e/\cos\theta_W$ is assumed unless otherwise stated. We list limits with the assumption $\rho = 1$ but with no further constraints on the Higgs sector. Values in parentheses assume stronger constraint on the Higgs sector motivated by superstring models. Values in brackets are from cosmological and astrophysical considerations and assume a light right-handed neutrino.

VALUE (GeV)	CL%	DOCUMENT ID		TECN	COMMENT
>3900	95	[1] AABOUD	17AT	ATLS	pp; $Z'_\eta \to e^+e^-$, $\mu^+\mu^-$
• • • We do not use the following data for averages, fits, limits, etc. • • •					
		[2] BOBOVNIKOV	18	RVUE	pp, $Z'_\eta \to W^+W^-$
>2810	95	[3] AABOUD	16U	ATLS	pp; $Z'_\eta \to e^+e^-$, $\mu^+\mu^-$
>1870	95	[4] AAD	12CC	ATLS	pp, $Z'_\eta \to e^+e^-$, $\mu^+\mu^-$
> 938	95	[5] AALTONEN	11I	CDF	$p\overline{p}$; $Z'_\eta \to \mu^+\mu^-$
> 923	95	[6] ABAZOV	11A	D0	$p\overline{p}$, $Z'_\eta \to e^+e^-$
> 488	95	[7] DEL-AGUILA	10	RVUE	Electroweak
> 877	95	[6] AALTONEN	09T	CDF	$p\overline{p}$, $Z'_\eta \to e^+e^-$
> 904	95	[8] AALTONEN	09V	CDF	Repl. by AALTONEN 11I
> 427	95	[9] ERLER	09	RVUE	Electroweak
> 891	95	[6] AALTONEN	07H	CDF	Repl. by AALTONEN 09T
> 350	95	SCHAEL	07A	ALEP	e^+e^-
> 360	95	[10] ABDALLAH	06C	DLPH	e^+e^-
> 745		[6] ABULENCIA	06L	CDF	Repl. by AALTONEN 07H
> 720	95	[11] ABULENCIA	05A	CDF	Repl. by AALTONEN 11I and AALTONEN 09T
> 515	95	[12] ABBIENDI	04G	OPAL	e^+e^-
>1600		[13] BARGER	03B	COSM	Nucleosynthesis; light ν_R
> 310	95	[14] ABREU	00S	DLPH	e^+e^-
> 329	95	[15] BARATE	00I	ALEP	Repl. by SCHAEL 07A
> 619	95	[16] CHO	00	RVUE	Electroweak
> 365	95	[17] ERLER	99	RVUE	Electroweak
> 87	95	[18] CONRAD	98	RVUE	$\nu_\mu N$ scattering
> 620	95	[19] ABE	97S	CDF	$p\overline{p}$; $Z'_\eta \to e^+e^-$, $\mu^+\mu^-$
> 100	95	[20] VILAIN	94B	CHM2	$\nu_\mu e \to \nu_\mu e$; $\overline{\nu}_\mu e \to \overline{\nu}_\mu e$
> 125	90	[21] ABE	90F	VNS	e^+e^-
[> 820]		[22] GONZALEZ...	90D	COSM	Nucleosynthesis; light ν_R
[> 3300]		[23] GRIFOLS	90	ASTR	SN 1987A; light ν_R
[> 1040]		[22] LOPEZ	90	COSM	Nucleosynthesis; light ν_R

[1] AABOUD 17AT search for resonances decaying to $\ell^+\ell^-$ in pp collisions at $\sqrt{s}$ = 13 TeV.

Downloaded from https://academic.oup.com/ptep/article/2022/8/083C01/6651666 by KIT Library user on 27 September 2022

[2] BOBOVNIKOV 18 use the ATLAS limits on $\sigma(pp \to Z')\cdot B(Z' \to W^+W^-)$ to constrain the Z-Z' mixing parameter ξ. See their Fig. 9 for limits in $M_{Z'} - \xi$ plane.

[3] AABOUD 16U search for resonances decaying to $\ell^+\ell^-$ in pp collisions at $\sqrt{s} = 13$ TeV.

[4] AAD 12CC search for resonances decaying to e^+e^-, $\mu^+\mu^-$ in pp collisions at $\sqrt{s} = 7$ TeV.

[5] AALTONEN 11I search for resonances decaying to $\mu^+\mu^-$ in $p\overline{p}$ collisions at $\sqrt{s} = 1.96$ TeV.

[6] ABAZOV 11A, AALTONEN 09T, AALTONEN 07H, and ABULENCIA 06L search for resonances decaying to e^+e^- in $p\overline{p}$ collisions at $\sqrt{s} = 1.96$ TeV.

[7] DEL-AGUILA 10 give 95% CL limit on the Z-Z' mixing $-0.0023 < \theta < 0.0027$.

[8] AALTONEN 09V search for resonances decaying to $\mu^+\mu^-$ in $p\overline{p}$ collisions at $\sqrt{s} = 1.96$ TeV.

[9] ERLER 09 give 95% CL limit on the Z-Z' mixing $-0.0047 < \theta < 0.0021$.

[10] ABDALLAH 06C give 95% CL limit $|\theta| < 0.0092$. See their Fig. 14 for limit contours in the mass-mixing plane.

[11] ABULENCIA 05A search for resonances decaying to electron or muon pairs in $p\overline{p}$ collisions at $\sqrt{s} = 1.96$ TeV.

[12] ABBIENDI 04G give 95% CL limit on Z-Z' mixing $-0.00447 < \theta < 0.00331$. See their Fig. 20 for the limit contour in the mass-mixing plane. $\sqrt{s} = 91$ to 207 GeV.

[13] BARGER 03B limit is from the nucleosynthesis bound on the effective number of light neutrino $\delta N_\nu < 1$. The quark-hadron transition temperature T_c=150 MeV is assumed. The limit with T_c=400 MeV is >3300 GeV.

[14] ABREU 00S give 95% CL limit on Z-Z' mixing $|\theta| < 0.0024$. See their Fig. 6 for the limit contour in the mass-mixing plane. $\sqrt{s}$=90 to 189 GeV.

[15] BARATE 00I search for deviations in cross section and asymmetries in $e^+e^- \to$ fermions at $\sqrt{s}$=90 to 183 GeV. Assume θ=0. Bounds in the mass-mixing plane are shown in their Figure 18.

[16] CHO 00 use various electroweak data to constrain Z' models assuming m_H=100 GeV. See Fig. 3 for limits in the mass-mixing plane.

[17] ERLER 99 give 90% CL limit on the Z-Z' mixing $-0.0062 < \theta < 0.0011$.

[18] CONRAD 98 limit is from measurements at CCFR, assuming no Z-Z' mixing.

[19] ABE 97S find $\sigma(Z')\times B(e^+e^-,\mu^+\mu^-) < 40$ fb for $m_{Z'} > 600$ GeV at $\sqrt{s}$= 1.8 TeV.

[20] VILAIN 94B assume m_t = 150 GeV and θ=0. See Fig. 2 for limit contours in the mass-mixing plane.

[21] ABE 90F use data for R, $R_{\ell\ell}$, and $A_{\ell\ell}$. ABE 90F fix $m_W = 80.49 \pm 0.43 \pm 0.24$ GeV and $m_Z = 91.13 \pm 0.03$ GeV.

[22] These authors claim that the nucleosynthesis bound on the effective number of light neutrinos ($\delta N_\nu < 1$) constrains Z' masses if ν_R is light ($\lesssim$ 1 MeV).

[23] GRIFOLS 90 limit holds for $m_{\nu_R} \lesssim$ 1 MeV. See also GRIFOLS 90D, RIZZO 91.

Limits for other Z'

VALUE (GeV)	CL%	DOCUMENT ID		TECN	COMMENT
none 800–3700	95	[1] SIRUNYAN	21X	CMS	$Z' \to HZ$
>2650	95	[2] AAD	20AJ	ATLS	$Z' \to HZ$
>3900	95	[3] AAD	20AM	ATLS	$Z' \to t\overline{t}$
>3900	95	[4] AAD	20AT	ATLS	$Z' \to WW$
none 1200–3500	95	[5] SIRUNYAN	20Q	CMS	$Z' \to WW$
none 580–3100	95	[6] AABOUD	19AS	ATLS	$Z' \to t\overline{t}$
none 1300–3100	95	[7] AAD	19D	ATLS	$Z' \to WW$
>3800	95	[8] SIRUNYAN	19AA	CMS	$Z' \to t\overline{t}$
>3700	95	[9] SIRUNYAN	19CP	CMS	$Z' \to WW$, HZ, $\ell^+\ell^-$
>1800	95	[10] SIRUNYAN	19I	CMS	$Z' \to HZ$
none 600–2100	95	[11] AABOUD	18AB	ATLS	$Z' \to b\overline{b}$
none 500–2830	95	[12] AABOUD	18AI	ATLS	$Z' \to HZ$
none 300–3000	95	[13] AABOUD	18AK	ATLS	$Z' \to WW$
>1300	95	[14] AABOUD	18B	ATLS	$Z' \to WW$
none 400–3000	95	[15] AABOUD	18BI	ATLS	$Z' \to t\overline{t}$
none 1200–2800	95	[16] AABOUD	18F	ATLS	$Z' \to WW$
>2300	95	[17] SIRUNYAN	18ED	CMS	$Z' \to HZ$
none 1200–2700	95	[18] SIRUNYAN	18P	CMS	$Z' \to WW$
>2900	95	[19] AABOUD	17AK	ATLS	$Z' \to q\overline{q}$
none 1100–2600	95	[20] AABOUD	17AO	ATLS	$Z' \to HZ$
>2300	95	[21] SIRUNYAN	17AK	CMS	$Z' \to WW$, HZ
>2500	95	[22] SIRUNYAN	17Q	CMS	$Z' \to t\overline{t}$
>1190	95	[23] SIRUNYAN	17R	CMS	$Z' \to HZ$
none 1210–2260	95	[23] SIRUNYAN	17R	CMS	$Z' \to HZ$
• • • We do not use the following data for averages, fits, limits, etc. • • •					
		[24] AAD	22	ATLS	$pp \to b\overline{b}Z' \to b\overline{b}b\overline{b}$
		[25] AAD	21AQ	ATLS	pp, $\ell^+\ell^-\ell^+\ell^-$
		[26] AAD	21AZ	ATLS	DM mediator Z'
		[27] AAD	21BB	ATLS	$Z' \to AH$
		[28] AAD	21D	ATLS	dark Higgs Z'
		[29] AAD	21K	ATLS	$Z' \to \chi\chi$
		[30] BURAS	21	RVUE	leptophilic Z'
		[31] CADEDDU	21	RVUE	ν-nucleus scattering
		[32] COLARESI	21	HPGE	ν-nucleus scattering
		[33] KRIBS	21	RVUE	ep scattering
		[34] TUMASYAN	21D	CMS	$Z' \to \chi\chi$
		[35] AAD	20AF	ATLS	$Z' \to H\gamma$
		[36] AAD	20T	ATLS	DM simplified Z'
		[37] AAD	20W	ATLS	DM simplified Z'
		[38] AAIJ	20AL	LHCB	$Z' \to \mu^+\mu^-$
		[39] ADACHI	20	BEL2	$e^+e^- \to \mu^+\mu^-Z'$, $e^\pm\mu^\mp Z'$
		[40] SIRUNYAN	20AI	CMS	$Z' \to q\overline{q}$
		[41] SIRUNYAN	20AQ	CMS	$Z' \to \mu^+\mu^-$
>4500	95	[42] SIRUNYAN	20M	CMS	$Z' \to q\overline{q}$
		[43] AABOUD	19AJ	ATLS	$Z' \to q\overline{q}$
		[44] AABOUD	19D	ATLS	$Z' \to q\overline{q}$
		[45] AABOUD	19V	ATLS	DM simplified Z'
		[46] AAD	19L	ATLS	$Z' \to e^+e^-$, $\mu^+\mu^-$
		[47] LONG	19	RVUE	Electroweak
		[48] PANDEY	19	RVUE	neutrino NSI
		[49] SIRUNYAN	19AL	CMS	$Z' \to tT$, $T \to Ht$, Zt, Wb
		[50] SIRUNYAN	19AN	CMS	DM simplified Z'
		[51] SIRUNYAN	19CB	CMS	$Z' \to q\overline{q}$
		[52] SIRUNYAN	19CD	CMS	$Z' \to q\overline{q}$
		[53] SIRUNYAN	19D	CMS	$Z' \to H\gamma$
		[54] AABOUD	18AA	ATLS	$Z' \to H\gamma$
>1580	95	[55] AABOUD	18CJ	ATLS	$Z' \to WW$,HZ, $\ell^+\ell^-$
		[56] AABOUD	18N	ATLS	$Z' \to q\overline{q}$
		[57] AAIJ	18AQ	LHCB	$Z' \to \mu^+\mu^-$
		[58] SIRUNYAN	18DR	CMS	$Z' \to \mu^+\mu^-$
		[59] SIRUNYAN	18G	CMS	$Z' \to q\overline{q}$
		[60] SIRUNYAN	18I	CMS	$Z' \to b\overline{b}$
>1700	95	[61] AABOUD	17B	ATLS	$Z' \to HZ$
		[62] KHACHATRY...	17AX	CMS	$Z' \to \ell\ell\ell\ell$
		[63] KHACHATRY...	17U	CMS	$Z' \to HZ$
		[64] SIRUNYAN	17A	CMS	$Z' \to WW$
		[65] SIRUNYAN	17AP	CMS	$Z' \to HA$
		[66] SIRUNYAN	17T	CMS	$Z' \to q\overline{q}$
		[67] SIRUNYAN	17V	CMS	$Z' \to Tt$
none 1100–1500	95	[68] AABOUD	16	ATLS	$Z' \to b\overline{b}$
		[69] AAD	16L	ATLS	$Z' \to a\gamma$, $a \to \gamma\gamma$
none 1500–2600	95	[70] AAD	16S	ATLS	$Z' \to q\overline{q}$
none 1000–1100, none 1300–1500	95	[71] KHACHATRY...	16AP	CMS	$Z' \to HZ$
>2400	95	[72] KHACHATRY...	16E	CMS	$Z' \to t\overline{t}$
		[73] AAD	15AO	ATLS	$Z' \to t\overline{t}$
		[74] AAD	15AT	ATLS	monotop
		[75] AAD	15CD	ATLS	$H \to ZZ'$, $Z'Z'$; $Z' \to \ell^+\ell^-$
		[76] KHACHATRY...	15F	CMS	monotop
		[77] KHACHATRY...	15O	CMS	$Z' \to HZ$
		[78] AAD	14AT	ATLS	$Z' \to Z\gamma$
		[79] KHACHATRY...	14A	CMS	$Z' \to VV$
		[80] MARTINEZ	14	RVUE	Electroweak
none 500–1740	95	[81] AAD	13AQ	ATLS	$Z' \to t\overline{t}$
>1320 or 1000–1280	95	[82] AAD	13G	ATLS	$Z' \to t\overline{t}$
> 915	95	[82] AALTONEN	13A	CDF	$Z' \to t\overline{t}$
>1300	95	[83] CHATRCHYAN	13AP	CMS	$Z' \to t\overline{t}$
>2100	95	[82] CHATRCHYAN	13BM	CMS	$Z' \to t\overline{t}$
		[84] AAD	12BV	ATLS	$Z' \to t\overline{t}$
		[85] AAD	12K	ATLS	$Z' \to t\overline{t}$
		[86] AALTONEN	12AR	CDF	Chromophilic
		[87] AALTONEN	12N	CDF	$Z' \to \overline{t}u$
> 835	95	[88] ABAZOV	12R	D0	$Z' \to t\overline{t}$
		[89] CHATRCHYAN	12AI	CMS	$Z' \to t\overline{u}$
		[90] CHATRCHYAN	12AQ	CMS	$Z' \to t\overline{t}$
>1490	95	[82] CHATRCHYAN	12BL	CMS	$Z' \to t\overline{t}$
		[91] AALTONEN	11AD	CDF	$Z' \to t\overline{t}$
		[92] AALTONEN	11AE	CDF	$Z' \to t\overline{t}$
		[93] CHATRCHYAN	11O	CMS	$pp \to tt$
		[94] AALTONEN	08D	CDF	$Z' \to t\overline{t}$
		[94] AALTONEN	08Y	CDF	$Z' \to t\overline{t}$
		[94] ABAZOV	08AA	D0	$Z' \to t\overline{t}$
		[95] ABAZOV	04A	D0	Repl. by ABAZOV 08AA
		[96] BARGER	03B	COSM	Nucleosynthesis; light ν_R
		[97] CHO	00	RVUE	E_6-motivated
		[98] CHO	98	RVUE	E_6-motivated
		[99] ABE	97G	CDF	$Z' \to \overline{q}q$

[1] SIRUNYAN 21X search for resonances decaying to HZ in pp collisions at $\sqrt{s} = 13$ TeV. The limit quoted above is for heavy-vector-triplet Z' with $g_V = 3$. The limit becomes $M_{Z'} > 3500$ GeV for $g_V = 1$.

[2] AAD 20AJ search for resonances decaying to HZ in pp collisions at $\sqrt{s} = 13$ TeV. The quoted limit is for heavy-vector-triplet Z' with $g_V = 3$. The limit becomes $M_{Z'} >$ 2200 GeV for $g_V = 1$. See their Fig. 6 for limits on $\sigma\cdot B$.

[3] AAD 20AM search for a resonance decaying to $t\overline{t}$ in pp collisions at $\sqrt{s} = 13$ TeV. The quoted limit is for a leptophobic top-color Z' with $\Gamma_{Z'}/M_{Z'} = 0.01$. The limit becomes $M_{Z'} > 4700$ GeV for $\Gamma_{Z'}/M_{Z'} = 0.03$.

[4] AAD 20AT search for resonances decaying to WW in pp collisions at $\sqrt{s} = 13$ TeV. The quoted limit is for heavy-vector-triplet Z' with $g_V = 3$. The limit becomes $M_{Z'} >$ 3500 GeV for $g_V = 1$. See their Fig. 14 for limits on $\sigma\cdot B$.

[5] SIRUNYAN 20Q search for resonances decaying to WW in pp collisions at $\sqrt{s} = 13$ TeV. The quoted limit is for heavy-vector-triplet Z' with $g_V = 3$.

[6] AABOUD 19AS search for a resonance decaying to $t\overline{t}$ in pp collisions at $\sqrt{s} = 13$ TeV. The quoted limit is for a top-color Z' with $\Gamma_{Z'}/M_{Z'} = 0.01$. Limits are also set on Z' masses in simplified Dark Matter models.

Downloaded from https://academic.oup.com/ptep/article/2022/8/083C01/6651666 by KIT Library user on 27 September 2022

[7] AAD 19D search for resonances decaying to WW in pp collisions at $\sqrt{s}$ = 13 TeV. The quoted limit is for heavy-vector-triplet Z' with $g_V = 3$. The limit becomes $M_{Z'} >$ 2900 GeV for $g_V = 1$. If we assume $M_{Z'} = M_{W'}$, the limit increases $M_{Z'} >$ 3800 GeV and $M_{Z'} >$ 3500 GeV for $g_V = 3$ and $g_V = 1$, respectively. See their Fig. 9 for limits on $\sigma \cdot B$.

[8] SIRUNYAN 19AA search for a resonance decaying to $t\overline{t}$ in pp collisions at $\sqrt{s}$ = 13 TeV. The quoted limit is for a leptophobic top-color Z' with $\Gamma_{Z'}/M_{Z'} = 0.01$.

[9] SIRUNYAN 19CP present a statistical combinations of searches for Z' decaying to pairs of bosons or leptons in pp collisions at $\sqrt{s}$ = 13 TeV. The quoted limit is for heavy-vector-triplet Z' with $g_V = 3$. If we assume $M_{Z'} = M_{W'}$, the limit becomes $M_{Z'} >$ 4500 GeV for $g_V = 3$ and $M_{Z'} >$ 5000 GeV for $g_V = 1$. See their Figs. 2 and 3 for limits on $\sigma \cdot B$.

[10] SIRUNYAN 19I search for resonances decaying to ZW in pp collisions at $\sqrt{s}$ = 13 TeV. The quoted limit is for heavy-vector-triplet Z' with $g_V = 3$. The limit becomes $M_{Z'} >$ 2800 GeV if we assume $M_{Z'} = M_{W'}$.

[11] AABOUD 18AB search for resonances decaying to $b\overline{b}$ in pp collisions at $\sqrt{s}$ = 13 TeV. The limit quoted above is for a leptophobic Z' with SM-like couplings to quarks. See their Fig. 6 for limits on $\sigma \cdot B$. Additional limits on a Z' axial-vector mediator in a simplified dark-matter model are shown in Fig. 7.

[12] AABOUD 18AI search for resonances decaying to HZ in pp collisions at $\sqrt{s}$ = 13 TeV. The quoted limit is for heavy-vector-triplet Z' with $g_V = 3$. The limit becomes $M_{Z'} >$ 2650 GeV for $g_V = 1$. If we assume $M_{W'} = M_{Z'}$, the limit increases $M_{Z'} >$ 2930 GeV and $M_{Z'} >$ 2800 GeV for $g_V = 3$ and $g_V = 1$, respectively. See their Fig. 5 for limits on $\sigma \cdot B$.

[13] AABOUD 18AK search for resonances decaying to WW in pp collisions at $\sqrt{s}$ =1 3 TeV. The limit quoted above is for heavy-vector-triplet Z' with $g_V = 3$. The limit becomes $M_{Z'} >$ 2750 GeV for $g_V = 1$.

[14] AABOUD 18B search for resonances decaying to WW in pp collisions at $\sqrt{s}$ = 13 TeV. The quoted limit is for heavy-vector-triplet Z' with $g_V = 1$. See their Fig.11 for limits on $\sigma \cdot B$.

[15] AABOUD 18BI search for a resonance decaying to $t\overline{t}$ in pp collisions at $\sqrt{s}$ = 13 TeV. The quoted limit is for a top-color assisted TC Z' with $\Gamma_{Z'}/M_{Z'} = 0.01$. The limits for wider resonances are available. See their Fig. 14 for limits on $\sigma \cdot B$.

[16] AABOUD 18F search for resonances decaying to WW in pp collisions at $\sqrt{s}$ = 13 TeV. The quoted limit is for heavy-vector-triplet Z' with $g_V = 3$. The limit becomes $M_{Z'} >$ 2200 GeV for $g_V = 1$. If we assume $M_{Z'} = M_{W'}$, the limit increases $M_{Z'} >$ 3500 GeV and $M_{Z'} >$ 3100 GeV for $g_V = 3$ and $g_V = 1$, respectively. See their Fig.5 for limits on $\sigma \cdot B$.

[17] SIRUNYAN 18ED search for resonances decaying to HZ in pp collisions at $\sqrt{s}$ = 13 TeV. The limit above is for heavy-vector-triplet Z' with $g_V = 3$. If we assume $M_{Z'} = M_{W'}$, the limit increases $M_{Z'} >$ 2900 GeV and $M_{Z'} >$ 2800 GeV for $g_V = 3$ and $g_V = 1$, respectively.

[18] SIRUNYAN 18P give this limit for a heavy-vector-triplet Z' with $g_V = 3$. If they assume $M_{Z'} = M_{W'}$, the limit increases to $M_{Z'} >$ 3800 GeV.

[19] AABOUD 17AK search for a new resonance decaying to dijets in pp collisions at $\sqrt{s}$ = 13 TeV. The limit quoted above is for a leptophobic Z' boson having axial-vector coupling strength with quarks $g_q = 0.2$. The limit is 2100 GeV if $g_q = 0.1$.

[20] AABOUD 17AO search for resonances decaying to HZ in pp collisions at $\sqrt{s}$ = 13 TeV. The limit quoted above is for a Z' in the heavy-vector-triplet model with $g_V = 3$. See their Fig.4 for limits on $\sigma \cdot B$.

[21] SIRUNYAN 17AK search for resonances decaying to WW or HZ in pp collisions at $\sqrt{s}$ = 8 and 13 TeV. The quoted limit is for heavy-vector-triplet Z' with $g_V = 3$. The limit becomes $M_{Z'} >$ 2200 GeV for g_V =1. If we assume $M_{Z'} = M_{W'}$, the limit increases $M_{Z'} >$ 2400 GeV for both $g_V = 3$ and $g_V = 1$. See their Fig.1 and 2 for limits on $\sigma \cdot B$.

[22] SIRUNYAN 17Q search for a resonance decaying to $t\overline{t}$ in pp collisions at $\sqrt{s}$ = 13 TeV. The limit quoted above is for a resonance with relative width $\Gamma_{Z'}$ / $M_{Z'}$ = 0.01. Limits for wider resonances are available. See their Fig.6 for limits on $\sigma \cdot B$.

[23] SIRUNYAN 17R search for resonances decaying to HZ in pp collisions at $\sqrt{s}$ = 13 TeV. The quoted limit is for heavy-vector-triplet Z' with $g_V = 3$. Mass regions $M_{Z'} <$ 1150 GeV and 1250 GeV $< M_{Z'} <$ 1670 GeV are excluded for $g_V = 1$. If we assume $M_{Z'} = M_{W'}$, the excluded mass regions are 1000 $< M_{Z'} <$ 2500 GeV and 2760 $< M_{Z'} <$ 3300 GeV for $g_V = 3$; 1000 $< M_{Z'} <$ 2430 GeV and 2810 $< M_{Z'} <$ 3130 GeV for $g_V = 1$. See their Fig.5 for limits on $\sigma \cdot B$.

[24] AAD 22 search for $b\overline{b}Z'$ productions in pp collisions at $\sqrt{s}$ = 13 TeV. Z' is assumed to decay into $b\overline{b}$. See their Fig.4 for limits on $\sigma \cdot B$.

[25] AAD 21AQ limits are for a $B - L$ gauge boson model derived from their measurements on four-lepton differential cross sections. See their Fig. 13 for exclusion limits on the $B - L$ breaking Higgs boson mass.

[26] AAD 21AZ search for DM mediator Z' produced in association with a SM Higgs boson in pp collisions at $\sqrt{s}$ = 13 TeV. Z' is assumed to decay invisibly $Z' \rightarrow \chi\chi$. See their Fig.7 for limits in $M_{Z'} - M_\chi$ plane.

[27] AAD 21BB search for Z' productions in pp collisions at $\sqrt{s}$ = 13 TeV. Z' is assumed to decay into a SM Higgs boson H and an invisible particle A. See their Fig.7 for limits in $M_{Z'} - M_A$ plane.

[28] AAD 21D set limits on a dark Higgs model with a spin-1 mediator Z' and a scalar dark Higgs boson s. Dark Higgs s is assumed to decay into WW or ZZ. See their Fig.4 for limits in $M_{Z'} - M_s$ plane.

[29] AAD 21K search for $\gamma + \not{E}_T$ events in pp collision at $\sqrt{s}$ = 13 TeV. See their Fig. 5 for limits on Z' particle invisibly decaying to $\chi\chi$.

[30] BURAS 21 performed global fit to leptophilic Z' models using a large number of observables.

[31] CADEDDU 21 obtain limits on Z' coupling $g_{Z'}$ from coherent ν-nucleus scattering data collected by COHERENT experiment. For limits in the $M_{Z'} - g_{Z'}$ plane, see their Figures 3 and 4 for the universal Z' model and Figures 5 and 6 for the $B - L$ model.

[32] COLARESI 21 obtain limits on Z' coupling from coherent ν-nucleus scattering data collected by a Ge detector at the Dresden-II power reactor. See their Fig.7 for limits in mass-coupling plane.

[33] KRIBS 21 set decay-agnostic limits on kinetic mixing parameter between $U(1)_Y$ field and new heavy abelian vector boson (dark photon) field using the HERA ep collision data. See their Fig. 3 for limits in mass-mixing plane.

[34] TUMASYAN 21D search for energetic jets + $\not{E}_T$ events in pp collisions at $\sqrt{s}$ = 13 TeV. Z' is assumed to decay into a pair of invisible particles $\chi\chi$. See their Fig. 7 for limits on signal strength in $M_{Z'} - M_\chi$ plane, and Fig. 8 for limits on signal strength in quark and dark matter coupling vs mediator mass.

[35] AAD 20AF search for resonances decaying to $H\gamma$ in pp collisions at $\sqrt{s}$ = 13 TeV. See their Fig. 1c for limits on $\sigma \cdot B$ for the mass range 0.7 $< m_{Z'} <$ 4 TeV.

[36] AAD 20T search for Dark Matter mediator Z' decaying invisibly or decaying to $q\overline{q}$ in pp collisions at $\sqrt{s}$ = 13 TeV. See their Fig. 5 for limits in $M_{Z'} - g_q$ plane from the inclusive category. See their Fig. 7(a) for limits on the product of the cross section, acceptance, b-tagging efficiency, and branching fraction from the 2 b-tag category.

[37] AAD 20W search for a Dark Matter (DM) simplified model Z' produced in association with W in pp collisions at $\sqrt{s}$ = 13 TeV. See their Fig. 5 for limits on Z' production cross section.

[38] AAIJ 20AL search for spin-0 and spin-1 resonances decaying to $\mu^+\mu^-$ in pp collisions at $\sqrt{s}$ = 13 TeV in the mass regions $M_{Z'} <$ 60 GeV, with non-negligible widths considered above 20 GeV. See their Figs. 7, 8, and 9 for limits on $\sigma \cdot B$.

[39] ADACHI 20 search for production of Z' in e^+e^- collisions. The Z' is assume to decay invisibly. See their Fig. 3 and Fig. 5 for limits on Z' coupling and $\sigma(e^+e^- \rightarrow e^\pm\mu^\mp Z')$.

[40] SIRUNYAN 20AI search for broad resonances decaying into dijets in pp collisions at $\sqrt{s}$ = 13 TeV. See their Fig. 11 for exclusion limits in mass-coupling plane.

[41] SIRUNYAN 20AQ search for a narrow resonance lighter than 200 GeV decaying to $\mu^+\mu^-$ in pp collisions at $\sqrt{s}$ = 13 TeV. See their Fig. 3 for limits on Z' kinetic mixing coefficient.

[42] SIRUNYAN 20M search for a narrow resonance with a mass between 350 and 700 GeV in pp collisions at $\sqrt{s}$ = 13 TeV. See their Fig.3 for exclusion limits in mass-coupling plane.

[43] AABOUD 19AJ search in pp collisions at $\sqrt{s}$ = 13 TeV for a new resonance decaying to $q\overline{q}$ and produced in association with a high p_T photon. For a leptophobic axial-vector Z' in the mass region 250 GeV $< M_{Z'} <$ 950 GeV, the Z' coupling with quarks g_q is constrained below 0.18. See their Fig.2 for limits in $M_{Z'} - g_q$ plane.

[44] AABOUD 19D search in pp collisions at $\sqrt{s}$ = 13 TeV for a new resonance decaying to $q\overline{q}$ and produced in association with a high-p_T photon or jet. For a leptophobic axial-vector Z' in the mass region 100 GeV $< M_{Z'} <$ 220 GeV, the Z' coupling with quarks g_q is constrained below 0.23. See their Fig. 6 for limits in $M_{Z'} - g_q$ plane.

[45] AABOUD 19V search for Dark Matter simplified Z' decaying invisibly or decaying to fermion pair in pp collisions at $\sqrt{s}$ = 13 TeV.

[46] AAD 19L search for resonances decaying to $\ell^+\ell^-$ in pp collisions at $\sqrt{s}$ = 13 TeV. See their Fig. 4 for limits in the heavy vector triplet model couplings.

[47] LONG 19 uses the weak charge data of Cesium and proton to constrain mass of Z' in the 3-3-1 models.

[48] PANDEY 19 obtain limits on Z' induced neutrino non-standard interaction (NSI) parameter ϵ from LHC and IceCube data. See their Fig.2 for limits in $M_{Z'} - \epsilon$ plane, where ϵ = $g_q\ g_\nu\ v^2$ / ($2\ M^2_{Z'}$).

[49] SIRUNYAN 19AL search for a new resonance decaying to a top quark and a heavy vector-like top partner in pp collisions at $\sqrt{s}$ = 13 TeV. See their Fig. 8 for limits on Z' production cross section.

[50] SIRUNYAN 19AN search for a Dark Matter (DM) simplified model Z' decaying to H DM DM in pp collisions at $\sqrt{s}$ = 13 TeV. See their Fig. 7 for limits on the signal strength modifiers.

[51] SIRUNYAN 19CB search in pp collisions at $\sqrt{s}$ = 13 TeV for a new resonance decaying to $q\overline{q}$. For a leptophobic Z' in the mass region 50–300 GeV, the Z' coupling with quarks g'_q is constrained below 0.2. See their Figs. 4 and 5 for limits on g'_q in the mass range 50 $< M_{Z'} <$ 450 GeV.

[52] SIRUNYAN 19CD search in pp collisions at $\sqrt{s}$=13 TeV for a leptophobic Z' produced in association of high p_T ISR photon and decaying to $q\overline{q}$. See their Fig. 2 for limits on the Z' coupling strength g'_q to $q\overline{q}$ in the mass range between 10 and 125 GeV.

[53] SIRUNYAN 19D search for a narrow neutral vector resonance decaying to $H\gamma$. See their Fig. 3 for exclusion limit in $M_{Z'} - \sigma \cdot B$ plane. Upper limits on the production of $H\gamma$ resonances are set as a function of the resonance mass in the range of 720–3250 GeV.

[54] AABOUD 18AA search for a narrow neutral vector boson decaying to $H\gamma$. See their Fig. 10 for the exclusion limit in $M_{Z'} - \sigma B$ plane.

[55] AABOUD 18CJ search for heavy-vector-triplet Z' in pp collisions at $\sqrt{s}$ = 13 TeV. The limit quoted above is for model with $g_V = 3$ assuming $M_{Z'} = M_{W'}$. The limit becomes $M_{Z'} >$ 5500 GeV for model with $g_V = 1$.

[56] AABOUD 18N search for a narrow resonance decaying to $q\overline{q}$ in pp collisions at $\sqrt{s}$ = 13 TeV using trigger level analysis to improve the low mass region sensitivity. See their Fig. 5 for limits in the mass-coupling plane in the Z' mass range 450–1800 GeV.

[57] AAIJ 18AQ search for spin-0 and spin-1 resonances decaying to $\mu^+\mu^-$ in pp collisions at $\sqrt{s}$ = 7 and 8 TeV in the mass region near 10 GeV. See their Figs. 4 and 5 for limits on $\sigma \cdot B$.

[58] SIRUNYAN 18DR searches for $\mu^+\mu^-$ resonances produced in association with b-jets in the pp collision data with $\sqrt{s}$ = 8 TeV and 13 TeV. An excess of events near $m_{\mu\mu}$ = 28 GeV is observed in the 8 TeV data. See their Fig. 3 for the measured fiducial signal cross sections at $\sqrt{s}$ = 8 TeV and the 95% CL upper limits at $\sqrt{s}$ = 13 TeV.

[59] SIRUNYAN 18G search for a new resonance decaying to dijets in pp collisions at $\sqrt{s}$ = 13 TeV in the mass range 50–300 GeV. See their Fig.7 for limits in the mass-coupling plane.

[60] SIRUNYAN 18I search for a narrow resonance decaying to $b\overline{b}$ in pp collisions at $\sqrt{s}$ = 8 TeV using dedicated b-tagged dijet triggers to improve the sensitivity in the low mass region. See their Fig. 3 for limits on $\sigma \cdot B$ in the Z' mass range 325–1200 GeV.

[61] AABOUD 17B search for resonances decaying to HZ ($H \rightarrow b\overline{b}, c\overline{c}$; $Z \rightarrow \ell^+\ell^-, \nu\overline{\nu}$) in pp collisions at $\sqrt{s}$ = 13 TeV. The quoted limit is for heavy-vector-triplet Z' with

Downloaded from https://academic.oup.com/ptep/article/2022/8/083C01/6651666 by KIT Library user on 27 September 2022

$g_V = 3$. The limit becomes $M_{Z'} > 1490$ GeV for $g_V = 1$. If we assume $M_{Z'} = M_{W'}$, the limit increases $M_{Z'} > 2310$ GeV and $M_{Z'} > 1730$ GeV for $g_V = 3$ and $g_V = 1$, respectively. See their Fig.3 for limits on $\sigma \cdot B$.

[62] KHACHATRYAN 17AX search for lepto-phobic resonances decaying to four leptons in pp collisions at $\sqrt{s} = 8$ TeV.

[63] KHACHATRYAN 17U search for resonances decaying to HZ ($H \to b\overline{b}$; $Z \to \ell^+\ell^-$, $\nu\overline{\nu}$) in pp collisions at $\sqrt{s} = 13$ TeV. The limit on the heavy-vector-triplet model is $M_{Z'} = M_{W'} > 2$ TeV for $g_V = 3$, in which constraints from the $W' \to HW$ ($H \to b\overline{b}$; $W \to \ell\nu$) are combined. See their Fig.3 and Fig.4 for limits on $\sigma \cdot B$.

[64] SIRUNYAN 17A search for resonances decaying to WW with $WW \to \ell\nu q\overline{q}$, $q\overline{q}q\overline{q}$ in pp collisions at $\sqrt{s} = 13$ TeV. The quoted limit is for heavy-vector-triplet Z' with $g_V = 3$. The limit becomes $M_{Z'} > 1600$ GeV for $g_V = 1$. If we assume $M_{Z'} = M_{W'}$, the limit increases $M_{Z'} > 2400$ GeV and $M_{Z'} > 2300$ GeV for $g_V = 3$ and $g_V = 1$, respectively. See their Fig.6 for limits on $\sigma \cdot B$.

[65] SIRUNYAN 17AP search for resonances decaying into a SM-like Higgs scalar H and a light pseudo scalar A. A is assumed to decay invisibly. See their Fig.9 for limits on $\sigma \cdot B$.

[66] SIRUNYAN 17T search for a new resonance decaying to dijets in pp collisions at $\sqrt{s} =$ 13 TeV in the mass range 100–300 GeV. See their Fig.3 for limits in the mass-coupling plane.

[67] SIRUNYAN 17V search for a new resonance decaying to a top quark and a heavy vector-like top partner T in pp collisions at $\sqrt{s} = 13$ TeV. See their table 5 for limits on the Z' production cross section for various values of $M_{Z'}$ and M_T in the range of $M_{Z'} =$ 1500–2500 GeV and $M_T =$ 700–1500 GeV.

[68] AABOUD 16 search for a narrow resonance decaying into $b\overline{b}$ in pp collisions at $\sqrt{s} = 13$ TeV. The limit quoted above is for a leptophobic Z' with SM-like couplings to quarks. See their Fig.6 for limits on $\sigma \cdot B$.

[69] AAD 16L search for $Z' \to a\gamma$, $a \to \gamma\gamma$ in pp collisions at $\sqrt{s} = 8$ TeV. See their Table 6 for limits on $\sigma \cdot B$.

[70] AAD 16S search for a new resonance decaying to dijets in pp collisions at $\sqrt{s} = 13$ TeV. The limit quoted above is for a leptophobic Z' having coupling strength with quark $g_q = 0.3$ and is taken from their Figure 3.

[71] KHACHATRYAN 16AP search for a resonance decaying to HZ in pp collisions at $\sqrt{s} = 8$ TeV. Both H and Z are assumed to decay to fat jets. The quoted limit is for heavy-vector-triplet Z' with $g_V = 3$.

[72] KHACHATRYAN 16E search for a leptophobic top-color Z' decaying to $t\overline{t}$ using pp collisions at $\sqrt{s} = 8$ TeV. The quoted limit assumes that $\Gamma_{Z'}/m_{Z'} = 0.012$. Also $m_{Z'} < 2.9$ TeV is excluded for wider topcolor Z' with $\Gamma_{Z'}/m_{Z'} = 0.1$.

[73] AAD 15AO search for narrow resonance decaying to $t\overline{t}$ using pp collisions at $\sqrt{s} = 8$ TeV. See Fig. 11 for limit on σB.

[74] AAD 15AT search for monotop production plus large missing E_T events in pp collisions at $\sqrt{s} = 8$ TeV and give constraints on a Z' model having $Z'u\overline{t}$ coupling. Z' is assumed to decay invisibly. See their Fig. 6 for limits on $\sigma \cdot B$.

[75] AAD 15CD search for decays of Higgs bosons to 4 ℓ states via Z' bosons, $H \to ZZ' \to 4\ell$ or $H \to Z'Z' \to 4\ell$. See Fig. 5 for the limit on the signal strength of the $H \to ZZ' \to 4\ell$ process and Fig. 16 for the limit on $H \to Z'Z' \to 4\ell$.

[76] KHACHATRYAN 15F search for monotop production plus large missing E_T events in pp collisions at $\sqrt{s} = 8$ TeV and give constraints on a Z' model having $Z'u\overline{t}$ coupling. Z' is assumed to decay invisibly. See Fig. 3 for limits on σB.

[77] KHACHATRYAN 15O search for narrow Z' resonance decaying to ZH in pp collisions at $\sqrt{s} = 8$ TeV. See their Fig. 6 for limit on σB.

[78] AAD 14AT search for a narrow neutral vector boson decaying to $Z\gamma$. See their Fig. 3b for the exclusion limit in $m_{Z'} - \sigma B$ plane.

[79] KHACHATRYAN 14A search for new resonance in the WW ($\ell\nu q\overline{q}$) and the ZZ ($\ell\ell q\overline{q}$) channels using pp collisions at $\sqrt{s}$=8 TeV. See their Fig.13 for the exclusion limit on the number of events in the mass-width plane.

[80] MARTINEZ 14 use various electroweak data to constrain the Z' boson in the 3-3-1 models.

[81] AAD 13AQ search for a leptophobic top-color Z' decaying to $t\overline{t}$. The quoted limit assumes that $\Gamma_{Z'}/m_{Z'} = 0.012$.

[82] CHATRCHYAN 13BM search for top-color Z' decaying to $t\overline{t}$ using pp collisions at $\sqrt{s}$=8 TeV. The quoted limit is for $\Gamma_{Z'}/m_{Z'} = 0.012$.

[83] CHATRCHYAN 13AP search for top-color leptophobic Z' decaying to $t\overline{t}$ using pp collisions at $\sqrt{s}$=7 TeV. The quoted limit is for $\Gamma_{Z'}/m_{Z'} = 0.012$.

[84] AAD 12BV search for narrow resonance decaying to $t\overline{t}$ using pp collisions at $\sqrt{s}$=7 TeV. See their Fig. 7 for limit on $\sigma \cdot$ B.

[85] AAD 12K search for narrow resonance decaying to $t\overline{t}$ using pp collisions at $\sqrt{s}$=7 TeV. See their Fig. 5 for limit on $\sigma \cdot$ B.

[86] AALTONEN 12AR search for chromophilic Z' in $p\overline{p}$ collisions at $\sqrt{s} = 1.96$ TeV. See their Fig. 5 for limit on $\sigma \cdot$ B.

[87] AALTONEN 12N search for $p\overline{p} \to tZ'$, $Z' \to \overline{t}u$ events in $p\overline{p}$ collisions. See their Fig. 3 for the limit on $\sigma \cdot$ B.

[88] ABAZOV 12R search for top-color Z' boson decaying exclusively to $t\overline{t}$. The quoted limit is for $\Gamma_{Z'}/m_{Z'}$= 0.012.

[89] CHATRCHYAN 12AI search for $pp \to tt$ events and give constraints on a Z' model having $Z'\overline{u}t$ coupling. See their Fig. 4 for the limit in mass-coupling plane.

[90] Search for resonance decaying to $t\overline{t}$. See their Fig. 6 for limit on $\sigma \cdot$ B.

[91] Search for narrow resonance decaying to $t\overline{t}$. See their Fig. 4 for limit on $\sigma \cdot$ B.

[92] Search for narrow resonance decaying to $t\overline{t}$. See their Fig. 3 for limit on $\sigma \cdot$ B.

[93] CHATRCHYAN 11O search for same-sign top production in pp collisions induced by a hypothetical FCNC Z' at $\sqrt{s} = 7$ TeV. See their Fig. 3 for limit in mass-coupling plane.

[94] Search for narrow resonance decaying to $t\overline{t}$. See their Fig. 3 for limit on $\sigma \cdot$ B.

[95] Search for narrow resonance decaying to $t\overline{t}$. See their Fig. 2 for limit on $\sigma \cdot$ B.

[96] BARGER 03B use the nucleosynthesis bound on the effective number of light neutrino δN_ν. See their Figs. 4–5 for limits in general E_6 motivated models.

[97] CHO 00 use various electroweak data to constrain Z' models assuming m_H=100 GeV. See Fig. 2 for limits in general E_6-motivated models.

[98] CHO 98 study constraints on four-Fermi contact interactions obtained from low-energy electroweak experiments, assuming no Z-Z' mixing.

[99] Search for Z' decaying to dijets at $\sqrt{s}$=1.8 TeV. For Z' with electromagnetic strength coupling, no bound is obtained.

Searches for Z' with Lepton-Flavor-Violating decays

The following limits are obtained from $p\overline{p}$ or $pp \to Z'X$ with Z' decaying to the mode indicated in the comments.

VALUE	DOCUMENT ID		TECN	COMMENT
• • • We do not use the following data for averages, fits, limits, etc. • • •				
	[1] AABOUD	18CM	ATLS	$Z' \to e\mu$, $e\tau$, $\mu\tau$
	[2] SIRUNYAN	18AT	CMS	$Z' \to e\mu$
	[3] AABOUD	16P	ATLS	$Z' \to e\mu$, $e\tau$, $\mu\tau$
	[4] KHACHATRY...	16BE	CMS	$Z' \to e\mu$
	[5] AAD	15O	ATLS	$Z' \to e\mu$, $e\tau$, $\mu\tau$
	[6] AAD	11H	ATLS	$Z' \to e\mu$
	[7] AAD	11Z	ATLS	$Z' \to e\mu$
	[8] ABULENCIA	06M	CDF	$Z' \to e\mu$

[1] AABOUD 18CM search for a new particle with lepton-flavor violating decay in pp collisions at $\sqrt{s} = 13$ TeV. See their Figs. 4, 5, and 6 for limits on $\sigma \cdot B$.

[2] SIRUNYAN 18AT search for a narrow resonance Z' decaying into $e\mu$ in pp collisions at $\sqrt{s} = 13$ TeV. See their Fig.5 for limit on $\sigma \cdot B$ in the range of 600 GeV $< M_{Z'} <$ 5000 GeV.

[3] AABOUD 16P search for new particle with lepton flavor violating decay in pp collisions at $\sqrt{s} = 13$ TeV. See their Figs.2, 3, and 4 for limits on $\sigma \cdot B$.

[4] KHACHATRYAN 16BE search for new particle Z' with lepton flavor violating decay in pp collisions at$\sqrt{s} = 8$ TeV in the range of 200 GeV $< M_{Z'} <$ 2000 GeV. See their Fig.4 for limits on $\sigma \cdot B$ and their Table 5 for bounds on various masses.

[5] AAD 15O search for new particle Z' with lepton flavor violating decay in pp collisions at $\sqrt{s} = 8$ TeV in the range of 500 GeV $< M_{Z'} <$ 3000 GeV. See their Fig. 2 for limits on σB.

[6] AAD 11H search for new particle Z' with lepton flavor violating decay in pp collisions at $\sqrt{s} = 7$ TeV in the range of 700 GeV $< M_{Z'} <$ 1000 GeV. See their Fig. 3 for limits on $\sigma \cdot B$.

[7] AAD 11Z search for new particle Z' with lepton flavor violating decay in pp collisions at $\sqrt{s} = 7$ TeV in the range 700 GeV $< M_{Z'} <$ 2000 GeV. See their Fig. 3 for limits on $\sigma \cdot B$.

[8] ABULENCIA 06M search for new particle Z' with lepton flavor violating decay in $p\overline{p}$ collisions at $\sqrt{s} = 1.96$ TeV in the range of 100 GeV $< M_{Z'} <$ 800 GeV. See their Fig. 4 for limits in the mass-coupling plane.

Indirect Constraints on Kaluza-Klein Gauge Bosons

Bounds on a Kaluza-Klein excitation of the Z boson or photon in d=1 extra dimension. These bounds can also be interpreted as a lower bound on $1/R$, the size of the extra dimension. Unless otherwise stated, bounds assume all fermions live on a single brane and all gauge fields occupy the 4+d-dimensional bulk. See also the section on "Extra Dimensions" in the "Searches" Listings in this *Review*.

VALUE (TeV)	CL%	DOCUMENT ID		TECN	COMMENT
• • • We do not use the following data for averages, fits, limits, etc. • • •					
> 4.7		[1] MUECK	02	RVUE	Electroweak
> 3.3	95	[2] CORNET	00	RVUE	$e\nu qq'$
>5000		[3] DELGADO	00	RVUE	ϵ_K
> 2.6	95	[4] DELGADO	00	RVUE	Electroweak
> 3.3	95	[5] RIZZO	00	RVUE	Electroweak
> 2.9	95	[6] MARCIANO	99	RVUE	Electroweak
> 2.5	95	[7] MASIP	99	RVUE	Electroweak
> 1.6	90	[8] NATH	99	RVUE	Electroweak
> 3.4	95	[9] STRUMIA	99	RVUE	Electroweak

[1] MUECK 02 limit is 2σ and is from global electroweak fit ignoring correlations among observables. Higgs is assumed to be confined on the brane and its mass is fixed. For scenarios of bulk Higgs, of brane-SU(2)$_L$, bulk-U(1)$_Y$, and of bulk-SU(2)$_L$, brane-U(1)$_Y$, the corresponding limits are > 4.6 TeV, > 4.3 TeV and > 3.0 TeV, respectively.

[2] Bound is derived from limits on $e\nu qq'$ contact interaction, using data from HERA and the Tevatron.

[3] Bound holds only if first two generations of quarks lives on separate branes. If quark mixing is not complex, then bound lowers to 400 TeV from Δm_K.

[4] See Figs. 1 and 2 of DELGADO 00 for several model variations. Special boundary conditions can be found which permit KK states down to 950 GeV and that agree with the measurement of Q_W(Cs). Quoted bound assumes all Higgs bosons confined to brane; placing one Higgs doublet in the bulk lowers bound to 2.3 TeV.

[5] Bound is derived from global electroweak analysis assuming the Higgs field is trapped on the matter brane. If the Higgs propagates in the bulk, the bound increases to 3.8 TeV.

[6] Bound is derived from global electroweak analysis but considering only presence of the KK W bosons.

[7] Global electroweak analysis used to obtain bound independent of position of Higgs on brane or in bulk.

[8] Bounds from effect of KK states on G_F, α, M_W, and M_Z. Hard cutoff at string scale determined using gauge coupling unification. Limits for d=2,3,4 rise to 3.5, 5.7, and 7.8 TeV.

[9] Bound obtained for Higgs confined to the matter brane with m_H=500 GeV. For Higgs in the bulk, the bound increases to 3.5 TeV.

See the related review(s):

Leptoquarks

MASS LIMITS for Leptoquarks from Pair Production

These limits rely only on the color or electroweak charge of the leptoquark.

VALUE (GeV)	CL%	DOCUMENT ID		TECN	COMMENT
>1480	95	[1] AAD	21AG	ATLS	Scalar LQ. B(te) = 1
>1470	95	[2] AAD	21AG	ATLS	Scalar LQ. B($t\mu$) = 1
>1190	95	[3] AAD	21AW	ATLS	Scalar LQ. B($b\tau$) = 1
>1030	95	[4] AAD	21AW	ATLS	Scalar LQ. B($t\tau$) = 1
>1760	95	[5] AAD	21AW	ATLS	Vector LQ. κ = 1. B($b\tau$) = 1

Downloaded from https://academic.oup.com/ptep/article/2022/8/083C01/6651666 by KIT Library user on 27 September 2022

>1260	95	[6] AAD	21S	ATLS	Scalar LQ. B($b\nu$) = 1
>1430	95	[7] AAD	21T	ATLS	Scalar LQ. B($t\tau$) = 1
> 950	95	[8] SIRUNYAN	21J	CMS	Scalar LQ. B($t\tau$)=B($b\nu$)=0.5
>1650	95	[9] SIRUNYAN	21J	CMS	Vector LQ. κ=1, B($t\nu$) = B($b\tau$) = 0.5
>1800	95	[10] AAD	20AK	ATLS	Scalar LQ. B(eq) = 1
>1700	95	[11] AAD	20AK	ATLS	Scalar LQ. B(μq) = 1
>1240	95	[12] AAD	20S	ATLS	Scalar LQ. B($t\nu$) = 1
>1185	95	[13] SIRUNYAN	20A	CMS	Scalar LQ. B(νb) = 1
>1140	95	[14] SIRUNYAN	20A	CMS	Scalar LQ. B(νt) = 1
>1140	95	[15] SIRUNYAN	20A	CMS	Scalar LQ. B(νq) = 1 with q = u, d, s, c
>1925	95	[16] SIRUNYAN	20A	CMS	Vector LQ. κ = 1. B(νb) = 1
>1825	95	[17] SIRUNYAN	20A	CMS	Vector LQ. κ = 1. B(νt) = 1
>1980	95	[18] SIRUNYAN	20A	CMS	Vector LQ. κ = 1. B(νq) = 1 with q = u, d, s, c
>1400	95	[19] AABOUD	19AX	ATLS	Scalar LQ. B(eq) = 1
>1560	95	[20] AABOUD	19AX	ATLS	Scalar LQ. B(μq) = 1
>1000	95	[21] AABOUD	19X	ATLS	Scalar LQ. B($t\nu$) = 1
>1030	95	[22] AABOUD	19X	ATLS	Scalar LQ. B($b\tau$) = 1
> 970	95	[23] AABOUD	19X	ATLS	Scalar LQ. B($b\nu$) = 1
> 920	95	[24] AABOUD	19X	ATLS	Scalar LQ. B($t\tau$) = 1
>1530	95	[25] SIRUNYAN	19BI	CMS	Scalar LQ. B(μq)+B(νq) = 1
>1435	95	[26] SIRUNYAN	19BJ	CMS	Scalar LQ. B(eq)+B(νq) = 1
>1020	95	[27] SIRUNYAN	19Y	CMS	Scalar LQ. B(τb) = 1
none 300–900	95	[28] SIRUNYAN	18CZ	CMS	Scalar LQ. B(τt) = 1
>1420	95	[29] SIRUNYAN	18EC	CMS	Scalar LQ. B(μt) = 1
>1190	95	[30] SIRUNYAN	18EC	CMS	Vector LQ. μt, τt, νb
>1100	95	[31] SIRUNYAN	18U	CMS	Scalar LQ. B(νb) = 1
> 980	95	[32] SIRUNYAN	18U	CMS	Scalar LQ. B(νq) = 1 with q = u,d,s,c
>1020	95	[33] SIRUNYAN	18U	CMS	Scalar LQ. B(νt) = 1
>1810	95	[34] SIRUNYAN	18U	CMS	Vector LQ. κ=1. LQ→ $b\nu$
>1790	95	[35] SIRUNYAN	18U	CMS	Vector LQ. κ=1. LQ→ $q\nu$ with q = u,d,s,c
>1780	95	[36] SIRUNYAN	18U	CMS	Vector LQ. κ=1. LQ→ $t\nu$
> 740	95	[37] KHACHATRY...	17J	CMS	Scalar LQ. B(τb) = 1
> 850	95	[38] SIRUNYAN	17H	CMS	Scalar LQ. B(τb) = 1
>1050	95	[39] AAD	16G	ATLS	Scalar LQ. B(eq) = 1
>1000	95	[40] AAD	16G	ATLS	Scalar LQ. B(μq) = 1
> 625	95	[41] AAD	16G	ATLS	Scalar LQ. B(νb) = 1
none 200–640	95	[42] AAD	16G	ATLS	Scalar LQ. B(νt) = 1
>1010	95	[43] KHACHATRY...	16AF	CMS	Scalar LQ. B(eq) = 1
>1080	95	[44] KHACHATRY...	16AF	CMS	Scalar LQ. B(μq) = 1
> 685	95	[45] KHACHATRY...	15AJ	CMS	Scalar LQ. B(τt) = 1
> 740	95	[46] KHACHATRY...	14T	CMS	Scalar LQ. B(τb) = 1
• • • We do not use the following data for averages, fits, limits, etc. • • •					
		[47] SIRUNYAN	19BC	CMS	Scalar LQ (→ μq) LQ (→ X + DM)
> 534	95	[48] AAD	13AE	ATLS	Third generation
> 525	95	[49] CHATRCHYAN	13M	CMS	Third generation
> 660	95	[50] AAD	12H	ATLS	First generation
> 685	95	[51] AAD	12O	ATLS	Second generation
> 830	95	[52] CHATRCHYAN	12AG	CMS	First generation
> 840	95	[53] CHATRCHYAN	12AG	CMS	Second generation
> 450	95	[54] CHATRCHYAN	12BO	CMS	Third generation
> 376	95	[55] AAD	11D	ATLS	Superseded by AAD 12H
> 422	95	[56] AAD	11D	ATLS	Superseded by AAD 12O
> 326	95	[57] ABAZOV	11V	D0	First generation
> 339	95	[58] CHATRCHYAN	11N	CMS	Superseded by CHATRCHYAN 12AG
> 384	95	[59] KHACHATRY...	11D	CMS	Superseded by CHATRCHYAN 12AG
> 394	95	[60] KHACHATRY...	11E	CMS	Superseded by CHATRCHYAN 12AG
> 247	95	[61] ABAZOV	10L	D0	Third generation
> 316	95	[62] ABAZOV	09	D0	Second generation
> 299	95	[63] ABAZOV	09AF	D0	Superseded by ABAZOV 11V
		[64] AALTONEN	08P	CDF	Third generation
> 153	95	[65] AALTONEN	08Z	CDF	Third generation
> 205	95	[66] ABAZOV	08AD	D0	All generations
> 210	95	[65] ABAZOV	08AN	D0	Third generation
> 229	95	[67] ABAZOV	07J	D0	Superseded by ABAZOV 10L
> 251	95	[68] ABAZOV	06A	D0	Superseded by ABAZOV 09
> 136	95	[69] ABAZOV	06L	D0	Superseded by ABAZOV 08AD
> 226	95	[70] ABULENCIA	06T	CDF	Second generation
> 256	95	[71] ABAZOV	05H	D0	First generation
> 117	95	[66] ACOSTA	05I	CDF	First generation
> 236	95	[72] ACOSTA	05P	CDF	First generation
> 99	95	[73] ABBIENDI	03R	OPAL	First generation
> 100	95	[73] ABBIENDI	03R	OPAL	Second generation
> 98	95	[73] ABBIENDI	03R	OPAL	Third generation
> 98	95	[74] ABAZOV	02	D0	All generations
> 225	95	[75] ABAZOV	01D	D0	First generation
> 85.8	95	[76] ABBIENDI	00M	OPAL	Superseded by ABBIENDI 03R
> 85.5	95	[76] ABBIENDI	00M	OPAL	Superseded by ABBIENDI 03R
> 82.7	95	[76] ABBIENDI	00M	OPAL	Superseded by ABBIENDI 03R
> 200	95	[77] ABBOTT	00C	D0	Second generation
> 123	95	[78] AFFOLDER	00K	CDF	Second generation
> 148	95	[79] AFFOLDER	00K	CDF	Third generation
> 160	95	[80] ABBOTT	99J	D0	Second generation
> 225	95	[81] ABBOTT	98E	D0	First generation
> 94	95	[82] ABBOTT	98J	D0	Third generation
> 202	95	[83] ABE	98S	CDF	Second generation
> 242	95	[84] GROSS-PILCH..98			First generation
> 99	95	[85] ABE	97F	CDF	Third generation
> 213	95	[86] ABE	97X	CDF	First generation
> 45.5	95	[87,88] ABREU	93J	DLPH	First + second generation
> 44.4	95	[89] ADRIANI	93M	L3	First generation
> 44.5	95	[89] ADRIANI	93M	L3	Second generation
> 45	95	[89] DECAMP	92	ALEP	Third generation
none 8.9–22.6	95	[90] KIM	90	AMY	First generation
none 10.2–23.2	95	[90] KIM	90	AMY	Second generation
none 5–20.8	95	[91] BARTEL	87B	JADE	
none 7–20.5	95	[92] BEHREND	86B	CELL	

[1] AAD 21AG search for scalar leptoquarks decaying to te. See their Fig. 6 for exclusion limit on B(te) as function of M_{LQ}.

[2] AAD 21AG search for scalar leptoquarks decaying to $t\mu$. See their Fig. 6 for exclusion limit on B($t\mu$) as function of M_{LQ}.

[3] AAD 21AW search for scalar leptoquarks decaying to $b\tau$. See their Fig. 9 for exclusion contour in B($b\tau$)−M_{LQ} plane.

[4] AAD 21AW search for scalar leptoquarks decaying to $t\tau$. See their Fig. 9 for exclusion contour in B($t\tau$)−M_{LQ} plane.

[5] AAD 21AW search for κ = 1 vector leptoquarks decaying to $b\tau$. See their Fig. 10 for exclusion contour in B($b\tau$)−M_{LQ} plane and for limit on κ = 0 vector leptoquarks.

[6] AAD 21S search for scalar leptoquarks decaying to $b\nu$ in pp collisions at $\sqrt{s}$ = 13 TeV. The limit above assumes B($b\nu$) = 1. For B($b\nu$) = 0.05, the limit becomes 400 GeV.

[7] AAD 21T search for scalar leptoquarks decaying to $t\tau$ in pp collisions at $\sqrt{s}$ = 13 TeV. The limit above assumes B($t\tau$) = 1. For B($t\tau$) = 0.5, the limit becomes 1220 GeV. See their Fig. 15b for limits on B($t\tau$) as a function of leptoquark mass.

[8] SIRUNYAN 21J search for scalar leptoquarks decaying to $t\tau$ and $b\nu$ in pp collisions at $\sqrt{s}$ = 13 TeV.

[9] SIRUNYAN 21J search for vector leptoquarks decaying to $t\nu$ and $b\tau$ in pp collisions at $\sqrt{s}$ = 13 TeV. The limit quoted above assumes κ = 1. If we assume κ = 0, the limit becomes M_{LQ} > 1290 GeV.

[10] AAD 20AK search for scalar leptoquarks decaying to eq, eb, ec, μq, μb, μc. The quoted limit assumes B(eq) = 1. See their Fig. 9 for limits on B(eq), B(eb), B(ec), B(μq), B(μb), B(μc) as a function of leptoquark mass.

[11] AAD 20AK search for scalar leptoquarks decaying to eq, eb, ec, μq, μb, μc. The quoted limit assumes B(μq) = 1. See their Fig. 9 for limits on B(eq), B(eb), B(ec), B(μq), B(μb), B(μc) as a function of leptoquark mass.

[12] AAD 20S search for scalar leptoquarks decaying to $t\nu$ in pp collisions at $\sqrt{s}$ = 13 TeV.

[13] SIRUNYAN 20A search for scalar and vector leptoquarks decaying to $t\nu$, $b\nu$, and $q\nu$ (q = u, d, s, c). The limit quoted above assumes scalar leptoquark with B(νb) = 1.

[14] SIRUNYAN 20A search for scalar and vector leptoquarks decaying to $t\nu$, $b\nu$, and $q\nu$ (q = u, d, s, c). The limit quoted above assumes scalar leptoquark with B(νt) = 1.

[15] SIRUNYAN 20A search for scalar and vector leptoquarks decaying to $t\nu$, $b\nu$, and $q\nu$ (q = u, d, s, c). The limit quoted above assumes scalar leptoquark with B(νq) = 1.

[16] SIRUNYAN 20A search for scalar and vector leptoquarks decaying to $t\nu$, $b\nu$, and $q\nu$ (q = u, d, s, c). The limit quoted above assumes vector leptoquark with B(νb) = 1 and κ = 1. If we assume κ = 0, the limit becomes M_{LQ} > 1560 GeV.

[17] SIRUNYAN 20A search for scalar and vector leptoquarks decaying to $t\nu$, $b\nu$, and $q\nu$ (q = u, d, s, c). The limit quoted above assumes vector leptoquark with B(νt) = 1 and κ = 1. If we assume κ = 0, the limit becomes M_{LQ} > 1475 GeV.

[18] SIRUNYAN 20A search for scalar and vector leptoquarks decaying to $t\nu$, $b\nu$, and $q\nu$ (q = u, d, s, c). The limit quoted above assumes vector leptoquark with B(νq) = 1 and κ = 1. If we assume κ = 0, the limit becomes M_{LQ} > 1560 GeV.

[19] AABOUD 19AX search for leptoquarks using $eejj$ events in pp collisions at $\sqrt{s}$ = 13 TeV. The limit above assumes B(eq) = 1.

[20] AABOUD 19AX search for leptoquarks using $\mu\mu jj$ events in pp collisions at $\sqrt{s}$ = 13 TeV. The limit above assumes B(μq) = 1.

[21] AABOUD 19X search for scalar leptoquarks decaying to $t\nu$ in pp collisions at $\sqrt{s}$ = 13 TeV.

[22] AABOUD 19X search for scalar leptoquarks decaying to $b\tau$ in pp collisions at $\sqrt{s}$ = 13 TeV.

[23] AABOUD 19X search for scalar leptoquarks decaying to $b\nu$ in pp collisions at $\sqrt{s}$ = 13 TeV.

[24] AABOUD 19X search for scalar leptoquarks decaying to $t\tau$ in pp collisions at $\sqrt{s}$ = 13 TeV.

[25] SIRUNYAN 19BI search for a pair of scalar leptoquarks decaying to $\mu\mu jj$ and to $\mu\nu jj$ final states in pp collisions at $\sqrt{s}$ = 13 TeV. Limits are shown as a function of β where β is the branching fraction to a muon and a quark. For β = 1.0 (0.5) LQ masses up to 1530 (1285) GeV are excluded. See Fig. 9 for exclusion limits in the plane of β and LQ mass.

[26] SIRUNYAN 19BJ search for a pair of scalar leptoquarks decaying to $eejj$ and $e\nu jj$ final states in pp collisions at $\sqrt{s}$ = 13 TeV. Limits are shown as a function of the branching fraction β to an electron and a quark. For β = 1.0 (0.5) LQ masses up to 1435 (1270) GeV are excluded. See Fig. 9 for exclusion limits in the plane of β and LQ mass.

[27] SIRUNYAN 19Y search for a pair of third generation scalar leptoquarks, each decaying to τ and a jet. Assuming B(τb) = 1, leptoquark masses below 1.02 TeV are excluded.

[28] SIRUNYAN 18CZ search for scalar leptoquarks decaying to τt in pp collisions at $\sqrt{s}$ = 13 TeV. The limit above assumes B(τt) = 1.

[29] SIRUNYAN 18EC set limits for scalar and vector leptoquarks decaying to μt, τt, and νb. The limit quoted above assumes scalar leptoquark with B(μt) = 1.

[30] SIRUNYAN 18EC set limits for scalar and vector leptoquarks decaying to μt, τt, and νb. The limit quoted above assumes vector leptoquark with all possible combinations of branching fractions to μt, τt, and νb.

[31] SIRUNYAN 18U set limits for scalar and vector leptoquarks decaying to $t\nu$, $b\nu$, and $q\nu$. The limit quoted above assumes scalar leptoquark with B($b\nu$) = 1. Vector leptoquarks with κ = 1 are excluded below masses of 1810 GeV.

Downloaded from https://academic.oup.com/ptep/article/2022/8/083C01/6651666 by KIT Library user on 27 September 2022

[32] SIRUNYAN 18U set limits for scalar and vector leptoquarks decaying to $t\nu$, $b\nu$, and $q\nu$. The limit quoted above assumes scalar leptoquark with $B(q\nu) = 1$. Vector leptoquarks with $\kappa = 1$ are excluded below masses of 1790 GeV.

[33] SIRUNYAN 18U set limits for scalar and vector leptoquarks decaying to $t\nu$, $b\nu$, and $q\nu$. The limit quoted above assumes scalar leptoquark with $B(\nu t) = 1$. Vector leptoquarks with $\kappa = 1$ are excluded below masses of 1780 GeV.

[34] SIRUNYAN 18U set limits for scalar and vector leptoquarks decaying to $t\nu$, $b\nu$, and $q\nu$. $\kappa = 1$ and LQ$\rightarrow$ $b\nu$ are assumed.

[35] SIRUNYAN 18U set limits for scalar and vector leptoquarks decaying to $t\nu$, $b\nu$, and $q\nu$. $\kappa = 1$ and LQ$\rightarrow$ $q\nu$ with $q = u,d,s,c$ are assumed.

[36] SIRUNYAN 18U set limits for scalar and vector leptoquarks decaying to $t\nu$, $b\nu$, and $q\nu$. $\kappa = 1$ and LQ$\rightarrow$ $t\nu$ are assumed.

[37] KHACHATRYAN 17J search for scalar leptoquarks decaying to τb using pp collisions at $\sqrt{s} = 13$ TeV. The limit above assumes $B(\tau b) = 1$.

[38] SIRUNYAN 17H search for scalar leptoquarks using $\tau\tau bb$ events in pp collisions at $\sqrt{s} = 8$ TeV. The limit above assumes $B(\tau b) = 1$.

[39] AAD 16G search for scalar leptoquarks using $eejj$ events in collisions at $\sqrt{s} = 8$ TeV. The limit above assumes $B(eq) = 1$.

[40] AAD 16G search for scalar leptoquarks using $\mu\mu jj$ events in collisions at $\sqrt{s} = 8$ TeV. The limit above assumes $B(\mu q) = 1$.

[41] AAD 16G search for scalar leptoquarks decaying to $b\nu$. The limit above assumes $B(b\nu) = 1$.

[42] AAD 16G search for scalar leptoquarks decaying to $t\nu$. The limit above assumes $B(t\nu) = 1$.

[43] KHACHATRYAN 16AF search for scalar leptoquarks using $eejj$ and $e\nu jj$ events in pp collisions at $\sqrt{s} = 8$ TeV. The limit above assumes $B(eq)= 1$. For $B(eq) = 0.5$, the limit becomes 850 GeV.

[44] KHACHATRYAN 16AF search for scalar leptoquarks using $\mu\mu jj$ and $\mu\nu jj$ events in pp collisions at $\sqrt{s} = 8$ TeV. The limit above assumes $B(\mu q) = 1$. For $B(\mu q) = 0.5$, the limit becomes 760 GeV.

[45] KHACHATRYAN 15AJ search for scalar leptoquarks using $\tau\tau tt$ events in pp collisions at $\sqrt{s} = 8$ TeV. The limit above assumes $B(\tau t) = 1$.

[46] KHACHATRYAN 14T search for scalar leptoquarks decaying to τb using pp collisions at $\sqrt{s} = 8$ TeV. The limit above assumes $B(\tau b) = 1$. See their Fig. 5 for the exclusion limit as function of $B(\tau b)$.

[47] SIRUNYAN 19BC search for scalar leptoquark (LQ) pair production in pp collisions at $\sqrt{s} = 13$ TeV. One LQ is assumed to decay to μq, while the other decays to dark matter pair and SM particles. See their Fig. 4 for limits in $M_{LQ}-M_{DM}$ plane.

[48] AAD 13AE search for scalar leptoquarks using $\tau\tau bb$ events in pp collisions at $E_{cm} =$ 7 TeV. The limit above assumes $B(\tau b) = 1$.

[49] CHATRCHYAN 13M search for scalar and vector leptoquarks decaying to τb in pp collisions at $E_{cm} = 7$ TeV. The limit above is for scalar leptoquarks with $B(\tau b) = 1$.

[50] AAD 12H search for scalar leptoquarks using $eejj$ and $e\nu jj$ events in pp collisions at $E_{cm} = 7$ TeV. The limit above assumes $B(eq) = 1$. For $B(eq) = 0.5$, the limit becomes 607 GeV.

[51] AAD 12O search for scalar leptoquarks using $\mu\mu jj$ and $\mu\nu jj$ events in pp collisions at $E_{cm} = 7$ TeV. The limit above assumes $B(\mu q) = 1$. For $B(\mu q) = 0.5$, the limit becomes 594 GeV.

[52] CHATRCHYAN 12AG search for scalar leptoquarks using $eejj$ and $e\nu jj$ events in pp collisions at $E_{cm} = 7$ TeV. The limit above assumes $B(eq) = 1$. For $B(eq) = 0.5$, the limit becomes 640 GeV.

[53] CHATRCHYAN 12AG search for scalar leptoquarks using $\mu\mu jj$ and $\mu\nu jj$ events in pp collisions at $E_{cm} = 7$ TeV. The limit above assumes $B(\mu q) = 1$. For $B(\mu q) = 0.5$, the limit becomes 650 GeV.

[54] CHATRCHYAN 12BO search for scalar leptoquarks decaying to νb in pp collisions at $\sqrt{s} = 7$ TeV. The limit above assumes $B(\nu b) = 1$.

[55] AAD 11D search for scalar leptoquarks using $eejj$ and $e\nu jj$ events in pp collisions at $E_{cm} = 7$ TeV.The limit above assumes $B(eq) = 1$. For $B(eq) = 0.5$, the limit becomes 319 GeV.

[56] AAD 11D search for scalar leptoquarks using $\mu\mu jj$ and $\mu\nu jj$ events in pp collisions at $E_{cm} = 7$ TeV. The limit above assumes $B(\mu q) = 1$. For $B(\mu q) = 0.5$, the limit becomes 362 GeV.

[57] ABAZOV 11V search for scalar leptoquarks using $e\nu jj$ events in $p\overline{p}$ collisions at $E_{cm} = 1.96$ TeV. The limit above assumes $B(eq) = 0.5$.

[58] CHATRCHYAN 11N search for scalar leptoquarks using $e\nu jj$ events in pp collisions at $E_{cm} = 7$ TeV. The limit above assumes $B(eq) = 0.5$.

[59] KHACHATRYAN 11D search for scalar leptoquarks using $eejj$ events in pp collisions at $E_{cm} = 7$ TeV. The limit above assumes $B(eq) = 1$.

[60] KHACHATRYAN 11E search for scalar leptoquarks using $\mu\mu jj$ events in pp collisions at $E_{cm} = 7$ TeV. The limit above assumes $B(\mu q) = 1$.

[61] ABAZOV 10L search for pair productions of scalar leptoquark state decaying to νb in $p\overline{p}$ collisions at $E_{cm} = 1.96$ TeV. The limit above assumes $B(\nu b) = 1$.

[62] ABAZOV 09 search for scalar leptoquarks using $\mu\mu jj$ and $\mu\nu jj$ events in $p\overline{p}$ collisions at $E_{cm} = 1.96$ TeV. The limit above assumes $B(\mu q) = 1$. For $B(\mu q) = 0.5$, the limit becomes 270 GeV.

[63] ABAZOV 09AF search for scalar leptoquarks using $eejj$ and $e\nu jj$ events in $p\overline{p}$ collisions at $E_{cm} = 1.96$ TeV. The limit above assumes $B(eq) = 1$. For $B(eq) = 0.5$ the bound becomes 284 GeV.

[64] AALTONEN 08P search for vector leptoquarks using $\tau^+\tau^- b\overline{b}$ events in $p\overline{p}$ collisions at $E_{cm} = 1.96$ TeV. Assuming Yang-Mills (minimal) couplings, the mass limit is >317 GeV (251 GeV) at 95% CL for $B(\tau b) = 1$.

[65] Search for pair production of scalar leptoquark state decaying to τb in $p\overline{p}$ collisions at $E_{cm}= 1.96$ TeV. The limit above assumes $B(\tau b) = 1$.

[66] Search for scalar leptoquarks using $\nu\nu jj$ events in $\overline{p}p$ collisions at $E_{cm} = 1.96$ TeV. The limit above assumes $B(\nu q) = 1$.

[67] ABAZOV 07J search for pair productions of scalar leptoquark state decaying to νb in $p\overline{p}$ collisions at $E_{cm} = 1.96$ TeV. The limit above assumes $B(\nu b) = 1$.

[68] ABAZOV 06A search for scalar leptoquarks using $\mu\mu jj$ events in $p\overline{p}$ collisions at E_{cm} = 1.8 TeV and 1.96 TeV. The limit above assumes $B(\mu q) = 1$. For $B(\mu q) = 0.5$, the limit becomes 204 GeV.

[69] ABAZOV 06L search for scalar leptoquarks using $\nu\nu jj$ events in $p\overline{p}$ collisions at $E_{cm} =$ 1.8 TeV and at 1.96 TeV. The limit above assumes $B(\nu q) = 1$.

[70] ABULENCIA 06T search for scalar leptoquarks using $\mu\mu jj$, $\mu\nu jj$, and $\nu\nu jj$ events in $p\overline{p}$ collisions at $E_{cm} = 1.96$ TeV. The quoted limit assumes $B(\mu q) = 1$. For $B(\mu q) =$ 0.5 or 0.1, the bound becomes 208 GeV or 143 GeV, respectively. See their Fig. 4 for the exclusion limit as a function of $B(\mu q)$.

[71] ABAZOV 05H search for scalar leptoquarks using $eejj$ and $e\nu jj$ events in $\overline{p}p$ collisions at $E_{cm} = 1.8$ TeV and 1.96 TeV. The limit above assumes $B(eq) = 1$. For $B(eq) =$ 0.5 the bound becomes 234 GeV.

[72] ACOSTA 05P search for scalar leptoquarks using $eejj$, $e\nu jj$ events in $\overline{p}p$ collisions at $E_{cm} = 1.96$TeV. The limit above assumes $B(eq) = 1$. For $B(eq) = 0.5$ and 0.1, the bound becomes 205 GeV and 145 GeV, respectively.

[73] ABBIENDI 03R search for scalar/vector leptoquarks in e^+e^- collisions at $\sqrt{s} = 189$–209 GeV. The quoted limits are for charge $-4/3$ isospin 0 scalar-leptoquark with $B(\ell q) = 1$. See their table 12 for other cases.

[74] ABAZOV 02 search for scalar leptoquarks using $\nu\nu jj$ events in $\overline{p}p$ collisions at E_{cm}=1.8 TeV. The bound holds for all leptoquark generations. Vector leptoquarks are likewise constrained to lie above 200 GeV.

[75] ABAZOV 01D search for scalar leptoquarks using $e\nu jj$, $eejj$, and $\nu\nu jj$ events in $p\overline{p}$ collisions at E_{cm}=1.8 TeV. The limit above assumes $B(eq)$=1. For $B(eq)$=0.5 and 0, the bound becomes 204 and 79 GeV, respectively. Bounds for vector leptoquarks are also given. Supersedes ABBOTT 98E.

[76] ABBIENDI 00M search for scalar/vector leptoquarks in e^+e^- collisions at $\sqrt{s}$=183 GeV. The quoted limits are for charge $-4/3$ isospin 0 scalar-leptoquarks with $B(\ell q)$=1. See their Table 8 and Figs. 6–9 for other cases.

[77] ABBOTT 00C search for scalar leptoquarks using $\mu\mu jj$, $\mu\nu jj$, and $\nu\nu jj$ events in $p\overline{p}$ collisions at E_{cm}=1.8 TeV. The limit above assumes $B(\mu q)$=1. For $B(\mu q)$=0.5 and 0, the bound becomes 180 and 79 GeV respectively. Bounds for vector leptoquarks are also given.

[78] AFFOLDER 00K search for scalar leptoquark using $\nu\nu cc$ events in $p\overline{p}$ collisions at E_{cm}=1.8 TeV. The quoted limit assumes $B(\nu c)$=1. Bounds for vector leptoquarks are also given.

[79] AFFOLDER 00K search for scalar leptoquark using $\nu\nu bb$ events in $p\overline{p}$ collisions at E_{cm}=1.8 TeV. The quoted limit assumes $B(\nu b)$=1. Bounds for vector leptoquarks are also given.

[80] ABBOTT 99J search for leptoquarks using $\mu\nu jj$ events in $p\overline{p}$ collisions at E_{cm}= 1.8TeV. The quoted limit is for a scalar leptoquark with $B(\mu q) = B(\nu q) = 0.5$. Limits on vector leptoquarks range from 240 to 290 GeV.

[81] ABBOTT 98E search for scalar leptoquarks using $e\nu jj$, $eejj$, and $\nu\nu jj$ events in $p\overline{p}$ collisions at E_{cm}=1.8 TeV. The limit above assumes $B(eq)$=1. For $B(eq)$=0.5 and 0, the bound becomes 204 and 79 GeV, respectively.

[82] ABBOTT 98J search for charge $-1/3$ third generation scalar and vector leptoquarks in $p\overline{p}$ collisions at E_{cm}= 1.8 TeV. The quoted limit is for scalar leptoquark with $B(\nu b)$=1.

[83] ABE 98S search for scalar leptoquarks using $\mu\mu jj$ events in $p\overline{p}$ collisions at E_{cm}= 1.8 TeV. The limit is for $B(\mu q)$= 1. For $B(\mu q)$=$B(\nu q)$=0.5, the limit is > 160 GeV.

[84] GROSS-PILCHER 98 is the combined limit of the CDF and DØ Collaborations as determined by a joint CDF/DØ working group and reported in this FNAL Technical Memo. Original data published in ABE 97X and ABBOTT 98E.

[85] ABE 97F search for third generation scalar and vector leptoquarks in $p\overline{p}$ collisions at $E_{cm} = 1.8$ TeV. The quoted limit is for scalar leptoquark with $B(\tau b) = 1$.

[86] ABE 97X search for scalar leptoquarks using $eejj$ events in $p\overline{p}$ collisions at E_{cm}=1.8 TeV. The limit is for $B(eq)$=1.

[87] Limit is for charge $-1/3$ isospin-0 leptoquark with $B(\ell q) = 2/3$.

[88] First and second generation leptoquarks are assumed to be degenerate. The limit is slightly lower for each generation.

[89] Limits are for charge $-1/3$, isospin-0 scalar leptoquarks decaying to $\ell^- q$ or νq with any branching ratio. See paper for limits for other charge-isospin assignments of leptoquarks.

[90] KIM 90 assume pair production of charge 2/3 scalar-leptoquark via photon exchange. The decay of the first (second) generation leptoquark is assumed to be any mixture of de^+ and $u\overline{\nu}$ ($s\mu^+$ and $c\overline{\nu}$). See paper for limits for specific branching ratios.

[91] BARTEL 87B limit is valid when a pair of charge 2/3 spinless leptoquarks X is produced with point coupling, and when they decay under the constraint $B(X \rightarrow c\overline{\nu}_\mu) + B(X \rightarrow s\mu^+) = 1$.

[92] BEHREND 86B assumed that a charge 2/3 spinless leptoquark, χ, decays either into $s\mu^+$ or $c\overline{\nu}$: $B(\chi \rightarrow s\mu^+) + B(\chi \rightarrow c\overline{\nu}) = 1$.

MASS LIMITS for Leptoquarks from Single Production

These limits depend on the q-ℓ-leptoquark coupling g_{LQ}. It is often assumed that $g^2_{LQ}/4\pi$=1/137. Limits shown are for a scalar, weak isoscalar, charge $-1/3$ leptoquark.

VALUE (GeV)	CL%	DOCUMENT ID		TECN	COMMENT
> 550	95	[1] SIRUNYAN	21J	CMS	Third generation
none 150–740	95	[2] SIRUNYAN	18BJ	CMS	Third generation
>1755	95	[3] KHACHATRY...	16AG	CMS	First generation
> 660	95	[4] KHACHATRY...	16AG	CMS	Second generation
> 304	95	[5] ABRAMOWICZ	12A	ZEUS	First generation
> 73	95	[6] ABREU	93J	DLPH	Second generation
• • • We do not use the following data for averages, fits, limits, etc. • • •					
		[7] TUMASYAN	21D	CMS	First generation
		[8] DEY	16	ICCB	$\nu q \rightarrow$ LQ $\rightarrow \nu q$
		[9] AARON	11A	H1	Lepton-flavor violation
> 300	95	[10] AARON	11B	H1	First generation
		[11] ABAZOV	07E	D0	Second generation
> 295	95	[12] AKTAS	05B	H1	First generation
		[13] CHEKANOV	05A	ZEUS	Lepton-flavor violation
> 298	95	[14] CHEKANOV	03B	ZEUS	First generation
> 197	95	[15] ABBIENDI	02B	OPAL	First generation
		[16] CHEKANOV	02	ZEUS	Repl. by CHEKANOV 05A
> 290	95	[17] ADLOFF	01C	H1	First generation
> 204	95	[18] BREITWEG	01	ZEUS	First generation
		[19] BREITWEG	00E	ZEUS	First generation
> 161	95	[20] ABREU	99G	DLPH	First generation
> 200	95	[21] ADLOFF	99	H1	First generation

Downloaded from https://academic.oup.com/ptep/article/2022/8/083C01/6651666 by KIT Library user on 27 September 2022

		[22] DERRICK	97	ZEUS	Lepton-flavor violation
> 168	95	[23] DERRICK	93	ZEUS	First generation

[1] SIRUNYAN 21J search for single production of charge $-1/3$ scalar leptoquarks decaying to $t\tau^-$ and $b\nu$, and charge 2/3 vector leptoquarks decaying to $t\nu$ and $b\tau^+$ in pp collisions at $\sqrt{s}$ = 13 TeV. The limit quoted above assumes a scalar leptoquark with B($t\tau$) = B($b\nu$) = 0.5 and the leptoquark coupling strength λ = 1.5. The limit becomes M_{LQ} > 750 GeV for λ = 2.5.

[2] SIRUNYAN 18BJ search for single production of charge 2/3 scalar leptoquarks decaying to τb in pp collisions at $\sqrt{s}$ = 13 TeV. The limit above assumes B(τb) =1 and the leptoquark coupling strength λ = 1.

[3] KHACHATRYAN 16AG search for single production of charge $\pm1/3$ scalar leptoquarks using eej events in pp collisions at $\sqrt{s}$ = 8 TeV. The limit above assumes B(eq) = 1 and the leptoquark coupling strength λ = 1.

[4] KHACHATRYAN 16AG search for single production of charge $\pm1/3$ scalar leptoquarks using $\mu\mu j$ events in pp collisions at $\sqrt{s}$ = 8 TeV. The limit above assumes B(μq) = 1 and the leptoquark coupling strength λ = 1.

[5] ABRAMOWICZ 12A limit is for a scalar, weak isoscalar, charge $-1/3$ leptoquark coupled with e_R. See their Figs. 12–17 and Table 4 for states with different quantum numbers.

[6] Limit from single production in Z decay. The limit is for a leptoquark coupling of electromagnetic strength and assumes B(ℓq) = 2/3. The limit is 77 GeV if first and second leptoquarks are degenerate.

[7] TUMASYAN 21D search for energetic jets + $\not{E}_T$ events in pp collisions at $\sqrt{s}$ = 13 TeV. The branching fraction for the decay of the leptoquark into an electron neutrino and up quark is assumed to be 100% (β = 0). See their Fig. 12 for exclusion limits in mass-coupling plane.

[8] DEY 16 use the 2010-2012 IceCube PeV energy data set to constrain the leptoquark production cross section through the $\nu q \rightarrow$ LQ $\rightarrow \nu q$ process. See their Figure 4 for the exclusion limit in the mass-coupling plane.

[9] AARON 11A search for various leptoquarks with lepton-flavor violating couplings. See their Figs. 2–3 and Tables 1–4 for detailed limits.

[10] The quoted limit is for a scalar, weak isoscalar, charge $-1/3$ leptoquark coupled with e_R. See their Figs. 3–5 for limits on states with different quantum numbers.

[11] ABAZOV 07E search for leptoquark single production through qg fusion process in $p\overline{p}$ collisions. See their Fig. 4 for exclusion plot in mass-coupling plane.

[12] AKTAS 05B limit is for a scalar, weak isoscalar, charge $-1/3$ leptoquark coupled with e_R. See their Fig. 3 for limits on states with different quantum numbers.

[13] CHEKANOV 05 search for various leptoquarks with lepton-flavor violating couplings. See their Figs.6–10 and Tables 1–8 for detailed limits.

[14] CHEKANOV 03B limit is for a scalar, weak isoscalar, charge $-1/3$ leptoquark coupled with e_R. See their Figs. 11–12 and Table 5 for limits on states with different quantum numbers.

[15] For limits on states with different quantum numbers and the limits in the mass-coupling plane, see their Fig. 4 and Fig. 5.

[16] CHEKANOV 02 search for various leptoquarks with lepton-flavor violating couplings. See their Figs. 6–7 and Tables 5–6 for detailed limits.

[17] For limits on states with different quantum numbers and the limits in the mass-coupling plane, see their Fig. 3.

[18] See their Fig. 14 for limits in the mass-coupling plane.

[19] BREITWEG 00E search for F=0 leptoquarks in e^+p collisions. For limits in mass-coupling plane, see their Fig. 11.

[20] ABREU 99G limit obtained from process $e\gamma \rightarrow LQ{+}q$. For limits on vector and scalar states with different quantum numbers and the limits in the coupling-mass plane, see their Fig. 4 and Table 2.

[21] For limits on states with different quantum numbers and the limits in the mass-coupling plane, see their Fig. 13 and Fig. 14. ADLOFF 99 also search for leptoquarks with lepton-flavor violating couplings. ADLOFF 99 supersedes AID 96B.

[22] DERRICK 97 search for various leptoquarks with lepton-flavor violating couplings. See their Figs. 5–8 and Table 1 for detailed limits.

[23] DERRICK 93 search for single leptoquark production in ep collisions with the decay eq and νq. The limit is for leptoquark coupling of electromagnetic strength and assumes B(eq) = B(νq) = 1/2. The limit for B(eq) = 1 is 176 GeV. For limits on states with different quantum numbers, see their Table 3.

Indirect Limits for Leptoquarks

VALUE (TeV)	CL%	DOCUMENT ID		TECN	COMMENT
• • • We do not use the following data for averages, fits, limits, etc. • • •					
		[1] CRIVELLIN	21A	RVUE	First generation
		[2] AEBISCHER	20	RVUE	B decays
		[3] DEPPISCH	20	RVUE	$K \rightarrow \pi\nu\nu$
> 3.1	95	[4] ABRAMOWICZ	19	ZEUS	First generation
		[5] MANDAL	19	RVUE	τ, μ, e, K
		[6] ZHANG	18A	RVUE	D decays
		[7] BARRANCO	16	RVUE	D decays
		[8] KUMAR	16	RVUE	neutral K mixing, rare K decays
		[9] BESSAA	15	RVUE	$q\overline{q} \rightarrow e^+e^-$
> 14	95	[10] SAHOO	15A	RVUE	$B_{s,d} \rightarrow \mu^+\mu^-$
		[11] SAKAKI	13	RVUE	$B \rightarrow D^{(*)}\tau\overline{\nu}$, $B \rightarrow X_s\nu\overline{\nu}$
		[12] KOSNIK	12	RVUE	$b \rightarrow s\ell^+\ell^-$
> 2.5	95	[13] AARON	11C	H1	First generation
		[14] DORSNER	11	RVUE	scalar, weak singlet, charge 4/3
		[15] AKTAS	07A	H1	Lepton-flavor violation
> 0.49	95	[16] SCHAEL	07A	ALEP	$e^+e^- \rightarrow q\overline{q}$
		[17] SMIRNOV	07	RVUE	$K \rightarrow e\mu$, $B \rightarrow e\tau$
		[18] CHEKANOV	05A	ZEUS	Lepton-flavor violation
> 1.7	96	[19] ADLOFF	03	H1	First generation
> 46	90	[20] CHANG	03	BELL	Pati-Salam type
		[21] CHEKANOV	02	ZEUS	Repl. by CHEKANOV 05A
> 1.7	95	[22] CHEUNG	01B	RVUE	First generation
> 0.39	95	[23] ACCIARRI	00P	L3	$e^+e^- \rightarrow qq$
> 1.5	95	[24] ADLOFF	00	H1	First generation
> 0.2	95	[25] BARATE	00I	ALEP	Repl. by SCHAEL 07A
		[26] BARGER	00	RVUE	Cs
		[27] GABRIELLI	00	RVUE	Lepton flavor violation
> 0.74	95	[28] ZARNECKI	00	RVUE	S_1 leptoquark
		[29] ABBIENDI	99	OPAL	
> 19.3	95	[30] ABE	98V	CDF	$B_s \rightarrow e^\pm\mu^\mp$, Pati-Salam type
		[31] ACCIARRI	98J	L3	$e^+e^- \rightarrow q\overline{q}$
		[32] ACKERSTAFF	98V	OPAL	$e^+e^- \rightarrow q\overline{q}$, $e^+e^- \rightarrow b\overline{b}$
> 0.76	95	[33] DEANDREA	97	RVUE	$\tilde{R}_2$ leptoquark
		[34] DERRICK	97	ZEUS	Lepton-flavor violation
		[35] GROSSMAN	97	RVUE	$B \rightarrow \tau^+\tau^-$(X)
		[36] JADACH	97	RVUE	$e^+e^- \rightarrow q\overline{q}$
>1200		[37] KUZNETSOV	95B	RVUE	Pati-Salam type
		[38] MIZUKOSHI	95	RVUE	Third generation scalar leptoquark
> 0.3	95	[39] BHATTACH...	94	RVUE	Spin-0 leptoquark coupled to $\overline{e}_R\, t_L$
		[40] DAVIDSON	94	RVUE	
> 18		[41] KUZNETSOV	94	RVUE	Pati-Salam type
> 0.43	95	[42] LEURER	94	RVUE	First generation spin-1 leptoquark
> 0.44	95	[42] LEURER	94B	RVUE	First generation spin-0 leptoquark
		[43] MAHANTA	94	RVUE	P and T violation
> 1		[44] SHANKER	82	RVUE	Nonchiral spin-0 leptoquark
> 125		[44] SHANKER	82	RVUE	Nonchiral spin-1 leptoquark

[1] CRIVELLIN 21A set limits on coupling strengths of scalar and vector leptoquarks using $K \rightarrow \pi\nu\nu$, $K \rightarrow \pi e^+e^-$, $K^0 - \overline{K}^0$ and $D^0 - \overline{D}^0$ mixings, and weak neutral current measurements. See their Fig. 2 and Fig. 3 for the limits in mass-coupling plane.

[2] AEBISCHER 20 explain the B decay anomalies using four-fermion operator Wilson coefficents. See their Table 1. These Wilson coefficients may be generated by a U_1 vector leptoquark with U_1 transforming as $(3,1)_{2/3}$ under the SM gauge group. See their Figures 6, 7, 8 for the regions of the LQ parameter space which explains the B anomalies and avoids the indirect low energy constraints.

[3] DEPPISCH 20 limits on the lepton-number-violating higher-dimensional-operators are derived from $K \rightarrow \pi\nu\nu$ in the standard model effective field theory. These higher-dimensional-operators may be induced from leptoquark-exchange diagrams.

[4] ABRAMOWICZ 19 obtain a limit on λ/M_{LQ} > 1.16 TeV^{-1} for weak isotriplet spin-0 leptoquark S_1^L. We obtain the limit quoted above by converting the limit on λ/M_{LQ} for S_1^L assuming $\lambda = \sqrt{4\pi}$. See their Table 5 for the limits of leptoquarks with different quantum numbers. These limits are derived from bounds of eq contact interactions.

[5] MANDAL 19 give bounds on leptoquarks from τ-decays, leptonic dipole moments, lepton-flavor-violating processes, and K decays.

[6] ZHANG 18A give bounds on leptoquark induced four-fermion interactions from $D \rightarrow K\ell\nu$. The authors inform us that the shape parameter of the vector form factor in both the abstract and the conclusions of ZHANG 18A should be r_{+1} = 2.16 ± 0.07 rather than ±0.007. The numbers listed in their Table 7 are correct.

[7] BARRANCO 16 give bounds on leptoquark induced four-fermion interactions from $D \rightarrow K\ell\nu$ and $D_s \rightarrow \ell\nu$.

[8] KUMAR 16 gives bound on SU(2) singlet scalar leptoquark with chrge $-1/3$ from $K^0 - \overline{K}^0$ mixing, $K \rightarrow \pi\nu\overline{\nu}$, $K_L^0 \rightarrow \mu^+\mu^-$, and $K_L^0 \rightarrow \mu^\pm e^\mp$ decays.

[9] BESSAA 15 obtain limit on leptoquark induced four-fermion interactions from the ATLAS and CMS limit on the $\overline{q}q\overline{e}e$ contact interactions.

[10] SAHOO 15A obtain limit on leptoquark induced four-fermion interactions from $B_{s,d} \rightarrow \mu^+\mu^-$ for $\lambda \simeq O(1)$.

[11] SAKAKI 13 explain the $B \rightarrow D^{(*)}\tau\overline{\nu}$ anomaly using Wilson coefficients of leptoquark-induced four-fermion operators.

[12] KOSNIK 12 obtains limits on leptoquark induced four-fermion interactions from $b \rightarrow s\ell^+\ell^-$ decays.

[13] AARON 11C limit is for weak isotriplet spin-0 leptoquark at strong coupling $\lambda = \sqrt{4\pi}$. For the limits of leptoquarks with different quantum numbers, see their Table 3. Limits are derived from bounds of eq contact intereactions.

[14] DORSNER 11 give bounds on scalar, weak singlet, charge 4/3 leptoquark from K, B, τ decays, meson mixings, LFV, $g-2$ and $Z \rightarrow b\overline{b}$.

[15] AKTAS 07A search for lepton-flavor violation in ep collision. See their Tables 4–7 for limits on lepton-flavor violating four-fermion interactions induced by various leptoquarks.

[16] SCHAEL 07A limit is for the weak-isoscalar spin-0 left-handed leptoquark with the coupling of electromagnetic strength. For the limits of leptoquarks with different quantum numbers, see their Table 35.

[17] SMIRNOV 07 obtains mass limits for the vector and scalar chiral leptoquark states from $K \rightarrow e\mu$, $B \rightarrow e\tau$ decays.

[18] CHEKANOV 05 search for various leptoquarks with lepton-flavor violating couplings. See their Figs.6–10 and Tables 1–8 for detailed limits.

[19] ADLOFF 03 limit is for the weak isotriplet spin-0 leptoquark at strong coupling $\lambda = \sqrt{4\pi}$. For the limits of leptoquarks with different quantum numbers, see their Table 3. Limits are derived from bounds on $e^\pm q$ contact interactions.

[20] The bound is derived from B($B^0 \rightarrow e^\pm\mu^\mp$) < 1.7×10^{-7}.

[21] CHEKANOV 02 search for lepton-flavor violation in ep collisions. See their Tables 1–4 for limits on lepton-flavor violating and four-fermion interactions induced by various leptoquarks.

[22] CHEUNG 01B quoted limit is for a scalar, weak isoscalar, charge $-1/3$ leptoquark with a coupling of electromagnetic strength. The limit is derived from bounds on contact interactions in a global electroweak analysis. For the limits of leptoquarks with different quantum numbers, see Table 5.

[23] ACCIARRI 00P limit is for the weak isoscalar spin-0 leptoquark with the coupling of electromagnetic strength. For the limits of leptoquarks with different quantum numbers, see their Table 4.

[24] ADLOFF 00 limit is for the weak isotriplet spin-0 leptoquark at strong coupling, $\lambda = \sqrt{4\pi}$. For the limits of leptoquarks with different quantum numbers, see their Table 2. ADLOFF 00 limits are from the Q^2 spectrum measurement of $e^+p \rightarrow e^+$X.

[25] BARATE 00I search for deviations in cross section and jet-charge asymmetry in $e^+e^- \rightarrow \overline{q}q$ due to t-channel exchange of a leptoquark at $\sqrt{s}$=130 to 183 GeV. Limits for other scalar and vector leptoquarks are also given in their Table 22.

Downloaded from https://academic.oup.com/ptep/article/2022/8/083C01/6651666 by KIT Library user on 27 September 2022

[26] BARGER 00 explain the deviation of atomic parity violation in cesium atoms from prediction is explained by scalar leptoquark exchange.

[27] GABRIELLI 00 calculate various process with lepton flavor violation in leptoquark models.

[28] ZARNECKI 00 limit is derived from data of HERA, LEP, and Tevatron and from various low-energy data including atomic parity violation. Leptoquark coupling with electromagnetic strength is assumed.

[29] ABBIENDI 99 limits are from $e^+e^- \rightarrow q\overline{q}$ cross section at 130–136, 161–172, 183 GeV. See their Fig. 8 and Fig. 9 for limits in mass-coupling plane.

[30] ABE 98V quoted limit is from $B(B_s \rightarrow e^{\pm}\mu^{\mp}) < 8.2 \times 10^{-6}$. ABE 98V also obtain a similar limit on $M_{LQ} > 20.4$ TeV from $B(B_d \rightarrow e^{\pm}\mu^{\mp}) < 4.5 \times 10^{-6}$. Both bounds assume the non-canonical association of the b quark with electrons or muons under SU(4).

[31] ACCIARRI 98J limit is from $e^+e^- \rightarrow q\overline{q}$ cross section at $\sqrt{s}$= 130–172 GeV which can be affected by the t- and u-channel exchanges of leptoquarks. See their Fig. 4 and Fig. 5 for limits in the mass-coupling plane.

[32] ACKERSTAFF 98V limits are from $e^+e^- \rightarrow q\overline{q}$ and $e^+e^- \rightarrow b\overline{b}$ cross sections at $\sqrt{s}$ = 130–172 GeV, which can be affected by the t- and u-channel exchanges of leptoquarks. See their Fig. 21 and Fig. 22 for limits of leptoquarks in mass-coupling plane.

[33] DEANDREA 97 limit is for $\widetilde{R}_2$ leptoquark obtained from atomic parity violation (APV). The coupling of leptoquark is assumed to be electromagnetic strength. See Table 2 for limits of the four-fermion interactions induced by various scalar leptoquark exchange. DEANDREA 97 combines APV limit and limits from Tevatron and HERA. See Fig. 1–4 for combined limits of leptoquark in mass-coupling plane.

[34] DERRICK 97 search for lepton-flavor violation in ep collision. See their Tables 2–5 for limits on lepton-flavor violating four-fermion interactions induced by various leptoquarks.

[35] GROSSMAN 97 estimate the upper bounds on the branching fraction $B \rightarrow \tau^+\tau^-(X)$ from the absence of the B decay with large missing energy. These bounds can be used to constrain leptoquark induced four-fermion interactions.

[36] JADACH 97 limit is from $e^+e^- \rightarrow q\overline{q}$ cross section at $\sqrt{s}$=172.3 GeV which can be affected by the t- and u-channel exchanges of leptoquarks. See their Fig. 1 for limits on vector leptoquarks in mass-coupling plane.

[37] KUZNETSOV 95B use π, K, B, τ decays and μe conversion and give a list of bounds on the leptoquark mass and the fermion mixing matrix in the Pati-Salam model. The quoted limit is from $K_L \rightarrow \mu e$ decay assuming zero mixing.

[38] MIZUKOSHI 95 calculate the one-loop radiative correction to the Z-physics parameters in various scalar leptoquark models. See their Fig. 4 for the exclusion plot of third generation leptoquark models in mass-coupling plane.

[39] BHATTACHARYYA 94 limit is from one-loop radiative correction to the leptonic decay width of the Z. m_H=250 GeV, $\alpha_s(m_Z)$=0.12, m_t=180 GeV, and the electroweak strength of leptoquark coupling are assumed. For leptoquark coupled to $\overline{e}_L\, t_R$, $\overline{\mu}t$, and $\overline{\tau}t$, see Fig. 2 in BHATTACHARYYA 94B erratum and Fig. 3.

[40] DAVIDSON 94 gives an extensive list of the bounds on leptoquark-induced four-fermion interactions from π, K, D, B, μ, τ decays and meson mixings, *etc.* See Table 15 of DAVIDSON 94 for detail.

[41] KUZNETSOV 94 gives mixing independent bound of the Pati-Salam leptoquark from the cosmological limit on $\pi^0 \rightarrow \overline{\nu}\nu$.

[42] LEURER 94, LEURER 94B limits are obtained from atomic parity violation and apply to any chiral leptoquark which couples to the first generation with electromagnetic strength. For a nonchiral leptoquark, universality in $\pi_{\ell 2}$ decay provides a much more stringent bound.

[43] MAHANTA 94 gives bounds of P- and T-violating scalar-leptoquark couplings from atomic and molecular experiments.

[44] From $(\pi \rightarrow e\nu)/(\pi \rightarrow \mu\nu)$ ratio. SHANKER 82 assumes the leptoquark induced four-fermion coupling $4g^2/M^2\ (\overline{\nu}_{eL}\ u_R)\ (\overline{d}_L\, e_R)$with g=0.004 for spin-0 leptoquark and $g^2/M^2\ (\overline{\nu}_{eL}\ \gamma_\mu u_L)\ (\overline{d}_R\ \gamma^\mu e_R)$ with $g \simeq$ 0.6 for spin-1 leptoquark.

MASS LIMITS for Diquarks

VALUE (GeV)	CL%	DOCUMENT ID		TECN	COMMENT
>7200 (CL = 95%) OUR LIMIT					
none 600–7200	95	[1] SIRUNYAN	18BO	CMS	E_6 diquark
none 600–6900	95	[2] KHACHATRY...	17W	CMS	E_6 diquark
none 1500–6000	95	[3] KHACHATRY...	16K	CMS	E_6 diquark
none 500–1600	95	[4] KHACHATRY...	16L	CMS	E_6 diquark
none 1200–4700	95	[5] KHACHATRY...	15V	CMS	E_6 diquark
• • • We do not use the following data for averages, fits, limits, etc. • • •					
>3750	95	[6] CHATRCHYAN	13A	CMS	E_6 diquark
none 1000–4280	95	[7] CHATRCHYAN	13AS	CMS	Superseded by KHACHATRYAN 15V
>3520	95	[8] CHATRCHYAN	11Y	CMS	Superseded by CHATRCHYAN 13A
none 970–1080, 1450–1600	95	[9] KHACHATRY...	10	CMS	Superseded by CHATRCHYAN 13A
none 290–630	95	[10] AALTONEN	09AC	CDF	E_6 diquark
none 290–420	95	[11] ABE	97G	CDF	E_6 diquark
none 15–31.7	95	[12] ABREU	94O	DLPH	SUSY E_6 diquark

[1] SIRUNYAN 18BO search for resonances decaying to dijets in pp collisions at $\sqrt{s}$ = 13 TeV.

[2] KHACHATRYAN 17W search for resonances decaying to dijets in pp collisions at $\sqrt{s}$ = 13 TeV.

[3] KHACHATRYAN 16K search for resonances decaying to dijets in pp collisions at $\sqrt{s}$ = 13 TeV.

[4] KHACHATRYAN 16L search for resonances decaying to dijets in pp collisions at $\sqrt{s}$ = 8 TeV with the data scouting technique, increasing the sensitivity to the low mass resonances.

[5] KHACHATRYAN 15V search for resonances decaying to dijets in pp collisions at $\sqrt{s}$ = 8 TeV.

[6] CHATRCHYAN 13A search for new resonance decaying to dijets in pp collisions at $\sqrt{s}$ = 7 TeV.

[7] CHATRCHYAN 13AS search for new resonance decaying to dijets in pp collisions at $\sqrt{s}$ = 8 TeV.

[8] CHATRCHYAN 11Y search for new resonance decaying to dijets in pp collisions at $\sqrt{s}$ = 7 TeV.

[9] KHACHATRYAN 10 search for new resonance decaying to dijets in pp collisions at $\sqrt{s}$ = 7 TeV.

[10] AALTONEN 09AC search for new narrow resonance decaying to dijets.

[11] ABE 97G search for new particle decaying to dijets.

[12] ABREU 94O limit is from $e^+e^- \rightarrow \overline{c}sc\,s$. Range extends up to 43 GeV if diquarks are degenerate in mass.

MASS LIMITS for g_A (axigluon) and Other Color-Octet Gauge Bosons

Axigluons are massive color-octet gauge bosons in chiral color models and have axial-vector coupling to quarks with the same coupling strength as gluons.

VALUE (GeV)	CL%	DOCUMENT ID		TECN	COMMENT
>6600 (CL = 95%) OUR LIMIT					
none 1800–6600	95	[1] SIRUNYAN	20AI	CMS	$pp \rightarrow g_A X$, $g_A \rightarrow 2j$
none 600–6100	95	[2] SIRUNYAN	18BO	CMS	$pp \rightarrow g_A X$, $g_A \rightarrow 2j$
none 600–5500	95	[3] KHACHATRY...	17W	CMS	$pp \rightarrow g_A X$, $g_A \rightarrow 2j$
none 1500–5100	95	[4] KHACHATRY...	16K	CMS	$pp \rightarrow g_A X$, $g_A \rightarrow 2j$
none 500–1600	95	[5] KHACHATRY...	16L	CMS	$pp \rightarrow g_A X$, $g_A \rightarrow 2j$
none 1300–3600	95	[6] KHACHATRY...	15V	CMS	$pp \rightarrow g_A X$, $g_A \rightarrow 2j$
• • • We do not use the following data for averages, fits, limits, etc. • • •					
		[7] KHACHATRY...	17Y	CMS	$pp \rightarrow g_A g_A \rightarrow 8j$
		[8] AAD	16W	ATLS	$pp \rightarrow g_A X$, $g_A \rightarrow b\overline{b}b\overline{b}$
>2800	95	[9] KHACHATRY...	16E	CMS	$pp \rightarrow g_{KK} X$, $g_{KK} \rightarrow t\overline{t}$
		[10] KHACHATRY...	15AV	CMS	$pp \rightarrow \Theta^0\Theta^0 \rightarrow b\overline{b}Zg$
		[11] AALTONEN	13R	CDF	$p\overline{p} \rightarrow g_A X$, $g_A \rightarrow \sigma\sigma$, $\sigma \rightarrow 2j$
>3360	95	[12] CHATRCHYAN	13A	CMS	$pp \rightarrow g_A X$, $g_A \rightarrow 2j$
none 1000–3270	95	[13] CHATRCHYAN	13AS	CMS	Superseded by KHACHATRYAN 15V
none 250–740	95	[14] CHATRCHYAN	13AU	CMS	$pp \rightarrow 2g_A X$,$g_A \rightarrow 2j$
> 775	95	[15] ABAZOV	12R	D0	$p\overline{p} \rightarrow g_A X$, $g_A \rightarrow t\overline{t}$
>2470	95	[16] CHATRCHYAN	11Y	CMS	Superseded by CHATRCHYAN 13A
		[17] AALTONEN	10L	CDF	$p\overline{p} \rightarrow g_A X$, $g_A \rightarrow t\overline{t}$
none 1470–1520	95	[18] KHACHATRY...	10	CMS	Superseded by CHATRCHYAN 13A
none 260–1250	95	[19] AALTONEN	09AC	CDF	$p\overline{p} \rightarrow g_A X$, $g_A \rightarrow 2j$
> 910	95	[20] CHOUDHURY	07	RVUE	$p\overline{p} \rightarrow t\overline{t}X$
> 365	95	[21] DONCHESKI	98	RVUE	$\Gamma(Z \rightarrow$ hadron)
none 200–980	95	[22] ABE	97G	CDF	$p\overline{p} \rightarrow g_A X$, $g_A \rightarrow 2j$
none 200–870	95	[23] ABE	95N	CDF	$p\overline{p} \rightarrow g_A X$, $g_A \rightarrow q\overline{q}$
none 240–640	95	[24] ABE	93G	CDF	$p\overline{p} \rightarrow g_A X$, $g_A \rightarrow 2j$
> 50	95	[25] CUYPERS	91	RVUE	$\sigma(e^+e^- \rightarrow$ hadrons)
none 120–210	95	[26] ABE	90H	CDF	$p\overline{p} \rightarrow g_A X$, $g_A \rightarrow 2j$
> 29		[27] ROBINETT	89	THEO	Partial-wave unitarity
none 150–310	95	[28] ALBAJAR	88B	UA1	$p\overline{p} \rightarrow g_A X$, $g_A \rightarrow 2j$
> 20		BERGSTROM	88	RVUE	$p\overline{p} \rightarrow \Upsilon X$ via $g_A g$
> 9		[29] CUYPERS	88	RVUE	Υ decay
> 25		[30] DONCHESKI	88B	RVUE	Υ decay

[1] SIRUNYAN 20AI search for resonances decaying into dijets in pp collisions at $\sqrt{s}$ = 13 TeV.

[2] SIRUNYAN 18BO search for resonances decaying to dijets in pp collisions at $\sqrt{s}$ = 13 TeV.

[3] KHACHATRYAN 17W search for resonances decaying to dijets in pp collisions at $\sqrt{s}$ = 13 TeV.

[4] KHACHATRYAN 16K search for resonances decaying to dijets in pp collisions at $\sqrt{s}$ = 13 TeV.

[5] KHACHATRYAN 16L search for resonances decaying to dijets in pp collisions at $\sqrt{s}$ = 8 TeV with the data scouting technique, increasing the sensitivity to the low mass resonances.

[6] KHACHATRYAN 15V search for resonances decaying to dijets in pp collisions at $\sqrt{s}$ = 8 TeV.

[7] KHACHATRYAN 17Y search for pair production of color-octet gauge boson g_A each decaying to $4j$ in pp collisions at $\sqrt{s}$ = 8 TeV.

[8] AAD 16W search for a new resonance decaying to a pair of b and B_H in pp collisions at $\sqrt{s}$ = 8 TeV. The vector-like quark B_H is assumed to decay to bH. See their Fig. 3 and Fig. 4 for limits on $\sigma \cdot B$.

[9] KHACHATRYAN 16E search for KK gluon decaying to $t\overline{t}$ in pp collisions at $\sqrt{s}$ = 8 TeV.

[10] KHACHATRYAN 15AV search for pair productions of neutral color-octet weak-triplet scalar particles (Θ^0), decaying to $b\overline{b}$, Zg or γg, in pp collisions at $\sqrt{s}$ = 8 TeV. The Θ^0 particle is often predicted in coloron (G', color-octet gauge boson) models and appear in the pp collisions through $G' \rightarrow \Theta^0\Theta^0$ decays. Assuming $B(\Theta^0 \rightarrow b\overline{b})$ = 0.5, they give limits $m_{\Theta^0} > 623$ GeV (426 GeV) for $m_{G'} = 2.3\ m_{\Theta^0}$ ($m_{G'} = 5\ m_{\Theta^0}$).

[11] AALTONEN 13R search for new resonance decaying to $\sigma\sigma$, with hypothetical strongly interacting σ particle subsequently decaying to 2 jets, in $p\overline{p}$ collisions at $\sqrt{s}$ = 1.96 TeV, using data corresponding to an integrated luminosity of 6.6 fb^{-1}. For 50 GeV $< m_\sigma < m_{g_A}/2$, axigluons in mass range 150–400 GeV are excluded.

[12] CHATRCHYAN 13A search for new resonance decaying to dijets in pp collisions at $\sqrt{s}$ = 7 TeV.

[13] CHATRCHYAN 13AS search for new resonance decaying to dijets in pp collisions at $\sqrt{s}$ = 8 TeV.

[14] CHATRCHYAN 13AU search for the pair produced color-octet vector bosons decaying to $q\overline{q}$ pairs in pp collisions. The quoted limit is for $B(g_A \rightarrow q\overline{q}) = 1$.

[15] ABAZOV 12R search for massive color octet vector particle decaying to $t\overline{t}$. The quoted limit assumes g_A couplings with light quarks are suppressed by 0.2.

[16] CHATRCHYAN 11Y search for new resonance decaying to dijets in pp collisions at $\sqrt{s}$ = 7 TeV.

Downloaded from https://academic.oup.com/ptep/article/2022/8/083C01/6651666 by KIT Library user on 27 September 2022

[17] AALTONEN 10L search for massive color octet non-chiral vector particle decaying into $t\overline{t}$ pair with mass in the range 400 GeV < M < 800 GeV. See their Fig. 6 for limit in the mass-coupling plane.
[18] KHACHATRYAN 10 search for new resonance decaying to dijets in pp collisions at $\sqrt{s} = 7$ TeV.
[19] AALTONEN 09AC search for new narrow resonance decaying to dijets.
[20] CHOUDHURY 07 limit is from the $t\overline{t}$ production cross section measured at CDF.
[21] DONCHESKI 98 compare α_s derived from low-energy data and that from $\Gamma(Z \to$ hadrons$)/\Gamma(Z \to$ leptons$)$.
[22] ABE 97G search for new particle decaying to dijets.
[23] ABE 95N assume axigluons decaying to quarks in the Standard Model only.
[24] ABE 93G assume $\Gamma(g_A) = N\alpha_s m_{g_A}/6$ with $N = 10$.
[25] CUYPERS 91 compare α_s measured in Υ decay and that from R at PEP/PETRA energies.
[26] ABE 90H assumes $\Gamma(g_A) = N\alpha_s m_{g_A}/6$ with $N = 5$ ($\Gamma(g_A) = 0.09 m_{g_A}$). For $N = 10$, the excluded region is reduced to 120–150 GeV.
[27] ROBINETT 89 result demands partial-wave unitarity of $J = 0$ $t\overline{t} \to t\overline{t}$ scattering amplitude and derives a limit $m_{g_A} > 0.5\, m_t$. Assumes $m_t > 56$ GeV.
[28] ALBAJAR 88B result is from the nonobservation of a peak in two-jet invariant mass distribution. $\Gamma(g_A) < 0.4\, m_{g_A}$ assumed. See also BAGGER 88.
[29] CUYPERS 88 requires $\Gamma(\Upsilon \to gg_A) < \Gamma(\Upsilon \to ggg)$. A similar result is obtained by DONCHESKI 88.
[30] DONCHESKI 88B requires $\Gamma(\Upsilon \to gq\overline{q})/\Gamma(\Upsilon \to ggg) < 0.25$, where the former decay proceeds via axigluon exchange. A more conservative estimate of < 0.5 leads to $m_{g_A} > 21$ GeV.

MASS LIMITS for Color-Octet Scalar Bosons

VALUE (GeV)	CL%	DOCUMENT ID		TECN	COMMENT
• • • We do not use the following data for averages, fits, limits, etc. • • •					
none 1800–3700	95	[1] SIRUNYAN	20AI	CMS	$pp \to S_8 X,\ S_8 \to gg$
none 600–3400	95	[2] SIRUNYAN	18BO	CMS	$pp \to S_8 X,\ S_8 \to gg$
		[3] KHACHATRY...	15AV	CMS	$pp \to \Theta^0 \Theta^0 \to b\overline{b}Zg$
none 150–287	95	[4] AAD	13K	ATLS	$pp \to S_8 S_8 X, S_8 \to$ 2 jets

[1] SIRUNYAN 20AI search for resonances decaying into dijets in pp collisions at $\sqrt{s} = 13$ TeV. The limit above assumes S_{8gg} coupling $k_s^2 = 1/2$.
[2] SIRUNYAN 18BO search for color octet scalar boson produced through gluon fusion process in pp collisions at $\sqrt{s} = 13$ TeV. The limit above assumes S_{8gg} coupling $k_s^2 = 1/2$.
[3] KHACHATRYAN 15AV search for pair productions of neutral color-octet weak-triplet scalar particles (Θ^0), decaying to $b\overline{b}$, Zg or γg, in pp collisions at $\sqrt{s} = 8$ TeV. The Θ^0 particle is often predicted in coloron (G', color-octet gauge boson) models and appear in the pp collisions through $G' \to \Theta^0 \Theta^0$ decays. Assuming B($\Theta^0 \to b\overline{b}$) = 0.5, they give limits $m_{\Theta^0} > 623$ GeV (426 GeV) for $m_{G'} = 2.3\, m_{\Theta^0}$ ($m_{G'} = 5\, m_{\Theta^0}$).
[4] AAD 13K search for pair production of color-octet scalar particles in pp collisions at $\sqrt{s} = 7$ TeV. Cross section limits are interpreted as mass limits on scalar partners of a Dirac gluino.

X^0 (Heavy Boson) Searches in Z Decays

Searches for radiative transition of Z to a lighter spin-0 state X^0 decaying to hadrons, a lepton pair, a photon pair, or invisible particles as shown in the comments. The limits are for the product of branching ratios.

VALUE	CL%	DOCUMENT ID		TECN	COMMENT
• • • We do not use the following data for averages, fits, limits, etc. • • •					
		[1] RAINBOLT	19	RVUE	$X^0 \to \ell^+\ell^-$
		[2] SIRUNYAN	19AZ	CMS	$X^0 \to \mu^+\mu^-$
		[3] BARATE	98U	ALEP	$X^0 \to \ell\overline{\ell}$, $q\overline{q}$, gg, $\gamma\gamma$, $\nu\overline{\nu}$
		[4] ACCIARRI	97Q	L3	$X^0 \to$ invisible particle(s)
		[5] ACTON	93E	OPAL	$X^0 \to \gamma\gamma$
		[6] ABREU	92D	DLPH	$X^0 \to$ hadrons
		[7] ADRIANI	92F	L3	$X^0 \to$ hadrons
		[8] ACTON	91	OPAL	$X^0 \to$ anything
$<1.1 \times 10^{-4}$	95	[9] ACTON	91B	OPAL	$X^0 \to e^+e^-$
$<9 \times 10^{-5}$	95	[9] ACTON	91B	OPAL	$X^0 \to \mu^+\mu^-$
$<1.1 \times 10^{-4}$	95	[9] ACTON	91B	OPAL	$X^0 \to \tau^+\tau^-$
$<2.8 \times 10^{-4}$	95	[10] ADEVA	91D	L3	$X^0 \to e^+e^-$
$<2.3 \times 10^{-4}$	95	[10] ADEVA	91D	L3	$X^0 \to \mu^+\mu^-$
$<4.7 \times 10^{-4}$	95	[11] ADEVA	91D	L3	$X^0 \to$ hadrons
$<8 \times 10^{-4}$	95	[12] AKRAWY	90J	OPAL	$X^0 \to$ hadrons

[1] RAINBOLT 19 limits are from B($Z \to \ell^+\ell^-\ell^+\ell^-$). See their Figs. 5 and 6 for limits in mass-coupling plane.
[2] SIRUNYAN 19AZ search for $pp \to Z \to X^0\mu^+\mu^- \to \mu^+\mu^-\mu^+\mu^-$ events in pp collisions at $\sqrt{s} = 13$ TeV. See their Fig. 5 for limits on $\sigma(pp \to X^0\mu^+\mu^-)\cdot$B($X^0 \to \mu^+\mu^-$).
[3] BARATE 98U obtain limits on B($Z \to \gamma X^0$)B($X^0 \to \ell\overline{\ell}$, $q\overline{q}$, gg, $\gamma\gamma$, $\nu\overline{\nu}$). See their Fig. 17.
[4] See Fig. 4 of ACCIARRI 97Q for the upper limit on B($Z \to \gamma X^0$; $E_\gamma > E_{\rm min}$) as a function of $E_{\rm min}$.
[5] ACTON 93E give $\sigma(e^+e^- \to X^0\gamma)\cdot$B($X^0 \to \gamma\gamma$)< 0.4 pb (95%CL) for m_{X^0}=60 ± 2.5 GeV. If the process occurs via s-channel γ exchange, the limit translates to $\Gamma(X^0)\cdot$B($X^0 \to \gamma\gamma$)^2 <20 MeV for m_{X^0} = 60 ± 1 GeV.
[6] ABREU 92D give $\sigma_Z \cdot$ B($Z \to \gamma X^0$) · B($X^0 \to$ hadrons) <(3–10) pb for m_{X^0} = 10–78 GeV. A very similar limit is obtained for spin-1 X^0.
[7] ADRIANI 92F search for isolated γ in hadronic Z decays. The limit $\sigma_Z \cdot$ B($Z \to \gamma X^0$) · B($X^0 \to$ hadrons) <(2–10) pb (95%CL) is given for m_{X^0} = 25–85 GeV.
[8] ACTON 91 searches for $Z \to Z^* X^0$, $Z^* \to e^+e^-$, $\mu^+\mu^-$, or $\nu\overline{\nu}$. Excludes any new scalar X^0 with $m_{X^0} < 9.5$ GeV/c if it has the same coupling to ZZ^* as the MSM Higgs boson.
[9] ACTON 91B limits are for m_{X^0} = 60–85 GeV.
[10] ADEVA 91D limits are for m_{X^0} = 30–89 GeV.
[11] ADEVA 91D limits are for m_{X^0} = 30–86 GeV.
[12] AKRAWY 90J give $\Gamma(Z \to \gamma X^0)\cdot$B($X^0 \to$ hadrons) < 1.9 MeV (95%CL) for m_{X^0} = 32–80 GeV. We divide by $\Gamma(Z)$ = 2.5 GeV to get product of branching ratios. For nonresonant transitions, the limit is B($Z \to \gamma q\overline{q}$) < 8.2 MeV assuming three-body phase space distribution.

MASS LIMITS for a Heavy Neutral Boson Coupling to e^+e^-

VALUE (GeV)	CL%	DOCUMENT ID		TECN	COMMENT
• • • We do not use the following data for averages, fits, limits, etc. • • •					
none 55–61		[1] ODAKA	89	VNS	$\Gamma(X^0 \to e^+e^-)\cdot$ B($X^0 \to$ had.) $\gtrsim$ 0.2 MeV
>45	95	[2] DERRICK	86	HRS	$\Gamma(X^0 \to e^+e^-)$=6 MeV
>46.6	95	[3] ADEVA	85	MRKJ	$\Gamma(X^0 \to e^+e^-)$=10 keV
>48	95	[3] ADEVA	85	MRKJ	$\Gamma(X^0 \to e^+e^-)$=4 MeV
		[4] BERGER	85B	PLUT	
none 39.8–45.5		[5] ADEVA	84	MRKJ	$\Gamma(X^0 \to e^+e^-)$=10 keV
>47.8	95	[5] ADEVA	84	MRKJ	$\Gamma(X^0 \to e^+e^-)$=4 MeV
none 39.8–45.2		[5] BEHREND	84C	CELL	
>47	95	[5] BEHREND	84C	CELL	$\Gamma(X^0 \to e^+e^-)$=4 MeV

[1] ODAKA 89 looked for a narrow or wide scalar resonance in $e^+e^- \to$ hadrons at $E_{\rm cm}$ = 55.0–60.8 GeV.
[2] DERRICK 86 found no deviation from the Standard Model Bhabha scattering at $E_{\rm cm}$= 29 GeV and set limits on the possible scalar boson e^+e^- coupling. See their figure 4 for excluded region in the $\Gamma(X^0 \to e^+e^-)$-m_{X^0} plane. Electronic chiral invariance requires a parity doublet of X^0, in which case the limit applies for $\Gamma(X^0 \to e^+e^-)$ = 3 MeV.
[3] ADEVA 85 first limit is from 2γ, $\mu^+\mu^-$, hadrons assuming X^0 is a scalar. Second limit is from e^+e^- channel. $E_{\rm cm}$ = 40–47 GeV. Supersedes ADEVA 84.
[4] BERGER 85B looked for effect of spin-0 boson exchange in $e^+e^- \to e^+e^-$ and $\mu^+\mu^-$ at $E_{\rm cm}$ = 34.7 GeV. See Fig. 5 for excluded region in the $m_{X^0} - \Gamma(X^0)$ plane.
[5] ADEVA 84 and BEHREND 84C have $E_{\rm cm}$ = 39.8–45.5 GeV. MARK-J searched X^0 in $e^+e^- \to$ hadrons, 2γ, $\mu^+\mu^-$, e^+e^- and CELLO in the same channels plus τ pair. No narrow or broad X^0 is found in the energy range. They also searched for the effect of X^0 with $m_X > E_{\rm cm}$. The second limits are from Bhabha data and for spin-0 singlet. The same limits apply for $\Gamma(X^0 \to e^+e^-)$ = 2 MeV if X^0 is a spin-0 doublet. The second limit of BEHREND 84C was read off from their figure 2. The original papers also list limits in other channels.

Search for X^0 Resonance in e^+e^- Collisions

The limit is for $\Gamma(X^0 \to e^+e^-)\cdot$B($X^0 \to f$), where f is the specified final state. Spin 0 is assumed for X^0.

VALUE (keV)	CL%	DOCUMENT ID		TECN	COMMENT
• • • We do not use the following data for averages, fits, limits, etc. • • •					
$<10^3$	95	[1] ABE	93C	VNS	$\Gamma(ee)$
<(0.4–10)	95	[2] ABE	93C	VNS	$f = \gamma\gamma$
<(0.3–5)	95	[3,4] ABE	93D	TOPZ	$f = \gamma\gamma$
<(2–12)	95	[3,4] ABE	93D	TOPZ	f = hadrons
<(4–200)	95	[4,5] ABE	93D	TOPZ	$f = ee$
<(0.1–6)	95	[4,5] ABE	93D	TOPZ	$f = \mu\mu$
<(0.5–8)	90	[6] STERNER	93	AMY	$f = \gamma\gamma$

[1] Limit is for $\Gamma(X^0 \to e^+e^-)$ m_{X^0} = 56–63.5 GeV for $\Gamma(X^0)$ = 0.5 GeV.
[2] Limit is for m_{X^0} = 56–61.5 GeV and is valid for $\Gamma(X^0) \ll 100$ MeV. See their Fig. 5 for limits for Γ = 1,2 GeV.
[3] Limit is for m_{X^0} = 57.2–60 GeV.
[4] Limit is valid for $\Gamma(X^0) \ll 100$ MeV. See paper for limits for Γ = 1 GeV and those for J = 2 resonances.
[5] Limit is for m_{X^0} = 56.6–60 GeV.
[6] STERNER 93 limit is for m_{X^0} = 57–59.6 GeV and is valid for $\Gamma(X^0)$<100 MeV. See their Fig. 2 for limits for Γ = 1,3 GeV.

Search for X^0 Resonance in ep Collisions

VALUE	DOCUMENT ID		TECN	COMMENT
• • • We do not use the following data for averages, fits, limits, etc. • • •				
	[1] CHEKANOV	02B	ZEUS	$X \to jj$

[1] CHEKANOV 02B search for photoproduction of X decaying into dijets in ep collisions. See their Fig. 5 for the limit on the photoproduction cross section.

Search for X^0 Resonance in $e^+e^- \to X^0\gamma$

VALUE (GeV)	DOCUMENT ID		TECN	COMMENT
• • • We do not use the following data for averages, fits, limits, etc. • • •				
	[1] ABBIENDI	03D	OPAL	$X^0 \to \gamma\gamma$
	[2] ABREU	00Z	DLPH	X^0 decaying invisibly
	[3] ADAM	96C	DLPH	X^0 decaying invisibly

Downloaded from https://academic.oup.com/ptep/article/2022/8/083C01/6651666 by KIT Library user on 27 September 2022

[1] ABBIENDI 03D measure the $e^+e^- \to \gamma\gamma\gamma$ cross section at $\sqrt{s}$=181–209 GeV. The upper bound on the production cross section, $\sigma(e^+e^- \to X^0\gamma)$ times the branching ratio for $X^0 \to \gamma\gamma$, is less than 0.03 pb at 95%CL for X^0 masses between 20 and 180 GeV. See their Fig. 9b for the limits in the mass-cross section plane.

[2] ABREU 00Z is from the single photon cross section at $\sqrt{s}$=183, 189 GeV. The production cross section upper limit is less than 0.3 pb for X^0 mass between 40 and 160 GeV. See their Fig. 4 for the limit in mass-cross section plane.

[3] ADAM 96C is from the single photon production cross at $\sqrt{s}$=130, 136 GeV. The upper bound is less than 3 pb for X^0 masses between 60 and 130 GeV. See their Fig. 5 for the exact bound on the cross section $\sigma(e^+e^- \to \gamma X^0)$.

Search for X^0 Resonance in $Z \to f\overline{f}X^0$

The limit is for $B(Z \to f\overline{f}X^0) \cdot B(X^0 \to F)$ where f is a fermion and F is the specified final state. Spin 0 is assumed for X^0.

VALUE	CL%	DOCUMENT ID		TECN	COMMENT
• • • We do not use the following data for averages, fits, limits, etc. • • •					
		[1] ABREU	96T	DLPH	f=e,μ,τ; F=$\gamma\gamma$
$<3.7 \times 10^{-6}$	95	[2] ABREU	96T	DLPH	f=ν; F=$\gamma\gamma$
		[3] ABREU	96T	DLPH	f=q; F=$\gamma\gamma$
$<6.8 \times 10^{-6}$	95	[2] ACTON	93E	OPAL	f=e,μ,τ; F=$\gamma\gamma$
$<5.5 \times 10^{-6}$	95	[2] ACTON	93E	OPAL	f=q; F=$\gamma\gamma$
$<3.1 \times 10^{-6}$	95	[2] ACTON	93E	OPAL	f=ν; F=$\gamma\gamma$
$<6.5 \times 10^{-6}$	95	[2] ACTON	93E	OPAL	f=e,μ; F=$\ell\overline{\ell}$, $q\overline{q}$, $\nu\overline{\nu}$
$<7.1 \times 10^{-6}$	95	[2] BUSKULIC	93F	ALEP	f=e,μ; F=$\ell\overline{\ell}$, $q\overline{q}$, $\nu\overline{\nu}$
		[4] ADRIANI	92F	L3	f=q; F=$\gamma\gamma$

[1] ABREU 96T obtain limit as a function of m_{X^0}. See their Fig. 6.

[2] Limit is for m_{X^0} around 60 GeV.

[3] ABREU 96T obtain limit as a function of m_{X^0}. See their Fig. 15.

[4] ADRIANI 92F give $\sigma_Z \cdot B(Z \to q\overline{q}X^0) \cdot B(X^0 \to \gamma\gamma)$<(0.75–1.5) pb (95%CL) for m_{X^0} = 10–70 GeV. The limit is 1 pb at 60 GeV.

Search for X^0 Resonance in WX^0 final state

VALUE (MeV)	DOCUMENT ID		TECN	COMMENT
• • • We do not use the following data for averages, fits, limits, etc. • • •				
	[1] AALTONEN	13AA	CDF	$X^0 \to jj$
	[2] CHATRCHYAN	12BR	CMS	$X^0 \to jj$
	[3] ABAZOV	11I	D0	$X^0 \to jj$
	[4] ABE	97W	CDF	$X^0 \to b\overline{b}$

[1] AALTONEN 13AA search for X^0 production associated with W (or Z) in $p\overline{p}$ collisions at E_{cm} = 1.96 TeV. The upper limit on the cross section $\sigma(p\overline{p} \to WX^0)$ is 2.2 pb for M_{X^0} = 145 GeV.

[2] CHATRCHYAN 12BR search for X^0 production associated with W in pp collisions at E_{cm} = 7 TeV. The upper limit on the cross section is 5.0 pb at 95% CL for m_{X^0} = 150 GeV.

[3] ABAZOV 11I search for X^0 production associated with W in $p\overline{p}$ collisions at E_{cm} = 1.96 TeV. The 95% CL upper limit on the cross section ranges from 2.57 to 1.28 pb for X^0 mass between 110 and 170 GeV.

[4] ABE 97W search for X^0 production associated with W in $p\overline{p}$ collisions at E_{cm}=1.8 TeV. The 95%CL upper limit on the production cross section times the branching ratio for $X^0 \to b\overline{b}$ ranges from 14 to 19 pb for X^0 mass between 70 and 120 GeV. See their Fig. 3 for upper limits of the production cross section as a function of m_{X^0}.

Search for X^0 Resonance in Quarkonium Decays

Limits are for branching ratios to modes shown. Spin 1 is assumed for X^0.

VALUE	CL%	DOCUMENT ID		TECN	COMMENT
• • • We do not use the following data for averages, fits, limits, etc. • • •					
$< 3 \times 10^{-5}$–6×10^{-3}	90	[1] BALEST	95	CLE2	$\Upsilon(1S) \to X^0\overline{X}^0\gamma$, m_{X^0} < 3.9 GeV

[1] BALEST 95 three-body limit is for phase-space photon energy distribution and angular distribution same as for $\Upsilon \to gg\gamma$.

Search for X^0 Resonance in $H(125)$ Decays

Spin 1 is assumed for X^0. See neutral Higgs search listing for pseudoscalar X^0.

VALUE	DOCUMENT ID		TECN	COMMENT
• • • We do not use the following data for averages, fits, limits, etc. • • •				
	[1] AABOUD	18AP	ATLS	$H(125) \to ZX^0$
	[2] AABOUD	18AP	ATLS	$H(125) \to X^0X^0$

[1] AABOUD 18AP use pp collision data at $\sqrt{s}$ = 13 TeV. $X^0 \to \ell^+\ell^-$ decay is assumed. See their Fig. 9 for limits on $\sigma_{H(125)} \cdot B(ZX^0)$.

[2] AABOUD 18AP use pp collision data at $\sqrt{s}$ = 13 TeV. $X^0 \to \ell^+\ell^-$ decay is assumed. See their Fig. 10 for limits on $\sigma_{H(125)} \cdot B(X^0X^0)$.

REFERENCES FOR Searches for New Heavy Bosons (W', Z', leptoquarks, etc.)

AAD	22	PR D105 012001	G. Aad *et al.*	(ATLAS Collab.)
AAD	21AG	EPJ C81 313	G. Aad *et al.*	(ATLAS Collab.)
AAD	21AQ	JHEP 2107 005	G. Aad *et al.*	(ATLAS Collab.)
AAD	21AW	PR D104 112005	G. Aad *et al.*	(ATLAS Collab.)
AAD	21AZ	JHEP 2110 013	G. Aad *et al.*	(ATLAS Collab.)
AAD	21BB	JHEP 2111 209	G. Aad *et al.*	(ATLAS Collab.)
AAD	21D	PRL 126 121802	G. Aad *et al.*	(ATLAS Collab.)
AAD	21K	JHEP 2102 226	G. Aad *et al.*	(ATLAS Collab.)
AAD	21S	JHEP 2105 093	G. Aad *et al.*	(ATLAS Collab.)
AAD	21T	JHEP 2106 179	G. Aad *et al.*	(ATLAS Collab.)
BURAS	21	JHEP 2106 068	A.J. Buras *et al.*	(TUM, CERN, ZURI+)
CADEDDU	21	JHEP 2101 116	M. Cadeddu *et al.*	(CAGLI, CAGL, INFN+)
COLARESI	21	PR D104 072003	J. Colaresi *et al.*	(MRION, FNAL, PNL+)
CRIVELLIN	21A	PR D103 115023	A. Crivellin, D. Mueller, L. Schnell	(CERN, ZURI+)
KRIBS	21	PRL 126 011801	G.D. Kribs, D. McKeen, N. Raj	(OREG, TRIU)
SIRUNYAN	21J	PL B819 136446	A.M. Sirunyan *et al.*	(CMS Collab.)
SIRUNYAN	21N	JHEP 2107 208	A.M. Sirunyan *et al.*	(CMS Collab.)
SIRUNYAN	21X	EPJ C81 688	A.M. Sirunyan *et al.*	(CMS Collab.)
SIRUNYAN	21Y	PL B820 136535	A.M. Sirunyan *et al.*	(CMS Collab.)
TUMASYAN	21D	JHEP 2111 153	A. Tumasyan *et al.*	(CMS Collab.)
AAD	20AD	PRL 125 131801	G. Aad *et al.*	(ATLAS Collab.)
AAD	20AF	PRL 125 251802	G. Aad *et al.*	(ATLAS Collab.)
AAD	20AJ	PR D102 112008	G. Aad *et al.*	(ATLAS Collab.)
AAD	20AK	JHEP 2010 112	G. Aad *et al.*	(ATLAS Collab.)
AAD	20AM	JHEP 2010 061	G. Aad *et al.*	(ATLAS Collab.)
AAD	20AT	EPJ C80 1165	G. Aad *et al.*	(ATLAS Collab.)
AAD	20S	EPJ C80 737	G. Aad *et al.*	(ATLAS Collab.)
AAD	20T	JHEP 2003 145	G. Aad *et al.*	(ATLAS Collab.)
AAD	20W	JHEP 2006 151	G. Aad *et al.*	(ATLAS Collab.)
AAIJ	20AL	JHEP 2010 156	R. Aaij *et al.*	(LHCb Collab.)
ADACHI	20	PRL 124 141801	I. Adachi *et al.*	(BELLE II Collab.)
AEBISCHER	20	EPJ C80 252	J. Aebischer *et al.*	(TUM, LAPTH, UCSC)
DEPPISCH	20	JHEP 2012 186	F.F. Deppisch, K. Fridell, J. Harz	(LOUC, TUM)
SIRUNYAN	20A	EPJ C80 3	A.M. Sirunyan *et al.*	(CMS Collab.)
SIRUNYAN	20AI	JHEP 2005 033	A.M. Sirunyan *et al.*	(CMS Collab.)
SIRUNYAN	20AQ	PRL 124 131802	A.M. Sirunyan *et al.*	(CMS Collab.)
SIRUNYAN	20M	PL B805 135448	A.M. Sirunyan *et al.*	(CMS Collab.)
SIRUNYAN	20Q	EPJ C80 237	A.M. Sirunyan *et al.*	(CMS Collab.)
AABOUD	19AJ	PL B795 56	M. Aaboud *et al.*	(ATLAS Collab.)
AABOUD	19AS	PR D99 092004	M. Aaboud *et al.*	(ATLAS Collab.)
AABOUD	19AX	EPJ C79 733	M. Aaboud *et al.*	(ATLAS Collab.)
AABOUD	19B	JHEP 1901 016	M. Aaboud *et al.*	(ATLAS Collab.)
AABOUD	19BB	PL B798 134942	M. Aaboud *et al.*	(ATLAS Collab.)
AABOUD	19D	PL B788 316	M. Aaboud *et al.*	(ATLAS Collab.)
AABOUD	19E	PL B788 347	M. Aaboud *et al.*	(ATLAS Collab.)
AABOUD	19V	JHEP 1905 142	M. Aaboud *et al.*	(ATLAS Collab.)
AABOUD	19X	JHEP 1906 144	M. Aaboud *et al.*	(ATLAS Collab.)
AAD	19C	PR D100 052013	G. Aad *et al.*	(ATLAS Collab.)
AAD	19D	JHEP 1909 091	G. Aad *et al.*	(ATLAS Collab.)
Also		JHEP 2006 042 (errat.)	G. Aad *et al.*	(ATLAS Collab.)
AAD	19L	PL B796 68	G. Aad *et al.*	(ATLAS Collab.)
ABRAMOWICZ	19	PR D99 092006	H. Abramowicz *et al.*	(ZEUS Collab.)
LONG	19	NP B943 114629	H.N. Long *et al.*	
MANDAL	19	JHEP 1912 089	R. Mandal, A. Pich	(VALE, SIEG)
PANDEY	19	JHEP 1911 046	S. Pandey, S. Karmakar, S. Rakshit	(IITI)
RAINBOLT	19	PR D99 013004	J.L. Rainbolt, M. Schmitt	(NWES)
SIRUNYAN	19AA	JHEP 1904 031	A.M. Sirunyan *et al.*	(CMS Collab.)
SIRUNYAN	19AL	EPJ C79 208	A.M. Sirunyan *et al.*	(CMS Collab.)
SIRUNYAN	19AN	EPJ C79 280	A.M. Sirunyan *et al.*	(CMS Collab.)
SIRUNYAN	19AY	PL B792 107	A.M. Sirunyan *et al.*	(CMS Collab.)
SIRUNYAN	19AZ	PL B792 345	A.M. Sirunyan *et al.*	(CMS Collab.)
SIRUNYAN	19BC	PL B795 76	A.M. Sirunyan *et al.*	(CMS Collab.)
SIRUNYAN	19BI	PR D99 032014	A.M. Sirunyan *et al.*	(CMS Collab.)
SIRUNYAN	19BJ	PR D99 052002	A.M. Sirunyan *et al.*	(CMS Collab.)
SIRUNYAN	19CB	PR D100 112007	A.M. Sirunyan *et al.*	(CMS Collab.)
SIRUNYAN	19CD	PRL 123 231803	A.M. Sirunyan *et al.*	(CMS Collab.)
SIRUNYAN	19CP	PL B798 134952	A.M. Sirunyan *et al.*	(CMS Collab.)
SIRUNYAN	19D	PRL 122 081804	A.M. Sirunyan *et al.*	(CMS Collab.)
SIRUNYAN	19I	JHEP 1901 051	A.M. Sirunyan *et al.*	(CMS Collab.)
SIRUNYAN	19V	JHEP 1903 127	A.M. Sirunyan *et al.*	(CMS Collab.)
SIRUNYAN	19Y	JHEP 1903 170	A.M. Sirunyan *et al.*	(CMS Collab.)
AABOUD	18AA	PR D98 032015	M. Aaboud *et al.*	(ATLAS Collab.)
AABOUD	18AB	PR D98 032016	M. Aaboud *et al.*	(ATLAS Collab.)
AABOUD	18AD	PL B779 24	M. Aaboud *et al.*	(ATLAS Collab.)
AABOUD	18AF	PL B781 327	M. Aaboud *et al.*	(ATLAS Collab.)
AABOUD	18AI	JHEP 1803 174	M. Aaboud *et al.*	(ATLAS Collab.)
Also		JHEP 1811 051 (errat.)	M. Aaboud *et al.*	(ATLAS Collab.)
AABOUD	18AK	JHEP 1803 042	M. Aaboud *et al.*	(ATLAS Collab.)
AABOUD	18AL	JHEP 1803 009	M. Aaboud *et al.*	(ATLAS Collab.)
AABOUD	18AP	JHEP 1806 166	M. Aaboud *et al.*	(ATLAS Collab.)
AABOUD	18B	EPJ C78 24	M. Aaboud *et al.*	(ATLAS Collab.)
AABOUD	18BG	EPJ C78 401	M. Aaboud *et al.*	(ATLAS Collab.)
AABOUD	18BI	EPJ C78 565	M. Aaboud *et al.*	(ATLAS Collab.)
AABOUD	18CH	PL B787 68	M. Aaboud *et al.*	(ATLAS Collab.)
AABOUD	18CJ	PR D98 052008	M. Aaboud *et al.*	(ATLAS Collab.)
AABOUD	18CM	PR D98 092008	M. Aaboud *et al.*	(ATLAS Collab.)
AABOUD	18F	PL B777 91	M. Aaboud *et al.*	(ATLAS Collab.)
AABOUD	18G	JHEP 1801 055	M. Aaboud *et al.*	(ATLAS Collab.)
AABOUD	18K	PRL 120 161802	M. Aaboud *et al.*	(ATLAS Collab.)
AABOUD	18N	PRL 121 081801	M. Aaboud *et al.*	(ATLAS Collab.)
AAIJ	18AQ	JHEP 1809 147	R. Aaij *et al.*	(LHCb Collab.)
BOBOVNIKOV	18	PR D98 095029	I.D. Bobovnikov, P. Osland, A.A. Pankov	(BERG+)
SIRUNYAN	18	PL B777 39	A.M. Sirunyan *et al.*	(CMS Collab.)
SIRUNYAN	18AT	JHEP 1804 073	A.M. Sirunyan *et al.*	(CMS Collab.)
SIRUNYAN	18AX	JHEP 1805 088	A.M. Sirunyan *et al.*	(CMS Collab.)
SIRUNYAN	18AZ	JHEP 1806 128	A.M. Sirunyan *et al.*	(CMS Collab.)
SIRUNYAN	18BB	JHEP 1806 120	A.M. Sirunyan *et al.*	(CMS Collab.)
SIRUNYAN	18BJ	JHEP 1807 115	A.M. Sirunyan *et al.*	(CMS Collab.)
SIRUNYAN	18BK	JHEP 1807 075	A.M. Sirunyan *et al.*	(CMS Collab.)
SIRUNYAN	18BO	JHEP 1808 130	A.M. Sirunyan *et al.*	(CMS Collab.)
SIRUNYAN	18CV	JHEP 1805 148	A.M. Sirunyan *et al.*	(CMS Collab.)
SIRUNYAN	18CZ	EPJ C78 707	A.M. Sirunyan *et al.*	(CMS Collab.)
SIRUNYAN	18DJ	JHEP 1809 101	A.M. Sirunyan *et al.*	(CMS Collab.)
SIRUNYAN	18DR	JHEP 1811 161	A.M. Sirunyan *et al.*	(CMS Collab.)
SIRUNYAN	18EC	PRL 121 241802	A.M. Sirunyan *et al.*	(CMS Collab.)
SIRUNYAN	18ED	JHEP 1811 172	A.M. Sirunyan *et al.*	(CMS Collab.)
SIRUNYAN	18G	JHEP 1801 097	A.M. Sirunyan *et al.*	(CMS Collab.)
SIRUNYAN	18I	PRL 120 201801	A.M. Sirunyan *et al.*	(CMS Collab.)
SIRUNYAN	18P	PR D97 072006	A.M. Sirunyan *et al.*	(CMS Collab.)
SIRUNYAN	18U	PR D98 032005	A.M. Sirunyan *et al.*	(CMS Collab.)
ZHANG	18A	EPJ C78 695	J. Zhang, C.-X. Yue, C.-H. Li	(LNUDA)
AABOUD	17AK	PR D96 052004	M. Aaboud *et al.*	(ATLAS Collab.)
AABOUD	17AO	PL B774 494	M. Aaboud *et al.*	(ATLAS Collab.)
AABOUD	17AT	JHEP 1710 182	M. Aaboud *et al.*	(ATLAS Collab.)
AABOUD	17B	PL B765 32	M. Aaboud *et al.*	(ATLAS Collab.)
KHACHATRY...	17AX	PL B773 563	V. Khachatryan *et al.*	(CMS Collab.)
KHACHATRY...	17H	JHEP 1702 048	V. Khachatryan *et al.*	(CMS Collab.)
KHACHATRY...	17J	JHEP 1703 077	V. Khachatryan *et al.*	(CMS Collab.)
KHACHATRY...	17T	PL B768 57	V. Khachatryan *et al.*	(CMS Collab.)
KHACHATRY...	17U	PL B768 137	V. Khachatryan *et al.*	(CMS Collab.)
KHACHATRY...	17W	PL B769 520	V. Khachatryan *et al.*	(CMS Collab.)
KHACHATRY...	17Y	PL B770 257	V. Khachatryan *et al.*	(CMS Collab.)
KHACHATRY...	17Z	PL B770 278	V. Khachatryan *et al.*	(CMS Collab.)
SIRUNYAN	17A	JHEP 1703 162	A.M. Sirunyan *et al.*	(CMS Collab.)
SIRUNYAN	17AK	PL B774 533	A.M. Sirunyan *et al.*	(CMS Collab.)
SIRUNYAN	17AP	JHEP 1710 180	A.M. Sirunyan *et al.*	(CMS Collab.)
SIRUNYAN	17H	JHEP 1707 121	A.M. Sirunyan *et al.*	(CMS Collab.)
SIRUNYAN	17I	JHEP 1708 029	A.M. Sirunyan *et al.*	(CMS Collab.)

Downloaded from https://academic.oup.com/ptep/article/2022/8/083C01/6651666 by KIT Library user on 27 September 2022

SIRUNYAN 17Q JHEP 1707 001 A.M. Sirunyan et al. (CMS Collab.)
SIRUNYAN 17R EPJ C77 636 A.M. Sirunyan et al. (CMS Collab.)
SIRUNYAN 17T PRL 119 111802 A.M. Sirunyan et al. (CMS Collab.)
SIRUNYAN 17V JHEP 1709 053 A.M. Sirunyan et al. (CMS Collab.)
AABOUD 16 PL B759 229 M. Aaboud et al. (ATLAS Collab.)
AABOUD 16AA EPJ C76 585 M. Aaboud et al. (ATLAS Collab.)
AABOUD 16AE JHEP 1609 173 M. Aaboud et al. (ATLAS Collab.)
AABOUD 16P EPJ C76 541 M. Aaboud et al. (ATLAS Collab.)
AABOUD 16U PL B761 372 M. Aaboud et al. (ATLAS Collab.)
AABOUD 16V PL B762 334 M. Aaboud et al. (ATLAS Collab.)
AAD 16G EPJ C76 5 G. Aad et al. (ATLAS Collab.)
AAD 16L EPJ C76 210 G. Aad et al. (ATLAS Collab.)
AAD 16R PL B755 285 G. Aad et al. (ATLAS Collab.)
AAD 16S PL B754 302 G. Aad et al. (ATLAS Collab.)
AAD 16W PL B758 249 G. Aad et al. (ATLAS Collab.)
BARRANCO 16 JP G43 115004 J. Barranco et al.
DEY 16 JHEP 1604 187 U.K. Dey, S. Mohanty
KHACHATRY... 16AF PR D93 032004 V. Khachatryan et al. (CMS Collab.)
KHACHATRY... 16AG PR D93 032005 V. Khachatryan et al. (CMS Collab.)
Also PR D95 039906 (errat.) V. Khachatryan et al. (CMS Collab.)
KHACHATRY... 16AO JHEP 1602 122 V. Khachatryan et al. (CMS Collab.)
KHACHATRY... 16AP JHEP 1602 145 V. Khachatryan et al. (CMS Collab.)
KHACHATRY... 16BD EPJ C76 237 V. Khachatryan et al. (CMS Collab.)
KHACHATRY... 16BE EPJ C76 317 V. Khachatryan et al. (CMS Collab.)
KHACHATRY... 16E PR D93 012001 V. Khachatryan et al. (CMS Collab.)
KHACHATRY... 16K PRL 116 071801 V. Khachatryan et al. (CMS Collab.)
KHACHATRY... 16L PRL 117 031802 V. Khachatryan et al. (CMS Collab.)
KHACHATRY... 16O PL B755 196 V. Khachatryan et al. (CMS Collab.)
KUMAR 16 PR D94 014022 G. Kumar
AAD 15AM JHEP 1507 157 G. Aad et al. (ATLAS Collab.)
AAD 15AO JHEP 1508 148 G. Aad et al. (ATLAS Collab.)
AAD 15AT EPJ C75 79 G. Aad et al. (ATLAS Collab.)
AAD 15AU EPJ C75 69 G. Aad et al. (ATLAS Collab.)
AAD 15AV EPJ C75 165 G. Aad et al. (ATLAS Collab.)
AAD 15AZ EPJ C75 209 G. Aad et al. (ATLAS Collab.)
Also EPJ C75 370 (errat.) G. Aad et al. (ATLAS Collab.)
AAD 15BB EPJ C75 263 G. Aad et al. (ATLAS Collab.)
AAD 15CD PR D92 092001 G. Aad et al. (ATLAS Collab.)
AAD 15CP JHEP 1512 055 G. Aad et al. (ATLAS Collab.)
AAD 15O PRL 115 031801 G. Aad et al. (ATLAS Collab.)
AAD 15R PL B743 235 G. Aad et al. (ATLAS Collab.)
AAD 15V PR D91 052007 G. Aad et al. (ATLAS Collab.)
AALTONEN 15C PRL 115 061801 T. Aaltonen et al. (CDF Collab.)
BESSAA 15 EPJ C75 97 A. Bessaa, S. Davidson
KHACHATRY... 15AE JHEP 1504 025 V. Khachatryan et al. (CMS Collab.)
KHACHATRY... 15AJ JHEP 1507 042 V. Khachatryan et al. (CMS Collab.)
KHACHATRY... 15AV JHEP 1509 201 V. Khachatryan et al. (CMS Collab.)
KHACHATRY... 15C PL B740 83 V. Khachatryan et al. (CMS Collab.)
KHACHATRY... 15F PRL 114 101801 V. Khachatryan et al. (CMS Collab.)
KHACHATRY... 15O PL B748 255 V. Khachatryan et al. (CMS Collab.)
KHACHATRY... 15T PR D91 092005 V. Khachatryan et al. (CMS Collab.)
KHACHATRY... 15V PR D91 052009 V. Khachatryan et al. (CMS Collab.)
SAHOO 15A PR D91 094019 S. Sahoo, R. Mohanta
AAD 14AI JHEP 1409 037 G. Aad et al. (ATLAS Collab.)
AAD 14AT PL B738 428 G. Aad et al. (ATLAS Collab.)
AAD 14S PL B737 223 G. Aad et al. (ATLAS Collab.)
AAD 14V PR D90 052005 G. Aad et al. (ATLAS Collab.)
KHACHATRY... 14 JHEP 1408 173 V. Khachatryan et al. (CMS Collab.)
KHACHATRY... 14A JHEP 1408 174 V. Khachatryan et al. (CMS Collab.)
KHACHATRY... 14O EPJ C74 3149 V. Khachatryan et al. (CMS Collab.)
KHACHATRY... 14T PL B739 229 V. Khachatryan et al. (CMS Collab.)
MARTINEZ 14 PR D90 015028 R. Martinez, F. Ochoa
PRIEELS 14 PR D90 112003 R. Prieels et al. (LOUV, ETH, PSI+)
AAD 13AE JHEP 1306 033 G. Aad et al. (ATLAS Collab.)
AAD 13AO PR D87 112006 G. Aad et al. (ATLAS Collab.)
AAD 13AQ PR D88 012004 G. Aad et al. (ATLAS Collab.)
AAD 13D JHEP 1301 029 G. Aad et al. (ATLAS Collab.)
AAD 13G JHEP 1301 116 G. Aad et al. (ATLAS Collab.)
AAD 13K EPJ C73 2263 G. Aad et al. (ATLAS Collab.)
AAD 13S PL B719 242 G. Aad et al. (ATLAS Collab.)
AALTONEN 13A PRL 110 121802 T. Aaltonen et al. (CDF Collab.)
AALTONEN 13AA PR D88 092004 T. Aaltonen et al. (CDF Collab.)
AALTONEN 13R PRL 111 031802 T. Aaltonen et al. (CDF Collab.)
CHATRCHYAN 13A JHEP 1301 013 S. Chatrchyan et al. (CMS Collab.)
CHATRCHYAN 13AF PL B720 63 S. Chatrchyan et al. (CMS Collab.)
CHATRCHYAN 13AJ PL B723 280 S. Chatrchyan et al. (CMS Collab.)
CHATRCHYAN 13AP PR D87 072002 S. Chatrchyan et al. (CMS Collab.)
CHATRCHYAN 13AQ PR D87 072005 S. Chatrchyan et al. (CMS Collab.)
CHATRCHYAN 13AS PR D87 114015 S. Chatrchyan et al. (CMS Collab.)
CHATRCHYAN 13AU PRL 110 141802 S. Chatrchyan et al. (CMS Collab.)
CHATRCHYAN 13BM PRL 111 211804 S. Chatrchyan et al. (CMS Collab.)
Also PRL 112 119903 (errat.) S. Chatrchyan et al. (CMS Collab.)
CHATRCHYAN 13E PL B718 1229 S. Chatrchyan et al. (CMS Collab.)
CHATRCHYAN 13M PRL 110 081801 S. Chatrchyan et al. (CMS Collab.)
CHATRCHYAN 13U JHEP 1302 036 S. Chatrchyan et al. (CMS Collab.)
SAKAKI 13 PR D88 094012 Y. Sakaki et al.
AAD 12AV PRL 109 081801 G. Aad et al. (ATLAS Collab.)
AAD 12BB PR D85 112012 G. Aad et al. (ATLAS Collab.)
AAD 12BV JHEP 1209 041 G. Aad et al. (ATLAS Collab.)
AAD 12CC JHEP 1211 138 G. Aad et al. (ATLAS Collab.)
AAD 12CK PR D86 091103 G. Aad et al. (ATLAS Collab.)
AAD 12CR EPJ C72 2241 G. Aad et al. (ATLAS Collab.)
AAD 12H PL B709 158 G. Aad et al. (ATLAS Collab.)
Also PL B711 442 (errat.) G. Aad et al. (ATLAS Collab.)
AAD 12K EPJ C72 2083 G. Aad et al. (ATLAS Collab.)
AAD 12M EPJ C72 2056 G. Aad et al. (ATLAS Collab.)
AAD 12O EPJ C72 2151 G. Aad et al. (ATLAS Collab.)
AALTONEN 12AR PR D86 112002 T. Aaltonen et al. (CDF Collab.)
AALTONEN 12N PRL 108 211805 T. Aaltonen et al. (CDF Collab.)
ABAZOV 12R PR D85 051101 V.M. Abazov et al. (D0 Collab.)
ABRAMOWICZ 12A PR D86 012005 H. Abramowicz et al. (ZEUS Collab.)
CHATRCHYAN 12AF PRL 109 141801 S. Chatrchyan et al. (CMS Collab.)
CHATRCHYAN 12AG PR D86 052013 S. Chatrchyan et al. (CMS Collab.)
CHATRCHYAN 12AI JHEP 1208 110 S. Chatrchyan et al. (CMS Collab.)
CHATRCHYAN 12AQ JHEP 1209 029 S. Chatrchyan et al. (CMS Collab.)
Also JHEP 1403 132 (errat.) S. Chatrchyan et al. (CMS Collab.)
CHATRCHYAN 12AR PL B717 351 S. Chatrchyan et al. (CMS Collab.)
CHATRCHYAN 12BG PRL 109 261802 S. Chatrchyan et al. (CMS Collab.)
CHATRCHYAN 12BL JHEP 1212 015 S. Chatrchyan et al. (CMS Collab.)
CHATRCHYAN 12BO JHEP 1212 055 S. Chatrchyan et al. (CMS Collab.)
CHATRCHYAN 12BR PRL 109 251801 S. Chatrchyan et al. (CMS Collab.)
CHATRCHYAN 12M PL B714 158 S. Chatrchyan et al. (CMS Collab.)
CHATRCHYAN 12O PL B716 82 S. Chatrchyan et al. (CMS Collab.)
KOSNIK 12 PR D86 055004 N. Kosnik (LALO, STFN)
AAD 11D PR D83 112006 G. Aad et al. (ATLAS Collab.)
AAD 11H PRL 106 251801 G. Aad et al. (ATLAS Collab.)
AAD 11Z EPJ C71 1809 G. Aad et al. (ATLAS Collab.)
AALTONEN 11AD PR D84 072003 T. Aaltonen et al. (CDF Collab.)
AALTONEN 11AE PR D84 072004 T. Aaltonen et al. (CDF Collab.)
AALTONEN 11C PR D83 031102 T. Aaltonen et al. (CDF Collab.)
AALTONEN 11I PRL 106 121801 T. Aaltonen et al. (CDF Collab.)
AARON 11A PL B701 20 F. D. Aaron et al. (H1 Collab.)
AARON 11B PL B704 388 F. D. Aaron et al. (H1 Collab.)
AARON 11C PL B705 52 F. D. Aaron et al. (H1 Collab.)
ABAZOV 11A PL B695 88 V.M. Abazov et al. (D0 Collab.)
ABAZOV 11H PRL 107 011801 V.M. Abazov et al. (D0 Collab.)
ABAZOV 11I PRL 107 011804 V.M. Abazov et al. (D0 Collab.)
ABAZOV 11L PL B699 145 V.M. Abazov et al. (D0 Collab.)
ABAZOV 11V PR D84 071104 V.M. Abazov et al. (D0 Collab.)
BUENO 11 PR D84 032005 J.F. Bueno et al. (TWIST Collab.)
Also PR D85 039908 (errat.) J.F. Bueno et al. (TWIST Collab.)
CHATRCHYAN 11N PL B703 246 S. Chatrchyan et al. (CMS Collab.)
CHATRCHYAN 11O JHEP 1108 005 S. Chatrchyan et al. (CMS Collab.)
CHATRCHYAN 11Y PL B704 123 S. Chatrchyan et al. (CMS Collab.)
DORSNER 11 JHEP 1111 002 I. Dorsner et al.
KHACHATRY... 11D PRL 106 201802 V. Khachatryan et al. (CMS Collab.)
KHACHATRY... 11E PRL 106 201803 V. Khachatryan et al. (CMS Collab.)
AALTONEN 10L PL B691 183 T. Aaltonen et al. (CDF Collab.)
AALTONEN 10N PRL 104 241801 T. Aaltonen et al. (CDF Collab.)
ABAZOV 10L PL B693 95 V.M. Abazov et al. (D0 Collab.)
DEL-AGUILA 10 JHEP 1009 033 F. del Aguila, J. de Blas, M. Perez-Victoria (GRAN)
KHACHATRY... 10 PRL 105 211801 V. Khachatryan et al. (CMS Collab.)
Also PRL 106 029902 V. Khachatryan et al. (CMS Collab.)
WAUTERS 10 PR C82 055502 F. Wauters et al. (REZ, TAMU)
AALTONEN 09AC PR D79 112002 T. Aaltonen et al. (CDF Collab.)
AALTONEN 09T PRL 102 031801 T. Aaltonen et al. (CDF Collab.)
AALTONEN 09V PRL 102 091805 T. Aaltonen et al. (CDF Collab.)
ABAZOV 09 PL B671 224 V.M. Abazov et al. (D0 Collab.)
ABAZOV 09AF PL B681 224 V.M. Abazov et al. (D0 Collab.)
ERLER 09 JHEP 0908 017 J. Erler et al.
AALTONEN 08D PR D77 051102 T. Aaltonen et al. (CDF Collab.)
AALTONEN 08P PR D77 091105 T. Aaltonen et al. (CDF Collab.)
AALTONEN 08Y PRL 100 231801 T. Aaltonen et al. (CDF Collab.)
AALTONEN 08Z PRL 101 071802 T. Aaltonen et al. (CDF Collab.)
ABAZOV 08AA PL B668 98 V.M. Abazov et al. (D0 Collab.)
ABAZOV 08AD PL B668 357 V.M. Abazov et al. (D0 Collab.)
ABAZOV 08AN PRL 101 241802 V.M. Abazov et al. (D0 Collab.)
ABAZOV 08C PRL 100 031804 V.M. Abazov et al. (D0 Collab.)
MACDONALD 08 PR D78 032010 R.P. MacDonald et al. (TWIST Collab.)
ZHANG 08 NP B802 247 Y. Zhang et al. (PKGU, UMD)
AALTONEN 07H PRL 99 171802 T. Aaltonen et al. (CDF Collab.)
ABAZOV 07E PL B647 74 V.M. Abazov et al. (D0 Collab.)
ABAZOV 07J PRL 99 061801 V.M. Abazov et al. (D0 Collab.)
AKTAS 07A EPJ C52 833 A. Aktas et al. (H1 Collab.)
CHOUDHURY 07 PL B657 69 D. Choudhury et al.
MELCONIAN 07 PL B649 370 D. Melconian et al. (TRIUMF)
SCHAEL 07A EPJ C49 411 S. Schael et al. (ALEPH Collab.)
SCHUMANN 07 PRL 99 191803 M. Schumann et al. (HEID, ILLG, KARL+)
SMIRNOV 07 MPL A22 2353 A.D. Smirnov
ABAZOV 06A PL B636 183 V.M. Abazov et al. (D0 Collab.)
ABAZOV 06L PL B640 230 V.M. Abazov et al. (D0 Collab.)
ABDALLAH 06C EPJ C45 589 J. Abdallah et al. (DELPHI Collab.)
ABULENCIA 06L PRL 96 211801 A. Abulencia et al. (CDF Collab.)
ABULENCIA 06M PRL 96 211802 A. Abulencia et al. (CDF Collab.)
ABULENCIA 06T PR D73 051102 A. Abulencia et al. (CDF Collab.)
ABAZOV 05H PR D71 071104 V.M. Abazov et al. (D0 Collab.)
ABULENCIA 05A PRL 95 252001 A. Abulencia et al. (CDF Collab.)
ACOSTA 05I PR D71 112001 D. Acosta et al. (CDF Collab.)
ACOSTA 05P PR D72 051107 D. Acosta et al. (CDF Collab.)
ACOSTA 05R PRL 95 131801 D. Acosta et al. (CDF Collab.)
AKTAS 05B PL B629 9 A. Aktas et al. (H1 Collab.)
CHEKANOV 05 PL B610 212 S. Chekanov et al. (HERA ZEUS Collab.)
CHEKANOV 05A EPJ C44 463 S. Chekanov et al. (ZEUS Collab.)
CYBURT 05 ASP 23 313 R.H. Cyburt et al.
ABAZOV 04A PRL 92 221801 V.M. Abazov et al. (D0 Collab.)
ABAZOV 04C PR D69 111101 V.M. Abazov et al. (D0 Collab.)
ABBIENDI 04G EPJ C33 173 G. Abbiendi et al. (OPAL Collab.)
ABBIENDI 03D EPJ C26 331 G. Abbiendi et al. (OPAL Collab.)
ABBIENDI 03R EPJ C31 281 G. Abbiendi et al. (OPAL)
ACOSTA 03B PRL 90 081802 D. Acosta et al. (CDF Collab.)
ADLOFF 03 PL B568 35 C. Adloff et al. (H1 Collab.)
BARGER 03B PR D67 075009 V. Barger, P. Langacker, H. Lee
CHANG 03 PR D68 111101 M.-C. Chang et al. (BELLE Collab.)
CHEKANOV 03B PR D68 052004 S. Chekanov et al. (ZEUS Collab.)
ABAZOV 02 PRL 88 191801 V.M. Abazov et al. (D0 Collab.)
ABBIENDI 02B PL B526 233 G. Abbiendi et al. (OPAL Collab.)
AFFOLDER 02C PRL 88 071806 T. Affolder et al. (CDF Collab.)
CHEKANOV 02 PR D65 092004 S. Chekanov et al. (ZEUS Collab.)
CHEKANOV 02B PL B531 9 S. Chekanov et al. (ZEUS Collab.)
MUECK 02 PR D65 085037 A. Mueck, A. Pilaftsis, R. Rueckl
ABAZOV 01B PRL 87 061802 V.M. Abazov et al. (D0 Collab.)
ABAZOV 01D PR D64 092004 V.M. Abazov et al. (D0 Collab.)
ADLOFF 01C PL B523 234 C. Adloff et al. (H1 Collab.)
AFFOLDER 01I PRL 87 231803 T. Affolder et al. (CDF Collab.)
BREITWEG 01 PR D63 052002 J. Breitweg et al. (ZEUS Collab.)
CHEUNG 01B PL B517 167 K. Cheung
THOMAS 01 NP A694 559 E. Thomas et al.
ABBIENDI 00M EPJ C13 15 G. Abbiendi et al. (OPAL Collab.)
ABBOTT 00C PRL 84 2088 B. Abbott et al. (D0 Collab.)
ABE 00 PRL 84 5716 F. Abe et al. (CDF Collab.)
ABREU 00S PL B485 45 P. Abreu et al. (DELPHI Collab.)
ABREU 00Z EPJ C17 53 P. Abreu et al. (DELPHI Collab.)
ACCIARRI 00P PL B489 81 M. Acciarri et al. (L3 Collab.)
ADLOFF 00 PL B479 358 C. Adloff et al. (H1 Collab.)
AFFOLDER 00K PRL 85 2056 T. Affolder et al. (CDF Collab.)
BARATE 00I EPJ C12 183 R. Barate et al. (ALEPH Collab.)
BARGER 00 PL B480 149 V. Barger, K. Cheung
BREITWEG 00E EPJ C16 253 J. Breitweg et al. (ZEUS Collab.)
CHAY 00 PR D61 035002 J. Chay, K.Y. Lee, S. Nam
CHO 00 MPL A15 311 G. Cho
CORNET 00 PR D61 037701 F. Cornet, M. Relano, J. Rico
DELGADO 00 JHEP 0001 030 A. Delgado, A. Pomarol, M. Quiros
ERLER 00 PRL 84 212 J. Erler, P. Langacker
GABRIELLI 00 PR D62 055009 E. Gabrielli
RIZZO 00 PR D61 016007 T.G. Rizzo, J.D. Wells
ROSNER 00 PR D61 016006 J.L. Rosner
ZARNECKI 00 EPJ C17 695 A. Zarnecki
ABBIENDI 99 EPJ C6 1 G. Abbiendi et al. (OPAL Collab.)
ABBOTT 99J PRL 83 2896 B. Abbott et al. (D0 Collab.)
ABREU 99G PL B446 62 P. Abreu et al. (DELPHI Collab.)
ACKERSTAFF 99D EPJ C8 3 K. Ackerstaff et al. (OPAL Collab.)
ADLOFF 99 EPJ C11 447 C. Adloff et al. (H1 Collab.)
Also EPJ C14 553 (errat.) C. Adloff et al. (H1 Collab.)
CASALBUONI 99 PL B460 135 R. Casalbuoni et al.
CZAKON 99 PL B458 355 M. Czakon, J. Gluza, M. Zralek
ERLER 99 PL B456 68 J. Erler, P. Langacker
MARCIANO 99 PR D60 093006 W. Marciano
MASIP 99 PR D60 096005 M. Masip, A. Pomarol
NATH 99 PR D60 116004 P. Nath, M. Yamaguchi
STRUMIA 99 PL B466 107 A. Strumia
ABBOTT 98E PRL 80 2051 B. Abbott et al. (D0 Collab.)
ABBOTT 98J PRL 81 38 B. Abbott et al. (D0 Collab.)
ABE 98S PRL 81 4806 F. Abe et al. (CDF Collab.)
ABE 98V PRL 81 5742 F. Abe et al. (CDF Collab.)

Downloaded from https://academic.oup.com/ptep/article/2022/8/083C01/6651666 by KIT Library user on 27 September 2022

ACCIARRI	98J	PL B433 163	M. Acciarri *et al.*	(L3 Collab.)
ACKERSTAFF	98V	EPJ C2 441	K. Ackerstaff *et al.*	(OPAL Collab.)
BARATE	98U	EPJ C4 571	R. Barate *et al.*	(ALEPH Collab.)
BARENBOIM	98	EPJ C1 369	G. Barenboim	
CHO	98	EPJ C5 155	G. Cho, K. Hagiwara, S. Matsumoto	
CONRAD	98	RMP 70 1341	J.M. Conrad, M.H. Shaevitz, T. Bolton	
DONCHESKI	98	PR D58 097702	M.A. Doncheski, R.W. Robinett	
GROSS-PILCH...	98	hep-ex/9810015	C. Grosso-Pilcher, G. Landsberg, M. Paterno	
ABE	97F	PRL 78 2906	F. Abe *et al.*	(CDF Collab.)
ABE	97G	PR D55 5263	F. Abe *et al.*	(CDF Collab.)
ABE	97S	PRL 79 2192	F. Abe *et al.*	(CDF Collab.)
ABE	97W	PRL 79 3819	F. Abe *et al.*	(CDF Collab.)
ABE	97X	PRL 79 4327	F. Abe *et al.*	(CDF Collab.)
ACCIARRI	97Q	PL B412 201	M. Acciarri *et al.*	(L3 Collab.)
ARIMA	97	PR D55 19	T. Arima *et al.*	(VENUS Collab.)
BARENBOIM	97	PR D55 4213	G. Barenboim *et al.*	(VALE, IFIC)
DEANDREA	97	PL B409 277	A. Deandrea	(MARS)
DERRICK	97	ZPHY C73 613	M. Derrick *et al.*	(ZEUS Collab.)
GROSSMAN	97	PR D55 2768	Y. Grossman, Z. Ligeti, E. Nardi	(REHO, CIT)
JADACH	97	PL B408 281	S. Jadach, B.F.L. Ward, Z. Was	(CERN, INPK+)
STAHL	97	ZPHY C74 73	A. Stahl, H. Voss	(BONN)
ABACHI	96C	PRL 76 3271	S. Abachi *et al.*	(D0 Collab.)
ABREU	96T	ZPHY C72 179	P. Abreu *et al.*	(DELPHI Collab.)
ADAM	96C	PL B380 471	W. Adam *et al.*	(DELPHI Collab.)
AID	96B	PL B369 173	S. Aid *et al.*	(H1 Collab.)
ALLET	96	PL B383 139	M. Allet *et al.*	(VILL, LEUV, LOUV, WISC)
ABACHI	95E	PL B358 405	S. Abachi *et al.*	(D0 Collab.)
ABE	95N	PRL 74 3538	F. Abe *et al.*	(CDF Collab.)
BALEST	95	PR D51 2053	R. Balest *et al.*	(CLEO Collab.)
KUZNETSOV	95	PRL 75 794	I.A. Kuznetsov *et al.*	(PNPI, KIAE, HARV+)
KUZNETSOV	95B	PAN 58 2113	A.V. Kuznetsov, N.V. Mikheev	(YARO)
		Translated from YAF 58 2228.		
MIZUKOSHI	95	NP B443 20	J.K. Mizukoshi, O.J.P. Eboli, M.C. Gonzalez-Garcia	
ABREU	94O	ZPHY C64 183	P. Abreu *et al.*	(DELPHI Collab.)
BHATTACH...	94	PL B336 100	G. Bhattacharyya, J. Ellis, K. Sridhar	(CERN)
Also		PL B338 522 (erratum)	G. Bhattacharyya, J. Ellis, K. Sridhar	(CERN)
BHATTACH...	94B	PL B338 522 (erratum)	G. Bhattacharyya, J. Ellis, K. Sridhar	(CERN)
DAVIDSON	94	ZPHY C61 613	S. Davidson, D. Bailey, B.A. Campbell	(CFPA+)
KUZNETSOV	94	PL B329 295	A.V. Kuznetsov, N.V. Mikheev	(YARO)
KUZNETSOV	94B	JETPL 60 315	I.A. Kuznetsov *et al.*	(PNPI, KIAE, HARV+)
		Translated from ZETFP 60 311.		
LEURER	94	PR D50 536	M. Leurer	(REHO)
LEURER	94B	PR D49 333	M. Leurer	(REHO)
Also		PRL 71 1324	M. Leurer	(REHO)
MAHANTA	94	PL B337 128	U. Mahanta	(MEHTA)
SEVERIJNS	94	PRL 73 611 (erratum)	N. Severijns *et al.*	(LOUV, WISC, LEUV+)
VILAIN	94B	PL B332 465	P. Vilain *et al.*	(CHARM II Collab.)
ABE	93C	PL B302 119	K. Abe *et al.*	(VENUS Collab.)
ABE	93D	PL B304 373	T. Abe *et al.*	(TOPAZ Collab.)
ABE	93G	PRL 71 2542	F. Abe *et al.*	(CDF Collab.)
ABREU	93J	PL B316 620	P. Abreu *et al.*	(DELPHI Collab.)
ACTON	93E	PL B311 391	P.D. Acton *et al.*	(OPAL Collab.)
ADRIANI	93M	PRPL 236 1	O. Adriani *et al.*	(L3 Collab.)
ALITTI	93	NP B400 3	J. Alitti *et al.*	(UA2 Collab.)
BHATTACH...	93	PR D47 3693	G. Bhattacharyya *et al.*	(CALC, JADA, ICTP+)
BUSKULIC	93F	PL B308 425	D. Buskulic *et al.*	(ALEPH Collab.)
DERRICK	93	PL B306 173	M. Derrick *et al.*	(ZEUS Collab.)
RIZZO	93	PR D48 4470	T.G. Rizzo	(ANL)
SEVERIJNS	93	PRL 70 4047	N. Severijns *et al.*	(LOUV, WISC, LEUV+)
Also		PRL 73 611 (erratum)	N. Severijns *et al.*	(LOUV, WISC, LEUV+)
STERNER	93	PL B303 385	K.L. Sterner *et al.*	(AMY Collab.)
ABREU	92D	ZPHY C53 555	P. Abreu *et al.*	(DELPHI Collab.)
ADRIANI	92F	PL B292 472	O. Adriani *et al.*	(L3 Collab.)
DECAMP	92	PRPL 216 253	D. Decamp *et al.*	(ALEPH Collab.)
IMAZATO	92	PRL 69 877	J. Imazato *et al.*	(KEK, INUS, TOKY+)
MISHRA	92	PRL 68 3499	S.R. Mishra *et al.*	(COLU, CHIC, FNAL+)
POLAK	92B	PR D46 3871	J. Polak, M. Zralek	(SILES)
ACTON	91	PL B268 122	D.P. Acton *et al.*	(OPAL Collab.)
ACTON	91B	PL B273 338	D.P. Acton *et al.*	(OPAL Collab.)
ADEVA	91D	PL B262 155	B. Adeva *et al.*	(L3 Collab.)
AQUINO	91	PL B261 280	M. Aquino, A. Fernandez, A. Garcia	(CINV, PUEB)
COLANGELO	91	PL B253 154	P. Colangelo, G. Nardulli	(BARI)
CUYPERS	91	PL B259 173	F. Cuypers, A.F. Falk, P.H. Frampton	(DURH, HARV+)
FARAGGI	91	MPL A6 61	A.E. Faraggi, D.V. Nanopoulos	(TAMU)
POLAK	91	NP B363 385	J. Polak, M. Zralek	(SILES)
RIZZO	91	PR D44 202	T.G. Rizzo	(WISC, ISU)
WALKER	91	APJ 376 51	T.P. Walker *et al.*	(HSCA, OSU, CHIC+)
ABE	90F	PL B246 297	K. Abe *et al.*	(VENUS Collab.)
ABE	90H	PR D41 1722	F. Abe *et al.*	(CDF Collab.)
AKRAWY	90J	PL B246 285	M.Z. Akrawy *et al.*	(OPAL Collab.)
GONZALEZ...	90D	PL B240 163	M.C. Gonzalez-Garcia, J.W.F. Valle	(VALE)
GRIFOLS	90	NP B331 244	J.A. Grifols, E. Masso	(BARC)
GRIFOLS	90D	PR D42 3293	J.A. Grifols, E. Masso, T.G. Rizzo	(BARC, CERN+)
KIM	90	PL B240 243	G.N. Kim *et al.*	(AMY Collab.)
LOPEZ	90	PL B241 392	J.L. Lopez, D.V. Nanopoulos	(TAMU)
BARBIERI	89B	PR D39 1229	R. Barbieri, R.N. Mohapatra	(PISA, UMD)
LANGACKER	89B	PR D40 1569	P. Langacker, S. Uma Sankar	(PENN)
ODAKA	89	JPSJ 58 3037	S. Odaka *et al.*	(VENUS Collab.)
ROBINETT	89	PR D39 834	R.W. Robinett	(PSU)
ALBAJAR	88B	PL B209 127	C. Albajar *et al.*	(UA1 Collab.)
BAGGER	88	PR D37 1188	J. Bagger, C. Schmidt, S. King	(HARV, BOST)
BALKE	88	PR D37 587	B. Balke *et al.*	(LBL, UCB, COLO, NWES+)
BERGSTROM	88	PL B212 386	L. Bergstrom	(STOH)
CUYPERS	88	PRL 60 1237	F. Cuypers, P.H. Frampton	(UNCCH)
DONCHESKI	88	PL B206 137	M.A. Doncheski, H. Grotch, R. Robinett	(PSU)
DONCHESKI	88B	PR D38 412	M.A. Doncheski, H. Grotch, R.W. Robinett	(PSU)
BARTEL	87B	ZPHY C36 15	W. Bartel *et al.*	(JADE Collab.)
BEHREND	86B	PL B178 452	H.J. Behrend *et al.*	(CELLO Collab.)
DERRICK	86	PL 166B 463	M. Derrick *et al.*	(HRS Collab.)
Also		PR D34 3286	M. Derrick *et al.*	(HRS Collab.)
JODIDIO	86	PR D34 1967	A. Jodidio *et al.*	(LBL, NWES, TRIU)
Also		PR D37 237 (erratum)	A. Jodidio *et al.*	(LBL, NWES, TRIU)
MOHAPATRA	86	PR D34 909	R.N. Mohapatra	(UMD)
ADEVA	85	PL 152B 439	B. Adeva *et al.*	(Mark-J Collab.)
BERGER	85B	ZPHY C27 341	C. Berger *et al.*	(PLUTO Collab.)
STOKER	85	PRL 54 1887	D.P. Stoker *et al.*	(LBL, NWES, TRIU)
ADEVA	84	PRL 53 134	B. Adeva *et al.*	(Mark-J Collab.)
BEHREND	84C	PL 140B 130	H.J. Behrend *et al.*	(CELLO Collab.)
BERGSMA	83	PL 122B 465	F. Bergsma *et al.*	(CHARM Collab.)
CARR	83	PRL 51 627	J. Carr *et al.*	(LBL, NWES, TRIU)
BEALL	82	PRL 48 848	G. Beall, M. Bander, A. Soni	(UCI, UCLA)
SHANKER	82	NP B204 375	O. Shanker	(TRIU)

Axions (A^0) and Other Very Light Bosons, Searches for

See the related review(s):

Axions and Other Similar Particles

A^0 (Axion) MASS LIMITS from Astrophysics and Cosmology

These bounds depend on model-dependent assumptions (i.e. — on a combination of axion parameters).

VALUE (MeV)	DOCUMENT ID		TECN	COMMENT
• • • We do not use the following data for averages, fits, limits, etc. • • •				
>0.2	BARROSO	82	ASTR	Standard Axion
>0.25	[1] RAFFELT	82	ASTR	Standard Axion
>0.2	[2] DICUS	78C	ASTR	Standard Axion
	MIKAELIAN	78	ASTR	Stellar emission
>0.3	[2] SATO	78	ASTR	Standard Axion
>0.2	VYSOTSKII	78	ASTR	Standard Axion

[1] Lower bound from 5.5 MeV γ-ray line from the sun.

[2] Lower bound from requiring the red giants' stellar evolution not be disrupted by axion emission.

A^0 (Axion) and Other Light Boson (X^0) Searches in Hadron Decays

Limits are for branching ratios.

VALUE	CL%	DOCUMENT ID		TECN	COMMENT
• • • We do not use the following data for averages, fits, limits, etc. • • •					
$<7 \times 10^{-13}$	95	[1] ABRATENKO	21	MCBN	$K^+ \to \pi^+ X^0$ ($X^0 \to e^+e^-$)
$<1.5 \times 10^{-7}$	90	[2] CORTINA-GIL	21	NA62	$K^+ \to \mu^+ \nu X^0$
$<5 \times 10^{-11}$	90	[3] CORTINA-GIL	21A	NA62	$K^+ \to \pi^+ X^0$
$<9 \times 10^{-10}$	90	[4] CORTINA-GIL	21C	NA62	$K^+ \to \pi^+ X^0$
$<1.5 \times 10^{-8}$	90	[5] PARK	21	BELL	$B^0 \to X^0 X^0$ ($X^0 \to e^+e^-$, $\mu^+\mu^-$, $\pi^+\pi^-$)
$<2.4 \times 10^{-9}$	90	[6] AHN	19	KOTO	$K^0_L \to \pi^0 X^0$, m_{X^0} = 135 MeV
$<2 \times 10^{-10}$	95	[7] AAIJ	17AQ	LHCB	$B^+ \to K^+ X^0$ ($X^0 \to \mu^+\mu^-$)
$<3.7 \times 10^{-8}$	90	[8] AHN	17	KOTO	$K^0_L \to \pi^0 X^0$, m_{X^0} = 135 MeV
$<6 \times 10^{-11}$	90	[9] BATLEY	17	NA48	$K^\pm \to \pi^\pm X^0$($X^0 \to \mu^+\mu^-$)
		[10] WON	16	BELL	$\eta \to \gamma X^0$ ($X^0 \to \pi^+\pi^-$)
$<1 \times 10^{-9}$	95	[11] AAIJ	15AZ	LHCB	$B^0 \to K^{*0} X^0$ ($X^0 \to \mu^+\mu^-$)
$<1.5 \times 10^{-6}$	90	[12] ADLARSON	13	WASA	$\pi^0 \to \gamma X^0$ ($X^0 \to e^+e^-$), m_{X^0} = 100 MeV
$<2 \times 10^{-8}$	90	[13] BABUSCI	13B	KLOE	$\phi \to \eta X^0$ ($X^0 \to e^+e^-$)
		[14] ARCHILLI	12	KLOE	$\phi \to \eta X^0$, $X^0 \to e^+e^-$
$<2 \times 10^{-15}$	90	[15] GNINENKO	12A	BDMP	$\pi^0 \to \gamma X^0$ ($X^0 \to e^+e^-$)
$<3 \times 10^{-14}$	90	[16] GNINENKO	12B	BDMP	$\eta(\eta') \to \gamma X^0$ ($X^0 \to e^+e^-$)
$<7 \times 10^{-10}$	90	[17] ADLER	04	B787	$K^+ \to \pi^+ X^0$
$<7.3 \times 10^{-11}$	90	[18] ANISIMOVSK...	04	B949	$K^+ \to \pi^+ X^0$
$<4.5 \times 10^{-11}$	90	[19] ADLER	02C	B787	$K^+ \to \pi^+ X^0$
$<4 \times 10^{-5}$	90	[20] ADLER	01	B787	$K^+ \to \pi^+ \pi^0 A^0$
$<4.9 \times 10^{-5}$	90	AMMAR	01B	CLEO	$B^\pm \to \pi^\pm (K^\pm) X^0$
$<5.3 \times 10^{-5}$	90	AMMAR	01B	CLEO	$B^0 \to K^0_S X^0$
$<3.3 \times 10^{-5}$	90	[21] ALTEGOER	98	NOMD	$\pi^0 \to \gamma X^0$, $m_{X^0} < 120$ MeV
$<5.0 \times 10^{-8}$	90	[22] KITCHING	97	B787	$K^+ \to \pi^+ X^0$ ($X^0 \to \gamma\gamma$)
$<5.2 \times 10^{-10}$	90	[23] ADLER	96	B787	$K^+ \to \pi^+ X^0$
$<2.8 \times 10^{-4}$	90	[24] AMSLER	96B	CBAR	$\pi^0 \to \gamma X^0$, $m_{X^0} < 65$ MeV
$<3 \times 10^{-4}$	90	[24] AMSLER	96B	CBAR	$\eta \to \gamma X^0$, m_{X^0}= 50–200 MeV
$<4 \times 10^{-5}$	90	[24] AMSLER	96B	CBAR	$\eta' \to \gamma X^0$, m_{X^0}= 50–925 MeV
$<6 \times 10^{-5}$	90	[24] AMSLER	94B	CBAR	$\pi^0 \to \gamma X^0$, m_{X^0}=65–125 MeV
$<6 \times 10^{-5}$	90	[24] AMSLER	94B	CBAR	$\eta \to \gamma X^0$, m_{X^0}=200–525 MeV
$<7 \times 10^{-3}$	90	[25] MEIJERDREES	94	CNTR	$\pi^0 \to \gamma X^0$, m_{X^0}=25 MeV
$<2 \times 10^{-3}$	90	[25] MEIJERDREES	94	CNTR	$\pi^0 \to \gamma X^0$, m_{X^0}=100 MeV
$<2 \times 10^{-7}$	90	[26] ATIYA	93B	B787	Sup. by ADLER 04
$<3 \times 10^{-13}$		[27] NG	93	COSM	$\pi^0 \to \gamma X^0$
$<1.1 \times 10^{-8}$	90	[28] ALLIEGRO	92	SPEC	$K^+ \to \pi^+ X^0$ ($X^0 \to e^+e^-$)
$<5 \times 10^{-4}$	90	[29] ATIYA	92	B787	$\pi^0 \to \gamma X^0$
$<1 \times 10^{-12}$	95	[30] BARABASH	92	BDMP	$\pi^\pm \to e^\pm \nu X^0$($X^0 \to e^+e^-$, $\gamma\gamma$), m_{X^0} = 8 MeV
$<1 \times 10^{-12}$	95	[31] BARABASH	92	BDMP	$K^\pm \to \pi^\pm X^0$($X^0 \to e^+e^-$, $\gamma\gamma$), m_{X^0} = 10 MeV
$<1 \times 10^{-11}$	95	[32] BARABASH	92	BDMP	$K^0_L \to \pi^0 X^0$($X^0 \to e^+e^-$, $\gamma\gamma$), m_{X^0} = 10 MeV
$<1 \times 10^{-14}$	95	[33] BARABASH	92	BDMP	$\eta' \to \eta X^0$($X^0 \to e^+e^-$, $\gamma\gamma$), m_{X^0} = 10 MeV
$<4 \times 10^{-6}$	90	[34] MEIJERDREES	92	SPEC	$\pi^0 \to \gamma X^0$ ($X^0 \to e^+e^-$), m_{X^0}= 100 MeV
$<1 \times 10^{-7}$	90	[35] ATIYA	90B	B787	Sup. by KITCHING 97
$<1.3 \times 10^{-8}$	90	[36] KORENCHE...	87	SPEC	$\pi^+ \to e^+ \nu A^0$ ($A^0 \to e^+e^-$)
$<1 \times 10^{-9}$	90	[37] EICHLER	86	SPEC	Stopped $\pi^+ \to e^+ \nu A^0$
$<2 \times 10^{-5}$	90	[38] YAMAZAKI	84	SPEC	For 160<m<260 MeV

Downloaded from https://academic.oup.com/ptep/article/2022/8/083C01/6651666 by KIT Library user on 27 September 2022

$<(1.5–4)\times10^{-6}$ 90	[38] YAMAZAKI	84	SPEC	K decay, $m_{X^0} \ll 100$ MeV
	[39] ASANO	82	CNTR	Stopped $K^+ \to \pi^+ X^0$
	[40] ASANO	81B	CNTR	Stopped $K^+ \to \pi^+ X^0$
	[41] ZHITNITSKII	79		Heavy axion

[1] ABRATENKO 21 quoted limit is for $m_{X^0} = 150$ MeV and the lifetime $c\tau_{X^0} = 80$ m. See their Fig. 4 for the limits in the range of $m_{X^0} = 10$–210 MeV.

[2] CORTINA-GIL 21 quoted limit is for $m_{X^0} = 370$ MeV. Limits from O(10^{-5}) and O(10^{-6}) are obtained for $m_{X^0} = 10$–370 MeV (see their Fig. 7).

[3] CORTINA-GIL 21A quoted limit is for $m_{X^0} = 160$–250 MeV. Limits between 5×10^{-11} and 2×10^{-10} are obtained in the range of $m_{X^0} = 0$–110 and 154–260 MeV, assuming stable or invisibly decaying X^0. See their Fig. 4 for mass- and lifetime-dependent limits.

[4] CORTINA-GIL 21C quoted limit is for $m_{X^0} = 130$–140 MeV, and limits of 9×10^{-10}–6×10^{-7} are obtained in the mass range of $m_{X^0} = 110$–155 MeV, assuming X^0 escapes detection. See their Fig. 6 for mass- and lifetime-dependent limits.

[5] PARK 21 look for dark photons produced by decays of B^0 through off-shell Higgs-dark Higgs mixing. See their Fig. 5 for limits in the range of $m_{X^0} = 0.01$–2.62 GeV.

[6] AHN 19 is an update of AHN 17 from a new data set. See their Fig. 4 for the limits in the range of $m_{X^0} = 0$–250 MeV.

[7] AAIJ 17AQ limit is for $\tau_{X^0} = 10$ ps. See their Fig. 4 for limits in the range of $m_{X^0} =$ 250–4700 MeV and $\tau_{X^0} = 0.1$–1000 ps.

[8] AHN 17 limit as a function of m_{X^0} from 0 to 250 MeV is provided in their Fig. 5.

[9] BATLEY 17 limit is for $m_{X^0} = 216$ MeV and $\tau_{X^0} \le 10$ ps. See their Fig. 4(c) for limits in the range of $m_{X^0} = 211$–354 MeV and longer lifetimes.

[10] WON 16 look for a vector boson coupled to baryon number. Derived limits on $\alpha' < 10^{-3}$–10^{-2} for $m_{X^0} = 290$–520 MeV at 95% CL. See their Fig. 4 for mass-dependent limits.

[11] AAIJ 15AZ limit is for $\tau_{X^0} = 10$ ps and $m_{X^0} = 214$–4350 MeV. See their Fig. 4 for mass- and lifetime-dependent limits.

[12] ADLARSON 13 limits between 2.0×10^{-5} and 1.5×10^{-6} are obtained for $m_{X^0} =$ 20–100 MeV (see their Fig. 8). Angular momentum conservation requires that X^0 has spin ≥ 1.

[13] BABUSCI 13B limit is for B($\phi \to \eta X^0$)·B($X^0 \to e^+e^-$) and applies to $m_{X^0} = 410$ MeV. It is derived by analyzing $\eta \to \pi^0\pi^0\pi^0$ and $\pi^-\pi^+\pi^0$. Limits between 1×10^{-6} and 2×10^{-8} are obtained for $m_{X^0} \le 450$ MeV (see their Fig. 6).

[14] ARCHILLI 12 analyzed $\eta \to \pi^+\pi^-\pi^0$ decays. Derived limits on $\alpha'/\alpha < 2\times10^{-5}$ for $m_{X^0} = 50$–420 MeV at 90% CL. See their Fig. 8 for mass-dependent limits.

[15] GNINENKO 12A limit is for B($\pi^0 \to \gamma X^0$)·B($X^0 \to e^+e^-$) and applies for $m_{X^0} =$ 90 MeV and $\tau_{X^0} \simeq 1\times10^{-8}$ sec. Limits between 10^{-8} and 2×10^{-15} are obtained for $m_{X^0} = 3$–120 MeV and $\tau_{X^0} = 1\times10^{-11}$–1 sec. See their Fig. 3 for limits at different masses and lifetimes.

[16] GNINENKO 12B limit is for B($\eta \to \gamma X^0$)·B($X^0 \to e^+e^-$) and applies for $m_{X^0} =$ 100 MeV and $\tau_{X^0} \simeq 6\times10^{-9}$ sec. Limits between 10^{-5} and 3×10^{-14} are obtained for $m_{X^0} \lesssim 550$ MeV and $\tau_{X^0} = 10^{-10}$–10 sec. See their Fig. 5 for limits at different mass and lifetime and for η' decays.

[17] ADLER 04 limit applies for a mass near 180 MeV. For other masses in the range $m_{X^0} =$ 150–250 MeV the limit is less restrictive, but still improves ADLER 02C and ATIYA 93B.

[18] ANISIMOVSKY 04 bound is for m_{X^0}=0.

[19] ADLER 02C bound is for m_{X^0} <60 MeV. See Fig. 2 for limits at higher masses.

[20] The quoted limit is for $m_{X^0} = 0$–80 MeV. See their Fig. 5 for the limit at higher mass. The branching fraction limit assumes pure phase space decay distributions.

[21] ALTEGOER 98 looked for X^0 from π^0 decay which penetrate the shielding and convert to π^0 in the external Coulomb field of a nucleus.

[22] KITCHING 97 limit is for B($K^+ \to \pi^+ X^0$)·B($X^0 \to \gamma\gamma$) and applies for $m_{X^0} \simeq 50$ MeV, $\tau_{X^0} < 10^{-10}$ s. Limits are provided for $0<m_{X^0}<100$ MeV, $\tau_{X^0} < 10^{-8}$ s.

[23] ADLER 96 looked for a peak in missing-mass distribution. This work is an update of ATIYA 93. The limit is for massless stable X^0 particles and extends to m_{X^0}=80 MeV at the same level. See paper for dependence on finite lifetime.

[24] AMSLER 94B and AMSLER 96B looked for a peak in missing-mass distribution.

[25] MEIJERDREES 94 limit is based on inclusive photon spectrum and is independent of X^0 decay modes. It applies to $\tau(X^0) > 10^{-23}$ sec.

[26] ATIYA 93B looked for a peak in missing mass distribution. The bound applies for stable X^0 of m_{X^0}=150–250 MeV, and the limit becomes stronger (10^{-8}) for m_{X^0}=180–240 MeV.

[27] NG 93 studied the production of X^0 via $\gamma\gamma \to \pi^0 \to \gamma X^0$ in the early universe at $T \simeq 1$ MeV. The bound on extra neutrinos from nucleosynthesis $\Delta N_\nu < 0.3$ (WALKER 91) is employed. It applies to $m_{X^0} \ll 1$ MeV in order to be relativistic down to nucleosynthesis temperature. See paper for heavier X^0.

[28] ALLIEGRO 92 limit applies for m_{X^0}=150–340 MeV and is the branching ratio times the decay probability. Limit is $< 1.5\times10^{-8}$ at 99%CL.

[29] ATIYA 92 looked for a peak in missing mass distribution. The limit applies to m_{X^0}=0–130 MeV in the narrow resonance limit. See paper for the dependence on lifetime. Covariance requires X^0 to be a vector particle.

[30] BARABASH 92 is a beam dump experiment that searched for a light Higgs. Limits between 1×10^{-12} and 1×10^{-7} are obtained for $3 < m_{X^0} < 40$ MeV.

[31] Limits between 1×10^{-12} and 1 are obtained for $4 < m_{X^0} < 69$ MeV.

[32] Limits between 1×10^{-11} and 5×10^{-3} are obtained for $4 < m_{X^0} < 63$ MeV.

[33] Limits between 1×10^{-14} and 1 are obtained for $3 < m_{X^0} < 82$ MeV.

[34] MEIJERDREES 92 limit applies for $\tau_{X^0} = 10^{-23}$–10^{-11} sec. Limits between 2×10^{-4} and 4×10^{-6} are obtained for $m_{X^0} = 25$–120 MeV. Angular momentum conservation requires that X^0 has spin ≥ 1.

[35] ATIYA 90B limit is for B($K^+ \to \pi^+ X^0$)·B($X^0 \to \gamma\gamma$) and applies for $m_{X^0} = 50$ MeV, $\tau_{X^0} < 10^{-10}$ s. Limits are also provided for $0 < m_{X^0} < 100$ MeV, $\tau_{X^0} < 10^{-8}$ s.

[36] KORENCHENKO 87 limit assumes $m_{A^0} = 1.7$ MeV, $\tau_{A^0} \lesssim 10^{-12}$ s, and B($A^0 \to e^+e^-$) = 1.

[37] EICHLER 86 looked for $\pi^+ \to e^+\nu A^0$ followed by $A^0 \to e^+e^-$. Limits on the branching fraction depend on the mass and and lifetime of A^0. The quoted limits are valid when $\tau(A^0) \gtrsim 3.\times10^{-10}$s if the decays are kinematically allowed.

[38] YAMAZAKI 84 looked for a discrete line in $K^+ \to \pi^+$X. Sensitive to wide mass range (5–300 MeV), independent of whether X decays promptly or not.

[39] ASANO 82 at KEK set limits for B($K^+ \to \pi^+ X^0$) for m_{X^0} <100 MeV as BR $< 4.\times10^{-8}$ for $\tau(X^0 \to n\gamma\text{'s}) > 1.\times10^{-9}$ s, BR $< 1.4\times10^{-6}$ for $\tau < 1.\times10^{-9}$s.

[40] ASANO 81B is KEK experiment. Set B($K^+ \to \pi^+ X^0$) $< 3.8\times10^{-8}$ at CL = 90%.

[41] ZHITNITSKII 79 argue that a heavy axion predicted by YANG 78 (3 <m <40 MeV) contradicts experimental muon anomalous magnetic moments.

A^0 (Axion) Searches in Quarkonium Decays

Decay or transition of quarkonium. Limits are for branching ratio.

VALUE	CL%	DOCUMENT ID		TECN	COMMENT
• • • We do not use the following data for averages, fits, limits, etc. • • •					
$<2.8\times10^{-8}$	90	[1] ABLIKIM	16E	BES3	$J/\psi \to A^0\gamma$ ($A^0 \to \mu^+\mu^-$)
$<4\times10^{-7}$	90	[2] ABLIKIM	12	BES3	$J/\psi \to A^0\gamma$ ($A^0 \to \mu^+\mu^-$)
$<4.0\times10^{-5}$	90	[3] ANTREASYAN	90C	CBAL	$\Upsilon(1S) \to A^0\gamma$
$<5\times10^{-5}$	90	[4] DRUZHININ	87	ND	$\phi \to A^0\gamma$ ($A^0 \to e^+e^-$)
$<2\times10^{-3}$	90	[5] DRUZHININ	87	ND	$\phi \to A^0\gamma$ ($A^0 \to \gamma\gamma$)
$<7\times10^{-6}$	90	[6] DRUZHININ	87	ND	$\phi \to A^0\gamma$ ($A^0 \to$ missing)
$<1.4\times10^{-5}$	90	[7] EDWARDS	82	CBAL	$J/\psi \to A^0\gamma$

[1] ABLIKIM 16E limits between 2.8–495.3$\times10^{-8}$ were obtained for 0.212 GeV $< m_{A^0} <$ 3.0 GeV. See their Fig. 5 for mass-dependent limits.

[2] ABLIKIM 12 derived limits between 4×10^{-7}–2.1×10^{-5} for 0.212 GeV $< m_{A^0} <$ 3.0 GeV. See their Fig. 2(c) for mass-dependent limits.

[3] ANTREASYAN 90C assume that A^0 does not decay in the detector.

[4] The first DRUZHININ 87 limit is valid when $\tau_{A^0}/m_{A^0} < 3\times10^{-13}$ s/MeV and $m_{A^0} < 20$ MeV.

[5] The second DRUZHININ 87 limit is valid when $\tau_{A^0}/m_{A^0} < 5\times10^{-13}$ s/MeV and $m_{A^0} < 20$ MeV.

[6] The third DRUZHININ 87 limit is valid when $\tau_{A^0}/m_{A^0} > 7\times10^{-12}$ s/MeV and $m_{A^0} < 200$ MeV.

[7] EDWARDS 82 looked for $J/\psi \to \gamma A^0$ decays by looking for events with a single γ [of energy $\sim 1/2$ the $J/\psi(1S)$ mass], plus nothing else in the detector. The limit is inconsistent with the axion interpretation of the FAISSNER 81B result.

A^0 (Axion) Searches in Positronium Decays

Decay or transition of positronium. Limits are for branching ratio.

VALUE	CL%	DOCUMENT ID		TECN	COMMENT
• • • We do not use the following data for averages, fits, limits, etc. • • •					
$<4.4\times10^{-5}$	90	[1] BADERT...	02	CNTR	o-Ps $\to \gamma X_1 X_2$, $m_{X_1}+m_{X_2} \le$ 900 keV
$<2\times10^{-4}$	90	MAENO	95	CNTR	o-Ps $\to A^0\gamma$ m_{A^0}=850–1013 keV
$<3.0\times10^{-4}$	90	[2] ASAI	94	CNTR	o-Ps $\to A^0\gamma$ m_{A^0}=30–500 keV
$<2.8\times10^{-5}$	90	[3] AKOPYAN	91	CNTR	o-Ps $\to A^0\gamma$ ($A^0 \to \gamma\gamma$), $m_{A^0} < 30$ keV
$<1.1\times10^{-6}$	90	[4] ASAI	91	CNTR	o-Ps $\to A^0\gamma$, $m_{A^0} < 800$ keV
$<3.8\times10^{-4}$	90	GNINENKO	90	CNTR	o-Ps $\to A^0\gamma$, $m_{A^0} < 30$ keV
$<(1–5)\times10^{-4}$	95	[5] TSUCHIAKI	90	CNTR	o-Ps $\to A^0\gamma$, m_{A^0} = 300–900 keV
$<6.4\times10^{-5}$	90	[6] ORITO	89	CNTR	o-Ps $\to A^0\gamma$, $m_{A^0} < 30$ keV
		[7] AMALDI	85	CNTR	Ortho-positronium
		[8] CARBONI	83	CNTR	Ortho-positronium

[1] BADERTSCHER 02 looked for a three-body decay of ortho-positronium into a photon and two penetrating (neutral or milli-charged) particles.

[2] The ASAI 94 limit is based on inclusive photon spectrum and is independent of A^0 decay modes.

[3] The AKOPYAN 91 limit applies for a short-lived A^0 with $\tau_{A^0} < 10^{-13}\ m_{A^0}$ [keV] s.

[4] ASAI 91 limit translates to $g^2_{A^0 e^+e^-}/4\pi < 1.1\times10^{-11}$ (90% CL) for $m_{A^0} < 800$ keV.

[5] The TSUCHIAKI 90 limit is based on inclusive photon spectrum and is independent of A^0 decay modes.

[6] ORITO 89 limit translates to $g^2_{A^0 ee}/4\pi < 6.2\times10^{-10}$. Somewhat more sensitive limits are obtained for larger m_{A^0}: $B < 7.6\times10^{-6}$ at 100 keV.

[7] AMALDI 85 set limits B($A^0\gamma$) / B($\gamma\gamma\gamma$) $<$ (1–5) $\times10^{-6}$ for m_{A^0} = 900–100 keV which are about 1/10 of the CARBONI 83 limits.

[8] CARBONI 83 looked for orthopositronium $\to A^0\gamma$. Set limit for A^0 electron coupling squared, $g(eeA^0)^2/(4\pi) < 6.\times10^{-10}$–$7.\times10^{-9}$ for m_{A^0} from 150–900 keV (CL = 99.7%). This is about 1/10 of the bound from g−2 experiments.

A^0 (Axion) Search in Photoproduction

VALUE	DOCUMENT ID	COMMENT
• • • We do not use the following data for averages, fits, limits, etc. • • •		
	[1] BASSOMPIE... 95	$m_{A^0} = 1.8 \pm 0.2$ MeV

Downloaded from https://academic.oup.com/ptep/article/2022/8/083C01/6651666 by KIT Library user on 27 September 2022

[1] BASSOMPIERRE 95 is an extension of BASSOMPIERRE 93. They looked for a peak in the invariant mass of e^+e^- pairs in the region $m_{e^+e^-} = 1.8 \pm 0.2$ MeV. They obtained bounds on the production rate A^0 for $\tau(A^0) = 10^{-18}$–10^{-9} sec. They also found an excess of events in the range $m_{e^+e^-} = 2.1$–3.5 MeV.

A^0 (Axion) Production in Hadron Collisions

Limits are for $\sigma(A^0)$ / $\sigma(\pi^0)$.

VALUE	CL%	EVTS	DOCUMENT ID		TECN	COMMENT
• • • We do not use the following data for averages, fits, limits, etc. • • •						
			[1] AAD	21F	ATLS	Monojet + missing p_T
			[2] AAD	21K	ATLS	Mono-γ + missing p_T
			[3] AAD	21N	ATLS	$\gamma\gamma$ scatt. in Pb+Pb
			[4] CARRA	21	ATLS	$pp \to A^{*0} \to WW$, $Z\gamma$
			[5] AAIJ	20AL	LHCB	$pp \to X^0 \to \mu^+\mu^-$
			[6] GAVELA	20	CMS	$pp \to A^{*0} \to \gamma\gamma$, ZZ
			[7] SIRUNYAN	19BQ	CMS	$X^0 \to \mu^+\mu^-$
			[8] JAIN	07	CNTR	$A^0 \to e^+e^-$
			[9] AHMAD	97	SPEC	e^+ production
			[10] LEINBERGER	97	SPEC	$A^0 \to e^+e^-$
			[11] GANZ	96	SPEC	$A^0 \to e^+e^-$
			[12] KAMEL	96	EMUL	^{32}S emulsion, $A^0 \to e^+e^-$
			[13] BLUEMLEIN	92	BDMP	$A^0 N_Z \to \ell^+\ell^- N_Z$
			[14] MEIJERDREES	92	SPEC	$\pi^- p \to nA^0$, $A^0 \to e^+e^-$
			[15] BLUEMLEIN	91	BDMP	$A^0 \to e^+e^-$, 2γ
			[16] FAISSNER	89	OSPK	Beam dump, $A^0 \to e^+e^-$
			[17] DEBOER	88	RVUE	$A^0 \to e^+e^-$
			[18] EL-NADI	88	EMUL	$A^0 \to e^+e^-$
			[19] FAISSNER	88	OSPK	Beam dump, $A^0 \to 2\gamma$
			[20] BADIER	86	BDMP	$A^0 \to e^+e^-$
$<2. \times 10^{-11}$	90	0	[21] BERGSMA	85	CHRM	CERN beam dump
$<1. \times 10^{-13}$	90	0	[21] BERGSMA	85	CHRM	CERN beam dump
		24	[22] FAISSNER	83	OSPK	Beam dump, $A^0 \to 2\gamma$
			[23] FAISSNER	83B	RVUE	LAMPF beam dump
			[24] FRANK	83B	RVUE	LAMPF beam dump
			[25] HOFFMAN	83	CNTR	$\pi p \to nA^0$ $(A^0 \to e^+e^-)$
			[26] FETSCHER	82	RVUE	See FAISSNER 81B
		12	[27] FAISSNER	81	OSPK	CERN PS ν wideband
		15	[28] FAISSNER	81B	OSPK	Beam dump, $A^0 \to 2\gamma$
		8	[29] KIM	81	OSPK	26 GeV $pN \to A^0X$
		0	[30] FAISSNER	80	OSPK	Beam dump, $A^0 \to e^+e^-$
$<1. \times 10^{-8}$	90		[31] JACQUES	80	HLBC	28 GeV protons
$<1. \times 10^{-14}$	90		[31] JACQUES	80	HLBC	Beam dump
			[32] SOUKAS	80	CALO	28 GeV p beam dump
			[33] BECHIS	79	CNTR	
$<1. \times 10^{-8}$	90		[34] COTEUS	79	OSPK	Beam dump
$<1. \times 10^{-3}$	95		[35] DISHAW	79	CALO	400 GeV pp
$<1. \times 10^{-8}$	90		ALIBRAN	78	HYBR	Beam dump
$<6. \times 10^{-9}$	95		ASRATYAN	78B	CALO	Beam dump
$<1.5 \times 10^{-8}$	90		[36] BELLOTTI	78	HLBC	Beam dump
$<5.4 \times 10^{-14}$	90		[36] BELLOTTI	78	HLBC	m_{A^0}=1.5 MeV
$<4.1 \times 10^{-9}$	90		[36] BELLOTTI	78	HLBC	m_{A^0}=1 MeV
$<1. \times 10^{-8}$	90		[37] BOSETTI	78B	HYBR	Beam dump
			[38] DONNELLY	78		
$<0.5 \times 10^{-8}$	90		HANSL	78D	WIRE	Beam dump
			[39] MICELMAC...	78		
			[40] VYSOTSKII	78		

[1] AAD 21F look for axion production with an energetic jet and large missing p_T, and set a limit on the axion coupling to gluons, $c_{\widetilde{G}}/f_{A^0} < 8 \times 10^{-6}$ GeV^{-1} at 95 % CL for $m_{A^0} = 1$ MeV. Using $c_{\widetilde{G}} = \alpha_s/8\pi$, we interpret the limit as $f_{A^0} > 0.4$ TeV for $\alpha_s \simeq 0.08$.

[2] AAD 21K look for axion production with an energetic photon and large missing p_T, and set a limit on the axion coupling to a Z boson and photon, $G_{AZ\gamma} < 5.1 \times 10^{-4}$ GeV^{-1} at 95 % CL for $m_{A^0} = 1$ MeV and assuming $G_{A\gamma\gamma} = 0$.

[3] AAD 21N look for axion production using the measurement of light-by-light scattering based on Pb+Pb collision data. They set the limit on the axion-photon coupling, $G_{A\gamma\gamma} < 5.3 \times 10^{-5}$–$3.4 \times 10^{-4}$ GeV^{-1} at 95 % CL for $m_{A^0} = 6$–100 GeV. Here we use $\Lambda_a = G_{A\gamma\gamma}{}^{-1}$ to translate their limits. See their Fig. 9 for mass-dependent limits.

[4] CARRA 21 is analogous to GAVELA 20, and they use the differential cross sections for WW and $Z\gamma$ production measured with the ATLAS detector to set limits on the product of the axion couplings to gauge bosons as $G_{AWW}\, G_{Agg} < 6.2 \times 10^{-7}$ GeV^{-2} and $G_{AZ\gamma}\, G_{Agg} < 3.7 \times 10^{-7}$ GeV^{-2} at 95 % CL for $m_{A^0} \lesssim 100$ GeV.

[5] AAIJ 20AL look for a light new boson decaying into a pair of muons using the LHCb data with an integrated luminosity of 5.1 fb^{-1}, and set limits on the cross section over a range of $m_{X^0} = 0.22$–3 and 20–60 GeV. See Figs. 8 and 9 for mass-dependent limits.

[6] GAVELA 20 focus on the axion production as an s-channel off shell mediator, and use the Run 2 CMS public data to set limits on the product of the axion couplings to gluons and photons as well as Z bosons as $G_{A\gamma\gamma}\, G_{Agg} < 2.8 \times 10^{-7}$ GeV^{-2} and $G_{AZZ}\, G_{Agg} < 9.8 \times 10^{-7}$ GeV^{-2} for $m_{A^0} \lesssim 200$ GeV. See their Fig.3 for the limits.

[7] SIRUNYAN 19BQ look for the pair production of a new light boson decaying into a pair of muons, and set limits on the product of the production cross section times branching fraction to dimuons squared times acceptance over a range of $m_{X^0} = 0.25$–8.5 GeV. See the right panel of their Fig. 1 for mass-dependent limits.

[8] JAIN 07 claims evidence for $A^0 \to e^+e^-$ produced in ^{207}Pb collision on nuclear emulsion (Ag/Br) for $m(A^0) = 7 \pm 1$ or 19 ± 1 MeV and $\tau(A^0) \leq 10^{-13}$ s.

[9] AHMAD 97 reports a result of APEX Collaboration which studied positron production in ^{238}U+^{232}Ta and ^{238}U+^{181}Ta collisions, without requiring a coincident electron. No narrow lines were found for $250 < E_{e^+} < 750$ keV.

[10] LEINBERGER 97 (ORANGE Collaboration) at GSI looked for a narrow sum-energy e^+e^--line at ~ 635 keV in ^{238}U+^{181}Ta collision. Limits on the production probability for a narrow sum-energy e^+e^- line are set. See their Table 2.

[11] GANZ 96 (EPos II Collaboration) has placed upper bounds on the production cross section of e^+e^- pairs from ^{238}U+^{181}Ta and ^{238}U+^{232}Th collisions at GSI. See Table 2 for limits both for back-to-back and isotropic configurations of e^+e^- pairs. These limits rule out the existence of peaks in the e^+e^- sum-energy distribution, reported by an earlier version of this experiment.

[12] KAMEL 96 looked for e^+e^- pairs from the collision of ^{32}S (200 GeV/nucleon) and emulsion. No evidence of mass peaks is found in the region of sensitivity $m_{ee} > 2$ MeV.

[13] BLUEMLEIN 92 is a proton beam dump experiment at Serpukhov with a secondary target to induce Bethe-Heitler production of e^+e^- or $\mu^+\mu^-$ from the produce A^0. See Fig. 5 for the excluded region in m_{A^0}-x plane. For the standard axion, $0.3 < x < 25$ is excluded at 95% CL. If combined with BLUEMLEIN 91, $0.008 < x < 32$ is excluded.

[14] MEIJERDREES 92 give $\Gamma(\pi^- p \to nA^0) \cdot B(A^0 \to e^+e^-)/\Gamma(\pi^- p \to \text{all}) < 10^{-5}$ (90% CL) for $m_{A^0} = 100$ MeV, $\tau_{A^0} = 10^{-11}$–10^{-23} sec. Limits ranging from 2.5×10^{-3} to 10^{-7} are given for $m_{A^0} = 25$–136 MeV.

[15] BLUEMLEIN 91 is a proton beam dump experiment at Serpukhov. No candidate event for $A^0 \to e^+e^-$, 2γ are found. Fig. 6 gives the excluded region in m_{A^0}-x plane ($x = \tan\beta = v_2/v_1$). Standard axion is excluded for $0.2 < m_{A^0} < 3.2$ MeV for most $x > 1$, 0.2–11 MeV for most $x < 1$.

[16] FAISSNER 89 searched for $A^0 \to e^+e^-$ in a proton beam dump experiment at SIN. No excess of events was observed over the background. A standard axion with mass $2m_e$–20 MeV is excluded. Lower limit on f_{A^0} of $\simeq 10^4$ GeV is given for $m_{A^0} = 2m_e$–20 MeV.

[17] DEBOER 88 reanalyze EL-NADI 88 data and claim evidence for three distinct states with mass ~ 1.1, ~ 2.1, and ~ 9 MeV, lifetimes 10^{-16}–10^{-15} s decaying to e^+e^- and note the similarity of the data with those of a cosmic-ray experiment by Bristol group (B.M. Anand, Proc. of the Royal Society of London, Section A **A22** 183 (1953)). For a criticism see PERKINS 89, who suggests that the events are compatible with π^0 Dalitz decay. DEBOER 89B is a reply which contests the criticism.

[18] EL-NADI 88 claim the existence of a neutral particle decaying into e^+e^- with mass 1.60 ± 0.59 MeV, lifetime $(0.15 \pm 0.01) \times 10^{-14}$ s, which is produced in heavy ion interactions with emulsion nuclei at ~ 4 GeV/c/nucleon.

[19] FAISSNER 88 is a proton beam dump experiment at SIN. They found no candidate event for $A^0 \to \gamma\gamma$. A standard axion decaying to 2γ is excluded except for a region $x \simeq 1$. Lower limit on f_{A^0} of 10^2–10^3 GeV is given for $m_{A^0} = 0.1$–1 MeV.

[20] BADIER 86 did not find long-lived A^0 in 300 GeV π^- Beam Dump Experiment that decays into e^+e^- in the mass range $m_{A^0} = (20$–$200)$ MeV, which excludes the A^0 decay constant $f(A^0)$ in the interval (60–600) GeV. See their figure 6 for excluded region on $f(A^0)$-m_{A^0} plane.

[21] BERGSMA 85 look for $A^0 \to 2\gamma$, e^+e^-, $\mu^+\mu^-$. First limit above is for $m_{A^0} = 1$ MeV; second is for 200 MeV. See their figure 4 for excluded region on f_{A^0}–m_{A^0} plane, where f_{A^0} is A^0 decay constant. For Peccei-Quinn PECCEI 77 A^0, $m_{A^0} < 180$ keV and $\tau > 0.037$ s. (CL = 90%). For the axion of FAISSNER 81B at 250 keV, BERGSMA 85 expect 15 events but observe zero.

[22] FAISSNER 83 observed 19 1-γ and 12 2-γ events where a background of 4.8 and 2.3 respectively is expected. A small-angle peak is observed even if iron wall is set in front of the decay region.

[23] FAISSNER 83B extrapolate SIN γ signal to LAMPF ν experimental condition. Resulting 370 γ's are not at variance with LAMPF upper limit of 450 γ's. Derived from LAMPF limit that $[d\sigma(A^0)/d\omega$ at $90°]\, m_{A^0}/\tau_{A^0} < 14 \times 10^{-35}$ cm^2 sr^{-1} MeV ms^{-1}. See comment on FRANK 83B.

[24] FRANK 83B stress the importance of LAMPF data bins with negative net signal. By statistical analysis say that LAMPF and SIN-A0 are at variance when extrapolation by phase-space model is done. They find LAMPF upper limit is 248 not 450 γ's. See comment on FAISSNER 83B.

[25] HOFFMAN 83 set CL = 90% limit $d\sigma/dt\, B(e^+e^-) < 3.5 \times 10^{-32}$ cm^2/GeV^2 for $140 < m_{A^0} < 160$ MeV. Limit assumes $\tau(A^0) < 10^{-9}$ s.

[26] FETSCHER 82 reanalyzes SIN beam-dump data of FAISSNER 81. Claims no evidence for axion since 2-γ peak rate remarkably decreases if iron wall is set in front of the decay region.

[27] FAISSNER 81 see excess μe events. Suggest axion interactions.

[28] FAISSNER 81B is SIN 590 MeV proton beam dump. Observed 14.5 ± 5.0 events of 2γ decay of long-lived neutral penetrating particle with $m_{2\gamma} \lesssim 1$ MeV. Axion interpretation with η-A^0 mixing gives $m_{A^0} = 250 \pm 25$ keV, $\tau_{(2\gamma)} = (7.3 \pm 3.7) \times 10^{-3}$ s from above rate. See critical remarks below in comments of FETSCHER 82, FAISSNER 83, FAISSNER 83B, FRANK 83B, and BERGSMA 85. Also see in the next subsection ALEKSEEV 82B, CAVAIGNAC 83, and ANANEV 85.

[29] KIM 81 analyzed 8 candidates for $A^0 \to 2\gamma$ obtained by Aachen-Padova experiment at CERN with 26 GeV protons on Be. Estimated axion mass is about 300 keV and lifetime is $(0.86 \sim 5.6) \times 10^{-3}$ s depending on models. Faissner (private communication), says axion production underestimated and mass overestimated. Correct value around 200 keV.

Downloaded from https://academic.oup.com/ptep/article/2022/8/083C01/6651666 by KIT Library user on 27 September 2022

[30] FAISSNER 80 is SIN beam dump experiment with 590 MeV protons looking for $A^0 \to e^+e^-$ decay. Assuming $A^0/\pi^0 = 5.5 \times 10^{-7}$, obtained decay rate limit 20/(A^0 mass) MeV/s (CL = 90%), which is about 10^{-7} below theory and interpreted as upper limit to $m_{A^0} < 2m_{e^-}$.

[31] JACQUES 80 is a BNL beam dump experiment. First limit above comes from nonobservation of excess neutral-current-type events [σ(production)σ(interaction) $< 7. \times 10^{-68}$ cm^4, CL = 90%]. Second limit is from nonobservation of axion decays into 2γ's or e^+e^-, and for axion mass a few MeV.

[32] SOUKAS 80 at BNL observed no excess of neutral-current-type events in beam dump.

[33] BECHIS 79 looked for the axion production in low energy electron Bremsstrahlung and the subsequent decay into either 2γ or e^+e^-. No signal found. CL = 90% limits for model parameter(s) are given.

[34] COTEUS 79 is a beam dump experiment at BNL.

[35] DISHAW 79 is a calorimetric experiment and looks for low energy tail of energy distributions due to energy lost to weakly interacting particles.

[36] BELLOTTI 78 first value comes from search for $A^0 \to e^+e^-$. Second value comes from search for $A^0 \to 2\gamma$, assuming mass $< 2m_{e^-}$. For any mass satisfying this, limit is above value$\times$(mass^{-4}). Third value uses data of PL 60B 401 and quotes σ(production)σ(interaction) $< 10^{-67}$ cm^4.

[37] BOSETTI 78B quotes σ(production)σ(interaction) $< 2. \times 10^{-67}$ cm^4.

[38] DONNELLY 78 examines data from reactor neutrino experiments of REINES 76 and GURR 74 as well as SLAC beam dump experiment. Evidence is negative.

[39] MICELMACHER 78 finds no evidence of axion existence in reactor experiments of REINES 76 and GURR 74. (See reference under DONNELLY 78 below).

[40] VYSOTSKII 78 derived lower limit for the axion mass 25 keV from luminosity of the sun and 200 keV from red supergiants.

A^0 (Axion) Searches in Reactor Experiments

VALUE	DOCUMENT ID		TECN	COMMENT
• • • We do not use the following data for averages, fits, limits, etc. • • •				
	[1] CHANG	07		Primakoff or Compton
	[2] ALTMANN	95	CNTR	Reactor; $A^0 \to e^+e^-$
	[3] KETOV	86	SPEC	Reactor, $A^0 \to \gamma\gamma$
	[4] KOCH	86	SPEC	Reactor; $A^0 \to \gamma\gamma$
	[5] DATAR	82	CNTR	Light water reactor
	[6] VUILLEUMIER	81	CNTR	Reactor, $A^0 \to 2\gamma$

[1] CHANG 07 looked for monochromatic photons from Primakoff or Compton conversion of axions from the Kuo-Sheng reactor due to axion coupling to photon or electron, respectively. The search places model-independent limits on the products $G_{A\gamma\gamma}G_{ANN}$ and $G_{Aee}G_{ANN}$ for $m(A^0)$ less than the MeV range.

[2] ALTMANN 95 looked for A^0 decaying into e^+e^- from the Bugey5 nuclear reactor. They obtain an upper limit on the A^0 production rate of $\omega(A^0)/\omega(\gamma) \times$B($A^0 \to e^+e^-$)$< 10^{-16}$ for $m_{A^0} = 1.5$ MeV at 90% CL. The limit is weaker for heavier A^0. In the case of a standard axion, this limit excludes a mass in the range $2m_e < m_{A^0} < 4.8$ MeV at 90% CL. See Fig. 5 of their paper for exclusion limits of axion-like resonances Z^0 in the (m_{X^0},f_{X^0}) plane.

[3] KETOV 86 searched for A^0 at the Rovno nuclear power plant. They found an upper limit on the A^0 production probability of 0.8 [100 keV/m_{A^0}]^6 $\times 10^{-6}$ per fission. In the standard axion model, this corresponds to $m_{A^0} > 150$ keV. Not valid for $m_{A^0} \gtrsim 1$ MeV.

[4] KOCH 86 searched for $A^0 \to \gamma\gamma$ at nuclear power reactor Biblis A. They found an upper limit on the A^0 production rate of $\omega(A^0)/\omega(\gamma(M1)) < 1.5 \times 10^{-10}$ (CL=95%). Standard axion with $m_{A^0} = 250$ keV gives 10^{-5} for the ratio. Not valid for $m_{A^0} > 1022$ keV.

[5] DATAR 82 looked for $A^0 \to 2\gamma$ in neutron capture ($np \to dA^0$) at Tarapur 500 MW reactor. Sensitive to sum of $l = 0$ and $l = 1$ amplitudes. With ZEHNDER 81 [($l = 0$) − ($l = 1$)] result, assert nonexistence of standard A^0.

[6] VUILLEUMIER 81 is at Grenoble reactor. Set limit $m_{A^0} < 280$ keV.

A^0 (Axion) and Other Light Boson (X^0) Searches in Nuclear Transitions

Limits are for branching ratio.

VALUE	CL%	DOCUMENT ID		TECN	COMMENT
• • • We do not use the following data for averages, fits, limits, etc. • • •					
$< 8.5 \times 10^{-6}$	90	[1] DERBIN	02	CNTR	^{125m}Te decay
		[2] DEBOER	97C	RVUE	M1 transitions
$< 5.5 \times 10^{-10}$	95	[3] TSUNODA	95	CNTR	^{252}Cf fission, $A^0 \to ee$
$< 1.2 \times 10^{-6}$	95	[4] MINOWA	93	CNTR	^{139}La* $\to$ ^{139}LaA^0
$< 2 \times 10^{-4}$	90	[5] HICKS	92	CNTR	^{35}S decay, $A^0 \to \gamma\gamma$
$< 1.5 \times 10^{-9}$	95	[6] ASANUMA	90	CNTR	^{241}Am decay
$<(0.4–10) \times 10^{-3}$	95	[7] DEBOER	90	CNTR	^{8}Be* $\to$ ^{8}BeA^0, $A^0 \to e^+e^-$
$<(0.2–1) \times 10^{-3}$	90	[8] BINI	89	CNTR	^{16}O* $\to$ ^{16}OX^0, $X^0 \to e^+e^-$
		[9] AVIGNONE	88	CNTR	Cu* $\to$ CuA^0 ($A^0 \to 2\gamma$, $A^0e \to \gamma e$, $A^0Z \to \gamma Z$)
$< 1.5 \times 10^{-4}$	90	[10] DATAR	88	CNTR	^{12}C* $\to$ ^{12}CA^0, $A^0 \to e^+e^-$
$< 5 \times 10^{-3}$	90	[11] DEBOER	88C	CNTR	^{16}O* $\to$ ^{16}OX^0, $X^0 \to e^+e^-$
$< 3.4 \times 10^{-5}$	95	[12] DOEHNER	88	SPEC	^{2}H*, $A^0 \to e^+e^-$
$< 4 \times 10^{-4}$	95	[13] SAVAGE	88	CNTR	Nuclear decay (isovector)
$< 3 \times 10^{-3}$	95	[13] SAVAGE	88	CNTR	Nuclear decay (isoscalar)
$<10.6 \times 10^{-2}$	90	[14] HALLIN	86	SPEC	^{6}Li isovector decay
<10.8	90	[14] HALLIN	86	SPEC	^{10}B isoscalar decays
< 2.2	90	[14] HALLIN	86	SPEC	^{14}N isoscalar decays
$< 4 \times 10^{-4}$	90	[15] SAVAGE	86B	CNTR	^{14}N*
		[16] ANANEV	85	CNTR	Li*, deut* $A^0 \to 2\gamma$
		[17] CAVAIGNAC	83	CNTR	^{97}Nb*, deut* transition $A^0 \to 2\gamma$
		[18] ALEKSEEV	82B	CNTR	Li*, deut* transition $A^0 \to 2\gamma$
		[19] LEHMANN	82	CNTR	Cu* $\to$ CuA^0 ($A^0 \to 2\gamma$)
		[20] ZEHNDER	82	CNTR	Li*, Nb* decay, n-capt.
		[21] ZEHNDER	81	CNTR	Ba* $\to$ BaA^0 ($A^0 \to 2\gamma$)
		[22] CALAPRICE	79		Carbon

[1] DERBIN 02 looked for the axion emission in an M1 transition in ^{125m}Te decay. They looked for a possible presence of a shifted energy spectrum in gamma rays due to the undetected axion.

[2] DEBOER 97C reanalyzed the existent data on Nuclear M1 transitions and find that a 9 MeV boson decaying into e^+e^- would explain the excess of events with large opening angles. See also DEBOER 01 for follow-up experiments.

[3] TSUNODA 95 looked for axion emission when ^{252}Cf undergoes a spontaneous fission, with the axion decaying into e^+e^-. The bound is for m_{A^0}=40 MeV. It improves to 2.5×10^{-5} for m_{A^0}=200 MeV.

[4] MINOWA 93 studied chain process, ^{139}Ce $\to$ ^{139}La* by electron capture and M1 transition of ^{139}La* to the ground state. It does not assume decay modes of A^0. The bound applies for $m_{A^0} < 166$ keV.

[5] HICKS 92 bound is applicable for $\tau_{X^0} < 4 \times 10^{-11}$ sec.

[6] The ASANUMA 90 limit is for the branching fraction of X^0 emission per ^{241}Am α decay and valid for $\tau_{X^0} < 3 \times 10^{-11}$ s.

[7] The DEBOER 90 limit is for the branching ratio ^{8}Be* (18.15 MeV, 1^+) $\to$ ^{8}BeA^0, $A^0 \to e^+e^-$ for the mass range $m_{A^0} = 4$–15 MeV.

[8] The BINI 89 limit is for the branching fraction of ^{16}O*(6.05 MeV, 0^+) $\to$ ^{16}OX^0, $X^0 \to e^+e^-$ for $m_X = 1.5$–3.1 MeV. $\tau_{X^0} \lesssim 10^{-11}$ s is assumed. The spin-parity of X is restricted to 0^+ or 1^-.

[9] AVIGNONE 88 looked for the 1115 keV transition C* $\to$ CuA^0, either from $A^0 \to 2\gamma$ in-flight decay or from the secondary A^0 interactions by Compton and by Primakoff processes. Limits for axion parameters are obtained for $m_{A^0} < 1.1$ MeV.

[10] DATAR 88 rule out light pseudoscalar particle emission through its decay $A^0 \to e^+e^-$ in the mass range 1.02–2.5 MeV and lifetime range 10^{-13}–10^{-8} s. The above limit is for $\tau = 5 \times 10^{-13}$ s and $m = 1.7$ MeV; see the paper for the τ-m dependence of the limit.

[11] The limit is for the branching fraction of ^{16}O*(6.05 MeV, 0^+) $\to$ ^{16}OX^0, $X^0 \to e^+e^-$ against internal pair conversion for $m_{X^0} = 1.7$ MeV and $\tau_{X^0} < 10^{-11}$ s. Similar limits are obtained for $m_{X^0} = 1.3$–3.2 MeV. The spin parity of X^0 must be either 0^+ or 1^-. The limit at 1.7 MeV is translated into a limit for the X^0-nucleon coupling constant: $g^2_{X^0NN}/4\pi < 2.3 \times 10^{-9}$.

[12] The DOEHNER 88 limit is for $m_{A^0} = 1.7$ MeV, $\tau(A^0) < 10^{-10}$ s. Limits less than 10^{-4} are obtained for $m_{A^0} = 1.2$–2.2 MeV.

[13] SAVAGE 88 looked for A^0 that decays into e^+e^- in the decay of the 9.17 MeV $J^P = 2^+$ state in ^{14}N, 17.64 MeV state $J^P = 1^+$ in ^{8}Be, and the 18.15 MeV state $J^P = 1^+$ in ^{8}Be. This experiment constrains the isovector coupling of A^0 to hadrons, if $m_{A^0} = (1.1 \to 2.2)$ MeV and the isoscalar coupling of A^0 to hadrons, if $m_{A^0} = (1.1 \to 2.6)$ MeV. Both limits are valid only if $\tau(A^0) \lesssim 1 \times 10^{-11}$ s.

[14] Limits are for $\Gamma(A^0(1.8\text{ MeV}))/\Gamma(\pi M1)$; i.e., for 1.8 MeV axion emission normalized to the rate for internal emission of e^+e^- pairs. Valid for $\tau_{A^0} < 2 \times 10^{-11}$s. ^{6}Li isovector decay data strongly disfavor PECCEI 86 model I, whereas the ^{10}B and ^{14}N isoscalar decay data strongly reject PECCEI 86 model II and III.

[15] SAVAGE 86B looked for A^0 that decays into e^+e^- in the decay of the 9.17 MeV $J^P = 2^+$ state in ^{14}N. Limit on the branching fraction is valid if $\tau_{A^0} \lesssim 1. \times 10^{-11}$s for $m_{A^0} = (1.1$–1.7) MeV. This experiment constrains the iso-vector coupling of A^0 to hadrons.

[16] ANANEV 85 with IBR-2 pulsed reactor exclude standard A^0 at CL = 95% masses below 470 keV (Li* decay) and below $2m_e$ for deuteron* decay.

[17] CAVAIGNAC 83 at Bugey reactor exclude axion at any $m_{^{97}\text{Nb*decay}}$ and axion with m_{A^0} between 275 and 288 keV (deuteron* decay).

[18] ALEKSEEV 82 with IBR-2 pulsed reactor exclude standard A^0 at CL = 95% mass-ranges $m_{A^0} < 400$ keV (Li* decay) and 330 keV $< m_{A^0} < 2.2$ MeV. (deuteron* decay).

[19] LEHMANN 82 obtained $A^0 \to 2\gamma$ rate $< 6.2 \times 10^{-5}$/s (CL = 95%) excluding m_{A^0} between 100 and 1000 keV.

[20] ZEHNDER 82 used Gosgen 2.8GW light-water reactor to check A^0 production. No 2γ peak in Li*, Nb* decay (both single p transition) nor in n capture (combined with previous Ba* negative result) rules out standard A^0. Set limit $m_{A^0} < 60$ keV for any A^0.

[21] ZEHNDER 81 looked for Ba* $\to$ A^0Ba transition with $A^0 \to 2\gamma$. Obtained 2γ coincidence rate $< 2.2 \times 10^{-5}$/s (CL = 95%) excluding $m_{A^0} > 160$ keV (or 200 keV depending on Higgs mixing). However, see BARROSO 81.

[22] CALAPRICE 79 saw no axion emission from excited states of carbon. Sensitive to axion mass between 1 and 15 MeV.

A^0 (Axion) Limits from Its Electron Coupling

Limits are for $\tau(A^0 \to e^+e^-)$.

VALUE (s)	CL%	DOCUMENT ID		TECN	COMMENT
• • • We do not use the following data for averages, fits, limits, etc. • • •					
		[1] ANDREEV	21	NA64	$eN \to eA^0N$ ($A^0 \to$ invisibles)

Downloaded from https://academic.oup.com/ptep/article/2022/8/083C01/6651666 by KIT Library user on 27 September 2022

		[2] ANDREEV	21B	NA64	$eN \to eA^0 N$ ($A^0 \to ee$)
none 4×10^{-16}–4.5×10^{-12}	90	[3] BROSS	91	BDMP	$eN \to eA^0 N$ ($A^0 \to ee$)
		[4] GUO	90	BDMP	$eN \to eA^0 N$ ($A^0 \to ee$)
		[5] BJORKEN	88	CALO	$A \to e^+e^-$ or 2γ
		[6] BLINOV	88	MD1	$ee \to eeA^0$ ($A^0 \to ee$)
none 1×10^{-14}–1×10^{-10}	90	[7] RIORDAN	87	BDMP	$eN \to eA^0 N$ ($A^0 \to ee$)
none 1×10^{-14}–1×10^{-11}	90	[8] BROWN	86	BDMP	$eN \to eA^0 N$ ($A^0 \to ee$)
none 6×10^{-14}–9×10^{-11}	95	[9] DAVIER	86	BDMP	$eN \to eA^0 N$ ($A^0 \to ee$)
none 3×10^{-13}–1×10^{-7}	90	[10] KONAKA	86	BDMP	$eN \to eA^0 N$ ($A^0 \to ee$)

[1] ANDREEV 21 look for invisible decays of axions coupled to electrons, and set limits on $g_{Aee} < 4.6\times10^{-6}$–$3.1\times10^{-3}$ for $m_{A^0} = 10^{-3}$–1 GeV. This limits the axion contribution to the electron $g-2$ to an order of magnitude less than the current experimental uncertainty. See their Figs. 3 and 4 for mass-dependent limits.

[2] ANDREEV 21B set limits on g_{Aee} in the range of 6.3×10^{-6}–1.6×10^{-3} for m_{A^0} = 2–17 MeV at 90% CL. This excludes $6.6\times10^{-5} < g_{Aee} < 1\times10^{-4}$ at m_{A^0} = 16.7 MeV corresponding to the ATOMKI anomaly. See their Fig. 2 for mass-dependent limits.

[3] The listed BROSS 91 limit is for $m_{A^0} = 1.14$ MeV. $B(A^0 \to e^+e^-) = 1$ assumed. Excluded domain in the τ_{A^0}–m_{A^0} plane extends up to $m_{A^0} \approx 7$ MeV (see Fig. 5). Combining with electron $g-2$ constraint, axions coupling only to e^+e^- ruled out for $m_{A^0} < 4.8$ MeV (90% CL).

[4] GUO 90 use the same apparatus as BROWN 86 and improve the previous limit in the shorter lifetime region. Combined with $g-2$ constraint, axions coupling only to e^+e^- are ruled out for $m_{A^0} < 2.7$ MeV (90% CL).

[5] BJORKEN 88 reports limits on axion parameters (f_A, m_A, τ_A) for $m_{A^0} < 200$ MeV from electron beam-dump experiment with production via Primakoff photoproduction, bremsstrahlung from electrons, and resonant annihilation of positrons on atomic electrons.

[6] BLINOV 88 assume zero spin, $m = 1.8$ MeV and lifetime $< 5\times10^{-12}$ s and find $\Gamma(A^0 \to \gamma\gamma)B(A^0 \to e^+e^-) < 2$ eV (CL=90%).

[7] Assumes $A^0\gamma\gamma$ coupling is small and hence Primakoff production is small. Their figure 2 shows limits on axions for $m_{A^0} < 15$ MeV.

[8] Uses electrons in hadronic showers from an incident 800 GeV proton beam. Limits for $m_{A^0} < 15$ MeV are shown in their figure 3.

[9] $m_{A^0} = 1.8$ MeV assumed. The excluded domain in the $\tau_{A^0}-m_{A^0}$ plane extends up to $m_{A^0} \approx 14$ MeV, see their figure 4.

[10] The limits are obtained from their figure 3. Also given is the limit on the $A^0\gamma\gamma$–$A^0e^+e^-$ coupling plane by assuming Primakoff production.

Search for A^0 (Axion) Resonance in Bhabha Scattering

The limit is for $\Gamma(A^0)[B(A^0 \to e^+e^-)]^2$.

VALUE (10^{-3} eV)	CL%	DOCUMENT ID		TECN	COMMENT
• • • We do not use the following data for averages, fits, limits, etc. • • •					
< 1.3	97	[1] HALLIN	92	CNTR	$m_{A^0} = 1.75$–1.88 MeV
none 0.0016–0.47	90	[2] HENDERSON	92C	CNTR	$m_{A^0} = 1.5$–1.86 MeV
< 2.0	90	[3] WU	92	CNTR	$m_{A^0} = 1.56$–1.86 MeV
< 0.013	95	TSERTOS	91	CNTR	$m_{A^0} = 1.832$ MeV
none 0.19–3.3	95	[4] WIDMANN	91	CNTR	$m_{A^0} = 1.78$–1.92 MeV
< 5	97	BAUER	90	CNTR	$m_{A^0} = 1.832$ MeV
none 0.09–1.5	95	[5] JUDGE	90	CNTR	$m_{A^0} = 1.832$ MeV, elastic
< 1.9	97	[6] TSERTOS	89	CNTR	$m_{A^0} = 1.82$ MeV
<(10–40)	97	[6] TSERTOS	89	CNTR	$m_{A^0} = 1.51$–1.65 MeV
<(1–2.5)	97	[6] TSERTOS	89	CNTR	$m_{A^0} = 1.80$–1.86 MeV
< 31	95	LORENZ	88	CNTR	$m_{A^0} = 1.646$ MeV
< 94	95	LORENZ	88	CNTR	$m_{A^0} = 1.726$ MeV
< 23	95	LORENZ	88	CNTR	$m_{A^0} = 1.782$ MeV
< 19	95	LORENZ	88	CNTR	$m_{A^0} = 1.837$ MeV
< 3.8	97	[7] TSERTOS	88	CNTR	$m_{A^0} = 1.832$ MeV
		[8] VANKLINKEN	88	CNTR	
		[9] MAIER	87	CNTR	
<2500	90	MILLS	87	CNTR	$m_{A^0} = 1.8$ MeV
		[10] VONWIMMER.	87	CNTR	

[1] HALLIN 92 quote limits on lifetime, 8×10^{-14} – 5×10^{-13} sec depending on mass, assuming $B(A^0 \to e^+e^-) = 100\%$. They say that TSERTOS 91 overstated their sensitivity by a factor of 3.

[2] HENDERSON 92C exclude axion with lifetime τ_{A^0}=1.4×10^{-12} – 4.0×10^{-10} s, assuming $B(A^0 \to e^+e^-)$=100%. HENDERSON 92C also exclude a vector boson with τ=1.4×10^{-12} – 6.0×10^{-10} s.

[3] WU 92 quote limits on lifetime $> 3.3\times10^{-13}$ s assuming $B(A^0 \to e^+e^-)$=100%. They say that TSERTOS 89 overestimate the limit by a factor of $\pi/2$. WU 92 also quote a bound for vector boson, $\tau > 8.2\times10^{-13}$ s.

[4] WIDMANN 91 bound applies exclusively to the case $B(A^0 \to e^+e^-)$=1, since the detection efficiency varies substantially as $\Gamma(A^0)_{total}$ changes. See their Fig. 6.

[5] JUDGE 90 excludes an elastic pseudoscalar e^+e^- resonance for 4.5×10^{-13} s $< \tau(A^0) < 7.5\times10^{-12}$ s (95% CL) at $m_{A^0} = 1.832$ MeV. Comparable limits can be set for $m_{A^0} = 1.776$–1.856 MeV.

[6] See also TSERTOS 88B in references.

[7] The upper limit listed in TSERTOS 88 is too large by a factor of 4. See TSERTOS 88B, footnote 3.

[8] VANKLINKEN 88 looked for relatively long-lived resonance ($\tau = 10^{-10}$–10^{-12} s). The sensitivity is not sufficient to exclude such a narrow resonance.

[9] MAIER 87 obtained limits $R\Gamma \lesssim 60$ eV (100 eV) at $m_{A^0} \simeq 1.64$ MeV (1.83 MeV) for energy resolution $\Delta E_{cm} \simeq 3$ keV, where R is the resonance cross section normalized to that of Bhabha scattering, and $\Gamma = \Gamma^2_{ee}/\Gamma_{total}$. For a discussion implying that $\Delta E_{cm} \simeq 10$ keV, see TSERTOS 89.

[10] VONWIMMERSPERG 87 measured Bhabha scattering for $E_{cm} = 1.37$–1.86 MeV and found a possible peak at 1.73 with $\int \sigma dE_{cm} = 14.5 \pm 6.8$ keV·b. For a comment and a reply, see VANKLINKEN 88B and VONWIMMERSPERG 88. Also see CONNELL 88.

Search for A^0 (Axion) Resonance in $e^+e^- \to \gamma\gamma$

The limit is for $\Gamma(A^0 \to e^+e^-)\cdot\Gamma(A^0 \to \gamma\gamma)/\Gamma_{total}$

VALUE (10^{-3} eV)	CL%	DOCUMENT ID		TECN	COMMENT
• • • We do not use the following data for averages, fits, limits, etc. • • •					
< 0.18	95	VO	94	CNTR	m_{A^0}=1.1 MeV
< 1.5	95	VO	94	CNTR	m_{A^0}=1.4 MeV
<12	95	VO	94	CNTR	m_{A^0}=1.7 MeV
< 6.6	95	[1] TRZASKA	91	CNTR	$m_{A^0} = 1.8$ MeV
< 4.4	95	WIDMANN	91	CNTR	m_{A^0}= 1.78–1.92 MeV
		[2] FOX	89	CNTR	
< 0.11	95	[3] MINOWA	89	CNTR	$m_{A^0} = 1.062$ MeV
<33	97	CONNELL	88	CNTR	$m_{A^0} = 1.580$ MeV
<42	97	CONNELL	88	CNTR	$m_{A^0} = 1.642$ MeV
<73	97	CONNELL	88	CNTR	$m_{A^0} = 1.782$ MeV
<79	97	CONNELL	88	CNTR	$m_{A^0} = 1.832$ MeV

[1] TRZASKA 91 also give limits in the range (6.6–30) $\times10^{-3}$ eV (95%CL) for m_{A^0} = 1.6–2.0 MeV.

[2] FOX 89 measured positron annihilation with an electron in the source material into two photons and found no signal at 1.062 MeV ($< 9\times10^{-5}$ of two-photon annihilation at rest).

[3] Similar limits are obtained for $m_{A^0} = 1.045$–1.085 MeV.

Search for X^0 (Light Boson) Resonance in $e^+e^- \to \gamma\gamma\gamma$

The limit is for $\Gamma(X^0 \to e^+e^-)\cdot\Gamma(X^0 \to \gamma\gamma\gamma)/\Gamma_{total}$. C invariance forbids spin-0 X^0 coupling to both e^+e^- and $\gamma\gamma\gamma$.

VALUE (10^{-3} eV)	CL%	DOCUMENT ID		TECN	COMMENT
• • • We do not use the following data for averages, fits, limits, etc. • • •					
< 0.2	95	[1] VO	94	CNTR	m_{X^0}=1.1–1.9 MeV
< 1.0	95	[2] VO	94	CNTR	m_{X^0}=1.1 MeV
< 2.5	95	[2] VO	94	CNTR	m_{X^0}=1.4 MeV
<120	95	[2] VO	94	CNTR	m_{X^0}=1.7 MeV
< 3.8	95	[3] SKALSEY	92	CNTR	m_{X^0}= 1.5 MeV

[1] VO 94 looked for $X^0 \to \gamma\gamma\gamma$ decaying at rest. The precise limits depend on m_{X^0}. See Fig. 2(b) in paper.

[2] VO 94 looked for $X^0 \to \gamma\gamma\gamma$ decaying in flight.

[3] SKALSEY 92 also give limits 4.3 for $m_{X^0} = 1.54$ and 7.5 for 1.64 MeV. The spin of X^0 is assumed to be one.

Light Boson (X^0) Search in Nonresonant e^+e^- Annihilation at Rest

Limits are for the ratio of $n\gamma + X^0$ production relative to $\gamma\gamma$.

VALUE (units 10^{-6})	CL%	DOCUMENT ID		TECN	COMMENT
• • • We do not use the following data for averages, fits, limits, etc. • • •					
< 4.2	90	[1] MITSUI	96	CNTR	γX^0
< 4	68	[2] SKALSEY	95	CNTR	γX^0
<40	68	[3] SKALSEY	95	RVUE	γX^0
< 0.18	90	[4] ADACHI	94	CNTR	$\gamma\gamma X^0$, $X^0 \to \gamma\gamma$
< 0.26	90	[5] ADACHI	94	CNTR	$\gamma\gamma X^0$, $X^0 \to \gamma\gamma$
< 0.33	90	[6] ADACHI	94	CNTR	γX^0, $X^0 \to \gamma\gamma\gamma$

[1] MITSUI 96 looked for a monochromatic γ. The bound applies for a vector X^0 with C=−1 and m_{X^0} <200 keV. They derive an upper bound on eeX^0 coupling and hence on the branching ratio $B(o\text{-Ps} \to \gamma\gamma X^0) < 6.2\times10^{-6}$. The bounds weaken for heavier X^0.

[2] SKALSEY 95 looked for a monochromatic γ without an accompanying γ in e^+e^- annihilation. The bound applies for scalar and vector X^0 with $C = -1$ and m_{X^0} = 100–1000 keV.

[3] SKALSEY 95 reinterpreted the bound on γA^0 decay of o-Ps by ASAI 91 where 3% of delayed annihilations are not from $^3S_1$ states. The bound applies for scalar and vector X^0 with $C = -1$ and m_{X^0} = 0–800 keV.

[4] ADACHI 94 looked for a peak in the $\gamma\gamma$ invariant mass distribution in $\gamma\gamma\gamma$ production from e^+e^- annihilation. The bound applies for m_{X^0} = 70–800 keV.

Downloaded from https://academic.oup.com/ptep/article/2022/8/083C01/6651666 by KIT Library user on 27 September 2022

[5] ADACHI 94 looked for a peak in the missing-mass mass distribution in $\gamma\gamma$ channel, using $\gamma\gamma\gamma\gamma$ production from e^+e^- annihilation. The bound applies for m_{X^0} <800 keV.

[6] ADACHI 94 looked for a peak in the missing mass distribution in $\gamma\gamma\gamma$ channel, using $\gamma\gamma\gamma\gamma$ production from e^+e^- annihilation. The bound applies for m_{X^0} = 200–900 keV.

Searches for Goldstone Bosons (X^0)

(Including Horizontal Bosons and Majorons.) Limits are for branching ratios.

VALUE	CL%	DOCUMENT ID		TECN	COMMENT
• • • We do not use the following data for averages, fits, limits, etc. • • •					
$<4.3\times10^{-6}$	90	[1] AGUILAR-AR...	21A	PIEN	$\pi\to\mu\nu X^0$, Majoron
$<5.2\times10^{-8}$	90	[2] AGUILAR-AR...	21A	PIEN	$\pi\to e\nu X^0$, Majoron
$<9\times10^{-6}$	90	[3] AGUILAR-AR...	20	PIEN	$\mu^+\to e^+X^0$, Familon
$<7\times10^{-12}$	90	[4] BALDINI	20	MEG	$\mu^+\to e^+X^0$ ($X^0\to\gamma\gamma$), Familon
$<9\times10^{-6}$	90	[5] BAYES	15	TWST	$\mu^+\to e^+X^0$, Familon
		[6] LATTANZI	13	COSM	Majoron dark matter decay
		[7] LESSA	07	RVUE	Meson, ℓ decays to Majoron
		[8] DIAZ	98	THEO	$H^0\to X^0X^0$, $A^0\to X^0X^0X^0$, Majoron
		[9] BOBRAKOV	91		Electron quasi-magnetic interaction
$<3.3\times10^{-2}$	95	[10] ALBRECHT	90E	ARG	$\tau\to\mu X^0$. Familon
$<1.8\times10^{-2}$	95	[10] ALBRECHT	90E	ARG	$\tau\to eX^0$. Familon
$<6.4\times10^{-9}$	90	[11] ATIYA	90	B787	$K^+\to\pi^+X^0$. Familon
$<1.4\times10^{-5}$	90	[12] BALKE	88	CNTR	$\mu^+\to e^+X^0$. Familon
$<1.1\times10^{-9}$	90	[13] BOLTON	88	CBOX	$\mu^+\to e^+\gamma X^0$. Familon
		[14] CHANDA	88	ASTR	Sun, Majoron
		[15] CHOI	88	ASTR	Majoron, SN 1987A
$<5\times10^{-6}$	90	[16] PICCIOTTO	88	CNTR	$\pi\to e\nu X^0$, Majoron
$<1.3\times10^{-9}$	90	[17] GOLDMAN	87	CNTR	$\mu\to e\gamma X^0$. Familon
$<3\times10^{-4}$	90	[18] BRYMAN	86B	RVUE	$\mu\to eX^0$. Familon
$<1\times10^{-10}$	90	[19] EICHLER	86	SPEC	$\mu^+\to e^+X^0$. Familon
$<2.6\times10^{-6}$	90	[20] JODIDIO	86	SPEC	$\mu^+\to e^+X^0$. Familon
		[21] BALTRUSAIT...	85	MRK3	$\tau\to\ell X^0$. Familon
		[22] DICUS	83	COSM	ν(hvy) $\to\nu$(light)X^0

[1] AGUILAR-AREVALO 21A quoted limit applies to m_{X^0} = 33.9 MeV. Limits between 4.3×10^{-6} and 7.5×10^{-5} are obtained for $0<m_{X^0}<33.9$ MeV. The lifetime of X^0 is assumed to be long enough. See their Fig. 6 for mass-dependent limits.

[2] AGUILAR-AREVALO 21A quoted limit applies to m_{X^0} = 85 MeV. Limits between 5.2×10^{-8} and 1.4×10^{-6} are obtained for $0<m_{X^0}<120$ MeV, which improve the limits of PICCIOTTO 88 by an order of magnitude. The lifetime of X^0 is assumed to be long enough. See their Fig. 4 for mass-dependent limits.

[3] AGUILAR-AREVALO 20 obtained limits of order 10^{-5} for m_{X^0} = 47.8–95.1 MeV. The quoted limit applies to m_{X^0} = 75 MeV. See their Fig. 1 for mass-dependent limits.

[4] BALDINI 20 obtained limits for m_{X^0} = 20–45 MeV and $\tau_{X^0}<40$ ps, and supersedes BOLTON 88 for m_{X^0} = 20–40 MeV. See their Fig. 17 for mass-dependent limits.

[5] BAYES 15 limits are the average over m_{X^0} = 13–80 MeV for the isotropic decay distribution of positrons. See their Fig. 4 and Table II for the mass-dependent limits as well as the dependence on the decay anisotropy. In particular, they find a limit $<58\times10^{-6}$ at 90% CL for massless familons and for the same asymmetry as normal muon decay, a case not covered by JODIDIO 86.

[6] LATTANZI 13 use WMAP 9 year data as well as X-ray and γ-ray observations to derive limits on decaying majoron dark matter. A limit on the decay width $\Gamma(X^0\to\nu\overline{\nu})<6.4\times10^{-19}$ s^{-1} at 95% CL is found if majorons make up all of the dark matter.

[7] LESSA 07 consider decays of the form Meson $\to\ell\nu$ Majoron and $\ell\to\ell'\nu\overline{\nu}$ Majoron and use existing data to derive limits on the neutrino-Majoron Yukawa couplings $g_{\alpha\beta}$ ($\alpha,\beta=e,\mu,\tau$). Their best limits are $|g_{e\alpha}|^2<5.5\times10^{-6}$, $|g_{\mu\alpha}|^2<4.5\times10^{-5}$, $|g_{\tau\alpha}|^2<5.5\times10^{-2}$ at CL = 90%.

[8] DIAZ 98 studied models of spontaneously broken lepton number with both singlet and triplet Higgses. They obtain limits on the parameter space from invisible decay $Z\to H^0A^0\to X^0X^0X^0X^0X^0$ and $e^+e^-\to ZH^0$ with $H^0\to X^0X^0$.

[9] BOBRAKOV 91 searched for anomalous magnetic interactions between polarized electrons expected from the exchange of a massless pseudoscalar boson (arion). A limit $x_e^2<2\times10^{-4}$ (95%CL) is found for the effective anomalous magneton parametrized as $x_e(G_F/8\pi\sqrt{2})^{1/2}$.

[10] ALBRECHT 90E limits are for $B(\tau\to\ell X^0)/B(\tau\to\ell\nu\overline{\nu})$. Valid for $m_{X^0}<100$ MeV. The limits rise to 7.1% (for μ), 5.0% (for e) for m_{X^0} = 500 MeV.

[11] ATIYA 90 limit is for m_{X^0} = 0. The limit $B<1\times10^{-8}$ holds for $m_{X^0}<95$ MeV. For the reduction of the limit due to finite lifetime of X^0, see their Fig. 3.

[12] BALKE 88 limits are for $B(\mu^+\to e^+X^0)$. Valid for $m_{X^0}<80$ MeV and $\tau_{X^0}>10^{-8}$ sec.

[13] BOLTON 88 limit corresponds to $F>3.1\times10^9$ GeV, which does not depend on the chirality property of the coupling.

[14] CHANDA 88 find $v_T<10$ MeV for the weak-triplet Higgs vacuum expectation value in Gelmini-Roncadelli model, and $v_S>5.8\times10^6$ GeV in the singlet Majoron model.

[15] CHOI 88 used the observed neutrino flux from the supernova SN1987A to exclude the neutrino Majoron Yukawa coupling h in the range $2\times10^{-5}<h<3\times10^{-4}$ for the interaction $L_{\rm int}=\frac{1}{2}ih\overline{\psi}^c_\nu\gamma_5\psi_\nu\phi_X$. For several families of neutrinos, the limit applies for $(\Sigma h_i^4)^{1/4}$.

[16] PICCIOTTO 88 limit applies when $m_{X^0}<55$ MeV and $\tau_{X^0}>2$ns, and it decreases to 4×10^{-7} at m_{X^0} = 125 MeV, beyond which no limit is obtained.

[17] GOLDMAN 87 limit corresponds to $F>2.9\times10^9$ GeV for the family symmetry breaking scale from the Lagrangian $L_{\rm int}=(1/F)\overline{\psi}_\mu\gamma^\mu(a+b\gamma_5)\psi_e\partial_\mu\phi_{X^0}$ with $a^2+b^2=1$. This is not as sensitive as the limit $F>9.9\times10^9$ GeV derived from the search for $\mu^+\to e^+X^0$ by JODIDIO 86, but does not depend on the chirality property of the coupling.

[18] Limits are for $\Gamma(\mu\to eX^0)/\Gamma(\mu\to e\nu\overline{\nu})$. Valid when m_{X^0} = 0–93.4, 98.1–103.5 MeV.

[19] EICHLER 86 looked for $\mu^+\to e^+X^0$ followed by $X^0\to e^+e^-$. Limits on the branching fraction depend on the mass and and lifetime of X^0. The quoted limits are valid when $\tau_{X^0}\lesssim3.\times10^{-10}$ s if the decays are kinematically allowed.

[20] JODIDIO 86 corresponds to $F>9.9\times10^9$ GeV for the family symmetry breaking scale with the parity-conserving effective Lagrangian $L_{\rm int}=(1/F)\overline{\psi}_\mu\gamma^\mu\psi_e\partial^\mu\phi_{X^0}$.

[21] BALTRUSAITIS 85 search for light Goldstone boson(X^0) of broken U(1). CL = 95% limits are $B(\tau\to\mu^+X^0)/B(\tau\to\mu^+\nu\nu)<0.125$ and $B(\tau\to e^+X^0)/B(\tau\to e^+\nu\nu)<0.04$. Inferred limit for the symmetry breaking scale is $m>3000$ TeV.

[22] The primordial heavy neutrino must decay into ν and familon, f_A, early so that the red-shifted decay products are below critical density, see their table. In addition, $K\to\pi f_A$ and $\mu\to ef_A$ are unseen. Combining these excludes $m_{{\rm heavy}\nu}$ between 5×10^{-5} and 5×10^{-4} MeV (μ decay) and $m_{{\rm heavy}\nu}$ between 5×10^{-5} and 0.1 MeV (K-decay).

Majoron Searches in Neutrinoless Double β Decay

Limits are for the half-life of neutrinoless $\beta\beta$ decay with a Majoron emission. No experiment currently claims any such evidence. Only the best or comparable limits for each isotope are reported.

$t_{1/2}(10^{21}$ yr)	CL%	ISOTOPE	TRANSITION	METHOD	DOCUMENT ID	
>7200	**90**	**^{128}Te**		**CNTR**	[1] BERNATOW...	92
• • • We do not use the following data for averages, fits, limits, etc. • • •						
>4300	90	^{136}Xe	$0\nu1\chi$	EXO-200	[2] AL-KHARUSI	21
> 4.4	90	^{100}Mo	$0\nu1\chi$	NEMO-3	[3] ARNOLD	19
> 37	90	^{82}Se	$0\nu1\chi$	NEMO-3	[4] ARNOLD	18
> 420	90	^{76}Ge	$0\nu1\chi$	GERDA	[5] AGOSTINI	15A
> 400	90	^{100}Mo	$0\nu1\chi$	NEMO-3	[6] ARNOLD	15
>1200	90	^{136}Xe	$0\nu1\chi$	EXO-200	[7] ALBERT	14A
>2600	90	^{136}Xe	$0\nu1\chi$	KamLAND-Zen	[8] GANDO	12
> 16	90	^{130}Te	$0\nu1\chi$	NEMO-3	[9] ARNOLD	11
> 1.9	90	^{96}Zr	$2\nu1\chi$	NEMO-3	[10] ARGYRIADES	10
> 1.52	90	^{150}Nd	$0\nu1\chi$	NEMO-3	[11] ARGYRIADES	09
> 27	90	^{100}Mo	$0\nu1\chi$	NEMO-3	[12] ARNOLD	06
> 15	90	^{82}Se	$0\nu1\chi$	NEMO-3	[13] ARNOLD	06
> 14	90	^{100}Mo	$0\nu1\chi$	NEMO-3	[14] ARNOLD	04
> 12	90	^{82}Se	$0\nu1\chi$	NEMO-3	[15] ARNOLD	04
> 2.2	90	^{130}Te	$0\nu1\chi$	Cryog. det.	[16] ARNABOLDI	03
> 0.9	90	^{130}Te	$0\nu2\chi$	Cryog. det.	[17] ARNABOLDI	03
> 8	90	^{116}Cd	$0\nu1\chi$	$CdWO_4$ scint.	[18] DANEVICH	03
> 0.8	90	^{116}Cd	$0\nu2\chi$	$CdWO_4$ scint.	[19] DANEVICH	03
> 500	90	^{136}Xe	$0\nu1\chi$	Liquid Xe Scint.	[20] BERNABEI	02D
> 5.8	90	^{100}Mo	$0\nu1\chi$	ELEGANT V	[21] FUSHIMI	02
> 0.32	90	^{100}Mo	$0\nu1\chi$	Liq. Ar ioniz.	[22] ASHITKOV	01
> 0.0035	90	^{160}Gd	$0\nu1\chi$	$^{160}Gd_2SiO_5$:Ce	[23] DANEVICH	01
> 0.013	90	^{160}Gd	$0\nu2\chi$	$^{160}Gd_2SiO_5$:Ce	[24] DANEVICH	01
> 2.3	90	^{82}Se	$0\nu1\chi$	NEMO 2	[25] ARNOLD	00
> 0.31	90	^{96}Zr	$0\nu1\chi$	NEMO 2	[26] ARNOLD	00
> 0.63	90	^{82}Se	$0\nu2\chi$	NEMO 2	[27] ARNOLD	00
> 0.063	90	^{96}Zr	$0\nu2\chi$	NEMO 2	[27] ARNOLD	00
> 0.16	90	^{100}Mo	$0\nu2\chi$	NEMO 2	[27] ARNOLD	00
> 2.4	90	^{82}Se	$0\nu1\chi$	NEMO 2	[28] ARNOLD	98
> 7.2	90	^{136}Xe	$0\nu2\chi$	TPC	[29] LUESCHER	98
> 7.91	90	^{76}Ge		SPEC	[30] GUENTHER	96
> 17	90	^{76}Ge		CNTR	BECK	93

[1] BERNATOWICZ 92 studied double-β decays of ^{128}Te and ^{130}Te, and found the ratio $\tau(^{130}{\rm Te})/\tau(^{128}{\rm Te})=(3.52\pm0.11)\times10^{-4}$ in agreement with relatively stable theoretical predictions. The bound is based on the requirement that Majoron-emitting decay cannot be larger than the observed double-beta rate of ^{128}Te of $(7.7\pm0.4)\times10^{24}$ year. We calculated 90% CL limit as $(7.7–1.28\times0.4=7.2)\times10^{24}$.

[2] AL-KHARUSI 21 utilize the complete dataset of the EXO-200 experiment, corresponding to an exposure of 234 kg yr, to place a limit on the one Majoron mode of the neutrinoless double beta decay of ^{136}Xe. Several limits are reported, the one given here corresponds to a spectral index of 1, resulting in a limit of $g_{\nu\chi}<0.4–0.9\times10^{-5}$ on the Majoron-neutrino coupling constant. The range reflects the spread of the nuclear matrix elements.

[3] ARNOLD 19 uses the NEMO-3 tracking calorimeter to determine limits for the Majoron emitting double beta decay, with spectral index n = 3. The limit corresponds to the range of the g_{ee} coupling of 0.013–0.035; dependimg on the nuclear matrix elements used.

[4] ARNOLD 18 use the NEMO-3 tracking detector. The limit corresponds to $\langle g_{ee}\rangle<3.2–8.0\times10^{-5}$; the range corresponds to different nuclear matrix element calculations.

[5] AGOSTINI 15A analyze a 20.3 kg yr of data set of the GERDA calorimeter to determine $g_{\nu\chi}<3.4–8.7\times10^{-5}$ on the Majoron-neutrino coupling constant. The range reflects the spread of the nuclear matrix elements.

[6] ARNOLD 15 use the NEMO-3 tracking calorimeter with 3.43 kg yr exposure to determine the limit on Majoron emission. The limit corresponds to $g_{\nu\chi}<1.6–3.0\times10^{-4}$. The spread reflects different nuclear matrix elements. Supersedes ARNOLD 06.

[7] ALBERT 14A utilize 100 kg yr of exposure of the EXO-200 tracking calorimeter to place a limit on the $g_{\nu\chi}<0.8–1.7\times10^{-5}$ on the Majoron-neutrino coupling constant. The range reflects the spread of the nuclear matrix elements.

Downloaded from https://academic.oup.com/ptep/article/2022/8/083C01/6651666 by KIT Library user on 27 September 2022

[8] GANDO 12 use the KamLAND-Zen detector to obtain the limit on the $0\nu\chi$ decay with Majoron emission. It implies that the coupling constant $g_{\nu\chi} < 0.8$–1.6×10^{-5} depending on the nuclear matrix elements used.

[9] ARNOLD 11 use the NEMO-3 detector to obtain the reported limit on Majoron emission. It implies that the coupling constant $g_{\nu\chi} < 0.6$–1.6×10^{-4} depending on the nuclear matrix element used. Supercedes ARNABOLDI 03.

[10] ARGYRIADES 10 use the NEMO-3 tracking detector and ^{96}Zr to derive the reported limit. No limit for the Majoron electron coupling is given.

[11] ARGYRIADES 09 use ^{150}Nd data taken with the NEMO-3 tracking detector. The reported limit corresponds to $\langle g_{\nu\chi} \rangle < 1.7$–$3.0 \times 10^{-4}$ using a range of nuclear matrix elements that include the effect of nuclear deformation.

[12] ARNOLD 06 use ^{100}Mo data taken with the NEMO-3 tracking detector. The reported limit corresponds to $\langle g_{\nu\chi} \rangle < (0.4$–$1.8) \times 10^{-4}$ using a range of matrix element calculations. Superseded by ARNOLD 15.

[13] NEMO-3 tracking calorimeter is used in ARNOLD 06 . Reported half-life limit for ^{82}Se corresponds to $\langle g_{\nu\chi} \rangle < (0.66$–$1.9) \times 10^{-4}$ using a range of matrix element calculations. Supersedes ARNOLD 04.

[14] ARNOLD 04 use the NEMO-3 tracking detector. The limit corresponds to $\langle g_{\nu\chi} \rangle < (0.5$–$0.9)10^{-4}$ using the matrix elements of SIMKOVIC 99, STOICA 01 and CIVITARESE 03. Superseded by ARNOLD 06.

[15] ARNOLD 04 use the NEMO-3 tracking detector. The limit corresponds to $\langle g_{\nu\chi} \rangle < (0.7$–$1.6)10^{-4}$ using the matrix elements of SIMKOVIC 99, STOICA 01 and CIVITARESE 03.

[16] Supersedes ALESSANDRELLO 00. Array of TeO_2 crystals in high resolution cryogenic calorimeter. Some enriched in ^{130}Te. Derive $\langle g_{\nu\chi} \rangle < 17$–$33 \times 10^{-5}$ depending on matrix element.

[17] Supersedes ALESSANDRELLO 00. Cryogenic calorimeter search.

[18] Limit for the $0\nu\chi$ decay with Majoron emission of ^{116}Cd using enriched $CdWO_4$ scintillators. $\langle g_{\nu\chi} \rangle < 4.6$–$8.1 \times 10^{-5}$ depending on the matrix element. Supersedes DANEVICH 00.

[19] Limit for the $0\nu2\chi$ decay of ^{116}Cd. Supersedes DANEVICH 00.

[20] BERNABEI 02D obtain limit for $0\nu\chi$ decay with Majoron emission of ^{136}Xe using liquid Xe scintillation detector. They derive $\langle g_{\nu\chi} \rangle < 2.0$–$3.0 \times 10^{-5}$ with several nuclear matrix elements.

[21] Replaces TANAKA 93. FUSHIMI 02 derive half-life limit for the $0\nu\chi$ decay by means of tracking calorimeter ELEGANT V. Considering various matrix element calculations, a range of limits for the Majoron-neutrino coupling is given: $\langle g_{\nu\chi} \rangle < (6.3$–$360) \times 10^{-5}$.

[22] ASHITKOV 01 result for $0\nu\chi$ of ^{100}Mo is less stringent than ARNOLD 00.

[23] DANEVICH 01 obtain limit for the $0\nu\chi$ decay with Majoron emission of ^{160}Gd using Gd_2SiO_5:Ce crystal scintillators.

[24] DANEVICH 01 obtain limit for the $0\nu2\chi$ decay with 2 Majoron emission of ^{160}Gd.

[25] ARNOLD 00 reports limit for the $0\nu\chi$ decay with Majoron emission derived from tracking calorimeter NEMO 2. Using ^{82}Se source: $\langle g_{\nu\chi} \rangle < 1.6 \times 10^{-4}$. Matrix element from GUENTHER 96.

[26] Using ^{96}Zr source: $\langle g_{\nu\chi} \rangle < 2.6 \times 10^{-4}$. Matrix element from ARNOLD 99.

[27] ARNOLD 00 reports limit for the $0\nu2\chi$ decay with two Majoron emission derived from tracking calorimeter NEMO 2.

[28] ARNOLD 98 determine the limit for $0\nu_\chi$ decay with Majoron emission of ^{82}Se using the NEMO-2 tracking detector. They derive $\langle g_{\nu_\chi} \rangle < 2.3$–$4.3 \times 10^{-4}$ with several nuclear matrix elements.

[29] LUESCHER 98 report a limit for the 0ν decay with Majoron emission of ^{136}Xe using Xe TPC. This result is more stringent than BARABASH 89. Using the matrix elements of ENGEL 88, they obtain a limit on $\langle g_{\nu\chi} \rangle$ of 2.0×10^{-4}.

[30] See Table 1 in GUENTHER 96 for limits on the Majoron coupling in different models.

Invisible A^0 (Axion) MASS LIMITS from Astrophysics and Cosmology

$\nu_1 = \nu_2$ is usually assumed (ν_i = vacuum expectation values). For a review of these limits, see RAFFELT 91 and TURNER 90. In the comment lines below, D and K refer to DFSZ and KSVZ axion types, discussed in the above minireview.

VALUE (eV)	CL%	DOCUMENT ID		TECN	COMMENT
• • • We do not use the following data for averages, fits, limits, etc. • • •					
$> 1.4 \times 10^{-21}$	95	[1] BANIK	21	ASTR	Fuzzy DM
$< 1.9 \times 10^{4}$		[2] BAUMHOLZ...	21	COSM	warm dark matter
		[3] CROON	21	ASTR	SN 1987A, axion-muon coupling
		[4] FUJIKURA	21	ASTR	Microlensing
		[5] MARTINCAM...	21	ASTR	SN 1987A, Λ decay
none 1.3–2.7×10^{-13}		[6] NG	21	ASTR	BH superradiance
$> 2 \times 10^{-20}$	95	[7] ROGERS	21	COSM	Lyman-α
none 0.8–6.5×10^{-13}	95	[8] TSUKADA	21	ASTR	BH superradiance
$> 2 \times 10^{-17}$		[9] IRSIC	20	COSM	Isocurvature fluctuations
$> 2.1 \times 10^{-21}$		[10] PODDAR	20	ASTR	Compact binary systems
none 6.4–8.0×10^{-13}	95	[11] SCHUTZ	20	COSM	Fuzzy DM
none 2.9–4.6×10^{-21}		[12] SUN	20	ASTR	BH superradiance
none 10^{-21}–6×10^{-20}		[13] DAVOUDIASL	19	ASTR	BH superradiance
none 1.1–4×10^{-13}	95	[14] MARSH	19	ASTR	Fuzzy DM
< 0.06		[15] PALOMBA	19	ASTR	BH superradiance
< 0.67	95	[16] CHANG	18	ASTR	K, SN 1987A
none 0.7–3×10^{5}		[17] ARCHIDIACO...	13A	COSM	K, hot dark matter
<105	90	[18] CADAMURO	11	COSM	D abundance
		[19] DERBIN	11A	CNTR	D, solar axion
		[20] ANDRIAMON...	10	CAST	K, solar axions
< 0.72	95	[21] HANNESTAD	10	COSM	K, hot dark matter
		[22] ANDRIAMON...	09	CAST	K, solar axions
<191	90	[23] DERBIN	09A	CNTR	K, solar axions
<334	95	[24] KEKEZ	09	HPGE	K, solar axions
< 1.02	95	[25] HANNESTAD	08	COSM	K, hot dark matter
< 1.2	95	[26] HANNESTAD	07	COSM	K, hot dark matter
< 0.42	95	[27] MELCHIORRI	07A	COSM	K, hot dark matter
< 1.05	95	[28] HANNESTAD	05A	COSM	K, hot dark matter
3 to 20		[29] MOROI	98	COSM	K, hot dark matter
< 0.007		[30] BORISOV	97	ASTR	D, neutron star
< 4		[31] KACHELRIESS	97	ASTR	D, neutron star cooling
$<(0.5$–$6) \times 10^{-3}$		[32] KEIL	97	ASTR	SN 1987A
< 0.018		[33] RAFFELT	95	ASTR	D, red giant
< 0.010		[34] ALTHERR	94	ASTR	D, red giants, white dwarfs
		[35] CHANG	93	ASTR	K, SN 1987A
< 0.01		WANG	92	ASTR	D, white dwarf
< 0.03		WANG	92C	ASTR	D, C-O burning
none 3–8		[36] BERSHADY	91	ASTR	D, K, intergalactic light
< 10		[37] KIM	91C	COSM	D, K, mass density of the universe, supersymmetry
		[38] RAFFELT	91B	ASTR	D,K, SN 1987A
$< 1 \times 10^{-3}$		[39] RESSELL	91	ASTR	K, intergalactic light
none 10^{-3}–3		BURROWS	90	ASTR	D,K, SN 1987A
		[40] ENGEL	90	ASTR	D,K, SN 1987A
< 0.02		[41] RAFFELT	90D	ASTR	D, red giant
$< 1 \times 10^{-3}$		[42] BURROWS	89	ASTR	D,K, SN 1987A
$<(1.4$–$10) \times 10^{-3}$		[43] ERICSON	89	ASTR	D,K, SN 1987A
$< 3.6 \times 10^{-4}$		[44] MAYLE	89	ASTR	D,K, SN 1987A
< 12		CHANDA	88	ASTR	D, Sun
$< 1 \times 10^{-3}$		RAFFELT	88	ASTR	D,K, SN 1987A
		[45] RAFFELT	88B	ASTR	red giant
< 0.07		FRIEMAN	87	ASTR	D, red giant
< 0.7		[46] RAFFELT	87	ASTR	K, red giant
< 2–5		TURNER	87	COSM	K, thermal production
< 0.01		[47] DEARBORN	86	ASTR	D, red giant
< 0.06		RAFFELT	86	ASTR	D, red giant
< 0.7		[48] RAFFELT	86	ASTR	K, red giant
< 0.03		RAFFELT	86B	ASTR	D, white dwarf
< 1		[49] KAPLAN	85	ASTR	K, red giant
< 0.003–0.02		IWAMOTO	84	ASTR	D, K, neutron star
$> 1 \times 10^{-5}$		ABBOTT	83	COSM	D,K, mass density of the universe
$> 1 \times 10^{-5}$		DINE	83	COSM	D,K, mass density of the universe
< 0.04		ELLIS	83B	ASTR	D, red giant
$> 1 \times 10^{-5}$		PRESKILL	83	COSM	D,K, mass density of the universe
< 0.1		BARROSO	82	ASTR	D, red giant
< 1		[50] FUKUGITA	82	ASTR	D, stellar cooling
< 0.07		FUKUGITA	82B	ASTR	D, red giant

[1] BANIK 21 use the subhalo mass function inferred from the analyses of the GD-1 and Pal 5 stellar streams. The limit is strengthened to 2.2×10^{-21} eV when adding dwarf satellite counts.

[2] BAUMHOLZER 21 study the freeze-in production of axion dark matter through couplings to photons, and set the limit using Lyman-α forest data and the observed number of Milky Way subhalos.

[3] CROON 21 study the supernova cooling effect of the axion-muon coupling, taking account of semi-Compton scattering and muon-proton bremsstrahlung, as well as the loop-induced axion-photon coupling, and exclude the range of $g_{A\mu\mu} \simeq 7 \times 10^{-3}$–$2 \times 10^{-10}$ for $m_{A^0} < 0.5$ GeV. See their Fig. 8 for mass-dependent limits.

[4] FUJIKURA 21 use the EROS-2 survey and the Subaru HSC observation to set limits on spherically symmetric axion clumps, taking account of the finite lens and source size effects. $f_{A^0} \gtrsim 10^{12}$ GeV can be constrained depending on the fraction of the axion dark matter collapsed into clumps, and the clump densities. See their Figs. 7–10 for the limits.

[5] MARTINCAMALICH 21 considered axion emission from a supernova core through the Λ hyperon decay, and set the limit on $B(\Lambda \to nA^0) \lesssim 8 \times 10^{-9}$, or equivalently, $f_{A^0}/C_{sd} \gtrsim 2.6 \times 10^{9}$ GeV in terms of the flavor-violating axion coupling to the down and strange quarks.

[6] NG 21 use the binary black holes reported by LIGO and Virgo to determine the black hole spin distribution at formation and the scalar boson mass simultaneously, neglecting the boson self-interaction.

[7] ROGERS 21 set the limit by using a framework involving Bayesian emulator optimization to accurately forward-model the Lyman-α flux power spectrum, and comparing this with small-scale data to constrain the predicted suppression of cosmic structure growth.

[8] TSUKADA 21 look for a stochastic GW background produced by extragalactic BH-hidden photon cloud systems through the superradiant instability. They assume a uniform spin distribution at birth of isolated BHs from 0 to 1.

[9] IRSIC 20 used the Lyman-α forest constraint on small-scale isocurvature perturbation to derive limits on the axion mass and decay constant, assuming that the axion makes up all dark matter in the post-inflationary scenario. See their Fig. 1 for other astrophysical limits as well as the limits on the case of the temperature-dependent axion mass.

[10] PODDAR 20 used the observed decay in orbital period of four compact binary systems to derive a limit on the emission of axions with $m_{A^0} < 1 \times 10^{-19}$ eV, assuming they couple to nucleons and the strong CP phase vanishes at the potential minimum. They exclude $f_{A^0} \lesssim 10^{11}$ GeV for such axions.

[11] SCHUTZ 20 set a limit on fuzzy dark matter based on the existing limits for warm dark matter derived from the inferred subhalo mass function.

[12] SUN 20 look for quasimonochromatic gravitational waves emitted from boson clouds around the Cygnus X-1 black hole. The quoted limit assume the black hole age of 5×10^{6} years. A mass range of 9.6–15.5×10^{-13} eV is disfavored when repeated induction of bosenova for string axions with decay constant $f_{A^0} \simeq 10^{15}$ GeV prevents the superradiance from being saturated.

Downloaded from https://academic.oup.com/ptep/article/2022/8/083C01/6651666 by KIT Library user on 27 September 2022

[13] DAVOUDIASL 19 used the observed data of M87* by the Event Horizon Telescope to set the limit. A mass range of 0.85–4.6 $\times 10^{-21}$ eV is disfavored for a spin-1 boson.

[14] MARSH 19 considered heating of star clusters due to the stochastic oscillations of the core and granular quasiparticles in the outer halo. The limit was derived by requiring the survival of the old star cluster in Eridanus II, where the lower end is set by the validity of diffusion approximation. The effect of tidal stripping is also discussed for lower masses.

[15] PALOMBA 19 used the LIGO O2 dataset to derive limits on nearly monochromatic gravitational waves emitted by boson clouds formed around a stellar-mass black hole. They exclude boson masses in a range of 1.1×10^{-13} and 4×10^{-13} eV for high initial black hole spin, and 1.2×10^{-13} and 1.8×10^{-13} eV for moderate spin. See their Figs. 2 and 3 for limits based on various values of black hole initial spin, boson cloud age, and distance.

[16] CHANG 18 update axion bremsstrahlung emission rates in nucleon-nucleon collisions, shifting the excluded mass range to higher values. They rule out the hadronic axion with mass up to a few hundred eV, closing the hadronic axion window. See their Fig. 11 for results based on several different choices of the temperature and density profile of the proto-neutron star.

[17] ARCHIDIACONO 13A is analogous to HANNESTAD 05A. The limit is based on the CMB temperature power spectrum of the Planck data, the CMB polarization from the WMAP 9-yr data, the matter power spectrum from SDSS-DR7, and the local Hubble parameter measurement by the Carnegie Hubble program.

[18] CADAMURO 11 use the deuterium abundance to show that the m_{A^0} range 0.7 eV – 300 keV is excluded for axions, complementing HANNESTAD 10.

[19] DERBIN 11A look for solar axions produced by Compton and bremsstrahlung processes, in the resonant excitation of ^{169}Tm, constraining the axion-electron $\times$ axion nucleon couplings.

[20] ANDRIAMONJE 10 search for solar axions produced from ^{7}Li (478 keV) and D(p,γ)^{3}He (5.5 MeV) nuclear transitions. They show limits on the axion-photon coupling for two reference values of the axion-nucleon coupling for $m_A < 100$ eV.

[21] This is an update of HANNESTAD 08 including 7 years of WMAP data.

[22] ANDRIAMONJE 09 look for solar axions produced from the thermally excited 14.4 keV level of ^{57}Fe. They show limits on the axion-nucleon $\times$ axion-photon coupling assuming $m_A < 0.03$ eV.

[23] DERBIN 09A look for Primakoff-produced solar axions in the resonant excitation of ^{169}Tm, constraining the axion-photon $\times$ axion-nucleon couplings.

[24] KEKEZ 09 look at axio-electric effect of solar axions in HPGe detectors. The one-loop axion-electron coupling for hadronic axions is used.

[25] This is an update of HANNESTAD 07 including 5 years of WMAP data.

[26] This is an update of HANNESTAD 05A with new cosmological data, notably WMAP (3 years) and baryon acoustic oscillations (BAO). Lyman-α data are left out, in contrast to HANNESTAD 05A and MELCHIORRI 07A, because it is argued that systematic errors are large. It uses Bayesian statistics and marginalizes over a possible neutrino hot dark matter component.

[27] MELCHIORRI 07A is analogous to HANNESTAD 05A, with updated cosmological data, notably WMAP (3 years). Uses Bayesian statistics and marginalizes over a possible neutrino hot dark matter component. Leaving out Lyman-α data, a conservative limit is 1.4 eV.

[28] HANNESTAD 05A puts an upper limit on the mass of hadronic axion because in this mass range it would have been thermalized and contribute to the hot dark matter component of the universe. The limit is based on the CMB anisotropy from WMAP, SDSS large scale structure, Lyman α, and the prior Hubble parameter from HST Key Project. A χ^2 statistic is used. Neutrinos are assumed not to contribute to hot dark matter.

[29] MOROI 98 points out that a KSVZ axion of this mass range (see CHANG 93) can be a viable hot dark matter of Universe, as long as the model-dependent $g_{A\gamma}$ is accidentally small enough as originally emphasized by KAPLAN 85; see Fig. 1.

[30] BORISOV 97 bound is on the axion-electron coupling $g_{ae} < 1 \times 10^{-13}$ from the photo-production of axions off of magnetic fields in the outer layers of neutron stars.

[31] KACHELRIESS 97 bound is on the axion-electron coupling $g_{ae} < 1 \times 10^{-10}$ from the production of axions in strongly magnetized neutron stars. The authors also quote a stronger limit, $g_{ae} < 9 \times 10^{-13}$ which is strongly dependent on the strength of the magnetic field in white dwarfs.

[32] KEIL 97 uses new measurements of the axial-vector coupling strength of nucleons, as well as a reanalysis of many-body effects and pion-emission processes in the core of the neutron star, to update limits on the invisible-axion mass.

[33] RAFFELT 95 reexamined the constraints on axion emission from red giants due to the axion-electron coupling. They improve on DEARBORN 86 by taking into proper account degeneracy effects in the bremsstrahlung rate. The limit comes from requiring the red giant core mass at helium ignition not to exceed its standard value by more than 5% (0.025 solar masses).

[34] ALTHERR 94 bound is on the axion-electron coupling $g_{ae} < 1.5 \times 10^{-13}$, from energy loss via axion emission.

[35] CHANG 93 updates ENGEL 90 bound with the Kaplan-Manohar ambiguity in $z = m_u/m_d$ (see the Note on the Quark Masses in the Quark Particle Listings). It leaves the window $f_A = 3\times10^5$–3×10^6 GeV open. The constraint from Big-Bang Nucleosynthesis is satisfied in this window as well.

[36] BERSHADY 91 searched for a line at wave length from 3100–8300 Å expected from 2γ decays of relic thermal axions in intergalactic light of three rich clusters of galaxies.

[37] KIM 91C argues that the bound from the mass density of the universe will change drastically for the supersymmetric models due to the entropy production of saxion (scalar component in the axionic chiral multiplet) decay. Note that it is an *upperbound* rather than a lowerbound.

[38] RAFFELT 91B argue that previous SN 1987A bounds must be relaxed due to corrections to nucleon bremsstrahlung processes.

[39] RESSELL 91 uses absence of any intracluster line emission to set limit.

[40] ENGEL 90 rule out $10^{-10} \lesssim g_{AN} \lesssim 10^{-3}$, which for a hadronic axion with EMC motivated axion-nucleon couplings corresponds to 2.5×10^{-3} eV $\lesssim m_{A^0} \lesssim 2.5 \times 10^4$ eV. The constraint is loose in the middle of the range, i.e. for $g_{AN} \sim 10^{-6}$.

[41] RAFFELT 90D is a re-analysis of DEARBORN 86.

[42] The region $m_{A^0} \gtrsim 2$ eV is also allowed.

[43] ERICSON 89 considered various nuclear corrections to axion emission in a supernova core, and found a reduction of the previous limit (MAYLE 88) by a large factor.

[44] MAYLE 89 limit based on naive quark model couplings of axion to nucleons. Limit based on couplings motivated by EMC measurements is 2–4 times weaker. The limit from axion-electron coupling is weak: see HATSUDA 88B.

[45] RAFFELT 88B derives a limit for the energy generation rate by exotic processes in helium-burning stars $\epsilon < 100$ erg g^{-1} s^{-1}, which gives a firmer basis for the axion limits based on red giant cooling.

[46] RAFFELT 87 also gives a limit $g_{A\gamma} < 1 \times 10^{-10}$ GeV^{-1}.

[47] DEARBORN 86 also gives a limit $g_{A\gamma} < 1.4 \times 10^{-11}$ GeV^{-1}.

[48] RAFFELT 86 gives a limit $g_{A\gamma} < 1.1\times10^{-10}$ GeV^{-1} from red giants and $< 2.4\times10^{-9}$ GeV^{-1} from the sun.

[49] KAPLAN 85 says $m_{A^0} < 23$ eV is allowed for a special choice of model parameters.

[50] FUKUGITA 82 gives a limit $g_{A\gamma} < 2.3 \times 10^{-10}$ GeV^{-1}.

Search for Relic Invisible Axions

Limits are for the dimensionless quantity $[G_{A\gamma\gamma}/m_{A^0}]^2\rho_A$ where $G_{A\gamma\gamma}$ denotes the axion two-photon coupling, $L_{\rm int} = -\frac{G_{A\gamma\gamma}}{4}\phi_A F_{\mu\nu}\tilde{F}^{\mu\nu} = G_{A\gamma\gamma}\phi_A \mathbf{E}\cdot\mathbf{B}$, and ρ_A is the axion energy density near the earth, unless otherwise stated. Notice that for QCD axions $G_{A\gamma\gamma}/m_{A^0}$ does not depend on m_{A^0}. For the reference values $m_{A^0} = 1$ μeV, $G_{A\gamma\gamma} = 3.9 \times 10^{-16}$ GeV^{-1} (that would apply to KSVZ axions at that mass), and $\rho_A = 300$ MeV/cm^3 one finds $[G_{A\gamma\gamma}/m_{A^0}]^2\rho_A = 3.5 \times 10^{-43}$.

VALUE	CL%	DOCUMENT ID		TECN	COMMENT
• • • We do not use the following data for averages, fits, limits, etc. • • •					
$<2.8 \times 10^{-4}$	95	[1] ADE	21	CMB	$m_{A^0} = 0.16$–4.8×10^{-20} eV
$<1.1 \times 10^{-41}$	90	[2] ALESINI	21	QUAX	$m_{A^0} = 43$ μeV
$<1 \times 10^{-44}$	90	[3] BARTRAM	21A	ADMX	$m_{A^0} = 3.3$–4.2 μeV
$<1.6 \times 10^{-29}$	95	[4] DEVLIN	21	TRAP	$m_{A^0} = 2.7906$–2.7914 neV
$<1.4 \times 10^{-23}$	95	[5] GRAMOLIN	21	SHFT	$m_{A^0} = 0.012$–12 neV
$<7 \times 10^{-43}$	90	[6] KWON	21	CASK	$m_{A^0} = 10.7126$–10.7186 μeV
$<4.6 \times 10^{-40}$	95	[7] MELCON	21	RADE	$m_{A^0} = 34.6738$–34.6771 μeV
$<3.5 \times 10^{-28}$	95	[8] SALEMI	21	ABRA	$m_{A^0} = 0.41$–8.27 neV
$<3 \times 10^{-3}$	95	[9] THOMSON	21		$m_{A^0} = 7.44$–19.38 neV
$<1 \times 10^{-2}$	95	[9] THOMSON	21		$m_{A^0} = 74.4$–74.5 μeV
		[10] YUAN	21	ASTR	$m_{A^0} = 10^{-20}$–10^{-17} eV
$<1.9 \times 10^{-44}$	90	[11] BRAINE	20	ADMX	$m_{A^0} = 2.81$–3.31 μeV
$<2 \times 10^{-35}$	90	[12] CRISOSTO	20	SLIC	$m_{A^0} = 180.07$–180.15 neV
$<4 \times 10^{-37}$	95	[13] DARLING	20A	ASTR	$m_{A^0} = 4.2$–165.6 μeV
$<3.2 \times 10^{-36}$	95	[14] FOSTER	20	ASTR	$m_{A^0} = 5$–7, 10–11 μeV
$<5.7 \times 10^{-41}$	90	[15] JEONG	20	CASK	$m_{A^0} = 13.0$–13.9 μeV
		[16] KENNEDY	20		$m_{S^0} = 10^{-19}$–10^{-17} eV
$<4.8 \times 10^{-42}$	90	[17] LEE	20A	CASK	$m_{A^0} = 6.62$–6.82 μeV
$<2.6 \times 10^{-39}$	95	[18] ALESINI	19	QUAX	$m_{A^0} = 37.5$ μeV
$<6 \times 10^{-5}$		[19] FUJITA	19	ASTR	$m_{A^0} < 10^{-21}$ eV
$<2 \times 10^{-27}$	95	[20] OUELLET	19A	ABRA	$m_{A^0} = 0.31$–8.3 neV
$<7.3 \times 10^{-40}$	90	[21] BOUTAN	18	ADMX	$m_{A^0} = 17.38$–17.57 μeV
$<1.8 \times 10^{-39}$	90	[21] BOUTAN	18	ADMX	$m_{A^0} = 21.03$–23.98 μeV
$<3.4 \times 10^{-39}$	90	[21] BOUTAN	18	ADMX	$m_{A^0} = 29.67$–29.79 μeV
$<1.4 \times 10^{-44}$	90	[22] DU	18	ADMX	$m_{A^0} = 2.66$–2.81 μeV
$<2.87 \times 10^{-42}$	90	[23] ZHONG	18	HYST	$m_{A^0} = 23.15$–24 μeV
		[24] BRANCA	17	AURG	$m_{S^0} = 3.5$–3.9 peV
$<3 \times 10^{-42}$	90	[25] BRUBAKER	17	HYST	$m_{A^0} = 23.55$–24.0 μeV
$<1.0 \times 10^{-29}$	95	[26] CHOI	17	CASK	$m_{A^0} = 24.7$–29.1 μeV
$<8.6 \times 10^{-42}$	90	[27] HOSKINS	16	ADMX	$m_{A^0} = 3.36$–3.52 or 3.55–3.69 μeV
		[28] BECK	13		$m_{A^0} = 0.11$ meV
$<3.5 \times 10^{-43}$		[29] HOSKINS	11	ADMX	$m_{A^0} = 3.3$–3.69×10^{-6} eV
$<2.9 \times 10^{-43}$	90	[30] ASZTALOS	10	ADMX	$m_{A^0} = 3.34$–3.53×10^{-6} eV
$<1.9 \times 10^{-43}$	97.7	[31] DUFFY	06	ADMX	$m_{A^0} = 1.98$–2.17×10^{-6} eV
$<5.5 \times 10^{-43}$	90	[32] ASZTALOS	04	ADMX	$m_{A^0} = 1.9$–3.3×10^{-6} eV
		[33] KIM	98	THEO	
$<2 \times 10^{-41}$		[34] HAGMANN	90	CNTR	$m_{A^0} = (5.4$–$5.9)10^{-6}$ eV
$<6.3 \times 10^{-42}$	95	[35] WUENSCH	89	CNTR	$m_{A^0} = (4.5$–$10.2)10^{-6}$ eV
$<5.4 \times 10^{-41}$	95	[35] WUENSCH	89	CNTR	$m_{A^0} = (11.3$–$16.3)10^{-6}$ eV

[1] ADE 21 looks for a time-variable global rotation of the CMB polarization induced by the harmonic oscillations of local axion-like dark matter and uses data from the 2012 observing season of the Keck Array, part of the BICEP program. The limits get 25% weaker for $m_{A^0} = 4.8 \times 10^{-20}$–$5.7 \times 10^{-19}$ eV. See their Eq. (80) and Fig. 6 for mass-dependent limits.

[2] ALESINI 21 is an update of ALESINI 19. See their Figs. 5 and 6 for the mass-dependent limits.

[3] BARTRAM 21A is analogous to DU 18. See their Fig.4 for mass-dependent limits.

[4] DEVLIN 21 use the superconducting resonant detection circuit of a cryogenic Penning trap with a single antiproton. See their Fig. 3 for mass-dependent limits.

[5] GRAMOLIN 21 use two detection channels, each consisting of two stacked toroids to look for the axion-induced oscillating magnetic field. The quoted limit applies at $m_{A^0} = 0.02$ neV. See their Fig. 4 for mass-dependent limits.

[6] KWON 21 is analogous to LEE 20A. They also obtain weaker limits in the range of $m_{A^0} = 10.16$–11.37 μeV. See their Fig. 4 for mass-dependent limits.

[7] MELCON 21 use a radio frequency cavity consisting of 5 sub-cavities coupled by inductive irises installed inside the CAST dipole magnet to look for higher axion masses. See their Fig. 9 for mass-dependent limits.

Downloaded from https://academic.oup.com/ptep/article/2022/8/083C01/6651666 by KIT Library user on 27 September 2022

[8] SALEMI 21 is an update of OUELLET 19A. See their Fig. 4 for mass-dependent limits.

[9] THOMSON 21 use a resonant cavity supporting two spatially overlapping microwave modes, which is sensitive to the axion mass corresponding to the sum or difference of the two resonant frequencies. The original limit was retracted due to a sign error. See their Fig. 2 in the erratum for the corrected limits.

[10] YUAN 21 use polarimetric observations of Sgr A* taken by the Event Horizon Telescope to search for periodic oscillation of the polarization induced by axion dark matter, assuming a solitonic core near the Galactic center. They obtained limits in the range of $G_{A\gamma\gamma} = 8\times10^{-13}$–$3\times10^{-11}$ GeV^{-1}.

[11] BRAINE 20 is analogous to DU 18. See Fig. 4 for their mass-dependent limits.

[12] CRISOSTO 20 used a resonant LC circuit to look for lighter axion dark matter. They obtained a similar, slightly weaker limit for $m_{A^0} = 174.98$–175.19 and 177.34–177.38 neV. See their Fig. 4 for mass-dependent limits.

[13] DARLING 20A use VLA data to look for radio-frequency radiation converted from axion dark matter in the magnetosphere of the Galactic Center magnetar PSR J1745-2900. They extended the results of DARLING 20, which used only data with the highest angular resolution, by adding sub-optimal data. They use $\rho_A = 6.5\times10^4$ GeV/cm^3 in the vicinity of the magnetar. See their Fig. 2 for mass-dependent limits.

[14] FOSTER 20 look for radio-frequency radiation converted from axion dark matter in the magnetic field around neutron stars. They use the observed data of isolated local neutron stars and in the Galactic center. The quoted limit applies to $m_{A^0} \simeq 7$ μeV. See their Fig. 2 for mass-dependent limits.

[15] JEONG 20 is analogous to LEE 20A, and they use a double-cell cavity to look for axions with mass > 10 μeV. See their Fig. 5 for mass-dependent limits.

[16] KENNEDY 20 is analogous to BRANCA 17, and they compare the frequency ratios of the Si cavity measured by a Sr optical lattice clock and by a H maser. Assuming the local density of moduli dark matter, $\rho_S = 0.3$ GeV/cm^3, they obtain a limit $G_{S\gamma\gamma} < 5.8\times10^{-24}$ GeV^{-1} at $m_{S^0} = 2\times10^{-19}$ eV. See their Fig. 2 for mass-dependent limits as well as limits on the modulus coupling to electrons.

[17] LEE 20A used a microwave cavity detector at the IBS/CAPP to search for dark matter axions. See Fig. 3 for the mass-dependent limits.

[18] ALESINI 19 used a superconducting resonant cavity made of NbTi to increase the quality factor. The limit applies to a mass range of 0.2 neV around $m_{A^0} = 37.5$ μeV.

[19] FUJITA 19 look for photon birefringence under the oscillating axion background using the polarimetric imaging observation of a protoplanetary disk, AB Aur. See their Fig. 2 for a more conservative limit taking account of possible systematic effects.

[20] OUELLET 19A look for the axion-induced oscillating magnetic field generated by a toroidal magnetic field. The quoted limit applies at $m_{A^0} = 8$ neV. See their Fig. 3 for the mass-dependent limits.

[21] BOUTAN 18 use a small high frequency cavity installed above the main ADMX cavity to look for heavier axion dark matter. See their Fig. 4 for mass-dependent limits.

[22] DU 18 is analogous to DUFFY 06. They upgraded a dilution refrigerator to reduce the system noise. The quoted limit is around $m_{A^0} = 2.69$ μeV for the boosted Maxwellian axion line shape. See Fig. 4 for their mass-dependent limits.

[23] ZHONG 18 is analogous to BRUBAKER 17. The quoted limit applies at $m_{A^0} = 23.76$ μeV. See Fig. 4 for their mass-dependent limits.

[24] BRANCA 17 look for modulations of the fine-structure constant and the electron mass due to moduli dark matter by using the cryogenic resonant-mass AURIGA detector. The limit on the assumed dilatonic coupling implies $G_{S\gamma\gamma} < 1.5\times10^{-24}$ GeV^{-1} for the scalar to two-photon coupling. See Fig. 5 for the mass-dependent limits.

[25] BRUBAKER 17 used a microwave cavity detector at the Yale Wright Laboratory to search for dark matter axions. See Fig. 3 for the mass-dependent limits.

[26] CHOI 17 used a microwave cavity detector with toroidal geometry. See Fig. 4 for their mass-dependent limits.

[27] HOSKINS 16 is analogous to DUFFY 06. See Fig. 12 for mass-dependent limits in terms of the local dark matter density.

[28] BECK 13 argues that dark-matter axions passing through Earth may generate a small observable signal in resonant S/N/S Josephson junctions. A measurement by HOFFMANN 04 [Physical Review **B70** 180503 (2004)] is interpreted in terms of subdominant dark matter axions with $m_{A^0} = 0.11$ meV.

[29] HOSKINS 11 is analogous to DUFFY 06. See Fig. 4 for the mass-dependent limit in terms of the local density.

[30] ASZTALOS 10 used the upgraded detector of ASZTALOS 04 to search for halo axions. See their Fig. 5 for the m_{A^0} dependence of the limit.

[31] DUFFY 06 used the upgraded detector of ASZTALOS 04, while assuming a smaller velocity dispersion than the isothermal model as in Eq. (8) of their paper. See Fig. 10 of their paper on the axion mass dependence of the limit.

[32] ASZTALOS 04 looked for a conversion of halo axions to microwave photons in magnetic field. At 90% CL, the KSVZ axion cannot have a local halo density more than 0.45 GeV/cm^3 in the quoted mass range. See Fig. 7 of their paper on the axion mass dependence of the limit.

[33] KIM 98 calculated the axion-to-photon couplings for various axion models and compared them to the HAGMANN 90 bounds. This analysis demonstrates a strong model dependence of $G_{A\gamma\gamma}$ and hence the bound from relic axion search.

[34] HAGMANN 90 experiment is based on the proposal of SIKIVIE 83.

[35] WUENSCH 89 looks for condensed axions near the earth that could be converted to photons in the presence of an intense electromagnetic field via the Primakoff effect, following the proposal of SIKIVIE 83. The theoretical prediction with $[G_{A\gamma\gamma}/m_{A^0}]^2 = 2\times10^{-14}$ MeV^{-4} (the three generation DFSZ model) and $\rho_A = 300$ MeV/cm^3 that makes up galactic halos gives $(G_{A\gamma\gamma}/m_{A^0})^2\,\rho_A = 4\times10^{-44}$. Note that our definition of $G_{A\gamma\gamma}$ is $(1/4\pi)$ smaller than that of WUENSCH 89.

Invisible A^0 (Axion) Limits from Photon Coupling

Limits are for the modulus of the axion-two-photon coupling $G_{A\gamma\gamma}$ defined by $L = -G_{A\gamma\gamma}\phi_A \mathbf{E}\cdot\mathbf{B}$. For scalars S^0 the limit is on the coupling constant in $L = G_{S\gamma\gamma}\phi_S(\mathbf{E}^2-\mathbf{B}^2)$. The relation between $G_{A\gamma\gamma}$ and m_{A^0} is not used unless stated otherwise, i.e., many of these bounds apply to low-mass axion-like particles (ALPs), not to QCD axions.

VALUE (GeV^{-1})	CL%	DOCUMENT ID		TECN	COMMENT
• • • We do not use the following data for averages, fits, limits, etc. • • •					
$<9.2\times10^{-11}$	95	[1] BASU	21	ASTR	$m_{A^0} = 3.6\times10^{-21}$ eV
$<1.8\times10^{-10}$	95	[2] BI	21	ASTR	$m_{A^0} = 2$–6×10^{-7} eV
$<1.6\times10^{-10}$	95	[3] DOLAN	21A	ASTR	$m_{A^0} = 1$–570 keV
$<5\times10^{-11}$	95	[4] GUO	21	ASTR	$m_{A^0} = 8$–23 neV
$<1.2\times10^{-4}$	95	[5] HOMMA	21	LASR	$m_{A^0} = 0.4$–600 meV
$<1.2\times10^{-11}$	95	[6] LI	21B	ASTR	$m_{A^0} = 0.5$–500 neV
		[7] LLOYD	21	ASTR	Magnetars
$<1\times10^{-13}$	95	[8] REGIS	21	ASTR	$m_{A^0} = 2.7$–5.3 eV
$<1.8\times10^{-11}$	95	[9] XIAO	21	ASTR	$m_{A^0} < 3.5\times10^{-11}$ eV
$<7\times10^{-4}$	95	[10] ABUDINEN	20	BEL2	$m_{A^0} = 0.2$–1 GeV
$<2\times10^{-4}$	90	[11] BANERJEE	20A	NA64	$m_{A^0} < 55$ MeV
$<1.0\times10^{-11}$	95	[12] BUEHLER	20	ASTR	$m_{A^0} < 3$ neV
$<5\times10^{-10}$		[13] CALORE	20	ASTR	$m_{A^0} \lesssim 10^{-11}$ eV
		[14] CARENZA	20	ASTR	Globular clusters
2–4×10^{-10}	95	[15] DENT	20A	ASTR	Solar axions
		[16] DEPTA	20	COSM	Axion-like particles
$<3.6\times10^{-12}$	95	[17] DESSERT	20A	ASTR	$m_{A^0} < 5\times10^{-11}$ eV
		[18] ESTEBAN	20	ANIT	Axion-like particles
4–6×10^{-10}	90	[19] GAO	20	ASTR	Solar axions
$<2.8\times10^{-11}$	95	[20] KOROCHKIN	20	ASTR	$m_{A^0} = 25$ eV
none 6.0×10^{-9}–1.3×10^{-5}		[21] LUCENTE	20A	ASTR	$m_{A^0} < 270$ MeV
$<2.6\times10^{-11}$	95	[22] MEYER	20	FLAT	$m_{A^0} < 3\times10^{-10}$ eV
$<8.4\times10^{-8}$	99	[23] YAMAMOTO	20	COSM	$m_{A^0} < 4\times10^{-6}$ eV
$<1\times10^{-3}$	95	[24] ALONI	19	PRMX	$m_{A^0} = 0.16$ GeV
$<1.4\times10^{-14}$	95	[25] CAPUTO	19	ASTR	$m_{A^0} = 5\times10^{-24}$ eV
$<9.6\times10^{-14}$	95	[26] FEDDERKE	19	CMB	$m_{A^0} = 10^{-22}$ eV
$<7\times10^{-13}$	95	[27] IVANOV	19	ASTR	$m_{A^0} = 5\times10^{-23}$ eV
$<4\times10^{-11}$	95	[28] LIANG	19	ASTR	$m_{A^0} = 1.2\times10^{-7}$ eV
		[29] FORTIN	18	ASTR	Axion-like particles
$<5.0\times10^{-3}$	90	[30] YAMAJI	18	LSW	$m_{A^0} = 46$–1020 eV
$<1\times10^{-11}$	99.9	[31] ZHANG	18	ASTR	$m_{A^0} = 0.6$–4 neV
		[32] ADE	17	CMB	Axion-like particles
$<6.6\times10^{-11}$	95	[33] ANASTASSO...	17	CAST	$m_{A^0} < 0.02$ eV
		[34] DOLAN	17	RVUE	Axion-like particles
$<2.51\times10^{-4}$	95	[35] INADA	17	LSW	$m_{A^0} < 0.1$ eV
$>1.5\times10^{-11}$	95	[36] KOHRI	17	ASTR	$m_{A^0} = 0.7$–50 neV
$<2.6\times10^{-12}$	95	[37] MARSH	17	ASTR	$m_{A^0} \leq 10^{-13}$ eV
$<6\times10^{-13}$		[38] TIWARI	17	COSM	$m_{A^0} \leq 10^{-15}$ eV
$<5\times10^{-12}$	95	[39] AJELLO	16	ASTR	$m_{A^0} = 0.5$–5 neV
$<1.2\times10^{-7}$	95	[40] DELLA-VALLE	16	LASR	$m_{A^0} = 1.3$ meV
$<7.2\times10^{-8}$	95	[41] DELLA-VALLE	16	LASR	$m_{A^0} < 0.5$ meV
$<8\times10^{-4}$		[42] JAECKEL	16	ALPS	$m_{A^0} = 0.1$–100 GeV
$<6\times10^{-21}$		[43] LEEFER	16		$m_{S^0} < 10^{-18}$ eV
		[44] ANASTASSO...	15	CAST	Chameleons
$<1.47\times10^{-10}$	95	[45] ARIK	15	CAST	$m_{A^0} = 0.39$–0.42 eV
$<3.5\times10^{-8}$	95	[46] BALLOU	15	LSW	$m_{A^0} < 2\times10^{-4}$ eV
		[47] BRAX	15	ASTR	$m_{S^0} < 4\times10^{-12}$ eV
$<5.42\times10^{-4}$	95	[48] HASEBE	15	LASR	$m_{A^0} = 0.15$ eV
		[49] MILLEA	15	COSM	Axion-like particles
		[50] VANTILBURG	15		Dilaton-like dark matter
$<4.1\times10^{-10}$	99.7	[51] VINYOLES	15	ASTR	$m_{A^0} = 0.6$–185 eV
$<3.3\times10^{-10}$	95	[52] ARIK	14	CAST	$m_{A^0} = 0.64$–1.17 eV
$<6.6\times10^{-11}$	95	[53] AYALA	14	ASTR	Globular clusters
$<1.4\times10^{-7}$	95	[54] DELLA-VALLE	14	LASR	$m_{A^0} = 1$ meV
		[55] EJLLI	14	COSM	$m_{A^0} = 2.66$–48.8 μeV
$<8\times10^{-8}$	95	[56] PUGNAT	14	LSW	$m_{A^0} < 0.3$ meV
$<1\times10^{-11}$		[57] REESMAN	14	ASTR	$m_{A^0} < 1\times10^{-10}$ eV
$<2.1\times10^{-11}$	95	[58] ABRAMOWSKI	13A	IACT	$m_{A^0} = 15$–60 neV
$<2.15\times10^{-9}$	95	[59] ARMENGAUD	13	EDEL	$m_{A^0} < 200$ eV
$<4.5\times10^{-8}$	95	[60] BETZ	13	LSW	$m_{A^0} = 7.2\times10^{-6}$ eV
$<8\times10^{-11}$		[61] FRIEDLAND	13	ASTR	Red giants
$>2\times10^{-11}$		[62] MEYER	13	ASTR	$m_{A^0} < 1\times10^{-7}$ eV
$<8.3\times10^{-12}$	95	[63] WOUTERS	13	ASTR	$m_{A^0} < 7\times10^{-12}$ eV
		[64] CADAMURO	12	COSM	Axion-like particles
$<2.5\times10^{-13}$	95	[65] PAYEZ	12	ASTR	$m_{A^0} < 4.2\times10^{-14}$ eV
$<2.3\times10^{-10}$	95	[66] ARIK	11	CAST	$m_{A^0} = 0.39$–0.64 eV
$<6.5\times10^{-8}$	95	[67] EHRET	10	ALPS	$m_{A^0} < 0.7$ meV
$<2.4\times10^{-9}$	95	[68] AHMED	09A	CDMS	$m_{A^0} < 100$ eV
<1.2–2.8×10^{-10}	95	[69] ARIK	09	CAST	$m_{A^0} = 0.02$–0.39 eV
		[70] CHOU	09		Chameleons
$<7\times10^{-10}$		[71] GONDOLO	09	ASTR	$m_{A^0} <$ few keV

Downloaded from https://academic.oup.com/ptep/article/2022/8/083C01/6651666 by KIT Library user on 27 September 2022

$<1.3 \times 10^{-6}$	95	[72] AFANASEV	08		$m_{S^0} < 1$ meV
$<3.5 \times 10^{-7}$	99.7	[73] CHOU	08		$m_{A^0} < 0.5$ meV
$<1.1 \times 10^{-6}$	99.7	[74] FOUCHE	08		$m_{A^0} < 1$ meV
< 5.6–13.4×10^{-10}	95	[75] INOUE	08		$m_{A^0} = 0.84$–1.00 eV
$<5 \times 10^{-7}$		[76] ZAVATTINI	08		$m_{A^0} < 1$ meV
$<8.8 \times 10^{-11}$	95	[77] ANDRIAMON..	07	CAST	$m_{A^0} < 0.02$ eV
$<1.25 \times 10^{-6}$	95	[78] ROBILLIARD	07		$m_{A^0} < 1$ meV
2–5×10^{-6}		[79] ZAVATTINI	06		$m_{A^0} = 1$–1.5 meV
$<1.1 \times 10^{-9}$	95	[80] INOUE	02		$m_{A^0} = 0.05$–0.27 eV
$<2.78 \times 10^{-9}$	95	[81] MORALES	02B		$m_{A^0} <1$ keV
$<1.7 \times 10^{-9}$	90	[82] BERNABEI	01B		$m_{A^0} <100$ eV
$<1.5 \times 10^{-4}$	90	[83] ASTIER	00B	NOMD	$m_{A^0} <40$ eV
		[84] MASSO	00	THEO	induced γ coupling
$<2.7 \times 10^{-9}$	95	[85] AVIGNONE	98	SLAX	$m_{A^0} < 1$ keV
$<6.0 \times 10^{-10}$	95	[86] MORIYAMA	98		$m_{A^0} < 0.03$ eV
$<3.6 \times 10^{-7}$	95	[87] CAMERON	93		$m_{A^0} < 10^{-3}$ eV, optical rotation
$<6.7 \times 10^{-7}$	95	[88] CAMERON	93		$m_{A^0} < 10^{-3}$ eV, photon regeneration
$<3.6 \times 10^{-9}$	99.7	[89] LAZARUS	92		$m_{A^0} < 0.03$ eV
$<7.7 \times 10^{-9}$	99.7	[89] LAZARUS	92		$m_{A^0} = 0.03$–0.11 eV
$<7.7 \times 10^{-7}$	99	[90] RUOSO	92		$m_{A^0} < 10^{-3}$ eV
$<2.5 \times 10^{-6}$		[91] SEMERTZIDIS	90		$m_{A^0} < 7 \times 10^{-4}$ eV

[1] BASU 21 searched for birefringence induced by axion dark matter using multiple images of the polarized source in the strongly gravitationally lensed system CLASS B1152+199. They assume the axion makes up all dark matter, and used the axion density in the emitting region, $\rho_A = 20$ GeV/cm^3. Limits between 9.2×10^{-11}–7.7×10^{-8} GeV^{-1} are obtained for $m_{A^0} = 3.6\times10^{-21}$–$4.6\times10^{-18}$eV. See their Fig. 2 for mass-dependent limits.

[2] BI 21 look for the gamma-ray spectral distortions induced by axion-photon oscillations in the presence of the Galactic magnetic field, using the measurements of sub-PeV gamma-rays from the Crab Nebula by the Tibet ASγ and HAWC experiments, together with MAGIC and HEGRA gamma-ray data. See their Fig. 3 for mass-dependent limits.

[3] DOLAN 21A study the effect of axion production on the evolution of asymptotic giant branch stars, and use the white-dwarf initial-final mass relation to set the limits. See their Fig. 1 for mass-dependent limits.

[4] GUO 21 is analogous to AJELLO 16, and use the Fermi-LAT and H.E.S.S. II measurements of PG 1553+113 and PKS 2155-304. See their Fig. 6 for mass-dependent limits.

[5] HOMMA 21 look for the production of axion resonance states and their subsequent stimulated decays by combining linearly polarized creation laser pulses and circularly polarized inducing laser pulses. The quoted limit is at $m_{A^0} \simeq 0.178$ eV. See their Fig. 14 for mass-dependent limits.

[6] LI 21B is analogous to AJELLO 16, and use the spectra of the blazar Mrk 421 measured by ARGO-YBJ and Fermi-LAT. They consider ALP-photon mixing in the magnetic fields of both the blazar jet and the Galaxy. The quoted limit applies to $m_{A^0} \simeq 1 \times 10^{-9}$ eV. See their Fig. 5 for mass-dependent limits.

[7] LLOYD 21 is analogous to FORTIN 18, and set limits on the product of the axion couplings to photons and nucleons as $g_{ANN}\, G_{A\gamma\gamma} \lesssim 4.6\times10^{-19}$ GeV^{-1} for $m_{A^0} \lesssim 10^{-5}$ eV by using the quiescent soft gamma-ray flux upper limits in five magnetars. We use $g_{ANN} = G_{AN}\, 2m_N$ to translate their limits. See their Table II and Fig. 3 for the limits.

[8] REGIS 21 look for monochromatic photons from axion decay, using the MUSE spectroscopic data on the Leo T dwarf spheroidal galaxy. They assume that axions make up all of dark matter and use the integrated dark matter density along the line of sight determined by observations.

[9] XIAO 21 use X-ray data from Betelgeuse to look for signals from axions produced in the stellar core that were converted to X-rays by the Galactic magnetic field. See their Fig. 1 for the mass-dependent limit.

[10] ABUDINEN 20 look for the process $e^+e^- \to \gamma A^0$ ($A^0 \to \gamma\gamma$) and set upper limits of around 10^{-3} over the mass range. The quoted limit is at $m_{A^0} = 0.3$ GeV. See their Fig. 5 for mass dependent limits.

[11] BANERJEE 20A look for axions produced from high-energy bremsstrahlung photons through the Primakoff effect with the electric field of the target nuclei. They exclude $G_{A\gamma\gamma} = 2 \times 10^{-4}$–$5 \times 10^{-2}$ GeV^{-1} for $m_{A^0} < 55$ MeV. See their Fig. 5 for mass-dependent limits.

[12] BUEHLER 20 look for the γ-ray transparency due to axion-photon oscillations using high-energy photon events from 79 sources in the Second Fermi-LAT Catalog of High-Energy Sources. The quoted limit is for the intergalactic magnetic field strength and coherence length of $B = 1$ nG and $s = 1$ Mpc. See their Figs. 4 and 5 for mass-dependent limits and for different magnetic-field parameters.

[13] CALORE 20 use the isotropic diffuse γ-ray background measured by the Fermi-LAT to constrain the γ-ray flux converted in the Galactic magnetic field from axions produced from past core-collapse supernovae. They also derive a limit on a heavier axion with $m_{A^0} \gtrsim$ keV decaying into two photons of $G_{A\gamma\gamma} \lesssim 5 \times 10^{-11}$ GeV^{-1} for $m_{A^0} = 5$ keV. See their Figs. 5 and 7 for the limits as well as limits in the presence of axion-nucleon couplings.

[14] CARENZA 20 extend the globular cluster bound of AYALA 14 to heavier masses ($m_{A^0} \leq$ a few 100 keV) by taking account of the coalescence process $\gamma + \gamma \to A^0$ as well as the decay of the ALP inside the stellar core. See their Fig.4 for mass-dependent limits.

[15] DENT 20A is analogous to GAO 20. The quoted limit is from their arXiv:2006.15118v3 (v2 is their published version), using the relativistic Hartree-Fock form factor. The limit is up to two times weaker than the published one. See Fig. 4 in their arXiv version 3 for the correlation between $G_{A\gamma\gamma}$ and g_{Aee} corresponding to the excess reported in APRILE 20.

[16] DEPTA 20 correct the underestimated D abundance in MILLEA 15, and derive robust cosmological bounds by allowing the reheating temperature, $N_{\rm eff}$, and neutrino chemical potential to vary. See their Fig. 6 for mass-dependent limits.

[17] DESSERT 20A use the NuSTAR data of the Quintuplet and Westerlund 1 super star clusters to look for X-rays converted in the Galactic magnetic field from the axions produced in stellar cores. See their Fig. 3 for the mass-dependent limits.

[18] ESTEBAN 20 show that the two anomalous ANITA events can be explained by the reflected radio pulses that are resonantly produced in the ionosphere via axion-photon conversion for $m_{A^0} \lesssim 1 \times 10^{-7}$ eV , if an axion clump passes the Earth about once a month. See their Fig.5 for the region consistent with this interpretation for different values of the axion density inside the clumps.

[19] GAO 20 correct the limit of APRILE 20 by including inverse Primakoff scattering in the XENON1T detector. The quoted limit is from their arXiv:2006.14598v4 (v3 is their published version), taking account of the atomic form factor of Xe as pointed out in ABE 20J. The limit is weaker by a factor of 1.5–2 than the published one. See Fig. 3 in their arXiv version 4 for correlation between $G_{A\gamma\gamma}$ and g_{Aee} corresponding to the excess reported in APRILE 20.

[20] KOROCHKIN 20 assume the axion makes up all dark matter, and look for a dip in the observed gamma-ray spectrum of the blazer 1ES 1218+304 by Fermi/LAT and VERITAS due to the extragalactic background light produced by the axion decay. Their analysis favors nonzero axion-induced absorption with $G_{A\gamma\gamma} = 3 \times 10^{-11}$–$2 \times 10^{-10}$ GeV^{-1} over a range of $m_{A^0} = 2$–18 eV. See their Fig. 1 for mass-dependent limits between $0.25 < m_{A^0} < 25$ eV.

[21] LUCENTE 20A study the SN 1987A energy-loss argument on the axion-like particle production. In addition to the Primakoff process, they take account of photon coalescence as well as gravitational trapping that become relevant at $m_{A^0} > 100$ MeV. See their Fig. 12 for the mass-dependent limit.

[22] MEYER 20 look for prompt γ-rays converted in the Galactic magnetic fields from axions produced via the Primakoff process in a sample of 20 extragalactic core-collapse supernovae. The limits assume a progenitor mass of 10 times the solar mass and certain models for the optical emission and the galactic magnetic field. See their Figs. 2 and 6 in the erratum for mass- and model-dependent limits.

[23] YAMAMOTO 20 look for X-ray photons converted by the Earth's magnetic field from the axions produced by the two-body decay of dark matter, and set the limits by using the Suzaku data. The quoted limit is for the monochromatic X-ray line from the galactic dark matter with lifetime $\tau = 4.32 \times 10^{17}$ sec. They also derive limits on the continuum spectrum from the extragalactic component. See their Fig. 7 for the limits.

[24] ALONI 19 used the data collected by the PRIMEX experiment to derive a limit based on a data-driven method. See their Fig. 2 for mass-dependent limits.

[25] CAPUTO 19 look for an oscillating variation of the polarization angle of the pulsar J0437-4715, where they assume the local axion energy density $\rho_A = 0.3$ GeV/cm^3. See their Fig. 2 for mass-dependent limits for 5×10^{-24} eV $\leq m_{A^0} \leq 2 \times 10^{-19}$ eV.

[26] FEDDERKE 19 look for a uniform reduction of the CMB polarization at large scales, which is induced by the oscillating axion background during CMB decoupling. The quoted limit is based on the assumption that axions make up all of the dark matter. See their Fig. 3 for mass-dependent limits for $m_{A^0} = 10^{-22}$–10^{-19} eV.

[27] IVANOV 19 look for the axion-induced periodic changes in the polarization angle of parsec-scale jets in active galactic nuclei observed by the MOJAVE program, where they use the axion energy density $\rho_A = 20$ GeV/cm^3. See their Fig. 6 for mass-dependent limits for 5×10^{-23} eV $\leq m_{A^0} \leq 1.2 \times 10^{-21}$ eV.

[28] LIANG 19 look for spectral irregularities in the spectrum of 10 bright H.E.S.S. sources in the Galactic plane, assuming photon-ALP mixing in the Galactic magnetic fields. See their Fig. 2 for mass-dependent limits with different Galactic magnetic field models.

[29] FORTIN 18 studied the conversion of axion-like particles produced in the core of a magnetar to hard X-rays in the magnetosphere. See their Fig. 5 for mass-dependent limits with different values of the magnetar core temperature.

[30] YAMAJI 18 search for axions with an x-ray LSW at Spring-8, using the Laue-case conversion in a silicon crystal. They also obtain $G_{A\gamma\gamma} < 4.2 \times 10^{-3}$ GeV^{-1} for $m_{A^0} < 10$ eV. See their Fig. 5 for mass-dependent limits.

[31] ZHANG 18 look for spectral irregularities in the spectrum of PKS 2155-304 measured by Fermi LAT, assuming photon-ALP mixing in the intercluster and Galactic magnetic fields. See their Figs. 2 and 3 for mass-dependent limits with different values of the intercluster magnetic field parameters.

[32] ADE 17 look for cosmic birefringence from axion-like particles using CMB polarization data taken by the BICEP2 and Keck Array experiments. They set a limit $G_{A\gamma\gamma} H_I < 7.2 \times 10^{-2}$ at 95 %CL for $m_{A^0} < 10^{-28}$ eV, where H_I is the Hubble parameter during inflation.

[33] ANASTASSOPOULOS 17 looked for solar axions by the CAST axion helioscope in the vacuum phase, and supersedes ANDRIAMONJE 07.

[34] DOLAN 17 update existing limits on $G_{A\gamma\gamma}$ for axion-like particles. The limits from the proton beam dump experiments in their Fig. 2 contained an error, and the corrected version is shown in Fig. 1 of DOLAN 21.

[35] INADA 17 search for axions with an x-ray LSW at Spring-8. See their Fig. 4 for mass-dependent limits.

[36] KOHRI 17 attributed to axion-photon oscillations the excess of cosmic infrared background observed by the CIBER experiment. See their Fig. 5 for the region preferred by their scenario.

[37] MARSH 17 is similar to WOUTERS 13, using Chandra observations of M87. See their Fig. 6 for mass-dependent limits.

[38] TIWARI 17 use observed limits of the cosmic distance-duality relation to constrain the photon-ALP mixing based on 3D simulations of the magnetic field configuration. The quoted value is for the averaged magnetic field of 1nG with a coherent length of 1 Mpc. See their Fig. 5 for mass-dependent limits.

[39] AJELLO 16 look for irregularities in the energy spectrum of the NGC1275 measured by Fermi LAT, assuming photon-ALP mixing in the intra-cluster and Galactic magnetic fields. See their Fig. 2 for mass-dependent limits.

[40] DELLA-VALLE 16 look for the birefringence induced by axion-like particles. See their Fig. 14 for mass-dependent limits.

[41] DELLA-VALLE 16 look for the dichroism induced by axion-like particles. See their Fig. 14 for mass-dependent limits.

[42] JAECKEL 16 use the LEP data of $Z \to 2\gamma$ and $Z \to 3\gamma$ to constrain the ALP production via $e^+e^- \to Z \to A^0\gamma$ ($A^0 \to \gamma\gamma$), assuming the ALP coupling with two hypercharge bosons. See their Fig. 4 for mass-dependent limits.

[43] LEEFER 16 derived limits by using radio-frequency spectroscopy of dysprosium and atomic clock measurements. See their Fig. 1 for mass-dependent limits as well as limits on Yukawa-type couplings of the scalar to the electron and nucleons.

Downloaded from https://academic.oup.com/ptep/article/2022/8/083C01/6651666 by KIT Library user on 27 September 2022

[44] ANASTASSOPOULOS 15 search for solar chameleons with CAST and derived limits on the chameleon coupling to photons and matter. See their Fig. 12 for the exclusion region.

[45] ARIK 15 is analogous to ARIK 09, and search for solar axions for m_{A^0} around 0.2 and 0.4 eV. See their Figs. 1 and 3 for the mass-dependent limits.

[46] Based on OSQAR photon regeneration experiment. See their Fig. 6 for mass-dependent limits on scalar and pseudoscalar bosons.

[47] BRAX 15 derived limits on conformal and disformal couplings of a scalar to photons by searching for a chaotic absorption pattern in the X-ray and UV bands of the Hydra A galaxy cluster and a BL lac object, respectively. See their Fig. 8.

[48] HASEBE 15 look for an axion via a four-wave mixing process at quasi-parallel colliding laser beams. They also derived limits on a scalar coupling to photons $G_{S\gamma\gamma} < 2.62 \times 10^{-4}$ GeV^{-1} at $m_{S^0} = 0.15$ eV. See their Figs. 11 and 12 for mass-dependent limits.

[49] MILLEA 15 is similar to CADAMURO 12, including the Planck data and the latest inferences of primordial deuterium abundance. See their Fig. 3 for mass-dependent limits.

[50] VANTILBURG 15 look for harmonic variations in the dyprosium transition frequency data, induced by coherent oscillations of the fine-structure constant due to dilaton-like dark matter, and set the limits, $G_{S\gamma\gamma} < 6 \times 10^{-27}$ GeV^{-1} at $m_{S^0} = 6 \times 10^{-23}$ eV. See their Fig. 4 for mass-dependent limits between $1 \times 10^{-24} < m_{S^0} < 1 \times 10^{-15}$ eV.

[51] VINYOLES 15 performed a global fit analysis based on helioseismology and solar neutrino observations. See their Fig. 9.

[52] ARIK 14 is similar to ARIK 11. See their Fig. 2 for mass-dependent limits.

[53] AYALA 14 derived the limit from the helium-burning lifetime of horizontal-branch stars based on number counts in globular clusters.

[54] DELLA-VALLE 14 use the new PVLAS apparatus to set a limit on vacuum magnetic birefringence induced by axion-like particles. See their Fig. 6 for the mass-dependent limits.

[55] EJLLI 14 set limits on a product of primordial magnetic field and the axion mass using CMB distortion induced by resonant axion production from CMB photons. See their Fig. 1 for limits applying specifically to the DFSZ and KSVZ axion models.

[56] PUGNAT 14 is analogous to EHRET 10. See their Fig. 5 for mass-dependent limits on scalar and pseudoscalar bosons.

[57] REESMAN 14 derive limits by requiring effects of axion-photon interconversion on gamma-ray spectra from distant blazars to be no larger than errors in the best-fit optical depth based on a certain extragalactic background light model. See their Fig. 5 for mass-dependent limits.

[58] ABRAMOWSKI 13A look for irregularities in the energy spectrum of the BL Lac object PKS 2155–304 measured by H.E.S.S. The limits depend on assumed magnetic field around the source. See their Fig. 7 for mass-dependent limits.

[59] ARMENGAUD 13 is analogous to AVIGNONE 98. See Fig. 6 for the limit.

[60] BETZ 13 performed a microwave-based light shining through the wall experiment. See their Fig. 13 for mass-dependent limits.

[61] FRIEDLAND 13 derived the limit by considering blue-loop suppression of the evolution of red giants with 7–12 solar masses.

[62] MEYER 13 attributed to axion-photon oscillations the observed excess of very high-energy γ-rays with respect to predictions based on extragalactic background light models. See their Fig.4 for mass-dependent lower limits for various magnetic field configurations.

[63] WOUTERS 13 look for irregularities in the X-ray spectrum of the Hydra cluster observed by Chandra. See their Fig. 4 for mass-dependent limits.

[64] CADAMURO 12 derived cosmological limits on $G_{A\gamma\gamma}$ for axion-like particles. See their Fig. 1 for mass-dependent limits.

[65] PAYEZ 12 derive limits from polarization measurements of quasar light (see their Fig. 3). The limits depend on assumed magnetic field strength in galaxy clusters. The limits depend on assumed magnetic field and electron density in the local galaxy supercluster.

[66] ARIK 11 search for solar axions using ^{3}He buffer gas in CAST, continuing from the ^{4}He version of ARIK 09. See Fig. 2 for the exact mass-dependent limits.

[67] ALPS is a photon regeneration experiment. See their Fig. 4 for mass-dependent limits on scalar and pseudoscalar bosons.

[68] AHMED 09A is analogous to AVIGNONE 98.

[69] ARIK 09 is the ^{4}He filling version of the CAST axion helioscope in analogy to INOUE 02 and INOUE 08. See their Fig. 7 for mass-dependent limits.

[70] CHOU 09 use the GammeV apparatus in the afterglow mode to search for chameleons, (pseudo)scalar bosons with a mass depending on the environment. For pseudoscalars they exclude at 3σ the range 2.6×10^{-7} GeV$^{-1} < G_{A\gamma\gamma} < 4.2 \times 10^{-6}$ GeV^{-1} for vacuum m_{A^0} roughly below 6 meV for density scaling index exceeding 0.8.

[71] GONDOLO 09 use the all-flavor measured solar neutrino flux to constrain solar interior temperature and thus energy losses.

[72] LIPSS photon regeneration experiment, assuming scalar particle S^0. See Fig. 4 for mass-dependent limits.

[73] CHOU 08 perform a variable-baseline photon regeneration experiment. See their Fig. 3 for mass-dependent limits. Excludes the PVLAS result of ZAVATTINI 06.

[74] FOUCHE 08 is an update of ROBILLIARD 07. See their Fig. 12 for mass-dependent limits.

[75] INOUE 08 is an extension of INOUE 02 to larger axion masses, using the Tokyo axion helioscope. See their Fig. 4 for mass-dependent limits.

[76] ZAVATTINI 08 is an upgrade of ZAVATTINI 06, see their Fig. 8 for mass-dependent limits. They now exclude the parameter range where ZAVATTINI 06 had seen a positive signature.

[77] ANDRIAMONJE 07 looked for Primakoff conversion of solar axions in 9T superconducting magnet into X-rays. Supersedes ZIOUTAS 05.

[78] ROBILLIARD 07 perform a photon regeneration experiment with a pulsed laser and pulsed magnetic field. See their Fig. 4 for mass-dependent limits. Excludes the PVLAS result of ZAVATTINI 06 with a CL exceeding 99.9%.

[79] ZAVATTINI 06 propagate a laser beam in a magnetic field and observe dichroism and birefringence effects that could be attributed to an axion-like particle. This result is now excluded by ROBILLIARD 07, ZAVATTINI 08, and CHOU 08.

[80] INOUE 02 looked for Primakoff conversion of solar axions in 4T superconducting magnet into X ray.

[81] MORALES 02B looked for the coherent conversion of solar axions to photons via the Primakoff effect in Germanium detector.

[82] BERNABEI 01B looked for Primakoff coherent conversion of solar axions into photons via Bragg scattering in NaI crystal in DAMA dark matter detector.

[83] ASTIER 00B looked for production of axions from the interaction of high-energy photons with the horn magnetic field and their subsequent re-conversion to photons via the interaction with the NOMAD dipole magnetic field.

[84] MASSO 00 studied limits on axion-proton coupling using the induced axion-photon coupling through the proton loop and CAMERON 93 bound on the axion-photon coupling using optical rotation. They obtained the bound $g_p^2/4\pi < 1.7 \times 10^{-9}$ for the coupling $g_p \overline{p} \gamma_5 p \phi_A$.

[85] AVIGNONE 98 result is based on the coherent conversion of solar axions to photons via the Primakoff effect in a single crystal germanium detector.

[86] Based on the conversion of solar axions to X-rays in a strong laboratory magnetic field.

[87] Experiment based on proposal by MAIANI 86.

[88] Experiment based on proposal by VANBIBBER 87.

[89] LAZARUS 92 experiment is based on proposal found in VANBIBBER 89.

[90] RUOSO 92 experiment is based on the proposal by VANBIBBER 87.

[91] SEMERTZIDIS 90 experiment is based on the proposal of MAIANI 86. The limit is obtained by taking the noise amplitude as the upper limit. Limits extend to $m_{A^0} = 4 \times 10^{-3}$ where $G_{A\gamma\gamma} < 1 \times 10^{-4}$ GeV^{-1}.

Limit on Invisible A^0 (Axion) Electron Coupling

The limit is for $g_{Aee}\, \phi_A\, \overline{e}(i\gamma_5)e$, or equivalently, the dipole-dipole potential $-\frac{g^2_{Aee}}{16\pi m^2_e}((\boldsymbol{\sigma}_1 \cdot \boldsymbol{\sigma}_2) - 3(\boldsymbol{\sigma}_1 \cdot \boldsymbol{n})(\boldsymbol{\sigma}_2 \cdot \boldsymbol{n}))/r^3$ where $\boldsymbol{n} = \boldsymbol{r}/r$ and the sign of the potential was corrected based on DAIDO 17.

VALUE	CL%	DOCUMENT ID		TECN	COMMENT
• • • We do not use the following data for averages, fits, limits, etc. • • •					
		[1] CALORE	21	ASTR	Core-collapse SNe
$<2.5 \times 10^{-10}$		[2] LUCENTE	21	ASTR	SN 1987A
$<3 \times 10^{-12}$	90	[3] AGOSTINI	20	HPGE	$m_{A^0} = 0.06$–1 MeV
$<1 \times 10^{-9}$	90	[4] AMARAL	20	SCDM	$m_{A^0} = 1.2$–50 eV
$<2 \times 10^{-14}$	90	[5] APRILE	20	XE1T	$m_{A^0} = 1$ keV
2.6–3.7×10^{-12}	90	[6] APRILE	20	XE1T	Solar axions
$<6 \times 10^{-13}$	90	[7] ARALIS	20	SCDM	$m_{A^0} = 0.04$–500 keV
$<1.3 \times 10^{-13}$	95	[8] CAPOZZI	20	ASTR	Tip of the Red Giant Branch
$<1.7 \times 10^{-11}$	95	[9] CRESCINI	20	QUAX	$m_{A^0} = 42.4$–43.1 μeV
$<1.8 \times 10^{-9}$		[10] GHOSH	20A	COSM	$m_{A^0} \lesssim 0.5$ MeV
$<1.48 \times 10^{-13}$	95	[11] STRANIERO	20	ASTR	Tip of the Red Giant Branch
$<2.48 \times 10^{-11}$	90	[12] WANG	20A	CDEX	Solar axions
$<4 \times 10^{-13}$	90	[13] WANG	20A	CDEX	$m_{A^0} = 1.5$ keV
$<1.7 \times 10^{-11}$	90	[14] ADHIKARI	19B	C100	Solar axions
$<2.3 \times 10^{-14}$	90	[15] APRILE	19D	XE1T	$m_{A^0} = 0.186$–1 keV
		[16] DESSERT	19	ASTR	Magnetic white dwarf
$<2.6 \times 10^{-10}$	95	[17] TERRANO	19		Torsion pendulum
$<1.5 \times 10^{-13}$	90	[18] ABE	18F	XMAS	$m_{A^0} = 40$–120 keV
$<1.1 \times 10^{-11}$	90	[19] ARMENGAUD	18	EDE3	Solar axions
$<4 \times 10^{-13}$	90	[20] ARMENGAUD	18	EDE3	$m_{A^0} = 0.8$–500 keV
$<4.9 \times 10^{-10}$	95	[21] CRESCINI	18	QUAX	$m_{A^0} = 58$ μeV
		[22] FICEK	18	THEO	$m_{A^0} < 10$ keV
$<4.5 \times 10^{-13}$	90	[23] ABGRALL	17	HPGE	$m_{A^0} = 11.8$ keV
$<3.5 \times 10^{-12}$	90	[24] AKERIB	17B	LUX	Solar axions
$<4.2 \times 10^{-13}$	90	[25] AKERIB	17B	LUX	$m_{A^0} = 1$–16 keV
$<2.3 \times 10^{-13}$	90	[26] APRILE	17B	X100	$m_{A^0} = 6$ keV
$<4 \times 10^{-4}$	90	[27] FICEK	17	THEO	$m_{A^0} < 1$ keV
$<4.35 \times 10^{-12}$	90	[28] FU	17A	PNDX	Solar axions
$<4.3 \times 10^{-14}$	90	[29] FU	17A	PNDX	$m_{A^0} = 2$ keV
$<5 \times 10^{-13}$	90	[30] LIU	17A	CDEX	$m_{A^0} = 13$ keV
$<2.5 \times 10^{-11}$	90	[31] LIU	17A	CDEX	Solar axions
<0.15	95	[32] LUO	17		$m_{A^0} = 300$ eV
$<3.3 \times 10^{-13}$	68	[33] BATTICH	16	ASTR	White dwarf cooling
$<7 \times 10^{-13}$		[34] CORSICO	16	ASTR	White dwarf cooling
$<1.39 \times 10^{-11}$	90	[35] YOON	16	KIMS	Solar axions
$<7.4 \times 10^{-9}$	95	[36] TERRANO	15		$m_{A^0} < 30$ μeV
$<8 \times 10^{-13}$	90	[37] ABE	14F	XMAS	$m_{A^0} = 60$ keV
$<7.7 \times 10^{-12}$	90	[38] APRILE	14B	X100	Solar axions
		[39] APRILE	14B	X100	$m_{A^0} = 5$–7 keV
< 0.96–8.2×10^{-8}	90	[40] DERBIN	14	CNTR	$m_{A^0} = 0.1$–1 MeV
$<2.8 \times 10^{-13}$	99	[41] MILLER-BER...	14	ASTR	White dwarf cooling
$<5.4 \times 10^{-11}$	90	[42] ABE	13D	XMAS	Solar axions
$<1.07 \times 10^{-12}$	90	[43] ARMENGAUD	13	EDEL	$m_{A^0} = 12.5$ keV
$<2.59 \times 10^{-11}$	90	[44] ARMENGAUD	13	EDEL	Solar axions
		[45] BARTH	13	CAST	Solar axions
< 1.4–9.7×10^{-7}	90	[46] DERBIN	13	CNTR	$m_{A^0} = 0.1$–1 MeV
$<1.5 \times 10^{-8}$	68	[47] HECKEL	13		$m_{A^0} \leq 0.1$ μeV
$<4.3 \times 10^{-13}$	95	[48] VIAUX	13A	ASTR	Low-mass red giants
$<7 \times 10^{-13}$	95	[49] CORSICO	12	ASTR	White dwarf cooling
$<2.2 \times 10^{-10}$	90	[50] DERBIN	12	CNTR	Solar axions
< 0.02–1×10^{-10}	90	[51] AALSETH	11	CNTR	$m_{A^0} = 0.3$–8 keV
$<1.4 \times 10^{-12}$	90	[52] AHMED	09A	CDMS	$m_{A^0} = 2.5$ keV
$<4 \times 10^{-9}$		[53] DAVOUDIASL	09	ASTR	Earth cooling

Downloaded from https://academic.oup.com/ptep/article/2022/8/083C01/6651666 by KIT Library user on 27 September 2022

$<2.7 \times 10^{-8}$	66	[54] NI	94		Induced magnetism
		[54] CHUI	93		Induced magnetism
$<3.6 \times 10^{-7}$	66	[55] PAN	92		Torsion pendulum
$<2.9 \times 10^{-8}$	95	[54] BOBRAKOV	91		Induced magnetism
$<1.9 \times 10^{-6}$	66	[56] WINELAND	91	NMR	
$<7 \times 10^{-7}$	66	[55] RITTER	90		Torsion pendulum
$<6.6 \times 10^{-8}$	95	[54] VOROBYOV	88		Induced magnetism

[1] CALORE 21 consider the production of axions from Galactic and extragalactic SNe via nucleon-nucleon bremsstrahlung and their subsequent decay into electron-positron pairs, and exclude the range of $g_{Aee} \simeq 10^{-19}$–10^{-11} at $g_{App} = 10^{-9}$ for $m_{A^0} = 3$–30 MeV. See their Fig. 7 for the limits.

[2] LUCENTE 21 study the axion production in a supernova via electron-proton bremsstrahlung and electron-positron fusion, and exclude the range of $g_{Aee} \simeq 10^{-10}$–10^{-8} for $m_{A^0} = 1$–160 MeV. The quoted limit is at $m_{A^0} = 120$ MeV. See their Fig. 12 for the mass-dependent limits.

[3] AGOSTINI 20 is analogous to AHMED 09A. The quoted limit applies to $m_{A^0} = 150$ keV. See their Fig.3 for mass-dependent limits.

[4] AMARAL 20 use a second-generation SuperCDMS high-voltage eV-resolution detector to set limits on dark-matter axion absorption. The quoted limit is for $m_{A^0} \simeq 17$ eV. The local density $\rho_{\gamma'} = 0.3$ GeV/cm^3 is assumed. See their Fig. 3 for mass-dependent limits.

[5] APRILE 20 is an update of APRILE 17B where they look for an absorption signal of axion dark matter. They obtained the limit, $g_{Aee} \lesssim 2 \times 10^{-14}$–$1 \times 10^{-12}$ at 90%CL for $m_{A^0} = 1$–200 keV. They also found an excess over known backgrounds, which favors the mass $m_{A^0} = 2.3 \pm 0.2$ keV with a 3 σ significance. See their Fig. 10 for mass-dependent limits.

[6] APRILE 20 look for solar axions from the ABC interactions, the Primakoff conversion, and the 14.4 keV M1 transition of ^{57}Fe, and set limits on g_{Aee}, $G_{A\gamma\gamma}$, g_{ANN}, and their products. An excess is observed at low energies between 2 and 3 keV. See their Fig.8 for correlation between the couplings. The quoted limit applies to the case of vanishing $G_{A\gamma\gamma}$ and g_{ANN}.

[7] ARALIS 20 is analogous to AHMED 09A. The quoted limit applies to $m_{A^0} = 0.3$ keV. The limits at masses above 3 keV in their Fig. 9 was later found to be incorrect due to an error in their analysis. See Fig. 2 in ARALIS 21 for the corrected limits.

[8] CAPOZZI 20 obtains a limit on the axion-electron coupling from the brightness of the tip of the red-giant branch in ω Centauri. A similar limit of $< 1.6 \times 10^{-13}$ is obtained in NGC 4258.

[9] CRESCINI 20 is an update of CRESCINI 18. They assume a local axion dark matter density, $\rho_A = 0.3$ GeV/cm^3. See their Fig.4 for the limits.

[10] GHOSH 20A study thermal production of axion via coupling to leptons in the early universe and estimate its contribution to $\Delta N_{\rm eff}$. The quoted limit is for $\Delta N_{\rm eff} < 0.5$. See their Fig. 7 for their mass-dependent limits.

[11] STRANIERO 20 is analogous to CAPOZZI 20, with 22 galactic globular clusters used to derive the limit.

[12] WANG 20A is an update of LIU 17A. See their Fig. 9.

[13] WANG 20A is an update of LIU 17A. They assume a local axion dark matter density, $\rho_A = 0.3$ GeV/cm^3. See their Fig. 10 for limits between $0.185 < m_{A^0} < 10$ keV.

[14] ADHIKARI 19B is analogous to LIU 17A.

[15] APRILE 19D is analogous to APRILE 17B, but they use only ionization signals. The quoted limit applies to $m_{A^0} = 0.7$ keV. See their Fig. 5(e) for mass-dependent limits.

[16] DESSERT 19 used the Suzaku observations of a magnetic white dwarf (RE J0317-853) to look for X-ray signatures converted from axions in the surrounding magnetic fields. They obtained the limit, $g_{Aee} \cdot G_{A\gamma\gamma} < 1.6 \times 10^{-24}$ GeV^{-1} at 95%CL for $m_{A^0} \lesssim 10^{-5}$ eV. See their Fig. 2 for mass-dependent limits.

[17] TERRANO 19 look for the axion-induced oscillating magnetic field acting on the electron spin, using data taken with a rotating torsion pendulum containing polarized electrons. The quoted limit applies to $m_{A^0} = 10^{-23}$–10^{-18} eV and assumes a local axion dark matter density, $\rho_A = 0.45$ GeV/cm^3. See their Fig. 5 for mass-dependent limits.

[18] ABE 18F is an update of ABE 14F. The quoted limit applies to $m_{A^0} = 60$ keV. See their Fig. 5 for mass-dependent limits.

[19] ARMENGAUD 18 is analogous to LIU 17A.

[20] ARMENGAUD 18 is analogous to AHMED 09A. See the left panel of Fig. 5 for mass-dependent limits.

[21] CRESCINI 18 look for collective excitations of the electron spins caused by dark matter axions. The quoted limit assumes the local dark matter density, $\rho_A = 0.45$ GeV/cm^3.

[22] FICEK 18 use the measurements of the hyperfine structure of antiprotonic helium to constrain a dipole-dipole potential between electron and antiproton. See their Fig. 3 for limits on various spin- and velocity-dependent potentials.

[23] ABGRALL 17 is analogous to AHMED 09A using the MAJORANA DEMONSTRATOR. See their Fig. 2 for limits between 6 keV $< m_{A^0} <$ 97 keV.

[24] AKERIB 17B is analogous to LIU 17A.

[25] AKERIB 17B is analogous to AHMED 09A. See their Fig. 7 for mass-dependent limits.

[26] APRILE 17B is analogous to AHMED 09A. They found a bug in their code and needed to correct the limits in Fig. 7 of APRILE 14B. See their Fig. 1 for the corrected limits between 1 keV $< m_{A^0} <$ 40 keV.

[27] FICEK 17 look for spin-dependent interactions between electrons by comparing precision spectroscopic measurements in ^{4}He with theoretical calculations. See their Fig. 1 for limits up to $m_{A^0} = 10$ keV.

[28] FU 17A is analogous to LIU 17A. See their Fig. 3 for mass-dependent limits.

[29] FU 17A is analogous to AHMED 09A. See their Fig. 4 for mass-dependent limits.

[30] LIU 17A is analogous to AHMED 09A. See their Fig. 9 for limits between 0.25 keV $< m_{A^0} <$ 20 keV.

[31] LIU 17A look for solar axions produced from Compton, bremsstrahlung, atomic-recombination and deexcitation channels, and set a limit for $m_{A^0} < 1$ keV.

[32] LUO 17 use a recent measurement of the dipole-dipole interaction between two iron atoms at the nanometer scale and set a limit for $m_{A^0} < 1$ keV. See their Fig. 3 for mass-dependent limits.

[33] BATTICH 16 is analogous to CORSICO 16 and used the pulsating DB white dwarf PG 1351+489.

[34] CORSICO 16 studied the cooling rate of the pulsating DA white dwarf L19-2 based on an asteroseismic model.

[35] YOON 16 look for solar axions with the axio-electric effect in CsI(Tl) crystals and set a limit for $m_{A^0} < 1$ keV.

[36] TERRANO 15 used a torsion pendulum and rotating attractor with 20-pole electron-spin distributions. See their Fig. 4 for a mass-dependent limit up to $m_{A^0} = 500$ μeV.

[37] ABE 14F set limits on the axioelectric effect in the XMASS detector assuming the pseudoscalar constitutes all the local dark matter. See their Fig. 3 for limits between $m_{A^0} = 40$–120 keV.

[38] APRILE 14B look for solar axions using the XENON100 detector.

[39] APRILE 14B is analogous to AHMED 09A. Their Fig. 7 was later found to be incorrect due to a bug in their code. See Fig. 1 in APRILE 17B for the corrected limits.

[40] DERBIN 14 is an update of DERBIN 13 with a BGO scintillating bolometer. See their Fig. 3 for mass-dependent limits.

[41] MILLER-BERTOLAMI 14 studied the impact of axion emission on white dwarf cooling in a self-consistent way.

[42] ABE 13D is analogous to DERBIN 12, using the XMASS detector.

[43] ARMENGAUD 13 is similar to AALSETH 11. See their Fig. 10 for limits between 3 keV $< m_{A^0} <$ 100 keV.

[44] ARMENGAUD 13 is similar to DERBIN 12, and take account of axio-recombination and axio-deexcitation effects. See their Fig. 12 for mass-dependent limits.

[45] BARTH 13 search for solar axions produced by axion-electron coupling, and obtained the limit, $g_{Aee} \cdot G_{A\gamma\gamma} < 8.1 \times 10^{-23}$ GeV^{-1} at 95%CL.

[46] DERBIN 13 looked for 5.5 MeV solar axions produced in $pd \rightarrow {}^3$He A^0 in a BGO detector through the axioelectric effect. See their Fig. 4 for mass-dependent limits.

[47] HECKEL 13 studied the influence of 2 or 4 stationary sources each containing 6.0×10^{24} polarized electrons, on a rotating torsion pendulum containing 9.8×10^{24} polarized electrons. See their Fig. 4 for mass-dependent limits.

[48] VIAUX 13A constrain axion emission using the observed brightness of the tip of the red-giant branch in the globular cluster M5.

[49] CORSICO 12 attributed the excessive cooling rate of the pulsating white dwarf R548 to emission of axions with $g_{Aee} \simeq 4.8 \times 10^{-13}$.

[50] DERBIN 12 look for solar axions with the axio-electric effect in a Si(Li) detector. The solar production is based on Compton and bremsstrahlung processes.

[51] AALSETH 11 is analogous to AHMED 09A. See their Fig. 4 for mass-dependent limits.

[52] AHMED 09A assume keV-mass pseudoscalars are the local dark matter and constrain the axio-electric effect in the CDMS detector. See their Fig. 5 for mass-dependent limits.

[53] DAVOUDIASL 09 use geophysical constraints on Earth cooling by axion emission.

[54] These experiments measured induced magnetization of a bulk material by the spin-dependent potential generated from other bulk material with aligned electron spins, where the magnetic field is shielded with superconductor. The sign of the limit set by CHUI 93 is opposite to that of the axion-mediated dipole-dipole potential.

[55] These experiments used a torsion pendulum to measure the potential between two bulk matter objects where the spins are polarized but without a net magnetic field in either of them. The limits reflect the corrected sign of the dipole-dipole potential.

[56] WINELAND 91 looked for an effect of bulk matter with aligned electron spins on atomic hyperfine splitting using nuclear magnetic resonance.

Invisible A^0 (Axion) Limits from Nucleon Coupling

Limits are for the axion mass in eV.

VALUE (eV)	CL%	DOCUMENT ID		TECN	COMMENT
• • • We do not use the following data for averages, fits, limits, etc. • • •					
		[1] AYBAS	21	CASP	Nucleon EDM
		[2] BHUSAL	21		Solar axion
		[3] JIANG	21	NMR	Axion dark matter
		[4] ROUSSY	21		Molecular EDM
		[5] ZHANG	21B	ASTR	Neutron star inspiral
< 24	90	[6] ABDELHAME...	20	CNTR	Solar axion
		[7] ABDELHAME...	20	CNTR	Solar axion
		[8] APRILE	20	XE1T	Solar axion
		[9] KLIMCHITSK...	20		Casimir effect
< 7.3	90	[10] WANG	20A	CDEX	Solar axion
< 0.03		[11] LEINSON	19	ASTR	Neutron star cooling
$< 9.6 \times 10^{-3}$	95	[12] LLOYD	19	ASTR	γ-rays from NS
		[13] SMORRA	19		$\overline{p}$ g-factor
		[14] WU	19	NMR	Axion dark matter
< 65	95	[15] AKHMATOV	18	CNTR	Solar axion
< 6.6	90	[16] ARMENGAUD	18	EDE3	Solar axion
< 0.085	90	[17] BEZNOGOV	18	ASTR	Neutron star cooling
< 12.7	95	[18] GAVRILYUK	18	CNTR	Solar axion
< 0.01		[19] HAMAGUCHI	18	ASTR	Neutron star cooling
		[20] ABEL	17		Neutron EDM
< 93	90	[21] ABGRALL	17	HPGE	Solar axion
< 4	90	[22] FU	17A	PNDX	Solar axion
		[23] KLIMCHITSK...	17A		Casimir effect
<177	90	[24] LIU	17A	CDEX	Solar axion
< 0.079	95	[25] BERENJI	16	ASTR	γ-rays from NS
<100	95	[26] GAVRILYUK	15	CNTR	Solar axion
		[27] KLIMCHITSK...	15		Casimir-less
		[28] BEZERRA	14		Casimir effect
		[29] BEZERRA	14A		Casimir effect
		[30] BEZERRA	14B		Casimir effect
		[31] BEZERRA	14C		Casimir effect
		[32] BLUM	14	COSM	^{4}He abundance

Downloaded from https://academic.oup.com/ptep/article/2022/8/083C01/6651666 by KIT Library user on 27 September 2022

<250		95		
<155		90		
< 8.6	$\times 10^3$	90		
< 1.4	$\times 10^4$	90		
<145		95		

[33] LEINSON	14	ASTR	Neutron star cooling	
[34] ALESSANDRIA	13	CNTR	Solar axion	
[35] ARMENGAUD	13	EDEL	Solar axion	
[36] BELLI	12	CNTR	Solar axion	
[37] BELLINI	12B	BORX	Solar axion	
[38] DERBIN	11	CNTR	Solar axion	
[39] BELLINI	08	CNTR	Solar axion	
[40] ADELBERGER	07		Test of Newton's law	

[1] AYBAS 21 limits the axion couplings to the nucleon EDM and the nucleons as $g_{ANN\gamma} < 9.5 \times 10^{-4}$ GeV^{-2} and $g_{ANN}/2m_N < 0.28$ GeV^{-1} (95 % CL) for $m_{A^0} = 162$–166 neV, based on a measurement of ^{207}Pb solid-state NMR in a polarized ferroelecrtric crystal. Here m_N is the nucleon mass and g_{ANN} is the dimensionless axion-nucleon coupling. They assume that axions make up all the dark matter with $\rho_A \simeq 0.46$ GeV/cm^3. See their Fig. 3 for the limits.

[2] BHUSAL 21 looked for 5.5 MeV solar axions produced by $pd \rightarrow {}^3$He A^0 through the axion-induced dissociation of deuterons by using SNO data, and set a limit on the isovector axion-nucleon coupling, $|g^3_{aN}| < 2\times10^{-5}$ GeV^{-1}, which is equivalent to $|g_{Ann} - g_{App}| < 4\times10^{-5}$ in terms of the dimensionless axion-nucleon couplings.

[3] JIANG 21 use the spin-amplifier based on hyperpolarized ^{129}Xe gas to set limits on the axion couplings to nucleons as $g_{ANN}/2m_N < 3.2\times10^{-9}$ GeV^{-1} (95 % CL) at $m_{A^0} = 52.94$ feV, and comparable limits in the mass range of 8.3–744 feV. Here m_N is the nucleon mass and g_{ANN} is the dimensionless axion-nucleon coupling. They assume that axions make up all the dark matter with $\rho_A \simeq 0.4$ GeV/cm^3. See their Fig. 4b for the limits.

[4] ROUSSY 21 look for a time-oscillating EDM of molecular ions HfF$^+$ induced by axion dark matter couplings to gluons. See their Fig. 3 for limits in the range of $m_{A^0} = 10^{-22}$–10^{-15} eV.

[5] ZHANG 21B use the gravitational waves from the binary neutron star inspiral GW170817 to look for a type of axion whose mass is suppressed due to cancellation with additional contributions. They exclude $1.6\times10^{16} < f_A < 10^{18}$ GeV at 3 σ for $m_{A^0} \lesssim 10^{-13}$ eV. See their Fig. 1 for mass-dependent limits.

[6] ABDELHAMEED 20 look for the resonant excitation of ^{169}Tm (8.41 keV) by solar axions produced via the Primakoff effect. The mass bound assumes the KSVZ axion model, $S = 0.5$, and $m_u/m_d = 0.56$. They set a limit on the product of axion couplings to photons and nucleons as $G_{A\gamma\gamma} \cdot g_{App} < 1.44\times10^{-14}$ GeV^{-1} (90 % CL).

[7] ABDELHAMEED 20 look for the resonant excitation of ^{169}Tm (8.41 keV) by solar axions produced via the axion-electron coupling. They set a limit on the product of axion couplings to electrons and nucleons as $g_{Aee} \cdot g_{App} < 2.81\times10^{-16}$ (90 % CL).

[8] APRILE 20 look for solar axions from the ABC interactions, the Primakoff conversion, and the 14.4 keV M1 transition of ^{57}Fe. An excess is observed at low energies between 2 and 3 keV. See their Fig.8 for correlation between the couplings.

[9] KLIMCHITSKAYA 20 use the measurement of the Casimir force between a Au-coated microsphere and a SiC plate to constrain the force due to two-axion exchange for 17.8 $< m_{A^0} <$ 100 eV. See their Fig. 2 for mass-dependent limits.

[10] WANG 20A is an update of LIU 17A. The limit assumes the DFSZ axion. See their Fig. 7 for the limit on product of axion couplings to electrons and nucleons.

[11] LEINSON 19 is analogous to BEZNOGOV 18, but estimating the axion luminosity based on the Tolman's analytic solution to the Einstein equations of spherical fluids in hydrostatic equilibrium. The dimensionless axion-neutron coupling is constrained as $g_{Ann} < 1.0\times10^{-10}$.

[12] LLOYD 19 is analogous to BERENJI 16. They highlight that the limit obtained with this technique strongly depends on the assumed NS core temperature.

[13] SMORRA 19 look for spin-precession effects from ultra-light axion dark matter in the $\overline{p}$ spin-flip resonance data. Assuming $\rho_A = 0.4$ GeV/cm^3, they constrain the dimensionless axion-antiproton coupling as $g_{A\overline{p}\overline{p}} < 2$–9 at 95% CL for $m_{A^0} = 2\times10^{-23}$–$4\times10^{-17}$ eV. See the right panel of their Fig. 3.

[14] WU 19 look for axion-induced time-oscillating features of the NMR spectrum of acetonitrile-2-^{13}C. Assuming $C_p = C_n$ and $\rho_A = 0.4$ GeV/cm^3, they constrain the dimensionless axion-nucleon coupling as $g_{ANN} < 6\times10^{-5}$ for $m_{A^0} = 10^{-21}$–1.3×10^{-17} eV. Note that the limits for $m_{A^0} < 10^{-21}$ eV in their Fig. 3(a) should be weaker than those for heavier masses. See ADELBERGER 19 and WU 19C on this issue.

[15] AKHMATOV 18 is an update of GAVRILYUK 15.

[16] ARMENGAUD 18 is analogous to ALESSANDRIA 13. The quoted limit assumes the DFSZ axion model. See their Fig. 4 for the limit on product of axion couplings to electrons and nucleons.

[17] BEZNOGOV 18 constrain the axion-neutron coupling by assuming that thermal evolution of the hot neutron star HESS J1731-347 is dominated by the lowest possible neutrino emission. The quoted limit assumes the KSVZ axion with the effective Peccei-Quinn charge of the neutron $C_n = -0.02$. The dimensionless axion-neutron couling is constrained as $g_{Ann} < 2.8\times10^{-10}$.

[18] GAVRILYUK 18 look for the resonant excitation of ^{83}Kr (9.4 keV) by solar axions produced via the Primakoff effect. The mass bound assumes $m_u/m_d = 0.56$ and $S = 0.5$.

[19] HAMAGUCHI 18 studied the axion emission from the neutron star in Cassiopeia A based on the minimal cooling scenario which explains the observed rapid cooling rate. The quoted limit corresponds to $f_A > 5\times10^8$ GeV obtained for the KSVZ axion with $C_p = -0.47$ and $C_n = -0.02$.

[20] ABEL 17 look for a time-oscillating neutron EDM and an axion-wind spin-precession effect respectively induced by axion dark matter couplings to gluons and nucleons. See their Fig. 4 for limits in the range of $m_{A^0} = 10^{-24}$–10^{-17} eV.

[21] ABGRALL 17 limit assumes the hadronic axion model used in ALESSANDRIA 13. See their Fig. 4 for the limit on product of axion couplings to electrons and nucleons.

[22] FU 17A look for the 14.4 keV ^{57}Fe solar axions. The limit assumes the DFSZ axion model. See their Fig. 3 for mass-dependent limits on the axion-electron coupling. Notice that in this figure the DFSZ and KSVZ lines should be interchanged.

[23] KLIMCHITSKAYA 17A use the differential measurement of the Casimir force between a Ni-coated sphere and Au and Ni sectors of the structured disc to constrain the axion coupling to nucleons for 2.61 meV $< m_{A^0} <$ 0.9 eV. See their Figs. 1 and 2 for mass dependent limits.

[24] LIU 17 is analogous to ALESSANDRIA 13. The limit assumes the hadronic axion model. See their Fig. 6(b) for the limit on product of axion couplings to electrons and nucleons.

[25] BERENJI 16 used the Fermi LAT observations of neutron stars to look for photons from axion decay. They assume the effective Peccei-Quinn charge of the neutron $C_n = 0.1$ and a neutron-star core temperature of 20 MeV.

[26] GAVRILYUK 15 look for solar axions emitted by the M1 transition of ^{83}Kr (9.4 keV). The mass bound assumes $m_u/m_d = 0.56$ and $S = 0.5$.

[27] KLIMCHITSKAYA 15 use the measurement of differential forces between a test mass and rotating source masses of Au and Si to constrain the force due to two-axion exchange for $1.7\times10^{-3} < m_{A^0} <$ 0.9 eV. See their Figs. 1 and 2 for mass dependent limits.

[28] BEZERRA 14 use the measurement of the thermal Casimir-Polder force between a Bose-Einstein condensate of ^{87}Rb atoms and a SiO_2 plate to constrain the force mediated by exchange of two pseudoscalars for 0.1 meV $< m_{A^0} <$ 0.3 eV. See their Fig. 2 for the mass-dependent limit on pseudoscalar coupling to nucleons.

[29] BEZERRA 14A is analogous to BEZERRA 14. They use the measurement of the Casimir pressure between two Au-coated plates to constrain pseudoscalar coupling to nucleons for 1×10^{-3} eV $< m_{A^0} <$ 15 eV. See their Figs. 1 and 2 for the mass-dependent limit.

[30] BEZERRA 14B is analogous to BEZERRA 14. BEZERRA 14B use the measurement of the normal and lateral Casimir forces between sinusoidally corrugated surfaces of a sphere and a plate to constrain pseudoscalar coupling to nucleons for 1 eV $< m_{A^0} <$ 20 eV. See their Figs. 1–3 for mass-dependent limits.

[31] BEZERRA 14C is analogous to BEZERRA 14. They use the measurement of the gradient of the Casimir force between Au- and Ni-coated surfaces of a sphere and a plate to constrain pseudoscalar coupling to nucleons for 3×10^{-5} eV $< m_{A_0} <$ 1 eV. See their Figs. 1, 3, and 4 for the mass-dependent limits.

[32] BLUM 14 studied effects of an oscillating strong *CP* phase induced by axion dark matter on the primordial ^{4}He abundance. See their Fig. 1 for mass-dependent limits.

[33] LEINSON 14 attributes the excessive cooling rate of the neutron star in Cassiopeia A to axion emission from the superfluid core, and found $C_n^2\, m^2_{A^0} \simeq 5.7\times10^{-6}$ eV^2, where C_n is the effective Peccei-Quinn charge of the neutron.

[34] ALESSANDRIA 13 used the CUORE experiment to look for 14.4 keV solar axions produced from the M1 transition of thermally excited ^{57}Fe nuclei in the solar core, using the axio-electric effect. The limit assumes the hadronic axion model. See their Fig. 4 for the limit on product of axion couplings to electrons and nucleons.

[35] ARMENGAUD 13 is analogous to ALESSANDRIA 13. The limit assumes the hadronic axion model. See their Fig. 8 for the limit on product of axion couplings to electrons and nucleons.

[36] BELLI 12 looked for solar axions emitted by the M1 transition of ^{7}Li* (478 keV) after the electron capture of ^{7}Be, using the resonant excitation ^{7}Li in the LiF crystal. The mass bound assumes $m_u/m_d = 0.55$, $m_u/m_s = 0.029$, and the flavor-singlet axial vector matrix element $S = 0.4$.

[37] BELLINI 12B looked for 5.5 MeV solar axions produced in the $pd \rightarrow {}^3$He A^0.The limit assumes the hadronic axion model. See their Figs. 6 and 7 for mass-dependent limits on productsof axion couplings to photons, electrons, and nucleons.

[38] DERBIN 11 looked for solar axions emitted by the M1 transition of thermally excited ^{57}Fe nuclei in the Sun, using their possible resonant capture on ^{57}Fe in the laboratory. The mass bound assumes $m_u/m_d = 0.56$ and the flavor-singlet axial vector matrix element $S = 3F - D \simeq 0.5$.

[39] BELLINI 08 consider solar axions emitted in the M1 transition of ^{7}Li* (478 keV) and look for a peak at 478 keV in the energy spectra of the Counting Test Facility (CTF), a Borexino prototype. For $m_{A^0} <$ 450 keV they find mass-dependent limits on products of axion couplings to photons, electrons, and nucleons.

[40] ADELBERGER 07 use precision tests of Newton's law to constrain a force contribution from the exchange of two pseudoscalars. See their Fig. 5 for limits on the pseudoscalar coupling to nucleons, relevant for m_{A^0} below about 1 meV.

Axion Limits from *T*-violating Medium-Range Forces

The limit is for the coupling $g = g_p\, g_s$ in a *T*-violating potential between nucleons or nucleon and electron of the form $V = \frac{g\hbar^2}{8\pi m_p}(\boldsymbol{\sigma}\cdot\hat{\boldsymbol{r}})\left(\frac{1}{r^2} + \frac{1}{\lambda r}\right) e^{-r/\lambda}$, where g_p and g_s are dimensionless scalar and pseudoscalar coupling constants and $\lambda = \hbar/(m_A c)$ is the range of the force.

VALUE	DOCUMENT ID		TECN	COMMENT
• • • We do not use the following data for averages, fits, limits, etc. • • •				
	[1] AFACH	21	GNME	Optical magnetometers
	[2] DZUBA	18	THEO	atomic EDM
	[3] STADNIK	18	THEO	atomic and molecular EDMs
	[4] CRESCINI	17	SQID	paramagnetic GSO crystal
	[5] AFACH	15		ultracold neutrons
	[6] STADNIK	15	THEO	nucleon spin contributions for nuclei
	[7] TERRANO	15		torsion pendulum
	[8] BULATOWICZ	13	NMR	polarized ^{129}Xe and ^{131}Xe
	[9] CHU	13		polarized ^{3}He
	[10] TULLNEY	13	SQID	polarized ^{3}He and ^{129}Xe
	[11] RAFFELT	12		stellar energy loss
	[12] HOEDL	11		torsion pendulum
	[13] PETUKHOV	10		polarized ^{3}He
	[14] SEREBROV	10		ultracold neutrons
	[15] IGNATOVICH	09	RVUE	ultracold neutrons
	[16] SEREBROV	09	RVUE	ultracold neutrons
	[17] BAESSLER	07		ultracold neutrons
	[18] HECKEL	06		torsion pendulum
	[19] NI	99		paramagnetic Tb F_3
	[20] POSPELOV	98	THEO	neutron EDM

Downloaded from https://academic.oup.com/ptep/article/2022/8/083C01/6651666 by KIT Library user on 27 September 2022

[21] YOUDIN	96		
[22] RITTER	93		torsion pendulum
[23] VENEMA	92		nuclear spin-precession frequencies
[24] WINELAND	91	NMR	

[1] AFACH 21 look for axion domain walls coupled to atomic spins by using the global network of optical magnetometers. Assuming that the axion domain walls make up all dark matter, they exclude the effective decay constant below 4×10^5 GeV for m_{A^0} in the range of 10^{-15}–10^{-11} eV. See their Fig. 4 for the mass-dependent limits.

[2] DZUBA 18 used atomic EDM measurements to derive limits on the product of the pseudoscalar coupling to nucleon and the scalar coupling to electron, which improved on the laboratory bounds for $m_{A^0} > 0.01$ eV. See their Fig. 1 for mass-dependent limits.

[3] STADNIK 18 used atomic and molecular EDM experiments to derive limits on the product of the pseudoscalar couplings to electron and the scalar coupling to nucleon and electron. See their Fig. 2 for mass-dependent limits, which improved on the laboratory bounds for $m_{A^0} > 0.01$ eV.

[4] CRESCINI 17 use the QUAX-$g_p g_s$ experiment to look for variation of a paramagnetic GSO crystal magnetization when rotating lead disks are positioned near the crystal, and find $g = g_p^e g_s^N < 4.3 \times 10^{-30}$ for $\lambda = 0.1$–0.2 m at 95% CL. See their Fig. 6 for limits as a function of λ.

[5] AFACH 15 look for a change of spin precession frequency of ultracold neutrons when a magnetic field with opposite directions is applied, and find $g < 2.2 \times 10^{-27}$ $(\mathrm{m}/\lambda)^2$ at 95% CL for 1 μm $< \lambda <$ 5 mm. See their Fig. 3 for their limits.

[6] STADNIK 15 studied proton and neutron spin contributions for nuclei and derive the limits $g < 10^{-28}$–10^{-23} for $\lambda > 3 \times 10^{-4}$ m using the data of TULLNEY 13. See their Figs. 1 and 2 for λ-dependent limits.

[7] TERRANO 15 used a torsion pendulum and rotating attractor, and derived a restrictive limit on the product of the pseudoscalar coupling to electron and the scalar coupling to nucleons, $g < 9 \times 10^{-29}$–5×10^{-26} for $m_{A^0} < 1.5$–400 μeV. See their Fig. 5 for mass-dependent limits.

[8] BULATOWICZ 13 looked for NMR frequency shifts in polarized ^{129}Xe and ^{131}Xe when a zirconia rod is positioned near the NMR cell, and find $g < 1 \times 10^{-19}$–1×10^{-24} for $\lambda = 0.01$–1 cm. See their Fig. 4 for their limits.

[9] CHU 13 look for a shift of the spin precession frequency of polarized ^{3}He in the presence of an unpolarized mass, in analogy to YOUDIN 96. See Fig. 3 for limits on g in the approximate m_{A^0} range 0.02–2 meV.

[10] TULLNEY 13 look for a shift of the precession frequency difference between the colocated ^{3}He and ^{129}Xe in the presence an unpolarized mass, and derive limits $g < 3 \times 10^{-29}$–2×10^{-22} for $\lambda > 3 \times 10^{-4}$ m. See their Fig. 3 for λ-dependent limits.

[11] RAFFELT 12 show that the pseudoscalar couplings to electron and nucleon and the scalar coupling to nucleon are individually constrained by stellar energy-loss arguments and searches for anomalous monopole-monopole forces, together providing restrictive constraints on g. See their Figs. 2 and 3 for results.

[12] HOEDL 11 use a novel torsion pendulum to study the force by the polarized electrons of an external magnet. In their Fig. 3 they show restrictive limits on g in the approximate m_{A^0} range 0.03–10 meV.

[13] PETUKHOV 10 use spin relaxation of polarized ^{3}He and find $g < 3 \times 10^{-23}$ $(\mathrm{cm}/\lambda)^2$ at 95% CL for the force range $\lambda = 10^{-4}$–1 cm.

[14] SEREBROV 10 use spin precession of ultracold neutrons close to bulk matter and find $g < 2 \times 10^{-21}$ $(\mathrm{cm}/\lambda)^2$ at 95% CL for the force range $\lambda = 10^{-4}$–1 cm.

[15] IGNATOVICH 09 use data on depolarization of ultracold neutrons in material traps. They show λ-dependent limits in their Fig. 1.

[16] SEREBROV 09 uses data on depolarization of ultracold neutrons stored in material traps and finds $g < 2.96 \times 10^{-21}$ $(\mathrm{cm}/\lambda)^2$ for the force range $\lambda = 10^{-3}$–1 cm and $g < 3.9 \times 10^{-22}$ $(\mathrm{cm}/\lambda)^2$ for $\lambda = 10^{-4}$–10^{-3} cm, each time at 95% CL, significantly improving on BAESSLER 07.

[17] BAESSLER 07 use the observation of quantum states of ultracold neutrons in the Earth's gravitational field to constrain g for an interaction range 1 μm–a few mm. See their Fig. 3 for results.

[18] HECKEL 06 studied the influence of unpolarized bulk matter, including the laboratory's surroundings or the Sun, on a torsion pendulum containing about 9×10^{22} polarized electrons. See their Fig. 4 for limits on g as a function of interaction range.

[19] NI 99 searched for a T-violating medium-range force acting on paramagnetic Tb F_3 salt. See their Fig. 1 for the result.

[20] POSPELOV 98 studied the possible contribution of T-violating Medium-Range Force to the neutron electric dipole moment, which is possible when axion interactions violate CP. The size of the force among nucleons must be smaller than gravity by a factor of 2×10^{-10} $(1\ \mathrm{cm}/\lambda_A)$, where $\lambda_A = \hbar/m_A c$.

[21] YOUDIN 96 compared the precession frequencies of atomic ^{199}Hg and Cs when a large mass is positioned near the cells, relative to an applied magnetic field. See Fig. 3 for their limits.

[22] RITTER 93 studied the influence of bulk mass with polarized electrons on an unpolarized torsion pendulum, providing limits in the interaction range from 1 to 100 cm.

[23] VENEMA 92 looked for an effect of Earth's gravity on nuclear spin-precession frequencies of ^{199}Hg and ^{201}Hg atoms.

[24] WINELAND 91 looked for an effect of bulk matter with aligned electron spins on atomic hyperfine resonances in stored ^{9}Be$^+$ ions using nuclear magnetic resonance.

Hidden Photons: Kinetic Mixing Parameter Limits

Limits are on the kinetic mixing parameter χ which is defined by the Lagrangian

$$L = -\frac{1}{4} F_{\mu\nu}F^{\mu\nu} - \frac{1}{4} F'_{\mu\nu}F'^{\mu\nu} - \frac{\chi}{2} F_{\mu\nu}F'^{\mu\nu} + \frac{m^2_{\gamma'}}{2} A'_\mu A'^\mu,$$

where A_μ and A'_μ are the photon and hidden-photon fields with field strengths $F_{\mu\nu}$ and $F'_{\mu\nu}$, respectively, and $m_{\gamma'}$ is the hidden-photon mass.

VALUE	CL%	DOCUMENT ID		TECN	COMMENT
• • • We do not use the following data for averages, fits, limits, etc. • • •					
		[1] LEES	22	BABR	$m_{\gamma'} = 1 \times 10^{-3}$–$3.16$ GeV
$<8 \times 10^{-6}$	90	[2] ANDREEV	21	NA64	$m_{\gamma'} = 1 \times 10^{-3}$–$1$ GeV
$<2.3 \times 10^{-4}$	90	[3] ANDREEV	21A	NA64	$m_{\gamma'} = 0.1$–0.35 GeV
$<1.6 \times 10^{-4}$	95	[4] BI	21	ASTR	$m_{\gamma'} = 0.03$–0.06 eV
$<3 \times 10^{-5}$	90	[5] CAZZANIGA	21	NA64	$m_{\gamma'} = 10$–390 MeV
$<1.68 \times 10^{-15}$	90	[6] DIXIT	21	CNTR	$m_{\gamma'} = 24.86$ μeV
$<2 \times 10^{-16}$	90	[7] GHOSH	21	RVUE	$m_{\gamma'} = 2$–30 μeV
$<1.8 \times 10^{-13}$		[8] GODFREY	21		$m_{\gamma'} = 0.2637$–0.2648 μeV
$<3 \times 10^{-12}$	95	[9] KOPYLOV	21A	CNTR	$m_{\gamma'} = 9$–40 eV
$<2 \times 10^{-2}$	95	[10] KRIBS	21		$m_{\gamma'} \lesssim 10$ GeV
		[11] SCHMIDT	21	THEO	$m_{\gamma'} < 0.6$ GeV
$<3 \times 10^{-8}$	90	[12] TSAI	21	BDMP	$m_{\gamma'} = 0.78$ GeV
$<1 \times 10^{-4}$	90	[13] AAIJ	20C	LHCB	$m_{\gamma'} = 214$ MeV
		[14] AAIJ	20C	LHCB	$m_{\gamma'} = 218$–315 MeV
		[15] ABLIKIM	20AB	BES3	$m_{\gamma'} = 0.2$–2.1 GeV
$<2.5 \times 10^{-12}$	90	[16] AGOSTINI	20	HPGE	$m_{\gamma'} = 60$ keV – 1 MeV
$<3.3 \times 10^{-14}$	90	[17] AMARAL	20	SCDM	$m_{\gamma'} = 1.2$–50 eV
$<1.2 \times 10^{-14}$	90	[18] AN	20	XE1T	$m_{\gamma'} = 200$ eV
$<6.72 \times 10^{-13}$	95	[19] ANDRIANAV...	20	FUNK	$m_{\gamma'} = 1.95$–8.55 eV
$<1 \times 10^{-16}$	90	[20] APRILE	20	XE1T	$m_{\gamma'} = 1$–200 keV
$<9 \times 10^{-16}$	90	[21] ARALIS	20	SCDM	$m_{\gamma'} = 0.04$–500 keV
$<3 \times 10^{-5}$	90	[22] ARGUELLES	20	THEO	$m_{\gamma'} = 0.01$ GeV
$<7 \times 10^{-14}$	90	[23] ARNAUD	20	EDEL	$m_{\gamma'} = 1$–40 eV
$<8.2 \times 10^{-5}$	90	[24] BANERJEE	20	NA64	$m_{\gamma'} = 1.5$–24 MeV
$<7 \times 10^{-15}$	90	[25] BARAK	20	SENS	$m_{\gamma'} = 1.2$–12.8 eV
		[26] KRASNIKOV	20	RVUE	$m_{\gamma'} = 16.7$ MeV
$<1.4 \times 10^{-14}$	90	[27] SHE	20	CDEX	$m_{\gamma'} = 10$–300 eV
$<1.3 \times 10^{-15}$	90	[28] SHE	20	CDEX	$m_{\gamma'} = 0.1$–4 keV
$<1 \times 10^{-3}$	90	[29] SIRUNYAN	20AQ	CMS	$m_{\gamma'} = 11.5$–75 GeV, 110–200 GeV
$<4.3 \times 10^{-10}$	95	[30] TOMITA	20		$m_{\gamma'} = 115.79$–115.85 μeV
$<9 \times 10^{-16}$	90	[31] WANG	20A	CDEX	$m_{\gamma'} = 0.185$–10 keV
		[32] AABOUD	19G	ATLS	$m_{\gamma'} = 20$–60 GeV
$<6 \times 10^{-3}$	90	[33] ABLIKIM	19A	BES3	$m_{\gamma'} = 0.01$–2.4 GeV
$<3.4 \times 10^{-3}$	90	[34] ABLIKIM	19H	BES3	$m_{\gamma'} = 0.1$–2.1 GeV
$<8 \times 10^{-15}$	90	[35] AGUILAR-AR...	19A	DAMC	$m_{\gamma'} = 1.2$–30 eV
$<9 \times 10^{-17}$	90	[36] APRILE	19D	XE1T	$m_{\gamma'} = 0.186$–5 keV
$<7.5 \times 10^{-6}$	90	[37] BANERJEE	19	NA64	$m_{\gamma'} = 1$–200 MeV
$<2 \times 10^{-11}$		[38] BHOONAH	19	ASTR	$m_{\gamma'} = 10^{-22}$–10^{-10} eV
$<5 \times 10^{-12}$	95	[39] BRUN	19	SHUK	$m_{\gamma'} = 20.8$–28.3 μeV
$<4.4 \times 10^{-4}$	90	[40] CORTINA-GIL	19	NA62	$m_{\gamma'} = 60$–110 MeV
$<3 \times 10^{-5}$	95	[41] DANILOV	19	TEXO	$m_{\gamma'} = 20$ eV - 1 MeV
$<6 \times 10^{-9}$	95	[42] HOCHBERG	19		$m_{\gamma'} = 0.8$–4 eV
$<1 \times 10^{-11}$	95	[43] KOPYLOV	19	CNTR	$m_{\gamma'} = 9$–40 eV
$<1.5 \times 10^{-9}$		[44] KOVETZ	19	COSM	$m_{\gamma'} = 10^{-23}$–10^{-13} eV
$<3 \times 10^{-14}$	95	[45] NGUYEN	19	WDMX	$m_{\gamma'} = 6$ neV – 2.07 μeV
$<4.5 \times 10^{-14}$	90	[46] ABE	18F	XMAS	$m_{\gamma'} = 40$–120 keV
$<2.5 \times 10^{-3}$	95	[47] ADRIAN	18	HPS	$m_{\gamma'} = 19$–81 MeV
$<4.4 \times 10^{-4}$	90	[48] ANASTASI	18B	KLOE	$m_{\gamma'} = 519$–987 MeV
$<4 \times 10^{-15}$	90	[49] ARMENGAUD	18	EDE3	$m_{\gamma'} = 0.8$–500 keV
		[50] BANERJEE	18	NA64	$m_{\gamma'} = 1$–23 MeV
$<1.8 \times 10^{-5}$	90	[51] BANERJEE	18A	NA64	$m_{\gamma'} = 1$–100 MeV
$<1 \times 10^{-8}$	90	[52] KNIRCK	18		$m_{\gamma'} = 0.67$–0.92 meV
$<3.1 \times 10^{-14}$	90	[53] ABGRALL	17	HPGE	$m_{\gamma'} = 11.8$ keV
$<6 \times 10^{-4}$	90	[54] ABLIKIM	17AA	BES3	$m_{\gamma'} = 1.5$–3.4 GeV
$<7 \times 10^{-15}$	90	[55] ANGLOHER	17	CRES	$m_{\gamma'} = 0.3$–0.7 keV
$<1.2 \times 10^{-4}$	90	[56] BANERJEE	17	NA64	$m_{\gamma'} = 0.002$–0.4 GeV
$<2 \times 10^{-11}$		[57] CHANG	17	ASTR	$m_{\gamma'} = 15$ MeV
$<4.5 \times 10^{-3}$	90	[58] DUBININA	17	EMUL	$m_{\gamma'} = 1.1$–24 MeV
$<4 \times 10^{-4}$	90	[59] LEES	17E	BABR	$m_{\gamma'} = 4.7$ GeV
		[60] AAD	16AG	ATLS	$m_{\gamma'} = 0.1$–2 GeV
$<4.4 \times 10^{-4}$	90	[61] ANASTASI	16	KLOE	$m_{\gamma'} = 527$–987 MeV
$<1.7 \times 10^{-6}$	95	[62] KHACHATRY...	16	CMS	$m_{\gamma'} = 2$ GeV
$<4 \times 10^{-2}$	95	[63] AAD	15CD	ATLS	$m_{\gamma'} = 15$–55 GeV
$<1.4 \times 10^{-3}$	90	[64] ADARE	15		$m_{\gamma'} = 30$–90 MeV
		[65] AN	15A		$m_{\gamma'} = 12$ eV - 40 keV
		[66] ANASTASI	15	KLOE	$m_{\gamma'} = 2m_\mu$ - 1 GeV

Downloaded from https://academic.oup.com/ptep/article/2022/8/083C01/6651666 by KIT Library user on 27 September 2022

$<1.7 \times 10^{-3}$	90	[67] ANASTASI	15A	KLOE	$m_{\gamma'} = 5$–320 MeV
$<4.2 \times 10^{-4}$	90	[68] BATLEY	15A	NA48	$m_{\gamma'} = 36$ MeV
		[69] JAEGLE	15	BELL	$m_{\gamma'} = 0.1$–3.5 GeV
$<3 \times 10^{-13}$		[70] KAZANAS	15	ASTR	$m_{\gamma'} = 2m_e$ – 100 MeV
$<6 \times 10^{-12}$		[71] SUZUKI	15		$m_{\gamma'} = 1.9$–4.3 eV
$<2.3 \times 10^{-13}$	99.7	[72] VINYOLES	15	ASTR	$m_{\gamma'} = 8$ eV
$<2 \times 10^{-13}$		[73] ABE	14F	XMAS	$m_{\gamma'} = 40$–120 keV
$<1.8 \times 10^{-3}$	90	[74] AGAKISHIEV	14	HDES	$m_{\gamma'} = 63$ MeV
$<9.0 \times 10^{-4}$	90	[75] BABUSCI	14	KLOE	$m_{\gamma'} = 969$ MeV
		[76] BATELL	14	BDMP	$m_{\gamma'} = 10^{-3}$–1 GeV
$<1.3 \times 10^{-7}$	95	[77] BLUEMLEIN	14	BDMP	$m_{\gamma'} = 0.6$ GeV
$<3 \times 10^{-18}$		[78] FRADETTE	14	COSM	$m_{\gamma'} = 50$–300 MeV
$<3.5 \times 10^{-4}$	90	[79] LEES	14J	BABR	$m_{\gamma'} = 0.2$ GeV
$<9 \times 10^{-4}$	95	[80] MERKEL	14	A1	$m_{\gamma'} = 40$–300 MeV
$<3 \times 10^{-15}$		[81] AN	13B	ASTR	$m_{\gamma'} = 2$ keV
$<7 \times 10^{-14}$		[82] AN	13C	XE10	$m_{\gamma'} = 100$ eV
$<8 \times 10^{-4}$		[83] DIAMOND	13	BDMP	$m_{\gamma'} = 30$–250 MeV
$<2 \times 10^{-3}$	90	[84] GNINENKO	13	BDMP	$m_{\gamma'} = 25$–120 MeV
$<2.2 \times 10^{-13}$		[85] HORVAT	13	HPGE	$m_{\gamma'} = 230$ eV
$<8.06 \times 10^{-5}$	95	[86] INADA	13	LSW	$m_{\gamma'} = 0.04$ eV–26 keV
$<2 \times 10^{-10}$	95	[87] MIZUMOTO	13		$m_{\gamma'} = 1$ eV
$<1.7 \times 10^{-7}$		[88] PARKER	13	LSW	$m_{\gamma'} = 53$ μeV
$<5.32 \times 10^{-15}$		[89] PARKER	13		$m_{\gamma'} = 53$ μeV
$<1 \times 10^{-15}$		[90] REDONDO	13	ASTR	$m_{\gamma'} = 2$ keV
$<8 \times 10^{-8}$	90	[91] GNINENKO	12A	BDMP	$m_{\gamma'} = 1$–135 MeV
$<1 \times 10^{-7}$	90	[92] GNINENKO	12B	CHRM	$m_{\gamma'} = 1$–500 MeV
$<1 \times 10^{-3}$	90	[93] ABRAHAMY...	11		$m_{\gamma'} = 175$–250 MeV
$<9 \times 10^{-8}$	95	[94] BLUEMLEIN	11	BDMP	$m_{\gamma'} = 70$ MeV
$<1 \times 10^{-7}$		[95] BJORKEN	09	BDMP	$m_{\gamma'} = 2$–400 MeV
$<5 \times 10^{-9}$		[96] BJORKEN	09	ASTR	$m_{\gamma'} = 2$–50 MeV

[1] LEES 22 look for a hidden fermion-fermion bound state decaying into three hidden photons, which subsequently decay into e^+e^-, $\mu^+\mu^-$, or $\pi^+\pi^-$. For the bound-state mass in the range of 0.05–9.5 GeV, limits at the level of 5×10^{-5}–1×10^{-3} are obtained. See their Fig. 6 for mass-dependent limits.

[2] ANDREEV 21 is analogous to BANERJEE 18A. The quoted limit applies to $m_{\gamma'} = 1$ MeV. See their Fig. 3 for mass-dependent limits.

[3] ANDREEV 21A extends the limits of BANERJEE 19 by taking account of production through the resonant annihilation of secondary positrons with atomic electrons. The quoted limit is at $m_{\gamma'} = 0.23$ GeV, assuming the fermion dark matter of mass $m_{\gamma'}/3$ and the hidden gauge coupling $\alpha_D = 0.1$. See their Fig.3 for mass-dependent limits.

[4] BI 21 look for the gamma-ray spectral attenuation due to scattering with hidden photons constituting all dark matter, using the measurements of sub-PeV gamma-rays from the Crab Nebula by the Tibet ASγ and HAWC experiments, together with MAGIC and HEGRA gamma-ray data. See their Fig. 4 for mass-dependent limits.

[5] CAZZANIGA 21 look for semi-visible decays of hidden photons, $\gamma' \to \chi_1\chi_2$ ($\chi_2 \to \chi_1 e^+e^-$), where χ_1 and χ_2 are hidden fermions. They exclude $3\times10^{-5} \lesssim \chi \lesssim 2\times10^{-2}$ assuming the hidden gauge coupling $\alpha_D = 0.1$, and the fermion masses $m_{\chi_1} = m_{\gamma'}/3$, $(m_{\chi_2} - m_{\chi_1})/m_{\chi_1} = 0.4$. See their Fig. 4 for mass-dependent limits.

[6] DIXIT 21 look for hidden photon dark matter by using a superconducting transmon qubit dispersively coupled to a high Q storage cavity. The local density $\rho_{\gamma'} = 0.4$ GeV/cm^3 is assumed. See their Fig.4 for mass-dependent limits.

[7] GHOSH 21 use existing haloscope axion search limits to set limits on hidden photon dark matter, considering the polarization of hidden photons. The quoted limit is at $m_{\gamma'} \simeq 3$ μeV. See their Fig. 1 for mass-dependent limits.

[8] GODFREY 21 look for hidden photon dark matter by using a wideband antenna, and set 5σ limits on χ. The local density $\rho_{\gamma'} = 0.38$ GeV/cm^3 is assumed. See their updated Fig. 12 in arXiv:2101.02805v4 for mass-dependent limits in the range of $m_{\gamma'} = 0.207$–1.24 μeV.

[9] KOPYLOV 21A is an update of KOPYLOV 19, but use Ne gas instead of Ar. The quoted limit applies to $m_{\gamma'} = 12$ eV. See their Fig. 4 for mass-dependent limits.

[10] KRIBS 21 used the HERA data on neutral current deep inelastic ep scattering to derive the limits, which become weaker for heavier masses. See their Fig. 3 for mass-dependent limits.

[11] SCHMIDT 21 use the microscopic Parton-Hadron-String Dynamics approach to extract limits by comparing the theoretically calculated dilepton spectra with the HADES data on the search for $\gamma' \to e^+e^-$. See their Fig. 5 for the mass-dependent limits for various allowed surplus of the hidden photon contribution over the standard model yield.

[12] TSAI 21 update the limits from the CHARM and NuCal experiments, taking account of additional production channels from proton bremsstrahlung and η meson decays, respectively. Limits between 3×10^{-8} and 1×10^{-4} are obtained for $0.01 < m_{\gamma'} < 0.8$ GeV (see their Fig. 1).

[13] AAIJ 20C look for hidden photons produced from the pp collision in the decay channel $\gamma' \to \mu^+\mu^-$. For prompt decaying hidden photons, limits at the level of 10^{-4}–10^{-3} are obtained for $m_{\gamma'} = 0.214$–30 GeV. See their Fig. 2 for mass-dependent limits.

[14] AAIJ 20C look for hidden photons produced from the pp collision in the decay channel $\gamma' \to \mu^+\mu^-$. For hidden photons with lifetimes of order ps, limits at the level of 10^{-5} are obtained for $m_{\gamma'} = 218$–315 MeV. See their Fig. 4 for mass-dependent limits.

[15] ABLIKIM 20AB search for $J/\psi \to \eta'\gamma'$ ($\gamma' \to \gamma\pi^0$), and set the upper limit on the product branching fraction of order 10^{-7}. See their Fig. 7 for mass-dependent limits.

[16] AGOSTINI 20 is analogous to ABE 14F. The quoted limit applies to $m_{\gamma'} = 120$ keV. The local density $\rho_{\gamma'} = 0.3$ GeV/cm^3 is assumed. See their Fig. 3 for mass-dependent limits.

[17] AMARAL 20 use a second-generation SuperCDMS high-voltage eV-resolution detector to set limits on dark-matter dark photon absorption. The quoted limit is for $m_{\gamma'} \simeq 17$ eV. The local density $\rho_{\gamma'} = 0.3$ GeV/cm^3 is assumed. See their Fig. 3 for mass-dependent limits.

[18] AN 20 updates the direct detection limit of AN 13C on solar flux of hidden photons; $\chi < 1.6\times10^{-12}$ (eV/$m_{\gamma'}$) for $m_{\gamma'} < 6$ eV (90% C.L.). For $m_{\gamma'} > 6$ eV, see their Fig. 1 for mass-dependent limits.

[19] ANDRIANAVALOMAHEFA 20 is analogous to SUZUKI 15, but uses a mirror that is about one order of magnitude larger than in similar studies in the past. Limits at the level of 10^{-12} are obtained for $m_{\gamma'} = 2.5$–7 eV. See their Fig.23 and Table III for mass-dependent limits.

[20] APRILE 20 is analogous to ABE 14F, and set limits $\chi \lesssim 10^{-16}$–10^{-12}. The quoted limit applies to $m_{\gamma'} = 1$ keV. They also found an excess over known backgrounds, which favors the mass $m_{\gamma'} = 2.3 \pm 0.2$ keV with a 3 σ significance. See their Fig. 10 for mass-dependent limits.

[21] ARALIS 20 is analogous to ABE 14F. The quoted limit applies to $m_{\gamma'} = 0.1$ keV. The local density $\rho_{\gamma'} = 0.3$ GeV/cm^3 is assumed. The limits at masses above 3 keV in their Fig. 10 was later found to be incorrect due to an error in their analysis. See Fig. 3 in ARALIS 21 for the corrected limits.

[22] ARGUELLES 20 examine hidden-photon production in atmospheric cosmic-ray showers and its decay in IceCube and Super-Kamiokande. The quoted limit assumes a lifetime of $c\tau = 0.1$ km. See their Fig. 16 for mass- and lifetime-dependent limits.

[23] ARNAUD 20 look for the absorption signal of hidden photon dark matter in a Ge detector. The quoted limit applies to $m_{\gamma'} \simeq 9$ eV. The local density $\rho_{\gamma'} = 0.3$ GeV/cm^3 is assumed. See their Fig. 3 for mass-dependent limits.

[24] BANERJEE 20 is an update of BANERJEE 18. They exclude $8.2\times10^{-5} \lesssim \chi \lesssim 1\times10^{-2}$ for $m_{\gamma'} = 1.5$–24 MeV. In particular, they exclude $\chi = 1.2\times10^{-4}$–6.8×10^{-4} for the 16.7 MeV gauge boson. See their Fig. 5 for mass-dependent limits.

[25] BARAK 20 is analogous to AGUILAR-AREVALO 19A, and look for hidden photon dark matter by using the Skipper CCD. The quoted limit applies to $m_{\gamma'} = 12.8$ eV. See their Fig. 4 for mass-dependent limits.

[26] KRASNIKOV 20 showed that the limit of BANERJEE 20 combined with the measured anomalous magnetic moment of the electron exclude the 16.7 MeV gauge boson suggested by the ATOMKI (KRASZNAHORKAY 16) experiment if it has pure vector or axial-vector interactions.

[27] SHE 20 look for solar hidden photons. The quoted limit applies to $m_{\gamma'} = 180$ eV. See their Fig. 4 for mass-dependent limits.

[28] SHE 20 look for hidden photon dark matter and set limits $\chi < 1.3\times10^{-15}$–2.8×10^{-14} for the quoted mass range. The local density $\rho_{\gamma'} = 0.3$ GeV/cm^3 is assumed. See their Fig. 6 for mass-dependent limits.

[29] SIRUNYAN 20AQ look for a narrow resonance decaying into a pair of muons. For $m_{\gamma'} < 45$ GeV, they use dedicated high-rate dimuon triggers to reduce the muon transverse momentum thresholds. The quoted limit applies to $m_{\gamma'} = 50$ GeV, and limits of order 10^{-3} are obtained for the quoted mass range. See their Fig. 3 for mass-dependent limits.

[30] TOMITA 20 look for hidden photon dark matter using a planar metal plate and cryogenic receiver and set limits $\chi < 1.8$–4.3×10^{-10} for the quoted mass range. The local density $\rho_{\gamma'} = 0.39$ GeV/cm^3 is assumed. See their Fig. 7 for mass-dependent limits.

[31] WANG 20A is analogous to ABE 14F. The quoted limit applies to $m_{\gamma'} = 185$ eV. The local density $\rho_{\gamma'} = 0.3$ GeV/cm^3 is assumed. See their Fig. 11 for mass-dependent limits.

[32] AABOUD 19G look for $h \to \gamma'\gamma'$ ($\gamma' \to \mu^+\mu^-$) and exclude a kinetic mixing around 10^{-9}–10^{-8} for B($h \to \gamma'\gamma'$) = 0.01 and 0.1. See their Fig. 9 for mass-dependent limits.

[33] ABLIKIM 19A look for $J/\psi \to \gamma'\eta$ ($\gamma' \to e^+e^-$). Limits between 6×10^{-3} and 5×10^{-2} are obtained (see their Fig. 8).

[34] ABLIKIM 19H look for $J/\psi \to \gamma'\eta'$ ($\gamma' \to e^+e^-$). Limits between 3.4×10^{-3} and 2.6×10^{-2} are obtained. See their Fig. 5 for mass-dependent limits.

[35] AGUILAR-AREVALO 19A look for the absorption signal of hidden photon dark matter by using a CCD. The quoted limit applies to $m_{\gamma'} = 17$ eV. The local density $\rho_{\gamma'} = 0.3$ GeV/cm^3 is assumed. See their Fig. 4 for mass-dependent limits.

[36] APRILE 19D is analogous to ABE 14F. The quoted limit applies to $m_{\gamma'} = 0.7$ keV. See their Fig. 5(f) for mass-dependent limits.

[37] BANERJEE 19 is an update of BANERJEE 18A. The quoted limit is at $m_{\gamma'} = 1$ MeV. See their Fig. 3 for mass-dependent limits.

[38] BHOONAH 19 examine heating of Galactic Center gas clouds by hidden photon dark matter. The quoted limit applies to $m_{\gamma'} \simeq 10^{-12}$ eV. See their Fig. 2 for mass-dependent limits.

[39] BRUN 19 is analogous to SUZUKI 15. The limit is derived under an assumption that hidden photons constitute the local dark matter density $\rho_{\gamma'} = 0.3$ GeV/cm^3.

[40] CORTINA-GIL 19 look for an invisible hidden photon in the reaction $K^+ \to \pi^+\pi^0$ ($\pi^0 \to \gamma\gamma'$). The quoted limit applies to $m_{\gamma'} = 62.5$–65 MeV. See their Figs. 6 and 7 for mass-dependent limits.

[41] DANILOV 19 examined the hidden photon production in nuclear reactors, correctly taking account of the effective photon mass in the reactor and detector. The limit gets weaker

Downloaded from https://academic.oup.com/ptep/article/2022/8/083C01/6651666 by KIT Library user on 27 September 2022

for $m_{\gamma'}$ less than the effective photon mass in proportion to $1/m^2_{\gamma'}$. See their Fig. 1 for mass-dependent limits.

[42] HOCHBERG 19 look for the absorption signal of hidden photon dark matter by using superconducting-nanowire single-photon detectors. The quoted limit applies to $m_{\gamma'} \simeq$ 1 eV. The local density $\rho_{\gamma'} = 0.3$ GeV/cm^3 is assumed. See their Fig. 4 for mass-dependent limits.

[43] KOPYLOV 19 look for hidden-photon dark matter using a counter with an aluminum cathode and derive limits assuming it constitute all the local dark matter. The quoted limit applies to $m_{\gamma'} = 12$ eV. See their Fig. 7 for mass-dependent limits.

[44] KOVETZ 19 examine heating of the early Universe plasma by hidden photon dark matter, and derive the limits by requiring that the cosmic mean 21 cm brightness temperature relative to the CMB temperature satisfy $T_{21} > -100$ mK. The quoted limit applies to $m_{\gamma'} \simeq 2 \times 10^{-14}$ eV. See their Fig. 3 for mass-dependent limits.

[45] NGUYEN 19 look for hidden photon dark matter with a resonant cavity, and set limits $\sim 10^{-12}$ for $m_{\gamma'} = 0.2$–2.07μeV. The quoted limit applies to $m_{\gamma'} = 1.3\ \mu$eV. The local density $\rho_{\gamma'} = 0.3$ GeV/cm^3 is assumed. See their Fig. 19 for mass-dependent limits.

[46] ABE 18F is an update of ABE 14F. The quoted limit applies to $m_{\gamma'} \simeq 40$ keV. See their Fig. 5 for mass-dependent limits.

[47] ADRIAN 18 look for a hidden photon resonance in the reaction $e^- Z \to e^- Z \gamma'$ ($\gamma' \to e^+ e^-$). The quoted limit applies to $m_{\gamma'} = 40$ MeV. See their Fig. 4 for mass-dependent limits.

[48] ANASTASI 18B look for a hidden photon resonance in the reaction $e^+ e^- \to \gamma' \gamma$ ($\gamma' \to \mu^+ \mu^-$). The quoted limit is obtained by combining the result of ANASTASI 16 and it applies to $m_{\gamma'} \simeq$ 519–987 MeV. See their Fig. 9 for mass-dependent limits.

[49] ARMENGAUD 18 is analogous to ABE 14F. The quoted limits applies to $m_{\gamma'} = 1.6$ keV. See the right panel of Fig. 5 for mass-dependent limits.

[50] BANERJEE 18 look for hidden photons produced in the reaction $e^- Z \to e^- Z \gamma'$ ($\gamma' \to e^+ e^-$), and exclude $9.2 \times 10^{-5} \lesssim \chi \lesssim 1 \times 10^{-2}$ for $m_{\gamma'} = 1$–23 MeV. They also set a limit on the electron coupling to a 16.7 MeV gauge boson suggested by the ATOMKI (KRASZNAHORKAY 16) experiment. See their Fig. 3 for mass-dependent limits.

[51] BANERJEE 18A look for invisible decays of hidden photons produced in the reaction $e^- Z \to e^- Z \gamma'$. The quoted limit is at $m_{\gamma'} = 1$ MeV. See their Fig. 15 for mass-dependent limits.

[52] KNIRCK 18 is analogous to SUZUKI 15. See their Fig. 5 for mass-dependent limits.

[53] ABGRALL 17 is analogous to ABE 14F using the MAJORANA DEMONSTRATOR. See their Fig. 3 for limits between 6 keV $< m_{\gamma'} <$ 97 keV.

[54] ABLIKIM 17AA look for $e^+ e^- \to \gamma \gamma'$ ($\gamma' \to e^+ e^-$ or $\mu^+ \mu^-$) . Limits between 10^{-3} and 10^{-4} are obtained (see their Fig. 3).

[55] ANGLOHER 17 is analogous to ABE 14F. The quoted limit is at $m_{\gamma'} = 0.7$ keV. See their Fig. 8 for mass-dependent limits.

[56] BANERJEE 17 look for invisible decays of hidden photons produced in the reaction $e^- Z \to e^- Z \gamma'$. The quoted limit applies to $m_{\gamma'} = 2$ MeV. See their Fig. 3 for mass-dependent limits.

[57] CHANG 17 examine the hidden photon emission from SN1987A, including the effects of finite temperature and density on χ and obtain limits $\chi\ (m_{\gamma'}/\text{MeV}) \lesssim 3 \times 10^{-9}$ for $m_{\gamma'} < 15$ MeV and $\chi \lesssim 10^{-9}$ for $m_{\gamma'} =$ 15–120 MeV.

[58] DUBININA 17 look for $\mu^+ \to e^+ \overline{\nu}_\mu \nu_e \gamma'$ ($\gamma' \to e^+ e^-$) in a nuclear photoemulsion. The quoted limit applies to $m_{\gamma'} = 1.1$ MeV. Limits between 4.5×10^{-3} and 10^{-2} are obtained (see their Fig. 3).

[59] LEES 17E look for invisible decays of hidden photons produced in the reaction $e^+ e^- \to \gamma \gamma'$. See their Fig. 5 for limits in the mass range $m_{\gamma'} \leq 8$ GeV.

[60] AAD 16AG look for hidden photons promptly decaying into collimated electrons and/or muons, assuming that they are produced in the cascade decays of squarks or the Higgs boson. See their Fig. 10 and Fig.13 for their limits on the cross section times branching fractions.

[61] ANASTASI 16 look for the decay $\gamma' \to \pi^+ \pi^-$ in the reaction $e^+ e^- \to \gamma \gamma'$. Limits between 4.3×10^{-3} and 4.4×10^{-4} are obtained for 527 $< m_{\gamma'} <$ 987 MeV (see their Fig. 9).

[62] KHACHATRYAN 16 look for $\gamma' \to \mu^+ \mu^-$ in a dark SUSY scenario where the SM-like Higgs boson decays into a pair of the visible lightest neutralinos with mass 10 GeV, both of which decay into γ' and a hidden neutralino with mass 1 GeV. See the right panel in their Fig. 2.

[63] AAD 15CD look for $H \to Z \gamma' \to 4\ell$ with the ATLAS detector at LHC and find $\chi < 4$–17×10^{-2} for $m_{\gamma'} =$ 15–55 GeV. See their Fig. 6.

[64] ADARE 15 look for a hidden photon in $\pi^0, \eta^0 \to \gamma e^+ e^-$ at the PHENIX experiment. See their Fig. 4 for mass-dependent limits.

[65] AN 15A derived limits from the absence of ionization signals in the XENON10 and XENON100 experiments, assuming hidden photons constitute all the local dark matter. Their best limit is $\chi < 1.3 \times 10^{-15}$ at $m_{\gamma'} = 18$ eV. See their Fig. 1 for mass-dependent limits.

[66] ANASTASI 15 look for a production of a hidden photon and a hidden Higgs boson with the KLOE detector at DAΦNE, where the hidden photon decays into a pair of muons and the hidden Higgs boson lighter than $m_{\gamma'}$ escape detection. See their Figs. 6 and 7 for mass-dependent limits on a product of the hidden fine structure constant and the kinetic mixing.

[67] ANASTASI 15A look for the decay $\gamma' \to e^+ e^-$ in the reaction $e^+ e^- \to e^+ e^- \gamma$. Limits between 1.7×10^{-3} and 1×10^{-2} are obtained for $m_{\gamma'} =$ 5–320 MeV (see their Fig. 7).

[68] BATLEY 15A look for $\pi^0 \to \gamma \gamma'$ ($\gamma' \to e^+ e^-$) at the NA48/2 experiment. Limits between 4.2×10^{-4} and 8.8×10^{-3} are obtained for $m_{\gamma'} =$ 9–120 MeV (see their Fig. 4).

[69] JAEGLE 15 look for the decay $\gamma' \to e^+ e^-$, $\mu^+ \mu^-$, or $\pi^+ \pi^-$ in the dark Higgstrahlung channel, $e^+ e^- \to \gamma' H'$ ($H' \to \gamma' \gamma'$) at the BELLE experiment. They set limits on a product of the branching fraction and the Born cross section as well as a product of the hidden fine structure constant and the kinetic mixing. See their Figs. 3 and 4.

[70] KAZANAS 15 set limits by studying the decay of hidden photons $\gamma' \to e^+ e^-$ inside and near the progenitor star of SN1987A. See their Fig. 6 for mass-dependent limits.

[71] SUZUKI 15 looked for hidden-photon dark matter with a dish antenna and derived limits assuming they constitute all the local dark matter. Their limits are $\chi < 6 \times 10^{-12}$ for $m_{\gamma'} =$ 1.9–4.3 eV. See their Fig. 7 for mass-dependent limits.

[72] VINYOLES 15 performed a global fit analysis based on helioseismology and solar neutrino observations, and set the limits $\chi m_{\gamma'} < 1.8 \times 10^{-12}$ eV for $m_{\gamma'} = 3 \times 10^{-5}$–8 eV. See their Fig. 11.

[73] ABE 14F look for the photoelectric-like interaction in the XMASS detector assuming the hidden photon constitutes all the local dark matter. Limits between 2×10^{-13} and 1×10^{-12} are obtained, where the relation $\chi^2 = \alpha'/\alpha$ is used to translate the original bound on the ratio of the hidden and EM fine-structure constants. See their Fig. 3 for mass-dependent limits.

[74] AGAKISHIEV 14 look for hidden photons $\gamma' \to e^+ e^-$ at the HADES experiment, and set limits on χ for $m_{\gamma'} =$ 0.02–0.6 GeV. See their Fig. 5 for mass-dependent limits.

[75] BABUSCI 14 look for the decay $\gamma' \to \mu^+ \mu^-$ in the reaction $e^+ e^- \to \mu^+ \mu^- \gamma$. Limits between 4×10^{-3} and 9.0×10^{-4} are obtained for 520 MeV $< m_{\gamma'} <$ 980 MeV (see their Fig. 7).

[76] BATELL 14 derived limits from the electron beam dump experiment at SLAC (E-137) by searching for events with recoil electrons by sub-GeV dark matter produced from the decay of the hidden photon. Limits at the level of 10^{-4}–10^{-1} are obtained for $m_{\gamma'} =$ 10^{-3}–1 GeV, depending on the dark matter mass and the hidden gauge coupling (see their Fig. 2).

[77] BLUEMLEIN 14 analyzed the beam dump data taken at the U-70 accelerator to look for γ'-bremsstrahlung and the subsequent decay into muon pairs and hadrons. See their Fig. 4 for mass-dependent excluded region.

[78] FRADETTE 14 studied effects of decay of relic hidden photons on BBN and CMB to set constraints on very small values of the kinetic mixing. See their Figs. 4 and 7 for mass-dependent excluded regions.

[79] LEES 14J look for hidden photons in the reaction $e^+ e^- \to \gamma \gamma'$ ($\gamma' \to e^+ e^-, \mu^+ \mu^-$). Limits at the level of 10^{-4}–10^{-3} are obtained for 0.02 GeV $< m_{\gamma'} <$ 10.2 GeV. See their Fig. 4 for mass-dependent limits.

[80] MERKEL 14 look for $\gamma' \to e^+ e^-$ at the A1 experiment at the Mainz Microtron (MAMI). See their Fig. 3 for mass-dependent limits.

[81] AN 13B examined the stellar production of hidden photons, correcting an important error of the production rate of the longitudinal mode which now dominates. See their Fig. 2 for mass-dependent limits based on solar energy loss.

[82] AN 13C use the solar flux of hidden photons to set a limit on the atomic ionization rate in the XENON10 experiment. They find $\chi\ m_{\gamma'} < 3 \times 10^{-12}$ eV for $m_{\gamma'} < 1$ eV. See their Fig. 2 for mass-dependent limits.

[83] DIAMOND 13 analyzed the beam dump data taken at the SLAC millicharge experiment to constrain a hidden photon invisibly decaying into lighter long-lived particles, which undergo elastic scattering off nuclei in the detector. Limits between 8×10^{-4}–2×10^{-2} are obtained. The quoted limit is applied when the dark gauge coupling is set equal to the electromagnetic coupling. See their Fig.4 for mass-dependent limits.

[84] GNINENKO 13 used the data taken at the SINDRUM experiment to constrain the decay, $\pi^0 \to \gamma \gamma'$ ($\gamma' \to e^+ e^-$) to derive limits. See their Fig. 2 for their mass-dependent excluded region.

[85] HORVAT 13 look for hidden-photo-electric effect in HPGe detectors induced by solar hidden photons. See their Fig. 3 for mass-dependent limits.

[86] INADA 13 search for hidden photons using an intense X-ray beamline at SPring-8. See their Fig. 4 for mass-dependent limits.

[87] MIZUMOTO 13 look for solar hidden photons. See their Fig. 5 for mass-dependent limits.

[88] PARKER 13 look for hidden photons using a cryogenic resonant microwave cavity. See their Fig.5 for mass-dependent limits.

[89] PARKER 13 derived a limit for the hidden photon CDM with a randomly oriented hidden photon field.

[90] REDONDO 13 examined the solar emission of hidden photons including the enhancement factor for the longitudinal mode pointed out by AN 13B, and also updated stellar-energy loss arguments. See their Fig.3 for mass-dependent limits, including a review of the currently best limits from other arguments.

[91] GNINENKO 12A obtained bounds on $B(\pi^0 \to \gamma \gamma') \cdot B(\gamma' \to e^+ e^-)$ from the NOMAD and PS191 neutrino experiments, and derived limits between 8×10^{-8}–2×10^{-4}. See their Fig.4 for mass-dependent excluded regions.

[92] GNINENKO 12B used the data taken at the CHARM experiment to constrain the decay, $\eta(\eta') \to \gamma \gamma'$ ($\gamma' \to e^+ e^-$), and derived limits between 1×10^{-7}–1×10^{-4}. See their Fig.4 for mass-dependent excluded region.

[93] ABRAHAMYAN 11 look for $\gamma' \to e^+ e^-$ in the electron-nucelon fixed-target experiment at the Jefferson Laboratory (APEX). See their Fig. 5 for mass-dependent limits.

[94] BLUEMLEIN 11 analyzed the beam dump data taken at the U-70 accelerator to look for $\pi^0 \to \gamma \gamma'$ ($\gamma' \to e^+ e^-$). See their Fig. 5 for mass-dependent limits.

[95] BJORKEN 09 analyzed the beam dump data taken at E137, E141, and E774 to constrain a hidden photon produced by bremsstrahlung, subsequently decaying into $e^+ e^-$, and derived limits between 10^{-7} and 10^{-2}. See their Fig. 1 for mass-dependent excluded region.

[96] BJORKEN 09 required the energy loss in the γ' emission from the core of SN1987A not to exceed 10^{53} erg/s, and derived limits between 5×10^{-9} and 2×10^{-6}. See their Fig. 1 for mass-dependent excluded region.

REFERENCES FOR Searches for Axions (A^0) and Other Very Light Bosons

LEES	22	PRL 128 021802	J.P. Lees *et al.*	(BABAR Collab.)
AAD	21F	PR D103 112006	G. Aad *et al.*	(ATLAS Collab.)
AAD	21K	JHEP 2102 226	G. Aad *et al.*	(ATLAS Collab.)
AAD	21N	JHEP 2103 243	G. Aad *et al.*	(ATLAS Collab.)
Also		JHEP 2111 050 (errat.)	G. Aad *et al.*	(ATLAS Collab.)

Downloaded from https://academic.oup.com/ptep/article/2022/8/083C01/6651666 by KIT Library user on 27 September 2022

See key on page 1127

Gauge & Higgs Boson Particle Listings

Axions (A^0) and Other Very Light Bosons

ABRATENKO	21	PRL 127 151803	P. Abratenko *et al.*	(MicroBooNE Collab.)
ADE	21	PR D103 042002	P.A.R. Ade *et al.*	(BICEP/Keck Collab.)
AFACH	21	NATP 17 1396	S. Afach *et al.*	(GNOME Collab.)
AGUILAR-AR...	21A	PR D103 052006	A. Aguilar-Arevalo *et al.*	(PIENU Collab.)
ALESINI	21	PR D103 102004	D. Alesini *et al.*	(QUAX Collab.)
AL-KHARUSI	21	PR D104 112002	S. Al Kharusi *et al.*	(EXO-200 Collab.)
ANDREEV	21	PRL 126 211802	Yu.M. Andreev *et al.*	(NA64 Collab.)
ANDREEV	21A	PR D104 L091701	Yu.M. Andreev *et al.*	(NA64 Collab.)
ANDREEV	21B	PR D104 L111102	Yu.M. Andreev *et al.*	(NA64 Collab.)
ARALIS	21	PR D103 039901 (errat.)	T. Aralis *et al.*	(SuperCDMS Collab.)
AYBAS	21	PRL 126 141802	D. Aybas *et al.*	(CASPEr Collab.)
BANIK	21	JCAP 2110 043	N. Banik *et al.*	
BARTRAM	21A	PRL 127 261803	C. Bartram *et al.*	(ADMX Collab.)
BASU	21	PRL 126 191102	A. Basu *et al.*	(BIEL, NAGO)
BAUMHOLZ...	21	JCAP 2105 004	S. Baumholzer, V. Brdar, E. Morgante	(MAINZ, FNAL+)
BHUSAL	21	PRL 126 091601	A. Bhusal, N. Houston, T. Li	(BEIJ)
BI	21	PR D103 043018	X.-J. Bi *et al.*	(BHEP, TSIN)
CALORE	21	PR D104 043016	F. Calore *et al.*	(HEID)
CARRA	21	PR D104 092005	S. Carra *et al.*	
CAZZANIGA	21	EPJ C81 959	C. Cazzaniga *et al.*	(NA64 Collab.)
CORTINA-GIL	21	PL B816 136259	E. Cortina Gil *et al.*	(NA62 Collab.)
CORTINA-GIL	21A	JHEP 2103 058	E. Cortina Gil *et al.*	(NA62 Collab.)
CORTINA-GIL	21C	JHEP 2102 201	E. Cortina Gil *et al.*	(NA62 Collab.)
CROON	21	JHEP 2101 107	D. Croon *et al.*	(TRIU, WASH, MIT, FNAL)
DEVLIN	21	PRL 126 041301	J.A. Devlin *et al.*	(BASE Collab.)
DIXIT	21	PRL 126 141302	A.V. Dixit *et al.*	(CHIC, RUTG, UCB+)
DOLAN	21	JHEP 2103 190 (errat.)	M.J. Dolan *et al.*	(MELB, BRCO, DESY)
DOLAN	21A	JCAP 2109 010	M.J. Dolan, F.J. Hiskens, R.R. Volkas	(MELB)
FUJIKURA	21	PR D104 123012	K. Fujikura *et al.*	
GHOSH	21	PR D104 092016	S. Ghosh *et al.*	
GODFREY	21	PR D104 012013	B. Godfrey *et al.*	(UCD, CSUS, STAN)
GRAMOLIN	21	NATP 17 79	A.V. Gramolin *et al.*	(SHAFT Collab.)
GUO	21	CP C45 025105	J.-G. Guo *et al.*	(BHEP)
HOMMA	21	JHEP 2112 108	K. Homa *et al.*	(SAPPHIRES Collab.)
JIANG	21	NATP 17 1402	M. Jiang *et al.*	
KOPYLOV	21A	PPN 52 31	A.V. Kopylov, I.V. Orekhov, V.V. Petukhov	(INRM)
KRIBS	21	PRL 126 011801	G.D. Kribs, D. McKeen, N. Raj	(OREG, TRIU)
KWON	21	PRL 126 191802	O. Kwon *et al.*	(CAPP-ACTION Collab.)
LI	21B	PR D103 083003	H.-J. Li *et al.*	(BHEP)
LLOYD	21	PR D103 023010	S.J. Lloyd *et al.*	(DURH, OKLA)
LUCENTE	21	PR D104 103007	G. Lucente, P. Carenza	(BARI)
MARTINCAM...	21	PR D103 L121301	J. Martin Camalich *et al.*	
MELCON	21	JHEP 2110 075	A.A. Melcon *et al.*	(CAST-RADES Collab.)
NG	21	PRL 126 151102	K.K.Y. Ng *et al.*	(MIT, ANIK, UTRE, LEUV)
PARK	21	JHEP 2104 191	S.-H. Park *et al.*	(BELLE Collab.)
REGIS	21	PL B814 136075	M. Regis *et al.*	(MUSE Collab.)
ROGERS	21	PRL 126 071302	K.K. Rogers, H.V. Peiris	(STOH, LOUC)
ROUSSY	21	PRL 126 171301	T.S. Roussy *et al.*	(COLO, MAINZ)
SALEMI	21	PRL 127 081801	C.P. Salemi *et al.*	(ABRACADABRA Collab.)
SCHMIDT	21	PR D104 015008	I. Schmidt *et al.*	(FRAN, GSI, +)
THOMSON	21	PRL 126 081803	C.A. Thomson *et al.*	(WAUS)
Also		PRL 127 019901 (errat.)	C.A. Thomson *et al.*	(WAUS)
TSAI	21	PRL 126 181801	Y.-D. Tsai, P. deNiverville, M.X. Liu	(FNAL+)
TSUKADA	21	PR D103 083005	L. Tsukada *et al.*	(ROMA, TOKY, WATER)
XIAO	21	PRL 126 031101	M. Xiao *et al.*	
YUAN	21	JCAP 2103 018	G.-W. Yuan *et al.*	(CST)
ZHANG	21B	PRL 127 161101	J. Zhang *et al.*	
AAIJ	20AL	JHEP 2010 156	R. Aaij *et al.*	(LHCb Collab.)
AAIJ	20C	PRL 124 041801	R. Aaij *et al.*	(LHCb Collab.)
ABDELHAME...	20	EPJ C80 376	A.H. Abdelhameed *et al.*	
ABE	20J	PL B815 136174	T. Abe, K. Hamaguchi, N. Nagata	(TOKY)
ABLIKIM	20AB	PR D102 052005	M. Ablikim *et al.*	(BESIII Collab.)
ABUDINEN	20	PRL 125 161806	F. Abudinen *et al.*	(BELLE II Collab.)
AGOSTINI	20	PRL 125 011801	M. Agostini *et al.*	(GERDA Collab.)
AGUILAR-AR...	20	PR D101 052014	A. Aguilar-Arevalo *et al.*	(PIENU Collab.)
AMARAL	20	PR D102 091101	D.W. Amaral *et al.*	(SuperCDMS Collab.)
AN	20	PR D102 115022	H. An *et al.*	(VIEN, MINN, VICT, TSIN)
ANDRIANAV...	20	PR D102 042001	A. Andrianavalomahefa *et al.*	(FUNK Collab.)
APRILE	20	PR D102 072004	E. Aprile *et al.*	(XENON Collab.)
ARALIS	20	PR D101 052008	T. Aralis *et al.*	(SuperCDMS Collab.)
Also		PR D103 039901 (errat.)	T. Aralis *et al.*	(SuperCDMS Collab.)
ARGUELLES	20	JHEP 2002 190	C. Arguelles *et al.*	(MIT, VALE)
ARNAUD	20	PRL 125 141301	Q. Arnaud *et al.*	(EDELWEISS Collab.)
BALDINI	20	EPJ C80 858	A.M. Baldini *et al.*	(MEG Collab.)
BANERJEE	20	PR D101 071101	D. Banerjee *et al.*	(NA64 Collab.)
BANERJEE	20A	PRL 125 081801	D. Banerjee *et al.*	(NA64 Collab.)
BARAK	20	PRL 125 171802	L. Barak *et al.*	(SENSEI Collab.)
BRAINE	20	PRL 124 101303	T. Braine *et al.*	(ADMX Collab.)
BUEHLER	20	JCAP 2009 027	R. Buehler *et al.*	(DESY, MADU)
CALORE	20	PR D102 123005	F. Calore *et al.*	(LAPP, BARI, HEID, +)
CAPOZZI	20	PR D102 083007	F. Capozzi, G. Raffelt	(MPIM)
CARENZA	20	PL B809 135709	P. Carenza *et al.*	
CRESCINI	20	PRL 124 171801	N. Crescini *et al.*	(QUAX Collab.)
CRISOSTO	20	PRL 124 241101	N. Crisosto *et al.*	(ADMX SLIC Collab.)
DARLING	20	PRL 125 121103	J. Darling	(COLO)
DARLING	20A	APJ 900 L28	J. Darling	(COLO)
DENT	20A	PRL 125 131805	J.B. Dent *et al.*	
DEPTA	20	JCAP 2005 009	P.F. Depta, M. Hufnagel, K. Schmidt-Hoberg	(DESY)
DESSERT	20A	PRL 125 261102	C. Dessert, J.W. Foster, B.R. Safdi	(MICH)
ESTEBAN	20	EPJ C80 259	I. Esteban *et al.*	
FOSTER	20	PRL 125 171301	J.W. Foster *et al.*	(MICH, ILL, TOKY+)
GAO	20	PRL 125 131806	C. Gao *et al.*	(FNAL, EFI, CHIC, ANL+)
GAVELA	20	PRL 124 051802	M.B. Gavela *et al.*	
GHOSH	20A	JCAP 2010 060	D. Ghosh, D. Sachdeva	
IRSIC	20	PR D101 123518	V. Irsic, H. Xiao, M. McQuinn	
JEONG	20	PRL 125 221302	J. Jeong *et al.*	
KENNEDY	20	PRL 125 201302	C.J. Kennedy *et al.*	(COLO, STAN)
KLIMCHITSK...	20	PR D101 056013	G.L. Klimchitskaya, P. Kuusk, V.M. Mostepanenko	
KOROCHKIN	20	JCAP 2003 064	A. Korochkin, A. Neronov, D. Semikoz	
KRASNIKOV	20	MPL A35 2050116	N.V. Krasnikov	
LEE	20A	PRL 124 101802	S .Lee *et al.*	(CULTASK Collab.)
LUCENTE	20A	JCAP 2012 008	G. Lucente *et al.*	
MEYER	20	PRL 124 231101	M. Meyer, T. Petrushevska	(Fermi-LAT Collab.)
Also		PRL 125 119901 (errat.)	M. Meyer, T. Petrushevska	(Fermi-LAT Collab.)
PODDAR	20	PR D101 083007	T.K. Poddar, S. Mohanty, S. Jana	
SCHUTZ	20	PR D101 123026	K. Schutz	(MIT)
SHE	20	PRL 124 111301	Z. She *et al.*	(CDEX Collab.)
SIRUNYAN	20AQ	PRL 124 131802	A.M. Sirunyan *et al.*	(CMS Collab.)
STRANIERO	20	AA 644 A166	O. Straniero *et al.*	(SASSO, BGNA, GRAN)
SUN	20	PR D101 063020	L. Sun, R. Brito, M. Isi	(CIT, ROMA1, MIT)
TOMITA	20	JCAP 2009 012	N. Tomita *et al.*	
WANG	20A	PR D101 052003	Y. Wang *et al.*	(CDEX Collab.)
YAMAMOTO	20	JCAP 2002 011	R. Yamamoto *et al.*	
AABOUD	19G	PR D99 012001	M. Aaboud *et al.*	(ATLAS Collab.)
ABLIKIM	19A	PR D99 012006	M. Ablikim *et al.*	(BESIII Collab.)
Also		PR D104 099901 (errat.)	M. Ablikim *et al.*	(BESIII Collab.)
ABLIKIM	19H	PR D99 012013	M. Ablikim *et al.*	(BESIII Collab.)
ADELBERGER	19	PRL 123 169001	E.G. Adelberger, W.A. Terrano	(WASH, PRIN)
ADHIKARI	19B	ASP 114 101	P. Adhikari *et al.*	(COSINE-100 Collab.)
AGUILAR-AR...	19A	PRL 123 181802	A. Aguilar-Arevalo *et al.*	(DAMIC Collab.)
AHN	19	PRL 122 021802	J.K. Ahn *et al.*	(KOTO Collab.)
ALESINI	19	PR D99 101101	D. Alesini *et al.*	(QUAX Collab.)
ALONI	19	PRL 123 071801	D. Aloni *et al.*	(REHO, MIT, CERN, HAIF)
APRILE	19D	PRL 123 251801	E. Aprile *et al.*	(XENON1T Collab.)
ARNOLD	19	EPJ C79 440	R. Arnold *et al.*	(NEMO-3 Collab.)
BANERJEE	19	PRL 123 121801	D. Banerjee *et al.*	(NA64 Collab.)
BHOONAH	19	PR D100 023001	A. Bhoonah *et al.*	
BRUN	19	PRL 122 201801	P. Brun, L. Chevalier, C. Flouzat	(SACL)
CAPUTO	19	PR D100 063515	A. Caputo *et al.*	
CORTINA-GIL	19	JHEP 1905 182	E. Cortina Gil *et al.*	(NA62 Collab.)
DANILOV	19	PRL 122 041801	M. Danilov, S. Demidov, D. Gorbunov	(LEBD, INRM+)
DAVOUDIASL	19	PRL 123 021102	H. Davoudiasl, P.B. Denton	(BNL)
DESSERT	19	PRL 123 061104	C. Dessert, A.J. Long, B.R. Safdi	(MICH)
FEDDERKE	19	PR D100 015040	M.A. Fedderke, P.W. Graham, S. Rajendran	(STAN+)
FUJITA	19	PRL 122 191101	T. Fujita, R. Tazaki, K. Toma	(KYOT, GEVA, TOHO)
HOCHBERG	19	PRL 123 151802	Y. Hochberg *et al.*	(HEBR, MIT, NIST)
IVANOV	19	JCAP 1902 059	M.M. Ivanov *et al.*	
KOPYLOV	19	JCAP 1907 008	A. Kopylov, I. Orekhov, V. Petukhov	(INRM)
KOVETZ	19	PR D99 123511	E.D. Kovetz, I. Cholis, D.E. Kaplan	(JHU)
LEINSON	19	JCAP 1911 031	L.B. Leinson	
LIANG	19	JCAP 1906 042	Y-F. Liang *et al.*	
LLOYD	19	PR D100 063005	S.J. Lloyd *et al.*	
MARSH	19	PRL 123 051103	D.J.E. Marsh, J.C. Niemeyer	(GOET)
NGUYEN	19	JCAP 1910 014	L.H. Nguyen, A. Lobanov, D. Horns	(WISPDMX Collab.)
OUELLET	19A	PRL 122 121802	J.L. Ouellet *et al.*	(ABRACADABRA Collab.)
PALOMBA	19	PRL 123 171101	C. Palomba *et al.*	
SIRUNYAN	19BQ	PL B796 131	A.M. Sirunyan *et al.*	(CMS Collab.)
SMORRA	19	NAT 575 310	C. Smorra *et al.*	
TERRANO	19	PRL 122 231301	W. Terrano *et al.*	(WASH)
WU	19	PRL 122 191302	T. Wu *et al.*	(CASPEr-ZULF Collab.)
WU	19C	PRL 123 169002	T. Wu *et al.*	(CASPEr-ZULF Collab.)
ABE	18F	PL B787 153	K. Abe *et al.*	(XMASS Collab.)
ADRIAN	18	PR D98 091101	P.H. Adrian *et al.*	(HPS Collab.)
AKHMATOV	18	PPN 49 599	Z.A. Akhmatov *et al.*	
ANASTASI	18B	PL B784 336	A. Anastasi *et al.*	(KLOE-2 Collab.)
ARMENGAUD	18	PR D98 082004	E. Armengaud *et al.*	(EDELWEISS-III Collab.)
ARNOLD	18	EPJ C78 821	R. Arnold *et al.*	(NEMO-3 Collab.)
BANERJEE	18	PRL 120 231802	D. Banerjee *et al.*	(NA64 Collab.)
BANERJEE	18A	PR D97 072002	D. Banerjee *et al.*	(NA64 Collab.)
BEZNOGOV	18	PR C98 035802	M.V. Beznogov *et al.*	
BOUTAN	18	PRL 121 261302	C. Boutan *et al.*	(ADMX Collab.)
CHANG	18	JHEP 1809 051	J.C. Chang, R. Essig, S.D. McDermott	
CRESCINI	18	EPJ C78 703	N. Crescini *et al.*	(QUAX Collab.)
DU	18	PRL 120 151301	N. Du *et al.*	(ADMX Collab.)
DZUBA	18	PR D98 035048	V.A. Dzuba *et al.*	
FICEK	18	PRL 120 183002	F. Ficek *et al.*	
FORTIN	18	JHEP 1806 048	J.-F. Fortin, K. Sinha	(LAVL, OKLA)
GAVRILYUK	18	JETPL 107 589	Yu.M. Gavrilyuk *et al.*	
HAMAGUCHI	18	PR D98 103015	K. Hamaguchi *et al.*	
KNIRCK	18	JCAP 1811 031	S. Knirck *et al.*	
STADNIK	18	PRL 120 013202	Y.V. Stadnik, V.A. Dzuba, V.V. Flambaum	
YAMAJI	18	PL B782 523	T. Yamaji *et al.*	(TOKY, RIKEN, KEK)
ZHANG	18	PR D97 063009	C. Zhang *et al.*	
ZHONG	18	PR D97 092001	L. Zhong *et al.*	(HAYSTAC Collab.)
AAIJ	17AQ	PR D95 071101	R. Aaij *et al.*	(LHCb Collab.)
ABEL	17	PR X7 041034	C. Abel *et al.*	(nEDM Collab.)
ABGRALL	17	PRL 118 161801	N. Abgrall *et al.*	(MAJORANA Collab.)
ABLIKIM	17AA	PL B774 252	M. Ablikim *et al.*	(BESIII Collab.)
ADE	17	PR D96 102003	P.A.R. Ade *et al.*	(BICEP2/Keck Array Collab.)
AHN	17	PTEP 2017 021C01	J.K. Ahn *et al.*	(KOTO Collab.)
AKERIB	17B	PRL 118 261301	D.S. Akerib *et al.*	(LUX Collab.)
ANASTASSO...	17	NATP 13 584	V. Anastassopoulos *et al.*	(CAST Collab.)
ANGLOHER	17	EPJ C77 299	G. Angloher *et al.*	(CRESST-II Collab.)
APRILE	17B	PR D95 029904	E. Aprile *et al.*	(XENON100 Collab.)
BANERJEE	17	PRL 118 011802	D. Banerjee *et al.*	(NA64 Collab.)
BATLEY	17	PL B769 67	J.R. Batley *et al.*	(NA48/2 Collab.)
BRANCA	17	PRL 118 021302	A. Branca *et al.*	(AURIGA Collab.)
BRUBAKER	17	PRL 118 061302	B.M. Brubaker *et al.*	(YALE, UCB, NIST+)
CHANG	17	JHEP 1701 107	J.H. Chang, R. Essig, S.D. McDermott	(STON)
CHOI	17	PR D96 061102	J. Choi *et al.*	(CAPP-ACTION Collab.)
CRESCINI	17	PL B773 677	N. Crescini *et al.*	(QUAX-gpgs Collab.)
DAIDO	17	PL B772 127	R. Daido, F. Takahashi	
DOLAN	17	JHEP 1712 094	M.J. Dolan *et al.*	
Also		JHEP 2103 190 (errat.)	M.J. Dolan *et al.*	(MELB, BRCO, DESY)
DUBININA	17	PAN 80 461	V.V. Dubinina *et al.*	
FICEK	17	PR A95 032505	F. Ficek *et al.*	
FU	17A	PRL 119 181806	C. Fu *et al.*	(PandaX-II Collab.)
INADA	17	PRL 118 071803	T. Inada *et al.*	
KLIMCHITSK...	17A	PR D95 123013	G.L. Klimchitskaya, V.M. Mostepanenko	
KOHRI	17	PR D96 051701	K. Kohri, H. Kodama	(KEK, KYOT)
LEES	17E	PRL 119 131804	J.P. Lees *et al.*	(BABAR Collab.)
LIU	17	PL B766 117	X.-H. Liu	(TINT)
LIU	17A	PR D95 052006	S.K. Liu *et al.*	(CDEX Collab.)
LUO	17	PR D96 055028	P. Luo *et al.*	
MARSH	17	JCAP 1712 036	M.C.D. Marsh *et al.*	
TIWARI	17	PR D95 023005	P. Tiwari	(Technion)
AAD	16AG	JHEP 1602 062	G. Aad *et al.*	(ATLAS Collab.)
ABLIKIM	16E	PR D93 052005	M. Ablikim *et al.*	(BESIII Collab.)
AJELLO	16	PRL 116 161101	M. Ajello *et al.*	(Fermi-LAT Collab.)
ANASTASI	16	PL B757 356	A. Anastasi *et al.*	(KLOE-2 Collab.)
BATTICH	16	JCAP 1608 062	T. Battich *et al.*	
BERENJI	16	PR D93 045019	B. Berenji *et al.*	
CORSICO	16	JCAP 1607 036	A.H. Corsico *et al.*	
DELLA-VALLE	16	EPJ C76 24	F. Della Valle *et al.*	(PVLAS Collab.)
HOSKINS	16	PR D94 082001	J. Hoskins *et al.*	(ADMX Collab.)
JAECKEL	16	PL B753 482	J. Jaeckel, M. Spannowsky	(HEID, DURH)
KHACHATRY...	16	PL B752 146	V. Khachatryan *et al.*	(CMS Collab.)
KRASZNAHO...	16	PRL 116 042501	A.J. Krasznahorkay *et al.*	(HINR, ANIK+)
LEEFER	16	PRL 117 271601	N. Leefer *et al.*	(MAINZ, BONN, LBL, UCB+)
WON	16	PR D94 092006	E. Won *et al.*	(BELLE Collab.)
YOON	16	JHEP 1606 011	Y.S. Yoon *et al.*	(KIMS Collab.)
AAD	15CD	PR D92 092001	G. Aad *et al.*	(ATLAS Collab.)
AAIJ	15AZ	PRL 115 161802	R. Aaij *et al.*	(LHCb Collab.)
ADARE	15	PR C91 031901	A. Adare *et al.*	(PHENIX Collab.)
AFACH	15	PL B745 58	S. Afach *et al.*	(ETH, PSI, CAEN, +)
AGOSTINI	15A	EPJ C75 416	M. Agostini *et al.*	(GERDA Collab.)
AN	15A	PL B747 331	H. An *et al.*	(CIT, VICT, VIEN)
ANASTASI	15	PL B747 365	A. Anastasi *et al.*	(KLOE-2 Collab.)
ANASTASI	15A	PL B750 633	A. Anastasi *et al.*	(KLOE-2 Collab.)
ANASTASSO...	15	PL B749 172	V. Anastassopoulos *et al.*	(CAST Collab.)
ARIK	15	PR D92 021101	M. Arik *et al.*	(CAST Collab.)
ARNOLD	15	PR D92 072011	R. Arnold *et al.*	(NEMO-3 Collab.)
BALLOU	15	PR D92 092002	R. Ballou *et al.*	(OSQAR Collab.)
BATLEY	15A	PL B746 178	J.R. Batley *et al.*	(NA48/2 Collab.)
BAYES	15	PR D91 052020	R. Bayes *et al.*	(TWIST Collab.)
BRAX	15	PR D92 083501	P. Brax, P. Brun, D. Wouters	(SACL, SACL5)
GAVRILYUK	15	JETPL 101 664	Yu.M. Gavrilyuk *et al.*	
		Translated from ZETFP 101 739.		
HASEBE	15	PTEP 2015 073C01	T. Hasebe *et al.*	
JAEGLE	15	PRL 114 211801	I. Jaegle *et al.*	(BELLE Collab.)
KAZANAS	15	NP B890 17	D. Kazanas *et al.*	
KLIMCHITSK...	15	EPJ C75 164	G.L. Klimchitskaya, V.M. Mostepanenko	
MILLEA	15	PR D92 023010	M. Millea, L. Knox, B. Fields	(UCD, ILL)
STADNIK	15	EPJ C75 110	Y.V. Stadnik, V.V. Flambaum	(SYDN)

Downloaded from https://academic.oup.com/ptep/article/2022/8/083C01/6651666 by KIT Library user on 27 September 2022

SUZUKI	15	JCAP 1509 042	J. Suzuki *et al.*	
TERRANO	15	PRL 115 201801	W.A. Terrano *et al.*	(WASH)
VANTILBURG	15	PRL 115 011802	K. Van Tilburg *et al.*	
VINYOLES	15	JCAP 1510 015	N. Vinyoles *et al.*	
ABE	14F	PRL 113 121301	K. Abe *et al.*	(XMASS Collab.)
AGAKISHIEV	14	PL B731 265	G. Agakishiev *et al.*	(HADES Collab.)
ALBERT	14A	PR D90 092004	J.B. Albert *et al.*	(EXO-200 Collab.)
APRILE	14B	PR D90 062009	E. Aprile *et al.*	(XENON100 Collab.)
ARIK	14	PRL 112 091302	M. Arik *et al.*	(CAST Collab.)
AYALA	14	PRL 113 191302	A. Ayala *et al.*	
BABUSCI	14	PL B736 459	D. Babusci *et al.*	(KLOE-2 Collab.)
BATELL	14	PRL 113 171802	B. Batell, R. Essig, Z. Surujon	(EFI, STON)
BEZERRA	14	PR D89 035010	V.B. Bezerra *et al.*	
BEZERRA	14A	EPJ C74 2859	V.B. Bezerra *et al.*	
BEZERRA	14B	PR D90 055013	V.B. Bezerra *et al.*	
BEZERRA	14C	PR D89 075002	V.B. Bezerra *et al.*	
BLUEMLEIN	14	PL B731 320	J. Bluemlein, J. Brunner	(CPPM, DESY)
BLUM	14	PL B737 30	K. Blum *et al.*	(IAS, PRIN)
DELLA-VALLE	14	PR D90 092003	F. Della Valle *et al.*	(PVLAS Collab.)
DERBIN	14	EPJ C74 3035	A.V. Derbin *et al.*	
EJLLI	14	PR D90 123527	D. Ejlli	
FRADETTE	14	PR D90 035022	A. Fradette *et al.*	
LEES	14J	PRL 113 201801	J.P. Lees *et al.*	(BABAR Collab.)
LEINSON	14	JCAP 1408 031	L. Leinson	
MERKEL	14	PRL 112 221802	H. Merkel *et al.*	(A1 at MAMI)
MILLER-BER...	14	JCAP 1410 069	M.M. Miller Bertolami *et al.*	
PUGNAT	14	EPJ C74 3027	P. Pugnat *et al.*	(OSQAR Collab.)
REESMAN	14	JCAP 1408 021	R. Reesman *et al.*	(OSU)
ABE	13D	PL B724 46	K. Abe *et al.*	(XMASS Collab.)
ABRAMOWSKI	13A	PR D88 102003	A. Abramowski *et al.*	(H.E.S.S. Collab.)
ADLARSON	13	PL B726 187	P. Adlarson *et al.*	(WASA-at-COSY Collab.)
ALESSANDRIA	13	JCAP 1305 007	F. Alessandria *et al.*	(CUORE Collab.)
AN	13B	PL B725 190	H. An, M. Pospelov, J. Pradler	
AN	13C	PRL 111 041302	H. An, M. Pospelov, J. Pradler	
ARCHIDIACO...	13A	JCAP 1310 020	M. Archidiacono *et al.*	
ARMENGAUD	13	JCAP 1311 067	E. Armengaud *et al.*	(EDELWEISS-II Collab.)
BABUSCI	13B	PL B720 111	D. Babusci *et al.*	(KLOE-2 Collab.)
BARTH	13	JCAP 1305 010	K. Barth *et al.*	(CAST Collab.)
BECK	13	PRL 111 231801	C. Beck	
BETZ	13	PR D88 075014	M. Betz *et al.*	(CROWS Collab.)
BULATOWICZ	13	PRL 111 102001	M. Bulatowicz *et al.*	
CHU	13	PR D87 011105	P.-H. Chu *et al.*	(DUKE, IND, SJTU)
DERBIN	13	EPJ C73 2490	A. V. Derbin *et al.*	
DIAMOND	13	PRL 111 221803	M.D. Diamond, P. Schuster	
FRIEDLAND	13	PRL 110 061101	A. Friedland, M. Giannotti, M. Wise	
GNINENKO	13	PR D87 035030	S.N. Gninenko	(INRM)
HECKEL	13	PRL 111 151802	B. R. Heckel *et al.*	
HORVAT	13	PL B721 220	R. Horvat *et al.*	
INADA	13	PL B722 301	T. Inada *et al.*	
LATTANZI	13	PR D88 063528	M. Lattanzi *et al.*	
MEYER	13	PR D87 035027	M. Meyer, D. Horns, M. Raue	
MIZUMOTO	13	JCAP 1307 013	T. Mizumoto *et al.*	
PARKER	13	PR D88 112004	S. Parker *et al.*	
REDONDO	13	JCAP 1308 034	J. Redondo, G. Raffelt	
TULLNEY	13	PRL 111 100801	K. Tullney *et al.*	
VIAUX	13A	PRL 111 231301	N. Viaux *et al.*	
WOUTERS	13	APJ 772 44	D. Wouters, P. Brun	(SACL)
ABLIKIM	12	PR D85 092012	M. Ablikim *et al.*	(BESIII Collab.)
ARCHILLI	12	PL B706 251	F. Archilli *et al.*	(KLOE-2 Collab.)
BELLI	12	PL B711 41	P. Belli *et al.*	(DAMA-KIEV)
BELLINI	12B	PR D85 092003	G. Bellini *et al.*	(Borexino Collab.)
CADAMURO	12	JCAP 1202 032	D. Cadamuro *et al.*	(MPIM)
CORSICO	12	JCAP 1212 010	A.H. Corsico *et al.*	(LAPL, RGSUL, WASH+)
DERBIN	12	JETPL 95 339	A.V. Derbin *et al.*	(PNPI)
		Translated from ZETFP 95 379.		
GANDO	12	PR C86 021601	A. Gando *et al.*	(KamLAND-Zen Collab.)
GNINENKO	12A	PR D85 055027	S.N. Gninenko	(INRM)
GNINENKO	12B	PL B713 244	S.N. Gninenko	(INRM)
PAYEZ	12	JCAP 1207 041	A. Payez *et al.*	(LIEG)
RAFFELT	12	PR D86 015001	G. Raffelt	(MPIM)
AALSETH	11	PRL 106 131301	C.E. Aalseth *et al.*	(CoGeNT Collab.)
ABRAHAMY...	11	PRL 107 191804	S. Abrahamyan *et al.*	
ARIK	11	PRL 107 261302	M. Arik *et al.*	(CAST Collab.)
ARNOLD	11	PRL 107 062504	R. Arnold *et al.*	(NEMO-3 Collab.)
BLUEMLEIN	11	PL B701 155	J. Bluemlein, J. Brunner	(DESY)
CADAMURO	11	JCAP 1102 003	D. Cadamuro *et al.*	(MPIM, AARHUS)
DERBIN	11	PAN 74 596	A.V. Derbin *et al.*	(PNPI)
		Translated from YAF 74 620.		
DERBIN	11A	PR D83 023505	A.V. Derbin *et al.*	(PNPI)
HOEDL	11	PRL 106 041801	S.A. Hoedl *et al.*	(WASH)
HOSKINS	11	PR D84 121302	J. Hoskins *et al.*	(ADMX Collab.)
ANDRIAMON...	10	JCAP 1003 032	S. Andriamonje *et al.*	(CAST Collab.)
ARGYRIADES	10	NP A847 168	J. Argyriades *et al.*	(NEMO-3 Collab.)
ASZTALOS	10	PRL 104 041301	S.J. Asztalos *et al.*	(ADMX Collab.)
EHRET	10	PL B689 149	K. Ehret *et al.*	(ALPS Collab.)
HANNESTAD	10	JCAP 1008 001	S. Hannestad *et al.*	
PETUKHOV	10	PRL 105 170401	A.K. Petukhov *et al.*	
SEREBROV	10	JETPL 91 6	A.P. Serebrov *et al.*	
		Translated from ZETFP 91 8.		
AHMED	09A	PRL 103 141802	Z. Ahmed *et al.*	(CDMS Collab.)
ANDRIAMON...	09	JCAP 0912 002	S. Andriamonje *et al.*	
ARGYRIADES	09	PR C80 032501	J. Argyriades *et al.*	(NEMO-3 Collab.)
ARIK	09	JCAP 0902 008	E. Arik *et al.*	(CAST Collab.)
BJORKEN	09	PR D80 075018	J. Bjorken *et al.*	
CHOU	09	PRL 102 030402	A.S. Chou *et al.*	(GammeV Collab.)
DAVOUDIASL	09	PR D79 095024	H. Davoudiasl, P. Huber	
DERBIN	09A	PL B678 181	A.V. Derbin *et al.*	
GONDOLO	09	PR D79 107301	P. Gondolo, G. Raffelt	(UTAH, MPIM)
IGNATOVICH	09	EPJ C64 19	V.K. Ignatovich, Y.N. Pokotilovski	(JINR)
KEKEZ	09	PL B671 345	D. Kekez *et al.*	
SEREBROV	09	PL B680 423	A.P. Serebrov	(PNPI)
AFANASEV	08	PRL 101 120401	A. Afanasev *et al.*	
BELLINI	08	EPJ C54 61	G. Bellini *et al.*	(Borexino Collab.)
CHOU	08	PRL 100 080402	A.S. Chou *et al.*	(GammeV Collab.)
FOUCHE	08	PR D78 032013	M. Fouche *et al.*	
HANNESTAD	08	JCAP 0804 019	S. Hannestad *et al.*	
INOUE	08	PL B668 93	Y. Inoue *et al.*	
ZAVATTINI	08	PR D77 032006	E. Zavattini *et al.*	(PVLAS Collab.)
ADELBERGER	07	PRL 98 131104	E.G. Adelberger *et al.*	
ANDRIAMON...	07	JCAP 0704 010	S. Andriamonje *et al.*	(CAST Collab.)
BAESSLER	07	PR D75 075006	S. Baessler *et al.*	
CHANG	07	PR D75 052004	H.M. Chang *et al.*	(TEXONO Collab.)
HANNESTAD	07	JCAP 0708 015	S. Hannestad *et al.*	
JAIN	07	JP G34 129	P.L. Jain, G. Singh	
LESSA	07	PR D75 094001	A.P. Lessa, O.L.G. Peres	
MELCHIORRI	07A	PR D76 041303	A. Melchiorri, O. Mena, A. Slosar	
ROBILLIARD	07	PRL 99 190403	C. Robilliard *et al.*	
ARNOLD	06	NP A765 483	R. Arnold *et al.*	(NEMO-3 Collab.)
DUFFY	06	PR D74 012006	L.D. Duffy *et al.*	
HECKEL	06	PRL 97 021603	B.R. Heckel *et al.*	
ZAVATTINI	06	PRL 96 110406	E. Zavattini *et al.*	(PVLAS Collab.)
HANNESTAD	05A	JCAP 0507 002	S. Hannestad, A. Mirizzi, G. Raffelt	
ZIOUTAS	05	PRL 94 121301	K. Zioutas *et al.*	(CAST Collab.)
ADLER	04	PR D70 037102	S. Adler *et al.*	(BNL E787 Collab.)
ANISIMOVSK...	04	PRL 93 031801	V.V. Anisimovsky *et al.*	(BNL E949 Collab.)
ARNOLD	04	JETPL 80 377	R. Arnold *et al.*	(NEMO-3 Collab.)
		Translated from ZETFP 80 429.		
ASZTALOS	04	PR D69 011101	S.J. Asztalos *et al.*	
HOFFMANN	04	PR B70 180503	C. Hoffmann *et al.*	
ARNABOLDI	03	PL B557 167	C. Arnaboldi *et al.*	
CIVITARESE	03	NP A729 867	O. Civitarese, J. Suhonen	
DANEVICH	03	PR C68 035501	F.A. Danevich *et al.*	
ADLER	02C	PL B537 211	S. Adler *et al.*	(BNL E787 Collab.)
BADERT...	02	PL B542 29	A. Badertscher *et al.*	
BERNABEI	02D	PL B546 23	R. Bernabei *et al.*	(DAMA Collab.)
DERBIN	02	PAN 65 1302	A.V. Derbin *et al.*	
		Translated from YAF 65 1335.		
FUSHIMI	02	PL B531 190	K. Fushimi *et al.*	(ELEGANT V Collab.)
INOUE	02	PL B536 18	Y. Inoue *et al.*	
MORALES	02B	ASP 16 325	A. Morales *et al.*	(COSME Collab.)
ADLER	01	PR D63 032004	S. Adler *et al.*	(BNL E787 Collab.)
AMMAR	01B	PRL 87 271801	R. Ammar *et al.*	(CLEO Collab.)
ASHITKOV	01	JETPL 74 529	V.D. Ashitkov *et al.*	
		Translated from ZETFP 74 601.		
BERNABEI	01B	PL B515 6	R. Bernabei *et al.*	(DAMA Collab.)
DANEVICH	01	NP A694 375	F.A. Danevich *et al.*	
DEBOER	01	JP G27 L29	F.W.N. de Boer *et al.*	
STOICA	01	NP A694 269	S. Stoica, H.V. Klapdor-Kleingrothous	
ALESSAND...	00	PL B486 13	A. Alessandrello *et al.*	
ARNOLD	00	NP A678 341	R. Arnold *et al.*	
ASTIER	00B	PL B479 371	P. Astier *et al.*	(NOMAD Collab.)
DANEVICH	00	PR C62 045501	F.A. Danevich *et al.*	
MASSO	00	PR D61 011701	E. Masso	
ARNOLD	99	NP A658 299	R. Arnold *et al.*	(NEMO Collab.)
NI	99	PRL 82 2439	W.-T. Ni *et al.*	
SIMKOVIC	99	PR C60 055502	F. Simkovic *et al.*	
ALTEGOER	98	PL B428 197	J. Altegoer *et al.*	
ARNOLD	98	NP A636 209	R. Arnold *et al.*	(NEMO-2 Collab.)
AVIGNONE	98	PRL 81 5068	F.T. Avignone *et al.*	(Solar Axion Experiment)
DIAZ	98	NP B527 44	M.A. Díaz *et al.*	
KIM	98	PR D58 055006	J.E. Kim	
LUESCHER	98	PL B434 407	R. Luescher *et al.*	
MORIYAMA	98	PL B434 147	S. Moriyama *et al.*	
MOROI	98	PL B440 69	T. Moroi, H. Murayama	
POSPELOV	98	PR D58 097703	M. Pospelov	
AHMAD	97	PRL 78 618	I. Ahmad *et al.*	(APEX Collab.)
BORISOV	97	JETP 83 868	A.V. Borisov, V.Y. Grishinia	(MOSU)
DEBOER	97C	JP G23 L85	F.W.N. de Boer *et al.*	
KACHELRIESS	97	PR D56 1313	M. Kachelriess, C. Wilke, G. Wunner	(BOCH)
KEIL	97	PR D56 2419	W. Keil *et al.*	
KITCHING	97	PRL 79 4079	P. Kitching *et al.*	(BNL E787 Collab.)
LEINBERGER	97	PL B394 16	U. Leinberger *et al.*	(ORANGE Collab.)
ADLER	96	PRL 76 1421	S. Adler *et al.*	(BNL E787 Collab.)
AMSLER	96B	ZPHY C70 219	C. Amsler *et al.*	(Crystal Barrel Collab.)
GANZ	96	PL B389 4	R. Ganz *et al.*	(GSI, HEID, FRAN, JAGL+)
GUENTHER	96	PR D54 3641	M. Gunther *et al.*	(MPIK, SASSO)
KAMEL	96	PL B368 291	S. Kamel	(SHAMS)
MITSUI	96	EPL 33 111	T. Mitsui *et al.*	(TOKY)
YOUDIN	96	PRL 77 2170	A.N. Youdin *et al.*	(AMHT, WASH)
ALTMANN	95	ZPHY C68 221	M. Altmann *et al.*	(TUM, LAPP, CPPM)
BASSOMPIE...	95	PL B355 584	G. Bassompierre *et al.*	(LAPP, LCGT, LYON)
MAENO	95	PL B351 574	T. Maeno *et al.*	(TOKY)
RAFFELT	95	PR D51 1495	G. Raffelt, A. Weiss	(MPIM, MPIG)
SKALSEY	95	PR D51 6292	M. Skalsey, R.S. Conti	(MICH)
TSUNODA	95	EPL 30 273	T. Tsunoda *et al.*	(TOKY)
ADACHI	94	PR A49 3201	S. Adachi *et al.*	(TMU)
ALTHERR	94	ASP 2 175	T. Altherr, E. Petitgirard, T. del Rio Gaztelurrutia	
AMSLER	94B	PL B333 271	C. Amsler *et al.*	(Crystal Barrel Collab.)
ASAI	94	PL B323 90	S. Asai *et al.*	(TOKY)
MEIJERDREES	94	PR D49 4937	M.R. Drees *et al.*	(BRCO, OREG, TRIU)
NI	94	Physica B194 153	W.T. Ni *et al.*	(NTHU)
VO	94	PR C49 1551	D.T. Vo *et al.*	(ISU, LBL, LLNL, UCD)
ATIYA	93	PRL 70 2521	M.S. Atiya *et al.*	(BNL E787 Collab.)
Also		PRL 71 305 (erratum)	M.S. Atiya *et al.*	(BNL E787 Collab.)
ATIYA	93B	PR D48 1	M.S. Atiya *et al.*	(BNL E787 Collab.)
BASSOMPIE...	93	EPL 22 239	G. Bassompierre *et al.*	(LAPP, TORI, LYON)
BECK	93	PRL 70 2853	M. Beck *et al.*	(MPIK, KIAE, SASSO)
CAMERON	93	PR D47 3707	R.E. Cameron *et al.*	(ROCH, BNL, FNAL+)
CHANG	93	PL B316 51	S. Chang, K. Choi	
CHUI	93	PRL 71 3247	T.C.P. Chui, W.T. Ni	(NTHU)
MINOWA	93	PRL 71 4120	M. Minowa *et al.*	(TOKY)
NG	93	PR D48 2941	K.W. Ng	(AST)
RITTER	93	PRL 70 701	R.C. Ritter *et al.*	
TANAKA	93	PR D48 5412	J. Tanaka, H. Ejiri	(OSAK)
ALLIEGRO	92	PRL 68 278	C. Alliegro *et al.*	(BNL, FNAL, PSI+)
ATIYA	92	PRL 69 733	M.S. Atiya *et al.*	(BNL, LANL, PRIN+)
BARABASH	92	PL B295 154	L.S. Barabash *et al.*	(JINR, CERN, SERP+)
BERNATOW...	92	PRL 69 2341	T. Bernatowicz *et al.*	(WUSL, TATA)
BLUEMLEIN	92	IJMP A7 3835	J. Bluemlein *et al.*	(BERL, BUDA, JINR+)
HALLIN	92	PR D45 3955	A.L. Hallin *et al.*	(PRIN)
HENDERSON	92C	PRL 69 1733	S.D. Henderson *et al.*	(YALE, BNL)
HICKS	92	PL B276 423	K.H. Hicks, D.E. Alburger	(OHIO, BNL)
LAZARUS	92	PRL 69 2333	D.M. Lazarus *et al.*	(BNL, ROCH, FNAL)
MEIJERDREES	92	PRL 68 3845	R. Meijer Drees *et al.*	(SINDRUM I Collab.)
PAN	92	MPL A7 1287	S.S. Pan, W.T. Ni, S.C. Chen	(NTHU)
RUOSO	92	ZPHY C56 505	G. Ruoso *et al.*	(ROCH, BNL, FNAL, TRST)
SKALSEY	92	PRL 68 456	M. Skalsey, J.J. Kolata	(MICH, NDAM)
VENEMA	92	PRL 68 135	B.J. Venema *et al.*	
WANG	92	MPL A7 1497	J. Wang	(ILL)
WANG	92C	PL B291 97	J. Wang	(ILL)
WU	92	PRL 69 1729	X.Y. Wu *et al.*	(BNL, YALE, CUNY)
AKOPYAN	91	PL B272 443	M.V. Akopyan *et al.*	(INRM)
ASAI	91	PRL 66 2440	S. Asai *et al.*	(ICEPP)
BERSHADY	91	PRL 66 1398	M.A. Bershady, M.T. Ressell, M.S. Turner	(CHIC+)
BLUEMLEIN	91	ZPHY C51 341	J. Bluemlein *et al.*	(BERL, BUDA, JINR+)
BOBRAKOV	91	JETPL 53 294	V.F. Bobrakov *et al.*	(PNPI)
		Translated from ZETFP 53 283.		
BROSS	91	PRL 67 2942	A.D. Bross *et al.*	(FNAL, ILL)
KIM	91C	PRL 67 3465	J.E. Kim	(SEOUL)
RAFFELT	91	PRPL 198 1	G.G. Raffelt	(MPIM)
RAFFELT	91B	PRL 67 2605	G. Raffelt, D. Seckel	(MPIM, BART)
RESSELL	91	PR D44 3001	M.T. Ressell	(CHIC, FNAL)
TRZASKA	91	PL B269 54	W.H. Trzaska *et al.*	(TAMU)
TSERTOS	91	PL B266 259	H. Tsertos *et al.*	(ILLG, GSI)
WALKER	91	APJ 376 51	T.P. Walker *et al.*	(HSCA, OSU, CHIC+)
WIDMANN	91	ZPHY A340 209	E. Widmann *et al.*	(STUT, GSI, STUTM)
WINELAND	91	PRL 67 1735	D.J. Wineland *et al.*	(NBSB)
ALBRECHT	90E	PL B246 278	H. Albrecht *et al.*	(ARGUS Collab.)
ANTREASYAN	90C	PL B251 204	D. Antreasyan *et al.*	(Crystal Ball Collab.)
ASANUMA	90	PL B237 588	T. Asanuma *et al.*	(TOKY)
ATIYA	90	PRL 64 21	M.S. Atiya *et al.*	(BNL E787 Collab.)
ATIYA	90B	PRL 65 1188	M.S. Atiya *et al.*	(BNL E787 Collab.)
BAUER	90	NIM B50 300	W. Bauer *et al.*	(STUT, VILL, GSI)
BURROWS	90	PR D42 3297	A. Burrows, M.T. Ressell, M.S. Turner	(ARIZ+)
DEBOER	90	JP G16 L1	F.W.N. de Boer, J. Lehmann, J. Steyaert	(LOUV)

Downloaded from https://academic.oup.com/ptep/article/2022/8/083C01/6651666 by KIT Library user on 27 September 2022

ENGEL	90	PRL 65 960	J. Engel, D. Seckel, A.C. Hayes	(BART, LANL)
GNINENKO	90	PL B237 287	S.N. Gninenko *et al.*	(INRM)
GUO	90	PR D41 2924	R. Guo *et al.*	(NIU, LANL, FNAL, CASE+)
HAGMANN	90	PR D42 1297	C. Hagmann *et al.*	(FLOR)
JUDGE	90	PRL 65 972	S.M. Judge *et al.*	(ILLG, GSI)
RAFFELT	90D	PR D41 1324	G.G. Raffelt	(MPIM)
RITTER	90	PR D42 977	R.C. Ritter *et al.*	(UVA)
SEMERTZIDIS	90	PRL 64 2988	Y.K. Semertzidis *et al.*	(ROCH, BNL, FNAL+)
TSUCHIAKI	90	PL B236 81	M. Tsuchiaki *et al.*	(ICEPP)
TURNER	90	PRPL 197 67	M.S. Turner	(FNAL)
BARABASH	89	PL B223 273	A.S. Barabash *et al.*	(ITEP, INRM)
BINI	89	PL B221 99	M. Bini *et al.*	(FIRZ, CERN, AARH)
BURROWS	89	PR D39 1020	A. Burrows, M.S. Turner, R.P. Brinkmann	(ARIZ+)
Also		PRL 60 1797	M.S. Turner	(FNAL, EFI)
DEBOER	89B	PRL 62 2639	F.W.N. de Boer, R. van Dantzig	(ANIK)
ERICSON	89	PL B219 507	T.E.O. Ericson, J.F. Mathiot	(CERN, IPN)
FAISSNER	89	ZPHY C44 557	H. Faissner *et al.*	(AACH3, BERL, PSI)
FOX	89	PR C39 288	J.D. Fox *et al.*	(FSU)
MAYLE	89	PL B219 515	R. Mayle *et al.*	(LLL, CERN, MINN, FNAL+)
Also		PL B203 188	R. Mayle *et al.*	(LLL, CERN, MINN, FNAL+)
MINOWA	89	PRL 62 1091	H. Minowa *et al.*	(ICEPP)
ORITO	89	PRL 63 597	S. Orito *et al.*	(ICEPP)
PERKINS	89	PRL 62 2638	D.H. Perkins	(OXF)
TSERTOS	89	PR D40 1397	H. Tsertos *et al.*	(GSI, ILLG)
VANBIBBER	89	PR D39 2089	K. van Bibber *et al.*	(LLL, TAMU, LBL)
WUENSCH	89	PR D40 3153	W.U. Wuensch *et al.*	(ROCH, BNL, FNAL)
Also		PRL 59 839	S. de Panfilis *et al.*	(ROCH, BNL, FNAL)
AVIGNONE	88	PR D37 618	F.T. Avignone *et al.*	(PRIN, SCUC, ORNL+)
BALKE	88	PR D37 587	B. Balke *et al.*	(LBL, UCB, COLO, NWES+)
BJORKEN	88	PR D38 3375	J.D. Bjorken *et al.*	(FNAL, SLAC, VPI)
BLINOV	88	SJNP 47 563	A.E. Blinov *et al.*	(NOVO)
		Translated from YAF 47 889.		
BOLTON	88	PR D38 2077	R.D. Bolton *et al.*	(LANL, STAN, CHIC+)
Also		PRL 56 2461	R.D. Bolton *et al.*	(LANL, STAN, CHIC+)
Also		PRL 57 3241	D. Grosnick *et al.*	(CHIC, LANL, STAN+)
CHANDA	88	PR D37 2714	R. Chanda, J.F. Nieves, P.B. Pal	(UMD, UPR+)
CHOI	88	PR D37 3225	K. Choi *et al.*	(JHU)
CONNELL	88	PRL 60 2242	S.H. Connell *et al.*	(WITW)
DATAR	88	PR C37 250	V.M. Datar *et al.*	(IPN)
DEBOER	88	PRL 61 1274	F.W.N. de Boer, R. van Dantzig	(ANIK)
Also		PRL 62 2644 (erratum)	F.W.N. de Boer, R. van Dantzig	(ANIK)
Also		PRL 62 2638	D.H. Perkins	(OXF)
Also		PRL 62 2639	F.W.N. de Boer, R. van Dantzig	(ANIK)
DEBOER	88C	JP G14 L131	F.W.N. de Boer *et al.*	(LOUV)
DOEHNER	88	PR D38 2722	J. Dohner *et al.*	(HEIDP, ANL, ILLG)
EL-NADI	88	PRL 61 1271	M. el Nadi, O.E. Badawy	(CAIR)
ENGEL	88	PR C37 731	J. Engel, P. Vogel, M.R. Zirnbauer	
FAISSNER	88	ZPHY C37 231	H. Faissner *et al.*	(AACH3, BERL, SIN)
HATSUDA	88B	PL B203 469	T. Hatsuda, M. Yoshimura	(KEK)
LORENZ	88	PL B214 10	E. Lorenz *et al.*	(MPIM, PSI)
MAYLE	88	PL B203 188	R. Mayle *et al.*	(LLL, CERN, MINN, FNAL+)
PICCIOTTO	88	PR D37 1131	C.E. Picciotto *et al.*	(TRIU, CNRC)
RAFFELT	88	PRL 60 1793	G. Raffelt, D. Seckel	(UCB, LLL, UCSC)
RAFFELT	88B	PR D37 549	G.G. Raffelt, D.S.P. Dearborn	(UCB, LLL)
SAVAGE	88	PR D37 1134	M.J. Savage, B.W. Filippone, L.W. Mitchell	(CIT)
TSERTOS	88	PL B207 273	A. Tsertos *et al.*	(GSI, ILLG)
TSERTOS	88B	ZPHY A331 103	A. Tsertos *et al.*	(GSI, ILLG)
VANKLINKEN	88	PL B205 223	J. van Klinken *et al.*	(GRON, GSI)
VANKLINKEN	88B	PRL 60 2442	J. van Klinken	(GRON)
VONWIMMER...	88	PRL 60 2443	U. von Wimmersperg	(BNL)
VOROBYOV	88	PL B208 146	P.V. Vorobiev, Y.I. Gitarts	(NOVO)
DRUZHININ	87	ZPHY C37 1	V.P. Druzhinin *et al.*	(NOVO)
FRIEMAN	87	PR D36 2201	J.A. Frieman, S. Dimopoulos, M.S. Turner	(SLAC+)
GOLDMAN	87	PR D36 1543	T. Goldman *et al.*	(LANL, CHIC, STAN+)
KORENCHE...	87	SJNP 46 192	S.M. Korenchenko *et al.*	(JINR)
		Translated from YAF 46 313.		
MAIER	87	ZPHY A326 527	K. Maier *et al.*	(STUT, GSI)
MILLS	87	PR D36 707	A.P. Mills, J. Levy	(BELL)
RAFFELT	87	PR D36 2211	G.G. Raffelt, D.S.P. Dearborn	(LLL, UCB)
RIORDAN	87	PRL 59 755	E.M. Riordan *et al.*	(ROCH, CIT+)
TURNER	87	PRL 59 2489	M.S. Turner	(FNAL, EFI)
VANBIBBER	87	PRL 59 759	K. van Bibber *et al.*	(LLL, CIT, MIT+)
VONWIMMER...	87	PRL 59 266	U. von Wimmersperg *et al.*	(WITW)
BADIER	86	ZPHY C31 21	J. Badier *et al.*	(NA3 Collab.)
BROWN	86	PRL 57 2101	C.N. Brown *et al.*	(FNAL, WASH, KYOT+)
BRYMAN	86B	PRL 57 2787	D.A. Bryman, E.T.H. Clifford	(TRIU)
DAVIER	86	PL B180 295	M. Davier, J. Jeanjean, H. Nguyen Ngoc	(LALO)
DEARBORN	86	PRL 56 26	D.S.P. Dearborn, D.N. Schramm, G. Steigman	(LLL+)
EICHLER	86	PL B175 101	R.A. Eichler *et al.*	(SINDRUM Collab.)
HALLIN	86	PRL 57 2105	A.L. Hallin *et al.*	(PRIN)
JODIDIO	86	PR D34 1967	A. Jodidio *et al.*	(LBL, NWES, TRIU)
Also		PR D37 237 (erratum)	A. Jodidio *et al.*	(LBL, NWES, TRIU)
KETOV	86	JETPL 44 146	S.N. Ketov *et al.*	(KIAE)
		Translated from ZETFP 44 114.		
KOCH	86	NC 96A 182	H.R. Koch, O.W.B. Schult	(JULI)
KONAKA	86	PRL 57 659	A. Konaka *et al.*	(KYOT, KEK)
MAIANI	86	PL B175 359	L. Maiani, R. Petronzio, E. Zavattini	(CERN)
PECCEI	86	PL B172 435	R.D. Peccei, T.T. Wu, T. Yanagida	(DESY)
RAFFELT	86	PR D33 897	G.G. Raffelt	(MPIM)
RAFFELT	86B	PL 166B 402	G.G. Raffelt	(MPIM)
SAVAGE	86B	PRL 57 178	M.J. Savage *et al.*	(CIT)
AMALDI	85	PL 153B 444	U. Amaldi *et al.*	(CERN)
ANANEV	85	SJNP 41 585	V.D. Ananev *et al.*	(JINR)
		Translated from YAF 41 912.		
BALTRUSAIT...	85	PRL 55 1842	R.M. Baltrusaitis *et al.*	(Mark III Collab.)
BERGSMA	85	PL 157B 458	F. Bergsma *et al.*	(CHARM Collab.)
KAPLAN	85	NP B260 215	D.B. Kaplan	(HARV)
IWAMOTO	84	PRL 53 1198	N. Iwamoto	(UCSB, WUSL)
YAMAZAKI	84	PRL 52 1089	T. Yamazaki *et al.*	(INUS, KEK)
ABBOTT	83	PL 120B 133	L.F. Abbott, P. Sikivie	(BRAN, FLOR)
CARBONI	83	PL 123B 349	G. Carboni, W. Dahme	(CERN, MUNI)
CAVAIGNAC	83	PL 121B 193	J.F. Cavaignac *et al.*	(ISNG, LAPP)
DICUS	83	PR D28 1778	D.A. Dicus, V.L. Teplitz	(TEXA, UMD)
DINE	83	PL 120B 137	M. Dine, W. Fischler	(IAS, PENN)
ELLIS	83B	NP B223 252	J. Ellis, K.A. Olive	(CERN)
FAISSNER	83	PR D28 1198	H. Faissner *et al.*	(AACH)
FAISSNER	83B	PR D28 1787	H. Faissner *et al.*	(AACH3)
FRANK	83B	PR D28 1790	J.S. Frank *et al.*	(LANL, YALE, LBL+)
HOFFMAN	83	PR D28 660	C.M. Hoffman *et al.*	(LANL, ARZS)
PRESKILL	83	PL 120B 127	J. Preskill, M.B. Wise, F. Wilczek	(HARV, UCSBT)
SIKIVIE	83	PRL 51 1415	P. Sikivie	(FLOR)
Also		PRL 52 695 (erratum)	P. Sikivie	(FLOR)
ALEKSEEV	82	JETP 55 591	E.A. Alekseeva *et al.*	(KIAE)
		Translated from ZETF 82 1007.		
ALEKSEEV	82B	JETPL 36 116	G.D. Alekseev *et al.*	(MOSU, JINR)
		Translated from ZETFP 36 94.		
ASANO	82	PL 113B 195	Y. Asano *et al.*	(KEK, TOKY, INUS, OSAK)
BARROSO	82	PL 116B 247	A. Barroso, G.C. Branco	(LISB)
DATAR	82	PL 114B 63	V.M. Datar *et al.*	(BHAB)
EDWARDS	82	PRL 48 903	C. Edwards *et al.*	(Crystal Ball Collab.)
FETSCHER	82	JP G8 L147	W. Fetscher	(ETH)
FUKUGITA	82	PRL 48 1522	M. Fukugita, S. Watamura, M. Yoshimura	(KEK)
FUKUGITA	82B	PR D26 1840	M. Fukugita, S. Watamura, M. Yoshimura	(KEK)
LEHMANN	82	PL 115B 270	P. Lehmann *et al.*	(SACL)
RAFFELT	82	PL 119B 323	G. Raffelt, L. Stodolsky	(MPIM)
ZEHNDER	82	PL 110B 419	A. Zehnder, K. Gabathuler, J.L. Vuilleumier	(ETH+)
ASANO	81B	PL 107B 159	Y. Asano *et al.*	(KEK, TOKY, INUS, OSAK)
BARROSO	81	PL 106B 91	A. Barroso, N.C. Mukhopadhyay	(SIN)
FAISSNER	81	ZPHY C10 95	H. Faissner *et al.*	(AACH3)
FAISSNER	81B	PL 103B 234	H. Faissner *et al.*	(AACH3)
KIM	81	PL 105B 55	B.R. Kim, C. Stamm	(AACH3)
VUILLEUMIER	81	PL 101B 341	J.L. Vuilleumier *et al.*	(CIT, MUNI)
ZEHNDER	81	PL 104B 494	A. Zehnder	(ETH)
FAISSNER	80	PL 96B 201	H. Faissner *et al.*	(AACH3)
JACQUES	80	PR D21 1206	P.F. Jacques *et al.*	(RUTG, STEV, COLU)
SOUKAS	80	PRL 44 564	A. Soukas *et al.*	(BNL, HARV, ORNL, PENN)
BECHIS	79	PRL 42 1511	D.J. Bechis *et al.*	(UMD, COLU, AFRR)
CALAPRICE	79	PR D20 2708	F.P. Calaprice *et al.*	(PRIN)
COTEUS	79	PRL 42 1438	P. Coteus *et al.*	(COLU, ILL, BNL)
DISHAW	79	PL 85B 142	J.P. Dishaw *et al.*	(SLAC, CIT)
ZHITNITSKII	79	SJNP 29 517	A.R. Zhitnitsky, Y.I. Skovpen	(NOVO)
		Translated from YAF 29 1001.		
ALIBRAN	78	PL 74B 134	P. Alibran *et al.*	(Gargamelle Collab.)
ASRATYAN	78B	PL 79B 497	A.E. Asratyan *et al.*	(ITEP, SERP)
BELLOTTI	78	PL 76B 223	E. Bellotti, E. Fiorini, L. Zanotti	(MILA)
BOSETTI	78B	PL 74B 143	P.C. Bosetti *et al.*	(BEBC Collab.)
DICUS	78C	PR D18 1829	D.A. Dicus *et al.*	(TEXA, VPI, STAN)
DONNELLY	78	PR D18 1607	T.W. Donnelly *et al.*	(STAN)
Also		PRL 37 315	F. Reines, H.S. Gurr, H.W. Sobel	(UCI)
Also		PRL 33 179	H.S. Gurr, F. Reines, H.W. Sobel	(UCI)
HANSL	78D	PL 74B 139	T. Hansl *et al.*	(CDHS Collab.)
MICELMAC...	78	LNC 21 441	G.V. Mitselmakher, B. Pontecorvo	(JINR)
MIKAELIAN	78	PR D18 3605	K.O. Mikaelian	(FNAL, NWES)
SATO	78	PTP 60 1942	K. Sato	(KYOT)
VYSOTSKII	78	JETPL 27 502	M.I. Vysotsky *et al.*	(ASCI)
		Translated from ZETFP 27 533.		
YANG	78	PRL 41 523	T.C. Yang	(MASA)
PECCEI	77	PR D16 1791	R.D. Peccei, H.R. Quinn	(STAN, SLAC)
Also		PRL 38 1440	R.D. Peccei, H.R. Quinn	(STAN, SLAC)
REINES	76	PRL 37 315	F. Reines, H.S. Gurr, H.W. Sobel	(UCI)
GURR	74	PRL 33 179	H.S. Gurr, F. Reines, H.W. Sobel	(UCI)
ANAND	53	PRSL A22 183	B.M. Anand	

OTHER RELATED PAPERS

SREDNICKI	85	NP B260 689	M. Srednicki	(UCSB)
BARDEEN	78	PL 74B 229	W.A. Bardeen, S.-H.H. Tye	(FNAL)

Downloaded from https://academic.oup.com/ptep/article/2022/8/083C01/6651666 by KIT Library user on 27 September 2022

Downloaded from https://academic.oup.com/ptep/article/2022/8/083C01/6651666 by KIT Library user on 27 September 2022

e 1239
μ 1240
τ 1245
Heavy Charged Lepton Searches 1272
Neutrino Properties 1273
Number of Neutrino Types 1282
Double-β Decay 1284
Neutrino Mixing 1288
Heavy Neutral Leptons, Searches for 1307

Notes in the Listings

Neutrino properties (rev.) 1273
Sum of neutrino masses (rev.) 1276
Number of light neutrino types from collider experiments 1282
Neutrinoless double-β decay 1284

Related Reviews in Volume 1

56. Muon anomalous magnetic moment (rev.) 796
57. Muon decay parameters (rev.) 800
58. τ branching fractions (rev.) 803
59. τ-lepton decay parameters (rev.) 806

Downloaded from https://academic.oup.com/ptep/article/2022/8/033C01/6651666 by KIT Library user on 27 September 2022

Downloaded from https://academic.oup.com/ptep/article/2022/8/083C01/6651666 by KIT Library user on 27 September 2022

LEPTONS

e

$J = \frac{1}{2}$

e MASS (atomic mass units u)

The primary determination of an electron's mass comes from measuring the ratio of the mass to that of a nucleus, so that the result is obtained in u (atomic mass units). The conversion factor to MeV is more uncertain than the mass of the electron in u; indeed, the recent improvements in the mass determination are not evident when the result is given in MeV. In this datablock we give the result in u, and in the following datablock in MeV.

VALUE (10^{-6} u)	DOCUMENT ID		TECN	COMMENT
548.579909065±0.000000016	TIESINGA	21	RVUE	2018 CODATA value
• • • We do not use the following data for averages, fits, limits, etc. • • •				
548.579909070±0.000000016	MOHR	16	RVUE	2014 CODATA value
548.57990946 ±0.00000022	MOHR	12	RVUE	2010 CODATA value
548.57990943 ±0.00000023	MOHR	08	RVUE	2006 CODATA value
548.57990945 ±0.00000024	MOHR	05	RVUE	2002 CODATA value
548.5799092 ±0.0000004	[1] BEIER	02	CNTR	Penning trap
548.5799110 ±0.0000012	MOHR	99	RVUE	1998 CODATA value
548.5799111 ±0.0000012	[2] FARNHAM	95	CNTR	Penning trap
548.579903 ±0.000013	COHEN	87	RVUE	1986 CODATA value

[1] BEIER 02 compares Larmor frequency of the electron bound in a $^{12}C^{5+}$ ion with the cyclotron frequency of a single trapped $^{12}C^{5+}$ ion.
[2] FARNHAM 95 compares cyclotron frequency of trapped electrons with that of a single trapped $^{12}C^{6+}$ ion.

e MASS

The mass is known more precisely in u (atomic mass units) than in MeV. The conversion is: 1 u = 931.494 102 42(28) MeV/c^2 (2018 CODATA value, TIESINGA 21). The conversion error dominates the uncertainty of the masses given below.

VALUE (MeV)	DOCUMENT ID		TECN	COMMENT
0.51099895000±0.00000000015	TIESINGA	21	RVUE	2018 CODATA value
• • • We do not use the following data for averages, fits, limits, etc. • • •				
0.5109989461 ±0.0000000031	MOHR	16	RVUE	2014 CODATA value
0.510998928 ±0.000000011	MOHR	12	RVUE	2010 CODATA value
0.510998910 ±0.000000013	MOHR	08	RVUE	2006 CODATA value
0.510998918 ±0.000000044	MOHR	05	RVUE	2002 CODATA value
0.510998901 ±0.000000020	[1,2] BEIER	02	CNTR	Penning trap
0.510998902 ±0.000000021	MOHR	99	RVUE	1998 CODATA value
0.510998903 ±0.000000020	[1,3] FARNHAM	95	CNTR	Penning trap
0.510998895 ±0.000000024	[1] COHEN	87	RVUE	1986 CODATA value
0.5110034 ±0.0000014	COHEN	73	RVUE	1973 CODATA value

[1] Converted to MeV using the 1998 CODATA value of the conversion constant, 931.494013 ± 0.000037 MeV/u.
[2] BEIER 02 compares Larmor frequency of the electron bound in a $^{12}C^{5+}$ ion with the cyclotron frequency of a single trapped $^{12}C^{5+}$ ion.
[3] FARNHAM 95 compares cyclotron frequency of trapped electrons with that of a single trapped $^{12}C^{6+}$ ion.

$(m_{e^+} - m_{e^-}) / m_{average}$

A test of *CPT* invariance.

VALUE	CL%	DOCUMENT ID		TECN	COMMENT
$<8 \times 10^{-9}$	90	[1] FEE	93	CNTR	Positronium spectroscopy
• • • We do not use the following data for averages, fits, limits, etc. • • •					
$<4 \times 10^{-23}$	90	[2] DOLGOV	14		From photon mass limit
$<4 \times 10^{-8}$	90	CHU	84	CNTR	Positronium spectroscopy

[1] FEE 93 value is obtained under the assumption that the positronium Rydberg constant is exactly half the hydrogen one.
[2] DOLGOV 14 result is obtained under the assumption that any mass difference between electron and positron would lead to a non-zero photon mass. The PDG 12 limit of 1×10^{-18} eV on the photon mass is in turn used to derive the value quoted here.

$|q_{e^+} + q_{e^-}|/e$

A test of *CPT* invariance. See also similar tests involving the proton.

VALUE	DOCUMENT ID		TECN	COMMENT
$<4 \times 10^{-8}$	[1] HUGHES	92	RVUE	
• • • We do not use the following data for averages, fits, limits, etc. • • •				
$<2 \times 10^{-18}$	[2] SCHAEFER	95	THEO	Vacuum polarization
$<1 \times 10^{-18}$	[3] MUELLER	92	THEO	Vacuum polarization

[1] HUGHES 92 uses recent measurements of Rydberg-energy and cyclotron-frequency ratios.
[2] SCHAEFER 95 removes model dependency of MUELLER 92.
[3] MUELLER 92 argues that an inequality of the charge magnitudes would, through higher-order vacuum polarization, contribute to the net charge of atoms.

e MAGNETIC MOMENT ANOMALY

$\mu_e/\mu_B - 1 = (g-2)/2$

VALUE (units 10^{-6})	DOCUMENT ID		TECN	CHG	COMMENT
1159.65218076±0.00000028 OUR AVERAGE					
1159.65218073±0.00000028	HANNEKE	08	MRS		Single electron
1159.6521884 ±0.0000043	VANDYCK	87	MRS	−	Single electron
• • • We do not use the following data for averages, fits, limits, etc. • • •					
1159.65218128±0.00000018	TIESINGA	21	RVUE		2018 CODATA value
1159.65218091±0.00000026	MOHR	16	RVUE		2014 CODATA value
1159.65218076±0.00000027	MOHR	12	RVUE		2010 CODATA value
1159.65218111±0.00000074	[1] MOHR	08	RVUE		2006 CODATA value
1159.65218085±0.00000076	[2] ODOM	06	MRS	−	Single electron
1159.6521859 ±0.0000038	MOHR	05	RVUE		2002 CODATA value
1159.6521869 ±0.0000041	MOHR	99	RVUE		1998 CODATA value
1159.652193 ±0.000010	COHEN	87	RVUE		1986 CODATA value
1159.6521879 ±0.0000043	[3] VANDYCK	87	MRS	+	Single positron

[1] MOHR 08 average is dominated by ODOM 06.
[2] Superseded by HANNEKE 08 per private communication with Gerald Gabrielse.
[3] This VANDYCK 87 reault is for a positron. We do not take it into account for the average to avoid the assumption of CPT invariance.

$(g_{e^+} - g_{e^-}) / g_{average}$

A test of *CPT* invariance.

VALUE (units 10^{-12})	CL%	DOCUMENT ID		TECN	COMMENT
− 0.5± 2.1		[1] VANDYCK	87	MRS	Penning trap
• • • We do not use the following data for averages, fits, limits, etc. • • •					
< 12	95	[2] VASSERMAN	87	CNTR	Assumes $m_{e^+} = m_{e^-}$
22 ±64		SCHWINBERG	81	MRS	Penning trap

[1] VANDYCK 87 measured $(g_-/g_+)-1$ and we converted it.
[2] VASSERMAN 87 measured $(g_+ - g_-)/(g-2)$. We multiplied by $(g-2)/g = 1.2 \times 10^{-3}$.

e ELECTRIC DIPOLE MOMENT (d)

A nonzero value is forbidden by both *T* invariance and *P* invariance.

VALUE (10^{-28} ecm)	CL%	DOCUMENT ID		TECN	COMMENT
< 0.11	90	[1] ANDREEV	18	CNTR	ThO molecules
• • • We do not use the following data for averages, fits, limits, etc. • • •					
< 1.3	90	[2] CAIRNCROSS	17	ESR	$^{180}Hf^{19}F$ molecules
− 5570 ± 7980 ±120		KIM	15	CNTR	$Gd_3Ga_5O_{12}$ molecules
< 0.87	90	[3] BARON	14	CNTR	ThO molecules
< 6050	90	[4] ECKEL	12	CNTR	$Eu_{0.5}Ba_{0.5}TiO_3$ molecules
< 10.5	90	[5] HUDSON	11	NMR	YbF molecules
6.9 ± 7.4		REGAN	02	MRS	^{205}Tl beams
18 ± 12 ± 10		[6] COMMINS	94	MRS	^{205}Tl beams
− 27 ± 83		[6] ABDULLAH	90	MRS	^{205}Tl beams
− 1400 ± 2400		CHO	89	NMR	TlF molecules
− 150 ± 550 ±150		MURTHY	89		Cs, no *B* field
− 5000 ±11000		LAMOREAUX	87	NMR	^{199}Hg
19000 ±34000	90	SANDARS	75	MRS	Thallium
7000 ±22000	90	PLAYER	70	MRS	Xenon
< 30000	90	WEISSKOPF	68	MRS	Cesium

[1] ANDREEV 18 gives a measurement corresponding to this limit as $(4.3 \pm 3.1 \pm 2.6) \times 10^{-30}$ ecm.
[2] CAIRNCROSS 17 gives a measurement corresponding to this limit as $(0.09 \pm 0.77 \pm 0.17) \times 10^{-28}$ ecm.
[3] BARON 14 gives a measurement corresponding to this limit as $(-0.21 \pm 0.37 \pm 0.25) \times 10^{-28}$ ecm.
[4] ECKEL 12 gives a measurement corresponding to this limit as $(-1.07 \pm 3.06 \pm 1.74) \times 10^{-25}$ ecm.
[5] HUDSON 11 gives a measurement corresponding to this limit as $(-2.4 \pm 5.7 \pm 1.5) \times 10^{-28}$ ecm.
[6] ABDULLAH 90, COMMINS 94, and REGAN 02 use the relativistic enhancement of a valence electron's electric dipole moment in a high-Z atom.

e^- MEAN LIFE / BRANCHING FRACTION

A test of charge conservation. See the "Note on Testing Charge Conservation and the Pauli Exclusion Principle" following this section in our 1992 edition (Physical Review **D45** S1 (1992), p. VI.10).

Most of these experiments are one of three kinds: Attempts to observe (a) the 255.5 keV gamma ray produced in $e^- \rightarrow \nu_e \gamma$, (b) the (K) shell x ray produced when an electron decays without additional energy deposit,

Downloaded from https://academic.oup.com/ptep/article/2022/8/083C01/6651666 by KIT Library user on 27 September 2022

e.g., $e^- \to \nu_e \overline{\nu}_e \nu_e$ ("disappearance" experiments), and (c) nuclear de-excitation gamma rays after the electron disappears from an atomic shell and the nucleus is left in an excited state. The last can include both weak boson and photon mediating processes. We use the best $e^- \to \nu_e \gamma$ limit for the Summary Tables.

Note that we use the mean life rather than the half life, which is often reported.

$e \to \nu_e \gamma$ and astrophysical limits

VALUE (yr)	CL%	DOCUMENT ID		TECN	COMMENT
$>6.6 \times 10^{28}$	90	AGOSTINI	15B	BORX	$e^- \to \nu\gamma$
• • • We do not use the following data for averages, fits, limits, etc. • • •					
$>1.2 \times 10^{24}$	90	ABGRALL	17	HPGE	electron decay to invisible
$>1.22 \times 10^{26}$	68	[1] KLAPDOR-K...	07	CNTR	$e^- \to \nu\gamma$
$>4.6 \times 10^{26}$	90	BACK	02	BORX	$e^- \to \nu\gamma$
$>3.4 \times 10^{26}$	68	BELLI	00B	DAMA	$e^- \to \nu\gamma$, liquid Xe
$>3.7 \times 10^{25}$	68	AHARONOV	95B	CNTR	$e^- \to \nu\gamma$
$>2.35 \times 10^{25}$	68	BALYSH	93	CNTR	$e^- \to \nu\gamma$, ^{76}Ge detector
$>1.5 \times 10^{25}$	68	AVIGNONE	86	CNTR	$e^- \to \nu\gamma$
$>1 \times 10^{39}$		[2] ORITO	85	ASTR	Astrophysical argument
$>3 \times 10^{23}$	68	BELLOTTI	83B	CNTR	$e^- \to \nu\gamma$

[1] The authors of A. Derbin et al, arXiv:0704.2047v1 argue that this limit is overestimated by at least a factor of 5.
[2] ORITO 85 assumes that electromagnetic forces extend out to large enough distances and that the age of our galaxy is 10^{10} years.

Disappearance and nuclear-de-excitation experiments

VALUE (yr)	CL%	DOCUMENT ID		TECN	COMMENT
$>6.4 \times 10^{24}$	68	[1] BELLI	99B	DAMA	De-excitation of ^{129}Xe
• • • We do not use the following data for averages, fits, limits, etc. • • •					
$>4.2 \times 10^{24}$	68	BELLI	99	DAMA	Iodine L-shell disappearance
$>2.4 \times 10^{23}$	90	[2] BELLI	99D	DAMA	De-excitation of ^{127}I (in NaI)
$>4.3 \times 10^{23}$	68	AHARONOV	95B	CNTR	Ge K-shell disappearance
$>2.7 \times 10^{23}$	68	REUSSER	91	CNTR	Ge K-shell disappearance
$>2 \times 10^{22}$	68	BELLOTTI	83B	CNTR	Ge K-shell disappearance

[1] BELLI 99B limit on charge nonconserving e^- capture involving excitation of the 236.1 keV nuclear state of ^{129}Xe; the 90% CL limit is 3.7×10^{24} yr. Less stringent limits for other states are also given.
[2] BELLI 99D limit on charge nonconserving e^- capture involving excitation of the 57.6 keV nuclear state of ^{127}I. Less stringent limits for the other states and for the state of ^{23}Na are also given.

LIMITS ON LEPTON-FLAVOR VIOLATION IN PRODUCTION

Forbidden by lepton family number conservation.

This section was added for the 2008 edition of this *Review* and is not complete. For a list of further measurements see references in the papers listed below.

$\sigma(e^+e^- \to e^\pm\tau^\mp) / \sigma(e^+e^- \to \mu^+\mu^-)$

VALUE	CL%	DOCUMENT ID		TECN	COMMENT
$<8.9 \times 10^{-6}$	95	AUBERT	07P	BABR	e^+e^- at $E_{cm} = 10.58$ GeV
• • • We do not use the following data for averages, fits, limits, etc. • • •					
$<1.8 \times 10^{-3}$	95	GOMEZ-CAD...	91	MRK2	e^+e^- at $E_{cm} = 29$ GeV

$\sigma(e^+e^- \to \mu^\pm\tau^\mp) / \sigma(e^+e^- \to \mu^+\mu^-)$

VALUE	CL%	DOCUMENT ID		TECN	COMMENT
$<4.0 \times 10^{-6}$	95	AUBERT	07P	BABR	e^+e^- at $E_{cm} = 10.58$ GeV
• • • We do not use the following data for averages, fits, limits, etc. • • •					
$<6.1 \times 10^{-3}$	95	GOMEZ-CAD...	91	MRK2	e^+e^- at $E_{cm} = 29$ GeV

e REFERENCES

TIESINGA	21	RMP 93 025010	E. Tiesinga *et al.*	(NIST)
ANDREEV	18	NAT 562 355	V. Andreev *et al.*	(ACME Collab.)
ABGRALL	17	PRL 118 161801	N. Abgrall *et al.*	(MAJORANA Collab.)
CAIRNCROSS	17	PRL 119 153001	W.B. Cairncross *et al.*	(NIST,COLO)
MOHR	16	RMP 88 035009	P.J. Mohr, D.B. Newell, B.N. Taylor	(NIST)
AGOSTINI	15B	PRL 115 231802	M. Agostini *et al.*	(Borexino Collab.)
KIM	15	PR D91 102004	Y.J. Kim *et al.*	(IND, YALE, LANL)
BARON	14	SCIENCE 343 269	J. Baron *et al.*	(ACME Collab.)
DOLGOV	14	PL B732 244	A.D. Dolgov, V.A. Novikov	
ECKEL	12	PRL 109 193003	S. Eckel, A.O. Sushkov, S.K. Lamoreaux	(YALE)
MOHR	12	RMP 84 1527	P.J. Mohr, B.N. Taylor, D.B. Newell	(NIST)
PDG	12	PR D86 010001	J. Beringer *et al.*	(PDG Collab.)
HUDSON	11	NAT 473 493	J.J. Hudson *et al.*	(LOIC)
HANNEKE	08	PRL 100 120801	D. Hanneke, S. Fogwell, G. Gabrielse	(HARV)
MOHR	08	RMP 80 633	P.J. Mohr, B.N. Taylor, D.B. Newell	(NIST)
AUBERT	07P	PR D75 031103	B. Aubert *et al.*	(BABAR Collab.)
KLAPDOR-K...	07	PL B644 109	H.V. Klapdor-Kleingrothaus, I.V. Krivosheina, I.V. Titkova	
ODOM	06	PRL 97 030801	B. Odom *et al.*	(HARV)
MOHR	05	RMP 77 1	P.J. Mohr, B.N. Taylor	(NIST)
BACK	02	PL B525 29	H.O. Back *et al.*	(Borexino/SASSO Collab.)
BEIER	02	PRL 88 011603	T. Beier *et al.*	
REGAN	02	PRL 88 071805	B.C. Regan *et al.*	
BELLI	00B	PR D61 117301	P. Belli *et al.*	(DAMA Collab.)
BELLI	99	PL B460 236	P. Belli *et al.*	(DAMA Collab.)
BELLI	99B	PL B465 315	P. Belli *et al.*	(DAMA Collab.)
BELLI	99D	PR C60 065501	P. Belli *et al.*	(DAMA Collab.)
MOHR	99	JPCRD 28 1713	P.J. Mohr, B.N. Taylor	(NIST)
Also		RMP 72 351	P.J. Mohr, B.N. Taylor	(NIST)
AHARONOV	95B	PR D52 3785	Y. Aharonov *et al.*	(SCUC, PNL, ZARA+)
Also		PL B353 168	Y. Aharonov *et al.*	(SCUC, PNL, ZARA+)
FARNHAM	95	PRL 75 3598	D.L. Farnham, R.S. van Dyck, P.B. Schwinberg	(WASH)
SCHAEFER	95	PR A51 838	A. Schaefer, J. Reinhardt	(FRAN)
COMMINS	94	PR A50 2960	E.D. Commins *et al.*	
BALYSH	93	PL B298 278	A. Balysh *et al.*	(KIAE, MPIK, SASSO)
FEE	93	PR A48 192	M.S. Fee *et al.*	
HUGHES	92	PRL 69 578	R.J. Hughes, B.I. Deutch	(LANL, AARH)
MUELLER	92	PRL 69 3432	B. Muller, M.H. Thoma	(DUKE)
PDG	92	PR D45 S1	K. Hikasa *et al.*	(KEK, LBL, BOST+)
GOMEZ-CAD...	91	PRL 66 1007	J.J. Gomez-Cadenas *et al.*	(SLAC MARK-2 Collab.)
REUSSER	91	PL B255 143	D. Reusser *et al.*	(NEUC, CIT, PSI)
ABDULLAH	90	PRL 65 2347	K. Abdullah *et al.*	(LBL, UCB)
CHO	89	PRL 63 2559	D. Cho, K. Sangster, E.A. Hinds	(YALE)
MURTHY	89	PRL 63 965	S.A. Murthy *et al.*	(AMHT)
COHEN	87	RMP 59 1121	E.R. Cohen, B.N. Taylor	(RISC, NBS)
LAMOREAUX	87	PRL 59 2275	S.K. Lamoreaux *et al.*	(WASH)
VANDYCK	87	PRL 59 26	R.S. van Dyck, P.B. Schwinberg, H.G. Dehmelt	(WASH)
VASSERMAN	87	PL B198 302	I.B. Vasserman *et al.*	(NOVO)
Also		PL B187 172	I.B. Vasserman *et al.*	(NOVO)
AVIGNONE	86	PR D34 97	F.T. Avignone *et al.*	(PNL, SCUC)
ORITO	85	PRL 54 2457	S. Orito, M. Yoshimura	(TOKY, KEK)
CHU	84	PRL 52 1689	S. Chu, A.P. Mills, J.L. Hall	(BELL, NBS, COLO)
BELLOTTI	83B	PL 124B 435	E. Bellotti *et al.*	(MILA)
SCHWINBERG	81	PRL 47 1679	P.B. Schwinberg, R.S. van Dyck, H.G. Dehmelt	(WASH)
SANDARS	75	PR A11 473	P.G.H. Sandars, D.M. Sternheimer	(OXF, BNL)
COHEN	73	JPCRD 2 664	E.R. Cohen, B.N. Taylor	(RISC, NBS)
PLAYER	70	JP B3 1620	M.A. Player, P.G.H. Sandars	(OXF)
WEISSKOPF	68	PRL 21 1645	M.C. Weisskopf *et al.*	(BRAN)

μ

$J = \frac{1}{2}$

μ MASS (atomic mass units u)

The muon's mass is obtained from the muon-electron mass ratio as determined from the measurement of Zeeman transition frequencies in muonium (μ^+e^- atom). Since the electron's mass is most accurately known in u, the muon's mass is also most accurately known in u. The conversion factor to MeV has approximately the same relative uncertainty as the mass of the muon in u. In this datablock we give the result in u, and in the following datablock in MeV.

VALUE (u)	DOCUMENT ID		TECN	COMMENT
0.1134289259 ± 0.0000000025	TIESINGA	21	RVUE	2018 CODATA value
• • • We do not use the following data for averages, fits, limits, etc. • • •				
0.1134289257 ± 0.0000000025	MOHR	16	RVUE	2014 CODATA value
0.1134289267 ± 0.0000000029	MOHR	12	RVUE	2010 CODATA value
0.1134289256 ± 0.0000000029	MOHR	08	RVUE	2006 CODATA value
0.1134289264 ± 0.0000000030	MOHR	05	RVUE	2002 CODATA value
0.1134289168 ± 0.0000000034	[1] MOHR	99	RVUE	1998 CODATA value
0.113428913 ± 0.000000017	[2] COHEN	87	RVUE	1986 CODATA value

[1] MOHR 99 make use of other 1998 CODATA entries below.
[2] COHEN 87 make use of other 1986 CODATA entries below.

μ MASS

The mass is known more precisely in u (atomic mass units) than in MeV. The conversion is: 1 u = 931.494 102 42(28) MeV/c^2 (2018 CODATA value, TIESINGA 21). The conversion error contributes significantly to the uncertainty of the masses given below.

VALUE (MeV)	DOCUMENT ID		TECN	CHG	COMMENT
105.6583755 ± 0.0000023	TIESINGA	21	RVUE		2018 CODATA value
• • • We do not use the following data for averages, fits, limits, etc. • • •					
105.6583745 ± 0.0000024	MOHR	16	RVUE		2014 CODATA value
105.6583715 ± 0.0000035	MOHR	12	RVUE		2010 CODATA value
105.6583668 ± 0.0000038	MOHR	08	RVUE		2006 CODATA value
105.6583692 ± 0.0000094	MOHR	05	RVUE		2002 CODATA value
105.6583568 ± 0.0000052	MOHR	99	RVUE		1998 CODATA value
105.658353 ± 0.000016	[1] COHEN	87	RVUE		1986 CODATA value
105.658386 ± 0.000044	[2] MARIAM	82	CNTR	+	
105.65836 ± 0.00026	[3] CROWE	72	CNTR		
105.65865 ± 0.00044	[4] CRANE	71	CNTR		

[1] Converted to MeV using the 1998 CODATA value of the conversion constant, 931.494013 ± 0.000037 MeV/u.
[2] MARIAM 82 give $m_\mu/m_e = 206.768259(62)$.
[3] CROWE 72 give $m_\mu/m_e = 206.7682(5)$.
[4] CRANE 71 give $m_\mu/m_e = 206.76878(85)$.

μ MEAN LIFE τ

Measurements with an error > 0.001×10^{-6} s have been omitted.

VALUE (10^{-6} s)	DOCUMENT ID		TECN	CHG	COMMENT
2.1969811 ± 0.0000022 OUR AVERAGE					
2.1969803 ± 0.0000021 ± 0.0000007	[1] TISHCHENKO	13	CNTR	+	Surface μ^+ at PSI
2.197083 ± 0.000032 ± 0.000015	BARCZYK	08	CNTR	+	Muons from π^+ decay at rest
2.197013 ± 0.000021 ± 0.000011	CHITWOOD	07	CNTR	+	Surface μ^+ at PSI
2.197078 ± 0.000073	BARDIN	84	CNTR	+	

Downloaded from https://academic.oup.com/ptep/article/2022/8/083C01/6651666 by KIT Library user on 27 September 2022

2.197025	±0.000155	BARDIN	84	CNTR	−
2.19695	±0.00006	GIOVANETTI	84	CNTR	+
2.19711	±0.00008	BALANDIN	74	CNTR	+
2.1973	±0.0003	DUCLOS	73	CNTR	+
• • • We do not use the following data for averages, fits, limits, etc. • • •					
2.1969803	±0.0000022	WEBBER	11	CNTR	+ Surface μ^+ at PSI

[1] TISHCHENKO 13 uses 1.6×10^{12} μ^+ events and supersedes WEBBER 11.

$\tau_{\mu^+}/\tau_{\mu^-}$ MEAN LIFE RATIO

A test of *CPT* invariance.

VALUE	DOCUMENT ID		TECN	COMMENT
1.000024±0.000078	BARDIN	84	CNTR	
• • • We do not use the following data for averages, fits, limits, etc. • • •				
1.0008 ±0.0010	BAILEY	79	CNTR	Storage ring
1.000 ±0.001	MEYER	63	CNTR	Mean life μ^+ / μ^-

$(\tau_{\mu^+} - \tau_{\mu^-}) / \tau_{\text{average}}$

A test of *CPT* invariance. Calculated from the mean-life ratio, above.

VALUE	DOCUMENT ID
(2±8) × 10^{-5} OUR EVALUATION	

μ/p MAGNETIC MOMENT RATIO

This ratio is used to obtain a precise value of the muon mass and to reduce experimental muon Larmor frequency measurements to the muon magnetic moment anomaly. Measurements with an error > 0.00001 have been omitted. By convention, the minus sign on this ratio is omitted. CODATA values were fitted using their selection of data, plus other data from multiparameter fits.

VALUE	DOCUMENT ID		TECN	CHG	COMMENT
3.183345142±0.000000071	TIESINGA	21	RVUE		2018 CODATA value
• • • We do not use the following data for averages, fits, limits, etc. • • •					
3.183345142±0.000000071	MOHR	16	RVUE		2014 CODATA value
3.183345107±0.000000084	MOHR	12	RVUE		2010 CODATA value
3.183345137±0.000000085	MOHR	08	RVUE		2006 CODATA value
3.183345118±0.000000089	MOHR	05	RVUE		2002 CODATA value
3.18334513 ±0.00000039	LIU	99	CNTR	+	HFS in muonium
3.18334539 ±0.00000010	MOHR	99	RVUE		1998 CODATA value
3.18334547 ±0.00000047	COHEN	87	RVUE		1986 CODATA value
3.1833441 ±0.0000017	KLEMPT	82	CNTR	+	Precession strob
3.1833461 ±0.0000011	MARIAM	82	CNTR	+	HFS splitting
3.1833448 ±0.0000029	CAMANI	78	CNTR	+	See KLEMPT 82
3.1833403 ±0.0000044	CASPERSON	77	CNTR	+	HFS splitting
3.1833402 ±0.0000072	COHEN	73	RVUE		1973 CODATA value
3.1833467 ±0.0000082	CROWE	72	CNTR	+	Precession phase

See the related review(s):
Muon Anomalous Magnetic Moment

μ MAGNETIC MOMENT ANOMALY

The parity-violating decay of muons in a storage ring is observed. The difference frequency ω_a between the muon spin precision and the orbital angular frequency $(e/m_\mu c)\langle B\rangle$ is measured, as is the free proton NMR frequency ω_p, thus determining the ratio $R=\omega_a/\omega_p$. Given the magnetic moment ratio $\lambda=\mu_\mu/\mu_p$ (from hyperfine structure in muonium), $(g-2)/2 = R/(\lambda-R)$.

$\mu_\mu/(e\hbar/2m_\mu)-1 = (g_\mu-2)/2$

VALUE (units 10^{-10})	DOCUMENT ID		TECN	CHG	COMMENT
11659206.1± 4.1	[1] ABI	21	MUG2	±	Combined FNAL and BNL values
• • • We do not use the following data for averages, fits, limits, etc. • • •					
11659204.0± 5.4	ABI	21	MUG2	+	Storage ring
11659208.0± 5.4±3.3	BENNETT	06	MUG2	±	Average μ^+ and μ^-
11659208 ± 6	BENNETT	04	MUG2	±	Average μ^+ and μ^-
11659214 ± 8 ±3	BENNETT	04	MUG2	−	Storage ring
11659203 ± 6 ±5	BENNETT	04	MUG2	+	Storage ring
11659204 ± 7 ±5	BENNETT	02	MUG2	+	Storage ring
11659202 ± 14 ±6	BROWN	01	MUG2	+	Storage ring
11659191 ± 59	BROWN	00	MUG2	+	
11659100 ± 110	[2] BAILEY	79	CNTR	+	Storage ring
11659360 ± 120	[2] BAILEY	79	CNTR	−	Storage ring
11659230 ± 85	[2] BAILEY	79	CNTR	±	Storage ring
11620000 ±5000	CHARPAK	62	CNTR	+	

[1] ABI 21 combined their value with the previous independent BNL measurement of BENNETT 06. ABI 21 also report that the difference of this combination with the standard model value of (11659181.0 ± 4.3) × 10^{-10} (AOYAMA 20) has a significance of 4.2 σ.
[2] BAILEY 79 values recalculated by HUGHES 99 using the COHEN 87 μ/p magnetic moment. The improved MOHR 99 value does not change the result.

$(g_{\mu^+} - g_{\mu^-}) / g_{\text{average}}$

A test of *CPT* invariance.

VALUE (units 10^{-8})	DOCUMENT ID		TECN
−0.11±0.12	BENNETT	04	MUG2
• • • We do not use the following data for averages, fits, limits, etc. • • •			
−2.6 ±1.6	BAILEY	79	CNTR

μ ELECTRIC DIPOLE MOMENT (d)

A nonzero value is forbidden by both *T* invariance and *P* invariance.

VALUE (10^{-19} ecm)	CL%	DOCUMENT ID		TECN	CHG	COMMENT
< 1.8	95	[1] BENNETT	09	MUG2	±	Storage ring
• • • We do not use the following data for averages, fits, limits, etc. • • •						
−0.1±1.0		[2] BENNETT	09	MUG2	+	Storage ring
−0.1±0.7		[3] BENNETT	09	MUG2	−	Storage ring
−3.7±3.4		[4] BAILEY	78	CNTR	±	Storage ring
8.6±4.5		BAILEY	78	CNTR	+	Storage ring
0.8±4.3		BAILEY	78	CNTR	−	Storage ring

[1] This is the combination of the two BENNETT 09 measurements quoted here separately for μ^+ and μ^-. The result is also presented as a measurement of $(0.0 \pm 0.9) \times 10^{-19}$ *e* cm.
[2] Also reported as the limit of $|d(\mu^+)| < 2.1 \times 10^{-19}$ *e* cm at 95% CL.
[3] Also reported as the limit of $|d(\mu^-)| < 1.5 \times 10^{-19}$ *e* cm at 95% CL.
[4] This is the combination of the two BAILEY 78 results quoted here separately for μ^+ and μ^-. BAILEY 78 uses the convention $d = 1/2 \cdot (d_{\mu^+} - d_{\mu^-})$ and reports 3.7 ± 3.4. We convert their result to use the same convention as BENNETT 09.

MUON-ELECTRON CHARGE RATIO ANOMALY $q_{\mu^+}/q_{e^-} + 1$

VALUE	DOCUMENT ID		TECN	CHG	COMMENT
(1.1±2.1) × 10^{-9}	[1] MEYER	00	CNTR	+	1s–2s muonium interval

[1] MEYER 00 measure the 1s–2s muonium interval, and then interpret the result in terms of muon-electron charge ratio q_{μ^+}/q_{e^-}.

μ^- DECAY MODES

μ^+ modes are charge conjugates of the modes below.

	Mode		Fraction (Γ_i/Γ)	Confidence level
Γ_1	$e^- \overline{\nu}_e \nu_\mu$		≈ 100%	
Γ_2	$e^- \overline{\nu}_e \nu_\mu \gamma$		[a] $(6.0\pm0.5) \times 10^{-8}$	
Γ_3	$e^- \overline{\nu}_e \nu_\mu e^+ e^-$		[b] $(3.4\pm0.4) \times 10^{-5}$	
	Lepton Family number (*LF*) violating modes			
Γ_4	$e^- \nu_e \overline{\nu}_\mu$	*LF*	[c] < 1.2 %	90%
Γ_5	$e^- \gamma$	*LF*	< 4.2 $\times 10^{-13}$	90%
Γ_6	$e^- e^+ e^-$	*LF*	< 1.0 $\times 10^{-12}$	90%
Γ_7	$e^- 2\gamma$	*LF*	< 7.2 $\times 10^{-11}$	90%

[a] This only includes events with energy of $e > 45$ MeV and energy of $\gamma > 40$ MeV. Since the $e^- \overline{\nu}_e \nu_\mu$ and $e^- \overline{\nu}_e \nu_\mu \gamma$ modes cannot be clearly separated, we regard the latter mode as a subset of the former.
[b] See the Particle Listings below for the energy limits used in this measurement.
[c] A test of additive vs. multiplicative lepton family number conservation.

μ^- BRANCHING RATIOS

$\Gamma(e^- \overline{\nu}_e \nu_\mu \gamma)/\Gamma_{\text{total}}$ — Γ_2/Γ

VALUE	EVTS	DOCUMENT ID		TECN	COMMENT
(6.03±0.14±0.53) × 10^{-8}	13k	[1] BALDINI	16A	SPEC	γ KE > 40 MeV
• • • We do not use the following data for averages, fits, limits, etc. • • •					
	862	BOGART	67	CNTR	γ KE > 14.5 MeV
(3.3 ±1.3) × 10^{-3}		CRITTENDEN	61	CNTR	γ KE > 20 MeV
(1.4 ±0.4) × 10^{-2}		CRITTENDEN	61	CNTR	γ KE > 10 MeV
	27	ASHKIN	59	CNTR	

[1] BALDINI 16 measurement refers to $\mu^+ \to e^+ \nu\overline{\nu}\gamma$ decay and requires energy of $e^+ >$ 45 MeV and energy $\gamma > 40$ MeV.

$\Gamma(e^- \overline{\nu}_e \nu_\mu e^+ e^-)/\Gamma_{\text{total}}$ — Γ_3/Γ

VALUE (units 10^{-5})	EVTS	DOCUMENT ID		TECN	CHG	COMMENT
3.4±0.2±0.3	7443	[1] BERTL	85	SPEC	+	SINDRUM
• • • We do not use the following data for averages, fits, limits, etc. • • •						
2.2±1.5	7	[2] CRITTENDEN	61	HLBC	+	E(e^+e^-) > 10 MeV
2	1	[3] GUREVICH	60	EMUL	+	

Downloaded from https://academic.oup.com/ptep/article/2022/8/083C01/6651666 by KIT Library user on 27 September 2022

1.5 ± 1.0	3	[4] LEE	59	HBC	+	

[1] BERTL 85 has transverse momentum cut $p_T > 17$ MeV/c. Systematic error was increased by us.
[2] CRITTENDEN 61 count only those decays where total energy of either (e^+, e^-) combination is >10 MeV.
[3] GUREVICH 60 interpret their event as either virtual or real photon conversion. e^+ and e^- energies not measured.
[4] In the three LEE 59 events, the sum of energies $E(e^+) + E(e^-) + E(e^+)$ was 51 MeV, 55 MeV, and 33 MeV.

$\Gamma(e^- \nu_e \overline{\nu}_\mu)/\Gamma_{total}$ — Γ_4/Γ

Forbidden by the additive conservation law for lepton family number. A multiplicative law predicts this branching ratio to be 1/2. For a review see NEMETHY 81.

VALUE	CL%	DOCUMENT ID		TECN	CHG	COMMENT
< 0.012	90	[1] FREEDMAN	93	CNTR	+	ν oscillation search
• • • We do not use the following data for averages, fits, limits, etc. • • •						
< 0.018	90	KRAKAUER	91B	CALO	+	
< 0.05	90	[2] BERGSMA	83	CALO		$\overline{\nu}_\mu e \rightarrow \mu^- \overline{\nu}_e$
< 0.09	90	JONKER	80	CALO		See BERGSMA 83
-0.001 ± 0.061		WILLIS	80	CNTR	+	
0.13 ± 0.15		BLIETSCHAU	78	HLBC	±	Avg. of 4 values
< 0.25	90	EICHTEN	73	HLBC	+	

[1] FREEDMAN 93 limit on $\overline{\nu}_e$ observation is here interpreted as a limit on lepton family number violation.
[2] BERGSMA 83 gives a limit on the inverse muon decay cross-section ratio $\sigma(\overline{\nu}_\mu e^- \rightarrow \mu^- \overline{\nu}_e)/\sigma(\nu_\mu e^- \rightarrow \mu^- \nu_e)$, which is essentially equivalent to $\Gamma(e^- \nu_e \overline{\nu}_\mu)/\Gamma_{total}$ for small values like that quoted.

$\Gamma(e^- \gamma)/\Gamma_{total}$ — Γ_5/Γ

Forbidden by lepton family number conservation.

VALUE (units 10^{-11})	CL%	DOCUMENT ID		TECN	CHG	COMMENT
< 0.042	90	BALDINI	16	SPEC	+	MEG at PSI
• • • We do not use the following data for averages, fits, limits, etc. • • •						
< 0.057	90	ADAM	13B	SPEC	+	MEG at PSI
< 0.24	90	ADAM	11	SPEC	+	MEG at PSI
< 2.8	90	ADAM	10	SPEC	+	MEG at PSI
< 1.2	90	AHMED	02	SPEC	+	MEGA
< 1.2	90	BROOKS	99	SPEC	+	LAMPF
< 4.9	90	BOLTON	88	CBOX	+	LAMPF
<100	90	AZUELOS	83	CNTR	+	TRIUMF
< 17	90	KINNISON	82	SPEC	+	LAMPF
<100	90	SCHAAF	80	ELEC	+	SIN

$\Gamma(e^- e^+ e^-)/\Gamma_{total}$ — Γ_6/Γ

Forbidden by lepton family number conservation.

VALUE (units 10^{-12})	CL%	DOCUMENT ID		TECN	CHG	COMMENT
< 1.0	90	[1] BELLGARDT	88	SPEC	+	SINDRUM
• • • We do not use the following data for averages, fits, limits, etc. • • •						
< 36	90	BARANOV	91	SPEC	+	ARES
< 35	90	BOLTON	88	CBOX	+	LAMPF
< 2.4	90	[1] BERTL	85	SPEC	+	SINDRUM
<160	90	[1] BERTL	84	SPEC	+	SINDRUM
<130	90	[1] BOLTON	84	CNTR		LAMPF

[1] These experiments assume a constant matrix element.

$\Gamma(e^- 2\gamma)/\Gamma_{total}$ — Γ_7/Γ

Forbidden by lepton family number conservation.

VALUE (units 10^{-11})	CL%	DOCUMENT ID		TECN	CHG	COMMENT
< 7.2	90	BOLTON	88	CBOX	+	LAMPF
• • • We do not use the following data for averages, fits, limits, etc. • • •						
< 1	90	[1] BALDINI	20	MEG		PSI
< 840	90	[2] AZUELOS	83	CNTR	+	TRIUMF
<5000	90	[3] BOWMAN	78	CNTR		DEPOMMIER 77 data

[1] BALDINI 20 uses 7.5×10^{14} stopped muons to obtain limits on $\mu \rightarrow eX$ decay mediated by a new light particle X with lifetimes < 40 ps, which decays to $\gamma\gamma$ for X-mass ranges 20–45 MeV. The limit of the order < 10^{-11} at 90% CL is for the mass range 20–30 MeV.
[2] AZUELOS 83 uses the phase space distribution of BOWMAN 78.
[3] BOWMAN 78 assumes an interaction Lagrangian local on the scale of the inverse μ mass.

LIMIT ON $\mu^- \rightarrow e^-$ CONVERSION

Forbidden by lepton family number conservation.

$\sigma(\mu^- {}^{32}S \rightarrow e^- {}^{32}S) / \sigma(\mu^- {}^{32}S \rightarrow \nu_\mu {}^{32}P^*)$

VALUE	CL%	DOCUMENT ID		TECN	COMMENT
$<7 \times 10^{-11}$	90	BADERT...	80	STRC	SIN
• • • We do not use the following data for averages, fits, limits, etc. • • •					
$<4 \times 10^{-10}$	90	BADERT...	77	STRC	SIN

$\sigma(\mu^- Cu \rightarrow e^- Cu) / \sigma(\mu^- Cu \rightarrow capture)$

VALUE	CL%	DOCUMENT ID		TECN
• • • We do not use the following data for averages, fits, limits, etc. • • •				
$<1.6 \times 10^{-8}$	90	BRYMAN	72	SPEC

$\sigma(\mu^- Ti \rightarrow e^- Ti) / \sigma(\mu^- Ti \rightarrow capture)$

VALUE	CL%	DOCUMENT ID		TECN	COMMENT
$<4.3 \times 10^{-12}$	90	[1] DOHMEN	93	SPEC	SINDRUM II
• • • We do not use the following data for averages, fits, limits, etc. • • •					
$<4.6 \times 10^{-12}$	90	AHMAD	88	TPC	TRIUMF
$<1.6 \times 10^{-11}$	90	BRYMAN	85	TPC	TRIUMF

[1] DOHMEN 93 assumes $\mu^- \rightarrow e^-$ conversion leaves the nucleus in its ground state, a process enhanced by coherence and expected to dominate.

$\sigma(\mu^- Pb \rightarrow e^- Pb) / \sigma(\mu^- Pb \rightarrow capture)$

VALUE	CL%	DOCUMENT ID		TECN	COMMENT
$<4.6 \times 10^{-11}$	90	HONECKER	96	SPEC	SINDRUM II
• • • We do not use the following data for averages, fits, limits, etc. • • •					
$<4.9 \times 10^{-10}$	90	AHMAD	88	TPC	TRIUMF

$\sigma(\mu^- Au \rightarrow e^- Au) / \sigma(\mu^- Au \rightarrow capture)$

VALUE	CL%	DOCUMENT ID		TECN	CHG	COMMENT
$<7 \times 10^{-13}$	90	BERTL	06	SPEC	−	SINDRUM II

LIMIT ON $\mu^- \rightarrow e^+$ CONVERSION

Forbidden by total lepton number conservation.

$\sigma(\mu^- {}^{32}S \rightarrow e^+ {}^{32}Si^*) / \sigma(\mu^- {}^{32}S \rightarrow \nu_\mu {}^{32}P^*)$

VALUE	CL%	DOCUMENT ID		TECN	COMMENT
<9 $\times 10^{-10}$	90	BADERT...	80	STRC	SIN
• • • We do not use the following data for averages, fits, limits, etc. • • •					
$<1.5 \times 10^{-9}$	90	BADERT...	78	STRC	SIN

$\sigma(\mu^- {}^{127}I \rightarrow e^+ {}^{127}Sb^*) / \sigma(\mu^- {}^{127}I \rightarrow anything)$

VALUE	CL%	DOCUMENT ID		TECN	COMMENT
$<3 \times 10^{-10}$	90	[1] ABELA	80	CNTR	Radiochemical tech.

[1] ABELA 80 is upper limit for $\mu^- e^+$ conversion leading to particle-stable states of ${}^{127}Sb$. Limit for total conversion rate is higher by a factor less than 4 (G. Backenstoss, private communication).

$\sigma(\mu^- Cu \rightarrow e^+ Co) / \sigma(\mu^- Cu \rightarrow \nu_\mu Ni)$

VALUE	CL%	DOCUMENT ID		TECN
• • • We do not use the following data for averages, fits, limits, etc. • • •				
$<2.6 \times 10^{-8}$	90	BRYMAN	72	SPEC
$<2.2 \times 10^{-7}$	90	CONFORTO	62	OSPK

$\sigma(\mu^- Ti \rightarrow e^+ Ca) / \sigma(\mu^- Ti \rightarrow capture)$

VALUE	CL%	EVTS	DOCUMENT ID		TECN	CHG	COMMENT
$<3.6 \times 10^{-11}$	90	1	[1,2] KAULARD	98	SPEC	−	SINDRUM II
• • • We do not use the following data for averages, fits, limits, etc. • • •							
$<1.7 \times 10^{-12}$	90	1	[2,3] KAULARD	98	SPEC	−	SINDRUM II
$<4.3 \times 10^{-12}$	90		[3] DOHMEN	93	SPEC		SINDRUM II
$<8.9 \times 10^{-11}$	90		[1] DOHMEN	93	SPEC		SINDRUM II
$<1.7 \times 10^{-10}$	90		[4] AHMAD	88	TPC		TRIUMF

[1] This limit assumes a giant resonance excitation of the daughter Ca nucleus (mean energy and width both 20 MeV).
[2] KAULARD 98 obtained these same limits using the unified classical analysis of FELDMAN 98.
[3] This limit assumes the daughter Ca nucleus is left in the ground state. However, the probability of this is unknown.
[4] Assuming a giant-resonance-excitation model.

LIMIT ON MUONIUM → ANTIMUONIUM CONVERSION

Forbidden by lepton family number conservation.

$R_g = G_C / G_F$

The effective Lagrangian for the $\mu^+ e^- \rightarrow \mu^- e^+$ conversion is assumed to be

$$\mathcal{L} = 2^{-1/2}\, G_C\, [\overline{\psi}_\mu \gamma_\lambda (1 - \gamma_5)\, \psi_e]\, [\overline{\psi}_\mu \gamma_\lambda (1 - \gamma_5)\, \psi_e] + \text{h.c.}$$

The experimental result is then an upper limit on G_C/G_F, where G_F is the Fermi coupling constant.

VALUE	CL%	EVTS	DOCUMENT ID		TECN	CHG	COMMENT
< 0.0030	90	1	[1] WILLMANN	99	SPEC	+	μ^+ at 26 GeV/c
• • • We do not use the following data for averages, fits, limits, etc. • • •							
< 0.14	90	1	[2] GORDEEV	97	SPEC	+	JINR phasotron
< 0.018	90	0	[3] ABELA	96	SPEC	+	μ^+ at 24 MeV
< 6.9	90		NI	93	CBOX		LAMPF
< 0.16	90		MATTHIAS	91	SPEC		LAMPF
< 0.29	90		HUBER	90B	CNTR		TRIUMF
<20	95		BEER	86	CNTR		TRIUMF
<42	95		MARSHALL	82	CNTR		

[1] WILLMANN 99 quote both probability $P_{M\overline{M}} < 8.3 \times 10^{-11}$ at 90%CL in a 0.1 T field and $R_g = G_C/G_F$.
[2] GORDEEV 97 quote limits on both $f = G_{MM}/GF$ and the probability $W_{MM} < 4.7 \times 10^{-7}$ (90% CL).
[3] ABELA 96 quote both probability $P_{M\overline{M}} < 8 \times 10^{-9}$ at 90% CL and $R_g = G_C/G_F$.

Downloaded from https://academic.oup.com/ptep/article/2022/8/083C01/6651666 by KIT Library user on 27 September 2022

See the related review(s):
Muon Decay Parameters

μ DECAY PARAMETERS

ρ PARAMETER

($V-A$) theory predicts $\rho = 0.75$.

VALUE	EVTS	DOCUMENT ID		TECN	CHG	COMMENT
0.74979±0.00026 OUR AVERAGE						
0.74977±0.00012±0.00023		[1] BAYES	11	TWST	+	Surface μ^+
0.7518 ±0.0026		DERENZO	69	RVUE		
• • • We do not use the following data for averages, fits, limits, etc. • • •						
0.75014±0.00017±0.00045		[2] MACDONALD	08	TWST	+	Surface μ^+
0.75080±0.00032±0.00100	6G	[3] MUSSER	05	TWST	+	Surface μ^+
0.72 ±0.06 ±0.08		AMORUSO	04	ICAR		Liquid Ar TPC
0.762 ±0.008	170k	[4] FRYBERGER	68	ASPK	+	25–53 MeV e^+
0.760 ±0.009	280k	[4] SHERWOOD	67	ASPK	+	25–53 MeV e^+
0.7503 ±0.0026	800k	[4] PEOPLES	66	ASPK	+	20–53 MeV e^+

[1] The quoted systematic error includes a contribution of 0.00013 (added in quadrature) from uncertainties on radiative corrections and on the Michel parameter η.
[2] The quoted systematic error includes a contribution of 0.00011 (added in quadrature) from the dependence on the Michel parameter η.
[3] The quoted systematic error includes a contribution of 0.00023 (added in quadrature) from the dependence on the Michel parameter η.
[4] η constrained = 0. These values incorporated into a two parameter fit to ρ and η by DERENZO 69.

η PARAMETER

($V-A$) theory predicts $\eta = 0$.

VALUE	EVTS	DOCUMENT ID		TECN	CHG	COMMENT
0.057 ±0.034 OUR AVERAGE						
0.071 ±0.037 ±0.005	30M	DANNEBERG	05	CNTR	+	7–53 MeV e^+
0.011 ±0.081 ±0.026	5.3M	[1] BURKARD	85B	CNTR	+	9–53 MeV e^+
−0.12 ±0.21	6346	DERENZO	69	HBC	+	1.6–6.8 MeV e^+
• • • We do not use the following data for averages, fits, limits, etc. • • •						
−0.0021±0.0070±0.0010	30M	[2] DANNEBERG	05	CNTR	+	7–53 MeV e^+
−0.012 ±0.015 ±0.003	5.3M	[2] BURKARD	85B	CNTR	+	9–53 MeV e^+
−0.007 ±0.013	5.3M	[3] BURKARD	85B	FIT	+	9–53 MeV e^+
−0.7 ±0.5	170k	[4] FRYBERGER	68	ASPK	+	25–53 MeV e^+
−0.7 ±0.6	280k	[4] SHERWOOD	67	ASPK	+	25–53 MeV e^+
0.05 ±0.5	800k	[4] PEOPLES	66	ASPK	+	20–53 MeV e^+
−2.0 ±0.9	9213	[5] PLANO	60	HBC	+	Whole spectrum

[1] Previously we used the global fit result from BURKARD 85B in OUR AVERAGE, we now only include their actual measurement.
[2] $\alpha = \alpha' = 0$ assumed.
[3] Global fit to all measured parameters. The fit correlation coefficients are given in BURKARD 85B.
[4] ρ constrained = 0.75.
[5] Two parameter fit to ρ and η; PLANO 60 discounts value for η.

δ PARAMETER

($V-A$) theory predicts $\delta = 0.75$.

VALUE	EVTS	DOCUMENT ID		TECN	CHG	COMMENT
0.75047±0.00034 OUR AVERAGE						
0.75049±0.00021±0.00027		[1] BAYES	11	TWST	+	Surface μ^+
0.7486 ±0.0026 ±0.0028		[2] BALKE	88	SPEC	+	Surface μ^+
• • • We do not use the following data for averages, fits, limits, etc. • • •						
0.75067±0.00030±0.00067		MACDONALD	08	TWST	+	Surface μ^+
0.74964±0.00066±0.00112	6G	GAPONENKO	05	TWST	+	Surface μ^+
		[3] VOSSLER	69			
0.752 ±0.009	490k	FRYBERGER	68	ASPK	+	25–53 MeV e^+
0.782 ±0.031		KRUGER	61			
0.78 ±0.05	8354	PLANO	60	HBC	+	Whole spectrum

[1] The quoted systematic error includes a contribution of 0.00006 (added in quadrature) from uncertainties on radiative corrections and on the Michel parameter η.
[2] BALKE 88 uses $\rho = 0.752 \pm 0.003$.
[3] VOSSLER 69 has measured the asymmetry below 10 MeV. See comments about radiative corrections in VOSSLER 69.

|(ξ PARAMETER)×(μ LONGITUDINAL POLARIZATION)|

($V-A$) theory predicts $\xi = 1$, longitudinal polarization = 1.

VALUE	DOCUMENT ID		TECN	CHG	COMMENT
1.0009 $^{+0.0016}_{-0.0007}$ OUR AVERAGE					
1.00084±0.00029$^{+0.00165}_{-0.00063}$	BUENO	11	TWST		Surface μ^+ beam
1.0027 ±0.0079 ±0.0030	BELTRAMI	87	CNTR		SIN, π decay in flight
• • • We do not use the following data for averages, fits, limits, etc. • • •					
1.0003 ±0.0006 ±0.0038	JAMIESON	06	TWST	+	surface μ^+ beam
1.0013 ±0.0030 ±0.0053	[1] IMAZATO	92	SPEC	+	$K^+ \rightarrow \mu^+ \nu_\mu$
0.975 ±0.015	AKHMANOV	68	EMUL		140 kG
0.975 ±0.030	GUREVICH	64	EMUL		See AKHMANOV 68
0.903 ±0.027	[2] ALI-ZADE	61	EMUL	+	27 kG
0.93 ±0.06	PLANO	60	HBC	+	8.8 kG
0.97 ±0.05	BARDON	59	CNTR		Bromoform target

[1] The corresponding 90% confidence limit from IMAZATO 92 is $|\xi P_\mu| > 0.990$. This measurement is of K^+ decay, not π^+ decay, so we do not include it in an average, nor do we yet set up a separate data block for K results.
[2] Depolarization by medium not known sufficiently well.

ξ × (μ LONGITUDINAL POLARIZATION) × δ / ρ

VALUE	CL%	DOCUMENT ID		TECN	CHG	COMMENT
1.00179$^{+0.00156}_{-0.00071}$		[1] BAYES	11	TWST	+	Surface μ^+ beam
• • • We do not use the following data for averages, fits, limits, etc. • • •						
>0.99682	90	[2] JODIDIO	86	SPEC	+	TRIUMF
>0.9966	90	[3] STOKER	85	SPEC	+	μ-spin rotation
>0.9959	90	CARR	83	SPEC	+	11 kG

[1] BAYES 11 obtains the limit > 0.99909 (90% CL) with the constraint that $\xi\times$(μ LONGITUDINAL POLARIZATION) $\times\ \delta/\rho \leq 1.0$.
[2] JODIDIO 86 includes data from CARR 83 and STOKER 85. The value here is from the erratum.
[3] STOKER 85 find ($\xi P_\mu \delta/\rho$) >0.9955 and >0.9966, where the first limit is from new μ spin-rotation data and the second is from combination with CARR 83 data. In $V-A$ theory, $(\delta/\rho) = 1.0$.

ξ' = LONGITUDINAL POLARIZATION OF e^+

($V-A$) theory predicts the longitudinal polarization = ±1 for $e^\pm$, respectively. We have flipped the sign for e^- so our programs can average.

VALUE	EVTS	DOCUMENT ID		TECN	CHG	COMMENT
1.00 ±0.04 OUR AVERAGE						
0.998±0.045	1M	BURKARD	85	CNTR	+	Bhabha + annihil
0.89 ±0.28	29k	SCHWARTZ	67	OSPK	−	Moller scattering
0.94 ±0.38		BLOOM	64	CNTR	+	Brems. transmiss.
1.04 ±0.18		DUCLOS	64	CNTR	+	Bhabha scattering
1.05 ±0.30		BUHLER	63	CNTR	+	Annihilation

ξ'' PARAMETER

VALUE	EVTS	DOCUMENT ID		TECN	CHG	COMMENT
0.98 ±0.04 OUR AVERAGE						
0.981±0.045±0.003	3.87M	PRIEELS	14	CNTR	+	Bhabha + annihil
0.65 ±0.36	326k	[1] BURKARD	85	CNTR	+	Bhabha + annihil

[1] BURKARD 85 measure (ξ''-$\xi\xi'$)/ξ and ξ' and set $\xi = 1$.

TRANSVERSE e^+ POLARIZATION IN PLANE OF μ SPIN, e^+ MOMENTUM

VALUE (units 10^{-3})	EVTS	DOCUMENT ID		TECN	CHG	COMMENT
7 ± 8 OUR AVERAGE						
6.3± 7.7± 3.4	30M	DANNEBERG	05	CNTR	+	7–53 MeV e^+
16 ±21 ±10	5.3M	BURKARD	85B	CNTR	+	Annihil 9–53 MeV

TRANSVERSE e^+ POLARIZATION NORMAL TO PLANE OF μ SPIN, e^+ MOMENTUM

Zero if T invariance holds.

VALUE (units 10^{-3})	EVTS	DOCUMENT ID		TECN	CHG	COMMENT
−2 ± 8 OUR AVERAGE						
−3.7± 7.7±3.4	30M	DANNEBERG	05	CNTR	+	7–53 MeV e^+
7 ±22 ±7	5.3M	BURKARD	85B	CNTR	+	Annihil 9–53 MeV

α/A

VALUE (units 10^{-3})	EVTS	DOCUMENT ID		TECN	CHG	COMMENT
0.4± 4.3		[1] BURKARD	85B	FIT		
• • • We do not use the following data for averages, fits, limits, etc. • • •						
15 ±50 ±14	5.3M	BURKARD	85B	CNTR	+	9–53 MeV e^+

[1] Global fit to all measured parameters. Correlation coefficients are given in BURKARD 85B.

α'/A

Zero if T invariance holds.

VALUE (units 10^{-3})	EVTS	DOCUMENT ID		TECN	CHG	COMMENT
−10 ±20 OUR AVERAGE						
− 3.4±21.3± 4.9	30M	DANNEBERG	05	CNTR	+	7–53 MeV e^+
−47 ±50 ±14	5.3M	[1] BURKARD	85B	CNTR	+	9–53 MeV e^+
• • • We do not use the following data for averages, fits, limits, etc. • • •						
− 0.2± 4.3		[2] BURKARD	85B	FIT		

[1] Previously we used the global fit result from BURKARD 85B in OUR AVERAGE, we now only include their actual measurement. BURKARD 85B measure e^+ polarizations P_{T_1} and P_{T_2} versus e^+ energy.
[2] Global fit to all measured parameters. The fit correlation coefficients are given in BURKARD 85B.

β/A

VALUE (units 10^{-3})	EVTS	DOCUMENT ID		TECN	CHG	COMMENT
3.9± 6.2		[1] BURKARD	85B	FIT		
• • • We do not use the following data for averages, fits, limits, etc. • • •						
2 ±17 ±6	5.3M	BURKARD	85B	CNTR	+	9–53 MeV e^+

[1] Global fit to all measured parameters. The fit correlation coefficients are given in BURKARD 85B.

β'/A

Zero if T invariance holds.

VALUE (units 10^{-3})	EVTS	DOCUMENT ID		TECN	CHG	COMMENT
2 ± 7 OUR AVERAGE						
− 0.5± 7.8±1.8	30M	DANNEBERG	05	CNTR	+	7–53 MeV e^+
17 ±17 ±6	5.3M	[1] BURKARD	85B	CNTR	+	9–53 MeV e^+

Downloaded from https://academic.oup.com/ptep/article/2022/8/083C01/6651666 by KIT Library user on 27 September 2022

• • • We do not use the following data for averages, fits, limits, etc. • • •

− 1.3± 3.5±0.6	30M	[2] DANNEBERG	05	CNTR	+	7–53 MeV e^+
1.5± 6.3		[3] BURKARD	85B	FIT		

[1] Previously we used the global fit result from BURKARD 85B in OUR AVERAGE, we now only include their actual measurement. BURKARD 85B measure e^+ polarizations P_{T_1} and P_{T_2} versus e^+ energy.

[2] $\alpha = \alpha' = 0$ assumed.

[3] Global fit to all measured parameters. The fit correlation coefficients are given in BURKARD 85B.

a/A

This comes from an alternative parameterization to that used in the Summary Table (see the "Note on Muon Decay Parameters" above).

VALUE (units 10^{-3})	CL%	DOCUMENT ID		TECN
• • • We do not use the following data for averages, fits, limits, etc. • • •				
<15.9	90	[1] BURKARD	85B	FIT

[1] Global fit to all measured parameters. Correlation coefficients are given in BURKARD 85B.

a′/A

This comes from an alternative parameterization to that used in the Summary Table (see the "Note on Muon Decay Parameters" above).

VALUE (units 10^{-3})	DOCUMENT ID		TECN
• • • We do not use the following data for averages, fits, limits, etc. • • •			
5.3±4.1	[1] BURKARD	85B	FIT

[1] Global fit to all measured parameters. Correlation coefficients are given in BURKARD 85B.

(b′+b)/A

This comes from an alternative parameterization to that used in the Summary Table (see the "Note on Muon Decay Parameters" above).

VALUE (units 10^{-3})	CL%	DOCUMENT ID		TECN
• • • We do not use the following data for averages, fits, limits, etc. • • •				
<1.04	90	[1] BURKARD	85B	FIT

[1] Global fit to all measured parameters. Correlation coefficients are given in BURKARD 85B.

c/A

This comes from an alternative parameterization to that used in the Summary Table (see the "Note on Muon Decay Parameters" above).

VALUE (units 10^{-3})	CL%	DOCUMENT ID		TECN
• • • We do not use the following data for averages, fits, limits, etc. • • •				
<6.4	90	[1] BURKARD	85B	FIT

[1] Global fit to all measured parameters. Correlation coefficients are given in BURKARD 85B.

c′/A

This comes from an alternative parameterization to that used in the Summary Table (see the "Note on Muon Decay Parameters" above).

VALUE (units 10^{-3})	DOCUMENT ID		TECN
• • • We do not use the following data for averages, fits, limits, etc. • • •			
3.5±2.0	[1] BURKARD	85B	FIT

[1] Global fit to all measured parameters. Correlation coefficients are given in BURKARD 85B.

$\overline{\eta}$ PARAMETER

$(V-A)$ theory predicts $\overline{\eta} = 0$. $\overline{\eta}$ affects spectrum of radiative muon decay.

VALUE	DOCUMENT ID		TECN	CHG	COMMENT
0.02 ±0.08 OUR AVERAGE					
−0.014±0.090	EICHENBER...	84	ELEC	+	ρ free
+0.09 ±0.14	BOGART	67	CNTR	+	
• • • We do not use the following data for averages, fits, limits, etc. • • •					
−0.035±0.098	EICHENBER...	84	ELEC	+	ρ=0.75 assumed

μ REFERENCES

ABI	21	PRL 126 141801	B. Abi et al.	(Muon g-2 Collab.)
TIESINGA	21	RMP 93 025010	E. Tiesinga et al.	(NIST)
AOYAMA	20	PRPL 887 1	T. Aoyama et al.	
BALDINI	20	EPJ C80 858	A.M. Baldini et al.	(MEG Collab.)
BALDINI	16	EPJ C76 434	A.M. Baldini et al.	(MEG Collab.)
BALDINI	16A	EPJ C76 108	A.M. Baldini et al.	(MEG Collab.)
MOHR	16	RMP 88 035009	P.J. Mohr, D.B. Newell, B.N. Taylor	(NIST)
PRIEELS	14	PR D90 112003	R. Prieels et al.	(LOUV, ETH, PSI+)
ADAM	13B	PRL 110 201801	J. Adam et al.	(MEG Collab.)
TISHCHENKO	13	PR D87 052003	V. Tishchenko et al.	(MuLan Collab.)
MOHR	12	RMP 84 1527	P.J. Mohr, B.N. Taylor, D.B. Newell	(NIST)
ADAM	11	PRL 107 171801	J. Adam et al.	(MEG Collab.)
BAYES	11	PRL 106 041804	R. Bayes et al.	(TWIST Collab.)
Also		PR D85 092013	A. Hillairet et al.	(TWIST Collab.)
BUENO	11	PR D84 032005	J.F. Bueno et al.	(TWIST Collab.)
Also		PR D85 039908 (errat.)	J.F. Bueno et al.	(TWIST Collab.)
WEBBER	11	PRL 106 041803	D.M. Webber et al.	(MuLan Collab.)
Also		PRL 106 079901 (errat.)	D.M. Webber et al.	(MuLan Collab.)
ADAM	10	NP B834 1	J. Adam et al.	(MEG Collab.)
BENNETT	09	PR D80 052008	G.W. Bennett et al.	(MUG-2 Collab.)
BARCZYK	08	PL B663 172	A. Barczyk et al.	(FAST Collab.)
MACDONALD	08	PR D78 032010	R.P. MacDonald et al.	(TWIST Collab.)
MOHR	08	RMP 80 633	P.J. Mohr, B.N. Taylor, D.B. Newell	(NIST)
CHITWOOD	07	PRL 99 032001	D.B. Chitwood et al.	(MULAN Collab.)
BENNETT	06	PR D73 072003	G.W. Bennett et al.	(MUG-2 Collab.)
BERTL	06	EPJ C47 337	W. Bertl et al.	(SINDRUM II Collab.)
JAMIESON	06	PR D74 072007	B. Jamieson et al.	(TWIST Collab.)
DANNEBERG	05	PRL 94 021802	N. Danneberg et al.	(ETH, JAGL, PSI+)
GAPONENKO	05	PR D71 071101	A. Gaponenko et al.	(TWIST Collab.)
MOHR	05	RMP 77 1	P.J. Mohr, B.N. Taylor	(NIST)
MUSSER	05	PRL 94 101805	J.R. Musser et al.	(TWIST Collab.)
AMORUSO	04	EPJ C33 233	S. Amoruso et al.	(ICARUS Collab.)
BENNETT	04	PRL 92 161802	G.W. Bennett et al.	(Muon(g-2) Collab.)
AHMED	02	PR D65 112002	M. Ahmed et al.	(MEGA Collab.)
BENNETT	02	PRL 89 101804	G.W. Bennett et al.	(Muon(g-2) Collab.)
BROWN	01	PRL 86 2227	H.N. Brown et al.	(Muon(g-2) Collab.)
BROWN	00	PR D62 091101	H.N. Brown et al.	(BNL/G-2 Collab.)
MEYER	00	PRL 84 1136	V. Meyer et al.	
BROOKS	99	PRL 83 1521	M.L. Brooks et al.	(MEGA/LAMPF Collab.)
HUGHES	99	RMP 71 S133	V.W. Hughes, T. Kinoshita	
LIU	99	PRL 82 711	W. Liu et al.	(LAMPF Collab.)
MOHR	99	JPCRD 28 1713	P.J. Mohr, B.N. Taylor	(NIST)
Also		RMP 72 351	P.J. Mohr, B.N. Taylor	(NIST)
WILLMANN	99	PRL 82 49	L. Willmann et al.	
FELDMAN	98	PR D57 3873	G.J. Feldman, R.D. Cousins	
KAULARD	98	PL B422 334	J. Kaulard et al.	(SINDRUM-II Collab.)
GORDEEV	97	PAN 60 1164	V.A. Gordeev et al.	(PNPI)
		Translated from YAF 60 1291.		
ABELA	96	PRL 77 1950	R. Abela et al.	(PSI, ZURI, HEIDH, TBIL+)
HONECKER	96	PRL 76 200	W. Honecker et al.	(SINDRUM II Collab.)
DOHMEN	93	PL B317 631	C. Dohmen et al.	(PSI SINDRUM-II Collab.)
FREEDMAN	93	PR D47 811	S.J. Freedman et al.	(LAMPF E645 Collab.)
NI	93	PR D48 1976	B. Ni et al.	(LAMPF Crystal-Box Collab.)
IMAZATO	92	PRL 69 877	J. Imazato et al.	(KEK, INUS, TOKY+)
BARANOV	91	SJNP 53 802	V.A. Baranov et al.	(JINR)
		Translated from YAF 53 1302.		
KRAKAUER	91B	PL B263 534	D.A. Krakauer et al.	(UMD, UCI, LANL)
MATTHIAS	91	PRL 66 2716	B.E. Matthias et al.	(YALE, HEIDP, WILL+)
Also		PRL 67 932 (erratum)	B.E. Matthias et al.	(YALE, HEIDP, WILL+)
HUBER	90B	PR D41 2709	T.M. Huber et al.	(WYOM, VICT, ARIZ+)
AHMAD	88	PR D38 2102	S. Ahmad et al.	(TRIU, VICT, VPI, BRCO+)
Also		PRL 59 970	S. Ahmad et al.	(TRIU, VPI, VICT, BRCO+)
BALKE	88	PR D37 587	B. Balke et al.	(LBL, UCB, COLO, NWES+)
BELLGARDT	88	NP B299 1	U. Bellgardt et al.	(SINDRUM Collab.)
BOLTON	88	PR D38 2077	R.D. Bolton et al.	(LANL, STAN, CHIC+)
Also		PRL 56 2461	R.D. Bolton et al.	(LANL, STAN, CHIC+)
Also		PRL 57 3241	D. Grosnick et al.	(CHIC, LANL, STAN+)
BELTRAMI	87	PL B194 326	I. Beltrami et al.	(ETH, SIN, MAINZ)
COHEN	87	RMP 59 1121	E.R. Cohen, B.N. Taylor	(RISC, NBS)
BEER	86	PRL 57 671	G.A. Beer et al.	(VICT, TRIU, WYOM)
JODIDIO	86	PR D34 1967	A. Jodidio et al.	(LBL, NWES, TRIU)
Also		PR D37 237 (erratum)	A. Jodidio et al.	(LBL, NWES, TRIU)
BERTL	85	NP B260 1	W. Bertl et al.	(SINDRUM Collab.)
BRYMAN	85	PRL 55 465	D.A. Bryman et al.	(TRIU, CNRC, BRCO+)
BURKARD	85	PL 150B 242	H. Burkhardt et al.	(ETH, SIN, MAINZ)
BURKARD	85B	PL 160B 343	H. Burkhardt et al.	(ETH, SIN, MAINZ)
Also		PR D24 2004	F. Corriveau et al.	(ETH, SIN, MAINZ)
Also		PL 129B 260	F. Corriveau et al.	(ETH, SIN, MAINZ)
STOKER	85	PRL 54 1887	D.P. Stoker et al.	(LBL, NWES, TRIU)
BARDIN	84	PL 137B 135	G. Bardin et al.	(SACL, CERN, BGNA, FIRZ)
BERTL	84	PL 140B 299	W. Bertl et al.	(SINDRUM Collab.)
BOLTON	84	PRL 53 1415	R.D. Bolton et al.	(LANL, CHIC, STAN+)
EICHENBER...	84	NP A412 523	W. Eichenberger, R. Engfer, A. van der Schaff	
GIOVANETTI	84	PR D29 343	K.L. Giovanetti et al.	(WILL)
AZUELOS	83	PRL 51 164	G. Azuelos et al.	(MONT, TRIU, BRCO)
Also		PRL 39 1113	P. Depommier et al.	(MONT, BRCO, TRIU+)
BERGSMA	83	PL 122B 465	F. Bergsma et al.	(CHARM Collab.)
CARR	83	PRL 51 627	J. Carr et al.	(LBL, NWES, TRIU)
KINNISON	82	PR D25 2846	W.W. Kinnison et al.	(EFI, STAN, LANL)
Also		PRL 42 556	J.D. Bowman et al.	(LASL, EFI, STAN)
KLEMPT	82	PR D25 652	E. Klempt et al.	(MAINZ, ETH)
MARIAM	82	PRL 49 993	F.G. Mariam et al.	(YALE, HEIDH, BERN)
MARSHALL	82	PR D25 1174	G.M. Marshall et al.	(BRCO)
NEMETHY	81	CNPP 10 147	P. Nemethy, V.W. Hughes	(LBL, YALE)
ABELA	80	PL 95B 318	R. Abela et al.	(BASL, KARLK, KARLE)
BADERT...	80	LNC 28 401	A. Badertscher et al.	(BERN)
Also		NP A377 406	A. Badertscher et al.	(BERN)
JONKER	80	PL 93B 203	M. Jonker et al.	(CHARM Collab.)
SCHAAF	80	NP A340 249	A. van der Schaaf et al.	(ZURI, ETH+)
Also		PL 72B 183	H.P. Povel et al.	(ZURI, ETH, SIN)
WILLIS	80	PRL 44 522	S.E. Willis et al.	(YALE, LBL, LASL+)
Also		PRL 45 1370	S.E. Willis et al.	(YALE, LBL, LASL+)
BAILEY	79	NP B150 1	J.M. Bailey	(CERN, DARE, MAINZ)
BADERT...	78	PL 79B 371	A. Badertscher et al.	(BERN)
BAILEY	78	JP G4 345	J.M. Bailey	(DARE, BERN, SHEF, MAINZ, RMCS+)
Also		NP B150 1	J.M. Bailey	(CERN, DARE, MAINZ)
BLIETSCHAU	78	NP B133 205	J. Blietschau et al.	(Gargamelle Collab.)
BOWMAN	78	PRL 41 442	J.D. Bowman et al.	(LASL, IAS, CMU+)
CAMANI	78	PL 77B 326	M. Camani et al.	(ETH, MAINZ)
BADERT...	77	PRL 39 1385	A. Badertscher et al.	(BERN)
CASPERSON	77	PRL 38 956	D.E. Casperson et al.	(BERN, HEIDH, LASL+)
DEPOMMIER	77	PRL 39 1113	P. Depommier et al.	(MONT, BRCO, TRIU+)
BALANDIN	74	JETP 40 811	M.P. Balandin et al.	(JINR)
		Translated from ZETF 67 1631.		
COHEN	73	JPCRD 2 664	E.R. Cohen, B.N. Taylor	(RISC, NBS)
DUCLOS	73	PL 47B 491	J. Duclos, A. Magnon, J. Picard	(SACL)
EICHTEN	73	PL 46B 281	T. Eichten et al.	(Gargamelle Collab.)
BRYMAN	72	PRL 28 1469	D.A. Bryman et al.	(VPI)
CROWE	72	PR D5 2145	K.M. Crowe et al.	(LBL, WASH)
CRANE	71	PRL 27 474	T. Crane et al.	(YALE)
DERENZO	69	PR 181 1854	S.E. Derenzo	(EFI)
VOSSLER	69	NC 63A 423	C. Vossler	(EFI)
AKHMANOV	68	SJNP 6 230	V.V. Akhmanov et al.	(KIAE)
		Translated from YAF 6 316.		
FRYBERGER	68	PR 166 1379	D. Fryberger	(EFI)
BOGART	67	PR 156 1405	E. Bogart et al.	(COLU)
SCHWARTZ	67	PR 162 1306	D.M. Schwartz	(EFI)
SHERWOOD	67	PR 156 1475	B.A. Sherwood	(EFI)
PEOPLES	66	Nevis 147 unpub.	J. Peoples	(COLU)
BLOOM	64	PL 8 87	S. Bloom et al.	(CERN)
DUCLOS	64	PL 9 62	J. Duclos et al.	(CERN)
GUREVICH	64	PL 11 185	I.I. Gurevich et al.	(KIAE)
BUHLER	63	PL 7 368	A. Buhler-Broglin et al.	(CERN)
MEYER	63	PR 132 2693	S.L. Meyer et al.	(COLU)
CHARPAK	62	PL 1 16	G. Charpak et al.	(CERN)
CONFORTO	62	NC 26 261	G. Conforto et al.	(INFN, ROMA, CERN)
ALI-ZADE	61	JETP 13 313	S.A. Ali-Zade, I.I. Gurevich, B.A. Nikolsky	
		Translated from ZETF 40 452.		
CRITTENDEN	61	PR 121 1823	R.R. Crittenden, W.D. Walker, J. Ballam	(WISC+)
KRUGER	61	UCRL 9322 unpub.	H. Kruger	(LRL)
GUREVICH	60	JETP 10 225	I.I. Gurevich, B.A. Nikolsky, L.V. Surkova	(ITEP)
		Translated from ZETF 37 318.		
PLANO	60	PR 119 1400	R.J. Plano	(COLU)
ASHKIN	59	NC 14 1266	J. Ashkin et al.	(CERN)
BARDON	59	PRL 2 56	M. Bardon, D. Berley, L.M. Lederman	(COLU)
LEE	59	PRL 3 55	J. Lee, N.P. Samios	(COLU)

Downloaded from https://academic.oup.com/ptep/article/2022/8/083C01/6651666 by KIT Library user on 27 September 2022

τ

$J = \frac{1}{2}$

τ discovery paper was PERL 75. $e^+e^- \to \tau^+\tau^-$ cross-section threshold behavior and magnitude are consistent with pointlike spin-1/2 Dirac particle. BRANDELIK 78 ruled out pointlike spin-0 or spin-1 particle. FELDMAN 78 ruled out $J = 3/2$. KIRKBY 79 also ruled out J=integer, $J = 3/2$.

τ MASS

VALUE (MeV)	EVTS	DOCUMENT ID		TECN	COMMENT
1776.86±0.12 OUR AVERAGE					
$1776.91 \pm 0.12^{+0.10}_{-0.13}$	1171	[1] ABLIKIM	14D	BES3	23.3 pb^{-1}, E^{ee}_{cm}= 3.54–3.60 GeV
$1776.68 \pm 0.12 \pm 0.41$	682k	[2] AUBERT	09AK	BABR	423 fb^{-1}, E^{ee}_{cm}=10.6 GeV
$1776.81^{+0.25}_{-0.23} \pm 0.15$	81	ANASHIN	07	KEDR	6.7 pb^{-1}, E^{ee}_{cm}= 3.54–3.78 GeV
$1776.61 \pm 0.13 \pm 0.35$		[2] BELOUS	07	BELL	414 fb^{-1} E^{ee}_{cm}=10.6 GeV
$1775.1 \pm 1.6 \pm 1.0$	13.3k	[3] ABBIENDI	00A	OPAL	1990–1995 LEP runs
$1778.2 \pm 0.8 \pm 1.2$		ANASTASSOV	97	CLEO	E^{ee}_{cm}= 10.6 GeV
$1776.96^{+0.18}_{-0.21} \pm^{0.25}_{-0.17}$	65	[4] BAI	96	BES	E^{ee}_{cm}= 3.54–3.57 GeV
$1776.3 \pm 2.4 \pm 1.4$	11k	[5] ALBRECHT	92M	ARG	E^{ee}_{cm}= 9.4–10.6 GeV
$1783 \pm^{3}_{-4}$	692	[6] BACINO	78B	DLCO	E^{ee}_{cm}= 3.1–7.4 GeV
• • • We do not use the following data for averages, fits, limits, etc. • • •					
$1777.8 \pm 0.7 \pm 1.7$	35k	[7] BALEST	93	CLEO	Repl. by ANASTASSOV 97
$1776.9 \pm^{0.4}_{-0.5} \pm 0.2$	14	[8] BAI	92	BES	Repl. by BAI 96

[1] ABLIKIM 14D fit $\sigma(e^+e^- \to \tau^+\tau^-)$ at different energies near threshold.
[2] AUBERT 09AK and BELOUS 07 fit τ pseudomass spectrum in $\tau \to \pi\pi^+\pi^-\nu_\tau$ decays. Result assumes $m_{\nu_\tau} = 0$.
[3] ABBIENDI 00A fit τ pseudomass spectrum in $\tau \to \pi^\pm \leq 2\pi^0\nu_\tau$ and $\tau \to \pi^\pm\pi^+\pi^- \leq 1\pi^0\nu_\tau$ decays. Result assumes m_{ν_τ}=0.
[4] BAI 96 fit $\sigma(e^+e^- \to \tau^+\tau^-)$ at different energies near threshold.
[5] ALBRECHT 92M fit τ pseudomass spectrum in $\tau^- \to 2\pi^-\pi^+\nu_\tau$ decays. Result assumes m_{ν_τ}=0.
[6] BACINO 78B value comes from $e^\pm X^\mp$ threshold. Published mass 1782 MeV increased by 1 MeV using the high precision $\psi(2S)$ mass measurement of ZHOLENTZ 80 to eliminate the absolute SPEAR energy calibration uncertainty.
[7] BALEST 93 fit spectra of minimum kinematically allowed τ mass in events of the type $e^+e^- \to \tau^+\tau^- \to (\pi^+ n\pi^0\nu_\tau)(\pi^- m\pi^0\nu_\tau)$ $n \leq 2$, $m \leq 2$, $1 \leq n+m \leq 3$. If $m_{\nu_\tau} \neq 0$, result increases by $(m^2_{\nu_\tau}/1100$ MeV).
[8] BAI 92 fit $\sigma(e^+e^- \to \tau^+\tau^-)$ near threshold using $e\mu$ events.

$(m_{\tau^+} - m_{\tau^-})/m_{\text{average}}$

A test of CPT invariance.

VALUE	CL%	DOCUMENT ID		TECN	COMMENT
$<2.8 \times 10^{-4}$	90	BELOUS	07	BELL	414 fb^{-1}, E^{ee}_{cm}=10.6 GeV
• • • We do not use the following data for averages, fits, limits, etc. • • •					
$<5.5 \times 10^{-4}$	90	[1] AUBERT	09AK	BABR	423 fb^{-1}, E^{ee}_{cm}=10.6 GeV
$<3.0 \times 10^{-3}$	90	ABBIENDI	00A	OPAL	1990–1995 LEP runs

[1] AUBERT 09AK quote both the listed upper limit and $(m_{\tau^+} - m_{\tau^-})/m_{\text{average}} = (-3.4 \pm 1.3 \pm 0.3) \times 10^{-4}$.

τ MEAN LIFE

VALUE (10^{-15} s)	EVTS	DOCUMENT ID		TECN	COMMENT
290.3 ± 0.5 OUR AVERAGE					
$290.17 \pm 0.53 \pm 0.33$	1.1M	BELOUS	14	BELL	711 fb^{-1} E^{ee}_{cm}=10.6 GeV
$290.9 \pm 1.4 \pm 1.0$		ABDALLAH	04T	DLPH	1991-1995 LEP runs
$293.2 \pm 2.0 \pm 1.5$		ACCIARRI	00B	L3	1991–1995 LEP runs
$290.1 \pm 1.5 \pm 1.1$		BARATE	97R	ALEP	1989–1994 LEP runs
$289.2 \pm 1.7 \pm 1.2$		ALEXANDER	96E	OPAL	1990–1994 LEP runs
$289.0 \pm 2.8 \pm 4.0$	57.4k	BALEST	96	CLEO	E^{ee}_{cm}= 10.6 GeV
• • • We do not use the following data for averages, fits, limits, etc. • • •					
$291.2 \pm 2.0 \pm 1.2$		BARATE	97I	ALEP	Repl. by BARATE 97R
291.4 ± 3.0		ABREU	96B	DLPH	Repl. by ABDALLAH 04T
290.1 ± 4.0	34k	ACCIARRI	96K	L3	Repl. by ACCIARRI 00B
$297 \pm 9 \pm 5$	1671	ABE	95Y	SLD	1992–1993 SLC runs
$304 \pm 14 \pm 7$	4100	BATTLE	92	CLEO	E^{ee}_{cm}= 10.6 GeV
301 ± 29	3780	KLEINWORT	89	JADE	E^{ee}_{cm}= 35–46 GeV
$288 \pm 16 \pm 17$	807	AMIDEI	88	MRK2	E^{ee}_{cm}= 29 GeV
$306 \pm 20 \pm 14$	695	BRAUNSCH...	88C	TASS	E^{ee}_{cm}= 36 GeV
$299 \pm 15 \pm 10$	1311	ABACHI	87C	HRS	E^{ee}_{cm}= 29 GeV
$295 \pm 14 \pm 11$	5696	ALBRECHT	87P	ARG	E^{ee}_{cm}= 9.3–10.6 GeV
$309 \pm 17 \pm 7$	3788	BAND	87B	MAC	E^{ee}_{cm}= 29 GeV
$325 \pm 14 \pm 18$	8470	BEBEK	87C	CLEO	E^{ee}_{cm}= 10.5 GeV
460 ± 190	102	FELDMAN	82	MRK2	E^{ee}_{cm}= 29 GeV

$(\tau_{\tau^+} - \tau_{\tau^-}) / \tau_{\text{average}}$

Test of CPT invariance.

VALUE	CL%	DOCUMENT ID		TECN	COMMENT
$<7.0 \times 10^{-3}$	90	[1] BELOUS	14	BELL	711 fb^{-1} E^{ee}_{cm} = 10.6 GeV

[1] BELOUS 14 quote limit on the absolute value of the relative lifetime difference.

τ MAGNETIC MOMENT ANOMALY

The q^2 dependence is expected to be small providing no thresholds are nearby.

$\mu_\tau/(e\hbar/2m_\tau)-1 = (g_\tau-2)/2$

For a theoretical calculation $[(g_\tau-2)/2 = 117\,721(5) \times 10^{-8}]$, see EIDELMAN 07.

VALUE	CL%	DOCUMENT ID		TECN	COMMENT
> -0.052 and < 0.013 (CL = 95%) OUR LIMIT					
> -0.052 and < 0.013	95	[1] ABDALLAH	04K	DLPH	$e^+e^- \to e^+e^-\tau^+\tau^-$ at LEP2
• • • We do not use the following data for averages, fits, limits, etc. • • •					
<0.107	95	[2] ACHARD	04G	L3	$e^+e^- \to e^+e^-\tau^+\tau^-$ at LEP2
> -0.007 and < 0.005	95	[3] GONZALEZ-S...	00	RVUE	$e^+e^- \to \tau^+\tau^-$ and $W \to \tau\nu_\tau$
> -0.052 and < 0.058	95	[4] ACCIARRI	98E	L3	1991–1995 LEP runs
> -0.068 and < 0.065	95	[5] ACKERSTAFF	98N	OPAL	1990–1995 LEP runs
> -0.004 and < 0.006	95	[6] ESCRIBANO	97	RVUE	$Z \to \tau^+\tau^-$ at LEP
<0.01	95	[7] ESCRIBANO	93	RVUE	$Z \to \tau^+\tau^-$ at LEP
<0.12	90	GRIFOLS	91	RVUE	$Z \to \tau\tau\gamma$ at LEP
<0.023	95	[8] SILVERMAN	83	RVUE	$e^+e^- \to \tau^+\tau^-$ at PETRA

[1] ABDALLAH 04K limit is derived from $e^+e^- \to e^+e^-\tau^+\tau^-$ total cross-section measurements at $\sqrt{s}$ between 183 and 208 GeV. In addition to the limits, the authors also quote a value of -0.018 ± 0.017.
[2] ACHARD 04G limit is derived from $e^+e^- \to e^+e^-\tau^+\tau^-$ total cross-section measurements at $\sqrt{s}$ between 189 and 206 GeV, and is on the absolute value of the magnetic moment anomaly.
[3] GONZALEZ-SPRINBERG 00 use data on tau lepton production at LEP1, SLC, and LEP2, and data from colliders and LEP2 to determine limits. Assume imaginary component is zero.
[4] ACCIARRI 98E use $Z \to \tau^+\tau^-\gamma$ events. In addition to the limits, the authors also quote a value of $0.004 \pm 0.027 \pm 0.023$.
[5] ACKERSTAFF 98N use $Z \to \tau^+\tau^-\gamma$ events. The limit applies to an average of the form factor for off-shell τ's having p^2 ranging from m^2_τ to $(M_Z-m_\tau)^2$.
[6] ESCRIBANO 97 use preliminary experimental results.
[7] ESCRIBANO 93 limit derived from $\Gamma(Z \to \tau^+\tau^-)$, and is on the absolute value of the magnetic moment anomaly.
[8] SILVERMAN 83 limit is derived from $e^+e^- \to \tau^+\tau^-$ total cross-section measurements for q^2 up to (37 GeV)^2.

τ ELECTRIC DIPOLE MOMENT (d_τ)

A nonzero value is forbidden by both T invariance and P invariance.

The q^2 dependence is expected to be small providing no thresholds are nearby.

Re(d_τ)

VALUE (10^{-16} e cm)	CL%	DOCUMENT ID		TECN	COMMENT
− 0.22 to 0.45	95	[1] INAMI	03	BELL	E^{ee}_{cm}= 10.6 GeV
• • • We do not use the following data for averages, fits, limits, etc. • • •					
< 2.3	90	[2] GROZIN	09A	RVUE	From e EDM limit
< 3.7	95	[3] ABDALLAH	04K	DLPH	$e^+e^- \to e^+e^-\tau^+\tau^-$ at LEP2
< 11.4	95	[4] ACHARD	04G	L3	$e^+e^- \to e^+e^-\tau^+\tau^-$ at LEP2
< 4.6	95	[5] ALBRECHT	00	ARG	E^{ee}_{cm}= 10.4 GeV
> -3.1 and < 3.1	95	ACCIARRI	98E	L3	1991–1995 LEP runs
> -3.8 and < 3.6	95	[6] ACKERSTAFF	98N	OPAL	1990–1995 LEP runs
< 0.11	95	[7,8] ESCRIBANO	97	RVUE	$Z \to \tau^+\tau^-$ at LEP
< 0.5	95	[9] ESCRIBANO	93	RVUE	$Z \to \tau^+\tau^-$ at LEP
< 7	90	GRIFOLS	91	RVUE	$Z \to \tau\tau\gamma$ at LEP
< 1.6	90	DELAGUILA	90	RVUE	$e^+e^- \to \tau^+\tau^-$ E^{ee}_{cm}= 35 GeV

[1] INAMI 03 use $e^+e^- \to \tau^+\tau^-$ events.
[2] GROZIN 09A calculate the contribution to the electron electric dipole moment from the τ electric dipole moment appearing in loops, which is $\Delta d_e = 6.9 \times 10^{-12}$ d_τ. Dividing the REGAN 02 upper limit $|d_e| \leq 1.6 \times 10^{-27}$ e cm at CL=90% by 6.9×10^{-12} gives this limit.
[3] ABDALLAH 04K limit is derived from $e^+e^- \to e^+e^-\tau^+\tau^-$ total cross-section measurements at $\sqrt{s}$ between 183 and 208 GeV and is on the absolute value of d_τ.
[4] ACHARD 04G limit is derived from $e^+e^- \to e^+e^-\tau^+\tau^-$ total cross-section measurements at $\sqrt{s}$ between 189 and 206 GeV, and is on the absolute value of d_τ.
[5] ALBRECHT 00 use $e^+e^- \to \tau^+\tau^-$ events. Limit is on the absolute value of Re(d_τ).
[6] ACKERSTAFF 98N use $Z \to \tau^+\tau^-\gamma$ events. The limit applies to an average of the form factor for off-shell τ's having p^2 ranging from m^2_τ to $(M_Z-m_\tau)^2$.
[7] ESCRIBANO 97 derive the relationship $|d_\tau| = \cot\theta_W |d^W_\tau|$ using effective Lagrangian methods, and use a conference result $|d^W_\tau| < 5.8 \times 10^{-18}$ $e$cm at 95% CL (L. Silvestris, ICHEP96) to obtain this result.
[8] ESCRIBANO 97 use preliminary experimental results.
[9] ESCRIBANO 93 limit derived from $\Gamma(Z \to \tau^+\tau^-)$, and is on the absolute value of the electric dipole moment.

Downloaded from https://academic.oup.com/ptep/article/2022/8/083C01/6651666 by KIT Library user on 27 September 2022

Im(d_τ)

VALUE (10^{-16} e cm)	CL%	DOCUMENT ID		TECN	COMMENT
−0.25 to 0.008	95	[1] INAMI	03	BELL	E^{ee}_{cm}= 10.6 GeV
• • • We do not use the following data for averages, fits, limits, etc. • • •					
< 1.8	95	[2] ALBRECHT	00	ARG	E^{ee}_{cm}= 10.4 GeV

[1] INAMI 03 use $e^+e^- \to \tau^+\tau^-$ events.
[2] ALBRECHT 00 use $e^+e^- \to \tau^+\tau^-$ events. Limit is on the absolute value of Im(d_τ).

τ WEAK DIPOLE MOMENT (d^W_τ)

A nonzero value is forbidden by *CP* invariance.

The q^2 dependence is expected to be small providing no thresholds are nearby.

Re(d^W_τ)

VALUE (10^{-17} e cm)	CL%	DOCUMENT ID		TECN	COMMENT
<0.50	95	[1] HEISTER	03F	ALEP	1990–1995 LEP runs
• • • We do not use the following data for averages, fits, limits, etc. • • •					
<3.0	90	[1] ACCIARRI	98C	L3	1991–1995 LEP runs
<0.56	95	ACKERSTAFF	97L	OPAL	1991–1995 LEP runs
<0.78	95	[2] AKERS	95F	OPAL	Repl. by ACKERSTAFF 97L
<1.5	95	[2] BUSKULIC	95C	ALEP	Repl. by HEISTER 03F
<7.0	95	[2] ACTON	92F	OPAL	$Z \to \tau^+\tau^-$ at LEP
<3.7	95	[2] BUSKULIC	92J	ALEP	Repl. by BUSKULIC 95C

[1] Limit is on the absolute value of the real part of the weak dipole moment.
[2] Limit is on the absolute value of the real part of the weak dipole moment, and applies for $q^2 = m^2_Z$.

Im(d^W_τ)

VALUE (10^{-17} e cm)	CL%	DOCUMENT ID		TECN	COMMENT
<1.1	95	[1] HEISTER	03F	ALEP	1990–1995 LEP runs
• • • We do not use the following data for averages, fits, limits, etc. • • •					
<1.5	95	ACKERSTAFF	97L	OPAL	1991–1995 LEP runs
<4.5	95	[2] AKERS	95F	OPAL	Repl. by ACKERSTAFF 97L

[1] HEISTER 03F limit is on the absolute value of the imaginary part of the weak dipole moment.
[2] Limit is on the absolute value of the imaginary part of the weak dipole moment, and applies for $q^2 = m^2_Z$.

τ WEAK ANOMALOUS MAGNETIC DIPOLE MOMENT (a^W_τ)

Electroweak radiative corrections are expected to contribute at the 10^{-6} level. See BERNABEU 95.

The q^2 dependence is expected to be small providing no thresholds are nearby.

Re(a^W_τ)

VALUE	CL%	DOCUMENT ID		TECN	COMMENT
$<1.1 \times 10^{-3}$	95	[1] HEISTER	03F	ALEP	1990–1995 LEP runs
• • • We do not use the following data for averages, fits, limits, etc. • • •					
> -0.0024 and < 0.0025	95	[2] GONZALEZ-S...	00	RVUE	$e^+e^- \to \tau^+\tau^-$ and $W \to \tau\nu_\tau$
$<4.5 \times 10^{-3}$	90	[1] ACCIARRI	98C	L3	1991–1995 LEP runs

[1] Limit is on the absolute value of the real part of the weak anomalous magnetic dipole moment.
[2] GONZALEZ-SPRINBERG 00 use data on tau lepton production at LEP1, SLC, and LEP2, and data from colliders and LEP2 to determine limits. Assume imaginary component is zero.

Im(a^W_τ)

VALUE	CL%	DOCUMENT ID		TECN	COMMENT
$<2.7 \times 10^{-3}$	95	[1] HEISTER	03F	ALEP	1990–1995 LEP runs
• • • We do not use the following data for averages, fits, limits, etc. • • •					
$<9.9 \times 10^{-3}$	90	[1] ACCIARRI	98C	L3	1991–1995 LEP runs

[1] Limit is on the absolute value of the imaginary part of the weak anomalous magnetic dipole moment.

τ^- DECAY MODES

τ^+ modes are charge conjugates of the modes below. "$h^\pm$" stands for $\pi^\pm$ or $K^\pm$. "ℓ" stands for e or μ. "Neutrals" stands for γ's and/or π^0's.

	Mode		Fraction (Γ_i/Γ)	Scale factor/ Confidence level
	Modes with one charged particle			
Γ_1	particle$^- \geq 0$ neutrals $\geq 0K^0\nu_\tau$ ("1-prong")		(85.24 ± 0.06) %	
Γ_2	particle$^- \geq 0$ neutrals $\geq 0K^0_L\nu_\tau$		(84.58 ± 0.06) %	
Γ_3	$\mu^-\overline{\nu}_\mu\nu_\tau$	[a]	(17.39 ± 0.04) %	
Γ_4	$\mu^-\overline{\nu}_\mu\nu_\tau\gamma$	[b]	(3.67 ± 0.08) $\times 10^{-3}$	
Γ_5	$e^-\overline{\nu}_e\nu_\tau$	[a]	(17.82 ± 0.04) %	
Γ_6	$e^-\overline{\nu}_e\nu_\tau\gamma$	[b]	(1.83 ± 0.05) %	
Γ_7	$h^- \geq 0K^0_L\ \nu_\tau$		(12.03 ± 0.05) %	
Γ_8	$h^-\nu_\tau$		(11.51 ± 0.05) %	
Γ_9	$\pi^-\nu_\tau$	[a]	(10.82 ± 0.05) %	
Γ_{10}	$K^-\nu_\tau$	[a]	(6.96 ± 0.10) $\times 10^{-3}$	
Γ_{11}	$h^- \geq 1$ neutralsν_τ		(37.01 ± 0.09) %	
Γ_{12}	$h^- \geq 1\pi^0\nu_\tau$(ex.K^0)		(36.51 ± 0.09) %	
Γ_{13}	$h^-\pi^0\nu_\tau$		(25.93 ± 0.09) %	
Γ_{14}	$\pi^-\pi^0\nu_\tau$	[a]	(25.49 ± 0.09) %	
Γ_{15}	$\pi^-\pi^0$non-$\rho(770)\nu_\tau$		(3.0 ± 3.2) $\times 10^{-3}$	
Γ_{16}	$K^-\pi^0\nu_\tau$	[a]	(4.33 ± 0.15) $\times 10^{-3}$	
Γ_{17}	$h^- \geq 2\pi^0\nu_\tau$		(10.81 ± 0.09) %	
Γ_{18}	$h^-2\pi^0\nu_\tau$		(9.48 ± 0.10) %	
Γ_{19}	$h^-2\pi^0\nu_\tau$(ex.K^0)		(9.32 ± 0.10) %	
Γ_{20}	$\pi^-2\pi^0\nu_\tau$(ex.K^0)	[a]	(9.26 ± 0.10) %	
Γ_{21}	$\pi^-2\pi^0\nu_\tau$(ex.K^0), scalar		< 9 $\times 10^{-3}$	CL=95%
Γ_{22}	$\pi^-2\pi^0\nu_\tau$(ex.K^0), vector		< 7 $\times 10^{-3}$	CL=95%
Γ_{23}	$K^-2\pi^0\nu_\tau$(ex.K^0)	[a]	(6.5 ± 2.2) $\times 10^{-4}$	
Γ_{24}	$h^- \geq 3\pi^0\nu_\tau$		(1.34 ± 0.07) %	
Γ_{25}	$h^- \geq 3\pi^0\nu_\tau$(ex. K^0)		(1.25 ± 0.07) %	
Γ_{26}	$h^-3\pi^0\nu_\tau$		(1.18 ± 0.07) %	
Γ_{27}	$\pi^-3\pi^0\nu_\tau$(ex.K^0)	[a]	(1.04 ± 0.07) %	
Γ_{28}	$K^-3\pi^0\nu_\tau$(ex.K^0, η)	[a]	(4.8 ± 2.1) $\times 10^{-4}$	
Γ_{29}	$h^-4\pi^0\nu_\tau$(ex.K^0)		(1.6 ± 0.4) $\times 10^{-3}$	
Γ_{30}	$h^-4\pi^0\nu_\tau$(ex.K^0,η)	[a]	(1.1 ± 0.4) $\times 10^{-3}$	
Γ_{31}	$a_1(1260)\nu_\tau \to \pi^-\gamma\nu_\tau$		(3.8 ± 1.5) $\times 10^{-4}$	
Γ_{32}	$K^- \geq 0\pi^0\ \geq 0K^0\ \geq 0\gamma\ \nu_\tau$		(1.552± 0.029) %	
Γ_{33}	$K^- \geq 1$ (π^0 or K^0 or γ) ν_τ		(8.59 ± 0.28) $\times 10^{-3}$	
	Modes with K^0's			
Γ_{34}	K^0_S(particles)$^-\nu_\tau$		(9.43 ± 0.28) $\times 10^{-3}$	
Γ_{35}	$h^-\overline{K}^0\nu_\tau$		(9.87 ± 0.14) $\times 10^{-3}$	
Γ_{36}	$\pi^-\overline{K}^0\nu_\tau$	[a]	(8.38 ± 0.14) $\times 10^{-3}$	
Γ_{37}	$\pi^-\overline{K}^0$(non-$K^*(892)^-)\nu_\tau$		(5.4 ± 2.1) $\times 10^{-4}$	
Γ_{38}	$K^-K^0\nu_\tau$	[a]	(1.486± 0.034) $\times 10^{-3}$	
Γ_{39}	$K^-K^0 \geq 0\pi^0\nu_\tau$		(2.99 ± 0.07) $\times 10^{-3}$	
Γ_{40}	$h^-\overline{K}^0\pi^0\nu_\tau$		(5.32 ± 0.13) $\times 10^{-3}$	
Γ_{41}	$\pi^-\overline{K}^0\pi^0\nu_\tau$	[a]	(3.82 ± 0.13) $\times 10^{-3}$	
Γ_{42}	$\overline{K}^0\rho^-\nu_\tau$		(2.2 ± 0.5) $\times 10^{-3}$	
Γ_{43}	$K^-K^0\pi^0\nu_\tau$	[a]	(1.50 ± 0.07) $\times 10^{-3}$	
Γ_{44}	$\pi^-\overline{K}^0 \geq 1\pi^0\nu_\tau$		(4.08 ± 0.25) $\times 10^{-3}$	
Γ_{45}	$\pi^-\overline{K}^0\pi^0\pi^0\nu_\tau$(ex.$K^0$)	[a]	(2.6 ± 2.3) $\times 10^{-4}$	
Γ_{46}	$K^-K^0\pi^0\pi^0\nu_\tau$		< 1.6 $\times 10^{-4}$	CL=95%
Γ_{47}	$\pi^-K^0\overline{K}^0\nu_\tau$		(1.55 ± 0.24) $\times 10^{-3}$	
Γ_{48}	$\pi^-K^0_SK^0_S\nu_\tau$	[a]	(2.35 ± 0.06) $\times 10^{-4}$	
Γ_{49}	$\pi^-K^0_SK^0_L\nu_\tau$	[a]	(1.08 ± 0.24) $\times 10^{-3}$	
Γ_{50}	$\pi^-K^0_LK^0_L\nu_\tau$		(2.35 ± 0.06) $\times 10^{-4}$	
Γ_{51}	$\pi^-K^0\overline{K}^0\pi^0\nu_\tau$		(3.6 ± 1.2) $\times 10^{-4}$	
Γ_{52}	$\pi^-K^0_SK^0_S\pi^0\nu_\tau$	[a]	(1.82 ± 0.21) $\times 10^{-5}$	
Γ_{53}	$K^{*-}K^0\pi^0\nu_\tau \to \pi^-K^0_SK^0_S\pi^0\nu_\tau$		(1.08 ± 0.21) $\times 10^{-5}$	
Γ_{54}	$f_1(1285)\pi^-\nu_\tau \to \pi^-K^0_SK^0_S\pi^0\nu_\tau$		(6.8 ± 1.5) $\times 10^{-6}$	
Γ_{55}	$f_1(1420)\pi^-\nu_\tau \to \pi^-K^0_SK^0_S\pi^0\nu_\tau$		(2.4 ± 0.8) $\times 10^{-6}$	
Γ_{56}	$\pi^-K^0_SK^0_L\pi^0\nu_\tau$	[a]	(3.2 ± 1.2) $\times 10^{-4}$	
Γ_{57}	$\pi^-K^0_LK^0_L\pi^0\nu_\tau$		(1.82 ± 0.21) $\times 10^{-5}$	
Γ_{58}	$K^-K^0_SK^0_S\nu_\tau$		< 6.3 $\times 10^{-7}$	CL=90%
Γ_{59}	$K^-K^0_SK^0_S\pi^0\nu_\tau$		< 4.0 $\times 10^{-7}$	CL=90%
Γ_{60}	$K^0h^+h^-h^- \geq 0$ neutrals ν_τ		< 1.7 $\times 10^{-3}$	CL=95%
Γ_{61}	$K^0h^+h^-h^-\nu_\tau$	[a]	(2.5 ± 2.0) $\times 10^{-4}$	
	Modes with three charged particles			
Γ_{62}	$h^-h^-h^+ \geq 0$ neutrals $\geq 0K^0_L\nu_\tau$		(15.20 ± 0.06) %	
Γ_{63}	$h^-h^-h^+ \geq 0$ neutrals ν_τ (ex. $K^0_S \to \pi^+\pi^-$) ("3-prong")		(14.55 ± 0.06) %	
Γ_{64}	$h^-h^-h^+\nu_\tau$		(9.80 ± 0.05) %	
Γ_{65}	$h^-h^-h^+\nu_\tau$(ex.K^0)		(9.46 ± 0.05) %	
Γ_{66}	$h^-h^-h^+\nu_\tau$(ex.K^0,ω)		(9.43 ± 0.05) %	
Γ_{67}	$\pi^-\pi^+\pi^-\nu_\tau$		(9.31 ± 0.05) %	
Γ_{68}	$\pi^-\pi^+\pi^-\nu_\tau$(ex.K^0)		(9.02 ± 0.05) %	
Γ_{69}	$\pi^-\pi^+\pi^-\nu_\tau$(ex.K^0), non-axial vector		< 2.4 %	CL=95%

Downloaded from https://academic.oup.com/ptep/article/2022/8/083C01/6651666 by KIT Library user on 27 September 2022

Γ_{70}	$\pi^-\pi^+\pi^-\nu_\tau$ (ex.K^0,ω)	[a]	(8.99 ± 0.05) %	
Γ_{71}	$h^-h^-h^+ \geq 1$ neutrals ν_τ		(5.29 ± 0.05) %	
Γ_{72}	$h^-h^-h^+ \geq 1\pi^0\nu_\tau$ (ex. K^0)		(5.09 ± 0.05) %	
Γ_{73}	$h^-h^-h^+\pi^0\nu_\tau$		(4.76 ± 0.05) %	
Γ_{74}	$h^-h^-h^+\pi^0\nu_\tau$ (ex.K^0)		(4.57 ± 0.05) %	
Γ_{75}	$h^-h^-h^+\pi^0\nu_\tau$ (ex. K^0, ω)		(2.79 ± 0.07) %	
Γ_{76}	$\pi^-\pi^+\pi^-\pi^0\nu_\tau$		(4.62 ± 0.05) %	
Γ_{77}	$\pi^-\pi^+\pi^-\pi^0\nu_\tau$ (ex.K^0)		(4.49 ± 0.05) %	
Γ_{78}	$\pi^-\pi^+\pi^-\pi^0\nu_\tau$ (ex.K^0,ω)	[a]	(2.74 ± 0.07) %	
Γ_{79}	$h^-\rho\pi^0\nu_\tau$			
Γ_{80}	$h^-\rho^+h^-\nu_\tau$			
Γ_{81}	$h^-\rho^-h^+\nu_\tau$			
Γ_{82}	$h^-h^-h^+ \geq 2\pi^0\nu_\tau$ (ex. K^0)		$(5.17 \pm 0.31) \times 10^{-3}$	
Γ_{83}	$h^-h^-h^+2\pi^0\nu_\tau$		$(5.05 \pm 0.31) \times 10^{-3}$	
Γ_{84}	$h^-h^-h^+2\pi^0\nu_\tau$ (ex.K^0)		$(4.95 \pm 0.31) \times 10^{-3}$	
Γ_{85}	$h^-h^-h^+2\pi^0\nu_\tau$ (ex.K^0,ω,η)	[a]	$(10 \pm 4) \times 10^{-4}$	
Γ_{86}	$h^-h^-h^+3\pi^0\nu_\tau$		$(2.13 \pm 0.30) \times 10^{-4}$	
Γ_{87}	$2\pi^-\pi^+3\pi^0\nu_\tau$ (ex.K^0)		$(1.95 \pm 0.30) \times 10^{-4}$	
Γ_{88}	$2\pi^-\pi^+3\pi^0\nu_\tau$ (ex.K^0, η, $f_1(1285)$)		$(1.7 \pm 0.4) \times 10^{-4}$	
Γ_{89}	$2\pi^-\pi^+3\pi^0\nu_\tau$ (ex.K^0, η, ω, $f_1(1285)$)	[a]	$(1.4 \pm 2.7) \times 10^{-5}$	
Γ_{90}	$K^-h^+h^- \geq 0$ neutrals ν_τ		$(6.29 \pm 0.14) \times 10^{-3}$	
Γ_{91}	$K^-h^+\pi^-\nu_\tau$ (ex.K^0)		$(4.37 \pm 0.07) \times 10^{-3}$	
Γ_{92}	$K^-h^+\pi^-\pi^0\nu_\tau$ (ex.K^0)		$(8.6 \pm 1.2) \times 10^{-4}$	
Γ_{93}	$K^-\pi^+\pi^- \geq 0$ neutrals ν_τ		$(4.77 \pm 0.14) \times 10^{-3}$	
Γ_{94}	$K^-\pi^+\pi^- \geq 0\pi^0\nu_\tau$ (ex.K^0)		$(3.73 \pm 0.13) \times 10^{-3}$	
Γ_{95}	$K^-\pi^+\pi^-\nu_\tau$		$(3.45 \pm 0.07) \times 10^{-3}$	
Γ_{96}	$K^-\pi^+\pi^-\nu_\tau$ (ex.K^0)		$(2.93 \pm 0.07) \times 10^{-3}$	
Γ_{97}	$K^-\pi^+\pi^-\nu_\tau$ (ex.K^0,ω)	[a]	$(2.93 \pm 0.07) \times 10^{-3}$	
Γ_{98}	$K^-\rho^0\nu_\tau \to K^-\pi^+\pi^-\nu_\tau$		$(1.4 \pm 0.5) \times 10^{-3}$	
Γ_{99}	$K^-\pi^+\pi^-\pi^0\nu_\tau$		$(1.31 \pm 0.12) \times 10^{-3}$	
Γ_{100}	$K^-\pi^+\pi^-\pi^0\nu_\tau$ (ex.K^0)		$(7.9 \pm 1.2) \times 10^{-4}$	
Γ_{101}	$K^-\pi^+\pi^-\pi^0\nu_\tau$ (ex.K^0,η)		$(7.6 \pm 1.2) \times 10^{-4}$	
Γ_{102}	$K^-\pi^+\pi^-\pi^0\nu_\tau$ (ex.K^0,ω)		$(3.7 \pm 0.9) \times 10^{-4}$	
Γ_{103}	$K^-\pi^+\pi^-\pi^0\nu_\tau$ (ex.K^0,ω,η)	[a]	$(3.9 \pm 1.4) \times 10^{-4}$	
Γ_{104}	$K^-\pi^+K^- \geq 0$ neut. ν_τ		$< 9 \times 10^{-4}$	CL=95%
Γ_{105}	$K^-K^+\pi^- \geq 0$ neut. ν_τ		$(1.496 \pm 0.033) \times 10^{-3}$	
Γ_{106}	$K^-K^+\pi^-\nu_\tau$	[a]	$(1.435 \pm 0.027) \times 10^{-3}$	
Γ_{107}	$K^-K^+\pi^-\pi^0\nu_\tau$	[a]	$(6.1 \pm 1.8) \times 10^{-5}$	
Γ_{108}	$K^-K^+K^-\nu_\tau$		$(2.2 \pm 0.8) \times 10^{-5}$	S=5.4
Γ_{109}	$K^-K^+K^-\nu_\tau$ (ex. ϕ)		$< 2.5 \times 10^{-6}$	CL=90%
Γ_{110}	$K^-K^+K^-\pi^0\nu_\tau$		$< 4.8 \times 10^{-6}$	CL=90%
Γ_{111}	$\pi^-K^+\pi^- \geq 0$ neut. ν_τ		$< 2.5 \times 10^{-3}$	CL=95%
Γ_{112}	$e^-e^-e^+\overline{\nu}_e\nu_\tau$		$(2.8 \pm 1.5) \times 10^{-5}$	
Γ_{113}	$\mu^-e^-e^+\overline{\nu}_\mu\nu_\tau$		$< 3.2 \times 10^{-5}$	CL=90%
Γ_{114}	$\pi^-e^-e^+\nu_\tau$		seen	
Γ_{115}	$\pi^-\mu^-\mu^+\nu_\tau$		$< 1.14 \times 10^{-5}$	CL=90%

Modes with five charged particles

Γ_{116}	$3h^-2h^+ \geq 0$ neutrals ν_τ (ex. $K^0_S \to \pi^-\pi^+$) ("5-prong")		$(9.9 \pm 0.4) \times 10^{-4}$	
Γ_{117}	$3h^-2h^+\nu_\tau$ (ex.K^0)		$(8.29 \pm 0.31) \times 10^{-4}$	
Γ_{118}	$3\pi^-2\pi^+\nu_\tau$ (ex.K^0, ω)		$(8.27 \pm 0.31) \times 10^{-4}$	
Γ_{119}	$3\pi^-2\pi^+\nu_\tau$ (ex.K^0, ω, $f_1(1285)$)	[a]	$(7.75 \pm 0.30) \times 10^{-4}$	
Γ_{120}	$K^-2\pi^-2\pi^+\nu_\tau$ (ex.K^0)	[a]	$(6 \pm 12) \times 10^{-7}$	
Γ_{121}	$K^+3\pi^-\pi^+\nu_\tau$		$< 5.0 \times 10^{-6}$	CL=90%
Γ_{122}	$K^+K^-2\pi^-\pi^+\nu_\tau$		$< 4.5 \times 10^{-7}$	CL=90%
Γ_{123}	$3h^-2h^+\pi^0\nu_\tau$ (ex.K^0)		$(1.65 \pm 0.11) \times 10^{-4}$	
Γ_{124}	$3\pi^-2\pi^+\pi^0\nu_\tau$ (ex.K^0)		$(1.63 \pm 0.11) \times 10^{-4}$	
Γ_{125}	$3\pi^-2\pi^+\pi^0\nu_\tau$ (ex.K^0, η, $f_1(1285)$)		$(1.11 \pm 0.10) \times 10^{-4}$	
Γ_{126}	$3\pi^-2\pi^+\pi^0\nu_\tau$ (ex.K^0, η, ω, $f_1(1285)$)	[a]	$(3.8 \pm 0.9) \times 10^{-5}$	
Γ_{127}	$K^-2\pi^-2\pi^+\pi^0\nu_\tau$ (ex.K^0)	[a]	$(1.1 \pm 0.6) \times 10^{-6}$	
Γ_{128}	$K^+3\pi^-\pi^+\pi^0\nu_\tau$		$< 8 \times 10^{-7}$	CL=90%
Γ_{129}	$3h^-2h^+2\pi^0\nu_\tau$		$< 3.4 \times 10^{-6}$	CL=90%

Miscellaneous other allowed modes

Γ_{130}	$(5\pi)^-\nu_\tau$		$(7.8 \pm 0.5) \times 10^{-3}$	
Γ_{131}	$4h^-3h^+ \geq 0$ neutrals ν_τ ("7-prong")		$< 3.0 \times 10^{-7}$	CL=90%
Γ_{132}	$4h^-3h^+\nu_\tau$		$< 4.3 \times 10^{-7}$	CL=90%
Γ_{133}	$4h^-3h^+\pi^0\nu_\tau$		$< 2.5 \times 10^{-7}$	CL=90%
Γ_{134}	$X^-(S=-1)\nu_\tau$		(2.92 ± 0.04) %	
Γ_{135}	$K^*(892)^- \geq 0$ neutrals $\geq 0K^0_L\nu_\tau$		(1.42 ± 0.18) %	S=1.4
Γ_{136}	$K^*(892)^-\nu_\tau$		(1.20 ± 0.07) %	S=1.8
Γ_{137}	$K^*(892)^-\nu_\tau \to \pi^-\overline{K}^0\nu_\tau$		$(7.82 \pm 0.26) \times 10^{-3}$	
Γ_{138}	$K^*(892)^0K^- \geq 0$ neutrals ν_τ		$(3.2 \pm 1.4) \times 10^{-3}$	
Γ_{139}	$K^*(892)^0K^-\nu_\tau$		$(2.1 \pm 0.4) \times 10^{-3}$	
Γ_{140}	$\overline{K}^*(892)^0\pi^- \geq 0$ neutrals ν_τ		$(3.8 \pm 1.7) \times 10^{-3}$	
Γ_{141}	$\overline{K}^*(892)^0\pi^-\nu_\tau$		$(2.2 \pm 0.5) \times 10^{-3}$	
Γ_{142}	$(\overline{K}^*(892)\pi)^-\nu_\tau \to \pi^-\overline{K}^0\pi^0\nu_\tau$		$(1.0 \pm 0.4) \times 10^{-3}$	
Γ_{143}	$K_1(1270)^-\nu_\tau$		$(4.7 \pm 1.1) \times 10^{-3}$	
Γ_{144}	$K_1(1400)^-\nu_\tau$		$(1.7 \pm 2.6) \times 10^{-3}$	S=1.7
Γ_{145}	$K^*(1410)^-\nu_\tau$		$(1.5 {}^{+1.4}_{-1.0}) \times 10^{-3}$	
Γ_{146}	$K^*_0(1430)^-\nu_\tau$		$< 5 \times 10^{-4}$	CL=95%
Γ_{147}	$K^*_2(1430)^-\nu_\tau$		$< 3 \times 10^{-3}$	CL=95%
Γ_{148}	$a_0(980)^- \geq 0$ neutrals ν_τ			
Γ_{149}	$\eta\pi^-\nu_\tau$		$< 9.9 \times 10^{-5}$	CL=95%
Γ_{150}	$\eta\pi^-\pi^0\nu_\tau$	[a]	$(1.39 \pm 0.07) \times 10^{-3}$	
Γ_{151}	$\eta\pi^-\pi^0\pi^0\nu_\tau$	[a]	$(2.0 \pm 0.4) \times 10^{-4}$	
Γ_{152}	$\eta K^-\nu_\tau$	[a]	$(1.55 \pm 0.08) \times 10^{-4}$	
Γ_{153}	$\eta K^*(892)^-\nu_\tau$		$(1.38 \pm 0.15) \times 10^{-4}$	
Γ_{154}	$\eta K^-\pi^0\nu_\tau$	[a]	$(4.8 \pm 1.2) \times 10^{-5}$	
Γ_{155}	$\eta K^-\pi^0$(non-$K^*(892)$)ν_τ		$< 3.5 \times 10^{-5}$	CL=90%
Γ_{156}	$\eta\overline{K}^0\pi^-\nu_\tau$	[a]	$(9.4 \pm 1.5) \times 10^{-5}$	
Γ_{157}	$\eta\overline{K}^0\pi^-\pi^0\nu_\tau$		$< 5.0 \times 10^{-5}$	CL=90%
Γ_{158}	$\eta K^-K^0\nu_\tau$		$< 9.0 \times 10^{-6}$	CL=90%
Γ_{159}	$\eta\pi^+\pi^-\pi^- \geq 0$ neutrals ν_τ		$< 3 \times 10^{-3}$	CL=90%
Γ_{160}	$\eta\pi^-\pi^+\pi^-\nu_\tau$ (ex.K^0)	[a]	$(2.20 \pm 0.13) \times 10^{-4}$	
Γ_{161}	$\eta\pi^-\pi^+\pi^-\nu_\tau$ (ex.K^0,$f_1(1285)$)		$(9.9 \pm 1.6) \times 10^{-5}$	
Γ_{162}	$\eta a_1(1260)^-\nu_\tau \to \eta\pi^-\rho^0\nu_\tau$		$< 3.9 \times 10^{-4}$	CL=90%
Γ_{163}	$\eta\eta\pi^-\nu_\tau$		$< 7.4 \times 10^{-6}$	CL=90%
Γ_{164}	$\eta\eta\pi^-\pi^0\nu_\tau$		$< 2.0 \times 10^{-4}$	CL=95%
Γ_{165}	$\eta\eta K^-\nu_\tau$		$< 3.0 \times 10^{-6}$	CL=90%
Γ_{166}	$\eta'(958)\pi^-\nu_\tau$		$< 4.0 \times 10^{-6}$	CL=90%
Γ_{167}	$\eta'(958)\pi^-\pi^0\nu_\tau$		$< 1.2 \times 10^{-5}$	CL=90%
Γ_{168}	$\eta'(958)K^-\nu_\tau$		$< 2.4 \times 10^{-6}$	CL=90%
Γ_{169}	$\phi\pi^-\nu_\tau$		$(3.4 \pm 0.6) \times 10^{-5}$	
Γ_{170}	$\phi K^-\nu_\tau$	[a]	$(4.4 \pm 1.6) \times 10^{-5}$	
Γ_{171}	$f_1(1285)\pi^-\nu_\tau$		$(3.9 \pm 0.5) \times 10^{-4}$	S=1.9
Γ_{172}	$f_1(1285)\pi^-\nu_\tau \to \eta\pi^-\pi^+\pi^-\nu_\tau$		$(1.18 \pm 0.07) \times 10^{-4}$	S=1.3
Γ_{173}	$f_1(1285)\pi^-\nu_\tau \to 3\pi^-2\pi^+\nu_\tau$	[a]	$(5.2 \pm 0.4) \times 10^{-5}$	
Γ_{174}	$\pi(1300)^-\nu_\tau \to (\rho\pi)^-\nu_\tau \to (3\pi)^-\nu_\tau$		$< 1.0 \times 10^{-4}$	CL=90%
Γ_{175}	$\pi(1300)^-\nu_\tau \to ((\pi\pi)_{S-\text{wave}}\pi)^-\nu_\tau \to (3\pi)^-\nu_\tau$		$< 1.9 \times 10^{-4}$	CL=90%
Γ_{176}	$h^-\omega \geq 0$ neutrals ν_τ		(2.40 ± 0.08) %	
Γ_{177}	$h^-\omega\nu_\tau$		(1.99 ± 0.06) %	
Γ_{178}	$\pi^-\omega\nu_\tau$	[a]	(1.95 ± 0.06) %	
Γ_{179}	$K^-\omega\nu_\tau$	[a]	$(4.1 \pm 0.9) \times 10^{-4}$	
Γ_{180}	$h^-\omega\pi^0\nu_\tau$	[a]	$(4.1 \pm 0.4) \times 10^{-3}$	
Γ_{181}	$h^-\omega 2\pi^0\nu_\tau$		$(1.4 \pm 0.5) \times 10^{-4}$	
Γ_{182}	$\pi^-\omega 2\pi^0\nu_\tau$	[a]	$(7.2 \pm 1.6) \times 10^{-5}$	
Γ_{183}	$h^-2\omega\nu_\tau$		$< 5.4 \times 10^{-7}$	CL=90%
Γ_{184}	$2h^-h^+\omega\nu_\tau$		$(1.20 \pm 0.22) \times 10^{-4}$	
Γ_{185}	$2\pi^-\pi^+\omega\nu_\tau$ (ex.K^0)	[a]	$(8.4 \pm 0.6) \times 10^{-5}$	

Lepton Family number (*LF*), Lepton number (*L*), or Baryon number (*B*) violating modes

L means lepton number violation (*e.g.* $\tau^- \to e^+\pi^-\pi^-$). Following common usage, *LF* means lepton family violation *and not* lepton number violation (*e.g.* $\tau^- \to e^-\pi^+\pi^-$). *B* means baryon number violation.

Γ_{186}	$e^-\gamma$	*LF*	$< 3.3 \times 10^{-8}$	CL=90%
Γ_{187}	$e^-\gamma\gamma$		$< 2.5 \times 10^{-4}$	CL=90%
Γ_{188}	$\mu^-\gamma$	*LF*	$< 4.2 \times 10^{-8}$	CL=90%
Γ_{189}	$\mu^-\gamma\gamma$		$< 5.8 \times 10^{-4}$	CL=90%
Γ_{190}	$e^-\pi^0$	*LF*	$< 8.0 \times 10^{-8}$	CL=90%
Γ_{191}	$\mu^-\pi^0$	*LF*	$< 1.1 \times 10^{-7}$	CL=90%
Γ_{192}	$e^-K^0_S$	*LF*	$< 2.6 \times 10^{-8}$	CL=90%
Γ_{193}	$\mu^-K^0_S$	*LF*	$< 2.3 \times 10^{-8}$	CL=90%
Γ_{194}	$e^-\eta$	*LF*	$< 9.2 \times 10^{-8}$	CL=90%

Downloaded from https://academic.oup.com/ptep/article/2022/8/083C01/6651666 by KIT Library user on 27 September 2022

Γ_{195}	$\mu^- \eta$	LF	<	6.5	$\times 10^{-8}$	CL=90%
Γ_{196}	$e^- \rho^0$	LF	<	1.8	$\times 10^{-8}$	CL=90%
Γ_{197}	$\mu^- \rho^0$	LF	<	1.2	$\times 10^{-8}$	CL=90%
Γ_{198}	$e^- \omega$	LF	<	4.8	$\times 10^{-8}$	CL=90%
Γ_{199}	$\mu^- \omega$	LF	<	4.7	$\times 10^{-8}$	CL=90%
Γ_{200}	$e^- K^*(892)^0$	LF	<	3.2	$\times 10^{-8}$	CL=90%
Γ_{201}	$\mu^- K^*(892)^0$	LF	<	5.9	$\times 10^{-8}$	CL=90%
Γ_{202}	$e^- \overline{K}^*(892)^0$	LF	<	3.4	$\times 10^{-8}$	CL=90%
Γ_{203}	$\mu^- \overline{K}^*(892)^0$	LF	<	7.0	$\times 10^{-8}$	CL=90%
Γ_{204}	$e^- \eta'(958)$	LF	<	1.6	$\times 10^{-7}$	CL=90%
Γ_{205}	$\mu^- \eta'(958)$	LF	<	1.3	$\times 10^{-7}$	CL=90%
Γ_{206}	$e^- f_0(980) \rightarrow e^- \pi^+ \pi^-$	LF	<	3.2	$\times 10^{-8}$	CL=90%
Γ_{207}	$\mu^- f_0(980) \rightarrow \mu^- \pi^+ \pi^-$	LF	<	3.4	$\times 10^{-8}$	CL=90%
Γ_{208}	$e^- \phi$	LF	<	3.1	$\times 10^{-8}$	CL=90%
Γ_{209}	$\mu^- \phi$	LF	<	8.4	$\times 10^{-8}$	CL=90%
Γ_{210}	$e^- e^+ e^-$	LF	<	2.7	$\times 10^{-8}$	CL=90%
Γ_{211}	$e^- \mu^+ \mu^-$	LF	<	2.7	$\times 10^{-8}$	CL=90%
Γ_{212}	$e^+ \mu^- \mu^-$	LF	<	1.7	$\times 10^{-8}$	CL=90%
Γ_{213}	$\mu^- e^+ e^-$	LF	<	1.8	$\times 10^{-8}$	CL=90%
Γ_{214}	$\mu^+ e^- e^-$	LF	<	1.5	$\times 10^{-8}$	CL=90%
Γ_{215}	$\mu^- \mu^+ \mu^-$	LF	<	2.1	$\times 10^{-8}$	CL=90%
Γ_{216}	$e^- \pi^+ \pi^-$	LF	<	2.3	$\times 10^{-8}$	CL=90%
Γ_{217}	$e^+ \pi^- \pi^-$	L	<	2.0	$\times 10^{-8}$	CL=90%
Γ_{218}	$\mu^- \pi^+ \pi^-$	LF	<	2.1	$\times 10^{-8}$	CL=90%
Γ_{219}	$\mu^+ \pi^- \pi^-$	L	<	3.9	$\times 10^{-8}$	CL=90%
Γ_{220}	$e^- \pi^+ K^-$	LF	<	3.7	$\times 10^{-8}$	CL=90%
Γ_{221}	$e^- \pi^- K^+$	LF	<	3.1	$\times 10^{-8}$	CL=90%
Γ_{222}	$e^+ \pi^- K^-$	L	<	3.2	$\times 10^{-8}$	CL=90%
Γ_{223}	$e^- K^0_S K^0_S$	LF	<	7.1	$\times 10^{-8}$	CL=90%
Γ_{224}	$e^- K^+ K^-$	LF	<	3.4	$\times 10^{-8}$	CL=90%
Γ_{225}	$e^+ K^- K^-$	L	<	3.3	$\times 10^{-8}$	CL=90%
Γ_{226}	$\mu^- \pi^+ K^-$	LF	<	8.6	$\times 10^{-8}$	CL=90%
Γ_{227}	$\mu^- \pi^- K^+$	LF	<	4.5	$\times 10^{-8}$	CL=90%
Γ_{228}	$\mu^+ \pi^- K^-$	L	<	4.8	$\times 10^{-8}$	CL=90%
Γ_{229}	$\mu^- K^0_S K^0_S$	LF	<	8.0	$\times 10^{-8}$	CL=90%
Γ_{230}	$\mu^- K^+ K^-$	LF	<	4.4	$\times 10^{-8}$	CL=90%
Γ_{231}	$\mu^+ K^- K^-$	L	<	4.7	$\times 10^{-8}$	CL=90%
Γ_{232}	$e^- \pi^0 \pi^0$	LF	<	6.5	$\times 10^{-6}$	CL=90%
Γ_{233}	$\mu^- \pi^0 \pi^0$	LF	<	1.4	$\times 10^{-5}$	CL=90%
Γ_{234}	$e^- \eta \eta$	LF	<	3.5	$\times 10^{-5}$	CL=90%
Γ_{235}	$\mu^- \eta \eta$	LF	<	6.0	$\times 10^{-5}$	CL=90%
Γ_{236}	$e^- \pi^0 \eta$	LF	<	2.4	$\times 10^{-5}$	CL=90%
Γ_{237}	$\mu^- \pi^0 \eta$	LF	<	2.2	$\times 10^{-5}$	CL=90%
Γ_{238}	$p e^- e^-$	L,B	<	3.0	$\times 10^{-8}$	CL=90%
Γ_{239}	$\overline{p} e^+ e^-$	L,B	<	3.0	$\times 10^{-8}$	CL=90%
Γ_{240}	$\overline{p} e^+ \mu^-$	L,B	<	2.0	$\times 10^{-8}$	CL=90%
Γ_{241}	$\overline{p} e^- \mu^+$	L,B	<	1.8	$\times 10^{-8}$	CL=90%
Γ_{242}	$p \mu^- \mu^-$	L,B	<	4.0	$\times 10^{-8}$	CL=90%
Γ_{243}	$\overline{p} \mu^+ \mu^-$	L,B	<	1.8	$\times 10^{-8}$	CL=90%
Γ_{244}	$\overline{p} \gamma$	L,B	<	3.5	$\times 10^{-6}$	CL=90%
Γ_{245}	$\overline{p} \pi^0$	L,B	<	1.5	$\times 10^{-5}$	CL=90%
Γ_{246}	$\overline{p} 2\pi^0$	L,B	<	3.3	$\times 10^{-5}$	CL=90%
Γ_{247}	$\overline{p} \eta$	L,B	<	8.9	$\times 10^{-6}$	CL=90%
Γ_{248}	$\overline{p} \pi^0 \eta$	L,B	<	2.7	$\times 10^{-5}$	CL=90%
Γ_{249}	$\Lambda \pi^-$	L,B	<	7.2	$\times 10^{-8}$	CL=90%
Γ_{250}	$\overline{\Lambda} \pi^-$	L,B	<	1.4	$\times 10^{-7}$	CL=90%
Γ_{251}	e^- light boson	LF	<	2.7	$\times 10^{-3}$	CL=95%
Γ_{252}	μ^- light boson	LF	<	5	$\times 10^{-3}$	CL=95%

[a] Basis mode for the τ.

[b] See the Particle Listings below for the energy limits used in this measurement.

CONSTRAINED FIT INFORMATION

An overall fit to 87 branching ratios uses 170 measurements and one constraint to determine 46 parameters. The overall fit has a $\chi^2 = 135.0$ for 125 degrees of freedom.

The following *off-diagonal* array elements are the correlation coefficients $\langle \delta x_i \delta x_j \rangle / (\delta x_i \cdot \delta x_j)$, in percent, from the fit to the branching fractions, $x_i \equiv \Gamma_i / \Gamma_{\text{total}}$.

	x_3	x_5	x_9	x_{10}	x_{14}	x_{16}	x_{20}	x_{23}	x_{27}	x_{28}
x_5	18									
x_9	2	−1								
x_{10}	3	4	5							
x_{14}	−18	−19	−17	−5						
x_{16}	−1	−1	0	−2	−9					
x_{20}	−11	−11	−14	−4	−46	−1				
x_{23}	−1	0	−2	−3	−1	−14	−10			
x_{27}	−6	−5	−10	−1	0	1	−39	1		
x_{28}	−1	−1	−1	−2	0	−13	−3	−23	−11	
x_{30}	−4	−3	−11	−1	−9	0	7	−2	−44	2
x_{36}	−2	−2	−3	−1	−1	−1	−2	0	−1	0
x_{38}	−1	−1	1	0	0	0	0	−2	0	−2
x_{41}	−2	−2	−2	−1	−1	0	−2	0	−1	0
x_{43}	−1	−1	−1	−1	0	−3	0	−5	0	−5
x_{45}	−5	−5	−5	−2	−3	−1	−5	−2	−1	−2
x_{48}	−1	−1	2	0	−1	2	−1	−1	0	−1
x_{49}	−5	−5	−5	−2	−3	−1	−5	−2	−1	−2
x_{52}	0	0	0	0	0	0	0	−1	0	−1
x_{56}	−2	−2	−2	−1	−1	−1	−2	−1	−1	−1
x_{61}	−5	−5	−5	−2	−3	−1	−4	−2	−1	−2
x_{70}	−7	−9	4	−2	−6	3	−12	−2	−7	−1
x_{78}	−4	−4	−5	0	−9	0	1	1	−1	1
x_{85}	0	0	−2	0	−2	0	0	0	2	0
x_{89}	0	0	0	0	0	0	0	0	0	0
x_{97}	−2	−2	−1	−1	−1	−1	−4	−1	−2	−1
x_{103}	1	1	0	−1	1	−1	−1	−1	0	−1
x_{106}	−1	−2	2	−1	−1	1	−2	−1	−1	−1
x_{107}	0	0	0	0	0	0	0	0	0	0
x_{119}	−1	−1	1	0	−1	1	−2	−1	−1	0
x_{120}	0	0	0	0	0	0	0	0	0	0
x_{126}	0	0	0	0	0	0	0	0	0	0
x_{127}	0	0	0	0	0	0	0	0	0	0
x_{150}	−1	−1	−1	0	−1	0	−2	−1	0	−1
x_{151}	−1	−1	0	0	−1	0	−1	0	0	0
x_{152}	0	0	0	0	0	0	0	−1	0	−1
x_{154}	0	0	0	0	0	0	0	0	0	0
x_{156}	0	0	0	0	0	0	0	0	0	0
x_{160}	−1	−1	1	0	−1	1	−1	0	−1	0
x_{170}	0	0	0	0	0	0	0	0	0	0
x_{173}	0	−1	1	0	0	1	−1	0	0	0
x_{178}	−3	−3	−3	−1	−4	−1	−1	0	−1	0
x_{179}	0	0	0	0	0	0	0	0	0	0
x_{180}	−2	−2	−5	−1	−3	0	−2	−1	2	−1
x_{182}	0	0	0	0	0	0	0	0	0	0
x_{185}	−1	−1	0	0	−1	1	−1	0	0	0

Downloaded from https://academic.oup.com/ptep/article/2022/8/083C01/6651666 by KIT Library user on 27 September 2022

	x_{30}	x_{36}	x_{38}	x_{41}	x_{43}	x_{45}	x_{48}	x_{49}	x_{52}	x_{56}
x_{36}	0									
x_{38}	0	−15								
x_{41}	0	−13	2							
x_{43}	0	−1	−14	−20						
x_{45}	0	−3	0	−6	0					
x_{48}	0	−2	3	−4	1	0				
x_{49}	0	−5	0	−4	−1	−10	−1			
x_{52}	0	1	5	−1	6	0	−7	0		
x_{56}	0	−2	0	−2	−1	−4	0	−8	0	
x_{61}	0	−2	0	−2	0	−4	0	−4	0	−2
x_{70}	−5	−3	3	−2	−1	−4	5	−4	0	−2
x_{78}	3	1	−1	1	0	2	−1	2	0	1
x_{85}	2	0	0	0	0	0	0	0	0	0
x_{89}	0	0	0	0	0	0	0	0	−1	0
x_{97}	−1	−1	0	−1	0	−2	0	−2	0	−1
x_{103}	−1	−1	0	−1	0	−1	0	−1	0	−1
x_{106}	−1	−1	1	0	0	−1	2	−1	0	−1
x_{107}	0	0	0	0	0	0	0	0	0	0
x_{119}	−1	−1	1	0	0	−1	2	−1	0	0
x_{120}	0	0	0	0	0	0	0	0	0	0
x_{126}	0	0	0	0	0	0	0	0	0	0
x_{127}	0	0	0	0	0	0	0	0	0	0
x_{150}	−2	−1	0	0	0	−1	0	−1	0	0
x_{151}	0	0	0	0	0	−1	0	−1	0	0
x_{152}	0	0	1	0	0	0	1	0	0	0
x_{154}	0	0	0	0	0	0	0	0	0	0
x_{156}	0	0	0	0	0	0	0	−1	0	0
x_{160}	−1	0	1	0	0	−1	1	−1	0	0
x_{170}	0	0	0	0	0	0	0	0	0	0
x_{173}	−1	0	1	0	0	0	1	0	0	0
x_{178}	1	0	0	0	0	−1	0	−1	0	0
x_{179}	0	0	0	0	0	0	0	0	0	0
x_{180}	2	−1	0	0	0	−1	0	−1	0	0
x_{182}	0	0	0	0	0	0	0	0	0	0
x_{185}	−1	0	1	0	0	0	1	−1	0	0

	x_{61}	x_{70}	x_{78}	x_{85}	x_{89}	x_{97}	x_{103}	x_{106}	x_{107}	x_{119}
x_{70}	−4									
x_{78}	2	−19								
x_{85}	0	−1	−8							
x_{89}	0	−1	−1	0						
x_{97}	−2	19	−6	0	0					
x_{103}	−1	−4	−14	−1	0	−1				
x_{106}	−1	15	−4	0	0	0	−1			
x_{107}	0	−1	−1	0	0	0	−3	0		
x_{119}	−1	3	−1	0	−4	−1	0	1	0	
x_{120}	0	0	0	0	0	0	0	0	0	−1
x_{126}	0	0	0	0	0	0	0	0	0	3
x_{127}	0	0	0	0	0	0	0	0	0	−1
x_{150}	−1	0	0	−5	0	0	0	0	0	0
x_{151}	−1	0	0	0	−11	0	0	0	0	9
x_{152}	0	2	0	0	0	0	−1	1	0	1
x_{154}	0	0	0	−1	0	0	0	0	0	0
x_{156}	0	0	0	0	−2	0	0	0	0	0
x_{160}	−1	1	−1	0	−8	−1	0	1	0	46
x_{170}	0	−1	0	0	0	1	0	1	0	0
x_{173}	0	1	0	0	−2	0	0	1	0	34
x_{178}	−1	−9	−67	−3	0	−2	10	−2	0	−1
x_{179}	0	0	12	0	0	−2	−58	0	0	0
x_{180}	−1	−2	−11	−64	−1	−1	−1	−1	0	0
x_{182}	0	0	0	0	−16	0	0	0	0	7
x_{185}	0	1	0	0	−4	0	0	1	0	39

	x_{120}	x_{126}	x_{127}	x_{150}	x_{151}	x_{152}	x_{154}	x_{156}	x_{160}	x_{170}
x_{126}	0									
x_{127}	0	−1								
x_{150}	0	0	0							
x_{151}	0	2	0	0						
x_{152}	0	0	0	4	0					
x_{154}	0	0	0	1	0	1				
x_{156}	0	0	0	2	−1	1	0			
x_{160}	−1	3	−1	0	25	0	0	0		
x_{170}	0	0	0	0	0	0	0	0	0	
x_{173}	−1	1	0	0	4	0	0	0	20	0
x_{178}	0	0	0	0	0	0	0	0	−1	0
x_{179}	0	0	0	0	0	0	0	0	0	0
x_{180}	0	0	0	0	0	0	0	0	0	0
x_{182}	0	2	0	0	10	0	0	−1	20	0
x_{185}	−1	−2	−1	0	17	0	0	0	38	0

	x_{173}	x_{178}	x_{179}	x_{180}	x_{182}
x_{178}	0				
x_{179}	0	−14			
x_{180}	0	−4	0		
x_{182}	3	0	0	0	
x_{185}	17	0	0	0	14

See the related review(s):

τ Branching Fractions

$(\Gamma(\tau^+) - \Gamma(\tau^-))$ / $(\Gamma(\tau^+) + \Gamma(\tau^-))$

$\tau^\pm \to \pi^\pm K^0_S \nu_\tau$ (RATE DIFFERENCE) / (RATE SUM)

VALUE (%)	DOCUMENT ID		TECN	COMMENT
−0.36±0.23±0.11	LEES	12M	BABR	476 fb^{-1} E^{ee}_{cm} = 10.6 GeV

τ^- BRANCHING RATIOS

$\Gamma(\text{particle}^- \geq 0 \text{ neutrals} \geq 0K^0\nu_\tau(\text{"1-prong"}))/\Gamma_{total}$ — Γ_1/Γ

$\Gamma_1/\Gamma = (\Gamma_3+\Gamma_5+\Gamma_9+\Gamma_{10}+\Gamma_{14}+\Gamma_{16}+\Gamma_{20}+\Gamma_{23}+\Gamma_{27}+\Gamma_{28}+\Gamma_{30}+\Gamma_{36}+\Gamma_{38}+\Gamma_{41}+\Gamma_{43}+\Gamma_{45}+\Gamma_{48}+\Gamma_{49}+\Gamma_{50}+\Gamma_{52}+\Gamma_{56}+\Gamma_{57}+0.7196\Gamma_{150}+0.7196\Gamma_{152}+0.7196\Gamma_{154}+0.7196\Gamma_{156}+0.339\Gamma_{170}+0.0835\Gamma_{178}+0.0835\Gamma_{179}+0.0835\Gamma_{180})/\Gamma$

The charged particle here can be e, μ, or hadron. In many analyses, the sum of the topological branching fractions (1, 3, and 5 prongs) is constrained to be unity. Since the 5-prong fraction is very small, the measured 1-prong and 3-prong fractions are highly correlated and cannot be treated as independent quantities in our overall fit. We arbitrarily choose to use the 3-prong fraction in our fit, and leave the 1-prong fraction out. We do, however, use these 1-prong measurements in our average below.

VALUE (%)	EVTS	DOCUMENT ID		TECN	COMMENT
85.24 ±0.06 OUR FIT					
85.26 ±0.13 OUR AVERAGE Error includes scale factor of 1.6. See the ideogram below.					
• • • We use the following data for averages but not for fits. • • •					
85.316±0.093±0.049	78k	[1] ABREU	01M	DLPH	1992–1995 LEP runs
85.274±0.105±0.073		[2] ACHARD	01D	L3	1992–1995 LEP runs
84.48 ±0.27 ±0.23		ACTON	92H	OPAL	1990–1991 LEP runs
• • • We do not use the following data for averages, fits, limits, etc. • • •					
85.45 $^{+0.69}_{-0.73}$ ±0.65		DECAMP	92C	ALEP	Repl. by SCHAEL 05C

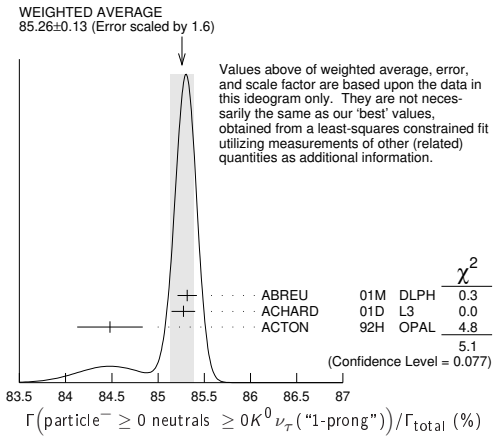

[1] The correlation coefficients between this measurement and the ABREU 01M measurements of B($\tau \to$ 3-prong) and B($\tau \to$ 5-prong) are −0.98 and −0.08 respectively.

Downloaded from https://academic.oup.com/ptep/article/2022/8/083C01/6651666 by KIT Library user on 27 September 2022

[2] The correlation coefficients between this measurement and the ACHARD 01D measurements of B($\tau \to$ "3-prong") and B($\tau \to$ "5-prong") are -0.978 and -0.082 respectively.

$\Gamma(\text{particle}^- \geq 0 \text{ neutrals } \geq 0 K^0_L \nu_\tau)/\Gamma_{\text{total}}$ — Γ_2/Γ

$\Gamma_2/\Gamma = (\Gamma_3+\Gamma_5+\Gamma_9+\Gamma_{10}+\Gamma_{14}+\Gamma_{16}+\Gamma_{20}+\Gamma_{23}+\Gamma_{27}+\Gamma_{28}+\Gamma_{30}+0.6534\Gamma_{36}+0.6534\Gamma_{38}+0.6534\Gamma_{41}+0.6534\Gamma_{43}+0.6534\Gamma_{45}+0.0942\Gamma_{48}+0.3069\Gamma_{49}+\Gamma_{50}+0.0942\Gamma_{52}+0.3069\Gamma_{56}+\Gamma_{57}+0.7196\Gamma_{150}+0.7196\Gamma_{152}+0.7196\Gamma_{154}+0.4702\Gamma_{156}+0.1049\Gamma_{170}+0.0835\Gamma_{178}+0.0835\Gamma_{179}+0.0835\Gamma_{180})/\Gamma$

VALUE (%)	EVTS	DOCUMENT ID		TECN	COMMENT
84.58±0.06 OUR FIT					
85.1 ±0.4 OUR AVERAGE					
• • • We use the following data for averages but not for fits. • • •					
85.6 ±0.6 ±0.3	3300	[1] ADEVA	91F	L3	E^{ee}_{cm}= 88.3–94.3 GeV
84.9 ±0.4 ±0.3		BEHREND	89B	CELL	E^{ee}_{cm}= 14–47 GeV
84.7 ±0.8 ±0.6		[2] AIHARA	87B	TPC	E^{ee}_{cm}= 29 GeV
• • • We do not use the following data for averages, fits, limits, etc. • • •					
86.4 ±0.3 ±0.3		ABACHI	89B	HRS	E^{ee}_{cm}= 29 GeV
87.1 ±1.0 ±0.7		[3] BURCHAT	87	MRK2	E^{ee}_{cm}= 29 GeV
87.2 ±0.5 ±0.8		SCHMIDKE	86	MRK2	E^{ee}_{cm}= 29 GeV
84.7 ±1.1 $^{+1.6}_{-1.3}$	169	[4] ALTHOFF	85	TASS	E^{ee}_{cm}= 34.5 GeV
86.1 ±0.5 ±0.9		BARTEL	85F	JADE	E^{ee}_{cm}= 34.6 GeV
87.8 ±1.3 ±3.9		[5] BERGER	85	PLUT	E^{ee}_{cm}= 34.6 GeV
86.7 ±0.3 ±0.6		FERNANDEZ	85	MAC	E^{ee}_{cm}= 29 GeV

[1] Not independent of ADEVA 91F $\Gamma(h^- h^- h^+ \geq 0 \text{ neutrals } \geq 0 K^0_L \nu_\tau)/\Gamma_{\text{total}}$ value.

[2] Not independent of AIHARA 87B $\Gamma(\mu^- \overline{\nu}_\mu \nu_\tau)/\Gamma_{\text{total}}$, $\Gamma(e^- \overline{\nu}_e \nu_\tau)/\Gamma_{\text{total}}$, and $\Gamma(h^- \geq 0 \text{ neutrals } \geq 0 K^0_L \nu_\tau)/\Gamma_{\text{total}}$ values.

[3] Not independent of SCHMIDKE 86 value (also not independent of BURCHAT 87 value for $\Gamma(h^- h^- h^+ \geq 0 \text{ neutrals } \geq 0 K^0_L \nu_\tau)/\Gamma_{\text{total}}$.

[4] Not independent of ALTHOFF 85 $\Gamma(\mu^- \overline{\nu}_\mu \nu_\tau)/\Gamma_{\text{total}}$, $\Gamma(e^- \overline{\nu}_e \nu_\tau)/\Gamma_{\text{total}}$, $\Gamma(h^- \geq 0 \text{ neutrals } \geq 0 K^0_L \nu_\tau)/\Gamma_{\text{total}}$, and $\Gamma(h^- h^- h^+ \geq 0 \text{ neutrals } \geq 0 K^0_L \nu_\tau)/\Gamma_{\text{total}}$ values.

[5] Not independent of (1-prong + $0\pi^0$) and (1-prong + $\geq 1\pi^0$) values.

$\Gamma(\mu^- \overline{\nu}_\mu \nu_\tau)/\Gamma_{\text{total}}$ — Γ_3/Γ

To minimize the effect of experiments with large systematic errors, we exclude experiments which together would contribute 5% of the weight in the average.

VALUE (%)	EVTS	DOCUMENT ID		TECN	COMMENT
17.39 ±0.04 OUR FIT					
17.33 ±0.05 OUR AVERAGE					
17.319±0.070±0.032	54k	[1] SCHAEL	05C	ALEP	1991-1995 LEP runs
17.34 ±0.09 ±0.06	31.4k	ABBIENDI	03	OPAL	1990-1995 LEP runs
17.342±0.110±0.067	21.5k	[2] ACCIARRI	01F	L3	1991-1995 LEP runs
17.325±0.095±0.077	27.7k	ABREU	99X	DLPH	1991-1995 LEP runs
• • • We use the following data for averages but not for fits. • • •					
17.37 ±0.08 ±0.18		[3] ANASTASSOV 97		CLEO	E^{ee}_{cm}= 10.6 GeV
• • • We do not use the following data for averages, fits, limits, etc. • • •					
17.31 ±0.11 ±0.05	20.7k	BUSKULIC	96C	ALEP	Repl. by SCHAEL 05C
17.02 ±0.19 ±0.24	6586	ABREU	95T	DLPH	Repl. by ABREU 99X
17.36 ±0.27	7941	AKERS	95I	OPAL	Repl. by ABBIENDI 03
17.6 ±0.4 ±0.4	2148	ADRIANI	93M	L3	Repl. by ACCIARRI 01F
17.4 ±0.3 ±0.5		[4] ALBRECHT	93G	ARG	E^{ee}_{cm}= 9.4–10.6 GeV
17.35 ±0.41 ±0.37		DECAMP	92C	ALEP	1989-1990 LEP runs
17.7 ±0.8 ±0.4	568	BEHREND	90	CELL	E^{ee}_{cm}= 35 GeV
17.4 ±1.0	2197	ADEVA	88	MRKJ	E^{ee}_{cm}= 14–16 GeV
17.7 ±1.2 ±0.7		AIHARA	87B	TPC	E^{ee}_{cm}= 29 GeV
18.3 ±0.9 ±0.8		BURCHAT	87	MRK2	E^{ee}_{cm}= 29 GeV
18.6 ±0.8 ±0.7	558	[5] BARTEL	86D	JADE	E^{ee}_{cm}= 34.6 GeV
12.9 ±1.7 $^{+0.7}_{-0.5}$		ALTHOFF	85	TASS	E^{ee}_{cm}= 34.5 GeV
18.0 ±0.9 ±0.5	473	[5] ASH	85B	MAC	E^{ee}_{cm}= 29 GeV
18.0 ±1.0 ±0.6		[6] BALTRUSAIT...85		MRK3	E^{ee}_{cm}= 3.77 GeV
19.4 ±1.6 ±1.7	153	BERGER	85	PLUT	E^{ee}_{cm}= 34.6 GeV
17.6 ±2.6 ±2.1	47	BEHREND	83C	CELL	E^{ee}_{cm}= 34 GeV
17.8 ±2.0 ±1.8		BERGER	81B	PLUT	E^{ee}_{cm}= 9–32 GeV

[1] See footnote to SCHAEL 05C $\Gamma(\tau^- \to e^- \overline{\nu}_e \nu_\tau)/\Gamma_{\text{total}}$ measurement for correlations with other measurements.

[2] The correlation coefficient between this measurement and the ACCIARRI 01F measurement of B($\tau^- \to e^- \overline{\nu}_e \nu_\tau$) is 0.08.

[3] The correlation coefficients between this measurement and the ANASTASSOV 97 measurements of B($e \overline{\nu}_e \nu_\tau$), B($\mu \overline{\nu}_\mu \nu_\tau$)/B($e \overline{\nu}_e \nu_\tau$), B($h^- \nu_\tau$), and B($h^- \nu_\tau$)/B($e \overline{\nu}_e \nu_\tau$) are 0.50, 0.58, 0.50, and 0.08 respectively.

[4] Not independent of ALBRECHT 92D $\Gamma(\mu^- \overline{\nu}_\mu \nu_\tau)/\Gamma(e^- \overline{\nu}_e \nu_\tau)$ and ALBRECHT 93G $\Gamma(\mu^- \overline{\nu}_\mu \nu_\tau) \times \Gamma(e^- \overline{\nu}_e \nu_\tau)/\Gamma^2_{\text{total}}$ values.

[5] Modified using B($e^- \overline{\nu}_e \nu_\tau$)/B("1 prong") and B("1 prong") ,= 0.855.

[6] Error correlated with BALTRUSAITIS 85 $e \nu \overline{\nu}$ value.

$\Gamma(\mu^- \overline{\nu}_\mu \nu_\tau \gamma)/\Gamma_{\text{total}}$ — Γ_4/Γ

VALUE (%)	EVTS	DOCUMENT ID		TECN	COMMENT
0.367±0.008 OUR AVERAGE					
0.363±0.002±0.015	22k	[1] SHIMIZU	18A	BELL	711 fb^{-1} E^{ee}_{cm}=10.6 GeV
0.369±0.003±0.010	16k	[2] LEES	15G	BABR	431 fb^{-1} E^{ee}_{cm}=10.6 GeV
0.361±0.016±0.035		[3] BERGFELD	00	CLEO	E^{ee}_{cm}= 10.6 GeV
• • • We do not use the following data for averages, fits, limits, etc. • • •					
0.30 ±0.04 ±0.05	116	[4] ALEXANDER	96S	OPAL	1991–1994 LEP runs
0.23 ±0.10	10	[5] WU	90	MRK2	E^{ee}_{cm}= 29 GeV

[1] SHIMIZU 18A impose requirements on detected γ's corresponding to a τ-rest-frame energy cutoff $E^*_\gamma > 10$ MeV.

[2] LEES 15G impose requirements on detected γ's corresponding to a τ-rest-frame energy cutoff $E^*_\gamma > 10$ MeV.

[3] BERGFELD 00 impose requirements on detected γ's corresponding to a τ-rest-frame energy cutoff $E^*_\gamma > 10$ MeV. For $E^*_\gamma > 20$ MeV, they quote $(3.04 \pm 0.14 \pm 0.30) \times 10^{-3}$.

[4] ALEXANDER 96S impose requirements on detected γ's corresponding to a τ-rest-frame energy cutoff E_γ >20 MeV.

[5] WU 90 reports $\Gamma(\mu^- \overline{\nu}_\mu \nu_\tau \gamma)/\Gamma(\mu^- \overline{\nu}_\mu \nu_\tau) = 0.013 \pm 0.006$, which is converted to $\Gamma(\mu^- \overline{\nu}_\mu \nu_\tau \gamma)/\Gamma_{\text{total}}$ using $\Gamma(\mu^- \overline{\nu}_\mu \nu_\tau \gamma)/\Gamma_{\text{total}} = 17.35\%$. Requirements on detected γ's correspond to a τ rest frame energy cutoff $E_\gamma > 37$ MeV.

$\Gamma(e^- \overline{\nu}_e \nu_\tau)/\Gamma_{\text{total}}$ — Γ_5/Γ

To minimize the effect of experiments with large systematic errors, we exclude experiments which together would contribute 5% of the weight in the average.

VALUE (%)	EVTS	DOCUMENT ID		TECN	COMMENT
17.82 ±0.04 OUR FIT					
17.82 ±0.05 OUR AVERAGE					
17.837±0.072±0.036	56k	[1] SCHAEL	05C	ALEP	1991-1995 LEP runs
17.806±0.104±0.076	24.7k	[2] ACCIARRI	01F	L3	1991–1995 LEP runs
17.81 ±0.09 ±0.06	33.1k	ABBIENDI	99H	OPAL	1991–1995 LEP runs
17.877±0.109±0.110	23.3k	ABREU	99X	DLPH	1991–1995 LEP runs
17.76 ±0.06 ±0.17		[3] ANASTASSOV 97		CLEO	E^{ee}_{cm}= 10.6 GeV
• • • We do not use the following data for averages, fits, limits, etc. • • •					
17.78 ±0.10 ±0.09	25.3k	ALEXANDER	96D	OPAL	Repl. by ABBIENDI 99H
17.79 ±0.12 ±0.06	20.6k	BUSKULIC	96C	ALEP	Repl. by SCHAEL 05C
17.51 ±0.23 ±0.31	5059	ABREU	95T	DLPH	Repl.. by ABREU 99X
17.9 ±0.4 ±0.4	2892	ADRIANI	93M	L3	Repl. by ACCIARRI 01F
17.5 ±0.3 ±0.5		[4] ALBRECHT	93G	ARG	E^{ee}_{cm}= 9.4–10.6 GeV
17.97 ±0.14 ±0.23	3970	AKERIB	92	CLEO	Repl. by ANASTASSOV 97
19.1 ±0.4 ±0.6	2960	[5] AMMAR	92	CLEO	E^{ee}_{cm}= 10.5–10.9 GeV
18.09 ±0.45 ±0.45		DECAMP	92C	ALEP	Repl. by SCHAEL 05C
17.0 ±0.5 ±0.6	1.7k	ABACHI	90	HRS	E^{ee}_{cm}= 29 GeV
18.4 ±0.8 ±0.4	644	BEHREND	90	CELL	E^{ee}_{cm}= 35 GeV
16.3 ±0.3 ±3.2		JANSSEN	89	CBAL	E^{ee}_{cm}= 9.4–10.6 GeV
18.4 ±1.2 ±1.0		AIHARA	87B	TPC	E^{ee}_{cm}= 29 GeV
19.1 ±0.8 ±1.1		BURCHAT	87	MRK2	E^{ee}_{cm}= 29 GeV
16.8 ±0.7 ±0.9	515	[5] BARTEL	86D	JADE	E^{ee}_{cm}= 34.6 GeV
20.4 ±3.0 $^{+1.4}_{-0.9}$		ALTHOFF	85	TASS	E^{ee}_{cm}= 34.5 GeV
17.8 ±0.9 ±0.6	390	[5] ASH	85B	MAC	E^{ee}_{cm}= 29 GeV
18.2 ±0.7 ±0.5		[6] BALTRUSAIT...85		MRK3	E^{ee}_{cm}= 3.77 GeV
13.0 ±1.9 ±2.9		BERGER	85	PLUT	E^{ee}_{cm}= 34.6 GeV
18.3 ±2.4 ±1.9	60	BEHREND	83C	CELL	E^{ee}_{cm}= 34 GeV
16.0 ±1.3	459	[7] BACINO	78B	DLCO	E^{ee}_{cm}= 3.1–7.4 GeV

[1] Correlation matrix for SCHAEL 05C branching fractions, in percent:

(1) $\Gamma(\tau^- \to e^- \overline{\nu}_e \nu_\tau)/\Gamma_{\text{total}}$
(2) $\Gamma(\tau^- \to \mu^- \overline{\nu}_\mu \nu_\tau)/\Gamma_{\text{total}}$
(3) $\Gamma(\tau^- \to \pi^- \nu_\tau)/\Gamma_{\text{total}}$
(4) $\Gamma(\tau^- \to \pi^- \pi^0 \nu_\tau)/\Gamma_{\text{total}}$
(5) $\Gamma(\tau^- \to \pi^- 2\pi^0 \nu_\tau (\text{ex.} K^0))/\Gamma_{\text{total}}$
(6) $\Gamma(\tau^- \to \pi^- 3\pi^0 \nu_\tau (\text{ex.} K^0))/\Gamma_{\text{total}}$
(7) $\Gamma(\tau^- \to h^- 4\pi^0 \nu_\tau (\text{ex.} K^0, \eta))/\Gamma_{\text{total}}$
(8) $\Gamma(\tau^- \to \pi^- \pi^+ \pi^- \nu_\tau (\text{ex.} K^0, \omega))/\Gamma_{\text{total}}$
(9) $\Gamma(\tau^- \to \pi^- \pi^+ \pi^- \pi^0 \nu_\tau (\text{ex.} K^0))/\Gamma_{\text{total}}$
(10) $\Gamma(\tau^- \to h^- h^- h^+ 2\pi^0 \nu_\tau (\text{ex.} K^0))/\Gamma_{\text{total}}$
(11) $\Gamma(\tau^- \to h^- h^- h^+ 3\pi^0 \nu_\tau)/\Gamma_{\text{total}}$
(12) $\Gamma(\tau^- \to 3h^- 2h^+ \nu_\tau (\text{ex.} K^0))/\Gamma_{\text{total}}$
(13) $\Gamma(\tau^- \to 3h^- 2h^+ \pi^0 \nu_\tau (\text{ex.} K^0))/\Gamma_{\text{total}}$

	(1)	(2)	(3)	(4)	(5)	(6)	(7)	(8)	(9)	(10)	(11)	(12)
(2)	-20											
(3)	-9	-6										
(4)	-16	-12	2									
(5)	-5	-5	-17	-37								
(6)	0	-4	-15	2	-27							
(7)	-2	-4	-24	-15	20	-47						
(8)	-14	-9	15	-5	-17	-14	-8					
(9)	-13	-12	-25	-30	4	-2	16	-15				
(10)	0	-2	-23	-14	4	10	13	-6	-17			
(11)	1	0	-5	1	4	6	0	-9	-2	-11		
(12)	0	1	9	4	-8	-4	-6	9	-5	-4	-2	
(13)	1	-4	-3	-5	3	2	-4	-3	-1	4	1	-24

Downloaded from https://academic.oup.com/ptep/article/2022/8/083C01/6651666 by KIT Library user on 27 September 2022

[2] The correlation coefficient between this measurement and the ACCIARRI 01F measurement of $B(\tau^- \to \mu^- \overline{\nu}_\mu \nu_\tau)$ is 0.08.

[3] The correlation coefficients between this measurement and the ANASTASSOV 97 measurements of $B(\mu\overline{\nu}_\mu\nu_\tau)$, $B(\mu\overline{\nu}_\mu\nu_\tau)/B(e\overline{\nu}_e\nu_\tau)$, $B(h^-\nu_\tau)$, and $B(h^-\nu_\tau)/B(e\overline{\nu}_e\nu_\tau)$ are 0.50, −0.42, 0.48, and −0.39 respectively.

[4] Not independent of ALBRECHT 92D $\Gamma(\mu^-\overline{\nu}_\mu\nu_\tau)/\Gamma(e^-\overline{\nu}_e\nu_\tau)$ and ALBRECHT 93G $\Gamma(\mu^-\overline{\nu}_\mu\nu_\tau)\times\Gamma(e^-\overline{\nu}_e\nu_\tau)/\Gamma^2_{\rm total}$ values.

[5] Modified using $B(e^-\overline{\nu}_e\nu_\tau)/B(\text{"1 prong"})$ and $B(\text{"1 prong"})$,= 0.855.

[6] Error correlated with BALTRUSAITIS 85 $\Gamma(\mu^-\overline{\nu}_\mu\nu_\tau)/\Gamma_{\rm total}$.

[7] BACINO 78B value comes from fit to events with $e^\pm$ and one other nonelectron charged prong.

$\Gamma(\mu^-\overline{\nu}_\mu\nu_\tau)/\Gamma(e^-\overline{\nu}_e\nu_\tau)$ — Γ_3/Γ_5

Standard Model prediction including mass effects is 0.9726.

VALUE (units 10^{-2})	EVTS	DOCUMENT ID		TECN	COMMENT
97.62±0.28 OUR FIT					
97.9 ±0.4 OUR AVERAGE					
97.96±0.16±0.36	731k	[1] AUBERT	10F	BABR	467 fb^{-1} $E^{ee}_{\rm cm}$= 10.6 GeV
97.77±0.63±0.87		[2] ANASTASSOV	97	CLEO	$E^{ee}_{\rm cm}$= 10.6 GeV
99.7 ±3.5 ±4.0		ALBRECHT	92D	ARG	$E^{ee}_{\rm cm}$= 9.4–10.6 GeV

[1] Correlation matrix for AUBERT 10F branching fractions:

(1) $\Gamma(\tau^- \to \mu^-\overline{\nu}_\mu\nu_\tau)$ / $\Gamma(\tau^- \to e^-\overline{\nu}_e\nu_\tau)$
(2) $\Gamma(\tau^- \to \pi^-\nu_\tau)$ / $\Gamma(\tau^- \to e^-\overline{\nu}_e\nu_\tau)$
(3) $\Gamma(\tau^- \to K^-\nu_\tau)$ / $\Gamma(\tau^- \to e^-\overline{\nu}_e\nu_\tau)$

	(1)	(2)
(2)	0.25	
(3)	0.12	0.33

[2] The correlation coefficients between this measurement and the ANASTASSOV 97 measurements of $B(\mu\overline{\nu}_\mu\nu_\tau)$, $B(e\overline{\nu}_e\nu_\tau)$, $B(h^-\nu_\tau)$, and $B(h^-\nu_\tau)/B(e\overline{\nu}_e\nu_\tau)$ are 0.58, −0.42, 0.07, and 0.45 respectively.

$\Gamma(e^-\overline{\nu}_e\nu_\tau\gamma)/\Gamma_{\rm total}$ — Γ_6/Γ

VALUE (%)	EVTS	DOCUMENT ID		TECN	COMMENT
1.83 ±0.05 OUR AVERAGE					
1.79 ±0.02 ±0.10	12k	[1] SHIMIZU	18A	BELL	711 fb^{-1} $E^{ee}_{\rm cm}$=10.6 GeV
1.847±0.015±0.052	18k	[2] LEES	15G	BABR	431 fb^{-1} $E^{ee}_{\rm cm}$=10.6 GeV
1.75 ±0.06 ±0.17		[3] BERGFELD	00	CLEO	$E^{ee}_{\rm cm}$= 10.6 GeV

[1] SHIMIZU 18A impose requirements on detected γ's corresponding to a τ-rest-frame energy cutoff $E^*_\gamma > 10$ MeV.

[2] LEES 15G impose requirements on detected γ's corresponding to a τ-rest-frame energy cutoff $E^*_\gamma > 10$ MeV.

[3] BERGFELD 00 impose requirements on detected γ's corresponding to a τ-rest-frame energy cutoff $E^*_\gamma > 10$ MeV.

$\Gamma(h^- \geq 0K^0_L\,\nu_\tau)/\Gamma_{\rm total}$ — Γ_7/Γ

$\Gamma_7/\Gamma = (\Gamma_9+\Gamma_{10}+\frac{1}{2}\Gamma_{36}+\frac{1}{2}\Gamma_{38}+\Gamma_{50})/\Gamma$

VALUE (%)	EVTS	DOCUMENT ID		TECN	COMMENT
12.03±0.05 OUR FIT					
12.2 ±0.4 OUR AVERAGE					
12.47±0.26±0.43	2967	[1] ACCIARRI	95	L3	1992 LEP run
12.4 ±0.7 ±0.7	283	[2] ABREU	92N	DLPH	1990 LEP run
12.1 ±0.7 ±0.5	309	ALEXANDER	91D	OPAL	1990 LEP run
• • • We use the following data for averages but not for fits. • • •					
11.3 ±0.5 ±0.8	798	[3] FORD	87	MAC	$E^{ee}_{\rm cm}$= 29 GeV
• • • We do not use the following data for averages, fits, limits, etc. • • •					
12.44±0.11±0.11	15k	[4] BUSKULIC	96	ALEP	Repl. by SCHAEL 05C
11.7 ±0.6 ±0.8		[5] ALBRECHT	92D	ARG	$E^{ee}_{\rm cm}$= 9.4–10.6 GeV
12.98±0.44±0.33		[6] DECAMP	92C	ALEP	Repl. by SCHAEL 05C
12.3 ±0.9 ±0.5	1338	BEHREND	90	CELL	$E^{ee}_{\rm cm}$= 35 GeV
11.1 ±1.1 ±1.4		[7] BURCHAT	87	MRK2	$E^{ee}_{\rm cm}$= 29 GeV
12.3 ±0.6 ±1.1	328	[8] BARTEL	86D	JADE	$E^{ee}_{\rm cm}$= 34.6 GeV
13.0 ±2.0 ±4.0		BERGER	85	PLUT	$E^{ee}_{\rm cm}$= 34.6 GeV
11.2 ±1.7 ±1.2	34	[9] BEHREND	83C	CELL	$E^{ee}_{\rm cm}$= 34 GeV

[1] ACCIARRI 95 with 0.65% added to remove their correction for $\pi^- K^0_L$ backgrounds.

[2] ABREU 92N with 0.5% added to remove their correction for $K^*(892)^-$ backgrounds.

[3] FORD 87 result for $B(\pi^-\nu_\tau)$ with 0.67% added to remove their K^- correction and adjusted for 1992 B("1 prong").

[4] BUSKULIC 96 quote 11.78 ± 0.11 ± 0.13 We add 0.66 to undo their correction for unseen K^0_L and modify the systematic error accordingly.

[5] Not independent of ALBRECHT 92D $\Gamma(\mu^-\overline{\nu}_\mu\nu_\tau)/\Gamma(e^-\overline{\nu}_e\nu_\tau)$, $\Gamma(\mu^-\overline{\nu}_\mu\nu_\tau)\times\Gamma(e^-\overline{\nu}_e\nu_\tau)$, and $\Gamma(h^- \geq 0K^0_L\nu_\tau)/\Gamma(e^-\overline{\nu}_e\nu_\tau)$ values.

[6] DECAMP 92C quote $B(h^- \geq 0K^0_L \geq 0\,(K^0_S \to \pi^+\pi^-)\,\nu_\tau) = 13.32 \pm 0.44 \pm 0.33$. We subtract 0.35 to correct for their inclusion of the K^0_S decays.

[7] BURCHAT 87 with 1.1% added to remove their correction for K^- and $K^*(892)^-$ backgrounds.

[8] BARTEL 86D result for $B(\pi^-\nu_\tau)$ with 0.59% added to remove their K^- correction and adjusted for 1992 B("1 prong").

[9] BEHREND 83C quote $B(\pi^-\nu_\tau) = 9.9 \pm 1.7 \pm 1.3$ after subtracting 1.3 ± 0.5 to correct for $B(K^-\nu_\tau)$.

$\Gamma(h^-\nu_\tau)/\Gamma_{\rm total}$ — $\Gamma_8/\Gamma = (\Gamma_9+\Gamma_{10})/\Gamma$

VALUE (%)	EVTS	DOCUMENT ID		TECN	COMMENT
11.51 ±0.05 OUR FIT					
11.63 ±0.12 OUR AVERAGE Error includes scale factor of 1.4. See the ideogram below.					
11.571±0.120±0.114	19k	[1] ABDALLAH	06A	DLPH	1992–1995 LEP runs
11.98 ±0.13 ±0.16		ACKERSTAFF	98M	OPAL	1991–1995 LEP runs
11.52 ±0.05 ±0.12		[2] ANASTASSOV	97	CLEO	$E^{ee}_{\rm cm}$= 10.6 GeV

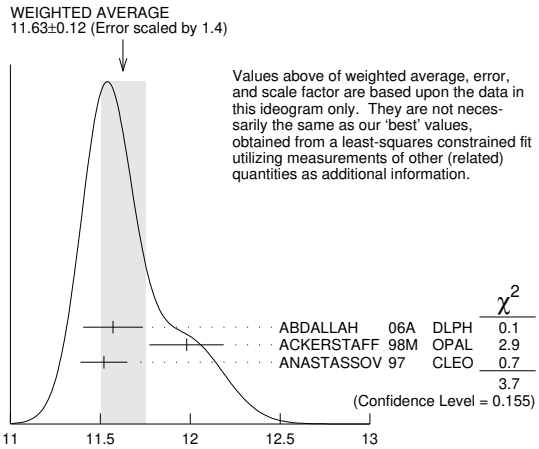

[1] Correlation matrix for ABDALLAH 06A branching fractions, in percent:

(1) $\Gamma(\tau^- \to h^-\nu_\tau)/\Gamma_{\rm total}$
(2) $\Gamma(\tau^- \to h^-\pi^0\nu_\tau)/\Gamma_{\rm total}$
(3) $\Gamma(\tau^- \to h^- \geq 1\pi^0\nu_\tau(\text{ex.}K^0))/\Gamma_{\rm total}$
(4) $\Gamma(\tau^- \to h^-2\pi^0\nu_\tau(\text{ex.}K^0))/\Gamma_{\rm total}$
(5) $\Gamma(\tau^- \to h^- \geq 3\pi^0\nu_\tau(\text{ex. }K^0))/\Gamma_{\rm total}$
(6) $\Gamma(\tau^- \to h^-h^-h^+\nu_\tau(\text{ex.}K^0))/\Gamma_{\rm total}$
(7) $\Gamma(\tau^- \to h^-h^-h^+\pi^0\nu_\tau(\text{ex.}K^0))/\Gamma_{\rm total}$
(8) $\Gamma(\tau^- \to h^-h^-h^+ \geq 1\pi^0\nu_\tau(\text{ex. }K^0))/\Gamma_{\rm total}$
(9) $\Gamma(\tau^- \to h^-h^-h^+ \geq 2\pi^0\nu_\tau(\text{ex. }K^0))/\Gamma_{\rm total}$
(10) $\Gamma(\tau^- \to 3h^-2h^+\nu_\tau(\text{ex.}K^0))/\Gamma_{\rm total}$
(11) $\Gamma(\tau^- \to 3h^-2h^+\pi^0\nu_\tau(\text{ex.}K^0))/\Gamma_{\rm total}$

	(1)	(2)	(3)	(4)	(5)	(6)	(7)	(8)	(9)	(10)
(2)	-34									
(3)	-47	56								
(4)	6	-66	15							
(5)	-6	38	11	-86						
(6)	-7	-8	15	0	-2					
(7)	-2	-1	-5	-3	3	-53				
(8)	-4	-4	-13	-4	-2	-56	75			
(9)	-1	-1	-4	3	-6	26	-78	-16		
(10)	-1	-1	1	0	0	-2	-3	-1	3	
(11)	0	0	0	0	0	1	0	-5	5	-57

[2] The correlation coefficients between this measurement and the ANASTASSOV 97 measurements of $B(\mu\overline{\nu}_\mu\nu_\tau)$, $B(e\overline{\nu}_e\nu_\tau)$, $B(\mu\overline{\nu}_\mu\nu_\tau)/B(e\overline{\nu}_e\nu_\tau)$, and $B(h^-\nu_\tau)/B(e\overline{\nu}_e\nu_\tau)$ are 0.50, 0.48, 0.07, and 0.63 respectively.

$\Gamma(h^-\nu_\tau)/\Gamma(e^-\overline{\nu}_e\nu_\tau)$ — $\Gamma_8/\Gamma_5 = (\Gamma_9+\Gamma_{10})/\Gamma_5$

VALUE (units 10^{-2})	EVTS	DOCUMENT ID		TECN	COMMENT
64.62±0.33 OUR FIT					
64.0 ±0.7 OUR AVERAGE Error includes scale factor of 1.6.					
• • • We use the following data for averages but not for fits. • • •					
63.33±0.14±0.61	394k	[1] AUBERT	10F	BABR	467 fb^{-1} $E^{ee}_{\rm cm}$=10.6 GeV
64.84±0.41±0.60		[2] ANASTASSOV	97	CLEO	$E^{ee}_{\rm cm}$= 10.6 GeV

[1] Not independent of AUBERT 10F $\Gamma(\tau^- \to \pi^-\nu_\tau)/\Gamma(\tau^- \to e^-\overline{\nu}_e\nu_\tau)$ and $\Gamma(\tau^- \to K^-\nu_\tau)/\Gamma(\tau^- \to e^-\overline{\nu}_e\nu_\tau)$.

[2] The correlation coefficients between this measurement and the ANASTASSOV 97 measurements of $B(\mu\overline{\nu}_\mu\nu_\tau)$, $B(e\overline{\nu}_e\nu_\tau)$, $B(\mu\overline{\nu}_\mu\nu_\tau)/B(e\overline{\nu}_e\nu_\tau)$, and $B(h^-\nu_\tau)$ are 0.08, −0.39, 0.45, and 0.63 respectively.

$\Gamma(\pi^-\nu_\tau)/\Gamma_{\rm total}$ — Γ_9/Γ

VALUE (%)	EVTS	DOCUMENT ID		TECN	COMMENT
10.82 ±0.05 OUR FIT					
10.828±0.070±0.078	38k	[1] SCHAEL	05C	ALEP	1991-1995 LEP runs
• • • We do not use the following data for averages, fits, limits, etc. • • •					
11.06 ±0.11 ±0.14		[2] BUSKULIC	96	ALEP	Repl. by SCHAEL 05C
11.7 ±0.4 ±1.8	1138	BLOCKER	82D	MRK2	$E^{ee}_{\rm cm}$= 3.5–6.7 GeV

[1] See footnote to SCHAEL 05C $\Gamma(\tau^- \to e^-\overline{\nu}_e\nu_\tau)/\Gamma_{\rm total}$ measurement for correlations with other measurements.

[2] Not independent of BUSKULIC 96 $B(h^-\nu_\tau)$ and $B(K^-\nu_\tau)$ values.

Downloaded from https://academic.oup.com/ptep/article/2022/8/033C01/6651666 by KIT Library user on 27 September 2022

$\Gamma(\pi^-\nu_\tau)/\Gamma(e^-\overline{\nu}_e\nu_\tau)$ — Γ_9/Γ_5

VALUE (units 10^{-2})	EVTS	DOCUMENT ID		TECN	COMMENT
60.71±0.32 OUR FIT					
59.45±0.14±0.61	369k	[1] AUBERT	10F	BABR	467 fb^{-1} E^{ee}_{cm} = 10.6 GeV

[1] See footnote to AUBERT 10F $\Gamma(\tau^- \to \mu^-\overline{\nu}_\mu\nu_\tau)/\Gamma(\tau^- \to e^-\overline{\nu}_e\nu_\tau)$ for correlations with other measurements.

$\Gamma(K^-\nu_\tau)/\Gamma_{total}$ — Γ_{10}/Γ

VALUE (%)	EVTS	DOCUMENT ID		TECN	COMMENT
0.696±0.010 OUR FIT					
0.685±0.023 OUR AVERAGE					
0.658±0.027±0.029		[1] ABBIENDI	01J	OPAL	1990–1995 LEP runs
0.696±0.025±0.014	2032	BARATE	99K	ALEP	1991–1995 LEP runs
0.85 ±0.18	27	ABREU	94K	DLPH	LEP 1992 Z data
0.66 ±0.07 ±0.09	99	BATTLE	94	CLEO	$E^{ee}_{cm} \approx$ 10.6 GeV
• • • We do not use the following data for averages, fits, limits, etc. • • •					
0.72 ±0.04 ±0.04	728	BUSKULIC	96	ALEP	Repl. by BARATE 99K
0.59 ±0.18	16	MILLS	84	DLCO	E^{ee}_{cm} = 29 GeV
1.3 ±0.5	15	BLOCKER	82B	MRK2	E^{ee}_{cm} = 3.9–6.7 GeV

[1] The correlation coefficient between this measurement and the ABBIENDI 01J $B(\tau^- \to K^- \geq 0\pi^0 \geq 0K^0 \geq 0\gamma\ \nu_\tau)$ is 0.60.

$\Gamma(K^-\nu_\tau)/\Gamma(e^-\overline{\nu}_e\nu_\tau)$ — Γ_{10}/Γ_5

VALUE (units 10^{-2})	EVTS	DOCUMENT ID		TECN	COMMENT
3.91 ±0.05 OUR FIT					
3.882±0.032±0.057	25k	[1] AUBERT	10F	BABR	467 fb^{-1} E^{ee}_{cm} = 10.6 GeV

[1] See footnote to AUBERT 10F $\Gamma(\tau^- \to \mu^-\overline{\nu}_\mu\nu_\tau)/\Gamma(\tau^- \to e^-\overline{\nu}_e\nu_\tau)$ for correlations with other measurements.

$\Gamma(K^-\nu_\tau)/\Gamma(\pi^-\nu_\tau)$ — Γ_{10}/Γ_9

VALUE (units 10^{-2})	DOCUMENT ID		TECN	COMMENT
6.44 ±0.09 OUR FIT				
• • • We use the following data for averages but not for fits. • • •				
6.531±0.056±0.093	[1] AUBERT	10F	BABR	467 fb^{-1} E^{ee}_{cm} = 10.6 GeV

[1] Not independent of AUBERT 10F $\Gamma(\tau^- \to \pi^-\nu_\tau)/\Gamma(\tau^- \to e^-\overline{\nu}_e\nu_\tau)$ and $\Gamma(\tau^- \to K^-\nu_\tau)/\Gamma(\tau^- \to e^-\overline{\nu}_e\nu_\tau)$.

$\Gamma(h^- \geq 1\ \text{neutrals}\ \nu_\tau)/\Gamma_{total}$ — Γ_{11}/Γ

$\Gamma_{11}/\Gamma = (\Gamma_{14}+\Gamma_{16}+\Gamma_{20}+\Gamma_{23}+\Gamma_{27}+\Gamma_{28}+\Gamma_{30}+0.15344\Gamma_{36}+0.15344\Gamma_{38}+0.15344\Gamma_{41}+0.15344\Gamma_{43}+0.0942\Gamma_{48}+0.0942\Gamma_{52}+0.7196\Gamma_{150}+0.7196\Gamma_{152}+0.7196\Gamma_{154}+0.1107\Gamma_{156}+0.0835\Gamma_{178}+0.0835\Gamma_{179}+0.0835\Gamma_{180})/\Gamma$

VALUE (%)	DOCUMENT ID		TECN	COMMENT
37.01±0.09 OUR FIT				
• • • We do not use the following data for averages, fits, limits, etc. • • •				
36.14±0.33±0.58	[1] AKERS	94E	OPAL	1991–1992 LEP runs
38.4 ±1.2 ±1.0	[2] BURCHAT	87	MRK2	E^{ee}_{cm} = 29 GeV
42.7 ±2.0 ±2.9	BERGER	85	PLUT	E^{ee}_{cm} = 34.6 GeV

[1] Not independent of ACKERSTAFF 98M $B(h^-\pi^0\nu_\tau)$ and $B(h^- \geq 2\pi^0\nu_\tau)$ values.
[2] BURCHAT 87 quote for $B(\pi^\pm \geq 1\ \text{neutral}\ \nu_\tau) = 0.378 \pm 0.012 \pm 0.010$. We add 0.006 to account for contribution from $(K^{*-}\nu_\tau)$ which they fixed at BR = 0.013.

$\Gamma(h^- \geq 1\pi^0\nu_\tau(\text{ex.}K^0))/\Gamma_{total}$ — Γ_{12}/Γ

$\Gamma_{12}/\Gamma = (\Gamma_{14}+\Gamma_{16}+\Gamma_{20}+\Gamma_{23}+\Gamma_{27}+\Gamma_{28}+\Gamma_{30}+0.3257\Gamma_{150}+0.3257\Gamma_{152}+0.3257\Gamma_{154})/\Gamma$

VALUE (%)	EVTS	DOCUMENT ID		TECN	COMMENT
36.51 ±0.09 OUR FIT					
• • • We use the following data for averages but not for fits. • • •					
36.641±0.155±0.127	45k	[1] ABDALLAH	06A	DLPH	1992–1995 LEP runs

[1] See footnote to ABDALLAH 06A $\Gamma(\tau^- \to h^-\nu_\tau)/\Gamma_{total}$ measurement for correlations with other measurements.

$\Gamma(h^-\pi^0\nu_\tau)/\Gamma_{total}$ — $\Gamma_{13}/\Gamma = (\Gamma_{14}+\Gamma_{16})/\Gamma$

VALUE (%)	EVTS	DOCUMENT ID		TECN	COMMENT
25.93 ±0.09 OUR FIT					
25.73 ±0.16 OUR AVERAGE					
25.67 ±0.01 ±0.39	5.4M	FUJIKAWA	08	BELL	72 fb^{-1} E^{ee}_{cm}=10.6GeV
25.740±0.201±0.138	35k	[1] ABDALLAH	06A	DLPH	1992–1995 LEP runs
25.89 ±0.17 ±0.29		ACKERSTAFF	98M	OPAL	1991–1995 LEP runs
25.05 ±0.35 ±0.50	6613	ACCIARRI	95	L3	1992 LEP run
25.87 ±0.12 ±0.42	51k	[2] ARTUSO	94	CLEO	E^{ee}_{cm} = 10.6 GeV
• • • We do not use the following data for averages, fits, limits, etc. • • •					
25.76 ±0.15 ±0.13	31k	BUSKULIC	96	ALEP	Repl. by SCHAEL 05C
25.98 ±0.36 ±0.52		[3] AKERS	94E	OPAL	Repl. by ACKERSTAFF 98M
22.9 ±0.8 ±1.3	283	[4] ABREU	92N	DLPH	E^{ee}_{cm} = 88.2–94.2 GeV
23.1 ±0.4 ±0.9	1249	[5] ALBRECHT	92Q	ARG	E^{ee}_{cm} = 10 GeV
25.02 ±0.64 ±0.88	1849	DECAMP	92C	ALEP	1989–1990 LEP runs
22.0 ±0.8 ±1.9	779	ANTREASYAN	91	CBAL	E^{ee}_{cm} = 9.4–10.6 GeV
22.6 ±1.5 ±0.7	1101	BEHREND	90	CELL	E^{ee}_{cm} = 35 GeV
23.1 ±1.9 ±1.6		BEHREND	84	CELL	E^{ee}_{cm} = 14,22 GeV

[1] See footnote to ABDALLAH 06A $\Gamma(\tau^- \to h^-\nu_\tau)/\Gamma_{total}$ measurement for correlations with other measurements.
[2] ARTUSO 94 reports the combined result from three independent methods, one of which (23% of the $\tau^- \to h^-\pi^0\nu_\tau$) is normalized to the inclusive one-prong branching fraction, taken as 0.854 ± 0.004. Renormalization to the present value causes negligible change.
[3] AKERS 94E quote $(26.25 \pm 0.36 \pm 0.52) \times 10^{-2}$; we subtract 0.27% from their number to correct for $\tau^- \to h^-K^0_L\nu_\tau$.
[4] ABREU 92N with 0.5% added to remove their correction for $K^*(892)^-$ backgrounds.
[5] ALBRECHT 92Q with 0.5% added to remove their correction for $\tau^- \to K^*(892)^-\nu_\tau$ background.

$\Gamma(\pi^-\pi^0\nu_\tau)/\Gamma_{total}$ — Γ_{14}/Γ

VALUE (%)	EVTS	DOCUMENT ID		TECN	COMMENT
25.49 ±0.09 OUR FIT					
25.46 ±0.12 OUR AVERAGE					
25.471±0.097±0.085	81k	[1] SCHAEL	05C	ALEP	1991-1995 LEP runs
• • • We use the following data for averages but not for fits. • • •					
25.36 ±0.44		[2] ARTUSO	94	CLEO	E^{ee}_{cm} = 10.6 GeV
• • • We do not use the following data for averages, fits, limits, etc. • • •					
25.30 ±0.15 ±0.13		[3] BUSKULIC	96	ALEP	Repl. by SCHAEL 05C
21.5 ±0.4 ±1.9	4400	[4,5] ALBRECHT	88L	ARG	E^{ee}_{cm} = 10 GeV
23.0 ±1.3 ±1.7	582	ADLER	87B	MRK3	E^{ee}_{cm} = 3.77 GeV
25.8 ±1.7 ±2.5		[6] BURCHAT	87	MRK2	E^{ee}_{cm} = 29 GeV
22.3 ±0.6 ±1.4	629	[5] YELTON	86	MRK2	E^{ee}_{cm} = 29 GeV

[1] See footnote to SCHAEL 05C $\Gamma(\tau^- \to e^-\overline{\nu}_e\nu_\tau)/\Gamma_{total}$ measurement for correlations with other measurements.
[2] Not independent of ARTUSO 94 $B(h^-\pi^0\nu_\tau)$ and BATTLE 94 $B(K^-\pi^0\nu_\tau)$ values.
[3] Not independent of BUSKULIC 96 $B(h^-\pi^0\nu_\tau)$ and $B(K^-\pi^0\nu_\tau)$ values.
[4] The authors divide by $(\Gamma_3+\Gamma_5+\Gamma_9+\Gamma_{10})/\Gamma = 0.467$ to obtain this result.
[5] Experiment had no hadron identification. Kaon corrections were made, but insufficient information is given to permit their removal.
[6] BURCHAT 87 value is not independent of YELTON 86 value. Nonresonant decays included.

$\Gamma(\pi^-\pi^0\ \text{non-}\rho(770)\nu_\tau)/\Gamma_{total}$ — Γ_{15}/Γ

VALUE (%)	DOCUMENT ID		TECN	COMMENT
0.3±0.1±0.3	[1] BEHREND	84	CELL	E^{ee}_{cm} = 14,22 GeV

[1] BEHREND 84 assume a flat nonresonant mass distribution down to the $\rho(770)$ mass, using events with mass above 1300 to set the level.

$\Gamma(K^-\pi^0\nu_\tau)/\Gamma_{total}$ — Γ_{16}/Γ

VALUE (%)	EVTS	DOCUMENT ID		TECN	COMMENT
0.433±0.015 OUR FIT					
0.426±0.016 OUR AVERAGE					
0.416±0.003±0.018	78k	AUBERT	07AP	BABR	230 fb^{-1} E^{ee}_{cm} = 10.6 GeV
0.471±0.059±0.023	360	ABBIENDI	04J	OPAL	1991-1995 LEP runs
0.444±0.026±0.024	923	BARATE	99K	ALEP	1991-1995 LEP runs
0.51 ±0.10 ±0.07	37	BATTLE	94	CLEO	$E^{ee}_{cm} \approx$ 10.6 GeV
• • • We do not use the following data for averages, fits, limits, etc. • • •					
0.52 ±0.04 ±0.05	395	BUSKULIC	96	ALEP	Repl. by BARATE 99K

$\Gamma(h^- \geq 2\pi^0\nu_\tau)/\Gamma_{total}$ — Γ_{17}/Γ

$\Gamma_{17}/\Gamma = (\Gamma_{20}+\Gamma_{23}+\Gamma_{27}+\Gamma_{28}+\Gamma_{30}+0.15344\Gamma_{36}+0.15344\Gamma_{38}+0.15344\Gamma_{41}+0.15344\Gamma_{43}+0.09419\Gamma_{48}+0.0942\Gamma_{52}+0.3257\Gamma_{150}+0.3257\Gamma_{152}+0.3257\Gamma_{154})/\Gamma$

VALUE (%)	EVTS	DOCUMENT ID		TECN	COMMENT
10.81±0.09 OUR FIT					
9.91±0.31±0.27		ACKERSTAFF	98M	OPAL	1991–1995 LEP runs
• • • We do not use the following data for averages, fits, limits, etc. • • •					
9.89±0.34±0.55		[1] AKERS	94E	OPAL	Repl. by ACKERSTAFF 98M
14.0 ±1.2 ±0.6	938	[2] BEHREND	90	CELL	E^{ee}_{cm} = 35 GeV
12.0 ±1.4 ±2.5		[3] BURCHAT	87	MRK2	E^{ee}_{cm} = 29 GeV
13.9 ±2.0 $^{+1.9}_{-2.2}$		[4] AIHARA	86E	TPC	E^{ee}_{cm} = 29 GeV

[1] AKERS 94E not independent of AKERS 94E $B(h^- \geq 1\pi^0\nu_\tau)$ and $B(h^-\pi^0\nu_\tau)$ measurements.
[2] No independent of BEHREND 90 $\Gamma(h^-2\pi^0\nu_\tau(\text{exp. } K^0))$ and $\Gamma(h^- \geq 3\pi^0\nu_\tau)$.
[3] Error correlated with BURCHAT 87 $\Gamma(\rho^-\nu_e)/\Gamma(\text{total})$ value.
[4] AIHARA 86E (TPC) quote $B(2\pi^0\pi^-\nu_\tau) + 1.6B(3\pi^0\pi^-\nu_\tau) + 1.1B(\pi^0\eta\pi^-\nu_\tau)$.

$\Gamma(h^-2\pi^0\nu_\tau)/\Gamma_{total}$ — Γ_{18}/Γ

$\Gamma_{18}/\Gamma = (\Gamma_{20}+\Gamma_{23}+0.15344\Gamma_{36}+0.15344\Gamma_{38})/\Gamma$

VALUE (%)	EVTS	DOCUMENT ID		TECN	COMMENT
9.48±0.10 OUR FIT					
• • • We do not use the following data for averages, fits, limits, etc. • • •					
9.48±0.13±0.10	12k	[1] BUSKULIC	96	ALEP	Repl. by SCHAEL 05C

[1] BUSKULIC 96 quote 9.29 ± 0.13 ± 0.10. We add 0.19 to undo their correction for $\tau^- \to h^-K^0\nu_\tau$.

$\Gamma(h^-2\pi^0\nu_\tau(\text{ex.}K^0))/\Gamma_{total}$ — Γ_{19}/Γ

$\Gamma_{19}/\Gamma = (\Gamma_{20}+\Gamma_{23})/\Gamma$

VALUE (%)	EVTS	DOCUMENT ID		TECN	COMMENT
9.32 ±0.10 OUR FIT					
9.17 ±0.27 OUR AVERAGE					

Downloaded from https://academic.oup.com/ptep/article/2022/8/083C01/6651666 by KIT Library user on 27 September 2022

9.498±0.320±0.275	9.5k	[1] ABDALLAH	06A	DLPH	1992–1995 LEP runs	
8.88 ±0.37 ±0.42	1060	ACCIARRI	95	L3	1992 LEP run	
• • • We use the following data for averages but not for fits. • • •						
8.96 ±0.16 ±0.44		[2] PROCARIO	93	CLEO	$E^{ee}_{cm} \approx$ 10.6 GeV	
• • • We do not use the following data for averages, fits, limits, etc. • • •						
10.38 ±0.66 ±0.82	809	[3] DECAMP	92C	ALEP	Repl. by SCHAEL 05C	
5.7 ±0.5 $^{+1.7}_{-1.0}$	133	[4] ANTREASYAN	91	CBAL	E^{ee}_{cm}= 9.4–10.6 GeV	
10.0 ±1.5 ±1.1	333	[5] BEHREND	90	CELL	E^{ee}_{cm}= 35 GeV	
8.7 ±0.4 ±1.1	815	[6] BAND	87	MAC	E^{ee}_{cm}= 29 GeV	
6.2 ±0.6 ±1.2		[7] GAN	87	MRK2	E^{ee}_{cm}= 29 GeV	
6.0 ±3.0 ±1.8		BEHREND	84	CELL	E^{ee}_{cm}= 14,22 GeV	

[1] See footnote to ABDALLAH 06A $\Gamma(\tau^- \to h^- \nu_\tau)/\Gamma_{total}$ measurement for correlations with other measurements.
[2] PROCARIO 93 entry is obtained from $B(h^- 2\pi^0 \nu_\tau)/B(h^- \pi^0 \nu_\tau)$ using ARTUSO 94 result for $B(h^- \pi^0 \nu_\tau)$.
[3] We subtract 0.0015 to account for $\tau^- \to K^*(892)^- \nu_\tau$ contribution.
[4] ANTREASYAN 91 subtract 0.001 to account for the $\tau^- \to K^*(892)^- \nu_\tau$ contribution.
[5] BEHREND 90 subtract 0.002 to account for the $\tau^- \to K^*(892)^- \nu_\tau$ contribution.
[6] BAND 87 assume $B(\pi^- 3\pi^0 \nu_\tau) = 0.01$ and $B(\pi^- \pi^0 \eta \nu_\tau) = 0.005$.
[7] GAN 87 analysis use photon multiplicity distribution.

$\Gamma(h^- 2\pi^0 \nu_\tau (\text{ex.}K^0))/\Gamma(h^- \pi^0 \nu_\tau)$ — Γ_{19}/Γ_{13}

$\Gamma_{19}/\Gamma_{13} = (\Gamma_{20}+\Gamma_{23})/(\Gamma_{14}+\Gamma_{16})$

VALUE (units 10^{-2})	DOCUMENT ID		TECN	COMMENT
36.0±0.4 OUR FIT				
34.2±0.6±1.6	[1] PROCARIO	93	CLEO	$E^{ee}_{cm} \approx$ 10.6 GeV

[1] PROCARIO 93 quote 0.345 ± 0.006 ± 0.016 after correction for 2 kaon backgrounds assuming $B(K^{*-}\nu_\tau)$=1.42 ± 0.18% and $B(h^- K^0 \pi^0 \nu_\tau)$=0.48 ± 0.48%. We multiply by 0.990 ± 0.010 to remove these corrections to $B(h^- \pi^0 \nu_\tau)$.

$\Gamma(\pi^- 2\pi^0 \nu_\tau (\text{ex.}K^0))/\Gamma_{total}$ — Γ_{20}/Γ

VALUE (%)	EVTS	DOCUMENT ID		TECN	COMMENT
9.26 ±0.10 OUR FIT					
9.239±0.086±0.090	31k	[1] SCHAEL	05C	ALEP	1991-1995 LEP runs
• • • We do not use the following data for averages, fits, limits, etc. • • •					
9.21 ±0.13 ±0.11		[2] BUSKULIC	96	ALEP	Repl. by SCHAEL 05C

[1] See footnote to SCHAEL 05C $\Gamma(\tau^- \to e^- \overline{\nu}_e \nu_\tau)/\Gamma_{total}$ measurement for correlations with other measurements.
[2] Not independent of BUSKULIC 96 $B(h^- 2\pi^0 \nu_\tau(\text{ex. } K^0))$ and $B(K^- 2\pi^0 \nu_\tau(\text{ex. } K^0))$ values.

$\Gamma(\pi^- 2\pi^0 \nu_\tau (\text{ex.}K^0), \text{scalar})/\Gamma(\pi^- 2\pi^0 \nu_\tau (\text{ex.}K^0))$ — Γ_{21}/Γ_{20}

VALUE	CL%	DOCUMENT ID		TECN	COMMENT
<0.094	95	[1] BROWDER	00	CLEO	4.7 fb^{-1} E^{ee}_{cm}= 10.6 GeV

[1] Model-independent limit from structure function analysis on contribution to $B(\tau^- \to \pi^- 2\pi^0 \nu_\tau(\text{ex. } K^0))$ from scalars.

$\Gamma(\pi^- 2\pi^0 \nu_\tau (\text{ex.}K^0), \text{vector})/\Gamma(\pi^- 2\pi^0 \nu_\tau (\text{ex.}K^0))$ — Γ_{22}/Γ_{20}

VALUE	CL%	DOCUMENT ID		TECN	COMMENT
<0.073	95	[1] BROWDER	00	CLEO	4.7 fb^{-1} E^{ee}_{cm}= 10.6 GeV

[1] Model-independent limit from structure function analysis on contribution to $B(\tau^- \to \pi^- 2\pi^0 \nu_\tau(\text{ex. } K^0))$ from vectors.

$\Gamma(K^- 2\pi^0 \nu_\tau (\text{ex.}K^0))/\Gamma_{total}$ — Γ_{23}/Γ

VALUE (units 10^{-4})	EVTS	DOCUMENT ID		TECN	COMMENT
6.5± 2.2 OUR FIT					
5.8± 2.4 OUR AVERAGE					
5.6± 2.0±1.5	131	BARATE	99K	ALEP	1991–1995 LEP runs
9 ±10 ±3	3	[1] BATTLE	94	CLEO	$E^{ee}_{cm} \approx$ 10.6 GeV
• • • We do not use the following data for averages, fits, limits, etc. • • •					
8 ± 2 ±2	59	BUSKULIC	96	ALEP	Repl. by BARATE 99K

[1] BATTLE 94 quote (14 ± 10 ± 3) × 10^{-4} or < 30 × 10^{-4} at 90% CL. We subtract (5 ± 2) × 10^{-4} to account for $\tau^- \to K^-(K^0 \to \pi^0\pi^0)\nu_\tau$ background.

$\Gamma(h^- \geq 3\pi^0 \nu_\tau)/\Gamma_{total}$ — Γ_{24}/Γ

$\Gamma_{24}/\Gamma = (\Gamma_{27}+\Gamma_{28}+\Gamma_{30}+0.15344\Gamma_{41}+0.15344\Gamma_{43}+0.0942\Gamma_{48}+0.0942\Gamma_{52}+0.3257\Gamma_{150}+0.3257\Gamma_{152}+0.3257\Gamma_{154}+0.0501\Gamma_{156})/\Gamma$

VALUE (%)	EVTS	DOCUMENT ID		TECN	COMMENT
1.34±0.07 OUR FIT					
• • • We do not use the following data for averages, fits, limits, etc. • • •					
1.53±0.40±0.46	186	DECAMP	92C	ALEP	Repl. by SCHAEL 05C
3.2 ±1.0 ±1.0		BEHREND	90	CELL	E^{ee}_{cm}= 35 GeV

$\Gamma(h^- \geq 3\pi^0 \nu_\tau (\text{ex. } K^0))/\Gamma_{total}$ — Γ_{25}/Γ

$\Gamma_{25}/\Gamma = (\Gamma_{27}+\Gamma_{28}+\Gamma_{30}+0.3257\Gamma_{150}+0.3257\Gamma_{152}+0.3257\Gamma_{154})/\Gamma$

VALUE (%)	EVTS	DOCUMENT ID		TECN	COMMENT
1.25 ±0.07 OUR FIT					
1.403±0.214±0.224	1.1k	[1] ABDALLAH	06A	DLPH	1992–1995 LEP runs

[1] See footnote to ABDALLAH 06A $\Gamma(\tau^- \to h^- \nu_\tau)/\Gamma_{total}$ measurement for correlations with other measurements.

$\Gamma(h^- 3\pi^0 \nu_\tau)/\Gamma_{total}$ — Γ_{26}/Γ

$\Gamma_{26}/\Gamma = (\Gamma_{27}+\Gamma_{28}+0.15344\Gamma_{41}+0.15344\Gamma_{43}+0.3257\Gamma_{152})/\Gamma$

VALUE (%)	EVTS	DOCUMENT ID		TECN	COMMENT
1.18±0.07 OUR FIT					
1.21±0.17 OUR AVERAGE Error includes scale factor of 1.2.					
1.70±0.24±0.38	293	ACCIARRI	95	L3	1992 LEP run
• • • We use the following data for averages but not for fits. • • •					
1.15±0.08±0.13		[1] PROCARIO	93	CLEO	$E^{ee}_{cm} \approx$ 10.6 GeV
• • • We do not use the following data for averages, fits, limits, etc. • • •					
1.24±0.09±0.11	2.3k	[2] BUSKULIC	96	ALEP	Repl. by SCHAEL 05C
0.0 $^{+1.4}_{-0.1}$ $^{+1.1}_{-0.1}$		[3] GAN	87	MRK2	E^{ee}_{cm}= 29 GeV

[1] PROCARIO 93 entry is obtained from $B(h^- 3\pi^0 \nu_\tau)/B(h^- \pi^0 \nu_\tau)$ using ARTUSO 94 result for $B(h^- \pi^0 \nu_\tau)$.
[2] BUSKULIC 96 quote $B(h^- 3\pi^0 \nu_\tau(\text{ex. } K^0))$ = 1.17 ± 0.09 ± 0.11. We add 0.07 to remove their correction for K^0 backgrounds.
[3] Highly correlated with GAN 87 $\Gamma(\eta\pi^- \pi^0 \nu_\tau)/\Gamma_{total}$ value. Authors quote $B(\pi^\pm 3\pi^0 \nu_\tau) + 0.67B(\pi^\pm \eta\pi^0 \nu_\tau)$ = 0.047 ± 0.010 ± 0.011.

$\Gamma(h^- 3\pi^0 \nu_\tau)/\Gamma(h^- \pi^0 \nu_\tau)$ — Γ_{26}/Γ_{13}

$\Gamma_{26}/\Gamma_{13} = (\Gamma_{27}+\Gamma_{28}+0.15344\Gamma_{41}+0.15344\Gamma_{43}+0.3257\Gamma_{152})/(\Gamma_{14}+\Gamma_{16})$

VALUE (units 10^{-2})	DOCUMENT ID		TECN	COMMENT
4.54±0.28 OUR FIT				
4.4 ±0.3 ±0.5	[1] PROCARIO	93	CLEO	$E^{ee}_{cm} \approx$ 10.6 GeV

[1] PROCARIO 93 quote 0.041 ± 0.003 ± 0.005 after correction for 2 kaon backgrounds assuming $B(K^{*-}\nu_\tau)$=1.42 ± 0.18% and $B(h^- K^0 \pi^0 \nu_\tau)$=0.48 ± 0.48%. We add 0.003 ± 0.003 and multiply the sum by 0.990 ± 0.010 to remove these corrections.

$\Gamma(\pi^- 3\pi^0 \nu_\tau (\text{ex.}K^0))/\Gamma_{total}$ — Γ_{27}/Γ

VALUE (%)	EVTS	DOCUMENT ID		TECN	COMMENT
1.04 ±0.07 OUR FIT					
0.977±0.069±0.058	6.1k	[1] SCHAEL	05C	ALEP	1991-1995 LEP runs

[1] See footnote to SCHAEL 05C $\Gamma(\tau^- \to e^- \overline{\nu}_e \nu_\tau)/\Gamma_{total}$ measurement for correlations with other measurements.

$\Gamma(K^- 3\pi^0 \nu_\tau (\text{ex.}K^0, \eta))/\Gamma_{total}$ — Γ_{28}/Γ

VALUE (units 10^{-4})	EVTS	DOCUMENT ID		TECN	COMMENT
4.8± 2.1 OUR FIT					
3.7± 2.1±1.1	22	BARATE	99K	ALEP	1991–1995 LEP runs
• • • We do not use the following data for averages, fits, limits, etc. • • •					
5 ±13		[1] BUSKULIC	94E	ALEP	Repl. by BARATE 99K

[1] BUSKULIC 94E quote $B(K^- \geq 0\pi^0 \geq 0K^0\nu_\tau) - [B(K^-\nu_\tau) + B(K^-\pi^0\nu_\tau) + B(K^-K^0\nu_\tau) + B(K^-\pi^0\pi^0\nu_\tau) + B(K^-\pi^0K^0\nu_\tau)]$ = (5 ± 13) × 10^{-4} accounting for common systematic errors in BUSKULIC 94E and BUSKULIC 94F measurements of these modes. We assume $B(K^- \geq 2K^0\nu_\tau)$ and $B(K^- \geq 4\pi^0\nu_\tau)$ are negligible.

$\Gamma(h^- 4\pi^0 \nu_\tau (\text{ex.}K^0))/\Gamma_{total}$ — Γ_{29}/Γ

$\Gamma_{29}/\Gamma = (\Gamma_{30}+0.3257\Gamma_{150}+0.3257\Gamma_{154})/\Gamma$

VALUE (%)	EVTS	DOCUMENT ID		TECN	COMMENT
0.16±0.04 OUR FIT					
0.16±0.05±0.05		[1] PROCARIO	93	CLEO	$E^{ee}_{cm} \approx$ 10.6 GeV
• • • We do not use the following data for averages, fits, limits, etc. • • •					
0.16±0.04±0.09	232	[2] BUSKULIC	96	ALEP	Repl. by SCHAEL 05C

[1] PROCARIO 93 quotes $B(h^- 4\pi^0 \nu_\tau)/B(h^- \pi^0 \nu_\tau)$ =0.006±0.002±0.002. We multiply by the ARTUSO 94 result for $B(h^- \pi^0 \nu_\tau)$ to obtain $B(h^- 4\pi^0 \nu_\tau)$. PROCARIO 93 assume $B(h^- \geq 5\ \pi^0 \nu_\tau)$ is small and do not correct for it.
[2] BUSKULIC 96 quote result for $\tau^- \to h^- \geq 4\pi^0 \nu_\tau$. We assume $B(h^- \geq 5\pi^0 \nu_\tau)$ is negligible.

$\Gamma(h^- 4\pi^0 \nu_\tau (\text{ex.}K^0, \eta))/\Gamma_{total}$ — Γ_{30}/Γ

VALUE (%)	EVTS	DOCUMENT ID		TECN	COMMENT
0.11 ±0.04 OUR FIT					
0.112±0.037±0.035	957	[1] SCHAEL	05C	ALEP	1991-1995 LEP runs

[1] See footnote to SCHAEL 05C $\Gamma(\tau^- \to e^- \overline{\nu}_e \nu_\tau)/\Gamma_{total}$ measurement for correlations with other measurements.

$\Gamma(a_1(1260)\nu_\tau \to \pi^- \gamma \nu_\tau)/\Gamma_{total}$ — $\Gamma_{31}/\Gamma = (0.0021\Gamma_{20}+0.0021\Gamma_{70})/\Gamma$

The uncertainty on $\Gamma(\tau^- \to a_1(1260)\nu_\tau \to \pi^-\gamma\nu_\tau)/\Gamma_{total}$ is the sum in quadrature of the uncertainty on the fit result for $\Gamma(\tau^- \to a_1(1260)\nu_\tau \to \pi^-\gamma\nu_\tau)/\Gamma_{total}$ and of the uncertainty on $\Gamma(a_1(1260) \to \pi\gamma)/\Gamma^{a_1(1260)}_{total} = ((2.1 \pm 0.8) \times 10^{-3})$ as reported in SCHAEL 05C, which is the coefficient of the relationship that defines $\Gamma(\tau^- \to a_1(1260)\nu_\tau \to \pi^-\gamma\nu_\tau)/\Gamma_{total}$ in terms of $\Gamma(\tau^- \to \pi^- 2\pi^0 \nu_\tau(\text{ex.}K^0))/\Gamma_{total}$ and $\Gamma(\tau^- \to \pi^-\pi^+\pi^-\nu_\tau(\text{ex.}K^0,\omega))/\Gamma_{total}$.

VALUE (units 10^{-4})	DOCUMENT ID
3.8±1.5 OUR FIT	

$\Gamma(K^- \geq 0\pi^0 \geq 0K^0 \geq 0\gamma \nu_\tau)/\Gamma_{total}$ — Γ_{32}/Γ

$\Gamma_{32}/\Gamma = (\Gamma_{10}+\Gamma_{16}+\Gamma_{23}+\Gamma_{28}+\Gamma_{38}+\Gamma_{43}+0.7196\Gamma_{152}+0.1049\Gamma_{170})/\Gamma$

VALUE (%)	EVTS	DOCUMENT ID		TECN	COMMENT
1.552±0.029 OUR FIT					
1.53 ±0.04 OUR AVERAGE					
1.528±0.039±0.040		[1] ABBIENDI	01J	OPAL	1990–1995 LEP runs

Downloaded from https://academic.oup.com/ptep/article/2022/8/033C01/6651666 by KIT Library user on 27 September 2022

1.54 ±0.24		ABREU	94K	DLPH	LEP 1992 Z data
1.70 ±0.12 ±0.19	202	[2] BATTLE	94	CLEO	$E^{ee}_{cm} \approx$ 10.6 GeV
• • • We use the following data for averages but not for fits. • • •					
1.520±0.040±0.041	4006	[3] BARATE	99K	ALEP	1991–1995 LEP runs
• • • We do not use the following data for averages, fits, limits, etc. • • •					
1.70 ±0.05 ±0.06	1610	[4] BUSKULIC	96	ALEP	Repl. by BARATE 99K
1.6 ±0.4 ±0.2	35	AIHARA	87B	TPC	E^{ee}_{cm}= 29 GeV
1.71 ±0.29	53	MILLS	84	DLCO	E^{ee}_{cm}= 29 GeV

[1] The correlation coefficient between this measurement and the ABBIENDI 01J B($\tau^- \to K^- \nu_\tau$) is 0.60.
[2] BATTLE 94 quote 1.60 ± 0.12 ± 0.19. We add 0.10 ± 0.02 to correct for their rejection of $K^0_S \to \pi^+\pi^-$ decays.
[3] Not independent of BARATE 99K B($K^-\nu_\tau$), B($K^-\pi^0\nu_\tau$), B($K^-2\pi^0\nu_\tau$(ex. K^0)), B($K^-3\pi^0\nu_\tau$(ex. K^0)), B($K^-K^0\nu_\tau$), and B($K^-K^0\pi^0\nu_\tau$) values.
[4] Not independent of BUSKULIC 96 B($K^-\nu_\tau$), B($K^-\pi^0\nu_\tau$), B($K^-2\pi^0\nu_\tau$), B($K^-K^0\nu_\tau$), and B($K^-K^0\pi^0\nu_\tau$) values.

$\Gamma(K^- \geq 1(\pi^0 \text{ or } K^0 \text{ or } \gamma)\nu_\tau)/\Gamma_{total}$ — Γ_{33}/Γ

$\Gamma_{33}/\Gamma = (\Gamma_{16}+\Gamma_{23}+\Gamma_{28}+\Gamma_{38}+\Gamma_{43}+0.7196\Gamma_{152}+0.7196\Gamma_{154}+0.1049\Gamma_{170})/\Gamma$

VALUE (%)	EVTS	DOCUMENT ID		TECN	COMMENT
0.859±0.028 OUR FIT					
0.86 ±0.05 OUR AVERAGE					
• • • We use the following data for averages but not for fits. • • •					
0.869±0.031±0.034		[1] ABBIENDI	01J	OPAL	1990–1995 LEP runs
0.69 ±0.25		[2] ABREU	94K	DLPH	LEP 1992 Z data
• • • We do not use the following data for averages, fits, limits, etc. • • •					
1.2 ±0.5 $^{+0.2}_{-0.4}$	9	AIHARA	87B	TPC	E^{ee}_{cm}= 29 GeV

[1] Not independent of ABBIENDI 01J B($\tau^- \to K^-\nu_\tau$) and B($\tau^- \to K^- \geq 0\pi^0 \geq 0K^0 \geq 0\gamma\ \nu_\tau$) values.
[2] Not independent of ABREU 94K B($K^-\nu_\tau$) and B($K^- \geq 0$ neutralsν_τ) measurements.

$\Gamma(K^0_S(\text{particles})^-\nu_\tau)/\Gamma_{total}$ — Γ_{34}/Γ

$\Gamma_{34}/\Gamma = (\frac{1}{2}\Gamma_{36}+\frac{1}{2}\Gamma_{38}+\frac{1}{2}\Gamma_{41}+\frac{1}{2}\Gamma_{43}+\frac{1}{2}\Gamma_{45}+\Gamma_{48}+\Gamma_{49}+\Gamma_{52}+\Gamma_{56}+0.3598\Gamma_{156}+0.339\Gamma_{170})/\Gamma$

VALUE (%)	EVTS	DOCUMENT ID		TECN	COMMENT
0.943±0.028 OUR FIT					
0.918±0.015 OUR AVERAGE					
0.970±0.058±0.062	929	BARATE	98E	ALEP	1991–1995 LEP runs
0.97 ±0.09 ±0.06	141	AKERS	94G	OPAL	E^{ee}_{cm}= 88–94 GeV
• • • We use the following data for averages but not for fits. • • •					
0.915±0.001±0.015	398k	[1] RYU	14	BELL	669 fb^{-1} E^{ee}_{cm}=10.6 GeV

[1] Not independent of RYU 14 measurements of B($\tau^- \to \pi^-\overline{K}^0\nu_\tau$), B($\tau^- \to K^-K^0\nu_\tau$), B($\tau^- \to \pi^-\overline{K}^0\pi^0\nu_\tau$), B($\tau^- \to K^-K^0\pi^0\nu_\tau$), B($\tau^- \to \pi^-K^0_S K^0_S\nu_\tau$), and B($\tau^- \to \pi^-K^0_S K^0_S\pi^0\nu_\tau$).

$\Gamma(h^-\overline{K}^0\nu_\tau)/\Gamma_{total}$ — $\Gamma_{35}/\Gamma = (\Gamma_{36}+\Gamma_{38})/\Gamma$

VALUE (%)	EVTS	DOCUMENT ID		TECN	COMMENT
0.987±0.014 OUR FIT					
0.90 ±0.07 OUR AVERAGE					
0.855±0.036±0.073	1242	COAN	96	CLEO	$E^{ee}_{cm} \approx$ 10.6 GeV
• • • We use the following data for averages but not for fits. • • •					
1.01 ±0.11 ±0.07	555	[1] BARATE	98E	ALEP	1991–1995 LEP runs

[1] Not independent of BARATE 98E B($\tau^- \to \pi^-\overline{K}^0\nu_\tau$) and B($\tau^- \to K^-K^0\nu_\tau$) values.

$\Gamma(\pi^-\overline{K}^0\nu_\tau)/\Gamma_{total}$ — Γ_{36}/Γ

VALUE (units 10^{-3})	EVTS	DOCUMENT ID		TECN	COMMENT
8.38±0.14 OUR FIT					
8.39±0.22 OUR AVERAGE Error includes scale factor of 1.5. See the ideogram below.					
8.32±0.02±0.16	158k	[1] RYU	14	BELL	669 fb^{-1} E^{ee}_{cm}=10.6 GeV
9.33±0.68±0.49	377	ABBIENDI	00C	OPAL	1991–1995 LEP runs
9.28±0.45±0.34	937	[2] BARATE	99K	ALEP	1991–1995 LEP runs
9.5 ±1.5 ±0.6		[3] ACCIARRI	95F	L3	1991–1993 LEP runs
• • • We use the following data for averages but not for fits. • • •					
8.55±1.17±0.66	509	[4] BARATE	98E	ALEP	1991–1995 LEP runs
7.04±0.41±0.72		[5] COAN	96	CLEO	$E^{ee}_{cm} \approx$ 10.6 GeV
• • • We do not use the following data for averages, fits, limits, etc. • • •					
8.08±0.04±0.26	53k	EPIFANOV	07	BELL	Repl. by RYU 14
7.9 ±1.0 ±0.9	98	[6] BUSKULIC	96	ALEP	Repl. by BARATE 99K

[1] RYU 14 reconstruct K^0's using $K^0_S \to \pi^+\pi^-$ decays.
[2] BARATE 99K measure K^0's by detecting K^0_L's in their hadron calorimeter.
[3] ACCIARRI 95F do not identify π^-/K^- and assume B($K^-K^0\nu_\tau$) = (0.29 ± 0.12)%.
[4] BARATE 98E reconstruct K^0's using $K^0_S \to \pi^+\pi^-$ decays. Not independent of BARATE 98E B(K^0particles$^-\nu_\tau$) value.
[5] Not independent of COAN 96 B($h^-K^0\nu_\tau$) and B($K^-K^0\nu_\tau$) measurements.
[6] BUSKULIC 96 measure K^0's by detecting K^0_L's in their hadron calorimeter.

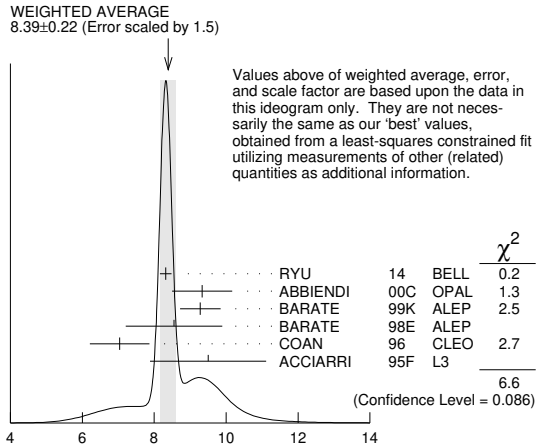

$\Gamma(\pi^-\overline{K}^0(\text{non-}K^*(892)^-)\nu_\tau)/\Gamma_{total}$ — Γ_{37}/Γ

VALUE (units 10^{-4})	CL%	DOCUMENT ID		TECN	COMMENT
5.4±2.1		[1] EPIFANOV	07	BELL	351 fb^{-1} E^{ee}_{cm}= 10.6 GeV
• • • We do not use the following data for averages, fits, limits, etc. • • •					
<17	95	ACCIARRI	95F	L3	1991–1993 LEP runs

[1] EPIFANOV 07 quote B($\tau^- \to K^*(892)^-\nu_\tau$) B($K^*(892)^- \to K^0_S\pi^-$) / B($\tau^- \to K^0_S\pi^-\nu_\tau$) = 0.933 ± 0.027. We multiply their B($\tau^- \to \overline{K}^0\pi^-\nu_\tau$) by [1−(0.933 ± 0.027)] to obtain this result.

$\Gamma(K^-K^0\nu_\tau)/\Gamma_{total}$ — Γ_{38}/Γ

VALUE (units 10^{-4})	EVTS	DOCUMENT ID		TECN	COMMENT
14.86±0.34 OUR FIT					
14.83±0.35 OUR AVERAGE					
14.78±0.22±0.40	29k	[1] LEES	18B	BABR	468 fb^{-1} E^{ee}_{cm}=10.6 GeV
14.80±0.14±0.54	33k	[2] RYU	14	BELL	669 fb^{-1} E^{ee}_{cm}=10.6 GeV
16.2 ±2.1 ±1.1	150	[3] BARATE	99K	ALEP	1991–1995 LEP runs
15.8 ±4.2 ±1.7	46	[4] BARATE	98E	ALEP	1991–1995 LEP runs
15.1 ±2.1 ±2.2	111	COAN	96	CLEO	$E^{ee}_{cm} \approx$ 10.6 GeV
• • • We do not use the following data for averages, fits, limits, etc. • • •					
26 ±9 ±2	13	[5] BUSKULIC	96	ALEP	Repl. by BARATE 99K

[1] LEES 18B reconstructs K^0_S's using $K^0_S \to \pi^+\pi^-$ decays.
[2] RYU 14 reconstruct K^0's using $K^0_S \to \pi^+\pi^-$ decays.
[3] BARATE 99K measure K^0's by detecting K^0_L's in their hadron calorimeter.
[4] BARATE 98E reconstruct K^0's using $K^0_S \to \pi^+\pi^-$ decays.
[5] BUSKULIC 96 measure K^0's by detecting K^0_L's in their hadron calorimeter.

$\Gamma(K^-K^0 \geq 0\pi^0\nu_\tau)/\Gamma_{total}$ — $\Gamma_{39}/\Gamma = (\Gamma_{38}+\Gamma_{43})/\Gamma$

VALUE (%)	EVTS	DOCUMENT ID		TECN	COMMENT
0.299±0.007 OUR FIT					
0.330±0.055±0.039	124	ABBIENDI	00C	OPAL	1991–1995 LEP runs

$\Gamma(h^-\overline{K}^0\pi^0\nu_\tau)/\Gamma_{total}$ — $\Gamma_{40}/\Gamma = (\Gamma_{41}+\Gamma_{43})/\Gamma$

VALUE (%)	EVTS	DOCUMENT ID		TECN	COMMENT
0.532±0.013 OUR FIT					
0.50 ±0.06 OUR AVERAGE Error includes scale factor of 1.2.					
0.562±0.050±0.048	264	COAN	96	CLEO	$E^{ee}_{cm} \approx$ 10.6 GeV
• • • We use the following data for averages but not for fits. • • •					
0.446±0.052±0.046	157	[1] BARATE	98E	ALEP	1991–1995 LEP runs

[1] Not independent of BARATE 98E B($\tau^- \to \pi^-\overline{K}^0\pi^0\tau$) and B($\tau^- \to K^-K^0\pi^0\nu_\tau$) values.

$\Gamma(\pi^-\overline{K}^0\pi^0\nu_\tau)/\Gamma_{total}$ — Γ_{41}/Γ

VALUE (%)	EVTS	DOCUMENT ID		TECN	COMMENT
0.382±0.013 OUR FIT					
0.383±0.014 OUR AVERAGE					
0.386±0.004±0.014	27k	[1] RYU	14	BELL	669 fb^{-1} E^{ee}_{cm}=10.6 GeV
0.347±0.053±0.037	299	[2] BARATE	99K	ALEP	1991–1995 LEP runs
0.294±0.073±0.037	142	[3] BARATE	98E	ALEP	1991–1995 LEP runs
0.41 ±0.12 ±0.03		[4] ACCIARRI	95F	L3	1991–1993 LEP runs
• • • We use the following data for averages but not for fits. • • •					
0.417±0.058±0.044		[5] COAN	96	CLEO	$E^{ee}_{cm} \approx$ 10.6 GeV
• • • We do not use the following data for averages, fits, limits, etc. • • •					
0.32 ±0.11 ±0.05	23	[6] BUSKULIC	96	ALEP	Repl. by BARATE 99K

[1] RYU 14 reconstruct K^0's using $K^0_S \to \pi^+\pi^-$ decays.
[2] BARATE 99K measure K^0's by detecting K^0_L's in their hadron calorimeter.
[3] BARATE 98E reconstruct K^0's using $K^0_S \to \pi^+\pi^-$ decays.
[4] ACCIARRI 95F do not identify π^-/K^- and assume B($K^-K^0\pi^0\nu_\tau$) = (0.05 ± 0.05)%.
[5] Not independent of COAN 96 B($h^-K^0\pi^0\nu_\tau$) and B($K^-K^0\pi^0\nu_\tau$) measurements.
[6] BUSKULIC 96 measure K^0's by detecting K^0_L's in their hadron calorimeter.

Downloaded from https://academic.oup.com/ptep/article/2022/8/083C01/6651666 by KIT Library user on 27 September 2022

$\Gamma(\overline{K}^0\rho^-\nu_\tau)/\Gamma_{total}$ — Γ_{42}/Γ

VALUE (%)	DOCUMENT ID		TECN	COMMENT
0.22 ±0.05 OUR AVERAGE				
0.250±0.057±0.044	[1] BARATE	99K	ALEP	1991–1995 LEP runs
0.188±0.054±0.038	[2] BARATE	98E	ALEP	1991–1995 LEP runs

[1] BARATE 99K measure K^0's by detecting K^0_L's in hadron calorimeter. They determine the $\overline{K}^0\rho^-$ fraction in $\tau^- \to \pi^-\overline{K}^0\pi^0\nu_\tau$ decays to be (0.72 ± 0.12 ± 0.10) and multiply their $B(\pi^-\overline{K}^0\pi^0\nu_\tau)$ measurement by this fraction to obtain the quoted result.

[2] BARATE 98E reconstruct K^0's using $K^0_S \to \pi^+\pi^-$ decays. They determine the $\overline{K}^0\rho^-$ fraction in $\tau^- \to \pi^-\overline{K}^0\pi^0\nu_\tau$ decays to be (0.64 ± 0.09 ± 0.10) and multiply their $B(\pi^-\overline{K}^0\pi^0\nu_\tau)$ measurement by this fraction to obtain the quoted result.

$\Gamma(K^-K^0\pi^0\nu_\tau)/\Gamma_{total}$ — Γ_{43}/Γ

VALUE (units 10^{-4})	EVTS	DOCUMENT ID		TECN	COMMENT
15.0 ±0.7 OUR FIT					
14.9 ±0.7 OUR AVERAGE					
14.96±0.20±0.74	8.3k	[1] RYU	14	BELL	669 fb^{-1} E^{ee}_{cm}=10.6 GeV
14.3 ±2.5 ±1.5	78	[2] BARATE	99K	ALEP	1991–1995 LEP runs
15.2 ±7.6 ±2.1	15	[3] BARATE	98E	ALEP	1991–1995 LEP runs
14.5 ±3.6 ±2.0	32	COAN	96	CLEO	$E^{ee}_{cm} \approx$ 10.6 GeV
• • • We do not use the following data for averages, fits, limits, etc. • • •					
10 ±5 ±3	5	[4] BUSKULIC	96	ALEP	Repl. by BARATE 99K

[1] RYU 14 reconstruct K^0's using $K^0_S \to \pi^+\pi^-$ decays.

[2] BARATE 99K measure K^0's by detecting K^0_L's in their hadron calorimeter.

[3] BARATE 98E reconstruct K^0's using $K^0_S \to \pi^+\pi^-$ decays.

[4] BUSKULIC 96 measure K^0's by detecting K^0_L's in their hadron calorimeter.

$\Gamma(\pi^-\overline{K}^0 \geq 1\pi^0\nu_\tau)/\Gamma_{total}$ — $\Gamma_{44}/\Gamma = (\Gamma_{41}+\Gamma_{45})/\Gamma$

VALUE (%)	EVTS	DOCUMENT ID		TECN	COMMENT
0.408±0.025 OUR FIT					
0.324±0.074±0.066	148	ABBIENDI	00C	OPAL	1991–1995 LEP runs

$\Gamma(\pi^-\overline{K}^0\pi^0\pi^0\nu_\tau(\text{ex}.K^0))/\Gamma_{total}$ — Γ_{45}/Γ

VALUE (units 10^{-3})	CL%	EVTS	DOCUMENT ID		TECN	COMMENT
0.26±0.23 OUR FIT						
0.26±0.24			[1] BARATE	99R	ALEP	1991–1995 LEP runs
• • • We do not use the following data for averages, fits, limits, etc. • • •						
<0.66	95	17	[2] BARATE	99K	ALEP	1991–1995 LEP runs
0.58±0.33±0.14		5	[3] BARATE	98E	ALEP	1991–1995 LEP runs

[1] BARATE 99R combine the BARATE 98E and BARATE 99K measurements to obtain this value.

[2] BARATE 99K measure K^0's by detecting K^0_L's in their hadron calorimeter.

[3] BARATE 98E reconstruct K^0's using $K^0_S \to \pi^+\pi^-$ decays.

$\Gamma(K^-K^0\pi^0\pi^0\nu_\tau)/\Gamma_{total}$ — Γ_{46}/Γ

VALUE	CL%	DOCUMENT ID		TECN	COMMENT
<0.16 × 10^{-3}	95	[1] BARATE	99R	ALEP	1991–1995 LEP runs
• • • We do not use the following data for averages, fits, limits, etc. • • •					
<0.18 × 10^{-3}	95	[2] BARATE	99K	ALEP	1991–1995 LEP runs
<0.39 × 10^{-3}	95	[3] BARATE	98E	ALEP	1991–1995 LEP runs

[1] BARATE 99R combine the BARATE 98E and BARATE 99K bounds to obtain this value.

[2] BARATE 99K measure K^0's by detecting K^0_L's in hadron calorimeter.

[3] BARATE 98E reconstruct K^0's using $K^0_S \to \pi^+\pi^-$ decays.

$\Gamma(\pi^-K^0\overline{K}^0\nu_\tau)/\Gamma_{total}$ — $\Gamma_{47}/\Gamma = (\Gamma_{48}+\Gamma_{49}+\Gamma_{50})/\Gamma$

VALUE (%)	EVTS	DOCUMENT ID		TECN	COMMENT
0.155±0.024 OUR FIT					
• • • We use the following data for averages but not for fits. • • •					
0.153±0.030±0.016	74	[1] BARATE	98E	ALEP	1991–1995 LEP runs
• • • We do not use the following data for averages, fits, limits, etc. • • •					
0.31 ±0.12 ±0.04		[2] ACCIARRI	95F	L3	1991–1993 LEP runs

[1] BARATE 98E obtain this value by adding twice their $B(\pi^-K^0_SK^0_S\nu_\tau)$ value to their $B(\pi^-K^0_SK^0_L\nu_\tau)$ value.

[2] ACCIARRI 95F assume $B(\pi^-K^0_SK^0_S\nu) = B(\pi^-K^0_SK^0_L\nu) = 1/2B(\pi^-K^0_SK^0_L\nu)$.

$\Gamma(\pi^-K^0_SK^0_S\nu_\tau)/\Gamma_{total}$ — Γ_{48}/Γ

Bose-Einstein correlations might make the mixing fraction different than 1/4.

VALUE (units 10^{-4})	EVTS	DOCUMENT ID		TECN	COMMENT
2.35±0.06 OUR FIT					
2.32±0.06 OUR AVERAGE					
2.33±0.03±0.09	6.7k	RYU	14	BELL	669 fb^{-1} E^{ee}_{cm}=10.6 GeV
2.31±0.04±0.08	5.0k	[1] LEES	12Y	BABR	468 fb^{-1} E^{ee}_{cm}=10.6 GeV
2.6 ±1.0 ±0.5	6	BARATE	98E	ALEP	1991–1995 LEP runs
2.3 ±0.5 ±0.3	42	COAN	96	CLEO	$E^{ee}_{cm} \approx$ 10.6 GeV

[1] The correlation coefficient between this measurement and the LEES 12Y $\Gamma(\tau^- \to \pi^-K^0_SK^0_S\pi^0\nu_\tau)/\Gamma_{total}$ one is 0.0828.

$\Gamma(\pi^-K^0_SK^0_L\nu_\tau)/\Gamma_{total}$ — Γ_{49}/Γ

VALUE (units 10^{-4})	EVTS	DOCUMENT ID		TECN	COMMENT
10.8±2.4 OUR FIT					
10.1±2.3±1.3	68	BARATE	98E	ALEP	1991–1995 LEP runs

$\Gamma(\pi^-K^0_LK^0_L\nu_\tau)/\Gamma_{total}$ — $\Gamma_{50}/\Gamma = \Gamma_{48}/\Gamma$

VALUE (units 10^{-4})	DOCUMENT ID
2.35±0.06 OUR FIT	

$\Gamma(\pi^-K^0\overline{K}^0\pi^0\nu_\tau)/\Gamma_{total}$ — $\Gamma_{51}/\Gamma = (\Gamma_{52}+\Gamma_{56}+\Gamma_{57})/\Gamma$

VALUE (units 10^{-4})	DOCUMENT ID		TECN	COMMENT
3.6±1.2 OUR FIT				
• • • We use the following data for averages but not for fits. • • •				
3.1±2.3	[1] BARATE	99R	ALEP	1991–1995 LEP runs

[1] BARATE 99R combine BARATE 98E $\Gamma(\pi^-K^0_SK^0_S\pi^0\nu_\tau)/\Gamma_{total}$ and $\Gamma(\pi^-K^0_SK^0_L\pi^0\nu_\tau)/\Gamma_{total}$ measurements to obtain this value.

$\Gamma(\pi^-K^0_SK^0_S\pi^0\nu_\tau)/\Gamma_{total}$ — Γ_{52}/Γ

VALUE (units 10^{-5})	CL%	EVTS	DOCUMENT ID		TECN	COMMENT
1.82±0.21 OUR FIT						
1.80±0.21 OUR AVERAGE						
2.00±0.22±0.20		303	RYU	14	BELL	669 fb^{-1} E^{ee}_{cm}=10.6 GeV
1.60±0.20±0.22		409	[1] LEES	12Y	BABR	468 fb^{-1} E^{ee}_{cm}=10.6 GeV
• • • We do not use the following data for averages, fits, limits, etc. • • •						
<20	95		BARATE	98E	ALEP	1991–1995 LEP runs

[1] The correlation coefficient between this measurement and the LEES 12Y $\Gamma(\tau^- \to \pi^-K^0_SK^0_S\nu_\tau)/\Gamma_{total}$ one is 0.0828.

$\Gamma(K^{*-}K^0\pi^0\nu_\tau \to \pi^-K^0_SK^0_S\pi^0\nu_\tau)/\Gamma_{total}$ — Γ_{53}/Γ

VALUE (units 10^{-6})	DOCUMENT ID		TECN	COMMENT
10.8±1.4±1.5	RYU	14	BELL	669 fb^{-1} E^{ee}_{cm}=10.6 GeV

$\Gamma(f_1(1285)\pi^-\nu_\tau \to \pi^-K^0_SK^0_S\pi^0\nu_\tau)/\Gamma_{total}$ — Γ_{54}/Γ

VALUE (units 10^{-6})	DOCUMENT ID		TECN	COMMENT
6.8±1.3±0.7	RYU	14	BELL	669 fb^{-1} E^{ee}_{cm}=10.6 GeV

$\Gamma(f_1(1420)\pi^-\nu_\tau \to \pi^-K^0_SK^0_S\pi^0\nu_\tau)/\Gamma_{total}$ — Γ_{55}/Γ

VALUE (units 10^{-6})	DOCUMENT ID		TECN	COMMENT
2.4±0.5±0.6	RYU	14	BELL	669 fb^{-1} E^{ee}_{cm}=10.6 GeV

$\Gamma(\pi^-K^0_SK^0_L\pi^0\nu_\tau)/\Gamma_{total}$ — Γ_{56}/Γ

VALUE (units 10^{-4})	EVTS	DOCUMENT ID		TECN	COMMENT
3.2±1.2 OUR FIT					
3.1±1.1±0.5	11	BARATE	98E	ALEP	1991–1995 LEP runs

$\Gamma(\pi^-K^0_LK^0_L\pi^0\nu_\tau)/\Gamma_{total}$ — $\Gamma_{57}/\Gamma = \Gamma_{52}/\Gamma$

VALUE (units 10^{-5})	DOCUMENT ID
1.82±0.21 OUR FIT	

$\Gamma(K^-K^0_SK^0_S\nu_\tau)/\Gamma_{total}$ — Γ_{58}/Γ

VALUE	CL%	DOCUMENT ID		TECN	COMMENT
<6.3 × 10^{-7}	90	LEES	12Y	BABR	468 fb^{-1} E^{ee}_{cm}=10.6 GeV

$\Gamma(K^-K^0_SK^0_S\pi^0\nu_\tau)/\Gamma_{total}$ — Γ_{59}/Γ

VALUE	CL%	DOCUMENT ID		TECN	COMMENT
<4.0 × 10^{-7}	90	LEES	12Y	BABR	468 fb^{-1} E^{ee}_{cm}=10.6 GeV

$\Gamma(K^0h^+h^-h^- \geq 0 \text{ neutrals } \nu_\tau)/\Gamma_{total}$ — Γ_{60}/Γ

VALUE (%)	CL%	DOCUMENT ID		TECN	COMMENT
<0.17	95	TSCHIRHART	88	HRS	E^{ee}_{cm}= 29 GeV
• • • We do not use the following data for averages, fits, limits, etc. • • •					
<0.27	90	BELTRAMI	85	HRS	E^{ee}_{cm}= 29 GeV

$\Gamma(K^0h^+h^-h^-\nu_\tau)/\Gamma_{total}$ — Γ_{61}/Γ

VALUE (units 10^{-4})	EVTS	DOCUMENT ID		TECN	COMMENT
2.5±2.0 OUR FIT					
2.3±1.9±0.7	6	[1] BARATE	98E	ALEP	1991–1995 LEP runs

[1] BARATE 98E reconstruct K^0's using $K^0_S \to \pi^+\pi^-$ decays.

$\Gamma(h^-h^-h^+ \geq 0 \text{ neutrals } \geq 0K^0_L\nu_\tau)/\Gamma_{total}$ — Γ_{62}/Γ

$\Gamma_{62}/\Gamma = (0.34598\Gamma_{36}+0.34598\Gamma_{38}+0.34598\Gamma_{41}+0.34598\Gamma_{43}+0.4247\Gamma_{48}+0.6920\Gamma_{49}+0.4247\Gamma_{52}+0.6920\Gamma_{56}+0.6534\Gamma_{61}+\Gamma_{70}+\Gamma_{78}+\Gamma_{85}+\Gamma_{86}+\Gamma_{97}+\Gamma_{103}+\Gamma_{106}+\Gamma_{107}+0.2804\Gamma_{150}+0.2804\Gamma_{152}+0.2804\Gamma_{154}+0.2628\Gamma_{156}+0.7259\Gamma_{170}+0.9078\Gamma_{178}+0.9078\Gamma_{179}+0.9078\Gamma_{180})/\Gamma$

VALUE (%)	EVTS	DOCUMENT ID		TECN	COMMENT
15.20± 0.06 OUR FIT					
14.8 ± 0.4 OUR AVERAGE					
14.4 ± 0.6 ±0.3		ADEVA	91F	L3	E^{ee}_{cm}= 88.3–94.3 GeV
15.0 ± 0.4 ±0.3		BEHREND	89B	CELL	E^{ee}_{cm}= 14–47 GeV
15.1 ± 0.8 ±0.6		AIHARA	87B	TPC	E^{ee}_{cm}= 29 GeV

Downloaded from https://academic.oup.com/ptep/article/2022/8/083C01/6651666 by KIT Library user on 27 September 2022

• • • We do not use the following data for averages, fits, limits, etc. • • •

13.5 ± 0.3 ±0.3		ABACHI	89B	HRS	E^{ee}_{cm}= 29 GeV
12.8 ± 1.0 ±0.7		[1] BURCHAT	87	MRK2	E^{ee}_{cm}= 29 GeV
12.1 ± 0.5 ±1.2		RUCKSTUHL	86	DLCO	E^{ee}_{cm}= 29 GeV
12.8 ± 0.5 ±0.8	1420	SCHMIDKE	86	MRK2	E^{ee}_{cm}= 29 GeV
15.3 ± 1.1 $^{+1.3}_{-1.6}$	367	ALTHOFF	85	TASS	E^{ee}_{cm}= 34.5 GeV
13.6 ± 0.5 ±0.8		BARTEL	85F	JADE	E^{ee}_{cm}= 34.6 GeV
12.2 ± 1.3 ±3.9		[2] BERGER	85	PLUT	E^{ee}_{cm}= 34.6 GeV
13.3 ± 0.3 ±0.6		FERNANDEZ	85	MAC	E^{ee}_{cm}= 29 GeV
24 ± 6	35	BRANDELIK	80	TASS	E^{ee}_{cm}= 30 GeV
32 ± 5	692	[3] BACINO	78B	DLCO	E^{ee}_{cm}= 3.1–7.4 GeV
35 ±11		[3] BRANDELIK	78	DASP	Assumes $V-A$ decay
18 ± 6.5	33	[3] JAROS	78	LGW	E^{ee}_{cm} > 6 GeV

[1] BURCHAT 87 value is not independent of SCHMIDKE 86 value.
[2] Not independent of BERGER 85 $\Gamma(\mu^-\overline{\nu}_\mu\nu_\tau)/\Gamma_{total}$, $\Gamma(e^-\overline{\nu}_e\nu_\tau)/\Gamma_{total}$, $\Gamma(h^- \geq 1$ neutrals$\nu_\tau)/\Gamma_{total}$, and $\Gamma(h^- \geq 0 K^0_L\ \nu_\tau)/\Gamma_{total}$, and therefore not used in the fit.
[3] Low energy experiments are not in average or fit because the systematic errors in background subtraction are judged to be large.

$\Gamma(h^-h^-h^+ \geq 0$ neutrals ν_τ(ex. $K^0_S \to \pi^+\pi^-)$("3-prong"))/Γ_{total} — Γ_{63}/Γ

$\Gamma_{63}/\Gamma = (\Gamma_{70}+\Gamma_{78}+\Gamma_{85}+\Gamma_{86}+\Gamma_{97}+\Gamma_{103}+\Gamma_{106}+\Gamma_{107}+0.2804\Gamma_{150}+0.2804\Gamma_{152}+0.2804\Gamma_{154}+0.491\Gamma_{170}+0.9078\Gamma_{178}+0.9078\Gamma_{179}+0.9078\Gamma_{180})/\Gamma$

VALUE (%)	EVTS	DOCUMENT ID		TECN	COMMENT
14.55 ±0.06 OUR FIT					
14.61 ±0.06 OUR AVERAGE					
14.556±0.105±0.076		[1] ACHARD	01D	L3	1992–1995 LEP runs
14.96 ±0.09 ±0.22	10.4k	AKERS	95Y	OPAL	1991–1994 LEP runs
• • • We use the following data for averages but not for fits. • • •					
14.652±0.067±0.086		SCHAEL	05C	ALEP	1991–1995 LEP runs
14.569±0.093±0.048	23k	[2] ABREU	01M	DLPH	1992–1995 LEP runs
14.22 ±0.10 ±0.37		[3] BALEST	95C	CLEO	$E^{ee}_{cm} \approx$ 10.6 GeV
• • • We do not use the following data for averages, fits, limits, etc. • • •					
15.26 ±0.26 ±0.22		ACTON	92H	OPAL	Repl. by AKERS 95Y
13.3 ±0.3 ±0.8		[4] ALBRECHT	92D	ARG	E^{ee}_{cm}= 9.4–10.6 GeV
14.35 $^{+0.40}_{-0.45}$ ±0.24		DECAMP	92C	ALEP	1989–1990 LEP runs

[1] The correlation coefficients between this measurement and the ACHARD 01D measurements of B($\tau \to$ "1-prong") and B($\tau \to$ "5-prong") are −0.978 and −0.19 respectively.
[2] The correlation coefficients between this measurement and the ABREU 01M measurements of B($\tau \to$ 1-prong) and B($\tau \to$ 5-prong) are −0.98 and −0.08 respectively.
[3] Not independent of BALEST 95C B($h^-h^-h^+\nu_\tau$) and B($h^-h^-h^+\pi^0\nu_\tau$) values, and BORTOLETTO 93 B($h^-h^-h^+2\pi^0\nu_\tau$)/B($h^-h^-h^+ \geq 0$ neutrals ν_τ) value.
[4] This ALBRECHT 92D value is not independent of their $\Gamma(\mu^-\overline{\nu}_\mu\nu_\tau)\Gamma(e^-\overline{\nu}_e\nu_\tau)/\Gamma^2_{total}$ value.

$\Gamma(h^-h^-h^+\nu_\tau)/\Gamma_{total}$ — Γ_{64}/Γ

$\Gamma_{64}/\Gamma = (0.34598\Gamma_{36}+0.34598\Gamma_{38}+\Gamma_{70}+\Gamma_{97}+\Gamma_{106}+0.491\Gamma_{170}+0.0153\Gamma_{178}+0.0153\Gamma_{179})/\Gamma$

VALUE (%)	EVTS	DOCUMENT ID		TECN	COMMENT
9.80±0.05 OUR FIT					
• • • We use the following data for averages but not for fits. • • •					
7.6 ±0.1 ±0.5	7.5k	[1] ALBRECHT	96E	ARG	E^{ee}_{cm}= 9.4–10.6 GeV
• • • We do not use the following data for averages, fits, limits, etc. • • •					
9.92±0.10±0.09	11.2k	[2] BUSKULIC	96	ALEP	Repl. by SCHAEL 05C
9.49±0.36±0.63		DECAMP	92C	ALEP	Repl. by SCHAEL 05C
8.7 ±0.7 ±0.3	694	[3] BEHREND	90	CELL	E^{ee}_{cm}= 35 GeV
7.0 ±0.3 ±0.7	1566	[4] BAND	87	MAC	E^{ee}_{cm}= 29 GeV
6.7 ±0.8 ±0.9		[5] BURCHAT	87	MRK2	E^{ee}_{cm}= 29 GeV
6.4 ±0.4 ±0.9		[6] RUCKSTUHL	86	DLCO	E^{ee}_{cm}= 29 GeV
7.8 ±0.5 ±0.8	890	SCHMIDKE	86	MRK2	E^{ee}_{cm}= 29 GeV
8.4 ±0.4 ±0.7	1255	[6] FERNANDEZ	85	MAC	E^{ee}_{cm}= 29 GeV
9.7 ±2.0 ±1.3		BEHREND	84	CELL	E^{ee}_{cm}= 14,22 GeV

[1] ALBRECHT 96E not independent of ALBRECHT 93C $\Gamma(h^-h^-h^+\nu_\tau$(ex. $K^0) \times \Gamma$(particle$^- \geq 0$ neutrals $\geq 0 K^0_L\nu_\tau)/\Gamma^2_{total}$ value.
[2] BUSKULIC 96 quote B($h^-h^-h^+\nu_\tau$(ex. K^0)) = 9.50 ± 0.10 ± 0.11. We add 0.42 to remove their K^0 correction and reduce the systematic error accordingly.
[3] BEHREND 90 subtract 0.3% to account for the $\tau^- \to K^*(892)^-\nu_\tau$ contribution to measured events.
[4] BAND 87 subtract for charged kaon modes; not independent of FERNANDEZ 85 value.
[5] BURCHAT 87 value is not independent of SCHMIDKE 86 value.
[6] Value obtained by multiplying paper's R = B($h^-h^-h^+\nu_\tau$)/B(3-prong) by B(3-prong) = 0.143 and subtracting 0.3% for $K^*(892)$ background.

$\Gamma(h^-h^-h^+\nu_\tau$(ex.K^0))/Γ_{total} — Γ_{65}/Γ

$\Gamma_{65}/\Gamma = (\Gamma_{70}+\Gamma_{97}+\Gamma_{106}+0.491\Gamma_{170}+0.0153\Gamma_{178}+0.0153\Gamma_{179})/\Gamma$

VALUE (%)	EVTS	DOCUMENT ID		TECN	COMMENT
9.46 ±0.05 OUR FIT					
9.44 ±0.14 OUR AVERAGE	Error includes scale factor of 1.4. See the ideogram below.				
9.317±0.090±0.082	12.2k	[1] ABDALLAH	06A	DLPH	1992–1995 LEP runs
9.51 ±0.07 ±0.20	37.7k	BALEST	95C	CLEO	$E^{ee}_{cm} \approx$ 10.6 GeV
• • • We use the following data for averages but not for fits. • • •					
9.87 ±0.10 ±0.24		[2] AKERS	95Y	OPAL	1991–1994 LEP runs
• • • We do not use the following data for averages, fits, limits, etc. • • •					
9.50 ±0.10 ±0.11	11.2k	[3] BUSKULIC	96	ALEP	Repl. by SCHAEL 05C

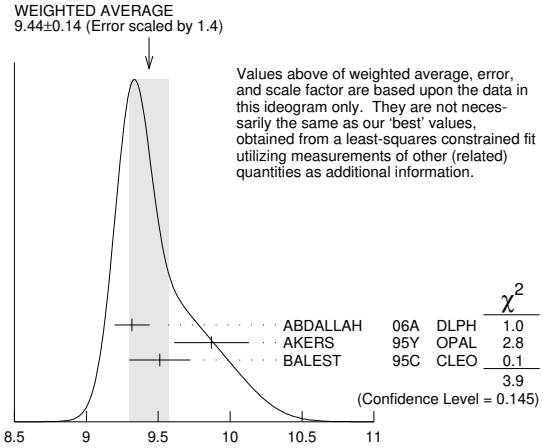

[1] See footnote to ABDALLAH 06A $\Gamma(\tau^- \to h^-\nu_\tau)/\Gamma_{total}$ measurement for correlations with other measurements.
[2] Not independent of AKERS 95Y B($h^-h^-h^+ \geq 0$ neutralsν_τ(ex. $K^0_S \to \pi^+\pi^-$)) and B($h^-h^-h^+\nu_\tau$(ex. K^0))/B($h^-h^-h^+ \geq 0$ neutralsν_τ(ex. $K^0_S \to \pi^+\pi^-$)) values.
[3] Not independent of BUSKULIC 96 B($h^-h^-h^+\nu_\tau$) value.

$\Gamma(h^-h^-h^+\nu_\tau$(ex.K^0))/$\Gamma(h^-h^-h^+ \geq 0$ neutrals ν_τ(ex. $K^0_S \to \pi^+\pi^-$) ("3-prong")) — Γ_{65}/Γ_{63}

$\Gamma_{65}/\Gamma_{63} = (\Gamma_{70}+\Gamma_{97}+\Gamma_{106}+0.491\Gamma_{170}+0.0153\Gamma_{178}+0.0153\Gamma_{179})/(0.4247\Gamma_{52}+\Gamma_{70}+\Gamma_{78}+\Gamma_{85}+\Gamma_{89}+\Gamma_{97}+\Gamma_{103}+\Gamma_{106}+\Gamma_{107}+0.2804\Gamma_{150}+0.2302\Gamma_{151}+0.2804\Gamma_{152}+0.2804\Gamma_{154}+0.1131\Gamma_{156}+0.3257\Gamma_{160}+0.491\Gamma_{170}+0.9078\Gamma_{178}+0.9078\Gamma_{179}+0.9078\Gamma_{180}+0.892\Gamma_{182})$

VALUE (units 10^{-2})	DOCUMENT ID		TECN	COMMENT
64.98±0.31 OUR FIT				
66.0 ±0.4 ±1.4	AKERS	95Y	OPAL	1991–1994 LEP runs

$\Gamma(h^-h^-h^+\nu_\tau$(ex.$K^0\omega$))/Γ_{total} — Γ_{66}/Γ

$\Gamma_{66}/\Gamma = (\Gamma_{70}+\Gamma_{97}+\Gamma_{106}+0.491\Gamma_{170})/\Gamma$

VALUE (%)	DOCUMENT ID
9.43±0.05 OUR FIT	

$\Gamma(\pi^-\pi^+\pi^-\nu_\tau)/\Gamma_{total}$ — $\Gamma_{67}/\Gamma = (0.34598\Gamma_{36}+\Gamma_{70}+0.0153\Gamma_{178})/\Gamma$

VALUE (%)	DOCUMENT ID
9.31±0.05 OUR FIT	

$\Gamma(\pi^-\pi^+\pi^-\nu_\tau$(ex.$K^0$))/$\Gamma_{total}$ — $\Gamma_{68}/\Gamma = (\Gamma_{70}+0.0153\Gamma_{178})/\Gamma$

VALUE (%)	EVTS	DOCUMENT ID		TECN	COMMENT
9.02±0.05 OUR FIT					
8.77±0.13 OUR AVERAGE	Error includes scale factor of 1.1.				
8.42±0.00$^{+0.26}_{-0.25}$	8.9M	[1] LEE	10	BELL	666 fb^{-1} E^{ee}_{cm} = 10.6 GeV
8.83±0.01±0.13	1.6M	[2] AUBERT	08	BABR	342 fb^{-1} E^{ee}_{cm} = 10.6 GeV
9.13±0.05±0.46	43k	[3] BRIERE	03	CLE3	E^{ee}_{cm}= 10.6 GeV

[1] Quoted statistical error is 0.003%. Correlation matrix for LEE 10 branching fractions:
(1) $\Gamma(\tau^- \to \pi^-\pi^+\pi^-\nu_\tau$(ex.$K^0$))/$\Gamma_{total}$
(2) $\Gamma(\tau^- \to K^-\pi^+\pi^-\nu_\tau$(ex.$K^0$))/$\Gamma_{total}$
(3) $\Gamma(\tau^- \to K^-K^+\pi^-\nu_\tau)/\Gamma_{total}$
(4) $\Gamma(\tau^- \to K^-K^+K^-\nu_\tau)/\Gamma_{total}$

	(1)	(2)	(3)
(2)	0.175		
(3)	0.049	0.080	
(4)	-0.053	0.035	-0.008

[2] Correlation matrix for AUBERT 08 branching fractions:
(1) $\Gamma(\tau^- \to \pi^-\pi^+\pi^-\nu_\tau$(ex.$K^0$))/$\Gamma_{total}$
(2) $\Gamma(\tau^- \to K^-\pi^+\pi^-\nu_\tau$(ex.$K^0$))/$\Gamma_{total}$
(3) $\Gamma(\tau^- \to K^-K^+\pi^-\nu_\tau)/\Gamma_{total}$
(4) $\Gamma(\tau^- \to K^-K^+K^-\nu_\tau)/\Gamma_{total}$

	(1)	(2)	(3)
(2)	0.544		
(3)	0.390	0.177	
(4)	0.031	0.093	0.087

[3] 47% correlated with BRIERE 03 $\tau^- \to K^-\pi^+\pi^-\nu_\tau$ and 71% correlated with $\tau^- \to K^-K^+\pi^-\nu_\tau$ because of a common 5% normalization error.

Downloaded from https://academic.oup.com/ptep/article/2022/8/083C01/6651666 by KIT Library user on 27 September 2022

$\Gamma(\pi^-\pi^+\pi^-\nu_\tau(\text{ex.}K^0),\text{non-axial vector})/\Gamma(\pi^-\pi^+\pi^-\nu_\tau(\text{ex.}K^0))$ — Γ_{69}/Γ_{68}

$\Gamma_{69}/\Gamma_{68} = \Gamma_{69}/(\Gamma_{70}+0.0153\Gamma_{177})$

VALUE	CL%	DOCUMENT ID	TECN	COMMENT
<0.261	95	[1] ACKERSTAFF 97R	OPAL	1992–1994 LEP runs

[1] Model-independent limit from structure function analysis on contribution to $B(\tau^- \to \pi^-\pi^+\pi^-\nu_\tau(\text{ex. } K^0))$ from non-axial vectors.

$\Gamma(\pi^-\pi^+\pi^-\nu_\tau(\text{ex.}K^0,\omega))/\Gamma_{\text{total}}$ — Γ_{70}/Γ

VALUE (%)	EVTS	DOCUMENT ID	TECN	COMMENT
8.99 ±0.05 OUR FIT				
9.041±0.060±0.076	29k	[1] SCHAEL 05C	ALEP	1991-1995 LEP runs

[1] See footnote to SCHAEL 05C $\Gamma(\tau^- \to e^-\overline{\nu}_e\nu_\tau)/\Gamma_{\text{total}}$ measurement for correlations with other measurements.

$\Gamma(h^-h^-h^+ \geq 1 \text{ neutrals } \nu_\tau)/\Gamma_{\text{total}}$ — Γ_{71}/Γ

$\Gamma_{71}/\Gamma = (0.34598\Gamma_{41}+0.34598\Gamma_{43}+0.4247\Gamma_{48}+0.4247\Gamma_{52}+\Gamma_{78}+\Gamma_{85}+\Gamma_{86}+\Gamma_{103}+\Gamma_{107}+0.2804\Gamma_{150}+0.2804\Gamma_{152}+0.2804\Gamma_{154}+0.2926\Gamma_{156}+0.892\Gamma_{178}+0.892\Gamma_{179}+0.9078\Gamma_{180})/\Gamma$

VALUE (%)	EVTS	DOCUMENT ID	TECN	COMMENT
5.29±0.05 OUR FIT				
• • • We do not use the following data for averages, fits, limits, etc. • • •				
5.6 ±0.7 ±0.3	352	[1] BEHREND 90	CELL	E^{ee}_{cm}= 35 GeV
4.2 ±0.5 ±0.9	203	[2] ALBRECHT 87L	ARG	E^{ee}_{cm}= 10 GeV
6.1 ±0.8 ±0.9		[3] BURCHAT 87	MRK2	E^{ee}_{cm}= 29 GeV
7.6 ±0.4 ±0.9		[4,5] RUCKSTUHL 86	DLCO	E^{ee}_{cm}= 29 GeV
4.7 ±0.5 ±0.8	530	[6] SCHMIDKE 86	MRK2	E^{ee}_{cm}= 29 GeV
5.6 ±0.4 ±0.7		[5] FERNANDEZ 85	MAC	E^{ee}_{cm}= 29 GeV
6.2 ±2.3 ±1.7		BEHREND 84	CELL	E^{ee}_{cm}= 14,22 GeV

[1] BEHREND 90 value is not independent of BEHREND 90 $B(3h\nu_\tau \geq 1 \text{ neutrals}) + B(5\text{-prong})$.
[2] ALBRECHT 87L measure the product of branching ratios $B(3\pi^\pm\pi^0\nu_\tau)\, B((e\overline{\nu}\text{ or }\mu\overline{\nu}\text{ or }\pi\text{ or }K\text{ or }\rho)\nu_\tau) = 0.029$ and use the PDG 86 values for the second branching ratio which sum to 0.69 ± 0.03 to get the quoted value.
[3] BURCHAT 87 value is not independent of SCHMIDKE 86 value.
[4] Contributions from kaons and from $>1\pi^0$ are subtracted. Not independent of (3-prong + $0\pi^0$) and (3-prong + $\geq 0\pi^0$) values.
[5] Value obtained using paper's $R = B(h^-h^-h^+\nu_\tau)/B(\text{3-prong})$ and current B(3-prong) = 0.143.
[6] Not independent of SCHMIDKE 86 $h^-h^-h^+\nu_\tau$ and $h^-h^-h^+(\geq 0\pi^0)\nu_\tau$ values.

$\Gamma(h^-h^-h^+ \geq 1\pi^0\nu_\tau(\text{ex. } K^0))/\Gamma_{\text{total}}$ — Γ_{72}/Γ

$\Gamma_{72}/\Gamma = (\Gamma_{78}+\Gamma_{85}+\Gamma_{86}+\Gamma_{103}+\Gamma_{107}+0.2302\Gamma_{150}+0.2302\Gamma_{152}+0.2302\Gamma_{154}+0.892\Gamma_{178}+0.892\Gamma_{179}+0.9078\Gamma_{180})/\Gamma$

VALUE (%)	EVTS	DOCUMENT ID	TECN	COMMENT
5.09 ±0.05 OUR FIT				
5.10 ±0.12 OUR AVERAGE				
• • • We use the following data for averages but not for fits. • • •				
5.106±0.083±0.103	10.1k	[1] ABDALLAH 06A	DLPH	1992–1995 LEP runs
5.09 ±0.10 ±0.23		[2] AKERS 95Y	OPAL	1991–1994 LEP runs
• • • We do not use the following data for averages, fits, limits, etc. • • •				
4.95 ±0.29 ±0.65	570	DECAMP 92C	ALEP	Repl. by SCHAEL 05C

[1] See footnote to ABDALLAH 06A $\Gamma(\tau^- \to h^-\nu_\tau)/\Gamma_{\text{total}}$ measurement for correlations with other measurements.
[2] Not independent of AKERS 95Y $B(h^-h^-h^+ \geq 0 \text{ neutrals}\,\nu_\tau(\text{ex. } K^0_S \to \pi^+\pi^-))$ and $B(h^-h^-h^+ \geq 0 \text{ neutrals}\,\nu_\tau(\text{ex. } K^0))/B(h^-h^-h^+ \geq 0 \text{ neutrals}\,\nu_\tau(\text{ex. } K^0_S \to \pi^+\pi^-))$ values.

$\Gamma(h^-h^-h^+\pi^0\nu_\tau)/\Gamma_{\text{total}}$ — Γ_{73}/Γ

$\Gamma_{73}/\Gamma = (0.34598\Gamma_{41}+0.34598\Gamma_{43}+\Gamma_{78}+\Gamma_{103}+\Gamma_{107}+0.2302\Gamma_{152}+0.892\Gamma_{178}+0.892\Gamma_{179}+0.0153\Gamma_{180})/\Gamma$

VALUE (%)	EVTS	DOCUMENT ID	TECN	COMMENT
4.76±0.05 OUR FIT				
• • • We do not use the following data for averages, fits, limits, etc. • • •				
4.45±0.09±0.07	6.1k	[1] BUSKULIC 96	ALEP	Repl. by SCHAEL 05C

[1] BUSKULIC 96 quote $B(h^-h^-h^+\pi^0\nu_\tau(\text{ex. } K^0)) = 4.30 \pm 0.09 \pm 0.09$. We add 0.15 to remove their K^0 correction and reduce the systematic error accordingly.

$\Gamma(h^-h^-h^+\pi^0\nu_\tau(\text{ex.}K^0))/\Gamma_{\text{total}}$ — Γ_{74}/Γ

$\Gamma_{74}/\Gamma = (\Gamma_{78}+\Gamma_{103}+\Gamma_{107}+0.2302\Gamma_{152}+0.892\Gamma_{178}+0.892\Gamma_{179}+0.0153\Gamma_{180})/\Gamma$

VALUE (%)	EVTS	DOCUMENT ID	TECN	COMMENT
4.57 ±0.05 OUR FIT				
4.45 ±0.14 OUR AVERAGE Error includes scale factor of 1.2.				
4.545±0.106±0.103	8.9k	[1] ABDALLAH 06A	DLPH	1992–1995 LEP runs
4.23 ±0.06 ±0.22	7.2k	BALEST 95C	CLEO	$E^{ee}_{\text{cm}} \approx$ 10.6 GeV

[1] See footnote to ABDALLAH 06A $\Gamma(\tau^- \to h^-\nu_\tau)/\Gamma_{\text{total}}$ measurement for correlations with other measurements.

$\Gamma(h^-h^-h^+\pi^0\nu_\tau(\text{ex. } K^0,\omega))/\Gamma_{\text{total}}$

$\Gamma_{75}/\Gamma = (\Gamma_{78}+\Gamma_{103}+\Gamma_{107}+0.2302\Gamma_{152})/\Gamma$

VALUE (%)	DOCUMENT ID
2.79±0.07 OUR FIT	

$\Gamma(\pi^-\pi^+\pi^-\pi^0\nu_\tau)/\Gamma_{\text{total}}$ — Γ_{76}/Γ

$\Gamma_{76}/\Gamma = (0.34598\Gamma_{41}+\Gamma_{78}+0.892\Gamma_{178}+0.0153\Gamma_{180})/\Gamma$

VALUE (%)	DOCUMENT ID
4.62±0.05 OUR FIT	

$\Gamma(\pi^-\pi^+\pi^-\pi^0\nu_\tau(\text{ex.}K^0))/\Gamma_{\text{total}}$ — Γ_{77}/Γ

$\Gamma_{77}/\Gamma = (\Gamma_{78}+0.892\Gamma_{178}+0.0153\Gamma_{180})/\Gamma$

VALUE (%)	EVTS	DOCUMENT ID	TECN	COMMENT
4.49 ±0.05 OUR FIT				
4.55 ±0.13 OUR AVERAGE Error includes scale factor of 1.6.				
4.598±0.057±0.064	16k	[1] SCHAEL 05C	ALEP	1991-1995 LEP runs
4.19 ±0.10 ±0.21		[2] EDWARDS 00A	CLEO	4.7 fb^{-1} E^{ee}_{cm}= 10.6 GeV

[1] SCHAEL 05C quote (4.590±0.057±0.064)%. We add 0.008% to remove their correction for $\tau^- \to \pi^-\pi^0\omega\nu_\tau \to \pi^-\pi^0\pi^+\pi^-\nu_\tau$ decays. See footnote to SCHAEL 05C $\Gamma(\tau^- \to e^-\overline{\nu}_e\nu_\tau)/\Gamma_{\text{total}}$ measurement for correlations with other measurements.
[2] EDWARDS 00A quote (4.19 ± 0.10) × 10^{-2} with a 5% systematic error.

$\Gamma(\pi^-\pi^+\pi^-\pi^0\nu_\tau(\text{ex.}K^0,\omega))/\Gamma_{\text{total}}$ — Γ_{78}/Γ

VALUE (%)	DOCUMENT ID
2.74±0.07 OUR FIT	

$\Gamma(h^-\rho\pi^0\nu_\tau)/\Gamma(h^-h^-h^+\pi^0\nu_\tau)$ — Γ_{79}/Γ_{73}

VALUE	EVTS	DOCUMENT ID	TECN	COMMENT
• • • We do not use the following data for averages, fits, limits, etc. • • •				
0.30±0.04±0.02	393	ALBRECHT 91D	ARG	E^{ee}_{cm}= 9.4–10.6 GeV

$\Gamma(h^-\rho^+h^-\nu_\tau)/\Gamma(h^-h^-h^+\pi^0\nu_\tau)$ — Γ_{80}/Γ_{73}

VALUE	EVTS	DOCUMENT ID	TECN	COMMENT
• • • We do not use the following data for averages, fits, limits, etc. • • •				
0.10±0.03±0.04	142	ALBRECHT 91D	ARG	E^{ee}_{cm}= 9.4–10.6 GeV

$\Gamma(h^-\rho^-h^+\nu_\tau)/\Gamma(h^-h^-h^+\pi^0\nu_\tau)$ — Γ_{81}/Γ_{73}

VALUE	EVTS	DOCUMENT ID	TECN	COMMENT
• • • We do not use the following data for averages, fits, limits, etc. • • •				
0.26±0.05±0.01	370	ALBRECHT 91D	ARG	E^{ee}_{cm}= 9.4–10.6 GeV

$\Gamma(h^-h^-h^+ \geq 2\pi^0\nu_\tau(\text{ex. } K^0))/\Gamma_{\text{total}}$ — Γ_{82}/Γ

$\Gamma_{82}/\Gamma = (\Gamma_{85}+\Gamma_{86}+0.2302\Gamma_{150}+0.2302\Gamma_{154}+0.892\Gamma_{180})/\Gamma$

VALUE (%)	EVTS	DOCUMENT ID	TECN	COMMENT
0.517±0.031 OUR FIT				
0.561±0.068±0.095	1.3k	[1] ABDALLAH 06A	DLPH	1992–1995 LEP runs

[1] See footnote to ABDALLAH 06A $\Gamma(\tau^- \to h^-\nu_\tau)/\Gamma_{\text{total}}$ measurement for correlations with other measurements.

$\Gamma(h^-h^-h^+2\pi^0\nu_\tau)/\Gamma_{\text{total}}$ — Γ_{83}/Γ

$\Gamma_{83}/\Gamma = (0.4247\Gamma_{48}+\Gamma_{85}+0.2302\Gamma_{150}+0.2302\Gamma_{154}+0.892\Gamma_{180})/\Gamma$

VALUE (%)	DOCUMENT ID
0.505±0.031 OUR FIT	

$\Gamma(h^-h^-h^+2\pi^0\nu_\tau(\text{ex.}K^0))/\Gamma_{\text{total}}$ — Γ_{84}/Γ

$\Gamma_{84}/\Gamma = (\Gamma_{85}+0.2302\Gamma_{150}+0.2302\Gamma_{154}+0.892\Gamma_{180})/\Gamma$

VALUE (%)	EVTS	DOCUMENT ID	TECN	COMMENT
0.495±0.031 OUR FIT				
0.435±0.030±0.035	2.6k	[1] SCHAEL 05C	ALEP	1991-1995 LEP runs
• • • We do not use the following data for averages, fits, limits, etc. • • •				
0.50 ±0.07 ±0.07	1.8k	BUSKULIC 96	ALEP	Repl. by SCHAEL 05C

[1] SCHAEL 05C quote (0.392 ± 0.030 ± 0.035)%. We add 0.043% to remove their correction for $\tau^- \to \pi^-\eta\pi^0\nu_\tau \to \pi^-\pi^+\pi^-2\pi^0\nu_\tau$ and $\tau^- \to K^*(892)^-\eta\nu_\tau \to K^-\pi^+\pi^-2\pi^0\nu_\tau$ decays. See footnote to SCHAEL 05C $\Gamma(\tau^- \to e^-\overline{\nu}_e\nu_\tau)/\Gamma_{\text{total}}$ measurement for correlations with other measurements.

$\Gamma(h^-h^-h^+2\pi^0\nu_\tau(\text{ex.}K^0))/\Gamma(h^-h^-h^+ \geq 0 \text{ neutrals} \geq 0K^0_L\nu_\tau)$ — Γ_{84}/Γ_{62}

$\Gamma_{84}/\Gamma_{62} = (\Gamma_{85}+0.2302\Gamma_{150}+0.2302\Gamma_{154}+0.892\Gamma_{180})/(0.34598\Gamma_{36}+0.34598\Gamma_{38}+0.34598\Gamma_{41}+0.34598\Gamma_{43}+0.4247\Gamma_{48}+0.6920\Gamma_{49}+0.8494\Gamma_{52}+0.6920\Gamma_{56}+0.6534\Gamma_{61}+\Gamma_{70}+\Gamma_{78}+\Gamma_{85}+\Gamma_{89}+\Gamma_{97}+\Gamma_{103}+\Gamma_{106}+\Gamma_{107}+0.2804\Gamma_{150}+0.2302\Gamma_{151}+0.2804\Gamma_{152}+0.2804\Gamma_{154}+0.3759\Gamma_{156}+0.3257\Gamma_{160}+0.7259\Gamma_{170}+0.9078\Gamma_{178}+0.9078\Gamma_{179}+0.9078\Gamma_{180}+0.892\Gamma_{182})$

VALUE (units 10^{-2})	EVTS	DOCUMENT ID	TECN	COMMENT
3.26±0.20 OUR FIT				
3.4 ±0.2 ±0.3	668	BORTOLETTO 93	CLEO	$E^{ee}_{\text{cm}} \approx$ 10.6 GeV

$\Gamma(h^-h^-h^+2\pi^0\nu_\tau(\text{ex.}K^0,\omega,\eta))/\Gamma_{\text{total}}$ — Γ_{85}/Γ

VALUE (units 10^{-4})	DOCUMENT ID
10±4 OUR FIT	

$\Gamma(h^-h^-h^+3\pi^0\nu_\tau)/\Gamma_{\text{total}}$ — $\Gamma_{86}/\Gamma = (0.4247\Gamma_{52}+\Gamma_{87}+0.1131\Gamma_{156})/\Gamma$

VALUE (units 10^{-4})	CL%	EVTS	DOCUMENT ID	TECN	COMMENT
2.13±0.30 OUR FIT					
2.2 ±0.3 ±0.4		139	ANASTASSOV 01	CLEO	E^{ee}_{cm}= 10.6 GeV

Downloaded from https://academic.oup.com/ptep/article/2022/8/083C01/6651666 by KIT Library user on 27 September 2022

• • • We do not use the following data for averages, fits, limits, etc. • • •

< 4.9	95	SCHAEL	05C	ALEP	1991-1995 LEP runs
$2.85 \pm 0.56 \pm 0.51$	57	ANDERSON	97	CLEO	Repl. by ANASTASSOV 01
$11 \pm 4 \pm 5$	440	[1] BUSKULIC	96	ALEP	Repl. by SCHAEL 05C

[1] BUSKULIC 96 state their measurement is for $B(h^- h^- h^+ \geq 3\pi^0 \nu_\tau)$. We assume that $B(h^- h^- h^+ \geq 4\pi^0 \nu_\tau)$ is very small.

$\Gamma(2\pi^- \pi^+ 3\pi^0 \nu_\tau (\text{ex.}K^0))/\Gamma_{total}$ — Γ_{87}/Γ

$\Gamma_{87}/\Gamma = (\Gamma_{89} + 0.2302\Gamma_{151} + 0.3257\Gamma_{160} + 0.892\Gamma_{182})/\Gamma$

VALUE (units 10^{-4})	DOCUMENT ID	TECN	COMMENT
1.95±0.30 OUR FIT			
• • • We use the following data for averages but not for fits. • • •			
2.07±0.18±0.37	[1] LEES 12X	BABR	468 fb^{-1} $E^{ee}_{cm} = 10.6$ GeV

[1] Not independent of LEES 12X $\Gamma(\tau^- \to \eta\pi^-\pi^+\pi^-\nu_\tau(\text{ex.}K^0))/\Gamma$, $\Gamma(\tau^- \to \eta\pi^-\pi^0\pi^0\nu_\tau)/\Gamma$, $\Gamma(\tau^- \to \pi^-\omega 2\pi^0\nu_\tau)/\Gamma$, and $\Gamma(\tau^- \to f_1(1285)\pi^-\nu_\tau \to \eta\pi^-\pi^+\pi^-\nu_\tau)/\Gamma$ values.

$\Gamma(2\pi^- \pi^+ 3\pi^0 \nu_\tau (\text{ex.}K^0, \eta, f_1(1285)))/\Gamma_{total}$ — Γ_{88}/Γ

VALUE (units 10^{-4})	DOCUMENT ID	TECN	COMMENT
1.69±0.08±0.43	LEES 12X	BABR	468 fb^{-1} $E^{ee}_{cm} = 10.6$ GeV

$\Gamma(2\pi^- \pi^+ 3\pi^0 \nu_\tau (\text{ex.}K^0, \eta, \omega, f_1(1285)))/\Gamma_{total}$ — Γ_{89}/Γ

VALUE (units 10^{-5})	DOCUMENT ID	TECN	COMMENT
1.4±2.7 OUR FIT			
1.0±0.8±3.0	[1] LEES 12X	BABR	468 fb^{-1} $E^{ee}_{cm} = 10.6$ GeV

[1] LEES 12X meaurement corresponds to the lower limit of $< 5.8 \times 10^{-5}$ at 90% CL.

$\Gamma(K^- h^+ h^- \geq 0 \text{ neutrals } \nu_\tau)/\Gamma_{total}$ — Γ_{90}/Γ

$\Gamma_{90}/\Gamma = (0.34598\Gamma_{38} + 0.34598\Gamma_{43} + \Gamma_{97} + \Gamma_{103} + \Gamma_{106} + \Gamma_{107} + 0.2804\Gamma_{152} + 0.491\Gamma_{170} + 0.9078\Gamma_{179})/\Gamma$

VALUE (%)	CL%	DOCUMENT ID	TECN	COMMENT
0.629±0.014 OUR FIT				
<0.6	90	AIHARA 84C	TPC	$E^{ee}_{cm} = 29$ GeV

$\Gamma(K^- h^+ \pi^- \nu_\tau (\text{ex.}K^0))/\Gamma_{total}$ — $\Gamma_{91}/\Gamma = (\Gamma_{97} + \Gamma_{106} + 0.0153\Gamma_{179})/\Gamma$

VALUE (%)	DOCUMENT ID
0.437±0.007 OUR FIT	

$\Gamma(K^- h^+ \pi^- \nu_\tau (\text{ex.}K^0))/\Gamma(\pi^- \pi^+ \pi^- \nu_\tau (\text{ex.}K^0))$ — Γ_{91}/Γ_{68}

$\Gamma_{91}/\Gamma_{68} = (\Gamma_{97} + \Gamma_{106} + 0.0153\Gamma_{179})/(\Gamma_{70} + 0.0153\Gamma_{178})$

VALUE (%)	EVTS	DOCUMENT ID	TECN	COMMENT
4.85±0.08 OUR FIT				
5.44±0.21±0.53	7.9k	RICHICHI 99	CLEO	$E^{ee}_{cm} = 10.6$ GeV

$\Gamma(K^- h^+ \pi^- \pi^0 \nu_\tau (\text{ex.}K^0))/\Gamma_{total}$ — Γ_{92}/Γ

$\Gamma_{92}/\Gamma = (\Gamma_{103} + \Gamma_{107} + 0.2302\Gamma_{152} + 0.892\Gamma_{179})/\Gamma$

VALUE (units 10^{-4})	DOCUMENT ID
8.6±1.2 OUR FIT	

$\Gamma(K^- h^+ \pi^- \pi^0 \nu_\tau (\text{ex.}K^0))/\Gamma(\pi^- \pi^+ \pi^- \pi^0 \nu_\tau (\text{ex.}K^0))$ — Γ_{92}/Γ_{77}

$\Gamma_{92}/\Gamma_{77} = (\Gamma_{103} + \Gamma_{107} + 0.2302\Gamma_{152} + 0.892\Gamma_{179})/(\Gamma_{78} + 0.892\Gamma_{178} + 0.0153\Gamma_{180})$

VALUE (%)	EVTS	DOCUMENT ID	TECN	COMMENT
1.91±0.26 OUR FIT				
2.61±0.45±0.42	719	RICHICHI 99	CLEO	$E^{ee}_{cm} = 10.6$ GeV

$\Gamma(K^- \pi^+ \pi^- \geq 0 \text{ neutrals } \nu_\tau)/\Gamma_{total}$ — Γ_{93}/Γ

$\Gamma_{93}/\Gamma = (0.34598\Gamma_{38} + 0.34598\Gamma_{43} + \Gamma_{97} + \Gamma_{103} + 0.2804\Gamma_{152} + 0.9078\Gamma_{179})/\Gamma$

VALUE (%)	EVTS	DOCUMENT ID	TECN	COMMENT
0.477±0.014 OUR FIT				
$0.58\ ^{+0.15}_{-0.13} \pm 0.12$	20	[1] BAUER 94	TPC	$E^{ee}_{cm} = 29$ GeV
• • • We do not use the following data for averages, fits, limits, etc. • • •				
$0.22\ ^{+0.16}_{-0.13} \pm 0.05$	9	[2] MILLS 85	DLCO	$E^{ee}_{cm} = 29$ GeV

[1] We multiply 0.58% by 0.20, the relative systematic error quoted by BAUER 94, to obtain the systematic error.
[2] Error correlated with MILLS 85 ($K K \pi \nu$) value. We multiply 0.22% by 0.23, the relative systematic error quoted by MILLS 85, to obtain the systematic error.

$\Gamma(K^- \pi^+ \pi^- \geq 0\pi^0 \nu_\tau (\text{ex.}K^0))/\Gamma_{total}$ — Γ_{94}/Γ

$\Gamma_{94}/\Gamma = (\Gamma_{97} + \Gamma_{103} + 0.2302\Gamma_{152} + 0.9078\Gamma_{179})/\Gamma$

VALUE (%)	DOCUMENT ID	TECN	COMMENT
0.373±0.013 OUR FIT			
0.30 ±0.05 OUR AVERAGE			
• • • We use the following data for averages but not for fits. • • •			
$0.343 \pm 0.073 \pm 0.031$	ABBIENDI 00D	OPAL	1990–1995 LEP runs
0.275 ± 0.064	[1] BARATE 98	ALEP	1991–1995 LEP runs

[1] Not independent of BARATE 98 $\Gamma(\tau^- \to K^-\pi^+\pi^-\nu_\tau)/\Gamma_{total}$ and $\Gamma(\tau^- \to K^-\pi^+\pi^-\pi^0\nu_\tau)/\Gamma_{total}$ values.

$\Gamma(K^- \pi^+ \pi^- \nu_\tau)/\Gamma_{total}$ — $\Gamma_{95}/\Gamma = (0.34598\Gamma_{38} + \Gamma_{97} + 0.0153\Gamma_{179})/\Gamma$

VALUE (%)	DOCUMENT ID
0.345±0.007 OUR FIT	

$\Gamma(K^- \pi^+ \pi^- \nu_\tau (\text{ex.}K^0))/\Gamma_{total}$ — $\Gamma_{96}/\Gamma = (\Gamma_{97} + 0.0153\Gamma_{179})/\Gamma$

VALUE (%)	EVTS	DOCUMENT ID	TECN	COMMENT
0.293±0.007 OUR FIT				
0.290±0.018 OUR AVERAGE		Error includes scale factor of 2.4. See the ideogram below.		
$0.330 \pm 0.001\ ^{+0.016}_{-0.017}$	794k	[1] LEE 10	BELL	666 fb^{-1} $E^{ee}_{cm} = 10.6$ GeV
$0.273 \pm 0.002 \pm 0.009$	70k	[2] AUBERT 08	BABR	342 fb^{-1} $E^{ee}_{cm} = 10.6$ GeV
$0.415 \pm 0.053 \pm 0.040$	269	ABBIENDI 04J	OPAL	1991-1995 LEP runs
$0.384 \pm 0.014 \pm 0.038$	3.5k	[3] BRIERE 03	CLE3	$E^{ee}_{cm} = 10.6$ GeV
$0.214 \pm 0.037 \pm 0.029$		BARATE 98	ALEP	1991–1995 LEP runs
• • • We use the following data for averages but not for fits. • • •				
$0.346 \pm 0.023 \pm 0.056$	158	[4] RICHICHI 99	CLEO	$E^{ee}_{cm} = 10.6$ GeV
• • • We do not use the following data for averages, fits, limits, etc. • • •				
$0.360 \pm 0.082 \pm 0.048$		ABBIENDI 00D	OPAL	1990–1995 LEP runs

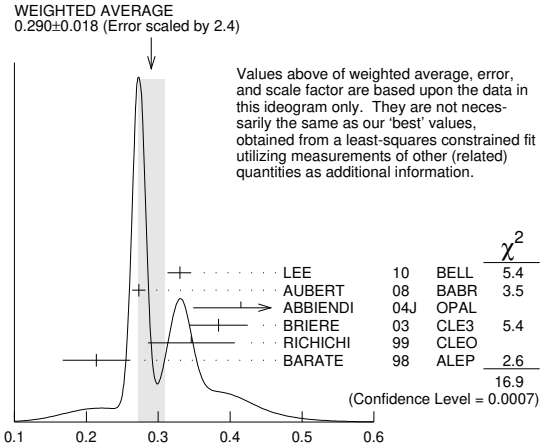

[1] See footnote to LEE 10 $\Gamma(\tau^- \to \pi^-\pi^+\pi^-\nu_\tau(\text{ex.}K^0))/\Gamma_{total}$ measurement for correlations with other measurements. Not independent of LEE 10 $\Gamma(\tau^- \to K^-\pi^+\pi^-\nu_\tau(\text{ex.}K^0))/\Gamma(\tau^- \to \pi^-\pi^+\pi^-\nu_\tau(\text{ex.}K^0))$ value.
[2] See footnote to AUBERT 08 $\Gamma(\tau^- \to \pi^-\pi^+\pi^-\nu_\tau(\text{ex.}K^0))/\Gamma_{total}$ measurement for correlations with other measurements.
[3] 47% correlated with BRIERE 03 $\tau^- \to \pi^-\pi^+\pi^-\nu_\tau$ and 34% correlated with $\tau^- \to K^-K^+\pi^-\nu_\tau$ because of a common 5% normalization error.
[4] Not independent of RICHICHI 99 $\Gamma(\tau^- \to K^-h^+\pi^-\nu_\tau(\text{ex.}K^0))/\Gamma(\tau^- \to \pi^-\pi^+\pi^-\nu_\tau(\text{ex.}K^0))$, $\Gamma(\tau^- \to K^-K^+\pi^-\nu_\tau)/\Gamma(\tau^- \to \pi^-\pi^+\pi^-\nu_\tau(\text{ex.}K^0))$ and BALEST 95C $\Gamma(\tau^- \to h^-h^-h^+\nu_\tau(\text{ex.}K^0))/\Gamma_{total}$ values.

$\Gamma(K^- \pi^+ \pi^- \nu_\tau (\text{ex.}K^0))/\Gamma(\pi^- \pi^+ \pi^- \nu_\tau (\text{ex.}K^0))$ — Γ_{96}/Γ_{68}

$\Gamma_{96}/\Gamma_{68} = (\Gamma_{97} + 0.0153\Gamma_{179})/(\Gamma_{70} + 0.0153\Gamma_{178})$

VALUE (units 10^{-2})	EVTS	DOCUMENT ID	TECN	COMMENT
3.25±0.07 OUR FIT				
• • • We use the following data for averages but not for fits. • • •				
$3.92 \pm 0.02\ ^{+0.15}_{-0.16}$	794k	[1] LEE 10	BELL	666 fb^{-1} $E^{ee}_{cm} = 10.6$ GeV

[1] Not independent of LEE 10 $\Gamma(\tau^- \to K^-\pi^+\pi^-\nu_\tau(\text{ex.}K^0))/\Gamma_{total}$ and $\Gamma(\tau^- \to \pi^-\pi^+\pi^-\nu_\tau(\text{ex.}K^0))/\Gamma_{total}$ values.

$\Gamma(K^- \pi^+ \pi^- \nu_\tau (\text{ex.}K^0, \omega))/\Gamma_{total}$ — Γ_{97}/Γ

VALUE (units 10^{-3})	DOCUMENT ID
2.93±0.07 OUR FIT	

$\Gamma(K^- \rho^0 \nu_\tau \to K^- \pi^+ \pi^- \nu_\tau)/\Gamma(K^- \pi^+ \pi^- \nu_\tau (\text{ex.}K^0))$ — Γ_{98}/Γ_{96}

VALUE	DOCUMENT ID	TECN	COMMENT
0.48±0.14±0.10	[1] ASNER 00B	CLEO	$E^{ee}_{cm} = 10.6$ GeV
• • • We do not use the following data for averages, fits, limits, etc. • • •			
0.39 ± 0.14	[2] BARATE 99R	ALEP	1991–1995 LEP runs

[1] ASNER 00B assume $\tau^- \to K^-\pi^+\pi^-\nu_\tau$ (ex. K^0) decays proceed only through $K\rho$ and $K^*\pi$ intermediate states. They assume the resonance structure of $\tau^- \to K^-\pi^+\pi^-\nu_\tau$ (ex. K^0) decays is dominated by $K_1(1270)^-$ and $K_1(1400)^-$ resonances, and assume $B(K_1(1270) \to K^*(892)\pi) = (16 \pm 5)\%$, $B(K_1(1270) \to K\rho) = (42 \pm 6)\%$, and $B(K_1(1400) \to K\rho) = 0$.
[2] BARATE 99R assume $\tau^- \to K^-\pi^+\pi^-\nu_\tau$ (ex. K^0) decays proceed only through $K\rho$ and $K^*\pi$ intermediate states. The quoted error is statistical only.

Downloaded from https://academic.oup.com/ptep/article/2022/8/083C01/6651666 by KIT Library user on 27 September 2022

$\Gamma(K^-\pi^+\pi^-\pi^0\nu_\tau)/\Gamma_{total}$ — Γ_{99}/Γ

$\Gamma_{99}/\Gamma = (0.34598\Gamma_{43}+\Gamma_{103}+0.2302\Gamma_{152}+0.892\Gamma_{179})/\Gamma$

VALUE (units 10^{-4})	DOCUMENT ID
13.1±1.2 OUR FIT	

$\Gamma(K^-\pi^+\pi^-\pi^0\nu_\tau(\text{ex.}K^0))/\Gamma_{total}$ — Γ_{100}/Γ

$\Gamma_{100}/\Gamma = (\Gamma_{103}+0.2302\Gamma_{152}+0.892\Gamma_{179})/\Gamma$

VALUE (units 10^{-4})	CL%	DOCUMENT ID		TECN	COMMENT
7.9±1.2 OUR FIT					
7.3±1.2 OUR AVERAGE					
7.4±0.8±1.1		[1] ARMS	05	CLE3	7.6 fb^{-1}, E^{ee}_{cm}= 10.6 GeV
6.1±3.9±1.8		BARATE	98	ALEP	1991–1995 LEP runs
• • • We use the following data for averages but not for fits. • • •					
7.5±2.6±1.8		[2] RICHICHI	99	CLEO	E^{ee}_{cm}= 10.6 GeV
• • • We do not use the following data for averages, fits, limits, etc. • • •					
<17	95	ABBIENDI	00D	OPAL	1990–1995 LEP runs

[1] Not independent of ARMS 05 $\Gamma(\tau^- \to K^-\pi^+\pi^-\pi^0\nu_\tau(\text{ex.}K^0,\omega))$ / Γ_{total} and $\Gamma(\tau^- \to K^-\omega\nu_\tau)$ / Γ_{total} values.

[2] Not independent of RICHICHI 99 $\Gamma(\tau^- \to K^-h^+\pi^-\nu_\tau(\text{ex.}K^0))/\Gamma(\tau^- \to \pi^-\pi^+\pi^-\nu_\tau(\text{ex.}K^0))$, $\Gamma(\tau^- \to K^-K^+\pi^-\nu_\tau)/\Gamma(\tau^- \to \pi^-\pi^+\pi^-\nu_\tau(\text{ex.}K^0))$ and BALEST 95C $\Gamma(\tau^- \to h^-h^-h^+\nu_\tau(\text{ex.}K^0))/\Gamma_{total}$ values.

$\Gamma(K^-\pi^+\pi^-\pi^0\nu_\tau(\text{ex.}K^0,\eta))/\Gamma_{total}$ — $\Gamma_{101}/\Gamma = (\Gamma_{103}+0.892\Gamma_{179})/\Gamma$

VALUE (units 10^{-4})	DOCUMENT ID
7.6±1.2 OUR FIT	

$\Gamma(K^-\pi^+\pi^-\pi^0\nu_\tau(\text{ex.}K^0,\omega))/\Gamma_{total}$ — Γ_{102}/Γ

VALUE (units 10^{-4})	EVTS	DOCUMENT ID		TECN	COMMENT
3.7±0.5±0.8	833	ARMS	05	CLE3	7.6 fb^{-1}, E^{ee}_{cm}= 10.6 GeV

$\Gamma(K^-\pi^+\pi^-\pi^0\nu_\tau(\text{ex.}K^0,\omega,\eta))/\Gamma_{total}$ — Γ_{103}/Γ

VALUE (units 10^{-4})	DOCUMENT ID
3.9±1.4 OUR FIT	

$\Gamma(K^-\pi^+K^- \geq 0 \text{ neut. } \nu_\tau)/\Gamma_{total}$ — Γ_{104}/Γ

VALUE (%)	CL%	DOCUMENT ID		TECN	COMMENT
<0.09	95	BAUER	94	TPC	E^{ee}_{cm}= 29 GeV

$\Gamma(K^-K^+\pi^- \geq 0 \text{ neut. } \nu_\tau)/\Gamma_{total}$ — $\Gamma_{105}/\Gamma = (\Gamma_{106}+\Gamma_{107})/\Gamma$

VALUE (%)	EVTS	DOCUMENT ID		TECN	COMMENT
0.1496±0.0033 OUR FIT					
0.203 ±0.031 OUR AVERAGE					
0.159 ±0.053 ±0.020		ABBIENDI	00D	OPAL	1990–1995 LEP runs
0.15 $^{+0.09}_{-0.07}$ ±0.03	4	[1] BAUER	94	TPC	E^{ee}_{cm}= 29 GeV
• • • We use the following data for averages but not for fits. • • •					
0.238 ±0.042		[2] BARATE	98	ALEP	1991–1995 LEP runs

[1] We multiply 0.15% by 0.20, the relative systematic error quoted by BAUER 94, to obtain the systematic error.

[2] Not independent of BARATE 98 $\Gamma(\tau^- \to K^-K^+\pi^-\nu_\tau)/\Gamma_{total}$ and $\Gamma(\tau^- \to K^-K^+\pi^-\pi^0\nu_\tau)/\Gamma_{total}$ values.

$\Gamma(K^-K^+\pi^-\nu_\tau)/\Gamma_{total}$ — Γ_{106}/Γ

VALUE (units 10^{-3})	EVTS	DOCUMENT ID		TECN	COMMENT
1.435±0.027 OUR FIT					
1.43 ±0.07 OUR AVERAGE	Error includes scale factor of 2.4. See the ideogram below.				
1.55 ±0.01 $^{+0.06}_{-0.05}$	108k	[1] LEE	10	BELL	666 fb^{-1} E^{ee}_{cm}=10.6 GeV
1.346±0.010±0.036	18k	[2] AUBERT	08	BABR	342 fb^{-1} E^{ee}_{cm}= 10.6 GeV
1.55 ±0.06 ±0.09	932	[3] BRIERE	03	CLE3	E^{ee}_{cm}= 10.6 GeV
1.63 ±0.21 ±0.17		BARATE	98	ALEP	1991–1995 LEP runs
• • • We use the following data for averages but not for fits. • • •					
0.87 ±0.56 ±0.40		ABBIENDI	00D	OPAL	1990–1995 LEP runs
1.45 ±0.13 ±0.28	2.3k	[4] RICHICHI	99	CLEO	E^{ee}_{cm}= 10.6 GeV
• • • We do not use the following data for averages, fits, limits, etc. • • •					
2.2 $^{+1.7}_{-1.1}$ ±0.5	9	[5] MILLS	85	DLCO	E^{ee}_{cm}= 29 GeV

[1] See footnote to LEE 10 $\Gamma(\tau^- \to \pi^-\pi^+\pi^-\nu_\tau(\text{ex.}K^0))/\Gamma_{total}$ measurement for correlations with other measurements. Not independent of LEE 10 $\Gamma(\tau^- \to K^-K^+\pi^-\nu_\tau)/\Gamma(\tau^- \to \pi^-\pi^+\pi^-\nu_\tau(\text{ex.}K^0))$ value.

[2] See footnote to AUBERT 08 $\Gamma(\tau^- \to \pi^-\pi^+\pi^-\nu_\tau(\text{ex.}K^0))/\Gamma_{total}$ measurement for correlations with other measurements.

[3] 71% correlated with BRIERE 03 $\tau^- \to \pi^-\pi^+\pi^-\nu_\tau$ and 34% correlated with $\tau \to K^-\pi^+\pi^-\nu_\tau$ because of a common 5% normalization error.

[4] Not independent of RICHICHI 99 $\Gamma(\tau^- \to K^-K^+\pi^-\nu_\tau)/\Gamma(\tau^- \to \pi^-\pi^+\pi^-\nu_\tau(\text{ex.}K^0))$ and BALEST 95C $\Gamma(\tau^- \to h^-h^-h^+\nu_\tau(\text{ex.}K^0))/\Gamma_{total}$ values.

[5] Error correlated with MILLS 85 ($K\pi\pi\pi^0\nu$) value. We multiply 0.22% by 0.23, the relative systematic error quoted by MILLS 85, to obtain the systematic error.

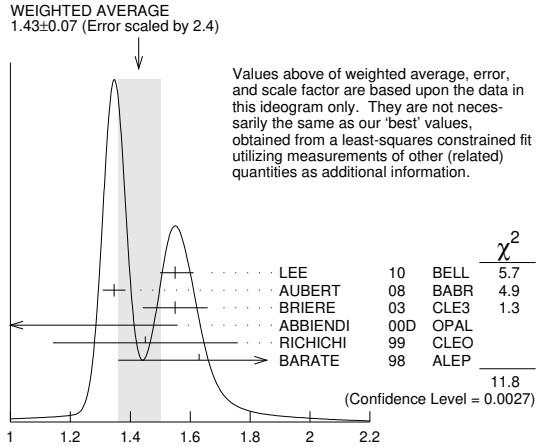

$\Gamma(K^-K^+\pi^-\nu_\tau)/\Gamma(\pi^-\pi^+\pi^-\nu_\tau(\text{ex.}K^0))$ — Γ_{106}/Γ_{68}

$\Gamma_{106}/\Gamma_{68} = \Gamma_{106}/(\Gamma_{70}+0.0153\Gamma_{178})$

VALUE (%)	EVTS	DOCUMENT ID		TECN	COMMENT
1.592±0.030 OUR FIT					
1.83 ±0.05 OUR AVERAGE					
1.60 ±0.15 ±0.30	2.3k	RICHICHI	99	CLEO	E^{ee}_{cm}= 10.6 GeV
• • • We use the following data for averages but not for fits. • • •					
1.84 ±0.01 ±0.05	108k	[1] LEE	10	BELL	666 fb^{-1} E^{ee}_{cm}= 10.6 GeV

[1] Not independent of LEE 10 $\Gamma(\tau^- \to K^-K^+\pi^-\nu_\tau)/\Gamma_{total}$ and $\Gamma(\tau^- \to \pi^-\pi^+\pi^-\nu_\tau(\text{ex.}K^0))/\Gamma_{total}$ values.

$\Gamma(K^-K^+\pi^-\pi^0\nu_\tau)/\Gamma_{total}$ — Γ_{107}/Γ

VALUE (units 10^{-4})	CL%	EVTS	DOCUMENT ID		TECN	COMMENT
0.61±0.18 OUR FIT						
0.60±0.18 OUR AVERAGE						
0.55±0.14±0.12		48	ARMS	05	CLE3	7.6 fb^{-1},E^{ee}_{cm}=10.6 GeV
7.5 ±2.9 ±1.5			BARATE	98	ALEP	1991–1995 LEP runs
• • • We use the following data for averages but not for fits. • • •						
3.3 ±1.8 ±0.7		158	[1] RICHICHI	99	CLEO	E^{ee}_{cm}= 10.6 GeV
• • • We do not use the following data for averages, fits, limits, etc. • • •						
<27	95		ABBIENDI	00D	OPAL	1990–1995 LEP runs

[1] Not independent of RICHICHI 99 $\Gamma(\tau^- \to K^-K^+\pi^-\nu_\tau)/\Gamma(\tau^- \to \pi^-\pi^+\pi^-\nu_\tau(\text{ex.}K^0))$ and BALEST 95C $\Gamma(\tau^- \to h^-h^-h^+\nu_\tau(\text{ex.}K^0))/\Gamma_{total}$ values.

$\Gamma(K^-K^+\pi^-\pi^0\nu_\tau)/\Gamma(\pi^-\pi^+\pi^-\pi^0\nu_\tau(\text{ex.}K^0))$ — Γ_{107}/Γ_{77}

$\Gamma_{107}/\Gamma_{77} = \Gamma_{107}/(\Gamma_{78}+0.892\Gamma_{178}+0.0153\Gamma_{180})$

VALUE (%)	EVTS	DOCUMENT ID		TECN	COMMENT
0.14±0.04 OUR FIT					
0.79±0.44±0.16	158	[1] RICHICHI	99	CLEO	E^{ee}_{cm}= 10.6 GeV

[1] RICHICHI 99 also quote a 95%CL upper limit of 0.0157 for this measurement.

$\Gamma(K^-K^+K^-\nu_\tau)/\Gamma_{total}$ — $\Gamma_{108}/\Gamma = 0.491\Gamma_{170}/\Gamma$

VALUE (units 10^{-5})	CL%	EVTS	DOCUMENT ID		TECN	COMMENT
2.2 ±0.8 OUR FIT	Error includes scale factor of 5.4.					
2.1 ±0.8 OUR AVERAGE	Error includes scale factor of 5.4.					
3.29±0.17$^{+0.19}_{-0.20}$		3.2k	[1] LEE	10	BELL	666 fb^{-1} E^{ee}_{cm} = 10.6 GeV
1.58±0.13±0.12		275	[2] AUBERT	08	BABR	342 fb^{-1} E^{ee}_{cm}= 10.6 GeV
• • • We do not use the following data for averages, fits, limits, etc. • • •						
< 3.7	90		BRIERE	03	CLE3	E^{ee}_{cm}= 10.6 GeV
< 19	90		BARATE	98	ALEP	1991–1995 LEP runs

[1] See footnote to LEE 10 $\Gamma(\tau^- \to \pi^-\pi^+\pi^-\nu_\tau(\text{ex.}K^0))/\Gamma_{total}$ measurement for correlations with other measurements. Not independent of LEE 10 $\Gamma(\tau^- \to K^-K^+K^-\nu_\tau)/\Gamma(\tau^- \to \pi^-\pi^+\pi^-\nu_\tau(\text{ex.}K^0))$ value.

[2] See footnote to AUBERT 08 $\Gamma(\tau^- \to \pi^-\pi^+\pi^-\nu_\tau(\text{ex.}K^0))/\Gamma_{total}$ measurement for correlations with other measurements.

$\Gamma(K^-K^+K^-\nu_\tau)/\Gamma(\pi^-\pi^+\pi^-\nu_\tau(\text{ex.}K^0))$ — Γ_{108}/Γ_{68}

VALUE (units 10^{-4})	EVTS	DOCUMENT ID		TECN	COMMENT
• • • We do not use the following data for averages, fits, limits, etc. • • •					
3.90±0.02$^{+0.22}_{-0.23}$	3.2k	[1] LEE	10	BELL	666 fb^{-1} E^{ee}_{cm} = 10.6 GeV

[1] Not independent of LEE 10 $\Gamma(\tau^- \to K^-K^+K^-\nu_\tau)/\Gamma_{total}$ and $\Gamma(\tau^- \to \pi^-\pi^+\pi^-\nu_\tau(\text{ex.}K^0))/\Gamma_{total}$ values.

Downloaded from https://academic.oup.com/ptep/article/2022/8/083C01/6651666 by KIT Library user on 27 September 2022

$\Gamma(K^- K^+ K^- \nu_\tau (\text{ex. } \phi))/\Gamma_{\text{total}}$ — Γ_{109}/Γ

VALUE	CL%	DOCUMENT ID		TECN	COMMENT
$<2.5 \times 10^{-6}$	90	AUBERT	08	BABR	342 fb^{-1} E^{ee}_{cm} = 10.6 GeV

$\Gamma(K^- K^+ K^- \pi^0 \nu_\tau)/\Gamma_{\text{total}}$ — Γ_{110}/Γ

VALUE	CL%	DOCUMENT ID		TECN	COMMENT
$<4.8 \times 10^{-6}$	90	ARMS	05	CLE3	7.6 fb^{-1}, E^{ee}_{cm} = 10.6 GeV

$\Gamma(\pi^- K^+ \pi^- \geq 0 \text{ neut. } \nu_\tau)/\Gamma_{\text{total}}$ — Γ_{111}/Γ

VALUE (%)	CL%	DOCUMENT ID		TECN	COMMENT
<0.25	95	BAUER	94	TPC	E^{ee}_{cm} = 29 GeV

$\Gamma(e^- e^- e^+ \overline{\nu}_e \nu_\tau)/\Gamma_{\text{total}}$ — Γ_{112}/Γ

VALUE (units 10^{-5})	EVTS	DOCUMENT ID		TECN	COMMENT
$2.8 \pm 1.4 \pm 0.4$	5	ALAM	96	CLEO	E^{ee}_{cm} = 10.6 GeV

$\Gamma(\mu^- e^- e^+ \overline{\nu}_\mu \nu_\tau)/\Gamma_{\text{total}}$ — Γ_{113}/Γ

VALUE (units 10^{-5})	CL%	DOCUMENT ID		TECN	COMMENT
<3.2	90	ALAM	96	CLEO	E^{ee}_{cm} = 10.6 GeV

$\Gamma(\pi^- e^- e^+ \nu_\tau)/\Gamma_{\text{total}}$ — Γ_{114}/Γ

VALUE (units 10^{-5})	EVTS	DOCUMENT ID		TECN	COMMENT
seen	400	[1] JIN	19	BELL	562 fb^{-1}, E^{ee}_{cm} = 10.6 GeV
• • • We do not use the following data for averages, fits, limits, etc. • • •					
$1.46 \pm 0.13 \pm 0.21$	400	[1] JIN	19	BELL	axial-vector, 562 fb^{-1}, E^{ee}_{cm} = 10.6 GeV
$3.01 \pm 0.27 \pm 0.43$	400	[1] JIN	19	BELL	vector, 562 fb^{-1}, E^{ee}_{cm} = 10.6 GeV

[1] JIN 19 measures $B(\tau^- \to \pi^- e^- e^+ \nu_\tau (m_{\pi^- e^- e^+} > 1.05 \text{ GeV}/c^2)) = (5.90 \pm 0.53 \pm 0.86) \times 10^{-6}$, which is only sensitive to the structure-dependent contribution, and assumes that the decay proceeds with either a pure axial-vector current or a pure vector current to obtain the two respective branching fraction measurements for this mode, which are 100% correlated.

$\Gamma(\pi^- \mu^- \mu^+ \nu_\tau)/\Gamma_{\text{total}}$ — Γ_{115}/Γ

VALUE	CL%	DOCUMENT ID		TECN	COMMENT
$<1.14 \times 10^{-5}$	90	JIN	19	BELL	562 fb^{-1}, E^{ee}_{cm} = 10.6 GeV

$\Gamma(3h^- 2h^+ \geq 0 \text{ neutrals } \nu_\tau (\text{ex. } K^0_S \to \pi^- \pi^+)(\text{"5-prong"}))/\Gamma_{\text{total}}$ — Γ_{116}/Γ

$\Gamma_{116}/\Gamma = (\Gamma_{117}+\Gamma_{123})/\Gamma$

VALUE (%)	EVTS	DOCUMENT ID		TECN	COMMENT
0.099±0.004 OUR FIT					
0.107±0.007 OUR AVERAGE		Error includes scale factor of 1.1.			
$0.170 \pm 0.022 \pm 0.026$		[1] ACHARD	01D	L3	1992–1995 LEP runs
$0.097 \pm 0.005 \pm 0.011$	419	GIBAUT	94B	CLEO	E^{ee}_{cm} = 10.6 GeV
0.102 ± 0.029	13	BYLSMA	87	HRS	E^{ee}_{cm} = 29 GeV
• • • We use the following data for averages but not for fits. • • •					
$0.093 \pm 0.009 \pm 0.012$		SCHAEL	05C	ALEP	1991-1995 LEP runs
$0.115 \pm 0.013 \pm 0.006$	112	[2] ABREU	01M	DLPH	1992–1995 LEP runs
$0.119 \pm 0.013 \pm 0.008$	119	[3] ACKERSTAFF	99E	OPAL	1991–1995 LEP runs
• • • We do not use the following data for averages, fits, limits, etc. • • •					
$0.26 \pm 0.06 \pm 0.05$		ACTON	92H	OPAL	E^{ee}_{cm} = 88.2–94.2 GeV
$0.10 \; {}^{+0.05}_{-0.04} \pm 0.03$		DECAMP	92C	ALEP	1989–1990 LEP runs
$0.16 \pm 0.13 \pm 0.04$		BEHREND	89B	CELL	E^{ee}_{cm} = 14–47 GeV
$0.3 \pm 0.1 \pm 0.2$		BARTEL	85F	JADE	E^{ee}_{cm} = 34.6 GeV
0.13 ± 0.04	10	BELTRAMI	85	HRS	Repl. by BYLSMA 87
$0.16 \pm 0.08 \pm 0.04$	4	BURCHAT	85	MRK2	E^{ee}_{cm} = 29 GeV
1.0 ± 0.4	10	BEHREND	82	CELL	Repl. by BEHREND 89B

[1] The correlation coefficients between this measurement and the ACHARD 01D measurements of $B(\tau \to$ "1-prong") and $B(\tau \to$ "3-prong") are -0.082 and -0.19 respectively.
[2] The correlation coefficients between this measurement and the ABREU 01M measurements of $B(\tau \to$ 1-prong) and $B(\tau \to$ 3-prong) are -0.08 and -0.08 respectively.
[3] Not independent of ACKERSTAFF 99E $B(\tau^- \to 3h^- 2h^+ \nu_\tau (\text{ex. } K^0))$ and $B(\tau^- \to 3h^- 2h^+ \pi^0 \nu_\tau (\text{ex. } K^0))$ measurements.

$\Gamma(3h^- 2h^+ \nu_\tau (\text{ex.} K^0))/\Gamma_{\text{total}}$ — $\Gamma_{117}/\Gamma = (\Gamma_{118}+\Gamma_{120}+0.0153\Gamma_{185})/\Gamma$

VALUE (units 10^{-4})	EVTS	DOCUMENT ID		TECN	COMMENT
8.29±0.31 OUR FIT					
8.32±0.35 OUR AVERAGE					
$9.7 \pm 1.5 \pm 0.5$	96	[1] ABDALLAH	06A	DLPH	1992–1995 LEP runs
$7.2 \pm 0.9 \pm 1.2$	165	[2] SCHAEL	05C	ALEP	1991-1995 LEP runs
$9.1 \pm 1.4 \pm 0.6$	97	ACKERSTAFF	99E	OPAL	1991–1995 LEP runs
$7.7 \pm 0.5 \pm 0.9$	295	GIBAUT	94B	CLEO	E^{ee}_{cm} = 10.6 GeV
$6.4 \pm 2.3 \pm 1.0$	12	ALBRECHT	88B	ARG	E^{ee}_{cm} = 10 GeV
5.1 ± 2.0	7	BYLSMA	87	HRS	E^{ee}_{cm} = 29 GeV
• • • We use the following data for averages but not for fits. • • •					
$8.56 \pm 0.05 \pm 0.42$	34k	AUBERT,B	05W	BABR	232 fb^{-1}, E^{ee}_{cm} = 10.6 GeV
• • • We do not use the following data for averages, fits, limits, etc. • • •					
$8.0 \pm 1.1 \pm 1.3$	58	BUSKULIC	96	ALEP	Repl. by SCHAEL 05C
6.7 ± 3.0	5	[3] BELTRAMI	85	HRS	Repl. by BYLSMA 87

[1] See footnote to ABDALLAH 06A $\Gamma(\tau^- \to h^- \nu_\tau)/\Gamma_{\text{total}}$ measurement for correlations with other measurements.
[2] See footnote to SCHAEL 05C $\Gamma(\tau^- \to e^- \overline{\nu}_e \nu_\tau)/\Gamma_{\text{total}}$ measurement for correlations with other measurements.
[3] The error quoted is statistical only.

$\Gamma(3\pi^- 2\pi^+ \nu_\tau (\text{ex.} K^0, \omega))/\Gamma_{\text{total}}$ — $\Gamma_{118}/\Gamma = (\Gamma_{119}+\Gamma_{173})/\Gamma$

VALUE (units 10^{-4})	DOCUMENT ID		TECN	COMMENT
8.27±0.31 OUR FIT				
• • • We use the following data for averages but not for fits. • • •				
8.33±0.04±0.43	[1] LEES	12X	BABR	468 fb^{-1} E^{ee}_{cm} = 10.6 GeV

[1] Not independent of LEES 12X $\Gamma(\tau^- \to f_1(1285) \pi^- \nu_\tau \to 3\pi^- 2\pi^+ \nu_\tau)/\Gamma$ and $\Gamma(\tau^- \to 3\pi^- 2\pi^+ \nu_\tau (\text{ex.} K^0, \omega, f_1(1285)))/\Gamma$ values.

$\Gamma(3\pi^- 2\pi^+ \nu_\tau (\text{ex.} K^0, \omega, f_1(1285)))/\Gamma_{\text{total}}$ — Γ_{119}/Γ

VALUE (units 10^{-4})	EVTS	DOCUMENT ID		TECN	COMMENT
7.75±0.30 OUR FIT					
7.68±0.04±0.40	69k	LEES	12X	BABR	468 fb^{-1} E^{ee}_{cm} = 10.6 GeV

$\Gamma(K^- 2\pi^- 2\pi^+ \nu_\tau (\text{ex.} K^0))/\Gamma_{\text{total}}$ — Γ_{120}/Γ

VALUE (units 10^{-6})	DOCUMENT ID		TECN	COMMENT
0.6±1.2 OUR FIT				
0.6±0.5±1.1	[1] LEES	12X	BABR	468 fb^{-1} E^{ee}_{cm} = 10.6 GeV

[1] LEES 12X meaurement corresponds to the lower limit of $< 2.4 \times 10^{-6}$ at 90% CL.

$\Gamma(K^+ 3\pi^- \pi^+ \nu_\tau)/\Gamma_{\text{total}}$ — Γ_{121}/Γ

VALUE	CL%	DOCUMENT ID		TECN	COMMENT
$<5.0 \times 10^{-6}$	90	LEES	12X	BABR	468 fb^{-1} E^{ee}_{cm} = 10.6 GeV

$\Gamma(K^+ K^- 2\pi^- \pi^+ \nu_\tau)/\Gamma_{\text{total}}$ — Γ_{122}/Γ

VALUE	CL%	DOCUMENT ID		TECN	COMMENT
$<4.5 \times 10^{-7}$	90	LEES	12X	BABR	468 fb^{-1} E^{ee}_{cm} = 10.6 GeV

$\Gamma(3h^- 2h^+ \pi^0 \nu_\tau (\text{ex.} K^0))/\Gamma_{\text{total}}$ — $\Gamma_{123}/\Gamma = (\Gamma_{124}+\Gamma_{127})/\Gamma$

VALUE (units 10^{-4})	EVTS	DOCUMENT ID		TECN	COMMENT
1.65±0.11 OUR FIT					
1.74±0.27 OUR AVERAGE					
$1.6 \pm 1.2 \pm 0.6$	13	[1] ABDALLAH	06A	DLPH	1992–1995 LEP runs
$2.1 \pm 0.7 \pm 0.9$	95	[2] SCHAEL	05C	ALEP	1991-1995 LEP runs
$1.7 \pm 0.2 \pm 0.2$	231	ANASTASSOV	01	CLEO	E^{ee}_{cm} = 10.6 GeV
$2.7 \pm 1.8 \pm 0.9$	23	ACKERSTAFF	99E	OPAL	1991–1995 LEP runs
• • • We do not use the following data for averages, fits, limits, etc. • • •					
$1.8 \pm 0.7 \pm 1.2$	18	BUSKULIC	96	ALEP	Repl. by SCHAEL 05C
$1.9 \pm 0.4 \pm 0.4$	31	GIBAUT	94B	CLEO	Repl. by ANASTASSOV 01
5.1 ± 2.2	6	BYLSMA	87	HRS	E^{ee}_{cm} = 29 GeV
6.7 ± 3.0	5	[3] BELTRAMI	85	HRS	Repl. by BYLSMA 87

[1] See footnote to ABDALLAH 06A $\Gamma(\tau^- \to h^- \nu_\tau)/\Gamma_{\text{total}}$ measurement for correlations with other measurements.
[2] SCHAEL 05C quote $(1.4 \pm 0.7 \pm 0.9) \times 10^{-4}$. We add 0.7×10^{-4} to remove their correction for $\tau^- \to \eta\pi^-\pi^+\pi^-\nu_\tau \to 3\pi^- 2\pi^+ \pi^0 \nu_\tau$ and $\tau^- \to K^*(892)^- \eta \nu_\tau \to 3\pi^- 2\pi^+ \pi^0 \nu_\tau$ decays. See footnote to SCHAEL 05C $\Gamma(\tau^- \to e^- \overline{\nu}_e \nu_\tau)/\Gamma_{\text{total}}$ measurement for correlations with other measurements.
[3] The error quoted is statistical only.

$\Gamma(3\pi^- 2\pi^+ \pi^0 \nu_\tau (\text{ex.} K^0))/\Gamma_{\text{total}}$ — Γ_{124}/Γ

$\Gamma_{124}/\Gamma = (\Gamma_{126}+0.2302\Gamma_{160}+0.892\Gamma_{185})/\Gamma$

VALUE (units 10^{-4})	DOCUMENT ID		TECN	COMMENT
1.63±0.11 OUR FIT				
• • • We use the following data for averages but not for fits. • • •				
1.65±0.05±0.09	[1] LEES	12X	BABR	468 fb^{-1} E^{ee}_{cm} = 10.6 GeV

[1] Not independent of LEES 12X measurements of $\Gamma(\tau^- \to 2\pi^-\pi^+\omega\nu_\tau (\text{ex.} K^0))/\Gamma$, $\Gamma(\tau^- \to \eta\pi^-\pi^+\pi^-\nu_\tau (\text{ex.} K^0))/\Gamma$, and $\Gamma(\tau^- \to 3\pi^- 2\pi^+ \pi^0 \nu_\tau (\text{ex.} K^0, \eta, \omega, f_1(1285)))/\Gamma$.

$\Gamma(3\pi^- 2\pi^+ \pi^0 \nu_\tau (\text{ex.} K^0, \eta, f_1(1285)))/\Gamma_{\text{total}}$ — Γ_{125}/Γ

VALUE (units 10^{-4})	DOCUMENT ID		TECN	COMMENT
1.11±0.04±0.09	[1] LEES	12X	BABR	468 fb^{-1} E^{ee}_{cm} = 10.6 GeV

[1] Not independent of LEES 12X $\Gamma(\tau^- \to 2\pi^-\pi^+\omega\nu_\tau (\text{ex.} K^0))/\Gamma$ and $\Gamma(\tau^- \to 3\pi^- 2\pi^+ \pi^0 \nu_\tau (\text{ex.} K^0, \eta, \omega, f_1(1285)))/\Gamma$ values.

$\Gamma(3\pi^- 2\pi^+ \pi^0 \nu_\tau (\text{ex.} K^0, \eta, \omega, f_1(1285)))/\Gamma_{\text{total}}$ — Γ_{126}/Γ

VALUE (units 10^{-4})	EVTS	DOCUMENT ID		TECN	COMMENT
0.38±0.09 OUR FIT					
0.36±0.03±0.09	7.3k	LEES	12X	BABR	468 fb^{-1} E^{ee}_{cm} = 10.6 GeV

$\Gamma(K^- 2\pi^- 2\pi^+ \pi^0 \nu_\tau (\text{ex.} K^0))/\Gamma_{\text{total}}$ — Γ_{127}/Γ

VALUE (units 10^{-6})	DOCUMENT ID		TECN	COMMENT
1.1±0.6 OUR FIT				
1.1±0.4±0.4	[1] LEES	12X	BABR	468 fb^{-1} E^{ee}_{cm} = 10.6 GeV

[1] LEES 12X meaurement corresponds to the lower limit of $< 1.9 \times 10^{-6}$ at 90% CL.

Downloaded from https://academic.oup.com/ptep/article/2022/8/083C01/6651666 by KIT Library user on 27 September 2022

$\Gamma(K^+ 3\pi^- \pi^+ \pi^0 \nu_\tau)/\Gamma_{total}$ — Γ_{128}/Γ

VALUE	CL%	DOCUMENT ID		TECN	COMMENT
$<8 \times 10^{-7}$	90	LEES	12X	BABR	468 fb^{-1} E^{ee}_{cm} = 10.6 GeV

$\Gamma(3h^- 2h^+ 2\pi^0 \nu_\tau)/\Gamma_{total}$ — Γ_{129}/Γ

VALUE	CL%	DOCUMENT ID		TECN	COMMENT
$<3.4 \times 10^{-6}$	90	AUBERT,B	06	BABR	232 fb^{-1} E^{ee}_{cm} = 10.6 GeV
• • • We do not use the following data for averages, fits, limits, etc. • • •					
$<1.1 \times 10^{-4}$	90	GIBAUT	94B	CLEO	E^{ee}_{cm} = 10.6 GeV

$\Gamma((5\pi)^- \nu_\tau)/\Gamma_{total}$ — Γ_{130}/Γ

$\Gamma_{130}/\Gamma = (\Gamma_{30}+\frac{1}{2}\Gamma_{45}+\Gamma_{48}+\frac{1}{2}\Gamma_{61}+\Gamma_{85}+\Gamma_{117}+0.5559\Gamma_{150}+0.892\Gamma_{180})/\Gamma$

VALUE (%)	DOCUMENT ID		TECN	COMMENT
0.78±0.05 OUR FIT				
• • • We use the following data for averages but not for fits. • • •				
0.61±0.06±0.08	[1] GIBAUT	94B	CLEO	E^{ee}_{cm} = 10.6 GeV

[1] Not independent of GIBAUT 94B B($3h^- 2h^+ \nu_\tau$), PROCARIO 93 B($h^- 4\pi^0 \nu_\tau$), and BORTOLETTO 93 B($2h^- h^+ 2\pi^0 \nu_\tau$)/B("3prong") measurements. Result is corrected for η contributions.

$\Gamma(4h^- 3h^+ \geq 0$ neutrals ν_τ ("7-prong"))/Γ_{total} — Γ_{131}/Γ

VALUE	CL%	DOCUMENT ID		TECN	COMMENT
$<3.0 \times 10^{-7}$	90	AUBERT,B	05F	BABR	232 fb^{-1}, E^{ee}_{cm} = 10.6 GeV
• • • We do not use the following data for averages, fits, limits, etc. • • •					
$<1.8 \times 10^{-5}$	95	ACKERSTAFF	97J	OPAL	1990–1995 LEP runs
$<2.4 \times 10^{-6}$	90	EDWARDS	97B	CLEO	E^{ee}_{cm} = 10.6 GeV
$<2.9 \times 10^{-4}$	90	BYLSMA	87	HRS	E^{ee}_{cm} = 29 GeV

$\Gamma(4h^- 3h^+ \nu_\tau)/\Gamma_{total}$ — Γ_{132}/Γ

VALUE	CL%	DOCUMENT ID		TECN	COMMENT
$<4.3 \times 10^{-7}$	90	AUBERT,B	05F	BABR	232 fb^{-1}, E^{ee}_{cm} = 10.6 GeV

$\Gamma(4h^- 3h^+ \pi^0 \nu_\tau)/\Gamma_{total}$ — Γ_{133}/Γ

VALUE	CL%	DOCUMENT ID		TECN	COMMENT
$<2.5 \times 10^{-7}$	90	AUBERT,B	05F	BABR	232 fb^{-1}, E^{ee}_{cm} = 10.6 GeV

$\Gamma(X^-(S{=}-1)\nu_\tau)/\Gamma_{total}$ — Γ_{134}/Γ

$\Gamma_{134}/\Gamma = (\Gamma_{10}+\Gamma_{16}+\Gamma_{23}+\Gamma_{28}+\Gamma_{36}+\Gamma_{41}+\Gamma_{45}+\Gamma_{61}+\Gamma_{97}+\Gamma_{103}+\Gamma_{120}+\Gamma_{127}+\Gamma_{152}+\Gamma_{154}+\Gamma_{156}+0.8312\Gamma_{170}+\Gamma_{179})/\Gamma$

VALUE (%)	DOCUMENT ID		TECN	COMMENT
2.92±0.04 OUR FIT				
• • • We use the following data for averages but not for fits. • • •				
2.87±0.12	[1] BARATE	99R	ALEP	1991–1995 LEP runs

[1] BARATE 99R perform a combined analysis of all ALEPH LEP 1 data on τ branching fraction measurements for decay modes having total strangeness equal to -1.

$\Gamma(K^*(892)^- \geq 0$ neutrals $\geq 0K^0_L \nu_\tau)/\Gamma_{total}$ — Γ_{135}/Γ

VALUE (%)	EVTS	DOCUMENT ID		TECN	COMMENT
1.42±0.18 OUR AVERAGE	Error includes scale factor of 1.4. See the ideogram below.				
$1.19 \pm 0.15^{+0.13}_{-0.18}$	104	ALBRECHT	95H	ARG	E^{ee}_{cm} = 9.4–10.6 GeV
1.94±0.27±0.15	74	[1] AKERS	94G	OPAL	E^{ee}_{cm} = 88–94 GeV
1.43±0.11±0.13	475	[2] GOLDBERG	90	CLEO	E^{ee}_{cm} = 9.4–10.9 GeV

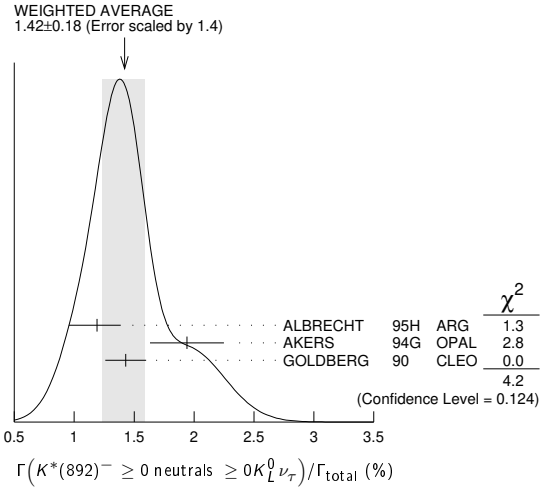

[1] AKERS 94G reject events in which a K^0_S accompanies the $K^*(892)^-$. We do not correct for them.

[2] GOLDBERG 90 estimates that 10% of observed $K^*(892)$ are accompanied by a π^0.

$\Gamma(K^*(892)^- \nu_\tau)/\Gamma_{total}$ — Γ_{136}/Γ

VALUE (%)	EVTS	DOCUMENT ID		TECN	COMMENT
1.20 ±0.07 OUR AVERAGE	Error includes scale factor of 1.8. See the ideogram below.				
1.131±0.006±0.051	49k	[1] EPIFANOV	07	BELL	351 fb^{-1} E^{ee}_{cm}=10.6 GeV
1.326±0.063		BARATE	99R	ALEP	1991–1995 LEP runs
1.11 ±0.12		[2] COAN	96	CLEO	$E^{ee}_{cm} \approx$ 10.6 GeV
1.42 ±0.22 ±0.09		[3] ACCIARRI	95F	L3	1991–1993 LEP runs
• • • We do not use the following data for averages, fits, limits, etc. • • •					
1.39 ±0.09 ±0.10		[4] BUSKULIC	96	ALEP	Repl. by BARATE 99R
1.45 ±0.13 ±0.11	273	[5] BUSKULIC	94F	ALEP	Repl. by BUSKULIC 96
1.23 ±0.21 $^{+0.11}_{-0.21}$	54	[6] ALBRECHT	88L	ARG	E^{ee}_{cm}= 10 GeV
1.9 ±0.3 ±0.4	44	[7] TSCHIRHART	88	HRS	E^{ee}_{cm}= 29 GeV
1.5 ±0.4 ±0.4	15	[8] AIHARA	87C	TPC	E^{ee}_{cm}= 29 GeV
1.3 ±0.3 ±0.3	31	YELTON	86	MRK2	E^{ee}_{cm}= 29 GeV
1.7 ±0.7	11	DORFAN	81	MRK2	E^{ee}_{cm}= 4.2–6.7 GeV

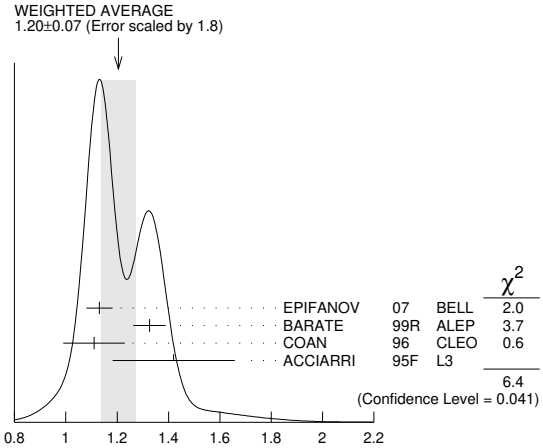

[1] EPIFANOV 07 quote B($\tau^- \to K^*(892)^- \nu_\tau$) B($K^*(892)^- \to K^0_S \pi^-$) = (3.77 ± 0.02(stat) ±0.12(syst) ±0.12(mod)) × 10^{-3}. We add the systematic and model uncertainties in quadrature and divide by B($K^*(892)^- \to K^0_S \pi^-$) = 0.3333.

[2] Not independent of COAN 96 B($\pi^- \overline{K}^0 \nu_\tau$) and BATTLE 94 B($K^- \pi^0 \nu_\tau$) measurements. $K\pi$ final states are consistent with and assumed to originate from $K^*(892)^-$ production.

[3] This result is obtained from their B($\pi^- \overline{K}^0 \nu_\tau$) assuming all those decays originate in $K^*(892)^-$ decays.

[4] Not independent of BUSKULIC 96 B($\pi^- \overline{K}^0 \nu_\tau$) and B($K^- \pi^0 \nu_\tau$) measurements.

[5] BUSKULIC 94F obtain this result from BUSKULIC 94F B($\overline{K}^0 \pi^- \nu_\tau$) and BUSKULIC 94E B($K^- \pi^0 \nu_\tau$) assuming all of those decays originate in $K^*(892)^-$ decays.

[6] The authors divide by Γ_2/Γ = 0.865 to obtain this result.

[7] Not independent of TSCHIRHART 88 $\Gamma(\tau^- \to h^- \overline{K}^0 \geq 0$ neutrals $\geq 0K^0_L \nu_\tau)$ / Γ.

[8] Decay π^- identified in this experiment, is assumed in the others.

$\Gamma(K^*(892)^- \nu_\tau)/\Gamma(\pi^- \pi^0 \nu_\tau)$ — Γ_{136}/Γ_{14}

VALUE	DOCUMENT ID		TECN	COMMENT
0.075±0.027	[1] ABREU	94K	DLPH	LEP 1992 Z data

[1] ABREU 94K quote B($\tau^- \to K^*(892)^- \nu_\tau$)B($K^*(892)^- \to K^- \pi^0$)/B($\tau^- \to \rho^- \nu_\tau$) = 0.025 ± 0.009. We divide by B($K^*(892)^- \to K^- \pi^0$) = 0.333 to obtain this result.

$\Gamma(K^*(892)^- \nu_\tau \to \pi^- \overline{K}^0 \nu_\tau)/\Gamma(\pi^- \overline{K}^0 \nu_\tau)$ — Γ_{137}/Γ_{36}

VALUE	EVTS	DOCUMENT ID		TECN	COMMENT
0.933±0.027	49k	EPIFANOV	07	BELL	351 fb^{-1} E^{ee}_{cm}= 10.6 GeV

$\Gamma(K^*(892)^0 K^- \geq 0$ neutrals $\nu_\tau)/\Gamma_{total}$ — Γ_{138}/Γ

VALUE (%)	EVTS	DOCUMENT ID		TECN	COMMENT
0.32±0.08±0.12	119	GOLDBERG	90	CLEO	E^{ee}_{cm}= 9.4–10.9 GeV

$\Gamma(K^*(892)^0 K^- \nu_\tau)/\Gamma_{total}$ — Γ_{139}/Γ

VALUE (%)	EVTS	DOCUMENT ID		TECN	COMMENT
0.21 ±0.04 OUR AVERAGE					
0.213±0.048		[1] BARATE	98	ALEP	1991–1995 LEP runs
0.20 ±0.05 ±0.04	47	ALBRECHT	95H	ARG	E^{ee}_{cm}= 9.4–10.6 GeV

[1] BARATE 98 measure the K^- ($\rho^0 \to \pi^+ \pi^-$) fraction in $\tau^- \to K^- \pi^+ \pi^- \nu_\tau$ decays to be (35 ± 11)% and derive this result from their measurement of $\Gamma(\tau^- \to K^- \pi^+ \pi^- \nu_\tau)/\Gamma_{total}$ assuming the intermediate states are all $K^- \rho$ and $K^- K^*(892)^0$.

$\Gamma(\overline{K}^*(892)^0 \pi^- \geq 0$ neutrals $\nu_\tau)/\Gamma_{total}$ — Γ_{140}/Γ

VALUE (%)	EVTS	DOCUMENT ID		TECN	COMMENT
0.38±0.11±0.13	105	GOLDBERG	90	CLEO	E^{ee}_{cm}= 9.4–10.9 GeV

Downloaded from https://academic.oup.com/ptep/article/2022/8/033C01/6651666 by KIT Library user on 27 September 2022

$\Gamma(\overline{K}^*(892)^0\pi^-\nu_\tau)/\Gamma_{total}$ — Γ_{141}/Γ

VALUE (%)	EVTS	DOCUMENT ID		TECN	COMMENT
0.22 ±0.05 OUR AVERAGE					
0.209±0.058		[1] BARATE	98	ALEP	1991–1995 LEP runs
0.25 ±0.10 ±0.05	27	ALBRECHT	95H	ARG	E^{ee}_{cm}= 9.4–10.6 GeV

[1] BARATE 98 measure the $K^-K^*(892)^0$ fraction in $\tau^- \to K^-K^+\pi^-\nu_\tau$ decays to be (87 ± 13)% and derive this result from their measurement of $\Gamma(\tau^- \to K^-K^+\pi^-\nu_\tau)/\Gamma_{total}$.

$\Gamma((\overline{K}^*(892)\pi)^-\nu_\tau \to \pi^-\overline{K}^0\pi^0\nu_\tau)/\Gamma_{total}$ — Γ_{142}/Γ

VALUE (%)	DOCUMENT ID		TECN	COMMENT
0.10 ±0.04 OUR AVERAGE				
0.097±0.044±0.036	[1] BARATE	99K	ALEP	1991–1995 LEP runs
0.106±0.037±0.032	[2] BARATE	98E	ALEP	1991–1995 LEP runs

[1] BARATE 99K measure K^0's by detecting K^0_L's in their hadron calorimeter. They determine the $\overline{K}^0\rho^-$ fraction in $\tau^- \to \pi^-\overline{K}^0\pi^0\nu_\tau$ decays to be (0.72 ± 0.12 ± 0.10) and multiply their $B(\pi^-\overline{K}^0\pi^0\nu_\tau)$ measurement by one minus this fraction to obtain the quoted result.

[2] BARATE 98E reconstruct K^0's using $K^0_S \to \pi^+\pi^-$ decays. They determine the $\overline{K}^0\rho^-$ fraction in $\tau^- \to \pi^-\overline{K}^0\pi^0\nu_\tau$ decays to be (0.64 ± 0.09 ± 0.10) and multiply their $B(\pi^-\overline{K}^0\pi^0\nu_\tau)$ measurement by one minus this fraction to obtain the quoted result.

$\Gamma(K_1(1270)^-\nu_\tau)/\Gamma_{total}$ — Γ_{143}/Γ

VALUE (%)	EVTS	DOCUMENT ID		TECN	COMMENT
0.47±0.11 OUR AVERAGE					
0.48±0.11		BARATE	99R	ALEP	1991–1995 LEP runs
$0.41^{+0.41}_{-0.35}\pm0.10$	5	[1] BAUER	94	TPC	E^{ee}_{cm}= 29 GeV

[1] We multiply 0.41% by 0.25, the relative systematic error quoted by BAUER 94, to obtain the systematic error.

$\Gamma(K_1(1400)^-\nu_\tau)/\Gamma_{total}$ — Γ_{144}/Γ

VALUE (%)	EVTS	DOCUMENT ID		TECN	COMMENT
0.17±0.26 OUR AVERAGE Error includes scale factor of 1.7.					
0.05±0.17		BARATE	99R	ALEP	1991–1995 LEP runs
$0.76^{+0.40}_{-0.33}\pm0.20$	11	[1] BAUER	94	TPC	E^{ee}_{cm}= 29 GeV

[1] We multiply 0.76% by 0.25, the relative systematic error quoted by BAUER 94, to obtain the systematic error.

$[\Gamma(K_1(1270)^-\nu_\tau)+\Gamma(K_1(1400)^-\nu_\tau)]/\Gamma_{total}$ — $(\Gamma_{143}+\Gamma_{144})/\Gamma$

VALUE (%)	EVTS	DOCUMENT ID		TECN	COMMENT
$\mathbf{1.17^{+0.41}_{-0.37}\pm0.29}$	16	[1] BAUER	94	TPC	E^{ee}_{cm}= 29 GeV

[1] We multiply 1.17% by 0.25, the relative systematic error quoted by BAUER 94, to obtain the systematic error. Not independent of BAUER 94 $B(K_1(1270)^-\nu_\tau)$ and BAUER 94 $B(K_1(1400)^-\nu_\tau)$ measurements.

$\Gamma(K_1(1270)^-\nu_\tau)/[\Gamma(K_1(1270)^-\nu_\tau)+\Gamma(K_1(1400)^-\nu_\tau)]$ — $\Gamma_{143}/(\Gamma_{143}+\Gamma_{144})$

VALUE	DOCUMENT ID		TECN	COMMENT
0.69±0.15 OUR AVERAGE				
0.71±0.16±0.11	[1] ABBIENDI	00D	OPAL	1990–1995 LEP runs
0.66±0.19±0.13	[2] ASNER	00B	CLEO	E^{ee}_{cm}= 10.6 GeV

[1] ABBIENDI 00D assume the resonance structure of $\tau^- \to K^-\pi^+\pi^-\nu_\tau$ decays is dominated by the $K_1(1270)^-$ and $K_1(1400)^-$ resonances.

[2] ASNER 00B assume the resonance structure of $\tau^- \to K^-\pi^+\pi^-\nu_\tau$ (ex. K^0) decays is dominated by $K_1(1270)^-$ and $K_1(1400)^-$ resonances.

$\Gamma(K^*(1410)^-\nu_\tau)/\Gamma_{total}$ — Γ_{145}/Γ

VALUE (units 10^{-3})	DOCUMENT ID		TECN	COMMENT
$\mathbf{1.5^{+1.4}_{-1.0}}$	BARATE	99R	ALEP	1991–1995 LEP runs

$\Gamma(K^*_0(1430)^-\nu_\tau)/\Gamma_{total}$ — Γ_{146}/Γ

VALUE (units 10^{-3})	CL%	DOCUMENT ID		TECN	COMMENT
<0.5	95	BARATE	99R	ALEP	1991–1995 LEP runs

$\Gamma(K^*_2(1430)^-\nu_\tau)/\Gamma_{total}$ — Γ_{147}/Γ

VALUE (%)	CL%	EVTS	DOCUMENT ID		TECN	COMMENT
<0.3	95		TSCHIRHART	88	HRS	E^{ee}_{cm}= 29 GeV
• • • We do not use the following data for averages, fits, limits, etc. • • •						
<0.33	95		[1] ACCIARRI	95F	L3	1991–1993 LEP runs
<0.9	95	0	DORFAN	81	MRK2	E^{ee}_{cm}= 4.2–6.7 GeV

[1] ACCIARRI 95F quote $B(\tau^- \to K^*(1430)^- \to \pi^-\overline{K}^0\nu_\tau) < 0.11\%$. We divide by $B(K^*(1430)^- \to \pi^-\overline{K}^0) = 0.33$ to obtain the limit shown.

$\Gamma(a_0(980)^- \geq 0 \text{ neutrals } \nu_\tau)/\Gamma_{total} \times B(a_0(980) \to K^0K^-)$ — $\Gamma_{148}/\Gamma \times B$

VALUE (units 10^{-4})	CL%	DOCUMENT ID		TECN	COMMENT
<2.8	90	GOLDBERG	90	CLEO	E^{ee}_{cm}= 9.4–10.9 GeV

$\Gamma(\eta\pi^-\nu_\tau)/\Gamma_{total}$ — Γ_{149}/Γ

VALUE (units 10^{-4})	CL%	EVTS	DOCUMENT ID		TECN	COMMENT
< 0.99	95		[1] DEL-AMO-SA...	11E	BABR	470 fb^{-1} E^{ee}_{cm}= 10.6 GeV
• • • We do not use the following data for averages, fits, limits, etc. • • •						
< 6.2	95		BUSKULIC	97C	ALEP	1991–1994 LEP runs
< 1.4	95	0	BARTELT	96	CLEO	$E^{ee}_{cm}\approx$ 10.6 GeV
< 3.4	95		ARTUSO	92	CLEO	$E^{ee}_{cm}\approx$ 10.6 GeV
< 90	95		ALBRECHT	88M	ARG	$E^{ee}_{cm}\approx$ 10 GeV
<140	90		BEHREND	88	CELL	E^{ee}_{cm}= 14–46.8 GeV
<180	95		BARINGER	87	CLEO	E^{ee}_{cm}= 10.5 GeV
<250	90	0	COFFMAN	87	MRK3	E^{ee}_{cm}= 3.77 GeV
510 ±100±120		65	DERRICK	87	HRS	E^{ee}_{cm}= 29 GeV
<100	95		GAN	87B	MRK2	E^{ee}_{cm}= 29 GeV

[1] DEL-AMO-SANCHEZ 11E also quote $B(\tau^- \to \eta\pi^-\nu_\tau) = (3.4 \pm 3.4 \pm 2.1) \times 10^{-5}$.

$\Gamma(\eta\pi^-\pi^0\nu_\tau)/\Gamma_{total}$ — Γ_{150}/Γ

VALUE (units 10^{-3})	CL%	EVTS	DOCUMENT ID		TECN	COMMENT
1.39± 0.07 OUR FIT						
1.38± 0.09 OUR AVERAGE Error includes scale factor of 1.2.						
1.35± 0.03± 0.07		6.0k	INAMI	09	BELL	490 fb^{-1} E^{ee}_{cm}= 10.6 GeV
1.8 ± 0.4 ± 0.2			BUSKULIC	97C	ALEP	1991–1994 LEP runs
1.7 ± 0.2 ± 0.2		125	ARTUSO	92	CLEO	$E^{ee}_{cm}\approx$ 10.6 GeV
• • • We do not use the following data for averages, fits, limits, etc. • • •						
< 11.0	95		ALBRECHT	88M	ARG	$E^{ee}_{cm}\approx$ 10 GeV
< 21.0	95		BARINGER	87	CLEO	E^{ee}_{cm}= 10.5 GeV
$42.0\ ^{+7.0}_{-12.0}\pm16.0$			[1] GAN	87	MRK2	E^{ee}_{cm}= 29 GeV

[1] Highly correlated with GAN 87 $\Gamma(\pi^-3\pi^0\nu_\tau)/\Gamma(\text{total})$ value.

$\Gamma(\eta\pi^-\pi^0\pi^0\nu_\tau)/\Gamma_{total}$ — Γ_{151}/Γ

VALUE (units 10^{-4})	CL%	EVTS	DOCUMENT ID		TECN	COMMENT
2.0 ±0.4 OUR FIT						
1.81±0.31 OUR AVERAGE						
2.01±0.34±0.22		381	LEES	12X	BABR	468 fb^{-1} E^{ee}_{cm} = 10.6 GeV
• • • We use the following data for averages but not for fits. • • •						
1.5 ±0.5		30	[1] ANASTASSOV	01	CLEO	E^{ee}_{cm}= 10.6 GeV
• • • We do not use the following data for averages, fits, limits, etc. • • •						
1.4 ±0.6 ±0.3		15	[2] BERGFELD	97	CLEO	Repl. by ANASTASSOV 01
< 4.3	95		ARTUSO	92	CLEO	$E^{ee}_{cm}\approx$ 10.6 GeV
<120	95		ALBRECHT	88M	ARG	$E^{ee}_{cm}\approx$ 10 GeV

[1] Weighted average of BERGFELD 97 and ANASTASSOV 01 value of $(1.5 \pm 0.6 \pm 0.3) \times 10^{-4}$ obtained using η's reconstructed from $\eta \to \pi^+\pi^-\pi^0$ decays.

[2] BERGFELD 97 reconstruct η's using $\eta \to \gamma\gamma$ decays.

$\Gamma(\eta K^-\nu_\tau)/\Gamma_{total}$ — Γ_{152}/Γ

VALUE (units 10^{-4})	CL%	EVTS	DOCUMENT ID		TECN	COMMENT
1.55±0.08 OUR FIT						
1.54±0.08 OUR AVERAGE						
1.42±0.11±0.07		690	DEL-AMO-SA...	11E	BABR	470 fb^{-1} E^{ee}_{cm}= 10.6 GeV
1.58±0.05±0.09		1.6k	INAMI	09	BELL	490 fb^{-1} E^{ee}_{cm}= 10.6 GeV
$2.9\ ^{+1.3}_{-1.2}\pm0.7$			BUSKULIC	97C	ALEP	1991–1994 LEP runs
2.6 ±0.5 ±0.5		85	BARTELT	96	CLEO	$E^{ee}_{cm}\approx$ 10.6 GeV
• • • We do not use the following data for averages, fits, limits, etc. • • •						
< 4.7	95		ARTUSO	92	CLEO	$E^{ee}_{cm}\approx$ 10.6 GeV

$\Gamma(\eta K^*(892)^-\nu_\tau)/\Gamma_{total}$ — Γ_{153}/Γ

VALUE (units 10^{-4})	EVTS	DOCUMENT ID		TECN	COMMENT
1.38±0.15 OUR AVERAGE					
1.34±0.12±0.09	245	[1] INAMI	09	BELL	490 fb^{-1} E^{ee}_{cm}= 10.6 GeV
2.90±0.80±0.42	25	BISHAI	99	CLEO	E^{ee}_{cm}= 10.6 GeV

[1] Not independent of INAMI 09 $B(\tau^- \to \eta K^-\pi^0\nu_\tau)$ and $B(\tau^- \to \eta\overline{K}^0\pi^-\nu_\tau)$ values.

$\Gamma(\eta K^-\pi^0\nu_\tau)/\Gamma_{total}$ — Γ_{154}/Γ

VALUE (units 10^{-4})	EVTS	DOCUMENT ID		TECN	COMMENT
0.48±0.12 OUR FIT					
0.48±0.12 OUR AVERAGE					
0.46±0.11±0.04	270	INAMI	09	BELL	490 fb^{-1} E^{ee}_{cm}= 10.6 GeV
1.77±0.56±0.71	36	BISHAI	99	CLEO	E^{ee}_{cm}= 10.6 GeV

$\Gamma(\eta K^-\pi^0(\text{non-}K^*(892))\nu_\tau)/\Gamma_{total}$ — Γ_{155}/Γ

VALUE	CL%	DOCUMENT ID		TECN	COMMENT
<3.5 × 10^{-5}	90	INAMI	09	BELL	490 fb^{-1} E^{ee}_{cm}= 10.6 GeV

Downloaded from https://academic.oup.com/ptep/article/2022/8/083C01/6651666 by KIT Library user on 27 September 2022

$\Gamma(\eta\overline{K}^0\pi^-\nu_\tau)/\Gamma_{total}$ — Γ_{156}/Γ

VALUE (units 10^{-4})	EVTS	DOCUMENT ID		TECN	COMMENT
0.94±0.15 OUR FIT					
0.93±0.15 OUR AVERAGE					
0.88±0.14±0.06	161	[1] INAMI	09	BELL	490 fb^{-1} E^{ee}_{cm}= 10.6 GeV
2.20±0.70±0.22	15	[2] BISHAI	99	CLEO	E^{ee}_{cm}= 10.6 GeV

[1] We multiply the INAMI 09 measurement B($\tau^- \to \eta K^0_S \pi^- \nu_\tau$) = (0.44 ± 0.07 ± 0.03) × 10^{-4} by 2 to obtain the listed value.
[2] We multiply the BISHAI 99 measurement B($\tau^- \to \eta K^0_S \pi^- \nu_\tau$) = (1.10 ± 0.35 ± 0.11) × 10^{-4} by 2 to obtain the listed value.

$\Gamma(\eta\overline{K}^0\pi^-\pi^0\nu_\tau)/\Gamma_{total}$ — Γ_{157}/Γ

VALUE	CL%	DOCUMENT ID		TECN	COMMENT
<5.0 × 10^{-5}	90	[1] INAMI	09	BELL	490 fb^{-1} E^{ee}_{cm}= 10.6 GeV

[1] We multiply the INAMI 09 measurement B($\tau^- \to \eta K^0_S \pi^- \pi^0 \nu_\tau$) < 2.5 × 10^{-5} by 2 to obtain the listed value.

$\Gamma(\eta K^- K^0\nu_\tau)/\Gamma_{total}$ — Γ_{158}/Γ

VALUE	CL%	DOCUMENT ID		TECN	COMMENT
<9.0 × 10^{-6}	90	[1] INAMI	09	BELL	490 fb^{-1} E^{ee}_{cm}= 10.6 GeV

[1] We multiply the INAMI 09 measurement B($\tau^- \to \eta K^- K^0_S \nu_\tau$) < 4.5 × 10^{-6} by 2 to obtain the listed value.

$\Gamma(\eta\pi^+\pi^-\pi^- \geq 0 \text{ neutrals } \nu_\tau)/\Gamma_{total}$ — Γ_{159}/Γ

VALUE (%)	CL%	DOCUMENT ID		TECN	COMMENT
<0.3	90	ABACHI	87B	HRS	E^{ee}_{cm}= 29 GeV

$\Gamma(\eta\pi^-\pi^+\pi^-\nu_\tau(\text{ex.}K^0))/\Gamma_{total}$ — Γ_{160}/Γ

VALUE (units 10^{-4})	EVTS	DOCUMENT ID		TECN	COMMENT
2.20±0.13 OUR FIT					
2.23±0.12 OUR AVERAGE					
2.10±0.09±0.13	2.9k	[1] LEES	12X	BABR	$\eta \to \gamma\gamma$
2.37±0.12±0.18	1.4k	[1] LEES	12X	BABR	$\eta \to \pi^+\pi^-\pi^0$
2.54±0.27±0.25	315	[1] LEES	12X	BABR	$\eta \to 3\pi^0$
• • • We use the following data for averages but not for fits. • • •					
2.3 ±0.5	170	[2] ANASTASSOV	01	CLEO	E^{ee}_{cm}= 10.6 GeV
• • • We do not use the following data for averages, fits, limits, etc. • • •					
1.60±0.05±0.11	1.8 k	AUBERT	08AE	BABR	Repl. by LEES 12X
3.4 $^{+0.6}_{-0.5}$ ±0.6	89	[3] BERGFELD	97	CLEO	Repl. by ANASTASSOV 01

[1] LEES 12X uses 468 fb^{-1} of data taken at E^{ee}_{cm} = 10.6 GeV. It gives the average of the three measurements listed here as (2.25 ± 0.07 ± 0.12) × 10^{-4}.
[2] Weighted average of BERGFELD 97 and ANASTASSOV 01 measurements using η's reconstructed from $\eta \to \pi^+\pi^-\pi^0$ and $\eta \to 3\pi^0$ decays.
[3] BERGFELD 97 reconstruct η's using $\eta \to \gamma\gamma$ and $\eta \to 3\pi^0$ decays.

$\Gamma(\eta\pi^-\pi^+\pi^-\nu_\tau(\text{ex.}K^0,f_1(1285)))/\Gamma_{total}$ — Γ_{161}/Γ

VALUE (units 10^{-4})	DOCUMENT ID		TECN	COMMENT
0.99±0.09±0.13	[1] LEES	12X	BABR	468 fb^{-1} E^{ee}_{cm} = 10.6 GeV

[1] LEES 12X obtain this result by subtracting their B($\tau^- \to f_1(1285)\pi^-\nu_\tau \to \eta\pi^-\pi^+\pi^-\nu_\tau$) measurement from their B($\tau^- \to \eta\pi^-\pi^+\pi^-\nu_\tau(\text{ex.}K^0)$) measurement.

$\Gamma(\eta a_1(1260)^-\nu_\tau \to \eta\pi^-\rho^0\nu_\tau)/\Gamma_{total}$ — Γ_{162}/Γ

VALUE	CL%	DOCUMENT ID		TECN	COMMENT
<3.9 × 10^{-4}	90	BERGFELD	97	CLEO	E^{ee}_{cm}= 10.6 GeV

$\Gamma(\eta\eta\pi^-\nu_\tau)/\Gamma_{total}$ — Γ_{163}/Γ

VALUE	CL%	DOCUMENT ID		TECN	COMMENT
<7.4 × 10^{-6}	90	INAMI	09	BELL	490 fb^{-1} E^{ee}_{cm}= 10.6 GeV
• • • We do not use the following data for averages, fits, limits, etc. • • •					
<1.1 × 10^{-4}	95	ARTUSO	92	CLEO	E^{ee}_{cm} ≈ 10.6 GeV
<8.3 × 10^{-3}	95	ALBRECHT	88M	ARG	E^{ee}_{cm} ≈ 10 GeV

$\Gamma(\eta\eta\pi^-\pi^0\nu_\tau)/\Gamma_{total}$ — Γ_{164}/Γ

VALUE (units 10^{-4})	CL%	DOCUMENT ID		TECN	COMMENT
< 2.0	95	ARTUSO	92	CLEO	E^{ee}_{cm} ≈ 10.6 GeV
• • • We do not use the following data for averages, fits, limits, etc. • • •					
<90	95	ALBRECHT	88M	ARG	E^{ee}_{cm} ≈ 10 GeV

$\Gamma(\eta\eta K^-\nu_\tau)/\Gamma_{total}$ — Γ_{165}/Γ

VALUE	CL%	DOCUMENT ID		TECN	COMMENT
<3.0 × 10^{-6}	90	INAMI	09	BELL	490 fb^{-1} E^{ee}_{cm}= 10.6 GeV

$\Gamma(\eta'(958)\pi^-\nu_\tau)/\Gamma_{total}$ — Γ_{166}/Γ

VALUE	CL%	DOCUMENT ID		TECN	COMMENT
<4.0 × 10^{-6}	90	LEES	12X	BABR	468 fb^{-1} E^{ee}_{cm} = 10.6 GeV
• • • We do not use the following data for averages, fits, limits, etc. • • •					
<7.2 × 10^{-6}	90	AUBERT	08AE	BABR	384 fb^{-1}, E^{ee}_{cm}= 10.6 GeV
<7.4 × 10^{-5}	90	BERGFELD	97	CLEO	E^{ee}_{cm}= 10.6 GeV

$\Gamma(\eta'(958)\pi^-\pi^0\nu_\tau)/\Gamma_{total}$ — Γ_{167}/Γ

VALUE	CL%	DOCUMENT ID		TECN	COMMENT
<1.2 × 10^{-5}	90	LEES	12X	BABR	468 fb^{-1} E^{ee}_{cm} = 10.6 GeV
• • • We do not use the following data for averages, fits, limits, etc. • • •					
<8.0 × 10^{-5}	90	BERGFELD	97	CLEO	E^{ee}_{cm}= 10.6 GeV

$\Gamma(\eta'(958)K^-\nu_\tau)/\Gamma_{total}$ — Γ_{168}/Γ

VALUE	CL%	DOCUMENT ID		TECN	COMMENT
<2.4 × 10^{-6}	90	LEES	12X	BABR	468 fb^{-1} E^{ee}_{cm} = 10.6 GeV

$\Gamma(\phi\pi^-\nu_\tau)/\Gamma_{total}$ — Γ_{169}/Γ

VALUE (units 10^{-5})	CL%	EVTS	DOCUMENT ID		TECN	COMMENT
3.42±0.55±0.25		344	AUBERT	08	BABR	342 fb^{-1} E^{ee}_{cm} = 10.6 GeV
• • • We do not use the following data for averages, fits, limits, etc. • • •						
< 20	90		[1] AVERY	97	CLEO	E^{ee}_{cm}= 10.6 GeV
< 35	90		ALBRECHT	95H	ARG	E^{ee}_{cm}= 9.4–10.6 GeV

[1] AVERY 97 limit varies from (1.2–2.0) × 10^{-4} depending on decay model assumptions.

$\Gamma(\phi K^-\nu_\tau)/\Gamma_{total}$ — Γ_{170}/Γ

VALUE (units 10^{-5})	CL%	EVTS	DOCUMENT ID		TECN	COMMENT
4.4 ±1.6 OUR FIT						
3.70±0.33 OUR AVERAGE Error includes scale factor of 1.3.						
• • • We use the following data for averages but not for fits. • • •						
3.39±0.20±0.28		274	AUBERT	08	BABR	342 fb^{-1} E^{ee}_{cm} = 10.6 GeV
4.05±0.25±0.26		551	INAMI	06	BELL	401 fb^{-1} E^{ee}_{cm}=10.6 GeV
• • • We do not use the following data for averages, fits, limits, etc. • • •						
<6.7	90		[1] AVERY	97	CLEO	E^{ee}_{cm}= 10.6 GeV

[1] AVERY 97 limit varies from (5.4–6.7) × 10^{-5} depending on decay model assumptions.

$\Gamma(f_1(1285)\pi^-\nu_\tau)/\Gamma_{total}$ — Γ_{171}/Γ

VALUE (units 10^{-4})	EVTS	DOCUMENT ID		TECN	COMMENT
3.9 ±0.5 OUR AVERAGE Error includes scale factor of 1.9.					
4.73±0.28±0.45	3.7k	[1] LEES	12X	BABR	468 fb^{-1} E^{ee}_{cm} = 10.6 GeV
3.60±0.18±0.23	2.5k	[2] LEES	12X	BABR	468 fb^{-1} E^{ee}_{cm} = 10.6 GeV
• • • We do not use the following data for averages, fits, limits, etc. • • •					
3.19±0.18±1.00	1.3 k	[3] AUBERT	08AE	BABR	Repl. by LEES 12X
3.9 ±0.7 ±0.5	1.4 k	[4] AUBERT,B	05W	BABR	Repl. by LEES 12X
5.8 $^{+1.4}_{-1.3}$ ±1.8	54	[5] BERGFELD	97	CLEO	E^{ee}_{cm}= 10.6 GeV

[1] LEES 12X obtain this value by dividing their B($\tau^- \to f_1(1285)\pi^-\nu_\tau \to 3\pi^-2\pi^+\nu_\tau$) measurement by the PDG 12 value of B($f_1(1285) \to 2\pi^+2\pi^-$) = 0.111 $^{+0.007}_{-0.006}$.
[2] LEES 12X obtain this value by dividing their B($\tau^- \to f_1(1285)\pi^-\nu_\tau \to \eta\pi^-\pi^+\pi^-\nu_\tau$) measurement by 2/3 of the PDG 12 value of B($f_1(1285) \to \eta\pi\pi$) = 0.524 $^{+0.019}_{-0.021}$.
[3] AUBERT 08AE obtain this value by dividing their B($\tau^- \to f_1(1285)\pi^-\nu_\tau \to \eta\pi^-\pi^+\pi^-\nu_\tau$) measurement by the PDG 06 value of B($f_1(1285) \to \eta\pi^-\pi^+$) = 0.35 ± 0.11. The quote (3.19 ± 0.18 ± 0.16 ± 0.99) × 10^{-4} where the final error is due to the uncertainty on B($f_1(1285) \to \eta\pi^-\pi^+$). We combine the two systematic errors in quadrature.
[4] AUBERT,B 05W use the $f_1(1285) \to 2\pi^+2\pi^-$ decay mode and the PDG 04 value of B($f_1(1285) \to 2\pi^+2\pi^-$) = 0.110 $^{+0.007}_{-0.006}$.
[5] BERGFELD 97 use the $f_1(1285) \to \eta\pi^+\pi^-$ decay mode.

$\Gamma(f_1(1285)\pi^-\nu_\tau \to \eta\pi^-\pi^+\pi^-\nu_\tau)/\Gamma_{total}$ — Γ_{172}/Γ

VALUE (units 10^{-4})	EVTS	DOCUMENT ID		TECN	COMMENT
1.18±0.07 OUR AVERAGE Error includes scale factor of 1.3.					
1.26±0.06±0.06	2.5k	LEES	12X	BABR	468 fb^{-1} E^{ee}_{cm} = 10.6 GeV
1.11±0.06±0.05	1.3 k	AUBERT	08AE	BABR	384 fb^{-1}, E^{ee}_{cm}= 10.6 GeV

$\Gamma(f_1(1285)\pi^-\nu_\tau \to \eta\pi^-\pi^+\pi^-\nu_\tau)/\Gamma(\eta\pi^-\pi^+\pi^-\nu_\tau(\text{ex.}K^0))$ — $\Gamma_{172}/\Gamma_{160}$

VALUE	DOCUMENT ID		TECN	COMMENT
0.69±0.01±0.05	[1] AUBERT	08AE	BABR	384 fb^{-1}, E^{ee}_{cm}= 10.6 GeV
• • • We do not use the following data for averages, fits, limits, etc. • • •				
0.55±0.14	BERGFELD	97	CLEO	E^{ee}_{cm}= 10.6 GeV

[1] Not independent of AUBERT 08AE B($\tau^- \to f_1(1285)\pi^-\nu_\tau \to \eta\pi^-\pi^+\pi^-\nu_\tau$) and B($\tau^- \to \eta\pi^-\pi^+\pi^-\nu_\tau(\text{ex.}K^0)$) values.

$\Gamma(f_1(1285)\pi^-\nu_\tau \to 3\pi^-2\pi^+\nu_\tau)/\Gamma_{total}$ — Γ_{173}/Γ

VALUE (units 10^{-4})	EVTS	DOCUMENT ID		TECN	COMMENT
0.52 ±0.04 OUR FIT					
0.520±0.031±0.037	3.7k	LEES	12X	BABR	468 fb^{-1} E^{ee}_{cm}=10.6 GeV

$\Gamma(\pi(1300)^-\nu_\tau \to (\rho\pi)^-\nu_\tau \to (3\pi)^-\nu_\tau)/\Gamma_{total}$ — Γ_{174}/Γ

VALUE	CL%	DOCUMENT ID		TECN	COMMENT
<1.0 × 10^{-4}	90	ASNER	00	CLEO	E^{ee}_{cm}= 10.6 GeV

Downloaded from https://academic.oup.com/ptep/article/2022/8/083C01/6651666 by KIT Library user on 27 September 2022

$\Gamma(\pi(1300)^- \nu_\tau \to ((\pi\pi)_{S-\text{wave}}\, \pi)^- \nu_\tau \to (3\pi)^- \nu_\tau)/\Gamma_{\text{total}}$ — Γ_{175}/Γ

VALUE	CL%	DOCUMENT ID		TECN	COMMENT
$<1.9 \times 10^{-4}$	90	ASNER	00	CLEO	$E^{ee}_{\text{cm}} = 10.6$ GeV

$\Gamma(h^- \omega \geq 0 \text{ neutrals } \nu_\tau)/\Gamma_{\text{total}}$ — Γ_{176}/Γ

$\Gamma_{176}/\Gamma = (\Gamma_{178}+\Gamma_{179}+\Gamma_{180})/\Gamma$

VALUE (%)	EVTS	DOCUMENT ID		TECN	COMMENT
2.40±0.08 OUR FIT					
• • • We use the following data for averages but not for fits. • • •					
1.65±0.3 ±0.2	1513	ALBRECHT	88M	ARG	$E^{ee}_{\text{cm}} \approx 10$ GeV

$\Gamma(h^- \omega \nu_\tau)/\Gamma_{\text{total}}$ — $\Gamma_{177}/\Gamma = (\Gamma_{178}+\Gamma_{179})/\Gamma$

VALUE (%)	EVTS	DOCUMENT ID		TECN	COMMENT
1.99±0.06 OUR FIT					
1.92±0.07 OUR AVERAGE					
1.91±0.07±0.06	5803	BUSKULIC	97C	ALEP	1991–1994 LEP runs
1.60±0.27±0.41	139	BARINGER	87	CLEO	$E^{ee}_{\text{cm}} = 10.5$ GeV
• • • We use the following data for averages but not for fits. • • •					
1.95±0.07±0.11	2223	[1] BALEST	95C	CLEO	$E^{ee}_{\text{cm}} \approx 10.6$ GeV

[1] Not independent of BALEST 95C $B(\tau^- \to h^- \omega \nu_\tau)/B(\tau^- \to h^- h^+ \pi^0 \nu_\tau)$ value.

$[\Gamma(\pi^- \omega \nu_\tau) + \Gamma(K^- \omega \nu_\tau)]/\Gamma(h^- h^- h^+ \pi^0 \nu_\tau (\text{ex.}K^0))$ — $(\Gamma_{178}+\Gamma_{179})/\Gamma_{74}$

$(\Gamma_{178}+\Gamma_{179})/\Gamma_{74} = (\Gamma_{178}+\Gamma_{179})/(\Gamma_{78}+\Gamma_{103}+\Gamma_{107}+0.2302\Gamma_{152}+0.892\Gamma_{178}+0.892\Gamma_{179}+0.0153\Gamma_{180})$

VALUE (units 10^{-2})	EVTS	DOCUMENT ID		TECN	COMMENT
43.5±1.4 OUR FIT					
45.3±1.9 OUR AVERAGE					
43.1±3.3	2350	[1] BUSKULIC	96	ALEP	LEP 1991–1993 data
46.4±1.6±1.7	2223	[2] BALEST	95C	CLEO	$E^{ee}_{\text{cm}} \approx 10.6$ GeV
• • • We do not use the following data for averages, fits, limits, etc. • • •					
37 ±5 ±2	458	[3] ALBRECHT	91D	ARG	$E^{ee}_{\text{cm}} = 9.4$–10.6 GeV

[1] BUSKULIC 96 quote the fraction of $\tau \to h^- h^- h^+ \pi^0 \nu_\tau$ (ex. K^0) decays which originate in a $h^- \omega$ final state = 0.383 ± 0.029. We divide this by the $\omega(782) \to \pi^+ \pi^- \pi^0$ branching fraction (0.888).

[2] BALEST 95C quote the fraction of $\tau^- \to h^- h^- h^+ \pi^0 \nu_\tau$ (ex. K^0) decays which originate in a $h^- \omega$ final state equals 0.412 ± 0.014 ± 0.015. We divide this by the $\omega(782) \to \pi^+ \pi^- \pi^0$ branching fraction (0.888).

[3] ALBRECHT 91D quote the fraction of $\tau^- \to h^- h^- h^+ \pi^0 \nu_\tau$ decays which originate in a $\pi^- \omega$ final state equals 0.33 ± 0.04 ± 0.02. We divide this by the $\omega(782) \to \pi^+ \pi^- \pi^0$ branching fraction (0.888).

$\Gamma(\pi^- \omega \nu_\tau)/\Gamma_{\text{total}}$ — Γ_{178}/Γ

VALUE (%)	DOCUMENT ID
1.95±0.06 OUR FIT	

$\Gamma(K^- \omega \nu_\tau)/\Gamma_{\text{total}}$ — Γ_{179}/Γ

VALUE (units 10^{-4})	EVTS	DOCUMENT ID		TECN	COMMENT
4.1±0.9 OUR FIT					
4.1±0.6±0.7	500	ARMS	05	CLE3	7.6 fb^{-1}, $E^{ee}_{\text{cm}} = 10.6$ GeV

$\Gamma(h^- \omega \pi^0 \nu_\tau)/\Gamma_{\text{total}}$ — Γ_{180}/Γ

VALUE (%)	EVTS	DOCUMENT ID		TECN	COMMENT
0.41±0.04 OUR FIT					
0.43±0.06±0.05	7283	BUSKULIC	97C	ALEP	1991–1994 LEP runs

$\Gamma(h^- \omega \pi^0 \nu_\tau)/\Gamma(h^- h^- h^+ \geq 0 \text{ neutrals } \geq 0 K^0_L \nu_\tau)$ — Γ_{180}/Γ_{62}

$\Gamma_{180}/\Gamma_{62} = \Gamma_{180}/(0.34598\Gamma_{36}+0.34598\Gamma_{38}+0.34598\Gamma_{41}+0.34598\Gamma_{43}+0.4247\Gamma_{48}+0.6920\Gamma_{49}+0.8494\Gamma_{52}+0.6920\Gamma_{56}+0.6534\Gamma_{61}+\Gamma_{70}+\Gamma_{78}+\Gamma_{85}+\Gamma_{89}+\Gamma_{97}+\Gamma_{103}+\Gamma_{106}+\Gamma_{107}+0.2804\Gamma_{150}+0.2302\Gamma_{151}+0.2804\Gamma_{152}+0.2804\Gamma_{154}+0.3759\Gamma_{156}+0.3257\Gamma_{160}+0.7259\Gamma_{170}+0.9078\Gamma_{178}+0.9078\Gamma_{179}+0.9078\Gamma_{180}+0.892\Gamma_{182})$

VALUE	EVTS	DOCUMENT ID		TECN	COMMENT
(2.69 ±0.28) $\times 10^{-2}$ OUR FIT					
• • • We use the following data for averages but not for fits. • • •					
0.028±0.003±0.003	430	[1] BORTOLETTO	93	CLEO	$E^{ee}_{\text{cm}} \approx 10.6$ GeV

[1] Not independent of BORTOLETTO 93 $\Gamma(\tau^- \to h^- \omega \pi^0 \nu_\tau)/\Gamma(\tau^- \to h^- h^- h^+ 2\pi^0 \nu_\tau (\text{ex.}K^0))$ value.

$\Gamma(h^- \omega \pi^0 \nu_\tau)/\Gamma(h^- h^- h^+ 2\pi^0 \nu_\tau (\text{ex.}K^0))$ — Γ_{180}/Γ_{84}

$\Gamma_{180}/\Gamma_{84} = \Gamma_{180}/(\Gamma_{85}+0.2302\Gamma_{150}+0.2302\Gamma_{154}+0.892\Gamma_{180})$

VALUE (units 10^{-2})	DOCUMENT ID		TECN	COMMENT
82±8 OUR FIT				
81±6±6	BORTOLETTO	93	CLEO	$E^{ee}_{\text{cm}} \approx 10.6$ GeV

$\Gamma(h^- \omega 2\pi^0 \nu_\tau)/\Gamma_{\text{total}}$ — Γ_{181}/Γ

VALUE (units 10^{-4})	EVTS	DOCUMENT ID		TECN	COMMENT
1.4 ±0.4 ±0.3	53	ANASTASSOV	01	CLEO	$E^{ee}_{\text{cm}} = 10.6$ GeV
• • • We do not use the following data for averages, fits, limits, etc. • • •					
$1.89^{+0.74}_{-0.67} \pm 0.40$	19	ANDERSON	97	CLEO	Repl. by ANASTASSOV 01

$\Gamma(\pi^- \omega 2\pi^0 \nu_\tau)/\Gamma_{\text{total}}$ — Γ_{182}/Γ

VALUE (units 10^{-4})	EVTS	DOCUMENT ID		TECN	COMMENT
0.72±0.16 OUR FIT					
0.73±0.12±0.12	1.1k	LEES	12X	BABR	468 fb^{-1} $E^{ee}_{\text{cm}} = 10.6$ GeV

$\Gamma(h^- 2\omega \nu_\tau)/\Gamma_{\text{total}}$ — Γ_{183}/Γ

VALUE	CL%	DOCUMENT ID		TECN	COMMENT
$<5.4 \times 10^{-7}$	90	AUBERT,B	06	BABR	232 fb^{-1} $E^{ee}_{\text{cm}} = 10.6$ GeV

$\Gamma(2h^- h^+ \omega \nu_\tau)/\Gamma_{\text{total}}$ — Γ_{184}/Γ

VALUE (units 10^{-4})	EVTS	DOCUMENT ID		TECN	COMMENT
1.2±0.2±0.1	110	ANASTASSOV	01	CLEO	$E^{ee}_{\text{cm}} = 10.6$ GeV

$\Gamma(2\pi^- \pi^+ \omega \nu_\tau (\text{ex.}K^0))/\Gamma_{\text{total}}$ — Γ_{185}/Γ

VALUE (units 10^{-4})	EVTS	DOCUMENT ID		TECN	COMMENT
0.84±0.06 OUR FIT					
0.84±0.04±0.06	2.4k	LEES	12X	BABR	468 fb^{-1} $E^{ee}_{\text{cm}} = 10.6$ GeV

$\Gamma(e^- \gamma)/\Gamma_{\text{total}}$ — Γ_{186}/Γ

Test of lepton family number conservation.

VALUE	CL%	DOCUMENT ID		TECN	COMMENT
$<3.3 \times 10^{-8}$	90	AUBERT	10B	BABR	516 fb^{-1}, $E^{ee}_{\text{cm}} = 10.6$ GeV
• • • We do not use the following data for averages, fits, limits, etc. • • •					
$<5.6 \times 10^{-8}$	90	UNO	21	BELL	988 fb^{-1}, $E^{ee}_{\text{cm}} = 10.6$ GeV
$<1.2 \times 10^{-7}$	90	HAYASAKA	08	BELL	535 fb^{-1}, $E^{ee}_{\text{cm}} = 10.6$ GeV
$<1.1 \times 10^{-7}$	90	AUBERT	06C	BABR	232 fb^{-1}, $E^{ee}_{\text{cm}} = 10.6$ GeV
$<3.9 \times 10^{-7}$	90	HAYASAKA	05	BELL	86.7 fb^{-1}, $E^{ee}_{\text{cm}} = 10.6$ GeV
$<2.7 \times 10^{-6}$	90	EDWARDS	97	CLEO	
$<1.1 \times 10^{-4}$	90	ABREU	95U	DLPH	1990–1993 LEP runs
$<1.2 \times 10^{-4}$	90	ALBRECHT	92K	ARG	$E^{ee}_{\text{cm}} = 10$ GeV
$<2.0 \times 10^{-4}$	90	KEH	88	CBAL	$E^{ee}_{\text{cm}} = 10$ GeV
$<6.4 \times 10^{-4}$	90	HAYES	82	MRK2	$E^{ee}_{\text{cm}} = 3.8$–6.8 GeV

$\Gamma(e^- \gamma\gamma)/\Gamma_{\text{total}}$ — Γ_{187}/Γ

VALUE	CL%	DOCUMENT ID		TECN	COMMENT
$<2.5 \times 10^{-4}$	90	[1] BRYMAN	21	RVUE	516 fb^{-1}, $E^{ee}_{\text{cm}} = 10.6$ GeV

[1] BRYMAN 21 reinterprets the upper limit result on $B(\tau^- \to e^- \gamma)$ and $B(\tau^- \to \mu^- \gamma)$ by AUBERT 10B, estimating with a simulation the efficiency for this decay mode to be detected as the corresponding AUBERT 10B decay mode.

$\Gamma(\mu^- \gamma)/\Gamma_{\text{total}}$ — Γ_{188}/Γ

Test of lepton family number conservation.

VALUE	CL%	DOCUMENT ID		TECN	COMMENT
$< 4.2 \times 10^{-8}$	90	UNO	21	BELL	988 fb^{-1}, $E^{ee}_{\text{cm}} = 10.6$ GeV
• • • We do not use the following data for averages, fits, limits, etc. • • •					
$< 4.4 \times 10^{-8}$	90	AUBERT	10B	BABR	516 fb^{-1}, $E^{ee}_{\text{cm}} = 10.6$ GeV
$< 4.5 \times 10^{-8}$	90	HAYASAKA	08	BELL	535 fb^{-1}, $E^{ee}_{\text{cm}} = 10.6$ GeV
$< 6.8 \times 10^{-8}$	90	AUBERT,B	05A	BABR	232 fb^{-1}, $E^{ee}_{\text{cm}} = 10.6$ GeV
$< 3.1 \times 10^{-7}$	90	ABE	04B	BELL	86.3 fb^{-1}, $E^{ee}_{\text{cm}} = 10.6$ GeV
$< 1.1 \times 10^{-6}$	90	AHMED	00	CLEO	$E^{ee}_{\text{cm}} = 10.6$ GeV
$< 3.0 \times 10^{-6}$	90	EDWARDS	97	CLEO	
$< 6.2 \times 10^{-5}$	90	ABREU	95U	DLPH	1990–1993 LEP runs
$< 0.42 \times 10^{-5}$	90	BEAN	93	CLEO	$E^{ee}_{\text{cm}} = 10.6$ GeV
$< 3.4 \times 10^{-5}$	90	ALBRECHT	92K	ARG	$E^{ee}_{\text{cm}} = 10$ GeV
$<55 \times 10^{-5}$	90	HAYES	82	MRK2	$E^{ee}_{\text{cm}} = 3.8$–6.8 GeV

$\Gamma(\mu^- \gamma\gamma)/\Gamma_{\text{total}}$ — Γ_{189}/Γ

VALUE	CL%	DOCUMENT ID		TECN	COMMENT
$<5.8 \times 10^{-4}$	90	[1] BRYMAN	21	RVUE	516 fb^{-1}, $E^{ee}_{\text{cm}} = 10.6$ GeV

[1] BRYMAN 21 reinterprets the upper limit result on $B(\tau^- \to e^- \gamma)$ and $B(\tau^- \to \mu^- \gamma)$ by AUBERT 10B, estimating with a simulation the efficiency for this decay mode to be detected as the corresponding AUBERT 10B decay mode.

$\Gamma(e^- \pi^0)/\Gamma_{\text{total}}$ — Γ_{190}/Γ

Test of lepton family number conservation.

VALUE	CL%	DOCUMENT ID		TECN	COMMENT
$< 8.0 \times 10^{-8}$	90	MIYAZAKI	07	BELL	401 fb^{-1}, $E^{ee}_{\text{cm}} = 10.6$ GeV
• • • We do not use the following data for averages, fits, limits, etc. • • •					
$< 1.3 \times 10^{-7}$	90	AUBERT	07I	BABR	339 fb^{-1}, $E^{ee}_{\text{cm}} = 10.6$ GeV
$< 1.9 \times 10^{-7}$	90	ENARI	05	BELL	154 fb^{-1}, $E^{ee}_{\text{cm}} = 10.6$ GeV
$< 3.7 \times 10^{-6}$	90	BONVICINI	97	CLEO	$E^{ee}_{\text{cm}} = 10.6$ GeV
$< 17 \times 10^{-5}$	90	ALBRECHT	92K	ARG	$E^{ee}_{\text{cm}} = 10$ GeV
$< 14 \times 10^{-5}$	90	KEH	88	CBAL	$E^{ee}_{\text{cm}} = 10$ GeV
$<210 \times 10^{-5}$	90	HAYES	82	MRK2	$E^{ee}_{\text{cm}} = 3.8$–6.8 GeV

Downloaded from https://academic.oup.com/ptep/article/2022/8/083C01/6651666 by KIT Library user on 27 September 2022

$\Gamma(\mu^- \pi^0)/\Gamma_{total}$ — Γ_{191}/Γ

Test of lepton family number conservation.

VALUE	CL%	DOCUMENT ID		TECN	COMMENT
$< 1.1 \times 10^{-7}$	90	AUBERT	07I	BABR	339 fb^{-1}, E^{ee}_{cm}=10.6 GeV
• • • We do not use the following data for averages, fits, limits, etc. • • •					
$< 1.2 \times 10^{-7}$	90	MIYAZAKI	07	BELL	401 fb^{-1}, E^{ee}_{cm}=10.6 GeV
$< 4.1 \times 10^{-7}$	90	ENARI	05	BELL	154 fb^{-1}, E^{ee}_{cm}= 10.6 GeV
$< 4.0 \times 10^{-6}$	90	BONVICINI	97	CLEO	E^{ee}_{cm}= 10.6 GeV
$< 4.4 \times 10^{-5}$	90	ALBRECHT	92K	ARG	E^{ee}_{cm}= 10 GeV
$<82 \times 10^{-5}$	90	HAYES	82	MRK2	E^{ee}_{cm}= 3.8–6.8 GeV

$\Gamma(e^- K^0_S)/\Gamma_{total}$ — Γ_{192}/Γ

Test of lepton family number conservation.

VALUE	CL%	DOCUMENT ID		TECN	COMMENT
$<2.6 \times 10^{-8}$	90	MIYAZAKI	10A	BELL	671 fb^{-1} E^{ee}_{cm} = 10.6 GeV
• • • We do not use the following data for averages, fits, limits, etc. • • •					
$<3.3 \times 10^{-8}$	90	AUBERT	09D	BABR	469 fb^{-1} E^{ee}_{cm} = 10.6 GeV
$<5.6 \times 10^{-8}$	90	MIYAZAKI	06A	BELL	281 fb^{-1} E^{ee}_{cm} = 10.6 GeV
$<9.1 \times 10^{-7}$	90	CHEN	02C	CLEO	E^{ee}_{cm}= 10.6 GeV
$<1.3 \times 10^{-3}$	90	HAYES	82	MRK2	E^{ee}_{cm}= 3.8–6.8 GeV

$\Gamma(\mu^- K^0_S)/\Gamma_{total}$ — Γ_{193}/Γ

Test of lepton family number conservation.

VALUE	CL%	DOCUMENT ID		TECN	COMMENT
$<2.3 \times 10^{-8}$	90	MIYAZAKI	10A	BELL	671 fb^{-1} E^{ee}_{cm} = 10.6 GeV
• • • We do not use the following data for averages, fits, limits, etc. • • •					
$<4.0 \times 10^{-8}$	90	AUBERT	09D	BABR	469 fb^{-1} E^{ee}_{cm} = 10.6 GeV
$<4.9 \times 10^{-8}$	90	MIYAZAKI	06A	BELL	281 fb^{-1} E^{ee}_{cm} = 10.6 GeV
$<9.5 \times 10^{-7}$	90	CHEN	02C	CLEO	E^{ee}_{cm}= 10.6 GeV
$<1.0 \times 10^{-3}$	90	HAYES	82	MRK2	E^{ee}_{cm}= 3.8–6.8 GeV

$\Gamma(e^- \eta)/\Gamma_{total}$ — Γ_{194}/Γ

Test of lepton family number conservation.

VALUE	CL%	DOCUMENT ID		TECN	COMMENT
$< 9.2 \times 10^{-8}$	90	MIYAZAKI	07	BELL	401 fb^{-1}, E^{ee}_{cm}=10.6 GeV
• • • We do not use the following data for averages, fits, limits, etc. • • •					
$< 1.6 \times 10^{-7}$	90	AUBERT	07I	BABR	339 fb^{-1}, E^{ee}_{cm}=10.6 GeV
$< 2.4 \times 10^{-7}$	90	ENARI	05	BELL	154 fb^{-1}, E^{ee}_{cm}= 10.6 GeV
$< 8.2 \times 10^{-6}$	90	BONVICINI	97	CLEO	E^{ee}_{cm}= 10.6 GeV
$< 6.3 \times 10^{-5}$	90	ALBRECHT	92K	ARG	E^{ee}_{cm}= 10 GeV
$<24 \times 10^{-5}$	90	KEH	88	CBAL	E^{ee}_{cm}= 10 GeV

$\Gamma(\mu^- \eta)/\Gamma_{total}$ — Γ_{195}/Γ

Test of lepton family number conservation.

VALUE	CL%	DOCUMENT ID		TECN	COMMENT
$<6.5 \times 10^{-8}$	90	MIYAZAKI	07	BELL	401 fb^{-1}, E^{ee}_{cm}=10.6 GeV
• • • We do not use the following data for averages, fits, limits, etc. • • •					
$<1.5 \times 10^{-7}$	90	AUBERT	07I	BABR	339 fb^{-1}, E^{ee}_{cm}=10.6 GeV
$<1.5 \times 10^{-7}$	90	ENARI	05	BELL	154 fb^{-1}, E^{ee}_{cm}= 10.6 GeV
$<3.4 \times 10^{-7}$	90	ENARI	04	BELL	84.3 fb^{-1}, E^{ee}_{cm}=10.6 GeV
$<9.6 \times 10^{-6}$	90	BONVICINI	97	CLEO	E^{ee}_{cm}= 10.6 GeV
$<7.3 \times 10^{-5}$	90	ALBRECHT	92K	ARG	E^{ee}_{cm}= 10 GeV

$\Gamma(e^- \rho^0)/\Gamma_{total}$ — Γ_{196}/Γ

Test of lepton family number conservation.

VALUE	CL%	DOCUMENT ID		TECN	COMMENT
$< 1.8 \times 10^{-8}$	90	MIYAZAKI	11	BELL	854 fb^{-1} E^{ee}_{cm} = 10.6 GeV
• • • We do not use the following data for averages, fits, limits, etc. • • •					
$< 4.6 \times 10^{-8}$	90	AUBERT	09W	BABR	451 fb^{-1} E^{ee}_{cm} = 10.6 GeV
$< 6.3 \times 10^{-8}$	90	NISHIO	08	BELL	543 fb^{-1} E^{ee}_{cm} = 10.6 GeV
$< 6.5 \times 10^{-7}$	90	YUSA	06	BELL	158 fb^{-1} E^{ee}_{cm} = 10.6 GeV
$< 2.0 \times 10^{-6}$	90	BLISS	98	CLEO	E^{ee}_{cm}= 10.6 GeV
$< 4.2 \times 10^{-6}$	90	[1] BARTELT	94	CLEO	Repl. by BLISS 98
$< 1.9 \times 10^{-5}$	90	ALBRECHT	92K	ARG	E^{ee}_{cm}= 10 GeV
$<37 \times 10^{-5}$	90	HAYES	82	MRK2	E^{ee}_{cm}= 3.8–6.8 GeV

[1] BARTELT 94 assume phase space decays.

$\Gamma(\mu^- \rho^0)/\Gamma_{total}$ — Γ_{197}/Γ

Test of lepton family number conservation.

VALUE	CL%	DOCUMENT ID		TECN	COMMENT
$< 1.2 \times 10^{-8}$	90	MIYAZAKI	11	BELL	854 fb^{-1} E^{ee}_{cm} = 10.6 GeV
• • • We do not use the following data for averages, fits, limits, etc. • • •					
$< 2.6 \times 10^{-8}$	90	AUBERT	09W	BABR	451 fb^{-1} E^{ee}_{cm} = 10.6 GeV
$< 6.8 \times 10^{-8}$	90	NISHIO	08	BELL	543 fb^{-1} E^{ee}_{cm} = 10.6 GeV
$< 2.0 \times 10^{-7}$	90	YUSA	06	BELL	158 fb^{-1} E^{ee}_{cm} = 10.6 GeV
$< 6.3 \times 10^{-6}$	90	BLISS	98	CLEO	E^{ee}_{cm}= 10.6 GeV
$< 5.7 \times 10^{-6}$	90	[1] BARTELT	94	CLEO	Repl. by BLISS 98
$< 2.9 \times 10^{-5}$	90	ALBRECHT	92K	ARG	E^{ee}_{cm}= 10 GeV
$<44 \times 10^{-5}$	90	HAYES	82	MRK2	E^{ee}_{cm}= 3.8–6.8 GeV

[1] BARTELT 94 assume phase space decays.

$\Gamma(e^- \omega)/\Gamma_{total}$ — Γ_{198}/Γ

VALUE	CL%	DOCUMENT ID		TECN	COMMENT
$<4.8 \times 10^{-8}$	90	MIYAZAKI	11	BELL	854 fb^{-1} E^{ee}_{cm} = 10.6 GeV
• • • We do not use the following data for averages, fits, limits, etc. • • •					
$<1.1 \times 10^{-7}$	90	AUBERT	08K	BABR	384 fb^{-1} E^{ee}_{cm} = 10.6 GeV
$<1.8 \times 10^{-7}$	90	NISHIO	08	BELL	543 fb^{-1} E^{ee}_{cm} = 10.6 GeV

$\Gamma(\mu^- \omega)/\Gamma_{total}$ — Γ_{199}/Γ

VALUE	CL%	DOCUMENT ID		TECN	COMMENT
$<4.7 \times 10^{-8}$	90	MIYAZAKI	11	BELL	854 fb^{-1} E^{ee}_{cm} = 10.6 GeV
• • • We do not use the following data for averages, fits, limits, etc. • • •					
$<1.0 \times 10^{-7}$	90	AUBERT	08K	BABR	384 fb^{-1} E^{ee}_{cm} = 10.6 GeV
$<8.9 \times 10^{-8}$	90	NISHIO	08	BELL	543 fb^{-1} E^{ee}_{cm} = 10.6 GeV

$\Gamma(e^- K^*(892)^0)/\Gamma_{total}$ — Γ_{200}/Γ

Test of lepton family number conservation.

VALUE	CL%	DOCUMENT ID		TECN	COMMENT
$<3.2 \times 10^{-8}$	90	MIYAZAKI	11	BELL	854 fb^{-1} E^{ee}_{cm} = 10.6 GeV
• • • We do not use the following data for averages, fits, limits, etc. • • •					
$<5.9 \times 10^{-8}$	90	AUBERT	09W	BABR	451 fb^{-1} E^{ee}_{cm} = 10.6 GeV
$<7.8 \times 10^{-8}$	90	NISHIO	08	BELL	543 fb^{-1} E^{ee}_{cm} = 10.6 GeV
$<3.0 \times 10^{-7}$	90	YUSA	06	BELL	158 fb^{-1} E^{ee}_{cm} = 10.6 GeV
$<5.1 \times 10^{-6}$	90	BLISS	98	CLEO	E^{ee}_{cm}= 10.6 GeV
$<6.3 \times 10^{-6}$	90	[1] BARTELT	94	CLEO	Repl. by BLISS 98
$<3.8 \times 10^{-5}$	90	ALBRECHT	92K	ARG	E^{ee}_{cm}= 10 GeV

[1] BARTELT 94 assume phase space decays.

$\Gamma(\mu^- K^*(892)^0)/\Gamma_{total}$ — Γ_{201}/Γ

Test of lepton family number conservation.

VALUE	CL%	DOCUMENT ID		TECN	COMMENT
$<5.9 \times 10^{-8}$	90	NISHIO	08	BELL	543 fb^{-1} E^{ee}_{cm} = 10.6 GeV
• • • We do not use the following data for averages, fits, limits, etc. • • •					
$<7.2 \times 10^{-8}$	90	MIYAZAKI	11	BELL	854 fb^{-1} E^{ee}_{cm} = 10.6 GeV
$<1.7 \times 10^{-7}$	90	AUBERT	09W	BABR	451 fb^{-1} E^{ee}_{cm} = 10.6 GeV
$<3.9 \times 10^{-7}$	90	YUSA	06	BELL	158 fb^{-1} E^{ee}_{cm} = 10.6 GeV
$<7.5 \times 10^{-6}$	90	BLISS	98	CLEO	E^{ee}_{cm}= 10.6 GeV
$<9.4 \times 10^{-6}$	90	[1] BARTELT	94	CLEO	Repl. by BLISS 98
$<4.5 \times 10^{-5}$	90	ALBRECHT	92K	ARG	E^{ee}_{cm}= 10 GeV

[1] BARTELT 94 assume phase space decays.

$\Gamma(e^- \overline{K}^*(892)^0)/\Gamma_{total}$ — Γ_{202}/Γ

Test of lepton family number conservation.

VALUE	CL%	DOCUMENT ID		TECN	COMMENT
$<3.4 \times 10^{-8}$	90	MIYAZAKI	11	BELL	854 fb^{-1} E^{ee}_{cm} = 10.6 GeV
• • • We do not use the following data for averages, fits, limits, etc. • • •					
$<4.6 \times 10^{-8}$	90	AUBERT	09W	BABR	451 fb^{-1} E^{ee}_{cm} = 10.6 GeV
$<7.7 \times 10^{-8}$	90	NISHIO	08	BELL	543 fb^{-1} E^{ee}_{cm} = 10.6 GeV
$<4.0 \times 10^{-7}$	90	YUSA	06	BELL	158 fb^{-1} E^{ee}_{cm} = 10.6 GeV
$<7.4 \times 10^{-6}$	90	BLISS	98	CLEO	E^{ee}_{cm}= 10.6 GeV
$<1.1 \times 10^{-5}$	90	[1] BARTELT	94	CLEO	Repl. by BLISS 98

[1] BARTELT 94 assume phase space decays.

$\Gamma(\mu^- \overline{K}^*(892)^0)/\Gamma_{total}$ — Γ_{203}/Γ

Test of lepton family number conservation.

VALUE	CL%	DOCUMENT ID		TECN	COMMENT
$<7.0 \times 10^{-8}$	90	MIYAZAKI	11	BELL	854 fb^{-1} E^{ee}_{cm} = 10.6 GeV
• • • We do not use the following data for averages, fits, limits, etc. • • •					
$<7.3 \times 10^{-8}$	90	AUBERT	09W	BABR	451 fb^{-1} E^{ee}_{cm} = 10.6 GeV
$<1.0 \times 10^{-7}$	90	NISHIO	08	BELL	543 fb^{-1} E^{ee}_{cm} = 10.6 GeV
$<4.0 \times 10^{-7}$	90	YUSA	06	BELL	158 fb^{-1} E^{ee}_{cm} = 10.6 GeV
$<7.5 \times 10^{-6}$	90	BLISS	98	CLEO	E^{ee}_{cm}= 10.6 GeV
$<8.7 \times 10^{-6}$	90	[1] BARTELT	94	CLEO	Repl. by BLISS 98

[1] BARTELT 94 assume phase space decays.

$\Gamma(e^- \eta'(958))/\Gamma_{total}$ — Γ_{204}/Γ

VALUE	CL%	DOCUMENT ID		TECN	COMMENT
$< 1.6 \times 10^{-7}$	90	MIYAZAKI	07	BELL	401 fb^{-1}, E^{ee}_{cm}=10.6 GeV
• • • We do not use the following data for averages, fits, limits, etc. • • •					
$< 2.4 \times 10^{-7}$	90	AUBERT	07I	BABR	339 fb^{-1}, E^{ee}_{cm}=10.6 GeV
$<10. \times 10^{-7}$	90	ENARI	05	BELL	154 fb^{-1}, E^{ee}_{cm}= 10.6 GeV

$\Gamma(\mu^- \eta'(958))/\Gamma_{total}$ — Γ_{205}/Γ

VALUE	CL%	DOCUMENT ID		TECN	COMMENT
$<1.3 \times 10^{-7}$	90	MIYAZAKI	07	BELL	401 fb^{-1}, E^{ee}_{cm}=10.6 GeV
• • • We do not use the following data for averages, fits, limits, etc. • • •					
$<1.4 \times 10^{-7}$	90	AUBERT	07I	BABR	339 fb^{-1}, E^{ee}_{cm}=10.6 GeV
$<4.7 \times 10^{-7}$	90	ENARI	05	BELL	154 fb^{-1}, E^{ee}_{cm}= 10.6 GeV

Downloaded from https://academic.oup.com/ptep/article/2022/8/033C01/6651666 by KIT Library user on 27 September 2022

$\Gamma(e^- f_0(980) \to e^- \pi^+ \pi^-)/\Gamma_{total}$ — Γ_{206}/Γ

VALUE	CL%	DOCUMENT ID		TECN	COMMENT
$<3.2 \times 10^{-8}$	90	MIYAZAKI	09	BELL	671 fb^{-1} E^{ee}_{cm} = 10.6 GeV

$\Gamma(\mu^- f_0(980) \to \mu^- \pi^+ \pi^-)/\Gamma_{total}$ — Γ_{207}/Γ

VALUE	CL%	DOCUMENT ID		TECN	COMMENT
$<3.4 \times 10^{-8}$	90	MIYAZAKI	09	BELL	671 fb^{-1} E^{ee}_{cm} = 10.6 GeV

$\Gamma(e^- \phi)/\Gamma_{total}$ — Γ_{208}/Γ

Test of lepton family number conservation.

VALUE	CL%	DOCUMENT ID		TECN	COMMENT
$<3.1 \times 10^{-8}$	90	MIYAZAKI	11	BELL	854 fb^{-1} E^{ee}_{cm} = 10.6 GeV
$<3.1 \times 10^{-8}$	90	AUBERT	09W	BABR	451 fb^{-1} E^{ee}_{cm} = 10.6 GeV
• • • We do not use the following data for averages, fits, limits, etc. • • •					
$<7.3 \times 10^{-8}$	90	NISHIO	08	BELL	543 fb^{-1} E^{ee}_{cm} = 10.6 GeV
$<7.3 \times 10^{-7}$	90	YUSA	06	BELL	158 fb^{-1} E^{ee}_{cm} = 10.6 GeV
$<6.9 \times 10^{-6}$	90	BLISS	98	CLEO	E^{ee}_{cm} = 10.6 GeV

$\Gamma(\mu^- \phi)/\Gamma_{total}$ — Γ_{209}/Γ

Test of lepton family number conservation.

VALUE	CL%	DOCUMENT ID		TECN	COMMENT
$<8.4 \times 10^{-8}$	90	MIYAZAKI	11	BELL	854 fb^{-1} E^{ee}_{cm} = 10.6 GeV
• • • We do not use the following data for averages, fits, limits, etc. • • •					
$<1.9 \times 10^{-7}$	90	AUBERT	09W	BABR	451 fb^{-1} E^{ee}_{cm} = 10.6 GeV
$<1.3 \times 10^{-7}$	90	NISHIO	08	BELL	543 fb^{-1} E^{ee}_{cm} = 10.6 GeV
$<7.7 \times 10^{-7}$	90	YUSA	06	BELL	158 fb^{-1} E^{ee}_{cm} = 10.6 GeV
$<7.0 \times 10^{-6}$	90	BLISS	98	CLEO	E^{ee}_{cm} = 10.6 GeV

$\Gamma(e^- e^+ e^-)/\Gamma_{total}$ — Γ_{210}/Γ

Test of lepton family number conservation.

VALUE	CL%	DOCUMENT ID		TECN	COMMENT
$< 2.7 \times 10^{-8}$	90	HAYASAKA	10	BELL	782 fb^{-1} E^{ee}_{cm} = 10.6 GeV
• • • We do not use the following data for averages, fits, limits, etc. • • •					
$< 2.9 \times 10^{-8}$	90	LEES	10A	BABR	468 fb^{-1} E^{ee}_{cm} = 10.6 GeV
$< 3.6 \times 10^{-8}$	90	MIYAZAKI	08	BELL	535 fb^{-1} E^{ee}_{cm} = 10.6 GeV
$< 4.3 \times 10^{-8}$	90	AUBERT	07BK	BABR	376 fb^{-1} E^{ee}_{cm} = 10.6 GeV
$< 2.0 \times 10^{-7}$	90	AUBERT	04J	BABR	91.5 fb^{-1} E^{ee}_{cm} = 10.6 GeV
$< 3.5 \times 10^{-7}$	90	YUSA	04	BELL	87.1 fb^{-1} E^{ee}_{cm} = 10.6 GeV
$< 2.9 \times 10^{-6}$	90	BLISS	98	CLEO	E^{ee}_{cm} = 10.6 GeV
$< 0.33 \times 10^{-5}$	90	[1] BARTELT	94	CLEO	Repl. by BLISS 98
$< 1.3 \times 10^{-5}$	90	ALBRECHT	92K	ARG	E^{ee}_{cm} = 10 GeV
$< 2.7 \times 10^{-5}$	90	BOWCOCK	90	CLEO	E^{ee}_{cm} = 10.4–10.9
$<40 \times 10^{-5}$	90	HAYES	82	MRK2	E^{ee}_{cm} = 3.8–6.8 GeV

[1] BARTELT 94 assume phase space decays.

$\Gamma(e^- \mu^+ \mu^-)/\Gamma_{total}$ — Γ_{211}/Γ

Test of lepton family number conservation.

VALUE	CL%	DOCUMENT ID		TECN	COMMENT
$< 2.7 \times 10^{-8}$	90	HAYASAKA	10	BELL	782 fb^{-1} E^{ee}_{cm} = 10.6 GeV
• • • We do not use the following data for averages, fits, limits, etc. • • •					
$< 3.2 \times 10^{-8}$	90	LEES	10A	BABR	468 fb^{-1} E^{ee}_{cm} = 10.6 GeV
$< 4.1 \times 10^{-8}$	90	MIYAZAKI	08	BELL	535 fb^{-1} E^{ee}_{cm} = 10.6 GeV
$< 3.7 \times 10^{-8}$	90	AUBERT	07BK	BABR	376 fb^{-1} E^{ee}_{cm} = 10.6 GeV
$< 3.3 \times 10^{-7}$	90	AUBERT	04J	BABR	91.5 fb^{-1} E^{ee}_{cm} = 10.6 GeV
$< 2.0 \times 10^{-7}$	90	YUSA	04	BELL	87.1 fb^{-1} E^{ee}_{cm} = 10.6 GeV
$< 1.8 \times 10^{-6}$	90	BLISS	98	CLEO	E^{ee}_{cm} = 10.6 GeV
$< 0.36 \times 10^{-5}$	90	[1] BARTELT	94	CLEO	Repl. by BLISS 98
$< 1.9 \times 10^{-5}$	90	ALBRECHT	92K	ARG	E^{ee}_{cm} = 10 GeV
$< 2.7 \times 10^{-5}$	90	BOWCOCK	90	CLEO	E^{ee}_{cm} = 10.4–10.9
$<33 \times 10^{-5}$	90	HAYES	82	MRK2	E^{ee}_{cm} = 3.8–6.8 GeV

[1] BARTELT 94 assume phase space decays.

$\Gamma(e^+ \mu^- \mu^-)/\Gamma_{total}$ — Γ_{212}/Γ

Test of lepton family number conservation.

VALUE	CL%	DOCUMENT ID		TECN	COMMENT
$<1.7 \times 10^{-8}$	90	HAYASAKA	10	BELL	782 fb^{-1} E^{ee}_{cm} = 10.6 GeV
• • • We do not use the following data for averages, fits, limits, etc. • • •					
$<2.6 \times 10^{-8}$	90	LEES	10A	BABR	468 fb^{-1} E^{ee}_{cm} = 10.6 GeV
$<2.3 \times 10^{-8}$	90	MIYAZAKI	08	BELL	535 fb^{-1} E^{ee}_{cm} = 10.6 GeV
$<5.6 \times 10^{-8}$	90	AUBERT	07BK	BABR	376 fb^{-1} E^{ee}_{cm} = 10.6 GeV
$<1.3 \times 10^{-7}$	90	AUBERT	04J	BABR	91.5 fb^{-1} E^{ee}_{cm} = 10.6 GeV
$<2.0 \times 10^{-7}$	90	YUSA	04	BELL	87.1 fb^{-1} E^{ee}_{cm} = 10.6 GeV
$<1.5 \times 10^{-6}$	90	BLISS	98	CLEO	E^{ee}_{cm} = 10.6 GeV
$<0.35 \times 10^{-5}$	90	[1] BARTELT	94	CLEO	Repl. by BLISS 98
$<1.8 \times 10^{-5}$	90	ALBRECHT	92K	ARG	E^{ee}_{cm} = 10 GeV
$<1.6 \times 10^{-5}$	90	BOWCOCK	90	CLEO	E^{ee}_{cm} = 10.4–10.9

[1] BARTELT 94 assume phase space decays.

$\Gamma(\mu^- e^+ e^-)/\Gamma_{total}$ — Γ_{213}/Γ

Test of lepton family number conservation.

VALUE	CL%	DOCUMENT ID		TECN	COMMENT
$< 1.8 \times 10^{-8}$	90	HAYASAKA	10	BELL	782 fb^{-1} E^{ee}_{cm} = 10.6 GeV
• • • We do not use the following data for averages, fits, limits, etc. • • •					
$< 2.2 \times 10^{-8}$	90	LEES	10A	BABR	468 fb^{-1} E^{ee}_{cm} = 10.6 GeV
$< 2.7 \times 10^{-8}$	90	MIYAZAKI	08	BELL	535 fb^{-1} E^{ee}_{cm} = 10.6 GeV
$< 8.0 \times 10^{-8}$	90	AUBERT	07BK	BABR	376 fb^{-1} E^{ee}_{cm} = 10.6 GeV
$< 2.7 \times 10^{-7}$	90	AUBERT	04J	BABR	91.5 fb^{-1} E^{ee}_{cm} = 10.6 GeV
$< 1.9 \times 10^{-7}$	90	YUSA	04	BELL	87.1 fb^{-1} E^{ee}_{cm} = 10.6 GeV
$< 1.7 \times 10^{-6}$	90	BLISS	98	CLEO	E^{ee}_{cm} = 10.6 GeV
$< 0.34 \times 10^{-5}$	90	[1] BARTELT	94	CLEO	Repl. by BLISS 98
$< 1.4 \times 10^{-5}$	90	ALBRECHT	92K	ARG	E^{ee}_{cm} = 10 GeV
$< 2.7 \times 10^{-5}$	90	BOWCOCK	90	CLEO	E^{ee}_{cm} = 10.4–10.9
$<44 \times 10^{-5}$	90	HAYES	82	MRK2	E^{ee}_{cm} = 3.8–6.8 GeV

[1] BARTELT 94 assume phase space decays.

$\Gamma(\mu^+ e^- e^-)/\Gamma_{total}$ — Γ_{214}/Γ

Test of lepton family number conservation.

VALUE	CL%	DOCUMENT ID		TECN	COMMENT
$<1.5 \times 10^{-8}$	90	HAYASAKA	10	BELL	782 fb^{-1} E^{ee}_{cm} = 10.6 GeV
• • • We do not use the following data for averages, fits, limits, etc. • • •					
$<1.8 \times 10^{-8}$	90	LEES	10A	BABR	468 fb^{-1} E^{ee}_{cm} = 10.6 GeV
$<2.0 \times 10^{-8}$	90	MIYAZAKI	08	BELL	535 fb^{-1} E^{ee}_{cm} = 10.6 GeV
$<5.8 \times 10^{-8}$	90	AUBERT	07BK	BABR	376 fb^{-1} E^{ee}_{cm} = 10.6 GeV
$<1.1 \times 10^{-7}$	90	AUBERT	04J	BABR	91.5 fb^{-1} E^{ee}_{cm} = 10.6 GeV
$<2.0 \times 10^{-7}$	90	YUSA	04	BELL	87.1 fb^{-1} E^{ee}_{cm} = 10.6 GeV
$<1.5 \times 10^{-6}$	90	BLISS	98	CLEO	E^{ee}_{cm} = 10.6 GeV
$<0.34 \times 10^{-5}$	90	[1] BARTELT	94	CLEO	Repl. by BLISS 98
$<1.4 \times 10^{-5}$	90	ALBRECHT	92K	ARG	E^{ee}_{cm} = 10 GeV
$<1.6 \times 10^{-5}$	90	BOWCOCK	90	CLEO	E^{ee}_{cm} = 10.4–10.9

[1] BARTELT 94 assume phase space decays.

$\Gamma(\mu^- \mu^+ \mu^-)/\Gamma_{total}$ — Γ_{215}/Γ

Test of lepton family number conservation.

VALUE	CL%	DOCUMENT ID		TECN	COMMENT
$< 2.1 \times 10^{-8}$	90	HAYASAKA	10	BELL	782 fb^{-1} E^{ee}_{cm} = 10.6 GeV
• • • We do not use the following data for averages, fits, limits, etc. • • •					
$< 8.0 \times 10^{-8}$	90	SIRUNYAN	21D	CMS	33.2 fb^{-1}, pp at 13 TeV
$< 3.8 \times 10^{-7}$	90	AAD	16BA	ATLS	20.3 fb^{-1}, pp at 8 TeV
$< 4.6 \times 10^{-8}$	90	AAIJ	15AI	LHCB	3.0 fb^{-1}, pp at 7, 8 TeV
$< 8.0 \times 10^{-8}$	90	[1] AAIJ	13AH	LHCB	1.0 fb^{-1}, pp at 7 TeV
$< 3.3 \times 10^{-8}$	90	LEES	10A	BABR	468 fb^{-1} E^{ee}_{cm} = 10.6 GeV
$< 3.2 \times 10^{-8}$	90	MIYAZAKI	08	BELL	535 fb^{-1} E^{ee}_{cm} = 10.6 GeV
$< 5.3 \times 10^{-8}$	90	AUBERT	07BK	BABR	376 fb^{-1} E^{ee}_{cm} = 10.6 GeV
$< 1.9 \times 10^{-7}$	90	AUBERT	04J	BABR	91.5 fb^{-1} E^{ee}_{cm} = 10.6 GeV
$< 2.0 \times 10^{-7}$	90	YUSA	04	BELL	87.1 fb^{-1} E^{ee}_{cm} = 10.6 GeV
$< 1.9 \times 10^{-6}$	90	BLISS	98	CLEO	E^{ee}_{cm} = 10.6 GeV
$< 0.43 \times 10^{-5}$	90	[2] BARTELT	94	CLEO	Repl. by BLISS 98
$< 1.9 \times 10^{-5}$	90	ALBRECHT	92K	ARG	E^{ee}_{cm} = 10 GeV
$< 1.7 \times 10^{-5}$	90	BOWCOCK	90	CLEO	E^{ee}_{cm} = 10.4–10.9
$<49 \times 10^{-5}$	90	HAYES	82	MRK2	E^{ee}_{cm} = 3.8–6.8 GeV

[1] Repl. by AAIJ 15AI.
[2] BARTELT 94 assume phase space decays.

$\Gamma(e^- \pi^+ \pi^-)/\Gamma_{total}$ — Γ_{216}/Γ

Test of lepton family number conservation.

VALUE	CL%	DOCUMENT ID		TECN	COMMENT
$<2.3 \times 10^{-8}$	90	MIYAZAKI	13	BELL	854 fb^{-1} E^{ee}_{cm} = 10.6 GeV
• • • We do not use the following data for averages, fits, limits, etc. • • •					
$<4.4 \times 10^{-8}$	90	MIYAZAKI	10	BELL	Repl. by MIYAZAKI 13
$<7.3 \times 10^{-7}$	90	YUSA	06	BELL	158 fb^{-1} E^{ee}_{cm} = 10.6 GeV
$<1.2 \times 10^{-7}$	90	AUBERT,BE	05D	BABR	221 fb^{-1}, E^{ee}_{cm} = 10.6 GeV
$<2.2 \times 10^{-6}$	90	BLISS	98	CLEO	E^{ee}_{cm} = 10.6 GeV
$<4.4 \times 10^{-6}$	90	[1] BARTELT	94	CLEO	Repl. by BLISS 98
$<2.7 \times 10^{-5}$	90	ALBRECHT	92K	ARG	E^{ee}_{cm} = 10 GeV
$<6.0 \times 10^{-5}$	90	BOWCOCK	90	CLEO	E^{ee}_{cm} = 10.4–10.9

[1] BARTELT 94 assume phase space decays.

$\Gamma(e^+ \pi^- \pi^-)/\Gamma_{total}$ — Γ_{217}/Γ

Test of lepton number conservation.

VALUE	CL%	DOCUMENT ID		TECN	COMMENT
$<2.0 \times 10^{-8}$	90	MIYAZAKI	13	BELL	854 fb^{-1} E^{ee}_{cm} = 10.6 GeV
• • • We do not use the following data for averages, fits, limits, etc. • • •					
$<8.8 \times 10^{-8}$	90	MIYAZAKI	10	BELL	Repl. by MIYAZAKI 13
$<2.0 \times 10^{-7}$	90	YUSA	06	BELL	158 fb^{-1} E^{ee}_{cm} = 10.6 GeV
$<2.7 \times 10^{-7}$	90	AUBERT,BE	05D	BABR	221 fb^{-1}, E^{ee}_{cm} = 10.6 GeV

Downloaded from https://academic.oup.com/ptep/article/2022/8/083C01/6651666 by KIT Library user on 27 September 2022

$<1.9\times10^{-6}$	90	BLISS	98	CLEO	$E^{ee}_{cm}=10.6$ GeV
$<4.4\times10^{-6}$	90	[1] BARTELT	94	CLEO	Repl. by BLISS 98
$<1.8\times10^{-5}$	90	ALBRECHT	92K	ARG	$E^{ee}_{cm}=10$ GeV
$<1.7\times10^{-5}$	90	BOWCOCK	90	CLEO	$E^{ee}_{cm}=10.4$–10.9

[1] BARTELT 94 assume phase space decays.

$\Gamma(\mu^-\pi^+\pi^-)/\Gamma_{total}$ — Γ_{218}/Γ

Test of lepton family number conservation.

VALUE	CL%	DOCUMENT ID		TECN	COMMENT
$<2.1\times10^{-8}$	90	MIYAZAKI	13	BELL	854 fb^{-1} $E^{ee}_{cm}=10.6$ GeV
• • • We do not use the following data for averages, fits, limits, etc. • • •					
$<3.3\times10^{-8}$	90	MIYAZAKI	10	BELL	Repl. by MIYAZAKI 13
$<4.8\times10^{-7}$	90	YUSA	06	BELL	158 fb^{-1} $E^{ee}_{cm}=10.6$ GeV
$<2.9\times10^{-7}$	90	AUBERT,BE	05D	BABR	221 fb^{-1}, $E^{ee}_{cm}=10.6$ GeV
$<8.2\times10^{-6}$	90	BLISS	98	CLEO	$E^{ee}_{cm}=10.6$ GeV
$<7.4\times10^{-6}$	90	[1] BARTELT	94	CLEO	Repl. by BLISS 98
$<3.6\times10^{-5}$	90	ALBRECHT	92K	ARG	$E^{ee}_{cm}=10$ GeV
$<3.9\times10^{-5}$	90	BOWCOCK	90	CLEO	$E^{ee}_{cm}=10.4$–10.9

[1] BARTELT 94 assume phase space decays.

$\Gamma(\mu^+\pi^-\pi^-)/\Gamma_{total}$ — Γ_{219}/Γ

Test of lepton number conservation.

VALUE	CL%	DOCUMENT ID		TECN	COMMENT
$<3.9\times10^{-8}$	90	MIYAZAKI	13	BELL	854 fb^{-1} $E^{ee}_{cm}=10.6$ GeV
• • • We do not use the following data for averages, fits, limits, etc. • • •					
$<3.7\times10^{-8}$	90	MIYAZAKI	10	BELL	Repl. by MIYAZAKI 13
$<3.4\times10^{-7}$	90	YUSA	06	BELL	158 fb^{-1} $E^{ee}_{cm}=10.6$ GeV
$<7\times10^{-8}$	90	AUBERT,BE	05D	BABR	221 fb^{-1}, $E^{ee}_{cm}=10.6$ GeV
$<3.4\times10^{-6}$	90	BLISS	98	CLEO	$E^{ee}_{cm}=10.6$ GeV
$<6.9\times10^{-6}$	90	[1] BARTELT	94	CLEO	Repl. by BLISS 98
$<6.3\times10^{-5}$	90	ALBRECHT	92K	ARG	$E^{ee}_{cm}=10$ GeV
$<3.9\times10^{-5}$	90	BOWCOCK	90	CLEO	$E^{ee}_{cm}=10.4$–10.9

[1] BARTELT 94 assume phase space decays.

$\Gamma(e^-\pi^+K^-)/\Gamma_{total}$ — Γ_{220}/Γ

Test of lepton family number conservation.

VALUE	CL%	DOCUMENT ID		TECN	COMMENT
$<3.7\times10^{-8}$	90	MIYAZAKI	13	BELL	854 fb^{-1} $E^{ee}_{cm}=10.6$ GeV
• • • We do not use the following data for averages, fits, limits, etc. • • •					
$<5.8\times10^{-8}$	90	MIYAZAKI	10	BELL	Repl. by MIYAZAKI 13
$<7.2\times10^{-7}$	90	YUSA	06	BELL	158 fb^{-1} $E^{ee}_{cm}=10.6$ GeV
$<3.2\times10^{-7}$	90	AUBERT,BE	05D	BABR	221 fb^{-1}, $E^{ee}_{cm}=10.6$ GeV
$<6.4\times10^{-6}$	90	BLISS	98	CLEO	$E^{ee}_{cm}=10.6$ GeV
$<7.7\times10^{-6}$	90	[1] BARTELT	94	CLEO	Repl. by BLISS 98
$<2.9\times10^{-5}$	90	ALBRECHT	92K	ARG	$E^{ee}_{cm}=10$ GeV
$<5.8\times10^{-5}$	90	BOWCOCK	90	CLEO	$E^{ee}_{cm}=10.4$–10.9

[1] BARTELT 94 assume phase space decays.

$\Gamma(e^-\pi^-K^+)/\Gamma_{total}$ — Γ_{221}/Γ

Test of lepton family number conservation.

VALUE	CL%	DOCUMENT ID		TECN	COMMENT
$<3.1\times10^{-8}$	90	MIYAZAKI	13	BELL	854 fb^{-1} $E^{ee}_{cm}=10.6$ GeV
• • • We do not use the following data for averages, fits, limits, etc. • • •					
$<5.2\times10^{-8}$	90	MIYAZAKI	10	BELL	Repl. by MIYAZAKI 13
$<1.6\times10^{-7}$	90	YUSA	06	BELL	158 fb^{-1} $E^{ee}_{cm}=10.6$ GeV
$<1.7\times10^{-7}$	90	AUBERT,BE	05D	BABR	221 fb^{-1}, $E^{ee}_{cm}=10.6$ GeV
$<3.8\times10^{-6}$	90	BLISS	98	CLEO	$E^{ee}_{cm}=10.6$ GeV
$<4.6\times10^{-6}$	90	[1] BARTELT	94	CLEO	Repl. by BLISS 98
$<5.8\times10^{-5}$	90	BOWCOCK	90	CLEO	$E^{ee}_{cm}=10.4$–10.9

[1] BARTELT 94 assume phase space decays.

$\Gamma(e^+\pi^-K^-)/\Gamma_{total}$ — Γ_{222}/Γ

Test of lepton number conservation.

VALUE	CL%	DOCUMENT ID		TECN	COMMENT
$<3.2\times10^{-8}$	90	MIYAZAKI	13	BELL	854 fb^{-1} $E^{ee}_{cm}=10.6$ GeV
• • • We do not use the following data for averages, fits, limits, etc. • • •					
$<6.7\times10^{-8}$	90	MIYAZAKI	10	BELL	Repl. by MIYAZAKI 13
$<1.9\times10^{-7}$	90	YUSA	06	BELL	158 fb^{-1} $E^{ee}_{cm}=10.6$ GeV
$<1.8\times10^{-7}$	90	AUBERT,BE	05D	BABR	221 fb^{-1}, $E^{ee}_{cm}=10.6$ GeV
$<2.1\times10^{-6}$	90	BLISS	98	CLEO	$E^{ee}_{cm}=10.6$ GeV
$<4.5\times10^{-6}$	90	[1] BARTELT	94	CLEO	Repl. by BLISS 98
$<2.0\times10^{-5}$	90	ALBRECHT	92K	ARG	$E^{ee}_{cm}=10$ GeV
$<4.9\times10^{-5}$	90	BOWCOCK	90	CLEO	$E^{ee}_{cm}=10.4$–10.9

[1] BARTELT 94 assume phase space decays.

$\Gamma(e^-K^0_SK^0_S)/\Gamma_{total}$ — Γ_{223}/Γ

Test of lepton family number conservation.

VALUE	CL%	DOCUMENT ID		TECN	COMMENT
$<7.1\times10^{-8}$	90	MIYAZAKI	10A	BELL	671 fb^{-1} $E^{ee}_{cm}=10.6$ GeV
• • • We do not use the following data for averages, fits, limits, etc. • • •					
$<2.2\times10^{-6}$	90	CHEN	02C	CLEO	$E^{ee}_{cm}=10.6$ GeV

$\Gamma(e^-K^+K^-)/\Gamma_{total}$ — Γ_{224}/Γ

Test of lepton family number conservation.

VALUE	CL%	DOCUMENT ID		TECN	COMMENT
$<3.4\times10^{-8}$	90	MIYAZAKI	13	BELL	854 fb^{-1} $E^{ee}_{cm}=10.6$ GeV
• • • We do not use the following data for averages, fits, limits, etc. • • •					
$<5.4\times10^{-8}$	90	MIYAZAKI	10	BELL	Repl. by MIYAZAKI 13
$<3.0\times10^{-7}$	90	YUSA	06	BELL	158 fb^{-1} $E^{ee}_{cm}=10.6$ GeV
$<1.4\times10^{-7}$	90	AUBERT,BE	05D	BABR	221 fb^{-1}, $E^{ee}_{cm}=10.6$ GeV
$<6.0\times10^{-6}$	90	BLISS	98	CLEO	$E^{ee}_{cm}=10.6$ GeV

$\Gamma(e^+K^-K^-)/\Gamma_{total}$ — Γ_{225}/Γ

Test of lepton number conservation.

VALUE	CL%	DOCUMENT ID		TECN	COMMENT
$<3.3\times10^{-8}$	90	MIYAZAKI	13	BELL	854 fb^{-1} $E^{ee}_{cm}=10.6$ GeV
• • • We do not use the following data for averages, fits, limits, etc. • • •					
$<6.0\times10^{-8}$	90	MIYAZAKI	10	BELL	Repl. by MIYAZAKI 13
$<3.1\times10^{-7}$	90	YUSA	06	BELL	158 fb^{-1} $E^{ee}_{cm}=10.6$ GeV
$<1.5\times10^{-7}$	90	AUBERT,BE	05D	BABR	221 fb^{-1}, $E^{ee}_{cm}=10.6$ GeV
$<3.8\times10^{-6}$	90	BLISS	98	CLEO	$E^{ee}_{cm}=10.6$ GeV

$\Gamma(\mu^-\pi^+K^-)/\Gamma_{total}$ — Γ_{226}/Γ

Test of lepton family number conservation.

VALUE	CL%	DOCUMENT ID		TECN	COMMENT
$<8.6\times10^{-8}$	90	MIYAZAKI	13	BELL	854 fb^{-1} $E^{ee}_{cm}=10.6$ GeV
• • • We do not use the following data for averages, fits, limits, etc. • • •					
$<1.6\times10^{-7}$	90	MIYAZAKI	10	BELL	Repl. by MIYAZAKI 13
$<2.7\times10^{-7}$	90	YUSA	06	BELL	158 fb^{-1} $E^{ee}_{cm}=10.6$ GeV
$<2.6\times10^{-7}$	90	AUBERT,BE	05D	BABR	221 fb^{-1}, $E^{ee}_{cm}=10.6$ GeV
$<7.5\times10^{-6}$	90	BLISS	98	CLEO	$E^{ee}_{cm}=10.6$ GeV
$<8.7\times10^{-6}$	90	[1] BARTELT	94	CLEO	Repl. by BLISS 98
$<11\times10^{-5}$	90	ALBRECHT	92K	ARG	$E^{ee}_{cm}=10$ GeV
$<7.7\times10^{-5}$	90	BOWCOCK	90	CLEO	$E^{ee}_{cm}=10.4$–10.9

[1] BARTELT 94 assume phase space decays.

$\Gamma(\mu^-\pi^-K^+)/\Gamma_{total}$ — Γ_{227}/Γ

Test of lepton family number conservation.

VALUE	CL%	DOCUMENT ID		TECN	COMMENT
$<4.5\times10^{-8}$	90	MIYAZAKI	13	BELL	854 fb^{-1} $E^{ee}_{cm}=10.6$ GeV
• • • We do not use the following data for averages, fits, limits, etc. • • •					
$<1.0\times10^{-7}$	90	MIYAZAKI	10	BELL	Repl. by MIYAZAKI 13
$<7.3\times10^{-7}$	90	YUSA	06	BELL	158 fb^{-1} $E^{ee}_{cm}=10.6$ GeV
$<3.2\times10^{-7}$	90	AUBERT,BE	05D	BABR	221 fb^{-1}, $E^{ee}_{cm}=10.6$ GeV
$<7.4\times10^{-6}$	90	BLISS	98	CLEO	$E^{ee}_{cm}=10.6$ GeV
$<1.5\times10^{-5}$	90	[1] BARTELT	94	CLEO	Repl. by BLISS 98
$<7.7\times10^{-5}$	90	BOWCOCK	90	CLEO	$E^{ee}_{cm}=10.4$–10.9

[1] BARTELT 94 assume phase space decays.

$\Gamma(\mu^+\pi^-K^-)/\Gamma_{total}$ — Γ_{228}/Γ

Test of lepton number conservation.

VALUE	CL%	DOCUMENT ID		TECN	COMMENT
$<4.8\times10^{-8}$	90	MIYAZAKI	13	BELL	854 fb^{-1} $E^{ee}_{cm}=10.6$ GeV
• • • We do not use the following data for averages, fits, limits, etc. • • •					
$<9.4\times10^{-8}$	90	MIYAZAKI	10	BELL	Repl. by MIYAZAKI 13
$<2.9\times10^{-7}$	90	YUSA	06	BELL	158 fb^{-1} $E^{ee}_{cm}=10.6$ GeV
$<2.2\times10^{-7}$	90	AUBERT,BE	05D	BABR	221 fb^{-1}, $E^{ee}_{cm}=10.6$ GeV
$<7.0\times10^{-6}$	90	BLISS	98	CLEO	$E^{ee}_{cm}=10.6$ GeV
$<2.0\times10^{-5}$	90	[1] BARTELT	94	CLEO	Repl. by BLISS 98
$<5.8\times10^{-5}$	90	ALBRECHT	92K	ARG	$E^{ee}_{cm}=10$ GeV
$<4.0\times10^{-5}$	90	BOWCOCK	90	CLEO	$E^{ee}_{cm}=10.4$–10.9

[1] BARTELT 94 assume phase space decays.

$\Gamma(\mu^-K^0_SK^0_S)/\Gamma_{total}$ — Γ_{229}/Γ

VALUE	CL%	DOCUMENT ID		TECN	COMMENT
$<8.0\times10^{-8}$	90	MIYAZAKI	10A	BELL	671 fb^{-1} $E^{ee}_{cm}=10.6$ GeV
• • • We do not use the following data for averages, fits, limits, etc. • • •					
$<3.4\times10^{-6}$	90	CHEN	02C	CLEO	$E^{ee}_{cm}=10.6$ GeV

Downloaded from https://academic.oup.com/ptep/article/2022/8/083C01/6651666 by KIT Library user on 27 September 2022

$\Gamma(\mu^- K^+ K^-)/\Gamma_{total}$ — Γ_{230}/Γ

Test of lepton family number conservation.

VALUE	CL%	DOCUMENT ID		TECN	COMMENT
$< 4.4 \times 10^{-8}$	90	MIYAZAKI	13	BELL	854 fb^{-1} $E^{ee}_{cm} = 10.6$ GeV
• • • We do not use the following data for averages, fits, limits, etc. • • •					
$< 6.8 \times 10^{-8}$	90	MIYAZAKI	10	BELL	Repl. by MIYAZAKI 13
$< 8.0 \times 10^{-7}$	90	YUSA	06	BELL	158 fb^{-1} $E^{ee}_{cm} = 10.6$ GeV
$< 2.5 \times 10^{-7}$	90	AUBERT,BE	05D	BABR	221 fb^{-1}, $E^{ee}_{cm} = 10.6$ GeV
$<15 \times 10^{-6}$	90	BLISS	98	CLEO	$E^{ee}_{cm} = 10.6$ GeV

$\Gamma(\mu^+ K^- K^-)/\Gamma_{total}$ — Γ_{231}/Γ

Test of lepton number conservation.

VALUE	CL%	DOCUMENT ID		TECN	COMMENT
$<4.7 \times 10^{-8}$	90	MIYAZAKI	13	BELL	854 fb^{-1} $E^{ee}_{cm} = 10.6$ GeV
• • • We do not use the following data for averages, fits, limits, etc. • • •					
$<9.6 \times 10^{-8}$	90	MIYAZAKI	10	BELL	Repl. by MIYAZAKI 13
$<4.4 \times 10^{-7}$	90	YUSA	06	BELL	158 fb^{-1} $E^{ee}_{cm} = 10.6$ GeV
$<4.8 \times 10^{-7}$	90	AUBERT,BE	05D	BABR	221 fb^{-1}, $E^{ee}_{cm} = 10.6$ GeV
$<6.0 \times 10^{-6}$	90	BLISS	98	CLEO	$E^{ee}_{cm} = 10.6$ GeV

$\Gamma(e^- \pi^0 \pi^0)/\Gamma_{total}$ — Γ_{232}/Γ

Test of lepton family number conservation.

VALUE	CL%	DOCUMENT ID		TECN	COMMENT
$<6.5 \times 10^{-6}$	90	BONVICINI	97	CLEO	$E^{ee}_{cm} = 10.6$ GeV

$\Gamma(\mu^- \pi^0 \pi^0)/\Gamma_{total}$ — Γ_{233}/Γ

Test of lepton family number conservation.

VALUE	CL%	DOCUMENT ID		TECN	COMMENT
$<14 \times 10^{-6}$	90	BONVICINI	97	CLEO	$E^{ee}_{cm} = 10.6$ GeV

$\Gamma(e^- \eta\eta)/\Gamma_{total}$ — Γ_{234}/Γ

Test of lepton family number conservation.

VALUE	CL%	DOCUMENT ID		TECN	COMMENT
$<35 \times 10^{-6}$	90	BONVICINI	97	CLEO	$E^{ee}_{cm} = 10.6$ GeV

$\Gamma(\mu^- \eta\eta)/\Gamma_{total}$ — Γ_{235}/Γ

Test of lepton family number conservation.

VALUE	CL%	DOCUMENT ID		TECN	COMMENT
$<60 \times 10^{-6}$	90	BONVICINI	97	CLEO	$E^{ee}_{cm} = 10.6$ GeV

$\Gamma(e^- \pi^0 \eta)/\Gamma_{total}$ — Γ_{236}/Γ

Test of lepton family number conservation.

VALUE	CL%	DOCUMENT ID		TECN	COMMENT
$<24 \times 10^{-6}$	90	BONVICINI	97	CLEO	$E^{ee}_{cm} = 10.6$ GeV

$\Gamma(\mu^- \pi^0 \eta)/\Gamma_{total}$ — Γ_{237}/Γ

Test of lepton family number conservation.

VALUE	CL%	DOCUMENT ID		TECN	COMMENT
$<22 \times 10^{-6}$	90	BONVICINI	97	CLEO	$E^{ee}_{cm} = 10.6$ GeV

$\Gamma(p e^- e^-)/\Gamma_{total}$ — Γ_{238}/Γ

VALUE	CL%	DOCUMENT ID		TECN	COMMENT
$<3.0 \times 10^{-8}$	90	SAHOO	20	BELL	921 fb^{-1} $E^{ee}_{cm} = 10.6$ GeV

$\Gamma(\overline{p} e^+ e^-)/\Gamma_{total}$ — Γ_{239}/Γ

VALUE	CL%	DOCUMENT ID		TECN	COMMENT
$<3.0 \times 10^{-8}$	90	SAHOO	20	BELL	921 fb^{-1} $E^{ee}_{cm} = 10.6$ GeV

$\Gamma(\overline{p} e^+ \mu^-)/\Gamma_{total}$ — Γ_{240}/Γ

VALUE	CL%	DOCUMENT ID		TECN	COMMENT
$<2.0 \times 10^{-8}$	90	SAHOO	20	BELL	921 fb^{-1} $E^{ee}_{cm} = 10.6$ GeV

$\Gamma(\overline{p} e^- \mu^+)/\Gamma_{total}$ — Γ_{241}/Γ

VALUE	CL%	DOCUMENT ID		TECN	COMMENT
$<1.8 \times 10^{-8}$	90	SAHOO	20	BELL	921 fb^{-1} $E^{ee}_{cm} = 10.6$ GeV

$\Gamma(p \mu^- \mu^-)/\Gamma_{total}$ — Γ_{242}/Γ

VALUE	CL%	DOCUMENT ID		TECN	COMMENT
$<4.0 \times 10^{-8}$	90	SAHOO	20	BELL	921 fb^{-1} $E^{ee}_{cm} = 10.6$ GeV
• • • We do not use the following data for averages, fits, limits, etc. • • •					
$<4.4 \times 10^{-7}$	90	AAIJ	13AH	LHCB	1.0 fb^{-1}, pp at 7 TeV

$\Gamma(\overline{p} \mu^+ \mu^-)/\Gamma_{total}$ — Γ_{243}/Γ

VALUE	CL%	DOCUMENT ID		TECN	COMMENT
$<1.8 \times 10^{-8}$	90	SAHOO	20	BELL	921 fb^{-1} $E^{ee}_{cm} = 10.6$ GeV
• • • We do not use the following data for averages, fits, limits, etc. • • •					
$<3.3 \times 10^{-7}$	90	AAIJ	13AH	LHCB	1.0 fb^{-1}, pp at 7 TeV

$\Gamma(\overline{p}\gamma)/\Gamma_{total}$ — Γ_{244}/Γ

Test of lepton number and baryon number conservation.

VALUE	CL%	DOCUMENT ID		TECN	COMMENT
$< 3.5 \times 10^{-6}$	90	GODANG	99	CLEO	$E^{ee}_{cm} = 10.6$ GeV
• • • We do not use the following data for averages, fits, limits, etc. • • •					
$<29 \times 10^{-5}$	90	ALBRECHT	92K	ARG	$E^{ee}_{cm} = 10$ GeV

$\Gamma(\overline{p}\pi^0)/\Gamma_{total}$ — Γ_{245}/Γ

Test of lepton number and baryon number conservation.

VALUE	CL%	DOCUMENT ID		TECN	COMMENT
$<15 \times 10^{-6}$	90	GODANG	99	CLEO	$E^{ee}_{cm} = 10.6$ GeV
• • • We do not use the following data for averages, fits, limits, etc. • • •					
$<66 \times 10^{-5}$	90	ALBRECHT	92K	ARG	$E^{ee}_{cm} = 10$ GeV

$\Gamma(\overline{p}2\pi^0)/\Gamma_{total}$ — Γ_{246}/Γ

Test of lepton number and baryon number conservation.

VALUE	CL%	DOCUMENT ID		TECN	COMMENT
$<33 \times 10^{-6}$	90	GODANG	99	CLEO	$E^{ee}_{cm} = 10.6$ GeV

$\Gamma(\overline{p}\eta)/\Gamma_{total}$ — Γ_{247}/Γ

Test of lepton number and baryon number conservation.

VALUE	CL%	DOCUMENT ID		TECN	COMMENT
$< 8.9 \times 10^{-6}$	90	GODANG	99	CLEO	$E^{ee}_{cm} = 10.6$ GeV
• • • We do not use the following data for averages, fits, limits, etc. • • •					
$<130 \times 10^{-5}$	90	ALBRECHT	92K	ARG	$E^{ee}_{cm} = 10$ GeV

$\Gamma(\overline{p}\pi^0\eta)/\Gamma_{total}$ — Γ_{248}/Γ

Test of lepton number and baryon number conservation.

VALUE	CL%	DOCUMENT ID		TECN	COMMENT
$<27 \times 10^{-6}$	90	GODANG	99	CLEO	$E^{ee}_{cm} = 10.6$ GeV

$\Gamma(\Lambda\pi^-)/\Gamma_{total}$ — Γ_{249}/Γ

Test of lepton number and baryon number conservation.

VALUE	CL%	DOCUMENT ID		TECN	COMMENT
$<0.72 \times 10^{-7}$	90	MIYAZAKI	06	BELL	154 fb^{-1}, $E^{ee}_{cm} = 10.6$ GeV

$\Gamma(\overline{\Lambda}\pi^-)/\Gamma_{total}$ — Γ_{250}/Γ

Test of lepton number and baryon number conservation.

VALUE	CL%	DOCUMENT ID		TECN	COMMENT
$<1.4 \times 10^{-7}$	90	MIYAZAKI	06	BELL	154 fb^{-1}, $E^{ee}_{cm} = 10.6$ GeV

$\Gamma(e^- \text{light boson})/\Gamma(e^- \overline{\nu}_e \nu_\tau)$ — Γ_{251}/Γ_5

Test of lepton family number conservation.

VALUE	CL%	DOCUMENT ID		TECN	COMMENT
<0.015	95	[1] ALBRECHT	95G	ARG	$E^{ee}_{cm} = 9.4$–10.6 GeV
• • • We do not use the following data for averages, fits, limits, etc. • • •					
<0.008	95	[2] BRYMAN	21	RVUE	
<0.018	95	[3] ALBRECHT	90E	ARG	$E^{ee}_{cm} = 9.4$–10.6 GeV
<0.040	95	[4] BALTRUSAIT...85		MRK3	$E^{ee}_{cm} = 3.77$ GeV

[1] ALBRECHT 95G limit holds for bosons with mass < 0.4 GeV. The limit rises to 0.036 for a mass of 1.0 GeV, then falls to 0.006 at the upper mass limit of 1.6 GeV.
[2] BRYMAN 21 reports indirect limits obtained from the consistency of the world averages of $B(\tau^- \to e^- \overline{\nu}_e \nu_\tau)$ and $B(\tau^- \to \mu^- \overline{\nu}_\mu \nu_\tau)$ with their Standard Model predictions, without a simulation of the efficiency as a function of the X mass for the searched decay modes to be detected as the corresponding Standard Model decay modes.
[3] ALBRECHT 90E limit applies for spinless boson with mass < 100 MeV, and rises to 0.050 for mass $= 500$ MeV.
[4] BALTRUSAITIS 85 limit applies for spinless boson with mass < 100 MeV.

$\Gamma(\mu^- \text{light boson})/\Gamma(e^- \overline{\nu}_e \nu_\tau)$ — Γ_{252}/Γ_5

Test of lepton family number conservation.

VALUE	CL%	DOCUMENT ID		TECN	COMMENT
<0.026	95	[1] ALBRECHT	95G	ARG	$E^{ee}_{cm} = 9.4$–10.6 GeV
• • • We do not use the following data for averages, fits, limits, etc. • • •					
<0.011	95	[2] BRYMAN	21	RVUE	
<0.033	95	[3] ALBRECHT	90E	ARG	$E^{ee}_{cm} = 9.4$–10.6 GeV
<0.125	95	[4] BALTRUSAIT...85		MRK3	$E^{ee}_{cm} = 3.77$ GeV

[1] ALBRECHT 95G limit holds for bosons with mass < 1.3 GeV. The limit rises to 0.034 for a mass of 1.4 GeV, then falls to 0.003 at the upper mass limit of 1.6 GeV.
[2] BRYMAN 21 reports indirect limits obtained from the consistency of the world averages of $B(\tau^- \to e^- \overline{\nu}_e \nu_\tau)$ and $B(\tau^- \to \mu^- \overline{\nu}_\mu \nu_\tau)$ with their Standard Model predictions, without a simulation of the efficiency as a function of the X mass for the searched decay modes to be detected as the corresponding Standard Model decay modes.
[3] ALBRECHT 90E limit applies for spinless boson with mass < 100 MeV, and rises to 0.071 for mass $= 500$ MeV.
[4] BALTRUSAITIS 85 limit applies for spinless boson with mass < 100 MeV.

Downloaded from https://academic.oup.com/ptep/article/2022/8/083C01/6651666 by KIT Library user on 27 September 2022

τ-DECAY PARAMETERS

See the related review(s):

τ-Lepton Decay Parameters

$\rho(e$ or $\mu)$ PARAMETER

$(V-A)$ theory predicts $\rho = 0.75$.

VALUE	EVTS	DOCUMENT ID		TECN	COMMENT
0.745±0.008 OUR FIT					
0.749±0.008 OUR AVERAGE					
0.742±0.014±0.006	81k	HEISTER	01E	ALEP	1991–1995 LEP runs
0.775±0.023±0.020	36k	ABREU	00L	DLPH	1992–1995 runs
0.781±0.028±0.018	46k	ACKERSTAFF	99D	OPAL	1990–1995 LEP runs
0.762±0.035	54k	ACCIARRI	98R	L3	1991–1995 LEP runs
0.731±0.031		[1] ALBRECHT	98	ARG	E^{ee}_{cm}= 9.5–10.6 GeV
0.72 ±0.09 ±0.03		[2] ABE	97O	SLD	1993–1995 SLC runs
0.747±0.010±0.006	55k	ALEXANDER	97F	CLEO	E^{ee}_{cm}= 10.6 GeV
0.79 ±0.10 ±0.10	3732	FORD	87B	MAC	E^{ee}_{cm}= 29 GeV
0.71 ±0.09 ±0.03	1426	BEHRENDS	85	CLEO	e^+e^- near $\Upsilon(4S)$
• • • We do not use the following data for averages, fits, limits, etc. • • •					
0.735±0.013±0.008	31k	AMMAR	97B	CLEO	Repl. by ALEXANDER 97F
0.794±0.039±0.031	18k	ACCIARRI	96H	L3	Repl. by ACCIARRI 98R
0.732±0.034±0.020	8.2k	[3] ALBRECHT	95	ARG	E^{ee}_{cm}= 9.5–10.6 GeV
0.738±0.038		[4] ALBRECHT	95C	ARG	Repl. by ALBRECHT 98
0.751±0.039±0.022		BUSKULIC	95D	ALEP	Repl. by HEISTER 01E
0.742±0.035±0.020	8000	ALBRECHT	90E	ARG	E^{ee}_{cm}= 9.4–10.6 GeV

[1] Combined fit to ARGUS tau decay parameter measurements in ALBRECHT 98, ALBRECHT 95C, ALBRECHT 93G, and ALBRECHT 94E. ALBRECHT 98 use tau pair events of the type $\tau^-\tau^+ \to (\ell^-\overline{\nu}_\ell\nu_\tau)(\pi^+\pi^0\overline{\nu}_\tau)$, and their charged conjugates.

[2] ABE 97O assume $\eta = 0$ in their fit. Letting η vary in the fit gives a ρ value of 0.69 ± 0.13 ± 0.05.

[3] Value is from a simultaneous fit for the ρ and η decay parameters to the lepton energy spectrum. Not independent of ALBRECHT 90E $\rho(e$ or $\mu)$ value which assumes $\eta = 0$. Result is strongly correlated with ALBRECHT 95C.

[4] Combined fit to ARGUS tau decay parameter measurements in ALBRECHT 95C, ALBRECHT 93G, and ALBRECHT 94E.

$\rho(e)$ PARAMETER

$(V-A)$ theory predicts $\rho = 0.75$.

VALUE	EVTS	DOCUMENT ID		TECN	COMMENT
0.747±0.010 OUR FIT					
0.744±0.010 OUR AVERAGE					
0.747±0.019±0.014	44k	HEISTER	01E	ALEP	1991–1995 LEP runs
0.744±0.036±0.037	17k	ABREU	00L	DLPH	1992–1995 runs
0.779±0.047±0.029	25k	ACKERSTAFF	99D	OPAL	1990–1995 LEP runs
0.68 ±0.04 ±0.07		[1] ALBRECHT	98	ARG	E^{ee}_{cm}= 9.5–10.6 GeV
0.71 ±0.14 ±0.05		ABE	97O	SLD	1993–1995 SLC runs
0.747±0.012±0.004	34k	ALEXANDER	97F	CLEO	E^{ee}_{cm}= 10.6 GeV
0.735±0.036±0.020	4.7k	[2] ALBRECHT	95	ARG	E^{ee}_{cm}= 9.5–10.6 GeV
0.79 ±0.08 ±0.06	3230	[3] ALBRECHT	93G	ARG	E^{ee}_{cm}= 9.4–10.6 GeV
0.64 ±0.06 ±0.07	2753	JANSSEN	89	CBAL	E^{ee}_{cm}= 9.4–10.6 GeV
0.62 ±0.17 ±0.14	1823	FORD	87B	MAC	E^{ee}_{cm}= 29 GeV
0.60 ±0.13	699	BEHRENDS	85	CLEO	e^+e^- near $\Upsilon(4S)$
0.72 ±0.10 ±0.11	594	BACINO	79B	DLCO	E^{ee}_{cm}= 3.5–7.4 GeV
• • • We do not use the following data for averages, fits, limits, etc. • • •					
0.732±0.014±0.009	19k	AMMAR	97B	CLEO	Repl. by ALEXANDER 97F
0.793±0.050±0.025		BUSKULIC	95D	ALEP	Repl. by HEISTER 01E
0.747±0.045±0.028	5106	ALBRECHT	90E	ARG	Repl. by ALBRECHT 95

[1] ALBRECHT 98 use tau pair events of the type $\tau^-\tau^+ \to (\ell^-\overline{\nu}_\ell\nu_\tau)(\pi^+\pi^0\overline{\nu}_\tau)$, and their charged conjugates.

[2] ALBRECHT 95 use tau pair events of the type $\tau^-\tau^+ \to (\ell^-\overline{\nu}_\ell\nu_\tau)(h^+h^-h^+(\pi^0)\overline{\nu}_\tau)$ and their charged conjugates.

[3] ALBRECHT 93G use tau pair events of the type $\tau^-\tau^+ \to (\mu^-\overline{\nu}_\mu\nu_\tau)(e^+\nu_e\overline{\nu}_\tau)$ and their charged conjugates.

$\rho(\mu)$ PARAMETER

$(V-A)$ theory predicts $\rho = 0.75$.

VALUE	EVTS	DOCUMENT ID		TECN	COMMENT
0.763±0.020 OUR FIT					
0.770±0.022 OUR AVERAGE					
0.776±0.045±0.019	46k	HEISTER	01E	ALEP	1991–1995 LEP runs
0.999±0.098±0.045	22k	ABREU	00L	DLPH	1992–1995 runs
0.777±0.044±0.016	27k	ACKERSTAFF	99D	OPAL	1990–1995 LEP runs
0.69 ±0.06 ±0.06		[1] ALBRECHT	98	ARG	E^{ee}_{cm}= 9.5–10.6 GeV
0.54 ±0.28 ±0.14		ABE	97O	SLD	1993–1995 SLC runs
0.750±0.017±0.045	22k	ALEXANDER	97F	CLEO	E^{ee}_{cm}= 10.6 GeV
0.76 ±0.07 ±0.08	3230	ALBRECHT	93G	ARG	E^{ee}_{cm}= 9.4–10.6 GeV
0.734±0.055±0.027	3041	ALBRECHT	90E	ARG	E^{ee}_{cm}= 9.4–10.6 GeV
0.89 ±0.14 ±0.08	1909	FORD	87B	MAC	E^{ee}_{cm}= 29 GeV
0.81 ±0.13	727	BEHRENDS	85	CLEO	e^+e^- near $\Upsilon(4S)$
• • • We do not use the following data for averages, fits, limits, etc. • • •					
0.747±0.048±0.044	13k	AMMAR	97B	CLEO	Repl. by ALEXANDER 97F
0.693±0.057±0.028		BUSKULIC	95D	ALEP	Repl. by HEISTER 01E

[1] ALBRECHT 98 use tau pair events of the type $\tau^-\tau^+ \to (\ell^-\overline{\nu}_\ell\nu_\tau)(\pi^+\pi^0\overline{\nu}_\tau)$, and their charged conjugates.

$\xi(e$ or $\mu)$ PARAMETER

$(V-A)$ theory predicts $\xi = 1$.

VALUE	EVTS	DOCUMENT ID		TECN	COMMENT
0.985±0.030 OUR FIT					
0.981±0.031 OUR AVERAGE					
0.986±0.068±0.031	81k	HEISTER	01E	ALEP	1991–1995 LEP runs
0.929±0.070±0.030	36k	ABREU	00L	DLPH	1992–1995 runs
0.98 ±0.22 ±0.10	46k	ACKERSTAFF	99D	OPAL	1990–1995 LEP runs
0.70 ±0.16	54k	ACCIARRI	98R	L3	1991–1995 LEP runs
1.03 ±0.11		[1] ALBRECHT	98	ARG	E^{ee}_{cm}= 9.5–10.6 GeV
1.05 ±0.35 ±0.04		[2] ABE	97O	SLD	1993–1995 SLC runs
1.007±0.040±0.015	55k	ALEXANDER	97F	CLEO	E^{ee}_{cm}= 10.6 GeV
• • • We do not use the following data for averages, fits, limits, etc. • • •					
0.94 ±0.21 ±0.07	18k	ACCIARRI	96H	L3	Repl. by ACCIARRI 98R
0.97 ±0.14		[3] ALBRECHT	95C	ARG	Repl. by ALBRECHT 98
1.18 ±0.15 ±0.16		BUSKULIC	95D	ALEP	Repl. by HEISTER 01E
0.90 ±0.15 ±0.10	3230	[4] ALBRECHT	93G	ARG	E^{ee}_{cm}= 9.4–10.6 GeV

[1] Combined fit to ARGUS tau decay parameter measurements in ALBRECHT 98, ALBRECHT 95C, ALBRECHT 93G, and ALBRECHT 94E. ALBRECHT 98 use tau pair events of the type $\tau^-\tau^+ \to (\ell^-\overline{\nu}_\ell\nu_\tau)(\pi^+\pi^0\overline{\nu}_\tau)$, and their charged conjugates.

[2] ABE 97O assume $\eta = 0$ in their fit. Letting η vary in the fit gives a ξ value of 1.02 ± 0.36 ± 0.05.

[3] Combined fit to ARGUS tau decay parameter measurements in ALBRECHT 95C, ALBRECHT 93G, and ALBRECHT 94E. ALBRECHT 95C uses events of the type $\tau^-\tau^+ \to (\ell^-\overline{\nu}_\ell\nu_\tau)(h^+h^-h^+\overline{\nu}_\tau)$ and their charged conjugates.

[4] ALBRECHT 93G measurement determines $|\xi|$ for the case $\xi(e) = \xi(\mu)$, but the authors point out that other LEP experiments determine the sign to be positive.

$\xi(e)$ PARAMETER

$(V-A)$ theory predicts $\xi = 1$.

VALUE	EVTS	DOCUMENT ID		TECN	COMMENT
0.994±0.040 OUR FIT					
1.00 ±0.04 OUR AVERAGE					
1.011±0.094±0.038	44k	HEISTER	01E	ALEP	1991–1995 LEP runs
1.01 ±0.12 ±0.05	17k	ABREU	00L	DLPH	1992–1995 runs
1.13 ±0.39 ±0.14	25k	ACKERSTAFF	99D	OPAL	1990–1995 LEP runs
1.11 ±0.20 ±0.08		[1] ALBRECHT	98	ARG	E^{ee}_{cm}= 9.5–10.6 GeV
1.16 ±0.52 ±0.06		ABE	97O	SLD	1993–1995 SLC runs
0.979±0.048±0.016	34k	ALEXANDER	97F	CLEO	E^{ee}_{cm}= 10.6 GeV
• • • We do not use the following data for averages, fits, limits, etc. • • •					
1.03 ±0.23 ±0.09		BUSKULIC	95D	ALEP	Repl. by HEISTER 01E

[1] ALBRECHT 98 use tau pair events of the type $\tau^-\tau^+ \to (\ell^-\overline{\nu}_\ell\nu_\tau)(\pi^+\pi^0\overline{\nu}_\tau)$, and their charged conjugates.

$\xi(\mu)$ PARAMETER

$(V-A)$ theory predicts $\xi = 1$.

VALUE	EVTS	DOCUMENT ID		TECN	COMMENT
1.030±0.059 OUR FIT					
1.06 ±0.06 OUR AVERAGE					
1.030±0.120±0.050	46k	HEISTER	01E	ALEP	1991–1995 LEP runs
1.16 ±0.19 ±0.06	22k	ABREU	00L	DLPH	1992–1995 runs
0.79 ±0.41 ±0.09	27k	ACKERSTAFF	99D	OPAL	1990–1995 LEP runs
1.26 ±0.27 ±0.14		[1] ALBRECHT	98	ARG	E^{ee}_{cm}= 9.5–10.6 GeV
0.75 ±0.50 ±0.14		ABE	97O	SLD	1993–1995 SLC runs
1.054±0.069±0.047	22k	ALEXANDER	97F	CLEO	E^{ee}_{cm}= 10.6 GeV
• • • We do not use the following data for averages, fits, limits, etc. • • •					
1.23 ±0.22 ±0.10		BUSKULIC	95D	ALEP	Repl. by HEISTER 01E

[1] ALBRECHT 98 use tau pair events of the type $\tau^-\tau^+ \to (\ell^-\overline{\nu}_\ell\nu_\tau)(\pi^+\pi^0\overline{\nu}_\tau)$, and their charged conjugates.

$\eta(e$ or $\mu)$ PARAMETER

$(V-A)$ theory predicts $\eta = 0$.

VALUE	EVTS	DOCUMENT ID		TECN	COMMENT
0.013±0.020 OUR FIT					
0.015±0.021 OUR AVERAGE					
0.012±0.026±0.004	81k	HEISTER	01E	ALEP	1991–1995 LEP runs
−0.005±0.036±0.037		ABREU	00L	DLPH	1992–1995 runs
0.027±0.055±0.005	46k	ACKERSTAFF	99D	OPAL	1990–1995 LEP runs
0.27 ±0.14	54k	ACCIARRI	98R	L3	1991–1995 LEP runs
−0.13 ±0.47 ±0.15		ABE	97O	SLD	1993–1995 SLC runs
−0.015±0.061±0.062	31k	AMMAR	97B	CLEO	E^{ee}_{cm}= 10.6 GeV
0.03 ±0.18 ±0.12	8.2k	ALBRECHT	95	ARG	E^{ee}_{cm}= 9.5–10.6 GeV
• • • We do not use the following data for averages, fits, limits, etc. • • •					
0.25 ±0.17 ±0.11	18k	ACCIARRI	96H	L3	Repl. by ACCIARRI 98R
−0.04 ±0.15 ±0.11		BUSKULIC	95D	ALEP	Repl. by HEISTER 01E

$\eta(\mu)$ PARAMETER

$(V-A)$ theory predicts $\eta = 0$.

VALUE	EVTS	DOCUMENT ID		TECN	COMMENT
0.094±0.073 OUR FIT					
0.17 ±0.15 OUR AVERAGE		Error includes scale factor of 1.2.			
0.160±0.150±0.060	46k	HEISTER	01E	ALEP	1991–1995 LEP runs
0.72 ±0.32 ±0.15		ABREU	00L	DLPH	1992–1995 runs
−0.59 ±0.82 ±0.45		[1] ABE	97O	SLD	1993–1995 SLC runs
0.010±0.149±0.171	13k	[2] AMMAR	97B	CLEO	E^{ee}_{cm}= 10.6 GeV

Downloaded from https://academic.oup.com/ptep/article/2022/8/083C01/6651666 by KIT Library user on 27 September 2022

• • • We do not use the following data for averages, fits, limits, etc. • • •

$0.010 \pm 0.065 \pm 0.001$	27k	[3] ACKERSTAFF	99D	OPAL	1990–1995 LEP runs
$-0.24 \pm 0.23 \pm 0.18$		BUSKULIC	95D	ALEP	Repl. by HEISTER 01E

[1] Highly correlated (corr. = 0.92) with ABE 97O $\rho(\mu)$ measurement.
[2] Highly correlated (corr. = 0.949) with AMMAR 97B $\rho(\mu)$ value.
[3] ACKERSTAFF 99D result is dominated by a constraint on η from the OPAL measurements of the τ lifetime and $B(\tau^- \to \mu^- \overline{\nu}_\mu \nu_\tau)$ assuming lepton universality for the total coupling strength.

$(\delta\xi)(e$ or $\mu)$ PARAMETER

($V-A$) theory predicts $(\delta\xi) = 0.75$.

VALUE	EVTS	DOCUMENT ID		TECN	COMMENT
0.746±0.021 OUR FIT					
0.744±0.022 OUR AVERAGE					
$0.776 \pm 0.045 \pm 0.024$	81k	HEISTER	01E	ALEP	1991–1995 LEP runs
$0.779 \pm 0.070 \pm 0.028$	36k	ABREU	00L	DLPH	1992–1995 runs
$0.65 \pm 0.14 \pm 0.07$	46k	ACKERSTAFF	99D	OPAL	1990–1995 LEP runs
0.70 ± 0.11	54k	ACCIARRI	98R	L3	1991–1995 LEP runs
0.63 ± 0.09		[1] ALBRECHT	98	ARG	E^{ee}_{cm}= 9.5–10.6 GeV
$0.88 \pm 0.27 \pm 0.04$		[2] ABE	97O	SLD	1993–1995 SLC runs
$0.745 \pm 0.026 \pm 0.009$	55k	ALEXANDER	97F	CLEO	E^{ee}_{cm}= 10.6 GeV
• • • We do not use the following data for averages, fits, limits, etc. • • •					
$0.81 \pm 0.14 \pm 0.06$	18k	ACCIARRI	96H	L3	Repl. by ACCIARRI 98R
0.65 ± 0.12		[3] ALBRECHT	95C	ARG	Repl. by ALBRECHT 98
$0.88 \pm 0.11 \pm 0.07$		BUSKULIC	95D	ALEP	Repl. by HEISTER 01E

[1] Combined fit to ARGUS tau decay parameter measurements in ALBRECHT 98, ALBRECHT 95C, ALBRECHT 93G, and ALBRECHT 94E. ALBRECHT 98 use tau pair events of the type $\tau^-\tau^+ \to (\ell^- \overline{\nu}_\ell \nu_\tau)(\pi^+\pi^0\overline{\nu}_\tau)$, and their charged conjugates.
[2] ABE 97O assume $\eta = 0$ in their fit. Letting η vary in the fit gives a $(\delta\xi)$ value of $0.87 \pm 0.27 \pm 0.04$.
[3] Combined fit to ARGUS tau decay parameter measurements in ALBRECHT 95C, ALBRECHT 93G, and ALBRECHT 94E. ALBRECHT 95C uses events of the type $\tau^-\tau^+ \to (\ell^- \overline{\nu}_\ell \nu_\tau)\ (h^+ h^- h^+ \overline{\nu}_\tau)$ and their charged conjugates.

$(\delta\xi)(e)$ PARAMETER

($V-A$) theory predicts $(\delta\xi) = 0.75$.

VALUE	EVTS	DOCUMENT ID		TECN	COMMENT
0.734±0.028 OUR FIT					
0.731±0.029 OUR AVERAGE					
$0.778 \pm 0.066 \pm 0.024$	44k	HEISTER	01E	ALEP	1991–1995 LEP runs
$0.85 \pm 0.12 \pm 0.04$	17k	ABREU	00L	DLPH	1992–1995 runs
$0.72 \pm 0.31 \pm 0.14$	25k	ACKERSTAFF	99D	OPAL	1990–1995 LEP runs
$0.56 \pm 0.14 \pm 0.06$		[1] ALBRECHT	98	ARG	E^{ee}_{cm}= 9.5–10.6 GeV
$0.85 \pm 0.43 \pm 0.08$		ABE	97O	SLD	1993–1995 SLC runs
$0.720 \pm 0.032 \pm 0.010$	34k	ALEXANDER	97F	CLEO	E^{ee}_{cm}= 10.6 GeV
• • • We do not use the following data for averages, fits, limits, etc. • • •					
$1.11 \pm 0.17 \pm 0.07$		BUSKULIC	95D	ALEP	Repl. by HEISTER 01E

[1] ALBRECHT 98 use tau pair events of the type $\tau^-\tau^+ \to (\ell^- \overline{\nu}_\ell \nu_\tau)(\pi^+\pi^0\overline{\nu}_\tau)$, and their charged conjugates.

$(\delta\xi)(\mu)$ PARAMETER

($V-A$) theory predicts $(\delta\xi) = 0.75$.

VALUE	EVTS	DOCUMENT ID		TECN	COMMENT
0.778±0.037 OUR FIT					
0.79 ±0.04 OUR AVERAGE					
$0.786 \pm 0.066 \pm 0.028$	46k	HEISTER	01E	ALEP	1991–1995 LEP runs
$0.86 \pm 0.13 \pm 0.04$	22k	ABREU	00L	DLPH	1992–1995 runs
$0.63 \pm 0.23 \pm 0.05$	27k	ACKERSTAFF	99D	OPAL	1990–1995 LEP runs
$0.73 \pm 0.18 \pm 0.10$		[1] ALBRECHT	98	ARG	E^{ee}_{cm}= 9.5–10.6 GeV
$0.82 \pm 0.32 \pm 0.07$		ABE	97O	SLD	1993–1995 SLC runs
$0.786 \pm 0.041 \pm 0.032$	22k	ALEXANDER	97F	CLEO	E^{ee}_{cm}= 10.6 GeV
• • • We do not use the following data for averages, fits, limits, etc. • • •					
$0.71 \pm 0.14 \pm 0.06$		BUSKULIC	95D	ALEP	Repl. by HEISTER 01E

[1] ALBRECHT 98 use tau pair events of the type $\tau^-\tau^+ \to (\ell^- \overline{\nu}_\ell \nu_\tau)(\pi^+\pi^0\overline{\nu}_\tau)$, and their charged conjugates.

$\xi(\pi)$ PARAMETER

($V-A$) theory predicts $\xi(\pi) = 1$.

VALUE	EVTS	DOCUMENT ID		TECN	COMMENT
0.993±0.022 OUR FIT					
0.994±0.023 OUR AVERAGE					
$0.994 \pm 0.020 \pm 0.014$	27k	HEISTER	01E	ALEP	1991–1995 LEP runs
$0.81 \pm 0.17 \pm 0.02$		ABE	97O	SLD	1993–1995 SLC runs
$1.03 \pm 0.06 \pm 0.04$	2.0k	COAN	97	CLEO	E^{ee}_{cm}= 10.6 GeV
• • • We do not use the following data for averages, fits, limits, etc. • • •					
$0.987 \pm 0.057 \pm 0.027$		BUSKULIC	95D	ALEP	Repl. by HEISTER 01E
$0.95 \pm 0.11 \pm 0.05$		[1] BUSKULIC	94D	ALEP	1990+1991 LEP run

[1] Superseded by BUSKULIC 95D.

$\xi(\rho)$ PARAMETER

($V-A$) theory predicts $\xi(\rho) = 1$.

VALUE	EVTS	DOCUMENT ID		TECN	COMMENT
0.994±0.008 OUR FIT					
0.994±0.009 OUR AVERAGE					
$0.987 \pm 0.012 \pm 0.011$	59k	HEISTER	01E	ALEP	1991–1995 LEP runs
$0.99 \pm 0.12 \pm 0.04$		ABE	97O	SLD	1993–1995 SLC runs
$0.995 \pm 0.010 \pm 0.003$	66k	ALEXANDER	97F	CLEO	E^{ee}_{cm}= 10.6 GeV
$1.022 \pm 0.028 \pm 0.030$	1.7k	[1] ALBRECHT	94E	ARG	E^{ee}_{cm}= 9.4–10.6 GeV
• • • We do not use the following data for averages, fits, limits, etc. • • •					
$1.045 \pm 0.058 \pm 0.032$		BUSKULIC	95D	ALEP	Repl. by HEISTER 01E
$1.03 \pm 0.11 \pm 0.05$		[2] BUSKULIC	94D	ALEP	1990+1991 LEP run

[1] ALBRECHT 94E measure the square of this quantity and use the sign determined by ALBRECHT 90I to obtain the quoted result.
[2] Superseded by BUSKULIC 95D.

$\xi(a_1)$ PARAMETER

($V-A$) theory predicts $\xi(a_1) = 1$.

VALUE	EVTS	DOCUMENT ID		TECN	COMMENT
1.001±0.027 OUR FIT					
1.002±0.028 OUR AVERAGE					
$1.000 \pm 0.016 \pm 0.024$	35k	[1] HEISTER	01E	ALEP	1991–1995 LEP runs
$1.02 \pm 0.13 \pm 0.03$	17.2k	ASNER	00	CLEO	E^{ee}_{cm}= 10.6 GeV
$1.29 \pm 0.26 \pm 0.11$	7.4k	[2] ACKERSTAFF	97R	OPAL	1992–1994 LEP runs
$0.85 \ ^{+0.15}_{-0.17} \pm 0.05$		ALBRECHT	95C	ARG	E^{ee}_{cm}= 9.5–10.6 GeV
$1.25 \pm 0.23 \ ^{+0.15}_{-0.08}$	7.5k	ALBRECHT	93C	ARG	E^{ee}_{cm}= 9.4–10.6 GeV
• • • We do not use the following data for averages, fits, limits, etc. • • •					
$1.08 \ ^{+0.46}_{-0.41} \ ^{+0.14}_{-0.25}$	2.6k	[3] AKERS	95P	OPAL	Repl. by ACKERSTAFF 97R
$0.937 \pm 0.116 \pm 0.064$		BUSKULIC	95D	ALEP	Repl. by HEISTER 01E

[1] HEISTER 01E quote $1.000 \pm 0.016 \pm 0.013 \pm 0.020$ where the errors are statistical, systematic, and an uncertainty due to the final state model. We combine the systematic error and model uncertainty.
[2] ACKERSTAFF 97R obtain this result with a model independent fit to the hadronic structure functions. Fitting with the model of Kuhn and Santamaria (ZPHY **C48**, 445 (1990)) gives $0.87 \pm 0.16 \pm 0.04$, and with the model of of Isgur *et al.* (PR **D39**,1357 (1989)) they obtain $1.20 \pm 0.21 \pm 0.14$.
[3] AKERS 95P obtain this result with a model independent fit to the hadronic structure functions. Fitting with the model of Kuhn and Santamaria (ZPHY **C48**, 445 (1990)) gives $0.87 \pm 0.27 \ ^{+0.05}_{-0.06}$, and with the model of of Isgur *et al.* (PR **D39**,1357 (1989)) they obtain $1.10 \pm 0.31 \ ^{+0.13}_{-0.14}$.

ξ(all hadronic modes) PARAMETER

($V-A$) theory predicts $\xi = 1$.

VALUE	EVTS	DOCUMENT ID		TECN	COMMENT
0.995±0.007 OUR FIT					
0.997±0.007 OUR AVERAGE					
$0.992 \pm 0.007 \pm 0.008$	102k	[1] HEISTER	01E	ALEP	1991–1995 LEP runs
$0.997 \pm 0.027 \pm 0.011$	39k	[2] ABREU	00L	DLPH	1992–1995 runs
$1.02 \pm 0.13 \pm 0.03$	17.2k	[3] ASNER	00	CLEO	E^{ee}_{cm}= 10.6 GeV
1.032 ± 0.031	37k	[4] ACCIARRI	98R	L3	1991–1995 LEP runs
$0.93 \pm 0.10 \pm 0.04$		ABE	97O	SLD	1993–1995 SLC runs
$1.29 \pm 0.26 \pm 0.11$	7.4k	[5] ACKERSTAFF	97R	OPAL	1992–1994 LEP runs
$0.995 \pm 0.010 \pm 0.003$	66k	[6] ALEXANDER	97F	CLEO	E^{ee}_{cm}= 10.6 GeV
$1.03 \pm 0.06 \pm 0.04$	2.0k	[7] COAN	97	CLEO	E^{ee}_{cm}= 10.6 GeV
1.017 ± 0.039		[8] ALBRECHT	95C	ARG	E^{ee}_{cm}= 9.5–10.6 GeV
$1.25 \pm 0.23 \ ^{+0.15}_{-0.08}$	7.5k	[9] ALBRECHT	93C	ARG	E^{ee}_{cm}= 9.4–10.6 GeV
• • • We do not use the following data for averages, fits, limits, etc. • • •					
$0.970 \pm 0.053 \pm 0.011$	14k	[10] ACCIARRI	96H	L3	Repl. by ACCIARRI 98R
$1.08 \ ^{+0.46}_{-0.41} \ ^{+0.14}_{-0.25}$	2.6k	[11] AKERS	95P	OPAL	Repl. by ACKERSTAFF 97R
$1.006 \pm 0.032 \pm 0.019$		[12] BUSKULIC	95D	ALEP	Repl. by HEISTER 01E
$1.022 \pm 0.028 \pm 0.030$	1.7k	[13] ALBRECHT	94E	ARG	E^{ee}_{cm}= 9.4–10.6 GeV
$0.99 \pm 0.07 \pm 0.04$		[14] BUSKULIC	94D	ALEP	1990+1991 LEP run
$1.14 \pm 0.34 \ ^{+0.34}_{-0.17}$	3.9k	[9] ALBRECHT	90I	ARG	Repl. by ALBRECHT 93C

[1] HEISTER 01E quote $0.992 \pm 0.007 \pm 0.006 \pm 0.005$ where the errors are statistical, systematic, and an uncertainty due to the final state model. We combine the systematic error and model uncertainty. They use $\tau \to \pi\nu_\tau$, $\tau \to K\nu_\tau$, $\tau \to \rho\nu_\tau$, and $\tau \to a_1\nu_\tau$ decays.
[2] ABREU 00L use $\tau^- \to h^- \geq 0\pi^0\nu_\tau$ decays.
[3] ASNER 00 use $\tau^- \to \pi^- 2\pi^0\nu_\tau$ decays.
[4] ACCIARRI 98R use $\tau \to \pi\nu_\tau$, $\tau \to K\nu_\tau$, and $\tau \to \rho\nu_\tau$ decays.
[5] ACKERSTAFF 97R use $\tau \to a_1\nu_\tau$ decays.
[6] ALEXANDER 97F use $\tau \to \rho\nu_\tau$ decays.
[7] COAN 97 use h^+h^- energy correlations.
[8] Combined fit to ARGUS tau decay parameter measurements in ALBRECHT 95C, ALBRECHT 93G, and ALBRECHT 94E.
[9] Uses $\tau \to a_1\nu_\tau$ decays. Replaced by ALBRECHT 95C.
[10] ACCIARRI 96H use $\tau \to \pi\nu_\tau$, $\tau \to K\nu_\tau$, and $\tau \to \rho\nu_\tau$ decays.
[11] AKERS 95P use $\tau \to a_1\nu_\tau$ decays.
[12] BUSKULIC 95D use $\tau \to \pi\nu_\tau$, $\tau \to \rho\nu_\tau$, and $\tau \to a_1\nu_\tau$ decays.
[13] ALBRECHT 94E measure the square of this quantity and use the sign determined by ALBRECHT 90I to obtain the quoted result. Uses $\tau \to a_1\nu_\tau$ decays. Replaced by ALBRECHT 95C.
[14] BUSKULIC 94D use $\tau \to \pi\nu_\tau$ and $\tau \to \rho\nu_\tau$ decays. Superseded by BUSKULIC 95D.

$\overline{\eta}(\mu)$ PARAMETER

($V-A$) theory predicts $\overline{\eta}(\mu) = 0$.

VALUE	EVTS	DOCUMENT ID		TECN	COMMENT
−1.3±1.5±0.8	71k	[1] SHIMIZU	18A	BELL	$\tau^- \to \nu_\tau \mu^- \overline{\nu}_\mu \gamma$

[1] SHIMIZU 18A measurement procedure fits a distribution affected by $\overline{\eta}(\mu)$, $\xi\kappa(\mu)$ and $\eta''(\mu)$, floating $\overline{\eta}(\mu)$ and $\xi\kappa(\mu)$ and fixing $\eta''(\mu) = 0$. The contribution of $\eta''(\mu)$ is suppressed by m_μ/m_τ.

Downloaded from https://academic.oup.com/ptep/article/2022/8/083C01/6651666 by KIT Library user on 27 September 2022

$(\xi\kappa)(e$ or $\mu)$ PARAMETER

$(V-A)$ theory predicts $(\xi\kappa)(e$ or $\mu) = 0$.

VALUE	EVTS	DOCUMENT ID		TECN	COMMENT
0.5±0.4±0.2	149k	[1,2] SHIMIZU	18A	BELL	$\tau^- \to \nu_\tau e^- \overline{\nu}_e \gamma$ and $\tau^- \to \nu_\tau \mu^- \overline{\nu}_\mu \gamma$

[1] SHIMIZU 18A measurement procedure fits a distribution of radiative tau decays into both electrons and muons affected by $\overline{\eta}(e$ or $\mu)$, $\xi\kappa(e$ or $\mu)$ and $\eta''(e$ or $\mu)$, floating $\overline{\eta}(e$ or $\mu)$ and $\xi\kappa(e$ or $\mu)$ and fixing $\eta''(e$ or $\mu) = 0$. The contribution of $\eta''(e$ or $\mu)$ is suppressed by m_e/m_τ for tau decaying to electrons and by m_μ/m_τ for tau decaying to muons.

[2] Error correlated with SHIMIZU 18A $(\xi\kappa)(e)$ and $(\xi\kappa)(\mu)$ values.

$(\xi\kappa)(e)$ PARAMETER

$(V-A)$ theory predicts $(\xi\kappa)(e) = 0$.

VALUE	EVTS	DOCUMENT ID		TECN	COMMENT
−0.4±0.8±0.9	78k	[1,2] SHIMIZU	18A	BELL	$\tau^- \to \nu_\tau e^- \overline{\nu}_e \gamma$

[1] SHIMIZU 18A measurement procedure fits a distribution affected by $\overline{\eta}(e)$, $(\xi\kappa)(e)$ and $\eta''(e)$, floating $(\xi\kappa)(e)$ and fixing $\overline{\eta}(e) = 0$ and $\eta''(e) = 0$. The contribution of $\eta''(e)$ is suppressed by m_e/m_τ.

[2] Error correlated with SHIMIZU 18A $(\xi\kappa)(e$ or $\mu)$ value.

$(\xi\kappa)(\mu)$ PARAMETER

$(V-A)$ theory predicts $(\xi\kappa)(\mu) = 0$.

VALUE	EVTS	DOCUMENT ID		TECN	COMMENT
0.8±0.5±0.3	71k	[1,2] SHIMIZU	18A	BELL	$\tau^- \to \nu_\tau \mu^- \overline{\nu}_\mu \gamma$

[1] SHIMIZU 18A measurement procedure fits a distribution affected by $\overline{\eta}(\mu)$, $\xi\kappa(\mu)$ and $\eta''(\mu)$, floating $\overline{\eta}(\mu)$ and $\xi\kappa(\mu)$ and fixing $\eta''(\mu) = 0$. The contribution of $\eta''(\mu)$ is suppressed by m_μ/m_τ.

[2] Error correlated with SHIMIZU 18A $(\xi\kappa)(e$ or $\mu)$ value.

τ REFERENCES

BRYMAN 21 PR D104 075032 D.A. Bryman, S. Ito, R. Shrock (BRCO, TRIU+)
SIRUNYAN 21D JHEP 2101 163 A.M. Sirunyan et al. (CMS Collab.)
UNO 21 JHEP 2110 019 K. Uno et al. (BELLE Collab.)
SAHOO 20 PR D102 111101 D. Sahoo et al. (BELLE Collab.)
JIN 19 PR D100 071101 Y. Jin et al. (BELLE Collab.)
LEES 18B PR D98 032010 J.P. Lees et al. (BABAR Collab.)
SHIMIZU 18A PTEP 2018 023C01 N. Shimizu et al. (BELLE Collab.)
AAD 16BA EPJ C76 232 G.Aad et al. (ATLAS Collab.)
AAIJ 15AI JHEP 1502 121 R. Aaij et al. (LHCb Collab.)
LEES 15G PR D91 051103 J.P. Lees et al. (BABAR Collab.)
ABLIKIM 14D PR D90 012001 M. Ablikim et al. (BESIII Collab.)
BELOUS 14 PRL 112 031801 K. Belous et al. (BELLE Collab.)
RYU 14 PR D89 072009 S. Ryu et al. (BELLE Collab.)
AAIJ 13AH PL B724 36 R. Aaij et al. (LHCb Collab.)
MIYAZAKI 13 PL B719 346 Y. Miyazaki et al. (BELLE Collab.)
LEES 12M PR D85 031102 J.P. Lees et al. (BABAR Collab.)
Also PR D85 099904 (errat.) J.P. Lees et al. (BABAR Collab.)
LEES 12X PR D86 092010 J.P. Lees et al. (BABAR Collab.)
LEES 12Y PR D86 092013 J.P. Lees et al. (BABAR Collab.)
PDG 12 PR D86 010001 J. Beringer et al. (PDG Collab.)
DEL-AMO-SA... 11E PR D83 032002 P. del Amo Sanchez et al. (BABAR Collab.)
MIYAZAKI 11 PL B699 251 Y. Miyazaki et al. (BELLE Collab.)
AUBERT 10B PRL 104 021802 B. Aubert et al. (BABAR Collab.)
AUBERT 10F PRL 105 051602 B. Aubert et al. (BABAR Collab.)
HAYASAKA 10 PL B687 139 K. Hayasaka et al. (BELLE Collab.)
LEE 10 PR D81 113007 M.J. Lee et al. (BELLE Collab.)
LEES 10A PR D81 111101 J.P. Lees et al. (BABAR Collab.)
MIYAZAKI 10 PL B682 355 Y. Miyazaki et al. (BELLE Collab.)
MIYAZAKI 10A PL B692 4 Y. Miyazaki et al. (BELLE Collab.)
AUBERT 09AK PR D80 092005 B. Aubert et al. (BABAR Collab.)
AUBERT 09D PR D79 012004 B. Aubert et al. (BABAR Collab.)
AUBERT 09W PRL 103 021801 B. Aubert et al. (BABAR Collab.)
GROZIN 09A PAN 72 1203 A.G. Grozin, I.B. Khriplovich, A.S. Rudenko (NOVO)
INAMI 09 PL B672 209 K. Inami et al. (BELLE Collab.)
MIYAZAKI 09 PL B672 317 Y. Miyazaki et al. (BELLE Collab.)
AUBERT 08 PRL 100 011801 B. Aubert et al. (BABAR Collab.)
AUBERT 08AE PR D77 112002 B. Aubert et al. (BABAR Collab.)
AUBERT 08K PRL 100 071802 B. Aubert et al. (BABAR Collab.)
FUJIKAWA 08 PR D78 072006 M. Fujikawa et al. (BELLE Collab.)
HAYASAKA 08 PL B666 16 K. Hayasaka et al. (BELLE Collab.)
MIYAZAKI 08 PL B660 154 Y. Miyazaki et al. (BELLE Collab.)
NISHIO 08 PL B664 35 Y. Nishio et al. (BELLE Collab.)
ANASHIN 07 JETPL 85 347 V.V. Anashin et al. (KEDR Collab.)
Translated from ZETFP 85 429.
AUBERT 07AP PR D76 051104 B. Aubert et al. (BABAR Collab.)
AUBERT 07BK PRL 99 251803 B. Aubert et al. (BABAR Collab.)
AUBERT 07I PRL 98 061803 B. Aubert et al. (BABAR Collab.)
BELOUS 07 PRL 99 011801 K. Belous et al. (BELLE Collab.)
EIDELMAN 07 MPL A22 159 S. Eidelman, M. Passera (NOVO, PADO)
EPIFANOV 07 PL B654 65 D. Epifanov et al. (BELLE Collab.)
MIYAZAKI 07 PL B648 341 Y. Miyazaki et al. (BELLE Collab.)
ABDALLAH 06A EPJ C46 1 J. Abdallah et al. (DELPHI Collab.)
AUBERT 06C PRL 96 041801 B. Aubert et al. (BABAR Collab.)
AUBERT,B 06 PR D73 112003 B. Aubert et al. (BABAR Collab.)
INAMI 06 PL B643 5 K. Inami et al. (BELLE Collab.)
MIYAZAKI 06 PL B632 51 Y. Miyazaki et al. (BELLE Collab.)
MIYAZAKI 06A PL B639 159 Y. Miyazaki et al. (BELLE Collab.)
PDG 06 JP G33 1 W.-M. Yao et al. (PDG Collab.)
YUSA 06 PL B640 138 Y. Yusa et al. (BELLE Collab.)
ARMS 05 PRL 94 241802 K. Arms et al. (CLEO Collab.)
AUBERT,B 05A PRL 95 041802 B. Aubert et al. (BABAR Collab.)
AUBERT,B 05F PR D72 012003 B. Aubert et al. (BABAR Collab.)
AUBERT,B 05W PR D72 072001 B. Aubert et al. (BABAR Collab.)
AUBERT,BE 05D PRL 95 191801 B. Aubert et al. (BABAR Collab.)
ENARI 05 PL B622 218 Y. Enari et al. (BELLE Collab.)
HAYASAKA 05 PL B613 20 K. Hayasaka et al. (BELLE Collab.)
SCHAEL 05C PRPL 421 191 S. Schael et al. (ALEPH Collab.)
ABBIENDI 04J EPJ C35 437 G. Abbiendi et al. (OPAL Collab.)
ABDALLAH 04K EPJ C35 159 J. Abdallah et al. (DELPHI Collab.)
ABDALLAH 04T EPJ C36 283 J. Abdallah et al. (DELPHI Collab.)
ABE 04B PRL 92 171802 K. Abe et al. (BELLE Collab.)
ACHARD 04G PL B585 53 P. Achard et al. (L3 Collab.)
AUBERT 04J PRL 92 121801 B. Aubert et al. (BABAR Collab.)
ENARI 04 PRL 93 081803 Y. Enari et al. (BELLE Collab.)
PDG 04 PL B592 1 S. Eidelman et al. (PDG Collab.)
YUSA 04 PL B589 103 Y. Yusa et al. (BELLE Collab.)
ABBIENDI 03 PL B551 35 G. Abbiendi et al. (OPAL Collab.)
BRIERE 03 PRL 90 181802 R. A. Briere et al. (CLEO Collab.)
HEISTER 03F EPJ C30 291 A. Heister et al. (ALEPH Collab.)
INAMI 03 PL B551 16 K. Inami et al. (BELLE Collab.)
CHEN 02C PR D66 071101 S. Chen et al. (CLEO Collab.)
REGAN 02 PRL 88 071805 B.C. Regan et al.
ABBIENDI 01J EPJ C19 653 G. Abbiendi et al. (OPAL Collab.)
ABREU 01M EPJ C20 617 P. Abreu et al. (DELPHI Collab.)
ACCIARRI 01F PL B507 47 M. Acciarri et al. (L3 Collab.)
ACHARD 01D PL B519 189 P. Achard et al. (L3 Collab.)
ANASTASSOV 01 PRL 86 4467 A. Anastassov et al. (CLEO Collab.)
HEISTER 01E EPJ C22 217 A. Heister et al. (ALEPH Collab.)
ABBIENDI 00A PL B492 23 G. Abbiendi et al. (OPAL Collab.)
ABBIENDI 00C EPJ C13 213 G. Abbiendi et al. (OPAL Collab.)
ABBIENDI 00D EPJ C13 197 G. Abbiendi et al. (OPAL Collab.)
ABREU 00L EPJ C16 229 P. Abreu et al. (DELPHI Collab.)
ACCIARRI 00B PL B479 67 M. Acciarri et al. (L3 Collab.)
AHMED 00 PR D61 071101 S. Ahmed et al. (CLEO Collab.)
ALBRECHT 00 PL B485 37 H. Albrecht et al. (ARGUS Collab.)
ASNER 00 PR D61 012002 D.M. Asner et al. (CLEO Collab.)
ASNER 00B PR D62 072006 D.M. Asner et al. (CLEO Collab.)
BERGFELD 00 PRL 84 830 T. Bergfeld et al. (CLEO Collab.)
BROWDER 00 PR D61 052004 T.E. Browder et al. (CLEO Collab.)
EDWARDS 00A PR D61 072003 K.W. Edwards et al. (CLEO Collab.)
GONZALEZ-S... 00 NP B582 3 G.A. Gonzalez-Sprinberg et al.
ABBIENDI 99H PL B447 134 G. Abbiendi et al. (OPAL Collab.)
ABREU 99X EPJ C10 201 P. Abreu et al. (DELPHI Collab.)
ACKERSTAFF 99D EPJ C8 3 K. Ackerstaff et al. (OPAL Collab.)
ACKERSTAFF 99E EPJ C8 183 K. Ackerstaff et al. (OPAL Collab.)
BARATE 99K EPJ C10 1 R. Barate et al. (ALEPH Collab.)
BARATE 99R EPJ C11 599 R. Barate et al. (ALEPH Collab.)
BISHAI 99 PRL 82 281 M. Bishai et al. (CLEO Collab.)
GODANG 99 PR D59 091303 R. Godang et al. (CLEO Collab.)
RICHICHI 99 PR D60 112002 S.J. Richichi et al. (CLEO Collab.)
ACCIARRI 98C PL B426 207 M. Acciarri et al. (L3 Collab.)
ACCIARRI 98E PL B434 169 M. Acciarri et al. (L3 Collab.)
ACCIARRI 98R PL B438 405 M. Acciarri et al. (L3 Collab.)
ACKERSTAFF 98M EPJ C4 193 K. Ackerstaff et al. (OPAL Collab.)
ACKERSTAFF 98N PL B431 188 K. Ackerstaff et al. (OPAL Collab.)
ALBRECHT 98 PL B431 179 H. Albrecht et al. (ARGUS Collab.)
BARATE 98 EPJ C1 65 R. Barate et al. (ALEPH Collab.)
BARATE 98E EPJ C4 29 R. Barate et al. (ALEPH Collab.)
BLISS 98 PR D57 5903 D.W. Bliss et al. (CLEO Collab.)
ABE 97O PRL 78 4691 K. Abe et al. (SLD Collab.)
ACKERSTAFF 97J PL B404 213 K. Ackerstaff et al. (OPAL Collab.)
ACKERSTAFF 97L ZPHY C74 403 K. Ackerstaff et al. (OPAL Collab.)
ACKERSTAFF 97R ZPHY C75 593 K. Ackerstaff et al. (OPAL Collab.)
ALEXANDER 97F PR D56 5320 J.P. Alexander et al. (CLEO Collab.)
AMMAR 97B PRL 78 4686 R. Ammar et al. (CLEO Collab.)
ANASTASSOV 97 PR D55 2559 A. Anastassov et al. (CLEO Collab.)
Also PR D58 119903 (erratum) A. Anastassov et al. (CLEO Collab.)
ANDERSON 97 PRL 79 3814 S. Anderson et al. (CLEO Collab.)
AVERY 97 PR D55 1119 P. Avery et al. (CLEO Collab.)
BARATE 97I ZPHY C74 387 R. Barate et al. (ALEPH Collab.)
BARATE 97R PL B414 362 R. Barate et al. (ALEPH Collab.)
BERGFELD 97 PRL 79 2406 T. Bergfeld et al. (CLEO Collab.)
BONVICINI 97 PRL 79 1221 G. Bonvicini et al. (CLEO Collab.)
BUSKULIC 97C ZPHY C74 263 D. Buskulic et al. (ALEPH Collab.)
COAN 97 PR D55 7291 T.E. Coan et al. (CLEO Collab.)
EDWARDS 97 PR D55 3919 K.W. Edwards et al. (CLEO Collab.)
EDWARDS 97B PR D56 5297 K.W. Edwards et al. (CLEO Collab.)
ESCRIBANO 97 PL B395 369 R. Escribano, E. Masso (BARC, PARIT)
ABREU 96B PL B365 448 P. Abreu et al. (DELPHI Collab.)
ACCIARRI 96H PL B377 313 M. Acciarri et al. (L3 Collab.)
ACCIARRI 96K PL B389 187 M. Acciarri et al. (L3 Collab.)
ALAM 96 PRL 76 2637 M.S. Alam et al. (CLEO Collab.)
ALBRECHT 96E PRPL 276 223 H. Albrecht et al. (ARGUS Collab.)
ALEXANDER 96D PL B369 163 G. Alexander et al. (OPAL Collab.)
ALEXANDER 96E PL B374 341 G. Alexander et al. (OPAL Collab.)
ALEXANDER 96S PL B388 437 G. Alexander et al. (OPAL Collab.)
BAI 96 PR D53 20 J.Z. Bai et al. (BES Collab.)
BALEST 96 PL B388 402 R. Balest et al. (CLEO Collab.)
BARTELT 96 PRL 76 4119 J.E. Bartelt et al. (CLEO Collab.)
BUSKULIC 96 ZPHY C70 579 D. Buskulic et al. (ALEPH Collab.)
BUSKULIC 96C ZPHY C70 561 D. Buskulic et al. (ALEPH Collab.)
COAN 96 PR D53 6037 T.E. Coan et al. (CLEO Collab.)
ABE 95Y PR D52 4828 K. Abe et al. (SLD Collab.)
ABREU 95T PL B357 715 P. Abreu et al. (DELPHI Collab.)
ABREU 95U PL B359 411 P. Abreu et al. (DELPHI Collab.)
ACCIARRI 95 PL B345 93 M. Acciarri et al. (L3 Collab.)
ACCIARRI 95F PL B352 487 M. Acciarri et al. (L3 Collab.)
AKERS 95F ZPHY C66 31 R. Akers et al. (OPAL Collab.)
AKERS 95I ZPHY C66 543 R. Akers et al. (OPAL Collab.)
AKERS 95P ZPHY C67 45 R. Akers et al. (OPAL Collab.)
AKERS 95Y ZPHY C68 555 R. Akers et al. (OPAL Collab.)
ALBRECHT 95 PL B341 441 H. Albrecht et al. (ARGUS Collab.)
ALBRECHT 95C PL B349 576 H. Albrecht et al. (ARGUS Collab.)
ALBRECHT 95G ZPHY C68 25 H. Albrecht et al. (ARGUS Collab.)
ALBRECHT 95H ZPHY C68 215 H. Albrecht et al. (ARGUS Collab.)
BALEST 95C PRL 75 3809 R. Balest et al. (CLEO Collab.)
BERNABEU 95 NP B436 474 J. Bernabeu et al.
BUSKULIC 95C PL B346 371 D. Buskulic et al. (ALEPH Collab.)
BUSKULIC 95D PL B346 379 D. Buskulic et al. (ALEPH Collab.)
Also PL B363 265 (erratum) D. Buskulic et al. (ALEPH Collab.)
ABREU 94K PL B334 435 P. Abreu et al. (DELPHI Collab.)
AKERS 94E PL B328 207 R. Akers et al. (OPAL Collab.)
AKERS 94G PL B339 278 R. Akers et al. (OPAL Collab.)
ALBRECHT 94E PL B337 383 H. Albrecht et al. (ARGUS Collab.)
ARTUSO 94 PRL 72 3762 M. Artuso et al. (CLEO Collab.)
BARTELT 94 PRL 73 1890 J.E. Bartelt et al. (CLEO Collab.)
BATTLE 94 PRL 73 1079 M. Battle et al. (CLEO Collab.)
BAUER 94 PR D50 13 D.A. Bauer et al. (TPC/2gamma Collab.)
BUSKULIC 94D PL B321 168 D. Buskulic et al. (ALEPH Collab.)
BUSKULIC 94E PL B332 209 D. Buskulic et al. (ALEPH Collab.)
BUSKULIC 94F PL B332 219 D. Buskulic et al. (ALEPH Collab.)
GIBAUT 94B PRL 73 934 D. Gibaut et al. (CLEO Collab.)
ADRIANI 93M PRPL 236 1 O. Adriani et al. (L3 Collab.)
ALBRECHT 93C ZPHY C58 61 H. Albrecht et al. (ARGUS Collab.)
ALBRECHT 93G PL B316 608 H. Albrecht et al. (ARGUS Collab.)
BALEST 93 PR D47 3671 R. Balest et al. (CLEO Collab.)
BEAN 93 PRL 70 138 A. Bean et al. (CLEO Collab.)
BORTOLETTO 93 PRL 71 1791 D. Bortoletto et al. (CLEO Collab.)
ESCRIBANO 93 PL B301 419 R. Escribano, E. Masso (BARC)
PROCARIO 93 PRL 70 1207 M. Procario et al. (CLEO Collab.)
ABREU 92N ZPHY C55 555 P. Abreu et al. (DELPHI Collab.)
ACTON 92F PL B281 405 D.P. Acton et al. (OPAL Collab.)
ACTON 92H PL B288 373 P.D. Acton et al. (OPAL Collab.)
AKERIB 92 PRL 69 3610 D.S. Akerib et al. (CLEO Collab.)
Also PRL 71 3395 (erratum) D.S. Akerib et al. (CLEO Collab.)
ALBRECHT 92D ZPHY C53 367 H. Albrecht et al. (ARGUS Collab.)
ALBRECHT 92K ZPHY C55 179 H. Albrecht et al. (ARGUS Collab.)
ALBRECHT 92M PL B292 221 H. Albrecht et al. (ARGUS Collab.)

Downloaded from https://academic.oup.com/ptep/article/2022/8/083C01/6651666 by KIT Library user on 27 September 2022

ALBRECHT	92Q	ZPHY C56 339	H. Albrecht *et al.*	(ARGUS Collab.)
AMMAR	92	PR D45 3976	R. Ammar *et al.*	(CLEO Collab.)
ARTUSO	92	PRL 69 3278	M. Artuso *et al.*	(CLEO Collab.)
BAI	92	PRL 69 3021	J.Z. Bai *et al.*	(BES Collab.)
BATTLE	92	PL B291 488	M. Battle *et al.*	(CLEO Collab.)
BUSKULIC	92J	PL B297 459	D. Buskulic *et al.*	(ALEPH Collab.)
DECAMP	92C	ZPHY C54 211	D. Decamp *et al.*	(ALEPH Collab.)
ADEVA	91F	PL B265 451	B. Adeva *et al.*	(L3 Collab.)
ALBRECHT	91D	PL B260 259	H. Albrecht *et al.*	(ARGUS Collab.)
ALEXANDER	91D	PL B266 201	G. Alexander *et al.*	(OPAL Collab.)
ANTREASYAN	91	PL B259 216	D. Antreasyan *et al.*	(Crystal Ball Collab.)
GRIFOLS	91	PL B255 611	J.A. Grifols, A. Mendez	(BARC)
ABACHI	90	PR D41 1414	S. Abachi *et al.*	(HRS Collab.)
ALBRECHT	90E	PL B246 278	H. Albrecht *et al.*	(ARGUS Collab.)
ALBRECHT	90I	PL B250 164	H. Albrecht *et al.*	(ARGUS Collab.)
BEHREND	90	ZPHY C46 537	H.J. Behrend *et al.*	(CELLO Collab.)
BOWCOCK	90	PR D41 805	T.J.V. Bowcock *et al.*	(CLEO Collab.)
DELAGUILA	90	PL B252 116	F. del Aguila, M. Sher	(BARC, WILL)
GOLDBERG	90	PL B251 223	M. Goldberg *et al.*	(CLEO Collab.)
WU	90	PR D41 2339	D.Y. Wu *et al.*	(Mark II Collab.)
ABACHI	89B	PR D40 902	S. Abachi *et al.*	(HRS Collab.)
BEHREND	89B	PL B222 163	H.J. Behrend *et al.*	(CELLO Collab.)
JANSSEN	89	PL B228 273	H. Janssen *et al.*	(Crystal Ball Collab.)
KLEINWORT	89	ZPHY C42 7	C. Kleinwort *et al.*	(JADE Collab.)
ADEVA	88	PR D38 2665	B. Adeva *et al.*	(Mark-J Collab.)
ALBRECHT	88B	PL B202 149	H. Albrecht *et al.*	(ARGUS Collab.)
ALBRECHT	88L	ZPHY C41 1	H. Albrecht *et al.*	(ARGUS Collab.)
ALBRECHT	88M	ZPHY C41 405	H. Albrecht *et al.*	(ARGUS Collab.)
AMIDEI	88	PR D37 1750	D. Amidei *et al.*	(Mark II Collab.)
BEHREND	88	PL B200 226	H.J. Behrend *et al.*	(CELLO Collab.)
BRAUNSCH...	88C	ZPHY C39 331	W. Braunschweig *et al.*	(TASSO Collab.)
KEH	88	PL B212 123	S. Keh *et al.*	(Crystal Ball Collab.)
TSCHIRHART	88	PL B205 407	R. Tschirhart *et al.*	(HRS Collab.)
ABACHI	87B	PL B197 291	S. Abachi *et al.*	(HRS Collab.)
ABACHI	87C	PRL 59 2519	S. Abachi *et al.*	(HRS Collab.)
ADLER	87B	PRL 59 1527	J. Adler *et al.*	(Mark III Collab.)
AIHARA	87B	PR D35 1553	H. Aihara *et al.*	(TPC Collab.)
AIHARA	87C	PRL 59 751	H. Aihara *et al.*	(TPC Collab.)
ALBRECHT	87L	PL B185 223	H. Albrecht *et al.*	(ARGUS Collab.)
ALBRECHT	87P	PL B199 580	H. Albrecht *et al.*	(ARGUS Collab.)
BAND	87	PL B198 297	H.R. Band *et al.*	(MAC Collab.)
BAND	87B	PRL 59 415	H.R. Band *et al.*	(MAC Collab.)
BARINGER	87	PRL 59 1993	P. Baringer *et al.*	(CLEO Collab.)
BEBEK	87C	PR D36 690	C. Bebek *et al.*	(CLEO Collab.)
BURCHAT	87	PR D35 27	P.R. Burchat *et al.*	(Mark II Collab.)
BYLSMA	87	PR D35 2269	B.G. Bylsma *et al.*	(HRS Collab.)
COFFMAN	87	PR D36 2185	D.M. Coffman *et al.*	(Mark III Collab.)
DERRICK	87	PL B189 260	M. Derrick *et al.*	(HRS Collab.)
FORD	87	PR D35 408	W.T. Ford *et al.*	(MAC Collab.)
FORD	87B	PR D36 1971	W.T. Ford *et al.*	(MAC Collab.)
GAN	87	PRL 59 411	K.K. Gan *et al.*	(Mark II Collab.)
GAN	87B	PL B197 561	K.K. Gan *et al.*	(Mark II Collab.)
AIHARA	86E	PRL 57 1836	H. Aihara *et al.*	(TPC Collab.)
BARTEL	86D	PL B182 216	W. Bartel *et al.*	(JADE Collab.)
PDG	86	PL 170B 1	M. Aguilar-Benitez *et al.*	(CERN, CIT+)
RUCKSTUHL	86	PRL 56 2132	W. Ruckstuhl *et al.*	(DELCO Collab.)
SCHMIDKE	86	PRL 57 527	W.B. Schmidke *et al.*	(Mark II Collab.)
YELTON	86	PRL 56 812	J.M. Yelton *et al.*	(Mark II Collab.)
ALTHOFF	85	ZPHY C26 521	M. Althoff *et al.*	(TASSO Collab.)
ASH	85B	PRL 55 2118	W.W. Ash *et al.*	(MAC Collab.)
BALTRUSAIT...	85	PRL 55 1842	R.M. Baltrusaitis *et al.*	(Mark III Collab.)
BARTEL	85F	PL 161B 188	W. Bartel *et al.*	(JADE Collab.)
BEHRENDS	85	PR D32 2468	S. Behrends *et al.*	(CLEO Collab.)
BELTRAMI	85	PRL 54 1775	I. Beltrami *et al.*	(HRS Collab.)
BERGER	85	ZPHY C28 1	C. Berger *et al.*	(PLUTO Collab.)
BURCHAT	85	PRL 54 2489	P.R. Burchat *et al.*	(Mark II Collab.)
FERNANDEZ	85	PRL 54 1624	E. Fernandez *et al.*	(MAC Collab.)
MILLS	85	PRL 54 624	G.B. Mills *et al.*	(DELCO Collab.)
AIHARA	84C	PR D30 2436	H. Aihara *et al.*	(TPC Collab.)
BEHREND	84	ZPHY C23 103	H.J. Behrend *et al.*	(CELLO Collab.)
MILLS	84	PRL 52 1944	G.B. Mills *et al.*	(DELCO Collab.)
BEHREND	83C	PL 127B 270	H.J. Behrend *et al.*	(CELLO Collab.)
SILVERMAN	83	PR D27 1196	D.J. Silverman, G.L. Shaw	(UCI)
BEHREND	82	PL 114B 282	H.J. Behrend *et al.*	(CELLO Collab.)
BLOCKER	82B	PRL 48 1586	C.A. Blocker *et al.*	(Mark II Collab.)
BLOCKER	82D	PL 109B 119	C.A. Blocker *et al.*	(Mark II Collab.) J
FELDMAN	82	PRL 48 66	G.J. Feldman *et al.*	(Mark II Collab.)
HAYES	82	PR D25 2869	K.G. Hayes *et al.*	(Mark II Collab.)
BERGER	81B	PL 99B 489	C. Berger *et al.*	(PLUTO Collab.)
DORFAN	81	PRL 46 215	J.M. Dorfan *et al.*	(Mark II Collab.)
BRANDELIK	80	PL 92B 199	R. Brandelik *et al.*	(TASSO Collab.)
ZHOLENTZ	80	PL 96B 214	A.A. Zholents *et al.*	(NOVO)
Also		SJNP 34 814	A.A. Zholents *et al.*	(NOVO)
		Translated from YAF 34 1471.		
BACINO	79B	PRL 42 749	W.J. Bacino *et al.*	(DELCO Collab.)
KIRKBY	79	SLAC-PUB-2419	J. Kirkby	(SLAC) J
Batavia Lepton Photon Conference.				
BACINO	78B	PRL 41 13	W.J. Bacino *et al.*	(DELCO Collab.) J
Also		Tokyo Conf. 249	J. Kirz	(STON)
Also		PL 96B 214	A.A. Zholents *et al.*	(NOVO)
BRANDELIK	78	PL 73B 109	R. Brandelik *et al.*	(DASP Collab.) J
FELDMAN	78	Tokyo Conf. 777	G.J. Feldman	(SLAC) J
JAROS	78	PRL 40 1120	J. Jaros *et al.*	(LGW Collab.)
PERL	75	PRL 35 1489	M.L. Perl *et al.*	(LBL, SLAC)

OTHER RELATED PAPERS

DAVIER	06	RMP 78 1043	M. Davier, A. Hocker, Z. Zhang	(LALO, PARIN+)
RAHAL-CAL...	98	IJMP A13 695	G. Rahal-Callot	(ETH)
GENTILE	96	PRPL 274 287	S. Gentile, M. Pohl	(ROMAI, ETH)
WEINSTEIN	93	ARNPS 43 457	A.J. Weinstein, R. Stroynowski	(CIT, SMU)
PERL	92	RPP 55 653	M.L. Perl	(SLAC)
PICH	90	MPL A5 1995	A. Pich	(VALE)
BARISH	88	PRPL 157 1	B.C. Barish, R. Stroynowski	(CIT)
GAN	88	IJMP A3 531	K.K. Gan, M.L. Perl	(SLAC)
HAYES	88	PR D38 3351	K.G. Hayes, M.L. Perl	(SLAC)
PERL	80	ARNPS 30 299	M.L. Perl	(SLAC)

Heavy Charged Lepton Searches

Charged Heavy Lepton MASS LIMITS

Sequential Charged Heavy Lepton ($L^{\pm}$) MASS LIMITS

These experiments assumed that a fourth generation $L^{\pm}$ decayed to a fourth generation ν_L (or L^0) where ν_L was stable, or that $L^{\pm}$ decays to a light ν_ℓ via mixing.

See the "Quark and Lepton Compositeness, Searches for" Listings for limits on radiatively decaying excited leptons, *i.e.* $\ell^* \rightarrow \ell\gamma$. See the "WIMPs and other Particle Searches" section for heavy charged particle search limits in which the charged particle could be a lepton.

VALUE (GeV)	CL%	DOCUMENT ID		TECN	COMMENT
>100.8	95	ACHARD	01B	L3	Decay to νW
>101.9	95	ACHARD	01B	L3	$m_L - m_{L^0} > 15$ GeV
• • • We do not use the following data for averages, fits, limits, etc. • • •					
> 81.5	95	ACKERSTAFF	98C	OPAL	Assumed $m_{L^{\pm}} - m_{L^0} > 8.4$ GeV
> 80.2	95	ACKERSTAFF	98C	OPAL	$m_{L^0} > m_{L^{\pm}}$ and $L^{\pm} \rightarrow \nu W$
< 48 or > 61	95	[1] ACCIARRI	96G	L3	
> 63.9	95	ALEXANDER	96P	OPAL	Decay to massless ν's
> 63.5	95	BUSKULIC	96S	ALEP	$m_L - m_{L^0} > 7$ GeV
> 65	95	BUSKULIC	96S	ALEP	Decay to massless ν's
none 10–225		[2] AHMED	94	CNTR	H1 Collab. at HERA
none 12.6–29.6	95	KIM	91B	AMY	Massless ν assumed
> 44.3	95	AKRAWY	90G	OPAL	
none 0.5–10	95	[3] RILES	90	MRK2	For (m_{L^0}-m_{L^0})> 0.25–0.4GeV
> 8		[4] STOKER	89	MRK2	For ($m_{L^+} - m_{L^0}$)= 0.4 GeV
> 12		[4] STOKER	89	MRK2	For m_{L^0}=0.9 GeV
none 18.4–27.6	95	[5] ABE	88	VNS	
> 25.5	95	[6] ADACHI	88B	TOPZ	
none 1.5–22.0	95	BEHREND	88C	CELL	
> 41	90	[7] ALBAJAR	87B	UA1	
> 22.5	95	[8] ADEVA	85	MRKJ	
> 18.0	95	[9] BARTEL	83	JADE	
none 4–14.5	95	[10] BERGER	81B	PLUT	
> 15.5	95	[11] BRANDELIK	81	TASS	
> 13.		[12] AZIMOV	80		
> 16.	95	[13] BARBER	80B	CNTR	
> 0.490		[14] ROTHE	69	RVUE	

[1] ACCIARRI 96G assumes LEP result that the associated neutral heavy lepton mass > 40 GeV.

[2] The AHMED 94 limits are from a search for neutral and charged sequential heavy leptons at HERA via the decay channels $L^- \rightarrow e\gamma$, $L^- \rightarrow \nu W^-$, $L^- \rightarrow eZ$; and $L^0 \rightarrow \nu\gamma$, $L^0 \rightarrow e^- W^+$, $L^- \rightarrow \nu Z$, where the W decays to $\ell\nu_\ell$, or to jets, and Z decays to $\ell^+\ell^-$ or jets.

[3] RILES 90 limits were the result of a special analysis of the data in the case where the mass difference $m_{L^-} - m_{L^0}$ was allowed to be quite small, where L^0 denotes the neutrino into which the sequential charged lepton decays. With a slightly reduced $m_{L^{\pm}}$ range, the mass difference extends to about 4 GeV.

[4] STOKER 89 (Mark II at PEP) gives bounds on charged heavy lepton (L^+) mass for the generalized case in which the corresponding neutral heavy lepton (L^0) in the SU(2) doublet is not of negligible mass.

[5] ABE 88 search for L^+ and $L^- \rightarrow$ hadrons looking for acoplanar jets. The bound is valid for $m_\nu < 10$ GeV.

[6] ADACHI 88B search for hadronic decays giving acoplanar events with large missing energy. $E_{cm}{}^{ee} = 52$ GeV.

[7] Assumes associated neutrino is approximately massless.

[8] ADEVA 85 analyze one-isolated-muon data and sensitive to τ <10 nanosec. Assume B(lepton) = 0.30. E_{cm} = 40–47 GeV.

[9] BARTEL 83 limit is from PETRA e^+e^- experiment with average E_{cm} = 34.2 GeV.

[10] BERGER 81B is DESY DORIS and PETRA experiment. Looking for $e^+e^- \rightarrow L^+L^-$.

[11] BRANDELIK 81 is DESY-PETRA experiment. Looking for $e^+e^- \rightarrow L^+L^-$.

[12] AZIMOV 80 estimated probabilities for $M + N$ type events in $e^+e^- \rightarrow L^+L^-$ deducing semi-hadronic decay multiplicities of L from e^+e^- annihilation data at $E_{cm} = (2/3)m_L$. Obtained above limit comparing these with e^+e^- data (BRANDELIK 80).

[13] BARBER 80B looked for $e^+e^- \rightarrow L^+L^-$, $L \rightarrow \nu_L^+ X$ with MARK-J at DESY-PETRA.

[14] ROTHE 69 examines previous data on μ pair production and π and K decays.

Stable Charged Heavy Lepton ($L^{\pm}$) MASS LIMITS

VALUE (GeV)	CL%	DOCUMENT ID		TECN
>102.6	95	ACHARD	01B	L3
• • • We do not use the following data for averages, fits, limits, etc. • • •				
> 28.2	95	[15] ADACHI	90C	TOPZ
none 18.5–42.8	95	AKRAWY	90O	OPAL
> 26.5	95	DECAMP	90F	ALEP
none m_μ–36.3	95	SODERSTROM	90	MRK2

[15] ADACHI 90C put lower limits on the mass of stable charged particles with electric charge Q satisfying $2/3 < Q/e < 4/3$ and with spin 0 or 1/2. We list here the special case for a stable charged heavy lepton.

Downloaded from https://academic.oup.com/ptep/article/2022/8/083C01/6651666 by KIT Library user on 27 September 2022

Charged Long-Lived Heavy Lepton MASS LIMITS

VALUE (GeV)	CL%	DOCUMENT ID		TECN	CHG	COMMENT
• • • We do not use the following data for averages, fits, limits, etc. • • •						
>574	95	CHATRCHYAN 13AB		CMS		Leptons singlet model
>102.0	95	ABBIENDI	03L	OPAL		pair produced in e^+e^-
> 0.1		[16] ANSORGE	73B	HBC	–	Long-lived
none 0.55–4.5		[17] BUSHNIN	73	CNTR	–	Long-lived
none 0.2–0.92		[18] BARNA	68	CNTR	–	Long-lived
none 0.97–1.03		[18] BARNA	68	CNTR	–	Long-lived

[16] ANSORGE 73B looks for electron pair production and electron-like Bremsstrahlung.
[17] BUSHNIN 73 is SERPUKHOV 70 GeV p experiment. Masses assume mean life above 7×10^{-10} and 3×10^{-8} respectively. Calculated from cross section (see "Charged Quasi-Stable Lepton Production Differential Cross Section" below) and 30 GeV muon pair production data.
[18] BARNA 68 is SLAC photoproduction experiment.

Doubly-Charged Heavy Lepton MASS LIMITS

VALUE (GeV)	CL%	DOCUMENT ID		TECN	CHG
• • • We do not use the following data for averages, fits, limits, etc. • • •					
none 1–9 GeV	90	[19] CLARK	81	SPEC	++

[19] CLARK 81 is FNAL experiment with 209 GeV muons. Bounds apply to μ_P which couples with full weak strength to muon. See also section on "Doubly-Charged Lepton Production Cross Section."

Doubly-Charged Lepton Production Cross Section (μN Scattering)

VALUE (cm^2)	EVTS	DOCUMENT ID		TECN	CHG
• • • We do not use the following data for averages, fits, limits, etc. • • •					
$<6. \times 10^{-38}$	0	[20] CLARK	81	SPEC	++

[20] CLARK 81 is FNAL experiment with 209 GeV muon. Looked for μ^+ nucleon $\rightarrow \overline{\mu}^0_P X$, $\overline{\mu}^0_P \rightarrow \mu^+\mu^-\overline{\nu}_\mu$ and $\mu^+ n \rightarrow \mu^{++}_P X$, $\mu^{++}_P \rightarrow 2\mu^+\nu_\mu$. Above limits are for $\sigma\times$BR taken from their mass-dependence plot figure 2.

REFERENCES FOR Heavy Charged Lepton Searches

CHATRCHYAN	13AB	JHEP 1307 122	S. Chatrchyan *et al.*	(CMS Collab.)
ABBIENDI	03L	PL B572 8	G. Abbiendi *et al.*	(OPAL Collab.)
ACHARD	01B	PL B517 75	P. Achard *et al.*	(L3 Collab.)
ACKERSTAFF	98C	EPJ C1 45	K. Ackerstaff *et al.*	(OPAL Collab.)
ACCIARRI	96G	PL B377 304	M. Acciarri *et al.*	(L3 Collab.)
ALEXANDER	96P	PL B385 433	G. Alexander *et al.*	(OPAL Collab.)
BUSKULIC	96S	PL B384 439	D. Buskulic *et al.*	(ALEPH Collab.)
AHMED	94	PL B340 205	T. Ahmed *et al.*	(H1 Collab.)
KIM	91B	IJMP A6 2583	G.N. Kim *et al.*	(AMY Collab.)
ADACHI	90C	PL B244 352	I. Adachi *et al.*	(TOPAZ Collab.)
AKRAWY	90G	PL B240 250	M.Z. Akrawy *et al.*	(OPAL Collab.)
AKRAWY	90O	PL B252 290	M.Z. Akrawy *et al.*	(OPAL Collab.)
DECAMP	90F	PL B236 511	D. Decamp *et al.*	(ALEPH Collab.)
RILES	90	PR D42 1	K. Riles *et al.*	(Mark II Collab.)
SODERSTROM	90	PRL 64 2980	E. Soderstrom *et al.*	(Mark II Collab.)
STOKER	89	PR D39 1811	D.P. Stoker *et al.*	(Mark II Collab.)
ABE	88	PRL 61 915	K. Abe *et al.*	(VENUS Collab.)
ADACHI	88B	PR D37 1339	I. Adachi *et al.*	(TOPAZ Collab.)
BEHREND	88C	ZPHY C41 7	H.J. Behrend *et al.*	(CELLO Collab.)
ALBAJAR	87B	PL B185 241	C. Albajar *et al.*	(UA1 Collab.)
ADEVA	85	PL 152B 439	B. Adeva *et al.*	(Mark-J Collab.)
Also		PRPL 109 131	B. Adeva *et al.*	(Mark-J Collab.)
BARTEL	83	PL 123B 353	W. Bartel *et al.*	(JADE Collab.)
BERGER	81B	PL 99B 489	C. Berger *et al.*	(PLUTO Collab.)
BRANDELIK	81	PL 99B 163	R. Brandelik *et al.*	(TASSO Collab.)
CLARK	81	PRL 46 299	A.R. Clark *et al.*	(UCB, LBL, FNAL+)
Also		PR D25 2762	W.H. Smith *et al.*	(LBL, FNAL, PRIN)
AZIMOV	80	JETPL 32 664	Y.I. Azimov, V.A. Khoze	(PNPI)
		Translated from ZETFP 32 677.		
BARBER	80B	PRL 45 1904	D.P. Barber *et al.*	(Mark-J Collab.)
BRANDELIK	80	PL 92B 199	R. Brandelik *et al.*	(TASSO Collab.)
ANSORGE	73B	PR D7 26	R.E. Ansorge *et al.*	(CAVE)
BUSHNIN	73	NP B58 476	Y.B. Bushnin *et al.*	(SERP)
Also		PL 42B 136	S.V. Golovkin *et al.*	(SERP)
ROTHE	69	NP B10 241	K.W. Rothe, A.M. Wolsky	(PENN)
BARNA	68	PR 173 1391	A. Barna *et al.*	(SLAC, STAN)

OTHER RELATED PAPERS

PERL	81	SLAC-PUB-2752	M.L. Perl	(SLAC)
Physics in Collision Conference.				

Neutrino Properties

NEUTRINO PROPERTIES

Revised July 2021 by P. Vogel (Caltech) and A. Piepke (University of Alabama).

The Neutrino Properties Listings concern measurements of various properties of neutrinos. Nearly all of the measurements, so far only limits, actually concern superpositions of the mass eigenstates ν_i, which are in turn related to the weak eigenstates ν_ℓ, via the neutrino mixing matrix

$$|\nu_\ell\rangle = \sum_i U_{\ell i}\,|\nu_i\rangle \ .$$

In the analogous case of quark mixing via the CKM matrix, the smallness of the off-diagonal terms (small mixing angles) permits a "dominant eigenstate" approximation. However, the results of neutrino oscillation searches show that the mixing matrix contains two large mixing angles and a third angle that is not exceedingly small. We cannot therefore associate any particular state $|\nu_i\rangle$ with any particular lepton label e, μ or τ. Nevertheless, note that in the standard labeling the $|\nu_1\rangle$ has the largest $|\nu_e\rangle$ component ($\sim 2/3$), $|\nu_2\rangle$ contains $\sim 1/3$ of the $|\nu_e\rangle$ component and $|\nu_3\rangle$ contains only a small $\sim 2.5\%$ $|\nu_e\rangle$ component.

Neutrinos are produced in weak decays with a definite lepton flavor, and are typically detected by the charged current weak interaction again associated with a specific lepton flavor. Hence, the listings for the neutrino mass that follow are separated into the three associated charged lepton categories. Other properties (mean lifetime, magnetic moment, charge and charge radius) are no longer separated this way. If needed, the associated lepton flavor is reported in the footnotes.

Measured quantities (mass-squared, magnetic moments, mean lifetimes, *etc.*) all depend upon the mixing parameters $|U_{\ell i}|^2$, but to some extent also on experimental conditions (e.g., on energy resolution). Many of these observables, in particular mass-squared, cannot distinguish between Dirac and Majorana neutrinos and are unaffected by CP phases.

Direct neutrino mass measurements are usually based on the analysis of the kinematics of charged particles (leptons, pions) emitted together with neutrinos (flavor states) in various weak decays. The most sensitive neutrino mass measurement to date, involving electron type antineutrinos, is based on fitting the shape of the beta spectrum. The quantity $m^{2(eff)}_{\nu_e} = \sum_i |U_{ei}|^2 m^2_{\nu_i}$ is determined or constrained, where the sum is over all mass eigenvalues m_{ν_i} that are too close together to be resolved experimentally. (The quantity $m^{eff}_{\nu_e} \equiv \sqrt{m^{2(eff)}_{\nu_e}}$ is often denoted $\langle m_\beta \rangle$ in the literature.) If the energy resolution is better than $\Delta m^2_{ij} \equiv m^2_{\nu_i} - m^2_{\nu_j}$, the corresponding heavier m_{ν_i} and mixing parameter could be determined by fitting the resulting spectral anomaly (step or kink).

The dependence of m_{ν_e} on the mass of the lightest neutrino is shown in Fig. 14.11 of the *Neutrino Masses, Mixing, and Oscillations* review. In the case of inverted ordering there is a minimum possible value of $m^{eff}_{\nu_e}$, approximately $\sqrt{(}\Delta m^2_{32}) \sim$ 50 meV. If $m^{eff}_{\nu_e}$ is found to be larger than this value, it is impossible, based on this information only, to decide which ordering is realized in nature. On the other hand, if the $m^{eff}_{\nu_e}$ is less than ~50 meV, only the normal mass ordering is possible.

A limit on $m^{2(eff)}_{\nu_e}$ implies an upper limit on the minimum value m^2_{min} of $m^2_{\nu_i}$, independent of the mixing parameters U_{ei}:

Downloaded from https://academic.oup.com/ptep/article/2022/8/083C01/6651666 by KIT Library user on 27 September 2022

$m^2_{min} \leq m^{2(eff)}_{\nu_e}$. However, if and when the value of $m^{2(eff)}_{\nu_e}$ is determined then its combination with the results derived from neutrino oscillations that give us the values of the neutrino mass-squared differences $\Delta m^2_{ij} \equiv m^2_i - m^2_j$, including eventually also their signs, and the mixing parameters $|U_{ei}|^2$, the individual neutrino mass squares $m^2_{\nu_j} = m^{2(eff)}_{\nu_e} - \sum_i |U_{ei}|^2 \Delta m^2_{ij}$ can be determined.

So far solar, reactor, atmospheric and accelerator neutrino oscillation experiments can be consistently described using three active neutrino flavors, i.e. two mass splittings and three mixing angles. However, several experiments with radioactive sources, reactors, and accelerators imply the possible existence of one or more non-interacting, i.e. sterile, neutrino species that might be observable since they couple, albeit weakly, to the flavor neutrinos $|\nu_l\rangle$. In that case, the neutrino mixing matrix would be $n \times n$ unitary matrix with $n > 3$.

Combined three neutrino analyses determine the squared mass differences and all three mixing angles to within reasonable accuracy. For given $|\Delta m^2_{ij}|$ a limit on $m^{2(eff)}_{\nu_e}$ from beta decay defines an upper limit on the maximum value m_{max} of m_{ν_i}: $m^2_{max} \leq m^{2(eff)}_{\nu_e} + \sum_{i<j} |\Delta m^2_{ij}|$. The analysis of the low energy beta decay of tritium, combined with the oscillation results, thus limits *all* active neutrino masses. Traditionally, experimental neutrino mass limits obtained from pion decay $\pi^+ \to \mu^+ + \nu_\mu$ or the shape of the spectrum of decay products of the τ lepton did not distinguish between flavor and mass eigenstates. These results are reported as limits of the μ and τ based neutrino mass. After the determination of the $|\Delta m^2_{ij}|$'s and the mixing angles θ_{ij}, the corresponding neutrino mass limits are no longer competitive with those derived from low energy beta decays.

The spread of arrival times of the neutrinos from SN1987A, coupled with the measured neutrino energies, provided a time-of-flight limit on a quantity similar to $\langle m_\beta \rangle \equiv \sqrt{m^{2(eff)}_{\nu_e}}$. This statement, clothed in various degrees of sophistication, has been the basis for a very large number of papers. The resulting limits, however, are no longer comparable with the limits from tritium beta decay.

Constraint, or eventually a value, of the sum of the neutrino masses m_{tot} can be determined from the analysis of the cosmic microwave background anisotropy, combined with the galaxy redshift surveys and other data. These limits are reported in a separate table (Sum of Neutrino Masses, m_{tot}). Obviously, m_{tot} represents an upper limit for all m_i values. Note that many reported m_{tot} limits are considerably more stringent than the listed $m^{eff}_{\nu_e}$ limits. Discussion concerning the model dependence of the m_{tot} limit is continuing.

$\overline{\nu}$ MASS (electron based)

Those limits given below are for the square root of $m^{2(\mathrm{eff})}_{\nu_e} \equiv \sum_i |U_{ei}|^2 m^2_{\nu_i}$. Limits that come from the kinematics of ^{3}H $\beta^- \overline{\nu}$ decay are the square roots of the limits for $m^{2(\mathrm{eff})}_{\nu_e}$. Obtained from the measurements reported in the Listings for "$\overline{\nu}$ Mass Squared," below.

VALUE (eV)	CL%	DOCUMENT ID		TECN	COMMENT
< 1.1	90	[1] AKER	19	SPEC	^{3}H β decay
• • • We do not use the following data for averages, fits, limits, etc. • • •					
< 2.05	95	[2] ASEEV	11	SPEC	^{3}H β decay
< 5.8	95	[3] PAGLIAROLI	10	ASTR	SN1987A
< 2.3	95	[4] KRAUS	05	SPEC	^{3}H β decay
<21.7	90	[5] ARNABOLDI	03A	BOLO	^{187}Re β decay
< 5.7	95	[6] LOREDO	02	ASTR	SN1987A
< 2.5	95	[7] LOBASHEV	99	SPEC	^{3}H β decay
< 2.8	95	[8] WEINHEIMER	99	SPEC	^{3}H β decay
< 4.35	95	[9] BELESEV	95	SPEC	^{3}H β decay
<12.4	95	[10] CHING	95	SPEC	^{3}H β decay
<92	95	[11] HIDDEMANN	95	SPEC	^{3}H β decay
15^{+32}_{-15}		HIDDEMANN	95	SPEC	^{3}H β decay
<19.6	95	KERNAN	95	ASTR	SN 1987A
< 7.0	95	[12] STOEFFL	95	SPEC	^{3}H β decay
< 7.2	95	[13] WEINHEIMER	93	SPEC	^{3}H β decay
<11.7	95	[14] HOLZSCHUH	92B	SPEC	^{3}H β decay
<13.1	95	[15] KAWAKAMI	91	SPEC	^{3}H β decay
< 9.3	95	[16] ROBERTSON	91	SPEC	^{3}H β decay
<14	95	AVIGNONE	90	ASTR	SN 1987A
<16		SPERGEL	88	ASTR	SN 1987A
17 to 40		[17] BORIS	87	SPEC	^{3}H β decay

[1] AKER 19 report a neutrino mass limit, derived from the first month of data collected by the KATRIN tritium endpoint experiment. The analysis of the electron kinematics shows no evidence for neutrino mass. The quoted result is based on a Bayesian analysis of the data. Using the method of Feldman and Cousins, the derived upper limit is < 0.8 eV at 90% C.L.

[2] ASEEV 11 report the analysis of the entire beta endpoint data, taken with the Troitsk integrating electrostatic spectrometer between 1997 and 2002 (some of the earlier runs were rejected), using a windowless gaseous tritium source. The fitted value of m_ν, based on the method of Feldman and Cousins, is obtained from the upper limit of the fit for m^2_ν. Previous analysis problems were resolved by careful monitoring of the tritium gas column density. Supersedes LOBASHEV 99 and BELESEV 95.

[3] PAGLIAROLI 10 is critical of the likelihood method used by LOREDO 02.

[4] KRAUS 05 is a continuation of the work reported in WEINHEIMER 99. This result represents the final analysis of data taken from 1997 to 2001. Various sources of systematic uncertainties have been identified and quantified. The background has been reduced compared to the initial running period. A spectral anomaly at the endpoint, reported in LOBASHEV 99, was not observed.

[5] ARNABOLDI 03A *et al.* report kinematical neutrino mass limit using β-decay of ^{187}Re. Bolometric $AgReO_4$ micro-calorimeters are used. Mass bound is substantially weaker than those derived from tritium β-decays but has different systematic uncertainties.

[6] LOREDO 02 updates LOREDO 89.

[7] LOBASHEV 99 report a new measurement which continues the work reported in BELESEV 95. This limit depends on phenomenological fit parameters used to derive their best fit to m^2_ν, making unambiguous interpretation difficult. See the footnote under "$\overline{\nu}$ Mass Squared."

[8] WEINHEIMER 99 presents two analyses which exclude the spectral anomaly and result in an acceptable m^2_ν. We report the most conservative limit, but the other is nearly the same. See the footnote under "$\overline{\nu}$ Mass Squared."

[9] BELESEV 95 (Moscow) use an integral electrostatic spectrometer with adiabatic magnetic collimation and a gaseous tritium sources. A fit to a normal Kurie plot above 18300–18350 eV (to avoid a low-energy anomaly) plus a monochromatic line 7–15 eV below the endpoint yields $m^2_\nu = -4.1 \pm 10.9$ eV^2, leading to this Bayesian limit.

[10] CHING 95 quotes results previously given by SUN 93; no experimental details are given. A possible explanation for consistently negative values of m^2_ν is given.

[11] HIDDEMANN 95 (Munich) experiment uses atomic tritium embedded in a metal-dioxide lattice. Bayesian limit calculated from the weighted mean $m^2_\nu = 221 \pm 4244$ eV^2 from the two runs listed below.

[12] STOEFFL 95 (LLNL) result is the Bayesian limit obtained from the m^2_ν errors given below but with m^2_ν set equal to 0. The anomalous endpoint accumulation leads to a value of m^2_ν which is negative by more than 5 standard deviations.

[13] WEINHEIMER 93 (Mainz) is a measurement of the endpoint of the tritium β spectrum using an electrostatic spectrometer with a magnetic guiding field. The source is molecular tritium frozen onto an aluminum substrate.

[14] HOLZSCHUH 92B (Zurich) result is obtained from the measurement $m^2_\nu = -24 \pm 48 \pm 61$ (1σ errors), in eV^2, using the PDG prescription for conversion to a limit in m_ν.

[15] KAWAKAMI 91 (Tokyo) experiment uses tritium-labeled arachidic acid. This result is the Bayesian limit obtained from the m^2_ν limit with the errors combined in quadrature. This was also done in ROBERTSON 91, although the authors report a different procedure.

[16] ROBERTSON 91 (LANL) experiment uses gaseous molecular tritium. The result is in strong disagreement with the earlier claims by the ITEP group [LUBIMOV 80, BORIS 87 (+ BORIS 88 erratum)] that m_ν lies between 17 and 40 eV. However, the probability of a positive m^2 is only 3% if statistical and systematic error are combined in quadrature.

[17] See also comment in BORIS 87B and erratum in BORIS 88.

Downloaded from https://academic.oup.com/ptep/article/2022/8/083C01/6651666 by KIT Library user on 27 September 2022

$\overline{\nu}$ MASS SQUARED (electron based)

Given troubling systematics which result in improbably negative estimators of $m^{2(\mathrm{eff})}_{\nu_e} \equiv \sum_i |U_{ei}|^2\ m^2_{\nu_i}$, in many experiments, we use only KRAUS 05, LOBASHEV 99, and AKER 19 for our average.

VALUE (eV^2)	DOCUMENT ID		TECN	COMMENT
$-0.9^{+0.8}_{-1.0}$ OUR AVERAGE				
$-1.0^{+0.9}_{-1.1}$	[1] AKER	19	SPEC	^{3}H β decay
-0.67 ± 2.53	[2] ASEEV	11	SPEC	^{3}H β decay
$-0.6 \pm 2.2 \pm 2.1$	[3] KRAUS	05	SPEC	^{3}H β decay
• • • We do not use the following data for averages, fits, limits, etc. • • •				
$-1.9 \pm 3.4 \pm 2.2$	[4] LOBASHEV	99	SPEC	^{3}H β decay
$-3.7 \pm 5.3 \pm 2.1$	[5] WEINHEIMER	99	SPEC	^{3}H β decay
-22 ± 4.8	[6] BELESEV	95	SPEC	^{3}H β decay
129 ± 6010	[7] HIDDEMANN	95	SPEC	^{3}H β decay
313 ± 5994	[7] HIDDEMANN	95	SPEC	^{3}H β decay
$-130 \pm 20 \pm 15$	[8] STOEFFL	95	SPEC	^{3}H β decay
$-31 \pm 75 \pm 48$	[9] SUN	93	SPEC	^{3}H β decay
$-39 \pm 34 \pm 15$	[10] WEINHEIMER	93	SPEC	^{3}H β decay
$-24 \pm 48 \pm 61$	[11] HOLZSCHUH	92B	SPEC	^{3}H β decay
$-65 \pm 85 \pm 65$	[12] KAWAKAMI	91	SPEC	^{3}H β decay
$-147 \pm 68 \pm 41$	[13] ROBERTSON	91	SPEC	^{3}H β decay

[1] AKER 19 use the first month of data collected by the KATRIN experiment to determine $m^2_{\overline{\nu}}$. The result is consistent with a neutrino mass of zero and is used to place a limit on m_ν.

[2] ASEEV 11 report the analysis of the entire beta endpoint data, taken with the Troitsk integrating electrostatic spectrometer between 1997 and 2002, using a windowless gaseous tritium source. The analysis does not use the two additional fit parameters (see LOBASHEV 99) for a step-like structure near the endpoint. Using only the runs where the tritium gas column density was carefully monitored the need for such parameters was eliminated. Supersedes LOBASHEV 99 and BELESEV 95.

[3] KRAUS 05 is a continuation of the work reported in WEINHEIMER 99. This result represents the final analysis of data taken from 1997 to 2001. Problems with significantly negative squared neutrino masses, observed in some earlier experiments, have been resolved in this work.

[4] LOBASHEV 99 report a new measurement which continues the work reported in BELESEV 95. The data were corrected for electron trapping effects in the source, eliminating the dependence of the fitted neutrino mass on the fit interval. The analysis assuming a pure beta spectrum yields significantly negative fitted $m^2_\nu \approx -(20\text{–}10)$ eV^2. This problem is attributed to a discrete spectral anomaly of about 6×10^{-11} intensity with a time-dependent energy of 5–15 eV below the endpoint. The data analysis accounts for this anomaly by introducing two extra phenomenological fit parameters resulting in a best fit of $m^2_\nu = -1.9 \pm 3.4 \pm 2.2\,eV^2$ which is used to derive a neutrino mass limit. However, the introduction of phenomenological fit parameters which are correlated with the derived m^2_ν limit makes unambiguous interpretation of this result difficult.

[5] WEINHEIMER 99 is a continuation of the work reported in WEINHEIMER 93 . Using a lower temperature of the frozen tritium source eliminated the dewetting of the T_2 film, which introduced a dependence of the fitted neutrino mass on the fit interval in the earlier work. An indication for a spectral anomaly reported in LOBASHEV 99 has been seen, but its time dependence does not agree with LOBASHEV 99. Two analyses, which exclude the spectral anomaly either by choice of the analysis interval or by using a particular data set which does not exhibit the anomaly, result in acceptable m^2_ν fits and are used to derive the neutrino mass limit published by the authors. We list the most conservative of the two.

[6] BELESEV 95 (Moscow) use an integral electrostatic spectrometer with adiabatic magnetic collimation and a gaseous tritium sources. This value comes from a fit to a normal Kurie plot above 18300–18350 eV (to avoid a low-energy anomaly), including the effects of an apparent peak 7–15 eV below the endpoint.

[7] HIDDEMANN 95 (Munich) experiment uses atomic tritium embedded in a metal-dioxide lattice. They quote measurements from two data sets.

[8] STOEFFL 95 (LLNL) uses a gaseous source of molecular tritium. An anomalous pileup of events at the endpoint leads to the negative value for m^2_ν. The authors acknowledge that "the negative value for the best fit of m^2_ν has no physical meaning" and discuss possible explanations for this effect.

[9] SUN 93 uses a tritiated hydrocarbon source. See also CHING 95.

[10] WEINHEIMER 93 (Mainz) is a measurement of the endpoint of the tritium β spectrum using an electrostatic spectrometer with a magnetic guiding field. The source is molecular tritium frozen onto an aluminum substrate.

[11] HOLZSCHUH 92B (Zurich) source is a monolayer of tritiated hydrocarbon.

[12] KAWAKAMI 91 (Tokyo) experiment uses tritium-labeled arachidic acid.

[13] ROBERTSON 91 (LANL) experiment uses gaseous molecular tritium. The result is in strong disagreement with the earlier claims by the ITEP group [LUBIMOV 80, BORIS 87 (+ BORIS 88 erratum)] that m_ν lies between 17 and 40 eV. However, the probability of a positive m^2_ν is only 3% if statistical and systematic error are combined in quadrature.

ν MASS (electron based)

These are measurement of m_ν (in contrast to $m_{\overline{\nu}}$, given above). The masses can be different for a Dirac neutrino in the absence of CPT invariance. The possible distinction between ν and $\overline{\nu}$ properties is usually ignored elsewhere in these Listings.

VALUE (eV)	CL%	DOCUMENT ID		TECN	COMMENT
<460	68	YASUMI	94	CNTR	^{163}Ho decay
<225	95	SPRINGER	87	CNTR	^{163}Ho decay

ν MASS (muon based)

Limits given below are for the square root of $m^{2(\mathrm{eff})}_{\nu_\mu} \equiv \sum_i |U_{\mu i}|^2\ m^2_{\nu_i}$.

In some of the COSM papers listed below, the authors did not distinguish between weak and mass eigenstates.

OUR EVALUATION is based on OUR AVERAGE for the $\pi^\pm$ mass and the ASSAMAGAN 96 value for the muon momentum for the π^+ decay at rest. The limit is calculated using the unified classical analysis of FELDMAN 98 for a Gaussian distribution near a physical boundary. WARNING: since $m^{2(\mathrm{eff})}_{\nu_\mu}$ is calculated from the differences of large numbers, it and the corresponding limits are extraordinarily sensitive to small changes in the pion mass, the decay muon momentum, and their errors. For example, the limits obtained using JECKELMANN 94, LENZ 98, and the weighted averages are 0.15, 0.29, and 0.19 MeV, respectively.

VALUE (MeV)	CL%	DOCUMENT ID		TECN	COMMENT
<0.19 (CL = 90%) OUR EVALUATION					
<0.17	90	[1] ASSAMAGAN	96	SPEC	$m^2_\nu = -0.016 \pm 0.023$
• • • We do not use the following data for averages, fits, limits, etc. • • •					
<0.15		[2] DOLGOV	95	COSM	Nucleosynthesis
<0.48		[3] ENQVIST	93	COSM	Nucleosynthesis
<0.3		[4] FULLER	91	COSM	Nucleosynthesis
<0.42		[4] LAM	91	COSM	Nucleosynthesis
<0.50	90	[5] ANDERHUB	82	SPEC	$m^2_\nu = -0.14 \pm 0.20$
<0.65	90	CLARK	74	ASPK	$K_{\mu 3}$ decay

[1] ASSAMAGAN 96 measurement of p_μ from $\pi^+ \to \mu^+\nu$ at rest combined with JECKELMANN 94 Solution B pion mass yields $m^2_\nu = -0.016 \pm 0.023$ with corresponding Bayesian limit listed above. If Solution A is used, $m^2_\nu = -0.143 \pm 0.024$ MeV^2. Replaces ASSAMAGAN 94.

[2] DOLGOV 95 removes earlier assumptions (DOLGOV 93) about thermal equilibrium below T_{QCD} for wrong-helicity Dirac neutrinos (ENQVIST 93, FULLER 91) to set more stringent limits.

[3] ENQVIST 93 bases limit on the fact that thermalized wrong-helicity Dirac neutrinos would speed up expansion of early universe, thus reducing the primordial abundance. FULLER 91 exploits the same mechanism but in the older calculation obtains a larger production rate for these states, and hence a lower limit. Neutrino lifetime assumed to exceed nucleosynthesis time, ~ 1 s.

[4] Assumes neutrino lifetime >1 s. For Dirac neutrinos only. See also ENQVIST 93.

[5] ANDERHUB 82 kinematics is insensitive to the pion mass.

ν MASS (tau based)

The limits given below are the square roots of limits for $m^{2(\mathrm{eff})}_{\nu_\tau} \equiv \sum_i |U_{\tau i}|^2\ m^2_{\nu_i}$.

In some of the ASTR and COSM papers listed below, the authors did not distinguish between weak and mass eigenstates.

VALUE (MeV)	CL%	EVTS	DOCUMENT ID		TECN	COMMENT
< 18.2	95		[1] BARATE	98F	ALEP	1991–1995 LEP runs
• • • We do not use the following data for averages, fits, limits, etc. • • •						
< 28	95		[2] ATHANAS	00	CLEO	$E^{ee}_{cm} = 10.6$ GeV
< 27.6	95		[3] ACKERSTAFF	98T	OPAL	1990–1995 LEP runs
< 30	95	473	[4] AMMAR	98	CLEO	$E^{ee}_{cm} = 10.6$ GeV
< 60	95		[5] ANASTASSOV	97	CLEO	$E^{ee}_{cm} = 10.6$ GeV
< 0.37 or >22			[6] FIELDS	97	COSM	Nucleosynthesis
< 68	95		[7] SWAIN	97	THEO	m_τ, τ_τ, τ partial widths
< 29.9	95		[8] ALEXANDER	96M	OPAL	1990–1994 LEP runs
<149			[9] BOTTINO	96	THEO	π, μ, τ leptonic decays
<1 or >25			[10] HANNESTAD	96C	COSM	Nucleosynthesis
< 71	95		[11] SOBIE	96	THEO	m_τ, τ_τ, $B(\tau^- \to e^- \overline{\nu}_e \nu_\tau)$
< 24	95	25	[12] BUSKULIC	95H	ALEP	1991–1993 LEP runs
< 0.19			[13] DOLGOV	95	COSM	Nucleosynthesis
< 3			[14] SIGL	95	ASTR	SN 1987A
< 0.4 or > 30			[15] DODELSON	94	COSM	Nucleosynthesis
< 0.1 or > 50			[16] KAWASAKI	94	COSM	Nucleosynthesis
155–225			[17] PERES	94	THEO	π, K, μ, τ weak decays
< 32.6	95	113	[18] CINABRO	93	CLEO	$E^{ee}_{cm} \approx 10.6$ GeV
< 0.3 or > 35			[19] DOLGOV	93	COSM	Nucleosynthesis
< 0.74			[20] ENQVIST	93	COSM	Nucleosynthesis

Downloaded from https://academic.oup.com/ptep/article/2022/8/083C01/6651666 by KIT Library user on 27 September 2022

$<$ 31	95	19	[21] ALBRECHT	92M	ARG	E^{ee}_{cm}= 9.4–10.6 GeV
$<$ 0.3			[22] FULLER	91	COSM	Nucleosynthesis
$<$ 0.5 or $>$ 25			[23] KOLB	91	COSM	Nucleosynthesis
$<$ 0.42			[22] LAM	91	COSM	Nucleosynthesis

[1] BARATE 98F result based on kinematics of 2939 $\tau^- \to 2\pi^-\pi^+\nu_\tau$ and 52 $\tau^- \to 3\pi^- 2\pi^+ (\pi^0)\nu_\tau$ decays. If possible 2.5% excited a_1 decay is included in 3-prong sample analysis, limit increases to 19.2 MeV.

[2] ATHANAS 00 bound comes from analysis of $\tau^- \to \pi^-\pi^+\pi^-\pi^0\nu_\tau$ decays.

[3] ACKERSTAFF 98T use $\tau \to 5\pi^\pm\nu_\tau$ decays to obtain a limit of 43.2 MeV (95%CL). They combine this with ALEXANDER 96M value using $\tau \to 3h^\pm\nu_\tau$ decays to obtain quoted limit.

[4] AMMAR 98 limit comes from analysis of $\tau^- \to 3\pi^- 2\pi^+\nu_\tau$ and $\tau^- \to 2\pi^-\pi^+ 2\pi^0\nu_\tau$ decay modes.

[5] ANASTASSOV 97 derive limit by comparing their m_τ measurement (which depends on m_{ν_τ}) to BAI 96 m_τ threshold measurement.

[6] FIELDS 97 limit for a Dirac neutrino. For a Majorana neutrino the mass region $<$ 0.93 or $>$31 MeV is excluded. These bounds assume N_ν <4 from nucleosynthesis; a wider excluded region occurs with a smaller N_ν upper limit.

[7] SWAIN 97 derive their limit from the Standard Model relationships between the tau mass, lifetime, branching fractions for $\tau^- \to e^-\overline{\nu}_e\nu_\tau$, $\tau^- \to \mu^-\overline{\nu}_\mu\nu_\tau$, $\tau^- \to \pi^-\nu_\tau$, and $\tau^- \to K^-\nu_\tau$, and the muon mass and lifetime by assuming lepton universality and using world average values. Limit is reduced to 48 MeV when the CLEO τ mass measurement (BALEST 93) is included; see CLEO's more recent m_{ν_τ} limit (ANASTASSOV 97). Consideration of mixing with a fourth generation heavy neutrino yields $\sin^2\theta_L < 0.016$ (95%CL).

[8] ALEXANDER 96M bound comes from analyses of $\tau^- \to 3\pi^- 2\pi^+\nu_\tau$ and $\tau^- \to h^- h^- h^+\nu_\tau$ decays.

[9] BOTTINO 96 assumes three generations of neutrinos with mixing, finds consistency with massless neutrinos with no mixing based on 1995 data for masses, lifetimes, and leptonic partial widths.

[10] HANNESTAD 96C limit is on the mass of a Majorana neutrino. This bound assumes $N_\nu < 4$ from nucleosynthesis. A wider excluded region occurs with a smaller N_ν upper limit. This paper is the corrected version of HANNESTAD 96; see the erratum: HANNESTAD 96B.

[11] SOBIE 96 derive their limit from the Standard Model relationship between the tau mass, lifetime, and leptonic branching fraction, and the muon mass and lifetime, by assuming lepton universality and using world average values.

[12] BUSKULIC 95H bound comes from a two-dimensional fit of the visible energy and invariant mass distribution of $\tau \to 5\pi(\pi^0)\nu_\tau$ decays. Replaced by BARATE 98F.

[13] DOLGOV 95 removes earlier assumptions (DOLGOV 93) about thermal equilibrium below T_{QCD} for wrong-helicity Dirac neutrinos (ENQVIST 93, FULLER 91) to set more stringent limits. DOLGOV 96 argues that a possible window near 20 MeV is excluded.

[14] SIGL 95 exclude massive Dirac or Majorana neutrinos with lifetimes between 10^{-3} and 10^8 seconds if the decay products are predominantly γ or e^+e^-.

[15] DODELSON 94 calculate constraints on ν_τ mass and lifetime from nucleosynthesis for 4 generic decay modes. Limits depend strongly on decay mode. Quoted limit is valid for all decay modes of Majorana neutrinos with lifetime greater than about 300 s. For Dirac neutrinos limits change to $<$ 0.3 or $>$ 33.

[16] KAWASAKI 94 excluded region is for Majorana neutrino with lifetime $>$1000 s. Other limits are given as a function of ν_τ lifetime for decays of the type $\nu_\tau \to \nu_\mu\phi$ where ϕ is a Nambu-Goldstone boson.

[17] PERES 94 used PDG 92 values for parameters to obtain a value consistent with mixing. Reexamination by BOTTINO 96 which included radiative corrections and 1995 PDG parameters resulted in two allowed regions, $m_3 < 70$ MeV and 140 MeV $m_3 < 149$ MeV.

[18] CINABRO 93 bound comes from analysis of $\tau^- \to 3\pi^- 2\pi^+\nu_\tau$ and $\tau^- \to 2\pi^-\pi^+ 2\pi^0\nu_\tau$ decay modes.

[19] DOLGOV 93 assumes neutrino lifetime $>$100 s. For Majorana neutrinos, the low mass limit is 0.5 MeV. KAWANO 92 points out that these bounds can be overcome for a Dirac neutrino if it possesses a magnetic moment. See also DOLGOV 96.

[20] ENQVIST 93 bases limit on the fact that thermalized wrong-helicity Dirac neutrinos would speed up expansion of early universe, thus reducing the primordial abundance. FULLER 91 exploits the same mechanism but in the older calculation obtains a larger production rate for these states, and hence a lower limit. Neutrino lifetime assumed to exceed nucleosynthesis time, $\sim$1 s.

[21] ALBRECHT 92M reports measurement of a slightly lower τ mass, which has the effect of reducing the ν_τ mass reported in ALBRECHT 88B. Bound is from analysis of $\tau^- \to 3\pi^- 2\pi^+\nu_\tau$ mode.

[22] Assumes neutrino lifetime $>$1 s. For Dirac neutrinos. See also ENQVIST 93.

[23] KOLB 91 exclusion region is for Dirac neutrino with lifetime $>$1 s; other limits are given.

Revised August 2021 by K.A. Olive (University of Minnesota).

Neutrinos decouple from thermal equilibrium in the early universe at temperatures $\mathcal{O}(1)$ MeV. The limits on low mass ($m_\nu \lesssim$ 1 MeV) neutrinos apply to m_{tot} given by

$$m_{tot} = \sum_\nu m_\nu \ .$$

Stable neutrinos in this mass range decouple from the thermal bath while still relativistic and make a contribution to the total energy density of the Universe which is given by

$$\rho_\nu = m_{tot} n_\nu \simeq m_{tot}(3/11)(3.045/3)^{3/4} n_\gamma \ ,$$

where the factor 3/11 is the ratio of (light) neutrinos to photons and the factor $(3.045/3)^{3/4}$ corrects for the fact that the effective number of neutrinos in the standard model is 3.045 when taking into account e^+e^- annihilation during neutrino decoupling. Writing $\Omega_\nu = \rho_\nu/\rho_c$, where ρ_c is the critical energy density of the Universe, and using $n_\gamma = 410.7$ cm^{-3}, we have

$$\Omega_\nu h^2 \simeq m_{tot}/(93 \text{ eV}) \ .$$

While an upper limit to the matter density of $\Omega_m h^2 < 0.12$ would constrain $m_{tot} < 11$ eV, much stronger constraints are obtained from the observations of the CMB, combined with lensing and baryon acoustic oscillations data. These combine to give an upper limit of around 0.12 eV, and may, in the near future, be able to provide a lower bound on the sum of the neutrino masses. The current lower bound of $m_{tot} > 0.06$ eV implies a lower limit of $\Omega_\nu h^2 > 6 \times 10^{-4}$. See our review on "Neutrinos in Cosmology" for more details.

SUM OF THE NEUTRINO MASSES, m_{tot}

This is a sum of the neutrino masses, m_{tot}, as defined in the above note, of effectively stable neutrinos, i.e. those with mean lifetimes on cosmological scales. When necessary, we have generalized the results reported so they apply to m_{tot}. For other limits, see SZALAY 76, VYSOTSKY 77, BERNSTEIN 81, FREESE 84, SCHRAMM 84, and COWSIK 85. For more information see a note on "Neutrinos in Cosmology" in this *Review*.

VALUE (eV)	CL%	DOCUMENT ID		TECN	COMMENT
• • • We do not use the following data for averages, fits, limits, etc. • • •					
$<$ 0.13	95	[1] ABBOTT	21A	COSM	DES and Planck
$<$ 0.12	95	[2] ALAM	21	COSM	
$<$ 0.09	95	[3] DI-VALENT...	21	COSM	
$<$ 0.16	95	[4] GARNY	21	COSM	
$<$ 0.06–0.14	95	[5] STOCKER	21	COSM	Normal mass ordering
$<$ 0.12	95	[6] AGHANIM	20	COSM	
$<$ 0.15	95	[7] CHOUDHURY	20	COSM	Normal mass hierarchy
$<$ 0.16	95	[8] IVANOV	20	COSM	Planck and BOSS
$<$ 0.11	95	[9] PALANQUE-...	20	COSM	Lyman alpha and CMB
$<$ 0.26	95	[10] LOUREIRO	19	COSM	
$<$ 0.18	95	[11] UPADHYE	19	COSM	BOSS and CMB
$<$ 0.152	95	[12] CHOUDHURY	18	COSM	
0.064 $^{+0.061}_{-0.005}$	95	[13] SIMPSON	17	COSM	
$<$ 0.151	95	[14] VAGNOZZI	17	COSM	
$<$ 0.14	95	[15] YECHE	17	COSM	BOSS and XQ-100
$<$ 0.0926	90	[16] DIVALENTINO	16	COSM	
$<$ 0.18	95	[17] HUANG	16	COSM	Normal mass hierarchy
$<$ 0.14	95	[18] ROSSI	15	COSM	
$<$ 0.23	95	[19] ADE	14	COSM	Planck
0.320 $\pm$0.081		[20] BATTYE	14	COSM	
0.35 $\pm$0.10		[21] BEUTLER	14	COSM	BOSS
0.22 $^{+0.09}_{-0.10}$		[22] COSTANZI	14	COSM	
$<$ 0.22	95	[23] GIUSARMA	14	COSM	
0.32 $\pm$0.11		[24] HOU	14	COSM	
$<$ 0.26	95	[25] LEISTEDT	14	COSM	
$<$ 0.18	95	[26] RIEMER-SOR...	14	COSM	
$<$ 0.24	68	[27] MORESCO	12	COSM	
$<$ 0.29	95	[28] XIA	12	COSM	
$<$ 0.81	95	[29] SAITO	11	COSM	SDSS
$<$ 0.44	95	[30] HANNESTAD	10	COSM	
$<$ 0.6	95	[31] SEKIGUCHI	10	COSM	
$<$ 0.28	95	[32] THOMAS	10	COSM	
$<$ 1.1		[33] ICHIKI	09	COSM	

Downloaded from https://academic.oup.com/ptep/article/2022/8/083C01/6651666 by KIT Library user on 27 September 2022

< 1.3	95	[34] KOMATSU	09	COSM	WMAP
< 1.2		[35] TERENO	09	COSM	
< 0.33		[36] VIKHLININ	09	COSM	
< 0.28		[37] BERNARDIS	08	COSM	
< 0.17–2.3		[38] FOGLI	07	COSM	
< 0.42	95	[39] KRISTIANSEN	07	COSM	
< 0.63–2.2		[40] ZUNCKEL	07	COSM	
< 0.24	95	[41] CIRELLI	06	COSM	
< 0.62	95	[42] HANNESTAD	06	COSM	
< 1.2		[43] SANCHEZ	06	COSM	
< 0.17	95	[41] SELJAK	06	COSM	
< 2.0	95	[44] ICHIKAWA	05	COSM	
< 0.75		[45] BARGER	04	COSM	
< 1.0		[46] CROTTY	04	COSM	
< 0.7		[47] SPERGEL	03	COSM	WMAP
< 0.9		[48] LEWIS	02	COSM	
< 4.2		[49] WANG	02	COSM	CMB
< 2.7		[50] FUKUGITA	00	COSM	
< 5.5		[51] CROFT	99	ASTR	Ly α power spec
<180		SZALAY	74	COSM	
<132		COWSIK	72	COSM	
<280		MARX	72	COSM	
<400		GERSHTEIN	66	COSM	

[1] ABBOTT 21A combines Dark Energy Survey (DES) year 3 results with Planck CMB lensing measurements.

[2] ALAM 21 limit on the sum of neutrino masses by the eBOSS collaboration is based on galaxy, quasar, and Lyman-α 3D clustering data combined with Planck temperature and polarization CMB and supernovae data.

[3] DI-VALENTINO 21 combines CMB temperature and polarization, SNIa luminosity distances and baryon acoustic oscillations data.

[4] GARNY 21 employs a model for the Lyman-α flux power spectrum to set a limit using BOSS data. When combined with Planck CMB temperature and polarization data, a 95% CL range 0.10–0.13 eV is found.

[5] STOCKER 21 use terrestrial and cosmological experiments to set a 95% CL range on the sum of neutrino masses of 0.058–0.139 eV for normal ordering and 0.098–0.174 eV for inverse ordering. They also set an upper limit of 0.037 eV (NO) and 0.042 eV (IO) for the lightest neutrino mass.

[6] AGHANIM 20 limit on the sum of neutrino masses from Planck data combined with lensing and baryon acoustic oscillations (BAO). Without BAO, the limit relaxes to <0.24 eV. Several other limits are quoted based on different combinations of data.

[7] CHOUDHURY 20 combines 2018 Planck CMB temperature and polarization data plus lensing, together with baryon acoustic oscillation data from BOSS, MGS, and 6dFGS. Assumes ΛCDM model. The upper limit is 0.17 eV for the inverted hierarchy, and 0.12 eV for degenerate neutrinos. Limits are also derived for extended cosmological models.

[8] IVANOV 20 combines 2018 Planck CMB data with baryon acoustic oscillation data from BOSS. This study is based on a full-shape likelhood for the redshift-space galaxy power spectrum of the BOSS data.

[9] PALANQUE-DELABROUILLE 20 combine Lyman alpha and Planck temperature and polarization data. Limit improves to 0.09 eV when CMB lensing and baryon acoustic oscillation data are included.

[10] LOUREIRO 19 combines data from large scale structure, cosmic microwave background, type Ia supernovae and big bang nucleosynthesis using physically motivated neutrino mass models.

[11] UPADHYE 19 uses the shape of the BOSS redshift-space galaxy power spectrum in combination with the CMB, and supernovae data. Limit weakens to < 0.54 eV if the dark energy equation of state is allowed to vary.

[12] CHOUDHURY 18 combines 2015 Planck CMB temperature data, information from the optical depth to reionization from Planck 2016 intermediate results together with baryon acoustic oscillation data from BOSS, MGS, and 6dFGS as well as supernovae Type Ia data from the Pantheon Sample. The limit is strengthened to 0.118 eV when high-l CMB polarization data is also included.

[13] SIMPSON 17 uses a combination of laboratory and cosmological measurements to determine the light neutrino masses and argue that there is strong evidence for the normal mass ordering.

[14] Combines temperature anisotropies of the CMB from Planck with data on baryon acoustic oscillations and the optical depth to reionization. Limit is strengthened to 0.118 when high multipole polarization data is included. Updates GIUSARMA 16.

[15] Constrains the total mass of neutrinos using the Lyman-alpha forest power spectrum with BOSS (mid-resolution), XQ-100 (high-resolution) and CMB. Without the CMB data, the limit relaxes to 0.8 eV. Supersedes PALANQUE-DELABROUILLE 15A.

[16] Constrains the total mass of neutrinos from Planck CMB data combined with baryon acoustic oscillation and Planck cluster data.

[17] Constrains the total mass of neutrinos from BAO data from SDSS-III/BOSS combined with CMB data from Planck. Limit quoted for normal mass hierarchy. The limit for the inverted mass hierarchy is 0.20 eV and for the degenerate mass hierarchy it is 0.15 eV.

[18] ROSSI 15 sets limits on the sum of neutrino masses using BOSS Lyman alpha forest data combined with Planck CMB data and baryon acoustic oscillations.

[19] Constrains the total mass of neutrinos from Planck CMB data along with WMAP polarization, high L, and BAO data.

[20] Finite neutrino mass fit to resolve discrepancy between CMB and lensing measurements.

[21] Fit to the total mass of neutrinos from BOSS data along with WMAP CMB data and data from other BAO constraints and weak lensing.

[22] Fit to the total mass of neutrinos from Planck CMB data along with BAO.

[23] Constrains the total mass of neutrinos from Planck CMB data combined with baryon acoustic oscillation data from BOSS and HST data on the Hubble parameter.

[24] Fit based on the SPT-SZ survey combined with CMB, BAO, and H_0 data.

[25] Constraints the total mass of neutrinos (marginalizing over the effective number of neutrino species) from CMB, CMB lensing, BAO, and galaxy clustering data.

[26] Constrains the total mass of neutrinos from Planck CMB data combined with baryon acoustic oscillation data from BOSS, 6dFGS, SDSS, WiggleZ data on the galaxy power spectrum, and HST data on the Hubble parameter. The limit is increased to 0.25 eV if a lower bound to the sum of neutrino masses of 0.04 eV is assumed.

[27] Constrains the total mass of neutrinos from observational Hubble parameter data with seven-year WMAP data and the most recent estimate of H_0.

[28] Constrains the total mass of neutrinos from the CFHTLS combined with seven-year WMAP data and a prior on the Hubble parameter. Limit is relaxed to 0.41 eV when small scales affected by non-linearities are removed.

[29] Constrains the total mass of neutrinos from the Sloan Digital Sky Survey and the five-year WMAP data.

[30] Constrains the total mass of neutrinos from the 7-year WMAP data including SDSS and HST data. Limit relaxes to 1.19 eV when CMB data is used alone. Supersedes HANNESTAD 06.

[31] Constrains the total mass of neutrinos from a combination of CMB data, a recent measurement of H_0 (SHOES), and baryon acoustic oscillation data from SDSS.

[32] Constrains the total mass of neutrinos from SDSS MegaZ LRG DR7 galaxy clustering data combined with CMB, HST, supernovae and baryon acoustic oscillation data. Limit relaxes to 0.47 eV when the equation of state parameter, $w \neq 1$.

[33] Constrains the total mass of neutrinos from weak lensing measurements when combined with CMB. Limit improves to 0.54 eV when supernovae and baryon acoustic oscillation observations are included. Assumes ΛCDM model.

[34] Constrains the total mass of neutrinos from five-year WMAP data. Limit improves to 0.67 eV when supernovae and baryon acoustic oscillation observations are included. Limits quoted assume the ΛCDM model. Supersedes SPERGEL 07.

[35] Constrains the total mass of neutrinos from weak lensing measurements when combined with CMB. Limit improves to $0.03 < \Sigma m_\nu < 0.54$ eV when supernovae and baryon acoustic oscillation observations are included. The slight preference for massive neutrinos at the two-sigma level disappears when systematic errors are taken into account. Assumes ΛCDM model.

[36] Constrains the total mass of neutrinos from recent Chandra X-ray observations of galaxy clusters when combined with CMB, supernovae, and baryon acoustic oscillation measurements. Assumes flat universe and constant dark-energy equation of state, w.

[37] Constraints the total mass of neutrinos from recent CMB and SOSS LRG power spectrum data along with bias mass relations from SDSS, DEEP2, and Lyman-Break Galaxies. It assumes ΛCDM model. Limit degrades to 0.59 eV in a more general wCDM model.

[38] Constrains the total mass of neutrinos from neutrino oscillation experiments and cosmological data. The most conservative limit uses only WMAP three-year data, while the most stringent limit includes CMB, large-scale structure, supernova, and Lyman-alpha data.

[39] Constrains the total mass of neutrinos from recent CMB, large scale structure, SN1a, and baryon acoustic oscillation data. The limit relaxes to 1.75 when WMAP data alone is used with no prior. Paper shows results with several combinations of data sets. Supersedes KRISTIANSEN 06.

[40] Constrains the total mass of neutrinos from the CMB and the large scale structure data. The most conservative limit is obtained when generic initial conditions are allowed.

[41] Constrains the total mass of neutrinos from recent CMB, large scale structure, Lyman-alpha forest, and SN1a data.

[42] Constrains the total mass of neutrinos from recent CMB and large scale structure data. See also GOOBAR 06. Superseded by HANNESTAD 10.

[43] Constrains the total mass of neutrinos from the CMB and the final 2dF Galaxy Redshift Survey.

[44] Constrains the total mass of neutrinos from the CMB experiments alone, assuming ΛCDM Universe. FUKUGITA 06 show that this result is unchanged by the 3-year WMAP data.

[45] Constrains the total mass of neutrinos from the power spectrum of fluctuations derived from the Sloan Digital Sky Survey and the 2dF galaxy redshift survey, WMAP and 27 other CMB experiments and measurements by the HST Key project.

[46] Constrains the total mass of neutrinos from the power spectrum of fluctuations derived from the Sloan Digital Sky Survey, the 2dF galaxy redshift survey, WMAP and ACBAR. The limit is strengthened to 0.6 eV when measurements by the HST Key project and supernovae data are included.

[47] Constrains the fractional contribution of neutrinos to the total matter density in the Universe from WMAP data combined with other CMB measurements, the 2dfGRS data, and Lyman α data. The limit does not noticeably change if the Lyman α data are not used.

[48] LEWIS 02 constrains the total mass of neutrinos from the power spectrum of fluctuations derived from the CMB, HST Key project, 2dF galaxy redshift survey, supernovae type Ia, and BBN.

[49] WANG 02 constrains the total mass of neutrinos from the power spectrum of fluctuations derived from the CMB and other cosmological data sets such as galaxy clustering and the Lyman α forest.

[50] FUKUGITA 00 is a limit on neutrino masses from structure formation. The constraint is based on the clustering scale σ_8 and the COBE normalization and leads to a conservative limit of 0.9 eV assuming 3 nearly degenerate neutrinos. The quoted limit is on the sum of the light neutrino masses.

[51] CROFT 99 result based on the power spectrum of the Ly α forest. If $\Omega_{\rm matter} < 0.5$, the limit is improved to $m_\nu < 2.4$ ($\Omega_{\rm matter}$/0.17–1) eV.

Limits on MASSES of Light Stable Right-Handed ν (with necessarily suppressed interaction strengths)

VALUE (eV)	DOCUMENT ID		TECN	COMMENT
• • • We do not use the following data for averages, fits, limits, etc. • • •				
<100–200	[1] OLIVE	82	COSM	Dirac ν
<200–2000	[1] OLIVE	82	COSM	Majorana ν

[1] Depending on interaction strength G_R where $G_R < G_F$.

Downloaded from https://academic.oup.com/ptep/article/2022/8/083C01/6651666 by KIT Library user on 27 September 2022

Limits on MASSES of Heavy Stable Right-Handed ν (with necessarily suppressed interaction strengths)

VALUE (GeV)	DOCUMENT ID		TECN	COMMENT
• • • We do not use the following data for averages, fits, limits, etc. • • •				
> 10	[1] OLIVE	82	COSM	G_R/G_F <0.1
>100	[1] OLIVE	82	COSM	G_R/G_F <0.01

[1] These results apply to heavy Majorana neutrinos and are summarized by the equation: m_ν >1.2 GeV (G_F/G_R). The bound saturates, and if G_R is too small no mass range is allowed.

ν CHARGE

e = electron charge is the unit of values listed below.

VALUE (e)	CL%	DOCUMENT ID		TECN	COMMENT
<4 $\times 10^{-35}$	95	[1] CAPRINI	05	COSM	charge neutral universe
• • • We do not use the following data for averages, fits, limits, etc. • • •					
$<5.4 \times 10^{-12}$	90	[2] ABE	20E	XMAS	solar neutrinos
$1.7–2.3 \times 10^{-12}$	68	[3] KHAN	20		spectral fit of XENON1T
$<3 \times 10^{-8}$	95	[4] DELLA-VALLE	16	LASR	magnetic dichroism
$<2.1 \times 10^{-12}$	90	[5] CHEN	14A	TEXO	nuclear reactor
$<1.5 \times 10^{-12}$	90	[6] STUDENIKIN	14		nuclear reactor
$<3.7 \times 10^{-12}$	90	[7] GNINENKO	07	RVUE	nuclear reactor
$<2 \times 10^{-14}$		[8] RAFFELT	99	ASTR	red giant luminosity
$<6 \times 10^{-14}$		[9] RAFFELT	99	ASTR	solar cooling
$<4 \times 10^{-4}$		[10] BABU	94	RVUE	BEBC beam dump
$<3 \times 10^{-4}$		[11] DAVIDSON	91	RVUE	SLAC e^- beam dump
$<2 \times 10^{-15}$		[12] BARBIELLINI	87	ASTR	SN 1987A
$<1 \times 10^{-13}$		[13] BERNSTEIN	63	ASTR	solar energy losses

[1] CAPRINI 05 limit derived from the lack of a charge asymmetry in the universe. Limit assumes that charge asymmetries between particles are not anti-correlated.

[2] ABE 20E obtains this result by assuming that the low-energy excess events in the XMASS detector are produced by neutrino millicharge which is common for all three neutrino flavors.

[3] KHAN 20 performed a constrained spectral fit analysis of the excess observed in the electron recoil energy spectrum by the XENON1T experiment. This range of neutrino millicharge values is one of the possible interpretations of these excess events. For the individual flavor constraints at 90% C.L. see the original reference.

[4] DELLA-VALLE 16 obtain a limit on the charge of neutrinos valid for masses of less than 10 meV. For heavier neutrinos the limit increases as a power of mass, reaching 10^{-6} e for $m = 100$ meV.

[5] CHEN 14A use the Multi-Configuration RRPA method to analyze reactor $\overline{\nu}_e$ scattering on Ge atoms with 300 eV recoil energy threshold to obtain this limit.

[6] STUDENIKIN 14 uses the limit on μ_ν from BEDA 13 and the 2.8 keV threshold of the electron recoil energy to obtain this limit.

[7] GNINENKO 07 use limit on $\overline{\nu}_e$ magnetic moment from LI 03B to derive this result. The limit is considerably weaker than the limits on the charge of ν_e and $\overline{\nu}_e$ from various astrophysics considerations.

[8] This RAFFELT 99 limit applies to all neutrino flavors which are light enough (<5 keV) to be emitted from globular-cluster red giants.

[9] This RAFFELT 99 limit is derived from the helioseismological limit on a new energy-loss channel of the Sun, and applies to all neutrino flavors which are light enough (<1 keV) to be emitted from the sun.

[10] BABU 94 use COOPER-SARKAR 92 limit on ν magnetic moment to derive quoted result. It applies to ν_τ.

[11] DAVIDSON 91 use data from early SLAC electron beam dump experiment to derive charge limit as a function of neutrino mass. It applies to ν_τ.

[12] Exact BARBIELLINI 87 limit depends on assumptions about the intergalactic or galactic magnetic fields and about the direct distance and time through the field. It applies to ν_e.

[13] The limit applies to all flavors.

ν (MEAN LIFE) / MASS

Measures $\left[\sum |U_{\ell j}|^2 \Gamma_j m_j\right]^{-1}$, where the sum is over mass eigenstates which cannot be resolved experimentally. Some of the limits constrain the radiative decay and are based on the limit of the corresponding photon flux. Other apply to the decay of a heavier neutrino into the lighter one and a Majoron or other invisible particle. Many of these limits apply to any ν within the indicated mass range.

Limits on the radiative decay are either directly based on the limits of the corresponding photon flux, or are derived from the limits on the neutrino magnetic moments. In the later case the transition rate for $\nu_i \to \nu_j + \gamma$ is constrained by $\Gamma_{ij} = \frac{1}{\tau_{ij}} = \frac{(m_i^2 - m_j^2)^3}{m_i^3} \mu_{ij}^2$ where μ_{ij} is the neutrino transition moment in the mass eigenstates basis. Typically, the limits on lifetime based on the magnetic moments are many orders of magnitude more restrictive than limits based on the nonobservation of photons.

VALUE (s/eV)	CL%	DOCUMENT ID		TECN	COMMENT
> 15.4	90	[1] KRAKAUER	91	CNTR	ν_μ, $\overline{\nu}_\mu$ at LAMPF
> 7 $\times 10^9$		[2] RAFFELT	85	ASTR	
> 300	90	[3] REINES	74	CNTR	$\overline{\nu}_e$
• • • We do not use the following data for averages, fits, limits, etc. • • •					
$> 8.08 \times 10^{-5}$	90	[4] AHARMIM	19	SNO	ν_2 invisible nonradiative decay
$> 1.92 \times 10^{-3}$	90	[5] AHARMIM	19	FIT	ν_2 invisible nonradiative decay
$6–26 \times 10^9$	95	[6] ESCUDERO	19	COSM	Invisible decay $m_\nu \geq$ 0.05 eV
$> 10^5 - 10^{10}$	95	[7] CECCHINI	11	ASTR	$\nu_2 \to \nu_1$ radiative decay
	90	[8] MIRIZZI	07	CMB	radiative decay
	90	[9] MIRIZZI	07	CIB	radiative decay
		[10] WONG	07	CNTR	Reactor $\overline{\nu}_e$
> 0.11	90	[11] XIN	05	CNTR	Reactor ν_e
		[12] XIN	05	CNTR	Reactor ν_e
> 0.004	90	[13] AHARMIM	04	SNO	quasidegen. ν masses
$> 4.4 \times 10^{-5}$	90	[13] AHARMIM	04	SNO	hierarchical ν masses
$\gtrsim 100$	95	[14] CECCHINI	04	ASTR	Radiative decay for ν mass > 0.01 eV
> 0.067	90	[15] EGUCHI	04	KLND	quasidegen. ν masses
$> 1.1 \times 10^{-3}$	90	[15] EGUCHI	04	KLND	hierarchical ν masses
$> 8.7 \times 10^{-5}$	99	[16] BANDYOPA...	03	FIT	nonradiative decay
≥ 4200	90	[17] DERBIN	02B	CNTR	Solar pp and Be ν
$> 2.8 \times 10^{-5}$	99	[18] JOSHIPURA	02B	FIT	nonradiative decay
		[19] DOLGOV	99	COSM	
		[20] BILLER	98	ASTR	m_ν= 0.05–1 eV
$> 2.8 \times 10^{15}$		[21,22] BLUDMAN	92	ASTR	$m_\nu < 50$ eV
none $10^{-12} - 5 \times 10^4$		[23] DODELSON	92	ASTR	m_ν=1–300 keV
$< 10^{-12}$ or $> 5 \times 10^4$		[23] DODELSON	92	ASTR	m_ν=1–300 keV
		[24] GRANEK	91	COSM	Decaying L^0
> 6.4	90	[25] KRAKAUER	91	CNTR	ν_e at LAMPF
$> 1.1 \times 10^{15}$		[26] WALKER	90	ASTR	m_ν= 0.03 – ~ 2 MeV
$> 6.3 \times 10^{15}$		[22,27] CHUPP	89	ASTR	$m_\nu < 20$ eV
$> 1.7 \times 10^{15}$		[22] KOLB	89	ASTR	$m_\nu < 20$ eV
		[28] RAFFELT	89	RVUE	$\overline{\nu}$ (Dirac, Majorana)
		[29] RAFFELT	89B	ASTR	
$> 8.3 \times 10^{14}$		[30] VONFEILIT...	88	ASTR	
> 22	68	[31] OBERAUER	87		$\overline{\nu}_R$ (Dirac)
> 38	68	[31] OBERAUER	87		$\overline{\nu}$ (Majorana)
> 59	68	[31] OBERAUER	87		$\overline{\nu}_L$ (Dirac)
> 30	68	KETOV	86	CNTR	$\overline{\nu}$ (Dirac)
> 20	68	KETOV	86	CNTR	$\overline{\nu}$ (Majorana)
		[32] BINETRUY	84	COSM	$m_\nu \sim$ 1 MeV
> 0.11	90	[33] FRANK	81	CNTR	$\nu\overline{\nu}$ LAMPF
$> 2 \times 10^{21}$		[34] STECKER	80	ASTR	m_ν= 10–100 eV
$> 1.0 \times 10^{-2}$	90	[33] BLIETSCHAU	78	HLBC	ν_μ, CERN GGM
$> 1.7 \times 10^{-2}$	90	[33] BLIETSCHAU	78	HLBC	$\overline{\nu}_\mu$, CERN GGM
$< 3 \times 10^{-11}$		[35] FALK	78	ASTR	m_ν <10 MeV
$> 2.2 \times 10^{-3}$	90	[33] BARNES	77	DBC	ν, ANL 12-ft
		[36] COWSIK	77	ASTR	
$> 3. \times 10^{-3}$	90	[33] BELLOTTI	76	HLBC	ν, CERN GGM
$> 1.3 \times 10^{-2}$	90	[33] BELLOTTI	76	HLBC	$\overline{\nu}$, CERN GGM

[1] KRAKAUER 91 quotes the limit $\tau/m_{\nu_1} > (0.75a^2 + 21.65a + 26.3)$ s/eV, where a is a parameter describing the asymmetry in the neutrino decay defined as $dN_\gamma/d\cos\theta = (1/2)(1 + a\cos\theta)$ The parameter $a = 0$ for a Majorana neutrino, but can vary from -1 to 1 for a Dirac neutrino. The bound given by the authors is the most conservative (which applies for $a = -1$).

[2] RAFFELT 85 limit on the radiative decay is from solar x- and γ-ray fluxes. Limit depends on ν flux from pp, now established from GALLEX and SAGE to be > 0.5 of expectation.

[3] REINES 74 looked for ν of nonzero mass decaying radiatively to a neutral of lesser mass + γ. Used liquid scintillator detector near fission reactor. Finds lab lifetime 6×10^7 s or more. Above value of (mean life)/mass assumes average effective neutrino energy of 0.2 MeV. To obtain the limit 6×10^7 s REINES 74 assumed that the full $\overline{\nu}_e$ reactor flux could be responsible for yielding decays with photon energies in the interval 0.1 MeV – 0.5 MeV. This represents some overestimate so their lower limit is an over-estimate of the lab lifetime (VOGEL 84). If so, OBERAUER 87 may be comparable or better.

[4] AHARMIM 19 quotes the limit τ/m_{ν_2} for invisible nonradiative decay of ν_2. They obtained this result by analyzing the entire SNO dataset, allowing for the decay of ν_2 which would cause an energy-dependent distortion of the survival probability of electron-type solar neutrinos.

[5] AHARMIM 19 quotes the limit τ/m_{ν_2} for invisible nonradiative decay of ν_2. They obtained this result by combining the τ/m_{ν_2} measurements from SNO and other solar neutrino experiments (Super-Kamiokande, KamLAND, and Borexino ^{8}B results; Borexino and KamLAND ^{7}Be results; the combined gallium interaction rate from GNO, GALLEX, and SAGE; and the chlorine interaction rate from Homestake). The quoted limit at 99% CL is $> 1.04 \times 10^{-3}$.

[6] ESCUDERO 19 sets limits on invisible neutrino decays using Planck 2018 data of $\tau > 1.3–0.3 \times 10^9$ s at 95% C.L. Values in the range $\tau = 2–16 \times 10^9$ s are preferred at 95% C.L. when Planck polarization data is included. Limits scale as $(m_\nu/0.05 \text{ eV})^3$.

[7] CECCHINI 11 search for radiative decays of solar neutrinos into visible photons during the 2006 total solar eclipse. The range of (mean life)/mass values corresponds to a range of ν_1 masses between 10^{-4} and 0.1 eV.

[8] MIRIZZI 07 determine a limit on the neutrino radiative decay from analysis of the maximum allowed distortion of the CMB spectrum as measured by the COBE/FIRAS. For the decay $\nu_2 \to \nu_1$ the lifetime limit is $\lesssim 4 \times 10^{20}$ s for $m_{min} \lesssim 0.14$ eV. For transition

Downloaded from https://academic.oup.com/ptep/article/2022/8/083C01/6651666 by KIT Library user on 27 September 2022

with the $|\Delta m_{31}|$ mass difference the lifetime limit is $\sim 2\times10^{19}$ s for $m_{min} \lesssim 0.14$ eV and $\sim 5\times10^{20}$ s for $m_{min} \gtrsim 0.14$ eV.

[9] MIRIZZI 07 determine a limit on the neutrino radiative decay from analysis of the cosmic infrared background (CIB) using the Spitzer Observatory data. For transition with the $|\Delta m_{31}|$ mass difference they obtain the lifetime limit $\sim 10^{20}$ s for $m_{min} \lesssim 0.14$ eV.

[10] WONG 07 use their limit on the neutrino magnetic moment together with the assumed experimental value of $\Delta m^2_{13} \sim 2\times10^{-3}$ eV^2 to obtain $\tau_{13}/m_1^3 > 3.2\times10^{27}$ s/eV^3 for the radiative decay in the case of the inverted mass hierarchy. Similarly to RAFFELT 89 this limit can be violated if electric and magnetic moments are equal to each other. Analogous, but numerically somewhat different limits are obtained for τ_{23} and τ_{21}.

[11] XIN 05 search for the γ from radiative decay of ν_e produced by the electron capture on ^{51}Cr. No events were seen and the limit on τ/m_ν was derived. This is a weaker limit on the decay of ν_e than KRAKAUER 91.

[12] XIN 05 use their limit on the neutrino magnetic moment of ν_e together with the assumed experimental value of $\Delta m^2_{1,3} \sim 2\times10^{-3}$ eV^2 to obtain $\tau_{13}/m_1^3 > 1\times10^{23}$ s/eV^3 for the radiative decay in the case of the inverted mass hierarchy. Similarly to RAFFELT 89 this limit can be violated if electric and magnetic moments are equal to each other. Analogous, but numerically somewhat different limits are obtained for τ_{23} and τ_{21}. Again, this limit is specific for ν_e.

[13] AHARMIM 04 obtained these results from the solar $\overline{\nu}_e$ flux limit set by the SNO measurement assuming ν_2 decay through nonradiative process $\nu_2 \rightarrow \overline{\nu}_1 X$, where X is a Majoron or other invisible particle. Limits are given for the cases of quasidegenerate and hierarchical neutrino masses.

[14] CECCHINI 04 obtained this bound through the observations performed on the occasion of the 21 June 2001 total solar eclipse, looking for visible photons from radiative decays of solar neutrinos. Limit is a τ/m_{ν_2} in $\nu_2 \rightarrow \nu_1\gamma$. Limit ranges from $\sim$ 100 to 10^7 s/eV for $0.01 < m_{\nu_1} < 0.1$ eV.

[15] EGUCHI 04 obtained these results from the solar $\overline{\nu}_e$ flux limit set by the KamLAND measurement assuming ν_2 decay through nonradiative process $\nu_2 \rightarrow \overline{\nu}_1 X$, where X is a Majoron or other invisible particle. Limits are given for the cases of quasidegenerate and hierarchical neutrino masses.

[16] The ratio of the lifetime over the mass derived by BANDYOPADHYAY 03 is for ν_2. They obtained this result using the following solar-neutrino data: total rates measured in Cl and Ga experiments, the Super-Kamiokande's zenith-angle spectra, and SNO's day and night spectra. They assumed that ν_1 is the lowest mass, stable or nearly stable neutrino state and ν_2 decays through nonradiative Majoron emission process, $\nu_2 \rightarrow \overline{\nu}_1 + J$, or through nonradiative process with all the final state particles being sterile. The best fit is obtained in the region of the LMA solution.

[17] DERBIN 02B (also BACK 03B) obtained this bound for the radiative decay from the results of background measurements with Counting Test Facility (the prototype of the Borexino detector). The laboratory gamma spectrum is given as $dN_\gamma/d\cos\theta = (1/2)\,(1 + \alpha\cos\theta)$ with α=0 for a Majorana neutrino, and α varying to -1 to 1 for a Dirac neutrino. The listed bound is for the case of α=0. The most conservative bound 1.5×10^3 s eV^{-1} is obtained for the case of α=-1.

[18] The ratio of the lifetime over the mass derived by JOSHIPURA 02B is for ν_2. They obtained this result from the total rates measured in all solar neutrino experiments. They assumed that ν_1 is the lowest mass, stable or nearly stable neutrino state and ν_2 decays through nonradiative process like Majoron emission decay, $\nu_2 \rightarrow \nu_1' + J$ where ν_1' state is sterile. The exact limit depends on the specific solution of the solar neutrino problem. The quoted limit is for the LMA solution.

[19] DOLGOV 99 places limits in the (Majorana) τ-associated ν mass-lifetime plane based on nucleosynthesis. Results would be considerably modified if neutrino oscillations exist.

[20] BILLER 98 use the observed TeV γ-ray spectra to set limits on the mean life of any radiatively decaying neutrino between 0.05 and 1 eV. Curve shows $\tau_\nu/B_\gamma > 0.15\times10^{21}$ s at 0.05 eV, $> 1.2\times10^{21}$ s at 0.17 eV, $> 3\times10^{21}$ s at 1 eV, where B_γ is the branching ratio to photons.

[21] BLUDMAN 92 sets additional limits by this method for higher mass ranges. Cosmological limits are also obtained.

[22] Limit on the radiative decay based on nonobservation of γ's in coincidence with ν's from SN 1987A.

[23] DODELSON 92 range is for wrong-helicity keV mass Dirac ν's from the core of neutron star in SN 1987A decaying to ν's that would have interacted in KAM2 or IMB detectors.

[24] GRANEK 91 considers heavy neutrino decays to $\gamma\nu_L$ and $3\nu_L$, where m_{ν_L} <100 keV. Lifetime is calculated as a function of heavy neutrino mass, branching ratio into $\gamma\nu_L$, and m_{ν_L}.

[25] KRAKAUER 91 quotes the limit for ν_e, $\tau/m_\nu > (0.3a^2 + 9.8a + 15.9)$ s/eV, where a is a parameter describing the asymmetry in the radiative neutrino decay defined as $dN_\gamma/d\cos\theta = (1/2)(1 + a\cos\theta)$ $a=0$ for a Majorana neutrino, but can vary from -1 to 1 for a Dirac neutrino. The bound given by the authors is the most conservative (which applies for $a = -1$).

[26] WALKER 90 uses SN 1987A γ flux limits after 289 days.

[27] CHUPP 89 should be multiplied by a branching ratio (about 1) and a detection efficiency (about 1/4), and pertains to radiative decay of any neutrino to a lighter or sterile neutrino.

[28] RAFFELT 89 uses KYULDJIEV 84 to obtain $\tau m^3 > 3\times10^{18}$ s eV^3 (based on $\overline{\nu}_e e^-$ cross sections). The bound for the radiative decay is not valid if electric and magnetic transition moments are equal for Dirac neutrinos.

[29] RAFFELT 89B analyze stellar evolution and exclude the region $3\times10^{12} < \tau m^3 < 3\times10^{21}$ s eV^3.

[30] Model-dependent theoretical analysis of SN 1987A neutrinos. Quoted limit is for $\left[\sum_j |U_{\ell j}|^2\, \Gamma_j\, m_j\right]^{-1}$, where ℓ=μ, τ. Limit is 3.3×10^{14} s/eV for ℓ=e.

[31] OBERAUER 87 looks for photons and e^+e^- pairs from radiative decays of reactor neutrinos.

[32] BINETRUY 84 finds $\tau < 10^8$ s for neutrinos in a radiation-dominated universe.

[33] These experiments look for $\nu_k \rightarrow \nu_j\gamma$ or $\overline{\nu}_k \rightarrow \overline{\nu}_j\gamma$.

[34] STECKER 80 limit based on UV background; result given is $\tau > 4\times10^{22}$ s at m_ν=20 eV.

[35] FALK 78 finds lifetime constraints based on supernova energetics.

[36] COWSIK 77 considers variety of scenarios. For neutrinos produced in the big bang, present limits on optical photon flux require $\tau > 10^{23}$ s for $m_\nu \sim 1$ eV. See also COWSIK 79 and GOLDMAN 79.

ν MAGNETIC MOMENT

The coupling of neutrinos to an electromagnetic field is a characterized by a 3×3 matrix λ of the magnetic (μ) and electric (d) dipole moments ($\lambda = \mu$ - id). For Majorana neutrinos the matrix λ is antisymmetric and only transition moments are allowed, while for Dirac neutrinos λ is a general 3×3 matrix. In the standard electroweak theory extended to include neutrino masses (see FUJIKAWA 80) $\mu_\nu = 3eG_F\, m_\nu/(8\pi^2\sqrt{2}) = 3.2\times10^{-19}(m_\nu/\text{eV})\mu_B$, i.e. it is unobservably small given the known small neutrino masses. In more general models there is no longer a proportionality between neutrino mass and its magnetic moment, even though only massive neutrinos have nonvanishing magnetic moments without fine tuning.

Laboratory bounds on λ are obtained via elastic ν-e scattering, where the scattered neutrino is not observed. The combinations of matrix elements of λ that are constrained by various experiments depend on the initial neutrino flavor and on its propagation between source and detector (e.g., solar ν_e and reactor $\overline{\nu}_e$ do not constrain the same combinations). The listings below therefore identify the initial neutrino flavor.

Other limits, e.g. from various stellar cooling processes, apply to all neutrino flavors. Analogous flavor independent, but weaker, limits are obtained from the analysis of $e^+e^- \rightarrow \nu\overline{\nu}\gamma$ collider experiments.

VALUE (10^{-10} μ_B)	CL%	DOCUMENT ID		TECN	COMMENT
0.14–0.29	90	[1] APRILE	20	XE1T	Solar ν spectrum
< 0.28	90	[2] AGOSTINI	17A	BORX	Solar ν spectrum
< 0.29	90	[3] BEDA	13	CNTR	Reactor $\overline{\nu}_e$
< 6.8	90	[4] AUERBACH	01	LSND	$\nu_e e$, $\nu_\mu e$ scattering
< 3900	90	[5] SCHWIENHO...	01	DONU	$\nu_\tau e^- \rightarrow \nu_\tau e^-$
• • • We do not use the following data for averages, fits, limits, etc. • • •					
< 1.8	90	[6] ABE	20E	XMAS	Solar ν spectrum
< 0.012	95	[7] CAPOZZI	20	ASTR	Tip of the Red-Giant Branch
0.2–0.4	68	[8] KHAN	20		Spectral fit of XENON1T
< 0.022	90	[9] ARCEO-DIAZ	15	ASTR	Red giants
< 0.1	95	[10] CORSICO	14	ASTR	
< 0.05	95	[11] MILLER-BER...	14B	ASTR	
< 0.045	95	[12] VIAUX	13A	ASTR	Globular cluster M5
< 0.32	90	[13] BEDA	10	CNTR	Reactor $\overline{\nu}_e$
< 2.2	90	[14] DENIZ	10	TEXO	Reactor $\overline{\nu}_e$
< 0.011–0.027		[15] KUZNETSOV	09	ASTR	$\nu_L \rightarrow \nu_R$ in SN1987A
< 0.54	90	[16] ARPESELLA	08A	BORX	Solar ν spectrum
< 0.58	90	[17] BEDA	07	CNTR	Reactor $\overline{\nu}_e$
< 0.74	90	[18] WONG	07	CNTR	Reactor $\overline{\nu}_e$
< 0.9	90	[19] DARAKTCH...	05		Reactor $\overline{\nu}_e$
< 130	90	[20] XIN	05	CNTR	Reactor ν_e
< 37	95	[21] GRIFOLS	04	FIT	Solar ^{8}B ν (SNO NC)
< 3.6	90	[22] LIU	04	SKAM	Solar ν spectrum
< 1.1	90	[23] LIU	04	SKAM	Solar ν spectrum (LMA region)
< 5.5	90	[24] BACK	03B	CNTR	Solar pp and Be ν
< 1.0	90	[25] DARAKTCH...	03		Reactor $\overline{\nu}_e$
< 1.3	90	[26] LI	03B	CNTR	Reactor $\overline{\nu}_e$
< 2	90	[27] GRIMUS	02	FIT	solar + reactor (Majorana ν)
<80000	90	[28] TANIMOTO	00	RVUE	$e^+e^- \rightarrow \nu\overline{\nu}\gamma$
< 0.01–0.04		[29] AYALA	99	ASTR	$\nu_L \rightarrow \nu_R$ in SN 1987A
< 1.5	90	[30] BEACOM	99	SKAM	Solar ν spectrum
< 0.03		[31] RAFFELT	99	ASTR	Red giant luminosity
< 4		[32] RAFFELT	99	ASTR	Solar cooling
<44000	90	ABREU	97J	DLPH	$e^+e^- \rightarrow \nu\overline{\nu}\gamma$ at LEP
<33000	90	[33] ACCIARRI	97Q	L3	$e^+e^- \rightarrow \nu\overline{\nu}\gamma$ at LEP
< 0.62		[34] ELMFORS	97	COSM	Depolarization in early universe plasma
<27000	95	[35] ESCRIBANO	97	RVUE	$\Gamma(Z \rightarrow \nu\nu)$ at LEP
< 30	90	VILAIN	95B	CHM2	$\nu_\mu e \rightarrow \nu_\mu e$
<55000	90	GOULD	94	RVUE	$e^+e^- \rightarrow \nu\overline{\nu}\gamma$ at LEP
< 1.9	95	[36] DERBIN	93	CNTR	Reactor $\overline{\nu}e \rightarrow \overline{\nu}e$
< 5400	90	[37] COOPER-...	92	BEBC	$\nu_\tau e^- \rightarrow \nu_\tau e^-$
< 2.4	90	[38] VIDYAKIN	92	CNTR	Reactor $\overline{\nu}e \rightarrow \overline{\nu}e$
<56000	90	DESHPANDE	91	RVUE	$e^+e^- \rightarrow \nu\overline{\nu}\gamma$
< 100	95	[39] DORENBOS...	91	CHRM	$\nu_\mu e \rightarrow \nu_\mu e$
< 8.5	90	AHRENS	90	CNTR	$\nu_\mu e \rightarrow \nu_\mu e$
< 10.8	90	[40] KRAKAUER	90	CNTR	LAMPF $\nu e \rightarrow \nu e$
< 7.4	90	[40] KRAKAUER	90	CNTR	LAMPF $(\nu_\mu, \overline{\nu}_\mu)e$ elast.
< 0.02		[41] RAFFELT	90	ASTR	Red giant luminosity
< 0.1		[42] RAFFELT	89B	ASTR	Cooling helium stars

Downloaded from https://academic.oup.com/ptep/article/2022/8/083C01/6651666 by KIT Library user on 27 September 2022

		[43] FUKUGITA	88	COSM	Primordial magn. fields
<40000	90	[44] GROTCH	88	RVUE	$e^+e^- \to \nu\overline{\nu}\gamma$
≤ .3		[42] RAFFELT	88B	ASTR	He burning stars
< 0.11		[42] FUKUGITA	87	ASTR	Cooling helium stars
< 0.0006		[45] NUSSINOV	87	ASTR	Cosmic EM backgrounds
< 0.1–0.2		MORGAN	81	COSM	[4]He abundance
< 0.85		BEG	78	ASTR	Stellar plasmons
< 0.6		[46] SUTHERLAND	76	ASTR	Red giants + degenerate dwarfs
< 81		[47] KIM	74	RVUE	$\overline{\nu}_\mu e \to \overline{\nu}_\mu e$
< 1		BERNSTEIN	63	ASTR	Solar cooling
< 14		COWAN	57	CNTR	Reactor $\overline{\nu}$

[1] APRILE 20 observed an excess of low-energy events in the XENON1T detector, which could be interpreted as a signal produced by a neutrino magnetic moment with this magnitude.

[2] AGOSTINI 17A obtained this limit using the shape of the recoil electron energy spectrum from the Borexino Phase-II 1291.5 live days of solar neutrino data and the constraints on the sum of the solar neutrino fluxes from the radiochemical gallium experiments SAGE, Gallex, and GNO. Without radiochemical constraints, the 90% C.L. limit of $< 4.0 \times 10^{-11} \mu_B$ is obtained.

[3] BEDA 13 report $\overline{\nu}_e e^-$ scattering results, using the Kalinin Nuclear Power Plant and a shielded Ge detector. The recoil electron spectrum is analyzed between 2.5 and 55 keV. Supersedes BEDA 07. Supersedes BEDA 10. This is the most stringent limit on the magnetic moment of reactor $\overline{\nu}_e$.

[4] AUERBACH 01 limit is based on the LSND ν_e and ν_μ electron scattering measurements. The limit is slightly more stringent than KRAKAUER 90.

[5] SCHWIENHORST 01 quote an experimental sensitivity of 4.9×10^{-7}.

[6] ABE 20E observed an excess of low-energy events in the XMASS detector, which could be interpreted as a signal produced by a neutrino magnetic moment with this magnitude.

[7] CAPOZZI 20 obtains a limit on the neutrino dipole moment from the brightness of the tip of the red-giant branch in ω Centauri. A similar limit of $\mu_\nu < 1.5 \times 10^{-12} \mu_B$ is obtained in NGC 4258.

[8] KHAN 20 performed a constrained spectral fit analysis of the excess observed in the electron recoil energy spectrum by the XENON1T experiment. This range of the μ_B values is one of the possible interpretations of these excess events. For the individual flavor constraints at 90% C.L. see the original reference.

[9] ARCEO-DIAZ 15 constrains the neutrino magnetic moment from observation of the tip of the red giant branch in the globular cluster ω-Centauri.

[10] CORSICO 14 constrains the neutrino magnetic moment from observations of white drarf pulsations.

[11] MILLER-BERTOLAMI 14B constrains the neutrino magnetic moment from observations of the white dwarf luminosity function of the Galactic disk.

[12] VIAUX 13A constrains the neutrino magnetic moment from observations of the globular cluster M5.

[13] BEDA 10 report $\overline{\nu}_e e^-$ scattering results, using the Kalinin Nuclear Power Plant and a shielded Ge detector. The recoil electron spectrum is analyzed between 2.9 and 45 keV. Supersedes BEDA 07. Superseded by BEDA 13.

[14] DENIZ 10 observe reactor $\overline{\nu}_e e$ scattering with recoil kinetic energies 3–8 MeV using CsI(Tl) detectors. The observed rate and spectral shape are consistent with the Standard Model prediction, leading to the reported constraint on $\overline{\nu}_e$ magnetic moment.

[15] KUZNETSOV 09 obtain a limit on the flavor averaged magnetic moment of Dirac neutrinos from the time averaged neutrino signal of SN1987A. Improves and supersedes the analysis of BARBIERI 88 and AYALA 99.

[16] ARPESELLA 08A obtained this limit using the shape of the recoil electron energy spectrum from the Borexino 192 live days of solar neutrino data.

[17] BEDA 07 performed search for electromagnetic $\overline{\nu}_e$-e scattering at Kalininskaya nuclear reactor. A Ge detector with active and passive shield was used and the electron recoil spectrum between 3.0 and 61.3 keV analyzed. Superseded by BEDA 10.

[18] WONG 07 performed search for non-standard $\overline{\nu}_e$-e scattering at the Kuo-Sheng nuclear reactor. Ge detector equipped with active anti-Compton shield is used. Most stringent laboratory limit on magnetic moment of reactor $\overline{\nu}_e$. Supersedes LI 03B.

[19] DARAKTCHIEVA 05 present the final analysis of the search for non-standard $\overline{\nu}_e$-e scattering component at Bugey nuclear reactor. Full kinematical event reconstruction of both the kinetic energy above 700 keV and scattering angle of the recoil electron, by use of TPC. Most stringent laboratory limit on magnetic moment. Supersedes DARAKTCHIEVA 03.

[20] XIN 05 evaluated the ν_e flux at the Kuo-Sheng nuclear reactor and searched for non-standard ν_e-e scattering. Ge detector equipped with active anti-Compton shield was used. This laboratory limit on magnetic moment is considerably less stringent than the limits for reactor $\overline{\nu}_e$, but is specific to ν_e.

[21] GRIFOLS 04 obtained this bound using the SNO data of the solar ^{8}B neutrino flux measured with deuteron breakup. This bound applies to $\mu_{\rm eff} = (\mu_{21}^2 + \mu_{22}^2 + \mu_{23}^2)^{1/2}$.

[22] LIU 04 obtained this limit using the shape of the recoil electron energy spectrum from the Super-Kamiokande-I 1496 days of solar neutrino data. Neutrinos are assumed to have only diagonal magnetic moments, $\mu_{\nu 1} = \mu_{\nu 2}$. This limit corresponds to the oscillation parameters in the vacuum oscillation region.

[23] LIU 04 obtained this limit using the shape of the recoil electron energy spectrum from the Super-Kamiokande-I 1496 live-day solar neutrino data, by limiting the oscillation parameter region in the LMA region allowed by solar neutrino experiments plus KamLAND. $\mu_{\nu 1} = \mu_{\nu 2}$ is assumed. In the LMA region, the same limit would be obtained even if neutrinos have off-diagonal magnetic moments.

[24] BACK 03B obtained this bound from the results of background measurements with Counting Test Facility (the prototype of the Borexino detector). Standard Solar Model flux was assumed. This μ_ν can be different from the reactor μ_ν in certain oscillation scenarios (see BEACOM 99).

[25] DARAKTCHIEVA 03 searched for non-standard $\overline{\nu}_e$-e scattering component at Bugey nuclear reactor. Full kinematical event reconstruction by use of TPC. Superseded by DARAKTCHIEVA 05.

[26] LI 03B used Ge detector in active shield near nuclear reactor to test for nonstandard $\overline{\nu}_e$-e scattering.

[27] GRIMUS 02 obtain stringent bounds on all Majorana neutrino transition moments from a simultaneous fit of LMA-MSW oscillation parameters and transition moments to global solar neutrino data + reactor data. Using only solar neutrino data, a 90% CL bound of $6.3 \times 10^{-10} \mu_B$ is obtained.

[28] TANIMOTO 00 combined $e^+e^- \to \nu\overline{\nu}\gamma$ data from VENUS, TOPAZ, and AMY.

[29] AYALA 99 improves the limit of BARBIERI 88.

[30] BEACOM 99 obtain the limit using the shape, but not the absolute magnitude which is affected by oscillations, of the solar neutrino spectrum obtained by Superkamiokande (825 days). This μ_ν can be different from the reactor μ_ν in certain oscillation scenarios.

[31] RAFFELT 99 is an update of RAFFELT 90. This limit applies to all neutrino flavors which are light enough (< 5 keV) to be emitted from globular-cluster red giants. This limit pertains equally to electric dipole moments and magnetic transition moments, and it applies to both Dirac and Majorana neutrinos.

[32] RAFFELT 99 is essentially an update of BERNSTEIN 63, but is derived from the helioseismological limit on a new energy-loss channel of the Sun. This limit applies to all neutrino flavors which are light enough (<1 keV) to be emitted from the Sun. This limit pertains equally to electric dipole and magnetic transition moments, and it applies to both Dirac and Majorana neutrinos.

[33] ACCIARRI 97Q result applies to both direct and transition magnetic moments and for q^2=0.

[34] ELMFORS 97 calculate the rate of depolarization in a plasma for neutrinos with a magnetic moment and use the constraints from a big-bang nucleosynthesis on additional degrees of freedom.

[35] Applies to absolute value of magnetic moment.

[36] DERBIN 93 determine the cross section for 0.6–2.0 MeV electron energy as $(1.28 \pm 0.63) \times \sigma_{\rm weak}$. However, the (reactor on − reactor off)/(reactor off) is only $\sim 1/100$.

[37] COOPER-SARKAR 92 assume $f_{D_s}/f_\pi = 2$ and D_s, $\overline{D}_s$ production cross section = 2.6 μb to calculate ν flux.

[38] VIDYAKIN 92 limit is from a $e\overline{\nu}_e$ elastic scattering experiment. No experimental details are given except for the cross section from which this limit is derived. Signal/noise was 1/10. The limit uses $\sin^2\theta_W = 0.23$ as input.

[39] DORENBOSCH 91 corrects an incorrect statement in DORENBOSCH 89 that the ν magnetic moment is $< 1 \times 10^{-9}$ at the 95%CL. DORENBOSCH 89 measures both $\nu_\mu e$ and $\overline{\nu} e$ elastic scattering and assume $\mu(\nu) = \mu(\overline{\nu})$.

[40] KRAKAUER 90 experiment fully reported in ALLEN 93.

[41] RAFFELT 90 limit applies for a diagonal magnetic moment of a Dirac neutrino, or for a transition magnetic moment of a Majorana neutrino. In the latter case, the same analysis gives $< 1.4 \times 10^{-12}$. Limit at 95%CL obtained from δM_c.

[42] Significant dependence on details of stellar models.

[43] FUKUGITA 88 find magnetic dipole moments of any two neutrino species are bounded by $\mu < 10^{-16}$ $[10^{-9}\ G/B_0]$ where B_0 is the present-day intergalactic field strength.

[44] GROTCH 88 combined data from MAC, ASP, CELLO, and Mark J.

[45] For m_ν = 8–200 eV. NUSSINOV 87 examines transition magnetic moments for $\nu_\mu \to \nu_e$ and obtain $< 3 \times 10^{-15}$ for $m_\nu > 16$ eV and $< 6 \times 10^{-14}$ for $m_\nu > 4$ eV.

[46] We obtain above limit from SUTHERLAND 76 using their limit $f < 1/3$.

[47] KIM 74 is a theoretical analysis of $\overline{\nu}_\mu$ reaction data.

NEUTRINO CHARGE RADIUS SQUARED

We report limits on the so-called neutrino charge radius squared. While the straight-forward definition of a neutrino charge radius has been proven to be gauge-dependent and, hence, unphysical (LEE 77C), there have been recent attempts to define a physically observable neutrino charge radius (BERNABEU 00, BERNABEU 02). The issue is still controversial (FUJIKAWA 03, BERNABEU 03). A more general interpretation of the experimental results is that they are limits on certain nonstandard contributions to neutrino scattering.

VALUE (10^{-32} cm^2)	*CL%*	*DOCUMENT ID*		*TECN*	*COMMENT*
− 2.1 to 3.3	90	[1] DENIZ	10	TEXO	Reactor $\overline{\nu}_e e$
• • • We do not use the following data for averages, fits, limits, etc. • • •					
−27.5 to 3	90	[2] CADEDDU	18		ν_μ coherent scat. on CsI
− 0.53 to 0.68	90	[3] HIRSCH	03		$\nu_\mu e$ scat.
− 8.2 to 9.9	90	[4] HIRSCH	03		anomalous $e^+e^- \to \nu\overline{\nu}\gamma$
− 2.97 to 4.14	90	[5] AUERBACH	01	LSND	$\nu_e e \to \nu_e e$
− 0.6 to 0.6	90	VILAIN	95B	CHM2	$\nu_\mu e$ elastic scat.
0.9 ±2.7		ALLEN	93	CNTR	LAMPF $\nu e \to \nu e$
< 2.3	95	MOURAO	92	ASTR	HOME/KAM2 ν rates
< 7.3	90	[6] VIDYAKIN	92	CNTR	Reactor $\overline{\nu} e \to \overline{\nu} e$
1.1 ±2.3		ALLEN	91	CNTR	Repl. by ALLEN 93
− 1.1 ±1.0		[7] AHRENS	90	CNTR	$\nu_\mu e$ elastic scat.

Downloaded from https://academic.oup.com/ptep/article/2022/8/083C01/6651666 by KIT Library user on 27 September 2022

– 0.3 ±1.5

[7] DORENBOS... 89 CHRM $\nu_\mu e$ elastic scat.

[8] GRIFOLS 89B ASTR SN 1987A

[1] DENIZ 10 observe reactor $\overline{\nu}_e e$ scattering with recoil kinetic energies 3–8 MeV using CsI(Tl) detectors. The observed rate and spectral shape are consistent with the Standard Model prediction, leading to the reported constraint on $\overline{\nu}_e$ charge radius.

[2] CADEDDU 18 use the data of the COHERENT experiment, AKIMOV 18. The limit is $\langle r^2_\nu \rangle$ for ν_μ obtained from the time-dependent data. Weaker limits were obtained for charge radii of ν_e and for transition charge radii. The published value was divided by 2 to conform to the convention of this table.

[3] Based on analysis of CCFR 98 results. Limit is on $\langle r^2_V \rangle + \langle r^2_A \rangle$. The CHARM II and E734 at BNL results are reanalyzed, and weaker bounds on the charge radius squared than previously published are obtained. The NuTeV result is discussed; when tentatively interpreted as ν_μ charge radius it implies $\langle r^2_V \rangle + \langle r^2_A \rangle = (4.20 \pm 1.64) \times 10^{-33}$ cm^2.

[4] Results of LEP-2 are interpreted as limits on the axial-vector charge radius squared of a Majorana ν_τ. Slightly weaker limits for both vector and axial-vector charge radius squared are obtained for the Dirac case, and somewhat weaker limits are obtained from the analysis of lower energy data (LEP-1.5 and TRISTAN).

[5] AUERBACH 01 measure $\nu_e e$ elastic scattering with LSND detector. The cross section agrees with the Standard Model expectation, including the charge and neutral current interference. The 90% CL applies to the range shown.

[6] VIDYAKIN 92 limit is from a $e\overline{\nu}$ elastic scattering experiment. No experimental details are given except for the cross section from which this limit is derived. Signal/noise was 1/10. The limit uses $\sin^2\theta_W = 0.23$ as input.

[7] Result is obtained from reanalysis given in ALLEN 91, followed by our reduction to obtain 1 σ errors.

[8] GRIFOLS 89B sets a limit of $\langle r^2 \rangle < 0.2 \times 10^{-32}$ cm^2 for right-handed neutrinos.

REFERENCES FOR Neutrino Properties

ABBOTT	21A	PR D105 023520	T.C.M. Abbott *et al.*	(DES Collab.)
ALAM	21	PR D103 083533	S. Alam *et al.*	(eBOSS Collab.)
DI-VALENT...	21	PR D 104 083504	E. Di Valentino, S. Gariazzo, O. Mena	(DURH+)
GARNY	21	JCAP 2103 049	M. Garny *et al.*	
STOCKER	21	PR D103 123508	P. Stocker *et al.*	(GAMBIT Collab.)
ABE	20E	PL B809 135741	K. Abe *et al.*	(XMASS Collab.)
AGHANIM	20	AA 641 A6	N. Aghanim *et al.*	(Planck Collab.)
APRILE	20	PR D102 072004	E. Aprile *et al.*	(XENON Collab.)
CAPOZZI	20	PR D102 083007	F. Capozzi, G. Raffelt	(MPIM)
CHOUDHURY	20	JCAP 2007 037	S.R. Choudhury, S. Hannestad	(IITB, AARH)
IVANOV	20	PR D101 083504	M.M. Ivanov, M. Simonovic, M. Zaldarriaga	(NYU,+)
KHAN	20	PL B809 135782	A.N. Khan	(MPIK)
PALANQUE-...	20	JCAP 2004 038	N. Palanque-Delabrouille *et al.*	(SACL+)
AHARMIM	19	PR D99 032013	B. Aharmim *et al.*	(SNO Collab.)
AKER	19	PRL 123 221802	M. Aker *et al.*	(KATRIN Collab.)
Also		PR D104 012005	M. Aker *et al.*	(KATRIN Collab.)
ESCUDERO	19	PR D100 103531	M. Escudero, M. Fairbairn	(LOKC)
LOUREIRO	19	PRL 123 081301	A. Loureiro *et al.*	
UPADHYE	19	JCAP 1905 041	A. Upadhye	(WISC)
AKIMOV	18	arXiv:1804.09459	D. Akimov *et al.*	(COHERENT Collab.)
CADEDDU	18	PR D98 113010	M. Cadeddu *et al.*	
Also		PR D101 059902 (errat.)	M. Cadeddu *et al.*	
CHOUDHURY	18	JCAP 1809 017	S.R. Choudhury, S. Choubey	
AGOSTINI	17A	PR D96 091103	M. Agostini *et al.*	(Borexino Collab.)
SIMPSON	17	JCAP 1706 029	F. Simpson *et al.*	(BARC)
VAGNOZZI	17	PR D96 123503	S. Vagnozzi *et al.*	
YECHE	17	JCAP 1706 047	C. Yeche *et al.*	
DELLA-VALLE	16	EPJ C76 24	F. Della Valle *et al.*	(PVLAS Collab.)
DIVALENTINO	16	PR D93 083527	E. Di Valentino *et al.*	
GIUSARMA	16	PR D94 083522	E. Guisarma *et al.*	
HUANG	16	EPJ C76 489	Q.-G. Huang, K. Wang, S. Wang	
ARCEO-DIAZ	15	ASP 70 1	S. Arceo-Diaz *et al.*	
PALANQUE-...	15A	JCAP 1511 011	N. Palanque-Delabrouille *et al.*	
ROSSI	15	PR D92 063505	G. Rossi *et al.*	
ADE	14	AA 571 A16	P.A.R. Ade *et al.*	(Planck Collab.)
BATTYE	14	PRL 112 051303	R.A. Battye, A. Moss	(MCHS, NOTT)
BEUTLER	14	MNRAS 444 3501	F. Beutler *et al.*	(BOSS Collab.)
CHEN	14A	PR D90 011301	J.-W. Chen *et al.*	(TEXONO Collab.)
CORSICO	14	JCAP 1408 054	A.H. Corsico	
COSTANZI	14	JCAP 1410 081	M. Costanzi *et al.*	(TRST, TRSTI)
GIUSARMA	14	PR D90 043507	E. Giusarma *et al.*	
HOU	14	APJ 782 74	Z. Hou *et al.*	
LEISTEDT	14	PRL 113 041301	B. Leistedt, H.V. Peiris, L. Verde	
MILLER-BER...	14B	AA 562 A123	M.M. Miller Bertolami	(MPIG, LAPL)
RIEMER-SOR...	14	PR D89 103505	S. Riemer-Sorensen, D. Parkinson, T.M. Davis	
STUDENIKIN	14	EPL 107 21001	A.I. Studenikin	
BEDA	13	PPNL 10 139	A.G. Beda *et al.*	(GEMMA Collab.)
VIAUX	13A	PRL 111 231301	N. Viaux *et al.*	
MORESCO	12	JCAP 1207 053	M. Moresco *et al.*	
XIA	12	JCAP 1206 010	J.-Q. Xia *et al.*	
ASEEV	11	PR D84 112003	V.N. Aseev *et al.*	
CECCHINI	11	ASP 34 486	S. Cecchini *et al.*	
SAITO	11	PR D83 043529	S. Saito, M. Takada, A. Taruya	
BEDA	10	PPNL 7 406	A.G. Beda *et al.*	(GEMMA Collab.)
DENIZ	10	PR D81 072001	M. Deniz *et al.*	(TEXONO Collab.)
HANNESTAD	10	JCAP 1008 001	S. Hannestad *et al.*	(AARH)
PAGLIAROLI	10	ASP 33 287	G. Pagliaroli, F. Rossi-Torres, E. Vissani	(INFN+)
SEKIGUCHI	10	JCAP 1003 015	T. Sekiguchi *et al.*	
THOMAS	10	PRL 105 031301	S.A. Thomas, F.B. Abdalla, O. Lahav	(LOUC)
ICHIKI	09	PR D79 023520	K. Ichiki, M. Takada, T. Takahashi	
KOMATSU	09	APJS 180 330	E. Komatsu *et al.*	
KUZNETSOV	09	IJMP A24 5977	A.V. Kuznetsov, N.V. Mikheev, A.A. Okrugin	(YARO)
TERENO	09	AA 500 657	I. Tereno *et al.*	
VIKHLININ	09	APJ 692 1060	A. Vikhlinin *et al.*	
ARPESELLA	08A	PRL 101 091302	C. Arpesella *et al.*	(Borexino Collab.)
BERNARDIS	08	PR D78 083535	F. De Bernardis *et al.*	
BEDA	07	PAN 70 1873	A.G. Beda *et al.*	
		Translated from YAF 70 1925.		
FOGLI	07	PR D75 053001	G.L. Fogli *et al.*	
GNINENKO	07	PR D75 075014	S.N. Gninenko, N.V. Krasnikov, A. Rubbia	
KRISTIANSEN	07	PR D75 083510	J. Kristiansen, O. Elgaroy, H. Dahle	
MIRIZZI	07	PR D76 053007	A. Mirizzi, D. Montanino, P.D. Serpico	
SPERGEL	07	APJS 170 377	D.N. Spergel *et al.*	
WONG	07	PR D75 012001	H.T. Wong *et al.*	(TEXONO Collab.)
ZUNCKEL	07	JCAP 0708 004	C. Zunckel, P. Ferreira	
CIRELLI	06	JCAP 0612 013	M. Cirelli *et al.*	
FUKUGITA	06	PR D74 027302	M. Fukugita *et al.*	
GOOBAR	06	JCAP 0606 019	A. Goobar *et al.*	
HANNESTAD	06	JCAP 0611 016	S. Hannestad, G. Raffelt	
KRISTIANSEN	06	PR D74 123005	J. Kristiansen, O. Elgaroy, H. Eriksen	
SANCHEZ	06	MNRAS 366 189	A.G. Sanchez *et al.*	
SELJAK	06	JCAP 0610 014	U. Seljak, A. Slosar, P. McDonald	
CAPRINI	05	JCAP 0502 006	C. Caprini, P.G. Ferreira	(GEVA, OXFTP)
DARAKTCH...	05	PL B615 153	Z. Daraktchieva *et al.*	(MUNU Collab.)
ICHIKAWA	05	PR D71 043001	K. Ichikawa, M. Fukugita, M. Kawasaki	(ICRR)
KRAUS	05	EPJ C40 447	Ch. Kraus *et al.*	
XIN	05	PR D72 012006	B. Xin *et al.*	(TEXONO Collab.)
AHARMIM	04	PR D70 093014	B. Aharmim *et al.*	(SNO Collab.)
BARGER	04	PL B595 55	V. Barger, D. Marfatia, A. Tregre	
CECCHINI	04	ASP 21 183	S. Cecchini *et al.*	(BGNA+)
CROTTY	04	PR D69 123007	P. Crotty, J. Lesgourgues, S. Pastor	
EGUCHI	04	PRL 92 071301	K. Eguchi *et al.*	(KamLAND Collab.)
GRIFOLS	04	PL B587 184	J.A. Grifols, E. Masso, S. Mohanty	(BARC, AHMED)
LIU	04	PRL 93 021802	D.W. Liu *et al.*	(Super-Kamiokande Collab.)
ARNABOLDI	03A	PRL 91 161802	C. Arnaboldi *et al.*	
BACK	03B	PL B563 35	H.O. Back *et al.*	(Borexino Collab.)
BANDYOPA...	03	PL B555 33	A. Bandyopadhyay, S. Choubey, S. Goswami	(SAHA+)
BERNABEU	03	hep-ph/0303202	J. Bernabeu, J. Papavassiliou, J. Vidal	
DARAKTCH...	03	PL B564 190	Z. Daraktchieva *et al.*	(MUNU Collab.)
FUJIKAWA	03	hep-ph/0303188	K. Fujikawa, R. Shrock	
HIRSCH	03	PR D67 033005	M. Hirsch, E. Nardi, D. Restrepo	
LI	03B	PRL 90 131802	H.B. Li *et al.*	(TEXONO Collab.)
SPERGEL	03	APJS 148 175	D.N. Spergel *et al.*	
BERNABEU	02	PRL 89 101802	J. Bernabeu, J. Papavassiliou, J. Vidal	
Also		PRL 89 229902 (errat.)	J. Bernabeu, J. Papavassiliou, J. Vidal	
DERBIN	02B	JETPL 76 409	A.V. Derbin, O.Ju. Smirnov	
		Translated from ZETFP 76 483.		
GRIMUS	02	NP B648 376	W. Grimus *et al.*	
JOSHIPURA	02B	PR D66 113008	A.S. Joshipura, E. Masso, S. Mohanty	
LEWIS	02	PR D66 103511	A. Lewis, S. Bridle	
LOREDO	02	PR D65 063002	T.J. Loredo, D.Q. Lamb	
WANG	02	PR D65 123001	X. Wang, M. Tegmark, M. Zaldarriaga	
AUERBACH	01	PR D63 112001	L.B. Auerbach *et al.*	(LSND Collab.)
SCHWIENHO...	01	PL B513 23	R. Schwienhorst *et al.*	(DONUT Collab.)
ATHANAS	00	PR D61 052002	M. Athanas *et al.*	(CLEO Collab.)
BERNABEU	00	PR D62 113012	J. Bernabeu *et al.*	
FUKUGITA	00	PRL 84 1082	M. Fukugita, G.C. Liu, N. Sugiyama	
TANIMOTO	00	PL B478 1	N. Tanimoto *et al.*	
AYALA	99	PR D59 111901	A. Ayala, J.C. D'Olivo, M. Torres	
BEACOM	99	PRL 83 5222	J.F. Beacom, P. Vogel	
CROFT	99	PRL 83 1092	R.A.C. Croft, W. Hu, R. Dave	
DOLGOV	99	NP B548 385	A.D. Dolgov *et al.*	
LOBASHEV	99	PL B460 227	V.M. Lobashev *et al.*	
RAFFELT	99	PRPL 320 319	G.G. Raffelt	
WEINHEIMER	99	PL B460 219	Ch. Weinheimer *et al.*	
ACKERSTAFF	98T	EPJ C5 229	K. Ackerstaff *et al.*	(OPAL Collab.)
AMMAR	98	PL B431 209	R. Ammar *et al.*	(CLEO Collab.)
BARATE	98F	EPJ C2 395	R. Barate *et al.*	(ALEPH Collab.)
BILLER	98	PRL 80 2992	S.D. Biller *et al.*	(WHIPPLE Collab.)
FELDMAN	98	PR D57 3873	G.J. Feldman, R.D. Cousins	
LENZ	98	PL B416 50	S. Lenz *et al.*	
ABREU	97J	ZPHY C74 577	P. Abreu *et al.*	(DELPHI Collab.)
ACCIARRI	97Q	PL B412 201	M. Acciarri *et al.*	(L3 Collab.)
ANASTASSOV	97	PR D55 2559	A. Anastassov *et al.*	(CLEO Collab.)
Also		PR D58 119903 (erratum)	A. Anastassov *et al.*	(CLEO Collab.)
ELMFORS	97	NP B503 3	P. Elmfors *et al.*	
ESCRIBANO	97	PL B395 369	R. Escribano, E. Masso	(BARC, PARIT)
FIELDS	97	ASP 6 169	B.D. Fields, K. Kainulainen, K.A. Olive	(NDAM+)
SWAIN	97	PR D55 1	J. Swain, L. Taylor	(NEAS)
ALEXANDER	96M	ZPHY C72 231	G. Alexander *et al.*	(OPAL Collab.)
ASSAMAGAN	96	PR D53 6065	K.A. Assamagan *et al.*	(PSI, ZURI, VILL+)
BAI	96	PR D53 20	J.Z. Bai *et al.*	(BES Collab.)
BOTTINO	96	PR D53 6361	A. Bottino *et al.*	
DOLGOV	96	PL B383 193	A.D. Dolgov, S. Pastor, J.W.F. Valle	(IFIC, VALE)
HANNESTAD	96	PRL 76 2848	S. Hannestad, J. Madsen	(AARH)
HANNESTAD	96B	PRL 77 5148 (erratum)	S. Hannestad, J. Madsen	(AARH)
HANNESTAD	96C	PR D54 7894	S. Hannestad, J. Madsen	(AARH)
SOBIE	96	ZPHY C70 383	R.J. Sobie, R.K. Keeler, I. Lawson	(VICT)
BELESEV	95	PL B350 263	A.I. Belesev *et al.*	(INRM, KIAE)
BUSKULIC	95H	PL B349 585	D. Buskulic *et al.*	(ALEPH Collab.)
CHING	95	IJMP A10 2841	C.R. Ching *et al.*	(CST, BEIJT, CIAE)
DOLGOV	95	PR D51 4129	A.D. Dolgov, K. Kainulainen, I.Z. Rothstein	(MICH+)
HIDDEMANN	95	JP G21 639	K.H. Hiddemann, H. Daniel, O. Schwentker	(TUM)
KERNAN	95	NP B437 243	P.J. Kernan, L.M. Krauss	(CASE)
SIGL	95	PR D51 1499	G. Sigl, M.S. Turner	(FNAL, EFI)
STOEFFL	95	PRL 75 3237	W. Stoeffl, D.J. Decman	(LLNL)
VILAIN	95B	PL B345 115	P. Vilain *et al.*	(CHARM II Collab.)
ASSAMAGAN	94	PL B335 231	K.A. Assamagan *et al.*	(PSI, ZURI, VILL+)
BABU	94	PL B321 140	K.S. Babu, T.M. Gould, I.Z. Rothstein	(BART+)
DODELSON	94	PR D49 5068	S. Dodelson, G. Gyuk, M.S. Turner	(FNAL, CHIC+)
GOULD	94	PL B333 545	T.M. Gould, I.Z. Rothstein	(JHU, MICH)
JECKELMANN	94	PL B335 326	B. Jeckelmann, P.F.A. Goudsmit, H.J. Leisi	(WABRN+)
KAWASAKI	94	NP B419 105	M. Kawasaki *et al.*	(OSU)
PERES	94	PR D50 513	O.L.G. Peres, V. Pleitez, R. Zukanovich Funchal	
YASUMI	94	PL B334 229	S. Yasumi *et al.*	(KEK, TSUK, KYOT+)
ALLEN	93	PR D47 11	R.C. Allen *et al.*	(UCI, LANL, ANL+)
BALEST	93	PR D47 3671	R. Balest *et al.*	(CLEO Collab.)
CINABRO	93	PRL 70 3700	D. Cinabro *et al.*	(CLEO Collab.)
DERBIN	93	JETPL 57 768	A.V. Derbin *et al.*	(PNPI)
		Translated from ZETFP 57 755.		
DOLGOV	93	PRL 71 476	A.D. Dolgov, I.Z. Rothstein	(MICH)
ENQVIST	93	PL B301 376	K. Enqvist, H. Uibo	(NORD)
SUN	93	CJNP 15 261	H.C. Sun *et al.*	(CIAE, CST, BEIJT)
WEINHEIMER	93	PL B300 210	C. Weinheimer *et al.*	(MAINZ)
ALBRECHT	92M	PL B292 221	H. Albrecht *et al.*	(ARGUS Collab.)
BLUDMAN	92	PR D45 4720	S.A. Bludman	(CFPA)
COOPER-...	92	PL B280 153	A.M. Cooper-Sarkar *et al.*	(BEBC WA66 Collab.)
DODELSON	92	PRL 68 2572	S. Dodelson, J.A. Frieman, M.S. Turner	(FNAL+)
HOLZSCHUH	92B	PL B287 381	E. Holzschuh, M. Fritschi, W. Kundig	(ZURI)
KAWANO	92	PL B275 487	L.H. Kawano *et al.*	(CIT, UCSD, LLL+)
MOURAO	92	PL B285 364	A.M. Mourao, J. Pulido, J.P. Ralston	(LISB, LISBT+)
PDG	92	PR D45 S1	K. Hikasa *et al.*	(KEK, LBL, BOST+)
VIDYAKIN	92	JETPL 55 206	G.S. Vidyakin *et al.*	(KIAE)
		Translated from ZETFP 55 212.		
ALLEN	91	PR D43 1	R.C. Allen *et al.*	(UCI, LANL, UMD)
DAVIDSON	91	PR D43 2314	S. Davidson, B.A. Campbell, D. Bailey	(ALBE+)
DESHPANDE	91	PR D43 943	N.G. Deshpande, K.V.L. Sarma	(OREG, TATA)
DORENBOS...	91	ZPHY C51 142 (erratum)	J. Dorenbosch *et al.*	(CHARM Collab.)
FULLER	91	PR D43 3136	G.M. Fuller, R.A. Malaney	(UCSD)
GRANEK	91	IJMP A6 2387	H. Granek, B.H.J. McKellar	(MELB)
KAWAKAMI	91	PL B256 105	H. Kawakami *et al.*	(INUS, TOHOK, TINT+)
KOLB	91	PRL 67 533	E.W. Kolb *et al.*	(FNAL, CHIC)
KRAKAUER	91	PR D44 6	D.A. Krakauer *et al.*	(LAMPF E225 Collab.)
LAM	91	PR D44 3345	W.P. Lam, K.W. Ng	(AST)
ROBERTSON	91	PRL 67 957	R.G.H. Robertson *et al.*	(LASL, LLL)
AHRENS	90	PR D41 3297	L.A. Ahrens *et al.*	(BNL, BROW, HIRO+)
AVIGNONE	90	PR D41 682	F.T. Avignone, J.I. Collar	(SCUC)
KRAKAUER	90	PL B252 177	D.A. Krakauer *et al.*	(LAMPF E225 Collab.)
RAFFELT	90	PRL 64 2856	G.G. Raffelt	(MPIM)

Downloaded from https://academic.oup.com/ptep/article/2022/8/083C01/6651666 by KIT Library user on 27 September 2022

WALKER	90	PR D41 689	T.P. Walker	(HARV)
CHUPP	89	PRL 62 505	E.L. Chupp, W.T. Vestrand, C. Reppin	(UNH, MPIM)
DORENBOS...	89	ZPHY C41 567	J. Dorenbosch *et al.*	(CHARM Collab.)
GRIFOLS	89B	PR D40 3819	J.A. Grifols, E. Masso	(BARC)
KOLB	89	PRL 62 509	E.W. Kolb, M.S. Turner	(CHIC, FNAL)
LOREDO	89	ANYAS 571 601	T.J. Loredo, D.Q. Lamb	(CHIC)
RAFFELT	89	PR D39 2066	G.G. Raffelt	(PRIN, UCB)
RAFFELT	89B	APJ 336 61	G. Raffelt, D. Dearborn, J. Silk	(UCB, LLL)
ALBRECHT	88B	PL B202 149	H. Albrecht *et al.*	(ARGUS Collab.)
BARBIERI	88	PRL 61 27	R. Barbieri, R.N. Mohapatra	(PISA, UMD)
BORIS	88	PRL 61 245 (erratum)	S.D. Boris *et al.*	(ITEP, ASCI)
FUKUGITA	88	PRL 60 879	M. Fukugita *et al.*	(KYOTU, MPIM, UCB)
GROTCH	88	ZPHY C39 553	H. Grotch, R.W. Robinett	(PSU)
RAFFELT	88B	PR D37 549	G.G. Raffelt, D.S.P. Dearborn	(UCB, LLL)
SPERGEL	88	PL B200 366	D.N. Spergel, J.N. Bahcall	(IAS)
VONFEILIT...	88	PL B200 580	F. von Feilitzsch, L. Oberauer	(TUM)
BARBIELLINI	87	NAT 329 21	G. Barbiellini, G. Cocconi	(CERN)
BORIS	87	PRL 58 2019	S.D. Boris *et al.*	(ITEP, ASCI)
Also		PRL 61 245 (erratum)	S.D. Boris *et al.*	(ITEP, ASCI)
BORIS	87B	JETPL 45 333	S.D. Boris *et al.*	(ITEP)
		Translated from ZETFP 45 267.		
FUKUGITA	87	PR D36 3817	M. Fukugita, S. Yazaki	(KYOTU, TOKY)
NUSSINOV	87	PR D36 2278	S. Nussinov, Y. Rephaeli	(TELA)
OBERAUER	87	PL B198 113	L.F. Oberauer, F. von Feilitzsch, R.L. Mossbauer	
SPRINGER	87	PR A35 679	P.T. Springer *et al.*	(LLNL)
KETOV	86	JETPL 44 146	S.N. Ketov *et al.*	(KIAE)
		Translated from ZETFP 44 114.		
COWSIK	85	PL 151B 62	R. Cowsik	(TATA)
RAFFELT	85	PR D31 3002	G.G. Raffelt	(MPIM)
BINETRUY	84	PL 134B 174	P. Binetruy, G. Girardi, P. Salati	(LAPP)
FREESE	84	NP B233 167	K. Freese, D.N. Schramm	(CHIC, FNAL)
KYULDJIEV	84	NP B243 387	A.V. Kyuldjiev	(SOFI)
SCHRAMM	84	PL 141B 337	D.N. Schramm, G. Steigman	(FNAL, BART)
VOGEL	84	PR D30 1505	P. Vogel	
ANDERHUB	82	PL 114B 76	H.B. Anderhub *et al.*	(ETH, SIN)
OLIVE	82	PR D25 213	K.A. Olive, M.S. Turner	(CHIC, UCSB)
BERNSTEIN	81	PL 101B 39	J. Bernstein, G. Feinberg	(STEV, COLU)
FRANK	81	PR D24 2001	J.S. Frank *et al.*	(LASL, YALE, MIT+)
MORGAN	81	PL 102B 247	J.A. Morgan	(SUSS)
FUJIKAWA	80	PRL 45 963	K. Fujikawa, R. Shrock	(STON)
LUBIMOV	80	PL 94B 266	V.A. Lyubimov *et al.*	(ITEP)
STECKER	80	PRL 45 1460	F.W. Stecker	(NASA)
COWSIK	79	PR D19 2219	R. Cowsik	(TATA)
GOLDMAN	79	PR D19 2215	T. Goldman, G.J. Stephenson	(LASL)
BEG	78	PR D17 1395	M.A.B. Beg, W.J. Marciano, M. Ruderman	(ROCK+)
BLIETSCHAU	78	NP B133 205	J. Blietschau *et al.*	(Gargamelle Collab.)
FALK	78	PL 79B 511	S.W. Falk, D.N. Schramm	(CHIC)
BARNES	77	PRL 38 1049	V.E. Barnes *et al.*	(PURD, ANL)
COWSIK	77	PRL 39 784	R. Cowsik	(MPIM, TATA)
LEE	77C	PR D16 1444	B.W. Lee, R.E. Shrock	(STON)
VYSOTSKY	77	JETPL 26 188	M.I. Vysotsky, A.D. Dolgov, Y.B. Zeldovich	(ITEP)
		Translated from ZETFP 26 200.		
BELLOTTI	76	LNC 17 553	E. Bellotti *et al.*	(MILA)
SUTHERLAND	76	PR D13 2700	P. Sutherland *et al.*	(PENN, COLU, NYU)
SZALAY	76	AA 49 437	A.S. Szalay, G. Marx	(EOTV)
CLARK	74	PR D9 533	A.R. Clark *et al.*	(LBL)
KIM	74	PR D9 3050	J.E. Kim, V.S. Mathur, S. Okubo	(ROCH)
REINES	74	PRL 32 180	F. Reines, H.W. Sobel, H.S. Gurr	(UCI)
SZALAY	74	APAH 35 8	A.S. Szalay, G. Marx	(EOTV)
COWSIK	72	PRL 29 669	R. Cowsik, J. McClelland	(UCB)
MARX	72	Nu Conf. Budapest	G. Marx, A.S. Szalay	(EOTV)
GERSHTEIN	66	JETPL 4 120	S.S. Gershtein, Y.B. Zeldovich	(KIAM)
		Translated from ZETFP 4 189.		
BERNSTEIN	63	PR 132 1227	J. Bernstein, M. Ruderman, G. Feinberg	(NYU+)
COWAN	57	PR 107 528	C.L. Cowan, F. Reines	(LANL)

Number of Neutrino Types

The neutrinos referred to in this section are those of the Standard SU(2)×U(1) Electroweak Model possibly extended to allow nonzero neutrino masses. Light neutrinos are those with $m < m_Z/2$. The limits are on the number of neutrino mass eigenstates, including ν_1, ν_2, and ν_3.

THE NUMBER OF LIGHT NEUTRINO TYPES FROM COLLIDER EXPERIMENTS

Revised June 2020 by C.-J. Lin (LBNL). Written by D. Karlen (University of Victoria and TRIUMF).

The most precise measurements of the number of light neutrino types, N_ν, come from studies of Z production in e^+e^- collisions. The invisible partial width, $\Gamma_{\rm inv}$, is determined by subtracting the measured visible partial widths, corresponding to Z decays into quarks and charged leptons, from the total Z width. The invisible width is assumed to be due to N_ν light neutrino species each contributing the neutrino partial width Γ_ν as given by the Standard Model. In order to reduce the model dependence, the Standard Model value for the ratio of the neutrino to charged leptonic partial widths, $(\Gamma_\nu/\Gamma_\ell)_{\rm SM} = 1.991 \pm 0.001$, is used instead of $(\Gamma_\nu)_{\rm SM}$ to determine the number of light neutrino types:

$$N_\nu = \frac{\Gamma_{\rm inv}}{\Gamma_\ell}\left(\frac{\Gamma_\ell}{\Gamma_\nu}\right)_{\rm SM} . \qquad (1)$$

The combined result from the four LEP experiments is $N_\nu = 2.984 \pm 0.008$ [1]. Recent analyses applied corrections to the LEP result [1] by including the effect of correlated luminosity systematics and also using an improved Bhabha cross section calculation [2,3] to obtain $N_\nu = 2.9963 \pm 0.0074$.

In the past, when only small samples of Z decays had been recorded by the LEP experiments and by the Mark II at SLC, the uncertainty in N_ν was reduced by using Standard Model fits to the measured hadronic cross sections at several center-of-mass energies near the Z resonance. Since this method is much more dependent on the Standard Model, the approach described above is favored.

Before SLC and LEP, limits on the number of neutrino generations were placed by experiments at lower-energy e^+e^- colliders by measuring the cross section of the process $e^+e^- \to \nu\overline{\nu}\gamma$. The ASP, CELLO, MAC, MARK J, and VENUS experiments observed a total of 3.9 events above background [4], leading to a 95% CL limit of $N_\nu < 4.8$. This process has a much larger cross section at center-of-mass energies near the Z mass and has been measured at LEP by the ALEPH, DELPHI, L3, and OPAL experiments [5]. These experiments have observed several thousand such events, and the combined result is $N_\nu = 3.00 \pm 0.08$. The same process has also been measured by the LEP experiments at much higher center-of-mass energies, between 130 and 208 GeV, in searches for new physics [6]. Combined with the lower energy data, the result is $N_\nu = 2.92 \pm 0.05$.

Experiments at $p\overline{p}$ colliders also placed limits on N_ν by determining the total Z width from the observed ratio of $W^\pm \to \ell^\pm\nu$ to $Z \to \ell^+\ell^-$ events [7]. This involved a calculation that assumed Standard Model values for the total W width and the ratio of W and Z leptonic partial widths, and used an estimate of the ratio of Z to W production cross sections. Now that the Z width is very precisely known from the LEP experiments, the approach is now one of those used to determine the W width.

References

1. ALEPH, DELPHI, L3, OPAL, and SLD Collaborations, and LEP Electroweak Working Group, and SLD Electroweak Group, and SLD Heavy Flavour Group, Phys. Reports **427**, 257 (2006).
2. P. Janot and S. Jadach, Phys. Lett. **B803**, 135319 (2020).
3. G. Voutsinas *et al.*, Phys. Lett. **B800**, 135068 (2020).
4. VENUS: K. Abe *et al.*, Phys. Lett. **B232**, 431 (1989); ASP: C. Hearty *et al.*, Phys. Rev. **D39**, 3207 (1989); CELLO: H.J. Behrend *et al.*, Phys. Lett. **B215**, 186 (1988); MAC: W.T. Ford *et al.*, Phys. Rev. **D33**, 3472 (1986); MARK J: H. Wu, Ph.D. Thesis, Univ. Hamburg (1986).
5. L3: M. Acciarri *et al.*, Phys. Lett. **B431**, 199 (1998); DELPHI: P. Abreu *et al.*, Z. Phys. **C74**, 577 (1997); OPAL: R. Akers *et al.*, Z. Phys. **C65**, 47 (1995); ALEPH: D. Buskulic *et al.*, Phys. Lett. **B313**, 520 (1993).
6. DELPHI: J. Abdallah *et al.*, Eur. Phys. J. **C38**, 395 (2005); L3: P. Achard *et al.*, Phys. Lett. **B587**, 16 (2004); ALEPH: A. Heister *et al.*, Eur. Phys. J. **C28**, 1 (2003); OPAL: G. Abbiendi *et al.*, Eur. Phys. J. **C18**, 253 (2000).

Downloaded from https://academic.oup.com/ptep/article/2022/8/083C01/6651666 by KIT Library user on 27 September 2022

7. UA1: C. Albajar *et al.*, Phys. Lett. **B198**, 271 (1987); UA2: R. Ansari *et al.*, Phys. Lett. **B186**, 440 (1987).

Number from e^+e^- Colliders

Number of Light ν Types

VALUE	DOCUMENT ID		TECN
2.9963±0.0074	[1] JANOT	20	
• • • We do not use the following data for averages, fits, limits, etc. • • •			
2.9918±0.0081	[2] VOUTSINAS	20	
2.9840±0.0082	[3] LEP-SLC	06	RVUE
3.00 ±0.05	[4] LEP	92	RVUE

[1] JANOT 20 applies a correction to LEP-SLC 06 using an updated Bhabha cross section calculation. This result also includes a correction to account for correlated luminosity bias as presented in VOUTSINAS 20.

[2] VOUTSINAS 20 applies a correction to LEP-SLC 06 to account for correlated luminosity bias.

[3] Combined fit from ALEPH, DELPHI, L3 and OPAL Experiments.

[4] Simultaneous fits to all measured cross section data from all four LEP experiments.

Number of Light ν Types from Direct Measurement of Invisible Z Width

In the following, the invisible Z width is obtained from studies of single-photon events from the reaction $e^+e^- \rightarrow \nu\overline{\nu}\gamma$. All are obtained from LEP runs in the E^{ee}_{cm} range 88–209 GeV.

VALUE	DOCUMENT ID		TECN	COMMENT
2.92±0.05 OUR AVERAGE Error includes scale factor of 1.2.				
2.84±0.10±0.14	ABDALLAH	05B	DLPH	$\sqrt{s}$ = 180–209 GeV
2.98±0.05±0.04	ACHARD	04E	L3	1990-2000 LEP runs
2.86±0.09	HEISTER	03C	ALEP	$\sqrt{s}$ = 189–209 GeV
2.69±0.13±0.11	ABBIENDI,G	00D	OPAL	1998 LEP run
2.89±0.32±0.19	ABREU	97J	DLPH	1993–1994 LEP runs
3.23±0.16±0.10	AKERS	95C	OPAL	1990–1992 LEP runs
2.68±0.20±0.20	BUSKULIC	93L	ALEP	1990–1991 LEP runs
• • • We do not use the following data for averages, fits, limits, etc. • • •				
2.84±0.15±0.14	ABREU	00Z	DLPH	1997–1998 LEP runs
3.01±0.08	ACCIARRI	99R	L3	1991–1998 LEP runs
3.1 ±0.6 ±0.1	ADAM	96C	DLPH	$\sqrt{s}$ = 130, 136 GeV

Limits from Astrophysics and Cosmology

Effective Number of Light ν Types

"Light" means here with a mass < about 1 MeV. The quoted values correspond to N_{eff}, where N_{eff} = 3.045 in the Standard Model with N_ν = 3. See also reviews on "Big-Bang Nucleosynthesis" and "Neutrinos in Cosmology."

VALUE	CL%	DOCUMENT ID		TECN	COMMENT
• • • We do not use the following data for averages, fits, limits, etc. • • •					
2.99±0.17	68	[1] AGHANIM	20	COSM	
2.84±0.15	68	[2] FIELDS	20	COSM	BBN
2.88±0.17	68	[3] IVANOV	20	COSM	Planck and BOSS
2.3–3.2	95	[4] VERDE	17	COSM	
2.88±0.16	68	[5] CYBURT	16	COSM	BBN
2.88±0.20	95	[6] ROSSI	15	COSM	
3.3 ±0.5	95	[7] ADE	14	COSM	Planck
$3.78^{+0.31}_{-0.30}$		[8] COSTANZI	14	COSM	
3.29±0.31		[9] HOU	14	COSM	
< 3.80	95	[10] LEISTEDT	14	COSM	
< 4.10	95	[11] MORESCO	12	COSM	
< 5.79	95	[12] XIA	12	COSM	
< 4.08	95	MANGANO	11	COSM	BBN
0.9–8.2		[13] ICHIKAWA	07	COSM	
3–7	95	[14] CIRELLI	06	COSM	
2.7–4.6	95	[15] HANNESTAD	06	COSM	
3.6–7.4	95	[14] SELJAK	06	COSM	
< 4.4		[16] CYBURT	05	COSM	
< 3.3		[17] BARGER	03C	COSM	
1.4–6.8		[18] CROTTY	03	COSM	
1.9–6.6		[18] PIERPAOLI	03	COSM	
2–4		LISI	99	COSM	BBN
< 4.3		OLIVE	99	COSM	BBN
< 4.9		COPI	97		Cosmology
< 3.6		HATA	97B		High D/H quasar abs.
< 4.0		OLIVE	97		BBN; high ^{4}He and ^{7}Li
< 4.7		CARDALL	96B	COSM	High D/H quasar abs.
< 3.9		FIELDS	96	COSM	BBN; high ^{4}He and ^{7}Li
< 4.5		KERNAN	96	COSM	High D/H quasar abs.
< 3.6		OLIVE	95		BBN; $\geq$ 3 massless ν
< 3.3		WALKER	91		Cosmology
< 3.4		OLIVE	90		Cosmology
< 4		YANG	84		Cosmology
< 4		YANG	79		Cosmology
< 7		STEIGMAN	77		Cosmology
		PEEBLES	71		Cosmology
<16		[19] SHVARTSMAN	69		Cosmology
		HOYLE	64		Cosmology

[1] AGHANIM 20 best fit on number of neutrino types is based on Planck data combined with lensing and baryon acoustic oscillations (BAO). Without BAO, they find $2.89^{+0.18}_{-0.19}$. Several other values are quoted using different combinations of data.

[2] FIELDS 20 combines Planck 2018 CMB data with BBN and observations of deuterium and Helium-4.

[3] IVANOV 20 combines 2018 Planck CMB data with baryon acoustic oscillation data from BOSS. This study is based on a full-shape likelihood for the redshift-space galaxy power spectrum of the BOSS data.

[4] Uses Planck Data combined with an independent standard measure of distance to the sound horizon to set a limit on the total number of neutrinos. Only CMB and early-time information are used.

[5] CYBURT 16 combines Planck 2015 CMB data with BBN and observations of deuterium and Helium-4.

[6] ROSSI 15 sets limits on the number of neutrino types using BOSS Lyman alpha forest data combined with Planck CMB data and baryon acoustic oscillations.

[7] Fit to the number of neutrino degrees of freedom from Planck CMB data along with WMAP polarization, high L, and BAO data.

[8] Fit to the number of neutrinos degrees of freedom from Planck CMB data along with BAO, shear and cluster data.

[9] Fit based on the SPT-SZ survey combined with CMB, BAO, and H_0 data.

[10] Constrains the number of neutrino degrees of freedom (marginalizing over the total mass) from CMB, CMB lensing, BAO, and galaxy clustering data.

[11] Limit on the number of light neutrino types from observational Hubble parameter data with seven-year WMAP data, SPT, and the most recent estimate of H_0. Best fit is 3.45 ± 0.65.

[12] Limit on the number of light neutrino types from the CFHTLS combined with seven-year WMAP data and a prior on the Hubble parameter. Best fit is $4.17^{+1.62}_{-1.26}$. Limit is relaxed to $3.98^{+2.02}_{-1.20}$ when small scales affected by non-linearities are removed.

[13] Constrains the number of neutrino types from recent CMB and large scale structure data. No priors on other cosmological parameters are used.

[14] Constrains the number of neutrino types from recent CMB, large scale structure, Lyman-alpha forest, and SN1a data. The slight preference for $N_\nu > 3$ comes mostly from the Lyman-alpha forest data.

[15] Constrains the number of neutrino types from recent CMB and large scale structure data. See also HAMANN 07.

[16] Limit on the number of neutrino types based on ^{4}He and D/H abundance assuming a baryon density fixed to the WMAP data. Limit relaxes to 4.6 if D/H is not used or to 5.8 if only D/H and the CMB are used. See also CYBURT 01 and CYBURT 03.

[17] Limit on the number of neutrino types based on combination of WMAP data and big-bang nucleosynthesis. The limit from WMAP data alone is 8.3. See also KNELLER 01. $N_\nu \geq 3$ is assumed to compute the limit.

[18] 95% confidence level range on the number of neutrino flavors from WMAP data combined with other CMB measurements, the 2dfGRS data, and HST data.

[19] SHVARTSMAN 69 limit inferred from his equations.

Number Coupling with Less Than Full Weak Strength

VALUE	DOCUMENT ID		TECN
• • • We do not use the following data for averages, fits, limits, etc. • • •			
<20	[1] OLIVE	81C	COSM
<20	[1] STEIGMAN	79	COSM

[1] Limit varies with strength of coupling. See also WALKER 91.

REFERENCES FOR Limits on Number of Neutrino Types

AGHANIM	20	AA 641 A6	N. Aghanim *et al.*	(Planck Collab.)
FIELDS	20	JCAP 2003 010	B. Fields *et al.*	(ILL, MINN)
Also		JCAP 2011 E02 (errat.)	B. Fields *et al.*	(ILL, MINN)
IVANOV	20	PR D101 083504	M.M. Ivanov, M. Simonovic, M. Zaldarriaga	(NYU,+)
JANOT	20	PL B803 135319	P. Janot, S. Jadach	(CERN, CRAC)
VOUTSINAS	20	PL B800 135068	G. Voutsinas *et al.*	(CERN, BOHR)
VERDE	17	JCAP 1704 023	L. Verde *et al.*	
CYBURT	16	RMP 88 015004	R.H. Cyburt *et al.*	(MSU, ILL, MINN)
ROSSI	15	PR D92 063505	G. Rossi *et al.*	
ADE	14	AA 571 A16	P.A.R. Ade *et al.*	(Planck Collab.)
COSTANZI	14	JCAP 1410 081	M. Costanzi *et al.*	(TRST, TRSTI)
HOU	14	APJ 782 74	Z. Hou *et al.*	
LEISTEDT	14	PRL 113 041301	B. Leistedt, H.V. Peiris, L. Verde	
MORESCO	12	JCAP 1207 053	M. Moresco *et al.*	
XIA	12	JCAP 1206 010	J.-Q. Xia *et al.*	
MANGANO	11	PL B701 296	G. Mangano, P. Serpico	
HAMANN	07	JCAP 0708 021	J. Hamann *et al.*	
ICHIKAWA	07	JCAP 0705 007	K. Ichikawa, M. Kawasaki, F. Takahashi	
CIRELLI	06	JCAP 0612 013	M. Cirelli *et al.*	
HANNESTAD	06	JCAP 0611 016	S. Hannestad, G. Raffelt	
LEP-SLC	06	PRPL 427 257	ALEPH, DELPHI, L3, OPAL, SLD and working groups	
SELJAK	06	JCAP 0610 014	U. Seljak, A. Slosar, P. McDonald	
ABDALLAH	05B	EPJ C38 395	J. Abdallah *et al.*	(DELPHI Collab.)
CYBURT	05	ASP 23 313	R.H. Cyburt *et al.*	
ACHARD	04E	PL B587 16	P. Achard *et al.*	(L3 Collab.)
BARGER	03C	PL B566 8	V. Barger *et al.*	
CROTTY	03	PR D67 123005	P. Crotty, J. Lesgourgues, S. Pastor	
CYBURT	03	PL B567 227	R.H. Cyburt, B.D. Fields, K.A. Olive	
HEISTER	03C	EPJ C28 1	A. Heister *et al.*	(ALEPH Collab.)
PIERPAOLI	03	MNRAS 342 L63	E. Pierpaoli	
CYBURT	01	ASP 17 87	R.H. Cyburt, B.D. Fields, K.A. Olive	
KNELLER	01	PR D64 123506	J.P. Kneller *et al.*	
ABBIENDI,G	00D	EPJ C18 253	G. Abbiendi *et al.*	(OPAL Collab.)

Downloaded from https://academic.oup.com/ptep/article/2022/8/083C01/6651666 by KIT Library user on 27 September 2022

ABREU	00Z	EPJ C17 53	P. Abreu *et al.*	(DELPHI Collab.)
ACCIARRI	99R	PL B470 268	M. Acciarri *et al.*	(L3 Collab.)
LISI	99	PR D59 123520	E. Lisi, S. Sarkar, F.L. Villante	
OLIVE	99	ASP 11 403	K.A. Olive, D. Thomas	
ABREU	97J	ZPHY C74 577	P. Abreu *et al.*	(DELPHI Collab.)
COPI	97	PR D55 3389	C.J. Copi, D.N. Schramm, M.S. Turner	(CHIC)
HATA	97B	PR D55 540	N. Hata *et al.*	(OSU, PENN)
OLIVE	97	ASP 7 27	K.A. Olive, D. Thomas	(MINN, FLOR)
ADAM	96C	PL B380 471	W. Adam *et al.*	(DELPHI Collab.)
CARDALL	96B	APJ 472 435	C.Y. Cardall, G.M. Fuller	(UCSD)
FIELDS	96	New Ast 1 77	B.D. Fields *et al.*	(NDAM, CERN, MINN+)
KERNAN	96	PR D54 3681	P.S. Kernan, S. Sarkar	(CASE, OXFTP)
AKERS	95C	ZPHY C65 47	R. Akers *et al.*	(OPAL Collab.)
OLIVE	95	PL B354 357	K.A. Olive, G. Steigman	(MINN, OSU)
BUSKULIC	93L	PL B313 520	D. Buskulic *et al.*	(ALEPH Collab.)
LEP	92	PL B276 247	LEP Collabs.	(LEP, ALEPH, DELPHI, L3, OPAL)
WALKER	91	APJ 376 51	T.P. Walker *et al.*	(HSCA, OSU, CHIC+)
OLIVE	90	PL B236 454	K.A. Olive *et al.*	(MINN, CHIC, OSU+)
YANG	84	APJ 281 493	J. Yang *et al.*	(CHIC, BART)
OLIVE	81C	NP B180 497	K.A. Olive, D.N. Schramm, G. Steigman	(EFI+)
STEIGMAN	79	PRL 43 239	G. Steigman, K.A. Olive, D.N. Schramm	(BART+)
YANG	79	APJ 227 697	J. Yang *et al.*	(CHIC, YALE, UVA)
STEIGMAN	77	PL 66B 202	G. Steigman, D.N. Schramm, J.E. Gunn	(YALE, CHIC+)
PEEBLES	71	Physical Cosmology Princeton Univ. Press (1971)	P.Z. Peebles	(PRIN)
SHVARTSMAN	69	JETPL 9 184 Translated from ZETFP 9 315.	V.F. Shvartsman	(MOSU)
HOYLE	64	NAT 203 1108	F. Hoyle, R.J. Tayler	(CAMB)

Double-β Decay

OMITTED FROM SUMMARY TABLE

NEUTRINOLESS DOUBLE-β DECAY

Revised August 2019 by A. Piepke (University of Alabama) and P. Vogel (Caltech) .

Observation of neutrinoless double-beta ($0\nu\beta\beta$) decay would signal violation of total lepton number conservation. The process can be mediated by an exchange of a light Majorana neutrino, or by an exchange of other particles. However, the existence of $0\nu\beta\beta$-decay requires a nonvanishing Majorana neutrino mass, no matter what the actual mechanism is. As long as only a limit on the lifetime is available, limits on the effective Majorana neutrino mass, on the lepton-number violating right-handed current or other possible mechanisms mediating $0\nu\beta\beta$ decay can be obtained, independently of the actual mechanism, by assuming that one of these "new physics" possibilities dominates. These limits are listed in the Double-β Decay Listings of the experimental measurements.

In the following we assume that the exchange of light Majorana neutrinos ($m_{\nu_i} \leq 10$ MeV) contributes dominantly to the decay rate. Besides a dependence on the phase space ($G^{0\nu}$) and the nuclear matrix element ($M^{0\nu}$), the observable $0\nu\beta\beta$-decay rate is proportional then to the square of the effective Majorana mass m_{ee}, $(T^{0\nu}_{1/2})^{-1} = G^{0\nu} \cdot |M^{0\nu}|^2 \cdot m^2_{ee}$, with $m^2_{ee} = |\sum_i U^2_{ei} m_{\nu_i}|^2$. The sum contains, in general, complex CP-phases in U^2_{ei}, i.e., cancellations may occur. For three neutrino flavors there are two physical phases for Majorana neutrinos (η_1, η_2) and one for Dirac neutrinos (δ_{CP}). The relevant Majorana phases affect only processes to which lepton-number changing amplitudes contribute. Given the general 3×3 mixing matrix for Majorana neutrinos, one can construct other analogous lepton number violating quantities, $m_{\ell\ell'} = \sum_i U_{\ell i} U_{\ell' i} m_{\nu_i}$($\ell$ or $\ell' \neq e$). However, these are currently much less constrained than m_{ee}.

Nuclear structure calculations are needed to deduce m_{ee} from the decay rate. While $G^{0\nu}$ can be calculated accurately, the computation of $M^{0\nu}$ is subject to uncertainty. Comparing different nuclear model evaluations indicates a factor ∼2-3 spread in the calculated nuclear matrix elements. Nuclear structure calculation consistently overestimate Gamow-Teller (axial current) matrix elements. This inability of the nuclear models to reproduce Gamow-Teller decay rates is often parametrized in form of a modified coupling constant g_A. Many nuclear theorists interpret this shortcoming as evidence that important physics is missing in the modeling of weak nuclear transitions. It is not clear how these observed uncertainties impact $0\nu\beta\beta$-matrix elements. Nevertheless, this constitutes an additional element of uncertainty. Recent work, [1] shows how the discrepancy between experimental and theoretical axial current matrix elements might be resolved. However, application of this approach to the $0\nu\beta\beta$ decay remains to be accomplished. The particle physics quantities to be determined are thus nuclear model-dependent, so the half-life measurements are listed first. Where possible, we reference the nuclear matrix elements used in the subsequent analysis. Since rates for the conventional $2\nu\beta\beta$ decay serve to constrain the nuclear theory models, results for this process are also given.

Oscillation experiments utilizing atmospheric, accelerator, solar, and reactor produced neutrinos and anti-neutrinos show that at least some neutrinos are massive. However, so far the inverted mass ordering (i.e., whether $\Delta m^2_{31} < 0$) is disfavored only by 2-3 σ compared to the normal mass ordering (when $\Delta m^2_{31} > 0$), while the absolute neutrino mass values or the properties of neutrinos under CPT-conjugation (Dirac or Majorana) remain undetermined. All confirmed oscillation experiments can be consistently described using three interacting neutrino species with two mass splittings and three mixing angles. (For values of the mixing angles and mass square differences see the corresponding tables.)

Based on the 3-neutrino analysis:
$m^2_{ee} = |\cos^2\theta_{13}\cos^2\theta_{12} m_1 + e^{2i(\eta_2-\eta_1)}\cos^2\theta_{13}\sin^2\theta_{12} m_2 + e^{-2i(\eta_1+\delta_{CP})}\sin^2\theta_{13} m_3|^2$, valid for both mass orderings. Given the present knowledge of the neutrino oscillation parameters one can derive a relation between the effective Majorana mass and the mass of the lightest neutrino, as illustrated in Figure 14.11 in the Neutrino Masses, Mixing and Oscillations review. The three mass orderings allowed by the oscillation data: normal ($m_1 < m_2 \ll m_3$), inverted ($m_3 \ll m_1 < m_2$), and degenerate ($m_1 \approx m_2 \approx m_3$), result in different projections. The width of the colored bands reflects the uncertainty introduced by the unknown Majorana and Dirac phases as well as the experimental errors of the oscillation parameters. The latter causes only minor broadening of the bands. Because of the overlap of the different mass scenarios, a measurement of m_{ee} would not reveal which mass ordering is applicable, provided the value of m_{ee} is in the overlapping range.

Analogous plots depict the relation of m_{ee} with the summed neutrino mass $m_{tot} = m_1 + m_2 + m_3$, constrained by observational cosmology, and m_{ee} as a function of the average mass

Downloaded from https://academic.oup.com/ptep/article/2022/8/083C01/6651666 by KIT Library user on 27 September 2022

$m_{\nu_e}^{eff} = [\Sigma|U_{ei}|^2 m_{\nu_i}^2]^{1/2}$ determined through the analysis of the electron energy distribution in low energy beta decays. (See Fig. 1 of [2].) The oscillation data thus allow to test whether observed values of m_{ee} and m_{tot} or $m_{\nu_e}^{eff}$ are consistent within the 3 neutrino framework. The rather large intrinsic width of the $\beta\beta$-decay constraints essentially does not allow to positively identify the mass ordering, and thus the sign of Δm_{31}^2, even in combination with these other observables. Naturally, if a value of $0 < m_{ee} \leq 0.01$ eV is ever established, then the normal mass ordering becomes the only possible scenario.

It should be noted that systematic uncertainties of the nuclear matrix elements and possible quenching of the axial current matrix elements are sometimes not folded into the mass limits reported by $\beta\beta$-decay experiments. Taking this additional uncertainty into account would further widen the projections. The plots are based on a 3-neutrino analysis. If it turns out that additional, i.e. sterile light neutrinos exist, the allowed regions would be modified substantially.

If neutrinoless double-beta decay is observed, it will be possible to fix a range of absolute values of the masses m_{ν_i}. Unlike the direct neutrino mass measurements, however, a limit on m_{ee} does not allow one to constrain the individual mass values m_{ν_i} even when the mass differences Δm_{ij}^2 are known.

Neutrino oscillation data imply the existence of a lower limit ~ 0.014 eV for the Majorana neutrino mass for the inverted mass ordering pattern, while m_{ee} could, by fine tuning, vanish in the case of the normal mass ordering. Several new double-beta searches have been proposed to probe the interesting m_{ee} mass range, with the prospect of full coverage of the inverted mass ordering region within the next decade.

The $0\nu\beta\beta$ decay mechanism discussed so far is not the only way in which the decay can occur. Numerous other possible scenarios have been proposed, however, all of them requiring new physics. It will be a challenging task to decide which mechanism was responsible once $0\nu\beta\beta$ decay is observed. LHC experiments may reveal corresponding signatures for new physics of lepton number violation. If lepton-number violating right-handed weak current interactions exist, its strength can be characterized by the phenomenological coupling constants η and λ (η describes the coupling between the right-handed lepton current and left-handed quark current while λ describes the coupling when both currents are right-handed). The $0\nu\beta\beta$ decay rate then depends on $\langle\eta\rangle = \eta \sum_i U_{ei} V_{ei}$ and $\langle\lambda\rangle = \lambda \sum_i U_{ei} V_{ei}$ that vanish for massless or unmixed neutrinos ($V_{\ell j}$ is a matrix analogous to $U_{\ell j}$ but describing the mixing with the hypothetical right-handed neutrinos). The observation of the single electron spectra could, in principle, allow to distinguish this mechanism of $0\nu\beta\beta$ from the light Majorana neutrino exchange driven mode. The limits on $\langle\eta\rangle$ and $\langle\lambda\rangle$ are listed in a separate table. The reader is cautioned that a number of earlier experiments did not distinguish between η and λ. In addition, see the section on Majoron searches for additional limits set by these experiments.

References

1. P. Gysbers *et al.*, Nature Phys. **15**, 5 (2019); [arXiv:1903.00047].
2. M.J. Dolinski, A.W.P. Poon and W. Rodejohann, Ann. Rev. Nucl. Part. Sci. **49**, 219 (2019); [arXiv:1902.04097].

Half-life 0ν double-β decay

In most cases the transitions (Z,A) $\rightarrow$ (Z+2,A) $+ 2e^-$ to the 0^+ ground state of the final nucleus are listed. We also list transitions that decrease the nuclear charge ($2e^+$, e^+ CC and double EC) and transitions to an excited state of the final nucleus (0_i^+, 2^+, and 2_i^+). In the following Listings only the best or comparable limits for the half-lives of each transition are reported and only those with about $T_{1/2} > 10^{23}$ years that are relevant for particle physics.

$t_{1/2}(10^{23}$ yr)	CL%	ISOTOPE	TRANSITION	METHOD	DOCUMENT ID	
• • • We do not use the following data for averages, fits, limits, etc. • • •						
> 59	90	^{130}Te	g.s. $\rightarrow 0_1^+$	CUORE	[1] ADAMS	21A
> 15	90	^{100}Mo		CUPID-Mo	[2] ARMENGAUD	21
> 39.9	90	^{76}Ge	g.s. $\rightarrow 0_1^+$	MAJORANA-Dem	[3] ARNQUIST	21
> 21.2	90	^{76}Ge	g.s. $\rightarrow 2_1^+$	MAJORANA-Dem	[4] ARNQUIST	21
> 9.7	90	^{76}Ge	g.s. $\rightarrow 2_2^+$	MAJORANA-Dem	[5] ARNQUIST	21
> 320	90	^{130}Te		CUORE	[6] ADAMS	20A
>1800	90	^{76}Ge		GERDA	[7] AGOSTINI	20B
> 900	90	^{76}Ge		GERDA	[8] AGOSTINI	19
> 14	90	^{130}Te	g.s. $\rightarrow 0_1^+$	CUORE-0	[9] ALDUINO	19
> 0.95	90	^{100}Mo		AMoRE	[10] ALENKOV	19
> 270	90	^{76}Ge		MAJORANA	[11] ALVIS	19
> 350	90	^{136}Xe		EXO-200	[12] ANTON	19
> 35	90	^{82}Se		CUPID-0	[13] AZZOLINI	19
> 2.4	90	^{136}Xe		PANDAX-II	[14] NI	19
> 190	90	^{76}Ge		MAJORANA	[15] AALSETH	18
> 800	90	^{76}Ge		GERDA	[16] AGOSTINI	18
> 180	90	^{136}Xe		EXO-200	[17] ALBERT	18
> 150	90	^{130}Te		CUORE	[18] ALDUINO	18
> 2.5	90	^{82}Se		NEMO-3	[19] ARNOLD	18
> 24	90	^{82}Se		CUPID-0	[20] AZZOLINI	18
> 0.81	90	^{82}Se	g.s. $\rightarrow 0_1^+$	CUPID-0	[21] AZZOLINI	18A
> 2.2	90	^{116}Cd		AURORA	[22] BARABASH	18
> 530	90	^{76}Ge		GERDA	[23] AGOSTINI	17
> 1.1	90	^{134}Xe		EXO-200	[24] ALBERT	17C
> 1	90	^{116}Cd		NEMO-3	[25] ARNOLD	17
> 40	90	^{130}Te		CUORE(CINO)	[26] ALDUINO	16
> 260	90	^{136}Xe	g.s.$\rightarrow 2_1^+$	KamLAND-Zen	[27] ASAKURA	16
> 260	90	^{136}Xe	g.s.$\rightarrow 2_2^+$	KamLAND-Zen	[28] ASAKURA	16
> 240	90	^{136}Xe	g.s.$\rightarrow 0_1^+$	KamLAND-Zen	[29] ASAKURA	16
>1070	90	^{136}Xe		KamLAND-Zen	[30] GANDO	16
> 11	90	^{100}Mo		NEMO-3	[31] ARNOLD	15
> 110	90	^{136}Xe		EXO-200	[32] ALBERT	14B
> 9.4	90	^{130}Te	g.s. $\rightarrow 0_1^+$	CUORICINO	[33] ANDREOTTI	12
> 3.6	90	^{82}Se		NEMO-3	[34] BARABASH	11A
> 30	90	^{130}Te		CUORICINO	[35] ARNABOLDI	08
> 0.58	90	^{48}Ca		CaF_2 scint.	[36] UMEHARA	08
> 0.89	90	^{100}Mo	g.s. $\rightarrow 0_1^+$	NEMO-3	[37] ARNOLD	07
> 1.6	90	^{100}Mo	g.s. $\rightarrow 2^+$	NEMO-3	[38] ARNOLD	07
> 1	90	^{82}Se		NEMO-3	[39] ARNOLD	05A
> 1.1	90	^{128}Te		Cryog. det.	[40] ARNABOLDI	03
> 1.7	90	^{116}Cd		$^{116}CdWO_4$ scint.	[41] DANEVICH	03
> 157	90	^{76}Ge		Enriched HPGe	[42] AALSETH	02B
> 190	90	^{76}Ge		Enriched HPGe	[43] KLAPDOR-K...	01

[1] ADAMS 21A et al. used 101.76 kg yr of ^{130}Te exposure of the CUORE (LNGS) bolometric detector to place a limit on the decay to the first excited state of ^{130}Xe, superseding ALDUINO 19 as the most restrictive bound on this particular decay.

[2] ARMENGAUD 21 use the CUPID-Mo 4.2 kg array of enriched $Li_2{}^{100}MoO_4$ scintillating bolometers, with 1.17 kg·yr exposure, to set this limit.

[3] ARNQUIST 21 use the MAJORANA demonstrator to set this limit for the 0ν $\beta\beta$ decay to the first excited 0^+ state, with a 41.9 kg yr isotopic exposure. The median sensitivity is 39.9×10^{23} yr.

[4] ARNQUIST 21 use the MAJORANA demonstrator to set this limit for the 0ν $\beta\beta$ decay to the first excited 2^+ state, with a 41.9 kg yr isotopic exposure. The median sensitivity is 21.2×10^{23} yr.

[5] ARNQUIST 21 use the MAJORANA demonstrator to set this limit for the 0ν $\beta\beta$ decay to the second excited 2^+ state, with a 41.9 kg yr isotopic exposure. The median sensitivity is 18.6×10^{23} yr.

Downloaded from https://academic.oup.com/ptep/article/2022/8/083C01/6651666 by KIT Library user on 27 September 2022

[6] ADAMS 20A use the CUORE detector to search for the $0\nu\ \beta\beta$ decay of ^{130}Te. The exposure was 372.5 kg·yr of TeO_2 corresponding to 103.6 kg·yr of ^{130}Te. The exclusion sensitivity is 1.7×10^{25}yr. Supersedes ALDUINO 18.

[7] AGOSTINI 20B present the final data set of the GERDA experiment, searching for $0\nu\ \beta\beta$ decay of ^{76}Ge with isotopically enriched, high resolution Ge detectors. A final exposure of 127.2 kg·yr is reported. The experiment reports the lowest background and longest half life limit ever achieved by any double beta decay experiment. The reported experiment sensitivity equals the limit. Supersedes AGOSTINI 19.

[8] AGOSTINI 19 use 82.4 kg·yr of data, collected by the GERDA experiment, to search for the $0\nu\ \beta\beta$ decay of ^{76}Ge. High resolution Ge-calorimeters, made from isotopically enriched Ge, are used. A median sensitivity of 1.1×10^{26} yr is reported. Supersedes AGOSTINI 18.

[9] ALDUINO 19 use the combined data of the CUORICINO and CUORE-0 experiments to place a lower limit on the half life of the $0\nu\ \beta\beta$ decay of ^{130}Te to the first excited 0^+ state of ^{130}Xe. Supersedes ANDREOTTI 12.

[10] ALENKOV 19 report the $0\nu\ \beta\beta$ decay half-life limit based on the 52.1 kg·d exposure of ^{100}Mo, of a a cryogenic dual heat and light detector in the Yangyang underground laboratory. The median sensitivity is 1.1×10^{23} years.

[11] ALVIS 19 use the MAJORANA Demonstrator with enriched in ^{76}Ge detectors to set this limit on $0\nu\ \beta\beta$ half-life of ^{76}Ge. The exposure is 26.0 kg yr. The sensitivity is 4.8×10^{25} yr.

[12] ANTON 19 uses he complete dataset of the EXO-200 detector to search for the $0\nu\ \beta\beta$ decay. The exposure is 234.1 kg yr. The median sensitivity is 5.0×10^{25} yr. Supersedes ALBERT 18 and ALBERT 14B.

[13] AZZOLINI 19 use the CPID-0 scintillating cryogenic bolometer to set this limit on $0\nu\ \beta\beta$ half-life of ^{82}Se. The exposure is 5.29 kg yr. The sensitivity is 5×10^{24} yr.

[14] NI 19 use the PandaX-II dual phase TPC at CJPL to search for the $0\nu\ \beta\beta$ decay of ^{136}Xe. The half-life limit 2.4×10^{23} yr is obtained from 22.2 kg yr exposure with a sensitivity of 1.9×10^{23} yr.

[15] AALSETH 18 uses the MAJORANA Demonstrator to search for the $0\nu\ \beta\beta$ decay. The exposure is 9.95 kg·year. The median sensitivity is 2.1×10^{25} yr.

[16] AGOSTINI 18 uses the GERDA detector to search for the $0\nu\ \beta\beta$ decay. The exposure is 46.7 kg·year. The median sensitivity is 5.8×10^{25} yr. Supersedes AGOSTINI 17.

[17] ALBERT 18 uses the EXO-200 detector to search for the $0\nu\ \beta\beta$ decay. The exposure is 177.6 kg·year. The median sensitivity is 3.7×10^{25} years.

[18] ALDUINO 18 uses the CUORE detector to search for the $0\nu\ \beta\beta$ decay of ^{130}Te. The exposure is 86.3 kg·year of natural TeO_2 corresponding to 24.0 kg·year for ^{130}Te. The median sensitivity is 0.7×10^{25} yr. The limit is obtained combining the new data from CUORE with those of CUORE0 (9.8 kg·year of ^{130}Te) and Cuoricino (19.8 kg·year of ^{130}Te).

[19] ARNOLD 18 use the NEMO-3 tracking detector to place a limit on the $0\nu\beta\beta$ decay of ^{82}Se. This is a slightly weaker limit than in BARABASH 11A, using the same detector. Supersedes ARNOLD 05A.

[20] AZZOLINI 18 uses CUPID-0 detector, a novel scintillating cryogenic calorimeter, operated in the LNGS. This results replaces BARABASH 11A (NEMO-3) as the most stringent limit on the $0\nu\ \beta\beta$-decay of ^{82}Se.

[21] AZZOLINI 18A data collected by CUPID-0 based on scintillating bolometers is used to derive a new most stringent limit on the $0\nu\beta\beta$-decay of ^{82}Se to the 0^+_1 state of ^{82}Kr.

[22] BARABASH 18 use 1.162 kg of $^{116}CdWO_4$ scintillating crystals to obtain this limit. Supersedes DANEVICH 03 with analogous source and is more sensitive than ARNOLD 17.

[23] AGOSTINI 17 result corresponds to data collected with GERDA phase 1 and first release of phase 2 for a total of 343 mol-yr exposure. Supersedes AGOSTINI 13A. The median sensitivity is 4.0 10^{25} yr.

[24] ALBERT 17C uses the EXO-200 detector that contains 19.098 $\pm$ 0.014% admixture of ^{134}Xe to search for the 0ν and $2\nu\ \beta\beta$ decay modes. The exposure is 29.6 kg·year. The median sensitivity is 1.9×10^{21} years.

[25] ARNOLD 17 use the NEMO-3 tracking calorimeter, containing 410 g of enriched ^{116}Cd exposed for 5.26 yr, to determine the half-life limit. Supersedes BARABASH 11A.

[26] ALDUINO 16 report result obtained with 9.8 kg y of data collected with the CUORE-0 bolometer, combined with data from the CUORICINO. Supersedes ALFONSO 15.

[27] ASAKURA 16 use the KamLAND-Zen liquid scintillator calorimeter (^{136}Xe 89.5 kg yr) to place a limit on the $0\nu\beta\beta$-decay into the first excited state of the daughter nuclide.

[28] ASAKURA 16 use the KamLAND-Zen liquid scintillator calorimeter (^{136}Xe 89.5 kg yr) to place a limit on the $0\nu\beta\beta$-decay into the second excited state of the daughter nuclide.

[29] ASAKURA 16 use the KamLAND-Zen liquid scintillator calorimeter (^{136}Xe 89.5 kg yr) to place a limit on the $0\nu\beta\beta$-decay into the third excited state of the daughter nuclide.

[30] GANDO 16 use the the KamLAND detector to search for the 0ν decay of ^{136}Xe. With a significant background reduction, the combination of results of the first (270.7 days) and the second phase (263.8 days) of the experiment leads to about six fold improvement over the previous limit. Supersedes GANDO 13A. The sensitivity is 5.6 10^{25} yr.

[31] ARNOLD 15 use the NEMO-3 tracking calorimeter with 34.3 kg yr exposure to determine the limit of $0\nu\beta\beta$-half life of ^{100}Mo. Supersedes ARNOLD 2005A and BARABASH 11A.

[32] ALBERT 14B use 100 kg yr of exposure of the EXO-200 tracking calorimeter to place a lower limit on the $0\nu\beta\beta$-half life of ^{136}Xe. Supersedes AUGER 12.

[33] ANDREOTTI 12 use high resolution TeO_2 bolometric calorimeter to search for the $0\nu\beta\beta$ decay of ^{130}Te leading to the excited 0^1_+ state at 1793.5 keV.

[34] BARABASH 11A use the NEMO-3 detector to measure $2\nu\beta\beta$ rates and place limits on $0\nu\beta\beta$ half lives for various nuclides. Supersedes ARNOLD 05A, ARNOLD 04, ARNOLD 98, and ELLIOTT 92.

[35] Supersedes ARNABOLDI 04. Bolometric TeO_2 detector array CUORICINO is used for high resolution search for $0\nu\beta\beta$ decay. The half-life limit is derived from 3.09 kg yr ^{130}Te exposure.

[36] UMEHARA 08 use CaF_2 scintillation calorimeter to search for double beta decay of ^{48}Ca. Limit is significantly more stringent than quoted sensitivity: 18×10^{21} years.

[37] Limit on 0ν-decay to the first excited 0^+_1-state of daughter nucleus using NEMO-3 tracking calorimeter. Supersedes DASSIE 95.

[38] Limit on 0ν-decay to the first excited 2^+-state of daughter nucleus using NEMO-3 tracking calorimeter.

[39] NEMO-3 tracking calorimeter is used in ARNOLD 05A to place limit on $0\nu\beta\beta$ half-life of ^{82}Se. Detector contains 0.93 kg of enriched ^{82}Se. Supersedes ARNOLD 04.

[40] Supersedes ALESSANDRELLO 00. Array of TeO_2 crystals in high resolution cryogenic calorimeter. Some enriched in ^{128}Te. Ground state to ground state decay.

[41] Limit on $0\nu\beta\beta$ decay of ^{116}Cd using enriched $CdWO_4$ scintillators. Supersedes DANEVICH 00.

[42] AALSETH 02B limit is based on 117 mol·yr of data using enriched Ge detectors. Background reduction by means of pulse shape analysis is applied to part of the data set. Reported limit is slightly less restrictive than that in KLAPDOR-KLEINGROTHAUS 01 However, it excludes part of the allowed half-life range reported in KLAPDOR-KLEINGROTHAUS 01B for the same nuclide. The analysis has been criticized in KLAPDOR-KLEINGROTHAUS 04B. The criticism was addressed and disputed in AALSETH 04.

[43] KLAPDOR-KLEINGROTHAUS 01 is a continuation of the work published in BAUDIS 99. Isotopically enriched Ge detectors are used in calorimetric measurement. The most stringent bound is derived from the data set in which pulse-shape analysis has been used to reduce background. Exposure time is 35.5 kg y. Supersedes BAUDIS 99 as most stringent result.

Half-life measurements of the two-neutrino double-β decay

The measured half-life values for the transitions (Z,A) $\rightarrow$ (Z+2,A) + $2e^-$ + $2\overline{\nu}_e$ to the 0^+ ground state of the final nucleus are listed. We also list the transitions to an excited state of the final nucleus (0^+_i, etc.). We report only the measuremetnts with the smallest (or comparable) uncertainty for each transition.

$t_{1/2}$ (10^{21} yr)			ISOTOPE	TRANSITION	METHOD	DOCUMENT ID	
• • • We do not use the following data for averages, fits, limits, etc. • • •							
0.771	$^{+0.008}_{-0.006}$	$^{+0.012}_{-0.015}$	^{130}Te		CUORE	[1] ADAMS	21
0.00712	$^{+0.00018}_{-0.00014}$	± 0.00010	^{100}Mo		CUPID-Mo	[2] ARMENGAUD	20
18	± 5	± 1	^{124}Xe	2νDEC	XENON1T	[3] APRILE	19E
0.00680	± 0.00001	$^{+0.00038}_{-0.00040}$	^{100}Mo		NEMO-3	[4] ARNOLD	19
0.0860	± 0.0003	$^{+0.0019}_{-0.0013}$	^{82}Se		CUPID-0	[5] AZZOLINI	19B
0.0939	± 0.0017	± 0.0058	^{82}Se		NEMO-3	[6] ARNOLD	18
0.0263	$^{+0.0011}_{-0.0012}$		^{116}Cd		AURORA	[7] BARABASH	18
> 0.87			^{134}Xe		EXO-200	[8] ALBERT	17C
0.82	± 0.02	± 0.06	^{130}Te		CUORE-0	[9] ALDUINO	17
0.00690	± 0.00015	± 0.00037	^{100}Mo		CUPID	[10] ARMENGAUD	17
0.0274	± 0.0004	± 0.0018	^{116}Cd		NEMO-3	[11] ARNOLD	17
0.064	$^{+0.007}_{-0.006}$	$^{+0.012}_{-0.009}$	^{48}Ca		NEMO-3	[12] ARNOLD	16
0.00934	± 0.00022	$^{+0.00062}_{-0.00060}$	^{150}Nd		NEMO-3	[13] ARNOLD	16A
1.926	± 0.094		^{76}Ge		GERDA	[14] AGOSTINI	15A
0.00693	± 0.00004		^{100}Mo		NEMO-3	[15] ARNOLD	15
2.165	± 0.016	± 0.059	^{136}Xe		EXO-200	[16] ALBERT	14
9.2	$^{+5.5}_{-2.6}$	± 1.3	^{78}Kr		BAKSAN	[17] GAVRILYAK	13
2.38	± 0.02	± 0.14	^{136}Xe		KamLAND-Zen	[18] GANDO	12A
0.7	± 0.09	± 0.11	^{130}Te		NEMO-3	[19] ARNOLD	11
0.0235	± 0.0014	± 0.0016	^{96}Zr		NEMO-3	[20] ARGYRIADES	10
0.69	$^{+0.10}_{-0.08}$	± 0.07	^{100}Mo	$0^+ \rightarrow 0^+_1$	Ge coinc.	[21] BELLI	10
0.57	$^{+0.13}_{-0.09}$	± 0.08	^{100}Mo	$0^+ \rightarrow 0^+_1$	NEMO-3	[22] ARNOLD	07
0.096	± 0.003	± 0.010	^{82}Se		NEMO-3	[23] ARNOLD	05A
0.029	$^{+0.004}_{-0.003}$		^{116}Cd		$CdWO_4$ scint.	[24] DANEVICH	03

[1] ADAMS 21 use 102.7 kg yr of ^{130}Te exposure, collected by the CUORE bolometric detector at LNGS, to perform the most precise measurement of $2\nu\ \beta\beta$ decay of this nuclide to date. The dataset is more than 10-times that used by the CUORE-0 experiment. Supersedes ALDUINO 17.

[2] ARMENGAUD 20 use the $Li_2{}^{100}MoO_4$ scintillating bolometers to determine the half-life of the $2\nu\ \beta\beta$ decay of ^{100}Mo. The total exposure was 42.235 kg·d. The single-state dominance for this decay is favored at $> 3\ \sigma$.

[3] APRILE 19E report first measurement of two-neutrino double electron capture in ^{124}Xe using the XENON1T detector with a 0.73 t-yr exposure. An excess of 126 $\pm$ 29 events is observed at 64.3 $\pm$ 0.6 keV decay energy, corresponding to $\sqrt{\Delta\chi^2} = 4.4$ with respect to the background-only hypothesis.

[4] ARNOLD 19 use the NEMO-3 tracking calorimeter with 34.3 kg y exposure to determine the $2\nu\ \beta\beta$ half-life of ^{100}Mo. Supersedes ARNOLD 15.

Downloaded from https://academic.oup.com/ptep/article/2022/8/083C01/6651666 by KIT Library user on 27 September 2022

[5] AZZOLINI 19B use the CUPID-0 experiment, utilizing ZnSe bolometers and an exposure of 9.95 kg·yr of $Zn^{82}Se$, to determine the half-life of the $2\nu\ \beta\beta$ decay of ^{82}Se. The analysis provides evidence for single state dominance showing that the higher state dominance is disfavored at the level of 5.5 σ .

[6] ARNOLD 18 use the NEMO-3 tracking detector to determine the $2\nu\beta\beta$ half-life of ^{82}Se. 0.93 kg of ^{82}Se was observed for 5.25 y. The half-life value was obtained based on the single-state-dominance (SSD) hypothesis, preferred in this case by about 2 σ. Supersedes ARNOLD 05A.

[7] BARABASH 18 use 1.162 kg of $^{116}CdWO_4$ scintillating crystals to obtain this value. Supersedes DANEVICH 03 with analogous source and agrees with ARNOLD 17 with the NEMO-3 detector.

[8] ALBERT 17C uses the EXO-200 detector that contains 19.098 $\pm$ 0.014% admixture of ^{134}Xe to search for the $2\nu\ \beta\beta$ decay mode. The exposure is 29.6 kg·year. The median sensitivity is 1.2×10^{21} years.

[9] ALDUINO 17 use the CUORE-0 detector containing 10.8 kg of ^{130}Te in 52 crystals of TeO_2. The exposure was 9.3 kg yr of ^{130}Te. This is a more accurate rate determination than in ARNOLD 11 and BARABASH 11A.

[10] ARMENGAUD 17 use 185.9 $\pm$ 0.1 g crystal of $Li_2{}^{100}MoO_4$ to determine the ^{100}Mo $2\nu\ \beta\beta$ half-life. The exposure was of 1303 $\pm$ 26 hours only, using novel technique.

[11] ARNOLD 17 use the NEMO-3 tracking calorimeter, containing 410 grams of enriched ^{116}Cd exposed for 5.26 years, to determine the half-life value.

[12] ARNOLD 16 use the NEMO-3 detector and a source of 6.99 g of ^{48}Ca. The half-life is based on 36.7 g year exposure. It is consistent, although somewhat longer, than the previous determinations of the half-life. Supersedes BARABASH 11A.

[13] ARNOLD 16A use the NEMO-3 tracking calorimeter, containing 36.6 g of ^{150}Nd exposed for 1918.5 days, to determine the half-life. Supersedes ARGYRIADES 09.

[14] AGOSTINI 15A use 17.9 kg yr exposure of the GERDA calorimeter to derive an improved measurement of the $2\nu\beta\beta$ decay half life of ^{76}Ge.

[15] ARNOLD 15 use the NEMO-3 tracking calorimeter with 34.3 kg yr exposure to determine the $2\nu\beta\beta$-half life of ^{100}Mo. Supersedes ARNOLD 05A and ARNOLD 04.

[16] ALBERT 14 use the EXO-200 tracking detector for a re-measurement of the $2\nu\beta\beta$-half life of ^{136}Xe. A nuclear matrix element of 0.0218 $\pm$ 0.0003 MeV^{-1} is derived from this data. Supersedes ACKERMAN 11.

[17] GAVRILYAK 13 use a proportional counter filled with Kr gas to search for the 2ν2K decay of ^{78}Kr. Data with the enriched and depleted Kr were used to determine signal and background. A 2.5σ excess of events obtained with the enriched sample is interpreted as an indication for the presence of this decay.

[18] GANDO 12A use a modification of the existing KamLAND detector. The $\beta\beta$ decay source/detector is 13 tons of enriched ^{136}Xe-loaded scintillator contained in an inner balloon. The $2\nu\beta\beta$ decay rate is derived from the fit to the spectrum between 0.5 and 4.8 MeV. This result is in agreement with ACKERMAN 11.

[19] ARNOLD 11 use enriched ^{130}Te in the NEMO-3 detector to measure the $2\nu\ \beta\beta$ decay rate. This result is in agreement with, but more accurate than ARNABOLDI 03.

[20] ARGYRIADES 10 use 9.4 $\pm$ 0.2 g of ^{96}Zr in NEMO-3 detector and identify its $2\nu\beta\beta$ decay. The result is in agreement and supersedes ARNOLD 99.

[21] BELLI 10 use enriched ^{100}Mo with 4 HP Ge detectors to record the 590.8 and 539.5 keV γ rays from the decay of the 0^+_1 state in ^{100}Ru both in singles and coincidences. This result confirms the measurement of KIDD 09 and ARNOLD 07 and supersedes them.

[22] First exclusive measurement of 2ν-decay to the first excited 0^+_1-state of daughter nucleus. ARNOLD 07 use the NEMO-3 tracking calorimeter to detect all particles emitted in decay. Result agrees with the inclusive ($0\nu + 2\nu$) measurement of DEBRAECKELEER 01.

[23] ARNOLD 05A use the NEMO-3 tracking detector to determine the $2\nu\beta\beta$ half-life of ^{82}Se with high statistics and low background (389 days of data taking). Supersedes ARNOLD 04.

[24] DANEVICH 03 is calorimetric measurement of $2\nu\beta\beta$ ground state decay of ^{116}Cd using enriched $CdWO_4$ scintillators. Agrees with EJIRI 95 and ARNOLD 96. Supersedes DANEVICH 00.

$\langle m_{ee} \rangle$, The Effective Weighted Sum of Majorana Neutrino Masses Contributing to Neutrinoless Double-β Decay

$\langle m_{ee} \rangle = |\Sigma U^2_{ei} m_{\nu_i}|$, i = 1,2,3. It is assumed that ν_i are Majorana particles and that the transition is dominated by the known (light) neutrinos. Note that U^2_{ei} and not $|U_{ei}|^2$ occur in the sum, and that consequently cancellations are possible. The experiments obtain the limits on $\langle m_\nu \rangle$ from the measured ones on $T_{1/2}$ using a range of nuclear matrix elements (NME), which is reflected in the spread of $\langle m_\nu \rangle$. Different experiments may choose different NME. All assume g_A = 1.27. In the following Listings, only the best or comparable limits for each isotope are reported. When not mentioned explicitly the transition is between ground states, but transitions between excited states are also reported.

VALUE (eV)	ISOTOPE	METHOD	DOCUMENT ID	
• • • We do not use the following data for averages, fits, limits, etc. • • •				
< 0.31–0.54	^{100}Mo	CUPID-Mo	[1] ARMENGAUD	21
< 0.075–0.35	^{130}Te	CUORE	[2] ADAMS	20A
< 0.079–0.180	^{76}Ge	GERDA	[3] AGOSTINI	20B
< 0.07–0.16	^{76}Ge	GERDA	[4] AGOSTINI	19
< 1.2–2.1	^{100}Mo	AMoRE	[5] ALENKOV	19
< 0.200–0.433	^{76}Ge	MAJORANA	[6] ALVIS	19
< 0.093–0.286	^{136}Xe	EXO-200	[7] ANTON	19
< 0.311–0.638	^{82}Se	CUPID-0	[8] AZZOLINI	19
< 1.3–3.5	^{136}Xe	PANDAX-II	[9] NI	19
< 0.24–0.52	^{76}Ge	MAJORANA Dem	[10] AALSETH	18
< 0.12–0.26	^{76}Ge	GERDA	[11] AGOSTINI	18
< 0.15–0.40	^{136}Xe	EXO-200	[12] ALBERT	18
< 0.11–0.52	^{130}Te	CUORE	[13] ALDUINO	18
< 1.2–3.0	^{82}Se	NEMO-3	[14] ARNOLD	18
< 0.376–0.770	^{82}Se	CUPID-0	[15] AZZOLINI	18
< 1.0–1.7	^{116}Cd	AURORA	[16] BARABASH	18
< 0.15–0.33	^{76}Ge	GERDA	[17] AGOSTINI	17
< 1.4–2.5	^{116}Cd	NEMO-3	[18] ARNOLD	17
< 0.27–0.76	^{130}Te	CUORE(CINO)	[19] ALDUINO	16
< 1.6–5.3	^{150}Nd	NEMO-3	[20] ARNOLD	16A
< 0.061–0.165	^{136}Xe	KamLAND-Zen	[21] GANDO	16
< 0.33–0.62	^{100}Mo	NEMO-3	[22] ARNOLD	15
< 0.19–0.45	^{136}Xe	EXO-200	[23] ALBERT	14B
< 0.89–2.43	^{82}Se	NEMO-3	[24] BARABASH	11A
< 7.2–19.5	^{96}Zr	NEMO-3	[25] ARGYRIADES	10
< 3.5–22	^{48}Ca	CaF_2 scint.	[26] UMEHARA	08
< 0.2–1.1	^{130}Te	Cryog. det.	[27] ARNABOLDI	05
< 0.37–1.9	^{130}Te	Cryog. det.	[28] ARNABOLDI	04
< 1.5–1.7	^{116}Cd	$^{116}CdWO_4$ scint.	[29] DANEVICH	03
< 0.350	^{76}Ge	Enriched HPGe	[30] KLAPDOR-K...	01
<8.3	^{48}Ca	CaF_2 scint.	YOU	91

[1] ARMENGAUD 21 use the CUPID-Mo demonstrator, with 1.17 kg·yr exposure of ^{100}Mo, to set this limit. The range reflects the estimated uncertainty of the calculated nuclear matrix elements.

[2] ADAMS 20A use the data of CUORE (372.5 kg·yr exposure of TeO_2) to obtain this limit.

[3] AGOSTINI 20B use the final data set of the GERDA experiment, representing an exposure of 127.2 kg·yr to derive an upper limit for $\langle m_{\beta\beta} \rangle$. Isotopically enriched Ge detectors were used. The range reflects the variability of the theoretically calculated nuclear matrix elements. Supersedes AGOSTINI 19.

[4] AGOSTINI 19 use 82.4 kg·yr of data collected by the isotopically enriched ^{76}Ge detectors of the GERDA experiment to derive an upper limit for $\langle m_{\beta\beta} \rangle$. The range reflects the variability of the theoretically calculated nuclear matrix elements. Supersedes AGOSTINI 18.

[5] ALENKOV 19 report the range of the effective masses $\langle m_{\beta\beta} \rangle$ corresponding to the $0\nu\ \beta\beta$ decay half-life limit. It is based on the 52.1 kg·d exposure of ^{100}Mo, in the Yangyang underground laboratory. The median sensitivity is 1.1×10^{23} years. The range of $\langle m_{\beta\beta} \rangle$ reflects the uncertainty of nuclear matrix elements.

[6] ALVIS 19 use the MAJORANA Demonstrator with enriched in ^{76}Ge detectors to set this limit. The exposure is 26.0 kg yr. The sensitivity is 4.8×10^{25} yr.

[7] ANTON 19 uses the complete dataset of the EXO-200 experiment to obtain these limits. The spread reflect the uncertainty in the nuclear matrix elements. Supersedes ALBERT 18 and ALBERT 14B.

[8] AZZOLINI 19 use the CPID-0 scintillating cryogenic bolometer to set this limit. The exposure is 5.29 kg yr. The sensitivity is 5×10^{24} yr.

[9] NI 19 use the PandaX-II dual phase TPC at CJPL to search for the $0\nu\ \beta\beta$ decay of ^{136}Xe with 22.2 kg yr exposure. The range in the $m_{\beta\beta}$ limit of 1.3–3.5 eV reflects the range of the calculated nuclear matrix elements. The sensitivity is 1.9×10^{23} yr.

[10] AALSETH 18 uses the MAJORANA Demonstrator detector to establish this limit.

[11] AGOSTINI 18 uses the GERDA detector to establish this limit.

[12] ALBERT 18 uses the EXO-200 experiment to obtain this limit.

[13] ALDUINO 18 use the combined data of CUORE, CUORE0, and Cuoricino to obtain this limit.

[14] ARNOLD 18 use the NEMO-3 tracking detector to constrain the $0\nu\beta\beta$ decay of ^{82}Se. The limit on $\langle m_{\beta\beta} \rangle$ is obtained assuming light neutrino exchange; the range reflects different calculations of the nuclear matrix elements. This is a somewhat weaker limit than in BARABASH 11A using the same detector.

[15] AZZOLINI 18 uses data collected by the CUPID-0 scintillating cryogenic calorimeter, operated in the LNGS, to derive a range of limits on $\langle m_\nu \rangle$. The reported range reflects the spread of the nuclear matrix element calculations considered in this work. Use g_A= 1.269.

[16] BARABASH 18 use 1.162 kg of $^{116}CdWO_4$ scintillating crystals to obtain these limits. The spread reflects the estimated uncertainty in the nuclear matrix element. Supersedes DANEVICH 03.

[17] AGOSTINI 17 is based on 343 mol yr of data from GERDA phase 1 and phase 2 first part and the corresponding limit on $T_{1/2}$ using the different nuclear matrix elements mentioned by the authors. Supersedes AGOSTINI 13A.

[18] ARNOLD 17 utilize NEMO-3 data, taken with enriched ^{116}Cd to limit the effective Majorana neutrino mass. The reported range results from the use of different nuclear matrix elements. Supersedes BARABASH 11A.

[19] ALDUINO 16 place a limit on the effective Majorana neutrino mass using the combined data of the CUORE-0 and CUORICINO experiments. The range reflects the authors' evaluation of the variability of the nuclear matrix elements. Supersededs ALFONSO 15.

[20] ARNOLD 16A limit is derived from data taken with the NEMO-3 detector and ^{150}Nd. A range of nuclear matrix elements that include the effect of nuclear deformation have been used. Supersedes ARGYRIADES 09.

[21] GANDO 16 result is based on the 2016 KamLAND-Zen half-life limit. The stated range reflects different nuclear matrix elements, an unquenched g_A = 1.27 is used. Supersedes GANDO 13A.

[22] ARNOLD 15 use the NEMO-3 tracking calorimeter with 34.3 kg yr exposure to determine the neutrino mass limit based on the $0\nu\beta\beta$-half life of ^{100}Mo. The spread range reflects different nuclear matrix elements. Supersedes ARNOLD 14 and BARABASH 11A.

[23] ALBERT 14B is based on 100 kg yr of exposure of the EXO-200 tracking calorimeter. The mass range reflects the nuclear matrix element calculations. Supersedes AUGER 12.

Downloaded from https://academic.oup.com/ptep/article/2022/8/083C01/6651666 by KIT Library user on 27 September 2022

[24] BARABASH 11A limit is based on NEMO-3 data for ^{82}Se. The reported range reflects different nuclear matrix elements. Supersedes ARNOLD 05A and ARNOLD 04.

[25] ARGYRIADES 10 use ^{96}Zr and the NEMO-3 tracking detector to obtain the reported mass limit. The range reflects the fluctuation of the nuclear matrix elements considered.

[26] Limit was obtained using CaF_2 scintillation calorimeter to search for double beta decay of ^{48}Ca. Reported range of limits reflects spread of QRPA and SM matrix element calculations used. Supersedes OGAWA 04.

[27] Supersedes ARNABOLDI 04. Reported range of limits due to use of different nuclear matrix element calculations.

[28] Supersedes ARNABOLDI 03. Reported range of limits due to use of different nuclear matrix element calculations.

[29] Limit for $\langle m_\nu \rangle$ is based on the nuclear matrix elements of STAUDT 90 and ARNOLD 96. Supersedes DANEVICH 00.

[30] KLAPDOR-KLEINGROTHAUS 01 uses the calculation by STAUDT 90. Using several other models in the literature could worsen the limit up to 1.2 eV. This is the most stringent experimental bound on m_ν. It supersedes BAUDIS 99B.

Limits on Lepton-Number Violating ($V+A$) Current Admixture

For reasons given in the discussion at the beginning of this section, we list only results from 1989 and later. $\langle\lambda\rangle = \lambda\sum U_{ej} V_{ej}$ and $\langle\eta\rangle = \eta\sum U_{ej} V_{ej}$, where the sum is over the number of neutrino generations. This sum vanishes for massless or unmixed neutrinos. In the following Listings, only best or comparable limits or lifetimes for each isotope are reported.

$\langle\lambda\rangle$ (10^{-6})	CL%	$\langle\eta\rangle$ (10^{-8})	CL%	ISOTOPE	METHOD	DOCUMENT ID	
• • • We do not use the following data for averages, fits, limits, etc. • • •							
< 2.2–2.6	90	< 1.7–2.1	90	^{82}Se	NEMO-3	[1] ARNOLD	18
< 1.8–22	90	< 1.6–21	90	^{116}Cd	AURORA	[2] BARABASH	18
< 0.9–1.3	90	< 0.5–0.8	90	^{100}Mo	NEMO-3	[3] ARNOLD	14
<120	90			^{100}Mo	$0^+ \to 2^+$	[4] ARNOLD	07
$0.692^{+0.058}_{-0.056}$	68	$0.305^{+0.026}_{-0.025}$	68	^{76}Ge	Enriched HPGe	[5] KLAPDOR-K...	06A
< 2.5	90			^{100}Mo	0ν, NEMO-3	[6] ARNOLD	05A
< 3.8	90			^{82}Se	0ν, NEMO-3	[7] ARNOLD	05A
< 1.5–2.0	90			^{100}Mo	0ν, NEMO-3	[8] ARNOLD	04
< 3.2–3.8	90			^{82}Se	0ν, NEMO-3	[9] ARNOLD	04
< 1.6–2.4	90	< 0.9–5.3	90	^{130}Te	Cryog. det.	[10] ARNABOLDI	03
< 2.2	90	<2.5	90	^{116}Cd	$^{116}CdWO_4$ scint.	[11] DANEVICH	03
< 3.2–4.7	90	< 2.4–2.7	90	^{100}Mo	ELEGANT V	[12] EJIRI	01
< 1.1	90	<0.64	90	^{76}Ge	Enriched HPGe	[13] GUENTHER	97
< 4.4	90	<2.3	90	^{136}Xe	TPC	[14] VUILLEUMIER	93
		<5.3		^{128}Te	Geochem	[15] BERNATOW...	92

[1] ARNOLD 18 use the NEMO03 tracking detector, with 0.93 kg of ^{82}Se mass and 5.25 y exposure to obtain the limits for the hypothetical right-handed currents. Supersedes ARNOLD 05A.

[2] BARABASH 18 use 1.162 kg of $^{116}CdWO_4$ scintillating crystals to obtain this limits for the hypothetical right-handed currents in the $0\nu\beta\beta$ decay of ^{116}Cd.

[3] ARNOLD 14 is based on 34.7 kg yr of exposure of the NEMO-3 tracking calorimeter. The reported range limit on $\langle\lambda\rangle$ and $\langle\eta\rangle$ reflects the nuclear matrix element uncertainty in ^{100}Mo.

[4] ARNOLD 07 use NEMO-3 half life limit for 0ν-decay of ^{100}Mo to the first excited 2^+-state of daughter nucleus to limit the right-right handed admixture of weak currents $\langle\lambda\rangle$. This limit is not competitive when compared to the decay to the ground state.

[5] Re-analysis of data originally published in KLAPDOR-KLEINGROTHAUS 04A. Modified pulse shape analysis leads the authors to claim 6σ statistical evidence for observation of 0ν-decay. Authors use matrix element of MUTO 89 to determine $\langle\lambda\rangle$ and $\langle\eta\rangle$. Uncertainty of nuclear matrix element is not reflected in stated errors.

[6] ARNOLD 05A derive limit for $\langle\lambda\rangle$ based on ^{100}Mo data collected with NEMO-3 detector. No limit for $\langle\eta\rangle$ is given. Supersedes ARNOLD 04.

[7] ARNOLD 05A derive limit for $\langle\lambda\rangle$ based on ^{82}Se data collected with NEMO-3 detector. No limit for $\langle\eta\rangle$ is given. Supersedes ARNOLD 04.

[8] ARNOLD 04 use the matrix elements of SUHONEN 94 to obtain a limit for $\langle\lambda\rangle$, no limit for $\langle\eta\rangle$ is given. This limit is more stringent than the limit in EJIRI 01 for the same nucleus.

[9] ARNOLD 04 use the matrix elements of TOMODA 91 and SUHONEN 91 to obtain a limit for $\langle\lambda\rangle$, no limit for $\langle\eta\rangle$ is given.

[10] Supersedes ALESSANDRELLO 00. Cryogenic calorimeter search. Reported a range reflecting uncertainty in nuclear matrix element calculations.

[11] Limits for $\langle\lambda\rangle$ and $\langle\eta\rangle$ are based on nuclear matrix elements of STAUDT 90. Supersedes DANEVICH 00.

[12] The range of the reported $\langle\lambda\rangle$ and $\langle\eta\rangle$ values reflects the spread of the nuclear matrix elements. On axis value assuming $\langle m_\nu\rangle$=0 and $\langle\lambda\rangle$=$\langle\eta\rangle$=0, respectively.

[13] GUENTHER 97 limits use the matrix elements of STAUDT 90. Supersedes BALYSH 95 and BALYSH 92.

[14] VUILLEUMIER 93 uses the matrix elements of MUTO 89. Based on a half-life limit 2.6×10^{23} y at 90%CL.

[15] BERNATOWICZ 92 takes the measured geochemical decay width as a limit on the 0ν width, and uses the SUHONEN 91 coefficients to obtain the least restrictive limit on η. Further details of the experiment are given in BERNATOWICZ 93.

Double-β Decay REFERENCES

ADAMS	21	PRL 126 171801	D.Q. Adams et al.	(CUORE Collab.)
ADAMS	21A	EPJ C81 567	D.Q. Adams et al.	(CUORE Collab.)
ARMENGAUD	21	PRL 126 181802	E. Armengaud et al.	(CUPID-Mo Collab.)
ARNQUIST	21	PR C103 015501	I.J. Arnquist et al.	(MAJORANA Collab.)
ADAMS	20A	PRL 124 122501	D.Q. Adams et al.	(CUORE Collab.)
AGOSTINI	20B	PRL 125 252502	M. Agostini et al.	(GERDA Collab.)
ARMENGAUD	20	EPJ C80 674	E. Armengaud et al.	(CUPID-Mo Collab.)
AGOSTINI	19	SCI 365 1445	M. Agostini et al.	(GERDA Collab.)
ALDUINO	19	EPJ C79 795	C. Alduino et al.	(CUORE Collab.)
ALENKOV	19	EPJ C79 791	V. Alenkov et al.	(AMoRE Collab.)
ALVIS	19	PR C100 025501	S.I. Alvis et al.	(MAJORANA Collab.)
ANTON	19	PRL 123 161802	G. Anton et al.	(EXO-200 Collab.)
APRILE	19E	NAT 568 532	E. Aprile et al.	(XENON1T Collab.)
ARNOLD	19	EPJ C79 440	R. Arnold et al.	(NEMO-3 Collab.)
AZZOLINI	19	PRL 123 032501	O. Azzolini et al.	(CUPID-0 Collab.)
AZZOLINI	19B	PRL 123 262501	O. Azzolini et al.	(CUPID-0 Collab.)
NI	19	CP C43 113001	K. Ni et al.	(PandaX-II Collab.)
AALSETH	18	PRL 120 132502	C.E. Aalseth et al.	(MAJORANA Collab.)
AGOSTINI	18	PRL 120 132503	M. Agostini et al.	(GERDA Collab.)
ALBERT	18	PRL 120 072701	J.B. Albert et al.	(EXO-200 Collab.)
ALDUINO	18	PRL 120 132501	C. Alduino et al.	(CUORE Collab.)
ARNOLD	18	EPJ C78 821	R. Arnold et al.	(NEMO-3 Collab.)
AZZOLINI	18	PRL 120 232502	O. Azzolini et al.	(CUPID-0 Collab.)
AZZOLINI	18A	EPJ C78 888	O. Azzolini et al.	(CUPID-0 Collab.)
BARABASH	18	PR D98 092007	A.S. Barabash et al.	(AURORA Collab.)
AGOSTINI	17	NAT 544 47	M. Agostini et al.	(GERDA Collab.)
ALBERT	17C	PR D96 092001	J.B. Albert et al.	(EXO-200 Collab.)
ALDUINO	17	EPJ C77 13	C. Alduino et al.	(CUORE Collab.)
ARMENGAUD	17	EPJ C77 785	E. Armengaud et al.	(CUPID Collab.)
ARNOLD	17	PR D95 012007	R. Arnold et al.	(NEMO-3 Collab.)
ALDUINO	16	PR C93 045503	C. Alduino et al.	(CUORE Collab.)
ARNOLD	16	PR D93 112008	R. Arnold et al.	(NEMO-3 Collab.)
ARNOLD	16A	PR D94 072003	R. Arnold et al.	(NEMO-3 Collab.)
ASAKURA	16	NP A946 171	K. Asakura et al.	(KamLAND-Zen Collab.)
GANDO	16	PRL 117 082503	A. Gando et al.	(KamLAND-Zen Collab.)
AGOSTINI	15A	EPJ C75 416	M. Agostini et al.	(GERDA Collab.)
ALFONSO	15	PRL 115 102502	K. Alfonso et al.	(CUORE Collab.)
ARNOLD	15	PR D92 072011	R. Arnold et al.	(NEMO-3 Collab.)
ALBERT	14	PR C89 015502	J. Albert et al.	(EXO-200 Collab.)
ALBERT	14B	NAT 510 229	J.B. Albert et al.	(EXO-200 Collab.)
ARNOLD	14	PR D89 111101	R. Arnold et al.	(NEMO-3 Collab.)
AGOSTINI	13A	PRL 111 122503	M. Agostini et al.	(GERDA Collab.)
GANDO	13A	PRL 110 062502	A. Gando et al.	(KamLAND-Zen Collab.)
GAVRILYAK	13	PR C87 035501	Yu.M. Gavrilyuk et al.	
ANDREOTTI	12	PR C85 045503	E. Andreotti et al.	(CUORICINO Collab.)
AUGER	12	PRL 109 032505	M. Auger et al.	(EXO-200 Collab.)
GANDO	12A	PR C85 045504	A. Gando et al.	(KamLAND-Zen Collab.)
ACKERMAN	11	PRL 107 212501	N. Ackerman et al.	(EXO Collab.)
ARNOLD	11	PRL 107 062504	R. Arnold et al.	(NEMO-3 Collab.)
BARABASH	11A	PAN 74 312	A.S. Barabash et al.	(NEMO-3 Collab.)
		Translated from YAF 74 330.		
ARGYRIADES	10	NP A847 168	J. Argyriades et al.	(NEMO-3 Collab.)
BELLI	10	NP A846 143	P. Belli et al.	(DAMA-INR Collab.)
ARGYRIADES	09	PR C80 032501	J. Argyriades et al.	(NEMO-3 Collab.)
KIDD	09	NP A821 251	M. Kidd et al.	
ARNABOLDI	08	PR C78 035502	C. Arnaboldi et al.	(CUORICINO Collab.)
UMEHARA	08	PR C78 058501	S. Umehara et al.	
ARNOLD	07	NP A781 209	R. Arnold et al.	(NEMO-3 Collab.)
KLAPDOR-K...	06A	MPL A21 1547	H.V. Klapdor-Kleingrothaus, I.V. Krivosheina	
ARNABOLDI	05	PRL 95 142501	C. Arnaboldi et al.	(CUORICINO Collab.)
ARNOLD	05A	PRL 95 182302	R. Arnold et al.	(NEMO-3 Collab.)
AALSETH	04	PR D70 078302	C.E. Aalseth et al.	
ARNABOLDI	04	PL B584 260	C. Arnaboldi et al.	
ARNOLD	04	JETPL 80 377	R. Arnold et al.	(NEMO-3 Collab.)
		Translated from ZETFP 80 429.		
KLAPDOR-K...	04A	PL B586 198	H.V. Klapdor-Kleingrothaus et al.	
KLAPDOR-K...	04B	PR D70 078301	H.V. Klapdor-Kleingrothaus, A. Dietz, I.V. Krivosheina	
OGAWA	04	NP A730 215	I. Ogawa et al.	
ARNABOLDI	03	PL B557 167	C. Arnaboldi et al.	
DANEVICH	03	PR C68 035501	F.A. Danevich et al.	
AALSETH	02B	PR D65 092007	C.E. Aalseth et al.	(IGEX Collab.)
DEBRAECKEL...	01	PRL 86 3510	L. De Braeckeleer et al.	
EJIRI	01	PR C63 065501	H. Ejiri et al.	
KLAPDOR-K...	01	EPJ A12 147	H.V. Klapdor-Kleingrothaus et al.	
KLAPDOR-K...	01B	MPL A16 2409	H.V. Klapdor-Kleingrothaus et al.	
ALESSAND...	00	PL B486 13	A. Alessandrello et al.	
DANEVICH	00	PR C62 045501	F.A. Danevich et al.	
ARNOLD	99	NP A658 299	R. Arnold et al.	(NEMO Collab.)
BAUDIS	99	PR D59 022001	L. Baudis et al.	(Heidelberg-Moscow Collab.)
BAUDIS	99B	PRL 83 41	L. Baudis et al.	(Heidelberg-Moscow Collab.)
ARNOLD	98	NP A636 209	R. Arnold et al.	(NEMO-2 Collab.)
GUENTHER	97	PR D55 54	M. Gunther et al.	(Heidelberg-Moscow Collab.)
ARNOLD	96	ZPHY C72 239	R. Arnold et al.	(BCEN, CAEN, JINR+)
BALYSH	95	PL B356 450	A. Balysh et al.	(Heidelberg-Moscow Collab.)
DASSIE	95	PR D51 2090	D. Dassie et al.	(NEMO Collab.)
EJIRI	95	JPSJ 64 339	H. Ejiri et al.	(OSAK, KIEV)
SUHONEN	94	PR C49 3055	J. Suhonen, O. Civitarese	
BERNATOW...	93	PR C47 806	T. Bernatowicz et al.	(WUSL, TATA)
VUILLEUMIER	93	PR D48 1009	J.C. Vuilleumier et al.	(NEUC, CIT, VILL)
BALYSH	92	PL B283 32	A. Balysh et al.	(MPIK, KIAE, SASSO)
BERNATOW...	92	PRL 69 2341	T. Bernatowicz et al.	(WUSL, TATA)
ELLIOTT	92	PR C46 1535	S.R. Elliott et al.	(UCI)
SUHONEN	91	NP A535 509	J. Suhonen, S.B. Khadkikar, A. Faessler	(JYV+)
TOMODA	91	RPP 54 53	T. Tomoda	
YOU	91	PL B265 53	K. You et al.	(BHEP, CAST+)
STAUDT	90	EPL 13 31	A. Staudt, K. Muto, H.V. Klapdor-Kleingrothaus	
MUTO	89	ZPHY A334 187	K. Muto, E. Bender, H.V. Klapdor	(TINT, MPIK)

Neutrino Mixing

With the possible exceptions of "short-baseline anomalies," such as LSND, all neutrino data can be described within the framework of a 3×3 mixing matrix between the mass eigenstates ν_1, ν_2, and ν_3, leading to the flavor eigenstates ν_e, ν_μ, and ν_τ, as described in the review *"Neutrino masses, mixing and oscillations."*

Downloaded from https://academic.oup.com/ptep/article/2022/8/083C01/6651666 by KIT Library user on 27 September 2022

The Listings are divided in the following sections:

(A) Neutrino fluxes and event ratios: shows measurements which correspond to various oscillation tests for Accelerator, Reactor, Atmospheric, and Solar neutrino experiments. Typically, ratios involve a measurement in a realm sensitive to oscillations compared to one for which no oscillation effect is expected.

(B) Neutrino mixing parameters: shows measurements of $\sin^2(\theta_{12})$, $\sin^2(\theta_{23})$, $\sin^2(\theta_{13})$, Δm^2_{21}, Δm^2_{32}, and δ_{CP} as extracted from the measured data in the quoted publications in the frame of the three-neutrino mixing scheme. The quoted averages are not the result of a global fit, as in the review *"Neutrino masses, mixing, and oscillations,"* and, as a consequence, might slightly differ from them. In some cases, measurements depend on the mass order (normal when $\Delta m^2_{32} > 0$ or inverted when $\Delta m^2_{32} < 0$) or octant of θ_{23} (lower when $\theta_{23} < 45°$ or upper when $\theta_{23} > 45°$).

(C) Other neutrino mixing results:

The LSND anomaly [AGUILAR 01], reported a signal which is consistent with $\overline{\nu}_\mu \to \overline{\nu}_e$ oscillations. In a three neutrino framework, this would be a measurement of θ_{12} and Δm^2_{21}. This does not appear to be consistent with the interpretation of other neutrino data. It has been interpreted as evidence for a 4th "sterile" neutrino. The following listings include results which might be relevant towards understanding this observation. They include searches for $\nu_\mu \to \nu_e$, $\overline{\nu}_\mu \to \overline{\nu}_e$, sterile neutrino oscillations, and others.

(A) Neutrino fluxes and event ratios

Events (observed/expected) from accelerator ν_μ experiments.

Some neutrino oscillation experiments compare the flux in two or more detectors. This is usually quoted as the ratio of the event rate in the far detector to the expected rate based on an extrapolation from the near detector in the absence of oscillations.

VALUE	DOCUMENT ID		TECN	COMMENT
• • • We do not use the following data for averages, fits, limits, etc. • • •				
1.01 ± 0.10	[1] ABE	14B	T2K	ν_e rate in T2K near detect.
0.71 ± 0.08	[2] AHN	06A	K2K	K2K to Super-K
0.64 ± 0.05	[3] MICHAEL	06	MINS	All charged current events
$0.71^{+0.08}_{-0.09}$	[4] ALIU	05	K2K	KEK to Super-K
$0.70^{+0.10}_{-0.11}$	[5] AHN	03	K2K	KEK to Super-K

[1] The rate of ν_e from μ decay was measured to be 0.68 ± 0.30 compared to the predicted flux. From K decay 1.10 ± 0.14 compared to the predicted flux.

[2] Based on the observation of 112 events when $158.1^{+9.2}_{-8.6}$ were expected without oscillations. Including not only the number of events but also the shape of the energy distribution, the evidence for oscillation is at the level of about 4.3 σ. Supersedes ALIU 05.

[3] This ratio is based on the observation of 215 events compared to an expectation of 336 ± 14 without oscillations. See also ADAMSON 08.

[4] This ratio is based on the observation of 107 events at the far detector 250 km away from KEK, and an expectation of 151^{+12}_{-10}.

[5] This ratio is based on the observation of 56 events with an expectation of $80.1^{+6.2}_{-5.4}$.

Events (observed/expected) from reactor $\overline{\nu}_e$ experiments.

The quoted values are the ratios of the measured reactor $\overline{\nu}_e$ event rate at the quoted distances, and the rate expected without oscillations. The expected rate is based on the experimental data for the most significant reactor fuels (^{235}U, ^{239}Pu, ^{241}Pu) and on calculations for ^{238}U.

A recent re-evaluation of the spectral conversion of electron to $\overline{\nu}_e$ in MUELLER 11 results in an upward shift of the reactor $\overline{\nu}_e$ spectrum by 3% and, thus, might require revisions to the ratios listed in this table.

VALUE	DOCUMENT ID		TECN	COMMENT
• • • We do not use the following data for averages, fits, limits, etc. • • •				
$0.948 \pm 0.008 \pm 0.033$	[1] ALMAZAN	20	RHF	RHF reactor at ILL
0.952 ± 0.027	[2] ADEY	19	DAYA	DayaBay, Ling Ao/Ao II reactors
	[3] AN	16	DAYA	DayaBay, Ling Ao/Ao II reactors
$1.08 \pm 0.21 \pm 0.16$	[4] DENIZ	10	TEXO	Kuo-Sheng reactor, 28 m
$0.658 \pm 0.044 \pm 0.047$	[5] ARAKI	05	KLND	Japanese react. $\sim$ 180 km
$0.611 \pm 0.085 \pm 0.041$	[6] EGUCHI	03	KLND	Japanese react. $\sim$ 180 km
$1.01 \pm 0.024 \pm 0.053$	[7] BOEHM	01		Palo Verde react. 0.75–0.89 km
$1.01 \pm 0.028 \pm 0.027$	[8] APOLLONIO	99	CHOZ	Chooz reactors 1 km
$0.987 \pm 0.006 \pm 0.037$	[9] GREENWOOD	96		Savannah River, 18.2 m
$0.988 \pm 0.004 \pm 0.05$	ACHKAR	95	CNTR	Bugey reactor, 15 m
$0.994 \pm 0.010 \pm 0.05$	ACHKAR	95	CNTR	Bugey reactor, 40 m
$0.915 \pm 0.132 \pm 0.05$	ACHKAR	95	CNTR	Bugey reactor, 95 m
$0.987 \pm 0.014 \pm 0.027$	[10] DECLAIS	94	CNTR	Bugey reactor, 15 m
$0.985 \pm 0.018 \pm 0.034$	KUVSHINN...	91	CNTR	Rovno reactor
$1.05 \pm 0.02 \pm 0.05$	VUILLEUMIER	82		Gösgen reactor
$0.955 \pm 0.035 \pm 0.110$	[11] KWON	81		$\overline{\nu}_e p \to e^+ n$
0.89 ± 0.15	[11] BOEHM	80		$\overline{\nu}_e p \to e^+ n$

[1] ALMAZAN 20 use the RHF research reactor at ILL to compare their measured antineutrino event rate to the calculation by HUBER 11. Reported $0.948 \pm 0.008 \pm 0.023 \pm 0.023$ measurement with uncertainties from statistics, systematic, and model. Note that this result is obtained for highly enriched ^{235}U reactor fuel while most other reactor experiments utilize a low-enrichment mix of fissile nuclides.

[2] ADEY 19 present a re-analysis of 1230 days of Daya Bay near detector data with reduced systematic uncertainties on the neutron detection efficiency. Note that ADEY 19 report the measured to predicted antineutrino ratio using the reactor model of MUELLER 11 (Huber-Mueller model). The ratio using the older ILL-Vogel model is $1.001 \pm 0.015 \pm 0.027$.

[3] AN 16 use 217 days of data (338k events) to determine the neutrino flux ratio relative to the prediction of Mueller-Huber and ILL-Vogel models (see AN 16 for details). The reported flux ratios were corrected for θ_{13} oscillation effect. The flux measurement is consistent with results from previous short-baseline reactor experiments. The measured inverse beta decay yield is $(1.55 \pm 0.04) \times 10^{-18}$ cm^2/(GW day) or $\sigma_f = (5.92 \pm 0.14) \times 10^{-43}$ cm^2/fission. About 4σ excess of events was observed in the 4–6 MeV prompt energy region.

[4] DENIZ 10 observe reactor $\overline{\nu}_e e$ scattering with recoil kinetic energies 3–8 MeV using CsI(Tl) detectors. The observed rate is consistent with the Standard Model prediction, leading to a constraint on $\sin^2\theta_W = 0.251 \pm 0.031(\text{stat}) \pm 0.024(\text{sys})$.

[5] Updated result of KamLAND, including the data used in EGUCHI 03. Note that the survival probabilities for different periods are not directly comparable because the effective baseline varies with power output of the reactor sources involved, and there were large variations in the reactor power production in Japan in 2003.

[6] EGUCHI 03 observe reactor neutrino disappearance at $\sim$ 180 km baseline to various Japanese nuclear power reactors.

[7] BOEHM 01 search for neutrino oscillations at 0.75 and 0.89 km distance from the Palo Verde reactors.

[8] APOLLONIO 99, APOLLONIO 98 search for neutrino oscillations at 1.1 km fixed distance from Chooz reactors. They use $\overline{\nu}_e p \to e^+ n$ in Gd-loaded scintillator target. APOLLONIO 99 supersedes APOLLONIO 98. See also APOLLONIO 03 for detailed description.

[9] GREENWOOD 96 search for neutrino oscillations at 18 m and 24 m from the reactor at Savannah River.

[10] DECLAIS 94 result based on integral measurement of neutrons only. Result is ratio of measured cross section to that expected in standard *V-A* theory. Replaced by ACHKAR 95.

[11] KWON 81 represents an analysis of a larger set of data from the same experiment as BOEHM 80.

Atmospheric neutrinos

Neutrinos and antineutrinos produced in the atmosphere induce μ-like and e-like events in underground detectors. The ratio of the numbers of the two kinds of events is defined as μ/e. It has the advantage that systematic effects, such as flux uncertainty, tend to cancel, for both experimental and theoretical values of the ratio. The "ratio of the ratios" of experimental to theoretical μ/e, $R(\mu/e)$, or that of experimental to theoretical μ/total, $R(\mu/\text{total})$ with total $= \mu + e$, is reported below. If the actual value is not unity, the value obtained in a given experiment may depend on the experimental conditions. In addition, the measured "up-down asymmetry" for μ ($N_{up}(\mu)/N_{down}(\mu)$) or e ($N_{up}(e)/N_{down}(e)$) is reported. The expected "up-down asymmetry" is nearly unity if there is no neutrino oscillation.

R(μ/e) = (Measured Ratio μ/e) / (Expected Ratio μ/e)

VALUE	DOCUMENT ID		TECN	COMMENT
• • • We do not use the following data for averages, fits, limits, etc. • • •				
$0.658 \pm 0.016 \pm 0.035$	[1] ASHIE	05	SKAM	sub-GeV
$0.702^{+0.032}_{-0.030} \pm 0.101$	[2] ASHIE	05	SKAM	multi-GeV
$0.69 \pm 0.10 \pm 0.06$	[3] SANCHEZ	03	SOU2	Calorimeter raw data
	[4] FUKUDA	96B	KAMI	Water Cherenkov

Downloaded from https://academic.oup.com/ptep/article/2022/8/083C01/6651666 by KIT Library user on 27 September 2022

$1.00 \pm 0.15 \pm 0.08$	[5] DAUM	95	FREJ	Calorimeter
$0.60 \ ^{+0.06}_{-0.05} \pm 0.05$	[6] FUKUDA	94	KAMI	sub-GeV
$0.57 \ ^{+0.08}_{-0.07} \pm 0.07$	[7] FUKUDA	94	KAMI	multi-Gev
	[8] BECKER-SZ...	92B	IMB	Water Cherenkov

[1] ASHIE 05 results are based on an exposure of 92 kton yr during the complete Super-Kamiokande I running period. The analyzed data sample consists of fully-contained single-ring e-like events with 0.1 GeV/c $< p_e$ and μ-like events 0.2 GeV/c $< p_\mu$, both having a visible energy $<$ 1.33 GeV. These criteria match the definition used by FUKUDA 94.

[2] ASHIE 05 results are based on an exposure of 92 kton yr during the complete Super-Kamiokande I running period. The analyzed data sample consists of fully-contained single-ring events with visible energy $>$ 1.33 GeV and partially-contained events. All partially-contained events are classified as μ-like.

[3] SANCHEZ 03 result is based on an exposure of 5.9 kton yr, and updates ALLISON 99 result. The analyzed data sample consists of fully-contained e-flavor and μ-flavor events having lepton momentum $>$ 0.3 GeV/c.

[4] FUKUDA 96B studied neutron background in the atmospheric neutrino sample observed in the Kamiokande detector. No evidence for the background contamination was found.

[5] DAUM 95 results are based on an exposure of 2.0 kton yr which includes the data used by BERGER 90B. This ratio is for the contained and semicontained events. DAUM 95 also report $R(\mu/e) = 0.99 \pm 0.13 \pm 0.08$ for the total neutrino induced data sample which includes upward going stopping muons and horizontal muons in addition to the contained and semicontained events.

[6] FUKUDA 94 result is based on an exposure of 7.7 kton yr and updates the HIRATA 92 result. The analyzed data sample consists of fully-contained e-like events with $0.1 < p_e < 1.33$ GeV/c and fully-contained μ-like events with $0.2 < p_\mu < 1.5$ GeV/c.

[7] FUKUDA 94 analyzed the data sample consisting of fully contained events with visible energy $>$ 1.33 GeV and partially contained μ-like events.

[8] BECKER-SZENDY 92B reports the fraction of nonshowering events (mostly muons from atmospheric neutrinos) as $0.36 \pm 0.02 \pm 0.02$, as compared with expected fraction $0.51 \pm 0.01 \pm 0.05$. After cutting the energy range to the Kamiokande limits, BEIER 92 finds $R(\mu/e)$ very close to the Kamiokande value.

R(ν_μ) = (Measured Flux of ν_μ) / (Expected Flux of ν_μ)

VALUE	DOCUMENT ID		TECN	COMMENT
• • • We do not use the following data for averages, fits, limits, etc. • • •				
0.84 ± 0.12	[1] ADAMSON	06	MINS	MINOS atmospheric
$0.72 \pm 0.026 \pm 0.13$	[2] AMBROSIO	01	MCRO	upward through-going
$0.57 \pm 0.05 \pm 0.15$	[3] AMBROSIO	00	MCRO	upgoing partially contained
$0.71 \pm 0.05 \pm 0.19$	[4] AMBROSIO	00	MCRO	downgoing partially contained + upgoing stopping
$0.74 \pm 0.036 \pm 0.046$	[5] AMBROSIO	98	MCRO	Streamer tubes
	[6] CASPER	91	IMB	Water Cherenkov
	[7] AGLIETTA	89	NUSX	
0.95 ± 0.22	[8] BOLIEV	81		Baksan
0.62 ± 0.17	CROUCH	78		Case Western/UCI

[1] ADAMSON 06 uses a measurement of 107 total neutrinos compared to an expected rate of 127 ± 13 without oscillations.

[2] AMBROSIO 01 result is based on the upward through-going muon tracks with $E_\mu > 1$ GeV. The data came from three different detector configurations, but the statistics is largely dominated by the full detector run, from May 1994 to December 2000. The total live time, normalized to the full detector configuration, is 6.17 years. The first error is the statistical error, the second is the systematic error, dominated by the theoretical error in the predicted flux.

[3] AMBROSIO 00 result is based on the upgoing partially contained event sample. It came from 4.1 live years of data taking with the full detector, from April 1994 to February 1999. The average energy of atmospheric muon neutrinos corresponding to this sample is 4 GeV. The first error is statistical, the second is the systematic error, dominated by the 25% theoretical error in the rate (20% in the flux and 15% in the cross section, added in quadrature). Within statistics, the observed deficit is uniform over the zenith angle.

[4] AMBROSIO 00 result is based on the combined samples of downgoing partially contained events and upgoing stopping events. These two subsamples could not be distinguished due to the lack of timing information. The result came from 4.1 live years of data taking with the full detector, from April 1994 to February 1999. The average energy of atmospheric muon neutrinos corresponding to this sample is 4 GeV. The first error is statistical, the second is the systematic error, dominated by the 25% theoretical error in the rate (20% in the flux and 15% in the cross section, added in quadrature). Within statistics, the observed deficit is uniform over the zenith angle.

[5] AMBROSIO 98 result is for all nadir angles and updates AHLEN 95 result. The lower cutoff on the muon energy is 1 GeV. In addition to the statistical and systematic errors, there is a Monte Carlo flux error (theoretical error) of ± 0.13. With a neutrino oscillation hypothesis, the fit either to the flux or zenith distribution independently yields $\sin^2 2\theta$=1.0 and $\Delta(m^2) \sim$ a few times 10^{-3} eV^2. However, the fit to the observed zenith distribution gives a maximum probability for χ^2 of only 5% for the best oscillation hypothesis.

[6] CASPER 91 correlates showering/nonshowering signature of single-ring events with parent atmospheric-neutrino flavor. They find nonshowering ($\approx \nu_\mu$ induced) fraction is $0.41 \pm 0.03 \pm 0.02$, as compared with expected 0.51 ± 0.05 (syst).

[7] AGLIETTA 89 finds no evidence for any anomaly in the neutrino flux. They define ρ = (measured number of ν_e's)/(measured number of ν_μ's). They report ρ(measured)=ρ(expected) $= 0.96 \ ^{+0.32}_{-0.28}$.

[8] From this data BOLIEV 81 obtain the limit $\Delta(m^2) \leq 6 \times 10^{-3}$ eV^2 for maximal mixing, $\nu_\mu \not\to \nu_\mu$ type oscillation.

R(μ/total) = (Measured Ratio μ/total) / (Expected Ratio μ/total)

VALUE	DOCUMENT ID		TECN	COMMENT
• • • We do not use the following data for averages, fits, limits, etc. • • •				
$1.1 \ ^{+0.07}_{-0.12} \pm 0.11$	[1] CLARK	97	IMB	multi-GeV

[1] CLARK 97 obtained this result by an analysis of fully contained and partially contained events in the IMB water-Cherenkov detector with visible energy $>$ 0.95 GeV.

$N_{up}(\mu)/N_{down}(\mu)$

VALUE	DOCUMENT ID		TECN	COMMENT
• • • We do not use the following data for averages, fits, limits, etc. • • •				
0.71 ± 0.06	[1] ADAMSON	12B	MINS	contained-vertex muons
$0.551 \ ^{+0.035}_{-0.033} \pm 0.004$	[2] ASHIE	05	SKAM	multi-GeV

[1] ADAMSON 12B reports the atmospheric neutrino results obtained with MINOS far detector in 2,553 live days (an exposure of 37.9 kton-yr). This result is obtained with a sample of high resolution contained-vertex muons. The quoted error is statistical only.

[2] ASHIE 05 results are based on an exposure of 92 kton yr during the complete Super-Kamiokande I running period. The analyzed data sample consists of fully-contained single-ring μ-like events with visible energy $>$ 1.33 GeV and partially-contained events. All partially-contained events are classified as μ-like. Upward-going events are those with $-1 <$ cos(zenith angle) < -0.2 and downward-going events are those with 0.2$<$ cos(zenith angle) $<$1. The μ-like up-down ratio for the multi-GeV data deviates from 1 (the expectation for no atmospheric ν_μ oscillations) by more than 12 standard deviations.

$N_{up}(e)/N_{down}(e)$

VALUE	DOCUMENT ID		TECN	COMMENT
• • • We do not use the following data for averages, fits, limits, etc. • • •				
$0.961 \ ^{+0.086}_{-0.079} \pm 0.016$	[1] ASHIE	05	SKAM	multi-GeV

[1] ASHIE 05 results are based on an exposure of 92 kton yr during the complete Super-Kamiokande I running period. The analyzed data sample consists of fully-contained single-ring e-like events with visible energy $>$ 1.33 GeV. Upward-going events are those with $-1 <$ cos(zenith angle) < -0.2 and downward-going events are those with 0.2 $<$ cos(zenith angle) $<$ 1. The e-like up-down ratio for the multi-GeV data is consistent with 1 (the expectation for no atmospheric ν_e oscillations).

R(up/down; μ) = (Measured up/down; μ) / (Expected up/down; μ)

VALUE	DOCUMENT ID		TECN	COMMENT
• • • We do not use the following data for averages, fits, limits, etc. • • •				
$0.62 \pm 0.05 \pm 0.02$	[1] ADAMSON	12B	MINS	contained-vertex muons
$0.62 \ ^{+0.19}_{-0.14} \pm 0.02$	[2] ADAMSON	06	MINS	atmospheric ν with far detector

[1] ADAMSON 12B reports the atmospheric neutrino results obtained with MINOS far detector in 2,553 live days (an exposure of 37.9 kton-yr). This result is obtained with a sample of high resolution contained-vertex muons. The expected ratio is calculated with no neutrino oscillation.

[2] ADAMSON 06 result is obtained with the MINOS far detector with an exposure of 4.54 kton yr. The expected ratio is calculated with no neutrino oscillation.

N(μ^+)/N(μ^-)

VALUE	DOCUMENT ID		TECN	COMMENT
• • • We do not use the following data for averages, fits, limits, etc. • • •				
$0.46 \ ^{+0.05}_{-0.04}$	[1,2] ADAMSON	12B	MINS	contained-vertex muons
$0.63 \ ^{+0.09}_{-0.08}$	[1,3] ADAMSON	12B	MINS	ν-induced rock-muons

[1] ADAMSON 12B reports the atmospheric neutrino results obtained with MINOS far detector in 2,553 live days (an exposure of 37.9 kton-yr). The muon charge ratio N(μ^+)/N(μ^-) represents the $\overline{\nu}_\mu/\nu_\mu$ ratio.

[2] This result is obtained with a charge-separated sample of high resolution contained-vertex muons. The quoted error is statistical only.

[3] This result is obtained with a charge-separated sample of high resolution neutrino-induced rock-muons. The quoted error is statistical only.

R(μ^+/μ^-) = (Measured N(μ^+)/N(μ^-)) / (Expected N(μ^+)/N(μ^-))

VALUE	DOCUMENT ID		TECN	COMMENT
• • • We do not use the following data for averages, fits, limits, etc. • • •				
$0.93 \pm 0.09 \pm 0.09$	[1,2] ADAMSON	12B	MINS	contained-vertex muons
$1.29 \ ^{+0.19}_{-0.17} \pm 0.16$	[1,3] ADAMSON	12B	MINS	ν-induced rock-muons
$1.03 \pm 0.08 \pm 0.08$	[1,4] ADAMSON	12B	MINS	contained
$1.39 \ ^{+0.35}_{-0.46} \ ^{+0.08}_{-0.14}$	[5] ADAMSON	07	MINS	Upward and horizontal μ with far detector
$0.96 \ ^{+0.38}_{-0.27} \pm 0.15$	[6] ADAMSON	06	MINS	atmospheric ν with far detector

[1] ADAMSON 12B reports the atmospheric neutrino results obtained with MINOS far detector in 2,553 live days (an exposure of 37.9 kton-yr). The muon charge ratio N(μ^+)/N(μ^-) represents the $\overline{\nu}_\mu/\nu_\mu$ ratio. As far as the same oscillation parameters are used for νs and $\overline{\nu}$s, the expected $\overline{\nu}_\mu/\nu_\mu$ ratio is almost entirely independent of any input oscillations.

Downloaded from https://academic.oup.com/ptep/article/2022/8/083C01/6651666 by KIT Library user on 27 September 2022

[2] This result is obtained with a charge-separated sample of high resolution contained-vertex muons.

[3] This result is obtained with a charge-separated sample of high resolution neutrino-induced rock-muons.

[4] The charge-separated samples of high resolution contained-vertex muons and neutrino-induced rock-muons are combined to obtain this result which is consistent with unity.

[5] ADAMSON 07 result is obtained with the MINOS far detector in 854.24 live days, based on neutrino-induced upward-going and horizontal muons. This result is consistent with *CPT* conservation.

[6] ADAMSON 06 result is obtained with the MINOS far detector with an exposure of 4.54 kton yr, based on contained events. The expected ratio is calculated by assuming the same oscillation parameters for neutrinos and antineutrinos.

Solar neutrinos

Solar neutrinos are produced by thermonuclear fusion reactions in the Sun. Radiochemical experiments measure particular combinations of fluxes from various neutrino-producing reactions, whereas water-Cherenkov experiments mainly measure a flux of neutrinos from decay of ^{8}B. Solar neutrino fluxes are composed of all active neutrino species, ν_e, ν_μ, and ν_τ. In addition, some other mechanisms may cause antineutrino components in solar neutrino fluxes. Each measurement method is sensitive to a particular component or a combination of components of solar neutrino fluxes.

ν_e Capture Rates from Radiochemical Experiments

1 SNU (Solar Neutrino Unit) = 10^{-36} captures per atom per second.

VALUE (SNU)	DOCUMENT ID		TECN	COMMENT
• • • We do not use the following data for averages, fits, limits, etc. • • •				
$73.4\ ^{+6.1}_{-6.0}\ ^{+3.7}_{-4.1}$	[1] KAETHER	10		GALX reanalysis
$67.6 \pm 4.0 \pm 3.2$	[2] KAETHER	10		GNO+GALX reanalysis combined
$65.4\ ^{+3.1}_{-3.0}\ ^{+2.6}_{-2.8}$	[3] ABDURASHI...	09	SAGE	^{71}Ga $\rightarrow$ ^{71}Ge
$62.9\ ^{+5.5}_{-5.3} \pm 2.5$	[4] ALTMANN	05	GNO	^{71}Ga $\rightarrow$ ^{71}Ge
$69.3 \pm 4.1 \pm 3.6$	[5] ALTMANN	05	GNO	GNO + GALX combined
$77.5 \pm 6.2\ ^{+4.3}_{-4.7}$	[6] HAMPEL	99	GALX	^{71}Ga $\rightarrow$ ^{71}Ge
$2.56 \pm 0.16 \pm 0.16$	[7] CLEVELAND	98	HOME	^{37}Cl $\rightarrow$ ^{37}Ar

[1] KAETHER 10 reports the reanalysis results of a complete GALLEX data (GALLEX I+II+III+IV, reported in HAMPEL 99) based on the event selection with a new pulse shape analysis, which provides a better background reduction than the rise time analysis adopted in HAMPEL 99.

[2] Combined result of GALLEX I+II+III+IV reanalysis and GNO I+II+III (ALTMANN 05).

[3] ABDURASHITOV 09 reports a combined analysis of 168 extractions of the SAGE solar neutrino experiment during the period January 1990 through December 2007, and updates the ABDURASHITOV 02 result. The data are consistent with the assumption that the solar neutrino production rate is constant in time. Note that a $\sim$ 15% systematic uncertainty in the overall normalization may be added to the ABDURASHITOV 09 result, because calibration experiments for gallium solar neutrino measurements using intense ^{51}Cr (twice by GALLEX and once by SAGE) and ^{37}Ar (by SAGE) result in an average ratio of 0.87 $\pm$ 0.05 of the observed to calculated rates.

[4] ALTMANN 05 reports the complete result from the GNO solar neutrino experiment (GNO I+II+III), which is the successor project of GALLEX. Experimental technique of GNO is essentially the same as that of GALLEX. The run data cover the period 20 May 1998 through 9 April 2003.

[5] Combined result of GALLEX I+II+III+IV (HAMPEL 99) and GNO I+II+III.

[6] HAMPEL 99 report the combined result for GALLEX I+II+III+IV (65 runs in total), which update the HAMPEL 96 result. The GALLEX IV result (12 runs) is 118.4 $\pm$ 17.8 $\pm$ 6.6 SNU. (HAMPEL 99 discuss the consistency of partial results with the mean.) The GALLEX experimental program has been completed with these runs. The total run data cover the period 14 May 1991 through 23 January 1997. A total of 300 ^{71}Ge events were observed. Note that a $\sim$ 15% systematic uncertainty in the overall normalization may be added to the HAMPEL 99 result, because calibration experiments for gallium solar neutrino measurements using intense ^{51}Cr (twice by GALLEX and once by SAGE) and ^{37}Ar (by SAGE) result in an average ratio of 0.87 $\pm$ 0.05 of the observed to calculated rates.

[7] CLEVELAND 98 is a detailed report of the ^{37}Cl experiment at the Homestake Mine. The average solar neutrino-induced ^{37}Ar production rate from 108 runs between 1970 and 1994 updates the DAVIS 89 result.

ϕ_{ES} (^{8}B)

^{8}B solar-neutrino flux measured via νe elastic scattering. This process is sensitive to all active neutrino flavors, but with reduced sensitivity to ν_μ, ν_τ due to the cross-section difference, $\sigma(\nu_{\mu,\tau} e) \sim 0.16\sigma(\nu_e e)$. If the ^{8}B solar-neutrino flux involves nonelectron flavor active neutrinos, their contribution to the flux is $\sim$ 0.16 times of ν_e.

VALUE (10^6 cm^{-2}s^{-1})	DOCUMENT ID		TECN	COMMENT
• • • We do not use the following data for averages, fits, limits, etc. • • •				
$2.57\ ^{+0.17}_{-0.18}\ ^{+0.07}_{-0.07}$	[1] AGOSTINI	20A	BORX	average flux
$2.53\ ^{+0.31}_{-0.28}\ ^{+0.13}_{-0.10}$	[2] ANDERSON	19	SNO+	Water phase; average flux
$2.57\ ^{+0.17}_{-0.18}\ ^{+0.07}_{-0.07}$	[3] AGOSTINI	18B	BORX	average flux
$2.345 \pm 0.014 \pm 0.036$	[4] ABE	16C	SKAM	SK-I+II+III+IV average flux
$2.308 \pm 0.020\ ^{+0.039}_{-0.040}$	[5] ABE	16C	SKAM	SK-IV average flux
$2.250\ ^{+0.030}_{-0.029} \pm 0.038$	[5] ABE	16C	SKAM	SK-IV day flux
$2.364 \pm 0.029 \pm 0.040$	[5] ABE	16C	SKAM	SK-IV night flux
$2.404 \pm 0.039 \pm 0.053$	[6] ABE	16C	SKAM	SK-III average flux
$2.41 \pm 0.05\ ^{+0.16}_{-0.15}$	[7] ABE	11	SKAM	SK-II average flux
$2.38 \pm 0.02 \pm 0.08$	[8] ABE	11	SKAM	SK-I average flux
$2.77 \pm 0.26 \pm 0.32$	[9] ABE	11B	KLND	average flux
$2.4 \pm 0.4 \pm 0.1$	[10] BELLINI	10A	BORX	average flux
$1.77\ ^{+0.24}_{-0.21}\ ^{+0.09}_{-0.10}$	[11] AHARMIM	08	SNO	Phase III
$2.38 \pm 0.05\ ^{+0.16}_{-0.15}$	[12] CRAVENS	08	SKAM	average flux
$2.35 \pm 0.02 \pm 0.08$	[13] HOSAKA	06	SKAM	average flux
$2.35 \pm 0.22 \pm 0.15$	[14] AHARMIM	05A	SNO	Salty D_2O; ^{8}B shape not constrained
$2.34 \pm 0.23\ ^{+0.15}_{-0.14}$	[14] AHARMIM	05A	SNO	Salty D_2O; ^{8}B shape constrained
$2.39\ ^{+0.24}_{-0.23} \pm 0.12$	[15] AHMAD	02	SNO	average flux
$2.39 \pm 0.34\ ^{+0.16}_{-0.14}$	[16] AHMAD	01	SNO	average flux
$2.80 \pm 0.19 \pm 0.33$	[17] FUKUDA	96	KAMI	average flux
2.70 ± 0.27	[17] FUKUDA	96	KAMI	day flux
$2.87\ ^{+0.27}_{-0.26}$	[17] FUKUDA	96	KAMI	night flux

[1] AGOSTINI 20A obtained this result from the $\nu_e e$ elastic scattering rate over the period between January 2008 and December 2016. Uses the same data as AGOSTINI 18B, but the analysis technique is significantly improved.

[2] ANDERSON 19 reports this result from the $\nu_e e$ elastic scattering rate using a 69.2 kton·day (or 114.7 days) of exposure from May through December, 2017 during the SNO+ detector's water commissioning phase. The events over the reconstructed electron kinetic energy range of 5–15 MeV were analyzed.

[3] AGOSTINI 18B obtained this result from the $\nu_e e$ elastic scattering rate over the period between January 2008 and December 2016.

[4] ABE 16C reports the combined results of the four phases of the Super-Kamiokande average flux measurements. Here the revised Super-Kamiokande-III result is used.

[5] ABE 16C reports the Super-Kamiokande-IV results for 1664 live days from September 2008 to February 2014. The analysis threshold is total electron energy of 4.0 MeV.

[6] ABE 16C revised the Super-Kamiokande-III average flux value reported in ABE 11. Super-Kamiokande-III results are for 548 live days from August 4, 2006 to August 18, 2008. The analysis threshold is 5.0 MeV, but the event sample in the 5.0–6.5 MeV total electron energy range has a total live time of 298 days.

[7] ABE 11 recalculated the Super-Kamiokande-II results using ^{8}B spectrum of WINTER 06A.

[8] ABE 11 recalculated the Super-Kamiokande-I results using ^{8}B spectrum of WINTER 06A.

[9] ABE 11B use a 123 kton·day exposure of the KamLAND liquid scintillation detector to measure the ^{8}B solar neutrino flux. They utilize $\nu - e$ elastic scattering above a reconstructed-energy threshold of 5.5 MeV, corresponding to 5 MeV electron recoil energy. 299 electron recoil candidate events are reported, of which 157 $\pm$ 23.6 are assigned to background.

[10] BELLINI 10A reports the Borexino result with 3 MeV energy threshold for scattered electrons. The data correspond to 345.3 live days with a target mass of 100 t, between July 15, 2007 and August 23, 2009.

[11] AHARMIM 08 reports the results from SNO Phase III measurement using an array of ^{3}He proportional counters to measure the rate of NC interactions in heavy water, over the period between November 27, 2004 and November 28, 2006, corresponding to 385.17 live days. A simultaneous fit was made for the number of NC events detected by the proportional counters and the numbers of NC, CC, and ES events detected by the PMTs, where the spectral distributions of the ES and CC events were not constrained to the ^{8}B shape.

[12] CRAVENS 08 reports the Super-Kamiokande-II results for 791 live days from December 2002 to October 2005. The photocathode coverage of the detector is 19% (reduced from 40% of that of Super-Kamiokande-I due to an accident in 2001). The analysis threshold for the average flux is 7 MeV.

[13] HOSAKA 06 reports the final results for 1496 live days with Super-Kamiokande-I between May 31, 1996 and July 15, 2001, and replace FUKUDA 02 results. The analysis threshold is 5 MeV except for the first 280 live days (6.5 MeV).

[14] AHARMIM 05A measurements were made with dissolved NaCl (0.195% by weight) in heavy water over the period between July 26, 2001 and August 28, 2003, corresponding to 391.4 live days, and update AHMED 04A. The *CC*, *ES*, and *NC* events were statistically separated. In one method, the ^{8}B energy spectrum was not constrained. In the other method, the constraint of an undistorted ^{8}B energy spectrum was added for comparison with AHMAD 02 results.

[15] AHMAD 02 reports the ^{8}B solar-neutrino flux measured via νe elastic scattering above the kinetic energy threshold of 5 MeV. The data correspond to 306.4 live days with SNO between November 2, 1999 and May 28, 2001, and updates AHMAD 01 results.

[16] AHMAD 01 reports the ^{8}B solar-neutrino flux measured via νe elastic scattering above the kinetic energy threshold of 6.75 MeV. The data correspond to 241 live days with SNO between November 2, 1999 and January 15, 2001.

[17] FUKUDA 96 results are for a total of 2079 live days with Kamiokande II and III from January 1987 through February 1995, covering the entire solar cycle 22, with threshold $E_e > 9.3$ MeV (first 449 days), > 7.5 MeV (middle 794 days), and > 7.0 MeV (last 836 days). These results update the HIRATA 90 result for the average ^{8}B solar-neutrino flux and HIRATA 91 result for the day-night variation in the ^{8}B solar-neutrino flux. The total

Downloaded from https://academic.oup.com/ptep/article/2022/8/083C01/6651666 by KIT Library user on 27 September 2022

data sample was also analyzed for short-term variations: within experimental errors, no strong correlation of the solar-neutrino flux with the sunspot numbers was found.

ϕ_{CC} (^{8}B)

^{8}B solar-neutrino flux measured with charged-current reaction which is sensitive exclusively to ν_e.

VALUE (10^6 cm^{-2}s^{-1})	DOCUMENT ID		TECN	COMMENT
• • • We do not use the following data for averages, fits, limits, etc. • • •				
$1.67^{+0.05}_{-0.04}{}^{+0.07}_{-0.08}$	[1] AHARMIM	08	SNO	Phase III
$1.68\pm0.06^{+0.08}_{-0.09}$	[2] AHARMIM	05A	SNO	Salty D_2O; ^{8}B shape not const.
$1.72\pm0.05\pm0.11$	[2] AHARMIM	05A	SNO	Salty D_2O; ^{8}B shape constrained
$1.76^{+0.06}_{-0.05}\pm0.09$	[3] AHMAD	02	SNO	average flux
$1.75\pm0.07^{+0.12}_{-0.11}\pm0.05$	[4] AHMAD	01	SNO	average flux

[1] AHARMIM 08 reports the results from SNO Phase III measurement using an array of ^{3}He proportional counters to measure the rate of NC interactions in heavy water, over the period between November 27, 2004 and November 28, 2006, corresponding to 385.17 live days. A simultaneous fit was made for the number of NC events detected by the proportional counters and the numbers of NC, CC, and ES events detected by the PMTs, where the spectral distributions of the ES and CC events were not constrained to the ^{8}B shape.

[2] AHARMIM 05A measurements were made with dissolved NaCl (0.195% by weight) in heavy water over the period between July 26, 2001 and August 28, 2003, corresponding to 391.4 live days, and update AHMED 04A. The *CC*, *ES*, and *NC* events were statistically separated. In one method, the ^{8}B energy spectrum was not constrained. In the other method, the constraint of an undistorted ^{8}B energy spectrum was added for comparison with AHMAD 02 results.

[3] AHMAD 02 reports the SNO result of the ^{8}B solar-neutrino flux measured with charged-current reaction on deuterium, $\nu_e d \rightarrow pp e^-$, above the kinetic energy threshold of 5 MeV. The data correspond to 306.4 live days with SNO between November 2, 1999 and May 28, 2001, and updates AHMAD 01 results. The complete description of the SNO Phase I data set is given in AHARMIM 07.

[4] AHMAD 01 reports the first SNO result of the ^{8}B solar-neutrino flux measured with the charged-current reaction on deuterium, $\nu_e d \rightarrow pp e^-$, above the kinetic energy threshold of 6.75 MeV. The data correspond to 241 live days with SNO between November 2, 1999 and January 15, 2001.

ϕ_{NC} (^{8}B)

^{8}B solar neutrino flux measured with neutral-current reaction, which is equally sensitive to ν_e, ν_μ, and ν_τ.

VALUE (10^6 cm^{-2}s^{-1})	DOCUMENT ID		TECN	COMMENT
• • • We do not use the following data for averages, fits, limits, etc. • • •				
$5.25\pm0.16^{+0.11}_{-0.13}$	[1] AHARMIM	13	SNO	All three phases combined
$5.140^{+0.160}_{-0.158}{}^{+0.132}_{-0.117}$	[2] AHARMIM	10	SNO	Phase I+II, low threshold
$5.54^{+0.33}_{-0.31}{}^{+0.36}_{-0.34}$	[3] AHARMIM	08	SNO	Phase III, prop. counter + PMT
$4.94\pm0.21^{+0.38}_{-0.34}$	[4] AHARMIM	05A	SNO	Salty D_2O; ^{8}B shape not const.
$4.81\pm0.19^{+0.28}_{-0.27}$	[4] AHARMIM	05A	SNO	Salty D_2O; ^{8}B shape constrained
$5.09^{+0.44}_{-0.43}{}^{+0.46}_{-0.43}$	[5] AHMAD	02	SNO	average flux; ^{8}B shape const.
$6.42\pm1.57^{+0.55}_{-0.58}$	[5] AHMAD	02	SNO	average flux; ^{8}B shape not const.

[1] AHARMIM 13 obtained this result from a combined analysis of the data from all three phases, SNO-I, II, and III. The measurement of the ^{8}B flux mostly comes from the NC signal, however, CC contribution is included in the fit.

[2] AHARMIM 10 reports this result from a joint analysis of SNO Phase I+II data with the "effective electron kinetic energy" threshold of 3.5 MeV. This result is obtained with a "binned-histogram unconstrained fit" where binned probability distribution functions of the neutrino signal observables were used without any model constraints on the shape of the neutrino spectrum.

[3] AHARMIM 08 reports the results from SNO Phase III measurement using an array of ^{3}He proportional counters to measure the rate of NC interactions in heavy water, over the period between November 27, 2004 and November 28, 2006, corresponding to 385.17 live days. A simultaneous fit was made for the number of NC events detected by the proportional counters and the numbers of NC, CC, and ES events detected by the PMTs, where the spectral distributions of the ES and CC events were not constrained to the ^{8}B shape.

[4] AHARMIM 05A measurements were made with dissolved NaCl (0.195% by weight) in heavy water over the period between July 26, 2001 and August 28, 2003, corresponding to 391.4 live days, and update AHMED 04A. The *CC*, *ES*, and *NC* events were statistically separated. In one method, the ^{8}B energy spectrum was not constrained. In the other method, the constraint of an undistorted ^{8}B energy spectrum was added for comparison with AHMAD 02 results.

[5] AHMAD 02 reports the first SNO result of the ^{8}B solar-neutrino flux measured with the neutral-current reaction on deuterium, $\nu_\ell d \rightarrow np\nu_\ell$, above the neutral-current reaction threshold of 2.2 MeV. The data correspond to 306.4 live days with SNO between November 2, 1999 and May 28, 2001. The complete description of the SNO Phase I data set is given in AHARMIM 07.

$\phi_{\nu_\mu+\nu_\tau}$ (^{8}B)

Nonelectron-flavor active neutrino component (ν_μ and ν_τ) in the ^{8}B solar-neutrino flux.

VALUE (10^6 cm^{-2}s^{-1})	DOCUMENT ID		TECN	COMMENT
• • • We do not use the following data for averages, fits, limits, etc. • • •				
$3.26\pm0.25^{+0.40}_{-0.35}$	[1] AHARMIM	05A	SNO	From ϕ_{NC}, ϕ_{CC}, and ϕ_{ES}; ^{8}B shape not const.
$3.09\pm0.22^{+0.30}_{-0.27}$	[1] AHARMIM	05A	SNO	From ϕ_{NC}, ϕ_{CC}, and ϕ_{ES}; ^{8}B shape constrained
$3.41\pm0.45^{+0.48}_{-0.45}$	[2] AHMAD	02	SNO	From ϕ_{NC}, ϕ_{CC}, and ϕ_{ES}
3.69 ± 1.13	[3] AHMAD	01		Derived from SNO+SuperKam, water Cherenkov

[1] AHARMIM 05A measurements were made with dissolved NaCl (0.195% by weight) in heavy water over the period between July 26, 2001 and August 28, 2003, corresponding to 391.4 live days, and update AHMED 04A. The *CC*, *ES*, and *NC* events were statistically separated. In one method, the ^{8}B energy spectrum was not constrained. In the other method, the constraint of an undistorted ^{8}B energy spectrum was added for comparison with AHMAD 02 results.

[2] AHMAD 02 deduced the nonelectron-flavor active neutrino component (ν_μ and ν_τ) in the ^{8}B solar-neutrino flux, by combining the charged-current result, the νe elastic-scattering result and the neutral-current result. The complete description of the SNO Phase I data set is given in AHARMIM 07.

[3] AHMAD 01 deduced the nonelectron-flavor active neutrino component (ν_μ and ν_τ) in the ^{8}B solar-neutrino flux, by combining the SNO charged-current result (AHMAD 01) and the Super-Kamiokande νe elastic-scattering result (FUKUDA 01).

Total Flux of Active *pp* Solar Neutrinos

Total flux of active neutrinos (ν_e,ν_μ,ν_τ).

VALUE (10^{10} cm^{-2}s^{-1})	DOCUMENT ID		TECN	COMMENT
• • • We do not use the following data for averages, fits, limits, etc. • • •				
$6.1\pm0.5^{+0.3}_{-0.5}$	[1] AGOSTINI	18B	BORX	Use $\nu_e e$ scattering rate

[1] AGOSTINI 18B obtained this result from the measured $\nu_e e$ elastic scattering rate over the period between December 2011 and May 2016, assuming the MSW-LMA oscillation parameters derived by ESTEBAN 17. Assuming a high-metalicity standard solar model, the electron neutrino survival probability for the *pp* solar neutrino is calculated to be 0.57 ± 0.09.

Total Flux of Active ^{7}Be Solar Neutrinos

Total flux of active neutrinos (ν_e,ν_μ,ν_τ).

VALUE (10^9 cm^{-2}s^{-1})	DOCUMENT ID		TECN	COMMENT
• • • We do not use the following data for averages, fits, limits, etc. • • •				
$4.99\pm0.11^{+0.06}_{-0.08}$	[1] AGOSTINI	18B	BORX	Use $\nu_e e$ scattering rate

[1] AGOSTINI 18B obtained this result from the measured $\nu_e e$ elastic scattering rate over the period between December 2011 and May 2016, assuming the MSW-LMA oscillation parameters derived by ESTEBAN 17. Assuming a high-metalicity standard solar model, the electron neutrino survival probability for the ^{7}Be solar neutrino is calculated to be 0.53 ± 0.05.

Total Flux of Active *pep* Solar Neutrinos

Total flux of active neutrinos (ν_e,ν_μ,ν_τ).

VALUE (10^8 cm^{-2}s^{-1})	DOCUMENT ID		TECN	COMMENT
• • • We do not use the following data for averages, fits, limits, etc. • • •				
$1.27\pm0.19^{+0.08}_{-0.12}$	[1] AGOSTINI	18B	BORX	Use $\nu_e e$ scattering rate

[1] AGOSTINI 18B obtained this result from the measured $\nu_e e$ elastic scattering rate over the period between December 2011 and May 2016, assuming the MSW-LMA oscillation parameters derived by ESTEBAN 17 and a high-metalicity standard solar model. The electron neutrino survival probability for the pep solar neutrino is calculated to be 0.43 ± 0.11.

Total Flux of Active ^{8}B Solar Neutrinos

Total flux of active neutrinos (ν_e, ν_μ, and ν_τ).

VALUE (10^6 cm^{-2}s^{-1})	DOCUMENT ID		TECN	COMMENT
• • • We do not use the following data for averages, fits, limits, etc. • • •				
$5.95^{+0.75}_{-0.71}{}^{+0.28}_{-0.30}$	[1] ANDERSON	19	SNO+	Water phase; $\nu_e e$ scattering rate
$5.68^{+0.39}_{-0.41}{}^{+0.03}_{-0.03}$	[2] AGOSTINI	18B	BORX	From $\nu_e e$ scattering rate
$5.25\pm0.16^{+0.11}_{-0.13}$	[3] AHARMIM	13	SNO	All three phases combined
$5.046^{+0.159}_{-0.152}{}^{+0.107}_{-0.123}$	[4] AHARMIM	10	SNO	From ϕ_{NC} in Phase I+II, low threshold
$5.54^{+0.33}_{-0.31}{}^{+0.36}_{-0.34}$	[5] AHARMIM	08	SNO	ϕ_{NC} in Phase III

Downloaded from https://academic.oup.com/ptep/article/2022/8/083C01/6651666 by KIT Library user on 27 September 2022

$4.94 \pm 0.21 {}^{+0.38}_{-0.34}$	[6] AHARMIM	05A	SNO	From ϕ_{NC}; ^{8}B shape not const.
$4.81 \pm 0.19 {}^{+0.28}_{-0.27}$	[6] AHARMIM	05A	SNO	From ϕ_{NC}; ^{8}B shape constrained
$5.09 {}^{+0.44}_{-0.43} {}^{+0.46}_{-0.43}$	[7] AHMAD	02	SNO	Direct measurement from ϕ_{NC}
5.44 ± 0.99	[8] AHMAD	01		Derived from SNO+SuperKam, water Cherenkov

[1] ANDERSON 19 reports this result from the measured $\nu_e e$ elastic scattering rate using a 69.2 kton·day (or 114.7 days) of exposure from May through December, 2017 during the SNO+ detector's water commissioning phase, assuming the neutrino mixing parameters given in PDG 16 and a standard solar model given in BAHCALL 05.

[2] AGOSTINI 18B obtained this result from the measured $\nu_e e$ elastic scattering rate over the period between January 2008 and December 2016, assuming the MSW-LMA oscillation parameters derived by ESTEBAN 17. Assuming a high-metalicity standard solar model, the electron neutrino survival probability for the ^{8}B solar neutrino is calculated to be 0.37 ± 0.08.

[3] AHARMIM 13 obtained this result from a combined analysis of the data from all three phases, SNO-I, II, and III. The measurement of the ^{8}B flux mostly comes from the NC signal, however, CC contribution is included in the fit.

[4] AHARMIM 10 reports this result from a joint analysis of SNO Phase I+II data with the "effective electron kinetic energy" threshold of 3.5 MeV. This result is obtained with the assumption of unitarity, which relates the NC, CC, and ES rates. The data were fit with the free parameters directly describing the total ^{8}B neutrino flux and the energy-dependent ν_e survival probability.

[5] AHARMIM 08 reports the results from SNO Phase III measurement using an array of ^{3}He proportional counters to measure the rate of NC interactions in heavy water, over the period between November 27, 2004 and November 28, 2006, corresponding to 385.17 live days. A simultaneous fit was made for the number of NC events detected by the proportional counters and the numbers of NC, CC, and ES events detected by the PMTs, where the spectral distributions of the ES and CC events were not constrained to the ^{8}B shape.

[6] AHARMIM 05A measurements were made with dissolved NaCl (0.195% by weight) in heavy water over the period between July 26, 2001 and August 28, 2003, corresponding to 391.4 live days, and update AHMED 04A. The CC, ES, and NC events were statistically separated. In one method, the ^{8}B energy spectrum was not constrained. In the other method, the constraint of an undistorted ^{8}B energy spectrum was added for comparison with AHMAD 02 results.

[7] AHMAD 02 determined the total flux of active ^{8}B solar neutrinos by directly measuring the neutral-current reaction, $\nu_\ell d \rightarrow n p \nu_\ell$, which is equally sensitive to ν_e, ν_μ, and ν_τ. The complete description of the SNO Phase I data set is given in AHARMIM 07.

[8] AHMAD 01 deduced the total flux of active ^{8}B solar neutrinos by combining the SNO charged-current result (AHMAD 01) and the Super-Kamiokande νe elastic-scattering result (FUKUDA 01).

Total Flux of Active CNO Solar Neutrinos

Total flux of active neutrinos (ν_e,ν_μ,ν_τ).

VALUE (10^8 cm^{-2} s^{-1})	CL%	DOCUMENT ID		TECN	COMMENT
• • • We do not use the following data for averages, fits, limits, etc. • • •					
<7.9	95	[1] AGOSTINI	18B	BORX	Use $\nu_e e$ scattering rate

[1] AGOSTINI 18B obtained this result from an upper limit of the $\nu_e e$ elastic scattering rate for the CNO neutrinos over the period between December 2011 and May 2016, assuming the MSW-LMA oscillation parameters derived by ESTEBAN 17.

Total Flux of Active hep Solar Neutrinos

Total flux of active neutrinos (ν_e,ν_μ,ν_τ).

VALUE (10^5 cm^{-2}s^{-1})	CL%	DOCUMENT ID		TECN	COMMENT
• • • We do not use the following data for averages, fits, limits, etc. • • •					
<1.8	90	[1] AGOSTINI	20A	BORX	Use $\nu_e e$ scattering and ^{12}C(ν,ν')^{12}C*
<0.3	90	[2] AHARMIM	20	SNO	CC, NC, $\nu_e e$ scattering
<2.2	90	[3] AGOSTINI	18B	BORX	Use $\nu_e e$ scattering rate

[1] AGOSTINI 20A obtained this result from an upper limit of the $\nu_e e$ elastic scattering rate and NC-mediated inelastic scattering on carbon nuclei with 15.1 MeV deexcitation γ-ray for the hep neutrino. The dataset corresponds to an effective exposure of 0.745 kt·yr from November 2009 to October 2017. A FADC DAQ system, optimized for the acquisition of high-energy events was used for data collection. The MSW-LMA oscillation parameters derived by ESTEBAN 17 were assumed.

[2] AHARMIM 20 uses the entire SNO dataset, corresponding to 2.47 kton·yrs of exposure after fiducialization. With the D_2O target, SNO was sensitive to charged current, neutral current, and elastic scattering channels.

[3] AGOSTINI 18B obtained this result from an upper limit of the $\nu_e e$ elastic scattering rate for the hep neutrino using the dataset corresponding to an exposure of 0.8 kt·yr and assuming the MSW-LMA oscillation parameters derived by ESTEBAN 17.

Day-Night Asymmetry (^{8}B)

$A = (\phi_{\rm night} - \phi_{\rm day}) / \phi_{\rm average}$

VALUE	DOCUMENT ID		TECN	COMMENT
$0.033 \pm 0.010 \pm 0.005$	[1] ABE	16C	SKAM	SK combined; Based on ϕ_{ES}
• • • We do not use the following data for averages, fits, limits, etc. • • •				
$0.036 \pm 0.016 \pm 0.006$	[2] ABE	16C	SKAM	SK-IV; Based on ϕ_{ES}
$0.032 \pm 0.011 \pm 0.005$	[3] RENSHAW	14	SKAM	Based on ϕ_{ES}
$0.063 \pm 0.042 \pm 0.037$	[4] CRAVENS	08	SKAM	Based on ϕ_{ES}
$0.021 \pm 0.020 {}^{+0.012}_{-0.013}$	[5] HOSAKA	06	SKAM	Based on ϕ_{ES}
$0.017 \pm 0.016 {}^{+0.012}_{-0.013}$	[6] HOSAKA	06	SKAM	Fitted in the LMA region
$-0.056 \pm 0.074 \pm 0.053$	[7] AHARMIM	05A	SNO	From salty SNO ϕ_{CC}
$-0.037 \pm 0.063 \pm 0.032$	[7] AHARMIM	05A	SNO	From salty SNO ϕ_{CC}; const. of no ϕ_{NC} asymmetry
$0.14 \pm 0.063 {}^{+0.015}_{-0.014}$	[8] AHMAD	02B	SNO	Derived from SNO ϕ_{CC}
$0.07 \pm 0.049 {}^{+0.013}_{-0.012}$	[9] AHMAD	02B	SNO	Const. of no ϕ_{NC} asymmetry

[1] ABE 16C reports the combined day-night flux asymmetry results of the four phases of the Super-Kamiokande measurements. Amplitude fit method is used. See footnote to RENSHAW 14.

[2] ABE 16C reports the Super-Kamiokande-IV results for 1664 live days from September 2008 to February 2014. The analysis threshold for day-night flux asymmetry is recoil electron energy of 4.49 MeV (total electron energy of 5.0 MeV). Amplitude fit method is used. See footnote to RENSHAW 14.

[3] RENSHAW 14 obtains this result by using the "amplitude fit" introduced in SMY 04. The data from the Super-Kamiokande(SK)-I, -II, -III, and 1306 live days of the SK-IV measurements are used. The analysis threshold is recoil-electron kinetic energy of 4.5 MeV for SK-III, and SK-IV except for 250 live days in SK-III (6.0 MeV). The analysis threshold for SK-I and SK-II is the same as in the previous reports. (Note that in the previous SK solar-neutrino results, the analysis threshold is quoted as recoil-electron total energy.) This day-night asymmetry result is consistent with neutrino oscillations for 4×10^{-5} eV^2 $< \Delta m^2_{21} < 7 \times 10^{-5}$ eV^2 and large mixing values of θ_{12} at the 68% CL.

[4] CRAVENS 08 reports the Super-Kamiokande-II results for 791 live days from December 2002 to October 2005. The photocathode coverage of the detector is 19% (reduced from 40% of that of Super-Kamiokande-I due to an accident in 2001). The analysis threshold for the day and night fluxes is 7.5 MeV except for the first 159 live days (8.0 MeV).

[5] HOSAKA 06 reports the final results for 1496 live days with Super-Kamiokande-I between May 31, 1996 and July 15, 2001, and replace FUKUDA 02 results. The analysis threshold is 5 MeV except for the first 280 live days (6.5 MeV).

[6] This result with reduced statistical uncertainty is obtained by assuming two-neutrino oscillations within the LMA (large mixing angle) region and by fitting the time variation of the solar neutrino flux measured via ν_e elastic scattering to the variations expected from neutrino oscillations. For details, see SMY 04. There is an additional small systematic error of ± 0.0004 coming from uncertainty of oscillation parameters.

[7] AHARMIM 05A measurements were made with dissolved NaCl (0.195% by weight) in heavy water over the period between July 26, 2001 and August 28, 2003, with 176.5 days of the live time recorded during the day and 214.9 days during the night. This result is obtained with the spectral distribution of the CC events not constrained to the ^{8}B shape.

[8] AHMAD 02B results are based on the charged-current interactions recorded between November 2, 1999 and May 28, 2001, with the day and night live times of 128.5 and 177.9 days, respectively. The complete description of the SNO Phase I data set is given in AHARMIM 07.

[9] AHMAD 02B results are derived from the charged-current interactions, neutral-current interactions, and νe elastic scattering, with the total flux of active neutrinos constrained to have no asymmetry. The data were recorded between November 2, 1999 and May 28, 2001, with the day and night live times of 128.5 and 177.9 days, respectively. The complete description of the SNO Phase I data set is given in AHARMIM 07.

ϕ_{ES} (^{7}Be)

^{7}Be solar-neutrino flux measured via ν_e elastic scattering. This process is sensitive to all active neutrino flavors, but with reduced sensitivity to ν_μ, ν_τ due to the cross-section difference, $\sigma(\nu_{\mu,\tau} e) \sim 0.2\ \sigma(\nu_e e)$. If the ^{7}Be solar-neutrino flux involves nonelectron flavor active neutrinos, their contribution to the flux is ~ 0.2 times that of ν_e.

VALUE (10^9 cm^{-2} s^{-1})	DOCUMENT ID		TECN	COMMENT
• • • We do not use the following data for averages, fits, limits, etc. • • •				
3.26 ± 0.52	[1] GANDO	15	KLND	average flux
3.10 ± 0.15	[2] BELLINI	11A	BORX	average flux

[1] GANDO 15 uses 165.4 kton·day exposure of the KamLAND liquid scintillator detector to measure the 862 keV ^{7}Be solar neutrino flux via $\nu - e$ elastic scattering

[2] BELLINI 11A reports the ^{7}Be solar neutrino flux measured via $\nu - e$ elastic scattering. The data correspond to 740.7 live days between May 16, 2007 and May 8, 2010, and also correspond to 153.6 ton-year fiducial exposure. BELLINI 11A measured the 862 keV ^{7}Be solar neutrino flux, which is an 89.6% branch of the ^{7}Be solar neutrino flux, to be $(2.78 \pm 0.13) \times 10^9$ cm^{-2}s^{-1}. Supercedes ARPESELLA 08A.

ϕ_{ES} (pep)

pep solar-neutrino flux measured via ν_e elastic scattering. This process is sensitive to all active neutrino flavors, but with reduced sensitivity to ν_μ, ν_τ due to the cross section difference, $\sigma(\nu_{\mu,\tau}\ e) \sim 0.2\ \sigma(\nu_e e)$. If the pep solar-neutrino flux involves non-electron flavor active neutrinos, their contribution to the flux is ~ 0.2 times that of ν_e.

VALUE (10^8 cm^{-2}s^{-1})	DOCUMENT ID		TECN	COMMENT
• • • We do not use the following data for averages, fits, limits, etc. • • •				
1.0 ± 0.2	[1] BELLINI	12A	BORX	average flux

[1] BELLINI 12A reports 1.44 MeV pep solar-neutrino flux measured via ν_e elastic scattering. The data were collected between January 13, 2008 and May 9, 2010, corresponding to 20,4009 ton·day fiducial exposure. The listed flux value is calculated from the observed

Downloaded from https://academic.oup.com/ptep/article/2022/8/083C01/6651666 by KIT Library user on 27 September 2022

rate of pep solar neutrino interactions in Borexino ($3.1 \pm 0.6 \pm 0.3$ counts/(day·100 ton)) and the corresponding rate expected for no neutrino flavor oscillations (4.47 ± 0.05 counts/(day·100 ton)), using the SSM prediction for the pep solar neutrino flux of $(1.441 \pm 0.012) \times 10^8$ cm^{-2}s^{-1}.

ϕ_{ES} (CNO)

CNO solar-neutrino flux measured via ν_e elastic scattering. This process is sensitive to all active neutrino flavors, but with reduced sensitivity to ν_μ, ν_τ due to the cross section difference, $\sigma(\nu_{\mu,\tau}\, e) \sim 0.2\, \sigma(\nu_e\, e)$. If the CNO solar-neutrino flux involves non-electron flavor active neutrinos, their contribution to the flux is $\sim$ 0.2 times that of ν_e.

VALUE (10^8 cm^{-2}s^{-1})	CL%	DOCUMENT ID		TECN	COMMENT
• • • We do not use the following data for averages, fits, limits, etc. • • •					
<7.7	90	[1] BELLINI	12A	BORX	MSW-LMA solution assumed

[1] BELLINI 12A reports an upper limit of the CNO solar neutrino flux measured via ν_e elastic scattering. The data were collected between January 13, 2008 and May 9, 2010, corresponding to 20,409 ton·day fiducial exposure.

$\phi_{ES}(pp)$

pp solar-neutrino flux measured via νe elastic scattering. This process is sensitive to all active neutrino flavors, but with reduced sensitivity to ν_μ, ν_τ due to the cross section difference, $\sigma(\nu_{\mu,\tau}\, e) \sim 0.3\, \sigma(\nu_e\, e)$. If the pp solar-neutrino flux involves nonelectron flavor active neutrinos, their contribution to the flux is $\sim$ 0.3 times of ν_e.

VALUE (10^{10} cm^{-2} s^{-1})	DOCUMENT ID		TECN	COMMENT
• • • We do not use the following data for averages, fits, limits, etc. • • •				
4.4 ± 0.5	[1] BELLINI	14A	BORX	average flux

[1] BELLINI 14A reports pp solar-neutrino flux measured via νe elastic scattering. The data were collected between January 2012 and May 2013, corresponding to 408 days of data. The pp neutrino interaction rate in Borexino is measured to be $144 \pm 13 \pm 10$ counts/(day·100 ton) by fitting the measured energy spectrum of events in the 165–590 keV recoil electron kinetic energy window with the expected signal + background spectrum. The listed flux value $\phi_{ES}(pp)$ is calculated from the observed rate and the number of $(3.307 \pm 0.003) \times 10^{31}$ electrons for 100 tons of the Borexino scintillator, and the $\nu_e e$ integrated cross section over the pp neutrino spectrum, $\sigma(\nu_e e) = 11.38 \times 10^{-46}$ cm^2.

$\phi_{CC}(pp)$

pp solar-neutrino flux measured with charged-current reaction which is sensitive exclusively to ν_e.

VALUE (10^{10} cm^{-2} s^{-1})	DOCUMENT ID		TECN	COMMENT
• • • We do not use the following data for averages, fits, limits, etc. • • •				
3.38 ± 0.47	[1] ABDURASHI...	09	FIT	Fit existing solar-ν data

[1] ABDURASHITOV 09 reports the pp solar-neutrino flux derived from the Ga solar neutrino capture rate by subtracting contributions from ^{8}B, ^{7}Be, pep and CNO solar neutrino fluxes determined by other solar neutrino experiments as well as neutrino oscillation parameters determined from available world neutrino oscillation data.

ϕ_{ES} (hep)

hep solar-neutrino flux measured via νe elastic scattering. This process is sensitive to all active neutrino flavors, but with reduced sensitivity to ν_μ, ν_τ due to the cross-section difference, $\sigma(\nu_{\mu,\tau}\, e) \sim 0.16\sigma(\nu_e\, e)$. If the hep solar-neutrino flux involves nonelectron flavor active neutrinos, their contribution to the flux is $\sim$ 0.16 times of ν_e.

VALUE (10^3 cm^{-2}s^{-1})	CL%	DOCUMENT ID		TECN
• • • We do not use the following data for averages, fits, limits, etc. • • •				
<73	90	[1] HOSAKA	06	SKAM

[1] HOSAKA 06 result is obtained from the recoil electron energy window of 18–21 MeV, and updates FUKUDA 01 result.

$\phi_{\overline{\nu}_e}$ (^{8}B)

Searches are made for electron antineutrino flux from the Sun. Flux limits listed here are derived relative to the BS05(OP) Standard Solar Model ^{8}B solar neutrino flux (5.69×10^6 cm^{-2} s^{-1}), with an assumption that solar $\overline{\nu}_e$s follow an unoscillated ^{8}B neutrino spectrum.

VALUE (%)	CL%	DOCUMENT ID		TECN	COMMENT
• • • We do not use the following data for averages, fits, limits, etc. • • •					
<0.0072	90	[1] AGOSTINI	21	BORX	$E_{\overline{\nu}_e} > 1.8$ MeV
<0.013	90	[2] BELLINI	11	BORX	$E_{\overline{\nu}_e} > 1.8$ MeV
<1.9	90	[3] BALATA	06	CNTR	$1.8 < E_{\overline{\nu}_e} < 20.0$ MeV
<0.72	90	AHARMIM	04	SNO	$4.0 < E_{\overline{\nu}_e} < 14.8$ MeV
<0.022	90	EGUCHI	04	KLND	$8.3 < E_{\overline{\nu}_e} < 14.8$ MeV
<0.7	90	GANDO	03	SKAM	$8.0 < E_{\overline{\nu}_e} < 20.0$ MeV
<1.7	90	AGLIETTA	96	LSD	$7 < E_{\overline{\nu}_e} < 17$ MeV

[1] AGOSTINI 21 derived this result relative to the Standard Solar Model ^{8}B solar neutrino flux, under an assumption of high solar metallicity, of $5.46\ (1 \pm 0.12) \times 10^6$ cm^{-2}s^{-1} (see VINYOLES 17).
[2] Superseded by AGOSTINI 21.
[3] BALATA 06 obtained this result from the search for $\overline{\nu}_e$ interactions with Counting Test Facility (the prototype of the Borexino detector).

(B) Three-neutrino mixing parameters

$\sin^2(\theta_{12})$

If an experiment reports $\sin^2(2\,\theta_{12})$ we convert the value to $\sin^2(\,\theta_{12})$.

VALUE	DOCUMENT ID		TECN	COMMENT
$\mathbf{0.307^{+0.013}_{-0.012}}$	[1] ABE	16C	FIT	KamLAND+global solar; 3ν
• • • We do not use the following data for averages, fits, limits, etc. • • •				
0.318 ± 0.016	[2] SALAS	21	FIT	global fit
0.304 ± 0.012	[3] ESTEBAN	20A	FIT	Global fit
$0.320^{+0.020}_{-0.016}$	DE-SALAS	18	FIT	Global fit
0.310 ± 0.014	[4] ABE	16C	FIT	SKAM+SNO; 3ν
$0.334^{+0.027}_{-0.023}$	[5] ABE	16C	FIT	SK-I+II+III+IV; 3ν
$0.327^{+0.026}_{-0.031}$	[6] ABE	16C	FIT	SK-IV; 3ν
0.323 ± 0.016	[7] FORERO	14	FIT	3ν
$0.304^{+0.013}_{-0.012}$	[8] GONZALEZ...	14	FIT	Either mass ordering; global fit
$0.299^{+0.014}_{-0.014}$	[9,10] AHARMIM	13	FIT	global solar: 2ν
$0.307^{+0.016}_{-0.013}$	[10,11] AHARMIM	13	FIT	global solar: 3ν
$0.304^{+0.022}_{-0.018}$	[10,12] AHARMIM	13	FIT	KamLAND + global solar: 3ν
$0.304^{+0.014}_{-0.013}$	[13] GANDO	13	FIT	KamLAND + global solar + SBL + accelerator: 3ν
$0.304^{+0.014}_{-0.013}$	[14] GANDO	13	FIT	KamLAND + global solar: 3ν
$0.325^{+0.039}_{-0.039}$	[15] GANDO	13	FIT	KamLAND: 3ν
$0.30^{+0.02}_{-0.01}$	[16] ABE	11	FIT	KamLAND + global solar: 2ν
$0.30^{+0.02}_{-0.01}$	[17] ABE	11	FIT	global solar: 2ν
$0.31^{+0.03}_{-0.02}$	[18] ABE	11	FIT	KamLAND + global solar: 3ν
$0.31^{+0.03}_{-0.03}$	[19] ABE	11	FIT	global solar: 3ν
$0.314^{+0.015}_{-0.012}$	[20] BELLINI	11A	FIT	KamLAND + global solar: 2ν
$0.319^{+0.017}_{-0.015}$	[21] BELLINI	11A	FIT	global solar: 2ν
$0.311^{+0.016}_{-0.016}$	[22] GANDO	11	FIT	KamLAND + solar: 3ν
$0.304^{+0.046}_{-0.042}$	[23] GANDO	11	FIT	KamLAND: 3ν
$0.314^{+0.018}_{-0.014}$	[24,25] AHARMIM	10	FIT	KamLAND + global solar: 2ν
$0.314^{+0.017}_{-0.020}$	[24,26] AHARMIM	10	FIT	global solar: 2ν
$0.319^{+0.019}_{-0.016}$	[24,27] AHARMIM	10	FIT	KamLAND + global solar: 3ν
$0.319^{+0.023}_{-0.024}$	[24,28] AHARMIM	10	FIT	global solar: 3ν
$0.36^{+0.05}_{-0.04}$	[29] ABE	08A	FIT	KamLAND
0.32 ± 0.03	[30] ABE	08A	FIT	KamLAND + global fit
0.32 ± 0.02	[31] AHARMIM	08	FIT	KamLAND + global solar
$0.31^{+0.04}_{-0.04}$	[32] HOSAKA	06	FIT	KamLAND + global solar
$0.31^{+0.04}_{-0.03}$	[33] HOSAKA	06	FIT	SKAM+SNO+KamLAND
$0.31^{+0.03}_{-0.04}$	[34] HOSAKA	06	FIT	SKAM+SNO
$0.31^{+0.02}_{-0.03}$	[35] AHARMIM	05A	FIT	KamLAND + global solar
0.25–0.39	[36] AHARMIM	05A	FIT	global solar
0.29 ± 0.03	[37] ARAKI	05	FIT	KamLAND + global solar
$0.29^{+0.03}_{-0.02}$	[38] AHMED	04A	FIT	KamLAND + global solar
0.23–0.37	[39] AHMED	04A	FIT	global solar
$0.31^{+0.04}_{-0.04}$	[40] SMY	04	FIT	KamLAND + global solar
$0.29^{+0.04}_{-0.04}$	[41] SMY	04	FIT	global solar
$0.32^{+0.06}_{-0.05}$	[42] SMY	04	FIT	SKAM + SNO
0.19–0.33	[43] AHMAD	02B	FIT	global solar
0.19–0.39	[44] FUKUDA	02	FIT	global solar

[1] ABE 16C obtained this result by a three-neutrino oscillation analysis, with a constraint of $\sin^2(\theta_{13}) = 0.0219 \pm 0.0014$ coming from reactor neutrino experiments, using all solar data and KamLAND data. CPT invariance is assumed.
[2] SALAS 21 reports results of a global fit to neutrino oscillation data available at the time of the Neutrino 2020 conference.
[3] ESTEBAN 20A reports results of a global fit to neutrino oscillation data available at the time of the Neutrino2020 conference.

Downloaded from https://academic.oup.com/ptep/article/2022/8/083C01/6651666 by KIT Library user on 27 September 2022

[4] ABE 16C obtained this result by a three-neutrino oscillation analysis, with a constraint of $\sin^2(\theta_{13}) = 0.0219 \pm 0.0014$ coming from reactor neutrino experiments, using Super-Kamiokande (I+II+III+IV) and SNO data.

[5] ABE 16C obtained this result by a three-neutrino oscillation analysis, with a constraint of $\sin^2(\theta_{13}) = 0.0219 \pm 0.0014$ coming from reactor neutrino experiments, by combining the four phases of the Super-Kamiokande solar data.

[6] ABE 16C obtained this result by a three-neutrino oscillation analysis, with a constraint of $\sin^2(\theta_{13}) = 0.0219 \pm 0.0014$ coming from reactor neutrino experiments, using the Super-Kamiokande-IV data.

[7] FORERO 14 performs a global fit to neutrino oscillations using solar, reactor, long-baseline accelerator, and atmospheric neutrino data.

[8] GONZALEZ-GARCIA 14 result comes from a frequentist global fit. The corresponding Bayesian global fit to the same data results are reported in BERGSTROM 15 as $0.304^{+0.013}_{-0.012}$ for normal and $0.305^{+0.012}_{-0.013}$ for inverted mass ordering.

[9] AHARMIM 13 obtained this result by a two-neutrino oscillation analysis using global solar neutrino data.

[10] AHARMIM 13 global solar neutrino data include SNO's all-phases-combined analysis results on the total active ^{8}B neutrino flux and energy-dependent ν_e survival probability parameters, measurements of Cl (CLEVELAND 98), Ga (ABDURASHITOV 09 which contains combined analysis with GNO (ALTMANN 05 and Ph.D. thesis of F. Kaether)), and ^{7}Be (BELLINI 11A) rates, and ^{8}B solar-neutrino recoil electron measurements of SK-I (HOSAKA 06) zenith, SK-II (CRAVENS 08) and SK-III (ABE 11) day/night spectra, and Borexino (BELLINI 10A) spectra.

[11] AHARMIM 13 obtained this result by a three-neutrino oscillation analysis with the value of Δm^2_{32} fixed to 2.45×10^{-3} eV^2, using global solar neutrino data.

[12] AHARMIM 13 obtained this result by a three-neutrino oscillation analysis with the value of Δm^2_{32} fixed to 2.45×10^{-3} eV^2, using global solar neutrino and KamLAND (GANDO 11) data. CPT invariance is assumed.

[13] GANDO 13 obtained this result by a three-neutrino oscillation analysis using KamLAND, global solar neutrino, short-baseline (SBL) reactor, and accelerator data, assuming *CPT* invariance. Supersedes GANDO 11.

[14] GANDO 13 obtained this result by a three-neutrino oscillation analysis using KamLAND and global solar neutrino data, assuming CPT invariance. Supersedes GANDO 11.

[15] GANDO 13 obtained this result by a three-neutrino oscillation analysis using KamLAND data. Supersedes GANDO 11.

[16] ABE 11 obtained this result by a two-neutrino oscillation analysis using solar neutrino data including Super-Kamiokande, SNO, Borexino (ARPESELLA 08A), Homestake, GALLEX/GNO, SAGE, and KamLAND data. CPT invariance is assumed.

[17] ABE 11 obtained this result by a two-neutrino oscillation analysis using solar neutrino data including Super-Kamiokande, SNO, Borexino (ARPESELLA 08A), Homestake, GALLEX/GNO, and SAGE data.

[18] ABE 11 obtained this result by a three-neutrino oscillation analysis with the value of Δm^2_{32} fixed to 2.4×10^{-3} eV^2, using solar neutrino data including Super-Kamiokande, SNO, Borexino (ARPESELLA 08A), Homestake, GALLEX/GNO, SAGE, and KamLAND data. The normal neutrino mass ordering and CPT invariance are assumed.

[19] ABE 11 obtained this result by a three-neutrino oscillation analysis with the value of Δm^2_{32} fixed to 2.4×10^{-3} eV^2, using solar neutrino data including Super-Kamiokande, SNO, Borexino (ARPESELLA 08A), Homestake, and GALLEX/GNO data. The normal neutrino mass ordering is assumed.

[20] BELLINI 11A obtained this result by a two-neutrino oscillation analysis using KamLAND, Homestake, SAGE, Gallex, GNO, Kamiokande, Super-Kamiokande, SNO, and Borexino (BELLINI 11A) data and the SSM flux prediction in SERENELLI 11 (Astrophysical Journal **743** 24 (2011)) with the exception that the ^{8}B flux was left free. CPT invariance is assumed.

[21] BELLINI 11A obtained this result by a two-neutrino oscillation analysis using Homestake, SAGE, Gallex, GNO, Kamiokande, Super-Kamiokande, SNO, and Borexino (BELLINI 11A) data and the SSM flux prediction in SERENELLI 11 (Astrophysical Journal **743** 24 (2011)) with the exception that the ^{8}B flux was left free.

[22] GANDO 11 obtain this result with three-neutrino fit using the KamLAND + solar data. Superseded by GANDO 13.

[23] GANDO 11 obtain this result with three-neutrino fit using the KamLAND data only. Superseded by GANDO 13.

[24] AHARMIM 10 global solar neutrino data include SNO's low-energy-threshold analysis survival probability day/night curves, SNO Phase III integral rates (AHARMIM 08), Cl (CLEVELAND 98), SAGE (ABDURASHITOV 09), Gallex/GNO (HAMPEL 99, ALTMANN 05), Borexino (ARPESELLA 08A), SK-I zenith (HOSAKA 06), and SK-II day/night spectra (CRAVENS 08).

[25] AHARMIM 10 obtained this result by a two-neutrino oscillation analysis using global solar neutrino data and KamLAND data (ABE 08A). *CPT* invariance is assumed.

[26] AHARMIM 10 obtained this result by a two-neutrino oscillation analysis using global solar neutrino data.

[27] AHARMIM 10 obtained this result by a three-neutrino oscillation analysis with the value of Δm^2_{31} fixed to 2.3×10^{-3} eV^2, using global solar neutrino data and KamLAND data (ABE 08A). *CPT* invariance is assumed.

[28] AHARMIM 10 obtained this result by a three-neutrino oscillation analysis with the value of Δm^2_{31} fixed to 2.3×10^{-3} eV^2, using global solar neutrino data.

[29] ABE 08A obtained this result by a rate + shape + time combined geoneutrino and reactor two-neutrino fit for Δm^2_{21} and $\tan^2\theta_{12}$, using KamLAND data only. Superseded by GANDO 11.

[30] ABE 08A obtained this result by means of a two-neutrino fit using KamLAND, Homestake, SAGE, GALLEX, GNO, SK (zenith angle and E-spectrum), the SNO χ^2-map, and solar flux data. *CPT* invariance is assumed. Superseded by GANDO 11.

[31] The result given by AHARMIM 08 is $\theta = (34.4^{+1.3}_{-1.2})^\circ$. This result is obtained by a two-neutrino oscillation analysis using solar neutrino data including those of Borexino (ARPESELLA 08A) and Super-Kamiokande-I (HOSAKA 06), and KamLAND data (ABE 08A). *CPT* invariance is assumed.

[32] HOSAKA 06 obtained this result by a two-neutrino oscillation analysis using SK ν_e data, CC data from other solar neutrino experiments, and KamLAND data (ARAKI 05). *CPT* invariance is assumed.

[33] HOSAKA 06 obtained this result by a two-neutrino oscillation analysis using the data from Super-Kamiokande, SNO (AHMAD 02 and AHMAD 02B), and KamLAND (ARAKI 05) experiments. *CPT* invariance is assumed.

[34] HOSAKA 06 obtained this result by a two-neutrino oscillation analysis using the Super-Kamiokande and SNO (AHMAD 02 and AHMAD 02B) solar neutrino data.

[35] The result given by AHARMIM 05A is $\theta = (33.9 \pm 1.6)^\circ$. This result is obtained by a two-neutrino oscillation analysis using SNO pure deuteron and salt phase data, SK ν_e data, Cl and Ga CC data, and KamLAND data (ARAKI 05). *CPT* invariance is assumed. AHARMIM 05A also quotes $\theta = (33.9^{+2.4}_{-2.2})^\circ$ as the error enveloping the 68% CL two-dimensional region. This translates into $\sin^2 2\,\theta = 0.86^{+0.05}_{-0.06}$.

[36] AHARMIM 05A obtained this result by a two-neutrino oscillation analysis using the data from all solar neutrino experiments. The listed range of the parameter envelops the 95% CL two-dimensional region shown in figure 35a of AHARMIM 05A. AHARMIM 05A also quotes $\tan^2\theta = 0.45^{+0.09}_{-0.08}$ as the error enveloping the 68% CL two-dimensional region. This translates into $\sin^2 2\,\theta = 0.86^{+0.05}_{-0.07}$.

[37] ARAKI 05 obtained this result by a two-neutrino oscillation analysis using KamLAND and solar neutrino data. *CPT* invariance is assumed. The 1σ error shown here is translated from the number provided by the KamLAND collaboration, $\tan^2\theta = 0.40^{+0.07}_{-0.05}$. The corresponding number quoted in ARAKI 05 is $\tan^2\theta = 0.40^{+0.10}_{-0.07}$ ($\sin^2 2\,\theta = 0.82 \pm 0.07$), which envelops the 68% CL two-dimensional region.

[38] The result given by AHMED 04A is $\theta = (32.5^{+1.7}_{-1.6})^\circ$. This result is obtained by a two-neutrino oscillation analysis using solar neutrino and KamLAND data (EGUCHI 03). *CPT* invariance is assumed. AHMED 04A also quotes $\theta = (32.5^{+2.4}_{-2.3})^\circ$ as the error enveloping the 68% CL two-dimensional region. This translates into $\sin^2 2\,\theta = 0.82 \pm 0.06$.

[39] AHMED 04A obtained this result by a two-neutrino oscillation analysis using the data from all solar neutrino experiments. The listed range of the parameter envelops the 95% CL two-dimensional region shown in Fig. 5(a) of AHMED 04A. The best-fit point is $\Delta(m^2) = 6.5 \times 10^{-5}$ eV^2, $\tan^2\theta = 0.40$ ($\sin^2 2\,\theta = 0.82$).

[40] The result given by SMY 04 is $\tan^2\theta = 0.44 \pm 0.08$. This result is obtained by a two-neutrino oscillation analysis using solar neutrino and KamLAND data (IANNI 03). *CPT* invariance is assumed.

[41] SMY 04 obtained this result by a two-neutrino oscillation analysis using the data from all solar neutrino experiments. The 1σ errors are read from Fig. 6(a) of SMY 04.

[42] SMY 04 obtained this result by a two-neutrino oscillation analysis using the Super-Kamiokande and SNO (AHMAD 02 and AHMAD 02B) solar neutrino data. The 1σ errors are read from Fig. 6(a) of SMY 04.

[43] AHMAD 02B obtained this result by a two-neutrino oscillation analysis using the data from all solar neutrino experiments. The listed range of the parameter envelops the 95% CL two-dimensional region shown in Fig. 4(b) of AHMAD 02B. The best fit point is $\Delta(m^2) = 5.0 \times 10^{-5}$ eV^2 and $\tan\theta = 0.34$ ($\sin^2 2\,\theta = 0.76$).

[44] FUKUDA 02 obtained this result by a two-neutrino oscillation analysis using the data from all solar neutrino experiments. The listed range of the parameter envelops the 95% CL two-dimensional region shown in Fig. 4 of FUKUDA 02. The best fit point is $\Delta(m^2) = 6.9 \times 10^{-5}$ eV^2 and $\tan^2\theta = 0.38$ ($\sin^2 2\,\theta = 0.80$).

Δm^2_{21}

VALUE (10^{-5} eV^2)	*DOCUMENT ID*		*TECN*	*COMMENT*
7.53±0.18	[1] GANDO	13	FIT	KamLAND + global solar + SBL + accelerator: 3ν
• • • We do not use the following data for averages, fits, limits, etc. • • •				
$7.50^{+0.22}_{-0.20}$	[2] SALAS	21	FIT	global fit
$7.42^{+0.21}_{-0.20}$	[3] ESTEBAN	20A	FIT	Global fit
$7.55^{+0.20}_{-0.16}$	DE-SALAS	18	FIT	Global fit
$7.49^{+0.19}_{-0.18}$	[4] ABE	16C	FIT	KamLAND+global solar; 3ν
$4.8^{+1.3}_{-0.6}$	[5] ABE	16C	FIT	SKAM+SNO; 3ν
$4.8^{+1.5}_{-0.8}$	[6] ABE	16C	FIT	SK-I+II+III+IV; 3ν
$3.2^{+2.8}_{-0.2}$	[7] ABE	16C	FIT	SK-IV; 3ν
$7.6^{+0.19}_{-0.18}$	[8] FORERO	14	FIT	3ν
$7.50^{+0.19}_{-0.17}$	[9] GONZALEZ...	14	FIT	Either mass ordering; global fit
$5.13^{+1.29}_{-0.96}$	[10,11] AHARMIM	13	FIT	global solar: 2ν
$5.13^{+1.49}_{-0.98}$	[11,12] AHARMIM	13	FIT	global solar: 3ν
$7.46^{+0.20}_{-0.19}$	[11,13] AHARMIM	13	FIT	KamLAND + global solar: 3ν
$7.53^{+0.19}_{-0.18}$	[14] GANDO	13	FIT	KamLAND + global solar: 3ν
$7.54^{+0.19}_{-0.18}$	[15] GANDO	13	FIT	KamLAND: 3ν
7.6 ± 0.2	[16] ABE	11	FIT	KamLAND + global solar: 2ν

Downloaded from https://academic.oup.com/ptep/article/2022/8/083C01/6651666 by KIT Library user on 27 September 2022

$6.2\ ^{+1.1}_{-1.9}$	[17] ABE	11	FIT	global solar: 2ν
$7.7\ \pm 0.3$	[18] ABE	11	FIT	KamLAND + global solar: 3ν
$6.0\ ^{+2.2}_{-2.5}$	[19] ABE	11	FIT	global solar: 3ν
$7.50^{+0.16}_{-0.24}$	[20] BELLINI	11A	FIT	KamLAND + global solar: 2ν
$5.2\ ^{+1.5}_{-0.9}$	[21] BELLINI	11A	FIT	global solar: 2ν
$7.50^{+0.19}_{-0.20}$	[22] GANDO	11	FIT	KamLAND + solar: 3ν
7.49 ± 0.20	[23] GANDO	11	FIT	KamLAND: 3ν
$7.59^{+0.20}_{-0.21}$	[24,25] AHARMIM	10	FIT	KamLAND + global solar: 2ν
$5.89^{+2.13}_{-2.16}$	[24,26] AHARMIM	10	FIT	global solar: 2ν
7.59 ± 0.21	[24,27] AHARMIM	10	FIT	KamLAND + global solar: 3ν
$6.31^{+2.49}_{-2.58}$	[24,28] AHARMIM	10	FIT	global solar: 3ν
$7.58^{+0.14}_{-0.13}\pm 0.15$	[29] ABE	08A	FIT	KamLAND
7.59 ± 0.21	[30] ABE	08A	FIT	KamLAND + global solar
$7.59^{+0.19}_{-0.21}$	[31] AHARMIM	08	FIT	KamLAND + global solar
$8.0\ \pm 0.3$	[32] HOSAKA	06	FIT	KamLAND + global solar
$8.0\ \pm 0.3$	[33] HOSAKA	06	FIT	SKAM+SNO+KamLAND
$6.3\ ^{+3.7}_{-1.5}$	[34] HOSAKA	06	FIT	SKAM+SNO
5–12	[35] HOSAKA	06	FIT	SKAM day/night in the LMA region
$8.0\ ^{+0.4}_{-0.3}$	[36] AHARMIM	05A	FIT	KamLAND + global solar LMA
3.3–14.4	[37] AHARMIM	05A	FIT	global solar
$7.9\ ^{+0.4}_{-0.3}$	[38] ARAKI	05	FIT	KamLAND + global solar
$7.1\ ^{+1.0}_{-0.3}$	[39] AHMED	04A	FIT	KamLAND + global solar
3.2–13.7	[40] AHMED	04A	FIT	global solar
$7.1\ ^{+0.6}_{-0.5}$	[41] SMY	04	FIT	KamLAND + global solar
$6.0\ ^{+1.7}_{-1.6}$	[42] SMY	04	FIT	global solar
$6.0\ ^{+2.5}_{-1.6}$	[43] SMY	04	FIT	SKAM + SNO
2.8–12.0	[44] AHMAD	02B	FIT	global solar
3.2–19.1	[45] FUKUDA	02	FIT	global solar

[1] GANDO 13 obtained this result by a three-neutrino oscillation analysis using KamLAND, global solar neutrino, short-baseline (SBL) reactor, and accelerator data, assuming CPT invariance. Supersedes GANDO 11.

[2] SALAS 21 reports results of a global fit to neutrino oscillation data available at the time of the Neutrino 2020 conference.

[3] ESTEBAN 20A reports results of a global fit to neutrino oscillation data available at the time of the Neutrino2020 conference.

[4] ABE 16C obtained this result by a three-neutrino oscillation analysis, with a constraint of $\sin^2(\theta_{13}) = 0.0219 \pm 0.0014$ coming from reactor neutrino experiments, using all solar data and KamLAND data. *CPT* invariance is assumed.

[5] ABE 16C obtained this result by a three-neutrino oscillation analysis, with a constraint of $\sin^2(\theta_{13}) = 0.0219 \pm 0.0014$ coming from reactor neutrino experiments, using Super-Kamiokande (I+II+III+IV) and SNO data.

[6] ABE 16C obtained this result by a three-neutrino oscillation analysis, with a constraint of $\sin^2(\theta_{13}) = 0.0219 \pm 0.0014$ coming from reactor neutrino experiments, by combining the four phases of the Super-Kamiokande solar data.

[7] ABE 16C obtained this result by a three-neutrino oscillation analysis, with a constraint of $\sin^2(\theta_{13}) = 0.0219 \pm 0.0014$ coming from reactor neutrino experiments, using the Super-Kamiokande-IV data.

[8] FORERO 14 performs a global fit to Δm^2_{21} using solar, reactor, long-baseline accelerator, and atmospheric neutrino data.

[9] GONZALEZ-GARCIA 14 result comes from a frequentist global fit. The corresponding Bayesian global fit to the same data results are reported in BERGSTROM 15 as $(7.50^{+0.19}_{-0.17}) \times 10^{-5}$ eV^2 for normal and $(7.50^{+0.18}_{-0.17}) \times 10^{-5}$ eV^2 for inverted mass ordering.

[10] AHARMIM 13 obtained this result by a two-neutrino oscillation analysis using global solar neutrino data.

[11] AHARMIM 13 global solar neutrino data include SNO's all-phases-combined analysis results on the total active ^{8}B neutrino flux and energy-dependent ν_e survival probability parameters, measurements of Cl (CLEVELAND 98), Ga (ABDURASHITOV 09 which contains combined analysis with GNO (ALTMANN 05 and Ph.D. thesis of F. Kaether)), and ^{7}Be (BELLINI 11A) rates, and ^{8}B solar-neutrino recoil electron measurements of SK-I (HOSAKA 06) zenith, SK-II (CRAVENS 08), and SK-III (ABE 11) day/night spectra, and Borexino (BELLINI 10A) spectra.

[12] AHARMIM 13 obtained this result by a three-neutrino oscillation analysis with the value of Δm^2_{31} fixed to 2.45×10^{-3} eV^2, using global solar neutrino data.

[13] AHARMIM 13 obtained this result by a three-neutrino oscillation analysis with the value of Δm^2_{31} fixed to 2.45×10^{-3} eV^2, using global solar neutrino and KamLAND data (GANDO 11). CPT invariance is assumed.

[14] GANDO 13 obtained this result by a three-neutrino oscillation analysis using KamLAND and global solar neutrino data, assuming CPT invariance. Supersedes GANDO 11.

[15] GANDO 13 obtained this result by a three-neutrino oscillation analysis using KamLAND data. Supersedes GANDO 11.

[16] ABE 11 obtained this result by a two-neutrino oscillation analysis using solar neutrino data including Super-Kamiokande, SNO, Borexino (ARPESELLA 08A), Homestake, GALLEX/GNO, SAGE, and KamLAND data. CPT invariance is assumed.

[17] ABE 11 obtained this result by a two-neutrino oscillation analysis using solar neutrino data including Super-Kamiokande, SNO, Borexino (ARPESELLA 08A), Homestake, GALLEX/GNO, and SAGE data.

[18] ABE 11 obtained this result by a three-neutrino oscillation analysis with the value of Δm^2_{32} fixed to 2.4×10^{-3} eV^2, using solar neutrino data including Super-Kamiokande, SNO, Borexino (ARPESELLA 08A), Homestake, GALLEX/GNO, SAGE, and KamLAND data. The normal neutrino mass ordering and CPT invariance are assumed.

[19] ABE 11 obtained this result by a three-neutrino oscillation analysis with the value of Δm^2_{32} fixed to 2.4×10^{-3} eV^2, using solar neutrino data including Super-Kamiokande, SNO, Borexino (ARPESELLA 08A), Homestake, and GALLEX/GNO data. The normal neutrino mass ordering is assumed.

[20] BELLINI 11A obtained this result by a two-neutrino oscillation analysis using KamLAND, Homestake, SAGE, Gallex, GNO, Kamiokande, Super-Kamiokande, SNO, and Borexino (BELLINI 11A) data and the SSM flux prediction in SERENELLI 11 (Astrophysical Journal **743** 24 (2011)) with the exception that the ^{8}B flux was left free. CPT invariance is assumed.

[21] BELLINI 11A obtained this result by a two-neutrino oscillation analysis using Homestake, SAGE, Gallex, GNO, Kamiokande, Super-Kamiokande, SNO, and Borexino (BELLINI 11A) data and the SSM flux prediction in SERENELLI 11 (Astrophysical Journal **743** 24 (2011)) with the exception that the ^{8}B flux was left free.

[22] GANDO 11 obtain this result with three-neutrino fit using the KamLAND + solar data. Superseded by GANDO 13.

[23] GANDO 11 obtain this result with three-neutrino fit using the KamLAND data only. Supersedes ABE 08A.

[24] AHARMIM 10 global solar neutrino data include SNO's low-energy-threshold analysis survival probability day/night curves, SNO Phase III integral rates (AHARMIM 08), Cl (CLEVELAND 98), SAGE (ABDURASHITOV 09), Gallex/GNO (HAMPEL 99, ALTMANN 05), Borexino (ARPESELLA 08A), SK-I zenith (HOSAKA 06), and SK-II day/night spectra (CRAVENS 08).

[25] AHARMIM 10 obtained this result by a two-neutrino oscillation analysis using global solar neutrino data and KamLAND data (ABE 08A). *CPT* invariance is assumed.

[26] AHARMIM 10 obtained this result by a two-neutrino oscillation analysis using global solar neutrino data.

[27] AHARMIM 10 obtained this result by a three-neutrino oscillation analysis with the value of Δm^2_{31} fixed to 2.3×10^{-3} eV^2, using global solar neutrino data and KamLAND data (ABE 08A). *CPT* invariance is assumed.

[28] AHARMIM 10 obtained this result by a three-neutrino oscillation analysis with the value of Δm^2_{31} fixed to 2.3×10^{-3} eV^2, using global solar neutrino data.

[29] ABE 08A obtained this result by a rate + shape + time combined geoneutrino and reactor two-neutrino fit for Δm^2_{21} and $\tan^2\theta_{12}$, using KamLAND data only. Superseded by GANDO 11.

[30] ABE 08A obtained this result by means of a two-neutrino fit using KamLAND, Homestake, SAGE, GALLEX, GNO, SK (zenith angle and E-spectrum), the SNO χ^2-map, and solar flux data. *CPT* invariance is assumed. Superseded by GANDO 11.

[31] AHARMIM 08 obtained this result by a two-neutrino oscillation analysis using all solar neutrino data including those of Borexino (ARPESELLA 08A) and Super-Kamiokande-I (HOSAKA 06), and KamLAND data (ABE 08A). *CPT* invariance is assumed.

[32] HOSAKA 06 obtained this result by a two-neutrino oscillation analysis using solar neutrino and KamLAND data (ARAKI 05). *CPT* invariance is assumed.

[33] HOSAKA 06 obtained this result by a two-neutrino oscillation analysis using the data from Super-Kamiokande, SNO (AHMAD 02 and AHMAD 02B), and KamLAND (ARAKI 05) experiments. *CPT* invariance is assumed.

[34] HOSAKA 06 obtained this result by a two-neutrino oscillation analysis using the Super-Kamiokande and SNO (AHMAD 02 and AHMAD 02B) solar neutrino data.

[35] HOSAKA 06 obtained this result from the consistency between the observed and expected day-night flux asymmetry amplitude. The listed 68% CL range is derived from the 1σ boundary of the amplitude fit to the data. Oscillation parameters are constrained to be in the LMA region. The mixing angle is fixed at $\tan^2\theta = 0.44$ because the fit depends only very weekly on it.

[36] AHARMIM 05A obtained this result by a two-neutrino oscillation analysis using solar neutrino and KamLAND data (ARAKI 05). *CPT* invariance is assumed. AHARMIM 05A also quotes $\Delta(m^2) = (8.0^{+0.6}_{-0.4}) \times 10^{-5}$ eV^2 as the error enveloping the 68% CL two-dimensional region.

[37] AHARMIM 05A obtained this result by a two-neutrino oscillation analysis using the data from all solar neutrino experiments. The listed range of the parameter envelops the 95% CL two-dimensional region shown in figure 35a of AHARMIM 05A. AHARMIM 05A also quotes $\Delta(m^2) = (6.5^{+4.4}_{-2.3}) \times 10^{-5}$ eV^2 as the error enveloping the 68% CL two-dimensional region.

[38] ARAKI 05 obtained this result by a two-neutrino oscillation analysis using KamLAND and solar neutrino data. *CPT* invariance is assumed. The 1σ error shown here is provided by the KamLAND collaboration. The error quoted in ARAKI 05, $\Delta(m^2) = (7.9^{+0.6}_{-0.5}) \times 10^{-5}$, envelops the 68% CL two-dimensional region.

[39] AHMED 04A obtained this result by a two-neutrino oscillation analysis using solar neutrino and KamLAND data (EGUCHI 03). *CPT* invariance is assumed. AHMED 04A also quotes $\Delta(m^2) = (7.1^{+1.2}_{-0.6}) \times 10^{-5}$ eV^2 as the error enveloping the 68% CL two-dimensional region.

[40] AHMED 04A obtained this result by a two-neutrino oscillation analysis using the data from all solar neutrino experiments. The listed range of the parameter envelops the 95% CL two-dimensional region shown in Fig. 5(a) of AHMED 04A. The best-fit point is $\Delta(m^2) = 6.5 \times 10^{-5}$ eV^2, $\tan^2\theta = 0.40$ ($\sin^2 2\,\theta = 0.82$).

Downloaded from https://academic.oup.com/ptep/article/2022/8/083C01/6651666 by KIT Library user on 27 September 2022

[41] SMY 04 obtained this result by a two-neutrino oscillation analysis using solar neutrino and KamLAND data (IANNI 03). *CPT* invariance is assumed.

[42] SMY 04 obtained this result by a two-neutrino oscillation analysis using the data from all solar neutrino experiments. The 1σ errors are read from Fig. 6(a) of SMY 04.

[43] SMY 04 obtained this result by a two-neutrino oscillation analysis using the Super-Kamiokande and SNO (AHMAD 02 and AHMAD 02B) solar neutrino data. The 1σ errors are read from Fig. 6(a) of SMY 04.

[44] AHMAD 02B obtained this result by a two-neutrino oscillation analysis using the data from all solar neutrino experiments. The listed range of the parameter envelops the 95% CL two-dimensional region shown in Fig. 4(b) of AHMAD 02B. The best fit point is $\Delta(m^2) = 5.0 \times 10^{-5}$ eV^2 and $\tan\theta = 0.34$ ($\sin^2 2\,\theta = 0.76$).

[45] FUKUDA 02 obtained this result by a two-neutrino oscillation analysis using the data from all solar neutrino experiments. The listed range of the parameter envelops the 95% CL two-dimensional region shown in Fig. 4 of FUKUDA 02. The best fit point is $\Delta(m^2) = 6.9 \times 10^{-5}$ eV^2 and $\tan^2\theta = 0.38$ ($\sin^2 2\,\theta = 0.80$).

$\sin^2(\theta_{23})$

The reported limits below correspond to the projection onto the $\sin^2(\theta_{23})$ axis of the 90% CL contours in the $\sin^2(\theta_{23}) - \Delta m^2_{32}$ plane presented by the authors. Unless otherwise specified, the limits are 90% CL and the reported uncertainties are 68% CL.

If an experiment reports $\sin^2(2\,\theta_{23})$ we convert the value to $\sin^2(\,\theta_{23})$.

VALUE	DOCUMENT ID		TECN	COMMENT
0.539±0.022 OUR FIT	Error includes scale factor of 1.1. Assuming inverted mass ordering			
0.546±0.021 OUR FIT	Assuming normal mass ordering			
$0.53^{+0.03}_{-0.04}$	[1] ABE	20F	T2K	Both mass orderings
$0.43^{+0.20}_{-0.04}$	[2] ADAMSON	20A	MINS	Normal mass ordering
$0.42^{+0.07}_{-0.03}$	[2] ADAMSON	20A	MINS	Inverted mass ordering
$0.56^{+0.04}_{-0.03}$	[3] ACERO	19	NOVA	Normal mass order; octant II for θ_{23}
$0.56^{+0.04}_{-0.03}$	[3,4] ACERO	19	NOVA	Inverted mass order; octant II for θ_{23}
$0.51^{+0.07}_{-0.09}$	[5] AARTSEN	18A	ICCB	Normal mass ordering
$0.588^{+0.031}_{-0.064}$	[6] ABE	18B	SKAM	Normal mass ordering, θ_{13} constrained
$0.575^{+0.036}_{-0.073}$	[6] ABE	18B	SKAM	Inverted mass ordering, θ_{13} constrained
• • • We do not use the following data for averages, fits, limits, etc. • • •				
$0.51^{+0.06}_{-0.07}$	[7] ABE	21A	T2K	ν_μ disappearance
$0.43^{+0.21}_{-0.05}$	[7] ABE	21A	T2K	$\overline{\nu}_\mu$ disappearance
0.574 ± 0.014	[8] SALAS	21	FIT	Normal mass ordering, global fit
$0.578^{+0.010}_{-0.017}$	[8] SALAS	21	FIT	Inverted mass ordering, global fit
0.455	[9] AARTSEN	20	ICCB	For both mass orderings
$0.573^{+0.016}_{-0.020}$	[10] ESTEBAN	20A	FIT	Normal mass ordering, global fit
$0.575^{+0.016}_{-0.019}$	[10] ESTEBAN	20A	FIT	Inverted mass ordering, global fit
$0.58^{+0.04}_{-0.13}$	[11] AARTSEN	19C	ICCB	
$0.48^{+0.04}_{-0.03}$	[3,4] ACERO	19	NOVA	Normal mass order; octant I for θ_{23}
$0.47^{+0.04}_{-0.03}$	[3,4] ACERO	19	NOVA	Inverted mass order; octant I for θ_{23}
$0.49^{+0.30}_{-0.28}$	AGAFONOVA	19	OPER	
$0.50^{+0.20}_{-0.19}$	[12] ALBERT	19	ANTR	Atmospheric ν, deep sea telescope
$0.587^{+0.036}_{-0.069}$	[13] ABE	18B	SKAM	3ν osc: normal mass ordering, θ_{13} free
$0.551^{+0.044}_{-0.075}$	[13] ABE	18B	SKAM	3ν osc: inverted mass ordering, θ_{13} free
$0.526^{+0.032}_{-0.036}$	[14] ABE	18G	T2K	Normal mass ordering, θ_{13} constrained
$0.530^{+0.030}_{-0.034}$	[14] ABE	18G	T2K	Inverted mass ordering, θ_{13} constrained
0.56 ± 0.04	[15] ACERO	18	NOVA	Normal mass order; octant II for θ_{23}
0.47 ± 0.04	[15] ACERO	18	NOVA	Normal mass order; octant I for θ_{23}
$0.547^{+0.020}_{-0.030}$	DE-SALAS	18	FIT	Normal mass ordering, global fit
$0.551^{+0.018}_{-0.030}$	DE-SALAS	18	FIT	Inverted mass order, global fit
$0.532^{+0.061}_{-0.087}$	[16] ABE	17A	T2K	Normal mass ordering
$0.534^{+0.061}_{-0.087}$	[16] ABE	17A	T2K	Inverted mass ordering
$0.51^{+0.08}_{-0.07}$	ABE	17C	T2K	Normal mass ordering with neutrinos
$0.42^{+0.25}_{-0.07}$	ABE	17C	T2K	Normal mass ordering with antineutrinos
$0.52^{+0.075}_{-0.09}$	ABE	17C	T2K	normal mass ordering with neutrinos and antineutrinos
$0.55^{+0.05}_{-0.09}$	[16] ABE	17F	T2K	Normal mass ordering
$0.55^{+0.05}_{-0.08}$	[16] ABE	17F	T2K	Inverted mass ordering
$0.404^{+0.022}_{-0.030}$	[17] ADAMSON	17A	NOVA	Normal mass ordering; octant I for θ_{23}
$0.624^{+0.022}_{-0.030}$	[17] ADAMSON	17A	NOVA	Normal mass ordering; octant II for θ_{23}
$0.398^{+0.030}_{-0.022}$	[17] ADAMSON	17A	NOVA	Inverted mass ordering; octant I for θ_{23}
$0.618^{+0.022}_{-0.030}$	[17] ADAMSON	17A	NOVA	Inverted mass ordering; octant II for θ_{23}
$0.45^{+0.19}_{-0.07}$	[18] ABE	16D	T2K	3ν osc; normal mass ordering; $\overline{\nu}$ beam
0.38 to 0.65	[19] ADAMSON	16A	NOVA	normal mass ordering
0.37 to 0.64	[19] ADAMSON	16A	NOVA	Inverted mass ordering
$0.53^{+0.09}_{-0.12}$	[20] AARTSEN	15A	ICCB	Normal mass ordering
$0.51^{+0.09}_{-0.11}$	[20] AARTSEN	15A	ICCB	Inverted mass ordering
$0.514^{+0.055}_{-0.056}$	[21] ABE	14	T2K	3ν osc.; normal mass ordering
0.511 ± 0.055	[21] ABE	14	T2K	3ν osc.; inverted mass ordering
$0.41^{+0.23}_{-0.06}$	[22] ADAMSON	14	MINS	Normal mass ordering
$0.41^{+0.26}_{-0.07}$	[22] ADAMSON	14	MINS	Inverted mass ordering
$0.567^{+0.032}_{-0.128}$	[23] FORERO	14	FIT	Normal mass ordering
$0.573^{+0.025}_{-0.043}$	[23] FORERO	14	FIT	Inverted mass ordering
$0.452^{+0.052}_{-0.028}$	[24] GONZALEZ...	14	FIT	Normal mass ordering; global fit
$0.579^{+0.025}_{-0.037}$	[24] GONZALEZ...	14	FIT	Inverted mass ordering; global fit
0.24 to 0.76	[25] AARTSEN	13B	ICCB	DeepCore, 2ν oscillation
0.514 ± 0.082	[26] ABE	13G	T2K	3ν osc.; normal mass ordering
$0.388^{+0.051}_{-0.053}$	[27] ADAMSON	13B	MINS	Beam + Atmospheric; identical ν & $\overline{\nu}$
0.3 to 0.7	[28] ABE	12A	T2K	Off-axis beam
0.28 to 0.72	[29] ADAMSON	12	MINS	$\overline{\nu}$ beam
0.25 to 0.75	[30,31] ADAMSON	12B	MINS	MINOS atmospheric
0.27 to 0.73	[30,32] ADAMSON	12B	MINS	MINOS pure atmospheric ν
0.21 to 0.79	[30,32] ADAMSON	12B	MINS	MINOS pure atmospheric $\overline{\nu}$
0.15 to 0.85	[33] ADRIAN-MAR..	12	ANTR	Atmospheric ν with deep see telescope
0.39 to 0.61	[34] ABE	11C	SKAM	Super-Kamiokande
0.34 to 0.66	ADAMSON	11	MINS	2ν osc.; maximal mixing
$0.31^{+0.10}_{-0.07}$	[35] ADAMSON	11B	MINS	$\overline{\nu}$ beam
0.41 to 0.59	[36] WENDELL	10	SKAM	3ν osc. with solar terms; θ_{13}=0
0.39 to 0.61	[37] WENDELL	10	SKAM	3ν osc.; normal mass ordering
0.37 to 0.63	[38] WENDELL	10	SKAM	3ν osc.; inverted mass ordering
0.31 to 0.69	ADAMSON	08A	MINS	MINOS
0.05 to 0.95	[39] ADAMSON	06	MINS	Atmospheric ν with far detector
0.18 to 0.82	[40] AHN	06A	K2K	KEK to Super-K
0.23 to 0.77	[41] MICHAEL	06	MINS	MINOS
0.18 to 0.82	[42] ALIU	05	K2K	KEK to Super-K
0.18 to 0.82	[43] ALLISON	05	SOU2	
0.36 to 0.64	[44] ASHIE	05	SKAM	Super-Kamiokande
0.28 to 0.72	[45] AMBROSIO	04	MCRO	MACRO
0.34 to 0.66	[46] ASHIE	04	SKAM	L/E distribution
0.08 to 0.92	[47] AHN	03	K2K	KEK to Super-K
0.13 to 0.87	[48] AMBROSIO	03	MCRO	MACRO
0.26 to 0.74	[49] AMBROSIO	03	MCRO	MACRO
0.15 to 0.85	[50] SANCHEZ	03	SOU2	Soudan-2 Atmospheric
0.28 to 0.72	[51] AMBROSIO	01	MCRO	Upward μ
0.29 to 0.71	[52] AMBROSIO	01	MCRO	Upward μ
0.13 to 0.87	[53] FUKUDA	99C	SKAM	Upward μ
0.23 to 0.77	[54] FUKUDA	99D	SKAM	Upward μ
0.08 to 0.92	[55] FUKUDA	99D	SKAM	Stop μ / through
0.29 to 0.71	[56] FUKUDA	98C	SKAM	Super-Kamiokande
0.08 to 0.92	[57] HATAKEYAMA	98	KAMI	Kamiokande
0.24 to 0.76	[58] HATAKEYAMA	98	KAMI	Kamiokande
0.20 to 0.80	[59] FUKUDA	94	KAMI	Kamiokande

[1] ABE 20F results are based on data collected between 2009 and 2018 in (anti)neutrino mode and include a neutrino beam exposure of 1.49×10^{21} (1.64×10^{21}) protons on target. Supersedes ABE 18G.

[2] ADAMSON 20A uses the complete dataset from MINOS and MINOS+ experiments. The data were collected using a total exposure of 23.76×10^{20} protons on target and 60.75 kton-yr exposure to atmospheric neutrinos. Supersedes ADAMSON 14.

[3] ACERO 19 is based on a sample size of 12.33×10^{20} protons on target. The fit combines both antineutrino and neutrino data to extract the oscillation parameters. The results favor the normal mass ordering by 1.9 σ and θ_{23} values in octant II by 1.6 σ. Supersedes ACERO 18.

[4] Errors are from normal mass ordering and θ_{13} octant II fits.

[5] AARTSEN 18A uses three years (April 2012 – May 2015) of neutrino data from full sky with reconstructed energies between 5.6 and 56 GeV, measured with the low-energy subdetector DeepCore of the IceCube neutrino telescope. AARTSEN 18A also reports the best fit result for the inverted mass ordering as $\Delta m^2_{32} = -2.32 \times 10^{-3}$ eV^2 and $\sin^2(\theta_{23}) = 0.51$. Uncertainties for the inverted mass ordering fits were not provided. Supersedes AARTSEN 15A.

[6] ABE 18B uses 328 kton-years of Super-Kamiokande I-IV atmospheric neutrino data to obtain this result. The fit is performed over the three parameters, Δm^2_{32}, $\sin^2(\theta_{23})$, and

Downloaded from https://academic.oup.com/ptep/article/2022/8/083C01/6651666 by KIT Library user on 27 September 2022

δ, while the solar parameters and $\sin^2(\theta_{13})$ are fixed to $\Delta m^2_{21} = (7.53 \pm 0.18) \times 10^{-5}$ eV^2, $\sin^2(\theta_{12}) = 0.304 \pm 0.014$, and $\sin^2(\theta_{13}) = 0.0219 \pm 0.0012$.

[7] ABE 21A results are based on 1.49×10^{21} POT in neutrino mode and 1.64×10^{21} POT in antineutrino mode.

[8] SALAS 21 reports results of a global fit to neutrino oscillation data available at the time of the Neutrino 2020 conference.

[9] AARTSEN 20 uses the data taken between May 2012 and April 2014 with the low-energy subdetector DeepCore of the IceCube neutrino telescope. The reconstructed energy range is between 4 (5) and 90 (80) GeV for the main (confirmatory) analysis. Though the observed best-fit is in the lower octant for both mass orderings, a substantial range of $\sin^2(\theta_{23}) > 0.5$ is still compatible with the observed data for both mass orderings.

[10] ESTEBAN 20A reports results of a global fit to neutrino oscillation data available at the time of the Neutrino2020 conference.

[11] AARTSEN 19C uses three years (April 2012 – May 2015) of neutrino data from full sky with reconstructed energies between 5.6 and 56 GeV, measured with the low-energy subdetector DeepCore of the IceCube neutrino telescope. AARTSEN 19C adopts looser event selection criteria to prioritize the efficiency of selecting neutrino events, different from tighter event selection criteria which closely follow the criteria used by AARTSEN 18A to measure the ν_μ disappearance.

[12] ALBERT 19 measured the oscillation parameters of atmospheric neutrinos with the ANTARES deep sea neutrino telescope using the data taken from 2007 to 2016 (2830 days of total live time). Supersedes ADRIAN-MARTINEZ 12.

[13] ABE 18B uses 328 kton-years of Super-Kamiokande I-IV atmospheric neutrino data to obtain this result. The fit is performed over the four parameters, Δm^2_{32}, $\sin^2\theta_{23}$, $\sin^2\theta_{13}$, and δ, while the solar parameters are fixed to $\Delta m^2_{21} = (7.53 \pm 0.18) \times 10^{-5}$ eV^2 and $\sin^2\theta_{12} = 0.304 \pm 0.014$.

[14] ABE 18G data prefers normal mass ordering is with a posterior probability of 87%. Supersedes ABE 17F.

[15] ACERO 18 performs a joint fit to the data for ν_μ disappearance and ν_e appearance. The overall best fit favors normal mass ordering and θ_{23} in octant II. No 1σ confidence intervals are presented for the inverted mass ordering scenarios. Superseded by ACERO 19.

[16] Errors are from the projections of the 68% contour on 2D plot of Δm^2 versus $\sin^2(\theta_{23})$. ABE 17F supersedes ABE 17A. Superseded by ABE 18G.

[17] Superseded by ACERO 18.

[18] ABE 16D reports oscillation results using $\overline{\nu}_\mu$ disappearance in an off-axis beam.

[19] ADAMSON 16A obtains $\sin^2(\theta_{23})$ in the 68% C.L. range [0.38, 0.65] ([0.37, 0.64]), with two statistically degenerate best-fit values of 0.44 and 0.59 (0.44 and 0.59) for normal (inverted) mass ordering. Superseded by ADAMSON 17A.

[20] AARTSEN 15A obtains this result by a three-neutrino oscillation analysis using 10–100 GeV muon neutrino sample from a total of 953 days of measurement with the low-energy subdetector DeepCore of the IceCube neutrino telescope. Superseded by AARTSEN 18A.

[21] ABE 14 results are based on ν_μ disappearance using three-neutrino oscillation fit. The confidence intervals are derived from one dimensional profiled likelihoods. Superseded by ABE 17A.

[22] ADAMSON 14 uses a complete set of accelerator and atmospheric data. The analysis combines the ν_μ disappearance and ν_e appearance data using three-neutrino oscillation fit. The fit results are obtained for normal and inverted mass ordering assumptions. The best fit is for first θ_{23} octant and inverted mass ordering.

[23] FORERO 14 performs a global fit to neutrino oscillations using solar, reactor, long-baseline accelerator, and atmospheric neutrino data.

[24] GONZALEZ-GARCIA 14 result comes from a frequentist global fit. The corresponding Bayesian global fit to the same data results are reported in BERGSTROM 15 as 68% CL intervals of 0.433–0.496 or 0.530–0.594 for normal and 0.514–0.612 for inverted mass ordering.

[25] AARTSEN 13B obtained this result by a two-neutrino oscillation analysis using 20–100 GeV muon neutrino sample from a total of 318.9 days of live-time measurement with the low-energy subdetector DeepCore of the IceCube neutrino telescope.

[26] The best fit value is $\sin^2(\theta_{23}) = 0.514 \pm 0.082$. Superseded by ABE 14.

[27] ADAMSON 13B obtained this result from ν_μ and $\overline{\nu}_\mu$ disappearance using ν_μ (10.71×10^{20} POT) and $\overline{\nu}_\mu$ (3.36×10^{20} POT) beams, and atmospheric (37.88kton-years) data from MINOS The fit assumed two-flavor neutrino hypothesis and identical ν_μ and $\overline{\nu}_\mu$ oscillation parameters. Superseded by ADAMSON 14.

[28] ABE 12A obtained this result by a two-neutrino oscillation analysis. The best-fit point is $\sin^2(2\theta_{23}) = 0.98$.

[29] ADAMSON 12 is a two-neutrino oscillation analysis using antineutrinos. The best fit value is $\sin^2(2\theta_{23}) = 0.95^{+0.10}_{-0.11} \pm 0.01$.

[30] ADAMSON 12B obtained this result by a two-neutrino oscillation analysis of the L/E distribution using 37.9 kton-yr atmospheric neutrino data with the MINOS far detector.

[31] The best fit point is $\Delta m^2 = 0.0019$ eV^2 and $\sin^2 2\theta = 0.99$. The 90% single-parameter confidence interval at the best fit point is $\sin^2 2\theta > 0.86$.

[32] The data are separated into pure samples of νs and $\overline{\nu}$s, and separate oscillation parameters for νs and $\overline{\nu}$s are fit to the data. The best fit point is (Δm^2, $\sin^2 2\theta$) = (0.0022 eV^2, 0.99) and ($\Delta\overline{m}^2$, $\sin^2 2\overline{\theta}$) = (0.0016 eV^2, 1.00). The quoted result is taken from the 90% C.L. contour in the (Δm^2, $\sin^2 2\theta$) plane obtained by minimizing the four parameter log-likelihood function with respect to the other oscillation parameters.

[33] ADRIAN-MARTINEZ 12 measured the oscillation parameters of atmospheric neutrinos with the ANTARES deep sea neutrino telescope using the data taken from 2007 to 2010 (863 days of total live time). Superseded by ALBERT 19.

[34] ABE 11C obtained this result by a two-neutrino oscillation analysis using the Super-Kamiokande-I+II+III atmospheric neutrino data. ABE 11C also reported results under a two-neutrino disappearance model with separate mixing parameters between ν and $\overline{\nu}$, and obtained $\sin^2 2\theta > 0.93$ for ν and $\sin^2 2\theta > 0.83$ for $\overline{\nu}$ at 90% C.L.

[35] ADAMSON 11B obtained this result by a two-neutrino oscillation analysis of antineutrinos in an antineutrino enhanced beam with 1.71×10^{20} protons on target. This results is consistent with the neutrino measurements of ADAMSON 11 at 2% C.L.

[36] WENDELL 10 obtained this result ($\sin^2\theta_{23} = 0.407$–$0.583$) by a three-neutrino oscillation analysis using the Super-Kamiokande-I+II+III atmospheric neutrino data, assuming $\theta_{13} = 0$ but including the solar oscillation parameters Δm^2_{21} and $\sin^2\theta_{12}$ in the fit.

[37] WENDELL 10 obtained this result ($\sin^2\theta_{23} = 0.43$–0.61) by a three-neutrino oscillation analysis with one mass scale dominance ($\Delta m^2_{21} = 0$) using the Super-Kamiokande-I+II+III atmospheric neutrino data, and updates the HOSAKA 06A result.

[38] WENDELL 10 obtained this result ($\sin^2\theta_{23} = 0.44$–0.63) by a three-neutrino oscillation analysis with one mass scale dominance ($\Delta m^2_{21} = 0$) using the Super-Kamiokande-I+II+III atmospheric neutrino data, and updates the HOSAKA 06A result.

[39] ADAMSON 06 obtained this result by a two-neutrino oscillation analysis of the L/E distribution using 4.54 kton yr atmospheric neutrino data with the MINOS far detector.

[40] Supercedes ALIU 05.

[41] MICHAEL 06 best fit is for maximal mixing. See also ADAMSON 08.

[42] The best fit is for maximal mixing.

[43] ALLISON 05 result is based upon atmospheric neutrino interactions including upward-stopping muons, with an exposure of 5.9 kton yr. From a two-flavor oscillation analysis the best-fit point is $\Delta m^2 = 0.0017$ eV^2 and $\sin^2(2\theta) = 0.97$.

[44] ASHIE 05 obtained this result by a two-neutrino oscillation analysis using 92 kton yr atmospheric neutrino data from the complete Super-Kamiokande I running period.

[45] AMBROSIO 04 obtained this result, without using the absolute normalization of the neutrino flux, by combining the angular distribution of upward through-going muon tracks with $E_\mu > 1$ GeV, N_{low} and N_{high}, and the numbers of InDown + UpStop and InUp events. Here, N_{low} and N_{high} are the number of events with reconstructed neutrino energies < 30 GeV and > 130 GeV, respectively. InDown and InUp represent events with downward and upward-going tracks starting inside the detector due to neutrino interactions, while UpStop represents entering upward-going tracks which stop in the detector. The best fit is for maximal mixing.

[46] ASHIE 04 obtained this result from the L(flight length)/E(estimated neutrino energy) distribution of ν_μ disappearance probability, using the Super-Kamiokande-I 1489 live-day atmospheric neutrino data.

[47] There are several islands of allowed region from this K2K analysis, extending to high values of Δm^2. We only include the one that overlaps atmospheric neutrino analyses. The best fit is for maximal mixing.

[48] AMBROSIO 03 obtained this result on the basis of the ratio $R = N_{low}/N_{high}$, where N_{low} and N_{high} are the number of upward through-going muon events with reconstructed neutrino energy < 30 GeV and > 130 GeV, respectively. The data came from the full detector run started in 1994. The method of FELDMAN 98 is used to obtain the limits.

[49] AMBROSIO 03 obtained this result by using the ratio R and the angular distribution of the upward through-going muons. R is given in the previous note and the angular distribution is reported in AMBROSIO 01. The method of FELDMAN 98 is used to obtain the limits. The best fit is to maximal mixing.

[50] SANCHEZ 03 is based on an exposure of 5.9 kton yr. The result is obtained using a likelihood analysis of the neutrino L/E distribution for a selection μ flavor sample while the e-flavor sample provides flux normalization. The method of FELDMAN 98 is used to obtain the allowed region. The best fit is $\sin^2(2\theta) = 0.97$.

[51] AMBROSIO 01 result is based on the angular distribution of upward through-going muon tracks with $E_\mu > 1$ GeV. The data came from three different detector configurations, but the statistics is largely dominated by the full detector run, from May 1994 to December 2000. The total live time, normalized to the full detector configuration is 6.17 years. The best fit is obtained outside the physical region. The method of FELDMAN 98 is used to obtain the limits. The best fit is for maximal mixing.

[52] AMBROSIO 01 result is based on the angular distribution and normalization of upward through-going muon tracks with $E_\mu > 1$ GeV. See the previous footnote.

[53] FUKUDA 99C obtained this result from a total of 537 live days of upward through-going muon data in Super-Kamiokande between April 1996 to January 1998. With a threshold of $E_\mu > 1.6$ GeV, the observed flux is $(1.74 \pm 0.07 \pm 0.02) \times 10^{-13}$ cm^{-2}s^{-1}sr^{-1}. The best fit is $\sin^2(2\theta) = 0.95$.

[54] FUKUDA 99D obtained this result from a simultaneous fitting to zenith angle distributions of upward-stopping and through-going muons. The flux of upward-stopping muons of minimum energy of 1.6 GeV measured between April 1996 and January 1998 is $(0.39 \pm 0.04 \pm 0.02) \times 10^{-13}$ cm^{-2}s^{-1}sr^{-1}. This is compared to the expected flux of $(0.73 \pm 0.16$ (theoretical error)$) \times 10^{-13}$ cm^{-2}s^{-1}sr^{-1}. The best fit is to maximal mixing.

[55] FUKUDA 99D obtained this result from the zenith dependence of the upward-stopping/through-going flux ratio. The best fit is to maximal mixing.

[56] FUKUDA 98C obtained this result by an analysis of 33.0 kton yr atmospheric neutrino data. The best fit is for maximal mixing.

[57] HATAKEYAMA 98 obtained this result from a total of 2456 live days of upward-going muon data in Kamiokande between December 1985 and May 1995. With a threshold of $E_\mu > 1.6$ GeV, the observed flux of upward through-going muons is $(1.94 \pm 0.10^{+0.07}_{-0.06}) \times 10^{-13}$ cm^{-2}s^{-1}sr^{-1}. This is compared to the expected flux of $(2.46 \pm 0.54$ (theoretical error)$) \times 10^{-13}$ cm^{-2}s^{-1}sr^{-1}. The best fit is for maximal mixing.

[58] HATAKEYAMA 98 obtained this result from a combined analysis of Kamiokande contained events (FUKUDA 94) and upward going muon events. The best fit is $\sin^2(2\theta) = 0.95$.

[59] FUKUDA 94 obtained the result by a combined analysis of sub- and multi-GeV atmospheric neutrino events in Kamiokande. The best fit is for maximal mixing.

Downloaded from https://academic.oup.com/ptep/article/2022/8/083C01/6651666 by KIT Library user on 27 September 2022

Δm^2_{32}

The sign of Δm^2_{32} is not known at this time. If given, values are shown separately for the normal and inverted mass ordering. Unless otherwise specified, the ranges below correspond to the projection onto the Δm^2_{32} axis of the 90% CL contours in the $\sin^2(2\theta_{23}) - \Delta m^2_{32}$ plane presented by the authors. If uncertainties are reported with the value, they correspond to one standard deviation uncertainty.

VALUE (10^{-3} eV^2)	DOCUMENT ID		TECN	COMMENT
-2.536 ± 0.034 OUR FIT	Assuming inverted ordering			
2.453 ± 0.033 OUR FIT	Assuming normal ordering			
2.45 ± 0.07	[1] ABE	20F	T2K	Normal mass ordering, θ_{13} constrained
-2.51 ± 0.07	[1,2] ABE	20F	T2K	Inverted mass ordering, θ_{13} constrained
$2.40 {}^{+0.08}_{-0.09}$	[3] ADAMSON	20A	MINS	Accel., atmospheric, normal mass ordering
$-2.45 {}^{+0.08}_{-0.07}$	[3] ADAMSON	20A	MINS	Accel., atmospheric, inverted mass ordering
$2.48 {}^{+0.11}_{-0.06}$	[4] ACERO	19	NOVA	Normal mass ordering, octant II for θ_{23}
$-2.54 {}^{+0.06}_{-0.11}$	[4] ACERO	19	NOVA	Inverted mass ordering, octant II for θ_{23}
$2.31 {}^{+0.11}_{-0.13}$	[5] AARTSEN	18A	ICCB	Normal mass ordering
$2.50 {}^{+0.13}_{-0.20}$	[6] ABE	18B	SKAM	Normal mass ordering, θ_{13} constrained
$-2.58 {}^{+0.08}_{-0.37}$	[6] ABE	18B	SKAM	Inverted mass ordering, θ_{13} constrained
$2.471 {}^{+0.068}_{-0.070}$	[7] ADEY	18A	DAYA	Normal mass ordering
$-2.575 {}^{+0.068}_{-0.070}$	[7] ADEY	18A	DAYA	Inverted mass ordering
2.63 ± 0.14	[8] BAK	18	RENO	Normal mass ordering
-2.73 ± 0.14	[8] BAK	18	RENO	Inverted mass ordering
• • • We do not use the following data for averages, fits, limits, etc. • • •				
$2.47 {}^{+0.08}_{-0.09}$	[9] ABE	21A	T2K	ν_μ disappearance
$2.50 {}^{+0.18}_{-0.13}$	[9] ABE	21A	T2K	$\overline{\nu}_\mu$ disappearance
$2.517 {}^{+0.026}_{-0.028}$	[10] ESTEBAN	20A	FIT	Normal mass ordering, global fit
$-2.498 {}^{+0.028}_{-0.028}$	[10] ESTEBAN	20A	FIT	Inverted mass ordering, global fit
$2.55 {}^{+0.12}_{-0.11}$	[11] AARTSEN	19C	ICCB	
< 4.1 at 90% CL	AGAFONOVA	19	OPER	
$2.0 {}^{+0.4}_{-0.3}$	[12] ALBERT	19	ANTR	Atmospheric ν, deep sea telescope
$2.50 {}^{+0.13}_{-0.31}$	[13] ABE	18B	SKAM	3ν osc: normal mass ordering, θ_{13} free
$-2.28 {}^{+0.33}_{-0.13}$	[13] ABE	18B	SKAM	3ν osc: inverted mass ordering, θ_{13} free
$2.463 {}^{+0.071}_{-0.070}$	[14] ABE	18G	T2K	Normal mass ordering, θ_{13} constrained
-2.507 ± 0.070	[14,15] ABE	18G	T2K	Inverted mass ordering, θ_{13} constrained
$2.44 {}^{+0.08}_{-0.07}$	[16] ACERO	18	NOVA	Normal mass order, octant II for θ_{23}
$2.45 {}^{+0.07}_{-0.08}$	[16,17] ACERO	18	NOVA	Normal mass order; octant I for θ_{23}
$2.7 {}^{+0.7}_{-0.6}$	[18] AGAFONOVA	18	OPER	OPERA ν_τ appearance
2.42 ± 0.03	DE-SALAS	18	FIT	Normal mass ordering, global fit
$-2.50 {}^{+0.03}_{-0.04}$	DE-SALAS	18	FIT	Inverted mass order, global fit
$2.57 {}^{+0.21}_{-0.23} {}^{+0.12}_{-0.13}$	[19] SEO	18	RENO	Normal mass ordering
$-2.67 {}^{+0.23}_{-0.21} {}^{+0.13}_{-0.12}$	[19] SEO	18	RENO	Inverted mass ordering
$2.53 {}^{+0.15}_{-0.13}$	ABE	17C	T2K	Normal mass ordering with neutrinos
$2.55 {}^{+0.33}_{-0.27}$	ABE	17C	T2K	Normal mass ordering with antineutrinos
$2.55 {}^{+0.08}_{-0.08}$	ABE	17C	T2K	Normal mass ordering with neutrinos and antineutrinos
$-2.63 {}^{+0.08}_{-0.08}$	ABE	17C	T2K	Inverted mass ordering with neutrinos and antineutrinos
2.54 ± 0.08	[20] ABE	17F	T2K	Normal mass ordering; $\nu+\overline{\nu}$
-2.51 ± 0.08	[20] ABE	17F	T2K	Inverted mass ordering; $\nu+\overline{\nu}$
2.67 ± 0.11	[21] ADAMSON	17A	NOVA	3ν osc; normal mass ordering
-2.72 ± 0.11	[21] ADAMSON	17A	NOVA	3ν osc; inverted mass ordering
$2.45 \pm 0.06 \pm 0.06$	[22] AN	17A	DAYA	Normal mass ordering
$-2.56 \pm 0.06 \pm 0.06$	[22] AN	17A	DAYA	Inverted mass ordering
$2.51 {}^{+0.29}_{-0.25}$	[23] ABE	16D	T2K	3ν osc.; normal mass ordering; $\overline{\nu}$ beam
$2.52 {}^{+0.20}_{-0.18}$	[24] ADAMSON	16A	NOVA	3ν osc; normal mass ordering
-2.56 ± 0.19	[24] ADAMSON	16A	NOVA	3ν osc; inverted mass ordering
$2.56 {}^{+0.21}_{-0.23} {}^{+0.12}_{-0.13}$	[25] CHOI	16	RENO	3ν osc; normal mass ordering
$-2.69 {}^{+0.23}_{-0.21} {}^{+0.13}_{-0.12}$	[25] CHOI	16	RENO	3ν osc; inverted mass ordering
$2.72 {}^{+0.19}_{-0.20}$	[26] AARTSEN	15A	ICCB	Normal mass ordering
$-2.73 {}^{+0.21}_{-0.18}$	[26] AARTSEN	15A	ICCB	Inverted mass ordering
2.0–5.0	[27] AGAFONOVA	15A	OPER	90% CL, 5 events
2.37 ± 0.11	[28] AN	15	DAYA	3ν osc.; normal mass ordering
-2.47 ± 0.11	[28] AN	15	DAYA	3ν osc.; inverted mass ordering
2.51 ± 0.10	[29] ABE	14	T2K	3ν osc.; normal mass ordering
-2.56 ± 0.10	[29] ABE	14	T2K	3ν osc.; inverted mass ordering
2.37 ± 0.09	[30] ADAMSON	14	MINS	Accel., atmospheric, normal mass ordering
$-2.41 {}^{+0.09}_{-0.12}$	[30] ADAMSON	14	MINS	Accel., atmsopheric, inverted mass ordering
$2.54 {}^{+0.19}_{-0.20}$	[31] AN	14	DAYA	3ν osc.; normal mass ordering
$-2.64 {}^{+0.20}_{-0.19}$	[31] AN	14	DAYA	3ν osc.; inverted mass ordering
$2.48 {}^{+0.05}_{-0.07}$	[32] FORERO	14	FIT	3ν; normal mass ordering
$-2.38 {}^{+0.06}_{-0.05}$	[32] FORERO	14	FIT	3ν; inverted mass ordering
2.457 ± 0.047	[33,34] GONZALEZ...	14	FIT	Normal mass ordering; global fit
$-2.449 {}^{+0.047}_{-0.048}$	[33] GONZALEZ...	14	FIT	Inverted mass ordering; global fit
$2.3 {}^{+0.6}_{-0.5}$	[35] AARTSEN	13B	ICCB	DeepCore, 2ν oscillation
$2.44 {}^{+0.17}_{-0.15}$	[36] ABE	13G	T2K	3ν osc.; normal mass ordering
$2.41 {}^{+0.09}_{-0.10}$	[37] ADAMSON	13B	MINS	2ν osc.; beam + atmospheric; identical ν & $\overline{\nu}$
2.2–3.1	[38] ABE	12A	T2K	off-axis beam
$2.62 {}^{+0.31}_{-0.28} \pm 0.09$	[39] ADAMSON	12	MINS	$\overline{\nu}$ beam
1.35–2.55	[40,41] ADAMSON	12B	MINS	MINOS atmospheric
1.4–5.6	[40,42] ADAMSON	12B	MINS	MINOS pure atmospheric ν
0.9–2.5	[40,42] ADAMSON	12B	MINS	MINOS pure atmospheric $\overline{\nu}$
1.8–5.0	[43] ADRIAN-MAR..	12	ANTR	Atmospheric ν with deep sea telescope
1.3–4.0	[44] ABE	11C	SKAM	atmospheric $\overline{\nu}$
$2.32 {}^{+0.12}_{-0.08}$	ADAMSON	11	MINS	2ν oscillation; maximal mixing
$3.36 {}^{+0.46}_{-0.40}$	[45] ADAMSON	11B	MINS	$\overline{\nu}$ beam
< 3.37	[46] ADAMSON	11C	MINS	MINOS
1.9–2.6	[47] WENDELL	10	SKAM	3ν osc.; normal mass ordering
$-1.7 - -2.7$	[47] WENDELL	10	SKAM	3ν osc.; inverted mass ordering
2.43 ± 0.13	ADAMSON	08A	MINS	MINOS
0.07–50	[48] ADAMSON	06	MINS	atmospheric ν with far detector
1.9–4.0	[49,50] AHN	06A	K2K	KEK to Super-K
2.2–3.8	[51] MICHAEL	06	MINS	MINOS
1.9–3.6	[49] ALIU	05	K2K	KEK to Super-K
0.3–12	[52] ALLISON	05	SOU2	
1.5–3.4	[53] ASHIE	05	SKAM	atmospheric neutrino
0.6–8.0	[54] AMBROSIO	04	MCRO	MACRO
1.9 to 3.0	[55] ASHIE	04	SKAM	L/E distribution
1.5–3.9	[56] AHN	03	K2K	KEK to Super-K
0.25–9.0	[57] AMBROSIO	03	MCRO	MACRO
0.6–7.0	[58] AMBROSIO	03	MCRO	MACRO
0.15–15	[59] SANCHEZ	03	SOU2	Soudan-2 Atmospheric
0.6–15	[60] AMBROSIO	01	MCRO	upward μ
1.0–6.0	[61] AMBROSIO	01	MCRO	upward μ
1.0–50	[62] FUKUDA	99C	SKAM	upward μ
1.5–15.0	[63] FUKUDA	99D	SKAM	upward μ
0.7–18	[64] FUKUDA	99D	SKAM	stop μ / through
0.5–6.0	[65] FUKUDA	98C	SKAM	Super-Kamiokande
0.55–50	[66] HATAKEYAMA	98	KAMI	Kamiokande
4–23	[67] HATAKEYAMA	98	KAMI	Kamiokande
5–25	[68] FUKUDA	94	KAMI	Kamiokande

[1] ABE 20F results are based on data collected between 2009 and 2018 in (anti)neutrino mode and include a neutrino beam exposure of 1.49×10^{21} (1.64×10^{21}) protons on target. Supersedes ABE 18G.

[2] ABE 20F reports $\Delta m^2_{13} = (2.43 \pm 0.07) \times 10^{-3}$ eV^2 for inverted mass ordering. We convert to Δm^2_{32} using PDG 20 value of $\Delta m^2_{21} = (7.53 \pm 0.18) \times 10^{-5}$ eV^2.

[3] ADAMSON 20A uses the complete dataset from MINOS and MINOS+ experiments. The data were collected using a total exposure of 23.76×10^{20} protons on target and 60.75 kton·yr exposure to atmospheric neutrinos. Supersedes ADAMSON 14.

[4] ACERO 19 is based on a sample size of 12.33×10^{20} protons on target. The fit combines both antineutrino and neutrino data to extract the oscillation parameters. The results favor the normal mass ordering by 1.9 σ and θ_{23} values in octant II by 1.6 σ. Supersedes ACERO 18.

[5] AARTSEN 18A uses three years (April 2012 – May 2015) of neutrino data from full sky with reconstructed energies between 5.6 and 56 GeV, measured with the low-energy subdetector DeepCore of the IceCube neutrino telescope. AARTSEN 18A also reports the best fit values for the inverted mass ordering as $\Delta m^2_{32} = -2.32 \times 10^{-3}$ eV^2 and $\sin^2(\theta_{23}) = 0.51$. Uncertainties for the inverted mass ordering fits were not provided. Supersedes AARTSEN 15A.

Downloaded from https://academic.oup.com/ptep/article/2022/8/083C01/6651666 by KIT Library user on 27 September 2022

[6] ABE 18B uses 328 kton-years of Super-Kamiokande I-IV atmospheric neutrino data to obtain this result. The fit is performed over the three parameters, Δm^2_{32}, $\sin^2(\theta_{23})$, and δ, while the solar parameters and $\sin^2(\theta_{13})$ are fixed to $\Delta m^2_{21} = (7.53 \pm 0.18) \times 10^{-5}$ eV^2, $\sin^2(\theta_{12}) = 0.304 \pm 0.014$, and $\sin^2(\theta_{13}) = 0.0219 \pm 0.0012$.

[7] ADEY 18A reports results from analysis of 1958 days of data taking with the Daya-Bay experiment, with 3.9×10^6 $\overline{\nu}_e$ candidates. The fit to the data gives $\Delta m^2_{ee} = (2.522^{+0.068}_{-0.070}) \times 10^{-3}$ eV^2. Solar oscillation parameters are fixed in the analysis using the global averages, $\sin^2(\theta_{12}) = 0.307^{+0.013}_{-0.012}$, $\Delta m^2_{21} = (7.53 \pm 0.18) \times 10^{-5}$ eV^2, from PDG 18. Supersedes AN 17A.

[8] BAK 18 reports results of the RENO experiment using about 2200 live-days of data taken with detectors placed at 410.6 and 1445.7 m from reactors of the Hanbit Nuclear Power Plant. We convert the results to Δm^2_{32} using the PDG 18 values of $\sin^2\theta_{12} = 0.307^{+0.013}_{-0.012}$ and $\Delta m^2_{21} = (7.53 \pm 0.18) \times 10^{-5}$ eV^2. Supersedes SEO 18.

[9] ABE 21A results are based on 1.49×10^{21} POT in neutrino mode and 1.64×10^{21} POT in antineutrino mode.

[10] ESTEBAN 20A reports results of a global fit to neutrino oscillation data available at the time of the Neutrino2020 conference.

[11] AARTSEN 19C uses three years (April 2012 – May 2015) of neutrino data from full sky with reconstructed energies between 5.6 and 56 GeV, measured with the low-energy sub-detector DeepCore of the IceCube neutrino telescope. AARTSEN 19C adopts looser event selection criteria to prioritize the efficiency of selecting neutrino events, different from tighter event selection criteria which closely follow the criteria used by AARTSEN 18A to measure the ν_μ disappearance.

[12] ALBERT 19 measured the oscillation parameters of atmospheric neutrinos with the ANTARES deep sea neutrino telescope using the data taken from 2007 to 2016 (2830 days of total live time). Supersedes ADRIAN-MARTINEZ 12.

[13] ABE 18B uses 328 kton-years of Super-Kamiokande I-IV atmospheric neutrino data to obtain this result. The fit is performed over the four parameters, Δm^2_{32}, $\sin^2\theta_{23}$, $\sin^2\theta_{13}$, and δ, while the solar parameters are fixed to $\Delta m^2_{21} = (7.53 \pm 0.18) \times 10^{-5}$ eV^2 and $\sin^2\theta_{12} = 0.304 \pm 0.014$.

[14] ABE 18G data prefers normal ordering with a posterior probability of 87%. Supersedes ABE 17F.

[15] ABE 18G reports Δm^2_{13}=$(2.432 \pm 0.070) \times 10^{-3}$ eV^2 for inverted mass ordering. We convert to Δm^2_{32} using PDG 18 value of Δm^2_{21}=$(7.53 \pm 0.18) \times 10^{-5}$ eV^2.

[16] ACERO 18 performs a joint fit to the data for ν_μ disappearance and ν_e appearance. The overall best fit favors normal mass ordering and θ_{23} in octant II. No 1σ confidence intervals are presented for the inverted mass ordering scenarios. Superseded by ACERO 19.

[17] The error for octant I is taken from the result for octant II.

[18] AGAFONOVA 18 assumes maximal θ_{23} mixing.

[19] SEO 18 reports result of the RENO experiment from a rate and shape analysis of 500 days of data. A simultaneous fit to θ_{13} and Δm^2_{ee} yields $\Delta m^2_{ee} = (2.62^{+0.21}_{-0.23}{}^{+0.12}_{-0.13}) \times 10^{-3}$ eV^2. We convert the results to Δm^2_{32} using the PDG 18 values of $\sin^2\theta_{12}$ and Δm^2_{21}. SEO 18 is a detailed description of the results published in CHOI 16, which it supersedes. Superseded by BAK 18

[20] ABE 17F confidence intervals are obtained using a frequentist analysis including θ_{13} constraint from reactor experiments. Bayesian intervals based on Markov Chain Monte Carlo method are also provided by the authors. Superseded by ABE 18G.

[21] Superseded by ACERO 18.

[22] AN 17A report results from combined rate and spectral shape analysis of 1230 days of data taken with the Daya Bay reactor experiment. The data set contains more than 2.5×10^6 inverse beta-decay events with neutron capture on Gd. The fit to the data gives Δ^2_{ee}=$(2.50 \pm 0.06 \pm 0.06) \times 10^{-3}$ eV. Superseded by ADEY 18A.

[23] ABE 16D reports oscillation results using $\overline{\nu}_\mu$ disappearance in an off-axis beam.

[24] Superseded by ADAMSON 17A.

[25] CHOI 16 reports result of the RENO experiment from a rate and shape analysis of 500 days of data. A simultaneous fit to θ_{13} and Δm^2_{ee} yields $\Delta m^2_{ee} = (2.62^{+0.21}_{-0.23}{}^{+0.12}_{-0.13}) \times 10^{-3}$ eV. We convert the results to Δm^2_{32} using PDG 18 values of $\sin^2(\theta_{12})$ and Δm^2_{21}.

[26] AARTSEN 15A obtains this result by a three-neutrino oscillation analysis using 10–100 GeV muon neutrino sample from a total of 953 days of measurements with the low-energy subdetector DeepCore of the IceCube neutrino telescope. Superseded by AARTSEN 18A.

[27] AGAFONOVA 15A result is based on 5 $\nu_\mu \rightarrow \nu_\tau$ appearance candidates with an expected background of 0.25 ± 0.05 events. The best fit is for Δm^2_{32}=3.3×10^{-3} eV^2.

[28] AN 15 uses all eight identical detectors, with four placed near the reactor cores and the remaining four at the far hall to determine prompt energy spectra. The results correspond to the exposure of 6.9×10^5 GW$_{th}$-ton-days. They derive $\Delta m^2_{ee} = (2.42 \pm 0.11) \times 10^{-3}$ eV^2. Assuming the normal (inverted) ordering, the fitted $\Delta m^2_{32} = (2.37 \pm 0.11) \times 10^{-3}$ $((2.47 \pm 0.11) \times 10^{-3})$ eV^2. Superseded by AN 17A.

[29] ABE 14 results are based on ν_μ disappearance using three-neutrino oscillation fit. The confidence intervals are derived from one dimensional profiled likelihoods. In ABE 14 the inverted mass ordering result is reported as $\Delta m^2_{13} = (2.48 \pm 0.10) \times 10^{-3}$ eV^2 which we converted to Δm^2_{32} by adding PDG 14 value of $\Delta m^2_{21} = (7.53 \pm 0.18) \times 10^{-5}$ eV^2. Superseded by ABE 17C.

[30] ADAMSON 14 uses a complete set of accelerator and atmospheric data. The analysis combines The analysis combines the ν_μ disappearance and ν_e appearance data using three-neutrino oscillation fit. The fit results are obtained for normal and inverted mass ordering assumptions.

[31] AN 14 uses six identical detectors, with three placed near the reactor cores (flux-weighted baselines of 512 and 561 m) and the remaining three at the far hall (at the flux averaged distance of 1579 m from all six reactor cores) to determine prompt energy spectra and derive $\Delta m^2_{ee} = (2.59^{+0.19}_{-0.20}) \times 10^{-3}$ eV^2. Assuming the normal (inverted) ordering, the fitted $\Delta m^2_{32} = (2.54^{+0.19}_{-0.20}) \times 10^{-3}$ $((2.64^{+0.19}_{-0.20}) \times 10^{-3})$ eV^2. Superseded by AN 15.

[32] FORERO 14 performs a global fit to Δm^2_{31} using solar, reactor, long-baseline accelerator, and atmospheric neutrino data.

[33] GONZALEZ-GARCIA 14 result comes from a frequentist global fit. The corresponding Bayesian global fit to the same data results are reported in BERGSTROM 15 as $(2.460 \pm 0.046) \times 10^{-3}$ eV^2 for normal and $(2.445^{+0.047}_{-0.045}) \times 10^{-3}$ eV^2 for inverted mass ordering.

[34] The value for normal mass ordering is actually a measurement of Δm^2_{31} which differs from Δm^2_{32} by a much smaller value of Δm^2_{12}.

[35] AARTSEN 13B obtained this result by a two-neutrino oscillation analysis using 20–100 GeV muon neutrino sample from a total of 318.9 days of live-time measurement with the low-energy subdetector DeepCore of the IceCube neutrino telescope.

[36] Based on the observation of 58 ν_μ events with 205 ± 17(syst) expected in the absence of neutrino oscillations. Superseded by ABE 14.

[37] ADAMSON 13B obtained this result from ν_μ and $\overline{\nu}_\mu$ disappearance using ν_μ (10.71×10^{20} POT) and $\overline{\nu}_\mu$ (3.36×10^{20} POT) beams, and atmospheric (37.88 kton-years) data from MINOS. The fit assumed two-flavor neutrino hypothesis and identical ν_μ and $\overline{\nu}_\mu$ oscillation parameters.

[38] ABE 12A obtained this result by a two-neutrino oscillation analysis. The best-fit point is $\Delta m^2_{32} = 2.65 \times 10^{-3}$ eV^2.

[39] ADAMSON 12 is a two-neutrino oscillation analysis using antineutrinos.

[40] ADAMSON 12B obtained this result by a two-neutrino oscillation analysis of the L/E distribution using 37.9 kton·yr atmospheric neutrino data with the MINOS far detector.

[41] The 90% single-parameter confidence interval at the best fit point is $\Delta m^2 = 0.0019 \pm 0.0004$ eV^2.

[42] The data are separated into pure samples of νs and $\overline{\nu}$s, and separate oscillation parameters for νs and $\overline{\nu}$s are fit to the data. The best fit point is (Δm^2, $\sin^2 2\theta$) = (0.0022 eV^2, 0.99) and ($\Delta\overline{m}^2$, $\sin^2 2\overline{\theta}$) = (0.0016 eV^2, 1.00). The quoted result is taken from the 90% C.L. contour in the (Δm^2, $\sin^2 2\theta$) plane obtained by minimizing the four parameter log-likelihood function with respect to the other oscillation parameters.

[43] ADRIAN-MARTINEZ 12 measured the oscillation parameters of atmospheric neutrinos with the ANTARES deep sea neutrino telescope using the data taken from 2007 to 2010 (863 days of total live time). Superseded by ALBERT 19

[44] ABE 11C obtained this result by a two-neutrino oscillation analysis with separate mixing parameters between neutrinos and antineutrinos, using the Super-Kamiokande-I+II+III atmospheric neutrino data. The corresponding 90% CL neutrino oscillation parameter range obtained from this analysis is $\Delta m^2 = 1.7$–3.0×10^{-3} eV^2.

[45] ADAMSON 11B obtained this result by a two-neutrino oscillation analysis of antineutrinos in an antineutrino enhanced beam with 1.71×10^{20} protons on target. This results is consistent with the neutrino measurements of ADAMSON 11 at 2% C.L.

[46] ADAMSON 11C obtains this result based on a study of antineutrinos in a neutrino beam and assumes maximal mixing in the two-flavor approximation.

[47] WENDELL 10 obtained this result by a three-neutrino oscillation analysis with one mass scale dominance ($\Delta m^2_{21} = 0$) using the Super-Kamiokande-I+II+III atmospheric neutrino data, and updates the HOSAKA 06A result.

[48] ADAMSON 06 obtained this result by a two-neutrino oscillation analysis of the L/E distribution using 4.54 kton yr atmospheric neutrino data with the MINOS far detector.

[49] The best fit in the physical region is for $\Delta m^2 = 2.8 \times 10^{-3}$ eV^2.

[50] Supercedes ALIU 05.

[51] MICHAEL 06 best fit is 2.74×10^{-3} eV^2. See also ADAMSON 08.

[52] ALLISON 05 result is based on an atmospheric neutrino observation with an exposure of 5.9 kton yr. From a two-flavor oscillation analysis the best-fit point is $\Delta m^2 = 0.0017$ eV^2 and $\sin^2 2\,\theta = 0.97$.

[53] ASHIE 05 obtained this result by a two-neutrino oscillation analysis using 92 kton yr atmospheric neutrino data from the complete Super-Kamiokande I running period. The best fit is for $\Delta m^2 = 2.1 \times 10^{-3}$ eV^2.

[54] AMBROSIO 04 obtained this result, without using the absolute normalization of the neutrino flux, by combining the angular distribution of upward through-going muon tracks with $E_\mu > 1$ GeV, N$_{low}$ and N$_{high}$, and the numbers of InDown + UpStop and InUp events. Here, N$_{low}$ and N$_{high}$ are the number of events with reconstructed neutrino energies < 30 GeV and > 130 GeV, respectively. InDown and InUp represent events with downward and upward-going tracks starting inside the detector due to neutrino interactions, while UpStop represents entering upward-going tracks which stop in the detector. The best fit is for $\Delta m^2 = 2.3 \times 10^{-3}$ eV^2.

[55] ASHIE 04 obtained this result from the L(flight length)/E(estimated neutrino energy) distribution of ν_μ disappearance probability, using the Super-Kamiokande-I 1489 live-day atmospheric neutrino data. The best fit is for $\Delta m^2 = 2.4 \times 10^{-3}$ eV^2.

[56] There are several islands of allowed region from this K2K analysis, extending to high values of Δm^2. We only include the one that overlaps atmospheric neutrino analyses. The best fit is for $\Delta m^2 = 2.8 \times 10^{-3}$ eV^2.

[57] AMBROSIO 03 obtained this result on the basis of the ratio R = N$_{low}$/N$_{high}$, where N$_{low}$ and N$_{high}$ are the number of upward through-going muon events with reconstructed neutrino energy < 30 GeV and > 130 GeV, respectively. The data came from the full detector run started in 1994. The method of FELDMAN 98 is used to obtain the limits. The best fit is for $\Delta m^2 = 2.5 \times 10^{-3}$ eV^2.

[58] AMBROSIO 03 obtained this result by using the ratio R and the angular distribution of the upward through-going muons. R is given in the previous note and the angular

Downloaded from https://academic.oup.com/ptep/article/2022/8/083C01/6651666 by KIT Library user on 27 September 2022

distribution is reported in AMBROSIO 01. The method of FELDMAN 98 is used to obtain the limits. The best fit is for $\Delta m^2 = 2.5 \times 10^{-3}$ eV^2.

[59] SANCHEZ 03 is based on an exposure of 5.9 kton yr. The result is obtained using a likelihood analysis of the neutrino L/E distribution for a selection μ flavor sample while the e-flavor sample provides flux normalization. The method of FELDMAN 98 is used to obtain the allowed region. The best fit is for $\Delta m^2 = 5.2 \times 10^{-3}$ eV^2.

[60] AMBROSIO 01 result is based on the angular distribution of upward through-going muon tracks with $E_\mu > 1$ GeV. The data came from three different detector configurations, but the statistics is largely dominated by the full detector run, from May 1994 to December 2000. The total live time, normalized to the full detector configuration is 6.17 years. The best fit is obtained outside the physical region. The method of FELDMAN 98 is used to obtain the limits.

[61] AMBROSIO 01 result is based on the angular distribution and normalization of upward through-going muon tracks with $E_\mu > 1$ GeV. See the previous footnote.

[62] FUKUDA 99C obtained this result from a total of 537 live days of upward through-going muon data in Super-Kamiokande between April 1996 to January 1998. With a threshold of $E_\mu > 1.6$ GeV, the observed flux is $(1.74 \pm 0.07 \pm 0.02) \times 10^{-13}$ cm^{-2}s^{-1}sr^{-1}. The best fit is for $\Delta m^2 = 5.9 \times 10^{-3}$ eV^2.

[63] FUKUDA 99D obtained this result from a simultaneous fitting to zenith angle distributions of upward-stopping and through-going muons. The flux of upward-stopping muons of minimum energy of 1.6 GeV measured between April 1996 and January 1998 is $(0.39 \pm 0.04 \pm 0.02) \times 10^{-13}$ cm^{-2}s^{-1}sr^{-1}. This is compared to the expected flux of $(0.73 \pm 0.16$ (theoretical error)$) \times 10^{-13}$ cm^{-2}s^{-1}sr^{-1}. The best fit is for $\Delta m^2 = 3.9 \times 10^{-3}$ eV^2.

[64] FUKUDA 99D obtained this result from the zenith dependence of the upward-stopping/through-going flux ratio. The best fit is for $\Delta m^2 = 3.1 \times 10^{-3}$ eV^2.

[65] FUKUDA 98C obtained this result by an analysis of 33.0 kton yr atmospheric neutrino data. The best fit is for $\Delta m^2 = 2.2 \times 10^{-3}$ eV^2.

[66] HATAKEYAMA 98 obtained this result from a total of 2456 live days of upward-going muon data in Kamiokande between December 1985 and May 1995. With a threshold of $E_\mu > 1.6$ GeV, the observed flux of upward through-going muons is $(1.94 \pm 0.10^{+0.07}_{-0.06}) \times 10^{-13}$ cm^{-2}s^{-1}sr^{-1}. This is compared to the expected flux of $(2.46 \pm 0.54$ (theoretical error)$) \times 10^{-13}$ cm^{-2}s^{-1}sr^{-1}. The best fit is for $\Delta m^2 = 2.2 \times 10^{-3}$ eV^2.

[67] HATAKEYAMA 98 obtained this result from a combined analysis of Kamiokande contained events (FUKUDA 94) and upward going muon events. The best fit is for $\Delta m^2 = 13 \times 10^{-3}$ eV^2.

[68] FUKUDA 94 obtained the result by a combined analysis of sub- and multi-GeV atmospheric neutrino events in Kamiokande. The best fit is for $\Delta m^2 = 16 \times 10^{-3}$ eV^2.

$\sin^2(\theta_{13})$

At present time direct measurements of $\sin^2(\theta_{13})$ are derived from the reactor $\overline{\nu}_e$ disappearance at distances corresponding to the Δm^2_{32} value, i.e. L $\sim$ 1km. Alternatively, limits can also be obtained from the analysis of the solar neutrino data and accelerator-based $\nu_\mu \rightarrow \nu_e$ experiments.

If an experiment reports $\sin^2(2\theta_{13})$ we convert the value to $\sin^2(\theta_{13})$.

VALUE (units 10^{-2})	CL%	DOCUMENT ID		TECN	COMMENT
2.20 ± 0.07 OUR AVERAGE					
2.70 ± 0.37		[1] DE-KERRET	20	DCHZ	Chooz reactors
2.22 ± 0.21 ±0.37		[2] SHIN	20	RENO	Yonggwang reactors
2.188± 0.076		[3] ADEY	18A	DAYA	DayaBay, LingAo/Ao II reactors
2.29 ± 0.18		[4] BAK	18	RENO	Yonggwang reactors
1.81 ± 0.29		[5] AN	16A	DAYA	DayaBay, Ling Ao/Ao II reactors
• • • We do not use the following data for averages, fits, limits, etc. • • •					
2.41 ± 0.45		[6] ABRAHAO	21	DCHZ	Chooz reactors
$2.200^{+0.069}_{-0.062}$		[7] SALAS	21	FIT	Normal mass ordering, global fit
$2.225^{+0.064}_{-0.070}$		[7] SALAS	21	FIT	Inverted mass ordering, global fit
$2.219^{+0.062}_{-0.063}$		[8] ESTEBAN	20A	FIT	Normal mass ordering, global fit
$2.238^{+0.063}_{-0.062}$		[8] ESTEBAN	20A	FIT	Inverted mass ordering, global fit
< 3.9	68	AGAFONOVA	19	OPER	
$1.8^{+2.9}_{-1.3}$		[9] ABE	18B	SKAM	3ν osc: normal mass ordering, θ_{13} free
$0.8^{+1.7}_{-0.7}$		[9] ABE	18B	SKAM	3ν osc: inverted mass ordering, θ_{13} free
<12	90	[10] AGAFONOVA	18A	OPER	OPERA: ν_e appearance
$2.160^{+0.083}_{-0.069}$		DE-SALAS	18	FIT	Normal mass ordering, global fit
$2.220^{+0.074}_{-0.076}$		DE-SALAS	18	FIT	Inverted mass ordering, global fit
2.09 ± 0.23 ±0.16		[11] SEO	18	RENO	Yonggwang reactors
2.7 ± 0.7		[12] ABE	17F	T2K	Normal mass ordering, T2K only
2.149± 0.071±0.050		[13] AN	17A	DAYA	DayaBay, LingAo/Ao II reactors
$2.25^{+0.87}_{-0.86}$		[14] ABE	16B	DCHZ	Chooz reactors
2.09 ± 0.23 ±0.16		[15] CHOI	16	RENO	Yonggwang reactors
2.15 ± 0.13		[16] AN	15	DAYA	DayaBay, Ling Ao/Ao II reactors
$2.6^{+1.2}_{-1.1}$		[17] ABE	14A	DCHZ	Chooz reactors
$3.0^{+1.3}_{-1.0}$		[18] ABE	14C	T2K	Inverted mass ordering
$3.6^{+1.0}_{-0.9}$		[18] ABE	14C	T2K	Normal mass ordering
$2.3^{+0.9}_{-0.8}$		[19] ABE	14H	DCHZ	Chooz reactors
2.3 ± 0.2		[20] AN	14	DAYA	DayaBay, Ling Ao/Ao II reactors
2.12 ± 0.47		[21] AN	14B	DAYA	DayaBay, Ling Ao/Ao II reactors
2.34 ± 0.20		[22] FORERO	14	FIT	Normal mass ordering
2.40 ± 0.19		[22] FORERO	14	FIT	Inverted mass ordering
2.18 ± 0.10		[23] GONZALEZ...	14	FIT	Normal mass ordering; global fit
$2.19^{+0.11}_{-0.10}$		[23] GONZALEZ...	14	FIT	Inverted mass ordering; global fit
2.5 ± 0.9 ±0.9		[24] ABE	13C	DCHZ	Chooz reactors
$2.3^{+1.3}_{-1.0}$		[25] ABE	13E	T2K	Normal mass ordering
$2.8^{+1.6}_{-1.2}$		[25] ABE	13E	T2K	Inverted mass ordering
$1.6^{+1.3}_{-0.9}$		[26] ADAMSON	13A	MINS	Normal mass ordering
$3.0^{+1.8}_{-1.6}$		[26] ADAMSON	13A	MINS	Inverted mass ordering
<13	90	AGAFONOVA	13	OPER	OPERA: 3ν
< 3.6	95	[27] AHARMIM	13	FIT	global solar: 3ν
2.3 ± 0.3 ±0.1		[28] AN	13	DAYA	DayaBay, LIng Ao/Ao II reactors
2.2 ± 1.1 ±0.8		[29] ABE	12	DCHZ	Chooz reactors
2.8 ± 0.8 ±0.7		[30] ABE	12B	DCHZ	Chooz reactors
2.9 ± 0.3 ±0.5		[31] AHN	12	RENO	Yonggwang reactors
2.4 ± 0.4 ±0.1		[32] AN	12	DAYA	DayaBay, Ling Ao/Ao II reactors
$2.5^{+1.8}_{-1.6}$		[33] ABE	11	FIT	KamLAND + global solar
< 6.1	95	[34] ABE	11	FIT	Global solar
1.3 to 5.6	68	[35] ABE	11A	T2K	Normal mass ordering
1.5 to 5.6	68	[36] ABE	11A	T2K	Inverted mass ordering
0.3 to 2.3	68	[37] ADAMSON	11D	MINS	Normal mass ordering
0.8 to 3.9	68	[38] ADAMSON	11D	MINS	Inverted mass ordering
8 ± 3		[39] FOGLI	11	FIT	Global neutrino data
7.8 ± 6.2		[40] GANDO	11	FIT	KamLAND + solar: 3ν
12.4 ±13.3		[41] GANDO	11	FIT	KamLAND: 3ν
3^{+9}_{-7}	90	[42] ADAMSON	10A	MINS	Normal mass ordering
6^{+14}_{-6}	90	[43] ADAMSON	10A	MINS	Inverted mass ordering
8^{+8}_{-7}		[44,45] AHARMIM	10	FIT	KamLAND + global solar: 3ν
< 30	95	[44,46] AHARMIM	10	FIT	global solar: 3ν
< 15	90	[47] WENDELL	10	SKAM	3ν osc.; normal m ordering
< 33	90	[47] WENDELL	10	SKAM	3ν osc.; inverted m ordering
11^{+11}_{-8}		[48] ADAMSON	09	MINS	Normal mass ordering
18^{+15}_{-11}		[49] ADAMSON	09	MINS	Inverted mass ordering
6 ± 4		[50] FOGLI	08	FIT	Global neutrino data
8 ± 7		[51] FOGLI	08	FIT	Solar + KamLAND data
5 ± 5		[52] FOGLI	08	FIT	Atmospheric + LBL + CHOOZ
< 36	90	[53] YAMAMOTO	06	K2K	Accelerator experiment
< 48	90	[54] AHN	04	K2K	Accelerator experiment
< 36	90	[55] BOEHM	01		Palo Verde react.
< 45	90	[56] BOEHM	00		Palo Verde react.
< 15	90	[57] APOLLONIO	99	CHOZ	Reactor Experiment

[1] DE-KERRET 20 uses 481 days of data from single detector operation and also 384 days of data with both near and far detectors operating. A rate and shape analysis is performed on combined neutron captures on H and Gd. Supersedes ABE 16B.

[2] SHIN 20 uses the RENO detector and 1500 live days of data. The near (far) detector observed 567,690 (90,747) $\overline{\nu}_e$ candidate events with a delayed neutron capture on hydrogen. The extracted value of $\sin^2\theta_{13}$ is consistent with the previous analysis with neutron capture on Gd in BAK 18.

[3] ADEY 18A reports results from analysis of 1958 days of data taking with the DayaBay experiment, with 3.9×10^6 $\overline{\nu}_e$ candidates. The fit to the data gives $\Delta m^2_{ee} = (2.522^{+0.068}_{-0.070}) \times 10^{-3}$ eV^2. Solar oscillation parameters are fixed in the analysis using the global averages, $\sin^2(\theta_{12}) = 0.307^{+0.013}_{-0.012}$, $\Delta m^2_{21} = (7.53 \pm 0.18) \times 10^{-5}$ eV^2, from PDG 18. Supersedes AN 17A.

[4] BAK 18 reports results of the RENO experiment using about 2200 live-days of data taken with detectors placed at 410.6 and 1445.7 m from reactors of the Hanbit Nuclear Power Plant. Supersedes SEO 18.

[5] AN 16A uses data from the eight antineutrino detectors (404 days) and six antineutrino detectors (217 days) runs to determine the mixing parameter $\sin^2(2\theta_{13})$ using the neutron capture on H only. Supersedes AN 14B.

Downloaded from https://academic.oup.com/ptep/article/2022/8/083C01/6651666 by KIT Library user on 27 September 2022

[6] ABRAHAO 21 uses 865 days of data collected in both near and far detectors with at least one reactor in operation. The analysis is based on a background model independent approach, so called Reactor Rate Modulation, to determine the mixing angle θ_{13}. Adding the background model reduces the uncertainty to 0.0041. Supersedes ABE 16B.

[7] SALAS 21 reports results of a global fit to neutrino oscillation data available at the time of the Neutrino 2020 conference.

[8] ESTEBAN 20A reports results of a global fit to neutrino oscillation data available at the time of the Neutrino2020 conference.

[9] ABE 18B uses 328 kton-years of Super-Kamiokande I-IV atmospheric neutrino data to obtain this result. The fit is performed over the four parameters, Δm^2_{32}, $\sin^2\theta_{23}$, $\sin^2\theta_{13}$, and δ, while the solar parameters are fixed to $\Delta m^2_{21} = (7.53 \pm 0.18) \times 10^{-5}$ eV^2 and $\sin^2\theta_{12} = 0.304 \pm 0.014$.

[10] AGAFONOVA 18A reports $\sin^2(2\theta_{13}) < 0.43$ at 90% C.L. The result on the sterile neutrino search in the context of 3+1 model is also reported. A 90% C.L. upper limit on $\sin^2(2\theta_{\mu e}) = 0.021$ for $\Delta m^2_{41} \geq 0.1$ eV^2 is set.

[11] SEO 18 reports results of the RENO experiment using about 500 days of data, performing a rate and shape analysis. Compared to AHN 12, a significant reduction of the systematic uncertainties is reported. A 3% excess of events near 5 MeV of the prompt energy is observed. SEO 18 is a detailed description of the results published in CHOI 16, which it supersedes. Superseded by BAK 18.

[12] Using T2K data only. For inverted mass ordering, all values of θ_{13} are ruled out at 68% CL.

[13] AN 17A reports results from combined rate and spectral shape analysis of 1230 days of data taken with the Daya Bay reactor experiment. The data set contains more than 2.5×10^6 inverse beta-decay events with neutron capture on Gd. A simultaneous fit to θ_{13} and Δm^2_{ee} is performed. Superseded by ADEY 18A.

[14] ABE 16B uses 455.57 live days of data from a detector 1050 m away from two reactor cores of the Chooz nuclear power station, to determine the mixing parameter $\sin^2(2\theta_{13})$. This analysis uses 7.15 reactor-off days for constraining backgrounds. A rate and shape analysis is performed on combined neutron captures on H and Gd. Supersedes ABE 14H and ABE 13C.

[15] CHOI 16 reports results of the RENO experiment using about 500 days of data, performing a rate and shape analysis. Compared to AHN 12, a significant reduction of the systematic uncertainties is reported. A 3% excess of events near 5 MeV of the prompt energy is observed. Supersedes AHN 12.

[16] AN 15 uses all eight identical detectors, with four placed near the reactor cores and the remaining four at the far hall to determine the mixing angle θ_{13} using the $\overline{\nu}_e$ observed interaction rates with neutron capture on Gd and energy spectra. The result corresponds to the exposure of 6.9×10^5 GW$_{th}$-ton-days. Superseded by AN 17A.

[17] ABE 14A uses 467.9 live days of one detector, 1050 m away from two reactor cores of the Chooz nuclear power station, to determine the mixing parameter $\sin^2(2\,\theta_{13})$. The Bugey4 data (DECLAIS 94) is used to constrain the neutrino flux. The data set includes 7.24 reactor-off days. A "rate-modulation" analysis is performed. Supercedes ABE 12B.

[18] ABE 14C result is for ν_e appearance and assumes $\Delta m^2_{32} = 2.4 \times 10^{-3}$ eV^2, $\sin^2(\,\theta_{23}) = 0.5$, and $\delta = 0$.

[19] ABE 14H uses 467.9 live days of one detector, 1050 m away from two reactor cores of the Chooz nuclear power station, to determine the mixing parameter $\sin^2(2\,\theta_{13})$. The Bugey4 data (DECLAIS 94) is used to constrain the neutrino flux. The data set includes 7.24 reactor-off days. A rate and shape analysis is performed. Superceded by ABE 16B.

[20] AN 14 uses six identical detectors, with three placed near the reactor cores (flux-weighted baselines of 512 and 561 m) and the remaining three at the far hall (at the flux averaged distance of 1579 m from all six reactor cores) to determine the mixing angle θ_{13} using the $\overline{\nu}_e$ observed interaction rates with neutron capture on Gd and energy spectra. Supersedes AN 13 and superseded by AN 15.

[21] AN 14B uses six identical anti-neutrino detectors with flux-weighted baselines of ~ 500 m and ~ 1.6 km to six power reactors. This rate analysis uses a 217-day data set and neutron capture on protons (not Gd) only. $\Delta m^2_{31} = 2.32 \times 10^{-3}$ eV^2 is assumed. Superseded by AN 16A.

[22] FORERO 14 performs a global fit to neutrino oscillations using solar, reactor, long-baseline accelerator, and atmospheric neutrino data.

[23] GONZALEZ-GARCIA 14 result comes from a frequentist global fit. The corresponding Bayesian global fit to the same data results are reported in BERGSTROM 15 as $(2.18^{+0.10}_{-0.11}) \times 10^{-2}$ eV^2 for normal and $(2.19^{+0.12}_{-0.10}) \times 10^{-2}$ eV^2 for inverted mass ordering.

[24] ABE 13C uses delayed neutron capture on hydrogen instead of on Gd used previously. The physical volume is thus three times larger. The fit is based on the rate and shape analysis as in ABE 12B. The Bugey4 data (DECLAIS 94) is used to constrain the neutrino flux. Superseded by ABE 16B.

[25] ABE 13E assumes maximal θ_{23} mixing and *CP* phase $\delta = 0$.

[26] ADAMSON 13A results obtained from ν_e appearance, assuming $\delta = 0$, and $\sin^2(2\,\theta_{23}) = 0.957$.

[27] AHARMIM 13 obtained this result by a three-neutrino oscillation analysis with the value of Δm^2_{32} fixed to 2.45×10^{-3} eV^2, using global solar neutrino data. AHARMIM 13 global solar neutrino data include SNO's all-phases-combined analysis results on the total active ^{8}B neutrino flux and energy-dependent ν_e survival probability parameters, measurements of Cl (CLEVELAND 98), Ga (ABDURASHITOV 09 which contains combined analysis with GNO (ALTMANN 05 and Ph.D. thesis of F. Kaether)), and ^{7}Be (BELLINI 11A) rates, and ^{8}B solar-neutrino recoil electron measurements of SK-I (HOSAKA 06) zenith, SK-II (CRAVENS 08) and SK-III (ABE 11) day/night spectra, and Borexino (BELLINI 10A) spectra. AHARMIM 13 also reported a result combining global solar and KamLAND data, which is $\sin^2(2\,\theta_{13}) = (9.1^{+2.9}_{-3.1}) \times 10^{-2}$.

[28] AN 13 uses six identical detectors, with three placed near the reactor cores (flux-weighted baselines of 498 and 555 m) and the remaining three at the far hall (at the flux averaged distance of 1628 m from all six reactor cores) to determine the $\overline{\nu}_e$ interaction rate ratios. Superseded by AN 14.

[29] ABE 12 determines the $\overline{\nu}_e$ interaction rate in a single detector, located 1050 m from the cores of two reactors. A rate and shape analysis is performed. The rate normalization is fixed by the results of the Bugey4 reactor experiment, thus avoiding any dependence on possible very short baseline oscillations. The value of $\Delta m^2_{31} = 2.4 \times 10^{-3}$ eV^2 is used in the analysis. Superseded by ABE 12B.

[30] ABE 12B determines the neutrino mixing angle θ_{13} using a single detector, located 1050 m from the cores of two reactors. This result is based on a spectral shape and rate analysis. The Bugey4 data (DECLAIS 94) is used to constrain the neutrino flux. Superseded by ABE 14A.

[31] AHN 12 uses two identical detectors, placed at flux weighted distances of 408.56 m and 1433.99 m from six reactor cores, to determine the mixing angle θ_{13}. This rate-only analysis excludes the no-oscillation hypothesis at 4.9 standard deviations. The value of $\Delta m^2_{31} = (2.32^{+0.12}_{-0.08}) \times 10^{-3}$ eV^2 was assumed in the analysis. Superseded by CHOI 16.

[32] AN 12 uses six identical detectors with three placed near the reactor cores (flux-weighted baselines of 470 m and 576 m) and the remaining three at the far hall (at the flux averaged distance of 1648 m from all six reactor cores) to determine the mixing angle θ_{13} using the $\overline{\nu}_e$ observed interaction rate ratios. This rate-only analysis excludes the no-oscillation hypothesis at 5.2 standard deviations. The value of $\Delta m^2_{31} = (2.32^{+0.12}_{-0.08}) \times 10^{-3}$ eV^2 was assumed in the analysis. Superseded by AN 13.

[33] ABE 11 obtained this result by a three-neutrino oscillation analysis with the value of Δm^2_{32} fixed to 2.4×10^{-3} eV^2, using solar neutrino data including Super-Kamiokande, SNO, Borexino (ARPESELLA 08A), Homestake, GALLEX/GNO, SAGE, and KamLAND data. This result implies an upper bound of $\sin^2\theta_{13} < 0.059$ (95% CL) or $\sin^2 2\theta_{13} < 0.22$ (95% CL). The normal neutrino mass ordering and CPT invariance are assumed.

[34] ABE 11 obtained this result by a three-neutrino oscillation analysis with the value of Δm^2_{32} fixed to 2.4×10^{-3} eV^2, using solar neutrino data including Super-Kamiokande, SNO, Borexino (ARPESELLA 08A), Homestake, and GALLEX/GNO data. The normal neutrino mass ordering is assumed.

[35] The quoted limit is for $\Delta m^2_{32} = 2.4 \times 10^{-3}$ eV^2, $\theta_{23} = \pi/2$, $\delta = 0$, and the normal mass ordering. For other values of δ, the 68% region spans from 0.03 to 0.25, and the 90% region from 0.02 to 0.32.

[36] The quoted limit is for $\Delta m^2_{32} = 2.4 \times 10^{-3}$ eV^2, $\theta_{23} = \pi/2$, $\delta = 0$, and the inverted mass ordering. For other values of δ, the 68% region spans from 0.04 to 0.30, and the 90% region from 0.02 to 0.39.

[37] The quoted limit is for $\Delta m^2_{32} = 2.32 \times 10^{-3}$ eV^2, $\theta_{23} = \pi/2$, $\delta = 0$, and the normal mass ordering. For other values of δ, the 68% region spans from 0.02 to 0.12, and the 90% region from 0 to 0.16.

[38] The quoted limit is for $\Delta m^2_{32} = 2.32 \times 10^{-3}$ eV^2, $\theta_{23} = \pi/2$, $\delta = 0$, and the inverted mass ordering. For other values of δ, the 68% region spans from 0.02 to 0.16, and the 90% region from 0 to 0.21.

[39] FOGLI 11 obtained this result from an analysis using the atmospheric, accelerator long baseline, CHOOZ, solar, and KamLAND data. Recently, MUELLER 11 suggested an average increase of about 3.5% in normalization of the reactor $\overline{\nu}_e$ fluxess, and using these fluxes, the fitted result becomes 0.10 ± 0.03.

[40] GANDO 11 report $\sin^2\theta_{13} = 0.020 \pm 0.016$. This result was obtained with three-neutrino fit using the KamLAND + solar data.

[41] GANDO 11 report $\sin^2\theta_{13} = 0.032 \pm 0.037$. This result was obtained with three-neutrino fit using the KamLAND data only.

[42] This result corresponds to the limit of <0.12 at 90% CL for $\Delta m^2_{32} = 2.43 \times 10^{-3}$ eV^2, $\theta_{23} = \pi/2$, and $\delta = 0$. For other values of δ, the 90% CL region spans from 0 to 0.16.

[43] This result corresponds to the limit of <0.20 at 90% CL for $\Delta m^2_{32} = 2.43 \times 10^{-3}$ eV^2, $\theta_{23} = \pi/2$, and $\delta = 0$. For other values of δ, the 90% CL region spans from 0 to 0.21.

[44] AHARMIM 10 global solar neutrino data include SNO's low-energy-threshold analysis survival probability day/night curves, SNO Phase III integral rates (AHARMIM 08), Cl (CLEVELAND 98), SAGE (ABDURASHITOV 09), Gallex/GNO (HAMPEL 99, ALTMANN 05), Borexino (ARPESELLA 08A), SK-I zenith (HOSAKA 06), and SK-II day/night spectra (CRAVENS 08).

[45] AHARMIM 10 obtained this result by a three-neutrino oscillation analysis with the value of Δm^2_{31} fixed to 2.3×10^{-3} eV^2, using global solar neutrino data and KamLAND data (ABE 08A). *CPT* invariance is assumed. This result implies an upper bound of $\sin^2\theta_{13} < 0.057$ (95% CL) or $\sin^2 2\theta_{13} < 0.22$ (95% CL).

[46] AHARMIM 10 obtained this result by a three-neutrino oscillation analysis with the value of Δm^2_{31} fixed to 2.3×10^{-3} eV^2, using global solar neutrino data.

[47] WENDELL 10 obtained this result by a three-neutrino oscillation analysis with one mass scale dominance ($\Delta m^2_{21} = 0$) using the Super-Kamiokande-I+II+III atmospheric neutrino data, and updates the HOSAKA 06A result.

[48] The quoted limit is for $\Delta m^2_{32} = 2.43 \times 10^{-3}$ eV^2, $\theta_{23} = \pi/2$, and $\delta = 0$. For other values of δ, the 68% CL region spans from 0.02 to 0.26.

[49] The quoted limit is for $\Delta m^2_{32} = 2.43 \times 10^{-3}$ eV^2, $\theta_{23} = \pi/2$, and $\delta = 0$. For other values of δ, the 68% CL region spans from 0.04 to 0.34.

[50] FOGLI 08 obtained this result from a global analysis of all neutrino oscillation data, that is, solar + KamLAND + atmospheric + accelerator long baseline + CHOOZ.

[51] FOGLI 08 obtained this result from an analysis using the solar and KamLAND neutrino oscillation data.

[52] FOGLI 08 obtained this result from an analysis using the atmospheric, accelerator long baseline, and CHOOZ neutrino oscillation data.

[53] YAMAMOTO 06 searched for $\nu_\mu \rightarrow \nu_e$ appearance. Assumes $2\,\sin^2(2\theta_{\mu e}) = \sin^2(2\theta_{13})$. The quoted limit is for $\Delta m^2_{32} = 1.9 \times 10^{-3}$ eV^2. That value of Δm^2_{32} is the one-σ low value for AHN 06A. For the AHN 06A best fit value of 2.8×10^{-3} eV^2, the $\sin^2(2\theta_{13})$ limit is < 0.26. Supersedes AHN 04.

Downloaded from https://academic.oup.com/ptep/article/2022/8/083C01/6651666 by KIT Library user on 27 September 2022

[54] AHN 04 searched for $\nu_\mu \rightarrow \nu_e$ appearance. Assuming $2 \sin^2(2\,\theta_{\mu_e}) = \sin^2(2\,\theta_{13})$, a limit on $\sin^2(2\,\theta_{\mu_e})$ is converted to a limit on $\sin^2(2\,\theta_{13})$.The quoted limit is for $\Delta m^2_{32} = 1.9 \times 10^{-3}$ eV^2. That value of Δm^2_{32} is the one-σ low value for ALIU 05. For the ALIU 05 best fit value of 2.8×10^{-3} eV^2, the $\sin^2(2\,\theta_{13})$ limit is < 0.30.

[55] The quoted limit is for $\Delta m^2_{32} = 1.9 \times 10^{-3}$ eV^2. That value of Δm^2_{32} is the 1-σ low value for ALIU 05. For the ALIU 05 best fit value of 2.8×10^{-3} eV^2, the $\sin^2 2\,\theta_{13}$ limit is < 0.19. In this range, the θ_{13} limit is larger for lower values of Δm^2_{32}, and smaller for higher values of Δm^2_{32}.

[56] The quoted limit is for $\Delta m^2_{32} = 1.9 \times 10^{-3}$ eV^2. That value of Δm^2_{32} is the 1-σ low value for ALIU 05. For the ALIU 05 best fit value of 2.8×10^{-3} eV^2, the $\sin^2 2\,\theta_{13}$ limit is < 0.23.

[57] The quoted limit is for $\Delta m^2_{32} = 2.43 \times 10^{-3}$ eV^2. That value of Δm^2_{32} is the central value for ADAMSON 08. For the ADAMSON 08 1-σ low value of 2.30×10^{-3} eV^2, the $\sin^2 2\,\theta_{13}$ limit is < 0.16. See also APOLLONIO 03 for a detailed description of the experiment.

CP violating phase

δ, *CP* violating phase

Measurements of δ come from atmospheric and accelarator experiments looking at ν_e appearance. We encode values between 0 and 2π, though it is equivalent to use $-\pi$ to π.

VALUE (π rad)	CL%	DOCUMENT ID		TECN	COMMENT
$1.36^{+0.20}_{-0.16}$ OUR AVERAGE					
$1.40^{+0.22}_{-0.18}$		[1] ABE	20F	T2K	Normal mass ordering
$0.0\ ^{+1.3}_{-0.4}$		[2] ACERO	19	NOVA	Normall mass ordering, octant II for θ_{23}
$1.33^{+0.45}_{-0.51}$		[3] ABE	18B	SKAM	Normal mass ordering, θ_{13} constrained
• • • We do not use the following data for averages, fits, limits, etc. • • •					
$1.08^{+0.13}_{-0.12}$		[4] SALAS	21	FIT	Normal mass ordering, global fit
$1.58^{+0.15}_{-0.16}$		[4] SALAS	21	FIT	Inverted mass ordering, global fit
$1.09^{+0.15}_{-0.13}$		[5] ESTEBAN	20A	FIT	Normal mass ordering, global fit
$1.57^{+0.14}_{-0.17}$		[5] ESTEBAN	20A	FIT	Inverted mass ordering, global fit
$1.33^{+0.46}_{-0.53}$		[6] ABE	18B	SKAM	3ν osc: normal mass ordering, θ_{13} free
$1.22^{+0.76}_{-0.67}$		[6] ABE	18B	SKAM	3ν osc: inverted mass ordering, θ_{13} free
$1.33^{+0.48}_{-0.53}$		[3] ABE	18B	SKAM	3ν osc: inverted mass ordering, θ_{13} constrained
1.40 ± 0.20		[7] ABE	18G	T2K	Normal mass ordering, θ_{13} constrained
$1.54^{+0.14}_{-0.12}$	95	[7] ABE	18G	T2K	Inverted mass ordering, θ_{13} constrained
$1.21^{+0.91}_{-0.30}$		[8] ACERO	18	NOVA	Normal mass ordering, octant II for θ_{23}
$1.46^{+0.56}_{-0.42}$		[8] ACERO	18	NOVA	Normal mass order; octant I for θ_{23}
$1.32^{+0.21}_{-0.15}$		DE-SALAS	18	FIT	Normal mass ordering, global fit
$1.56^{+0.13}_{-0.15}$		DE-SALAS	18	FIT	Inverted mass ordering, global fit
$1.45^{+0.27}_{-0.26}$		[9] ABE	17F	T2K	Normal mass ordering
$1.54^{+0.22}_{-0.23}$		[9] ABE	17F	T2K	Inverted mass ordering
$1.50^{+0.53}_{-0.57}$		[10] ADAMSON	17B	NOVA	Inverted mass ordering; θ_{23} in octant II
$0.74^{+0.57}_{-0.93}$		[10] ADAMSON	17B	NOVA	Normal mass ordering; θ_{23} in octant II
$1.48^{+0.69}_{-0.58}$		[10] ADAMSON	17B	NOVA	Normal mass ordering; θ_{23} in octant I
0.0 to 0.1, 0.5 to 2.0	90	[10,11] ADAMSON	16	NOVA	Inverted mass ordering
0.0 to 2.0	90	[11] ADAMSON	16	NOVA	Normal mass ordering
0 to 0.15, 0.83 to 2	90	ABE	15D	T2K	Normal mass ordering
1.09 to 1.92	90	ABE	15D	T2K	Inverted mass ordering
0.05 to 1.2	90	[12] ADAMSON	14	MINS	Normal mass ordering
$1.34^{+0.64}_{-0.38}$		FORERO	14	FIT	Normal mass ordering
$1.48^{+0.34}_{-0.32}$		FORERO	14	FIT	Inverted mass ordering
$1.70^{+0.22}_{-0.39}$		[13] GONZALEZ...	14	FIT	Normal mass ordering; global fit
$1.41^{+0.35}_{-0.34}$		[13] GONZALEZ...	14	FIT	Inverted mass ordering; global fit
0 to 1.5 or 1.9 to 2	90	[14] ADAMSON	13A	MINS	Normal mass ordering

[1] ABE 20F results are based on data collected between 2009 and 2018 in (anti)neutrino mode and include a neutrino beam exposure of 1.49×10^{21} (1.64×10^{21}) protons on target. For inverted mass ordering, the quoted result is $1.56^{+0.15}_{-0.17}$ π rad. Supersedes ABE 18G.

[2] ACERO 19 is based on a sample size of 1.33×10^{20} protons on target with combined antineutrino and neutrino data. Supersedes ACERO 18.

[3] ABE 18B uses 328 kton-years of Super-Kamiokande I-IV atmospheric neutrino data to obtain this result. The fit is performed over the three parameters, Δm^2_{32}, $\sin^2\theta_{23}$, and δ, while the solar parameters and $\sin^2\theta_{23}$ are fixed to $\Delta m^2_{21} = (7.53 \pm 0.18) \times 10^{-5}$ eV^2, $\sin^2\theta_{12} = 0.304 \pm 0.014$, and $\sin^2\theta_{13} = 0.0219 \pm 0.0012$.

[4] SALAS 21 reports results of a global fit to neutrino oscillation data available at the time of the Neutrino 2020 conference.

[5] ESTEBAN 20A reports results of a global fit to neutrino oscillation data available at the time of the Neutrino 2020 conference.

[6] ABE 18B uses 328 kton-years of Super-Kamiokande I-IV atmospheric neutrino data to obtain this result. The fit is performed over the four parameters, Δm^2_{32}, $\sin^2\theta_{23}$, $\sin^2\theta_{13}$, and δ, while the solar parameters are fixed to $\Delta m^2_{21} = (7.53 \pm 0.18) \times 10^{-5}$ eV^2 and $\sin^2\theta_{12} = 0.304 \pm 0.014$.

[7] ABE 18G confidence intervals are marginalized over both mass orderings. Normal order preferred with a posterior probability of 87%. The 1-sigma result for normal mass ordering used in the average was provided by the experiment via private communications. Supersedes ABE 17F.

[8] ACERO 18 performs a joint fit to the data for ν_μ disappearance and ν_e appearance. The overall best fit favors normal mass ordering and θ_{23} in octant II. No 1σ confidence intervals are presented for the inverted mass ordering scenarios. Superseded by ACERO 19.

[9] ABE 17F confidence intervals are obtained using a frequentist analysis including θ_{13} constraint from reactor experiments. Bayesian intervals based on Markov Chain Monte Carlo method are also provided by the authors. Superseded by ABE 18G.

[10] Errors are projections of 68% C.L. curve of δ_{CP} vs. $\sin^2\theta_{23}$.

[11] ADAMSON 16 result is based on a data sample with 2.74×10^{20} protons on target. The likelihood-based analysis observed 6 ν_e events with an expected background of 0.99 ± 0.11 events.

[12] ADAMSON 14 result is based on three-flavor formalism and $\theta_{23} > \pi/4$. Likelihood as a function of δ is also shown for the other three combinations of hierarchy and θ_{23} octants; all values of δ are allowed at 90% C.L.

[13] GONZALEZ-GARCIA 14 result comes from a frequentist global fit. The corresponding Bayesian global fit to the same data results are reported in BERGSTROM 15 as 68% CL intervals of 1.24–1.94 for normal and 1.15–1.77 for inverted mass ordering.

[14] ADAMSON 13A result is based on ν_e appearance in MINOS and the calculated $\sin^2(2\theta_{23}) = 0.957, \theta_{23} > \pi/4$, and normal mass hierarchy. Likelihood as a function of δ is also shown for the other three combinations of hierarchy and θ_{23} octants; all values of δ are allowed at 90% C.L.

(C) Other neutrino mixing results

The LSND collaboration reported in AGUILAR 01 a signal which is consistent with $\overline{\nu}_\mu \rightarrow \overline{\nu}_e$ oscillations. In a three neutrino framework, this would be a measurement of θ_{12} and Δm^2_{21}. This does not appear to be consistent with most of the other neutrino data. The following listings include results from $\nu_\mu \rightarrow \nu_e$, $\overline{\nu}_\mu \rightarrow \overline{\nu}_e$ appearance and ν_μ, $\overline{\nu}_\mu$, ν_e, and $\overline{\nu}_e$ disappearance experiments, and searches for *CPT* violation.

$\Delta(m^2)$ for $\sin^2(2\theta) = 1$ $(\nu_\mu \rightarrow \nu_e)$

VALUE (eV^2)	CL%	DOCUMENT ID		TECN	COMMENT
• • • We do not use the following data for averages, fits, limits, etc. • • •					
0.03 to 0.55	90	[1] AGUILAR-AR...	21	MBNE	MiniBooNE $\nu,\overline{\nu}$ combined
0.03 to 0.05	90	[2] AGUILAR-AR...	18C	MBNE	MiniBooNE $\nu,\overline{\nu}$ combined
0.015 to 0.050	90	[3] AGUILAR-AR...	13A	MBNE	MiniBooNE
<0.34	90	[4] MAHN	12	MBNE	MiniBooNE/SciBooNE
<0.034	90	AGUILAR-AR...	07	MBNE	MiniBooNE
<0.0008	90	AHN	04	K2K	Water Cherenkov
<0.4	90	ASTIER	03	NOMD	CERN SPS
<2.4	90	AVVAKUMOV	02	NTEV	NUTEV FNAL
		[5] AGUILAR	01	LSND	$\nu\mu \rightarrow \nu_e$ osc.prob.
0.03 to 0.3	95	[6] ATHANASSO...	98	LSND	$\nu_\mu \rightarrow \nu_e$
<2.3	90	[7] LOVERRE	96		CHARM/CDHS
<0.9	90	VILAIN	94C	CHM2	CERN SPS
<0.09	90	ANGELINI	86	HLBC	BEBC CERN PS

[1] AGUILAR-AREVALO 21 result is based on a total of 18.75×10^{20} POT in neutrino mode, and 11.27×10^{20} POT in anti-neutrino mode. Best fit at 0.043 eV^2. The allowed region does not extend to large Δm^2. The quoted value is the entire allowed region of Δm^2 at 90% C.L. for all values of $\sin^2(2\theta)$. Supersedes AGUILAR-AREVALO 18C.

[2] AGUILAR-AREVALO 18C result is based on $\nu_\mu \rightarrow \nu_e$ appearance of 460.5 ± 99.0 events; The best fit value is $\Delta m^2 = 0.041$ eV^2. Superseded by AGUILAR-AREVALO 21.

[3] AGUILAR-AREVALO 13A result is based on $\nu_\mu \rightarrow \nu_e$ appearance of 162.0 ± 47.8 events; marginally compatible with twoneutrino oscillations. The best fit value is $\Delta m^2 = 3.14$ eV^2.

[4] MAHN 12 is a combined spectral fit of MiniBooNE and SciBooNE neutrino data with the range of Δm^2 up to 25 eV^2. The best limit is 0.04 at 7 eV^2.

Downloaded from https://academic.oup.com/ptep/article/2022/8/083C01/6651666 by KIT Library user on 27 September 2022

[5] AGUILAR 01 is the final analysis of the LSND full data set. Search is made for the $\nu_\mu \rightarrow \nu_e$ oscillations using ν_μ from π^+ decay in flight by observing beam-on electron events from $\nu_e C \rightarrow e^- X$. Present analysis results in $8.1 \pm 12.2 \pm 1.7$ excess events in the $60 < E_e < 200$ MeV energy range, corresponding to oscillation probability of $0.10 \pm 0.16 \pm 0.04$%. This is consistent, though less significant, with the previous result of ATHANASSOPOULOS 98, which it supersedes. The present analysis uses selection criteria developed for the decay at rest region, and is less effective in removing the background above 60 MeV than ATHANASSOPOULOS 98.

[6] ATHANASSOPOULOS 98 is a search for the $\nu_\mu \rightarrow \nu_e$ oscillations using ν_μ from π^+ decay in flight. The 40 observed beam-on electron events are consistent with $\nu_e C \rightarrow e^- X$; the expected background is 21.9 ± 2.1. Authors interpret this excess as evidence for an oscillation signal corresponding to oscillations with probability $(0.26 \pm 0.10 \pm 0.05)$%. Although the significance is only $2.3\,\sigma$, this measurement is an important and consistent cross check of ATHANASSOPOULOS 96 who reported evidence for $\overline{\nu}_\mu \rightarrow \overline{\nu}_e$ oscillations from μ^+ decay at rest. See also ATHANASSOPOULOS 98B.

[7] LOVERRE 96 uses the charged-current to neutral-current ratio from the combined CHARM (ALLABY 86) and CDHS (ABRAMOWICZ 86) data from 1986.

$\sin^2(2\theta)$ for "Large" $\Delta(m^2)$ $(\nu_\mu \rightarrow \nu_e)$

VALUE (units 10^{-3})	CL%	DOCUMENT ID		TECN	COMMENT
• • • We do not use the following data for averages, fits, limits, etc. • • •					
6 to 1000	90	[1] AGUILAR-AR...	21	MBNE	MiniBooNE; $\nu + \overline{\nu}$
< 5	90	[2] AGUILAR-AR...	18C	MBNE	MiniBooNE; $\nu + \overline{\nu}$
< 7.2	90	AGAFONOVA	13	OPER	$\Delta(m^2) > 0.1$ eV^2
0.8 to 3	90	[3] AGUILAR-AR...	13A	MBNE	MiniBooNE
< 11	90	[4] ANTONELLO	13	ICAR	$\nu_\mu \rightarrow \nu_e$
< 6.8	90	[5] ANTONELLO	13A	ICAR	$\nu_\mu \rightarrow \nu_e$
<100	90	[6] MAHN	12	MBNE	MiniBooNE/SciBooNE
< 1.8	90	[7] AGUILAR-AR...	07	MBNE	MiniBooNE
<110	90	[8] AHN	04	K2K	Water Cherenkov
< 1.4	90	ASTIER	03	NOMD	CERN SPS
< 1.6	90	AVVAKUMOV	02	NTEV	NUTEV FNAL
		[9] AGUILAR	01	LSND	$\nu_\mu \rightarrow \nu_e$ osc.prob.
0.5 to 30	95	[10] ATHANASSO...	98	LSND	$\nu_\mu \rightarrow \nu_e$
< 3.0	90	[11] LOVERRE	96		CHARM/CDHS
< 9.4	90	VILAIN	94C	CHM2	CERN SPS
< 5.6	90	[12] VILAIN	94C	CHM2	CERN SPS

[1] AGUILAR-AREVALO 21 result is based on a total of 18.75×10^{20} POT in neutrino mode, and 11.27×10^{20} POT in anti-neutrino mode. The best fit value is $\sin^2(2\theta)$=0.807. The allowed region does not extend to large Δm^2. The quoted value is the entire allowed region of $\sin^2(2\theta)$ at 90% C.L. for all values of Δm^2. Supersedes AGUILAR-AREVALO 18C.

[2] AGUILAR-AREVALO 18C result is based on $\nu_\mu \rightarrow \nu_e$ appearance of 460.5 ± 99.0 events; The best fit value is $\sin^2(2\theta) = 0.92$. The quoted limit for the two-neutrino mixing angle θ is valid above $\Delta m^2 = 0.59$ eV^2. Superseded by AGUILAR-AREVALO 21.

[3] AGUILAR-AREVALO 13A result is based on $\nu_\mu \rightarrow \nu_e$ appearance of 162.0 ± 47.8 events; marginally compatible with two neutrino oscillations. The best fit value is $\sin^2(2\theta) = 0.002$.

[4] ANTONELLO 13 use the ICARUS T600 detector at LNGS and ~ 20 GeV beam of ν_μ from CERN 730 km away to search for an excess of ν_e events. Two events are found with 3.7 ± 0.6 expected from conventional sources. This result excludes some parts of the parameter space expected by LSND. Superseded by ANTONELLO 13A.

[5] Based on four events with a background of 6.4 ± 0.9 from conventional sources with an average energy of 20 GeV and 730 km from the source of ν_μ.

[6] MAHN 12 is a combined fit of MiniBooNE and SciBooNE neutrino data.

[7] The limit is $\sin^2 2\theta < 0.9 \times 10^{-3}$ at $\Delta m^2 = 2$ eV^2. That value of Δm^2 corresponds to the smallest mixing angle consistent with the reported signal from LSND in AGUILAR 01.

[8] The limit becomes $\sin^2 2\theta < 0.15$ at $\Delta m^2 = 2.8 \times 10^{-3}$ eV^2, the bets-fit value of the ν_μ disappearance analysis in K2K.

[9] AGUILAR 01 is the final analysis of the LSND full data set of the search for the $\nu_\mu \rightarrow \nu_e$ oscillations. See footnote in preceding table for further details.

[10] ATHANASSOPOULOS 98 report $(0.26 \pm 0.10 \pm 0.05)$% for the oscillation probability; the value of $\sin^2 2\theta$ for large Δm^2 is deduced from this probability. See footnote in preceding table for further details, and see the paper for a plot showing allowed regions. If effect is due to oscillation, it is most likely to be intermediate $\sin^2 2\theta$ and Δm^2. See also ATHANASSOPOULOS 98B.

[11] LOVERRE 96 uses the charged-current to neutral-current ratio from the combined CHARM (ALLABY 86) and CDHS (ABRAMOWICZ 86) data from 1986.

[12] VILAIN 94C limit derived by combining the ν_μ and $\overline{\nu}_\mu$ data assuming *CP* conservation.

$\Delta(m^2)$ for $\sin^2(2\theta) = 1$ $(\overline{\nu}_\mu \rightarrow \overline{\nu}_e)$

VALUE (eV^2)	CL%	DOCUMENT ID		TECN	COMMENT
• • • We do not use the following data for averages, fits, limits, etc. • • •					
0.023 to 0.060	90	[1] AGUILAR-AR...	13A	MBNE	MiniBooNE
<0.16	90	[2] CHENG	12	MBNE	MiniBooNE/SciBooNE
0.03–0.09	90	[3] AGUILAR-AR...	10	MBNE	$E_\nu > 475$ MeV
0.03–0.07	90	[4] AGUILAR-AR...	10	MBNE	$E_\nu > 200$ MeV
<0.06	90	AGUILAR-AR...	09B	MBNE	MiniBooNE
<0.055	90	[5] ARMBRUSTER	02	KAR2	Liquid Sci. calor.
<2.6	90	AVVAKUMOV	02	NTEV	NUTEV FNAL
0.03–0.05		[6] AGUILAR	01	LSND	LAMPF
0.05–0.08	90	[7] ATHANASSO...	96	LSND	LAMPF
0.048–0.090	80	[8] ATHANASSO...	95		
<0.07	90	[9] HILL	95		
<0.9	90	VILAIN	94C	CHM2	CERN SPS
<0.14	90	[10] FREEDMAN	93	CNTR	LAMPF

[1] Based on $\overline{\nu}_\mu \rightarrow \overline{\nu}_e$ appearance of 78.4 ± 28.5 events. The best fit values are $\Delta m^2 = 0.043$ eV^2 and $\sin^2 2\theta = 0.88$.

[2] CHENG 12 is a combined fit of MiniBooNE and SciBooNE antineutrino data.

[3] This value is for a two neutrino oscillation analysis for excess antineutrino events with $E_\nu > 475$ MeV. The best fit is at 0.07. The allowed region is consistent with LSND reported by AGUILAR 01. Supercedes AGUILAR-AREVALO 09B.

[4] This value is for a two neutrino oscillation analysis for excess antineutrino events with $E_\nu > 200$ MeV with subtraction of the expected 12 events low energy excess seen in the neutrino component of the beam. The best fit value is 0.007 for $\Delta(m^2) = 4.4$ eV^2.

[5] ARMBRUSTER 02 is the final analysis of the KARMEN 2 data for 17.7 m distance from the ISIS stopped pion and muon neutrino source. It is a search for $\overline{\nu}_e$, detected by the inverse β-decay reaction on protons and ^{12}C. 15 candidate events are observed, and 15.8 ± 0.5 background events are expected, hence no oscillation signal is detected. The results exclude large regions of the parameter area favored by the LSND experiment.

[6] AGUILAR 01 is the final analysis of the LSND full data set. It is a search for $\overline{\nu}_e$ 30 m from LAMPF beam stop. Neutrinos originate mainly for π^+ decay at rest. $\overline{\nu}_e$ are detected through $\overline{\nu}_e p \rightarrow e^+ n$ ($20 < E_{e^+} < 60$ MeV) in delayed coincidence with $np \rightarrow d\gamma$. Authors observe $87.9 \pm 22.4 \pm 6.0$ total excess events. The observation is attributed to $\overline{\nu}_\mu \rightarrow \overline{\nu}_e$ oscillations with the oscillation probability of $0.264 \pm 0.067 \pm 0.045$%, consistent with the previously published result. Taking into account all constraints, the most favored allowed region of oscillation parameters is a band of $\Delta(m^2)$ from 0.2–2.0 eV^2. Supersedes ATHANASSOPOULOS 95, ATHANASSOPOULOS 96, and ATHANASSOPOULOS 98.

[7] ATHANASSOPOULOS 96 is a search for $\overline{\nu}_e$ 30 m from LAMPF beam stop. Neutrinos originate mainly from π^+ decay at rest. $\overline{\nu}_e$ could come from either $\overline{\nu}_\mu \rightarrow \overline{\nu}_e$ or $\nu_e \rightarrow \overline{\nu}_e$; our entry assumes the first interpretation. They are detected through $\overline{\nu}_e p \rightarrow e^+ n$ (20 MeV $< E_{e^+} <$60 MeV) in delayed coincidence with $np \rightarrow d\gamma$. Authors observe $51 \pm 20 \pm 8$ total excess events over an estimated background 12.5 ± 2.9. ATHANASSOPOULOS 96B is a shorter version of this paper.

[8] ATHANASSOPOULOS 95 error corresponds to the 1.6σ band in the plot. The expected background is 2.7 ± 0.4 events. Corresponds to an oscillation probability of $(0.34^{+0.20}_{-0.18} \pm 0.07)$%. For a different interpretation, see HILL 95. Replaced by ATHANASSOPOULOS 96.

[9] HILL 95 is a report by one member of the LSND Collaboration, reporting a different conclusion from the analysis of the data of this experiment (see ATHANASSOPOULOS 95). Contrary to the rest of the LSND Collaboration, Hill finds no evidence for the neutrino oscillation $\overline{\nu}_\mu \rightarrow \overline{\nu}_e$ and obtains only upper limits.

[10] FREEDMAN 93 is a search at LAMPF for $\overline{\nu}_e$ generated from any of the three neutrino types ν_μ, $\overline{\nu}_\mu$, and ν_e which come from the beam stop. The $\overline{\nu}_e$'s would be detected by the reaction $\overline{\nu}_e p \rightarrow e^+ n$. FREEDMAN 93 replaces DURKIN 88.

$\sin^2(2\theta)$ for "Large" $\Delta(m^2)$ $(\overline{\nu}_\mu \rightarrow \overline{\nu}_e)$

VALUE (units 10^{-3})	CL%	DOCUMENT ID		TECN	COMMENT
• • • We do not use the following data for averages, fits, limits, etc. • • •					
<640	90	[1] ANTONELLO	13A	ICAR	$\overline{\nu}_e$ appearance
<150	90	[2] CHENG	12	MBNE	MiniBooNE/SciBooNE
0.4–9.0	99	[3] AGUILAR-AR...	10	MBNE	$E_\nu > 475$ MeV
0.4–9.0	99	[4] AGUILAR-AR...	10	MBNE	$E_\nu > 200$ MeV
< 3.3	90	[5] AGUILAR-AR...	09B	MBNE	MiniBooNE
< 1.7	90	[6] ARMBRUSTER	02	KAR2	Liquid Sci. calor.
< 1.1	90	AVVAKUMOV	02	NTEV	NUTEV FNAL
$5.3 \pm 1.3 \pm 9.0$		[7] AGUILAR	01	LSND	LAMPF
$6.2 \pm 2.4 \pm 1.0$		[8] ATHANASSO...	96	LSND	LAMPF
3–12	80	[9] ATHANASSO...	95		
< 6	90	[10] HILL	95		

[1] ANTONELLO 13A obtained the limit by assuming $\overline{\nu}_\mu \rightarrow \overline{\nu}_e$ oscillation from the ~ 2% of $\overline{\nu}_\mu$ evnets contamination in the CNGS beam.

[2] CHENG 12 is a combined fit of MiniBooNE and SciBooNE antineutrino data.

[3] This value is for a two neutrino oscillation analysis for excess antineutrino events with $E_\nu > 475$ MeV. At 90% CL there is no solution at high $\Delta(m^2)$. The best fit is at maximal mixing. The allowed region is consistent with LSND reported by AGUILAR 01. Supercedes AGUILAR-AREVALO 09B.

[4] This value is for a two neutrino oscillation analysis for excess antineutrino events with $E_\nu > 200$ MeV with subtraction of the expected 12 events low energy excess seen in the neutrino component of the beam. At 90% CL there is no solution at high $\Delta(m^2)$. The best fit value is 0.007 for $\Delta(m^2) = 4.4$ eV^2.

[5] This result is inconclusive with respect to small amplitude mixing suggested by LSND.

[6] ARMBRUSTER 02 is the final analysis of the KARMEN2 data. See footnote in the preceding table for further details, and the paper for the exclusion plot.

[7] AGUILAR 01 is the final analysis of the LSND full data set. The deduced oscillation probability is $0.264 \pm 0.067 \pm 0.045$%; the value of $\sin^2 2\theta$ for large $\Delta(m^2)$ is twice this probability (although these values are excluded by other constraints). See footnote in preceding table for further details, and the paper for a plot showing allowed regions. Supersedes ATHANASSOPOULOS 95, ATHANASSOPOULOS 96, and ATHANASSOPOULOS 98.

Downloaded from https://academic.oup.com/ptep/article/2022/8/083C01/6651666 by KIT Library user on 27 September 2022

[8] ATHANASSOPOULOS 96 reports $(0.31 \pm 0.12 \pm 0.05)$% for the oscillation probability; the value of $\sin^2 2\theta$ for large $\Delta(m^2)$ should be twice this probability. See footnote in preceding table for further details, and see the paper for a plot showing allowed regions.

[9] ATHANASSOPOULOS 95 error corresponds to the 1.6σ band in the plot. The expected background is 2.7 ± 0.4 events. Corresponds to an oscillation probability of $(0.34^{+0.20}_{-0.18} \pm 0.07)$%. For a different interpretation, see HILL 95. Replaced by ATHANASSOPOULOS 96.

[10] HILL 95 is a report by one member of the LSND Collaboration, reporting a different conclusion from the analysis of the data of this experiment (see ATHANASSOPOULOS 95). Contrary to the rest of the LSND Collaboration, Hill finds no evidence for the neutrino oscillation $\overline{\nu}_\mu \rightarrow \overline{\nu}_e$ and obtains only upper limits.

$\Delta(m^2)$ for $\sin^2(2\theta) = 1$ $(\nu_\mu(\overline{\nu}_\mu) \rightarrow \nu_e(\overline{\nu}_e))$

VALUE (eV^2)	CL%	DOCUMENT ID		TECN	COMMENT
<0.075	90	BORODOV...	92	CNTR	BNL E776
• • • We do not use the following data for averages, fits, limits, etc. • • •					
<1.6	90	[1] ROMOSAN	97	CCFR	FNAL

[1] ROMOSAN 97 uses wideband beam with a 0.5 km decay region.

$\sin^2(2\theta)$ for "Large" $\Delta(m^2)$ $(\nu_\mu(\overline{\nu}_\mu) \rightarrow \nu_e(\overline{\nu}_e))$

VALUE (units 10^{-3})	CL%	DOCUMENT ID		TECN	COMMENT
<1.8	90	[1] ROMOSAN	97	CCFR	FNAL
• • • We do not use the following data for averages, fits, limits, etc. • • •					
<3.8	90	[2] MCFARLAND	95	CCFR	FNAL
<3	90	BORODOV...	92	CNTR	BNL E776

[1] ROMOSAN 97 uses wideband beam with a 0.5 km decay region.

[2] MCFARLAND 95 state that "This result is the most stringent to date for 250< $\Delta(m^2)$ <450 eV^2 and also excludes at 90%CL much of the high $\Delta(m^2)$ region favored by the recent LSND observation." See ATHANASSOPOULOS 95 and ATHANASSOPOULOS 96.

$\Delta(m^2)$ for $\sin^2(2\theta) = 1$ $(\overline{\nu}_e \not\rightarrow \overline{\nu}_e)$

VALUE (eV^2)	CL%	DOCUMENT ID		TECN	COMMENT
• • • We do not use the following data for averages, fits, limits, etc. • • •					
<0.01	90	[1] ACHKAR	95	CNTR	Bugey reactor

[1] ACHKAR 95 bound is for L=15, 40, and 95 m.

$\sin^2(2\theta)$ for "Large" $\Delta(m^2)$ $(\overline{\nu}_e \not\rightarrow \overline{\nu}_e)$

VALUE	CL%	DOCUMENT ID		TECN	COMMENT
• • • We do not use the following data for averages, fits, limits, etc. • • •					
<0.02	90	[1] ACHKAR	95	CNTR	For $\Delta(m^2) = 0.6$ eV^2

[1] ACHKAR 95 bound is from data for L=15, 40, and 95 m distance from the Bugey reactor.

Sterile neutrino limits

$\Delta(m^2)$ for $\sin^2(2\theta) = 1$ $(\nu_\mu \rightarrow \nu_s)$

ν_s means ν_τ or any sterile (noninteracting) ν.

VALUE (10^{-5} eV^2)	CL%	DOCUMENT ID		TECN	COMMENT
• • • We do not use the following data for averages, fits, limits, etc. • • •					
<3000 (or <550)	90	[1] OYAMA	89	KAMI	Water Cherenkov
< 4.2 or > 54.	90	BIONTA	88	IMB	Flux has ν_μ, $\overline{\nu}_\mu$, ν_e, and $\overline{\nu}_e$

[1] OYAMA 89 gives a range of limits, depending on assumptions in their analysis. They argue that the region $\Delta(m^2) = (100\text{–}1000) \times 10^{-5}$ eV^2 is not ruled out by any data for large mixing.

Search for ν_μ or $\nu_e \rightarrow \nu_s$

VALUE	CL%	DOCUMENT ID		TECN	COMMENT
• • • We do not use the following data for averages, fits, limits, etc. • • •					
<0.05	95	[1] ANDRIAMIR...	21		PROSPECT
<0.005	95	[2] SEREBROV	21		Neutrino-4
<0.008	95	[3] SKROBOVA	20		DANSS
<0.01	90	[4] ALEKSEEV	18		DANSS
<0.06	90	[5] ALMAZAN	18		STEREO
<0.1	95	[6] ASHENFELT...	18		PROSPECT
<0.4	90	[7] AARTSEN	17B	ICCB	IceCube-DeepCore
$<8 \times 10^{-3}$	95	[8] ABDURASHI...	17		T β decay
$<1 \times 10^{-2}$	90	[9] KO	17	NEOS	
$<2 \times 10^{-2}$	90	[10] AARTSEN	16	ICCB	IceCube
$<4.5 \times 10^{-4}$	95	[11] ADAMSON	16B		MINOS, DayaBay
$<8.6 \times 10^{-2}$	95	[12] ADAMSON	16C	MINS	
$<1.1 \times 10^{-2}$	95	[13] AN	16B	DAYA	
		[14] AMBROSIO	01	MCRO	matter effects
		[15] FUKUDA	00	SKAM	neutral currents + matter effects

[1] ANDRIAMIRADO 21 reports a search for $\overline{\nu}_e \rightarrow \overline{\nu}_s$ oscillations at the HFIR research reactor, at baselines from 6.7 to 9.2 m. The reactor has a ^{235}U core. 4 tons of ^{6}Li-doped liquid scintillator are used in a segmented detector. Oscillations into sterile neutrinos are disfavored. The stated limit for $\sin^2(2\theta_{14})$ is for $\Delta m^2_{41} \sim 2$ eV^2 where the sensitivity is maximal.

[2] SEREBROV 21 searches for $\overline{\nu}_e \rightarrow \overline{\nu}_s$ oscillations with a moveable detector with baseline 6–12 m from the SM-3 research reactor with highly enriched ^{235}U fuel. Analyzing the L/E dependence a χ^2 minimum is found at $\Delta m^2_{41} = 7.3 \pm 0.13 \pm 1.16$ eV^2 and $\sin^2(2\theta_{14}) = 0.36 \pm 0.12$. The quoted limit of 0.005 for $\sin^2(2\theta_{14})$ corresponds to $\Delta m^2_{41} \sim 2$ eV^2. This is the result from 720 days of reactor ON and 860 days of reactor OFF measurements. The significance of the χ^2 minimum is 2.9 σ. Supersedes SEREBROV 20, SEREBROV 19 and SEREBROV 18A.

[3] SKROBOVA 20 searches for $\overline{\nu}_e - \overline{\nu}_s$ oscillations using the DANSS detector at 10.7, 11.2, and 12.7 m from the 3.1 GW$_{th}$ power reactor. The DANSS detector is highly segmented and moveable; the positions are changed usually 3 times a week. The analysis is based on the ratio of the events at top and bottom position; the middle position is used for checks of consistency. No evidence for sterile neutrinos is found. The quoted limit 0.008, the smallest excluded $\sin^2(2\theta_{14})$, corresponds to $\Delta m^2_{41} \sim 1.0$ eV^2. Supersedes ALEKSEEV 18.

[4] ALEKSEEV 18 searches for $\overline{\nu}_e \rightarrow \overline{\nu}_s$ oscillations using the DANSS detector at 10.7, 11.2, and 12.7 m from the 3.1 GW$_{th}$ power reactor. The DANSS detector is highly segmented and moveable; the positions are changed usually 3 times a week. The analysis is based on the ratio of the events at top and bottom position; the middle position is used for checks of consistency. The best fit point is at $\Delta m^2_{41} = 1.4$ eV^2 and $\sin^2(2\theta_{14}) = 0.05$ with $\Delta\chi^2 = 13.1$ (statistical errors only) compared to the fit with 3 active neutrinos only. The quoted limit of 0.01 for $\sin^2(2\theta_{14})$ corresponds to $\Delta m^2_{41} \sim 1.0$ eV^2. Superseded by SKROBOVA 20.

[5] ALMAZAN 18 searches for the $\overline{\nu}_e \rightarrow \overline{\nu}_s$ oscillations with baseline from 9.4 to 11.1 m from the ILL research reactor with highly enriched ^{235}U fuel. The STEREO detector consists of six separated cells with Gd loaded scintillator, with 15 m water equivalent overburden. The detected rate is 396.3 ± 4.7 $\overline{\nu}_e$/day with signal to background ratio of about 0.9. The reported results corresponds to 66 days of reactor-on. The analysis uses the relative rates normalized to the cell number 1. No indication of the oscillation to the sterile neutrinos is found, the stated limit on $\sin^2(2\theta_{14})$ correspond to $\Delta m^2_{41} \sim$ 3.5 eV^2 where the exclusion is maximal.

[6] ASHENFELTER 18 searches for the $\overline{\nu}_e \rightarrow \overline{\nu}_s$ oscillations at baseline from 6.7 to 9.2 m from the 85 MW research reactor with pure ^{235}U core. The segmented 4 ton ^{6}Li-doped liquid scintillator is operated with about 1 m water equivalent overburden and recorded 25461 ± 283 IBD events. No indication of oscillations into sterile neutrinos was observed. The stated limit for $\sin^2(2\theta_{14})$ is for $\Delta m^2_{41} \sim 2$ eV^2 where the sensitivity is maximal.

[7] AARTSEN 17B uses three years of upward-going atmospheric neutrino data in the energy range of 10-60 GeV to constrain their disappearance into light sterile neutrinos. The reported limit $\sin^2\theta_{24} < 0.11$ at 90% C.L. is for $\Delta m^2_{41} = 1.0$ eV^2. We convert the result to $\sin^2 2\theta_{24}$ for the listing. AARTSEN 17B also reports $\cos^2\theta_{24} \cdot \sin^2\theta_{34} < 0.15$ at 90% C.L. for $\Delta m^2_{41} = 1.0$ eV^2.

[8] ABDURASHITOV 17 use the Troitsk nu-mass experiment to search for sterile neutrinos with mass 0.1 - 2 keV. We convert the reported limit from U^2_{e4} <0.002 to $\sin^2 2\theta_{14}$ <0.008 assume $U_{e4} \sim \sin\theta_{14}$. The stated limit corresponds to the smallest U^2_{e4}. The exclusion curve begins at U^2_{e4} of 0.02 for $m_4 = 0.1$ keV.

[9] KO 17 reports on short baseline reactor oscillation search ($\overline{\nu}_e \rightarrow \overline{\nu}_s$), motivated be the so-called "reactor antineutrino anomaly". The experiment is conducted at 23.7 m from the core of unit 5 of the Hanbit Nuclear Power Complex in Korea. the reported limited on $\sin^2(2\theta_{41})$ for sterile neutrinos was determined using the reactor antineutrino spectrum determined by the Daya Bay experiment for Δm^2_{14} around 0.55 eV^2 where the sensitivity is maximal. A fraction of the parameter space derived from the "reactor antineutrino anomaly" is excluded by this work. Compared to reactor models an event excess is observed at about 5 MeV, in agreement with other experiments.

[10] AARTSEN 16 use one year of upward-going atmospheric muon neutrino data in the energy range of 320 GeV to 20 TeV to constrain their disappearance into light sterile neutrinos. Sterile neutrinos are expected to produce distinctive zenith distribution for these energies for $0.01 \leq \Delta m^2 \leq 10$ eV^2. The stated limit is for $\sin^2 2\theta_{24}$ at Δm^2 around 0.3 eV^2.

[11] ADAMSON 16B combine the results of AN 16B, ADAMSON 16C, and Bugey-3 reactor experiments to constrain ν_μ to ν_e mixing through oscillations into light sterile neutrinos. The stated limit for $\sin^2 2\theta_{\mu e}$ is at $|\Delta m^2_{41}| = 1.2$ eV^2.

[12] ADAMSON 16C use the NuMI beam and exposure of 10.56×10^{20} protons on target to search for the oscillation of ν_μ dominated beam into light sterile neutrinos with detectors at 1.04 and 735 km. The reported limit $\sin^2(\theta_{24}) < 0.022$ at 95% C.L. is for $|\Delta m^2_{41}|$ = 0.5 eV^2. We convert the result to $\sin^2(2\theta_{24})$ for the listing.

[13] AN 16B utilize 621 days of data to place limits on the $\overline{\nu}_e$ disappearance into a light sterile neutrino. The stated limit corresponds to the smallest $\sin^2(2\theta_{14})$ at $|\Delta m^2_{41}| \sim 3 \times 10^{-2}$ eV^2 (obtained from Figure 3 in AN 16B). The exclusion curve begins at $|\Delta m^2_{41}| \sim 1.5 \times 10^{-4}$ eV^2 and extends to ~ 0.25 eV^2. The analysis assumes $\sin^2(2\theta_{12})$ = 0.846 ± 0.021, $\Delta m^2_{21} = (7.53 \pm 0.18) \times 10^{-5}$ eV^2, and $|\Delta m^2_{32}| = (2.44 \pm 0.06) \times 10^{-3}$ eV^2.

[14] AMBROSIO 01 tested the pure 2-flavor $\nu_\mu \rightarrow \nu_s$ hypothesis using matter effects which change the shape of the zenith-angle distribution of upward through-going muons. With maximum mixing and Δm^2around 0.0024 eV^2, the $\nu_\mu \rightarrow \nu_s$ oscillation isdisfavored with 99% confidence level with respect to the $\nu_\mu \rightarrow \nu_\tau$ hypothesis.

[15] FUKUDA 00 tested the pure 2-flavor $\nu_\mu \rightarrow \nu_s$ hypothesis using three complementary atmospheric-neutrino data samples. With this hypothesis, zenith-angle distributions are expected to show characteristic behavior due to neutral currents and matter effects. In the

Downloaded from https://academic.oup.com/ptep/article/2022/8/083C01/6651666 by KIT Library user on 27 September 2022

Δm^2 and $\sin^2 2\theta$ region preferred by the Super-Kamiokande data, the $\nu_\mu \to \nu_s$ hypothesis isrejected at the 99% confidence level, while the $\nu_\mu \to \nu_\tau$ hypothesis consistently fits all of the data sample.

CPT tests

$\langle \Delta m^2_{21} - \Delta \overline{m}^2_{21} \rangle$

VALUE (10^{-4} eV^2)	*CL%*	*DOCUMENT ID*		*TECN*	*COMMENT*
<1.1	99.7	[1] DEGOUVEA	05	FIT	solar vs. reactor

[1] DEGOUVEA 05 obtained this bound at the 3σ CL from the KamLAND (ARAKI 05) and solar neutrino data.

$\langle \Delta m^2_{32} - \Delta \overline{m}^2_{32} \rangle$

VALUE (10^{-3} eV^2)	*CL%*	*DOCUMENT ID*		*TECN*	*COMMENT*
$\mathbf{-0.12^{+0.26}_{-0.24}}$		[1] ADAMSON	13B	MINS	beam and atmosperic
• • • We do not use the following data for averages, fits, limits, etc. • • •					
$0.6\ ^{+2.4}_{-0.8}$	90	[2] ADAMSON	12B	MINS	MINOS atmospheric

[1] ADAMSON 13B quotes this difference as a negative of our convention.

[2] The quoted result is the single-parameter 90% C.L. interval determined from the 90% C.L. contour in the (Δm^2, $\Delta \overline{m}^2$) plane, which is obtained by minimizing the four parameter log-likelihood function with respect to the other oscillation parameters.

REFERENCES FOR Neutrino Mixing

ABE 21A PR D103 L011101 K. Abe et al. (T2K Collab.)
ABRAHAO 21 JHEP 2101 190 T. Abrahao et al. (Double Chooz Collab.)
AGOSTINI 21 ASP 125 102509 M. Agostini et al. (Borexino Collab.)
AGUILAR-AR... 21 PR D103 052002 A.A. Aguilar-Arevalo et al. (MiniBooNE Collab.)
ANDRIAMIR... 21 PR D103 032001 M. Andriamirado et al. (PROSPECT Collab.)
SALAS 21 JHEP 2102 071 P.F. de Salas et al. (STOH, VALE, INFN+)
SEREBROV 21 PR D104 032003 A.P. Serebrov et al. (Neutrino-4 Collab.)
AARTSEN 20 EPJ C80 9 M.G. Aartsen et al. (IceCube Collab.)
ABE 20F NAT 580 339 K. Abe et al. (T2K Collab.)
Also PR D103 112008 K. Abe et al. (T2K Collab.)
ADAMSON 20A PRL 125 131802 P. Adamson et al. (MINOS+ Collab.)
AGOSTINI 20A PR D101 062001 M. Agostini et al. (Borexino Collab.)
AHARMIM 20 PR D102 062006 B. Aharmim et al. (SNO Collab.)
ALMAZAN 20 PRL 125 201801 H. Almazan et al. (STEREO Collab.)
DE-KERRET 20 NATP 16 558 H. de Karret et al. (Double Chooz Collab.)
ESTEBAN 20A JHEP 2009 178 I. Esteban et al. (NuFIT Collab.)
PDG 20 PTEP 2020 083C01 P.A. Zyla et al. (PDG Collab.)
SEREBROV 20 JETPL 112 199 A.P. Serebrov, R.M. Samoilov (PNPI)
Translated from ZETFP 112 211.
SHIN 20 JHEP 2004 029 C.D. Shin et al. (RENO Collab.)
SKROBOVA 20 IJMP A35 2044015 N. Skrobova (DANSS Collab.)
AARTSEN 19C PR D99 032007 M.G. Aartsen et al. (IceCube Collab.)
ACERO 19 PRL 123 151803 M.A. Acero et al. (NOvA Collab.)
ADEY 19 PR D100 052004 D. Adey et al. (Daya Bay Collab.)
AGAFONOVA 19 PR D100 051301 N. Agafonova et al. (OPERA Collab.)
ALBERT 19 JHEP 1906 113 A. Albert et al. (ANTARES Collab.)
ANDERSON 19 PR D99 012012 M. Anderson et al. (SNO+ Collab.)
SEREBROV 19 JETPL 109 213 A.P. Serebrov et al. (Neutrino-4 Collab.)
AARTSEN 18A PRL 120 071801 M.G. Aartsen et al. (IceCube Collab.)
ABE 18B PR D97 072001 K. Abe et al. (Super-Kamiokande Collab.)
ABE 18G PRL 121 171802 K. Abe et al. (T2K Collab.)
ACERO 18 PR D98 032012 M.A. Acero et al. (NOvA Collab.)
ADEY 18A PRL 121 241805 D. Adey et al. (Daya Bay Collab.)
AGAFONOVA 18 PRL 120 211801 N. Agafonova et al. (OPERA Collab.)
AGAFONOVA 18A JHEP 1806 151 N. Agafonova et al. (OPERA Collab.)
AGOSTINI 18B NAT 562 505 M. Agostini et al. (Borexino Collab.)
AGUILAR-AR... 18C PRL 121 221801 A.A. Aguilar-Arevalo et al. (MiniBooNE Collab.)
ALEKSEEV 18 PL B787 56 I. Alekseev et al. (DANSS Collab.)
ALMAZAN 18 PRL 121 161801 H. Almazan et al. (STEREO Collab.)
ASHENFELT... 18 PRL 121 251802 J. Ashenfelter et al. (PROSPECT Collab.)
BAK 18 PRL 121 201801 G. Bak et al. (RENO Collab.)
DE-SALAS 18 PL B782 633 P.F. de Salas et al.
PDG 18 PR D98 030001 M. Tanabashi et al. (PDG Collab.)
SEO 18 PR D98 012002 S.H. Seo et al. (RENO Collab.)
SEREBROV 18A PPN 49 701 A.P. Serebrov et al. (Neutrino-4 Collab.)
AARTSEN 17B PR D95 112002 M.G. Aartsen et al. (IceCube Collab.)
ABDURASHI... 17 JETPL 105 753 J.N. Abdurashitov et al. (Troitsk nu-mass Collab.)
ABE 17A PRL 118 151801 K. Abe et al. (T2K Collab.)
ABE 17C PR D96 011102 K. Abe et al. (T2K Collab.)
ABE 17F PR D96 092006 K. Abe et al. (T2K Collab.)
Also PR D98 019902 (errat.) K. Abe et al. (T2K Collab.)
ADAMSON 17A PRL 118 151802 P. Adamson et al. (NOvA Collab.)
ADAMSON 17B PRL 118 231801 P. Adamson et al. (NOvA Collab.)
AN 17A PR D95 072006 F.P. An et al. (Daya Bay Collab.)
ESTEBAN 17 JHEP 1701 087 I. Esteban et al.
KO 17 PRL 118 121802 Y.J. Ko et al. (NEOS Collab.)
VINYOLES 17 APJ 835 202 N. Vinyoles et al.
AARTSEN 16 PRL 117 071801 M.G. Aartsen et al. (IceCube Collab.)
ABE 16B JHEP 1601 163 Y. Abe et al. (Double Chooz Collab.)
ABE 16C PR D94 052010 K. Abe et al. (Super-Kamiokande Collab.)
ABE 16D PRL 116 181801 K. Abe et al. (T2K Collab.)
ADAMSON 16 PRL 116 151806 P. Adamson et al. (NOvA Collab.)
ADAMSON 16A PR D93 051104 P. Adamson et al. (NOvA Collab.)
ADAMSON 16B PRL 117 151801 P. Adamson et al. (Daya Bay and MINOS Collab.)
ADAMSON 16C PRL 117 151803 P. Adamson et al. (MINOS Collab.)
AN 16 PRL 116 061801 F.P. An et al. (Daya Bay Collab.)
AN 16A PR D93 072011 F.P. An et al. (Daya Bay Collab.)
AN 16B PRL 117 151802 F.P. An et al. (Daya Bay Collab.)
CHOI 16 PRL 116 211801 J.H. Choi et al. (RENO Collab.)
PDG 16 CP C40 100001 C. Patrignani et al. (PDG Collab.)
AARTSEN 15A PR D91 072004 M.G. Aartsen (IceCube Collab.)
ABE 15D PR D91 072010 K. Abe et al. (T2K Collab.)
AGAFONOVA 15A PRL 115 121802 N. Agafonova et al. (OPERA Collab.)
AN 15 PRL 115 111802 F.P. An et al. (Daya Bay Collab.)
BERGSTROM 15 JHEP 1509 200 J. Bergstrom et al. (BARC, STON, MADU+)
GANDO 15 PR C92 055808 A. Gando et al. (KamLAND Collab.)
ABE 14 PRL 112 181801 K. Abe et al. (T2K Collab.)
Also PR D91 072010 K. Abe et al. (T2K Collab.)
ABE 14A PL B735 51 Y. Abe et al. (Double Chooz Collab.)
ABE 14B PR D89 092003 K. Abe et al. (T2K Collab.)
ABE 14C PRL 112 061802 K. Abe et al. (T2K Collab.)
ABE 14H JHEP 1410 086 Y. Abe et al. (Double Chooz Collab.)
Also JHEP 1502 074 (errat.) Y. Abe et al. (Double Chooz Collab.)
ADAMSON 14 PRL 112 191801 P. Adamson et al. (MINOS Collab.)
AN 14 PRL 112 061801 F.P. An et al. (Daya Bay Collab.)
AN 14B PR D90 071101 F.P. An et al. (Daya Bay Collab.)
BELLINI 14A NAT 512 383 G. Bellini et al. (Borexino Collab.)
FORERO 14 PR D90 093006 D.V. Forero, M. Tortola, J.W.F. Valle
GONZALEZ... 14 JHEP 1411 052 M.C. Gonzalez-Garcia, M. Maltoni, T. Schwetz
PDG 14 CP C38 070001 K. Olive et al. (PDG Collab.)
RENSHAW 14 PRL 112 091805 A. Renshaw et al. (Super-Kamiokande Collab.)
AARTSEN 13B PRL 111 081801 M.G. Aartsen et al. (IceCube Collab.)
ABE 13C PL B723 66 Y. Abe et al. (Double Chooz Collab.)
ABE 13E PR D88 032002 K. Abe et al. (T2K Collab.)
ABE 13G PRL 111 211803 K. Abe et al. (T2K Collab.)
ADAMSON 13A PRL 110 171801 P. Adamson et al. (MINOS Collab.)
ADAMSON 13B PRL 110 251801 P. Adamson et al. (MINOS Collab.)
AGAFONOVA 13 JHEP 1307 004 N. Agafonova et al. (OPERA Collab.)
AGUILAR-AR... 13A PRL 110 161801 A.A. Aguilar-Arevalo et al. (MiniBooNE Collab.)
AHARMIM 13 PR C88 025501 B. Aharmim et al. (SNO Collab.)
AN 13 CP C37 011001 F.P. An et al. (Daya Bay Collab.)
ANTONELLO 13 EPJ C73 2345 M. Antonello et al. (ICARUS Collab.)
ANTONELLO 13A EPJ C73 2599 M. Antonello et al. (ICARUS Collab.)
GANDO 13 PR D88 033001 A. Gando et al. (KamLAND Collab.)
ABE 12 PRL 108 131801 Y. Abe et al. (Double Chooz Collab.)
ABE 12A PR D85 031103 K. Abe et al. (T2K Collab.)
ABE 12B PR D86 052008 Y. Abe et al. (Double Chooz Collab.)
ADAMSON 12 PRL 108 191801 P. Adamson et al. (MINOS Collab.)
ADAMSON 12B PR D86 052007 P. Adamson et al. (MINOS Collab.)
ADRIAN-MAR... 12 PL B714 224 S. Adrian-Martinez et al. (ANTARES Collab.)
AHN 12 PRL 108 191802 J.K. Ahn et al. (RENO Collab.)
AN 12 PRL 108 171803 F.P. An et al. (Daya Bay Collab.)
BELLINI 12A PRL 108 051302 G. Bellini et al. (Borexino Collab.)
CHENG 12 PR D86 052009 G. Cheng et al. (MiniBooNE/SciBooNE Collab.)
MAHN 12 PR D85 032007 K.B.M. Mahn et al. (MiniBooNE/SciBooNE Collab.)
ABE 11 PR D83 052010 K. Abe et al. (Super-Kamiokande Collab.)
ABE 11A PRL 107 041801 K. Abe et al. (T2K Collab.)
ABE 11B PR C84 035804 S. Abe et al. (KamLAND Collab.)
ABE 11C PRL 107 241801 K. Abe et al. (Super-Kamiokande Collab.)
ADAMSON 11 PRL 106 181801 P. Adamson et al. (MINOS Collab.)
ADAMSON 11B PRL 107 021801 P. Adamson et al. (MINOS Collab.)
ADAMSON 11C PR D84 071103 P. Adamson et al. (MINOS Collab.)
ADAMSON 11D PRL 107 181802 P. Adamson et al. (MINOS Collab.)
BELLINI 11 PL B696 191 G. Bellini et al. (Borexino Collab.)
BELLINI 11A PRL 107 141302 G. Bellini et al. (Borexino Collab.)
FOGLI 11 PR D84 053007 G.L. Fogli et al.
GANDO 11 PR D83 052002 A. Gando et al. (KamLAND Collab.)
HUBER 11 PR C84 024617 P. Huber (VPI)
Also PR C85 029901 (errat.) P. Huber (VPI)
MUELLER 11 PR C83 054615 Th.A Mueller et al.
SERENELLI 11 APJ 743 24 A.M. Serenelli, W.C. Haxton, C. Pena-Garay
ADAMSON 10A PR D82 051102 P. Adamson et al. (MINOS Collab.)
AGUILAR-AR... 10 PRL 105 181801 A.A. Aguillar-Arevalo et al. (MiniBooNE Collab.)
AHARMIM 10 PR C81 055504 B. Aharmim et al. (SNO Collab.)
BELLINI 10A PR D82 033006 G. Bellini et al. (Borexino Collab.)
DENIZ 10 PR D81 072001 M. Deniz et al. (TEXONO Collab.)
KAETHER 10 PL B685 47 F. Kaether et al.
WENDELL 10 PR D81 092004 R. Wendell et al. (Super-Kamiokande Collab.)
ABDURASHI... 09 PR C80 015807 J.N. Abdurashitov et al. (SAGE Collab.)
ADAMSON 09 PRL 103 261802 P. Adamson et al. (MINOS Collab.)
AGUILAR-AR... 09B PRL 103 111801 A.A. Aguilar-Arevalo et al. (MiniBooNE Collab.)
ABE 08A PRL 100 221803 S. Abe et al. (KamLAND Collab.)
Also PRL 101 119904E S. Abe et al. (KamLAND Collab.)
ADAMSON 08 PR D77 072002 P. Adamson et al. (MINOS Collab.)
ADAMSON 08A PRL 101 131802 P. Adamson et al. (MINOS Collab.)
AHARMIM 08 PRL 101 111301 B. Aharmim et al. (SNO Collab.)
Also PR C87 015502 B. Aharmim et al. (SNO Collab.)
ARPESELLA 08A PRL 101 091302 C. Arpesella et al. (Borexino Collab.)
CRAVENS 08 PR D78 032002 J.P. Cravens et al. (Super-Kamiokande Collab.)
FOGLI 08 PRL 101 141801 G.L. Fogli
ADAMSON 07 PR D75 092003 P. Adamson et al. (MINOS Collab.)
AGUILAR-AR... 07 PRL 98 231801 A.A. Aguilar-Arevalo et al. (MiniBooNE Collab.)
AHARMIM 07 PR C75 045502 B. Aharmim et al. (SNO Collab.)
ADAMSON 06 PR D73 072002 P. Adamson et al. (MINOS Collab.)
AHN 06A PR D74 072003 M.H. Ahn et al. (K2K Collab.)
BALATA 06 EPJ C47 21 M. Balata et al. (Borexino Collab.)
HOSAKA 06 PR D73 112001 J. Hosaka et al. (Super-Kamiokande Collab.)
HOSAKA 06A PR D74 032002 J. Hosaka et al. (Super-Kamiokande Collab.)
MICHAEL 06 PRL 97 191801 D. Michael et al. (MINOS Collab.)
WINTER 06A PR C73 025503 W.T. Winter et al.
YAMAMOTO 06 PRL 96 181801 S. Yamamoto et al. (K2K Collab.)
AHARMIM 05A PR C72 055502 B. Aharmim et al. (SNO Collab.)
ALIU 05 PRL 94 081802 E. Aliu et al. (K2K Collab.)
ALLISON 05 PR D72 052005 W.W.M. Allison et al. (SOUDAN-2 Collab.)
ALTMANN 05 PL B616 174 M. Altmann et al. (GNO Collab.)
ARAKI 05 PRL 94 081801 T. Araki et al. (KamLAND Collab.)
ASHIE 05 PR D71 112005 Y. Ashie et al. (Super-Kamiokande Collab.)
BAHCALL 05 APJ 621 L85 J.N. Bahcall, A.M. Serenelli, S. Basu (IAS+)
DEGOUVEA 05 PR D71 093002 A. de Gouvea, C. Pena-Garay
AHARMIM 04 PR D70 093014 B. Aharmim et al. (SNO Collab.)
AHMED 04A PRL 92 181301 S.N. Ahmed et al. (SNO Collab.)
AHN 04 PRL 93 051801 M.H. Ahn et al. (K2K Collab.)
AMBROSIO 04 EPJ C36 323 M. Ambrosio et al. (MACRO Collab.)
ASHIE 04 PRL 93 101801 Y. Ashie et al. (Super-Kamiokande Collab.)
EGUCHI 04 PRL 92 071301 K. Eguchi et al. (KamLAND Collab.)
SMY 04 PR D69 011104 M.B. Smy et al. (Super-Kamiokande Collab.)
AHN 03 PRL 90 041801 M.H. Ahn et al. (K2K Collab.)
AMBROSIO 03 PL B566 35 M. Ambrosio et al. (MACRO Collab.)
APOLLONIO 03 EPJ C27 331 M. Apollonio et al. (CHOOZ Collab.)
ASTIER 03 PL B570 19 P. Astier et al. (NOMAD Collab.)
EGUCHI 03 PRL 90 021802 K. Eguchi et al. (KamLAND Collab.)
GANDO 03 PRL 90 171302 Y. Gando et al. (Super-Kamiokande Collab.)
IANNI 03 JP G29 2107 A. Ianni (INFN Gran Sasso)
SANCHEZ 03 PR D68 113004 M. Sanchez et al. (Soudan 2 Collab.)
ABDURASHI... 02 JETP 95 181 J.N. Abdurashitov et al. (SAGE Collab.)
Translated from ZETF 122 211.
AHMAD 02 PRL 89 011301 Q.R. Ahmad et al. (SNO Collab.)
AHMAD 02B PRL 89 011302 Q.R. Ahmad et al. (SNO Collab.)
ARMBRUSTER 02 PR D65 112001 B. Armbruster et al. (KARMEN 2 Collab.)
AVVAKUMOV 02 PRL 89 011804 S. Avvakumov et al. (NuTeV Collab.)
FUKUDA 02 PL B539 179 S. Fukuda et al. (Super-Kamiokande Collab.)
AGUILAR 01 PR D64 112007 A. Aguilar et al. (LSND Collab.)
AHMAD 01 PRL 87 071301 Q.R. Ahmad et al. (SNO Collab.)
AMBROSIO 01 PL B517 59 M. Ambrosio et al. (MACRO Collab.)
BOEHM 01 PR D64 112001 F. Boehm et al.
FUKUDA 01 PRL 86 5651 S. Fukuda et al. (Super-Kamiokande Collab.)
AMBROSIO 00 PL B478 5 M. Ambrosio et al. (MACRO Collab.)
BOEHM 00 PRL 84 3764 F. Boehm et al.
FUKUDA 00 PRL 85 3999 S. Fukuda et al. (Super-Kamiokande Collab.)
ALLISON 99 PL B449 137 W.W.M. Allison et al. (Soudan 2 Collab.)
APOLLONIO 99 PL B466 415 M. Apollonio et al. (CHOOZ Collab.)
Also PL B472 434 (errat.) M. Apollonio et al. (CHOOZ Collab.)

Downloaded from https://academic.oup.com/ptep/article/2022/8/083C01/6651666 by KIT Library user on 27 September 2022

FUKUDA	99C	PRL 82 2644	Y. Fukuda *et al.*	(Super-Kamiokande Collab.)
FUKUDA	99D	PL B467 185	Y. Fukuda *et al.*	(Super-Kamiokande Collab.)
HAMPEL	99	PL B447 127	W. Hampel *et al.*	(GALLEX Collab.)
AMBROSIO	98	PL B434 451	M. Ambrosio *et al.*	(MACRO Collab.)
APOLLONIO	98	PL B420 397	M. Apollonio *et al.*	(CHOOZ Collab.)
ATHANASSO...	98	PRL 81 1774	C. Athanassopoulos *et al.*	(LSND Collab.)
ATHANASSO...	98B	PR C58 2489	C. Athanassopoulos *et al.*	(LSND Collab.)
CLEVELAND	98	APJ 496 505	B.T. Cleveland *et al.*	(Homestake Collab.)
FELDMAN	98	PR D57 3873	G.J. Feldman, R.D. Cousins	
FUKUDA	98C	PRL 81 1562	Y. Fukuda *et al.*	(Super-Kamiokande Collab.)
HATAKEYAMA	98	PRL 81 2016	S. Hatakeyama *et al.*	(Kamiokande Collab.)
CLARK	97	PRL 79 345	R. Clark *et al.*	(IMB Collab.)
ROMOSAN	97	PRL 78 2912	A. Romosan *et al.*	(CCFR Collab.)
AGLIETTA	96	JETPL 63 791	M. Aglietta *et al.*	(LSD Collab.)
		Translated from ZETFP 63 753.		
ATHANASSO...	96	PR C54 2685	C. Athanassopoulos *et al.*	(LSND Collab.)
ATHANASSO...	96B	PRL 77 3082	C. Athanassopoulos *et al.*	(LSND Collab.)
FUKUDA	96	PRL 77 1683	Y. Fukuda *et al.*	(Kamiokande Collab.)
FUKUDA	96B	PL B388 397	Y. Fukuda *et al.*	(Kamiokande Collab.)
GREENWOOD	96	PR D53 6054	Z.D. Greenwood *et al.*	(UCI, SVR, SCUC)
HAMPEL	96	PL B388 384	W. Hampel *et al.*	(GALLEX Collab.)
LOVERRE	96	PL B370 156	P.F. Loverre	
ACHKAR	95	NP B434 503	B. Achkar *et al.*	(SING, SACLD, CPPM, CDEF+)
AHLEN	95	PL B357 481	S.P. Ahlen *et al.*	(MACRO Collab.)
ATHANASSO...	95	PRL 75 2650	C. Athanassopoulos *et al.*	(LSND Collab.)
DAUM	95	ZPHY C66 417	K. Daum *et al.*	(FREJUS Collab.)
HILL	95	PRL 75 2654	J.E. Hill	(PENN)
MCFARLAND	95	PRL 75 3993	K.S. McFarland *et al.*	(CCFR Collab.)
DECLAIS	94	PL B338 383	Y. Declais *et al.*	
FUKUDA	94	PL B335 237	Y. Fukuda *et al.*	(Kamiokande Collab.)
VILAIN	94C	ZPHY C64 539	P. Vilain *et al.*	(CHARM II Collab.)
FREEDMAN	93	PR D47 811	S.J. Freedman *et al.*	(LAMPF E645 Collab.)
BECKER-SZ...	92B	PR D46 3720	R.A. Becker-Szendy *et al.*	(IMB Collab.)
BEIER	92	PL B283 446	E.W. Beier *et al.*	(KAM2 Collab.)
Also		PTRSL A346 63	E.W. Beier, E.D. Frank	(PENN)
BORODOV...	92	PRL 68 274	L. Borodovsky *et al.*	(COLU, JHU, ILL)
HIRATA	92	PL B280 146	K.S. Hirata *et al.*	(Kamiokande II Collab.)
CASPER	91	PRL 66 2561	D. Casper *et al.*	(IMB Collab.)
HIRATA	91	PRL 66 9	K.S. Hirata *et al.*	(Kamiokande II Collab.)
KUVSHINN...	91	JETPL 54 253	A.A. Kuvshinnikov *et al.*	(KIAE)
BERGER	90B	PL B245 305	C. Berger *et al.*	(FREJUS Collab.)
HIRATA	90	PRL 65 1297	K.S. Hirata *et al.*	(Kamiokande II Collab.)
AGLIETTA	89	EPL 8 611	M. Aglietta *et al.*	(FREJUS Collab.)
DAVIS	89	ARNPS 39 467	R. Davis, A.K. Mann, L. Wolfenstein	(BNL, PENN+)
OYAMA	89	PR D39 1481	Y. Oyama *et al.*	(Kamiokande II Collab.)
BIONTA	88	PR D38 768	R.M. Bionta *et al.*	(IMB Collab.)
DURKIN	88	PRL 61 1811	L.S. Durkin *et al.*	(OSU, ANL, CIT+)
ABRAMOWICZ	86	PRL 57 298	H. Abramowicz *et al.*	(CDHS Collab.)
ALLABY	86	PL B177 446	J.V. Allaby *et al.*	(CHARM Collab.)
ANGELINI	86	PL B179 307	C. Angelini *et al.*	(PISA, ATHU, PADO+)
VUILLEUMIER	82	PL 114B 298	J.L. Vuilleumier *et al.*	(CIT, SIN, MUNI)
BOLIEV	81	SJNP 34 787	M.M. Boliev *et al.*	(INRM)
		Translated from YAF 34 1418.		
KWON	81	PR D24 1097	H. Kwon *et al.*	(CIT, ISNG, MUNI)
BOEHM	80	PL 97B 310	F. Boehm *et al.*	(ILLG, CIT, ISNG, MUNI)
CROUCH	78	PR D18 2239	M.F. Crouch *et al.*	(CASE, UCI, WITW)

Heavy Neutral Leptons, Searches for

OMITTED FROM SUMMARY TABLE

We define searches for Heavy Neutral Leptons (HNLs) as searches for Dirac or Majorana fermions with sterile neutrino quantum numbers, that are heavy enough to not disrupt the simplest Big Bang Nucleosynthesis bounds and/or unstable on cosmological timescales: Typically HNLs have mass $\sim$ MeV or higher.

Searches for these particles generically set bounds on the mixing between the HNL and the active neutrinos, as parametrized by the extended 3×4 PMNS matrix elements $U_{\ell x}$ (see the "Neutrino mass, mixing and oscillations" review) where $\ell = e, \mu$ or τ, and we denote the HNL as ν_x. While many measurements may be interpreted to place bounds on various combinations of these matrix elements, we quote below limits only for those cases in which one matrix element is assumed to be much larger than the other two, i.e. $|U_{\ell x}| \gg |U_{\ell' x}|$ for $\ell' \neq \ell$.

Experimental searches make use of various different strategies, including e.g. resonance searches in missing mass decay distributions or specific final states, searches for lepton number violating decays, and trilepton signatures. The resulting bounds on $U_{\ell x}$ are typically dependent on the HNL mass. The quoted limits below are either the best limit near an experimental kinematic threshold, or a characteristic value in the mass range of the experimental sensitivity.

Limits on heavy neutral lepton mixing parameters

Limits on $|U_{ex}|^2$

Quoted limits are either the best limit near the kinematic threshold of the experiment, or a characteristic value in the mass range of the experimental sensitivity

VALUE	CL%	DOCUMENT ID		TECN	COMMENT
$<2\times10^{-4}$	95	[1] FRIEDRICH	21		Near $m_{^7\mathrm{Be}} - m_{^7\mathrm{Li}}$ kin. thres.
$<1\times10^{-9}$	90	[2] CORTINA-GIL	20	NA62	$m_{\nu_x} \sim$ 150–400 MeV
$<2\times10^{-5}$	95	[3] AAD	19F	ATLS	$m_{\nu_x} \sim$ 15–40 GeV
$<1\times10^{-9}$	90	[4] ABE	19B	T2K	Near $m_K - m_e$ kin. thres.
$<1\times10^{-4}$	90	[5] ABLIKIM	19AL	BES3	$m_{\nu_x} \sim$ 0.3–0.7 GeV
$<1\times10^{-8}$	90	[6] AGUILAR-AR...	18A	PIEN	$m_{\nu_x} \sim$ 60–120 MeV ¡br¿
$<3\times10^{-7}$	90	[7] CORTINA-GIL	18	NA62	$m_{\nu_x} \sim$ 200–400 MeV
$<1\times10^{-6}$	90	[8] PARK	16	BELL	$m_{\nu_x} \sim$ 1.4 GeV
$<3\times10^{-5}$	90	[9] LIVENTSEV	13	BELL	Near $m_{\nu_x} \sim$ 2–2.5 GeV
$<3\times10^{-5}$	95	[10] ABREU	97I	DLPH	$m_{\nu_x} \sim$ 6–50 GeV
$<2\times10^{-5}$	95	[11] ABREU	97I	DLPH	Near $m_{\nu_x} \sim$ 3.5 GeV
$<1\times10^{-5}$	90	[12] BARANOV	93		Near $m_\pi - m_e$ kin. thres.
$<2\times10^{-7}$	90	[12] BARANOV	93		Near $m_K - m_e$ kin. thres.
$<1\times10^{-7}$		[13,14] BERNARDI	88	CNTR	Near $m_\pi - m_e$ kin. thres.
$<2\times10^{-9}$		[14,15] BERNARDI	88	CNTR	Near $m_K - m_e$ kin. thres.
$<1\times10^{-7}$	90	[16] DORENBOS...	86	CHRM	Near $m_D - m_e$ kin. thres.
$<1\times10^{-7}$	90	[17] COOPER-...	85	BEBC	Near $m_D - m_e$ kin. thres.

[1] Search in electron capture decay $^7\mathrm{Be} \to {}^7\mathrm{Li}\,\nu_x$. Kinematic threshold is $\sim$ 850 keV.

[2] Search for $K^+ \to e^+\nu_x$. Assumes lifetime of $\nu_x > 50$ ns.

[3] Limit from prompt lepton number violating trilepton search.

[4] $K^+ \to e^+\nu_x$, with ν_x decay through U_{ex}. ABE 19B also considers bounds on $|U_{\ell x}\, U_{\ell' x}|$ for combinations of lepton flavors in the ν_x decay final state.

[5] Searches for a Majorana Heavy Neutral Lepton producing a $\pi^- e^+$ resonance in the same sign dilepton decay $D \to K\pi^- e^+ e^+$.

[6] Search for $\pi^+ \to e^+\nu_x$.

[7] Search for $K^+ \to e^+\nu_x$.

[8] PARK 16 quotes an approximate limit $B(B^+ \to e^+\nu_x) < 3\times10^{-6}$ in the mass range $m_{\nu_x} \sim$ 0.2–1.4 GeV.

[9] Search for $B^+ \to e^+\nu_x$.

[10] Search for prompt ν_x decay signatures.

[11] Search for displaced ν_x decay signatures.

[12] Searches for K or $\pi \to e^+\nu_x$, $\nu_x \to e^+e^-\nu_e$ using a beam dump experiment at the 70 GeV Serpukhov proton synchrotron. BARANOV 93 also considers limits for $|U_{ex}\, U_{\mu x}|$ from K or $\pi \to \mu^+\nu_x$, $\nu_x \to e^+e^-\nu_e$.

[13] $\pi^+ \to e^+\nu_x$, with ν_x decay through U_{ex}.

[14] BERNARDI 88 also considers bounds on $|U_{ex}\, U_{\mu x}|$.

[15] $K^+ \to e^+\nu_x$, with ν_x decay through U_{ex}.

[16] $D^+ \to e^+\nu_x$, with $\nu_x \to e^-\ell^+\nu_\ell$.

[17] $D^+ \to e^+\nu_x$, with $\nu_x \to e^-\ell^+\nu_\ell$ or $\nu_x \to e^-\pi^+$.

Limits on $|U_{\mu x}|^2$

Quoted limits are either the best limit near the kinematic threshold of the experiment, or a characteristic value in the mass range of the experimental sensitivity

VALUE	CL%	DOCUMENT ID		TECN	COMMENT
$<1\times10^{-3}$	95	[1] AAIJ	21AA	LHCB	$m_{\nu_x} \sim$ 5–50 GeV, pp at 7, 8 TeV
$<2\times10^{-4}$	95	[2] AAIJ	21AA	LHCB	$m_{\nu_x} \sim$ 5–50 GeV, pp at 7, 8 TeV
$<5\times10^{-9}$	90	[3,4] CORTINA-GIL	21	NA62	Near $m_K - m_\mu$ kin. thres.
$<1\times10^{-7}$	90	[5] ABRATENKO	20	MBNE	Near $m_K - m_\mu$ kin. thres.
$<2\times10^{-2}$	90	[6] PRIM	20	BELL	$m_{\nu_x} \sim$ 1 GeV
$<2\times10^{-5}$	95	[7] AAD	19F	ATLS	$m_{\nu_x} \sim$ 10–50 GeV
$<2\times10^{-6}$	95	[8] AAD	19F	ATLS	$m_{\nu_x} \sim$ 10 GeV
$<1\times10^{-9}$	90	[9] ABE	19B	T2K	Near $m_K - m_\mu$ kin. thres.
$<5\times10^{-6}$	90	[10,11] AGUILAR-AR...	19B	PIEN	$m_{\nu_x} \sim$ 16–30 MeV
$<1\times10^{-5}$	90	[11] AGUILAR-AR...	19B	PIEN	Near $m_\pi - m_\mu$ kin. thres.
$<3\times10^{-7}$	90	[3] CORTINA-GIL	18	NA62	$m_{\nu_x} \sim$ 250–350 MeV
$<3\times10^{-6}$	90	[3] LAZZERONI	17A	NA62	Near $m_K - m_\mu$ kin. thres.
$<5\times10^{-2}$	90	[12] PARK	16	BELL	$m_{\nu_x} \sim$ 1.4 GeV
$<1\times10^{-8}$	90	[3] ARTAMONOV	15A	B949	$m_{\nu_x} \sim$ 200–300 MeV
$<3\times10^{-5}$	90	[13] LIVENTSEV	13	BELL	Near $m_{\nu_x} \sim$ 2–2.5 GeV
$<2.0\times10^{-8}$	95	[14] DAUM	00	KARM	$m_{\nu_x} = 33.905$ MeV
$<8\times10^{-8}$	90	[15] VAITAITIS	99	CCFR	Near $m_K - m_\mu$ kin. thres.
$<6\times10^{-8}$	90	[16] VAITAITIS	99	CCFR	Near $m_{D_s} - m_\mu$ kin. thres.
$<3\times10^{-5}$	95	[17] ABREU	97I	DLPH	$m_{\nu_x} \sim$ 6–50 GeV
$<2\times10^{-5}$	95	[18] ABREU	97I	DLPH	Near $m_{\nu_x} \sim$ 3.5 GeV
$<3\times10^{-5}$	90	[19] VILAIN	95C	CHM2	Near $m_K - m_\mu$ kin. thres.
$<3\times10^{-8}$		[20,21] BERNARDI	88	CNTR	Near $m_\mu + m_\pi$ kin. thres.
$<2\times10^{-9}$		[21,22] BERNARDI	88	CNTR	Near $m_K - m_\mu$ kin. thres.
$<1\times10^{-7}$	90	[23] DORENBOS...	86	CHRM	Near $m_D - m_\mu$ kin. thres.
$<1\times10^{-7}$	90	[24] COOPER-...	85	BEBC	Near $m_D - m_\mu$ kin. thres.

[1] Limit from prompt lepton number conserving $W \to \mu\mu j$ search.

[2] Limit from prompt lepton number violating $W \to \mu\mu j$ search .

[3] Search for $K^+ \to \mu^+\nu_x$.

[4] Assumes a lifetime exceeding 50 ns, and searches over m_{ν_x} range 200–384 MeV.

Downloaded from https://academic.oup.com/ptep/article/2022/8/083C01/6651666 by KIT Library user on 27 September 2022

[5] $K^+ \to \mu^+ \nu_X$, with $\nu_X \to \mu^- \pi^+$, in the mass range $m_{\nu_X} \sim$ 260–385 MeV. ABRATENKO 20 also considers $\nu_X \to \mu^+ \pi^-$ for the case of Majorana HNL.

[6] Search for $B^+ \to \mu^+ \nu_X$ in the mass range $m_{\nu_X} \sim$ 0–1.5 GeV .

[7] Limit from prompt lepton number violating trilepton search.

[8] Limit from displaced lepton violating or conserving trilepton searches.

[9] $K^+ \to \mu^+ \nu_X$, with ν_X decay through $U_{\mu X}$. ABE 19B also considers bounds on $|U_{\ell X}\ U_{\ell' X}|$ for combinations of lepton flavors in the ν_X decay final state.

[10] Limit requires muon kinetic energy > 1.2 MeV.

[11] Search for $\pi^+ \to \mu^+ \nu_X$.

[12] PARK 16 quotes an approximate limit $B(B^+ \to \mu^+ \nu_X) < 3 \times 10^{-6}$ in the mass range $m_{\nu_X} \sim$ 0.2–1.4 GeV.

[13] Search for $B^+ \to \mu^+ \nu_X$.

[14] DAUM 00 quotes a branching ratio bound $B(\pi^+ \to \mu^+ \nu_X) < 6.0 \times 10^{-10}$ at 95% CL.

[15] $K^+ \to \mu^+ \nu_X$, with $\nu_X \to \mu X$.

[16] $D_s \to \mu^+ \nu_X$, with $\nu_X \to \mu X$.

[17] Search for prompt ν_X decay signatures.

[18] Search for displaced ν_X decay signatures.

[19] Search for Heavy Neutral Leptons produced by neutral current muon neutrino interactions, with $\nu_X \to \mu^+ \mu^- \nu_\mu$.

[20] $K^+ \to \mu^+ \nu_X$, with ν_X decay through $U_{\mu X}$ and $m_{\nu_X} < m_\mu + m_\pi$.

[21] BERNARDI 88 also considers bounds on $|U_{eX}\ U_{\mu X}|$.

[22] $K^+ \to \mu^+ \nu_X$, with $\nu_X \to \mu^- \pi^+$.

[23] $D^+ \to \mu^+ \nu_X$, with $\nu_X \to \mu^- \ell^+ \nu_\ell$.

[24] $D^+ \to \mu^+ \nu_X$, with $\nu_X \to \mu^- \ell^+ \nu_\ell$ or $\nu_X \to \mu^- \pi^+$.

Limits on $|U_{\tau X}|^2$

Quoted limits are either the best limit near the kinematic threshold of the experiment, or a characteristic value in the mass range of the experimental sensitivity

VALUE	CL%	DOCUMENT ID		TECN	COMMENT
$<3 \times 10^{-4}$	90	[1] ACCIARRI	21	ARNT	Near $m_{\nu_X} \lesssim$ 970 MeV
$<3 \times 10^{-6}$	90	[2] BOIARSKA	21	RVUE	Near $m_{\nu_X} \sim$ 0.8–1.6 GeV
$<2 \times 10^{-4}$	90	[3] ORLOFF	02	CHRM	Near $m_D - m_\tau$ kin. thres.
$<1 \times 10^{-4}$	90	[4] ORLOFF	02	CHRM	$m_{\nu_X} \sim$ 200–250 MeV
$<3 \times 10^{-5}$	95	[5] ABREU	97I	DLPH	$m_{\nu_X} \sim$ 6–50 GeV
$<2 \times 10^{-5}$	95	[6] ABREU	97I	DLPH	Near $m_{\nu_X} \sim$ 3.5 GeV

[1] Search for $\nu_X \to \mu^+ \mu^- \nu$.

[2] Reanalysis of CHARM results (cf. ORLOFF 02) to include searches for $\nu_X \to \nu \ell^+ \ell^-$ decays, and including the production of HNLs from τ decays.

[3] $D_s \to \tau^+ \nu_X$, with ν_X decay via $U_{\tau X}$.

[4] $D_s \to \nu_\tau \tau^+$, $\tau^+ \to \nu_X X$, with ν_X decay via $U_{\tau X}$.

[5] Search for prompt ν_X decay signatures.

[6] Search for displaced ν_X decay signatures. Kinematical suppression of $\nu_X \to \tau X$ at lower masses leads to rapid loosening of the $|U_{\tau X}|$ bound compared to that for $|U_{eX}|$ and $|U_{\mu X}|$.

REFERENCES FOR Heavy Neutral Leptons, Searches for

AAIJ	21AA	EPJ C81 248	R. Aaij *et al.*	(LHCb Collab.)
ACCIARRI	21	PRL 127 121801	R. Acciarri *et al.*	(ArgoNeuT Collab.)
BOIARSKA	21	PR D104 095019	I. Boiarska *et al.*	(BOHR, LEID)
CORTINA-GIL	21	PL B816 136259	E. Cortina Gil *et al.*	(NA62 Collab.)
FRIEDRICH	21	PRL 126 021803	S. Friedrich *et al.*	(BeEST Collab.)
ABRATENKO	20	PR D101 052001	P. Abratenko *et al.*	(MiniBooNE Collab.)
CORTINA-GIL	20	PL B807 135599	E. Cortina Gil *et al.*	(NA62 Collab.)
PRIM	20	PR D101 032007	M.T. Prim *et al.*	(BELLE Collab.)
AAD	19F	JHEP 1910 265	G. Aad *et al.*	(ATLAS Collab.)
ABE	19B	PR D100 052006	K. Abe *et al.*	(T2K Collab.)
ABLIKIM	19AL	PR D99 112002	M. Ablikim *et al.*	(BESIII Collab.)
AGUILAR-AR...	19B	PL B798 134980	A. Aguilar-Arevalo *et al.*	(PIENU Collab.)
AGUILAR-AR...	18A	PR D97 072012	A. Aguilar-Arevalo *et al.*	(PIENU Collab.)
CORTINA-GIL	18	PL B778 137	E. Cortina Gil *et al.*	(NA62 Collab.)
LAZZERONI	17A	PL B772 712	C. Lazzeroni *et al.*	(NA62 Collab.)
PARK	16	PR D94 012003	C.-S. Park *et al.*	(BELLE Collab.)
ARTAMONOV	15A	PR D91 052001	A.V. Artamanov *et al.*	(E949 Collab.)
LIVENTSEV	13	PR D87 071102	D. Liventsev *et al.*	(BELLE Collab.)
Also		PR D95 099903 (errat.)	D. Liventsev *et al.*	(BELLE Collab.)
ORLOFF	02	PL B550 8	J. Orloff *et al.*	(CHARM Collab.)
DAUM	00	PRL 85 1815	M. Daum *et al.*	(KARMEN Collab.)
VAITAITIS	99	PRL 83 4943	A. Vaitaitis *et al.*	(CCFR Collab.)
ABREU	97I	ZPHY C74 57	P. Abreu *et al.*	(DELPHI Collab.)
Also		ZPHY C75 580 (errat.)	P. Abreu *et al.*	(DELPHI Collab.)
VILAIN	95C	PL B351 387	P. Vilain *et al.*	(CHARM II Collab.)
Also		PL B343 453	P. Vilain *et al.*	(CHARM II Collab.)
BARANOV	93	PL B302 336	S.A. Baranov *et al.*	(JINR, SERP, BUDA)
BERNARDI	88	PL B203 332	G. Bernardi *et al.*	(PARIN, CERN, INFN+)
DORENBOS...	86	PL 166B 473	J. Dorenbosch *et al.*	(CHARM Collab.)
COOPER-...	85	PL 160B 207	A.M. Cooper-Sarkar *et al.*	(CERN, LOIC+)

Downloaded from https://academic.oup.com/ptep/article/2022/8/083C01/6651666 by KIT Library user on 27 September 2022

u 1311
d 1311
s 1311
c 1315
b 1317
t 1319
b' (Fourth Generation) Quark 1337
t' (Fourth Generation) Quark 1339
Free Quark Searches 1341

Related Reviews in Volume 1

60. Quark masses (rev.) 808
61. Top quark (rev.) 817

Downloaded from https://academic.oup.com/ptep/article/2022/8/083C01/6651666 by KIT Library user on 27 September 2022

Downloaded from https://academic.oup.com/ptep/article/2022/8/083C01/6651666 by KIT Library user on 27 September 2022

QUARKS

See the related review(s):

Quark Masses

u

$I(J^P) = \frac{1}{2}(\frac{1}{2}^+)$

Mass $m = 2.16^{+0.49}_{-0.26}$ MeV Charge $= \frac{2}{3}\ e$ $I_z = +\frac{1}{2}$

$m_u/m_d = 0.474^{+0.056}_{-0.074}$

d

$I(J^P) = \frac{1}{2}(\frac{1}{2}^+)$

Mass $m = 4.67^{+0.48}_{-0.17}$ MeV Charge $= -\frac{1}{3}\ e$ $I_z = -\frac{1}{2}$

$m_s/m_d = 17$–22

$\overline{m} = (m_u + m_d)/2 = 3.45^{+0.35}_{-0.15}$ MeV

s

$I(J^P) = 0(\frac{1}{2}^+)$

Mass $m = 93.4^{+8.6}_{-3.4}$ MeV Charge $= -\frac{1}{3}\ e$ Strangeness $= -1$

$(m_s - (m_u + m_d)/2)/(m_d - m_u) = 27.33^{+0.67}_{-0.77}$

Light Quarks (u, d, s)

OMITTED FROM SUMMARY TABLE

u-QUARK MASS

The u-, d-, and s-quark masses are estimates of so-called "current-quark masses," in a mass- independent subtraction scheme such as $\overline{\text{MS}}$. The ratios m_u/m_d and m_s/m_d are extracted from pion and kaon masses using chiral symmetry. The estimates of d and u masses are not without controversy and remain under active investigation. Within the literature there are even suggestions that the u quark could be essentially massless. The s-quark mass is estimated from SU(3) splittings in hadron masses.

We have normalized the $\overline{\text{MS}}$ masses at a renormalization scale of $\mu = 2$ GeV. Results quoted in the literature at $\mu = 1$ GeV have been rescaled by dividing by 1.35. The values of "Our Evaluation" were determined in part via Figures 1 and 2.

$\overline{\text{MS}}$ MASS (MeV)	DOCUMENT ID		TECN
$2.16^{+0.49}_{-0.26}$ OUR EVALUATION	See the ideogram below.		
2.6 ±0.4	[1] DOMINGUEZ	19	THEO
2.130±0.041	[2] BAZAVOV	18	LATT
2.27 ±0.06 ±0.06	[3] FODOR	16	LATT
2.36 ±0.24	[4] CARRASCO	14	LATT
2.57 ±0.26 ±0.07	[5] AOKI	12	LATT
2.24 ±0.10 ±0.34	[6] BLUM	10	LATT
2.01 ±0.14	[7] MCNEILE	10	LATT
• • • We do not use the following data for averages, fits, limits, etc. • • •			
2.15 ±0.03 ±0.10	[8] DURR	11	LATT
1.9 ±0.2	[9] BAZAVOV	10	LATT
2.01 ±0.14	[7] DAVIES	10	LATT
2.9 ±0.2	[10] DOMINGUEZ	09	THEO
2.9 ±0.8	[11] DEANDREA	08	THEO
3.02 ±0.33	[12] BLUM	07	LATT
2.7 ±0.4	[13] JAMIN	06	THEO
1.9 ±0.2	[14] MASON	06	LATT
2.8 ±0.2	[15] NARISON	06	THEO
1.7 ±0.3	[16] AUBIN	04A	LATT

[1] DOMINGUEZ 19 determine the quark mass from a QCD finite energy sum rule for the divergence of the axial current.

[2] BAZAVOV 18 determine the quark masses using a lattice computation with staggered fermions and four active quark flavors.

[3] FODOR 16 is a lattice simulation with $n_f = 2 + 1$ dynamical flavors and includes partially quenched QED effects.

[4] CARRASCO 14 is a lattice QCD computation of light quark masses using $2 + 1 + 1$ dynamical quarks, with $m_u = m_d \neq m_s \neq m_c$. The u and d quark masses are obtained separately by using the K meson mass splittings and lattice results for the electromagnetic contributions.

[5] AOKI 12 is a lattice computation using $1 + 1 + 1$ dynamical quark flavors.

[6] BLUM 10 determines light quark masses using a QCD plus QED lattice computation of the electromagnetic mass splittings of the low-lying hadrons. The lattice simulations use 2+1 dynamical quark flavors.

[7] DAVIES 10 and MCNEILE 10 determine $\overline{m}_c(\mu)/\overline{m}_s(\mu) = 11.85 \pm 0.16$ using a lattice computation with $n_f = 2 + 1$ dynamical fermions of the pseudoscalar meson masses. Mass m_u is obtained from this using the value of m_c from ALLISON 08 or MCNEILE 10 and the BAZAVOV 10 values for the light quark mass ratios, $m_s/\overline{m}$ and m_u/m_d.

[8] DURR 11 determine quark mass from a lattice computation of the meson spectrum using $n_f = 2 + 1$ dynamical flavors. The lattice simulations were done at the physical quark mass, so that extrapolation in the quark mass was not needed. The individual m_u, m_d values are obtained using the lattice determination of the average mass m_{ud} and of the ratio m_s/m_{ud} and the value of $Q = (m_s^2 - m_{\text{ud}}^2)\ /\ (m_d^2 - m_u^2)$ as determined from $\eta \to 3\pi$ decays.

[9] BAZAVOV 10 is a lattice computation using 2+1 dynamical quark flavors.

[10] DOMINGUEZ 09 use QCD finite energy sum rules for the two-point function of the divergence of the axial vector current computed to order α_s^4.

[11] DEANDREA 08 determine $m_u - m_d$ from $\eta \to 3\pi^0$, and combine with the PDG 06 lattice average value of $m_u + m_d = 7.6 \pm 1.6$ to determine m_u and m_d.

[12] BLUM 07 determine quark masses from the pseudoscalar meson masses using a QED plus QCD lattice computation with two dynamical quark flavors.

[13] JAMIN 06 determine m_u(2 GeV) by combining the value of m_s obtained from the spectral function for the scalar $K\pi$ form factor with other determinations of the quark mass ratios.

[14] MASON 06 extract light quark masses from a lattice simulation using staggered fermions with an improved action, and three dynamical light quark flavors with degenerate u and d quarks. Perturbative corrections were included at NNLO order. The quark masses m_u and m_d were determined from their $(m_u + m_d)/2$ measurement and AUBIN 04A m_u/m_d value.

[15] NARISON 06 uses sum rules for $e^+e^- \to$ hadrons to order α_s^3 to determine m_s combined with other determinations of the quark mass ratios.

[16] AUBIN 04A employ a partially quenched lattice calculation of the pseudoscalar meson masses.

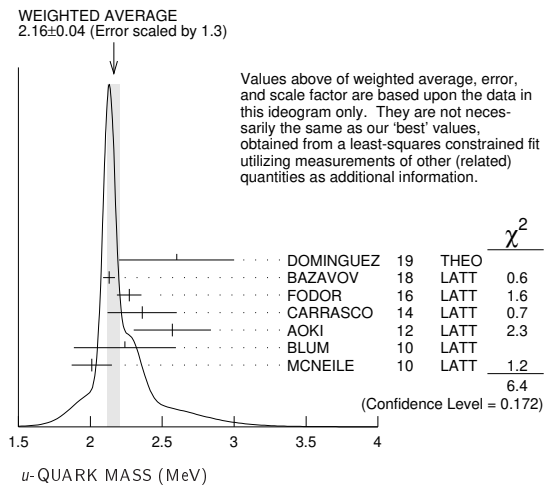

d-QUARK MASS

See the comment for the u quark above.

We have normalized the $\overline{\text{MS}}$ masses at a renormalization scale of $\mu = 2$ GeV. Results quoted in the literature at $\mu = 1$ GeV have been rescaled by dividing by 1.35. The values of "Our Evaluation" were determined in part via Figures 1 and 2.

$\overline{\text{MS}}$ MASS (MeV)	DOCUMENT ID		TECN
$4.67^{+0.48}_{-0.17}$ OUR EVALUATION	See the ideogram below.		
5.3 ±0.4	[1] DOMINGUEZ	19	THEO
4.675±0.056	[2] BAZAVOV	18	LATT
4.67 ±0.06 ±0.06	[3] FODOR	16	LATT
5.03 ±0.26	[4] CARRASCO	14	LATT
3.68 ±0.29 ±0.10	[5] AOKI	12	LATT
4.65 ±0.15 ±0.32	[6] BLUM	10	LATT
4.77 ±0.15	[7] MCNEILE	10	LATT
• • • We do not use the following data for averages, fits, limits, etc. • • •			
4.79 ±0.07 ±0.12	[8] DURR	11	LATT
4.6 ±0.3	[9] BAZAVOV	10	LATT
4.79 ±0.16	[7] DAVIES	10	LATT
5.3 ±0.4	[10] DOMINGUEZ	09	THEO
4.7 ±0.8	[11] DEANDREA	08	THEO
5.49 ±0.39	[12] BLUM	07	LATT
4.8 ±0.5	[13] JAMIN	06	THEO
4.4 ±0.3	[14] MASON	06	LATT
5.1 ±0.4	[15] NARISON	06	THEO
3.9 ±0.5	[16] AUBIN	04A	LATT

[1] DOMINGUEZ 19 determine the quark mass from a QCD finite energy sum rule for the divergence of the axial current.

[2] BAZAVOV 18 determine the quark masses using a lattice computation with staggered fermions and four active quark flavors.

[3] FODOR 16 is a lattice simulation with $n_f = 2 + 1$ dynamical flavors and includes partially quenched QED effects.

Downloaded from https://academic.oup.com/ptep/article/2022/8/083C01/6651666 by KIT Library user on 27 September 2022

[4] CARRASCO 14 is a lattice QCD computation of light quark masses using $2+1+1$ dynamical quarks, with $m_u = m_d \neq m_s \neq m_c$. The u and d quark masses are obtained separately by using the K meson mass splittings and lattice results for the electromagnetic contributions.

[5] AOKI 12 is a lattice computation using $1+1+1$ dynamical quark flavors.

[6] BLUM 10 determines light quark masses using a QCD plus QED lattice computation of the electromagnetic mass splittings of the low-lying hadrons. The lattice simulations use 2+1 dynamical quark flavors.

[7] DAVIES 10 and MCNEILE 10 determine $\overline{m}_c(\mu)/\overline{m}_s(\mu) = 11.85 \pm 0.16$ using a lattice computation with $n_f = 2+1$ dynamical fermions of the pseudoscalar meson masses. Mass m_d is obtained from this using the value of m_c from ALLISON 08 or MCNEILE 10 and the BAZAVOV 10 values for the light quark mass ratios, $m_s/\overline{m}$ and m_u/m_d.

[8] DURR 11 determine quark mass from a lattice computation of the meson spectrum using $n_f = 2+1$ dynamical flavors. The lattice simulations were done at the physical quark mass, so that extrapolation in the quark mass was not needed. The individual m_u, m_d values are obtained using the lattice determination of the average mass $m_{\rm ud}$ and of the ratio $m_s/m_{\rm ud}$ and the value of $Q = (m_s^2 - m_{\rm ud}^2)\ /\ (m_d^2 - m_u^2)$ as determined from $\eta \to 3\pi$ decays.

[9] BAZAVOV 10 is a lattice computation using 2+1 dynamical quark flavors.

[10] DOMINGUEZ 09 use QCD finite energy sum rules for the two-point function of the divergence of the axial vector current computed to order α_s^4.

[11] DEANDREA 08 determine $m_u - m_d$ from $\eta \to 3\pi^0$, and combine with the PDG 06 lattice average value of $m_u + m_d = 7.6 \pm 1.6$ to determine m_u and m_d.

[12] BLUM 07 determine quark masses from the pseudoscalar meson masses using a QED plus QCD lattice computation with two dynamical quark flavors.

[13] JAMIN 06 determine m_d(2 GeV) by combining the value of m_s obtained from the spectral function for the scalar $K\pi$ form factor with other determinations of the quark mass ratios.

[14] MASON 06 extract light quark masses from a lattice simulation using staggered fermions with an improved action, and three dynamical light quark flavors with degenerate u and d quarks. Perturbative corrections were included at NNLO order. The quark masses m_u and m_d were determined from their $(m_u + m_d)/2$ measurement and AUBIN 04A m_u/m_d value.

[15] NARISON 06 uses sum rules for $e^+e^- \to$ hadrons to order α_s^3 to determine m_s combined with other determinations of the quark mass ratios.

[16] AUBIN 04A perform three flavor dynamical lattice calculation of pseudoscalar meson masses, with continuum estimate of electromagnetic effects in the kaon masses, and one-loop perturbative renormalization constant.

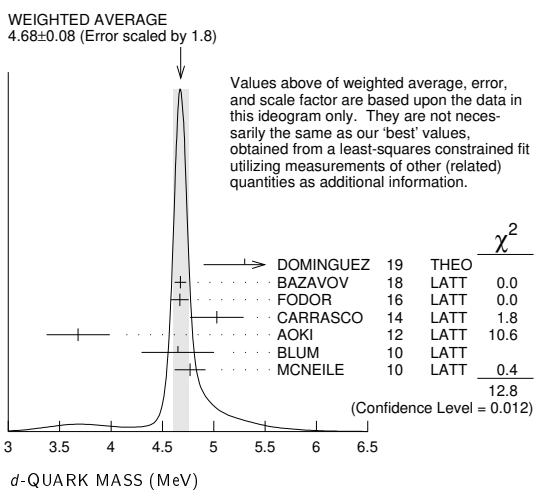

$\overline{m} = (m_u + m_d)/2$

See the comments for the u quark above.

We have normalized the $\overline{\rm MS}$ masses at a renormalization scale of $\mu = 2$ GeV. Results quoted in the literature at $\mu = 1$ GeV have been rescaled by dividing by 1.35. The values of "Our Evaluation" were determined in part via Figures 1 and 2.

$\overline{\rm MS}$ MASS (MeV)	DOCUMENT ID		TECN
$3.45\ ^{+0.35}_{-0.15}$ OUR EVALUATION	See the ideogram below.		
$3.636 \pm 0.066\ ^{+0.060}_{-0.057}$	[1] ALEXANDROU	21	LATT
$3.54 \pm 0.12 \pm 0.09$	[2] BRUNO	20	LATT
3.9 ± 0.3	[3] DOMINGUEZ	19	THEO
$4.7\ ^{+0.8}_{-0.7}$	[4] YUAN	17	THEO
3.70 ± 0.17	[5] CARRASCO	14	LATT
3.45 ± 0.12	[6] ARTHUR	13	LATT
$3.469 \pm 0.047 \pm 0.048$	[7] DURR	11	LATT
3.6 ± 0.2	[8] BLOSSIER	10	LATT
3.39 ± 0.06	[9] MCNEILE	10	LATT
• • • We do not use the following data for averages, fits, limits, etc. • • •			
3.59 ± 0.21	[10] AOKI	11A	LATT
3.40 ± 0.07	[9] DAVIES	10	LATT
4.1 ± 0.2	[11] DOMINGUEZ	09	THEO
3.72 ± 0.41	[12] ALLTON	08	LATT
$3.85 \pm 0.12 \pm 0.4$	[13] BLOSSIER	08	LATT
$\geq 4.85 \pm 0.20$	[14] DOMINGUEZ...	08B	THEO
$3.55\ ^{+0.65}_{-0.28}$	[15] ISHIKAWA	08	LATT
4.026 ± 0.048	[16] NAKAMURA	08	LATT
4.25 ± 0.35	[17] BLUM	07	LATT
$4.08 \pm 0.25 \pm 0.42$	[18] GOCKELER	06	LATT
$4.7 \pm 0.2 \pm 0.3$	[19] GOCKELER	06A	LATT
3.2 ± 0.3	[20] MASON	06	LATT
3.95 ± 0.3	[21] NARISON	06	THEO
2.8 ± 0.3	[22] AUBIN	04	LATT
$4.29 \pm 0.14 \pm 0.65$	[23] AOKI	03	LATT
3.223 ± 0.3	[24] AOKI	03B	LATT
$4.4 \pm 0.1 \pm 0.4$	[25] BECIREVIC	03	LATT
$4.1 \pm 0.3 \pm 1.0$	[26] CHIU	03	LATT

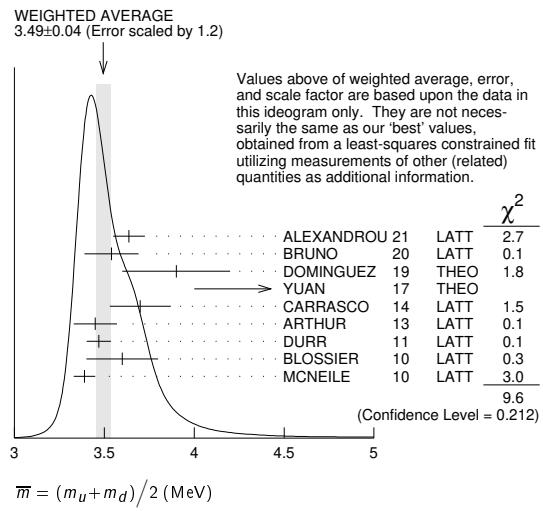

[1] ALEXANDROU 21 determines the quark mass using a lattice calculation of the meson and baryon masses with a twisted mass fermion action. The simulations are carried out using 2+1+1 dynamical quarks with $m_u = m_d \neq m_s \neq m_c$, including gauge ensembles close to the physical pion point.

[2] BRUNO 20 determines the light quark mass using a lattice calculation with $n_f = 2+1$ flavors of Wilson fermions. The scale has been set from f_π and f_K. The tuning was done using the masses of the lightest (π) and strange (K) pseudoscalar mesons.

[3] DOMINGUEZ 19 determine the quark mass from a QCD finite energy sum rule for the divergence of the axial current.

[4] YUAN 17 determine $\overline{m}$ using QCD sum rules in the isospin $I=0$ scalar channel. At the end of the "Numerical Results" section of YUAN 17 the authors discuss the significance of their larger value of the light quark mass compared to previous determinations.

[5] CARRASCO 14 is a lattice QCD computation of light quark masses using $2+1+1$ dynamical quarks, with $m_u = m_d \neq m_s \neq m_c$. The u and d quark masses are obtained separately by using the K meson mass splittings and lattice results for the electromagnetic contributions.

[6] ARTHUR 13 is a lattice computation using 2+1 dynamical domain wall fermions. Masses at $\mu = 3$ GeV have been converted to $\mu = 2$ GeV using conversion factors given in their paper.

[7] DURR 11 determine quark mass from a lattice computation of the meson spectrum using $n_f = 2+1$ dynamical flavors. The lattice simulations were done at the physical quark mass, so that extrapolation in the quark mass was not needed.

[8] BLOSSIER 10 determines quark masses from a computation of the hadron spectrum using n_f=2 dynamical twisted-mass Wilson fermions.

[9] DAVIES 10 and MCNEILE 10 determine $\overline{m}_c(\mu)/\overline{m}_s(\mu) = 11.85 \pm 0.16$ using a lattice computation with $n_f = 2+1$ dynamical fermions of the pseudoscalar meson masses. Mass $\overline{m}$ is obtained from this using the value of m_c from ALLISON 08 or MCNEILE 10 and the BAZAVOV 10 values for the light quark mass ratio, $m_s/\overline{m}$.

[10] AOKI 11A determine quark masses from a lattice computation of the hadron spectrum using $n_f = 2+1$ dynamical flavors of domain wall fermions.

[11] DOMINGUEZ 09 use QCD finite energy sum rules for the two-point function of the divergence of the axial vector current computed to order α_s^4.

[12] ALLTON 08 use a lattice computation of the π, K, and Ω masses with 2+1 dynamical flavors of domain wall quarks, and non-perturbative renormalization.

[13] BLOSSIER 08 use a lattice computation of pseudoscalar meson masses and decay constants with 2 dynamical flavors and non-perturbative renormalization.

[14] DOMINGUEZ-CLARIMON 08B obtain an inequality from sum rules for the scalar two-point correlator.

Downloaded from https://academic.oup.com/ptep/article/2022/8/083C01/6651666 by KIT Library user on 27 September 2022

[15] ISHIKAWA 08 use a lattice computation of the light meson spectrum with 2+1 dynamical flavors of $\mathcal{O}(a)$ improved Wilson quarks, and one-loop perturbative renormalization.

[16] NAKAMURA 08 do a lattice computation using quenched domain wall fermions and non-perturbative renormalization.

[17] BLUM 07 determine quark masses from the pseudoscalar meson masses using a QED plus QCD lattice computation with two dynamical quark flavors.

[18] GOCKELER 06 use an unquenched lattice computation of the axial Ward Identity with $n_f = 2$ dynamical light quark flavors, and non-perturbative renormalization, to obtain $\overline{m}(2\text{ GeV}) = 4.08 \pm 0.25 \pm 0.19 \pm 0.23$ MeV, where the first error is statistical, the second and third are systematic due to the fit range and force scale uncertainties, respectively. We have combined the systematic errors linearly.

[19] GOCKELER 06A use an unquenched lattice computation of the pseudoscalar meson masses with $n_f = 2$ dynamical light quark flavors, and non-perturbative renormalization.

[20] MASON 06 extract light quark masses from a lattice simulation using staggered fermions with an improved action, and three dynamical light quark flavors with degenerate u and d quarks. Perturbative corrections were included at NNLO order.

[21] NARISON 06 uses sum rules for $e^+ e^- \to$ hadrons to order α_s^3 to determine m_s combined with other determinations of the quark mass ratios.

[22] AUBIN 04 perform three flavor dynamical lattice calculation of pseudoscalar meson masses, with one-loop perturbative renormalization constant.

[23] AOKI 03 uses quenched lattice simulation of the meson and baryon masses with degenerate light quarks. The extrapolations are done using quenched chiral perturbation theory.

[24] The errors given in AOKI 03B were $^{+0.046}_{-0.069}$. We changed them to ± 0.3 for calculating the overall best values. AOKI 03B uses lattice simulation of the meson and baryon masses with two dynamical light quarks. Simulations are performed using the $\mathcal{O}(a)$ improved Wilson action.

[25] BECIREVIC 03 perform quenched lattice computation using the vector and axial Ward identities. Uses $\mathcal{O}(a)$ improved Wilson action and nonperturbative renormalization.

[26] CHIU 03 determines quark masses from the pion and kaon masses using a lattice simulation with a chiral fermion action in quenched approximation.

m_u/m_d MASS RATIO

VALUE	DOCUMENT ID		TECN	COMMENT
$0.474\ ^{+0.056}_{-0.074}$ OUR EVALUATION	See the ideogram below.			
$0.485 \pm 0.011 \pm 0.016$	[1] FODOR	16	LATT	
$0.4482\ ^{+0.0173}_{-0.0206}$	[2] BASAK	15	LATT	
0.470 ± 0.056	[3] CARRASCO	14	LATT	
0.698 ± 0.051	[4] AOKI	12	LATT	
$0.42 \pm 0.01 \pm 0.04$	[5] BAZAVOV	10	LATT	
$0.4818 \pm 0.0096 \pm 0.0860$	[6] BLUM	10	LATT	
• • • We do not use the following data for averages, fits, limits, etc. • • •				
0.550 ± 0.031	[7] BLUM	07	LATT	
0.43 ± 0.08	[8] AUBIN	04A	LATT	
0.410 ± 0.036	[9] NELSON	03	LATT	
0.553 ± 0.043	[10] LEUTWYLER	96	THEO	Compilation

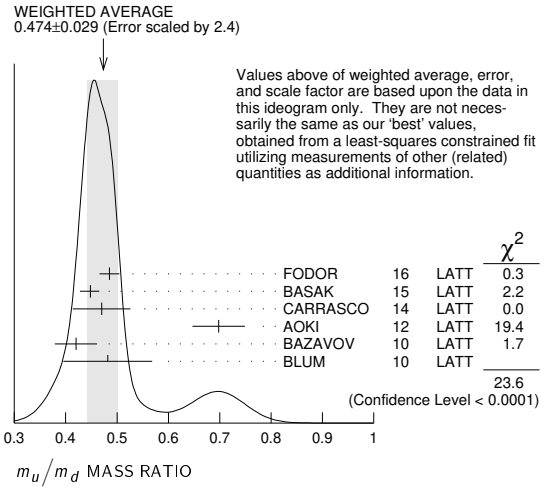

[1] FODOR 16 is a lattice simulation with $n_f = 2 + 1$ dynamical flavors and includes partially quenched QED effects.

[2] BASAK 15 is a lattice computation using 2+1 dynamical quark flavors.

[3] CARRASCO 14 is a lattice QCD computation of light quark masses using $2 + 1 + 1$ dynamical quarks, with $m_u = m_d \neq m_s \neq m_c$. The u and d quark masses are obtained separately by using the K meson mass splittings and lattice results for the electromagnetic contributions.

[4] AOKI 12 is a lattice computation using $1 + 1 + 1$ dynamical quark flavors.

[5] BAZAVOV 10 is a lattice computation using 2+1 dynamical quark flavors.

[6] BLUM 10 is a lattice computation using 2+1 dynamical quark flavors.

[7] BLUM 07 determine quark masses from the pseudoscalar meson masses using a QED plus QCD lattice computation with two dynamical quark flavors.

[8] AUBIN 04A perform three flavor dynamical lattice calculation of pseudoscalar meson masses, with continuum estimate of electromagnetic effects in the kaon masses.

[9] NELSON 03 computes coefficients in the order p^4 chiral Lagrangian using a lattice calculation with three dynamical flavors. The ratio m_u/m_d is obtained by combining this with the chiral perturbation theory computation of the meson masses to order p^4.

[10] LEUTWYLER 96 uses a combined fit to $\eta \to 3\pi$ and $\psi' \to J/\psi\ (\pi,\eta)$ decay rates, and the electromagnetic mass differences of the π and K.

s-QUARK MASS

See the comment for the u quark above.

We have normalized the $\overline{\text{MS}}$ masses at a renormalization scale of $\mu = 2$ GeV. Results quoted in the literature at $\mu = 1$ GeV have been rescaled by dividing by 1.35.

$\overline{\text{MS}}$ MASS (MeV)	DOCUMENT ID		TECN
$93.4\ ^{+8.6}_{-3.4}$ OUR EVALUATION	See the ideogram below.		
$98.7 \pm 2.4\ ^{+4.0}_{-3.2}$	[1] ALEXANDROU	21	LATT
$95.7 \pm 2.5 \pm 2.4$	[2] BRUNO	20	LATT
92.47 ± 0.69	[3] BAZAVOV	18	LATT
93.85 ± 0.75	[4] LYTLE	18	LATT
87.6 ± 6.0	[5] ANANTHANA..	16	THEO
99.6 ± 4.3	[6] CARRASCO	14	LATT
94.4 ± 2.3	[7] ARTHUR	13	LATT
94 ± 9	[8] BODENSTEIN	13	THEO
$102 \pm 3 \pm 1$	[9] FRITZSCH	12	LATT
$95.5 \pm 1.1 \pm 1.5$	[10] DURR	11	LATT
• • • We do not use the following data for averages, fits, limits, etc. • • •			
93.6 ± 0.8	[11] CHAKRABOR..	15	LATT
96.2 ± 2.7	[12] AOKI	11A	LATT
95 ± 6	[13] BLOSSIER	10	LATT
$97.6 \pm 2.9 \pm 5.5$	[14] BLUM	10	LATT
92.4 ± 1.5	[15] DAVIES	10	LATT
92.2 ± 1.3	[15] MCNEILE	10	LATT
107.3 ± 11.7	[16] ALLTON	08	LATT
$105 \pm 3 \pm 9$	[17] BLOSSIER	08	LATT
102 ± 8	[18] DOMINGUEZ	08A	THEO
$90.1\ ^{+17.2}_{-6.1}$	[19] ISHIKAWA	08	LATT
105.6 ± 1.2	[20] NAKAMURA	08	LATT
119.5 ± 9.3	[21] BLUM	07	LATT
$105 \pm 6 \pm 7$	[22] CHETYRKIN	06	THEO
$111 \pm 6 \pm 10$	[23] GOCKELER	06	LATT
$119 \pm 5 \pm 8$	[24] GOCKELER	06A	LATT
92 ± 9	[25] JAMIN	06	THEO
87 ± 6	[26] MASON	06	LATT
104 ± 15	[27] NARISON	06	THEO
$\geq 71 \pm 4,\ \leq 151 \pm 14$	[28] NARISON	06	THEO
$96\ ^{+5}_{-3}\ ^{+16}_{-18}$	[29] BAIKOV	05	THEO
81 ± 22	[30] GAMIZ	05	THEO
125 ± 28	[31] GORBUNOV	05	THEO
93 ± 32	[32] NARISON	05	THEO
76 ± 8	[33] AUBIN	04	LATT
$116 \pm 6 \pm 0.65$	[34] AOKI	03	LATT
$84.5\ ^{+12}_{-1.7}$	[35] AOKI	03B	LATT
$106 \pm 2 \pm 8$	[36] BECIREVIC	03	LATT
$92 \pm 9 \pm 16$	[37] CHIU	03	LATT
117 ± 17	[38] GAMIZ	03	THEO
103 ± 17	[39] GAMIZ	03	THEO

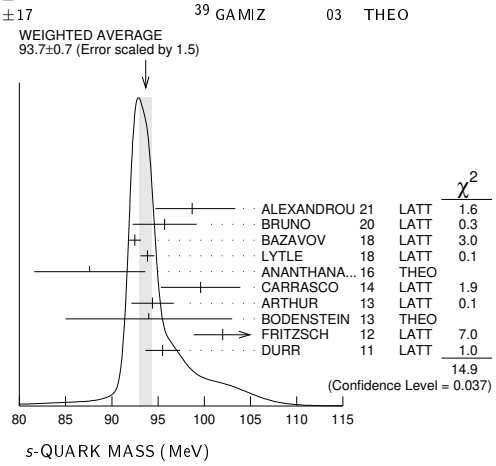

Downloaded from https://academic.oup.com/ptep/article/2022/8/083C01/6651666 by KIT Library user on 27 September 2022

[1] ALEXANDROU 21 determines the quark mass using a lattice calculation of the meson and baryon masses with a twisted mass fermion action. The simulations are carried out using 2+1+1 dynamical quarks with $m_u = m_d \neq m_s \neq m_c$, including gauge ensembles close to the physical pion point.

[2] BRUNO 20 determines the light quark mass using a lattice calculation with $n_f = 2+1$ flavors of Wilson fermions. The scale has been set from f_π and f_K. The tuning was done using the masses of the lightest (π) and strange (K) pseudoscalar mesons.

[3] BAZAVOV 18 determine the quark masses using a lattice computation with staggered fermions and four active quark flavors.

[4] LYTLE 18 combined with CHAKRABORTY 2015 determine $\overline{m}_s(3\text{ GeV}) = 84.78 \pm 0.65$ MeV from a lattice simulation with $n_f = 2+1+1$ flavors. They also determine the quoted value $\overline{m}_s(2\text{ GeV})$ for $n_f = 4$ dynamical flavors.

[5] ANANTHANARAYAN 16 determine $\overline{m}_s(2\text{ GeV}) = 106.70 \pm 9.36$ MeV and 74.47 ± 7.77 MeV from fits to ALEPH and OPAL τ decay data, respectively. We have used the weighted average of the two.

[6] CARRASCO 14 is a lattice QCD computation of light quark masses using $2 + 1 + 1$ dynamical quarks, with $m_u = m_d \neq m_s \neq m_c$. The u and d quark masses are obtained separately by using the K meson mass splittings and lattice results for the electromagnetic contributions.

[7] ARTHUR 13 is a lattice computation using 2+1 dynamical domain wall fermions. Masses at $\mu = 3$ GeV have been converted to $\mu = 2$ GeV using conversion factors given in their paper.

[8] BODENSTEIN 13 determines m_s from QCD finite energy sum rules, and the perturbative computation of the pseudoscalar correlator to five-loop order.

[9] FRITZSCH 12 determine m_s using a lattice computation with $n_f = 2$ dynamical flavors.

[10] DURR 11 determine quark mass from a lattice computation of the meson spectrum using $n_f = 2 + 1$ dynamical flavors. The lattice simulations were done at the physical quark mass, so that extrapolation in the quark mass was not needed.

[11] CHAKRABORTY 15 is a lattice QCD computation that determines m_c and m_c/m_s using pseudoscalar mesons masses tuned on gluon field configurations with 2+1+1 dynamical flavors of HISQ quarks with u/d masses down to the physical value.

[12] AOKI 11A determine quark masses from a lattice computation of the hadron spectrum using $n_f = 2 + 1$ dynamical flavors of domain wall fermions.

[13] BLOSSIER 10 determines quark masses from a computation of the hadron spectrum using n_f=2 dynamical twisted-mass Wilson fermions.

[14] BLUM 10 determines light quark masses using a QCD plus QED lattice computation of the electromagnetic mass splittings of the low-lying hadrons. The lattice simulations use 2+1 dynamical quark flavors.

[15] DAVIES 10 and MCNEILE 10 determine $\overline{m}_c(\mu)/\overline{m}_s(\mu) = 11.85 \pm 0.16$ using a lattice computation with $n_f = 2 + 1$ dynamical fermions of the pseudoscalar meson masses. Mass m_s is obtained from this using the value of m_c from ALLISON 08 or MCNEILE 10.

[16] ALLTON 08 use a lattice computation of the π, K, and Ω masses with 2+1 dynamical flavors of domain wall quarks, and non-perturbative renormalization.

[17] BLOSSIER 08 use a lattice computation of pseudoscalar meson masses and decay constants with 2 dynamical flavors and non-perturbative renormalization.

[18] DOMINGUEZ 08A make determination from QCD finite energy sum rules for the pseudoscalar two-point function computed to order α_s^4.

[19] ISHIKAWA 08 use a lattice computation of the light meson spectrum with 2+1 dynamical flavors of $\mathcal{O}(a)$ improved Wilson quarks, and one-loop perturbative renormalization.

[20] NAKAMURA 08 do a lattice computation using quenched domain wall fermions and non-perturbative renormalization.

[21] BLUM 07 determine quark masses from the pseudoscalar meson masses using a QED plus QCD lattice computation with two dynamical quark flavors.

[22] CHETYRKIN 06 use QCD sum rules in the pseudoscalar channel to order α_s^4.

[23] GOCKELER 06 use an unquenched lattice computation of the axial Ward Identity with $n_f = 2$ dynamical light quark flavors, and non-perturbative renormalization, to obtain $\overline{m}_s(2\text{ GeV}) = 111 \pm 6 \pm 4 \pm 6$ MeV, where the first error is statistical, the second and third are systematic due to the fit range and force scale uncertainties, respectively. We have combined the systematic errors linearly.

[24] GOCKELER 06A use an unquenched lattice computation of the pseudoscalar meson masses with $n_f = 2$ dynamical light quark flavors, and non-perturbative renormalization.

[25] JAMIN 06 determine $\overline{m}_s(2\text{ GeV})$ from the spectral function for the scalar $K\pi$ form factor.

[26] MASON 06 extract light quark masses from a lattice simulation using staggered fermions with an improved action, and three dynamical light quark flavors with degenerate u and d quarks. Perturbative corrections were included at NNLO order.

[27] NARISON 06 uses sum rules for $e^+e^- \to$ hadrons to order α_s^3.

[28] NARISON 06 obtains the quoted range from positivity of the spectral functions.

[29] BAIKOV 05 determines $\overline{m}_s(M_\tau) = 100^{+5}_{-3}{}^{+17}_{-19}$ from sum rules using the strange spectral function in τ decay. The computations were done to order α_s^3, with an estimate of the α_s^4 terms. We have converted the result to $\mu = 2$ GeV.

[30] GAMIZ 05 determines $\overline{m}_s(2\text{ GeV})$ from sum rules using the strange spectral function in τ decay. The computations were done to order α_s^2, with an estimate of the α_s^3 terms.

[31] GORBUNOV 05 use hadronic tau decays to N3LO, including power corrections.

[32] NARISON 05 determines $\overline{m}_s(2\text{ GeV})$ from sum rules using the strange spectral function in τ decay. The computations were done to order α_s^3.

[33] AUBIN 04 perform three flavor dynamical lattice calculation of pseudoscalar meson masses, with one-loop perturbative renormalization constant.

[34] AOKI 03 uses quenched lattice simulation of the meson and baryon masses with degenerate light quarks. The extrapolations are done using quenched chiral perturbation theory. Determines $m_s = 113.8 \pm 2.3^{+5.8}_{-2.9}$ using K mass as input and $m_s = 142.3 \pm 5.8^{+22}_{-0}$ using ϕ mass as input. We have performed a weighted average of these values.

[35] AOKI 03B uses lattice simulation of the meson and baryon masses with two dynamical light quarks. Simulations are performed using the $\mathcal{O}(a)$ improved Wilson action.

[36] BECIREVIC 03 perform quenched lattice computation using the vector and axial Ward identities. Uses $\mathcal{O}(a)$ improved Wilson action and nonperturbative renormalization. They also quote $\overline{m}/m_s = 24.3 \pm 0.2 \pm 0.6$.

[37] CHIU 03 determines quark masses from the pion and kaon masses using a lattice simulation with a chiral fermion action in quenched approximation.

[38] GAMIZ 03 determines m_s from SU(3) breaking in the τ hadronic width. The value of V_{us} is chosen to satisfy ČKM unitarity.

[39] GAMIZ 03 determines m_s from SU(3) breaking in the τ hadronic width. The value of V_{us} is taken from the PDG.

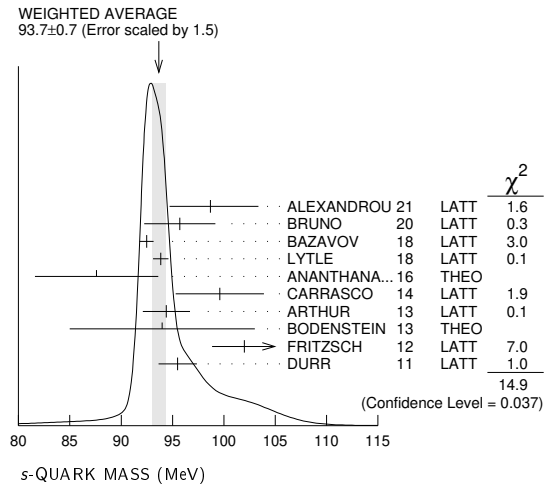

OTHER LIGHT QUARK MASS RATIOS

m_s/m_d MASS RATIO

VALUE	DOCUMENT ID		TECN	COMMENT
17–22 OUR EVALUATION				
20.0	[1] GAO	97	THEO	
18.9±0.8	[2] LEUTWYLER	96	THEO	Compilation
21	[3] DONOGHUE	92	THEO	
18	[4] GERARD	90	THEO	
18 to 23	[5] LEUTWYLER	90B	THEO	

[1] GAO 97 uses electromagnetic mass splittings of light mesons.

[2] LEUTWYLER 96 uses a combined fit to $\eta \to 3\pi$ and $\psi' \to J/\psi\,(\pi,\eta)$ decay rates, and the electromagnetic mass differences of the π and K.

[3] DONOGHUE 92 result is from a combined analysis of meson masses, $\eta \to 3\pi$ using second-order chiral perturbation theory including nonanalytic terms, and $(\psi(2S) \to J/\psi(1S)\,\pi)/(\psi(2S) \to J/\psi(1S)\,\eta)$.

[4] GERARD 90 uses large N and η-η' mixing.

[5] LEUTWYLER 90B determines quark mass ratios using second-order chiral perturbation theory for the meson and baryon masses, including nonanalytic corrections. Also uses Weinberg sum rules to determine L_7.

$m_s/\overline{m}$ MASS RATIO

$\overline{m} \equiv (m_u + m_d)/2$

VALUE	DOCUMENT ID		TECN
$27.33^{+0.67}_{-0.77}$ OUR EVALUATION	See the ideogram below.		
$27.17 \pm 0.32^{+0.56}_{-0.38}$	[1] ALEXANDROU	21	LATT
27.0 ±1.0 ±0.4	[2] BRUNO	20	LATT
$27.35 \pm 0.05^{+0.10}_{-0.07}$	[3] BAZAVOV	14A	LATT
26.66±0.32	[4] CARRASCO	14	LATT
27.36±0.54	[5] ARTHUR	13	LATT
27.53±0.20±0.08	[6] DURR	11	LATT
• • • We do not use the following data for averages, fits, limits, etc. • • •			
26.8 ±1.4	[7] AOKI	11A	LATT
27.3 ±0.9	[8] BLOSSIER	10	LATT
28.8 ±1.65	[9] ALLTON	08	LATT
27.3 ±0.3 ±1.2	[10] BLOSSIER	08	LATT
23.5 ±1.5	[11] OLLER	07A	THEO
27.4 ±0.4	[12] AUBIN	04	LATT

[1] ALEXANDROU 21 determines the quark mass using a lattice calculation of the meson and baryon masses with a twisted mass fermion action. The simulations are carried out using 2+1+1 dynamical quarks with $m_u = m_d \neq m_s \neq m_c$, including gauge ensembles close to the physical pion point.

[2] BRUNO 20 determines the light quark mass using a lattice calculation with $n_f = 2+1$ flavors of Wilson fermions. The scale has been set from f_π and f_K. The tuning was done using the masses of the lightest (π) and strange (K) pseudoscalar mesons.

[3] BAZAVOV 14A is a lattice computation using 4 dynamical flavors of HISQ fermions.

[4] CARRASCO 14 is a lattice QCD computation of light quark masses using $2 + 1 + 1$ dynamical quarks, with $m_u = m_d \neq m_s \neq m_c$. The u and d quark masses are obtained separately by using the K meson mass splittings and lattice results for the electromagnetic contributions.

[5] ARTHUR 13 is a lattice computation using 2+1 dynamical domain wall fermions.

[6] DURR 11 determine quark mass from a lattice computation of the meson spectrum using $n_f = 2 + 1$ dynamical flavors. The lattice simulations were done at the physical quark mass, so that extrapolation in the quark mass was not needed.

[7] AOKI 11A determine quark masses from a lattice computation of the hadron spectrum using $n_f = 2 + 1$ dynamical flavors of domain wall fermions.

[8] BLOSSIER 10 determines quark masses from a computation of the hadron spectrum using n_f=2 dynamical twisted-mass Wilson fermions.

Downloaded from https://academic.oup.com/ptep/article/2022/8/083C01/6651666 by KIT Library user on 27 September 2022

[9] ALLTON 08 use a lattice computation of the π, K, and Ω masses with 2+1 dynamical flavors of domain wall quarks, and non-perturbative renormalization.

[10] BLOSSIER 08 use a lattice computation of pseudoscalar meson masses and decay constants with 2 dynamical flavors and non-perturbative renormalization.

[11] OLLER 07A use unitarized chiral perturbation theory to order p^4.

[12] Three flavor dynamical lattice calculation of pseudoscalar meson masses.

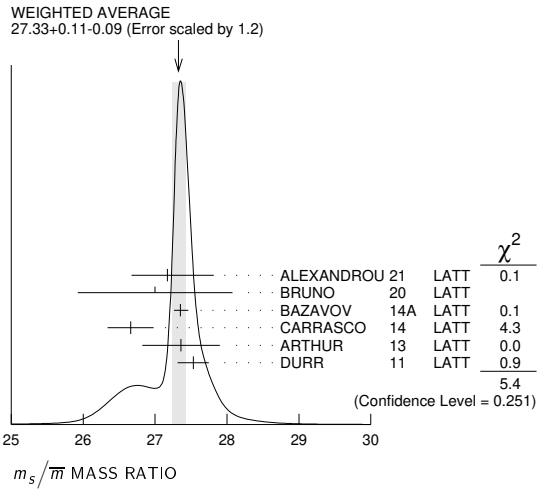

Q MASS RATIO

$$Q \equiv \sqrt{(m^2{}_s - \overline{m}^2)/(m^2{}_d - m^2{}_u)}; \quad \overline{m} \equiv (m_u + m_d)/2$$

VALUE	DOCUMENT ID		TECN
• • • We do not use the following data for averages, fits, limits, etc. • • •			
22.1±0.7	[1] COLANGELO	18	THEO
22.0±0.7	[2] COLANGELO	17	THEO
21.6±1.1	[3] GUO	17	THEO
23.4±0.4±0.5	[4] FODOR	16	LATT
21.4±0.4	[5] GUO	15F	THEO
22.8±0.4	[6] MARTEMYA...	05	THEO
22.7±0.8	[7] ANISOVICH	96	THEO

[1] COLANGELO 18 obtain Q from a dispersive analysis of $\eta \to 3\pi$ decay.

[2] COLANGELO 17 obtain Q from a dispersive analysis of KLOE collaboration data on $\eta \to \pi^+\pi^-\pi^0$ decays and chiral perturbation theory input.

[3] GUO 17 determine Q from a dispersive model fit to KLOE and WASA-at-COSY data on $\eta \to \pi^+\pi^-\pi^0$ decay and matching to chiral perturbation theory .

[4] FODOR 16 is a lattice simulation with $n_f = 2 + 1$ dynamical flavors and includes partially quenched QED effects.

[5] GUO 15F determine Q from a Khuri-Treiman analysis of $\eta \to 3\pi$ decays.

[6] MARTEMYANOV 05 determine Q from $\eta \to 3\pi$ decay.

[7] ANISOVICH 96 find Q from $\eta \to \pi^+\pi^-\pi^0$ decay using dispersion relations and chiral perturbation theory.

LIGHT QUARKS (u, d, s) REFERENCES

ALEXANDROU	21	PR D104 074515	C. Alexandrou *et al.*	(ETM Collab.)
BRUNO	20	EPJ C80 169	M. Bruno *et al.*	(ALPHA Collab.)
DOMINGUEZ	19	JHEP 1902 057	C.A. Dominguez, A. Mes, K. Schilcher	(CAPE, MAINZ)
BAZAVOV	18	PR D98 054517	A. Bazavov *et al.*	(Fermilab Lattice, MILC, TUMQCD)
COLANGELO	18	EPJ C78 947	G. Colangelo *et al.*	
LYTLE	18	PR D98 014513	A.T. Lytle *et al.*	(HPQCD Collab.)
COLANGELO	17	PRL 118 022001	G. Colangelo *et al.*	(BERN, IND, JLAB)
GUO	17	PL B771 497	P. Guo *et al.*	
YUAN	17	PR D96 014034	J.-M. Yuan *et al.*	
ANANTHANA...	16	PR D94 116014	B. Ananthanarayan, D. Das	(BANG, AHMED)
FODOR	16	PRL 117 082001	Z. Fodor *et al.*	(BMW Collab.)
BASAK	15	JPCS 640 012052	S. Basak *et al.*	(MILC Collab.)
CHAKRABOR...	15	PR D91 054508	B. Chakraborty *et al.*	(HPQCD Collab.)
GUO	15F	PR D92 054016	P. Guo *et al.*	
BAZAVOV	14A	PR D90 074509	A. Bazavov *et al.*	(Fermi-LAT and MILC Collabs.)
CARRASCO	14	NP B887 19	N. Carrasco *et al.*	(European Twisted Mass Collab.)
ARTHUR	13	PR D87 094514	R. Arthur *et al.*	(RBC and UKQCD Collabs.)
BODENSTEIN	13	JHEP 1307 138	S. Bodenstein, C.A. Dominguez, K. Schilcher	
AOKI	12	PR D86 034507	S. Aoki *et al.*	(PACS-CS Collab.)
FRITZSCH	12	NP B865 397	P. Fritzsch *et al.*	(ALPHA Collab.)
AOKI	11A	PR D83 074508	Y. Aoki *et al.*	(RBC-UKQCD Collab.)
DURR	11	PL B701 265	S. Durr *et al.*	(BMW Collab.)
BAZAVOV	10	RMP 82 1349	A. Bazavov *et al.*	(MILC Collab.)
BLOSSIER	10	PR D82 114513	B. Blossier *et al.*	(ETM Collab.)
BLUM	10	PR D82 094508	T. Blum *et al.*	
DAVIES	10	PRL 104 132003	C.T.H. Davies *et al.*	(HPQCD Collab.)
MCNEILE	10	PR D82 034512	C. McNeile *et al.*	(HPQCD Collab.)
DOMINGUEZ	09	PR D79 014009	C.A. Dominguez *et al.*	
ALLISON	08	PR D78 054513	I. Allison *et al.*	(HPQCD Collab.)
ALLTON	08	PR D78 114509	C. Allton *et al.*	(RBC and UKQCD Collabs.)
BLOSSIER	08	JHEP 0804 020	B. Blossier *et al.*	(ETM Collab.)
DEANDREA	08	PR D78 034032	A. Deandrea, A. Nehme, P. Talavera	
DOMINGUEZ	08A	JHEP 0805 020	C.A. Dominguez *et al.*	
DOMINGUEZ...	08B	PL B660 49	A. Dominguez-Clarimon, E. de Rafael, J. Taron	
ISHIKAWA	08	PR D78 011502	T. Ishikawa *et al.*	(CP-PACS and JLQCD Collabs.)
NAKAMURA	08	PR D78 034502	Y. Nakamura *et al.*	(CP-PACS Collab.)
BLUM	07	PR D76 114508	T. Blum *et al.*	(RBC Collab.)
OLLER	07A	EPJ A34 371	J.A. Oller, L. Roca	
CHETYRKIN	06	EPJ C46 721	K.G. Chetyrkin, A. Khodjamirian	
GOCKELER	06	PR D73 054508	M. Gockeler *et al.*	(QCDSF and UKQCD Collabs)
GOCKELER	06A	PL B639 307	M. Gockeler *et al.*	(QCDSF and UKQCD Collabs)
JAMIN	06	PR D74 074009	M. Jamin, J.A. Oller, A. Pich	
MASON	06	PR D73 114501	Q. Mason *et al.*	(HPQCD Collab.)
NARISON	06	PR D74 034013	S. Narison	
PDG	06	JP G33 1	W.-M. Yao *et al.*	(PDG Collab.)
BAIKOV	05	PRL 95 012003	P.A. Baikov, K.G. Chetyrkin, J.H. Kuhn	
GAMIZ	05	PRL 94 011803	E. Gamiz *et al.*	
GORBUNOV	05	PR D71 013002	D.S. Gorbunov, A.A. Pivovarov	
MARTEMYA...	05	PR D71 017501	B.V. Martemyanov, V.S. Sopov	
NARISON	05	PL B626 101	S. Narison	
AUBIN	04	PR D70 031504	C. Aubin *et al.*	(HPQCD, MILC, UKQCD Collabs.)
AUBIN	04A	PR D70 114501	C. Aubin *et al.*	(MILC Collab.)
AOKI	03	PR D67 034503	S. Aoki *et al.*	(CP-PACS Collab.)
AOKI	03B	PR D68 054502	S. Aoki *et al.*	(CP-PACS Collab.)
BECIREVIC	03	PL B558 69	D. Becirevic, V. Lubicz, C. Tarantino	
CHIU	03	NP B673 217	T.-W. Chiu, T.-H. Hsieh	
GAMIZ	03	JHEP 0301 060	E. Gamiz *et al.*	
NELSON	03	PRL 90 021601	D. Nelson, G.T. Fleming, G.W. Kilcup	
GAO	97	PR D56 4115	D.-N. Gao, B.A. Li, M.-L. Yan	
ANISOVICH	96	PL B375 335	A.V. Anisovich, H. Leutwyler	
LEUTWYLER	96	PL B378 313	H. Leutwyler	
DONOGHUE	92	PRL 69 3444	J.F. Donoghue, B.R. Holstein, D. Wyler	(MASA+)
GERARD	90	MPL A5 391	J.M. Gerard	(MPIM)
LEUTWYLER	90B	NP B337 108	H. Leutwyler	(BERN)

c

$$I(J^P) = 0(\tfrac{1}{2}^+)$$

Charge $= \frac{2}{3}\, e$ Charm $= +1$

c-QUARK MASS

The c-quark mass corresponds to the "running" mass m_c ($\mu = m_c$) in the $\overline{\text{MS}}$ scheme. We have converted masses in other schemes to the $\overline{\text{MS}}$ scheme using two-loop QCD perturbation theory with $\alpha_s(\mu{=}m_c) = 0.38 \pm 0.03$. The value 1.27 ± 0.02 GeV for the $\overline{\text{MS}}$ mass corresponds to 1.67 ± 0.07 GeV for the pole mass (see the "Note on Quark Masses").

$\overline{\text{MS}}$ MASS (GeV)		DOCUMENT ID		TECN
1.27 ±0.02 OUR EVALUATION		See the ideogram below.		
1.316 ±0.022	$^{+0.019}_{-0.010}$	[1] ALEXANDROU	21	LATT
1.296 ±0.019		[2] HEITGER	21	LATT
1.2723±0.0078		[3] HATTON	20	LATT
1.266 ±0.006		[4] NARISON	20	THEO
1.290	$^{+0.077}_{-0.053}$	[5] ABRAMOWICZ	18	HERA
1.273 ±0.010		[6] BAZAVOV	18	LATT
1.2737±0.0077		[7] LYTLE	18	LATT
1.223 ±0.033		[8] PESET	18	THEO
1.279 ±0.008		[9] CHETYRKIN	17	THEO
1.272 ±0.008		[10] ERLER	17	THEO
1.246 ±0.023		[11] KIYO	16	THEO
1.288 ±0.020		[12] DEHNADI	15	THEO
1.348 ±0.046		[13] CARRASCO	14	LATT
1.24 ±0.03	$^{+0.03}_{-0.07}$	[14] ALEKHIN	13	THEO
1.159 ±0.075		[15] SAMOYLOV	13	NOMD
1.278 ±0.009		[16] BODENSTEIN	11	THEO
1.28	$^{+0.07}_{-0.06}$	[17] LASCHKA	11	THEO
1.196 ±0.059	±0.050	[18] AUBERT	10A	BABR
1.25 ±0.04		[19] SIGNER	09	THEO
• • • We do not use the following data for averages, fits, limits, etc. • • •				
1.263 ±0.014		[20] NARISON	18A	THEO
1.264 ±0.006		[21] NARISON	18B	THEO
1.335 ±0.043	$^{+0.040}_{-0.011}$	[22] BERTONE	16	THEO
1.2715±0.0095		[23] CHAKRABOR...	15	LATT
1.26 ±0.05	±0.04	[24] ABRAMOWICZ	13C	COMB
1.282 ±0.011	±0.022	[25] DEHNADI	13	THEO
1.286 ±0.066		[26] NARISON	13	THEO
1.36 ±0.04	±0.10	[27] ALEKHIN	12	THEO
1.261 ±0.016		[28] NARISON	12A	THEO
1.01 ±0.09	±0.03	[29] ALEKHIN	11	THEO
1.28 ±0.04		[30] BLOSSIER	10	LATT
1.299 ±0.026		[31] BODENSTEIN	10	THEO
1.273 ±0.006		[32] MCNEILE	10	LATT
1.261 ±0.018		[33] NARISON	10	THEO
1.279 ±0.013		[34] CHETYRKIN	09	THEO
1.268 ±0.009		[35] ALLISON	08	LATT
1.286 ±0.013		[36] KUHN	07	THEO
1.295 ±0.015		[37] BOUGHEZAL	06	THEO
1.24 ±0.09		[38] BUCHMUEL...	06	THEO
1.224 ±0.017	±0.054	[39] HOANG	06	THEO
1.33 ±0.10		[40] AUBERT	04X	THEO
1.29 ±0.07		[41] HOANG	04	THEO
1.319 ±0.028		[42] DEDIVITIIS	03	LATT
1.19 ±0.11		[43] EIDEMULLER	03	THEO
1.289 ±0.043		[44] ERLER	03	THEO
1.26 ±0.02		[45] ZYABLYUK	03	THEO

[1] ALEXANDROU 21 determines the quark mass using a lattice calculation of the meson and baryon masses with a twisted mass fermion action. We have converted $\overline{m}_c(3\text{ GeV}) = 1.036 \pm 0.017 ^{+0.015}_{-0.008}$ to $\overline{m}_c(\overline{m}_c)$. The simulations are carried out using 2+1+1 dynamical quarks with $m_u = m_d \neq m_s \neq m_c$, including gauge ensembles close to the physical pion point.

Downloaded from https://academic.oup.com/ptep/article/2022/8/083C01/6651666 by KIT Library user on 27 September 2022

[2] HEITGER 21 determines the charm quark mass using a $n_f = 2+1$ flavor lattice QCD simulation with non-perturbatively O(a) improved Wilson fermions. They also determine $\overline{m}_c(3\text{ GeV}) = 1.007 \pm 0.016$ GeV.

[3] HATTON 20 determine the charm quark mass using a $n_f = 2+1+1$ flavor lattice simulation with the HISQ action of ground state charmonium mesons. They also determine $\overline{m}_c(3\text{ GeV}) = 0.9841 \pm 0.0051$ GeV.

[4] NARISON 20 determines the quark mass using QCD Laplace sum rules from the B_c mass, combined with previous determinations of the QCD condensates and c and b masses.

[5] ABRAMOWICZ 18 determine $\overline{m}_c(\overline{m}_c) = 1.290^{+0.046+0.062+0.003}_{-0.041-0.014-0.031}$ from the production of c quarks in ep collisions at HERA using combined H1 and ZEUS data. The experimental/fitting errors, and those from modeling and parameterization have been combined in quadrature.

[6] BAZAVOV 18 determine the quark masses using a lattice computation with staggered fermions and four active quark flavors.

[7] LYTLE 18 combined with CHAKRABORTY 15 determine $\overline{m}_c(3\text{ GeV}) = 0.9874(48)$ GeV from a lattice simulation with $n_f = 2+1+1$ flavors. They also determine the quoted value $\overline{m}_c(\overline{m}_c)$ for $n_f = 4$ dynamical flavors.

[8] PESET 18 determine $\overline{m}_c(\overline{m}_c)$ and $\overline{m}_b(\overline{m}_b)$ using an N3LO calculation of the η_c, η_b and B_c masses.

[9] CHETYRKIN 17 determine $\overline{m}_c(\mu = 3\text{ GeV}) = 0.993 \pm 0.008$ GeV and $\overline{m}_c(\overline{m}_c)$ from a four-loop sum-rule computation of the cross-section for $e^+e^- \to$ hadrons in the charm threshold region.

[10] ERLER 17 determine $\overline{m}_c(\overline{m}_c) = 1.272 \pm 0.008$ GeV from a three-loop QCD sum-rule computation of the vector current correlator. This result is for fixed $\alpha_s(M_Z) = 0.1182$. Including an α_s uncertainty of ± 0.0016, the charm mass error increases from 8 to 9 MeV.

[11] KIYO 16 determine $\overline{m}_c(\overline{m}_c)$ from the $J/\psi(1S)$ mass at order α_s^3 (N3LO).

[12] DEHNADI 15 determine $\overline{m}_c(\overline{m}_c)$ using sum rules for $e^+e^- \to$ hadrons at order α_s^3 (N3LO), and fitting to both experimental data and lattice results.

[13] CARRASCO 14 is a lattice QCD computation of light quark masses using $2+1+1$ dynamical quarks, with $m_u = m_d \neq m_s \neq m_c$. The u and d quark masses are obtained separately by using the K meson mass splittings and lattice results for the electromagnetic contributions.

[14] ALEKHIN 13 determines m_c from charm production in deep inelastic scattering at HERA using approximate NNLO QCD.

[15] SAMOYLOV 13 determines m_c from a study of charm dimuon production in neutrino-iron scattering using the NLO QCD result for the charm quark production cross section.

[16] BODENSTEIN 11 determine $\overline{m}_c(3\text{ GeV}) = 0.987 \pm 0.009$ GeV and $\overline{m}_c(\overline{m}_c) = 1.278 \pm 0.009$ GeV using QCD sum rules for the charm quark vector current correlator.

[17] LASCHKA 11 determine the c mass from the charmonium spectrum. The theoretical computation uses the heavy $Q\overline{Q}$ potential to order $1/m_Q$ obtained by matching the short-distance perturbative result onto lattice QCD result at larger scales.

[18] AUBERT 10A determine the b- and c-quark masses from a fit to the inclusive decay spectra in semileptonic B decays in the kinetic scheme (and convert it to the $\overline{\text{MS}}$ scheme).

[19] SIGNER 09 determines the c-quark mass using non-relativistic sum rules to analyze the $e^+e^- \to c\overline{c}$ cross-section near threshold. Also determine the PS mass $m_{PS}(\mu_F = 0.7\text{ GeV}) = 1.50 \pm 0.04$ GeV.

[20] NARISON 18A determines simultaneously $\overline{m}_c(\overline{m}_c)$ and the 4-dimension gluon condensate using QCD exponential sum rules and their ratios evaluated at the optimal scale $\mu = 2.85$ GeV at N2LO-N3LO of perturbative QCD and including condensates up to dimension 6–8 in the (axial-)vector and (pseudo-)scalar charmonium channels.

[21] NARISON 18B determines $\overline{m}_c(\overline{m}_c)$ using QCD vector moment sum rules and their ratios at N2LO-N3LO of perturbative QCD and including condensates up to dimension 8.

[22] BERTONE 16 determine $\overline{m}_c(\overline{m}_c)$ from HERA deep inelastic scattering data using the FONLL scheme. Also determine $\overline{m}_c(\overline{m}_c) = 1.318 \pm 0.054^{+0.490}_{-0.022}$ using the fixed flavor number scheme.

[23] CHAKRABORTY 15 is a lattice QCD computation using $2+1+1$ dynamical flavors. Moments of pseudoscalar current-current correlators are matched to α_s^3-accurate QCD perturbation theory with the η_c meson mass tuned to experiment.

[24] ABRAMOWICZ 13C determines m_c from charm production in deep inelastic ep scattering, using the QCD prediction at NLO order. The uncertainties from model and parameterization assumptions, and the value of α_s, of ± 0.03, ± 0.02, and ± 0.02 respectively, have been combined in quadrature.

[25] DEHNADI 13 determines m_c using QCD sum rules for the charmonium spectrum and charm continuum to order α_s^3 (N3LO). The statistical and systematic experimental errors of ± 0.006 and ± 0.009 have been combined in quadrature. The theoretical uncertainties ± 0.019 from truncation of the perturbation series, ± 0.010 from α_s, and ± 0.002 from the gluon condensate have been combined in quadrature.

[26] NARISON 13 determines m_c using QCD spectral sum rules to order α_s^2 (NNLO) and including condensates up to dimension 6.

[27] ALEKHIN 12 determines m_c from heavy quark production in deep inelastic scattering at HERA using approximate NNLO QCD.

[28] NARISON 12A determines m_c using sum rules for the vector current correlator to order α_s^3, including the effect of gluon condensates up to dimension eight.

[29] ALEKHIN 11 determines m_c from heavy quark production in deep inelastic scattering using fixed target and HERA data, and approximate NNLO QCD.

[30] BLOSSIER 10 determines quark masses from a computation of the hadron spectrum using n_f=2 dynamical twisted-mass Wilson fermions.

[31] BODENSTEIN 10 determines $\overline{m}_c(3\text{ GeV}) = 1.008 \pm 0.026$ GeV using finite energy sum rules for the vector current correlator. The authors have converted this to $\overline{m}_c(\overline{m}_c)$ using $\alpha_s(M_Z) = 0.1189 \pm 0.0020$.

[32] MCNEILE 10 determines m_c by comparing the order α_s^3 perturbative results for the pseudo-scalar current to lattice simulations with $n_f = 2+1$ sea-quarks by the HPQCD collaboration.

[33] NARISON 10 determines m_c from ratios of moments of vector current correlators computed to order α_s^3 and including the dimension-six gluon condensate.

[34] CHETYRKIN 09 determine m_c and m_b from the $e^+e^- \to Q\overline{Q}$ cross-section and sum rules, using an order α_s^3 computation of the heavy quark vacuum polarization. They also determine $m_c(3\text{ GeV}) = 0.986 \pm 0.013$GeV.

[35] ALLISON 08 determine m_c by comparing four-loop perturbative results for the pseudo-scalar current correlator to lattice simulations by the HPQCD collaboration. The result has been updated in MCNEILE 10.

[36] KUHN 07 determine $\overline{m}_c(\mu = 3\text{ GeV}) = 0.986 \pm 0.013$ GeV and $\overline{m}_c(\overline{m}_c)$ from a four-loop sum-rule computation of the cross-section for $e^+e^- \to$ hadrons in the charm threshold region.

[37] BOUGHEZAL 06 result comes from the first moment of the hadronic production cross-section to order α_s^3.

[38] BUCHMUELLER 06 determine m_b and m_c by a global fit to inclusive B decay spectra.

[39] HOANG 06 determines $\overline{m}_c(\overline{m}_c)$ from a global fit to inclusive B decay data. The B decay distributions were computed to order $\alpha_s^2\beta_0$, and the conversion between different m_c mass schemes to order α_s^3.

[40] AUBERT 04X obtain m_c from a fit to the hadron mass and lepton energy distributions in semileptonic B decay. The paper quotes values in the kinetic scheme. The $\overline{\text{MS}}$ value has been provided by the BABAR collaboration.

[41] HOANG 04 determines $\overline{m}_c(\overline{m}_c)$ from moments at order α_s^2 of the charm production cross-section in e^+e^- annihilation.

[42] DEDIVITIIS 03 use a quenched lattice computation of heavy-heavy and heavy-light meson masses.

[43] EIDEMULLER 03 determines m_b and m_c using QCD sum rules.

[44] ERLER 03 determines m_b and m_c using QCD sum rules. Includes recent BES data.

[45] ZYABLYUK 03 determines m_c by using QCD sum rules in the pseudoscalar channel and comparing with the η_c mass.

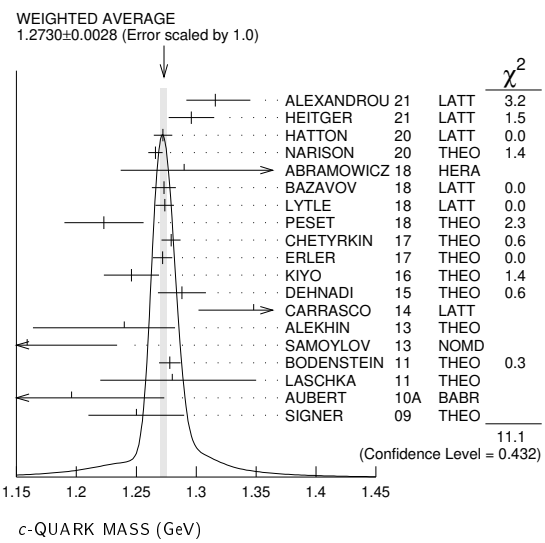

m_c/m_s MASS RATIO

The ratio is that of the $\overline{\text{MS}}$ masses at a common scale, for four dynamical quark flavors.

VALUE	DOCUMENT ID		TECN
$11.76^{+0.05}_{-0.10}$ OUR EVALUATION	See the ideogram below.		
$11.48 \pm 0.12^{+0.25}_{-0.19}$	[1] ALEXANDROU	21	LATT
11.783 ± 0.025	[2] BAZAVOV	18	LATT
11.652 ± 0.065	[3] CHAKRABOR..	15	LATT
11.62 ± 0.16	[4] CARRASCO	14	LATT
$11.27 \pm 0.30 \pm 0.26$	[5] DURR	12	LATT
11.85 ± 0.16	[6] DAVIES	10	LATT
• • • We do not use the following data for averages, fits, limits, etc. • • •			
$11.747 \pm 0.019^{+0.059}_{-0.043}$	[7] BAZAVOV	14A	LATT
12.0 ± 0.3	[8] BLOSSIER	10	LATT

[1] ALEXANDROU 21 determines the quark mass using a lattice calculation of the meson and baryon masses with a twisted mass fermion action. The simulations are carried out using 2+1+1 dynamical quarks with $m_u = m_d \neq m_s \neq m_c$, including gauge ensembles close to the physical pion point.

[2] BAZAVOV 18 determine the quark masses using a lattice computation with staggered fermions and four active quark flavors.

[3] CHAKRABORTY 15 is a lattice QCD computation on gluon field configurations with 2+1+1 dynamical flavors of HISQ quarks with u/d masses down to the physical value. m_c and m_s are tuned from pseudoscalar meson masses.

[4] CARRASCO 14 is a lattice QCD computation of light quark masses using $2+1+1$ dynamical quarks, with $m_u = m_d \neq m_s \neq m_c$. The u and d quark masses are obtained separately by using the K meson mass splittings and lattice results for the electromagnetic contributions.

[5] DURR 12 determine m_c/m_s using a lattice computation with $n_f = 2$ dynamical fermions. The result is combined with other determinations of m_c to obtain $m_s(2\text{ GeV}) = 97.0 \pm 2.6 \pm 2.5$ MeV.

[6] DAVIES 10 determine m_c/m_s from meson masses calculated on gluon fields including u, d, and s sea quarks with lattice spacing down to 0.045 fm. The Highly Improved Staggered quark formalism is used for the valence quarks.

[7] BAZAVOV 14A is a lattice computation using 4 dynamical flavors of HISQ fermions.

Downloaded from https://academic.oup.com/ptep/article/2022/8/083C01/6651666 by KIT Library user on 27 September 2022

[8] BLOSSIER 10 determine m_c/m_s from a computation of the hadron spectrum using $n_f = 2$ dynamical twisted-mass Wilson fermions.

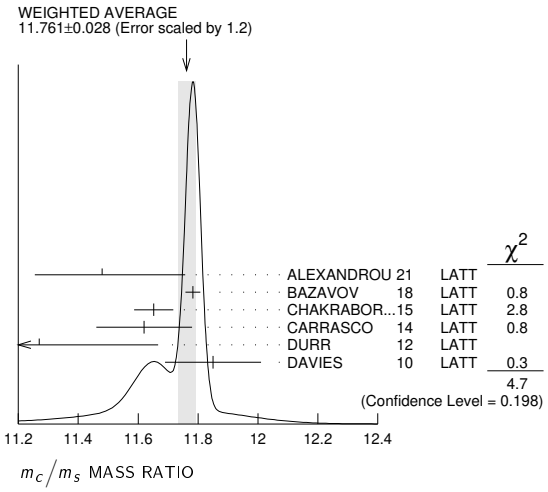

m_b/m_c MASS RATIO

The ratio is that of the $\overline{\text{MS}}$ masses at a common scale, for four dynamical quark flavors.

VALUE	DOCUMENT ID		TECN
4.58 ±0.01 OUR EVALUATION			
4.577±0.008 OUR AVERAGE	See the ideogram below.		
4.578±0.008	[1] BAZAVOV	18	LATT
4.528±0.054	[2] CHAKRABOR..	15	LATT

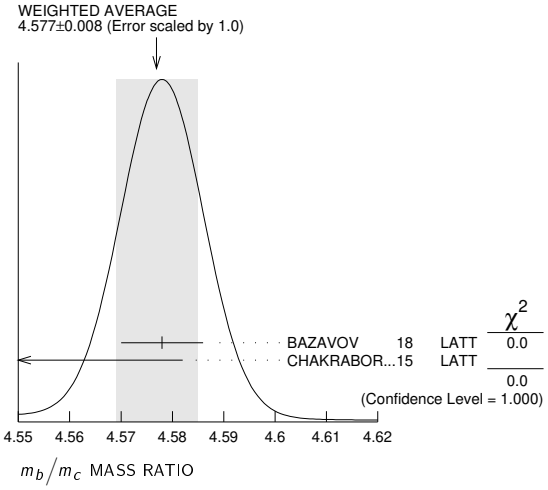

[1] BAZAVOV 18 determine the quark masses using a lattice computation with staggered fermions and four active quark flavors for the u, d, s, c quarks and five active flavors for the b quark.

[2] CHAKRABORTY 15 is a lattice computation using 4 dynamical quark flavors.

$m_b - m_c$ QUARK MASS DIFFERENCE

VALUE (GeV)	DOCUMENT ID		TECN
3.45 ±0.05 OUR EVALUATION			
• • • We do not use the following data for averages, fits, limits, etc. • • •			
3.472±0.032	[1] AUBERT	10A	BABR
3.42 ±0.06	[2] ABDALLAH	06B	DLPH
3.44 ±0.03	[3] AUBERT	04X	BABR
3.41 ±0.01	[3] BAUER	04	THEO

[1] AUBERT 10A determine the b- and c-quark masses from a fit to the inclusive decay spectra in semileptonic B decays in the kinetic scheme.

[2] ABDALLAH 06B determine $m_b - m_c$ from moments of the hadron invariant mass and lepton energy spectra in semileptonic inclusive B decays.

[3] Determine $m_b - m_c$ from a global fit to inclusive B decay spectra.

c-QUARK REFERENCES

ALEXANDROU	21	PR D104 074515	C. Alexandrou et al.	(ETM Collab.)
HEITGER	21	JHEP 2105 288	J. Heitger, F. Joswig, S. Kuberski	(ALPHA Collab.)
HATTON	20	PR D102 054511	D. Hatton et al.	(HPQCD Collab.)
NARISON	20	PL B802 135221	S. Narison	(MONP)
ABRAMOWICZ	18	EPJ C78 473	H. Abramowicz et al.	(H1 and ZEUS Collabs.)
BAZAVOV	18	PR D98 054517	A. Bazavov et al.	(Fermilab Lattice, MILC, TUMQCD)
LYTLE	18	PR D98 014513	A.T. Lytle et al.	(HPQCD Collab.)
NARISON	18A	IJMP A33 1850045	S. Narison	(MONP)
NARISON	18B	PL B784 261	S. Narison	(MONP)
PESET	18	JHEP 1809 167	C. Peset, A. Pineda, J. Segovia	(BARC, TUM)
CHETYRKIN	17	PR D96 116007	K.G. Chetyrkin et al.	
ERLER	17	EPJ C77 99	J. Erler, P. Masjuan, H. Spiesberger	
BERTONE	16	JHEP 1608 050	V. Bertone et al.	(xFitter Developers)
KIYO	16	PL B752 122	Y. Kiyo, G. Mishima, Y. Sumino	
CHAKRABOR...	15	PR D91 054508	B. Chakraborty et al.	(HPQCD Collab.)
DEHNADI	15	JHEP 1508 155	B. Dehnadi, A.H. Hoang, V. Mateu	
BAZAVOV	14A	PR D90 074509	A. Bazavov et al.	(Fermi-LAT and MILC Collabs.)
CARRASCO	14	NP B887 19	N. Carrasco et al.	(European Twisted Mass Collab.)
ABRAMOWICZ	13C	EPJ C73 2311	H. Abramovicz et al.	(H1 and Zeus Collabs.)
ALEKHIN	13	PL B720 172	S. Alekhin et al.	(SERP, DESYZ, WUPP+)
DEHNADI	13	JHEP 1309 103	B. Dehnadi et al.	(SHRZ, VIEN, MPIM+)
NARISON	13	PL B718 1321	S. Narison	(MONP)
SAMOYLOV	13	NP B876 339	O. Samoylov et al.	(NOMAD Collab.)
ALEKHIN	12	PL B718 550	S. Alekhin et al.	(SERP, WUPP, DESY+)
DURR	12	PRL 108 122003	S. Durr, G. Koutsou	(WUPP, JULI, CYPR)
NARISON	12A	PL B706 412	S. Narison	(MONP)
ALEKHIN	11	PL B699 345	S. Alekhin, S. Moch	(DESY, SERP)
BODENSTEIN	11	PR D83 074014	S. Bodenstein et al.	
LASCHKA	11	PR D83 094002	A. Laschka, N. Kaiser, W. Weise	
AUBERT	10A	PR D81 032003	B. Aubert et al.	(BABAR Collab.)
BLOSSIER	10	PR D82 114513	B. Blossier et al.	(ETM Collab.)
BODENSTEIN	10	PR D82 114013	S. Bodenstein et al.	
DAVIES	10	PRL 104 132003	C.T.H. Davies et al.	(HPQCD Collab.)
MCNEILE	10	PR D82 034512	C. McNeile et al.	(HPQCD Collab.)
NARISON	10	PL B693 559	S. Narison	(MONP)
Also		PL B705 544 (errat.)	S. Narison	(MONP)
CHETYRKIN	09	PR D80 074010	K.G. Chetyrkin et al.	(KARL, BNL)
SIGNER	09	PL B672 333	A. Signer	(DURH)
ALLISON	08	PR D78 054513	I. Allison et al.	(HPQCD Collab.)
KUHN	07	NP B778 192	J.H. Kuhn, M. Steinhauser, C. Sturm	
ABDALLAH	06B	EPJ C45 35	J. Abdallah et al.	(DELPHI Collab.)
BOUGHEZAL	06	PR D74 074006	R. Boughezal, M. Czakon, T. Schutzmeier	
BUCHMUEL...	06	PR D73 073008	O.L. Buchmueller, H.U. Flacher	(RHBL)
HOANG	06	PL B633 526	A.H. Hoang, A.V. Manohar	
AUBERT	04X	PRL 93 011803	B. Aubert et al.	(BABAR Collab.)
BAUER	04	PR D70 094017	C. Bauer et al.	
HOANG	04	PL B594 127	A.H. Hoang, M. Jamin	
DEDIVITIIS	03	NP B675 309	G.M. de Divitiis et al.	
EIDEMULLER	03	PR D67 113002	M. Eidemuller	
ERLER	03	PL B558 125	J. Erler, M. Luo	
ZYABLYUK	03	JHEP 0301 081	K.N. Zyablyuk	(ITEP)

b

$I(J^P) = 0(\frac{1}{2}^+)$

Charge $= -\frac{1}{3}\ e$ Bottom $= -1$

b-QUARK MASS

b-quark mass corresponds to the "running mass" $\overline{m}_b(\mu = \overline{m}_b)$ in the $\overline{\text{MS}}$ scheme. We have converted masses in other schemes to the $\overline{\text{MS}}$ mass using two-loop QCD perturbation theory with $\alpha_s(\mu = \overline{m}_b) = 0.223 \pm 0.008$. The value $4.18^{+0.04}_{-0.03}$ GeV for the $\overline{\text{MS}}$ mass corresponds to 4.78 ± 0.06 GeV for the pole mass, using the two-loop conversion formula. A discussion of masses in different schemes can be found in the "Note on Quark Masses."

$\overline{\text{MS}}$ MASS (GeV)	DOCUMENT ID		TECN
$4.18^{+0.03}_{-0.02}$ OUR EVALUATION	of $\overline{\text{MS}}$ Mass. See the ideogram below.		
4.197±0.008	[1] NARISON	20	THEO
$4.049^{+0.138}_{-0.118}$	[2] ABRAMOWICZ	18	HERA
4.195±0.014	[3] BAZAVOV	18	LATT
4.186±0.037	[4] PESET	18	THEO
4.197±0.022	[5] KIYO	16	THEO
4.183±0.037	[6] ALBERTI	15	THEO
$4.203^{+0.016}_{-0.034}$	[7] BENEKE	15	THEO
4.196±0.023	[8] COLQUHOUN	15	LATT
4.176±0.023	[9] DEHNADI	15	THEO
4.21 ±0.11	[10] BERNARDONI	14	LATT
4.169±0.002±0.008	[11] PENIN	14	THEO
4.166±0.043	[12] LEE	13O	LATT
4.247±0.034	[13] LUCHA	13	THEO
4.171±0.009	[14] BODENSTEIN	12	THEO
4.29 ±0.14	[15] DIMOPOUL...	12	LATT
$4.18^{+0.05}_{-0.04}$	[16] LASCHKA	11	THEO
4.186±0.044±0.015	[17] AUBERT	10A	BABR
4.163±0.016	[18] CHETYRKIN	09	THEO
4.243±0.049	[19] SCHWANDA	08	BELL
• • • We do not use the following data for averages, fits, limits, etc. • • •			
4.184±0.011	[20] NARISON	18A	THEO
4.188±0.008	[21] NARISON	18B	THEO
4.07 ±0.17	[22] ABRAMOWICZ	14A	ZEUS
4.201±0.043	[23] AYALA	14A	THEO
4.236±0.069	[24] NARISON	13	THEO
4.213±0.059	[25] NARISON	13A	THEO
4.235±0.003±0.055	[26] HOANG	12	THEO
4.212±0.032	[27] NARISON	12	THEO
4.177±0.011	[28] NARISON	12	THEO
4.171±0.014	[29] NARISON	12A	THEO
4.164±0.023	[30] MCNEILE	10	LATT
4.173±0.010	[31] NARISON	10	THEO
5.26 ±1.2	[32] ABDALLAH	08D	DLPH
4.42 ±0.06 ±0.08	[33] GUAZZINI	08	LATT
4.347±0.048±0.08	[34] DELLA-MOR...	07	LATT
4.164±0.025	[35] KUHN	07	THEO

Downloaded from https://academic.oup.com/ptep/article/2022/8/083C01/6651666 by KIT Library user on 27 September 2022

4.19 ±0.40	[36] ABDALLAH	06D	DLPH
4.205±0.058	[37] BOUGHEZAL	06	THEO
4.20 ±0.04	[38] BUCHMUEL...	06	THEO
4.19 ±0.06	[39] PINEDA	06	THEO
4.4 ±0.3	[40] GRAY	05	LATT
4.22 ±0.06	[41] AUBERT	04X	THEO
4.17 ±0.03	[42] BAUER	04	THEO
4.22 ±0.11	[43] HOANG	04	THEO
4.25 ±0.11	[44] MCNEILE	04	LATT
4.22 ±0.09	[45] BAUER	03	THEO
4.19 ±0.05	[46] BORDES	03	THEO
4.20 ±0.09	[47] CORCELLA	03	THEO
4.33 ±0.10	[48] DEDIVITIIS	03	LATT
4.24 ±0.10	[49] EIDEMULLER	03	THEO
4.207±0.03	[50] ERLER	03	THEO
4.33 ±0.06 ±0.10	[51] MAHMOOD	03	CLEO
4.190±0.032	[52] BRAMBILLA	02	THEO
4.346±0.070	[53] PENIN	02	THEO

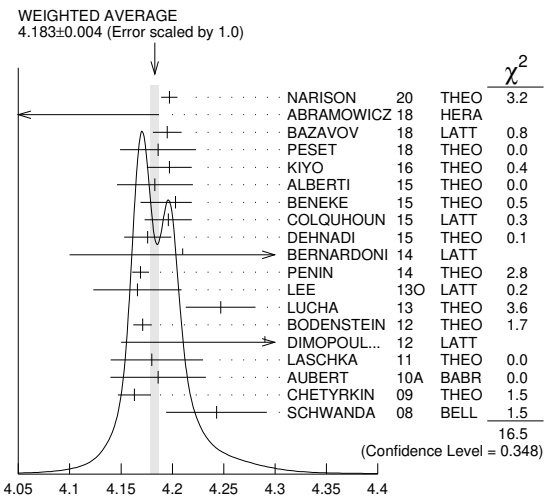

[1] NARISON 20 determines the quark mass using QCD Laplace sum rules from the B_c mass, combined with previous determinations of the QCD condensates and c and b masses.

[2] ABRAMOWICZ 18 determine $\overline{m}_b(\overline{m}_b) = 4.049^{+0.104+0.090+0.001}_{-0.109-0.032-0.031}$ from the production of b quarks in ep collisions at HERA using combined H1 and ZEUS data. The experimental/fitting errors, and those from modeling and parameterization have been combined in quadrature.

[3] BAZAVOV 18 determine the b mass using a lattice computation with staggered fermions and five active quark flavors.

[4] PESET 18 determine $\overline{m}_c(\overline{m}_c)$ and $\overline{m}_b(\overline{m}_b)$ using an N3LO calculation of the η_c, η_b and B_c masses.

[5] KIYO 16 determine $\overline{m}_b(\overline{m}_b)$ from the $\Upsilon(1S)$ mass at order α_s^3 (N3LO).

[6] ALBERTI 15 determine $\overline{m}_b(\overline{m}_b)$ from fits to inclusive $B \to X_c e \overline{\nu}$ decay. They also find $m_b^{\rm kin}(1\ {\rm GeV}) = 4.553 \pm 0.020$ GeV.

[7] BENEKE 15 determine $\overline{m}_b(\overline{m}_b)$ using sum rules for $e^+e^- \to$ hadrons at order N3LO including finite m_c effects. They find $m_b^{\rm PS}(2\ {\rm GeV}) = 4.532^{+0.013}_{-0.039}$ GeV, and $\overline{m}_b(\overline{m}_b) = 4.193^{+0.022}_{-0.035}$ GeV. The value quoted is obtained using the four-loop conversion given in BENEKE 16.

[8] COLQUHOUN 15 determine $\overline{m}_b(\overline{m}_b)$ from moments of the vector current correlator computed with a lattice simulation using the NRQCD action.

[9] DEHNADI 15 determine $\overline{m}_b(\overline{m}_b)$ using sum rules for $e^+e^- \to$ hadrons at order α_s^3 (N3LO), and fitting to both experimental data and lattice results.

[10] BERNARDONI 14 determine m_b from $n_f = 2$ lattice calculations using heavy quark effective theory non-perturbatively renormalized and matched to QCD at $1/m$ order.

[11] PENIN 14 determine $\overline{m}_b(\overline{m}_b) = 4.169 \pm 0.008 \pm 0.002 \pm 0.002$ using an estimate of the order α_s^3 b-quark vacuum polarization function in the threshold region, including finite m_c effects. The errors of ± 0.008 from theoretical uncertainties, and ± 0.002 from α_s have been combined in quadrature.

[12] LEE 13O determines m_b using lattice calculations of the Υ and B_s binding energies in NRQCD, including three light dynamical quark flavors. The quark mass shift in NRQCD is determined to order α_s^2, with partial α_s^3 contributions.

[13] LUCHA 13 determines m_b from QCD sum rules for heavy-light currents using the lattice value for f_B of 191.5 ± 7.3 GeV.

[14] BODENSTEIN 12 determine m_b using sum rules for the vector current correlator and the $e^+e^- \to Q\overline{Q}$ total cross-section.

[15] DIMOPOULOS 12 determine quark masses from a lattice computation using $n_f = 2$ dynamical flavors of twisted mass fermions.

[16] LASCHKA 11 determine the b mass from the charmonium spectrum. The theoretical computation uses the heavy $Q\overline{Q}$ potential to order $1/m_Q$ obtained by matching the short-distance perturbative result onto lattice QCD result at larger scales.

[17] AUBERT 10A determine the b- and c-quark masses from a fit to the inclusive decay spectra in semileptonic B decays in the kinetic scheme (and convert it to the $\overline{\rm MS}$ scheme).

[18] CHETYRKIN 09 determine m_c and m_b from the $e^+e^- \to Q\overline{Q}$ cross-section and sum rules, using an order α_s^3 (N3LO) computation of the heavy quark vacuum polarization.

[19] SCHWANDA 08 measure moments of the inclusive photon spectrum in $B \to X_s\gamma$ decay to determine m_b^{1S}. We have converted this to $\overline{\rm MS}$ scheme.

[20] NARISON 18A determines $\overline{m}_b(\overline{m}_b)$ as a function of α_s using QCD exponential sum rules and their ratios evaluated at the optimal scale $\mu = 9.5$ GeV at N2LO-N3LO of perturbative QCD and including condensates up to dimension 6–8 in the (axial-)vector and (pseudo-)scalar bottomonium channels.

[21] NARISON 18B determines $\overline{m}_b(\overline{m}_b)$ using QCD vector moment sum rules and their ratios at N2LO-N3LO of perturbative QCD and including condensates up to dimension 8.

[22] ABRAMOWICZ 14A determine $\overline{m}_b(\overline{m}_b) = 4.07 \pm 0.14^{+0.01+0.05+0.08}_{-0.07-0.00-0.05}$ from the production of b quarks in ep collisions at HERA. The errors due to fitting, modeling, PDF parameterization, and theoretical QCD uncertainties due to the values of α_s, m_c, and the renormalization scale μ have been combined in quadrature.

[23] AYALA 14A determine $\overline{m}_b(\overline{m}_b)$ from the $\Upsilon(1S)$ mass computed to N3LO order in perturbation theory using a renormalon subtracted scheme.

[24] NARISON 13 determines m_b using QCD spectral sum rules to order α_s^2 (NNLO) and including condensates up to dimension 6.

[25] NARISON 13A determines m_b using HQET sum rules to order α_s^2 (NNLO) and the B meson mass and decay constant.

[26] HOANG 12 determine m_b using non-relativistic sum rules for the Υ system at order α_s^2 (NNLO) with renormalization group improvement.

[27] NARISON 12 determines m_b using exponential sum rules for the vector current correlator to order α_s^3, including the effect of gluon condensates up to dimension eight.

[28] Determines m_b to order α_s^3 (N3LO), including the effect of gluon condensates up to dimension eight combining the methods of NARISON 12 and NARISON 12A.

[29] NARISON 12A determines m_b using sum rules for the vector current correlator to order α_s^3, including the effect of gluon condensates up to dimension eight.

[30] MCNEILE 10 determines m_b by comparing order α_s^3 (N3LO) perturbative results for the pseudo-scalar current to lattice simulations with $n_f = 2+1$ sea-quarks by the HPQCD collaboration.

[31] NARISON 10 determines m_b from ratios of moments of vector current correlators computed to order α_s^3 and including the dimension-six gluon condensate. These values are taken from the erratum to that reference.

[32] ABDALLAH 08D determine $\overline{m}_b(M_Z) = 3.76 \pm 1.0$ GeV from a leading order study of four-jet rates at LEP.

[33] GUAZZINI 08 determine $\overline{m}_b(\overline{m}_b)$ from a quenched lattice simulation of heavy meson masses. The ±0.08 is an estimate of the quenching error.

[34] DELLA-MORTE 07 determine $\overline{m}_b(\overline{m}_b)$ from a computation of the spin-averaged B meson mass using quenched lattice HQET at order $1/m$. The ±0.08 is an estimate of the quenching error.

[35] KUHN 07 determine $\overline{m}_b(\mu = 10\ {\rm GeV}) = 3.609 \pm 0.025$ GeV and $\overline{m}_b(\overline{m}_b)$ from a four-loop sum-rule computation of the cross-section for $e^+e^- \to$ hadrons in the bottom threshold region.

[36] ABDALLAH 06D determine $m_b(M_Z) = 2.85 \pm 0.32$ GeV from Z-decay three-jet events containing a b-quark.

[37] BOUGHEZAL 06 $\overline{\rm MS}$ scheme result comes from the first moment of the hadronic production cross-section to order α_s^3.

[38] BUCHMUELLER 06 determine m_b and m_c by a global fit to inclusive B decay spectra.

[39] PINEDA 06 $\overline{\rm MS}$ scheme result comes from a partial NNLL evaluation (complete at order α_s^2 (NNLO)) of sum rules of the bottom production cross-section in e^+e^- annihilation.

[40] GRAY 05 determines $\overline{m}_b(\overline{m}_b)$ from a lattice computation of the Υ spectrum. The simulations have 2+1 dynamical light flavors. The b quark is implemented using NRQCD.

[41] AUBERT 04X obtain m_b from a fit to the hadron mass and lepton energy distributions in semileptonic B decay. The paper quotes values in the kinetic scheme. The $\overline{\rm MS}$ value has been provided by the BABAR collaboration.

[42] BAUER 04 determine m_b, m_c and $m_b - m_c$ by a global fit to inclusive B decay spectra.

[43] HOANG 04 determines $\overline{m}_b(\overline{m}_b)$ from moments at order α_s^2 of the bottom production cross-section in e^+e^- annihilation.

[44] MCNEILE 04 use lattice QCD with dynamical light quarks and a static heavy quark to compute the masses of heavy-light mesons.

[45] BAUER 03 determine the b quark mass by a global fit to B decay observables. The experimental data includes lepton energy and hadron invariant mass moments in semileptonic $B \to X_c \ell \nu_\ell$ decay, and the inclusive photon spectrum in $B \to X_s\gamma$ decay. The theoretical expressions used are of order $1/{\rm m}^3$, and $\alpha_s^2\beta_0$.

[46] BORDES 03 determines m_b using QCD finite energy sum rules to order α_s^2.

[47] CORCELLA 03 determines $\overline{m}_b$ using sum rules computed to order α_s^2. Includes charm quark mass effects.

[48] DEDIVITIIS 03 use a quenched lattice computation of heavy-heavy and heavy-light meson masses.

[49] EIDEMULLER 03 determines $\overline{m}_b$ and $\overline{m}_c$ using QCD sum rules.

[50] ERLER 03 determines $\overline{m}_b$ and $\overline{m}_c$ using QCD sum rules. Includes recent BES data.

[51] MAHMOOD 03 determines m_b^{1S} by a fit to the lepton energy moments in $B \to X_c \ell \nu_\ell$ decay. The theoretical expressions used are of order $1/{\rm m}^3$ and $\alpha_s^2\beta_0$. We have converted their result to the $\overline{\rm MS}$ scheme.

[52] BRAMBILLA 02 determine $\overline{m}_b(\overline{m}_b)$ from a computation of the $\Upsilon(1S)$ mass to order α_s^4, including finite m_c corrections.

[53] PENIN 02 determines $\overline{m}_b$ from the spectrum of the Υ system.

m_b/m_s MASS RATIO

VALUE	DOCUMENT ID		TECN
53.94±0.12	[1] BAZAVOV	18	LATT

[1] BAZAVOV 18 determine the quark masses using a lattice computation with staggered fermions and four active quark flavors for the u, d, s, c quarks and five active flavors for the b quark.

Downloaded from https://academic.oup.com/ptep/article/2022/8/083C01/6651666 by KIT Library user on 27 September 2022

b-QUARK REFERENCES

NARISON	20	PL B802 135221	S. Narison	(MONP)
ABRAMOWICZ	18	EPJ C78 473	H. Abramowicz *et al.*	(H1 and ZEUS Collabs.)
BAZAVOV	18	PR D98 054517	A. Bazavov *et al.*	(Fermilab Lattice, MILC, TUMQCD)
NARISON	18A	IJMP A33 1850045	S. Narison	(MONP)
NARISON	18B	PL B784 261	S. Narison	(MONP)
PESET	18	JHEP 1809 167	C. Peset, A. Pineda, J. Segovia	(BARC, TUM)
BENEKE	16	PoS RADCOR2015 035	M. Beneke *et al.*	
KIYO	16	PL B752 122	Y. Kiyo, G. Mishima, Y. Sumino	
ALBERTI	15	PRL 114 061802	A. Alberti *et al.*	
BENEKE	15	NP B891 42	M. Beneke *et al.*	
COLQUHOUN	15	PR D91 074514	B. Colquhoun *et al.*	(HPQCD Collab.)
DEHNADI	15	JHEP 1508 155	B. Dehnadi, A.H. Hoang, V. Mateu	
ABRAMOWICZ	14A	JHEP 1409 127	H. Abramowicz *et al.*	(ZEUS Collab.)
AYALA	14A	JHEP 1409 045	C. Ayala, G. Cvetic, A. Pineda	
BERNARDONI	14	PL B730 171	F. Bernardoni *et al.*	(ALPHA Collab.)
PENIN	14	JHEP 1404 120	A.A. Penin, N. Zerf	
LEE	13O	PR D87 074018	A.J. Lee *et al.*	(HPQCD Collab.)
LUCHA	13	PR D88 056011	W. Lucha, D. Melikhov, S. Simula	(VIEN, MOSU+)
NARISON	13	PL B718 1321	S. Narison	(MONP)
NARISON	13A	PL B721 269	S. Narison	(MONP)
BODENSTEIN	12	PR D85 034003	S. Bodenstein *et al.*	(CAPE, VALE, MAINZ+)
DIMOPOUL...	12	JHEP 1201 046	P. Dimopoulos *et al.*	(ETM Collab.)
HOANG	12	JHEP 1210 188	A.H. Hoang, P. Ruiz-Femenia, M. Stahlhofen	(WIEN+)
NARISON	12	PL B707 259	S. Narison	(MONP)
NARISON	12A	PL B706 412	S. Narison	(MONP)
LASCHKA	11	PR D83 094002	A. Laschka, N. Kaiser, W. Weise	
AUBERT	10A	PR D81 032003	B. Aubert *et al.*	(BABAR Collab.)
MCNEILE	10	PR D82 034512	C. McNeile *et al.*	(HPQCD Collab.)
NARISON	10	PL B693 559	S. Narison	(MONP)
Also		PL B705 544 (errat.)	S. Narison	(MONP)
CHETYRKIN	09	PR D80 074010	K.G. Chetyrkin *et al.*	(KARL, BNL)
ABDALLAH	08D	EPJ C55 525	J. Abdallah *et al.*	(DELPHI Collab.)
GUAZZINI	08	JHEP 0801 076	D. Guazzini, R. Sommer, N. Tantalo	
SCHWANDA	08	PR D78 032016	C. Schwanda *et al.*	(BELLE Collab.)
DELLA-MOR...	07	JHEP 0701 007	M. Della Morte *et al.*	
KUHN	07	NP B778 192	J.H. Kuhn, M. Steinhauser, C. Sturm	
ABDALLAH	06D	EPJ C46 569	J. Abdallah *et al.*	(DELPHI Collab.)
BOUGHEZAL	06	PR D74 074006	R. Boughezal, M. Czakon, T. Schutzmeier	
BUCHMUEL...	06	PR D73 073008	O.L. Buchmueller, H.U. Flacher	(RHBL)
PINEDA	06	PR D73 111501	A. Pineda, A. Signer	
GRAY	05	PR D72 094507	A. Gray *et al.*	(HPQCD and UKQCD Collab.)
AUBERT	04X	PRL 93 011803	B. Aubert *et al.*	(BABAR Collab.)
BAUER	04	PR D70 094017	C. Bauer *et al.*	
HOANG	04	PL B594 127	A.H. Hoang, M. Jamin	
MCNEILE	04	PL B600 77	C. McNeile, C. Michael, G. Thompson	(UKQCD Collab.)
BAUER	03	PR D67 054012	C.W. Bauer *et al.*	
BORDES	03	PL B562 81	J. Bordes, J. Penarrocha, K. Schilcher	
CORCELLA	03	PL B554 133	G. Corcella, A.H. Hoang	
DEDIVITIIS	03	NP B675 309	G.M. de Divitiis *et al.*	
EIDEMULLER	03	PR D67 113002	M. Eidemuller	
ERLER	03	PL B558 125	J. Erler, M. Luo	
MAHMOOD	03	PR D67 072001	A.H. Mahmood *et al.*	(CLEO Collab.)
BRAMBILLA	02	PR D65 034001	N. Brambilla, Y. Sumino, A. Vairo	
PENIN	02	PL B538 335	A. Penin, M. Steinhauser	

t

$I(J^P) = 0(\frac{1}{2}^+)$

Charge $= \frac{2}{3}\ e$ Top $= +1$

See the related review(s):

Top Quark

t-QUARK MASS

We first list the direct measurements of the top quark mass which employ the event kinematics and then list the measurements which extract a top quark mass from the measured $t\bar{t}$ cross-section using theory calculations. A discussion of the definition of the top quark mass in these measurements can be found in the review "The Top Quark."

For earlier search limits see PDG 96, Physical Review **D54** 1 (1996). We no longer include a compilation of indirect top mass determinations from Standard Model Electroweak fits in the Listings (our last compilation can be found in the Listings of the 2007 partial update). For a discussion of current results see the reviews "The Top Quark" and "Electroweak Model and Constraints on New Physics."

t-Quark Mass (Direct Measurements)

The following measurements extract a *t*-quark mass from the kinematics of $t\bar{t}$ events. They are sensitive to the top quark mass used in the MC generator that is usually interpreted as the pole mass, but the theoretical uncertainty in this interpretation is hard to quantify. See the review "The Top Quark" and references therein for more information.

OUR AVERAGE of 172.69 ± 0.30 GeV is an average of top mass measurements from LHC and Tevatron Runs. The latest Tevatron average, 174.30 ± 0.35 ± 0.54 GeV, was provided by the Tevatron Electroweak Working Group (TEVEWWG).

VALUE (GeV)	*DOCUMENT ID*		*TECN*	*COMMENT*
172.69± 0.30 OUR AVERAGE	Error includes scale factor of 1.3. See the ideogram below.			
$172.13^{+0.76}_{-0.77}$	[1] TUMASYAN	21G	CMS	*t*-channel single top production
172.6 ± 2.5	[2] SIRUNYAN	20AR	CMS	jet mass from boosted top
172.69± 0.25± 0.41	[3] AABOUD	19AC	ATLS	7, 8 TeV ATLAS combination
172.26± 0.07± 0.61	[4] SIRUNYAN	19AP	CMS	lepton+jets, all-jets channels
$172.33\pm 0.14^{+0.66}_{-0.72}$	[5] SIRUNYAN	19AR	CMS	dilepton channel ($e\mu$, $2e$, 2μ)
172.44± 0.13± 0.47	[6] KHACHATRY...	16AK	CMS	7, 8 TeV CMS combination
174.30± 0.35± 0.54	[7] TEVEWWG	16	TEVA	Tevatron combination
• • • We do not use the following data for averages, fits, limits, etc. • • •				
172.08± 0.39± 0.82	[8] AABOUD	19AC	ATLS	$\ell + \geq 4$j ($2b$)
172.34± 0.20± 0.70	[9] SIRUNYAN	19AP	CMS	≥ 6 jets ($\geq 2b$)
172.25± 0.08± 0.62	[10] SIRUNYAN	18DE	CMS	$\ell + \geq 4$j ($2b$)
173.72± 0.55± 1.01	[11] AABOUD	17AH	ATLS	≥ 5 jets ($2b$)
174.95± 0.40± 0.64	[12] ABAZOV	17B	D0	ℓ + jets and dilepton channels
$172.95\pm 0.77^{+0.97}_{-0.93}$	[13] SIRUNYAN	17L	CMS	*t*-channel single top production
170.8 ± 9.0	[14] SIRUNYAN	17N	CMS	jet mass in highly-boosted $t\bar{t}$ events
$172.22\pm 0.18^{+0.89}_{-0.93}$	[15] SIRUNYAN	17O	CMS	Dilepton channel
172.99± 0.41± 0.74	[16] AABOUD	16T	ATLS	dilepton channel
172.84± 0.34± 0.61	[17] AABOUD	16T	ATLS	combination of ATLAS
173.32± 1.36± 0.85	[18] ABAZOV	16	D0	$\ell\ell + \not{E}_T + \geq 2$j ($\geq 2b$)
173.93± 1.61± 0.88	[19] ABAZOV	16D	D0	$\ell\ell + \not{E}_T + \geq 2$j ($\geq 2b$)
172.35± 0.16± 0.48	[20,21] KHACHATRY...	16AK	CMS	$\ell + \geq 4$j ($2b$)
172.32± 0.25± 0.59	[20,21] KHACHATRY...	16AK	CMS	≥ 6 jets ($2b$)
172.82± 0.19± 1.22	[20,22] KHACHATRY...	16AK	CMS	$(ee/\mu\mu)+\not{E}_T+ \geq 2b, e\mu+ \geq 2b$
$173.68\pm 0.20^{+1.58}_{-0.97}$	[23] KHACHATRY...	16AL	CMS	semi- + di-leptonic channels
173.5 ± 3.0 ± 0.9	[24] KHACHATRY...	16CB	CMS	$t \to (W \to \ell\nu)(b \to J/\psi X \to \mu^+\mu^- X)$
175.1 ± 1.4 ± 1.2	[25] AAD	15AW	ATLS	small $\not{E}_T$, ≥ 6 jets ($2b$-tag)
172.99± 0.48± 0.78	[26] AAD	15BF	ATLS	ℓ + jets and dilepton
171.5 ± 1.9 ± 2.5	[27] AALTONEN	15D	CDF	$\ell\ell + \not{E}_T + \geq 2$j
$175.07\pm 1.19^{+1.55}_{-1.58}$	[28] AALTONEN	14N	CDF	small $\not{E}_T$, 6–8 jets ($\geq 1b$-tag)
174.98± 0.58± 0.49	[29] ABAZOV	14C	D0	$\ell + \not{E}_T + 4$ jets (≥ 1 b-tag)
173.49± 0.69± 1.21	[30] CHATRCHYAN	14C	CMS	≥ 6 jets (≥ 2 b-tag)
173.93± 1.64± 0.87	[31] AALTONEN	13H	CDF	$\not{E}_T + \geq 4$ jets (≥ 1 b)
$173.9 \pm 0.9 ^{+1.7}_{-2.1}$	[32] CHATRCHYAN	13S	CMS	$\ell\ell+\not{E}_T+ \geq 2b$-tag ($MT2_{(T)}$)
174.5 ± 0.6 ± 2.3	[33] AAD	12I	ATLS	$\ell+\not{E}_T+ \geq 4$ jets (≥ 1 b), MT
172.85± 0.71± 0.85	[34] AALTONEN	12AI	CDF	$\ell+\not{E}_T+ \geq 4$j (0,1,2b) template
172.7 ± 9.3 ± 3.7	[35] AALTONEN	12AL	CDF	$\tau_h + \not{E}_T + 4$j ($\geq 1b$)
173.18± 0.56± 0.75	[36] AALTONEN	12AP	TEVA	CDF, D0 combination
172.5 ± 1.4 ± 1.5	[37] AALTONEN	12G	CDF	6–8 jets with ≥ 1 b
173.7 ± 2.8 ± 1.5	[38] ABAZOV	12AB	D0	$\ell\ell + \not{E}_T + \geq 2$ j (νWT)
173.9 ± 1.9 ± 1.6	[39] ABAZOV	12AB	D0	$\ell\ell+\not{E}_T+ \geq 2$j ($\nu$WT+MWT)
172.5 ± 0.4 ± 1.5	[40] CHATRCHYAN	12BA	CMS	$\ell\ell+\not{E}_T+ \geq 2$j ($\geq 1b$), AMWT
173.49± 0.43± 0.98	[41] CHATRCHYAN	12BP	CMS	$\ell+\not{E}_T+ \geq 4$j ($\geq 2b$)
172.4 ± 1.4 ± 1.3	[42] AALTONEN	11AC	CDF	$\ell + \not{E}_T + 4$ jets (≥ 1 b-tag)
172.3 ± 2.4 ± 1.0	[43] AALTONEN	11AK	CDF	Repl. by AALTONEN 13H
172.1 ± 1.1 ± 0.9	[44] AALTONEN	11E	CDF	ℓ + jets and dilepton
176.9 ± 8.0 ± 2.7	[45] AALTONEN	11T	CDF	$\ell + \not{E}_T + 4$ jets (≥ 1 b-tag), $p_T(\ell)$ shape
174.94± 0.83± 1.24	[46] ABAZOV	11P	D0	$\ell + \not{E}_T + 4$ jets (≥ 1 b-tag)
174.0 ± 1.8 ± 2.4	[47] ABAZOV	11R	D0	dilepton + $\not{E}_T + \geq 2$ jets
175.5 ± 4.6 ± 4.6	[48] CHATRCHYAN	11F	CMS	dilepton + $\not{E}_T$ + jets
173.0 ± 0.9 ± 0.9	[49] AALTONEN	10AE	CDF	$\ell + \not{E}_T + 4$ jets (≥ 1 b-tag), ME method
169.3 ± 2.7 ± 3.2	[50] AALTONEN	10C	CDF	dilepton + b-tag (MT2+NWA)
170.7 ± 6.3 ± 2.6	[51] AALTONEN	10D	CDF	$\ell + \not{E}_T + 4$ jets (b-tag)
$174.8 \pm 2.4 ^{+1.2}_{-1.0}$	[52] AALTONEN	10E	CDF	≥ 6 jets, vtx b-tag
180.5 ±12.0 ± 3.6	[53] AALTONEN	09AK	CDF	$\ell + \not{E}_T$ + jets (soft μ b-tag)
172.7 ± 1.8 ± 1.2	[54] AALTONEN	09J	CDF	$\ell + \not{E}_T + 4$ jets (b-tag)
171.1 ± 3.7 ± 2.1	[55] AALTONEN	09K	CDF	6 jets, vtx b-tag
171.9 ± 1.7 ± 1.1	[56] AALTONEN	09L	CDF	ℓ + jets, $\ell\ell$ + jets
171.2 ± 2.7 ± 2.9	[57] AALTONEN	09O	CDF	dilepton
$165.5 ^{+3.4}_{-3.3} \pm 3.1$	[58] AALTONEN	09X	CDF	$\ell\ell + \not{E}_T$ ($\nu\phi$ weighting)
174.7 ± 4.4 ± 2.0	[59] ABAZOV	09AH	D0	dilepton + b-tag (νWT+MWT)
$170.7 ^{+4.2}_{-3.9} \pm 3.5$	[60,61] AALTONEN	08C	CDF	dilepton, $\sigma_{t\bar{t}}$ constrained
171.5 ± 1.8 ± 1.1	[62] ABAZOV	08AH	D0	$\ell + \not{E}_T + 4$ jets
177.1 ± 4.9 ± 4.7	[63,64] AALTONEN	07	CDF	6 jets with ≥ 1 b vtx
$172.3 ^{+10.8}_{-9.6} \pm 10.8$	[65] AALTONEN	07B	CDF	≥ 4 jets (b-tag)
174.0 ± 2.2 ± 4.8	[66] AALTONEN	07D	CDF	≥ 6 jets, vtx b-tag
170.8 ± 2.2 ± 1.4	[67,68] AALTONEN	07I	CDF	lepton + jets (b-tag)
$173.7 \pm 4.4 ^{+2.1}_{-2.0}$	[64,69] ABAZOV	07F	D0	lepton + jets
176.2 ± 9.2 ± 3.9	[70] ABAZOV	07W	D0	dilepton (MWT)
179.5 ± 7.4 ± 5.6	[70] ABAZOV	07W	D0	dilepton (νWT)
164.5 ± 3.9 ± 3.9	[68,71] ABULENCIA	07D	CDF	dilepton
$180.7 ^{+15.5}_{-13.4} \pm 8.6$	[72] ABULENCIA	07J	CDF	lepton + jets
$170.3 ^{+4.1}_{-4.5} ^{+1.2}_{-1.8}$	[68,73] ABAZOV	06U	D0	lepton + jets (b-tag)
$173.2 ^{+2.6}_{-2.4} \pm 3.2$	[74,75] ABULENCIA	06D	CDF	lepton + jets
$173.5 ^{+3.7}_{-3.6} \pm 1.3$	[61,74] ABULENCIA	06D	CDF	lepton + jets
165.2 ± 6.1 ± 3.4	[68,76] ABULENCIA	06G	CDF	dilepton
170.1 ± 6.0 ± 4.1	[61,77] ABULENCIA	06V	CDF	dilepton
178.5 ±13.7 ± 7.7	[78,79] ABAZOV	05	D0	6 or more jets
180.1 ± 3.6 ± 3.9	[80,81] ABAZOV	04G	D0	lepton + jets
176.1 ± 5.1 ± 5.3	[82] AFFOLDER	01	CDF	lepton + jets
176.1 ± 6.6	[83] AFFOLDER	01	CDF	dilepton, lepton+jets, all-jets
172.1 ± 5.2 ± 4.9	[84] ABBOTT	99G	D0	di-lepton, lepton+jets
176.0 ± 6.5	[85,86] ABE	99B	CDF	dilepton, lepton+jets, all-jets
167.4 ±10.3 ± 4.8	[86,87] ABE	99B	CDF	dilepton
168.4 ±12.3 ± 3.6	[81] ABBOTT	98D	D0	dilepton
173.3 ± 5.6 ± 5.5	[81,88] ABBOTT	98F	D0	lepton + jets
175.9 ± 4.8 ± 5.3	[87,89] ABE	98E	CDF	lepton + jets

Downloaded from https://academic.oup.com/ptep/article/2022/8/083C01/6651666 by KIT Library user on 27 September 2022

161	±17	±10	[87] ABE	98F	CDF	dilepton
172.1	± 5.2	± 4.9	[90] BHAT	98B	RVUE	dilepton and lepton+jets
173.8	± 5.0		[91] BHAT	98B	RVUE	dilepton, lepton+jets, all-jets
173.3	± 5.6	± 6.2	[81] ABACHI	97E	D0	lepton + jets
186	±10	± 5.7	[87,92] ABE	97R	CDF	6 or more jets
199	$^{+19}_{-21}$	±22	ABACHI	95	D0	lepton + jets
176	± 8	±10	ABE	95F	CDF	lepton + b-jet
174	±10	$^{+13}_{-12}$	ABE	94E	CDF	lepton + b-jet

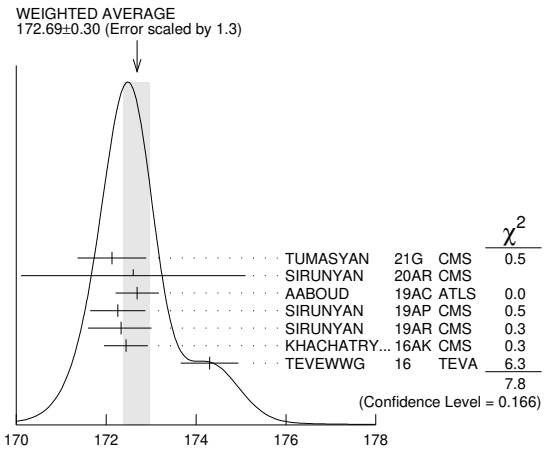

t-Quark Mass (Direct Measurements) (GeV)

[1] TUMASYAN 21G based on 35.9 fb^{-1} of pp data at $\sqrt{s}$ = 13 TeV. Events are selected by requiring 1ℓ + 2jets($1b$ jet) final state.

[2] SIRUNYAN 20AR based on 35.9 fb^{-1} of pp data at $\sqrt{s}$ = 13 TeV. The products of the hadronic decay of a top quark with p_T > 400 GeV, in the ℓ + jets channel of $t\overline{t}$ are reconstructed as a single jet. The top quark mass is determined from the normalized differential cross section measurement in the $m_{\rm jet}$ distribution.

[3] AABOUD 19AC is an ATLAS combination of 7 and 8 TeV top-quark mass determination in the dilepton, lepton + jets, and all jets channels.

[4] SIRUNYAN 19AP based on 35.9 fb^{-1} of pp data at $\sqrt{s}$ = 13 TeV. A combined measurement using the lepton+jets and all-jets channels through a single likelihood function. See SIRUNYAN 18DE and SIRUNYAN 19AP below.

[5] SIRUNYAN 19AR based on 35.9 fb^{-1} of pp data at $\sqrt{s}$ = 13 TeV. Obtained from a simultaneous fit of the cross section and the top quark mass in the POWHEG simulation. The cross section is used also to extract the $\overline{\rm MS}$ mass and the strong coupling constant for different PDF sets.

[6] KHACHATRYAN 16AK based on 19.7 fb^{-1} of pp data at $\sqrt{s}$ = 8 TeV. Combination of the three top mass measurements in KHACHATRYAN 16AK and with the CMS results at $\sqrt{s}$ = 7 TeV.

[7] TEVEWWG 16 is the latest Tevatron average (July 2016) provided by the Tevatron Electroweak Working Group. It takes correlated uncertainties into account and has a χ^2 of 10.8 for 11 degrees of freedom.

[8] AABOUD 19AC based on 20.2 fb^{-1} in pp collisions at $\sqrt{s}$ = 8 TeV. Uses optimized event selection to suppress less-well-reconstructed events and template fits to determine m_t together with a global jet energy scale factor and a relative b-to-light-jet energy scale factor.

[9] SIRUNYAN 19AP based on 35.9 fb^{-1} of pp data at $\sqrt{s}$ = 13 TeV. A kinematical fit is applied to each event assuming the signal event topology. m_t is determined simultaneously with a jet energy scale factor (JSF). The second error represents stat.+JSF. Modeling uncertainties are larger than in the measurements at $\sqrt{s}$ = 7 and 8 TeV because of the use of new alternative color reconnection models.

[10] SIRUNYAN 18DE based on 35.9 fb^{-1} of pp data at $\sqrt{s}$ = 13 TeV. m_t is determined simultaneously with an overall jet energy scale factor constrained by the mass of the hadronically decayed W. Compared to the Run 1 analysis a more advanced treatment of modeling uncertainties are employed, in particular concerning color-reconnection models.

[11] AABOUD 17AH based on 20.2 fb^{-1} of pp data at $\sqrt{s}$ = 8 TeV. Uses template fits to the ratio of the masses of three-jets (from t candidate) and dijets (from W candidate), to suppress jet energy scale uncertainty. Large QCD background is modelled using a data-driven method.

[12] ABAZOV 17B is a combination of measurements of the top quark mass by D0 in the lepton+jets and dilepton channels, using all data collected in Run I (1992–1996) at $\sqrt{s}$ = 1.8 TeV and Run II (2001–2011) at $\sqrt{s}$ = 1.96 TeV of the Tevatron, corresponding to integrated luminosities of 0.1 fb^{-1} and 9.7 fb^{-1}, respectively.

[13] SIRUNYAN 17L based on 19.7 fb^{-1} of pp data at $\sqrt{s}$ = 8 TeV. m_t is reconstructed from a fit to the invariant mass distribution of $\mu\nu b$, where p_T^{miss} and W mass constraint are used to reconstruct ν momentum. The number of events for various contributions, except for the t-channel single top one, are fixed to the values extracted from simulation. Superseded by TUMASYAN 21G.

[14] SIRUNYAN 17N based on 19.7 fb^{-1} of pp data at $\sqrt{s}$ = 8 TeV. The fully hadronic decay of a highly-boosted t is reconstructed in the ℓ+jets channel and unfolded at the particle level. The sensitivity of the peak position of the m_{jet} distribution is used to test quality of the modelling by the simulation.

[15] SIRUNYAN 17O based on 19.7 fb^{-1} of pp data at $\sqrt{s}$ = 8 TeV. Analysis is based on the kinematical observables $M(b\ell)$, M_{T2} and $M(b\ell\nu)$. A fit is performed to determine m_t and an overall jet energy scale factor simultaneously.

[16] AABOUD 16T based on 20.2 fb^{-1} of pp data at $\sqrt{s}$ = 8 TeV. The analysis is refined using the p_T and invariant mass distributions of ℓ+b-jet system. A combination with measurements from $\sqrt{s}$ = 7 TeV data in the dilepton and lepton+jets channels gives 172.84 ± 0.34 ± 0.61 GeV.

[17] AABOUD 16T is an ATLAS combination of 8 TeV top-quark mass in the dilepton channel with previous measurements from $\sqrt{s}$ = 7 TeV data in the dilepton and lepton + jets channels.

[18] ABAZOV 16 based on 9.7 fb^{-1} of data in $p\overline{p}$ collisions at $\sqrt{s}$ = 1.96 TeV. Employs improved fit to minimize statistical errors and improved jet energy calibration, using lepton + jets mode, which reduces error of jet energy scale. Based on previous determination in ABAZOV 12AB with increased integrated luminosity and improved fit and calibrations.

[19] ABAZOV 16D based on 9.7 fb^{-1} of data in $p\overline{p}$ collisions at $\sqrt{s}$ = 1.96 TeV, using the matrix element technique. Based on previous determination in ABAZOV 11R with increased integrated luminosity. There is a strong correlation with the determination in ABAZOV 16. (See ABAZOV 17B.)

[20] KHACHATRYAN 16AK based on 19.7 fb^{-1} of pp data at $\sqrt{s}$ = 8 TeV. Combination of the three top mass measurements in KHACHATRYAN 16AK and with the CMS results at $\sqrt{s}$ = 7 TeV gives 172.44 ± 0.13 ± 0.47 GeV.

[21] The top mass and jet energy scale factor are determined by a fit.

[22] Uses the analytical matrix weighting technique method.

[23] KHACHATRYAN 16AL based on 19.7 fb^{-1} in pp collisions at $\sqrt{s}$ = 8 TeV. Determined from the invariant mass distribution of leptons and reconstructed secondary vertices from b decays using only charged particles. The uncertainty is dominated by modeling of b fragmentation and top p_T distribution.

[24] KHACHATRYAN 16CB based on 666 candidate reconstructed events corresponding to 19.7 fb^{-1} of pp data at $\sqrt{s}$ = 8 TeV. The measurement exploits correlation of m_t with M($J/\psi\ell$) in the same top quark decay, using a high-purity event sample. A study on modeling of b-quark fragmentation is given in Sec. 3.3.

[25] AAD 15AW based on 4.6 fb^{-1} of pp data at $\sqrt{s}$ = 7 TeV. Uses template fits to the ratio of the masses of three-jets (from t candidate) and dijets (from W candidate). Large background from multijet production is modeled with data-driven methods.

[26] AAD 15BF based on 4.6 fb^{-1} in pp collisions at $\sqrt{s}$ = 7 TeV. Using a three-dimensional template likelihood technique the lepton plus jets (≥ 1b-tagged) channel gives 172.33 ± 0.75 ± 1.02 GeV, while exploiting a one dimensional template method using $m_{\ell b}$ the dilepton channel (1 or 2b-tags) gives 173.79 ± 0.54 ± 1.30 GeV. The results are combined.

[27] AALTONEN 15D based on 9.1 fb^{-1} of $p\overline{p}$ data at $\sqrt{s}$ = 1.96 TeV. Uses a template technique to fit a distribution of a variable defined by a linear combination of variables sensitive and insensitive to jet energy scale to optimize reduction of systematic errors. b-tagged and non-b-tagged events are separately analyzed and combined.

[28] Based on 9.3 fb^{-1} of $p\overline{p}$ data at $\sqrt{s}$ = 1.96 TeV. Multivariate algorithm is used to discriminate signal from backgrounds, and templates are used to measure m_t.

[29] Based on 9.7 fb^{-1} of $p\overline{p}$ data at $\sqrt{s}$ = 1.96 TeV. A matrix element method is used to calculate the probability of an event to be signal or background, and the overall jet energy scale is constrained *in situ* by m_W. See ABAZOV 15G for further details.

[30] Based on 3.54 fb^{-1} of pp data at $\sqrt{s}$ = 7 TeV. The mass is reconstructed for each event employing a kinematic fit of the jets to a ttbar hypothesis. The combination with the pervious CMS measurements in the dilepton and the lepton+jets channels gives 173.54 ± 0.33 ± 0.96 GeV.

[31] Based on 8.7 fb^{-1} in $p\overline{p}$ collisions at $\sqrt{s}$ = 1.96 TeV. Events with an identified charged lepton or small $\not{E}_T$ are rejected from the event sample, so that the measurement is statistically independent from those in the ℓ + jets and all hadronic channels while being sensitive to those events with a τ lepton in the final state.

[32] Based on 5.0 fb^{-1} of pp data at $\sqrt{s}$ = 7 TeV. CHATRCHYAN 13S studied events with di-lepton + $\not{E}_T$ + ≥ 2 b-jets, and looked for kinematical endpoints of MT2, MT2$_T$, and subsystem variables.

[33] AAD 12I based on 1.04 fb^{-1} of pp data at $\sqrt{s}$ = 7 TeV. Uses 2d-template analysis (MT) with m_t and jet energy scale factor (JSF) from m_W mass fit.

[34] Based on 8.7 fb^{-1} of data in $p\overline{p}$ collisions at 1.96 TeV. The JES is calibrated by using the dijet mass from the W boson decay.

[35] Use the ME method based on 2.2 fb^{-1} of data in $p\overline{p}$ collisions at 1.96 TeV.

[36] Combination based on up to 5.8 fb^{-1} of data in $p\overline{p}$ collisions at 1.96 TeV.

[37] Based on 5.8 fb^{-1} of data in $p\overline{p}$ collisions at 1.96 TeV the quoted value is m_t = 172.5 ± 1.4(stat) ± 1.0(JES) ± 1.1(syst) GeV. The measurement is performed with a liklihood fit technique which simultaneously determines m_t and JES (Jet Energy Scale).

[38] Based on 4.3 fb^{-1} of data in p-pbar collisions at 1.96 TeV. The measurement reduces the JES uncertainty by using the single lepton channel study of ABAZOV 11P.

[39] Combination with the result in 1 fb^{-1} of preceding data reported in ABAZOV 09AH as well as the MWT result of ABAZOV 11R with a statistical correlation of 60%.

[40] Based on 5.0 fb^{-1} of pp data at $\sqrt{s}$ = 7 TeV. Uses an analytical matrix weighting technique (AMWT) and full kinematic analysis (KIN).

[41] Based on 5.0 fb^{-1} of pp data at $\sqrt{s}$ = 7 TeV. The first error is statistical and JES combined, and the second is systematic. Ideogram method is used to obtain 2D liklihood for the kinematical fit with two parameters mtop and JES.

[42] Based on 3.2 fb^{-1} in $p\overline{p}$ collisions at $\sqrt{s}$ = 1.96 TeV. The first error is from statistics and JES combined, and the latter is from the other systematic uncertainties. The result is obtained using an unbinned maximum likelihood method where the top quark mass and the JES are measured simultaneously, with Δ_{JES} = 0.3 ± 0.3(stat).

[43] Based on 5.7 fb^{-1} in $p\overline{p}$ collisions at $\sqrt{s}$ = 1.96 TeV. Events with an identified charged lepton or small $\not{E}_T$ are rejected from the event sample, so that the measurement is statistically independent from those in the ℓ + jets and all hadronic channels while being sensitive to those events with a τ lepton in the final state. Supersedes AALTONEN 07B.

[44] AALTONEN 11E based on 5.6 fb^{-1} in $p\overline{p}$ collisions at $\sqrt{s}$ = 1.96 TeV. Employs a multi-dimensional template likelihood technique where the lepton plus jets (one or two b-tags) channel gives 172.2 ± 1.2 ± 0.9 GeV while the dilepton channel yields 170.3 ± 2.0 ± 3.1 GeV. The results are combined. OUR EVALUATION includes the measurement in the dilepton channel only.

[45] Uses a likelihood fit of the lepton p_T distribution based on 2.7 fb^{-1} in $p\overline{p}$ collisions at $\sqrt{s}$ = 1.96 TeV.

[46] Based on 3.6 fb^{-1} in $p\overline{p}$ collisions at $\sqrt{s}$ = 1.96 TeV. ABAZOV 11P reports 174.94 ± 0.83 ± 0.78 ± 0.96 GeV, where the first uncertainty is from statistics, the second from JES, and the last from other systematic uncertainties. We combine the JES and systematic uncertainties. A matrix-element method is used where the JES uncertainty is constrained by the W mass. ABAZOV 11P describes a measurement based on 2.6 fb^{-1} that is combined with ABAZOV 08AH, which employs an independent 1 fb^{-1} of data.

[47] Based on a matrix-element method which employs 5.4 fb^{-1} in $p\overline{p}$ collisions at $\sqrt{s}$ = 1.96 TeV. Superseded by ABAZOV 12AB.

[48] Based on 36 pb^{-1} of pp collisions at $\sqrt{s}$ = 7 TeV. A Kinematic Method using b-tagging and an analytical Matrix Weighting Technique give consistent results and are combined. Superseded by CHATRCHYAN 12BA.

Downloaded from https://academic.oup.com/ptep/article/2022/8/083C01/6651666 by KIT Library user on 27 September 2022

[49] Based on 5.6 fb^{-1} in $p\overline{p}$ collisions at $\sqrt{s}$ = 1.96 TeV. The likelihood calculated using a matrix element method gives m_t = 173.0 ± 0.7(stat)±0.6(JES)±0.9(syst) GeV, for a total uncertainty of 1.2 GeV.

[50] Based on 3.4 fb^{-1} of $p\overline{p}$ collisions at $\sqrt{s}$ = 1.96 TeV. The result is obtained by combining the MT2 variable method and the NWA (Neutrino Weighting Algorithm). The MT2 method alone gives $m_t = 168.0^{+4.8}_{-4.0}$(stat)±2.9(syst) GeV with smaller systematic error due to small JES uncertainty.

[51] Based on 1.9 fb^{-1} in $p\overline{p}$ collisions at $\sqrt{s}$ = 1.96 TeV. The result is from the measurement using the transverse decay length of b-hadrons and that using the transverse momentum of the W decay muons, which are both insensitive to the JES (jet energy scale) uncertainty. OUR EVALUATION uses only the measurement exploiting the decay length significance which yields $166.9^{+9.5}_{-8.5}$(stat)±2.9 (syst) GeV. The measurement that uses the lepton transverse momentum is excluded from the average because of a statistical correlation with other samples.

[52] Based on 2.9 fb^{-1} of $p\overline{p}$ collisions at $\sqrt{s}$ = 1.96 TeV. The first error is from statistics and JES uncertainty, and the latter is from the other systematics. Neural-network-based kinematical selection of 6 highest E_T jets with a vtx b-tag is used to distinguish signal from background. Superseded by AALTONEN 12G.

[53] Based on 2 fb^{-1} of data at $\sqrt{s}$ = 1.96 TeV. The top mass is obtained from the measurement of the invariant mass of the lepton (e or μ) from W decays and the soft μ in b-jet. The result is insensitive to jet energy scaling.

[54] Based on 1.9 fb^{-1} of data at $\sqrt{s}$ = 1.96 TeV. The first error is from statistics and jet energy scale uncertainty, and the latter is from the other systematics. Matrix element method with effective propagators.

[55] Based on 943 pb^{-1} of data at $\sqrt{s}$ = 1.96 TeV. The first error is from statistical and jet-energy-scale uncertainties, and the latter is from other systematics. AALTONEN 09K selected 6 jet events with one or more vertex b-tags and used the tree-level matrix element to construct template models of signal and background.

[56] Based on 1.9 fb^{-1} of data at $\sqrt{s}$ = 1.96 TeV. The first error is from statistical and jet-energy-scale (JES) uncertainties, and the second is from other systematics. Events with lepton + jets and those with dilepton + jets were simultaneously fit to constrain m_t and JES. Lepton + jets data only give m_t = 171.8 ± 2.2 GeV, and dilepton data only give $m_t = 171.2^{+5.3}_{-5.1}$ GeV.

[57] Based on 2 fb^{-1} of data at $\sqrt{s}$ = 1.96 TeV. Matrix Element method. Optimal selection criteria for candidate events with two high p_T leptons, high $\not{E}_T$, and two or more jets with and without b-tag are obtained by neural network with neuroevolution technique to minimize the statistical error of m_t.

[58] Based on 2.9 fb^{-1} of data at $\sqrt{s}$ = 1.96 TeV. Mass m_t is estimated from the likelihood for the eight-fold kinematical solutions in the plane of the azimuthal angles of the two neutrino momenta.

[59] Based on 1 fb^{-1} of data at $\sqrt{s}$ = 1.96 TeV. Events with two identified leptons, and those with one lepton plus one isolated track and a b-tag were used to constrain m_t. The result is a combination of the νWT (ν Weighting Technique) result of 176.2 ± 4.8 ± 2.1 GeV and the MWT (Matrix-element Weighting Technique) result of 173.2 ± 4.9 ± 2.0 GeV.

[60] Reports measurement of $170.7^{+4.2}_{-3.9}$ ± 2.6 ± 2.4 GeV based on 1.2 fb^{-1} of data at $\sqrt{s}$ = 1.96 TeV. The last error is due to the theoretical uncertainty on $\sigma_{t\overline{t}}$. Without the cross-section constraint a top mass of $169.7^{+5.2}_{-4.9}$ ± 3.1 GeV is obtained.

[61] Template method.

[62] Result is based on 1 fb^{-1} of data at $\sqrt{s}$ = 1.96 TeV. The first error is from statistics and jet energy scale uncertainty, and the latter is from the other systematics.

[63] Based on 310 pb^{-1} of data at $\sqrt{s}$ = 1.96 TeV.

[64] Ideogram method.

[65] Based on 311 pb^{-1} of data at $\sqrt{s}$ = 1.96 TeV. Events with 4 or more jets with E_T > 15 GeV, significant missing E_T, and secondary vertex b-tag are used in the fit. About 44% of the signal acceptance is from $\tau\nu$ + 4 jets. Events with identified e or μ are vetoed to provide a statistically independent measurement.

[66] Based on 1.02 fb^{-1} of data at $\sqrt{s}$ = 1.96 TeV. Superseded by AALTONEN 12G.

[67] Based on 955 pb^{-1} of data $\sqrt{s}$ = 1.96 TeV. m_t and JES (Jet Energy Scale) are fitted simultaneously, and the first error contains the JES contribution of 1.5 GeV.

[68] Matrix element method.

[69] Based on 425 pb^{-1} of data at $\sqrt{s}$ = 1.96 TeV. The first error is a combination of statistics and JES (Jet Energy Scale) uncertainty, which has been measured simultaneously to give JES = 0.989 ± 0.029(stat).

[70] Based on 370 pb^{-1} of data at $\sqrt{s}$ = 1.96 TeV. Combined result of MWT (Matrix-element Weighting Technique) and νWT (ν Weighting Technique) analyses is 178.1 ± 6.7 ± 4.8 GeV.

[71] Based on 1.0 fb^{-1} of data at $\sqrt{s}$ = 1.96 TeV. ABULENCIA 07D improves the matrix element description by including the effects of initial-state radiation.

[72] Based on 695 pb^{-1} of data at $\sqrt{s}$ = 1.96 TeV. The transverse decay length of the b hadron is used to determine m_t, and the result is free from the JES (jet energy scale) uncertainty.

[73] Based on ∼ 400 pb^{-1} of data at $\sqrt{s}$ = 1.96 TeV. The first error includes statistical and systematic jet energy scale uncertainties, the second error is from the other systematics. The result is obtained with the b-tagging information. The result without b-tagging is $169.2^{+5.0}_{-7.4}{}^{+1.5}_{-1.4}$ GeV. Superseded by ABAZOV 08AH.

[74] Based on 318 pb^{-1} of data at $\sqrt{s}$ = 1.96 TeV.

[75] Dynamical likelihood method.

[76] Based on 340 pb^{-1} of data at $\sqrt{s}$ = 1.96 TeV.

[77] Based on 360 pb^{-1} of data at $\sqrt{s}$ = 1.96 TeV.

[78] Based on 110.2 ± 5.8 pb^{-1} at $\sqrt{s}$ = 1.8 TeV.

[79] Based on the all hadronic decays of $t\overline{t}$ pairs. Single b-quark tagging via the decay chain $b \to c \to \mu$ was used to select signal enriched multijet events. The result was obtained by the maximum likelihood method after bias correction.

[80] Obtained by re-analysis of the lepton + jets candidate events that led to ABBOTT 98F. It is based upon the maximum likelihood method which makes use of the leading order matrix elements.

[81] Based on 125 ± 7 pb^{-1} of data at $\sqrt{s}$ = 1.8 TeV.

[82] Based on ∼ 106 pb^{-1} of data at $\sqrt{s}$= 1.8 TeV.

[83] Obtained by combining the measurements in the lepton + jets [AFFOLDER 01], all-jets [ABE 97R, ABE 99B], and dilepton [ABE 99B] decay topologies.

[84] Obtained by combining the D0 result m_t (GeV) = 168.4 ± 12.3 ± 3.6 from 6 di-lepton events (see also ABBOTT 98D) and m_t (GeV) = 173.3 ± 5.6 ± 5.5 from lepton+jet events (ABBOTT 98F).

[85] Obtained by combining the CDF results of m_t (GeV)=167.4 ± 10.3 ± 4.8 from 8 dilepton events, m_t (GeV)=175.9 ± 4.8 ± 5.3 from lepton+jet events (ABE 98E), and m_t (GeV)=186.0 ± 10.0 ± 5.7 from all-jet events (ABE 97R). The systematic errors in the latter two measurements are changed in this paper.

[86] See AFFOLDER 01 for details of systematic error re-evaluation.

[87] Based on 109 ± 7 pb^{-1} of data at $\sqrt{s}$ = 1.8 TeV.

[88] See ABAZOV 04G.

[89] The updated systematic error is listed. See AFFOLDER 01, appendix C.

[90] Obtained by combining the DØ results of m_t(GeV)=168.4 ± 12.3 ± 3.6 from 6 dilepton events and m_t(GeV)=173.3 ± 5.6 ± 5.5 from 77 lepton+jet events.

[91] Obtained by combining the DØ results from dilepton and lepton+jet events, and the CDF results (ABE 99B) from dilepton, lepton+jet events, and all-jet events.

[92] Based on the first observation of all hadronic decays of $t\overline{t}$ pairs. Single b-quark tagging with jet-shape variable constraints was used to select signal enriched multi-jet events. The updated systematic error is listed. See AFFOLDER 01, appendix C.

t-Quark Mass from Cross-Section Measurements

The top quark $\overline{\text{MS}}$ or pole mass can be extracted from a measurement of $\sigma(t\overline{t})$ by using theory calculations. We quote below the $\overline{\text{MS}}$ mass. See the review "The Top Quark" and references therein for more information.

VALUE (GeV)	DOCUMENT ID		TECN	COMMENT
$162.5^{+2.1}_{-1.5}$ OUR AVERAGE				
$162.9 \pm 0.5 \pm 1.0^{+2.1}_{-1.2}$	[1] AAD	19G	ATLS	$\ell + \not{E}_T + \geq 5\ j\ (2b\text{-}j)$
$160.0^{+4.8}_{-4.3}$	[2] ABAZOV	11S	D0	$\sigma(t\overline{t})$ + theory
• • • We do not use the following data for averages, fits, limits, etc. • • •				
	[3] ABAZOV	09AG	D0	cross sects, theory + exp
	[4] ABAZOV	09R	D0	cross sects, theory + exp

[1] AAD 19G based on 20.2 fb^{-1} of data in pp collisions at $\sqrt{s}$ = 8 TeV. Normalized $t\overline{t}$ + 1-jet differential cross section as a function of $t\overline{t}j$ invariant mass is measured in the ℓ + jets mode. The unfolded parton-level distribution is compared with the NLO QCD prediction. The three errors are from statitics, systematics, and theory.

[2] Based on 5.3 fb^{-1} in $p\overline{p}$ collisions at $\sqrt{s}$ = 1.96 TeV. ABAZOV 11S uses the measured $t\overline{t}$ production cross section of $8.13^{+1.02}_{-0.90}$ pb [ABAZOV 11E] in the lepton plus jets channel to obtain the top quark $\overline{\text{MS}}$ mass by using an approximate NNLO computation (MOCH 08, LANGENFELD 09). The corresponding top quark pole mass is $167.5^{+5.4}_{-4.9}$ GeV. A different theory calculation (AHRENS 10, AHRENS 10A) is also used and yields $m_t^{\overline{\text{MS}}} = 154.5^{+5.0}_{-4.3}$ GeV.

[3] Based on 1 fb^{-1} of data at $\sqrt{s}$ = 1.96 TeV. Uses the ℓ + jets, $\ell\ell$, and $\ell\tau$ + jets channels. ABAZOV 09AG extract the pole mass of the top quark using two different calculations that yield $169.1^{+5.9}_{-5.2}$ GeV (MOCH 08, LANGENFELD 09) and $168.2^{+5.9}_{-5.4}$ GeV (KIDONAKIS 08).

[4] Based on 1 fb^{-1} of data at $\sqrt{s}$ = 1.96 TeV. Uses the $\ell\ell$ and $\ell\tau$ + jets channels. ABAZOV 09R extract the pole mass of the top quark using two different calculations that yield $173.3^{+9.8}_{-8.6}$ GeV (MOCH 08, LANGENFELD 09) and $171.5^{+9.9}_{-8.8}$ GeV (CACCIARI 08).

t-Quark Pole Mass from Cross-Section Measurements

VALUE (GeV)	DOCUMENT ID		TECN	COMMENT
172.5 ± 0.7 OUR AVERAGE				
$173.1^{+2.0}_{-2.1}$	[1] AAD	20Q	ATLS	$e + \mu$ + 1 or 2 b-jets
$171.1 \pm 0.4 \pm 0.9^{+0.7}_{-0.3}$	[2] AAD	19G	ATLS	$\ell + \not{E}_T + \geq 5\ j\ (2b\text{-}j)$
$173.2 \pm 0.9 \pm 0.8 \pm 1.2$	[3] AABOUD	17BC	ATLS	$e + \mu + \geq 1b$ jets
170.6 ± 2.7	[4] SIRUNYAN	17W	CMS	$\ell + \geq 1$j
$172.8 \pm 1.1^{+3.3}_{-3.1}$	[5] ABAZOV	16F	D0	$\ell\ell$, ℓ+jets channels
$173.8^{+1.7}_{-1.8}$	[6] KHACHATRY...	16AW	CMS	$e + \mu + \not{E}_T + \geq 0$j
$173.7^{+2.3}_{-2.1}$	[7] AAD	15BW	ATLS	$\ell + \not{E}_T + \geq 5$j (2$b$-tag)
$172.9^{+2.5}_{-2.6}$	[8] AAD	14AY	ATLS	pp at $\sqrt{s}$ = 7, 8 TeV
• • • We do not use the following data for averages, fits, limits, etc. • • •				
170.5 ± 0.8	[9] SIRUNYAN	20BV	CMS	$t\overline{t}$ normalized multi-differential cross sections
$176.7^{+3.0}_{-2.8}$	[10] CHATRCHYAN	14	CMS	pp at $\sqrt{s}$ = 7 TeV

[1] AAD 20Q based on 36.1 fb^{-1} of pp data at $\sqrt{s}$ = 13 TeV. The result is obtained from the inclusive cross section measurement and the NNLO+NNLL prediction.

[2] AAD 19G based on 20.2 fb^{-1} of data in pp collisions at $\sqrt{s}$ = 8 TeV. Normalized $t\overline{t}$ + 1-jet differential cross section as a function of $t\overline{t}j$ invariant mass is measured in the ℓ + jets mode. The unfolded parton-level distribution is compared with the NLO QCD prediction. The three errors are from statitics, systematics, and theory.

[3] AABOUD 17BC based on 20.2 fb^{-1} of pp data at $\sqrt{s}$ = 8 TeV. The pole mass is extracted from a fit of NLO predictions to eight single lepton and dilepton differential distributions, while simultaneously constraining uncertainties due to PDFs and QCD scales. The three reported uncertainties come from statistics, experimental systematics, and theoretical sources.

[4] SIRUNYAN 17W based on 2.2 fb^{-1} of pp data at $\sqrt{s}$ = 13 TeV. Events are categorized according to the jet multiplicity and the number of b-tagged jets. The pole mass is obtained from the inclusive cross section measurement and the NNLO prediction.

[5] ABAZOV 16F based on 9.7 fb^{-1} of data in $p\overline{p}$ collisions at $\sqrt{s}$ = 1.96 TeV. The result is obtained from the inclusive cross section measurement and the NNLO+NNLL prediction.

Downloaded from https://academic.oup.com/ptep/article/2022/8/083C01/6651666 by KIT Library user on 27 September 2022

[6] KHACHATRYAN 16AW based on 5.0 fb^{-1} of pp collisions at 7 TeV and 19.7 fb^{-1} at 8 TeV. The 7 TeV data include those used in CHATRCHYAN 14. The result is obtained from the inclusive cross sections.

[7] AAD 15BW based on 4.6 fb^{-1} of pp data at $\sqrt{s}$ = 7 TeV. Uses normalized differential cross section for $t\overline{t}$ + 1 jet as a function of the inverse of the invariant mass of the $t\overline{t}$ + 1 jet system. The measured cross section is corrected to the parton level. Then a fit to the data using NLO + parton shower prediction is performed.

[8] AAD 14AY used $\sigma(t\overline{t})$ for $e\mu$ events. The result is a combination of the measurements m_t = 171.4 ± 2.6 GeV based on 4.6 fb^{-1} of data at 7 TeV and m_t = 174.1 ± 2.6 GeV based on 20.3 fb^{-1} of data at 8 TeV.

[9] SIRUNYAN 20BV based on 35.9 fb^{-1} of pp data at $\sqrt{s}$ = 13 TeV. The error accounts for both experimental and theoretical uncertainties. Events containing two oppositely charged leptons are used. The pole mass is particularly sensitive to the $t\overline{t}$ invariant mass distribution close to the threshold. However, the Coulomb and soft gluon resummation effects are not taken into account, hence, an additional theoretical uncertainty of order +1 GeV is assumed.

[10] CHATRCHYAN 14 used $\sigma(t\overline{t})$ from pp collisions at $\sqrt{s}$ = 7 TeV measured in CHATRCHYAN 12AX to obtain m_t(pole) for $\alpha_s(m_Z)$ = 0.1184 ± 0.0007. The errors have been corrected in KHACHATRYAN 14K.

$m_t - m_{\overline{t}}$

Test of CPT conservation. OUR AVERAGE assumes that the systematic uncertainties are uncorrelated.

VALUE (GeV)	DOCUMENT ID		TECN	COMMENT
−0.15 ± 0.20 OUR AVERAGE	Error includes scale factor of 1.1.			
$0.83^{+1.79}_{-1.35}$	[1] TUMASYAN	21G	CMS	t-channel single top production
−0.15 ± 0.19 ± 0.09	[2] CHATRCHYAN	17	CMS	$\ell + \not{E}_T + \geq$ 4j ($\geq$ 1b j)
0.67 ± 0.61 ± 0.41	[3] AAD	14	ATLS	$\ell + \not{E}_T + \geq$ 4j ($\geq$ 2 b-tags)
−1.95 ± 1.11 ± 0.59	[4] AALTONEN	13E	CDF	$\ell + \not{E}_T + \geq$ 4j (0,1,2 b-tags)
−0.44 ± 0.46 ± 0.27	[5] CHATRCHYAN	12Y	CMS	$\ell + \not{E}_T + \geq$ 4j
0.8 ± 1.8 ± 0.5	[6] ABAZOV	11T	D0	$\ell + \not{E}_T$ + 4 jets ($\geq$ 1 b-tag)
• • • We do not use the following data for averages, fits, limits, etc. • • •				
−3.3 ± 1.4 ± 1.0	[7] AALTONEN	11K	CDF	Repl. by AALTONEN 13E
3.8 ± 3.4 ± 1.2	[8] ABAZOV	09AA	D0	$\ell + \not{E}_T$ + 4 jets ($\geq$ 1 b-tag)

[1] TUMASYAN 21G based on 35.9 fb^{-1} of pp data at $\sqrt{s}$ = 13 TeV. Events are selected by requiring 1ℓ + 2jets(1b jet) final state. An average top mass of $172.13^{+0.76}_{-0.77}$ GeV/c^2 is obtained.

[2] CHATRCHYAN 17 based on 19.6 fb^{-1} of pp data at $\sqrt{s}$ = 8 TeV and an average top mass of 172.84 ± 0.10(stat) GeV is obtained.

[3] Based on 4.7 fb^{-1} of pp data at $\sqrt{s}$ = 7 TeV and an average top mass of 172.5 GeV/c^2.

[4] Based on 8.7 fb^{-1} of $p\overline{p}$ collisions at $\sqrt{s}$ = 1.96 TeV and an average top mass of 172.5 GeV/c^2.

[5] Based on 4.96 fb^{-1} of pp data at $\sqrt{s}$ = 7 TeV. Based on the fitted m_t for ℓ^+ and ℓ^- events using the Ideogram method.

[6] Based on a matrix-element method which employs 3.6 fb^{-1} in $p\overline{p}$ collisions at $\sqrt{s}$ = 1.96 TeV.

[7] Based on a template likelihood technique which employs 5.6 fb^{-1} in $p\overline{p}$ collisions at $\sqrt{s}$ = 1.96 TeV.

[8] Based on 1 fb^{-1} of data in $p\overline{p}$ collisions at $\sqrt{s}$ = 1.96 TeV.

t-quark DECAY WIDTH

VALUE (GeV)	CL%	DOCUMENT ID		TECN	COMMENT
$1.42^{+0.19}_{-0.15}$ OUR AVERAGE		Error includes scale factor of 1.4.			
$1.76 \pm 0.33^{+0.79}_{-0.68}$		[1] AABOUD	18AZ	ATLS	$\ell + \not{E}_T + \geq$ 4j ($\geq$ 1 b)
$1.36 \pm 0.02^{+0.14}_{-0.11}$		[2] KHACHATRY...	14E	CMS	$\ell\ell + \not{E}_T$ + 2-4jets (0-2b-tag)
$2.00^{+0.47}_{-0.43}$		[3] ABAZOV	12T	D0	$\Gamma(t \to bW)/B(t \to bW)$
• • • We do not use the following data for averages, fits, limits, etc. • • •					
< 6.38	95	[4] AALTONEN	13Z	CDF	$\ell + \not{E}_T + \geq$ 4j ($\geq$ 0 b), direct
$1.99^{+0.69}_{-0.55}$		[5] ABAZOV	11B	D0	Repl. by ABAZOV 12T
> 1.21	95	[5] ABAZOV	11B	D0	$\Gamma(t \to Wb)$
< 7.6	95	[6] AALTONEN	10AC	CDF	ℓ + jets, direct
<13.1	95	[7] AALTONEN	09M	CDF	m_t(rec) distribution

[1] Based on 20.2 fb^{-1} of pp data at $\sqrt{s}$ = 8 TeV. Γ_t is measured using a template fit to the reconstructed invariant mass of the b-jet of the semileptonically decaying top quark and the corresponding lepton, and the angular distance between j_b and j_l in hadronic top decay. Signal templates are generated by reweighting events at parton-level to Breit-Wigner distribution with different Γ_t hypotheses for m_t = 172.5 GeV. The result is consistent with the NNLO SM prediction of 1.322 GeV.

[2] Based on 19.7 fb^{-1} of pp data at $\sqrt{s}$ = 8 TeV. The result is obtained by combining the measurement of $R = \Gamma(t \to Wb)/\Gamma(t \to Wq\ (q{=}b,s,d))$ and a previous CMS measurement of the t-channel single top production cross section of CHATRCHYAN 12BQ, by using the theoretical calculation of $\Gamma(t \to Wb)$ for m_t = 172.5 GeV.

[3] Based on 5.4 fb^{-1} of data in $p\overline{p}$ collisions at 1.96 TeV. $\Gamma(t \to bW) = 1.87^{+0.44}_{-0.40}$ GeV is obtained from the observed t-channel single top quark production cross section, whereas $B(t \to bW) = 0.90 \pm 0.04$ is used assuming $\sum_q B(t \to qW) = 1$. The result is valid for m_t = 172.5 GeV. See the paper for the values for m_t = 170 or 175 GeV.

[4] Based on 8.7 fb^{-1} of data. The two sided 68% CL interval is 1.10 GeV < Γ_t < 4.05 GeV for m_t = 172.5 GeV.

[5] Based on 2.3 fb^{-1} in $p\overline{p}$ collisions at $\sqrt{s}$ = 1.96 TeV. ABAZOV 11B extracted Γ_t from the partial width $\Gamma(t \to Wb) = 1.92^{+0.58}_{-0.51}$ GeV measured using the t-channel single top production cross section, and the branching fraction br$t \to Wb$ = $0.962^{+0.068}_{-0.066}$(stat)$^{+0.064}_{-0.052}$(syst). The $\Gamma(t \to Wb)$ measurement gives the 95% CL lowerbound of $\Gamma(t \to Wb)$ and hence that of Γ_t.

[6] Results are based on 4.3 fb^{-1} of data in $p\overline{p}$ collisions at $\sqrt{s}$ = 1.96 TeV. The top quark mass and the hadronically decaying W boson mass are reconstructed for each candidate events and compared with templates of different top quark width. The two sided 68% CL interval is 0.3 GeV< Γ_t < 4.4 GeV for m_t = 172.5 GeV.

[7] Based on 955 pb^{-1} of $p\overline{p}$ collision data at $\sqrt{s}$ = 1.96 TeV. AALTONEN 09M selected $t\overline{t}$ candidate events for the $\ell + \not{E}_T$ + jets channel with one or two b-tags, and examine the decay width dependence of the reconstructed m_t distribution. The result is for m_t =175 GeV, whereas the upper limit is lower for smaller m_t.

t DECAY MODES

	Mode	Fraction (Γ_i/Γ)	Confidence level
Γ_1	$Wq\,(q = b, s, d)$		
Γ_2	Wb		
Γ_3	$e\nu_e b$	(11.10 ± 0.30) %	
Γ_4	$\mu\nu_\mu b$	(11.40 ± 0.20) %	
Γ_5	$\tau\nu_\tau b$	(10.7 ± 0.5) %	
Γ_6	$q\overline{q}b$	(66.5 ± 1.4) %	
Γ_7	$\gamma q\,(q{=}u,c)$	[a] < 1.8 $\times 10^{-4}$	95%
Γ_8	$H^+ b,\ H^+ \to \tau\nu_\tau$		
	ΔT = 1 weak neutral current ($T1$) modes		
Γ_9	$Zq\,(q{=}u,c)$ $T1$	[b] < 5 $\times 10^{-4}$	95%
Γ_{10}	Hu $T1$	< 1.2 $\times 10^{-3}$	95%
Γ_{11}	Hc $T1$	< 1.1 $\times 10^{-3}$	95%
Γ_{12}	$\ell^+\overline{q}q'\,(q{=}d,s,b;\ q'{=}u,c)$ $T1$	< 1.6 $\times 10^{-3}$	95%

[a] This limit is for $\Gamma(t \to \gamma q)/\Gamma(t \to Wb)$.

[b] This limit is for $\Gamma(t \to Zq)/\Gamma(t \to Wb)$.

t BRANCHING RATIOS

$\Gamma(Wb)/\Gamma(Wq(q=b,s,d))$ — Γ_2/Γ_1

OUR AVERAGE assumes that the systematic uncertainties are uncorrelated.

VALUE	DOCUMENT ID		TECN	COMMENT
0.957 ± 0.034 OUR AVERAGE	Error includes scale factor of 1.5. See the ideogram below.			
0.87 ± 0.07	[1] AALTONEN	14G	CDF	$\ell\ell + \not{E}_T + \geq$ 2j (0,1,2 b-tag)
1.014 ± 0.003 ± 0.032	[2] KHACHATRY...	14E	CMS	$\ell\ell + \not{E}_T$ + 2,3,4j (0–2b-tag)
0.94 ± 0.09	[3] AALTONEN	13G	CDF	$\ell + \not{E}_T + \geq$ 3jets ($\geq$ 1b-tag)
0.90 ± 0.04	[4] ABAZOV	11X	D0	
• • • We do not use the following data for averages, fits, limits, etc. • • •				
$0.97^{+0.09}_{-0.08}$	[5] ABAZOV	08M	D0	ℓ + n jets with 0,1,2 b-tag
$1.03^{+0.19}_{-0.17}$	[6] ABAZOV	06K	D0	
$1.12^{+0.21}_{-0.19}{}^{+0.17}_{-0.13}$	[7] ACOSTA	05A	CDF	Repl. by AALTONEN 13G
$0.94^{+0.26}_{-0.21}{}^{+0.17}_{-0.12}$	[8] AFFOLDER	01C	CDF	

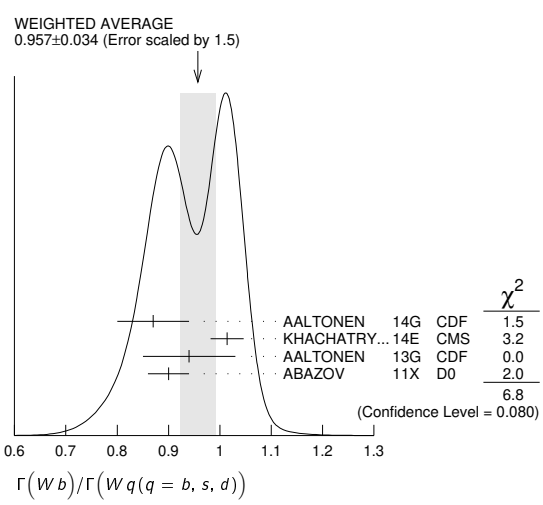

[1] Based on 8.7 fb^{-1} of data. This measurement gives $|V_{tb}| = 0.93 \pm 0.04$ and $|V_{tb}| >$ 0.85 (95% CL) in the SM.

[2] Based on 19.7 fb^{-1} of pp data at $\sqrt{s}$ = 8 TeV. The result is obtained by counting the number of b jets per $t\overline{t}$ signal events in the dilepton channel. The $t\overline{t}$ production cross section is measured to be $\sigma(t\overline{t})$ = 238 ± 1 ± 15 pb, in good agreement with the SM prediction and the latest CMS measurement of CHATRCHYAN 14F. The measurement gives R > 0.995 (95% CL), or $|V_{tb}|$ > 0.975 (95% CL) in the SM, requiring $R \leq 1$.

[3] Based on 8.7 fb^{-1} of $p\overline{p}$ collisions at $\sqrt{s}$ = 1.96 TeV. Measure the fraction of $t \to Wb$ decays simultaneously with the $t\overline{t}$ cross section. The correlation coefficient between

Downloaded from https://academic.oup.com/ptep/article/2022/8/083C01/6651666 by KIT Library user on 27 September 2022

those two measurements is -0.434. Assume unitarity of the 3×3 CKM matrix and set $|V_{tb}| > 0.89$ at 95% CL.

[4] Based on 5.4 fb^{-1} of data. The error is statistical and systematic combined. The result is a combination of 0.95 ± 0.07 from ℓ + jets channel and 0.86 ± 0.05 from $\ell\ell$ channel. $|V^{tb}| = 0.95 \pm 0.02$ follows from the result by assuming unitarity of the 3x3 CKM matrix.

[5] Result is based on 0.9 fb^{-1} of data. The 95% CL lower bound R > 0.79 gives $|V_{tb}| > 0.89$ (95% CL).

[6] ABAZOV 06K result is from the analysis of $t\overline{t} \rightarrow \ell\nu + \geq 3$ jets with 230 pb^{-1} of data at $\sqrt{s} = 1.96$ TeV. It gives R > 0.61 and $|V_{tb}|$ >0.78 at 95% CL. Superseded by ABAZOV 08M.

[7] ACOSTA 05A result is from the analysis of lepton + jets and di-lepton + jets final states of $t\overline{t}$ candidate events with $\sim$ 162 pb^{-1} of data at $\sqrt{s} = 1.96$ TeV. The first error is statistical and the second systematic. It gives R > 0.61, or $|V_{tb}| > 0.78$ at 95% CL.

[8] AFFOLDER 01C measures the top-quark decay width ratio $R = \Gamma(Wb)/\Gamma(Wq)$, where q is a d, s, or b quark, by using the number of events with multiple b tags. The first error is statistical and the second systematic. A numerical integration of the likelihood function gives $R > 0.61$ (0.56) at 90% (95%) CL. By assuming three generation unitarity, $|V_{tb}| = 0.97^{+0.16}_{-0.12}$ or $|V_{tb}| > 0.78$ (0.75) at 90% (95%) CL is obtained. The result is based on 109 pb^{-1} of data at $\sqrt{s} = 1.8$ TeV.

$\Gamma(e\nu_e b)/\Gamma_{total}$ — Γ_3/Γ

VALUE	DOCUMENT ID		TECN	COMMENT
0.111±0.003	[1] AAD	15CC	ATLS	ℓ+jets, $\ell\ell$+jets, $\ell\tau_h$+jets

[1] AAD 15CC based on 4.6 fb^{-1} of pp data at $\sqrt{s} = 7$ TeV. The original value is given by $13.3 \pm 0.4 \pm 0.5$%, which includes electrons from the decay of τ leptons. It is assumed that the top branching ratios to leptons and jets add up to one and that only SM processes contribute to the background. The event selection criteria are optimized for the $\ell\tau_h$ + jets channel. We have converted the original value to eliminate contributions of electrons from τ's, by using the AAD 15CC measurements of the branching ratios to μ and τ channels, as well as the PDG values of τ branching ratios into e and μ channels.

$\Gamma(\mu\nu_\mu b)/\Gamma_{total}$ — Γ_4/Γ

VALUE	DOCUMENT ID		TECN	COMMENT
0.114±0.002	[1] AAD	15CC	ATLS	ℓ+jets, $\ell\ell$+jets, $\ell\tau_h$+jets

[1] AAD 15CC based on 4.6 fb^{-1} of pp data at $\sqrt{s} = 7$ TeV. The original value is given by $13.4 \pm 0.3 \pm 0.5$%, which includes muons from the decay of τ leptons. It is assumed that the top branching ratios to leptons and jets add up to one and that only SM processes contribute to the background. The event selection criteria are optimized for the $\ell\tau_h$ + jets channel. We have converted the original value to eliminate contributions of muons from τ's, by using the AAD 15CC measurements of the branching ratios to μ and τ channels, as well as the PDG values of τ branching ratios into e and τ channels.

$\Gamma(\tau\nu_\tau b)/\Gamma_{total}$ — Γ_5/Γ

VALUE	DOCUMENT ID		TECN	COMMENT
0.107 ±0.005 OUR AVERAGE				
0.1050±0.0009±0.0071	[1] SIRUNYAN	20V	CMS	$\ell\tau_h$ + $\geq$ 3 jets ($\geq$ 1b-tag)
0.112 ±0.009	[2] AAD	15CC	ATLS	ℓ+jets, $\ell\ell$+jets, $\ell\tau_h$+jets
0.096 ±0.028	[3] AALTONEN	14A	CDF	ℓ+τ_h+ $\geq$ 2jets ($\geq$ 1b-tag)
• • • We do not use the following data for averages, fits, limits, etc. • • •				
	[4] ABULENCIA	06R	CDF	$\ell\tau$ + jets
	[5] ABE	97V	CDF	$\ell\tau$ + jets

[1] SIRUNYAN 20V based on 35.9 fb^{-1} of pp data at $\sqrt{s} = 13$ TeV. $t\overline{t}$ events are selected in the $t\overline{t} \rightarrow (\ell\nu_\ell)(\tau_h\nu_\tau)b\overline{b}$ mode, where τ_h refers to the hadronic decays of τ. The branching ratio is determined with respect to the $t\overline{t}$ inclusive cross section extrapolated from the light dilepton mode. The ratio of the $t\overline{t}$ production cross sections in the $\ell\tau_h$ and $\ell\ell$ channels yields $0.973 \pm 0.009 \pm 0.066$, consistent with lepton universality.

[2] AAD 15CC based on 4.6 fb^{-1} of pp data at $\sqrt{s} = 7$ TeV. The original value is given by $7.0 \pm 0.3 \pm 0.5$%, which includes only the hadronic decay of τ leptons. It is assumed that the top branching ratios to leptons and jets add up to one and that only SM processes contribute to the background. The event selection criteria are optimized for the $\ell\tau_h$ + jets channel. We have converted the original value to include leptonic decays of τ's, by using the AAD 15CC measurements of the branching ratios to e and μ channels, as well as the PDG values of τ branching ratios into e and μ channels.

[3] Based on 9 fb^{-1} of data. The measurement is in the channel $t\overline{t} \rightarrow (b\ell\nu)(b\tau\nu)$, where τ decays into hadrons (τ_h), and ℓ (e or μ) include ℓ from τ decays (τ_ℓ). The result is consistent with lepton universality.

[4] ABULENCIA 06R looked for $t\overline{t} \rightarrow (\ell\nu_\ell)(\tau\nu_\tau)b\overline{b}$ events in 194 pb^{-1} of $p\overline{p}$ collisions at $\sqrt{s} = 1.96$ TeV. 2 events are found where 1.00 ± 0.17 signal and 1.29 ± 0.25 background events are expected, giving a 95% CL upper bound for the partial width ratio $\Gamma(t \rightarrow \tau\nu q) / \Gamma_{SM}(t \rightarrow \tau\nu q) < 5.2$.

[5] ABE 97V searched for $t\overline{t} \rightarrow (\ell\nu_\ell)(\tau\nu_\tau)b\overline{b}$ events in 109 pb^{-1} of $p\overline{p}$ collisions at $\sqrt{s} = 1.8$ TeV. They observed 4 candidate events where one expects $\sim$1 signal and $\sim$2 background events. Three of the four observed events have jets identified as b candidates.

$\Gamma(q\overline{q}b)/\Gamma_{total}$ — Γ_6/Γ

VALUE	DOCUMENT ID		TECN	COMMENT
0.665±0.004±0.013	[1] AAD	15CC	ATLS	ℓ+jets, $\ell\ell$+jets, $\ell\tau_h$+jets

[1] AAD 15CC based on 4.6 fb^{-1} of pp data at $\sqrt{s} = 7$ TeV. Branching ratio of top quark into b and jets. It is assumed that the top branching ratios to leptons and jets add up to one and that only SM processes contribute to the background. The event selection criteria are optimized for the $\ell\tau_h$ + jets channel.

$\Gamma(\gamma q(q{=}u,c))/\Gamma_{total}$ — Γ_7/Γ

VALUE	CL%	DOCUMENT ID		TECN	COMMENT
<2.8 $\times 10^{-5}$	95	[1] AAD	20B	ATLS	B($t \rightarrow \gamma u$), left-handed $tu\gamma$ coupling
<6.1 $\times 10^{-5}$	95	[1] AAD	20B	ATLS	B($t \rightarrow \gamma u$), right-handed $tu\gamma$ coupling
<2.2 $\times 10^{-4}$	95	[1] AAD	20B	ATLS	B($t \rightarrow \gamma c$), left-handed $tc\gamma$ coupling
<1.8 $\times 10^{-4}$	95	[1] AAD	20B	ATLS	B($t \rightarrow \gamma c$), right-handed $tc\gamma$ coupling
<1.3 $\times 10^{-4}$	95	[2] KHACHATRY...16AS		CMS	B($t \rightarrow \gamma u$)
<1.7 $\times 10^{-3}$	95	[2] KHACHATRY...16AS		CMS	B($t \rightarrow \gamma c$)
<5.9 $\times 10^{-3}$	95	[3] CHEKANOV	03	ZEUS	B($t \rightarrow \gamma u$)
• • • We do not use the following data for averages, fits, limits, etc. • • •					
<0.0064	95	[4] AARON	09A	H1	$t \rightarrow \gamma u$
<0.0465	95	[5] ABDALLAH	04C	DLPH	B(γc or γu)
<0.0132	95	[6] AKTAS	04	H1	B($t \rightarrow \gamma u$)
<0.041	95	[7] ACHARD	02J	L3	B($t \rightarrow \gamma c$ or γu)
<0.032	95	[8] ABE	98G	CDF	$t\overline{t} \rightarrow (Wb)(\gamma c$ or $\gamma u)$

[1] AAD 20B based on 81 fb^{-1} of data in pp collisions at $\sqrt{s} = 13$ TeV. FCNC through single top production in association with a photon is searched for in the mode $\ell\gamma + \not{E}_T$ + 1j (b-tag). Anomalous FCNC left-handed and right-handed couplings are searched for, which result in different kinematical properties of top decay such as the lepton distribution. Limits are set on the $tq\gamma$ couplings in an effective field theory.

[2] KHACHATRYAN 16AS based on 19.8 fb^{-1} of data in pp collisions at $\sqrt{s} = 8$ TeV. FCNC through single top production in association with a photon is searched for in the mode $\mu + \gamma + \not{E}_T + \geq$ 1j (0,1b). Bounds on the anomalous FCNC couplings are given by $\kappa_{tu\gamma} < 0.025$ and $\kappa_{tc\gamma} < 0.091$.

[3] CHEKANOV 03 looked for single top production via FCNC in the reaction $e^{\pm}p \rightarrow e^{\pm}$ (t or $\overline{t}$) X in 130.1 pb^{-1} of data at $\sqrt{s}$=300–318 GeV. No evidence for top production and its decay into bW was found. The result is obtained for m_t=175 GeV when B(γc)=B(Zq)=0, where q is a u or c quark. Bounds on the effective t-u-γ and t-u-Z couplings are found in their Fig. 4. The conversion to the constraint listed is from private communication, E. Gallo, January 2004.

[4] AARON 09A looked for single top production via FCNC in $e^{\pm}p$ collisions at HERA with 474 pb^{-1}. The upper bound of the cross section gives the bound on the FCNC coupling $\kappa_{tu\gamma}/\Lambda < 1.03$ TeV^{-1}, which corresponds to the result for m_t = 175 GeV.

[5] ABDALLAH 04C looked for single top production via FCNC in the reaction $e^+e^- \rightarrow \overline{t}c$ or $\overline{t}u$ in 541 pb^{-1} of data at $\sqrt{s}$=189–208 GeV. No deviation from the SM is found, which leads to the bound on B($t \rightarrow \gamma q$), where q is a u or a c quark, for m_t = 175 GeV when B($t \rightarrow Zq$)=0 is assumed. The conversion to the listed bound is from private communication, O. Yushchenko, April 2005. The chiral couplings to maximize the negative interference between the virtual γ and Z exchange amplitudes.

[6] AKTAS 04 looked for single top production via FCNC in $e^{\pm}$ collisions at HERA with 118.3 pb^{-1}, and found 5 events in the e or μ channels. By assuming that they are due to statistical fluctuation, the upper bound on the $tu\gamma$ coupling $\kappa_{tu\gamma} < 0.27$ (95% CL) is obtained. The conversion to the partial width limit, when B(γc) = B(Zu) = B(Zc) = 0, is from private communication, E. Perez, May 2005.

[7] ACHARD 02J looked for single top production via FCNC in the reaction $e^+e^- \rightarrow \overline{t}c$ or $\overline{t}u$ in 634 pb^{-1} of data at $\sqrt{s}$= 189–209 GeV. No deviation from the SM is found, which leads to a bound on the top-quark decay branching fraction B(γq), where q is a u or c quark. The bound assumes B(Zq)=0 and is for m_t= 175 GeV; bounds for m_t=170 GeV and 180 GeV and B(Zq) $\neq$ 0 are given in Fig. 5 and Table 7.

[8] ABE 98G looked for $t\overline{t}$ events where one t decays into $q\gamma$ while the other decays into bW. The quoted bound is for $\Gamma(\gamma q)/\Gamma(Wb)$.

$\Gamma(H^+b,\ H^+ \rightarrow \tau\nu_\tau)/\Gamma_{total}$ — Γ_8/Γ

VALUE (%)	CL%	DOCUMENT ID		TECN
<0.25	95	[1] AABOUD	18BW	ATLS

[1] AABOUD 18BW based on 36.1 fb^{-1} of pp data at $\sqrt{s} = 13$ TeV. In the mass range of m_{H^+} = 90–160 GeV, assuming the SM cross section for the $t\overline{t}$ production, the upper limit for the branching fraction B($t \rightarrow bH^+$) $\times$ B($H^+ \rightarrow \tau\nu_\tau$) ranges between 0.25% and 0.031%.

$\Gamma(Zq(q{=}u,c))/\Gamma_{total}$ — Γ_9/Γ

Test for ΔT=1 weak neutral current. Allowed by higher-order electroweak interaction.

VALUE (units 10^{-3})	CL%	DOCUMENT ID		TECN	COMMENT
< 0.17	95	[1] AABOUD	18AT	ATLS	$t \rightarrow Zu$
< 0.24	95	[1] AABOUD	18AT	ATLS	$t \rightarrow Zc$
< 0.22	95	[2] SIRUNYAN	17E	CMS	$t \rightarrow Zu$
< 0.49	95	[2] SIRUNYAN	17E	CMS	$t \rightarrow Zc$
< 0.7	95	[3] AAD	16D	ATLS	$t \rightarrow Zq$ (q = u, c)
< 0.5	95	[4] CHATRCHYAN	14S	CMS	$t \rightarrow Zq$ (q = u, c)
• • • We do not use the following data for averages, fits, limits, etc. • • •					
< 0.6	95	[5] CHATRCHYAN	14S	CMS	$t \rightarrow Zq$ (q = u, c)
< 2.1	95	[6] CHATRCHYAN	13F	CMS	$t \rightarrow Zq$ (q = u, c)
< 7.3	95	[7] AAD	12BT	ATLS	$t\overline{t} \rightarrow \ell^+\ell^-\ell'^{\pm} + \not{E}_T$ + jets
<32	95	[8] ABAZOV	11M	D0	$t \rightarrow Zq$ (q = u, c)
<83	95	[9] AALTONEN	09AL	CDF	$t \rightarrow Zq$ (q=c)
<37	95	[10] AALTONEN	08AD	CDF	$t \rightarrow Zq$ (q = u, c)
< 1.59 $\times 10^2$	95	[11] ABDALLAH	04C	DLPH	$e^+e^- \rightarrow \overline{t}c$ or $\overline{t}u$
< 1.37 $\times 10^2$	95	[12] ACHARD	02J	L3	$e^+e^- \rightarrow \overline{t}c$ or $\overline{t}u$
< 1.4 $\times 10^2$	95	[13] HEISTER	02Q	ALEP	$e^+e^- \rightarrow \overline{t}c$ or $\overline{t}u$
< 1.37 $\times 10^2$	95	[14] ABBIENDI	01T	OPAL	$e^+e^- \rightarrow \overline{t}c$ or $\overline{t}u$
< 1.7 $\times 10^2$	95	[15] BARATE	00S	ALEP	$e^+e^- \rightarrow \overline{t}c$ or $\overline{t}u$
< 3.3 $\times 10^2$	95	[16] ABE	98G	CDF	$t\overline{t} \rightarrow (Wb)(Zc$ or $Zu)$

[1] Based on 36.1 fb^{-1} of pp data at $\sqrt{s} = 13$ TeV. The final states $t\overline{t} \rightarrow \ell^+\ell^-\ell'^{\pm}\nu$ + jets (ℓ, ℓ' = e, μ) are investigated and no significant excess over the SM background contributions is observed.

[2] SIRUNYAN 17E based on 19.7 fb^{-1} of pp data at $\sqrt{s} = 8$ TeV. The final states $t\overline{t} \rightarrow \ell^+\ell^-\ell'^{\pm}\nu$ + jets (ℓ, ℓ' = e, μ) are investigated and the cross section $\sigma(pp \rightarrow tZq \rightarrow \ell\nu b\ell^+\ell^-q) = 10^{+8}_{-7}$ fb is measured, giving no sign of FCNC decays of the top quark.

Downloaded from https://academic.oup.com/ptep/article/2022/8/083C01/6651666 by KIT Library user on 27 September 2022

[3] AAD 16D based on 20.3 fb^{-1} of pp data at $\sqrt{s}$ = 8 TeV. The FCNC decay is searched for in $t\overline{t}$ events in the final state $(bW)(qZ)$ when both W and Z decay leptonically, giving 3 charged leptons.

[4] CHATRCHYAN 14S combined search limit from this and CHATRCHYAN 13F data.

[5] Based on 19.7 fb^{-1} of pp data at $\sqrt{s}$ = 8 TeV. The flavor changing decay is searched for in $t\overline{t}$ events in the final state $(bW)(qZ)$ when both W and Z decay leptoically, giving 3 charged leptons.

[6] Based on 5.0 fb^{-1} of pp data at $\sqrt{s}$ = 7 TeV. Search for FCNC decays of the top quark in $t\overline{t} \rightarrow \ell^+\ell^-\ell'^{\pm}\nu$ + jets (ℓ, ℓ' = e, μ) final states found no excess of signal events.

[7] Based on 2.1 fb^{-1} of pp data at $\sqrt{s}$ = 7 TeV.

[8] Based on 4.1 fb^{-1} of data. ABAZOV 11M searched for FCNC decays of the top quark in $t\overline{t} \rightarrow \ell^+\ell^-\ell'^{\pm}\nu$ + jets (ℓ, ℓ' = e, μ) final states, and absence of the signal gives the bound.

[9] Based on $p\overline{p}$ data of 1.52 fb^{-1}. AALTONEN 09AL compared $t\overline{t} \rightarrow WbWb \rightarrow \ell\nu bjjb$ and $t\overline{t} \rightarrow ZcWb \rightarrow \ell\ell cjjb$ decay chains, and absence of the latter signal gives the bound. The result is for 100% longitudinally polarized Z boson and the theoretical $t\overline{t}$ production cross section The results for different Z polarizations and those without the cross section assumption are given in their Table XII.

[10] Result is based on 1.9 fb^{-1} of data at $\sqrt{s}$ = 1.96 TeV. $t\overline{t} \rightarrow WbZq$ or $ZqZq$ processes have been looked for in $Z + \geq 4$ jet events with and without b-tag. No signal leads to the bound B($t \rightarrow Zq$) < 0.037 (0.041) for m_t = 175 (170) GeV.

[11] ABDALLAH 04C looked for single top production via FCNC in the reaction $e^+e^- \rightarrow \overline{t}c$ or $\overline{t}u$ in 541 pb^{-1} of data at $\sqrt{s}$=189–208 GeV. No deviation from the SM is found, which leads to the bound on B($t \rightarrow Zq$), where q is a u or a c quark, for m_t = 175 GeV when B($t \rightarrow \gamma q$)=0 is assumed. The conversion to the listed bound is from private communication, O. Yushchenko, April 2005. The bounds on the effective t-q-γ and t-q-Z couplings are given in their Fig. 7 and Table 4, for m_t = 170–180 GeV, where most conservative bounds are found by choosing the chiral couplings to maximize the negative interference between the virtual γ and Z exchange amplitudes.

[12] ACHARD 02J looked for single top production via FCNC in the reaction $e^+e^- \rightarrow \overline{t}c$ or $\overline{t}u$ in 634 pb^{-1} of data at $\sqrt{s}$= 189–209 GeV. No deviation from the SM is found, which leads to a bound on the top-quark decay branching fraction B(Zq), where q is a u or c quark. The bound assumes B(γq)=0 and is for m_t= 175 GeV; bounds for m_t=170 GeV and 180 GeV and B(γq) $\neq$0 are given in Fig. 5 and Table 7. Table 6 gives constraints on t-c-e-e four-fermi contact interactions.

[13] HEISTER 02Q looked for single top production via FCNC in the reaction $e^+e^- \rightarrow \overline{t}c$ or $\overline{t}u$ in 214 pb^{-1} of data at $\sqrt{s}$= 204–209 GeV. No deviation from the SM is found, which leads to a bound on the branching fraction B(Zq), where q is a u or c quark. The bound assumes B(γq)=0 and is for m_t= 174 GeV. Bounds on the effective t- (c or u)-γ and t- (c or u)- Z couplings are given in their Fig. 2.

[14] ABBIENDI 01T looked for single top production via FCNC in the reaction $e^+e^- \rightarrow \overline{t}c$ or $\overline{t}u$ in 600 pb^{-1} of data at $\sqrt{s}$= 189–209 GeV. No deviation from the SM is found, which leads to bounds on the branching fractions B(Zq) and B(γq), where q is a u or c quark. The result is obtained for m_t= 174 GeV. The upper bound becomes 9.7% (20.6%) for m_t= 169 (179) GeV. Bounds on the effective t- (c or u)-γ and t- (c or u)-Z couplings are given in their Fig. 4.

[15] BARATE 00S looked for single top production via FCNC in the reaction $e^+e^- \rightarrow \overline{t}c$ or $\overline{t}u$ in 411 pb^{-1} of data at c.m. energies between 189 and 202 GeV. No deviation from the SM is found, which leads to a bound on the branching fraction. The bound assumes B(γq)=0. Bounds on the effective t- (c or u)-γ and t- (c or u)-Z couplings are given in their Fig. 4.

[16] ABE 98G looked for $t\overline{t}$ events where one t decays into three jets and the other decays into qZ with $Z \rightarrow \ell\ell$. The quoted bound is for $\Gamma(Zq)/\Gamma(Wb)$.

$\Gamma(Hu)/\Gamma_{total}$ — Γ_{10}/Γ

VALUE (units 10^{-3})	CL%	DOCUMENT ID		TECN	COMMENT
<1.2	95	[1] AABOUD	19S	ATLS	combination of $t \rightarrow Hu$ ($H \rightarrow WW$, ZZ, $\tau\tau$, $\gamma\gamma$, $b\overline{b}$)
• • • We do not use the following data for averages, fits, limits, etc. • • •					
<5.2	95	[2] AABOUD	19S	ATLS	$t \rightarrow Hu$ ($H \rightarrow bb$)
<1.7	95	[3] AABOUD	19S	ATLS	$t \rightarrow Hu$ ($H \rightarrow \tau\tau$)
<1.9	95	[4] AABOUD	18X	ATLS	$t \rightarrow Hu$ ($H \rightarrow WW$, ZZ, $\tau\tau$)
<4.7	95	[5] SIRUNYAN	18BC	CMS	$t \rightarrow Hu$ ($H \rightarrow bb$)
<2.4	95	[6] AABOUD	17AV	ATLS	$t \rightarrow Hu$ ($H \rightarrow \gamma\gamma$)
<5.5	95	[7] KHACHATRY...17I		CMS	$t \rightarrow Hu$ ($H \rightarrow WW$, ZZ, $\tau\tau$, $\gamma\gamma$, $b\overline{b}$)
<6.1	95	[8] AAD	15CO	ATLS	$t \rightarrow Hu$ ($H \rightarrow bb$)
<7.9	95	[9] AAD	14AA	ATLS	$t \rightarrow Hq$ (q=u,c; $H \rightarrow \gamma\gamma$)

[1] AABOUD 19S based on 36.1 fb^{-1} at $\sqrt{s}$ = 13 TeV of pp data. The searches using $H \rightarrow bb$ and $H \rightarrow \tau_h\tau_h$ are combined with searches in diphoton and multilepton final states. The upper limit on the Yukawa coupling $|Y_{tuH}|$ < 0.066 (95% CL) is obtained.

[2] AABOUD 19S based on 36.1 fb^{-1} at $\sqrt{s}$ = 13 TeV of pp data. Uses events with one isolated lepton and multiple jets (several of them b-tagged with high purity). A multivariate analysis is performed to distinguish the signal from backgrounds.

[3] AABOUD 19S based on 36.1 fb^{-1} at $\sqrt{s}$ = 13 TeV of pp data. Uses events with one or two hadronically decaying τ and multiple jets. A multivariate analysis is performed to distinguish the signal from backgrounds.

[4] AABOUD 18X based on 36.1 fb^{-1} at $\sqrt{s}$ = 13 TeV of pp data. $\ell\ell$(same sign) + $\geq$4j mode and $\ell\ell\ell$ + $\geq$2j mode are targeted and specialized boosted decision trees are used to distinguish signals from backgrounds.

[5] SIRUNYAN 18BC based on 35.9 fb^{-1} at $\sqrt{s}$ = 13 TeV of pp data. Two channels $pp \rightarrow tH$ and $pp \rightarrow t\overline{t}$ in final states with one isolated lepton and >=2 b jets are considered assuming a single tHu FCNC coupling. Reconstructed kinematical variables are fed into a multivariate analysis and no significant deviation is observed from the predicted background.

[6] AABOUD 17AV based on 36.1 fb^{-1} at $\sqrt{s}$ = 13 TeV of pp data. Search for $t\overline{t}$ events, where the other top quark decays hadronically or semi-leptonically.

[7] KHACHATRYAN 17I based on 19.7 fb^{-1} of pp data at $\sqrt{s}$ = 8 TeV, using the topologies $t\overline{t} \rightarrow Hq$+$Wb$, where q=u, c.

[8] AAD 15CO based on 20.3 fb^{-1} at $\sqrt{s}$ = 8 TeV of pp data. Searches for $t\overline{t}$ events, where the other top quark decays semi-leptonically. Exploits high multiplicity of b-jets and uses a likelihood discriminant. Combining with other ATLAS searches for different Higgs decay modes, B($t \rightarrow Hc$) < 0.46% and B($t \rightarrow Hu$) < 0.45% are obtained.

[9] AAD 14AA based on 4.7 fb^{-1} at $\sqrt{s}$ = 7 TeV and 20.3 fb^{-1} at $\sqrt{s}$ = 8 TeV of pp data. The upper-bound is for the sum of Br($t \rightarrow Hc$) and Br($t \rightarrow Hu$). Search for $t\overline{t}$ events, where the other top quark decays hadronically or semi-leptonically. The upper bound constrains the H-t-c Yukawa couplings $\sqrt{|Y^H_{tc_L}|^2 + |Y^H_{tc_R}|^2}$ < 0.17 (95% CL).

$\Gamma(Hc)/\Gamma_{total}$ — Γ_{11}/Γ

VALUE (units 10^{-3})	CL%	DOCUMENT ID		TECN	COMMENT
< 1.1	95	[1] AABOUD	19S	ATLS	combination of $t \rightarrow Hc$ ($H \rightarrow WW$, ZZ, $\tau\tau$, $\gamma\gamma$, $b\overline{b}$)
• • • We do not use the following data for averages, fits, limits, etc. • • •					
< 4.2	95	[2] AABOUD	19S	ATLS	$t \rightarrow Hc$ ($H \rightarrow bb$)
< 1.9	95	[3] AABOUD	19S	ATLS	$t \rightarrow Hc$ ($H \rightarrow \tau\tau$)
< 1.6	95	[4] AABOUD	18X	ATLS	$t \rightarrow Hc$ ($H \rightarrow WW$, ZZ, $\tau\tau$)
< 4.7	95	[5] SIRUNYAN	18BC	CMS	$t \rightarrow Hc$ ($H \rightarrow bb$)
< 2.2	95	[6] AABOUD	17AV	ATLS	$t \rightarrow Hc$ ($H \rightarrow \gamma\gamma$)
< 4	95	[7] KHACHATRY...17I		CMS	$t \rightarrow Hc$ ($H \rightarrow WW$, ZZ, $\tau\tau$, $\gamma\gamma$, $b\overline{b}$)
< 5.6	95	[8] AAD	15CO	ATLS	$t \rightarrow Hc$ ($H \rightarrow bb$)
< 7.9	95	[9] AAD	14AA	ATLS	$t \rightarrow Hq$ (q=u,c; $H \rightarrow \gamma\gamma$)
<13	95	[10] CHATRCHYAN	14R	CMS	$t \rightarrow Hc$ ($H \rightarrow \geq 2\ \ell$)
< 5.6	95	[11] KHACHATRY...14Q		CMS	$t \rightarrow Hc$ ($H \rightarrow \gamma\gamma$ or leptons)

[1] AABOUD 19S based on 36.1 fb^{-1} at $\sqrt{s}$ = 13 TeV of pp data. The searches using $H \rightarrow bb$ and $H \rightarrow \tau_h\tau_h$ are combined with searches in diphoton and multilepton final states. The upper limit on the Yukawa coupling $|Y_{tcH}|$ < 0.064 (95% CL) is obtained.

[2] AABOUD 19S based on 36.1 fb^{-1} at $\sqrt{s}$ = 13 TeV of pp data. Uses events with one isolated lepton and multiple jets (several of them b-tagged with high purity). A multivariate analysis is performed to distinguish the signal from backgrounds.

[3] AABOUD 19S based on 36.1 fb^{-1} at $\sqrt{s}$ = 13 TeV of pp data. Uses events with one or two hadronically decaying τ and multiple jets. A multivariate analysis is performed to distinguish the signal from backgrounds.

[4] AABOUD 18X based on 36.1 fb^{-1} at $\sqrt{s}$ = 13 TeV of pp data. $\ell\ell$(same sign) + $\geq$4j mode and $\ell\ell\ell$ + $\geq$2j mode are targeted and specialized boosted decision trees are used to distinguish signals from backgrounds.

[5] SIRUNYAN 18BC based on 35.9 fb^{-1} at $\sqrt{s}$ = 13 TeV of pp data. Two channels $pp \rightarrow tH$ and $pp \rightarrow t\overline{t}$ in final states with one isolated lepton and >=3 jets with >=2 b jets are considered assuming a single tHc FCNC coupling. Reconstructed kinematical variables are fed into a multivariate analysis and no significant deviation is observed from the predicted background.

[6] AABOUD 17AV based on 36.1 fb^{-1} at $\sqrt{s}$ = 13 TeV of pp data. Search for $t\overline{t}$ events, where the other top quark decays hadronically or semi-leptonically. The upper bound on the H-t-c Yukawa couplings is 0.090 (95% CL).

[7] KHACHATRYAN 17I based on 19.7 fb^{-1} of pp data at $\sqrt{s}$ = 8 TeV, using the topologies $t\overline{t} \rightarrow Hq$+$Wb$, where q=u, c.

[8] AAD 15CO based on 20.3 fb^{-1} at $\sqrt{s}$ = 8 TeV of pp data. Searches for $t\overline{t}$ events, where the other top quark decays semi-leptonically. Exploits high multiplicity of b-jets and uses a likelihood discriminant. Combining with other ATLAS searches for different Higgs decay modes, B($t \rightarrow Hc$) < 0.46% and B($t \rightarrow Hu$) < 0.45% are obtained.

[9] AAD 14AA based on 4.7 fb^{-1} at $\sqrt{s}$ = 7 TeV and 20.3 fb^{-1} at $\sqrt{s}$ = 8 TeV of pp data. The upper-bound is for the sum of Br($t \rightarrow Hc$) and Br($t \rightarrow Hu$). Search for $t\overline{t}$ events, where the other top quark decays hadronically or semi-leptonically. The upper bound constrains the H-t-c Yukawa couplings $\sqrt{|Y^H_{tc_L}|^2 + |Y^H_{tc_R}|^2}$ < 0.17 (95% CL).

[10] Based on 19.5 fb^{-1} of pp data at $\sqrt{s}$ = 8 TeV. Search for final states with 3 or more isolated high E_T charged leptons (ℓ = e, μ) bounds the $t \rightarrow Hc$ decay in $t\overline{t}$ events when H decays contain a pair of leptons. The upper bound constrains the H-t-c Yukawa couplings $\sqrt{|Y^H_{tc_L}|^2 + |Y^H_{tc_R}|^2}$ < 0.21 (95% CL).

[11] KHACHATRYAN 14Q based on 19.5 fb^{-1} at $\sqrt{s}$ = 8 TeV of pp data. Search for final states with $\geq$ 3 isolated charged leptons or with a photon pair accompanied by $\geq$ 1 lepton(s).

$\Gamma(\ell^+\overline{q}q'$ (q=d,s,b; q'=u,c))/Γ_{total} — Γ_{12}/Γ

VALUE	CL%	DOCUMENT ID		TECN	COMMENT
<1.6 × 10^{-3}	95	[1] CHATRCHYAN	14O	CMS	μ + dijets
• • • We do not use the following data for averages, fits, limits, etc. • • •					
<1.7 × 10^{-3}	95	[1] CHATRCHYAN	14O	CMS	e + dijets

[1] Based on 19.5 fb^{-1} of pp data at $\sqrt{s}$ = 8 TeV. Baryon number violating decays of the top quark are searched for in $t\overline{t}$ production events where one of the pair decays into hadronic three jets.

t-quark EW Couplings

W helicity fractions in top decays. F_0 is the fraction of longitudinal and F_+ the fraction of right-handed W bosons. F_{V+A} is the fraction of V+A current in top decays. The effective Lagrangian (cited by ABAZOV 08AI) has terms f_1^L and f_1^R for $V-A$ and $V+A$ couplings, f_2^L and f_2^R for tensor couplings with b_R and b_L respectively.

F_0

VALUE	DOCUMENT ID		TECN	COMMENT
0.693±0.013 OUR AVERAGE				
0.693±0.009±0.011	[1] AAD	20Y	LHC	ATLAS+CMS combined
0.726±0.066±0.067	[2] AALTONEN	13D	CDF	F_0 = B($t \rightarrow W_0 b$)
0.682±0.030±0.033	[3] CHATRCHYAN	13BH	CMS	F_0 = B($t \rightarrow W_0 b$)
0.67 ±0.07	[4] AAD	12BG	ATLS	F_0 = B($t \rightarrow W_0 b$)

Downloaded from https://academic.oup.com/ptep/article/2022/8/083C01/6651666 by KIT Library user on 27 September 2022

$0.722 \pm 0.062 \pm 0.052$	[5] AALTONEN	12Z	TEVA	$F_0 = B(t \to W_0 b)$
$0.669 \pm 0.078 \pm 0.065$	[6] ABAZOV	11C	D0	$F_0 = B(t \to W_0 b)$
$0.91 \pm 0.37 \pm 0.13$	[7] AFFOLDER	00B	CDF	$F_0 = B(t \to W_0 b)$
• • • We do not use the following data for averages, fits, limits, etc. • • •				
0.70 ± 0.05	[8] AABOUD	17BB	ATLS	$F_0 = 1 - f_1$, Repl by AAD 20Y
$0.681 \pm 0.012 \pm 0.023$	[9] KHACHATRY...	16BU	CMS	$F_0 = B(t \to W_0 b)$, Repl by AAD 20Y
$0.70 \pm 0.07 \pm 0.04$	[10] AALTONEN	10Q	CDF	Repl. by AALTONEN 12Z
$0.62 \pm 0.10 \pm 0.05$	[11] AALTONEN	09Q	CDF	Repl. by AALTONEN 10Q
$0.425 \pm 0.166 \pm 0.102$	[12] ABAZOV	08B	D0	Repl. by ABAZOV 11C
$0.85 \; {}^{+0.15}_{-0.22} \pm 0.06$	[13] ABULENCIA	07I	CDF	$F_0 = B(t \to W_0 b)$
$0.74 \; {}^{+0.22}_{-0.34}$	[14] ABULENCIA	06U	CDF	$F_0 = B(t \to W_0 b)$
0.56 ± 0.31	[15] ABAZOV	05G	D0	$F_0 = B(t \to W_0 b)$

[1] AAD 20Y based on about 20 fb^{-1} of pp data at $\sqrt{s} = 8$ TeV for each experiment. The first error stands for the sum of the statistical and background uncertainties, and the second error for the remaining systematic uncertainties. The measurements used events with one lepton and different jet multiplicities in the final state. The result is consistent with the NNLO SM prediction of 0.687 ± 0.005 for $m_t = 172.8 \pm 1.3$ GeV.

[2] Based on 8.7 fb^{-1} of data in $p\overline{p}$ collisions at $\sqrt{s} = 1.96$ TeV using $t\overline{t}$ events with $\ell + \not{E}_T + \geq 4$ jets(≥ 1 b), and under the constraint $F_0 + F_+ + F_- = 1$. The statstical errors of F_0 and F_+ are correlated with correlation coefficient $\rho(F_0, F_+) = -0.69$.

[3] Based on 5.0 fb^{-1} of pp data at $\sqrt{s} = 7$ TeV. CHATRCHYAN 13BH studied tt events with large $\not{E}_T$ and $\ell + \geq 4$ jets using a constrained kinematic fit.

[4] Based on 1.04 fb^{-1} of pp data at $\sqrt{s} = 7$ TeV. AAD 12BG studied tt events with large $\not{E}_T$ and either $\ell + \geq 4$j or $\ell\ell + \geq 2$j. The uncertainties are not independent, $\rho(F_0, F_-) = -0.96$.

[5] Based on 2.7 and 5.1 fb^{-1} of CDF data in $\ell +$ jets and dilepton channels, and 5.4 fb^{-1} of D0 data in $\ell +$ jets and dilepton channels. $F_0 = 0.682 \pm 0.035 \pm 0.046$ if $F_+ = 0.0017(1)$, while $F_+ = -0.015 \pm 0.018 \pm 0.030$ if $F_0 = 0.688(4)$, where the assumed fixed values are the SM prediction for $m_t = 173.3 \pm 1.1$ GeV and $m_W = 80.399 \pm 0.023$ GeV.

[6] Results are based on 5.4 fb^{-1} of data in $p\overline{p}$ collisions at 1.96 TeV, including those of ABAZOV 08B. Under the SM constraint of $f_0 = 0.698$ (for $m_t = 173.3$ GeV, $m_W = 80.399$ GeV), $f_+ = 0.010 \pm 0.022 \pm 0.030$ is obtained.

[7] AFFOLDER 00B studied the angular distribution of leptonic decays of W bosons in $t \to Wb$ events. The ratio F_0 is the fraction of the helicity zero (longitudinal) W bosons in the decaying top quark rest frame. $B(t \to W_+ b)$ is the fraction of positive helicity (right-handed) positive charge W bosons in the top quark decays. It is obtained by assuming the Standard Model value of F_0.

[8] AABOUD 17BB based on 20.2 fb^{-1} of pp data at $\sqrt{s} = 8$ TeV. Triple-differential decay rate of top quark in the t-channel single-top production is used to simultaneously determine five generalized Wtb couplings as well as the top polarization. No assumption is made for the other couplings. See this paper for constraints on other couplings not included here. The paper reported f_1, and we converted it to F_0.

[9] KHACHATRYAN 16BU based on 19.8 fb^{-1} of pp data at $\sqrt{s} = 8$ TeV using $t\overline{t}$ events with $\ell + \not{E}_T + \geq 4$ jets(≥ 2 b). The errors of F_0 and F_- are correlated with a correlation coefficient $\rho(F_0, F_-) = -0.87$. The result is consistent with the NNLO SM prediction of 0.687 ± 0.005 for $m_t = 172.8 \pm 1.3$ GeV.

[10] Results are based on 2.7 fb^{-1} of data in $p\overline{p}$ collisions at $\sqrt{s} = 1.96$ TeV. F_0 result is obtained by assuming $F_+ = 0$, while F_+ result is obtained for $F_0 = 0.70$, the SM value. Model independent fits for the two fractions give $F_0 = 0.88 \pm 0.11 \pm 0.06$ and $F_+ = -0.15 \pm 0.07 \pm 0.06$ with correlation coefficient of -0.59. The results are for $m_t = 175$ GeV.

[11] Results are based on 1.9 fb^{-1} of data in $p\overline{p}$ collisions at $\sqrt{s} = 1.96$ TeV. F_0 result is obtained assuming $F_+ = 0$, while F_+ result is obtained for $F_0 = 0.70$, the SM values. Model independent fits for the two fractions give $F_0 = 0.66 \pm 0.16 \pm 0.05$ and $F_+ = -0.03 \pm 0.06 \pm 0.03$.

[12] Based on 1 fb^{-1} at $\sqrt{s} = 1.96$ TeV.

[13] Based on 318 pb^{-1} of data at $\sqrt{s} = 1.96$ TeV.

[14] Based on 200 pb^{-1} of data at $\sqrt{s} = 1.96$ TeV. $t \to Wb \to \ell\nu b$ ($\ell = e$ or μ). The errors are stat + syst.

[15] ABAZOV 05G studied the angular distribution of leptonic decays of W bosons in $t\overline{t}$ candidate events with lepton + jets final states, and obtained the fraction of longitudinally polarized W under the constraint of no right-handed current, $F_+ = 0$. Based on 125 pb^{-1} of data at $\sqrt{s} = 1.8$ TeV.

F_-

VALUE	CL%	DOCUMENT ID		TECN	COMMENT
0.315 ± 0.010 OUR AVERAGE					
$0.315 \pm 0.006 \pm 0.009$		[1] AAD	20Y	LHC	ATLAS+CMS combined
$0.310 \pm 0.022 \pm 0.022$		[2] CHATRCHYAN	13BH	CMS	$F_- = B(t \to W_- b)$
0.32 ± 0.04		[3] AAD	12BG	ATLS	$F_- = B(t \to W_- b)$
• • • We do not use the following data for averages, fits, limits, etc. • • •					
$> 0.264 \pm 0.044$	95	[4] AABOUD	17BB	ATLS	$F_- = f_1(1 - f_1^+)$, Repl. by AAD 20Y
$0.323 \pm 0.008 \pm 0.014$		[5] KHACHATRY...	16BU	CMS	$F_- = B(t \to W_- b)$, Repl. by AAD 20Y

[1] AAD 20Y based on about 20 fb^{-1} of pp data at $\sqrt{s} = 8$ TeV for each experiment. The first error stands for the sum of the statistical and background uncertainties, and the second error for the remaining systematic uncertainties. The measurements used events with one lepton and different jet multiplicities in the final state. The result is consistent with the NNLO SM prediction of 0.311 ± 0.005 for $m_t = 172.8 \pm 1.3$ GeV.

[2] Based on 5.0 fb^{-1} of pp data at $\sqrt{s} = 7$ TeV. CHATRCHYAN 13BH studied tt events with large $\not{E}_T$ and $\ell + \geq 4$ jets using a constrained kinematic fit.

[3] Based on 1.04 fb^{-1} of pp data at $\sqrt{s} = 7$ TeV. AAD 12BG studied tt events with large $\not{E}_T$ and either $\ell + \geq 4$j or $\ell\ell + \geq 2$j. The uncertainties are not independent, $\rho(F_0, F_-) = -0.96$.

[4] AABOUD 17BB based on 20.2 fb^{-1} of pp data at $\sqrt{s} = 8$ TeV. Triple-differential decay rate of top quark in the t-channel single-top production is used to simultaneously determine five generalized Wtb couplings as well as the top polarization. No assumption is made for the other couplings. The authors reported $f_1 = 0.30 \pm 0.05$ and $f_1^+ < 0.120$ which we converted to $F_- = f_1(1 - f_1^+)$. See this paper for constraints on other couplings not included here.

[5] KHACHATRYAN 16BU based on 19.8 fb^{-1} of pp data at $\sqrt{s} = 8$ TeV using $t\overline{t}$ events with $\ell + \not{E}_T + \geq 4$ jets(≥ 2 b). The errors of F_0 and F_- are correlated with a correlation coefficient $\rho(F_0, F_-) = -0.87$. The result is consistent with the NNLO SM prediction of 0.311 ± 0.005 for $m_t = 172.8 \pm 1.3$ GeV.

F_+

VALUE	CL%	DOCUMENT ID		TECN	COMMENT
-0.005 ± 0.007 OUR AVERAGE					
$-0.008 \pm 0.005 \pm 0.006$		[1] AAD	20Y	LHC	ATLAS+CMS combined
$-0.045 \pm 0.044 \pm 0.058$		[2] AALTONEN	13D	CDF	$F_+ = B(t \to W_+ b)$
$0.008 \pm 0.012 \pm 0.014$		[3] CHATRCHYAN	13BH	CMS	$F_+ = B(t \to W_+ b)$
0.01 ± 0.05		[4] AAD	12BG	ATLS	$F_+ = B(t \to W_+ b)$
$0.023 \pm 0.041 \pm 0.034$		[5] ABAZOV	11C	D0	$F_+ = B(t \to W_+ b)$
0.11 ± 0.15		[6] AFFOLDER	00B	CDF	$F_+ = B(t \to W_+ b)$
• • • We do not use the following data for averages, fits, limits, etc. • • •					
$< 0.036 \pm 0.006$	95	[7] AABOUD	17BB	ATLS	$F_+ = f_1 f_1^+$, Repl. by AAD 20Y
$-0.004 \pm 0.005 \pm 0.014$		[8] KHACHATRY...	16BU	CMS	$F_+ = B(t \to W_+ b)$, Repl. by AAD 20Y
$-0.033 \pm 0.034 \pm 0.031$		[9] AALTONEN	12Z	TEVA	$F_+ = B(t \to W_+ b)$
$-0.01 \pm 0.02 \pm 0.05$		[10] AALTONEN	10Q	CDF	Repl. by AALTONEN 13D
$-0.04 \pm 0.04 \pm 0.03$		[11] AALTONEN	09Q	CDF	Repl. by AALTONEN 10Q
$0.119 \pm 0.090 \pm 0.053$		[12] ABAZOV	08B	D0	Repl. by ABAZOV 11C
$0.056 \pm 0.080 \pm 0.057$		[13] ABAZOV	07D	D0	$F_+ = B(t \to W_+ b)$
$0.05 \; {}^{+0.11}_{-0.05} \pm 0.03$		[14] ABULENCIA	07I	CDF	$F_+ = B(t \to W_+ b)$
< 0.26	95	[14] ABULENCIA	07I	CDF	$F_+ = B(t \to W_+ b)$
< 0.27	95	[15] ABULENCIA	06U	CDF	$F_+ = B(t \to W_+ b)$
$0.00 \pm 0.13 \pm 0.07$		[16] ABAZOV	05L	D0	$F_+ = B(t \to W_+ b)$
< 0.25	95	[16] ABAZOV	05L	D0	$F_+ = B(t \to W_+ b)$
< 0.24	95	[17] ACOSTA	05D	CDF	$F_+ = B(t \to W_+ b)$

[1] AAD 20Y based on about 20 fb^{-1} of pp data at $\sqrt{s} = 8$ TeV for each experiment. The first error stands for the sum of the statistical and background uncertainties, and the second error for the remaining systematic uncertainties. The measurements used events with one lepton and different jet multiplicities in the final state. The result is estimated from the measurements of F_0 and F_- assuming unitarity. The value is consistent with the NNLO SM prediction of 0.0017 ± 0.0001 for $m_t = 172.8 \pm 1.3$ GeV.

[2] Based on 8.7 fb^{-1} of data in $p\overline{p}$ collisions at $\sqrt{s} = 1.96$ TeV using $t\overline{t}$ events with $\ell + \not{E}_T + \geq 4$ jets(≥ 1 b), and under the constraint $F_0 + F_+ + F_- = 1$. The statstical errors of F_0 and F_+ are correlated with correlation coefficient $\rho(F_0, F_+) = -0.69$.

[3] Based on 5.0 fb^{-1} of pp data at $\sqrt{s} = 7$ TeV. CHATRCHYAN 13BH studied tt events with large $\not{E}_T$ and $\ell + \geq 4$ jets using a constrained kinematic fit.

[4] Based on 1.04 fb^{-1} of pp data at $\sqrt{s} = 7$ TeV. AAD 12BG studied tt events with large $\not{E}_T$ and either $\ell + \geq 4$j or $\ell\ell + \geq 2$j.

[5] Results are based on 5.4 fb^{-1} of data in $p\overline{p}$ collisions at 1.96 TeV, including those of ABAZOV 08B. Under the SM constraint of $f_0 = 0.698$ (for $m_t = 173.3$ GeV, $m_W = 80.399$ GeV), $f_+ = 0.010 \pm 0.022 \pm 0.030$ is obtained.

[6] AFFOLDER 00B studied the angular distribution of leptonic decays of W bosons in $t \to Wb$ events. The ratio F_0 is the fraction of the helicity zero (longitudinal) W bosons in the decaying top quark rest frame. $B(t \to W_+ b)$ is the fraction of positive helicity (right-handed) positive charge W bosons in the top quark decays. It is obtained by assuming the Standard Model value of F_0.

[7] AABOUD 17BB based on 20.2 fb^{-1} of pp data at $\sqrt{s} = 8$ TeV. Triple-differential decay rate of top quark in the t-channel single-top production is used to simultaneously determine five generalized Wtb couplings as well as the top polarization. No assumption is made for the other couplings. The authors reported $f_1 = 0.30 \pm 0.05$ and $f_1^+ < 0.120$ which we converted to $F_+ = f_1 f_1^+$. See this paper for constraints on other couplings not included here.

[8] KHACHATRYAN 16BU based on 19.8 fb^{-1} of pp data at $\sqrt{s} = 8$ TeV using $t\overline{t}$ events with $\ell + \not{E}_T + \geq 4$ jets(≥ 2 b). The result is consistent with the NNLO SM prediction of 0.0017 ± 0.0001 for $m_t = 172.8 \pm 1.3$ GeV.

[9] Based on 2.7 and 5.1 fb^{-1} of CDF data in $\ell +$ jets and dilepton channels, and 5.4 fb^{-1} of D0 data in $\ell +$ jets and dilepton channels. $F_0 = 0.682 \pm 0.035 \pm 0.046$ if $F_+ = 0.0017(1)$, while $F_+ = -0.015 \pm 0.018 \pm 0.030$ if $F_0 = 0.688(4)$, where the assumed fixed values are the SM prediction for $m_t = 173.3 \pm 1.1$ GeV and $m_W = 80.399 \pm 0.023$ GeV.

[10] Results are based on 2.7 fb^{-1} of data in $p\overline{p}$ collisions at $\sqrt{s} = 1.96$ TeV. F_0 result is obtained by assuming $F_+ = 0$, while F_+ result is obtained for $F_0 = 0.70$, the SM value. Model independent fits for the two fractions give $F_0 = 0.88 \pm 0.11 \pm 0.06$ and $F_+ = -0.15 \pm 0.07 \pm 0.06$ with correlation coefficient of -0.59. The results are for $m_t = 175$ GeV.

[11] Results are based on 1.9 fb^{-1} of data in $p\overline{p}$ collisions at $\sqrt{s} = 1.96$ TeV. F_0 result is obtained assuming $F_+ = 0$, while F_+ result is obtained for $F_0 = 0.70$, the SM values. Model independent fits for the two fractions give $F_0 = 0.66 \pm 0.16 \pm 0.05$ and $F_+ = -0.03 \pm 0.06 \pm 0.03$.

[12] Based on 1 fb^{-1} at $\sqrt{s} = 1.96$ TeV.

[13] Based on 370 pb^{-1} of data at $\sqrt{s} = 1.96$ TeV, using the $\ell +$ jets and dilepton decay channels. The result assumes $F_0 = 0.70$, and it gives $F_+ < 0.23$ at 95% CL.

[14] Based on 318 pb^{-1} of data at $\sqrt{s} = 1.96$ TeV.

[15] Based on 200 pb^{-1} of data at $\sqrt{s} = 1.96$ TeV. $t \to Wb \to \ell\nu b$ ($\ell = e$ or μ). The errors are stat + syst.

Downloaded from https://academic.oup.com/ptep/article/2022/8/083C01/6651666 by KIT Library user on 27 September 2022

[16] ABAZOV 05L studied the angular distribution of leptonic decays of W bosons in $t\overline{t}$ events, where one of the W's from t or $\overline{t}$ decays into e or μ and the other decays hadronically. The fraction of the "+" helicity W boson is obtained by assuming $F_0 = 0.7$, which is the generic prediction for any linear combination of V and A currents. Based on 230 ± 15 pb^{-1} of data at $\sqrt{s} = 1.96$ TeV.

[17] ACOSTA 05D measures the $m^2_{\ell+b}$ distribution in $t\overline{t}$ production events where one or both W's decay leptonically to $\ell = e$ or μ, and finds a bound on the V+A coupling of the tbW vertex. By assuming the SM value of the longitudinal W fraction $F_0 = B(t \to W_0 b) = 0.70$, the bound on F_+ is obtained. If the results are combined with those of AFFOLDER 00B, the bounds become $F_{V+A} < 0.61$ (95% CL) and $F_+ < 0.18$ (95 %CL), respectively. Based on 109 ± 7 pb^{-1} of data at $\sqrt{s} = 1.8$ TeV (run I).

F_{V+A}

VALUE	CL%	DOCUMENT ID		TECN	COMMENT
< 0.29	95	[1] ABULENCIA	07G	CDF	$F_{V+A} = B(t \to Wb_R)$
• • • We do not use the following data for averages, fits, limits, etc. • • •					
$-0.06 \pm 0.22 \pm 0.12$		[1] ABULENCIA	07G	CDF	$F_{V+A} = B(t \to Wb_R)$
< 0.80	95	[2] ACOSTA	05D	CDF	$F_{V+A} = B(t \to Wb_R)$

[1] Based on 700 pb^{-1} of data at $\sqrt{s} = 1.96$ TeV.

[2] ACOSTA 05D measures the $m^2_{\ell+b}$ distribution in $t\overline{t}$ production events where one or both W's decay leptonically to $\ell = e$ or μ, and finds a bound on the V+A coupling of the tbW vertex. By assuming the SM value of the longitudinal W fraction $F_0 = B(t \to W_0 b) = 0.70$, the bound on F_+ is obtained. If the results are combined with those of AFFOLDER 00B, the bounds become $F_{V+A} < 0.61$ (95% CL) and $F_+ < 0.18$ (95 %CL), respectively. Based on 109 ± 7 pb^{-1} of data at $\sqrt{s} = 1.8$ TeV (run I).

f_1^R

VALUE	CL%	DOCUMENT ID		TECN	COMMENT
• • • We do not use the following data for averages, fits, limits, etc. • • •					
$-0.11 < f_1^R < 0.16$	95	[1] AAD	20Y	LHC	ATLAS+CMS combined
$\lvert f_1^R/f_2^L\rvert < 0.37$	95	[2] AABOUD	17BB	ATLS	t-channel single top
$\lvert f_1^R\rvert < 0.16$	95	[3] KHACHATRY...	17G	CMS	t-channel single-t prod.
$-0.20 < \mathrm{Re}(V_{tb} f_1^R) < 0.23$	95	[4] AAD	12BG	ATLS	Constr. on Wtb vtx
$(V_{tb} f_1^R)^2 < 0.93$	95	[5] ABAZOV	12E	D0	Single-top
$\lvert f_1^R\rvert^2 < 0.30$	95	[6] ABAZOV	12I	D0	single-t + W helicity
$\lvert f_1^R\rvert^2 < 1.01$	95	[7] ABAZOV	09J	D0	$\lvert f_1^L\rvert = 1$, $\lvert f_2^L\rvert = \lvert f_2^R\rvert = 0$
$\lvert f_1^R\rvert^2 < 2.5$	95	[8] ABAZOV	08AI	D0	$\lvert f_1^L\rvert^2 = 1.8^{+1.0}_{-1.3}$

[1] AAD 20Y based on about 20 fb^{-1} of pp data at $\sqrt{s} = 8$ TeV for each experiment. The measurements used events with one lepton and different jet multiplicities in the final state. The measurements of F_0 and F_- are used to set the limit. The limit is obtained by assuming the other couplings to have their SM values.

[2] AABOUD 17BB based on 20.2 fb^{-1} of pp data at $\sqrt{s} = 8$ TeV. Triple-differential decay rate of top quark is used to simultaneously determine five generalized Wtb couplings as well as the top polarization. No assumption is made for the other couplings. See this paper for constraints on other couplings not included here.

[3] KHACHATRYAN 17G based on 5.0 and 19.7 fb^{-1} of pp data at $\sqrt{s} = 7$ and 8 TeV, respectively. A Bayesian neural network technique is used to discriminate between signal and backgrounds. This is a 95% CL exclusion limit obtained by a three-dimensional fit with simultaneous variation of (f_1^L, f_1^R, f_2^R).

[4] Based on 1.04 fb^{-1} of pp data at $\sqrt{s} = 7$ TeV. AAD 12BG studied tt events with large $\not{E}_T$ and either $\ell + \geq 4$j or $\ell\ell + \geq 2$j.

[5] Based on 5.4 fb^{-1} of data. For each value of the form factor quoted the other two are assumed to have their SM value. Their Fig. 4 shows two-dimensional posterior probability density distributions for the anomalous couplings.

[6] Based on 5.4 fb^{-1} of data in $p\overline{p}$ collisions at 1.96 TeV. Results are obtained by combining the limits from the W helicity measurements and those from the single top quark production.

[7] Based on 1 fb^{-1} of data at $p\overline{p}$ collisions $\sqrt{s} = 1.96$ TeV. Combined result of the W helicity measurement in $t\overline{t}$ events (ABAZOV 08B) and the search for anomalous tbW couplings in the single top production (ABAZOV 08AI). Constraints when f_1^L and one of the anomalous couplings are simultaneously allowed to vary are given in their Fig. 1 and Table 1.

[8] Result is based on 0.9 fb^{-1} of data at $\sqrt{s} = 1.96$ TeV. Single top quark production events are used to measure the Lorentz structure of the tbW coupling. The upper bounds on the non-standard couplings are obtained when only one non-standard coupling is allowed to be present together with the SM one, $f_1^L = V^*_{tb}$.

f_2^L

VALUE	CL%	DOCUMENT ID		TECN	COMMENT
• • • We do not use the following data for averages, fits, limits, etc. • • •					
$-0.08 < f_2^L < 0.05$	95	[1] AAD	20Y	LHC	ATLAS+CMS combined
$\lvert f_2^L/f_1^L\rvert < 0.29$	95	[2] AABOUD	17BB	ATLS	t-channel single top
$\lvert f_2^L\rvert < 0.057$	95	[3] KHACHATRY...	17G	CMS	t-channel single-t prod.
$-0.14 < \mathrm{Re}(f_2^L) < 0.11$	95	[4] AAD	12BG	ATLS	Constr. on Wtb vtx
$(V_{tb} f_2^L)^2 < 0.13$	95	[5] ABAZOV	12E	D0	Single-top
$\lvert f_2^L\rvert^2 < 0.05$	95	[6] ABAZOV	12I	D0	single-t + W helicity
$\lvert f_2^L\rvert^2 < 0.28$	95	[7] ABAZOV	09J	D0	$\lvert f_1^L\rvert = 1$, $\lvert f_1^R\rvert = \lvert f_2^R\rvert = 0$
$\lvert f_2^L\rvert^2 < 0.5$	95	[8] ABAZOV	08AI	D0	$\lvert f_1^L\rvert^2 = 1.4^{+0.6}_{-0.5}$

[1] AAD 20Y based on about 20 fb^{-1} of pp data at $\sqrt{s} = 8$ TeV for each experiment. The measurements used events with one lepton and different jet multiplicities in the final state. The measurements of F_0 and F_- are used to set the limit. The limit is obtained by assuming the other couplings to have their SM values.

[2] AABOUD 17BB based on 20.2 fb^{-1} of pp data at $\sqrt{s} = 8$ TeV. Triple-differential decay rate of top quark is used to simultaneously determine five generalized Wtb couplings as well as the top polarization. No assumption is made for the other couplings. See this paper for constraints on other couplings not included here.

[3] KHACHATRYAN 17G based on 5.0 and 19.7 fb^{-1} of pp data at $\sqrt{s} = 7$ and 8 TeV, respectively. A Bayesian neural network technique is used to discriminate between signal and backgrounds. This is a 95% CL exclusion limit obtained by a three-dimensional fit with simultaneous variation of (f_1^L, f_2^L, f_2^R).

[4] Based on 1.04 fb^{-1} of pp data at $\sqrt{s} = 7$ TeV. AAD 12BG studied tt events with large $\not{E}_T$ and either $\ell + \geq 4$j or $\ell\ell + \geq 2$j.

[5] Based on 5.4 fb^{-1} of data. For each value of the form factor quoted the other two are assumed to have their SM value. Their Fig. 4 shows two-dimensional posterior probability density distributions for the anomalous couplings.

[6] Based on 5.4 fb^{-1} of data in $p\overline{p}$ collisions at 1.96 TeV. Results are obtained by combining the limits from the W helicity measurements and those from the single top quark production.

[7] Based on 1 fb^{-1} of data at $p\overline{p}$ collisions $\sqrt{s} = 1.96$ TeV. Combined result of the W helicity measurement in $t\overline{t}$ events (ABAZOV 08B) and the search for anomalous tbW couplings in the single top production (ABAZOV 08AI). Constraints when f_1^L and one of the anomalous couplings are simultaneously allowed to vary are given in their Fig. 1 and Table 1.

[8] Result is based on 0.9 fb^{-1} of data at $\sqrt{s} = 1.96$ TeV. Single top quark production events are used to measure the Lorentz structure of the tbW coupling. The upper bounds on the non-standard couplings are obtained when only one non-standard coupling is allowed to be present together with the SM one, $f_1^L = V^*_{tb}$.

f_2^R

VALUE	CL%	DOCUMENT ID		TECN	COMMENT
• • • We do not use the following data for averages, fits, limits, etc. • • •					
$-0.04 < f_2^R < 0.02$	95	[1] AAD	20Y	LHC	ATLAS+CMS combined
$-0.12 < \mathrm{Re}(f_2^R/f_1^L) < 0.17$	95	[2] AABOUD	17BB	ATLS	t-channel single top
$-0.07 < \mathrm{Im}(f_2^R/f_1^L) < 0.06$	95	[2] AABOUD	17BB	ATLS	t-channel single top
$-0.18 < \mathrm{Im}(f_2^R) < 0.06$	95	[3] AABOUD	17I	ATLS	t-channel single top
$-0.049 < f_2^R < 0.048$	95	[4] KHACHATRY...	17G	CMS	t-channel single top
$-0.36 < \mathrm{Re}(f_2^R/f_1^L) < 0.10$	95	[5] AAD	16AK	ATLS	Single-top
$-0.17 < \mathrm{Im}(f_2^R/f_1^L) < 0.23$	95	[5] AAD	16AK	ATLS	Single-top
$-0.08 < \mathrm{Re}(f_2^R) < 0.04$	95	[6] AAD	12BG	ATLS	Constr. on Wtb vtx
$(V_{tb} f_2^R)^2 < 0.06$	95	[7] ABAZOV	12E	D0	Single-top
$\lvert f_2^R\rvert^2 < 0.12$	95	[8] ABAZOV	12I	D0	single-t + W helicity
$\lvert f_2^R\rvert^2 < 0.23$	95	[9] ABAZOV	09J	D0	$\lvert f_1^L\rvert = 1$, $\lvert f_1^R\rvert = \lvert f_2^L\rvert = 0$
$\lvert f_2^R\rvert^2 < 0.3$	95	[10] ABAZOV	08AI	D0	$\lvert f_1^L\rvert^2 = 1.4^{+0.9}_{-0.8}$

[1] AAD 20Y based on about 20 fb^{-1} of pp data at $\sqrt{s} = 8$ TeV for each experiment. The measurements used events with one lepton and different jet multiplicities in the final state. The measurements of F_0 and F_- are used to set the limit. The limit is obtained by assuming the other couplings to have their SM values.

[2] AABOUD 17BB based on 20.2 fb^{-1} of pp data at $\sqrt{s} = 8$ TeV. Triple-differential decay rate of top quark is used to simultaneously determine five generalized Wtb couplings as well as the top polarization. No assumption is made for the other couplings. See this paper for constraints on other couplings not included here.

[3] AABOUD 17I based on 20.2 fb^{-1} of pp data at $\sqrt{s} = 8$ TeV. A cut-based analysis is used to discriminate between signal and backgrounds. All anomalous couplings other than $\mathrm{Im}(f)_2^R$ are assumed to be zero. See this paper for a number of other asymmetries and measurements that are not included here.

[4] KHACHATRYAN 17G based on 5.0 and 19.7 fb^{-1} of pp data at $\sqrt{s} = 7$ and 8 TeV, respectively. A Bayesian neural network technique is used to discriminate between signal and backgrounds. This is a 95% CL exclusion limit obtained by a three-dimensional fit with simultaneous variation of (f_1^L, f_2^L, f_2^R).

[5] AAD 16AK based on 4.6 fb^{-1} of pp data at $\sqrt{s} = 7$ TeV. The results are obtained from an analysis of angular distributions of the decay products of single top quarks, assuming $f_1^R = f_2^L = 0$. The fraction of decays containing transversely polarized W is measured to be $F_+ + F_- = 0.37 \pm 0.07$.

[6] Based on 1.04 fb^{-1} of pp data at $\sqrt{s} = 7$ TeV. AAD 12BG studied tt events with large $\not{E}_T$ and either $\ell + \geq 4$j or $\ell\ell + \geq 2$j.

[7] Based on 5.4 fb^{-1} of data. For each value of the form factor quoted the other two are assumed to have their SM value. Their Fig. 4 shows two-dimensional posterior probability density distributions for the anomalous couplings.

[8] Based on 5.4 fb^{-1} of data in $p\overline{p}$ collisions at 1.96 TeV. Results are obtained by combining the limits from the W helicity measurements and those from the single top quark production.

[9] Based on 1 fb^{-1} of data at $p\overline{p}$ collisions $\sqrt{s} = 1.96$ TeV. Combined result of the W helicity measurement in $t\overline{t}$ events (ABAZOV 08B) and the search for anomalous tbW couplings in the single top production (ABAZOV 08AI). Constraints when f_1^L and one of the anomalous couplings are simultaneously allowed to vary are given in their Fig. 1 and Table 1.

[10] Result is based on 0.9 fb^{-1} of data at $\sqrt{s} = 1.96$ TeV. Single top quark production events are used to measure the Lorentz structure of the tbW coupling. The upper bounds on the non-standard couplings are obtained when only one non-standard coupling is allowed to be present together with the SM one, $f_1^L = V^*_{tb}$.

$|f_{LV} V_{tb}|$

Assumed that the top-quark-related CKM matrix elements obey the relation $|V_{td}|$, $|V_{ts}| \ll |V_{tb}|$ and a form factor f_{LV} is determined for each production mode and centre-of-mass energy.

VALUE	DOCUMENT ID		TECN	COMMENT
0.995 ± 0.021 OUR AVERAGE				
0.988 ± 0.024	[1] SIRUNYAN	20AZ	CMS	13 TeV, t-channel single top
1.02 ± 0.04 ± 0.02	[2] AABOUD	19R	LHC	ATLAS + CMS at 7, 8 TeV

Downloaded from https://academic.oup.com/ptep/article/2022/8/083C01/6651666 by KIT Library user on 27 September 2022

[1] SIRUNYAN 20AZ based on 35.9 fb^{-1} of pp data at $\sqrt{s}$ = 13 TeV. Final states enriched in single top quark t-channel events are used. Several theories beyond the standard model are considered, and by releasing all constraints among the involved parameters. Under the standard model assumption of CKM unitarity, the values are found to be $|V_{tb}| > 0.970$ and $|V_{td}|^2 + |V_{ts}|^2 < 0.057$, both at 95% CL.

[2] The combination of single-top production cross-section measurements in the t-channel, tW, and s-channel production modes from ATLAS and CMS at $\sqrt{s}$ = 7 and 8 TeV.

$|f_{LV}\sqrt{|V_{td}|^2 + |V_{ts}|^2}|$

Assumed that the top-quark-related CKM matrix elements obey the relation $|V_{td}|,|V_{ts}| \ll |V_{tb}|$ and a form factor f_{LV} is determined for each production mode andcentre-of-mass energy.

VALUE	DOCUMENT ID	TECN	COMMENT
• • • We do not use the following data for averages, fits, limits, etc. • • •			
0.24±0.12	[1] SIRUNYAN 20AZ	CMS	t-channel single top

[1] We report the square root of SIRUNYAN 20AZ result based on 35.9 fb^{-1} of pp data at $\sqrt{s}$ = 13 TeV measured $|V_{td}|^2 + |V_{ts}|^2 = 0.06 \pm 0.06$ using final states enriched in single top quark t-channel events by releasing all constraints from unitarity of the CKM matrix within the SM. Under the standard model assumption of CKM unitarity,the values are found to be $|V_{tb}| > 0.970$ and $|V_{td}|^2 + |V_{ts}|^2 < 0.057$, both at 95% CL.

Chromo-magnetic dipole moment $\mu_t = g_s\hat{\mu}_t/m_t$

VALUE	CL%	DOCUMENT ID	TECN	COMMENT
• • • We do not use the following data for averages, fits, limits, etc. • • •				
$-0.024^{+0.013}_{-0.009}{}^{+0.016}_{-0.011}$		[1] SIRUNYAN 20AM	CMS	ℓ+jets
$-0.014 < \hat{\mu}_t < 0.004$	95	[2] SIRUNYAN 19BX	CMS	$\ell\ell + \geq 2j$ ($\geq 1b$)
$-0.053 < \mathrm{Re}(\hat{\mu}_t) < 0.026$	95	[3] KHACHATRY...16AI	CMS	$\ell\ell + \geq 2j$ ($\geq 1b$)

[1] SIRUNYAN 20AM based on 35.9 fb^{-1} of pp data at $\sqrt{s}$ = 13 TeV. $t\overline{t}$ with low and high boosts are reconstructed through a fit of the kinematic distributions. The $q\overline{q}$ initial subprocess is separated using different dependencies of the distributions on the initial states, and the linearized forward-backward asymmetry is measured to be $A^{(1)}_{FB} = 0.048^{+0.095}_{-0.087}{}^{+0.020}_{-0.029}$.

[2] SIRUNYAN 19BX based on 35.9 fb^{-1} of pp data at $\sqrt{s}$ = 13 TeV. A set of parton-level normalized differential cross sections is measured to extract coefficients of the spin-dependent $t\overline{t}$ production density matrix. The coefficients are compared with the NLO MC simulations and with the NLO QCD calculation including EW corrections.

[3] KHACHATRYAN 16AI based on 19.5 fb^{-1} of pp data at $\sqrt{s}$ = 8 TeV, using lepton angular distributions as a function of the $t\overline{t}$-system kinematical variables.

Chromo-electric dipole moment $d_t = g_s\hat{d}_t/m_t$

VALUE	CL%	DOCUMENT ID	TECN	COMMENT
• • • We do not use the following data for averages, fits, limits, etc. • • •				
$|\hat{d}_t| < 0.03$	95	[1] SIRUNYAN 20AM	CMS	ℓ+jets
$-0.020 < \hat{d}_t < 0.012$	95	[2] SIRUNYAN 19BX	CMS	$\ell\ell + \geq 2j$ ($\geq 1b$)
$-0.068 < \mathrm{Im}(\hat{d}_t) < 0.067$	95	[3] KHACHATRY...16AI	CMS	$\ell\ell + \geq 2j$ ($\geq 1b$)

[1] SIRUNYAN 20AM based on 35.9 fb^{-1} of pp data at $\sqrt{s}$ = 13 TeV. $t\overline{t}$ with low and high boosts are reconstructed through a fit of the kinematic distributions. The $q\overline{q}$ initial subprocess is separated using different dependences of the distributions on the initial states, and the linearized forward-backward asymmetry is measured to be $A^{(1)}_{FB} = 0.048^{+0.095}_{-0.087}{}^{+0.020}_{-0.029}$.

[2] SIRUNYAN 19BX based on 35.9 fb^{-1} of pp data at $\sqrt{s}$ = 13 TeV. A set of parton-level normalized differential cross sections is measured to extract coefficients of the spin-dependent $t\overline{t}$ production density matrix and constrain the anomalous chromomagnetic and chromoelectric dipole moments of the top quark. The coefficients are compared with the NLO MC simulations and with the NLO QCD calculation including EW corrections.

[3] KHACHATRYAN 16AI based on 19.5 fb^{-1} of pp data at $\sqrt{s}$ = 8 TeV, using lepton angular distributions as a function of the $t\overline{t}$-system kinematical variables.

Spin Correlation in $t\overline{t}$ Production in $p\overline{p}$ Collisions

C is the correlation strength parameter, f is the ratio of events with correlated t and $\overline{t}$ spins (SM prediction: f = 1), and κ is the spin correlation coefficient. See "The Top Quark" review for more information.

VALUE	DOCUMENT ID	TECN	COMMENT
• • • We do not use the following data for averages, fits, limits, etc. • • •			
0.89±0.22	[1] ABAZOV 16A	D0	f ($\ell\ell + \geq 2$ jets, $\ell + \geq 4$ jets)
0.85±0.29	[2] ABAZOV 12B	D0	f ($\ell\ell + \geq 2$ jets, $\ell + \geq 4$ jets)
$1.15^{+0.42}_{-0.43}$	[3] ABAZOV 12B	D0	f ($\ell + \not{E}_T + \geq 4$ jets)
$0.60^{+0.50}_{-0.16}$	[4] AALTONEN 11AR	CDF	κ ($\ell + \not{E}_T + \geq 4$ jets)
$0.74^{+0.40}_{-0.41}$	[5] ABAZOV 11AE	D0	f ($\ell\ell + \not{E}_T + \geq 2$ jets)
0.10±0.45	[6] ABAZOV 11AF	D0	C ($\ell\ell + \not{E}_T + \geq 2$ jets)

[1] ABAZOV 16A based on 9.7 fb^{-1} of data. A matrix element method is used. It corresponds to evidence of spin correlation at 4.2σ and is in agreement with the NLO SM prediction $0.80^{+0.01}_{-0.02}$.

[2] This is a combination of the lepton + jets analysis presented in ABAZOV 12B and the dilepton measurement of ABAZOV 11AE. It provides a 3.1 σ evidence for the $t\overline{t}$ spin correlation.

[3] Based on 5.3 fb^{-1} of data. The error is statistical and systematic combined. A matrix element method is used.

[4] Based on 4.3 fb^{-1} of data. The measurement is based on the angular study of the top quark decay products in the helicity basis.The theory prediction is $\kappa \approx 0.40$.

[5] Based on 5.4 fb^{-1} of data using a matrix element method. The error is statistical and systematic combined. The no-correlation hypothesis is excluded at the 97.7% CL.

[6] Based on 5.4 fb^{-1} of data. The error is statistical and systematic combined. The NLO QCD prediction is C = 0.78 ± 0.03. The neutrino weighting method is used for reconstruction of kinematics.

Spin Correlation in $t\overline{t}$ Production in pp Collisions

Spin correlation, f_{SM}, measures the strength of the correlation between the spins of the pair produced $t\overline{t}$. f_{SM} =1 for the SM, while f_{SM} =0 for no spin correlation.

VALUE	DOCUMENT ID	TECN	COMMENT
• • • We do not use the following data for averages, fits, limits, etc. • • •			
0.90±0.07±0.09±0.01	[1] SIRUNYAN 19BX	CMS	C_{kk} in $\ell\ell + \geq 2j$ ($\geq 1b$)
$1.13\pm0.32\pm0.32^{+0.10}_{-0.13}$	[1] SIRUNYAN 19BX	CMS	C_{rr} in $\ell\ell + \geq 2j$ ($\geq 1b$)
1.01±0.04±0.05±0.01	[1] SIRUNYAN 19BX	CMS	C_{nn} in $\ell\ell + \geq 2j$ ($\geq 1b$)
0.94±0.17±0.26±0.01	[1] SIRUNYAN 19BX	CMS	$C_{rk}+C_{kr}$ in $\ell\ell + \geq 2j$ ($\geq 1b$)
0.98±0.03±0.04±0.01	[1] SIRUNYAN 19BX	CMS	$(C_{kk}+C_{rr}+C_{nn})/3$ in $\ell\ell + \geq 2j$ ($\geq 1b$)
$0.74\pm0.07\pm0.19^{+0.06}_{-0.08}$	[1] SIRUNYAN 19BX	CMS	$A^{lab}_{cos\phi}$ in $\ell\ell + \geq 2j$ ($\geq 1b$)
$1.05\pm0.03\pm0.08^{+0.09}_{-0.12}$	[1] SIRUNYAN 19BX	CMS	$A_{\lvert\Delta\phi(\ell\ell)\rvert}$ in $\ell\ell + \geq 2j$ ($\geq 1b$)
$1.12^{+0.12}_{-0.15}$	[2] KHACHATRY...16AI	CMS	$\ell\ell + \geq 2j$ ($\geq 1b$)
$0.72\pm0.08^{+0.15}_{-0.13}$	[3] KHACHATRY...16X	CMS	μ + 4,5j
1.20±0.05±0.13	[4] AAD 15J	ATLS	$\Delta\phi(\ell\ell)$ in $\ell\ell + \geq 2j$($\geq 1b$)
1.19±0.09±0.18	[5] AAD 14BB	ATLS	$\Delta\phi(\ell\ell)$ in $\ell\ell + \geq 2j$ events
1.12±0.11±0.22	[5] AAD 14BB	ATLS	$\Delta\phi(\ell j)$ in $\ell + \geq 4j$ events
0.87±0.11±0.14	[5,6] AAD 14BB	ATLS	S-ratio in $\ell\ell + \geq 2j$ events
0.75±0.19±0.23	[5,7] AAD 14BB	ATLS	$\cos\theta(\ell^+)\cos\theta(\ell^-)$ in $\ell\ell + \geq 2j$ events
0.83±0.14±0.18	[5,8] AAD 14BB	ATLS	$\cos\theta(\ell^+)\cos\theta(\ell^-)$ in $\ell\ell + \geq 2j$ events

[1] SIRUNYAN 19BX based on 35.9 fb^{-1} of pp data at $\sqrt{s}$ = 13 TeV. A set of parton-level normalized differential cross sections sensitive to coefficients of the spin-dependent $t\overline{t}$ production density matrix is measured. The distributions and coefficients are compared with the NLO MC simulations and with the NLO QCD calculation including EW corrections. Three errors are from statistics, experimental systematics, and theory.

[2] KHACHATRYAN 16AI based on 19.5 fb^{-1} of pp data at $\sqrt{s}$ = 8 TeV, using lepton angular distributions as a function of the $t\overline{t}$-system kinematical variables.

[3] KHACHATRYAN 16X based on 19.7 fb^{-1} of pp data at $\sqrt{s}$ = 8 TeV. Uses a template fit method. Spin correlation strength in the helicity basis is given by $A_{\rm hel} = 0.23 \pm 0.03^{+0.05}_{-0.04}$.

[4] AAD 15J based on 20.3 fb^{-1} of pp data at $\sqrt{s}$ = 8 TeV. Uses a fit including a linear superposition of $\Delta\phi$ distribution from the SM NLO simulation with coefficient f_{SM} and from $t\overline{t}$ simulation without spin correlation with coefficient $(1 - f_{SM})$.

[5] Based on 4.6 fb^{-1} of pp data at $\sqrt{s}$ =7 TeV. The results are for m_t = 172.5 GeV.

[6] The S-ratio is defined as the SM spin correlation in the like-helicity gluon-gluon collisions normalized to the no spin correlation case; see eq.(6) for the LO expression.

[7] The polar angle correlation along the helicity axis.

[8] The polar angle correlation along the direction which maximizes the correlation.

t-quark FCNC Couplings κ^{utg}/Λ and κ^{ctg}/Λ

VALUE (TeV^{-1})	CL%	DOCUMENT ID	TECN	COMMENT
• • • We do not use the following data for averages, fits, limits, etc. • • •				
<0.0041	95	[1] KHACHATRY...17G	CMS	$\lvert\kappa^{tug}\rvert/\Lambda$
<0.018	95	[1] KHACHATRY...17G	CMS	$\lvert\kappa^{tcg}\rvert/\Lambda$
<0.0058	95	[2] AAD 16AS	ATLS	κ^{tug}/Λ
<0.013	95	[2] AAD 16AS	ATLS	κ^{tcg}/Λ
<0.0069	95	[3] AAD 12BP	ATLS	t^{tug}/Λ (t^{tcg} = 0)
<0.016	95	[3] AAD 12BP	ATLS	t^{tcg}/Λ (t^{tug} = 0)
<0.013	95	[4] ABAZOV 10K	D0	κ^{tug}/Λ
<0.057	95	[4] ABAZOV 10K	D0	κ^{tcg}/Λ
<0.018	95	[5] AALTONEN 09N	CDF	κ^{tug}/Λ (κ^{tcg} = 0)
<0.069	95	[5] AALTONEN 09N	CDF	κ^{tcg}/Λ (κ^{tug} = 0)
<0.037	95	[6] ABAZOV 07V	D0	κ^{utg}/Λ
<0.15	95	[6] ABAZOV 07V	D0	κ^{ctg}/Λ

[1] KHACHATRYAN 17G based on 5.0 and 19.7 fb^{-1} of pp data at $\sqrt{s}$ = 7 and 8 TeV, respectively. t-channel single top production is used. The result corresponds to $B(t \to ug) < 2.0 \times 10^{-5}$ or $B(t \to cg) < 4.1 \times 10^{-4}$.

[2] AAD 16AS based on 20.3 fb^{-1} of pp data at $\sqrt{s}$ = 8 TeV. The results are obtained from the 95% CL upper limit on the single top-quark production $\sigma(qg \to t)\cdot B(t \to bW) < 3.4$ pb, $B(t \to ug) < 4.0 \times 10^{-5}$ and $B(t \to cg) < 20 \times 10^{-5}$.

[3] Based on 2.05 fb^{-1} of pp data at $\sqrt{s}$ = 7 TeV. The results are obtained from the 95% CL upper limit on the single top-quark production $\sigma(qg \to t)\cdot B(t \to bW) < 3.9$ pb, for q=u or q=c, $B(t \to ug) < 5.7 \times 10^{-5}$ and $B(t \to ug) < 2.7 \times 10^{-4}$.

[4] Based on 2.3 fb^{-1} of data in $p\overline{p}$ collisions at $\sqrt{s}$ = 1.96 TeV. Upper limit of single top quark production cross section 0.20 pb and 0.27 pb via FCNC t-u-g and t-c-g couplings, respectively, lead to the bounds without assuming the absence of the other coupling. $B(t \to u + g) < 2.0 \times 10^{-4}$ and $B(t \to c + g) < 3.9 \times 10^{-3}$ follow.

[5] Based on 2.2 fb^{-1} of data in $p\overline{p}$ collisions at $\sqrt{s}$ = 1.96 TeV. Upper limit of single top quark production cross section $\sigma(u(c) + g \to t) < 1.8$ pb (95% CL) via FCNC t-u-g and t-c-g couplings lead to the bounds. $B(t \to u + g) < 3.9 \times 10^{-4}$ and $B(t \to c + g) < 5.7 \times 10^{-3}$ follow.

[6] Result is based on 230 pb^{-1} of data at $\sqrt{s}$ = 1.96 TeV. Absence of single top quark production events via FCNC t-u-g and t-c-g couplings lead to the upper bounds on the dimensionled couplings, κ^{utg}/Λ and κ^{ctg}/Λ, respectively.

Downloaded from https://academic.oup.com/ptep/article/2022/8/083C01/6651666 by KIT Library user on 27 September 2022

t-Quark Yukawa Coupling from $t\overline{t}$ Kinematic Distributions in pp Collisions

The ratio of t-quark Yukawa coupling to its standard model predicted value.

VALUE	DOCUMENT ID		TECN	COMMENT
• • • We do not use the following data for averages, fits, limits, etc. • • •				
$1.16^{+0.24}_{-0.35}$	[1] SIRUNYAN	20BH	CMS	$\ell\ell$ (ℓ=e,μ) + jets ($\geq$ 2bj) + $\not{E}_T$
$1.07^{+0.34}_{-0.43}$	[2] SIRUNYAN	19BY	CMS	ℓ+jets, $t\overline{t}$ threshold

[1] SIRUNYAN 20BH based on 137 fb^{-1} of data at $\sqrt{s}$ = 13 TeV. Kinematic distributions of $t\overline{t}$ are compared with predictions by different values of the top Yukawa coupling in loop corrections, where the scaling of the SM coupling is used within the κ-framework. The $\not{E}_T$ cut applies only to the same-flavor dilepton, not $e\mu$ events.

[2] SIRUNYAN 19BY based on 35.8 fb^{-1} of data at $\sqrt{s}$ = 13 TeV. Experimental sensitivity is enhanced in the low $M_{t\overline{t}}$ region. The distributions of $M_{t\overline{t}}$, $|y_t - y_{\overline{t}}|$, and the number of reconstructed jets are compared with predictions by different Yukawa couplings which include NNLO QCD and NLO EW corrections.

$\sigma(Ht\overline{t})$ /$\sigma(Ht\overline{t})_{SM}$

VALUE	CL%	DOCUMENT ID		TECN	COMMENT
• • • We do not use the following data for averages, fits, limits, etc. • • •					
$1.43^{+0.33}_{-0.31}{}^{+0.21}_{-0.15}$		[1] AAD	20Z	ATLS	$Ht\overline{t}$ ($H \to \gamma\gamma$)
$1.38^{+0.29}_{-0.27}{}^{+0.21}_{-0.11}$		[2] SIRUNYAN	20AS	CMS	$Ht\overline{t}$ ($H \to \gamma\gamma$)
$0.72 \pm 0.24 \pm 0.38$		[3] SIRUNYAN	19R	CMS	$Ht\overline{t}$ ($H \to b\overline{b}$, $t\overline{t} \to$ ℓ+jets or dilepton)
$0.9 \pm 0.7 \pm 1.3$		[4] SIRUNYAN	18BD	CMS	$Ht\overline{t}$ ($H \to b\overline{b}$, $t\overline{t} \to$ all jets)
$1.26^{+0.31}_{-0.26}$		[5] SIRUNYAN	18L	CMS	combination of CMS
<6.7	95	[6] AAD	15	ATLS	$Ht\overline{t}$; $H \to \gamma\gamma$
2.8 ± 1.0		[7] KHACHATRY..	14H	CMS	$H \to b\overline{b}$, $\tau_h\tau_h$, $\gamma\gamma$, WW/ZZ(leptons)

[1] AAD 20Z based on 139 fb^{-1} of pp data at 13 TeV. Assuming a CP-even coupling the $t\overline{t}H$ process is observed with a significance of 5.2 σ, and the measured $\sigma_{t\overline{t}H} \cdot B_{\gamma\gamma} = 1.64^{+0.38}_{-0.36}{}^{+0.17}_{-0.14}$ fb. A CP-mixing angle $|\alpha| > 43^\circ$ is excluded at 95% CL.

[2] SIRUNYAN 20AS based on 137 fb^{-1} of pp data at 13 TeV. The $t\overline{t}H$ process is observed with a significance of 6.6 σ, and the measured $\sigma_{t\overline{t}H} \cdot B_{\gamma\gamma} = 1.56^{+0.33}_{-0.30}{}^{+0.09}_{-0.08}$ fb. The fractional contribution of the CP-odd component is measured to be $f_{CP}^{t\overline{t}H} = 0.00 \pm 0.33$.

[3] SIRUNYAN 19R based on 35.9 fb^{-1} of pp data at 13 TeV. Multivariate techniques are employed to separate the signal from the dominant $t\overline{t}$+jets background. The result is for m_H = 125 GeV. The measured ratio corresponds to a signal significance of 1.6σ above the background-only hypothesis.

[4] SIRUNYAN 18BD based on 35.9 fb^{-1} of pp data at 13 TeV. A combined fit of signal and background templates to data is performed in six event categories separated by jet and b-jet multiplicities. An upper limit of 3.8 is obtained for the cross section ratio.

[5] SIRUNYAN 18L based on up to 5.1, 19.7, and 35.9 fb^{-1} of pp data at 7, 8, and 13 TeV, respectively. An excess of events is observed, with a significance of 5.2 standard deviations, over the expectation from the background-only hypothesis. The result is for the Higgs boson mass of 125.09 GeV.

[6] Based on 4.5 fb^{-1} of data at 7 TeV and 20.3 fb^{-1} at 8 TeV. The result is for m_H = 125.4 GeV. The measurement constrains the top quark Yukawa coupling strength parameter $\kappa_t = Y_t/Y_t^{SM}$ to be $-1.3 < \kappa_t < 8.0$ (95% CL).

[7] Based on 5.1 fb^{-1} of pp data at 7 TeV and 19.7 fb^{-1} at 8 TeV. The results are obtained by assuming the SM decay branching fractions for the Higgs boson of mass 125.6 GeV. The signal strength for individual Higgs decay channels are given in Fig. 13, and the preferred region in the (κ_V, κ_f) space is given in Fig. 14.

Single t-Quark Production Cross Section in $p\overline{p}$ Collisions at $\sqrt{s}$ = 1.8 TeV

Direct probe of the tbW coupling and possible new physics at $\sqrt{s}$ = 1.8 TeV.

VALUE (pb)	CL%	DOCUMENT ID		TECN	COMMENT
• • • We do not use the following data for averages, fits, limits, etc. • • •					
<24	95	[1] ACOSTA	04H	CDF	$p\overline{p} \to tb + X$, $tqb + X$
<18	95	[2] ACOSTA	02	CDF	$p\overline{p} \to tb + X$
<13	95	[3] ACOSTA	02	CDF	$p\overline{p} \to tqb + X$

[1] ACOSTA 04H bounds single top-quark production from the s-channel W-exchange process, $q'\overline{q} \to t\overline{b}$, and the t-channel W-exchange process, $q'g \to qt\overline{b}$. Based on $\sim$ 106 pb^{-1} of data.

[2] ACOSTA 02 bounds the cross section for single top-quark production via the s-channel W-exchange process, $q'\overline{q} \to t\overline{b}$. Based on $\sim$ 106 pb^{-1} of data.

[3] ACOSTA 02 bounds the cross section for single top-quark production via the t-channel W-exchange process, $q'g \to qt\overline{b}$. Based on $\sim$ 106 pb^{-1} of data.

Single t-Quark Production Cross Section in $p\overline{p}$ Collisions at $\sqrt{s}$ = 1.96 TeV

Direct probes of the tbW coupling and possible new physics at $\sqrt{s}$ = 1.96 TeV.
OUR AVERAGE assumes that the systematic uncertainties are uncorrelated.

VALUE (pb)	CL%	DOCUMENT ID		TECN	COMMENT
• • • We do not use the following data for averages, fits, limits, etc. • • •					
$3.53^{+1.25}_{-1.16}$		[1] AALTONEN	16	CDF	s- + t-channels (0ℓ+$\not{E}_T$ + 2,3j ($\geq$ 1b-tag))
$2.25^{+0.29}_{-0.31}$		[2] AALTONEN	15H	TEVA	t-channel
$3.30^{+0.52}_{-0.40}$		[2,3] AALTONEN	15H	TEVA	s- + t-channels
$1.12^{+0.61}_{-0.57}$		[4] AALTONEN	14K	CDF	s-channel (0ℓ+$\not{E}_T$+2,3j ($\geq$ 1b-tag))
$1.41^{+0.44}_{-0.42}$		[5] AALTONEN	14L	CDF	s-channel (ℓ+$\not{E}_T$+2j ($\geq$ 1b-tag))
$1.29^{+0.26}_{-0.24}$		[6] AALTONEN	14M	TEVA	s-channel (CDF + D0)
$3.04^{+0.57}_{-0.53}$		[7] AALTONEN	14O	CDF	$s + t + Wt$ ($\ell + \not{E}_T$ + 2 or 3 jets ($\geq$ 1b-tag))
$1.10^{+0.33}_{-0.31}$		[8] ABAZOV	13O	D0	s-channel
$3.07^{+0.54}_{-0.49}$		[8] ABAZOV	13O	D0	t-channel
$4.11^{+0.60}_{-0.55}$		[8] ABAZOV	13O	D0	s- + t-channels
0.98 ± 0.63		[9] ABAZOV	11AA	D0	s-channel
2.90 ± 0.59		[9] ABAZOV	11AA	D0	t-channel
$3.43^{+0.73}_{-0.74}$		[10] ABAZOV	11AD	D0	s- + t-channels
$1.8 \ ^{+0.7}_{-0.5}$		[11] AALTONEN	10AB	CDF	s-channel
0.8 ± 0.4		[11] AALTONEN	10AB	CDF	t-channel
$4.9 \ ^{+2.5}_{-2.2}$		[12] AALTONEN	10U	CDF	$\not{E}_T$ + jets decay
$3.14^{+0.94}_{-0.80}$		[13] ABAZOV	10	D0	t-channel
1.05 ± 0.81		[13] ABAZOV	10	D0	s-channel
< 7.3	95	[14] ABAZOV	10J	D0	τ + jets decay
$2.3 \ ^{+0.6}_{-0.5}$		[15] AALTONEN	09AT	CDF	s- + t-channel
3.94 ± 0.88		[16] ABAZOV	09Z	D0	s- + t-channel
$2.2 \ ^{+0.7}_{-0.6}$		[17] AALTONEN	08AH	CDF	s- + t-channel
4.7 ± 1.3		[18] ABAZOV	08I	D0	s- + t-channel
4.9 ± 1.4		[19] ABAZOV	07H	D0	s- + t-channel
< 6.4	95	[20] ABAZOV	05P	D0	$p\overline{p} \to tb + X$
< 5.0	95	[20] ABAZOV	05P	D0	$p\overline{p} \to tqb + X$
<10.1	95	[21] ACOSTA	05N	CDF	$p\overline{p} \to tqb + X$
<13.6	95	[21] ACOSTA	05N	CDF	$p\overline{p} \to tb + X$
<17.8	95	[21] ACOSTA	05N	CDF	$p\overline{p} \to tb + X$, $tqb + X$

[1] AALTONEN 16 based on 9.5 fb^{-1} of data. This includes, as a part, the result of AALTONEN 14K. Combination of this result with that of AALTONEN 14O gives a $s + t$ cross section of $3.02^{+0.49}_{-0.48}$ pb and $|V_{tb}| > 0.84$ (95% CL).

[2] AALTONEN 15H based on 9.7 fb^{-1} of data per experiment. The result is for m_t = 172.5 GeV, and is a combination of the CDF measurements (AALTONEN 16) and the D0 measurements (ABAZOV 13O) on the t-channel single t-quark production cross section. The result is consistent with the NLO+NNLL SM prediction and gives $|V_{tb}| = 1.02^{+0.06}_{-0.05}$ and $|V_{tb}| > 0.92$ (95% CL).

[3] AALTONEN 15H is a combined measurement of s-channel single top cross section by CDF + D0. AALTONEN 14M is not included.

[4] Based on 9.45 fb^{-1} of data, using neural networks to separate signal from backgrounds. The result is for m_t = 172.5 GeV. Combination of this result with the CDF measurement in the 1 lepton channel AALTONEN 14L gives $1.36^{+0.37}_{-0.32}$ pb, consistent with the SM prediction, and is 4.2 sigma away from the background only hypothesis.

[5] Based on 9.4 fb^{-1} of data, using neural networks to separate signal from backgrounds. The result is for m_t = 172.5 GeV. The result is 3.8 sigma away from the background only hypothesis.

[6] Based on 9.7 fb^{-1} of data per experiment. The result is for m_t = 172.5 GeV, and is a combination of the CDF measurements AALTONEN 14L, AALTONEN 14K and the D0 measurement ABAZOV 13O on the s-channel single t-quark production cross section. The result is consistent with the SM prediction of 1.05 $\pm$ 0.06 pb and the significance of the observation is of 6.3 standard deviations.

[7] Based on 7.5 fb^{-1} of data. Neural network is used to discriminate signals (s-, t- and Wt-channel single top production) from backgrounds. The result is consistent with the SM prediction, and gives $|V_{tb}| = 0.95 \pm 0.09$(stat + syst)± 0.05(theory) and $|V_{tb}| > 0.78$ (95% CL). The result is for m_t = 172.5 GeV.

[8] Based on 9.7 fb^{-1} of data. Events with $\ell + \not{E}_T$ + 2 or 3 jets (1 or 2 b-tag) are analysed, assuming m_t = 172.5 GeV. The combined s- + t-channel cross section gives $|V_{tb}\ f_1^L| = 1.12^{+0.09}_{-0.08}$, or $|V_{tb}| > 0.92$ at 95% CL for $f_1^L = 1$ and a flat prior within $0 \leq |V_{tb}|^2 \leq 1$.

[9] Based on 5.4 fb^{-1} of data. The error is statistical + systematic combined. The results are for m_t = 172.5 GeV. Results for other m_t values are given in Table 2 of ABAZOV 11AA.

[10] Based on 5.4 fb^{-1} of data and for m_t = 172.5 GeV. The error is statistical + systematic combined. Results for other m_t values are given in Table III of ABAZOV 11AD. The result is obtained by assuming the SM ratio between tb (s-channel) and tqb (t-channel) productions, and gives $|V_{tb}\ f_1^L| = 1.02^{+0.10}_{-0.11}$, or $|V_{tb}| > 0.79$ at 95% CL for a flat prior within $0 < |V_{tb}|^2 < 1$.

[11] Based on 3.2 fb^{-1} of data. For combined s- + t-channel result see AALTONEN 09AT.

[12] Result is based on 2.1 fb^{-1} of data. Events with large missing E_T and jets with at least one b-jet without identified electron or muon are selected. Result is obtained when observed 2.1 σ excess over the background originates from the signal for m_t = 175 GeV, giving $|V_{tb}| = 1.24^{+0.34}_{-0.29} \pm 0.07$(theory).

[13] Result is based on 2.3 fb^{-1} of data. Events with isolated $\ell + \not{E}_T$ + 2 ,3, 4 jets with one or two b-tags are selected. The analysis assumes m_t = 170 GeV.

[14] Result is based on 4.8 fb^{-1} of data. Events with an isolated reconstructed tau lepton, missing E_T + 2, 3 jets with one or two b-tags are selected. When combined with ABAZOV 09Z result for $e + \mu$ channels, the s- and t-channels combined cross section is $3.84^{+0.89}_{-0.83}$ pb.

[15] Based on 3.2 fb^{-1} of data. Events with isolated $\ell + \not{E}_T$ + jets with at least one b-tag are analyzed and s- and t-channel single top events are selected by using the likelihood function, matrix element, neural-network, boosted decision tree, likelihood function optimized for s-channel process, and neural-networked based analysis of events with $\not{E}_T$ that has sensitivity for $W \to \tau\nu$ decays. The result is for m_t = 175 GeV, and the mean value decreases by 0.02 pb/GeV for smaller m_t. The signal has 5.0

Downloaded from https://academic.oup.com/ptep/article/2022/8/083C01/6651666 by KIT Library user on 27 September 2022

sigma significance. The result gives $|V_{tb}| = 0.91 \pm 0.11$ (stat+syst) ± 0.07 (theory), or $|V_{tb}| > 0.71$ at 95% CL.

[16] Based on 2.3 fb^{-1} of data. Events with isolated $\ell + \not{E}_T + \geq 2$ jets with 1 or 2 b-tags are analyzed and s- and t-channel single top events are selected by using boosted decision tree, Bayesian neural networks and the matrix element method. The signal has 5.0 sigma significance. The result gives $|V_{tb}| = 1.07 \pm 0.12$, or $|V_{tb}| > 0.78$ at 95% CL. The analysis assumes $m_t = 170$ GeV.

[17] Result is based on 2.2 fb^{-1} of data. Events with isolated $\ell + \not{E}_T + 2$, 3 jets with at least one b-tag are selected, and s- and t-channel single top events are selected by using likelihood, matrix element, and neural network discriminants. The result can be interpreted as $|V_{tb}| = 0.88^{+0.13}_{-0.12}$(stat + syst) ± 0.07(theory), and $|V_{tb}| > 0.66$ (95% CL) under the $|V_{tb}| < 1$ constraint.

[18] Result is based on 0.9 fb^{-1} of data. Events with isolated $\ell + \not{E}_T + 2$, 3, 4 jets with one or two b-vertex-tag are selected, and contributions from W + jets, $t\overline{t}$, s- and t-channel single top events are identified by using boosted decision trees, Bayesian neural networks, and matrix element analysis. The result can be interpreted as the measurement of the CKM matrix element $|V_{tb}| = 1.31^{+0.25}_{-0.21}$, or $|V_{tb}| > 0.68$ (95% CL) under the $|V_{tb}| < 1$ constraint.

[19] Result is based on 0.9 fb^{-1} of data. This result constrains V_{tb} to $0.68 < |V_{tb}| \leq 1$ at 95% CL.

[20] ABAZOV 05P bounds single top-quark production from either the s-channel W-exchange process, $q'\overline{q} \rightarrow t\overline{b}$, or the t-channel W-exchange process, $q'g \rightarrow q\,t\overline{b}$, based on ~ 230 pb^{-1} of data.

[21] ACOSTA 05N bounds single top-quark production from the t-channel W-exchange process ($q'g \rightarrow q\,t\overline{b}$), the s-channel W-exchange process ($q'\overline{q} \rightarrow t\overline{b}$), and from the combined cross section of t- and s-channel. Based on $\sim$ 162 pb^{-1} of data.

t-channel Single t Production Cross Section in pp Collisions at $\sqrt{s} = 7$ TeV

Direct probe of the $t\,b\,W$ coupling and possible new physics at $\sqrt{s} = 7$ TeV.

VALUE (pb)	DOCUMENT ID		TECN	COMMENT
• • • We do not use the following data for averages, fits, limits, etc. • • •				
67.5 ± 5.7	[1] AABOUD	19R	LHC	combination of ATLAS+CMS
68 ± 2 ± 8	[2] AAD	14BI	ATLS	$\ell + \not{E}_T$ + 2j or 3j
83 ± 4 $^{+20}_{-19}$	[3] AAD	12CH	ATLS	t-channel $\ell + \not{E}_T$+ (2,3)j (1b)
67.2 ± 6.1	[4] CHATRCHYAN	12BQ	CMS	t-channel $\ell + \not{E}_T$+ $\geq$ 2j (1b)
83.6 ± 29.8 ± 3.3	[5] CHATRCHYAN	11R	CMS	t-channel

[1] AABOUD 19R based on 1.17 to 5.1 fb^{-1} of data from ATLAS and CMS at 7 TeV.

[2] Based on 4.59 fb^{-1} of data, using neural networks for signal and background separation. $\sigma(tq) = 46 \pm 1 \pm 6$ pb and $\sigma(\overline{t}q) = 23 \pm 1 \pm 3$ pb are separately measured, as well as their ratio $R = \sigma(tq)/\sigma(\overline{t}q) = 2.04 \pm 0.13 \pm 0.12$. The results are for $m_t = 172.5$ GeV, and those for other m_t values are given by eq.(4) and Table IV. The measurements give $|V_{tb}| = 1.02 \pm 0.07$ or $|V_{tb}| > 0.88$ (95% CL).

[3] Based on 1.04 fb^{-1} of data. The result gives $|V_{tb}| = 1.13^{+0.14}_{-0.13}$ from the ratio σ(exp)/σ(th), where σ(th) is the SM prediction for $|V_{tb}| = 1$. The 95% CL lower bound of $|V_{tb}| > 0.75$ is found if $|V_{tb}| < 1$ is assumed. $\sigma(t) = 59^{+18}_{-16}$ pb and $\sigma(\overline{t}) = 33^{+13}_{-12}$ pb are found for the separate single t and $\overline{t}$ production cross sections, respectively. The results assume $m_t = 172.5$ GeV for the acceptance.

[4] Based on 1.17 fb^{-1} of data for $\ell = \mu$, 1.56 fb^{-1} of data for $\ell = e$ at 7 TeV collected during 2011. The result gives $|V_{tb}| = 1.020 \pm 0.046$(meas) ± 0.017(th). The 95% CL lower bound of $|V_{tb}| > 0.92$ is found if $|V_{tb}| < 1$ is assumed. The results assume $m_t = 172.5$ GeV for the acceptance.

[5] Based on 36 pb^{-1} of data. The first error is statistical + systematic combined, the second is luminosity. The result gives $|V_{tb}| = 1.114 \pm 0.22$(exp) ± 0.02(th) from the ratio σ(exp)/σ(th), where σ(th) is the SM prediction for $|V_{tb}| = 1$. The 95% CL lower bound of $|V_{tb}| > 0.62$ (0.68) is found from the 2D (BDT) analysis under the constraint $0 < |V_{tb}|^2 < 1$.

t-channel Single t Production Cross Section in pp Collisions at $\sqrt{s} = 8$ TeV

VALUE (pb)	DOCUMENT ID		TECN	COMMENT
• • • We do not use the following data for averages, fits, limits, etc. • • •				
87.7 ± 5.8	[1] AABOUD	19R	LHC	combination of ATLAS+CMS
89.6 $^{+7.1}_{-6.3}$	[2] AABOUD	17T	ATLS	ℓ+$\not{E}_T$+2 j (1b j)
83.6 ± 2.3 ± 7.4	[3] KHACHATRY...	14F	CMS	ℓ+$\not{E}_T$+ $\geq$ 2 j (1,2 b, 1 forward j)

[1] AABOUD 19R based on 12.2 to 20.3 fb^{-1} of data from ATLAS and CMS at 8 TeV.

[2] AABOUD 17T based on 20.2 fb^{-1} of data. A maximum-likelihood fit to neural-network discriminant distributions is used to separate signal and background events. Individual cross sections are measured as $\sigma(tq) = 56.7^{+4.3}_{-3.8}$ pb and $\sigma(\overline{t}q) = 32.9^{+3.0}_{-2.7}$ pb, while their ratio is given by $\sigma(tq)/\sigma(\overline{t}q) = 1.72 \pm 0.09$. A lower limit $|V_{tb}| > 0.92$ (95% CL) is obtained. Measured total and differential cross sections are described well by the SM.

[3] Based on 19.7 fb^{-1} of data. The t and $\overline{t}$ production cross sections are measured separately as $\sigma_{t-ch.}(t) = 53.8 \pm 1.5 \pm 4.4$ pb and $\sigma_{t-ch.}(\overline{t}) = 27.6 \pm 1.3 \pm 3.7$ pb, respectively, as well as their ratio $R_{t-ch} = \sigma_{t-ch.}(t)/\sigma_{t-ch.}(\overline{t}) = 1.95 \pm 0.10 \pm 0.19$, in agreement with the SM predictions. Combination with a previous CMS result at $\sqrt{s}$ = 7 TeV [CHATRCHYAN 12BQ] gives $|V_{tb}| = 0.998 \pm 0.038 \pm 0.016$. Also obtained is the ratio $R_{8/7} = \sigma_{t-ch.}(8\text{TeV})/\sigma_{t-ch.}(7\text{TeV}) = 1.24 \pm 0.08 \pm 0.12$.

s-channel Single t Production Cross Section in pp Collisions at $\sqrt{s} = 8$ TeV

VALUE (pb)	DOCUMENT ID		TECN	COMMENT
• • • We do not use the following data for averages, fits, limits, etc. • • •				
4.9 ± 1.4	[1] AABOUD	19R	LHC	ATLAS + CMS
4.8 ± 0.8 $^{+1.6}_{-1.3}$	[2] AAD	16U	ATLS	$\ell + \not{E}_T + 2b$
13.4 ± 7.3	[3] KHACHATRY...	16AZ	CMS	$\ell + \not{E}_T + 2b$
5.0 ± 4.3	[4] AAD	15A	ATLS	$\ell + \not{E}_T + 2b$

[1] AABOUD 19R based on 12.2 to 20.3 fb^{-1} of data from ATLAS and CMS at 8 TeV.

[2] AAD 16U based on 20.3 fb^{-1} of data, using a maximum-likelihood fit of a matrix element method discriminant. The same data set as in AAD 15A is used. The result corresponds to an observed significance of 3.2σ.

[3] KHACHATRYAN 16AZ based on 19.7 fb^{-1} of data, using a multivariate analysis to separate signal and backgrounds. The same method is applied to 5.1 fb^{-1} of data at $\sqrt{s} = 7$ TeV, giving 7.1 ± 8.1 pb. Combining both measurements, the observed significance is 2.5σ. A best fit value of 2.0 ± 0.9 is obtained for the combined ratio of the measured values and SM expectations.

[4] AAD 15A based on 20.3 fb^{-1} of data, using a multivariate analysis to separate signal and backgrounds. The 95% CL upper bound of the cross section is 14.6 pb. The results are consistent with the SM prediction of 5.61 ± 0.22 pb at approximate NNLO.

t-channel Single t Production Cross Section in pp Collisions at $\sqrt{s} = 13$ TeV

VALUE (pb)	DOCUMENT ID		TECN	COMMENT
• • • We do not use the following data for averages, fits, limits, etc. • • •				
130 ± 1 ± 19	[1] SIRUNYAN	20D	CMS	$\sigma(tq)$, ℓ+$\not{E}_T$+ $\geq 2\,j$
77 ± 1 ± 12	[1] SIRUNYAN	20D	CMS	$\sigma(\overline{t}q)$, ℓ+$\not{E}_T$+ $\geq 2\,j$
156 ± 5 ± 27 ± 3	[2] AABOUD	17H	ATLS	$\sigma(tq)$, ℓ+$\not{E}_T$+2 j (1b, 1 forward j)
91 ± 4 ± 18 ± 2	[2] AABOUD	17H	ATLS	$\sigma(\overline{t}q)$, ℓ+$\not{E}_T$+2 j (1b, 1 forward j)
154 ± 8 ± 9 ± 19 ± 4	[3] SIRUNYAN	17AA	CMS	$\sigma(tq)$, μ+ $\geq$ 2 j (1b)
85 ± 10 ± 4 ± 11 ± 2	[3] SIRUNYAN	17AA	CMS	$\sigma(\overline{t}q)$, μ+ $\geq$ 2 j (1b)

[1] SIRUNYAN 20D based on 35.9 fb^{-1} of data. Different categories of jet and b jet multiplicity and multivariate discriminators are used to separate signal and background events. The cross section ratio is measured to be $\sigma(tq)/\sigma(\overline{t}q) = 1.68 \pm 0.02 \pm 0.05$. CKM matrix element is obtained as $|f_{LV} V_{tb}| = 0.98 \pm 0.07$(exp) ± 0.02(theo) where f_{LV} is an anomalous form factor. All results are in agreement with the SM.

[2] AABOUD 17H based on 3.2 fb^{-1} of data. A maximum-likelihood fit to neural-network discriminant distributions is used to separate signal and background events. The third error is for luminosity. The cross section ratio is measured to be $\sigma(tq)/\sigma(\overline{t}q) = 1.72 \pm 0.09 \pm 0.18$. A lower limit $|V_{tb}| > 0.84$ (95% CL) is obtained. All results are in agreement with the SM.

[3] SIRUNYAN 17AA based on 2.2 fb^{-1} of data. A multivariate discriminator is used to separate signal and background events. The four errors are from statitics, experimental systematics, theory, and luminosity. The cross section ratio is measured to be $\sigma(tq)/\sigma(\overline{t}q) = 1.81 \pm 0.18 \pm 0.15$. CKM matrix element is obtained as $|V_{tb}| = 1.05 \pm 0.07$(exp) ± 0.02(theo). All results are in agreement with the SM.

$t\overline{t}H$ Production Cross Section in pp Collisions at $\sqrt{s} = 13$ TeV

VALUE (fb)	DOCUMENT ID		TECN	COMMENT
• • • We do not use the following data for averages, fits, limits, etc. • • •				
670 ± 90 $^{+110}_{-100}$	[1] AABOUD	18BK	ATLS	$H \rightarrow b\overline{b}$, WW^* $\tau\tau$, $\gamma\gamma$, ZZ^*

[1] AABOUD 18BK based on 79.8 fb^{-1} of data. The observed significance is 5.8σ relative to the background-only hypothesis. The measurement is consistent with the NLO SM prediction of 507 $^{+35}_{-50}$ fb. See Table 3 and Fig. 5 for measurements of individual modes. Combined with the measurements at 7 and 8 TeV, the observed significance is 6.3σ.

Wt Production Cross Section in pp Collisions at $\sqrt{s} = 7$ TeV

VALUE (pb)	DOCUMENT ID		TECN	COMMENT
• • • We do not use the following data for averages, fits, limits, etc. • • •				
16.3 ± 4.1	[1] AABOUD	19R	LHC	ATLAS + CMS combined
16 $^{+5}_{-4}$	[2] CHATRCHYAN	13C	CMS	t+W channel, 2ℓ+$\not{E}_T$+1b

[1] AABOUD 19R based on 1.17 to 5.1 fb^{-1} of data from ATLAS and CMS at 7 TeV.

[2] Based on 4.9 fb^{-1} of data. The result gives $V_{tb} = 1.01^{+0.16}_{-0.13}$(exp) $^{+0.03}_{-0.04}$(th). $V_{tb} > 0.79$ (95% CL) if $V_{tb} < 1$ is assumed. The results assume $m_t = 172.5$ GeV for the acceptance.

Wt Production Cross Section in pp Collisions at $\sqrt{s} = 8$ TeV

VALUE (pb)	DOCUMENT ID		TECN	COMMENT
• • • We do not use the following data for averages, fits, limits, etc. • • •				
26 ± 7	[1] AAD	21AT	ATLS	ℓ+ $\geq$ 3j
23.1 ± 3.6	[2] AABOUD	19R	LHC	ATLAS + CMS combined
23.0 ± 1.3 $^{+3.2}_{-3.5}$ ± 1.1	[3] AAD	16B	ATLS	2ℓ+$\not{E}_T$+1b
23.4 ± 5.4	[4] CHATRCHYAN	14AC	CMS	t+W channel, 2ℓ+$\not{E}_T$+1b

[1] AAD 21AT based on 20.2 fb^{-1} of data. In this single lepton channel, only single neutrino is emitted, so that both W and t can be reconstructed. A neural network is trained to separate signal from background. The measured cross section agrees with the NLO+NNLL SM prediction of 22.4 ± 0.6(scale) ± 1.4(PDF) pb.

[2] AABOUD 19R based on 12.2 to 20.3 fb^{-1} of data from ATLAS and CMS at 8 TeV.

[3] AAD 16B based on 20.3 fb^{-1} of data. The result gives $|V_{tb}| = 1.01 \pm 0.10$ and $|V_{tb}| > 0.80$ (95% CL) without assuming unitarity of the CKM matrix. The results assume m_t = 172.5 GeV for the acceptance.

[4] Based on 12.2 fb^{-1} of data. Events with two oppositely charged leptons, large $\not{E}_T$ and a b-tagged jet are selected, and a multivariate analysis is used to separate the signal from the backgrounds. The result is consistent with the SM prediction of 22.2 ± 0.6(scale) ± 1.4(PDF) pb at approximate NNLO.

Wt Production Cross Section in pp Collisions at $\sqrt{s} = 13$ TeV

VALUE (pb)	DOCUMENT ID		TECN	COMMENT
• • • We do not use the following data for averages, fits, limits, etc. • • •				
89 ± 4 ± 12	[1] TUMASYAN	21E	CMS	1ℓ + jets
94 ± 10 $^{+28}_{-22}$ ± 2	[2] AABOUD	18H	ATLS	$\ell^+\ell^-$ + $\geq$ 1j
63.1 ± 1.8 ± 6.4 ± 2.1	[3] SIRUNYAN	18DL	CMS	$e^{\pm}\mu^{\mp}$ + $\geq$ 1j(b-tag)

Downloaded from https://academic.oup.com/ptep/article/2022/8/083C01/6651666 by KIT Library user on 27 September 2022

[1] TUMASYAN 21E based on 36 fb^{-1} of data. A boosted decision tree is used to separate the signal from the dominant $t\overline{t}$ backgrounds. The result corresponds to an observation with a significance exceeding 5 σ and is consistent with the NNLO QCD prediction of 71.7 $\pm$ 1.8(scale) $\pm$ 3.4(PDF) pb or with the approximate NNNLO SM prediction of 79.5 $^{+1.9}_{-1.8}$(scale) $^{+2.0}_{-1.4}$(PDF) pb.

[2] AABOUD 18H based on 3.2 fb^{-1} of data. The last error is from luminosity. A multivariate analysis is used to separate the signal from the backgrounds. The result is consistent with the NLO+NNLL SM prediction of 71.7 $\pm$ 1.8(scale) $\pm$ 3.4(PDF) pb.

[3] SIRUNYAN 18DL based on 35.9 fb^{-1} of data. The last error is from luminosity. A multivariate analysis is used to separate the signal from the backgrounds. The result is consistent with the NLO+NNLL SM prediction of 71.7 $\pm$ 1.8(scale) $\pm$ 3.4(PDF) pb.

Zt Production Cross Section in pp Collisions at $\sqrt{s}$ = 13 TeV

VALUE (fb)	DOCUMENT ID		TECN	COMMENT
• • • We do not use the following data for averages, fits, limits, etc. • • •				
97 $\pm$ 13 $\pm$ 7	[1] AAD	20AB	ATLS	3ℓ + 1,2j + 1bj
111 $\pm$ 13 $^{+11}_{-9}$	[2] SIRUNYAN	19BF	CMS	3ℓ + $\geq$ 2j ($\geq$ 1bj)
600 $\pm$ 170 $\pm$ 140	[3] AABOUD	18AE	ATLS	3ℓ + 1j + 1bj
123 $^{+33}_{-31}$ $^{+29}_{-23}$	[4] SIRUNYAN	18Z	CMS	3ℓ + 1j + 1bj

[1] AAD 20AB based on 139 fb^{-1} of data at 13 TeV. Neural networks are used to discriminate tZq signal from backgrounds. The result is for the cross section $\sigma(pp \rightarrow t\ell^+\ell^- q)$, including non-resonant dilepton pairs, for dilepton invariant masses above 30 GeV and is consistent with the NLO SM prediction of 102 $^{+5}_{-2}$ fb.

[2] SIRUNYAN 19BF based on 77.4 fb^{-1} of data. Two BDT's are used in the analysis: one to discriminate prompt leptons from non-prompt ones; and one to discriminate tZq signal from backgrounds. The result is for the cross section $\sigma(pp \rightarrow tZq \rightarrow t\ell^+\ell^- q)$ for dilepton invariant masses above 30 GeV and is consistent with the NLO SM prediction of 94.2 $\pm$ 3.1 fb.

[3] AABOUD 18AE based on 36.1 fb^{-1} of data. A multivariate analysis is used to separate the signal from the backgrounds. The result is consistent with the NLO SM prediction of 800 fb with a scale uncertainty of $^{+6.1}_{-7.4}$%.

[4] SIRUNYAN 18Z based on 35.9 fb^{-1} of data. A multivariate analysis is used to separate the signal from the backgrounds. The result is for the cross section $\sigma(pp \rightarrow tZq \rightarrow Wb\ell^+\ell^- q)$ and is consistent with the NLO SM prediction of 94.2 $^{+1.9}_{-1.8}$(scale) $\pm$ 2.5(PDF) fb. Superseded by SIRUNYAN 19BF.

Single t-Quark Production Cross Section in ep Collisions

VALUE (pb)	CL%	DOCUMENT ID		TECN	COMMENT
• • • We do not use the following data for averages, fits, limits, etc. • • •					
<0.25	95	[1] AARON	09A	H1	$e^\pm p \rightarrow e^\pm tX$
<0.55	95	[2] AKTAS	04	H1	$e^\pm p \rightarrow e^\pm tX$
<0.225	95	[3] CHEKANOV	03	ZEUS	$e^\pm p \rightarrow e^\pm tX$

[1] AARON 09A looked for single top production via FCNC in $e^\pm p$ collisions at HERA with 474 pb^{-1} of data at $\sqrt{s}$ = 301–319 GeV. The result supersedes that of AKTAS 04.

[2] AKTAS 04 looked for single top production via FCNC in $e^\pm$ collisions at HERA with 118.3 pb^{-1}, and found 5 events in the e or μ channels while 1.31 $\pm$ 0.22 events are expected from the Standard Model background. No excess was found for the hadronic channel. The observed cross section of $\sigma(ep \rightarrow etX)$ = 0.29 $^{+0.15}_{-0.14}$ pb at $\sqrt{s}$ = 319 GeV gives the quoted upper bound if the observed events are due to statistical fluctuation.

[3] CHEKANOV 03 looked in 130.1 pb^{-1} of data at $\sqrt{s}$ = 301 and 318 GeV. The limit is for $\sqrt{s}$ = 318 GeV and assumes m_t = 175 GeV.

$t\overline{t}$ Production Cross Section in $p\overline{p}$ Collisions at $\sqrt{s}$ = 1.8 TeV

Only the final combined $t\overline{t}$ production cross sections obtained from Tevatron Run I by the CDF and D0 experiments are quoted below.

VALUE (pb)	DOCUMENT ID		TECN	COMMENT
• • • We do not use the following data for averages, fits, limits, etc. • • •				
5.69 $\pm$ 1.21 $\pm$ 1.04	[1] ABAZOV	03A	D0	Combined Run I data
6.5 $^{+1.7}_{-1.4}$	[2] AFFOLDER	01A	CDF	Combined Run I data

[1] Combined result from 110 pb^{-1} of Tevatron Run I data. Assume m_t = 172.1 GeV.

[2] Combined result from 105 pb^{-1} of Tevatron Run I data. Assume m_t = 175 GeV.

$t\overline{t}$ Production Cross Section in $p\overline{p}$ Collisions at $\sqrt{s}$ = 1.96 TeV

Unless otherwise noted the first quoted error is from statistics, the second from systematic uncertainties, and the third from luminosity. If only two errors are quoted the luminosity is included in the systematic uncertainties.

VALUE (pb)	DOCUMENT ID		TECN	COMMENT
• • • We do not use the following data for averages, fits, limits, etc. • • •				
7.26 $\pm$ 0.13 $^{+0.57}_{-0.50}$	[1] ABAZOV	16F	D0	$\ell\ell$, ℓ+jets channels
8.1 $\pm$ 2.1	[2] AALTONEN	14A	CDF	$\ell + \tau_h$ + $\geq$ 2jets ($\geq$ 1b-tag)
7.60 $\pm$ 0.20 $\pm$ 0.29 $\pm$ 0.21	[3] AALTONEN	14H	TEVA	$\ell\ell$, ℓ+jets, all-jets channels
8.0 $\pm$ 0.7 $\pm$ 0.6 $\pm$ 0.5	[4] ABAZOV	14K	D0	ℓ+$\not{E}_T$+ $\geq$ 4 jets ($\geq$ 1b-tag)
7.09 $\pm$ 0.84	[5] AALTONEN	13AB	CDF	$\ell\ell + \not{E}_T$ + $\geq$ 2 jets
7.5 $\pm$ 1.0	[6] AALTONEN	13G	CDF	$\ell + \not{E}_T$ + $\geq$ 3jets ($\geq$ 1b-tag)
8.8 $\pm$ 3.3 $\pm$ 2.2	[7] AALTONEN	12AL	CDF	$\tau_h + \not{E}_T$ +4j ($\geq$ 1b)
8.5 $\pm$ 0.6 $\pm$ 0.7	[8] AALTONEN	11D	CDF	$\ell + \not{E}_T$ + jets ($\geq$ 1b-tag)
7.64 $\pm$ 0.57 $\pm$ 0.45	[9] AALTONEN	11W	CDF	$\ell + \not{E}_T$ + jets ($\geq$ 1b-tag)
7.99 $\pm$ 0.55 $\pm$ 0.76 $\pm$ 0.46	[10] AALTONEN	11Y	CDF	$\not{E}_T$ + $\geq$ 4jets (0,1,2 b-tag)
7.78 $^{+0.77}_{-0.64}$	[11] ABAZOV	11E	D0	$\ell + \not{E}_T$ + $\geq$ 2 jets
7.56 $^{+0.63}_{-0.56}$	[12] ABAZOV	11Z	D0	Combination
6.27 $\pm$ 0.73 $\pm$ 0.63 $\pm$ 0.39	[13] AALTONEN	10AA	CDF	Repl. by AALTONEN 13AB
7.2 $\pm$ 0.5 $\pm$ 1.0 $\pm$ 0.4	[14] AALTONEN	10E	CDF	$\geq$ 6 jets, vtx b-tag
7.8 $\pm$ 2.4 $\pm$ 1.6 $\pm$ 0.5	[15] AALTONEN	10V	CDF	ℓ + $\geq$ 3 jets, soft-e b-tag
7.70 $\pm$ 0.52	[16] AALTONEN	10W	CDF	$\ell + \not{E}_T$ + $\geq$ 3 jets + b-tag, norm. to $\sigma(Z \rightarrow \ell\ell)_{TH}$
6.9 $\pm$ 2.0	[17] ABAZOV	10I	D0	$\geq$ 6 jets with 2 b-tags
6.9 $\pm$ 1.2 $^{+0.8}_{-0.7}$ $\pm$ 0.4	[18] ABAZOV	10Q	D0	τ_h + jets
9.6 $\pm$ 1.2 $^{+0.6}_{-0.5}$ $\pm$ 0.6	[19] AALTONEN	09AD	CDF	$\ell\ell + \not{E}_T$ / vtx b-tag
9.1 $\pm$ 1.1 $^{+1.0}_{-0.9}$ $\pm$ 0.6	[20] AALTONEN	09H	CDF	ℓ + $\geq$ 3 jets+$\not{E}_T$/soft μ b-tag
8.18 $^{+0.98}_{-0.87}$	[21] ABAZOV	09AG	D0	ℓ + jets, $\ell\ell$ and $\ell\tau$ + jets
7.5 $\pm$ 1.0 $^{+0.7}_{-0.6}$ $^{+0.6}_{-0.5}$	[22] ABAZOV	09R	D0	$\ell\ell$ and $\ell\tau$ + jets
8.18 $^{+0.90}_{-0.84}$ $\pm$ 0.50	[23] ABAZOV	08M	D0	ℓ + n jets with 0,1,2 b-tag
7.62 $\pm$ 0.85	[24] ABAZOV	08N	D0	ℓ + n jets + b-tag or kinematics
8.5 $^{+2.7}_{-2.2}$	[25] ABULENCIA	08	CDF	$\ell^+\ell^-$ (ℓ = e, μ)
8.3 $\pm$ 1.0 $^{+2.0}_{-1.5}$ $\pm$ 0.5	[26] AALTONEN	07D	CDF	$\geq$ 6 jets, vtx b-tag
7.4 $\pm$ 1.4 $\pm$ 1.0	[27] ABAZOV	07O	D0	$\ell\ell$ + jets, vtx b-tag
4.5 $^{+2.0}_{-1.9}$ $^{+1.4}_{-1.1}$ $\pm$ 0.3	[28] ABAZOV	07P	D0	$\geq$ 6 jets, vtx b-tag
6.4 $^{+1.3}_{-1.2}$ $\pm$ 0.7 $\pm$ 0.4	[29] ABAZOV	07R	D0	ℓ + $\geq$ 4 jets
6.6 $\pm$ 0.9 $\pm$ 0.4	[30] ABAZOV	06X	D0	ℓ + jets, vtx b-tag
8.7 $\pm$ 0.9 $^{+1.1}_{-0.9}$	[31] ABULENCIA	06Z	CDF	ℓ + jets, vtx b-tag
5.8 $\pm$ 1.2 $^{+0.9}_{-0.7}$	[32] ABULENCIA,A	06C	CDF	missing E_T + jets, vtx b-tag
7.5 $\pm$ 2.1 $^{+3.3}_{-2.2}$ $^{+0.5}_{-0.4}$	[33] ABULENCIA,A	06E	CDF	6–8 jets, b-tag
8.9 $\pm$ 1.0 $^{+1.1}_{-1.0}$	[34] ABULENCIA,A	06F	CDF	ℓ + $\geq$ 3 jets, b-tag
8.6 $^{+1.6}_{-1.5}$ $\pm$ 0.6	[35] ABAZOV	05Q	D0	ℓ + n jets
8.6 $^{+3.2}_{-2.7}$ $\pm$ 1.1 $\pm$ 0.6	[36] ABAZOV	05R	D0	di-lepton + n jets
6.7 $^{+1.4}_{-1.3}$ $^{+1.6}_{-1.1}$ $\pm$ 0.4	[37] ABAZOV	05X	D0	ℓ + jets / kinematics
5.3 $\pm$ 3.3 $^{+1.3}_{-1.0}$	[38] ACOSTA	05S	CDF	ℓ + jets / soft μ b-tag
6.6 $\pm$ 1.1 $\pm$ 1.5	[39] ACOSTA	05T	CDF	ℓ + jets / kinematics
6.0 $^{+1.5}_{-1.6}$ $^{+1.2}_{-1.3}$	[40] ACOSTA	05U	CDF	ℓ + jets/kinematics + vtx b-tag
5.6 $^{+1.2}_{-1.1}$ $^{+0.9}_{-0.6}$	[41] ACOSTA	05V	CDF	ℓ + n jets
7.0 $^{+2.4}_{-2.1}$ $^{+1.6}_{-1.1}$ $\pm$ 0.4	[42] ACOSTA	04I	CDF	di-lepton + jets + missing ET

[1] ABAZOV 16F based on 9.7 fb^{-1} of data. The result is for m_t = 172.5 GeV, and the m_t dependence is shown in Table V and Fig. 9. The result agrees with the NNLO+NNLL SM prediction of 7.35 $^{+0.23}_{-0.27}$ pb.

[2] Based on 9 fb^{-1} of data. The measurement is in the channel $t\overline{t} \rightarrow (b\ell\nu)(b\tau\nu)$, where τ decays into hadrons (τ_h), and ℓ (e or μ) include ℓ from τ decays (τ_ℓ). The result is for m_t = 173 GeV.

[3] Based on 8.8 fb^{-1} of data. Combination of CDF and D0 measurements given, respectively, by $\sigma(t\overline{t}$; CDF) = 7.63 $\pm$ 0.31 $\pm$ 0.36 $\pm$ 0.16 pb, $\sigma(t\overline{t}$; D0) = 7.56 $\pm$ 0.20 $\pm$ 0.32 $\pm$ 0.46 pb. All the results are for m_t = 172.5 GeV. The m_t dependence of the mean value is parametrized in eq. (1) and shown in Fig. 2.

[4] Based on 9.7 fb^{-1} of data. Differential cross sections with respect to m_{tt}, $|y(\text{top})|$, E_T(top) are shown in Figs. 9, 10, 11, respectively, and are compared to the predictions of MC models.

[5] Based on 8.8 fb^{-1} of $p\overline{p}$ collisions at $\sqrt{s}$ = 1.96 TeV.

[6] Based on 8.7 fb^{-1} of $p\overline{p}$ collisions at $\sqrt{s}$ = 1.96 TeV. Measure the $t\overline{t}$ cross section simultaneously with the fraction of $t \rightarrow Wb$ decays. The correlation coefficient between those two measurements is -0.434. Assume unitarity of the 3×3 CKM matrix and set $|V_{tb}| > 0.89$ at 95% CL.

[7] Based on 2.2 fb^{-1} of data in $p\overline{p}$ collisions at 1.96 TeV. The result assumes the acceptance for m_t = 172.5 GeV.

[8] Based on 1.12 fb^{-1} and assumes m_t = 175 GeV, where the cross section changes by $\pm$0.1 pb for every $\mp$1 GeV shift in m_t. AALTONEN 11D fits simultaneously the $t\overline{t}$ production cross section and the b-tagging efficiency and find improvements in both measurements.

[9] Based on 2.7 fb^{-1}. The first error is from statistics and systematics, the second is from luminosity. The result is for m_t = 175 GeV. AALTONEN 11W fits simultaneously a jet flavor discriminator between b-, c-, and light-quarks, and find significant reduction in the systematic error.

[10] Based on 2.2 fb^{-1}. The result is for m_t = 172.5 GeV. AALTONEN 11Y selects multi-jet events with large $\not{E}_T$, and vetoes identified electrons and muons.

[11] Based on 5.3 fb^{-1}. The error is statistical + systematic + luminosity combined. The result is for m_t = 172.5 GeV. The results for other m_t values are given in Table XII and eq.(10) of ABAZOV 11E.

[12] Combination of a dilepton measurement presented in ABAZOV 11Z (based on 5.4 fb^{-1}), which yields 7.36 $^{+0.90}_{-0.79}$ (stat+syst) pb, and the lepton + jets measurement of ABAZOV 11E. The result is for m_t = 172.5 GeV. The results for other m_t values is given by eq.(5) of ABAZOV 11A.

[13] Based on 2.8 fb^{-1}. The result is for m_t = 175 GeV.

[14] Based on 2.9 fb^{-1}. Result is obtained from the fraction of signal events in the top quark mass measurement in the all hadronic decay channel.

[15] Based on 1.7 fb^{-1}. The result is for m_t = 175 GeV. AALTONEN 10V uses soft electrons from b-hadron decays to suppress W+jets background events.

[16] Based on 4.6 fb^{-1}. The result is for m_t = 172.5 GeV. The ratio $\sigma(t\overline{t} \rightarrow \ell$+jets) / $\sigma(Z/\gamma^* \rightarrow \ell\ell)$ is measured and then multiplied by the theoretical $Z/\gamma^* \rightarrow \ell\ell$ cross section of $\sigma(Z/\gamma^* \rightarrow \ell\ell)$ = 251.3 $\pm$ 5.0 pb, which is free from the luminosity error.

Downloaded from https://academic.oup.com/ptep/article/2022/8/083C01/6651666 by KIT Library user on 27 September 2022

[17] Based on 1 fb^{-1}. The result is for m_t = 175 GeV. 7.9 ± 2.3 pb is found for m_t = 170 GeV. ABAZOV 10I uses a likelihood discriminant to separate signal from background, where the background model was created from lower jet-multiplicity data.

[18] Based on 1 fb^{-1}. The result is for m_t = 170 GeV. For m_t = 175 GeV, the result is $6.3^{+1.2}_{-1.1}$(stat)±0.7(syst)±0.4(lumi) pb. Cross section of $t\overline{t}$ production has been measured in the $t\overline{t} \to \tau_h +$ jets topology, where τ_h denotes hadronically decaying τ leptons. The result for the cross section times the branching ratio is $\sigma(t\overline{t}) \cdot B(t\overline{t} \to \tau_h +$ jets$) = 0.60^{+0.23}_{-0.22}{}^{+0.15}_{-0.14} \pm 0.04$ pb for m_t = 170 GeV.

[19] Based on 1.1 fb^{-1}. The result is for $B(W \to \ell\nu)$ = 10.8% and m_t = 175 GeV; the mean value is 9.8 for m_t = 172.5 GeV and 10.1 for m_t = 170 GeV. AALTONEN 09AD used high p_T e or μ with an isolated track to select $t\overline{t}$ decays into dileptons including $\ell = \tau$. The result is based on the candidate event samples with and without vertex b-tag.

[20] Based on 2 fb^{-1}. The result is for m_t = 175 GeV; the mean value is 3% higher for m_t = 170 GeV and 4% lower for m_t = 180 GeV.

[21] Result is based on 1 fb^{-1} of data. The result is for m_t = 170 GeV, and the mean value decreases with increasing m_t; see their Fig. 2. The result is obtained after combining ℓ + jets, $\ell\ell$, and $\ell\tau$ final states, and the ratios of the extracted cross sections are $R^{\ell\ell/\ell j} = 0.86^{+0.19}_{-0.17}$ and $R^{\ell\tau/\ell\ell-\ell j} = 0.97^{+0.32}_{-0.29}$, consistent with the SM expectation of R = 1. This leads to the upper bound of $B(t \to bH^+)$ as a function of m_{H^+}. Results are shown in their Fig. 1 for $B(H^+ \to \tau\nu) = 1$ and $B(H^+ \to c\overline{s}) = 1$ cases. Comparison of the m_t dependence of the extracted cross section and a partial NNLO prediction gives $m_t = 169.1^{+5.9}_{-5.2}$ GeV.

[22] Result is based on 1 fb^{-1} of data. The result is for m_t = 170 GeV, and the mean value changes by −0.07 [m_t(GeV)−170] pb near the reference m_t value. Comparison of the m_t dependence of the extracted cross section and a partial NNLO QCD prediction gives $m_t = 171.5^{+9.9}_{-8.8}$ GeV. The $\ell\tau$ channel alone gives $7.6^{+4.9}_{-4.3}{}^{+3.5}_{-3.4}{}^{+1.4}_{-0.9}$ pb and the $\ell\ell$ channel gives $7.5^{+1.2}_{-1.1}{}^{+0.7}_{-0.6}{}^{+0.7}_{-0.5}$ pb.

[23] Result is based on 0.9 fb^{-1} of data. The first error is from stat + syst, while the latter error is from luminosity. The result is for m_t=175 GeV, and the mean value changes by −0.09 pb·[m_t(GeV)−175].

[24] Result is based on 0.9 fb^{-1} of data. The cross section is obtained from the $\ell + \geq 3$jet event rates with 1 or 2 b-tag, and also from the kinematical likelihood analysis of the ℓ + 3, 4 jet events. The result is for m_t= 172.6 GeV, and its m_t dependence shown in Fig. 3 leads to the constraint $m_t = 170 \pm 7$ GeV when compared to the SM prediction.

[25] Result is based on 360 pb^{-1} of data. Events with high p_T oppositely charged dileptons $\ell^+\ell^-$ ($\ell = e, \mu$) are used to obtain cross sections for $t\overline{t}$, W^+W^-, and $Z \to \tau^+\tau^-$ production processes simultaneously. The other cross sections are given in Table IV.

[26] Based on 1.02 fb^{-1} of data. Result is for m_t = 175 GeV. Secondary vertex b-tag and neural network selections are used to achieve a signal-to-background ratio of about 1/2.

[27] Based on 425 pb^{-1} of data. Result is for m_t = 175 GeV. For m_t = 170.9 GeV, 7.8 ± 1.8(stat + syst) pb is obtained.

[28] Based on 405 ± 25 pb^{-1} of data. Result is for m_t = 175 GeV. The last error is for luminosity. Secondary vertex b-tag and neural network are used to separate the signal events from the background.

[29] Based on 425 pb^{-1} of data. Assumes m_t = 175 GeV.

[30] Based on ∼ 425 pb^{-1}. Assuming m_t = 175 GeV. The first error is combined statistical and systematic, the second one is luminosity.

[31] Based on ∼ 318 pb^{-1}. Assuming m_t = 178 GeV. The cross section changes by ±0.08 pb for each ∓ GeV change in the assumed m_t. Result is for at least one b-tag. For at least two b-tagged jets, $t\overline{t}$ signal of significance greater than 5σ is found, and the cross section is $10.1^{+1.6}_{-1.4}{}^{+2.0}_{-1.3}$ pb for m_t = 178 GeV.

[32] Based on ∼ 311 pb^{-1}. Assuming m_t = 178 GeV. For m_t = 175 GeV, the result is $6.0 \pm 1.2^{+0.9}_{-0.7}$. This is the first CDF measurement without lepton identification, and hence it has sensitivity to the $W \to \tau\nu$ mode.

[33] ABULENCIA,A 06E measures the $t\overline{t}$ production cross section in the all hadronic decay mode by selecting events with 6 to 8 jets and at least one b-jet. S/B = 1/5 has been achieved. Based on 311 pb^{-1}. Assuming m_t = 178 GeV.

[34] Based on ∼ 318 pb^{-1}. Assuming m_t = 178 GeV. Result is for at least one b-tag. For at least two b-tagged jets, the cross section is $11.1^{+2.3}_{-1.9}{}^{+2.5}_{-1.9}$ pb.

[35] ABAZOV 05Q measures the top-quark pair production cross section with ∼ 230 pb^{-1} of data, based on the analysis of W plus n-jet events where W decays into e or μ plus neutrino, and at least one of the jets is b-jet like. The first error is statistical and systematic, and the second accounts for the luminosity uncertainty. The result assumes m_t = 175 GeV; the mean value changes by (175−m_t(GeV)) × 0.06 pb in the mass range 160 to 190 GeV.

[36] ABAZOV 05R measures the top-quark pair production cross section with 224–243 pb^{-1} of data, based on the analysis of events with two charged leptons in the final state. The result assumes m_t = 175 GeV; the mean value changes by (175−m_t(GeV)) × 0.08 pb in the mass range 160 to 190 GeV.

[37] Based on 230 pb^{-1}. Assuming m_t = 175 GeV.

[38] Based on 194 pb^{-1}. Assuming m_t = 175 GeV.

[39] Based on 194 ± 11 pb^{-1}. Assuming m_t = 175 GeV.

[40] Based on 162 ± 10 pb^{-1}. Assuming m_t = 175 GeV.

[41] ACOSTA 05V measures the top-quark pair production cross section with ∼ 162 pb^{-1} data, based on the analysis of W plus n-jet events where W decays into e or μ plus neutrino, and at least one of the jets is b-jet like. Assumes m_t = 175 GeV.

[42] ACOSTA 04I measures the top-quark pair production cross section with 197 ± 12 pb^{-1} data, based on the analysis of events with two charged leptons in the final state. Assumes m_t = 175 GeV.

Ratio of the Production Cross Sections of $t\overline{t}\gamma$ to $t\overline{t}$ at $\sqrt{s}$ = 1.96 TeV

VALUE	DOCUMENT ID		TECN	COMMENT
• • • We do not use the following data for averages, fits, limits, etc. • • •				
0.024±0.009	[1] AALTONEN	11Z	CDF	$E_T(\gamma) > 10$ GeV, $\lvert\eta(\gamma)\rvert < 1.0$

[1] Based on 6.0 fb^{-1} of data. The error is statistical and systematic combined. Events with lepton + $\not{E}_T$ + ≥ 3 jets(≥ 1b) with and without central, high E_T photon are measured. The result is consistent with the SM prediction of 0.024 ± 0.005. The absolute production cross section is measured to be 0.18 ± 0.08 fb. The statistical significance is 3.0 standard deviations.

tt Production Cross Section in pp Collisions at $\sqrt{s}$ = 7 TeV

VALUE (pb)	CL%	DOCUMENT ID		TECN	COMMENT
• • • We do not use the following data for averages, fits, limits, etc. • • •					
<1.7	95	[1] AAD	12BE	ATLS	$\ell^+\ell^+ + \not{E}_T + \geq 2$j +HT

[1] Based on 1.04 fb^{-1} of pp data at $\sqrt{s}$ = 7 TeV. The upper bounds are the same for LL, LR and RR chiral components of the two top quarks.

$t\overline{t}$ Production Cross Section in pp Collisions at $\sqrt{s}$ = 5.02 TeV

Unless otherwise noted the first quoted error is from statistics, the second from systematic uncertainties, and the third from luminosity. If only two errors are quoted the luminosity is included in the systematic uncertainties.

VALUE (pb)	DOCUMENT ID		TECN	COMMENT
• • • We do not use the following data for averages, fits, limits, etc. • • •				
69.5±6.1±5.6±1.6	[1] SIRUNYAN	18AQ	CMS	ℓ+jets, $\ell\ell$+jets

[1] SIRUNYAN 18AQ based on 27.4 pb^{-1} of data from pp collisions at $\sqrt{s}$ = 5.02 TeV. The result is in agreement with the NNLO SM prediction $68.9^{+1.9}_{-2.3}$(scale)±2.3(PDF)$^{+1.4}_{-1.0}$(α_s) pb.

$t\overline{t}$ Production Cross Section in pp Collisions at $\sqrt{s}$ = 7 TeV

Unless otherwise noted the first quoted error is from statistics, the second from systematic uncertainties, and the third from luminosity. If only two errors are quoted the luminosity is included in the systematic uncertainties.

VALUE (pb)	DOCUMENT ID		TECN	COMMENT
• • • We do not use the following data for averages, fits, limits, etc. • • •				
161.7± 6.0±12.0± 3.6	[1] KHACHATRY...17B		CMS	$\ell + \not{E}_T + \geq 4$j (≥ 1$b$)
173.6± 2.1$^{+4.5}_{-4.0}$± 3.8	[2] KHACHATRY...16AW		CMS	$e + \mu + \not{E}_T + \geq 0$j
181.2± 2.8$^{+10.8}_{-10.6}$	[3] AAD	15BO	ATLS	$e + \mu + \not{E}_T + \geq 0$j
178 ± 3 ±16 ± 3	[4] AAD	15CC	ATLS	ℓ+jets, $\ell\ell$+jets, $\ell\tau_h$+jets
	[5] AAIJ	15R	LHCB	$\mu + \geq 1$j(b-tag) forward region
182.9± 3.1± 6.4	[6] AAD	14AY	ATLS	$e + \mu$ + 1 or 2b jets
194 ±18 ±46	[7] AAD	13X	ATLS	$\tau_h + \not{E}_T + \geq 5$j (≥ 2$b$)
139 ±10 ±26	[8] CHATRCHYAN	13AY	CMS	≥ 6 jets with 2 b-tags
158.1± 2.1±10.8	[9] CHATRCHYAN	13BB	CMS	$\ell + \not{E}_T$ + jets(≥ 1 b-tag)
152 ±12 ±32	[10] CHATRCHYAN	13BE	CMS	$\tau_h + \not{E}_T + \geq 4$ jets (≥ 1 b)
177 ±20 ±14 ± 7	[11] AAD	12B	ATLS	Repl. by AAD 12BF
176 ± 5 $^{+14}_{-11}$ ± 8	[12] AAD	12BF	ATLS	$\ell\ell + \not{E}_T + \geq 2$j
187 ±11 $^{+18}_{-17}$ ± 6	[13] AAD	12BO	ATLS	$\ell + \not{E}_T + \geq 3$j with b-tag
186 ±13 ±20 ± 7	[14] AAD	12CG	ATLS	$\ell + \tau_h + \not{E}_T + \geq 2$j (≥ 1$b$)
143 ±14 ±22 ± 3	[15] CHATRCHYAN	12AC	CMS	$\ell + \tau_h + \not{E}_T + \geq 2$j (≥ 1$b$)
161.9± 2.5$^{+5.1}_{-5.0}$± 3.6	[16] CHATRCHYAN	12AX	CMS	$\ell\ell + \not{E}_T + \geq 2b$
145 ±31 $^{+42}_{-27}$	[17] AAD	11A	ATLS	$\ell + \not{E}_T + \geq 4$j, $\ell\ell + \not{E}_T + \geq 2$j
173 $^{+39}_{-32}$ ± 7	[18] CHATRCHYAN	11AA	CMS	$\ell + \not{E}_T + \geq 3$ jets
168 ±18 ±14 ± 7	[19] CHATRCHYAN	11F	CMS	$\ell\ell + \not{E}_T$ + jets
154 ±17 ± 6	[20] CHATRCHYAN	11Z	CMS	Combination
194 ±72 ±24 ±21	[21] KHACHATRY...11A		CMS	$\ell\ell + \not{E}_T + \geq 2$ jets

[1] KHACHATRYAN 17B based on 5.0 fb^{-1} of data, using a binned likelihood fit of templates to the data. Also the ratio $\sigma(t\overline{t}; 8\text{ TeV})/\sigma(t\overline{t}; 7\text{ TeV}) = 1.43 \pm 0.04 \pm 0.07 \pm 0.05$ is reported. The results are in agreement with NNLO SM predictions.

[2] KHACHATRYAN 16AW based on 5.0 fb^{-1} of data, using a binned likelihood fit to differential distributions of b-tagged and non-b-tagged jets. The result is in good agreement with NNLO SM predictions.

[3] Based on 4.6 fb^{-1} of data. Uses a template fit to distributions of $\not{E}_T$ and jet multiplicities to measure simultaneously $t\overline{t}$, WW, and $Z/\gamma^* \to \tau\tau$ cross sections, assuming m_t = 172.5 GeV.

[4] AAD 15CC based on 4.6 fb^{-1} of data. The event selection criteria are optimized for the $\ell\tau_h$ + jets channel. Using only this channel 183 ± 9 ± 23 ± 3 pb is derived for the cross section.

[5] AAIJ 15R, based on 1.0 fb^{-1} of data, reports 0.239 ± 0.053 ± 0.033 ± 0.024 pb cross section for the forward fiducial region $p_T(\mu) > 25$ GeV, $2.0 < \eta(\mu) < 4.5$, 50 GeV < $p_T(b) < 100$ GeV, $2.2 < \eta(b) < 4.2$, $\Delta R(\mu,b) > 0.5$, and $p_T(\mu+b) > 20$ GeV. The three errors are from statistics, systematics, and theory. The result agrees with the SM NLO prediction.

[6] AAD 14AY reports 182.9 ± 3.1 ± 4.2 ± 3.6 ± 3.3 pb value based on 4.6 fb^{-1} of data. The four errors are from statistics, systematic, luminosity, and the 0.66% beam energy uncertainty. We have combined the systematic uncertainties in quadrature. The result is for m_t = 172.5GeV; for other m_t, $\sigma(m_t) = \sigma(172.5\text{GeV}) \times [1 - 0.0028 \times (m_t - 172.5\text{GeV})]$. The result is consistent with the SM prediction at NNLO.

[7] Based on 1.67 fb^{-1} of data. The result uses the acceptance for m_t = 172.5 GeV.

[8] Based on 3.54 fb^{-1} of data.

[9] Based on 2.3 fb^{-1} of data.

[10] Based on 3.9 fb^{-1} of data.

[11] Based on 35 pb^{-1} of data for an assumed top quark mass of m_t = 172.5 GeV.

[12] Based on 0.70 fb^{-1} of data. The 3 errors are from statistics, systematics, and luminosity. The result uses the acceptance for m_t = 172.5 GeV.

[13] Based on 35 pb^{-1} of data. The 3 errors are from statistics, systematics, and luminosity. The result uses the acceptance for m_t = 172.5 GeV and $173 \pm 17^{+18}_{-16} \pm 6$ pb is found without the b-tag.

[14] Based on 2.05 fb^{-1} of data. The hadronic τ candidates are selected using a BDT technique. The 3 errors are from statistics, systematics, and luminosity. The result uses the acceptance for m_t = 172.5 GeV.

[15] Based on 2.0 fb^{-1} and 2.2 fb^{-1} of data for $\ell = e$ and $\ell = \mu$, respectively. The 3 errors are from statistics, systematics, and luminosity. The result uses the acceptance for m_t = 172.5 GeV.

Downloaded from https://academic.oup.com/ptep/article/2022/8/083C01/6651666 by KIT Library user on 27 September 2022

[16] Based on 2.3 fb^{-1} of data. The 3 errors are from statistics, systematics, and luminosity. The result uses the profile likelihood-ratio (PLB) method and an assumed m_t of 172.5 GeV.

[17] Based on 2.9 pb^{-1} of data. The result for single lepton channels is $142 \pm 34^{+50}_{-31}$ pb, while for the dilepton channels is 151^{+78+37}_{-62-24} pb.

[18] Result is based on 36 pb^{-1} of data. The first uncertainty corresponds to the statistical and systematic uncertainties, and the second corresponds to the luminosity.

[19] Based on 36 pb^{-1} of data. The ratio of $t\overline{t}$ and Z/γ^* cross sections is measured as $\sigma(pp \to t\overline{t})/\sigma(pp \to Z/\gamma^* \to e^+e^-/\mu^+\mu^-) = 0.175 \pm 0.018(\text{stat}) \pm 0.015(\text{syst})$ for $60 < m_{\ell\ell} < 120$ GeV, for which they use an NNLO prediction for the denominator cross section of 972 ± 42 pb.

[20] Result is based on 36 pb^{-1} of data. The first error is from statistical and systematic uncertainties, and the second from luminosity. This is a combination of a measurement in the dilepton channel (CHATRCHYAN 11F) and the measurement in the ℓ + jets channel (CHATRCHYAN 11Z) which yields $150 \pm 9 \pm 17 \pm 6$ pb.

[21] Result is based on 3.1 $\pm$ 0.3 pb^{-1} of data.

$t\overline{t}$ Production Cross Section in pp Collisions at $\sqrt{s} = 8$ TeV

Unless otherwise noted the first quoted error is from statistics, the second from systematic uncertainties, and the third from luminosity. If only two errors are quoted the luminosity is included in the systematic uncertainties.

VALUE (pb)	DOCUMENT ID		TECN	COMMENT
• • • We do not use the following data for averages, fits, limits, etc. • • •				
$248.3 \pm 0.7 \pm 13.4 \pm 4.7$	[1] AABOUD	18BH	ATLS	$\ell + \not{E}_T + \geq 4$j ($\geq 1b$)
$239 \pm 4 \pm 28 \pm 5$	[2] AABOUD	17Z	ATLS	$\tau_h + \not{E}_T + \geq 2$j ($\geq 2b$)
$228.5 \pm 3.8 \pm 13.7 \pm 6.0$	[3] KHACHATRY...	17B	CMS	$\ell + \not{E}_T + \geq 4$j ($\geq 1b$)
$242.9 \pm 1.7 \pm 8.6$	[4] AAD	16BK	ATLS	$e + \mu + 1$ or $2b$ jets
$244.9 \pm 1.4^{+6.3}_{-5.5} \pm 6.4$	[5] KHACHATRY...	16AW	CMS	$e + \mu + \not{E}_T + \geq 0$j
$275.6 \pm 6.1 \pm 37.8 \pm 7.2$	[6] KHACHATRY...	16BC	CMS	≥ 6j ($\geq 2b$)
$260 \pm 1 \pm^{24}_{-25}$	[7] AAD	15BP	ATLS	$\ell + \not{E}_T + \geq 3$j ($\geq 1b$)
	[8] AAIJ	15R	LHCB	$\mu + \geq 1$j(b-tag) forward region
$242.4 \pm 1.7 \pm 10.2$	[9] AAD	14AY	ATLS	$e + \mu + 1$ or $2b$ jets
$239 \pm 2 \pm 11 \pm 6$	[10] CHATRCHYAN	14F	CMS	$\ell\ell + \not{E}_T + \geq 2$j (≥ 1 b-tag)
$257 \pm 3 \pm 24 \pm 7$	[11] KHACHATRY...	14S	CMS	$\ell + \tau_h + \not{E}_T + \geq 2$j ($\geq 1b$)

[1] AABOUD 18BH based on 20.2 fb^{-1} of data. The result is for $m_t = 172.5$ GeV. To reduce effects of uncertainties in the jet energy scale and b-tagging efficiency, they are included as nuisance parameters in the fit of discriminant distributions, after separating selected events into three regions. Furthermore the W+jets background distribution is modelled using Z+jets event data.

[2] AABOUD 17Z based on 20.2 fb^{-1} of data, using the mode $t\overline{t} \to \tau\nu q'\overline{q}b\overline{b}$ with τ decaying hadronically. Single prong and 3 prong decays of τ are separately analyzed. The result is consistent with the SM. The third quoted uncertainty is due to luminosity.

[3] KHACHATRYAN 17B based on 19.6 fb^{-1} of data, using a binned likelihood fit of templates to the data. Also the ratio $\sigma(t\overline{t}; 8\text{ TeV})/\sigma(t\overline{t}; 7\text{ TeV}) = 1.43 \pm 0.04 \pm 0.07 \pm 0.05$ is reported. The results are in agreement with NNLO SM predictions.

[4] AAD 16BK is an update of the value from AAD 14AY using the improved luminosity calibration. The value $242.9 \pm 1.7 \pm 5.5 \pm 5.1 \pm 4.2$ pb is reported, where we have combined the systematic uncertainties in quadrature. Also the ratio $\sigma(t\overline{t}; 8\text{TeV})/\sigma(t\overline{t}; 7\text{TeV}) = 1.328 \pm 0.024 \pm 0.015 \pm 0.038 \pm 0.001$ has been updated. The former result is consistent with the SM predictions at NNLO, while the latter result is 2.1 σ below the expectation.

[5] KHACHATRYAN 16AW based on 19.7 fb^{-1} of data, using a binned likelihood fit to differential distributions of b-tagged and non-b-tagged jets. The result is in good agreement with NNLO SM predictions.

[6] KHACHATRYAN 16BC based on 18.4 fb^{-1} of data. The last uncertainty is due to luminosity. Cuts on kinematical fit probability and $\Delta R(b,b)$ are imposed. The major QCD background is determined from the data. The result is for $m_t = 172.5$ GeV and in agreement with the SM prediction. The top quark p_T spectra, also measured, are significantly softer than theoretical predictions.

[7] AAD 15BP based on 20.3 fb^{-1} of data. The result is for $m_t = 172.5$ GeV and in agreement with the SM prediction 253^{+13}_{-15} pb at NNLO+NNLL. Superseded by AABOUD 18BH.

[8] AAIJ 15R, based on 2.0 fb^{-1} of data, reports $0.289 \pm 0.043 \pm 0.040 \pm 0.029$ pb cross section for the forward fiducial region $p_T(\mu) > 25$ GeV, $2.0 < \eta(\mu) < 4.5$, 50 GeV $< p_T(b) < 100$ GeV, $2.2 < \eta(b) < 4.2$, $\Delta R(\mu,b) > 0.5$, and $p_T(\mu+b) > 20$ GeV. The three errors are from statistics, systematics, and theory. The result agrees with the SM NLO prediction.

[9] AAD 14AY reports $242.4 \pm 1.7 \pm 5.5 \pm 7.5 \pm 4.2$ pb value based on 20.3 fb^{-1} of data. The four errors are from statistics, systematic, luminosity, and the 0.66% beam energy uncertainty. We have combined the systematic uncertainties in quadrature. The result is for $m_t = 172.5$GeV; for other m_t, $\sigma(m_t) = \sigma(172.5\text{GeV}) \times [1 - 0.0028 \times (m_t - 172.5\text{GeV})]$. Also measured is the ratio $\sigma(t\overline{t}; 8\text{TeV})/\sigma(t\overline{t}; 7\text{TeV}) = 1.326 \pm 0.024 \pm 0.015 \pm 0.049 \pm 0.001$. The results are consistent with the SM predictions at NNLO.

[10] Based on 5.3 fb^{-1} of data. The result is for $m_t = 172.5$ GeV, and a parametrization is given in eq.(6.1) for the mean value at other m_t values. The result is in agreement with the SM prediction $252.9^{+6.4}_{-8.6}$ pb at NNLO.

[11] Based on 19.6 fb^{-1} of data. The measurement is in the channel $t\overline{t} \to (b\ell\nu)(b\tau\nu)$, where τ decays into hadrons (τ_h). The result is for $m_t = 172.5$ GeV. For $m_t = 173.3$ GeV, the cross section is lower by 3.1 pb.

$t\overline{t}$ Production Cross Section in pp Collisions at $\sqrt{s} = 13$ TeV

VALUE (pb)	DOCUMENT ID		TECN	COMMENT
• • • We do not use the following data for averages, fits, limits, etc. • • •				
$791 \pm 1 \pm 21 \pm 14$	[1] TUMASYAN	21J	CMS	1ℓ + jets
$830 \pm 0.4 \pm 36 \pm 14$	[2] AAD	20AH	ATLS	ℓ + ≥ 4 jets ($\geq 1b$-tag)
$826.4 \pm 3.6 \pm 11.5 \pm 15.8$	[3] AAD	20Q	ATLS	$e\mu$ + 1 or 2 b-jets
$781 \pm 7 \pm 62 \pm 20$	[4] SIRUNYAN	20V	CMS	$\ell\tau_h$ + ≥ 3 jets ($\geq 1b$-tag)
$803 \pm 2 \pm 25 \pm 20$	[5] SIRUNYAN	19AR	CMS	dilepton channel ($e\mu$,2e,2μ)
	[6] SIRUNYAN	19P	CMS	dilepton channel
$815 \pm 9 \pm 38 \pm 19$	[7] KHACHATRY...	17N	CMS	$e\mu$ + ≥ 2j ($\geq 1b$ j)
$888 \pm 2 \pm^{26}_{-28} \pm 20$	[8] SIRUNYAN	17W	CMS	ℓ + ≥ 1j
$818 \pm 8 \pm 35$	[9] AABOUD	16R	ATLS	$e + \mu + 1$ or $2b$ jets
$746 \pm 58 \pm 53 \pm 36$	[10] KHACHATRY...	16J	CMS	$e + \mu$ + ≥ 2j

[1] TUMASYAN 21J result is based on 137 fb^{-1} of data. The last uncertainty is due to the beam luminosity. The result is in agreement with the SM prediction of 832^{+40}_{-46} pb at NNLO+NNLL. Measurements of differential and double-differential cross sections are also presented.

[2] AAD 20AH based on 139 fb^{-1} of data. The last quoted uncertainty is due to the beam luminosity. The result is for $m_t = 172.5$ GeV and in agreement with the SM prediction of $832^{+20}_{-29}(\text{scale}) \pm 35(\text{PDF}+\alpha(\text{s}))$ pb at NNLO+NNLL.

[3] AAD 20Q reports $826.4 \pm 3.6 \pm 11.5 \pm 15.7 \pm 1.9$ pb based on 36.1 fb^{-1} of data at 13 TeV. The four errors stem from statistics, systematic effects, luminosity, and beam energy, respectively. We have combined luminosity and beam energy uncertainties in quadrature. The result is in agreement with the SM prediction $832^{+20}_{-29}(\text{scale}) \pm 35(\text{PDF}+\alpha(\text{s}))$ pb at NNLO+NNLL for $m_t = 172.5$ GeV .

[4] SIRUNYAN 20V based on 35.9 fb^{-1} of pp data at $\sqrt{s} = 13$ TeV. The last uncertainty is due to beam luminosity. The $t\overline{t}$ production cross section is measured in the $t\overline{t} \to (\ell\nu_\ell)(\tau_h\nu_\tau)b\overline{b}$ final state, where τ_h refers to the hadronic decays of τ. The result is for $m_t = 172.5$ GeV and in agreement with the SM prediction at NNLO+NNLL.

[5] SIRUNYAN 19AR based on 35.9 fb^{-1} of data. Obtained from the visible cross section measured using a template fit to multidifferential distributions categorized according to the b-tagged jet multiplicity. The result is for $m_t = 172.5$ GeV and in agreement with the SM prediction at NNLO+NNLL.

[6] SIRUNYAN 19P reports differential $t\overline{t}$ cross sections measured using dilepton events at 13 TeV with 35.9 fb^{-1} and compared to NLO predictions.

[7] KHACHATRYAN 17N based on 2.2 fb^{-1} of data. The last quoted uncertainty is due to the beam luminosity. This measurement supersedes that of KHACHATRYAN 16J.

[8] SIRUNYAN 17W based on 2.2 fb^{-1} of pp data at $\sqrt{s} = 13$ TeV. Events are categorized according to the jet multiplicity and the number of b-tagged jets. A likelihood fit is performed to the event distributions to compare to the NNLO+NNLL prediction.

[9] AABOUD 16R reported value $818 \pm 8 \pm 27 \pm 19 \pm 12$ pb based on 3.2 fb^{-1} of data. The four errors are from statistics, systematic, luminosity, and beam energy. We have combined the systematic uncertainties in quadrature. The result is in agreement with the SM prediction $832^{+20}_{-29}(\text{scale}) \pm 35(\text{PDF}+\alpha(\text{s}))$ pb at NNLO+NNLL for $m_t = 172.5$ GeV .

[10] KHACHATRYAN 16J based on 43 pb^{-1} of data. The last uncertainty is due to luminosity. The result is for $m_t = 172.5$ GeV and in agreement with the SM prediction $832^{+20}_{-29}(\text{scale}) \pm 35(\text{PDF}+\alpha(\text{s}))$ pb at NNLO+NNLL.

$t\overline{t}$ Production Cross Section in Nucleus-Nucleus Collisions

VALUE (μbarn)	DOCUMENT ID		TECN	COMMENT
• • • We do not use the following data for averages, fits, limits, etc. • • •				
$2.03^{+0.71}_{-0.64}$	[1] SIRUNYAN	20BC	CMS	Pb-Pb collisions, dilepton + b-jets
$2.54^{+0.84}_{-0.74}$	[2] SIRUNYAN	20BC	CMS	Pb-Pb collisions, dilepton only

[1] SIRUNYAN 20BC based on (1.7 ± 0.1) nb^{-1} of lead-lead collision data at a nucleon-nucleon c.m. energy of 5.02 TeV. It makes use of the final-state dilepton kinematic properties together with requirements on the number of b-jets. The measured value is compatible with QCD predictions.

[2] SIRUNYAN 20BC based on (1.7 ± 0.1) nb^{-1} of lead-lead collision data at a nucleon-nucleon c.m. energy of 5.02 TeV. It makes use of the final-state dilepton kinematic properties alone. The measured value is compatible with QCD predictions.

$t\overline{t}\,t\overline{t}$ Production Cross Section in pp Collisions at $\sqrt{s} = 8$ TeV

VALUE (fb)	CL%	DOCUMENT ID		TECN	COMMENT
• • • We do not use the following data for averages, fits, limits, etc. • • •					
<23	95	[1] AAD	15AR	ATLS	$\ell + \not{E}_T + \geq 5$j (≥ 2 b)
<70	95	[2] AAD	15BY	ATLS	$\geq 2\ell + \not{E}_T + \geq 2$j (≥ 1 b)
<32	95	[3] KHACHATRY...	14R	CMS	$\ell + \not{E}_T + \geq 6$j (≥ 2 b)

[1] AAD 15AR based on 20.3 fb^{-1} of data. A fit to H_T distributions in multi-channels classified by the number of jets and of b-tagged jets is performed.

[2] AAD 15BY based on 20.3 fb^{-1} of data. A same-sign lepton pair is required. An excess over the SM prediction reaches 2.5σ for hypotheses involving heavy resonances decaying into $t\overline{t}\,t\overline{t}$.

[3] Based on 19.6 fb^{-1} of data, using a multivariate analysis to separate signal from backgrounds. About $\sigma(t\overline{t}\,t\overline{t}) = 1$ fb is expected in the SM.

$t\overline{t}\,t\overline{t}$ Production Cross Section in pp Collisions at $\sqrt{s} = 13$ TeV

VALUE (fb)	CL%	DOCUMENT ID		TECN	COMMENT
• • • We do not use the following data for averages, fits, limits, etc. • • •					
26^{+17}_{-15}		[1] AAD	21BC	ATLS	ℓ or $\ell^+\ell^-$ + jets
24^{+7}_{-6}		[2] AAD	21BC	ATLS	combination of $1\ell/2\ell$(OS) and 2ℓ(SS)/3ℓ
24^{+7}_{-6}		[3] AAD	20AR	ATLS	(same-sign 2ℓ) or $\geq 3\ell$ + jets
$12.6^{+5.8}_{-5.2}$		[4] SIRUNYAN	20C	CMS	(same-sign 2ℓ) or 3ℓ + jets
<47	95	[5] AABOUD	19AP	ATLS	$\ell + \ell^+\ell^-$ channels
<49	95	[6] AABOUD	19AP	ATLS	combination of ATLAS

Downloaded from https://academic.oup.com/ptep/article/2022/8/083C01/6651666 by KIT Library user on 27 September 2022

13^{+11}_{-9}		[7] SIRUNYAN	19CN	CMS	combination of CMS
<48	95	[8] SIRUNYAN	19CN	CMS	ℓ+jets, $\ell^+\ell^-$+jets channels
<69	95	[9] AABOUD	18CE	ATLS	$\geq 2\ell$(same sign) + $\not{E}_T$ + $\geq 1b$j
$16.9^{+13.8}_{-11.4}$		[10] SIRUNYAN	18BU	CMS	$t\overline{t}t\overline{t} \rightarrow$ (same sign 2ℓ or $\geq 3\ell$) + ≥ 4 j ($\geq 2b$)
<94	95	[11] SIRUNYAN	17AB	CMS	ℓ+jets, $\ell^+\ell^-$+jets channels
<42	95	[12] SIRUNYAN	17S	CMS	(same sign 2ℓ)+$\not{E}_T$+ $\geq$ 2j

[1] AAD 21BC result is based on 139 fb^{-1} of data. The events are categorized according to the number of jets and how likely to contain b-hadrons and a multivariate analysis is used to discriminate the signal from backgrounds. The result corresponds to observed significance of 1.9 σ.

[2] AAD 21BC combines the results of the four-top-quark production cross section measured from the 1ℓ/opposite-sign 2ℓ channel with that from the same-sign $2\ell/3\ell$ channel (AAD 20AR). The result corresponds to observed significance of 4.7 σ and is consistent within 2.0 σ with the NLO (QCD+EW) SM prediction of 12.0 $\pm$ 2.4 fb.

[3] AAD 20AR based on 139 fb^{-1} of data. Jet multiplicity, jet flavor and event kinematics are used in a multivariate analysis to discriminate the signal from backgrounds. The result corresponds to observed significance of 4.3σ and is consistent within 1.7σ with the NLO (QCD+EW) SM prediction of 12.0 $\pm$ 2.4 fb.

[4] SIRUNYAN 20C based on 137 fb^{-1} of data. Both cut-based and multivariate approaches are taken to discriminate the signal from backgrounds. The result is in agreement with the NLO (QCD+EW) SM prediction of $12.0^{+2.2}_{-2.5}$ fb. The measurement constrains the top quark Yukawa coupling strength parameter to be $|Y_t/Y_t^{SM}| < 1.7$ (95% CL). It is also used to constrain an oblique parameter of the Higgs boson.

[5] AABOUD 19AP based on 36.1 fb^{-1} of data. The upper limit corresponds to 5.1 times the NLO SM cross section.

[6] AABOUD 19AP limit from data combined with AABOUD 18CE. The upper limit corresponds to 5.3 times the NLO SM cross section. Also a limit on the four-top-quark contact interaction of $|C_{4t}|/\Lambda^2 < 1.9$ TeV^{-2} (95% CL) is obtained in an EFT model.

[7] SIRUNYAN 19CN based on 35.8 fb^{-1} of data, combined with SIRUNYAN 18BU. The results are also interpreted in the effective field theory framework.

[8] SIRUNYAN 19CN based on 35.8 fb^{-1} of data. A multivariate analysis using global event and jet propoerties is performed to discriminate from $t\overline{t}$ background.

[9] AABOUD 18CE based on 36.1 fb^{-1} of proton-proton data taken at $\sqrt{s} = 13$ TeV. Events including a same-sign lepton pair are used. The result is consistent with the NLO SM cross section of 9.2 fb.

[10] SIRUNYAN 18BU based on 35.9 fb^{-1} of proton-proton data taken at $\sqrt{s} = 13$ TeV. Yields from signal regions and control regions defined based on N_{jets}, N_b and N_l are combined in a maximum-likelihood fit. The result is in agreement with the NLO SM prediction $9.2^{+2.9}_{-2.4}$ fb. The measurement constrains the top quark Yukawa coupling strength parameter to be $|Y_t/Y_t^{SM}| < 2.1$ (95% CL).

[11] SIRUNYAN 17AB based on 2.6 fb^{-1} of data. A multivariate analysis is used to discriminate between $t\overline{t}t\overline{t}$ signal and $t\overline{t}$ background. A combination with a previous search (CMS, KHACHATRYAN 16BJ) in the same-sign dilepton channel gives an upper limit of 69 fb (95% CL), corresponding to 7.4·(SM prediction).

[12] SIRUNYAN 17S based on 35.9 fb^{-1}. The limit is in agreement with the NLO SM prediction $9.2^{+2.9}_{-2.4}$ fb. Superseded by SIRUNYAN 18BU. The signal events are also used to constrain various new physics models.

$t\overline{t}W$ Production Cross Section in pp Collisions at $\sqrt{s} = 8$ TeV

VALUE (fb)	DOCUMENT ID		TECN	COMMENT
• • • We do not use the following data for averages, fits, limits, etc. • • •				
$170^{+90}_{-80}\pm70$	[1] KHACHATRY...14N		CMS	$t\overline{t}W \rightarrow$ same sign dilepton + $\not{E}_T$ + jets

[1] Based on 19.5 fb^{-1} of data. The result is consistent with the SM prediction of $\sigma(t\overline{t}W) = 206^{+21}_{-23}$ fb.

$t\overline{t}W$ Production Cross Section in pp Collisions at $\sqrt{s} = 13$ TeV

VALUE (pb)	DOCUMENT ID		TECN	COMMENT
• • • We do not use the following data for averages, fits, limits, etc. • • •				
$0.87\pm0.13\pm0.14$	[1] AABOUD	19AR	ATLS	2,3,4ℓ + $\not{E}_T$ + jets
$0.77^{+0.12}_{-0.11}\pm0.13$	[2] SIRUNYAN	18BS	CMS	$t\overline{t}W \rightarrow$ same sign dilepton + $\not{E}_T$ + jets

[1] AABOUD 19AR based on 35.9 fb^{-1} of data. $t\overline{t}W$ and $t\overline{t}Z$ cross sections are simultaneously measured using a combined fit to the events divided into multiple regions. The result is consistent with the SM prediction at NLO $0.60^{+0.08}_{-0.07}$ pb. It is also used to constrain the Wilson coefficients for dimension-six operators which modify the $t\overline{t}Z$ vertex.

[2] Based on 35.9 fb^{-1} of proton-proton data taken at $\sqrt{s} = 13$ TeV. The result is consistent with the SM prediction and is used to constrain the Wilson coefficients for dimension-six operators describing new interactions. The result is consistent with the SM prediction at NLO 0.628 $\pm$ 0.082 pb.

$t\overline{t}Z$ Production Cross Section in pp Collisions at $\sqrt{s} = 8$ TeV

VALUE (fb)	DOCUMENT ID		TECN	COMMENT
• • • We do not use the following data for averages, fits, limits, etc. • • •				
200^{+80+40}_{-70-30}	[1] KHACHATRY...14N		CMS	$t\overline{t}Z \rightarrow 3,4\ \ell + \not{E}_T$ + jets

[1] Based on 19.5 fb^{-1} of data. The result is consistent with the SM prediction of $\sigma(t\overline{t}Z) = 197^{+22}_{-25}$ fb.

$t\overline{t}Z$ Production Cross Section in pp Collisions at $\sqrt{s} = 13$ TeV

VALUE (pb)	DOCUMENT ID		TECN	COMMENT
• • • We do not use the following data for averages, fits, limits, etc. • • •				
$0.99\pm0.05\pm0.08$	[1] AAD	21AS	ATLS	3,4ℓ + jets
$0.95\pm0.05\pm0.06$	[2] SIRUNYAN	20AB	CMS	3,4ℓ + jets
$0.95\pm0.08\pm0.10$	[3] AABOUD	19AR	ATLS	2,3,4ℓ + $\not{E}_T$ + jets
$0.99^{+0.09+0.12}_{-0.08-0.10}$	[4] SIRUNYAN	18BS	CMS	$t\overline{t}Z \rightarrow 3,4\ \ell + \not{E}_T$ + jets

[1] AAD 21AS based on 139 fb^{-1} of data. The result is consistent with the SM prediction of $0.88^{+0.09}_{-0.10}$ pb which includes NLO QCD+EW corrections. Also overall the differential cross sections are in good agreement with the SM predictions.

[2] SIRUNYAN 20AB based on 77.5 fb^{-1} of data at 13 TeV. The result is consistent with the NLO SM prediction of 0.84 $\pm$ 0.10 pb. Differential cross sections are measured and used to constrain the anomalous couplings and Wilson coefficients for the $t\overline{t}Z$ interaction.

[3] AABOUD 19AR based on 35.9 fb^{-1} of data. $t\overline{t}W$ and $t\overline{t}Z$ cross sections are simultaneously measured using a combined fit to the events divided into multiple regions. The result is consistent with the SM prediction at NLO $0.88^{+0.09}_{-0.11}$ pb. It is also used to constrain the Wilson coefficients for dimension-six operators which modify the $t\overline{t}Z$ vertex.

[4] Based on 35.9 fb^{-1} of proton-proton data taken at $\sqrt{s} = 13$ TeV. The result is consistent with the SM prediction and is used to constrain the Wilson coefficients for dimension-six operators describing new interactions. The result is consistent with the SM prediction at NLO 0.839 $\pm$ 0.101 pb.

$t\overline{t}\gamma$ Production Cross Section in pp Collisions at $\sqrt{s} = 13$ TeV

VALUE (pb)	DOCUMENT ID		TECN	COMMENT
• • • We do not use the following data for averages, fits, limits, etc. • • •				
	[1] TUMASYAN	21H	CMS	$pp \rightarrow t\overline{t}\gamma$
	[2] AABOUD	19AD	ATLS	$pp \rightarrow t\overline{t}\gamma$

[1] TUMASYAN 21H measured fiducial inclusive and differential cross-sections for $pp \rightarrow t\overline{t}\gamma$ at 13 TeV with 137 fb^{-1} of data. The results are in agreement with the SM predictions. The results are used to constrain anomalous couplings of the top quark in the SMEFT framework.

[2] AABOUD 19AD measured fiducial inclusive and differential cross-sections for $pp \rightarrow t\overline{t}\gamma$ at 13 TeV with 36.1 fb^{-1} of data. The results are in agreement with the theoretical predictions.

f(Q_0): $t\overline{t}$ Fraction of Events with a Veto on Additional Central Jet Activity in pp Collisions at $\sqrt{s} = 7$ TeV

Q_0 denotes the threshold of the additional jet p_T.

VALUE (%)	DOCUMENT ID		TECN	COMMENT
• • • We do not use the following data for averages, fits, limits, etc. • • •				
$80.0\pm1.1\pm1.6$	[1] CHATRCHYAN	14AE	CMS	Q_0 = 75 GeV (|y| <2.4)
$92.0\pm0.7\pm0.8$	[1] CHATRCHYAN	14AE	CMS	Q_0= 150 GeV (|y| <2.4)
$98.0\pm0.3\pm0.3$	[1] CHATRCHYAN	14AE	CMS	Q_0= 300 GeV (|y| <2.4)
$56.4\pm1.3^{+2.6}_{-2.8}$	[2] AAD	12BL	ATLS	Q_0 = 25 GeV (|y| <2.1)
$84.7\pm0.9\pm1.0$	[2] AAD	12BL	ATLS	Q_0 = 75 GeV (|y| <2.1)
$95.2^{+0.5}_{-0.6}\pm0.4$	[2] AAD	12BL	ATLS	Q_0= 150 GeV (|y| <2.1)

[1] CHATRCHYAN 15 based on 5.0 fb^{-1} of data. The $t\overline{t}$ events are selected in the dilepton and lepton + jets decay channels. For other values of Q_0 see Table 5.

[2] Based on 2.05 fb^{-1} of data. The $t\overline{t}$ events are selected in the dilepton decay channel with two identified b-jets.

Fraction of $t\overline{t}$ + multi-jet Events in pp Collisions at $\sqrt{s} = 7$ TeV

VALUE	DOCUMENT ID		TECN	COMMENT
• • • We do not use the following data for averages, fits, limits, etc. • • •				
	[1] AAD	15D	ATLS	ℓ+$\not{E}_T$ + nj (n=3 to 8)
0.332 ± 0.090	[2] CHATRCHYAN	14AE	CMS	$t\overline{t}(\ell\ell)$ + 0 jet (E_T > 30GeV)
0.436 ± 0.098	[2] CHATRCHYAN	14AE	CMS	$t\overline{t}(\ell\ell)$ + 1 jet (E_T > 30GeV)
0.232 ± 0.125	[2] CHATRCHYAN	14AE	CMS	$t\overline{t}(\ell\ell)$ + $\geq$ 2 jet (E_T > 30GeV)

[1] Based on 4.6 fb^{-1} of data. Fiducial $t\overline{t}$ production cross section is presented as a function of the jet multiplicity for up to eight jets with the jet p_T threshold of 25, 40, 60, and 80 GeV, and as a function of jet p_T up to the 5th jet. MC models can be discriminated by using data for high jet multiplicity and by p_T distributions of the leading and 5th jet.

[2] Based on 5.0 fb^{-1} of data. Events with two oppositely charged leptons, large $\not{E}_T$ and jets with at least 1 b-tag are used to measure the fraction of $t\overline{t}$ plus additional jets. The gap fraction (n=0 jet rate) as a function of the jet p_T and that of H_T, the scalar sum of the p_T's of additional jets, is shown in Fig. 8.

$t\overline{t}$ Charge Asymmetry (A_C) in pp Collisions at $\sqrt{s} = 7$ TeV

A_C = (N(Δ|y| >0) − N(Δ|y| <0)) / (N(Δ|y| >0) + N(Δ|y| <0)) where Δ|y| = $|y_t| - |y_{\overline{t}}|$ is the difference between the absolute values of the top and antitop rapidities and N is the number of events with Δ|y| positive or negative.

VALUE (%)	DOCUMENT ID		TECN	COMMENT
• • • We do not use the following data for averages, fits, limits, etc. • • •				
$0.5\pm0.7\pm0.6$	[1] AABOUD	18AM	LHC	ATLAS+CMS combination (lepton + jets)
$2.1\pm2.5\pm1.7$	[2] AAD	15AJ	ATLS	$\ell\ell$ + $\not{E}_T$ + $\geq$ 2j
0.6 ± 1.0	[3] AAD	14I	ATLS	ℓ + $\not{E}_T$ + $\geq$ 4j ($\geq$ 1b)
$-1.0\pm1.7\pm0.8$	[4] CHATRCHYAN	14D	CMS	$\ell\ell$ + $\not{E}_T$ + $\geq$ 2j ($\geq$ 1b)
$-1.9\pm2.8\pm2.4$	[5] AAD	12BK	ATLS	ℓ + $\not{E}_T$ + $\geq$ 4j ($\geq$ 1b)
$0.4\pm1.0\pm1.1$	[6] CHATRCHYAN	12BB	CMS	ℓ + $\not{E}_T$ + $\geq$ 4j ($\geq$ 1b)
$-1.3\pm2.8^{+2.9}_{-3.1}$	[7] CHATRCHYAN	12BS	CMS	ℓ + $\not{E}_T$ + $\geq$ 4j ($\geq$ 1b)

[1] ATLAS and CMS combination based on the data of AAD 14I and CHATRCHYAN 12BB. It takes into account the correlations of the measurements and systematic errors. The result is in agreement with the SM prediction (NLO QCD + NLO EW).

[2] AAD 15AJ based on 4.6 fb^{-1} of data. After kinematic reconstruction the top quark momenta are corrected for detector resolution and acceptance effects by unfolding, using parton level information of the MC generators. The lepton charge asymmetry is measured

Downloaded from https://academic.oup.com/ptep/article/2022/8/083C01/6651666 by KIT Library user on 27 September 2022

as $A_C^\ell = 0.024 \pm 0.015 \pm 0.009$. All the measurements are consistent with the SM predictions.

[3] Based on 4.7 fb^{-1} of data. The result is consistent with the SM prediction of $A_C = 0.0123 \pm 0.0005$. The asymmetry is 0.011 ± 0.018 if restricted to those events where $\beta_Z(t\overline{t}) > 0.6$, which is also consistent with the SM prediction of $0.020^{+0.006}_{-0.007}$.

[4] Based on 5.0 fb^{-1} of data. The lepton charge asymmetry is measured as $A_C^\ell = 0.009 \pm 0.0010 \pm 0.006$. A_C^ℓ dependences on $m_{t\overline{t}}$, $|y(t\overline{t})|$, and $p_T(t\overline{t})$ are given in Fig. 5. All measurements are consistent with the SM predictions.

[5] Based on 1.04 fb^{-1} of data. The result is consistent with $A_C = 0.006 \pm 0.002$ (MC at NLO). No significant dependence of A_C on $m_{t\overline{t}}$ is observed.

[6] Based on 5.0 fb^{-1} of data at 7 TeV.

[7] Based on 1.09 fb^{-1} of data. The result is consistent with the SM predictions.

$t\overline{t}$ Charge Asymmetry (A_C) in pp Collisions at $\sqrt{s} = 8$ TeV

VALUE (%)	DOCUMENT ID		TECN	COMMENT
• • • We do not use the following data for averages, fits, limits, etc. • • •				
$0.55 \pm 0.23 \pm 0.25$	[1] AABOUD	18AM	LHC	ATLAS+CMS combination (lepton + jets)
2.1 ± 1.6	[2] AAD	16AE	ATLS	$\ell\ell + \not{E}_T + \geq 2j$
0.9 ± 0.5	[3] AAD	16AZ	ATLS	$\ell + \not{E}_T + \geq 4j$
4.2 ± 3.2	[4] AAD	16T	ATLS	$m_{t\overline{t}} > 0.75$ TeV, $\|\|y_t\| - \|y_{\overline{t}}\|\| < 2$, $\ell + \not{E}_T$ + jets
$1.1 \pm 1.1 \pm 0.7$	[5] KHACHATRY...16AD		CMS	$\ell\ell + \not{E}_T + \geq 2j$ ($\geq 1b$)
$0.33 \pm 0.26 \pm 0.33$	[6] KHACHATRY...16AH		CMS	$\ell + \not{E}_T + \geq 4j$ ($\geq 1b$)
$0.10 \pm 0.68 \pm 0.37$	[7] KHACHATRY...16T		CMS	$\ell + \not{E}_T + \geq 4j$ ($\geq 1b$)

[1] ATLAS and CMS combination based on the data of AAD 16AZ and KHACHATRYAN 16AH. It takes into account the correlations of the measurements and systematic errors. A combination of the differential measurements of the charge asymmetry is also presented. The results are in agreement with the SM prediction (NNLO QCD + NLO EW).

[2] AAD 16AE is based on 20.3 fb^{-1} of data. After kinematic reconstruction, the top quark momenta are corrected for detector resolution and acceptance effects by unfolding, using parton level information of the MC generators. The lepton charge asymmetry is measured as $A_C^{\ell\ell} = 0.008 \pm 0.006$. All the measurements are consistent with the SM predictions.

[3] AAD 16AZ based on 20.3 fb^{-1} of data. All the differential and inclusive measurements are statistically limited and consistent with the SM predictions.

[4] AAD 16T based on 20.3 fb^{-1} of data. Uses reconstruction techniques for the decay topology of highly boosted top quarks. The observed asymmetry is transformed by unfolding to a parton-level result in the shown fiducial region. The result is consistent with the NLO SM prediction.

[5] KHACHATRYAN 16AD based on 19.5 fb^{-1} of data. The lepton charge asymmetry is measured as $A_C^{\ell\ell} = 0.003 \pm 0.006 \pm 0.003$. All the measurements are consistent with the SM predictions.

[6] KHACHATRYAN 16AH based on 19.6 fb^{-1} of data. The same data set as in KHACHATRYAN 16T is used. A template technique is used, which is sensitive to the charge anti-symmetric component of the $t\overline{t}$ rapidity distributions and statistically advantageous. The result is consistent with the SM predictions.

[7] KHACHATRYAN 16T based on 19.7 fb^{-1} of data. The same data set as in KHACHATRYAN 16AH is used. After kinematic reconstruction the top quark momenta are corrected for detector resolution and acceptance effects by unfolding, using parton level information of the MC generators. All the measurements are consistent with the SM predictions.

t-quark Polarization in $t\overline{t}$ Events in $p\overline{p}$ Collisions at $\sqrt{s} = 1.96$ TeV

VALUE	DOCUMENT ID		TECN	COMMENT
• • • We do not use the following data for averages, fits, limits, etc. • • •				
0.070 ± 0.055	[1] ABAZOV	17	D0	$\ell + \not{E}_T + \geq 3j$($\geq 1b$)
-0.102 ± 0.061	[2] ABAZOV	17	D0	$\ell + \not{E}_T + \geq 3j$($\geq 1b$)
0.040 ± 0.035	[3] ABAZOV	17	D0	$\ell + \not{E}_T + \geq 3j$($\geq 1b$)
$0.113 \pm 0.091 \pm 0.019$	[4] ABAZOV	15K	D0	A_{FB}^ℓ in $\ell\ell + \not{E}_T + \geq 2j$($\geq 1b$)

[1] ABAZOV 17 based on 9.7 fb^{-1} of data. The value is top quark polarization times spin analyzing power in the beam basis. Combination with the result of ABAZOV 15K yields 0.081 ± 0.048. This result together with the helicity polarization is shown in a 2-dimensional plot in Fig.4. These results are consistent with the SM prediction.

[2] ABAZOV 17 based on 9.7 fb^{-1} of data. The value is top quark polarization times spin analyzing power in the helicity basis. The result is consistent with the SM prediction. This result together with the beam polarization is shown in a 2-dimensional plot in Fig.4.

[3] ABAZOV 17 based on 9.7 fb^{-1} of data. The value is top quark polarization times spin analyzing power in the transverse basis. The result is consistent with the SM prediction.

[4] ABAZOV 15K based on 9.7 fb^{-1} of data. The value is top quark polarization times spin analyzing power in the beam basis. The result is consistent with the SM prediction of -0.0019 ± 0.0005.

t-quark Polarization in $t\overline{t}$ Events in pp Collisions at $\sqrt{s} = 7$ TeV

The double differential distribution in polar angles, θ_1 (θ_2) of the decay particle of the top (anti-top) decay products, is parametrized as $(1/\sigma)d\sigma/(d\cos\theta_1\ d\cos\theta_2) = (1/4)\ (1 + A_t \cos\theta_1 + A_{\overline{t}} \cos\theta_2 - C \cos\theta_1 \cos\theta_2)$. The charged lepton is used to tag t or $\overline{t}$. The coefficient A_t and $A_{\overline{t}}$ measure the average helicity of t and $\overline{t}$, respectively. $A_{CPC} = A_t = A_{\overline{t}}$ assumes CP conservation, whereas $A_{CPV} = A_t = -A_{\overline{t}}$ corresponds to maximal CP violation.

VALUE	DOCUMENT ID		TECN	COMMENT
• • • We do not use the following data for averages, fits, limits, etc. • • •				
$-0.035 \pm 0.014 \pm 0.037$	[1] AAD	13BE	ATLS	A_{CPC}
$0.020 \pm 0.016^{+0.013}_{-0.017}$	[1] AAD	13BE	ATLS	A_{CPV}

[1] Based on 4.7 fb^{-1} of data using the final states containing one or two isolated electrons or muons and jets with at least one b-tag.

t-quark Polarization in $t\overline{t}$ Events in pp Collisions at $\sqrt{s} = 8$ TeV

A_t, $A_{\overline{t}}$, A_{CPC}, A_{CPV}, and A_C are defined in header texts in the subsections, just above.

VALUE	DOCUMENT ID		TECN	COMMENT
• • • We do not use the following data for averages, fits, limits, etc. • • •				
$-0.044 \pm 0.038 \pm 0.027$	[1] AABOUD	17G	ATLS	A_t
$-0.064 \pm 0.040 \pm 0.027$	[1] AABOUD	17G	ATLS	$A_{\overline{t}}$
$0.296 \pm 0.093 \pm 0.037$	[1] AABOUD	17G	ATLS	A_C
-0.022 ± 0.058	[2] KHACHATRY...16AI		CMS	A_{CPC}
0.000 ± 0.016	[2] KHACHATRY...16AI		CMS	A_{CPV}

[1] AABOUD 17G based on 20.2 fb^{-1} of pp data, using events with two leptons and two or more jets with at least one b-tag. Determined from measurements of 15 top quark spin observables. The second error corresponds to a variation of m_t about 172.5 GeV by 0.7 GeV. The values are consistent with the NLO SM predictions.

[2] KHACHATRYAN 16AI based on 19.5 fb^{-1} of pp data at $\sqrt{s} = 8$ TeV, using events with two leptons and two or more jets with at least one b-tag. Determined from the lepton angular distributions as a function of the $t\overline{t}$-system kinematical variables.

t-quark Polarization in Single Top Events in pp Collisions at $\sqrt{s} = 8$ TeV

VALUE	CL%	DOCUMENT ID		TECN	COMMENT
• • • We do not use the following data for averages, fits, limits, etc. • • •					
>0.72	95	[1] AABOUD	17BB	ATLS	$\alpha_\ell P$; t-channel
$0.97 \pm 0.05 \pm 0.11$		[2] AABOUD	17I	ATLS	$\alpha_\ell P$; t-channel
$0.25 \pm 0.08 \pm 0.14$		[3] AABOUD	17I	ATLS	$(F_+ + F_-)P$; t-channel
$0.26 \pm 0.03 \pm 0.10$		[4] KHACHATRY...16BO		CMS	$(\alpha_\mu P)/2$; t-channel

[1] AABOUD 17BB based on 20.2 fb^{-1} of pp data. Triple-differential decay rate of top quark is used to simultaneously determine five generalized Wtb couplings as well as the top polarization. α_ℓ denotes the spin analyzing power of charged lepton, and the spin axis of the top polarization P is taken along the spectator-quark momentum in the top rest frame. The value is compatible with the SM prediction of about 0.9.

[2] AABOUD 17I based on 20.2 fb^{-1} of pp data. A cut-based analysis is used to discriminate between signal and backgrounds. α_ℓ denotes the spin analyzing power of charged lepton, and the spin axis of the top polarization P is taken along the spectator-quark momentum in the top rest frame. See this paper for a number of other asymmetries and measurements that are not included here.

[3] AABOUD 17I based on 20.2 fb^{-1} of pp data. A cut-based analysis is used to discriminate between signal and backgrounds. $F_\pm$ denotes W helicity fraction, and the spin axis of the top polarization P is taken along the spectator-quark momentum in the top rest frame. See this paper for a number of other asymmetries and measurements that are not included here.

[4] KHACHATRYAN 16BO based on 19.7 fb^{-1} of data. A high-purity sample with a muon is selected by a multivariate analysis. The value is the top spin asymmetry, given by one half of the spin analyzing power α_μ (=1 at LO of SM) times the top polarization, P, where the spin axis is defined as the direction of the untagged jet in the top rest frame. The value is compatible with the SM prediction of 0.44 with a 2.0σ deviation.

t-quark Polarization in Single Top Events in pp Collisions at $\sqrt{s} = 13$ TeV

VALUE	DOCUMENT ID		TECN	COMMENT
• • • We do not use the following data for averages, fits, limits, etc. • • •				
0.440 ± 0.070	[1] SIRUNYAN	20R	CMS	$(\alpha_\ell P)/2$; t-channel

[1] SIRUNYAN 20R based on 36.1 fb^{-1} of data. Differential cross sections for t-channel single top production are measured using 1ℓ + 2,3-jet mode and found to be in good agreement with SM predictions. The value is the top spin asymmetry, given by 1/2 of the spin analyzing power α_ℓ (=1 at LO of SM) times the top polarization P, where the spin axis is defined as the direction of the spectator quark in the top rest frame at the parton level. It is in good agreement with the NLO SM prediction of 0.436.

$gg \rightarrow t\overline{t}$ Fraction in $p\overline{p}$ Collisions at $\sqrt{s} = 1.96$ TeV

VALUE	CL%	DOCUMENT ID		TECN	COMMENT
• • • We do not use the following data for averages, fits, limits, etc. • • •					
<0.33	68	[1] AALTONEN	09F	CDF	$t\overline{t}$ correlations
$0.07 \pm 0.14 \pm 0.07$		[2] AALTONEN	08AG	CDF	low p_T number of tracks

[1] Based on 955 pb^{-1}. AALTONEN 09F used differences in the $t\overline{t}$ production angular distribution and polarization correlation to descriminate between $gg \rightarrow t\overline{t}$ and $q\overline{q} \rightarrow t\overline{t}$ subprocesses. The combination with the result of AALTONEN 08AG gives $0.07^{+0.15}_{-0.07}$.

[2] Result is based on 0.96 fb^{-1} of data. The contribution of the subprocesses $gg \rightarrow t\overline{t}$ and $q\overline{q} \rightarrow t\overline{t}$ is distinguished by using the difference between quark and gluon initiated jets in the number of small p_T (0.3 GeV $< p_T <$ 3 GeV) charged particles in the central region ($|\eta| < 1.1$).

A_{FB} of $t\overline{t}$ in $p\overline{p}$ Collisions at $\sqrt{s} = 1.96$ TeV

A_{FB} = Forward-backward asymmetry.

VALUE (%)	DOCUMENT ID		TECN	COMMENT
• • • We do not use the following data for averages, fits, limits, etc. • • •				
$12.8 \pm 2.1 \pm 1.4$	[1] AALTONEN	18	TEVA	CDF, D0 combination
$17.5 \pm 5.6 \pm 3.1$	[2] ABAZOV	15K	D0	A_{FB}^ℓ in $\ell\ell + \not{E}_T + \geq 2j$($\geq 1b$)
7.2 ± 6.0	[3] AALTONEN	14F	CDF	A_{FB}^ℓ in dilepton channel ($\ell\ell + \not{E}_T + \geq 2j$)
7.6 ± 8.2	[3] AALTONEN	14F	CDF	$A_{FB}^{\ell\ell}$ in dilepton channel ($\ell\ell + \not{E}_T + \geq 2j$)
$4.2 \pm 2.3^{+1.7}_{-2.0}$	[4] ABAZOV	14G	D0	A_{FB}^ℓ ($\ell + \not{E}_T + \geq 3j$ (0,1 $\geq 2b$))
10.6 ± 3.0	[5] ABAZOV	14H	D0	A_{FB} ($\ell + \not{E}_T + \geq 3j$ ($\geq 1b$))
20.1 ± 6.7	[6] AALTONEN	13AD	CDF	a_1/a_0 in $\ell + \not{E}_T + \geq 4j$ ($\geq 1b$)
-0.2 ± 3.1	[6] AALTONEN	13AD	CDF	a_3, a_5, a_7 in $\ell + \not{E}_T + \geq 4j$ ($\geq 1b$)
16.4 ± 4.7	[7] AALTONEN	13S	CDF	$\ell + \not{E}_T + \geq 4$ jets($\geq 1b$-tag)

Downloaded from https://academic.oup.com/ptep/article/2022/8/083C01/6651666 by KIT Library user on 27 September 2022

$9.4^{+3.2}_{-2.9}$	[8] AALTONEN	13X	CDF	$\ell + \not{E}_T + \geq 4$ jets (≥ 1 b-tag)
11.8 ± 3.2	[9] ABAZOV	13A	D0	$\ell\ell$ & $\ell+$ jets comb.
-11.6 ± 15.3	[10] AALTONEN	11F	CDF	$m_{t\overline{t}} < 450$ GeV
47.5 ± 11.4	[10] AALTONEN	11F	CDF	$m_{t\overline{t}} > 450$ GeV
19.6 ± 6.5	[11] ABAZOV	11AH	D0	$\ell + \not{E}_T + \geq 4$ jets($\geq 1b$-tag)
17 ± 8	[12] AALTONEN	08AB	CDF	$p\overline{p}$ frame
24 ± 14	[12] AALTONEN	08AB	CDF	$t\overline{t}$ frame
$12 \pm 8 \pm 1$	[13] ABAZOV	08L	D0	$\ell + \not{E}_T + \geq 4$ jets

[1] AALTONEN 18 based on 9–10 fb^{-1} of $p\overline{p}$ data at $\sqrt{s} = 1.96$ TeV. The value is the asymmetry in the number of reconstructed $t\overline{t}$ events with rapidity $y_t > y_{\overline{t}}$ and those with $y_t < y_{\overline{t}}$. The combined fits to CDF and D0 single lepton and $\ell\ell$ asymmetries give $A^{\ell}_{FB} = 0.073 \pm 0.016 \pm 0.012$ and $A^{\ell\ell}_{FB} = 0.108 \pm 0.043 \pm 0.016$, respectively. The results are consistent with the SM predictions.

[2] ABAZOV 15K based on 9.7 fb^{-1} of data. The result is consistent with the SM predictions. By combining with the previous D0 measurement in the ℓ + jet channel ABAZOV 14H, $A^{\ell}_{FB} = 0.118 \pm 0.025 \pm 0.013$ is obtained.

[3] AALTONEN 14F based on 9.1 fb^{-1} of data. A^{ℓ}_{FB} and $A^{\ell\ell}_{FB}$ denote, respectively, the asymmetries $(N(x>0) - N(x<0))/N_{tot}$ for $x = q_\ell \eta_\ell$ (q_ℓ is the charge of ℓ) and $x = \eta_{\ell^+} - \eta_{\ell^-}$. Both results are consistent with the SM predictions. By combining with the previous CDF measurement in the ℓ+jet channel AALTONEN 13X, $A^{\ell}_{FB} = 0.098^{+0.028}_{-0.026}$ is obtained. The combined result is about two sigma larger than the SM prediction of $A^{\ell}_{FB} = 0.038 \pm 0.003$.

[4] Based on 9.7 fb^{-1} of $p\overline{p}$ data at $\sqrt{s} = 1.96$ TeV. The asymmetry is corrected for the production level for events with $|y_l| < 1.5$. Asymmetry as functions of $E_T(\ell)$ and $|y_l|$ are given in Figs. 7 and 8, respectively. Combination with the asymmetry measured in the dilepton channel [ABAZOV 13P] gives $A^{\ell}_{FB} = 4.2 \pm 2.0 \pm 1.4$ %, in agreement with the SM prediction of 2.0%.

[5] Based on 9.7 fb^{-1} of data of $p\overline{p}$ data at $\sqrt{s}$=1.96 TeV. The measured asymmetry is in agreement with the SM predictions of 8.8 ± 0.9 % [BERNREUTHER 12], which includes the EW effects. The dependences of the asymmetry on $|y(t) - y(\overline{t})|$ and $m_{t\overline{t}}$ are shown in Figs. 9 and 10, respectively.

[6] Based on 9.4 fb^{-1} of data. Reported A_{FB} values come from the determination of a_i coefficients of $d\sigma/d(\cos\theta_t) = \Sigma_i\ a_i P_i(\cos(\theta_t))$ measurement. The result of $a_1/a_0 = (40 \pm 12)$% seems higher than the NLO SM prediction of (15^{+7}_{-3})%.

[7] Based on 9.4 fb^{-1} of data. The quoted result is the asymmetry at the parton level.

[8] Based on 9.4 fb^{-1} of data. The observed asymmetry is to be compared with the SM prediction of $A^{\ell}_{FB} = 0.038 \pm 0.003$.

[9] Based on 5.4 fb^{-1} of data. ABAZOV 13A studied the dilepton channel of the $t\overline{t}$ events and measured the leptonic forward-backward asymmetry to be $A^{\ell}_{FB} = 5.8 \pm 5.1 \pm 1.3$%, which is consistent with the SM (QCD+EW) prediction of 4.7 ± 0.1%. The result is obtained after combining the measurement (15.2 ± 4.0)% in the ℓ + jets channel ABAZOV 11AH. The top quark helicity is measured by using the neutrino weighting method to be consistent with zero in both dilepton and ℓ + jets channels.

[10] Based on 5.3 fb^{-1} of data. The error is statistical and systematic combined. Events with lepton + $\not{E}_T$ + $\geq$ 4jets($\geq 1b$) are used. AALTONEN 11F also measures the asymmetry as a function of the rapidity difference $|y_t - y_{\overline{t}}|$. The NLO QCD predictions [MCFM] are (4.0 ± 0.6)% and (8.8 ± 1.3)% for $m_{t\overline{t}} < 450$ and > 450 GeV, respectively.

[11] Based on 5.4 fb^{-1} of data. The error is statistical and systematic combined. The quoted asymmetry is obtained after unfolding to be compared with the MC@NLO prediction of (5.0 ± 0.1)%. No significant difference between the $m_{t\overline{t}} < 450$ and > 450 GeV data samples is found. A corrected asymmetry based on the lepton from a top quark decay of (15.2 ± 4.0)% is measured to be compared to the MC@NLO prediction of (2.1 ± 0.1)%.

[12] Result is based on 1.9 fb^{-1} of data. The *FB* asymmetry in the $t\overline{t}$ events has been measured in the ℓ + jets mode, where the lepton charge is used as the flavor tag. The asymmetry in the $p\overline{p}$ frame is defined in terms of $\cos(\theta)$ of hadronically decaying t-quark momentum, whereas that in the $t\overline{t}$ frame is defined in terms of the t and $\overline{t}$ rapidity difference. The results are consistent ($\leq 2\ \sigma$) with the SM predictions.

[13] Result is based on 0.9 fb^{-1} of data. The asymmetry in the number of $t\overline{t}$ events with $y_t > y_{\overline{t}}$ and those with $y_t < y_{\overline{t}}$ has been measured in the lepton + jets final state. The observed value is consistent with the SM prediction of 0.8% by MC@NLO, and an upper bound on the $Z' \rightarrow t\overline{t}$ contribution for the SM Z-like couplings is given in in Fig. 2 for 350 GeV $< m_{Z'} < 1$ TeV.

t-Quark Electric Charge

VALUE	DOCUMENT ID		TECN	COMMENT
0.64±0.02±0.08	[1] AAD	13AY	ATLS	$\ell + \not{E}_T + \geq 4$ jets (≥ 1 b)
• • • We do not use the following data for averages, fits, limits, etc. • • •				
	[2] ABAZOV	14D	D0	$\ell + \not{E}_T + \geq 4$ jets (≥ 2 b)
	[3] AALTONEN	13J	CDF	$p\overline{p}$ at 1.96 TeV
	[4] AALTONEN	10S	CDF	Repl. by AALTONEN 13J
	[5] ABAZOV	07C	D0	fraction of $\|q\|$=4e/3 pair

[1] AAD 13AY result is based on 2.05 fb^{-1} of pp data at $\sqrt{s} = 7$ TeV, the result is obtained by reconstructing $t\overline{t}$ events in the lepton + jets final state, where b-jet charges are tagged by the jet-charge algorithm. This measurement excludes the charge $-4/3$ assignment to the top quark at more than 8 standard deviations.

[2] ABAZOV 14D result is based on 5.3 fb^{-1} of $p\overline{p}$ data at $\sqrt{s}$=1.96 TeV. The electric charge of $b + W$ system in $t\overline{t}$ candidate events is measured from the charges of the leptons from W decay and in b jets. Under the assumption that the $b + W$ system consists of the sum of the top quark and the charge $-4/3$ quark b'(-4/3) of the same mass, the top quark fraction is found to be $f = 0.88 \pm 0.13$ (stat)± 0.11 (syst), or the upper bound for the b'(-4/3) contamination of $1 - f < 0.46$ (95% CL).

[3] AALTONEN 13J excludes the charge $-4/3$ assignment to the top quark at 99% CL, using 5.6 fb^{-1} of data in $p\overline{p}$ collisions at $\sqrt{s} = 1.96$ TeV. Result is obtained by reconstructing $t\overline{t}$ events in the lepton + jets final state, where b-jet charges are tagged by the jet-charge algorithm.

[4] AALTONEN 10S excludes the charge $-4/3$ assignment for the top quark [CHANG 99] at 95%CL, using 2.7 fb^{-1} of data in $p\overline{p}$ collisions at $\sqrt{s} = 1.96$ TeV. Result is obtained by reconstructing $t\overline{t}$ events in the lepton + jets final state, where b-jet charges are tagged by the SLT (soft lepton tag) algorithm.

[5] ABAZOV 07C reports an upper limit $\rho < 0.80$ (90% CL) on the fraction ρ of exotic quark pairs $Q\overline{Q}$ with electric charge $|q| = 4e/3$ in $t\overline{t}$ candidate events with high p_T lepton, missing E_T and ≥ 4 jets. The result is obtained by measuring the fraction of events in which the quark pair decays into $W^- + b$ and $W^+ + \overline{b}$, where b and $\overline{b}$ jets are discriminated by using the charge and momenta of tracks within the jet cones. The maximum CL at which the model of CHANG 99 can be excluded is 92%. Based on 370 pb^{-1} of data at $\sqrt{s} = 1.96$ TeV.

t-Quark REFERENCES

AAD	21AS	EPJ C81 737	G. Aad *et al.*	(ATLAS Collab.)
AAD	21AT	EPJ C81 720	G. Aad *et al.*	(ATLAS Collab.)
AAD	21BC	JHEP 2111 118	G. Aad *et al.*	(ATLAS Collab.)
TUMASYAN	21E	JHEP 2111 111	A. Tumasyan *et al.*	(CMS Collab.)
TUMASYAN	21G	JHEP 2112 161	A. Tumasyan *et al.*	(CMS Collab.)
TUMASYAN	21H	JHEP 2112 180	A. Tumasyan *et al.*	(CMS Collab.)
TUMASYAN	21J	PR D104 092013	A. Tumasyan *et al.*	(CMS Collab.)
AAD	20AB	JHEP 2007 124	G. Aad *et al.*	(ATLAS Collab.)
AAD	20AH	PL B810 135797	G. Aad *et al.*	(ATLAS Collab.)
AAD	20AR	EPJ C80 1085	G. Aad *et al.*	(ATLAS Collab.)
AAD	20B	PL B800 135082	G. Aad *et al.*	(ATLAS Collab.)
AAD	20Q	EPJ C80 528	G. Aad *et al.*	(ATLAS Collab.)
AAD	20Y	JHEP 2008 051	G. Aad *et al.*	(ATLAS and CMS Collabs.)
AAD	20Z	PRL 125 061802	G. Aad *et al.*	(ATLAS Collab.)
SIRUNYAN	20AB	JHEP 2003 056	A.M. Sirunyan *et al.*	(CMS Collab.)
SIRUNYAN	20AM	JHEP 2006 146	A.M. Sirunyan *et al.*	(CMS Collab.)
SIRUNYAN	20AR	PRL 124 202001	A.M. Sirunyan *et al.*	(CMS Collab.)
SIRUNYAN	20AS	PRL 125 061801	A.M. Sirunyan *et al.*	(CMS Collab.)
SIRUNYAN	20AZ	PL B808 135609	A.M. Sirunyan *et al.*	(CMS Collab.)
SIRUNYAN	20BC	PRL 125 222001	A.M. Sirunyan	(CMS Collab.)
SIRUNYAN	20BH	PR D102 092013	A.M. Sirunyan *et al.*	(CMS Collab.)
SIRUNYAN	20BV	EPJ C80 658	A.M. Sirunyan *et al.*	(CMS Collab.)
SIRUNYAN	20C	EPJ C80 75	A.M. Sirunyan *et al.*	(CMS Collab.)
SIRUNYAN	20D	PL B800 135042	A.M. Sirunyan *et al.*	(CMS Collab.)
SIRUNYAN	20R	EPJ C80 370	A.M. Sirunyan *et al.*	(CMS Collab.)
SIRUNYAN	20V	JHEP 2002 191	A.M. Sirunyan *et al.*	(CMS Collab.)
AABOUD	19AC	EPJ C79 290	M. Aaboud *et al.*	(ATLAS Collab.)
AABOUD	19AD	EPJ C79 382	M. Aaboud *et al.*	(ATLAS Collab.)
AABOUD	19AP	PR D99 052009	M. Aaboud *et al.*	(ATLAS Collab.)
AABOUD	19AR	PR D99 072009	M. Aaboud *et al.*	(ATLAS Collab.)
AABOUD	19R	JHEP 1905 088	M. Aaboud *et al.*	(ATLAS and CMS Collabs.)
AABOUD	19S	JHEP 1905 123	M. Aaboud *et al.*	(ATLAS Collab.)
AAD	19G	JHEP 1911 150	G. Aad *et al.*	(ATLAS Collab.)
SIRUNYAN	19AP	EPJ C79 313	A.M. Sirunyan *et al.*	(CMS Collab.)
SIRUNYAN	19AR	EPJ C79 368	A.M. Sirunyan *et al.*	(CMS Collab.)
SIRUNYAN	19BF	PRL 122 132003	A.M. Sirunyan *et al.*	(CMS Collab.)
SIRUNYAN	19BX	PR D100 072002	A.M. Sirunyan *et al.*	(CMS Collab.)
SIRUNYAN	19BY	PR D100 072007	A.M. Sirunyan *et al.*	(CMS Collab.)
SIRUNYAN	19CN	JHEP 1911 082	A.M. Sirunyan *et al.*	(CMS Collab.)
SIRUNYAN	19P	JHEP 1902 149	A.M. Sirunyan *et al.*	(CMS Collab.)
SIRUNYAN	19R	JHEP 1903 026	A.M. Sirunyan *et al.*	(CMS Collab.)
AABOUD	18AE	PL B780 557	M. Aaboud *et al.*	(ATLAS Collab.)
AABOUD	18AM	JHEP 1804 033	M. Aaboud *et al.*	(ATLAS and CMS Collabs.)
AABOUD	18AT	JHEP 1807 176	M. Aaboud *et al.*	(ATLAS Collab.)
AABOUD	18AZ	EPJ C78 129	M. Aaboud *et al.*	(ATLAS Collab.)
AABOUD	18BH	EPJ C78 487	M. Aaboud *et al.*	(ATLAS Collab.)
AABOUD	18BK	PL B784 173	M. Aaboud *et al.*	(ATLAS Collab.)
AABOUD	18BW	JHEP 1809 139	M. Aaboud *et al.*	(ATLAS Collab.)
AABOUD	18CE	JHEP 1812 039	M. Aaboud *et al.*	(ATLAS Collab.)
AABOUD	18H	JHEP 1801 063	M. Aaboud *et al.*	(ATLAS Collab.)
AABOUD	18X	PR D98 032002	M. Aaboud *et al.*	(ATLAS Collab.)
AALTONEN	18	PRL 120 042001	T. Aaltonen *et al.*	(CDF and D0 Collabs.)
SIRUNYAN	18AQ	JHEP 1803 115	A.M. Sirunyan *et al.*	(CMS Collab.)
SIRUNYAN	18BC	JHEP 1806 102	A.M. Sirunyan *et al.*	(CMS Collab.)
SIRUNYAN	18BD	JHEP 1806 101	A.M. Sirunyan *et al.*	(CMS Collab.)
SIRUNYAN	18BS	JHEP 1808 011	A.M. Sirunyan *et al.*	(CMS Collab.)
SIRUNYAN	18BU	EPJ C78 140	A.M. Sirunyan *et al.*	(CMS Collab.)
SIRUNYAN	18DE	EPJ C78 891	A.M. Sirunyan *et al.*	(CMS Collab.)
SIRUNYAN	18DL	JHEP 1810 117	A.M. Sirunyan *et al.*	(CMS Collab.)
SIRUNYAN	18L	PRL 120 231801	A.M. Sirunyan *et al.*	(CMS Collab.)
SIRUNYAN	18Z	PL B779 358	A.M. Sirunyan *et al.*	(CMS Collab.)
AABOUD	17AH	JHEP 1709 118	M. Aaboud *et al.*	(ATLAS Collab.)
AABOUD	17AV	JHEP 1710 129	M. Aaboud *et al.*	(ATLAS Collab.)
AABOUD	17BB	JHEP 1712 017	M. Aaboud *et al.*	(ATLAS Collab.)
AABOUD	17BC	EPJ C77 804	M. Aaboud *et al.*	(ATLAS Collab.)
AABOUD	17G	JHEP 1703 113	M. Aaboud *et al.*	(ATLAS Collab.)
AABOUD	17H	JHEP 1704 086	M. Aaboud *et al.*	(ATLAS Collab.)
AABOUD	17I	JHEP 1704 124	M. Aaboud *et al.*	(ATLAS Collab.)
AABOUD	17T	EPJ C77 531	M. Aaboud *et al.*	(ATLAS Collab.)
AABOUD	17Z	PR D95 072003	M. Aaboud *et al.*	(ATLAS Collab.)
ABAZOV	17	PR D95 011101	V.M. Abazov *et al.*	(D0 Collab.)
ABAZOV	17B	PR D95 112004	V.M. Abazov *et al.*	(D0 Collab.)
CHATRCHYAN	17	PL B770 50	S. Chatrchyan *et al.*	(CMS Collab.)
KHACHATRY...	17B	EPJ C77 15	V. Khachatryan *et al.*	(CMS Collab.)
KHACHATRY...	17G	JHEP 1702 028	V. Khachatryan *et al.*	(CMS Collab.)
KHACHATRY...	17I	JHEP 1702 079	V. Khachatryan *et al.*	(CMS Collab.)
KHACHATRY...	17N	EPJ C77 172	V. Khachatryan *et al.*	(CMS Collab.)
SIRUNYAN	17AA	PL B772 752	A.M. Sirunyan *et al.*	(CMS Collab.)
SIRUNYAN	17AB	PL B772 336	A.M. Sirunyan *et al.*	(CMS Collab.)
SIRUNYAN	17E	JHEP 1707 003	A.M. Sirunyan *et al.*	(CMS Collab.)
SIRUNYAN	17L	EPJ C77 354	A.M. Sirunyan *et al.*	(CMS Collab.)
SIRUNYAN	17N	EPJ C77 467	A.M. Sirunyan *et al.*	(CMS Collab.)
SIRUNYAN	17O	PR D96 032002	A.M. Sirunyan *et al.*	(CMS Collab.)
SIRUNYAN	17S	EPJ C77 578	A.M. Sirunyan *et al.*	(CMS Collab.)
SIRUNYAN	17W	JHEP 1709 051	A.M. Sirunyan *et al.*	(CMS Collab.)
AABOUD	16R	PL B761 136	M. Aaboud *et al.*	(ATLAS Collab.)
AABOUD	16T	PL B761 350	M. Aaboud *et al.*	(ATLAS Collab.)
AAD	16AE	PR D94 032006	G. Aad *et al.*	(ATLAS Collab.)
AAD	16AK	JHEP 1604 023	G. Aad *et al.*	(ATLAS Collab.)
AAD	16AS	EPJ C76 55	G. Aad *et al.*	(ATLAS Collab.)
AAD	16AZ	EPJ C76 87	G. Aad *et al.*	(ATLAS Collab.)
AAD	16B	JHEP 1601 064	G. Aad *et al.*	(ATLAS Collab.)
AAD	16BK	EPJ C76 642	G. Aad *et al.*	(ATLAS Collab.)
AAD	16D	EPJ C76 12	G. Aad *et al.*	(ATLAS Collab.)
AAD	16T	PL B756 52	G. Aad *et al.*	(ATLAS Collab.)
AAD	16U	PL B756 228	G. Aad *et al.*	(ATLAS Collab.)
AALTONEN	16	PR D93 032011	T. Aaltonen *et al.*	(CDF Collab.)
ABAZOV	16	PL B752 18	V.M. Abazov *et al.*	(D0 Collab.)
ABAZOV	16A	PL B757 199	V.M. Abazov *et al.*	(D0 Collab.)
ABAZOV	16D	PR D94 032004	V.M. Abazov *et al.*	(D0 Collab.)
ABAZOV	16F	PR D94 092004	V.M. Abazov *et al.*	(D0 Collab.)
KHACHATRY...	16AD	PL B760 365	V. Khachatryan *et al.*	(CMS Collab.)
KHACHATRY...	16AH	PR D93 034014	V. Khachatryan *et al.*	(CMS Collab.)

Downloaded from https://academic.oup.com/ptep/article/2022/8/083C01/6651666 by KIT Library user on 27 September 2022

KHACHATRY... 16AI PR D93 052007 V. Khachatryan *et al.* (CMS Collab.)
KHACHATRY... 16AK PR D93 072004 V. Khachatryan *et al.* (CMS Collab.)
KHACHATRY... 16AL PR D93 092006 V. Khachatryan *et al.* (CMS Collab.)
KHACHATRY... 16AS JHEP 1604 035 V. Khachatryan *et al.* (CMS Collab.)
KHACHATRY... 16AW JHEP 1608 029 V. Khachatryan *et al.* (CMS Collab.)
KHACHATRY... 16AZ JHEP 1609 027 V. Khachatryan *et al.* (CMS Collab.)
KHACHATRY... 16BC EPJ C76 128 V. Khachatryan *et al.* (CMS Collab.)
KHACHATRY... 16BJ EPJ C76 439 V. Khachatryan *et al.* (CMS Collab.)
KHACHATRY... 16BO JHEP 1604 073 V. Khachatryan *et al.* (CMS Collab.)
KHACHATRY... 16BU PL B762 512 V. Khachatryan *et al.* (CMS Collab.)
KHACHATRY... 16CB JHEP 1612 123 V. Khachatryan *et al.* (CMS Collab.)
KHACHATRY... 16J PRL 116 052002 V. Khachatryan *et al.* (CMS Collab.)
KHACHATRY... 16T PL B757 154 V. Khachatryan *et al.* (CMS Collab.)
KHACHATRY... 16X PL B758 321 V. Khachatryan *et al.* (CMS Collab.)
TEVEWWG 16 arXiv:1608.01881 Tevatron Electroweak Working Group
AAD 15 PL B740 222 G. Aad *et al.* (ATLAS Collab.)
AAD 15A PL B740 118 G. Aad *et al.* (ATLAS Collab.)
AAD 15AJ JHEP 1505 061 G. Aad *et al.* (ATLAS Collab.)
AAD 15AR JHEP 1508 105 G. Aad *et al.* (ATLAS Collab.)
AAD 15AW EPJ C75 158 G. Aad *et al.* (ATLAS Collab.)
AAD 15BF EPJ C75 330 G. Aad *et al.* (ATLAS Collab.)
AAD 15BO PR D91 052005 G. Aad *et al.* (ATLAS Collab.)
AAD 15BP PR D91 112013 G. Aad *et al.* (ATLAS Collab.)
AAD 15BW JHEP 1510 121 G. Aad *et al.* (ATLAS Collab.)
AAD 15BY JHEP 1510 150 G. Aad *et al.* (ATLAS Collab.)
AAD 15CC PR D92 072005 G. Aad *et al.* (ATLAS Collab.)
AAD 15CO JHEP 1512 061 G. Aad *et al.* (ATLAS Collab.)
AAD 15D JHEP 1501 020 G. Aad *et al.* (ATLAS Collab.)
AAD 15J PRL 114 142001 G. Aad *et al.* (ATLAS Collab.)
AAIJ 15R PRL 115 112001 R. Aaij *et al.* (LHCb Collab.)
AALTONEN 15D PR D92 032003 T. Aaltonen *et al.* (CDF Collab.)
AALTONEN 15H PRL 115 152003 T. Aaltonen *et al.* (CDF, D0 Collab.)
ABAZOV 15G PR D91 112003 V.M. Abazov *et al.* (D0 Collab.)
ABAZOV 15K PR D92 052007 V.M. Abazov *et al.* (D0 Collab.)
CHATRCHYAN 15 EPJ C75 216 (errat.) S. Chatrchyan *et al.* (CMS Collab.)
AAD 14 PL B728 363 G. Aad *et al.* (ATLAS Collab.)
AAD 14AA JHEP 1406 008 G. Aad *et al.* (ATLAS Collab.)
AAD 14AY EPJ C74 3109 G. Aad *et al.* (ATLAS Collab.)
AAD 14BB PR D90 112016 G. Aad *et al.* (ATLAS Collab.)
AAD 14BI PR D90 112006 G. Aad *et al.* (ATLAS Collab.)
AAD 14I JHEP 1402 107 G. Aad *et al.* (ATLAS Collab.)
AALTONEN 14A PR D89 091101 T. Aaltonen *et al.* (CDF Collab.)
AALTONEN 14F PRL 113 042001 T. Aaltonen *et al.* (CDF Collab.)
Also PRL 117 199901 (errat.) T. Aaltonen *et al.* (CDF Collab.)
AALTONEN 14G PRL 112 221801 T. Aaltonen *et al.* (CDF Collab.)
AALTONEN 14H PR D89 072001 T. Aaltonen *et al.* (CDF and D0 Collab.)
AALTONEN 14K PRL 112 231805 T. Aaltonen *et al.* (CDF Collab.)
AALTONEN 14L PRL 112 231804 T. Aaltonen *et al.* (CDF Collab.)
AALTONEN 14M PRL 112 231803 T. Aaltonen *et al.* (CDF and D0 Collab.)
AALTONEN 14N PR D90 091101 T. Aaltonen *et al.* (CDF Collab.)
AALTONEN 14O PRL 113 261804 T. Aaltonen *et al.* (CDF Collab.)
ABAZOV 14C PRL 113 032002 V.M. Abazov *et al.* (D0 Collab.)
Also PR D91 112003 V.M. Abazov *et al.* (D0 Collab.)
ABAZOV 14D PR D90 051101 V.M. Abazov *et al.* (D0 Collab.)
ABAZOV 14G PR D90 072001 V.M. Abazov *et al.* (D0 Collab.)
ABAZOV 14H PR D90 072011 V.M. Abazov *et al.* (D0 Collab.)
ABAZOV 14K PR D90 092006 V.M. Abazov *et al.* (D0 Collab.)
CHATRCHYAN 14 PL B728 496 S. Chatrchyan *et al.* (CMS Collab.)
CHATRCHYAN 14AC PRL 112 231802 S. Chatrchyan *et al.* (CMS Collab.)
CHATRCHYAN 14AE EPJ C74 3014 S. Chatrchyan *et al.* (CMS Collab.)
Also EPJ C75 216 (errat.) S. Chatrchyan *et al.* (CMS Collab.)
CHATRCHYAN 14C EPJ C74 2758 S. Chatrchyan *et al.* (CMS Collab.)
CHATRCHYAN 14D JHEP 1404 191 S. Chatrchyan *et al.* (CMS Collab.)
CHATRCHYAN 14F JHEP 1402 024 S. Chatrchyan *et al.* (CMS Collab.)
CHATRCHYAN 14O PL B731 173 S. Chatrchyan *et al.* (CMS Collab.)
CHATRCHYAN 14R PR D90 032006 S. Chatrchyan *et al.* (CMS Collab.)
CHATRCHYAN 14S PRL 112 171802 S. Chatrchyan *et al.* (CMS Collab.)
KHACHATRY... 14E PL B736 33 V. Khachartryan *et al.* (CMS Collab.)
KHACHATRY... 14F JHEP 1406 090 V. Khachartryan *et al.* (CMS Collab.)
KHACHATRY... 14H JHEP 1409 087 V. Khachartryan *et al.* (CMS Collab.)
KHACHATRY... 14K PL B738 526 (errat.) S. Chatrchyan *et al.* (CMS Collab.)
KHACHATRY... 14N EPJ C74 3060 V. Khachartryan *et al.* (CMS Collab.)
KHACHATRY... 14Q PR D90 112013 V. Khachartryan *et al.* (CMS Collab.)
KHACHATRY... 14R JHEP 1411 154 V. Khachartryan *et al.* (CMS Collab.)
KHACHATRY... 14S PL B739 23 V. Khachartryan *et al.* (CMS Collab.)
AAD 13AY JHEP 1311 031 G. Aad *et al.* (ATLAS Collab.)
AAD 13BE PRL 111 232002 G. Aad *et al.* (ATLAS Collab.)
AAD 13X EPJ C73 2328 G. Aad *et al.* (ATLAS Collab.)
AALTONEN 13AB PR D88 091103 T. Aaltonen *et al.* (CDF Collab.)
AALTONEN 13AD PRL 111 182002 T. Aaltonen *et al.* (CDF Collab.)
AALTONEN 13D PR D87 031104 T. Aaltonen *et al.* (CDF Collab.)
AALTONEN 13E PR D87 052013 T. Aaltonen *et al.* (CDF Collab.)
AALTONEN 13G PR D87 111101 T. Aaltonen *et al.* (CDF Collab.)
AALTONEN 13H PR D88 011101 T. Aaltonen *et al.* (CDF Collab.)
AALTONEN 13J PR D88 032003 T. Aaltonen *et al.* (CDF Collab.)
AALTONEN 13S PR D87 092002 T. Aaltonen *et al.* (CDF Collab.)
AALTONEN 13X PR D88 072003 T. Aaltonen *et al.* (CDF Collab.)
AALTONEN 13Z PRL 111 202001 T. Aaltonen *et al.* (CDF Collab.)
ABAZOV 13A PR D87 011103 V.M. Abazov *et al.* (D0 Collab.)
ABAZOV 13O PL B726 656 V.M. Abazov *et al.* (D0 Collab.)
ABAZOV 13P PR D88 112002 V.M. Abazov *et al.* (D0 Collab.)
CHATRCHYAN 13AY JHEP 1305 065 S. Chatrchyan *et al.* (CMS Collab.)
CHATRCHYAN 13BB PL B720 83 S. Chatrchyan *et al.* (CMS Collab.)
CHATRCHYAN 13BE EPJ C73 2386 S. Chatrchyan *et al.* (CMS Collab.)
CHATRCHYAN 13BH JHEP 1310 167 S. Chatrchyan *et al.* (CMS Collab.)
CHATRCHYAN 13C PRL 110 022003 S. Chatrchyan *et al.* (CMS Collab.)
CHATRCHYAN 13F PL B718 1252 S. Chatrchyan *et al.* (CMS Collab.)
CHATRCHYAN 13S EPJ C73 2494 S. Chatrchyan *et al.* (CMS Collab.)
AAD 12B PL B707 459 G. Aad *et al.* (ATLAS Collab.)
AAD 12BE JHEP 1204 069 G. Aad *et al.* (ATLAS Collab.)
AAD 12BF JHEP 1205 059 G. Aad *et al.* (ATLAS Collab.)
AAD 12BG JHEP 1206 088 G. Aad *et al.* (ATLAS Collab.)
AAD 12BK EPJ C72 2039 G. Aad *et al.* (ATLAS Collab.)
AAD 12BL EPJ C72 2043 G. Aad *et al.* (ATLAS Collab.)
AAD 12BO PL B711 244 G. Aad *et al.* (ATLAS Collab.)
AAD 12BP PL B712 351 G. Aad *et al.* (ATLAS Collab.)
AAD 12BT JHEP 1209 139 G. Aad *et al.* (ATLAS Collab.)
AAD 12CG PL B717 89 G. Aad *et al.* (ATLAS Collab.)
AAD 12CH PL B717 330 G. Aad *et al.* (ATLAS Collab.)
AAD 12I EPJ C72 2046 G. Aad *et al.* (ATLAS Collab.)
AALTONEN 12AI PRL 109 152003 T. Aaltonen *et al.* (CDF Collab.)
AALTONEN 12AL PRL 109 192001 T. Aaltonen *et al.* (CDF Collab.)
AALTONEN 12AP PR D86 092003 T. Aaltonen *et al.* (CDF, D0 Collab.)
AALTONEN 12G PL B714 24 T. Aaltonen *et al.* (CDF Collab.)
AALTONEN 12Z PR D85 071106 T. Aaltonen *et al.* (CDF, D0 Collab.)
ABAZOV 12AB PR D86 051103 V.M. Abazov *et al.* (D0 Collab.)
ABAZOV 12B PRL 108 032004 V.M. Abazov *et al.* (D0 Collab.)
ABAZOV 12E PL B708 21 V.M. Abazov *et al.* (D0 Collab.)
ABAZOV 12I PL B713 165 V.M. Abazov *et al.* (D0 Collab.)
ABAZOV 12T PR D85 091104 V.M. Abazov *et al.* (D0 Collab.)
BERNREUTH... 12 PR D86 034026 W. Bernreuther, Z.-G. Si (AACH, SHDN)
CHATRCHYAN 12AC PR D85 112007 S. Chatrchyan *et al.* (CMS Collab.)
CHATRCHYAN 12AX JHEP 1211 067 S. Chatrchyan *et al.* (CMS Collab.)
CHATRCHYAN 12BA EPJ C72 2202 S. Chatrchyan *et al.* (CMS Collab.)
CHATRCHYAN 12BB PL B717 129 S. Chatrchyan *et al.* (CMS Collab.)
CHATRCHYAN 12BP JHEP 1212 105 S. Chatrchyan *et al.* (CMS Collab.)
CHATRCHYAN 12BQ JHEP 1212 035 S. Chatrchyan *et al.* (CMS Collab.)
CHATRCHYAN 12BS PL B709 28 S. Chatrchyan *et al.* (CMS Collab.)
CHATRCHYAN 12Y JHEP 1206 109 S. Chatrchyan *et al.* (CMS Collab.)
AAD 11A EPJ C71 1577 G. Aad *et al.* (ATLAS Collab.)
AALTONEN 11AC PR D84 071105 T. Aaltonen *et al.* (CDF Collab.)
AALTONEN 11AK PRL 107 232002 T. Aaltonen *et al.* (CDF Collab.)
AALTONEN 11AR PR D83 031104 T. Aaltonen *et al.* (CDF Collab.)
AALTONEN 11D PR D83 071102 T. Aaltonen *et al.* (CDF Collab.)
AALTONEN 11E PR D83 111101 T. Aaltonen *et al.* (CDF Collab.)
AALTONEN 11F PR D83 112003 T. Aaltonen *et al.* (CDF Collab.)
AALTONEN 11K PRL 106 152001 T. Aaltonen *et al.* (CDF Collab.)
AALTONEN 11T PL B698 371 T. Aaltonen *et al.* (CDF Collab.)
AALTONEN 11W PR D84 031101 T. Aaltonen *et al.* (CDF Collab.)
AALTONEN 11Y PR D84 032003 T. Aaltonen *et al.* (CDF Collab.)
AALTONEN 11Z PR D84 031104 T. Aaltonen *et al.* (CDF Collab.)
ABAZOV 11A PL B695 88 V.M. Abazov *et al.* (D0 Collab.)
ABAZOV 11AA PL B705 313 V.M. Abazov *et al.* (D0 Collab.)
ABAZOV 11AD PR D84 112001 V.M. Abazov *et al.* (D0 Collab.)
ABAZOV 11AE PRL 107 032001 V.M. Abazov *et al.* (D0 Collab.)
ABAZOV 11AF PL B702 16 V.M. Abazov *et al.* (D0 Collab.)
ABAZOV 11AH PR D84 112005 V.M. Abazov *et al.* (D0 Collab.)
ABAZOV 11B PRL 106 022001 V.M. Abazov *et al.* (D0 Collab.)
ABAZOV 11C PR D83 032009 V.M. Abazov *et al.* (D0 Collab.)
ABAZOV 11E PR D84 012008 V.M. Abazov *et al.* (D0 Collab.)
ABAZOV 11M PL B701 313 V.M. Abazov *et al.* (D0 Collab.)
ABAZOV 11P PR D84 032004 V.M. Abazov *et al.* (D0 Collab.)
ABAZOV 11R PRL 107 082004 V.M. Abazov *et al.* (D0 Collab.)
ABAZOV 11S PL B703 422 V.M. Abazov *et al.* (D0 Collab.)
ABAZOV 11T PR D84 052005 V.M. Abazov *et al.* (D0 Collab.)
ABAZOV 11X PRL 107 121802 V.M. Abazov *et al.* (D0 Collab.)
ABAZOV 11Z PL B704 403 V.M. Abazov *et al.* (D0 Collab.)
CHATRCHYAN 11AA EPJ C71 1721 S. Chatrchyan *et al.* (CMS Collab.)
CHATRCHYAN 11F JHEP 1107 049 S. Chatrchyan *et al.* (CMS Collab.)
CHATRCHYAN 11R PRL 107 091802 S. Chatrchyan *et al.* (CMS Collab.)
CHATRCHYAN 11Z PR D84 092004 S. Chatrchyan *et al.* (CMS Collab.)
KHACHATRY... 11A PL B695 424 V. Khachatryan *et al.* (CMS Collab.)
AALTONEN 10AA PR D82 052002 T. Aaltonen *et al.* (CDF Collab.)
AALTONEN 10AB PR D82 112005 T. Aaltonen *et al.* (CDF Collab.)
AALTONEN 10AC PRL 105 232003 T. Aaltonen *et al.* (CDF Collab.)
AALTONEN 10AE PRL 105 252001 T. Aaltonen *et al.* (CDF Collab.)
AALTONEN 10C PR D81 031102 T. Aaltonen *et al.* (CDF Collab.)
AALTONEN 10D PR D81 032002 T. Aaltonen *et al.* (CDF Collab.)
AALTONEN 10E PR D81 052011 T. Aaltonen *et al.* (CDF Collab.)
AALTONEN 10Q PRL 105 042002 T. Aaltonen *et al.* (CDF Collab.)
AALTONEN 10S PRL 105 101801 T. Aaltonen *et al.* (CDF Collab.)
AALTONEN 10U PR D81 072003 T. Aaltonen *et al.* (CDF Collab.)
AALTONEN 10V PR D81 092002 T. Aaltonen *et al.* (CDF Collab.)
AALTONEN 10W PRL 105 012001 T. Aaltonen *et al.* (CDF Collab.)
ABAZOV 10 PL B682 363 V.M. Abazov *et al.* (D0 Collab.)
ABAZOV 10I PR D82 032002 V.M. Abazov *et al.* (D0 Collab.)
ABAZOV 10J PL B690 5 V.M. Abazov *et al.* (D0 Collab.)
ABAZOV 10K PL B693 81 V.M. Abazov *et al.* (D0 Collab.)
ABAZOV 10Q PR D82 071102 V.M. Abazov *et al.* (D0 Collab.)
AHRENS 10 JHEP 1009 097 V. Ahrens *et al.* (MAINZ, HEIDH)
AHRENS 10A NPBPS 205-206 48 V. Ahrens *et al.* (MAINZ, HEIDH)
AALTONEN 09AD PR D79 112007 T. Aaltonen *et al.* (CDF Collab.)
AALTONEN 09AK PR D80 051104 T. Aaltonen *et al.* (CDF Collab.)
AALTONEN 09AL PR D80 052001 T. Aaltonen *et al.* (CDF Collab.)
AALTONEN 09AT PRL 103 092002 T. Aaltonen *et al.* (CDF Collab.)
AALTONEN 09F PR D79 031101 T. Aaltonen *et al.* (CDF Collab.)
AALTONEN 09H PR D79 052007 T. Aaltonen *et al.* (CDF Collab.)
AALTONEN 09J PR D79 072001 T. Aaltonen *et al.* (CDF Collab.)
AALTONEN 09K PR D79 072010 T. Aaltonen *et al.* (CDF Collab.)
AALTONEN 09L PR D79 092005 T. Aaltonen *et al.* (CDF Collab.)
AALTONEN 09M PRL 102 042001 T. Aaltonen *et al.* (CDF Collab.)
AALTONEN 09N PRL 102 151801 T. Aaltonen *et al.* (CDF Collab.)
AALTONEN 09O PRL 102 152001 T. Aaltonen *et al.* (CDF Collab.)
AALTONEN 09Q PL B674 160 T. Aaltonen *et al.* (CDF Collab.)
AALTONEN 09X PR D79 072005 T. Aaltonen *et al.* (CDF Collab.)
AARON 09A PL B678 450 F.D. Aaron *et al.* (H1 Collab.)
ABAZOV 09AA PRL 103 132001 V.M. Abazov *et al.* (D0 Collab.)
ABAZOV 09AG PR D80 071102 V.M. Abazov *et al.* (D0 Collab.)
ABAZOV 09AH PR D80 092006 V.M. Abazov *et al.* (D0 Collab.)
ABAZOV 09J PRL 102 092002 V.M. Abazov *et al.* (D0 Collab.)
ABAZOV 09R PL B679 177 V.M. Abazov *et al.* (D0 Collab.)
ABAZOV 09Z PRL 103 092001 V.M. Abazov *et al.* (D0 Collab.)
LANGENFELD 09 PR D80 054009 U. Langenfeld, S. Moch, P. Uwer
AALTONEN 08AB PRL 101 202001 T. Aaltonen *et al.* (CDF Collab.)
AALTONEN 08AD PRL 101 192002 T. Aaltonen *et al.* (CDF Collab.)
AALTONEN 08AG PR D78 111101 T. Aaltonen *et al.* (CDF Collab.)
AALTONEN 08AH PRL 101 252001 T. Aaltonen *et al.* (CDF Collab.)
AALTONEN 08C PRL 100 062005 T. Aaltonen *et al.* (CDF Collab.)
ABAZOV 08AH PRL 101 182001 V.M. Abazov *et al.* (D0 Collab.)
ABAZOV 08AI PRL 101 221801 V.M. Abazov *et al.* (D0 Collab.)
ABAZOV 08B PRL 100 062004 V.M. Abazov *et al.* (D0 Collab.)
ABAZOV 08I PR D78 012005 V.M. Abazov *et al.* (D0 Collab.)
ABAZOV 08L PRL 100 142002 V.M. Abazov *et al.* (D0 Collab.)
ABAZOV 08M PRL 100 192003 V.M. Abazov *et al.* (D0 Collab.)
ABAZOV 08N PRL 100 192004 V.M. Abazov *et al.* (D0 Collab.)
ABULENCIA 08 PR D78 012003 A. Abulencia *et al.* (CDF Collab.)
CACCIARI 08 JHEP 0809 127 M. Cacciari *et al.*
KIDONAKIS 08 PR D78 074005 N. Kidonakis, R. Vogt
MOCH 08 PR D78 034003 S. Moch, P. Uwer (BERL, KARLE)
AALTONEN 07 PRL 98 142001 T. Aaltonen *et al.* (CDF Collab.)
AALTONEN 07B PR D75 111103 T. Aaltonen *et al.* (CDF Collab.)
AALTONEN 07D PR D76 072009 T. Aaltonen *et al.* (CDF Collab.)
AALTONEN 07I PRL 99 182002 T. Aaltonen *et al.* (CDF Collab.)
ABAZOV 07C PRL 98 041801 V.M. Abazov *et al.* (D0 Collab.)
ABAZOV 07D PR D75 031102 V.M. Abazov *et al.* (D0 Collab.)
ABAZOV 07F PR D75 092001 V.M. Abazov *et al.* (D0 Collab.)
ABAZOV 07H PRL 98 181802 V.M. Abazov *et al.* (D0 Collab.)
ABAZOV 07O PR D76 052006 V.M. Abazov *et al.* (D0 Collab.)
ABAZOV 07P PR D76 072007 V.M. Abazov *et al.* (D0 Collab.)
ABAZOV 07R PR D76 092007 V.M. Abazov *et al.* (D0 Collab.)
ABAZOV 07V PRL 99 191802 V.M. Abazov *et al.* (D0 Collab.)
ABAZOV 07W PL B655 7 V.M. Abazov *et al.* (D0 Collab.)
ABULENCIA 07D PR D75 031105 A. Abulencia *et al.* (CDF Collab.)
ABULENCIA 07G PRL 98 072001 A. Abulencia *et al.* (CDF Collab.)
ABULENCIA 07I PR D75 052001 A. Abulencia *et al.* (CDF Collab.)
ABULENCIA 07J PR D75 071102 A. Abulencia *et al.* (CDF Collab.)
ABAZOV 06K PL B639 616 V.M. Abazov *et al.* (D0 Collab.)
ABAZOV 06U PR D74 092005 V.M. Abazov *et al.* (D0 Collab.)
ABAZOV 06X PR D74 112004 V.M. Abazov *et al.* (D0 Collab.)
ABULENCIA 06D PRL 96 022004 A. Abulencia *et al.* (CDF Collab.)
Also PR D73 032003 A. Abulencia *et al.* (CDF Collab.)
Also PR D73 092002 A. Abulencia *et al.* (CDF Collab.)

Downloaded from https://academic.oup.com/ptep/article/2022/8/083C01/6651666 by KIT Library user on 27 September 2022

ABULENCIA	06G	PRL 96 152002	A. Abulencia *et al.*	(CDF Collab.)
Also		PR D74 032009	A. Abulencia *et al.*	(CDF Collab.)
ABULENCIA	06R	PL B639 172	A. Abulencia *et al.*	(CDF Collab.)
ABULENCIA	06U	PR D73 111103	A. Abulencia *et al.*	(CDF Collab.)
ABULENCIA	06V	PR D73 112006	A. Abulencia *et al.*	(CDF Collab.)
ABULENCIA	06Z	PRL 97 082004	A. Abulencia *et al.*	(CDF Collab.)
ABULENCIA,A	06C	PRL 96 202002	A. Abulencia *et al.*	(CDF Collab.)
ABULENCIA,A	06E	PR D74 072005	A. Abulencia *et al.*	(CDF Collab.)
ABULENCIA,A	06F	PR D74 072006	A. Abulencia *et al.*	(CDF Collab.)
ABAZOV	05	PL B606 25	V.M. Abazov *et al.*	(D0 Collab.)
ABAZOV	05G	PL B617 1	V.M. Abazov *et al.*	(D0 Collab.)
ABAZOV	05L	PR D72 011104	V.M. Abazov *et al.*	(D0 Collab.)
ABAZOV	05P	PL B622 265	V.M. Abazov *et al.*	(D0 Collab.)
Also		PL B517 282	V.M. Abazov *et al.*	(D0 Collab.)
Also		PR D63 031101	B. Abbott *et al.*	(D0 Collab.)
Also		PR D75 092007	V.M. Abazov *et al.*	(D0 Collab.)
ABAZOV	05Q	PL B626 35	V.M. Abazov *et al.*	(D0 Collab.)
ABAZOV	05R	PL B626 55	V.M. Abazov *et al.*	(D0 Collab.)
ABAZOV	05X	PL B626 45	V.M. Abazov *et al.*	(D0 Collab.)
ACOSTA	05A	PRL 95 102002	D. Acosta *et al.*	(CDF Collab.)
ACOSTA	05D	PR D71 031101	D. Acosta *et al.*	(CDF Collab.)
ACOSTA	05N	PR D71 012005	D. Acosta *et al.*	(CDF Collab.)
ACOSTA	05S	PR D72 032002	D. Acosta *et al.*	(CDF Collab.)
ACOSTA	05T	PR D72 052003	D. Acosta *et al.*	(CDF Collab.)
ACOSTA	05U	PR D71 072005	D. Acosta *et al.*	(CDF Collab.)
ACOSTA	05V	PR D71 052003	D. Acosta *et al.*	(CDF Collab.)
ABAZOV	04G	NAT 429 638	V.M. Abazov *et al.*	(D0 Collab.)
ABDALLAH	04C	PL B590 21	J. Abdallah *et al.*	(DELPHI Collab.)
ACOSTA	04H	PR D69 052003	D. Acosta *et al.*	(CDF Collab.)
ACOSTA	04I	PRL 93 142001	D. Acosta *et al.*	(CDF Collab.)
AKTAS	04	EPJ C33 9	A. Aktas *et al.*	(H1 Collab.)
ABAZOV	03A	PR D67 012004	V.M. Abazov *et al.*	(D0 Collab.)
CHEKANOV	03	PL B559 153	S. Chekanov *et al.*	(ZEUS Collab.)
ACHARD	02J	PL B549 290	P. Achard *et al.*	(L3 Collab.)
ACOSTA	02	PR D65 091102	D. Acosta *et al.*	(CDF Collab.)
HEISTER	02Q	PL B543 173	A. Heister *et al.*	(ALEPH Collab.)
ABBIENDI	01T	PL B521 181	G. Abbiendi *et al.*	(OPAL Collab.)
AFFOLDER	01	PR D63 032003	T. Affolder *et al.*	(CDF Collab.)
AFFOLDER	01A	PR D64 032002	T. Affolder *et al.*	(CDF Collab.)
AFFOLDER	01C	PRL 86 3233	T. Affolder *et al.*	(CDF Collab.)
AFFOLDER	00B	PRL 84 216	T. Affolder *et al.*	(CDF Collab.)
BARATE	00S	PL B494 33	S. Barate *et al.*	(ALEPH Collab.)
ABBOTT	99G	PR D60 052001	B. Abbott *et al.*	(D0 Collab.)
ABE	99B	PRL 82 271	F. Abe *et al.*	(CDF Collab.)
Also		PRL 82 2808 (erratum)	F. Abe *et al.*	(CDF Collab.)
CHANG	99	PR D59 091503	D. Chang, W. Chang, E. Ma	
ABBOTT	98D	PRL 80 2063	B. Abbott *et al.*	(D0 Collab.)
ABBOTT	98F	PR D58 052001	B. Abbott *et al.*	(D0 Collab.)
ABE	98E	PRL 80 2767	F. Abe *et al.*	(CDF Collab.)
ABE	98F	PRL 80 2779	F. Abe *et al.*	(CDF Collab.)
ABE	98G	PRL 80 2525	F. Abe *et al.*	(CDF Collab.)
BHAT	98B	IJMP A13 5113	P.C. Bhat, H.B. Prosper, S.S. Snyder	
ABACHI	97E	PRL 79 1197	S. Abachi *et al.*	(D0 Collab.)
ABE	97R	PRL 79 1992	F. Abe *et al.*	(CDF Collab.)
ABE	97V	PRL 79 3585	F. Abe *et al.*	(CDF Collab.)
PDG	96	PR D54 1	R. M. Barnett *et al.*	(PDG Collab.)
ABACHI	95	PRL 74 2632	S. Abachi *et al.*	(D0 Collab.)
ABE	95F	PRL 74 2626	F. Abe *et al.*	(CDF Collab.)
ABE	94E	PR D50 2966	F. Abe *et al.*	(CDF Collab.)
Also		PRL 73 225	F. Abe *et al.*	(CDF Collab.)

b' (4th Generation) Quark, Searches for

$b'(-1/3)$-quark/hadron mass limits in $p\overline{p}$ and pp collisions

VALUE (GeV)	CL%	DOCUMENT ID		TECN	COMMENT
>1570	95	[1] SIRUNYAN	20BI	CMS	$B(b' \to Hb) = 1$
>1390	95	[1] SIRUNYAN	20BI	CMS	$B(b' \to Zb) = 1$
>1130	95	[2] SIRUNYAN	19AQ	CMS	$B(b' \to Zb) = 1$
>1230	95	[3] SIRUNYAN	19BW	CMS	$B(b' \to Wt) = 1$
>1350	95	[4] AABOUD	18AW	ATLS	$B(b' \to Wt) = 1$
>1000	95	[5] AABOUD	18CE	ATLS	$\geq 2\ell + \not{E}_T + \geq 1$bj
> 950	95	[6] AABOUD	18CL	ATLS	Wt, Zb, hb modes
>1010	95	[7,8] AABOUD	18CP	ATLS	$2,3\ell$, singlet model
>1140	95	[6,9] AABOUD	18CP	ATLS	$2,3\ell$, doublet model
>1220	95	[10,11] AABOUD	18CR	ATLS	singlet b'. ATLAS Combination
>1370	95	[10,12] AABOUD	18CR	ATLS	b' in a weak isospin doublet (t',b'). ATLAS combination.
> 910	95	[13] SIRUNYAN	18BM	CMS	Wt, Zb, hb modes
> 845	95	[14] SIRUNYAN	18Q	CMS	$B(b' \to Wu) = 1$
> 730	95	[15] SIRUNYAN	17AU	CMS	
> 880	95	[16] KHACHATRY...	16AN	CMS	$B(b' \to Wt) = 1$
> 620	95	[17] AAD	15BY	ATLS	Wt, Zb, hb modes
> 730	95	[18] AAD	15BY	ATLS	$B(b' \to Wt) = 1$
> 810	95	[19] AAD	15Z	ATLS	
> 755	95	[20] AAD	14AZ	ATLS	$B(b' \to Wt) = 1$
> 675	95	[21] CHATRCHYAN	13I	CMS	$B(b' \to Wt) = 1$
> 190	95	[22] ABAZOV	08X	D0	$c\tau$= 200mm
> 190	95	[23] ACOSTA	03	CDF	quasi-stable b'
• • • We do not use the following data for averages, fits, limits, etc. • • •					
<350, 580–635, >700	95	[24] AAD	15AR	ATLS	$B(b' \to Hb) = 1$
> 690	95	[25] AAD	15CN	ATLS	$B(b' \to Wq) = 1$ (q=u)
> 480	95	[26] AAD	12AT	ATLS	$B(b' \to Wt) = 1$
> 400	95	[27] AAD	12AU	ATLS	$B(b' \to Zb) = 1$
> 350	95	[28] AAD	12BC	ATLS	$B(b' \to Wq) = 1$ (q=u,c)
> 450	95	[29] AAD	12BE	ATLS	$B(b' \to Wt) = 1$
> 685	95	[30] CHATRCHYAN	12BH	CMS	$m_{t'} = m_{b'}$
> 611	95	[31] CHATRCHYAN	12X	CMS	$B(b' \to Wt) = 1$
> 372	95	[32] AALTONEN	11J	CDF	$b' \to Wt$
> 361	95	[33] CHATRCHYAN	11L	CMS	Repl. by CHATRCHYAN 12X
> 338	95	[34] AALTONEN	10H	CDF	$b' \to Wt$
> 380–430	95	[35] FLACCO	10	RVUE	$m_{b'} > m_{t'}$
> 268	95	[36,37] AALTONEN	07C	CDF	$B(b' \to Zb) = 1$
> 199	95	[38] AFFOLDER	00	CDF	NC: $b' \to Zb$
> 148	95	[39] ABE	98N	CDF	NC: $b' \to Zb$ + vertex
> 96	95	[40] ABACHI	97D	D0	NC: $b' \to b\gamma$
> 128	95	[41] ABACHI	95F	D0	$\ell\ell$ + jets, ℓ + jets
> 75	95	[42] MUKHOPAD...	93	RVUE	NC: $b' \to b\ell\ell$
> 85	95	[43] ABE	92	CDF	CC: $\ell\ell$
> 72	95	[44] ABE	90B	CDF	CC: $e + \mu$
> 54	95	[45] AKESSON	90	UA2	CC: e + jets + $\not{E}_T$
> 43	95	[46] ALBAJAR	90B	UA1	CC: μ + jets
> 34	95	[47] ALBAJAR	88	UA1	CC: e or μ + jets

[1] SIRUNYAN 20BI based on 137 fb^{-1} of pp data at $\sqrt{s}$ = 13 TeV. Pair production of vector-like b' is seached for with each b' decaying into Zb or hb. Analysis focuses on final states consisting of jets from six quarks. Mass limits are obtained for a variety of branching ratios of b' decays.

[2] SIRUNYAN 19AQ based on 35.9 fb^{-1} of pp data at $\sqrt{s}$ = 13 TeV. Pair production of vector-like b' is seached for with one b' decaying into Zb and the other b' decaying into Wt, Zb, hb. Events with an opposite-sign lepton pair consistent with coming from Z and jets are used. Mass limits are obtained for a variety of branching ratios of b'.

[3] SIRUNYAN 19BW based on 35.9 fb^{-1} of pp data at $\sqrt{s}$ = 13 TeV. The limit is for the pair-produced vector-like b' using all-hadronic final state. The analysis is made for the Zb, Wt, hb modes and mass limits are obtained for a variety of branching ratios.

[4] AABOUD 18AW based on 36.1 fb^{-1} of pp data at $\sqrt{s}$ = 13 TeV. The limit is for the pair-produced vector-like b' using lepton-plus-jets final state. The search is also sensitive to the decays into Zb and Hb final states.

[5] AABOUD 18CE based on 36.1 fb^{-1} of proton-proton data taken at $\sqrt{s}$ = 13 TeV. Events including a same-sign lepton pair are used. The limit is for a singlet model, assuming the branching ratios of b' into Zb, Wt and Hb as predicted by the model.

[6] AABOUD 18CL, AABOUD 18CP based on 36.1 fb^{-1} of pp data at $\sqrt{s}$ = 13 TeV. The limit is for the pair-produced vector-like b' using all-hadronic final state. The analysis is particularly powerful for the $b' \to hb$ mode. Assuming the pure decay only in this mode sets a limit $m_{b'} > 1010$ GeV.

[7] AABOUD 18CP based on 36.1 fb^{-1} of pp data at $\sqrt{s}$ = 13 TeV. Pair and single production of vector-like b' are seached for with at least one b' decaying into Zb. In the case of $B(b' \to Zb) = 1$, the limit is $m_{b'} > 1220$ GeV.

[8] The limit is for the singlet model, assuming that the branching ratios into Wt, Zb, hb add up to one.

[9] The limit is for the doublet model, assuming that the branching ratios into Wt, Zb, hb add up to one.

[10] AABOUD 18CR based on 36.1 fb^{-1} of pp data at $\sqrt{s}$ = 13 TeV. A combination of searches for the pair-produced vector-like b' in various decay channels ($b' \to Wt$, Zb, hb). Also a model-independent limit is obtained as $m_{b'} > 1.03$ TeV, assuming that the branching ratios into Zb, Wt, and hb add up to one.

[11] The limit is for the singlet b'.

[12] The limit is for b' in a weak isospin doublet (t',b') and $|V_{t'b}| \ll |V_{tb'}|$. For a b' in a doublet with a charge $-4/3$ vector-like quark, the limit $m_{b'} > 1.14$ TeV is obtained.

[13] SIRUNYAN 18BM based on 35.9 fb^{-1} of pp data at $\sqrt{s}$ = 13 TeV. The limit is for the pair-produced vector-like b'. Three channels (single lepton, same-charge 2 leptons, or at least 3 leptons) are considered for various branching fraction combinations. Assuming $B(tW) = 1$, the limit is 1240 GeV and for $B(bZ) = 1$ it is 960 GeV.

[14] SIRUNYAN 18Q based on 19.7 fb^{-1} of pp data at $\sqrt{s}$ = 8 TeV. The limit is for the pair-produced vector-like b' that couple only to light quarks. Upper cross section limits on the single production of a b' and constraints for other decay channels (Zq and Hq) are also given in the paper.

[15] SIRUNYAN 17AU based on 2.3–2.6 fb^{-1} of pp data at $\sqrt{s}$ = 13 TeV. Limit on pair-produced singlet vector-like b' using one lepton and several jets. The mass bound is given for a b' transforming as a singlet under the electroweak symmetry group, assumed to decay through W, Z or Higgs boson (which decays to jets) and to a third generation quark.

[16] KHACHATRYAN 16AN based on 19.7 fb^{-1} of pp data at $\sqrt{s}$ = 8 TeV. Limit on pair-produced vector-like b' using 1, 2, and >2 leptons as well as fully hadronic final states. Other limits depending on the branching fractions to tW, bZ, and bH are given in Table IX.

[17] AAD 15BY based on 20.3 fb^{-1} of pp data at $\sqrt{s}$ = 8 TeV. Limit on pair-produced vector-like b' assuming the branching fractions to W, Z, and h modes of the singlet model. Used events containing $\geq 2\ell + \not{E}_T + \geq 2$j ($\geq 1$ b) and including a same-sign lepton pair.

[18] AAD 15BY based on 20.3 fb^{-1} of pp data at $\sqrt{s}$ = 8 TeV. Limit on pair-produced chiral b'-quark. Used events containing $\geq 2\ell + \not{E}_T + \geq 2$j ($\geq 1$ b) and including a same-sign lepton pair.

[19] AAD 15Z based on 20.3 fb^{-1} of pp data at $\sqrt{s}$ = 8 TeV. Used events with $\ell + \not{E}_T + \geq 6$j ($\geq 1$ b) and at least one pair of jets from weak boson decay, primarily designed to select the signature $b'\overline{b}' \to WWt\overline{t} \to WWWWb\overline{b}$. This is a limit on pair-produced vector-like b'. The lower mass limit is 640 GeV for a vector-like singlet b'.

[20] Based on 20.3 fb^{-1} of pp data at $\sqrt{s}$ = 8 TeV. No significant excess over SM expectation is found in the search for pair production or single production of b' in the events with dilepton from a high p_T Z and additional jets ($\geq$ 1 b-tag). If instead of $B(b' \to Wt) = 1$ an electroweak singlet with $B(b' \to Wt) \sim 0.45$ is assumed, the limit reduces to 685 GeV.

[21] Based on 5.0 fb^{-1} of pp data at $\sqrt{s}$ = 7 TeV. CHATRCHYAN 13I looked for events with one isolated electron or muon, large $\not{E}_T$, and at least four jets with large transverse momenta, where one jet is likely to originate from the decay of a bottom quark.

Downloaded from https://academic.oup.com/ptep/article/2022/8/083C01/6651666 by KIT Library user on 27 September 2022

[22] Result is based on 1.1 fb^{-1} of data. No signal is found for the search of long-lived particles which decay into final states with two electrons or photons, and upper bound on the cross section times branching fraction is obtained for $2 < c\tau < 7000$ mm; see Fig. 3. 95% CL excluded region of b' lifetime and mass is shown in Fig. 4.

[23] ACOSTA 03 looked for long-lived fourth generation quarks in the data sample of 90 pb^{-1} of $\sqrt{s}$=1.8 TeV $p\overline{p}$ collisions by using the muon-like penetration and anomalously high ionization energy loss signature. The corresponding lower mass bound for the charge (2/3)e quark (t') is 220 GeV. The t' bound is higher than the b' bound because t' is more likely to produce charged hadrons than b'. The 95% CL upper bounds for the production cross sections are given in their Fig. 3.

[24] AAD 15AR based on 20.3 fb^{-1} of pp data at $\sqrt{s}$ = 8 TeV. Used lepton-plus-jets final state. See Fig. 24 for mass limits in the plane of B($b' \rightarrow Wt$) vs. B($b' \rightarrow Hb$) from $b'\overline{b}' \rightarrow Hb + X$ searches.

[25] AAD 15CN based on 20.3 fb^{-1} of pp data at $\sqrt{s}$ = 8 TeV. Limit on pair-production of chiral b'-quark. Used events with $\ell + \not{E}_T + \geq 4$j (non-$b$-tagged). Limits on a heavy vector-like quark, which decays into Wq, Zq, hq, are presented in the plane B($Q \rightarrow Wq$) vs. B($Q \rightarrow hq$) in Fig. 12.

[26] Based on 1.04 fb^{-1} of pp data at $\sqrt{s}$ = 7 TeV. No signal is found for the search of heavy quark pair production that decay into W and a t quark in the events with a high p_T isolated lepton, large $\not{E}_T$, and at least 6 jets in which one, two or more dijets are from W.

[27] Based on 2.0 fb^{-1} of pp data at $\sqrt{s}$ = 7 TeV. No $b' \rightarrow Zb$ invariant mass peak is found in the search of heavy quark pair production that decay into Z and a b quark in events with $Z \rightarrow e^+e^-$ and at least one b-jet. The lower mass limit is 358 GeV for a vector-like singlet b' mixing solely with the third SM generation.

[28] Based on 1.04 fb^{-1} of pp data at $\sqrt{s}$ = 7 TeV. No signal is found for the search of heavy quark pair production that decay into W and a quark in the events with dileptons, large $\not{E}_T$, and ≥ 2 jets.

[29] Based on 1.04 fb^{-1} of pp data at $\sqrt{s}$ = 7 TeV. AAD 12BE looked for events with two isolated like-sign leptons and at least 2 jets, large $\not{E}_T$ and H_T > 350 GeV.

[30] Based on 5 fb^{-1} of pp data at $\sqrt{s}$ = 7 TeV. CHATRCHYAN 12BH searched for QCD and EW production of single and pair of degenerate 4'th generation quarks that decay to bW or tW. Absence of signal in events with one lepton, same-sign dileptons or tri-leptons gives the bound. With a mass difference of 25 GeV/c^2 between $m_{t'}$ and $m_{b'}$, the corresponding limit shifts by about $\pm$20 GeV/c^2.

[31] Based on 4.9 fb^{-1} of pp data at $\sqrt{s}$ = 7 TeV. CHATRCHYAN 12X looked for events with trileptons or same-sign dileptons and at least one b jet.

[32] Based on 4.8 fb^{-1} of data in $p\overline{p}$ collisions at 1.96 TeV. AALTONEN 11J looked for events with $\ell + \not{E}_T + \geq 5$j ($\geq 1$ b or c). No signal is observed and the bound $\sigma(b'\overline{b}')$ < 30 fb for $m_{b'}$ > 375 GeV is found for B($b' \rightarrow Wt$) = 1.

[33] Based on 34 pb^{-1} of data in pp collisions at 7 TeV. CHATRCHYAN 11L looked for multi-jet events with trileptons or same-sign dileptons. No excess above the SM background excludes $m_{b'}$ between 255 and 361 GeV at 95% CL for B($b' \rightarrow Wt$) = 1.

[34] Based on 2.7 fb^{-1} of data in $p\overline{p}$ collisions at $\sqrt{s}$ = 1.96 TeV. AALTONEN 10H looked for pair production of heavy quarks which decay into tW^- or tW^+, in events with same sign dileptons (e or μ), several jets and large missing E_T. The result is obtained for b' which decays into tW^-. For the charge 5/3 quark ($T_{5/3}$) which decays into tW^+, $m_{T_{5/3}}$ > 365 GeV (95% CL) is found when it has the charge $-1/3$ partner B of the same mass.

[35] FLACCO 10 result is obtained from AALTONEN 10H result of $m_{b'}$ > 338 GeV, by relaxing the condition B($b' \rightarrow Wt$) = 100% when $m_{b'} > m_{t'}$.

[36] Result is based on 1.06 fb^{-1} of data. No excess from the SM Z+jet events is found when Z decays into ee or $\mu\mu$. The $m_{b'}$ bound is found by comparing the resulting upper bound on $\sigma(b'\overline{b}')$ [1-(1-B($b' \rightarrow Zb$))^2] and the LO estimate of the b' pair production cross section shown in Fig. 38 of the article.

[37] HUANG 08 reexamined the b' mass lower bound of 268 GeV obtained in AALTONEN 07C that assumes B($b' \rightarrow Zb$) = 1, which does not hold for $m_{b'}$ > 255 GeV. The lower mass bound is given in the plane of sin$^2(\theta_{tb'})$ and $m_{b'}$.

[38] AFFOLDER 00 looked for b' that decays in to b+Z. The signal searched for is $bbZZ$ events where one Z decays into e^+e^- or $\mu^+\mu^-$ and the other Z decays hadronically. The bound assumes B($b' \rightarrow Zb$)= 100%. Between 100 GeV and 199 GeV, the 95%CL upper bound on $\sigma(b' \rightarrow \overline{b}')\times$B^2($b' \rightarrow Zb$) is also given (see their Fig. 2).

[39] ABE 98N looked for $Z \rightarrow e^+e^-$ decays with displaced vertices. Quoted limit assumes B($b' \rightarrow Zb$)=1 and $c\tau_{b'}$=1 cm. The limit is lower than m_Z+m_b ($\sim$ 96 GeV) if $c\tau$> 22 cm or $c\tau$< 0.009 cm. See their Fig. 4.

[40] ABACHI 97D searched for b' that decays mainly via FCNC. They obtained 95%CL upper bounds on B($b'\overline{b}' \rightarrow \gamma$+ 3 jets) and B($b'\overline{b}' \rightarrow 2\gamma$+ 2 jets), which can be interpreted as the lower mass bound $m_{b'} > m_Z+m_b$.

[41] ABACHI 95F bound on the top-quark also applies to b' and t' quarks that decay predominantly into W. See FROGGATT 97.

[42] MUKHOPADHYAYA 93 analyze CDF dilepton data of ABE 92G in terms of a new quark decaying via flavor-changing neutral current. The above limit assumes B($b' \rightarrow b\ell^+\ell^-$)=1%. For an exotic quark decaying only via virtual Z [B($b\ell^+\ell^-$) = 3%], the limit is 85 GeV.

[43] ABE 92 dilepton analysis limit of >85 GeV at CL=95% also applies to b' quarks, as discussed in ABE 90B.

[44] ABE 90B exclude the region 28–72 GeV.

[45] AKESSON 90 searched for events having an electron with p_T > 12 GeV, missing momentum > 15 GeV, and a jet with E_T > 10 GeV, $|\eta|$ < 2.2, and excluded $m_{b'}$ between 30 and 69 GeV.

[46] For the reduction of the limit due to non-charged-current decay modes, see Fig. 19 of ALBAJAR 90B.

[47] ALBAJAR 88 study events at E_{cm} = 546 and 630 GeV with a muon or isolated electron, accompanied by one or more jets and find agreement with Monte Carlo predictions for the production of charm and bottom, without the need for a new quark. The lower mass limit is obtained by using a conservative estimate for the $b'\overline{b}'$ production cross section and by assuming that it cannot be produced in W decays. The value quoted here is revised using the full $O(\alpha_s^3)$ cross section of ALTARELLI 88.

$b'(-1/3)$ mass limits from single production in $p\overline{p}$ and pp collisions

VALUE (GeV)	CL%	DOCUMENT ID		TECN	COMMENT
>1500	95	[1] AAD	16AH	ATLS	$gb \rightarrow b' \rightarrow tW$, B($b' \rightarrow tW$)=1
>1390	95	[2] KHACHATRY...	16I	CMS	$gb \rightarrow b' \rightarrow tW$, B($b' \rightarrow tW$)=1
>1430	95	[3] KHACHATRY...	16I	CMS	$gb \rightarrow b' \rightarrow tW$, B($b' \rightarrow tW$)=1
>1530	95	[4] KHACHATRY...	16I	CMS	$gb \rightarrow b' \rightarrow tW$, B($b' \rightarrow tW$)=1
> 693	95	[5] ABAZOV	11F	D0	$qu \rightarrow q'b' \rightarrow q'(Wu)$ $\widetilde{\kappa}_{ub'}$=1, B($b' \rightarrow Wu$)=1
> 430	95	[5] ABAZOV	11F	D0	$qd \rightarrow qb' \rightarrow q(Zd)$ $\widetilde{\kappa}_{db'}$=$\sqrt{2}$, B($b' \rightarrow Zd$)=1
• • • We do not use the following data for averages, fits, limits, etc. • • •					
		[6] SIRUNYAN	19AI	CMS	$bZ/tW \rightarrow b' \rightarrow tW$

[1] AAD 16AH based on 20.3 fb^{-1} of data in pp collisions at 8 TeV. No significant excess over SM expectation is found in the search for a vector-like b' in the single-lepton and dilepton channels (ℓ or $\ell\ell$) + 1,2,3 j ($\geq 1b$). The model assumes that the b' has the excited quark couplings.

[2] Based on 19.7 fb^{-1} of data in pp collisions at 8 TeV. Limit on left-handed b' assuming 100% decay to tW and using all-hadronic, lepton + jets, and dilepton final states.

[3] Based on 19.7 fb^{-1} of data in pp collisions at 8 TeV. Limit on right-handed b' assuming 100% decay to tW and using all-hadronic, lepton + jets, and dilepton final states.

[4] Based on 19.7 fb^{-1} of data in pp collisions at 8 TeV. Limit on vector-like b' assuming 100% decay to tW and using all-hadronic, lepton+jets, and dilepton final states.

[5] Based on 5.4 fb^{-1} of data in ppbar collisions at 1.96 TeV. ABAZOV 11F looked for single production of b' via the W or Z coupling to the first generation up or down quarks, respectively. Model independent cross section limits for the single production processes $p\overline{p} \rightarrow b'q \rightarrow Wuq$, and $p\overline{p} \rightarrow b'q \rightarrow Zdq$ are given in Figs. 3 and 4, respectively, and the mass limits are obtained for the model of ATRE 09 with degenerate bi-doublets of vector-like quarks.

[6] SIRUNYAN 19AI based on 35.9 fb^{-1} of pp data at $\sqrt{s}$ = 13 TeV. Exclusion limits are set on the product of the production cross section and branching fraction for the $b'(-1/3)$ + b and $b'(-1/3)$ + t modes as a function of the vector-like quark mass in Figs. 7 and 8 and in Tab. 2 for relative vector-like quark widths between 1 and 30% for left- and right-handed vector-like quark couplings. No significant deviation from the SM prediction is observed.

MASS LIMITS for b' (4th Generation) Quark or Hadron in e^+e^- Collisions

Search for hadrons containing a fourth-generation $-1/3$ quark denoted b'.

The last column specifies the assumption for the decay mode (CC denotes the conventional charged-current decay) and the event signature which is looked for.

VALUE (GeV)	CL%	DOCUMENT ID		TECN	COMMENT
>46.0	95	[1] DECAMP	90F	ALEP	any decay
• • • We do not use the following data for averages, fits, limits, etc. • • •					
none 96–103	95	[2] ABDALLAH	07	DLPH	$b' \rightarrow bZ$, cW
		[3] ADRIANI	93G	L3	Quarkonium
>44.7	95	ADRIANI	93M	L3	$\Gamma(Z)$
>45	95	ABREU	91F	DLPH	$\Gamma(Z)$
none 19.4–28.2	95	ABE	90D	VNS	Any decay; event shape
>45.0	95	ABREU	90D	DLPH	B(CC) = 1; event shape
>44.5	95	[4] ABREU	90D	DLPH	$b' \rightarrow cH^-$, $H^- \rightarrow \overline{c}s$, $\tau^-\nu$
>40.5	95	[5] ABREU	90D	DLPH	$\Gamma(Z \rightarrow$ hadrons)
>28.3	95	ADACHI	90	TOPZ	B(FCNC)=100%; isol. γ or 4 jets
>41.4	95	[6] AKRAWY	90B	OPAL	Any decay; acoplanarity
>45.2	95	[6] AKRAWY	90B	OPAL	B(CC) = 1; acoplanarity
>46	95	[7] AKRAWY	90J	OPAL	$b' \rightarrow \gamma$ + any
>27.5	95	[8] ABE	89E	VNS	B(CC) =1; μ, e
none 11.4–27.3	95	[9] ABE	89G	VNS	B($b' \rightarrow b\gamma$) > 10%; isolated γ
>44.7	95	[10] ABRAMS	89C	MRK2	B(CC)= 100%; isol. track
>42.7	95	[10] ABRAMS	89C	MRK2	B(bg)= 100%; event shape
>42.0	95	[10] ABRAMS	89C	MRK2	Any decay; event shape
>28.4	95	[11,12] ADACHI	89C	TOPZ	B(CC) =1; μ
>28.8	95	[13] ENO	89	AMY	B(CC) $\gtrsim$ 90%; μ, e
>27.2	95	[13,14] ENO	89	AMY	any decay; event shape
>29.0	95	[13] ENO	89	AMY	B($b' \rightarrow bg$) $\gtrsim$ 85%; event shape
>24.4	95	[15] IGARASHI	88	AMY	μ,e
>23.8	95	[16] SAGAWA	88	AMY	event shape
>22.7	95	[17] ADEVA	86	MRKJ	μ
>21		[18] ALTHOFF	84C	TASS	R, event shape
>19		[19] ALTHOFF	84I	TASS	Aplanarity

[1] DECAMP 90F looked for isolated charged particles, for isolated photons, and for four-jet final states. The modes $b' \rightarrow bg$ for B($b' \rightarrow bg$) > 65% $b' \rightarrow b\gamma$ for B($b' \rightarrow b\gamma$) > 5% are excluded. Charged Higgs decay were not discussed.

[2] ABDALLAH 07 searched for b' pair production at E_{cm}=196–209 GeV, with 420 pb^{-1}. No signal leads to the 95% CL upper limits on B($b' \rightarrow bZ$) and B($b' \rightarrow cW$) for $m_{b'}$ = 96 to 103 GeV.

[3] ADRIANI 93G search for vector quarkonium states near Z and give limit on quarkonium-Z mixing parameter δm^2 <(10–30) GeV^2 (95%CL) for the mass 88–94.5 GeV. Using

Downloaded from https://academic.oup.com/ptep/article/2022/8/083C01/6651666 by KIT Library user on 27 September 2022

Richardson potential, a 1S ($b'\overline{b}'$) state is excluded for the mass range 87.7–94.7 GeV. This range depends on the potential choice.

[4] ABREU 90D assumed $m_{H^-} < m_{b'} - 3$ GeV.

[5] Superseded by ABREU 91F.

[6] AKRAWY 90B search was restricted to data near the Z peak at $E_{cm} = 91.26$ GeV at LEP. The excluded region is between 23.6 and 41.4 GeV if no H^+ decays exist. For charged Higgs decays the excluded regions are between (m_{H^+} + 1.5 GeV) and 45.5 GeV.

[7] AKRAWY 90J search for isolated photons in hadronic Z decay and derive $B(Z \rightarrow b'\overline{b}')\cdot B(b' \rightarrow \gamma X)/B(Z \rightarrow \text{hadrons}) < 2.2 \times 10^{-3}$. Mass limit assumes $B(b' \rightarrow \gamma X) > 10\%$.

[8] ABE 89E search at $E_{cm} = 56$–57 GeV at TRISTAN for multihadron events with a spherical shape (using thrust and acoplanarity) or containing isolated leptons.

[9] ABE 89G search was at $E_{cm} = 55$–60.8 GeV at TRISTAN.

[10] If the photonic decay mode is large ($B(b' \rightarrow b\gamma) > 25\%$), the ABRAMS 89C limit is 45.4 GeV. The limit for for Higgs decay ($b' \rightarrow cH^-$, $H^- \rightarrow \overline{c}s$) is 45.2 GeV.

[11] ADACHI 89C search was at $E_{cm} = 56.5$–60.8 GeV at TRISTAN using multi-hadron events accompanying muons.

[12] ADACHI 89C also gives limits for any mixture of CC and bg decays.

[13] ENO 89 search at $E_{cm} = 50$–60.8 at TRISTAN.

[14] ENO 89 considers arbitrary mixture of the charged current, bg, and $b\gamma$ decays.

[15] IGARASHI 88 searches for leptons in low-thrust events and gives $\Delta R(b') < 0.26$ (95% CL) assuming charged current decay, which translates to $m_{b'} > 24.4$ GeV.

[16] SAGAWA 88 set limit $\sigma(\text{top}) < 6.1$ pb at CL=95% for top-flavored hadron production from event shape analyses at $E_{cm} = 52$ GeV. By using the quark parton model cross-section formula near threshold, the above limit leads to lower mass bounds of 23.8 GeV for charge $-1/3$ quarks.

[17] ADEVA 86 give 95%CL upper bound on an excess of the normalized cross section, ΔR, as a function of the minimum c.m. energy (see their figure 3). Production of a pair of 1/3 charge quarks is excluded up to $E_{cm} = 45.4$ GeV.

[18] ALTHOFF 84C narrow state search sets limit $\Gamma(e^+e^-)B(\text{hadrons}) < 2.4$ keV CL = 95% and heavy charge 1/3 quark pair production $m > 21$ GeV, CL = 95%.

[19] ALTHOFF 84I exclude heavy quark pair production for $7 < m < 19$ GeV (1/3 charge) using aplanarity distributions (CL = 95%).

REFERENCES FOR Searches for (Fourth Generation) b' Quark

SIRUNYAN	20BI	PR D102 112004	A.M. Sirunyan et al.	(CMS Collab.)
SIRUNYAN	19AI	EPJ C79 90	A.M. Sirunyan et al.	(CMS Collab.)
SIRUNYAN	19AQ	EPJ C79 364	A.M. Sirunyan et al.	(CMS Collab.)
SIRUNYAN	19BW	PR D100 072001	A.M. Sirunyan et al.	(CMS Collab.)
AABOUD	18AW	JHEP 1808 048	M. Aaboud et al.	(ATLAS Collab.)
AABOUD	18CE	JHEP 1812 039	M. Aaboud et al.	(ATLAS Collab.)
AABOUD	18CL	PR D98 092005	M. Aaboud et al.	(ATLAS Collab.)
AABOUD	18CP	PR D98 112010	M. Aaboud et al.	(ATLAS Collab.)
AABOUD	18CR	PRL 121 211801	M. Aaboud et al.	(ATLAS Collab.)
SIRUNYAN	18BM	JHEP 1808 177	A.M. Sirunyan et al.	(CMS Collab.)
SIRUNYAN	18Q	PR D97 072008	A.M. Sirunyan et al.	(CMS Collab.)
SIRUNYAN	17AU	JHEP 1711 085	A.M. Sirunyan et al.	(CMS Collab.)
AAD	16AH	JHEP 1602 110	G. Aad et al.	(ATLAS Collab.)
KHACHATRY...	16AN	PR D93 112009	V. Khachatryan et al.	(CMS Collab.)
KHACHATRY...	16I	JHEP 1601 166	V. Khachatryan et al.	(CMS Collab.)
AAD	15AR	JHEP 1508 105	G. Aad et al.	(ATLAS Collab.)
AAD	15BY	JHEP 1510 150	G. Aad et al.	(ATLAS Collab.)
AAD	15CN	PR D92 112007	G. Aad et al.	(ATLAS Collab.)
AAD	15Z	PR D91 112011	G. Aad et al.	(ATLAS Collab.)
AAD	14AZ	JHEP 1411 104	G. Aad et al.	(ATLAS Collab.)
CHATRCHYAN	13I	JHEP 1301 154	S. Chatrchyan et al.	(CMS Collab.)
AAD	12AT	PRL 109 032001	G. Aad et al.	(ATLAS Collab.)
AAD	12AU	PRL 109 071801	G. Aad et al.	(ATLAS Collab.)
AAD	12BC	PR D86 012007	G. Aad et al.	(ATLAS Collab.)
AAD	12BE	JHEP 1204 069	G. Aad et al.	(ATLAS Collab.)
CHATRCHYAN	12BH	PR D86 112003	S. Chatrchyan et al.	(CMS Collab.)
CHATRCHYAN	12X	JHEP 1205 123	S. Chatrchyan et al.	(CMS Collab.)
AALTONEN	11J	PRL 106 141803	T. Aaltonen et al.	(CDF Collab.)
ABAZOV	11F	PRL 106 081801	V.M. Abazov et al.	(D0 Collab.)
CHATRCHYAN	11L	PL B701 204	S. Chatrchyan et al.	(CMS Collab.)
AALTONEN	10H	PRL 104 091801	T. Aaltonen et al.	(CDF Collab.)
FLACCO	10	PRL 105 111801	C.J. Flacco et al.	(UCI, HAIF)
ATRE	09	PR D79 054018	A. Atre et al.	
ABAZOV	08X	PRL 101 111802	V.M. Abazov et al.	(D0 Collab.)
HUANG	08	PR D77 037302	P.Q. Hung, M. Sher	(UVA, WILL)
AALTONEN	07C	PR D76 072006	T. Aaltonen et al.	(CDF Collab.)
ABDALLAH	07	EPJ C50 507	J. Abdallah et al.	(DELPHI Collab.)
ACOSTA	03	PRL 90 131801	D. Acosta et al.	(CDF Collab.)
AFFOLDER	00	PRL 84 835	A. Affolder et al.	(CDF Collab.)
ABE	98N	PR D58 051102	F. Abe et al.	(CDF Collab.)
ABACHI	97D	PRL 78 3818	S. Abachi et al.	(D0 Collab.)
FROGGATT	97	ZPHY C73 333	C.D. Froggatt, D.J. Smith, H.B. Nielsen	(GLAS+)
ABACHI	95F	PR D52 4877	S. Abachi et al.	(D0 Collab.)
ADRIANI	93G	PL B313 326	O. Adriani et al.	(L3 Collab.)
ADRIANI	93M	PRPL 236 1	O. Adriani et al.	(L3 Collab.)
MUKHOPAD...	93	PR D48 2105	B. Mukhopadhyaya, D.P. Roy	(TATA)
ABE	92	PRL 68 447	F. Abe et al.	(CDF Collab.)
Also		PR D45 3921	F. Abe et al.	(CDF Collab.)
ABE	92G	PR D45 3921	F. Abe et al.	(CDF Collab.)
ABREU	91F	NP B367 511	P. Abreu et al.	(DELPHI Collab.)
ABE	90B	PRL 64 147	F. Abe et al.	(CDF Collab.)
ABE	90D	PL B234 382	K. Abe et al.	(VENUS Collab.)
ABREU	90D	PL B242 536	P. Abreu et al.	(DELPHI Collab.)
ADACHI	90	PL B234 197	I. Adachi et al.	(TOPAZ Collab.)
AKESSON	90	ZPHY C46 179	T. Akesson et al.	(UA2 Collab.)
AKRAWY	90B	PL B236 364	M.Z. Akrawy et al.	(OPAL Collab.)
AKRAWY	90J	PL B246 285	M.Z. Akrawy et al.	(OPAL Collab.)
ALBAJAR	90B	ZPHY C48 1	C. Albajar et al.	(UA1 Collab.)
DECAMP	90F	PL B236 511	D. Decamp et al.	(ALEPH Collab.)
ABE	89E	PR D39 3524	K. Abe et al.	(VENUS Collab.)
ABE	89G	PRL 63 1776	K. Abe et al.	(VENUS Collab.)
ABRAMS	89C	PRL 63 2447	G.S. Abrams et al.	(Mark II Collab.)
ADACHI	89C	PL B229 427	I. Adachi et al.	(TOPAZ Collab.)
ENO	89	PRL 63 1910	S. Eno et al.	(AMY Collab.)
ALBAJAR	88	ZPHY C37 505	C. Albajar et al.	(UA1 Collab.)
ALTARELLI	88	NP B308 724	G. Altarelli et al.	(CERN, ROMA, ETH)
IGARASHI	88	PRL 60 2359	S. Igarashi et al.	(AMY Collab.)
SAGAWA	88	PRL 60 93	H. Sagawa et al.	(AMY Collab.)
ADEVA	86	PR D34 681	B. Adeva et al.	(Mark-J Collab.)
ALTHOFF	84C	PL 138B 441	M. Althoff et al.	(TASSO Collab.)
ALTHOFF	84I	ZPHY C22 307	M. Althoff et al.	(TASSO Collab.)

t' (4th Generation) Quark, Searches for

t'(2/3)-quark/hadron mass limits in $p\overline{p}$ and pp collisions

VALUE (GeV)	CL%	DOCUMENT ID		TECN	COMMENT
>1280	95	[1] SIRUNYAN	19AQ	CMS	$B(t' \rightarrow Zt) = 1$
>1370	95	[2] SIRUNYAN	19BW	CMS	$B(t' \rightarrow ht) = 1$
> 980	95	[3] AABOUD	18CE	ATLS	$\geq 2\ell + \not{E}_T + \geq 1bj$
>1010	95	[4] AABOUD	18CL	ATLS	$B(t' \rightarrow ht) = 1$
>1030	95	[5,6] AABOUD	18CP	ATLS	2,3ℓ, singlet model
>1210	95	[5,7] AABOUD	18CP	ATLS	2,3ℓ, doublet model
>1310	95	[8,9] AABOUD	18CR	ATLS	singlet t'. ATLAS combination
>1370	95	[8,10] AABOUD	18CR	ATLS	t' in a weak isospin doublet (t',b'). ATLAS combination.
>1140	95	[11] SIRUNYAN	18BM	CMS	Wb, Zt, ht modes
> 845	95	[12] SIRUNYAN	18Q	CMS	$B(t' \rightarrow Wq) = 1$ (q=d,s)
>1295	95	[13] SIRUNYAN	18W	CMS	$B(t' \rightarrow Wb) = 1$
>1160	95	[14] AABOUD	17L	ATLS	$B(t' \rightarrow Zt) = 1$
> 860	95	[15] SIRUNYAN	17AU	CMS	
> 770	95	[16] AAD	15AR	ATLS	$B(t' \rightarrow Wb) = 1$
> 590	95	[17] AAD	15BY	ATLS	Wb, Zt, ht modes
> 745	95	[18] KHACHATRY...	15AI	CMS	$B(t' \rightarrow ht) = 1$
> 735	95	[19] AAD	14AZ	ATLS	$B(b' \rightarrow Wt) = 1$
> 700	95	[20] CHATRCHYAN	14A	CMS	$B(t' \rightarrow Wb) = 1$
> 706	95	[20] CHATRCHYAN	14A	CMS	$B(t' \rightarrow Zt) = 1$
> 782	95	[20] CHATRCHYAN	14A	CMS	$B(t' \rightarrow ht) = 1$
> 350	95	[21] AAD	12BC	ATLS	$B(t' \rightarrow Wq)$=1 (q=d,s,b)
> 420	95	[22] AAD	12C	ATLS	$t' \rightarrow Xt$ ($m_X < 140$ GeV)
> 685	95	[23] CHATRCHYAN	12BH	CMS	$m_{b'} = m_{t'}$
> 557	95	[24] CHATRCHYAN	12P	CMS	$t'\overline{t}' \rightarrow W^+ b W^- \overline{b} \rightarrow b\ell^+\nu\overline{b}\ell^-\overline{\nu}$
• • • We do not use the following data for averages, fits, limits, etc. • • •					
> 656	95	[25] AAD	13F	ATLS	$B(t' \rightarrow Wb) = 1$
> 625	95	[26] CHATRCHYAN	13I	CMS	$B(t' \rightarrow Zt) = 1$
> 404	95	[27] AAD	12AR	ATLS	$B(t' \rightarrow Wb) = 1$
> 570	95	[28] CHATRCHYAN	12BC	CMS	$t'\overline{t}' \rightarrow W^+ b W^- \overline{b}$
> 400	95	[29] AALTONEN	11AH	CDF	$t' \rightarrow Xt$ ($m_X < 70$ GeV)
> 358	95	[30] AALTONEN	11AL	CDF	$t' \rightarrow Wb$
> 340	95	[30] AALTONEN	11AL	CDF	$t' \rightarrow Wq$ (q=d,s,b)
> 360	95	[31] AALTONEN	11O	CDF	$t' \rightarrow Xt$ ($m_X < 100$ GeV)
> 285	95	[32] ABAZOV	11Q	D0	$t' \rightarrow Wq$ (q=d,s,b)
> 256	95	[33,34] AALTONEN	08H	CDF	$t' \rightarrow Wq$

[1] SIRUNYAN 19AQ based on 35.9 fb^{-1} of pp data at $\sqrt{s} = 13$ TeV. Pair production of vector-like t' is seached for with one t' decaying into Zt and the other t' decaying into Wb, Zt, ht. Events with an opposite-sign lepton pair consistent with coming from Z and jets are used. Mass limits are obtained for a variety of branching ratios of t'.

[2] SIRUNYAN 19BW based on 35.9 fb^{-1} of pp data at $\sqrt{s} = 13$ TeV. The limit is for the pair-produced vector-like t' using all-hadronic final state. The analysis is made for the Wb, Zt, ht modes and mass limits are obtained for a variety of branching ratios.

[3] AABOUD 18CE based on 36.1 fb^{-1} of proton-proton data taken at $\sqrt{s} = 13$ TeV. Events including a same-sign lepton pair are used. The limit is for a singlet model, assuming the branching ratios of t' into Zt, Wb and Ht as predicted by the model.

[4] AABOUD 18CL based on 36.1 fb^{-1} of pp data at $\sqrt{s} = 13$ TeV. The limit is for the pair-produced vector-like t' using all-hadronic final state. The analysis is also made for the Wb, Zt, ht modes and mass limits are obtained for a variety of branching ratios.

[5] AABOUD 18CP based on 36.1 fb^{-1} of pp data at $\sqrt{s} = 13$ TeV. Pair and single production of vector-like t' are seached for with at least one t' decaying into Zt. In the case of $B(t' \rightarrow Zt) = 1$, the limit is $m_{t'} > 1340$ GeV.

[6] The limit is for the singlet model, assuming that the branching ratios into Zt, Wb, and Ht add up to one.

[7] The limit is for the doublet model, assuming that the branching ratios into Zt, Wb, and Ht add up to one.

[8] AABOUD 18CR based on 36.1 fb^{-1} of pp data at $\sqrt{s} = 13$ TeV. A combination of searches for the pair-produced vector-like t' in various decay channels ($t' \rightarrow Wb$, Zt, ht). Also a model-independent limit is obtained as $m_{t'} > 1.31$ TeV, assuming that the branching ratios into Zt, Wb and ht add up to one.

[9] The limit is for the singlet t'.

[10] The limit is for t' in a weak isospin doublet (t',b') and $|V_{t'b}| \ll |V_{tb'}|$.

[11] SIRUNYAN 18BM based on 35.9 fb^{-1} of pp data at $\sqrt{s} = 13$ TeV. The limit is for the pair-produced vector-like t'. Three channels (single lepton, same-charge 2 leptons, or at least 3 leptons) are considered for various branching fraction combinations. Assuming $B(tH) = 1$, the limit is 1270 GeV and for $B(tZ) = 1$ it is 1300 GeV.

[12] SIRUNYAN 18Q based on 19.7 fb^{-1} of pp data at $\sqrt{s} = 8$ TeV. The limit is for the pair-produced vector-like t' that couple only to light quarks. Constraints for other decay channels (Zq and Hq) are also given in the paper.

[13] SIRUNYAN 18W based on 35.8 fb^{-1} of pp data at $\sqrt{s} = 13$ TeV. The limit is for the vector-like t' pair-produced by strong interaction using lepton-plus-jets mode and assuming that $B(t' \rightarrow Wb)$ is 100product of the production cross section and branching faction to Wb for any new pair-produced heavy quark decaying to this channel as a narrow resonance.

[14] AABOUD 17L based on 36.1 fb^{-1} of pp data at $\sqrt{s} = 13$ TeV. No signal is found in the search for heavy quark pair production that decay into Zt followed by $Z \rightarrow \nu\nu$ in

Downloaded from https://academic.oup.com/ptep/article/2022/8/083C01/6651666 by KIT Library user on 27 September 2022

the events with one lepton, large $\not{E}_T$, and ≥ 4 jets. The lower mass limit 0.87 (1.05) TeV is obtained for the singlet (doublet) model with other possible decay modes.

[15] SIRUNYAN 17AU based on 2.3-2.6 fb^{-1} of pp data at $\sqrt{s}$ = 13 TeV. Limit on pair-produced singlet vector-like t' using one lepton and several jets. The mass bound is given for a t' transforming as a singlet under the electroweak symmetry group, assumed to decay through W, Z or Higgs boson (which decays to jets) and to a third generation quark. For a doublet, the limit is >830 GeV. Other limits are also given in the paper.

[16] AAD 15AR based on 20.3 fb^{-1} of pp data at $\sqrt{s}$ = 8 TeV. Used lepton-plus-jets final state. See Fig. 20 for mass limits in the plane of B($t' \rightarrow Ht$) vs. B($t' \rightarrow Wb$) from a combination of $t'\overline{t}' \rightarrow Wb + X$ and $t'\overline{t}' \rightarrow Ht + X$ searches. Any branching ratio scenario is excluded for mass below 715 GeV.

[17] AAD 15BY based on 20.3 fb^{-1} of pp data at $\sqrt{s}$ = 8 TeV. Limit on pair-produced vector-like t' assuming the branching fractions to W, Z, and h modes of the singlet model. Used events containing $\geq 2\ell + \not{E}_T + \geq 2$j (≥ 1 b) and including a same-sign lepton pair.

[18] KHACHATRYAN 15AI based on 19.7 fb^{-1} of pp data at $\sqrt{s}$ = 8 TeV. The search exploits all-hadronic final states by tagging boosted Higgs boson using jet substructure and b-tagging.

[19] Based on 20.3 fb^{-1} of pp data at $\sqrt{s}$ = 8 TeV. No significant excess over SM expectation is found in the search for pair production or single production of t' in the events with dilepton from a high p_T Z and additional jets ($\geq$ 1 b-tag). If instead of B($b' \rightarrow Wt$) = 1 an electroweak singlet with B($b' \rightarrow Wt$) $\sim$ 0.45 is assumed, the limit reduces to 685 GeV.

[20] Based on 19.5 fb^{-1} of pp data at $\sqrt{s}$ = 8TeV. The t' quark is pair produced and is assumed to decay into three different final states of bW, tZ, and th. The search is carried out using events with at least one isolated lepton.

[21] Based on 1.04 fb^{-1} of pp data at $\sqrt{s}$ = 7 TeV. No signal is found for the search of heavy quark pair production that decay into W and a quark in the events with dileptons, large $\not{E}_T$, and ≥ 2 jets.

[22] Based on 1.04 fb^{-1} of data in pp collisions at 7 TeV. AAD 12C looked for $t'\overline{t}'$ production followed by t' decaying into a top quark and X, an invisible particle, in a final state with an isolated high-P$_T$ lepton, four or more jets, and a large missing transverse energy. No excess over the SM $t\overline{t}$ production gives the upper limit on $t'\overline{t}'$ production cross section as a function of $m_{t'}$ and m_X. The result is obtained for B($t' \rightarrow Wt$) = 1.

[23] Based on 5 fb^{-1} of pp data at $\sqrt{s}$ = 7 TeV. CHATRCHYAN 12BH searched for QCD and EW production of single and pair of degenerate 4'th generation quarks that decay to Wb or Wt. Absence of signal in events with one lepton, same-sign dileptons or tri-leptons gives the bound. With a mass difference of 25 GeV/c^2 between $m_{t'}$ and $m_{b'}$, the corresponding limit shifts by about $\pm$20 GeV/c^2.

[24] Based on 5.0 fb^{-1} of pp data at $\sqrt{s}$ = 7 TeV. CHATRCHYAN 12P looked for $t'\overline{t}'$ production events with two isolated high p_T leptons, large $\not{E}_T$, and 2 high p_T jets with b-tag. The absence of signal above the SM background gives the limit for B($t' \rightarrow Wb$) = 1.

[25] Based on 4.7 fb^{-1} of pp data at $\sqrt{s}$ = 7 TeV. No signal is found for the search of heavy quark pair production that decay into W and a b quark in the events with a high p_T isolated lepton, large $\not{E}_T$ and at least 3 jets ($\geq$ 1 b-tag). Vector-like quark of charge 2/3 with 400 < $m_{t'}$ < 550 GeV and B($t' \rightarrow Wb$) > 0.63 is excluded at 95% CL.

[26] Based on 5.0 fb^{-1} of pp data at $\sqrt{s}$ = 7 TeV. CHATRCHYAN 13I looked for events with one isolated electron or muon, large $\not{E}_T$, and at least four jets with large transverse momenta, where one jet is likely to originate from the decay of a bottom quark.

[27] Based on 1.04 fb^{-1} of pp data at $\sqrt{s}$ = 7 TeV. No signal is found in the search for pair produced heavy quarks that decay into W boson and a b quark in the events with a high p_T isolated lepton, large $\not{E}_T$ and at least 3 jets ($\geq$ 1 b-tag).

[28] Based on 5.0 fb^{-1} of pp data at $\sqrt{s}$ = 7 TeV. CHATRCHYAN 12BC looked for $t'\overline{t}'$ production events with a single isolated high p_T lepton, large $\not{E}_T$ and at least 4 high p_T jets with a b-tag. The absence of signal above the SM background gives the limit for B($t' \rightarrow Wb$) = 1.

[29] Based on 5.7 fb^{-1} of data in $p\overline{p}$ collisions at 1.96 TeV. AALTONEN 11AH looked for $t'\overline{t}'$ production followed by t' decaying into a top quark and X, an invisible particle, in the all hadronic decay mode of $t\overline{t}$. No excess over the SM $t\overline{t}$ production gives the upper limit on $t'\overline{t}'$ production cross section as a function of $m_{t'}$ and m_X. The result is obtained for B($t' \rightarrow Xt$) = 1.

[30] Based on 5.6 fb^{-1} of data in ppbar collisions at 1.96 TeV. AALTONEN 11AL looked for $\ell + \geq 4$j events and set upper limits on $\sigma(t'\overline{t}')$ as functions of $m_{t'}$.

[31] Based on 4.8 fb^{-1} of data in $p\overline{p}$ collisions at 1.96 TeV. AALTONEN 11O looked for $t'\overline{t}'$ production signal when t' decays into a top quark and X, an invisible particle, in $\ell + \not{E}_T$ + jets channel. No excess over the SM $t\overline{t}$ production gives the upper limit on $t'\overline{t}'$ production cross section as a function of $m_{t'}$ and m_X. The result is obtained for B($t' \rightarrow Xt$) = 1.

[32] Based on 5.3 fb^{-1} of data in $p\overline{p}$ collisions at 1.96 TeV. ABAZOV 11Q looked for $\ell + \not{E}_T + \geq 4$j events and set upper limits on $\sigma(t'\overline{t}')$ as functions of $m_{t'}$.

[33] Searches for pair production of a new heavy top-like quark t' decaying to a W boson and another quark by fitting the observed spectrum of total transverse energy and reconstructed t' mass in the lepton + jets events.

[34] HUANG 08 reexamined the t' mass lower bound of 256 GeV obtained in AALTONEN 08H that assumes B($b' \rightarrow qZ$) = 1 for $q = u, c$ which does not hold when $m_{b'} < m_{t'} - m_W$ or the mixing sin$^2(\theta_{bt'})$ is so tiny that the decay occurs outside of the vertex detector. Fig. 1 gives that lower bound on $m_{t'}$ in the plane of sin$^2(\theta_{bt'})$ and $m_{b'}$.

t'(5/3)-quark/hadron mass limits in $p\overline{p}$ and pp collisions

VALUE (GeV)	CL%	DOCUMENT ID		TECN	COMMENT
>1330	95	[1] SIRUNYAN	19T	CMS	$t'_R(5/3) \rightarrow tW^+$
>1300	95	[1] SIRUNYAN	19T	CMS	$t'_L(5/3) \rightarrow tW^+$
>1350	95	[2] AABOUD	18AW	ATLS	$t'(5/3) \rightarrow tW^+$
>1190	95	[3] AABOUD	18CE	ATLS	$\geq 2\ell + \not{E}_T + \geq 1bj$
>1020	95	[4] SIRUNYAN	17J	CMS	$t'_R(5/3) \rightarrow tW^+$
> 990	95	[4] SIRUNYAN	17J	CMS	$t'_L(5/3) \rightarrow tW^+$
> 750	95	[5] AAD	15BY	ATLS	$t'(5/3) \rightarrow tW^+$
> 840	95	[6] AAD	15Z	ATLS	$t'(5/3) \rightarrow tW^+$
> 800	95	[7] CHATRCHYAN	14T	CMS	$t'(5/3) \rightarrow tW^+$

[1] SIRUNYAN 19T based on 35.9 fb^{-1} of pp data at $\sqrt{s}$ = 13 TeV. Signals are searched in the final states of t' pair production, with same-sign leptons (which come from a t' decay) or a single lepton (which comes from a W out of 4Ws), along with jets, and no excess over the SM expectation is found.

[2] AABOUD 18AW based on 36.1 fb^{-1} of pp data at $\sqrt{s}$ = 13 TeV. Limit on $t'(5/3)$ in pair production assuming its coupling to Wt is equal to one. Lepton-plus-jets final state is used, characterized by $\ell + \not{E}_T$ + jets (≥ 1 b-tagged).

[3] AABOUD 18CE based on 36.1 fb^{-1} of proton-proton data taken at $\sqrt{s}$ = 13 TeV. Events including a same-sign lepton pair are used. The limit is for the pair-produced vector-like t'. With single t' production included, assuming $t'tW$ coupling of one, the limit is $m_{t'}$ > 1.6 TeV.

[4] SIRUNYAN 17J based on 2.3 fb^{-1} of pp data at $\sqrt{s}$ = 13 TeV. Signals are searched in the final states of t' pair production, with same-sign leptons (which come from a t' decay) or a single lepton (which comes from a W out of 4Ws), along with jets, and no excess over the SM expectation is found.

[5] AAD 15BY based on 20.3 fb^{-1} of pp data at $\sqrt{s}$ = 8 TeV. Limit on $t'(5/3)$ in pair and single production assuming its coupling to Wt is equal to one. Used events containing $\geq 2\ell + \not{E}_T + \geq 2$j (≥ 1 b) and including a same-sign lepton pair.

[6] AAD 15Z based on 20.3 fb^{-1} of pp data at $\sqrt{s}$ = 8 TeV. Used events with $\ell + \not{E}_T + \geq 6$j (≥ 1 b) and at least one pair of jets from weak boson decay, sensitive to the final state $b\overline{b}W^+W^-W^+W^-$.

[7] CHATRCHYAN 14T based on 19.5 fb^{-1} of pp data at $\sqrt{s}$ = 8 TeV. Non-observation of anomaly in H_T distribution in the same-sign dilepton events leads to the limit when pair produced $t'(5/3)$ quark decays exclusively into t and W^+, resulting in the final state with $b\overline{b}W^+W^-W^+W^-$.

t'(2/3) mass limits from single production in $p\overline{p}$ and pp collisions

VALUE (GeV)	CL%	DOCUMENT ID		TECN	COMMENT
>950	95	[1] AAD	16AV	ATLS	$qg \rightarrow q't'b$, B($t' \rightarrow Wb$)=0.5
>403	95	[2] ABAZOV	11F	D0	$qd \rightarrow q't' \rightarrow q'(Wd)$ $\tilde{\kappa}_{dt'}$=1, B($t' \rightarrow Wd$)=1
>551	95	[2] ABAZOV	11F	D0	$qu \rightarrow q't' \rightarrow q(Zu)$ $\tilde{\kappa}_{ut'}$=$\sqrt{2}$, B($t' \rightarrow Zu$)=1

[1] AAD 16AV based on 20.3 fb^{-1} of pp data at $\sqrt{s}$ = 8 TeV. No significant excess over SM expectation is found in the search for a fully reconstructed vector-like t' in the mode $\ell + \not{E}_T + \geq 2j$ ($\geq 1b$). A veto on massive large-radius jets is used to reject the $t\overline{t}$ background.

[2] Based on 5.4 fb^{-1} of data in ppbar collisions at 1.96 TeV. ABAZOV 11F looked for single production of t' via the Z or E coupling to the first generation up or down quarks, respectively. Model independent cross section limits for the single production processes $p\overline{p} \rightarrow t'q \rightarrow (Wd)q$, and $p\overline{p} \rightarrow t'q \rightarrow (Zd)q$ are given in Figs. 3 and 4, respectively, and the mass limits are obtained for the model of ATRE 09 with degenerate bi-doublets of vector-like quarks.

t'(5/3) mass limits from single production in $p\overline{p}$ and pp collisions

VALUE (GeV)	DOCUMENT ID		TECN	COMMENT
• • • We do not use the following data for averages, fits, limits, etc. • • •				
	[1] SIRUNYAN	19AI	CMS	$tW \rightarrow t'(5/3) \rightarrow tW$

[1] SIRUNYAN 19AI based on 35.9 fb^{-1} of pp data at $\sqrt{s}$ = 13 TeV. Exclusion limits are set on the product of the production cross section and branching fraction for the $b'(-1/3) + t$ and $t'(5/3) + t$ modes as a function of the vector-like quark mass in Fig. 8 and Tab. 2 for relative vector-like quark widths between 1 and 30% for left- and right-handed vector-like quark couplings. No significant deviation from the SM prediction is observed.

REFERENCES FOR Searches for (Fourth Generation) t' Quark

SIRUNYAN	19AI	EPJ C79 90	A.M. Sirunyan et al.	(CMS Collab.)
SIRUNYAN	19AQ	EPJ C79 364	A.M. Sirunyan et al.	(CMS Collab.)
SIRUNYAN	19BW	PR D100 072001	A.M. Sirunyan et al.	(CMS Collab.)
SIRUNYAN	19T	JHEP 1903 082	A.M. Sirunyan et al.	(CMS Collab.)
AABOUD	18AW	JHEP 1808 048	M. Aaboud et al.	(ATLAS Collab.)
AABOUD	18CE	JHEP 1812 039	M. Aaboud et al.	(ATLAS Collab.)
AABOUD	18CL	PR D98 092005	M. Aaboud et al.	(ATLAS Collab.)
AABOUD	18CP	PR D98 112010	M. Aaboud et al.	(ATLAS Collab.)
AABOUD	18CR	PRL 121 211801	M. Aaboud et al.	(ATLAS Collab.)
SIRUNYAN	18BM	JHEP 1808 177	A.M. Sirunyan et al.	(CMS Collab.)
SIRUNYAN	18Q	PR D97 072008	A.M. Sirunyan et al.	(CMS Collab.)
SIRUNYAN	18W	PL B779 82	A.M. Sirunyan et al.	(CMS Collab.)
AABOUD	17L	JHEP 1708 052	M. Aaboud et al.	(ATLAS Collab.)
SIRUNYAN	17AU	JHEP 1711 085	A.M. Sirunyan et al.	(CMS Collab.)
SIRUNYAN	17J	JHEP 1708 073	A.M. Sirunyan et al.	(CMS Collab.)
AAD	16AV	EPJ C76 442	G. Aad et al.	(ATLAS Collab.)
AAD	15AR	JHEP 1508 105	G. Aad et al.	(ATLAS Collab.)
AAD	15BY	JHEP 1510 150	G. Aad et al.	(ATLAS Collab.)
AAD	15Z	PR D91 112011	G. Aad et al.	(ATLAS Collab.)
KHACHATRY...	15AI	JHEP 1506 080	V. Khachatryan et al.	(CMS Collab.)
AAD	14AZ	JHEP 1411 104	G. Aad et al.	(ATLAS Collab.)
CHATRCHYAN	14A	PL B729 149	S. Chatrchyan et al.	(CMS Collab.)
CHATRCHYAN	14T	PRL 112 171801	S. Chatrchyan et al.	(CMS Collab.)
AAD	13F	PL B718 1284	G. Aad et al.	(ATLAS Collab.)
CHATRCHYAN	13I	JHEP 1301 154	S. Chatrchyan et al.	(CMS Collab.)
AAD	12AR	PRL 108 261802	G. Aad et al.	(ATLAS Collab.)
AAD	12BC	PR D86 012007	G. Aad et al.	(ATLAS Collab.)
AAD	12C	PRL 108 041805	G. Aad et al.	(ATLAS Collab.)
CHATRCHYAN	12BC	PL B718 307	S. Chatrchyan et al.	(CMS Collab.)
CHATRCHYAN	12BH	PR D86 112003	S. Chatrchyan et al.	(CMS Collab.)
CHATRCHYAN	12P	PL B716 103	S. Chatrchyan et al.	(CMS Collab.)
AALTONEN	11AH	PRL 107 191803	T. Aaltonen et al.	(CDF Collab.)
AALTONEN	11AL	PRL 107 261801	T. Aaltonen et al.	(CDF Collab.)
AALTONEN	11O	PRL 106 191801	T. Aaltonen et al.	(CDF Collab.)
ABAZOV	11F	PRL 106 081801	V.M. Abazov et al.	(D0 Collab.)
ABAZOV	11Q	PRL 107 082001	V.M. Abazov et al.	(D0 Collab.)

Downloaded from https://academic.oup.com/ptep/article/2022/8/083C01/6651666 by KIT Library user on 27 September 2022

ATRE	09	PR D79 054018	A. Atre *et al.*	
AALTONEN	08H	PRL 100 161803	T. Aaltonen *et al.*	(CDF Collab.)
HUANG	08	PR D77 037302	P.Q. Hung, M. Sher	(UVA, WILL)

Free Quark Searches

FREE QUARK SEARCHES

The basis for much of the theory of particle scattering and hadron spectroscopy is the construction of the hadrons from a set of fractionally charged constituents (quarks). A central element of Quantum Chromodynamics is that quarks cannot be observed as free particles but are confined to mesons and baryons. Experiments have produced no evidence for free quarks.

This compilation is only a guide to the literature, since the quoted experimental limits are often only indicative. Reviews can be found in Refs. 1–4.

References

1. M.L. Perl, E.R. Lee, and D. Lomba, Mod. Phys. Lett. **A19**, 2595 (2004).
2. P.F. Smith, Ann. Rev. Nucl. and Part. Sci. **39**, 73 (1989).
3. L. Lyons, Phys. Reports **129**, 225 (1985).
4. M. Marinelli and G. Morpurgo, Phys. Reports **85**, 161 (1982).

Quark Production Cross Section — Accelerator Searches

X-SECT (cm^2)	CHG ($e/3$)	MASS (GeV)	ENERGY (GeV)	BEAM	EVTS	DOCUMENT ID		TECN
<1.7-2.3E−39	±2	100–600	7000	pp	0	[1] CHATRCHYAN	13AR	CMS
<14-5.4E−39	±1	100–600	7000	pp	0	[1] CHATRCHYAN	13AR	CMS
<1.3E−36	±2	45–84	130–172	e^+e^-	0	ABREU	97D	DLPH
<2.E−35	+2	250	1800	$p\overline{p}$	0	[2] ABE	92J	CDF
<1.E−35	+4	250	1800	$p\overline{p}$	0	[2] ABE	92J	CDF
<3.8E−28			14.5A	^{28}Si–Pb	0	[3] HE	91	PLAS
<3.2E−28			14.5A	^{28}Si–Cu	0	[3] HE	91	PLAS
<1.E−40	±1,2	<10		$p,\nu,\overline{\nu}$	0	BERGSMA	84B	CHRM
<1.E−36	±1,2	<9	200	μ	0	AUBERT	83C	SPEC
<2.E−10	±2,4	1–3	200	p	0	[4] BUSSIERE	80	CNTR
<5.E−38	+1,2	>5	300	p	0	[5,6] STEVENSON	79	CNTR
<1.E−33	±1	<20	52	pp	0	BASILE	78	SPEC
<9.E−39	±1,2	<6	400	p	0	[5] ANTREASYAN	77	SPEC
<8.E−35	+1,2	<20	52	pp	0	[7] FABJAN	75	CNTR
<5.E−38	−1,2	4–9	200	p	0	NASH	74	CNTR
<1.E−32	+2,4	4–24	52	pp	0	ALPER	73	SPEC
<5.E−31	+1,2,4	<12	300	p	0	LEIPUNER	73	CNTR
<6.E−34	±1,2	<13	52	pp	0	BOTT	72	CNTR
<1.E−36	−4	4	70	p	0	ANTIPOV	71	CNTR
<1.E−35	±1,2	2	28	p	0	[8] ALLABY	69B	CNTR
<4.E−37	−2	<5	70	p	0	[4] ANTIPOV	69	CNTR
<3.E−37	−1,2	2–5	70	p	0	[8] ANTIPOV	69B	CNTR
<1.E−35	+1,2	<7	30	p	0	DORFAN	65	CNTR
<2.E−35	−2	< 2.5–5	30	p	0	[9] FRANZINI	65B	CNTR
<5.E−35	+1,2	<2.2	21	p	0	BINGHAM	64	HLBC
<1.E−32	+1,2	<4.0	28	p	0	BLUM	64	HBC
<1.E−35	+1,2	<2.5	31	p	0	[9] HAGOPIAN	64	HBC
<1.E−34	+1	<2	28	p	0	LEIPUNER	64	CNTR
<1.E−33	+1,2	<2.4	24	p	0	MORRISON	64	HBC

[1] CHATRCHYAN 13AR limits assume pair-produced long-lived spin-1/2 particles neutral under $SU(3)_C$ and $SU(2)_L$.
[2] ABE 92J flux limits decrease as the mass increases from 50 to 500 GeV.
[3] HE 91 limits are for charges of the form $N\pm1/3$ from 23/3 to 38/3.
[4] Hadronic or leptonic quarks.
[5] Cross section cm^2/GeV^2.
[6] 3×10^{-5} <lifetime $< 1\times10^{-3}$ s.
[7] Includes BOTT 72 results.
[8] Assumes isotropic cm production.
[9] Cross section inferred from flux.

Quark Differential Production Cross Section — Accelerator Searches

X-SECT ($cm^2sr^{-1}GeV^{-1}$)	CHG ($e/3$)	MASS (GeV)	ENERGY (GeV)	BEAM	EVTS	DOCUMENT ID		TECN
<4.E−36	−2,4	1.5–6	70	p	0	BALDIN	76	CNTR
<2.E−33	±4	5–20	52	pp	0	ALBROW	75	SPEC
<5.E−34	<7	7–15	44	pp	0	JOVANOV...	75	CNTR
<5.E−35			20	γ	0	[1] GALIK	74	CNTR
<9.E−35	−1,2		200	p	0	NASH	74	CNTR
<4.E−36	−4	2.3–2.7	70	p	0	ANTIPOV	71	CNTR
<3.E−35	±1,2	<2.7	27	p	0	ALLABY	69B	CNTR
<7.E−38	−1,2	<2.5	70	p	0	ANTIPOV	69B	CNTR

[1] Cross section in cm^2/sr/equivalent quanta.

Quark Flux — Accelerator Searches

The definition of FLUX depends on the experiment

(a) is the ratio of measured free quarks to predicted free quarks if there is no "confinement."
(b) is the probability of fractional charge on nuclear fragments. Energy is in GeV/nucleon.
(c) is the 90%CL upper limit on fractionally-charged particles produced per interaction.
(d) is quarks per collision.
(e) is inclusive quark-production cross-section ratio to $\sigma(e^+e^-\to\mu^+\mu^-)$.
(f) is quark flux per charged particle.
(g) is the flux per ν-event.
(h) is quark yield per π^- yield.
(i) is 2-body exclusive quark-production cross-section ratio to $\sigma(e^+e^-\to\mu^+\mu^-)$.

FLUX		CHG ($e/3$)	MASS (GeV)	ENRGY (GeV)	BEAM	EVTS	DOCUMENT ID		TECN
<1.6E−3	b	see note		200	^{32}S–Pb	0	[1] HUENTRUP	96	PLAS
<6.2E−4	b	see note		10.6	^{32}S–Pb	0	[1] HUENTRUP	96	PLAS
<0.94E−4	e	±2	2–30	88–94	e^+e^-	0	AKERS	95R	OPAL
<1.7E−4	e	±2	30–40	88–94	e^+e^-	0	AKERS	95R	OPAL
<3.6E−4	e	±4	5–30	88–94	e^+e^-	0	AKERS	95R	OPAL
<1.9E−4	e	±4	30–45	88–94	e^+e^-	0	AKERS	95R	OPAL
<2.E−3	e	+1	5–40	88–94	e^+e^-	0	[2] BUSKULIC	93C	ALEP
<6.E−4	e	+2	5–30	88–94	e^+e^-	0	[2] BUSKULIC	93C	ALEP
<1.2E−3	e	+4	15–40	88–94	e^+e^-	0	[2] BUSKULIC	93C	ALEP
<3.6E−4	i	+4	5.0–10.2	88–94	e^+e^-	0	BUSKULIC	93C	ALEP
<3.6E−4	i	+4	16.5–26.0	88–94	e^+e^-	0	BUSKULIC	93C	ALEP
<6.9E−4	i	+4	26.0–33.3	88–94	e^+e^-	0	BUSKULIC	93C	ALEP
<9.1E−4	i	+4	33.3–38.6	88–94	e^+e^-	0	BUSKULIC	93C	ALEP
<1.1E−3	i	+4	38.6–44.9	88–94	e^+e^-	0	BUSKULIC	93C	ALEP
<1.6E−4	b	see note		see note		0	[3] CECCHINI	93	PLAS
	b	4,5,7,8		2.1A	^{16}O	0,2,0,6	[4] GHOSH	92	EMUL
<6.4E−5	g	1			$\nu,\overline{\nu}$	1	[5] BASILE	91	CNTR
<3.7E−5	g	2			$\nu,\overline{\nu}$	0	[5] BASILE	91	CNTR
<3.9E−5	g	1			$\nu,\overline{\nu}$	1	[6] BASILE	91	CNTR
<2.8E−5	g	2			$\nu,\overline{\nu}$	0	[6] BASILE	91	CNTR
<1.9E−4	c			14.5A	^{28}Si–Pb	0	[7] HE	91	PLAS
<3.9E−4	c			14.5A	^{28}Si–Cu	0	[7] HE	91	PLAS
<1.E−9	c	±1,2,4		14.5A	^{16}O–Ar	0	MATIS	91	MDRP
<5.1E−10	c	±1,2,4		14.5A	^{16}O–Hg	0	MATIS	91	MDRP
<8.1E−9	c	±1,2,4		14.5A	Si–Hg	0	MATIS	91	MDRP
<1.7E−6	c	±1,2,4		60A	^{16}O–Hg	0	MATIS	91	MDRP
<3.5E−7	c	±1,2,4		200A	^{16}O–Hg	0	MATIS	91	MDRP
<1.3E−6	c	±1,2,4		200A	S–Hg	0	MATIS	91	MDRP
<5E−2	e	2	19–27	52–60	e^+e^-	0	ADACHI	90C	TOPZ
<5E−2	e	4	<24	52–60	e^+e^-	0	ADACHI	90C	TOPZ
<1.E−4	e	+2	<3.5	10	e^+e^-	0	BOWCOCK	89B	CLEO
<1.E−6	d	±1,2		60	^{16}O–Hg	0	CALLOWAY	89	MDRP
<3.5E−7	d	±1,2		200	^{16}O–Hg	0	CALLOWAY	89	MDRP
<1.3E−6	d	±1,2		200	S–Hg	0	CALLOWAY	89	MDRP
<1.2E−10	d	±1	1	800	p–Hg	0	MATIS	89	MDRP
<1.1E−10	d	±2	1	800	p–Hg	0	MATIS	89	MDRP
<1.2E−10	d	±1	1	800	p–N_2	0	MATIS	89	MDRP
<7.7E−11	d	±2	1	800	p–N_2	0	MATIS	89	MDRP
<6.E−9	h	−5	0.9–2.3	12	p	0	NAKAMURA	89	SPEC
<5.E−5	g	1,2	<0.5		$\nu,\overline{\nu}d$	0	ALLASIA	88	BEBC
<3.E−4	b	See note		14.5	^{16}O–Pb	0	[8] HOFFMANN	88	PLAS
<2.E−4	b	See note		200	^{16}O–Pb	0	[9] HOFFMANN	88	PLAS
<8E−5	b	19,20,22,23		200A			GERBIER	87	PLAS
<2.E−4	a	±1,2	<300	320	$\overline{p}p$	0	LYONS	87	MLEV
<1.E−9	c	±1,2,4,5		14.5	^{16}O–Hg	0	SHAW	87	MDRP
<3.E−3	d	−1,2,3,4,6	<5	2	Si–Si	0	[10] ABACHI	86C	CNTR
<1.E−4	e	±1,2,4	<4	10	e^+e^-	0	ALBRECHT	85G	ARG
<6.E−5	b	±1,2	1	540	$p\overline{p}$	0	BANNER	85	UA2
<5.E−3	e	−4	1–8	29	e^+e^-	0	AIHARA	84	TPC
<1.E−2	e	±1,2	1–13	29	e^+e^-	0	AIHARA	84B	TPC
<2.E−4	b	±1		72	^{40}Ar	0	[11] BARWICK	84	CNTR
<1.E−4	e	±2	<0.4	1.4	e^+e^-	0	BONDAR	84	OLYA
<5.E−1	e	±1,2	<13	29	e^+e^-	0	GURYN	84	CNTR
<3.E−3	b	±1,2	<2	540	$p\overline{p}$	0	BANNER	83	CNTR
<1.E−4	b	±1,2		106	^{56}Fe	0	LINDGREN	83	CNTR
<3.E−3	b	>|±0.1|		74	^{40}Ar	0	[11] PRICE	83	PLAS
<1.E−2	e	±1,2	<14	29	e^+e^-	0	MARINI	82B	CNTR
<8.E−2	e	±1,2	<12	29	e^+e^-	0	ROSS	82	CNTR
<3.E−4	e	±2	1.8–2	7	e^+e^-	0	WEISS	81	MRK2
<5.E−2	e	+1,2,4,5	2–12	27	e^+e^-	0	BARTEL	80	JADE

Downloaded from https://academic.oup.com/ptep/article/2022/8/083C01/6651666 by KIT Library user on 27 September 2022

<2.E−5	g	1,2			ν	0	[5,6] BASILE	80	CNTR
<3.E−10	f	±2,4	1–3	200	p	0	[12] BOZZOLI	79	CNTR
<6.E−11	f	±1	<21	52	pp	0	BASILE	78	SPEC
<5.E−3	g				ν_μ	0	BASILE	78B	CNTR
<2.E−9	f	±1	<26	62	pp	0	BASILE	77	SPEC
<7.E−10	f	+1,2	<20	52	p	0	[13] FABJAN	75	CNTR
		+1,2	>4.5		γ	0	[5,6] GALIK	74	CNTR
		+1,2	>1.5	12	e^-	0	[5,6] BELLAMY	68	CNTR
		+1,2	>0.9		γ	0	[6] BATHOW	67	CNTR
		+1,2	>0.9	6	γ	0	[6] FOSS	67	CNTR

[1] HUENTRUP 96 quote 95% CL limits for production of fragments with charge differing by as much as ±1/3 (in units of e) for charge $6 \leq Z \leq 10$.
[2] BUSKULIC 93C limits for inclusive quark production are more conservative if the ALEPH hadronic fragmentation function is assumed.
[3] CECCHINI 93 limit at 90%CL for $23/3 \leq Z \leq 40/3$, for 16*A* GeV O, 14.5*A* Si, and 200*A* S incident on Cu target. Other limits are 2.3×10^{-4} for $17/3 \leq Z \leq 20/3$ and 1.2×10^{-4} for $20/3 \leq Z \leq 23/3$.
[4] GHOSH 92 reports measurement of spallation fragment charge based on ionization in emulsion. Out of 650 measured tracks, 2 were consistent with charge $5e/3$, and 4 with $7e/3$.
[5] Hadronic quark.
[6] Leptonic quark.
[7] HE 91 limits are for charges of the form $N \pm 1/3$ from 23/3 to 38/3, and correspond to cross-section limits of 380μb (Pb) and 320μb (Cu).
[8] The limits apply to projectile fragment charges of 17, 19, 20, 22, 23 in units of $e/3$.
[9] The limits apply to projectile fragment charges of 16, 17, 19, 20, 22, 23 in units of $e/3$.
[10] Flux limits and mass range depend on charge.
[11] Bound to nuclei.
[12] Quark lifetimes $> 1 \times 10^{-8}$ s.
[13] One candidate m <0.17 GeV.

Quark Flux — Cosmic Ray Searches

Shielding values followed with an asterisk indicate altitude in km. Shielding values not followed with an asterisk indicate sea level in kg/cm^2.

FLUX (cm^{-2}sr^{-1}s^{-1})	CHG ($e/3$)	MASS (GeV)	SHIELDING	DOCUMENT ID		TECN
< 1.E−8	±1/6–1/10			[1] AGNESE	15	CDMS
< 9.2E−15	±1		3800	[2] AMBROSIO	00C	MCRO
<2.1E−15	±1			MORI	91	KAM2
<2.3E−15	±2			MORI	91	KAM2
<2.E−10	±1,2		0.3	WADA	88	CNTR
	±4		0.3	[3] WADA	88	CNTR
	±4		0.3	[4] WADA	86	CNTR
<1.E−12	±2,3/2		−70.	[5] KAWAGOE	84B	PLAS
<9.E−10	±1,2		0.3	WADA	84B	CNTR
<4.E−9	±4		0.3	WADA	84B	CNTR
<2.E−12	±1,2,3		−0.3 *	MASHIMO	83	CNTR
<3.E−10	±1,2		0.3	MARINI	82	CNTR
<2.E−11	±1,2			MASHIMO	82	CNTR
<8.E−10	±1,2		0.3	[5] NAPOLITANO	82	CNTR
				[6] YOCK	78	CNTR
<1.E−9				[7] BRIATORE	76	ELEC
<2.E−11	+1			[8] HAZEN	75	CC
<2.E−10	+1,2			KRISOR	75	CNTR
<1.E−7	+1,2			[8,9] CLARK	74B	CC
<3.E−10	+1	>20		KIFUNE	74	CNTR
<8.E−11	+1			[8] ASHTON	73	CNTR
<2.E−8	+1,2			HICKS	73B	CNTR
<5.E−10	+4		2.8 *	BEAUCHAMP	72	CNTR
<1.E−10	+1,2			[8] BOHM	72B	CNTR
<1.E−10	+1,2		2.8 *	COX	72	ELEC
<3.E−10	+2			CROUCH	72	CNTR
<3.E−8			7	[7] DARDO	72	CNTR
<4.E−9	+1			[8] EVANS	72	CC
<2.E−9		>10		[7] TONWAR	72	CNTR
<2.E−10	+1		2.8 *	CHIN	71	CNTR
<3.E−10	+1,2			[8] CLARK	71B	CC
<1.E−10	+1,2			[8] HAZEN	71	CC
<5.E−10	+1,2		3.5 *	BOSIA	70	CNTR
	+1,2	<6.5		[8] CHU	70	HLBC
<2.E−9	+1			FAISSNER	70B	CNTR
<2.E−10	+1,2		0.8 *	KRIDER	70	CNTR
<5.E−11	+2			CAIRNS	69	CC
<8.E−10	+1,2	<10		FUKUSHIMA	69	CNTR
	+2			[8,10] MCCUSKER	69	CC
<1.E−10		>5	1.7,3.6	[7] BJORNBOE	68	CNTR
<1.E−8	±1,2,4		6.3,.2 *	[5] BRIATORE	68	CNTR
<3.E−8		>2		FRANZINI	68	CNTR
<9.E−11	±1,2			GARMIRE	68	CNTR
<4.E−10	±1			HANAYAMA	68	CNTR
<3.E−8		>15		KASHA	68	OSPK
<2.E−10	+2			KASHA	68B	CNTR
<2.E−10	+4			KASHA	68C	CNTR
<2.E−10	+2		6	BARTON	67	CNTR
<2.E−7	+4		0.008,0.5 *	BUHLER	67	CNTR
<5.E−10	1,2		0.008,0.5 *	BUHLER	67B	CNTR
<4.E−10	+1,2			GOMEZ	67	CNTR
<2.E−9	+2			KASHA	67	CNTR
<2.E−10	+2		220	BARTON	66	CNTR
<2.E−9	+1,2		0.5 *	BUHLER	66	CNTR
<3.E−9	+1,2			KASHA	66	CNTR
<2.E−9	+1,2			LAMB	66	CNTR
<2.E−8	+1,2	>7	2.8 *	DELISE	65	CNTR
<5.E−8	+2	>2.5	0.5 *	MASSAM	65	CNTR
<2.E−8	+1		2.5 *	BOWEN	64	CNTR
<2.E−7	+1		0.8	SUNYAR	64	CNTR

[1] See AGNESE 15 Fig.6 for limits on vertical density as function of charge extending to $|q|/e < 1/10$.
[2] AMBROSIO 00C limit is below 11×10^{-15} for $0.25 < q/e < 0.5$, and is changing rapidly near q/e=2/3, where it is 2×10^{-14}.
[3] Distribution in celestial sphere was described as anisotropic.
[4] With telescope axis at zenith angle 40° to the south.
[5] Leptonic quarks.
[6] Lifetime $> 10^{-8}$ s; charge ±0.70, 0.68, 0.42; and mass >4.4, 4.8, and 20 GeV, respectively.
[7] Time delayed air shower search.
[8] Prompt air shower search.
[9] Also $e/4$ and $e/6$ charges.
[10] No events in subsequent experiments.

Quark Density — Matter Searches

QUARKS/ NUCLEON	CHG ($e/3$)	MASS (GeV)	MATERIAL/METHOD	EVTS	DOCUMENT ID	
<1.17E−22			silicone oil drops	0	[1] LEE	02
<4.71E−22			silicone oil drops	1	[2] HALYO	00
<4.7E−21	±1,2		silicone oil drops	0	MAR	96
<8.E−22	+2		Si/infrared photoionization	0	PERERA	93
<5.E−27	±1,2		sea water/levitation	0	HOMER	92
<4.E−20	±1,2		meteorites/mag. levitation	0	JONES	89
<1.E−19	±1,2		various/spectrometer	0	MILNER	87
<5.E−22	±1,2		W/levitation	0	SMITH	87
<3.E−20	+1,2		org liq/droplet tower	0	VANPOLEN	87
<6.E−20	−1,2		org liq/droplet tower	0	VANPOLEN	87
<3.E−21	±1		Hg drops-untreated	0	SAVAGE	86
<3.E−22	±1,2		levitated niobium	0	SMITH	86
<2.E−26	±1,2		^{4}He/levitation	0	SMITH	86B
<2.E−20	>±1	0.2–250	niobium+tungs/ion	0	MILNER	85
<1.E−21	±1		levitated niobium	0	SMITH	85
	+1,2	<100	niobium/mass spec	0	KUTSCHERA	84
<5.E−22			levitated steel	0	MARINELLI	84
<9.E−20	± <13		water/oil drop	0	JOYCE	83
<2.E−21	> | ± 1/2|		levitated steel	0	LIEBOWITZ	83
<1.E−19	±1,2		photo ion spec	0	VANDESTEEG	83
<2.E−20			mercury/oil drop	0	[3] HODGES	81
1.E−20	+1		levitated niobium	4	[4] LARUE	81
1.E−20	−1		levitated niobium	4	[4] LARUE	81
<1.E−21			levitated steel	0	MARINELLI	80B
<6.E−16			helium/mass spec	0	BOYD	79
1.E−20	+1		levitated niobium	2	[4] LARUE	79
<4.E−28			earth+/ion beam	0	OGOROD...	79
<5.E−15	+1		tungs./mass spec	0	BOYD	78
<5.E−16	+3	<1.7	hydrogen/mass spec	0	BOYD	78B
<1.E−21	±2,4		water/ion beam	0	LUND	78
<6.E−15	>1/2		levitated tungsten	0	PUTT	78
<1.E−22			metals/mass spec	0	SCHIFFER	78
<5.E−15			levitated tungsten ox	0	BLAND	77
<3.E−21			levitated iron	0	GALLINARO	77
2.E−21	−1		levitated niobium	1	[4] LARUE	77
4.E−21	+1		levitated niobium	2	[4] LARUE	77
<1.E−13	+3	<7.7	hydrogen/mass spec	0	MULLER	77
<5.E−27			water+/ion beam	0	OGOROD...	77
<1.E−21			lunar+/ion spec	0	STEVENS	76
<1.E−15	+1	<60	oxygen+/ion spec	0	ELBERT	70
<5.E−19			levitated graphite	0	MORPURGO	70
<5.E−23			water+/atom beam	0	COOK	69
<1.E−17	±1,2		levitated graphite	0	BRAGINSK	68
<1.E−17			water+/uv spec	0	RANK	68
<3.E−19	±1		levitated iron	0	STOVER	67
<1.E−10			sun/uv spec	0	[5] BENNETT	66
<1.E−17	+1,2		meteorites+/ion beam	0	CHUPKA	66
<1.E−16	±1		levitated graphite	0	GALLINARO	66
<1.E−22			argon/electrometer	0	HILLAS	59
	−2		levitated oil	0	MILLIKAN	10

[1] 95% CL limit for fractional charge particles with $0.18e \leq |Q_{residual}| \leq 0.82e$ in total of 70.1 mg of silicone oil.
[2] 95% CL limit for particles with fractional charge $|Q_{residual}|$ >0.16e in total of 17.4 mg of silicone oil.
[3] Also set limits for $Q = \pm e/6$.
[4] Note that in PHILLIPS 88 these authors report a subtle magnetic effect which could account for the apparent fractional charges.
[5] Limit inferred by JONES 77B.

Downloaded from https://academic.oup.com/ptep/article/2022/8/083C01/6651666 by KIT Library user on 27 September 2022

REFERENCES FOR Free Quark Searches

AGNESE	15	PRL 114 111302	R. Agnese *et al.*	(CDMS Collab.)
CHATRCHYAN	13AR	PR D87 092008	S. Chatrchyan *et al.*	(CMS Collab.)
LEE	02	PR D66 012002	I.T. Lee *et al.*	
AMBROSIO	00C	PR D62 052003	M. Ambrosio *et al.*	(MACRO Collab.)
HALYO	00	PRL 84 2576	V. Halyo *et al.*	
ABREU	97D	PL B396 315	P. Abreu *et al.*	(DELPHI Collab.)
HUENTRUP	96	PR C53 358	G. Huentrup *et al.*	(SIEG)
MAR	96	PR D53 6017	N.M. Mar *et al.*	(SLAC, SCHAF, LANL, UCI)
AKERS	95R	ZPHY C67 203	R. Akers *et al.*	(OPAL Collab.)
BUSKULIC	93C	PL B303 198	D. Buskulic *et al.*	(ALEPH Collab.)
CECCHINI	93	ASP 1 369	S. Cecchini *et al.*	
PERERA	93	PRL 70 1053	A.G.U. Perera *et al.*	(PITT)
ABE	92J	PR D46 1889	F. Abe *et al.*	(CDF Collab.)
GHOSH	92	NC 105A 99	D. Ghosh *et al.*	(JADA, BANGB)
HOMER	92	ZPHY C55 549	G.J. Homer *et al.*	(RAL, SHMP, LOQM)
BASILE	91	NC 104A 405	M. Basile *et al.*	(BGNA, INFN, CERN, PLRM+)
HE	91	PR C44 1672	Y.B. He, P.B. Price	(UCB)
MATIS	91	NP A525 513	H.S. Matis *et al.*	(LBL, SFSU, UCI+)
MORI	91	PR D43 2843	M. Mori *et al.*	(Kamiokande II Collab.)
ADACHI	90C	PL B244 352	I. Adachi *et al.*	(TOPAZ Collab.)
BOWCOCK	89B	PR D40 263	T.J.V. Bowcock *et al.*	(CLEO Collab.)
CALLOWAY	89	PL B232 549	D. Calloway *et al.*	(SFSU, UCI, LBL+)
JONES	89	ZPHY C43 349	W.G. Jones *et al.*	(LOIC, RAL)
MATIS	89	PR D39 1851	H.S. Matis *et al.*	(LBL, SFSU, UCI+)
NAKAMURA	89	PR D39 1261	T.T. Nakamura *et al.*	(KYOT, TMTC)
ALLASIA	88	PR D37 219	D. Allasia *et al.*	(WA25 Collab.)
HOFFMANN	88	PL B200 583	A. Hofmann *et al.*	(SIEG, USF)
PHILLIPS	88	NIM A264 125	J.D. Phillips, W.M. Fairbank, J. Navarro	(STAN)
WADA	88	NC 11C 229	T. Wada, Y. Yamashita, I. Yamamoto	(OKAY)
GERBIER	87	PRL 59 2535	G. Gerbier *et al.*	(UCB, CERN)
LYONS	87	ZPHY C36 363	L. Lyons *et al.*	(OXF, RAL, LOIC)
MILNER	87	PR D36 37	R.E. Milner *et al.*	(CIT)
SHAW	87	PR D36 3533	G.L. Shaw *et al.*	(UCI, LBL, LANL, SFSU)
SMITH	87	PL B197 447	P.F. Smith *et al.*	(RAL, LOIC)
VANPOLEN	87	PR D36 1983	J. van Polen, R.T. Hagstrom, G. Hirsch	(ANL+)
ABACHI	86C	PR D33 2733	S. Abachi *et al.*	(UCLA, LBL, UCD)
SAVAGE	86	PL 167B 481	M.L. Savage *et al.*	(SFSU)
SMITH	86	PL B171 129	P.F. Smith *et al.*	(RAL, LOIC)
SMITH	86B	PL B181 407	P.F. Smith *et al.*	(RAL, LOIC)
WADA	86	NC 9C 358	T. Wada	(OKAY)
ALBRECHT	85G	PL 156B 134	H. Albrecht *et al.*	(ARGUS Collab.)
BANNER	85	PL 156B 129	M. Banner *et al.*	(UA2 Collab.)
MILNER	85	PRL 54 1472	R.E. Milner *et al.*	(CIT)
SMITH	85	PL 153B 188	P.F. Smith *et al.*	(RAL, LOIC)
AIHARA	84	PRL 52 168	H. Aihara *et al.*	(TPC Collab.)
AIHARA	84B	PRL 52 2332	H. Aihara *et al.*	(TPC Collab.)
BARWICK	84	PR D30 691	S.W. Barwick, J.A. Musser, J.D. Stevenson	(UCB)
BERGSMA	84B	ZPHY C24 217	F. Bergsma *et al.*	(CHARM Collab.)
BONDAR	84	JETPL 40 1265	A.E. Bondar *et al.*	(NOVO)
		Translated from ZETFP 40 440.		
GURYN	84	PL 139B 313	W. Guryn *et al.*	(FRAS, LBL, NWES, STAN+)
KAWAGOE	84B	LNC 41 604	K. Kawagoe *et al.*	(TOKY)
KUTSCHERA	84	PR D29 791	W. Kutschera *et al.*	(ANL, FNAL)
MARINELLI	84	PL 137B 439	M. Marinelli, G. Morpurgo	(GENO)
WADA	84B	LNC 40 329	T. Wada, Y. Yamashita, I. Yamamoto	(OKAY)
AUBERT	83C	PL 133B 461	J.J. Aubert *et al.*	(EMC Collab.)
BANNER	83	PL 121B 187	M. Banner *et al.*	(UA2 Collab.)
JOYCE	83	PRL 51 731	D.C. Joyce *et al.*	(SFSU)
LIEBOWITZ	83	PRL 50 1640	D. Liebowitz, M. Binder, K.O.H. Ziock	(UVA)
LINDGREN	83	PRL 51 1621	M.A. Lindgren *et al.*	(SFSU, UCR, UCI+)
MASHIMO	83	PL 128B 327	T. Mashimo *et al.*	(ICEPP)
PRICE	83	PRL 50 566	P.B. Price *et al.*	(UCB)
VANDESTEEG	83	PRL 50 1234	M.J.H. van de Steeg, H.W.H.M. Jongbloets, P. Wyder	
MARINI	82	PR D26 1777	A. Marini *et al.*	(FRAS, LBL, NWES, STAN+)
MARINI	82B	PRL 48 1649	A. Marini *et al.*	(FRAS, LBL, NWES, STAN+)
MASHIMO	82	JPSJ 51 3067	T. Mashimo, K. Kawagoe, M. Koshiba	(INUS)
NAPOLITANO	82	PR D25 2837	J. Napolitano *et al.*	(STAN, FRAS, LBL+)
ROSS	82	PL 118B 199	M.C. Ross *et al.*	(FRAS, LBL, NWES, STAN+)
HODGES	81	PRL 47 1651	C.L. Hodges *et al.*	(UCR, SFSU)
LARUE	81	PRL 46 967	G.S. Larue, J.D. Phillips, W.M. Fairbank	(STAN)
WEISS	81	PL 101B 439	J.M. Weiss *et al.*	(SLAC, LBL, UCB)
BARTEL	80	ZPHY C6 295	W. Bartel *et al.*	(JADE Collab.)
BASILE	80	LNC 29 251	M. Basile *et al.*	(BGNA, CERN, FRAS, ROMA+)
BUSSIERE	80	NP B174 1	A. Bussiere *et al.*	(BGNA, SACL, LAPP)
MARINELLI	80B	PL 94B 433	M. Marinelli, G. Morpurgo	(GENO)
Also		PL 94B 427	M. Marinelli, G. Morpurgo	(GENO)
BOYD	79	PRL 43 1288	R.N. Boyd *et al.*	(OSU)
BOZZOLI	79	NP B159 363	W. Bozzoli *et al.*	(BGNA, LAPP, SACL+)
LARUE	79	PRL 42 142	G.S. Larue, W.M. Fairbank, J.D. Phillips	(STAN)
Also		PRL 42 1019	G.S. Larue, W.M. Fairbank, J.D. Phillips	
OGOROD...	79	JETP 49 953	D.D. Ogorodnikov, I.M. Samoilov, A.M. Solntsev	
		Translated from ZETF 76 1881.		
STEVENSON	79	PR D20 82	M.L. Stevenson	(LBL)
BASILE	78	NC 45A 171	M. Basile *et al.*	(CERN, BGNA)
BASILE	78B	NC 45A 281	M. Basile *et al.*	(CERN, BGNA)
BOYD	78	PRL 40 216	R.N. Boyd *et al.*	(ROCH)
BOYD	78B	PL 72B 484	R.N. Boyd *et al.*	(ROCH)
LUND	78	RA 25 75	T. Lund, R. Brandt, Y. Fares	(MARB)
PUTT	78	PR D17 1466	G.D. Putt, P.C.M. Yock	(AUCK)
SCHIFFER	78	PR D17 2241	J.P. Schiffer *et al.*	(CHIC, ANL)
YOCK	78	PR D18 641	P.C.M. Yock	(AUCK)
ANTREASYAN	77	PRL 39 513	D. Antreasyan *et al.*	(EFI, PRIN)
BASILE	77	NC 40A 41	M. Basile *et al.*	(CERN, BGNA)
BLAND	77	PRL 39 369	R.W. Bland *et al.*	(SFSU)
GALLINARO	77	PRL 38 1255	G. Gallinaro, M. Marinelli, G. Morpurgo	(GENO)
JONES	77B	RMP 49 717	L.W. Jones	
LARUE	77	PRL 38 1011	G.S. Larue, W.M. Fairbank, A.F. Hebard	(STAN)
MULLER	77	SCI 196 521	R.A. Muller *et al.*	(LBL)
OGOROD...	77	JETP 45 857	D.D. Ogorodnikov, I.M. Samoilov, A.M. Solntsev	
		Translated from ZETF 72 1633.		
BALDIN	76	SJNP 22 264	B.Y. Baldin *et al.*	(JINR)
		Translated from YAF 22 512.		
BRIATORE	76	NC 31A 553	L. Briatore *et al.*	(LCGT, FRAS, FREIB)
STEVENS	76	PR D14 716	C.M. Stevens, J.P. Schiffer, W. Chupka	(ANL)
ALBROW	75	NP B97 189	M.G. Albrow *et al.*	(CERN, DARE, FOM+)
FABJAN	75	NP B101 349	C.W. Fabjan *et al.*	(CERN, MPIM)
HAZEN	75	NP B95 189	W.E. Hazen *et al.*	(MICH, LEED)
JOVANOV...	75	PL 56B 105	J.V. Jovanovich *et al.*	(MANI, AACH, CERN+)
KRISOR	75	NC 27A 132	K. Krisor	(AACH3)
CLARK	74B	PR D10 2721	A.F. Clark *et al.*	(LLL)
GALIK	74	PR D9 1856	R.S. Galik *et al.*	(SLAC, FNAL)
KIFUNE	74	JPSJ 36 629	T. Kifune *et al.*	(TOKY, KEK)
NASH	74	PRL 32 858	T. Nash *et al.*	(FNAL, CORN, NYU)
ALPER	73	PL 46B 265	B. Alper *et al.*	(CERN, LIVP, LUND, BOHR+)
ASHTON	73	JP A6 577	F. Ashton *et al.*	(DURH)
HICKS	73B	NC 14A 65	R.B. Hicks, R.W. Flint, S. Standil	(MANI)
LEIPUNER	73	PRL 31 1226	L.B. Leipuner *et al.*	(BNL, YALE)
BEAUCHAMP	72	PR D6 1211	W.T. Beauchamp *et al.*	(ARIZ)
BOHM	72B	PRL 28 326	A. Bohm *et al.*	(AACH)
BOTT	72	PL 40B 693	M. Bott-Bodenhausen *et al.*	(CERN, MPIM)
COX	72	PR D6 1203	A.J. Cox *et al.*	(ARIZ)
CROUCH	72	PR D5 2667	M.F. Crouch, K. Mori, G.R. Smith	(CASE)
DARDO	72	NC 9A 319	M. Dardo *et al.*	(TORI)
EVANS	72	PRSE A70 143	G.R. Evans *et al.*	(EDIN, LEED)
TONWAR	72	JP A5 569	S.C. Tonwar, S. Naranan, B.V. Sreekantan	(TATA)
ANTIPOV	71	NP B29 374	Y.M. Antipov *et al.*	(SERP)
CHIN	71	NC 2A 419	S. Chin *et al.*	(OSAK)
CLARK	71B	PRL 27 51	A.F. Clark *et al.*	(LLL, LBL)
HAZEN	71	PRL 26 582	W.E. Hazen	(MICH)
BOSIA	70	NC 66A 167	G.F. Bosia, L. Briatore	(TORI)
CHU	70	PRL 24 917	W.T. Chu *et al.*	(OSU, ROSE, KANS)
Also		PRL 25 550	W.W.M. Allison *et al.*	(ANL)
ELBERT	70	NP B20 217	J.W. Elbert *et al.*	(WISC)
FAISSNER	70B	PRL 24 1357	H. Faissner *et al.*	(AACH3)
KRIDER	70	PR D1 835	E.P. Krider, T. Bowen, R.M. Kalbach	(ARIZ)
MORPURGO	70	NIM 79 95	G. Morpurgo, G. Gallinaro, G. Palmieri	(GENO)
ALLABY	69B	NC 64A 75	J.V. Allaby *et al.*	(CERN)
ANTIPOV	69	PL 29B 245	Y.M. Antipov *et al.*	(SERP)
ANTIPOV	69B	PL 30B 576	Y.M. Antipov *et al.*	(SERP)
CAIRNS	69	PR 186 1394	I. Cairns *et al.*	(SYDN)
COOK	69	PR 188 2092	D.D. Cook *et al.*	(ILL)
FUKUSHIMA	69	PR 178 2058	Y. Fukushima *et al.*	(TOKY)
MCCUSKER	69	PRL 23 658	C.B.A. McCusker, I. Cairns	(SYDN)
BELLAMY	68	PR 166 1391	E.H. Bellamy *et al.*	(STAN, SLAC)
BJORNBOE	68	NC B53 241	J. Bjornboe *et al.*	(BOHR, TATA, BERN+)
BRAGINSK	68	JETP 27 51	V.B. Braginsky *et al.*	(MOSU)
		Translated from ZETF 54 91.		
BRIATORE	68	NC 57A 850	L. Briatore *et al.*	(TORI, CERN, BGNA)
FRANZINI	68	PRL 21 1013	P. Franzini, S. Shulman	(COLU)
GARMIRE	68	PR 166 1280	G. Garmire, C. Leong, V. Sreekantan	(MIT)
HANAYAMA	68	CJP 46 S734	Y. Hanayama *et al.*	(OSAK)
KASHA	68	PR 172 1297	H. Kasha, R.J. Stefanski	(BNL, YALE)
KASHA	68B	PRL 20 217	H. Kasha *et al.*	(BNL, YALE)
KASHA	68C	CJP 46 S730	H. Kasha *et al.*	(BNL, YALE)
RANK	68	PR 176 1635	D. Rank	(MICH)
BARTON	67	PRSL 90 87	J.C. Barton	(NPOL)
BATHOW	67	PL 25B 163	G. Bathow *et al.*	(DESY)
BUHLER	67	NC 49A 209	A. Buhler-Broglin *et al.*	(CERN, BGNA)
BUHLER	67B	NC 51A 837	A. Buhler-Broglin *et al.*	(CERN, BGNA+)
FOSS	67	PL 25B 166	J. Foss *et al.*	(MIT)
GOMEZ	67	PRL 18 1022	R. Gomez *et al.*	(CIT)
KASHA	67	PR 154 1263	H. Kasha *et al.*	(BNL, YALE)
STOVER	67	PR 164 1599	R.W. Stover, T.I. Moran, J.W. Trischka	(SYRA)
BARTON	66	PL 21 360	J.C. Barton, C.T. Stockel	(NPOL)
BENNETT	66	PRL 17 1196	W.R. Bennett	(YALE)
BUHLER	66	NC 45A 520	A. Buhler-Broglin *et al.*	(CERN, BGNA+)
CHUPKA	66	PRL 17 60	W.A. Chupka, J.P. Schiffer, C.M. Stevens	(ANL)
GALLINARO	66	PL 23 609	G. Gallinaro, G. Morpurgo	(GENO)
KASHA	66	PR 150 1140	H. Kasha, L.B. Leipuner, R.K. Adair	(BNL, YALE)
LAMB	66	PRL 17 1068	R.C. Lamb *et al.*	(ANL)
DELISE	65	PR 140 B458	D.A. de Lise, T. Bowen	(ARIZ)
DORFAN	65	PRL 14 999	D.E. Dorfan *et al.*	(COLU)
FRANZINI	65B	PRL 14 196	P. Franzini *et al.*	(BNL, COLU)
MASSAM	65	NC 40A 589	T. Massam, T. Muller, A. Zichichi	(CERN)
BINGHAM	64	PL 9 201	H.H. Bingham *et al.*	(CERN, EPOL)
BLUM	64	PRL 13 353A	W. Blum *et al.*	(CERN)
BOWEN	64	PRL 13 728	T. Bowen *et al.*	(ARIZ)
HAGOPIAN	64	PRL 13 280	V. Hagopian *et al.*	(PENN, BNL)
LEIPUNER	64	PRL 12 423	L.B. Leipuner *et al.*	(BNL, YALE)
MORRISON	64	PL 9 199	D.R.O. Morrison	(CERN)
SUNYAR	64	PR 136 B1157	A.W. Sunyar, A.Z. Schwarzschild, P.I. Connors	(BNL)
HILLAS	59	NAT 184 B92	A.M. Hillas, T.E. Cranshaw	(AERE)
MILLIKAN	10	Phil Mag 19 209	R.A. Millikan	(CHIC)

OTHER RELATED PAPERS

LYONS	85	PRPL C129 225	L. Lyons	(OXF)
Review				
MARINELLI	82	PRPL 85 161	M. Marinelli, G. Morpurgo	(GENO)
Review				

Downloaded from https://academic.oup.com/ptep/article/2022/8/083C01/6651666 by KIT Library user on 27 September 2022

Downloaded from https://academic.oup.com/ptep/article/2022/8/083C01/6651666 by KIT Library user on 27 September 2022

- $\pi^{\pm}$ . . . 1349
- π^0 . . . 1352
- η . . . 1354
- $f_0(500)$ aka σ; was $f_0(600)$ . . . 1359
- $\rho(770)$ . . . 1361
- $\omega(782)$ . . . 1367
- $\eta'(958)$ . . . 1373
- $f_0(980)$ . . . 1379
- $a_0(980)$ . . . 1382
- $\phi(1020)$ . . . 1383
- $h_1(1170)$ . . . 1391
- $b_1(1235)$ . . . 1391
- $a_1(1260)$ . . . 1392
- $f_2(1270)$ . . . 1395
- $f_1(1285)$ . . . 1398
- $\eta(1295)$ . . . 1401
- $\pi(1300)$ . . . 1402
- $a_2(1320)$ . . . 1402
- $f_0(1370)$ . . . 1406
- $\pi_1(1400)$ . . . 1409
- $\eta(1405)$ . . . 1410
- $h_1(1415)$ . . . 1412
- $h_1(1415)$ was $h_1(1380)$ . . . 1412
- $f_1(1420)$ . . . 1413
- $\omega(1420)$ . . . 1414
  $f_2(1430)$ . . . 1416
- $a_0(1450)$ . . . 1416
- $\rho(1450)$ . . . 1417
- $\eta(1475)$ . . . 1420
- $f_0(1500)$ . . . 1421
  $f_1(1510)$ . . . 1424
- $f_2'(1525)$ . . . 1425
  $f_2(1565)$ . . . 1429
  $\rho(1570)$ . . . 1430
  $h_1(1595)$ . . . 1430
- $\pi_1(1600)$ . . . 1430
- $a_1(1640)$ . . . 1431
  $f_2(1640)$ . . . 1432
- $\eta_2(1645)$ . . . 1432
- $\omega(1650)$ . . . 1433
- $\omega_3(1670)$ . . . 1434
- $\pi_2(1670)$ . . . 1435
- $\phi(1680)$ . . . 1437
- $\rho_3(1690)$ . . . 1438
- $\rho(1700)$ . . . 1441
- $a_2(1700)$ . . . 1445
- $f_0(1710)$ . . . 1446
  $X(1750)$ . . . 1449
  $\eta(1760)$ . . . 1449
- $\pi(1800)$ . . . 1450
  $f_2(1810)$ . . . 1451
  $X(1835)$ . . . 1452
- $\phi_3(1850)$ . . . 1453
- $\eta_2(1870)$ . . . 1453
- $\pi_2(1880)$ . . . 1454
  $\rho(1900)$ . . . 1455
  $f_2(1910)$ . . . 1455
  $a_0(1950)$ . . . 1456
- $f_2(1950)$ . . . 1456
- $a_4(1970)$ was $a_4(2040)$ . . . 1458
  $\rho_3(1990)$ . . . 1458
  $\pi_2(2005)$ . . . 1459
- $f_2(2010)$ . . . 1459
  $f_0(2020)$ . . . 1459
- $f_4(2050)$ . . . 1460
  $\pi_2(2100)$ . . . 1461
  $f_0(2100)$ . . . 1462
  $f_2(2150)$ . . . 1462
  $\rho(2150)$ . . . 1464
- $\phi(2170)$ . . . 1465
  $f_0(2200)$ . . . 1466
  $f_J(2220)$ . . . 1467
  $\eta(2225)$ . . . 1468
  $\rho_3(2250)$ . . . 1468
- $f_2(2300)$ . . . 1469
  $f_4(2300)$ . . . 1469
  $f_0(2330)$ . . . 1470
- $f_2(2340)$ . . . 1470
  $\rho_5(2350)$ . . . 1471
  $X(2370)$ . . . 1471
  $f_6(2510)$ . . . 1472

- $K^{\pm}$ . . . 1473
- K^0 . . . 1488
- K^0_S . . . 1489
- K^0_L . . . 1493
- $K^*_0(700)$ aka κ; was $K^*_0(800)$ . . . 1508
- $K^*(892)$ . . . 1509
- $K_1(1270)$ . . . 1512
- $K_1(1400)$ . . . 1513
- $K^*(1410)$ . . . 1514
- $K^*_0(1430)$ . . . 1515
- $K^*_2(1430)$ . . . 1516
  $K(1460)$ . . . 1518
  $K_2(1580)$ . . . 1519
  $K(1630)$ . . . 1519
- $K_1(1650)$ . . . 1519
- $K^*(1680)$ . . . 1519
- $K_2(1770)$ . . . 1520
- $K^*_3(1780)$ . . . 1521
- $K_2(1820)$ . . . 1522
  $K(1830)$ . . . 1523
  $K^*_0(1950)$ . . . 1523
- $K^*_2(1980)$ . . . 1523
- $K^*_4(2045)$ . . . 1524
  $K_2(2250)$ . . . 1525
  $K_3(2320)$ . . . 1525
  $K^*_5(2380)$ . . . 1525
  $K_4(2500)$ . . . 1525
  $K(3100)$ . . . 1526

- $D^{\pm}$ . . . 1527
- D^0 . . . 1543
- $D^*(2007)^0$ . . . 1578
- $D^*(2010)^{\pm}$ . . . 1578
- $D^*_0(2300)$ was $D^*_0(2400)$ . . . 1580
- $D_1(2420)$ . . . 1580
- $D_1(2430)^0$ . . . 1582
- $D^*_2(2460)$ . . . 1582

(Continued on the next page)

• Indicates the particle is in the Meson Summary Table

Downloaded from https://academic.oup.com/ptep/article/2022/8/083C01/6651666 by KIT Library user on 27 September 2022

$D_0(2550)^0$ . . . 1584
$D_1^*(2600)^0$ was $D(2600)$ . . . 1584
$D^*(2640)^\pm$ . . . 1585
$D_2(2740)^0$ was $D(2740)^0$ . . . 1585
• $D_3^*(2750)$ . . . 1586
$D_1^*(2760)^0$ . . . 1586
$D(3000)^0$ . . . 1587

• $D_s^\pm$ . . . 1588
• $D_s^{*\pm}$ . . . 1601
• $D_{s0}^*(2317)^\pm$ . . . 1601
• $D_{s1}(2460)^\pm$ . . . 1602
• $D_{s1}(2536)^\pm$ . . . 1604
• $D_{s2}^*(2573)$ . . . 1605
$D_{s0}(2590)^+$ . . . 1605
• $D_{s1}^*(2700)^\pm$ . . . 1606
$D_{s1}^*(2860)^\pm$ . . . 1606
• $D_{s3}^*(2860)^\pm$ . . . 1607
$X_0(2900)$ . . . 1607
$X_1(2900)$ . . . 1607
$D_{sJ}(3040)^\pm$ . . . 1608

• $B^\pm$ . . . 1610
• B^0 . . . 1675
• $B^\pm/B^0$ ADMIXTURE . . . 1750
• $B^\pm/B^0/B_s^0/b$-baryon ADMIXTURE . . . 1772
V_{cb} and V_{ub} CKM Matrix Elements . . . 1780
• B^* . . . 1781
• $B_1(5721)$ . . . 1782
$B_J^*(5732)$ aka B^{**} . . . 1782
• $B_2^*(5747)$ . . . 1783
$B_J(5840)$ . . . 1783
• $B_J(5970)$ . . . 1784

• B_s^0 . . . 1786
• B_s^* . . . 1810
$X(5568)^\pm$ . . . 1810
• $B_{s1}(5830)^0$ . . . 1811
• $B_{s2}^*(5840)^0$ . . . 1811
$B_{sJ}^*(5850)$ . . . 1811

• B_c^+ . . . 1813
$B_c(2S)^\pm$ . . . 1817

• $\eta_c(1S)$ . . . 1818
• $J/\psi(1S)$ . . . 1826
• $\chi_{c0}(1P)$ . . . 1851
• $\chi_{c1}(1P)$ . . . 1861
• $h_c(1P)$ . . . 1870
• $\chi_{c2}(1P)$ . . . 1872
• $\eta_c(2S)$ . . . 1883
• $\psi(2S)$ . . . 1886
• $\psi(3770)$ . . . 1903
• $\psi_2(3823)$ was $\psi(3823)$, $X(3823)$ . . . 1910
• $\psi_3(3842)$ . . . 1911
$\chi_{c0}(3860)$ . . . 1911
• $\chi_{c1}(3872)$ aka $X(3872)$ . . . 1911
• $Z_c(3900)$ was $X(3900)$ . . . 1915
• $\chi_{c0}(3915)$ was $X(3915)$ . . . 1916
• $\chi_{c2}(3930)$ . . . 1917
$X(3940)$ . . . 1918
• $X(4020)^\pm$ . . . 1918
• $\psi(4040)$ . . . 1919
$X(4050)^\pm$ . . . 1921
$X(4055)^\pm$ . . . 1922
$X(4100)^\pm$ . . . 1922
• $\chi_{c1}(4140)$ was $X(4140)$ . . . 1922
• $\psi(4160)$ . . . 1923
$X(4160)$ . . . 1926
$Z_c(4200)$ was $X(4200)^\pm$ . . . 1926
$R_{c0}(4240)$ was $X(4240)^\pm$ . . . 1931
$X(4250)^\pm$ . . . 1932
• $\psi(4230)$ aka $Y(4260)$; was $X(4260)$ . . . 1927
• $\chi_{c1}(4274)$ was $X(4274)$ . . . 1932
$X(4350)$ . . . 1932
• $\psi(4360)$ aka $Y(4360)$; was $X(4360)$ . . . 1933
was $X(4390)$ . . . .
• $\psi(4415)$ . . . 1934
• $Z_c(4430)$ was $X(4430)^\pm$ . . . 1936
$\chi_{c0}(4500)$ was $X(4500)$ . . . 1936
$X(4630)$ . . . 1937
• $\psi(4660)$ aka $Y(4660)$; was $X(4660)$ . . . 1937
$\chi_{c1}(4685)$ . . . 1939
$\chi_{c0}(4700)$ was $X(4700)$ . . . 1939

• $\eta_b(1S)$ . . . 1940
• $\Upsilon(1S)$ . . . 1942
• $\chi_{b0}(1P)$ . . . 1948
• $\chi_{b1}(1P)$ . . . 1950
• $h_b(1P)$ . . . 1952
• $\chi_{b2}(1P)$ . . . 1952
$\eta_b(2S)$ . . . 1954
• $\Upsilon(2S)$ . . . 1954
• $\Upsilon_2(1D)$ was $\Upsilon(1D)$ . . . 1959
• $\chi_{b0}(2P)$ . . . 1960
• $\chi_{b1}(2P)$ . . . 1961
• $h_b(2P)$ . . . 1964
• $\chi_{b2}(2P)$ . . . 1964
• $\Upsilon(3S)$ . . . 1966
• $\chi_{b1}(3P)$ . . . 1969
• $\chi_{b2}(3P)$ . . . 1970
• $\Upsilon(4S)$ aka $\Upsilon(10580)$ . . . 1970
• $Z_b(10610)$ was $X(10610)$ . . . 1972
• $Z_b(10650)$ was $X(10650)^\pm$ . . . 1973
$\Upsilon(10753)$ . . . 1974
• $\Upsilon(10860)$ . . . 1975
• $\Upsilon(11020)$ . . . 1978

Further States . . . 1980

Notes in the Listings

Charged kaon mass . . . 1473
Dalitz plot parameters for $K \to 3\pi$ decays . . . 1482
CP-violation in $K_S \to 3\pi$ . . . 1492
Heavy Flavor Averaging Group (rev.) . . . 1609
Charmonium system (rev.) . . . 1818
Branching ratios of $\psi(2S)$ and $\chi_{c0,1,2}$ (rev.) . . . 1850
Bottomonium system (rev.) . . . 1940
Width determination of the Υ states . . . 1940

(Continued on next page.)

• Indicates the particle is in the Meson Summary Table

Downloaded from https://academic.oup.com/ptep/article/2022/8/083C01/6651666 by KIT Library user on 27 September 2022

Related Reviews in Volume 1

62. Form factors for semileptonic kaon ($K_{\ell 3}$), radiative pion ($\pi_{\ell 2\gamma}$) & kaon ($K_{\ell 2\gamma}$) decays (rev.) 842
63. Spectroscopy of light meson resonances (new) 845
64. Scalar mesons below 1 GeV (rev.) 858
65. Rare kaon decays (rev.) 865
66. CPT invariance tests in neutral kaon decay (rev.) 871
67. V_{ud}, V_{us}, Cabibbo angle, and CKM unitarity (rev.) 873
68. CP-violation in K_L decays (rev.) 877
69. Review of multibody charm analyses (rev.) 880
70. D^0–$\overline{D}^0$ mixing (rev.) 885
71. D_s^+ branching fractions (rev.) 895
72. Leptonic decays of charged pseudoscalar mesons (rev.) . . . 897
73. Production and decay of b-flavored hadrons (rev.) 908
74. Polarization in B decays (rev.) 919
75. B^0–$\overline{B}^0$ mixing (rev.) 923
76. Semileptonic B decays, V_{cb} and V_{ub} (rev.) 930
77. CKM angles from B hadrons, determination of (rev.) . . . 946
78. Spectroscopy of mesons containing two heavy quarks (rev.) . 951
79. Heavy non-$q\overline{q}$ mesons (rev.) 959

Downloaded from https://academic.oup.com/ptep/article/2022/8/083C01/6651666 by KIT Library user on 27 September 2022

Downloaded from https://academic.oup.com/ptep/article/2022/8/083C01/6651666 by KIT Library user on 27 September 2022

LIGHT UNFLAVORED MESONS ($S = C = B = 0$)

For $I = 1$ (π, b, ρ, a): $u\overline{d}$, $(u\overline{u}-d\overline{d})/\sqrt{2}$, $d\overline{u}$;
for $I = 0$ (η, η', h, h', ω, ϕ, f, f'): $c_1(u\overline{u} + d\overline{d}) + c_2(s\overline{s})$

$\pi^{\pm}$

$I^G(J^P) = 1^-(0^-)$

We have omitted some results that have been superseded by later experiments. The omitted results may be found in our 1988 edition Physics Letters **B204** 1 (1988).

$\pi^{\pm}$ MASS

The most accurate charged pion mass measurements are based upon x-ray wavelength measurements for transitions in π^--mesonic atoms. The observed line is the blend of three components, corresponding to different K-shell occupancies. JECKELMANN 94 revisits the occupancy question, with the conclusion that two sets of occupancy ratios, resulting in two different pion masses (Solutions A and B), are equally probable. We choose the higher Solution B since only this solution is consistent with a positive mass-squared for the muon neutrino, given the precise muon momentum measurements now available (DAUM 91, ASSAMAGAN 94, and ASSAMAGAN 96) for the decay of pions at rest. Earlier mass determinations with pi-mesonic atoms may have used incorrect K-shell screening corrections.

Measurements with an error of > 0.005 MeV have been omitted from this Listing.

VALUE (MeV)	DOCUMENT ID		TECN	CHG	COMMENT
139.57039±0.00018 OUR FIT	Error includes scale factor of 1.8.				
139.57039±0.00017 OUR AVERAGE	Error includes scale factor of 1.6. See the ideogram below.				
139.57021±0.00014	[1] DAUM	19	SPEC		$\pi^+ \to \mu^+\nu_\mu$
139.57077±0.00018	[2] TRASSINELLI	16	CNTR		X-ray transitions in pionic N2
139.57071±0.00053	[3] LENZ	98	CNTR	−	pionic N2-atoms gas target
139.56995±0.00035	[4] JECKELMANN	94	CNTR	−	π^- atom, Soln. B
• • • We do not use the following data for averages, fits, limits, etc. • • •					
139.57022±0.00014	[5] ASSAMAGAN	96	SPEC	+	$\pi^+ \to \mu^+\nu_\mu$
139.56782±0.00037	[6] JECKELMANN	94	CNTR	−	π^- atom, Soln. A
139.56996±0.00067	[7] DAUM	91	SPEC	+	$\pi^+ \to \mu^+\nu$
139.56752±0.00037	[8] JECKELMANN	86B	CNTR	−	Mesonic atoms
139.5704 ±0.0011	[7] ABELA	84	SPEC	+	See DAUM 91
139.5664 ±0.0009	[9] LU	80	CNTR	−	Mesonic atoms
139.5686 ±0.0020	CARTER	76	CNTR	−	Mesonic atoms
139.5660 ±0.0024	[9,10] MARUSHEN...	76	CNTR	−	Mesonic atoms

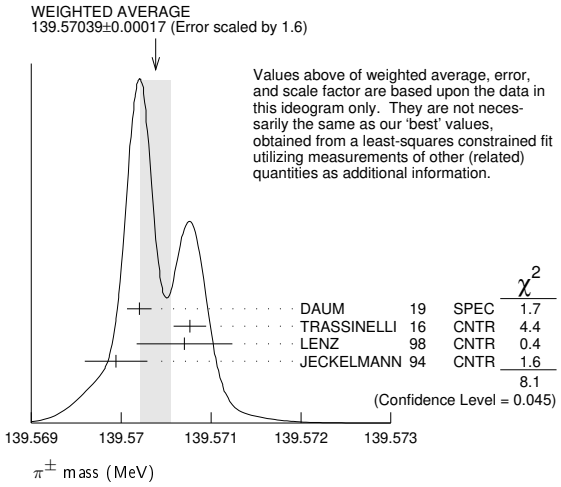

[1] DAUM 19 value is based on their previous (1991+1996) measurements of the μ^+ momentum of 29.79200 ± 0.00011 MeV for π^+ decay at rest. It also uses m_μ = 105.658 3745 ± 0.0000024 MeV, and assumes conservatively m_{ν_μ} = 2.0 ± 2.0 MeV. It is the most precise charged pion mass determination.

[2] TRASSINELLI 16 use the muonic oxygen line for online energy calibration of the pionic line.

[3] LENZ 98 result does not suffer K-electron configuration uncertainties as does JECKELMANN 94.

[4] JECKELMANN 94 Solution B (dominant 2-electron K-shell occupancy), chosen for consistency with positive $m^2_{\nu_\mu}$.

[5] ASSAMAGAN 96 measures the μ^+ momentum p_μ in $\pi^+ \to \mu^+\nu_\mu$ decay at rest to be 29.79200 ± 0.00011 MeV/c. Combined with the μ^+ mass and the assumption m_{ν_μ} = 0, this gives the π^+ mass above; if $m_{\nu_\mu} > 0$, m_{π^+} given above is a lower limit. Combined instead with m_μ and (assuming CPT) the π^- mass of JECKELMANN 94, p_μ gives an upper limit on m_{ν_μ} (see the ν_μ).

[6] JECKELMANN 94 Solution A (small 2-electron K-shell occupancy) in combination with either the DAUM 91 or ASSAMAGAN 94 pion decay muon momentum measurement yields a significantly negative $m^2_{\nu_\mu}$. It is accordingly not used in our fits.

[7] The DAUM 91 value includes the ABELA 84 result. The value is based on a measurement of the μ^+ momentum for π^+ decay at rest, p_μ = 29.79179 ± 0.00053 MeV, uses m_μ = 105.658389 ± 0.000034 MeV, and assumes that m_{ν_μ} = 0. The last assumption means that in fact the value is a lower limit.

[8] JECKELMANN 86B gives m_π/m_e = 273.12677(71). We use m_e = 0.51099906(15) MeV from COHEN 87. The authors note that two solutions for the probability distribution of K-shell occupancy fit equally well, and use other data to choose the lower of the two possible $\pi^{\pm}$ masses.

[9] These values are scaled with a new wavelength-energy conversion factor $V\lambda$ = 1.23984244(37) × 10^{-6} eV m from COHEN 87. The LU 80 screening correction relies upon a theoretical calculation of inner-shell refilling rates.

[10] This MARUSHENKO 76 value used at the authors' request to use the accepted set of calibration γ energies. Error increased from 0.0017 MeV to include QED calculation error of 0.0017 MeV (12 ppm).

$m_{\pi^+} - m_{\mu^+}$

Measurements with an error $>$ 0.05 MeV have been omitted from this Listing.

VALUE (MeV)	EVTS	DOCUMENT ID		TECN	CHG	COMMENT
• • • We do not use the following data for averages, fits, limits, etc. • • •						
33.91157±0.00067		[1] DAUM	91	SPEC	+	$\pi^+ \to \mu^+\nu$
33.9111 ±0.0011		ABELA	84	SPEC		See DAUM 91
33.925 ±0.025		BOOTH	70	CNTR	+	Magnetic spect.
33.881 ±0.035	145	HYMAN	67	HEBC	+	K^- He

[1] The DAUM 91 value assumes that m_{ν_μ} = 0 and uses our m_μ = 105.658389 ± 0.000034 MeV.

$(m_{\pi^+} - m_{\pi^-}) / m_{\text{average}}$

A test of CPT invariance.

VALUE (units 10^{-4})	DOCUMENT ID		TECN
2±5	AYRES	71	CNTR

$\pi^{\pm}$ MEAN LIFE

Measurements with an error $> 0.02 \times 10^{-8}$ s have been omitted.

VALUE (10^{-8} s)	DOCUMENT ID		TECN	CHG	COMMENT
2.6033 ±0.0005 OUR AVERAGE	Error includes scale factor of 1.2.				
2.60361±0.00052	[1] KOPTEV	95	SPEC	+	Surface μ^+'s
2.60231±0.00050±0.00084	NUMAO	95	SPEC	+	Surface μ^+'s
2.609 ±0.008	DUNAITSEV	73	CNTR	+	
2.602 ±0.004	AYRES	71	CNTR	±	
2.604 ±0.005	NORDBERG	67	CNTR	+	
2.602 ±0.004	ECKHAUSE	65	CNTR	+	
• • • We do not use the following data for averages, fits, limits, etc. • • •					
2.640 ±0.008	[2] KINSEY	66	CNTR	+	

[1] KOPTEV 95 combines the statistical and systematic errors; the statistical error dominates.

[2] Systematic errors in the calibration of this experiment are discussed by NORDBERG 67.

$(\tau_{\pi^+} - \tau_{\pi^-}) / \tau_{\text{average}}$

A test of CPT invariance.

VALUE (units 10^{-4})	DOCUMENT ID		TECN
5.5± 7.1	AYRES	71	CNTR
• • • We do not use the following data for averages, fits, limits, etc. • • •			
−14 ±29	PETRUKHIN	68	CNTR
40 ±70	BARDON	66	CNTR
23 ±40	[1] LOBKOWICZ	66	CNTR

[1] This is the most conservative value given by LOBKOWICZ 66.

π ELECTRIC POLARIZABILITY α_π

See HOLSTEIN 14 for a general review on hadron polarizability.

VALUE (10^{-4} fm^3)	EVTS	DOCUMENT ID		TECN	COMMENT
2.0±0.6±0.7	63k	[1] ADOLPH	15A	SPEC	$\pi^-\gamma \to \pi^-\gamma$ Compton scatt.

[1] Value is derived assuming $\alpha_\pi = -\beta_\pi$.

Downloaded from https://academic.oup.com/ptep/article/2022/8/083C01/6651666 by KIT Library user on 27 September 2022

π^+ DECAY MODES

π^- modes are charge conjugates of the modes below.

For decay limits to particles which are not established, see the section on Searches for Axions and Other Very Light Bosons.

	Mode		Fraction (Γ_i/Γ)	Confidence level
Γ_1	$\mu^+\nu_\mu$	[a]	(99.98770 ± 0.00004) %	
Γ_2	$\mu^+\nu_\mu\gamma$	[b]	$(2.00\pm0.25)\times10^{-4}$	
Γ_3	$e^+\nu_e$	[a]	$(1.230\pm0.004)\times10^{-4}$	
Γ_4	$e^+\nu_e\gamma$	[b]	$(7.39\pm0.05)\times10^{-7}$	
Γ_5	$e^+\nu_e\pi^0$		$(1.036\pm0.006)\times10^{-8}$	
Γ_6	$e^+\nu_e e^+e^-$		$(3.2\pm0.5)\times10^{-9}$	
Γ_7	$\mu^+\nu_\mu\nu\overline{\nu}$		$<9\times10^{-6}$	90%
Γ_8	$e^+\nu_e\nu\overline{\nu}$		$<1.6\times10^{-7}$	90%
	Lepton Family number (*LF*) or Lepton number (*L*) violating modes			
Γ_9	$\mu^+\overline{\nu}_e$	*L* [c]	$<1.5\times10^{-3}$	90%
Γ_{10}	$\mu^+\nu_e$	*LF* [c]	$<8.0\times10^{-3}$	90%
Γ_{11}	$\mu^-e^+e^+\nu$	*LF*	$<1.6\times10^{-6}$	90%

[a] Measurements of $\Gamma(e^+\nu_e)/\Gamma(\mu^+\nu_\mu)$ always include decays with γ's, and measurements of $\Gamma(e^+\nu_e\gamma)$ and $\Gamma(\mu^+\nu_\mu\gamma)$ never include low-energy γ's. Therefore, since no clean separation is possible, we consider the modes with γ's to be subreactions of the modes without them, and let $[\Gamma(e^+\nu_e)+\Gamma(\mu^+\nu_\mu)]/\Gamma_{total}=100\%$.

[b] See the Particle Listings below for the energy limits used in this measurement; low-energy γ's are not included.

[c] Derived from an analysis of neutrino-oscillation experiments.

π^+ BRANCHING RATIOS

$\Gamma(e^+\nu_e)/\Gamma_{total}$ — Γ_3/Γ

See note [a] in the list of π^+ decay modes just above, and see also the next block of data. See also the note on "Decay Constants of Charged Pseudoscalar Mesons" in the D_s^+ Listings.

VALUE (units 10^{-4})	DOCUMENT ID
1.230±0.004 OUR EVALUATION	

$[\Gamma(e^+\nu_e)+\Gamma(e^+\nu_e\gamma)]/[\Gamma(\mu^+\nu_\mu)+\Gamma(\mu^+\nu_\mu\gamma)]$ — $(\Gamma_3+\Gamma_4)/(\Gamma_1+\Gamma_2)$

See note [a] in the list of π^+ decay modes above. See NUMAO 92 for a discussion of e-μ universality. See also the note on "Decay Constants of Charged Pseudoscalar Mesons" in the D_s^+ Listings.

VALUE (units 10^{-4})	EVTS	DOCUMENT ID		TECN	CHG	COMMENT
1.2327±0.0023 OUR AVERAGE						
1.2344±0.0023±0.0019	400k	AGUILAR-AR...	15	CNTR	+	Stopping π^+
1.2346±0.0035±0.0036	120k	CZAPEK	93	CALO		Stopping π^+
1.2265±0.0034±0.0044	190k	BRITTON	92	CNTR		Stopping π^+
1.218 ±0.014	32k	BRYMAN	86	CNTR		Stopping π^+
• • • We do not use the following data for averages, fits, limits, etc. • • •						
1.273 ±0.028	11k	[1] DICAPUA	64	CNTR		
1.21 ±0.07		ANDERSON	60	SPEC		

[1] DICAPUA 64 has been updated using the current mean life.

$\Gamma(\mu^+\nu_\mu\gamma)/\Gamma_{total}$ — Γ_2/Γ

Note that measurements here do not cover the full kinematic range.

VALUE (units 10^{-4})	EVTS	DOCUMENT ID		TECN	CHG	COMMENT
2.0 ±0.24±0.08		[1] BRESSI	98	CALO	+	Stopping π^+
• • • We do not use the following data for averages, fits, limits, etc. • • •						
1.24±0.25	26	CASTAGNOLI	58	EMUL		$KE_\mu < 3.38$ MeV

[1] BRESSI 98 result is given for $E_\gamma > 1$ MeV only. Result agrees with QED expectation, 2.283×10^{-4} and does not confirm discrepancy of earlier experiment CASTAGNOLI 58.

$\Gamma(e^+\nu_e\gamma)/\Gamma_{total}$ — Γ_4/Γ

The very different values reflect the very different kinematic ranges covered (bigger range, bigger value). And none of them covers the whole kinematic range.

VALUE (units 10^{-8})	EVTS	DOCUMENT ID		TECN	COMMENT
73.86±0.54	65k	[1] BYCHKOV	09	PIBE	$e^+\nu\gamma$ at rest
• • • We do not use the following data for averages, fits, limits, etc. • • •					
16.1 ±2.3		[2] BOLOTOV	90B	SPEC	17 GeV $\pi^-\to e^-\overline{\nu}_e\gamma$
5.6 ±0.7	226	[3] STETZ	78	SPEC	$P_e > 56$ MeV/c
3.0	143	DEPOMMIER	63B	CNTR	$(KE)_{e^+\gamma} > 48$ MeV

[1] This BYCHKOV 09 value is for $E_\gamma > 10$ MeV and $\Theta_{e^+\gamma} > 40°$.

[2] BOLOTOV 90B is for $E_\gamma > 21$ MeV, $E_e > 70 - 0.8\,E_\gamma$.

[3] STETZ 78 is for an $e^-\gamma$ opening angle $> 132°$. Obtains 3.7 when using same cutoffs as DEPOMMIER 63B.

$\Gamma(e^+\nu_e\pi^0)/\Gamma_{total}$ — Γ_5/Γ

VALUE (units 10^{-8})	EVTS	DOCUMENT ID		TECN	CHG	COMMENT
1.036±0.006 OUR AVERAGE						
1.036±0.006	64k	[1,2] POCANIC	04	PIBE	+	π decay at rest
1.026±0.039	1224	[3] MCFARLANE	85	CNTR	+	Decay in flight
1.00 $^{+0.08}_{-0.10}$	332	DEPOMMIER	68	CNTR	+	
1.07 ±0.21	38	[4] BACASTOW	65	OSPK	+	
1.10 ±0.26		[4] BERTRAM	65	OSPK	+	
1.1 ±0.2	43	[4] DUNAITSEV	65	CNTR	+	
0.97 ±0.20	36	[4] BARTLETT	64	OSPK	+	
• • • We do not use the following data for averages, fits, limits, etc. • • •						
1.15 ±0.22	52	[4] DEPOMMIER	63	CNTR	+	See DEPOMMIER 68

[1] POCANIC 04 normalizes to $e^+\nu_e$ decays, using the PDG 2004 value $B(\pi^+\to e^+\nu_e) = (1.230\pm0.004)\times10^{-4}$. We add their statistical (0.004×10^{-8}), systematic (0.004×10^{-8}) and systematic error due to the uncertainty of $B(\pi^+\to e^+\nu_e)$ (0.003×10^{-8}) in quadrature.

[2] This result can be used to calculate V_{ud} from pion beta decay: $V_{ud}^{PIBETA} = 0.9728\pm0.0030$.

[3] MCFARLANE 85 combines a measured rate (0.394 ± 0.015)/s with 1982 PDG mean life.

[4] DEPOMMIER 68 says the result of DEPOMMIER 63 is at least 10% too large because of a systematic error in the π^0 detection efficiency, and that this may be true of all the previous measurements (also V. Soergel, private communication, 1972).

$\Gamma(e^+\nu_e e^+e^-)/\Gamma(\mu^+\nu_\mu)$ — Γ_6/Γ_1

VALUE (units 10^{-9})	CL%	EVTS	DOCUMENT ID		TECN	COMMENT
3.2 ±0.5 ±0.2		98	EGLI	89	SPEC	Uses $R_{PCAC}=0.068\pm0.004$
• • • We do not use the following data for averages, fits, limits, etc. • • •						
0.46±0.16±0.07		7	[1] BARANOV	92	SPEC	Stopped π^+
< 4.8	90		KORENCHE...	76B	SPEC	
<34	90		KORENCHE...	71	OSPK	

[1] This measurement by BARANOV 92 is of the structure-dependent part of the decay. The value depends on values assumed for ratios of form factors.

$\Gamma(\mu^+\nu_\mu\nu\overline{\nu})/\Gamma(\mu^+\nu_\mu)$ — Γ_7/Γ_1

VALUE	CL%	EVTS	DOCUMENT ID		TECN	COMMENT
<8.6 × 10^{-6}	90	9.1M	AGUILAR-AR...	20A	SPEC	fit E_μ spectrum

$\Gamma(e^+\nu_e\nu\overline{\nu})/\Gamma_{total}$ — Γ_8/Γ

VALUE	CL%	EVTS	DOCUMENT ID		TECN	COMMENT
<1.6 × 10^{-7}	90	1.3M	AGUILAR-AR...	20A	SPEC	fit E_e spectrum
• • • We do not use the following data for averages, fits, limits, etc. • • •						
<5 × 10^{-6}	90		PICCIOTTO	88	SPEC	

$\Gamma(\mu^+\overline{\nu}_e)/\Gamma_{total}$ — Γ_9/Γ

Forbidden by total lepton number conservation. See the note on "Decay Constants of Charged Pseudoscalar Mesons" in the D_s^+ Listings.

VALUE (units 10^{-3})	CL%	DOCUMENT ID		TECN	COMMENT
<1.5	90	[1] COOPER	82	HLBC	Wideband ν beam

[1] COOPER 82 limit on $\overline{\nu}_e$ observation is here interpreted as a limit on lepton number violation.

$\Gamma(\mu^+\nu_e)/\Gamma_{total}$ — Γ_{10}/Γ

Forbidden by lepton family number conservation.

VALUE (units 10^{-3})	CL%	DOCUMENT ID		TECN	COMMENT
<8.0	90	[1] COOPER	82	HLBC	Wideband ν beam

[1] COOPER 82 limit on ν_e observation is here interpreted as a limit on lepton family number violation.

$\Gamma(\mu^-e^+e^+\nu)/\Gamma_{total}$ — Γ_{11}/Γ

Forbidden by lepton family number conservation.

VALUE (units 10^{-6})	CL%	DOCUMENT ID		TECN	CHG
<1.6	90	BARANOV	91B	SPEC	+
• • • We do not use the following data for averages, fits, limits, etc. • • •					
<7.7	90	KORENCHE...	87	SPEC	+

π^+ — POLARIZATION OF EMITTED μ^+

$\pi^+\to\mu^+\nu$

Tests the Lorentz structure of leptonic charged weak interactions.

VALUE	CL%	DOCUMENT ID		TECN	CHG	COMMENT
• • • We do not use the following data for averages, fits, limits, etc. • • •						
<(−0.9959)	90	[1] FETSCHER	84	RVUE	+	
−0.99±0.16		[2] ABELA	83	SPEC	−	μ X-rays

[1] FETSCHER 84 uses only the measurement of CARR 83.

[2] Sign of measurement reversed in ABELA 83 to compare with μ^+ measurements.

See the related review(s):

Form Factors for Semileptonic Kaon ($K_{\ell3}$), Radiative Pion ($\pi_{\ell2\gamma}$) and Kaon ($K_{\ell2\gamma}$) Decays

Downloaded from https://academic.oup.com/ptep/article/2022/8/083C01/6651666 by KIT Library user on 27 September 2022

$\pi^{\pm}$ FORM FACTORS

F_V, VECTOR FORM FACTOR

VALUE	EVTS	DOCUMENT ID		TECN	COMMENT
0.0254±0.0017 OUR AVERAGE					
0.0258±0.0017	65k	[1] BYCHKOV	09	PIBE	$e^+\nu\gamma$ at rest
0.014 ±0.009		[2] BOLOTOV	90B	SPEC	17 GeV $\pi^- \to e^-\overline{\nu}_e\gamma$
$0.023\ ^{+0.015}_{-0.013}$	98	EGLI	89	SPEC	$\pi^+ \to e^+\nu_e e^+ e^-$

[1] The BYCHKOV 09 F_A and F_V results are highly (anti-)correlated: $F_A + 1.0286\ F_V = 0.03853 \pm 0.00014$.
[2] BOLOTOV 90B only determines the absolute value.

F_A, AXIAL-VECTOR FORM FACTOR

VALUE	EVTS	DOCUMENT ID		TECN	COMMENT
0.0119±0.0001	65k	[1,2] BYCHKOV	09	PIBE	$e^+\nu\gamma$ at rest
• • • We do not use the following data for averages, fits, limits, etc. • • •					
0.0115±0.0004	41k	[1,3] FRLEZ	04	PIBE	$\pi^+ \to e^+\nu\gamma$ at rest
0.0106±0.0060		[1,4] BOLOTOV	90B	SPEC	17 GeV $\pi^- \to e^-\overline{\nu}_e\gamma$
$0.021\ ^{+0.011}_{-0.013}$	98	EGLI	89	SPEC	$\pi^+ \to e^+\nu_e e^+ e^-$
0.0135±0.0016		[1,4] BAY	86	SPEC	$\pi^+ \to e^+\nu\gamma$
0.006 ±0.003		[1,4] PIILONEN	86	SPEC	$\pi^+ \to e^+\nu\gamma$
0.011 ±0.003		[1,4,5] STETZ	78	SPEC	$\pi^+ \to e^+\nu\gamma$

[1] These values come from fixing the vector form factor at the CVC prediction, $F_V = 0.0259 \pm 0.0005$.
[2] When F_V is released, the BYCHKOV 09 F_A is 0.0117 ± 0.0017, and F_A and F_V results are highly (anti-)correlated: $F_A + 1.0286\ F_V = 0.03853 \pm 0.00014$.
[3] The sign of $\gamma = F_A / F_V$ is determined to be positive.
[4] Only the absolute value of F_A is determined.
[5] The result of STETZ 78 has a two-fold ambiguity. We take the solution compatible with later determinations.

VECTOR FORM FACTOR SLOPE PARAMETER *a*

This is a in $F_V(q^2) = F_V(0)\ (1 + a\ q^2)$

VALUE	EVTS	DOCUMENT ID		TECN	COMMENT
0.10±0.06	65k	BYCHKOV	09	PIBE	$e^+\nu\gamma$ at rest

R, SECOND AXIAL-VECTOR FORM FACTOR

VALUE	EVTS	DOCUMENT ID		TECN	COMMENT
$\mathbf{0.059^{+0.009}_{-0.008}}$	98	EGLI	89	SPEC	$\pi^+ \to e^+\nu_e e^+ e^-$

$\pi^{\pm}$ CHARGE RADIUS

The charge radius of the pion $\sqrt{\langle r^2_\pi \rangle}$ is defined in relation to the form factor of the pion electromagnetic vertex, called vector form factor VFF, F^V_π. The VFF is a function of the squared four-momentum transfer t, or of the squared c.m. energy s, depending on the channel in which the photon exchange takes place. In both cases, it is related to the slope of the VFF at zero, namely

$$\langle r^2_\pi \rangle = 6\ \frac{dF^V_\pi(q)}{dq}(q{=}0) \text{ where } q = t,\ s.$$

The quantity cannot be measured directly. It can be extracted from the cross sections of three processes: pion electroproduction, $eN \to eN\pi$, and pion electron scattering $e\pi \to e\pi$, for the t channel, and positron electron annihilation into two charged pions, $e^+e^- \to \pi^+\pi^-$, for the s channel. We encode all measurements, but we do not use electroproduction data in averaging because the extraction of the pion radius involves, in this case, theoretical uncertainties that cannot be controlled at the needed level of accuracy. In case of analyses based on the same data set, as ANANTHANARAYAN 17 and COLANGELO 19, which cannot be averaged, we combine the results into a common value, with the uncertainty range chosen to cover both analyses. Note that for consistency the form factor needs to be defined in both channels with the vacuum polarisation removed. For details see COLANGELO 19 or Appendix B of ANANTHANARAYAN 16A.

VALUE (fm)		DOCUMENT ID		TECN	COMMENT
0.659 ±0.004 OUR AVERAGE					
0.656 ±0.005		[1] PDG	19	FIT	
0.65 ±0.05	±0.06	ESCHRICH	01	CNTR	$\pi e \to \pi e$
0.663 ±0.006		AMENDOLIA	86	CNTR	$\pi e \to \pi e$
0.663 ±0.023		DALLY	82	CNTR	$\pi e \to \pi e$
• • • We do not use the following data for averages, fits, limits, etc. • • •					
0.640 ±0.007		[2] CUI	21A	FIT	Fit existing data
0.655 ±0.004		[3] COLANGELO	19	FIT	Fit existing data
0.657 ±0.003		[4] ANANTHANA..	17	FIT	Fit existing data
0.6603±0.0005	±0.0004	[5] HANHART	17	FIT	Fit existing data
0.740 ±0.031		[6] LIESENFELD	99	CNTR	$ep \to e\pi^+ n$
0.661 ±0.012		[7] BIJNENS	98	CNTR	χPT extraction
0.660 ±0.024		AMENDOLIA	84	CNTR	$\pi e \to \pi e$
0.711 ±0.009	±0.016	[6] BEBEK	78	CNTR	$eN \to e\pi N$
0.678 ±0.004	±0.008	[8] QUENZER	78	CNTR	$e^+e^- \to \pi^+\pi^-$
$0.78\ ^{+0.09}_{-0.10}$		ADYLOV	77	CNTR	$\pi e \to \pi e$
$0.74\ ^{+0.11}_{-0.13}$		BARDIN	77	CNTR	$ep \to e\pi^+ n$
0.56 ±0.04		DALLY	77	CNTR	$\pi e \to \pi e$

[1] This value combines the measurements of ANANTHANARAYAN 17 and COLANGELO 19 which are based on the same data set. The uncertainty range is chosen to cover both results.
[2] CUI 21A perform a fit including spacelike data only. Employ a new mathematical procedure based on interpolation via continued fractions augmented by statistical sampling. Also do not impose the charge conserving normalization condition F(0) = 1.
[3] COLANGELO 19 fit existing F_V data, using an extended Omnes dispersive representation. This analysis is based on the same data set of ANANTHANARAYAN 17 . Accordingly, they cannot be averaged. We combine the results into a common value, with the uncertainty range chosen to cover the uncertainty ranges of both analyses.
[4] ANANTHANARAYAN 17 fit existing F_V data, using a mixed phase-modulus dispersive representation. This analysis is based on the same data set of COLANGELO 19. Accordingly, they cannot be averaged. We combine the results into a common value, with the uncertainty range chosen to cover the uncertainty ranges of both analyses.
[5] According to the authors the uncertainty could be underestimated. The value quoted omits the BaBar data AUBERT 09.
[6] The extractions could contain an additional theoretical uncertainty which cannot be sufficiently quantified.
[7] BIJNENS 98 fits existing data.
[8] The extraction is based on a parametrization that does not have correct analytic properties.

$\pi^{\pm}$ REFERENCES

We have omitted some papers that have been superseded by later experiments. The omitted papers may be found in our 1988 edition Physics Letters **B204** 1 (1988).

CUI	21A	PL B822 136631	Z.-F. Cui *et al.*	(NJU, ECT, HZDR)
AGUILAR-AR...	20A	PR D102 012001	A. Aguilar-Arevalo *et al.*	(PIENU Collab.)
COLANGELO	19	JHEP 1902 006	G. Colangelo, M. Hoferichter, P. Stoffer	(BERN+)
DAUM	19	PL B796 11	M. Daum, R. Frosch, P.-R. Kettle	(PSI)
PDG	19	RPP 2019 at pdg.lbl.gov	M. Tanabashi *et al.*	(PDG Collab.)
ANANTHANA...	17	PRL 119 132002	B. Ananthanarayan, I. Caprini, D. Das	
HANHART	17	EPJ C77 98	C. Hanhart *et al.*	
ANANTHANA...	16A	PR D93 116007	B. Ananthanarayan *et al.*	
TRASSINELLI	16	PL B759 583	M. Trassinelli *et al.*	
ADOLPH	15A	PRL 114 062002	C. Adolph *et al.*	(COMPASS Collab.)
AGUILAR-AR...	15	PRL 115 071801	A. Aguilar-Arevalo *et al.*	(PIENU Collab.)
HOLSTEIN	14	ARNPS 64 51	B. Holstein, S. Scherer	(MASA, MAINZ)
AUBERT	09	PR D79 011102	B. Aubert *et al.*	(BABAR Collab.)
BYCHKOV	09	PRL 103 051802	M. Bychkov *et al.*	(PSI PIBETA Collab.)
FRLEZ	04	PRL 93 181804	E. Frlez *et al.*	(PSI PIBETA Collab.)
POCANIC	04	PRL 93 181803	D. Pocanic *et al.*	(PSI PIBETA Collab.)
ESCHRICH	01	PL B522 233	I. Eschrich *et al.*	(FNAL SELEX Collab.)
LIESENFELD	99	PL B468 20	A. Liesenfeld *et al.*	
BIJNENS	98	JHEP 9805 014	J. Bijnens *et al.*	
BRESSI	98	NP B513 555	G. Bressi *et al.*	
LENZ	98	PL B416 50	S. Lenz *et al.*	
ASSAMAGAN	96	PR D53 6065	K.A. Assamagan *et al.*	(PSI, ZURI, VILL+)
KOPTEV	95	JETPL 61 877	V.P. Koptev *et al.*	(PNPI)
		Translated from ZETFP 61 865.		
NUMAO	95	PR D52 4855	T. Numao *et al.*	(TRIU, BRCO)
ASSAMAGAN	94	PL B335 231	K.A. Assamagan *et al.*	(PSI, ZURI, VILL+)
JECKELMANN	94	PL B335 326	B. Jeckelmann, P.F.A. Goudsmit, H.J. Leisi	(WABRN+)
CZAPEK	93	PRL 70 17	G. Czapek *et al.*	(BERN, VILL)
BARANOV	92	SJNP 55 1644	V.A. Baranov *et al.*	(JINR)
		Translated from YAF 55 2940.		
BRITTON	92	PRL 68 3000	D.I. Britton *et al.*	(TRIU, CARL)
Also		PR D49 28	D.I. Britton *et al.*	(TRIU, CARL)
NUMAO	92	MPL A7 3357	T. Numao	(TRIU)
BARANOV	91B	SJNP 54 790	V.A. Baranov *et al.*	(JINR)
		Translated from YAF 54 1298.		
DAUM	91	PL B265 425	M. Daum *et al.*	(VILL)
BOLOTOV	90B	PL B243 308	V.N. Bolotov *et al.*	(INRM)
EGLI	89	PL B222 533	S. Egli *et al.*	(SINDRUM Collab.)
Also		PL B175 97	S. Egli *et al.*	(AACH3, ETH, SIN, ZURI)
PDG	88	PL B204 1	G.P. Yost *et al.*	(LBL+)
PICCIOTTO	88	PR D37 1131	C.E. Picciotto *et al.*	(TRIU, CNRC)
COHEN	87	RMP 59 1121	E.R. Cohen, B.N. Taylor	(RISC, NBS)
KORENCHE...	87	SJNP 46 192	S.M. Korenchenko *et al.*	(JINR)
		Translated from YAF 46 313.		
AMENDOLIA	86	NP B277 168	S.R. Amendolia *et al.*	(CERN NA7 Collab.)
BAY	86	PL B174 445	A. Bay *et al.*	(LAUS, ZURI)
BRYMAN	86	PR D33 1211	D.A. Bryman *et al.*	(TRIU, CNRC)
Also		PRL 50 7	D.A. Bryman *et al.*	(TRIU, CNRC)
JECKELMANN	86B	NP A457 709	B. Jeckelmann *et al.*	(ETH, FRIB)
Also		PRL 56 1444	B. Jeckelmann *et al.*	(ETH, FRIB)
PIILONEN	86	PRL 57 1402	L.E. Piilonen *et al.*	(LANL, TEMP, CHIC)
MCFARLANE	85	PR D32 547	W.K. McFarlane *et al.*	(TEMP, LANL)
ABELA	84	PL 146B 431	R. Abela *et al.*	(SIN)
Also		PL 74B 126	M. Daum *et al.*	(SIN)
Also		PR D20 2692	M. Daum *et al.*	(SIN)
AMENDOLIA	84	PL 146B 116	S.R. Amendolia *et al.*	(CERN NA7 Collab.)
FETSCHER	84	PL 140B 117	W. Fetscher	(ETH)
ABELA	83	NP A395 413	R. Abela *et al.*	(BASL, KARLK, KARLE)
CARR	83	PRL 51 627	J. Carr *et al.*	(LBL, NWES, TRIU)
COOPER	82	PL 112B 97	A.M. Cooper *et al.*	(RL)
DALLY	82	PRL 48 375	E.B. Dally *et al.*	
LU	80	PRL 45 1066	D.C. Lu *et al.*	(YALE, COLU, JHU)
BEBEK	78	PR D17 1693	C.J. Bebek *et al.*	
QUENZER	78	PL 76B 512	A. Quenzer *et al.*	(LALO)
STETZ	78	NP B138 285	A.W. Stetz *et al.*	(LBL, UCLA)
ADYLOV	77	NP B128 461	G.T. Adylov *et al.*	
BARDIN	77	NP B120 45	G. Bardin *et al.*	
DALLY	77	PRL 39 1176	E.B. Dally *et al.*	
CARTER	76	PRL 37 1380	A.L. Carter *et al.*	(CARL, CNRC, CHIC+)
KORENCHE...	76B	JETP 44 35	S.M. Korenchenko *et al.*	(JINR)
		Translated from ZETF 71 69.		
MARUSHEN...	76	JETPL 23 72	V.I. Marushenko *et al.*	(PNPI)
		Translated from ZETFP 23 80.		
Also		Private Comm.	R.E. Shafer	(FNAL)
Also		Private Comm.	A. Smirnov	(PNPI)
DUNAITSEV	73	SJNP 16 292	A.F. Dunaitsev *et al.*	(SERP)
		Translated from YAF 16 524.		
AYRES	71	PR D3 1051	D.S. Ayres *et al.*	(LRL, UCSB)
Also		PR 157 1288	D.S. Ayres *et al.*	(LRL)
Also		PRL 21 261	D.S. Ayres *et al.*	(LRL, UCSB)
Also		Thesis UCRL 18369	D.S. Ayres	(LRL)
Also		PRL 23 1267	A.J. Greenberg *et al.*	(LRL, UCSB)
KORENCHE...	71	SJNP 13 189	S.M. Korenchenko *et al.*	(JINR)
		Translated from YAF 13 339.		
BOOTH	70	PL 32B 723	P.S.L. Booth *et al.*	(LIVP)
DEPOMMIER	68	NP B4 189	P. Depommier *et al.*	(CERN)
PETRUKHIN	68	JINR P1 3862	V.I. Petrukhin *et al.*	(JINR)
HYMAN	67	PL 25B 376	L.G. Hyman *et al.*	(ANL, CMU, NWES)

Downloaded from https://academic.oup.com/ptep/article/2022/8/083C01/6651666 by KIT Library user on 27 September 2022

NORDBERG	67	PL 24B 594	M.E. Nordberg, F. Lobkowicz, R.L. Burman	(ROCH)
BARDON	66	PRL 16 775	M. Bardon *et al.*	(COLU)
KINSEY	66	PR 144 1132	K.F. Kinsey, F. Lobkowicz, M.E. Nordberg	(ROCH)
LOBKOWICZ	66	PRL 17 548	F. Lobkowicz *et al.*	(ROCH, BNL)
BACASTOW	65	PR 139 B407	R.B. Bacastow *et al.*	(LRL, SLAC)
BERTRAM	65	PR 139 B617	W.K. Bertram *et al.*	(MICH, CMU)
DUNAITSEV	65	JETP 20 58	A.F. Dunaitsev *et al.*	(JINR)
		Translated from ZETF 47 84.		
ECKHAUSE	65	PL 19 348	M. Eckhause *et al.*	(WILL)
BARTLETT	64	PR 136 B1452	D. Bartlett *et al.*	(COLU)
DICAPUA	64	PR 133 B1333	M. di Capua *et al.*	(COLU)
Also		Private Comm.	L. Pondrom	(WISC)
DEPOMMIER	63	PL 5 61	P. Depommier *et al.*	(CERN)
DEPOMMIER	63B	PL 7 285	P. Depommier *et al.*	(CERN)
ANDERSON	60	PR 119 2050	H.L. Anderson *et al.*	(EFI)
CASTAGNOLI	58	PR 112 1779	C. Castagnoli, M. Muchnik	(ROMA)

π^0

$$I^G(J^{PC}) = 1^-(0^{-+})$$

We have omitted some results that have been superseded by later experiments. The omitted results may be found in our 1988 edition Physics Letters **B204** 1 (1988).

π^0 MASS

The value is calculated from $m_{\pi^\pm}$ and $(m_{\pi^\pm} - m_{\pi^0})$. See also the notes under the $\pi^\pm$ Mass Listings.

VALUE (MeV)	DOCUMENT ID
134.9768±0.0005 OUR FIT	Error includes scale factor of 1.1.

$m_{\pi^\pm} - m_{\pi^0}$

Measurements with an error > 0.01 MeV have been omitted.

VALUE (MeV)	DOCUMENT ID		TECN	COMMENT
4.5936 ±0.0005 OUR FIT				
4.5936 ±0.0005 OUR AVERAGE				
4.59364±0.00048	CRAWFORD	91	CNTR	$\pi^- p \to \pi^0 n$, n TOF
4.5930 ±0.0013	CRAWFORD	86	CNTR	$\pi^- p \to \pi^0 n$, n TOF
• • • We do not use the following data for averages, fits, limits, etc. • • •				
4.59366±0.00048	CRAWFORD	88B	CNTR	See CRAWFORD 91
4.6034 ±0.0052	VASILEVSKY	66	CNTR	
4.6056 ±0.0055	CZIRR	63	CNTR	

π^0 MEAN LIFE

Most experiments measure the π^0 width which we convert to a lifetime. ATHERTON 85 is the only direct measurement of the π^0 lifetime. The two Primakoff measurements from 1970 have been excluded from our average because they suffered model-related systematics unknown at the time. More information on the π^0 lifetime can be found in BERNSTEIN 13.

VALUE (10^{-17} s)	EVTS	DOCUMENT ID		TECN	COMMENT
8.43 ±0.13 OUR AVERAGE		Error includes scale factor of 1.2.			
8.337±0.056±0.112		[1] LARIN	20	PRMX	Primakoff effect
8.5 ±1.1		[2] BYCHKOV	09	PIBE	$\pi^+ \to e^+ \nu\gamma$ at rest
8.4 ±0.5 ±0.5	1182	[3] WILLIAMS	88	CBAL	$e^+ e^- \to e^+ e^- \pi^0$
8.97 ±0.22 ±0.17		ATHERTON	85	CNTR	Direct measurement
8.2 ±0.4		[4] BROWMAN	74	CNTR	Primakoff effect
• • • We do not use the following data for averages, fits, limits, etc. • • •					
8.32 ±0.15 ±0.18		[5] LARIN	11	PRMX	Primakoff effect
5.6 ±0.6		BELLETTINI	70	CNTR	Primakoff effect
9 ±0.68		KRYSHKIN	70	CNTR	Primakoff effect
7.3 ±1.1		BELLETTINI	65B	CNTR	Primakoff effect

[1] LARIN 20 reported this lifetime value from a measurement of $\Gamma(\pi^0 \to \gamma\gamma) = 7.802 \pm 0.052 \pm 0.105$ eV, combining data from PrimEX-II on 12C and 28Si targets with previous PrimEx-I LARIN 11 measurements. This result supersedes LARIN 11.

[2] BYCHKOV 09 obtains this using the conserved-vector-current relation between the vector form factor F_V and the π^0 lifetime.

[3] WILLIAMS 88 gives $\Gamma(\gamma\gamma) = 7.7 \pm 0.5 \pm 0.5$ eV. We give here $\tau = \hbar/\Gamma(\text{total})$.

[4] BROWMAN 74 gives a π^0 width $\Gamma = 8.02 \pm 0.42$ eV. The mean life is $\hbar/\Gamma$.

[5] LARIN 11 reported $\Gamma(\pi^0 \to \gamma\gamma) = 7.82 \pm 0.14 \pm 0.17$ eV which we converted to mean life $\tau = \hbar/\Gamma(\text{total})$.

π^0 DECAY MODES

For decay limits to particles which are not established, see the appropriate Search sections (A^0 (axion) and Other Light Boson (X^0) Searches, etc.).

	Mode	Fraction (Γ_i/Γ)	Scale factor/ Confidence level
Γ_1	2γ	(98.823±0.034) %	S=1.5
Γ_2	$e^+ e^- \gamma$	(1.174±0.035) %	S=1.5
Γ_3	γ positronium	(1.82 ±0.29) $\times 10^{-9}$	
Γ_4	$e^+ e^+ e^- e^-$	(3.34 ±0.16) $\times 10^{-5}$	
Γ_5	$e^+ e^-$	(6.46 ±0.33) $\times 10^{-8}$	
Γ_6	4γ	< 2 $\times 10^{-8}$	CL=90%
Γ_7	$\nu\overline{\nu}$	[a] < 4.4 $\times 10^{-9}$	CL=90%
Γ_8	$\nu_e\overline{\nu}_e$	< 1.7 $\times 10^{-6}$	CL=90%
Γ_9	$\nu_\mu\overline{\nu}_\mu$	< 1.6 $\times 10^{-6}$	CL=90%
Γ_{10}	$\nu_\tau\overline{\nu}_\tau$	< 2.1 $\times 10^{-6}$	CL=90%
Γ_{11}	$\gamma\nu\overline{\nu}$	< 1.9 $\times 10^{-7}$	CL=90%
	Charge conjugation (C) or Lepton Family number (LF) violating modes		
Γ_{12}	3γ	C < 3.1 $\times 10^{-8}$	CL=90%
Γ_{13}	$\mu^+ e^-$	LF < 3.8 $\times 10^{-10}$	CL=90%
Γ_{14}	$\mu^- e^+$	LF < 3.2 $\times 10^{-10}$	CL=90%
Γ_{15}	$\mu^+ e^- + \mu^- e^+$	LF < 3.6 $\times 10^{-10}$	CL=90%

[a] Astrophysical and cosmological arguments give limits of order 10^{-13}, but they are model dependent and for the summary value we use the best laboratory limit, which includes any final state of invisible particles.

CONSTRAINED FIT INFORMATION

An overall fit to 2 branching ratios uses 6 measurements and one constraint to determine 3 parameters. The overall fit has a $\chi^2 = 4.6$ for 4 degrees of freedom.

The following *off-diagonal* array elements are the correlation coefficients $\langle \delta x_i \delta x_j \rangle / (\delta x_i \cdot \delta x_j)$, in percent, from the fit to the branching fractions, $x_i \equiv \Gamma_i/\Gamma_{\text{total}}$. The fit constrains the x_i whose labels appear in this array to sum to one.

	x_1	x_2
x_2	−100	
x_4	0	−1

π^0 BRANCHING RATIOS

$\Gamma(e^+ e^- \gamma)/\Gamma(2\gamma)$ — Γ_2/Γ_1

VALUE (%)	EVTS	DOCUMENT ID		TECN	COMMENT
1.188 ±0.035 OUR FIT		Error includes scale factor of 1.5.			
1.188 ±0.034 OUR AVERAGE		Error includes scale factor of 1.4. See the ideogram below.			
1.140 ±0.024 ±0.033	12.5k	[1] BEDDALL	08	ALEP	$e^+ e^- \to Z \to$ hadrons
1.25 ±0.04		SCHARDT	81	SPEC	$\pi^- p \to n\pi^0$
1.166 ±0.047	3k	[2] SAMIOS	61	HBC	$\pi^- p \to n\pi^0$
1.17 ±0.15	27	BUDAGOV	60	HBC	
• • • We do not use the following data for averages, fits, limits, etc. • • •					
1.1559±0.0047±0.0106	60k	[3] ABOUZAID	19	KTEV	$K_L \to 3\pi^0$ in flight
1.196		JOSEPH	60	THEO	QED calculation

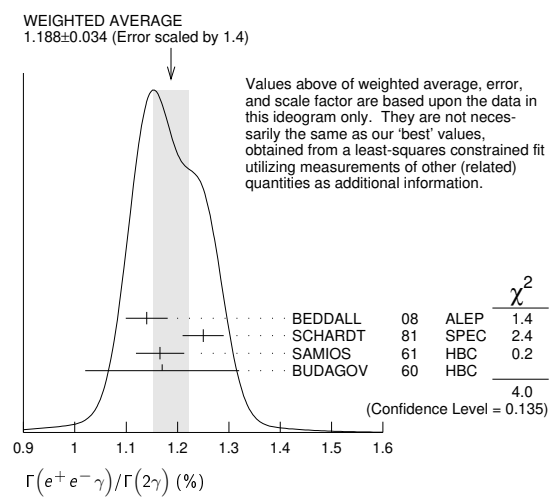

[1] BEDDALL 08 value is obtained from ALEPH archived data.

[2] SAMIOS 61 value uses a Panofsky ratio = 1.62.

[3] ABOUZAID 19 measured a value of (0.3920 ± 0.0016 ± 0.0036)% from 1999 KTEV data in $K_L \to 3\pi^0 \to 5\gamma e^+ e^-$ decays, normalised to $K_L \to 3\pi^0$, for m(ee) > 15 MeV and then extrapolated it to the full m(ee) range using the Mikaelian and Smith predictions for the mass spectrum.

$\Gamma(\gamma\text{positronium})/\Gamma(2\gamma)$ — Γ_3/Γ_1

VALUE (units 10^{-9})	EVTS	DOCUMENT ID		TECN	COMMENT
1.84±0.29	277	AFANASYEV	90	CNTR	pC 70 GeV

Downloaded from https://academic.oup.com/ptep/article/2022/8/083C01/6651666 by KIT Library user on 27 September 2022

$\Gamma(e^+e^+e^-e^-)/\Gamma(2\gamma)$ — Γ_4/Γ_1

VALUE (units 10^{-5})	EVTS	DOCUMENT ID		TECN	COMMENT
3.38±0.16 OUR FIT					
3.38±0.16 OUR AVERAGE					
3.46±0.19	30.5k	[1] ABOUZAID	08D	KTEV	$K^0_L \to \pi^0\pi^0\pi^0_{DD}$
3.18±0.30	146	[2] SAMIOS	62B	HBC	

[1] This ABOUZAID 08D value includes all radiative final states. The error includes both statistical and systematic errors. The correlation between the Dalitz-pair planes gives a direct measurement of the π^0 parity. The $\pi^0 2\gamma^*$ form factor is measured and limits are placed on a scalar contribution to the decay.

[2] SAMIOS 62B value uses a Panofsky ratio = 1.62.

$\Gamma(e^+e^-)/\Gamma_{total}$ — Γ_5/Γ

Experimental results are listed; branching ratios corrected for radiative effects are given in the footnotes. BERMAN 60 found $B(\pi^0 \to e^+e^-) \geq 4.69 \times 10^{-8}$ via an exact QED calculation.

VALUE (units 10^{-8})	EVTS	DOCUMENT ID		TECN	CHG	COMMENT
6.46±0.33 OUR AVERAGE						
6.44±0.25±0.22	794	[1] ABOUZAID	07	KTEV		$K^0_L \to 3\pi^0$ in flight
6.9 ±2.3 ±0.6	21	[2] DESHPANDE	93	SPEC		$K^+ \to \pi^+\pi^0$
7.6 $^{+2.9}_{-2.8}$ ±0.5	8	[3] MCFARLAND	93	SPEC		$K^0_L \to 3\pi^0$ in flight
• • • We do not use the following data for averages, fits, limits, etc. • • •						
6.09±0.40±0.24	275	[4] ALAVI-HARATI	99C	SPEC	0	Repl. by ABOUZAID 07

[1] ABOUZAID 07 result is for $m_{e^+e^-}/m_{\pi^0} > 0.95$. With radiative corrections the result becomes $(7.48 \pm 0.29 \pm 0.25) \times 10^{-8}$.

[2] The DESHPANDE 93 result with bremsstrahlung radiative corrections is $(8.0 \pm 2.6 \pm 0.6) \times 10^{-8}$.

[3] The MCFARLAND 93 result is for $B[\pi^0 \to e^+e^-, (m_{e^+e^-}/m_{\pi^0})^2 > 0.95]$. With radiative corrections it becomes $(8.8^{+4.5}_{-3.2} \pm 0.6) \times 10^{-8}$.

[4] ALAVI-HARATI 99C quote result for $B[\pi^0 \to e^+e^-, (m_{e^+e^-}/m_{\pi^0})^2 > 0.95]$ to minimize radiative contributions from $\pi^0 \to e^+e^-\gamma$. After radiative corrections they obtain $(7.04 \pm 0.46 \pm 0.28) \times 10^{-8}$.

$\Gamma(e^+e^-)/\Gamma(2\gamma)$ — Γ_5/Γ_1

VALUE (units 10^{-7})	CL%	EVTS	DOCUMENT ID		TECN	COMMENT
• • • We do not use the following data for averages, fits, limits, etc. • • •						
<1.3	90		NIEBUHR	89	SPEC	$\pi^-p \to \pi^0 n$ at rest
<5.3	90		ZEPHAT	87	SPEC	$\pi^-p \to \pi^0 n$ 0.3 GeV/c
1.7 ±0.6 ±0.3		59	FRANK	83	SPEC	$\pi^-p \to n\pi^0$
1.8 ±0.6		58	MISCHKE	82	SPEC	See FRANK 83
$2.23^{+2.40}_{-1.10}$	90	8	FISCHER	78B	SPRK	$K^+ \to \pi^+\pi^0$

$\Gamma(4\gamma)/\Gamma_{total}$ — Γ_6/Γ

VALUE (units 10^{-8})	CL%	EVTS	DOCUMENT ID		TECN	COMMENT
< 2	90		MCDONOUGH	88	CBOX	π^-p at rest
• • • We do not use the following data for averages, fits, limits, etc. • • •						
<160	90		BOLOTOV	86C	CALO	
<440	90	0	AUERBACH	80	CNTR	

$\Gamma(\nu\overline{\nu})/\Gamma_{total}$ — Γ_7/Γ

The astrophysical and cosmological limits are many orders of magnitude lower, but they are model dependent and for the summary value we use the best laboratory limit, which includes any final state of invisible particles.

VALUE (units 10^{-6})	CL%	DOCUMENT ID		TECN	COMMENT
< 4.4 $\times 10^{-3}$	90	[1] CORTINA-GIL	21C	SPEC	$K^+ \to \pi^+\pi^0(\gamma)$
• • • We do not use the following data for averages, fits, limits, etc. • • •					
< 0.27	90	[1] ARTAMONOV	05A	B949	$K^+ \to \pi^+\pi^0$
< 0.83	90	[1] ATIYA	91	B787	$K^+ \to \pi^+\nu\nu'$
< 2.9 $\times 10^{-7}$		[2] LAM	91		Cosmological limit
< 3.2 $\times 10^{-7}$		[3] NATALE	91		SN 1987A
< 6.5	90	DORENBOS...	88	CHRM	Beam dump, prompt ν
<24	90	[1] HERCZEG	81	RVUE	$K^+ \to \pi^+\nu\nu'$

[1] This limit applies to all possible "invisible" channels.

[2] LAM 91 considers the production of right-handed neutrinos produced from the cosmic thermal background at the temperature of about the pion mass through the reaction $\gamma\gamma \to \pi^0 \to \nu\overline{\nu}$.

[3] NATALE 91 considers the excess energy-loss rate from SN 1987A if the process $\gamma\gamma \to \pi^0 \to \nu\overline{\nu}$ occurs, permitted if the neutrinos have a right-handed component. As pointed out in LAM 91 (and confirmed by Natale), there is a factor 4 error in the NATALE 91 published result (0.8×10^{-7}).

$\Gamma(\nu_e\overline{\nu}_e)/\Gamma_{total}$ — Γ_8/Γ

VALUE (units 10^{-6})	CL%	DOCUMENT ID		TECN	COMMENT
<1.7	90	DORENBOS...	88	CHRM	Beam dump, prompt ν
• • • We do not use the following data for averages, fits, limits, etc. • • •					
<3.1	90	[1] HOFFMAN	88	RVUE	Beam dump, prompt ν

[1] HOFFMAN 88 analyzes data from a 400-GeV BEBC beam-dump experiment.

$\Gamma(\nu_\mu\overline{\nu}_\mu)/\Gamma_{total}$ — Γ_9/Γ

VALUE (units 10^{-6})	CL%	EVTS	DOCUMENT ID		TECN	COMMENT
<1.6	90	8.7	AUERBACH	04	LSND	800 MeV p on Cu
<3.1	90		[1] HOFFMAN	88	RVUE	Beam dump, prompt ν
• • • We do not use the following data for averages, fits, limits, etc. • • •						
<7.8	90		DORENBOS...	88	CHRM	Beam dump, prompt ν

[1] HOFFMAN 88 analyzes data from a 400-GeV BEBC beam-dump experiment.

$\Gamma(\nu_\tau\overline{\nu}_\tau)/\Gamma_{total}$ — Γ_{10}/Γ

VALUE (units 10^{-6})	CL%	DOCUMENT ID		TECN	COMMENT
<2.1	90	[1] HOFFMAN	88	RVUE	Beam dump, prompt ν
• • • We do not use the following data for averages, fits, limits, etc. • • •					
<4.1	90	DORENBOS...	88	CHRM	Beam dump, prompt ν

[1] HOFFMAN 88 analyzes data from a 400-GeV BEBC beam-dump experiment.

$\Gamma(\gamma\nu\overline{\nu})/\Gamma_{total}$ — Γ_{11}/Γ

Standard Model prediction is 6×10^{-18}.

VALUE	CL%	DOCUMENT ID		TECN	COMMENT
<1.9 × 10^{-7}	90	CORTINA-GIL	19	SPEC	$K^+ \to \pi^+\gamma\nu\overline{\nu}$
• • • We do not use the following data for averages, fits, limits, etc. • • •					
<6 $\times 10^{-4}$	90	ATIYA	92	CNTR	$K^+ \to \gamma\nu\overline{\nu}\pi^+$

$\Gamma(3\gamma)/\Gamma_{total}$ — Γ_{12}/Γ

Forbidden by C invariance.

VALUE (units 10^{-8})	CL%	EVTS	DOCUMENT ID		TECN	COMMENT
< 3.1	90		MCDONOUGH	88	CBOX	π^-p at rest
• • • We do not use the following data for averages, fits, limits, etc. • • •						
< 38	90	0	HIGHLAND	80	CNTR	
<150	90	0	AUERBACH	78	CNTR	
<490	90	0	[1] DUCLOS	65	CNTR	
<490	90		[1] KUTIN	65	CNTR	

[1] These experiments give $B(3\gamma/2\gamma) < 5.0 \times 10^{-6}$.

$\Gamma(\mu^+e^-)/\Gamma_{total}$ — Γ_{13}/Γ

Forbidden by lepton family number conservation.

VALUE (units 10^{-9})	CL%	EVTS	DOCUMENT ID		TECN	COMMENT
< 0.38	90	0	APPEL	00	SPEC	$K^+ \to \pi^+\mu^+e^-$
• • • We do not use the following data for averages, fits, limits, etc. • • •						
<16	90		LEE	90	SPEC	$K^+ \to \pi^+\mu^+e^-$
<78	90		CAMPAGNARI	88	SPEC	See LEE 90

$\Gamma(\mu^-e^+)/\Gamma_{total}$ — Γ_{14}/Γ

Forbidden by lepton family number conservation.

VALUE	CL%	DOCUMENT ID		TECN	COMMENT
<3.2 × 10^{-10}	90	ALIBERTI	21	NA62	$K^+ \to \pi^+e^+\mu^-$
• • • We do not use the following data for averages, fits, limits, etc. • • •					
<3.4 $\times 10^{-9}$	90	APPEL	00B	B865	$K^+ \to \pi^+e^+\mu^-$

$[\Gamma(\mu^+e^-) + \Gamma(\mu^-e^+)]/\Gamma_{total}$ — Γ_{15}/Γ

Forbidden by lepton family number conservation.

VALUE (units 10^{-9})	CL%	DOCUMENT ID		TECN	COMMENT
< 0.36	90	ABOUZAID	08C	KTEV	$K^0_L \to 2\pi^0\mu^\pm e^\mp$
• • • We do not use the following data for averages, fits, limits, etc. • • •					
< 17.2	90	KROLAK	94	E799	In $K^0_L \to 3\pi^0$
<140		HERCZEG	84	RVUE	$K^+ \to \pi^+\mu e$
< 2 $\times 10^{-6}$		HERCZEG	84	THEO	$\mu^- \to e^-$ conversion
< 70	90	BRYMAN	82	RVUE	$K^+ \to \pi^+\mu e$

π^0 ELECTROMAGNETIC FORM FACTOR

The amplitude for the process $\pi^0 \to e^+e^-\gamma$ contains a form factor $F(x)$ at the $\pi^0\gamma\gamma$ vertex, where $x = [m_{e^+e^-}/m_{\pi^0}]^2$. The parameter a in the linear expansion $F(x) = 1 + ax$ is listed below.

All the measurements except that of BEHREND 91 are in the time-like region of momentum transfer.

LINEAR COEFFICIENT OF π^0 ELECTROMAGNETIC FORM FACTOR

VALUE (units 10^{-2})	EVTS	DOCUMENT ID		TECN	COMMENT
3.35± 0.31 OUR AVERAGE					
3.68± 0.51±0.25	1.1M	LAZZERONI	17	SPEC	$K^\pm \to \pi^0\pi^\pm$; $\pi^0 \to e^+e^-\gamma$
2.6 ± 2.4 ±4.8	7.5k	FARZANPAY	92	SPEC	$\pi^-p \to \pi^0 n$ at rest
2.5 ± 1.4 ±2.6	54k	MEIJERDREES	92B	SPEC	$\pi^-p \to \pi^0 n$ at rest
3.26± 0.26±0.26	127	[1] BEHREND	91	CELL	$e^+e^- \to e^+e^-\pi^0$
−11 ± 3 ±8	32k	FONVIEILLE	89	SPEC	Radiation corr.
• • • We do not use the following data for averages, fits, limits, etc. • • •					
12 $^{+5}_{-4}$		[2] TUPPER	83	THEO	FISCHER 78 data
10 ± 3	31k	[3] FISCHER	78	SPEC	Radiation corr.
1 ±11	2.2k	DEVONS	69	OSPK	No radiation corr.
−15 ±10	7.6k	KOBRAK	61	HBC	No radiation corr.
−24 ±16	3.0k	SAMIOS	61	HBC	No radiation corr.

Downloaded from https://academic.oup.com/ptep/article/2022/8/083C01/6651666 by KIT Library user on 27 September 2022

[1] BEHREND 91 estimates that their systematic error is of the same order of magnitude as their statistical error, and so we have included a systematic error of this magnitude. The value of a is obtained by extrapolation from the region of large space-like momentum transfer assuming vector dominance.

[2] TUPPER 83 is a theoretical analysis of FISCHER 78 including 2-photon exchange in the corrections.

[3] The FISCHER 78 error is statistical only. The result without radiation corrections is $+0.05 \pm 0.03$.

π^0 REFERENCES

We have omitted some papers that have been superseded by later experiments. The omitted papers may be found in our 1988 edition Physics Letters **B204** 1 (1988).

ALIBERTI	21	PRL 127 131802	R. Aliberti *et al.*	(NA62 Collab.)
CORTINA-GIL	21C	JHEP 2102 201	E. Cortina Gil *et al.*	(NA62 Collab.)
LARIN	20	SCI 368 506	I. Larin *et al.*	(PrimEx II Collab.)
ABOUZAID	19	PR D100 032003	E. Abouzaid *et al.*	(KTeV Collab.)
CORTINA-GIL	19	JHEP 1905 182	E. Cortina Gil *et al.*	(NA62 Collab.)
LAZZERONI	17	PL B768 38	C. Lazzeroni *et al.*	(NA62 Collab.)
BERNSTEIN	13	RMP 85 49	A.M. Bernstein, B. R. Holstein	(AMHT, MIT)
LARIN	11	PRL 106 162303	I. Larin *et al.*	(PrimEx Collab.)
BYCHKOV	09	PRL 103 051802	M. Bychkov *et al.*	(PSI PIBETA Collab.)
ABOUZAID	08C	PRL 100 131803	E. Abouzaid *et al.*	(FNAL KTeV Collab.)
ABOUZAID	08D	PRL 100 182001	E. Abouzaid *et al.*	(FNAL KTeV Collab.)
BEDDALL	08	EPJ C54 365	A. Beddall, A. Beddall	(UGAZ)
ABOUZAID	07	PR D75 012004	E. Abouzaid *et al.*	(KTeV Collab.)
ARTAMONOV	05A	PR D72 091102	A.V. Artamonov *et al.*	(BNL E949 Collab.)
AUERBACH	04	PRL 92 091801	L.B. Auerbach *et al.*	(LSND Collab.)
APPEL	00	PRL 85 2450	R. Appel *et al.*	(BNL 865 Collab.)
Also		Thesis, Yale Univ.	D.R. Bergman	
Also		Thesis, Univ. Zurich	S. Pislak	
APPEL	00B	PRL 85 2877	R. Appel *et al.*	(BNL 865 Collab.)
ALAVI-HARATI	99C	PRL 83 922	A. Alavi-Harati *et al.*	(FNAL KTeV Collab.)
KROLAK	94	PL B320 407	P. Krolak *et al.*	(EFI, UCLA, COLO, ELMT+)
DESHPANDE	93	PRL 71 27	A. Deshpande *et al.*	(BNL E851 Collab.)
MCFARLAND	93	PRL 71 31	K.S. McFarland *et al.*	(EFI, UCLA, COLO+)
ATIYA	92	PRL 69 733	M.S. Atiya *et al.*	(BNL, LANL, PRIN+)
FARZANPAY	92	PL B278 413	F. Farzanpay *et al.*	(ORST, TRIU, BRCO+)
MEIJERDREES	92B	PR D45 1439	R. Meijer Drees *et al.*	(PSI SINDRUM-I Collab.)
ATIYA	91	PRL 66 2189	M.S. Atiya *et al.*	(BNL, LANL, PRIN+)
BEHREND	91	ZPHY C49 401	H.J. Behrend *et al.*	(CELLO Collab.)
CRAWFORD	91	PR D43 46	J.F. Crawford *et al.*	(VILL, UVA)
LAM	91	PR D44 3345	W.P. Lam, K.W. Ng	(AST)
NATALE	91	PL B258 227	A.A. Natale	(SPIFT)
AFANASYEV	90	PL B236 116	L.G. Afanasyev *et al.*	(JINR, MOSU, SERP)
Also		SJNP 51 664	L.G. Afanasyev *et al.*	(JINR)
		Translated from YAF 51 1040.		
LEE	90	PRL 64 165	A.M. Lee *et al.*	(BNL, FNAL, VILL, WASH+)
FONVIEILLE	89	PL B233 65	H. Fonvieille *et al.*	(CLER, LYON, SACL)
NIEBUHR	89	PR D40 2796	C. Niebuhr *et al.*	(SINDRUM Collab.)
CAMPAGNARI	88	PRL 61 2062	C. Campagnari *et al.*	(BNL, FNAL, PSI+)
CRAWFORD	88B	PL B213 391	J.F. Crawford *et al.*	(PSI, UVA)
DORENBOS...	88	ZPHY C40 497	J. Dorenbosch *et al.*	(CHARM Collab.)
HOFFMAN	88	PL B208 149	C.M. Hoffman	(LANL)
MCDONOUGH	88	PR D38 2121	J.M. McDonough *et al.*	(TEMP, LANL, CHIC)
PDG	88	PL B204 1	G.P. Yost *et al.*	(LBL+)
WILLIAMS	88	PR D38 1365	D.A. Williams *et al.*	(Crystal Ball Collab.)
ZEPHAT	87	JP G13 1375	A.G. Zephat *et al.*	(OMICRON Collab.)
BOLOTOV	86C	JETPL 43 520	V.N. Bolotov *et al.*	(INRM)
		Translated from ZETFP 43 405.		
CRAWFORD	86	PRL 56 1043	J.F. Crawford *et al.*	(SIN, UVA)
ATHERTON	85	PL 158B 81	H.W. Atherton *et al.*	(CERN, ISU, LUND+)
HERCZEG	84	PR D29 1954	P. Herczeg, C.M. Hoffman	(LANL)
FRANK	83	PR D28 423	J.S. Frank *et al.*	(LANL, ARZS)
TUPPER	83	PR D28 2905	G.B. Tupper, T.R. Grose, M.A. Samuel	(OKSU)
BRYMAN	82	PR D26 2538	D.A. Bryman	(TRIU)
MISCHKE	82	PRL 48 1153	R.E. Mischke *et al.*	(LANL, ARZS)
HERCZEG	81	PL 100B 347	P. Herczeg, C.M. Hoffman	(LANL)
SCHARDT	81	PR D23 639	M.A. Schardt *et al.*	(ARZS, LANL)
AUERBACH	80	PL 90B 317	L.B. Auerbach *et al.*	(TEMP, LASL)
HIGHLAND	80	PRL 44 628	V.L. Highland *et al.*	(TEMP, LASL)
AUERBACH	78	PRL 41 275	L.B. Auerbach *et al.*	(TEMP, LASL)
FISCHER	78	PL 73B 359	J. Fischer *et al.*	(GEVA, SACL)
FISCHER	78B	PL 73B 364	J. Fischer *et al.*	(GEVA, SACL)
BROWMAN	74	PRL 33 1400	A. Browman *et al.*	(CORN, BING)
BELLETTINI	70	NC 66A 243	G. Bellettini *et al.*	(PISA, BONN)
KRYSHKIN	70	JETP 30 1037	V.I. Kryshkin, A.G. Sterligov, Y.P. Usov	(TMSK)
		Translated from ZETF 57 1917.		
DEVONS	69	PR 184 1356	S. Devons *et al.*	(COLU, ROMA)
VASILEVSKY	66	PL 23 281	I.M. Vasilevsky *et al.*	(JINR)
BELLETTINI	65B	NC 40A 1139	G. Bellettini *et al.*	(PISA, FIRZ)
DUCLOS	65	PL 19 253	J. Duclos *et al.*	(CERN, HEID)
KUTIN	65	JETPL 2 243	V.M. Kutjin, V.I. Petrukhin, Y.D. Prokoshkin	(JINR)
		Translated from ZETFP 2 387.		
CZIRR	63	PR 130 341	J.B. Czirr	(LRL)
SAMIOS	62B	PR 126 1844	N.P. Samios *et al.*	(COLU, BNL)
KOBRAK	61	NC 20 1115	H. Kobrak	(EFI)
SAMIOS	61	PR 121 275	N.P. Samios	(COLU, BNL)
BERMAN	60	NC 18 1192	S. Berman, D. Geffen	
BUDAGOV	60	JETP 11 755	Y.A. Budagov *et al.*	(JINR)
		Translated from ZETF 38 1047.		
JOSEPH	60	NC 16 997	D.W. Joseph	(EFI)

η

$I^G(J^{PC}) = 0^+(0^{-+})$

We have omitted some results that have been superseded by later experiments. The omitted results may be found in our 1988 edition Physics Letters **B204** (1988).

η MASS

Recent measurements resolve the obvious inconsistency in previous η mass measurements in favor of the higher value first reported by NA48 (LAI 02). We use only precise measurements consistent with this higher mass value for our η mass average.

VALUE (MeV)	EVTS	DOCUMENT ID		TECN	COMMENT
547.862±0.017 OUR AVERAGE					
547.865±0.031±0.062		NIKOLAEV	14	CRYB	$\gamma p \to p\eta$
547.873±0.005±0.027	1M	GOSLAWSKI	12	SPEC	$dp \to {}^3\mathrm{He}\,\eta$
547.874±0.007±0.029		AMBROSINO	07B	KLOE	$e^+e^- \to \phi \to \eta\gamma$
547.785±0.017±0.057	16k	MILLER	07	CLEO	$\psi(2S) \to J/\psi\eta$
547.843±0.030±0.041	1134	LAI	02	NA48	$\eta \to 3\pi^0$
• • • We do not use the following data for averages, fits, limits, etc. • • •					
547.311±0.028±0.032		[1] ABDEL-BARY	05	SPEC	$dp \to {}^3\mathrm{He}\,\eta$
547.12 ±0.06 ±0.25		KRUSCHE	95D	SPEC	$\gamma p \to \eta p$, threshold
547.30 ±0.15		PLOUIN	92	SPEC	$dp \to {}^3\mathrm{He}\,\eta$
547.45 ±0.25		DUANE	74	SPEC	$\pi^- p \to n$ neutrals
548.2 ±0.65		FOSTER	65C	HBC	
549.0 ±0.7	148	FOELSCHE	64	HBC	
548.0 ±1.0	91	ALFF-...	62	HBC	
549.0 ±1.2	53	BASTIEN	62	HBC	

[1] ABDEL-BARY 05 disagrees significantly with recent measurements of similar or better precision. See comment in the header.

η WIDTH

This is the partial decay rate $\Gamma(\eta \to \gamma\gamma)$ divided by the fitted branching fraction for that mode. See the note at the start of the $\Gamma(2\gamma)$ data block, next below.

VALUE (keV)	DOCUMENT ID
1.31±0.05 OUR FIT	

η DECAY MODES

	Mode	Fraction (Γ_i/Γ)	Scale factor/ Confidence level
	Neutral modes		
Γ_1	neutral modes	(71.96±0.30) %	S=1.3
Γ_2	2γ	(39.36±0.18) %	S=1.1
Γ_3	$3\pi^0$	(32.57±0.21) %	S=1.2
Γ_4	$\pi^0 2\gamma$	$(2.55\pm0.22)\times10^{-4}$	
Γ_5	$2\pi^0 2\gamma$	$<1.2\times10^{-3}$	CL=90%
Γ_6	4γ	$<2.8\times10^{-4}$	CL=90%
Γ_7	invisible	$<1.0\times10^{-4}$	CL=90%
	Charged modes		
Γ_8	charged modes	(28.04±0.30) %	S=1.3
Γ_9	$\pi^+\pi^-\pi^0$	(23.02±0.25) %	S=1.2
Γ_{10}	$\pi^+\pi^-\gamma$	(4.28±0.07) %	S=1.1
Γ_{11}	$e^+e^-\gamma$	$(6.9\pm0.4)\times10^{-3}$	S=1.2
Γ_{12}	$\mu^+\mu^-\gamma$	$(3.1\pm0.4)\times10^{-4}$	
Γ_{13}	e^+e^-	$<7\times10^{-7}$	CL=90%
Γ_{14}	$\mu^+\mu^-$	$(5.8\pm0.8)\times10^{-6}$	
Γ_{15}	$2e^+2e^-$	$(2.40\pm0.22)\times10^{-5}$	
Γ_{16}	$\pi^+\pi^-e^+e^-(\gamma)$	$(2.68\pm0.11)\times10^{-4}$	
Γ_{17}	$e^+e^-\mu^+\mu^-$	$<1.6\times10^{-4}$	CL=90%
Γ_{18}	$2\mu^+2\mu^-$	$<3.6\times10^{-4}$	CL=90%
Γ_{19}	$\mu^+\mu^-\pi^+\pi^-$	$<3.6\times10^{-4}$	CL=90%
Γ_{20}	$\pi^+e^-\overline{\nu}_e$ + c.c.	$<1.7\times10^{-4}$	CL=90%
Γ_{21}	$\pi^+\pi^-2\gamma$	$<2.1\times10^{-3}$	
Γ_{22}	$\pi^+\pi^-\pi^0\gamma$	$<6\times10^{-4}$	CL=90%
Γ_{23}	$\pi^0\mu^+\mu^-\gamma$	$<3\times10^{-6}$	CL=90%
	Charge conjugation (C), Parity (P), Charge conjugation × Parity (CP), or Lepton Family number (LF) violating modes		
Γ_{24}	$\pi^0\gamma$	C [a] $<9\times10^{-5}$	CL=90%
Γ_{25}	$\pi^+\pi^-$	P,CP $<4.4\times10^{-6}$	CL=90%
Γ_{26}	$2\pi^0$	P,CP $<3.5\times10^{-4}$	CL=90%
Γ_{27}	$2\pi^0\gamma$	C $<5\times10^{-4}$	CL=90%
Γ_{28}	$3\pi^0\gamma$	C $<6\times10^{-5}$	CL=90%
Γ_{29}	3γ	C $<1.6\times10^{-5}$	CL=90%
Γ_{30}	$4\pi^0$	P,CP $<6.9\times10^{-7}$	CL=90%
Γ_{31}	$\pi^0e^+e^-$	C [b] $<8\times10^{-6}$	CL=90%
Γ_{32}	$\pi^0\mu^+\mu^-$	C [b] $<5\times10^{-6}$	CL=90%
Γ_{33}	$\mu^+e^- + \mu^-e^+$	LF $<6\times10^{-6}$	CL=90%

[a] Forbidden by angular momentum conservation.

[b] C parity forbids this to occur as a single-photon process.

Downloaded from https://academic.oup.com/ptep/article/2022/8/083C01/6651666 by KIT Library user on 27 September 2022

CONSTRAINED FIT INFORMATION

An overall fit to 2 decay rate and 22 branching ratios uses 54 measurements and one constraint to determine 9 parameters. The overall fit has a $\chi^2 = 46.2$ for 46 degrees of freedom.

The following *off-diagonal* array elements are the correlation coefficients $\langle \delta x_i \delta x_j \rangle / (\delta x_i \cdot \delta x_j)$, in percent, from the fit to the branching fractions, $x_i \equiv \Gamma_i/\Gamma_{total}$. The fit constrains the x_i whose labels appear in this array to sum to one.

	x_2	x_3	x_4	x_9	x_{10}	x_{11}	x_{12}	x_{16}
x_3	12							
x_4	4	0						
x_9	−69	−76	−3					
x_{10}	−48	−52	−2	53				
x_{11}	−8	−7	0	−4	−3			
x_{12}	−1	−1	0	0	0	0		
x_{16}	0	0	0	0	0	0	0	
Γ	−13	−1	−32	9	6	1	0	0

	Mode	Rate (keV)	Scale factor
Γ_2	2γ	0.515 ± 0.018	
Γ_3	$3\pi^0$	0.426 ± 0.015	
Γ_4	$\pi^0 2\gamma$	(3.34 ± 0.28) × 10^{-4}	
Γ_9	$\pi^+\pi^-\pi^0$	0.301 ± 0.011	
Γ_{10}	$\pi^+\pi^-\gamma$	0.0559 ± 0.0022	
Γ_{11}	$e^+e^-\gamma$	0.0090 ± 0.0006	1.2
Γ_{12}	$\mu^+\mu^-\gamma$	(4.1 ± 0.5) × 10^{-4}	
Γ_{16}	$\pi^+\pi^-e^+e^-(\gamma)$	(3.50 ± 0.19) × 10^{-4}	

η DECAY RATES

$\Gamma(2\gamma)$ — Γ_2

See the table immediately above giving the fitted decay rates. Following the advice of NEFKENS 02, we have removed the Primakoff-effect measurement from the average. See also the "Note on the Decay Width $\Gamma(\eta \to \gamma\gamma)$," in our 1994 edition, Phys. Rev. **D50**, 1 August 1994, Part I, p. 1451, for a discussion of the various measurements.

VALUE (keV)	EVTS	DOCUMENT ID		TECN	COMMENT
0.515±0.018 OUR FIT					
0.516±0.018 OUR AVERAGE					
0.520±0.020±0.013		BABUSCI	13A	KLOE	$e^+e^- \to e^+e^-\eta$
0.51 ±0.12 ±0.05	36	BARU	90	MD1	$e^+e^- \to e^+e^-\eta$
0.490±0.010±0.048	2287	ROE	90	ASP	$e^+e^- \to e^+e^-\eta$
0.514±0.017±0.035	1295	WILLIAMS	88	CBAL	$e^+e^- \to e^+e^-\eta$
0.53 ±0.04 ±0.04		BARTEL	85E	JADE	$e^+e^- \to e^+e^-\eta$
• • • We do not use the following data for averages, fits, limits, etc. • • •					
0.476±0.062		[1] RODRIGUES	08	CNTR	Reanalysis
0.64 ±0.14 ±0.13		AIHARA	86	TPC	$e^+e^- \to e^+e^-\eta$
0.56 ±0.16	56	WEINSTEIN	83	CBAL	$e^+e^- \to e^+e^-\eta$
0.324±0.046		BROWMAN	74B	CNTR	Primakoff effect
1.00 ±0.22		[2] BEMPORAD	67	CNTR	Primakoff effect

[1] RODRIGUES 08 uses a more sophisticated calculation for the inelastic background due to incoherent photoproduction to reanalyze the η photoproduction data on Be and Cu at 9 GeV from BROWMAN 74B. This brings the value of $\Gamma(\eta \to 2\gamma)$ in line with direct measurements of the width. The error here is only statistical.

[2] BEMPORAD 67 gives $\Gamma(2\gamma) = 1.21 \pm 0.26$ keV assuming $\Gamma(2\gamma)/\Gamma(\text{total}) = 0.314$. Bemporad private communication gives $\Gamma(2\gamma)^2/\Gamma(\text{total}) = 0.380 \pm 0.083$. We evaluate this using $\Gamma(2\gamma)/\Gamma(\text{total}) = 0.38 \pm 0.01$. Not included in average because the uncertainty resulting from the separation of the coulomb and nuclear amplitudes has apparently been underestimated.

$\Gamma(\pi^0 2\gamma)$ — Γ_4

VALUE (eV)	EVTS	DOCUMENT ID		TECN	COMMENT
0.334±0.028 OUR FIT					
0.33 ±0.03	1200	NEFKENS	14	CRYB	$\gamma p \to \eta p$

η BRANCHING RATIOS

Neutral modes

$\Gamma(\text{neutral modes})/\Gamma_{total}$ — $\Gamma_1/\Gamma = (\Gamma_2+\Gamma_3+\Gamma_4)/\Gamma$

VALUE	EVTS	DOCUMENT ID		TECN	COMMENT
0.7196±0.0030 OUR FIT Error includes scale factor of 1.3.					
0.705 ±0.008	16k	BASILE	71D	CNTR	MM spectrometer
• • • We do not use the following data for averages, fits, limits, etc. • • •					
0.79 ±0.08		BUNIATOV	67	OSPK	

$\Gamma(2\gamma)/\Gamma_{total}$ — Γ_2/Γ

VALUE (units 10^{-2})	EVTS	DOCUMENT ID		TECN	COMMENT
39.36±0.18 OUR FIT Error includes scale factor of 1.1.					
39.53±0.33 OUR AVERAGE					
39.86±0.04±0.99	2m	[1] ABLIKIM	21AM	BES3	$J/\psi \to \gamma\eta$
39.49±0.17±0.30	65k	ABEGG	96	SPEC	$pd \to {}^3\text{He}\eta$
• • • We do not use the following data for averages, fits, limits, etc. • • •					
38.45±0.40±0.36	14k	[2] LOPEZ	07	CLEO	$\psi(2S) \to J/\psi\eta$

[1] ABLIKIM 21AM normalize the branching ratio $(\eta \to \gamma\gamma)$ to $B(J/\psi \to \gamma\eta)$, which they measured absolutely.

[2] Not independent of other results listed for LOPEZ 07. Assuming decays of $\eta \to \gamma\gamma$, $3\pi^0$, $\pi^+\pi^-\pi^0$, $\pi^+\pi^-\gamma$, and $e^+e^-\gamma$ account for all η decays within a contribution of 0.3% to the systematic error.

$\Gamma(2\gamma)/\Gamma(\text{neutral modes})$ — $\Gamma_2/\Gamma_1 = \Gamma_2/(\Gamma_2+\Gamma_3+\Gamma_4)$

VALUE	EVTS	DOCUMENT ID		TECN	COMMENT
0.5470±0.0018 OUR FIT					
0.548 ±0.023 OUR AVERAGE Error includes scale factor of 1.5.					
0.535 ±0.018		BUTTRAM	70	OSPK	
0.59 ±0.033		BUNIATOV	67	OSPK	
• • • We do not use the following data for averages, fits, limits, etc. • • •					
0.52 ±0.09	88	ABROSIMOV	80	HLBC	
0.60 ±0.14	113	KENDALL	74	OSPK	
0.57 ±0.09		STRUGALSKI	71	HLBC	
0.579 ±0.052		FELDMAN	67	OSPK	
0.416 ±0.044		DIGIUGNO	66	CNTR	Error doubled
0.44 ±0.07		GRUNHAUS	66	OSPK	
0.39 ±0.06		[1] JONES	66	CNTR	

[1] This result from combining cross sections from two different experiments.

$\Gamma(3\pi^0)/\Gamma_{total}$ — Γ_3/Γ

VALUE (units 10^{-2})	EVTS	DOCUMENT ID		TECN	COMMENT
32.57±0.21 OUR FIT Error includes scale factor of 1.2.					
31.96±0.07±0.84	280k	[1] ABLIKIM	21AM	BES3	$J/\psi \to \gamma\eta$
• • • We do not use the following data for averages, fits, limits, etc. • • •					
34.03±0.56±0.49	1821	[2] LOPEZ	07	CLEO	$\psi(2S) \to J/\psi\eta$

[1] ABLIKIM 21AM normalize the branching ratio $(\eta \to 3\pi^0)$ to $B(J/\psi \to \gamma\eta)$, which they measured absolutely.

[2] Not independent of other results listed for LOPEZ 07. Assuming decays of $\eta \to \gamma\gamma$, $3\pi^0$, $\pi^+\pi^-\pi^0$, $\pi^+\pi^-\gamma$, and $e^+e^-\gamma$ account for all η decays within a contribution of 0.3% to the systematic error.

$\Gamma(3\pi^0)/\Gamma(\text{neutral modes})$ — $\Gamma_3/\Gamma_1 = \Gamma_3/(\Gamma_2+\Gamma_3+\Gamma_4)$

VALUE	EVTS	DOCUMENT ID		TECN	COMMENT
0.4526±0.0019 OUR FIT					
0.439 ±0.024		BUTTRAM	70	OSPK	
• • • We do not use the following data for averages, fits, limits, etc. • • •					
0.44 ±0.08	75	ABROSIMOV	80	HLBC	
0.32 ±0.09		STRUGALSKI	71	HLBC	
0.41 ±0.033		BUNIATOV	67	OSPK	Not indep. of $\Gamma(2\gamma)/\Gamma(\text{neutral modes})$
0.177 ±0.035		FELDMAN	67	OSPK	
0.209 ±0.054		DIGIUGNO	66	CNTR	Error doubled
0.29 ±0.10		GRUNHAUS	66	OSPK	

$\Gamma(3\pi^0)/\Gamma(2\gamma)$ — Γ_3/Γ_2

VALUE	EVTS	DOCUMENT ID		TECN	COMMENT
0.827±0.006 OUR FIT					
0.829±0.007 OUR AVERAGE					
0.884±0.022±0.019	1821	LOPEZ	07	CLEO	$\psi(2S) \to J/\psi\eta$
0.817±0.012±0.032	17.4k	[1] AKHMETSHIN	05	CMD2	$e^+e^- \to \phi \to \eta\gamma$
0.826±0.024		ACHASOV	00D	SND	$e^+e^- \to \phi \to \eta\gamma$
0.832±0.005±0.012		KRUSCHE	95D	SPEC	$\gamma p \to \eta p$, threshold
0.841±0.034		AMSLER	93	CBAR	$\bar{p}p \to \pi^+\pi^-\eta$ at rest
0.822±0.009		ALDE	84	GAM2	
• • • We do not use the following data for averages, fits, limits, etc. • • •					
0.796±0.016±0.016		ACHASOV	00	SND	See ACHASOV 00D
0.91 ±0.14		COX	70B	HBC	
0.75 ±0.09		DEVONS	70	OSPK	
0.88 ±0.16		BALTAY	67D	DBC	
1.1 ±0.2		CENCE	67	OSPK	
1.25 ±0.39		BACCI	63	CNTR	Inverse BR reported

[1] Uses result from AKHMETSHIN 01B.

$\Gamma(\pi^0 2\gamma)/\Gamma_{total}$ — Γ_4/Γ

Early results are summarized in the review by LANDSBERG 85.

VALUE (units 10^{-4})	CL%	EVTS	DOCUMENT ID		TECN	COMMENT
2.55±0.22 OUR FIT						
2.21±0.24±0.47		≈ 500	[1] PRAKHOV	08	CRYB	$\pi^-p \to \eta n \approx$ threshold
• • • We do not use the following data for averages, fits, limits, etc. • • •						
3.5 ±0.7 ±0.6		1.6k	[2,3] PRAKHOV	05	CRYB	See PRAKHOV 08
<8.4	90	7	ACHASOV	01D	SND	$e^+e^- \to \phi \to \eta\gamma$
<30	90	0	DAVYDOV	81	GAM2	$\pi^-p \to \eta n$

[1] PRAKHOV 08 is a reanalysis of the data of PRAKHOV 05, using for the first time the invariant-mass spectrum of the two photons.

[2] Normalized using $\Gamma(\eta \to 2\gamma)/\Gamma = 0.3943 \pm 0.0026$.

[3] This measurement and the independent analysis of the same data by KNECHT 04 both imply a lower value of $\Gamma(\pi^0 2\gamma)$ than the one obtained by ALDE 84 from $\Gamma(\pi^0 2\gamma)/\Gamma(2\gamma)$.

$\Gamma(\pi^0 2\gamma)/\Gamma(2\gamma)$ — Γ_4/Γ_2

VALUE (units 10^{-3})	EVTS	DOCUMENT ID		TECN	CHG	COMMENT
0.65±0.06 OUR FIT						
1.8 ±0.4		ALDE	84	GAM2	0	

Downloaded from https://academic.oup.com/ptep/article/2022/8/083C01/6651666 by KIT Library user on 27 September 2022

• • • We do not use the following data for averages, fits, limits, etc. • • •

2.5 ±0.6	70	BINON	82	GAM2 See ALDE 84

$\Gamma(\pi^0 2\gamma)/\Gamma(3\pi^0)$ — Γ_4/Γ_3

VALUE (units 10^{-4})	DOCUMENT ID		TECN	COMMENT
7.8±0.7 OUR FIT				
• • • We do not use the following data for averages, fits, limits, etc. • • •				
8.3±2.8±1.4	[1] KNECHT	04	CRYB	$\pi^- p \to n\eta$

[1] Independent analysis of same data as PRAKHOV 05.

$\Gamma(2\pi^0 2\gamma)/\Gamma_{total}$ — Γ_5/Γ

VALUE	CL%	DOCUMENT ID		TECN	COMMENT
$<1.2\times10^{-3}$	90	[1] NEFKENS	05A	CRYB	p(720 MeV/c) $\pi^- \to n\eta$
• • • We do not use the following data for averages, fits, limits, etc. • • •					
$<4.0\times10^{-3}$	90	BLIK	07	GAM4	$\pi^- p \to \eta n$

[1] Measurement is done in limited $\gamma\gamma$ energy range.

$\Gamma(4\gamma)/\Gamma_{total}$ — Γ_6/Γ

VALUE	CL%	DOCUMENT ID		TECN	COMMENT
$<2.8\times10^{-4}$	90	BLIK	07	GAM4	$\pi^- p \to \eta n$

$\Gamma(\text{invisible})/\Gamma(2\gamma)$ — Γ_7/Γ_2

VALUE	CL%	DOCUMENT ID		TECN	COMMENT
$<2.6\times10^{-4}$	90	[1] ABLIKIM	13	BES3	$J/\psi \to \phi\eta$
• • • We do not use the following data for averages, fits, limits, etc. • • •					
$<1.65\times10^{-3}$	90	[2] ABLIKIM	06Q	BES2	$J/\psi \to \phi\eta$

[1] Based on 225M J/ψ decays.
[2] Based on 58M J/ψ decays.

Charged modes

$\Gamma(\text{charged modes})/\Gamma_{total}$ — $\Gamma_8/\Gamma = (\Gamma_9+\Gamma_{10}+\Gamma_{11}+\Gamma_{12}+\Gamma_{16})/\Gamma$

VALUE	DOCUMENT ID
0.2804±0.0030 OUR FIT Error includes scale factor of 1.3.	

$\Gamma(\pi^+\pi^-\pi^0)/\Gamma_{total}$ — Γ_9/Γ

VALUE (units 10^{-2})	EVTS	DOCUMENT ID		TECN	COMMENT
23.02±0.25 OUR FIT Error includes scale factor of 1.2.					
23.04±0.03±0.54	60k	[1] ABLIKIM	21AM	BES3	$J/\psi \to \gamma\eta$
• • • We do not use the following data for averages, fits, limits, etc. • • •					
22.60±0.35±0.29	3915	[2] LOPEZ	07	CLEO	$\psi(2S) \to J/\psi\eta$

[1] ABLIKIM 21AM normalize the branching ratio ($\eta \to \pi^+\pi^-\pi^0$) to B($J/\psi \to \gamma\eta$), which they measured absolutely.
[2] Not independent of other results listed for LOPEZ 07. Assuming decays of $\eta \to \gamma\gamma$, $3\pi^0$, $\pi^+\pi^-\pi^0$, $\pi^+\pi^-\gamma$, and $e^+e^-\gamma$ account for all η decays within a contribution of 0.3% to the systematic error.

$\Gamma(\text{neutral modes})/\Gamma(\pi^+\pi^-\pi^0)$ — $\Gamma_1/\Gamma_9 = (\Gamma_2+\Gamma_3+\Gamma_4)/\Gamma_9$

VALUE	EVTS	DOCUMENT ID		TECN
3.13±0.05 OUR FIT Error includes scale factor of 1.3.				
3.26±0.30 OUR AVERAGE				
2.54±1.89	74	KENDALL	74	OSPK
3.4 ±1.1	29	AGUILAR-...	72B	HBC
2.83±0.80	70	[1] BLOODWO...	72B	HBC
3.6 ±0.6	244	FLATTE	67B	HBC
2.89±0.56		ALFF-...	66	HBC
3.6 ±0.8	50	KRAEMER	64	DBC
3.8 ±1.1		PAULI	64	DBC

[1] Error increased from published value 0.5 by Bloodworth (private communication).

$\Gamma(2\gamma)/\Gamma(\pi^+\pi^-\pi^0)$ — Γ_2/Γ_9

VALUE	EVTS	DOCUMENT ID		TECN	COMMENT
1.710±0.025 OUR FIT Error includes scale factor of 1.2.					
1.70 ±0.04 OUR AVERAGE					
1.704±0.032±0.026	3915	[1] LOPEZ	07	CLEO	$\psi(2S) \to J/\psi\eta$
1.61 ±0.14		ABLIKIM	06E	BES2	$e^+e^- \to J/\psi \to \eta\gamma$
1.78 ±0.10 ±0.13	1077	AMSLER	95	CBAR	$\bar{p}p \to \pi^+\pi^-\eta$ at rest
1.72 ±0.25	401	BAGLIN	69	HLBC	
1.61 ±0.39		FOSTER	65	HBC	

[1] LOPEZ 07 reports $\Gamma(\eta \to \pi^+\pi^-\pi^0)$ / $\Gamma(\eta \to 2\gamma) = \Gamma_9/\Gamma_2 = 0.587 \pm 0.011 \pm 0.009$.

$\Gamma(3\pi^0)/\Gamma(\pi^+\pi^-\pi^0)$ — Γ_3/Γ_9

VALUE	EVTS	DOCUMENT ID		TECN	COMMENT
1.415±0.023 OUR FIT Error includes scale factor of 1.2.					
1.48 ±0.05 OUR AVERAGE					
1.46 ±0.03 ±0.09		ACHASOV	06A	SND	$e^+e^- \to \eta\gamma$
1.52 ±0.04 ±0.08	23k	[1] AKHMETSHIN	01B	CMD2	$e^+e^- \to \phi \to \eta\gamma$
1.44 ±0.09 ±0.10	1627	AMSLER	95	CBAR	$\bar{p}p \to \pi^+\pi^-\eta$ at rest
$1.50\ ^{+0.15}_{-0.29}$	199	BAGLIN	69	HLBC	
$1.47\ ^{+0.20}_{-0.17}$		BULLOCK	68	HLBC	
• • • We do not use the following data for averages, fits, limits, etc. • • •					
1.3 ±0.4		BAGLIN	67B	HLBC	
0.90 ±0.24		FOSTER	65	HBC	
2.0 ±1.0		FOELSCHE	64	HBC	
0.83 ±0.32		CRAWFORD	63	HBC	

[1] AKHMETSHIN 01B uses results from AKHMETSHIN 99F.

$\Gamma(\pi^+\pi^-\pi^0)/[\Gamma(2\gamma)+\Gamma(3\pi^0)]$ — $\Gamma_9/(\Gamma_2+\Gamma_3)$

VALUE	DOCUMENT ID		TECN	COMMENT
0.320 ±0.005 OUR FIT Error includes scale factor of 1.2.				
0.304 ±0.012	ACHASOV	00D	SND	$e^+e^- \to \phi \to \eta\gamma$
• • • We do not use the following data for averages, fits, limits, etc. • • •				
0.3141±0.0081±0.0058	ACHASOV	00B	SND	See ACHASOV 00D

$\Gamma(\pi^+\pi^-\gamma)/\Gamma_{total}$ — Γ_{10}/Γ

VALUE (units 10^{-2})	EVTS	DOCUMENT ID		TECN	COMMENT
4.28±0.07 OUR FIT Error includes scale factor of 1.1.					
4.38±0.02±0.10	200k	[1] ABLIKIM	21AM	BES3	$J/\psi \to \gamma\eta$
• • • We do not use the following data for averages, fits, limits, etc. • • •					
3.96±0.14±0.14	859	[2] LOPEZ	07	CLEO	$\psi(2S) \to J/\psi\eta$

[1] ABLIKIM 21AM normalize the branching ratio ($\eta \to \pi^+\pi^-\gamma$) to B($J/\psi \to \gamma\eta$), which they measured absolutely.
[2] Not independent of other results listed for LOPEZ 07. Assuming decays of $\eta \to \gamma\gamma$, $3\pi^0$, $\pi^+\pi^-\pi^0$, $\pi^+\pi^-\gamma$, and $e^+e^-\gamma$ account for all η decays within a contribution of 0.3% to the systematic error.

$\Gamma(\pi^+\pi^-\gamma)/\Gamma(\pi^+\pi^-\pi^0)$ — Γ_{10}/Γ_9

VALUE	EVTS	DOCUMENT ID		TECN	COMMENT
0.1858±0.0025 OUR FIT					
0.1847±0.0030 OUR AVERAGE Error includes scale factor of 1.1.					
0.1856±0.0005±0.0028	200k	BABUSCI	13	KLOE	$e^+e^- \to \phi \to \eta\gamma$
0.175 ±0.007 ±0.006	859	LOPEZ	07	CLEO	$\psi(2S) \to J/\psi\eta$
• • • We do not use the following data for averages, fits, limits, etc. • • •					
0.209 ±0.004	18k	THALER	73	ASPK	
0.201 ±0.006	7250	GORMLEY	70	ASPK	
0.28 ±0.04		BALTAY	67B	DBC	
0.25 ±0.035		LITCHFIELD	67	DBC	
0.30 ±0.06		CRAWFORD	66	HBC	
0.196 ±0.041		FOSTER	65C	HBC	

$\Gamma(e^+e^-\gamma)/\Gamma_{total}$ — Γ_{11}/Γ

VALUE (units 10^{-3})	EVTS	DOCUMENT ID		TECN	COMMENT
6.9 ±0.4 OUR FIT Error includes scale factor of 1.2.					
6.7 ±0.5 OUR AVERAGE Error includes scale factor of 1.2.					
6.6 ±0.4 ±0.4	1345	BERGHAUSER	11	SPEC	$\gamma p \to p\eta$
7.8 ±0.5 ±0.8	435 ± 31	BERLOWSKI	08	WASA	$pd \to {}^3\text{He}\,\eta$
5.15±0.62±0.74	283	ACHASOV	01B	SND	$e^+e^- \to \phi \to \eta\gamma$
7.10±0.64±0.46	323	AKHMETSHIN	01	CMD2	$e^+e^- \to \phi \to \eta\gamma$
• • • We do not use the following data for averages, fits, limits, etc. • • •					
9.4 ±0.7 ±0.5	172	[1] LOPEZ	07	CLEO	$\psi(2S) \to J/\psi\eta$

[1] Not independent of other results listed for LOPEZ 07. Assuming decays of $\eta \to \gamma\gamma$, $3\pi^0$, $\pi^+\pi^-\pi^0$, $\pi^+\pi^-\gamma$, and $e^+e^-\gamma$ account for all η decays within a contribution of 0.3% to the systematic error.

$\Gamma(e^+e^-\gamma)/\Gamma(\pi^+\pi^-\gamma)$ — Γ_{11}/Γ_{10}

VALUE	EVTS	DOCUMENT ID		TECN	COMMENT
0.161±0.010 OUR FIT Error includes scale factor of 1.2.					
0.237±0.021±0.015	172	LOPEZ	07	CLEO	$\psi(2S) \to J/\psi\eta$

$\Gamma(e^+e^-\gamma)/\Gamma(\pi^+\pi^-\pi^0)$ — Γ_{11}/Γ_9

VALUE (units 10^{-2})	EVTS	DOCUMENT ID		TECN	COMMENT
2.98±0.19 OUR FIT Error includes scale factor of 1.3.					
2.1 ±0.5	80	JANE	75B	OSPK	See the erratum

$\Gamma(\text{neutral modes})/[\Gamma(\pi^+\pi^-\pi^0)+\Gamma(\pi^+\pi^-\gamma)+\Gamma(e^+e^-\gamma)]$ — $\Gamma_1/(\Gamma_9+\Gamma_{10}+\Gamma_{11}) = (\Gamma_2+\Gamma_3+\Gamma_4)/(\Gamma_9+\Gamma_{10}+\Gamma_{11})$

VALUE	EVTS	DOCUMENT ID		TECN
2.57±0.04 OUR FIT Error includes scale factor of 1.3.				
2.64±0.23		BALTAY	67B	DBC
• • • We do not use the following data for averages, fits, limits, etc. • • •				
4.5 ±1.0	280	[1] JAMES	66	HBC
3.20±1.26	53	[1] BASTIEN	62	HBC
2.5 ±1.0	10	[1] PICKUP	62	HBC

[1] These experiments are not used in the averages as they do not separate clearly $\eta \to \pi^+\pi^-\pi^0$ and $\eta \to \pi^+\pi^-\gamma$ from each other. The reported values thus probably contain some unknown fraction of $\eta \to \pi^+\pi^-\gamma$.

$\Gamma(2\gamma)/[\Gamma(\pi^+\pi^-\pi^0)+\Gamma(\pi^+\pi^-\gamma)+\Gamma(e^+e^-\gamma)]$ — $\Gamma_2/(\Gamma_9+\Gamma_{10}+\Gamma_{11})$

VALUE	EVTS	DOCUMENT ID		TECN
1.407±0.020 OUR FIT Error includes scale factor of 1.2.				
1.1 ±0.4 OUR AVERAGE				
1.51 ±0.93	75	KENDALL	74	OSPK
0.99 ±0.48		CRAWFORD	63	HBC

$\Gamma(\mu^+\mu^-\gamma)/\Gamma_{total}$ — Γ_{12}/Γ

VALUE (units 10^{-4})	EVTS	DOCUMENT ID		TECN	COMMENT
3.1±0.4 OUR FIT					
3.1±0.4	600	DZHELYADIN	80	SPEC	$\pi^- p \to \eta n$
• • • We do not use the following data for averages, fits, limits, etc. • • •					
1.5±0.75	100	BUSHNIN	78	SPEC	See DZHELYADIN 80

Downloaded from https://academic.oup.com/ptep/article/2022/8/083C01/6651666 by KIT Library user on 27 September 2022

$\Gamma(e^+e^-)/\Gamma_{total}$ — Γ_{13}/Γ

VALUE	CL%	DOCUMENT ID		TECN	COMMENT
<7 $\times 10^{-7}$	90	ACHASOV	18B	CNTR	Inverse reaction $e^+e^- \to \eta$
• • • We do not use the following data for averages, fits, limits, etc. • • •					
<2.3 $\times 10^{-6}$	90	AGAKISHIEV	14		$pp \to \eta + X$
<5.6 $\times 10^{-6}$	90	[1] AGAKISHIEV	12A	SPEC	$pp \to \eta + X$
<2.7 $\times 10^{-5}$	90	BERLOWSKI	08	WASA	$pd \to {}^3$He η
<0.77 $\times 10^{-4}$	90	BROWDER	97B	CLE2	$e^+e^- \simeq 10.5$ GeV
<2 $\times 10^{-4}$	90	WHITE	96	SPEC	$pd \to \eta\, {}^3$He
<3 $\times 10^{-4}$	90	DAVIES	74	RVUE	Uses ESTEN 67

[1] AGAKISHIEV 12A uses a data sample of 3.5 GeV proton beam collisions on liquid hydrogen target collected by the HADES detector.

$\Gamma(\mu^+\mu^-)/\Gamma_{total}$ — Γ_{14}/Γ

VALUE (units 10^{-6})	CL%	EVTS	DOCUMENT ID		TECN	COMMENT
5.8±0.8 OUR AVERAGE						
5.7±0.7±0.5		114	ABEGG	94	SPEC	$pd \to \eta\, {}^3$He
6.5±2.1		27	DZHELYADIN	80B	SPEC	$\pi^- p \to \eta n$
• • • We do not use the following data for averages, fits, limits, etc. • • •						
$5.6^{+0.6}_{-0.7}$±0.5		100	KESSLER	93	SPEC	See ABEGG 94
< 20	95	0	WEHMANN	68	OSPK	

$\Gamma(\mu^+\mu^-)/\Gamma(2\gamma)$ — Γ_{14}/Γ_2

VALUE (units 10^{-5})	DOCUMENT ID		TECN
• • • We do not use the following data for averages, fits, limits, etc. • • •			
5.9±2.2	HYAMS	69	OSPK

$\Gamma(2e^+2e^-)/\Gamma_{total}$ — Γ_{15}/Γ

VALUE (units 10^{-5})	CL%	EVTS	DOCUMENT ID		TECN	COMMENT
2.4±0.2±0.1		362	[1] AMBROSINO	11B	KLOE	$e^+e^- \to \phi \to \eta\gamma$
• • • We do not use the following data for averages, fits, limits, etc. • • •						
<9.7	90		BERLOWSKI	08	WASA	$pd \to {}^3$He η
<6.9	90		AKHMETSHIN	01	CMD2	$e^+e^- \to \phi \to \eta\gamma$

[1] This measurement is fully inclusive (includes "$2e^+2e^-\gamma$" channel).

$\Gamma(\pi^+\pi^-e^+e^-(\gamma))/\Gamma_{total}$ — Γ_{16}/Γ

VALUE (units 10^{-4})	EVTS	DOCUMENT ID		TECN	COMMENT
2.68±0.11 OUR FIT					
2.68±0.09±0.07	1555 ± 52	[1] AMBROSINO	09B	KLOE	$e^+e^- \to \phi \to \eta\gamma$
• • • We do not use the following data for averages, fits, limits, etc. • • •					
4.3 $^{+2.0}_{-1.6}$ ±0.4	16	BERLOWSKI	08	WASA	$pd \to {}^3$He η
4.3 ±1.3 ±0.4	16	BARGHOLTZ	07	CNTR	See BERLOWSKI 08
3.7 $^{+2.5}_{-1.8}$ ±0.3	4	AKHMETSHIN	01	CMD2	$e^+e^- \to \phi \to \eta\gamma$

[1] This AMBROSINO 09B value includes radiative events.

$\Gamma(e^+e^-\mu^+\mu^-)/\Gamma_{total}$ — Γ_{17}/Γ

VALUE	CL%	DOCUMENT ID		TECN	COMMENT
<1.6 $\times 10^{-4}$	90	BERLOWSKI	08	WASA	$pd \to {}^3$He η

$\Gamma(2\mu^+2\mu^-)/\Gamma_{total}$ — Γ_{18}/Γ

VALUE	CL%	DOCUMENT ID		TECN	COMMENT
<3.6 $\times 10^{-4}$	90	BERLOWSKI	08	WASA	$pd \to {}^3$He η

$\Gamma(\mu^+\mu^-\pi^+\pi^-)/\Gamma_{total}$ — Γ_{19}/Γ

VALUE	CL%	DOCUMENT ID		TECN	COMMENT
<3.6 $\times 10^{-4}$	90	BERLOWSKI	08	WASA	$pd \to {}^3$He η

$\Gamma(\pi^+e^-\overline{\nu}_e + \text{c.c.})/\Gamma(\pi^+\pi^-\pi^0)$ — Γ_{20}/Γ_9

VALUE	CL%	DOCUMENT ID		TECN	COMMENT
<7.3 $\times 10^{-4}$	90	ABLIKIM	13G	BES3	$J/\psi \to \phi\eta$

$\Gamma(\pi^+\pi^-2\gamma)/\Gamma(\pi^+\pi^-\pi^0)$ — Γ_{21}/Γ_9

VALUE	CL%	DOCUMENT ID		TECN
< 9 $\times 10^{-3}$		PRICE	67	HBC
• • • We do not use the following data for averages, fits, limits, etc. • • •				
<16 $\times 10^{-3}$	95	BALTAY	67B	DBC

$\Gamma(\pi^+\pi^-\pi^0\gamma)/\Gamma(\pi^+\pi^-\pi^0)$ — Γ_{22}/Γ_9

VALUE	CL%	EVTS	DOCUMENT ID		TECN
<0.24 $\times 10^{-2}$	90	0	THALER	73	ASPK
• • • We do not use the following data for averages, fits, limits, etc. • • •					
<1.7 $\times 10^{-2}$	90		ARNOLD	68	HLBC
<1.6 $\times 10^{-2}$	95		BALTAY	67B	DBC
<7.0 $\times 10^{-2}$			FLATTE	67	HBC
<0.9 $\times 10^{-2}$			PRICE	67	HBC

$\Gamma(\pi^0\mu^+\mu^-\gamma)/\Gamma_{total}$ — Γ_{23}/Γ

VALUE	CL%	DOCUMENT ID		TECN	COMMENT
<3 $\times 10^{-6}$	90	DZHELYADIN	81	SPEC	$\pi^- p \to \eta n$

Forbidden modes

$\Gamma(\pi^0\gamma)/\Gamma_{total}$ — Γ_{24}/Γ

Forbidden by angular momentum conservation.

VALUE	CL%	DOCUMENT ID		TECN	COMMENT
<9 $\times 10^{-5}$	90	NEFKENS	05A	CRYB	p(720 MeV/c) $\pi^- \to n\eta$

$\Gamma(\pi^+\pi^-)/\Gamma_{total}$ — Γ_{25}/Γ

Forbidden by P and CP invariance.

VALUE	CL%	EVTS	DOCUMENT ID		TECN	COMMENT
< 4.4 $\times 10^{-6}$	90	83M	[1] BABUSCI	20A	KLOE	$e^+e^- \to \phi \to \eta\gamma$
• • • We do not use the following data for averages, fits, limits, etc. • • •						
< 5.3 $\times 10^{-17}$			[2] ZHEVLAKOV	19	THEO	from nEDM limits
< 1.6 $\times 10^{-5}$	90	25M	AAIJ	17D	LHCB	in $D \to \pi\pi\pi$ decays
< 3.9 $\times 10^{-4}$	90	225M	ABLIKIM	11G	BES3	$e^+e^- \to J/\psi \to \eta\gamma$
< 1.3 $\times 10^{-5}$	90	16M	AMBROSINO	05A	KLOE	$e^+e^- \to \phi \to \eta\gamma$
< 3.3 $\times 10^{-4}$	90		AKHMETSHIN	99B	CMD2	$e^+e^- \to \phi \to \eta\gamma$
< 9 $\times 10^{-4}$	90		AKHMETSHIN	97C	CMD2	See AKHMETSHIN 99B
<15 $\times 10^{-4}$		0	THALER	73	ASPK	

[1] BABUSCI 20A combines new data with the previous AMBROSINO 05A data, and thus supersedes AMBROSINO 05A.

[2] ZHEVLAKOV 19 derives the value from the experimental limits of nEDM by a calculation using an effective Lagrangian.

$\Gamma(2\pi^0)/\Gamma_{total}$ — Γ_{26}/Γ

Forbidden by P and CP invariance.

VALUE	CL%	EVTS	DOCUMENT ID		TECN	COMMENT
<3.5 $\times 10^{-4}$	90		BLIK	07	GAM4	$\pi^- p \to \eta n$
• • • We do not use the following data for averages, fits, limits, etc. • • •						
<2.7 $\times 10^{-17}$			[1] ZHEVLAKOV	19	THEO	from nEDM limits
<6.9 $\times 10^{-4}$	90	225M	ABLIKIM	11G	BES3	$e^+e^- \to J/\psi \to \eta\gamma$
<4.3 $\times 10^{-4}$	90		AKHMETSHIN	99C	CMD2	$e^+e^- \to \phi \to \eta\gamma$
<6 $\times 10^{-4}$	90		[2] ACHASOV	98	SND	$e^+e^- \to \phi \to \eta\gamma$

[1] ZHEVLAKOV 19 derives the value from the experimental limits of nEDM by a calculation using an effective Lagrangian.

[2] ACHASOV 98 observes one event in a $\pm 3\sigma$ region around the η mass, while a Monte Carlo calculation gives 10 ± 5 events. The limit here is the Poisson upper limit for one observed event and no background.

$\Gamma(2\pi^0\gamma)/\Gamma_{total}$ — Γ_{27}/Γ

Forbidden by C invariance.

VALUE	CL%	DOCUMENT ID		TECN	CHG	COMMENT
< 5 $\times 10^{-4}$	90	NEFKENS	05	CRYB	0	p(720 MeV/c) $\pi^- \to n\eta$
• • • We do not use the following data for averages, fits, limits, etc. • • •						
<17 $\times 10^{-4}$	90	BLIK	07	GAM4		$\pi^- p \to \eta n$

$\Gamma(3\pi^0\gamma)/\Gamma_{total}$ — Γ_{28}/Γ

Forbidden by C invariance.

VALUE	CL%	DOCUMENT ID		TECN	CHG	COMMENT
< 6 $\times 10^{-5}$	90	NEFKENS	05	CRYB	0	p(720 MeV/c) $\pi^- \to n\eta$
• • • We do not use the following data for averages, fits, limits, etc. • • •						
<24 $\times 10^{-5}$	90	BLIK	07	GAM4		$\pi^- p \to \eta n$

$\Gamma(3\gamma)/\Gamma_{total}$ — Γ_{29}/Γ

Forbidden by C invariance.

VALUE	CL%	DOCUMENT ID		TECN	COMMENT
• • • We do not use the following data for averages, fits, limits, etc. • • •					
<16 $\times 10^{-5}$	90	BLIK	07	GAM4	$\pi^- p \to \eta n$
< 4 $\times 10^{-5}$	90	NEFKENS	05A	CRYB	p(720 MeV/c) $\pi^- \to n\eta$

$\Gamma(3\gamma)/\Gamma(2\gamma)$ — Γ_{29}/Γ_2

VALUE	CL%	DOCUMENT ID		TECN	CHG
<1.2 $\times 10^{-3}$	95	ALDE	84	GAM2	0

$\Gamma(3\gamma)/\Gamma(3\pi^0)$ — Γ_{29}/Γ_3

VALUE	CL%	DOCUMENT ID		TECN	COMMENT
<4.9 $\times 10^{-5}$	90	ALOISIO	04	KLOE	$\phi \to \eta\gamma$

$\Gamma(4\pi^0)/\Gamma_{total}$ — Γ_{30}/Γ

Forbidden by P and CP invariance.

VALUE	CL%	DOCUMENT ID		TECN	COMMENT
< 6.9 $\times 10^{-7}$	90	PRAKHOV	00	CRYB	$\pi^- p \to n\eta$, 720 MeV/c
• • • We do not use the following data for averages, fits, limits, etc. • • •					
<200 $\times 10^{-7}$	90	BLIK	07	GAM4	$\pi^- p \to \eta n$

$\Gamma(\pi^0e^+e^-)/\Gamma_{total}$ — Γ_{31}/Γ

C parity forbids this to occur as a single-photon process.

VALUE	CL%	DOCUMENT ID		TECN	COMMENT
• • • We do not use the following data for averages, fits, limits, etc. • • •					
< 7.5 $\times 10^{-6}$	90	ADLARSON	18C	WASA	$pd \to \eta\, {}^3$He
< 1.6 $\times 10^{-4}$	90	MARTYNOV	76	HLBC	
< 8.4 $\times 10^{-4}$	90	BAZIN	68	DBC	
<70 $\times 10^{-4}$		RITTENBERG	65	HBC	

Downloaded from https://academic.oup.com/ptep/article/2022/8/083C01/6651666 by KIT Library user on 27 September 2022

$\Gamma(\pi^0 e^+ e^-)/\Gamma(\pi^+\pi^-\pi^0)$ — Γ_{31}/Γ_9

C parity forbids this to occur as a single-photon process.

VALUE	CL%	DOCUMENT ID		TECN	COMMENT
< 3.28 × 10⁻⁵	90	ADLARSON	18C	WASA	$pd \to \eta\, {}^3$He
• • • We do not use the following data for averages, fits, limits, etc. • • •					
$< 1.9 \times 10^{-4}$	90	JANE	75	OSPK	
$< 42 \times 10^{-4}$	90	BAGLIN	67	HLBC	
$< 16 \times 10^{-4}$	90	BILLING	67	HLBC	
$< 77 \times 10^{-4}$		FOSTER	65B	HBC	
$<110 \times 10^{-4}$		PRICE	65	HBC	

$\Gamma(\pi^0\mu^+\mu^-)/\Gamma_{total}$ — Γ_{32}/Γ

C parity forbids this to occur as a single-photon process.

VALUE	CL%	DOCUMENT ID		TECN	COMMENT
$< 5 \times 10^{-6}$	90	DZHELYADIN	81	SPEC	$\pi^- p \to \eta n$
• • • We do not use the following data for averages, fits, limits, etc. • • •					
$<500 \times 10^{-6}$		WEHMANN	68	OSPK	

$[\Gamma(\mu^+ e^-) + \Gamma(\mu^- e^+)]/\Gamma_{total}$ — Γ_{33}/Γ

Forbidden by lepton family number conservation.

VALUE	CL%	DOCUMENT ID		TECN	COMMENT
$<6 \times 10^{-6}$	90	WHITE	96	SPEC	$pd \to \eta\, {}^3$He

η C-NONCONSERVING DECAY PARAMETERS

$\pi^+\pi^-\pi^0$ LEFT-RIGHT ASYMMETRY PARAMETER

Measurements with an error > 1.0×10^{-2} have been omitted.

VALUE (units 10^{-2})	EVTS	DOCUMENT ID		TECN
$0.09^{+0.11}_{-0.12}$ OUR AVERAGE				
$+0.09 \pm 0.10^{+0.09}_{-0.14}$	1.34M	AMBROSINO	08D	KLOE
0.28 ± 0.26	165k	JANE	74	OSPK
-0.05 ± 0.22	220k	LAYTER	72	ASPK
• • • We do not use the following data for averages, fits, limits, etc. • • •				
1.5 ± 0.5	37k	[1] GORMLEY	68C	ASPK

[1] The GORMLEY 68C asymmetry is probably due to unmeasured ($\mathbf{E} \times \mathbf{B}$) spark chamber effects. New experiments with ($\mathbf{E} \times \mathbf{B}$) controls don't observe an asymmetry.

$\pi^+\pi^-\pi^0$ SEXTANT ASYMMETRY PARAMETER

Measurements with an error > 2.0×10^{-2} have been omitted.

VALUE (units 10^{-2})	EVTS	DOCUMENT ID		TECN
$0.12^{+0.10}_{-0.11}$ OUR AVERAGE				
$+0.08 \pm 0.10^{+0.08}_{-0.13}$	1.34M	AMBROSINO	08D	KLOE
0.20 ± 0.25	165k	JANE	74	OSPK
0.10 ± 0.22	220k	LAYTER	72	ASPK
0.5 ± 0.5	37k	GORMLEY	68C	WIRE

$\pi^+\pi^-\pi^0$ QUADRANT ASYMMETRY PARAMETER

VALUE (units 10^{-2})	EVTS	DOCUMENT ID		TECN
-0.09 ± 0.09 OUR AVERAGE				
$-0.05 \pm 0.10^{+0.03}_{-0.05}$	1.34M	AMBROSINO	08D	KLOE
-0.30 ± 0.25	165k	JANE	74	OSPK
-0.07 ± 0.22	220k	LAYTER	72	ASPK

$\pi^+\pi^-\gamma$ LEFT-RIGHT ASYMMETRY PARAMETER

Measurements with an error > 2.0×10^{-2} have been omitted.

VALUE (units 10^{-2})	EVTS	DOCUMENT ID		TECN
0.9 ± 0.4 OUR AVERAGE				
1.2 ± 0.6	35k	JANE	74B	OSPK
0.5 ± 0.6	36k	THALER	72	ASPK
1.22 ± 1.56	7257	GORMLEY	70	ASPK

$\pi^+\pi^-\gamma$ PARAMETER β (D-wave)

Sensitive to a D-wave contribution: $dN/d\cos\theta = \sin^2\theta\ (1 + \beta\ \cos^2\theta)$.

VALUE	EVTS	DOCUMENT ID		TECN
-0.02 ± 0.07 OUR AVERAGE Error includes scale factor of 1.3.				
0.11 ± 0.11	35k	JANE	74B	OSPK
-0.060 ± 0.065	7250	GORMLEY	70	WIRE
• • • We do not use the following data for averages, fits, limits, etc. • • •				
0.12 ± 0.06		[1] THALER	72	ASPK

[1] The authors don't believe this indicates D-wave because the dependence of β on the γ energy is inconsistent with the theoretical prediction. A $\cos^2\theta$ dependence can also come from P- and F-wave interference.

η CP-NONCONSERVING DECAY PARAMETER

$\pi^+\pi^- e^+ e^-$ DECAY-PLANE ASYMMETRY PARAMETER A_ϕ

In the η rest frame, the total momentum of the e^+e^- pair is equal and opposite to that of the $\pi^+\pi^-$ pair. Let $\hat{z}$ be the unit vector along the momentum of the e^+e^- pair; let $\hat{n}_{ee}$ and $\hat{n}_{\pi\pi}$ be the unit vectors normal to the e^+e^- and $\pi^+\pi^-$ planes; and let ϕ be the angle between the two normals. Then

$$\sin\phi\,\cos\phi = [(\hat{n}_{ee} \times \hat{n}_{\pi\pi}) \cdot \hat{z}]\,(\hat{n}_{ee} \cdot \hat{n}_{\pi\pi})\ ,$$

and

$$A_\phi \equiv \frac{N_{\sin\phi\cos\phi>0} - N_{\sin\phi\cos\phi<0}}{N_{\sin\phi\cos\phi>0} + N_{\sin\phi\cos\phi<0}}\ .$$

VALUE (units 10^{-2})	EVTS	DOCUMENT ID		TECN	COMMENT
$-0.6 \pm 2.5 \pm 1.8$	1555 ± 52	AMBROSINO	09B	KLOE	$e^+e^- \to \phi \to \eta\gamma$

ENERGY DEPENDENCE OF $\eta \to 3\pi$ DALITZ PLOTS

PARAMETERS FOR $\eta \to \pi^+\pi^-\pi^0$

See the "Note on η Decay Parameters," page 1454, in our 1994 edition (Physical Review **D50** 1173 (1994)). The following experiments fit to one or more of the coefficients a, b, c, d, e, f or g for $|\text{matrix element}|^2 = 1 + ay + by^2 + cx + dx^2 + exy + fy^3 + gx^2y$.

VALUE	EVTS	DOCUMENT ID		TECN	COMMENT
• • • We do not use the following data for averages, fits, limits, etc. • • •					
	4.7M	[1] ANASTASI	16A	KLOE	$e^+e^- \to \phi \to \eta\gamma$
	79k	ABLIKIM	15G	BES3	$e^+e^- \to J/\psi \to \gamma\eta$
	174k	ADLARSON	14A	WASA	$pd \to \eta\, {}^3$He
	1.34M	AMBROSINO	08D	KLOE	
	3230	[2] ABELE	98D	CBAR	$\bar{p}p \to \pi^0\pi^0\eta$ at rest
	1077	[3] AMSLER	95	CBAR	$\bar{p}p \to \pi^+\pi^-\eta$ at rest
	81k	LAYTER	73	ASPK	
	220k	LAYTER	72	ASPK	
	1138	CARPENTER	70	HBC	
	349	DANBURG	70	DBC	
	7250	GORMLEY	70	WIRE	
	526	BAGLIN	69	HLBC	
	7170	CNOPS	68	OSPK	
	37k	GORMLEY	68C	WIRE	
	1300	CLPWY	66	HBC	
	705	LARRIBE	66	HBC	

[1] ANASTASI 16A measure the Dalitz parameters a, b, d, f, and g. This is the first measurement of g.
[2] ABELE 98D obtains $a = -1.22 \pm 0.07$ and $b = 0.22 \pm 0.11$ when c (or d) is fixed at 0.06.
[3] AMSLER 95 fits to $(1+ay+by^2)$ and obtains $a = -0.94 \pm 0.15$ and $b = 0.11 \pm 0.27$.

α PARAMETER FOR $\eta \to 3\pi^0$

See the "Note on η Decay Parameters" in our 1994 edition, Phys. Rev. **D50**, 1 August 1994, Part I, p. 1454. The value here is of α in $|\text{matrix element}|^2 = 1 + 2\alpha z$.

VALUE	EVTS	DOCUMENT ID		TECN	COMMENT
-0.0288 ± 0.0012 OUR AVERAGE Error includes scale factor of 1.1.					
$-0.0265 \pm 0.0010 \pm 0.0009$	7M	PRAKHOV	18	CRYB	$\gamma p \to p\eta$
$-0.055 \pm 0.014 \pm 0.004$	33k	ABLIKIM	15G	BES3	$e^+e^- \to J/\psi \to \gamma\eta$
$-0.0301 \pm 0.0035^{+0.0022}_{-0.0035}$	512k	AMBROSINO	10A	KLOE	$e^+e^- \to \phi \to \eta\gamma$
$-0.027 \pm 0.008 \pm 0.005$	120k	[1] ADOLPH	09	WASA	$pp \to pp\eta$
$-0.0322 \pm 0.0012 \pm 0.0022$	3M	[2] PRAKHOV	09	CRYB	$\gamma p \to p\eta$
$-0.032 \pm 0.002 \pm 0.002$	1.8M	[2] UNVERZAGT	09	CRYB	$\gamma p \to p\eta$
$-0.026 \pm 0.010 \pm 0.010$	75k	BASHKANOV	07	WASA	$pp \to pp\eta$
$-0.010 \pm 0.021 \pm 0.010$	12k	ACHASOV	01C	SND	$e^+e^- \to \phi \to \eta\gamma$
-0.031 ± 0.004	1M	TIPPENS	01	CRYB	$\pi^- p \to n\eta$, 720 MeV
$-0.052 \pm 0.017 \pm 0.010$	98k	ABELE	98C	CBAR	$\bar{p}p \to 5\pi^0$
-0.022 ± 0.023	50k	ALDE	84	GAM2	
• • • We do not use the following data for averages, fits, limits, etc. • • •					
$-0.038 \pm 0.003\ ^{+0.012}_{-0.008}$	1.34M	[3] AMBROSINO	08D	KLOE	
-0.32 ± 0.37	192	BAGLIN	70	HLBC	

[1] This ADOLPH 09 result is independent of the BASHKANOV 07 result.
[2] The PRAKHOV 09 and UNVERZAGT 09 results are independent.
[3] This AMBROSINO 08D value is an indirect result using $\eta \to \pi^+\pi^0\pi^-$ events and a rescattering matrix that mixes isospin decay amplitudes.

PARAMETER Λ IN $\eta \to \ell^+\ell^-\gamma$ DECAY

In the pole approximation the electromagnetic transition form factor for a resonance of mass M is given by the expression:

$$|F|^2 = (1 - M^2_{\ell\ell}/\Lambda^2)^{-2},$$

where for the parameter Λ vector dominance predicts $\Lambda \approx 0.770$ GeV.

VALUE (GeV/c²)	EVTS	DOCUMENT ID		TECN	COMMENT
0.716 ± 0.011 OUR AVERAGE					
0.712 ± 0.020		[1] ADLARSON	17B	A2MM	$\gamma p \to \eta p$
$0.7191 \pm 0.0125 \pm 0.0093$		[2] ARNALDI	16	NA60	400 GeV p-A collisions
$0.716 \pm 0.031 \pm 0.009$		[3] ARNALDI	09	NA60	158A In−In collisions
0.72 ± 0.09	600	DZHELYADIN	80	SPEC	$\pi^- p \to \eta n$, $\eta \to \gamma\mu^+\mu^-$

[1] ADLARSON 17B reports $\Lambda^{-2}(\eta \to \gamma e^+e^-) = 1.97 \pm 0.11$ (GeV/c²)$^{-2}$ which we converted to the quoted Λ value and uncertainty (total=statistical plus systematic).
[2] ARNALDI 16 reports $\Lambda^{-2}(\eta \to \gamma\mu^+\mu^-) = 1.934 \pm 0.067 \pm 0.050$ (GeV/c²)$^{-2}$ which we converted to the quoted Λ value.
[3] ARNALDI 09 reports $\Lambda^{-2}(\eta \to \gamma\mu^+\mu^-) = 1.95 \pm 0.17 \pm 0.05$ (GeV/c²)$^{-2}$ which we converted to the quoted Λ value.

Downloaded from https://academic.oup.com/ptep/article/2022/8/083C01/6651666 by KIT Library user on 27 September 2022

η REFERENCES

ABLIKIM	21AM	PR D104 092004	M. Ablikim et al.	(BESIII Collab.)
BABUSCI	20A	JHEP 2010 047	D. Babusci et al.	(KLOE-2 Collab.)
ZHEVLAKOV	19	PR D99 031703	A.S. Zhevlakov et al.	(TMSK, MAINZ, TUBIN+)
ACHASOV	18B	PR D98 052007	M.N. Achasov et al.	(SND Collab.)
ADLARSON	18C	PL B784 378	P. Adlarson et al.	(WASA-at-COSY Collab.)
PRAKHOV	18	PR C97 065203	S. Prakhov et al.	(A2 Collab. at MAMI)
AAIJ	17D	PL B764 233	R. Aaij et al.	(LHCb Collab.)
ADLARSON	17B	PR C95 035208	P. Adlarson et al.	(A2 Collab. at MAMI)
ANASTASI	16A	JHEP 1605 019	A. Anastasi et al.	(KLOE-2 Collab.)
ARNALDI	16	PL B757 437	R. Arnaldi et al.	(NA60 Collab.)
ABLIKIM	15G	PR D92 012014	M. Ablikim et al.	(BESIII Collab.)
ADLARSON	14A	PR C90 045207	P. Adlarson et al.	(WASA-at-COSY Collab.)
AGAKISHIEV	14	PL B731 265	G. Agakishiev et al.	(HADES Collab.)
NEFKENS	14	PR C90 025206	B.M.K. Nefkens et al.	(A2 Collab. at MAMI)
NIKOLAEV	14	EPJ A50 58	A. Nikolaev et al.	(MAMI-B, MAINZ, BONN)
ABLIKIM	13	PR D87 012009	M. Ablikim et al.	(BESIII Collab.)
ABLIKIM	13G	PR D87 032006	M. Ablikim et al.	(BESIII Collab.)
BABUSCI	13	PL B718 910	D. Babusci et al.	(KLOE/KLOE-2 Collab.)
BABUSCI	13A	JHEP 1301 119	D. Babusci et al.	(KLOE-2 Collab.)
AGAKISHIEV	12A	EPJ A48 64	G. Agakishiev et al.	(HADES Collab.)
GOSLAWSKI	12	PR D85 112011	P. Goslawski et al.	(COSY-ANKE Collab.)
ABLIKIM	11G	PR D84 032006	M. Ablikim et al.	(BESIII Collab.)
AMBROSINO	11B	PL B702 324	F. Ambrosino et al.	(KLOE Collab.)
BERGHAUSER	11	PL B701 562	H. Berghauser et al.	(GIES, UCLA, GUTE)
AMBROSINO	10A	PL B694 16	F. Ambrosino et al.	(KLOE Collab.)
ADOLPH	09	PL B677 24	C. Adolph et al.	(WASA-at-COSY Collab.)
AMBROSINO	09B	PL B675 283	F. Ambrosino et al.	(KLOE Collab.)
ARNALDI	09	PL B677 260	R. Arnaldi et al.	(NA60 Collab.)
PRAKHOV	09	PR C79 035204	S. Prakhov et al.	(MAMI-C Crystal Ball Collab.)
UNVERZAGT	09	EPJ A39 169	M. Unverzagt et al.	(MAMI-B Crystal Ball Collab.)
AMBROSINO	08D	JHEP 0805 006	F. Ambrosino et al.	(DAPHNE KLOE Collab.)
BERLOWSKI	08	PR D77 032004	M. Berlowski et al.	(CELSIUS/WASA Collab.)
PRAKHOV	08	PR C78 015206	S. Prakhov et al.	(BNL Crystal Ball Collab.)
RODRIGUES	08	PRL 101 012301	T.E. Rodrigues et al.	(USP, FESP, UNESP+)
AMBROSINO	07B	JHEP 0712 073	F. Ambrosino et al.	(KLOE Collab.)
BARGHOLTZ	07	PL B644 299	Chr. Bargholtz et al.	(CELSIUS/WASA Collab.)
BASHKANOV	07	PR C76 048201	M. Bashkanov et al.	(CELSIUS/WASA Collab.)
BLIK	07	PAN 70 693	A.M. Blik et al.	(GAMS Collab.)
		Translated from YAF 70 724.		
LOPEZ	07	PRL 99 122001	A. Lopez et al.	(CLEO Collab.)
MILLER	07	PRL 99 122002	D.H. Miller et al.	(CLEO Collab.)
ABLIKIM	06E	PR D73 052008	M. Ablikim et al.	(BES Collab.)
ABLIKIM	06Q	PRL 97 202002	M. Ablikim et al.	(BES Collab.)
ACHASOV	06A	PR D74 014016	M.N. Achasov et al.	(SND Collab.)
ABDEL-BARY	05	PL B619 281	M. Abdel-Bary et al.	(GEM Collab.)
AKHMETSHIN	05	PL B605 26	R.R. Akhmetshin et al.	(Novosibirsk CMD-2 Collab.)
AMBROSINO	05A	PL B606 276	F. Ambrosino et al.	(KLOE Collab.)
NEFKENS	05	PRL 94 041601	B.M.K. Nefkens et al.	(BNL Crystal Ball Collab.)
NEFKENS	05A	PR C72 035212	B.M.K. Nefkens et al.	(BNL Crystal Ball Collab.)
PRAKHOV	05	PR C72 025201	S. Prakhov et al.	(BNL Crystal Ball Collab.)
ALOISIO	04	PL B591 49	A. Aloisio et al.	(KLOE Collab.)
KNECHT	04	PL B589 14	N. Knecht et al.	
LAI	02	PL B533 196	A. Lai et al.	(CERN NA48 Collab.)
NEFKENS	02	PS T99 114	B.M.K. Nefkens, J.W. Price	(UCLA)
ACHASOV	01B	PL B504 275	M.N. Achasov et al.	(Novosibirsk SND Collab.)
ACHASOV	01C	JETPL 73 451	M.N. Achasov et al.	(Novosibirsk SND Collab.)
		Translated from ZETFP 73 511.		
ACHASOV	01D	NP B600 3	M.N. Achasov et al.	(Novosibirsk SND Collab.)
AKHMETSHIN	01	PL B501 191	R.R. Akhmetshin et al.	(Novosibirsk CMD-2 Collab.)
AKHMETSHIN	01B	PL B509 217	R.R. Akhmetshin et al.	(Novosibirsk CMD-2 Collab.)
TIPPENS	01	PRL 87 192001	W.B. Tippens et al.	(BNL Crystal Ball Collab.)
ACHASOV	00	EPJ C12 25	M.N. Achasov et al.	(Novosibirsk SND Collab.)
ACHASOV	00B	JETP 90 17	M.N. Achasov et al.	(Novosibirsk SND Collab.)
		Translated from ZETF 117 22.		
ACHASOV	00D	JETPL 72 282	M.N. Achasov et al.	(Novosibirsk SND Collab.)
		Translated from ZETFP 72 411.		
PRAKHOV	00	PRL 84 4802	S. Prakhov et al.	(BNL Crystal Ball Collab.)
AKHMETSHIN	99B	PL B462 371	R.R. Akhmetshin et al.	(Novosibirsk CMD-2 Collab.)
AKHMETSHIN	99C	PL B462 380	R.R. Akhmetshin et al.	(Novosibirsk CMD-2 Collab.)
AKHMETSHIN	99F	PL B460 242	R.R. Akhmetshin et al.	(Novosibirsk CMD-2 Collab.)
ABELE	98C	PL B417 193	A. Abele et al.	(Crystal Barrel Collab.)
ABELE	98D	PL B417 197	A. Abele et al.	(Crystal Barrel Collab.)
ACHASOV	98	PL B425 388	M.N. Achasov et al.	(Novosibirsk SND Collab.)
AKHMETSHIN	97C	PL B415 452	R.R. Akhmetshin et al.	(Novosibirsk CMD-2 Collab.)
BROWDER	97B	PR D56 5359	T.E. Browder et al.	(CLEO Collab.)
ABEGG	96	PR D53 11	R. Abegg et al.	(Saturne SPES2 Collab.)
WHITE	96	PR D53 6658	D.B. White et al.	(Saturne SPES2 Collab.)
AMSLER	95	PL B346 203	C. Amsler et al.	(Crystal Barrel Collab.)
KRUSCHE	95D	ZPHY A351 237	B. Krusche et al.	(TAPS + A2 Collab.)
ABEGG	94	PR D50 92	R. Abegg et al.	(Saturne SPES2 Collab.)
PDG	94	PR D50 1173	L. Montanet et al.	(CERN, LBL, BOST+)
AMSLER	93	ZPHY C58 175	C. Amsler et al.	(Crystal Barrel Collab.)
KESSLER	93	PRL 70 892	R.S. Kessler et al.	(Saturne SPES2 Collab.)
PLOUIN	92	PL B276 526	F. Plouin et al.	(Saturne SPES4 Collab.)
BARU	90	ZPHY C48 581	S.E. Baru et al.	(MD-1 Collab.)
ROE	90	PR D41 17	N.A. Roe et al.	(ASP Collab.)
WILLIAMS	88	PR D38 1365	D.A. Williams et al.	(Crystal Ball Collab.)
AIHARA	86	PR D33 844	H. Aihara et al.	(TPC-2γ Collab.)
BARTEL	85E	PL 160B 421	W. Bartel et al.	(JADE Collab.)
LANDSBERG	85	PRPL 128 301	L.G. Landsberg	(SERP)
ALDE	84	ZPHY C25 225	D.M. Alde et al.	(SERP, BELG, LAPP)
Also		SJNP 40 918	D.M. Alde et al.	(SERP, BELG, LAPP)
		Translated from YAF 40 1447.		
WEINSTEIN	83	PR D28 2896	A.J. Weinstein et al.	(Crystal Ball Collab.)
BINON	82	SJNP 36 391	F.G. Binon et al.	(SERP, BELG, LAPP+)
		Translated from YAF 36 670.		
Also		NC 71A 497	F.G. Binon et al.	(SERP, BELG, LAPP+)
DAVYDOV	81	LNC 32 45	V.A. Davydov et al.	(SERP, BELG, LAPP+)
Also		SJNP 33 825	V.A. Davydov et al.	(SERP, BELG, LAPP+)
		Translated from YAF 33 1534.		
DZHELYADIN	81	PL 105B 239	R.I. Dzhelyadin et al.	(SERP)
Also		SJNP 33 822	R.I. Dzhelyadin et al.	(SERP)
		Translated from YAF 33 1529.		
ABROSIMOV	80	SJNP 31 195	A.T. Abrosimov et al.	(JINR)
		Translated from YAF 31 371.		
DZHELYADIN	80	PL 94B 548	R.I. Dzhelyadin et al.	(SERP)
Also		SJNP 32 516	R.I. Dzhelyadin et al.	(SERP)
		Translated from YAF 32 998.		
DZHELYADIN	80B	PL 97B 471	R.I. Dzhelyadin et al.	(SERP)
Also		SJNP 32 518	R.I. Dzhelyadin et al.	(SERP)
		Translated from YAF 32 1002.		
BUSHNIN	78	PL 79B 147	Y.B. Bushnin et al.	(SERP)
Also		SJNP 28 775	Y.B. Bushnin et al.	(SERP)
		Translated from YAF 28 1507.		
MARTYNOV	76	SJNP 23 48	A.S. Martynov et al.	(JINR)
		Translated from YAF 23 93.		
JANE	75	PL 59B 99	M.R. Jane et al.	(RHEL, LOWC)
JANE	75B	PL 59B 103	M.R. Jane et al.	(RHEL, LOWC)
Also		PL 73B 503	M.R. Jane	
		Erratum in private communication.		
BROWMAN	74B	PRL 32 1067	A. Browman et al.	(CORN, BING)
DAVIES	74	NC 24A 324	J.D. Davies, J.G. Guy, R.K.P. Zia	(BIRM, RHEL+)
DUANE	74	PRL 32 425	A. Duane et al.	(LOIC, SHMP)
JANE	74	PL 48B 260	M.R. Jane et al.	(RHEL, LOWC, SUSS)
JANE	74B	PL 48B 265	M.R. Jane et al.	(RHEL, LOWC, SUSS)
KENDALL	74	NC 21A 387	B.N. Kendall et al.	(BROW, BARI, MIT)
LAYTER	73	PR D7 2565	J.G. Layter et al.	(COLU)
THALER	73	PR D7 2569	J.J. Thaler et al.	(COLU)
AGUILAR-...	72B	PR D6 29	M. Aguilar-Benitez et al.	(BNL)
BLOODWO...	72B	NP B39 525	I.J. Bloodworth et al.	(TNTO)
LAYTER	72	PRL 29 316	J.G. Layter et al.	(COLU)
THALER	72	PRL 29 313	J.J. Thaler et al.	(COLU)
BASILE	71D	NC 3A 796	M. Basile et al.	(CERN, BGNA, STRB)
STRUGALSKI	71	NP B27 429	Z.S. Strugalski et al.	(JINR)
BAGLIN	70	NP B22 66	C. Baglin et al.	(EPOL, MADR, STRB)
BUTTRAM	70	PRL 25 1358	M.T. Buttram, M.N. Kreisler, R.E. Mischke	(PRIN)
CARPENTER	70	PR D1 1303	D.W. Carpenter et al.	(DUKE)
COX	70B	PRL 24 534	B. Cox, L. Fortney, J.P. Golson	(DUKE)
DANBURG	70	PR D2 2564	J.S. Danburg et al.	(LRL)
DEVONS	70	PR D1 1936	S. Devons et al.	(COLU, SYRA)
GORMLEY	70	PR D2 501	M. Gormley et al.	(COLU, BNL)
Also		Thesis Nevis 181	M. Gormley	(COLU)
BAGLIN	69	PL 29B 445	C. Baglin et al.	(EPOL, UCB, MADR, STRB)
Also		NP B22 66	C. Baglin et al.	(EPOL, MADR, STRB)
HYAMS	69	PL 29B 128	B.D. Hyams et al.	(CERN, MPIM)
ARNOLD	68	PL 27B 466	R.G. Arnold et al.	(STRB, MADR, EPOL+)
BAZIN	68	PRL 20 895	M.J. Bazin et al.	(PRIN, QUKI)
BULLOCK	68	PL 27B 402	F.W. Bullock et al.	(LOUC)
CNOPS	68	PRL 21 1609	A.M. Cnops et al.	(BNL, ORNL, UCND+)
GORMLEY	68C	PRL 21 402	M. Gormley et al.	(COLU, BNL)
WEHMANN	68	PRL 20 748	A.W. Wehmann et al.	(HARV, CASE, SLAC+)
BAGLIN	67	PL 24B 637	C. Baglin et al.	(EPOL, UCB)
BAGLIN	67B	BAPS 12 567	C. Baglin et al.	(EPOL, UCB)
BALTAY	67B	PRL 19 1498	C. Baltay et al.	(COLU, STON)
BALTAY	67D	PRL 19 1495	C. Baltay et al.	(COLU, BRAN)
BEMPORAD	67	PL 25B 380	C. Bemporad et al.	(PISA, BONN)
Also		Private Comm.	I. Ion	
BILLING	67	PL 25B 435	K.D. Billing et al.	(LOUC, OXF)
BUNIATOV	67	PL 25B 560	S.A. Bunyatov et al.	(CERN, KARL)
CENCE	67	PRL 19 1393	R.J. Cence et al.	(HAWA, LRL)
ESTEN	67	PL 24B 115	M.J. Esten et al.	(LOUC, OXF)
FELDMAN	67	PRL 18 868	M. Feldman et al.	(PENN)
FLATTE	67	PRL 18 976	S.M. Flatte	(LRL)
FLATTE	67B	PR 163 1441	S.M. Flatte, C.G. Wohl	(LRL)
LITCHFIELD	67	PL 24B 486	P.J. Litchfield et al.	(RHEL, SACL)
PRICE	67	PRL 18 1207	L.R. Price, F.S. Crawford	(LRL)
ALFF-...	66	PR 145 1072	C. Alff-Steinberger et al.	(COLU, RUTG)
CLPWY	66	PR 149 1044	C. Baltay	(SCUC, LRL, PURD, WISC, YALE)
CRAWFORD	66	PRL 16 333	F.S. Crawford, L.R. Price	(LRL)
DIGIUGNO	66	PRL 16 767	G. di Giugno et al.	(NAPL, TRST, FRAS)
GRUNHAUS	66	Thesis	J. Grunhaus	(COLU)
JAMES	66	PR 142 896	F.E. James, H.L. Kraybill	(YALE, BNL)
JONES	66	PL 23 597	W.G. Jones et al.	(LOIC, RHEL)
LARRIBE	66	PL 23 600	A. Larribe et al.	(SACL, RHEL)
FOSTER	65	PR 138 B652	M. Foster et al.	(WISC, PURD)
FOSTER	65B	Athens Conf.	M. Foster, M. Good, M. Meer	(WISC)
FOSTER	65C	Thesis	M. Foster	(WISC)
PRICE	65	PRL 15 123	L.R. Price, F.S. Crawford	(LRL)
RITTENBERG	65	PRL 15 556	A. Rittenberg, G.R. Kalbfleisch	(LRL, BNL)
FOELSCHE	64	PR 134 B1138	H.W.J. Foelsche, H.L. Kraybill	(YALE)
KRAEMER	64	PR 136 B496	R.W. Kraemer et al.	(JHU, NWES, WOOD)
PAULI	64	PL 13 351	E. Pauli, A. Muller	(SACL)
BACCI	63	PRL 11 37	C. Bacci et al.	(ROMA, FRAS)
CRAWFORD	63	PRL 10 546	F.S.Jr. Crawford, L.J. Lloyd, E.C. Fowler	(LRL+)
Also		PRL 16 907	F.S. Crawford, L.J. Lloyd, E.C. Fowler	(LRL+)
ALFF-...	62	PRL 9 322	C. Alff-Steinberger et al.	(COLU, RUTG)
BASTIEN	62	PRL 8 114	P.L. Bastien et al.	(LRL)
PICKUP	62	PRL 8 329	E. Pickup, D.K. Robinson, E.O. Salant	(CNRC+)

$f_0(500)$

$I^G(J^{PC}) = 0^+(0^{++})$

also known as σ; was $f_0(600)$

See the related review(s):

Scalar Mesons below 1 GeV

$f_0(500)$ T-MATRIX POLE $\sqrt{s}$

Note that $\Gamma \approx 2\ \mathrm{Im}(\sqrt{s_{\mathrm{pole}}})$.

VALUE (MeV)	*DOCUMENT ID*		*TECN*	*COMMENT*
(400–550)−i(200–350) OUR ESTIMATE (see Fig. 64.3 in the review)				
• • • We do not use the following data for averages, fits, limits, etc. • • •				
$(410 \pm 20) - i(240 \pm 15)$	SARANTSEV	21	RVUE	$J/\psi(1S) \to \gamma(\pi\pi, K\overline{K}, \eta\eta, \omega\phi)$
$(512 \pm 15) - i(188 \pm 12)$	[1] ABLIKIM	17	BES3	$J/\psi \to \gamma 3\pi$
$(440 \pm 10) - i(238 \pm 10)$	[2] ALBALADEJO	12	RVUE	Compilation
$(445 \pm 25) - i(278^{+22}_{-18})$	[3,4] GARCIA-MAR..	11	RVUE	Compilation
$(457^{+14}_{-13}) - i(279^{+11}_{-7})$	[3,5] GARCIA-MAR..	11	RVUE	Compilation
$(442^{+5}_{-8}) - i(274^{+6}_{-5})$	[6] MOUSSALLAM	11	RVUE	Compilation
$(452 \pm 13) - i(259 \pm 16)$	[7] MENNESSIER	10	RVUE	Compilation
$(448 \pm 43) - i(266 \pm 43)$	[8] MENNESSIER	10	RVUE	Compilation
$(455 \pm 6^{+31}_{-13}) - i(278 \pm 6^{+34}_{-43})$	[9] CAPRINI	08	RVUE	Compilation
$(463 \pm 6^{+31}_{-17}) - i(259 \pm 6^{+33}_{-34})$	[10] CAPRINI	08	RVUE	Compilation
$(552^{+84}_{-106}) - i(232^{+81}_{-72})$	[11] ABLIKIM	07A	BES2	$\psi(2S) \to \pi^+\pi^- J/\psi$
$(466 \pm 18) - i(223 \pm 28)$	[12] BONVICINI	07	CLEO	$D^+ \to \pi^-\pi^+\pi^+$
$(472 \pm 30) - i(271 \pm 30)$	[13] BUGG	07A	RVUE	Compilation
$(484 \pm 17) - i(255 \pm 10)$	GARCIA-MAR..	07	RVUE	Compilation
$(430) - i(325)$	[14] ANISOVICH	06	RVUE	Compilation
$(441^{+16}_{-8}) - i(272^{+9}_{-12.5})$	[15] CAPRINI	06	RVUE	$\pi\pi \to \pi\pi$
$(470 \pm 50) - i(285 \pm 25)$	[16] ZHOU	05	RVUE	
$(541 \pm 39) - i(252 \pm 42)$	[17] ABLIKIM	04A	BES2	$J/\psi \to \omega\pi^+\pi^-$
$(528 \pm 32) - i(207 \pm 23)$	[18] GALLEGOS	04	RVUE	Compilation
$(533 \pm 25) - i(249 \pm 25)$	[19] BUGG	03	RVUE	

Downloaded from https://academic.oup.com/ptep/article/2022/8/083C01/6651666 by KIT Library user on 27 September 2022

$517 - i240$	BLACK	01	RVUE	$\pi\pi \to \pi\pi$
$(470 \pm 30) - i(295 \pm 20)$	[15] COLANGELO	01	RVUE	$\pi\pi \to \pi\pi$
$(535^{+48}_{-36}) - i(155^{+76}_{-53})$	[20] ISHIDA	01		$\Upsilon(3S) \to \Upsilon\pi\pi$
$610 \pm 14 - i(310 \pm 13)$	[21] SUROVTSEV	01	RVUE	$\pi\pi \to \pi\pi$, $K\overline{K}$
$(540^{+36}_{-29}) - i(193^{+32}_{-40})$	ISHIDA	00B		$p\overline{p} \to \pi^0\pi^0\pi^0$
$445 - i235$	HANNAH	99	RVUE	π scalar form factor
$(523 \pm 12) - i(259 \pm 7)$	KAMINSKI	99	RVUE	$\pi\pi \to \pi\pi$, $K\overline{K}$, $\sigma\sigma$
$442 - i\ 227$	OLLER	99	RVUE	$\pi\pi \to \pi\pi$, $K\overline{K}$
$469 - i203$	OLLER	99B	RVUE	$\pi\pi \to \pi\pi$, $K\overline{K}$
$445 - i221$	OLLER	99C	RVUE	$\pi\pi \to \pi\pi$, $K\overline{K}$, $\eta\eta$
$420 - i\ 212$	LOCHER	98	RVUE	$\pi\pi \to \pi\pi$, $K\overline{K}$
$440 - i245$	[22] DOBADO	97	RVUE	Compilation
$(602 \pm 26) - i(196 \pm 27)$	[23] ISHIDA	97		$\pi\pi \to \pi\pi$
$(537 \pm 20) - i(250 \pm 17)$	[24] KAMINSKI	97B	RVUE	$\pi\pi \to \pi\pi$, $K\overline{K}$, 4π
$470 - i250$	[25,26] TORNQVIST	96	RVUE	$\pi\pi \to \pi\pi$, $K\overline{K}$, $K\pi$, $\eta\pi$
$387 - i305$	[26,27] JANSSEN	95	RVUE	$\pi\pi \to \pi\pi$, $K\overline{K}$
$420 - i370$	[28] ACHASOV	94	RVUE	$\pi\pi \to \pi\pi$
$(506 \pm 10) - i(247 \pm 3)$	KAMINSKI	94	RVUE	$\pi\pi \to \pi\pi$, $K\overline{K}$
$370 - i356$	[29] ZOU	94B	RVUE	$\pi\pi \to \pi\pi$, $K\overline{K}$
$408 - i342$	[26,29] ZOU	93	RVUE	$\pi\pi \to \pi\pi$, $K\overline{K}$
$470 - i208$	[30] VANBEVEREN	86	RVUE	$\pi\pi \to \pi\pi$, $K\overline{K}$, $\eta\eta$, ...
$(750 \pm 50) - i(450 \pm 50)$	[31] ESTABROOKS	79	RVUE	$\pi\pi \to \pi\pi$, $K\overline{K}$
$(660 \pm 100) - i(320 \pm 70)$	PROTOPOP...	73	HBC	$\pi\pi \to \pi\pi$, $K\overline{K}$
$650 - i370$	[32] BASDEVANT	72	RVUE	$\pi\pi \to \pi\pi$

[1] S-matrix pole; 8595 events.
[2] Applying the chiral unitary approach at NLO to the K_{e4} data of BATLEY 10 and $\pi N \to \pi\pi N$ data of HYAMS 73, GRAYER 74, and PROTOPOPESCU 73.
[3] Uses the K_{e4} data of BATLEY 10C and the $\pi N \to \pi\pi N$ data of HYAMS 73, GRAYER 74, and PROTOPOPESCU 73.
[4] Analytic continuation using Roy equations.
[5] Analytic continuation using GKPY equations.
[6] Using Roy equations.
[7] Average of three variants of the analytic K-matrix model. Uses the K_{e4} data of BATLEY 08A and the $\pi N \to \pi\pi N$ data of HYAMS 73 and GRAYER 74.
[8] Average of the analyses of three data sets in the K-matrix model. Uses the data of BATLEY 08A, HYAMS 73, and GRAYER 74, partially of COHEN 80 or ETKIN 82B.
[9] From the K_{e4} data of BATLEY 08A and $\pi N \to \pi\pi N$ data of HYAMS 73.
[10] From the K_{e4} data of BATLEY 08A and $\pi N \to \pi\pi N$ data of PROTOPOPESCU 73, GRAYER 74, and ESTABROOKS 74.
[11] From a mean of three different $f_0(500)$ parametrizations. Uses 40k events.
[12] From an isobar model using 2.6k events.
[13] Reanalysis of ABLIKIM 04A, PISLAK 01, and HYAMS 73 data.
[14] Using the N/D method.
[15] From the solution of the Roy equation (ROY 71) for the isoscalar S-wave and using a phase-shift analysis of HYAMS 73 and PROTOPOPESCU 73 data.
[16] Reanalysis of the data from PROTOPOPESCU 73, ESTABROOKS 74, GRAYER 74, ROSSELET 77, PISLAK 03, and AKHMETSHIN 04.
[17] From a mean of six different analyses and $f_0(500)$ parameterizations.
[18] Using data on $\psi(2S) \to J/\psi\pi\pi$ from BAI 00E and on $\Upsilon(nS) \to \Upsilon(mS)\pi\pi$ from BUTLER 94B and ALEXANDER 98.
[19] From a combined analysis of HYAMS 73, AUGUSTIN 89, AITALA 01B, and PISLAK 01.
[20] A similar analysis (KOMADA 01) finds $(580^{+79}_{-30}) - i(190^{+107}_{-49})$ MeV.
[21] Coupled channel reanalysis of BATON 70, BENSINGER 71, BAILLON 72, HYAMS 73, HYAMS 75, ROSSELET 77, COHEN 80, and ETKIN 82B using the uniformizing variable.
[22] Using the inverse amplitude method and data of ESTABROOKS 73, GRAYER 74, and PROTOPOPESCU 73.
[23] Reanalysis of data from HYAMS 73, GRAYER 74, SRINIVASAN 75, and ROSSELET 77 using the interfering amplitude method.
[24] Average and spread of 4 variants ("up" and "down") of KAMINSKI 97B 3-channel model.
[25] Uses data from BEIER 72B, OCHS 73, HYAMS 73, GRAYER 74, ROSSELET 77, CASON 83, ASTON 88, and ARMSTRONG 91B. Coupled channel analysis with flavor symmetry and all light two-pseudoscalars systems.
[26] Demonstrates explicitly that $f_0(500)$ and $f_0(1370)$ are two different poles.
[27] Analysis of data from FALVARD 88.
[28] Analysis of data from OCHS 73, ESTABROOKS 75, ROSSELET 77, and MUKHIN 80.
[29] Analysis of data from OCHS 73, GRAYER 74, and ROSSELET 77.
[30] Coupled-channel analysis using data from PROTOPOPESCU 73, HYAMS 73, HYAMS 75, GRAYER 74, ESTABROOKS 74, ESTABROOKS 75, FROGGATT 77, CORDEN 79, BISWAS 81.
[31] Analysis of data from APEL 72C, GRAYER 74, CASON 76, PAWLICKI 77. Includes spread and errors of 4 solutions.
[32] Analysis of data from BATON 70, BENSINGER 71, COLTON 71, BAILLON 72,PROTOPOPESCU 73, and WALKER 67.

$f_0(500)$ BREIT-WIGNER MASS

VALUE (MeV)	DOCUMENT ID		TECN	COMMENT
400 to 800 OUR ESTIMATE				
• • • We do not use the following data for averages, fits, limits, etc. • • •				
513 ± 32	[33] MURAMATSU	02	CLEO	$e^+e^- \approx 10$ GeV
$478^{+24}_{-23} \pm 17$	AITALA	01B	E791	$D^+ \to \pi^-\pi^+\pi^+$
563^{+58}_{-29}	[34] ISHIDA	01		$\Upsilon(3S) \to \Upsilon\pi\pi$
555	[35] ASNER	00	CLE2	$\tau^- \to \pi^-\pi^0\pi^0\nu_\tau$
540 ± 36	ISHIDA	00B		$p\overline{p} \to \pi^0\pi^0\pi^0$
750 ± 4	ALEKSEEV	99	SPEC	$1.78\ \pi^-\ p_{\rm polar} \to \pi^-\pi^+ n$
744 ± 5	ALEKSEEV	98	SPEC	$1.78\ \pi^-\ p_{\rm polar} \to \pi^-\pi^+ n$
759 ± 5	[36] TROYAN	98		$5.2\ np \to np\pi^+\pi^-$
780 ± 30	ALDE	97	GAM2	$450\ pp \to pp\pi^0\pi^0$
585 ± 20	[37] ISHIDA	97		$\pi\pi \to \pi\pi$
761 ± 12	[38] SVEC	96	RVUE	6–$17\ \pi N_{\rm polar} \to \pi^+\pi^- N$
~ 860	[39,40] TORNQVIST	96	RVUE	$\pi\pi \to \pi\pi$, $K\overline{K}$, $K\pi$, $\eta\pi$
1165 ± 50	[41,42] ANISOVICH	95	RVUE	$\pi^- p \to \pi^0\pi^0 n$, $\overline{p}p \to \pi^0\pi^0\pi^0$, $\pi^0\pi^0\eta$, $\pi^0\eta\eta$
414 ± 20	[38] AUGUSTIN	89	DM2	

[33] Statistical uncertainty only.
[34] A similar analysis (KOMADA 01) finds 526^{+48}_{-37} MeV.
[35] From the best fit of the Dalitz plot.
[36] 6σ effect, no PWA.
[37] Reanalysis of data from HYAMS 73, GRAYER 74, SRINIVASAN 75, and ROSSELET 77 using the interfering amplitude method.
[38] Breit-Wigner fit to S-wave intensity measured in $\pi N \to \pi^-\pi^+ N$ on polarized targets. The fit does not include $f_0(980)$.
[39] Uses data from ASTON 88, OCHS 73, HYAMS 73, ARMSTRONG 91B, GRAYER 74, CASON 83, ROSSELET 77, and BEIER 72B. Coupled channel analysis with flavor symmetry and all light two-pseudoscalars systems.
[40] Also observed by ASNER 00 in $\tau^- \to \pi^-\pi^0\pi^0\nu_\tau$ decays.
[41] Uses $\pi^0\pi^0$ data from ANISOVICH 94, AMSLER 94D, and ALDE 95B, $\pi^+\pi^-$ data from OCHS 73, GRAYER 74 and ROSSELET 77, and $\eta\eta$ data from ANISOVICH 94.
[42] The pole is on Sheet III. Demonstrates explicitly that $f_0(500)$ and $f_0(1370)$ are two different poles.

$f_0(500)$ BREIT-WIGNER WIDTH

VALUE (MeV)	DOCUMENT ID		TECN	COMMENT
100 to 800 OUR ESTIMATE				
• • • We do not use the following data for averages, fits, limits, etc. • • •				
335 ± 67	[43] MURAMATSU	02	CLEO	$e^+e^- \approx 10$ GeV
$324^{+42}_{-40} \pm 21$	AITALA	01B	E791	$D^+ \to \pi^-\pi^+\pi^+$
372^{+229}_{-95}	[44] ISHIDA	01		$\Upsilon(3S) \to \Upsilon\pi\pi$
540	[45] ASNER	00	CLE2	$\tau^- \to \pi^-\pi^0\pi^0\nu_\tau$
372 ± 80	ISHIDA	00B		$p\overline{p} \to \pi^0\pi^0\pi^0$
119 ± 13	ALEKSEEV	99	SPEC	$1.78\ \pi^-\ p_{\rm polar} \to \pi^-\pi^+ n$
77 ± 22	ALEKSEEV	98	SPEC	$1.78\ \pi^-\ p_{\rm polar} \to \pi^-\pi^+ n$
35 ± 12	[46] TROYAN	98		$5.2\ np \to np\pi^+\pi^-$
780 ± 60	ALDE	97	GAM2	$450\ pp \to pp\pi^0\pi^0$
385 ± 70	[47] ISHIDA	97		$\pi\pi \to \pi\pi$
290 ± 54	[48] SVEC	96	RVUE	6–$17\ \pi N_{\rm polar} \to \pi^+\pi^- N$
~ 880	[49,50] TORNQVIST	96	RVUE	$\pi\pi \to \pi\pi$, $K\overline{K}$, $K\pi$, $\eta\pi$
460 ± 40	[51,52] ANISOVICH	95	RVUE	$\pi^- p \to \pi^0\pi^0 n$, $\overline{p}p \to \pi^0\pi^0\pi^0$, $\pi^0\pi^0\eta$, $\pi^0\eta\eta$
494 ± 58	[48] AUGUSTIN	89	DM2	

[43] Statistical uncertainty only.
[44] A similar analysis (KOMADA 01) finds 301^{+145}_{-100} MeV.
[45] From the best fit of the Dalitz plot.
[46] 6σ effect, no PWA.
[47] Reanalysis of data from HYAMS 73, GRAYER 74, SRINIVASAN 75, and ROSSELET 77 using the interfering amplitude method.
[48] Breit-Wigner fit to S-wave intensity measured in $\pi N \to \pi^-\pi^+ N$ on polarized targets. The fit does not include $f_0(980)$.
[49] Uses data from ASTON 88, OCHS 73, HYAMS 73, ARMSTRONG 91B, GRAYER 74, CASON 83, ROSSELET 77, and BEIER 72B. Coupled channel analysis with flavor symmetry and all light two-pseudoscalars systems.
[50] Also observed by ASNER 00 in $\tau^- \to \pi^-\pi^0\pi^0\nu_\tau$ decays.
[51] Uses $\pi^0\pi^0$ data from ANISOVICH 94, AMSLER 94D, and ALDE 95B, $\pi^+\pi^-$ data from OCHS 73, GRAYER 74 and ROSSELET 77, and $\eta\eta$ data from ANISOVICH 94.
[52] The pole is on Sheet III. Demonstrates explicitly that $f_0(500)$ and $f_0(1370)$ are two different poles.

$f_0(500)$ DECAY MODES

	Mode	Fraction (Γ_i/Γ)
Γ_1	$\pi\pi$	seen
Γ_2	$\gamma\gamma$	seen

$f_0(500)$ PARTIAL WIDTHS

$\Gamma(\gamma\gamma)$ Γ_2

VALUE (keV)	DOCUMENT ID		TECN	COMMENT
• • • We do not use the following data for averages, fits, limits, etc. • • •				
2.05 ± 0.21	[53] DAI	14A	RVUE	Compilation
1.7 ± 0.4	[54] HOFERICHT...	11	RVUE	Compilation
3.08 ± 0.82	[55] MENNESSIER	11	RVUE	Compilation
$2.08 \pm 0.2\ ^{+0.07}_{-0.04}$	[56] MOUSSALLAM	11	RVUE	Compilation
2.08	[57] MAO	09	RVUE	Compilation
1.2 ± 0.4	[58] BERNABEU	08	RVUE	
3.9 ± 0.6	[55] MENNESSIER	08	RVUE	$\gamma\gamma \to \pi^+\pi^-$, $\pi^0\pi^0$

Downloaded from https://academic.oup.com/ptep/article/2022/8/083C01/6651666 by KIT Library user on 27 September 2022

1.8 ±0.4	[59] OLLER	08	RVUE	Compilation	
1.68±0.15	[59,60] OLLER	08A	RVUE	Compilation	
3.1 ±0.5	[61,62] PENNINGTON	08	RVUE	Compilation	
2.4 ±0.4	[62,63] PENNINGTON	08	RVUE	Compilation	
4.1 ±0.3	[64] PENNINGTON	06	RVUE	$\gamma\gamma \to \pi^0\pi^0$	
3.8 ±1.5	[65,66] BOGLIONE	99	RVUE	$\gamma\gamma \to \pi^+\pi^-, \pi^0\pi^0$	
5.4 ±2.3	[65] MORGAN	90	RVUE	$\gamma\gamma \to \pi^+\pi^-, \pi^0\pi^0$	
10 ±6	COURAU	86	DM1	$e^+e^- \to \pi^+\pi^-e^+e^-$	

[53] Using dispersive analysis with phases from GARCIA-MARTIN 11A and BUETTIKER 04 as input.

[54] Using Roy-Steiner equations with $\pi\pi$ phase shifts from an update of COLANGELO 01 and from GARCIA-MARTIN 11A.

[55] Using an analytic K-matrix model.

[56] Using dispersion integral with phase input from Roy equations and data from MARSISKE 90, BOYER 90, BEHREND 92, UEHARA 08A, and MORI 07.

[57] Used dispersion theory. The value quoted used the $f_0(500)$ pole position of $457 - i276$ MeV.

[58] Using p, n polarizabilities from PDG 06 and fitting to $\pi\pi$ phase motion from GARCIA-MARTIN 07 and σ-poles from GARCIA-MARTIN 07 and CAPRINI 06.

[59] Using twice-subtracted dispersion integrals.

[60] Supersedes OLLER 08.

[61] Solution A (preferred solution based on χ^2-analysis).

[62] Dispersion theory based amplitude analysis of BOYER 90, MARSISKE 90, BEHREND 92, and MORI 07.

[63] Solution B (worse than solution A; still acceptable when systematic uncertainties are included).

[64] Using unitarity and the σ pole position from CAPRINI 06.

[65] This width could equally well be assigned to the $f_0(1370)$. The authors analyse data from BOYER 90 and MARSISKE 90 and report strong correlation with $\gamma\gamma$ width of $f_2(1270)$.

[66] Supersedes MORGAN 90.

$f_0(500)$ REFERENCES

SARANTSEV	21	PL B816 136227	A.V. Sarantsev *et al.*	(BONN, PNPI)
ABLIKIM	17	PRL 118 012001	M. Ablikim *et al.*	(BESIII Collab.)
DAI	14A	PR D90 036004	L.-Y. Dai, M.R. Pennington	(CEBAF)
ALBALADEJO	12	PR D86 034003	M. Albaladejo, J.A. Oller	(MURC)
GARCIA-MAR...	11	PRL 107 072001	R. Garcia-Martin *et al.*	(MADR, CRAC)
GARCIA-MAR...	11A	PR D83 074004	R. Garcia-Martin *et al.*	(MADR, CRAC)
HOFERICHT...	11	EPJ C71 1743	M. Hoferichter, D.R. Phillips, C. Schat	(BONN+)
MENNESSIER	11	PL B696 40	G. Mennessier, S. Narison, X.-G. Wang	
MOUSSALLAM	11	EPJ C71 1814	B. Moussallam	
BATLEY	10	PL B686 101	J.R. Batley *et al.*	(CERN NA48/2 Collab.)
BATLEY	10C	EPJ C70 635	J.R. Batley *et al.*	(CERN NA48/2 Collab.)
MENNESSIER	10	PL B688 59	G. Mennessier, S. Narison, X.-G. Wang	
MAO	09	PR D79 116008	Y. Mao *et al.*	
BATLEY	08A	EPJ C54 411	J.R. Batley *et al.*	(CERN NA48/2 Collab.)
BERNABEU	08	PRL 100 241804	J. Bernabeu, J. Prades	(IFIC, GRAN)
CAPRINI	08	PR D77 114019	I. Caprini	
MENNESSIER	08	PL B665 205	G. Mennessier, S. Narison, W. Ochs	
OLLER	08	PL B659 201	J.A. Oller, L. Roca, C. Schat	(MURC, UBA)
OLLER	08A	EPJ A37 15	J.A. Oller, L. Roca	(MURC)
PENNINGTON	08	EPJ C56 1	M.R. Pennington *et al.*	
UEHARA	08A	PR D78 052004	S. Uehara *et al.*	(BELLE Collab.)
ABLIKIM	07A	PL B645 19	M. Ablikim *et al.*	(BES Collab.)
BONVICINI	07	PR D76 012001	G. Bonvicini *et al.*	(CLEO Collab.)
BUGG	07A	JP G34 151	D.V. Bugg *et al.*	
GARCIA-MAR...	07	PR D76 074034	R. Garcia-Martin, J.R. Pelaez, F.J. Yndurain	
MORI	07	PR D75 051101	T. Mori *et al.*	(BELLE Collab.)
ANISOVICH	06	IJMP A21 3615	V.V. Anisovich	
CAPRINI	06	PRL 96 132001	I. Caprini, G. Colangelo, H. Leutwyler	(BCIP+)
PDG	06	JP G33 1	W.-M. Yao *et al.*	(PDG Collab.)
PENNINGTON	06	PRL 97 011601	M.R. Pennington	
ZHOU	05	JHEP 0502 043	Z.Y. Zhou *et al.*	
ABLIKIM	04A	PL B598 149	M. Ablikim *et al.*	(BES Collab.)
AKHMETSHIN	04	PL B578 285	R.R. Akhmetshin *et al.*	(Novosibirsk CMD-2 Collab.)
BUETTIKER	04	EPJ C33 409	P. Buettiker, S. Descotes-Genon, B. Moussallam	
GALLEGOS	04	PR D69 074033	A. Gallegos *et al.*	
BUGG	03	PL B572 1	D.V. Bugg	
PISLAK	03	PR D67 072004	S. Pislak *et al.*	(BNL E865 Collab.)
Also		PR D81 119903E	S. Pislak *et al.*	(BNL E865 Collab.)
MURAMATSU	02	PRL 89 251802	H. Muramatsu *et al.*	(CLEO Collab.)
Also		PRL 90 059901 (errat.)	H. Muramatsu *et al.*	(CLEO Collab.)
AITALA	01B	PRL 86 770	E.M. Aitala *et al.*	(FNAL E791 Collab.)
BLACK	01	PR D64 014031	D. Black *et al.*	
COLANGELO	01	NP B603 125	G. Colangelo, J. Gasser, H. Leytwyler	
ISHIDA	01	PL B518 47	M. Ishida *et al.*	
KOMADA	01	PL B508 31	T. Komada *et al.*	
PISLAK	01	PRL 87 221801	S. Pislak *et al.*	(BNL E865 Collab.)
Also		PR D67 072004	S. Pislak *et al.*	(BNL E865 Collab.)
Also		PRL 105 019901E	S. Pislak *et al.*	(BNL E865 Collab.)
SUROVTSEV	01	PR D63 054024	Y.S. Surovtsev, D. Krupa, M. Nagy	
ASNER	00	PR D61 012002	D.M. Asner *et al.*	(CLEO Collab.)
BAI	00E	PR D62 032002	J. Bai *et al.*	(BES Collab.)
ISHIDA	00B	PTP 104 203	M. Ishida *et al.*	
ALEKSEEV	99	NP B541 3	I.G. Alekseev *et al.*	
BOGLIONE	99	EPJ C9 11	M. Boglione, M.R. Pennington	
HANNAH	99	PR D60 017502	T. Hannah	
KAMINSKI	99	EPJ C9 141	R. Kaminski, L. Lesniak, B. Loiseau	(CRAC, PARIN)
OLLER	99	PR D60 099906 (erratum)	J.A. Oller *et al.*	
OLLER	99B	NP A652 407 (erratum)	J.A. Oller, E. Oset	
OLLER	99C	PR D60 074023	J.A. Oller, E. Oset	
ALEKSEEV	98	PAN 61 174	I.G. Alekseev *et al.*	
ALEXANDER	98	PR D58 052004	J.P. Alexander *et al.*	(CLEO Collab.)
LOCHER	98	EPJ C4 317	M.P. Locher *et al.*	(PSI)
TROYAN	98	JINRRC 5-91 33	Yu. Troyan *et al.*	
ALDE	97	PL B397 350	D.M. Alde *et al.*	(GAMS Collab.)
DOBADO	97	PR D56 3057	A. Dobado, J.R. Pelaez	
ISHIDA	97	PTP 98 1005	S. Ishida *et al.*	(TOKY, MIYA, KEK)
KAMINSKI	97B	PL B413 130	R. Kaminski, L. Lesniak, B. Loiseau	(CRAC, IPN)
Also		PTP 95 745	S. Ishida *et al.*	(TOKY, MIYA, KEK)
SVEC	96	PR D53 2343	M. Svec	(MCGI)
TORNQVIST	96	PRL 76 1575	N.A. Tornqvist, M. Roos	(HELS)
ALDE	95B	ZPHY C66 375	D.M. Alde *et al.*	(GAMS Collab.)
ANISOVICH	95	PL B355 363	V.V. Anisovich *et al.*	(PNPI, SERP)
JANSSEN	95	PR D52 2690	G. Janssen *et al.*	(STON, ADLD, JULI)
ACHASOV	94	PR D49 5779	N.N. Achasov, G.N. Shestakov	(NOVM)
AMSLER	94D	PL B333 277	C. Amsler *et al.*	(Crystal Barrel Collab.)
ANISOVICH	94	PL B323 233	V.V. Anisovich *et al.*	(Crystal Barrel Collab.)
BUTLER	94B	PR D49 40	F. Butler *et al.*	(CLEO Collab.)
KAMINSKI	94	PR D50 3145	R. Kaminski, L. Lesniak, J.P. Maillet	(CRAC+)
ZOU	94B	PR D50 591	B.S. Zou, D.V. Bugg	(LOQM)
ZOU	93	PR D48 3948	B.S. Zou, D.V. Bugg	(LOQM)
BEHREND	92	ZPHY C56 381	H.J. Behrend	(CELLO Collab.)
ARMSTRONG	91B	ZPHY C52 389	T.A. Armstrong *et al.*	(ATHU, BARI, BIRM+)
BOYER	90	PR D42 1350	J. Boyer *et al.*	(Mark II Collab.)
MARSISKE	90	PR D41 3324	H. Marsiske *et al.*	(Crystal Ball Collab.)
MORGAN	90	ZPHY C48 623	D. Morgan, M.R. Pennington	(RAL, DURH)
AUGUSTIN	89	NP B320 1	J.E. Augustin, G. Cosme	(DM2 Collab.)
ASTON	88	NP B296 493	D. Aston *et al.*	(SLAC, NAGO, CINC, INUS)
FALVARD	88	PR D38 2706	A. Falvard *et al.*	(CLER, FRAS, LALO+)
COURAU	86	NP B271 1	A. Courau *et al.*	(CLER, LALO)
VANBEVEREN	86	ZPHY C30 615	E. van Beveren *et al.*	(NIJM, BIEL)
CASON	83	PR D28 1586	N.M. Cason *et al.*	(NDAM, ANL)
ETKIN	82B	PR D25 1786	A. Etkin *et al.*	(BNL, CUNY, TUFTS, VAND)
BISWAS	81	PRL 47 1378	N.N. Biswas *et al.*	(NDAM, ANL)
COHEN	80	PR D22 2595	D. Cohen *et al.*	(ANL) IJP
MUKHIN	80	JETPL 32 601	K.N. Mukhin *et al.*	(KIAE)
		Translated from ZETFP 32 616.		
CORDEN	79	NP B157 250	M.J. Corden *et al.*	(BIRM, RHEL, TELA+) JP
ESTABROOKS	79	PR D19 2678	P. Estabrooks	(CARL)
FROGGATT	77	NP B129 89	C.D. Froggatt, J.L. Petersen	(GLAS, NORD)
PAWLICKI	77	PR D15 3196	A.J. Pawlicki *et al.*	(ANL) IJ
ROSSELET	77	PR D15 574	L. Rosselet *et al.*	(GEVA, SACL)
CASON	76	PRL 36 1485	N.M. Cason *et al.*	(NDAM, ANL) IJ
ESTABROOKS	75	NP B95 322	P.G. Estabrooks, A.D. Martin	(DURH)
HYAMS	75	NP B100 205	B.D. Hyams *et al.*	(CERN, MPIM)
SRINIVASAN	75	PR D12 681	V. Srinivasan *et al.*	(NDAM, ANL)
ESTABROOKS	74	NP B79 301	P.G. Estabrooks, A.D. Martin	(DURH)
GRAYER	74	NP B75 189	G. Grayer *et al.*	(CERN, MPIM)
ESTABROOKS	73	Tallahassee	P.G. Estabrooks *et al.*	(CERN, MPIM)
HYAMS	73	NP B64 134	B.D. Hyams *et al.*	(CERN, MPIM)
OCHS	73	Thesis	W. Ochs	(MPIM, MUNI)
PROTOPOP...	73	PR D7 1279	S.D. Protopopescu *et al.*	(LBL)
APEL	72C	PL 41B 542	W.D. Apel *et al.*	(KARLK, KARLE, PISA)
BAILLON	72	PL 38B 555	P.H. Baillon *et al.*	(SLAC)
BASDEVANT	72	PL 41B 178	J.L. Basdevant, C.D. Froggatt, J.L. Petersen	(CERN)
BEIER	72B	PRL 29 511	E.W. Beier *et al.*	(PENN)
BENSINGER	71	PL 36B 134	J.R. Bensinger *et al.*	(WISC)
COLTON	71	PR D3 2028	E.P. Colton *et al.*	(LBL, FNAL, UCLA+)
ROY	71	PL 36B 353	S.M. Roy	
BATON	70	PL 33B 528	J.P. Baton, G. Laurens, J. Reignier	(SACL)
WALKER	67	RMP 39 695	W.D. Walker	(WISC)

$\rho(770)$

$I^G(J^{PC}) = 1^+(1^{--})$

$\rho(770)$ T-MATRIX POLE $\sqrt{s}$

VALUE (MeV)	DOCUMENT ID		TECN	COMMENT
• • • We do not use the following data for averages, fits, limits, etc. • • •				
$(761^{+4}_{-3}) - i(71.7^{+1.9}_{-2.3})$	[1] GARCIA-MAR...	11	RVUE	Compilation
$(763.7^{+1.7}_{-1.5}) - i(73.2^{+1.0}_{-1.1})$	[2] GARCIA-MAR...	11	RVUE	Compilation
$(754 \pm 18) - i(74 \pm 10)$	[3] PELAEZ	04A	RVUE	$\pi\pi \to \pi\pi$

[1] Reanalysis of the K_{e4} data of BATLEY 10C and the $\pi N \to \pi\pi N$ data of HYAMS 73, GRAYER 74, and PROTOPOPESCU 73 using Roy equations.

[2] Reanalysis of the K_{e4} data of BATLEY 10C and the $\pi N \to \pi\pi N$ data of HYAMS 73, GRAYER 74, and PROTOPOPESCU 73 using GKPY equations.

[3] Reanalysis of data from PROTOPOPESCU 73, ESTABROOKS 74, GRAYER 74, and COHEN 80 in the unitarized ChPT model.

$\rho(770)$ MASS

We no longer list S-wave Breit-Wigner fits, or data with high combinatorial background.

NEUTRAL ONLY, e^+e^-

VALUE (MeV)	EVTS	DOCUMENT ID		TECN	COMMENT
775.26±0.23 OUR AVERAGE					
775.3 ±0.5 ±0.6		[1] ACHASOV	21	SND	$e^+e^- \to \pi^+\pi^-$
775.02±0.35		[2] LEES	12G	BABR	$e^+e^- \to \pi^+\pi^-\gamma$
775.97±0.46±0.70	900k	[3] AKHMETSHIN	07		$e^+e^- \to \pi^+\pi^-$
774.6 ±0.4 ±0.5	800k	[4,5] ACHASOV	06	SND	$e^+e^- \to \pi^+\pi^-$
775.65±0.64±0.50	114k	[6,7] AKHMETSHIN	04	CMD2	$e^+e^- \to \pi^+\pi^-$
775.9 ±0.5 ±0.5	1.98M	[8] ALOISIO	03	KLOE	$1.02\ e^+e^- \to \pi^+\pi^-\pi^0$
775.8 ±0.9 ±2.0	500k	[8] ACHASOV	02	SND	$1.02\ e^+e^- \to \pi^+\pi^-\pi^0$
775.9 ±1.1		[9] BARKOV	85	OLYA	$e^+e^- \to \pi^+\pi^-$
• • • We do not use the following data for averages, fits, limits, etc. • • •					
763.49±0.53		[10] BARTOS	17	RVUE	$e^+e^- \to \pi^+\pi^-$
758.23±0.46		[11] BARTOS	17A	RVUE	$e^+e^- \to \pi^+\pi^-$
775.8 ±0.5 ±0.3	1.98M	[12] ALOISIO	03	KLOE	$1.02\ e^+e^- \to \pi^+\pi^-\pi^0$
775.9 ±0.6 ±0.5	1.98M	[13] ALOISIO	03	KLOE	$1.02\ e^+e^- \to \pi^+\pi^-\pi^0$
775.0 ±0.6 ±1.1	500k	[14] ACHASOV	02	SND	$1.02\ e^+e^- \to \pi^+\pi^-\pi^0$
775.1 ±0.7 ±5.3		[15] BENAYOUN	98	RVUE	$e^+e^- \to \pi^+\pi^-$, $\mu^+\mu^-$
770.5 ±1.9 ±5.1		[16] GARDNER	98	RVUE	0.28–0.92 $e^+e^- \to \pi^+\pi^-$
764.1 ±0.7		[17] O'CONNELL	97	RVUE	$e^+e^- \to \pi^+\pi^-$
757.5 ±1.5		[18] BERNICHA	94	RVUE	$e^+e^- \to \pi^+\pi^-$
768 ±1		[19] GESHKEN...	89	RVUE	$e^+e^- \to \pi^+\pi^-$

[1] From a fit of the cross section in the energy range $0.525 < \sqrt{s} < 0.883$ GeV parameterized by the sum of the Breit-Wigner amplitudes for the $\rho(770)$, ω and $\rho(1450)$ resonances.

[2] Using the GOUNARIS 68 parametrization with the complex phase of the $\rho-\omega$ interference and leaving the masses and widths of the $\rho(1450)$, $\rho(1700)$, and $\rho(2150)$ resonances as free parameters of the fit.

[3] A combined fit of AKHMETSHIN 07, AULCHENKO 06, and AULCHENKO 05.

Downloaded from https://academic.oup.com/ptep/article/2022/8/083C01/6651666 by KIT Library user on 27 September 2022

[4] Supersedes ACHASOV 05A.
[5] A fit of the SND data from 400 to 1000 MeV using parameters of the $\rho(1450)$ and $\rho(1700)$ from a fit of the data of BARKOV 85, BISELLO 89 and ANDERSON 00A.
[6] Using the GOUNARIS 68 parametrization with the complex phase of the ρ-ω interference.
[7] Update of AKHMETSHIN 02.
[8] Assuming $m_{\rho^+} = m_{\rho^-}$, $\Gamma_{\rho^+} = \Gamma_{\rho^-}$.
[9] From the GOUNARIS 68 parametrization of the pion form factor.
[10] Applies the Unitary & Analytic Model of the pion electromagnetic form factor of DUBNICKA 10 to analyze the data of LEES 12G and ABLIKIM 16C.
[11] Applies the Unitary & Analytic Model of the pion electromagnetic form factor of DUBNICKA 10 to analyze the data of ACHASOV 06, AKHMETSHIN 07, AUBERT 09AS, and AMBROSINO 11A.
[12] Assuming $m_{\rho^+} = m_{\rho^-} = m_{\rho^0}$, $\Gamma_{\rho^+} = \Gamma_{\rho^-} = \Gamma_{\rho^0}$.
[13] Without limitations on masses and widths.
[14] Assuming $m_{\rho^0} = m_{\rho^\pm}$, $g_{\rho^0\pi\pi} = g_{\rho^\pm\pi\pi}$.
[15] Using the data of BARKOV 85 in the hidden local symmetry model.
[16] From the fit to $e^+e^- \to \pi^+\pi^-$ data from the compilations of HEYN 81 and BARKOV 85, including the GOUNARIS 68 parametrization of the pion form factor.
[17] A fit of BARKOV 85 data assuming the direct $\omega\pi\pi$ coupling.
[18] Applying the S-matrix formalism to the BARKOV 85 data.
[19] Includes BARKOV 85 data. Model-dependent width definition.

CHARGED ONLY, τ DECAYS and e^+e^-

VALUE (MeV)	EVTS	DOCUMENT ID		TECN	CHG	COMMENT
775.11±0.34 OUR AVERAGE						
774.6 ±0.2 ±0.5	5.4M	[1,2] FUJIKAWA	08	BELL	±	$\tau^- \to \pi^-\pi^0\nu_\tau$
775.5 ±0.7		[2,3] SCHAEL	05C	ALEP		$\tau^- \to \pi^-\pi^0\nu_\tau$
775.5 ±0.5 ±0.4	1.98M	[4] ALOISIO	03	KLOE		1.02 $e^+e^- \to \pi^+\pi^-\pi^0$
775.1 ±1.1 ±0.5	87k	[5,6] ANDERSON	00A	CLE2		$\tau^- \to \pi^-\pi^0\nu_\tau$
• • • We do not use the following data for averages, fits, limits, etc. • • •						
761.60±0.95		[7] BARTOS	17A	RVUE		$\tau^- \to \pi^-\pi^0\nu_\tau$
774.8 ±0.6 ±0.4	1.98M	[8] ALOISIO	03	KLOE	−	1.02 $e^+e^- \to \pi^+\pi^-\pi^0$
776.3 ±0.6 ±0.7	1.98M	[8] ALOISIO	03	KLOE	+	1.02 $e^+e^- \to \pi^+\pi^-\pi^0$
773.9 ±2.0 $^{+0.3}_{-1.0}$		[9] SANZ-CILLERO	03	RVUE		$\tau^- \to \pi^-\pi^0\nu_\tau$
774.5 ±0.7 ±1.5	500k	[4] ACHASOV	02	SND	±	1.02 $e^+e^- \to \pi^+\pi^-\pi^0$
775.1 ±0.5		[10] PICH	01	RVUE		$\tau^- \to \pi^-\pi^0\nu_\tau$

[1] $|F_\pi(0)|^2$ fixed to 1.
[2] From the GOUNARIS 68 parametrization of the pion form factor.
[3] The error combines statistical and systematic uncertainties. Supersedes BARATE 97M.
[4] Assuming $m_{\rho^+} = m_{\rho^-}$, $\Gamma_{\rho^+} = \Gamma_{\rho^-}$.
[5] $\rho(1700)$ mass and width fixed at 1700 MeV and 235 MeV respectively.
[6] From the GOUNARIS 68 parametrization of the pion form factor. The second error is a model error taking into account different parametrizations of the pion form factor.
[7] Applies the Unitary & Analytic Model of the pion electromagnetic form factor of DUBNICKA 10 to analyze the data of FUJIKAWA 08.
[8] Without limitations on masses and widths.
[9] Using the data of BARATE 97M and the effective chiral Lagrangian.
[10] From a fit of the model-independent parameterization of the pion form factor to the data of BARATE 97M.

MIXED CHARGES, OTHER REACTIONS

VALUE (MeV)	EVTS	DOCUMENT ID		TECN	CHG	COMMENT
763.0±0.3±1.2	600k	[1] ABELE	99E	CBAR	0±	0.0 $\overline{p}p \to \pi^+\pi^-\pi^0$

[1] Assuming the equality of ρ^+ and ρ^- masses and widths.

CHARGED ONLY, HADROPRODUCED

VALUE (MeV)	EVTS	DOCUMENT ID		TECN	CHG	COMMENT
766.5±1.1 OUR AVERAGE						
763.7±3.2		ABELE	97	CBAR		$\overline{p}n \to \pi^-\pi^0\pi^0$
768 ±9		AGUILAR-...	91	EHS		400 pp
767 ±3	2935	[1] CAPRARO	87	SPEC	−	200 π^-Cu $\to \pi^-\pi^0$Cu
761 ±5	967	[1] CAPRARO	87	SPEC	−	200 π^-Pb $\to \pi^-\pi^0$Pb
771 ±4		HUSTON	86	SPEC	+	202 π^+A $\to \pi^+\pi^0$A
766 ±7	6500	[2] BYERLY	73	OSPK	−	5 π^-p
766.8±1.5	9650	[3] PISUT	68	RVUE	−	1.7–3.2 π^-p, t <10
767 ±6	900	[1] EISNER	67	HBC	−	4.2 π^-p, t <10

[1] Mass errors enlarged by us to $\Gamma/\sqrt{N}$; see the note with the $K^*(892)$ mass.
[2] Phase shift analysis. Systematic errors added corresponding to spread of different fits.
[3] From fit of 3-parameter relativistic P-wave Breit-Wigner to total mass distribution. Includes BATON 68, MILLER 67B, ALFF-STEINBERGER 66, HAGOPIAN 66, HAGOPIAN 66B, JACOBS 66B, JAMES 66, WEST 66, BLIEDEN 65 and CARMONY 64.

NEUTRAL ONLY, PHOTOPRODUCED

VALUE (MeV)	EVTS	DOCUMENT ID		TECN	COMMENT
769.2± 0.9 OUR AVERAGE					
770.8± 1.3 $^{+2.3}_{-2.4}$	900k	ANDREEV	20	H1	$ep \to e\pi^+\pi^-p$
771 ± 2 $^{+2}_{-1}$	63.5k	[1] ABRAMOWICZ	12	ZEUS	$ep \to e\pi^+\pi^-p$
770 ± 2 ±1	79k	[2] BREITWEG	98B	ZEUS	50–100 γp
767.6± 2.7		BARTALUCCI	78	CNTR	$\gamma p \to e^+e^-p$
775 ± 5		GLADDING	73	CNTR	2.9–4.7 γp
767 ± 4	1930	BALLAM	72	HBC	2.8 γp
770 ± 4	2430	BALLAM	72	HBC	4.7 γp
765 ±10		ALVENSLEB...	70	CNTR	γA, t <0.01
767.7± 1.9	140k	BIGGS	70	CNTR	<4.1 γC $\to \pi^+\pi^-$C
765 ± 5	4000	ASBURY	67B	CNTR	γ + Pb
• • • We do not use the following data for averages, fits, limits, etc. • • •					
771 ± 2	79k	[3] BREITWEG	98B	ZEUS	50–100 γp

[1] Using the KUHN 90 parametrization of the pion form factor, neglecting ρ–ω interference.
[2] From the parametrization according to SOEDING 66.
[3] From the parametrization according to ROSS 66.

NEUTRAL ONLY, OTHER REACTIONS

VALUE (MeV)	EVTS	DOCUMENT ID		TECN	COMMENT
769.0 ±0.9 OUR AVERAGE		Error includes scale factor of 1.4. See the ideogram below.			
765 ±6		BERTIN	97C	OBLX	0.0 $\overline{p}p \to \pi^+\pi^-\pi^0$
773 ±1.6		WEIDENAUER	93	ASTE	$\overline{p}p \to \pi^+\pi^-\omega$
762.6 ±2.6		AGUILAR-...	91	EHS	400 pp
770 ±2		[1] HEYN	81	RVUE	Pion form factor
768 ±4		[2,3] BOHACIK	80	RVUE	
769 ±3		[4] WICKLUND	78	ASPK	3,4,6 $\pi^\pm N$
768 ±1	76k	DEUTSCH...	76	HBC	16 π^+p
767 ±4	4100	ENGLER	74	DBC	6 $\pi^+n \to \pi^+\pi^-p$
775 ±4	32k	[2] PROTOPOP...	73	HBC	7.1 π^+p, t <0.4
764 ±3	6.8k	[5] RATCLIFF	72	ASPK	15 π^-p, t <0.3
774 ±3	1.7k	REYNOLDS	69	HBC	2.26 π^-p
769.2 ±1.5	13.3k	[6] PISUT	68	RVUE	1.7–3.2 π^-p, t <10
• • • We do not use the following data for averages, fits, limits, etc. • • •					
774.34±0.18±0.35	970k	[7] ABLIKIM	18C	BES3	$\eta'(958) \to \gamma\pi^+\pi^-$
772.93±0.18±0.34	970k	[8] ABLIKIM	18C	BES3	$\eta'(958) \to \gamma\pi^+\pi^-$
773.5 ±2.5		[9] COLANGELO	01	RVUE	$\pi\pi \to \pi\pi$
762.3 ±0.5 ±1.2	600k	[10] ABELE	99E	CBAR	0.0 $\overline{p}p \to \pi^+\pi^-\pi^0$
777 ±2	4.9k	[11] ADAMS	97	E665	470 $\mu p \to \mu XB$
770 ±2		[12] BOGOLYUB...	97	MIRA	32 $\overline{p}p \to \pi^+\pi^-$X
768 ±8		[12] BOGOLYUB...	97	MIRA	32 $pp \to \pi^+\pi^-$X
761.1 ±2.9		DUBNICKA	89	RVUE	π form factor
777.4 ±2.0		[13] CHABAUD	83	ASPK	17 π^-p polarized
769.5 ±0.7		[2,3] LANG	79	RVUE	
770 ±9		[3] ESTABROOKS	74	RVUE	17 $\pi^-p \to \pi^+\pi^-n$
773.5 ±1.7	11.2k	[14] JACOBS	72	HBC	2.8 π^-p
775 ±3	2.2k	[15] HYAMS	68	OSPK	11.2 π^-p

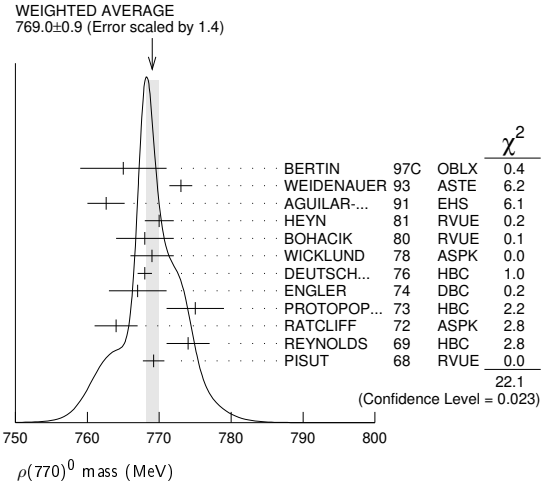

[1] HEYN 81 includes all spacelike and timelike F_π values until 1978.
[2] From pole extrapolation.
[3] From phase shift analysis of GRAYER 74 data.
[4] Phase shift analysis. Systematic errors added corresponding to spread of different fits.
[5] Published values contain misprints. Corrected by private communication RATCLIFF 74.
[6] Includes MALAMUD 69, ARMENISE 68, BACON 67, HUWE 67, MILLER 67B, ALFF-STEINBERGER 66, HAGOPIAN 66, HAGOPIAN 66B, JACOBS 66B, JAMES 66, WEST 66, GOLDHABER 64, ABOLINS 63.
[7] From a fit to $\pi^+\pi^-$ mass using $\rho(770)$ (parametrized with the Gounaris-Sakurai approach), $\omega(782)$, and box anomaly components.
[8] From a fit to $\pi^+\pi^-$ mass using $\rho(770)$ (parametrized with the Gounaris-Sakurai approach), $\omega(782)$, and $\rho(1450)$ components.
[9] Breit-Wigner mass from a phase-shift analysis of HYAMS 73 and PROTOPOPESCU 73 data.
[10] Using relativistic Breit-Wigner and taking into account ρ-ω interference.
[11] Systematic errors not evaluated.
[12] Systematic effects not studied.
[13] From fit of 3-parameter relativistic Breit-Wigner to helicity-zero part of P-wave intensity. CHABAUD 83 includes data of GRAYER 74.
[14] Mass errors enlarged by us to $\Gamma/\sqrt{N}$; see the note with the $K^*(892)$ mass.
[15] Of HYAMS 68 six parametrizations, this is theoretically soundest. MR

Downloaded from https://academic.oup.com/ptep/article/2022/8/083C01/6651666 by KIT Library user on 27 September 2022

$m_{\rho(770)^0} - m_{\rho(770)^\pm}$

VALUE (MeV)	EVTS	DOCUMENT ID		TECN	CHG	COMMENT
−0.7 ±0.8 OUR AVERAGE		Error includes scale factor of 1.5. See the ideogram below.				
−2.4 ±0.8		[1] SCHAEL	05C	ALEP		$\tau^- \to \pi^- \pi^0 \nu_\tau$
0.4 ±0.7 ±0.6	1.98M	[2] ALOISIO	03	KLOE		1.02 $e^+e^- \to \pi^+\pi^-\pi^0$
1.3 ±1.1 ±2.0	500k	[2] ACHASOV	02	SND		1.02 $e^+e^- \to \pi^+\pi^-\pi^0$
1.6 ±0.6 ±1.7	600k	ABELE	99E	CBAR	±0	0.0 $\overline{p}p \to \pi^+\pi^-\pi^0$
−4 ±4	3000	[3] REYNOLDS	69	HBC	−0	2.26 $\pi^- p$
−5 ±5	3600	[3] FOSTER	68	HBC	±0	0.0 $\overline{p}p$
2.4 ±2.1	22950	[4] PISUT	68	RVUE		$\pi N \to \rho N$
• • • We do not use the following data for averages, fits, limits, etc. • • •						
−3.37±1.06		[5] BARTOS	17A	RVUE		$e^+e^- \to \pi^+\pi^-$, $\tau^- \to \pi^-\pi^0\nu_\tau$

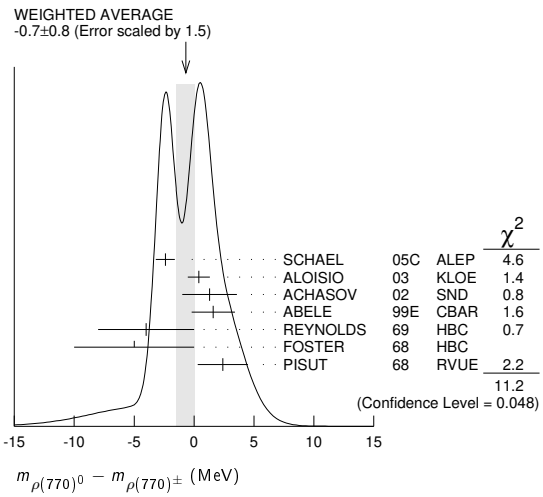

[1] From the combined fit of the τ^- data from ANDERSON 00A and SCHAEL 05C and e^+e^- data from the compilation of BARKOV 85, AKHMETSHIN 04, and ALOISIO 05. Supersedes BARATE 97M.

[2] Assuming $m_{\rho^+} = m_{\rho^-}$, $\Gamma_{\rho^+} = \Gamma_{\rho^-}$.

[3] From quoted masses of charged and neutral modes.

[4] Includes MALAMUD 69, ARMENISE 68, BATON 68, BACON 67, HUWE 67, MILLER 67B, ALFF-STEINBERGER 66, HAGOPIAN 66, HAGOPIAN 66B, JACOBS 66B, JAMES 66, WEST 66, BLIEDEN 65, CARMONY 64, GOLDHABER 64, ABOLINS 63.

[5] Applies the Unitary & Analytic Model of the pion electromagnetic form factor of DUBNICKA 10 to analyze the data of ACHASOV 06, AKHMETSHIN 07, AUBERT 09AS, AMBROSINO 11A, and FUJIKAWA 08.

$m_{\rho(770)^+} - m_{\rho(770)^-}$

VALUE (MeV)	EVTS	DOCUMENT ID		TECN	COMMENT
• • • We do not use the following data for averages, fits, limits, etc. • • •					
1.5±0.8±0.7	1.98M	[1] ALOISIO	03	KLOE	1.02 $e^+e^- \to \pi^+\pi^-\pi^0$

[1] Without limitations on masses and widths.

$\rho(770)$ RANGE PARAMETER

The range parameter R enters an energy-dependent correction to the width, of the form $(1 + q_r^2 R^2) / (1 + q^2 R^2)$, where q is the momentum of one of the pions in the $\pi\pi$ rest system. At resonance, $q = q_r$.

VALUE (GeV^{-1})	DOCUMENT ID		TECN	CHG	COMMENT
$\mathbf{5.3^{+0.9}_{-0.7}}$	[1] CHABAUD	83	ASPK	0	17 $\pi^- p$ polarized

[1] The old PISUT 68 value, properly corrected, was 3.2 ± 0.6.

$\rho(770)$ WIDTH

We no longer list S-wave Breit-Wigner fits, or data with high combinatorial background.

NEUTRAL ONLY, e^+e^-

VALUE (MeV)	EVTS	DOCUMENT ID		TECN	COMMENT
147.4 ±0.8 OUR AVERAGE		Error includes scale factor of 2.0. See the ideogram below.			
145.6 ±0.6 ±0.8		[1] ACHASOV	21	SND	$e^+e^- \to \pi^+\pi^-$
149.59±0.67		[2] LEES	12G	BABR	$e^+e^- \to \pi^+\pi^-\gamma$
145.98±0.75±0.50	900k	[3] AKHMETSHIN	07		$e^+e^- \to \pi^+\pi^-$
146.1 ±0.8 ±1.5	800k	[4,5] ACHASOV	06	SND	$e^+e^- \to \pi^+\pi^-$
143.85±1.33±0.80	114k	[6,7] AKHMETSHIN	04	CMD2	$e^+e^- \to \pi^+\pi^-$
147.3 ±1.5 ±0.7	1.98M	[8] ALOISIO	03	KLOE	1.02 $e^+e^- \to \pi^+\pi^-\pi^0$
151.1 ±2.6 ±3.0	500k	[8] ACHASOV	02	SND	1.02 $e^+e^- \to \pi^+\pi^-\pi^0$
150.5 ±3.0		[9] BARKOV	85	OLYA	$e^+e^- \to \pi^+\pi^-$
• • • We do not use the following data for averages, fits, limits, etc. • • •					
144.06±0.85		[10] BARTOS	17	RVUE	$e^+e^- \to \pi^+\pi^-$
144.56±0.80		[11] BARTOS	17A	RVUE	$e^+e^- \to \pi^+\pi^-$
143.9 ±1.3 ±1.1	1.98M	[12] ALOISIO	03	KLOE	1.02 $e^+e^- \to \pi^+\pi^-\pi^0$
147.4 ±1.5 ±0.7	1.98M	[13] ALOISIO	03	KLOE	1.02 $e^+e^- \to \pi^+\pi^-\pi^0$
149.8 ±2.2 ±2.0	500k	[14] ACHASOV	02	SND	1.02 $e^+e^- \to \pi^+\pi^-\pi^0$
147.9 ±1.5 ±7.5		[15] BENAYOUN	98	RVUE	$e^+e^- \to \pi^+\pi^-$, $\mu^+\mu^-$
153.5 ±1.3 ±4.6		[16] GARDNER	98	RVUE	0.28–0.92 $e^+e^- \to \pi^+\pi^-$
145.0 ±1.7		[17] O'CONNELL	97	RVUE	$e^+e^- \to \pi^+\pi^-$
142.5 ±3.5		[18] BERNICHA	94	RVUE	$e^+e^- \to \pi^+\pi^-$
138 ±1		[19] GESHKEN...	89	RVUE	$e^+e^- \to \pi^+\pi^-$

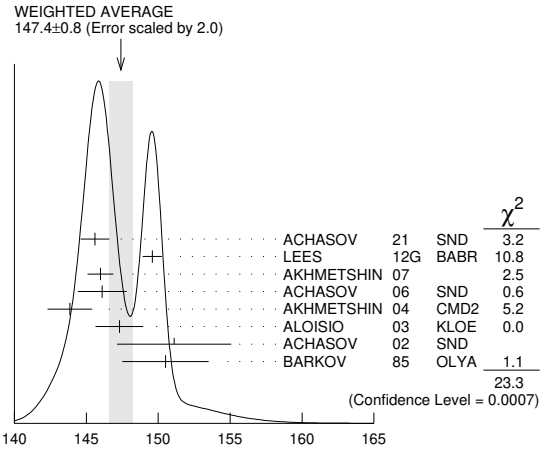

[1] From a fit of the cross section in the energy range $0.525 < \sqrt{s} < 0.883$ GeV parameterized by the sum of the Breit-Wigner amplitudes for the $\rho(770)$, ω and $\rho(1450)$ resonances.

[2] Using the GOUNARIS 68 parametrization with the complex phase of the $\rho-\omega$ interference and leaving the masses and widths of the $\rho(1450)$, $\rho(1700)$, and $\rho(2150)$ resonances as free parameters of the fit.

[3] A combined fit of AKHMETSHIN 07, AULCHENKO 06, and AULCHENKO 05.

[4] Supersedes ACHASOV 05A.

[5] A fit of the SND data from 400 to 1000 MeV using parameters of the $\rho(1450)$ and $\rho(1700)$ from a fit of the data of BARKOV 85, BISELLO 89 and ANDERSON 00A.

[6] Using the GOUNARIS 68 parametrization with the complex phase of the ρ-ω interference.

[7] From a fit in the energy range 0.61 to 0.96 GeV. Update of AKHMETSHIN 02.

[8] Assuming $m_{\rho^+} = m_{\rho^-}$, $\Gamma_{\rho^+} = \Gamma_{\rho^-}$.

[9] From the GOUNARIS 68 parametrization of the pion form factor.

[10] Applies the Unitary & Analytic Model of the pion electromagnetic form factor of DUBNICKA 10 to analyze the data of LEES 12G and ABLIKIM 16C.

[11] Applies the Unitary & Analytic Model of the pion electromagnetic form factor of DUBNICKA 10 to analyze the data of ACHASOV 06, AKHMETSHIN 07, AUBERT 09AS, and AMBROSINO 11A.

[12] Assuming $m_{\rho^+} = m_{\rho^-} = m_{\rho^0}$, $\Gamma_{\rho^+} = \Gamma_{\rho^-} = \Gamma_{\rho^0}$.

[13] Without limitations on masses and widths.

[14] Assuming $m_{\rho^0} = m_{\rho^\pm}$, $g_{\rho^0\pi\pi} = g_{\rho^\pm\pi\pi}$.

[15] Using the data of BARKOV 85 in the hidden local symmetry model.

[16] From the fit to $e^+e^- \to \pi^+\pi^-$ data from the compilations of HEYN 81 and BARKOV 85, including the GOUNARIS 68 parametrization of the pion form factor.

[17] A fit of BARKOV 85 data assuming the direct $\omega\pi\pi$ coupling.

[18] Applying the S-matrix formalism to the BARKOV 85 data.

[19] Includes BARKOV 85 data. Model-dependent width definition.

CHARGED ONLY, τ DECAYS and e^+e^-

VALUE (MeV)	EVTS	DOCUMENT ID		TECN	CHG	COMMENT
149.1 ±0.8 OUR FIT						
149.1 ±0.8 OUR AVERAGE						
148.1 ±0.4 ±1.7	5.4M	[1,2] FUJIKAWA	08	BELL	±	$\tau^- \to \pi^-\pi^0\nu_\tau$
149.0 ±1.2		[2,3] SCHAEL	05C	ALEP		$\tau^- \to \pi^-\pi^0\nu_\tau$
149.9 ±2.3 ±2.0	500k	[4] ACHASOV	02	SND	±	1.02 $e^+e^- \to \pi^+\pi^-\pi^0$
150.4 ±1.4 ±1.4	87k	[5,6] ANDERSON	00A	CLE2		$\tau^- \to \pi^-\pi^0\nu_\tau$
• • • We do not use the following data for averages, fits, limits, etc. • • •						
139.90±0.46		[7] BARTOS	17A	RVUE		$\tau^- \to \pi^-\pi^0\nu_\tau$
143.7 ±1.3 ±1.2	1.98M	[4] ALOISIO	03	KLOE	±	1.02 $e^+e^- \to \pi^+\pi^-\pi^0$

Downloaded from https://academic.oup.com/ptep/article/2022/8/083C01/6651666 by KIT Library user on 27 September 2022

142.9 ±1.3 ±1.4 1.98M	[8] ALOISIO	03	KLOE	−	1.02 $e^+e^- \to \pi^+\pi^-\pi^0$
144.7 ±1.4 ±1.2 1.98M	[8] ALOISIO	03	KLOE	+	1.02 $e^+e^- \to \pi^+\pi^-\pi^0$
150.2 ±2.0 $^{+0.7}_{-1.6}$	[9] SANZ-CILLERO	03	RVUE		$\tau^- \to \pi^-\pi^0\nu_\tau$
150.9 ±2.2 ±2.0 500k	[10] ACHASOV	02	SND		1.02 $e^+e^- \to \pi^+\pi^-\pi^0$

[1] $|F_\pi(0)|^2$ fixed to 1.
[2] From the GOUNARIS 68 parametrization of the pion form factor.
[3] The error combines statistical and systematic uncertainties. Supersedes BARATE 97M.
[4] Assuming $m_{\rho^+} = m_{\rho^-}$, $\Gamma_{\rho^+} = \Gamma_{\rho^-}$.
[5] $\rho(1700)$ mass and width fixed at 1700 MeV and 235 MeV respectively.
[6] From the GOUNARIS 68 parametrization of the pion form factor. The second error is a model error taking into account different parametrizations of the pion form factor.
[7] Applies the Unitary & Analytic Model of the pion electromagnetic form factor of DUBNICKA 10 to analyze the data of FUJIKAWA 08.
[8] Without limitations on masses and widths.
[9] Using the data of BARATE 97M and the effective chiral Lagrangian.
[10] Assuming $m_{\rho^0} = m_{\rho^\pm}$, $g_{\rho^0\pi\pi} = g_{\rho^\pm\pi\pi}$.

MIXED CHARGES, OTHER REACTIONS

VALUE (MeV)	EVTS	DOCUMENT ID		TECN	CHG	COMMENT
149.5±1.3	600k	[1] ABELE	99E	CBAR	0±	0.0 $\overline{p}p \to \pi^+\pi^-\pi^0$

[1] Assuming the equality of ρ^+ and ρ^- masses and widths.

CHARGED ONLY, HADROPRODUCED

VALUE (MeV)	EVTS	DOCUMENT ID		TECN	CHG	COMMENT
150.2± 2.4 OUR FIT						
150.2± 2.4 OUR AVERAGE						
152.8± 4.3		ABELE	97	CBAR		$\overline{p}n \to \pi^-\pi^0\pi^0$
155 ±11	2.9k	[1] CAPRARO	87	SPEC	−	200 π^-Cu $\to \pi^-\pi^0$Cu
154 ±20	967	[1] CAPRARO	87	SPEC	−	200 π^-Pb $\to \pi^-\pi^0$Pb
150 ± 5		HUSTON	86	SPEC	+	202 π^+A $\to \pi^+\pi^0$A
146 ±12	6.5k	[2] BYERLY	73	OSPK	−	5 π^-p
148.2± 4.1	9.6k	[3] PISUT	68	RVUE	−	1.7–3.2 π^-p, $t<10$
146 ±13	900	EISNER	67	HBC	−	4.2 π^-p, $t<10$
• • • We do not use the following data for averages, fits, limits, etc. • • •						
137.0± 0.4		[4] ABLIKIM	17	BES3		$J/\psi \to \gamma 3\pi$

[1] Width errors enlarged by us to $4\Gamma/\sqrt{N}$; see the note with the $K^*(892)$ mass.
[2] Phase shift analysis. Systematic errors added corresponding to spread of different fits.
[3] From fit of 3-parameter relativistic P-wave Breit-Wigner to total mass distribution. Includes BATON 68, MILLER 67B, ALFF-STEINBERGER 66, HAGOPIAN 66, HAGOPIAN 66B, JACOBS 66B, JAMES 66, WEST 66, BLIEDEN 65 and CARMONY 64.
[4] S-matrix pole at a fixed ρ meson mass of 775.49 MeV.

NEUTRAL ONLY, PHOTOPRODUCED

VALUE (MeV)	EVTS	DOCUMENT ID		TECN	COMMENT
$151.5^{+1.9}_{-2.1}$ OUR AVERAGE					
151.3± 2.2$^{+1.6}_{-2.8}$	900k	ANDREEV	20	H1	$ep \to e\pi^+\pi^-p$
155 ± 5 ± 2	63.5k	[1] ABRAMOWICZ	12	ZEUS	$ep \to e\pi^+\pi^-p$
146 ± 3 ±13	79k	[2] BREITWEG	98B	ZEUS	50–100 γp
150.9± 3.0		BARTALUCCI	78	CNTR	$\gamma p \to e^+e^-p$
• • • We do not use the following data for averages, fits, limits, etc. • • •					
138 ± 3	79k	[3] BREITWEG	98B	ZEUS	50–100 γp
147 ±11		GLADDING	73	CNTR	2.9–4.7 γp
155 ±12	2430	BALLAM	72	HBC	4.7 γp
145 ±13	1930	BALLAM	72	HBC	2.8 γp
140 ± 5		ALVENSLEB...	70	CNTR	γA, $t<0.01$
146.1± 2.9	140k	BIGGS	70	CNTR	$<4.1\ \gamma$C $\to \pi^+\pi^-$C
160 ±10		LANZEROTTI	68	CNTR	γp
130 ± 5	4000	ASBURY	67B	CNTR	$\gamma +$ Pb

[1] Using the KUHN 90 parametrization of the pion form factor, neglecting $\rho-\omega$ interference.
[2] From the parametrization according to SOEDING 66.
[3] From the parametrization according to ROSS 66.

NEUTRAL ONLY, OTHER REACTIONS

VALUE (MeV)	EVTS	DOCUMENT ID		TECN	COMMENT
150.9 ± 1.7 OUR AVERAGE		Error includes scale factor of 1.1.			
122 ±20		BERTIN	97C	OBLX	0.0 $\overline{p}p \to \pi^+\pi^-\pi^0$
145.7 ± 5.3		WEIDENAUER	93	ASTE	$\overline{p}p \to \pi^+\pi^-\omega$
144.9 ± 3.7		DUBNICKA	89	RVUE	π form factor
148 ± 6		[1,2] BOHACIK	80	RVUE	
152 ± 9		[3] WICKLUND	78	ASPK	3,4,6 $\pi^\pm pN$
154 ± 2	76k	DEUTSCH...	76	HBC	16 π^+p
157 ± 8	6.8k	[4] RATCLIFF	72	ASPK	15 π^-p, $t<0.3$
143 ± 8	1.7k	REYNOLDS	69	HBC	2.26 π^-p
• • • We do not use the following data for averages, fits, limits, etc. • • •					
150.85± 0.55±0.67	970k	[5] ABLIKIM	18C	BES3	$\eta'(958) \to \gamma\pi^+\pi^-$
150.18± 0.55±0.65	970k	[6] ABLIKIM	18C	BES3	$\eta'(958) \to \gamma\pi^+\pi^-$
147.0 ± 2.5	600k	[7] ABELE	99E	CBAR	0.0 $\overline{p}p \to \pi^+\pi^-\pi^0$
146 ± 3	4.9k	[8] ADAMS	97	E665	470 $\mu p \to \mu XB$
160.0 $^{+4.1}_{-4.0}$		[9] CHABAUD	83	ASPK	17 π^-p polarized
155 ± 1		[10] HEYN	81	RVUE	π form factor
148.0 ± 1.3		[1,2] LANG	79	RVUE	
146 ±14	4.1k	ENGLER	74	DBC	6 $\pi^+n \to \pi^+\pi^-p$
143 ±13		[2] ESTABROOKS	74	RVUE	17 $\pi^-p \to \pi^+\pi^-n$
160 ±10	32k	[1] PROTOPOP...	73	HBC	7.1 π^+p, $t<0.4$
145 ±12	2.2k	[3,11] HYAMS	68	OSPK	11.2 π^-p
163 ±15	13.3k	[12] PISUT	68	RVUE	1.7–3.2 π^-p, $t<10$

[1] From pole extrapolation.
[2] From phase shift analysis of GRAYER 74 data.
[3] Width errors enlarged by us to $4\Gamma/\sqrt{N}$; see the note with the $K^*(892)$ mass.
[4] Published values contain misprints. Corrected by private communication RATCLIFF 74.
[5] From a fit to $\pi^+\pi^-$ mass using $\rho(770)$ (parametrized with the Gounaris-Sakurai approach), $\omega(782)$, and box anomaly components.
[6] From a fit to $\pi^+\pi^-$ mass using $\rho(770)$ (parametrized with the Gounaris-Sakurai approach), $\omega(782)$, and $\rho(1450)$ components.
[7] Using relativistic Breit-Wigner and taking into account ρ-ω interference.
[8] Systematic errors not evaluated.
[9] From fit of 3-parameter relativistic Breit-Wigner to helicity-zero part of P-wave intensity. CHABAUD 83 includes data of GRAYER 74.
[10] HEYN 81 includes all spacelike and timelike F_π values until 1978.
[11] Of HYAMS 68 six parametrizations this is theoretically soundest. MR
[12] Includes MALAMUD 69, ARMENISE 68, BACON 67, HUWE 67, MILLER 67B, ALFF-STEINBERGER 66, HAGOPIAN 66, HAGOPIAN 66B, JACOBS 66B, JAMES 66, WEST 66, GOLDHABER 64, ABOLINS 63.

$\Gamma_{\rho(770)^0} - \Gamma_{\rho(770)^\pm}$

VALUE (MeV)	EVTS	DOCUMENT ID		TECN	COMMENT
0.3 ±1.3 OUR AVERAGE		Error includes scale factor of 1.4.			
−0.2 ±1.0		[1] SCHAEL	05C	ALEP	$\tau^- \to \pi^-\pi^0\nu_\tau$
3.6 ±1.8 ±1.7	1.98M	[2] ALOISIO	03	KLOE	1.02 $e^+e^- \to \pi^+\pi^-\pi^0$
• • • We do not use the following data for averages, fits, limits, etc. • • •					
4.66±0.85		[3] BARTOS	17A	RVUE	$e^+e^- \to \pi^+\pi^-$, $\tau^- \to \pi^-\pi^0\nu_\tau$

[1] From the combined fit of the τ^- data from ANDERSON 00A and SCHAEL 05C and e^+e^- data from the compilation of BARKOV 85, AKHMETSHIN 04, and ALOISIO 05. Supersedes BARATE 97M.
[2] Assuming $m_{\rho^+} = m_{\rho^-}$, $\Gamma_{\rho^+} = \Gamma_{\rho^-}$.
[3] Applies the Unitary & Analytic Model of the pion electromagnetic form factor of DUBNICKA 10 to analyze the data of ACHASOV 06, AKHMETSHIN 07, AUBERT 09AS, AMBROSINO 11A, and FUJIKAWA 08.

$\Gamma_{\rho(770)^+} - \Gamma_{\rho(770)^-}$

VALUE	EVTS	DOCUMENT ID		TECN	COMMENT
1.8±2.0±0.5	1.98M	[1] ALOISIO	03	KLOE	1.02 $e^+e^- \to \pi^+\pi^-\pi^0$

[1] Without limitations on masses and widths.

$\rho(770)$ DECAY MODES

	Mode	Fraction (Γ_i/Γ)	Scale factor/ Confidence level
Γ_1	$\pi\pi$	~ 100 %	
Γ_2	$K\overline{K}$		
	$\rho(770)^\pm$ decays		
Γ_3	$\pi^\pm\pi^0$	~ 100 %	
Γ_4	$\pi^\pm\gamma$	(4.5 ±0.5) $\times 10^{-4}$	S=2.2
Γ_5	$\pi^\pm\eta$	< 6 $\times 10^{-3}$	CL=84%
Γ_6	$\pi^\pm\pi^+\pi^-\pi^0$	< 2.0 $\times 10^{-3}$	CL=84%
	$\rho(770)^0$ decays		
Γ_7	$\pi^+\pi^-$	~ 100 %	
Γ_8	$\pi^+\pi^-\gamma$	(9.9 ±1.6) $\times 10^{-3}$	
Γ_9	$\pi^0\gamma$	(4.7 ±0.8) $\times 10^{-4}$	S=1.7
Γ_{10}	$\eta\gamma$	(3.00±0.21) $\times 10^{-4}$	
Γ_{11}	$\pi^0\pi^0\gamma$	(4.5 ±0.8) $\times 10^{-5}$	
Γ_{12}	$\mu^+\mu^-$	[a] (4.55±0.28) $\times 10^{-5}$	
Γ_{13}	e^+e^-	[a] (4.72±0.05) $\times 10^{-5}$	
Γ_{14}	$\pi^+\pi^-\pi^0$	($1.01^{+0.54}_{-0.36}$±0.34) $\times 10^{-4}$	
Γ_{15}	$\pi^+\pi^-\pi^+\pi^-$	(1.8 ±0.9) $\times 10^{-5}$	
Γ_{16}	$\pi^+\pi^-\pi^0\pi^0$	(1.6 ±0.8) $\times 10^{-5}$	
Γ_{17}	$\pi^0e^+e^-$	< 1.2 $\times 10^{-5}$	CL=90%
Γ_{18}	ηe^+e^-		

[a] The $\omega\rho$ interference is then due to $\omega\rho$ mixing only, and is expected to be small. If $e\mu$ universality holds, $\Gamma(\rho^0 \to \mu^+\mu^-) = \Gamma(\rho^0 \to e^+e^-) \times 0.99785$.

CONSTRAINED FIT INFORMATION

An overall fit to the total width and a partial width uses 10 measurements and one constraint to determine 3 parameters. The overall fit has a $\chi^2 = 10.7$ for 8 degrees of freedom.

Downloaded from https://academic.oup.com/ptep/article/2022/8/083C01/6651666 by KIT Library user on 27 September 2022

The following *off-diagonal* array elements are the correlation coefficients $\langle \delta p_i \delta p_j \rangle / (\delta p_i \cdot \delta p_j)$, in percent, from the fit to parameters p_i, including the branching fractions, $x_i \equiv \Gamma_i/\Gamma_{total}$. The fit constrains the x_i whose labels appear in this array to sum to one.

	x_3	x_4
x_4	−100	
Γ	15	−15

	Mode	Rate (MeV)	Scale factor
Γ_3	$\pi^\pm\pi^0$	150.2 ±2.4	
Γ_4	$\pi^\pm\gamma$	0.068±0.007	2.3

CONSTRAINED FIT INFORMATION

An overall fit to the total width, a partial width, and 7 branching ratios uses 21 measurements and one constraint to determine 9 parameters. The overall fit has a χ^2 = 9.5 for 13 degrees of freedom.

The following *off-diagonal* array elements are the correlation coefficients $\langle \delta p_i \delta p_j \rangle / (\delta p_i \cdot \delta p_j)$, in percent, from the fit to parameters p_i, including the branching fractions, $x_i \equiv \Gamma_i/\Gamma_{total}$. The fit constrains the x_i whose labels appear in this array to sum to one.

	x_7	x_8	x_9	x_{10}	x_{11}	x_{12}	x_{13}	x_{15}
x_8	−100							
x_9	−5	0						
x_{10}	−1	0	1					
x_{11}	−1	0	0	0				
x_{12}	2	−3	0	0	0			
x_{13}	0	0	−6	−9	0	0		
x_{15}	−1	0	0	0	0	0	0	
Γ	0	0	3	5	0	0	−54	0

	Mode		Rate (MeV)	Scale factor
Γ_7	$\pi^+\pi^-$		147.5 ±0.9	
Γ_8	$\pi^+\pi^-\gamma$		1.48 ±0.24	
Γ_9	$\pi^0\gamma$		0.070 ±0.012	1.7
Γ_{10}	$\eta\gamma$		0.0447 ±0.0032	
Γ_{11}	$\pi^0\pi^0\gamma$		0.0066 ±0.0012	
Γ_{12}	$\mu^+\mu^-$	[a]	0.0068 ±0.0004	
Γ_{13}	e^+e^-	[a]	0.00704±0.00006	
Γ_{15}	$\pi^+\pi^-\pi^+\pi^-$		0.0027 ±0.0014	

$\rho(770)$ PARTIAL WIDTHS

$\Gamma(\pi^\pm\gamma)$ — Γ_4

VALUE (keV)	DOCUMENT ID		TECN	CHG	COMMENT
68 ±7 OUR FIT Error includes scale factor of 2.3.					
68 ±7 OUR AVERAGE Error includes scale factor of 2.2. See the ideogram below.					
81 ±4 ±4	CAPRARO	87	SPEC	−	200 π^-A → $\pi^-\pi^0$A
59.8±4.0	HUSTON	86	SPEC	+	202 π^+A → $\pi^+\pi^0$A
71 ±7	JENSEN	83	SPEC	−	156–260 π^-A → $\pi^-\pi^0$A

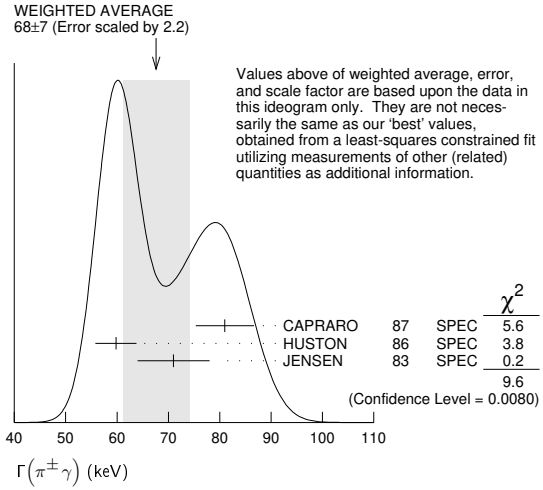

$\Gamma(\pi^0\gamma)$ — Γ_9

VALUE (keV)	EVTS	DOCUMENT ID		TECN	COMMENT
• • • We do not use the following data for averages, fits, limits, etc. • • •					
77±17±11	36500	[1] ACHASOV	03	SND	0.60–0.97 e^+e^- → $\pi^0\gamma$
121±31		DOLINSKY	89	ND	e^+e^- → $\pi^0\gamma$

[1] Using Γ_{total}= 147.9 ± 1.3 MeV and B(ρ → $\pi^0\gamma$) from ACHASOV 03.

$\Gamma(\eta\gamma)$ — Γ_{10}

VALUE (keV)	DOCUMENT ID		TECN	COMMENT
• • • We do not use the following data for averages, fits, limits, etc. • • •				
62±17	[1] DOLINSKY	89	ND	e^+e^- → $\eta\gamma$

[1] Solution corresponding to constructive ω-ρ interference.

$\Gamma(e^+e^-)$ — Γ_{13}

VALUE (keV)	EVTS	DOCUMENT ID		TECN	COMMENT
7.04 ±0.06 OUR FIT					
7.04 ±0.06 OUR AVERAGE					
7.048±0.057±0.050	900k	[1] AKHMETSHIN	07		e^+e^- → $\pi^+\pi^-$
7.06 ±0.11 ±0.05	114k	[2,3] AKHMETSHIN	04	CMD2	e^+e^- → $\pi^+\pi^-$
6.77 ±0.10 ±0.30		BARKOV	85	OLYA	e^+e^- → $\pi^+\pi^-$
• • • We do not use the following data for averages, fits, limits, etc. • • •					
7.12 ±0.02 ±0.11	800k	[4] ACHASOV	06	SND	e^+e^- → $\pi^+\pi^-$
6.3 ±0.1		[5] BENAYOUN	98	RVUE	e^+e^- → $\pi^+\pi^-$, $\mu^+\mu^-$

[1] A combined fit of AKHMETSHIN 07, AULCHENKO 06, and AULCHENKO 05.
[2] Using the GOUNARIS 68 parametrization with the complex phase of the ρ-ω interference.
[3] From a fit in the energy range 0.61 to 0.96 GeV. Update of AKHMETSHIN 02.
[4] Supersedes ACHASOV 05A.
[5] Using the data of BARKOV 85 in the hidden local symmetry model.

$\Gamma(\pi^+\pi^-\pi^+\pi^-)$ — Γ_{15}

VALUE (keV)	EVTS	DOCUMENT ID		TECN	COMMENT
• • • We do not use the following data for averages, fits, limits, etc. • • •					
2.8±1.4±0.5	153	AKHMETSHIN	00	CMD2	0.6–0.97 e^+e^- → $\pi^+\pi^-\pi^+\pi^-$

$\rho(770)$ $\Gamma(e^+e^-)\Gamma(i)/\Gamma^2(total)$

$\Gamma(e^+e^-)/\Gamma_{total} \times \Gamma(\pi^+\pi^-)/\Gamma_{total}$ — $\Gamma_{13}/\Gamma \times \Gamma_7/\Gamma$

VALUE (units 10^{-5})	EVTS	DOCUMENT ID		TECN	COMMENT
4.89 ±0.04 OUR AVERAGE					
4.889±0.015±0.039		[1] ACHASOV	21	SND	e^+e^- → $\pi^+\pi^-$
4.876±0.023±0.064	800k	[2,3] ACHASOV	06	SND	e^+e^- → $\pi^+\pi^-$
• • • We do not use the following data for averages, fits, limits, etc. • • •					
4.72 ±0.02		[4] BENAYOUN	10	RVUE	0.4–1.05 e^+e^-

[1] From a fit of the cross section in the energy range 0.525 < $\sqrt{s}$ < 0.883 GeV parameterized by the sum of the Breit-Wigner amplitudes for the $\rho(770)$, ω and $\rho(1450)$ resonances.
[2] Supersedes ACHASOV 05A.
[3] A fit of the SND data from 400 to 1000 MeV using parameters of the $\rho(1450)$ and $\rho(1700)$ from a fit of the data of BARKOV 85, BISELLO 89 and ANDERSON 00A.
[4] A simultaneous fit of e^+e^- → $\pi^+\pi^-$, $\pi^+\pi^-\pi^0$, $\pi^0\gamma$, $\eta\gamma$ data.

$\Gamma(e^+e^-)/\Gamma_{total} \times \Gamma(\eta\gamma)/\Gamma_{total}$ — $\Gamma_{13}/\Gamma \times \Gamma_{10}/\Gamma$

VALUE (units 10^{-8})	EVTS	DOCUMENT ID		TECN	COMMENT
1.42±0.10 OUR FIT					
1.45±0.12 OUR AVERAGE					
1.32±0.14±0.08	33k	[1] ACHASOV	07B	SND	0.6–1.38 e^+e^- → $\eta\gamma$
1.50±0.65±0.09	17.4k	[2] AKHMETSHIN	05	CMD2	0.60-1.38 e^+e^- → $\eta\gamma$
1.61±0.20±0.11	23k	[3,4] AKHMETSHIN	01B	CMD2	e^+e^- → $\eta\gamma$
1.85±0.49		[5] DOLINSKY	89	ND	e^+e^- → $\eta\gamma$
• • • We do not use the following data for averages, fits, limits, etc. • • •					
1.05±0.02		[6] BENAYOUN	10	RVUE	0.4–1.05 e^+e^-

[1] From a combined fit of $\sigma(e^+e^-$ → $\eta\gamma)$ with η → $3\pi^0$ and η → $\pi^+\pi^-\pi^0$, and fixing B(η → $3\pi^0$) / B(η → $\pi^+\pi^-\pi^0$) = 1.44 ± 0.04. Recalculated by us from the cross section at the peak. Supersedes ACHASOV 00D and ACHASOV 06A.
[2] From the η → 2γ decay and using B(η → $\gamma\gamma$)= 39.43 ± 0.26%.
[3] From the η → $3\pi^0$ decay and using B(η → $3\pi^0$)= (32.24 ± 0.29) × 10^{-2}.
[4] The combined fit from 600 to 1380 MeV taking into account $\rho(770)$, $\omega(782)$, $\phi(1020)$, and $\rho(1450)$ (mass and width fixed at 1450 MeV and 310 MeV respectively).
[5] Recalculated by us from the cross section in the peak.
[6] A simultaneous fit of e^+e^- → $\pi^+\pi^-$, $\pi^+\pi^-\pi^0$, $\pi^0\gamma$, $\eta\gamma$ data.

$\Gamma(e^+e^-)/\Gamma_{total} \times \Gamma(\pi^0\gamma)/\Gamma_{total}$ — $\Gamma_{13}/\Gamma \times \Gamma_9/\Gamma$

VALUE (units 10^{-8})	EVTS	DOCUMENT ID		TECN	COMMENT
2.2 ±0.4 OUR FIT Error includes scale factor of 1.7.					
2.21 ±0.34 OUR AVERAGE Error includes scale factor of 1.6. See the ideogram below.					
1.98 ±0.22 ±0.10		[1] ACHASOV	16A	SND	0.60-1.38 e^+e^- → $\pi^0\gamma$
2.90 $^{+0.60}_{-0.55}$ ±0.18	18k	AKHMETSHIN	05	CMD2	0.60-1.38 e^+e^- → $\pi^0\gamma$
3.61 ±0.74 ±0.49	10k	[2] DOLINSKY	89	ND	e^+e^- → $\pi^0\gamma$
• • • We do not use the following data for averages, fits, limits, etc. • • •					
1.875±0.026		[3] BENAYOUN	10	RVUE	0.4–1.05 e^+e^-
2.37 ±0.53 ±0.33	36k	[4] ACHASOV	03	SND	0.60–0.97 e^+e^- → $\pi^0\gamma$

Downloaded from https://academic.oup.com/ptep/article/2022/8/083C01/6651666 by KIT Library user on 27 September 2022

[1] From the VMD model with the prho(770), $\omega(782)$, $\phi(1020)$ resonances, and an additional resonance describing the total contribution of the $\rho(1450)$ and $\omega(1420)$ states. Supersedes ACHASOV 03.
[2] Recalculated by us from the cross section in the peak.
[3] A simultaneous fit of $e^+e^- \to \pi^+\pi^-$, $\pi^+\pi^-\pi^0$, $\pi^0\gamma$, $\eta\gamma$ data.
[4] Using $\sigma_{\phi \to \pi^0\gamma}$ from ACHASOV 00 and m_ρ = 775.97 MeV in the model with the energy-independent phase of ρ-ω interferenceequal to $(-10.2 \pm 7.0)^\circ$.

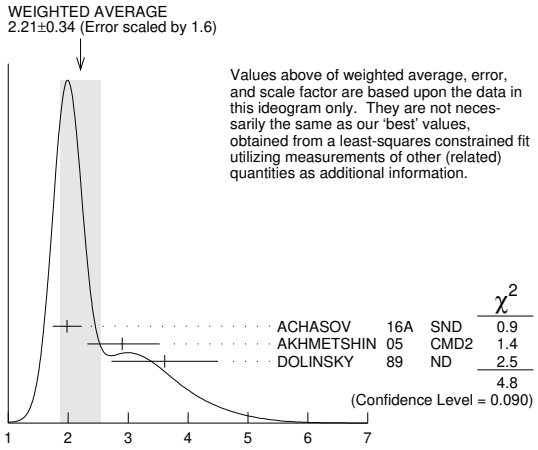

$\Gamma(e^+e^-)/\Gamma_{total} \times \Gamma(\pi^+\pi^-\pi^0)/\Gamma_{total}$ — $\Gamma_{13}/\Gamma \times \Gamma_{14}/\Gamma$

VALUE (units 10^{-9})	EVTS	DOCUMENT ID		TECN	COMMENT
• • • We do not use the following data for averages, fits, limits, etc. • • •					
0.903 ± 0.076		[1] BENAYOUN	10	RVUE	0.4–1.05 e^+e^-
$4.58^{+2.46}_{-1.64} \pm 1.56$	1.2M	[2] ACHASOV	03D	RVUE	0.44–2.00 $e^+e^- \to \pi^+\pi^-\pi^0$

[1] A simultaneous fit of $e^+e^- \to \pi^+\pi^-$, $\pi^+\pi^-\pi^0$, $\pi^0\gamma$, $\eta\gamma$ data.
[2] Statistical significance is less than 3σ.

$\rho(770)$ BRANCHING RATIOS

$\Gamma(\pi^\pm\eta)/\Gamma(\pi\pi)$ — Γ_5/Γ_1

VALUE (units 10^{-4})	CL%	DOCUMENT ID		TECN	CHG	COMMENT
<60	84	FERBEL	66	HBC	±	$\pi^\pm p$ above 2.5

$\Gamma(\pi^\pm\pi^+\pi^-\pi^0)/\Gamma(\pi\pi)$ — Γ_6/Γ_1

VALUE (units 10^{-4})	CL%	DOCUMENT ID		TECN	CHG	COMMENT
<20	84	FERBEL	66	HBC	±	$\pi^\pm p$ above 2.5
• • • We do not use the following data for averages, fits, limits, etc. • • •						
35 ± 40		JAMES	66	HBC	+	2.1 $\pi^+ p$

$\Gamma(\pi^+\pi^-\gamma)/\Gamma_{total}$ — Γ_8/Γ

VALUE	CL%	DOCUMENT ID		TECN	COMMENT
0.0099±0.0016 OUR FIT					
0.0099±0.0016		[1] DOLINSKY	91	ND	$e^+e^- \to \pi^+\pi^-\gamma$
• • • We do not use the following data for averages, fits, limits, etc. • • •					
0.0111 ± 0.0014		[2] VASSERMAN	88	ND	$e^+e^- \to \pi^+\pi^-\gamma$
<0.005	90	[3] VASSERMAN	88	ND	$e^+e^- \to \pi^+\pi^-\gamma$

[1] Bremsstrahlung from a decay pion and for photon energy above 50 MeV.
[2] Superseded by DOLINSKY 91.
[3] Structure radiation due to quark rearrangement in the decay.

$\Gamma(\pi^0\gamma)/\Gamma_{total}$ — Γ_9/Γ

VALUE (units 10^{-4})	EVTS	DOCUMENT ID		TECN	COMMENT
• • • We do not use the following data for averages, fits, limits, etc. • • •					
4.20 ± 0.52		[1] ACHASOV	16A	SND	0.60–1.38 $e^+e^- \to \pi^0\gamma$
$6.21^{+1.28}_{-1.18} \pm 0.39$	18k	[2,3] AKHMETSHIN	05	CMD2	0.60-1.38 $e^+e^- \to \pi^0\gamma$
$5.22 \pm 1.17 \pm 0.75$	36k	[3,4] ACHASOV	03	SND	0.60–0.97 $e^+e^- \to \pi^0\gamma$
6.8 ± 1.7		[5] BENAYOUN	96	RVUE	0.54-1.04 $e^+e^- \to \pi^0\gamma$
7.9 ± 2.0		[3] DOLINSKY	89	ND	$e^+e^- \to \pi^0\gamma$

[1] Using $B(\rho \to e^+e^-)$ from PDG 15. Supersedes ACHASOV 03.
[2] Using $B(\rho \to e^+e^-) = (4.67 \pm 0.09) \times 10^{-5}$.
[3] Not independent of the corresponding $\Gamma(e^+e^-) \times \Gamma(\pi^0\gamma)/\Gamma^2_{total}$.
[4] Using $B(\rho \to e^+e^-) = (4.54 \pm 0.10) \times 10^{-5}$.
[5] Reanalysis of DRUZHININ 84, DOLINSKY 89, and DOLINSKY 91 taking into account a triangle anomaly contribution.

$\Gamma(\eta\gamma)/\Gamma_{total}$ — Γ_{10}/Γ

VALUE (units 10^{-4})	EVTS	DOCUMENT ID		TECN	CHG	COMMENT
3.00±0.21 OUR FIT						
2.90±0.32 OUR AVERAGE						
$2.79 \pm 0.34 \pm 0.03$	33k	[1] ACHASOV	07B	SND		0.6–1.38 $e^+e^- \to \eta\gamma$
3.6 ± 0.9		[2] ANDREWS	77	CNTR	0	6.7–10 γCu
• • • We do not use the following data for averages, fits, limits, etc. • • •						
$3.21 \pm 1.39 \pm 0.20$	17.4k	[3,4] AKHMETSHIN	05	CMD2		0.60-1.38 $e^+e^- \to \eta\gamma$
$3.39 \pm 0.42 \pm 0.23$		[2,5,6] AKHMETSHIN	01B	CMD2		$e^+e^- \to \eta\gamma$
$1.9^{+0.6}_{-0.8}$		[7] BENAYOUN	96	RVUE		0.54-1.04 $e^+e^- \to \eta\gamma$
4.0 ± 1.1		[2,4] DOLINSKY	89	ND		$e^+e^- \to \eta\gamma$

[1] ACHASOV 07B reports $[\Gamma(\rho(770) \to \eta\gamma)/\Gamma_{total}] \times [B(\rho(770) \to e^+e^-)] = (1.32 \pm 0.14 \pm 0.08) \times 10^{-8}$ which we divide by our best value $B(\rho(770) \to e^+e^-) = (4.72 \pm 0.05) \times 10^{-5}$. Our first error is their experiment's error and our second error is the systematic error from using our best value. Supersedes ACHASOV 00D and ACHASOV 06A.
[2] Solution corresponding to constructive ω-ρ interference.
[3] Using $B(\rho \to e^+e^-) = (4.67 \pm 0.09) \times 10^{-5}$ and $B(\eta \to \gamma\gamma) = 39.43 \pm 0.26\%$.
[4] Not independent of the corresponding $\Gamma(e^+e^-) \times \Gamma(\eta\gamma)/\Gamma^2_{total}$.
[5] The combined fit from 600 to 1380 MeV taking into account $\rho(770)$, $\omega(782)$, $\phi(1020)$, and $\rho(1450)$ (mass and width fixed at 1450 MeV and 310 MeV respectively).
[6] Using $B(\rho \to e^+e^-) = (4.75 \pm 0.10) \times 10^{-5}$ from AKHMETSHIN 02 and $B(\eta \to 3\pi^0) = (32.24 \pm 0.29) \times 10^{-2}$.
[7] Reanalysis of DRUZHININ 84, DOLINSKY 89, and DOLINSKY 91 taking into account a triangle anomaly contribution. Constructive ρ-ω interference solution.

$\Gamma(\pi^0\pi^0\gamma)/\Gamma_{total}$ — Γ_{11}/Γ

VALUE (units 10^{-5})	EVTS	DOCUMENT ID		TECN	COMMENT
4.5±0.8 OUR FIT					
$4.5^{+0.9}_{-0.8}$ OUR AVERAGE					
$5.2^{+1.5}_{-1.3} \pm 0.6$	190	[1] AKHMETSHIN	04B	CMD2	0.6–0.97 $e^+e^- \to \pi^0\pi^0\gamma$
$4.1^{+1.0}_{-0.9} \pm 0.3$	295	[2] ACHASOV	02F	SND	0.36–0.97 $e^+e^- \to \pi^0\pi^0\gamma$
• • • We do not use the following data for averages, fits, limits, etc. • • •					
$4.8^{+3.4}_{-1.8} \pm 0.5$	63	[3] ACHASOV	00G	SND	$e^+e^- \to \pi^0\pi^0\gamma$

[1] This branching ratio includes the conventional VMD mechanism $\rho \to \omega\pi^0$, $\omega \to \pi^0\gamma$, and the new decay mode $\rho \to f_0(500)\gamma$, $f_0(500) \to \pi^0\pi^0$ with a branching ratio $(2.0^{+1.1}_{-0.9} \pm 0.3) \times 10^{-5}$ differing from zero by 2.0 standard deviations.
[2] This branching ratio includes the conventional VMD mechanism $\rho \to \omega\pi^0$, $\omega \to \pi^0\gamma$ and the new decay mode $\rho \to f_0(500)\gamma$, $f_0(500) \to \pi^0\pi^0$ with a branching ratio $(1.9^{+0.9}_{-0.8} \pm 0.4) \times 10^{-5}$ differing from zero by 2.4 standard deviations. Supersedes ACHASOV 00G.
[3] Superseded by ACHASOV 02F.

$\Gamma(\mu^+\mu^-)/\Gamma(\pi^+\pi^-)$ — Γ_{12}/Γ_7

VALUE (units 10^{-5})	DOCUMENT ID		TECN	COMMENT
4.60±0.28 OUR FIT				
4.6 ±0.2 ±0.2	ANTIPOV	89	SIGM	π^-Cu $\to \mu^+\mu^-\pi^-$Cu
• • • We do not use the following data for averages, fits, limits, etc. • • •				
$8.2^{+1.6}_{-3.6}$	[1] ROTHWELL	69	CNTR	Photoproduction
5.6 ± 1.5	[2] WEHMANN	69	OSPK	12 π^-C, Fe
$9.7^{+3.1}_{-3.3}$	[3,4] HYAMS	67	OSPK	11 π^-Li, H

[1] Possibly large ρ-ω interference leads us to increase the minus error.
[2] Result contains 11 ± 11% correction using SU(3) for central value. The error on the correction takes account of possible ρ-ω interference and the upper limit agrees with the upper limit of $\omega \to \mu^+\mu^-$ from this experiment.
[3] But he even enlarges his error to take residual ω contamination into account. Since his value is high, seems the other experiments also can't have too many ω's. But maybe Hyams has additional μ's from $\rho \to \pi\pi$, decaying π's.
[4] HYAMS 67's mass resolution is 20 MeV. The ω region was excluded.

$\Gamma(e^+e^-)/\Gamma(\pi\pi)$ — Γ_{13}/Γ_1

VALUE (units 10^{-4})	DOCUMENT ID		TECN	COMMENT
• • • We do not use the following data for averages, fits, limits, etc. • • •				
0.40 ± 0.05	[1,2] BENAKSAS	72	OSPK	$e^+e^- \to \pi^+\pi^-$

[1] The ρ' contribution is not taken into account.
[2] Barkov excludes Auslender and Benaksas for large statistical and systematic errors.

$\Gamma(\pi^+\pi^-\pi^0)/\Gamma_{total}$ — Γ_{14}/Γ

VALUE (units 10^{-4})	CL%	EVTS	DOCUMENT ID		TECN	COMMENT
0.88±0.23±0.30			[1] LEES	21B	BABR	10.5 $e^+e^- \to \pi^+\pi^-\pi^0\gamma$
• • • We do not use the following data for averages, fits, limits, etc. • • •						
$1.01^{+0.54}_{-0.36} \pm 0.34$		1.2M	[2] ACHASOV	03D	RVUE	0.44–2.00 $e^+e^- \to \pi^+\pi^-\pi^0$
<1.2	90		VASSERMAN	88B	ND	$e^+e^- \to \pi^+\pi^-\pi^0$

[1] From the cross section for $e^+e^- \to \pi^+\pi^-\pi^0$ with contributions from $\rho(770)$, $\omega(782)$, $\phi(1020)$, $\omega(1420)$, and $\omega(1650)$. Statistical evidence is more than 6 σ.
[2] Statistical significance is less than 3σ.

Downloaded from https://academic.oup.com/ptep/article/2022/8/083C01/6651666 by KIT Library user on 27 September 2022

$\Gamma(\pi^+\pi^-\pi^0)/\Gamma(\pi\pi)$ — Γ_{14}/Γ_1

VALUE	CL%	DOCUMENT ID		TECN	CHG	COMMENT
• • • We do not use the following data for averages, fits, limits, etc. • • •						
~ 0.01		BRAMON	86	RVUE	0	$J/\psi \to \omega\pi^0$
<0.01	84	[1] ABRAMS	71	HBC	0	3.7 $\pi^+ p$

[1] Model dependent, assumes $I = 1$, 2, or 3 for the 3π system.

$\Gamma(\pi^+\pi^-\pi^+\pi^-)/\Gamma_{total}$ — Γ_{15}/Γ

VALUE (units 10^{-5})	CL%	EVTS	DOCUMENT ID		TECN	COMMENT
1.8±0.9 OUR FIT						
1.8±0.9±0.3		153	AKHMETSHIN	00	CMD2	0.6–0.97 $e^+e^- \to \pi^+\pi^-\pi^+\pi^-$
• • • We do not use the following data for averages, fits, limits, etc. • • •						
<20	90		KURDADZE	88	OLYA	$e^+e^- \to \pi^+\pi^-\pi^+\pi^-$

$\Gamma(\pi^+\pi^-\pi^+\pi^-)/\Gamma(\pi\pi)$ — Γ_{15}/Γ_1

VALUE (units 10^{-4})	CL%	DOCUMENT ID		TECN	CHG	COMMENT
• • • We do not use the following data for averages, fits, limits, etc. • • •						
<15	90	ERBE	69	HBC	0	2.5–5.8 γp
<20		CHUNG	68	HBC	0	3.2,4.2 $\pi^- p$
<20	90	HUSON	68	HLBC	0	16.0 $\pi^- p$
<80		JAMES	66	HBC	0	2.1 $\pi^+ p$

$\Gamma(\pi^+\pi^-\pi^0\pi^0)/\Gamma_{total}$ — Γ_{16}/Γ

VALUE (units 10^{-5})	CL%	DOCUMENT ID		TECN	COMMENT
1.60±0.74±0.18		[1] ACHASOV	09A	SND	$e^+e^- \to \pi^+\pi^-\pi^0\pi^0$
• • • We do not use the following data for averages, fits, limits, etc. • • •					
< 4	90	AULCHENKO	87C	ND	$e^+e^- \to \pi^+\pi^-\pi^0\pi^0$
<20	90	KURDADZE	86	OLYA	$e^+e^- \to \pi^+\pi^-\pi^0\pi^0$

[1] Assuming no interference between the ρ and ω contributions.

$\Gamma(\pi^0 e^+ e^-)/\Gamma_{total}$ — Γ_{17}/Γ

VALUE (units 10^{-5})	CL%	DOCUMENT ID		TECN	COMMENT
<1.2	90	ACHASOV	08	SND	0.36–0.97 $e^+e^- \to \pi^0 e^+ e^-$
• • • We do not use the following data for averages, fits, limits, etc. • • •					
<1.6		AKHMETSHIN	05A	CMD2	0.72-0.84 e^+e^-

$\Gamma(\eta e^+ e^-)/\Gamma_{total}$ — Γ_{18}/Γ

VALUE (units 10^{-5})	DOCUMENT ID		TECN	COMMENT
• • • We do not use the following data for averages, fits, limits, etc. • • •				
<0.7	AKHMETSHIN	05A	CMD2	0.72-0.84 e^+e^-

$\rho(770)$ REFERENCES

ACHASOV 21 JHEP 2101 113 M.N. Achasov et al. (SND Collab.)
LEES 21B PR D104 112003 J.P. Lees et al. (BABAR Collab.)
ANDREEV 20 EPJ C80 1189 V. Andreev et al. (H1 Collab.)
ABLIKIM 18C PRL 120 242003 M. Ablikim et al. (BESIII Collab.)
ABLIKIM 17 PRL 118 012001 M. Ablikim et al. (BESIII Collab.)
BARTOS 17 PR D96 113004 E. Bartos et al.
BARTOS 17A IJMP A32 1750154 E. Bartos et al.
ABLIKIM 16C PL B753 629 M. Ablikim et al. (BESIII Collab.)
ACHASOV 16A PR D93 092001 M.N. Achasov et al. (SND Collab.)
PDG 15 RPP 2015 at pdg.lbl.gov (PDG Collab.)
ABRAMOWICZ 12 EPJ C72 1869 H. Abramowicz et al. (ZEUS Collab.)
LEES 12G PR D86 032013 J.P. Lees et al. (BABAR Collab.)
AMBROSINO 11A PL B700 102 F. Ambrosino et al. (KLOE Collab.)
GARCIA-MAR... 11 PRL 107 072001 R. Garcia-Martin et al. (MADR, CRAC)
BATLEY 10C EPJ C70 635 J.R. Batley et al. (CERN NA48/2 Collab.)
BENAYOUN 10 EPJ C65 211 M. Benayoun et al.
DUBNICKA 10 APS 60 1 S. Dubnicka, A.Z. Dubnickova
ACHASOV 09A JETP 109 379 M.N. Achasov et al. (SND Collab.)
Translated from ZETF 136 442.
AUBERT 09AS PRL 103 231801 B. Aubert et al. (BABAR Collab.)
ACHASOV 08 JETP 107 61 M.N. Achasov et al. (SND Collab.)
Translated from ZETF 134 80.
FUJIKAWA 08 PR D78 072006 M. Fujikawa et al. (BELLE Collab.)
ACHASOV 07B PR D76 077101 M.N. Achasov et al. (SND Collab.)
AKHMETSHIN 07 PL B648 28 R.R. Akhmetshin et al. (Novosibirsk CMD-2 Collab.)
ACHASOV 06 JETP 103 380 M.N. Achasov et al. (Novosibirsk SND Collab.)
Translated from ZETF 130 437.
ACHASOV 06A PR D74 014016 M.N. Achasov et al. (SND Collab.)
AULCHENKO 06 JETPL 84 413 V.M. Aulchenko et al. (Novosibirsk CMD-2 Collab.)
Translated from ZETFP 84 491.
ACHASOV 05A JETP 101 1053 M.N. Achasov et al. (Novosibirsk SND Collab.)
Translated from ZETF 128 1201.
AKHMETSHIN 05 PL B605 26 R.R. Akhmetshin et al. (Novosibirsk CMD-2 Collab.)
AKHMETSHIN 05A PL B613 29 R.R. Akhmetshin et al. (Novosibirsk CMD-2 Collab.)
ALOISIO 05 PL B606 12 A. Aloisio et al. (KLOE Collab.)
AULCHENKO 05 JETPL 82 743 V.M. Aulchenko et al. (Novosibirsk CMD-2 Collab.)
Translated from ZETFP 82 841.
SCHAEL 05C PRPL 421 191 S. Schael et al. (ALEPH Collab.)
AKHMETSHIN 04 PL B578 285 R.R. Akhmetshin et al. (Novosibirsk CMD-2 Collab.)
AKHMETSHIN 04B PL B580 119 R.R. Akhmetshin et al. (Novosibirsk CMD-2 Collab.)
PELAEZ 04A MPL A19 2879 J.R. Pelaez (MADU)
ACHASOV 03 PL B559 171 M.N. Achasov et al. (Novosibirsk SND Collab.)
ACHASOV 03D PR D68 052006 M.N. Achasov et al. (Novosibirsk SND Collab.)
ALOISIO 03 PL B561 55 A. Aloisio et al. (KLOE Collab.)
SANZ-CILLERO 03 EPJ C27 587 J.J. Sanz-Cillero, A. Pich
ACHASOV 02 PR D65 032002 M.N. Achasov et al. (Novosibirsk SND Collab.)
ACHASOV 02F PL B537 201 M.N. Achasov et al. (Novosibirsk SND Collab.)
AKHMETSHIN 02 PL B527 161 R.R. Akhmetshin et al. (Novosibirsk CMD-2 Collab.)
AKHMETSHIN 01B PL B509 217 R.R. Akhmetshin et al. (Novosibirsk CMD-2 Collab.)
COLANGELO 01 NP B603 125 G. Colangelo, J. Gasser, H. Leytwyler
PICH 01 PR D63 093005 A. Pich, J. Portoles
ACHASOV 00 EPJ C12 25 M.N. Achasov et al. (Novosibirsk SND Collab.)
ACHASOV 00D JETPL 72 282 M.N. Achasov et al. (Novosibirsk SND Collab.)
Translated from ZETFP 72 411.
ACHASOV 00G JETPL 71 355 M.N. Achasov et al. (Novosibirsk SND Collab.)
Translated from ZETFP 71 519.
AKHMETSHIN 00 PL B475 190 R.R. Akhmetshin et al. (Novosibirsk CMD-2 Collab.)
ANDERSON 00A PR D61 112002 S. Anderson et al. (CLEO Collab.)
ABELE 99E PL B469 270 A. Abele et al. (Crystal Barrel Collab.)
BENAYOUN 98 EPJ C2 269 M. Benayoun et al. (IPNP, NOVO, ADLD+)
BREITWEG 98B EPJ C2 247 J. Breitweg et al. (ZEUS Collab.)
GARDNER 98 PR D57 2716 S. Gardner, H.B. O'Connell
Also PR D62 019903 (errat.) S. Gardner, H.B. O'Connell
ABELE 97 PL B391 191 A. Abele et al. (Crystal Barrel Collab.)
ADAMS 97 ZPHY C74 237 M.R. Adams et al. (E665 Collab.)
BARATE 97M ZPHY C76 15 R. Barate et al. (ALEPH Collab.)
BERTIN 97C PL B408 476 A. Bertin et al. (OBELIX Collab.)
BOGOLYUB... 97 PAN 60 46 M.Y. Bogolyubsky et al. (MOSU, SERP)
Translated from YAF 60 53.
O'CONNELL 97 NP A623 559 H.B. O'Connell et al. (ADLD)
BENAYOUN 96 ZPHY C72 221 M. Benayoun et al. (IPNP, NOVO)
BERNICHA 94 PR D50 4454 A. Bernicha, G. Lopez Castro, J. Pestieau (LOUV+)
WEIDENAUER 93 ZPHY C59 387 P. Weidenauer et al. (ASTERIX Collab.)
AGUILAR-... 91 ZPHY C50 405 M. Aguilar-Benitez et al. (LEBC-EHS Collab.)
DOLINSKY 91 PRPL 202 99 S.I. Dolinsky et al. (NOVO)
KUHN 90 ZPHY C48 445 J.H. Kuhn et al. (MPIM)
ANTIPOV 89 ZPHY C42 185 Y.M. Antipov et al. (SERP, JINR, BGNA+)
BISELLO 89 PL B220 321 D. Bisello et al. (DM2 Collab.)
DOLINSKY 89 ZPHY C42 511 S.I. Dolinsky et al. (NOVO)
DUBNICKA 89 JP G15 1349 S. Dubnicka et al. (JINR, SLOV)
GESHKEN... 89 ZPHY C45 351 B.V. Geshkenbein (ITEP)
KURDADZE 88 JETPL 47 512 L.M. Kurdadze et al. (NOVO)
Translated from ZETFP 47 432.
VASSERMAN 88 SJNP 47 1035 I.B. Vasserman et al. (NOVO)
Translated from YAF 47 1635.
VASSERMAN 88B SJNP 48 480 I.B. Vasserman et al. (NOVO)
Translated from YAF 48 753.
AULCHENKO 87C IYF 87-90 Preprint V.M. Aulchenko et al. (NOVO)
CAPRARO 87 NP B288 659 L. Capraro et al. (CLER, FRAS, MILA+)
BRAMON 86 PL B173 97 A. Bramon, J. Casulleras (BARC)
HUSTON 86 PR D33 3199 J. Huston et al. (ROCH, FNAL, MINN)
KURDADZE 86 JETPL 43 643 L.M. Kurdadze et al. (NOVO)
Translated from ZETFP 43 497.
BARKOV 85 NP B256 365 L.M. Barkov et al. (NOVO)
DRUZHININ 84 PL 144B 136 V.P. Druzhinin et al. (NOVO)
CHABAUD 83 NP B223 1 V. Chabaud et al. (CERN, CRAC, MPIM)
JENSEN 83 PR D27 26 T. Jensen et al. (ROCH, FNAL, MINN)
HEYN 81 ZPHY C7 169 M.F. Heyn, C.B. Lang (GRAZ)
BOHACIK 80 PR D21 1342 J. Bohacik, H. Kuhnelt (SLOV, WIEN)
COHEN 80 PR D22 2595 D. Cohen et al. (ANL)
LANG 79 PR D19 956 C.B. Lang, A. Mas-Parareda (GRAZ)
BARTALUCCI 78 NC 44A 587 S. Bartalucci et al. (DESY, FRAS)
WICKLUND 78 PR D17 1197 A.B. Wicklund et al. (ANL)
ANDREWS 77 PRL 38 198 D.E. Andrews et al. (ROCH)
DEUTSCH... 76 NP B103 426 M. Deutschmann et al. (AACH3, BERL, BONN+)
ENGLER 74 PR D10 2070 A. Engler et al. (CMU, CASE)
ESTABROOKS 74 NP B79 301 P.G. Estabrooks, A.D. Martin (DURH)
GRAYER 74 NP B75 189 G. Grayer et al. (CERN, MPIM)
RATCLIFF 74 Private Comm.
BYERLY 73 PR D7 637 W.L. Byerly et al. (MICH)
GLADDING 73 PR D8 3721 G.E. Gladding et al. (HARV)
HYAMS 73 NP B64 134 B.D. Hyams et al. (CERN, MPIM)
PROTOPOP... 73 PR D7 1279 S.D. Protopopescu et al. (LBL)
BALLAM 72 PR D5 545 J. Ballam et al. (SLAC, LBL, TUFTS)
BENAKSAS 72 PL 39B 289 D. Benaksas et al. (ORSAY)
JACOBS 72 PR D6 1291 L.D. Jacobs (SACL)
RATCLIFF 72 PL 38B 345 B.N. Ratcliff et al. (SLAC)
ABRAMS 71 PR D4 653 G.S. Abrams et al. (LBL)
ALVENSLEB... 70 PRL 24 786 H. Alvensleben et al. (DESY)
BIGGS 70 PRL 24 1197 P.J. Biggs et al. (DARE)
ERBE 69 PR 188 2060 R. Erbe et al. (German Bubble Chamber Collab.)
MALAMUD 69 Argonne Conf. 93 E.I. Malamud, P.E. Schlein (UCLA)
REYNOLDS 69 PR 184 1424 B.G. Reynolds et al. (FSU)
ROTHWELL 69 PRL 23 1521 P.L. Rothwell et al. (NEAS)
WEHMANN 69 PR 178 2095 A.A. Wehmann et al. (HARV, CASE, SLAC+)
ARMENISE 68 NC 54A 999 N. Armenise et al. (BARI, BGNA, FIRZ+)
BATON 68 PR 176 1574 J.P. Baton, G. Laurens (SACL)
CHUNG 68 PR 165 1491 S.U. Chung et al. (LRL)
FOSTER 68 NP B6 107 M. Foster et al. (CERN, CDEF)
GOUNARIS 68 PRL 21 244 G.J. Gounaris, J.J. Sakurai
HUSON 68 PL 28B 208 R. Huson et al. (ORSAY, MILA, UCLA)
HYAMS 68 NP B7 1 B.D. Hyams et al. (CERN, MPIM)
LANZEROTTI 68 PR 166 1365 L.J. Lanzerotti et al. (HARV)
PISUT 68 NP B6 325 J. Pisut, M. Roos (CERN)
ASBURY 67B PRL 19 865 J.G. Asbury et al. (DESY, COLU)
BACON 67 PR 157 1263 T.C. Bacon et al. (BNL)
EISNER 67 PR 164 1699 R.L. Eisner et al. (PURD)
HUWE 67 PL 24B 252 D.O. Huwe et al. (COLU)
HYAMS 67 PL 24B 634 B.D. Hyams et al. (CERN, MPIM)
MILLER 67B PR 153 1423 D.H. Miller et al. (PURD)
ALFF-... 66 PR 145 1072 C. Alff-Steinberger et al. (COLU, RUTG)
FERBEL 66 PL 21 111 T. Ferbel (ROCH)
HAGOPIAN 66 PR 145 1128 V. Hagopian et al. (PENN, SACL)
HAGOPIAN 66B PR 152 1183 V. Hagopian, Y.L. Pan (PENN, LRL)
JACOBS 66B UCRL 16877 L.D. Jacobs (LRL)
JAMES 66 PR 142 896 F.E. James, H.L. Kraybill (YALE, BNL)
ROSS 66 PR 149 1172 M. Ross, L. Stodolsky
SOEDING 66 PL B19 702 P. Soeding
WEST 66 PR 149 1089 E. West et al. (WISC)
BLIEDEN 65 PL 19 444 H.R. Blieden et al. (CERN MMS Collab.)
CARMONY 64 PRL 12 254 D.D. Carmony et al. (UCB)
GOLDHABER 64 PRL 12 336 G. Goldhaber et al. (LRL, UCB)
ABOLINS 63 PRL 11 381 M.A. Abolins et al. (UCSD)

$\omega(782)$

$I^G(J^{PC}) = 0^-(1^{--})$

$\omega(782)$ MASS

VALUE (MeV)	EVTS	DOCUMENT ID		TECN	COMMENT
782.66±0.13 OUR AVERAGE		Error includes scale factor of 2.0. See the ideogram below.			
777.9 $\pm 2.2\ ^{+4.3}_{-2.2}$	900k	ANDREEV	20	H1	$ep \to e\pi^+\pi^-p$
783.20±0.13±0.16	18680	AKHMETSHIN	05	CMD2	0.60-1.38 $e^+e^- \to \pi^0\gamma$
782.68±0.09±0.04	11200	[1] AKHMETSHIN	04	CMD2	$e^+e^- \to \pi^+\pi^-\pi^0$
782.79±0.08±0.09	1.2M	[2] ACHASOV	03D	RVUE	0.44–2.00 $e^+e^- \to \pi^+\pi^-\pi^0$
781.96±0.17±0.80	11k	[3] AMSLER	94C	CBAR	0.0 $\bar{p}p \to \omega\eta\pi^0$

Downloaded from https://academic.oup.com/ptep/article/2022/8/083C01/6651666 by KIT Library user on 27 September 2022

$782.08 \pm 0.36 \pm 0.82$	3463	[4] AMSLER	94C	CBAR	$0.0\ \overline{p}p \to \omega\eta\pi^0$
$781.96 \pm 0.13 \pm 0.17$	15k	AMSLER	93B	CBAR	$0.0\ \overline{p}p \to \omega\pi^0\pi^0$
782.4 ± 0.2	270k	WEIDENAUER	93	ASTE	$\overline{p}p \to 2\pi^+ 2\pi^- \pi^0$
782.4 ± 0.5	7000	[5] KEYNE	76	CNTR	$\pi^- p \to \omega n$
• • • We do not use the following data for averages, fits, limits, etc. • • •					
$782.58 \pm 0.03 \pm 0.01$		[6] HOID	20	RVUE	$e^+e^- \to \pi^0\gamma$
$781.68 \pm 0.09 \pm 0.03$		[7] COLANGELO	19	RVUE	$e^+e^- \to \pi^+\pi^-$
$782.63 \pm 0.03 \pm 0.01$		[8] HOFERICHT...	19	RVUE	$e^+e^- \to \pi^+\pi^-\pi^0$
781.91 ± 0.24		[9] LEES	12G	BABR	$e^+e^- \to \pi^+\pi^-\gamma$
$782.7 \pm 0.1 \pm 1.5$	19500	[10] WURZINGER	95	SPEC	$1.33\ pd \to {}^3\mathrm{He}\omega$
781.78 ± 0.10		[10] BARKOV	87	CMD	$e^+e^- \to \pi^+\pi^-\pi^0$
782.2 ± 0.4	1488	[11] KURDADZE	83B	OLYA	$e^+e^- \to \pi^+\pi^-\pi^0$
783.3 ± 0.4	433	CORDIER	80	DM1	$e^+e^- \to \pi^+\pi^-\pi^0$
782.5 ± 0.8	33260	ROOS	80	RVUE	0.0–$3.6\ \overline{p}p$
782.6 ± 0.8	3000	BENKHEIRI	79	OMEG	9–$12\ \pi^\pm p$
781.8 ± 0.6	1430	COOPER	78B	HBC	0.7–$0.8\ \overline{p}p \to 5\pi$
782.7 ± 0.9	535	VANAPEL...	78	HBC	$7.2\ \overline{p}p \to \overline{p}p\omega$
783.5 ± 0.8	2100	GESSAROLI	77	HBC	$11\ \pi^- p \to \omega n$
782.5 ± 0.8	418	AGUILAR-...	72B	HBC	$3.9, 4.6\ K^- p$
783.4 ± 1.0	248	BIZZARRI	71	HBC	$0.0\ p\overline{p} \to K^+K^-\omega$
781.0 ± 0.6	510	BIZZARRI	71	HBC	$0.0\ p\overline{p} \to K_1 K_1 \omega$
783.7 ± 1.0	3583	[12] COYNE	71	HBC	$3.7\ \pi^+ p \to p\pi^+\pi^+\pi^-\pi^0$
784.1 ± 1.2	750	ABRAMOVI...	70	HBC	$3.9\ \pi^- p$
783.2 ± 1.6		[13] BIGGS	70B	CNTR	$<4.1\ \gamma\mathrm{C} \to \pi^+\pi^-\mathrm{C}$
782.4 ± 0.5	2400	BIZZARRI	69	HBC	$0.0\ \overline{p}p$

[1] Update of AKHMETSHIN 00C.
[2] From the combined fit of ANTONELLI 92, ACHASOV 01E, ACHASOV 02E, and ACHASOV 03D data on the $\pi^+\pi^-\pi^0$ and ANTONELLI 92 on the $\omega\pi^+\pi^-$ final states. Supersedes ACHASOV 99E and ACHASOV 02E.
[3] From the $\eta \to \gamma\gamma$ decay.
[4] From the $\eta \to 3\pi^0$ decay.
[5] Observed by threshold-crossing technique. Mass resolution = 4.8 MeV FWHM.
[6] The values were extracted from a dispersively improved Breit-Wigner parameterization and do not include vacuum polarization. Inclusion of vacuum polarization gives 782.736 ± 0.024 MeV.
[7] The ω mass was extracted from a dispersively improved Breit-Wigner parameterization, the ω width fixed at 8.49 ± 0.08 MeV. The value does not include vacuum polarization which would shift the mass to $781.81 \pm 0.09 \pm 0.03$ MeV. The mixing parameter is assumed real valued.
[8] The values were extracted from a dispersively improved Breit-Wigner parameterization and do not include vacuum polarization.
[9] From the $\rho-\omega$ interference in the $\pi^+\pi^-$ mass spectrum using the Breit-Wigner for the ω and leaving its mass and width as free parameters of the fit.
[10] Systematic uncertainties underestimated.
[11] Systematic uncertainties not estimated.
[12] From best-resolution sample of COYNE 71.
[13] From ω-ρ interference in the $\pi^+\pi^-$ mass spectrum assuming ω width 12.6 MeV.

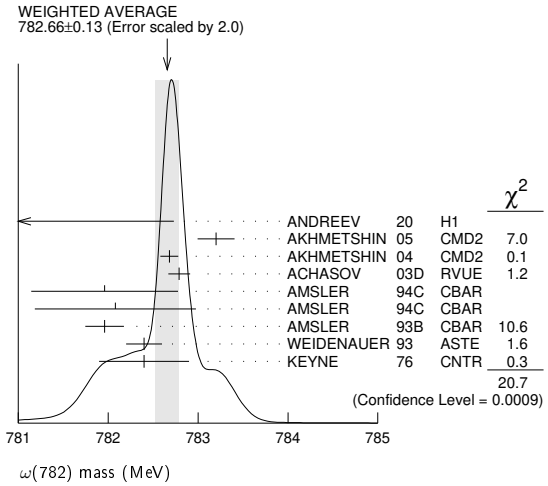

$\omega(782)$ WIDTH

VALUE (MeV)	EVTS	DOCUMENT ID		TECN	COMMENT
8.68 ± 0.13 OUR AVERAGE					
$8.68 \pm 0.23 \pm 0.10$	11200	[1] AKHMETSHIN	04	CMD2	$e^+e^- \to \pi^+\pi^-\pi^0$
$8.68 \pm 0.04 \pm 0.15$	1.2M	[2] ACHASOV	03D	RVUE	0.44–$2.00\ e^+e^- \to \pi^+\pi^-\pi^0$
• • • We do not use the following data for averages, fits, limits, etc. • • •					
$8.65 \pm 0.06 \pm 0.01$		[3] HOID	20	RVUE	$e^+e^- \to \pi^0\gamma$
$8.71 \pm 0.04 \pm 0.04$		[4] HOFERICHT...	19	RVUE	$e^+e^- \to \pi^+\pi^-\pi^0$
8.13 ± 0.45		[5] LEES	12G	BABR	$e^+e^- \to \pi^+\pi^-\gamma$
8.2 ± 0.3	19500	[6] WURZINGER	95	SPEC	$1.33\ pd \to {}^3\mathrm{He}\omega$
8.4 ± 0.1		[7] AULCHENKO	87	ND	$e^+e^- \to \pi^+\pi^-\pi^0$
8.30 ± 0.40		[6] BARKOV	87	CMD	$e^+e^- \to \pi^+\pi^-\pi^0$
9.8 ± 0.9	1488	[8] KURDADZE	83B	OLYA	$e^+e^- \to \pi^+\pi^-\pi^0$
9.0 ± 0.8	433	[6] CORDIER	80	DM1	$e^+e^- \to \pi^+\pi^-\pi^0$
12 ± 2	1430	COOPER	78B	HBC	0.7–$0.8\ \overline{p}p \to 5\pi$
9.4 ± 2.5	2100	GESSAROLI	77	HBC	$11\ \pi^- p \to \omega n$
10.22 ± 0.43	20000	[9] KEYNE	76	CNTR	$\pi^- p \to \omega n$
13.3 ± 2	418	AGUILAR-...	72B	HBC	$3.9, 4.6\ K^- p$
9.1 ± 0.8	451	[6] BENAKSAS	72B	OSPK	$e^+e^- \to \pi^+\pi^-\pi^0$
10.5 ± 1.5		BORENSTEIN	72	HBC	$2.18\ K^- p$
$7.70 \pm 0.9 \pm 1.15$	940	BROWN	72	MMS	$2.5\ \pi^- p \to n\mathrm{MM}$
10.3 ± 1.4	510	BIZZARRI	71	HBC	$0.0\ p\overline{p} \to K_1 K_1 \omega$
12.8 ± 3.0	248	BIZZARRI	71	HBC	$0.0\ p\overline{p} \to K^+K^-\omega$
9.5 ± 1.0	3583	COYNE	71	HBC	$3.7\ \pi^+ p \to p\pi^+\pi^+\pi^-\pi^0$

[1] Update of AKHMETSHIN 00C.
[2] From the combined fit of ANTONELLI 92, ACHASOV 01E, ACHASOV 02E, and ACHASOV 03D data on the $\pi^+\pi^-\pi^0$ and ANTONELLI 92 on the $\omega\pi^+\pi^-$ final states. Supersedes ACHASOV 99E and ACHASOV 02E.
[3] The values were extracted from a dispersively improved Breit-Wigner parameterization and do not include vacuum polarization. Inclusion of vacuum polarization gives 8.63 ± 0.05 MeV.
[4] The values were extracted from a dispersively improved Breit-Wigner parameterization and do not include vacuum polarization.
[5] From the $\rho-\omega$ interference in the $\pi^+\pi^-$ mass spectrum using the Breit-Wigner for the ω and leaving its mass and width as free parameters of the fit.
[6] Systematic uncertainties underestimated.
[7] Relativistic Breit-Wigner includes radiative corrections. Systematic uncertainties not estimated.
[8] Systematic uncertainties not estimated.
[9] Observed by threshold-crossing technique. Mass resolution = 4.8 MeV FWHM.

$\omega(782)$ DECAY MODES

	Mode	Fraction (Γ_i/Γ)	Scale factor/ Confidence level
Γ_1	$\pi^+\pi^-\pi^0$	(89.2 ± 0.7) %	
Γ_2	$\pi^0\gamma$	(8.35 ± 0.27) %	S=2.2
Γ_3	$\pi^+\pi^-$	$(1.53^{+0.11}_{-0.13})$ %	S=1.2
Γ_4	neutrals (excluding $\pi^0\gamma$)	$(7\ ^{+8}_{-4}) \times 10^{-3}$	S=1.1
Γ_5	$\eta\gamma$	$(4.5 \pm 0.4) \times 10^{-4}$	S=1.1
Γ_6	$\pi^0 e^+e^-$	$(7.7 \pm 0.6) \times 10^{-4}$	
Γ_7	$\pi^0\mu^+\mu^-$	$(1.34 \pm 0.18) \times 10^{-4}$	S=1.5
Γ_8	ηe^+e^-		
Γ_9	e^+e^-	$(7.38 \pm 0.22) \times 10^{-5}$	S=1.9
Γ_{10}	$\pi^+\pi^-\pi^0\pi^0$	$< 2 \times 10^{-4}$	CL=90%
Γ_{11}	$\pi^+\pi^-\gamma$	$< 3.6 \times 10^{-3}$	CL=95%
Γ_{12}	$\pi^+\pi^-\pi^+\pi^-$	$< 1 \times 10^{-3}$	CL=90%
Γ_{13}	$\pi^0\pi^0\gamma$	$(6.7 \pm 1.1) \times 10^{-5}$	
Γ_{14}	$\eta\pi^0\gamma$	$< 3.3 \times 10^{-5}$	CL=90%
Γ_{15}	$\mu^+\mu^-$	$(7.4 \pm 1.8) \times 10^{-5}$	
Γ_{16}	3γ	$< 1.9 \times 10^{-4}$	CL=95%
	Charge conjugation (C) violating modes		
Γ_{17}	$\eta\pi^0$ C	$< 2.1 \times 10^{-4}$	CL=90%
Γ_{18}	$2\pi^0$ C	$< 2.2 \times 10^{-4}$	CL=90%
Γ_{19}	$3\pi^0$ C	$< 2.3 \times 10^{-4}$	CL=90%
Γ_{20}	invisible	$< 7 \times 10^{-5}$	CL=90%

CONSTRAINED FIT INFORMATION

An overall fit to 15 branching ratios uses 48 measurements and one constraint to determine 10 parameters. The overall fit has a $\chi^2 = 48.0$ for 39 degrees of freedom.

The following *off-diagonal* array elements are the correlation coefficients $\langle \delta x_i \delta x_j \rangle / (\delta x_i \cdot \delta x_j)$, in percent, from the fit to the branching fractions, $x_i \equiv \Gamma_i/\Gamma_{\mathrm{total}}$. The fit constrains the x_i whose labels appear in this array to sum to one.

	x_1	x_2	x_3	x_4	x_5	x_6	x_7	x_9	x_{13}
x_2	23								
x_3	−18	−4							
x_4	−92	−55	1						
x_5	7	23	−1	−15					
x_6	−1	0	0	0	0				
x_7	0	0	0	0	0	0			
x_9	−24	−73	4	47	−31	0	0		
x_{13}	1	4	0	−2	1	0	0	−3	
x_{15}	0	0	0	0	0	0	0	0	0

Downloaded from https://academic.oup.com/ptep/article/2022/8/083C01/6651666 by KIT Library user on 27 September 2022

$\omega(782)$ PARTIAL WIDTHS

$\Gamma(\pi^0\gamma)$ — Γ_2

VALUE (keV)	EVTS	DOCUMENT ID		TECN	COMMENT
• • • We do not use the following data for averages, fits, limits, etc. • • •					
880±50	7815	[1] ACHASOV	13	SND	1.05–2.00 $e^+e^- \to \pi^0\pi^0\gamma$
788±12±27	36500	[2] ACHASOV	03	SND	0.60–0.97 $e^+e^- \to \pi^0\gamma$
764±51	10625	DOLINSKY	89	ND	$e^+e^- \to \pi^0\gamma$

[1] Systematic uncertainty not estimated.
[2] Using $\Gamma_\omega = 8.44 \pm 0.09$ MeV and $B(\omega \to \pi^0\gamma)$ from ACHASOV 03.

$\Gamma(\eta\gamma)$ — Γ_5

VALUE (keV)	DOCUMENT ID		TECN	COMMENT
• • • We do not use the following data for averages, fits, limits, etc. • • •				
6.1±2.5	[1] DOLINSKY	89	ND	$e^+e^- \to \eta\gamma$

[1] Using $\Gamma_\omega = 8.4 \pm 0.1$ MeV and $B(\omega \to \eta\gamma)$ from DOLINSKY 89.

$\Gamma(e^+e^-)$ — Γ_9

VALUE (keV)	EVTS	DOCUMENT ID		TECN	COMMENT
0.60 ±0.02 OUR EVALUATION					
• • • We do not use the following data for averages, fits, limits, etc. • • •					
0.591±0.015	11200	[1,2] AKHMETSHIN	04	CMD2	$e^+e^- \to \pi^+\pi^-\pi^0$
0.653±0.003±0.021	1.2M	[3] ACHASOV	03D	RVUE	0.44–2.00 $e^+e^- \to \pi^+\pi^-\pi^0$
0.600±0.031	10625	DOLINSKY	89	ND	$e^+e^- \to \pi^0\gamma$

[1] Using $B(\omega \to \pi^+\pi^-\pi^0) = 0.891 \pm 0.007$ and $\Gamma_{total} = 8.44 \pm 0.09$ MeV.
[2] Update of AKHMETSHIN 00C.
[3] Using ACHASOV 03, ACHASOV 03D and $B(\omega \to \pi^+\pi^-) = (1.70 \pm 0.28)\%$.

$\omega(782)\ \Gamma(i)\Gamma(e^+e^-)/\Gamma(total)$

$\Gamma(\pi^+\pi^-\pi^0) \times \Gamma(e^+e^-)/\Gamma_{total}$ — $\Gamma_1\Gamma_9/\Gamma$

VALUE (eV)	DOCUMENT ID		TECN	COMMENT
569.8±3.1±8.2	[1] LEES	21B	BABR	10.5 $e^+e^- \to \pi^+\pi^-\pi^0\gamma$

[1] From the cross section for $e^+e^- \to \pi^+\pi^-\pi^0$ with contributions from $\rho(770)$, $\omega(782)$, $\phi(1020)$, $\omega(1420)$, and $\omega(1650)$.

$\omega(782)\ \Gamma(e^+e^-)\Gamma(i)/\Gamma^2(total)$

$\Gamma(e^+e^-)/\Gamma_{total} \times \Gamma(\pi^+\pi^-\pi^0)/\Gamma_{total}$ — $\Gamma_9/\Gamma \times \Gamma_1/\Gamma$

VALUE (units 10^{-5})	EVTS	DOCUMENT ID		TECN	COMMENT
6.59±0.19 OUR FIT Error includes scale factor of 2.1.					
6.36±0.14 OUR AVERAGE Error includes scale factor of 1.3. See the ideogram below.					
6.24±0.11±0.08	11.2k	[1] AKHMETSHIN	04	CMD2	$e^+e^- \to \pi^+\pi^-\pi^0$
6.74±0.04±0.24	1.2M	[2,3] ACHASOV	03D	RVUE	0.44–2.00 $e^+e^- \to \pi^+\pi^-\pi^0$
6.37±0.35		[2] DOLINSKY	89	ND	$e^+e^- \to \pi^+\pi^-\pi^0$
• • • We do not use the following data for averages, fits, limits, etc. • • •					
6.20±0.13		[4] BENAYOUN	10	RVUE	0.4–1.05 e^+e^-
6.70±0.06±0.27		[5] AUBERT,B	04N	BABR	10.6 $e^+e^- \to \pi^+\pi^-\pi^0\gamma$
6.45±0.24		[6] BARKOV	87	CMD	$e^+e^- \to \pi^+\pi^-\pi^0$
5.79±0.42	1488	[7] KURDADZE	83B	OLYA	$e^+e^- \to \pi^+\pi^-\pi^0$
5.89±0.54	433	[6] CORDIER	80	DM1	$e^+e^- \to \pi^+\pi^-\pi^0$
7.54±0.84	451	[6] BENAKSAS	72B	OSPK	$e^+e^- \to \pi^+\pi^-\pi^0$

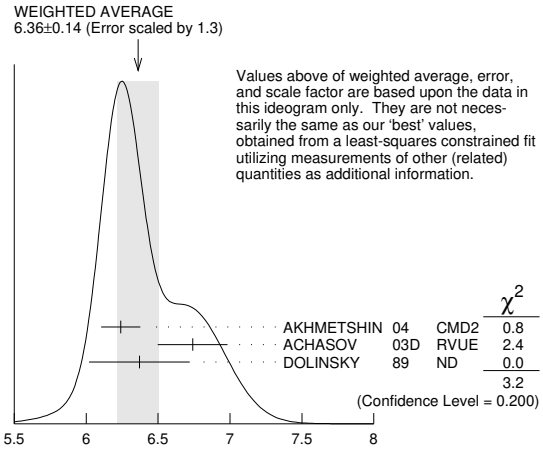

[1] Update of AKHMETSHIN 00C.
[2] Recalculated by us from the cross section in the peak.
[3] From the combined fit of ANTONELLI 92, ACHASOV 01E, ACHASOV 02E, and ACHASOV 03D data on the $\pi^+\pi^-\pi^0$ and ANTONELLI 92 on the $\omega\pi^+\pi^-$ final states. Supersedes ACHASOV 99E and ACHASOV 02E.
[4] A simultaneous fit of $e^+e^- \to \pi^+\pi^-$, $\pi^+\pi^-\pi^0$, $\pi^0\gamma$, $\eta\gamma$ data.
[5] Superseeded by LEES 21B.
[6] Recalculated by us from the cross section in the peak. Systematic uncertainties underestimated.
[7] Recalculated by us from the cross section in the peak. Systematic uncertainties not estimated.

$\Gamma(e^+e^-)/\Gamma_{total} \times \Gamma(\pi^0\gamma)/\Gamma_{total}$ — $\Gamma_9/\Gamma \times \Gamma_2/\Gamma$

VALUE (units 10^{-6})	EVTS	DOCUMENT ID		TECN	COMMENT
6.16 ±0.14 OUR FIT Error includes scale factor of 1.8.					
6.34 ±0.10 OUR AVERAGE					
6.336±0.056±0.089		[1] ACHASOV	16A	SND	0.60–1.38 $e^+e^- \to \pi^0\gamma$
6.47 ±0.14 ±0.39	18k	AKHMETSHIN	05	CMD2	0.60-1.38 $e^+e^- \to \pi^0\gamma$
6.34 ±0.21 ±0.21	10k	[2] DOLINSKY	89	ND	$e^+e^- \to \pi^0\gamma$
• • • We do not use the following data for averages, fits, limits, etc. • • •					
6.80 ±0.13		[3] BENAYOUN	10	RVUE	0.4–1.05 e^+e^-
6.50 ±0.11 ±0.20	36k	[4] ACHASOV	03	SND	0.60–0.97 $e^+e^- \to \pi^0\gamma$

[1] From the VMD model with the interfering $\rho(770)$, $\omega(782)$, $\phi(1020)$, and an additional resonance describing the total contribution of the $\rho(1450)$ and $\omega(1420)$ states. Supersedes ACHASOV 03.
[2] Recalculated by us from the cross section in the peak.
[3] A simultaneous fit of $e^+e^- \to \pi^+\pi^-$, $\pi^+\pi^-\pi^0$, $\pi^0\gamma$, $\eta\gamma$ data.
[4] Using $\sigma(\phi \to \pi^0\gamma)$ from ACHASOV 00 and $m_\omega = 782.57$ MeV in the model with the energy-independent phase of ρ-ω interferenceequal to $(-10.2 \pm 7.0)^\circ$.

$\Gamma(e^+e^-)/\Gamma_{total} \times \Gamma(\pi^+\pi^-)/\Gamma_{total}$ — $\Gamma_9/\Gamma \times \Gamma_3/\Gamma$

VALUE (units 10^{-6})	EVTS	DOCUMENT ID		TECN	COMMENT
1.28 ±0.05 OUR AVERAGE					
1.318±0.051±0.021		[1] ACHASOV	21	SND	$e^+e^- \to \pi^+\pi^-$
1.225±0.058±0.041	800k	[2] ACHASOV	06	SND	$e^+e^- \to \pi^+\pi^-$
• • • We do not use the following data for averages, fits, limits, etc. • • •					
1.166±0.036		[3] BENAYOUN	13	RVUE	0.4–1.05 e^+e^-
1.05 ±0.08		[4] DAVIER	13	RVUE	$e^+e^- \to \pi^+\pi^-(\gamma)$

[1] From a fit of the cross section in the energy range $0.525 < \sqrt{s} < 0.883$ GeV parameterized by the sum of the Breit-Wigner amplitudes for the $\rho(770)$, ω and $\rho(1450)$ resonances. The measured phase of the $\rho(770)$—ω interference is $(110.7 \pm 1.5 \pm 1.0)^\circ$.
[2] Supersedes ACHASOV 05A.
[3] A simultaneous fit to $e^+e^- \to \pi^+\pi^-$, $\pi^+\pi^-\pi^0$, $\pi^0\gamma$, $\eta\gamma$, $K\overline{K}$, and $\tau^- \to \pi^-\pi^0\nu_\tau$ data. Supersedes BENAYOUN 10.
[4] From $e^+e^- \to \pi^+\pi^-(\gamma)$ data of LEES 12G.

$\Gamma(e^+e^-)/\Gamma_{total} \times \Gamma(\eta\gamma)/\Gamma_{total}$ — $\Gamma_9/\Gamma \times \Gamma_5/\Gamma$

VALUE (units 10^{-8})	EVTS	DOCUMENT ID		TECN	COMMENT
3.32±0.28 OUR FIT Error includes scale factor of 1.1.					
3.18±0.28 OUR AVERAGE					
3.10±0.31±0.11	33k	[1] ACHASOV	07B	SND	0.6–1.38 $e^+e^- \to \eta\gamma$
$3.17^{+1.85}_{-1.31}$±0.21	17.4k	[2] AKHMETSHIN	05	CMD2	0.60-1.38 $e^+e^- \to \eta\gamma$
3.41±0.52±0.21	23k	[3,4] AKHMETSHIN	01B	CMD2	$e^+e^- \to \eta\gamma$
• • • We do not use the following data for averages, fits, limits, etc. • • •					
4.50±0.10		[5] BENAYOUN	10	RVUE	0.4–1.05 e^+e^-

[1] From a combined fit of $\sigma(e^+e^- \to \eta\gamma)$ with $\eta \to 3\pi^0$ and $\eta \to \pi^+\pi^-\pi^0$, and fixing $B(\eta \to 3\pi^0)$ / $B(\eta \to \pi^+\pi^-\pi^0) = 1.44 \pm 0.04$. Recalculated by us from the cross section at the peak. Supersedes ACHASOV 00D and ACHASOV 06A.
[2] From the $\eta \to 2\gamma$ decay and using $B(\eta \to \gamma\gamma) = 39.43 \pm 0.26\%$.
[3] From the $\eta \to 3\pi^0$ decay and using $B(\eta \to 3\pi^0) = (32.24 \pm 0.29) \times 10^{-2}$.
[4] The combined fit from 600 to 1380 MeV taking into account $\rho(770)$, $\omega(782)$, $\phi(1020)$, and $\rho(1450)$ (mass and width fixed at 1450 MeV and 310 MeV respectively).
[5] A simultaneous fit of $e^+e^- \to \pi^+\pi^-$, $\pi^+\pi^-\pi^0$, $\pi^0\gamma$, $\eta\gamma$ data.

$\Gamma(e^+e^-)/\Gamma_{total} \times \Gamma(\mu^+\mu^-)/\Gamma_{total}$ — $\Gamma_9/\Gamma \times \Gamma_{15}/\Gamma$

VALUE (units 10^{-9})	EVTS	DOCUMENT ID		TECN	COMMENT
4.3±1.8±2.2	4.5 M	[1] ANASTASI	17	KLOE	$e^+e^- \to \mu^+\mu^-\gamma$

[1] From a fit of the real part of the vacuum polarization by a sum of the leptonic and hadronic contributions, where the hadronic contribution is parametrized as a sum of Breit-Wigner resonances $\omega(782)$, $\phi(1020)$ and using a GOUNARIS 68 parametrization for the $\rho(770)$, and a non-resonant term.

$\omega(782)$ BRANCHING RATIOS

$\Gamma(\pi^+\pi^-\pi^0)/\Gamma_{total}$ — Γ_1/Γ

NIECKNIG 12 describes final-state interactions between the three pions in a dispersive framework using data on the $\pi\pi$ P-wave scattering phase shift.

VALUE	EVTS	DOCUMENT ID		TECN	COMMENT
• • • We do not use the following data for averages, fits, limits, etc. • • •					
0.9024±0.0019		[1] AMBROSINO	08G	KLOE	1.0–1.03 $e^+e^- \to \pi^+\pi^-2\pi^0$, $2\pi^0\gamma$
0.8965±0.0016±0.0048	1.2M	[2,3] ACHASOV	03D	RVUE	0.44–2.00 $e^+e^- \to \pi^+\pi^-\pi^0$
0.880 ±0.020 ±0.032	11200	[3,4] AKHMETSHIN	00C	CMD2	$e^+e^- \to \pi^+\pi^-\pi^0$
0.8942±0.0062		[3] DOLINSKY	89	ND	$e^+e^- \to \pi^+\pi^-\pi^0$

[1] Not independent of $\Gamma(\pi^0\gamma)$ / $\Gamma(\pi^+\pi^-\pi^0)$ from AMBROSINO 08G.
[2] Using ACHASOV 03, ACHASOV 03D and $B(\omega \to \pi^+\pi^-) = (1.70 \pm 0.28)\%$.
[3] Not independent of the corresponding $\Gamma(e^+e^-) \times \Gamma(\pi^+\pi^-\pi^0)/\Gamma^2_{total}$.
[4] Using $\Gamma(e^+e^-) = 0.60 \pm 0.02$ keV.

Downloaded from https://academic.oup.com/ptep/article/2022/8/083C01/6651666 by KIT Library user on 27 September 2022

$\Gamma(\pi^0\gamma)/\Gamma_{total}$ — Γ_2/Γ

VALUE (units 10^{-2})	EVTS	DOCUMENT ID		TECN	COMMENT
• • • We do not use the following data for averages, fits, limits, etc. • • •					
8.88±0.18		[1] ACHASOV	16A	SND	0.60–1.38 $e^+e^- \to \pi^0\gamma$
8.09±0.14		[2] AMBROSINO	08G	KLOE	$e^+e^- \to \pi^+\pi^-2\pi^0, 2\pi^0\gamma$
9.06±0.20±0.57	18k	[3,4] AKHMETSHIN	05	CMD2	0.60-1.38 $e^+e^- \to \pi^0\gamma$
9.34±0.15±0.31	36k	[4] ACHASOV	03	SND	0.60–0.97 $e^+e^- \to \pi^0\gamma$
8.65±0.16±0.42	1.2M	[5,6] ACHASOV	03D	RVUE	0.44–2.00 $e^+e^- \to \pi^+\pi^-\pi^0$
8.39±0.24	9k	[7] BENAYOUN	96	RVUE	$e^+e^- \to \pi^0\gamma$
8.88±0.62	10k	[4] DOLINSKY	89	ND	$e^+e^- \to \pi^0\gamma$

[1] Using $B(\omega \to e^+e^-)$ from PDG 15. Supersedes ACHASOV 03.
[2] Not independent of $\Gamma(\pi^0\gamma)\ /\ \Gamma(\pi^+\pi^-\pi^0)$ from AMBROSINO 08G.
[3] Using $B(\omega \to e^+e^-) = (7.14 \pm 0.13) \times 10^{-5}$.
[4] Not independent of the corresponding $\Gamma(e^+e^-) \times \Gamma(\pi^0\gamma)/\Gamma^2_{total}$.
[5] Using ACHASOV 03, ACHASOV 03D and $B(\omega \to \pi^+\pi^-) = (1.70 \pm 0.28)\%$.
[6] Not independent of the corresponding $\Gamma(e^+e^-) \times \Gamma(\pi^+\pi^-\pi^0)/\Gamma^2_{total}$.
[7] Reanalysis of DRUZHININ 84, DOLINSKY 89, DOLINSKY 91 taking into account the triangle anomaly contributions.

$\Gamma(\pi^0\gamma)/\Gamma(\pi^+\pi^-\pi^0)$ — Γ_2/Γ_1

VALUE (units 10^{-2})	DOCUMENT ID		TECN	COMMENT
9.35±0.30 OUR FIT Error includes scale factor of 2.4.				
9.05±0.27 OUR AVERAGE Error includes scale factor of 1.8.				
8.97±0.16	AMBROSINO	08G	KLOE	$e^+e^- \to \pi^+\pi^-2\pi^0, 2\pi^0\gamma$
9.94±0.36±0.38	[1] AULCHENKO	00A	SND	$e^+e^- \to \pi^+\pi^-2\pi^0, 2\pi^0\gamma$
8.4 ±1.3	KEYNE	76	CNTR	$\pi^-p \to \omega n$
10.9 ±2.5	BENAKSAS	72C	OSPK	$e^+e^- \to \pi^0\gamma$
8.1 ±2.0	BALDIN	71	HLBC	2.9 π^+p
13 ±4	JACQUET	69B	HLBC	2.05 $\pi^+p \to \pi^+p\omega$
• • • We do not use the following data for averages, fits, limits, etc. • • •				
9.7 ±0.2 ±0.5	[2,3] ACHASOV	03D	RVUE	0.44–2.00 $e^+e^- \to \pi^+\pi^-\pi^0$
9.9 ±0.7	[2] DOLINSKY	89	ND	$e^+e^- \to \pi^0\gamma$

[1] From $\sigma_0^{\omega\pi^0 \to \pi^0\pi^0\gamma}(m_\phi)/\sigma_0^{\omega\pi^0 \to \pi^+\pi^-\pi^0\pi^0}(m_\phi)$ with a phase-space correction factor of 1/1.023.
[2] Not independent of the corresponding $\Gamma(e^+e^-) \times \Gamma(\pi^0\gamma)/\Gamma^2_{total}$.
[3] Using ACHASOV 03. Based on 1.2M events.

$\Gamma(\pi^+\pi^-)/\Gamma_{total}$ — Γ_3/Γ

See also $\Gamma(\pi^+\pi^-)/\Gamma(\pi^+\pi^-\pi^0)$.

VALUE (units 10^{-2})	EVTS	DOCUMENT ID		TECN	COMMENT
$1.53^{+0.11}_{-0.13}$ OUR FIT Error includes scale factor of 1.2.					
1.49±0.13 OUR AVERAGE Error includes scale factor of 1.3. See the ideogram below.					
1.46±0.12±0.02	900k	[1] AKHMETSHIN	07		$e^+e^- \to \pi^+\pi^-$
1.30±0.24±0.05	11.2k	[2] AKHMETSHIN	04	CMD2	$e^+e^- \to \pi^+\pi^-$
$2.38^{+1.77}_{-0.90}$±0.18	5.4k	[3] ACHASOV	02E	SND	1.1–1.38 $e^+e^- \to \pi^+\pi^-\pi^0$
2.3 ±0.5		BARKOV	85	OLYA	$e^+e^- \to \pi^+\pi^-$
1.6 $^{+0.9}_{-0.7}$		QUENZER	78	DM1	$e^+e^- \to \pi^+\pi^-$
3.6 ±1.9		BENAKSAS	72	OSPK	$e^+e^- \to \pi^+\pi^-$
• • • We do not use the following data for averages, fits, limits, etc. • • •					
1.29±0.22±0.03	970k	[4,5] ABLIKIM	18C	BES3	$\eta'(958) \to \gamma\pi^+\pi^-$
1.28±0.22±0.03	970k	[6,7] ABLIKIM	18C	BES3	$\eta'(958) \to \gamma\pi^+\pi^-$
1.52±0.08		[8] HANHART	18	RVUE	$e^+e^- \to \pi^+\pi^-$
1.75±0.11	4.5M	[9] ACHASOV	05A	SND	$e^+e^- \to \pi^+\pi^-$
2.01±0.29		[10] BENAYOUN	03	RVUE	$e^+e^- \to \pi^+\pi^-$
1.9 ±0.3		[11] GARDNER	99	RVUE	$e^+e^- \to \pi^+\pi^-$
2.3 ±0.4		[12] BENAYOUN	98	RVUE	$e^+e^- \to \pi^+\pi^-, \mu^+\mu^-$
1.0 ±0.11		[13] WICKLUND	78	ASPK	3,4,6 $\pi^\pm N$
1.22±0.30		ALVENSLEB...	71C	CNTR	Photoproduction
1.3 $^{+1.2}_{-0.9}$		MOFFEIT	71	HBC	2.8,4.7 γp
0.80$^{+0.28}_{-0.20}$		[14] BIGGS	70B	CNTR	4.2γC $\to \pi^+\pi^-$ C

[1] A combined fit of AKHMETSHIN 07, AULCHENKO 06, and AULCHENKO 05.
[2] Update of AKHMETSHIN 02.
[3] From the $m_{\pi^+\pi^-}$ spectrum taking into account the interference of the $\rho\pi$ and $\omega\pi$ amplitudes.
[4] From a fit to $\pi^+\pi^-$ mass using $\rho(770)$ (parametrized with the Gounaris-Sakurai approach), $\omega(782)$, and box anomaly components.
[5] ABLIKIM 18C reports $[\Gamma(\omega(782) \to \pi^+\pi^-)/\Gamma_{total}] \times [B(\eta'(958) \to \omega\gamma)] = (3.25 \pm 0.21 \pm 0.52) \times 10^{-4}$ which we divide by our best value $B(\eta'(958) \to \omega\gamma) = (2.52 \pm 0.07) \times 10^{-2}$. Our first error is their experiment's error and our second error is the systematic error from using our best value.
[6] From a fit to $\pi^+\pi^-$ mass using $\rho(770)$ (parametrized with the Gounaris-Sakurai approach), $\omega(782)$, and $\rho(1450)$ components.
[7] ABLIKIM 18C reports $[\Gamma(\omega(782) \to \pi^+\pi^-)/\Gamma_{total}] \times [B(\eta'(958) \to \omega\gamma)] = (3.22 \pm 0.21 \pm 0.52) \times 10^{-4}$ which we divide by our best value $B(\eta'(958) \to \omega\gamma) = (2.52 \pm 0.07) \times 10^{-2}$. Our first error is their experiment's error and our second error is the systematic error from using our best value.
[8] Dispersive analysis. Value extracted from average of data from AUBERT 09AS, AKHMETSHIN 07, ACHASOV 06, AMBROSINO 11A, BABUSCI 13D, ABLIKIM 16B normalised by PDG 16 evaluation for $\Gamma(\omega \to e^+e^-)$.
[9] Using $\Gamma(\omega \to e^+e^-)$ from the 2004 Edition of this Review (PDG 04).
[10] Using the data of AKHMETSHIN 02 in the hidden local symmetry model.
[11] Using the data of BARKOV 85.
[12] Using the data of BARKOV 85 in the hidden local symmetry model.
[13] From a model-dependent analysis assuming complete coherence.
[14] Re-evaluated under $\Gamma(\pi^+\pi^-)/\Gamma(\pi^+\pi^-\pi^0)$ by BEHREND 71 using more accurate $\omega \to \rho$ photoproduction cross-section ratio.

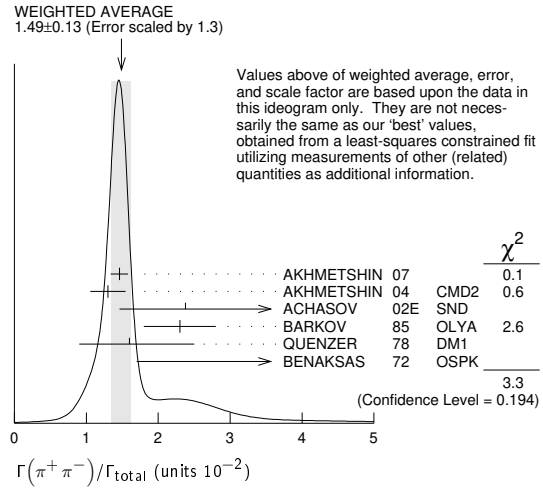

$\Gamma(\pi^+\pi^-)/\Gamma(\pi^+\pi^-\pi^0)$ — Γ_3/Γ_1

See also $\Gamma(\pi^+\pi^-)/\Gamma_{total}$.

VALUE	DOCUMENT ID		TECN	COMMENT
0.0172±0.0014 OUR FIT Error includes scale factor of 1.2.				
0.026 ±0.005 OUR AVERAGE				
0.021 $^{+0.028}_{-0.009}$	[1,2] RATCLIFF	72	ASPK	15 $\pi^-p \to n2\pi$
0.028 ±0.006	[1] BEHREND	71	ASPK	Photoproduction
0.022 $^{+0.009}_{-0.01}$	[3] ROOS	70	RVUE	

[1] The fitted width of these data is 160 MeV in agreement with present average, thus the ω contribution is overestimated. Assuming ρ width 145 MeV.
[2] Significant interference effect observed. NB of $\omega \to 3\pi$ comes from an extrapolation.
[3] ROOS 70 combines ABRAMOVICH 70 and BIZZARRI 70.

$\Gamma(\pi^+\pi^-)/\Gamma(\pi^0\gamma)$ — Γ_3/Γ_2

VALUE	EVTS	DOCUMENT ID		TECN	COMMENT
0.20±0.04	1.98M	[1] ALOISIO	03	KLOE	1.02 $e^+e^- \to \pi^+\pi^-\pi^0$

[1] Using the data of ALOISIO 02D.

$\Gamma(\text{neutrals})/\Gamma_{total}$ — $(\Gamma_2+\Gamma_4)/\Gamma$

VALUE	EVTS	DOCUMENT ID		TECN	COMMENT
0.091±0.006 OUR FIT					
0.081±0.011 OUR AVERAGE					
0.075±0.025		BIZZARRI	71	HBC	0.0 $p\overline{p}$
0.079±0.019		DEINET	69B	OSPK	1.5 π^-p
0.084±0.015		BOLLINI	68C	CNTR	2.1 π^-p
• • • We do not use the following data for averages, fits, limits, etc. • • •					
0.073±0.018	42	BASILE	72B	CNTR	1.67 π^-p

$\Gamma(\text{neutrals})/\Gamma(\pi^+\pi^-\pi^0)$ — $(\Gamma_2+\Gamma_4)/\Gamma_1$

VALUE	EVTS	DOCUMENT ID		TECN	COMMENT
0.102±0.008 OUR FIT					
$0.103^{+0.011}_{-0.010}$ OUR AVERAGE					
0.15 ±0.04	46	AGUILAR-...	72B	HBC	3.9,4.6 K^-p
0.10 ±0.03	19	BARASH	67B	HBC	0.0 $\overline{p}p$
0.134±0.026	850	DIGIUGNO	66B	CNTR	1.4 π^-p
0.097±0.016	348	FLATTE	66	HBC	1.4 – 1.7 $K^-p \to \Lambda$MM
0.06 $^{+0.05}_{-0.02}$		JAMES	66	HBC	2.1 π^+p
0.08 ±0.03	35	KRAEMER	64	DBC	1.2 π^+d
• • • We do not use the following data for averages, fits, limits, etc. • • •					
0.11 ±0.02	20	BUSCHBECK	63	HBC	1.5 K^-p

$\Gamma(\pi^0\gamma)/\Gamma(\text{neutrals})$ — $\Gamma_2/(\Gamma_2+\Gamma_4)$

VALUE	CL%	DOCUMENT ID		TECN	COMMENT
• • • We do not use the following data for averages, fits, limits, etc. • • •					
0.78±0.07		[1] DAKIN	72	OSPK	1.4 $\pi^-p \to n$MM
>0.81	90	DEINET	69B	OSPK	

[1] Error statistical only. Authors obtain good fit also assuming $\pi^0\gamma$ as the only neutral decay.

Downloaded from https://academic.oup.com/ptep/article/2022/8/083C01/6651666 by KIT Library user on 27 September 2022

$\Gamma(\text{neutrals})/\Gamma(\text{charged particles})$ — $(\Gamma_2+\Gamma_4)/(\Gamma_1+\Gamma_3)$

VALUE	DOCUMENT ID		TECN	COMMENT
0.100±0.008 OUR FIT				
0.124±0.021	FELDMAN	67C	OSPK	1.2 $\pi^- p$

$\Gamma(\eta\gamma)/\Gamma_{total}$ — Γ_5/Γ

VALUE (units 10^{-4})	EVTS	DOCUMENT ID		TECN	COMMENT
4.5 ±0.4 OUR FIT Error includes scale factor of 1.1.					
6.3 ±1.3 OUR AVERAGE Error includes scale factor of 1.2.					
6.6 ±1.7		[1] ABELE	97E	CBAR	0.0 $\overline{p}p \to 5\gamma$
8.3 ±2.1		ALDE	93	GAM2	38 $\pi^- p \to \omega n$
$3.0\ ^{+2.5}_{-1.8}$		[2] ANDREWS	77	CNTR	6.7–10 γ Cu
• • • We do not use the following data for averages, fits, limits, etc. • • •					
4.2 ±0.4 ±0.1	33k	[3] ACHASOV	07B	SND	0.6–1.38 $e^+e^- \to \eta\gamma$
$4.44^{+2.59}_{-1.83}\pm0.28$	17.4k	[4,5] AKHMETSHIN	05	CMD2	0.60-1.38 $e^+e^- \to \eta\gamma$
5.10±0.72±0.34	23k	[6] AKHMETSHIN	01B	CMD2	$e^+e^- \to \eta\gamma$
0.7 to 5.5		[7] CASE	00	CBAR	0.0 $p\overline{p} \to \eta\eta\gamma$
$6.56^{+2.41}_{-2.55}$	3525	[2,8] BENAYOUN	96	RVUE	$e^+e^- \to \eta\gamma$
7.3 ±2.9		[2,4] DOLINSKY	89	ND	$e^+e^- \to \eta\gamma$

[1] No flat $\eta\eta\gamma$ background assumed.
[2] Solution corresponding to constructive ω-ρ interference.
[3] ACHASOV 07B reports $[\Gamma(\omega(782) \to \eta\gamma)/\Gamma_{total}] \times [B(\omega(782) \to e^+e^-)] = (3.10 \pm 0.31 \pm 0.11) \times 10^{-8}$ which we divide by our best value $B(\omega(782) \to e^+e^-) = (7.38 \pm 0.22) \times 10^{-5}$. Our first error is their experiment's error and our second error is the systematic error from using our best value. Supersedes ACHASOV 00D and ACHASOV 06A.
[4] Not independent of the corresponding $\Gamma(e^+e^-) \times \Gamma(\eta\gamma)/\Gamma^2_{total}$.
[5] Using $B(\omega \to e^+e^-) = (7.14 \pm 0.13) \times 10^{-5}$ and $B(\eta \to \gamma\gamma) = 39.43 \pm 0.26\%$.
[6] Using $B(\omega \to e^+e^-) = (7.07 \pm 0.19) \times 10^{-5}$ and using $B(\eta \to 3\pi^0) = (32.24 \pm 0.29) \times 10^{-2}$. Solution corresponding to constructive ω-ρ interference. The combined fit from 600 to 1380 MeV taking into account $\rho(770)$, $\omega(782)$, $\phi(1020)$, and $\rho(1450)$ (mass and width fixed at 1450 MeV and 310 MeV respectively). Not independent of the corresponding $\Gamma(e^+e^-) \times \Gamma(\eta\gamma)/\Gamma^2_{total}$.
[7] Depending on the degree of coherence with the flat $\eta\eta\gamma$ background and using $B(\omega \to \pi^0\gamma) = (8.5 \pm 0.5) \times 10^{-2}$.
[8] Reanalysis of DRUZHININ 84, DOLINSKY 89, DOLINSKY 91 taking into account the triangle anomaly contributions.

$\Gamma(\eta\gamma)/\Gamma(\pi^0\gamma)$ — Γ_5/Γ_2

VALUE	DOCUMENT ID		TECN	COMMENT
• • • We do not use the following data for averages, fits, limits, etc. • • •				
0.0098±0.0024	[1] ALDE	93	GAM2	38 $\pi^- p \to \omega n$
0.0082±0.0033	[2] DOLINSKY	89	ND	$e^+e^- \to \eta\gamma$
0.010 ±0.045	APEL	72B	OSPK	4–8 $\pi^- p \to n3\gamma$

[1] Model independent determination.
[2] Solution corresponding to constructive ω-ρ interference.

$\Gamma(\pi^0 e^+e^-)/\Gamma_{total}$ — Γ_6/Γ

VALUE (units 10^{-4})	EVTS	DOCUMENT ID		TECN	COMMENT
7.7 ±0.6 OUR FIT					
7.7 ±0.6 OUR AVERAGE					
7.61±0.53±0.64		ACHASOV	08	SND	0.36–0.97 $e^+e^- \to \pi^0 e^+e^-$
8.19±0.71±0.62		AKHMETSHIN	05A	CMD2	0.72-0.84 e^+e^-
5.9 ±1.9	43	DOLINSKY	88	ND	$e^+e^- \to \pi^0 e^+e^-$

$\Gamma(\pi^0\mu^+\mu^-)/\Gamma_{total}$ — Γ_7/Γ

VALUE (units 10^{-4})	EVTS	DOCUMENT ID		TECN	COMMENT
1.34±0.18 OUR FIT Error includes scale factor of 1.5.					
1.34±0.19 OUR AVERAGE Error includes scale factor of 1.5. See the ideogram below.					
1.41±0.09±0.15		ARNALDI	16	NA60	400 GeV (p-A) collisions
1.72±0.25±0.14	3k	ARNALDI	09	NA60	158A In–In collisions
0.96±0.23		DZHELYADIN	81B	CNTR	25–33 $\pi^- p \to \omega n$

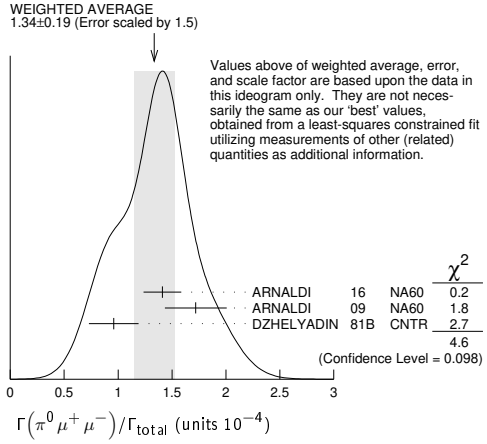

$\Gamma(\eta e^+e^-)/\Gamma_{total}$ — Γ_8/Γ

VALUE (units 10^{-5})	DOCUMENT ID		TECN	COMMENT
• • • We do not use the following data for averages, fits, limits, etc. • • •				
<1.1	AKHMETSHIN	05A	CMD2	0.72-0.84 e^+e^-

$\Gamma(e^+e^-)/\Gamma_{total}$ — Γ_9/Γ

VALUE (units 10^{-4})	EVTS	DOCUMENT ID		TECN	COMMENT
0.738±0.022 OUR FIT Error includes scale factor of 1.9.					
• • • We do not use the following data for averages, fits, limits, etc. • • •					
0.700±0.016	11200	[1,2] AKHMETSHIN	04	CMD2	$e^+e^- \to \pi^+\pi^-\pi^0$
0.752±0.004±0.024	1.2M	[2,3] ACHASOV	03D	RVUE	0.44–2.00 $e^+e^- \to \pi^+\pi^-\pi^0$
0.714±0.036		[2] DOLINSKY	89	ND	$e^+e^- \to \pi^+\pi^-\pi^0$
0.72 ±0.03		[2] BARKOV	87	CMD	$e^+e^- \to \pi^+\pi^-\pi^0$
0.64 ±0.04	1488	[2] KURDADZE	83B	OLYA	$e^+e^- \to \pi^+\pi^-\pi^0$
0.675±0.069	433	[2] CORDIER	80	DM1	$e^+e^- \to \pi^+\pi^-\pi^0$
0.83 ±0.10	451	[2] BENAKSAS	72B	OSPK	$e^+e^- \to \pi^+\pi^-\pi^0$
0.77 ±0.06		[4] AUGUSTIN	69D	OSPK	$e^+e^- \to \pi^+\pi^-\pi^0$
0.65 ±0.13	33	[5] ASTVACAT...	68	OSPK	Assume SU(3)+mixing

[1] Using $B(\omega \to \pi^+\pi^-\pi^0) = 0.891 \pm 0.007$. Update of AKHMETSHIN 00C.
[2] Not independent of the corresponding $\Gamma(e^+e^-) \times \Gamma(\pi^+\pi^-\pi^0)/\Gamma^2_{total}$.
[3] Using ACHASOV 03, ACHASOV 03D and $B(\omega \to \pi^+\pi^-) = (1.70 \pm 0.28)\%$.
[4] Rescaled by us to correspond to ω width 8.4 MeV. Systematic errors underestimated.
[5] Not resolved from ρ decay. Error statistical only.

$\Gamma(\pi^+\pi^-\pi^0\pi^0)/\Gamma_{total}$ — Γ_{10}/Γ

VALUE (units 10^{-4})	CL%	DOCUMENT ID		TECN	COMMENT
< 2	90	ACHASOV	09A	SND	$e^+e^- \to \pi^+\pi^-\pi^0\pi^0$
• • • We do not use the following data for averages, fits, limits, etc. • • •					
<200	90	KURDADZE	86	OLYA	$e^+e^- \to \pi^+\pi^-\pi^0\pi^0$

$\Gamma(\pi^+\pi^-\gamma)/\Gamma_{total}$ — Γ_{11}/Γ

VALUE	CL%	DOCUMENT ID		TECN	COMMENT
<0.0036	95	WEIDENAUER	90	ASTE	$p\overline{p} \to \pi^+\pi^-\pi^+\pi^-\gamma$
• • • We do not use the following data for averages, fits, limits, etc. • • •					
<0.004	95	BITYUKOV	88B	SPEC	32 $\pi^- p \to \pi^+\pi^-\gamma X$

$\Gamma(\pi^+\pi^-\gamma)/\Gamma(\pi^+\pi^-\pi^0)$ — Γ_{11}/Γ_1

VALUE	CL%	DOCUMENT ID		TECN	COMMENT
• • • We do not use the following data for averages, fits, limits, etc. • • •					
<0.066	90	KALBFLEISCH	75	HBC	2.18 $K^- p \to \Lambda\pi^+\pi^-\gamma$
<0.05	90	FLATTE	66	HBC	1.2 – 1.7 $K^- p \to \Lambda\pi^+\pi^-\gamma$

$\Gamma(\pi^+\pi^-\pi^+\pi^-)/\Gamma_{total}$ — Γ_{12}/Γ

VALUE	CL%	DOCUMENT ID		TECN	COMMENT
<1 × 10^{-3}	90	KURDADZE	88	OLYA	$e^+e^- \to \pi^+\pi^-\pi^+\pi^-$

$\Gamma(\pi^0\pi^0\gamma)/\Gamma_{total}$ — Γ_{13}/Γ

VALUE (units 10^{-5})	EVTS	DOCUMENT ID		TECN	COMMENT
6.7±1.1 OUR FIT					
6.5±1.2 OUR AVERAGE					
$6.4^{+2.4}_{-2.0}\pm0.8$	190	[1] AKHMETSHIN	04B	CMD2	0.6–0.97 $e^+e^- \to \pi^0\pi^0\gamma$
$6.6^{+1.4}_{-1.3}\pm0.6$	295	ACHASOV	02F	SND	0.36–0.97 $e^+e^- \to \pi^0\pi^0\gamma$
• • • We do not use the following data for averages, fits, limits, etc. • • •					
$11.8^{+2.1}_{-1.9}\pm1.4$	190	[2] AKHMETSHIN	04B	CMD2	0.6–0.97 $e^+e^- \to \pi^0\pi^0\gamma$
7.8±2.7±2.0	63	[1,3] ACHASOV	00G	SND	$e^+e^- \to \pi^0\pi^0\gamma$
12.7±2.3±2.5	63	[2,3] ACHASOV	00G	SND	$e^+e^- \to \pi^0\pi^0\gamma$

[1] In the model assuming the $\rho \to \pi^0\pi^0\gamma$ decay via the $\omega\pi$ and $f_0(500)\gamma$ mechanisms.
[2] In the model assuming the $\rho \to \pi^0\pi^0\gamma$ decay via the $\omega\pi$ mechanism only.
[3] Superseded by ACHASOV 02F.

$\Gamma(\pi^0\pi^0\gamma)/\Gamma(\pi^+\pi^-\pi^0)$ — Γ_{13}/Γ_1

VALUE	CL%	DOCUMENT ID		TECN	COMMENT
<0.00045	90	DOLINSKY	89	ND	$e^+e^- \to \pi^0\pi^0\gamma$
• • • We do not use the following data for averages, fits, limits, etc. • • •					
<0.08	95	JACQUET	69B	HLBC	2.05 $\pi^+ p \to \pi^+ p\omega$

$\Gamma(\pi^0\pi^0\gamma)/\Gamma(\pi^0\gamma)$ — Γ_{13}/Γ_2

VALUE (units 10^{-4})	CL%	EVTS	DOCUMENT ID		TECN	COMMENT
8.0±1.3 OUR FIT						
8.5±2.9		40 ± 14	ALDE	94B	GAM2	38 $\pi^- p \to \pi^0\pi^0\gamma n$
• • • We do not use the following data for averages, fits, limits, etc. • • •						
< 50	90		DOLINSKY	89	ND	$e^+e^- \to \pi^0\pi^0\gamma$
<1800	95		KEYNE	76	CNTR	$\pi^- p \to \omega n$
<1500	90		BENAKSAS	72C	OSPK	e^+e^-
<1400			BALDIN	71	HLBC	2.9 $\pi^+ p$
<1000	90		BARMIN	64	HLBC	1.3–2.8 $\pi^- p$

Downloaded from https://academic.oup.com/ptep/article/2022/8/083C01/6651666 by KIT Library user on 27 September 2022

$\Gamma(\pi^0\pi^0\gamma)/\Gamma(\text{neutrals})$ — $\Gamma_{13}/(\Gamma_2+\Gamma_4)$

VALUE	CL%	DOCUMENT ID		TECN	COMMENT
• • • We do not use the following data for averages, fits, limits, etc. • • •					
0.22 ± 0.07		[1] DAKIN	72	OSPK	$1.4\ \pi^- p \to n$MM
<0.19	90	DEINET	69B	OSPK	

[1] See $\Gamma(\pi^0\gamma)/\Gamma(\text{neutrals})$.

$\Gamma(\eta\pi^0\gamma)/\Gamma_{\text{total}}$ — Γ_{14}/Γ

VALUE (units 10^{-5})	CL%	DOCUMENT ID		TECN	COMMENT
<3.3	90	AKHMETSHIN	04B	CMD2	0.6–0.97 $e^+e^- \to \eta\pi^0\gamma$

$\Gamma(\mu^+\mu^-)/\Gamma_{\text{total}}$ — Γ_{15}/Γ

VALUE (units 10^{-5})	EVTS	DOCUMENT ID		TECN	COMMENT
7.4±1.8 OUR FIT					
7.4±1.8 OUR AVERAGE					
$6.6\pm1.4\pm1.7$	4.5 M	[1] ANASTASI	17	KLOE	$e^+e^- \to \mu^+\mu^-\gamma$
$9.0\pm2.9\pm1.1$	18	HEISTER	02C	ALEP	$Z \to \mu^+\mu^- + X$

[1] Assuming lepton universality in the decay $\omega \to \ell^+\ell^-$ and correcting for different phase space between electron and muon final states.

$\Gamma(\mu^+\mu^-)/\Gamma(\pi^+\pi^-\pi^0)$ — Γ_{15}/Γ_1

VALUE (units 10^{-3})	CL%	DOCUMENT ID		TECN	COMMENT
<0.2	90	WILSON	69	OSPK	$12\ \pi^- C \to$ Fe
• • • We do not use the following data for averages, fits, limits, etc. • • •					
<1.7	74	FLATTE	66	HBC	1.2 – 1.7 $K^- p \to \Lambda\mu^+\mu^-$
<1.2		BARBARO-...	65	HBC	2.7 $K^- p$

$\Gamma(\pi^0\mu^+\mu^-)/\Gamma(\mu^+\mu^-)$ — Γ_7/Γ_{15}

VALUE	EVTS	DOCUMENT ID		TECN	COMMENT
• • • We do not use the following data for averages, fits, limits, etc. • • •					
1.2 ± 0.6	30	[1] DZHELYADIN	79	CNTR	25–33 $\pi^- p$

[1] Superseded by DZHELYADIN 81B result above.

$\Gamma(3\gamma)/\Gamma_{\text{total}}$ — Γ_{16}/Γ

VALUE (units 10^{-4})	CL%	DOCUMENT ID		TECN	COMMENT
<1.9	95	[1] ABELE	97E	CBAR	0.0 $\overline{p}p \to 5\gamma$
• • • We do not use the following data for averages, fits, limits, etc. • • •					
<2	90	[1] PROKOSHKIN	95	GAM2	38 $\pi^- p \to 3\gamma n$

[1] From direct 3γ decay search.

$\Gamma(\eta\pi^0)/\Gamma_{\text{total}}$ — Γ_{17}/Γ

Violates C conservation.

VALUE	CL%	DOCUMENT ID		TECN	COMMENT
• • • We do not use the following data for averages, fits, limits, etc. • • •					
<0.001	90	ALDE	94B	GAM2	$38\pi^- p \to \eta\pi^0 n$

$[\Gamma(\eta\gamma)+\Gamma(\eta\pi^0)]/\Gamma(\pi^+\pi^-\pi^0)$ — $(\Gamma_5+\Gamma_{17})/\Gamma_1$

VALUE	CL%	DOCUMENT ID		TECN	COMMENT
<0.016	90	[1] FLATTE	66	HBC	1.2 – 1.7 $K^- p \to \Lambda\pi^+\pi^-$ MM
• • • We do not use the following data for averages, fits, limits, etc. • • •					
<0.045	95	JACQUET	69B	HLBC	2.05 $\pi^+ p \to \pi^+ p\omega$

[1] Restated by us using $B(\eta \to \text{charged modes}) = 29.2\%$.

$\Gamma(\eta\pi^0)/\Gamma(\pi^0\gamma)$ — Γ_{17}/Γ_2

Violates C conservation.

VALUE (units 10^{-3})	CL%	DOCUMENT ID		TECN	COMMENT
<2.6	90	[1] STAROSTIN	09	CRYM	$\gamma p \to \eta\pi^0 p$

[1] STAROSTIN 09 reports $[\Gamma(\omega(782) \to \eta\pi^0)/\Gamma(\omega(782) \to \pi^0\gamma)] \times [B(\eta \to 2\gamma)] < 1.01\times10^{-3}$ which we divide by our best value $B(\eta \to 2\gamma) = 39.36\times10^{-2}$.

$\Gamma(2\pi^0)/\Gamma(\pi^0\gamma)$ — Γ_{18}/Γ_2

Violates C conservation and Bose-Einstein statistics.

VALUE (units 10^{-3})	CL%	DOCUMENT ID		TECN	COMMENT
<2.59	90	STAROSTIN	09	CRYM	$\gamma p \to 2\pi^0 p$

$\Gamma(3\pi^0)/\Gamma_{\text{total}}$ — Γ_{19}/Γ

Violates C conservation.

VALUE	CL%	DOCUMENT ID		TECN	COMMENT
• • • We do not use the following data for averages, fits, limits, etc. • • •					
$<3\times10^{-4}$	90	PROKOSHKIN	95	GAM2	38 $\pi^- p \to 3\pi^0 n$

$\Gamma(3\pi^0)/\Gamma(\pi^0\gamma)$ — Γ_{19}/Γ_2

Violates C conservation.

VALUE (units 10^{-3})	CL%	DOCUMENT ID		TECN	COMMENT
<2.72	90	STAROSTIN	09	CRYM	$\gamma p \to 3\pi^0 p$

$\Gamma(3\pi^0)/\Gamma(\pi^+\pi^-\pi^0)$ — Γ_{19}/Γ_1

Violates C conservation.

VALUE	CL%	DOCUMENT ID		COMMENT
• • • We do not use the following data for averages, fits, limits, etc. • • •				
<0.009	90	BARBERIS	01	450 $pp \to p_f 3\pi^0 p_s$

$\Gamma(\text{invisible})/\Gamma(\pi^+\pi^-\pi^0)$ — Γ_{20}/Γ_1

VALUE	CL%	DOCUMENT ID		TECN	COMMENT
$<8.1\times10^{-5}$	90	ABLIKIM	18S	BES3	$J/\psi \to \omega\eta \to \omega\pi^+\pi^-\pi^0$

PARAMETER Λ IN $\omega \to \pi^0\ell^+\ell^-$ DECAY

In the pole approximation the electromagnetic transition form factor for a resonance of mass M is given by the expression:

$$|F|^2 = (1 - M^2/\Lambda^2)^{-2},$$

where for the parameter Λ vector dominance predicts $\Lambda = M_\rho \approx 0.770$ GeV. The ARNALDI 09 measurement is in obvious conflict with this expectation. Note that for $\eta \to \gamma\mu^+\mu^-$ decay ARNALDI 09 and DZHELYADIN 80 obtain the value of Λ consistent with vector dominance.

PARAMETER Λ IN $\omega \to \pi^0\mu^+\mu^-$ DECAY

VALUE (GeV)	EVTS	DOCUMENT ID		TECN	COMMENT
0.670 ±0.006 OUR AVERAGE					
$0.6707\pm0.0039\pm0.0056$		[1] ARNALDI	16	NA60	400 GeV (p-A) collisions
$0.668\ \pm0.009\ \pm0.003$	3k	[2] ARNALDI	09	NA60	158A In−In collisions
• • • We do not use the following data for averages, fits, limits, etc. • • •					
$0.65\ \pm0.03$		DZHELYADIN	81B	CNTR	25–33 $\pi^- p \to \omega n$

[1] ARNALDI 16 reports $\Lambda^{-2}(\omega) = 2.223 \pm 0.026 \pm 0.037$ GeV^{-2} which we converted to the quoted Λ value.

[2] ARNALDI 09 reports $\Lambda^{-2}(\omega) = 2.24 \pm 0.06 \pm 0.02$ GeV^{-2} which we converted to the quoted Λ value.

PARAMETER Λ IN $\omega \to \pi^0 e^+e^-$ DECAY

VALUE (GeV)	EVTS	DOCUMENT ID		TECN	COMMENT
0.709±0.037	1.1k	[1] ADLARSON	17B	A2MM	$\gamma p \to \omega p$

[1] ADLARSON 17B reports $\Lambda^{-2}(\omega\pi^0) = 1.99 \pm 0.21$ GeV^{-2} that we converted to the quoted Λ value.

ENERGY DEPENDENCE OF $\omega \to \pi^+\pi^-\pi^0$ DALITZ PLOT

The following experiments fit to one or more of the coefficients α, β, γ for $|\text{matrix element}|^2 \propto P\,(1 + 2\alpha Z + 2\beta Z^{3/2}\sin(3\phi) + 2\gamma Z^2 + O(Z^{5/2}))$ where P is the P-wave phase-space factor and Z, ϕ are kinematical variables as defined in ADLARSON 17.

VALUE	EVTS	DOCUMENT ID		TECN	COMMENT
0.133 ±0.008 OUR AVERAGE					
$0.1321\pm0.0067\pm0.0046$	260k	[1] ABLIKIM	18AD	BES3	$J/\psi \to \omega\eta$
$0.147\ \pm0.036$	44k	ADLARSON	17	WASA	α in $pd \to {}^3$He ω, $pp \to pp\omega$

[1] Keeping a term linear in Z only. A fit with the terms proportional to Z and $Z^{3/2}$ gives $\alpha = 0.133 \pm 0.041$ and $\beta = 0.037 \pm 0.054$.

$\omega(782)$ REFERENCES

ACHASOV	21	JHEP 2101 113	M.N. Achasov *et al.*	(SND Collab.)
LEES	21B	PR D104 112003	J.P. Lees *et al.*	(BABAR Collab.)
ANDREEV	20	EPJ C80 1189	V. Andreev *et al.*	(H1 Collab.)
HOID	20	EPJ C80 988	B.-L. Hoid, M. Hoferichter, B. Kubis	(BONN, BERN)
COLANGELO	19	JHEP 1902 006	G. Colangelo, M. Hoferichter, P. Stoffer	(BERN+)
HOFERICHT...	19	JHEP 1908 137	M. Hoferichter, B.-L. Hoid, B. Kubis	(WASH, BONN)
ABLIKIM	18AD	PR D98 112007	M. Ablikim *et al.*	(BESIII Collab.)
ABLIKIM	18C	PRL 120 242003	M. Ablikim *et al.*	(BESIII Collab.)
ABLIKIM	18S	PR D98 032001	M. Ablikim *et al.*	(BESIII Collab.)
HANHART	18	EPJ C78 450	C. Hanhart *et al.*	
ADLARSON	17	PL B770 418	P. Adlarson *et al.*	(WASA-at-COSY Collab.)
ADLARSON	17B	PR C95 035208	P. Adlarson *et al.*	(A2 Collab. at MAMI)
ANASTASI	17	PL B767 485	A. Anastasi *et al.*	(KLOE-2 Collab.)
ABLIKIM	16B	PL B753 103	M. Ablikim *et al.*	(BESIII Collab.)
ACHASOV	16A	PR D93 092001	M.N. Achasov *et al.*	(SND Collab.)
ARNALDI	16	PL B757 437	R. Arnaldi *et al.*	(NA60 Collab.)
PDG	16	CP C40 100001	C. Patrignani *et al.*	(PDG Collab.)
PDG	15	RPP 2015 at pdg.lbl.gov		(PDG Collab.)
ACHASOV	13	PR D88 054013	M.N. Achasov *et al.*	(SND Collab.)
BABUSCI	13D	PL B720 336	D. Babusci *et al.*	(CATA, CALB, BARI)
BENAYOUN	13	EPJ C73 2453	M. Benayoun, P. David, L. DelBuono	(PARIN, BERLIN+)
DAVIER	13	EPJ C73 2597	M. Davier *et al.*	
LEES	12G	PR D86 032013	J.P. Lees *et al.*	(BABAR Collab.)
NIECKNIG	12	EPJ C72 2014	F. Niecknig, B. Kubis, S.P. Schneider	(BONN)
AMBROSINO	11A	PL B700 102	F. Ambrosino *et al.*	(KLOE Collab.)
BENAYOUN	10	EPJ C65 211	M. Benayoun *et al.*	
ACHASOV	09A	JETP 109 379	M.N. Achasov *et al.*	(SND Collab.)
		Translated from ZETF 136 442.		
ARNALDI	09	PL B677 260	R. Arnaldi *et al.*	(NA60 Collab.)
AUBERT	09AS	PRL 103 231801	B. Aubert *et al.*	(BABAR Collab.)
STAROSTIN	09	PR C79 065201	A. Starostin *et al.*	(Crystal Ball Collab. at MAMI)
ACHASOV	08	JETP 107 61	M.N. Achasov *et al.*	(SND Collab.)
		Translated from ZETF 134 80.		
AMBROSINO	08G	PL B669 223	F. Ambrosino *et al.*	(KLOE Collab.)
ACHASOV	07B	PR D76 077101	M.N. Achasov *et al.*	(SND Collab.)
AKHMETSHIN	07	PL B648 28	R.R. Akhmetshin *et al.*	(Novosibirsk CMD-2 Collab.)
ACHASOV	06	JETP 103 380	M.N. Achasov *et al.*	(Novosibirsk SND Collab.)
		Translated from ZETF 130 437.		
ACHASOV	06A	PR D74 014016	M.N. Achasov *et al.*	(SND Collab.)
AULCHENKO	06	JETPL 84 413	V.M. Aulchenko *et al.*	(Novosibirsk CMD-2 Collab.)
		Translated from ZETFP 84 491.		
ACHASOV	05A	JETP 101 1053	M.N. Achasov *et al.*	(Novosibirsk SND Collab.)
		Translated from ZETF 128 1201.		
AKHMETSHIN	05	PL B605 26	R.R. Akhmetshin *et al.*	(Novosibirsk CMD-2 Collab.)
AKHMETSHIN	05A	PL B613 29	R.R. Akhmetshin *et al.*	(Novosibirsk CMD-2 Collab.)
AULCHENKO	05	JETPL 82 743	V.M. Aulchenko *et al.*	(Novosibirsk CMD-2 Collab.)
		Translated from ZETFP 82 841.		
AKHMETSHIN	04	PL B578 285	R.R. Akhmetshin *et al.*	(Novosibirsk CMD-2 Collab.)
AKHMETSHIN	04B	PL B580 119	R.R. Akhmetshin *et al.*	(Novosibirsk CMD-2 Collab.)
AUBERT,B	04N	PR D70 072004	B. Aubert *et al.*	(BABAR Collab.)
PDG	04	PL B592 1	S. Eidelman *et al.*	(PDG Collab.)
ACHASOV	03	PL B559 171	M.N. Achasov *et al.*	(Novosibirsk SND Collab.)
ACHASOV	03D	PR D68 052006	M.N. Achasov *et al.*	(Novosibirsk SND Collab.)

Downloaded from https://academic.oup.com/ptep/article/2022/8/083C01/6651666 by KIT Library user on 27 September 2022

ALOISIO	03	PL B561 55	A. Aloisio *et al.*	(KLOE Collab.)
BENAYOUN	03	EPJ C29 397	M. Benayoun *et al.*	
ACHASOV	02E	PR D66 032001	M.N. Achasov *et al.*	(Novosibirsk SND Collab.)
ACHASOV	02F	PL B537 201	M.N. Achasov *et al.*	(Novosibirsk SND Collab.)
AKHMETSHIN	02	PL B527 161	R.R. Akhmetshin *et al.*	(Novosibirsk CMD-2 Collab.)
ALOISIO	02D	PL B537 21	A. Aloisio *et al.*	(KLOE Collab.)
HEISTER	02C	PL B528 19	A. Heister *et al.*	(ALEPH Collab.)
ACHASOV	01E	PR D63 072002	M.N. Achasov *et al.*	(Novosibirsk SND Collab.)
AKHMETSHIN	01B	PL B509 217	R.R. Akhmetshin *et al.*	(Novosibirsk CMD-2 Collab.)
BARBERIS	01	PL B507 14	D. Barberis *et al.*	
ACHASOV	00	EPJ C12 25	M.N. Achasov *et al.*	(Novosibirsk SND Collab.)
ACHASOV	00D	JETPL 72 282	M.N. Achasov *et al.*	(Novosibirsk SND Collab.)
		Translated from ZETFP 72 411.		
ACHASOV	00G	JETPL 71 355	M.N. Achasov *et al.*	(Novosibirsk SND Collab.)
		Translated from ZETFP 71 519.		
AKHMETSHIN	00C	PL B476 33	R.R. Akhmetshin *et al.*	(Novosibirsk CMD-2 Collab.)
AULCHENKO	00A	JETP 90 927	V.M. Aulchenko *et al.*	(Novosibirsk SND Collab.)
		Translated from ZETF 117 1067.		
CASE	00	PR D61 032002	T. Case *et al.*	(Crystal Barrel Collab.)
ACHASOV	99E	PL B462 365	M.N. Achasov *et al.*	(Novosibirsk SND Collab.)
GARDNER	99	PR D59 076002	S. Gardner, H.B. O'Connell	
BENAYOUN	98	EPJ C2 269	M. Benayoun *et al.*	(IPNP, NOVO, ADLD+)
ABELE	97E	PL B411 361	A. Abele *et al.*	(Crystal Barrel Collab.)
BENAYOUN	96	ZPHY C72 221	M. Benayoun *et al.*	(IPNP, NOVO)
PROKOSHKIN	95	PD 40 273	Y.D. Prokoshkin, V.D. Samoilenko	(SERP)
		Translated from DANS 342 610.		
WURZINGER	95	PR C51 443	R. Wurzinger *et al.*	(BONN, ORSAY, SACL+)
ALDE	94B	PL B340 122	D.M. Alde *et al.*	(SERP, BELG, LANL, LAPP+)
AMSLER	94C	PL B327 425	C. Amsler *et al.*	(Crystal Barrel Collab.)
ALDE	93	PAN 56 1229	D.M. Alde *et al.*	(SERP, LAPP, LANL, BELG+)
		Translated from YAF 56 137.		
Also		ZPHY C61 35	D.M. Alde *et al.*	(SERP, LAPP, LANL, BELG+)
AMSLER	93B	PL B311 362	C. Amsler *et al.*	(Crystal Barrel Collab.)
WEIDENAUER	93	ZPHY C59 387	P. Weidenauer *et al.*	(ASTERIX Collab.)
ANTONELLI	92	ZPHY C56 15	A. Antonelli *et al.*	(DM2 Collab.)
DOLINSKY	91	PRPL 202 99	S.I. Dolinsky *et al.*	(NOVO)
WEIDENAUER	90	ZPHY C47 353	P. Weidenauer *et al.*	(ASTERIX Collab.)
DOLINSKY	89	ZPHY C42 511	S.I. Dolinsky *et al.*	(NOVO)
BITYUKOV	88B	SJNP 47 800	S.I. Bityukov *et al.*	(SERP)
		Translated from YAF 47 1258.		
DOLINSKY	88	SJNP 48 277	S.I. Dolinsky *et al.*	(NOVO)
		Translated from YAF 48 442.		
KURDADZE	88	JETPL 47 512	L.M. Kurdadze *et al.*	(NOVO)
		Translated from ZETFP 47 432.		
AULCHENKO	87	PL B186 432	V.M. Aulchenko *et al.*	(NOVO)
BARKOV	87	JETPL 46 164	L.M. Barkov *et al.*	(NOVO)
		Translated from ZETFP 46 132.		
KURDADZE	86	JETPL 43 643	L.M. Kurdadze *et al.*	(NOVO)
		Translated from ZETFP 43 497.		
BARKOV	85	NP B256 365	L.M. Barkov *et al.*	(NOVO)
DRUZHININ	84	PL 144B 136	V.P. Druzhinin *et al.*	(NOVO)
KURDADZE	83B	JETPL 36 274	A.M. Kurdadze *et al.*	(NOVO)
		Translated from ZETFP 36 221.		
DZHELYADIN	81B	PL 102B 296	R.I. Dzhelyadin *et al.*	(SERP)
CORDIER	80	NP B172 13	A. Cordier *et al.*	(LALO)
DZHELYADIN	80	PL 94B 548	R.I. Dzhelyadin *et al.*	(SERP)
ROOS	80	LNC 27 321	M. Roos, A. Pellinen	(HELS)
BENKHEIRI	79	NP B150 268	P. Benkheiri *et al.*	(EPOL, CERN, CDEF+)
DZHELYADIN	79	PL 84B 143	R.I. Dzhelyadin *et al.*	(SERP)
COOPER	78B	NP B146 1	A.M. Cooper *et al.*	(TATA, CERN, CDEF+)
QUENZER	78	PL 76B 512	A. Quenzer *et al.*	(LALO)
VANAPEL...	78	NP B133 245	G.W. van Apeldoorn *et al.*	(ZEEM)
WICKLUND	78	PR D17 1197	A.B. Wicklund *et al.*	(ANL)
ANDREWS	77	PRL 38 198	D.E. Andrews *et al.*	(ROCH)
GESSAROLI	77	NP B126 382	R. Gessaroli *et al.*	(BGNA, FIRZ, GENO+)
KEYNE	76	PR D14 28	J. Keyne *et al.*	(LOIC, SHMP)
Also		PR D8 2789	D.M. Binnie *et al.*	(LOIC, SHMP)
KALBFLEISCH	75	PR D11 987	G.R. Kalbfleisch, R.C. Strand, J.W. Chapman	(BNL+)
AGUILAR-...	72B	PR D6 29	M. Aguilar-Benitez *et al.*	(BNL)
APEL	72B	PL 41B 234	W.D. Apel *et al.*	(KARLK, KARLE, PISA)
BASILE	72B	Phil. Conf. 153	M. Basile *et al.*	(CERN)
BENAKSAS	72	PL 39B 289	D. Benaksas *et al.*	(ORSAY)
BENAKSAS	72B	PL 42B 507	D. Benaksas *et al.*	(ORSAY)
BENAKSAS	72C	PL 42B 511	D. Benaksas *et al.*	(ORSAY)
BORENSTEIN	72	PR D5 1559	S.R. Borenstein *et al.*	(BNL, MICH)
BROWN	72	PL 42B 117	R.M. Brown *et al.*	(ILL, ILLC)
DAKIN	72	PR D6 2321	J.T. Dakin *et al.*	(PRIN)
RATCLIFF	72	PL 38B 345	B.N. Ratcliff *et al.*	(SLAC)
ALVENSLEB...	71C	PRL 27 888	H. Alvensleben *et al.*	(DESY)
BALDIN	71	SJNP 13 758	A.B. Baldin *et al.*	(ITEP)
		Translated from YAF 13 1318.		
BEHREND	71	PRL 27 61	H.J. Behrend *et al.*	(ROCH, CORN, FNAL)
BIZZARRI	71	NP B27 140	R. Bizzarri *et al.*	(CERN, CDEF)
COYNE	71	NP B32 333	D.G. Coyne *et al.*	(LRL)
MOFFEIT	71	NP B29 349	K.C. Moffeit *et al.*	(LRL, UCB, SLAC+)
ABRAMOVI...	70	NP B20 209	M. Abramovich *et al.*	(CERN)
BIGGS	70B	PRL 24 1201	P.J. Biggs *et al.*	(DARE)
BIZZARRI	70	PRL 25 1385	R. Bizzarri *et al.*	(ROMA, SYRA)
ROOS	70	DNPL/R7 173	M. Roos	(CERN)
Proc. Daresbury Study Weekend No. 1.				
AUGUSTIN	69D	PL 28B 513	J.E. Augustin *et al.*	(ORSAY)
BIZZARRI	69	NP B14 169	R. Bizzarri *et al.*	(CERN, CDEF)
DEINET	69B	PL 30B 426	W. Deinet *et al.*	(KARL, CERN)
JACQUET	69B	NC 63A 743	F. Jacquet *et al.*	(EPOL, BERG)
WILSON	69	Private Comm.	R. Wilson	(HARV)
Also		PR 178 2095	A.A. Wehmann *et al.*	(HARV, CASE, SLAC+)
ASTVACAT...	68	PL 27B 45	R.G. Astvatsaturov *et al.*	(JINR, MOSU)
BOLLINI	68C	NC 56A 531	D. Bollini *et al.*	(CERN, BGNA, STRB)
GOUNARIS	68	PRL 21 244	G.J. Gounaris, J.J. Sakurai	
BARASH	67B	PR 156 1399	N. Barash *et al.*	(COLU)
FELDMAN	67C	PR 159 1219	M. Feldman *et al.*	(PENN)
DIGIUGNO	66B	NC 44A 1272	G. Di Giugno *et al.*	(NAPL, FRAS, TRST)
FLATTE	66	PR 145 1050	S.M. Flatte *et al.*	(LRL)
JAMES	66	PR 142 896	F.E. James, H.L. Kraybill	(YALE, BNL)
BARBARO-...	65	PRL 14 279	A. Barbaro-Galtieri, R.D. Tripp	(LRL)
BARMIN	64	JETP 18 1289	V.V. Barmin *et al.*	(ITEP)
		Translated from ZETF 45 1879.		
KRAEMER	64	PR 136 B496	R.W. Kraemer *et al.*	(JHU, NWES, WOOD)
BUSCHBECK	63	Siena Conf. 1 166	B. Buschbeck *et al.*	(VIEN, CERN, ANIK)

$\eta'(958)$

$I^G(J^{PC}) = 0^+(0^{-+})$

$\eta'(958)$ MASS

VALUE (MeV)	EVTS	DOCUMENT ID		TECN	COMMENT
957.78 ±0.06 OUR AVERAGE					
957.793±0.054±0.036	3.9k	LIBBY	08	CLEO	$J/\psi \to \gamma\eta'$
957.9 ±0.2 ±0.6	4800	WURZINGER	96	SPEC	1.68 $pd \to {}^3$Heη'
957.46 ±0.33		DUANE	74	MMS	$\pi^- p \to n$MM
958.2 ±0.5	1414	DANBURG	73	HBC	2.2 $K^- p \to \Lambda\eta'$
958 ±1	400	JACOBS	73	HBC	2.9 $K^- p \to \Lambda\eta'$
956.1 ±1.1	3415	[1] BASILE	71	CNTR	1.6 $\pi^- p \to n\eta'$
• • • We do not use the following data for averages, fits, limits, etc. • • •					
957.5 ±0.2		BAI	04J	BES2	$J/\psi \to \gamma\gamma\pi^+\pi^-$
959 ±1	630	[2] BELADIDZE	92C	VES	36 π^-Be $\to \pi^-\eta'\eta$Be
958 ±1	340	[2] ARMSTRONG	91B	OMEG	300 $pp \to pp\eta\pi^+\pi^-$
958.2 ±0.4	622	[2] AUGUSTIN	90	DM2	$J/\psi \to \gamma\eta\pi^+\pi^-$
957.8 ±0.2	2420	[2] AUGUSTIN	90	DM2	$J/\psi \to \gamma\gamma\pi^+\pi^-$
956.3 ±1.0	143	[2] GIDAL	87	MRK2	$e^+e^- \to e^+e^-\eta\pi^+\pi^-$
957.4 ±1.4	535	[3] BASILE	71	CNTR	1.6 $\pi^- p \to n\eta'$
957 ±1		RITTENBERG	69	HBC	1.7–2.7 $K^- p$

[1] Using all η' decays.
[2] Systematic uncertainty not estimated.
[3] Using η' decays into neutrals. Not independent of the other listed BASILE 71 η' mass measurement.

$\eta'(958)$ WIDTH

VALUE (MeV)	EVTS	DOCUMENT ID		TECN	CHG	COMMENT
0.188±0.006 OUR FIT						
0.230±0.021 OUR AVERAGE						
0.226±0.017±0.014	2300	CZERWINSKI	10	MMS		$pp \to pp\eta'$
0.40 ±0.22	4800	WURZINGER	96	SPEC		1.68 $pd \to {}^3$Heη'
0.28 ±0.10	1000	BINNIE	79	MMS	0	$\pi^- p \to n$MM
• • • We do not use the following data for averages, fits, limits, etc. • • •						
0.20 ±0.04		BAI	04J	BES2		$J/\psi \to \gamma\gamma\pi^+\pi^-$

$\eta'(958)$ DECAY MODES

	Mode	Fraction (Γ_i/Γ)	Confidence level
Γ_1	$\pi^+\pi^-\eta$	(42.5 ±0.5) %	
Γ_2	$\rho^0\gamma$(including non-resonant $\pi^+\pi^-\gamma$)	(29.5 ±0.4) %	
Γ_3	$\rho^0\gamma$		
Γ_4	$\pi^0\pi^0\eta$	(22.4 ±0.5) %	
Γ_5	$\omega\gamma$	(2.52 ±0.07) %	
Γ_6	ωe^+e^-	(2.0 ±0.4) $\times 10^{-4}$	
Γ_7	$\gamma\gamma$	(2.307±0.033) %	
Γ_8	$3\pi^0$	(2.50 ±0.17) $\times 10^{-3}$	
Γ_9	$\mu^+\mu^-\gamma$	(1.13 ±0.28) $\times 10^{-4}$	
Γ_{10}	$\pi^+\pi^-\mu^+\mu^-$	(2.0 ±0.4) $\times 10^{-5}$	
Γ_{11}	$\pi^+\pi^-\pi^0$	(3.61 ±0.17) $\times 10^{-3}$	
Γ_{12}	$(\pi^+\pi^-\pi^0)$ S-wave	(3.8 ±0.5) $\times 10^{-3}$	
Γ_{13}	$\pi^\mp\rho^\pm$	(7.4 ±2.3) $\times 10^{-4}$	
Γ_{14}	$\pi^0\rho^0$	< 4 %	90%
Γ_{15}	$2(\pi^+\pi^-)$	(8.4 ±0.9) $\times 10^{-5}$	
Γ_{16}	$\pi^+\pi^-2\pi^0$	(1.8 ±0.4) $\times 10^{-4}$	
Γ_{17}	$2(\pi^+\pi^-)$ neutrals	< 1 %	95%
Γ_{18}	$2(\pi^+\pi^-)\pi^0$	< 1.8 $\times 10^{-3}$	90%
Γ_{19}	$2(\pi^+\pi^-)2\pi^0$	< 1 %	95%
Γ_{20}	$3(\pi^+\pi^-)$	< 3.1 $\times 10^{-5}$	90%
Γ_{21}	$K^\pm\pi^\mp$	< 4 $\times 10^{-5}$	90%
Γ_{22}	$\pi^+\pi^-e^+e^-$	(2.42 ±0.10) $\times 10^{-3}$	
Γ_{23}	$\pi^+e^-\nu_e$ + c.c.	< 2.1 $\times 10^{-4}$	90%
Γ_{24}	γe^+e^-	(4.91 ±0.27) $\times 10^{-4}$	
Γ_{25}	$\pi^0\gamma\gamma$	(3.20 ±0.24) $\times 10^{-3}$	
Γ_{26}	$\pi^0\gamma\gamma$(non resonant)	(6.2 ±0.9) $\times 10^{-4}$	
Γ_{27}	$\eta\gamma\gamma$	< 1.33 $\times 10^{-4}$	90%
Γ_{28}	$4\pi^0$	< 4.94 $\times 10^{-5}$	90%
Γ_{29}	e^+e^-	< 5.6 $\times 10^{-9}$	90%
Γ_{30}	invisible	< 6 $\times 10^{-4}$	90%
	Charge conjugation (C), Parity (P), Lepton family number (LF) violating modes		
Γ_{31}	$\pi^+\pi^-$	P,CP < 1.8 $\times 10^{-5}$	90%
Γ_{32}	$\pi^0\pi^0$	P,CP < 4 $\times 10^{-4}$	90%
Γ_{33}	$\pi^0e^+e^-$	C [a] < 1.4 $\times 10^{-3}$	90%
Γ_{34}	ηe^+e^-	C [a] < 2.4 $\times 10^{-3}$	90%
Γ_{35}	3γ	C < 1.0 $\times 10^{-4}$	90%
Γ_{36}	$\mu^+\mu^-\pi^0$	C [a] < 6.0 $\times 10^{-5}$	90%
Γ_{37}	$\mu^+\mu^-\eta$	C [a] < 1.5 $\times 10^{-5}$	90%
Γ_{38}	$e\mu$	LF < 4.7 $\times 10^{-4}$	90%

[a] C parity forbids this to occur as a single-photon process.

Downloaded from https://academic.oup.com/ptep/article/2022/8/083C01/6651666 by KIT Library user on 27 September 2022

CONSTRAINED FIT INFORMATION

An overall fit to the total width, a partial width, 2 combinations of partial widths obtained from integrated cross section, and 20 branching ratios uses 52 measurements and one constraint to determine 9 parameters. The overall fit has a $\chi^2 = 69.5$ for 44 degrees of freedom.

The following *off-diagonal* array elements are the correlation coefficients $\langle \delta p_i \delta p_j \rangle / (\delta p_i \cdot \delta p_j)$, in percent, from the fit to parameters p_i, including the branching fractions, $x_i \equiv \Gamma_i/\Gamma_{total}$. The fit constrains the x_i whose labels appear in this array to sum to one.

	x_1	x_2	x_4	x_5	x_7	x_8	x_{11}	x_{22}
x_2	−25							
x_4	−75	−43						
x_5	−7	−6	−2					
x_7	−11	−7	9	−1				
x_8	−17	−10	19	0	2			
x_{11}	−1	−1	−1	0	0	0		
x_{22}	−8	30	−14	−2	−2	−3	0	
Γ	11	−10	−1	1	−40	0	0	−3

	Mode	Rate (MeV)
Γ_1	$\pi^+\pi^-\eta$	0.0799 ±0.0029
Γ_2	$\rho^0\gamma$ (including non-resonant $\pi^+\pi^-\gamma$)	0.0554 ±0.0019
Γ_4	$\pi^0\pi^0\eta$	0.0421 ±0.0017
Γ_5	$\omega\gamma$	0.00474 ± 0.00020
Γ_7	$\gamma\gamma$	0.00434 ± 0.00013
Γ_8	$3\pi^0$	(4.7 ±0.4) × 10^{-4}
Γ_{11}	$\pi^+\pi^-\pi^0$	(6.8 ±0.4) × 10^{-4}
Γ_{22}	$\pi^+\pi^-e^+e^-$	(4.54 ±0.23) × 10^{-4}

$\eta'(958)$ PARTIAL WIDTHS

$\Gamma(\gamma\gamma)$ — Γ_7

VALUE (keV)	EVTS	DOCUMENT ID		TECN	COMMENT
4.34±0.14 OUR FIT					
4.28±0.19 OUR AVERAGE					
4.17±0.10±0.27	2000	[1] ACCIARRI	98Q	L3	$e^+e^- \to e^+e^-\pi^+\pi^-\gamma$
4.53±0.29±0.51	266	KARCH	92	CBAL	$e^+e^- \to e^+e^-\eta\pi^0\pi^0$
3.61±0.13±0.48		[2] BEHREND	91	CELL	$e^+e^- \to e^+e^-\eta'(958)$
4.6 ±1.1 ±0.6	23	BARU	90	MD1	$e^+e^- \to e^+e^-\pi^+\pi^-\gamma$
4.57±0.25±0.44		BUTLER	90	MRK2	$e^+e^- \to e^+e^-\eta'(958)$
5.08±0.24±0.71	547	[3] ROE	90	ASP	$e^+e^- \to e^+e^-2\gamma$
3.8 ±0.7 ±0.6	34	AIHARA	88C	TPC	$e^+e^- \to e^+e^-\eta\pi^+\pi^-$
4.9 ±0.5 ±0.5	136	[4] WILLIAMS	88	CBAL	$e^+e^- \to e^+e^-2\gamma$
• • • We do not use the following data for averages, fits, limits, etc. • • •					
4.7 ±0.6 ±0.9	143	[5] GIDAL	87	MRK2	$e^+e^- \to e^+e^-\eta\pi^+\pi^-$
4.0 ±0.9		[6] BARTEL	85E	JADE	$e^+e^- \to e^+e^-2\gamma$

[1] No non-resonant $\pi^+\pi^-$ contribution found.
[2] Reevaluated by us using $B(\eta' \to \rho(770)\gamma) = (30.2 \pm 1.3)\%$.
[3] Reevaluated by us using $B(\eta' \to \gamma\gamma) = (2.11 \pm 0.13)\%$.
[4] Reevaluated by us using $B(\eta' \to \gamma\gamma) = (2.11 \pm 0.13)\%$.
[5] Superseded by BUTLER 90.
[6] Systematic error not evaluated.

$\Gamma(e^+e^-)$ — Γ_{29}

VALUE (eV)	CL%	DOCUMENT ID		TECN	COMMENT
<1.1 × 10^{-3}	90	[1,2] ACHASOV	15	SND	$0.958\ e^+e^- \to \pi\pi\eta$
• • • We do not use the following data for averages, fits, limits, etc. • • •					
<2.0 × 10^{-3}	90	[2] ACHASOV	15	SND	$0.958\ e^+e^- \to \pi\pi\eta$
<2.4 × 10^{-3}	90	[2] AKHMETSHIN	15	CMD3	$0.958\ e^+e^- \to \pi^+\pi^-\eta$

[1] Combining data of ACHASOV 15 and AKHMETSHIN 15.
[2] Using η and η' branching fractions from PDG 14.

$\eta'(958)$ $\Gamma(i)\Gamma(\gamma\gamma)/\Gamma(total)$

This combination of a partial width with the partial width into $\gamma\gamma$ and with the total width is obtained from the integrated cross section into channel(i) in the $\gamma\gamma$ annihilation.

$\Gamma(\gamma\gamma) \times \Gamma(\rho^0\gamma(\text{including non-resonant } \pi^+\pi^-\gamma))/\Gamma_{total}$ — $\Gamma_7\Gamma_2/\Gamma$

VALUE (keV)	EVTS	DOCUMENT ID		TECN	COMMENT
1.28±0.04 OUR FIT					
1.26±0.07 OUR AVERAGE	Error includes scale factor of 1.2.				
1.09±0.04±0.13		BEHREND	91	CELL	$e^+e^- \to e^+e^-\rho(770)^0\gamma$
1.35±0.09±0.21		AIHARA	87	TPC	$e^+e^- \to e^+e^-\rho\gamma$
1.13±0.04±0.13	867	ALBRECHT	87B	ARG	$e^+e^- \to e^+e^-\rho\gamma$
1.53±0.09±0.21		ALTHOFF	84E	TASS	$e^+e^- \to e^+e^-\rho\gamma$
1.14±0.08±0.11	243	BERGER	84B	PLUT	$e^+e^- \to e^+e^-\rho\gamma$
1.73±0.34±0.35	95	JENNI	83	MRK2	$e^+e^- \to e^+e^-\rho\gamma$
1.49±0.13±0.027	213	BARTEL	82B	JADE	$e^+e^- \to e^+e^-\rho\gamma$
• • • We do not use the following data for averages, fits, limits, etc. • • •					
1.85±0.31±0.24	43	BEHREND	82C	CELL	$e^+e^- \to e^+e^-\rho\gamma$

$\Gamma(\gamma\gamma) \times \Gamma(\pi^0\pi^0\eta)/\Gamma_{total}$ — $\Gamma_7\Gamma_4/\Gamma$

VALUE (keV)	DOCUMENT ID		TECN	COMMENT
0.97±0.04 OUR FIT	Error includes scale factor of 1.1.			
0.92±0.06±0.11	[1] KARCH	92	CBAL	$e^+e^- \to e^+e^-\eta\pi^0\pi^0$
• • • We do not use the following data for averages, fits, limits, etc. • • •				
0.95±0.05±0.08	[2] KARCH	90	CBAL	$e^+e^- \to e^+e^-\eta\pi^0\pi^0$
1.00±0.08±0.10	[2,3] ANTREASYAN	87	CBAL	$e^+e^- \to e^+e^-\eta\pi^0\pi^0$

[1] Reevaluated by us using $B(\eta \to \gamma\gamma) = (39.21 \pm 0.34)\%$. Supersedes ANTREASYAN 87 and KARCH 90.
[2] Superseded by KARCH 92.
[3] Using $BR(\eta \to 2\gamma) = (38.9 \pm 0.5)\%$.

$\eta'(958)$ $\Gamma(i)\Gamma(e^+e^-)/\Gamma(total)$

$\Gamma(\pi^+\pi^-\eta) \times \Gamma(e^+e^-)/\Gamma_{total}$ — $\Gamma_1\Gamma_{29}/\Gamma$

VALUE (10^{-3} eV)	CL%	DOCUMENT ID		TECN	COMMENT
<1.0	90	[1] AKHMETSHIN	15	CMD3	$0.958\ e^+e^- \to \pi^+\pi^-\eta$

[1] AKHMETSHIN 15 reports $[\Gamma(\eta'(958) \to \pi^+\pi^-\eta) \times \Gamma(\eta'(958) \to e^+e^-)/\Gamma_{total}] \times [B(\eta \to 2\gamma)] < 4.1 \times 10^{-4}$ eV which we divide by our best value $B(\eta \to 2\gamma) = 39.36 \times 10^{-2}$.

$\eta'(958)$ BRANCHING RATIOS

$\Gamma(\pi^+\pi^-\eta)/\Gamma_{total}$ — Γ_1/Γ

VALUE (units 10^{-2})	EVTS	DOCUMENT ID		TECN	COMMENT
42.5 ±0.5 OUR FIT	Error includes scale factor of 1.1.				
41.24±0.08±1.24	312k	ABLIKIM	19T	BES	$J/\psi \to \gamma\eta'$
• • • We do not use the following data for averages, fits, limits, etc. • • •					
42.4 ±1.1 ±0.4	1.2k	[1] PEDLAR	09	CLEO	$J/\psi \to \gamma\eta'$

[1] Not independent of other η' branching fractions and ratios in PEDLAR 09.

$\Gamma(\pi^+\pi^-\eta(\text{charged decay}))/\Gamma_{total}$ — $0.2804\Gamma_1/\Gamma$

VALUE	EVTS	DOCUMENT ID		TECN	COMMENT
0.1191±0.0015 OUR FIT	Error includes scale factor of 1.1.				
• • • We do not use the following data for averages, fits, limits, etc. • • •					
0.123 ±0.014	107	RITTENBERG	69	HBC	1.7–2.7 K^-p
0.10 ±0.04	10	LONDON	66	HBC	2.24 $K^-p \to \Lambda 2\pi^+ 2\pi^-\pi^0$
0.07 ±0.04	7	BADIER	65B	HBC	3 K^-p

$\Gamma(\pi^+\pi^-\eta(\text{neutral decay}))/\Gamma_{total}$ — $0.7196\Gamma_1/\Gamma$

VALUE	EVTS	DOCUMENT ID		TECN	COMMENT
0.306±0.004 OUR FIT	Error includes scale factor of 1.1.				
• • • We do not use the following data for averages, fits, limits, etc. • • •					
0.314±0.026	281	RITTENBERG	69	HBC	1.7–2.7 K^-p

$\Gamma(\rho^0\gamma(\text{including non-resonant } \pi^+\pi^-\gamma))/\Gamma_{total}$ — Γ_2/Γ

VALUE (units 10^{-2})	EVTS	DOCUMENT ID		TECN	COMMENT
29.5 ± 0.4 OUR FIT	Error includes scale factor of 1.1.				
29.90± 0.03±0.55	913k	ABLIKIM	19T	BES	$J/\psi \to \gamma\eta'$
• • • We do not use the following data for averages, fits, limits, etc. • • •					
28.7 ± 0.7 ±0.4	0.2k	[1] PEDLAR	09	CLEO	$J/\psi \to \gamma\eta'$
32.9 ± 3.3	298	RITTENBERG	69	HBC	1.7–2.7 K^-p
20 ±10	20	LONDON	66	HBC	2.24 $K^-p \to \Lambda\pi^+\pi^-\gamma$
34 ± 9	35	BADIER	65B	HBC	3 K^-p

[1] Not independent of other η' branching fractions and ratios in PEDLAR 09.

$\Gamma(\rho^0\gamma)/\Gamma_{total}$ — Γ_3/Γ

VALUE (%)	EVTS	DOCUMENT ID		TECN	COMMENT
• • • We do not use the following data for averages, fits, limits, etc. • • •					
33.34±0.06±1.60	970k	[1] ABLIKIM	18C	BES3	$\eta'(958) \to \gamma\pi^+\pi^-$
34.43±0.52±1.97	970k	[2] ABLIKIM	18C	BES3	$\eta'(958) \to \gamma\pi^+\pi^-$

[1] From a fit to $\pi^+\pi^-$ mass using $\rho(770)$, $\omega(782)$, and box anomaly components.
[2] From a fit to $\pi^+\pi^-$ mass using $\rho(770)$, $\omega(782)$, and $\rho(1450)$ components.

$\Gamma(\rho^0\gamma(\text{including non-resonant } \pi^+\pi^-\gamma))/\Gamma(\pi^+\pi^-\eta)$ — Γ_2/Γ_1

VALUE	DOCUMENT ID		TECN	COMMENT
0.694±0.014 OUR FIT	Error includes scale factor of 1.1.			
0.683±0.020 OUR AVERAGE				
0.677±0.024±0.011	PEDLAR	09	CLE3	$J/\psi \to \eta'\gamma$
0.69 ±0.03	ABLIKIM	06E	BES2	$J/\psi \to \eta'\gamma$

$\Gamma(\rho^0\gamma(\text{including non-resonant } \pi^+\pi^-\gamma))/\Gamma(\pi^+\pi^-\eta(\text{neutral decay}))$ — $\Gamma_2/0.714\Gamma_1$

VALUE	EVTS	DOCUMENT ID		TECN	COMMENT
0.972±0.020 OUR FIT	Error includes scale factor of 1.1.				
0.97 ±0.09 OUR AVERAGE					
0.70 ±0.22		AMSLER	04B	CBAR	$0\ \bar{p}p \to \pi^+\pi^-\eta$

Downloaded from https://academic.oup.com/ptep/article/2022/8/083C01/6651666 by KIT Library user on 27 September 2022

1.07 ±0.17		BELADIDZE	92C	VES	36 $\pi^- \mathrm{Be} \to \pi^- \eta' \eta \mathrm{Be}$
0.92 ±0.14	473	DANBURG	73	HBC	2.2 $K^- p \to \Lambda X^0$
1.11 ±0.18	192	JACOBS	73	HBC	2.9 $K^- p \to \Lambda X^0$

$\Gamma(\pi^0\pi^0\eta)/\Gamma_{total}$ — Γ_4/Γ

VALUE (units 10^{-2})	EVTS	DOCUMENT ID		TECN	COMMENT
22.4 ±0.6 OUR FIT	Error includes scale factor of 1.1.				
21.36±0.10±0.92	52k	ABLIKIM	19T	BES	$J/\psi \to \gamma\eta'$
• • • We do not use the following data for averages, fits, limits, etc. • • •					
23.5 ±1.3 ±0.4	3.2k	[1] PEDLAR	09	CLEO	$J/\psi \to \gamma\eta'$

[1] Not independent of other η' branching fractions and ratios in PEDLAR 09.

$\Gamma(\pi^0\pi^0\eta(3\pi^0 \text{ decay}))/\Gamma_{total}$ — $0.321\Gamma_4/\Gamma$

VALUE	EVTS	DOCUMENT ID		TECN	COMMENT
0.0718±0.0018 OUR FIT	Error includes scale factor of 1.1.				
• • • We do not use the following data for averages, fits, limits, etc. • • •					
0.11 ±0.06	4	BENSINGER	70	DBC	2.2 $\pi^+ d$

$\Gamma(\pi^0\pi^0\eta)/\Gamma(\pi^+\pi^-\eta)$ — Γ_4/Γ_1

VALUE	DOCUMENT ID		TECN	COMMENT
0.527±0.019 OUR FIT	Error includes scale factor of 1.1.			
0.555±0.043±0.013	PEDLAR	09	CLE3	$J/\psi \to \eta'\gamma$

$\Gamma(\rho^0\gamma(\text{including non-resonant } \pi^+\pi^-\gamma))/\Gamma(\pi\pi\eta)$ — $\Gamma_2/(\Gamma_1+\Gamma_4)$

VALUE	DOCUMENT ID		TECN	COMMENT
0.454±0.009 OUR FIT	Error includes scale factor of 1.1.			
0.43 ±0.02 ±0.02	BARBERIS	98C	OMEG	450 $pp \to p_f \eta' p_s$
• • • We do not use the following data for averages, fits, limits, etc. • • •				
0.31 ±0.15	DAVIS	68	HBC	5.5 $K^- p$

$\Gamma(\omega\gamma)/\Gamma_{total}$ — Γ_5/Γ

VALUE (units 10^{-2})	EVTS	DOCUMENT ID		TECN	COMMENT
2.52 ±0.07 OUR FIT					
2.50 ±0.07 OUR AVERAGE					
2.489±0.018±0.074	23k	ABLIKIM	19T	BES	$J/\psi \to \gamma\eta'$
2.55 ±0.03 ±0.16	33.2k	[1] ABLIKIM	15AD	BES3	$J/\psi \to \eta'\gamma$
• • • We do not use the following data for averages, fits, limits, etc. • • •					
2.34 ±0.30 ±0.04	70	[2] PEDLAR	09	CLEO	$J/\psi \to \gamma\eta'$

[1] Using $B(J/\psi \to \eta'\gamma) = (5.15 \pm 0.16) \times 10^{-3}$ and $B(\omega \to \pi^+\pi^-\pi^0) = (89.2 \pm 0.7)\%$.
[2] Not independent of other η' branching fractions and ratios in PEDLAR 09.

$\Gamma(\omega\gamma)/\Gamma(\pi^+\pi^-\eta)$ — Γ_5/Γ_1

VALUE	EVTS	DOCUMENT ID		TECN	COMMENT
0.0593±0.0018 OUR FIT	Error includes scale factor of 1.1.				
0.055 ±0.007 ±0.001		PEDLAR	09	CLE3	$J/\psi \to \eta'\gamma$
• • • We do not use the following data for averages, fits, limits, etc. • • •					
0.068 ±0.013	68	ZANFINO	77	ASPK	8.4 $\pi^- p$

$\Gamma(\omega\gamma)/\Gamma(\pi^0\pi^0\eta)$ — Γ_5/Γ_4

VALUE	DOCUMENT ID		TECN	COMMENT
0.113±0.004 OUR FIT				
0.147±0.016	ALDE	87B	GAM2	38 $\pi^- p \to n 4\gamma$

$\Gamma(\omega e^+e^-)/\Gamma(\omega\gamma)$ — Γ_6/Γ_5

VALUE (units 10^{-3})	DOCUMENT ID		TECN	COMMENT
• • • We do not use the following data for averages, fits, limits, etc. • • •				
7.71±1.34±0.54	[1] ABLIKIM	15AD	BES3	$J/\psi \to \eta'\gamma$

[1] Obtained from other ABLIKIM 15AD meausurements with common systematics taken into account.

$\Gamma(\omega e^+e^-)/\Gamma_{total}$ — Γ_6/Γ

VALUE (units 10^{-4})	EVTS	DOCUMENT ID		TECN	COMMENT
1.97±0.34±0.17	66	[1] ABLIKIM	15AD	BES3	$J/\psi \to \eta'\gamma$

[1] Using $B(J/\psi \to \eta'\gamma) = (5.15 \pm 0.16) \times 10^{-3}$ and $B(\omega \to \pi^+\pi^-\pi^0) = (89.2 \pm 0.7)\%$.

$\Gamma(\rho^0\gamma(\text{including non-resonant } \pi^+\pi^-\gamma))/[\Gamma(\pi^+\pi^-\eta)+\Gamma(\pi^0\pi^0\eta)+\Gamma(\omega\gamma)]$ — $\Gamma_2/(\Gamma_1+\Gamma_4+\Gamma_5)$

VALUE	DOCUMENT ID		TECN	COMMENT
0.437±0.008 OUR FIT	Error includes scale factor of 1.1.			
• • • We do not use the following data for averages, fits, limits, etc. • • •				
0.25 ±0.14	DAUBER	64	HBC	1.95 $K^- p$

$[\Gamma(\pi^0\pi^0\eta(\text{charged decay}))+\Gamma(\omega(\text{charged decay})\gamma)]/\Gamma_{total}$ — $(0.286\Gamma_4+0.89\Gamma_5)/\Gamma$

VALUE	EVTS	DOCUMENT ID		TECN	COMMENT
0.0864±0.0017 OUR FIT	Error includes scale factor of 1.1.				
• • • We do not use the following data for averages, fits, limits, etc. • • •					
0.045 ±0.029	42	RITTENBERG	69	HBC	1.7–2.7 $K^- p$

$\Gamma(\pi^+\pi^-\text{neutrals})/\Gamma_{total}$ — $(0.714\Gamma_1+0.286\Gamma_4+0.89\Gamma_5)/\Gamma$

VALUE	EVTS	DOCUMENT ID		TECN	COMMENT
0.3897±0.0028 OUR FIT	Error includes scale factor of 1.1.				
• • • We do not use the following data for averages, fits, limits, etc. • • •					
0.4 ±0.1	39	LONDON	66	HBC	2.24 $K^- p \to \Lambda\pi^+\pi^-$ neutrals
0.35 ±0.06	33	BADIER	65B	HBC	3 $K^- p$

$\Gamma(\gamma\gamma)/\Gamma_{total}$ — Γ_7/Γ

VALUE (units 10^{-2})	EVTS	DOCUMENT ID		TECN	COMMENT
2.307±0.035 OUR FIT	Error includes scale factor of 1.1.				
2.31 ±0.06 OUR AVERAGE	Error includes scale factor of 1.8.				
2.331±0.012±0.035	71k	ABLIKIM	19T	BES	$J/\psi \to \gamma\eta'$
1.99 $^{+0.31}_{-0.27}$ ±0.07	114	[1] WICHT	08	BELL	$B^\pm \to K^\pm\gamma\gamma$
2.00 ±0.18		[2] STANTON	80	SPEC	8.45 $\pi^- p \to n\pi^+\pi^- 2\gamma$
• • • We do not use the following data for averages, fits, limits, etc. • • •					
2.25 ±0.16 ±0.03	0.3k	[3] PEDLAR	09	CLEO	$J/\psi \to \gamma\eta'$
1.8 ±0.2	6000	[4] APEL	79	NICE	15–40 $\pi^- p \to n 2\gamma$
2.5 ±0.7		DUANE	74	MMS	$\pi^- p \to n$MM
1.71 ±0.33	68	DALPIAZ	72	CNTR	1.6 $\pi^- p \to n X^0$
2.0 $^{+0.8}_{-0.6}$	31	HARVEY	71	OSPK	3.65 $\pi^- p \to n X^0$

[1] WICHT 08 reports $[\Gamma(\eta'(958) \to \gamma\gamma)/\Gamma_{total}] \times [B(B^+ \to \eta' K^+)] = (1.40^{+0.16+0.15}_{-0.15-0.12}) \times 10^{-6}$ which we divide by our best value $B(B^+ \to \eta' K^+) = (7.04 \pm 0.25) \times 10^{-5}$. Our first error is their experiment's error and our second error is the systematic error from using our best value.
[2] Includes APEL 79 result.
[3] Not independent of other η' branching fractions and ratios in PEDLAR 09.
[4] Data is included in STANTON 80 evaluation.

$\Gamma(\gamma\gamma)/\Gamma(\pi^+\pi^-\eta)$ — Γ_7/Γ_1

VALUE	DOCUMENT ID		TECN	COMMENT
0.0543±0.0012 OUR FIT	Error includes scale factor of 1.1.			
0.053 ±0.004 ±0.001	PEDLAR	09	CLE3	$J/\psi \to \eta'\gamma$

$\Gamma(\gamma\gamma)/\Gamma(\rho^0\gamma(\text{including non-resonant } \pi^+\pi^-\gamma))$ — Γ_7/Γ_2

VALUE	DOCUMENT ID		TECN	COMMENT
0.0783±0.0016 OUR FIT	Error includes scale factor of 1.1.			
0.080 ±0.008	ABLIKIM	06E	BES2	$J/\psi \to \eta'\gamma$

$\Gamma(\gamma\gamma)/\Gamma(\pi^0\pi^0\eta)$ — Γ_7/Γ_4

VALUE	DOCUMENT ID		TECN	COMMENT
0.1031±0.0028 OUR FIT				
0.105 ±0.010 OUR AVERAGE	Error includes scale factor of 1.9.			
0.091 ±0.009	AMSLER	93	CBAR	0.0 $\bar{p}p$
0.112 ±0.002 ±0.006	ALDE	87B	GAM2	38 $\pi^- p \to n 2\gamma$

$\Gamma(\gamma\gamma)/\Gamma(\pi^0\pi^0\eta(\text{neutral decay}))$ — $\Gamma_7/0.714\Gamma_4$

VALUE	EVTS	DOCUMENT ID		TECN	COMMENT
0.144±0.004 OUR FIT					
• • • We do not use the following data for averages, fits, limits, etc. • • •					
0.188±0.058	16	APEL	72	OSPK	3.8 $\pi^- p \to n X^0$

$\Gamma(\text{neutrals})/\Gamma_{total}$ — $(0.714\Gamma_4+0.09\Gamma_5+\Gamma_7)/\Gamma$

VALUE	EVTS	DOCUMENT ID		TECN	COMMENT
0.185±0.004 OUR FIT	Error includes scale factor of 1.1.				
• • • We do not use the following data for averages, fits, limits, etc. • • •					
0.185±0.022	535	BASILE	71	CNTR	1.6 $\pi^- p \to n X^0$
0.189±0.026	123	RITTENBERG	69	HBC	1.7–2.7 $K^- p$

$\Gamma(3\pi^0)/\Gamma_{total}$ — Γ_8/Γ

VALUE (units 10^{-3})	EVTS	DOCUMENT ID		TECN	COMMENT
2.50 ±0.17 OUR FIT					
3.57 ±0.26 OUR AVERAGE					
3.522±0.082±0.254	2015	ABLIKIM	17	BES3	$J/\psi \to \gamma(3\pi^0)$
4.79 ±0.59 ±1.14	183	[1] ABLIKIM	15P	BES3	$J/\psi \to K^+K^-3\pi$
• • • We do not use the following data for averages, fits, limits, etc. • • •					
3.56 ±0.22 ±0.34	309	[2] ABLIKIM	12E	BES3	$J/\psi \to \gamma(3\pi^0)$

[1] We have added all systematic uncertainties in quadrature to a single value.
[2] Superseded by ABLIKIM 17.

$\Gamma(3\pi^0)/\Gamma(\pi^0\pi^0\eta)$ — Γ_8/Γ_4

VALUE (units 10^{-4})	EVTS	DOCUMENT ID		TECN	COMMENT
112± 8 OUR FIT					
78±10 OUR AVERAGE					
86±19	235	BLIK	08	GAMS	32 $\pi^- p \to \eta' n$
74±15		ALDE	87B	GAM2	38 $\pi^- p \to n 6\gamma$
75±18		BINON	84	GAM2	30–40 $\pi^- p \to n 6\gamma$

$\Gamma(\mu^+\mu^-\gamma)/\Gamma(\gamma\gamma)$ — Γ_9/Γ_7

VALUE (units 10^{-3})	EVTS	DOCUMENT ID		TECN	COMMENT
4.9±1.2	33	VIKTOROV	80	CNTR	25,33 $\pi^- p \to 2\mu\gamma$

Downloaded from https://academic.oup.com/ptep/article/2022/8/083C01/6651666 by KIT Library user on 27 September 2022

$\Gamma(\pi^+\pi^-\mu^+\mu^-)/\Gamma_{total}$ — Γ_{10}/Γ

VALUE (units 10^{-5})	CL%	EVTS	DOCUMENT ID		TECN	COMMENT
1.95±0.37±0.03		53	[1] ABLIKIM	21I	BES3	$J/\psi \to \gamma\eta'(958)$
• • • We do not use the following data for averages, fits, limits, etc. • • •						
< 2.9	90		[2] ABLIKIM	13O	BES3	$J/\psi \to \gamma\eta'$
<24	90		[3] NAIK	09	CLEO	$J/\psi \to \gamma\eta'$

[1] ABLIKIM 21I reports $(1.97 \pm 0.33 \pm 0.19) \times 10^{-5}$ from a measurement of $[\Gamma(\eta'(958) \to \pi^+\pi^-\mu^+\mu^-)/\Gamma_{total}] \times [B(J/\psi(1S) \to \gamma\eta'(958))]$ assuming $B(J/\psi(1S) \to \gamma\eta'(958)) = (5.21 \pm 0.17) \times 10^{-3}$, which we rescale to our best value $B(J/\psi(1S) \to \gamma\eta'(958)) = (5.25 \pm 0.07) \times 10^{-3}$. Our first error is their experiment's error and our second error is the systematic error from using our best value.
[2] Using $\Gamma_2/\Gamma = (29.3 \pm 0.6)\%$ from PDG 12.
[3] Not independent of measured value of Γ_{10}/Γ_1 from NAIK 09.

$\Gamma(\pi^+\pi^-\mu^+\mu^-)/\Gamma(\pi^+\pi^-\eta)$ — Γ_{10}/Γ_1

VALUE (units 10^{-3})	CL%	DOCUMENT ID		TECN	COMMENT
<0.5	90	[1] NAIK	09	CLEO	$J/\psi \to \gamma\eta'$

[1] NAIK 09 reports $[\Gamma(\eta'(958) \to \pi^+\pi^-\mu^+\mu^-)/\Gamma(\eta'(958) \to \pi^+\pi^-\eta)] / [B(\eta \to 2\gamma)] < 1.3 \times 10^{-3}$ which we multiply by our best value $B(\eta \to 2\gamma) = 39.36 \times 10^{-2}$.

$\Gamma(\pi^+\pi^-\mu^+\mu^-)/\Gamma(\rho^0\gamma(\text{including non-resonant } \pi^+\pi^-\gamma))$ — Γ_{10}/Γ_2

VALUE (units 10^{-4})	CL%	DOCUMENT ID		TECN	COMMENT
<1.0	90	ABLIKIM	13O	BES3	$J/\psi \to \gamma\eta'$

$\Gamma(\pi^+\pi^-\pi^0)/\Gamma_{total}$ — Γ_{11}/Γ

VALUE (units 10^{-3})	EVTS	DOCUMENT ID		TECN	COMMENT
3.61 ±0.18 OUR FIT					
3.61 ±0.18 OUR AVERAGE					
3.591±0.054±0.174	6067	ABLIKIM	17	BES3	$J/\psi \to \gamma(\pi^+\pi^-\pi^0)$
4.28 ±0.49 ±1.11	78	[1] ABLIKIM	15P	BES3	$J/\psi \to K^+K^-3\pi$
3.7 $^{+1.1}_{-0.9}$ ±0.4		[2] NAIK	09	CLEO	$J/\psi \to \gamma\eta'$
• • • We do not use the following data for averages, fits, limits, etc. • • •					
3.83 ±0.15 ±0.39	1014	[3] ABLIKIM	12E	BES3	$J/\psi \to \gamma(\pi^+\pi^-\pi^0)$

[1] We have added all systematic uncertainties in quadrature to a single value.
[2] Not independent of measured value of Γ_{11}/Γ_1 from NAIK 09.
[3] Superseded by ABLIKIM 17.

$\Gamma((\pi^+\pi^-\pi^0)\text{ S-wave})/\Gamma_{total}$ — Γ_{12}/Γ

VALUE (units 10^{-4})	EVTS	DOCUMENT ID		TECN	COMMENT
37.63±0.77±5.00	6580	[1] ABLIKIM	17	BES3	$J/\psi \to \gamma(\pi^+\pi^-\pi^0)$

[1] We have added all systematic uncertainties in quadrature .

$\Gamma(\pi^\mp\rho^\pm)/\Gamma_{total}$ — Γ_{13}/Γ

VALUE (units 10^{-4})	EVTS	DOCUMENT ID		TECN	COMMENT
7.44±0.60±2.23	1231	[1] ABLIKIM	17	BES3	$J/\psi \to \gamma(\pi^\mp\rho^\pm)$

[1] We have added all systematic uncertainties in quadrature .

$\Gamma(\pi^+\pi^-\pi^0)/\Gamma(\pi^+\pi^-\eta)$ — Γ_{11}/Γ_1

VALUE (units 10^{-3})	EVTS	DOCUMENT ID		TECN	COMMENT
8.5 ±0.4 OUR FIT Error includes scale factor of 1.1.					
8.27$^{+2.49}_{-2.12}$±0.04	20	[1] NAIK	09	CLEO	$J/\psi \to \gamma\eta'$

[1] NAIK 09 reports $[\Gamma(\eta'(958) \to \pi^+\pi^-\pi^0)/\Gamma(\eta'(958) \to \pi^+\pi^-\eta)] / [B(\eta \to 2\gamma)] = (21^{+6}_{-5} \pm 2) \times 10^{-3}$ which we multiply by our best value $B(\eta \to 2\gamma) = (39.36 \pm 0.18) \times 10^{-2}$. Our first error is their experiment's error and our second error is the systematic error from using our best value.

$\Gamma(\pi^0\rho^0)/\Gamma_{total}$ — Γ_{14}/Γ

VALUE	CL%	DOCUMENT ID		TECN	COMMENT
<0.04	90	RITTENBERG	65	HBC	2.7 K^-p

$\Gamma(2(\pi^+\pi^-))/\Gamma_{total}$ — Γ_{15}/Γ

VALUE (units 10^{-5})	CL%	EVTS	DOCUMENT ID		TECN	COMMENT
8.4±0.9±0.1		199	[1] ABLIKIM	14M	BES3	$J/\psi \to \gamma\eta'$
• • • We do not use the following data for averages, fits, limits, etc. • • •						
< 24	90		[2] NAIK	09	CLEO	$J/\psi \to \gamma\eta'$
<1000	90		RITTENBERG	69	HBC	1.7–2.7 K^-p

[1] ABLIKIM 14M reports $[\Gamma(\eta'(958) \to 2(\pi^+\pi^-))/\Gamma_{total}] \times [B(J/\psi(1S) \to \gamma\eta'(958))] = (4.40 \pm 0.35 \pm 0.30) \times 10^{-7}$ which we divide by our best value $B(J/\psi(1S) \to \gamma\eta'(958)) = (5.25 \pm 0.07) \times 10^{-3}$. Our first error is their experiment's error and our second error is the systematic error from using our best value.
[2] Not independent of measured value of Γ_{15}/Γ_1 from NAIK 09.

$\Gamma(2(\pi^+\pi^-))/\Gamma(\pi^+\pi^-\eta)$ — Γ_{15}/Γ_1

VALUE (units 10^{-3})	CL%	DOCUMENT ID		TECN	COMMENT
<0.6	90	[1] NAIK	09	CLEO	$J/\psi \to \gamma\eta'$

[1] NAIK 09 reports $[\Gamma(\eta'(958) \to 2(\pi^+\pi^-))/\Gamma(\eta'(958) \to \pi^+\pi^-\eta)] / [B(\eta \to 2\gamma)] < 1.4 \times 10^{-3}$ which we multiply by our best value $B(\eta \to 2\gamma) = 39.36 \times 10^{-2}$.

$\Gamma(\pi^+\pi^-2\pi^0)/\Gamma_{total}$ — Γ_{16}/Γ

VALUE (units 10^{-4})	CL%	EVTS	DOCUMENT ID		TECN	COMMENT
1.79±0.38±0.02		84	[1] ABLIKIM	14M	BES3	$J/\psi \to \gamma\eta'$
• • • We do not use the following data for averages, fits, limits, etc. • • •						
<27	90		[2] NAIK	09	CLEO	$J/\psi \to \gamma\eta'$

[1] ABLIKIM 14M reports $[\Gamma(\eta'(958) \to \pi^+\pi^-2\pi^0)/\Gamma_{total}] \times [B(J/\psi(1S) \to \gamma\eta'(958))] = (9.38 \pm 1.79 \pm 0.89) \times 10^{-7}$ which we divide by our best value $B(J/\psi(1S) \to \gamma\eta'(958)) = (5.25 \pm 0.07) \times 10^{-3}$. Our first error is their experiment's error and our second error is the systematic error from using our best value.
[2] Not independent of measured value of Γ_{16}/Γ_1 from NAIK 09.

$\Gamma(\pi^+\pi^-2\pi^0)/\Gamma(\pi^+\pi^-\eta)$ — Γ_{16}/Γ_1

VALUE (units 10^{-3})	CL%	DOCUMENT ID		TECN	COMMENT
<6	90	[1] NAIK	09	CLEO	$J/\psi \to \gamma\eta'$

[1] NAIK 09 reports $[\Gamma(\eta'(958) \to \pi^+\pi^-2\pi^0)/\Gamma(\eta'(958) \to \pi^+\pi^-\eta)] / [B(\eta \to 2\gamma)] < 15 \times 10^{-3}$ which we multiply by our best value $B(\eta \to 2\gamma) = 39.36 \times 10^{-2}$.

$\Gamma(2(\pi^+\pi^-)\text{ neutrals})/\Gamma_{total}$ — Γ_{17}/Γ

VALUE	CL%	DOCUMENT ID		TECN	COMMENT
<0.01	95	DANBURG	73	HBC	2.2 $K^-p \to \Lambda X^0$
• • • We do not use the following data for averages, fits, limits, etc. • • •					
<0.01	90	RITTENBERG	69	HBC	1.7–2.7 K^-p

$\Gamma(2(\pi^+\pi^-)\pi^0)/\Gamma_{total}$ — Γ_{18}/Γ

VALUE	CL%	DOCUMENT ID		TECN	COMMENT
• • • We do not use the following data for averages, fits, limits, etc. • • •					
<0.002	90	[1] NAIK	09	CLEO	$J/\psi \to \gamma\eta'$
<0.01	90	RITTENBERG	69	HBC	1.7–2.7 K^-p

[1] Not independent of measured value of Γ_{18}/Γ_1 from NAIK 09.

$\Gamma(2(\pi^+\pi^-)\pi^0)/\Gamma(\pi^+\pi^-\eta)$ — Γ_{18}/Γ_1

VALUE (units 10^{-3})	CL%	DOCUMENT ID		TECN	COMMENT
<4	90	[1] NAIK	09	CLEO	$J/\psi \to \gamma\eta'$

[1] NAIK 09 reports $[\Gamma(\eta'(958) \to 2(\pi^+\pi^-)\pi^0)/\Gamma(\eta'(958) \to \pi^+\pi^-\eta)] / [B(\eta \to 2\gamma)] < 11 \times 10^{-3}$ which we multiply by our best value $B(\eta \to 2\gamma) = 39.36 \times 10^{-2}$.

$\Gamma(2(\pi^+\pi^-)2\pi^0)/\Gamma_{total}$ — Γ_{19}/Γ

VALUE	CL%	DOCUMENT ID		TECN	COMMENT
<0.01	95	KALBFLEISCH	64B	HBC	$K^-p \to \Lambda 2(\pi^+\pi^-)$+MM
• • • We do not use the following data for averages, fits, limits, etc. • • •					
<0.01	90	LONDON	66	HBC	Compilation

$\Gamma(3(\pi^+\pi^-))/\Gamma_{total}$ — Γ_{20}/Γ

VALUE (units 10^{-5})	CL%	DOCUMENT ID		TECN	COMMENT
< 3.1	90	[1] ABLIKIM	13U	BES3	$J/\psi \to \gamma 3(\pi^+\pi^-)$
• • • We do not use the following data for averages, fits, limits, etc. • • •					
< 53	90	[2] NAIK	09	CLEO	$J/\psi \to \gamma\eta'$
<500	95	KALBFLEISCH	64B	HBC	$K^-p \to \Lambda 2(\pi^+\pi^-)$

[1] Using $B(J/\psi \to \gamma\eta'(958)) = (5.16 \pm 0.15) \times 10^{-3}$.
[2] Not independent of measured value of Γ_{20}/Γ_1 from NAIK 09.

$\Gamma(3(\pi^+\pi^-))/\Gamma(\pi^+\pi^-\eta)$ — Γ_{20}/Γ_1

VALUE (units 10^{-3})	CL%	DOCUMENT ID		TECN	COMMENT
<1.2	90	[1] NAIK	09	CLEO	$J/\psi \to \gamma\eta'$

[1] NAIK 09 reports $[\Gamma(\eta'(958) \to 3(\pi^+\pi^-))/\Gamma(\eta'(958) \to \pi^+\pi^-\eta)] / [B(\eta \to 2\gamma)] < 3.0 \times 10^{-3}$ which we multiply by our best value $B(\eta \to 2\gamma) = 39.36 \times 10^{-2}$.

$\Gamma(K^\pm\pi^\mp)/\Gamma(\rho^0\gamma(\text{including non-resonant } \pi^+\pi^-\gamma))$ — Γ_{21}/Γ_2

VALUE	CL%	DOCUMENT ID		TECN	COMMENT
<1.3 × 10^{-4}	90	ABLIKIM	16M	BES3	$e^+e^- \to J/\psi \to$ hadrons

$\Gamma(\pi^+\pi^-e^+e^-)/\Gamma_{total}$ — Γ_{22}/Γ

VALUE (units 10^{-3})	CL%	EVTS	DOCUMENT ID		TECN	COMMENT
2.42±0.10 OUR FIT						
• • • We do not use the following data for averages, fits, limits, etc. • • •						
2.11±0.12±0.14		429	[1] ABLIKIM	13O	BES3	$J/\psi \to \gamma\eta'$
2.5 $^{+1.2}_{-0.9}$ ±0.5			[2] NAIK	09	CLEO	$J/\psi \to \gamma\eta'$
<6	90		RITTENBERG	65	HBC	2.7 K^-p

[1] Using $\Gamma_2/\Gamma = (29.3 \pm 0.6)\%$ from PDG 12.
[2] Not independent of measured value of Γ_{22}/Γ_1 from NAIK 09.

$\Gamma(\pi^+\pi^-e^+e^-)/\Gamma(\pi^+\pi^-\eta)$ — Γ_{22}/Γ_1

VALUE (units 10^{-3})	EVTS	DOCUMENT ID		TECN	COMMENT
5.69±0.25 OUR FIT					
5.51$^{+3.00}_{-2.30}$±0.03	8	[1] NAIK	09	CLEO	$J/\psi \to \gamma\eta'$

[1] NAIK 09 reports $[\Gamma(\eta'(958) \to \pi^+\pi^-e^+e^-)/\Gamma(\eta'(958) \to \pi^+\pi^-\eta)] / [B(\eta \to 2\gamma)] = (14^{+7}_{-5} \pm 3) \times 10^{-3}$ which we multiply by our best value $B(\eta \to 2\gamma) = (39.36 \pm 0.18) \times 10^{-2}$. Our first error is their experiment's error and our second error is the systematic error from using our best value.

Downloaded from https://academic.oup.com/ptep/article/2022/8/083C01/6651666 by KIT Library user on 27 September 2022

$\Gamma(\pi^+\pi^-e^+e^-)/\Gamma(\rho^0\gamma$(including non-resonant $\pi^+\pi^-\gamma$)) — Γ_{22}/Γ_2

VALUE (units 10^{-3})	EVTS	DOCUMENT ID		TECN	COMMENT
8.20±0.31 OUR FIT					
8.20±0.16±0.27	2584	ABLIKIM	21J	BES3	$J/\psi \to \gamma\eta'$
• • • We do not use the following data for averages, fits, limits, etc. • • •					
7.2 ±0.4 ±0.5	429	[1] ABLIKIM	13O	BES3	$J/\psi \to \gamma\eta'$

[1] Superseded by ABLIKIM 21J.

$\Gamma(\pi^+e^-\nu_e+$c.c.$)/\Gamma(\pi^+\pi^-\eta)$ — Γ_{23}/Γ_1

VALUE (units 10^{-4})	CL%	DOCUMENT ID		TECN	COMMENT
<5.0	90	ABLIKIM	13G	BES3	$J/\psi \to \phi\eta'$

$\Gamma(\gamma e^+e^-)/\Gamma_{total}$ — Γ_{24}/Γ

VALUE (units 10^{-3})	CL%	DOCUMENT ID		TECN	COMMENT
• • • We do not use the following data for averages, fits, limits, etc. • • •					
<0.9	90	BRIERE	00	CLEO	10.6 e^+e^-

$\Gamma(\gamma e^+e^-)/\Gamma(\gamma\gamma)$ — Γ_{24}/Γ_7

VALUE (units 10^{-2})	EVTS	DOCUMENT ID		TECN	COMMENT
2.13±0.09±0.07	864	ABLIKIM	15O	BES3	$J/\psi \to \gamma e^+e^-$

$\Gamma(\pi^0\gamma\gamma)/\Gamma_{total}$ — Γ_{25}/Γ

VALUE (units 10^{-3})	EVTS	DOCUMENT ID		TECN	COMMENT
3.20±0.07±0.23	3.4k	ABLIKIM	17T	BES3	$J/\psi \to \gamma\eta'$

$\Gamma(\pi^0\gamma\gamma$(non resonant))$/\Gamma_{total}$ — Γ_{26}/Γ

VALUE (units 10^{-4})	EVTS	DOCUMENT ID		TECN	COMMENT
6.16±0.64±0.67	655	ABLIKIM	17T	BES3	$J/\psi \to \gamma\eta'$

$\Gamma(\pi^0\gamma\gamma)/\Gamma(\pi^0\pi^0\eta)$ — Γ_{25}/Γ_4

VALUE (units 10^{-4})	CL%	DOCUMENT ID		TECN	COMMENT
<37	90	ALDE	87B	GAM2	38 $\pi^-p \to n4\gamma$

$\Gamma(\eta\gamma\gamma)/\Gamma_{total}$ — Γ_{27}/Γ

VALUE	CL%	DOCUMENT ID		TECN	COMMENT
$<1.33\times10^{-4}$	90	ABLIKIM	19AW	BES3	$J/\psi \to \gamma\eta' \to \gamma\gamma\gamma 2\gamma$

$\Gamma(4\pi^0)/\Gamma_{total}$ — Γ_{28}/Γ

VALUE	CL%	DOCUMENT ID		TECN	COMMENT
$<4.94\times10^{-5}$	90	ABLIKIM	20E	BES3	$J/\psi \to \eta'\gamma$
• • • We do not use the following data for averages, fits, limits, etc. • • •					
$<3.2\ \times10^{-4}$	90	DONSKOV	14	GAM4	32.5 $\pi^-p \to \eta' n$

$\Gamma(4\pi^0)/\Gamma(\pi^0\pi^0\eta)$ — Γ_{28}/Γ_4

VALUE (units 10^{-4})	CL%	DOCUMENT ID		TECN	COMMENT
• • • We do not use the following data for averages, fits, limits, etc. • • •					
<23	90	ALDE	87B	GAM2	38 $\pi^-p \to n8\gamma$

$\Gamma(e^+e^-)/\Gamma_{total}$ — Γ_{29}/Γ

VALUE	CL%	DOCUMENT ID		TECN	COMMENT
$<5.6\times10^{-9}$	90	[1] ACHASOV	15	SND	0.958 $e^+e^- \to \pi\pi\eta$
• • • We do not use the following data for averages, fits, limits, etc. • • •					
$<12\ \times10^{-9}$	90	[2] AKHMETSHIN	15	CMD3	0.958 $e^+e^- \to \pi^+\pi^-\eta$
$<2.1\times10^{-7}$	90	VOROBYEV	88	ND	$e^+e^- \to \pi^+\pi^-\eta$

[1] Combining data of ACHASOV 15 and AKHMETSHIN 15 and using $\Gamma(\eta')=0.198\pm0.009$ MeV.
[2] Using $\Gamma_{\eta'(958)}=198\pm9$ keV, $B(\eta'(958)\to\pi^+\pi^-\eta)=(42.9\pm0.7)\%$, and $B(\eta\to\gamma\gamma)=(39.41\pm0.20)\%$.

Γ(invisible)$/\Gamma_{total}$ — Γ_{30}/Γ

VALUE (units 10^{-4})	CL%	DOCUMENT ID		TECN	COMMENT
• • • We do not use the following data for averages, fits, limits, etc. • • •					
<9.5	90	[1] NAIK	09	CLEO	$J/\psi \to \gamma\eta'$

[1] Not independent of measured value of Γ_{30}/Γ_1 from NAIK 09.

Γ(invisible)$/\Gamma(\gamma\gamma)$ — Γ_{30}/Γ_7

VALUE (units 10^{-2})	CL%	DOCUMENT ID		TECN	COMMENT
<2.4	90	ABLIKIM	13	BES3	$J/\psi \to \phi\eta'$
• • • We do not use the following data for averages, fits, limits, etc. • • •					
<6.69	90	ABLIKIM	06Q	BES	$J/\psi \to \phi\eta'$

Γ(invisible)$/\Gamma(\pi^+\pi^-\eta)$ — Γ_{30}/Γ_1

VALUE (units 10^{-3})	CL%	DOCUMENT ID		TECN	COMMENT
• • • We do not use the following data for averages, fits, limits, etc. • • •					
<2.1	90	[1] NAIK	09	CLEO	$J/\psi \to \gamma\eta'$

[1] NAIK 09 reports $[\Gamma(\eta'(958)\to$ invisible$)/\Gamma(\eta'(958)\to\pi^+\pi^-\eta)]$ / $[B(\eta\to2\gamma)]$ $<5.4\times10^{-3}$ which we multiply by our best value $B(\eta\to2\gamma)=39.36\times10^{-2}$.

$\Gamma(\pi^+\pi^-)/\Gamma_{total}$ — Γ_{31}/Γ

VALUE (units 10^{-4})	CL%	DOCUMENT ID		TECN	COMMENT
< 0.18	90	[1] AAIJ	17D	LHCB	$D^+_{(s)} \to \pi^+\pi^-\pi^+$
• • • We do not use the following data for averages, fits, limits, etc. • • •					
< 0.5	90	[2] ABLIKIM	11G	BES3	$J/\psi \to \gamma\pi^+\pi^-$
< 29	90	[3] MORI	07A	BELL	$\gamma\gamma \to \pi^+\pi^-$
< 3.3	90	[4] MORI	07A	BELL	$\gamma\gamma \to \pi^+\pi^-$
<800	95	DANBURG	73	HBC	2.2 $K^-p \to \Lambda X^0$
<200	90	RITTENBERG	69	HBC	1.7–2.7 K^-p

[1] Using branching fractions of $D^+_{(s)}$ decays from PDG 15.
[2] ABLIKIM 11G reports $[\Gamma(\eta'(958)\to\pi^+\pi^-)/\Gamma_{total}]\times[B(J/\psi(1S)\to\gamma\eta'(958))]<2.84\times10^{-7}$ which we divide by our best value $B(J/\psi(1S)\to\gamma\eta'(958))=5.25\times10^{-3}$.
[3] Taking into account interference with the $\gamma\gamma\to\pi^+\pi^-$ continuum.
[4] Without interference with the $\gamma\gamma\to\pi^+\pi^-$ continuum.

$\Gamma(\pi^0\pi^0)/\Gamma_{total}$ — Γ_{32}/Γ

VALUE	CL%	DOCUMENT ID		TECN	COMMENT
$<4\times10^{-4}$	90	[1] ABLIKIM	11G	BES3	$J/\psi \to \gamma\pi^0\pi^0$

[1] ABLIKIM 11G reports $[\Gamma(\eta'(958)\to\pi^+\pi^-)/\Gamma_{total}]\times[B(J/\psi(1S)\to\gamma\eta'(958))]<2.84\times10^{-7}$ which we divide by our best value $B(J/\psi(1S)\to\gamma\eta'(958))=5.25\times10^{-3}$.

$\Gamma(\pi^0\pi^0)/\Gamma(\pi^0\pi^0\eta)$ — Γ_{32}/Γ_4

VALUE (units 10^{-4})	CL%	DOCUMENT ID		TECN	COMMENT
<45	90	ALDE	87B	GAM2	38 $\pi^-p \to n4\gamma$

$\Gamma(\pi^0e^+e^-)/\Gamma_{total}$ — Γ_{33}/Γ

VALUE (units 10^{-3})	CL%	DOCUMENT ID		TECN	COMMENT
< 1.4	90	BRIERE	00	CLEO	10.6 e^+e^-
• • • We do not use the following data for averages, fits, limits, etc. • • •					
<13	90	RITTENBERG	65	HBC	2.7 K^-p

$\Gamma(\eta e^+e^-)/\Gamma_{total}$ — Γ_{34}/Γ

VALUE (units 10^{-3})	CL%	DOCUMENT ID		TECN	COMMENT
< 2.4	90	BRIERE	00	CLEO	10.6 e^+e^-
• • • We do not use the following data for averages, fits, limits, etc. • • •					
<11	90	RITTENBERG	65	HBC	2.7 K^-p

$\Gamma(3\gamma)/\Gamma(\pi^0\pi^0\eta)$ — Γ_{35}/Γ_4

VALUE (units 10^{-4})	CL%	DOCUMENT ID		TECN	COMMENT
<4.6	90	ALDE	87B	GAM2	38 $\pi^-p \to n3\gamma$

$\Gamma(\mu^+\mu^-\pi^0)/\Gamma_{total}$ — Γ_{36}/Γ

VALUE (units 10^{-5})	CL%	DOCUMENT ID		TECN	COMMENT
<6.0	90	DZHELYADIN	81	CNTR	30 $\pi^-p \to \eta' n$

$\Gamma(\mu^+\mu^-\eta)/\Gamma_{total}$ — Γ_{37}/Γ

VALUE (units 10^{-5})	CL%	DOCUMENT ID		TECN	COMMENT
<1.5	90	DZHELYADIN	81	CNTR	30 $\pi^-p \to \eta' n$

$\Gamma(e\mu)/\Gamma_{total}$ — Γ_{38}/Γ

VALUE (units 10^{-4})	CL%	DOCUMENT ID		TECN	COMMENT
<4.7	90	BRIERE	00	CLEO	10.6 e^+e^-

$\eta'(958) \to \eta\pi\pi$ DECAY PARAMETERS

$|\text{MATRIX ELEMENT}|^2 = |1+\alpha Y|^2 + CX + DX^2$

X and Y are Dalitz variables; α is complex and C, and D are real-valued. Parameters C and D are not necessarily equal to c and d, respectively, in the generalized parameterization following this one. May be different for $\eta'(958)\to\eta\pi^+\pi^-$ and $\eta'(958)\to\eta\pi^0\pi^0$ decays. Because of different initial assumptions and strong correlations of the parameters we do not average the parameters in the section below.

$Re(\alpha)$ decay parameter

VALUE	EVTS	DOCUMENT ID		TECN	COMMENT
• • • We do not use the following data for averages, fits, limits, etc. • • •					
$-0.034\pm0.002\pm0.002$	351k	ABLIKIM	18	BES3	$\eta' \to \eta\pi^+\pi^-$
$-0.054\pm0.004\pm0.001$	56k	ABLIKIM	18	BES3	$\eta' \to \eta\pi^0\pi^0$
$-0.033\pm0.005\pm0.003$	44k	[1] ABLIKIM	11	BES3	$J/\psi \to \gamma\eta\pi^+\pi^-$
$-0.072\pm0.012\pm0.006$	7k	[2] AMELIN	05A	VES	28 $\pi^-A \to \eta\pi^+\pi^-\pi^-A^*$
$-0.021\pm0.018\pm0.017$	6.7k	[3] BRIERE	00	CLEO	10.6 $e^+e^- \to \eta\pi^+\pi^-X$
$-0.058\pm0.013\pm0.003$	5.4k	[4] ALDE	86	GAM2	38 $\pi^-p \to n\eta\pi^0\pi^0$
$-0.08\ \pm0.03$		[4,5] KALBFLEISCH	74	RVUE	$\eta' \to \eta\pi^+\pi^-$

[1] See ABLIKIM 11 for the full correlation matrix.
[2] Superseded by DOROFEEV 07, which found this parameterization unacceptable. See below.
[3] Assuming $\mathrm{Im}(\alpha)=0$, $C=0$, and $D=0$.
[4] Assuming $C=0$.
[5] From the data of DAUBER 64, RITTENBERG 69, AGUILAR-BENITEZ 72B, JACOBS 73, and DANBURG 73.

Downloaded from https://academic.oup.com/ptep/article/2022/8/083C01/6651666 by KIT Library user on 27 September 2022

Im(α) decay parameter

VALUE	EVTS	DOCUMENT ID		TECN	COMMENT
• • • We do not use the following data for averages, fits, limits, etc. • • •					
$0.000 \pm 0.019 \pm 0.001$	351k	ABLIKIM	18	BES3	$\eta' \to \eta\pi^+\pi^-$
$0.000 \pm 0.038 \pm 0.002$	56k	ABLIKIM	18	BES3	$\eta' \to \eta\pi^0\pi^0$
$0.000 \pm 0.049 \pm 0.001$	44k	[1] ABLIKIM	11	BES3	$J/\psi \to \gamma\eta\pi^+\pi^-$
$0.0 \pm 0.1 \pm 0.0$	7k	[2] AMELIN	05A	VES	$28\ \pi^- A \to \eta\pi^+\pi^-\pi^- A^*$
$-0.00 \pm 0.13 \pm 0.00$	5.4k	[3] ALDE	86	GAM2	$38\ \pi^- p \to n\eta\pi^0\pi^0$
0.0 ± 0.3		[3,4] KALBFLEISCH	74	RVUE	$\eta' \to \eta\pi^+\pi^-$

[1] See ABLIKIM 11 for the full correlation matrix.
[2] Superseded by DOROFEEV 07, which found this parameterization unacceptable. See below.
[3] Assuming $C = 0$.
[4] From the data of DAUBER 64, RITTENBERG 69, AGUILAR-BENITEZ 72B, JACOBS 73, and DANBURG 73.

C decay parameter

VALUE	EVTS	DOCUMENT ID		TECN	COMMENT
• • • We do not use the following data for averages, fits, limits, etc. • • •					
$0.0027 \pm 0.0024 \pm 0.0015$	351k	ABLIKIM	18	BES3	$\eta' \to \eta\pi^+\pi^-$
$0.018 \pm 0.009 \pm 0.003$	44k	[1] ABLIKIM	11	BES3	$J/\psi \to \gamma\eta\pi^+\pi^-$
$0.020 \pm 0.018 \pm 0.004$	7k	[2] AMELIN	05A	VES	$28\ \pi^- A \to \eta\pi^+\pi^-\pi^- A^*$

[1] See ABLIKIM 11 for the full correlation matrix.
[2] Superseded by DOROFEEV 07, which found this parameterization unacceptable. See below.

D decay parameter

VALUE	EVTS	DOCUMENT ID		TECN	COMMENT
• • • We do not use the following data for averages, fits, limits, etc. • • •					
$-0.053 \pm 0.004 \pm 0.004$	351k	ABLIKIM	18	BES3	$\eta' \to \eta\pi^+\pi^-$
$-0.061 \pm 0.009 \pm 0.005$	56k	ABLIKIM	18	BES3	$\eta' \to \eta\pi^0\pi^0$
$-0.059 \pm 0.012 \pm 0.004$	44k	[1] ABLIKIM	11	BES3	$J/\psi \to \gamma\eta\pi^+\pi^-$
$-0.066 \pm 0.030 \pm 0.015$	7k	[2] AMELIN	05A	VES	$28\ \pi^- A \to \eta\pi^+\pi^-\pi^- A^*$
$0.00 \pm 0.03 \pm 0.00$	5.4k	[3] ALDE	86	GAM2	$38\ \pi^- p \to n\eta\pi^0\pi^0$
0		[3,4] KALBFLEISCH	74	RVUE	$\eta' \to \eta\pi^+\pi^-$

[1] See ABLIKIM 11 for the full correlation matrix.
[2] Superseded by DOROFEEV 07, which found this parameterization unacceptable. See below.
[3] Assuming $C = 0$.
[4] From the data of DAUBER 64, RITTENBERG 69, AGUILAR-BENITEZ 72B, JACOBS 73, and DANBURG 73.

$\eta'(958) \to \eta\pi\pi$ DECAY PARAMETERS

$|\text{MATRIX ELEMENT}|^2 \propto 1 + a\,Y + b\,Y^2 + c\,X + d\,X^2$

X and Y are Dalitz variables and a, b, c, and d are real-valued parameters. May be different for $\eta'(958) \to \eta\pi^+\pi^-$ and $\eta'(958) \to \eta\pi^0\pi^0$ decays. We do not average measurements in the section below because parameter values from each experiment are strongly correlated.

a decay parameter

VALUE	EVTS	DOCUMENT ID		TECN	COMMENT
• • • We do not use the following data for averages, fits, limits, etc. • • •					
$-0.056 \pm 0.004 \pm 0.002$	351k	ABLIKIM	18	BES3	$\eta' \to \eta\pi^+\pi^-$
$-0.087 \pm 0.009 \pm 0.006$	56k	ABLIKIM	18	BES3	$\eta' \to \eta\pi^0\pi^0$
$-0.074 \pm 0.008 \pm 0.006$	124k	ADLARSON	18A	A2MM	$\eta' \to \eta\pi^0\pi^0$
$-0.072 \pm 0.007 \pm 0.008$		[1] GONZALEZ-S...	18A	RVUE	$\eta' \to \eta\pi^0\pi^0$
$-0.047 \pm 0.011 \pm 0.003$	44k	[2] ABLIKIM	11	BES3	$J/\psi \to \gamma\eta\pi^+\pi^-$
$-0.066 \pm 0.016 \pm 0.003$	15k	[3] BLIK	09	GAM4	$32.5\ \pi^- p \to \eta' n$
$-0.127 \pm 0.016 \pm 0.008$	20k	[4] DOROFEEV	07	VES	$27\ \pi^- p \to \eta' n$, $\pi^- A \to \eta'\pi^- A^*$

[1] Theoretical analysis of ADLARSON 18A using resonance chiral perturbation theory to one loop.
[2] See ABLIKIM 11 for the full correlation matrix.
[3] From $\eta' \to \eta\pi^0\pi^0$ decay.
[4] From $\eta' \to \eta\pi^+\pi^-$ decay.

b decay parameter

VALUE	EVTS	DOCUMENT ID		TECN	COMMENT
• • • We do not use the following data for averages, fits, limits, etc. • • •					
$-0.049 \pm 0.006 \pm 0.006$	351k	ABLIKIM	18	BES3	$\eta' \to \eta\pi^+\pi^-$
$-0.073 \pm 0.014 \pm 0.005$	56k	ABLIKIM	18	BES3	$\eta' \to \eta\pi^0\pi^0$
$-0.063 \pm 0.014 \pm 0.005$	124k	ADLARSON	18A	A2MM	$\eta' \to \eta\pi^0\pi^0$
$-0.052 \pm 0.001 \pm 0.002$		[1] GONZALEZ-S...	18A	RVUE	$\eta' \to \eta\pi^0\pi^0$
$-0.069 \pm 0.019 \pm 0.009$	44k	[2] ABLIKIM	11	BES3	$J/\psi \to \gamma\eta\pi^+\pi^-$
$-0.063 \pm 0.028 \pm 0.004$	15k	[3] BLIK	09	GAM4	$32.5\ \pi^- p \to \eta' n$
$-0.106 \pm 0.028 \pm 0.014$	20k	[4] DOROFEEV	07	VES	$27\ \pi^- p \to \eta' n$, $\pi^- A \to \eta'\pi^- A^*$

[1] Theoretical analysis of ADLARSON 18A using resonance chiral perturbation theory to one loop.
[2] See ABLIKIM 11 for the full correlation matrix.
[3] From $\eta' \to \eta\pi^0\pi^0$ decay.
[4] From $\eta' \to \eta\pi^+\pi^-$ decay.

c decay parameter

VALUE	EVTS	DOCUMENT ID		TECN	COMMENT
• • • We do not use the following data for averages, fits, limits, etc. • • •					
$0.0027 \pm 0.0024 \pm 0.0018$	351k	ABLIKIM	18	BES3	$\eta' \to \eta\pi^+\pi^-$
$0.019 \pm 0.011 \pm 0.003$	44k	[1] ABLIKIM	11	BES3	$J/\psi \to \gamma\eta\pi^+\pi^-$
$-0.107 \pm 0.096 \pm 0.003$	15k	[2] BLIK	09	GAM4	$32.5\ \pi^- p \to \eta' n$
$0.015 \pm 0.011 \pm 0.014$	20k	[3] DOROFEEV	07	VES	$27\ \pi^- p \to \eta' n$, $\pi^- A \to \eta'\pi^- A^*$

[1] See ABLIKIM 11 for the full correlation matrix.
[2] From $\eta' \to \eta\pi^0\pi^0$ decay.
[3] From $\eta' \to \eta\pi^+\pi^-$ decay.

d decay parameter

VALUE	EVTS	DOCUMENT ID		TECN	COMMENT
• • • We do not use the following data for averages, fits, limits, etc. • • •					
$-0.063 \pm 0.004 \pm 0.003$	351k	ABLIKIM	18	BES3	$\eta' \to \eta\pi^+\pi^-$
$-0.074 \pm 0.009 \pm 0.004$	56k	ABLIKIM	18	BES3	$\eta' \to \eta\pi^0\pi^0$
$-0.050 \pm 0.009 \pm 0.005$	124k	ADLARSON	18A	A2MM	$\eta' \to \eta\pi^0\pi^0$
$-0.051 \pm 0.008 \pm 0.006$		[1] GONZALEZ-S...	18A	RVUE	$\eta' \to \eta\pi^0\pi^0$
$-0.073 \pm 0.012 \pm 0.003$	44k	[2] ABLIKIM	11	BES3	$J/\psi \to \gamma\eta\pi^+\pi^-$
$0.018 \pm 0.078 \pm 0.006$	15k	[3] BLIK	09	GAM4	$32.5\ \pi^- p \to \eta' n$
$-0.082 \pm 0.017 \pm 0.008$	20k	[4] DOROFEEV	07	VES	$27\ \pi^- p \to \eta' n$, $\pi^- A \to \eta'\pi^- A^*$

[1] Theoretical analysis of ADLARSON 18A using resonance chiral perturbation theory to one loop.
[2] See ABLIKIM 11 for the full correlation matrix.
[3] From $\eta' \to \eta\pi^0\pi^0$ decay. If $c \equiv 0$ from Bose-Einstein symmetry, $d = -0.067 \pm 0.020 \pm 0.003$.
[4] From $\eta' \to \eta\pi^+\pi^-$ decay.

$\eta'(958)$ β PARAMETER

$|\text{MATRIX ELEMENT}|^2 = (1 + 2\beta Z)$

See the "Note on η Decay Parameters" in our 1994 edition Physical Review **D50** 1173 (1994), p. 1454.

β decay parameter

VALUE	EVTS	DOCUMENT ID		TECN	COMMENT
-0.61 ± 0.08 OUR AVERAGE		Error includes scale factor of 1.2.			
$-0.640 \pm 0.046 \pm 0.047$	1.8k	ABLIKIM	15G	BES3	$J/\psi \to \gamma(\pi^0\pi^0\pi^0)$
-0.59 ± 0.18	235	BLIK	08	GAMS	$32\ \pi^- p \to \eta' n$
-0.1 ± 0.3		ALDE	87B	GAM2	$38\ \pi^- p \to n3\pi^0$

$\eta'(958)$ *C*-NONCONSERVING DECAY PARAMETER

See the note on η decay parameters in the Stable Particle Particle Listings for definition of this parameter.

DECAY ASYMMETRY PARAMETER FOR $\pi^+\pi^-\gamma$

VALUE	EVTS	DOCUMENT ID		TECN	COMMENT
-0.03 ± 0.04 OUR AVERAGE					
-0.019 ± 0.056		AIHARA	87	TPC	$2\gamma \to \pi^+\pi^-\gamma$
-0.069 ± 0.078	295	GRIGORIAN	75	STRC	$2.1\ \pi^- p$
0.00 ± 0.10	103	KALBFLEISCH	75	HBC	$2.18\ K^- p \to \Lambda\pi^+\pi^-\gamma$
• • • We do not use the following data for averages, fits, limits, etc. • • •					
0.07 ± 0.08	152	RITTENBERG	65	HBC	2.1–2.7 $K^- p$

$\eta'(958) \to \gamma\ell^+\ell^-$ TRANSITION FORM FACTOR SLOPE

Related to the effective virtual meson mass Λ, via slope $\approx \Lambda^{-2}$. See e.g. LANDSBERG 85, eq. (3.8), for a detailed definition.

VALUE (GeV^{-2})	EVTS	DOCUMENT ID		TECN	COMMENT
1.62 ± 0.17 OUR AVERAGE					
$1.60 \pm 0.17 \pm 0.08$	864	[1] ABLIKIM	15O	BES3	$J/\psi \to \gamma e^+e^-$
1.7 ± 0.4	33	[1] VIKTOROV	80		$25,33\ \pi^- p \to 2\mu\gamma$

[1] In the single-pole Ansatz where slope $= 1/(\Lambda^2 + \gamma^2)$ with Λ, γ being a Breit-Wigner mass, width for the effective contributing vector meson.

$\eta'(958)$ REFERENCES

ABLIKIM	21I	PR D103 072006	M. Ablikim *et al.*	(BESIII Collab.)
ABLIKIM	21J	PR D103 092005	M. Ablikim *et al.*	(BESIII Collab.)
ABLIKIM	20E	PR D101 032001	M. Ablikim *et al.*	(BESIII Collab.)
ABLIKIM	19AW	PR D100 052015	M. Ablikim *et al.*	(BESIII Collab.)
ABLIKIM	19T	PRL 122 142002	M. Ablikim *et al.*	(BESIII Collab.)
ABLIKIM	18	PR D97 012003	M. Ablikim *et al.*	(BESIII Collab.)
ABLIKIM	18C	PRL 120 242003	M. Ablikim *et al.*	(BESIII Collab.)
ADLARSON	18A	PR D98 012001	P. Adlarson *et al.*	(A2 Collab. at MAMI)
GONZALEZ-S...	18A	EPJ C78 758	S. Gonzalez-Solís, E. Passemar	(BEIJ, IND+)
AAIJ	17D	PL B764 233	R. Aaij *et al.*	(LHCb Collab.)
ABLIKIM	17	PRL 118 012001	M. Ablikim *et al.*	(BESIII Collab.)
ABLIKIM	17T	PR D96 012005	M. Ablikim *et al.*	(BESIII Collab.)
ABLIKIM	16M	PR D93 072008	M. Ablikim *et al.*	(BESIII Collab.)
ABLIKIM	15AD	PR D92 051101	M. Ablikim *et al.*	(BESIII Collab.)
ABLIKIM	15G	PR D92 012014	M. Ablikim *et al.*	(BESIII Collab.)
ABLIKIM	15O	PR D92 012001	M. Ablikim *et al.*	(BESIII Collab.)
ABLIKIM	15P	PR D92 012007	M. Ablikim *et al.*	(BESIII Collab.)
ACHASOV	15	PR D91 092010	M.N. Achasov *et al.*	(SND Collab.)
AKHMETSHIN	15	PL B740 273	R.R. Akhmetshin *et al.*	(CMD-3 Collab.)
PDG	15	RPP 2015 at pdg.lbl.gov		(PDG Collab.)
ABLIKIM	14M	PRL 112 251801	M. Ablikim *et al.*	(BESIII Collab.)

Downloaded from https://academic.oup.com/ptep/article/2022/8/083C01/6651666 by KIT Library user on 27 September 2022

DONSKOV	14	MPL A29 1450213	S. Donskov *et al.*	(GAMS-4π Collab.)
PDG	14	CP C38 070001	K. Olive *et al.*	(PDG Collab.)
ABLIKIM	13	PR D87 012009	M. Ablikim *et al.*	(BESIII Collab.)
ABLIKIM	13G	PR D87 032006	M. Ablikim *et al.*	(BESIII Collab.)
ABLIKIM	13O	PR D87 092011	M. Ablikim *et al.*	(BESIII Collab.)
ABLIKIM	13U	PR D88 091502	M. Ablikim *et al.*	(BESIII Collab.)
ABLIKIM	12E	PRL 108 182001	M. Ablikim *et al.*	(BESIII Collab.)
PDG	12	PR D86 010001	J. Beringer *et al.*	(PDG Collab.)
ABLIKIM	11	PR D83 012003	M. Ablikim *et al.*	(BESIII Collab.)
ABLIKIM	11G	PR D84 032006	M. Ablikim *et al.*	(BESIII Collab.)
CZERWINSKI	10	PRL 105 122001	E. Czerwinski *et al.*	(COSY-11 Collab.)
BLIK	09	PAN 72 231	A.M. Blik *et al.*	(IHEP (Protvino))
		Translated from YAF 72 258.		
NAIK	09	PRL 102 061801	P. Naik *et al.*	(CLEO Collab.)
PEDLAR	09	PR D79 111101	T.K. Pedlar *et al.*	(CLEO Collab.)
BLIK	08	PAN 71 2124	A. Blik *et al.*	(GAMS-4π Collab.)
		Translated from YAF 71 2161.		
LIBBY	08	PRL 101 182002	J. Libby *et al.*	(CLEO Collab.)
WICHT	08	PL B662 323	J. Wicht *et al.*	(BELLE Collab.)
DOROFEEV	07	PL B651 22	V. Dorofeev *et al.*	(VES Collab.)
MORI	07A	JPSJ 76 074102	T. Mori *et al.*	(BELLE Collab.)
ABLIKIM	06E	PR D73 052008	M. Ablikim *et al.*	(BES Collab.)
ABLIKIM	06Q	PRL 97 202002	M. Ablikim *et al.*	(BES Collab.)
AMELIN	05A	PAN 68 372	D.V. Amelin *et al.*	(VES Collab.)
		Translated from YAF 68 401.		
AMSLER	04B	EPJ C33 23	C. Amsler *et al.*	(Crystal Barrel Collab.)
BAI	04J	PL B594 47	J.Z. Bai *et al.*	(BES Collab.)
BRIERE	00	PRL 84 26	R. Briere *et al.*	(CLEO Collab.)
ACCIARRI	98Q	PL B418 399	M. Acciarri *et al.*	(L3 Collab.)
BARBERIS	98C	PL B440 225	D. Barberis *et al.*	(WA 102 Collab.)
WURZINGER	96	PL B374 283	R. Wurzinger *et al.*	(BONN, ORSAY, SACL+)
PDG	94	PR D50 1173	L. Montanet *et al.*	(CERN, LBL, BOST+)
AMSLER	93	ZPHY C58 175	C. Amsler *et al.*	(Crystal Barrel Collab.)
BELADIDZE	92C	SJNP 55 1535	G.M. Beladidze, S.I. Bityukov, G.V. Borisov	(SERP+)
		Translated from YAF 55 2748.		
KARCH	92	ZPHY C54 33	K. Karch *et al.*	(Crystal Ball Collab.)
ARMSTRONG	91B	ZPHY C52 389	T.A. Armstrong *et al.*	(ATHU, BARI, BIRM+)
BEHREND	91	ZPHY C49 401	H.J. Behrend *et al.*	(CELLO Collab.)
AUGUSTIN	90	PR D42 10	J.E. Augustin *et al.*	(DM2 Collab.)
BARU	90	ZPHY C48 581	S.E. Baru *et al.*	(MD-1 Collab.)
BUTLER	90	PR D42 1368	F. Butler *et al.*	(Mark II Collab.)
KARCH	90	PL B249 353	K. Karch *et al.*	(Crystal Ball Collab.)
ROE	90	PR D41 17	N.A. Roe *et al.*	(ASP Collab.)
AIHARA	88C	PR D38 1	H. Aihara *et al.*	(TPC-2γ Collab.)
VOROBYEV	88	SJNP 48 273	P.V. Vorobiev *et al.*	(NOVO)
		Translated from YAF 48 436.		
WILLIAMS	88	PR D38 1365	D.A. Williams *et al.*	(Crystal Ball Collab.)
AIHARA	87	PR D35 2650	H. Aihara *et al.*	(TPC-2γ Collab.) JP
ALBRECHT	87B	PL B199 457	H. Albrecht *et al.*	(ARGUS Collab.)
ALDE	87B	ZPHY C36 603	D.M. Alde *et al.*	(LANL, BELG, SERP, LAPP)
ANTREASYAN	87	PR D36 2633	D. Antreasyan *et al.*	(Crystal Ball Collab.)
GIDAL	87	PRL 59 2012	G. Gidal *et al.*	(LBL, SLAC, HARV)
ALDE	86	PL B177 115	D.M. Alde *et al.*	(SERP, BELG, LANL, LAPP)
BARTEL	85E	PL 160B 421	W. Bartel *et al.*	(JADE Collab.)
LANDSBERG	85	PRPL 128 301	L.G. Landsberg	(SERP)
ALTHOFF	84E	PL 147B 487	M. Althoff *et al.*	(TASSO Collab.)
BERGER	84B	PL 142B 125	C. Berger	(PLUTO Collab.)
BINON	84	PL 140B 264	F.G. Binon *et al.*	(SERP, BELG, LAPP+)
JENNI	83	PR D27 1031	P. Jenni *et al.*	(SLAC, LBL)
BARTEL	82B	PL 113B 190	W. Bartel *et al.*	(JADE Collab.)
BEHREND	82C	PL 114B 378	H.J. Behrend *et al.*	(CELLO Collab.)
Also		PL 125B 518 (erratum)	H.J. Behrend *et al.*	(CELLO Collab.)
DZHELYADIN	81	PL 105B 239	R.I. Dzhelyadin *et al.*	(SERP)
STANTON	80	PL B92 353	N.R. Stanton *et al.*	(OSU, CARL, MCGI+)
VIKTOROV	80	SJNP 32 520	V.A. Viktorov *et al.*	(SERP)
		Translated from YAF 32 1005.		
APEL	79	PL 83B 131	W.D. Apel, K.H. Augenstein, E. Bertolucci	(KARLK+)
BINNIE	79	PL 83B 141	D.M. Binnie *et al.*	(LOIC)
ZANFINO	77	PRL 38 930	C. Zanfino *et al.*	(CARL, MCGI, OHIO+)
GRIGORIAN	75	NP B91 232	A. Grigorian *et al.*	(+)
KALBFLEISCH	75	PR D11 987	G.R. Kalbfleisch, R.C. Strand, J.W. Chapman	(BNL+)
DUANE	74	PRL 32 425	A. Duane *et al.*	(LOIC, SHMP)
KALBFLEISCH	74	PR D10 916	G.R. Kalbfleisch	(BNL)
DANBURG	73	PR D8 3744	J.S. Danburg *et al.*	(BNL, MICH) JP
JACOBS	73	PR D8 18	S.M. Jacobs *et al.*	(BRAN, UMD, SYRA+) JP
AGUILAR-...	72B	PR D6 29	M. Aguilar-Benitez *et al.*	(BNL)
APEL	72	PL 40B 680	W.D. Apel *et al.*	(KARLK, KARLE, PISA)
DALPIAZ	72	PL 42B 377	P.F. Dalpiaz *et al.*	(CERN)
BASILE	71	NC 3A 371	M. Basile *et al.*	(CERN, BGNA, STRB)
HARVEY	71	PRL 27 885	E.H. Harvey *et al.*	(MINN, MICH)
BENSINGER	70	PL 33B 505	J.R. Bensinger *et al.*	(WISC)
RITTENBERG	69	Thesis UCRL 18863	A. Rittenberg	(LRL) I
DAVIS	68	PL 27B 532	R. Davis *et al.*	(NWES, ANL)
LONDON	66	PR 143 1034	G.W. London *et al.*	(BNL, SYRA) IJP
BADIER	65B	PL 17 337	J. Badier *et al.*	(EPOL, SACL, AMST)
RITTENBERG	65	PRL 15 556	A. Rittenberg, G.R. Kalbfleisch	(LRL, BNL)
DAUBER	64	PRL 13 449	P.M. Dauber *et al.*	(UCLA) JP
KALBFLEISCH	64B	PRL 13 349	G.R. Kalbfleisch, O.I. Dahl, A. Rittenberg	(LRL) JP

$f_0(980)$

$I^G(J^{PC}) = 0^+(0^{++})$

See the related review(s):

Scalar Mesons below 1 GeV

$f_0(980)$ T-MATRIX POLE $\sqrt{s}$

VALUE (MeV)	DOCUMENT ID		TECN	COMMENT
(980–1010) − i (20–35) OUR ESTIMATE (see Fig. 64.4 in the review)				
• • • We do not use the following data for averages, fits, limits, etc. • • •				
$(1014 \pm 8) - i(35 \pm 5)$	SARANTSEV	21	RVUE	$J/\psi(1S) \to \gamma(\pi\pi, K\overline{K}, \eta\eta, \omega\phi)$
$(992.8 \pm 1.3) - i(30.7 \pm 2.3)$	[1] ALBRECHT	20	RVUE	$0.9\ \overline{p}p \to \pi^0\pi^0\eta$, $\pi^0\eta\eta$, $\pi^0 K^+K^-$
$(1003^{+5}_{-27}) - i(21^{+10}_{-8})$	[2] GARCIA-MAR..	11	RVUE	Compilation
$(996 \pm 7) - i(25^{+10}_{-6})$	[3] GARCIA-MAR..	11	RVUE	Compilation
$(996^{+4}_{-14}) - i(24^{+11}_{-3})$	[4] MOUSSALLAM	11	RVUE	Compilation
$(981 \pm 43) - i(18 \pm 11)$	[5] MENNESSIER	10	RVUE	Compilation
$(1030^{+30}_{-10}) - i(35^{+10}_{-16})$	[6] ANISOVICH	09	RVUE	$0.0\ \overline{p}p$, πN
$(973^{+39}_{-127}) - i(11^{+189}_{-11})$	[7] PELAEZ	04A	RVUE	$\pi\pi \to \pi\pi$

[1] 5 poles, 5 channels, including scattering data from HYAMS 75 ($\pi\pi$), LONGACRE 86 ($K\overline{K}$), BINON 83 ($\eta\eta$), and BINON 84C ($\eta\eta'$). Based on 18.5k events. Second solution 977.8 ± 1.7 MeV.

[2] Reanalysis of the K_{e4} data of BATLEY 10C and the $\pi N \to \pi\pi N$ data of HYAMS 73, GRAYER 74, and PROTOPOPESCU 73 using Roy equations.

[3] Reanalysis of the K_{e4} data of BATLEY 10C and the $\pi N \to \pi\pi N$ data of HYAMS 73, GRAYER 74, and PROTOPOPESCU 73 using GKPY equations.

[4] Uses Roy equations.

[5] Average of the analyses of three data sets in the K-matrix model. Uses the data of BATLEY 08A, HYAMS 73 , and GRAYER 74 , partially of COHEN 80 or ETKIN 82B.

[6] On sheet II in a 2-pole solution. The other pole is found on sheet III at $(850 - i\,100)$ MeV.

[7] Reanalysis of data from PROTOPOPESCU 73, ESTABROOKS 74, GRAYER 74, and COHEN 80 in the unitarized ChPT model.

$f_0(980)$ MASS

VALUE (MeV)	EVTS	DOCUMENT ID		TECN	COMMENT
990 ±20 OUR ESTIMATE					
• • • We do not use the following data for averages, fits, limits, etc. • • •					
$992.0^{+8.5}_{-7.5} \pm 8.6$		[1] AAIJ	19H	LHCB	$pp \to D^\pm X$
989.4 ± 1.3	424	ABLIKIM	15P	BES3	$J/\psi \to K^+K^-3\pi$
989.9 ± 0.4	706	ABLIKIM	12E	BES3	$J/\psi \to \gamma 3\pi$
$977\ ^{+11}_{-9} \pm 1$	44	[2] ECKLUND	09	CLEO	$4.17\ e^+e^- \to D_s^- D_s^{*+}$ + c.c.
$982.2 \pm 1.0^{+8.1}_{-8.0}$		[3] UEHARA	08A	BELL	$10.6\ e^+e^- \to e^+e^-\pi^0\pi^0$
$976.8 \pm 0.3^{+10.1}_{-0.6}$	64k	[4] AMBROSINO	07	KLOE	$1.02\ e^+e^- \to \pi^0\pi^0\gamma$
$984.7 \pm 0.4^{+2.4}_{-3.7}$	64k	[5] AMBROSINO	07	KLOE	$1.02\ e^+e^- \to \pi^0\pi^0\gamma$
973 ± 3	262 ± 30	[6] AUBERT	07AK	BABR	$10.6\ e^+e^- \to \phi\pi^+\pi^-\gamma$
970 ± 7	54 ± 9	[6] AUBERT	07AK	BABR	$10.6\ e^+e^- \to \phi\pi^0\pi^0\gamma$
953 ± 20	2.6k	[7] BONVICINI	07	CLEO	$D^+ \to \pi^-\pi^+\pi^+$
$985.6^{+1.2}_{-1.5} \pm 1.1 \pm 1.6$		[8] MORI	07	BELL	$10.6\ e^+e^- \to e^+e^-\pi^+\pi^-$
$983.0 \pm 0.6^{+4.0}_{-3.0}$		[9] AMBROSINO	06B	KLOE	$1.02\ e^+e^- \to \pi^+\pi^-\gamma$
$977.3 \pm 0.9^{+3.7}_{-4.3}$		[10] AMBROSINO	06B	KLOE	$1.02\ e^+e^- \to \pi^+\pi^-\gamma$
950 ± 9	4286	[11] GARMASH	06	BELL	$B^+ \to K^+\pi^+\pi^-$
965 ± 10		[12] ABLIKIM	05	BES2	$J/\psi \to \phi\pi^+\pi^-$, ϕK^+K^-
1031 ± 8		[13] ANISOVICH	03	RVUE	
1037 ± 31		TIKHOMIROV	03	SPEC	$40.0\ \pi^- C \to K_S^0 K_S^0 K_L^0 X$
973 ± 1	2438	[14] ALOISIO	02D	KLOE	$e^+e^- \to \pi^0\pi^0\gamma$
$977 \pm 3 \pm 2$	848	[15] AITALA	01A	E791	$D_s^+ \to \pi^-\pi^+\pi^+$
969.8 ± 4.5	419	[16] ACHASOV	00H	SND	$e^+e^- \to \pi^0\pi^0\gamma$
$985\ ^{+16}_{-12}$	419	[17,18] ACHASOV	00H	SND	$e^+e^- \to \pi^0\pi^0\gamma$
$976 \pm 5 \pm 6$		[19] AKHMETSHIN	99B	CMD2	$e^+e^- \to \pi^+\pi^-\gamma$
$977 \pm 3 \pm 6$	268	[19] AKHMETSHIN	99C	CMD2	$e^+e^- \to \pi^0\pi^0\gamma$
$975 \pm 4 \pm 6$		[20] AKHMETSHIN	99C	CMD2	$e^+e^- \to \pi^0\pi^0\gamma$
$975 \pm 4 \pm 6$		[21] AKHMETSHIN	99C	CMD2	$e^+e^- \to \pi^+\pi^-\gamma$, $\pi^0\pi^0\gamma$
985 ± 10		BARBERIS	99	OMEG	$450\ pp \to p_s p_f K^+K^-$
982 ± 3		BARBERIS	99B	OMEG	$450\ pp \to p_s p_f \pi^+\pi^-$
982 ± 3		BARBERIS	99C	OMEG	$450\ pp \to p_s p_f \pi^0\pi^0$
$987 \pm 6 \pm 6$		[22] BARBERIS	99D	OMEG	$450\ pp \to K^+K^-$, $\pi^+\pi^-$
989 ± 15		BELLAZZINI	99	GAM4	$450\ pp \to pp\pi^0\pi^0$
991 ± 3		[23] KAMINSKI	99	RVUE	$\pi\pi \to \pi\pi$, $K\overline{K}$, $\sigma\sigma$
~ 980		[23] OLLER	99	RVUE	$\pi\pi \to \pi\pi$, $K\overline{K}$
~ 993.5		OLLER	99B	RVUE	$\pi\pi \to \pi\pi$, $K\overline{K}$
~ 987		[23] OLLER	99C	RVUE	$\pi\pi \to \pi\pi$, $K\overline{K}$, $\eta\eta$
957 ± 6		[24] ACKERSTAFF	98Q	OPAL	$Z \to f_0 X$
960 ± 10		ALDE	98	GAM4	
1015 ± 15		[23] ANISOVICH	98B	RVUE	Compilation
1008		[25] LOCHER	98	RVUE	$\pi\pi \to \pi\pi$, $K\overline{K}$
955 ± 10		[24] ALDE	97	GAM2	$450\ pp \to pp\pi^0\pi^0$
994 ± 9		[26] BERTIN	97C	OBLX	$0.0\ \overline{p}p \to \pi^+\pi^-\pi^0$
$993.2 \pm 6.5 \pm 6.9$		[27] ISHIDA	96	RVUE	$\pi\pi \to \pi\pi$, $K\overline{K}$
1006		TORNQVIST	96	RVUE	$\pi\pi \to \pi\pi$, $K\overline{K}$, $K\pi$, $\eta\pi$
997 ± 5	3k	[28] ALDE	95B	GAM2	$38\ \pi^-p \to \pi^0\pi^0 n$
960 ± 10	10k	[29] ALDE	95B	GAM2	$38\ \pi^-p \to \pi^0\pi^0 n$
994 ± 5		AMSLER	95B	CBAR	$0.0\ \overline{p}p \to 3\pi^0$
~ 996		[30] AMSLER	95D	CBAR	$0.0\ \overline{p}p \to \pi^0\pi^0\pi^0$, $\pi^0\eta\eta$, $\pi^0\pi^0\eta$
987 ± 6		[31] ANISOVICH	95	RVUE	
1015		JANSSEN	95	RVUE	$\pi\pi \to \pi\pi$, $K\overline{K}$
983		[32] BUGG	94	RVUE	$\overline{p}p \to \eta 2\pi^0$
973 ± 2		[33] KAMINSKI	94	RVUE	$\pi\pi \to \pi\pi$, $K\overline{K}$

Downloaded from https://academic.oup.com/ptep/article/2022/8/083C01/6651666 by KIT Library user on 27 September 2022

988	[34] ZOU	94B	RVUE	
988 ±10	[35] MORGAN	93	RVUE	$\pi\pi(K\overline{K}) \to \pi\pi(K\overline{K})$, $J/\psi \to \phi\pi\pi(K\overline{K})$, $D_s \to \pi(\pi\pi)$
971.1± 4.0	[24] AGUILAR-...	91	EHS	400 pp
979 ± 4	[36] ARMSTRONG	91	OMEG	300 $pp \to pp\pi\pi$, $pp K\overline{K}$
956 ±12	BREAKSTONE	90	SFM	$pp \to pp\pi^+\pi^-$
959.4± 6.5	[24] AUGUSTIN	89	DM2	$J/\psi \to \omega\pi^+\pi^-$
978 ± 9	[24] ABACHI	86B	HRS	$e^+e^- \to \pi^+\pi^- X$
$985.0^{+9.0}_{-39.0}$	ETKIN	82B	MPS	23 $\pi^- p \to n2K^0_S$
974 ± 4	[36] GIDAL	81	MRK2	$J/\psi \to \pi^+\pi^- X$
975	[37] ACHASOV	80	RVUE	
986 ±10	[36] AGUILAR-...	78	HBC	0.7 $\overline{p}p \to K^0_S K^0_S$
969 ± 5	[36] LEEPER	77	ASPK	2–2.4 $\pi^- p \to \pi^+\pi^- n$, $K^+K^- n$
987 ± 7	[36] BINNIE	73	CNTR	$\pi^- p \to n$MM
1012 ± 6	[38] GRAYER	73	ASPK	17 $\pi^- p \to \pi^+\pi^- n$
1007 ±20	[38] HYAMS	73	ASPK	17 $\pi^- p \to \pi^+\pi^- n$
997 ± 6	[38] PROTOPOP...	73	HBC	7 $\pi^+ p \to \pi^+ p\pi^+\pi^-$

[1] From the $D^\pm \to K^\pm K^+ K^-$ Dalitz plot fit with the Triple-M amplitude in the multi-meson model of AOUDE 18.
[2] Using a relativistic Breit-Wigner function and taking into account the finite D_s mass.
[3] Breit-Wigner mass. Using finite width corrections according to FLATTE 76 and ACHASOV 05, and the ratio $g_{f_0 KK}/g_{f_0\pi\pi} = 0$.
[4] In the kaon-loop fit.
[5] In the no-structure fit.
[6] Systematic errors not estimated.
[7] FLATTE 76 parameterization. $g_{f_0\pi\pi} = 329 \pm 96$ MeV/c^2 assuming $g_{f_0 K\overline{K}}/g_{f_0\pi\pi}$=2.
[8] Breit-Wigner mass. Using finite width corrections according to FLATTE 76 and ACHASOV 05, and the ratio $g_{f_0 KK}/g_{f_0\pi\pi} = 4.21 \pm 0.25 \pm 0.21$ from ABLIKIM 05.
[9] In the kaon-loop fit following formalism of ACHASOV 89.
[10] In the no-structure fit assuming a direct coupling of ϕ to $f_0\gamma$.
[11] FLATTE 76 parameterization. Supersedes GARMASH 05.
[12] FLATTE 76 parameterization, $g_{f_0 K\overline{K}}/g_{f_0\pi\pi} = 4.21 \pm 0.25 \pm 0.21$.
[13] K-matrix pole from combined analysis of $\pi^- p \to \pi^0\pi^0 n$, $\pi^- p \to K\overline{K} n$, $\pi^+\pi^- \to \pi^+\pi^-$, $\overline{p}p \to \pi^0\pi^0\pi^0$, $\pi^0\eta\eta$, $\pi^0\pi^0\eta$, $\pi^+\pi^-\pi^0$, $K^+K^-\pi^0$, $K^0_S K^0_S \pi^0$, $K^+K^0_S\pi^-$ at rest, $\overline{p}n \to \pi^-\pi^-\pi^+$, $K^0_S K^-\pi^0$, $K^0_S K^0_S \pi^-$ at rest.
[14] From the negative interference with the $f_0(500)$ meson of AITALA 01B using the ACHASOV 89 parameterization for the $f_0(980)$, a Breit-Wigner for the $f_0(500)$, and ACHASOV 01F for the $\rho\pi$ contribution.
[15] Coupled-channel Breit-Wigner, couplings g_π=0.09±0.01±0.01, g_K=0.02±0.04±0.03.
[16] Supersedes ACHASOV 98I. Using the model of ACHASOV 89.
[17] Supersedes ACHASOV 98I.
[18] In the "narrow resonance" approximation.
[19] Assuming $\Gamma(f_0)$= 40 MeV.
[20] From a narrow pole fit taking into account $f_0(980)$ and $f_0(1200)$ intermediate mechanisms.
[21] From the combined fit of the photon spectra in the reactions $e^+e^- \to \pi^+\pi^-\gamma$, $\pi^0\pi^0\gamma$.
[22] Supersedes BARBERIS 99 and BARBERIS 99B
[23] T-matrix pole.
[24] From invariant mass fit.
[25] On sheet II in a 2 pole solution. The other pole is found on sheet III at (1039−93i) MeV.
[26] On sheet II in a 2 pole solution. The other pole is found on sheet III at (963-29i) MeV.
[27] Reanalysis of data from HYAMS 73, GRAYER 74, SRINIVASAN 75, and ROSSELET 77 using the interfering amplitude method.
[28] At high $|t|$.
[29] At low $|t|$.
[30] On sheet II in a 4-pole solution, the other poles are found on sheet III at (953−55i) MeV and on sheet IV at (938−35i) MeV.
[31] Combined fit of ALDE 95B, ANISOVICH 94, AMSLER 94D.
[32] On sheet II in a 2 pole solution. The other pole is found on sheet III at (996−103i) MeV.
[33] From sheet II pole position.
[34] On sheet II in a 2 pole solution. The other pole is found on sheet III at (797−185i) MeV and can be interpreted as a shadow pole.
[35] On sheet II in a 2 pole solution. The other pole is found on sheet III at (978−28i) MeV.
[36] From coupled channel analysis.
[37] Coupled channel analysis with finite width corrections.
[38] Included in AGUILAR-BENITEZ 78 fit.

$f_0(980)$ WIDTH

Width determination very model dependent. Peak width in $\pi\pi$ is about 50 MeV, but decay width can be much larger.

VALUE (MeV)	EVTS	DOCUMENT ID		TECN	COMMENT
10 to 100 OUR ESTIMATE					
• • • We do not use the following data for averages, fits, limits, etc. • • •					
15.3± 4.7	424	ABLIKIM	15P	BES3	$J/\psi \to K^+K^- 3\pi$
9.5± 1.1	706	ABLIKIM	12E	BES3	$J/\psi \to \gamma 3\pi$
$91^{+30}_{-22} \pm 3$	44	[1] ECKLUND	09	CLEO	4.17 $e^+e^- \to D^-_s D^{*+}_s$ + c.c.
$66.9 \pm 2.2^{+17.6}_{-12.5}$		[2] UEHARA	08A	BELL	10.6 $e^+e^- \to e^+e^-\pi^0\pi^0$
65 ± 13	262 ± 30	[3] AUBERT	07AK	BABR	10.6 $e^+e^- \to \phi\pi^+\pi^-\gamma$
81 ± 21	54 ± 9	[3] AUBERT	07AK	BABR	10.6 $e^+e^- \to \phi\pi^0\pi^0\gamma$
$51.3^{+20.8}_{-17.7} {}^{+13.2}_{-3.8}$		[4] MORI	07	BELL	10.6 $e^+e^- \to e^+e^-\pi^+\pi^-$
$61 \pm 9 {}^{+14}_{-8}$	2584	[5] GARMASH	05	BELL	$B^+ \to K^+\pi^+\pi^-$
64 ± 16		[6] ANISOVICH	03	RVUE	
121 ± 23		TIKHOMIROV	03	SPEC	40.0 $\pi^- C \to K^0_S K^0_S K^0_L X$
∼ 70		[7] BRAMON	02	RVUE	1.02 $e^+e^- \to \pi^0\pi^0\gamma$
44 ± 2 ± 2	848	[8] AITALA	01A	E791	$D^+_s \to \pi^-\pi^+\pi^+$
201 ± 28	419	[9] ACHASOV	00H	SND	$e^+e^- \to \pi^0\pi^0\gamma$
122 ± 13	419	[10,11] ACHASOV	00H	SND	$e^+e^- \to \pi^0\pi^0\gamma$
56 ± 20		[12] AKHMETSHIN	99C	CMD2	$e^+e^- \to \pi^0\pi^0\gamma$
65 ± 20		BARBERIS	99	OMEG	450 $pp \to p_s p_f K^+K^-$
80 ± 10		BARBERIS	99B	OMEG	450 $pp \to p_s p_f \pi^+\pi^-$
80 ± 10		BARBERIS	99C	OMEG	450 $pp \to p_s p_f \pi^0\pi^0$
48 ± 12 ± 8		[13] BARBERIS	99D	OMEG	450 $pp \to K^+K^-$, $\pi^+\pi^-$
65 ± 25		BELLAZZINI	99	GAM4	450 $pp \to pp\pi^0\pi^0$
71 ± 14		[14] KAMINSKI	99	RVUE	$\pi\pi \to \pi\pi$, $K\overline{K}$, $\sigma\sigma$
∼ 28		[14] OLLER	99	RVUE	$\pi\pi \to \pi\pi$, $K\overline{K}$
∼ 25		OLLER	99B	RVUE	$\pi\pi \to \pi\pi$, $K\overline{K}$
∼ 14		[14] OLLER	99C	RVUE	$\pi\pi \to \pi\pi$, $K\overline{K}$, $\eta\eta$
70 ± 20		ALDE	98	GAM4	
86 ± 16		[14] ANISOVICH	98B	RVUE	Compilation
54		[15] LOCHER	98	RVUE	$\pi\pi \to \pi\pi$, $K\overline{K}$
69 ± 15		[16] ALDE	97	GAM2	450 $pp \to pp\pi^0\pi^0$
38 ± 20		[17] BERTIN	97C	OBLX	0.0 $\overline{p}p \to \pi^+\pi^-\pi^0$
∼ 100		[18] ISHIDA	96	RVUE	$\pi\pi \to \pi\pi$, $K\overline{K}$
34		TORNQVIST	96	RVUE	$\pi\pi \to \pi\pi$, $K\overline{K}$, $K\pi$, $\eta\pi$
48 ± 10	3k	[19] ALDE	95B	GAM2	38 $\pi^- p \to \pi^0\pi^0 n$
95 ± 20	10k	[20] ALDE	95B	GAM2	38 $\pi^- p \to \pi^0\pi^0 n$
26 ± 10		AMSLER	95B	CBAR	0.0 $\overline{p}p \to 3\pi^0$
∼ 112		[21] AMSLER	95D	CBAR	0.0 $\overline{p}p \to \pi^0\pi^0\pi^0$, $\pi^0\eta\eta$, $\pi^0\pi^0\eta$
80 ± 12		[22] ANISOVICH	95	RVUE	
30		JANSSEN	95	RVUE	$\pi\pi \to \pi\pi$, $K\overline{K}$
74		[23] BUGG	94	RVUE	$\overline{p}p \to \eta 2\pi^0$
29 ± 2		[24] KAMINSKI	94	RVUE	$\pi\pi \to \pi\pi$, $K\overline{K}$
46		[25] ZOU	94B	RVUE	
48 ± 12		[26] MORGAN	93	RVUE	$\pi\pi(K\overline{K}) \to \pi\pi(K\overline{K})$, $J/\psi \to \phi\pi\pi(K\overline{K})$, $D_s \to \pi(\pi\pi)$
37.4± 10.6		[16] AGUILAR-...	91	EHS	400 pp
72 ± 8		[27] ARMSTRONG	91	OMEG	300 $pp \to pp\pi\pi$, $pp K\overline{K}$
110 ± 30		BREAKSTONE	90	SFM	$pp \to pp\pi^+\pi^-$
29 ± 13		[16] ABACHI	86B	HRS	$e^+e^- \to \pi^+\pi^- X$
120 ±281 ±20		ETKIN	82B	MPS	23 $\pi^- p \to n2K^0_S$
28 ± 10		[27] GIDAL	81	MRK2	$J/\psi \to \pi^+\pi^- X$
70 to 300		[28] ACHASOV	80	RVUE	
100 ± 80		[29] AGUILAR-...	78	HBC	0.7 $\overline{p}p \to K^0_S K^0_S$
30 ± 8		[27] LEEPER	77	ASPK	2–2.4 $\pi^- p \to \pi^+\pi^- n$, $K^+K^- n$
48 ± 14		[27] BINNIE	73	CNTR	$\pi^- p \to n$MM
32 ± 10		[30] GRAYER	73	ASPK	17 $\pi^- p \to \pi^+\pi^- n$
30 ± 10		[30] HYAMS	73	ASPK	17 $\pi^- p \to \pi^+\pi^- n$
54 ± 16		[30] PROTOPOP...	73	HBC	7 $\pi^+ p \to \pi^+ p\pi^+\pi^-$

[1] Using a relativistic Breit-Wigner function and taking into account the finite D_s mass.
[2] Breit-Wigner $\pi\pi$ width. Using finite width corrections according to FLATTE 76 and ACHASOV 05, and the ratio $g_{f_0 KK}/g_{f_0\pi\pi} = 0$.
[3] Systematic errors not estimated.
[4] Breit-Wigner $\pi\pi$ width. Using finite width corrections according to FLATTE 76 and ACHASOV 05, and the ratio $g_{f_0 KK}/g_{f_0\pi\pi} = 4.21 \pm 0.25 \pm 0.21$ from ABLIKIM 05.
[5] Breit-Wigner, solution 1, PWA ambiguous.
[6] K-matrix pole from combined analysis of $\pi^- p \to \pi^0\pi^0 n$, $\pi^- p \to K\overline{K} n$, $\pi^+\pi^- \to \pi^+\pi^-$, $\overline{p}p \to \pi^0\pi^0\pi^0$, $\pi^0\eta\eta$, $\pi^0\pi^0\eta$, $\pi^+\pi^-\pi^0$, $K^+K^-\pi^0$, $K^0_S K^0_S \pi^0$, $K^+K^0_S\pi^-$ at rest, $\overline{p}n \to \pi^-\pi^-\pi^+$, $K^0_S K^-\pi^0$, $K^0_S K^0_S \pi^-$ at rest.
[7] Using the data of AKHMETSHIN 99C, ACHASOV 00H, and ALOISIO 02D.
[8] Breit-Wigner width.
[9] Supersedes ACHASOV 98I. Using the model of ACHASOV 89.
[10] Supersedes ACHASOV 98I.
[11] In the "narrow resonance" approximation.
[12] From the combined fit of the photon spectra in the reactions $e^+e^- \to \pi^+\pi^-\gamma$, $\pi^0\pi^0\gamma$.

Downloaded from https://academic.oup.com/ptep/article/2022/8/083C01/6651666 by KIT Library user on 27 September 2022

[13] Supersedes BARBERIS 99 and BARBERIS 99B
[14] T-matrix pole.
[15] On sheet II in a 2 pole solution. The other pole is found on sheet III at (1039−93i) MeV.
[16] From invariant mass fit.
[17] On sheet II in a 2 pole solution. The other pole is found on sheet III at (963-29i) MeV.
[18] Reanalysis of data from HYAMS 73, GRAYER 74, SRINIVASAN 75, and ROSSELET 77 using the interfering amplitude method.
[19] At high $|t|$.
[20] At low $|t|$.
[21] On sheet II in a 4-pole solution, the other poles are found on sheet III at (953−55i) MeV and on sheet IV at (938−35i) MeV.
[22] Combined fit of ALDE 95B, ANISOVICH 94,
[23] On sheet II in a 2 pole solution. The other pole is found on sheet III at (996−103i) MeV.
[24] From sheet II pole position.
[25] On sheet II in a 2 pole solution. The other pole is found on sheet III at (797−185i) MeV and can be interpreted as a shadow pole.
[26] On sheet II in a 2 pole solution. The other pole is found on sheet III at (978−28i) MeV.
[27] From coupled channel analysis.
[28] Coupled channel analysis with finite width corrections.
[29] From coupled channel fit to the HYAMS 73 and PROTOPOPESCU 73 data. With a simultaneous fit to the $\pi\pi$ phase-shifts, inelasticity and to the $K^0_S K^0_S$ invariant mass.
[30] Included in AGUILAR-BENITEZ 78 fit.

$f_0(980)$ DECAY MODES

	Mode	Fraction (Γ_i/Γ)
Γ_1	$\pi\pi$	seen
Γ_2	$K\overline{K}$	seen
Γ_3	$\gamma\gamma$	seen
Γ_4	e^+e^-	

$f_0(980)$ PARTIAL WIDTHS

$\Gamma(\gamma\gamma)$ — Γ_3

VALUE (keV)	DOCUMENT ID		TECN	COMMENT
$0.29^{+0.11}_{-0.06}$ OUR AVERAGE				
$0.286\pm0.017^{+0.211}_{-0.070}$	[1] UEHARA	08A	BELL	$10.6\ e^+e^- \to e^+e^-\pi^0\pi^0$
$0.205^{+0.095}_{-0.083}{}^{+0.147}_{-0.117}$	[2] MORI	07	BELL	$10.6\ e^+e^- \to e^+e^-\pi^+\pi^-$
$0.42 \pm0.06 \pm0.18$	[3] OEST	90	JADE	$e^+e^- \to e^+e^-\pi^0\pi^0$
• • • We do not use the following data for averages, fits, limits, etc. • • •				
0.32 ± 0.05	[4] DAI	14A	RVUE	Compilation
0.16 ± 0.01	[5] MENNESSIER	11	RVUE	
$0.29 \pm0.21\ ^{+0.02}_{-0.07}$	[6] MOUSSALLAM	11	RVUE	Compilation
0.42	[7,8] PENNINGTON	08	RVUE	Compilation
0.10	[8,9] PENNINGTON	08	RVUE	Compilation
$0.28\ ^{+0.09}_{-0.13}$	[10] BOGLIONE	99	RVUE	$\gamma\gamma \to \pi^+\pi^-, \pi^0\pi^0$
$0.29 \pm0.07 \pm0.12$	[11,12] BOYER	90	MRK2	$e^+e^- \to e^+e^-\pi^+\pi^-$
$0.31 \pm0.14 \pm0.09$	[11,12] MARSISKE	90	CBAL	$e^+e^- \to e^+e^-\pi^0\pi^0$
0.63 ± 0.14	[13] MORGAN	90	RVUE	$\gamma\gamma \to \pi^+\pi^-, \pi^0\pi^0$

[1] Using finite width corrections according to FLATTE 76 and ACHASOV 05, and the ratio $g_{f_0 KK}/g_{f_0\pi\pi} = 0$.
[2] Using finite width corrections according to FLATTE 76 and ACHASOV 05, and the ratio $g_{f_0 KK}/g_{f_0\pi\pi} = 4.21 \pm 0.25 \pm 0.21$ from ABLIKIM 05.
[3] OEST 90 quote systematic errors $^{+0.08}_{-0.18}$. We use ±0.18. Observed 60 events.
[4] Using dispersive analysis with phases from GARCIA-MARTIN 11A and BUETTIKER 04 as input.
[5] Uses an analytic K-matrix model. Compilation.
[6] Using dispersion integral with phase input from Roy equations and data from MARSISKE 90, BOYER 90, BEHREND 92, UEHARA 08A, and MORI 07.
[7] Solution A (preferred solution based on χ^2-analysis).
[8] Dispersion theory based amplitude analysis of BOYER 90, MARSISKE 90, BEHREND 92, and MORI 07.
[9] Solution B (worse than solution A; still acceptable when systematic uncertainties are included).
[10] Supersedes MORGAN 90.
[11] From analysis allowing arbitrary background unconstrained by unitarity.
[12] Data included in MORGAN 90, BOGLIONE 99 analyses.
[13] From amplitude analysis of BOYER 90 and MARSISKE 90, data corresponds to resonance parameters $m = 989$ MeV, $\Gamma = 61$ MeV.

$\Gamma(e^+e^-)$ — Γ_4

VALUE (eV)	CL%	DOCUMENT ID		TECN	COMMENT
<8.4	90	VOROBYEV	88	ND	$e^+e^- \to \pi^0\pi^0$

$f_0(980)$ BRANCHING RATIOS

$\Gamma(\pi\pi)/[\Gamma(\pi\pi)+\Gamma(K\overline{K})]$ — $\Gamma_1/(\Gamma_1+\Gamma_2)$

VALUE	EVTS	DOCUMENT ID		TECN	COMMENT
• • • We do not use the following data for averages, fits, limits, etc. • • •					
0.52 ± 0.12	9.9k	[1] AUBERT	06O	BABR	$B^\pm \to K^\pm\pi^\pm\pi^\mp$
$0.75\ ^{+0.11}_{-0.13}$		[2] ABLIKIM	05Q	BES2	$\chi_{c0} \to 2\pi^+2\pi^-$, $\pi^+\pi^-K^+K^-$
0.84 ± 0.02		[3] ANISOVICH	02D	SPEC	Combined fit
~ 0.68		OLLER	99B	RVUE	$\pi\pi \to \pi\pi, K\overline{K}$
0.67 ± 0.09		[4] LOVERRE	80	HBC	$4\ \pi^-p \to n2K^0_S$
$0.81\ ^{+0.09}_{-0.04}$		[4] CASON	78	STRC	$7\ \pi^-p \to n2K^0_S$
0.78 ± 0.03		[4] WETZEL	76	OSPK	$8.9\ \pi^-p \to n2K^0_S$

[1] Recalculated by us using $\Gamma(K^+K^-)\ /\ \Gamma(\pi^+\pi^-) = 0.69 \pm 0.32$ from AUBERT 06O and isospin relations.
[2] Using data from ABLIKIM 04G.
[3] From a combined K-matrix analysis of Crystal Barrel ($p\overline{p} \to \pi^0\pi^0\pi^0, \pi^0\eta\eta, \pi^0\pi^0\eta$), GAMS ($\pi p \to \pi^0\pi^0 n, \eta\eta n, \eta\eta' n$), and BNL ($\pi p \to K\overline{K}n$) data.
[4] Measure $\pi\pi$ elasticity assuming two resonances coupled to the $\pi\pi$ and $K\overline{K}$ channels only.

$f_0(980)$ REFERENCES

SARANTSEV 21 PL B816 136227 A.V. Sarantsev et al. (BONN, PNPI)
ALBRECHT 20 EPJ C80 453 M. Albrecht et al. (Crystal Barrel Collab.)
AAIJ 19H JHEP 1904 063 R. Aaij et al. (LHCb Collab.)
AOUDE 18 PR D98 056021 R.T. Aoude et al.
ABLIKIM 15P PR D92 012007 M. Ablikim et al. (BESIII Collab.)
DAI 14A PR D90 036004 L.-Y. Dai, M.R. Pennington (CEBAF)
ABLIKIM 12E PRL 108 182001 M. Ablikim et al. (BESIII Collab.)
GARCIA-MAR... 11 PRL 107 072001 R. Garcia-Martin et al. (MADR, CRAC)
GARCIA-MAR... 11A PR D83 074004 R. Garcia-Martin et al. (MADR, CRAC)
MENNESSIER 11 PL B696 40 G. Mennessier, S. Narison, X.-G. Wang
MOUSSALLAM 11 EPJ C71 1814 B. Moussallam
BATLEY 10C EPJ C70 635 J.R. Batley et al. (CERN NA48/2 Collab.)
MENNESSIER 10 PL B688 59 G. Mennessier, S. Narison, X.-G. Wang
ANISOVICH 09 IJMP A24 2481 V.V. Anisovich, A.V. Sarantsev
ECKLUND 09 PR D80 052009 K.M. Ecklund et al. (CLEO Collab.)
BATLEY 08A EPJ C54 411 J.R. Batley et al. (CERN NA48/2 Collab.)
PENNINGTON 08 EPJ C56 1 M.R. Pennington et al.
UEHARA 08A PR D78 052004 S. Uehara et al. (BELLE Collab.)
AMBROSINO 07 EPJ C49 473 F. Ambrosino et al. (KLOE Collab.)
AUBERT 07AK PR D76 012008 B. Aubert et al. (BABAR Collab.)
BONVICINI 07 PR D76 012001 G. Bonvicini et al. (CLEO Collab.)
MORI 07 PR D75 051101 T. Mori et al. (BELLE Collab.)
AMBROSINO 06B PL B634 148 F. Ambrosino et al. (KLOE Collab.)
AUBERT 06O PR D74 032003 B. Aubert et al. (BABAR Collab.)
GARMASH 06 PRL 96 251803 A. Garmash et al. (BELLE Collab.)
ABLIKIM 05 PL B607 243 M. Ablikim et al. (BES Collab.)
ABLIKIM 05Q PR D72 092002 M. Ablikim et al. (BES Collab.)
ACHASOV 05 PR D72 013006 N.N. Achasov, G.N. Shestakov
GARMASH 05 PR D71 092003 A. Garmash et al. (BELLE Collab.)
ABLIKIM 04G PR D70 092002 M. Ablikim et al. (BES Collab.)
BUETTIKER 04 EPJ C33 409 P. Buettiker, S. Descotes-Genon, B. Moussallam
PELAEZ 04A MPL A19 2879 J.R. Pelaez (MADU)
ANISOVICH 03 EPJ A16 229 V.V. Anisovich et al.
TIKHOMIROV 03 PAN 66 828 G.D. Tikhomirov et al.
Translated from YAF 66 860.
ALOISIO 02D PL B537 21 A. Aloisio et al. (KLOE Collab.)
ANISOVICH 02D PAN 65 1545 V.V. Anisovich et al.
Translated from YAF 65 1583.
BRAMON 02 EPJ C26 253 A. Bramon et al.
ACHASOV 01F PR D63 094007 N.N. Achasov, V.V. Gubin (Novosibirsk SND Collab.)
AITALA 01A PRL 86 765 E.M. Aitala et al. (FNAL E791 Collab.)
AITALA 01B PRL 86 770 E.M. Aitala et al. (FNAL E791 Collab.)
ACHASOV 00H PL B485 349 M.N. Achasov et al. (Novosibirsk SND Collab.)
AKHMETSHIN 99B PL B462 371 R.R. Akhmetshin et al. (Novosibirsk CMD-2 Collab.)
AKHMETSHIN 99C PL B462 380 R.R. Akhmetshin et al. (Novosibirsk CMD-2 Collab.)
BARBERIS 99 PL B453 305 D. Barberis et al. (Omega Expt.)
BARBERIS 99B PL B453 316 D. Barberis et al. (Omega Expt.)
BARBERIS 99C PL B453 325 D. Barberis et al. (Omega Expt.)
BARBERIS 99D PL B462 462 D. Barberis et al. (Omega Expt.)
BELLAZZINI 99 PL B467 296 R. Bellazzini et al.
BOGLIONE 99 EPJ C9 11 M. Boglione, M.R. Pennington
KAMINSKI 99 EPJ C9 141 R. Kaminski, L. Lesniak, B. Loiseau (CRAC, PARIN)
OLLER 99 PR D60 099906 (erratum) J.A. Oller et al.
OLLER 99B NP A652 407 (erratum) J.A. Oller, E. Oset
OLLER 99C PR D60 074023 J.A. Oller, E. Oset
ACHASOV 98I PL B440 442 M.N. Achasov et al.
ACKERSTAFF 98Q EPJ C4 19 K. Ackerstaff et al. (OPAL Collab.)
ALDE 98 EPJ A3 361 D. Alde et al. (GAM4 Collab.)
Also PAN 62 405 D. Alde et al. (GAMS Collab.)
Translated from YAF 62 446.
ANISOVICH 98B SPU 41 419 V.V. Anisovich et al.
Translated from UFN 168 481.
LOCHER 98 EPJ C4 317 M.P. Locher et al. (PSI)
ALDE 97 PL B397 350 D.M. Alde et al. (GAMS Collab.)
BERTIN 97C PL B408 476 A. Bertin et al. (OBELIX Collab.)
ISHIDA 96 PTP 95 745 S. Ishida et al. (TOKY, MIYA, KEK)
TORNQVIST 96 PRL 76 1575 N.A. Tornqvist, M. Roos (HELS)
ALDE 95B ZPHY C66 375 D.M. Alde et al. (GAMS Collab.)
AMSLER 95B PL B342 433 C. Amsler et al. (Crystal Barrel Collab.)
AMSLER 95D PL B355 425 C. Amsler et al. (Crystal Barrel Collab.)
ANISOVICH 95 PL B355 363 V.V. Anisovich et al. (PNPI, SERP)
JANSSEN 95 PR D52 2690 G. Janssen et al. (STON, ADLD, JULI)
AMSLER 94D PL B333 277 C. Amsler et al. (Crystal Barrel Collab.)
ANISOVICH 94 PL B323 233 V.V. Anisovich et al. (Crystal Barrel Collab.)
BUGG 94 PR D50 4412 D.V. Bugg et al. (LOQM)
KAMINSKI 94 PR D50 3145 R. Kaminski, L. Lesniak, J.P. Maillet (CRAC+)
ZOU 94B PR D50 591 B.S. Zou, D.V. Bugg (LOQM)
MORGAN 93 PR D48 1185 D. Morgan, M.R. Pennington (RAL, DURH)
BEHREND 92 ZPHY C56 381 H.J. Behrend (CELLO Collab.)
AGUILAR-... 91 ZPHY C50 405 M. Aguilar-Benitez et al. (LEBC-EHS Collab.)
ARMSTRONG 91 ZPHY C51 351 T.A. Armstrong et al. (ATHU, BARI, BIRM+)
BOYER 90 PR D42 1350 J. Boyer et al. (Mark II Collab.)
BREAKSTONE 90 ZPHY C48 569 A.M. Breakstone et al. (ISU, BGNA, CERN+)
MARSISKE 90 PR D41 3324 H. Marsiske et al. (Crystal Ball Collab.)
MORGAN 90 ZPHY C48 623 D. Morgan, M.R. Pennington (RAL, DURH)
OEST 90 ZPHY C47 343 T. Oest et al. (JADE Collab.)
ACHASOV 89 NP B315 465 N.N. Achasov, V.N. Ivanchenko
AUGUSTIN 89 NP B320 1 J.E. Augustin, G. Cosme (DM2 Collab.)
VOROBYEV 88 SJNP 48 273 P.V. Vorobiev et al. (NOVO)
Translated from YAF 48 436.
ABACHI 86B PRL 57 1990 S. Abachi et al. (PURD, ANL, IND, MICH+)
LONGACRE 86 PL B177 223 R.S. Longacre et al. (BNL, BRAN, CUNY+)
BINON 84C NC 80A 363 F.G. Binon et al. (BELG, LAPP, SERP+)
BINON 83 NC 78A 313 F.G. Binon et al. (BELG, LAPP, SERP+)
ETKIN 82B PR D25 1786 A. Etkin et al. (BNL, CUNY, TUFTS, VAND)
GIDAL 81 PL 107B 153 G. Gidal et al. (SLAC, LBL)
ACHASOV 80 SJNP 32 566 N.N. Achasov, S.A. Devyanin, G.N. Shestakov (NOVM)
Translated from YAF 32 1098.

Downloaded from https://academic.oup.com/ptep/article/2022/8/083C01/6651666 by KIT Library user on 27 September 2022

COHEN	80	PR D22 2595	D. Cohen *et al.*	(ANL) IJP
LOVERRE	80	ZPHY C6 187	P.F. Loverre *et al.*	(CERN, CDEF, MADR+) IJP
AGUILAR-...	78	NP B140 73	M. Aguilar-Benitez *et al.*	(MADR, BOMB+)
CASON	78	PRL 41 271	N.M. Cason *et al.*	(NDAM, ANL)
LEEPER	77	PR D16 2054	R.J. Leeper *et al.*	(ISU)
ROSSELET	77	PR D15 574	L. Rosselet *et al.*	(GEVA, SACL)
FLATTE	76	PL 63B 224	S.M. Flatte	(CERN)
WETZEL	76	NP B115 208	W. Wetzel *et al.*	(ETH, CERN, LOIC)
HYAMS	75	NP B100 205	B.D. Hyams *et al.*	(CERN, MPIM)
SRINIVASAN	75	PR D12 681	V. Srinivasan *et al.*	(NDAM, ANL)
ESTABROOKS	74	NP B79 301	P.G. Estabrooks, A.D. Martin	(DURH)
GRAYER	74	NP B75 189	G. Grayer *et al.*	(CERN, MPIM)
BINNIE	73	PRL 31 1534	D.M. Binnie *et al.*	(LOIC, SHMP)
GRAYER	73	Tallahassee	G. Grayer *et al.*	(CERN, MPIM)
HYAMS	73	NP B64 134	B.D. Hyams *et al.*	(CERN, MPIM)
PROTOPOP...	73	PR D7 1279	S.D. Protopopescu *et al.*	(LBL)

$a_0(980)$

$I^G(J^{PC}) = 1^-(0^{++})$

See the related review(s):
Scalar Mesons below 1 GeV

$a_0(980)$ T-MATRIX POLE $\sqrt{s}$

VALUE (MeV)	DOCUMENT ID		TECN	COMMENT
(960–1030) − i (20–70) OUR ESTIMATE (see Fig. 64.2 in the review)				
• • • We do not use the following data for averages, fits, limits, etc. • • •				
$(989 \pm 5) - i(40 \pm 5)$	[1] BUGG	08A	RVUE	$\overline{p}p$ annihilation data
$(1117^{+24}_{-320}) - i(12^{+43}_{-12})$	[2] PELAEZ	04A	RVUE	$\pi\pi \to \pi\pi, \pi K \to \pi K$
$(982 \pm 3) - i(46 \pm 4)$	[3] ABELE	98	CBAR	$0.0\ \overline{p}p \to K^0_L K^\pm \pi^\mp$

[1] T-matrix pole on sheet II. Parameterizes couplings to $\overline{K}K$, $\pi\eta$, and $\pi\eta'$. Uses AMSLER 94D and ABELE 98.
[2] Reanalysis of data from LINGLIN 73, ESTABROOKS 78, and ASTON 88 in the unitarized ChPT model.
[3] T-matrix pole on sheet II; the pole on sheet III is at $(1006 - i\ 49)$ MeV.

$a_0(980)$ MASS

VALUE (MeV)	DOCUMENT ID		TECN	COMMENT
980 ±20 OUR ESTIMATE Mass determination very model dependent				
• • • We do not use the following data for averages, fits, limits, etc. • • •				
$1000.7^{+12.9}_{-0.7}$	[1] LU	20	RVUE	$\gamma\gamma \to \pi^0\eta,\ K^0_S K^0_S$

[1] T-matrix pole on sheet II.

$\eta\pi$ FINAL STATE ONLY

VALUE (MeV)	EVTS	DOCUMENT ID		TECN	CHG	COMMENT
• • • We do not use the following data for averages, fits, limits, etc. • • •						
1004.1 ± 1.5 ±6.5		[1] ALBRECHT	20	CBAR		$0.9\ \overline{p}p \to \pi^0\pi^0\eta$, $\pi^0\eta\eta$, $\pi^0 K^+ K^-$
982.5 ± 1.6 ±1.1	16.9k	[2] AMBROSINO	09F	KLOE		$1.02\ e^+e^- \to \eta\pi^0\gamma$
986 ± 4		ANISOVICH	09	RVUE		$0.0\ \overline{p}p, \pi N$
$982.3^{+0.6}_{-0.7}\ ^{+3.1}_{-4.7}$		[3] UEHARA	09A	BELL		$\gamma\gamma \to \pi^0\eta$
985 ± 4 ±6	318	ACHARD	02B	L3		183–209 $e^+e^- \to e^+e^-\eta\pi^+\pi^-$
$995\ ^{+52}_{-10}$	36	[4] ACHASOV	00F	SND		$e^+e^- \to \eta\pi^0\gamma$
$994\ ^{+33}_{-8}$	36	[5] ACHASOV	00F	SND		$e^+e^- \to \eta\pi^0\gamma$
975 ± 7		BARBERIS	00H			$450\ pp \to p_f\eta\pi^0 p_s$
988 ± 8		BARBERIS	00H			$450\ pp \to \Delta^{++}_f\eta\pi^- p_s$
~ 1055		[6] OLLER	99	RVUE		$\eta\pi, K\overline{K}$
~ 1009.2		[6] OLLER	99B	RVUE		$\pi\pi \to \pi\pi, K\overline{K}$
993.1 ± 2.1		[7] TEIGE	99	B852		$18.3\ \pi^-p \to \eta\pi^+\pi^-n$
988 ± 6		[6] ANISOVICH	98B	RVUE		Compilation
987		TORNQVIST	96	RVUE		$\pi\pi \to \pi\pi, K\overline{K}, K\pi, \eta\pi$
991		JANSSEN	95	RVUE		$\eta\pi \to \eta\pi, K\overline{K}, K\pi, \eta\pi$
984.45 ± 1.23 ±0.34		AMSLER	94C	CBAR		$0.0\ \overline{p}p \to \omega\eta\pi^0$
982 ± 2		[8] AMSLER	92	CBAR		$0.0\ \overline{p}p \to \eta\eta\pi^0$
984 ± 4	1040	[8] ARMSTRONG	91B	OMEG ±		$300\ pp \to pp\eta\pi^+\pi^-$
976 ± 6		ATKINSON	84E	OMEG ±		25–55 $\gamma p \to \eta\pi n$
986 ± 3	500	[9] EVANGELIS...	81	OMEG ±		$12\ \pi^-p \to \eta\pi^+\pi^-\pi^-p$
990 ± 7	145	[9] GURTU	79	HBC ±		$4.2\ K^-p \to \Lambda\eta 2\pi$
980 ±11	47	CONFORTO	78	OSPK −		$4.5\ \pi^-p \to pX^-$
978 ±16	50	CORDEN	78	OMEG ±		12–15 $\pi^-p \to n\eta 2\pi$
977 ± 7		GRASSLER	77	HBC −		$16\ \pi^\mp p \to p\eta 3\pi$
989 ± 4	70	WELLS	75	HBC −		3.1–6 $K^-p \to \Lambda\eta 2\pi$
972 ±10	150	DEFOIX	72	HBC ±		$0.7\ \overline{p}p \to 7\pi$
970 ±15	20	BARNES	69C	HBC −		4–5 $K^-p \to \Lambda\eta 2\pi$
980 ±10		CAMPBELL	69	DBC ±		$2.7\ \pi^+d$
980 ±10	15	MILLER	69B	HBC −		$4.5\ K^-N \to \eta\pi\Lambda$
980 ±10	30	AMMAR	68	HBC ±		$5.5\ K^-p \to \Lambda\eta 2\pi$

[1] T-matrix pole with 2 poles, 2 channels, pole mass on adjacent sheet $1002.4 \pm 1.4 \pm 6.6$ MeV.
[2] Using the model of ACHASOV 89 and ACHASOV 03B.
[3] From a fit with the S-wave amplitude including two interfering Breit-Wigners plus a background term.
[4] Using the model of ACHASOV 89. Supersedes ACHASOV 98B.
[5] Using the model of JAFFE 77. Supersedes ACHASOV 98B.
[6] T-matrix pole.
[7] Breit-Wigner fit, average between $a_0^\pm$ and a_0^0. The fit favors a slightly heavier $a_0^\pm$.
[8] From a single Breit-Wigner fit.
[9] From $f_1(1285)$ decay.

$K\overline{K}$ ONLY

VALUE (MeV)	EVTS	DOCUMENT ID		TECN	COMMENT
• • • We do not use the following data for averages, fits, limits, etc. • • •					
$947.7^{+5.5}_{-5.0} \pm 6.6$		[1] AAIJ	19H	LHCB	$pp \to D^\pm X$
925 ± 5 ±8	190k	[2] AAIJ	16N	LHCB	$D^0 \to K^0_S K^\pm \pi^\mp$
~ 1053		[3] OLLER	99C	RVUE	$\pi\pi \to \pi\pi, K\overline{K}$
975 ±15		BERTIN	98B	OBLX	$0.0\ \overline{p}p \to K^\pm K_S \pi^\mp$
970 ±10	316	DEBILLY	80	HBC	1.2–2 $\overline{p}p \to f_1(1285)\omega$
1016 ±10	100	[4] ASTIER	67	HBC	$0.0\ \overline{p}p$
1003.3 ± 7.0	143	[5,6] ROSENFELD	65	RVUE	

[1] From the $D^\pm \to K^\pm K^+ K^-$ Dalitz plot fit with the Triple-M amplitude in the multi-meson model of AOUDE 18.
[2] Using a two-channel resonance parametrization with couplings fixed to ABELE 98.
[3] T-matrix pole.
[4] ASTIER 67 includes data of BARLOW 67, CONFORTO 67, ARMENTEROS 65.
[5] Note on J^P. Main argument for 0^+ is small Q value. Isotropy of decay distribution in $\overline{p}p$ at rest proves nothing. See discussion by Rosenfeld (Oxford) and Butterworth (Heidelberg).
[6] Plus systematic errors.

$a_0(980)$ WIDTH

VALUE (MeV)	EVTS	DOCUMENT ID		TECN	CHG	COMMENT
50 to 100 OUR ESTIMATE Width determination very model dependent. Peak width in $\eta\pi$ is about 60 MeV, but decay width can be much larger.						
• • • We do not use the following data for averages, fits, limits, etc. • • •						
97.2 ± 1.9 ± 5.7		[1] ALBRECHT	20	CBAR		$0.9\ \overline{p}p \to \pi^0\pi^0\eta$, $\pi^0\eta\eta$, $\pi^0 K^+ K^-$
$73.2\ ^{+25.4}_{-5.2}$		[2] LU	20	RVUE		$\gamma\gamma \to \pi^0\eta,\ K^0_S K^0_S$
$75.6 \pm 1.6\ ^{+17.4}_{-10.0}$		[3] UEHARA	09A	BELL		$\gamma\gamma \to \pi^0\eta$
50 ±13 ± 4	318	ACHARD	02B	L3		183–209 $e^+e^- \to e^+e^-\eta\pi^+\pi^-$
72 ±16		BARBERIS	00H			$450\ pp \to p_f\eta\pi^0 p_s$
61 ±19		BARBERIS	00H			$450\ pp \to \Delta^{++}_f\eta\pi^- p_s$
~ 42		[4] OLLER	99	RVUE		$\eta\pi, K\overline{K}$
~ 112		[4] OLLER	99B	RVUE		$\pi\pi \to \eta\pi, K\overline{K}$
71 ± 7		TEIGE	99	B852		$18.3\ \pi^-p \to \eta\pi^+\pi^-n$
92 ±20		[4] ANISOVICH	98B	RVUE		Compilation
65 ±10		[5] BERTIN	98B	OBLX ±		$0.0\ \overline{p}p \to K^\pm K_S \pi^\mp$
~ 100		TORNQVIST	96	RVUE		$\pi\pi \to \pi\pi, K\overline{K}, K\pi, \eta\pi$
202		JANSSEN	95	RVUE		$\eta\pi \to \eta\pi, K\overline{K}, K\pi, \eta\pi$
54.12 ± 0.34 ± 0.12		AMSLER	94C	CBAR		$0.0\ \overline{p}p \to \omega\eta\pi^0$
54 ±10		[6] AMSLER	92	CBAR		$0.0\ \overline{p}p \to \eta\eta\pi^0$
95 ±14	1040	[6] ARMSTRONG	91B	OMEG ±		$300\ pp \to pp\eta\pi^+\pi^-$
62 ±15	500	[7] EVANGELIS...	81	OMEG ±		$12\ \pi^-p \to \eta\pi^+\pi^-\pi^-p$
60 ±20	145	[7] GURTU	79	HBC ±		$4.2\ K^-p \to \Lambda\eta 2\pi$
$60\ ^{+50}_{-30}$	47	CONFORTO	78	OSPK −		$4.5\ \pi^-p \to pX^-$
$86.0\ ^{+60.0}_{-50.0}$	50	CORDEN	78	OMEG ±		12–15 $\pi^-p \to n\eta 2\pi$
44 ±22		GRASSLER	77	HBC −		$16\ \pi^\mp p \to p\eta 3\pi$
80 to 300		[8] FLATTE	76	RVUE −		$4.2\ K^-p \to \Lambda\eta 2\pi$
$16.0\ ^{+25.0}_{-16.0}$	70	[9] WELLS	75	HBC −		3.1–6 $K^-p \to \Lambda\eta 2\pi$
30 ± 5	150	[10] DEFOIX	72	HBC ±		$0.7\ \overline{p}p \to 7\pi$
40 ±15		CAMPBELL	69	DBC ±		$2.7\ \pi^+d$
60 ±30	15	MILLER	69B	HBC −		$4.5\ K^-N \to \eta\pi\Lambda$
80 ±30	30	AMMAR	68	HBC ±		$5.5\ K^-p \to \Lambda\eta 2\pi$

[1] T-matrix pole with 2 poles, 2 channels, pole width on adjacent sheet $127.0 \pm 2.3 \pm 6.7$ MeV.
[2] T-matrix pole on sheet II.
[3] From a fit with the S-wave amplitude including two interfering Breit-Wigners plus a background term.
[4] T-matrix pole.
[5] The $\eta\pi$ width.
[6] From a single Breit-Wigner fit.
[7] From $f_1(1285)$ decay.
[8] Using a two-channel resonance parametrization of GAY 76B data.
[9] Weak evidence only for $a_0(980)^+$ production.
[10] This number has very little meaning. Error is much too small. Vlada

Downloaded from https://academic.oup.com/ptep/article/2022/8/083C01/6651666 by KIT Library user on 27 September 2022

$K\overline{K}$ ONLY

VALUE (MeV)	EVTS	DOCUMENT ID		TECN	CHG	COMMENT
• • • We do not use the following data for averages, fits, limits, etc. • • •						
~ 48		[1] OLLER	99C	RVUE		$\pi\pi \to \pi\pi$, $K\overline{K}$
~ 25	100	[2] ASTIER	67	HBC	±	
57±13	143	[3] ROSENFELD	65	RVUE	±	

[1] T-matrix pole.
[2] ASTIER 67 includes data of BARLOW 67, CONFORTO 67, ARMENTEROS 65.
[3] Plus systematic errors.

$a_0(980)$ DECAY MODES

	Mode	Fraction (Γ_i/Γ)
Γ_1	$\eta\pi$	seen
Γ_2	$K\overline{K}$	seen
Γ_3	$\eta'\pi$	seen
Γ_4	$\rho\pi$	not seen
Γ_5	$\gamma\gamma$	seen
Γ_6	e^+e^-	

$a_0(980)$ PARTIAL WIDTHS

$\Gamma(\gamma\gamma)$ — Γ_5

VALUE (keV)	DOCUMENT ID		TECN
• • • We do not use the following data for averages, fits, limits, etc. • • •			
0.30±0.10	[1] AMSLER	98	RVUE

[1] Using $\Gamma_{\gamma\gamma}B(a0(980) \to \eta\pi)$ =0.24 ± 0.08 keV.

$a_0(980)$ $\Gamma(i)\Gamma(\gamma\gamma)/\Gamma(\text{total})$

$\Gamma(\eta\pi) \times \Gamma(\gamma\gamma)/\Gamma_{\text{total}}$ — $\Gamma_1\Gamma_5/\Gamma$

VALUE (keV)	EVTS	DOCUMENT ID		TECN	COMMENT
0.21 $^{+0.08}_{-0.04}$ OUR AVERAGE					
$0.128^{+0.003}_{-0.002}{}^{+0.502}_{-0.043}$		[1] UEHARA	09A	BELL	$\gamma\gamma \to \pi^0\eta$
0.28 ±0.04 ±0.10	44	OEST	90	JADE	$e^+e^- \to e^+e^-\pi^0\eta$
0.19 ±0.07 $^{+0.10}_{-0.07}$		ANTREASYAN	86	CBAL	$e^+e^- \to e^+e^-\pi^0\eta$

[1] From a fit with the S-wave amplitude including two interfering Breit-Wigners plus a background term.

$\Gamma(\eta\pi) \times \Gamma(e^+e^-)/\Gamma_{\text{total}}$ — $\Gamma_1\Gamma_6/\Gamma$

VALUE (eV)	CL%	DOCUMENT ID		TECN	COMMENT
<1.5	90	VOROBYEV	88	ND	$e^+e^- \to \pi^0\eta$

$a_0(980)$ BRANCHING RATIOS

$\Gamma(K\overline{K})/\Gamma(\eta\pi)$ — Γ_2/Γ_1

VALUE	DOCUMENT ID		TECN	CHG	COMMENT
0.177±0.024 OUR AVERAGE Error includes scale factor of 1.2.					
0.23 ±0.05	[1] ABELE	98	CBAR		0.0 $\overline{p}p \to K^0_L K^\pm\pi^\mp$
0.166±0.01 ±0.02	[2] BARBERIS	98C	OMEG		450 $pp \to p_f f_1(1285) p_s$
• • • We do not use the following data for averages, fits, limits, etc. • • •					
0.138±0.001±0.035	[3] ALBRECHT	20	CBAR		0.9 $\overline{p}p \to \pi^0\pi^0\eta$, $\pi^0\eta\eta$, $\pi^0K^+K^-$
1.20 ±0.15	[4] ANISOVICH	09	RVUE		0.0 $\overline{p}p$, πN
1.05 ±0.07 ±0.05	[5] BUGG	08A	RVUE	0	$\overline{p}p \to \pi^0\pi^0\eta$
0.57 ±0.16	[6] BARGIOTTI	03	OBLX		$\overline{p}p$
~ 0.60	OLLER	99B	RVUE		$\pi\pi \to \eta\eta$, $K\overline{K}$
0.7 ±0.3	[2] CORDEN	78	OMEG		12–15 $\pi^-p \to n\eta 2\pi$
0.25 ±0.08	[2] DEFOIX	72	HBC	±	0.7 $\overline{p} \to 7\pi$

[1] Using $\pi^0\pi^0\eta$ from AMSLER 94D.
[2] From the decay of $f_1(1285)$.
[3] Residues from T-matrix pole with 2 poles, 2 channels. Solution on adjacent sheet 0.149 ± 0.001 ± 0.039.
[4] This is a ratio of couplings.
[5] A ratio of couplings, using AMSLER 94D and ABELE 98. Supersedes BUGG 94.
[6] Coupled channel analysis of $\pi^+\pi^-\pi^0$, $K^+K^-\pi^0$, and $K^\pm K^0_S\pi^\mp$.

$\Gamma(\eta'\pi)/\Gamma_{\text{total}}$ — Γ_3/Γ

VALUE	EVTS	DOCUMENT ID		TECN	COMMENT
seen	116k	[1] CHEN	20A	BELL	$D^0 \to K^-\pi^+\eta$

[1] From an amplitude analysis of the $D^0 \to K^-\pi^+\eta$ decay in a three-channel Flatte model with a 10.1 σ significance. Earlier observed by ABLIKIM 17K in the $\chi_{c1} \to \eta\pi^+\pi^-$ decay with a 8.9 σ significance.

$\Gamma(\rho\pi)/\Gamma(\eta\pi)$ — Γ_4/Γ_1

$\rho\pi$ forbidden.

VALUE	CL%	DOCUMENT ID		TECN	CHG	COMMENT
• • • We do not use the following data for averages, fits, limits, etc. • • •						
<0.25	70	[1] AMMAR	70	HBC	±	4.1,5.5 $K^-p \to \Lambda\eta 2\pi$

[1] Not clear if they really observed the $a_0(980)$ 3 standard deviations.

$a_0(980)$ REFERENCES

ALBRECHT	20	EPJ C80 453	M. Albrecht et al.	(Crystal Barrel Collab.)
CHEN	20A	PR D102 012002	Y.Q. Chen et al.	(BELLE Collab.)
LU	20	EPJ C80 436	J. Lu, B. Moussallam	
AAIJ	19H	JHEP 1904 063	R. Aaij et al.	(LHCb Collab.)
AOUDE	18	PR D98 056021	R.T. Aoude et al.	
ABLIKIM	17K	PR D95 032002	M. Ablikim et al.	(BESIII Collab.)
AAIJ	16N	PR D93 052018	R. Aaij et al.	(LHCb Collab.)
AMBROSINO	09F	PL B681 5	F. Ambrosino et al.	(KLOE Collab.)
ANISOVICH	09	IJMP A24 2481	V.V. Anisovich, A.V. Sarantsev	
UEHARA	09A	PR D80 032001	S. Uehara et al.	(BELLE Collab.)
BUGG	08A	PR D78 074023	D.V. Bugg	(LOQM)
PELAEZ	04A	MPL A19 2879	J.R. Pelaez	(MADU)
ACHASOV	03B	PR D68 014006	N.N. Achsaov, A.V. Kiselev	
BARGIOTTI	03	EPJ C26 371	M. Bargiotti et al.	(OBELIX Collab.)
ACHARD	02B	PL B526 269	P. Achard et al.	(L3 Collab.)
ACHASOV	00F	PL B479 53	M.N. Achasov et al.	(Novosibirsk SND Collab.)
BARBERIS	00H	PL B488 225	D. Barberis et al.	(WA 102 Collab.)
OLLER	99	PR D60 099906 (erratum)	J.A. Oller et al.	
OLLER	99B	NP A652 407 (erratum)	J.A. Oller, E. Oset	
OLLER	99C	PR D60 074023	J.A. Oller, E. Oset	
TEIGE	99	PR D59 012001	S. Teige et al.	(BNL E852 Collab.)
ABELE	98	PR D57 3860	A. Abele et al.	(Crystal Barrel Collab.)
ACHASOV	98B	PL B438 441	M.N. Achasov et al.	(Novosibirsk SND Collab.)
AMSLER	98	RMP 70 1293	C. Amsler	
ANISOVICH	98B	SPU 41 419	V.V. Anisovich et al.	
		Translated from UFN 168 481.		
BARBERIS	98C	PL B440 225	D. Barberis et al.	(WA 102 Collab.)
BERTIN	98B	PL B434 180	A. Bertin et al.	(OBELIX Collab.)
TORNQVIST	96	PRL 76 1575	N.A. Tornqvist, M. Roos	(HELS)
JANSSEN	95	PR D52 2690	G. Janssen et al.	(STON, ADLD, JULI)
AMSLER	94C	PL B327 425	C. Amsler et al.	(Crystal Barrel Collab.)
AMSLER	94D	PL B333 277	C. Amsler et al.	(Crystal Barrel Collab.)
BUGG	94	PR D50 4412	D.V. Bugg et al.	(LOQM)
AMSLER	92	PL B291 347	C. Amsler et al.	(Crystal Barrel Collab.)
ARMSTRONG	91B	ZPHY C52 389	T.A. Armstrong et al.	(ATHU, BARI, BIRM+)
OEST	90	ZPHY C47 343	T. Oest et al.	(JADE Collab.)
ACHASOV	89	NP B315 465	N.N. Achasov, V.N. Ivanchenko	
ASTON	88	NP B296 493	D. Aston et al.	(SLAC, NAGO, CINC, INUS)
VOROBYEV	88	SJNP 48 273	P.V. Vorobiev et al.	(NOVO)
		Translated from YAF 48 436.		
ANTREASYAN	86	PR D33 1847	D. Antreasyan et al.	(Crystal Ball Collab.)
ATKINSON	84E	PL 138B 459	M. Atkinson et al.	(BONN, CERN, GLAS+)
EVANGELIS...	81	NP B178 197	C. Evangelista et al.	(BARI, BONN, CERN+)
DEBILLY	80	NP B176 1	L. de Billy et al.	(CURIN, LAUS, NEUC+)
GURTU	79	NP B151 181	A. Gurtu et al.	(CERN, ZEEM, NIJM, OXF)
CONFORTO	78	LNC 23 419	B. Conforto et al.	(RHEL, TNTO, CHIC+)
CORDEN	78	NP B144 253	M.J. Corden et al.	(BIRM, RHEL, TELA+)
ESTABROOKS	78	NP B133 490	P.G. Estabrooks et al.	(MCGI, CARL, DURH+)
GRASSLER	77	NP B121 189	H. Grassler et al.	(AACH3, BERL, BONN+)
JAFFE	77	PR D15 267,281	R. Jaffe	(MIT)
FLATTE	76	PL 63B 224	S.M. Flatte	(CERN)
GAY	76B	PL 63B 220	J.B. Gay et al.	(CERN, AMST, NIJM) JP
WELLS	75	NP B101 333	J. Wells et al.	(OXF)
LINGLIN	73	NP B55 408	D. Linglin	(CERN)
DEFOIX	72	NP B44 125	C. Defoix et al.	(CDEF, CERN)
AMMAR	70	PR D2 430	R. Ammar et al.	(KANS, NWES, ANL, WISC)
BARNES	69C	PRL 23 610	V.E. Barnes et al.	(BNL, SYRA)
CAMPBELL	69	PRL 22 1204	J.H. Campbell et al.	(PURD)
MILLER	69B	PL 29B 255	D.H. Miller et al.	(PURD)
Also		PR 188 2011	W.L. Yen et al.	(PURD)
AMMAR	68	PRL 21 1832	R. Ammar et al.	(NWES, ANL)
ASTIER	67	PL 25B 294	A. Astier et al.	(CDEF, CERN, IRAD)
Includes data of BARLOW 67, CONFORTO 67, and ARMENTEROS 65.				
BARLOW	67	NC 50A 701	J. Barlow et al.	(CERN, CDEF, IRAD, LIVP)
CONFORTO	67	NP B3 469	G. Conforto et al.	(CERN, CDEF, IPNP+)
ARMENTEROS	65	PL 17 344	R. Armenteros et al.	(CERN, CDEF)
ROSENFELD	65	Oxford Conf. 58	A.H. Rosenfeld	(LRL)

$\phi(1020)$

$I^G(J^{PC}) = 0^-(1^{--})$

$\phi(1020)$ MASS

VALUE (MeV)	EVTS	DOCUMENT ID		TECN	COMMENT
1019.461±0.016 OUR AVERAGE					
1019.463±0.061	2.3M	[1] KOZYREV	18	CMD3	$e^+e^- \to K^+K^-$, $K^0_S K^0_L$
1019.462±0.042±0.056	28k	[2] LEES	14H	BABR	$e^+e^- \to K^0_S K^0_L \gamma$
1019.51 ±0.02 ±0.05		[3] LEES	13Q	BABR	$e^+e^- \to K^+K^-\gamma$
1019.30 ±0.02 ±0.10	105k	AKHMETSHIN	06	CMD2	0.98–1.06 $e^+e^- \to \pi^+\pi^-\pi^0$
1019.52 ±0.05 ±0.05	17.4k	AKHMETSHIN	05	CMD2	0.60-1.38 $e^+e^- \to \eta\gamma$
1019.483±0.011±0.025	272k	[4] AKHMETSHIN	04	CMD2	$e^+e^- \to K^0_L K^0_S$
1019.42 ±0.05	1900k	[5] ACHASOV	01E	SND	$e^+e^- \to K^+K^-$, $K_S K_L$, $\pi^+\pi^-\pi^0$
1019.40 ±0.04 ±0.05	23k	AKHMETSHIN	01B	CMD2	$e^+e^- \to \eta\gamma$
1019.36 ±0.12		[6] ACHASOV	00B	SND	$e^+e^- \to \eta\gamma$
1019.38 ±0.07 ±0.08	2200	[7] AKHMETSHIN	99F	CMD2	$e^+e^- \to \pi^+\pi^- \geq 2\gamma$
1019.51 ±0.07 ±0.10	11169	AKHMETSHIN	98	CMD2	$e^+e^- \to \pi^+\pi^-\pi^0$
1019.5 ±0.4		BARBERIS	98	OMEG	450 $pp \to pp2K^+2K^-$
1019.42 ±0.06	55600	AKHMETSHIN	95	CMD2	$e^+e^- \to$ hadrons
1019.7 ±0.3	2012	DAVENPORT	86	MPSF	400 $pA \to 4KX$
1019.7 ±0.1 ±0.1	5079	ALBRECHT	85D	ARG	10 $e^+e^- \to K^+K^-X$
1019.3 ±0.1	1500	ARENTON	82	AEMS	11.8 polar. $pp \to KK$
1019.67 ±0.17	25080	[8] PELLINEN	82	RVUE	
1019.52 ±0.13	3681	BUKIN	78C	OLYA	$e^+e^- \to$ hadrons
• • • We do not use the following data for averages, fits, limits, etc. • • •					
1018.4 ±0.5 ±0.1		[9] ALBRECHT	20	CBAR	0.9 $\overline{p}p \to K^+K^-\pi^0$

Downloaded from https://academic.oup.com/ptep/article/2022/8/083C01/6651666 by KIT Library user on 27 September 2022

1019.21 ±0.04 ±0.03			[10] HOID	20	RVUE $e^+e^- \to \pi^0\gamma$
1019.54 ±0.10 ±0.51			[11] AAIJ	19H	LHCB $pp \to D^\pm X$
1019.20 ±0.02 ±0.01			[12] HOFERICHT...	19	RVUE $e^+e^- \to \pi^+\pi^-\pi^0$
1019.469±0.061	1.7M		KOZYREV	18	CMD3 $e^+e^- \to K^+K^-$
1019.457±0.061	610k		KOZYREV	16	CMD3 $e^+e^- \to K^0_S K^0_L$
1019.48 ±0.01			LEES	13F	BABR $D^+ \to K^+K^-\pi^+$
1019.441±0.008±0.080	542k		[13] AKHMETSHIN	08	CMD2 1.02 $e^+e^- \to K^+K^-$
1019.63 ±0.07	12540		[14] AUBERT,B	05J	BABR $D^0 \to \overline{K}^0 K^+K^-$
1019.8 ±0.7			ARMSTRONG	86	OMEG 85 $\pi^+/pp \to \pi^+/p4Kp$
1020.1 ±0.11	5526		[14] ATKINSON	86	OMEG 20–70 γp
1019.7 ±1.0			BEBEK	86	CLEO $e^+e^- \to \Upsilon(4S)$
1019.411±0.008	642k		[15] DIJKSTRA	86	SPEC 100–200 $\pi^\pm$, $\overline{p}$, p, $K^\pm$, on Be
1020.9 ±0.2			[14] FRAME	86	OMEG 13 $K^+p \to \phi K^+p$
1021.0 ±0.2			[14] ARMSTRONG	83B	OMEG 18.5 $K^-p \to K^-K^+\Lambda$
1020.0 ±0.5			[14] ARMSTRONG	83B	OMEG 18.5 $K^-p \to K^-K^+\Lambda$
1019.7 ±0.3			[14] BARATE	83	GOLI 190 π^-Be $\to 2\mu$X
1019.8 ±0.2 ±0.5	766		IVANOV	81	OLYA 1–1.4 $e^+e^- \to K^+K^-$
1019.4 ±0.5	337		COOPER	78B	HBC 0.7–0.8 $\overline{p}p \to K^0_S K^0_L \pi^+\pi^-$
1020 ±1	383		[14] BALDI	77	CNTR 10 $\pi^-p \to \pi^-\phi p$
1018.9 ±0.6	800		COHEN	77	ASPK 6 $\pi^\pm N \to K^+K^-N$
1019.7 ±0.5	454		KALBFLEISCH	76	HBC 2.18 $K^-p \to \Lambda K\overline{K}$
1019.4 ±0.8	984		BESCH	74	CNTR 2 $\gamma p \to pK^+K^-$
1020.3 ±0.4	100		BALLAM	73	HBC 2.8–9.3 γp
1019.4 ±0.7			BINNIE	73B	CNTR $\pi^-p \to \phi n$
1019.6 ±0.5	120		[16] AGUILAR-...	72B	HBC 3.9,4.6 $K^-p \to \Lambda K^+K^-$
1019.9 ±0.5	100		[16] AGUILAR-...	72B	HBC 3.9,4.6 $K^-p \to K^-pK^+K^-$
1020.4 ±0.5	131		COLLEY	72	HBC 10 $K^+p \to K^+p\phi$
1019.9 ±0.3	410		STOTTLE...	71	HBC 2.9 $K^-p \to \Sigma/\Lambda K\overline{K}$

[1] Average of KOZYREV 16 and KOZYREV 18 values taking into account the correlated uncertainties. Supersedes individual KOZYREV 16 and KOZYREV 18 results.
[2] Using a vector meson dominance model with contribution from $\phi(1020)$ and higher mass excitations of $\rho(770)$, $\omega(782)$, and $\phi(1020)$.
[3] Using a phenomenological model based on KUHN 90 with a sum of Breit-Wigner resonances for $\rho(770)$, $\omega(782)$, $\phi(1020)$ and their higher mass excitations.
[4] Update of AKHMETSHIN 99D
[5] From the combined fit assuming that the total $\phi(1020)$ production cross section is saturated by those of K^+K^-, K_SK_L, $\pi^+\pi^-\pi^0$, and $\eta\gamma$ decays modes and using ACHASOV 00B for the $\eta\gamma$ decay mode.
[6] Using a total width of 4.43 ± 0.05 MeV. Systematic uncertainty included.
[7] Using a total width of 4.43 ± 0.05 MeV.
[8] PELLINEN 82 review includes AKERLOF 77, DAUM 81, BALDI 77, AYRES 74, DEGROOT 74.
[9] Width fixed at 4.2 MeV.
[10] The values were extracted from a dispersively improved Breit-Wigner parameterization and do not include vacuum polarization. Inclusion of vacuum polarization gives 1019.457 ± 0.020 MeV.
[11] From the $D^\pm \to K^\pm K^+K^-$ Dalitz plot fit with the Triple-M amplitude in the multi-meson model of AOUDE 18.
[12] The values were extracted from a dispersively improved Breit-Wigner parameterization and do not include vacuum polarization.
[13] Strongly correlated with AKHMETSHIN 04.
[14] Systematic errors not evaluated.
[15] Weighted and scaled average of 12 measurements of DIJKSTRA 86.
[16] Mass errors enlarged by us to $\Gamma/\sqrt{N}$; see the note with the $K^*(892)$ mass.

$\phi(1020)$ WIDTH

VALUE (MeV)	EVTS	DOCUMENT ID		TECN	COMMENT
4.249±0.013 OUR AVERAGE		Error includes scale factor of 1.1.			
4.245±0.013	2.3M	[1] KOZYREV	18	CMD3	$e^+e^- \to K^+K^-$, $K^0_SK^0_L$
4.205±0.103±0.067	28k	[2] LEES	14H	BABR	$e^+e^- \to K^0_SK^0_L\gamma$
4.29 ±0.04 ±0.07		[3] LEES	13Q	BABR	$e^+e^- \to K^+K^-\gamma$
4.30 ±0.06 ±0.17	105k	AKHMETSHIN	06	CMD2	0.98–1.06 $e^+e^- \to \pi^+\pi^-\pi^0$
4.280±0.033±0.025	272k	[4] AKHMETSHIN	04	CMD2	$e^+e^- \to K^0_LK^0_S$
4.21 ±0.04	1900k	[5] ACHASOV	01E	SND	$e^+e^- \to K^+K^-$, K_SK_L, $\pi^+\pi^-\pi^0$
4.44 ±0.09	55600	AKHMETSHIN	95	CMD2	$e^+e^- \to$ hadrons
4.5 ±0.7	1500	ARENTON	82	AEMS	11.8 polar. $pp \to KK$
4.2 ±0.6	766	[6] IVANOV	81	OLYA	1–1.4 $e^+e^- \to K^+K^-$
4.3 ±0.6		[6] CORDIER	80	DM1	$e^+e^- \to \pi^+\pi^-\pi^0$
4.36 ±0.29	3681	[6] BUKIN	78C	OLYA	$e^+e^- \to$ hadrons
4.4 ±0.6	984	[6] BESCH	74	CNTR	2 $\gamma p \to pK^+K^-$
4.67 ±0.72	681	[6] BALAKIN	71	OSPK	$e^+e^- \to$ hadrons
4.09 ±0.29		BIZOT	70	OSPK	$e^+e^- \to$ hadrons
• • • We do not use the following data for averages, fits, limits, etc. • • •					
4.07 ±0.13 ±0.01		[7] HOID	20	RVUE	$e^+e^- \to \pi^0\gamma$
4.23 ±0.04 ±0.02		[8] HOFERICHT...	19	RVUE	$e^+e^- \to \pi^+\pi^-\pi^0$
4.249±0.015	1.7M	KOZYREV	18	CMD3	$e^+e^- \to K^+K^-$
4.240±0.017	610k	KOZYREV	16	CMD3	$e^+e^- \to K^0_SK^0_L$
4.37 ±0.02		LEES	13F	BABR	$D^+ \to K^+K^-\pi^+$
4.24 ±0.02 ±0.03	542k	[9] AKHMETSHIN	08	CMD2	1.02 $e^+e^- \to K^+K^-$
4.28 ±0.13	12540	[10] AUBERT,B	05J	BABR	$D^0 \to \overline{K}^0K^+K^-$
4.45 ±0.06	271k	DIJKSTRA	86	SPEC	100 π^-Be
3.6 ±0.8	337	[6] COOPER	78B	HBC	0.7–0.8 $\overline{p}p \to K^0_SK^0_L\pi^+\pi^-$
4.5 ±0.50	1300	[6,10] AKERLOF	77	SPEC	400 $pA \to K^+K^-X$
4.5 ±0.8	500	[6,10] AYRES	74	ASPK	3–6 $\pi^-p \to K^+K^-n$, $K^-p \to K^+K^-\Lambda/\Sigma^0$
3.81 ±0.37		COSME	74B	OSPK	$e^+e^- \to K^0_LK^0_S$
3.8 ±0.7	454	[6] BORENSTEIN	72	HBC	2.18 $K^-p \to K\overline{K}n$

[1] Average of KOZYREV 16 and KOZYREV 18 values taking into account the correlated uncertainties. Supersedes individual KOZYREV 16 and KOZYREV 18 results.
[2] Using a vector meson dominance model with contribution from $\phi(1020)$ and higher mass excitations of $\rho(770)$, $\omega(782)$, and $\phi(1020)$.
[3] Using a phenomenological model based on KUHN 90 with a sum of Breit-Wigner resonances for $\rho(770)$, $\omega(782)$, $\phi(1020)$ and their higher mass excitations.
[4] Update of AKHMETSHIN 99D
[5] From the combined fit assuming that the total $\phi(1020)$ production cross section is saturated by those of K^+K^-, K_SK_L, $\pi^+\pi^-\pi^0$, and $\eta\gamma$ decays modes and using ACHASOV 00B for the $\eta\gamma$ decay mode.
[6] Width errors enlarged by us to $4\Gamma/\sqrt{N}$; see the note with the $K^*(892)$ mass.
[7] The values were extracted from a dispersively improved Breit-Wigner parameterization.
[8] The values were extracted from a dispersively improved Breit-Wigner parameterization and do not include vacuum polarization.
[9] Strongly correlated with AKHMETSHIN 04.
[10] Systematic errors not evaluated.

$\phi(1020)$ DECAY MODES

	Mode	Fraction (Γ_i/Γ)	Scale factor/ Confidence level
Γ_1	K^+K^-	(49.1 ±0.5) %	S=1.3
Γ_2	$K^0_LK^0_S$	(33.9 ±0.4) %	S=1.2
Γ_3	$\rho\pi + \pi^+\pi^-\pi^0$	(15.4 ±0.4) %	S=1.2
Γ_4	$\rho\pi$		
Γ_5	$\pi^+\pi^-\pi^0$		
Γ_6	$\eta\gamma$	(1.301±0.025) %	S=1.2
Γ_7	$\pi^0\gamma$	(1.32 ±0.05) $\times 10^{-3}$	
Γ_8	$\ell^+\ell^-$	—	
Γ_9	e^+e^-	(2.979±0.033) $\times 10^{-4}$	S=1.3
Γ_{10}	$\mu^+\mu^-$	(2.85 ±0.19) $\times 10^{-4}$	
Γ_{11}	ηe^+e^-	(1.08 ±0.04) $\times 10^{-4}$	
Γ_{12}	$\pi^+\pi^-$	(7.3 ±1.3) $\times 10^{-5}$	
Γ_{13}	$\omega\pi^0$	(4.7 ±0.5) $\times 10^{-5}$	
Γ_{14}	$\omega\gamma$	< 5 %	CL=84%
Γ_{15}	$\rho\gamma$	< 1.2 $\times 10^{-5}$	CL=90%
Γ_{16}	$\pi^+\pi^-\gamma$	(4.1 ±1.3) $\times 10^{-5}$	
Γ_{17}	$f_0(980)\gamma$	(3.22 ±0.19) $\times 10^{-4}$	S=1.1
Γ_{18}	$\pi^0\pi^0\gamma$	(1.12 ±0.06) $\times 10^{-4}$	
Γ_{19}	$\pi^+\pi^-\pi^+\pi^-$	(3.9 $^{+2.8}_{-2.2}$) $\times 10^{-6}$	
Γ_{20}	$\pi^+\pi^+\pi^-\pi^-\pi^0$	< 4.6 $\times 10^{-6}$	CL=90%
Γ_{21}	$\pi^0e^+e^-$	(1.33 $^{+0.07}_{-0.10}$) $\times 10^{-5}$	
Γ_{22}	$\pi^0\eta\gamma$	(7.27 ±0.30) $\times 10^{-5}$	S=1.5
Γ_{23}	$a_0(980)\gamma$	(7.6 ±0.6) $\times 10^{-5}$	
Γ_{24}	$K^0\overline{K}^0\gamma$	< 1.9 $\times 10^{-8}$	CL=90%
Γ_{25}	$\eta'(958)\gamma$	(6.21 ±0.21) $\times 10^{-5}$	
Γ_{26}	$\eta\pi^0\pi^0\gamma$	< 2 $\times 10^{-5}$	CL=90%
Γ_{27}	$\mu^+\mu^-\gamma$	(1.4 ±0.5) $\times 10^{-5}$	
Γ_{28}	$\rho\gamma\gamma$	< 1.2 $\times 10^{-4}$	CL=90%
Γ_{29}	$\eta\pi^+\pi^-$	< 1.8 $\times 10^{-5}$	CL=90%
Γ_{30}	$\eta\mu^+\mu^-$	< 9.4 $\times 10^{-6}$	CL=90%
Γ_{31}	$\eta U \to \eta e^+e^-$	< 1 $\times 10^{-6}$	CL=90%
Γ_{32}	invisible	< 1.7 $\times 10^{-4}$	CL=90%
	Lepton Family number (LF) violating modes		
Γ_{33}	$e^\pm\mu^\mp$ *LF*	< 2 $\times 10^{-6}$	CL=90%

Downloaded from https://academic.oup.com/ptep/article/2022/8/083C01/6651666 by KIT Library user on 27 September 2022

CONSTRAINED FIT INFORMATION

An overall fit to 30 branching ratios uses 80 measurements and one constraint to determine 14 parameters. The overall fit has a $\chi^2 = 61.8$ for 67 degrees of freedom.

The following *off-diagonal* array elements are the correlation coefficients $\langle \delta x_i \delta x_j \rangle / (\delta x_i \cdot \delta x_j)$, in percent, from the fit to the branching fractions, $x_i \equiv \Gamma_i/\Gamma_{total}$. The fit constrains the x_i whose labels appear in this array to sum to one.

	x_1	x_2	x_3	x_6	x_7	x_9	x_{10}	x_{12}	x_{13}	x_{17}
x_2	−73									
x_3	−60	−10								
x_6	−21	18	2							
x_7	−11	11	2	8						
x_9	48	−51	−8	−37	−22					
x_{10}	−6	6	1	4	3	−12				
x_{12}	−3	3	0	2	1	−6	1			
x_{13}	−4	4	1	3	2	−8	1	0		
x_{17}	0	0	0	0	0	0	0	0	0	
x_{18}	−10	10	1	18	4	−19	2	1	2	0
x_{19}	−1	1	0	1	0	−2	0	0	0	0
x_{23}	0	0	0	0	0	0	0	0	0	0
x_{25}	−7	6	1	33	3	−12	1	1	1	0

	x_{18}	x_{19}	x_{23}
x_{19}	0		
x_{23}	0	0	
x_{25}	6	0	0

$\phi(1020)$ PARTIAL WIDTHS

$\Gamma(\eta\gamma)$ — Γ_6

VALUE (keV)	DOCUMENT ID		TECN	COMMENT
• • • We do not use the following data for averages, fits, limits, etc. • • •				
$58.9 \pm 0.5 \pm 2.4$	ACHASOV	00	SND	$e^+e^- \to \eta\gamma$

$\Gamma(\pi^0\gamma)$ — Γ_7

VALUE (keV)	DOCUMENT ID		TECN	COMMENT
• • • We do not use the following data for averages, fits, limits, etc. • • •				
$5.40 \pm 0.16 {}^{+0.43}_{-0.40}$	ACHASOV	00	SND	$e^+e^- \to \pi^0\gamma$

$\Gamma(\ell^+\ell^-)$ — Γ_8

VALUE (keV)	DOCUMENT ID		TECN	COMMENT
• • • We do not use the following data for averages, fits, limits, etc. • • •				
$1.320 \pm 0.017 \pm 0.015$	[1] AMBROSINO	05	KLOE	$1.02\ e^+e^- \to \mu^+\mu^-$

[1] Weighted average of Γ_{ee} and $\sqrt{\Gamma_{ee}\Gamma_{\mu\mu}}$ from AMBROSINO 05 assuming lepton universality.

$\Gamma(e^+e^-)$ — Γ_9

VALUE (keV)	DOCUMENT ID		TECN	COMMENT
1.27 ±0.04 OUR EVALUATION				
1.251±0.021 OUR AVERAGE Error includes scale factor of 1.1.				
$1.235 \pm 0.006 \pm 0.022$	[1] AKHMETSHIN	11	CMD2	$1.02\ e^+e^- \to \phi$
$1.32 \pm 0.05 \pm 0.03$	[2] AMBROSINO	05	KLOE	$1.02\ e^+e^- \to e^+e^-$
1.28 ± 0.05	AKHMETSHIN	95	CMD2	$1.02\ e^+e^- \to \phi$

[1] Combined analysis of the CMD-2 data on $\phi \to K^+K^-$, $K^0_S K^0_L$, $\pi^+\pi^-\pi^0$, $\eta\gamma$ assuming that the sum of their branching fractions is 0.99741 ± 0.00007.

[2] From forward-backward asymmetry and using $\Gamma_{total} = 4.26 \pm 0.05$ MeV from the 2004 edition of this Review.

$(\Gamma(e^+e^-) \times \Gamma(\mu^+\mu^-))^{1/2}$ — $(\Gamma_9\Gamma_{10})^{1/2}$

VALUE (keV)	DOCUMENT ID		TECN	COMMENT
1.320±0.018±0.017	AMBROSINO	05	KLOE	$1.02\ e^+e^- \to \mu^+\mu^-$

$\phi(1020)\ \Gamma(i)\Gamma(e^+e^-)/\Gamma(total)$

$\Gamma(K^+K^-) \times \Gamma(e^+e^-)/\Gamma_{total}$ — $\Gamma_1\Gamma_9/\Gamma$

VALUE (keV)	EVTS	DOCUMENT ID		TECN	COMMENT
0.6340±0.0070±0.0039		[1] LEES	13Q	BABR	$e^+e^- \to K^+K^-\gamma$
• • • We do not use the following data for averages, fits, limits, etc. • • •					
$0.669 \pm 0.001 \pm 0.023$	1.7M	KOZYREV	18	CMD3	$e^+e^- \to K^+K^-$

[1] Using a phenomenological model based on KUHN 90 with a sum of Breit-Wigner resonances for $\rho(770)$, $\omega(782)$, $\phi(1020)$ and their higher mass excitations. The first error combines statistical and systematic uncertainties. The second one is due to the parametrization of the charged kaon form factor and mass calibration.

$\Gamma(K^0_L K^0_S) \times \Gamma(e^+e^-)/\Gamma_{total}$ — $\Gamma_2\Gamma_9/\Gamma$

VALUE (keV)	EVTS	DOCUMENT ID		TECN	COMMENT
0.4200±0.0033±0.0123	28k	[1] LEES	14H	BABR	$e^+e^- \to K^0_S K^0_L \gamma$

[1] Using a vector meson dominance model with contribution from $\phi(1020)$ and higher mass excitations of $\rho(770)$, $\omega(782)$, and $\phi(1020)$.

$[\Gamma(\rho\pi) + \Gamma(\pi^+\pi^-\pi^0)] \times \Gamma(e^+e^-)/\Gamma_{total}$ — $\Gamma_3\Gamma_9/\Gamma$

VALUE (eV)	DOCUMENT ID		TECN	COMMENT
184.1±2.1±8.0	[1] LEES	21B	BABR	$10.5\ e^+e^- \to \pi^+\pi^-\pi^0\gamma$

[1] From the cross section for $e^+e^- \to \pi^+\pi^-\pi^0$ with contributions from $\rho(770)$, $\omega(782)$, $\phi(1020)$, $\omega(1420)$, and $\omega(1650)$.

$\phi(1020)\ \Gamma(i)\Gamma(e^+e^-)/\Gamma^2(total)$

$\Gamma(K^+K^-)/\Gamma_{total} \times \Gamma(e^+e^-)/\Gamma_{total}$ — $\Gamma_1/\Gamma \times \Gamma_9/\Gamma$

VALUE (units 10^{-5})	EVTS	DOCUMENT ID		TECN	COMMENT
14.64 ±0.28 OUR FIT Error includes scale factor of 1.4.					
14.6 ±0.5 OUR AVERAGE Error includes scale factor of 1.8. See the ideogram below.					
15.789 ± 0.541	1.7M	KOZYREV	18	CMD3	$e^+e^- \to K^+K^-$
$14.27 \pm 0.05 \pm 0.31$	542k	AKHMETSHIN	08	CMD2	$1.02\ e^+e^- \to K^+K^-$
$13.93 \pm 0.14 \pm 0.99$	1000k	[1] ACHASOV	01E	SND	$e^+e^- \to K^+K^-$, $K_S K_L$, $\pi^+\pi^-\pi^0$

[1] From the combined fit assuming that the total $\phi(1020)$ production cross section is saturated by those of K^+K^-, $K_S K_L$, $\pi^+\pi^-\pi^0$, and $\eta\gamma$ decays modes and using ACHASOV 00B for the $\eta\gamma$ decay mode.

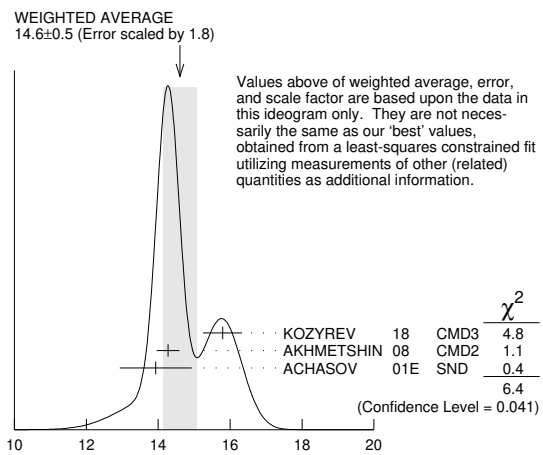

$\Gamma(K^0_L K^0_S)/\Gamma_{total} \times \Gamma(e^+e^-)/\Gamma_{total}$ — $\Gamma_2/\Gamma \times \Gamma_9/\Gamma$

VALUE (units 10^{-5})	EVTS	DOCUMENT ID		TECN	COMMENT
10.11 ±0.12 OUR FIT					
10.07 ±0.13 OUR AVERAGE					
10.078 ± 0.223	610k	[1] KOZYREV	16	CMD3	$e^+e^- \to K^0_S K^0_L$
$10.01 \pm 0.04 \pm 0.17$	272k	[2] AKHMETSHIN	04	CMD2	$e^+e^- \to K^0_L K^0_S$
$10.27 \pm 0.07 \pm 0.34$	500k	[3] ACHASOV	01E	SND	$e^+e^- \to K^+K^-$, $K_S K_L$, $\pi^+\pi^-\pi^0$

[1] KOZYREV 16 also reports $\Gamma(e^+e^-)\ B(\phi \to K^0_S K^0_L) = (0.428 \pm 0.001 \pm 0.009)$ keV.

[2] Update of AKHMETSHIN 99D

[3] From the combined fit assuming that the total $\phi(1020)$ production cross section is saturated by those of K^+K^-, $K_S K_L$, $\pi^+\pi^-\pi^0$, and $\eta\gamma$ decays modes and using ACHASOV 00B for the $\eta\gamma$ decay mode.

$[\Gamma(\rho\pi) + \Gamma(\pi^+\pi^-\pi^0)]/\Gamma_{total} \times \Gamma(e^+e^-)/\Gamma_{total}$ — $\Gamma_3/\Gamma \times \Gamma_9/\Gamma$

VALUE (units 10^{-5})	EVTS	DOCUMENT ID		TECN	COMMENT
4.58 ±0.11 OUR FIT Error includes scale factor of 1.1.					
4.51 ±0.14 OUR AVERAGE					
$4.51 \pm 0.16 \pm 0.11$	105k	AKHMETSHIN	06	CMD2	0.98–1.06 $e^+e^- \to \pi^+\pi^-\pi^0$
$4.665 \pm 0.042 \pm 0.261$	400k	[1] ACHASOV	01E	SND	$e^+e^- \to K^+K^-$, $K_S K_L$, $\pi^+\pi^-\pi^0$
$4.35 \pm 0.27 \pm 0.08$	11169	[2] AKHMETSHIN	98	CMD2	$e^+e^- \to \pi^+\pi^-\pi^0$
• • • We do not use the following data for averages, fits, limits, etc. • • •					
4.38 ± 0.12		BENAYOUN	10	RVUE	0.4–1.05 e^+e^-
$4.30 \pm 0.08 \pm 0.21$		[3] AUBERT,B	04N	BABR	10.6 $e^+e^- \to \pi^+\pi^-\pi^0\gamma$

[1] From the combined fit assuming that the total $\phi(1020)$ production cross section is saturated by those of K^+K^-, $K_S K_L$, $\pi^+\pi^-\pi^0$, and $\eta\gamma$ decays modes and using ACHASOV 00B for the $\eta\gamma$ decay mode.

[2] Recalculated by us from the cross section in the peak.

[3] Superseeded by LEES 21B.

Downloaded from https://academic.oup.com/ptep/article/2022/8/083C01/6651666 by KIT Library user on 27 September 2022

$\Gamma(\eta\gamma)/\Gamma_{total} \times \Gamma(e^+e^-)/\Gamma_{total}$ — $\Gamma_6/\Gamma \times \Gamma_9/\Gamma$

VALUE (units 10^{-6})	EVTS	DOCUMENT ID		TECN	COMMENT
3.88 ±0.07 OUR FIT Error includes scale factor of 1.2.					
3.93 ±0.09 OUR AVERAGE Error includes scale factor of 1.3. See the ideogram below.					
$4.050 \pm 0.067 \pm 0.118$	33k	[1] ACHASOV	07B	SND	0.6–1.38 $e^+e^- \to \eta\gamma$
$4.093^{+0.040}_{-0.043} \pm 0.247$	17.4k	[2] AKHMETSHIN	05	CMD2	0.60-1.38 $e^+e^- \to \eta\gamma$
$3.850 \pm 0.041 \pm 0.159$	23k	[3,4] AKHMETSHIN	01B	CMD2	$e^+e^- \to \eta\gamma$
$4.00 \pm 0.04 \pm 0.11$		[5] ACHASOV	00	SND	$e^+e^- \to \eta\gamma$
$3.53 \pm 0.08 \pm 0.17$	2200	[6,7] AKHMETSHIN	99F	CMD2	$e^+e^- \to \eta\gamma$
• • • We do not use the following data for averages, fits, limits, etc. • • •					
4.19 ± 0.06		[8] BENAYOUN	10	RVUE	0.4–1.05 e^+e^-

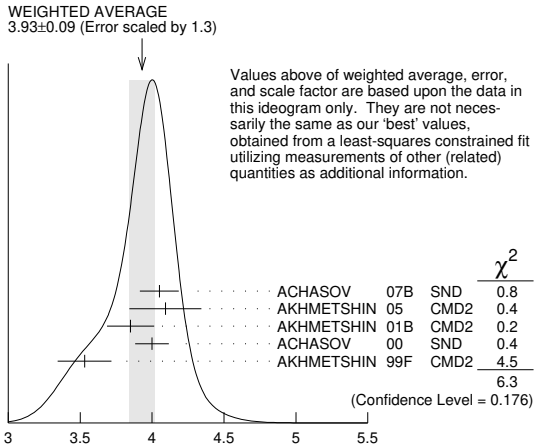

[1] From a combined fit of $\sigma(e^+e^- \to \eta\gamma)$ with $\eta \to 3\pi^0$ and $\eta \to \pi^+\pi^-\pi^0$, and fixing $B(\eta \to 3\pi^0)$ / $B(\eta \to \pi^+\pi^-\pi^0) = 1.44 \pm 0.04$. Recalculated by us from the cross section at the peak. Supersedes ACHASOV 00D and ACHASOV 06A.
[2] From the $\eta \to 2\gamma$ decay and using $B(\eta \to \gamma\gamma) = 39.43 \pm 0.26\%$.
[3] From the $\eta \to 3\pi^0$ decay and using $B(\eta \to 3\pi^0) = (32.24 \pm 0.29) \times 10^{-2}$.
[4] The combined fit from 600 to 1380 MeV taking into account $\rho(770)$, $\omega(782)$, $\phi(1020)$, and $\rho(1450)$ (mass and width fixed at 1450 MeV and 310 MeV respectively).
[5] From the $\eta \to 2\gamma$ decay and using $B(\eta \to 2\gamma) = (39.21 \pm 0.34) \times 10^{-2}$.
[6] Recalculated by the authors from the cross section in the peak.
[7] From the $\eta \to \pi^+\pi^-\pi^0$ decay and using $B(\eta \to \pi^+\pi^-\pi^0) = (23.1 \pm 0.5) \times 10^{-2}$.
[8] A simultaneous fit of $e^+e^- \to \pi^+\pi^-$, $\pi^+\pi^-\pi^0$, $\pi^0\gamma$, $\eta\gamma$ data.

$\Gamma(\pi^0\gamma)/\Gamma_{total} \times \Gamma(e^+e^-)/\Gamma_{total}$ — $\Gamma_7/\Gamma \times \Gamma_9/\Gamma$

VALUE (units 10^{-7})	EVTS	DOCUMENT ID		TECN	COMMENT
3.94±0.16 OUR FIT					
3.95±0.17 OUR AVERAGE					
$4.04 \pm 0.09 \pm 0.19$		[1] ACHASOV	16A	SND	0.60–1.38 $e^+e^- \to \pi^0\gamma$
$3.75 \pm 0.11 \pm 0.29$	18k	AKHMETSHIN	05	CMD2	0.60-1.38 $e^+e^- \to \pi^0\gamma$
• • • We do not use the following data for averages, fits, limits, etc. • • •					
4.29 ± 0.11		[2] BENAYOUN	10	RVUE	0.4–1.05 e^+e^-
$3.67 \pm 0.10^{+0.27}_{-0.25}$		[3] ACHASOV	00	SND	$e^+e^- \to \pi^0\gamma$

[1] From the VMD model with the interfering $\rho(770)$, $\omega(782)$, $\phi(1020)$ resonances, and an additional resonance describing the total contribution of the $\rho(1450)$ and $\omega(1420)$ states. Supersedes ACHASOV 00.
[2] A simultaneous fit of $e^+e^- \to \pi^+\pi^-$, $\pi^+\pi^-\pi^0$, $\pi^0\gamma$, $\eta\gamma$ data.
[3] From the $\pi^0 \to 2\gamma$ decay and using $B(\pi^0 \to 2\gamma) = (98.798 \pm 0.032) \times 10^{-2}$.

$\Gamma(\mu^+\mu^-)/\Gamma_{total} \times \Gamma(e^+e^-)/\Gamma_{total}$ — $\Gamma_{10}/\Gamma \times \Gamma_9/\Gamma$

VALUE (units 10^{-8})	DOCUMENT ID		TECN	COMMENT
8.5 ±0.6 OUR FIT				
8.8 ±0.9 OUR AVERAGE Error includes scale factor of 1.5. See the ideogram below.				
$8.36 \pm 0.59 \pm 0.37$	ACHASOV	01G	SND	$e^+e^- \to \mu^+\mu^-$
$9.9 \pm 1.4 \pm 0.9$	[1] ACHASOV	99C	SND	$e^+e^- \to \mu^+\mu^-$
14.4 ± 3.0	[2] VASSERMAN	81	OLYA	$e^+e^- \to \mu^+\mu^-$
8.6 ± 5.9	[2] AUGUSTIN	73	OSPK	$e^+e^- \to \mu^+\mu^-$

[1] Recalculated by the authors from the cross section in the peak.
[2] Recalculated by us from the cross section in the peak.

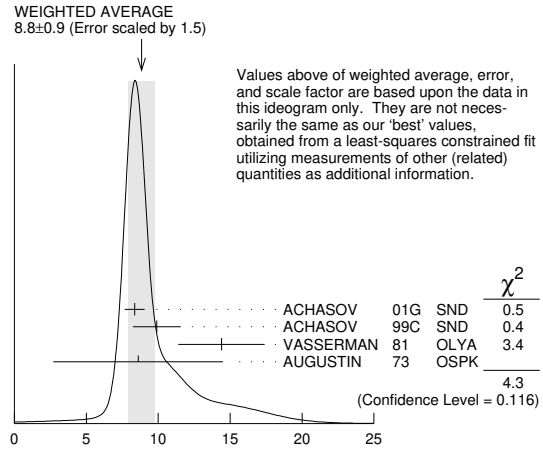

$\Gamma(\pi^+\pi^-)/\Gamma_{total} \times \Gamma(e^+e^-)/\Gamma_{total}$ — $\Gamma_{12}/\Gamma \times \Gamma_9/\Gamma$

VALUE (units 10^{-8})	DOCUMENT ID		TECN	COMMENT
2.2 ±0.4 OUR FIT				
2.2 ±0.4 OUR AVERAGE				
$2.1 \pm 0.3 \pm 0.3$	[1] ACHASOV	00C	SND	$e^+e^- \to \pi^+\pi^-$
$1.95^{+1.15}_{-0.87}$	[2] GOLUBEV	86	ND	$e^+e^- \to \pi^+\pi^-$
$6.01^{+3.19}_{-2.51}$	[2] VASSERMAN	81	OLYA	$e^+e^- \to \pi^+\pi^-$
• • • We do not use the following data for averages, fits, limits, etc. • • •				
3.31 ± 0.99	[3] BENAYOUN	13	RVUE	0.4–1.05 e^+e^-

[1] Recalculated by the authors from the cross section in the peak.
[2] Recalculated by us from the cross section in the peak.
[3] A simultaneous fit to $e^+e^- \to \pi^+\pi^-$, $\pi^+\pi^-\pi^0$, $\pi^0\gamma$, $\eta\gamma$, $K\overline{K}$, and $\tau^- \to \pi^-\pi^0\nu_\tau$ data.

$\Gamma(\omega\pi^0)/\Gamma_{total} \times \Gamma(e^+e^-)/\Gamma_{total}$ — $\Gamma_{13}/\Gamma \times \Gamma_9/\Gamma$

VALUE (units 10^{-8})	DOCUMENT ID		TECN	COMMENT
1.40±0.15 OUR FIT				
1.37±0.17±0.01	[1,2] AMBROSINO	08G	KLOE	$e^+e^- \to \pi^+\pi^-2\pi^0$, $2\pi^0\gamma$

[1] Recalculated by the authors from the cross section at the peak.
[2] AMBROSINO 08G reports $[\Gamma(\phi(1020) \to \omega\pi^0)/\Gamma_{total} \times \Gamma(\phi(1020) \to e^+e^-)/\Gamma_{total}] \times [B(\omega(782) \to \pi^+\pi^-\pi^0)] = (1.22 \pm 0.13 \pm 0.08) \times 10^{-8}$ which we divide by our best value $B(\omega(782) \to \pi^+\pi^-\pi^0) = (89.2 \pm 0.7) \times 10^{-2}$. Our first error is their experiment's error and our second error is the systematic error from using our best value.

$\Gamma(\pi^0\pi^0\gamma)/\Gamma_{total} \times \Gamma(e^+e^-)/\Gamma_{total}$ — $\Gamma_{18}/\Gamma \times \Gamma_9/\Gamma$

VALUE (units 10^{-8})	DOCUMENT ID		TECN	COMMENT
3.34±0.17 OUR FIT				
$\mathbf{3.33^{+0.04}_{-0.09} \pm 0.19_{-0.20}}$	[1] AMBROSINO	07	KLOE	$e^+e^- \to \pi^0\pi^0\gamma$

[1] Calculated by the authors from the cross section at the peak.

$\Gamma(\pi^+\pi^-\pi^+\pi^-)/\Gamma_{total} \times \Gamma(e^+e^-)/\Gamma_{total}$ — $\Gamma_{19}/\Gamma \times \Gamma_9/\Gamma$

VALUE (units 10^{-9})	EVTS	DOCUMENT ID		TECN	COMMENT
$\mathbf{1.2^{+0.8}_{-0.7}}$ **OUR FIT**					
1.17±0.52±0.64	3285	[1] AKHMETSHIN	00E	CMD2	$e^+e^- \to \pi^+\pi^-\pi^+\pi^-$

[1] Recalculated by the authors from the cross section in the peak.

$\phi(1020)$ BRANCHING RATIOS

$\Gamma(K^+K^-)/\Gamma_{total}$ — Γ_1/Γ

VALUE	EVTS	DOCUMENT ID		TECN	COMMENT
0.491±0.005 OUR FIT Error includes scale factor of 1.3.					
0.493±0.010 OUR AVERAGE					
0.492 ± 0.012	2913	AKHMETSHIN	95	CMD2	$e^+e^- \to K^+K^-$
0.44 ± 0.05	321	KALBFLEISCH	76	HBC	2.18 $K^-p \to \Lambda K^+K^-$
0.49 ± 0.06	270	DEGROOT	74	HBC	4.2 $K^-p \to \Lambda\phi$
0.540 ± 0.034	565	BALAKIN	71	OSPK	$e^+e^- \to K^+K^-$
0.48 ± 0.04	252	LINDSEY	66	HBC	2.1–2.7 $K^-p \to \Lambda K^+K^-$
• • • We do not use the following data for averages, fits, limits, etc. • • •					
$0.493 \pm 0.003 \pm 0.007$		[1] AKHMETSHIN	11	CMD2	1.02 $e^+e^- \to K^+K^-$
0.476 ± 0.017	1000k	[2] ACHASOV	01E	SND	$e^+e^- \to K^+K^-$, K_SK_L, $\pi^+\pi^-\pi^0$

[1] Combined analysis of the CMD-2 data on $\phi \to K^+K^-$, $K^0_SK^0_L$, $\pi^+\pi^-\pi^0$, $\eta\gamma$ assuming that the sum of their branching fractions is 0.99741 ± 0.00007.
[2] Using $B(\phi \to e^+e^-) = (2.93 \pm 0.14) \times 10^{-4}$.

Downloaded from https://academic.oup.com/ptep/article/2022/8/083C01/6651666 by KIT Library user on 27 September 2022

$\Gamma(K^0_L K^0_S)/\Gamma_{total}$ — Γ_2/Γ

VALUE	EVTS	DOCUMENT ID		TECN	COMMENT
0.339±0.004 OUR FIT	Error includes scale factor of 1.2.				
0.331±0.009 OUR AVERAGE					
0.335±0.010	40644	AKHMETSHIN	95	CMD2	$e^+e^- \to K^0_L K^0_S$
0.326±0.035		DOLINSKY	91	ND	$e^+e^- \to K^0_L K^0_S$
0.310±0.024		DRUZHININ	84	ND	$e^+e^- \to K^0_L K^0_S$
• • • We do not use the following data for averages, fits, limits, etc. • • •					
0.336±0.002±0.006		[1] AKHMETSHIN	11	CMD2	1.02 $e^+e^- \to K^0_S K^0_L$
0.351±0.013	500k	[2] ACHASOV	01E	SND	$e^+e^- \to K^+K^-$, $K_S K_L$, $\pi^+\pi^-\pi^0$
0.27 ±0.03	133	KALBFLEISCH	76	HBC	2.18 $K^-p \to \Lambda K^0_L K^0_S$
0.257±0.030	95	[3] BALAKIN	71	OSPK	$e^+e^- \to K^0_L K^0_S$
0.40 ±0.04	167	LINDSEY	66	HBC	2.1–2.7 $K^-p \to \Lambda K^0_L K^0_S$

[1] Combined analysis of the CMD-2 data on $\phi \to K^+K^-$, $K^0_S K^0_L$, $\pi^+\pi^-\pi^0$, $\eta\gamma$ assuming that the sum of their branching fractions is 0.99741 ± 0.00007.
[2] Using $B(\phi \to e^+e^-) = (2.93 \pm 0.14) \times 10^{-4}$.
[3] Balakin error increased by Paul.

$\Gamma(K^0_L K^0_S)/\Gamma(K^+K^-)$ — Γ_2/Γ_1

VALUE	EVTS	DOCUMENT ID		TECN	COMMENT
0.690±0.015 OUR FIT	Error includes scale factor of 1.3.				
0.740±0.031 OUR AVERAGE					
0.70 ±0.06	2732	BUKIN	78C	OLYA	$e^+e^- \to K^0_L K^0_S$
0.82 ±0.08		LOSTY	78	HBC	4.2 $K^-p \to \phi$hyperon
0.71 ±0.05		LAVEN	77	HBC	10 $K^-p \to K^+K^-\Lambda$
0.71 ±0.08		LYONS	77	HBC	3–4 $K^-p \to \Lambda\phi$
0.89 ±0.10	144	AGUILAR-...	72B	HBC	3.9,4.6 K^-p
• • • We do not use the following data for averages, fits, limits, etc. • • •					
0.638±0.022	2.3M	[1] KOZYREV	18	CMD3	$e^+e^- \to K^0_L K^0_S$, K^+K^-
0.68 ±0.03		[2] AKHMETSHIN	95	CMD2	$e^+e^- \to K^0_L K^0_S$, K^+K^-

[1] The prediction taking into account phase-space difference, radiative corrections, isospin breaking, and the Sommerfeld-Gamow-Sakharov factor gives 0.630.
[2] Theoretical analysis of BRAMON 00 taking into account phase-space difference, electromagnetic radiative corrections, as well as isospin breaking, predicts 0.62. FLOREZ-BAEZ 08 predicts 0.63 considering also structure-dependent radiative corrections. FISCHBACH 02 calculates additional corrections caused by the close threshold and predicts 0.68. See also BENAYOUN 01 and DUBYNSKIY 07. BENAYOUN 12 obtains 0.71±0.01 in the HLS model.

$\Gamma(K^0_L K^0_S)/\Gamma(K\overline{K})$ — $\Gamma_2/(\Gamma_1+\Gamma_2)$

VALUE	EVTS	DOCUMENT ID		TECN	COMMENT
0.408±0.005 OUR FIT	Error includes scale factor of 1.3.				
0.45 ±0.04 OUR AVERAGE					
0.44 ±0.07		[1] LONDON	66	HBC	2.24 $K^-p \to \Lambda K\overline{K}$
0.48 ±0.07	52	BADIER	65B	HBC	3 K^-p
0.40 ±0.10	34	SCHLEIN	63	HBC	1.95 $K^-p \to \Lambda K\overline{K}$

[1] This is probably not affected by their controversial background subtraction; the value is from their numbers of $K_1 K_2$ vs K^+K^- events.

$[\Gamma(\rho\pi) + \Gamma(\pi^+\pi^-\pi^0)]/\Gamma_{total}$ — Γ_3/Γ

VALUE	EVTS	DOCUMENT ID		TECN	COMMENT
0.154±0.004 OUR FIT	Error includes scale factor of 1.2.				
0.151±0.009 OUR AVERAGE	Error includes scale factor of 1.7.				
0.161±0.008	11761	AKHMETSHIN	95	CMD2	$e^+e^- \to \pi^+\pi^-\pi^0$
0.143±0.007		DOLINSKY	91	ND	$e^+e^- \to \pi^+\pi^-\pi^0$
• • • We do not use the following data for averages, fits, limits, etc. • • •					
0.155±0.002±0.005		[1] AKHMETSHIN	11	CMD2	1.02 $e^+e^- \to \pi^+\pi^-\pi^0$
0.159±0.008	400k	[2] ACHASOV	01E	SND	$e^+e^- \to K^+K^-$, $K_S K_L$, $\pi^+\pi^-\pi^0$
0.145±0.009±0.003	11169	[3] AKHMETSHIN	98	CMD2	$e^+e^- \to \pi^+\pi^-\pi^0$
0.139±0.007		[4] PARROUR	76B	OSPK	e^+e^-

[1] Combined analysis of the CMD-2 data on $\phi \to K^+K^-$, $K^0_S K^0_L$, $\pi^+\pi^-\pi^0$, $\eta\gamma$ assuming that the sum of their branching fractions is 0.99741 ± 0.00007.
[2] Using $B(\phi \to e^+e^-) = (2.93 \pm 0.14) \times 10^{-4}$.
[3] Using $B(\phi \to e^+e^-) = (2.99 \pm 0.08) \times 10^{-4}$.
[4] Using $\Gamma(\phi) = 4.1$ MeV. If interference between the $\rho\pi$ and 3π modes is neglected, the fraction of the $\rho\pi$ is more than 80% at the 90% confidence level.

$[\Gamma(\rho\pi) + \Gamma(\pi^+\pi^-\pi^0)]/\Gamma(K^+K^-)$ — Γ_3/Γ_1

VALUE	EVTS	DOCUMENT ID		TECN	COMMENT
0.313±0.010 OUR FIT	Error includes scale factor of 1.2.				
0.28 ±0.09	34	AGUILAR-...	72B	HBC	3.9,4.6 K^-p

$[\Gamma(\rho\pi) + \Gamma(\pi^+\pi^-\pi^0)]/\Gamma(K\overline{K})$ — $\Gamma_3/(\Gamma_1+\Gamma_2)$

VALUE	DOCUMENT ID		TECN	COMMENT
0.185±0.005 OUR FIT	Error includes scale factor of 1.2.			
0.24 ±0.04 OUR AVERAGE				
0.237±0.039	CERRADA	77B	HBC	4.2 $K^-p \to \Lambda 3\pi$
0.30 ±0.15	LONDON	66	HBC	2.24 $K^-p \to \Lambda\pi^+\pi^-\pi^0$

$[\Gamma(\rho\pi) + \Gamma(\pi^+\pi^-\pi^0)]/\Gamma(K^0_L K^0_S)$ — Γ_3/Γ_2

VALUE	EVTS	DOCUMENT ID		TECN	COMMENT
0.453±0.012 OUR FIT	Error includes scale factor of 1.1.				
0.51 ±0.05 OUR AVERAGE					
0.56 ±0.07	3681	BUKIN	78C	OLYA	$e^+e^- \to K^0_L K^0_S$, $\pi^+\pi^-\pi^0$
0.47 ±0.06	516	COSME	74	OSPK	$e^+e^- \to \pi^+\pi^-\pi^0$

$\Gamma(\pi^+\pi^-\pi^0)/\Gamma_{total}$ — Γ_5/Γ

VALUE	CL%	EVTS	DOCUMENT ID		TECN	COMMENT
• • • We do not use the following data for averages, fits, limits, etc. • • •						
≃ 0.0087		1.98M	[1,2] ALOISIO	03	KLOE	1.02 $e^+e^- \to \pi^+\pi^-\pi^0$
<0.0006	90		[3] ACHASOV	02	SND	1.02 $e^+e^- \to \pi^+\pi^-\pi^0$
<0.23	90		[3] CORDIER	80	DM1	$e^+e^- \to \pi^+\pi^-\pi^0$
<0.20	90		[3] PARROUR	76B	OSPK	$e^+e^- \to \pi^+\pi^-\pi^0$

[1] From a fit without limitations on charged and neutral ρ masses and widths.
[2] Adding the direct and $\omega\pi$ contributions and considering the interference between the $\rho\pi$ and $\pi^+\pi^-\pi^0$.
[3] Neglecting the interference between the $\rho\pi$ and $\pi^+\pi^-\pi^0$.

$\Gamma(\eta\gamma)/\Gamma_{total}$ — Γ_6/Γ

VALUE (units 10^{-2})	EVTS	DOCUMENT ID		TECN	COMMENT
1.301±0.025 OUR FIT	Error includes scale factor of 1.2.				
1.26 ±0.04 OUR AVERAGE					
1.246±0.025±0.057	10k	[1] ACHASOV	98F	SND	$e^+e^- \to 7\gamma$
1.18 ±0.11	279	[2] AKHMETSHIN	95	CMD2	$e^+e^- \to \pi^+\pi^-3\gamma$
1.30 ±0.06		[3] DRUZHININ	84	ND	$e^+e^- \to 3\gamma$
1.4 ±0.2		[4] DRUZHININ	84	ND	$e^+e^- \to 6\gamma$
0.88 ±0.20	290	KURDADZE	83C	OLYA	$e^+e^- \to 3\gamma$
1.35 ±0.29		ANDREWS	77	CNTR	6.7–10 γCu
1.5 ±0.4	54	[3] COSME	76	OSPK	e^+e^-
• • • We do not use the following data for averages, fits, limits, etc. • • •					
1.38 ±0.02 ±0.02		[5] AKHMETSHIN	11	CMD2	1.02 $e^+e^- \to \eta\gamma$
1.36 ±0.05 ±0.02	33k	[6] ACHASOV	07B	SND	0.6–1.38 $e^+e^- \to \eta\gamma$
1.373±0.014±0.085	17.4k	[7,8] AKHMETSHIN	05	CMD2	0.60-1.38 $e^+e^- \to \eta\gamma$
1.287±0.013±0.063		[9,10] AKHMETSHIN	01B	CMD2	$e^+e^- \to \eta\gamma$
1.338±0.012±0.052		[11] ACHASOV	00	SND	$e^+e^- \to \eta\gamma$
1.18 ±0.03 ±0.06	2200	[12] AKHMETSHIN	99F	CMD2	$e^+e^- \to \eta\gamma$
1.21 ±0.07		[13] BENAYOUN	96	RVUE	0.54-1.04 $e^+e^- \to \eta\gamma$

[1] Using $B(\phi \to e^+e^-) = (2.99 \pm 0.08) \times 10^{-4}$ and $B(\eta \to 3\pi^0) = (32.2 \pm 0.4) \times 10^{-2}$.
[2] From $\pi^+\pi^-\pi^0$ decay mode of η.
[3] From 2γ decay mode of η.
[4] From $3\pi^0$ decay mode of η.
[5] Combined analysis of the CMD-2 data on $\phi \to K^+K^-$, $K^0_S K^0_L$, $\pi^+\pi^-\pi^0$, $\eta\gamma$ assuming that the sum of their branching fractions is 0.99741 ± 0.00007.
[6] ACHASOV 07B reports $[\Gamma(\phi(1020) \to \eta\gamma)/\Gamma_{total}] \times [B(\phi(1020) \to e^+e^-)] = (4.050 \pm 0.067 \pm 0.118) \times 10^{-6}$ which we divide by our best value $B(\phi(1020) \to e^+e^-) = (2.979 \pm 0.033) \times 10^{-4}$. Our first error is their experiment's error and our second error is the systematic error from using our best value. Supersedes ACHASOV 00D and ACHASOV 06A.
[7] Using $B(\phi \to e^+e^-) = (2.98 \pm 0.04) \times 10^{-4}$ and $B(\eta \to \gamma\gamma) = 39.43 \pm 0.26\%$.
[8] Not independent of the corresponding $\Gamma(e^+e^-) \times \Gamma(\eta\gamma)/\Gamma^2_{total}$.
[9] Using $B(\phi \to e^+e^-) = (2.99 \pm 0.08) \times 10^{-4}$ and $B(\eta \to 3\pi^0) = (32.24 \pm 0.29) \times 10^{-2}$.
[10] The combined fit from 600 to 1380 MeV taking into account $\rho(770)$, $\omega(782)$, $\phi(1020)$, and $\rho(1450)$ (mass and width fixed at 1450 MeV and 310 MeV respectively).
[11] From the $\eta \to 2\gamma$ decay and using $B(\phi \to e^+e^-) = (2.99 \pm 0.08) \times 10^{-4}$.
[12] From $\pi^+\pi^-\pi^0$ decay mode of η and using $B(\phi \to e^+e^-) = (2.99 \pm 0.08) \times 10^{-4}$.
[13] Reanalysis of DRUZHININ 84, DOLINSKY 89, and DOLINSKY 91 taking into account a triangle anomaly contribution.

$\Gamma(\pi^0\gamma)/\Gamma_{total}$ — Γ_7/Γ

VALUE (units 10^{-3})	EVTS	DOCUMENT ID		TECN	COMMENT
1.32 ±0.05 OUR FIT					
1.31 ±0.13 OUR AVERAGE					
1.30 ±0.13		DRUZHININ	84	ND	$e^+e^- \to 3\gamma$
1.4 ±0.5	32	COSME	76	OSPK	e^+e^-
• • • We do not use the following data for averages, fits, limits, etc. • • •					
1.367±0.072		[1] ACHASOV	16A	SND	0.60–1.38 $e^+e^- \to \pi^0\gamma$
1.258±0.037±0.077	18k	[2,3] AKHMETSHIN	05	CMD2	0.60-1.38 $e^+e^- \to \pi^0\gamma$
$1.226 \pm 0.036^{+0.096}_{-0.089}$		[4] ACHASOV	00	SND	$e^+e^- \to \pi^0\gamma$
1.26 ±0.17		[5] BENAYOUN	96	RVUE	0.54-1.04 $e^+e^- \to \pi^0\gamma$

[1] Using $B(\phi \to e^+e^-)$ from PDG 15. Supersedes ACHASOV 00.
[2] Using $B(\phi \to e^+e^-) = (2.98 \pm 0.04) \times 10^{-4}$.
[3] Not independent of the corresponding $\Gamma(e^+e^-) \times \Gamma(\pi^0\gamma)/\Gamma^2_{total}$.
[4] From the $\pi^0 \to 2\gamma$ decay and using $B(\phi \to e^+e^-) = (2.99 \pm 0.08) \times 10^{-4}$.
[5] Reanalysis of DRUZHININ 84, DOLINSKY 89, and DOLINSKY 91 taking into account a triangle anomaly contribution.

$\Gamma(\eta\gamma)/\Gamma(\pi^0\gamma)$ — Γ_6/Γ_7

VALUE	DOCUMENT ID		TECN	COMMENT
• • • We do not use the following data for averages, fits, limits, etc. • • •				
$10.9 \pm 0.3^{+0.7}_{-0.8}$	ACHASOV	00	SND	$e^+e^- \to \eta\gamma, \pi^0\gamma$

Downloaded from https://academic.oup.com/ptep/article/2022/8/083C01/6651666 by KIT Library user on 27 September 2022

$\Gamma(e^+e^-)/\Gamma_{total}$ — Γ_9/Γ

VALUE (units 10^{-4})	EVTS	DOCUMENT ID		TECN	COMMENT
2.979±0.033 OUR FIT	Error includes scale factor of 1.3.				
2.98 ±0.07 OUR AVERAGE	Error includes scale factor of 1.1.				
2.93 ±0.14	1900k	[1] ACHASOV	01E	SND	$e^+e^- \to K^+K^-$, K_SK_L, $\pi^+\pi^-\pi^0$
2.88 ±0.09	55600	AKHMETSHIN	95	CMD2	$e^+e^- \to$ hadrons
3.00 ±0.21	3681	BUKIN	78C	OLYA	$e^+e^- \to$ hadrons
3.10 ±0.14		[2] PARROUR	76	OSPK	e^+e^-
3.3 ±0.3		COSME	74	OSPK	$e^+e^- \to$ hadrons
2.81 ±0.25	681	BALAKIN	71	OSPK	$e^+e^- \to$ hadrons
3.50 ±0.27		CHATELUS	71	OSPK	e^+e^-

[1] From the combined fit assuming that the total $\phi(1020)$ production cross section is saturated by those of K^+K^-, K_SK_L, $\pi^+\pi^-\pi^0$, and $\eta\gamma$ decays modes and using ACHASOV 00B for the $\eta\gamma$ decay mode.
[2] Using total width 4.2 MeV. They detect 3π mode and observe significant interference with ω tail. This is accounted for in the result quoted above.

$\Gamma(\mu^+\mu^-)/\Gamma_{total}$ — Γ_{10}/Γ

VALUE (units 10^{-4})	DOCUMENT ID		TECN	COMMENT
2.85±0.19 OUR FIT				
2.5 ±0.4 OUR AVERAGE				
2.69±0.46	[1] HAYES	71	CNTR	8.3,9.8 $\gamma C \to \mu^+\mu^- X$
2.17±0.60	[1] EARLES	70	CNTR	6.0 $\gamma C \to \mu^+\mu^- X$
• • • We do not use the following data for averages, fits, limits, etc. • • •				
2.87±0.20±0.14	[2] ACHASOV	01G	SND	$e^+e^- \to \mu^+\mu^-$
3.30±0.45±0.32	[3] ACHASOV	99C	SND	$e^+e^- \to \mu^+\mu^-$
4.83±1.02	[4] VASSERMAN	81	OLYA	$e^+e^- \to \mu^+\mu^-$
2.87±1.98	[4] AUGUSTIN	73	OSPK	$e^+e^- \to \mu^+\mu^-$

[1] Neglecting interference between resonance and continuum.
[2] Using $B(\phi \to e^+e^-) = (2.91 \pm 0.07) \times 10^{-4}$.
[3] Using $B(\phi \to e^+e^-) = (2.99 \pm 0.08) \times 10^{-4}$.
[4] Recalculated by us using $B(\phi \to e^+e^-) = (2.99 \pm 0.08) \times 10^{-4}$.

$\Gamma(\eta e^+e^-)/\Gamma_{total}$ — Γ_{11}/Γ

VALUE (units 10^{-4})	EVTS	DOCUMENT ID		TECN	COMMENT
1.08 ±0.04 OUR AVERAGE					
1.075±0.007±0.038	30k	[1] BABUSCI	15	KLOE	$1.02\ e^+e^- \to \eta e^+e^-$
1.19 ±0.19 ±0.12	213	[2] ACHASOV	01B	SND	$e^+e^- \to \eta e^+e^-$
1.14 ±0.10 ±0.06	355	[3] AKHMETSHIN	01	CMD2	$e^+e^- \to \eta e^+e^-$
• • • We do not use the following data for averages, fits, limits, etc. • • •					
1.13 ±0.14 ±0.07	183	[4] AKHMETSHIN	01	CMD2	$e^+e^- \to \eta e^+e^-$
1.21 ±0.14 ±0.09	130	[5] AKHMETSHIN	01	CMD2	$e^+e^- \to \eta e^+e^-$
1.04 ±0.20 ±0.08	42	[6] AKHMETSHIN	01	CMD2	$e^+e^- \to \eta e^+e^-$
$1.3\ ^{+0.8}_{-0.6}$	7	GOLUBEV	85	ND	$e^+e^- \to \eta e^+e^-$

[1] Using $B(\eta \to 3\pi^0) = (32.57 \pm 0.23)\%$ from PDG 12.
[2] Using $B(\eta \to \gamma\gamma) = (39.25 \pm 0.32)\%$, $B(\phi \to \eta\gamma) = (1.26 \pm 0.06)\%$, and $B(\phi \to e^+e^-) = (3.00 \pm 0.06) \times 10^{-4}$.
[3] The average of the branching ratios separately obtained from the $\eta \to \gamma\gamma$, $3\pi^0$, $\pi^+\pi^-\pi^0$ decays.
[4] From $\eta \to \gamma\gamma$ decays and using $B(\eta \to \gamma\gamma) = (39.33 \pm 0.25) \times 10^{-2}$, $B(\eta \to \pi^+\pi^-\gamma) = (4.75 \pm 11) \times 10^{-2}$, and $B(\phi \to \eta\gamma) = (1.297 \pm 0.033) \times 10^{-2}$.
[5] From $\eta \to 3\pi^0$ decays and using $B(\pi^0 \to \gamma\gamma) = (98.798 \pm 0.033) \times 10^{-2}$, $B(\eta \to 3\pi^0) = (32.24 \pm 0.29) \times 10^{-2}$, $B(\eta \to \pi^+\pi^-\gamma) = (4.75 \pm 0.11) \times 10^{-2}$, and $B(\phi \to \eta\gamma) = (1.297 \pm 0.033) \times 10^{-2}$.
[6] From $\eta \to \pi^+\pi^-\pi^0$ decays and using $B(\pi^0 \to \gamma\gamma) = (98.798 \pm 0.033) \times 10^{-2}$, $B(\pi^0 \to e^+e^-\gamma) = (1.198 \pm 0.032) \times 10^{-2}$, $B(\eta \to \pi^+\pi^-\pi^0) = (23.0 \pm 0.4) \times 10^{-2}$, $B(\phi \to \pi^+\pi^-\pi^0) = (15.5 \pm 0.6) \times 10^{-2}$, and $B(\phi \to \eta\gamma) = (1.297 \pm 0.033) \times 10^{-2}$.

$\Gamma(\pi^+\pi^-)/\Gamma_{total}$ — Γ_{12}/Γ

VALUE (units 10^{-4})	CL%	DOCUMENT ID		TECN	COMMENT
• • • We do not use the following data for averages, fits, limits, etc. • • •					
0.71±0.11±0.09		[1] ACHASOV	00C	SND	$e^+e^- \to \pi^+\pi^-$
$0.65\ ^{+0.38}_{-0.29}$		[1] GOLUBEV	86	ND	$e^+e^- \to \pi^+\pi^-$
$2.01\ ^{+1.07}_{-0.84}$		[1] VASSERMAN	81	OLYA	$e^+e^- \to \pi^+\pi^-$
<6.6	95	BUKIN	78B	OLYA	$e^+e^- \to \pi^+\pi^-$
<2.7	95	ALVENSLEB...	72	CNTR	$6.7\ \gamma C \to C\pi^+\pi^-$

[1] Using $B(\phi \to e^+e^-) = (2.99 \pm 0.08) \times 10^{-4}$.

$\Gamma(\omega\pi^0)/\Gamma_{total}$ — Γ_{13}/Γ

VALUE (units 10^{-5})	DOCUMENT ID		TECN	COMMENT
4.7±0.5 OUR FIT				
$\mathbf{5.2^{+1.3}_{-1.1}}$	[1,2] AULCHENKO	00A	SND	$e^+e^- \to \pi^+\pi^-\pi^0\pi^0$
• • • We do not use the following data for averages, fits, limits, etc. • • •				
4.4±0.6	[3] AMBROSINO	08G	KLOE	$e^+e^- \to \pi^+\pi^-2\pi^0$, $2\pi^0\gamma$
~5.4	[4] ACHASOV	00E	SND	$e^+e^- \to \pi^0\pi^0\gamma$
$5.5\ ^{+1.6}_{-1.4}\pm0.3$	[2,5] AULCHENKO	00A	SND	$e^+e^- \to \pi^+\pi^-\pi^0\pi^0$
$4.8\ ^{+1.9}_{-1.7}\pm0.8$	[4] ACHASOV	99	SND	$e^+e^- \to \pi^+\pi^-\pi^0\pi^0$

[1] Using the 1996 and 1998 data.
[2] (2.3 ± 0.3)% correction for other decay modes of the $\omega(782)$ applied.
[3] Not independent of the corresponding $\Gamma(\omega\pi^0) \times \Gamma(e^+e^-) / \Gamma^2(\text{total})$.
[4] Using the 1996 data.
[5] Using the 1998 data.

$\Gamma(\omega\gamma)/\Gamma_{total}$ — Γ_{14}/Γ

VALUE	CL%	DOCUMENT ID		TECN	COMMENT
<0.05	84	LINDSEY	66	HBC	2.1–2.7 $K^-p \to \Lambda\pi^+\pi^-$ neutrals

$\Gamma(\rho\gamma)/\Gamma_{total}$ — Γ_{15}/Γ

VALUE (units 10^{-4})	CL%	DOCUMENT ID		TECN	COMMENT
< 0.12	90	[1] AKHMETSHIN	99B	CMD2	$e^+e^- \to \pi^+\pi^-\gamma$
• • • We do not use the following data for averages, fits, limits, etc. • • •					
< 7	90	AKHMETSHIN	97C	CMD2	$e^+e^- \to \pi^+\pi^-\gamma$
<200	84	LINDSEY	66	HBC	2.1–2.7 $K^-p \to \Lambda\pi^+\pi^-$ neutrals

[1] Supersedes AKHMETSHIN 97C.

$\Gamma(\pi^+\pi^-\gamma)/\Gamma_{total}$ — Γ_{16}/Γ

VALUE (units 10^{-4})	CL%	EVTS	DOCUMENT ID		TECN	COMMENT
0.41±0.12±0.04		30175	[1] AKHMETSHIN	99B	CMD2	$e^+e^- \to \pi^+\pi^-\gamma$
• • • We do not use the following data for averages, fits, limits, etc. • • •						
< 0.3	90		[2] AKHMETSHIN	97C	CMD2	$e^+e^- \to \pi^+\pi^-\gamma$
<600	90		KALBFLEISCH	75	HBC	2.18 $K^-p \to \Lambda\pi^+\pi^-\gamma$
< 70	90		COSME	74	OSPK	$e^+e^- \to \pi^+\pi^-\gamma$
<400	90		LINDSEY	65	HBC	2.1–2.7 $K^-p \to \Lambda\pi^+\pi^-$ neutrals

[1] For $E_\gamma > 20$ MeV and assuming that $B(\phi(1020) \to f_0(980)\gamma)$ is negligible. Supersedes AKHMETSHIN 97C.
[2] For $E_\gamma > 20$ MeV and assuming that $B(\phi(1020) \to f_0(980)\gamma)$ is negligible.

$\Gamma(f_0(980)\gamma)/\Gamma_{total}$ — Γ_{17}/Γ

VALUE (units 10^{-4})	CL%	EVTS	DOCUMENT ID		TECN	COMMENT
3.22±0.19 OUR FIT	Error includes scale factor of 1.1.					
3.21±0.19 OUR AVERAGE						
$3.21\ ^{+0.03}_{-0.09}\pm0.18$			[1] AMBROSINO	07	KLOE	$e^+e^- \to \pi^0\pi^0\gamma$
2.90±0.21±1.54			[2] AKHMETSHIN	99C	CMD2	$e^+e^- \to \pi^+\pi^-\gamma$, $\pi^0\pi^0\gamma$
• • • We do not use the following data for averages, fits, limits, etc. • • •						
4.47±0.21		2438	[3] ALOISIO	02D	KLOE	$e^+e^- \to \pi^0\pi^0\gamma$
$3.5\ \pm0.3\ ^{+1.3}_{-0.5}$		419	[4,5] ACHASOV	00H	SND	$e^+e^- \to \pi^0\pi^0\gamma$
1.93±0.46±0.50		27188	[6] AKHMETSHIN	99B	CMD2	$e^+e^- \to \pi^+\pi^-\gamma$
3.05±0.25±0.72		268	[7] AKHMETSHIN	99C	CMD2	$e^+e^- \to \pi^0\pi^0\gamma$
1.5 ±0.5		268	[8] AKHMETSHIN	99C	CMD2	$e^+e^- \to \pi^0\pi^0\gamma$
3.42±0.30±0.36		164	[4] ACHASOV	98I	SND	$e^+e^- \to 5\gamma$
< 1	90		[9] AKHMETSHIN	97C	CMD2	$e^+e^- \to \pi^+\pi^-\gamma$
< 7	90		[10] AKHMETSHIN	97C	CMD2	$e^+e^- \to \pi^+\pi^-\gamma$
< 20	90		DRUZHININ	87	ND	$e^+e^- \to \pi^0\pi^0\gamma$

[1] Obtained by the authors taking into account the $\pi^+\pi^-$ decay mode. Includes a component due to $\pi\pi$ production via the $f_0(500)$ meson. Supersedes ALOISIO 02D.
[2] From the combined fit of the photon spectra in the reactions $e^+e^- \to \pi^+\pi^-\gamma$, $\pi^0\pi^0\gamma$.
[3] From the negative interference with the $f_0(500)$ meson of AITALA 01B using the ACHASOV 89 parameterization for the $f_0(980)$, a Breit-Wigner for the $f_0(500)$, and ACHASOV 01F for the $\rho\pi$ contribution. Superseded by AMBROSINO 07.
[4] Assuming that the $\pi^0\pi^0\gamma$ final state is completely determined by the $f_0\gamma$ mechanism, neglecting the decay $B(\phi \to K\overline{K}\gamma)$ and using $B(f_0 \to \pi^+\pi^-) = 2B(f_0 \to \pi^0\pi^0)$.
[5] Using the value $B(\phi \to \eta\gamma) = (1.338 \pm 0.053) \times 10^{-2}$.
[6] For $E_\gamma > 20$ MeV. Supersedes AKHMETSHIN 97C.
[7] Neglecting other intermediate mechanisms ($\rho\pi$, $\sigma\gamma$).
[8] A narrow pole fit taking into account $f_0(980)$ and $f_0(1200)$ intermediate mechanisms.
[9] For destructive interference with the Bremsstrahlung process
[10] For constructive interference with the Bremsstrahlung process

$\Gamma(f_0(980)\gamma)/\Gamma(\eta\gamma)$ — Γ_{17}/Γ_6

VALUE (units 10^{-2})	EVTS	DOCUMENT ID		TECN	COMMENT
2.48±0.15 OUR FIT	Error includes scale factor of 1.1.				
$\mathbf{2.6\ \pm0.2\ ^{+0.8}_{-0.3}}$	419	[1] ACHASOV	00H	SND	$e^+e^- \to \pi^0\pi^0\gamma$

[1] Assuming that the $\pi^0\pi^0\gamma$ final state is completely determined by the $f_0\gamma$ mechanism, neglecting the decay $B(\phi \to K\overline{K}\gamma)$ and using $B(f_0 \to \pi^+\pi^-) = 2B(f_0 \to \pi^0\pi^0)$.

$\Gamma(\pi^0\pi^0\gamma)/\Gamma_{total}$ — Γ_{18}/Γ

VALUE (units 10^{-4})	CL%	EVTS	DOCUMENT ID		TECN	COMMENT
1.07 ±0.06 OUR AVERAGE						
$1.07\ ^{+0.01}_{-0.03}\ ^{+0.06}_{-0.06}$			[1] AMBROSINO	07	KLOE	$e^+e^- \to \pi^0\pi^0\gamma$
1.08 ±0.17 ±0.09		268	AKHMETSHIN	99C	CMD2	$e^+e^- \to \pi^0\pi^0\gamma$

Downloaded from https://academic.oup.com/ptep/article/2022/8/083C01/6651666 by KIT Library user on 27 September 2022

• • • We do not use the following data for averages, fits, limits, etc. • • •

1.09 ±0.03 ±0.05	2438	ALOISIO	02D	KLOE	$e^+e^- \to \pi^0\pi^0\gamma$
1.158±0.093±0.052	419	[2,3] ACHASOV	00H	SND	$e^+e^- \to \pi^0\pi^0\gamma$
<10	90	DRUZHININ	87	ND	$e^+e^- \to 5\gamma$

[1] Supersedes ALOISIO 02D.
[2] Using the value B($\phi \to \eta\gamma$)=(1.338 ± 0.053) × 10^{-2}.
[3] Supersedes ACHASOV 98I. Excluding $\omega\pi^0$.

$\Gamma(\pi^0\pi^0\gamma)/\Gamma(\eta\gamma)$ — Γ_{18}/Γ_6

VALUE (units 10^{-2})	EVTS	DOCUMENT ID		TECN	COMMENT
0.86 ±0.04 OUR FIT					
0.865±0.070±0.017	419	[1] ACHASOV	00H	SND	$e^+e^- \to \pi^0\pi^0\gamma$
• • • We do not use the following data for averages, fits, limits, etc. • • •					
0.90 ±0.08 ±0.07	164	ACHASOV	98I	SND	$e^+e^- \to 5\gamma$

[1] Supersedes ACHASOV 98I. Excluding $\omega\pi^0$.

$\Gamma(\pi^+\pi^-\pi^+\pi^-)/\Gamma_{total}$ — Γ_{19}/Γ

VALUE (units 10^{-6})	CL%	EVTS	DOCUMENT ID		TECN	COMMENT
6.5 ±2.7 ±1.6		6.8k	[1] AKHMETSHIN	17	CMD3	$e^+e^- \to \pi^+\pi^-\pi^+\pi^-$
• • • We do not use the following data for averages, fits, limits, etc. • • •						
3.93±1.74±2.14		3.3k	AKHMETSHIN	00E	CMD2	$e^+e^- \to \pi^+\pi^-\pi^+\pi^-$
< 870	90		CORDIER	79	WIRE	$e^+e^- \to \pi^+\pi^-\pi^+\pi^-$

[1] Using the cross section at the ϕ meson peak $\sigma(\phi) = 4172 \pm 42$ nb, the nonresonant cross section $\sigma(0) = 1.263 \pm 0.027$ nb and Re(Z) = 0.146 ± 0.030, Im(Z) = −0.002 ± 0.024 for the complex amplitude of the $\phi \to \pi^+\pi^-\pi^+\pi^-$ transition.

$\Gamma(\pi^+\pi^+\pi^-\pi^-\pi^0)/\Gamma_{total}$ — Γ_{20}/Γ

VALUE (units 10^{-6})	CL%	DOCUMENT ID		TECN	COMMENT
< 4.6	90	AKHMETSHIN	00E	CMD2	$e^+e^- \to \pi^+\pi^-\pi^+\pi^-\pi^0$
• • • We do not use the following data for averages, fits, limits, etc. • • •					
<150	95	BARKOV	88	CMD	$e^+e^- \to \pi^+\pi^-\pi^+\pi^-\pi^0$

$\Gamma(\pi^0 e^+e^-)/\Gamma_{total}$ — Γ_{21}/Γ

VALUE (units 10^{-5})	CL%	EVTS	DOCUMENT ID		TECN	COMMENT
$1.33^{+0.07}_{-0.10}$ OUR AVERAGE						
$1.35\pm0.05^{+0.05}_{-0.10}$		9.5k	[1] ANASTASI	16B	KLOE	$e^+e^- \to \pi^0 e^+e^-$
1.01±0.28±0.29		52	[2] ACHASOV	02D	SND	$e^+e^- \to \pi^0 e^+e^-$
1.22±0.34±0.21		46	[3] AKHMETSHIN	01C	CMD2	$e^+e^- \to \pi^0 e^+e^-$
• • • We do not use the following data for averages, fits, limits, etc. • • •						
<12	90		DOLINSKY	88	ND	$e^+e^- \to \pi^0 e^+e^-$

[1] Using B($\pi^0 \to \gamma\gamma$) from the 2014 Edition of this Review (PDG 14).
[2] Using various branching ratios from the 2000 Edition of this Review (PDG 00).
[3] Using B($\pi^0 \to \gamma\gamma$) = 0.98798 ± 0.00032, B($\phi \to \eta\gamma$) = (1.297 ± 0.033) × 10^{-2}, and B($\eta \to \pi^+\pi^-\gamma$) = (4.75 ± 0.11) × 10^{-2}.

$\Gamma(\pi^0\eta\gamma)/\Gamma_{total}$ — Γ_{22}/Γ

VALUE (units 10^{-5})	CL%	EVTS	DOCUMENT ID		TECN	COMMENT
7.27±0.30 OUR AVERAGE Error includes scale factor of 1.5. See the ideogram below.						
7.06±0.22		16.9k	[1] AMBROSINO	09F	KLOE	$1.02\ e^+e^- \to \eta\pi^0\gamma$
8.51±0.51±0.57		607	[2] ALOISIO	02C	KLOE	$e^+e^- \to \eta\pi^0\gamma$
7.96±0.60±0.40		197	[3] ALOISIO	02C	KLOE	$e^+e^- \to \eta\pi^0\gamma$
8.8 ±1.4 ±0.9		36	[4] ACHASOV	00F	SND	$e^+e^- \to \eta\pi^0\gamma$
9.0 ±2.4 ±1.0		80	AKHMETSHIN	99C	CMD2	$e^+e^- \to \eta\pi^0\gamma$
• • • We do not use the following data for averages, fits, limits, etc. • • •						
7.01±0.10±0.20		13.3k	[2,5] AMBROSINO	09F	KLOE	$1.02\ e^+e^- \to \eta\pi^0\gamma$
7.12±0.13±0.22		3.6k	[3,6] AMBROSINO	09F	KLOE	$1.02\ e^+e^- \to \eta\pi^0\gamma$
8.3 ±2.3 ±1.2		20	ACHASOV	98B	SND	$e^+e^- \to 5\gamma$
<250	90		DOLINSKY	91	ND	$e^+e^- \to \pi^0\eta\gamma$

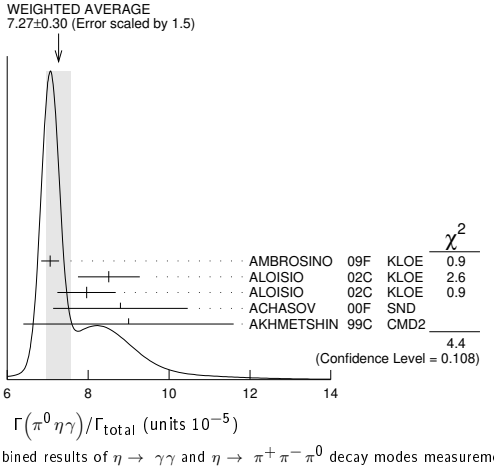

[1] Combined results of $\eta \to \gamma\gamma$ and $\eta \to \pi^+\pi^-\pi^0$ decay modes measurements.
[2] From the decay mode $\eta \to \gamma\gamma$.
[3] From the decay mode $\eta \to \pi^+\pi^-\pi^0$.
[4] Supersedes ACHASOV 98B.
[5] Using B($\phi \to \eta\gamma$) = (1.304 ± 0.025)%, B($\eta \to 3\pi^0$) = (32.56 ± 0.23)%, and B($\eta \to \gamma\gamma$) = (39.31 ± 0.20)%.
[6] Using B($\phi \to \eta\gamma$) = (1.304 ± 0.025)%, B($\eta \to 3\pi^0$) = (32.56 ± 0.23)%, and B($\eta \to \pi^+\pi^-\pi^0$) = (22.73 ± 0.28)%.

$\Gamma(a_0(980)\gamma)/\Gamma_{total}$ — Γ_{23}/Γ

VALUE (units 10^{-5})	CL%	EVTS	DOCUMENT ID		TECN	COMMENT
7.6±0.6 OUR FIT						
7.6±0.6 OUR AVERAGE						
7.4±0.7			[1] ALOISIO	02C	KLOE	$e^+e^- \to \eta\pi^0\gamma$
8.8±1.7		36	[2] ACHASOV	00F	SND	$e^+e^- \to \eta\pi^0\gamma$
• • • We do not use the following data for averages, fits, limits, etc. • • •						
11 ±2			[3] GOKALP	02	RVUE	$e^+e^- \to \eta\pi^0\gamma$
<500	90		DOLINSKY	91	ND	$e^+e^- \to \pi^0\eta\gamma$

[1] Using $M_{a_0(980)}$=984.8 MeV and assuming $a_0(980)\gamma$ dominance.
[2] Assuming $a_0(980)\gamma$ dominance in the $\eta\pi^0\gamma$ final state.
[3] Using data of ACHASOV 00F.

$\Gamma(f_0(980)\gamma)/\Gamma(a_0(980)\gamma)$ — Γ_{17}/Γ_{23}

VALUE	DOCUMENT ID		TECN	COMMENT
6.1±0.6	[1] ALOISIO	02C	KLOE	$e^+e^- \to \eta\pi^0\gamma$

[1] Using results of ALOISIO 02D and assuming that $f_0(980)$ decays into $\pi\pi$ only and $a_0(980)$ into $\eta\pi$ only.

$\Gamma(K^0\overline{K}^0\gamma)/\Gamma_{total}$ — Γ_{24}/Γ

VALUE	CL%	DOCUMENT ID		TECN	COMMENT
<1.9 × 10^{-8}	90	AMBROSINO	09C	KLOE	$e^+e^- \to K^0_S K^0_S \gamma$

$\Gamma(\eta'(958)\gamma)/\Gamma_{total}$ — Γ_{25}/Γ

VALUE (units 10^{-5})	CL%	EVTS	DOCUMENT ID		TECN	COMMENT
6.21±0.21 OUR FIT						
6.21±0.30 OUR AVERAGE						
6.21±0.27±0.12		3407	[1] AMBROSINO	07A	KLOE	$1.02\ e^+e^- \to \pi^+\pi^-7\gamma$
$6.7\ ^{+2.8}_{-2.4}$ ±0.8		12	[2] AULCHENKO	03B	SND	$e^+e^- \to \eta'\gamma$
• • • We do not use the following data for averages, fits, limits, etc. • • •						
$6.7\ ^{+5.0}_{-4.2}$ ±1.5		7	AULCHENKO	03B	SND	$e^+e^- \to 7\gamma$
6.10±0.61±0.43		120	[3] ALOISIO	02E	KLOE	$1.02\ e^+e^- \to \pi^+\pi^-3\gamma$
$8.2\ ^{+2.1}_{-1.9}$ ±1.1		21	[4] AKHMETSHIN	00B	CMD2	$e^+e^- \to \pi^+\pi^-3\gamma$
$4.9\ ^{+2.2}_{-1.8}$ ±0.6		9	[5] AKHMETSHIN	00F	CMD2	$e^+e^- \to \pi^+\pi^-\pi^+\pi^- \geq 2\gamma$
6.4 ±1.6		30	[6] AKHMETSHIN	00F	CMD2	$e^+e^- \to \eta'(958)\gamma$
$6.7\ ^{+3.4}_{-2.9}$ ±1.0		5	[7] AULCHENKO	99	SND	$e^+e^- \to \pi^+\pi^-3\gamma$
<11	90		AULCHENKO	98	SND	$e^+e^- \to 7\gamma$
$12\ ^{+7}_{-5}$ ±2		6	[4] AKHMETSHIN	97B	CMD2	$e^+e^- \to \pi^+\pi^-3\gamma$
<41	90		DRUZHININ	87	ND	$e^+e^- \to \gamma\eta\pi^+\pi^-$

[1] AMBROSINO 07A reports [$\Gamma(\phi(1020) \to \eta'(958)\gamma)/\Gamma_{total}$] / [B($\phi(1020) \to \eta\gamma$)] = (4.77 ± 0.09 ± 0.19) × 10^{-3} which we multiply by our best value B($\phi(1020) \to \eta\gamma$) = (1.301 ± 0.025) × 10^{-2}. Our first error is their experiment's error and our second error is the systematic error from using our best value.
[2] Averaging AULCHENKO 03B with AULCHENKO 99.
[3] Using B($\phi \to \eta\gamma$)= (1.297 ± 0.033)%.
[4] Using the value B($\phi \to \eta\gamma$) = (1.26 ± 0.06) × 10^{-2}.
[5] Using B($\phi \to K^0_L K^0_S$) = (33.8 ± 0.6)%.
[6] Averaging AKHMETSHIN 00B with AKHMETSHIN 00F.
[7] Using the value B($\eta' \to \eta\pi^+\pi^-$)= (43.7 ± 1.5) × 10^{-2} and B($\eta \to \gamma\gamma$)= (39.25 ± 0.31) × 10^{-2}.

$\Gamma(\eta'(958)\gamma)/\Gamma(K^0_L K^0_S)$ — Γ_{25}/Γ_2

VALUE (units 10^{-4})	EVTS	DOCUMENT ID		TECN	COMMENT
1.83±0.06 OUR FIT					
$1.46^{+0.64}_{-0.54}$±0.18	9	[1] AKHMETSHIN	00F	CMD2	$e^+e^- \to \pi^+\pi^-\pi^+\pi^- \geq 2\gamma$

[1] Using various branching ratios of K^0_S, K^0_L, η, η' from the 2000 edition (The European Physical Journal **C15** 1 (2000)) of this Review.

$\Gamma(\eta'(958)\gamma)/\Gamma(\eta\gamma)$ — Γ_{25}/Γ_6

VALUE (units 10^{-3})	EVTS	DOCUMENT ID		TECN	COMMENT
4.77±0.15 OUR FIT					
4.78±0.20 OUR AVERAGE					
4.77±0.09±0.19	3407	AMBROSINO	07A	KLOE	$1.02\ e^+e^- \to \pi^+\pi^-7\gamma$
4.70±0.47±0.31	120	[1] ALOISIO	02E	KLOE	$1.02\ e^+e^- \to \pi^+\pi^-3\gamma$
$6.5\ ^{+1.7}_{-1.5}$ ±0.8	21	AKHMETSHIN	00B	CMD2	$e^+e^- \to \pi^+\pi^-3\gamma$
• • • We do not use the following data for averages, fits, limits, etc. • • •					
$9.5\ ^{+5.2}_{-4.0}$ ±1.4	6	[2] AKHMETSHIN	97B	CMD2	$e^+e^- \to \pi^+\pi^-3\gamma$

[1] From the decay mode $\eta' \to \eta\pi^+\pi^-$, $\eta \to \gamma\gamma$.
[2] Superseded by AKHMETSHIN 00B.

Downloaded from https://academic.oup.com/ptep/article/2022/8/083C01/6651666 by KIT Library user on 27 September 2022

$\Gamma(\eta\pi^0\pi^0\gamma)/\Gamma_{total}$ — Γ_{26}/Γ

VALUE (units 10^{-5})	CL%	DOCUMENT ID		TECN	COMMENT
<2	90	AULCHENKO	98	SND	$e^+e^- \to 7\gamma$

$\Gamma(\mu^+\mu^-\gamma)/\Gamma_{total}$ — Γ_{27}/Γ

VALUE (units 10^{-5})	EVTS	DOCUMENT ID		TECN	COMMENT
1.43±0.45±0.14	27188	[1] AKHMETSHIN	99B	CMD2	$e^+e^- \to \mu^+\mu^-\gamma$
• • • We do not use the following data for averages, fits, limits, etc. • • •					
2.3 ±1.0	824 ± 33	[2] AKHMETSHIN	97C	CMD2	$e^+e^- \to \mu^+\mu^-\gamma$

[1] For $E_\gamma > 20$ MeV. Supersedes AKHMETSHIN 97C.
[2] For $E_\gamma > 20$ MeV.

$\Gamma(\rho\gamma\gamma)/\Gamma_{total}$ — Γ_{28}/Γ

VALUE (units 10^{-4})	CL%	DOCUMENT ID		TECN	COMMENT
<1.2	90	AULCHENKO	08	CMD2	$\phi \to \pi^+\pi^-\gamma\gamma$
• • • We do not use the following data for averages, fits, limits, etc. • • •					
<5	90	AKHMETSHIN	98	CMD2	$e^+e^- \to \pi^+\pi^-\gamma\gamma$

$\Gamma(\eta\pi^+\pi^-)/\Gamma_{total}$ — Γ_{29}/Γ

VALUE (units 10^{-5})	CL%	DOCUMENT ID		TECN	COMMENT
< 1.8	90	AKHMETSHIN	00E	CMD2	$e^+e^- \to \pi^+\pi^-\pi^+\pi^-\pi^0$
• • • We do not use the following data for averages, fits, limits, etc. • • •					
< 6.1	90	AULCHENKO	08	CMD2	$\phi \to \eta\pi^+\pi^-$
<30	90	AKHMETSHIN	98	CMD2	$e^+e^- \to \pi^+\pi^-\gamma\gamma$

$\Gamma(\eta\mu^+\mu^-)/\Gamma_{total}$ — Γ_{30}/Γ

VALUE (units 10^{-6})	CL%	DOCUMENT ID		TECN	COMMENT
<9.4	90	AKHMETSHIN	01	CMD2	$e^+e^- \to \eta e^+e^-$

$\Gamma(\eta U \to \eta e^+e^-)/\Gamma_{total}$ — Γ_{31}/Γ

VALUE	CL%	DOCUMENT ID		TECN	COMMENT
$<1\times10^{-6}$	90	[1] BABUSCI	13B	KLOE	$1.02\ e^+e^- \to \eta e^+e^-$

[1] For a narrow vector U with mass between 5 and 470 MeV, from the combined analysis of $\eta \to \pi^+\pi^-\pi^0$ and $\eta \to \pi^0\pi^0\pi^0$ from ARCHILLI 12. Measured 90% CL limits as a function of m_U range from 2.2×10^{-8} to 10^{-6}.

$\Gamma(\text{invisible})/\Gamma(K^+K^-)$ — Γ_{32}/Γ_1

VALUE	CL%	DOCUMENT ID		TECN	COMMENT
$<3.4\times10^{-4}$	90	ABLIKIM	18S	BES3	$J/\psi \to \phi\eta \to \phi\pi^+\pi^-\pi^0$

Lepton Family number (LF) violating modes

$\Gamma(e^\pm\mu^\mp)/\Gamma_{total}$ — Γ_{33}/Γ

VALUE	CL%	DOCUMENT ID		TECN	COMMENT
$<2\times10^{-6}$	90	ACHASOV	10A	SND	$e^+e^- \to e^\pm\mu^\mp$

$\pi^+\pi^-\pi^0$ / $\rho\pi$ AMPLITUDE RATIO a_1 IN DECAY OF $\phi \to \pi^+\pi^-\pi^0$

NIECKNIG 12 describes final-state interactions between the three pions in a dispersive framework using data on the $\pi\pi$ P-wave scattering phase shift.

VALUE (units 10^{-2})	CL%	EVTS	DOCUMENT ID		TECN	COMMENT
9.1±1.2 OUR AVERAGE						
10.1±4.4±1.7		80k	[1] AKHMETSHIN	06	CMD2	1.017–1.021 $e^+e^- \to \pi^+\pi^-\pi^0$
9.0±1.1±0.6		1.98M	[2,3] ALOISIO	03	KLOE	$1.02\ e^+e^- \to \pi^+\pi^-\pi^0$
• • • We do not use the following data for averages, fits, limits, etc. • • •						
$-6 < a_1 < 6$		500k	[3] ACHASOV	02	SND	$e^+e^- \to \pi^+\pi^-\pi^0$
$-16 < a_1 < 11$	90	9.8k	[1,4] AKHMETSHIN	98	CMD2	$e^+e^- \to \pi^+\pi^-\gamma\gamma$

[1] Dalitz plot analysis taking into account interference between the contact and $\rho\pi$ amplitudes.
[2] From a fit without limitations on charged and neutral ρ masses and widths.
[3] Recalculated by us to match the notations of AKHMETSHIN 98.
[4] Assuming zero phase for the contact term.

PARAMETER β IN $\phi \to Pe^+e^-$ DECAYS

In the one-pole approximation the electromagnetic transition form factor for $\phi \to Pe^+e^-$ ($P = \pi,\eta$) is given as a function of the e^+e^- invariant mass squared, q^2, by the expression:

$$|F(q^2)|^2 = (1 - q^2/\Lambda^2)^{-2},$$

where vector meson dominance predicts parameter $\Lambda \approx 0.770$ GeV ($\Lambda^{-2} \approx 1.687$ GeV^{-2}). The slope of this form factor, $\beta = dF/dq^2(q^2{=}0)$, equals Λ^{-2} in this approximation.

The measurements below obtain β in the one-pole approximation.

PARAMETER β IN $\phi \to \pi^0e^+e^-$ DECAY

VALUE (GeV^{-2})	EVTS	DOCUMENT ID		TECN	COMMENT
2.02±0.11	9.5k	[1] ANASTASI	16B	KLOE	$1.02\ e^+e^- \to \pi^0e^+e^-$

[1] The error combines statistical and systematic uncertainties.

PARAMETER β IN $\phi \to \eta e^+e^-$ DECAY

VALUE (GeV^{-2})	EVTS	DOCUMENT ID		TECN	COMMENT
1.29±0.13 OUR AVERAGE					
$1.28\pm0.10^{+0.09}_{-0.08}$	30k	BABUSCI	15	KLOE	$1.02\ e^+e^- \to \eta e^+e^-$
3.8 ±1.8	213	[1] ACHASOV	01B	SND	$1.02\ e^+e^- \to \eta e^+e^-$

[1] The uncertainty is statistical only. The systematic one is negligible, in comparison.

$\phi(1020)$ REFERENCES

LEES 21B PR D104 112003 J.P. Lees et al. (BABAR Collab.)
ALBRECHT 20 EPJ C80 453 M. Albrecht et al. (Crystal Barrel Collab.)
HOID 20 EPJ C80 988 B.-L. Hoid, M. Hoferichter, B. Kubis (BONN, BERN)
AAIJ 19H JHEP 1904 063 R. Aaij et al. (LHCb Collab.)
HOFERICHT... 19 JHEP 1908 137 M. Hoferichter, B.-L. Hoid, B. Kubis (WASH, BONN)
ABLIKIM 18S PR D98 032001 M. Ablikim et al. (BESIII Collab.)
AOUDE 18 PR D98 056021 R.T. Aoude et al.
KOZYREV 18 PL B779 64 E.A. Kozyrev et al. (CMD-3 Collab.)
AKHMETSHIN 17 PL B768 345 R.R. Akhmetshin et al. (CMD-3 Collab.)
ACHASOV 16A PR D93 092001 M.N. Achasov et al. (SND Collab.)
ANASTASI 16B PL B757 362 A. Anastasi et al. (KLOE-2 Collab.)
KOZYREV 16 PL B760 314 E.A. Kozyrev et al. (CMD-3 Collab.)
BABUSCI 15 PL B742 1 D. Babusci et al. (KLOE-2 Collab.)
PDG 15 RPP 2015 at pdg.lbl.gov (PDG Collab.)
LEES 14H PR D89 092002 J.P. Lees et al. (BABAR Collab.)
PDG 14 CP C38 070001 K. Olive et al. (PDG Collab.)
BABUSCI 13B PL B720 111 D. Babusci et al. (KLOE-2 Collab.)
BENAYOUN 13 EPJ C73 2453 M. Benayoun, P. David, L. DelBuono (PARIN, BERLIN+)
LEES 13F PR D87 052010 J.P. Lees et al. (BABAR Collab.)
LEES 13Q PR D88 032013 J.P. Lees et al. (BABAR Collab.)
ARCHILLI 12 PL B706 251 F. Archilli et al. (KLOE-2 Collab.)
BENAYOUN 12 EPJ C72 1848 M. Benayoun et al.
NIECKNIG 12 EPJ C72 2014 F. Niecknig, B. Kubis, S.P. Schneider (BONN)
PDG 12 PR D86 010001 J. Beringer et al. (PDG Collab.)
AKHMETSHIN 11 PL B695 412 R.R. Akhmetshin et al. (CMD-2 Collab.)
ACHASOV 10A PR D81 057102 M.N. Achasov et al. (Novosibirsk SND Collab.)
BENAYOUN 10 EPJ C65 211 M. Benayoun et al.
AMBROSINO 09C PL B679 10 F. Ambrosino et al. (KLOE Collab.)
AMBROSINO 09F PL B681 5 F. Ambrosino et al. (KLOE Collab.)
AKHMETSHIN 08 PL B669 217 R.R. Akhmetshin et al. (CMD-2 Collab.)
AMBROSINO 08G PL B669 223 F. Ambrosino et al. (KLOE Collab.)
AULCHENKO 08 JETPL 88 85 V. Aulchenko et al. (CMD-2 Collab.)
Translated from ZETFP 88 93.
FLOREZ-BAEZ 08 PR D78 077301 F.V. Florez-Baez, G. Lopez Castro
ACHASOV 07B PR D76 077101 M.N. Achasov et al. (SND Collab.)
AMBROSINO 07 EPJ C49 473 F. Ambrosino et al. (KLOE Collab.)
AMBROSINO 07A PL B648 267 F. Ambrosino et al. (KLOE Collab.)
DUBYNSKIY 07 PR D75 113001 S. Dubynskiy et al.
ACHASOV 06A PR D74 014016 M.N. Achasov et al. (SND Collab.)
AKHMETSHIN 06 PL B642 203 R.R. Akhmetshin et al. (CMD-2 Collab.)
AKHMETSHIN 05 PL B605 26 R.R. Akhmetshin et al. (Novosibirsk CMD-2 Collab.)
AMBROSINO 05 PL B608 199 F. Ambrosino et al. (KLOE Collab.)
AUBERT,B 05J PR D72 052008 B. Aubert et al. (BABAR Collab.)
AKHMETSHIN 04 PL B578 285 R.R. Akhmetshin et al. (Novosibirsk CMD-2 Collab.)
AUBERT,B 04N PR D70 072004 B. Aubert et al. (BABAR Collab.)
ALOISIO 03 PL B561 55 A. Aloisio et al. (KLOE Collab.)
AULCHENKO 03B JETP 97 24 V.M. Aulchenko et al. (Novosibirsk SND Collab.)
Translated from ZETF 124 28.
ACHASOV 02 PR D65 032002 M.N. Achasov et al. (Novosibirsk SND Collab.)
ACHASOV 02D JETPL 75 449 M.N. Achasov et al. (Novosibirsk SND Collab.)
Translated from ZETFP 75 539.
ALOISIO 02C PL B536 209 A. Aloisio et al. (KLOE Collab.)
ALOISIO 02D PL B537 21 A. Aloisio et al. (KLOE Collab.)
ALOISIO 02E PL B541 45 A. Aloisio et al. (KLOE Collab.)
FISCHBACH 02 PL B526 355 E. Fischbach, A.W. Overhauser, B. Woodahl
GOKALP 02 JP G28 2783 A. Gokalp et al.
ACHASOV 01B PL B504 275 M.N. Achasov et al. (Novosibirsk SND Collab.)
ACHASOV 01E PR D63 072002 M.N. Achasov et al. (Novosibirsk SND Collab.)
ACHASOV 01F PR D63 094007 N.N. Achasov, V.V. Gubin (Novosibirsk SND Collab.)
ACHASOV 01G PRL 86 1698 M.N. Achasov et al. (Novosibirsk SND Collab.)
AITALA 01B PRL 86 770 E.M. Aitala et al. (FNAL E791 Collab.)
AKHMETSHIN 01 PL B501 191 R.R. Akhmetshin et al. (Novosibirsk CMD-2 Collab.)
AKHMETSHIN 01B PL B509 217 R.R. Akhmetshin et al. (Novosibirsk CMD-2 Collab.)
AKHMETSHIN 01C PL B503 237 R.R. Akhmetshin et al. (Novosibirsk CMD-2 Collab.)
BENAYOUN 01 EPJ C22 503 M. Benayoun, H.B. O'Connell
ACHASOV 00 EPJ C12 25 M.N. Achasov et al. (Novosibirsk SND Collab.)
ACHASOV 00B JETP 90 17 M.N. Achasov et al. (Novosibirsk SND Collab.)
Translated from ZETF 117 22.
ACHASOV 00C PL B474 188 M.N. Achasov et al. (Novosibirsk SND Collab.)
ACHASOV 00D JETPL 72 282 M.N. Achasov et al. (Novosibirsk SND Collab.)
Translated from ZETFP 72 411.
ACHASOV 00E NP B569 158 M.N. Achasov et al. (Novosibirsk SND Collab.)
ACHASOV 00F PL B479 53 M.N. Achasov et al. (Novosibirsk SND Collab.)
ACHASOV 00H PL B485 349 M.N. Achasov et al. (Novosibirsk SND Collab.)
AKHMETSHIN 00B PL B473 337 R.R. Akhmetshin et al. (Novosibirsk CMD-2 Collab.)
AKHMETSHIN 00E PL B491 81 R.R. Akhmetshin et al. (Novosibirsk CMD-2 Collab.)
AKHMETSHIN 00F PL B494 26 R.R. Akhmetshin et al. (Novosibirsk CMD-2 Collab.)
AULCHENKO 00A JETP 90 927 V.M. Aulchenko et al. (Novosibirsk SND Collab.)
Translated from ZETF 117 1067.
BRAMON 00 PL B486 406 A. Bramon et al.
PDG 00 EPJ C15 1 D.E. Groom et al. (PDG Collab.)
ACHASOV 99 PL B449 122 M.N. Achasov et al.
ACHASOV 99C PL B456 304 M.N. Achasov et al.
AKHMETSHIN 99B PL B462 371 R.R. Akhmetshin et al. (Novosibirsk CMD-2 Collab.)
AKHMETSHIN 99C PL B462 380 R.R. Akhmetshin et al. (Novosibirsk CMD-2 Collab.)
AKHMETSHIN 99D PL B466 385 R.R. Akhmetshin et al.
Also PL B508 217 (errat.) R.R. Akhmetshin et al. (Novosibirsk CMD-2 Collab.)
AKHMETSHIN 99F PL B460 242 R.R. Akhmetshin et al. (Novosibirsk CMD-2 Collab.)
AULCHENKO 99 JETPL 69 97 V.M. Aulchenko et al.
Translated from ZETFP 69 87.
ACHASOV 98B PL B438 441 M.N. Achasov et al. (Novosibirsk SND Collab.)
ACHASOV 98F JETPL 68 573 M.N. Achasov et al. (Novosibirsk SND Collab.)
ACHASOV 98I PL B440 442 M.N. Achasov et al.
AKHMETSHIN 98 PL B434 426 R.R. Akhmetshin et al. (CMD-2 Collab.)
AULCHENKO 98 PL B436 199 V.M. Aulchenko et al. (Novosibirsk SND Collab.)
BARBERIS 98 PL B432 436 D. Barberis et al. (Omega Expt.)
AKHMETSHIN 97B PL B415 445 R.R. Akhmetshin et al. (NOVO, BOST, PITT+)
AKHMETSHIN 97C PL B415 452 R.R. Akhmetshin et al. (Novosibirsk CMD-2 Collab.)
BENAYOUN 96 ZPHY C72 221 M. Benayoun et al. (IPNP, NOVO)
AKHMETSHIN 95 PL B364 199 R.R. Akhmetshin et al. (Novosibirsk CMD-2 Collab.)
DOLINSKY 91 PRPL 202 99 S.I. Dolinsky et al. (NOVO)
KUHN 90 ZPHY C48 445 J.H. Kuhn et al. (MPIM)
ACHASOV 89 NP B315 465 N.N. Achasov, V.N. Ivanchenko
DOLINSKY 89 ZPHY C42 511 S.I. Dolinsky et al. (NOVO)
BARKOV 88 SJNP 47 248 L.M. Barkov et al. (NOVO)
Translated from YAF 47 393.
DOLINSKY 88 SJNP 48 277 S.I. Dolinsky et al. (NOVO)
Translated from YAF 48 442.

Downloaded from https://academic.oup.com/ptep/article/2022/8/083C01/6651666 by KIT Library user on 27 September 2022

DRUZHININ	87	ZPHY C37 1	V.P. Druzhinin *et al.*	(NOVO)
ARMSTRONG	86	PL 166B 245	T.A. Armstrong *et al.*	(ATHU, BARI, BIRM+)
ATKINSON	86	ZPHY C30 521	M. Atkinson *et al.*	(BONN, CERN, GLAS+)
BEBEK	86	PRL 56 1893	C. Bebek *et al.*	(CLEO Collab.)
DAVENPORT	86	PR D33 2519	T.F. Davenport	(TUFTS, ARIZ, FNAL, FSU, NDAM+)
DIJKSTRA	86	ZPHY C31 375	H. Dijkstra *et al.*	(ANIK, BRIS, CERN+)
FRAME	86	NP B276 667	D. Frame *et al.*	(GLAS)
GOLUBEV	86	SJNP 44 409	V.B. Golubev *et al.*	(NOVO)
		Translated from YAF 44 633.		
ALBRECHT	85D	PL 153B 343	H. Albrecht *et al.*	(ARGUS Collab.)
GOLUBEV	85	SJNP 41 756	V.B. Golubev *et al.*	(NOVO)
		Translated from YAF 41 1183.		
DRUZHININ	84	PL 144B 136	V.P. Druzhinin *et al.*	(NOVO)
ARMSTRONG	83B	NP B224 193	T.A. Armstrong *et al.*	(BARI, BIRM, CERN+)
BARATE	83	PL 121B 449	R. Barate *et al.*	(SACL, LOIC, SHMP, IND)
KURDADZE	83C	JETPL 38 366	L.M. Kurdadze *et al.*	(NOVO)
		Translated from ZETFP 38 306.		
ARENTON	82	PR D25 2241	M.W. Arenton *et al.*	(ANL, ILL)
PELLINEN	82	PS 25 599	A. Pellinen, M. Roos	(HELS)
DAUM	81	PL 100B 439	C. Daum *et al.*	(AMST, BRIS, CERN, CRAC+)
IVANOV	81	PL 107B 297	P.M. Ivanov *et al.*	(NOVO)
Also		Private Comm.	S.I. Eidelman	(NOVO)
VASSERMAN	81	PL 99B 62	I.B. Vasserman *et al.*	(NOVO)
Also		SJNP 35 240	L.M. Kurdadze *et al.*	
		Translated from YAF 35 352.		
CORDIER	80	NP B172 13	A. Cordier *et al.*	(LALO)
CORDIER	79	PL 81B 389	A. Cordier *et al.*	(LALO)
BUKIN	78B	SJNP 27 521	A.D. Bukin *et al.*	(NOVO)
		Translated from YAF 27 985.		
BUKIN	78C	SJNP 27 516	A.D. Bukin *et al.*	(NOVO)
		Translated from YAF 27 976.		
COOPER	78B	NP B146 1	A.M. Cooper *et al.*	(TATA, CERN, CDEF+)
LOSTY	78	NP B133 38	M.J. Losty *et al.*	(CERN, AMST, NIJM+)
AKERLOF	77	PRL 39 861	C.W. Akerlof *et al.*	(FNAL, MICH, PURD)
ANDREWS	77	PRL 38 198	D.E. Andrews *et al.*	(ROCH)
BALDI	77	PL 68B 381	R. Baldi *et al.*	(GEVA)
CERRADA	77B	NP B126 241	M. Cerrada *et al.*	(AMST, CERN, NIJM+)
COHEN	77	PRL 38 269	D. Cohen *et al.*	(ANL)
LAVEN	77	NP B127 43	H. Laven *et al.*	(AACH3, BERL, CERN, LOIC+)
LYONS	77	NP B125 207	L. Lyons, A.M. Cooper, A.G. Clark	(OXF)
COSME	76	PL 63B 352	G. Cosme *et al.*	(ORSAY)
KALBFLEISCH	76	PR D13 22	G.R. Kalbfleisch, R.C. Strand, J.W. Chapman	(BNL+)
PARROUR	76	PL 63B 357	G. Parrour *et al.*	(ORSAY)
PARROUR	76B	PL 63B 362	G. Parrour *et al.*	(ORSAY)
KALBFLEISCH	75	PR D11 987	G.R. Kalbfleisch, R.C. Strand, J.W. Chapman	(BNL+)
AYRES	74	PRL 32 1463	D.S. Ayres *et al.*	(ANL)
BESCH	74	NP B70 257	H.J. Besch *et al.*	(BONN)
COSME	74	PL 48B 155	G. Cosme *et al.*	(ORSAY)
COSME	74B	PL 48B 159	G. Cosme *et al.*	(ORSAY)
DEGROOT	74	NP B74 77	A.J. de Groot *et al.*	(AMST, NIJM)
AUGUSTIN	73	PRL 30 462	J.E. Augustin *et al.*	(ORSAY)
BALLAM	73	PR D7 3150	J. Ballam *et al.*	(SLAC, LBL)
BINNIE	73B	PR D8 2789	D.M. Binnie *et al.*	(LOIC, SHMP)
AGUILAR-...	72B	PR D6 29	M. Aguilar-Benitez *et al.*	(BNL)
ALVENSLEB...	72	PRL 28 66	H. Alvensleben *et al.*	(MIT, DESY)
BORENSTEIN	72	PR D5 1559	S.R. Borenstein *et al.*	(BNL, MICH)
COLLEY	72	NP B50 1	D.C. Colley *et al.*	(BIRM, GLAS)
BALAKIN	71	PL 34B 328	V.E. Balakin *et al.*	(NOVO)
CHATELUS	71	Thesis LAL 1247	Y. Chatelus	(STRB)
Also		PL 32B 416	J.C. Bizot *et al.*	(ORSAY)
HAYES	71	PR D4 899	S. Hayes *et al.*	(CORN)
STOTTLE...	71	Thesis ORO 2504 170	A.R. Stottlemyer	(UMD)
BIZOT	70	PL 32B 416	J.C. Bizot *et al.*	(ORSAY)
Also		Liverpool Sym. 69	J.P. Perez-y-Jorba	
EARLES	70	PRL 25 1312	D.R. Earles *et al.*	(NEAS)
LINDSEY	66	PR 147 913	J.S. Lindsey, G. Smith	(LRL)
LONDON	66	PR 143 1034	G.W. London *et al.*	(BNL, SYRA) IGJPC
BADIER	65B	PL 17 337	J. Badier *et al.*	(EPOL, SACL, AMST)
LINDSEY	65	PRL 15 221	J.S. Lindsey, G.A. Smith	(LRL)
LINDSEY 65 data included in LINDSEY 66.				
SCHLEIN	63	PRL 10 368	P.E. Schlein *et al.*	(UCLA) IGJP

$h_1(1170)$

$I^G(J^{PC}) = 0^-(1^{+-})$

$h_1(1170)$ MASS

VALUE (MeV)		DOCUMENT ID		TECN	CHG	COMMENT
1166± 5±3		[1] ANDO	92	SPEC		$8\ \pi^- p \to \pi^+\pi^-\pi^0 n$
• • • We do not use the following data for averages, fits, limits, etc. • • •						
1168± 4		ANDO	92	SPEC		$8\ \pi^- p \to \pi^+\pi^-\pi^0 n$
1190±60		[2] DANKOWY...	81	SPEC	0	$8\ \pi p \to 3\pi n$

[1] Average and spread of values using 2 variants of the model of BOWLER 75.
[2] Uses the model of BOWLER 75.

$h_1(1170)$ WIDTH

VALUE (MeV)		DOCUMENT ID		TECN	CHG	COMMENT
375± 6±34		[3] ANDO	92	SPEC		$8\ \pi^- p \to \pi^+\pi^-\pi^0 n$
• • • We do not use the following data for averages, fits, limits, etc. • • •						
345± 6		ANDO	92	SPEC		$8\ \pi^- p \to \pi^+\pi^-\pi^0 n$
320±50		[4] DANKOWY...	81	SPEC	0	$8\ \pi p \to 3\pi n$

[3] Average and spread of values using 2 variants of the model of BOWLER 75.
[4] Uses the model of BOWLER 75.

$h_1(1170)$ DECAY MODES

	Mode	Fraction (Γ_i/Γ)
Γ_1	$\rho\pi$	seen

$h_1(1170)$ BRANCHING RATIOS

$\Gamma(\rho\pi)/\Gamma_{total}$ — Γ_1/Γ

VALUE	DOCUMENT ID		TECN	COMMENT
• • • We do not use the following data for averages, fits, limits, etc. • • •				
seen	ANDO	92	SPEC	$8\ \pi^- p \to \pi^+\pi^-\pi^0 n$
seen	ATKINSON	84	OMEG	20–70 $\gamma p \to \pi^+\pi^-\pi^0 p$
seen	DANKOWY...	81	SPEC	$8\ \pi p \to 3\pi n$

$h_1(1170)$ REFERENCES

ANDO	92	PL B291 496	A. Ando *et al.*	(KEK, KYOT, NIRS, SAGA+)
ATKINSON	84	NP B231 15	M. Atkinson *et al.*	(BONN, CERN, GLAS+)
DANKOWY...	81	PRL 46 580	J.A. Dankowych *et al.*	(TNTO, BNL, CARL+)
BOWLER	75	NP B97 227	M.G. Bowler *et al.*	(OXFTP, DARE)

$b_1(1235)$

$I^G(J^{PC}) = 1^+(1^{+-})$

$b_1(1235)$ MASS

VALUE (MeV)	EVTS	DOCUMENT ID		TECN	CHG	COMMENT
1229.5± 3.2 OUR AVERAGE		Error includes scale factor of 1.6.				See the ideogram below.
1225 ± 5		WEIDENAUER	93	ASTE		$\bar{p}p \to 2\pi^+2\pi^-\pi^0$
1235 ±15		ALDE	92C	GAM2		38,100 $\pi^- p \to \omega\pi^0 n$
1236 ±16		FUKUI	91	SPEC		8.95 $\pi^- p \to \omega\pi^0 n$
1222 ± 6		ATKINSON	84E	OMEG	±	25–55 $\gamma p \to \omega\pi X$
1237 ± 7		ATKINSON	84E	OMEG	0	25–55 $\gamma p \to \omega\pi X$
1239 ± 5		EVANGELIS...	81	OMEG	−	12 $\pi^- p \to \omega\pi p$
1251 ± 8	450	GESSAROLI	77	HBC	−	11 $\pi^- p \to \pi^-\omega p$
1245 ±11	890	FLATTE	76C	HBC	−	4.2 $K^- p \to \pi^-\omega\Sigma^+$
1222 ± 4	1400	CHALOUPKA	74	HBC	−	3.9 $\pi^- p$
1220 ± 7	600	KARSHON	74B	HBC	+	4.9 $\pi^+ p$
• • • We do not use the following data for averages, fits, limits, etc. • • •						
1190 ±10		AUGUSTIN	89	DM2	±	$e^+e^- \to 5\pi$
1213 ± 5		ATKINSON	84C	OMEG	0	20–70 γp
1271 ±11		COLLICK	84	SPEC	+	200 $\pi^+ Z \to Z\pi\omega$

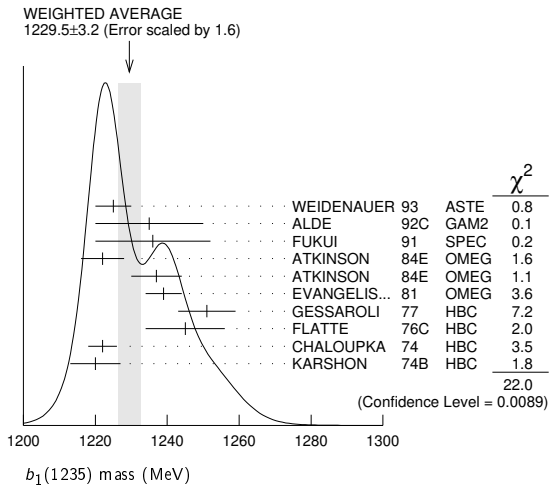

$b_1(1235)$ WIDTH

VALUE (MeV)	EVTS	DOCUMENT ID		TECN	CHG	COMMENT
142± 9 OUR AVERAGE		Error includes scale factor of 1.2.				
113±12		WEIDENAUER	93	ASTE		$\bar{p}p \to 2\pi^+2\pi^-\pi^0$
160±30		ALDE	92C	GAM2		38,100 $\pi^- p \to \omega\pi^0 n$
151±31		FUKUI	91	SPEC		8.95 $\pi^- p \to \omega\pi^0 n$
170±15		EVANGELIS...	81	OMEG	−	12 $\pi^- p \to \omega\pi p$
170±50	225	BALTAY	78B	HBC	+	15 $\pi^+ p \to p4\pi$
155±32	450	GESSAROLI	77	HBC	−	11 $\pi^- p \to \pi^-\omega p$
182±45	890	FLATTE	76C	HBC	−	4.2 $K^- p \to \pi^-\omega\Sigma^+$
135±20	1400	CHALOUPKA	74	HBC	−	3.9 $\pi^- p$
156±22	600	KARSHON	74B	HBC	+	4.9 $\pi^+ p$
• • • We do not use the following data for averages, fits, limits, etc. • • •						
210±19		AUGUSTIN	89	DM2	±	$e^+e^- \to 5\pi$
231±14		ATKINSON	84C	OMEG	0	20–70 γp
232±29		COLLICK	84	SPEC	+	200 $\pi^+ Z \to Z\pi\omega$

Downloaded from https://academic.oup.com/ptep/article/2022/8/083C01/6651666 by KIT Library user on 27 September 2022

$b_1(1235)$ DECAY MODES

	Mode	Fraction (Γ_i/Γ)	Confidence level
Γ_1	$\omega\pi$ [D/S amplitude ratio = 0.277 ± 0.027]	seen	
Γ_2	$\pi^\pm\gamma$	$(1.6\pm0.4)\times10^{-3}$	
Γ_3	$\eta\rho$	seen	
Γ_4	$\pi^+\pi^+\pi^-\pi^0$	<50 %	84%
Γ_5	$K^*(892)^\pm K^\mp$	seen	
Γ_6	$(K\overline{K})^\pm\pi^0$	<8 %	90%
Γ_7	$K^0_S K^0_L \pi^\pm$	<6 %	90%
Γ_8	$K^0_S K^0_S \pi^\pm$	<2 %	90%
Γ_9	$\phi\pi$	<1.5 %	84%

$b_1(1235)$ PARTIAL WIDTHS

$\Gamma(\pi^\pm\gamma)$ — Γ_2

VALUE (keV)	DOCUMENT ID		TECN	CHG	COMMENT
230±60	COLLICK	84	SPEC	+	200 $\pi^+ Z \to Z\pi\omega$

$b_1(1235)$ D-wave/S-wave AMPLITUDE RATIO IN DECAY OF $b_1(1235) \to \omega\pi$

VALUE	EVTS	DOCUMENT ID		TECN	CHG	COMMENT
0.277±0.027 OUR AVERAGE		Error includes scale factor of 2.4. See the ideogram below.				
0.269±0.009±0.010		NOZAR	02	MPS	−	18 $\pi^- p \to \omega\pi^- p$
0.23 ±0.03		AMSLER	94C	CBAR		0.0 $\overline{p}p \to \omega\eta\pi^0$
0.45 ±0.04		AMSLER	93B	CBAR		0.0 $\overline{p}p \to \omega\pi^0\pi^0$
0.235±0.047		ATKINSON	84C	OMEG		20–70 γp
$0.4\ ^{+0.1}_{-0.1}$		GESSAROLI	77	HBC	−	11 $\pi^- p \to \pi^-\omega p$
0.21 ±0.08		CHUNG	75B	HBC	+	7.1 $\pi^+ p$
0.3 ±0.1		CHALOUPKA	74	HBC	−	3.9–7.5 $\pi^- p$
0.35 ±0.25	600	KARSHON	74B	HBC	+	4.9 $\pi^+ p$

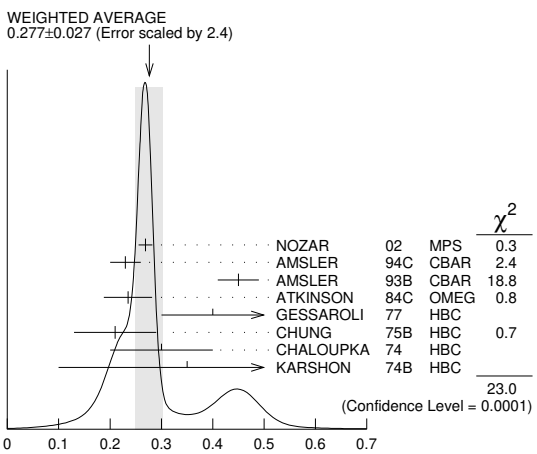

$b_1(1235)$ D-wave/S-wave amplitude ratio in decay of $b_1(1235) \to \omega\pi$

$b_1(1235)$ D-wave/S-wave AMPLITUDE PHASE DIFFERENCE IN DECAY OF $b_1(1235) \to \omega\pi$

VALUE (°)	DOCUMENT ID		TECN	CHG	COMMENT
10.5±2.4±3.9	NOZAR	02	MPS	−	18 $\pi^- p \to \omega\pi^- p$

$b_1(1235)$ BRANCHING RATIOS

$\Gamma(\eta\rho)/\Gamma(\omega\pi)$ — Γ_3/Γ_1

VALUE	DOCUMENT ID		TECN	COMMENT
<0.10	ATKINSON	84D	OMEG	20–70 γp

$\Gamma(\pi^+\pi^+\pi^-\pi^0)/\Gamma(\omega\pi)$ — Γ_4/Γ_1

VALUE	DOCUMENT ID		TECN	CHG	COMMENT
<0.5	ABOLINS	63	HBC	+	3.5 $\pi^+ p$

$\Gamma(K^*(892)^\pm K^\mp)/\Gamma_{total}$ — Γ_5/Γ

VALUE	DOCUMENT ID		TECN	COMMENT
seen	[1] ABLIKIM	10E	BES2	$J/\psi \to K^\pm K^0_S \pi^\mp \pi^0$

[1] From a fit including ten additional resonances and energy-independent Breit-Wigner width.

$\Gamma((K\overline{K})^\pm\pi^0)/\Gamma(\omega\pi)$ — Γ_6/Γ_1

VALUE	CL%	DOCUMENT ID		TECN	CHG	COMMENT
<0.08	90	BALTAY	67	HBC	±	0.0 $\overline{p}p$

$\Gamma(K^0_S K^0_L \pi^\pm)/\Gamma(\omega\pi)$ — Γ_7/Γ_1

VALUE	CL%	DOCUMENT ID		TECN	CHG	COMMENT
<0.06	90	BALTAY	67	HBC	±	0.0 $\overline{p}p$

$\Gamma(K^0_S K^0_S \pi^\pm)/\Gamma(\omega\pi)$ — Γ_8/Γ_1

VALUE	CL%	DOCUMENT ID		TECN	CHG	COMMENT
<0.02	90	BALTAY	67	HBC	±	0.0 $\overline{p}p$

$\Gamma(\phi\pi)/\Gamma(\omega\pi)$ — Γ_9/Γ_1

VALUE	CL%	DOCUMENT ID		TECN	CHG	COMMENT
<0.004	95	VIKTOROV	96	SPEC	0	32.5 $\pi^- p \to K^+ K^- \pi^0 n$
• • • We do not use the following data for averages, fits, limits, etc. • • •						
<0.04	95	BIZZARRI	69	HBC	±	0.0 $\overline{p}p$
<0.015		DAHL	67	HBC		1.6–4.2 $\pi^- p$

$b_1(1235)$ REFERENCES

ABLIKIM	10E	PL B693 88	M. Ablikim *et al.*	(BES II Collab.)
NOZAR	02	PL B541 35	M. Nozar *et al.*	
VIKTOROV	96	PAN 59 1184	V.A. Viktorov *et al.*	(SERP)
		Translated from YAF 59 1239.		
AMSLER	94C	PL B327 425	C. Amsler *et al.*	(Crystal Barrel Collab.)
AMSLER	93B	PL B311 362	C. Amsler *et al.*	(Crystal Barrel Collab.)
WEIDENAUER	93	ZPHY C59 387	P. Weidenauer *et al.*	(ASTERIX Collab.)
ALDE	92C	ZPHY C54 553	D.M. Alde *et al.*	(BELG, SERP, KEK, LANL+)
FUKUI	91	PL B257 241	S. Fukui *et al.*	(SUGI, NAGO, KEK, KYOT+)
AUGUSTIN	89	NP B320 1	J.E. Augustin, G. Cosme	(DM2 Collab.)
ATKINSON	84C	NP B243 1	M. Atkinson *et al.*	(BONN, CERN, GLAS+) JP
ATKINSON	84D	NP B242 269	M. Atkinson *et al.*	(BONN, CERN, GLAS+)
ATKINSON	84E	PL 138B 459	M. Atkinson *et al.*	(BONN, CERN, GLAS+)
COLLICK	84	PRL 53 2374	B. Collick *et al.*	(MINN, ROCH, FNAL)
EVANGELIS...	81	NP B178 197	C. Evangelista *et al.*	(BARI, BONN, CERN+)
BALTAY	78B	PR D17 62	C. Baltay *et al.*	(COLU, BING)
GESSAROLI	77	NP B126 382	R. Gessaroli *et al.*	(BGNA, FIRZ, GENO+) JP
FLATTE	76C	PL 64B 225	S.M. Flatte *et al.*	(CERN, AMST, NIJM+) JP
CHUNG	75B	PR D11 2426	S.U. Chung *et al.*	(BNL, LBL, UCSC) JP
CHALOUPKA	74	PL 51B 407	V. Chaloupka *et al.*	(CERN) JP
KARSHON	74B	PR D10 3608	U. Karshon *et al.*	(REHO) JP
BIZZARRI	69	NP B14 169	R. Bizzarri *et al.*	(CERN, CDEF)
BALTAY	67	PRL 18 93	C. Baltay *et al.*	(COLU)
DAHL	67	PR 163 1377	O.I. Dahl *et al.*	(LRL)
ABOLINS	63	PRL 11 381	M.A. Abolins *et al.*	(UCSD)

$a_1(1260)$

$I^G(J^{PC}) = 1^-(1^{++})$

See also our review under the $a_1(1260)$ in PDG 06, Journal of Physics **G33** 1 (2006).

$a_1(1260)$ MASS

VALUE (MeV)	EVTS	DOCUMENT ID		TECN	COMMENT
1230 ±40 OUR ESTIMATE					
1299 $^{+12}_{-28}$	46M	[1] AGHASYAN	18B	COMP	190 $\pi^- p \to \pi^-\pi^+\pi^- p$
• • • We do not use the following data for averages, fits, limits, etc. • • •					
1195.05± 1.05± 6.33	894k	AAIJ	18AI	LHCB	$D^0 \to K^\mp\pi^\pm\pi^\pm\pi^\mp$
1209 ± 4 $^{+12}_{-9}$		[2] MIKHASENKO	18	RVUE	$\tau^- \to \pi^-\pi^+\pi^-\nu_\tau$
1225 ± 9 ±20	7k	[3] DARGENT	17	RVUE	$D^0 \to \pi^-\pi^+\pi^-\pi^+$
1255 ± 6 $^{+7}_{-17}$	420k	[4] ALEKSEEV	10	COMP	190 $\pi^- Pb \to \pi^-\pi^-\pi^+ Pb'$
1243 ±12 ±20		[5] AUBERT	07AU	BABR	10.6 $e^+e^- \to \rho^0\rho^\pm\pi^\mp\gamma$
1230–1270	6360	[6] LINK	07A	FOCS	$D^0 \to \pi^-\pi^+\pi^-\pi^+$
1203 ± 3		[7] GOMEZ-DUM...04		RVUE	$\tau^+ \to \pi^+\pi^+\pi^-\nu_\tau$
1330 ±24	90k	SALVINI	04	OBLX	$\overline{p}p \to 2\pi^+2\pi^-$
1331 ±10 ± 3	37k	[8] ASNER	00	CLE2	10.6 $e^+e^- \to \tau^+\tau^-$, $\tau^- \to \pi^-\pi^0\pi^0\nu_\tau$
1255 ± 7 ± 6	5904	[9] ABREU	98G	DLPH	e^+e^-
1207 ± 5 ± 8	5904	[10] ABREU	98G	DLPH	e^+e^-
1196 ± 4 ± 5	5904	[11,12] ABREU	98G	DLPH	e^+e^-
1240 ±10		BARBERIS	98B		450 $pp \to p_f\pi^+\pi^-\pi^0 p_s$
1262 ± 9 ± 7		[9,13] ACKERSTAFF	97R	OPAL	E^{ee}_{cm}= 88–94, $\tau \to 3\pi\nu$
1210 ± 7 ± 2		[10,13] ACKERSTAFF	97R	OPAL	E^{ee}_{cm}= 88–94, $\tau \to 3\pi\nu$
1211 ± 7 $^{+50}_{-0}$		[10] ALBRECHT	93C	ARG	$\tau^+ \to \pi^+\pi^+\pi^-\nu$
1121 ± 8		[14] ANDO	92	SPEC	8 $\pi^- p \to \pi^+\pi^-\pi^0 n$
1242 ±37		[15] IVANOV	91	RVUE	$\tau \to \pi^+\pi^+\pi^-\nu$
1260 ±14		[16] IVANOV	91	RVUE	$\tau \to \pi^+\pi^+\pi^-\nu$
1250 ± 9		[17] IVANOV	91	RVUE	$\tau \to \pi^+\pi^+\pi^-\nu$
1208 ±15		ARMSTRONG	90	OMEG	300.0 $pp \to pp\pi^+\pi^-\pi^0$

Downloaded from https://academic.oup.com/ptep/article/2022/8/083C01/6651666 by KIT Library user on 27 September 2022

1220	±15			[18] ISGUR	89	RVUE	$\tau^+ \to \pi^+\pi^+\pi^-\nu$
1260	±25			[19] BOWLER	88	RVUE	
1166	±18	±11		BAND	87	MAC	$\tau^+ \to \pi^+\pi^+\pi^-\nu$
1164	±41	±23		BAND	87	MAC	$\tau^+ \to \pi^+\pi^0\pi^0\nu$
1250	±40			[18] TORNQVIST	87	RVUE	
1046	±11			ALBRECHT	86B	ARG	$\tau^+ \to \pi^+\pi^+\pi^-\nu$
1056	±20	±15		RUCKSTUHL	86	DLCO	$\tau^+ \to \pi^+\pi^+\pi^-\nu$
1194	±14	±10		SCHMIDKE	86	MRK2	$\tau^+ \to \pi^+\pi^+\pi^-\nu$
1255	±23			BELLINI	85	SPEC	$40\ \pi^- A \to \pi^-\pi^+\pi^- A$
1240	±80			[20] DANKOWY...	81	SPEC	$8.45\ \pi^- p \to n3\pi$
1280	±30			[20] DAUM	81B	CNTR	$63,94\ \pi^- p \to p3\pi$
1041	±13			[21] GAVILLET	77	HBC	$4.2\ K^- p \to \Sigma 3\pi$

[1] Statistical error negligible.
[2] From the pole position. Using an amplitude analysis based on approximate three-body unitary of τ data from SCHAEL 05C.
[3] Reanalysis of CLEO data using Breit-Wigner parameterization.
[4] Superseded by AGHASYAN 2018B.
[5] The $\rho^\pm\pi^\mp$ state can be also due to the $\pi(1300)$.
[6] Using the Breit-Wigner parameterization; strong correlation between mass and width.
[7] Using the data of BARATE 98R.
[8] From a fit to the 3π mass spectrum including the $K\overline{K}^*(892)$ threshold.
[9] Uses the model of KUHN 90.
[10] Uses the model of ISGUR 89.
[11] Includes the effect of a possible a_1' state.
[12] Uses the model of FEINDT 90.
[13] Supersedes AKERS 95P.
[14] Average and spread of values using 2 variants of the model of BOWLER 75.
[15] Reanalysis of RUCKSTUHL 86.
[16] Reanalysis of SCHMIDKE 86.
[17] Reanalysis of ALBRECHT 86B.
[18] From a combined reanalysis of ALBRECHT 86B, SCHMIDKE 86, and RUCKSTUHL 86.
[19] From a combined reanalysis of ALBRECHT 86B and DAUM 81B.
[20] Uses the model of BOWLER 75.
[21] Produced in K^- backward scattering.

$a_1(1260)$ WIDTH

VALUE (MeV)		EVTS	DOCUMENT ID		TECN	COMMENT
250 to 600 OUR ESTIMATE						
420 ± 35 OUR AVERAGE						
380 ± 80		46M	[1] AGHASYAN	18B	COMP	$190\ \pi^- p \to \pi^-\pi^+\pi^- p$
430 ± 24	± 31		DARGENT	17	RVUE	$D^0 \to \pi^-\pi^+\pi^-\pi^+$
• • • We do not use the following data for averages, fits, limits, etc. • • •						
422.01 ± 2.10	± 12.72	894k	AAIJ	18AI	LHCB	$D^0 \to K^\mp\pi^\pm\pi^\pm\pi^\mp$
576 ± 11	$^{+89}_{-20}$		[2] MIKHASENKO	18	RVUE	$\tau^- \to \pi^-\pi^+\pi^-\nu_\tau$
367 ± 9	$^{+28}_{-25}$	420k	[3] ALEKSEEV	10	COMP	$190\ \pi^- Pb \to \pi^-\pi^-\pi^+ Pb'$
410 ± 31	± 30		[4] AUBERT	07AU	BABR	$10.6\ e^+e^- \to \rho^0\rho^\pm\pi^\mp\gamma$
520–680		6360	[5] LINK	07A	FOCS	$D^0 \to \pi^-\pi^+\pi^-\pi^+$
480 ± 20			[6] GOMEZ-DUM..	04	RVUE	$\tau^+ \to \pi^+\pi^+\pi^-\nu_\tau$
580 ± 41		90k	SALVINI	04	OBLX	$\overline{p}p \to 2\pi^+2\pi^-$
460 ± 85		205	[7] DRUTSKOY	02	BELL	$B \to D^{(*)}K^-K^{*0}$
814 ± 36	± 13	37k	[8] ASNER	00	CLE2	$10.6\ e^+e^- \to \tau^+\tau^-,\ \tau^- \to \pi^-\pi^0\pi^0\nu_\tau$
450 ± 50		22k	[9] AKHMETSHIN	99E	CMD2	$1.05–1.38\ e^+e^- \to \pi^+\pi^-\pi^0\pi^0$
570 ± 10			[10] BONDAR	99	RVUE	$e^+e^- \to 4\pi,\ \tau \to 3\pi\nu_\tau$
587 ± 27	± 21	5904	[11] ABREU	98G	DLPH	e^+e^-
478 ± 3	± 15	5904	[12] ABREU	98G	DLPH	e^+e^-
425 ± 14	± 8	5904	[13,14] ABREU	98G	DLPH	e^+e^-
400 ± 35			BARBERIS	98B		$450\ pp \to p_f\pi^+\pi^-\pi^0 p_s$
621 ± 32	± 58		[11,15] ACKERSTAFF	97R	OPAL	$E^{ee}_{cm} = 88–94,\ \tau \to 3\pi\nu$
457 ± 15	± 17		[12,15] ACKERSTAFF	97R	OPAL	$E^{ee}_{cm} = 88–94,\ \tau \to 3\pi\nu$
446 ± 21	$^{+140}_{-0}$		[12] ALBRECHT	93C	ARG	$\tau^+ \to \pi^+\pi^+\pi^-\nu$
239 ± 11			ANDO	92	SPEC	$8\ \pi^- p \to \pi^+\pi^-\pi^0 n$
266 ± 13	± 4		[16] ANDO	92	SPEC	$8\ \pi^- p \to \pi^+\pi^-\pi^0 n$
465	$^{+228}_{-143}$		[17] IVANOV	91	RVUE	$\tau \to \pi^+\pi^+\pi^-\nu$
298	$^{+40}_{-34}$		[18] IVANOV	91	RVUE	$\tau \to \pi^+\pi^+\pi^-\nu$
488 ± 32			[19] IVANOV	91	RVUE	$\tau \to \pi^+\pi^+\pi^-\nu$
430 ± 50			ARMSTRONG	90	OMEG	$300.0 pp \to pp\pi^+\pi^-\pi^0$
420 ± 40			[20] ISGUR	89	RVUE	$\tau^+ \to \pi^+\pi^+\pi^-\nu$
396 ± 43			[21] BOWLER	88	RVUE	
405 ± 75	± 25		BAND	87	MAC	$\tau^+ \to \pi^+\pi^+\pi^-\nu$
419 ± 108	± 57		BAND	87	MAC	$\tau^+ \to \pi^+\pi^0\pi^0\nu$
521 ± 27			ALBRECHT	86B	ARG	$\tau^+ \to \pi^+\pi^+\pi^-\nu$
476	$^{+132}_{-120}$ ± 54		RUCKSTUHL	86	DLCO	$\tau^+ \to \pi^+\pi^+\pi^-\nu$
462 ± 56	± 30		SCHMIDKE	86	MRK2	$\tau^+ \to \pi^+\pi^+\pi^-\nu$
292 ± 40			BELLINI	85	SPEC	$40\ \pi^- A \to \pi^-\pi^+\pi^- A$
380 ± 100			[22] DANKOWY...	81	SPEC	$8.45\ \pi^- p \to n3\pi$
300 ± 50			[22] DAUM	81B	CNTR	$63,94\ \pi^- p \to p3\pi$
230 ± 50			[23] GAVILLET	77	HBC	$4.2\ K^- p \to \Sigma 3\pi$

[1] Statistical error negligible.
[2] From the pole position. Using an amplitude analysis based on approximate three-body unitary of τ data from SCHAEL 05C.
[3] Superseded by AGHASYAN 2018B.
[4] The $\rho^\pm\pi^\mp$ state can be also due to the $\pi(1300)$.
[5] Using the Breit-Wigner parameterization; strong correlation between mass and width.
[6] Using the data of BARATE 98R.
[7] From a fit of the K^-K^{*0} distribution assuming $m_{a_1} = 1230$ MeV and purely resonant production of the K^-K^{*0} system.
[8] From a fit to the 3π mass spectrum including the $K\overline{K}^*(892)$ threshold.
[9] Using the $a_1(1260)$ mass of 1230 MeV.
[10] From AKHMETSHIN 99E and ASNER 00 data using the $a_1(1260)$ mass of 1230 MeV.
[11] Uses the model of KUHN 90.
[12] Uses the model of ISGUR 89.
[13] Includes the effect of a possible a_1' state.
[14] Uses the model of FEINDT 90.
[15] Supersedes AKERS 95P.
[16] Average and spread of values using 2 variants of the model of BOWLER 75.
[17] Reanalysis of RUCKSTUHL 86.
[18] Reanalysis of SCHMIDKE 86.
[19] Reanalysis of ALBRECHT 86B.
[20] From a combined reanalysis of ALBRECHT 86B, SCHMIDKE 86, and RUCKSTUHL 86.
[21] From a combined reanalysis of ALBRECHT 86B and DAUM 81B.
[22] Uses the model of BOWLER 75.
[23] Produced in K^- backward scattering.

$a_1(1260)$ DECAY MODES

	Mode	Fraction (Γ_i/Γ)
Γ_1	3π	seen
Γ_2	$(\rho\pi)_{S-\text{wave}},\ \rho \to \pi\pi$	seen
Γ_3	$(\rho\pi)_{D-\text{wave}},\ \rho \to \pi\pi$	seen
Γ_4	$(\rho(1450)\pi)_{S-\text{wave}},\ \rho \to \pi\pi$	seen
Γ_5	$(\rho(1450)\pi)_{D-\text{wave}},\ \rho \to \pi\pi$	seen
Γ_6	$f_0(500)\pi,\ f_0 \to \pi\pi$	seen
Γ_7	$f_0(980)\pi,\ f_0 \to \pi\pi$	not seen
Γ_8	$f_0(1370)\pi,\ f_0 \to \pi\pi$	seen
Γ_9	$f_2(1270)\pi,\ f_2 \to \pi\pi$	seen
Γ_{10}	$\pi^+\pi^-\pi^0$	seen
Γ_{11}	$\pi^0\pi^0\pi^0$	not seen
Γ_{12}	$KK\pi$	seen
Γ_{13}	$K^*(892)K$	seen
Γ_{14}	$\pi\gamma$	seen

$a_1(1260)$ PARTIAL WIDTHS

$\Gamma(\pi\gamma)$ — Γ_{14}

VALUE (keV)	DOCUMENT ID		TECN	COMMENT
640±246	ZIELINSKI	84C	SPEC	$200\ \pi^+ Z \to Z3\pi$

D-wave/S-wave AMPLITUDE RATIO IN DECAY OF $a_1(1260) \to \rho\pi$

VALUE	DOCUMENT ID		TECN	COMMENT
−0.062±0.020 OUR AVERAGE	Error includes scale factor of 2.3. See the ideogram below.			
−0.043±0.009±0.005	LINK	07A	FOCS	$D^0 \to \pi^-\pi^+\pi^-\pi^+$
−0.14 ±0.04 ±0.07	[1] CHUNG	02	B852	$18.3\ \pi^- p \to \pi^+\pi^-\pi^- p$
−0.10 ±0.02 ±0.02	[2,3] ACKERSTAFF	97R	OPAL	$E^{ee}_{cm} = 88–94,\ \tau \to 3\pi\nu$
−0.11 ±0.02	[2] ALBRECHT	93C	ARG	$\tau^+ \to \pi^+\pi^+\pi^-\nu$

[1] Deck-type background not subtracted.
[2] Uses the model of ISGUR 89.
[3] Supersedes AKERS 95P.

Downloaded from https://academic.oup.com/ptep/article/2022/8/083C01/6651666 by KIT Library user on 27 September 2022

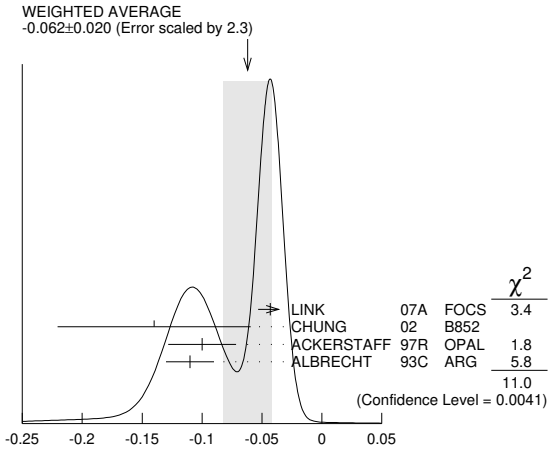

D-wave/S-wave AMPLITUDE RATIO IN DECAY OF $a_1(1260) \to \rho\pi$

$a_1(1260)$ BRANCHING RATIOS

$\Gamma((\rho\pi)_{S\text{-wave}}, \rho\to\pi\pi)/\Gamma_{total}$ — Γ_2/Γ

VALUE (units 10^{-2})	EVTS	DOCUMENT ID		TECN	COMMENT
• • • We do not use the following data for averages, fits, limits, etc. • • •					
60.19	37k	[1] ASNER	00	CLE2	10.6 $e^+e^-\to\tau^+\tau^-$, $\tau^-\to\pi^-\pi^0\pi^0\nu_\tau$

$\Gamma((\rho\pi)_{D\text{-wave}}, \rho\to\pi\pi)/\Gamma_{total}$ — Γ_3/Γ

VALUE (units 10^{-2})	EVTS	DOCUMENT ID		TECN	COMMENT
• • • We do not use the following data for averages, fits, limits, etc. • • •					
1.30±0.60±0.22	37k	[1] ASNER	00	CLE2	10.6 $e^+e^-\to\tau^+\tau^-$, $\tau^-\to\pi^-\pi^0\pi^0\nu_\tau$

$\Gamma((\rho(1450)\pi)_{S\text{-wave}}, \rho\to\pi\pi)/\Gamma_{total}$ — Γ_4/Γ

VALUE (units 10^{-2})	EVTS	DOCUMENT ID		TECN	COMMENT
• • • We do not use the following data for averages, fits, limits, etc. • • •					
0.56±0.84±0.32	37k	[1,2] ASNER	00	CLE2	10.6 $e^+e^-\to\tau^+\tau^-$, $\tau^-\to\pi^-\pi^0\pi^0\nu_\tau$

$\Gamma((\rho(1450)\pi)_{D\text{-wave}}, \rho\to\pi\pi)/\Gamma_{total}$ — Γ_5/Γ

VALUE (units 10^{-2})	EVTS	DOCUMENT ID		TECN	COMMENT
• • • We do not use the following data for averages, fits, limits, etc. • • •					
2.04±1.20±0.28	37k	[1,2] ASNER	00	CLE2	10.6 $e^+e^-\to\tau^+\tau^-$, $\tau^-\to\pi^-\pi^0\pi^0\nu_\tau$

$\Gamma(f_0(500)\pi, f_0\to\pi\pi)/\Gamma_{total}$ — Γ_6/Γ

VALUE (units 10^{-2})	EVTS	DOCUMENT ID		TECN	COMMENT
• • • We do not use the following data for averages, fits, limits, etc. • • •					
seen		CHUNG	02	B852	18.3 $\pi^-p\to\pi^+\pi^-\pi^-p$
18.76±4.29±1.48	37k	[1,3] ASNER	00	CLE2	10.6 $e^+e^-\to\tau^+\tau^-$, $\tau^-\to\pi^-\pi^0\pi^0\nu_\tau$

$\Gamma(f_0(500)\pi, f_0\to\pi\pi)/\Gamma((\rho\pi)_{S\text{-wave}}, \rho\to\pi\pi)$ — Γ_6/Γ_2

VALUE	EVTS	DOCUMENT ID		TECN	COMMENT
• • • We do not use the following data for averages, fits, limits, etc. • • •					
0.06 ±0.05	90k	SALVINI	04	OBLX	$\overline{p}p\to 2\pi^+2\pi^-$
∼ 0.3	28k	AKHMETSHIN	99E	CMD2	1.05–1.38 $e^+e^-\to\pi^+\pi^-\pi^+\pi^-$
0.003±0.003		[4] LONGACRE	82	RVUE	

$\Gamma(f_0(980)\pi, f_0\to\pi\pi)/\Gamma_{total}$ — Γ_7/Γ

VALUE (units 10^{-2})	EVTS	DOCUMENT ID		TECN	COMMENT
• • • We do not use the following data for averages, fits, limits, etc. • • •					
not seen	37k	ASNER	00	CLE2	10.6 $e^+e^-\to\tau^+\tau^-$, $\tau^-\to\pi^-\pi^0\pi^0\nu_\tau$

$\Gamma(f_0(1370)\pi, f_0\to\pi\pi)/\Gamma_{total}$ — Γ_8/Γ

VALUE (units 10^{-2})	EVTS	DOCUMENT ID		TECN	COMMENT
• • • We do not use the following data for averages, fits, limits, etc. • • •					
7.40±2.71±1.26	37k	[1,5] ASNER	00	CLE2	10.6 $e^+e^-\to\tau^+\tau^-$, $\tau^-\to\pi^-\pi^0\pi^0\nu_\tau$

$\Gamma(f_2(1270)\pi, f_2\to\pi\pi)/\Gamma_{total}$ — Γ_9/Γ

VALUE (units 10^{-2})	EVTS	DOCUMENT ID		TECN	COMMENT
• • • We do not use the following data for averages, fits, limits, etc. • • •					
1.19±0.49±0.17	37k	[1,6] ASNER	00	CLE2	10.6 $e^+e^-\to\tau^+\tau^-$, $\tau^-\to\pi^-\pi^0\pi^0\nu_\tau$

$\Gamma(\pi^+\pi^-\pi^0)/\Gamma_{total}$ — Γ_{10}/Γ

VALUE	DOCUMENT ID		COMMENT
seen	BARBERIS	98B	450 $pp\to p_f\pi^+\pi^-\pi^0p_s$

$\Gamma(\pi^0\pi^0\pi^0)/\Gamma(\pi^+\pi^-\pi^0)$ — Γ_{11}/Γ_{10}

VALUE	CL%	DOCUMENT ID		COMMENT
• • • We do not use the following data for averages, fits, limits, etc. • • •				
<0.008	90	[7] BARBERIS	01	450 $pp\to p_f3\pi^0p_s$

$\Gamma(K^*(892)K)/\Gamma_{total}$ — Γ_{13}/Γ

VALUE (units 10^{-2})	EVTS	DOCUMENT ID		TECN	COMMENT
• • • We do not use the following data for averages, fits, limits, etc. • • •					
2.2±0.5	2255	[8] COAN	04	CLEO	$\tau^-\to K^-\pi^-K^+\nu_\tau$
8 to 15	205	[9] DRUTSKOY	02	BELL	$B\to D^{(*)}K^-K^{*0}$
3.3±0.5±0.1	37k	[10] ASNER	00	CLE2	10.6 $e^+e^-\to\tau^+\tau^-$, $\tau^-\to\pi^-\pi^0\pi^0\nu_\tau$
2.6±0.3		[11] BARATE	99R	ALEP	$\tau\to K\overline{K}\pi\nu_\tau$

[1] From a fit to the Dalitz plot.
[2] Assuming for $\rho(1450)$ mass and width of 1370 and 386 MeV respectively.
[3] Assuming for $f_0(500)$ (σ) mass and width of 860 and 880 MeV respectively.
[4] Uses multichannel Aitchison-Bowler model (BOWLER 75). Uses data from GAVILLET 77, DAUM 80, and DANKOWYCH 81.
[5] Assuming for $f_0(1370)$ mass and width of 1186 and 350 MeV respectively.
[6] Assuming for $f_2(1270)$ mass and width of 1275 and 185 MeV respectively.
[7] Inconsistent with observations of $\sigma\pi$, $f_0(1370)\pi$, and $f_2(1270)\pi$ decay modes.
[8] Using structure functions from KUHN 92 and DECKER 93A and $B(\tau^-\to K^-\pi^-K^+\nu_\tau) = (0.155 \pm 0.006 \pm 0.009)\%$ from BRIERE 03.
[9] From a comparison to ALAM 94 assuming purely resonant production of the K^-K^{*0} system.
[10] From a fit to the 3π mass spectrum including the $K\overline{K}^*(892)$ threshold.
[11] Assuming $a_1(1260)$ dominance and taking $B(\tau\to a_1(1260)\nu_\tau)$ from BUSKULIC 96.

$a_1(1260)$ REFERENCES

AAIJ 18AI EPJ C78 443 R. Aaij et al. (LHCb Collab.)
AGHASYAN 18B PR D98 092003 M. Aghasyan et al. (COMPASS Collab.)
MIKHASENKO 18 PR D98 096021 M. Mikhasenko et al. (JPAC Collab.)
DARGENT 17 JHEP 1705 143 P. dArgent et al. (HEID, BRIS)
ALEKSEEV 10 PRL 104 241803 M.G. Alekseev et al. (COMPASS Collab.)
AUBERT 07AU PR D76 092005 B. Aubert et al. (BABAR Collab.)
LINK 07A PR D75 052003 J.M. Link et al. (FNAL FOCUS Collab.)
PDG 06 JP G33 1 W.-M. Yao et al. (PDG Collab.)
SCHAEL 05C PRPL 421 191 S. Schael et al. (ALEPH Collab.)
COAN 04 PRL 92 232001 T.E. Coan et al. (CLEO Collab.)
GOMEZ-DUM... 04 PR D69 073002 D. Gomez Dumm, A. Pich, J. Portoles
SALVINI 04 EPJ C35 21 P. Salvini et al. (OBELIX Collab.)
BRIERE 03 PRL 90 181802 R. A. Briere et al. (CLEO Collab.)
CHUNG 02 PR D65 072001 S.U. Chung et al. (BNL E852 Collab.)
DRUTSKOY 02 PL B542 171 A. Drutskoy et al. (BELLE Collab.)
BARBERIS 01 PL B507 14 D. Barberis et al.
ASNER 00 PR D61 012002 D.M. Asner et al. (CLEO Collab.)
AKHMETSHIN 99E PL B466 392 R.R. Akhmetshin et al. (Novosibirsk CMD-2 Collab.)
BARATE 99R EPJ C11 599 R. Barate et al. (ALEPH Collab.)
BONDAR 99 PL B466 403 A.E. Bondar et al. (Novosibirsk CMD-2 Collab.)
ABREU 98G PL B426 411 P. Abreu et al. (DELPHI Collab.)
BARATE 98R EPJ C4 409 R. Barate et al. (ALEPH Collab.)
BARBERIS 98B PL B422 399 D. Barberis et al. (WA 102 Collab.)
ACKERSTAFF 97R ZPHY C75 593 K. Ackerstaff et al. (OPAL Collab.)
BUSKULIC 96 ZPHY C70 579 D. Buskulic et al. (ALEPH Collab.)
AKERS 95P ZPHY C67 45 R. Akers et al. (OPAL Collab.)
ALAM 94 PR D50 43 M.S. Alam et al. (CLEO Collab.)
ALBRECHT 93C ZPHY C58 61 H. Albrecht et al. (ARGUS Collab.)
DECKER 93A ZPHY C58 445 R. Decker et al.
ANDO 92 PL B291 496 A. Ando et al. (KEK, KYOT, NIRS, SAGA+)
KUHN 92 ZPHY C56 661 J.H. Kuhn, E. Mirkes
IVANOV 91 ZPHY C49 563 Y.P. Ivanov, A.A. Osipov, M.K. Volkov (JINR)
ARMSTRONG 90 ZPHY C48 213 T.A. Armstrong, M. Benayoun, W. Beusch (WA76 Coll.)
FEINDT 90 ZPHY C48 681 M. Feindt (HAMB)
KUHN 90 ZPHY C48 445 J.H. Kuhn et al. (MPIM)
ISGUR 89 PR D39 1357 N. Isgur, C. Morningstar, C. Reader (TNTO)
BOWLER 88 PL B209 99 M.G. Bowler (OXF)
BAND 87 PL B198 297 H.R. Band et al. (MAC Collab.)
TORNQVIST 87 ZPHY C36 695 N.A. Tornqvist (HELS)
ALBRECHT 86B ZPHY C33 7 H. Albrecht et al. (ARGUS Collab.)
RUCKSTUHL 86 PRL 56 2132 W. Ruckstuhl et al. (DELCO Collab.)
SCHMIDKE 86 PRL 57 527 W.B. Schmidke et al. (Mark II Collab.)
BELLINI 85 SJNP 41 781 D. Bellini et al.
Translated from YAF 41 1223.
ZIELINSKI 84C PRL 52 1195 M. Zielinski et al. (ROCH, MINN, FNAL)
LONGACRE 82 PR D26 82 R.S. Longacre (BNL)
DANKOWY... 81 PRL 46 580 J.A. Dankowych et al. (TNTO, BNL, CARL+)
DAUM 81B NP B182 269 C. Daum et al. (AMST, CERN, CRAC, MPIM+)
DAUM 80 PL 89B 281 C. Daum et al. (AMST, CERN, CRAC, MPIM+) JP
GAVILLET 77 PL 69B 119 P. Gavillet et al. (AMST, CERN, NIJM+) JP
BOWLER 75 NP B97 227 M.G. Bowler et al. (OXFTP, DARE)

Downloaded from https://academic.oup.com/ptep/article/2022/8/083C01/6651666 by KIT Library user on 27 September 2022

$f_2(1270)$

$I^G(J^{PC}) = 0^+(2^{++})$

$f_2(1270)$ MASS

VALUE (MeV)	EVTS	DOCUMENT ID		TECN	COMMENT
1275.5± 0.8 OUR AVERAGE					
1275.8± 1.0±0.4		[1] BOGOLYUB...	13	SPEC	$7\pi^+(K^+,p)A \to n\gamma + X$
1262 $^{+1}_{-2}$ ±8		[2] ABLIKIM	06V	BES2	$e^+e^- \to J/\psi \to \gamma\pi^+\pi^-$
1275 ±15		ABLIKIM	05	BES2	$J/\psi \to \phi\pi^+\pi^-$
1283 ± 5		ALDE	98	GAM4	$100\ \pi^-p \to \pi^0\pi^0 n$
1278 ± 5		[3] BERTIN	97C	OBLX	$0.0\ \overline{p}p \to \pi^+\pi^-\pi^0$
1272 ± 8	200k	PROKOSHKIN	94	GAM2	$38\ \pi^-p \to \pi^0\pi^0 n$
1269.7± 5.2	5730	AUGUSTIN	89	DM2	$e^+e^- \to 5\pi$
1283 ± 8	400	[4] ALDE	87	GAM4	$100\ \pi^-p \to 4\pi^0 n$
1274 ± 5		[4] AUGUSTIN	87	DM2	$J/\psi \to \gamma\pi^+\pi^-$
1283 ± 6		[5] LONGACRE	86	MPS	$22\ \pi^-p \to n2K^0_S$
1276 ± 7		COURAU	84	DLCO	$e^+e^- \to e^+e^-\pi^+\pi^-$
1273.3± 2.3		[6] CHABAUD	83	ASPK	$17\ \pi^-p$ polarized
1280 ± 4		[7] CASON	82	STRC	$8\ \pi^+p \to \Delta^{++}\pi^0\pi^0$
1281 ± 7	11600	GIDAL	81	MRK2	J/ψ decay
1282 ± 5		[8] CORDEN	79	OMEG	12–$15\ \pi^-p \to n2\pi$
1269 ± 4	10k	APEL	75	NICE	$40\ \pi^-p \to n2\pi^0$
1272 ± 4	4600	ENGLER	74	DBC	$6\ \pi^+n \to \pi^+\pi^-p$
1277 ± 4	5300	FLATTE	71	HBC	$7.0\ \pi^+p$
1273 ± 8		[4] STUNTEBECK	70	HBC	$8\ \pi^-p$, $5.4\ \pi^+d$
1265 ± 8		BOESEBECK	68	HBC	$8\ \pi^+p$
• • • We do not use the following data for averages, fits, limits, etc. • • •					
1268 ± 8		[9] RODAS	22	RVUE	$J/\psi(1S) \to \gamma\ (\pi\pi,\ K\overline{K})$
1263 ±12		CARVER	21	CLAS	$\gamma p \to \pi^0\pi^0 p$
1263.3± 0.2±1.5		[10] ALBRECHT	20	RVUE	$0.9\ \overline{p}p \to \pi^0\pi^0\eta,\ \pi^0\eta\eta,\ \pi^0K^+K^-$
1259 ± 4 ±4	1.7k	[11,12] DOBBS	15		$J/\psi \to \gamma\pi^+\pi^-$
1267 ± 4 ±3	1.5k	[11,12] DOBBS	15		$\psi(2S) \to \gamma\pi^+\pi^-$
1270 ± 8		[13] ANISOVICH	09	RVUE	$0.0\ \overline{p}p,\ \pi N$
1277 ± 6	870	[14] SCHEGELSKY	06A	RVUE	$\gamma\gamma \to K^0_S K^0_S$
1251 ±10		TIKHOMIROV	03	SPEC	$40.0\ \pi^-C \to K^0_S K^0_S K^0_L X$
1260 ±10		[15] ALDE	97	GAM2	$450\ pp \to pp\pi^0\pi^0$
1278 ± 6		[15] GRYGOREV	96	SPEC	$40\ \pi^-N \to K^0_S K^0_S X$
1262 ±11		AGUILAR-...	91	EHS	$400\ pp$
1275 ±10		AKER	91	CBAR	$0.0\ \overline{p}p \to 3\pi^0$
1220 ±10		BREAKSTONE	90	SFM	$pp \to pp\pi^+\pi^-$
1288 ±12		ABACHI	86B	HRS	$e^+e^- \to \pi^+\pi^-X$
1284 ±30	3k	BINON	83	GAM2	$38\ \pi^-p \to n2\eta$
1280 ±20	3k	APEL	82	CNTR	$25\ \pi^-p \to n2\pi^0$
1284 ±10	16000	DEUTSCH...	76	HBC	$16\ \pi^+p$
1258 ±10	600	TAKAHASHI	72	HBC	$8\ \pi^-p \to n2\pi$
1275 ±13		ARMENISE	70	HBC	$9\ \pi^+n \to p\pi^+\pi^-$
1261 ± 5	1960	[4] ARMENISE	68	DBC	$5.1\ \pi^+n \to p\pi^+MM^-$
1270 ±10	360	[4] ARMENISE	68	DBC	$5.1\ \pi^+n \to p\pi^0MM$
1268 ± 6		[16] JOHNSON	68	HBC	3.7–$4.2\ \pi^-p$

[1] Averaged over six nuclear targets, no statistically significant dependence on target nucleus observed.
[2] Breit-Wigner mass.
[3] T-matrix pole.
[4] Mass errors enlarged by us to $\Gamma/\sqrt{N}$; see the note with the $K^*(892)$ mass.
[5] From a partial-wave analysis of data using a K-matrix formalism with 5 poles.
[6] From an energy-independent partial-wave analysis.
[7] From an amplitude analysis of the reaction $\pi^+\pi^- \to 2\pi^0$.
[8] From an amplitude analysis of $\pi^+\pi^- \to \pi^+\pi^-$ scattering data.
[9] T-matrix pole from coupled channel K-matrix fit to data on $J/\psi \to \gamma\pi^0\pi^0$ (ABLIKIM 15AE) and $J/\psi \to \gamma K^0_S K^0_S$ (ABLIKIM 18AA).
[10] T-matrix pole, 5 poles, 5 channels, including scattering data from HYAMS 75 ($\pi\pi$), LONGACRE 86 ($K\overline{K}$), BINON 83 ($\eta\eta$).
[11] Using CLEO-c data but not authored by the CLEO Collaboration.
[12] From a fit to a Breit-Wigner line shape with fixed $\Gamma = 185$ MeV.
[13] 4-poles, 5-channel K matrix fit.
[14] From analysis of L3 data at 91 and 183–209 GeV.
[15] Systematic uncertainties not estimated.
[16] JOHNSON 68 includes BONDAR 63, LEE 64, DERADO 65, EISNER 67.

$f_2(1270)$ WIDTH

VALUE (MeV)	EVTS	DOCUMENT ID		TECN	COMMENT
186.7$^{+2.2}_{-2.5}$ OUR FIT Error includes scale factor of 1.4.					
185.9$^{+2.8}_{-2.1}$ OUR AVERAGE Error includes scale factor of 1.6. See the ideogram below.					
190.3± 1.9± 1.8		[1] BOGOLYUB...	13	SPEC	$7\pi^+(K^+,p)A \to n\gamma + X$
175 $^{+6}_{-4}$ ±10		[2] ABLIKIM	06V	BES2	$e^+e^- \to J/\psi \to \gamma\pi^+\pi^-$
190 ±20		ABLIKIM	05	BES2	$J/\psi \to \phi\pi^+\pi^-$
171 ±10		ALDE	98	GAM4	$100\ \pi^-p \to \pi^0\pi^0 n$
204 ±20		[3] BERTIN	97C	OBLX	$0.0\ \overline{p}p \to \pi^+\pi^-\pi^0$
192 ± 5	200k	PROKOSHKIN	94	GAM2	$38\ \pi^-p \to \pi^0\pi^0 n$
180 ±24		AGUILAR-...	91	EHS	$400\ pp$
169 ± 9	5730	[4] AUGUSTIN	89	DM2	$e^+e^- \to 5\pi$
150 ±30	400	[4] ALDE	87	GAM4	$100\ \pi^-p \to 4\pi^0 n$
186 $^{+9}_{-2}$		[5] LONGACRE	86	MPS	$22\ \pi^-p \to n2K^0_S$
179.2$^{+6.9}_{-6.6}$		[6] CHABAUD	83	ASPK	$17\ \pi^-p$ polarized
160 ±11		DENNEY	83	LASS	$10\ \pi^+N$
196 ±10	3k	APEL	82	CNTR	$25\ \pi^-p \to n2\pi^0$
152 ± 9		[7] CASON	82	STRC	$8\ \pi^+p \to \Delta^{++}\pi^0\pi^0$
186 ±27	11600	GIDAL	81	MRK2	J/ψ decay
216 ±13		[8] CORDEN	79	OMEG	12–$15\ \pi^-p \to n2\pi$
190 ±10	10k	APEL	75	NICE	$40\ \pi^-p \to n2\pi^0$
192 ±16	4600	ENGLER	74	DBC	$6\ \pi^+n \to \pi^+\pi^-p$
183 ±15	5300	FLATTE	71	HBC	$7\ \pi^+p \to \Delta^{++}f_2$
196 ±30		[4] STUNTEBECK	70	HBC	$8\ \pi^-p$, $5.4\ \pi^+d$
216 ±20	1960	[4] ARMENISE	68	DBC	$5.1\ \pi^+n \to p\pi^+MM^-$
128 ±27		[4] BOESEBECK	68	HBC	$8\ \pi^+p$
176 ±21		[4,9] JOHNSON	68	HBC	3.7–$4.2\ \pi^-p$
• • • We do not use the following data for averages, fits, limits, etc. • • •					
201 ±11		[10] RODAS	22	RVUE	$J/\psi(1S) \to \gamma\ (\pi\pi,\ K\overline{K})$
183 ± 2		CARVER	21	CLAS	$\gamma p \to \pi^0\pi^0 p$
193.7± 0.4± 1.6		[11] ALBRECHT	20	RVUE	$0.9\ \overline{p}p \to \pi^0\pi^0\eta,\ \pi^0\eta\eta,\ \pi^0K^+K^-$
194 ±36		[12] ANISOVICH	09	RVUE	$0.0\ \overline{p}p,\ \pi N$
195 ±15	870	[13] SCHEGELSKY	06A	RVUE	$\gamma\gamma \to K^0_S K^0_S$
121 ±26		TIKHOMIROV	03	SPEC	$40.0\ \pi^-C \to K^0_S K^0_S K^0_L X$
187 ±20		[14] ALDE	97	GAM2	$450\ pp \to pp\pi^0\pi^0$
184 ±10		[14] GRYGOREV	96	SPEC	$40\ \pi^-N \to K^0_S K^0_S X$
200 ±10		AKER	91	CBAR	$0.0\ \overline{p}p \to 3\pi^0$
240 ±40	3k	BINON	83	GAM2	$38\ \pi^-p \to n2\eta$
187 ±30	650	[4] ANTIPOV	77	CIBS	$25\ \pi^-p \to p3\pi$
225 ±38	16000	DEUTSCH...	76	HBC	$16\ \pi^+p$
166 ±28	600	[4] TAKAHASHI	72	HBC	$8\ \pi^-p \to n2\pi$
173 ±53		[4] ARMENISE	70	HBC	$9\ \pi^+n \to p\pi^+\pi^-$

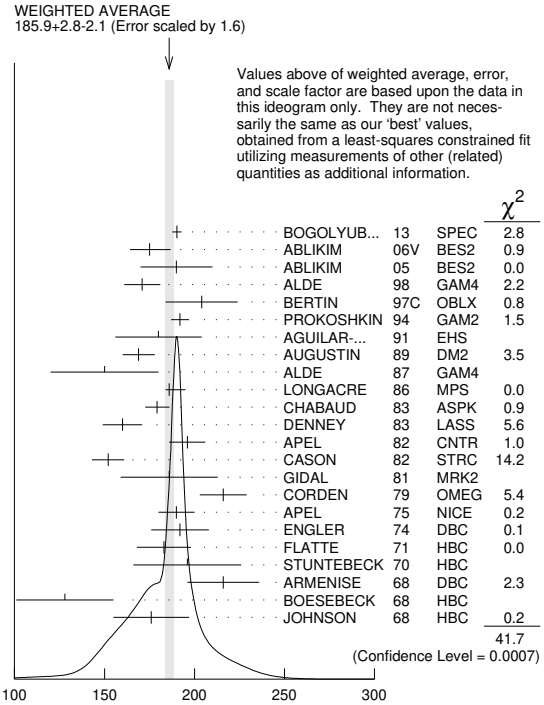

[1] Averaged over six nuclear targets, no statistically significant dependence on target nucleus observed.
[2] Breit-Wigner width
[3] T-matrix pole.
[4] Width errors enlarged by us to $4\Gamma/\sqrt{N}$; see the note with the $K^*(892)$ mass.
[5] From a partial-wave analysis of data using a K-matrix formalism with 5 poles.
[6] From an energy-independent partial-wave analysis.
[7] From an amplitude analysis of the reaction $\pi^+\pi^- \to 2\pi^0$.
[8] From an amplitude analysis of $\pi^+\pi^- \to \pi^+\pi^-$ scattering data.
[9] JOHNSON 68 includes BONDAR 63, LEE 64, DERADO 65, EISNER 67.

Downloaded from https://academic.oup.com/ptep/article/2022/8/083C01/6651666 by KIT Library user on 27 September 2022

[10] T-matrix pole from coupled channel K-matrix fit to data on $J/\psi \to \gamma\pi^0\pi^0$ (ABLIKIM 15AE) and $J/\psi \to \gamma K^0_S K^0_S$ (ABLIKIM 18AA).
[11] T-matrix pole, 4 poles, 4 channels, including scattering data from HYAMS 75 ($\pi\pi$), LONGACRE 86 ($K\overline{K}$), BINON 83 ($\eta\eta$).
[12] 4-poles, 5-channel K matrix fit.
[13] From analysis of L3 data at 91 and 183–209 GeV.
[14] Systematic uncertainties not estimated.

$f_2(1270)$ DECAY MODES

	Mode	Fraction (Γ_i/Γ)	Scale factor/ Confidence level
Γ_1	$\pi\pi$	$(84.2\ ^{+2.9}_{-0.9})$ %	S=1.1
Γ_2	$\pi^+\pi^-2\pi^0$	$(7.7\ ^{+1.1}_{-3.2})$ %	S=1.2
Γ_3	$K\overline{K}$	$(4.6\ ^{+0.5}_{-0.4})$ %	S=2.7
Γ_4	$2\pi^+2\pi^-$	(2.8 ± 0.4) %	S=1.2
Γ_5	$\eta\eta$	$(4.0 \pm 0.8) \times 10^{-3}$	S=2.1
Γ_6	$4\pi^0$	$(3.0 \pm 1.0) \times 10^{-3}$	
Γ_7	$\gamma\gamma$	$(1.42 \pm 0.24) \times 10^{-5}$	S=1.4
Γ_8	$\eta\pi\pi$	$< 8 \times 10^{-3}$	CL=95%
Γ_9	$K^0K^-\pi^+ +$ c.c.	$< 3.4 \times 10^{-3}$	CL=95%
Γ_{10}	e^+e^-	$< 6 \times 10^{-10}$	CL=90%

CONSTRAINED FIT INFORMATION

An overall fit to the total width, 4 partial widths, a combination of partial widths obtained from integrated cross sections, and 6 branching ratios uses 45 measurements and one constraint to determine 8 parameters. The overall fit has a $\chi^2 = 83.0$ for 38 degrees of freedom.

The following *off-diagonal* array elements are the correlation coefficients $\langle \delta p_i \delta p_j \rangle / (\delta p_i \cdot \delta p_j)$, in percent, from the fit to parameters p_i, including the branching fractions, $x_i \equiv \Gamma_i/\Gamma_{total}$. The fit constrains the x_i whose labels appear in this array to sum to one.

	x_1	x_2	x_3	x_4	x_5	x_6	x_7
x_2	−90						
x_3	10	−39					
x_4	10	−38	1				
x_5	1	−6	0	0			
x_6	0	−7	0	0	0		
x_7	3	1	−15	0	0	0	
Γ	−71	65	−10	−7	−1	0	−6

	Mode	Rate (MeV)	Scale factor
Γ_1	$\pi\pi$	$157.2\ ^{+4.0}_{-1.1}$	
Γ_2	$\pi^+\pi^-2\pi^0$	$14.4\ ^{+2.1}_{-6.0}$	1.2
Γ_3	$K\overline{K}$	8.5 ± 0.8	2.8
Γ_4	$2\pi^+2\pi^-$	5.2 ± 0.7	1.2
Γ_5	$\eta\eta$	0.75 ± 0.14	2.1
Γ_6	$4\pi^0$	0.56 ± 0.19	
Γ_7	$\gamma\gamma$	0.0026 ± 0.0005	1.4

$f_2(1270)$ PARTIAL WIDTHS

$\Gamma(\pi\pi)$ — Γ_1

VALUE (MeV)	EVTS	DOCUMENT ID		TECN	COMMENT
$157.2\ ^{+4.0}_{-1.1}$ OUR FIT					
$157.0\ ^{+6.0}_{-1.0}$		[1] LONGACRE	86	MPS	$22\ \pi^-p \to n2K^0_S$
• • • We do not use the following data for averages, fits, limits, etc. • • •					
152 ± 8	870	[2] SCHEGELSKY	06A	RVUE	$\gamma\gamma \to K^0_S K^0_S$

[1] From a partial-wave analysis of data using a K-matrix formalism with 5 poles.
[2] From analysis of L3 data at 91 and 183–209 GeV and using SU(3) relations.

$\Gamma(K\overline{K})$ — Γ_3

VALUE (MeV)	EVTS	DOCUMENT ID		TECN	COMMENT
8.5 ± 0.8 OUR FIT Error includes scale factor of 2.8.					
$9.0\ ^{+0.7}_{-0.3}$		[1] LONGACRE	86	MPS	$22\ \pi^-p \to n2K^0_S$
• • • We do not use the following data for averages, fits, limits, etc. • • •					
7.5 ± 2.0	870	[2] SCHEGELSKY	06A	RVUE	$\gamma\gamma \to K^0_S K^0_S$

[1] From a partial-wave analysis of data using a K-matrix formalism with 5 poles.
[2] From analysis of L3 data at 91 and 183–209 GeV and using SU(3) relations.

$\Gamma(\eta\eta)$ — Γ_5

VALUE (MeV)	EVTS	DOCUMENT ID		TECN	COMMENT
0.75 ± 0.14 OUR FIT Error includes scale factor of 2.1.					
1.0 ± 0.1		[1] LONGACRE	86	MPS	$22\ \pi^-p \to n2K^0_S$
• • • We do not use the following data for averages, fits, limits, etc. • • •					
1.8 ± 0.4	870	[2] SCHEGELSKY	06A	RVUE	$\gamma\gamma \to K^0_S K^0_S$

[1] From a partial-wave analysis of data using a K-matrix formalism with 5 poles.
[2] From analysis of L3 data at 91 and 183–209 GeV and using SU(3) relations.

$\Gamma(\gamma\gamma)$ — Γ_7

The value of this width depends on the theoretical model used. Unitary approaches with scalars typically (with exception of PENNINGTON 08) give values clustering around 2.6 keV; without an *S*-wave contribution, values are systematically higher (typically around 3 keV).

VALUE (keV)	EVTS	DOCUMENT ID		TECN	COMMENT
2.6 ± 0.5 OUR FIT Error includes scale factor of 1.4.					
2.93 ± 0.40		[1] DAI	14A	RVUE	Compilation
• • • We do not use the following data for averages, fits, limits, etc. • • •					
3.14 ± 0.20		[2,3] PENNINGTON	08	RVUE	Compilation
3.82 ± 0.30		[3,4] PENNINGTON	08	RVUE	Compilation
2.55 ± 0.15	870	[5] SCHEGELSKY	06A	RVUE	$\gamma\gamma \to K^0_S K^0_S$
2.84 ± 0.35		BOGLIONE	99	RVUE	$\gamma\gamma \to \pi^+\pi^-, \pi^0\pi^0$
$2.93 \pm 0.23 \pm 0.32$		[6] YABUKI	95	VNS	
$2.58 \pm 0.13\ ^{+0.36}_{-0.27}$		[7] BEHREND	92	CELL	$e^+e^- \to e^+e^-\pi^+\pi^-$
$3.10 \pm 0.35 \pm 0.35$		[8] BLINOV	92	MD1	$e^+e^- \to e^+e^-\pi^+\pi^-$
$2.27 \pm 0.47 \pm 0.11$		ADACHI	90D	TOPZ	$e^+e^- \to e^+e^-\pi^+\pi^-$
$3.15 \pm 0.04 \pm 0.39$		BOYER	90	MRK2	$e^+e^- \to e^+e^-\pi^+\pi^-$
$3.19 \pm 0.16\ ^{+0.29}_{-0.28}$		MARSISKE	90	CBAL	$e^+e^- \to e^+e^-\pi^0\pi^0$
2.35 ± 0.65		[9] MORGAN	90	RVUE	$\gamma\gamma \to \pi^+\pi^-, \pi^0\pi^0$
$3.19 \pm 0.09\ ^{+0.22}_{-0.38}$	2177	OEST	90	JADE	$e^+e^- \to e^+e^-\pi^0\pi^0$
$3.2 \pm 0.1 \pm 0.4$		[10] AIHARA	86B	TPC	$e^+e^- \to e^+e^-\pi^+\pi^-$
$2.5 \pm 0.1 \pm 0.5$		BEHREND	84B	CELL	$e^+e^- \to e^+e^-\pi^+\pi^-$
$2.85 \pm 0.25 \pm 0.5$		[11] BERGER	84	PLUT	$e^+e^- \to e^+e^-2\pi$
$2.70 \pm 0.05 \pm 0.20$		COURAU	84	DLCO	$e^+e^- \to e^+e^-\pi^+\pi^-$
$2.52 \pm 0.13 \pm 0.38$		[12] SMITH	84C	MRK2	$e^+e^- \to e^+e^-\pi^+\pi^-$
$2.7 \pm 0.2 \pm 0.6$		EDWARDS	82F	CBAL	$e^+e^- \to e^+e^-2\pi^0$
$2.9\ ^{+0.6}_{-0.4} \pm 0.6$		[13] EDWARDS	82F	CBAL	$e^+e^- \to e^+e^-2\pi^0$
$3.2 \pm 0.2 \pm 0.6$		BRANDELIK	81B	TASS	$e^+e^- \to e^+e^-\pi^+\pi^-$
$3.6 \pm 0.3 \pm 0.5$		ROUSSARIE	81	MRK2	$e^+e^- \to e^+e^-\pi^+\pi^-$
2.3 ± 0.8		[14] BERGER	80B	PLUT	e^+e^-

[1] Based on a *K*-matrix analysis of BELLE data from MORI 07, UEHARA 08A, UEHARA 09 and UEHARA 13. The width is derived for the pole on the third sheet which is closest to the physical axis. Supersedes PENNINGTON 08.
[2] Solution A (preferred solution based on χ^2-analysis).
[3] Dispersion theory based amplitude analysis of BOYER 90, MARSISKE 90, BEHREND 92, and MORI 07.
[4] Solution B (worse than solution A; still acceptable when systematic uncertainties are included).
[5] From analysis of L3 data at 91 and 183–209 GeV and using SU(3) relations.
[6] With a narrow scalar state around 1220 MeV.
[7] Using a unitarized model with a 300 - 500 keV wide scalar at 1100 MeV.
[8] Using the unitarized model of LYTH 85.
[9] Error includes spread of different solutions. Data of MARK2 and CRYSTAL BALL used in the analysis. Authors report strong correlations with $\gamma\gamma$ width of $f_0(1370)$: $\Gamma(f_2) + 1/4\ \Gamma(f^0) = 3.6 \pm 0.3$ KeV.
[10] Radiative corrections modify the partial widths; for instance the COURAU 84 value becomes 2.66 ± 0.21 in the calculation of LANDRO 86.
[11] Using the MENNESSIER 83 model.
[12] Superseded by BOYER 90.
[13] If helicity = 2 assumption is not made.
[14] Using mass, width and $B(f_2(1270) \to 2\pi)$ from PDG 78.

$\Gamma(e^+e^-)$ — Γ_{10}

VALUE (eV)	CL%	DOCUMENT ID		TECN	COMMENT
<0.11	90	ACHASOV	00K	SND	$e^+e^- \to \pi^0\pi^0$
• • • We do not use the following data for averages, fits, limits, etc. • • •					
<1.7	90	VOROBYEV	88	ND	$e^+e^- \to \pi^0\pi^0$

$f_2(1270)$ $\Gamma(i)\Gamma(\gamma\gamma)/\Gamma(total)$

$\Gamma(K\overline{K}) \times \Gamma(\gamma\gamma)/\Gamma_{total}$ — $\Gamma_3\Gamma_7/\Gamma$

VALUE (keV)	DOCUMENT ID		TECN	COMMENT
0.121 ± 0.020 OUR FIT Error includes scale factor of 1.3.				
$0.091 \pm 0.007 \pm 0.027$	[1] ALBRECHT	90G	ARG	$e^+e^- \to e^+e^-K^+K^-$
• • • We do not use the following data for averages, fits, limits, etc. • • •				
$0.104 \pm 0.007 \pm 0.072$	[2] ALBRECHT	90G	ARG	$e^+e^- \to e^+e^-K^+K^-$

[1] Using an incoherent background.
[2] Using a coherent background.

Downloaded from https://academic.oup.com/ptep/article/2022/8/083C01/6651666 by KIT Library user on 27 September 2022

$\Gamma(\eta\eta) \times \Gamma(\gamma\gamma)/\Gamma_{total}$ — $\Gamma_5\Gamma_7/\Gamma$

VALUE (eV)	DOCUMENT ID		TECN	COMMENT
$11.5^{+1.8+4.5}_{-2.0-3.7}$	[1] UEHARA	10A	BELL	10.6 $e^+e^- \to e^+e^-\eta\eta$

[1] Including interference with the $f'_2(1525)$ (parameters fixed to the values from the 2008 edition of this review, PDG 08) and $f_0(Y)$.

Helicity-0/Helicity-2 RATIO IN $\gamma\gamma \to f_2(1270) \to \pi\pi$

VALUE (units 10^{-2})	DOCUMENT ID		TECN	COMMENT
$3.7\pm0.3^{+15.9}_{-2.9}$	UEHARA	08A	BELL	10.6 $e^+e^- \to e^+e^-\pi^0\pi^0$
• • • We do not use the following data for averages, fits, limits, etc. • • •				
9.5 ± 1.8	[1] DAI	14A	RVUE	Compilation
13	[2,3] PENNINGTON	08	RVUE	Compilation
26	[3,4] PENNINGTON	08	RVUE	Compilation

[1] Based on a K-matrix analysis of BELLE data from MORI 07, UEHARA 08A, UEHARA 09 and UEHARA 13. The width is derived for the pole on the third sheet which is closest to the physical axis.
[2] Solution A (preferred solution based on χ^2-analysis).
[3] Dispersion theory based amplitude analysis of BOYER 90, MARSISKE 90, BEHREND 92, and MORI 07.
[4] Solution B (worse than solution A; still acceptable when systematic uncertainties are included).

$f_2(1270)$ BRANCHING RATIOS

$\Gamma(\pi\pi)/\Gamma_{total}$ — Γ_1/Γ

VALUE	EVTS	DOCUMENT ID		TECN	COMMENT
$0.842^{+0.029}_{-0.009}$ **OUR FIT**	Error includes scale factor of 1.1.				
0.837±0.020 OUR AVERAGE					
0.849 ± 0.025		CHABAUD	83	ASPK	17 π^-p polarized
$0.85\ \pm0.05$	250	BEAUPRE	71	HBC	8 $\pi^+p \to \Delta^{++}f_2$
$0.8\ \pm0.04$	600	OH	70	HBC	1.26 $\pi^-p \to \pi^+\pi^-n$
• • • We do not use the following data for averages, fits, limits, etc. • • •					
$0.856\pm0.001\pm0.05$		[1] ALBRECHT	20	RVUE	0.9 $\overline{p}p \to \pi^0\pi^0\eta$, $\pi^0\eta\eta$, $\pi^0K^+K^-$

[1] Residue from T-matrix pole, 4 poles, 4 channels, including scattering data from HYAMS 75 ($\pi\pi$), LONGACRE 86 ($K\overline{K}$), BINON 83 ($\eta\eta$).

$\Gamma(\pi^+\pi^-2\pi^0)/\Gamma(\pi\pi)$ — Γ_2/Γ_1

Should be twice $\Gamma(2\pi^+2\pi^-)/\Gamma(\pi\pi)$ if decay is $\rho\rho$. (See ASCOLI 68D.)

VALUE	EVTS	DOCUMENT ID		TECN	COMMENT
$0.091^{+0.014}_{-0.040}$ **OUR FIT**	Error includes scale factor of 1.2.				
0.15 ±0.06	600	EISENBERG	74	HBC	4.9 $\pi^+p \to \Delta^{++}f_2$
• • • We do not use the following data for averages, fits, limits, etc. • • •					
0.07		EMMS	75D	DBC	4 $\pi^+n \to pf_2$

$\Gamma(K\overline{K})/\Gamma_{total}$ — Γ_3/Γ

VALUE	DOCUMENT ID		TECN	COMMENT
• • • We do not use the following data for averages, fits, limits, etc. • • •				
$0.033\pm0.001\pm0.005$	[1] ALBRECHT	20	RVUE	0.9 $\overline{p}p \to \pi^0\pi^0\eta$, $\pi^0\eta\eta$, $\pi^0K^+K^-$

[1] Residue from T-matrix pole, 4 poles, 4 channels, including scattering data from HYAMS 75 ($\pi\pi$), LONGACRE 86 ($K\overline{K}$), BINON 83 ($\eta\eta$).

$\Gamma(K\overline{K})/\Gamma(\pi\pi)$ — Γ_3/Γ_1

We average only experiments which either take into account $f_2(1270)$-$a_2(1320)$ interference explicitly or demonstrate that $a_2(1320)$ production is negligible.

VALUE	EVTS	DOCUMENT ID		TECN	COMMENT
$0.054^{+0.005}_{-0.006}$ **OUR FIT**	Error includes scale factor of 2.7.				
$0.041^{+0.004}_{-0.005}$ **OUR AVERAGE**					
0.045 ± 0.01		[1] BARGIOTTI	03	OBLX	$\overline{p}p$
$0.037^{+0.008}_{-0.021}$		ETKIN	82B	MPS	23 $\pi^-p \to n2K^0_S$
0.045 ± 0.009		CHABAUD	81	ASPK	17 π^-p polarized
0.039 ± 0.008		LOVERRE	80	HBC	4 $\pi^-p \to K\overline{K}N$
• • • We do not use the following data for averages, fits, limits, etc. • • •					
0.052 ± 0.025		ABLIKIM	04E	BES2	$J/\psi \to \omega K^+K^-$
0.036 ± 0.005		[2] COSTA	80	OMEG	1–2.2 $\pi^-p \to K^+K^-n$
0.030 ± 0.005		[3] MARTIN	79	RVUE	
0.027 ± 0.009		[4] POLYCHRO...	79	STRC	7 $\pi^-p \to n2K^0_S$
0.025 ± 0.015		EMMS	75D	DBC	4 $\pi^+n \to pf_2$
0.031 ± 0.012	20	ADERHOLZ	69	HBC	8 $\pi^+p \to K^+K^-\pi^+p$

[1] Coupled channel analysis of $\pi^+\pi^-\pi^0$, $K^+K^-\pi^0$, and $K^\pm K^0_S\pi^\mp$.
[2] Re-evaluated by CHABAUD 83.
[3] Includes PAWLICKI 77 data.
[4] Takes into account the $f_2(1270)$-$f'_2(1525)$ interference.

$\Gamma(2\pi^+2\pi^-)/\Gamma(\pi\pi)$ — Γ_4/Γ_1

VALUE	EVTS	DOCUMENT ID		TECN	COMMENT
0.033±0.005 OUR FIT	Error includes scale factor of 1.2.				
0.033±0.004 OUR AVERAGE	Error includes scale factor of 1.1.				
0.024 ± 0.006	160	EMMS	75D	DBC	4 $\pi^+n \to pf_2$
0.051 ± 0.025	70	EISENBERG	74	HBC	4.9 $\pi^+p \to \Delta^{++}f_2$
$0.043^{+0.007}_{-0.011}$	285	[1] LOUIE	74	HBC	3.9 $\pi^-p \to nf_2$
0.037 ± 0.007	154	ANDERSON	73	DBC	6 $\pi^+n \to pf_2$
0.047 ± 0.013		OH	70	HBC	1.26 $\pi^-p \to \pi^+\pi^-n$

[1] LOUIE 74 was quoted as 0.065 in PDG 74. Factor 2/3 to go from $\pi^+\pi^- \to \pi\pi$ forgotten. Mike L.

$\Gamma(\eta\eta)/\Gamma_{total}$ — Γ_5/Γ

VALUE (units 10^{-3})	DOCUMENT ID		TECN	COMMENT
4.0±0.8 OUR FIT	Error includes scale factor of 2.1.			
2.9±0.5 OUR AVERAGE				
2.7 ± 0.7	BINON	05	GAMS	33 $\pi^-p \to \eta\eta n$
2.8 ± 0.7	ALDE	86D	GAM4	100 $\pi^-p \to 2\eta n$
5.2 ± 1.7	BINON	83	GAM2	38 $\pi^-p \to 2\eta n$
• • • We do not use the following data for averages, fits, limits, etc. • • •				
$4.0\pm1.0\pm2.0$	[1] ALBRECHT	20	RVUE	0.9 $\overline{p}p \to \pi^0\pi^0\eta$, $\pi^0\eta\eta$, $\pi^0K^+K^-$

[1] Residue from T-matrix pole, 4 poles, 4 channels, including scattering data from HYAMS 75 ($\pi\pi$), LONGACRE 86 ($K\overline{K}$), BINON 83 ($\eta\eta$).

$\Gamma(\eta\eta)/\Gamma(\pi\pi)$ — Γ_5/Γ_1

VALUE	CL%	DOCUMENT ID		TECN	COMMENT
0.003±0.001		BARBERIS	00E		450 $pp \to p_f\eta\eta p_s$
• • • We do not use the following data for averages, fits, limits, etc. • • •					
<0.05	95	EDWARDS	82F	CBAL	$e^+e^- \to e^+e^-2\eta$
<0.016	95	EMMS	75D	DBC	4 $\pi^+n \to pf_2$
<0.09	95	EISENBERG	74	HBC	4.9 $\pi^+p \to \Delta^{++}f_2$

$\Gamma(4\pi^0)/\Gamma_{total}$ — Γ_6/Γ

VALUE	EVTS	DOCUMENT ID		TECN	COMMENT
0.0030±0.0010 OUR FIT					
0.003 ±0.001	400 ± 50	ALDE	87	GAM4	100 $\pi^-p \to 4\pi^0n$

$\Gamma(\gamma\gamma)/\Gamma_{total}$ — Γ_7/Γ

VALUE (units 10^{-5})	DOCUMENT ID		TECN	COMMENT
• • • We do not use the following data for averages, fits, limits, etc. • • •				
$1.57\pm0.01^{+1.39}_{-0.14}$	UEHARA	08A	BELL	10.6 $e^+e^- \to e^+e^-\pi^0\pi^0$

$\Gamma(\eta\pi\pi)/\Gamma(\pi\pi)$ — Γ_8/Γ_1

VALUE	CL%	DOCUMENT ID		TECN	COMMENT
<0.010	95	EMMS	75D	DBC	4 $\pi^+n \to pf_2$

$\Gamma(K^0K^-\pi^+ + c.c.)/\Gamma(\pi\pi)$ — Γ_9/Γ_1

VALUE	CL%	DOCUMENT ID		TECN	COMMENT
<0.004	95	EMMS	75D	DBC	4 $\pi^+n \to pf_2$

$\Gamma(e^+e^-)/\Gamma_{total}$ — Γ_{10}/Γ

VALUE (units 10^{-10})	CL%	DOCUMENT ID		TECN	COMMENT
<6	90	ACHASOV	00K	SND	$e^+e^- \to \pi^0\pi^0$

$f_2(1270)$ REFERENCES

RODAS 22 EPJ C82 80 A. Rodas et al. (JPAC Collab.)
CARVER 21 PRL 126 082002 M. Carver et al. (CLAS Collab.)
ALBRECHT 20 EPJ C80 453 M. Albrecht et al. (Crystal Barrel Collab.)
ABLIKIM 18AA PR D98 072003 M. Ablikim et al. (BESIII Collab.)
ABLIKIM 15AE PR D92 052003 M. Ablikim et al. (BESIII Collab.)
DOBBS 15 PR D91 052006 S. Dobbs et al. (NWES)
DAI 14A PR D90 036004 L.-Y. Dai, M.R. Pennington (CEBAF)
BOGOLYUB... 13 PAN 76 1324 M.Yu. Bogolyubsky et al. (HYPERON-M Collab.)
Translated from YAF 76 1389.
UEHARA 13 PTEP 2013 123C01 S. Uehara et al. (BELLE Collab.)
UEHARA 10A PR D82 114031 S. Uehara et al. (BELLE Collab.)
ANISOVICH 09 IJMP A24 2481 V.V. Anisovich, A.V. Sarantsev
UEHARA 09 PR D79 052009 S. Uehara et al. (BELLE Collab.)
PDG 08 PL B667 1 C. Amsler et al. (PDG Collab.)
PENNINGTON 08 EPJ C56 1 M.R. Pennington et al.
UEHARA 08A PR D78 052004 S. Uehara et al. (BELLE Collab.)
MORI 07 PR D75 051101 T. Mori et al. (BELLE Collab.)
ABLIKIM 06V PL B642 441 M. Ablikim et al. (BES Collab.)
SCHEGELSKY 06A EPJ A27 207 V.A. Schegelsky et al.
ABLIKIM 05 PL B607 243 M. Ablikim et al. (BES Collab.)
BINON 05 PAN 68 960 F. Binon et al.
Translated from YAF 68 998.
ABLIKIM 04E PL B603 138 M. Ablikim et al. (BES Collab.)
BARGIOTTI 03 EPJ C26 371 M. Bargiotti et al. (OBELIX Collab.)
TIKHOMIROV 03 PAN 66 828 G.D. Tikhomirov et al.
Translated from YAF 66 860.
ACHASOV 00K PL B492 8 M.N. Achasov et al. (Novosibirsk SND Collab.)
BARBERIS 00E PL B479 59 D. Barberis et al. (WA 102 Collab.)
BOGLIONE 99 EPJ C9 11 M. Boglione, M.R. Pennington
ALDE 98 EPJ A3 361 D. Alde et al. (GAM4 Collab.)
Also PAN 62 405 D. Alde et al. (GAMS Collab.)
Translated from YAF 62 446.
ALDE 97 PL B397 350 D.M. Alde et al. (GAMS Collab.)
BERTIN 97C PL B408 476 A. Bertin et al. (OBELIX Collab.)
GRYGOREV 96 PAN 59 2105 V.K. Grigoriev, O.N. Baloshin, B.P. Barkov (ITEP)
Translated from YAF 59 2187.

Downloaded from https://academic.oup.com/ptep/article/2022/8/083C01/6651666 by KIT Library user on 27 September 2022

YABUKI	95	JPSJ 64 435	F. Yabuki *et al.*	(VENUS Collab.)
PROKOSHKIN	94	PD 39 420	Y.D. Prokoshkin, A.A. Kondashov	(SERP)
		Translated from DANS 336 613.		
BEHREND	92	ZPHY C56 381	H.J. Behrend	(CELLO Collab.)
BLINOV	92	ZPHY C53 33	A.E. Blinov *et al.*	(NOVO)
AGUILAR-...	91	ZPHY C50 405	M. Aguilar-Benitez *et al.*	(LEBC-EHS Collab.)
AKER	91	PL B260 249	E. Aker *et al.*	(Crystal Barrel Collab.)
ADACHI	90D	PL B234 185	I. Adachi *et al.*	(TOPAZ Collab.)
ALBRECHT	90G	ZPHY C48 183	H. Albrecht *et al.*	(ARGUS Collab.)
BOYER	90	PR D42 1350	J. Boyer *et al.*	(Mark II Collab.)
BREAKSTONE	90	ZPHY C48 569	A.M. Breakstone *et al.*	(ISU, BGNA, CERN+)
MARSISKE	90	PR D41 3324	H. Marsiske *et al.*	(Crystal Ball Collab.)
MORGAN	90	ZPHY C48 623	D. Morgan, M.R. Pennington	(RAL, DURH)
OEST	90	ZPHY C47 343	T. Oest *et al.*	(JADE Collab.)
AUGUSTIN	89	NP B320 1	J.E. Augustin, G. Cosme	(DM2 Collab.)
VOROBYEV	88	SJNP 48 273	P.V. Vorobiev *et al.*	(NOVO)
		Translated from YAF 48 436.		
ALDE	87	PL B198 286	D.M. Alde *et al.*	(LANL, BRUX, SERP, LAPP)
AUGUSTIN	87	ZPHY C36 369	J.E. Augustin *et al.*	(LALO, CLER, FRAS+)
ABACHI	86B	PRL 57 1990	S. Abachi *et al.*	(PURD, ANL, IND, MICH+)
AIHARA	86B	PRL 57 404	H. Aihara *et al.*	(TPC-2γ Collab.)
ALDE	86D	NP B269 485	D.M. Alde *et al.*	(BELG, LAPP, SERP, CERN+)
LANDRO	86	PL B172 445	M. Landro, K.J. Mork, H.A. Olsen	(UTRO)
LONGACRE	86	PL B177 223	R.S. Longacre *et al.*	(BNL, BRAN, CUNY+)
LYTH	85	JP G11 459	D.H. Lyth	
BEHREND	84B	ZPHY C23 223	H.J. Behrend *et al.*	(CELLO Collab.)
BERGER	84	ZPHY C26 199	C. Berger *et al.*	(PLUTO Collab.)
COURAU	84	PL 147B 227	A. Courau *et al.*	(CIT, SLAC)
SMITH	84C	PR D30 851	J.R. Smith *et al.*	(SLAC, LBL, HARV)
BINON	83	NC 78A 313	F.G. Binon *et al.*	(BELG, LAPP, SERP+)
Also		SJNP 38 561	F.G. Binon *et al.*	(BELG, LAPP, SERP+)
		Translated from YAF 38 934.		
CHABAUD	83	NP B223 1	V. Chabaud *et al.*	(CERN, CRAC, MPIM)
DENNEY	83	PR D28 2726	D.L. Denney *et al.*	(IOWA, MICH)
MENNESSIER	83	ZPHY C16 241	G. Mennessier	(MONP)
APEL	82	NP B201 197	W.D. Apel *et al.*	(KARLK, KARLE, PISA, SERP+)
CASON	82	PRL 48 1316	N.M. Cason *et al.*	(NDAM, ANL)
EDWARDS	82F	PL 110B 82	C. Edwards *et al.*	(CIT, HARV, PRIN+)
ETKIN	82B	PR D25 1786	A. Etkin *et al.*	(BNL, CUNY, TUFTS, VAND)
BRANDELIK	81B	ZPHY C10 117	R. Brandelik *et al.*	(TASSO Collab.)
CHABAUD	81	APP B12 575	V. Chabaud *et al.*	(CERN, CRAC, MPIM)
GIDAL	81	PL 107B 153	G. Gidal *et al.*	(SLAC, LBL)
ROUSSARIE	81	PL 105B 304	A. Roussarie *et al.*	(SLAC, LBL)
BERGER	80B	PL 94B 254	C. Berger *et al.*	(PLUTO Collab.)
COSTA	80	NP B175 402	G. Costa *et al.*	(BARI, BONN, CERN, GLAS+)
LOVERRE	80	ZPHY C6 187	P.F. Loverre *et al.*	(CERN, CDEF, MADR+)
CORDEN	79	NP B157 250	M.J. Corden *et al.*	(BIRM, RHEL, TELA+)
MARTIN	79	NP B158 520	A.D. Martin, E.N. Ozmutlu	(DURH)
POLYCHRO...	79	PR D19 1317	V.A. Polychronakos *et al.*	(NDAM, ANL)
PDG	78	PL 75B 1	C. Bricman *et al.*	
ANTIPOV	77	NP B119 45	Y.M. Antipov *et al.*	(SERP, GEVA)
PAWLICKI	77	PR D15 3196	A.J. Pawlicki *et al.*	(ANL)
DEUTSCH...	76	NP B103 426	M. Deutschmann *et al.*	(AACH3, BERL, BONN+)
APEL	75	PL 57B 398	W.D. Apel *et al.*	(KARLK, KARLE, PISA, SERP+)
EMMS	75D	NP B96 155	M.J. Emms *et al.*	(BIRM, DURH, RHEL)
HYAMS	75	NP B100 205	B.D. Hyams *et al.*	(CERN, MPIM)
EISENBERG	74	PL 52B 239	Y. Eisenberg *et al.*	(REHO)
ENGLER	74	PR D10 2070	A. Engler *et al.*	(CMU, CASE)
LOUIE	74	PL 48B 385	J. Louie *et al.*	(SACL, CERN)
PDG	74	PL 50B 1	V. Chaloupka *et al.*	
ANDERSON	73	PRL 31 562	J.C. Anderson *et al.*	(CMU, CASE)
TAKAHASHI	72	PR D6 1266	K. Takahashi *et al.*	(TOHOK, PENN, NDAM+)
BEAUPRE	71	NP B28 77	J.V. Beaupre *et al.*	(AACH, BERL, CERN)
FLATTE	71	PL 34B 551	S.M. Flatte *et al.*	(LBL)
ARMENISE	70	LNC 4 199	N. Armenise *et al.*	(BARI, BGNA, FIRZ)
OH	70	PR D1 2494	B.Y. Oh *et al.*	(WISC, TNTO) JP
STUNTEBECK	70	PL 32B 391	P.H. Stuntebeck *et al.*	(NDAM)
ADERHOLZ	69	NP B11 259	M. Aderholz *et al.*	(AACH3, BERL, CERN+)
ARMENISE	68	NC 54A 999	N. Armenise *et al.*	(BARI, BGNA, FIRZ+)
ASCOLI	68D	PRL 21 1712	G. Ascoli *et al.*	(ILL)
BOESEBECK	68	NP B4 501	K. Boesebeck *et al.*	(AACH, BERL, CERN)
JOHNSON	68	PR 176 1651	P.B. Johnson *et al.*	(NDAM, PURD, SLAC)
EISNER	67	PR 164 1699	R.L. Eisner *et al.*	(PURD)
DERADO	65	PRL 14 872	I. Derado *et al.*	(NDAM)
LEE	64	PRL 12 342	Y.Y. Lee *et al.*	(MICH)
BONDAR	63	PL 5 153	L. Bondar *et al.*	(AACH, BIRM, BONN, DESY+)

$f_1(1285)$

$I^G(J^{PC}) = 0^+(1^{++})$

$f_1(1285)$ MASS

VALUE (MeV)	EVTS	DOCUMENT ID		TECN	COMMENT
1281.9 ± 0.5 OUR AVERAGE		Error includes scale factor of 1.8. See the ideogram below.			
1281.0 ± 0.8		DICKSON	16	CLAS	2.55 $\gamma p \to \eta\pi^+\pi^- p$
1287.4 ± 3.0	87	ABLIKIM	15P	BES3	$J/\psi \to K^+K^-3\pi$
1281.16 ± 0.39 ± 0.45		[1] LEES	12X	BABR	$\tau^- \to \pi^- f_1(1285)\nu_\tau$
1285.1 ± 1.0 $^{+1.6}_{-0.3}$		[2] ABLIKIM	11J	BES3	$J/\psi \to \omega(\eta\pi^+\pi^-)$
1281 ± 2 ± 1		AUBERT	07AU	BABR	10.6 $e^+e^- \to f_1(1285)\pi^+\pi^-\gamma$
1276.1 ± 8.1 ± 8.0	203	BAI	04J	BES2	$J/\psi \to \gamma\gamma\pi^+\pi^-$
1274 ± 6	237	ABDALLAH	03H	DLPH	91.2 $e^+e^- \to K^0_S K^\pm\pi^\mp + X$
1280 ± 4		ACCIARRI	01G	L3	
1288 ± 4 ± 5	20k	ADAMS	01B	B852	18 GeV $\pi^- p \to K^+K^-\pi^0 n$
1284 ± 6	1400	ALDE	97B	GAM4	100 $\pi^- p \to \eta\pi^0\pi^0 n$
1281 ± 1		BARBERIS	97B	OMEG	450 $pp \to pp2(\pi^+\pi^-)$
1281 ± 1		BARBERIS	97C	OMEG	450 $pp \to pp K^0_S K^\pm\pi^\mp$
1280 ± 2		[3] ANTINORI	95	OMEG	300,450 $pp \to pp2(\pi^+\pi^-)$
1282.2 ± 1.5		LEE	94	MPS2	18 $\pi^- p \to K^+\overline{K}^0 2\pi^- p$
1279 ± 5		FUKUI	91C	SPEC	8.95 $\pi^- p \to \eta\pi^+\pi^- n$
1278 ± 2	140	ARMSTRONG	89	OMEG	300 $pp \to K\overline{K}\pi pp$
1278 ± 2		ARMSTRONG	89G	OMEG	85 $\pi^+ p \to 4\pi\pi p$, $pp \to 4\pi pp$
1280.1 ± 2.1	60	RATH	89	MPS	21.4 $\pi^- p \to K^0_S K^0_S \pi^0 n$
1285 ± 1	4750	[4] BIRMAN	88	MPS	8 $\pi^- p \to K^+\overline{K}^0\pi^- n$
1280 ± 1	504	BITYUKOV	88	SPEC	32.5 $\pi^- p \to K^+K^-\pi^0 n$
1280 ± 4		ANDO	86	SPEC	8 $\pi^- p \to \eta\pi^+\pi^- n$
1277 ± 2	420	REEVES	86	SPEC	6.6 $p\overline{p} \to KK\pi X$
1285 ± 2		CHUNG	85	SPEC	8 $\pi^- p \to NK\overline{K}\pi$
1279 ± 2	604	ARMSTRONG	84	OMEG	85 $\pi^+ p \to K\overline{K}\pi\pi p$, $pp \to K\overline{K}\pi pp$
1286 ± 1		CHAUVAT	84	SPEC	ISR 31.5 pp
1278 ± 4		EVANGELIS...	81	OMEG	12 $\pi^- p \to \eta\pi^+\pi^-\pi^- p$
1283 ± 3	103	DIONISI	80	HBC	4 $\pi^- p \to K\overline{K}\pi n$
1282 ± 2	320	NACASCH	78	HBC	0.7,0.76 $\overline{p}p \to K\overline{K}3\pi$
1279 ± 5	210	GRASSLER	77	HBC	16 $\pi^\mp p$
1286 ± 3	180	DUBOC	72	HBC	1.2 $\overline{p}p \to 2K4\pi$
1283 ± 5		DAHL	67	HBC	1.6–4.2 $\pi^- p$
• • • We do not use the following data for averages, fits, limits, etc. • • •					
1289.3 ± 2.8	234	ABLIKIM	19BA	BES3	$e^+e^- \to \psi(2S)$
1284.2 ± 2.2		[5] AAIJ	14Y	LHCB	$\overline{B}^0_{(s)} \to J/\psi 2(\pi^+\pi^-)$
1281.9 ± 0.5		[5] SOSA	99	SPEC	$pp \to p_{slow}(K^0_S K^+\pi^-) p_{fast}$
1282.8 ± 0.6		[5] SOSA	99	SPEC	$pp \to p_{slow}(K^0_S K^-\pi^+) p_{fast}$
1270 ±10		AMELIN	95	VES	37 $\pi^- N \to \pi^-\pi^+\pi^-\gamma N$
1280 ± 2		ABATZIS	94	OMEG	450 $pp \to pp2(\pi^+\pi^-)$
1282 ± 4		ARMSTRONG	93C	E760	$\overline{p}p \to \pi^0\eta\eta \to 6\gamma$
1270 ± 6 ±10		ARMSTRONG	92C	OMEG	300 $pp \to pp\pi^+\pi^-\gamma$
1281 ± 1		ARMSTRONG	89E	OMEG	300 $pp \to pp2(\pi^+\pi^-)$
1279 ± 6 ±10	16	BECKER	87	MRK3	$e^+e^- \to \phi K\overline{K}\pi$
1286 ± 9		GIDAL	87	MRK2	$e^+e^- \to e^+e^-\eta\pi^+\pi^-$
1287 ± 5	353	BITYUKOV	84B	SPEC	32 $\pi^- p \to K^+K^-\pi^0 n$
~ 1279		[6] TORNQVIST	82B	RVUE	
1275 ± 6	31	BROMBERG	80	SPEC	100 $\pi^- p \to K\overline{K}\pi X$
1288 ± 9	200	GURTU	79	HBC	4.2 $K^- p \to n\eta 2\pi$
~ 1275.0	46	[7] STANTON	79	CNTR	8.5 $\pi^- p \to n2\gamma 2\pi$
1271 ±10	34	CORDEN	78	OMEG	12–15 $\pi^- p \to K^+K^-\pi n$
1295 ±12	85	CORDEN	78	OMEG	12–15 $\pi^- p \to n5\pi$
1292 ±10	150	DEFOIX	72	HBC	0.7 $\overline{p}p \to 7\pi$
1280 ± 3	500	[8] THUN	72	MMS	13.4 $\pi^- p$
1303 ± 8		BARDADIN-...	71	HBC	8 $\pi^+ p \to p6\pi$
1283 ± 6		BOESEBECK	71	HBC	16.0 $\pi p \to p5\pi$
1270 ±10		CAMPBELL	69	DBC	2.7 $\pi^+ d$
1285 ± 7		LORSTAD	69	HBC	0.7 $\overline{p}p$, 4,5-body
1290 ± 7		D'ANDLAU	68	HBC	1.2 $\overline{p}p$, 5–6 body

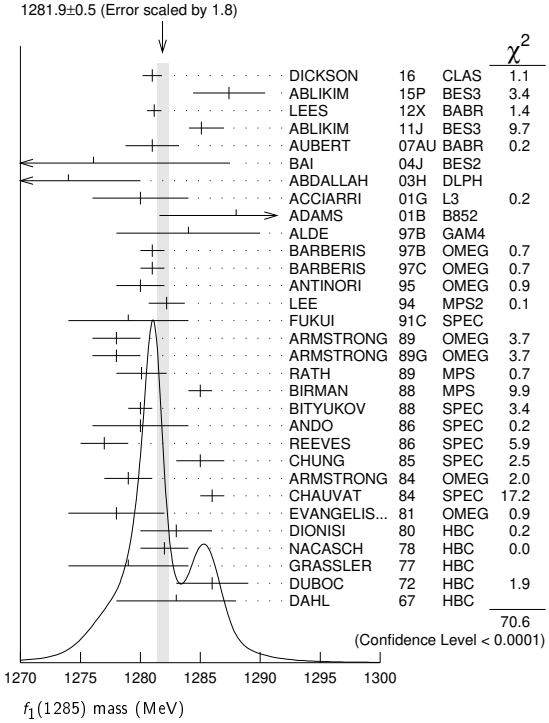

[1] Using the $2\pi^+2\pi^-$ and $\pi^+\pi^-\eta$ modes of $f_1(1285)$ decay.

Downloaded from https://academic.oup.com/ptep/article/2022/8/083C01/6651666 by KIT Library user on 27 September 2022

[2] The selected process is $J/\psi \to \omega a_0(980)\pi$.
[3] Supersedes ABATZIS 94, ARMSTRONG 89E.
[4] From partial wave analysis of $K^+\overline{K}^0\pi^-$ system.
[5] No systematic error given.
[6] From a unitarized quark-model calculation.
[7] From phase shift analysis of $\eta\pi^+\pi^-$ system.
[8] Seen in the missing mass spectrum.

$f_1(1285)$ WIDTH

Only experiments giving width error less than 20 MeV are kept for averaging.

VALUE (MeV)	EVTS	DOCUMENT ID		TECN	COMMENT
22.7± 1.1 OUR AVERAGE		Error includes scale factor of 1.5. See the ideogram below.			
18.4± 1.4		DICKSON	16	CLAS	2.55 $\gamma p \to \eta\pi^+\pi^- p$
18.3± 6.3	87	ABLIKIM	15P	BES3	$J/\psi \to K^+K^-3\pi$
22.0± 3.1$^{+2.0}_{-1.5}$		[1] ABLIKIM	11J	BES3	$J/\psi \to \omega(\eta\pi^+\pi^-)$
35 ± 6 ± 4		AUBERT	07AU	BABR	10.6 $e^+e^- \to f_1(1285)\pi^+\pi^-\gamma$
40.0± 8.6± 9.3	203	BAI	04J	BES2	$J/\psi \to \gamma\gamma\pi^+\pi^-$
29 ±12	237	ABDALLAH	03H	DLPH	91.2 $e^+e^- \to K^0_S K^\pm\pi^\mp + X$
45 ± 9 ± 7	20k	ADAMS	01B	B852	18 GeV $\pi^- p \to K^+K^-\pi^0 n$
55 ±18	1400	ALDE	97B	GAM4	100 $\pi^- p \to \eta\pi^0\pi^0 n$
24 ± 3		BARBERIS	97B	OMEG	450 $pp \to pp2(\pi^+\pi^-)$
20 ± 2		BARBERIS	97C	OMEG	450 $pp \to pp K^0_S K^\pm\pi^\mp$
36 ± 5		[2] ANTINORI	95	OMEG	300,450 $pp \to pp2(\pi^+\pi^-)$
29.0± 4.1		LEE	94	MPS2	18 $\pi^- p \to K^+\overline{K}^0 2\pi^- p$
25 ± 4	140	ARMSTRONG	89	OMEG	300 $pp \to K\overline{K}\pi pp$
22 ± 2	4750	[3] BIRMAN	88	MPS	8 $\pi^- p \to K^+\overline{K}^0\pi^- n$
25 ± 4	504	BITYUKOV	88	SPEC	32.5 $\pi^- p \to K^+K^-\pi^0 n$
19 ± 5		ANDO	86	SPEC	8 $\pi^- p \to \eta\pi^+\pi^- n$
32 ± 8	420	REEVES	86	SPEC	6.6 $p\overline{p} \to KK\pi X$
22 ± 2		CHUNG	85	SPEC	8 $\pi^- p \to NK\overline{K}\pi$
32 ± 3	604	ARMSTRONG	84	OMEG	85 $\pi^+ p \to K\overline{K}\pi\pi p$, $pp \to K\overline{K}\pi pp$
24 ± 3		CHAUVAT	84	SPEC	ISR 31.5 pp
29 ±10	103	DIONISI	80	HBC	4 $\pi^- p \to K\overline{K}\pi n$
28.3± 6.7	320	NACASCH	78	HBC	0.7,0.76 $\overline{p}p \to K\overline{K}3\pi$
• • • We do not use the following data for averages, fits, limits, etc. • • •					
17.1± 3.4	234	ABLIKIM	19BA	BES3	$e^+e^- \to \psi(2S)$
32.4± 5.8		[4] AAIJ	14Y	LHCB	$\overline{B}^0_{(s)} \to J/\psi 2(\pi^+\pi^-)$
18.2± 1.2		[4] SOSA	99	SPEC	$pp \to p_{slow}(K^0_S K^+\pi^-)p_{fast}$
19.4± 1.5		[4] SOSA	99	SPEC	$pp \to p_{slow}(K^0_S K^-\pi^+)p_{fast}$
40 ± 5		ABATZIS	94	OMEG	450 $pp \to pp2(\pi^+\pi^-)$
31 ± 5		ARMSTRONG	89E	OMEG	300 $pp \to pp2(\pi^+\pi^-)$
41 ±12		ARMSTRONG	89G	OMEG	85 $\pi^+ p \to 4\pi\pi p$, $pp \to 4\pi pp$
17.9±10.9	60	RATH	89	MPS	21.4 $\pi^- p \to K^0_S K^0_S \pi^0 n$
14 $^{+20}_{-14}$ ±10	16	BECKER	87	MRK3	$e^+e^- \to \phi K\overline{K}\pi$
26 ±12		EVANGELIS...	81	OMEG	12 $\pi^- p \to \eta\pi^+\pi^-\pi^- p$
25 ±15	200	GURTU	79	HBC	4.2 $K^- p \to n\eta 2\pi$
~ 10		[5] STANTON	79	CNTR	8.5 $\pi^- p \to n2\gamma 2\pi$
24 ±18	210	GRASSLER	77	HBC	16 $\pi^\mp p$
28 ± 5	150	[6] DEFOIX	72	HBC	0.7 $\overline{p}p \to 7\pi$
46 ± 9	180	[6] DUBOC	72	HBC	1.2 $\overline{p}p \to 2K4\pi$
37 ± 5	500	[7] THUN	72	MMS	13.4 $\pi^- p$
10 ±10		BOESEBECK	71	HBC	16.0 $\pi p \to p5\pi$
30 ±15		CAMPBELL	69	DBC	2.7 $\pi^+ d$
60 ±15		[6] LORSTAD	69	HBC	0.7 $\overline{p}p$, 4,5-body
35 ±10		[6] DAHL	67	HBC	1.6–4.2 $\pi^- p$

[1] The selected process is $J/\psi \to \omega a_0(980)\pi$.
[2] Supersedes ABATZIS 94, ARMSTRONG 89E.
[3] From partial wave analysis of $K^+\overline{K}^0\pi^-$ system.
[4] No systematic error given.
[5] From phase shift analysis of $\eta\pi^+\pi^-$ system.
[6] Resolution is not unfolded.
[7] Seen in the missing mass spectrum.

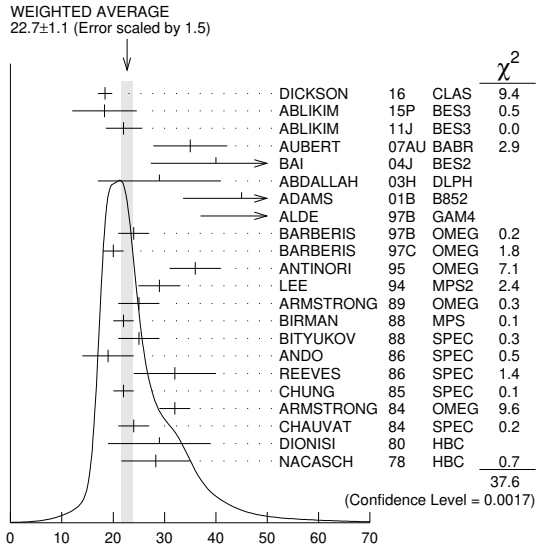

$f_1(1285)$ DECAY MODES

	Mode	Fraction (Γ_i/Γ)	Scale factor/ Confidence level
Γ_1	4π	(32.7± 1.9) %	S=1.2
Γ_2	$\pi^0\pi^0\pi^+\pi^-$	(21.8± 1.3) %	S=1.2
Γ_3	$2\pi^+2\pi^-$	(10.9± 0.6) %	S=1.2
Γ_4	$\rho^0\pi^+\pi^-$	(10.9± 0.6) %	S=1.2
Γ_5	$\rho^0\rho^0$	seen	
Γ_6	$4\pi^0$	$< 7 \times 10^{-4}$	CL=90%
Γ_7	$\eta\pi^+\pi^-$	(35 ±15) %	
Γ_8	$\eta\pi\pi$	(52.2± 2.0) %	S=1.2
Γ_9	$a_0(980)\pi$ [ignoring $a_0(980) \to K\overline{K}$]	(38 ± 4) %	
Γ_{10}	$\eta\pi\pi$ [excluding $a_0(980)\pi$]	(14 ± 4) %	
Γ_{11}	$K\overline{K}\pi$	(9.0± 0.4) %	S=1.1
Γ_{12}	$K\overline{K}^*(892)$	not seen	
Γ_{13}	$\pi^+\pi^-\pi^0$	(3.0± 0.9) $\times 10^{-3}$	
Γ_{14}	$\rho^\pm\pi^\mp$	$< 3.1 \times 10^{-3}$	CL=95%
Γ_{15}	$\gamma\rho^0$	(6.1± 1.0) %	S=1.7
Γ_{16}	$\phi\gamma$	(7.4± 2.6) $\times 10^{-4}$	
Γ_{17}	e^+e^-	$< 9.4 \times 10^{-9}$	CL=90%
Γ_{18}	$\gamma\gamma^*$		
Γ_{19}	$\gamma\gamma$		

CONSTRAINED FIT INFORMATION

An overall fit to 6 branching ratios uses 18 measurements and one constraint to determine 5 parameters. The overall fit has a $\chi^2 = 24.0$ for 14 degrees of freedom.

The following *off-diagonal* array elements are the correlation coefficients $\langle \delta x_i \delta x_j \rangle / (\delta x_i \cdot \delta x_j)$, in percent, from the fit to the branching fractions, $x_i \equiv \Gamma_i/\Gamma_{total}$. The fit constrains the x_i whose labels appear in this array to sum to one.

	x_1	x_9	x_{10}	x_{11}
x_9	−30			
x_{10}	−12	−88		
x_{11}	22	−10	−4	
x_{15}	−25	−7	−3	−27

$f_1(1285)$ $\Gamma(i)\Gamma(\gamma\gamma)/\Gamma(total)$

$\Gamma(\eta\pi\pi) \times \Gamma(\gamma\gamma)/\Gamma_{total}$

$\Gamma_8\Gamma_{19}/\Gamma = (\Gamma_9+\Gamma_{10})\Gamma_{19}/\Gamma$

VALUE (keV)	CL%	DOCUMENT ID		TECN	COMMENT
<0.62	95	GIDAL	87	MRK2	$e^+e^- \to e^+e^-\eta\pi^+\pi^-$

Downloaded from https://academic.oup.com/ptep/article/2022/8/083C01/6651666 by KIT Library user on 27 September 2022

$\Gamma(\eta\pi\pi) \times \Gamma(\gamma\gamma^*)/\Gamma_{total}$ — $\Gamma_8\Gamma_{18}/\Gamma = (\Gamma_9+\Gamma_{10})\Gamma_{18}/\Gamma$

VALUE (keV)	EVTS	DOCUMENT ID		TECN	COMMENT
1.4 ±0.4 OUR AVERAGE	Error includes scale factor of 1.4.				
1.18±0.25±0.20	26	[1,2] AIHARA	88B	TPC	$e^+e^- \to e^+e^-\eta\pi^+\pi^-$
2.30±0.61±0.42		[1,3] GIDAL	87	MRK2	$e^+e^- \to e^+e^-\eta\pi^+\pi^-$
• • • We do not use the following data for averages, fits, limits, etc. • • •					
1.8 ±0.3 ±0.3	420	[4] ACHARD	02B	L3	183–209 $e^+e^- \to e^+e^-\eta\pi^+\pi^-$

[1] Assuming a ρ-pole form factor.
[2] Published value multiplied by $\eta\pi\pi$ branching ratio 0.49.
[3] Published value divided by 2 and multiplied by the $\eta\pi\pi$ branching ratio 0.49.
[4] Published value multiplied by the $\eta\pi\pi$ branching ratio 0.52.

$f_1(1285)$ BRANCHING RATIOS

$\Gamma(K\overline{K}\pi)/\Gamma(4\pi)$ — Γ_{11}/Γ_1

VALUE	DOCUMENT ID		TECN	COMMENT
0.274±0.017 OUR FIT	Error includes scale factor of 1.4.			
0.271±0.016 OUR AVERAGE	Error includes scale factor of 1.2.			
0.265±0.014	[1] BARBERIS	97C	OMEG	450 $pp \to pp K^0_S K^\pm\pi^\mp$
0.28 ±0.05	[2] ARMSTRONG	89E	OMEG	300 $pp \to pp f_1(1285)$
0.37 ±0.03 ±0.05	[3] ARMSTRONG	89G	OMEG	85 $\pi p \to 4\pi X$

[1] Using $2(\pi^+\pi^-)$ data from BARBERIS 97B.
[2] Assuming $\rho\pi\pi$ and $a_0(980)\pi$ intermediate states.
[3] 4π consistent with being entirely $\rho\pi\pi$.

$\Gamma(\pi^0\pi^0\pi^+\pi^-)/\Gamma_{total}$ — $\Gamma_2/\Gamma = \frac{2}{3}\Gamma_1/\Gamma$

VALUE	DOCUMENT ID
0.218±0.013 OUR FIT Error includes scale factor of 1.2.	

$\Gamma(2\pi^+2\pi^-)/\Gamma_{total}$ — $\Gamma_3/\Gamma = \frac{1}{3}\Gamma_1/\Gamma$

VALUE	DOCUMENT ID
0.109±0.006 OUR FIT Error includes scale factor of 1.2.	

$\Gamma(\rho^0\pi^+\pi^-)/\Gamma_{total}$ — $\Gamma_4/\Gamma = \frac{1}{3}\Gamma_1/\Gamma$

VALUE	DOCUMENT ID
0.109±0.006 OUR FIT Error includes scale factor of 1.2.	

$\Gamma(\rho^0\pi^+\pi^-)/\Gamma(2\pi^+2\pi^-)$ — Γ_4/Γ_3

VALUE	DOCUMENT ID		TECN	COMMENT
• • • We do not use the following data for averages, fits, limits, etc. • • •				
1.0±0.4	GRASSLER	77	HBC	16 GeV $\pi^\pm p$

$\Gamma(\rho^0\rho^0)/\Gamma_{total}$ — Γ_5/Γ

VALUE	DOCUMENT ID		COMMENT
seen	BARBERIS	00C	450 $pp \to p_f 4\pi p_s$

$\Gamma(4\pi^0)/\Gamma_{total}$ — Γ_6/Γ

VALUE (units 10^{-4})	CL%	DOCUMENT ID		TECN	COMMENT
<7	90	ALDE	87	GAM4	100 $\pi^- p \to 4\pi^0 n$

$\Gamma(\pi^+\pi^-\pi^0)/\Gamma(\eta\pi^+\pi^-)$ — Γ_{13}/Γ_7

VALUE (%)	EVTS	DOCUMENT ID		TECN	COMMENT
0.86±0.16±0.20	2.3k	[1] DOROFEEV	11	VES	$\pi^- N \to \pi^- f_1(1285) N$

[1] Value obtained selecting the region corresponding to $f_0(980)$ in the $\pi^+\pi^-$ mass spectrum.

$\Gamma(\eta\pi\pi)/\Gamma_{total}$ — $\Gamma_8/\Gamma = (\Gamma_9+\Gamma_{10})/\Gamma$

VALUE	DOCUMENT ID
0.522±0.020 OUR FIT Error includes scale factor of 1.2.	

$\Gamma(4\pi)/\Gamma(\eta\pi\pi)$ — $\Gamma_1/\Gamma_8 = \Gamma_1/(\Gamma_9+\Gamma_{10})$

VALUE	DOCUMENT ID		TECN	COMMENT
0.63±0.06 OUR FIT Error includes scale factor of 1.3.				
0.41±0.14 OUR AVERAGE				
0.37±0.11±0.11	BOLTON	92	MRK3	$J/\psi \to \gamma f_1(1285)$
0.64±0.40	GURTU	79	HBC	4.2 $K^- p$
• • • We do not use the following data for averages, fits, limits, etc. • • •				
0.93±0.30	[1] GRASSLER	77	HBC	16 $\pi^\mp p$

[1] Assuming $\rho\pi\pi$ and $a_0(980)\pi$ intermediate states.

$\Gamma(2\pi^+2\pi^-)/\Gamma(\eta\pi\pi)$ — Γ_3/Γ_8

VALUE	DOCUMENT ID		TECN	COMMENT
0.28±0.02±0.02	[1] LEES	12X	BABR	$\tau^- \to \pi^- f_1(1285)\nu_\tau$

[1] Assuming $B(f_1(1285) \to \pi\pi\eta) = 3/2\, B(f_1(1285) \to \pi^+\pi^-\eta)$.

$\Gamma(a_0(980)\pi$ [ignoring $a_0(980) \to K\overline{K}$])$/\Gamma(\eta\pi\pi)$ — $\Gamma_9/\Gamma_8 = \Gamma_9/(\Gamma_9+\Gamma_{10})$

VALUE	CL%	DOCUMENT ID		TECN	COMMENT
0.72±0.08 OUR FIT					
0.72±0.07 OUR AVERAGE					
0.74±0.02±0.09		DICKSON	16	CLAS	$\gamma p \to f_1(1285) p$
0.72±0.15		GURTU	79	HBC	4.2 $K^- p$
$0.6\ ^{+0.3}_{-0.2}$		CORDEN	78	OMEG	12–15 $\pi^- p$
• • • We do not use the following data for averages, fits, limits, etc. • • •					
>0.69	95	ACHARD	02B	L3	183–209 $e^+e^- \to e^+e^-\eta\pi^+\pi^-$
0.28±0.07		ALDE	97B	GAM4	100 $\pi^- p \to \eta\pi^0\pi^0 n$
1.0 ±0.3		GRASSLER	77	HBC	16 $\pi^\mp p$

$\Gamma(K\overline{K}\pi)/\Gamma(\eta\pi\pi)$ — $\Gamma_{11}/\Gamma_8 = \Gamma_{11}/(\Gamma_9+\Gamma_{10})$

VALUE	DOCUMENT ID		TECN	COMMENT
0.172±0.012 OUR FIT Error includes scale factor of 1.1.				
0.176±0.012 OUR AVERAGE				
0.216±0.010±0.031	DICKSON	16	CLAS	$\gamma p \to f_1(1285) p$
0.166±0.01 ±0.008	BARBERIS	98C	OMEG	450 $pp \to p_f f_1(1285) p_s$
0.42 ±0.15	GURTU	79	HBC	4.2 $K^- p$
0.5 ±0.2	[1] CORDEN	78	OMEG	12–15 $\pi^- p$
0.20 ±0.08	[2] DEFOIX	72	HBC	0.7 $\overline{p}p \to 7\pi$
0.16 ±0.08	CAMPBELL	69	DBC	2.7 $\pi^+ d$

[1] CORDEN 78 assumes low-mass $\eta\pi\pi$ region is dominantly 1^{++}. See BARBERIS 98C and MANAK 00A for discussion.
[2] $K\overline{K}$ system characterized by the $I = 1$ threshold enhancement. (See under $a_0(980)$).

$\Gamma(K\overline{K}^*(892))/\Gamma_{total}$ — Γ_{12}/Γ

VALUE	DOCUMENT ID		TECN	COMMENT
not seen	NACASCH	78	HBC	0.7,0.76 $\overline{p}p \to K\overline{K}3\pi$
• • • We do not use the following data for averages, fits, limits, etc. • • •				
seen	[1] ACHARD	07	L3	183–209 $e^+e^- \to e^+e^- K^0_S K^\pm\pi^\mp$

[1] A clear signal of 19.8 ± 4.4 events observed at high Q^2.

$\Gamma(\pi^+\pi^-\pi^0)/\Gamma_{total}$ — Γ_{13}/Γ

VALUE (%)	EVTS	DOCUMENT ID		TECN	COMMENT
0.30±0.055±0.074	2.3k	[1] DOROFEEV	11	VES	$\pi^- N \to \pi^- f_1(1285) N$

[1] Value obtained selecting the region corresponding to $f_0(980)$ in the $\pi^+\pi^-$ mass spectrum. The sytematic error includes the uncertainty on the partial width $f_1 \to \eta\pi\pi$ obtained from PDG 10 data.

$\Gamma(\rho^\pm\pi^\mp)/\Gamma_{total}$ — Γ_{14}/Γ

VALUE (%)	CL%	DOCUMENT ID		TECN	COMMENT
<0.31	95	DOROFEEV	11	VES	$\pi^- N \to \pi^- f_1(1285) N$

$\Gamma(\gamma\rho^0)/\Gamma_{total}$ — Γ_{15}/Γ

VALUE (units 10^{-2})	CL%	DOCUMENT ID		TECN	COMMENT
6.1±1.0 OUR FIT Error includes scale factor of 1.7.					
• • • We do not use the following data for averages, fits, limits, etc. • • •					
2.8±0.7±0.6		[1] AMELIN	95	VES	37 $\pi^- N \to \pi^-\pi^+\pi^-\gamma N$
<5	95	BITYUKOV	91B	SPEC	32 $\pi^- p \to \pi^+\pi^-\gamma n$

[1] Not an independent measurement.

$\Gamma(\gamma\rho^0)/\Gamma(2\pi^+2\pi^-)$ — $\Gamma_{15}/\Gamma_3 = \Gamma_{15}/\frac{1}{3}\Gamma_1$

VALUE	DOCUMENT ID		TECN	COMMENT
0.55±0.10 OUR FIT Error includes scale factor of 1.5.				
0.45±0.18	[1] COFFMAN	90	MRK3	$J/\psi \to \gamma\gamma\pi^+\pi^-$

[1] Using $B(J/\psi \to \gamma f_1(1285) \to \gamma\gamma\rho^0)=0.25\times10^{-4}$ and $B(J/\psi \to \gamma f_1(1285) \to \gamma 2\pi^+2\pi^-)=0.55\times10^{-4}$ given by MIR 88.

$\Gamma(\eta\pi\pi)/\Gamma(\gamma\rho^0)$ — $\Gamma_8/\Gamma_{15} = (\Gamma_9+\Gamma_{10})/\Gamma_{15}$

VALUE	DOCUMENT ID		TECN	COMMENT
8.6±1.6 OUR FIT Error includes scale factor of 1.9.				
8.5±2.0 OUR AVERAGE Error includes scale factor of 2.2. See the ideogram below.				
21.3±4.4	DICKSON	16	CLAS	$\gamma p \to f_1(1285) p$
10.0±1.0±2.0	BARBERIS	98C	OMEG	450 $pp \to p_f f_1(1285) p_s$
7.5±1.0	[1] ARMSTRONG	92C	OMEG	300 $pp \to pp\pi^+\pi^-\gamma$, $pp\eta\pi^+\pi^-$

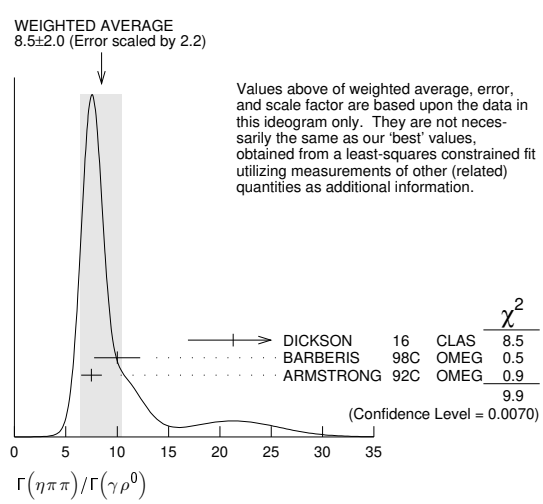

[1] Published value multiplied by 1.5.

Downloaded from https://academic.oup.com/ptep/article/2022/8/083C01/6651666 by KIT Library user on 27 September 2022

$\Gamma(\gamma\rho^0)/\Gamma(K\overline{K}\pi)$ — Γ_{15}/Γ_{11}

VALUE	CL%	DOCUMENT ID		TECN	COMMENT
• • • We do not use the following data for averages, fits, limits, etc. • • •					
>0.035	90	[1] COFFMAN	90	MRK3	$J/\psi \to \gamma\gamma\pi^+\pi^-$

[1] Using $B(J/\psi \to \gamma f_1(1285) \to \gamma\gamma\rho^0) = 0.25 \times 10^{-4}$ and $B(J/\psi \to \gamma f_1(1285) \to \gamma K\overline{K}\pi) = < 0.72 \times 10^{-3}$.

$\Gamma(\phi\gamma)/\Gamma(K\overline{K}\pi)$ — Γ_{16}/Γ_{11}

VALUE (units 10^{-2})	CL%	EVTS	DOCUMENT ID		TECN	COMMENT
0.82±0.21±0.20		19	BITYUKOV	88	SPEC	32.5 $\pi^- p \to K^+ K^- \pi^0 n$
• • • We do not use the following data for averages, fits, limits, etc. • • •						
<0.50	95		BARBERIS	98C	OMEG	450 $pp \to p_f f_1(1285) p_s$
<0.93	95		AMELIN	95	VES	37 $\pi^- N \to \pi^-\pi^+\pi^-\gamma N$

$\Gamma(e^+e^-)/\Gamma_{total}$ — Γ_{17}/Γ

VALUE	CL%	DOCUMENT ID		TECN	COMMENT
<9.4 × 10^{-9}	90	[1] ACHASOV	20	SND	$e^+e^- \to \eta\pi^0\pi^0$

[1] ACHASOV 20 reports two candidate events corresponding to a significance of 2.5 σ and the branching fraction of $(5.1^{+3.7}_{-2.7}) \times 10^{-9}$.

$f_1(1285)$ REFERENCES

ACHASOV	20	PL B800 135074	M.N. Achasov *et al.*	(SND Collab.)
ABLIKIM	19BA	PR D100 092003	M. Ablikim *et al.*	(BESIII Collab.)
DICKSON	16	PR C93 065202	R. Dickson *et al.*	(JLab CLAS Collab.)
ABLIKIM	15P	PR D92 012007	M. Ablikim *et al.*	(BESIII Collab.)
AAIJ	14Y	PRL 112 091802	R. Aaij *et al.*	(LHCb Collab.)
LEES	12X	PR D86 092010	J.P. Lees *et al.*	(BABAR Collab.)
ABLIKIM	11J	PRL 107 182001	M. Ablikim *et al.*	(BESIII Collab.)
DOROFEEV	11	EPJ A47 68	V. Dorofeev *et al.*	(SERP, MIPT)
PDG	10	JP G37 075021	K. Nakamura *et al.*	(PDG Collab.)
ACHARD	07	JHEP 0703 018	P. Achard *et al.*	(L3 Collab.)
AUBERT	07AU	PR D76 092005	B. Aubert *et al.*	(BABAR Collab.)
BAI	04J	PL B594 47	J.Z. Bai *et al.*	(BES Collab.)
ABDALLAH	03H	PL B569 129	J. Abdallah *et al.*	(DELPHI Collab.)
ACHARD	02B	PL B526 269	P. Achard *et al.*	(L3 Collab.)
ACCIARRI	01G	PL B501 1	M. Acciarri *et al.*	(L3 Collab.)
ADAMS	01B	PL B516 264	G.S. Adams *et al.*	(BNL E852 Collab.)
BARBERIS	00C	PL B471 440	D. Barberis *et al.*	(WA 102 Collab.)
MANAK	00A	PR D62 012003	J.J. Manak *et al.*	(BNL E852 Collab.)
SOSA	99	PRL 83 913	M. Sosa *et al.*	
BARBERIS	98C	PL B440 225	D. Barberis *et al.*	(WA 102 Collab.)
ALDE	97B	PAN 60 386	D. Alde *et al.*	(GAMS Collab.)
		Translated from YAF 60 458.		
BARBERIS	97B	PL B413 217	D. Barberis *et al.*	(WA 102 Collab.)
BARBERIS	97C	PL B413 225	D. Barberis *et al.*	(WA 102 Collab.)
AMELIN	95	ZPHY C66 71	D.V. Amelin *et al.*	(VES Collab.)
ANTINORI	95	PL B353 589	F. Antinori *et al.*	(ATHU, BARI, BIRM+)
ABATZIS	94	PL B324 509	S. Abatzis *et al.*	(ATHU, BARI, BIRM+)
LEE	94	PL B323 227	J.H. Lee *et al.*	(BNL, IND, KYUN, MASD+)
ARMSTRONG	93C	PL B307 394	T.A. Armstrong *et al.*	(FNAL, FERR, GENO+)
ARMSTRONG	92C	ZPHY C54 371	T.A. Armstrong *et al.*	(ATHU, BARI, BIRM+)
BOLTON	92	PL B278 495	T. Bolton *et al.*	(Mark III Collab.)
BITYUKOV	91B	SJNP 54 318	S.I. Bityukov *et al.*	(SERP)
		Translated from YAF 54 529.		
FUKUI	91C	PL B267 293	S. Fukui *et al.*	(SUGI, NAGO, KEK, KYOT+)
COFFMAN	90	PR D41 1410	D.M. Coffman *et al.*	(Mark III Collab.)
ARMSTRONG	89	PL B221 216	T.A. Armstrong *et al.*	(CERN, CDEF, BIRM+) JPC
ARMSTRONG	89E	PL B228 536	T.A. Armstrong, M. Benayoun	(ATHU, BARI, BIRM+)
ARMSTRONG	89G	ZPHY C43 55	T.A. Armstrong *et al.*	(CERN, BIRM, BARI+)
RATH	89	PR D40 693	M.G. Rath *et al.*	(NDAM, BRAN, BNL, CUNY+)
AIHARA	88B	PL B209 107	H. Aihara *et al.*	(TPC-2γ Collab.)
BIRMAN	88	PRL 61 1557	A. Birman *et al.*	(BNL, FSU, IND, MASD) JP
BITYUKOV	88	PL B203 327	S.I. Bityukov *et al.*	(SERP)
MIR	88	Photon-Photon 88, 126	R. Mir	(Mark III Collab.)
Conference				
ALDE	87	PL B198 286	D.M. Alde *et al.*	(LANL, BRUX, SERP, LAPP)
BECKER	87	PRL 59 186	J.J. Becker *et al.*	(Mark III Collab.)
GIDAL	87	PRL 59 2012	G. Gidal *et al.*	(LBL, SLAC, HARV)
ANDO	86	PRL 57 1296	A. Ando *et al.*	(KEK, KYOT, NIRS, SAGA+) IJP
REEVES	86	PR D34 1960	D.F. Reeves *et al.*	(FLOR, BNL, IND+) JP
CHUNG	85	PRL 55 779	S.U. Chung *et al.*	(BNL, FLOR, IND+) JP
ARMSTRONG	84	PL 146B 273	T.A. Armstrong *et al.*	(ATHU, BARI, BIRM+) JP
BITYUKOV	84B	PL 144B 133	S.I. Bityukov *et al.*	(SERP)
CHAUVAT	84	PL 148B 382	P. Chauvat *et al.*	(CERN, CLER, UCLA+)
TORNQVIST	82B	NP B203 268	N.A. Tornqvist	(HELS)
EVANGELIS...	81	NP B178 197	C. Evangelista *et al.*	(BARI, BONN, CERN+)
BROMBERG	80	PR D22 1513	C.M. Bromberg *et al.*	(CIT, FNAL, ILLC+)
DIONISI	80	NP B169 1	C. Dionisi *et al.*	(CERN, MADR, CDEF+)
GURTU	79	NP B151 181	A. Gurtu *et al.*	(CERN, ZEEM, NIJM, OXF)
STANTON	79	PRL 42 346	N.R. Stanton *et al.*	(OSU, CARL, MCGI+) JP
CORDEN	78	NP B144 253	M.J. Corden *et al.*	(BIRM, RHEL, TELA+) JP
NACASCH	78	NP B135 203	R. Nacasch *et al.*	(PARIS, MADR, CERN)
GRASSLER	77	NP B121 189	H. Grassler *et al.*	(AACH3, BERL, BONN+)
DEFOIX	72	NP B44 125	C. Defoix *et al.*	(CDEF, CERN)
DUBOC	72	NP B46 429	J. Duboc *et al.*	(PARIS, LIVP)
THUN	72	PRL 28 1733	R. Thun *et al.*	(STON, NEAS)
BARDADIN-...	71	PR D4 2711	M. Bardadin-Otwinowska *et al.*	(WARS)
BOESEBECK	71	PL 34B 659	K. Boesebeck (AACH, BERL, BONN, CERN, CRAC+)	
CAMPBELL	69	PRL 22 1204	J.H. Campbell *et al.*	(PURD)
LORSTAD	69	NP B14 63	B. Lorstad *et al.*	(CDEF, CERN) JP
D'ANDLAU	68	NP B5 693	C. d'Andlau *et al.*	(CDEF, CERN, IRAD+) IJP
DAHL	67	PR 163 1377	O.I. Dahl *et al.*	(LRL) IJP

$\eta(1295)$

$I^G(J^{PC}) = 0^+(0^{-+})$

See the review on "Spectroscopy of Light Meson Resonances."

$\eta(1295)$ MASS

VALUE (MeV)	EVTS	DOCUMENT ID		TECN	COMMENT
1294±4 OUR AVERAGE Error includes scale factor of 1.6. See the ideogram below.					
1302±9±8	20k	ADAMS	01B	B852	18 GeV $\pi^- p \to K^+K^-\pi^0 n$
1282±5	9082	MANAK	00A	MPS	18 $\pi^- p \to \eta\pi^+\pi^- n$
1299±4	2100	ALDE	97B	GAM4	100 $\pi^- p \to \eta\pi^0\pi^0 n$
1295±4		FUKUI	91C	SPEC	8.95 $\pi^- p \to \eta\pi^+\pi^- n$
• • • We do not use the following data for averages, fits, limits, etc. • • •					
1264±8		[1] AUGUSTIN	90	DM2	$J/\psi \to \gamma\eta\pi^+\pi^-$
~ 1275		STANTON	79	CNTR	8.4 $\pi^- p \to n\eta 2\pi$

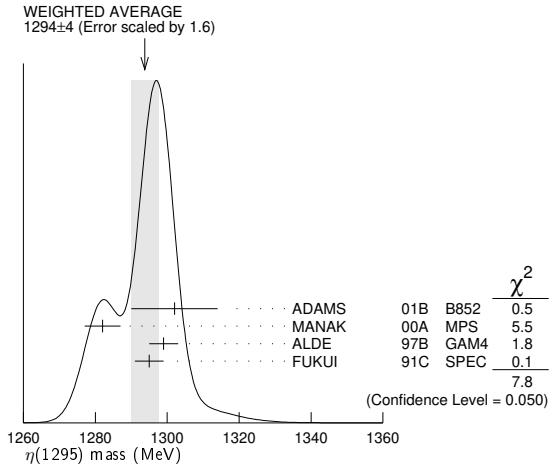

[1] PWA analysis of AUGUSTIN 92 assigns 0^{-+} quantum numbers to this state rather than 1^{++} as before.

$\eta(1295)$ WIDTH

VALUE (MeV)	EVTS	DOCUMENT ID		TECN	COMMENT
55± 5 OUR AVERAGE					
57±23±21	20k	ADAMS	01B	B852	18 GeV $\pi^- p \to K^+K^-\pi^0 n$
66±13	9082	MANAK	00A	MPS	18 $\pi^- p \to \eta\pi^+\pi^- n$
53± 6		FUKUI	91C	SPEC	8.95 $\pi^- p \to \eta\pi^+\pi^- n$
• • • We do not use the following data for averages, fits, limits, etc. • • •					
<40	2100	ALDE	97B	GAM4	100 $\pi^- p \to \eta\pi^0\pi^0 n$
44±20		[2] AUGUSTIN	90	DM2	$J/\psi \to \gamma\eta\pi^+\pi^-$
~ 70		STANTON	79	CNTR	8.4 $\pi^- p \to n\eta 2\pi$

[2] PWA analysis of AUGUSTIN 92 assigns 0^{-+} quantum numbers to this state rather than 1^{++} as before.

$\eta(1295)$ DECAY MODES

	Mode	Fraction (Γ_i/Γ)
Γ_1	$\eta\pi^+\pi^-$	seen
Γ_2	$a_0(980)\pi$	seen
Γ_3	$\gamma\gamma$	
Γ_4	$\eta\pi^0\pi^0$	seen
Γ_5	$\eta(\pi\pi)_{S\text{-wave}}$	seen
Γ_6	$\sigma\eta$	
Γ_7	$K\overline{K}\pi$	

$\eta(1295)$ $\Gamma(i)\Gamma(\gamma\gamma)/\Gamma(total)$

$\Gamma(\eta\pi^+\pi^-) \times \Gamma(\gamma\gamma)/\Gamma_{total}$ — $\Gamma_1\Gamma_3/\Gamma$

VALUE (keV)	CL%	DOCUMENT ID		TECN	COMMENT
<0.066	95	ACCIARRI	01G	L3	183–202 $e^+e^- \to e^+e^-\eta\pi^+\pi^-$
• • • We do not use the following data for averages, fits, limits, etc. • • •					
<0.6	90	AIHARA	88C	TPC	$e^+e^- \to e^+e^-\eta\pi^+\pi^-$
<0.3		ANTREASYAN	87	CBAL	$e^+e^- \to e^+e^-\eta\pi\pi$

$\Gamma(K\overline{K}\pi) \times \Gamma(\gamma\gamma)/\Gamma_{total}$ — $\Gamma_7\Gamma_3/\Gamma$

VALUE (keV)	CL%	DOCUMENT ID		TECN	COMMENT
• • • We do not use the following data for averages, fits, limits, etc. • • •					
<0.014	90	[3,4] AHOHE	05	CLE2	10.6 $e^+e^- \to e^+e^- K^0_S K^\pm\pi^\mp$

[3] Using $\eta(1295)$ mass and width 1294 MeV and 55 MeV, respectively.
[4] Assuming three-body phase-space decay to $K^0_S K^\pm\pi^\mp$.

Downloaded from https://academic.oup.com/ptep/article/2022/8/083C01/6651666 by KIT Library user on 27 September 2022

$\eta(1295)$ BRANCHING RATIOS

$\Gamma(a_0(980)\pi)/\Gamma_{total}$ — Γ_2/Γ

VALUE	DOCUMENT ID		TECN	COMMENT
• • • We do not use the following data for averages, fits, limits, etc. • • •				
not seen	BERTIN	97	OBLX	0.0 $\overline{p}p \to K^{\pm}(K^0)\pi^{\mp}\pi^+\pi^-$
seen	BIRMAN	88	MPS	8 $\pi^- p \to K^+\overline{K}^0\pi^- n$
large	ANDO	86	SPEC	8 $\pi^- p \to \eta\pi^+\pi^- n$
large	STANTON	79	CNTR	8.4 $\pi^- p \to n\eta 2\pi$

$\Gamma(a_0(980)\pi)/\Gamma(\eta\pi^0\pi^0)$ — Γ_2/Γ_4

VALUE	DOCUMENT ID		TECN	COMMENT
0.65±0.10	[5] ALDE	97B	GAM4	100 $\pi^- p \to \eta\pi^0\pi^0 n$

[5] Assuming that $a_0(980)$ decays only to $\eta\pi$.

$\Gamma(\eta(\pi\pi)_{S\text{-wave}})/\Gamma(\eta\pi^0\pi^0)$ — Γ_5/Γ_4

VALUE	DOCUMENT ID		TECN	COMMENT
0.35±0.10	ALDE	97B	GAM4	100 $\pi^- p \to \eta\pi^0\pi^0 n$

$\Gamma(a_0(980)\pi)/\Gamma(\sigma\eta)$ — Γ_2/Γ_6

VALUE	EVTS	DOCUMENT ID		TECN	COMMENT
0.48±0.22	9082	MANAK	00A	MPS	18 $\pi^- p \to \eta\pi^+\pi^- n$

$\eta(1295)$ REFERENCES

AHOHE	05	PR D71 072001	R. Ahohe *et al.*	(CLEO Collab.)
ACCIARRI	01G	PL B501 1	M. Acciarri *et al.*	(L3 Collab.)
ADAMS	01B	PL B516 264	G.S. Adams *et al.*	(BNL E852 Collab.)
MANAK	00A	PR D62 012003	J.J. Manak *et al.*	(BNL E852 Collab.)
ALDE	97B	PAN 60 386 Translated from YAF 60 458.	D. Alde *et al.*	(GAMS Collab.)
BERTIN	97	PL B400 226	A. Bertin *et al.*	(OBELIX Collab.)
AUGUSTIN	92	PR D46 1951	J.E. Augustin, G. Cosme	(DM2 Collab.)
FUKUI	91C	PL B267 293	S. Fukui *et al.*	(SUGI, NAGO, KEK, KYOT+)
AUGUSTIN	90	PR D42 10	J.E. Augustin *et al.*	(DM2 Collab.)
AIHARA	88C	PR D38 1	H. Aihara *et al.*	(TPC-2γ Collab.)
BIRMAN	88	PRL 61 1557	A. Birman *et al.*	(BNL, FSU, IND, MASD) JP
ANTREASYAN	87	PR D36 2633	D. Antreasyan *et al.*	(Crystal Ball Collab.)
ANDO	86	PRL 57 1296	A. Ando *et al.*	(KEK, KYOT, NIRS, SAGA+) IJP
STANTON	79	PRL 42 346	N.R. Stanton *et al.*	(OSU, CARL, MCGI+) JP

$\pi(1300)$

$I^G(J^{PC}) = 1^-(0^{-+})$

$\pi(1300)$ MASS

VALUE (MeV)	EVTS	DOCUMENT ID		TECN	COMMENT
1300±100 OUR ESTIMATE					
• • • We do not use the following data for averages, fits, limits, etc. • • •					
1128± 26±70		DARGENT	17	RVUE	$D^0 \to \pi^-\pi^+\pi^-\pi^+$
1345± 8±10	18k	[1] SCHEGELSKY	06	RVUE	$\gamma\gamma \to \pi^+\pi^-\pi^0$
1200± 40	90k	SALVINI	04	OBLX	$\overline{p}p \to 2\pi^+ 2\pi^-$
1343± 15±24		CHUNG	02	B852	18.3 $\pi^- p \to \pi^+\pi^-\pi^- p$
1375± 40		ABELE	01	CBAR	0.0 $\overline{p}d \to \pi^- 4\pi^0 p$
1275± 15		BERTIN	97D	OBLX	0.05 $\overline{p}p \to 2\pi^+ 2\pi^-$
~ 1114		ABELE	96	CBAR	0.0 $\overline{p}p \to 5\pi^0$
1190± 30		ZIELINSKI	84	SPEC	200 $\pi^+ Z \to Z 3\pi$
1240± 30		BELLINI	82	SPEC	40 $\pi^- A \to A 3\pi$
1273± 50		[2] AARON	81	RVUE	
1342± 20		BONESINI	81	OMEG	12 $\pi^- p \to p 3\pi$
~ 1400		DAUM	81B	SPEC	63,94 $\pi^- p$

[1] From analysis of L3 data at 183–209 GeV.
[2] Uses multichannel Aitchison-Bowler model (BOWLER 75). Uses data from DAUM 80 and DANKOWYCH 81.

$\pi(1300)$ WIDTH

VALUE (MeV)	EVTS	DOCUMENT ID		TECN	COMMENT
200 to 600 OUR ESTIMATE					
• • • We do not use the following data for averages, fits, limits, etc. • • •					
314± 39±66		DARGENT	17	RVUE	$D^0 \to \pi^-\pi^+\pi^-\pi^+$
260± 20±30	18k	[3] SCHEGELSKY	06	RVUE	$\gamma\gamma \to \pi^+\pi^-\pi^0$
470±120	90k	SALVINI	04	OBLX	$\overline{p}p \to 2\pi^+ 2\pi^-$
449± 39±47		CHUNG	02	B852	18.3 $\pi^- p \to \pi^+\pi^-\pi^- p$
268± 50		ABELE	01	CBAR	0.0 $\overline{p}d \to \pi^- 4\pi^0 p$
218±100		BERTIN	97D	OBLX	0.05 $\overline{p}p \to 2\pi^+ 2\pi^-$
~ 340		ABELE	96	CBAR	0.0 $\overline{p}p \to 5\pi^0$
440± 80		ZIELINSKI	84	SPEC	200 $\pi^+ Z \to Z 3\pi$
360±120		BELLINI	82	SPEC	40 $\pi^- A \to A 3\pi$
580±100		[4] AARON	81	RVUE	
220± 70		BONESINI	81	OMEG	12 $\pi^- p \to p 3\pi$
~ 600		DAUM	81B	SPEC	63,94 $\pi^- p$

[3] From analysis of L3 data at 183–209 GeV.
[4] Uses multichannel Aitchison-Bowler model (BOWLER 75). Uses data from DAUM 80 and DANKOWYCH 81.

$\pi(1300)$ DECAY MODES

	Mode	Fraction (Γ_i/Γ)
Γ_1	$\rho\pi$	seen
Γ_2	$\pi(\pi\pi)_{S\text{-wave}}$	seen
Γ_3	$\gamma\gamma$	

$\pi(1300)$ $\Gamma(i)\Gamma(\gamma\gamma)/\Gamma(\text{total})$

$\Gamma(\rho\pi) \times \Gamma(\gamma\gamma)/\Gamma_{total}$ — $\Gamma_1\Gamma_3/\Gamma$

VALUE (keV)	CL%	DOCUMENT ID		TECN	COMMENT
<0.085	90	ACCIARRI	97T	L3	$e^+e^- \to e^+e^-\pi^+\pi^-\pi^0$
• • • We do not use the following data for averages, fits, limits, etc. • • •					
<0.8	95	[5] SCHEGELSKY	06	RVUE	$\gamma\gamma \to \pi^+\pi^-\pi^0$
<0.54	90	ALBRECHT	97B	ARG	$e^+e^- \to e^+e^-\pi^+\pi^-\pi^0$

[5] From analysis of L3 data at 183–209 GeV.

$\pi(1300)$ BRANCHING RATIOS

$\Gamma(\pi(\pi\pi)_{S\text{-wave}})/\Gamma(\rho\pi)$ — Γ_2/Γ_1

VALUE	CL%	EVTS	DOCUMENT ID		TECN	COMMENT
• • • We do not use the following data for averages, fits, limits, etc. • • •						
2.2 ±0.4		90k	SALVINI	04	OBLX	$\overline{p}p \to 2\pi^+ 2\pi^-$
seen			CHUNG	02	B852	18.3 $\pi^- p \to \pi^+ 2\pi^- p$
<0.15	90		ABELE	01	CBAR	0.0 $\overline{p}d \to \pi^- 4\pi^0 p$
2.12			[6] AARON	81	RVUE	

[6] Uses multichannel Aitchison-Bowler model (BOWLER 75). Uses data from DAUM 80 and DANKOWYCH 81.

$\pi(1300)$ REFERENCES

DARGENT	17	JHEP 1705 143	P. dArgent *et al.*	(HEID, BRIS)
SCHEGELSKY	06	EPJ A27 199	V.A. Schegelsky *et al.*	
SALVINI	04	EPJ C35 21	P. Salvini *et al.*	(OBELIX Collab.)
CHUNG	02	PR D65 072001	S.U. Chung *et al.*	(BNL E852 Collab.)
ABELE	01	EPJ C19 667	A. Abele *et al.*	(Crystal Barrel Collab.)
ACCIARRI	97T	PL B413 147	M. Acciarri *et al.*	(L3 Collab.)
ALBRECHT	97B	ZPHY C74 469	H. Albrecht *et al.*	(ARGUS Collab.)
BERTIN	97D	PL B414 220	A. Bertin *et al.*	(OBELIX Collab.)
ABELE	96	PL B380 453	A. Abele *et al.*	(Crystal Barrel Collab.)
ZIELINSKI	84	PR D30 1855	M. Zielinski *et al.*	(ROCH, MINN, FNAL)
BELLINI	82	PRL 48 1697	G. Bellini *et al.*	(MILA, BGNA, JINR)
AARON	81	PR D24 1207	R.A. Aaron, R.S. Longacre	(NEAS, BNL)
BONESINI	81	PL 103B 75	M. Bonesini *et al.*	(MILA, LIVP, DARE+)
DANKOWY...	81	PRL 46 580	J.A. Dankowych *et al.*	(TNTO, BNL, CARL+)
DAUM	81B	NP B182 269	C. Daum *et al.*	(AMST, CERN, CRAC, MPIM+)
DAUM	80	PL 89B 281	C. Daum *et al.*	(AMST, CERN, CRAC, MPIM+)
BOWLER	75	NP B97 227	M.G. Bowler *et al.*	(OXFTP, DARE)

$a_2(1320)$

$I^G(J^{PC}) = 1^-(2^{++})$

$a_2(1320)$ MASS

VALUE (MeV)	DOCUMENT ID
1318.2±0.6 OUR AVERAGE Includes data from the 4 datablocks that follow this one. Error includes scale factor of 1.2.	

3π MODE

VALUE (MeV)	EVTS	DOCUMENT ID		TECN	CHG	COMMENT
The data in this block is included in the average printed for a previous datablock.						
1318.6± 1.3 OUR AVERAGE Error includes scale factor of 1.4. See the ideogram below.						
$1314.5^{+4.0}_{-3.3}$	46M	[1] AGHASYAN	18B	COMP		190 $\pi^- p \to \pi^-\pi^+\pi^- p$
1326 ± 2 ±2		CHUNG	02	B852		18.3 $\pi^- p \to \pi^+\pi^-\pi^- p$
1317 ± 3		BARBERIS	98B			450 $pp \to p_f\pi^+\pi^-\pi^0 p_s$
1323 ± 4 ±3		ACCIARRI	97T	L3		$e^+e^- \to e^+e^-\pi^+\pi^-\pi^0$
1320 ± 7		ALBRECHT	97B	ARG		$e^+e^- \to e^+e^-\pi^+\pi^-\pi^0$
1311.3± 1.6±3.0	72.4k	AMELIN	96	VES		36 $\pi^- p \to \pi^+\pi^-\pi^0 n$
1310 ± 5		ARMSTRONG	90	OMEG	0	300.0$pp \to pp\pi^+\pi^-\pi^0$
1323.8± 2.3	4022	AUGUSTIN	89	DM2	±	$J/\psi \to \rho^{\pm} a_2^{\mp}$
1320.6± 3.1	3562	AUGUSTIN	89	DM2	0	$J/\psi \to \rho^0 a_2^0$
1317 ± 2	25k	[2] DAUM	80C	SPEC	−	63,94 $\pi^- p \to 3\pi p$
1320 ±10	1097	[2] BALTAY	78B	HBC	+0	15 $\pi^+ p \to p 4\pi$
1306 ± 8		FERRERSORIA	78	OMEG	−	9 $\pi^- p \to p 3\pi$
1318 ± 7	1.6k	[2] EMMS	75	DBC	0	4 $\pi^+ n \to p(3\pi)^0$
1315 ± 5		[2] ANTIPOV	73C	CNTR	−	25,40 $\pi^- p \to p\eta\pi^-$
1306 ± 9	1580	CHALOUPKA	73	HBC	−	3.9 $\pi^- p$

Downloaded from https://academic.oup.com/ptep/article/2022/8/083C01/6651666 by KIT Library user on 27 September 2022

• • • We do not use the following data for averages, fits, limits, etc. • • •

1321 ± 1 $^{+0}_{-7}$	420k	[3] ALEKSEEV	10	COMP		190 $\pi^- Pb \to \pi^-\pi^-\pi^+ Pb'$
1300 ± 2 ±4	18k	[4] SCHEGELSKY	06	RVUE	0	$\gamma\gamma \to \pi^+\pi^-\pi^0$
1305 ±14		CONDO	93	SHF		$\gamma p \to n\pi^+\pi^+\pi^-$
1310 ± 2		[2] EVANGELIS...	81	OMEG	–	12 $\pi^- p \to 3\pi p$
1343 ±11	490	BALTAY	78B	HBC	0	15 $\pi^+ p \to \Delta 3\pi$
1309 ± 5	5k	BINNIE	71	MMS	–	$\pi^- p$ near a_2 threshold
1299 ± 6	28k	BOWEN	71	MMS	–	5 $\pi^- p$
1300 ± 6	24k	BOWEN	71	MMS	+	5 $\pi^+ p$
1309 ± 4	17k	BOWEN	71	MMS	–	7 $\pi^- p$
1306 ± 4	941	ALSTON-...	70	HBC	+	7.0 $\pi^+ p \to 3\pi p$

[1] Statistical error negligible.
[2] From a fit to $J^P = 2^+$ $\rho\pi$ partial wave.
[3] Superseded by AGHASYAN 2018B.
[4] From analysis of L3 data at 183–209 GeV.

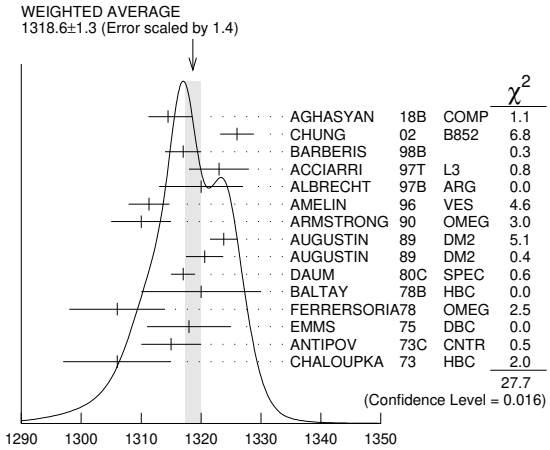

$a_2(1320)$ mass, 3π mode (MeV)

$K\overline{K}$ MODE

VALUE (MeV)	EVTS	DOCUMENT ID		TECN	CHG	COMMENT
The data in this block is included in the average printed for a previous datablock.						
1318.1± 0.7 OUR AVERAGE						
1319 ± 5	4700	[1,2] CLELAND	82B	SPEC	+	50 $\pi^+ p \to K^0_S K^+ p$
1324 ± 6	5200	[1,2] CLELAND	82B	SPEC	–	50 $\pi^- p \to K^0_S K^- p$
1320 ± 2	4000	CHABAUD	80	SPEC	–	17 $\pi^- A \to K^0_S K^- A$
1312 ± 4	11000	CHABAUD	78	SPEC	–	9.8 $\pi^- p \to K^- K^0_S p$
1316 ± 2	4730	CHABAUD	78	SPEC	–	18.8 $\pi^- p \to K^- K^0_S p$
1318 ± 1		[1,3] MARTIN	78D	SPEC	–	10 $\pi^- p \to K^0_S K^- p$
1320 ± 2	2724	MARGULIE	76	SPEC	–	23 $\pi^- p \to K^- K^0_S p$
1313 ± 4	730	FOLEY	72	CNTR	–	20.3 $\pi^- p \to K^- K^0_S p$
1319 ± 3	1500	[3] GRAYER	71	ASPK	–	17.2 $\pi^- p \to K^- K^0_S p$
• • • We do not use the following data for averages, fits, limits, etc. • • •						
1304 ±10	870	[4] SCHEGELSKY	06A	RVUE	0	$\gamma\gamma \to K^0_S K^0_S$
1330 ±11	1000	[1,2] CLELAND	82B	SPEC	+	30 $\pi^+ p \to K^0_S K^+ p$
1324 ± 5	350	HYAMS	78	ASPK	+	12.7 $\pi^+ p \to K^+ K^0_S p$

[1] From a fit to $J^P = 2^+$ partial wave.
[2] Number of events evaluated by us.
[3] Systematic error in mass scale subtracted.
[4] From analysis of L3 data at 91 and 183–209 GeV.

$\eta\pi$ MODE

VALUE (MeV)	EVTS	DOCUMENT ID		TECN	CHG	COMMENT
The data in this block is included in the average printed for a previous datablock.						
1317.7± 1.4 OUR AVERAGE						
1308 ± 9		BARBERIS	00H			450 $pp \to p_f \eta\pi^0 p_s$
1316 ± 9		BARBERIS	00H			450 $pp \to \Delta^{++}_f \eta\pi^- p_s$
1317 ± 1 ±2		THOMPSON	97	MPS		18 $\pi^- p \to \eta\pi^- p$
1315 ± 5 ±2		[1] AMSLER	94D	CBAR		0.0 $\overline{p}p \to \pi^0\pi^0\eta$
1325.1± 5.1		AOYAGI	93	BKEI		$\pi^- p \to \eta\pi^- p$
1317.7± 1.4±2.0		BELADIDZE	93	VES		37$\pi^- N \to \eta\pi^- N$
1323 ± 8	1000	[2] KEY	73	OSPK	–	6 $\pi^- p \to p\pi^- \eta$
• • • We do not use the following data for averages, fits, limits, etc. • • •						
1318.7± 1.9$^{+1.3}_{-1.3}$		[3] KOPF	21	RVUE		0.9 $p\overline{p} \to \pi^0\pi^0\eta$, $\pi^0\eta\eta$, $\pi^0 K^+ K^-$ and 191 $\pi^- p \to \pi^-\pi^-\pi^+ p$
1312.5± 0.7±2.6		[4] ALBRECHT	20	RVUE		0.9 $\overline{p}p \to \pi^0\pi^0\eta$, $\pi^0\eta\eta$, $\pi^0 K^+ K^-$
1306.0± 0.8±1.3		[5] RODAS	19	JPAC		191 $\pi^- p \to \eta^{(\prime)}\pi^- p$
1307 ± 1 ±6		[6] JACKURA	18	JPAC		$\pi^- p \to \eta\pi^- p$
1315 ±12		[7] ADOLPH	15	COMP		191 $\pi^- p \to \eta^{(\prime)}\pi^- p$
1309 ± 4		ANISOVICH	09	RVUE		$\overline{p}p$, πN
1324 ± 5		ARMSTRONG	93C	E760	0	$\overline{p}p \to \pi^0\eta\eta \to 6\gamma$
1336.2± 1.7	2561	DELFOSSE	81	SPEC	+	$\pi^\pm p \to p\pi^\pm\eta$
1330.7± 2.4	1653	DELFOSSE	81	SPEC	–	$\pi^\pm p \to p\pi^\pm\eta$
1324 ± 8	6200	[2,8] CONFORTO	73	OSPK	–	6 $\pi^- p \to p$MM$^-$

[1] The systematic error of 2 MeV corresponds to the spread of solutions.
[2] Error includes 5 MeV systematic mass-scale error.
[3] From T-matrix pole based on combined fit of Crystal Barrel and $\pi\pi$ scattering data (ALBRECHT 20), and COMPASS data (ADOLPH 15), using a coupled-channel model of $\eta\pi$, $\eta'\pi$ and $K\overline{K}$ systems.
[4] T-matrix pole with 2 poles, 2 channels ($\pi^0\eta$ and $K\overline{K}$).
[5] The coupled-channel analysis of both the $\eta\pi$ and $\eta'\pi$ systems using ADOLPH 15 data. The mass is extracted from the T-matrix pole.
[6] Superseded by RODAS 19.
[7] ADOLPH 15 value is derived from a Breit-Wigner fit with mass-dependent width taking the $\eta\pi$ and $\rho\pi$ channels into account.
[8] Missing mass with enriched MMS = $\eta\pi^-$, $\eta = 2\gamma$.

$\eta'\pi$ MODE

VALUE (MeV)	DOCUMENT ID		TECN	COMMENT
The data in this block is included in the average printed for a previous datablock.				
1322 ± 7 OUR AVERAGE				
1318 ± 8 $^{+3}_{-5}$	IVANOV	01	B852	18 $\pi^- p \to \eta'\pi^- p$
1327.0±10.7	BELADIDZE	93	VES	37$\pi^- N \to \eta'\pi^- N$

$a_2(1320)$ WIDTH

3π MODE

VALUE (MeV)	EVTS	DOCUMENT ID		TECN	CHG	COMMENT
105.0$^{+1.7}_{-1.9}$ OUR AVERAGE						
106.6$^{+3.4}_{-7.0}$	46M	[1] AGHASYAN	18B	COMP		190 $\pi^- p \to \pi^-\pi^+\pi^- p$
108 ± 3 ±15		CHUNG	02	B852		18.3 $\pi^- p \to \pi^+\pi^-\pi^- p$
120 ±10		BARBERIS	98B			450 $pp \to p_f\pi^+\pi^-\pi^0 p_s$
105 ±10 ±11		ACCIARRI	97T	L3		$e^+e^- \to e^+e^-\pi^+\pi^-\pi^0$
120 ±10		ALBRECHT	97B	ARG		$e^+e^- \to e^+e^-\pi^+\pi^-\pi^0$
103.0± 6.0± 3.3	72.4k	AMELIN	96	VES		36 $\pi^- p \to \pi^+\pi^-\pi^0 n$
120 ±10		ARMSTRONG	90	OMEG	0	300.0$pp \to pp\pi^+\pi^-\pi^0$
107.0± 9.7	4022	AUGUSTIN	89	DM2	±	$J/\psi \to \rho^\pm a_2^\mp$
118.5±12.5	3562	AUGUSTIN	89	DM2	0	$J/\psi \to \rho^0 a_2^0$
97 ± 5		[2] EVANGELIS...	81	OMEG	–	12 $\pi^- p \to 3\pi p$
96 ± 9	25k	[2] DAUM	80C	SPEC	–	63,94 $\pi^- p \to 3\pi p$
110 ±15	1097	[2] BALTAY	78B	HBC	+0	15 $\pi^+ p \to p4\pi$
112 ±18	1.6k	[2] EMMS	75	DBC	0	4 $\pi^+ n \to p(3\pi)^0$
122 ±14	1.2k	[2,3] WAGNER	75	HBC	0	7 $\pi^+ p \to \Delta^{++}(3\pi)^0$
115 ±15		[2] ANTIPOV	73C	CNTR	–	25,40 $\pi^- p \to p\eta\pi^-$
99 ±15	1580	CHALOUPKA	73	HBC	–	3.9 $\pi^- p$
105 ± 5	28k	BOWEN	71	MMS	–	5 $\pi^- p$
99 ± 5	24k	BOWEN	71	MMS	+	5 $\pi^+ p$
103 ± 5	17k	BOWEN	71	MMS	–	7 $\pi^- p$
• • • We do not use the following data for averages, fits, limits, etc. • • •						
110 ± 2 $^{+2}_{-15}$	420k	[4] ALEKSEEV	10	COMP		190 $\pi^- Pb \to \pi^-\pi^-\pi^+ Pb'$
117 ± 6 ±20	18k	[5] SCHEGELSKY	06	RVUE	0	$\gamma\gamma \to \pi^+\pi^-\pi^0$
120 ±40		CONDO	93	SHF		$\gamma p \to n\pi^+\pi^+\pi^-$
115 ±14	490	BALTAY	78B	HBC	0	15 $\pi^+ p \to \Delta 3\pi$
72 ±16	5k	BINNIE	71	MMS	–	$\pi^- p$ near a_2 threshold
79 ±12	941	ALSTON-...	70	HBC	+	7.0 $\pi^+ p \to 3\pi p$

[1] Statistical error negligible.
[2] From a fit to $J^P = 2^+$ $\rho\pi$ partial wave.
[3] Width errors enlarged by us to $4\Gamma/\sqrt{N}$; see the note with the $K^*(892)$ mass.
[4] Superseded by AGHASYAN 2018B.
[5] From analysis of L3 data at 183–209 GeV.

$K\overline{K}$ AND $\eta\pi$ MODES

VALUE (MeV)	DOCUMENT ID
107 ±5 OUR ESTIMATE	
110.4±1.7 OUR AVERAGE	Includes data from the 2 datablocks that follow this one.

Downloaded from https://academic.oup.com/ptep/article/2022/8/083C01/6651666 by KIT Library user on 27 September 2022

$K\overline{K}$ MODE

VALUE (MeV)	EVTS	DOCUMENT ID		TECN	CHG	COMMENT
The data in this block is included in the average printed for a previous datablock.						
109.8± 2.4 OUR AVERAGE						
112 ±20	4700	[1,2] CLELAND	82B	SPEC	+	$50\ \pi^+ p \to K^0_S K^+ p$
120 ±25	5200	[1,2] CLELAND	82B	SPEC	−	$50\ \pi^- p \to K^0_S K^- p$
106 ± 4	4000	CHABAUD	80	SPEC	−	$17\ \pi^- A \to K^0_S K^- A$
126 ±11	11000	CHABAUD	78	SPEC	−	$9.8\ \pi^- p \to K^- K^0_S p$
101 ± 8	4730	CHABAUD	78	SPEC	−	$18.8\ \pi^- p \to K^- K^0_S p$
113 ± 4		[1,3] MARTIN	78D	SPEC	−	$10\ \pi^- p \to K^0_S K^- p$
105 ± 8	2724	[3] MARGULIE	76	SPEC	−	$23\ \pi^- p \to K^- K^0_S p$
113 ±19	730	FOLEY	72	CNTR	−	$20.3\ \pi^- p \to K^- K^0_S p$
123 ±13	1500	[3] GRAYER	71	ASPK	−	$17.2\ \pi^- p \to K^- K^0_S p$
• • • We do not use the following data for averages, fits, limits, etc. • • •						
120 ±15	870	[4] SCHEGELSKY	06A	RVUE	0	$\gamma\gamma \to K^0_S K^0_S$
121 ±51	1000	[1,2] CLELAND	82B	SPEC	+	$30\ \pi^+ p \to K^0_S K^+ p$
110 ±18	350	HYAMS	78	ASPK	+	$12.7\ \pi^+ p \to K^+ K^0_S p$

[1] From a fit to $J^P = 2^+$ partial wave.
[2] Number of events evaluated by us.
[3] Width errors enlarged by us to $4\Gamma/\sqrt{N}$; see the note with the $K^*(892)$ mass.
[4] From analysis of L3 data at 91 and 183–209 GeV.

$\eta\pi$ MODE

VALUE (MeV)	EVTS	DOCUMENT ID		TECN	CHG	COMMENT
The data in this block is included in the average printed for a previous datablock.						
111.1± 2.4 OUR AVERAGE						
115 ±20		BARBERIS	00H			$450\ pp \to p_f \eta\pi^0 p_s$
112 ±14		BARBERIS	00H			$450\ pp \to \Delta_f^{++} \eta\pi^- p_s$
112 ± 3 ±2		[1] AMSLER	94D	CBAR		$0.0\ \overline{p}p \to \pi^0\pi^0\eta$
103 ± 6 ±3		BELADIDZE	93	VES		$37\pi^- N \to \eta\pi^- N$
112.2± 5.7	2561	DELFOSSE	81	SPEC	+	$\pi^\pm p \to p\pi^\pm\eta$
116.6± 7.7	1653	DELFOSSE	81	SPEC	−	$\pi^\pm p \to p\pi^\pm\eta$
108 ± 9	1000	KEY	73	OSPK	−	$6\ \pi^- p \to p\pi^-\eta$
• • • We do not use the following data for averages, fits, limits, etc. • • •						
$107.5\pm 4.6^{+3.3}_{-1.8}$		[2] KOPF	21	RVUE		$0.9\ p\overline{p} \to \pi^0\pi^0\eta$, $\pi^0\eta\eta$, $\pi^0 K^+ K^-$ and $191\ \pi^- p \to \pi^-\pi^-\pi^+ p$
106.9± 1.2±3.7		[3] ALBRECHT	20	RVUE		$0.9\ \overline{p}p \to \pi^0\pi^0\eta$, $\pi^0\eta\eta$, $\pi^0 K^+ K^-$
114.4± 1.6±0.0		[4] RODAS	19	JPAC		$191\ \pi^- p \to \eta^{(\prime)}\pi^- p$
112 ± 1 ±8		[5] JACKURA	18	JPAC		$\pi^- p \to \eta\pi^- p$
119 ±14		[6] ADOLPH	15	COMP		$191\ \pi^- p \to \eta^{(\prime)}\pi^- p$
110 ± 4		ANISOVICH	09	RVUE		$\overline{p}p$, πN
127 ± 2 ±2		[7] THOMPSON	97	MPS		$18\ \pi^- p \to \eta\pi^- p$
118 ±10		ARMSTRONG	93C	E760	0	$\overline{p}p \to \pi^0\eta\eta \to 6\gamma$
104 ± 9	6200	[8] CONFORTO	73	OSPK	−	$6\ \pi^- p \to p\,\mathrm{MM}^-$

[1] The systematic error of 2 MeV corresponds to the spread of solutions.
[2] From T-matrix pole based on combined fit of Crystal Barrel and $\pi\pi$ scattering data (ALBRECHT 20), and COMPASS data (ADOLPH 15), using a coupled-channel model of $\eta\pi$, $\eta'\pi$ and $K\overline{K}$ systems.
[3] T-matrix pole with 2 poles, 2 channels ($\pi^0\eta$ and $K\overline{K}$).
[4] The coupled-channel analysis of both the $\eta\pi$ and $\eta'\pi$ systems using ADOLPH 15 data. The width is extracted from the T-matrix pole.
[5] Superseded by RODAS 19.
[6] ADOLPH 15 value is derived from a Breit-Wigner fit with mass-dependent width taking the $\eta\pi$ and $\rho\pi$ channels into account.
[7] Resolution is not unfolded.
[8] Missing mass with enriched MMS $= \eta\pi^-$, $\eta = 2\gamma$.

$\eta'\pi$ MODE

VALUE (MeV)	DOCUMENT ID		TECN	COMMENT
119±25 OUR AVERAGE				
140±35±20	IVANOV	01	B852	$18\ \pi^- p \to \eta'\pi^- p$
106±32	BELADIDZE	93	VES	$37\pi^- N \to \eta'\pi^- N$

$a_2(1320)$ DECAY MODES

	Mode	Fraction (Γ_i/Γ)	Scale factor/ Confidence level
Γ_1	3π	(70.1 ±2.7) %	S=1.2
Γ_2	$\rho(770)\pi$		
Γ_3	$f_2(1270)\pi$		
Γ_4	$\rho(1450)\pi$		
Γ_5	$\eta\pi$	(14.5 ±1.2) %	
Γ_6	$\omega\pi\pi$	(10.6 ±3.2) %	S=1.3
Γ_7	$K\overline{K}$	(4.9 ±0.8) %	
Γ_8	$\eta'(958)\pi$	$(5.5 \pm 0.9) \times 10^{-3}$	
Γ_9	$\pi^\pm\gamma$	$(2.91\pm0.27) \times 10^{-3}$	
Γ_{10}	$\gamma\gamma$	$(9.4 \pm 0.7) \times 10^{-6}$	
Γ_{11}	e^+e^-	$< 5 \times 10^{-9}$	CL=90%

CONSTRAINED FIT INFORMATION

An overall fit to 5 branching ratios uses 18 measurements and one constraint to determine 4 parameters. The overall fit has a $\chi^2 = 9.3$ for 15 degrees of freedom.

The following *off-diagonal* array elements are the correlation coefficients $\langle \delta x_i \delta x_j \rangle / (\delta x_i \cdot \delta x_j)$, in percent, from the fit to the branching fractions, $x_i \equiv \Gamma_i/\Gamma_{\rm total}$. The fit constrains the x_i whose labels appear in this array to sum to one.

	x_1	x_5	x_6
x_5	10		
x_6	−89	−46	
x_7	−1	−2	−24

$a_2(1320)$ PARTIAL WIDTHS

$\Gamma(\eta\pi)$ — Γ_5

VALUE (MeV)	EVTS	DOCUMENT ID		TECN	CHG	COMMENT
• • • We do not use the following data for averages, fits, limits, etc. • • •						
18.5±3.0	870	[1] SCHEGELSKY	06A	RVUE	0	$\gamma\gamma \to K^0_S K^0_S$

[1] From analysis of L3 data at 91 and 183–209 GeV, using $\Gamma(a_2(1320) \to \gamma\gamma) = 0.91$ keV and SU(3) relations.

$\Gamma(K\overline{K})$ — Γ_7

VALUE (MeV)	EVTS	DOCUMENT ID		TECN	CHG	COMMENT
• • • We do not use the following data for averages, fits, limits, etc. • • •						
$7.0^{+2.0}_{-1.5}$	870	[1] SCHEGELSKY	06A	RVUE	0	$\gamma\gamma \to K^0_S K^0_S$

[1] From analysis of L3 data at 91 and 183–209 GeV, using $\Gamma(a_2(1320) \to \gamma\gamma) = 0.91$ keV and SU(3) relations.

$\Gamma(\pi^\pm\gamma)$ — Γ_9

VALUE (keV)	EVTS	DOCUMENT ID		TECN	CHG	COMMENT
311± 25 OUR AVERAGE						
358± 6±42		[1] ADOLPH	14	COMP	−	$190\ \pi^- \mathrm{Pb} \to \pi^+\pi^-\pi^- \mathrm{Pb}'$
284± 25±25	7.1k	MOLCHANOV	01	SELX		$600\ \pi^- A \to \pi^+\pi^-\pi^- A$
295± 60		CIHANGIR	82	SPEC	+	$200\ \pi^+ A$
• • • We do not use the following data for averages, fits, limits, etc. • • •						
461±110		[2] MAY	77	SPEC	±	$9.7\ \gamma A$

[1] Primakoff reaction using $a_2(1320) \to 3\pi$ branching ratio of 70.1%.
[2] Assuming one-pion exchange.

$\Gamma(\gamma\gamma)$ — Γ_{10}

VALUE (keV)	EVTS	DOCUMENT ID		TECN	CHG	COMMENT
1.00±0.06 OUR AVERAGE						
0.98±0.05±0.09		ACCIARRI	97T	L3		$e^+e^- \to e^+e^-\pi^+\pi^-\pi^0$
0.96±0.03±0.13		ALBRECHT	97B	ARG		$e^+e^- \to e^+e^-\pi^+\pi^-\pi^0$
1.26±0.26±0.18	36	BARU	90	MD1		$e^+e^- \to e^+e^-\pi^+\pi^-\pi^0$
1.00±0.07±0.15	415	BEHREND	90C	CELL	0	$e^+e^- \to e^+e^-\pi^+\pi^-\pi^0$
1.03±0.13±0.21		BUTLER	90	MRK2		$e^+e^- \to e^+e^-\pi^+\pi^-\pi^0$
1.01±0.14±0.22	85	OEST	90	JADE		$e^+e^- \to e^+e^-\pi^0\eta$
0.90±0.27±0.15	56	[1] ALTHOFF	86	TASS	0	$e^+e^- \to e^+e^-3\pi$
1.14±0.20±0.26		[2] ANTREASYAN	86	CBAL	0	$e^+e^- \to e^+e^-\pi^0\eta$
1.06±0.18±0.19		BERGER	84C	PLUT	0	$e^+e^- \to e^+e^-3\pi$
• • • We do not use the following data for averages, fits, limits, etc. • • •						
$0.81\pm0.19^{+0.42}_{-0.11}$	35	[1] BEHREND	82C	CELL	0	$e^+e^- \to e^+e^-3\pi$
0.77±0.18±0.27	22	[2] EDWARDS	82F	CBAL	0	$e^+e^- \to e^+e^-\pi^0\eta$

[1] From $\rho\pi$ decay mode.
[2] From $\eta\pi^0$ decay mode.

$\Gamma(e^+e^-)$ — Γ_{11}

VALUE (eV)	CL%	DOCUMENT ID		TECN	COMMENT
< 0.56	90	ACHASOV	00K	SND	$e^+e^- \to \pi^0\pi^0$
• • • We do not use the following data for averages, fits, limits, etc. • • •					
<25	90	VOROBYEV	88	ND	$e^+e^- \to \pi^0\eta$

Downloaded from https://academic.oup.com/ptep/article/2022/8/083C01/6651666 by KIT Library user on 27 September 2022

$a_2(1320)$ $\Gamma(i)\Gamma(\gamma\gamma)/\Gamma(\text{total})$

$\Gamma(3\pi) \times \Gamma(\gamma\gamma)/\Gamma_{\text{total}}$ — $\Gamma_1\Gamma_{10}/\Gamma$

VALUE (keV)	EVTS	DOCUMENT ID		TECN	COMMENT
• • • We do not use the following data for averages, fits, limits, etc. • • •					
$0.65 \pm 0.02 \pm 0.02$	18k	[1] SCHEGELSKY	06	RVUE	$\gamma\gamma \to \pi^+\pi^-\pi^0$

[1] From analysis of L3 data at 183–209 GeV.

$\Gamma(\eta\pi) \times \Gamma(\gamma\gamma)/\Gamma_{\text{total}}$ — $\Gamma_5\Gamma_{10}/\Gamma$

VALUE (keV)	DOCUMENT ID		TECN	COMMENT
• • • We do not use the following data for averages, fits, limits, etc. • • •				
$0.145^{+0.097}_{-0.034}$	[1] UEHARA	09A	BELL	$e^+e^- \to e^+e^-\eta\pi^0$

[1] From the D_2-wave. The fraction of the D_0-wave is $3.4^{+2.3}_{-1.1}$%.

$\Gamma(K\overline{K}) \times \Gamma(\gamma\gamma)/\Gamma_{\text{total}}$ — $\Gamma_7\Gamma_{10}/\Gamma$

VALUE (keV)	DOCUMENT ID		TECN	COMMENT
$0.126 \pm 0.007 \pm 0.028$	[1] ALBRECHT	90G	ARG	$e^+e^- \to e^+e^-K^+K^-$
• • • We do not use the following data for averages, fits, limits, etc. • • •				
$0.081 \pm 0.006 \pm 0.027$	[2] ALBRECHT	90G	ARG	$e^+e^- \to e^+e^-K^+K^-$

[1] Using an incoherent background.
[2] Using a coherent background.

$a_2(1320)$ BRANCHING RATIOS

$[\Gamma(f_2(1270)\pi) + \Gamma(\rho(1450)\pi)]/\Gamma(\rho(770)\pi)$ — $(\Gamma_3+\Gamma_4)/\Gamma_2$

VALUE	CL%	DOCUMENT ID		TECN	CHG	COMMENT
<0.12	90	ABRAMOVI...	70B	HBC	–	$3.93\ \pi^- p$

$\Gamma(\rho(770)\pi)/\Gamma(f_2(1270)\pi)$ — Γ_2/Γ_3

VALUE	EVTS	DOCUMENT ID		TECN	COMMENT
$16.5^{+1.2}_{-2.4}$	46M	[1] AGHASYAN	18B	COMP	$190\ \pi^- p \to \pi^-\pi^+\pi^- p$

[1] Statistical error negligible.

$\Gamma(\eta\pi)/\Gamma(3\pi)$ — Γ_5/Γ_1

VALUE	EVTS	DOCUMENT ID		TECN	CHG	COMMENT
0.207 ± 0.018 OUR FIT						
0.213 ± 0.020 OUR AVERAGE						
0.18 ± 0.05		FORINO	76	HBC		$11\ \pi^- p$
0.22 ± 0.05	52	ANTIPOV	73	CNTR	–	$40\ \pi^- p$
0.211 ± 0.044	149	CHALOUPKA	73	HBC	–	$3.9\ \pi^- p$
0.246 ± 0.042	167	ALSTON-...	71	HBC	+	$7.0\ \pi^+ p$
0.25 ± 0.09	15	BOECKMANN	70	HBC	+	$5.0\ \pi^+ p$
0.23 ± 0.08	22	ASCOLI	68	HBC	–	$5\ \pi^- p$
0.12 ± 0.08		CHUNG	68	HBC	–	$3.2\ \pi^- p$
0.22 ± 0.09		CONTE	67	HBC	–	$11.0\ \pi^- p$

$\Gamma(\omega\pi\pi)/\Gamma(3\pi)$ — Γ_6/Γ_1

VALUE	EVTS	DOCUMENT ID		TECN	CHG	COMMENT
0.15 ± 0.05 OUR FIT Error includes scale factor of 1.3.						
0.15 ± 0.05 OUR AVERAGE Error includes scale factor of 1.3. See the ideogram below.						
0.28 ± 0.09	60	DIAZ	74	DBC	0	$6\ \pi^+ n$
0.18 ± 0.08		[1] KARSHON	74	HBC		Avg. of above two
0.10 ± 0.05	279	[2] CHALOUPKA	73	HBC	–	$3.9\ \pi^- p$
• • • We do not use the following data for averages, fits, limits, etc. • • •						
0.29 ± 0.08	140	[1] KARSHON	74	HBC	0	$4.9\ \pi^+ p$
0.10 ± 0.04	60	[1] KARSHON	74	HBC	+	$4.9\ \pi^+ p$
0.19 ± 0.08		DEFOIX	73	HBC	0	$0.7\ \overline{p}p$

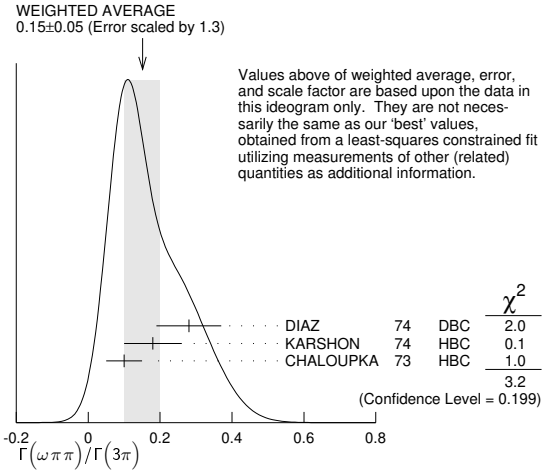

[1] KARSHON 74 suggest an additional $I = 0$ state strongly coupled to $\omega\pi\pi$ which could explain discrepancies in branching ratios and masses. We use a central value and a systematic spread.

[2] Decays to $b_1(1040)\pi$, $b_1 \to \omega\pi$. Error increased to account for possible systematic errors of complicated analysis.

$\Gamma(K\overline{K})/\Gamma(3\pi)$ — Γ_7/Γ_1

VALUE	EVTS	DOCUMENT ID		TECN	CHG	COMMENT
0.070 ± 0.012 OUR FIT						
0.078 ± 0.017		CHABAUD	78	RVUE		
• • • We do not use the following data for averages, fits, limits, etc. • • •						
0.011 ± 0.003		[1] BERTIN	98B	OBLX		$0.0\ \overline{p}p \to K^\pm K_S \pi^\mp$
0.056 ± 0.014	50	[2] CHALOUPKA	73	HBC	–	$3.9\ \pi^- p$
0.097 ± 0.018	113	[2] ALSTON-...	71	HBC	+	$7.0\ \pi^+ p$
0.06 ± 0.03		[2] ABRAMOVI...	70B	HBC	–	$3.93\ \pi^- p$
0.054 ± 0.022		[2] CHUNG	68	HBC	–	$3.2\ \pi^- p$

[1] Using 4π data from BERTIN 97D.
[2] Included in CHABAUD 78 review.

$\Gamma(K\overline{K})/\Gamma(\eta\pi)$ — Γ_7/Γ_5

VALUE	DOCUMENT ID		TECN	COMMENT
• • • We do not use the following data for averages, fits, limits, etc. • • •				
$0.31 \pm 0.22\ ^{+0.09}_{-0.11}$	[1] KOPF	21	RVUE	$0.9\ p\overline{p} \to \pi^0\pi^0\eta,\ \pi^0\eta\eta,\ \pi^0 K^+K^-$ and $191\ \pi^- p \to \pi^-\pi^-\pi^+ p$
$0.352 \pm 0.011 \pm 0.175$	[2] ALBRECHT	20	RVUE	$0.9\ \overline{p}p \to \pi^0\pi^0\eta,\ \pi^0\eta\eta,\ \pi^0 K^+K^-$
0.08 ± 0.02	[3] BERTIN	98B	OBLX	$0.0\ \overline{p}p \to K^\pm K_S \pi^\mp$

[1] From T-matrix pole based on combined fit of Crystal Barrel and $\pi\pi$ scattering data (ALBRECHT 20), and COMPASS data (ADOLPH 15), using a coupled-channel model of $\eta\pi$, $\eta'\pi$ and $K\overline{K}$ systems.
[2] Residues from T-matrix pole with 2 poles, 2 channels ($\pi^0\eta$ and $K\overline{K}$).
[3] Using $\eta\pi\pi$ data from AMSLER 94D.

$\Gamma(\eta\pi)/[\Gamma(3\pi) + \Gamma(\eta\pi) + \Gamma(K\overline{K})]$ — $\Gamma_5/(\Gamma_1+\Gamma_5+\Gamma_7)$

VALUE	EVTS	DOCUMENT ID		TECN	CHG	COMMENT
0.162 ± 0.012 OUR FIT						
0.140 ± 0.028 OUR AVERAGE						
0.13 ± 0.04		ESPIGAT	72	HBC	±	$0.0\ \overline{p}p$
0.15 ± 0.04	34	BARNHAM	71	HBC	+	$3.7\ \pi^+ p$

$\Gamma(K\overline{K})/[\Gamma(3\pi) + \Gamma(\eta\pi) + \Gamma(K\overline{K})]$ — $\Gamma_7/(\Gamma_1+\Gamma_5+\Gamma_7)$

VALUE	EVTS	DOCUMENT ID		TECN	CHG	COMMENT
0.054 ± 0.009 OUR FIT						
0.048 ± 0.012 OUR AVERAGE						
0.05 ± 0.02		TOET	73	HBC	+	$5\ \pi^+ p$
0.09 ± 0.04		TOET	73	HBC	0	$5\ \pi^+ p$
0.03 ± 0.02	8	[1] DAMERI	72	HBC	–	$11\ \pi^- p$
0.06 ± 0.03	17	BARNHAM	71	HBC	+	$3.7\ \pi^+ p$
• • • We do not use the following data for averages, fits, limits, etc. • • •						
0.020 ± 0.004		[2] ESPIGAT	72	HBC	±	$0.0\ \overline{p}p$

[1] Montanet agrees. Vlada.
[2] Not averaged because of discrepancy between masses from $K\overline{K}$ and $\rho\pi$ modes.

$\Gamma(\eta'(958)\pi)/\Gamma_{\text{total}}$ — Γ_8/Γ

VALUE	CL%	DOCUMENT ID		TECN	CHG	COMMENT
• • • We do not use the following data for averages, fits, limits, etc. • • •						
<0.006	95	ALDE	92B	GAM2		$38,100\ \pi^- p \to \eta'\pi^0 n$
<0.02	97	BARNHAM	71	HBC	+	$3.7\ \pi^+ p$
0.004 ± 0.004		[1] BOESEBECK	68	HBC	+	$8\ \pi^+ p$

[1] No longer valid since $\Gamma(K\overline{K})/\Gamma(3\pi)$ value has changed (MORRISON 71).

$\Gamma(\eta'(958)\pi)/\Gamma(3\pi)$ — Γ_8/Γ_1

VALUE	CL%	DOCUMENT ID		TECN	CHG	COMMENT
• • • We do not use the following data for averages, fits, limits, etc. • • •						
<0.011	90	EISENSTEIN	73	HBC	–	$5\ \pi^- p$
<0.04		ALSTON-...	71	HBC	+	$7.0\ \pi^+ p$
$0.04\ ^{+0.03}_{-0.04}$		BOECKMANN	70	HBC	0	$5.0\ \pi^+ p$

$\Gamma(\eta'(958)\pi)/\Gamma(\eta\pi)$ — Γ_8/Γ_5

VALUE	DOCUMENT ID		TECN	COMMENT
0.038 ± 0.005 OUR AVERAGE				
0.05 ± 0.02	ADOLPH	15	COMP	$191\ \pi^- p \to \eta^{(\prime)}\pi^- p$
0.032 ± 0.009	ABELE	97C	CBAR	$0.0\ \overline{p}p \to \pi^0\pi^0\eta'$
$0.047 \pm 0.010 \pm 0.004$	[1] BELADIDZE	93	VES	$37\pi^- N \to a_2^- N$
$0.034 \pm 0.008 \pm 0.005$	BELADIDZE	92	VES	$36\pi^- C \to a_2^- C$
• • • We do not use the following data for averages, fits, limits, etc. • • •				
$0.046 \pm 0.015\ ^{+0.07}_{-0.006}$	[2] KOPF	21	RVUE	$0.9\ p\overline{p} \to \pi^0\pi^0\eta,\ \pi^0\eta\eta,\ \pi^0 K^+K^-$ and $191\ \pi^- p \to \pi^-\pi^-\pi^+ p$

[1] Using $B(\eta' \to \pi^+\pi^-\eta) = 0.441$, $B(\eta \to \gamma\gamma) = 0.389$ and $B(\eta \to \pi^+\pi^-\pi^0) = 0.236$.
[2] From T-matrix pole based on combined fit of Crystal Barrel and $\pi\pi$ scattering data (ALBRECHT 20), and COMPASS data (ADOLPH 15), using a coupled-channel model of $\eta\pi$, $\eta'\pi$ and $K\overline{K}$ systems.

Downloaded from https://academic.oup.com/ptep/article/2022/8/083C01/6651666 by KIT Library user on 27 September 2022

$\Gamma(\pi^\pm\gamma)/\Gamma_{total}$ — Γ_9/Γ

VALUE	DOCUMENT ID		TECN	COMMENT
• • • We do not use the following data for averages, fits, limits, etc. • • •				
$0.005^{+0.005}_{-0.003}$	[1] EISENBERG	72	HBC	4.3,5.25,7.5 γp

[1] Pion-exchange model used in this estimation.

$\Gamma(e^+e^-)/\Gamma_{total}$ — Γ_{11}/Γ

VALUE (units 10^{-9})	CL%	DOCUMENT ID		TECN	COMMENT
• • • We do not use the following data for averages, fits, limits, etc. • • •					
<6	90	ACHASOV	00K	SND	$e^+e^- \to \pi^0\pi^0$

$a_2(1320)$ REFERENCES

KOPF	21	EPJ C81 1056	B. Kopf et al.	(BOCH)
ALBRECHT	20	EPJ C80 453	M. Albrecht et al.	(Crystal Barrel Collab.)
RODAS	19	PRL 122 042002	A. Rodas et al.	(JPAC Collab.)
AGHASYAN	18B	PR D98 092003	M. Aghasyan et al.	(COMPASS Collab.)
JACKURA	18	PL B779 464	A. Jackura et al.	(JPAC and COMPASS Collab.)
ADOLPH	15	PL B740 303	M. Adolph et al.	(COMPASS Collab.)
ADOLPH	14	EPJ A50 79	C. Adolph et al.	(COMPASS Collab.)
ALEKSEEV	10	PRL 104 241803	M.G. Alekseev et al.	(COMPASS Collab.)
ANISOVICH	09	IJMP A24 2481	V.V. Anisovich, A.V. Sarantsev	
UEHARA	09A	PR D80 032001	S. Uehara et al.	(BELLE Collab.)
SCHEGELSKY	06	EPJ A27 199	V.A. Schegelsky et al.	
SCHEGELSKY	06A	EPJ A27 207	V.A. Schegelsky et al.	
CHUNG	02	PR D65 072001	S.U. Chung et al.	(BNL E852 Collab.)
IVANOV	01	PRL 86 3977	E.I. Ivanov et al.	(BNL E852 Collab.)
MOLCHANOV	01	PL B521 171	V.V. Molchanov et al.	(FNAL SELEX Collab.)
ACHASOV	00K	PL B492 8	M.N. Achasov et al.	(Novosibirsk SND Collab.)
BARBERIS	00H	PL B488 225	D. Barberis et al.	(WA 102 Collab.)
BARBERIS	98B	PL B422 399	D. Barberis et al.	(WA 102 Collab.)
BERTIN	98B	PL B434 180	A. Bertin et al.	(OBELIX Collab.)
ABELE	97C	PL B404 179	A. Abele et al.	(Crystal Barrel Collab.)
ACCIARRI	97T	PL B413 147	M. Acciarri et al.	(L3 Collab.)
ALBRECHT	97B	ZPHY C74 469	H. Albrecht et al.	(ARGUS Collab.)
THOMPSON	97	PRL 79 1630	D.R. Thompson et al.	(BNL E852 Collab.)
AMELIN	96	ZPHY C70 71	D.V. Amelin et al.	(SERP, TBIL)
AMSLER	94D	PL B333 277	C. Amsler et al.	(Crystal Barrel Collab.)
AOYAGI	93	PL B314 246	H. Aoyagi et al.	(BKEI Collab.)
ARMSTRONG	93C	PL B307 394	T.A. Armstrong et al.	(FNAL, FERR, GENO+)
BELADIDZE	93	PL B313 276	G.M. Beladidze et al.	(VES Collab.)
CONDO	93	PR D48 3045	G.T. Condo et al.	(SLAC Hybrid Collab.)
ALDE	92B	ZPHY C54 549	D.M. Alde et al.	(SERP, BELG, LANL, LAPP+)
BELADIDZE	92	ZPHY C54 235	G.M. Beladidze et al.	(VES Collab.)
ALBRECHT	90G	ZPHY C48 183	H. Albrecht et al.	(ARGUS Collab.)
ARMSTRONG	90	ZPHY C48 213	T.A. Armstrong, M. Benayoun, W. Beusch	(WA76 Coll.)
BARU	90	ZPHY C48 581	S.E. Baru et al.	(MD-1 Collab.)
BEHREND	90C	ZPHY C46 583	H.J. Behrend et al.	(CELLO Collab.)
BUTLER	90	PR D42 1368	F. Butler et al.	(Mark II Collab.)
OEST	90	ZPHY C47 343	T. Oest et al.	(JADE Collab.)
AUGUSTIN	89	NP B320 1	J.E. Augustin, G. Cosme	(DM2 Collab.)
VOROBYEV	88	SJNP 48 273	P.V. Vorobiev et al.	(NOVO)
		Translated from YAF 48 436.		
ALTHOFF	86	ZPHY C31 537	M. Althoff et al.	(TASSO Collab.)
ANTREASYAN	86	PR D33 1847	D. Antreasyan et al.	(Crystal Ball Collab.)
BERGER	84C	PL 149B 427	C. Berger et al.	(PLUTO Collab.)
BEHREND	82C	PL 114B 378	H.J. Behrend et al.	(CELLO Collab.)
Also		PL 125B 518 (erratum)	H.J. Behrend et al.	(CELLO Collab.)
CIHANGIR	82	PL 117B 123	S. Cihangir et al.	(FNAL, MINN, ROCH)
CLELAND	82B	NP B208 228	W.E. Cleland et al.	(DURH, GEVA, LAUS+)
EDWARDS	82F	PL 110B 82	C. Edwards et al.	(CIT, HARV, PRIN+)
DELFOSSE	81	NP B183 349	A. Delfosse et al.	(GEVA, LAUS)
EVANGELIS...	81	NP B178 197	C. Evangelista et al.	(BARI, BONN, CERN+)
CHABAUD	80	NP B175 189	V. Chabaud et al.	(CERN, MPIM, AMST)
DAUM	80C	PL 89B 276	C. Daum et al.	(AMST, CERN, CRAC, MPIM+) JP
BALTAY	78B	PR D17 62	C. Baltay et al.	(COLU, BING)
CHABAUD	78	NP B145 349	V. Chabaud et al.	(CERN, MPIM)
FERRERSORIA	78	PL 74B 287	A. Ferrer Soria et al.	(ORSAY, CERN, CDEF+)
HYAMS	78	NP B146 303	B.D. Hyams et al.	(CERN, MPIM, ATEN)
MARTIN	78D	PL 74B 417	A.D. Martin et al.	(DURH, GEVA) JP
MAY	77	PR D16 1983	E.N. May et al.	(ROCH, CORN)
FORINO	76	NC 35A 465	A. Forino et al.	(BGNA, FIRZ, GENO, MILA+)
MARGULIE	76	PR D14 667	M. Margulies et al.	(BNL, CUNY)
EMMS	75	PL 58B 117	M.J. Emms et al.	(BIRM, DURH, RHEL) JP
WAGNER	75	PL 58B 201	F. Wagner, M. Tabak, D.M. Chew	(LBL) JP
DIAZ	74	PRL 32 260	J. Diaz et al.	(CASE, CMU)
KARSHON	74	PRL 32 852	U. Karshon et al.	(REHO)
ANTIPOV	73	NP B63 175	Y.M. Antipov et al.	(CERN, SERP) JP
ANTIPOV	73C	NP B63 153	Y.M. Antipov et al.	(CERN, SERP) JP
CHALOUPKA	73	PL 44B 211	V. Chaloupka et al.	(CERN)
CONFORTO	73	PL 45B 154	G. Conforto et al.	(EFI, FNAL, TNTO+)
DEFOIX	73	PL 43B 141	C. Defoix et al.	(CDEF)
EISENSTEIN	73	PR D7 278	L. Eisenstein et al.	(ILL)
KEY	73	PRL 30 503	A.W. Key et al.	(TNTO, EFI, FNAL, WISC)
TOET	73	NP B63 248	D.Z. Toet et al.	(NIJM, BONN, DURH, TORI)
DAMERI	72	NC 9A 1	M. Dameri et al.	(GENO, MILA, SACL)
EISENBERG	72	PR D5 15	Y. Eisenberg et al.	(REHO, SLAC, TELA)
ESPIGAT	72	NP B36 93	P. Espigat et al.	(CERN, CDEF)
FOLEY	72	PR D6 747	K.J. Foley et al.	(BNL, CUNY)
ALSTON-...	71	PL 34B 156	M. Alston-Garnjost et al.	(LRL)
BARNHAM	71	PRL 26 1494	K.W.J. Barnham et al.	(LBL)
BINNIE	71	PL 36B 257	D.M. Binnie et al.	(LOIC, SHMP)
BOWEN	71	PRL 26 1663	D.R. Bowen et al.	(NEAS, STON)
GRAYER	71	PL 34B 333	G. Grayer et al.	(CERN, MPIM)
ABRAMOVI...	70B	NP B23 466	M. Abramovich et al.	(CERN) JP
ALSTON-...	70	PL 33B 607	M. Alston-Garnjost et al.	(LRL)
BOECKMANN	70	NP B16 221	K. Boeckmann et al.	(BONN, DURH, NIJM+)
ASCOLI	68	PRL 20 1321	G. Ascoli et al.	(ILL) JP
BOESEBECK	68	NP B4 501	K. Boesebeck et al.	(AACH, BERL, CERN)
CHUNG	68	PR 165 1491	S.U. Chung et al.	(LRL)
CONTE	67	NC 51A 175	F. Conte et al.	(GENO, HAMB, MILA, SACL)

$f_0(1370)$

$I^G(J^{PC}) = 0^+(0^{++})$

See the review on "Spectroscopy of Light Meson Resonances" and a note on "Non-$q\overline{q}$ Candidates" in PDG 06, Journal of Physics **G33** 1 (2006).

$f_0(1370)$ T-MATRIX POLE POSITION

Note that $\Gamma \approx 2\,\mathrm{Im}(\sqrt{s_{pole}})$.

VALUE (MeV)	DOCUMENT ID		TECN	COMMENT
(1200–1500)−i(150–250) OUR ESTIMATE				
• • • We do not use the following data for averages, fits, limits, etc. • • •				
$(1370 \pm 40) - i(195 \pm 20)$	SARANTSEV	21	RVUE	$J/\psi(1S) \to \gamma\,(\pi\pi,\ K\overline{K},\ \eta\eta,\ \omega\phi)$
$(1280.6 \pm 1.6 \pm 47.4) - i(205.2 \pm 1.7 \pm 20.7)$	[1] ALBRECHT	20	RVUE	$0.9\,\overline{p}p \to \pi^0\pi^0\eta,\ \pi^0\eta\eta,\ \pi^0 K^+K^-$
$(1290 \pm 50) - i(170^{+20}_{-40})$	[2] ANISOVICH	09	RVUE	$0.0\,\overline{p}p,\ \pi N$
$(1373 \pm 15) - i(137 \pm 10)$	[3] BARGIOTTI	03	OBLX	$\overline{p}p$
$(1302 \pm 17) - i(166 \pm 18)$	[4] BARBERIS	00C		$450\,pp \to p_f 4\pi p_s$
$(1312 \pm 25 \pm 10) - i(109 \pm 22 \pm 15)$	BARBERIS	99D	OMEG	$450\,pp \to K^+K^-,\ \pi^+\pi^-$
$(1406 \pm 19) - i(80 \pm 6)$	[5] KAMINSKI	99	RVUE	$\pi\pi \to \pi\pi,\ K\overline{K},\ \sigma\sigma$
$(1300 \pm 20) - i(120 \pm 20)$	ANISOVICH	98B	RVUE	Compilation
$(1290 \pm 15) - i(145 \pm 15)$	BARBERIS	97B	OMEG	$450\,pp \to pp2(\pi^+\pi^-)$
$(1548 \pm 40) - i(560 \pm 40)$	BERTIN	97C	OBLX	$0.0\,\overline{p}p \to \pi^+\pi^-\pi^0$
$(1380 \pm 40) - i(180 \pm 25)$	ABELE	96B	CBAR	$0.0\,\overline{p}p \to \pi^0 K^0_L K^0_L$
$(1300 \pm 15) - i(115 \pm 8)$	BUGG	96	RVUE	
$(1330 \pm 50) - i(150 \pm 40)$	[6] AMSLER	95B	CBAR	$\overline{p}p \to 3\pi^0$
$(1360 \pm 35) - i(150–300)$	[6] AMSLER	95C	CBAR	$\overline{p}p \to \pi^0\eta\eta$
$(1390 \pm 30) - i(190 \pm 40)$	[7] AMSLER	95D	CBAR	$\overline{p}p \to 3\pi^0,\ \pi^0\eta\eta,\ \pi^0\pi^0\eta$
$1346 - i249$	[8,9] JANSSEN	95	RVUE	$\pi\pi \to \pi\pi,\ K\overline{K}$
$1214 - i168$	[9,10] TORNQVIST	95	RVUE	$\pi\pi \to \pi\pi,\ K\overline{K},\ K\pi,\ \eta\pi$
$1364 - i139$	AMSLER	94D	CBAR	$\overline{p}p \to \pi^0\pi^0\eta$
$(1365^{+20}_{-55}) - i(134 \pm 35)$	ANISOVICH	94	CBAR	$\overline{p}p \to 3\pi^0, \pi^0\eta\eta$
$(1340 \pm 40) - i(127^{+30}_{-20})$	[11] BUGG	94	RVUE	$\overline{p}p \to 3\pi^0,\ \eta\eta\pi^0,\ \eta\pi^0\pi^0$
$(1430 \pm 5) - i(73 \pm 13)$	[12] KAMINSKI	94	RVUE	$\pi\pi \to \pi\pi,\ K\overline{K}$
$1420 - i220$	[13] AU	87	RVUE	$\pi\pi \to \pi\pi,\ K\overline{K}$

[1] T-matrix pole, 5 poles, 5 channels, including scattering data from HYAMS 75 ($\pi\pi$), LONGACRE 86 ($K\overline{K}$), BINON 83 ($\eta\eta$), and BINON 84C ($\eta\eta'$).
[2] Another pole is found at $(1510 \pm 130) - i\,(800^{+100}_{-150})$ MeV.
[3] Coupled channel analysis of $\pi^+\pi^-\pi^0$, $K^+K^-\pi^0$, and $K^\pm K^0_S\pi^\mp$.
[4] Average between $\pi^+\pi^-2\pi^0$ and $2(\pi^+\pi^-)$.
[5] T-matrix pole on sheet − − −.
[6] Supersedes ANISOVICH 94.
[7] Coupled-channel analysis of $\overline{p}p \to 3\pi^0$, $\pi^0\eta\eta$, and $\pi^0\pi^0\eta$ on sheet IV. Demonstrates explicitly that $f_0(500)$ and $f_0(1370)$ are two different poles.
[8] Analysis of data from FALVARD 88.
[9] The pole is on Sheet III. Demonstrates explicitly that $f_0(500)$ and $f_0(1370)$ are two different poles.
[10] Uses data from BEIER 72B, OCHS 73, HYAMS 73, GRAYER 74, ROSSELET 77, CASON 83, ASTON 88, and ARMSTRONG 91B. Coupled channel analysis with flavor symmetry and all light two-pseudoscalars systems.
[11] Reanalysis of ANISOVICH 94 data.
[12] T-matrix pole on sheet III.
[13] Analysis of data from OCHS 73,GRAYER 74, BECKER 79, and CASON 83.

$f_0(1370)$ BREIT-WIGNER MASS

VALUE (MeV)	DOCUMENT ID
1200 to 1500 OUR ESTIMATE	

$\pi\pi$ MODE

VALUE (MeV)	EVTS	DOCUMENT ID		TECN	COMMENT
• • • We do not use the following data for averages, fits, limits, etc. • • •					
1400 ± 40		[1] AUBERT	09L	BABR	$B^\pm \to \pi^\pm\pi^\pm\pi^\mp$
$1470^{+\ 6+72}_{-\ 7-255}$		[2] UEHARA	08A	BELL	$10.6\,e^+e^- \to e^+e^-\pi^0\pi^0$
1259 ± 55	2.6k	BONVICINI	07	CLEO	$D^+ \to \pi^-\pi^+\pi^+$
$1309 \pm\ 1 \pm\ 15$		[3] BUGG	07A	RVUE	$0.0\,p\overline{p} \to 3\pi^0$
1449 ± 13	4.3k	[4] GARMASH	06	BELL	$B^+ \to K^+\pi^+\pi^-$
1350 ± 50		ABLIKIM	05	BES2	$J/\psi \to \phi\pi^+\pi^-$
$1265 \pm 30^{+\ 20}_{-\ 35}$		ABLIKIM	05Q	BES2	$\psi(2S) \to \gamma\pi^+\pi^-K^+K^-$
$1434 \pm 18 \pm\ \ 9$	848	AITALA	01A	E791	$D^+_s \to \pi^-\pi^+\pi^+$
1308 ± 10		BARBERIS	99B	OMEG	$450\,pp \to p_s p_f \pi^+\pi^-$

Downloaded from https://academic.oup.com/ptep/article/2022/8/083C01/6651666 by KIT Library user on 27 September 2022

1315 ± 50	BELLAZZINI	99	GAM4	450 $pp \to pp\pi^0\pi^0$
1315 ± 30	ALDE	98	GAM4	100 $\pi^- p \to \pi^0\pi^0 n$
1280 ± 55	BERTIN	98	OBLX	0.05–0.405 $\overline{n}p \to \pi^+\pi^+\pi^-$
1186	[5,6] TORNQVIST	95	RVUE	$\pi\pi \to \pi\pi$, $K\overline{K}$, $K\pi$, $\eta\pi$
1472 ± 12	ARMSTRONG	91	OMEG	300 $pp \to pp\pi\pi$, $ppK\overline{K}$
1275 ± 20	BREAKSTONE	90	SFM	62 $pp \to pp\pi^+\pi^-$
1420 ± 20	AKESSON	86	SPEC	63 $pp \to pp\pi^+\pi^-$
1256	FROGGATT	77	RVUE	$\pi^+\pi^-$ channel

[1] Breit-Wigner mass.
[2] Breit-Wigner mass. May also be the $f_0(1500)$.
[3] Reanalysis of ABELE 96C data.
[4] Also observed by GARMASH 07 in $B^0 \to K^0_S\pi^+\pi^-$ decays. Supersedes GARMASH 05.
[5] Uses data from BEIER 72B, OCHS 73, HYAMS 73, GRAYER 74, ROSSELET 77, CASON 83, ASTON 88, and ARMSTRONG 91B. Coupled channel analysis with flavor symmetry and all light two-pseudoscalars systems.
[6] Also observed by ASNER 00 in $\tau^- \to \pi^-\pi^0\pi^0\nu_\tau$ decays

$K\overline{K}$ MODE

VALUE (MeV)	EVTS	DOCUMENT ID		TECN	COMMENT
• • • We do not use the following data for averages, fits, limits, etc. • • •					
1422 ± 15 ± 28		[1] AAIJ	19H	LHCB	$pp \to D^\pm X$
1360 ± 31 ± 28	430	[2,3] DOBBS	15		$J/\psi \to \gamma K^+K^-$
1350 ± 48 ± 15	168	[2,3] DOBBS	15		$\psi(2S) \to \gamma K^+K^-$
1440 ± 6		VLADIMIRSK...06		SPEC	40 $\pi^- p \to K^0_S K^0_S n$
1391 ± 10		TIKHOMIROV	03	SPEC	40.0 $\pi^- C \to K^0_S K^0_S K^0_L X$
1440 ± 50		BOLONKIN	88	SPEC	40 $\pi^- p \to K^0_S K^0_S n$
1463 ± 9		ETKIN	82B	MPS	23 $\pi^- p \to n2K^0_S$
1425 ± 15		WICKLUND	80	SPEC	6 $\pi N \to K^+K^-N$
~ 1300		POLYCHRO...	79	STRC	7 $\pi^- p \to n2K^0_S$

[1] From the $D^\pm \to K^\pm K^+K^-$ Dalitz plot fit with the isobar model A.
[2] Using CLEO-c data but not authored by the CLEO Collaboration.
[3] From a fit to a Breit-Wigner line shape with fixed Γ = 346 MeV.

4π MODE $2(\pi\pi)_S+\rho\rho$

VALUE (MeV)	EVTS	DOCUMENT ID		TECN	COMMENT
• • • We do not use the following data for averages, fits, limits, etc. • • •					
1395 ± 40		ABELE	01	CBAR	0.0 $\overline{p}d \to \pi^-4\pi^0 p$
1374 ± 38		AMSLER	94	CBAR	0.0 $\overline{p}p \to \pi^+\pi^-3\pi^0$
1345 ± 12		ADAMO	93	OBLX	$\overline{n}p \to 3\pi^+2\pi^-$
1386 ± 30		GASPERO	93	DBC	0.0 $\overline{p}n \to 2\pi^+3\pi^-$
~ 1410	5751	[1] BETTINI	66	DBC	0.0 $\overline{p}n \to 2\pi^+3\pi^-$

[1] $\rho\rho$ dominant.

$\eta\eta$ MODE

VALUE (MeV)	DOCUMENT ID		TECN	COMMENT
• • • We do not use the following data for averages, fits, limits, etc. • • •				
$1262^{+51}_{-78}{}^{+82}_{-103}$	[1] UEHARA	10A	BELL	10.6 $e^+e^- \to e^+e^-\eta\eta$
1430	AMSLER	92	CBAR	0.0 $\overline{p}p \to \pi^0\eta\eta$
1220 ± 40	ALDE	86D	GAM4	100 $\pi^- p \to n2\eta$

[1] Breit-Wigner mass. May also be the $f_0(1500)$.

COUPLED CHANNEL MODE

VALUE (MeV)	DOCUMENT ID		TECN	COMMENT
• • • We do not use the following data for averages, fits, limits, etc. • • •				
$1330.2^{+5.9}_{-6.5} \pm 5.1$	[1] AAIJ	19H	LHCB	$pp \to D^\pm X$
1306 ± 20	[2] ANISOVICH	03	RVUE	

[1] From the $D^\pm \to K^\pm K^+K^-$ Dalitz plot fit with the Triple-M amplitude in the multi-meson model of AOUDE 18.
[2] K-matrix pole from combined analysis of $\pi^- p \to \pi^0\pi^0 n$, $\pi^- p \to K\overline{K}n$, $\pi^+\pi^- \to \pi^+\pi^-$, $\overline{p}p \to \pi^0\pi^0\pi^0$, $\pi^0\eta\eta$, $\pi^0\pi^0\eta$, $\pi^+\pi^-\pi^0$, $K^+K^-\pi^0$, $K^0_S K^0_S\pi^0$, $K^+K^0_S\pi^-$ at rest, $\overline{p}n \to \pi^-\pi^-\pi^+$, $K^0_S K^-\pi^0$, $K^0_S K^0_S\pi^-$ at rest.

$f_0(1370)$ BREIT-WIGNER WIDTH

VALUE (MeV)	DOCUMENT ID
200 to 500 OUR ESTIMATE	

$\pi\pi$ MODE

VALUE (MeV)	EVTS	DOCUMENT ID		TECN	COMMENT
• • • We do not use the following data for averages, fits, limits, etc. • • •					
300 ± 80		[1] AUBERT	09L	BABR	$B^\pm \to \pi^\pm\pi^\pm\pi^\mp$
$90^{+2}_{-1}{}^{+50}_{-22}$		[2] UEHARA	08A	BELL	10.6 $e^+e^- \to e^+e^-\pi^0\pi^0$
298 ± 21	2.6k	BONVICINI	07	CLEO	$D^+ \to \pi^-\pi^+\pi^+$
126 ± 25	4286	[3] GARMASH	06	BELL	$B^+ \to K^+\pi^+\pi^-$
265 ± 40		ABLIKIM	05	BES2	$J/\psi \to \phi\pi^+\pi^-$
$350 \pm 100^{+105}_{-60}$		ABLIKIM	05Q	BES2	$\psi(2S) \to \gamma\pi^+\pi^-K^+K^-$
173 ± 32 ± 6	848	AITALA	01A	E791	$D^+_s \to \pi^-\pi^+\pi^+$
222 ± 20		BARBERIS	99B	OMEG	450 $pp \to p_s p_f \pi^+\pi^-$
255 ± 60		BELLAZZINI	99	GAM4	450 $pp \to pp\pi^0\pi^0$
190 ± 50		ALDE	98	GAM4	100 $\pi^- p \to \pi^0\pi^0 n$
323 ± 13		BERTIN	98	OBLX	0.05–0.405 $\overline{n}p \to \pi^+\pi^+\pi^-$
350		[4,5] TORNQVIST	95	RVUE	$\pi\pi \to \pi\pi$, $K\overline{K}$, $K\pi$, $\eta\pi$
195 ± 33		ARMSTRONG	91	OMEG	300 $pp \to pp\pi\pi$, $ppK\overline{K}$
285 ± 60		BREAKSTONE	90	SFM	62 $pp \to pp\pi^+\pi^-$
460 ± 50		AKESSON	86	SPEC	63 $pp \to pp\pi^+\pi^-$
~ 400		[6] FROGGATT	77	RVUE	$\pi^+\pi^-$ channel

[1] The systematic errors are not reported.
[2] Breit-Wigner width. May also be the $f_0(1500)$.
[3] Also observed by GARMASH 07 in $B^0 \to K^0_S\pi^+\pi^-$ decays. Supersedes GARMASH 05.
[4] Uses data from BEIER 72B, OCHS 73, HYAMS 73, GRAYER 74, ROSSELET 77, CASON 83, ASTON 88, and ARMSTRONG 91B. Coupled channel analysis with flavor symmetry and all light two-pseudoscalars systems.
[5] Also observed by ASNER 00 in $\tau^- \to \pi^-\pi^0\pi^0\nu_\tau$ decays
[6] Width defined as distance between 45 and 135° phase shift.

$K\overline{K}$ MODE

VALUE (MeV)	DOCUMENT ID		TECN	COMMENT
• • • We do not use the following data for averages, fits, limits, etc. • • •				
324 ± 38 ± 42	[1] AAIJ	19H	LHCB	$pp \to D^\pm X$
121 ± 15	VLADIMIRSK...06		SPEC	40 $\pi^- p \to K^0_S K^0_S n$
55 ± 26	TIKHOMIROV	03	SPEC	40.0 $\pi^- C \to K^0_S K^0_S K^0_L X$
250 ± 80	BOLONKIN	88	SPEC	40 $\pi^- p \to K^0_S K^0_S n$
118^{+138}_{-16}	ETKIN	82B	MPS	23 $\pi^- p \to n2K^0_S$
160 ± 30	WICKLUND	80	SPEC	6 $\pi N \to K^+K^-N$
~ 150	POLYCHRO...	79	STRC	7 $\pi^- p \to n2K^0_S$

[1] From the $D^\pm \to K^\pm K^+K^-$ Dalitz plot fit with the isobar model A.

4π MODE $2(\pi\pi)_S+\rho\rho$

VALUE (MeV)	EVTS	DOCUMENT ID		TECN	COMMENT
• • • We do not use the following data for averages, fits, limits, etc. • • •					
275 ± 55		ABELE	01	CBAR	0.0 $\overline{p}d \to \pi^-4\pi^0 p$
375 ± 61		AMSLER	94	CBAR	0.0 $\overline{p}p \to \pi^+\pi^-3\pi^0$
398 ± 26		ADAMO	93	OBLX	$\overline{n}p \to 3\pi^+2\pi^-$
310 ± 50		GASPERO	93	DBC	0.0 $\overline{p}n \to 2\pi^+3\pi^-$
~ 90	5751	[1] BETTINI	66	DBC	0.0 $\overline{p}n \to 2\pi^+3\pi^-$

[1] $\rho\rho$ dominant.

$\eta\eta$ MODE

VALUE (MeV)	DOCUMENT ID		TECN	COMMENT
• • • We do not use the following data for averages, fits, limits, etc. • • •				
$484^{+246}_{-170}{}^{+246}_{-263}$	[1] UEHARA	10A	BELL	10.6 $e^+e^- \to e^+e^-\eta\eta$
250	AMSLER	92	CBAR	0.0 $\overline{p}p \to \pi^0\eta\eta$
320 ± 40	ALDE	86D	GAM4	100 $\pi^- p \to n2\eta$

[1] Breit-Wigner width. May also be the $f_0(1500)$.

COUPLED CHANNEL MODE

VALUE (MeV)	DOCUMENT ID		TECN
• • • We do not use the following data for averages, fits, limits, etc. • • •			
147^{+30}_{-50}	[1] ANISOVICH	03	RVUE

[1] K-matrix pole from combined analysis of $\pi^- p \to \pi^0\pi^0 n$, $\pi^- p \to K\overline{K}n$, $\pi^+\pi^- \to \pi^+\pi^-$, $\overline{p}p \to \pi^0\pi^0\pi^0$, $\pi^0\eta\eta$, $\pi^0\pi^0\eta$, $\pi^+\pi^-\pi^0$, $K^+K^-\pi^0$, $K^0_S K^0_S\pi^0$, $K^+K^0_S\pi^-$ at rest, $\overline{p}n \to \pi^-\pi^-\pi^+$, $K^0_S K^-\pi^0$, $K^0_S K^0_S\pi^-$ at rest.

$f_0(1370)$ DECAY MODES

	Mode	Fraction (Γ_i/Γ)
Γ_1	$\pi\pi$	seen
Γ_2	4π	seen
Γ_3	$4\pi^0$	seen
Γ_4	$2\pi^+2\pi^-$	seen
Γ_5	$\pi^+\pi^-2\pi^0$	seen
Γ_6	$\rho\rho$	seen
Γ_7	$2(\pi\pi)_S$-wave	seen
Γ_8	$\pi(1300)\pi$	seen
Γ_9	$a_1(1260)\pi$	seen
Γ_{10}	$\eta\eta$	seen
Γ_{11}	$K\overline{K}$	seen
Γ_{12}	$K\overline{K}n\pi$	not seen
Γ_{13}	6π	not seen
Γ_{14}	$\omega\omega$	not seen
Γ_{15}	$\gamma\gamma$	seen
Γ_{16}	e^+e^-	not seen

$f_0(1370)$ PARTIAL WIDTHS

$\Gamma(\gamma\gamma)$ Γ_{15}

See $\gamma\gamma$ widths under $f_0(500)$ and MORGAN 90.

Downloaded from https://academic.oup.com/ptep/article/2022/8/083C01/6651666 by KIT Library user on 27 September 2022

$\Gamma(e^+e^-)$ — Γ_{16}

VALUE (eV)	CL%	DOCUMENT ID		TECN	COMMENT
<20	90	VOROBYEV	88	ND	$e^+e^- \to \pi^0\pi^0$

$f_0(1370)$ $\Gamma(i)\Gamma(\gamma\gamma)/\Gamma(\text{total})$

$\Gamma(\eta\eta) \times \Gamma(\gamma\gamma)/\Gamma_{\text{total}}$ — $\Gamma_{10}\Gamma_{15}/\Gamma$

VALUE (eV)	DOCUMENT ID		TECN	COMMENT
• • • We do not use the following data for averages, fits, limits, etc. • • •				
$121^{+133+169}_{-\ 53-106}$	[1] UEHARA	10A	BELL	10.6 $e^+e^- \to e^+e^-\eta\eta$

[1] Including interference with the $f'_2(1525)$ (parameters fixed to the values from the 2008 edition of this review, PDG 08) and $f_2(1270)$. May also be the $f_0(1500)$.

$f_0(1370)$ BRANCHING RATIOS

$\Gamma(\pi\pi)/\Gamma_{\text{total}}$ — Γ_1/Γ

VALUE	CL%	DOCUMENT ID		TECN	COMMENT
• • • We do not use the following data for averages, fits, limits, etc. • • •					
<0.10	95	OCHS	13	RVUE	
0.26±0.09		BUGG	96	RVUE	
<0.15		[1] AMSLER	94	CBAR	$\overline{p}p \to \pi^+\pi^-3\pi^0$
<0.06		GASPERO	93	DBC	0.0 $\overline{p}n \to$ hadrons

[1] Using AMSLER 95B ($3\pi^0$).

$\Gamma(4\pi)/\Gamma_{\text{total}}$ — $\Gamma_2/\Gamma = (\Gamma_3+\Gamma_4+\Gamma_5)/\Gamma$

VALUE	DOCUMENT ID		TECN	COMMENT
• • • We do not use the following data for averages, fits, limits, etc. • • •				
>0.72	GASPERO	93	DBC	0.0 $\overline{p}n \to$ hadrons

$\Gamma(4\pi^0)/\Gamma(4\pi)$ — Γ_3/Γ_2

VALUE	DOCUMENT ID		TECN	COMMENT
• • • We do not use the following data for averages, fits, limits, etc. • • •				
seen	ABELE	96	CBAR	0.0 $\overline{p}p \to 5\pi^0$
0.068±0.005	[1] GASPERO	93	DBC	0.0 $\overline{p}n \to$ hadrons

[1] Model-dependent evaluation.

$\Gamma(2\pi^+2\pi^-)/\Gamma(4\pi)$ — $\Gamma_4/\Gamma_2 = \Gamma_4/(\Gamma_3+\Gamma_4+\Gamma_5)$

VALUE	DOCUMENT ID		TECN	COMMENT
• • • We do not use the following data for averages, fits, limits, etc. • • •				
0.420±0.014	[1] GASPERO	93	DBC	0.0 $\overline{p}n \to 2\pi^+3\pi^-$

[1] Model-dependent evaluation.

$\Gamma(\pi^+\pi^-2\pi^0)/\Gamma(4\pi)$ — $\Gamma_5/\Gamma_2 = \Gamma_5/(\Gamma_3+\Gamma_4+\Gamma_5)$

VALUE	DOCUMENT ID		TECN	COMMENT
• • • We do not use the following data for averages, fits, limits, etc. • • •				
0.512±0.019	[1] GASPERO	93	DBC	0.0 $\overline{p}n \to$ hadrons

[1] Model-dependent evaluation.

$\Gamma(\rho\rho)/\Gamma(4\pi)$ — Γ_6/Γ_2

VALUE	DOCUMENT ID		TECN	COMMENT
• • • We do not use the following data for averages, fits, limits, etc. • • •				
0.26±0.07	ABELE	01B	CBAR	0.0 $\overline{p}d \to 5\pi p$

$\Gamma(2(\pi\pi)_{S\text{-wave}})/\Gamma(\pi\pi)$ — Γ_7/Γ_1

VALUE	DOCUMENT ID		TECN	COMMENT
• • • We do not use the following data for averages, fits, limits, etc. • • •				
5.6±2.6	[1] ABELE	01	CBAR	0.0 $\overline{p}d \to \pi^-4\pi^0p$

[1] From the combined data of ABELE 96 and ABELE 96C.

$\Gamma(2(\pi\pi)_{S\text{-wave}})/\Gamma(4\pi)$ — Γ_7/Γ_2

VALUE	DOCUMENT ID		TECN	COMMENT
• • • We do not use the following data for averages, fits, limits, etc. • • •				
0.51±0.09	ABELE	01B	CBAR	0.0 $\overline{p}d \to 5\pi p$

$\Gamma(\rho\rho)/\Gamma(2(\pi\pi)_{S\text{-wave}})$ — Γ_6/Γ_7

VALUE	DOCUMENT ID		TECN	COMMENT
• • • We do not use the following data for averages, fits, limits, etc. • • •				
large	BARBERIS	00C		450 $pp \to p_f 4\pi p_s$
1.6 ±0.2	AMSLER	94	CBAR	$\overline{p}p \to \pi^+\pi^-3\pi^0$
~ 0.65	GASPERO	93	DBC	0.0 $\overline{p}n \to$ hadrons

$\Gamma(\pi(1300)\pi)/\Gamma(4\pi)$ — Γ_8/Γ_2

VALUE	DOCUMENT ID		TECN	COMMENT
• • • We do not use the following data for averages, fits, limits, etc. • • •				
0.17±0.06	ABELE	01B	CBAR	0.0 $\overline{p}d \to 5\pi p$

$\Gamma(a_1(1260)\pi)/\Gamma(4\pi)$ — Γ_9/Γ_2

VALUE	DOCUMENT ID		TECN	COMMENT
• • • We do not use the following data for averages, fits, limits, etc. • • •				
0.06±0.02	ABELE	01B	CBAR	0.0 $\overline{p}d \to 5\pi p$

$\Gamma(\eta\eta)/\Gamma(4\pi)$ — $\Gamma_{10}/\Gamma_2 = \Gamma_{10}/(\Gamma_3+\Gamma_4+\Gamma_5)$

VALUE	DOCUMENT ID		TECN	COMMENT
• • • We do not use the following data for averages, fits, limits, etc. • • •				
$(28 \pm 11) \times 10^{-3}$	[1] ANISOVICH	02D	SPEC	Combined fit
$(4.7 \pm 2.0) \times 10^{-3}$	BARBERIS	00E		450 $pp \to p_f\eta\eta p_s$

[1] From a combined K-matrix analysis of Crystal Barrel (0. $p\overline{p} \to \pi^0\pi^0\pi^0$, $\pi^0\eta\eta$, $\pi^0\pi^0\eta$), GAMS ($\pi p \to \pi^0\pi^0 n$, $\eta\eta n$, $\eta\eta' n$), and BNL ($\pi p \to K\overline{K}n$) data.

$\Gamma(K\overline{K})/\Gamma_{\text{total}}$ — Γ_{11}/Γ

VALUE	DOCUMENT ID		TECN
• • • We do not use the following data for averages, fits, limits, etc. • • •			
0.35±0.13	BUGG	96	RVUE

$\Gamma(K\overline{K})/\Gamma(\pi\pi)$ — Γ_{11}/Γ_1

VALUE	DOCUMENT ID		TECN	COMMENT
• • • We do not use the following data for averages, fits, limits, etc. • • •				
0.08±0.08	ABLIKIM	05	BES2	$J/\psi \to \phi\pi^+\pi^-$, ϕK^+K^-
0.91±0.20	[1] BARGIOTTI	03	OBLX	$\overline{p}p$
0.12±0.06	[2] ANISOVICH	02D	SPEC	Combined fit
0.46±0.15±0.11	BARBERIS	99D	OMEG	450 $pp \to K^+K^-, \pi^+\pi^-$

[1] Coupled channel analysis of $\pi^+\pi^-\pi^0$, $K^+K^-\pi^0$, and $K^\pm K^0_S\pi^\mp$.

[2] From a combined K-matrix analysis of Crystal Barrel (0. $p\overline{p} \to \pi^0\pi^0\pi^0$, $\pi^0\eta\eta$, $\pi^0\pi^0\eta$), GAMS ($\pi p \to \pi^0\pi^0 n$, $\eta\eta n$, $\eta\eta' n$), and BNL ($\pi p \to K\overline{K}n$) data.

$\Gamma(K\overline{K}n\pi)/\Gamma_{\text{total}}$ — Γ_{12}/Γ

VALUE	DOCUMENT ID		TECN	COMMENT
• • • We do not use the following data for averages, fits, limits, etc. • • •				
<0.03	GASPERO	93	DBC	0.0 $\overline{p}n \to$ hadrons

$\Gamma(6\pi)/\Gamma_{\text{total}}$ — Γ_{13}/Γ

VALUE	DOCUMENT ID		TECN	COMMENT
• • • We do not use the following data for averages, fits, limits, etc. • • •				
<0.22	GASPERO	93	DBC	0.0 $\overline{p}n \to$ hadrons

$\Gamma(\omega\omega)/\Gamma_{\text{total}}$ — Γ_{14}/Γ

VALUE	DOCUMENT ID		TECN	COMMENT
• • • We do not use the following data for averages, fits, limits, etc. • • •				
<0.13	GASPERO	93	DBC	0.0 $\overline{p}n \to$ hadrons

$f_0(1370)$ REFERENCES

SARANTSEV	21	PL B816 136227	A.V. Sarantsev *et al.*	(BONN, PNPI)
ALBRECHT	20	EPJ C80 453	M. Albrecht *et al.*	(Crystal Barrel Collab.)
AAIJ	19H	JHEP 1904 063	R. Aaij *et al.*	(LHCb Collab.)
AOUDE	18	PR D98 056021	R.T. Aoude *et al.*	
DOBBS	15	PR D91 052006	S. Dobbs *et al.*	(NWES)
OCHS	13	JP G40 043001	W. Ochs	
UEHARA	10A	PR D82 114031	S. Uehara *et al.*	(BELLE Collab.)
ANISOVICH	09	IJMP A24 2481	V.V. Anisovich, A.V. Sarantsev	
AUBERT	09L	PR D79 072006	B. Aubert *et al.*	(BABAR Collab.)
PDG	08	PL B667 1	C. Amsler *et al.*	(PDG Collab.)
UEHARA	08A	PR D78 052004	S. Uehara *et al.*	(BELLE Collab.)
BONVICINI	07	PR D76 012001	G. Bonvicini *et al.*	(CLEO Collab.)
BUGG	07A	JP G34 151	D.V. Bugg *et al.*	
GARMASH	07	PR D75 012006	A. Garmash *et al.*	(BELLE Collab.)
GARMASH	06	PRL 96 251803	A. Garmash *et al.*	(BELLE Collab.)
PDG	06	JP G33 1	W.-M. Yao *et al.*	(PDG Collab.)
VLADIMIRSK...	06	PAN 69 493	V.V. Vladimirsky *et al.*	(ITEP, Moscow)
		Translated from YAF 69 515.		
ABLIKIM	05	PL B607 243	M. Ablikim *et al.*	(BES Collab.)
ABLIKIM	05Q	PR D72 092002	M. Ablikim *et al.*	(BES Collab.)
GARMASH	05	PR D71 092003	A. Garmash *et al.*	(BELLE Collab.)
ANISOVICH	03	EPJ A16 229	V.V. Anisovich *et al.*	
BARGIOTTI	03	EPJ C26 371	M. Bargiotti *et al.*	(OBELIX Collab.)
TIKHOMIROV	03	PAN 66 828	G.D. Tikhomirov *et al.*	
		Translated from YAF 66 860.		
ANISOVICH	02D	PAN 65 1545	V.V. Anisovich *et al.*	
		Translated from YAF 65 1583.		
ABELE	01	EPJ C19 667	A. Abele *et al.*	(Crystal Barrel Collab.)
ABELE	01B	EPJ C21 261	A. Abele *et al.*	(Crystal Barrel Collab.)
AITALA	01A	PRL 86 765	E.M. Aitala *et al.*	(FNAL E791 Collab.)
ASNER	00	PR D61 012002	D.M. Asner *et al.*	(CLEO Collab.)
BARBERIS	00C	PL B471 440	D. Barberis *et al.*	(WA 102 Collab.)
BARBERIS	00E	PL B479 59	D. Barberis *et al.*	(WA 102 Collab.)
BARBERIS	99B	PL B453 316	D. Barberis *et al.*	(Omega Expt.)
BARBERIS	99D	PL B462 462	D. Barberis *et al.*	(Omega Expt.)
BELLAZZINI	99	PL B467 296	R. Bellazzini *et al.*	
KAMINSKI	99	EPJ C9 141	R. Kaminski, L. Lesniak, B. Loiseau	(CRAC, PARIN)
ALDE	98	EPJ A3 361	D. Alde *et al.*	(GAM4 Collab.)
Also		PAN 62 405	D. Alde *et al.*	(GAMS Collab.)
		Translated from YAF 62 446.		
ANISOVICH	98B	SPU 41 419	V.V. Anisovich *et al.*	
		Translated from UFN 168 481.		
BERTIN	98	PR D57 55	A. Bertin *et al.*	(OBELIX Collab.)
BARBERIS	97B	PL B413 217	D. Barberis *et al.*	(WA 102 Collab.)
BERTIN	97C	PL B408 476	A. Bertin *et al.*	(OBELIX Collab.)
ABELE	96	PL B380 453	A. Abele *et al.*	(Crystal Barrel Collab.)
ABELE	96B	PL B385 425	A. Abele *et al.*	(Crystal Barrel Collab.)
ABELE	96C	NP A609 562	A. Abele *et al.*	(Crystal Barrel Collab.)
BUGG	96	NP B471 59	D.V. Bugg, A.V. Sarantsev, B.S. Zou	(LOQM, PNPI)
AMSLER	95B	PL B342 433	C. Amsler *et al.*	(Crystal Barrel Collab.)
AMSLER	95C	PL B353 571	C. Amsler *et al.*	(Crystal Barrel Collab.)
AMSLER	95D	PL B355 425	C. Amsler *et al.*	(Crystal Barrel Collab.)
JANSSEN	95	PR D52 2690	G. Janssen *et al.*	(STON, ADLD, JULI)
TORNQVIST	95	ZPHY C68 647	N.A. Tornqvist	(HELS)
AMSLER	94	PL B322 431	C. Amsler *et al.*	(Crystal Barrel Collab.) JPC
AMSLER	94D	PL B333 277	C. Amsler *et al.*	(Crystal Barrel Collab.)
ANISOVICH	94	PL B323 233	V.V. Anisovich *et al.*	(Crystal Barrel Collab.) JPC
BUGG	94	PR D50 4412	D.V. Bugg *et al.*	(LOQM)

Downloaded from https://academic.oup.com/ptep/article/2022/8/083C01/6651666 by KIT Library user on 27 September 2022

KAMINSKI	94	PR D50 3145	R. Kaminski, L. Lesniak, J.P. Maillet	(CRAC+)
ADAMO	93	NP A558 13C	A. Adamo *et al.*	(OBELIX Collab.) JPC
GASPERO	93	NP A562 407	M. Gaspero	(ROMAI) JPC
AMSLER	92	PL B291 347	C. Amsler *et al.*	(Crystal Barrel Collab.)
ARMSTRONG	91	ZPHY C51 351	T.A. Armstrong *et al.*	(ATHU, BARI, BIRM+)
ARMSTRONG	91B	ZPHY C52 389	T.A. Armstrong *et al.*	(ATHU, BARI, BIRM+)
BREAKSTONE	90	ZPHY C48 569	A.M. Breakstone *et al.*	(ISU, BGNA, CERN+)
MORGAN	90	ZPHY C48 623	D. Morgan, M.R. Pennington	(RAL, DURH)
ASTON	88	NP B296 493	D. Aston *et al.*	(SLAC, NAGO, CINC, INUS)
BOLONKIN	88	NP B309 426	B.V. Bolonkin *et al.*	(ITEP, SERP)
FALVARD	88	PR D38 2706	A. Falvard *et al.*	(CLER, FRAS, LALO+)
VOROBYEV	88	SJNP 48 273	P.V. Vorobiev *et al.*	(NOVO)
		Translated from YAF 48 436.		
AU	87	PR D35 1633	K.L. Au, D. Morgan, M.R. Pennington	(DURH, RAL)
AKESSON	86	NP B264 154	T. Akesson *et al.*	(Axial Field Spec. Collab.)
ALDE	86D	NP B269 485	D.M. Alde *et al.*	(BELG, LAPP, SERP, CERN+)
LONGACRE	86	PL B177 223	R.S. Longacre *et al.*	(BNL, BRAN, CUNY+)
BINON	84C	NC 80A 363	F.G. Binon *et al.*	(BELG, LAPP, SERP+)
BINON	83	NC 78A 313	F.G. Binon *et al.*	(BELG, LAPP, SERP+)
CASON	83	PR D28 1586	N.M. Cason *et al.*	(NDAM, ANL)
ETKIN	82B	PR D25 1786	A. Etkin *et al.*	(BNL, CUNY, TUFTS, VAND)
WICKLUND	80	PRL 45 1469	A.B. Wicklund *et al.*	(ANL)
BECKER	79	NP B151 46	H. Becker *et al.*	(MPIM, CERN, ZEEM, CRAC)
POLYCHRO...	79	PR D19 1317	V.A. Polychronakos *et al.*	(NDAM, ANL)
FROGGATT	77	NP B129 89	C.D. Froggatt, J.L. Petersen	(GLAS, NORD)
ROSSELET	77	PR D15 574	L. Rosselet *et al.*	(GEVA, SACL)
HYAMS	75	NP B100 205	B.D. Hyams *et al.*	(CERN, MPIM)
GRAYER	74	NP B75 189	G. Grayer *et al.*	(CERN, MPIM)
HYAMS	73	NP B64 134	B.D. Hyams *et al.*	(CERN, MPIM)
OCHS	73	Thesis	W. Ochs	(MPIM, MUNI)
BEIER	72B	PRL 29 511	E.W. Beier *et al.*	(PENN)
BETTINI	66	NC 42A 695	A. Bettini *et al.*	(PADO, PISA)

$\pi_1(1400)$

$I^G(J^{PC}) = 1^-(1^{-+})$

Coupled channel analyses favor the existence of only one broad 1^{-+} isovector state consistent with $\pi_1(1600)$ in the 1400–1600 MeV region. See the review on "Spectroscopy of Light Meson Resonances." See also $\pi_1(1600)$.

$\pi_1(1400)$ MASS

VALUE (MeV)	EVTS	DOCUMENT ID		TECN	CHG	COMMENT
1354 ±25 OUR AVERAGE		Error includes scale factor of 1.8. See the ideogram below.				
1257 ±20 ±25	23.5k	ADAMS	07B	B852		$18\ \pi^- p \to \eta\pi^0 n$
1384 ±20 ±35	90k	SALVINI	04	OBLX		$\overline{p}p \to 2\pi^+ 2\pi^-$
1360 ±25		ABELE	99	CBAR		$0.0\ \overline{p}p \to \pi^0\pi^0\eta$
1400 ±20 ±20		ABELE	98B	CBAR		$0.0\ \overline{p}n \to \pi^-\pi^0\eta$
1370 ±16 $^{+50}_{-30}$		[1] THOMPSON	97	MPS		$18\ \pi^- p \to \eta\pi^- p$
• • • We do not use the following data for averages, fits, limits, etc. • • •						
1404.7± 3.5 $^{+15.1}_{-17.7}$		[2] ALBRECHT	20	RVUE		$0.9\ \overline{p}p \to \pi^0\pi^0\eta$
1323.1± 4.6		[3] AOYAGI	93	BKEI		$\pi^- p \to \eta\pi^- p$
1406 ±20		[4] ALDE	88B	GAM4	0	$100\ \pi^- p \to \eta\pi^0 n$

[1] Natural parity exchange, questioned by DZIERBA 03.
[2] T-matrix pole, 1 pole, 2 channels ($\pi\eta$, $\pi\eta'$ for unitarity).
[3] Unnatural parity exchange.
[4] Seen in the P_0-wave intensity of the $\eta\pi^0$ system, unnatural parity exchange.

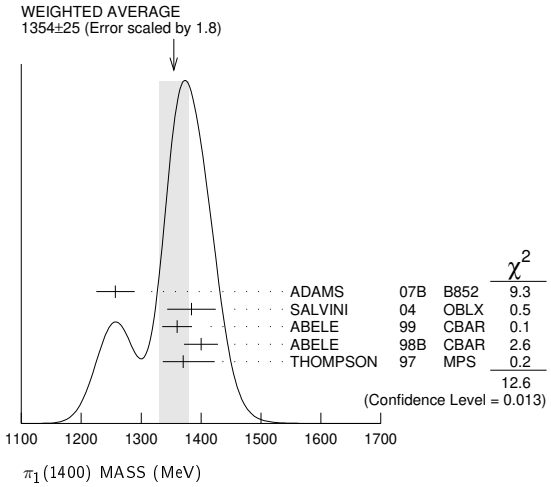

$\pi_1(1400)$ WIDTH

VALUE (MeV)	EVTS	DOCUMENT ID		TECN	CHG	COMMENT
330 ±35 OUR AVERAGE						
354 ±64 ± 58	23.5k	ADAMS	07B	B852		$18\ \pi^- p \to \eta\pi^0 n$
378 ±50 ± 50	90k	SALVINI	04	OBLX		$\overline{p}p \to 2\pi^+ 2\pi^-$
220 ±90		ABELE	99	CBAR		$0.0\ \overline{p}p \to \pi^0\pi^0\eta$
310 ±50 $^{+50}_{-30}$		ABELE	98B	CBAR		$0.0\ \overline{p}n \to \pi^-\pi^0\eta$
385 ±40 $^{+65}_{-105}$		[1] THOMPSON	97	MPS		$18\ \pi^- p \to \eta\pi^- p$
• • • We do not use the following data for averages, fits, limits, etc. • • •						
628.3±27.1 $^{+35.8}_{-138.2}$		[2] ALBRECHT	20	RVUE		$0.9\ \overline{p}p \to \pi^0\pi^0\eta$
143.2±12.5		[3] AOYAGI	93	BKEI		$\pi^- p \to \eta\pi^- p$
180 ±20		[4] ALDE	88B	GAM4	0	$100\ \pi^- p \to \eta\pi^0 n$

[1] Resolution is not unfolded, natural parity exchange, questioned by DZIERBA 03.
[2] T-matrix pole, 1 pole, 2 channels ($\pi\eta$, $\pi\eta'$ for unitarity).
[3] Unnatural parity exchange.
[4] Seen in the P_0-wave intensity of the $\eta\pi^0$ system, unnatural parity exchange.

$\pi_1(1400)$ DECAY MODES

	Mode	Fraction (Γ_i/Γ)
Γ_1	$\eta\pi^0$	seen
Γ_2	$\eta\pi^-$	seen
Γ_3	$\eta'\pi$	
Γ_4	$\rho(770)\pi$	not seen

$\pi_1(1400)$ BRANCHING RATIOS

$\Gamma(\eta\pi^0)/\Gamma_{total}$ — Γ_1/Γ

VALUE	DOCUMENT ID		TECN	CHG	COMMENT
• • • We do not use the following data for averages, fits, limits, etc. • • •					
not seen	PROKOSHKIN	95B	GAM4		$100\ \pi^- p \to \eta\pi^0 n$
not seen	[1] BUGG	94	RVUE		$\overline{p}p \to \eta 2\pi^0$
not seen	[2] APEL	81	NICE	0	$40\ \pi^- p \to \eta\pi^0 n$

[1] Using Crystal Barrel data.
[2] A general fit allowing S, D, and P waves (including m=0) is not done because of limited statistics.

$\Gamma(\eta\pi^-)/\Gamma_{total}$ — Γ_2/Γ

VALUE	DOCUMENT ID		TECN	COMMENT
• • • We do not use the following data for averages, fits, limits, etc. • • •				
possibly seen	BELADIDZE	93	VES	$37\pi^- N \to \eta\pi^- N$

$\Gamma(\eta'\pi)/\Gamma(\eta\pi^0)$ — Γ_3/Γ_1

VALUE	CL%	DOCUMENT ID		TECN	COMMENT
• • • We do not use the following data for averages, fits, limits, etc. • • •					
<0.80	95	BOUTEMEUR	90	GAM4	$100\ \pi^- p \to 4\gamma n$

$\Gamma(\rho(770)\pi)/\Gamma_{total}$ — Γ_4/Γ

VALUE	DOCUMENT ID		TECN	COMMENT
not seen	AGHASYAN	18B	COMP	$190\ \pi^- p \to \pi^-\pi^+\pi^- p$

$\pi_1(1400)$ REFERENCES

ALBRECHT	20	EPJ C80 453	M. Albrecht *et al.*	(Crystal Barrel Collab.)
AGHASYAN	18B	PR D98 092003	M. Aghasyan *et al.*	(COMPASS Collab.)
ADAMS	07B	PL B657 27	G.S. Adams *et al.*	(BNL E852 Collab.)
SALVINI	04	EPJ C35 21	P. Salvini *et al.*	(OBELIX Collab.)
DZIERBA	03	PR D67 094015	A.R. Dzierba *et al.*	
ABELE	99	PL B446 349	A. Abele *et al.*	(Crystal Barrel Collab.)
ABELE	98B	PL B423 175	A. Abele *et al.*	(Crystal Barrel Collab.)
THOMPSON	97	PRL 79 1630	D.R. Thompson *et al.*	(BNL E852 Collab.)
PROKOSHKIN	95B	PAN 58 606	Y.D. Prokoshkin, S.A. Sadovsky	(SERP)
		Translated from YAF 58 662.		
BUGG	94	PR D50 4412	D.V. Bugg *et al.*	(LOQM)
AOYAGI	93	PL B314 246	H. Aoyagi *et al.*	(BKEI Collab.)
BELADIDZE	93	PL B313 276	G.M. Beladidze *et al.*	(VES Collab.)
BOUTEMEUR	90	Hadron 89 Conf. p 119	M. Boutemeur, M. Poulet	(SERP, BELG, LANL+)
ALDE	88B	PL B205 397	D.M. Alde *et al.*	(SERP, BELG, LANL, LAPP) IGJPC
APEL	81	NP B193 269	W.D. Apel *et al.*	(SERP, CERN)

Downloaded from https://academic.oup.com/ptep/article/2022/8/083C01/6651666 by KIT Library user on 27 September 2022

$\eta(1405)$

$I^G(J^{PC}) = 0^+(0^{-+})$

See also the $\eta(1475)$.

$\eta(1405)$ MASS

VALUE (MeV)	DOCUMENT ID
1408.8±2.0 OUR AVERAGE Includes data from the 2 datablocks that follow this one. Error includes scale factor of 2.2. See the ideogram below.	

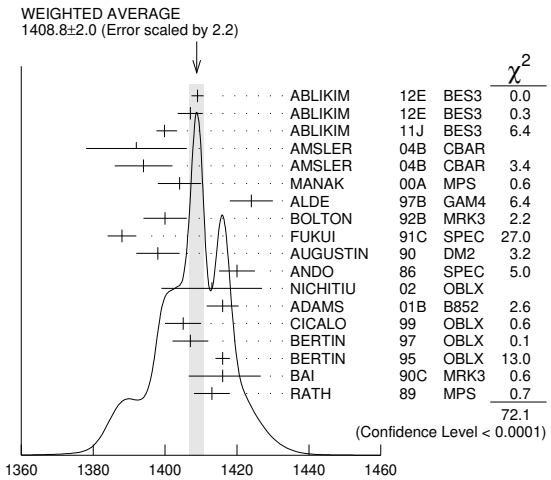

$\eta\pi\pi$ MODE

VALUE (MeV)	EVTS	DOCUMENT ID		TECN	COMMENT
The data in this block is included in the average printed for a previous datablock.					
1405.8± 2.6 OUR AVERAGE Error includes scale factor of 2.3. See the ideogram below.					
1409.0± 1.7	743	ABLIKIM	12E	BES3	$J/\psi \to \gamma(\pi^+\pi^-\pi^0)$
1407.0± 3.5	198	ABLIKIM	12E	BES3	$J/\psi \to \gamma(\pi^0\pi^0\pi^0)$
1399.8± $2.2^{+2.8}_{-0.1}$		[1] ABLIKIM	11J	BES3	$J/\psi \to \omega(\eta\pi^+\pi^-)$
1392 ±14	900 ± 375	AMSLER	04B	CBAR	$0\,\overline{p}p \to \pi^+\pi^-\pi^+\pi^-\eta$
1394 ± 8	6.6 ± 2.0k	AMSLER	04B	CBAR	$0\,\overline{p}p \to \pi^+\pi^-\pi^0\pi^0\eta$
1404 ± 6	9082	MANAK	00A	MPS	$18\,\pi^-p \to \eta\pi^+\pi^-n$
1424 ± 6	2200	ALDE	97B	GAM4	$100\,\pi^-p \to \eta\pi^0\pi^0n$
1400 ± 6		[2] BOLTON	92B	MRK3	$J/\psi \to \gamma\eta\pi^+\pi^-$
1388 ± 4		FUKUI	91C	SPEC	$8.95\,\pi^-p \to \eta\pi^+\pi^-n$
1398 ± 6	261	[3] AUGUSTIN	90	DM2	$J/\psi \to \gamma\eta\pi^+\pi^-$
1420 ± 5		ANDO	86	SPEC	$8\,\pi^-p \to \eta\pi^+\pi^-n$
• • • We do not use the following data for averages, fits, limits, etc. • • •					
1404.0±11.0	195	ABLIKIM	19BA	BES3	$e^+e^- \to \psi(2S)$
1385 ± 7		BAI	99	BES	$J/\psi \to \gamma\eta\pi^+\pi^-$
1409 ± 3		[4] AMSLER	95F	CBAR	$0\,\overline{p}p \to \pi^+\pi^-\pi^0\pi^0\eta$

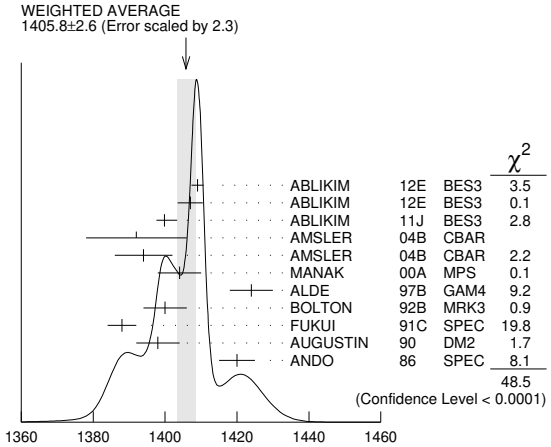

[1] The selected process is $J/\psi \to \omega a_0(980)\pi$.

[2] From fit to the $a_0(980)\pi\ 0^{-+}$ partial wave.

[3] Best fit with a single Breit Wigner.

[4] Superseded by AMSLER 04B.

$K\overline{K}\pi$ MODE ($a_0(980)\pi$ or direct $K\overline{K}\pi$)

VALUE (MeV)	EVTS	DOCUMENT ID		TECN	COMMENT
The data in this block is included in the average printed for a previous datablock.					
1413.9± 1.7 OUR AVERAGE Error includes scale factor of 1.1.					
1413 ±14	3651	[1] NICHITIU	02	OBLX	$0\,\overline{p}p \to K^+K^-\pi^+\pi^-\pi^0$
1416 ± 4 ±2	20k	ADAMS	01B	B852	18 GeV $\pi^-p \to K^+K^-\pi^0n$
1405 ± 5		[2] CICALO	99	OBLX	$0\,\overline{p}p \to K^\pm K^0_S\pi^\mp\pi^+\pi^-$
1407 ± 5		[2] BERTIN	97	OBLX	$0\,\overline{p}p \to K^\pm(K^0)\pi^\mp\pi^+\pi^-$
1416 ± 2		[2] BERTIN	95	OBLX	$0\,\overline{p}p \to K\overline{K}\pi\pi\pi$
1416 ± 8 $^{+7}_{-5}$	700	[3] BAI	90C	MRK3	$J/\psi \to \gamma K^0_S K^\pm\pi^\mp$
1413 ± 5		[3] RATH	89	MPS	$21.4\,\pi^-p \to nK^0_S K^0_S\pi^0$
• • • We do not use the following data for averages, fits, limits, etc. • • •					
1459 ± 5		[4] AUGUSTIN	92	DM2	$J/\psi \to \gamma K\overline{K}\pi$

[1] Decaying dominantly directly to $K^+K^-\pi^0$.

[2] Decaying into $(K\overline{K})_S\pi$, $(K\pi)_S\overline{K}$, and $a_0(980)\pi$.

[3] From fit to the $a_0(980)\pi\ 0^{-+}$ partial wave. Cannot rule out a $a_0(980)\pi\ 1^{++}$ partial wave.

[4] Excluded from averaging because averaging would be meaningless.

$\pi\pi\gamma$ MODE

VALUE (MeV)	EVTS	DOCUMENT ID		TECN	COMMENT
1403±17 OUR AVERAGE Error includes scale factor of 1.8.					
1390±12	235 ± 91	AMSLER	04B	CBAR	$0\,\overline{p}p \to \pi^+\pi^-\pi^+\pi^-\eta$
1424±10±11	547	BAI	04J	BES2	$J/\psi \to \gamma\gamma\pi^+\pi^-$
• • • We do not use the following data for averages, fits, limits, etc. • • •					
1401±18		[1,2] AUGUSTIN	90	DM2	$J/\psi \to \pi^+\pi^-\gamma\gamma$
1432± 8		[2] COFFMAN	90	MRK3	$J/\psi \to \pi^+\pi^-2\gamma$

[1] Best fit with a single Breit Wigner.

[2] This peak in the $\gamma\rho$ channel may not be related to the $\eta(1405)$.

4π MODE

VALUE (MeV)	EVTS	DOCUMENT ID		TECN	COMMENT
• • • We do not use the following data for averages, fits, limits, etc. • • •					
1420±20		BUGG	95	MRK3	$J/\psi \to \gamma\pi^+\pi^-\pi^+\pi^-$
1489±12	3270	[1] BISELLO	89B	DM2	$J/\psi \to 4\pi\gamma$

[1] Estimated by us from various fits.

$K\overline{K}\pi$ MODE (unresolved)

VALUE (MeV)	EVTS	DOCUMENT ID		TECN	COMMENT
• • • We do not use the following data for averages, fits, limits, etc. • • •					
1452.7± 3.3	191	[1,2] ABLIKIM	13M	BES3	$\psi(2S) \to \omega K K\pi$
1437.6± 3.2	249 ± 35	[1,2] ABLIKIM	08E	BES2	$J/\psi \to \omega K^0_S K^+\pi^-$ + c.c.
1445.9± 5.7	62 ± 18	[1,2] ABLIKIM	08E	BES2	$J/\psi \to \omega K^+K^-\pi^0$
1442 ±10	410	[1] BAI	98C	BES	$J/\psi \to \gamma K^+K^-\pi^0$
1445 ± 8	693	[1] AUGUSTIN	90	DM2	$J/\psi \to \gamma K^0_S K^\pm\pi^\mp$
1433 ± 8	296	[1] AUGUSTIN	90	DM2	$J/\psi \to \gamma K^+K^-\pi^0$
1413 ± 8	500	[1] DUCH	89	ASTE	$\overline{p}p \to \pi^+\pi^-K^\pm\pi^\mp K^0$
1453 ± 7	170	[1] RATH	89	MPS	$21.4\,\pi^-p \to K^0_S K^0_S\pi^0n$
1419 ± 1	8800	[1] BIRMAN	88	MPS	$8\,\pi^-p \to K^+\overline{K}^0\pi^-n$
1424 ± 3	620	[1] REEVES	86	SPEC	$6.6\,p\overline{p} \to K\overline{K}\pi X$
1421 ± 2		[1] CHUNG	85	SPEC	$8\,\pi^-p \to K\overline{K}\pi n$
1440 $^{+20}_{-15}$	174	[1] EDWARDS	82E	CBAL	$J/\psi \to \gamma K^+K^-\pi^0$
1440 $^{+10}_{-15}$		[1] SCHARRE	80	MRK2	$J/\psi \to \gamma K^0_S K^\pm\pi^\mp$
1425 ± 7	800	[1,3] BAILLON	67	HBC	$0\,\overline{p}p \to K\overline{K}\pi\pi\pi$

[1] These experiments identify only one pseudoscalar in the 1400–1500 range. Data could also refer to $\eta(1475)$.

[2] Systematic uncertainty not evaluated.

[3] From best fit of 0^{-+} partial wave , 50% $K^*(892)K$, 50% $a_0(980)\pi$.

$\eta(1405)$ WIDTH

VALUE (MeV)	DOCUMENT ID
50.1±2.6 OUR AVERAGE Includes data from the 2 datablocks that follow this one. Error includes scale factor of 1.7. See the ideogram below.	

Downloaded from https://academic.oup.com/ptep/article/2022/8/083C01/6651666 by KIT Library user on 27 September 2022

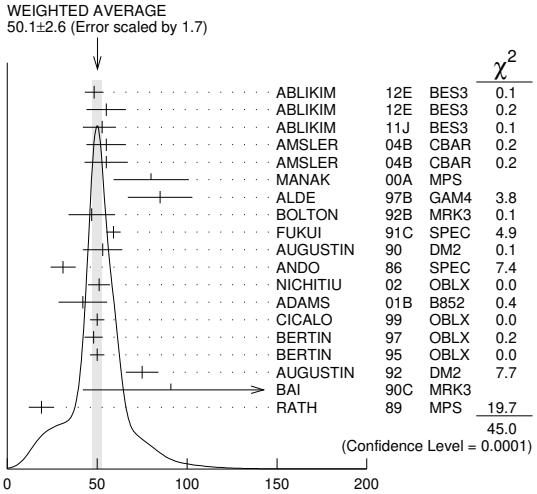

$\eta\pi\pi$ MODE

VALUE (MeV)	EVTS	DOCUMENT ID		TECN	COMMENT
The data in this block is included in the average printed for a previous datablock.					
52.6± 3.2 OUR AVERAGE	Error includes scale factor of 1.3. See the ideogram below.				
48.3± 5.2	743	ABLIKIM	12E	BES3	$J/\psi \to \gamma(\pi^+\pi^-\pi^0)$
55.0±11.0	198	ABLIKIM	12E	BES3	$J/\psi \to \gamma(\pi^0\pi^0\pi^0)$
$52.8\pm 7.6^{+0.1}_{-7.6}$		[1] ABLIKIM	11J	BES3	$J/\psi \to \omega(\eta\pi^+\pi^-)$
55 ±11	900	AMSLER	04B	CBAR	$0\,\overline{p}p \to \pi^+\pi^-\pi^+\pi^-\eta$
55 ±12	6.6k	AMSLER	04B	CBAR	$0\,\overline{p}p \to \pi^+\pi^-\pi^0\pi^0\gamma$
80 ±21	9.0k	MANAK	00A	MPS	$18\,\pi^-p \to \eta\pi^+\pi^-n$
85 ±18	2.2k	ALDE	97B	GAM4	$100\,\pi^-p \to \eta\pi^0\pi^0n$
47 ±13		[2] BOLTON	92B	MRK3	$J/\psi \to \gamma\eta\pi^+\pi^-$
59 ± 4		FUKUI	91C	SPEC	$8.95\,\pi^-p \to \eta\pi^+\pi^-n$
53 ±11		[3] AUGUSTIN	90	DM2	$J/\psi \to \gamma\eta\pi^+\pi^-$
31 ± 7		ANDO	86	SPEC	$8\,\pi^-p \to \eta\pi^+\pi^-n$
• • • We do not use the following data for averages, fits, limits, etc. • • •					
79.0±16.0	195	ABLIKIM	19BA	BES3	$e^+e^- \to \psi(2S)$
86 ±10		[4] AMSLER	95F	CBAR	$0\,\overline{p}p \to \pi^+\pi^-\pi^0\pi^0\eta$

[1] The selected process is $J/\psi \to \omega a_0(980)\pi$.
[2] From fit to the $a_0(980)\pi\ 0^{-+}$ partial wave.
[3] From $\eta\pi^+\pi^-$ mass distribution - mainly $a_0(980)\pi$ - no spin–parity determination available.
[4] Superseded by AMSLER 04B.

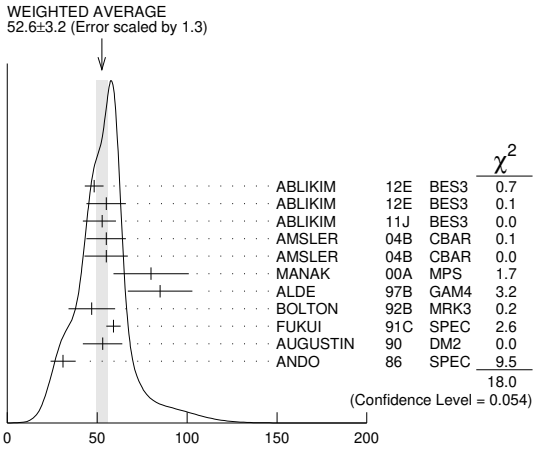

$K\overline{K}\pi$ MODE ($a_0(980)\pi$ or direct $K\overline{K}\pi$)

VALUE (MeV)	EVTS	DOCUMENT ID		TECN	COMMENT
The data in this block is included in the average printed for a previous datablock.					
48± 4 OUR AVERAGE	Error includes scale factor of 2.1. See the ideogram below.				
51± 6	3651	[1] NICHITIU	02	OBLX	$0\,\overline{p}p \to K^+K^-\pi^+\pi^-\pi^0$
42±10± 9	20k	ADAMS	01B	B852	18 GeV $\pi^-p \to K^+K^-\pi^0n$
50± 4		CICALO	99	OBLX	$0\,\overline{p}p \to K^\pm K^0_S\pi^\mp\pi^+\pi^-$
48± 5		[2] BERTIN	97	OBLX	$0.0\,\overline{p}p \to K^\pm(K^0)\pi^\mp\pi^+\pi^-$
50± 4		[2] BERTIN	95	OBLX	$0\,\overline{p}p \to K\overline{K}\pi\pi\pi$
75± 9		AUGUSTIN	92	DM2	$J/\psi \to \gamma K\overline{K}\pi$
91^{+67+15}_{-31-38}		[3] BAI	90C	MRK3	$J/\psi \to \gamma K^0_S K^\pm\pi^\mp$
19± 7		[3] RATH	89	MPS	$21.4\,\pi^-p \to nK^0_S K^0_S\pi^0$

[1] Decaying dominantly directly to $K^+K^-\pi^0$.
[2] Decaying into $(K\overline{K})_S\pi$, $(K\pi)_S\overline{K}$, and $a_0(980)\pi$.
[3] From fit to the $a_0(980)\pi\ 0^{-+}$ partial wave, but $a_0(980)\pi\ 1^{++}$ cannot be excluded.

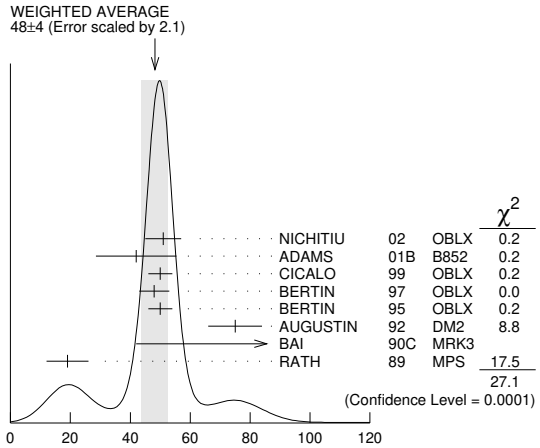

$\pi\pi\gamma$ MODE

VALUE (MeV)	EVTS	DOCUMENT ID		TECN	COMMENT
89 ±17 OUR AVERAGE	Error includes scale factor of 1.7.				
64 ±18	235 ± 91	AMSLER	04B	CBAR	$0\,\overline{p}p \to \pi^+\pi^-\pi^+\pi^-\gamma$
101.0± 8.8±8.8	547	BAI	04J	BES2	$J/\psi \to \gamma\gamma\pi^+\pi^-$
• • • We do not use the following data for averages, fits, limits, etc. • • •					
174 ±44		AUGUSTIN	90	DM2	$J/\psi \to \pi^+\pi^-\gamma\gamma$
90 ±26		[1] COFFMAN	90	MRK3	$J/\psi \to \pi^+\pi^-2\gamma$

[1] This peak in the $\gamma\rho$ channel may not be related to the $\eta(1405)$.

4π MODE

VALUE (MeV)	EVTS	DOCUMENT ID		TECN	COMMENT
• • • We do not use the following data for averages, fits, limits, etc. • • •					
160±30		BUGG	95	MRK3	$J/\psi \to \gamma\pi^+\pi^-\pi^+\pi^-$
144±13	3270	[1] BISELLO	89B	DM2	$J/\psi \to 4\pi\gamma$

[1] Estimated by us from various fits.

$K\overline{K}\pi$ MODE (unresolved)

VALUE (MeV)	EVTS	DOCUMENT ID		TECN	COMMENT
• • • We do not use the following data for averages, fits, limits, etc. • • •					
45.9± 8.2	191	[1,2] ABLIKIM	13M	BES3	$\psi(2S) \to \omega K K\pi$
48.9± 9.0	249 ± 35	[1,2] ABLIKIM	08E	BES2	$J/\psi \to \omega K^0_S K^+\pi^-$ + c.c.
34.2±18.5	62 ± 18	[1,2] ABLIKIM	08E	BES2	$J/\psi \to \omega K^+K^-\pi^0$
93 ±14	296	[1] AUGUSTIN	90	DM2	$J/\psi \to \gamma K^+K^-\pi^0$
105 ±10	693	[1] AUGUSTIN	90	DM2	$J/\psi \to \gamma K^0_S K^\pm\pi^\mp$
62 ±16	500	[1] DUCH	89	ASTE	$\overline{p}p \to K\overline{K}\pi\pi\pi$
100 ±11	170	[1] RATH	89	MPS	$21.4\,\pi^-p \to K^0_S K^0_S\pi^0n$
66 ± 2	8800	[1] BIRMAN	88	MPS	$8\,\pi^-p \to K^+\overline{K}^0\pi^-n$
60 ±10	620	[1] REEVES	86	SPEC	$6.6\,p\overline{p} \to KK\pi X$
60 ±10		[1] CHUNG	85	SPEC	$8\,\pi^-p \to K\overline{K}\pi n$
55^{+20}_{-30}	174	[1] EDWARDS	82E	CBAL	$J/\psi \to \gamma K^+K^-\pi^0$
50^{+30}_{-20}		[1] SCHARRE	80	MRK2	$J/\psi \to \gamma K^0_S K^\pm\pi^\mp$
80 ±10	800	[1,3] BAILLON	67	HBC	$0.0\,\overline{p}p \to K\overline{K}\pi\pi\pi$

[1] These experiments identify only one pseudoscalar in the 1400–1500 range. Data could also refer to $\eta(1475)$.
[2] Systematic uncertainty not evaluated.
[3] From best fit to 0^{-+} partial wave, 50% $K^*(892)K$, 50% $a_0(980)\pi$.

$\eta(1405)$ DECAY MODES

	Mode	Fraction (Γ_i/Γ)	Confidence level
Γ_1	$K\overline{K}\pi$	seen	
Γ_2	$\eta\pi\pi$	seen	
Γ_3	$a_0(980)\pi$	seen	
Γ_4	$\eta(\pi\pi)_S$-wave	seen	
Γ_5	$f_0(980)\pi^0 \to \pi^+\pi^-\pi^0$	not seen	
Γ_6	$f_0(980)\eta$	seen	

Downloaded from https://academic.oup.com/ptep/article/2022/8/083C01/6651666 by KIT Library user on 27 September 2022

Γ_7	4π	seen	
Γ_8	$\rho\rho$	<58 %	99.85%
Γ_9	$\gamma\gamma$		
Γ_{10}	$\rho^0\gamma$	seen	
Γ_{11}	$\phi\gamma$		
Γ_{12}	$K^*(892)K$	seen	

$\eta(1405)$ $\Gamma(i)\Gamma(\gamma\gamma)/\Gamma(\text{total})$

$\Gamma(K\overline{K}\pi) \times \Gamma(\gamma\gamma)/\Gamma_{\text{total}}$ — $\Gamma_1\Gamma_9/\Gamma$

VALUE (keV)	CL%	DOCUMENT ID		TECN	COMMENT
• • • We do not use the following data for averages, fits, limits, etc. • • •					
<0.035	90	[1,2] AHOHE	05	CLE2	10.6 $e^+e^- \to e^+e^- K^0_S K^\pm\pi^\mp$

[1] Using $\eta(1405)$ mass and width 1410 MeV and 51 MeV, respectively.
[2] Assuming three-body phase-space decay to $K^0_S K^\pm\pi^\mp$.

$\Gamma(\eta\pi\pi) \times \Gamma(\gamma\gamma)/\Gamma_{\text{total}}$ — $\Gamma_2\Gamma_9/\Gamma$

VALUE (keV)	CL%	DOCUMENT ID		TECN	COMMENT
<0.095	95	ACCIARRI	01G	L3	183–202 $e^+e^- \to e^+e^-\eta\pi^+\pi^-$

$\Gamma(\rho^0\gamma) \times \Gamma(\gamma\gamma)/\Gamma_{\text{total}}$ — $\Gamma_{10}\Gamma_9/\Gamma$

VALUE (keV)	CL%	DOCUMENT ID		TECN	COMMENT
• • • We do not use the following data for averages, fits, limits, etc. • • •					
<1.5	95	ALTHOFF	84E	TASS	$e^+e^- \to e^+e^-\pi^+\pi^-\gamma$

$\eta(1405)$ BRANCHING RATIOS

$\Gamma(\eta\pi\pi)/\Gamma(K\overline{K}\pi)$ — Γ_2/Γ_1

VALUE	CL%	DOCUMENT ID		TECN	COMMENT
1.09±0.48		[1] AMSLER	04B	CBAR	0 $\overline{p}p \to \pi^+\pi^-\pi^+\pi^-\eta$
• • • We do not use the following data for averages, fits, limits, etc. • • •					
<0.5	90	EDWARDS	83B	CBAL	$J/\psi \to \eta\pi\pi\gamma$
<1.1	90	SCHARRE	80	MRK2	$J/\psi \to \eta\pi\pi\gamma$
<1.5	95	FOSTER	68B	HBC	0.0 $\overline{p}p$

[1] Using the data of BAILLON 67 on $\overline{p}p \to K\overline{K}\pi$.

$\Gamma(\rho^0\gamma)/\Gamma(\eta\pi\pi)$ — Γ_{10}/Γ_2

VALUE	DOCUMENT ID		TECN	COMMENT
0.111±0.064	AMSLER	04B	CBAR	0 $\overline{p}p$

$\Gamma(a_0(980)\pi)/\Gamma(K\overline{K}\pi)$ — Γ_3/Γ_1

VALUE	EVTS	DOCUMENT ID		TECN	COMMENT
• • • We do not use the following data for averages, fits, limits, etc. • • •					
∼ 0.15		[1] BERTIN	95	OBLX	0 $\overline{p}p \to K\overline{K}\pi\pi\pi$
∼ 0.8	500	[1] DUCH	89	ASTE	$\overline{p}p \to \pi^+\pi^- K^\pm\pi^\mp K^0$
∼ 0.75		[1] REEVES	86	SPEC	6.6 $p\overline{p} \to K K\pi X$

[1] Assuming that the $a_0(980)$ decays only into $K\overline{K}$.

$\Gamma(a_0(980)\pi)/\Gamma(\eta\pi\pi)$ — Γ_3/Γ_2

VALUE	EVTS	DOCUMENT ID		TECN	COMMENT
• • • We do not use the following data for averages, fits, limits, etc. • • •					
0.29±0.10		ABELE	98E	CBAR	0 $p\overline{p} \to \eta\pi^0\pi^0\pi^0$
0.19±0.04	2200	[1] ALDE	97B	GAM4	100 $\pi^- p \to \eta\pi^0\pi^0 n$
0.56±0.04±0.03		[1] AMSLER	95F	CBAR	0 $\overline{p}p \to \pi^+\pi^-\pi^0\pi^0\eta$

[1] Assuming that the $a_0(980)$ decays only into $\eta\pi$.

$\Gamma(a_0(980)\pi)/\Gamma(\eta(\pi\pi)_{S\text{-wave}})$ — Γ_3/Γ_4

VALUE	EVTS	DOCUMENT ID		TECN	COMMENT
• • • We do not use the following data for averages, fits, limits, etc. • • •					
0.91±0.12		ANISOVICH	01	SPEC	0.0 $\overline{p}p \to \eta\pi^+\pi^-\pi^+\pi^-$
0.15±0.04	9082	[1] MANAK	00A	MPS	18 $\pi^- p \to \eta\pi^+\pi^- n$
0.70±0.12±0.20		[2] BAI	99	BES	$J/\psi \to \gamma\eta\pi^+\pi^-$

[1] Statistical error only.
[2] Assuming that the $a_0(980)$ decays only into $\eta\pi$.

$\Gamma(\rho^0\gamma)/\Gamma(K\overline{K}\pi)$ — Γ_{10}/Γ_1

VALUE	DOCUMENT ID		TECN	COMMENT
0.0152±0.0038	[1] COFFMAN	90	MRK3	$J/\psi \to \gamma\gamma\pi^+\pi^-$

[1] Using $B(J/\psi \to \gamma\eta(1405) \to \gamma K\overline{K}\pi)=4.2\times10^{-3}$ and $B(J/\psi \to \gamma\eta(1405) \to \gamma\gamma\rho^0)=6.4\times10^{-5}$.

$\Gamma(\gamma\gamma)/\Gamma(K\overline{K}\pi)$ — Γ_9/Γ_1

VALUE	CL%	DOCUMENT ID		TECN	COMMENT
<1.78 × 10^{-3}	90	[1] ABLIKIM	18O	BES3	$\psi(2S) \to \pi^+\pi^-\gamma\gamma\gamma$

[1] Using results from BAI 00D.

$\Gamma(\eta(\pi\pi)_{S\text{-wave}})/\Gamma(\eta\pi\pi)$ — Γ_4/Γ_2

VALUE	EVTS	DOCUMENT ID		TECN	COMMENT
• • • We do not use the following data for averages, fits, limits, etc. • • •					
0.81±0.04	2200	ALDE	97B	GAM4	100 $\pi^- p \to \eta\pi^0\pi^0 n$

$\Gamma(f_0(980)\eta)/\Gamma(\eta\pi\pi)$ — Γ_6/Γ_2

VALUE	DOCUMENT ID		TECN	COMMENT
• • • We do not use the following data for averages, fits, limits, etc. • • •				
0.32±0.07	[1] ANISOVICH	00	SPEC	0.9–1.2 $\overline{p}p \to \eta 3\pi^0$

[1] Using preliminary Crystal Barrel data.

$\Gamma(f_0(980)\pi^0 \to \pi^+\pi^-\pi^0)/\Gamma_{\text{total}}$ — Γ_5/Γ

VALUE	DOCUMENT ID		TECN	COMMENT
not seen	[1] ABLIKIM	17AJ	BES3	$\psi(2S) \to \gamma\pi^+\pi^-\pi^0$

[1] ABLIKIM 17AJ reports $B(\psi(2S) \to \gamma\eta(1405) \to \gamma f_0(980)\pi^0 \to \gamma\pi^+\pi^-\pi^0) < 5.0\times10^{-7}$.

$\Gamma(\rho\rho)/\Gamma_{\text{total}}$ — Γ_8/Γ

VALUE	CL%	DOCUMENT ID		TECN	COMMENT
<0.58	99.85	[1,2] AMSLER	04B	CBAR	0 $\overline{p}p$

[1] Assuming that the $\eta(1405)$ decays are saturated by the $\pi\pi\eta$, $K\overline{K}\pi$ and $\rho\rho$ modes.
[2] Using the data of BAILLON 67 on $\overline{p}p \to K\overline{K}\pi$.

$\Gamma(K^*(892)K)/\Gamma(a_0(980)\pi)$ — Γ_{12}/Γ_3

VALUE	DOCUMENT ID		TECN	COMMENT
• • • We do not use the following data for averages, fits, limits, etc. • • •				
0.084±0.024	[1] ADAMS	01B	B852	18 GeV $\pi^- p \to K^+K^-\pi^0 n$

[1] Statistical error only.

$\Gamma(\phi\gamma)/\Gamma(\rho^0\gamma)$ — Γ_{11}/Γ_{10}

VALUE	CL%	DOCUMENT ID		TECN	COMMENT
• • • We do not use the following data for averages, fits, limits, etc. • • •					
0.09±0.03		[1] ABLIKIM	18I	BES3	$J/\psi \to \gamma\gamma\phi(1020)$
0.13±0.04		[2] ABLIKIM	18I	BES3	$J/\psi \to \gamma\gamma\phi(1020)$
<0.77	95	[3] BAI	04J	BES2	$J/\psi \to \gamma\gamma K^+K^-$

[1] Constructive interference between $X(1835)$ and $\eta(1405)/\eta(1475)$ decays to $\gamma\phi$ is assumed. Also see $\eta(1475)$. ABLIKIM 18I reports the inverse as 11.10 ± 3.5.
[2] Destructive interference between $X(1835)$ and $\eta(1405)/\eta(1475)$ decays to $\gamma\phi$ is assumed. Also see $\eta(1475)$. ABLIKIM 18I reports the inverse as 7.53 ± 2.49.
[3] Calculated by us from $B(J/\psi \to \eta(1405)\gamma \to \phi\gamma\gamma) < 0.82\times10^{-4}$ and $B(J/\psi \to \eta(1405)\gamma \to \rho^0\gamma\gamma) = (1.07 \pm 0.17 \pm 0.11)\times10^{-4}$.

$\eta(1405)$ REFERENCES

ABLIKIM	19BA	PR D100 092003	M. Ablikim et al.	(BESIII Collab.)
ABLIKIM	18I	PR D97 051101	M. Ablikim et al.	(BESIII Collab.)
ABLIKIM	18O	PR D97 072014	M. Ablikim et al.	(BESIII Collab.)
ABLIKIM	17AJ	PR D96 112008	M. Ablikim et al.	(BESIII Collab.)
ABLIKIM	13M	PR D87 092006	M. Ablikim et al.	(BESIII Collab.)
ABLIKIM	12E	PRL 108 182001	M. Ablikim et al.	(BESIII Collab.)
ABLIKIM	11J	PRL 107 182001	M. Ablikim et al.	(BESIII Collab.)
ABLIKIM	08E	PR D77 032005	M. Ablikim et al.	(BES Collab.)
AHOHE	05	PR D71 072001	R. Ahohe et al.	(CLEO Collab.)
AMSLER	04B	EPJ C33 23	C. Amsler et al.	(Crystal Barrel Collab.)
BAI	04J	PL B594 47	J.Z. Bai et al.	(BES Collab.)
NICHITIU	02	PL B545 261	F. Nichitiu et al.	(OBELIX Collab.)
ACCIARRI	01G	PL B501 1	M. Acciarri et al.	(L3 Collab.)
ADAMS	01B	PL B516 264	G.S. Adams et al.	(BNL E852 Collab.)
ANISOVICH	01	NP A690 567	A.V. Anisovich et al.	
ANISOVICH	00	PL B472 168	A.V. Anisovich et al.	
BAI	00D	PL B476 25	J.Z. Bai et al.	(BES Collab.)
MANAK	00A	PR D62 012003	J.J. Manak et al.	(BNL E852 Collab.)
BAI	99	PL B446 356	J.Z. Bai et al.	(BES Collab.)
CICALO	99	PL B462 453	C. Cicalo et al.	(OBELIX Collab.)
ABELE	98E	NP B514 45	A. Abele et al.	(Crystal Barrel Collab.)
BAI	98C	PL B440 217	J.Z. Bai et al.	(BES Collab.)
ALDE	97B	PAN 60 386	D. Alde et al.	(GAMS Collab.)
		Translated from YAF 60 458.		
BERTIN	97	PL B400 226	A. Bertin et al.	(OBELIX Collab.)
AMSLER	95F	PL B358 389	C. Amsler et al.	(Crystal Barrel Collab.)
BERTIN	95	PL B361 187	A. Bertin et al.	(OBELIX Collab.)
BUGG	95	PL B353 378	D.V. Bugg et al.	(LOQM, PNPI, WASH)
AUGUSTIN	92	PR D46 1951	J.E. Augustin, G. Cosme	(DM2 Collab.)
BOLTON	92B	PRL 69 1328	T. Bolton et al.	(Mark III Collab.)
FUKUI	91C	PL B267 293	S. Fukui et al.	(SUGI, NAGO, KEK, KYOT+)
AUGUSTIN	90	PR D42 10	J.E. Augustin et al.	(DM2 Collab.)
BAI	90C	PRL 65 2507	Z. Bai et al.	(Mark III Collab.)
COFFMAN	90	PR D41 1410	D.M. Coffman et al.	(Mark III Collab.)
BISELLO	89B	PR D39 701	G. Busetto et al.	(DM2 Collab.)
DUCH	89	ZPHY C45 223	K.D. Duch et al.	(ASTERIX Collab.) JP
RATH	89	PR D40 693	M.G. Rath et al.	(NDAM, BRAN, BNL, CUNY+)
BIRMAN	88	PRL 61 1557	A. Birman et al.	(BNL, FSU, IND, MASD) JP
ANDO	86	PRL 57 1296	A. Ando et al.	(KEK, KYOT, NIRS, SAGA+) IJP
REEVES	86	PR D34 1960	D.F. Reeves et al.	(FLOR, BNL, IND+) JP
CHUNG	85	PRL 55 779	S.U. Chung et al.	(BNL, FLOR, IND+) JP
ALTHOFF	84E	PL 147B 487	M. Althoff et al.	(TASSO Collab.)
EDWARDS	83B	PRL 51 859	C. Edwards et al.	(CIT, HARV, PRIN+)
EDWARDS	82E	PRL 49 259	C. Edwards et al.	(CIT, HARV, PRIN+)
Also		PRL 50 219	C. Edwards et al.	(CIT, HARV, PRIN+)
SCHARRE	80	PL 97B 329	D.L. Scharre et al.	(SLAC, LBL)
FOSTER	68B	NP B8 174	M. Foster et al.	(CERN, CDEF)
BAILLON	67	NC 50A 393	P.H. Baillon et al.	(CERN, CDEF, IRAD)

$h_1(1415)$

$I^G(J^{PC}) = 0^-(1^{+-})$

was $h_1(1380)$

$h_1(1415)$ MASS

VALUE (MeV)	EVTS	DOCUMENT ID		TECN	COMMENT
1416± 8 OUR AVERAGE		Error includes scale factor of 1.5. See the ideogram below.			
1423± 2.1±7.3	2.2k	[1] ABLIKIM	18AB	BES3	$J/\psi \to \eta' h_1 \to \eta' K^*\overline{K}$

Downloaded from https://academic.oup.com/ptep/article/2022/8/083C01/6651666 by KIT Library user on 27 September 2022

1412± 4 ±8	[1] ABLIKIM	15M	BES3	$\psi(2S) \to \gamma\chi_{c1,2} \to \gamma\phi(h_1 \to K^*\overline{K})$
1440±60	ABELE	97H	CBAR	$\overline{p}p \to K^0_L K^0_S \pi^0\pi^0$
1380±20	ASTON	88C	LASS	11 $K^- p \to K^0_S K^\pm\pi^\mp \Lambda$

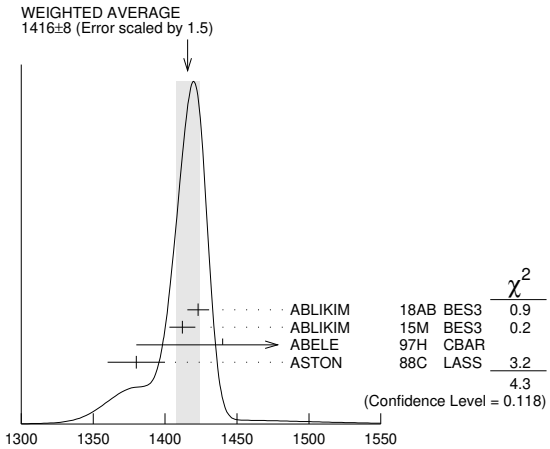

[1] Final states $K^+K^-\pi^0$ and $K^0_S K^\pm\pi^\mp$.

$h_1(1415)$ WIDTH

VALUE (MeV)	EVTS	DOCUMENT ID		TECN	COMMENT
90 ±15 OUR AVERAGE					
90.3± 9.8±17.5	2.2k	[1] ABLIKIM	18AB	BES3	$J/\psi \to \eta' h_1 \to \eta' K^*\overline{K}$
84 ±12 ±40		[1] ABLIKIM	15M	BES3	$\psi(2S) \to \gamma\chi_{c1,2} \to \gamma\phi(h_1 \to K^*\overline{K})$
170 ±80		ABELE	97H	CBAR	$\overline{p}p \to K^0_L K^0_S \pi^0\pi^0$
80 ±30		ASTON	88C	LASS	11 $K^- p \to K^0_S K^\pm\pi^\mp \Lambda$

[1] Final states $K^+K^-\pi^0$ and $K^0_S K^\pm\pi^\mp$.

$h_1(1415)$ DECAY MODES

	Mode
Γ_1	$K\overline{K}^*(892)+$ c.c.

$h_1(1415)$ REFERENCES

ABLIKIM	18AB	PR D98 072005	M. Ablikim *et al.*	(BESIII Collab.)
ABLIKIM	15M	PR D91 112008	M. Ablikim *et al.*	(BESIII Collab.)
ABELE	97H	PL B415 280	A. Abele *et al.*	(Crystal Barrel Collab.)
ASTON	88C	PL B201 573	D. Aston *et al.*	(SLAC, NAGO, CINC, INUS)

$f_1(1420)$

$I^G(J^{PC}) = 0^+(1^{++})$

See the review on "Spectroscopy of Light Meson Resonances."

$f_1(1420)$ MASS

VALUE (MeV)	EVTS	DOCUMENT ID		TECN	COMMENT
1426.3± 0.9 OUR AVERAGE		Error includes scale factor of 1.1.			
1434 ± 5 ± 5	133	[1] ACHARD	07	L3	183–209 $e^+e^- \to e^+e^- K^0_S K^\pm\pi^\mp$
1426 ± 6	711	ABDALLAH	03H	DLPH	91.2 $e^+e^- \to K^0_S K^\pm\pi^\mp + X$
1420 ±14	3651	NICHITIU	02	OBLX	0 $\overline{p}p \to K^+K^-\pi^+\pi^-\pi^0$
1428 ± 4 ± 2	20k	ADAMS	01B	B852	18 GeV $\pi^- p \to K^+K^-\pi^0 n$
1426 ± 1		BARBERIS	97C	OMEG	450 $pp \to pp K^0_S K^\pm\pi^\mp$
1425 ± 8		BERTIN	97	OBLX	0.0 $\overline{p}p \to K^\pm(K^0)\pi^\mp\pi^+\pi^-$
1430 ± 4		[2] ARMSTRONG	92E	OMEG	85,300 π^+p, $pp \to \pi^+p$, $pp(K\overline{K}\pi)$
1462 ±20		[3] AUGUSTIN	92	DM2	$J/\psi \to \gamma K\overline{K}\pi$
1443 $^{+7}_{-6}$ $^{+3}_{-2}$	1100	BAI	90C	MRK3	$J/\psi \to \gamma K^0_S K^\pm\pi^\mp$
1425 ±10	17	BEHREND	89	CELL	$\gamma\gamma \to K^0_S K^\pm\pi^\mp$
1442 ± 5 $^{+10}_{-17}$	111	BECKER	87	MRK3	e^+e^-, $\omega K\overline{K}\pi$
1423 ± 4		GIDAL	87B	MRK2	$e^+e^- \to e^+e^- K\overline{K}\pi$
1417 ±13	13	AIHARA	86C	TPC	$e^+e^- \to e^+e^- K\overline{K}\pi$
1422 ± 3		CHAUVAT	84	SPEC	ISR 31.5 pp
1440 ±10		[4] BROMBERG	80	SPEC	100 $\pi^- p \to K\overline{K}\pi X$
1426 ± 6	221	DIONISI	80	HBC	4 $\pi^- p \to K\overline{K}\pi n$
1420 ±20		DAHL	67	HBC	1.6–4.2 $\pi^- p$
• • • We do not use the following data for averages, fits, limits, etc. • • •					
1430.8± 0.9		[5] SOSA	99	SPEC	$pp \to p_{slow}(K^0_S K^+\pi^-)\, p_{fast}$
1433.4± 0.8		[5] SOSA	99	SPEC	$pp \to p_{slow}(K^0_S K^-\pi^+)\, p_{fast}$
1435 ± 9		PROKOSHKIN	97B	GAM4	100 $\pi^- p \to \eta\pi^0\pi^0 n$
1429 ± 3	389	ARMSTRONG	89	OMEG	300 $pp \to K\overline{K}\pi pp$
1425 ± 2	1520	ARMSTRONG	84	OMEG	85 π^+p, $pp \to (\pi^+,p)(K\overline{K}\pi)p$
~ 1420		BITYUKOV	84	SPEC	32 $K^- p \to K^+K^-\pi^0 Y$

[1] From a fit with a width fixed at 55 MeV.
[2] This result supersedes ARMSTRONG 84, ARMSTRONG 89.
[3] From fit to the $K^*(892)K$ 1^{++} partial wave.
[4] Mass error increased to account for $a_0(980)$ mass cut uncertainties.
[5] No systematic error given.

$f_1(1420)$ WIDTH

VALUE (MeV)	EVTS	DOCUMENT ID		TECN	COMMENT
54.5± 2.6 OUR AVERAGE					
51 ±14	711	ABDALLAH	03H	DLPH	91.2 $e^+e^- \to K^0_S K^\pm\pi^\mp + X$
61 ± 8	3651	NICHITIU	02	OBLX	0 $\overline{p}p \to K^+K^-\pi^+\pi^-\pi^0$
38 ± 9 ± 6	20k	ADAMS	01B	B852	18 GeV $\pi^- p \to K^+K^-\pi^0 n$
58 ± 4		BARBERIS	97C	OMEG	450 $pp \to pp K^0_S K^\pm\pi^\mp$
45 ±10		BERTIN	97	OBLX	0.0 $\overline{p}p \to K^\pm(K^0)\pi^\mp\pi^+\pi^-$
58 ±10		[6] ARMSTRONG	92E	OMEG	85,300 π^+p, $pp \to \pi^+p$, $pp(K\overline{K}\pi)$
129 ±41		[7] AUGUSTIN	92	DM2	$J/\psi \to \gamma K\overline{K}\pi$
68 $^{+29}_{-18}$ $^{+8}_{-9}$	1100	BAI	90C	MRK3	$J/\psi \to \gamma K^0_S K^\pm\pi^\mp$
42 ±22	17	BEHREND	89	CELL	$\gamma\gamma \to K^0_S K^\pm\pi^\mp$
40 $^{+17}_{-13}$ ±5	111	BECKER	87	MRK3	$e^+e^- \to \omega K\overline{K}\pi$
35 $^{+47}_{-20}$	13	AIHARA	86C	TPC	$e^+e^- \to e^+e^- K\overline{K}\pi$
47 ±10		CHAUVAT	84	SPEC	ISR 31.5 pp
62 ±14		BROMBERG	80	SPEC	100 $\pi^- p \to K\overline{K}\pi X$
40 ±15	221	DIONISI	80	HBC	4 $\pi^- p \to K\overline{K}\pi n$
60 ±20		DAHL	67	HBC	1.6–4.2 $\pi^- p$
• • • We do not use the following data for averages, fits, limits, etc. • • •					
68.7± 2.9		[8] SOSA	99	SPEC	$pp \to p_{slow}(K^0_S K^+\pi^-)\, p_{fast}$
58.8± 3.3		[8] SOSA	99	SPEC	$pp \to p_{slow}(K^0_S K^-\pi^+)\, p_{fast}$
90 ±25		PROKOSHKIN	97B	GAM4	100 $\pi^- p \to \eta\pi^0\pi^0 n$
58 ± 8	389	ARMSTRONG	89	OMEG	300 $pp \to K\overline{K}\pi pp$
62 ± 5	1520	ARMSTRONG	84	OMEG	85 π^+p, $pp \to (\pi^+,p)(K\overline{K}\pi)p$
~ 50		BITYUKOV	84	SPEC	32 $K^- p \to K^+K^-\pi^0 Y$

[6] This result supersedes ARMSTRONG 84, ARMSTRONG 89.
[7] From fit to the $K^*(892)K$ 1^{++} partial wave.
[8] No systematic error given.

$f_1(1420)$ DECAY MODES

	Mode	Fraction (Γ_i/Γ)
Γ_1	$K\overline{K}\pi$	seen
Γ_2	$K\overline{K}^*(892)+$ c.c.	seen
Γ_3	$\eta\pi\pi$	possibly seen
Γ_4	$a_0(980)\pi$	
Γ_5	$\pi\pi\rho$	
Γ_6	4π	
Γ_7	$\rho^0\gamma$	
Γ_8	$\phi\gamma$	seen

Downloaded from https://academic.oup.com/ptep/article/2022/8/083C01/6651666 by KIT Library user on 27 September 2022

$f_1(1420)$ $\Gamma(i)\Gamma(\gamma\gamma)/\Gamma(\text{total})$

$\Gamma(K\overline{K}\pi) \times \Gamma(\gamma\gamma^*)/\Gamma_{\text{total}}$

VALUE (keV)	CL%	EVTS	DOCUMENT ID		TECN	COMMENT
1.9±0.4 OUR AVERAGE						
3.2±0.6±0.7		133	[9,10] ACHARD	07	L3	183–209 $e^+e^- \to e^+e^- K^0_S K^\pm \pi^\mp$
3.0±0.9±0.7			[11,12] BEHREND	89	CELL	$e^+e^- \to e^+e^- K^0_S K\pi$
$2.3^{+1.0}_{-0.9}\pm0.8$			HILL	89	JADE	$e^+e^- \to e^+e^- K^\pm K^0_S \pi^\mp$
1.3±0.5±0.3			AIHARA	88B	TPC	$e^+e^- \to e^+e^- K^\pm K^0_S \pi^\mp$
1.6±0.7±0.3			[11,13] GIDAL	87B	MRK2	$e^+e^- \to e^+e^- K\overline{K}\pi$
• • • We do not use the following data for averages, fits, limits, etc. • • •						
<8.0	95		JENNI	83	MRK2	$e^+e^- \to e^+e^- K\overline{K}\pi$

[9] From a fit with a width fixed at 55 MeV.
[10] The form factor parameter from the fit is 926 ± 78 MeV.
[11] Assume a ρ-pole form factor.
[12] A ϕ - pole form factor gives considerably smaller widths.
[13] Published value divided by 2.

$f_1(1420)$ BRANCHING RATIOS

$\Gamma(K\overline{K}^*(892)+\text{c.c.})/\Gamma(K\overline{K}\pi)$ — Γ_2/Γ_1

VALUE	DOCUMENT ID		TECN	COMMENT
• • • We do not use the following data for averages, fits, limits, etc. • • •				
0.76±0.06	BROMBERG	80	SPEC	100 $\pi^- p \to K\overline{K}\pi X$
0.86±0.12	DIONISI	80	HBC	4 $\pi^- p \to K\overline{K}\pi n$

$\Gamma(\pi\pi\rho)/\Gamma(K\overline{K}\pi)$ — Γ_5/Γ_1

VALUE	CL%	DOCUMENT ID		TECN	COMMENT
• • • We do not use the following data for averages, fits, limits, etc. • • •					
<0.3	95	CORDEN	78	OMEG	12–15 $\pi^- p$
<2.0		DAHL	67	HBC	1.6–4.2 $\pi^- p$

$\Gamma(\eta\pi\pi)/\Gamma(K\overline{K}\pi)$ — Γ_3/Γ_1

VALUE	CL%	DOCUMENT ID		TECN	COMMENT
<0.1	95	ARMSTRONG	91B	OMEG	300 $pp \to pp\eta\pi^+\pi^-$
• • • We do not use the following data for averages, fits, limits, etc. • • •					
1.35±0.75		KOPKE	89	MRK3	$J/\psi \to \omega\eta\pi\pi(K\overline{K}\pi)$
<0.6	90	GIDAL	87	MRK2	$e^+e^- \to e^+e^-\eta\pi^+\pi^-$
<0.5	95	CORDEN	78	OMEG	12–15 $\pi^- p$
1.5 ±0.8		DEFOIX	72	HBC	0.7 $\overline{p}p$

$\Gamma(a_0(980)\pi)/\Gamma(\eta\pi\pi)$ — Γ_4/Γ_3

VALUE	CL%	DOCUMENT ID		TECN	COMMENT
• • • We do not use the following data for averages, fits, limits, etc. • • •					
>0.1	90	PROKOSHKIN	97B	GAM4	100 $\pi^- p \to \eta\pi^0\pi^0 n$
not seen in either mode		ANDO	86	SPEC	8 $\pi^- p$
not seen in either mode		CORDEN	78	OMEG	12–15 $\pi^- p$
0.4±0.2		DEFOIX	72	HBC	0.7 $\overline{p}p \to 7\pi$

$\Gamma(4\pi)/\Gamma(K\overline{K}^*(892)+\text{c.c.})$ — Γ_6/Γ_2

VALUE	CL%	DOCUMENT ID		TECN	COMMENT
• • • We do not use the following data for averages, fits, limits, etc. • • •					
<0.90	95	DIONISI	80	HBC	4 $\pi^- p$

$\Gamma(K\overline{K}\pi)/[\Gamma(K\overline{K}^*(892)+\text{c.c.})+\Gamma(a_0(980)\pi)]$ — $\Gamma_1/(\Gamma_2+\Gamma_4)$

VALUE	DOCUMENT ID		TECN	COMMENT
• • • We do not use the following data for averages, fits, limits, etc. • • •				
0.65±0.27	[14] DIONISI	80	HBC	4 $\pi^- p$

[14] Calculated using $\Gamma(K\overline{K})/\Gamma(\eta\pi) = 0.24 \pm 0.07$ for $a_0(980)$ fractions.

$\Gamma(a_0(980)\pi)/\Gamma(K\overline{K}^*(892)+\text{c.c.})$ — Γ_4/Γ_2

VALUE	CL%	DOCUMENT ID		TECN	COMMENT
0.042±0.014 OUR AVERAGE					
0.44 ±0.19		ABLIKIM	21U	BES3	$D_s^+ \to f_1(1420)\pi^+$
0.04 ±0.01 ±0.01		BARBERIS	98C	OMEG	450 $pp \to p_f f_1(1420) p_s$
• • • We do not use the following data for averages, fits, limits, etc. • • •					
<0.04	68	ARMSTRONG	84	OMEG	85 $\pi^+ p$

$\Gamma(4\pi)/\Gamma(K\overline{K}\pi)$ — Γ_6/Γ_1

VALUE	CL%	DOCUMENT ID		TECN	COMMENT
<0.62	95	ARMSTRONG	89G	OMEG	85 $\pi p \to 4\pi X$

$\Gamma(\rho^0\gamma)/\Gamma_{\text{total}}$ — Γ_7/Γ

VALUE	CL%	DOCUMENT ID		TECN	COMMENT
<0.08	95	[15] ARMSTRONG	92C	SPEC	300 $pp \to pp\pi^+\pi^-\gamma$

[15] Using the data on the $\overline{K}K\pi$ mode from ARMSTRONG 89.

$\Gamma(\rho^0\gamma)/\Gamma(K\overline{K}\pi)$ — Γ_7/Γ_1

VALUE	CL%	DOCUMENT ID		TECN	COMMENT
<0.02	95	BARBERIS	98C	OMEG	450 $pp \to p_f f_1(1420) p_s$

$\Gamma(\phi\gamma)/\Gamma(K\overline{K}\pi)$ — Γ_8/Γ_1

VALUE	DOCUMENT ID		TECN	COMMENT
0.003±0.001±0.001	BARBERIS	98C	OMEG	450 $pp \to p_f f_1(1420) p_s$

$f_1(1420)$ REFERENCES

ABLIKIM	21U	PR D104 032011	M. Ablikim et al.	(BESIII Collab.)
ACHARD	07	JHEP 0703 018	P. Achard et al.	(L3 Collab.)
ABDALLAH	03H	PL B569 129	J. Abdallah et al.	(DELPHI Collab.)
NICHITIU	02	PL B545 261	F. Nichitiu et al.	(OBELIX Collab.)
ADAMS	01B	PL B516 264	G.S. Adams et al.	(BNL E852 Collab.)
SOSA	99	PRL 83 913	M. Sosa et al.	
BARBERIS	98C	PL B440 225	D. Barberis et al.	(WA 102 Collab.)
BARBERIS	97C	PL B413 225	D. Barberis et al.	(WA 102 Collab.)
BERTIN	97	PL B400 226	A. Bertin et al.	(OBELIX Collab.)
PROKOSHKIN	97B	PD 42 298	Yu.D. Prokoshkin, S.A. Sadovsky	
		Translated from DANS 354 751.		
ARMSTRONG	92C	ZPHY C54 371	T.A. Armstrong et al.	(ATHU, BARI, BIRM+)
ARMSTRONG	92E	ZPHY C56 29	T.A. Armstrong et al.	(ATHU, BARI, BIRM+) JPC
AUGUSTIN	92	PR D46 1951	J.E. Augustin, G. Cosme	(DM2 Collab.)
ARMSTRONG	91B	ZPHY C52 389	T.A. Armstrong et al.	(ATHU, BARI, BIRM+)
BAI	90C	PRL 65 2507	Z. Bai et al.	(Mark III Collab.)
ARMSTRONG	89	PL B221 216	T.A. Armstrong et al.	(CERN, CDEF, BIRM+) JPC
ARMSTRONG	89G	ZPHY C43 55	T.A. Armstrong et al.	(CERN, BIRM, BARI+)
BEHREND	89	ZPHY C42 367	H.J. Behrend et al.	(CELLO Collab.)
HILL	89	ZPHY C42 355	P. Hill et al.	(JADE Collab.) JP
KOPKE	89	PRPL 174 67	L. Kopke et al.	(CERN)
AIHARA	88B	PL B209 107	H. Aihara et al.	(TPC-2γ Collab.)
BECKER	87	PRL 59 186	J.J. Becker et al.	(Mark III Collab.) JP
GIDAL	87	PRL 59 2012	G. Gidal et al.	(LBL, SLAC, HARV)
GIDAL	87B	PRL 59 2016	G. Gidal et al.	(LBL, SLAC, HARV)
AIHARA	86C	PRL 57 2500	H. Aihara et al.	(TPC-2γ Collab.) JP
ANDO	86	PRL 57 1296	A. Ando et al.	(KEK, KYOT, NIRS, SAGA+)
ARMSTRONG	84	PL 146B 273	T.A. Armstrong et al.	(ATHU, BARI, BIRM+) JP
BITYUKOV	84	SJNP 39 735	S. Bityukov et al.	(SERP)
		Translated from YAF 39 1165.		
CHAUVAT	84	PL 148B 382	P. Chauvat et al.	(CERN, CLER, UCLA+)
JENNI	83	PR D27 1031	P. Jenni et al.	(SLAC, LBL)
BROMBERG	80	PR D22 1513	C.M. Bromberg et al.	(CIT, FNAL, ILLC+)
DIONISI	80	NP B169 1	C. Dionisi et al.	(CERN, MADR, CDEF+) IJP
CORDEN	78	NP B144 253	M.J. Corden et al.	(BIRM, RHEL, TELA+)
DEFOIX	72	NP B44 125	C. Defoix et al.	(CDEF, CERN)
DAHL	67	PR 163 1377	O.I. Dahl et al.	(LRL) IJP
Also		PRL 14 1074	D.H. Miller et al.	(LRL, UCB)

$\omega(1420)$

$I^G(J^{PC}) = 0^-(1^{--})$

See also the $\omega(1650)$ particle listing.

$\omega(1420)$ MASS

VALUE (MeV)	EVTS	DOCUMENT ID		TECN	COMMENT
1410± 60 OUR ESTIMATE					
• • • We do not use the following data for averages, fits, limits, etc. • • •					
1418± 30± 10	824	[1] AKHMETSHIN	17A	CMD3	1.4–2.0 $e^+e^- \to \omega\eta$
1470± 50	13.1k	[2] AULCHENKO	15A	SND	1.05–1.80 $e^+e^- \to \pi^+\pi^-\pi^0$
1382± 23± 70		AUBERT	07AU	BABR	10.6 $e^+e^- \to \omega\pi^+\pi^-\gamma$
1350± 20± 20		AUBERT,B	04N	BABR	10.6 $e^+e^- \to \pi^+\pi^-\pi^0\gamma$
1400± 50±130	1.2M	[3] ACHASOV	03D	RVUE	0.44–2.00 $e^+e^- \to \pi^+\pi^-\pi^0$
1450± 10		[4] HENNER	02	RVUE	1.2–2.0 $e^+e^- \to \rho\pi, \omega\pi\pi$
1373± 70	177	[5] AKHMETSHIN	00D	CMD2	1.2–1.38 $e^+e^- \to \omega\pi^+\pi^-$
1370± 25	5095	ANISOVICH	00H	SPEC	0.0 $p\overline{p} \to \omega\pi^0\pi^0\pi^0$
1400^{+100}_{-200}		[6] ACHASOV	98H	RVUE	$e^+e^- \to \pi^+\pi^-\pi^0$
~ 1400		[7] ACHASOV	98H	RVUE	$e^+e^- \to \omega\pi^+\pi^-$
~ 1460		[8] ACHASOV	98H	RVUE	$e^+e^- \to K^+K^-$
1440± 70		[9] CLEGG	94	RVUE	
1419± 31	315	[10] ANTONELLI	92	DM2	1.34–2.4 $e^+e^- \to \rho\pi$

[1] From a fit of the interfering $\omega(1420)$ and $\omega(1650)$ with a relative phase of π and other parameters floating.
[2] From a fit with contributions from $\omega(782)$, $\phi(1020)$, $\omega(1420)$, and $\omega(1650)$. See ACHASOV 20A for a further analysis of the $\pi^+\pi^-\pi^0$ data.
[3] From the combined fit of ANTONELLI 92, ACHASOV 01E, ACHASOV 02E, and ACHASOV 03D data on the $\pi^+\pi^-\pi^0$ and ANTONELLI 92 on the $\omega\pi^+\pi^-$ final states. Supersedes ACHASOV 99E and ACHASOV 02E.
[4] Using results of CORDIER 81 and preliminary data of DOLINSKY 91 and ANTONELLI 92.
[5] Using the data of AKHMETSHIN 00D and ANTONELLI 92. The $\rho\pi$ dominance for the energy dependence of the $\omega(1420)$ and $\omega(1650)$ width assumed.
[6] Using data from BARKOV 87, DOLINSKY 91, and ANTONELLI 92.
[7] Using the data from ANTONELLI 92.
[8] Using the data from IVANOV 81 and BISELLO 88B.
[9] From a fit to two Breit-Wigner functions and using the data of DOLINSKY 91 and ANTONELLI 92.
[10] From a fit to two Breit-Wigner functions interfering between them and with the ω,ϕ tails with fixed (+,−,+) phases.

Downloaded from https://academic.oup.com/ptep/article/2022/8/083C01/6651666 by KIT Library user on 27 September 2022

$\omega(1420)$ WIDTH

VALUE (MeV)	EVTS	DOCUMENT ID		TECN	COMMENT
290±190 OUR ESTIMATE					
• • • We do not use the following data for averages, fits, limits, etc. • • •					
440±125	267	[1] ACHASOV	20B	SND	$e^+e^- \to \omega\eta \to \eta\pi^0\gamma$
104± 35± 10	824	[2] AKHMETSHIN	17A	CMD3	1.4–2.0 $e^+e^- \to \omega\eta$
880±170	13.1k	[3] AULCHENKO	15A	SND	1.05–1.80 $e^+e^- \to \pi^+\pi^-\pi^0$
480±180		[4] ACHASOV	10D	SND	1.075–2.0 $e^+e^- \to \pi^0\gamma$
130± 50±100		AUBERT	07AU	BABR	10.6 $e^+e^- \to \omega\pi^+\pi^-\gamma$
450± 70± 70		AUBERT,B	04N	BABR	10.6 $e^+e^- \to \pi^+\pi^-\pi^0\gamma$
870^{+500}_{-300}±450	1.2M	[5] ACHASOV	03D	RVUE	0.44–2.00 $e^+e^- \to \pi^+\pi^-\pi^0$
199± 15		[6] HENNER	02	RVUE	1.2–2.0 $e^+e^- \to \rho\pi, \omega\pi\pi$
188± 45	177	[7] AKHMETSHIN	00D	CMD2	1.2–1.38 $e^+e^- \to \omega\pi^+\pi^-$
360^{+100}_{-60}	5095	ANISOVICH	00H	SPEC	0.0 $p\overline{p} \to \omega\pi^0\pi^0\pi^0$
240± 70		[8] CLEGG	94	RVUE	
174± 59	315	[9] ANTONELLI	92	DM2	1.34–2.4 $e^+e^- \to \rho\pi$

[1] From a fit with contributions from $\omega(1420)$, $\omega(1650)$, and $\phi(1680)$. The mass of $\omega(1420)$ is fixed to the PDG 18 value of 1420 MeV.
[2] From a fit of the interfering $\omega(1420)$ and $\omega(1650)$ with a relative phase of π and other parameters floating.
[3] From a fit with contributions from $\omega(782)$, $\phi(1020)$, $\omega(1420)$, and $\omega(1650)$. See ACHASOV 20A for a further analysis of the $\pi^+\pi^-\pi^0$ data.
[4] From a fit of a VMD model with two effective resonances with masses of 1450 MeV and 1700 MeV to describe the excited vector states $\omega(1420)$, $\rho(1450)$, $\omega(1650)$, and $\rho(1700)$. Systematic errors not evaluated.
[5] From the combined fit of ANTONELLI 92, ACHASOV 01E, ACHASOV 02E, and ACHASOV 03D data on the $\pi^+\pi^-\pi^0$ and ANTONELLI 92 on the $\omega\pi^+\pi^-$ final states. Supersedes ACHASOV 99E and ACHASOV 02E.
[6] Using results of CORDIER 81 and preliminary data of DOLINSKY 91 and ANTONELLI 92.
[7] Using the data of AKHMETSHIN 00D and ANTONELLI 92. The $\rho\pi$ dominance for the energy dependence of the $\omega(1420)$ and $\omega(1650)$ width assumed.
[8] From a fit to two Breit-Wigner functions and using the data of DOLINSKY 91 and ANTONELLI 92.
[9] From a fit to two Breit-Wigner functions interfering between them and with the ω,ϕ tails with fixed $(+,-,+)$ phases.

$\omega(1420)$ DECAY MODES

	Mode	Fraction (Γ_i/Γ)
Γ_1	$\rho\pi$	seen
Γ_2	$\omega\pi\pi$	seen
Γ_3	$\omega\eta$	
Γ_4	$b_1(1235)\pi$	seen
Γ_5	e^+e^-	seen
Γ_6	$\pi^0\gamma$	

$\omega(1420)$ $\Gamma(i)\Gamma(e^+e^-)/\Gamma^2(\text{total})$

$\Gamma(\rho\pi)/\Gamma_{\text{total}} \times \Gamma(e^+e^-)/\Gamma_{\text{total}}$ — $\Gamma_1/\Gamma \times \Gamma_5/\Gamma$

VALUE (units 10^{-6})	EVTS	DOCUMENT ID		TECN	COMMENT
• • • We do not use the following data for averages, fits, limits, etc. • • •					
0.73 ±0.08	13.1k	[1] AULCHENKO	15A	SND	1.05–1.80 $e^+e^- \to \pi^+\pi^-\pi^0$
0.82 ±0.05 ±0.06		AUBERT,B	04N	BABR	10.6 $e^+e^- \to \pi^+\pi^-\pi^0\gamma$
0.65 ±0.13 ±0.21	1.2M	[2,3] ACHASOV	03D	RVUE	0.44–2.00 $e^+e^- \to \pi^+\pi^-\pi^0$
0.625±0.160		[4,5] CLEGG	94	RVUE	
0.466±0.178		[6,7] ANTONELLI	92	DM2	1.34–2.4 $e^+e^- \to \rho\pi$

[1] From a fit with contributions from $\omega(782)$, $\phi(1020)$, $\omega(1420)$, and $\omega(1650)$. See ACHASOV 20A for a further analysis of the $\pi^+\pi^-\pi^0$ data.
[2] Calculated by us from the cross section at the peak.
[3] From the combined fit of ANTONELLI 92, ACHASOV 01E, ACHASOV 02E, and ACHASOV 03D data on the $\pi^+\pi^-\pi^0$ and ANTONELLI 92 on the $\omega\pi^+\pi^-$ final states. Supersedes ACHASOV 99E and ACHASOV 02E.
[4] From a fit to two Breit-Wigner functions and using the data of DOLINSKY 91 and ANTONELLI 92.
[5] From the partial and leptonic width given by the authors.
[6] From a fit to two Breit-Wigner functions interfering between them and with the ω,ϕ tails with fixed $(+,-,+)$ phases.
[7] From the product of the leptonic width and partial branching ratio given by the authors.

$\Gamma(\omega\pi\pi)/\Gamma_{\text{total}} \times \Gamma(e^+e^-)/\Gamma_{\text{total}}$ — $\Gamma_2/\Gamma \times \Gamma_5/\Gamma$

VALUE (units 10^{-8})	DOCUMENT ID		TECN	COMMENT
• • • We do not use the following data for averages, fits, limits, etc. • • •				
19.7±5.7	AUBERT	07AU	BABR	10.6 $e^+e^- \to \omega\pi^+\pi^-\gamma$
1.9±1.9	[1] AKHMETSHIN	00D	CMD2	1.2–2.4 $e^+e^- \to \omega\pi^+\pi^-$

[1] Using the data of AKHMETSHIN 00D and ANTONELLI 92. The $\rho\pi$ dominance for the energy dependence of the $\omega(1420)$ and $\omega(1650)$ width assumed.

$\Gamma(\omega\eta)/\Gamma_{\text{total}} \times \Gamma(e^+e^-)/\Gamma_{\text{total}}$ — $\Gamma_3/\Gamma \times \Gamma_5/\Gamma$

VALUE (units 10^{-8})	EVTS	DOCUMENT ID		TECN	COMMENT
• • • We do not use the following data for averages, fits, limits, etc. • • •					
2.5±0.6	267	[1] ACHASOV	20B	SND	$e^+e^- \to \omega\eta \to \eta\pi^0\gamma$
$2.1^{+1.0}_{-0.8}$		ACHASOV	19	SND	$e^+e^- \to \pi^+\pi^-\pi^0\eta$
5.0±2.6±0.3	824	[2] AKHMETSHIN	17A	CMD3	1.4–2.0 $e^+e^- \to \omega\eta$
$1.6^{+0.9}_{-0.7}$	898	[3] ACHASOV	16B	SND	1.34–2.00 $e^+e^- \to \omega\eta$

[1] From a fit with contributions from $\omega(1420)$, $\omega(1650)$, and $\phi(1680)$. The mass of $\omega(1420)$ is fixed to the PDG 18 value of 1420 MeV. Fixing also the width of $\omega(1420)$ to the PDG 18 value of 220 MeV results in $(3.0 \pm 1.6) \times 10^{-8}$ measurement.
[2] From a fit of the interfering $\omega(1420)$ and $\omega(1650)$ with a relative phase of π and other parameters floating. From an alternative fit $\Gamma(\omega(1420) \to \omega\eta)/\Gamma_{\text{total}} \times \Gamma(\omega(1420) \to e^+e^-) = 5.3 \pm 1.6$ eV.
[3] From a fit with contributions from $\omega(1420)$, $\omega(1650)$, and $\phi(1680)$. The mass and the width of $\omega(1420)$ are fixed to the 2014 edition (PDG 14) of this review.

$\Gamma(\pi^0\gamma)/\Gamma_{\text{total}} \times \Gamma(e^+e^-)/\Gamma_{\text{total}}$ — $\Gamma_6/\Gamma \times \Gamma_5/\Gamma$

VALUE (units 10^{-8})	DOCUMENT ID		TECN	COMMENT
• • • We do not use the following data for averages, fits, limits, etc. • • •				
0.23±0.14	[1] ACHASOV	10D	SND	1.075–2.0 $e^+e^- \to \pi^0\gamma$
$2.03^{+0.70}_{-0.75}$	[2] AKHMETSHIN	05	CMD2	0.60–1.38 $e^+e^- \to \pi^0\gamma$

[1] From a fit of a VMD model with two effective resonances with masses of 1450 MeV and 1700 MeV to describe the excited vector states $\omega(1420)$, $\rho(1450)$, $\omega(1650)$, and $\rho(1700)$. Systematic errors not evaluated.
[2] Using 1420 MeV and 220 MeV for the $\omega(1420)$ mass and width.

$\omega(1420)$ BRANCHING RATIOS

$\Gamma(\omega\pi\pi)/\Gamma_{\text{total}}$ — Γ_2/Γ

VALUE	DOCUMENT ID		TECN	COMMENT
• • • We do not use the following data for averages, fits, limits, etc. • • •				
0.301±0.029	[1] HENNER	02	RVUE	1.2–2.0 $e^+e^- \to \rho\pi, \omega\pi\pi$
possibly seen	AKHMETSHIN	00D	CMD2	$e^+e^- \to \omega\pi^+\pi^-$

$\Gamma(\omega\pi\pi)/\Gamma(b_1(1235)\pi)$ — Γ_2/Γ_4

VALUE	EVTS	DOCUMENT ID		TECN	COMMENT
• • • We do not use the following data for averages, fits, limits, etc. • • •					
0.60±0.16	5095	ANISOVICH	00H	SPEC	0.0 $p\overline{p} \to \omega\pi^0\pi^0\pi^0$

$\Gamma(\rho\pi)/\Gamma_{\text{total}}$ — Γ_1/Γ

VALUE	DOCUMENT ID		TECN	COMMENT
• • • We do not use the following data for averages, fits, limits, etc. • • •				
seen	ACHASOV	20A	SND	1.15–2.00 $e^+e^- \to \pi^+\pi^-\pi^0$
0.699±0.029	[1] HENNER	02	RVUE	1.2–2.0 $e^+e^- \to \rho\pi, \omega\pi\pi$

$\Gamma(e^+e^-)/\Gamma_{\text{total}}$ — Γ_5/Γ

VALUE (units 10^{-7})	EVTS	DOCUMENT ID		TECN	COMMENT
• • • We do not use the following data for averages, fits, limits, etc. • • •					
~ 6.6	1.2M	[2,3] ACHASOV	03D	RVUE	0.44–2.00 $e^+e^- \to \pi^+\pi^-\pi^0$
23 ±1		[1] HENNER	02	RVUE	1.2–2.0 $e^+e^- \to \rho\pi, \omega\pi\pi$

[1] Assuming that the $\omega(1420)$ decays into $\rho\pi$ and $\omega\pi\pi$ only.
[2] Calculated by us from the cross section at the peak.
[3] Assuming that the $\omega(1420)$ decays into $\rho\pi$ only.

$\omega(1420)$ REFERENCES

ACHASOV 20A EPJ C80 993 M.N. Achasov et al. (SND Collab.)
ACHASOV 20B EPJ C80 1008 M.N. Achasov et al. (SND Collab.)
ACHASOV 19 PR D99 112004 M.N. Achasov et al. (SND Collab.)
PDG 18 PR D98 030001 M. Tanabashi et al. (PDG Collab.)
AKHMETSHIN 17A PL B773 150 R.R. Akhmetshin et al. (CMD-3 Collab.)
ACHASOV 16B PR D94 092002 M.N. Achasov et al. (SND Collab.)
AULCHENKO 15A JETP 121 27 V.M. Aulchenko et al. (SND Collab.)
Translated from ZETF 148 34.
PDG 14 CP C38 070001 K. Olive et al. (PDG Collab.)
ACHASOV 10D PR D98 112001 M.N. Achasov et al. (SND Collab.)
AUBERT 07AU PR D76 092005 B. Aubert et al. (BABAR Collab.)
AKHMETSHIN 05 PL B605 26 R.R. Akhmetshin et al. (Novosibirsk CMD-2 Collab.)
AUBERT,B 04N PR D70 072004 B. Aubert et al. (BABAR Collab.)
ACHASOV 03D PR D68 052006 M.N. Achasov et al. (Novosibirsk SND Collab.)
ACHASOV 02E PR D66 032001 M.N. Achasov et al. (Novosibirsk SND Collab.)
HENNER 02 EPJ C26 3 V.K. Henner et al.
ACHASOV 01E PR D63 072002 M.N. Achasov et al. (Novosibirsk SND Collab.)
AKHMETSHIN 00D PL B489 125 R.R. Akhmetshin et al. (Novosibirsk CMD-2 Collab.)
ANISOVICH 00H PL B485 341 A.V. Anisovich et al.
ACHASOV 99E PL B462 365 M.N. Achasov et al. (Novosibirsk SND Collab.)
ACHASOV 98H PR D57 4334 N.N. Achasov, A.A. Kozhevnikov
CLEGG 94 ZPHY C62 455 A.B. Clegg, A. Donnachie (LANC, MCHS)
ANTONELLI 92 ZPHY C56 15 A. Antonelli et al. (DM2 Collab.)
DOLINSKY 91 PRPL 202 99 S.I. Dolinsky et al. (NOVO)
BISELLO 88B ZPHY C39 13 D. Bisello et al. (PADO, CLER, FRAS+)
BARKOV 87 JETPL 46 164 L.M. Barkov et al. (NOVO)
Translated from ZETFP 46 132.
CORDIER 81 PL 106B 155 A. Cordier et al. (ORSAY)
IVANOV 81 PL 107B 297 P.M. Ivanov et al. (NOVO)

Downloaded from https://academic.oup.com/ptep/article/2022/8/083C01/6651666 by KIT Library user on 27 September 2022

$f_2(1430)$

$I^G(J^{PC}) = 0^+(2^{++})$

OMITTED FROM SUMMARY TABLE

This entry lists nearby peaks observed in the D wave of the $K\overline{K}$ and $\pi^+\pi^-$ systems. Needs confirmation.

$f_2(1430)$ MASS

VALUE (MeV)	DOCUMENT ID		TECN	COMMENT
≈ 1430 OUR ESTIMATE				
• • • We do not use the following data for averages, fits, limits, etc. • • •				
$1440 \pm 11 \pm 3$	LEES	21A	BABR	$\gamma\gamma \to \eta_c(1S) \to \eta'\pi^+\pi^-$
1453 ± 4	[1] VLADIMIRSK...	01	SPEC	$40\ \pi^- p \to K^0_S K^0_S n$
1421 ± 5	AUGUSTIN	87	DM2	$J/\psi \to \gamma\pi^+\pi^-$
1480 ± 50	AKESSON	86	SPEC	$pp \to pp\pi^+\pi^-$
1436^{+26}_{-16}	DAUM	84	CNTR	17–18 $\pi^- p \to K^+K^- n$
1412 ± 3	DAUM	84	CNTR	63 $\pi^- p \to K^0_S K^0_S n$, $K^+K^- n$
1439^{+5}_{-6}	[2] BEUSCH	67	OSPK	5,7,12 $\pi^- p \to K^0_S K^0_S n$

[1] $J^{PC} = 0^{++}$ or 2^{++}.
[2] Not seen by WETZEL 76.

$f_2(1430)$ WIDTH

VALUE (MeV)	DOCUMENT ID		TECN	COMMENT
• • • We do not use the following data for averages, fits, limits, etc. • • •				
$46 \pm 15 \pm 5$	LEES	21A	BABR	$\gamma\gamma \to \eta_c(1S) \to \eta'\pi^+\pi^-$
13 ± 5	[3] VLADIMIRSK...	01	SPEC	$40\ \pi^- p \to K^0_S K^0_S n$
30 ± 9	AUGUSTIN	87	DM2	$J/\psi \to \gamma\pi^+\pi^-$
150 ± 50	AKESSON	86	SPEC	$pp \to pp\pi^+\pi^-$
81^{+56}_{-29}	DAUM	84	CNTR	17–18 $\pi^- p \to K^+K^- n$
14 ± 6	DAUM	84	CNTR	63 $\pi^- p \to K^0_S K^0_S n$, $K^+K^- n$
43^{+17}_{-18}	[4] BEUSCH	67	OSPK	5,7,12 $\pi^- p \to K^0_S K^0_S n$

[3] $J^{PC} = 0^{++}$ or 2^{++}.
[4] Not seen by WETZEL 76.

$f_2(1430)$ DECAY MODES

	Mode
Γ_1	$K\overline{K}$
Γ_2	$\pi\pi$

$f_2(1430)$ REFERENCES

LEES	21A	PR D104 072002	J.P. Lees *et al.*	(BABAR Collab.)
VLADIMIRSK...	01	PAN 64 1895	V.V. Vladimirsky *et al.*	
		Translated from YAF 64 1979.		
AUGUSTIN	87	ZPHY C36 369	J.E. Augustin *et al.*	(LALO, CLER, FRAS+)
AKESSON	86	NP B264 154	T. Akesson *et al.*	(Axial Field Spec. Collab.)
DAUM	84	ZPHY C23 339	C. Daum *et al.*	(AMST, CERN, CRAC, MPIM+) JP
WETZEL	76	NP B115 208	W. Wetzel *et al.*	(ETH, CERN, LOIC)
BEUSCH	67	PL 25B 357	W. Beusch *et al.*	(ETH, CERN)

$a_0(1450)$

$I^G(J^{PC}) = 1^-(0^{++})$

See the review on "Spectroscopy of Light Meson Resonances."

$a_0(1450)$ MASS

VALUE (MeV)	EVTS	DOCUMENT ID		TECN	COMMENT
1474 ±19 OUR AVERAGE					
1480 ±30		ABELE	98	CBAR	$0.0\ \overline{p}p \to K^0_L K^\pm\pi^\mp$
1470 ±25		[1] AMSLER	95D	CBAR	$0.0\ \overline{p}p \to \pi^0\pi^0\pi^0$, $\pi^0\eta\eta$, $\pi^0\pi^0\eta$
• • • We do not use the following data for averages, fits, limits, etc. • • •					
$1302.1 \pm 1.1 \pm 3.9$		[2] ALBRECHT	20	RVUE	$0.9\ \overline{p}p \to \pi^0\pi^0\eta$, $\pi^0\eta\eta$, $\pi^0 K^+K^-$
1458 ±14 ±15	190k	[3] AAIJ	16N	LHCB	$D^0 \to K^0_S K^\pm\pi^\mp$
1515 ±30		[4] ANISOVICH	09	RVUE	$0.0\ \overline{p}p$, πN
$1316.8^{+0.7+24.7}_{-1.0-4.6}$		[5] UEHARA	09A	BELL	$\gamma\gamma \to \pi^0\eta$
1432 ±13 ±25		[6] BUGG	08A	RVUE	$\overline{p}p$
1477 ±10	80k	[7] UMAN	06	E835	$5.2\ \overline{p}p \to \eta\eta\pi^0$
1441^{+40}_{-15}	35k	[4] BAKER	03	SPEC	$\overline{p}p \to \omega\pi^+\pi^-\pi^0$
1303 ±16		[8] BARGIOTTI	03	OBLX	$\overline{p}p$
1296 ±10		[9] AMSLER	02	CBAR	$0.9\ \overline{p}p \to \pi^0\pi^0\eta$
1565 ±30		[9] ANISOVICH	98B	RVUE	Compilation
1290 ±10		[10] BERTIN	98B	OBLX	$0.0\ \overline{p}p \to K^\pm K_S\pi^\mp$
1450 ±40		AMSLER	94D	CBAR	$0.0\ \overline{p}p \to \pi^0\pi^0\eta$
1410 ±25		ETKIN	82C	MPS	$23\ \pi^- p \to n2K^0_S$
~ 1300		MARTIN	78	SPEC	$10\ K^\pm p \to K^0_S\pi p$
1255 ± 5		[11] CASON	76		

[1] Coupled-channel analysis of AMSLER 95B, AMSLER 95C, and AMSLER 94D.
[2] T-matrix pole, 2 poles, 2 channels ($\pi\eta$, $K\overline{K}$).
[3] Using a model with Gaussian constraints to the PDG averaged values .
[4] From the pole position.
[5] May be a different state.
[6] Using data from AMSLER 94D, ABELE 98, and BAKER 03. Supersedes BUGG 94.
[7] Statistical error only.
[8] Coupled channel analysis of $\pi^+\pi^-\pi^0$, $K^+K^-\pi^0$, and $K^\pm K^0_S\pi^\mp$.
[9] T-matrix pole.
[10] Not confirmed by BUGG 08A.
[11] Isospin 0 not excluded.

$a_0(1450)$ WIDTH

VALUE (MeV)	EVTS	DOCUMENT ID		TECN	COMMENT
265 ±13 OUR AVERAGE					
265 ±15		ABELE	98	CBAR	$0.0\ \overline{p}p \to K^0_L K^\pm\pi^\mp$
265 ±30		[1] AMSLER	95D	CBAR	$0.0\ \overline{p}p \to \pi^0\pi^0\pi^0$, $\pi^0\eta\eta$, $\pi^0\pi^0\eta$
• • • We do not use the following data for averages, fits, limits, etc. • • •					
$112.4 \pm 1.4 \pm 3.4$		[2] ALBRECHT	20	RVUE	$0.9\ \overline{p}p \to \pi^0\pi^0\eta$, $\pi^0\eta\eta$, $\pi^0 K^+K^-$
282 ±12 ±13	190k	[3] AAIJ	16N	LHCB	$D^0 \to K^0_S K^\pm\pi^\mp$
230 ±36		[4] ANISOVICH	09	RVUE	$0.0\ \overline{p}p$, πN
$65.0^{+2.1+99.1}_{-5.4-32.6}$		[5] UEHARA	09A	BELL	$\gamma\gamma \to \pi^0\eta$
196 ±10 ±10		[6] BUGG	08A	RVUE	$\overline{p}p$
267 ±11	80k	[7] UMAN	06	E835	$5.2\ \overline{p}p \to \eta\eta\pi^0$
110 ±14	35k	[4] BAKER	03	SPEC	$\overline{p}p \to \omega\pi^+\pi^-\pi^0$
92 ±16		[8] BARGIOTTI	03	OBLX	$\overline{p}p$
81 ±21		[9] AMSLER	02	CBAR	$0.9\ \overline{p}p \to \pi^0\pi^0\eta$
292 ±40		[9] ANISOVICH	98B	RVUE	Compilation
80 ± 5		[10] BERTIN	98B	OBLX	$0.0\ \overline{p}p \to K^\pm K_S\pi^\mp$
270 ±40		AMSLER	94D	CBAR	$0.0\ \overline{p}p \to \pi^0\pi^0\eta$
230 ±30		ETKIN	82C	MPS	$23\ \pi^- p \to n2K^0_S$
~ 250		MARTIN	78	SPEC	$10\ K^\pm p \to K^0_S\pi p$
79 ±10		[11] CASON	76		

[1] Coupled-channel analysis of AMSLER 95B, AMSLER 95C, and AMSLER 94D.
[2] T-matrix pole, 2 poles, 2 channels ($\pi\eta$, $K\overline{K}$).
[3] Using a model with Gaussian constraints to the PDG averaged values .
[4] From the pole position.
[5] May be a different state.
[6] Using data from AMSLER 94D, ABELE 98, and BAKER 03. Supersedes BUGG 94.
[7] Statistical error only.
[8] Coupled channel analysis of $\pi^+\pi^-\pi^0$, $K^+K^-\pi^0$, and $K^\pm K^0_S\pi^\mp$.
[9] T-matrix pole.
[10] Not confirmed by BUGG 08A.
[11] Isospin 0 not excluded.

$a_0(1450)$ DECAY MODES

Branching fractions are given relative to the one **DEFINED AS 1**.

	Mode	Fraction (Γ_i/Γ)
Γ_1	$\pi\eta$	0.093 ± 0.020
Γ_2	$\pi\eta'(958)$	0.033 ± 0.017
Γ_3	$K\overline{K}$	0.082 ± 0.028
Γ_4	$\omega\pi\pi$	**DEFINED AS 1**
Γ_5	$a_0(980)\pi\pi$	seen
Γ_6	$\gamma\gamma$	seen

$a_0(1450)$ $\Gamma(i)\Gamma(\gamma\gamma)/\Gamma(\text{total})$

$\Gamma(\pi\eta) \times \Gamma(\gamma\gamma)/\Gamma_{\text{total}}$ — $\Gamma_1\Gamma_6/\Gamma$

VALUE (eV)	DOCUMENT ID		TECN	COMMENT
• • • We do not use the following data for averages, fits, limits, etc. • • •				
$432 \pm 6^{+1073}_{-256}$	[1] UEHARA	09A	BELL	$\gamma\gamma \to \pi^0\eta$

[1] May be a different state.

Downloaded from https://academic.oup.com/ptep/article/2022/8/083C01/6651666 by KIT Library user on 27 September 2022

$a_0(1450)$ BRANCHING RATIOS

$\Gamma(\pi\eta'(958))/\Gamma(\pi\eta)$ — Γ_2/Γ_1

VALUE	DOCUMENT ID		TECN	COMMENT
0.35±0.16	[1] ABELE	98	CBAR	$0.0\ \overline{p}p \to K^0_L K^\pm \pi^\mp$
• • • We do not use the following data for averages, fits, limits, etc. • • •				
0.43±0.19	ABELE	97C	CBAR	$0.0\ \overline{p}p \to \pi^0\pi^0\eta'$

[1] Using $\pi^0\eta$ from AMSLER 94D.

$\Gamma(K\overline{K})/\Gamma(\pi\eta)$ — Γ_3/Γ_1

VALUE	DOCUMENT ID		TECN	COMMENT
0.88 ±0.23	[1] ABELE	98	CBAR	$0.0\ \overline{p}p \to K^0_L K^\pm \pi^\mp$
• • • We do not use the following data for averages, fits, limits, etc. • • •				
1.887±0.041±0.97	[2] ALBRECHT	20	RVUE	$0.9\ \overline{p}p \to \pi^0\pi^0\eta$, $\pi^0\eta\eta$, $\pi^0 K^+K^-$

[1] Using $\pi^0\eta$ from AMSLER 94D.
[2] Residues from T-matrix pole, 2 poles, 2 channels ($\pi\eta$, $K\overline{K}$).

$\Gamma(\omega\pi\pi)/\Gamma(\pi\eta)$ — Γ_4/Γ_1

VALUE	EVTS	DOCUMENT ID		TECN	COMMENT
10.7±2.3	35280	[1] BAKER	03	SPEC	$\overline{p}p \to \omega\pi^+\pi^-\pi^0$

[1] Using results on $\overline{p}p \to a_0(1450)^0\pi^0$, $a_0(1450) \to \eta\pi^0$ from ABELE 96C and assuming the $\omega\rho$ mechanism for the $\omega\pi\pi$ state.

$\Gamma(a_0(980)\pi\pi)/\Gamma_{total}$ — Γ_5/Γ

VALUE	DOCUMENT ID		TECN	COMMENT
seen	BUGG	08A	RVUE	$\overline{p}p$

$\Gamma(a_0(980)\pi\pi)/\Gamma(\pi\eta)$ — Γ_5/Γ_1

VALUE	DOCUMENT ID		TECN	CHG	COMMENT
• • • We do not use the following data for averages, fits, limits, etc. • • •					
≤ 4.3	ANISOVICH	01	RVUE	0	$\overline{p}p \to \eta 2\pi^+ 2\pi^-$

$\Gamma(\gamma\gamma)/\Gamma_{total}$ — Γ_6/Γ

VALUE	DOCUMENT ID		TECN	COMMENT
seen	[1] UEHARA	09A	BELL	$\gamma\gamma \to \pi^0\eta$

[1] May be a different state.

$a_0(1450)$ REFERENCES

ALBRECHT	20	EPJ C80 453	M. Albrecht *et al.*	(Crystal Barrel Collab.)
AAIJ	16N	PR D93 052018	R. Aaij *et al.*	(LHCb Collab.)
ANISOVICH	09	IJMP A24 2481	V.V. Anisovich, A.V. Sarantsev	
UEHARA	09A	PR D80 032001	S. Uehara *et al.*	(BELLE Collab.)
BUGG	08A	PR D78 074023	D.V. Bugg	(LOQM)
UMAN	06	PR D73 052009	I. Uman *et al.*	(FNAL E835)
BAKER	03	PL B563 140	C.A. Baker *et al.*	
BARGIOTTI	03	EPJ C26 371	M. Bargiotti *et al.*	(OBELIX Collab.)
AMSLER	02	EPJ C23 29	C. Amsler *et al.*	
ANISOVICH	01	NP A690 567	A.V. Anisovich *et al.*	
ABELE	98	PR D57 3860	A. Abele *et al.*	(Crystal Barrel Collab.)
ANISOVICH	98B	SPU 41 419 Translated from UFN 168 481.	V.V. Anisovich *et al.*	
BERTIN	98B	PL B434 180	A. Bertin *et al.*	(OBELIX Collab.)
ABELE	97C	PL B404 179	A. Abele *et al.*	(Crystal Barrel Collab.)
ABELE	96C	NP A609 562	A. Abele *et al.*	(Crystal Barrel Collab.)
AMSLER	95B	PL B342 433	C. Amsler *et al.*	(Crystal Barrel Collab.)
AMSLER	95C	PL B353 571	C. Amsler *et al.*	(Crystal Barrel Collab.)
AMSLER	95D	PL B355 425	C. Amsler *et al.*	(Crystal Barrel Collab.)
AMSLER	94D	PL B333 277	C. Amsler *et al.*	(Crystal Barrel Collab.) IGJPC
BUGG	94	PR D50 4412	D.V. Bugg *et al.*	(LOQM)
ETKIN	82C	PR D25 2446	A. Etkin *et al.*	(BNL, CUNY, TUFTS, VAND)
MARTIN	78	NP B134 392	A.D. Martin *et al.*	(DURH, GEVA)
CASON	76	PRL 36 1485	N.M. Cason *et al.*	(NDAM, ANL)

$\rho(1450)$

$I^G(J^{PC}) = 1^+(1^{--})$

$\rho(1450)$ MASS

$\rho(1450)$ MASS

VALUE (MeV)	DOCUMENT ID
1465±25 OUR ESTIMATE This is only an educated guess; the error given is larger than the error on the average of the published values.	

$\eta\rho^0$ MODE

VALUE (MeV)	EVTS	DOCUMENT ID		TECN	COMMENT
• • • We do not use the following data for averages, fits, limits, etc. • • •					
1506±11	13.4k	[1] GRIBANOV	20	CMD3	1.1–2.0 $e^+e^- \to \eta\pi^+\pi^-$
1500±10	7.4k	[2] ACHASOV	18	SND	1.22–2.00 $e^+e^- \to \eta\pi^+\pi^-$
1497±14		[3] AKHMETSHIN	01B	CMD2	$e^+e^- \to \eta\gamma$
1421±15		[4] AKHMETSHIN	00D	CMD2	$e^+e^- \to \eta\pi^+\pi^-$
1470±20		ANTONELLI	88	DM2	$e^+e^- \to \eta\pi^+\pi^-$
1446±10		FUKUI	88	SPEC	8.95 $\pi^-p \to \eta\pi^+\pi^-n$

[1] Mass and width of the $\rho(770)$ fixed at 775 and 149 MeV, respectively; solution 2 of model 2, $\eta \to \gamma\gamma$ decays used.
[2] From the combined fit of AULCHENKO 15 and ACHASOV 18 in the model with the interfering $\rho(1450)$, $\rho(1700)$ and $\rho(2150)$ with the parameters of the $\rho(1450)$ and $\rho(1700)$ floating and the mass and width of the $\rho(2150)$ fixed at 2155 MeV and 320 MeV, respectively. The phases of the resonances are π, 0 and π, respectively.
[3] Using the data of AKHMETSHIN 01B on $e^+e^- \to \eta\gamma$, AKHMETSHIN 00D and ANTONELLI 88 on $e^+e^- \to \eta\pi^+\pi^-$.
[4] Using the data of ANTONELLI 88, DOLINSKY 91, and AKHMETSHIN 00D. The energy-independent width of the $\rho(1450)$ and $\rho(1700)$ mesons assumed.

$\omega\pi$ MODE

VALUE (MeV)	EVTS	DOCUMENT ID		TECN	COMMENT
• • • We do not use the following data for averages, fits, limits, etc. • • •					
1510± 7	10.2k	[1] ACHASOV	16D	SND	1.05–2.00 $e^+e^- \to \pi^0\pi^0\gamma$
$1544\pm22^{+11}_{-46}$	821	[2] MATVIENKO	15	BELL	$\overline{B}^0 \to D^{*+}\omega\pi^-$
1491±19	7815	[3] ACHASOV	13	SND	1.05–2.00 $e^+e^- \to \pi^0\pi^0\gamma$
1582±17±25	2382	[4] AKHMETSHIN	03B	CMD2	$e^+e \to \pi^0\pi^0\gamma$
$1349\pm25^{+10}_{-5}$	341	[5] ALEXANDER	01B	CLE2	$B \to D^{(*)}\omega\pi^-$
1523±10		[6] EDWARDS	00A	CLE2	$\tau^- \to \omega\pi^-\nu_\tau$
1463±25		[7] CLEGG	94	RVUE	
1250		[8] ASTON	80C	OMEG	20–70 $\gamma p \to \omega\pi^0 p$
1290±40		[8] BARBER	80C	SPEC	3–5 $\gamma p \to \omega\pi^0 p$

[1] From a phenomenological model based on vector meson dominance with interfering $\rho(770)$, $\rho(1450)$, and $\rho(1700)$. The $\rho(1700)$ mass and width are fixed at 1720 MeV and 250 MeV, respectively. Systematic uncertainties not estimated. Supersedes ACHASOV 13.
[2] Using Breit-Wigner parameterization of the $\rho(1450)$ and assuming equal probabilities of the $\rho(1450) \to \pi\pi$ and $\rho(1450) \to \omega\pi$ decays.
[3] From a phenomenological model based on vector meson dominance with the interfering $\rho(1450)$ and $\rho(1700)$ and their widths fixed at 400 and 250 MeV, respectively. Systematic uncertainty not estimated.
[4] Using the data of AKHMETSHIN 03B and BISELLO 91B assuming the $\omega\pi^0$ and $\pi^+\pi^-$ mass dependence of the total width. $\rho(1700)$ mass and width fixed at 1700 MeV and 240 MeV, respectively.
[5] Using Breit-Wigner parameterization of the $\rho(1450)$ and assuming the $\omega\pi^-$ mass dependence for the total width.
[6] Mass-independent width parameterization. $\rho(1700)$ mass and width fixed at 1700 MeV and 235 MeV respectively.
[7] Using data from BISELLO 91B, DOLINSKY 86 and ALBRECHT 87L.
[8] Not separated from $b_1(1235)$, not pure $J^P = 1^-$ effect.

4π MODE

VALUE (MeV)	DOCUMENT ID		TECN	COMMENT
• • • We do not use the following data for averages, fits, limits, etc. • • •				
1435±40	ABELE	01B	CBAR	$0.0\ \overline{p}n \to 2\pi^-2\pi^0\pi^+$
1350±50	ACHASOV	97	RVUE	$e^+e^- \to 2(\pi^+\pi^-)$
1449± 4	[1] ARMSTRONG	89E	OMEG	300 $pp \to pp2(\pi^+\pi^-)$

[1] Not clear whether this observation has I=1 or 0.

$\pi\pi$ MODE

VALUE (MeV)	EVTS	DOCUMENT ID		TECN	COMMENT
• • • We do not use the following data for averages, fits, limits, etc. • • •					
1326.35± 3.46		[1] BARTOS	17	RVUE	$e^+e^- \to \pi^+\pi^-$
1342.31±46.62		[2] BARTOS	17A	RVUE	$e^+e^- \to \pi^+\pi^-$
1373.83±11.37		[3] BARTOS	17A	RVUE	$\tau^- \to \pi^-\pi^0\nu_\tau$
1429 ±41	20k	[4] LEES	17C	BABR	$J/\psi \to \pi^+\pi^-\pi^0$
1350 ±20 $^{+20}_{-30}$	63.5k	[5] ABRAMOWICZ	12	ZEUS	$ep \to e\pi^+\pi^-p$
1493 ±15		[6] LEES	12G	BABR	$e^+e^- \to \pi^+\pi^-\gamma$
1446 ± 7 ±28	5.4M	[7,8] FUJIKAWA	08	BELL	$\tau^- \to \pi^-\pi^0\nu_\tau$
1328 ±15		[9] SCHAEL	05C	ALEP	$\tau^- \to \pi^-\pi^0\nu_\tau$
1406 ±15	87k	[7,10] ANDERSON	00A	CLE2	$\tau^- \to \pi^-\pi^0\nu_\tau$
∼ 1368		[11] ABELE	99C	CBAR	$0.0\ \overline{p}d \to \pi^+\pi^-\pi^-p$
1348 ±33		BERTIN	98	OBLX	0.05–0.405 $\overline{n}p \to 2\pi^+\pi^-$
1411 ±14		[12] ABELE	97	CBAR	$\overline{p}n \to \pi^-\pi^0\pi^0$
1370 $^{+90}_{-70}$		ACHASOV	97	RVUE	$e^+e^- \to \pi^+\pi^-$
1359 ±40		[10] BERTIN	97C	OBLX	$0.0\ \overline{p}p \to \pi^+\pi^-\pi^0$
1282 ±37		BERTIN	97D	OBLX	0.05 $\overline{p}p \to 2\pi^+2\pi^-$
1424 ±25		BISELLO	89	DM2	$e^+e^- \to \pi^+\pi^-$
1265.5 ±75.3		DUBNICKA	89	RVUE	$e^+e^- \to \pi^+\pi^-$
1292 ±17		[13] KURDADZE	83	OLYA	0.64–1.4 $e^+e^- \to \pi^+\pi^-$

[1] Applies the Unitary & Analytic Model of the pion electromagnetic form factor of DUBNICKA 10 to analyze the data of LEES 12G and ABLIKIM 16C.
[2] Applies the Unitary & Analytic Model of the pion electromagnetic form factor of DUBNICKA 10 to analyze the data of ACHASOV 06, AKHMETSHIN 07, AUBERT 09AS, and AMBROSINO 11A.
[3] Applies the Unitary & Analytic Model of the pion electromagnetic form factor of DUBNICKA 10 to analyze the data of FUJIKAWA 08.
[4] From a Dalitz plot analysis in an isobar model with $\rho(1450)$ and $\rho(1700)$ masses and widths floating.
[5] Using the KUHN 90 parametrization of the pion form factor, neglecting $\rho-\omega$ interference.
[6] Using the GOUNARIS 68 parametrization of the pion form factor leaving the masses and widths of the $\rho(1450)$, $\rho(1700)$, and $\rho(2150)$ resonances as free parameters of the fit.
[7] From the GOUNARIS 68 parametrization of the pion form factor.
[8] $|F_\pi(0)|^2$ fixed to 1.
[9] From the combined fit of the τ^- data from ANDERSON 00A and SCHAEL 05C and e^+e^- data from the compilation of BARKOV 85, AKHMETSHIN 04, and ALOISIO 05.

Downloaded from https://academic.oup.com/ptep/article/2022/8/083C01/6651666 by KIT Library user on 27 September 2022

$\rho(1700)$ mass and width fixed at 1713 MeV and 235 MeV, respectively. Supersedes BARATE 97M.
[10] $\rho(1700)$ mass and width fixed at 1700 MeV and 235 MeV, respectively.
[11] $\rho(1700)$ mass and width fixed at 1780 MeV and 275 MeV respectively.
[12] T-matrix pole.
[13] Using for $\rho(1700)$ mass and width 1600 ± 20 and 300 ± 10 MeV respectively.

$K\overline{K}$ MODE

VALUE (MeV)	EVTS	DOCUMENT ID		TECN	CHG	COMMENT
• • • We do not use the following data for averages, fits, limits, etc. • • •						
$1208 \pm 8 \pm 9$	190k	[1] AAIJ	16N	LHCB		$D^0 \to K^0_S K^\pm \pi^\mp$
1422.8 ± 6.5	27k	[2] ABELE	99D	CBAR	$\pm$	$0.0\ \overline{p}p \to K^+ K^- \pi^0$

[1] Using the GOUNARIS 68 parameterization with fixed width.
[2] K-matrix pole. Isospin not determined, could be $\omega(1420)$.

$K\overline{K}^*(892)$ + c.c. MODE

VALUE (MeV)	DOCUMENT ID		TECN	COMMENT
• • • We do not use the following data for averages, fits, limits, etc. • • •				
$1505 \pm 19 \pm 7$	AUBERT	08S	BABR	$10.6\ e^+e^- \to K\overline{K}^*(892)\gamma$

$m_{\rho(1450)^0} - m_{\rho(1450)^\pm}$

VALUE (MeV)	DOCUMENT ID		TECN	COMMENT
• • • We do not use the following data for averages, fits, limits, etc. • • •				
-31.53 ± 47.99	[1] BARTOS	17A	RVUE	$e^+e^- \to \pi^+\pi^-$, $\tau^- \to \pi^-\pi^0\nu_\tau$

[1] Applies the Unitary & Analytic Model of the pion electromagnetic form factor of DUBNICKA 10 to analyze the data of ACHASOV 06, AKHMETSHIN 07, AUBERT 09AS, AMBROSINO 11A, and FUJIKAWA 08.

$\rho(1450)$ WIDTH

$\rho(1450)$ WIDTH

VALUE (MeV)	DOCUMENT ID		TECN	COMMENT
400± 60 OUR ESTIMATE This is only an educated guess; the error given is larger than the error on the average of the published values.				
• • • We do not use the following data for averages, fits, limits, etc. • • •				
480 ± 180	[1] ACHASOV	10D	SND	1.075–$2.0\ e^+e^- \to \pi^0\gamma$

[1] From a fit of a VMD model with two effective resonances with masses of 1450 MeV and 1700 MeV to describe the excited vector states $\omega(1420)$, $\rho(1450)$, $\omega(1650)$, and $\rho(1700)$. Systematic errors not evaluated.

$\eta\rho^0$ MODE

VALUE (MeV)	EVTS	DOCUMENT ID		TECN	COMMENT
• • • We do not use the following data for averages, fits, limits, etc. • • •					
321 ± 27	13.4k	[1] GRIBANOV	20	CMD3	1.1–$2.0\ e^+e^- \to \eta\pi^+\pi^-$
280 ± 20	7.4k	[2] ACHASOV	18	SND	1.22–$2.00\ e^+e^- \to \eta\pi^+\pi^-$
226 ± 44		[3] AKHMETSHIN	01B	CMD2	$e^+e^- \to \eta\gamma$
211 ± 31		[4] AKHMETSHIN	00D	CMD2	$e^+e^- \to \eta\pi^+\pi^-$
230 ± 30		ANTONELLI	88	DM2	$e^+e^- \to \eta\pi^+\pi^-$
60 ± 15		FUKUI	88	SPEC	$8.95\ \pi^- p \to \eta\pi^+\pi^- n$

[1] Mass and width of the $\rho(770)$ fixed at 775 and 149 MeV, respectively; solution 2 of model 2, $\eta \to \gamma\gamma$ decays used.
[2] From the combined fit of AULCHENKO 15 and ACHASOV 18 in the model with the interfering $\rho(1450)$, $\rho(1700)$ and $\rho(2150)$ with the parameters of the $\rho(1450)$ and $\rho(1700)$ floating and the mass and width of the $\rho(2150)$ fixed at 2155 MeV and 320 MeV, respectively. The phases of the resonances are π, 0 and π, respectively.
[3] Using the data of AKHMETSHIN 01B on $e^+e^- \to \eta\gamma$, AKHMETSHIN 00D and ANTONELLI 88 on $e^+e^- \to \eta\pi^+\pi^-$.
[4] Using the data of ANTONELLI 88, DOLINSKY 91, and AKHMETSHIN 00D. The energy-independent width of the $\rho(1450)$ and $\rho(1700)$ mesons assumed.

$\omega\pi$ MODE

VALUE (MeV)	EVTS	DOCUMENT ID		TECN	COMMENT
• • • We do not use the following data for averages, fits, limits, etc. • • •					
440 ± 40	10.2k	[1] ACHASOV	16D	SND	1.05–$2.00\ e^+e^- \to \pi^0\pi^0\gamma$
303^{+31+69}_{-52-7}	821	[2] MATVIENKO	15	BELL	$\overline{B}^0 \to D^{*+}\omega\pi^-$
$429 \pm 42 \pm 10$	2382	[3] AKHMETSHIN	03B	CMD2	$e^+e^- \to \pi^0\pi^0\gamma$
$547 \pm 86^{+46}_{-45}$	341	[4] ALEXANDER	01B	CLE2	$B \to D^{(*)}\omega\pi^-$
400 ± 35		[5] EDWARDS	00A	CLE2	$\tau^- \to \omega\pi^-\nu_\tau$
311 ± 62		[6] CLEGG	94	RVUE	
300		[7] ASTON	80C	OMEG	20–$70\ \gamma p \to \omega\pi^0 p$
320 ± 100		[7] BARBER	80C	SPEC	3–$5\ \gamma p \to \omega\pi^0 p$

[1] From a phenomenological model based on vector meson dominance with interfering $\rho(770)$, $\rho(1450)$, and $\rho(1700)$. The $\rho(1700)$ mass and width are fixed at 1720 MeV and 250 MeV, respectively. Systematic uncertainties not estimated. Supersedes ACHASOV 13.
[2] Using Breit-Wigner parameterization of the $\rho(1450)$ and assuming equal probabilities of the $\rho(1450) \to \pi\pi$ and $\rho(1450) \to \omega\pi$ decays.
[3] Using the data of AKHMETSHIN 03B and BISELLO 91B assuming the $\omega\pi^0$ and $\pi^+\pi^-$ mass dependence of the total width. $\rho(1700)$ mass and width fixed at 1700 MeV and 240 MeV, respectively.
[4] Using Breit-Wigner parameterization of the $\rho(1450)$ and assuming the $\omega\pi^-$ mass dependence for the total width.
[5] Mass-independent width parameterization. $\rho(1700)$ mass and width fixed at 1700 MeV and 235 MeV respectively.
[6] Using data from BISELLO 91B, DOLINSKY 86 and ALBRECHT 87L.
[7] Not separated from $b_1(1235)$, not pure $J^P = 1^-$ effect.

4π MODE

VALUE (MeV)	DOCUMENT ID		TECN	COMMENT
• • • We do not use the following data for averages, fits, limits, etc. • • •				
325 ± 100	ABELE	01B	CBAR	$0.0\ \overline{p}n \to 2\pi^- 2\pi^0 \pi^+$

$\pi\pi$ MODE

VALUE (MeV)	EVTS	DOCUMENT ID		TECN	COMMENT
• • • We do not use the following data for averages, fits, limits, etc. • • •					
324.13 ± 12.01		[1] BARTOS	17	RVUE	$e^+e^- \to \pi^+\pi^-$
492.17 ± 138.38		[2] BARTOS	17A	RVUE	$e^+e^- \to \pi^+\pi^-$
340.87 ± 23.84		[3] BARTOS	17A	RVUE	$\tau^- \to \pi^-\pi^0\nu_\tau$
576 ± 29	20k	[4] LEES	17C	BABR	$J/\psi \to \pi^+\pi^-\pi^0$
$460 \pm 30^{+40}_{-45}$	63.5k	[5] ABRAMOWICZ	12	ZEUS	$ep \to e\pi^+\pi^- p$
427 ± 31		[6] LEES	12G	BABR	$e^+e^- \to \pi^+\pi^-\gamma$
$434 \pm 16 \pm 60$	5.4M	[7,8] FUJIKAWA	08	BELL	$\tau^- \to \pi^-\pi^0\nu_\tau$
468 ± 41		[9] SCHAEL	05C	ALEP	$\tau^- \to \pi^-\pi^0\nu_\tau$
455 ± 41	87k	[7,10] ANDERSON	00A	CLE2	$\tau^- \to \pi^-\pi^0\nu_\tau$
~ 374		[11] ABELE	99C	CBAR	$0.0\ \overline{p}d \to \pi^+\pi^-\pi^- p$
275 ± 10		BERTIN	98	OBLX	0.05–$0.405\ \overline{n}p \to \pi^+\pi^+\pi^-$
343 ± 20		[12] ABELE	97	CBAR	$\overline{p}n \to \pi^-\pi^0\pi^0$
310 ± 40		[10] BERTIN	97C	OBLX	$0.0\ \overline{p}p \to \pi^+\pi^-\pi^0$
236 ± 36		BERTIN	97D	OBLX	$0.05\ \overline{p}p \to 2\pi^+ 2\pi^-$
269 ± 31		BISELLO	89	DM2	$e^+e^- \to \pi^+\pi^-$
391 ± 70		DUBNICKA	89	RVUE	$e^+e^- \to \pi^+\pi^-$
218 ± 46		[13] KURDADZE	83	OLYA	0.64–$1.4\ e^+e^- \to \pi^+\pi^-$

[1] Applies the Unitary & Analytic Model of the pion electromagnetic form factor of DUBNICKA 10 to analyze the data of LEES 12G and ABLIKIM 16C.
[2] Applies the Unitary & Analytic Model of the pion electromagnetic form factor of DUBNICKA 10 to analyze the data of ACHASOV 06, AKHMETSHIN 07, AUBERT 09AS, and AMBROSINO 11A.
[3] Applies the Unitary & Analytic Model of the pion electromagnetic form factor of DUBNICKA 10 to analyze the data of FUJIKAWA 08.
[4] From a Dalitz plot analysis in an isobar model with $\rho(1450)$ and $\rho(1700)$ masses and widths floating.
[5] Using the KUHN 90 parametrization of the pion form factor, neglecting ρ–ω interference.
[6] Using the GOUNARIS 68 parametrization of the pion form factor leaving the masses and widths of the $\rho(1450)$, $\rho(1700)$, and $\rho(2150)$ resonances as free parameters of the fit.
[7] From the GOUNARIS 68 parametrization of the pion form factor.
[8] $|F_\pi(0)|^2$ fixed to 1.
[9] From the combined fit of the τ^- data from ANDERSON 00A and SCHAEL 05C and e^+e^- data from the compilation of BARKOV 85, AKHMETSHIN 04, and ALOISIO 05. $\rho(1700)$ mass and width fixed at 1713 MeV and 235 MeV, respectively. Supersedes BARATE 97M.
[10] $\rho(1700)$ mass and width fixed at 1700 MeV and 235 MeV, respectively.
[11] $\rho(1700)$ mass and width fixed at 1780 MeV and 275 MeV respectively.
[12] T-matrix pole.
[13] Using for $\rho(1700)$ mass and width 1600 ± 20 and 300 ± 10 MeV respectively.

$K\overline{K}$ MODE

VALUE (MeV)	EVTS	DOCUMENT ID		TECN	CHG	COMMENT
• • • We do not use the following data for averages, fits, limits, etc. • • •						
$410 \pm 19 \pm 35$	190k	[1] AAIJ	16N	LHCB		$D^0 \to K^0_S K^\pm \pi^\mp$
146.5 ± 10.5	27k	[2] ABELE	99D	CBAR	$\pm$	$0.0\ \overline{p}p \to K^+ K^- \pi^0$

[1] Using the GOUNARIS 68 parameterization with fixed mass.
[2] K-matrix pole. Isospin not determined, could be $\omega(1420)$.

$K\overline{K}^*(892)$ + c.c. MODE

VALUE (MeV)	DOCUMENT ID		TECN	COMMENT
• • • We do not use the following data for averages, fits, limits, etc. • • •				
$418 \pm 25 \pm 4$	AUBERT	08S	BABR	$10.6\ e^+e^- \to K\overline{K}^*(892)\gamma$

$\Gamma_{\rho(1450)^0} - \Gamma_{\rho(1450)^\pm}$

VALUE (MeV)	DOCUMENT ID		TECN	COMMENT
• • • We do not use the following data for averages, fits, limits, etc. • • •				
151.30 ± 140.42	[1] BARTOS	17A	RVUE	$e^+e^- \to \pi^+\pi^-$, $\tau^- \to \pi^-\pi^0\nu_\tau$

[1] Applies the Unitary & Analytic Model of the pion electromagnetic form factor of DUBNICKA 10 to analyze the data of ACHASOV 06, AKHMETSHIN 07, AUBERT 09AS, AMBROSINO 11A, and FUJIKAWA 08.

$\rho(1450)$ DECAY MODES

	Mode	Fraction (Γ_i/Γ)
Γ_1	$\pi\pi$	seen
Γ_2	$\pi^+\pi^-$	seen
Γ_3	4π	seen
Γ_4	$\omega\pi$	
Γ_5	$a_1(1260)\pi$	
Γ_6	$h_1(1170)\pi$	
Γ_7	$\pi(1300)\pi$	
Γ_8	$\rho\rho$	

Downloaded from https://academic.oup.com/ptep/article/2022/8/083C01/6651666 by KIT Library user on 27 September 2022

Γ_9	$\rho(\pi\pi)$ S-wave	
Γ_{10}	e^+e^-	seen
Γ_{11}	$\eta\rho$	seen
Γ_{12}	$a_2(1320)\pi$	not seen
Γ_{13}	$K\overline{K}$	seen
Γ_{14}	K^+K^-	seen
Γ_{15}	$K\overline{K}^*(892)+$ c.c.	possibly seen
Γ_{16}	$\pi^0\gamma$	
Γ_{17}	$\eta\gamma$	seen
Γ_{18}	$f_0(500)\gamma$	not seen
Γ_{19}	$f_0(980)\gamma$	not seen
Γ_{20}	$f_0(1370)\gamma$	not seen
Γ_{21}	$f_2(1270)\gamma$	not seen

$\rho(1450)$ $\Gamma(i)\Gamma(e^+e^-)/\Gamma(\text{total})$

$\Gamma(\pi\pi) \times \Gamma(e^+e^-)/\Gamma_{\text{total}}$ — $\Gamma_1\Gamma_{10}/\Gamma$

VALUE (keV)	DOCUMENT ID		TECN	COMMENT
• • • We do not use the following data for averages, fits, limits, etc. • • •				
0.12	[1] DIEKMAN	88	RVUE	$e^+e^- \to \pi^+\pi^-$
$0.027^{+0.015}_{-0.010}$	[2] KURDADZE	83	OLYA	0.64–1.4 $e^+e^- \to \pi^+\pi^-$

[1] Using total width = 235 MeV.
[2] Using for $\rho(1700)$ mass and width 1600 ± 20 and 300 ± 10 MeV respectively.

$\Gamma(\eta\rho) \times \Gamma(e^+e^-)/\Gamma_{\text{total}}$ — $\Gamma_{11}\Gamma_{10}/\Gamma$

VALUE (eV)	EVTS	DOCUMENT ID		TECN	COMMENT
• • • We do not use the following data for averages, fits, limits, etc. • • •					
335±27±20	13.4k	[1] GRIBANOV	20	CMD3	1.1–2.0 $e^+e^- \to \eta\pi^+\pi^-$
210±24±10		[2] LEES	18	BABR	$e^+e^- \to \eta\pi^+\pi^-$
74±20		[3] AKHMETSHIN	00D	CMD2	$e^+e^- \to \eta\pi^+\pi^-$
91±19		ANTONELLI	88	DM2	$e^+e^- \to \eta\pi^+\pi^-$

[1] Mass and width of the $\rho(770)$ fixed at 775 and 149 MeV, respectively; solution 2 of model 2, $\eta \to \gamma\gamma$ decays used.
[2] Includes non-resonant contribution. The selected fit model includes three ρ excited states. Model uncertainty is 20%.
[3] Using the data of ANTONELLI 88, DOLINSKY 91, and AKHMETSHIN 00D. The energy-independent width of the $\rho(1450)$ and $\rho(1700)$ mesons assumed.

$\Gamma(\eta\gamma) \times \Gamma(e^+e^-)/\Gamma_{\text{total}}$ — $\Gamma_{17}\Gamma_{10}/\Gamma$

VALUE (eV)	DOCUMENT ID		TECN	COMMENT
• • • We do not use the following data for averages, fits, limits, etc. • • •				
<16.4	[1] AKHMETSHIN	05	CMD2	0.60-1.38 $e^+e^- \to \eta\gamma$
2.2±0.5±0.3	[2] AKHMETSHIN	01B	CMD2	$e^+e^- \to \eta\gamma$

[1] From 2γ decay mode of η using 1465 MeV and 310 MeV for the $\rho(1450)$ mass and width. Recalculated by us.
[2] Using the data of AKHMETSHIN 01B on $e^+e^- \to \eta\gamma$, AKHMETSHIN 00D and ANTONELLI 88 on $e^+e^- \to \eta\pi^+\pi^-$. Recalculated by us using width of 226 MeV.

$\Gamma(K\overline{K}^*(892)+\text{c.c.}) \times \Gamma(e^+e^-)/\Gamma_{\text{total}}$ — $\Gamma_{15}\Gamma_{10}/\Gamma$

VALUE (eV)	DOCUMENT ID		TECN	COMMENT
• • • We do not use the following data for averages, fits, limits, etc. • • •				
127±15±6	AUBERT	08S	BABR	10.6 $e^+e^- \to K\overline{K}^*(892)\gamma$

$\rho(1450)$ $\Gamma(i)/\Gamma(\text{total}) \times \Gamma(e^+e^-)/\Gamma(\text{total})$

$\Gamma(\omega\pi)/\Gamma_{\text{total}} \times \Gamma(e^+e^-)/\Gamma_{\text{total}}$ — $\Gamma_4/\Gamma \times \Gamma_{10}/\Gamma$

VALUE (units 10^{-6})	EVTS	DOCUMENT ID		TECN	COMMENT
• • • We do not use the following data for averages, fits, limits, etc. • • •					
2.1±0.4	10.2k	[1] ACHASOV	16D	SND	1.05–2.00 $e^+e^- \to \pi^0\pi^0\gamma$
5.3±0.4	7815	[2] ACHASOV	13	SND	1.05–2.00 $e^+e^- \to \pi^0\pi^0\gamma$

[1] From a phenomenological model based on vector meson dominance with interfering $\rho(770)$, $\rho(1450)$, and $\rho(1700)$. The $\rho(1700)$ mass and width are fixed at 1720 MeV and 250 MeV, respectively. Systematic uncertainties not estimated. Supersedes ACHASOV 13.
[2] From a phenomenological model based on vector meson dominance with the interfering $\rho(1450)$ and $\rho(1700)$ and their widths fixed at 400 and 250 MeV, respectively. Systematic uncertainty not estimated.

$\Gamma(\eta\rho)/\Gamma_{\text{total}} \times \Gamma(e^+e^-)/\Gamma_{\text{total}}$ — $\Gamma_{11}/\Gamma \times \Gamma_{10}/\Gamma$

VALUE (units 10^{-7})	EVTS	DOCUMENT ID		TECN	COMMENT
• • • We do not use the following data for averages, fits, limits, etc. • • •					
7.3±0.3	7.4k	[1] ACHASOV	18	SND	1.22–2.00 $e^+e^- \to \eta\pi^+\pi^-$
$4.3^{+1.1}_{-0.9}$±0.2	4.9k	[2] AULCHENKO	15	SND	1.22–2.00 $e^+e^- \to \eta\pi^+\pi^-$

[1] From the combined fit of AULCHENKO 15 and ACHASOV 18 in the model with the interfering $\rho(1450)$, $\rho(1700)$ and $\rho(2150)$ with the parameters of the $\rho(1450)$ and $\rho(1700)$ floating and the mass and width of the $\rho(2150)$ fixed at 2155 MeV and 320 MeV, respectively. The phases of the resonances are π, 0 and π, respectively.
[2] From a fit to the $e^+e^- \to \eta\pi^+\pi^-$ cross section with vector meson dominance model including $\rho(770)$, $\rho(1450)$, and $\rho(1700)$ decaying exclusively via $\eta\rho(770)$. Masses and widths of vector states are fixed to PDG 14. Coupling constants are assumed to be real.

$\Gamma(f_0(500)\gamma)/\Gamma_{\text{total}} \times \Gamma(e^+e^-)/\Gamma_{\text{total}}$ — $\Gamma_{18}/\Gamma \times \Gamma_{10}/\Gamma$

VALUE (units 10^{-9})	CL%	DOCUMENT ID		TECN	COMMENT
<4.0	90	ACHASOV	11	SND	$e^+e^- \to \pi^0\pi^0\gamma$

$\Gamma(\pi^0\gamma)/\Gamma_{\text{total}} \times \Gamma(e^+e^-)/\Gamma_{\text{total}}$ — $\Gamma_{16}/\Gamma \times \Gamma_{10}/\Gamma$

VALUE (units 10^{-9})	DOCUMENT ID		TECN	COMMENT
• • • We do not use the following data for averages, fits, limits, etc. • • •				
2.3±1.4	[1] ACHASOV	10D	SND	1.075–2.0 $e^+e^- \to \pi^0\gamma$

[1] From a fit of a VMD model with two effective resonances with masses of 1450 MeV and 1700 MeV to describe the excited vector states $\omega(1420)$, $\rho(1450)$, $\omega(1650)$, and $\rho(1700)$. Systematic errors not evaluated.

$\Gamma(f_0(980)\gamma)/\Gamma_{\text{total}} \times \Gamma(e^+e^-)/\Gamma_{\text{total}}$ — $\Gamma_{19}/\Gamma \times \Gamma_{10}/\Gamma$

VALUE (units 10^{-9})	CL%	DOCUMENT ID		TECN	COMMENT
<2.6	90	ACHASOV	11	SND	$e^+e^- \to \pi^0\pi^0\gamma$

$\Gamma(f_0(1370)\gamma)/\Gamma_{\text{total}} \times \Gamma(e^+e^-)/\Gamma_{\text{total}}$ — $\Gamma_{20}/\Gamma \times \Gamma_{10}/\Gamma$

VALUE (units 10^{-9})	CL%	DOCUMENT ID		TECN	COMMENT
<3.5	90	ACHASOV	11	SND	$e^+e^- \to \pi^0\pi^0\gamma$

$\Gamma(f_2(1270)\gamma)/\Gamma_{\text{total}} \times \Gamma(e^+e^-)/\Gamma_{\text{total}}$ — $\Gamma_{21}/\Gamma \times \Gamma_{10}/\Gamma$

VALUE (units 10^{-9})	CL%	DOCUMENT ID		TECN	COMMENT
<0.8	90	[1] ACHASOV	11	SND	$e^+e^- \to \pi^0\pi^0\gamma$

[1] Using Breit-Wigner parametrization of the $\rho(1450)$ with mass and width of 1465 MeV and 400 MeV, respectively.

$\rho(1450)$ BRANCHING RATIOS

$\Gamma(\pi\pi)/\Gamma(4\pi)$ — Γ_1/Γ_3

VALUE	DOCUMENT ID		TECN	COMMENT
• • • We do not use the following data for averages, fits, limits, etc. • • •				
0.37±0.10	[1,2] ABELE	01B	CBAR	0.0 $\overline{p}n \to 5\pi$

[1] $\omega\pi$ not included.
[2] Using ABELE 97.

$\Gamma(K^+K^-)/\Gamma(\pi^+\pi^-)$ — Γ_{14}/Γ_2

VALUE (%)	EVTS	DOCUMENT ID		TECN	COMMENT
30.7±8.4±8.2	20k	[1] LEES	17C	BABR	$J/\psi \to h^+h^-\pi^0$

[1] From Dalitz plot analyses in isobar models.

$\Gamma(\omega\pi)/\Gamma_{\text{total}}$ — Γ_4/Γ

VALUE	EVTS	DOCUMENT ID		TECN	COMMENT
• • • We do not use the following data for averages, fits, limits, etc. • • •					
seen	821	[1] MATVIENKO	15	BELL	$\overline{B}^0 \to D^{*+}\omega\pi^-$
seen	1.6k	ACHASOV	12	SND	$e^+e^- \to \pi^0\pi^0\gamma$
~ 0.21		CLEGG	94	RVUE	

[1] Using Breit-Wigner parameterization of the $\rho(1450)$ and assuming equal probabilities of the $\rho(1450) \to \pi\pi$ and $\rho(1450) \to \omega\pi$ decays.

$\Gamma(\pi\pi)/\Gamma(\omega\pi)$ — Γ_1/Γ_4

VALUE	DOCUMENT ID		TECN
• • • We do not use the following data for averages, fits, limits, etc. • • •			
~ 0.32	CLEGG	94	RVUE

$\Gamma(\omega\pi)/\Gamma(4\pi)$ — Γ_4/Γ_3

VALUE	DOCUMENT ID		TECN
• • • We do not use the following data for averages, fits, limits, etc. • • •			
<0.14	CLEGG	88	RVUE

$\Gamma(a_1(1260)\pi)/\Gamma(4\pi)$ — Γ_5/Γ_3

VALUE	DOCUMENT ID		TECN	COMMENT
• • • We do not use the following data for averages, fits, limits, etc. • • •				
0.27±0.08	[1] ABELE	01B	CBAR	0.0 $\overline{p}n \to 5\pi$

[1] $\omega\pi$ not included.

$\Gamma(h_1(1170)\pi)/\Gamma(4\pi)$ — Γ_6/Γ_3

VALUE	DOCUMENT ID		TECN	COMMENT
• • • We do not use the following data for averages, fits, limits, etc. • • •				
0.08±0.04	[1] ABELE	01B	CBAR	0.0 $\overline{p}n \to 5\pi$

[1] $\omega\pi$ not included.

$\Gamma(\pi(1300)\pi)/\Gamma(4\pi)$ — Γ_7/Γ_3

VALUE	DOCUMENT ID		TECN	COMMENT
• • • We do not use the following data for averages, fits, limits, etc. • • •				
0.37±0.13	[1] ABELE	01B	CBAR	0.0 $\overline{p}n \to 5\pi$

[1] $\omega\pi$ not included.

$\Gamma(\rho\rho)/\Gamma(4\pi)$ — Γ_8/Γ_3

VALUE	DOCUMENT ID		TECN	COMMENT
• • • We do not use the following data for averages, fits, limits, etc. • • •				
0.11±0.05	[1] ABELE	01B	CBAR	0.0 $\overline{p}n \to 5\pi$

[1] $\omega\pi$ not included.

Downloaded from https://academic.oup.com/ptep/article/2022/8/083C01/6651666 by KIT Library user on 27 September 2022

$\Gamma(\rho(\pi\pi)_{S\text{-wave}})/\Gamma(4\pi)$ — Γ_9/Γ_3

VALUE	DOCUMENT ID	TECN	COMMENT
• • • We do not use the following data for averages, fits, limits, etc. • • •			
0.17 ± 0.09	[1] ABELE 01B	CBAR	$0.0\ \overline{p}n \to 5\pi$

[1] $\omega\pi$ not included.

$\Gamma(\eta\rho)/\Gamma_{\text{total}}$ — Γ_{11}/Γ

VALUE	EVTS	DOCUMENT ID	TECN	COMMENT
seen	35	[1] ACHASOV 14	SND	1.15–$2.00\ e^+e^- \to \eta\gamma$
• • • We do not use the following data for averages, fits, limits, etc. • • •				
<0.04		DONNACHIE 87B	RVUE	

[1] From a phenomenological model based on vector meson dominance with $\rho(1450)$ and $\phi(1680)$ masses and widths from the PDG 12.

$\Gamma(\eta\rho)/\Gamma(\omega\pi)$ — Γ_{11}/Γ_4

VALUE	DOCUMENT ID	TECN	COMMENT
• • • We do not use the following data for averages, fits, limits, etc. • • •			
0.081 ± 0.020	[1,2] AULCHENKO 15	SND	1.22–$2.00\ e^+e^- \to \eta\pi^+\pi^-$
~ 0.24	[3] DONNACHIE 91	RVUE	
>2	FUKUI 91	SPEC	$8.95\ \pi^-p \to \omega\pi^0 n$

[1] From a fit to the $e^+e^- \to \eta\pi^+\pi^-$ cross section with vector meson dominance model including $\rho(770)$, $\rho(1450)$, and $\rho(1700)$ decaying exclusively via $\eta\rho(770)$. Masses and widths of vector states are fixed to PDG 14. Coupling constants are assumed to be real.
[2] Reports the inverse of the quoted value as 12.3 ± 3.1.
[3] Using data from BISELLO 91B, DOLINSKY 86 and ALBRECHT 87L.

$\Gamma(\pi\pi)/\Gamma(\eta\rho)$ — Γ_1/Γ_{11}

VALUE	DOCUMENT ID	TECN	COMMENT
• • • We do not use the following data for averages, fits, limits, etc. • • •			
1.3 ± 0.4	[1] AULCHENKO 15	SND	1.22–$2.00\ e^+e^- \to \eta\pi^+\pi^-$

[1] From a fit to the $e^+e^- \to \eta\pi^+\pi^-$ cross section with vector meson dominance model including $\rho(770)$, $\rho(1450)$, and $\rho(1700)$ decaying exclusively via $\eta\rho(770)$. Masses and widths of vector states are fixed to PDG 14. Coupling constants are assumed to be real.

$\Gamma(a_2(1320)\pi)/\Gamma_{\text{total}}$ — Γ_{12}/Γ

VALUE	DOCUMENT ID	TECN	COMMENT
• • • We do not use the following data for averages, fits, limits, etc. • • •			
not seen	AMELIN 00	VES	$37\ \pi^-p \to \eta\pi^+\pi^-n$

$\Gamma(K\overline{K})/\Gamma(\omega\pi)$ — Γ_{13}/Γ_4

VALUE	DOCUMENT ID	TECN
• • • We do not use the following data for averages, fits, limits, etc. • • •		
<0.08	[1] DONNACHIE 91	RVUE

[1] Using data from BISELLO 91B, DOLINSKY 86 and ALBRECHT 87L.

$\Gamma(K\overline{K}^*(892)+\text{c.c.})/\Gamma_{\text{total}}$ — Γ_{15}/Γ

VALUE	DOCUMENT ID	TECN	COMMENT
• • • We do not use the following data for averages, fits, limits, etc. • • •			
possibly seen	COAN 04	CLEO	$\tau^- \to K^-\pi^-K^+\nu_\tau$

$\Gamma(\eta\gamma)/\Gamma_{\text{total}}$ — Γ_{17}/Γ

VALUE	EVTS	DOCUMENT ID	TECN	COMMENT
seen	35	[1] ACHASOV 14	SND	1.15–$2.00\ e^+e^- \to \eta\gamma$

[1] From a phenomenological model based on vector meson dominance with $\rho(1450)$ and $\phi(1680)$ masses and widths from the PDG 12.

$\rho(1450)$ REFERENCES

GRIBANOV	20	JHEP 2001 112	S.S. Gribanov *et al.*	(CMD-3 Collab.)
ACHASOV	18	PR D97 012008	M.N. Achasov *et al.*	(SND Collab.)
LEES	18	PR D97 052007	J.P. Lees *et al.*	(BABAR Collab.)
BARTOS	17	PR D96 113004	E. Bartos *et al.*	
BARTOS	17A	IJMP A32 1750154	E. Bartos *et al.*	
LEES	17C	PR D95 072007	J.P. Lees *et al.*	(BABAR Collab.)
AAIJ	16N	PR D93 052018	R. Aaij *et al.*	(LHCb Collab.)
ABLIKIM	16C	PL B753 629	M. Ablikim *et al.*	(BESIII Collab.)
ACHASOV	16D	PR D94 112001	M.N. Achasov *et al.*	(SND Collab.)
AULCHENKO	15	PR D91 052013	V.M. Aulchenko *et al.*	(SND Collab.)
MATVIENKO	15	PR D92 012013	D. Matvienko *et al.*	(BELLE Collab.)
ACHASOV	14	PR D90 032002	M.N. Achasov *et al.*	(SND Collab.)
PDG	14	CP C38 070001	K. Olive *et al.*	(PDG Collab.)
ACHASOV	13	PR D88 054013	M.N. Achasov *et al.*	(SND Collab.)
ABRAMOWICZ	12	EPJ C72 1869	H. Abramowicz *et al.*	(ZEUS Collab.)
ACHASOV	12	JETPL 94 734	M.N. Achasov *et al.*	
		Translated from ZETFP 94 796.		
LEES	12G	PR D86 032013	J.P. Lees *et al.*	(BABAR Collab.)
PDG	12	PR D86 010001	J. Beringer *et al.*	(PDG Collab.)
ACHASOV	11	JETP 113 75	M.N. Achasov *et al.*	(SND Collab.)
		Translated from ZETF 140 87.		
AMBROSINO	11A	PL B700 102	F. Ambrosino *et al.*	(KLOE Collab.)
ACHASOV	10D	PR D98 112001	M.N. Achasov *et al.*	(SND Collab.)
DUBNICKA	10	APS 60 1	S. Dubnicka, A.Z. Dubnickova	
AUBERT	09AS	PRL 103 231801	B. Aubert *et al.*	(BABAR Collab.)
AUBERT	08S	PR D77 092002	B. Aubert *et al.*	(BABAR Collab.)
FUJIKAWA	08	PR D78 072006	M. Fujikawa *et al.*	(BELLE Collab.)
AKHMETSHIN	07	PL B648 28	R.R. Akhmetshin *et al.*	(Novosibirsk CMD-2 Collab.)
ACHASOV	06	JETP 103 380	M.N. Achasov *et al.*	(Novosibirsk SND Collab.)
		Translated from ZETF 130 437.		
AKHMETSHIN	05	PL B605 26	R.R. Akhmetshin *et al.*	(Novosibirsk CMD-2 Collab.)
ALOISIO	05	PL B606 12	A. Aloisio *et al.*	(KLOE Collab.)
SCHAEL	05C	PRPL 421 191	S. Schael *et al.*	(ALEPH Collab.)
AKHMETSHIN	04	PL B578 285	R.R. Akhmetshin *et al.*	(Novosibirsk CMD-2 Collab.)
COAN	04	PRL 92 232001	T.E. Coan *et al.*	(CLEO Collab.)
AKHMETSHIN	03B	PL B562 173	R.R. Akhmetshin *et al.*	(Novosibirsk CMD-2 Collab.)
ABELE	01B	EPJ C21 261	A. Abele *et al.*	(Crystal Barrel Collab.)
AKHMETSHIN	01B	PL B509 217	R.R. Akhmetshin *et al.*	(Novosibirsk CMD-2 Collab.)
ALEXANDER	01B	PR D64 092001	J.P. Alexander *et al.*	(CLEO Collab.)
AKHMETSHIN	00D	PL B489 125	R.R. Akhmetshin *et al.*	(Novosibirsk CMD-2 Collab.)
AMELIN	00	NP A668 83	D. Amelin *et al.*	(VES Collab.)
ANDERSON	00A	PR D61 112002	S. Anderson *et al.*	(CLEO Collab.)
EDWARDS	00A	PR D61 072003	K.W. Edwards *et al.*	(CLEO Collab.)
ABELE	99C	PL B450 275	A. Abele *et al.*	(Crystal Barrel Collab.)
ABELE	99D	PL B468 178	A. Abele *et al.*	(Crystal Barrel Collab.)
BERTIN	98	PR D57 55	A. Bertin *et al.*	(OBELIX Collab.)
ABELE	97	PL B391 191	A. Abele *et al.*	(Crystal Barrel Collab.)
ACHASOV	97	PR D55 2663	N.N. Achasov *et al.*	(NOVM)
BARATE	97M	ZPHY C76 15	R. Barate *et al.*	(ALEPH Collab.)
BERTIN	97C	PL B408 476	A. Bertin *et al.*	(OBELIX Collab.)
BERTIN	97D	PL B414 220	A. Bertin *et al.*	(OBELIX Collab.)
CLEGG	94	ZPHY C62 455	A.B. Clegg, A. Donnachie	(LANC, MCHS)
BISELLO	91B	NPBPS B21 111	D. Bisello	(DM2 Collab.)
DOLINSKY	91	PRPL 202 99	S.I. Dolinsky *et al.*	(NOVO)
DONNACHIE	91	ZPHY C51 689	A. Donnachie, A.B. Clegg	(MCHS, LANC)
FUKUI	91	PL B257 241	S. Fukui *et al.*	(SUGI, NAGO, KEK, KYOT+)
KUHN	90	ZPHY C48 445	J.H. Kuhn *et al.*	(MPIM)
ARMSTRONG	89E	PL B228 536	T.A. Armstrong, M. Benayoun	(ATHU, BARI, BIRM+)
BISELLO	89	PL B220 321	D. Bisello *et al.*	(DM2 Collab.)
DUBNICKA	89	JP G15 1349	S. Dubnicka *et al.*	(JINR, SLOV)
ANTONELLI	88	PL B212 133	A. Antonelli *et al.*	(DM2 Collab.)
CLEGG	88	ZPHY C40 313	A.B. Clegg, A. Donnachie	(MCHS, LANC)
DIEKMAN	88	PRPL 159 99	B. Diekmann	(BONN)
FUKUI	88	PL B202 441	S. Fukui *et al.*	(SUGI, NAGO, KEK, KYOT+)
ALBRECHT	87L	PL B185 223	H. Albrecht *et al.*	(ARGUS Collab.)
DONNACHIE	87B	ZPHY C34 257	A. Donnachie, A.B. Clegg	(MCHS, LANC)
DOLINSKY	86	PL B174 453	S.I. Dolinsky *et al.*	(NOVO)
BARKOV	85	NP B256 365	L.M. Barkov *et al.*	(NOVO)
KURDADZE	83	JETPL 37 733	L.M. Kurdadze *et al.*	(NOVO)
		Translated from ZETFP 37 613.		
ASTON	80C	PL 92B 211	D. Aston	(BONN, CERN, EPOL, GLAS, LANC+)
BARBER	80C	ZPHY C4 169	D.P. Barber *et al.*	(DARE, LANC, SHEF)
GOUNARIS	68	PRL 21 244	G.J. Gounaris, J.J. Sakurai	

$\eta(1475)$

$I^G(J^{PC}) = 0^+(0^{-+})$

See the $\eta(1405)$ and the related review on "Spectroscopy of Light Meson Resonances."

$\eta(1475)$ MASS

VALUE (MeV)	EVTS	DOCUMENT ID		TECN	COMMENT
1475 ± 4 OUR AVERAGE		Error includes scale factor of 1.4. See the ideogram below.			
$1469\pm14\pm13$	74	ACHARD	07	L3	183–$209\ e^+e^- \to e^+e^-K^0_S K^\pm\pi^\mp$
1460 ± 12	3651	NICHITIU	02	OBLX	$0\ \overline{p}p \to K^+K^-\pi^+\pi^-\pi^0$
$1485\pm8\pm5$	20k	ADAMS	01B	B852	18 GeV $\pi^-p \to K^+K^-\pi^0 n$
1500 ± 10		CICALO	99	OBLX	$0\ \overline{p}p \to K^\pm K^0_S\pi^\mp\pi^+\pi^-$
1464 ± 10		BERTIN	97	OBLX	$0\ \overline{p}p \to K^\pm(K^0)\pi^\mp\pi^+\pi^-$
1460 ± 10		BERTIN	95	OBLX	$0\ \overline{p}p \to K\overline{K}\pi\pi\pi$
$1490^{+14}_{-8}{}^{+3}_{-16}$	1100	BAI	90C	MRK3	$J/\psi \to \gamma K^0_S K^\pm\pi^\mp$
1475 ± 4		RATH	89	MPS	$21.4\ \pi^-p \to nK^0_S K^0_S\pi^0$
• • • We do not use the following data for averages, fits, limits, etc. • • •					
$1477\pm7\pm13$		[1] ABLIKIM	18I	BES3	$J/\psi \to \gamma\gamma\phi(1020)$
$1565\pm8^{+0}_{-63}$		[2] ABLIKIM	15T	BES3	$J/\psi \to \gamma K^0_S K^0_S\eta$
1421 ± 14		AUGUSTIN	92	DM2	$J/\psi \to \gamma K\overline{K}\pi$

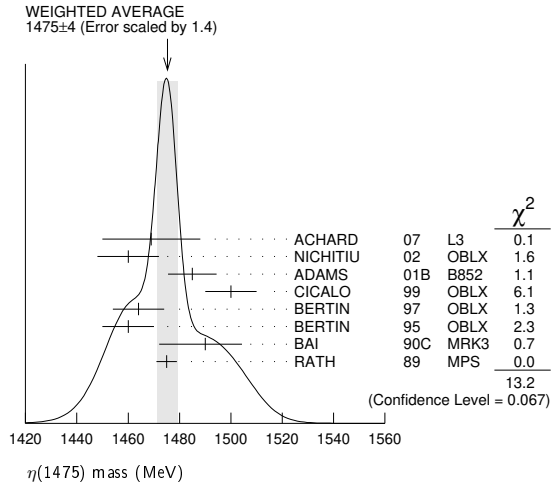

[1] From a fit to $\gamma\phi$ invariant mass. Angular analysis consistent with $J^{PC} = 0^{-+}$. Other J^{PC} not excluded.
[2] Could also be the $\eta(1405)$.

Downloaded from https://academic.oup.com/ptep/article/2022/8/083C01/6651666 by KIT Library user on 27 September 2022

$\eta(1475)$ WIDTH

VALUE (MeV)	EVTS	DOCUMENT ID		TECN	COMMENT
90± 9 OUR AVERAGE		Error includes scale factor of 1.6. See the ideogram below.			
67±18± 7	74	ACHARD	07	L3	183–209 $e^+e^- \to e^+e^- K^0_S K^\pm \pi^\mp$
120±15	3651	NICHITIU	02	OBLX	0 $\overline{p}p \to K^+K^-\pi^+\pi^-\pi^0$
98±18± 3	20k	ADAMS	01B	B852	18 GeV $\pi^- p \to K^+K^-\pi^0 n$
100±20		CICALO	99	OBLX	0 $\overline{p}p \to K^\pm K^0_S \pi^\mp \pi^+\pi^-$
105±15		BERTIN	97	OBLX	0.0 $\overline{p}p \to K^\pm (K^0) \pi^\mp \pi^+\pi^-$
105±15		BERTIN	95	OBLX	0 $\overline{p}p \to K\overline{K}\pi\pi\pi$
54^{+37+13}_{-21-24}		BAI	90C	MRK3	$J/\psi \to \gamma K^0_S K^\pm \pi^\mp$
51±13		RATH	89	MPS	21.4 $\pi^- p \to n K^0_S K^0_S \pi^0$
• • • We do not use the following data for averages, fits, limits, etc. • • •					
118±22±17		[1] ABLIKIM	18I	BES3	$J/\psi \to \gamma\gamma\phi(1020)$
45^{+14+21}_{-13-28}		[2] ABLIKIM	15T	BES3	$J/\psi \to \gamma K^0_S K^0_S \eta$
63±18		AUGUSTIN	92	DM2	$J/\psi \to \gamma K\overline{K}\pi$

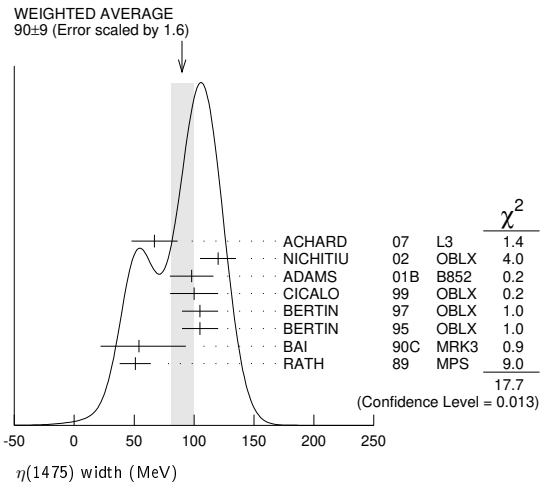

[1] From a fit to $\gamma\phi$ invariant mass. Angular analysis consistent with $J^{PC} = 0^{-+}$. Other J^{PC} not excluded.

[2] Could also be the $\eta(1405)$.

$\eta(1475)$ DECAY MODES

	Mode	Fraction (Γ_i/Γ)
Γ_1	$K\overline{K}\pi$	seen
Γ_2	$K\overline{K}^*(892)+$ c.c.	seen
Γ_3	$a_0(980)\pi$	seen
Γ_4	$\gamma\gamma$	seen
Γ_5	$K^0_S K^0_S \eta$	possibly seen
Γ_6	$\gamma\phi(1020)$	possibly seen

$\eta(1475)$ $\Gamma(i)\Gamma(\gamma\gamma)/\Gamma(\text{total})$

$\Gamma(K\overline{K}\pi) \times \Gamma(\gamma\gamma)/\Gamma_{\text{total}}$ — $\Gamma_1\Gamma_4/\Gamma$

VALUE (keV)	CL%	EVTS	DOCUMENT ID		TECN	COMMENT
0.23±0.05±0.05		74	[1] ACHARD	07	L3	183–209 $e^+e^- \to e^+e^- K^0_S K^\pm \pi^\mp$
• • • We do not use the following data for averages, fits, limits, etc. • • •						
< 0.089	90		[2,3] AHOHE	05	CLE2	10.6 $e^+e^- \to e^+e^- K^0_S K^\pm \pi^\mp$

[1] Supersedes ACCIARRI 01G. Using $B(K^0_S \to \pi^+\pi^-) = 0.6895$.

[2] Using $\eta(1475)$ mass of 1481 MeV and width of 48 MeV. The upper limit increases to 0.140 keV if the world average value, 87 MeV, of the width is used.

[3] Assuming three-body phase-space decay to $K^0_S K^\pm \pi^\mp$.

$\eta(1475)$ BRANCHING RATIOS

$\Gamma(K\overline{K}^*(892)+\text{c.c.})/\Gamma(K\overline{K}\pi)$ — Γ_2/Γ_1

VALUE	DOCUMENT ID		TECN	COMMENT
• • • We do not use the following data for averages, fits, limits, etc. • • •				
0.50±0.10	[1] BAILLON	67	HBC	0.0 $\overline{p}p \to K\overline{K}\pi\pi\pi$

[1] Data could also refer to $\eta(1405)$.

$\Gamma(K\overline{K}^*(892)+\text{c.c.})/[\Gamma(K\overline{K}^*(892)+\text{c.c.}) + \Gamma(a_0(980)\pi)]$ — $\Gamma_2/(\Gamma_2+\Gamma_3)$

VALUE	CL%	DOCUMENT ID		TECN	COMMENT
• • • We do not use the following data for averages, fits, limits, etc. • • •					
<0.25	90	EDWARDS	82E	CBAL	$J/\psi \to K^+K^-\pi^0\gamma$

$\Gamma(\gamma\gamma)/\Gamma(K\overline{K}\pi)$ — Γ_4/Γ_1

VALUE	CL%	DOCUMENT ID		TECN	COMMENT
<1.27 × 10⁻³	90	[1] ABLIKIM	18O	BES3	$\psi(2S) \to \pi^+\pi^-\gamma\gamma\gamma$

[1] Using results from BAI 00D.

$\Gamma(\gamma\phi(1020))/\Gamma_{\text{total}}$ — Γ_6/Γ

VALUE	DOCUMENT ID		TECN	COMMENT
possibly seen	[1] ABLIKIM	18I	BES3	$J/\psi \to \gamma\gamma\phi(1020)$

[1] Seen as a peak in $\gamma\phi$ invariant mass. Angular analysis consistent with $J^{PC} = 0^{-+}$. Other J^{PC} not excluded. Also see $\eta(1405)$.

$\eta(1475)$ REFERENCES

ABLIKIM	18I	PR D97 051101	M. Ablikim et al.	(BESIII Collab.)
ABLIKIM	18O	PR D97 072014	M. Ablikim et al.	(BESIII Collab.)
ABLIKIM	15T	PRL 115 091803	M. Ablikim et al.	(BESIII Collab.)
ACHARD	07	JHEP 0703 018	P. Achard et al.	(L3 Collab.)
AHOHE	05	PR D71 072001	R. Ahohe et al.	(CLEO Collab.)
NICHITIU	02	PL B545 261	F. Nichitiu et al.	(OBELIX Collab.)
ACCIARRI	01G	PL B501 1	M. Acciarri et al.	(L3 Collab.)
ADAMS	01B	PL B516 264	G.S. Adams et al.	(BNL E852 Collab.)
BAI	00D	PL B476 25	J.Z. Bai et al.	(BES Collab.)
CICALO	99	PL B462 453	C. Cicalo et al.	(OBELIX Collab.)
BERTIN	97	PL B400 226	A. Bertin et al.	(OBELIX Collab.)
BERTIN	95	PL B361 187	A. Bertin et al.	(OBELIX Collab.)
AUGUSTIN	92	PR D46 1951	J.E. Augustin, G. Cosme	(DM2 Collab.)
BAI	90C	PRL 65 2507	Z. Bai et al.	(Mark III Collab.)
RATH	89	PR D40 693	M.G. Rath et al.	(NDAM, BRAN, BNL, CUNY+)
EDWARDS	82E	PRL 49 259	C. Edwards et al.	(CIT, HARV, PRIN+)
BAILLON	67	NC 50A 393	P.H. Baillon et al.	(CERN, CDEF, IRAD)

$f_0(1500)$

$I^G(J^{PC}) = 0^+(0^{++})$

See the review on "Spectroscopy of Light Meson Resonances."

$f_0(1500)$ MASS

VALUE (MeV)	EVTS	DOCUMENT ID		TECN	COMMENT
1506 ± 6 OUR AVERAGE		Error includes scale factor of 1.4. See the ideogram below.			
1515 ±12		[1] BARBERIS	00A		450 $pp \to p_f \eta\eta p_s$
1511 ± 9		[1,2] BARBERIS	00C		450 $pp \to p_f 4\pi p_s$
1510 ± 8		[1] BARBERIS	00E		450 $pp \to p_f \eta\eta p_s$
1522 ±25		[1] BERTIN	98	OBLX	0.05–0.405 $\overline{n}p \to \pi^+\pi^+\pi^-$
1449 ±20		[1] BERTIN	97C	OBLX	0.0 $\overline{p}p \to \pi^+\pi^-\pi^0$
1500 ±10		[3] AMSLER	95D	CBAR	0.0 $\overline{p}p \to \pi^0\pi^0\pi^0$, $\pi^0\eta\eta$, $\pi^0\pi^0\eta$
• • • We do not use the following data for averages, fits, limits, etc. • • •					
1450 ±10		[4] RODAS	22	RVUE	$J/\psi(1S) \to \gamma(\pi\pi, K\overline{K})$
1483 ±15		[1] SARANTSEV	21	RVUE	$J/\psi(1S) \to \gamma(\pi\pi, K\overline{K}, \eta\eta, \omega\phi)$
1496 ± $1.2^{+4.4}_{-26.4}$		[5] ALBRECHT	20	RVUE	0.9 $\overline{p}p \to \pi^0\pi^0\eta$, $\pi^0\eta\eta$, $\pi^0K^+K^-$
1465 ±18		[6] ROPERTZ	18	RVUE	$\overline{B}^0_s \to J/\psi(\pi^+\pi^-/K^+K^-)$
1447 ±16 ± 13	163	[7,8] DOBBS	15		$J/\psi \to \gamma\pi^+\pi^-$
1442 ± 9 ± 4	261	[7,8] DOBBS	15		$\psi(2S) \to \gamma\pi^+\pi^-$
1460.9± 2.9		[9] AAIJ	14BR	LHCB	$\overline{B}^0_s \to J/\psi\pi^+\pi^-$
1468 $^{+14}_{-15}$ $^{+23}_{-74}$	5.5k	[10] ABLIKIM	13N	BES3	$e^+e^- \to J/\psi \to \gamma\eta\eta$
1486 ±10		[1] ANISOVICH	09	RVUE	0.0 $\overline{p}p$, πN
1470 ±60	568	[11] KLEMPT	08	E791	$D^+_s \to \pi^-\pi^+\pi^+$
1470 $^{+6}_{-7}$ $^{+72}_{-255}$		[12] UEHARA	08A	BELL	10.6 $e^+e^- \to e^+e^-\pi^0\pi^0$
1466 ± 6 ± 20		[13] ABLIKIM	06V	BES2	$e^+e^- \to J/\psi \to \gamma\pi^+\pi^-$
1495 ± 4		AMSLER	06	CBAR	0.9 $\overline{p}p \to K^+K^-\pi^0$
1539 ±20	9.9k	AUBERT	06O	BABR	$B^+ \to K^+K^+K^-$
1473 ± 5	80k	[13,14] UMAN	06	E835	5.2 $\overline{p}p \to \eta\eta\pi^0$
1478 ± 6		VLADIMIRSK...06		SPEC	40 $\pi^-p \to K^0_S K^0_S n$
1493 ± 7		[13] BINON	05	GAMS	33 $\pi^-p \to \eta\eta n$
1524 ±14	1400	[15] GARMASH	05	BELL	$B^+ \to K^+K^+K^-$
1489 $^{+8}_{-4}$		[16] ANISOVICH	03	RVUE	
1490 ±30		[13] ABELE	01	CBAR	0.0 $\overline{p}d \to \pi^-4\pi^0 p$
1497 ±10		[13] BARBERIS	99	OMEG	450 $pp \to p_s p_f K^+K^-$
1502 ±10		[13] BARBERIS	99B	OMEG	450 $pp \to p_s p_f \pi^+\pi^-$
1502 ±12 ± 10		[17] BARBERIS	99D	OMEG	450 $pp \to K^+K^-$, $\pi^+\pi^-$
1530 ±45		[13] BELLAZZINI	99	GAM4	450 $pp \to pp\pi^0\pi^0$
1505 ±18		[13] FRENCH	99		300 $pp \to p_f(K^+K^-)p_s$
1447 ±27		[18] KAMINSKI	99	RVUE	$\pi\pi \to \pi\pi$, $K\overline{K}$, $\sigma\sigma$
1580 ±80		[13] ALDE	98	GAM4	100 $\pi^-p \to \pi^0\pi^0 n$
1499 ± 8		[1] ANISOVICH	98B	RVUE	Compilation
~ 1520		REYES	98	SPEC	800 $pp \to p_s p_f K^0_S K^0_S$

Downloaded from https://academic.oup.com/ptep/article/2022/8/083C01/6651666 by KIT Library user on 27 September 2022

1510 ±20			[1] BARBERIS	97B	OMEG	450 $pp \to pp2(\pi^+\pi^-)$
~ 1475			FRABETTI	97D	E687	$D_s^\pm \to \pi^\mp\pi^\pm\pi^\pm$
~ 1505			ABELE	96	CBAR	0.0 $\overline{p}p \to 5\pi^0$
1515 ±20			ABELE	96B	CBAR	0.0 $\overline{p}p \to \pi^0 K_L^0 K_L^0$
1500 ± 8			[1] ABELE	96C	RVUE	Compilation
1460 ±20		120	[13] AMELIN	96B	VES	37 $\pi^- A \to \eta\eta\pi^- A$
1500 ± 8			BUGG	96	RVUE	
1500 ±15			[19] AMSLER	95B	CBAR	0.0 $\overline{p}p \to 3\pi^0$
1505 ±15			[20] AMSLER	95C	CBAR	0.0 $\overline{p}p \to \eta\eta\pi^0$
1445 ± 5			[21] ANTINORI	95	OMEG	300,450 $pp \to pp2(\pi^+\pi^-)$
1497 ±30			[13] ANTINORI	95	OMEG	300,450 $pp \to pp\pi^+\pi^-$
~ 1505			BUGG	95	MRK3	$J/\psi \to \gamma\pi^+\pi^-\pi^+\pi^-$
1446 ± 5			[13] ABATZIS	94	OMEG	450 $pp \to pp2(\pi^+\pi^-)$
1545 ±25			[13] AMSLER	94E	CBAR	0.0 $\overline{p}p \to \pi^0\eta\eta'$
1520 ±25			[1,22] ANISOVICH	94	CBAR	0.0 $\overline{p}p \to 3\pi^0, \pi^0\eta\eta$
1505 ±20			[1,23] BUGG	94	RVUE	$\overline{p}p \to 3\pi^0, \eta\eta\pi^0, \eta\pi^0\pi^0$
1560 ±25			[13] AMSLER	92	CBAR	0.0 $\overline{p}p \to \pi^0\eta\eta$
1550 ±45	± 30		[13] BELADIDZE	92C	VES	36 π^-Be $\to \pi^-\eta'\eta$Be
1449 ± 4			[13] ARMSTRONG	89E	OMEG	300 $pp \to pp2(\pi^+\pi^-)$
1610 ±20			[13] ALDE	88	GAM4	300 $\pi^- N \to \pi^- N2\eta$
~ 1525			ASTON	88D	LASS	11 $K^- p \to K_S^0 K_S^0 \Lambda$
1570 ±20		600	[13] ALDE	87	GAM4	100 $\pi^- p \to 4\pi^0 n$
1575 ±45			[24] ALDE	86D	GAM4	100 $\pi^- p \to 2\eta n$
1568 ±33			[13] BINON	84C	GAM2	38 $\pi^- p \to \eta\eta' n$
1592 ±25			[13] BINON	83	GAM2	38 $\pi^- p \to 2\eta n$
1525 ± 5			[13] GRAY	83	DBC	0.0 $\overline{p}N \to 3\pi$

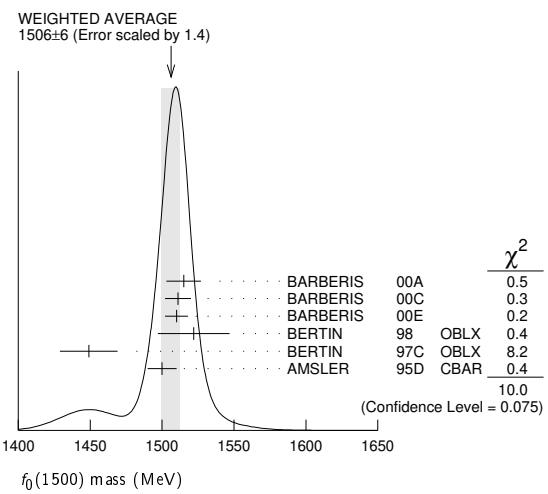

[1] T-matrix pole.
[2] Average between $\pi^+\pi^- 2\pi^0$ and $2(\pi^+\pi^-)$.
[3] T-matrix pole. Coupled-channel analysis of AMSLER 95B, AMSLER 95C, and AMSLER 94D.
[4] T-matrix pole from coupled channel K-matrix fit to data on $J/\psi \to \gamma\pi^0\pi^0$ (ABLIKIM 15AE) and $J/\psi \to \gamma K_S^0 K_S^0$ (ABLIKIM 18AA).
[5] T-matrix pole, 5 poles, 5 channels, including scattering data from HYAMS 75 ($\pi\pi$), LONGACRE 86 ($K\overline{K}$), BINON 83 ($\eta\eta$), and BINON 84C ($\eta\eta'$).
[6] T-matrix pole of 3 channel unitary model fit to data from AAIJ 14BR and AAIJ 17V extracted using Pade approximants.
[7] Using CLEO-c data but not authored by the CLEO Collaboration.
[8] From a fit to a Breit-Wigner line shape with fixed $\Gamma = 109$ MeV.
[9] Solution I, statistical error only.
[10] From partial wave analysis including all possible combinations of 0^{++}, 2^{++}, and 4^{++} resonances.
[11] Reanalysis of AITALA 01A data. This state could also be $f_0(1370)$.
[12] Breit-Wigner mass. May also be the $f_0(1370)$.
[13] Breit-Wigner mass.
[14] Statistical error only.
[15] Breit-Wigner, solution 1, PWA ambiguous.
[16] K-matrix pole from combined analysis of $\pi^- p \to \pi^0\pi^0 n$, $\pi^- p \to K\overline{K}n$, $\pi^+\pi^- \to \pi^+\pi^-$, $\overline{p}p \to \pi^0\pi^0\pi^0$, $\pi^0\eta\eta$, $\pi^0\pi^0\eta$, $\pi^+\pi^-\pi^0$, $K^+K^-\pi^0$, $K_S^0 K_S^0\pi^0$, $K^+K_S^0\pi^-$ at rest, $\overline{p}n \to \pi^-\pi^-\pi^+$, $K_S^0 K^-\pi^0$, $K_S^0 K_S^0\pi^-$ at rest.
[17] Supersedes BARBERIS 99 and BARBERIS 99B.
[18] T-matrix pole on sheet $- - +$.
[19] T-matrix pole, supersedes ANISOVICH 94.
[20] T-matrix pole, supersedes ANISOVICH 94 and AMSLER 92.
[21] Supersedes ABATZIS 94, ARMSTRONG 89E. Breit-Wigner mass.
[22] From a simultaneous analysis of the annihilations $\overline{p}p \to 3\pi^0, \pi^0\eta\eta$.
[23] Reanalysis of ANISOVICH 94 data.
[24] From central value and spread of two solutions. Breit-Wigner mass.

$f_0(1500)$ WIDTH

VALUE (MeV)	EVTS	DOCUMENT ID		TECN	COMMENT
112 ± 9 OUR AVERAGE					
110 ± 24		[1] BARBERIS	00A		450 $pp \to p_f\eta\eta p_s$
102 ± 18		[1,2] BARBERIS	00C		450 $pp \to p_f 4\pi p_s$
110 ± 16		[1] BARBERIS	00E		450 $pp \to p_f\eta\eta p_s$
108 ± 33		[1] BERTIN	98	OBLX	0.05–0.405 $\overline{n}p \to \pi^+\pi^+\pi^-$
114 ± 30		[1] BERTIN	97C	OBLX	0.0 $\overline{p}p \to \pi^+\pi^-\pi^0$
154 ± 30		[3] AMSLER	95D	CBAR	0.0 $\overline{p}p \to \pi^0\pi^0\pi^0$, $\pi^0\eta\eta$, $\pi^0\pi^0\eta$
• • • We do not use the following data for averages, fits, limits, etc. • • •					
106 ± 16		[4] RODAS	22	RVUE	$J/\psi(1S) \to \gamma(\pi\pi, K\overline{K})$
116 ± 12		[1] SARANTSEV	21	RVUE	$J/\psi(1S) \to \gamma(\pi\pi, K\overline{K}, \eta\eta, \omega\phi)$
$80.8 \pm 0.6^{+20.0}_{-5.0}$		[5] ALBRECHT	20	RVUE	0.9 $\overline{p}p \to \pi^0\pi^0\eta$, $\pi^0\eta\eta$, $\pi^0 K^+K^-$
100 ± 18		[6] ROPERTZ	18	RVUE	$\overline{B}_s^0 \to J/\psi(\pi^+\pi^-/K^+K^-)$
124 ± 7		[7] AAIJ	14BR	LHCB	$\overline{B}_s^0 \to J/\psi\pi^+\pi^-$
$136^{+41}_{-26}{}^{+28}_{-100}$	5.5k	[8] ABLIKIM	13N	BES3	$e^+e^- \to J/\psi \to \gamma\eta\eta$
114 ± 10		[1] ANISOVICH	09	RVUE	0.0 $\overline{p}p$, πN
$90^{+2}_{-1}{}^{+50}_{-22}$		[9] UEHARA	08A	BELL	10.6 $e^+e^- \to e^+e^-\pi^0\pi^0$
$108^{+14}_{-11} \pm 25$		[10] ABLIKIM	06V	BES2	$e^+e^- \to J/\psi \to \gamma\pi^+\pi^-$
121 ± 8		AMSLER	06	CBAR	0.9 $\overline{p}p \to K^+K^-\pi^0$
257 ± 33	9.9k	AUBERT	06O	BABR	$B^+ \to K^+K^+K^-$
108 ± 9	80k	[10,11] UMAN	06	E835	5.2 $\overline{p}p \to \eta\eta\pi^0$
119 ± 10		VLADIMIRSK...	06	SPEC	40 $\pi^- p \to K_S^0 K_S^0 n$
90 ± 15		[10] BINON	05	GAMS	33 $\pi^- p \to \eta\eta n$
136 ± 23	1400	[12] GARMASH	05	BELL	$B^+ \to K^+K^+K^-$
102 ± 10		[13] ANISOVICH	03	RVUE	
140 ± 40		[10] ABELE	01	CBAR	0.0 $\overline{p}d \to \pi^- 4\pi^0 p$
104 ± 25		[10] BARBERIS	99	OMEG	450 $pp \to p_s p_f K^+K^-$
131 ± 15		[10] BARBERIS	99B	OMEG	450 $pp \to p_s p_f \pi^+\pi^-$
98 ± 18 ± 16		[14] BARBERIS	99D	OMEG	450 $pp \to K^+K^-$, $\pi^+\pi^-$
160 ± 50		[10] BELLAZZINI	99	GAM4	450 $pp \to pp\pi^0\pi^0$
100 ± 33		[10] FRENCH	99		300 $pp \to p_f(K^+K^-)p_s$
108 ± 46		[15] KAMINSKI	99	RVUE	$\pi\pi \to \pi\pi$, $K\overline{K}$, $\sigma\sigma$
280 ±100		[10] ALDE	98	GAM4	100 $\pi^- p \to \pi^0\pi^0 n$
130 ± 20		[1] ANISOVICH	98B	RVUE	Compilation
120 ± 35		[1] BARBERIS	97B	OMEG	450 $pp \to pp2(\pi^+\pi^-)$
~ 100		FRABETTI	97D	E687	$D_s^\pm \to \pi^\mp\pi^\pm\pi^\pm$
~ 169		ABELE	96	CBAR	0.0 $\overline{p}p \to 5\pi^0$
105 ± 15		ABELE	96B	CBAR	0.0 $\overline{p}p \to \pi^0 K_L^0 K_L^0$
100 ± 30	120	[10] AMELIN	96B	VES	37 $\pi^- A \to \eta\eta\pi^- A$
132 ± 15		BUGG	96	RVUE	
120 ± 25		[16] AMSLER	95B	CBAR	0.0 $\overline{p}p \to 3\pi^0$
120 ± 30		[17] AMSLER	95C	CBAR	0.0 $\overline{p}p \to \eta\eta\pi^0$
65 ± 10		[18] ANTINORI	95	OMEG	300,450 $pp \to pp2(\pi^+\pi^-)$
199 ± 30		[10] ANTINORI	95	OMEG	300,450 $pp \to pp\pi^+\pi^-$
56 ± 12		[10] ABATZIS	94	OMEG	450 $pp \to pp2(\pi^+\pi^-)$
100 ± 40		[10] AMSLER	94E	CBAR	0.0 $\overline{p}p \to \pi^0\eta\eta'$
148^{+20}_{-25}		[1,19] ANISOVICH	94	CBAR	0.0 $\overline{p}p \to 3\pi^0, \pi^0\eta\eta$
150 ± 20		[1,20] BUGG	94	RVUE	$\overline{p}p \to 3\pi^0$, $\eta\eta\pi^0$, $\eta\pi^0\pi^0$
245 ± 50		[10] AMSLER	92	CBAR	0.0 $\overline{p}p \to \pi^0\eta\eta$
153 ± 67 ± 50		[10] BELADIDZE	92C	VES	36 π^-Be $\to \pi^-\eta'\eta$Be
78 ± 18		[10] ARMSTRONG	89E	OMEG	300 $pp \to pp2(\pi^+\pi^-)$
170 ± 40		[10] ALDE	88	GAM4	300 $\pi^- N \to \pi^- N2\eta$
150 ± 20	600	[10] ALDE	87	GAM4	100 $\pi^- p \to 4\pi^0 n$
265 ± 65		[21] ALDE	86D	GAM4	100 $\pi^- p \to 2\eta n$
260 ± 60		[10] BINON	84C	GAM2	38 $\pi^- p \to \eta\eta' n$
210 ± 40		[10] BINON	83	GAM2	38 $\pi^- p \to 2\eta n$
101 ± 13		[10] GRAY	83	DBC	0.0 $\overline{p}N \to 3\pi$

[1] T-matrix pole.
[2] Average between $\pi^+\pi^- 2\pi^0$ and $2(\pi^+\pi^-)$.
[3] T-matrix pole. Coupled-channel analysis of AMSLER 95B, AMSLER 95C, and AMSLER 94D.
[4] T-matrix pole from coupled channel K-matrix fit to data on $J/\psi \to \gamma\pi^0\pi^0$ (ABLIKIM 15AE) and $J/\psi \to \gamma K_S^0 K_S^0$ (ABLIKIM 18AA).
[5] T-matrix pole, 5 poles, 5 channels, including scattering data from HYAMS 75 ($\pi\pi$), LONGACRE 86 ($K\overline{K}$), BINON 83 ($\eta\eta$), and BINON 84C ($\eta\eta'$).
[6] T-matrix pole of 3 channel unitary model fit to data from AAIJ 14BR and AAIJ 17V extracted using Pade approximants.
[7] Solution I, statistical error only.

Downloaded from https://academic.oup.com/ptep/article/2022/8/083C01/6651666 by KIT Library user on 27 September 2022

[8] From partial wave analysis including all possible combinations of 0^{++}, 2^{++}, and 4^{++} resonances.
[9] Breit-Wigner width. May also be the $f_0(1370)$.
[10] Breit-Wigner width.
[11] Statistical error only.
[12] Breit-Wigner, solution 1, PWA ambiguous.
[13] K-matrix pole from combined analysis of $\pi^- p \to \pi^0\pi^0 n$, $\pi^- p \to K\overline{K} n$, $\pi^+\pi^- \to \pi^+\pi^-$, $\overline{p}p \to \pi^0\pi^0\pi^0$, $\pi^0\eta\eta$, $\pi^0\pi^0\eta$, $\pi^+\pi^-\pi^0$, $K^+K^-\pi^0$, $K^0_S K^0_S \pi^0$, $K^+K^0_S\pi^-$ at rest, $\overline{p}n \to \pi^-\pi^-\pi^+$, $K^0_S K^-\pi^0$, $K^0_S K^0_S \pi^-$ at rest.
[14] Supersedes BARBERIS 99 and BARBERIS 99B.
[15] T-matrix pole on sheet $- - +$.
[16] T-matrix pole, supersedes ANISOVICH 94.
[17] T-matrix pole, supersedes ANISOVICH 94 and AMSLER 92.
[18] Supersedes ABATZIS 94, ARMSTRONG 89E. Breit-Wigner mass.
[19] From a simultaneous analysis of the annihilations $\overline{p}p \to 3\pi^0, \pi^0\eta\eta$.
[20] Reanalysis of ANISOVICH 94 data.
[21] From central value and spread of two solutions. Breit-Wigner mass.

$f_0(1500)$ DECAY MODES

	Mode	Fraction (Γ_i/Γ)	Scale factor
Γ_1	$\pi\pi$	(34.5 ± 2.2) %	1.2
Γ_2	$\pi^+\pi^-$	seen	
Γ_3	$2\pi^0$	seen	
Γ_4	4π	(48.9 ± 3.3) %	1.2
Γ_5	$4\pi^0$	seen	
Γ_6	$2\pi^+2\pi^-$	seen	
Γ_7	$2(\pi\pi)_S$-wave	seen	
Γ_8	$\rho\rho$	seen	
Γ_9	$\pi(1300)\pi$	seen	
Γ_{10}	$a_1(1260)\pi$	seen	
Γ_{11}	$\eta\eta$	(6.0 ± 0.9) %	1.1
Γ_{12}	$\eta\eta'(958)$	(2.2 ± 0.8) %	1.4
Γ_{13}	$K\overline{K}$	(8.5 ± 1.0) %	1.1
Γ_{14}	$\gamma\gamma$	not seen	

CONSTRAINED FIT INFORMATION

An overall fit to 6 branching ratios uses 10 measurements and one constraint to determine 5 parameters. The overall fit has a $\chi^2 = 5.6$ for 6 degrees of freedom.

The following *off-diagonal* array elements are the correlation coefficients $\langle \delta x_i \delta x_j \rangle / (\delta x_i \cdot \delta x_j)$, in percent, from the fit to the branching fractions, $x_i \equiv \Gamma_i/\Gamma_{total}$. The fit constrains the x_i whose labels appear in this array to sum to one.

x_4	−88			
x_{11}	27	−56		
x_{12}	3	−32	26	
x_{13}	43	−64	20	2
	x_1	x_4	x_{11}	x_{12}

$f_0(1500)$ $\Gamma(i)\Gamma(\gamma\gamma)/\Gamma(\text{total})$

$\Gamma(\pi\pi) \times \Gamma(\gamma\gamma)/\Gamma_{total}$ — $\Gamma_1\Gamma_{14}/\Gamma$

VALUE (eV)	CL%	DOCUMENT ID		TECN	COMMENT
• • • We do not use the following data for averages, fits, limits, etc. • • •					
$33^{+12+1809}_{-\ 6-\ 21}$		[1] UEHARA	08A	BELL	$10.6\ e^+e^- \to e^+e^-\pi^0\pi^0$
not seen		ACCIARRI	01H	L3	$\gamma\gamma \to K^0_S K^0_S$, $E^{ee}_{cm}=$ 91, 183–209 GeV
<460	95	BARATE	00E	ALEP	$\gamma\gamma \to \pi^+\pi^-$

[1] May also be the $f_0(1370)$. Multiplied by us by 3 to obtain the $\pi\pi$ value.

$f_0(1500)$ BRANCHING RATIOS

$\Gamma(\pi\pi)/\Gamma_{total}$ — Γ_1/Γ

VALUE	DOCUMENT ID		TECN
• • • We do not use the following data for averages, fits, limits, etc. • • •			
0.454 ± 0.104	BUGG	96	RVUE

$\Gamma(\pi^+\pi^-)/\Gamma_{total}$ — Γ_2/Γ

VALUE	DOCUMENT ID		TECN	COMMENT
seen	BERTIN	98	OBLX	0.05–0.405 $\overline{n}p \to \pi^+\pi^+\pi^-$
• • • We do not use the following data for averages, fits, limits, etc. • • •				
possibly seen	FRABETTI	97D	E687	$D^\pm_s \to \pi^\mp\pi^\pm\pi^\pm$

$\Gamma(4\pi)/\Gamma(\pi\pi)$ — Γ_4/Γ_1

VALUE	DOCUMENT ID		TECN	COMMENT
1.42±0.18 OUR FIT Error includes scale factor of 1.2.				
1.42±0.18 OUR AVERAGE Error includes scale factor of 1.2.				
1.37 ± 0.16	BARBERIS	00D		450 $pp \to p_f 4\pi p_s$
$2.1\ \pm0.6$	[1] AMSLER	98	RVUE	
• • • We do not use the following data for averages, fits, limits, etc. • • •				
$2.1\ \pm0.2$	[2] ANISOVICH	02D	SPEC	Combined fit
$3.4\ \pm0.8$	[1] ABELE	96	CBAR	0.0 $\overline{p}p \to 5\pi^0$

[1] Excluding $\rho\rho$ contribution to 4π.
[2] From a combined K-matrix analysis of Crystal Barrel (0. $p\overline{p} \to \pi^0\pi^0\pi^0$, $\pi^0\eta\eta$, $\pi^0\pi^0\eta$), GAMS ($\pi p \to \pi^0\pi^0 n$, $\eta\eta n$, $\eta\eta' n$), and BNL ($\pi p \to K\overline{K} n$) data.

$\Gamma(2(\pi\pi)_S\text{-wave})/\Gamma(\pi\pi)$ — Γ_7/Γ_1

VALUE	DOCUMENT ID		TECN	COMMENT
• • • We do not use the following data for averages, fits, limits, etc. • • •				
0.42 ± 0.26	[1] ABELE	01	CBAR	0.0 $\overline{p}d \to \pi^-4\pi^0 p$

[1] From the combined data of ABELE 96 and ABELE 96C.

$\Gamma(2(\pi\pi)_S\text{-wave})/\Gamma(4\pi)$ — Γ_7/Γ_4

VALUE	DOCUMENT ID		TECN	COMMENT
• • • We do not use the following data for averages, fits, limits, etc. • • •				
0.26 ± 0.07	ABELE	01B	CBAR	0.0 $\overline{p}d \to 5\pi p$

$\Gamma(\rho\rho)/\Gamma(4\pi)$ — Γ_8/Γ_4

VALUE	DOCUMENT ID		TECN	COMMENT
• • • We do not use the following data for averages, fits, limits, etc. • • •				
0.13 ± 0.08	ABELE	01B	CBAR	0.0 $\overline{p}d \to 5\pi p$

$\Gamma(\rho\rho)/\Gamma(2(\pi\pi)_S\text{-wave})$ — Γ_8/Γ_7

VALUE	DOCUMENT ID		COMMENT
2.87±0.34 OUR AVERAGE Error includes scale factor of 1.1.			
$3.3\ \pm0.5$	BARBERIS	00C	450 $pp \to p_f \pi^+\pi^- 2\pi^0 p_s$
$2.6\ \pm0.4$	BARBERIS	00C	450 $pp \to p_f 2(\pi^+\pi^-) p_s$

$\Gamma(\pi(1300)\pi)/\Gamma(4\pi)$ — Γ_9/Γ_4

VALUE	DOCUMENT ID		TECN	COMMENT
• • • We do not use the following data for averages, fits, limits, etc. • • •				
0.50 ± 0.25	ABELE	01B	CBAR	0.0 $\overline{p}d \to 5\pi p$

$\Gamma(a_1(1260)\pi)/\Gamma(4\pi)$ — Γ_{10}/Γ_4

VALUE	DOCUMENT ID		TECN	COMMENT
• • • We do not use the following data for averages, fits, limits, etc. • • •				
0.12 ± 0.05	ABELE	01B	CBAR	0.0 $\overline{p}d \to 5\pi p$

$\Gamma(\eta\eta)/\Gamma_{total}$ — Γ_{11}/Γ

VALUE	DOCUMENT ID		TECN	COMMENT
• • • We do not use the following data for averages, fits, limits, etc. • • •				
large	ALDE	88	GAM4	300 $\pi^- N \to \eta\eta\pi^- N$
large	BINON	83	GAM2	38 $\pi^- p \to 2\eta n$

$\Gamma(\eta\eta)/\Gamma(\pi\pi)$ — Γ_{11}/Γ_1

VALUE	DOCUMENT ID		TECN	COMMENT
0.173±0.024 OUR FIT Error includes scale factor of 1.1.				
0.175±0.027 OUR AVERAGE				
$0.18\ \pm0.03$	BARBERIS	00E		450 $pp \to p_f \eta\eta p_s$
0.157 ± 0.060	[1] AMSLER	95D	CBAR	0.0 $\overline{p}p \to \pi^0\pi^0\pi^0$, $\pi^0\eta\eta$, $\pi^0\pi^0\eta$
• • • We do not use the following data for averages, fits, limits, etc. • • •				
0.080 ± 0.033	AMSLER	02	CBAR	0.9 $\overline{p}p \to \pi^0\eta\eta$, $\pi^0\pi^0\pi^0$
$0.11\ \pm0.03$	[2] ANISOVICH	02D	SPEC	Combined fit
0.078 ± 0.013	[3] ABELE	96C	RVUE	Compilation
0.230 ± 0.097	[4] AMSLER	95C	CBAR	0.0 $\overline{p}p \to \eta\eta\pi^0$

[1] Coupled-channel analysis of AMSLER 95B, AMSLER 95C, and AMSLER 94D.
[2] From a combined K-matrix analysis of Crystal Barrel (0. $p\overline{p} \to \pi^0\pi^0\pi^0$, $\pi^0\eta\eta$, $\pi^0\pi^0\eta$), GAMS ($\pi p \to \pi^0\pi^0 n$, $\eta\eta n$, $\eta\eta' n$), and BNL ($\pi p \to K\overline{K} n$) data.
[3] 2π width determined to be 60 ± 12 MeV.
[4] Using AMSLER 95B ($3\pi^0$).

$\Gamma(4\pi^0)/\Gamma(\eta\eta)$ — Γ_5/Γ_{11}

VALUE	DOCUMENT ID		TECN	COMMENT
• • • We do not use the following data for averages, fits, limits, etc. • • •				
0.8 ± 0.3	ALDE	87	GAM4	100 $\pi^- p \to 4\pi^0 n$

$\Gamma(\eta\eta'(958))/\Gamma(\pi\pi)$ — Γ_{12}/Γ_1

VALUE	DOCUMENT ID		TECN	COMMENT
0.064±0.022 OUR FIT Error includes scale factor of 1.4.				
0.095±0.026	BARBERIS	00A		450 $pp \to p_f \eta\eta p_s$
• • • We do not use the following data for averages, fits, limits, etc. • • •				
0.005 ± 0.003	[1] ANISOVICH	02D	SPEC	Combined fit

[1] From a combined K-matrix analysis of Crystal Barrel (0. $p\overline{p} \to \pi^0\pi^0\pi^0$, $\pi^0\eta\eta$, $\pi^0\pi^0\eta$), GAMS ($\pi p \to \pi^0\pi^0 n$, $\eta\eta n$, $\eta\eta' n$), and BNL ($\pi p \to K\overline{K} n$) data.

Downloaded from https://academic.oup.com/ptep/article/2022/8/083C01/6651666 by KIT Library user on 27 September 2022

$\Gamma(\eta\eta'(958))/\Gamma(\eta\eta)$ — Γ_{12}/Γ_{11}

VALUE	DOCUMENT ID		TECN	COMMENT
0.37±0.13 OUR FIT	Error includes scale factor of 1.5.			
0.29±0.10	[1] AMSLER	95C	CBAR	$0.0\ \overline{p}p \to \eta\eta\pi^0$
• • • We do not use the following data for averages, fits, limits, etc. • • •				
0.05±0.03	[2] ANISOVICH	02D	SPEC	Combined fit
0.84±0.23	ABELE	96C	RVUE	Compilation
2.7 ±0.8	BINON	84C	GAM2	$38\ \pi^- p \to \eta\eta' n$

[1] Using AMSLER 94E ($\eta\eta'\pi^0$).
[2] From a combined K-matrix analysis of Crystal Barrel (0. $p\overline{p} \to \pi^0\pi^0\pi^0$, $\pi^0\eta\eta$, $\pi^0\pi^0\eta$), GAMS ($\pi p \to \pi^0\pi^0 n$, $\eta\eta n$, $\eta\eta' n$), and BNL ($\pi p \to K\overline{K}n$) data.

$\Gamma(K\overline{K})/\Gamma_{total}$ — Γ_{13}/Γ

VALUE	DOCUMENT ID		TECN
• • • We do not use the following data for averages, fits, limits, etc. • • •			
0.044±0.021	BUGG	96	RVUE

$\Gamma(K\overline{K})/\Gamma(\pi\pi)$ — Γ_{13}/Γ_1

VALUE	DOCUMENT ID		TECN	COMMENT
0.246±0.025 OUR FIT				
0.236±0.026 OUR AVERAGE				
0.25 ±0.03	[1] BARGIOTTI	03	OBLX	$\overline{p}p$
0.19 ±0.07	[2] ABELE	98	CBAR	$0.0\ \overline{p}p \to K^0_L K^\pm\pi^\mp$
0.20 ±0.08	[3] ABELE	96B	CBAR	$0.0\ \overline{p}p \to \pi^0 K^0_L K^0_L$
• • • We do not use the following data for averages, fits, limits, etc. • • •				
0.16 ±0.05	[4] ANISOVICH	02D	SPEC	Combined fit
0.33 ±0.03 ±0.07	BARBERIS	99D	OMEG	$450\ pp \to K^+K^-, \pi^+\pi^-$

[1] Coupled channel analysis of $\pi^+\pi^-\pi^0$, $K^+K^-\pi^0$, and $K^\pm K^0_S\pi^\mp$.
[2] Using $\pi^0\pi^0$ from AMSLER 95B.
[3] Using AMSLER 95B ($3\pi^0$), AMSLER 94C ($2\pi^0\eta$) and SU(3).
[4] From a combined K-matrix analysis of Crystal Barrel (0. $p\overline{p} \to \pi^0\pi^0\pi^0$, $\pi^0\eta\eta$, $\pi^0\pi^0\eta$), GAMS ($\pi p \to \pi^0\pi^0 n$, $\eta\eta n$, $\eta\eta' n$), and BNL ($\pi p \to K\overline{K}n$) data.

$\Gamma(K\overline{K})/\Gamma(\eta\eta)$ — Γ_{13}/Γ_{11}

VALUE	CL%	DOCUMENT ID		TECN	COMMENT
1.43±0.24 OUR FIT	Error includes scale factor of 1.1.				
1.85±0.41		BARBERIS	00E		$450\ pp \to p_f\eta\eta p_s$
• • • We do not use the following data for averages, fits, limits, etc. • • •					
1.5 ±0.6		[1] ANISOVICH	02D	SPEC	Combined fit
<0.4	90	[2] PROKOSHKIN	91	GAM4	$300\ \pi^- p \to \pi^- p\eta\eta$
<0.6		[3] BINON	83	GAM2	$38\ \pi^- p \to 2\eta n$

[1] From a combined K-matrix analysis of Crystal Barrel (0. $p\overline{p} \to \pi^0\pi^0\pi^0$, $\pi^0\eta\eta$, $\pi^0\pi^0\eta$), GAMS ($\pi p \to \pi^0\pi^0 n$, $\eta\eta n$, $\eta\eta' n$), and BNL ($\pi p \to K\overline{K}n$) data.
[2] Combining results of GAM4 with those of WA76 on $K\overline{K}$ central production.
[3] Using ETKIN 82B and COHEN 80.

$f_0(1500)$ REFERENCES

RODAS	22	EPJ C82 80	A. Rodas *et al.*	(JPAC Collab.)
SARANTSEV	21	PL B816 136227	A.V. Sarantsev *et al.*	(BONN, PNPI)
ALBRECHT	20	EPJ C80 453	M. Albrecht *et al.*	(Crystal Barrel Collab.)
ABLIKIM	18AA	PR D98 072003	M. Ablikim *et al.*	(BESIII Collab.)
ROPERTZ	18	EPJ C78 1000	S. Ropertz, C. Hanhart, B. Kubis	(BONN, JULI)
AAIJ	17V	JHEP 1708 037	R. Aaij *et al.*	(LHCb Collab.)
ABLIKIM	15AE	PR D92 052003	M. Ablikim *et al.*	(BESIII Collab.)
DOBBS	15	PR D91 052006	S. Dobbs *et al.*	(NWES)
AAIJ	14BR	PR D89 092006	R. Aaij *et al.*	(LHCb Collab.)
ABLIKIM	13N	PR D87 092009	M. Ablikim *et al.*	(BESIII Collab.)
ANISOVICH	09	IJMP A24 2481	V.V. Anisovich, A.V. Sarantsev	
KLEMPT	08	EPJ C55 39	E. Klempt, M. Matveev, A.V. Sarantsev	(BONN+)
UEHARA	08A	PR D78 052004	S. Uehara *et al.*	(BELLE Collab.)
ABLIKIM	06V	PL B642 441	M. Ablikim *et al.*	(BES Collab.)
AMSLER	06	PL B639 165	C. Amsler *et al.*	(Crystal Barrel Collab.)
AUBERT	06O	PR D74 032003	B. Aubert *et al.*	(BABAR Collab.)
UMAN	06	PR D73 052009	I. Uman *et al.*	(FNAL E835)
VLADIMIRSK...	06	PAN 69 493	V.V. Vladimirsky *et al.*	(ITEP, Moscow)
		Translated from YAF 69 515.		
BINON	05	PAN 68 960	F. Binon *et al.*	
		Translated from YAF 68 998.		
GARMASH	05	PR D71 092003	A. Garmash *et al.*	(BELLE Collab.)
ANISOVICH	03	EPJ A16 229	V.V. Anisovich *et al.*	
BARGIOTTI	03	EPJ C26 371	M. Bargiotti *et al.*	(OBELIX Collab.)
AMSLER	02	EPJ C23 29	C. Amsler *et al.*	
ANISOVICH	02D	PAN 65 1545	V.V. Anisovich *et al.*	
		Translated from YAF 65 1583.		
ABELE	01	EPJ C19 667	A. Abele *et al.*	(Crystal Barrel Collab.)
ABELE	01B	EPJ C21 261	A. Abele *et al.*	(Crystal Barrel Collab.)
ACCIARRI	01H	PL B501 173	M. Acciarri *et al.*	(L3 Collab.)
AITALA	01A	PRL 86 765	E.M. Aitala *et al.*	(FNAL E791 Collab.)
BARATE	00E	PL B472 189	R. Barate *et al.*	(ALEPH Collab.)
BARBERIS	00A	PL B471 429	D. Barberis *et al.*	(WA 102 Collab.)
BARBERIS	00C	PL B471 440	D. Barberis *et al.*	(WA 102 Collab.)
BARBERIS	00D	PL B474 423	D. Barberis *et al.*	(WA 102 Collab.)
BARBERIS	00E	PL B479 59	D. Barberis *et al.*	(WA 102 Collab.)
BARBERIS	99	PL B453 305	D. Barberis *et al.*	(Omega Expt.)
BARBERIS	99B	PL B453 316	D. Barberis *et al.*	(Omega Expt.)
BARBERIS	99D	PL B462 462	D. Barberis *et al.*	(Omega Expt.)
BELLAZZINI	99	PL B467 296	R. Bellazzini *et al.*	
FRENCH	99	PL B460 213	B. French *et al.*	(WA76 Collab.)
KAMINSKI	99	EPJ C9 141	R. Kaminski, L. Lesniak, B. Loiseau	(CRAC, PARIN)
ABELE	98	PR D57 3860	A. Abele *et al.*	(Crystal Barrel Collab.)
ALDE	98	EPJ A3 361	D. Alde *et al.*	(GAM4 Collab.)
Also		PAN 62 405	D. Alde *et al.*	(GAMS Collab.)
		Translated from YAF 62 446.		
AMSLER	98	RMP 70 1293	C. Amsler	
ANISOVICH	98B	SPU 41 419	V.V. Anisovich *et al.*	
		Translated from UFN 168 481.		
BERTIN	98	PR D57 55	A. Bertin *et al.*	(OBELIX Collab.)
REYES	98	PRL 81 4079	M.A. Reyes *et al.*	
BARBERIS	97B	PL B413 217	D. Barberis *et al.*	(WA 102 Collab.)
BERTIN	97C	PL B408 476	A. Bertin *et al.*	(OBELIX Collab.)
FRABETTI	97D	PL B407 79	P.L. Frabetti *et al.*	(FNAL E687 Collab.)
ABELE	96	PL B380 453	A. Abele *et al.*	(Crystal Barrel Collab.)
ABELE	96B	PL B385 425	A. Abele *et al.*	(Crystal Barrel Collab.)
ABELE	96C	NP A609 562	A. Abele *et al.*	(Crystal Barrel Collab.)
AMELIN	96B	PAN 59 976	D.V. Amelin *et al.*	(SERP, TBIL)
		Translated from YAF 59 1021.		
BUGG	96	NP B471 59	D.V. Bugg, A.V. Sarantsev, B.S. Zou	(LOQM, PNPI)
AMSLER	95B	PL B342 433	C. Amsler *et al.*	(Crystal Barrel Collab.)
AMSLER	95C	PL B353 571	C. Amsler *et al.*	(Crystal Barrel Collab.)
AMSLER	95D	PL B355 425	C. Amsler *et al.*	(Crystal Barrel Collab.)
ANTINORI	95	PL B353 589	F. Antinori *et al.*	(ATHU, BARI, BIRM+)
BUGG	95	PL B353 378	D.V. Bugg *et al.*	(LOQM, PNPI, WASH)
ABATZIS	94	PL B324 509	S. Abatzis *et al.*	(ATHU, BARI, BIRM+)
AMSLER	94C	PL B327 425	C. Amsler *et al.*	(Crystal Barrel Collab.)
AMSLER	94D	PL B333 277	C. Amsler *et al.*	(Crystal Barrel Collab.)
AMSLER	94E	PL B340 259	C. Amsler *et al.*	(Crystal Barrel Collab.)
ANISOVICH	94	PL B323 233	V.V. Anisovich *et al.*	(Crystal Barrel Collab.)
BUGG	94	PR D50 4412	D.V. Bugg *et al.*	(LOQM)
AMSLER	92	PL B291 347	C. Amsler *et al.*	(Crystal Barrel Collab.)
BELADIDZE	92C	SJNP 55 1535	G.M. Beladidze, S.I. Bityukov, G.V. Borisov	(SERP+)
		Translated from YAF 55 2748.		
PROKOSHKIN	91	SPD 36 155	Y.D. Prokoshkin	(GAM2 and GAM4 Collab.)
		Translated from DANS 316 900.		
ARMSTRONG	89E	PL B228 536	T.A. Armstrong, M. Benayoun	(ATHU, BARI, BIRM+)
ALDE	88	PL B201 160	D.M. Alde *et al.*	(SERP, BELG, LANL, LAPP+)
ASTON	88D	NP B301 525	D. Aston *et al.*	(SLAC, NAGO, CINC, INUS)
ALDE	87	PL B198 286	D.M. Alde *et al.*	(LANL, BRUX, SERP, LAPP)
ALDE	86D	NP B269 485	D.M. Alde *et al.*	(BELG, LAPP, SERP, CERN+)
LONGACRE	86	PL B177 223	R.S. Longacre *et al.*	(BNL, BRAN, CUNY+)
BINON	84C	NC 80A 363	F.G. Binon *et al.*	(BELG, LAPP, SERP+)
BINON	83	NC 78A 313	F.G. Binon *et al.*	(BELG, LAPP, SERP+)
Also		SJNP 38 561	F.G. Binon *et al.*	(BELG, LAPP, SERP+)
		Translated from YAF 38 934.		
GRAY	83	PR D27 307	L. Gray *et al.*	(SYRA)
ETKIN	82B	PR D25 1786	A. Etkin *et al.*	(BNL, CUNY, TUFTS, VAND)
COHEN	80	PR D22 2595	D. Cohen *et al.*	(ANL)
HYAMS	75	NP B100 205	B.D. Hyams *et al.*	(CERN, MPIM)

$f_1(1510)$

$I^G(J^{PC}) = 0^+(1^{++})$

OMITTED FROM SUMMARY TABLE

See the review on "Spectroscopy of Light Meson Resonances."

$f_1(1510)$ MASS

VALUE (MeV)	EVTS	DOCUMENT ID		TECN	COMMENT
1518± 5 OUR AVERAGE	Error includes scale factor of 1.7. See the ideogram below.				
1530±10		ASTON	88C	LASS	$11\ K^- p \to K^0_S K^\pm\pi^\mp\Lambda$
1512± 4	600	[1] BIRMAN	88	MPS	$8\ \pi^- p \to K^+\overline{K}^0\pi^- n$
1526± 6	271	GAVILLET	82	HBC	$4.2\ K^- p \to \Lambda K K\pi$
• • • We do not use the following data for averages, fits, limits, etc. • • •					
~ 1525		[2] BAUER	93B		$\gamma\gamma^* \to \pi^+\pi^-\pi^0\pi^0$

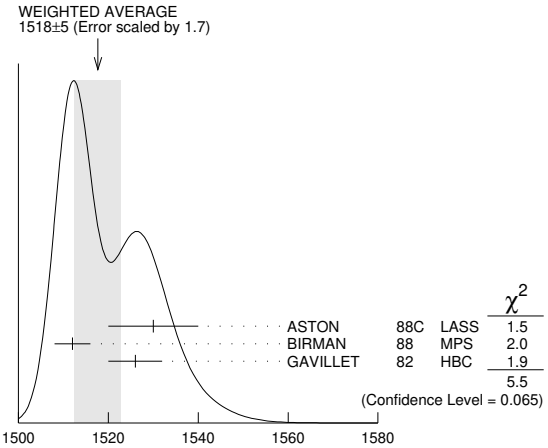

[1] From partial wave analysis of $K^+\overline{K}^0\pi^-$ state.
[2] Not seen by AIHARA 88C in the $K^0_S K^\pm\pi^\mp$ final state.

$f_1(1510)$ WIDTH

VALUE (MeV)	EVTS	DOCUMENT ID		TECN	COMMENT
73±25 OUR AVERAGE	Error includes scale factor of 2.5. See the ideogram below.				
100±40		ASTON	88C	LASS	$11\ K^- p \to K^0_S K^\pm\pi^\mp\Lambda$
35±15	600	[3] BIRMAN	88	MPS	$8\ \pi^- p \to K^+\overline{K}^0\pi^- n$
107±15	271	GAVILLET	82	HBC	$4.2\ K^- p \to \Lambda K K\pi$

Downloaded from https://academic.oup.com/ptep/article/2022/8/083C01/6651666 by KIT Library user on 27 September 2022

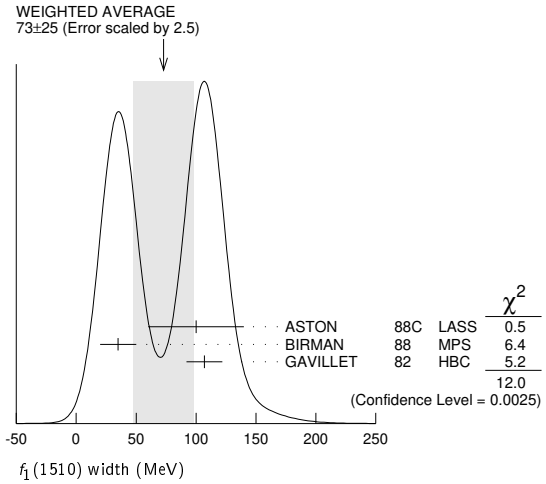

[3] From partial wave analysis of $K^+\overline{K}^0\pi^-$ state.

$f_1(1510)$ DECAY MODES

	Mode	Fraction (Γ_i/Γ)
Γ_1	$K\overline{K}^*(892)+$ c.c.	seen
Γ_2	$\pi^+\pi^-\eta'$	seen

$f_1(1510)$ BRANCHING RATIOS

$\Gamma(\pi^+\pi^-\eta')/\Gamma_{total}$ — Γ_2/Γ

VALUE	EVTS	DOCUMENT ID		TECN	COMMENT
seen	230	ABLIKIM	11C	BES3	$J/\psi \to \gamma\pi^+\pi^-\eta'$

$f_1(1510)$ REFERENCES

ABLIKIM	11C	PRL 106 072002	M. Ablikim et al.	(BESIII Collab.)
BAUER	93B	PR D48 3976	D.A. Bauer et al.	(SLAC)
AIHARA	88C	PR D38 1	H. Aihara et al.	(TPC-2γ Collab.)
ASTON	88C	PL B201 573	D. Aston et al.	(SLAC, NAGO, CINC, INUS) JP
BIRMAN	88	PRL 61 1557	A. Birman et al.	(BNL, FSU, IND, MASD) JP
GAVILLET	82	ZPHY C16 119	P. Gavillet et al.	(CERN, CDEF, PADO+)

$f'_2(1525)$

$I^G(J^{PC}) = 0^+(2^{++})$

$f'_2(1525)$ MASS

VALUE (MeV)	DOCUMENT ID
1517.4±2.5 OUR AVERAGE	Includes data from the 6 datablocks that follow this one. Error includes scale factor of 2.8. See the ideogram below.

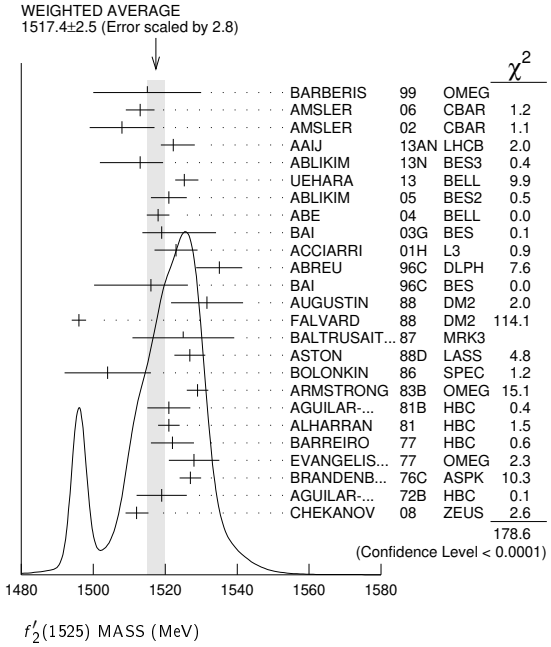

PRODUCED BY PION BEAM

VALUE (MeV)	EVTS	DOCUMENT ID		TECN	COMMENT
The data in this block is included in the average printed for a previous datablock.					
• • • We do not use the following data for averages, fits, limits, etc. • • •					
1521 ± 13		TIKHOMIROV	03	SPEC	$40.0\ \pi^-C \to K^0_S K^0_S K^0_L X$
1547^{+10}_{-2}		[1] LONGACRE	86	MPS	$22\ \pi^- p \to K^0_S K^0_S n$
1496^{+9}_{-8}		[2] CHABAUD	81	ASPK	$6\ \pi^- p \to K^+K^- n$
1497^{+8}_{-9}		CHABAUD	81	ASPK	$18.4\ \pi^- p \to K^+K^- n$
1492 ± 29		GORLICH	80	ASPK	$17\ \pi^- p$polarized $\to K^+K^- n$
1502 ± 25		[3] CORDEN	79	OMEG	12–$15\ \pi^- p \to \pi^+\pi^- n$
1480	14	CRENNELL	66	HBC	$6.0\ \pi^- p \to K^0_S K^0_S n$

[1] From a partial-wave analysis of data using a K-matrix formalism with 5 poles.
[2] CHABAUD 81 is a reanalysis of PAWLICKI 77 data.
[3] From an amplitude analysis where the $f'_2(1525)$ width and elasticity are in complete disagreement with the values obtained from $K\overline{K}$ channel, making the solution dubious.

PRODUCED BY $K^\pm$ BEAM

VALUE (MeV)	EVTS	DOCUMENT ID		TECN	COMMENT
The data in this block is included in the average printed for a previous datablock.					
1518.1± 2.8 OUR AVERAGE		Includes data from the datablock that follows this one. Error includes scale factor of 3.0. See the ideogram below.			
1526.8 ± 4.3		ASTON	88D	LASS	$11\ K^-p \to K^0_S K^0_S \Lambda$
1504 ± 12		BOLONKIN	86	SPEC	$40\ K^-p \to K^0_S K^0_S Y$
1529 ± 3		ARMSTRONG	83B	OMEG	$18.5\ K^-p \to K^-K^+\Lambda$
1521 ± 6	650	AGUILAR-...	81B	HBC	$4.2\ K^-p \to \Lambda K^+K^-$
1521 ± 3	572	ALHARRAN	81	HBC	$8.25\ K^-p \to \Lambda K\overline{K}$
1522 ± 6	123	BARREIRO	77	HBC	$4.15\ K^-p \to \Lambda K^0_S K^0_S$
1528 ± 7	166	EVANGELIS...	77	OMEG	$10\ K^-p \to K^+K^-(\Lambda,\Sigma)$
1527 ± 3	120	BRANDENB...	76C	ASPK	$13\ K^-p \to K^+K^-(\Lambda,\Sigma)$
1519 ± 7	100	AGUILAR-...	72B	HBC	$3.9,4.6\ K^-p \to K\overline{K}(\Lambda,\Sigma)$
• • • We do not use the following data for averages, fits, limits, etc. • • •					
1514 ± 8	61	BINON	07	GAMS	$32.5\ K^-p \to \eta\eta(\Lambda/\Sigma^0)$
1513 ± 10		[1] BARKOV	99	SPEC	$40\ K^-p \to K^0_S K^0_S y$

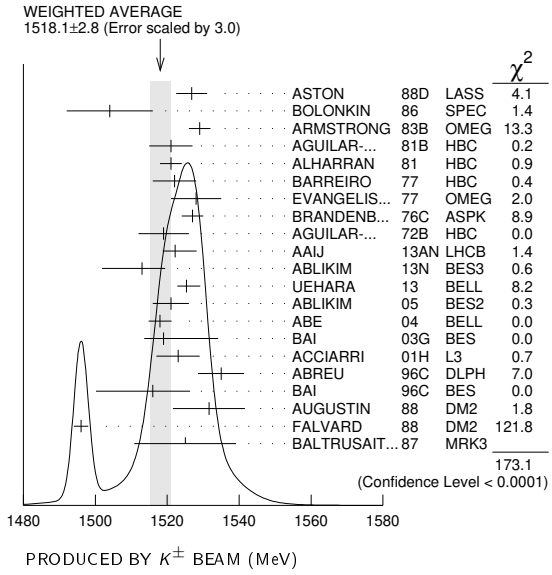

[1] Systematic errors not estimated.

PRODUCED IN e^+e^- ANNIHILATION AND PARTICLE DECAYS

VALUE (MeV)	EVTS	DOCUMENT ID		TECN	COMMENT
The data in this block is included in the average printed for a previous datablock.					
1514 $^{+5}_{-4}$ OUR AVERAGE		Error includes scale factor of 3.8. See the ideogram below.			
$1522.2\pm2.8^{+5.3}_{-2.0}$		AAIJ	13AN	LHCB	$\overline{B}^0_s \to J/\psi K^+K^-$
$1513\pm5\ ^{+4}_{-10}$	5.5k	[1] ABLIKIM	13N	BES3	$e^+e^- \to J/\psi \to \gamma\eta\eta$
$1525.3^{+1.2}_{-1.4}{}^{+3.7}_{-2.1}$		UEHARA	13	BELL	$\gamma\gamma \to K^0_S K^0_S$
1521 ± 5		ABLIKIM	05	BES2	$J/\psi \to \phi K^+K^-$
$1518\pm1\pm3$		ABE	04	BELL	$10.6\ e^+e^- \to e^+e^-K^+K^-$
$1519\pm2\ ^{+15}_{-5}$		BAI	03G	BES	$J/\psi \to \gamma K\overline{K}$

Downloaded from https://academic.oup.com/ptep/article/2022/8/083C01/6651666 by KIT Library user on 27 September 2022

1523 ± 6	331	[2] ACCIARRI	01H	L3	91, 183–209 $e^+e^- \to e^+e^- K^0_S K^0_S$
1535 ± 5 ± 4		ABREU	96C	DLPH	$Z^0 \to K^+K^- + X$
1516 ± 5 $^{+9}_{-15}$		BAI	96C	BES	$J/\psi \to \gamma K^+K^-$
1531.6 ± 10.0		AUGUSTIN	88	DM2	$J/\psi \to \gamma K^+K^-$
1496 ± 2		[3] FALVARD	88	DM2	$J/\psi \to \phi K^+K^-$
1525 ±10 ±10		BALTRUSAIT...	87	MRK3	$J/\psi \to \gamma K^+K^-$
• • • We do not use the following data for averages, fits, limits, etc. • • •					
1503 ±11		[4] RODAS	22	RVUE	$J/\psi(1S) \to \gamma(\pi\pi,\ K\overline{K})$
1532 ± 3 ± 6	644	[5,6] DOBBS	15		$J/\psi \to \gamma K^+K^-$
1557 ± 9 ± 3	113	[5,6] DOBBS	15		$\psi(2S) \to \gamma K^+K^-$
1526 ± 7	29	[7] LEES	14H	BABR	$e^+e^- \to K^0_S K^0_S K^+K^-\gamma$
1523 ± 5	870	[8] SCHEGELSKY	06A	RVUE	$\gamma\gamma \to K^0_S K^0_S$
1515 ± 5		[9] FALVARD	88	DM2	$J/\psi \to \phi K^+K^-$

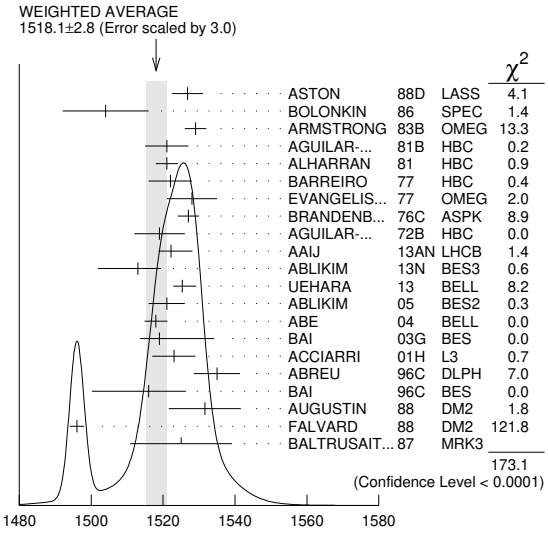

PRODUCED BY $K^\pm$ BEAM (MeV)

[1] From partial wave analysis including all possible combinations of 0^{++}, 2^{++}, and 4^{++} resonances.
[2] Supersedes ACCIARRI 95J.
[3] From an analysis including interference with $f_0(1710)$.
[4] T-matrix pole from coupled channel K-matrix fit to data on $J/\psi \to \gamma\pi^0\pi^0$ (ABLIKIM 15AE) and $J/\psi \to \gamma K^0_S K^0_S$ (ABLIKIM 18AA).
[5] Using CLEO-c data but not authored by the CLEO Collaboration.
[6] From a fit to a Breit-Wigner line shape with fixed $\Gamma = 73$ MeV.
[7] From a fit to a Breit-Wigner line shape plus a second-order polynomial function. Systematic errors not evaluated.
[8] From analysis of L3 data at 91 and 183–209 GeV.
[9] From an analysis ignoring interference with $f_0(1710)$.

PRODUCED IN $\overline{p}p$ ANNIHILATION

VALUE (MeV)	DOCUMENT ID		TECN	COMMENT
The data in this block is included in the average printed for a previous datablock.				
1512 ± 4 OUR AVERAGE				
1513 ± 4	AMSLER	06	CBAR	0.9 $\overline{p}p \to K^+K^-\pi^0$
1508 ± 9	[1] AMSLER	02	CBAR	0.9 $\overline{p}p \to \pi^0\eta\eta,\ \pi^0\pi^0\pi^0$
• • • We do not use the following data for averages, fits, limits, etc. • • •				
1495.0 ± 1.1 ± 8.1	[2] ALBRECHT	20	RVUE	0.9 $\overline{p}p \to \pi^0\pi^0\eta,\ \pi^0\eta\eta,\ \pi^0K^+K^-$
1530 ±12	[3] ANISOVICH	09	RVUE	0.0 $\overline{p}p,\ \pi N$

[1] T-matrix pole.
[2] T-matrix pole, 4 poles, 4 channels, including scattering data from HYAMS 75 ($\pi\pi$), LONGACRE 86 ($K\overline{K}$), BINON 83 ($\eta\eta$).
[3] 4-poles, 5-channel K matrix fit.

CENTRAL PRODUCTION

VALUE (MeV)	DOCUMENT ID		TECN	COMMENT
The data in this block is included in the average printed for a previous datablock.				
1515 ± 15	BARBERIS	99	OMEG	450 $pp \to p_s p_f K^+K^-$

PRODUCED IN ep COLLISIONS

VALUE (MeV)	EVTS	DOCUMENT ID		TECN	COMMENT
The data in this block is included in the average printed for a previous datablock.					
1512 ± 3 $^{+1.4}_{-0.5}$		[1] CHEKANOV	08	ZEUS	$ep \to K^0_S K^0_S X$
• • • We do not use the following data for averages, fits, limits, etc. • • •					
1537 $^{+9}_{-8}$	84	[2] CHEKANOV	04	ZEUS	$ep \to K^0_S K^0_S X$

[1] In the SU(3) based model with a specific interference pattern of the $f_2(1270)$, $a^0_2(1320)$, and $f'_2(1525)$ mesons incoherently added to the $f_0(1710)$ and non-resonant background.
[2] Systematic errors not estimated.

$f'_2(1525)$ WIDTH

VALUE (MeV)	DOCUMENT ID		COMMENT
86 ± 5 OUR FIT Error includes scale factor of 2.2.			
86.9 $^{+2.3}_{-2.1}$	PDG	18	Average of width measurements

PRODUCED BY PION BEAM

VALUE (MeV)	DOCUMENT ID		TECN	COMMENT
86.9 $^{+2.3}_{-2.1}$ OUR AVERAGE Includes data from the 5 datablocks that follow this one. Error includes scale factor of 1.4. See the ideogram below.				
• • • We do not use the following data for averages, fits, limits, etc. • • •				
102 ±42	TIKHOMIROV	03	SPEC	40.0 $\pi^- C \to K^0_S K^0_S K^0_L X$
108 $^{+5}_{-2}$	[1] LONGACRE	86	MPS	22 $\pi^- p \to K^0_S K^0_S n$
69 $^{+22}_{-16}$	[2] CHABAUD	81	ASPK	6 $\pi^- p \to K^+K^- n$
137 $^{+23}_{-21}$	CHABAUD	81	ASPK	18.4 $\pi^- p \to K^+K^- n$
150 $^{+83}_{-50}$	GORLICH	80	ASPK	17 $\pi^- p$ polarized $\to K^+K^- n$
165 ±42	[3] CORDEN	79	OMEG	12–15 $\pi^- p \to \pi^+\pi^- n$
92 $^{+39}_{-22}$	[4] POLYCHRO...	79	STRC	7 $\pi^- p \to n K^0_S K^0_S$

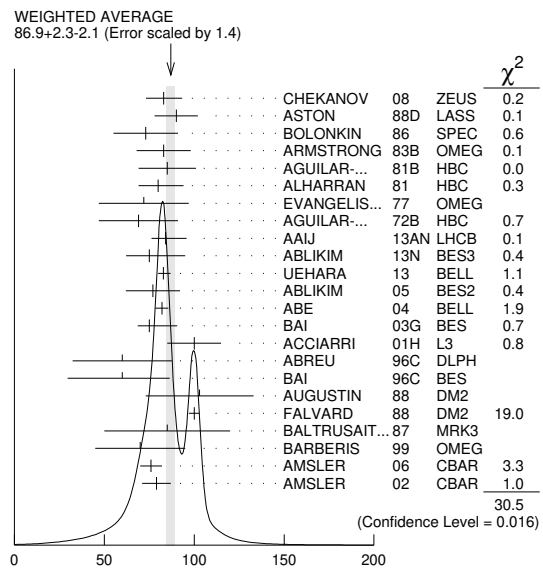

$f'_2(1525)$ WIDTH (MeV)

[1] From a partial-wave analysis of data using a K-matrix formalism with 5 poles.
[2] CHABAUD 81 is a reanalysis of PAWLICKI 77 data.
[3] From an amplitude analysis where the $f'_2(1525)$ width and elasticity are in complete disagreement with the values obtained from $K\overline{K}$ channel, making the solution dubious.
[4] From a fit to the D with $f_2(1270)$-$f'_2(1525)$ interference. Mass fixed at 1516 MeV.

PRODUCED BY $K^\pm$ BEAM

VALUE (MeV)	EVTS	DOCUMENT ID		TECN	COMMENT
The data in this block is included in the average printed for a previous datablock.					
82 ± 6 OUR AVERAGE					
90 ±12		ASTON	88D	LASS	11 $K^-p \to K^0_S K^0_S \Lambda$
73 ±18		BOLONKIN	86	SPEC	40 $K^-p \to K^0_S K^0_S Y$
83 ±15		ARMSTRONG	83B	OMEG	18.5 $K^-p \to K^-K^+\Lambda$
85 ±16	650	AGUILAR-...	81B	HBC	4.2 $K^-p \to \Lambda K^+K^-$
80 $^{+14}_{-11}$	572	ALHARRAN	81	HBC	8.25 $K^-p \to \Lambda K\overline{K}$
72 ±25	166	EVANGELIS...	77	OMEG	10 $K^-p \to K^+K^-(\Lambda,\Sigma)$
69 ±22	100	AGUILAR-...	72B	HBC	3.9,4.6 $K^-p \to K\overline{K}(\Lambda,\Sigma)$
• • • We do not use the following data for averages, fits, limits, etc. • • •					
92 $^{+25}_{-16}$	61	BINON	07	GAMS	32.5 $K^-p \to \eta\eta(\Lambda/\Sigma^0)$
75 ±20		[1] BARKOV	99	SPEC	40 $K^-p \to K^0_S K^0_S y$
62 $^{+19}_{-14}$	123	BARREIRO	77	HBC	4.15 $K^-p \to \Lambda K^0_S K^0_S$
61 ± 8	120	BRANDENB...	76C	ASPK	13 $K^-p \to K^+K^-(\Lambda,\Sigma)$

[1] Systematic errors not estimated.

Downloaded from https://academic.oup.com/ptep/article/2022/8/083C01/6651666 by KIT Library user on 27 September 2022

PRODUCED IN e^+e^- ANNIHILATION AND PARTICLE DECAYS

VALUE (MeV)	EVTS	DOCUMENT ID		TECN	COMMENT
The data in this block is included in the average printed for a previous datablock.					
$89.2^{+3.4}_{-3.0}$ OUR AVERAGE		Error includes scale factor of 1.8. See the ideogram below.			
$84 \pm 6^{+10}_{-5}$		AAIJ	13AN	LHCB	$\overline{B}^0_s \to J/\psi K^+ K^-$
$75^{+12}_{-10}{}^{+16}_{-8}$	5.5k	[1] ABLIKIM	13N	BES3	$e^+e^- \to J/\psi \to \gamma\eta\eta$
$82.9^{+2.1}_{-2.2}{}^{+3.3}_{-2.0}$		UEHARA	13	BELL	$\gamma\gamma \to K^0_S K^0_S$
77 ± 15		ABLIKIM	05	BES2	$J/\psi \to \phi K^+ K^-$
$82 \pm 2 \pm 3$		ABE	04	BELL	10.6 $e^+e^- \to e^+e^- K^+ K^-$
$75 \pm 4^{+15}_{-5}$		BAI	03G	BES	$J/\psi \to \gamma K\overline{K}$
100 ± 15	331	[2] ACCIARRI	01H	L3	91, 183–209 $e^+e^- \to e^+e^- K^0_S K^0_S$
$60 \pm 20 \pm 19$		ABREU	96C	DLPH	$Z^0 \to K^+K^- + X$
$60 \pm 23^{+13}_{-20}$		BAI	96C	BES	$J/\psi \to \gamma K^+ K^-$
103 ± 30		AUGUSTIN	88	DM2	$J/\psi \to \gamma K^+ K^-$
100 ± 3		[3] FALVARD	88	DM2	$J/\psi \to \phi K^+ K^-$
85 ± 35		BALTRUSAIT...87		MRK3	$J/\psi \to \gamma K^+ K^-$
• • • We do not use the following data for averages, fits, limits, etc. • • •					
84 ± 15		[4] RODAS	22	RVUE	$J/\psi(1S) \to \gamma(\pi\pi, K\overline{K})$
37 ± 12	29	[5] LEES	14H	BABR	$e^+e^- \to K^0_S K^0_S K^+K^-\gamma$
104 ± 10	870	[6] SCHEGELSKY	06A	RVUE	$\gamma\gamma \to K^0_S K^0_S$
62 ± 10		[7] FALVARD	88	DM2	$J/\psi \to \phi K^+ K^-$

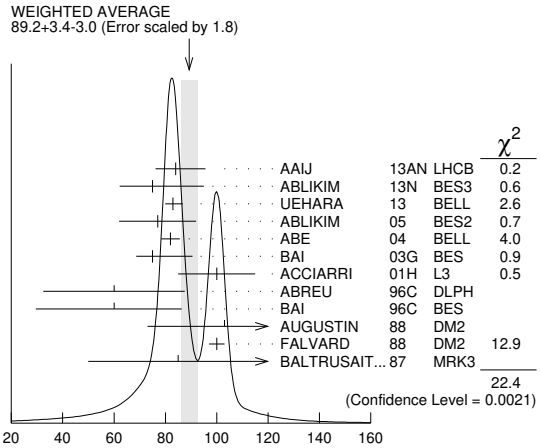

$f_2'(1525)$ width, e^+e^- annihilation and particle decays (MeV)

[1] From partial wave analysis including all possible combinations of 0^{++}, 2^{++}, and 4^{++} resonances.
[2] Supersedes ACCIARRI 95J.
[3] From an analysis including interference with $f_0(1710)$.
[4] T-matrix pole from coupled channel K-matrix fit to data on $J/\psi \to \gamma\pi^0\pi^0$ (ABLIKIM 15AE) and $J/\psi \to \gamma K^0_S K^0_S$ (ABLIKIM 18AA).
[5] From a fit to a Breit-Wigner line shape plus a second-order polynomial function. Systematic errors not evaluated.
[6] From analysis of L3 data at 91 and 183–209 GeV.
[7] From an analysis ignoring interference with $f_0(1710)$.

PRODUCED IN $\overline{p}p$ ANNIHILATION

VALUE (MeV)	DOCUMENT ID		TECN	COMMENT
The data in this block is included in the average printed for a previous datablock.				
77 ± 5 OUR AVERAGE				
76 ± 6	AMSLER	06	CBAR	0.9 $\overline{p}p \to K^+K^-\pi^0$
79 ± 8	[1] AMSLER	02	CBAR	0.9 $\overline{p}p \to \pi^0\eta\eta$, $\pi^0\pi^0\pi^0$
• • • We do not use the following data for averages, fits, limits, etc. • • •				
$104.8 \pm 0.9 \pm 9.8$	[2] ALBRECHT	20	RVUE	0.9 $\overline{p}p \to \pi^0\pi^0\eta$, $\pi^0\eta\eta$, $\pi^0K^+K^-$
128 ± 20	[3] ANISOVICH	09	RVUE	0.0 $\overline{p}p$, πN

[1] T-matrix pole.
[2] T-matrix pole, 4 poles, 4 channels, including scattering data from HYAMS 75 ($\pi\pi$), LONGACRE 86 ($K\overline{K}$), BINON 83 ($\eta\eta$).
[3] K-matrix, 4-poles, 5-channel fit.

CENTRAL PRODUCTION

VALUE (MeV)	DOCUMENT ID		TECN	COMMENT
The data in this block is included in the average printed for a previous datablock.				
70 ± 25	BARBERIS	99	OMEG	450 $pp \to p_s p_f K^+K^-$

PRODUCED IN ep COLLISIONS

VALUE (MeV)	EVTS	DOCUMENT ID		TECN	COMMENT
The data in this block is included in the average printed for a previous datablock.					
$83 \pm 9^{+5}_{-4}$		[1] CHEKANOV	08	ZEUS	$ep \to K^0_S K^0_S X$
• • • We do not use the following data for averages, fits, limits, etc. • • •					
50^{+34}_{-22}	84	[2] CHEKANOV	04	ZEUS	$ep \to K^0_S K^0_S X$

[1] In the SU(3) based model with a specific interference pattern of the $f_2(1270)$, $a^0_2(1320)$, and $f_2'(1525)$ mesons incoherently added to the $f_0(1710)$ and non-resonant background.
[2] Systematic errors not estimated.

$f_2'(1525)$ DECAY MODES

	Mode	Fraction (Γ_i/Γ)	Scale factor
Γ_1	$K\overline{K}$	(87.6 ± 2.2) %	1.1
Γ_2	$\eta\eta$	(11.6 ± 2.2) %	1.1
Γ_3	$\pi\pi$	$(8.3 \pm 1.6) \times 10^{-3}$	
Γ_4	$K\overline{K}^*(892) +$ c.c.		
Γ_5	$\pi K\overline{K}$		
Γ_6	$\pi\pi\eta$		
Γ_7	$\pi^+\pi^+\pi^-\pi^-$		
Γ_8	$\gamma\gamma$	$(9.5 \pm 1.1) \times 10^{-7}$	1.1

CONSTRAINED FIT INFORMATION

An overall fit to the total width, 2 partial widths, a combination of partial widths obtained from integrated cross sections, and 3 branching ratios uses 17 measurements and one constraint to determine 5 parameters. The overall fit has a $\chi^2 = 18.2$ for 13 degrees of freedom.

The following *off-diagonal* array elements are the correlation coefficients $\langle \delta p_i \delta p_j \rangle / (\delta p_i \cdot \delta p_j)$, in percent, from the fit to parameters p_i, including the branching fractions, $x_i \equiv \Gamma_i/\Gamma_{total}$. The fit constrains the x_i whose labels appear in this array to sum to one.

	x_1	x_2	x_3	x_8
x_2	−100			
x_3	−6	−1		
x_8	−19	19	1	
Γ	−4	4	0	−44

	Mode	Rate (MeV)	Scale factor
Γ_1	$K\overline{K}$	75 ± 4	1.8
Γ_2	$\eta\eta$	9.9 ± 1.9	1.1
Γ_3	$\pi\pi$	0.71 ± 0.14	1.1
Γ_8	$\gamma\gamma$	$(8.2 \pm 0.9) \times 10^{-5}$	

$f_2'(1525)$ PARTIAL WIDTHS

$\Gamma(K\overline{K})$ — Γ_1

VALUE (MeV)	DOCUMENT ID		TECN	COMMENT
75 ± 4 OUR FIT	Error includes scale factor of 1.8.			
63^{+6}_{-5}	[1] LONGACRE	86	MPS	22 $\pi^- p \to K^0_S K^0_S n$

[1] From a partial-wave analysis of data using a K-matrix formalism with 5 poles.

$\Gamma(\eta\eta)$ — Γ_2

VALUE (MeV)	EVTS	DOCUMENT ID		TECN	COMMENT
9.9 ± 1.9 OUR FIT	Error includes scale factor of 1.1.				
• • • We do not use the following data for averages, fits, limits, etc. • • •					
5.0 ± 0.8	870	[1] SCHEGELSKY	06A	RVUE	$\gamma\gamma \to K^0_S K^0_S$
24^{+3}_{-1}		[2] LONGACRE	86	MPS	22 $\pi^- p \to K^0_S K^0_S n$

[1] From analysis of L3 data at 91 and 183–209 GeV, using $\Gamma(f_2'(1525) \to K\overline{K}) = 68$ MeV and SU(3) relations.
[2] From a partial-wave analysis of data using a K-matrix formalism with 5 poles.

$\Gamma(\pi\pi)$ — Γ_3

VALUE (MeV)	EVTS	DOCUMENT ID		TECN	COMMENT
0.71 ± 0.14 OUR FIT	Error includes scale factor of 1.1.				
$1.4^{+1.0}_{-0.5}$		[1] LONGACRE	86	MPS	22 $\pi^- p \to K^0_S K^0_S n$
• • • We do not use the following data for averages, fits, limits, etc. • • •					
$0.2^{+1.0}_{-0.2}$	870	[2] SCHEGELSKY	06A	RVUE	$\gamma\gamma \to K^0_S K^0_S$

[1] From a partial-wave analysis of data using a K-matrix formalism with 5 poles.
[2] From analysis of L3 data at 91 and 183–209 GeV, using $\Gamma(f_2'(1525) \to K\overline{K}) = 68$ MeV and SU(3) relations.

Downloaded from https://academic.oup.com/ptep/article/2022/8/083C01/6651666 by KIT Library user on 27 September 2022

$\Gamma(\gamma\gamma)$ — Γ_8

VALUE (keV)	EVTS	DOCUMENT ID		TECN	COMMENT
0.082±0.009 OUR FIT					
• • • We do not use the following data for averages, fits, limits, etc. • • •					
0.13 ±0.03	870	[1] SCHEGELSKY	06A	RVUE	$\gamma\gamma \to K^0_S K^0_S$

[1] From analysis of L3 data at 91 and 183–209 GeV, using $\Gamma(f'_2(1525) \to K\overline{K}) = 68$ MeV and SU(3) relations.

$\Gamma(K\overline{K})/\Gamma_{total}$ — Γ_1/Γ

VALUE	DOCUMENT ID		TECN	COMMENT
• • • We do not use the following data for averages, fits, limits, etc. • • •				
$0.746 \pm 0.002^{+0.166}_{-0.162}$	[1] ALBRECHT	20	RVUE	$0.9\ \overline{p}p \to \pi^0\pi^0\eta$, $\pi^0\eta\eta$, $\pi^0 K^+K^-$

[1] Residue from T-matrix pole, 4 poles, 4 channels, including scattering data from HYAMS 75 ($\pi\pi$), LONGACRE 86 ($K\overline{K}$), BINON 83 ($\eta\eta$).

$f'_2(1525)$ $\Gamma(i)\Gamma(\gamma\gamma)/\Gamma(total)$

$\Gamma(K\overline{K}) \times \Gamma(\gamma\gamma)/\Gamma_{total}$ — $\Gamma_1\Gamma_8/\Gamma$

VALUE (keV)	EVTS	DOCUMENT ID		TECN	COMMENT
0.072 ±0.007 OUR FIT					
0.072 ±0.007 OUR AVERAGE					
$0.048\ ^{+0.067}_{-0.008}\ ^{+0.108}_{-0.012}$		UEHARA	13	BELL	$\gamma\gamma \to K^0_S K^0_S$
0.0564±0.0048±0.0116		ABE	04	BELL	10.6 $e^+e^- \to e^+e^-K^+K^-$
0.076 ±0.006 ±0.011	331	[1] ACCIARRI	01H	L3	$e^+e^- \to e^+e^-K^0_S K^0_S$
0.067 ±0.008 ±0.015		[2] ALBRECHT	90G	ARG	$e^+e^- \to e^+e^-K^+K^-$
$0.11\ ^{+0.03}_{-0.02}$ ±0.02		BEHREND	89C	CELL	$e^+e^- \to e^+e^-K^0_S K^0_S$
$0.10\ ^{+0.04}_{-0.03}\ ^{+0.03}_{-0.02}$		BERGER	88	PLUT	$e^+e^- \to e^+e^-K^0_S K^0_S$
0.12 ±0.07 ±0.04		[2] AIHARA	86B	TPC	$e^+e^- \to e^+e^-K^+K^-$
0.11 ±0.02 ±0.04		[2] ALTHOFF	83	TASS	$e^+e^- \to e^+e^-K\overline{K}$
• • • We do not use the following data for averages, fits, limits, etc. • • •					
0.0314±0.0050±0.0077		[3] ALBRECHT	90G	ARG	$e^+e^- \to e^+e^-K^+K^-$

[1] Supersedes ACCIARRI 95J. From analysis of L3 data at 91 and 183–209 GeV,
[2] Using an incoherent background.
[3] Using a coherent background.

$f'_2(1525)$ BRANCHING RATIOS

$\Gamma(\eta\eta)/\Gamma_{total}$ — Γ_2/Γ

VALUE	DOCUMENT ID		TECN	COMMENT
• • • We do not use the following data for averages, fits, limits, etc. • • •				
0.059±0.003±0.026	[1] ALBRECHT	20	RVUE	$0.9\ \overline{p}p \to \pi^0\pi^0\eta$, $\pi^0\eta\eta$, $\pi^0 K^+K^-$
seen	UEHARA	10A	BELL	10.6 $e^+e^- \to e^+e^-\eta\eta$
0.10 ±0.03	[2] PROKOSHKIN	91	GAM4	300 $\pi^-p \to \pi^-p\eta\eta$

[1] Residue from T-matrix pole, 4 poles, 4 channels, including scattering data from HYAMS 75 ($\pi\pi$), LONGACRE 86 ($K\overline{K}$), BINON 83 ($\eta\eta$).
[2] Combining results of GAM4 with those of WA76 on $K\overline{K}$ central production and results of CBAL, MRK3 and DM2 on $J/\psi \to \gamma\eta\eta$.

$\Gamma(\eta\eta)/\Gamma(K\overline{K})$ — Γ_2/Γ_1

VALUE	CL%	EVTS	DOCUMENT ID		TECN	COMMENT
0.132±0.028 OUR FIT						
0.115±0.028 OUR AVERAGE						
0.119±0.015±0.036		61	[1] BINON	07	GAMS	32.5 $K^-p \to \eta\eta(\Lambda/\Sigma^0)$
0.11 ±0.04			[2] PROKOSHKIN	91	GAM4	300 $\pi^-p \to \pi^-p\eta\eta$
• • • We do not use the following data for averages, fits, limits, etc. • • •						
< 0.14	90		BARBERIS	00E		450 $pp \to p_f\eta\eta p_s$
< 0.50			BARNES	67	HBC	4.6,5.0 K^-p

[1] Using the compilation of the cross sections for $f'_2(1525)$ production in K^-p collisions from ASTON 88D.
[2] Combining results of GAM4 with those of WA76 on $K\overline{K}$ central production and results of CBAL, MRK3 and DM2 on $J/\psi \to \gamma\eta\eta$.

$\Gamma(\pi\pi)/\Gamma_{total}$ — Γ_3/Γ

VALUE (units 10^{-2})	CL%	DOCUMENT ID		TECN	COMMENT
0.83±0.16 OUR FIT					
0.75±0.16 OUR AVERAGE					
0.7 ±0.2		COSTA	80	OMEG	10 $\pi^-p \to K^+K^-n$
$2.7\ ^{+7.1}_{-1.3}$		[1] GORLICH	80	ASPK	17,18 π^-p
0.75±0.25		[1,2] MARTIN	79	RVUE	
• • • We do not use the following data for averages, fits, limits, etc. • • •					
3.4 ±1.5 ±1.0		[3] ALBRECHT	20	RVUE	$0.9\ \overline{p}p \to \pi^0\pi^0\eta$, $\pi^0\eta\eta$, $\pi^0 K^+K^-$
< 6	95	AGUILAR-...	81B	HBC	4.2 $K^-p \to \Lambda K^+K^-$
19 ±3		CORDEN	79	OMEG	12–15 $\pi^-p \to \pi^+\pi^-n$
< 4.5	95	BARREIRO	77	HBC	4.15 $K^-p \to \Lambda K^0_S K^0_S$
1.2 ±0.4		[1] PAWLICKI	77	SPEC	6 $\pi N \to K^+K^-N$
< 6.3	90	BRANDENB...	76C	ASPK	13 $K^-p \to K^+K^-(\Lambda,\Sigma)$
< 0.86		[1] BEUSCH	75B	OSPK	8.9 $\pi^-p \to K^0\overline{K}^0n$

[1] Assuming that the $f'_2(1525)$ is produced by an one-pion exchange production mechanism.
[2] MARTIN 79 uses the PAWLICKI 77 data with different input value of the $f'_2(1525) \to K\overline{K}$ branching ratio.
[3] Residue from T-matrix pole, 4 poles, 4 channels, including scattering data from HYAMS 75 ($\pi\pi$), LONGACRE 86 ($K\overline{K}$), BINON 83 ($\eta\eta$).

$\Gamma(\pi\pi)/\Gamma(K\overline{K})$ — Γ_3/Γ_1

VALUE	DOCUMENT ID		TECN	COMMENT
0.0094±0.0018 OUR FIT				
0.075 ±0.035	AUGUSTIN	87	DM2	$J/\psi \to \gamma\pi^+\pi^-$

$[\Gamma(K\overline{K}^*(892)+c.c.) + \Gamma(\pi K\overline{K})]/\Gamma(K\overline{K})$ — $(\Gamma_4+\Gamma_5)/\Gamma_1$

VALUE	CL%	DOCUMENT ID		TECN	COMMENT
• • • We do not use the following data for averages, fits, limits, etc. • • •					
<0.35	95	AGUILAR-...	72B	HBC	3.9,4.6 K^-p
<0.4	67	AMMAR	67	HBC	

$\Gamma(\pi\pi\eta)/\Gamma(K\overline{K})$ — Γ_6/Γ_1

VALUE	CL%	DOCUMENT ID		TECN	COMMENT
• • • We do not use the following data for averages, fits, limits, etc. • • •					
<0.41	95	AGUILAR-...	72B	HBC	3.9,4.6 K^-p
<0.3	67	AMMAR	67	HBC	

$\Gamma(\pi^+\pi^+\pi^-\pi^-)/\Gamma(K\overline{K})$ — Γ_7/Γ_1

VALUE	CL%	DOCUMENT ID		TECN	COMMENT
• • • We do not use the following data for averages, fits, limits, etc. • • •					
<0.32	95	AGUILAR-...	72B	HBC	3.9,4.6 K^-p

$f'_2(1525)$ REFERENCES

RODAS	22	EPJ C82 80	A. Rodas *et al.*	(JPAC Collab.)
ALBRECHT	20	EPJ C80 453	M. Albrecht *et al.*	(Crystal Barrel Collab.)
ABLIKIM	18AA	PR D98 072003	M. Ablikim *et al.*	(BESIII Collab.)
PDG	18	PR D98 030001	M. Tanabashi *et al.*	(PDG Collab.)
ABLIKIM	15AE	PR D92 052003	M. Ablikim *et al.*	(BESIII Collab.)
DOBBS	15	PR D91 052006	S. Dobbs *et al.*	(NWES)
LEES	14H	PR D89 092002	J.P. Lees *et al.*	(BABAR Collab.)
AAIJ	13AN	PR D87 072004	R. Aaij *et al.*	(LHCb Collab.)
ABLIKIM	13N	PR D87 092009	M. Ablikim *et al.*	(BESIII Collab.)
UEHARA	13	PTEP 2013 123C01	S. Uehara *et al.*	(BELLE Collab.)
UEHARA	10A	PR D82 114031	S. Uehara *et al.*	(BELLE Collab.)
ANISOVICH	09	IJMP A24 2481	V.V. Anisovich, A.V. Sarantsev	
CHEKANOV	08	PRL 101 112003	S. Chekanov *et al.*	(ZEUS Collab.)
BINON	07	PAN 70 1713	F. Binon *et al.*	(GAMS Collab.)
		Translated from YAF 70 1758.		
AMSLER	06	PL B639 165	C. Amsler *et al.*	(Crystal Barrel Collab.)
SCHEGELSKY	06A	EPJ A27 207	V.A. Schegelsky *et al.*	
ABLIKIM	05	PL B607 243	M. Ablikim *et al.*	(BES Collab.)
ABE	04	EPJ C32 323	K. Abe *et al.*	(BELLE Collab.)
CHEKANOV	04	PL B578 33	S. Chekanov *et al.*	(ZEUS Collab.)
BAI	03G	PR D68 052003	J.Z. Bai *et al.*	(BES Collab.)
TIKHOMIROV	03	PAN 66 828	G.D. Tikhomirov *et al.*	
		Translated from YAF 66 860.		
AMSLER	02	EPJ C23 29	C. Amsler *et al.*	
ACCIARRI	01H	PL B501 173	M. Acciarri *et al.*	(L3 Collab.)
BARBERIS	00E	PL B479 59	D. Barberis *et al.*	(WA 102 Collab.)
BARBERIS	99	PL B453 305	D. Barberis *et al.*	(Omega Expt.)
BARKOV	99	JETPL 70 248	B.P. Barkov *et al.*	
		Translated from ZETFP 70 242.		
ABREU	96C	PL B379 309	P. Abreu *et al.*	(DELPHI Collab.)
BAI	96C	PRL 77 3959	J.Z. Bai *et al.*	(BES Collab.)
ACCIARRI	95J	PL B363 118	M. Acciarri *et al.*	(L3 Collab.)
PROKOSHKIN	91	SPD 36 155	Y.D. Prokoshkin	(GAM2 and GAM4 Collab.)
		Translated from DANS 316 900.		
ALBRECHT	90G	ZPHY C48 183	H. Albrecht *et al.*	(ARGUS Collab.)
BEHREND	89C	ZPHY C43 91	H.J. Behrend *et al.*	(CELLO Collab.)
ASTON	88D	NP B301 525	D. Aston *et al.*	(SLAC, NAGO, CINC, INUS)
AUGUSTIN	88	PRL 60 2238	J.E. Augustin *et al.*	(DM2 Collab.)
BERGER	88	ZPHY C37 329	C. Berger *et al.*	(PLUTO Collab.)
FALVARD	88	PR D38 2706	A. Falvard *et al.*	(CLER, FRAS, LALO+)
AUGUSTIN	87	ZPHY C36 369	J.E. Augustin *et al.*	(LALO, CLER, FRAS+)
BALTRUSAIT...	87	PR D35 2077	R.M. Baltrusaitis *et al.*	(Mark III Collab.)
AIHARA	86B	PRL 57 404	H. Aihara *et al.*	(TPC-2γ Collab.)
BOLONKIN	86	SJNP 43 776	B.V. Bolonkin *et al.*	(ITEP) JP
		Translated from YAF 43 1211.		
LONGACRE	86	PL B177 223	R.S. Longacre *et al.*	(BNL, BRAN, CUNY+)
ALTHOFF	83	PL 121B 216	M. Althoff *et al.*	(TASSO Collab.)
ARMSTRONG	83B	NP B224 193	T.A. Armstrong *et al.*	(BARI, BIRM, CERN+)
BINON	83	NC 78A 313	F.G. Binon *et al.*	(BELG, LAPP, SERP+)
AGUILAR-...	81B	ZPHY C8 313	M. Aguilar-Benitez *et al.*	(CERN, CDEF+)
ALHARRAN	81	NP B191 26	S. Al-Harran *et al.*	(BIRM, CERN, GLAS+)
CHABAUD	81	APP B12 575	V. Chabaud *et al.*	(CERN, CRAC, MPIM)
COSTA	80	NP B175 402	G. Costa *et al.*	(BARI, BONN, CERN, GLAS+)
GORLICH	80	NP B174 16	L. Gorlich *et al.*	(CRAC, MPIM, CERN+)
CORDEN	79	NP B157 250	M.J. Corden *et al.*	(BIRM, RHEL, TELA+) JP
MARTIN	79	NP B158 520	A.D. Martin, E.N. Ozmutlu	(DURH)
POLYCHRO...	79	PR D19 1317	V.A. Polychronakos *et al.*	(NDAM, ANL)
BARREIRO	77	NP B121 237	F. Barreiro *et al.*	(CERN, AMST, NIJM+)
EVANGELIS...	77	NP B127 384	C. Evangelista *et al.*	(BARI, BONN, CERN+)
PAWLICKI	77	PR D15 3196	A.J. Pawlicki *et al.*	(ANL) IJP
BRANDENB...	76C	NP B104 413	G.W. Brandenburg *et al.*	(SLAC)
BEUSCH	75B	PL 60B 101	W. Beusch *et al.*	(CERN, ETH)
HYAMS	75	NP B100 205	B.D. Hyams *et al.*	(CERN, MPIM)
AGUILAR-...	72B	PR D6 29	M. Aguilar-Benitez *et al.*	(BNL)
AMMAR	67	PRL 19 1071	R. Ammar *et al.*	(NWES, ANL) JP
BARNES	67	PRL 19 964	V.E. Barnes *et al.*	(BNL, SYRA) IJPC
CRENNELL	66	PRL 16 1025	D.J. Crennell *et al.*	(BNL) I

Downloaded from https://academic.oup.com/ptep/article/2022/8/083C01/6651666 by KIT Library user on 27 September 2022

$f_2(1565)$

$I^G(J^{PC}) = 0^+(2^{++})$

OMITTED FROM SUMMARY TABLE

Seen mostly in antinucleon-nucleon annihilation. Needs confirmation in other channels. See the review on "Spectroscopy of Light Meson Resonances."

$f_2(1565)$ MASS

VALUE (MeV)	DOCUMENT ID		TECN	COMMENT
1542±19 OUR AVERAGE	Error includes scale factor of 2.2. See the ideogram below.			
1552±13	[1] AMSLER	02	CBAR	0.9 $\overline{p}p \to \pi^0\eta\eta$, $\pi^0\pi^0\pi^0$
1575±18	[1] BERTIN	98	OBLX	0.05–0.405 $\overline{n}p \to \pi^+\pi^+\pi^-$
1507±15	[1] BERTIN	97C	OBLX	0.0 $\overline{p}p \to \pi^+\pi^-\pi^0$
• • • We do not use the following data for averages, fits, limits, etc. • • •				
1560±15	[2] ANISOVICH	09	RVUE	0.0 $\overline{p}p$, πN
1590±10	[3,4] AMELIN	06	VES	36 $\pi^- p \to \omega\omega n$
1550±10±20	[4] AMELIN	00	VES	37 $\pi^- p \to \eta\pi^+\pi^- n$
1598±11± 9	BAKER	99B	SPEC	0 $\overline{p}p \to \omega\omega\pi^0$
1534±20	[5] ABELE	96C	RVUE	Compilation
∼ 1552	[6] AMSLER	95D	CBAR	0.0 $\overline{p}p \to \pi^0\pi^0\pi^0$, $\pi^0\eta\eta$, $\pi^0\pi^0\eta$
1598±72	BALOSHIN	95	SPEC	40 $\pi^- C \to K^0_S K^0_S X$
1566^{+80}_{-50}	[7] ANISOVICH	94	CBAR	0.0 $\overline{p}p \to 3\pi^0, \eta\eta\pi^0$
1502± 9	ADAMO	93	OBLX	$\overline{n}p \to \pi^+\pi^+\pi^-$
1488±10	[8] ARMSTRONG	93C	E760	$\overline{p}p \to \pi^0\eta\eta \to 6\gamma$
1508±10	[8] ARMSTRONG	93D	E760	$\overline{p}p \to 3\pi^0 \to 6\gamma$
1525±10	[8] ARMSTRONG	93D	E760	$\overline{p}p \to \eta\pi^0\pi^0 \to 6\gamma$
∼ 1504	[9] WEIDENAUER	93	ASTE	0.0 $\overline{p}N \to 3\pi^- 2\pi^+$
1540±15	[8] ADAMO	92	OBLX	$\overline{n}p \to \pi^+\pi^+\pi^-$
1515±10	[10] AKER	91	CBAR	0.0 $\overline{p}p \to 3\pi^0$
1565±20	MAY	90	ASTE	0.0 $\overline{p}p \to \pi^+\pi^-\pi^0$
1477± 5	BRIDGES	86C	DBC	0.0 $\overline{p}N \to 3\pi^- 2\pi^+$

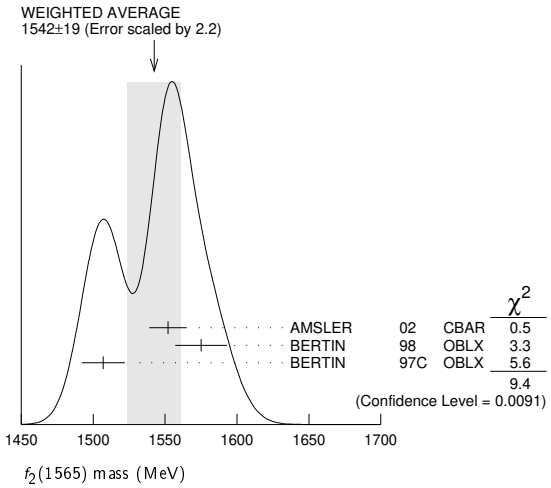

[1] T-matrix pole.
[2] On sheet II in a two-pole solution.
[3] Supersedes the $\omega\omega$ state of BELADIDZE 92B earlier assigned to the $f_2(1640)$.
[4] Breit-Wigner width.
[5] T-matrix pole, large coupling to $\rho\rho$ and $\omega\omega$, could be $f_2(1640)$.
[6] Coupled-channel analysis of AMSLER 95B, AMSLER 95C, and AMSLER 94D.
[7] From a simultaneous analysis of the annihilations $\overline{p}p \to 3\pi^0, \pi^0\eta\eta$ including AKER 91 data.
[8] J^P not determined, could be partly $f_0(1500)$.
[9] J^P not determined.
[10] Superseded by AMSLER 95B.

$f_2(1565)$ WIDTH

VALUE (MeV)	DOCUMENT ID		TECN	COMMENT
122± 13 OUR AVERAGE				
113± 23	[11] AMSLER	02	CBAR	0.9 $\overline{p}p \to \pi^0\eta\eta$, $\pi^0\pi^0\pi^0$
119± 24	[11] BERTIN	98	OBLX	0.05–0.405 $\overline{n}p \to \pi^+\pi^+\pi^-$
130± 20	[11] BERTIN	97C	OBLX	0.0 $\overline{p}p \to \pi^+\pi^-\pi^0$
• • • We do not use the following data for averages, fits, limits, etc. • • •				
280± 40	[12] ANISOVICH	09	RVUE	0.0 $\overline{p}p$, πN
140± 11	[13,14] AMELIN	06	VES	36 $\pi^- p \to \omega\omega n$
130± 20±40	[14] AMELIN	00	VES	37 $\pi^- p \to \eta\pi^+\pi^- n$
180± 60	[15] ABELE	96C	RVUE	Compilation
∼ 142	[16] AMSLER	95D	CBAR	0.0 $\overline{p}p \to \pi^0\pi^0\pi^0$, $\pi^0\eta\eta$, $\pi^0\pi^0\eta$
263±101	BALOSHIN	95	SPEC	40 $\pi^- C \to K^0_S K^0_S X$
166^{+80}_{-20}	[17] ANISOVICH	94	CBAR	0.0 $\overline{p}p \to 3\pi^0, \eta\eta\pi^0$
130± 10	[18] ADAMO	93	OBLX	$\overline{n}p \to \pi^+\pi^+\pi^-$
148± 27	[19] ARMSTRONG	93C	E760	$\overline{p}p \to \pi^0\eta\eta \to 6\gamma$
103± 15	[19] ARMSTRONG	93D	E760	$\overline{p}p \to 3\pi^0 \to 6\gamma$
111± 10	[19] ARMSTRONG	93D	E760	$\overline{p}p \to \eta\pi^0\pi^0 \to 6\gamma$
∼ 206	[20] WEIDENAUER	93	ASTE	0.0 $\overline{p}N \to 3\pi^- 2\pi^+$
132± 37	[19] ADAMO	92	OBLX	$\overline{n}p \to \pi^+\pi^+\pi^-$
120± 10	[21] AKER	91	CBAR	0.0 $\overline{p}p \to 3\pi^0$
170± 40	MAY	90	ASTE	0.0 $\overline{p}p \to \pi^+\pi^-\pi^0$
116± 9	BRIDGES	86C	DBC	0.0 $\overline{p}N \to 3\pi^- 2\pi^+$

[11] T-matrix pole.
[12] On sheet II in a two-pole solution.
[13] Supersedes the $\omega\omega$ state of BELADIDZE 92B earlier assigned to the $f_2(1640)$.
[14] Breit-Wigner width.
[15] T-matrix pole, large coupling to $\rho\rho$ and $\omega\omega$, could be $f_2(1640)$.
[16] Coupled-channel analysis of AMSLER 95B, AMSLER 95C, and AMSLER 94D.
[17] From a simultaneous analysis of the annihilations $\overline{p}p \to 3\pi^0, \pi^0\eta\eta$ including AKER 91 data.
[18] Supersedes ADAMO 92.
[19] J^P not determined, could be partly $f_0(1500)$.
[20] J^P not determined.
[21] Superseded by AMSLER 95B.

$f_2(1565)$ DECAY MODES

	Mode	Fraction (Γ_i/Γ)
Γ_1	$\pi\pi$	seen
Γ_2	$\pi^+\pi^-$	seen
Γ_3	$\pi^0\pi^0$	seen
Γ_4	$\rho^0\rho^0$	seen
Γ_5	$2\pi^+2\pi^-$	seen
Γ_6	$\eta\eta$	seen
Γ_7	$\omega\omega$	seen
Γ_8	$K\overline{K}$	seen
Γ_9	$\gamma\gamma$	seen

$f_2(1565)$ PARTIAL WIDTHS

$\Gamma(\eta\eta)$ — Γ_6

VALUE (MeV)	EVTS	DOCUMENT ID		TECN	COMMENT
• • • We do not use the following data for averages, fits, limits, etc. • • •					
1.2±0.3	870	[22] SCHEGELSKY	06A	RVUE	$\gamma\gamma \to K^0_S K^0_S$

$\Gamma(K\overline{K})$ — Γ_8

VALUE (MeV)	EVTS	DOCUMENT ID		TECN	COMMENT
• • • We do not use the following data for averages, fits, limits, etc. • • •					
2.0±1.0	870	[22] SCHEGELSKY	06A	RVUE	$\gamma\gamma \to K^0_S K^0_S$

$\Gamma(\gamma\gamma)$ — Γ_9

VALUE (keV)	EVTS	DOCUMENT ID		TECN	COMMENT
• • • We do not use the following data for averages, fits, limits, etc. • • •					
0.70±0.14	870	[22] SCHEGELSKY	06A	RVUE	$\gamma\gamma \to K^0_S K^0_S$

[22] From analysis of L3 data at 91 and 183–209 GeV, using $f_2(1565)$ mass of 1570 MeV, width of 160 MeV, $\Gamma(\pi\pi) = 25$ MeV, and SU(3) relations.

$f_2(1565)$ BRANCHING RATIOS

$\Gamma(\pi\pi)/\Gamma_{total}$ — Γ_1/Γ

VALUE	DOCUMENT ID		TECN	COMMENT
• • • We do not use the following data for averages, fits, limits, etc. • • •				
seen	BAKER	99B	SPEC	0 $\overline{p}p \to \omega\omega\pi^0$

$\Gamma(\pi^+\pi^-)/\Gamma_{total}$ — Γ_2/Γ

VALUE	DOCUMENT ID		TECN	COMMENT
• • • We do not use the following data for averages, fits, limits, etc. • • •				
seen	BERTIN	98	OBLX	0.05–0.405 $\overline{n}p \to \pi^+\pi^+\pi^-$
not seen	[23] ANISOVICH	94B	RVUE	$\overline{p}p \to \pi^+\pi^-\pi^0$
seen	MAY	89	ASTE	$\overline{p}p \to \pi^+\pi^-\pi^0$

[23] ANISOVICH 94B is from a reanalysis of MAY 90.

$\Gamma(\pi^0\pi^0)/\Gamma_{total}$ — Γ_3/Γ

VALUE	DOCUMENT ID		TECN	COMMENT
seen	AMSLER	95B	CBAR	0.0 $\overline{p}p \to 3\pi^0$

Downloaded from https://academic.oup.com/ptep/article/2022/8/083C01/6651666 by KIT Library user on 27 September 2022

$\Gamma(\pi^+\pi^-)/\Gamma(\rho^0\rho^0)$ — Γ_2/Γ_4

VALUE	DOCUMENT ID		TECN	COMMENT
• • • We do not use the following data for averages, fits, limits, etc. • • •				
0.042±0.013	BRIDGES	86B	DBC	$\overline{p}N \to 3\pi^- 2\pi^+$

$\Gamma(\eta\eta)/\Gamma(\pi^0\pi^0)$ — Γ_6/Γ_3

VALUE	DOCUMENT ID		TECN	COMMENT
• • • We do not use the following data for averages, fits, limits, etc. • • •				
0.024±0.005±0.012	[24] ARMSTRONG	93C	E760	$\overline{p}p \to \pi^0\eta\eta \to 6\gamma$

[24] J^P not determined, could be partly $f_0(1500)$.

$\Gamma(\omega\omega)/\Gamma_{total}$ — Γ_7/Γ

VALUE	DOCUMENT ID		TECN	COMMENT
• • • We do not use the following data for averages, fits, limits, etc. • • •				
seen	BAKER	99B	SPEC	$0\,\overline{p}p \to \omega\omega\pi^0$

$f_2(1565)$ REFERENCES

ANISOVICH	09	IJMP A24 2481	V.V. Anisovich, A.V. Sarantsev	
AMELIN	06	PAN 69 690	D.V. Amelin *et al.*	(VES Collab.)
		Translated from YAF 69 715.		
SCHEGELSKY	06A	EPJ A27 207	V.A. Schegelsky *et al.*	
AMSLER	02	EPJ C23 29	C. Amsler *et al.*	
AMELIN	00	NP A668 83	D. Amelin *et al.*	(VES Collab.)
BAKER	99B	PL B467 147	C.A. Baker *et al.*	
BERTIN	98	PR D57 55	A. Bertin *et al.*	(OBELIX Collab.)
BERTIN	97C	PL B408 476	A. Bertin *et al.*	(OBELIX Collab.)
ABELE	96C	NP A609 562	A. Abele *et al.*	(Crystal Barrel Collab.)
AMSLER	95B	PL B342 433	C. Amsler *et al.*	(Crystal Barrel Collab.)
AMSLER	95C	PL B353 571	C. Amsler *et al.*	(Crystal Barrel Collab.)
AMSLER	95D	PL B355 425	C. Amsler *et al.*	(Crystal Barrel Collab.)
BALOSHIN	95	PAN 58 46	O.N. Baloshin *et al.*	(ITEP)
		Translated from YAF 58 50.		
AMSLER	94D	PL B333 277	C. Amsler *et al.*	(Crystal Barrel Collab.)
ANISOVICH	94	PL B323 233	V.V. Anisovich *et al.*	(Crystal Barrel Collab.)
ANISOVICH	94B	PR D50 1972	V.V. Anisovich *et al.*	(LOQM)
ADAMO	93	NP A558 13C	A. Adamo *et al.*	(OBELIX Collab.)
ARMSTRONG	93C	PL B307 394	T.A. Armstrong *et al.*	(FNAL, FERR, GENO+)
ARMSTRONG	93D	PL B307 399	T.A. Armstrong *et al.*	(FNAL, FERR, GENO+)
WEIDENAUER	93	ZPHY C59 387	P. Weidenauer *et al.*	(ASTERIX Collab.)
ADAMO	92	PL B287 368	A. Adamo *et al.*	(OBELIX Collab.)
BELADIDZE	92B	ZPHY C54 367	G.M. Beladidze *et al.*	(VES Collab.)
AKER	91	PL B260 249	E. Aker *et al.*	(Crystal Barrel Collab.)
MAY	90	ZPHY C46 203	B. May *et al.*	(ASTERIX Collab.)
MAY	89	PL B225 450	B. May *et al.*	(ASTERIX Collab.) IJP
BRIDGES	86B	PRL 56 215	D.L. Bridges *et al.*	(SYRA, CASE)
BRIDGES	86C	PRL 57 1534	D.L. Bridges *et al.*	(SYRA)

$\rho(1570)$ — $I^G(J^{PC}) = 1^+(1^{--})$

OMITTED FROM SUMMARY TABLE

May be an OZI-violating decay mode of $\rho(1700)$. See the review on "Spectroscopy of Light Meson Resonances."

$\rho(1570)$ MASS

VALUE (MeV)	EVTS	DOCUMENT ID		TECN	COMMENT
1570±36±62	54	[1] AUBERT	08S	BABR	$10.6\ e^+e^- \to \phi\pi^0\gamma$
• • • We do not use the following data for averages, fits, limits, etc. • • •					
1585±15		[2] ACHASOV	20C	SND	$1.3–2.0\ e^+e^- \to K^+K^-\pi^0$
1480±40		[3] BITYUKOV	87	SPEC	$32.5\ \pi^-p \to \phi\pi^0 n$

[1] From the fit with two resonances.
[2] From a fit using a two resonance model in which the mass and width of the other resonance are fixed at the $\rho(1700)$ values from PDG 20.
[3] Systematic errors not estimated.

$\rho(1570)$ WIDTH

VALUE (MeV)	EVTS	DOCUMENT ID		TECN	COMMENT
144±75±43	54	[4] AUBERT	08S	BABR	$10.6\ e^+e^- \to \phi\pi^0\gamma$
• • • We do not use the following data for averages, fits, limits, etc. • • •					
75±30		[5] ACHASOV	20C	SND	$1.3–2.0\ e^+e^- \to K^+K^-\pi^0$
130±60		[6] BITYUKOV	87	SPEC	$32.5\ \pi^-p \to \phi\pi^0 n$

[4] From the fit with two resonances.
[5] From a fit using a two resonance model in which the mass and width of the other resonance are fixed at the $\rho(1700)$ values from PDG 20.
[6] Systematic errors not estimated.

$\rho(1570)$ DECAY MODES

	Mode	Fraction (Γ_i/Γ)
Γ_1	e^+e^-	
Γ_2	$\phi\pi$	not seen
Γ_3	$\omega\pi$	

$\rho(1570)$ $\Gamma(i)\Gamma(e^+e^-)/\Gamma(total)$

$\Gamma(\phi\pi) \times \Gamma(e^+e^-)/\Gamma_{total}$ — $\Gamma_2\Gamma_1/\Gamma$

VALUE (eV)	CL%	EVTS	DOCUMENT ID		TECN	COMMENT
3.5±0.9±0.3		54	[7] AUBERT	08S	BABR	$10.6\ e^+e^- \to \phi\pi^0\gamma$
• • • We do not use the following data for averages, fits, limits, etc. • • •						
<70	90		[8] AULCHENKO	87B	ND	$e^+e^- \to K^0_S K^0_L \pi^0$

[7] From the fit with two resonances.
[8] Using mass and width of BITYUKOV 87.

$\rho(1570)$ BRANCHING RATIOS

$\Gamma(\phi\pi)/\Gamma_{total}$ — Γ_2/Γ

VALUE	DOCUMENT ID		TECN	COMMENT
not seen	ABELE	97H	CBAR	$\overline{p}p \to K^0_L K^0_S \pi^0\pi^0$
• • • We do not use the following data for averages, fits, limits, etc. • • •				
<0.01	[9] DONNACHIE	91	RVUE	

[9] Using data from BISELLO 91B, DOLINSKY 86, and ALBRECHT 87L.

$\Gamma(\phi\pi)/\Gamma(\omega\pi)$ — Γ_2/Γ_3

VALUE	CL%	DOCUMENT ID		TECN	COMMENT
• • • We do not use the following data for averages, fits, limits, etc. • • •					
>0.5	95	BITYUKOV	87	SPEC	$32.5\ \pi^-p \to \phi\pi^0 n$

$\rho(1570)$ REFERENCES

ACHASOV	20C	EPJ C80 1139	M.N. Achasov *et al.*	(SND Collab.)
PDG	20	PTEP 2020 083C01	P.A. Zyla *et al.*	(PDG Collab.)
AUBERT	08S	PR D77 092002	B. Aubert *et al.*	(BABAR Collab.)
ABELE	97H	PL B415 280	A. Abele *et al.*	(Crystal Barrel Collab.)
BISELLO	91B	NPBPS B21 111	D. Bisello	(DM2 Collab.)
DONNACHIE	91	ZPHY C51 689	A. Donnachie, A.B. Clegg	(MCHS, LANC)
ALBRECHT	87L	PL B185 223	H. Albrecht *et al.*	(ARGUS Collab.)
AULCHENKO	87B	JETPL 45 145	V.M. Aulchenko *et al.*	(NOVO)
		Translated from ZETFP 45 118.		
BITYUKOV	87	PL B188 383	S.I. Bityukov *et al.*	(SERP)
DOLINSKY	86	PL B174 453	S.I. Dolinsky *et al.*	(NOVO)

$h_1(1595)$ — $I^G(J^{PC}) = 0^-(1^{+-})$

OMITTED FROM SUMMARY TABLE

Seen in a partial-wave analysis of the $\omega\eta$ system produced in the reaction $\pi^-p \to \omega\eta n$ at 18 GeV/c.

$h_1(1595)$ MASS

VALUE (MeV)	DOCUMENT ID		TECN	COMMENT
$1594 \pm 15^{+10}_{-60}$	EUGENIO	01	SPEC	$18\ \pi^-p \to \omega\eta n$

$h_1(1595)$ WIDTH

VALUE (MeV)	DOCUMENT ID		TECN	COMMENT
$384 \pm 60^{+70}_{-100}$	EUGENIO	01	SPEC	$18\ \pi^-p \to \omega\eta n$

$h_1(1595)$ DECAY MODES

	Mode	Fraction (Γ_i/Γ)
Γ_1	$\omega\eta$	seen

$h_1(1595)$ REFERENCES

EUGENIO	01	PL B497 190	P. Eugenio *et al.*

$\pi_1(1600)$ — $I^G(J^{PC}) = 1^-(1^{-+})$

See the review on "Spectroscopy of Light Meson Resonances" and a note in PDG 06, Journal of Physics **G33** 1 (2006).

$\pi_1(1600)$ T-Matrix Pole $\sqrt{s}$

VALUE (MeV)	DOCUMENT ID		TECN	COMMENT
• • • We do not use the following data for averages, fits, limits, etc. • • •				
$(1623 \pm 47^{+24}_{-75}) - i\,(228 \pm 44^{+72}_{-88})$	[1] KOPF	21	RVUE	$0.9\ p\overline{p} \to \pi^0\pi^0\eta$, $\pi^0\eta\eta$, $\pi^0K^+K^-$ and $191\ \pi^-p \to \pi^-\pi^-\pi^+p$

Downloaded from https://academic.oup.com/ptep/article/2022/8/083C01/6651666 by KIT Library user on 27 September 2022

$(1564 \pm 24 \pm 86) - i\,(246 \pm 27 \pm 51)$	[2] RODAS	19	JPAC	191 $\pi^- p \to \eta^{(\prime)} \pi^- p$	

[1] From T-matrix pole based on combined fit of Crystal Barrel and $\pi\pi$ scattering data (ALBRECHT 20), and COMPASS data (ADOLPH 15), using a coupled-channel model of $\eta\pi$, $\eta'\pi$ and $K\overline{K}$ systems.
[2] The coupled-channel analysis of both the $\eta\pi$ and $\eta'\pi$ systems using ADOLPH 15 data.

$\pi_1(1600)$ MASS

VALUE (MeV)	EVTS	DOCUMENT ID		TECN	COMMENT
1661^{+15}_{-11} OUR AVERAGE		Error includes scale factor of 1.2.			
1600^{+110}_{-60}	46M	[1] AGHASYAN	18B	COMP	190 $\pi^- p \to \pi^-\pi^+\pi^- p$
$1664 \pm 8 \pm 10$	145k	[2] LU	05	B852	18 $\pi^- p \to \omega\pi^-\pi^0 p$
$1709 \pm 24 \pm 41$	69k	[3] KUHN	04	B852	18 $\pi^- p \to \eta\pi^+\pi^-\pi^- p$
$1597 \pm 10^{+45}_{-10}$		[3] IVANOV	01	B852	18 $\pi^- p \to \eta'\pi^- p$
• • • We do not use the following data for averages, fits, limits, etc. • • •					
$1660 \pm 10^{+0}_{-64}$	420k	[4] ALEKSEEV	10	COMP	190 $\pi^- Pb \to \pi^-\pi^-\pi^+ Pb'$
$1593 \pm 8^{+29}_{-47}$		[3,5] ADAMS	98B	B852	18.3 $\pi^- p \to \pi^+\pi^-\pi^- p$

[1] Statistical error negligible. See also the review ALEXEEV 22.
[2] May be a different state: natural and unnatural parity exchanges.
[3] Natural parity exchange.
[4] Superseded by AGHASYAN 2018B.
[5] Superseded by DZIERBA 06 excluding this state in a more refined PWA analysis, with 2.6 M events of $\pi^- p \to \pi^-\pi^-\pi^+ p$ and 3 M events of $\pi^- p \to \pi^-\pi^0\pi^0 p$ of E852 data.

$\pi_1(1600)$ WIDTH

VALUE (MeV)	EVTS	DOCUMENT ID		TECN	COMMENT
240 ± 50 OUR AVERAGE		Error includes scale factor of 1.7. See the ideogram below.			
580^{+100}_{-230}	46M	[1] AGHASYAN	18B	COMP	190 $\pi^- p \to \pi^-\pi^+\pi^- p$
$185 \pm 25 \pm 28$	145k	[2] LU	05	B852	18 $\pi^- p \to \omega\pi^-\pi^0 p$
$403 \pm 80 \pm 115$	69k	[3] KUHN	04	B852	18 $\pi^- p \to \eta\pi^+\pi^-\pi^- p$
$340 \pm 40 \pm 50$		[3] IVANOV	01	B852	18 $\pi^- p \to \eta'\pi^- p$
• • • We do not use the following data for averages, fits, limits, etc. • • •					
$269 \pm 21^{+42}_{-64}$	420k	[4] ALEKSEEV	10	COMP	190 $\pi^- Pb \to \pi^-\pi^-\pi^+ Pb'$
$168 \pm 20^{+150}_{-12}$		[3,5] ADAMS	98B	B852	18.3 $\pi^- p \to \pi^+\pi^-\pi^- p$

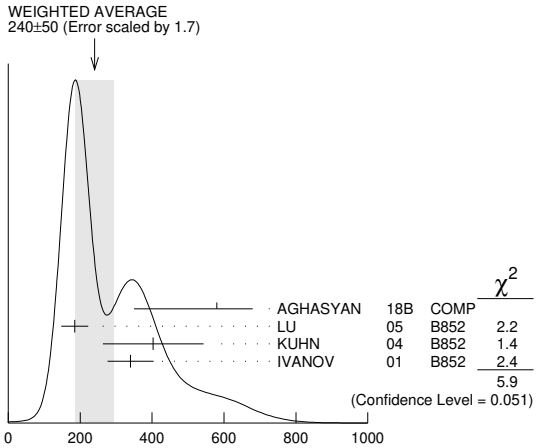

[1] Statistical error negligible. See also the review ALEXEEV 22.
[2] May be a different state: natural and unnatural parity exchanges.
[3] Natural parity exchange.
[4] Superseded by AGHASYAN 2018B.
[5] Superseded by DZIERBA 06 excluding this state in a more refined PWA analysis, with 2.6 M events of $\pi^- p \to \pi^-\pi^-\pi^+ p$ and 3 M events of $\pi^- p \to \pi^-\pi^0\pi^0 p$ of E852 data.

$\pi_1(1600)$ DECAY MODES

	Mode	Fraction (Γ_i/Γ)
Γ_1	$\pi\pi\pi$	seen
Γ_2	$\rho^0\pi^-$	seen
Γ_3	$f_2(1270)\pi^-$	not seen
Γ_4	$b_1(1235)\pi$	seen
Γ_5	$\eta'(958)\pi^-$	seen
Γ_6	$\eta\pi$	
Γ_7	$f_1(1285)\pi$	seen

$\pi_1(1600)$ BRANCHING RATIOS

$\Gamma(\rho^0\pi^-)/\Gamma_{total}$ — Γ_2/Γ

VALUE	DOCUMENT ID		TECN	COMMENT
seen	ALEKSEEV	10	COMP	190 $\pi^- Pb \to \pi^-\pi^-\pi^+ Pb'$
• • • We do not use the following data for averages, fits, limits, etc. • • •				
not seen	NOZAR	09	CLAS	$\gamma p \to 2\pi^+\pi^- n$
not seen	[1] DZIERBA	06	B852	18 $\pi^- p$

[1] From the PWA analysis of 2.6 M $\pi^- p \to \pi^-\pi^-\pi^+ p$ and 3 M events of $\pi^- p \to \pi^-\pi^0\pi^0 p$ of E852 data. Supersedes ADAMS 98B.

$\Gamma(f_2(1270)\pi^-)/\Gamma_{total}$ — Γ_3/Γ

VALUE	DOCUMENT ID		TECN	COMMENT
not seen	[1] DZIERBA	06	B852	18 $\pi^- p$

[1] From the PWA analysis of 2.6 M $\pi^- p \to \pi^-\pi^-\pi^+ p$ and 3 M events of $\pi^- p \to \pi^-\pi^0\pi^0 p$ of E852 data. Supersedes CHUNG 02.

$\Gamma(b_1(1235)\pi)/\Gamma_{total}$ — Γ_4/Γ

VALUE	EVTS	DOCUMENT ID		TECN	COMMENT
seen	35280	[1] BAKER	03	SPEC	$\overline{p}p \to \omega\pi^+\pi^-\pi^0$
• • • We do not use the following data for averages, fits, limits, etc. • • •					
seen	145k	LU	05	B852	18 $\pi^- p \to \omega\pi^-\pi^0 p$

[1] $B((b_1\pi)_{D-wave})/B((b_1\pi)_{S\text{-wave}}) = 0.3 \pm 0.1$.

$\Gamma(\eta'(958)\pi^-)/\Gamma_{total}$ — Γ_5/Γ

VALUE	DOCUMENT ID		TECN	COMMENT
seen	IVANOV	01	B852	18 $\pi^- p \to \eta'\pi^- p$

$\Gamma(\eta'(958)\pi^-)/\Gamma(\eta\pi)$ — Γ_5/Γ_6

VALUE	DOCUMENT ID		TECN	COMMENT
• • • We do not use the following data for averages, fits, limits, etc. • • •				
$5.54 \pm 1.1^{+1.8}_{-0.27}$	[1] KOPF	21	RVUE	0.9 $p\overline{p} \to \pi^0\pi^0\eta$, $\pi^0\pi^0\eta\eta$, $\pi^0 K^+ K^-$ and 191 $\pi^- p \to \pi^-\pi^-\pi^+ p$

[1] From T-matrix pole based on combined fit of Crystal Barrel and $\pi\pi$ scattering data (ALBRECHT 20), and COMPASS data (ADOLPH 15), using a coupled-channel model of $\eta\pi$, $\eta'\pi$ and $K\overline{K}$ systems.

$\Gamma(f_1(1285)\pi)/\Gamma(\eta'(958)\pi^-)$ — Γ_7/Γ_5

VALUE	EVTS	DOCUMENT ID		TECN	COMMENT
3.80±0.78	69k	[1] KUHN	04	B852	18 $\pi^- p \to \eta\pi^+\pi^-\pi^- p$

[1] Using $\eta'(958)\pi$ data from IVANOV 01.

$\pi_1(1600)$ REFERENCES

ALEXEEV	22	PR D105 012005	G.D. Alexeev *et al.*	(COMPASS Collab.)
KOPF	21	EPJ C81 1056	B. Kopf *et al.*	(BOCH)
ALBRECHT	20	EPJ C80 453	M. Albrecht *et al.*	(Crystal Barrel Collab.)
RODAS	19	PRL 122 042002	A. Rodas *et al.*	(JPAC Collab.)
AGHASYAN	18B	PR D98 092003	M. Aghasyan *et al.*	(COMPASS Collab.)
ADOLPH	15	PL B740 303	M. Adolph *et al.*	(COMPASS Collab.)
ALEKSEEV	10	PRL 104 241803	M.G. Alekseev *et al.*	(COMPASS Collab.)
NOZAR	09	PRL 102 102002	M. Nozar *et al.*	(JLab CLAS Collab.)
DZIERBA	06	PR D73 072001	A.R. Dzierba *et al.*	(BNL E852 Collab.)
PDG	06	JP G33 1	W.-M. Yao *et al.*	(PDG Collab.)
LU	05	PRL 94 032002	M. Lu *et al.*	(BNL E852 Collab.)
KUHN	04	PL B595 109	J. Kuhn *et al.*	(BNL E852 Collab.)
BAKER	03	PL B563 140	C.A. Baker *et al.*	
CHUNG	02	PR D65 072001	S.U. Chung *et al.*	(BNL E852 Collab.)
IVANOV	01	PRL 86 3977	E.I. Ivanov *et al.*	(BNL E852 Collab.)
ADAMS	98B	PRL 81 5760	G.S. Adams *et al.*	(BNL E852 Collab.)

$a_1(1640)$

$I^G(J^{PC}) = 1^-(1^{++})$

Possibly seen in the study of the hadronic structure in decay $\tau \to 3\pi\nu_\tau$ (ABREU 98G and ASNER 00).

$a_1(1640)$ MASS

VALUE (MeV)	EVTS	DOCUMENT ID		TECN	COMMENT
1655 ± 16 OUR AVERAGE		Error includes scale factor of 1.2.			
1700^{+35}_{-130}	46M	[1] AGHASYAN	18B	COMP	190 $\pi^- p \to \pi^-\pi^+\pi^- p$
$1691 \pm 18 \pm 30$		DARGENT	17	RVUE	$D^0 \to \pi^-\pi^+\pi^-\pi^+$
1630 ± 20	35k	[2] BAKER	03	SPEC	$\overline{p}p \to \omega\pi^+\pi^-\pi^0$
$1714 \pm 9 \pm 36$		CHUNG	02	B852	18.3 $\pi^- p \to \pi^+\pi^-\pi^- p$
$1640 \pm 12 \pm 30$		BAKER	99	SPEC	1.94 $\overline{p}p \to 4\pi^0$

Downloaded from https://academic.oup.com/ptep/article/2022/8/083C01/6651666 by KIT Library user on 27 September 2022

• • • We do not use the following data for averages, fits, limits, etc. • • •

1670 ± 90	BELLINI	85	SPEC	$40\ \pi^- A \to \pi^- \pi^+ \pi^- A$

[1] Statistical error negligible.
[2] Using the $a_1(1260)$ mass and width results of BOWLER 88.

$a_1(1640)$ WIDTH

VALUE (MeV)	EVTS	DOCUMENT ID		TECN	COMMENT
254 ± 40 OUR AVERAGE		Error includes scale factor of 1.8. See the ideogram below.			
510^{+170}_{-90}	46M	[1] AGHASYAN	18B	COMP	$190\ \pi^- p \to \pi^- \pi^+ \pi^- p$
171 ± 33 ± 40		DARGENT	17	RVUE	$D^0 \to \pi^- \pi^+ \pi^- \pi^+$
225 ± 30	35k	[2] BAKER	03	SPEC	$\overline{p}p \to \omega \pi^+ \pi^- \pi^0$
308 ± 37 ± 62		CHUNG	02	B852	$18.3\ \pi^- p \to \pi^+ \pi^- \pi^- p$
300 ± 22 ± 40		BAKER	99	SPEC	$1.94\ \overline{p}p \to 4\pi^0$
• • • We do not use the following data for averages, fits, limits, etc. • • •					
300 ± 100		BELLINI	85	SPEC	$40\ \pi^- A \to \pi^- \pi^+ \pi^- A$

[1] Statistical error negligible.
[2] Using the $a_1(1260)$ mass and width results of BOWLER 88.

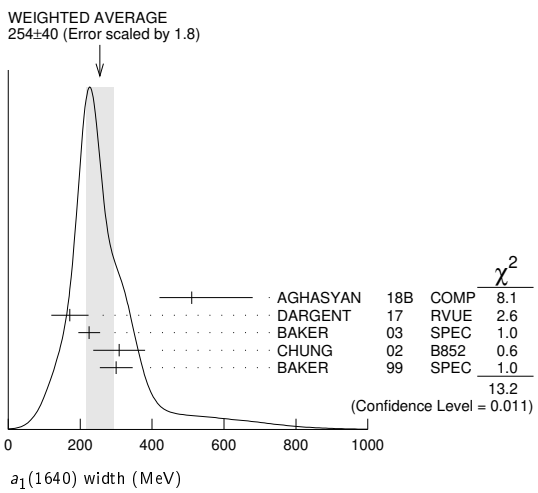

$a_1(1640)$ DECAY MODES

	Mode	Fraction (Γ_i/Γ)
Γ_1	$\pi\pi\pi$	seen
Γ_2	$f_2(1270)\pi$	seen
Γ_3	$\sigma\pi$	seen
Γ_4	$\rho\pi_{S-wave}$	seen
Γ_5	$\rho\pi_{D-wave}$	seen
Γ_6	$\omega\pi\pi$	seen
Γ_7	$f_1(1285)\pi$	seen
Γ_8	$a_1(1260)\eta$	not seen

$a_1(1640)$ BRANCHING RATIOS

$\Gamma(f_2(1270)\pi)/\Gamma(\sigma\pi)$ — Γ_2/Γ_3

VALUE	DOCUMENT ID		TECN	COMMENT
0.24 ± 0.07	BAKER	99	SPEC	$1.94\ \overline{p}p \to 4\pi^0$

$\Gamma(\rho\pi_{D-wave})/\Gamma_{total}$ — Γ_5/Γ

VALUE	DOCUMENT ID		TECN	COMMENT
• • • We do not use the following data for averages, fits, limits, etc. • • •				
seen	CHUNG	02	B852	$18.3\ \pi^- p \to \pi^+ \pi^- \pi^- p$
seen	AMELIN	95B	VES	$36\ \pi^- A \to \pi^+ \pi^- \pi^- A$

$\Gamma(\omega\pi\pi)/\Gamma_{total}$ — Γ_6/Γ

VALUE	EVTS	DOCUMENT ID		TECN	COMMENT
• • • We do not use the following data for averages, fits, limits, etc. • • •					
seen	35280	[1] BAKER	03	SPEC	$\overline{p}p \to \omega \pi^+ \pi^- \pi^0$

[1] Assuming the $\omega\rho$ mechanism for the $\omega\pi\pi$ state.

$\Gamma(f_1(1285)\pi)/\Gamma_{total}$ — Γ_7/Γ

VALUE	DOCUMENT ID		TECN	COMMENT
• • • We do not use the following data for averages, fits, limits, etc. • • •				
not seen	KUHN	04	B852	$18\ \pi^- p \to \eta \pi^+ \pi^- \pi^- p$
seen	LEE	94	MPS2	$18\ \pi^- p \to K^+ \overline{K}^0 \pi^- \pi^- p$

$\Gamma(a_1(1260)\eta)/\Gamma_{total}$ — Γ_8/Γ

VALUE	DOCUMENT ID		TECN	COMMENT
not seen	KUHN	04	B852	$18\ \pi^- p \to \eta \pi^+ \pi^- \pi^- p$

$a_1(1640)$ REFERENCES

AGHASYAN	18B	PR D98 092003	M. Aghasyan et al.	(COMPASS Collab.)
DARGENT	17	JHEP 1705 143	P. dArgent et al.	(HEID, BRIS)
KUHN	04	PL B595 109	J. Kuhn et al.	(BNL E852 Collab.)
BAKER	03	PL B563 140	C.A. Baker et al.	
CHUNG	02	PR D65 072001	S.U. Chung et al.	(BNL E852 Collab.)
ASNER	00	PR D61 012002	D.M. Asner et al.	(CLEO Collab.)
BAKER	99	PL B449 114	C.A. Baker et al.	
ABREU	98G	PL B426 411	P. Abreu et al.	(DELPHI Collab.)
AMELIN	95B	PL B356 595	D.V. Amelin et al.	(SERP, TBIL)
LEE	94	PL B323 227	J.H. Lee et al.	(BNL, IND, KYUN, MASD+)
BOWLER	88	PL B209 99	M.G. Bowler	(OXF)
BELLINI	85	SJNP 41 781	D. Bellini et al.	
		Translated from YAF 41 1223.		

$f_2(1640)$

$I^G(J^{PC}) = 0^+(2^{++})$

OMITTED FROM SUMMARY TABLE

$f_2(1640)$ MASS

VALUE (MeV)	DOCUMENT ID		TECN	COMMENT
1639 ± 6 OUR AVERAGE	Error includes scale factor of 1.2.			
1620 ± 16	BUGG	95	MRK3	$J/\psi \to \gamma \pi^+ \pi^- \pi^+ \pi^-$
1647 ± 7	ADAMO	92	OBLX	$\overline{n}p \to 3\pi^+ 2\pi^-$
1635 ± 7	ALDE	90	GAM2	$38\ \pi^- p \to \omega\omega n$
• • • We do not use the following data for averages, fits, limits, etc. • • •				
1640 ± 5	AMSLER	06	CBAR	$0.9\ \overline{p}p \to K^+ K^- \pi^0$
1659 ± 6	VLADIMIRSK...	06	SPEC	$40\ \pi^- p \to K^0_S K^0_S n$
1643 ± 7	[1] ALDE	89B	GAM2	$38\ \pi^- p \to \omega\omega n$

[1] Superseded by ALDE 90.

$f_2(1640)$ WIDTH

VALUE (MeV)	CL%	DOCUMENT ID		TECN	COMMENT
99^{+60}_{-40} OUR AVERAGE		Error includes scale factor of 2.9.			
140^{+60}_{-20}		BUGG	95	MRK3	$J/\psi \to \gamma \pi^+ \pi^- \pi^+ \pi^-$
58 ± 20		ADAMO	92	OBLX	$\overline{n}p \to 3\pi^+ 2\pi^-$
• • • We do not use the following data for averages, fits, limits, etc. • • •					
44 ± 9		AMSLER	06	CBAR	$0.9\ \overline{p}p \to K^+ K^- \pi^0$
152 ± 18		VLADIMIRSK...	06	SPEC	$40\ \pi^- p \to K^0_S K^0_S n$
< 70	90	ALDE	90	GAM2	$38\ \pi^- p \to \omega\omega n$

$f_2(1640)$ DECAY MODES

	Mode	Fraction (Γ_i/Γ)
Γ_1	$\omega\omega$	seen
Γ_2	4π	seen
Γ_3	$K\overline{K}$	seen

$f_2(1640)$ BRANCHING RATIOS

$\Gamma(K\overline{K})/\Gamma_{total}$ — Γ_3/Γ

VALUE	DOCUMENT ID		TECN	COMMENT
seen	AMSLER	06	CBAR	$0.9\ \overline{p}p \to K^+ K^- \pi^0$

$f_2(1640)$ REFERENCES

AMSLER	06	PL B639 165	C. Amsler et al.	(Crystal Barrel Collab.)
VLADIMIRSK...	06	PAN 69 493	V.V. Vladimirsky et al.	(ITEP, Moscow)
		Translated from YAF 69 515.		
BUGG	95	PL B353 378	D.V. Bugg et al.	(LOQM, PNPI, WASH) JP
ADAMO	92	PL B287 368	A. Adamo et al.	(OBELIX Collab.)
ALDE	90	PL B241 600	D.M. Alde et al.	(SERP, BELG, LANL, LAPP+)
ALDE	89B	PL B216 451	D.M. Alde et al.	(SERP, BELG, LANL, LAPP+) IGJPC

$\eta_2(1645)$

$I^G(J^{PC}) = 0^+(2^{-+})$

$\eta_2(1645)$ MASS

VALUE (MeV)	DOCUMENT ID		TECN	CHG	COMMENT
1617 ± 5 OUR AVERAGE					
1613 ± 8	BARBERIS	00B			$450\ pp \to p_f \eta \pi^+ \pi^- p_s$
1617 ± 8	BARBERIS	00C			$450\ pp \to p_f 4\pi p_s$
1620 ± 20	BARBERIS	97B	OMEG		$450\ pp \to pp2(\pi^+ \pi^-)$
1645 ± 14 ± 15	ADOMEIT	96	CBAR	0	$1.94\ \overline{p}p \to \eta 3\pi^0$

Downloaded from https://academic.oup.com/ptep/article/2022/8/083C01/6651666 by KIT Library user on 27 September 2022

• • • We do not use the following data for averages, fits, limits, etc. • • •

1645 ± 6 ± 20	ANISOVICH	00E	SPEC	0.9–1.94 $\overline{p}p \to \eta 3\pi^0$

$\eta_2(1645)$ WIDTH

VALUE (MeV)	DOCUMENT ID		TECN	CHG	COMMENT
181±11 OUR AVERAGE					
185 ± 17	BARBERIS	00B			450 $pp \to p_f \eta \pi^+ \pi^- p_s$
177 ± 18	BARBERIS	00C			450 $pp \to p_f 4\pi p_s$
180 ± 25	BARBERIS	97B	OMEG		450 $pp \to pp2(\pi^+\pi^-)$
$180^{+40}_{-21} \pm 25$	ADOMEIT	96	CBAR	0	1.94 $\overline{p}p \to \eta 3\pi^0$

• • • We do not use the following data for averages, fits, limits, etc. • • •

200 ± 25	ANISOVICH	00E	SPEC	0.9–1.94 $\overline{p}p \to \eta 3\pi^0$

$\eta_2(1645)$ DECAY MODES

	Mode	Fraction (Γ_i/Γ)
Γ_1	$a_2(1320)\pi$	seen
Γ_2	$K\overline{K}\pi$	seen
Γ_3	$K^*\overline{K}$	seen
Γ_4	$\eta\pi^+\pi^-$	seen
Γ_5	$a_0(980)\pi$	seen
Γ_6	$f_2(1270)\eta$	not seen

$\eta_2(1645)$ BRANCHING RATIOS

$\Gamma(K\overline{K}\pi)/\Gamma(a_2(1320)\pi)$ — Γ_2/Γ_1

VALUE	DOCUMENT ID		TECN	COMMENT
0.07±0.03	[1] BARBERIS	97C	OMEG	450 $pp \to pp K\overline{K}\pi$

[1] Using $2(\pi^+\pi^-)$ data from BARBERIS 97B.

$\Gamma(a_2(1320)\pi)/\Gamma(a_0(980)\pi)$ — Γ_1/Γ_5

VALUE	DOCUMENT ID		TECN	COMMENT
13.1±2.3 OUR AVERAGE				
13.5 ± 4.6	[2] ANISOVICH	11	SPEC	0.9–1.94 $p\overline{p}$
13.0 ± 2.7	BARBERIS	00B		450 $pp \to p_f \eta \pi^+ \pi^- p_s$

[2] Reanalysis of ADOMEIT 96 and ANISOVICH 00E.

$\Gamma(f_2(1270)\eta)/\Gamma_{total}$ — Γ_6/Γ

VALUE	DOCUMENT ID		COMMENT
• • • We do not use the following data for averages, fits, limits, etc. • • •			
not seen	BARBERIS	00B	450 $pp \to p_f \eta \pi^+ \pi^- p_s$

$\eta_2(1645)$ REFERENCES

ANISOVICH	11	EPJ C71 1511	A.V. Anisovich *et al.*	(LOQM, RAL, PNPI)
ANISOVICH	00E	PL B477 19	A.V. Anisovich *et al.*	
BARBERIS	00B	PL B471 435	D. Barberis *et al.*	(WA 102 Collab.)
BARBERIS	00C	PL B471 440	D. Barberis *et al.*	(WA 102 Collab.)
BARBERIS	97B	PL B413 217	D. Barberis *et al.*	(WA 102 Collab.)
BARBERIS	97C	PL B413 225	D. Barberis *et al.*	(WA 102 Collab.)
ADOMEIT	96	ZPHY C71 227	J. Adomeit *et al.*	(Crystal Barrel Collab.)

$\omega(1650)$

$I^G(J^{PC}) = 0^-(1^{--})$

See also the $\omega(1420)$ particle listing.

$\omega(1650)$ MASS

VALUE (MeV)	EVTS	DOCUMENT ID		TECN	COMMENT
1670± 30 OUR ESTIMATE					
• • • We do not use the following data for averages, fits, limits, etc. • • •					
1698 ± 10	267	[1] ACHASOV	20B	SND	$e^+e^- \to \omega\eta \to \eta\pi^0\gamma$
$1651 \pm 3^{+16}_{-6}$	183k	[2] ABLIKIM	19AQ	BES	$J/\psi \to K^+K^-\pi^0$
1673^{+6}_{-7}		ACHASOV	19	SND	$e^+e^- \to \pi^+\pi^-\pi^0\eta$
1671 ± 6 ± 10	824	[3] AKHMETSHIN	17A	CMD3	1.4–2.0 $e^+e^- \to \omega\eta$
1660 ± 10	898	[4] ACHASOV	16B	SND	1.34–2.00 $e^+e^- \to \omega\eta$
1680 ± 10	13.1k	[5] AULCHENKO	15A	SND	1.05–1.80 $e^+e^- \to \pi^+\pi^-\pi^0$
1667 ± 13 ± 6		AUBERT	07AU	BABR	10.6 $e^+e^- \to \omega\pi^+\pi^-\gamma$
1645 ± 8	13	AUBERT	06D	BABR	10.6 $e^+e^- \to \omega\eta\gamma$
1660 ± 10 ± 2		AUBERT,B	04N	BABR	10.6 $e^+e^- \to \pi^+\pi^-\pi^0\gamma$
1770 ± 50 ± 60	1.2M	[6] ACHASOV	03D	RVUE	0.44–2.00 $e^+e^- \to \pi^+\pi^-\pi^0$
1619 ± 5		[7] HENNER	02	RVUE	1.2–2.0 $e^+e^- \to \rho\pi, \omega\pi\pi$
1700 ± 20		EUGENIO	01	SPEC	18 $\pi^-p \to \omega\eta n$
1705 ± 26	612	[8] AKHMETSHIN	00D	CMD2	$e^+e^- \to \omega\pi^+\pi^-$
1820^{+190}_{-150}		[9] ACHASOV	98H	RVUE	$e^+e^- \to \pi^+\pi^-\pi^0$
1840^{+100}_{-70}		[10] ACHASOV	98H	RVUE	$e^+e^- \to \omega\pi^+\pi^-$
1780^{+170}_{-300}		[11] ACHASOV	98H	RVUE	$e^+e^- \to K^+K^-$
~ 2100		[12] ACHASOV	98H	RVUE	$e^+e^- \to K^0_S K^\pm\pi^\mp$
1606 ± 9		[13] CLEGG	94	RVUE	
1662 ± 13	750	[14] ANTONELLI	92	DM2	1.34–2.4 $e^+e^- \to \rho\pi, \omega\pi\pi$
1670 ± 20		ATKINSON	83B	OMEG	20–70 $\gamma p \to 3\pi X$
1657 ± 13		CORDIER	81	DM1	$e^+e^- \to \omega 2\pi$
1679 ± 34	21	ESPOSITO	80	FRAM	$e^+e^- \to 3\pi$
1652 ± 17		COSME	79	OSPK	$e^+e^- \to 3\pi$

[1] From a fit with contributions from $\omega(1420)$, $\omega(1650)$, and $\phi(1680)$. The mass of $\omega(1420)$ is fixed to the PDG 18 value of 1420 MeV. Fixing also the width of $\omega(1420)$ to the PDG 18 value of 220 MeV results in 1694 ± 9 MeV measurement.

[2] Could also be $\rho(1700)$. Branching ratio $J/\psi \to X\pi^0 \to K^+K^-\pi^0 = (5.3 \pm 0.3^{+0.6}_{-0.5}) \times 10^{-5}$.

[3] From a fit of the interfering $\omega(1420)$ and $\omega(1650)$ with a relative phase of π and other parameters floating.

[4] From a fit with contributions from $\omega(1420)$, $\omega(1650)$, and $\phi(1680)$.

[5] From a fit with contributions from $\omega(782)$, $\phi(1020)$, $\omega(1420)$, and $\omega(1650)$. See ACHASOV 20A for a further analysis of the $\pi^+\pi^-\pi^0$ data.

[6] From the combined fit of ANTONELLI 92, ACHASOV 01E, ACHASOV 02E, and ACHASOV 03D data on the $\pi^+\pi^-\pi^0$ and ANTONELLI 92 on the $\omega\pi^+\pi^-$ final states. Supersedes ACHASOV 99E and ACHASOV 02E.

[7] Using results of CORDIER 81 and preliminary data of DOLINSKY 91 and ANTONELLI 92.

[8] Using the data of AKHMETSHIN 00D and ANTONELLI 92. The $\rho\pi$ dominance for the energy dependence of the $\omega(1420)$ and $\omega(1650)$ width assumed.

[9] Using data from BARKOV 87, DOLINSKY 91, and ANTONELLI 92.

[10] Using the data from ANTONELLI 92.

[11] Using the data from IVANOV 81 and BISELLO 88B.

[12] Using the data from BISELLO 91C.

[13] From a fit to two Breit-Wigner functions and using the data of DOLINSKY 91 and ANTONELLI 92.

[14] From the combined fit of the $\rho\pi$ and $\omega\pi\pi$ final states.

$\omega(1650)$ WIDTH

VALUE (MeV)	EVTS	DOCUMENT ID		TECN	COMMENT
315± 35 OUR ESTIMATE					
• • • We do not use the following data for averages, fits, limits, etc. • • •					
110 ± 16	267	[1] ACHASOV	20B	SND	$e^+e^- \to \omega\eta \to \eta\pi^0\gamma$
$194 \pm 8^{+15}_{-7}$	183k	[2] ABLIKIM	19AQ	BES	$J/\psi \to K^+K^-\pi^0$
95 ± 11		ACHASOV	19	SND	$e^+e^- \to \pi^+\pi^-\pi^0\eta$
113 ± 9 ± 10	824	[3] AKHMETSHIN	17A	CMD3	1.4–2.0 $e^+e^- \to \omega\eta$
110 ± 20	898	[4] ACHASOV	16B	SND	1.34–2.00 $e^+e^- \to \omega\eta$
310 ± 30	13.1k	[5] AULCHENKO	15A	SND	1.05–1.80 $e^+e^- \to \pi^+\pi^-\pi^0$
222 ± 25 ± 20		AUBERT	07AU	BABR	10.6 $e^+e^- \to \omega\pi^+\pi^-\gamma$
114 ± 14	13	AUBERT	06D	BABR	10.6 $e^+e^- \to \omega\eta\gamma$
230 ± 30 ± 20		AUBERT,B	04N	BABR	10.6 $e^+e^- \to \pi^+\pi^-\pi^0\gamma$
$490^{+200}_{-150} \pm 130$	1.2M	[6] ACHASOV	03D	RVUE	0.44–2.00 $e^+e^- \to \pi^+\pi^-\pi^0$
250 ± 14		[7] HENNER	02	RVUE	1.2–2.0 $e^+e^- \to \rho\pi, \omega\pi\pi$
250 ± 50		EUGENIO	01	SPEC	18 $\pi^-p \to \omega\eta n$
370 ± 25	612	[8] AKHMETSHIN	00D	CMD2	$e^+e^- \to \omega\pi^+\pi^-$
113 ± 20		[9] CLEGG	94	RVUE	
280 ± 24	750	[10] ANTONELLI	92	DM2	1.34–2.4 $e^+e^- \to \rho\pi, \omega\pi\pi$
160 ± 20		ATKINSON	83B	OMEG	20–70 $\gamma p \to 3\pi X$
136 ± 46		CORDIER	81	DM1	$e^+e^- \to \omega 2\pi$
99 ± 49	21	ESPOSITO	80	FRAM	$e^+e^- \to 3\pi$
42 ± 17		COSME	79	OSPK	$e^+e^- \to 3\pi$

[1] From a fit with contributions from $\omega(1420)$, $\omega(1650)$, and $\phi(1680)$. The mass of $\omega(1420)$ is fixed to the PDG 18 value of 1420 MeV. Fixing also the width of $\omega(1420)$ to the PDG 18 value of 220 MeV results in 94 ± 13 MeV measurement.

[2] Could also be $\rho(1700)$. Branching ratio $J/\psi \to X\pi^0 \to K^+K^-\pi^0 = (5.3 \pm 0.3^{+0.6}_{-0.5}) \times 10^{-5}$.

[3] From a fit of the interfering $\omega(1420)$ and $\omega(1650)$ with a relative phase of π and other parameters floating.

[4] From a fit with contributions from $\omega(1420)$, $\omega(1650)$, and $\phi(1680)$.

[5] From a fit with contributions from $\omega(782)$, $\phi(1020)$, $\omega(1420)$, and $\omega(1650)$. See ACHASOV 20A for a further analysis of the $\pi^+\pi^-\pi^0$ data.

[6] From the combined fit of ANTONELLI 92, ACHASOV 01E, ACHASOV 02E, and ACHASOV 03D data on the $\pi^+\pi^-\pi^0$ and ANTONELLI 92 on the $\omega\pi^+\pi^-$ final states. Supersedes ACHASOV 99E and ACHASOV 02E.

[7] Using results of CORDIER 81 and preliminary data of DOLINSKY 91 and ANTONELLI 92.

[8] Using the data of AKHMETSHIN 00D and ANTONELLI 92. The $\rho\pi$ dominance for the energy dependence of the $\omega(1420)$ and $\omega(1650)$ width assumed.

[9] From a fit to two Breit-Wigner functions and using the data of DOLINSKY 91 and ANTONELLI 92.

[10] From the combined fit of the $\rho\pi$ and $\omega\pi\pi$ final states.

Downloaded from https://academic.oup.com/ptep/article/2022/8/083C01/6651666 by KIT Library user on 27 September 2022

$\omega(1650)$ DECAY MODES

	Mode	Fraction (Γ_i/Γ)
Γ_1	$\rho\pi$	seen
Γ_2	$\rho(1450)\pi$	seen
Γ_3	$\omega\pi\pi$	seen
Γ_4	$\omega\eta$	seen
Γ_5	e^+e^-	seen
Γ_6	$\pi^0\gamma$	not seen

$\omega(1650)$ $\Gamma(i)\Gamma(e^+e^-)/\Gamma^2(\text{total})$

$\Gamma(\rho\pi)/\Gamma_{\text{total}} \times \Gamma(e^+e^-)/\Gamma_{\text{total}}$ — $\Gamma_1/\Gamma \times \Gamma_5/\Gamma$

VALUE (units 10^{-6})	EVTS	DOCUMENT ID		TECN	COMMENT
• • • We do not use the following data for averages, fits, limits, etc. • • •					
1.56 ±0.23	13.1k	[1] AULCHENKO	15A	SND	1.05–1.80 $e^+e^- \to \pi^+\pi^-\pi^0$
1.3 ±0.1 ±0.1		AUBERT,B	04N	BABR	10.6 $e^+e^- \to \pi^+\pi^-\pi^0\gamma$
1.2 $^{+0.4}_{-0.1}$ ±0.8	1.2M	[2,3] ACHASOV	03D	RVUE	0.44–2.00 $e^+e^- \to \pi^+\pi^-\pi^0$
0.921±0.230		[4,5] CLEGG	94	RVUE	
0.479±0.050	750	[6,7] ANTONELLI	92	DM2	1.34–2.4 $e^+e^- \to \rho\pi, \omega\pi\pi$

[1] From a fit with contributions from $\omega(782)$, $\phi(1020)$, $\omega(1420)$, and $\omega(1650)$. See ACHASOV 20A for a further analysis of the $\pi^+\pi^-\pi^0$ data.
[2] Calculated by us from the cross section at the peak.
[3] From the combined fit of ANTONELLI 92, ACHASOV 01E, ACHASOV 02E, and ACHASOV 03D data on the $\pi^+\pi^-\pi^0$ and ANTONELLI 92 on the $\omega\pi^+\pi^-$ final states. Supersedes ACHASOV 99E and ACHASOV 02E.
[4] From a fit to two Breit-Wigner functions and using the data of DOLINSKY 91 and ANTONELLI 92.
[5] From the partial and leptonic width given by the authors.
[6] From the combined fit of the $\rho\pi$ and $\omega\pi\pi$ final states.
[7] From the product of the leptonic width and partial branching ratio given by the authors.

$\Gamma(\omega\pi\pi)/\Gamma_{\text{total}} \times \Gamma(e^+e^-)/\Gamma_{\text{total}}$ — $\Gamma_3/\Gamma \times \Gamma_5/\Gamma$

VALUE (units 10^{-7})	EVTS	DOCUMENT ID		TECN	COMMENT
• • • We do not use the following data for averages, fits, limits, etc. • • •					
7.0 ±0.5		AUBERT	07AU	BABR	10.6 $e^+e^- \to \omega\pi^+\pi^-\gamma$
4.1 ±0.9 ±1.3	1.2M	[1,2] ACHASOV	03D	RVUE	0.44–2.00 $e^+e^- \to \pi^+\pi^-\pi^0$
5.40±0.95		[3] AKHMETSHIN	00D	CMD2	1.2–1.38 $e^+e^- \to \omega\pi^+\pi^-$
3.18±0.80		[4,5] CLEGG	94	RVUE	
6.07±0.61	750	[6,7] ANTONELLI	92	DM2	1.34–2.4 $e^+e^- \to \rho\pi, \omega\pi\pi$

[1] Calculated by us from the cross section at the peak.
[2] From the combined fit of ANTONELLI 92, ACHASOV 01E, ACHASOV 02E, and ACHASOV 03D data on the $\pi^+\pi^-\pi^0$ and ANTONELLI 92 on the $\omega\pi^+\pi^-$ final states. Supersedes ACHASOV 99E and ACHASOV 02E.
[3] Using the data of AKHMETSHIN 00D and ANTONELLI 92. The $\rho\pi$ dominance for the energy dependence of the $\omega(1420)$ and $\omega(1650)$ width assumed.
[4] From a fit to two Breit-Wigner functions and using the data of DOLINSKY 91 and ANTONELLI 92.
[5] From the partial and leptonic width given by the authors.
[6] From the combined fit of the $\rho\pi$ and $\omega\pi\pi$ final states.
[7] From the product of the leptonic width and partial branching ratio given by the authors.

$\Gamma(\omega\eta)/\Gamma_{\text{total}} \times \Gamma(e^+e^-)/\Gamma_{\text{total}}$ — $\Gamma_4/\Gamma \times \Gamma_5/\Gamma$

VALUE (units 10^{-7})	EVTS	DOCUMENT ID		TECN	COMMENT
• • • We do not use the following data for averages, fits, limits, etc. • • •					
6.4 ±0.9	267	[1] ACHASOV	20B	SND	$e^+e^- \to \omega\eta \to \eta\pi^0\gamma$
$5.62^{+0.45}_{-0.42}$		ACHASOV	19	SND	$e^+e^- \to \pi^+\pi^-\pi^0\eta$
4.5 ±0.3 ±0.3	824	[2] AKHMETSHIN	17A	CMD3	1.4–2.0 $e^+e^- \to \omega\eta$
4.4 ±0.5	898	[3] ACHASOV	16B	SND	1.34–2.00 $e^+e^- \to \omega\eta$
5.7 ±0.6	13	AUBERT	06D	BABR	10.6 $e^+e^- \to \omega\eta\gamma$
< 60 at 90% CL		[4] AKHMETSHIN	03B	CMD2	$e^+e \to \eta\pi^0\gamma$

[1] From a fit with contributions from $\omega(1420)$, $\omega(1650)$, and $\phi(1680)$. The mass of $\omega(1420)$ is fixed to the PDG 18 value of 1420 MeV. Fixing also the width of $\omega(1420)$ to the PDG 18 value of 220 MeV results in $(5.4 \pm 0.6) \times 10^{-7}$ measurement.
[2] From a fit of the interfering $\omega(1420)$ and $\omega(1650)$ with a relative phase of π and other parameters floating. From an alternative fit $\Gamma(\omega(1650) \to \omega\eta)/\Gamma_{\text{total}} \times \Gamma(\omega(1650) \to e^+e^-) = 51 \pm 3$ eV.
[3] From a fit with contributions from $\omega(1420)$, $\omega(1650)$, and $\phi(1680)$.
[4] $\omega(1650)$ mass and width fixed at 1700 MeV and 250 MeV, respectively.

$\omega(1650)$ BRANCHING RATIOS

$\Gamma(\rho\pi)/\Gamma_{\text{total}}$ — Γ_1/Γ

VALUE	EVTS	DOCUMENT ID		TECN	COMMENT
• • • We do not use the following data for averages, fits, limits, etc. • • •					
~ 0.65	1.2M	[1] ACHASOV	03D	RVUE	0.44–2.00 $e^+e^- \to \pi^+\pi^-\pi^0$
0.380±0.014		[2] HENNER	02	RVUE	1.2–2.0 $e^+e^- \to \rho\pi, \omega\pi\pi$

[1] From the combined fit of ANTONELLI 92, ACHASOV 01E, ACHASOV 02E, and ACHASOV 03D data on the $\pi^+\pi^-\pi^0$ and ANTONELLI 92 on the $\omega\pi^+\pi^-$ final states. Supersedes ACHASOV 99E and ACHASOV 02E.
[2] Assuming that the $\omega(1650)$ decays into $\rho\pi$ and $\omega\pi\pi$ only.

$\Gamma(\rho(1450)\pi)/\Gamma_{\text{total}}$ — Γ_2/Γ

VALUE	DOCUMENT ID		TECN	COMMENT
seen	ACHASOV	20A	SND	1.15–2.00 $e^+e^- \to \pi^+\pi^-\pi^0$

$\Gamma(\omega\pi\pi)/\Gamma_{\text{total}}$ — Γ_3/Γ

VALUE	EVTS	DOCUMENT ID		TECN	COMMENT
• • • We do not use the following data for averages, fits, limits, etc. • • •					
~ 0.35	1.2M	[1] ACHASOV	03D	RVUE	0.44–2.00 $e^+e^- \to \pi^+\pi^-\pi^0$
0.620±0.014		[2] HENNER	02	RVUE	1.2–2.0 $e^+e^- \to \rho\pi, \omega\pi\pi$

[1] From the combined fit of ANTONELLI 92, ACHASOV 01E, ACHASOV 02E, and ACHASOV 03D data on the $\pi^+\pi^-\pi^0$ and ANTONELLI 92 on the $\omega\pi^+\pi^-$ final states. Supersedes ACHASOV 99E and ACHASOV 02E.
[2] Assuming that the $\omega(1650)$ decays into $\rho\pi$ and $\omega\pi\pi$ only.

$\Gamma(e^+e^-)/\Gamma_{\text{total}}$ — Γ_5/Γ

VALUE (units 10^{-7})	EVTS	DOCUMENT ID		TECN	COMMENT
• • • We do not use the following data for averages, fits, limits, etc. • • •					
~ 18	1.2M	[1,2] ACHASOV	03D	RVUE	0.44–2.00 $e^+e^- \to \pi^+\pi^-\pi^0$
32±1		[2] HENNER	02	RVUE	1.2–2.0 $e^+e^- \to \rho\pi, \omega\pi\pi$

[1] Calculated by us from the cross section at the peak.
[2] Assuming that the $\omega(1650)$ decays into $\rho\pi$ and $\omega\pi\pi$ only.

$\Gamma(\pi^0\gamma)/\Gamma_{\text{total}}$ — Γ_6/Γ

VALUE	DOCUMENT ID		TECN	COMMENT
not seen	[1] ACHASOV	10D	SND	1.075–2.0 $e^+e^- \to \pi^0\gamma$

[1] From a fit of a VMD model with two effective resonances with masses of 1450 MeV and 1700 MeV to describe the excited vector states $\omega(1420)$, $\rho(1450)$, $\omega(1650)$, and $\rho(1700)$. The width of the highest mass effective resonance is fixed at 315 MeV.

$\omega(1650)$ REFERENCES

ACHASOV	20A	EPJ C80 993	M.N. Achasov *et al.*	(SND Collab.)
ACHASOV	20B	EPJ C80 1008	M.N. Achasov *et al.*	(SND Collab.)
ABLIKIM	19AQ	PR D100 032004	M. Ablikim *et al.*	(BESIII Collab.)
ACHASOV	19	PR D99 112004	M.N. Achasov *et al.*	(SND Collab.)
PDG	18	PR D98 030001	M. Tanabashi *et al.*	(PDG Collab.)
AKHMETSHIN	17A	PL B773 150	R.R. Akhmetshin *et al.*	(CMD-3 Collab.)
ACHASOV	16B	PR D94 092002	M.N. Achasov *et al.*	(SND Collab.)
AULCHENKO	15A	JETP 121 27	V.M. Aulchenko *et al.*	(SND Collab.)
		Translated from ZETF 148 34.		
ACHASOV	10D	PR D98 112001	M.N. Achasov *et al.*	(SND Collab.)
AUBERT	07AU	PR D76 092005	B. Aubert *et al.*	(BABAR Collab.)
AUBERT	06D	PR D73 052003	B. Aubert *et al.*	(BABAR Collab.)
AUBERT,B	04N	PR D70 072004	B. Aubert *et al.*	(BABAR Collab.)
ACHASOV	03D	PR D68 052006	M.N. Achasov *et al.*	(Novosibirsk SND Collab.)
AKHMETSHIN	03B	PL B562 173	R.R. Akhmetshin *et al.*	(Novosibirsk CMD-2 Collab.)
ACHASOV	02E	PR D66 032001	M.N. Achasov *et al.*	(Novosibirsk SND Collab.)
HENNER	02	EPJ C26 3	V.K. Henner *et al.*	
ACHASOV	01E	PR D63 072002	M.N. Achasov *et al.*	(Novosibirsk SND Collab.)
EUGENIO	01	PL B497 190	P. Eugenio *et al.*	
AKHMETSHIN	00D	PL B489 125	R.R. Akhmetshin *et al.*	(Novosibirsk CMD-2 Collab.)
ACHASOV	99E	PL B462 365	M.N. Achasov *et al.*	(Novosibirsk SND Collab.)
ACHASOV	98H	PR D57 4334	N.N. Achasov, A.A. Kozhevnikov	
CLEGG	94	ZPHY C62 455	A.B. Clegg, A. Donnachie	(LANC, MCHS)
ANTONELLI	92	ZPHY C56 15	A. Antonelli *et al.*	(DM2 Collab.)
BISELLO	91C	ZPHY C52 227	D. Bisello *et al.*	(DM2 Collab.)
DOLINSKY	91	PRPL 202 99	S.I. Dolinsky *et al.*	(NOVO)
BISELLO	88B	ZPHY C39 13	D. Bisello *et al.*	(PADO, CLER, FRAS+)
BARKOV	87	JETPL 46 164	L.M. Barkov *et al.*	(NOVO)
		Translated from ZETFP 46 132.		
ATKINSON	83B	PL 127B 132	M. Atkinson *et al.*	(BONN, CERN, GLAS+)
CORDIER	81	PL 106B 155	A. Cordier *et al.*	(ORSAY)
IVANOV	81	PL 107B 297	P.M. Ivanov *et al.*	(NOVO)
ESPOSITO	80	LNC 28 195	B. Esposito *et al.*	(FRAS, NAPL, PADO+)
COSME	79	NP B152 215	G. Cosme *et al.*	(IPN)

$\omega_3(1670)$

$I^G(J^{PC}) = 0^-(3^{--})$

$\omega_3(1670)$ MASS

VALUE (MeV)	EVTS	DOCUMENT ID		TECN	COMMENT
1667 ± 4 OUR AVERAGE					
1665.3± 5.2±4.5	23400	AMELIN	96	VES	36 $\pi^-p \to \pi^+\pi^-\pi^0 n$
1685 ±20	60	BAUBILLIER	79	HBC	8.2 K^-p backward
1673 ±12	430	[1,2] BALTAY	78E	HBC	15 $\pi^+p \to \Delta 3\pi$
1650 ±12		CORDEN	78B	OMEG	8–12 $\pi^-p \to N3\pi$
1669 ±11	600	[2] WAGNER	75	HBC	7 $\pi^+p \to \Delta^{++}3\pi$
1678 ±14	500	DIAZ	74	DBC	6 $\pi^+n \to p3\pi^0$
1660 ±13	200	DIAZ	74	DBC	6 $\pi^+n \to p\omega\pi^0\pi^0$
1679 ±17	200	MATTHEWS	71D	DBC	7.0 $\pi^+n \to p3\pi^0$
1670 ±20		KENYON	69	DBC	8 $\pi^+n \to p3\pi^0$
• • • We do not use the following data for averages, fits, limits, etc. • • •					
~ 1700	110	[1] CERRADA	77B	HBC	4.2 $K^-p \to \Lambda 3\pi$
1695 ±20		BARNES	69B	HBC	4.6 $K^-p \to \omega 2\pi X$
1636 ±20		ARMENISE	68B	DBC	5.1 $\pi^+n \to p3\pi^0$

[1] Phase rotation seen for $J^P = 3^-$ $\rho\pi$ wave.
[2] From a fit to $I(J^P) = 0(3^-)$ $\rho\pi$ partial wave.

Downloaded from https://academic.oup.com/ptep/article/2022/8/083C01/6651666 by KIT Library user on 27 September 2022

$\omega_3(1670)$ WIDTH

VALUE (MeV)	EVTS	DOCUMENT ID		TECN	COMMENT
168±10 OUR AVERAGE					
149±19±7	23400	AMELIN	96	VES	36 $\pi^- p \to \pi^+\pi^-\pi^0 n$
160±80	60	[3] BAUBILLIER	79	HBC	8.2 $K^- p$ backward
173±16	430	[4,5] BALTAY	78E	HBC	15 $\pi^+ p \to \Delta 3\pi$
253±39		CORDEN	78B	OMEG	8–12 $\pi^- p \to N 3\pi$
173±28	600	[3,5] WAGNER	75	HBC	7 $\pi^+ p \to \Delta^{++} 3\pi$
167±40	500	DIAZ	74	DBC	6 $\pi^+ n \to p 3\pi^0$
122±39	200	DIAZ	74	DBC	6 $\pi^+ n \to p\omega\pi^0\pi^0$
155±40	200	[3] MATTHEWS	71D	DBC	7.0 $\pi^+ n \to p 3\pi^0$
• • • We do not use the following data for averages, fits, limits, etc. • • •					
90±20		BARNES	69B	HBC	4.6 $K^- p \to \omega 2\pi$
100±40		KENYON	69	DBC	8 $\pi^+ n \to p 3\pi^0$
112±60		ARMENISE	68B	DBC	5.1 $\pi^+ n \to p 3\pi^0$

[3] Width errors enlarged by us to $4\Gamma/\sqrt{N}$; see the note with the $K^*(892)$ mass.
[4] Phase rotation seen for $J^P = 3^-$ $\rho\pi$ wave.
[5] From a fit to $I(J^P) = 0(3^-)$ $\rho\pi$ partial wave.

$\omega_3(1670)$ DECAY MODES

	Mode	Fraction (Γ_i/Γ)
Γ_1	$\rho\pi$	seen
Γ_2	$\omega\pi\pi$	seen
Γ_3	$b_1(1235)\pi$	possibly seen

$\omega_3(1670)$ BRANCHING RATIOS

$\Gamma(\omega\pi\pi)/\Gamma(\rho\pi)$ — Γ_2/Γ_1

VALUE	EVTS	DOCUMENT ID		TECN	COMMENT
• • • We do not use the following data for averages, fits, limits, etc. • • •					
0.71±0.27	100	DIAZ	74	DBC	6 $\pi^+ n \to p 5\pi^0$

$\Gamma(b_1(1235)\pi)/\Gamma(\rho\pi)$ — Γ_3/Γ_1

VALUE	DOCUMENT ID		TECN	COMMENT
possibly seen	DIAZ	74	DBC	6 $\pi^+ n \to p 5\pi^0$

$\Gamma(b_1(1235)\pi)/\Gamma(\omega\pi\pi)$ — Γ_3/Γ_2

VALUE	CL%	DOCUMENT ID		TECN	COMMENT
• • • We do not use the following data for averages, fits, limits, etc. • • •					
>0.75	68	BAUBILLIER	79	HBC	8.2 $K^- p$ backward

$\omega_3(1670)$ REFERENCES

AMELIN	96	ZPHY C70 71	D.V. Amelin *et al.*	(SERP, TBIL)
BAUBILLIER	79	PL 89B 131	M. Baubillier *et al.*	(BIRM, CERN, GLAS+)
BALTAY	78E	PRL 40 87	C. Baltay, C.V. Cautis, M. Kalelkar	(COLU) JP
CORDEN	78B	NP B138 235	M.J. Corden *et al.*	(BIRM, RHEL, TELA+)
CERRADA	77B	NP B126 241	M. Cerrada *et al.*	(AMST, CERN, NIJM+) JP
WAGNER	75	PL 58B 201	F. Wagner, M. Tabak, D.M. Chew	(LBL) JP
DIAZ	74	PRL 32 260	J. Diaz *et al.*	(CASE, CMU)
MATTHEWS	71D	PR D3 2561	J.A.J. Matthews *et al.*	(TNTO, WISC)
BARNES	69B	PRL 23 142	V.E. Barnes *et al.*	(BNL)
KENYON	69	PRL 23 146	I.R. Kenyon *et al.*	(BNL, UCND, ORNL)
ARMENISE	68B	PL 26B 336	N. Armenise *et al.*	(BARI, BGNA, FIRZ+)

$\pi_2(1670)$

$I^G(J^{PC}) = 1^-(2^{-+})$

$\pi_2(1670)$ MASS

VALUE (MeV)	EVTS	DOCUMENT ID		TECN	CHG	COMMENT
$1670.6^{+2.9}_{-1.2}$ OUR AVERAGE Error includes scale factor of 1.3. See the ideogram below.						
1642^{+12}_{-1}	46M	[1] AGHASYAN	18B	COMP		190 $\pi^- p \to \pi^-\pi^+\pi^- p$
1749 ±10 ±100	145k	LU	05	B852		18 $\pi^- p \to \omega\pi^-\pi^0 p$
1676 ± 3 ± 8		[2] CHUNG	02	B852		18.3 $\pi^- p \to \pi^+\pi^-\pi^- p$
1685 ±10 ± 30		BARBERIS	01			450 $pp \to p_f 3\pi^0 p_s$
1687 ± 9 ± 15		AMELIN	99	VES		37 $\pi^- A \to \omega\pi^-\pi^0 A^*$
1669 ± 4		BARBERIS	98B			450 $pp \to p_f \rho\pi p_s$
1670 ± 4		BARBERIS	98B			450 $pp \to p_f f_2(1270)\pi p_s$
1690 ±14		[3] BERDNIKOV	94	VES		37 $\pi^- A \to K^+K^-\pi^- A$
1710 ±20	700	ANTIPOV	87	SIGM	−	50 π^- Cu $\to \mu^+\mu^-\pi^-$ Cu
1676 ± 6		[3] EVANGELIS...	81	OMEG	−	12 $\pi^- p \to 3\pi p$
1657 ±14		[3,4] DAUM	80D	SPEC	−	63–94 $\pi p \to 3\pi X$
1662 ±10	2000	[3] BALTAY	77	HBC	+	15 $\pi^+ p \to p 3\pi$
• • • We do not use the following data for averages, fits, limits, etc. • • •						
1658 ± 3 $^{+24}_{-8}$	420k	[5] ALEKSEEV	10	COMP		190 $\pi^- Pb \to \pi^-\pi^-\pi^+ Pb'$
1730 ±20		[6] AMELIN	95B	VES		36 $\pi^- A \to \pi^+\pi^-\pi^- A$
1742 ±31 ± 49		ANTREASYAN	90	CBAL		$e^+e^- \to e^+e^-\pi^0\pi^0\pi^0$
1624 ±21		[2] BELLINI	85	SPEC		40 $\pi^- A \to \pi^-\pi^+\pi^- A$
1622 ±35		[7] BELLINI	85	SPEC		40 $\pi^- A \to \pi^-\pi^+\pi^- A$
1693 ±28		[8] BELLINI	85	SPEC		40 $\pi^- A \to \pi^-\pi^+\pi^- A$
1710 ±20		[9] DAUM	81B	SPEC	−	63,94 $\pi^- p$
1660 ±10		[3] ASCOLI	73	HBC	−	5–25 $\pi^- p \to p\pi_2$

[1] Statistical error negligible.
[2] From $f_2(1270)\pi$ decay.
[3] From a fit to $J^P = 2^-S$-wave $f_2(1270)\pi$ partial wave.
[4] Clear phase rotation seen in 2^-S, 2^-P, 2^-D waves. We quote central value and spread of single-resonance fits to three channels.
[5] Superseded by AGHASYAN 2018B.
[6] J^{PC} ambiguous.
[7] From $\rho\pi$ decay.
[8] From $\sigma\pi$ decay.
[9] From a two-resonance fit to four 2^-0^+ waves. This should not be averaged with all the single resonance fits.

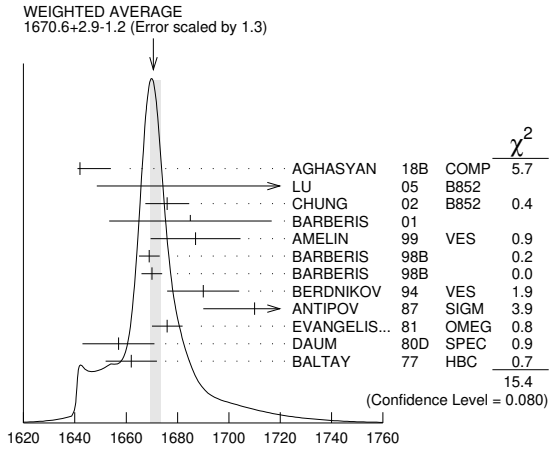

$\pi_2(1670)$ WIDTH

VALUE (MeV)	EVTS	DOCUMENT ID		TECN	CHG	COMMENT
258^{+8}_{-9} OUR AVERAGE Error includes scale factor of 1.2.						
311^{+12}_{-23}	46M	[10] AGHASYAN	18B	COMP		190 $\pi^- p \to \pi^-\pi^+\pi^- p$
408± 60±250	145k	LU	05	B852		18 $\pi^- p \to \omega\pi^-\pi^0 p$
254± 3± 31		[11] CHUNG	02	B852		18.3 $\pi^- p \to \pi^+\pi^-\pi^- p$
265± 30± 40		BARBERIS	01			450 $pp \to p_f 3\pi^0 p_s$
168± 43± 53		AMELIN	99	VES		37 $\pi^- A \to \omega\pi^-\pi^0 A^*$
268± 15		BARBERIS	98B			450 $pp \to p_f \rho\pi p_s$
256± 15		BARBERIS	98B			450 $pp \to p_f f_2(1270)\pi p_s$
190± 50		[12] BERDNIKOV	94	VES		37 $\pi^- A \to K^+K^-\pi^- A$
170± 80	700	ANTIPOV	87	SIGM	−	50 π^- Cu $\to \mu^+\mu^-\pi^-$ Cu
260± 20		[12] EVANGELIS...	81	OMEG	−	12 $\pi^- p \to 3\pi p$
219± 20		[12,13] DAUM	80D	SPEC	−	63–94 $\pi p \to 3\pi X$
285± 60	2000	[12] BALTAY	77	HBC	+	15 $\pi^+ p \to p 3\pi$
• • • We do not use the following data for averages, fits, limits, etc. • • •						
271± 9^{+22}_{-24}	420k	[14] ALEKSEEV	10	COMP		190 $\pi^- Pb \to \pi^-\pi^-\pi^+ Pb'$
310± 20		[15] AMELIN	95B	VES		36 $\pi^- A \to \pi^+\pi^-\pi^- A$
236± 49± 36		ANTREASYAN	90	CBAL		$e^+e^- \to e^+e^-\pi^0\pi^0\pi^0$
304± 22		[11] BELLINI	85	SPEC		40 $\pi^- A \to \pi^-\pi^+\pi^- A$
404±108		[16] BELLINI	85	SPEC		40 $\pi^- A \to \pi^-\pi^+\pi^- A$
330± 90		[17] BELLINI	85	SPEC		40 $\pi^- A \to \pi^-\pi^+\pi^- A$
312± 50		[18] DAUM	81B	SPEC	−	63,94 $\pi^- p$
270± 60		[12] ASCOLI	73	HBC	−	5–25 $\pi^- p \to p\pi_2$

[10] Statistical error negligible.

Downloaded from https://academic.oup.com/ptep/article/2022/8/083C01/6651666 by KIT Library user on 27 September 2022

[11] From $f_2(1270)\pi$ decay.
[12] From a fit to $J^P = 2^-$ $f_2(1270)\pi$ partial wave.
[13] Clear phase rotation seen in 2^-S, 2^-P, 2^-D waves. We quote central value and spread of single-resonance fits to three channels.
[14] Superseded by AGHASYAN 2018B.
[15] J^{PC} ambiguous.
[16] From $\rho\pi$ decay.
[17] From $\sigma\pi$ decay.
[18] From a two-resonance fit to four 2^-0^+ waves. This should not be averaged with all the single resonance fits.

$\pi_2(1670)$ DECAY MODES

	Mode	Fraction (Γ_i/Γ)	Confidence level
Γ_1	3π	(95.8 ± 1.4) %	
Γ_2	$\pi^+\pi^-\pi^0$		
Γ_3	$\pi^0\pi^0\pi^0$		
Γ_4	$f_2(1270)\pi$	(56.3 ± 3.2) %	
Γ_5	$\rho\pi$	$(31\ \pm4\ )$ %	
Γ_6	$\sigma\pi$	$(10\ \pm4\ )$ %	
Γ_7	$\pi(\pi\pi)_{S\text{-wave}}$	$(\ 8.7\pm3.4)$ %	
Γ_8	$\pi^\pm\pi^+\pi^-$	$(53\ \pm4\ )$ %	
Γ_9	$K\overline{K}^*(892)+$ c.c.	$(\ 4.2\pm1.4)$ %	
Γ_{10}	$\omega\rho$	$(\ 2.7\pm1.1)$ %	
Γ_{11}	$\pi^\pm\gamma$	$(\ 7.0\pm1.2)\times10^{-4}$	
Γ_{12}	$\gamma\gamma$	$<\ 2.8\ \times10^{-7}$	90%
Γ_{13}	$\eta\pi$	$<\ 5$ %	
Γ_{14}	$\pi^\pm2\pi^+2\pi^-$	$<\ 5$ %	
Γ_{15}	$\rho(1450)\pi$	$<\ 3.6\ \times10^{-3}$	97.7%
Γ_{16}	$b_1(1235)\pi$	$<\ 1.9\ \times10^{-3}$	97.7%
Γ_{17}	$\eta3\pi$		
Γ_{18}	$f_1(1285)\pi$	possibly seen	
Γ_{19}	$a_2(1320)\pi$	not seen	

CONSTRAINED FIT INFORMATION

An overall fit to 4 branching ratios uses 6 measurements and one constraint to determine 4 parameters. The overall fit has a $\chi^2 = 1.9$ for 3 degrees of freedom.

The following *off-diagonal* array elements are the correlation coefficients $\langle\delta x_i\delta x_j\rangle/(\delta x_i\cdot\delta x_j)$, in percent, from the fit to the branching fractions, $x_i \equiv \Gamma_i/\Gamma_{\text{total}}$. The fit constrains the x_i whose labels appear in array to sum to one.

x_5	−53		
x_7	−29	−59	
x_9	−8	−21	−9
	x_4	x_5	x_7

$\pi_2(1670)$ PARTIAL WIDTHS

$\Gamma(\pi^\pm\gamma)$ — Γ_{11}

VALUE (keV)	DOCUMENT ID		TECN	CHG	COMMENT
181±11±27	[19] ADOLPH	14	COMP	−	190 π^-Pb $\to$ $\pi^+\pi^-\pi^-$Pb$'$

[19] Primakoff reaction. Assumes incoherent $f_2(1270)\pi$ contribution to 3π final state and uses $B(\pi_2(1670) \to f_2\pi) = 56\%$.

$\Gamma(\gamma\gamma)$ — Γ_{12}

VALUE (keV)	CL%	DOCUMENT ID		TECN	CHG	COMMENT
<0.072	90	[20] ACCIARRI	97T	L3		$e^+e^-\to e^+e^-\pi^+\pi^-\pi^0$
• • • We do not use the following data for averages, fits, limits, etc. • • •						
<0.19	90	[20] ALBRECHT	97B	ARG		$e^+e^-\to e^+e^-\pi^+\pi^-\pi^0$
1.41 ±0.23±0.28		ANTREASYAN	90	CBAL	0	$e^+e^-\to e^+e^-\pi^0\pi^0\pi^0$
0.8 ±0.3 ±0.12		[21] BEHREND	90C	CELL	0	$e^+e^-\to e^+e^-\pi^+\pi^-\pi^0$
1.3 ±0.3 ±0.2		[22] BEHREND	90C	CELL	0	$e^+e^-\to e^+e^-\pi^+\pi^-\pi^0$

[20] Decaying into $f_2(1270)\pi$ and $\rho\pi$.
[21] Constructive interference between $f_2(1270)\pi$,$\rho\pi$ and background.
[22] Incoherent Ansatz.

$\pi_2(1670)$ $\Gamma(i)\Gamma(\gamma\gamma)/\Gamma(\text{total})$

$\Gamma(\pi^+\pi^-\pi^0)\times\Gamma(\gamma\gamma)/\Gamma_{\text{total}}$ — $\Gamma_2\Gamma_{12}/\Gamma$

VALUE (keV)	CL%	DOCUMENT ID		TECN	COMMENT
<0.1	95	[23] SCHEGELSKY	06	RVUE	$\gamma\gamma\to\pi^+\pi^-\pi^0$

[23] From analysis of L3 data at 183–209 GeV.

$\pi_2(1670)$ BRANCHING RATIOS

$\Gamma(3\pi)/\Gamma_{\text{total}}$ — $\Gamma_1/\Gamma = (\Gamma_4+\Gamma_5+\Gamma_7)/\Gamma$

VALUE	DOCUMENT ID
0.958±0.014 OUR FIT	

$\Gamma(\pi^0\pi^0\pi^0)/\Gamma(\pi^+\pi^-\pi^0)$ — Γ_3/Γ_2

VALUE	DOCUMENT ID		COMMENT
0.29±0.03±0.05	BARBERIS	01	450 $pp\to p_f3\pi^0p_s$

$\Gamma(\rho\pi)/0.565\Gamma(f_2(1270)\pi)$ — $\Gamma_5/0.565\Gamma_4$

(With $f_2(1270)\to\pi^+\pi^-$.)

VALUE	DOCUMENT ID		TECN	COMMENT
0.97±0.09 OUR AVERAGE	Error includes scale factor of 1.9.			
0.76±0.07±0.10	CHUNG	02	B852	18.3 $\pi^-p\to\pi^+\pi^-\pi^-p$
1.01±0.05	BARBERIS	98B		450 $pp\to p_f\pi^+\pi^-\pi^0p_s$

$\Gamma(\sigma\pi)/\Gamma(f_2(1270)\pi)$ — Γ_6/Γ_4

VALUE	DOCUMENT ID		TECN	COMMENT
0.17±0.02±0.07	CHUNG	02	B852	18.3 $\pi^-p\to\pi^+\pi^-\pi^-p$
• • • We do not use the following data for averages, fits, limits, etc. • • •				
0.24±0.10	[24,25] BAKER	99	SPEC	1.94 $\overline{p}p\to4\pi^0$

$\frac{1}{2}\Gamma(\rho\pi)/\Gamma(\pi^\pm\pi^+\pi^-)$ — $\frac{1}{2}\Gamma_5/\Gamma_8 = \frac{1}{2}\Gamma_5/(0.565\Gamma_4+\frac{1}{2}\Gamma_5+0.624\Gamma_7)$

VALUE	DOCUMENT ID		TECN	CHG	COMMENT
0.29±0.04 OUR FIT					
0.29±0.05	[26] DAUM	81B	SPEC		63,94 π^-p
• • • We do not use the following data for averages, fits, limits, etc. • • •					
<0.3	BARTSCH	68	HBC	+	8 $\pi^+p\to3\pi p$

$0.565\Gamma(f_2(1270)\pi)/\Gamma(\pi^\pm\pi^+\pi^-)$ — $0.565\Gamma_4/\Gamma_8 = 0.565\Gamma_4/(0.565\Gamma_4+\frac{1}{2}\Gamma_5+0.624\Gamma_7)$

(With $f_2(1270)\to\pi^+\pi^-$.)

VALUE	DOCUMENT ID		TECN	CHG	COMMENT
0.604±0.035 OUR FIT					
0.60 ±0.05 OUR AVERAGE	Error includes scale factor of 1.3.				
0.61 ±0.04	[26] DAUM	81B	SPEC		63,94 π^-p
0.76 $^{+0.24}_{-0.34}$	ARMENISE	69	DBC	+	5.1 $\pi^+d\to d3\pi$
0.35 ±0.20	BALTAY	68	HBC	+	7–8.5 π^+p
• • • We do not use the following data for averages, fits, limits, etc. • • •					
0.59	BARTSCH	68	HBC	+	8 $\pi^+p\to3\pi p$

$0.624\Gamma(\pi(\pi\pi)_{S\text{-wave}})/\Gamma(\pi^\pm\pi^+\pi^-)$ — $0.624\Gamma_7/\Gamma_8 = 0.624\Gamma_7/(0.565\Gamma_4+\frac{1}{2}\Gamma_5+0.624\Gamma_7)$

(With $(\pi\pi)_{S\text{-wave}}\to\pi^+\pi^-$.)

VALUE	DOCUMENT ID		TECN	COMMENT
0.10±0.04 OUR FIT				
0.10±0.05	[26] DAUM	81B	SPEC	63,94 π^-p

$\Gamma(K\overline{K}^*(892)+\text{c.c.})/\Gamma(f_2(1270)\pi)$ — Γ_9/Γ_4

VALUE	DOCUMENT ID		TECN	CHG	COMMENT
0.075±0.025 OUR FIT					
0.075±0.025	[27] ARMSTRONG	82B	OMEG	−	16 $\pi^-p\to K^+K^-\pi^-p$

$\Gamma(\omega\rho)/\Gamma_{\text{total}}$ — Γ_{10}/Γ

VALUE	DOCUMENT ID		TECN	COMMENT
0.027±0.004±0.010	[28] AMELIN	99	VES	37 $\pi^-A\to\omega\pi^-\pi^0A^*$

$\Gamma(\eta\pi)/\Gamma(\pi^\pm\pi^+\pi^-)$ — $\Gamma_{13}/\Gamma_8 = \Gamma_{13}/(0.565\Gamma_4+\frac{1}{2}\Gamma_5+0.624\Gamma_7)$

(All η decays.)

VALUE	DOCUMENT ID		TECN	CHG	COMMENT
<0.09	BALTAY	68	HBC	+	7–8.5 π^+p
• • • We do not use the following data for averages, fits, limits, etc. • • •					
<0.10	CRENNELL	70	HBC	−	6 $\pi^-p\to f_2\pi^-N$

$\Gamma(\pi^\pm2\pi^+2\pi^-)/\Gamma(\pi^\pm\pi^+\pi^-)$ — $\Gamma_{14}/\Gamma_8 = \Gamma_{14}/(0.565\Gamma_4+\frac{1}{2}\Gamma_5+0.624\Gamma_7)$

VALUE	DOCUMENT ID		TECN	CHG	COMMENT
<0.10	CRENNELL	70	HBC	−	6 $\pi^-p\to f_2\pi^-N$
• • • We do not use the following data for averages, fits, limits, etc. • • •					
<0.1	BALTAY	68	HBC	+	7,8.5 π^+p

$\Gamma(\rho(1450)\pi)/\Gamma_{\text{total}}$ — Γ_{15}/Γ

VALUE	CL%	DOCUMENT ID		TECN	COMMENT
<0.0036	97.7	AMELIN	99	VES	37 $\pi^-A\to\omega\pi^-\pi^0A^*$

$\Gamma(b_1(1235)\pi)/\Gamma_{\text{total}}$ — Γ_{16}/Γ

VALUE	CL%	DOCUMENT ID		TECN	COMMENT
<0.0019	97.7	AMELIN	99	VES	37 $\pi^-A\to\omega\pi^-\pi^0A^*$

$\Gamma(f_1(1285)\pi)/\Gamma_{\text{total}}$ — Γ_{18}/Γ

VALUE	EVTS	DOCUMENT ID		TECN	COMMENT
possibly seen	69k	KUHN	04	B852	18 $\pi^-p\to\eta\pi^+\pi^-\pi^-p$

Downloaded from https://academic.oup.com/ptep/article/2022/8/083C01/6651666 by KIT Library user on 27 September 2022

$\Gamma(a_2(1320)\pi)/\Gamma_{total}$ — Γ_{19}/Γ

VALUE	EVTS	DOCUMENT ID		TECN	COMMENT
not seen	69k	KUHN	04	B852	18 $\pi^- p \to \eta\pi^+\pi^-\pi^- p$

D-wave/S-wave RATIO FOR $\pi_2(1670) \to f_2(1270)\pi$

VALUE	DOCUMENT ID		TECN	COMMENT
−0.18±0.06	[24] BAKER	99	SPEC	1.94 $\overline{p}p \to 4\pi^0$
• • • We do not use the following data for averages, fits, limits, etc. • • •				
0.22±0.10	[26] DAUM	81B	SPEC	63,94 $\pi^- p$

F-wave/P-wave RATIO FOR $\pi_2(1670) \to \rho\pi$

VALUE	DOCUMENT ID		TECN	COMMENT
−0.72±0.07±0.14	CHUNG	02	B852	18.3 $\pi^- p \to \pi^+\pi^-\pi^- p$

[24] Using preliminary CBAR data.
[25] With the $\sigma\pi$ in L=2 and the $f_2(1270)\pi$ in L=0.
[26] From a two-resonance fit to four 2^-0^+ waves.
[27] From a partial-wave analysis of $K^+K^-\pi^-$ system.
[28] Normalized to the B($\pi_2(1670) \to f_2\pi$).

$\pi_2(1670)$ REFERENCES

AGHASYAN	18B	PR D98 092003	M. Aghasyan et al.	(COMPASS Collab.)
ADOLPH	14	EPJ A50 79	C. Adolph et al.	(COMPASS Collab.)
ALEKSEEV	10	PRL 104 241803	M.G. Alekseev et al.	(COMPASS Collab.)
SCHEGELSKY	06	EPJ A27 199	V.A. Schegelsky et al.	
LU	05	PRL 94 032002	M. Lu et al.	(BNL E852 Collab.)
KUHN	04	PL B595 109	J. Kuhn et al.	(BNL E852 Collab.)
CHUNG	02	PR D65 072001	S.U. Chung et al.	(BNL E852 Collab.)
BARBERIS	01	PL B507 14	D. Barberis et al.	
AMELIN	99	PAN 62 445	D.V. Amelin et al.	(VES Collab.)
		Translated from YAF 62 487.		
BAKER	99	PL B449 114	C.A. Baker et al.	
BARBERIS	98B	PL B422 399	D. Barberis et al.	(WA 102 Collab.)
ACCIARRI	97T	PL B413 147	M. Acciarri et al.	(L3 Collab.)
ALBRECHT	97B	ZPHY C74 469	H. Albrecht et al.	(ARGUS Collab.)
AMELIN	95B	PL B356 595	D.V. Amelin et al.	(SERP, TBIL)
BERDNIKOV	94	PL B337 219	E.B. Berdnikov et al.	(SERP, TBIL)
ANTREASYAN	90	ZPHY C48 561	D. Antreasyan et al.	(Crystal Ball Collab.)
BEHREND	90C	ZPHY C46 583	H.J. Behrend et al.	(CELLO Collab.)
ANTIPOV	87	EPL 4 403	Y.M. Antipov et al.	(SERP, JINR, INRM+)
BELLINI	85	SJNP 41 781	D. Bellini et al.	
		Translated from YAF 41 1223.		
ARMSTRONG	82B	NP B202 1	T.A. Armstrong, B. Baccari	(AACH3, BARI, BONN+)
DAUM	81B	NP B182 269	C. Daum et al.	(AMST, CERN, CRAC, MPIM+)
EVANGELIS...	81	NP B178 197	C. Evangelista et al.	(BARI, BONN, CERN+)
Also		NP B186 594	C. Evangelista	
DAUM	80D	PL 89B 285	C. Daum et al.	(AMST, CERN, CRAC, MPIM+) JP
BALTAY	77	PRL 39 591	C. Baltay, C.V. Cautis, M. Kalelkar	(COLU) JP
ASCOLI	73	PR D7 669	G. Ascoli	(ILL, TNTO, GENO, HAMB, MILA+) JP
CRENNELL	70	PRL 24 781	D.J. Crennell et al.	(BNL)
ARMENISE	69	LNC 2 501	N. Armenise et al.	(BARI, BGNA, FIRZ)
BALTAY	68	PRL 20 887	C. Baltay et al.	(COLU, ROCH, RUTG, YALE) I
BARTSCH	68	NP B7 345	J. Bartsch et al.	(AACH, BERL, CERN) JP

$\phi(1680)$

$I^G(J^{PC}) = 0^-(1^{--})$

$\phi(1680)$ MASS

e^+e^- PRODUCTION

VALUE (MeV)	EVTS	DOCUMENT ID		TECN	COMMENT
1680±20 OUR ESTIMATE					
• • • We do not use the following data for averages, fits, limits, etc. • • •					
$1680^{+12}_{-13}\pm21$	1.8k	[1] ABLIKIM	20F	BES3	$\psi(2S) \to K^+K^-\eta$
1662±20		[2] ACHASOV	20C	SND	1.3–2.0 $e^+e^- \to K^+K^-\pi^0$
1641^{+24}_{-18}		ACHASOV	19	SND	$e^+e^- \to \pi^+\pi^-\pi^0\eta$
1667± 5±11	3k	[3] IVANOV	19A	CMD3	1.59–2.007 $e^+e^- \to K^+K^-\eta$
1700±23	2k	[4] ACHASOV	18A	SND	1.3–2.0 $e^+e^- \to K^0_S K^0_L \pi^0$
1674±12± 6	6.2k	[5] LEES	14H	BABR	$e^+e^- \to K^0_S K^0_L \gamma$
1733±10±10		[6] LEES	12F	BABR	10.6 $e^+e^- \to \phi\pi^+\pi^-\gamma$
1689± 7±10	4.8k	[7] SHEN	09	BELL	10.6 $e^+e^- \to K^+K^-\pi^+\pi^-\gamma$
1709±20±43		[8] AUBERT	08S	BABR	10.6 $e^+e^- \to$ hadrons
1623±20	948	[9] AKHMETSHIN	03	CMD2	1.05–1.38 $e^+e^- \to K^0_L K^0_S$
∼ 1500		[10] ACHASOV	98H	RVUE	$e^+e^- \to \pi^+\pi^-\pi^0$, $\omega\pi^+\pi^-$, K^+K^-
∼ 1900		[11] ACHASOV	98H	RVUE	$e^+e^- \to K^0_S K^\pm\pi^\mp$
1700±20		[12] CLEGG	94	RVUE	$e^+e^- \to K^+K^-$, $K^0_S K\pi$
1657±27	367	BISELLO	91C	DM2	$e^+e^- \to K^0_S K^\pm\pi^\mp$
1655±17		[13] BISELLO	88B	DM2	$e^+e^- \to K^+K^-$
1680±10		[14] BUON	82	DM1	$e^+e^- \to$ hadrons
1677±12		[15] MANE	82	DM1	$e^+e^- \to K^0_S K\pi$

[1] Seen in $\psi(2S)$ decay with branching ratio $\psi(2S) \to X\eta \to K^+K^-\eta = (12.0 \pm 1.3^{+6.5}_{-6.9}) \times 10^{-6}$.
[2] From a fit using a vector meson dominance model with contribution from $\rho(770)$, $\omega(782)$, $\phi(1020)$, $\omega(1420)$, $\rho(1450)$.
[3] From a fit with coherent interference of the $\phi(1680)$ with a non-resonant contribution.
[4] Assuming the $K\overline{K}^*(892)+$ c.c. dynamics. Systematic uncertainties not estimated.
[5] Using a vector meson dominance model with contribution from $\phi(1020)$, $\phi(1680)$, and higher mass excitations of $\rho(770)$ and $\omega(782)$.
[6] Using events with $\pi\pi$ invariant mass less than 0.85 GeV.
[7] From a fit with two incoherent Breit-Wigners.
[8] From the simultaneous fit to the $K\overline{K}^*(892)+$ c.c. and $\phi\eta$ data from AUBERT 08S using the results of AUBERT 07AK.
[9] From the combined fit of AKHMETSHIN 03 and MANE 81 also including ρ, ω, and ϕ. Neither isospin nor flavor structure known.
[10] Using data from IVANOV 81, BARKOV 87, BISELLO 88B, DOLINSKY 91, and ANTONELLI 92.
[11] Using the data from BISELLO 91C.
[12] Using BISELLO 88B and MANE 82 data.
[13] From global fit including ρ, ω, ϕ and $\rho(1700)$ assume mass 1570 MeV and width 510 MeV for ρ radial excitation.
[14] From global fit of ρ, ω, ϕ and their radial excitations to channels $\omega\pi^+\pi^-$, K^+K^-, $K^0_S K^0_L$, $K^0_S K^\pm\pi^\mp$. Assume mass 1570 MeV and width 510 MeV for ρ radial excitations, mass 1570 and width 500 MeV for ω radial excitation.
[15] Fit to one channel only, neglecting interference with ω, $\rho(1700)$.

$p\overline{p}$ ANNIHILATION

VALUE (MeV)	DOCUMENT ID		TECN	COMMENT
• • • We do not use the following data for averages, fits, limits, etc. • • •				
1700±8	[1] AMSLER	06	CBAR	0.9 $\overline{p}p \to K^+K^-\pi^0$

[1] Could also be $\rho(1700)$.

$\phi(1680)$ WIDTH

e^+e^- PRODUCTION

VALUE (MeV)	EVTS	DOCUMENT ID		TECN	COMMENT
150±50 OUR ESTIMATE This is only an educated guess; the error given is larger than the error on the average of the published values.					
• • • We do not use the following data for averages, fits, limits, etc. • • •					
$185^{+30}_{-26}\pm^{25}_{47}$	1.8k	[1] ABLIKIM	20F	BES3	$\psi(2S) \to K^+K^-\eta$
159±32		[2] ACHASOV	20C	SND	1.3–2.0 $e^+e^- \to K^+K^-\pi^0$
103^{+26}_{-24}		ACHASOV	19	SND	$e^+e^- \to \pi^+\pi^-\pi^0\eta$
176±23± 38	3k	[3] IVANOV	19A	CMD3	1.59–2.007 $e^+e^- \to K^+K^-\eta$
300±50	2k	[4] ACHASOV	18A	SND	1.3–2.0 $e^+e^- \to K^0_S K^0_L \pi^0$
165±38± 70	6.2k	[5] LEES	14H	BABR	$e^+e^- \to K^0_S K^0_L \gamma$
300±15± 37		[6] LEES	12F	BABR	10.6 $e^+e^- \to \phi\pi^+\pi^-\gamma$
211±14± 19	4.8k	[7] SHEN	09	BELL	10.6 $e^+e^- \to K^+K^-\pi^+\pi^-\gamma$
322±77±160		[8] AUBERT	08S	BABR	10.6 $e^+e^- \to$ hadrons
139±60	948	[9] AKHMETSHIN	03	CMD2	1.05–1.38 $e^+e^- \to K^0_L K^0_S$
300±60		[10] CLEGG	94	RVUE	$e^+e^- \to K^+K^-$, $K^0_S K\pi$
146±55	367	BISELLO	91C	DM2	$e^+e^- \to K^0_S K^\pm\pi^\mp$
207±45		[11] BISELLO	88B	DM2	$e^+e^- \to K^+K^-$
185±22		[12] BUON	82	DM1	$e^+e^- \to$ hadrons
102±36		[13] MANE	82	DM1	$e^+e^- \to K^0_S K\pi$

[1] Seen in $\psi(2S)$ decay with branching ratio $\psi(2S) \to X\eta \to K^+K^-\eta = (12.0 \pm 1.3^{+6.5}_{-6.9}) \times 10^{-6}$.
[2] From a fit using a vector meson dominance model with contribution from $\rho(770)$, $\omega(782)$, $\phi(1020)$, $\omega(1420)$, $\rho(1450)$.
[3] From a fit with coherent interference of the $\phi(1680)$ with a non-resonant contribution.
[4] Assuming the $K\overline{K}^*(892)+$ c.c. dynamics. Systematic uncertainties not estimated.
[5] Using a vector meson dominance model with contribution from $\phi(1020)$, $\phi(1680)$, and higher mass excitations of $\rho(770)$ and $\omega(782)$.
[6] Using events with $\pi\pi$ invariant mass less than 0.85 GeV.
[7] From a fit with two incoherent Breit-Wigners.
[8] From the simultaneous fit to the $K\overline{K}^*(892)+$ c.c. and $\phi\eta$ data from AUBERT 08S using the results of AUBERT 07AK.
[9] From the combined fit of AKHMETSHIN 03 and MANE 81 also including ρ, ω, and ϕ. Neither isospin nor flavor structure known.
[10] Using BISELLO 88B and MANE 82 data.
[11] From global fit including ρ, ω, ϕ and $\rho(1700)$
[12] From global fit of ρ, ω, ϕ and their radial excitations to channels $\omega\pi^+\pi^-$, K^+K^-, $K^0_S K^0_L$, $K^0_S K^\pm\pi^\mp$. Assume mass 1570 MeV and width 510 MeV for ρ radial excitations, mass 1570 and width 500 MeV for ω radial excitation.
[13] Fit to one channel only, neglecting interference with ω, $\rho(1700)$.

$p\overline{p}$ ANNIHILATION

VALUE (MeV)	DOCUMENT ID		TECN	COMMENT
• • • We do not use the following data for averages, fits, limits, etc. • • •				
143±24	[1] AMSLER	06	CBAR	0.9 $\overline{p}p \to K^+K^-\pi^0$

[1] Could also be $\rho(1700)$.

$\phi(1680)$ DECAY MODES

	Mode	Fraction (Γ_i/Γ)
Γ_1	$K\overline{K}^*(892)+$ c.c.	seen
Γ_2	$K^0_S K\pi$	seen
Γ_3	$K\overline{K}$	seen
Γ_4	$K^0_L K^0_S$	
Γ_5	e^+e^-	seen
Γ_6	$\omega\pi\pi$	not seen

Downloaded from https://academic.oup.com/ptep/article/2022/8/083C01/6651666 by KIT Library user on 27 September 2022

Γ_7	$\phi\pi\pi$	
Γ_8	$K^+K^-\pi^+\pi^-$	seen
Γ_9	$\eta\phi$	seen
Γ_{10}	$K^+K^-\eta$	
Γ_{11}	$\eta\gamma$	seen
Γ_{12}	$K^+K^-\pi^0$	

$\phi(1680)$ $\Gamma(i)\Gamma(e^+e^-)/\Gamma(\text{total})$

This combination of a partial width with the partial width into e^+e^- and with the total width is obtained from the integrated cross section into channel (I) in e^+e^- annihilation. We list only data that have not been used to determine the partial width $\Gamma(I)$ or the branching ratio $\Gamma(I)/\text{total}$.

$\Gamma(K^0_L K^0_S) \times \Gamma(e^+e^-)/\Gamma_{\text{total}}$ — $\Gamma_4\Gamma_5/\Gamma$

VALUE (eV)	EVTS	DOCUMENT ID		TECN	COMMENT
• • • We do not use the following data for averages, fits, limits, etc. • • •					
$14.3\pm2.4\pm6.2$	6.2k	[1] LEES	14H	BABR	$e^+e^- \to K^0_S K^0_L \gamma$

[1] Using a vector meson dominance model with contribution from $\phi(1020)$, $\phi(1680)$, and higher mass excitations of $\rho(770)$ and $\omega(782)$.

$\Gamma(\phi\pi\pi) \times \Gamma(e^+e^-)/\Gamma_{\text{total}}$ — $\Gamma_7\Gamma_5/\Gamma$

VALUE (10^{-2} keV)	DOCUMENT ID		TECN	COMMENT
• • • We do not use the following data for averages, fits, limits, etc. • • •				
$4.2\pm0.2\pm0.3$	LEES	12F	BABR	$10.6\ e^+e^- \to \phi\pi^+\pi^-\gamma$

$\Gamma(\eta\phi) \times \Gamma(e^+e^-)/\Gamma_{\text{total}}$ — $\Gamma_9\Gamma_5/\Gamma$

VALUE (eV)	EVTS	DOCUMENT ID		TECN	COMMENT
• • • We do not use the following data for averages, fits, limits, etc. • • •					
$94\pm13\pm15$	3k	[1] IVANOV	19A	CMD3	1.59–$2.007\ e^+e^- \to K^+K^-\eta$

[1] From a fit with coherent interference of the $\phi(1680)$ with a non-resonant contribution.

$\phi(1680)$ $\Gamma(i)\Gamma(e^+e^-)/\Gamma^2(\text{total})$

This combination of a branching ratio into channel (i) and branching ratio into e^+e^- is directly measured and obtained from the cross section at the peak. We list only data that have not been used to determine the branching ratio into (i) or e^+e^-.

$\Gamma(K^0_L K^0_S)/\Gamma_{\text{total}} \times \Gamma(e^+e^-)/\Gamma_{\text{total}}$ — $\Gamma_4/\Gamma \times \Gamma_5/\Gamma$

VALUE (units 10^{-6})	EVTS	DOCUMENT ID		TECN	COMMENT
• • • We do not use the following data for averages, fits, limits, etc. • • •					
0.131 ± 0.059	948	[1] AKHMETSHIN	03	CMD2	1.05–$1.38\ e^+e^- \to K^0_L K^0_S$

[1] From the combined fit of AKHMETSHIN 03 and MANE 81 also including ρ, ω, and ϕ. Neither isospin nor flavor structure known. Recalculated by us.

$\Gamma(K\overline{K}^*(892)+\text{c.c.})/\Gamma_{\text{total}} \times \Gamma(e^+e^-)/\Gamma_{\text{total}}$ — $\Gamma_1/\Gamma \times \Gamma_5/\Gamma$

VALUE (units 10^{-6})	EVTS	DOCUMENT ID		TECN	COMMENT
• • • We do not use the following data for averages, fits, limits, etc. • • •					
$1.15\pm0.16\pm0.01$		[1] AUBERT	08S	BABR	$10.6\ e^+e^- \to K\overline{K}^*(892)\gamma +$ c.c.
3.29 ± 1.57	367	[2] BISELLO	91C	DM2	1.35–$2.40\ e^+e^- \to K^0_S K^\pm\pi^\mp$

[1] From the simultaneous fit to the $K\overline{K}^*(892)+$ c.c. and $\phi\eta$ data from AUBERT 08S using the results of AUBERT 07AK.
[2] Recalculated by us with the published value of $B(K\overline{K}^*(892) +$ c.c.$) \times \Gamma(e^+e^-)$.

$\Gamma(\phi\pi\pi)/\Gamma_{\text{total}} \times \Gamma(e^+e^-)/\Gamma_{\text{total}}$ — $\Gamma_7/\Gamma \times \Gamma_5/\Gamma$

VALUE (units 10^{-7})	EVTS	DOCUMENT ID		TECN	COMMENT
• • • We do not use the following data for averages, fits, limits, etc. • • •					
$1.86\pm0.14\pm0.21$	4.8k	[1] SHEN	09	BELL	$10.6\ e^+e^- \to K^+K^-\pi^+\pi^-\gamma$

[1] Multiplied by 3/2 to take into account the $\phi\pi^0\pi^0$ mode. Using $B(\phi \to K^+K^-) = (49.2 \pm 0.6)\%$.

$\Gamma(\eta\phi)/\Gamma_{\text{total}} \times \Gamma(e^+e^-)/\Gamma_{\text{total}}$ — $\Gamma_9/\Gamma \times \Gamma_5/\Gamma$

VALUE (units 10^{-7})	EVTS	DOCUMENT ID		TECN	COMMENT
• • • We do not use the following data for averages, fits, limits, etc. • • •					
$5.64^{+1.74}_{-1.80}$		ACHASOV	19	SND	$e^+e^- \to \pi^+\pi^-\pi^0\eta$
$5.3\ \pm0.6\ \pm0.9$	3k	[1] IVANOV	19A	CMD3	1.59–$2.007\ e^+e^- \to K^+K^-\eta$
$4.3\ \pm1.0\ \pm0.9$		[2] AUBERT	08S	BABR	$10.6\ e^+e^- \to \phi\eta\gamma$

[1] From a fit with coherent interference of the $\phi(1680)$ with a non-resonant contribution.
[2] From the simultaneous fit to the $K\overline{K}^*(892)+$ c.c. and $\phi\eta$ data from AUBERT 08S using the results of AUBERT 07AK.

$\phi(1680)$ BRANCHING RATIOS

$\Gamma(K\overline{K}^*(892)+\text{c.c.})/\Gamma(K^0_S K\pi)$ — Γ_1/Γ_2

VALUE	DOCUMENT ID		TECN	COMMENT
dominant	MANE	82	DM1	$e^+e^- \to K^0_S K^\pm\pi^\mp$

$\Gamma(K\overline{K})/\Gamma(K\overline{K}^*(892)+\text{c.c.})$ — Γ_3/Γ_1

VALUE	DOCUMENT ID		TECN	COMMENT
• • • We do not use the following data for averages, fits, limits, etc. • • •				
0.07 ± 0.01	BUON	82	DM1	e^+e^-

$\Gamma(\omega\pi\pi)/\Gamma(K\overline{K}^*(892)+\text{c.c.})$ — Γ_6/Γ_1

VALUE	DOCUMENT ID		TECN	COMMENT
<0.10	BUON	82	DM1	e^+e^-

$\Gamma(\eta\phi)/\Gamma_{\text{total}}$ — Γ_9/Γ

VALUE	EVTS	DOCUMENT ID		TECN	COMMENT
seen	35	[1] ACHASOV	14	SND	1.15–$2.00\ e^+e^- \to \eta\gamma$

[1] From a phenomenological model based on vector meson dominance with $\rho(1450)$ and $\phi(1680)$ masses and widths from the PDG 12.

$\Gamma(\eta\phi)/\Gamma(K\overline{K}^*(892)+\text{c.c.})$ — Γ_9/Γ_1

VALUE	DOCUMENT ID		TECN	COMMENT
• • • We do not use the following data for averages, fits, limits, etc. • • •				
≈ 0.37	[1] AUBERT	08S	BABR	$10.6\ e^+e^- \to$ hadrons

[1] From the fit including data from AUBERT 07AK.

$\Gamma(\eta\gamma)/\Gamma_{\text{total}}$ — Γ_{11}/Γ

VALUE	EVTS	DOCUMENT ID		TECN	COMMENT
seen	35	[1] ACHASOV	14	SND	1.15–$2.00\ e^+e^- \to \eta\gamma$

[1] From a phenomenological model based on vector meson dominance with $\rho(1450)$ and $\phi(1680)$ masses and widths from the PDG 12.

$\phi(1680)$ REFERENCES

ABLIKIM	20F	PR D101 032008	M. Ablikim *et al.*	(BESIII Collab.)
ACHASOV	20C	EPJ C80 1139	M.N. Achasov *et al.*	(SND Collab.)
ACHASOV	19	PR D99 112004	M.N. Achasov *et al.*	(SND Collab.)
IVANOV	19A	PL B798 134946	V.L. Ivanov *et al.*	(CMD-3 Collab.)
ACHASOV	18A	PR D97 032011	M.N. Achasov *et al.*	(SND Collab.)
ACHASOV	14	PR D90 032002	M.N. Achasov *et al.*	(SND Collab.)
LEES	14H	PR D89 092002	J.P. Lees *et al.*	(BABAR Collab.)
LEES	12F	PR D86 012008	J.P. Lees *et al.*	(BABAR Collab.)
PDG	12	PR D86 010001	J. Beringer *et al.*	(PDG Collab.)
SHEN	09	PR D80 031101	C.P. Shen *et al.*	(BELLE Collab.)
AUBERT	08S	PR D77 092002	B. Aubert *et al.*	(BABAR Collab.)
AUBERT	07AK	PR D76 012008	B. Aubert *et al.*	(BABAR Collab.)
AMSLER	06	PL B639 165	C. Amsler *et al.*	(Crystal Barrel Collab.)
AKHMETSHIN	03	PL B551 27	R.R. Akhmetshin *et al.*	(Novosibirsk CMD-2 Collab.)
Also		PAN 65 1222	E.V. Anashkin, V.M. Aulchenko, R.R. Akhmetshin	
		Translated from YAF 65 1255.		
ACHASOV	98H	PR D57 4334	N.N. Achasov, A.A. Kozhevnikov	
CLEGG	94	ZPHY C62 455	A.B. Clegg, A. Donnachie	(LANC, MCHS)
ANTONELLI	92	ZPHY C56 15	A. Antonelli *et al.*	(DM2 Collab.)
BISELLO	91C	ZPHY C52 227	D. Bisello *et al.*	(DM2 Collab.)
DOLINSKY	91	PRPL 202 99	S.I. Dolinsky *et al.*	(NOVO)
BISELLO	88B	ZPHY C39 13	D. Bisello *et al.*	(PADO, CLER, FRAS+)
BARKOV	87	JETPL 46 164	L.M. Barkov *et al.*	(NOVO)
		Translated from ZETFP 46 132.		
BUON	82	PL 118B 221	J. Buon *et al.*	(LALO, MONP)
MANE	82	PL 112B 178	F. Mane *et al.*	(LALO)
IVANOV	81	PL 107B 297	P.M. Ivanov *et al.*	(NOVO)
MANE	81	PL 99B 261	F. Mane *et al.*	(ORSAY)

$\rho_3(1690)$

$I^G(J^{PC}) = 1^+(3^{--})$

$\rho_3(1690)$ MASS

VALUE (MeV)	DOCUMENT ID
1688.8±2.1 OUR AVERAGE	Includes data from the 5 datablocks that follow this one.

2π MODE

VALUE (MeV)	EVTS	DOCUMENT ID		TECN	CHG	COMMENT
The data in this block is included in the average printed for a previous datablock.						
1686± 4 OUR AVERAGE						
1677 ± 14		EVANGELIS...	81	OMEG	−	$12\ \pi^-p \to 2\pi p$
1679 ± 11	476	BALTAY	78B	HBC	0	$15\ \pi^+p \to \pi^+\pi^-n$
1678 ± 12	175	[1] ANTIPOV	77	CIBS	0	$25\ \pi^-p \to p3\pi$
$1690\pm\ 7$	600	[1] ENGLER	74	DBC	0	$6\ \pi^+n \to \pi^+\pi^-p$
$1693\pm\ 8$		[2] GRAYER	74	ASPK	0	$17\ \pi^-p \to \pi^+\pi^-n$
1678 ± 12		MATTHEWS	71C	DBC	0	$7\ \pi^+N$
• • • We do not use the following data for averages, fits, limits, etc. • • •						
1734 ± 10		[3] CORDEN	79	OMEG		12–$15\ \pi^-p \to n2\pi$
1692 ± 12		[2,4] ESTABROOKS	75	RVUE		$17\ \pi^-p \to \pi^+\pi^-n$
1737 ± 23		ARMENISE	70	DBC	0	$9\ \pi^+N$
1650 ± 35	122	BARTSCH	70B	HBC	+	$8\ \pi^+p \to N2\pi$
1687 ± 21		STUNTEBECK	70	HDBC	0	$8\ \pi^-p$, $5.4\ \pi^+d$
1683 ± 13		ARMENISE	68	DBC	0	$5.1\ \pi^+d$
1670 ± 30		GOLDBERG	65	HBC	0	$6\ \pi^+d$, $8\ \pi^-p$

[1] Mass errors enlarged by us to $\Gamma/\sqrt{N}$; see the note with the $K^*(892)$ mass.
[2] Uses same data as HYAMS 75.
[3] From a phase shift solution containing a $f'_2(1525)$ width two times larger than the $K\overline{K}$ result.
[4] From phase-shift analysis. Error takes account of spread of different phase-shift solutions.

Downloaded from https://academic.oup.com/ptep/article/2022/8/083C01/6651666 by KIT Library user on 27 September 2022

$K\overline{K}$ AND $K\overline{K}\pi$ MODES

VALUE (MeV)	EVTS	DOCUMENT ID		TECN	CHG	COMMENT
The data in this block is included in the average printed for a previous datablock.						
1696± 4 OUR AVERAGE						
1699± 5		ALPER	80	CNTR	0	62 $\pi^- p \to K^+ K^- n$
1698±12	6k	[5,6] MARTIN	78D	SPEC		10 $\pi p \to K^0_S K^- p$
1692± 6		BLUM	75	ASPK	0	18.4 $\pi^- p \to n K^+ K^-$
1690±16		ADERHOLZ	69	HBC	+	8 $\pi^+ p \to K\overline{K}\pi$
• • • We do not use the following data for averages, fits, limits, etc. • • •						
1694± 8		[7] COSTA	80	OMEG		10 $\pi^- p \to K^+ K^- n$

[5] From a fit to $J^P = 3^-$ partial wave.
[6] Systematic error on mass scale subtracted.
[7] They cannot distinguish between $\rho_3(1690)$ and $\omega_3(1670)$.

$(4\pi)^\pm$ MODE

VALUE (MeV)	EVTS	DOCUMENT ID		TECN	CHG	COMMENT
The data in this block is included in the average printed for a previous datablock.						
1686± 5 OUR AVERAGE Error includes scale factor of 1.1.						
1694± 6		[8] EVANGELIS...	81	OMEG	−	12 $\pi^- p \to p 4\pi$
1665±15	177	BALTAY	78B	HBC	+	15 $\pi^+ p \to p 4\pi$
1670±10		THOMPSON	74	HBC	+	13 $\pi^+ p$
1687±20		CASON	73	HBC	−	8,18.5 $\pi^- p$
1685±14		[9] CASON	73	HBC	−	8,18.5 $\pi^- p$
1680±40	144	BARTSCH	70B	HBC	+	8 $\pi^+ p \to N 4\pi$
1689±20	102	[9] BARTSCH	70B	HBC	+	8 $\pi^+ p \to N 2\rho$
1705±21		CASO	70	HBC	−	11.2 $\pi^- p \to n\rho 2\pi$
• • • We do not use the following data for averages, fits, limits, etc. • • •						
1718±10		[10] EVANGELIS...	81	OMEG	−	12 $\pi^- p \to p 4\pi$
1673± 9		[11] EVANGELIS...	81	OMEG	−	12 $\pi^- p \to p 4\pi$
1733± 9	66	[9] KLIGER	74	HBC	−	4.5 $\pi^- p \to p 4\pi$
1630±15		HOLMES	72	HBC	+	10–12 $K^+ p$
1720±15		BALTAY	68	HBC	+	7, 8.5 $\pi^+ p$

[8] From $\rho^- \rho^0$ mode, not independent of the other two EVANGELISTA 81 entries.
[9] From $\rho^\pm \rho^0$ mode.
[10] From $a_2(1320)^- \pi^0$ mode, not independent of the other two EVANGELISTA 81 entries.
[11] From $a_2(1320)^0 \pi^-$ mode, not independent of the other two EVANGELISTA 81 entries.

$\omega\pi$ MODE

VALUE (MeV)	DOCUMENT ID		TECN	CHG	COMMENT
The data in this block is included in the average printed for a previous datablock.					
1681± 7 OUR AVERAGE					
1670±25	[12] ALDE	95	GAM2		38 $\pi^- p \to \omega\pi^0 n$
1690±15	EVANGELIS...	81	OMEG	−	12 $\pi^- p \to \omega\pi p$
1666±14	GESSAROLI	77	HBC		11 $\pi^- p \to \omega\pi p$
1686± 9	THOMPSON	74	HBC	+	13 $\pi^+ p$
• • • We do not use the following data for averages, fits, limits, etc. • • •					
1654±24	BARNHAM	70	HBC	+	10 $K^+ p \to \omega\pi X$

[12] Supersedes ALDE 92C.

$\eta\pi^+\pi^-$ MODE

(For difficulties with MMS experiments, see the $a_2(1320)$ mini-review in the 1973 edition.)

VALUE (MeV)	DOCUMENT ID		TECN	CHG	COMMENT
The data in this block is included in the average printed for a previous datablock.					
1682±12 OUR AVERAGE					
1685±10±20	AMELIN	00	VES		37 $\pi^- p \to \eta\pi^+\pi^- n$
1680±15	FUKUI	88	SPEC	0	8.95 $\pi^- p \to \eta\pi^+\pi^- n$
• • • We do not use the following data for averages, fits, limits, etc. • • •					
1700±47	[13] ANDERSON	69	MMS	−	16 $\pi^- p$ backward
1632±15	[13,14] FOCACCI	66	MMS	−	7–12 $\pi^- p \to p$MM
1700±15	[13,14] FOCACCI	66	MMS	−	7–12 $\pi^- p \to p$MM
1748±15	[13,14] FOCACCI	66	MMS	−	7–12 $\pi^- p \to p$MM

[13] Seen in 2.5–3 GeV/c $\overline{p}p$. $2\pi^+ 2\pi^-$, with 0, 1, 2 $\pi^+\pi^-$ pairs in ρ band not seen by OREN 74 (2.3 GeV/c $\overline{p}p$) with more statistics. (Jan. 1976)
[14] Not seen by BOWEN 72.

$\rho_3(1690)$ WIDTH

2π, $K\overline{K}$, AND $K\overline{K}\pi$ MODES

VALUE (MeV)	DOCUMENT ID
161±10 OUR AVERAGE Includes data from the 5 datablocks that follow this one. Error includes scale factor of 1.5. See the ideogram below.	

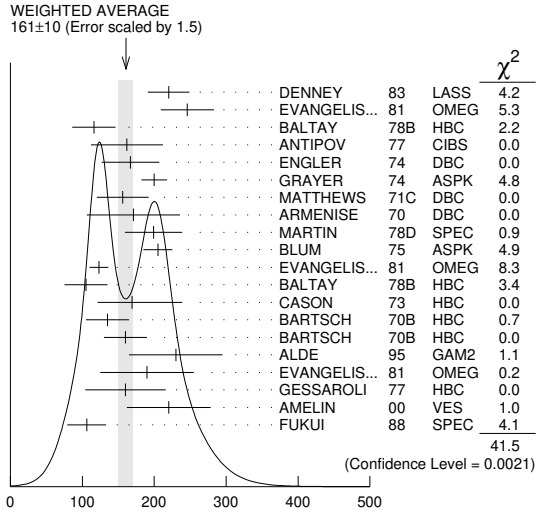

$\rho_3(1690)$ width, 2π, $K\overline{K}$, and $K\overline{K}\pi$ modes (MeV)

2π MODE

VALUE (MeV)	EVTS	DOCUMENT ID		TECN	CHG	COMMENT
The data in this block is included in the average printed for a previous datablock.						
186±14 OUR AVERAGE Error includes scale factor of 1.3. See the ideogram below.						
220±29		DENNEY	83	LASS		10 $\pi^+ N$
246±37		EVANGELIS...	81	OMEG	−	12 $\pi^- p \to 2\pi p$
116±30	476	BALTAY	78B	HBC	0	15 $\pi^+ p \to \pi^+\pi^- n$
162±50	175	[15] ANTIPOV	77	CIBS	0	25 $\pi^- p \to p 3\pi$
167±40	600	ENGLER	74	DBC	0	6 $\pi^+ n \to \pi^+\pi^- p$
200±18		[16] GRAYER	74	ASPK	0	17 $\pi^- p \to \pi^+\pi^- n$
156±36		MATTHEWS	71C	DBC	0	7 $\pi^+ N$
171±65		ARMENISE	70	DBC	0	9 $\pi^+ d$
• • • We do not use the following data for averages, fits, limits, etc. • • •						
322±35		[17] CORDEN	79	OMEG		12–15 $\pi^- p \to n 2\pi$
240±30		[16,18] ESTABROOKS	75	RVUE		17 $\pi^- p \to \pi^+\pi^- n$
180±30	122	BARTSCH	70B	HBC	+	8 $\pi^+ p \to N 2\pi$
267^{+72}_{-46}		STUNTEBECK	70	HDBC	0	8 $\pi^- p$, 5.4 $\pi^+ d$
188±49		ARMENISE	68	DBC	0	5.1 $\pi^+ d$
180±40		GOLDBERG	65	HBC	0	6 $\pi^+ d$, 8 $\pi^- p$

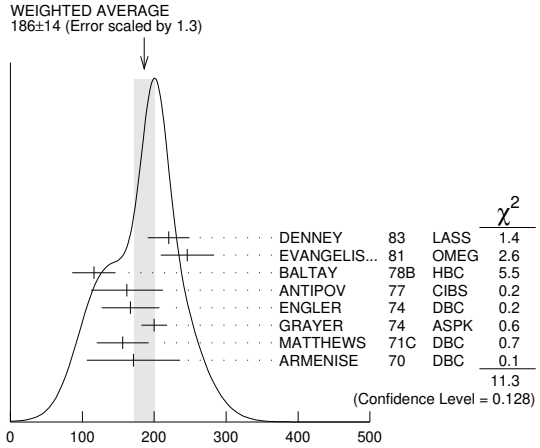

$\rho_3(1690)$ width, 2π mode (MeV)

[15] Width errors enlarged by us to $4\Gamma/\sqrt{N}$; see the note with the $K^*(892)$ mass.
[16] Uses same data as HYAMS 75 and BECKER 79.
[17] From a phase shift solution containing a $f'_2(1525)$ width two times larger than the $K\overline{K}$ result.
[18] From phase-shift analysis. Error takes account of spread of different phase-shift solutions.

$K\overline{K}$ AND $K\overline{K}\pi$ MODES

VALUE (MeV)	EVTS	DOCUMENT ID		TECN	CHG	COMMENT
The data in this block is included in the average printed for a previous datablock.						
204±18 OUR AVERAGE						
199±40	6000	[19] MARTIN	78D	SPEC		10 $\pi p \to K^0_S K^- p$
205±20		BLUM	75	ASPK	0	18.4 $\pi^- p \to n K^+ K^-$

Downloaded from https://academic.oup.com/ptep/article/2022/8/083C01/6651666 by KIT Library user on 27 September 2022

• • • We do not use the following data for averages, fits, limits, etc. • • •

219± 4		ALPER	80	CNTR	0	62 $\pi^- p \to K^+ K^- n$
186±11	[20]	COSTA	80	OMEG		10 $\pi^- p \to K^+ K^- n$
112±60		ADERHOLZ	69	HBC	+	8 $\pi^+ p \to K\overline{K}\pi$

[19] From a fit to $J^P = 3^-$ partial wave.
[20] They cannot distinguish between $\rho_3(1690)$ and $\omega_3(1670)$.

$(4\pi)^\pm$ MODE

VALUE (MeV)	EVTS	DOCUMENT ID		TECN	CHG	COMMENT
The data in this block is included in the average printed for a previous datablock.						
129±10 OUR AVERAGE						
123±13		[21] EVANGELIS...	81	OMEG	−	12 $\pi^- p \to p4\pi$
105±30	177	BALTAY	78B	HBC	+	15 $\pi^+ p \to p4\pi$
169^{+70}_{-48}		CASON	73	HBC	−	8,18.5 $\pi^- p$
135±30	144	BARTSCH	70B	HBC	+	8 $\pi^+ p \to N4\pi$
160±30	102	BARTSCH	70B	HBC	+	8 $\pi^+ p \to N2\rho$
• • • We do not use the following data for averages, fits, limits, etc. • • •						
230±28		[22] EVANGELIS...	81	OMEG	−	12 $\pi^- p \to p4\pi$
184±33		[23] EVANGELIS...	81	OMEG	−	12 $\pi^- p \to p4\pi$
150	66	[24] KLIGER	74	HBC	−	4.5 $\pi^- p \to p4\pi$
106±25		THOMPSON	74	HBC	+	13 $\pi^+ p$
125^{+83}_{-35}		[24] CASON	73	HBC	−	8,18.5 $\pi^- p$
130±30		HOLMES	72	HBC	+	10–12 $K^+ p$
180±30	90	[24] BARTSCH	70B	HBC	+	8 $\pi^+ p \to N a_2 \pi$
100±35		BALTAY	68	HBC	+	7, 8.5 $\pi^+ p$

[21] From $\rho^- \rho^0$ mode, not independent of the other two EVANGELISTA 81 entries.
[22] From $a_2(1320)^- \pi^0$ mode, not independent of the other two EVANGELISTA 81 entries.
[23] From $a_2(1320)^0 \pi^-$ mode, not independent of the other two EVANGELISTA 81 entries.
[24] From $\rho^\pm \rho^0$ mode.

$\omega\pi$ MODE

VALUE (MeV)	DOCUMENT ID		TECN	CHG	COMMENT
The data in this block is included in the average printed for a previous datablock.					
190±40 OUR AVERAGE					
230±65	[25] ALDE	95	GAM2		38 $\pi^- p \to \omega\pi^0 n$
190±65	EVANGELIS...	81	OMEG	−	12 $\pi^- p \to \omega\pi p$
160±56	GESSAROLI	77	HBC		11 $\pi^- p \to \omega\pi p$
• • • We do not use the following data for averages, fits, limits, etc. • • •					
89±25	THOMPSON	74	HBC	+	13 $\pi^+ p$
130^{+73}_{-43}	BARNHAM	70	HBC	+	10 $K^+ p \to \omega\pi X$

[25] Supersedes ALDE 92C.

$\eta\pi^+\pi^-$ MODE

(For difficulties with MMS experiments, see the $a_2(1320)$ mini-review in the 1973 edition.)

VALUE (MeV)	DOCUMENT ID		TECN	CHG	COMMENT
The data in this block is included in the average printed for a previous datablock.					
126±40 OUR AVERAGE Error includes scale factor of 1.8.					
220±30±50	AMELIN	00	VES		37 $\pi^- p \to \eta\pi^+\pi^- n$
106±27	FUKUI	88	SPEC	0	8.95 $\pi^- p \to \eta\pi^+\pi^- n$
• • • We do not use the following data for averages, fits, limits, etc. • • •					
195	[26] ANDERSON	69	MMS	−	16 $\pi^- p$ backward
< 21	[26,27] FOCACCI	66	MMS	−	7–12 $\pi^- p \to p$MM
< 30	[26,27] FOCACCI	66	MMS	−	7–12 $\pi^- p \to p$MM
< 38	[26,27] FOCACCI	66	MMS	−	7–12 $\pi^- p \to p$MM

[26] Seen in 2.5–3 GeV/c $\overline{p}p$. $2\pi^+2\pi^-$, with 0, 1, 2 $\pi^+\pi^-$ pairs in ρ^0 band not seen by OREN 74 (2.3 GeV/c $\overline{p}p$) with more statistics. (Jan. 1979)
[27] Not seen by BOWEN 72.

$\rho_3(1690)$ DECAY MODES

	Mode	Fraction (Γ_i/Γ)	Scale factor
Γ_1	4π	(71.1 ± 1.9) %	
Γ_2	$\pi^\pm\pi^+\pi^-\pi^0$	(67 ±22) %	
Γ_3	$\omega\pi$	(16 ± 6) %	
Γ_4	$\pi\pi$	(23.6 ± 1.3) %	
Γ_5	$K\overline{K}\pi$	(3.8 ± 1.2) %	
Γ_6	$K\overline{K}$	(1.58± 0.26) %	1.2
Γ_7	$\eta\pi^+\pi^-$	seen	
Γ_8	$\rho(770)\eta$	seen	
Γ_9	$\pi\pi\rho$	seen	
Γ_{10}	$a_2(1320)\pi$	seen	
Γ_{11}	$\rho\rho$	seen	
Γ_{12}	$\phi\pi$		
Γ_{13}	$\eta\pi$		
Γ_{14}	$\pi^\pm 2\pi^+ 2\pi^- \pi^0$		

CONSTRAINED FIT INFORMATION

An overall fit to 5 branching ratios uses 10 measurements and one constraint to determine 4 parameters. The overall fit has a χ^2 = 14.7 for 7 degrees of freedom.

The following *off-diagonal* array elements are the correlation coefficients $\langle \delta x_i \delta x_j \rangle / (\delta x_i \cdot \delta x_j)$, in percent, from the fit to the branching fractions, $x_i \equiv \Gamma_i/\Gamma_{total}$. The fit constrains the x_i whose labels appear in this array to sum to one.

	x_1	x_4	x_5
x_4	−77		
x_5	−74	17	
x_6	−15	2	0

$\rho_3(1690)$ BRANCHING RATIOS

$\Gamma(\pi\pi)/\Gamma_{total}$ — Γ_4/Γ

VALUE	DOCUMENT ID		TECN	CHG	COMMENT
0.236±0.013 OUR FIT					
0.243±0.013 OUR AVERAGE					
$0.259^{+0.018}_{-0.019}$	BECKER	79	ASPK	0	17 $\pi^- p$ polarized
0.23 ±0.02	CORDEN	79	OMEG		12–15 $\pi^- p \to n2\pi$
0.22 ±0.04	[28] MATTHEWS	71C	HDBC	0	7 $\pi^+ n \to \pi^- p$
• • • We do not use the following data for averages, fits, limits, etc. • • •					
0.245±0.006	[29] ESTABROOKS	75	RVUE		17 $\pi^- p \to \pi^+\pi^- n$

[28] One-pion-exchange model used in this estimation.
[29] From phase-shift analysis of HYAMS 75 data.

$\Gamma(\pi\pi)/\Gamma(\pi^\pm\pi^+\pi^-\pi^0)$ — Γ_4/Γ_2

VALUE	DOCUMENT ID		TECN	CHG	COMMENT
0.35±0.11	CASON	73	HBC	−	8,18.5 $\pi^- p$
• • • We do not use the following data for averages, fits, limits, etc. • • •					
<0.2	HOLMES	72	HBC	+	10–12 $K^+ p$
<0.12	BALLAM	71B	HBC	−	16 $\pi^- p$

$\Gamma(\pi\pi)/\Gamma(4\pi)$ — Γ_4/Γ_1

VALUE	DOCUMENT ID		TECN	CHG	COMMENT
0.332±0.026 OUR FIT Error includes scale factor of 1.1.					
0.30 ±0.10	BALTAY	78B	HBC	0	15 $\pi^+ p \to p4\pi$

$\Gamma(K\overline{K})/\Gamma(\pi\pi)$ — Γ_6/Γ_4

VALUE	DOCUMENT ID		TECN	CHG	COMMENT
0.067±0.011 OUR FIT Error includes scale factor of 1.2.					
$\mathbf{0.118^{+0.040}_{-0.032}}$ **OUR AVERAGE** Error includes scale factor of 1.7. See the ideogram below.					
$0.191^{+0.040}_{-0.037}$	GORLICH	80	ASPK	0	17,18 $\pi^- p$ polarized
0.08 ±0.03	BARTSCH	70B	HBC	+	8 $\pi^+ p$
$0.08^{+0.08}_{-0.03}$	CRENNELL	68B	HBC		6.0 $\pi^- p$

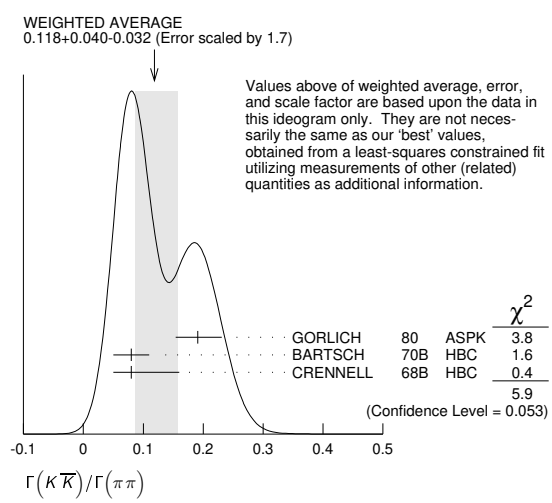

$\Gamma(K\overline{K}\pi)/\Gamma(\pi\pi)$ — Γ_5/Γ_4

VALUE	DOCUMENT ID		TECN	CHG	COMMENT
0.16±0.05 OUR FIT					
0.16±0.05	[30] BARTSCH	70B	HBC	+	8 $\pi^+ p$

[30] Increased by us to correspond to B($\rho_3(1690) \to \pi\pi$)=0.24.

Downloaded from https://academic.oup.com/ptep/article/2022/8/083C01/6651666 by KIT Library user on 27 September 2022

$[\Gamma(\pi\pi\rho)+\Gamma(a_2(1320)\pi)+\Gamma(\rho\rho)]/\Gamma(\pi^\pm\pi^+\pi^-\pi^0)$ $(\Gamma_9+\Gamma_{10}+\Gamma_{11})/\Gamma_2$

VALUE	DOCUMENT ID		TECN	CHG	COMMENT
0.94±0.09 OUR AVERAGE					
0.96±0.21	BALTAY	78B	HBC	+	15 $\pi^+ p \to p4\pi$
0.88±0.15	BALLAM	71B	HBC	−	16 $\pi^- p$
1 ±0.15	BARTSCH	70B	HBC	+	8 $\pi^+ p$
consistent with 1	CASO	68	HBC	−	11 $\pi^- p$

$\Gamma(\rho\rho)/\Gamma(\pi^\pm\pi^+\pi^-\pi^0)$ Γ_{11}/Γ_2

VALUE	EVTS	DOCUMENT ID		TECN	CHG	COMMENT
• • • We do not use the following data for averages, fits, limits, etc. • • •						
0.12±0.11		BALTAY	78B	HBC	+	15 $\pi^+ p \to p4\pi$
0.56	66	KLIGER	74	HBC	−	4.5 $\pi^- p \to p4\pi$
0.13±0.09		[31] THOMPSON	74	HBC	+	13 $\pi^+ p$
0.7 ±0.15		BARTSCH	70B	HBC	+	8 $\pi^+ p$

[31] $\rho\rho$ and $a_2(1320)\pi$ modes are indistinguishable.

$\Gamma(\rho\rho)/[\Gamma(\pi\pi\rho)+\Gamma(a_2(1320)\pi)+\Gamma(\rho\rho)]$ $\Gamma_{11}/(\Gamma_9+\Gamma_{10}+\Gamma_{11})$

VALUE	DOCUMENT ID		TECN	CHG	COMMENT
• • • We do not use the following data for averages, fits, limits, etc. • • •					
0.48±0.16	CASO	68	HBC	−	11 $\pi^- p$

$\Gamma(a_2(1320)\pi)/\Gamma(\pi^\pm\pi^+\pi^-\pi^0)$ Γ_{10}/Γ_2

VALUE	DOCUMENT ID		TECN	CHG	COMMENT
• • • We do not use the following data for averages, fits, limits, etc. • • •					
0.66±0.08	BALTAY	78B	HBC	+	15 $\pi^+ p \to p4\pi$
0.36±0.14	[32] THOMPSON	74	HBC	+	13 $\pi^+ p$
not seen	CASON	73	HBC	−	8,18.5 $\pi^- p$
0.6 ±0.15	BARTSCH	70B	HBC	+	8 $\pi^+ p$
0.6	BALTAY	68	HBC	+	7,8.5 $\pi^+ p$

[32] $\rho\rho$ and $a_2(1320)\pi$ modes are indistinguishable.

$\Gamma(\omega\pi)/\Gamma(\pi^\pm\pi^+\pi^-\pi^0)$ Γ_3/Γ_2

VALUE	CL%	DOCUMENT ID		TECN	CHG	COMMENT
0.23±0.05 OUR AVERAGE		Error includes scale factor of 1.2.				
0.33±0.07		THOMPSON	74	HBC	+	13 $\pi^+ p$
0.12±0.07		BALLAM	71B	HBC	−	16 $\pi^- p$
0.25±0.10		BALTAY	68	HBC	+	7,8.5 $\pi^+ p$
0.25±0.10		JOHNSTON	68	HBC	−	7.0 $\pi^- p$
• • • We do not use the following data for averages, fits, limits, etc. • • •						
<0.11	95	BALTAY	78B	HBC	+	15 $\pi^+ p \to p4\pi$
<0.09		KLIGER	74	HBC	−	4.5 $\pi^- p \to p4\pi$

$\Gamma(\phi\pi)/\Gamma(\pi^\pm\pi^+\pi^-\pi^0)$ Γ_{12}/Γ_2

VALUE	DOCUMENT ID		TECN	CHG	COMMENT
• • • We do not use the following data for averages, fits, limits, etc. • • •					
<0.11	BALTAY	68	HBC	+	7,8.5 $\pi^+ p$

$\Gamma(\pi^\pm 2\pi^+ 2\pi^-\pi^0)/\Gamma(\pi^\pm\pi^+\pi^-\pi^0)$ Γ_{14}/Γ_2

VALUE	DOCUMENT ID		TECN	CHG	COMMENT
• • • We do not use the following data for averages, fits, limits, etc. • • •					
<0.15	BALTAY	68	HBC	+	7,8.5 $\pi^+ p$

$\Gamma(\eta\pi)/\Gamma(\pi^\pm\pi^+\pi^-\pi^0)$ Γ_{13}/Γ_2

VALUE	DOCUMENT ID		TECN	CHG	COMMENT
• • • We do not use the following data for averages, fits, limits, etc. • • •					
<0.02	THOMPSON	74	HBC	+	13 $\pi^+ p$

$\Gamma(K\overline{K})/\Gamma_{total}$ Γ_6/Γ

VALUE	DOCUMENT ID		TECN	CHG	COMMENT
0.0158±0.0026 OUR FIT	Error includes scale factor of 1.2.				
0.0130±0.0024 OUR AVERAGE					
0.013 ±0.003	COSTA	80	OMEG	0	10 $\pi^- p \to K^+ K^- n$
0.013 ±0.004	[33] MARTIN	78B	SPEC	−	10 $\pi p \to K^0_S K^- p$

[33] From $(\Gamma_4\Gamma_6)^{1/2} = 0.056 \pm 0.034$ assuming $B(\rho_3(1690) \to \pi\pi) = 0.24$.

$\Gamma(\omega\pi)/[\Gamma(\omega\pi)+\Gamma(\rho\rho)]$ $\Gamma_3/(\Gamma_3+\Gamma_{11})$

VALUE	DOCUMENT ID		TECN	CHG	COMMENT
• • • We do not use the following data for averages, fits, limits, etc. • • •					
0.22±0.08	CASON	73	HBC	−	8,18.5 $\pi^- p$

$\Gamma(\eta\pi^+\pi^-)/\Gamma_{total}$ Γ_7/Γ

VALUE	DOCUMENT ID		TECN	COMMENT
seen	FUKUI	88	SPEC	8.95 $\pi^- p \to \eta\pi^+\pi^- n$

$\Gamma(a_2(1320)\pi)/\Gamma(\rho(770)\eta)$ Γ_{10}/Γ_8

VALUE	DOCUMENT ID		TECN	COMMENT
5.5±2.0	AMELIN	00	VES	37 $\pi^- p \to \eta\pi^+\pi^- n$

$\rho_3(1690)$ REFERENCES

AMELIN 00 NP A668 83 D. Amelin et al. (VES Collab.)
ALDE 95 ZPHY C66 379 D.M. Alde et al. (GAMS Collab.) JP
ALDE 92C ZPHY C54 553 D.M. Alde et al. (BELG, SERP, KEK, LANL+)
FUKUI 88 PL B202 441 S. Fukui et al. (SUGI, NAGO, KEK, KYOT+)
DENNEY 83 PR D28 2726 D.L. Denney et al. (IOWA, MICH)
EVANGELIS... 81 NP B178 197 C. Evangelista et al. (BARI, BONN, CERN+)
ALPER 80 PL 94B 422 B. Alper et al. (AMST, CERN, CRAC, MPIM+)
COSTA 80 NP B175 402 G. Costa et al. (BARI, BONN, CERN, GLAS+)
GORLICH 80 NP B174 16 L. Gorlich et al. (CRAC, MPIM, CERN+)
BECKER 79 NP B151 46 H. Becker et al. (MPIM, CERN, ZEEM, CRAC)
CORDEN 79 NP B157 250 M.J. Corden et al. (BIRM, RHEL, TELA+) JP
BALTAY 78B PR D17 62 C. Baltay et al. (COLU, BING)
MARTIN 78B NP B140 158 A.D. Martin et al. (DURH, GEVA)
MARTIN 78D PL 74B 417 A.D. Martin et al. (DURH, GEVA)
ANTIPOV 77 NP B119 45 Y.M. Antipov et al. (SERP, GEVA)
GESSAROLI 77 NP B126 382 R. Gessaroli et al. (BGNA, FIRZ, GENO+)
BLUM 75 PL 57B 403 W. Blum et al. (CERN, MPIM) JP
ESTABROOKS 75 NP B95 322 P.G. Estabrooks, A.D. Martin (DURH)
HYAMS 75 NP B100 205 B.D. Hyams et al. (CERN, MPIM)
ENGLER 74 PR D10 2070 A. Engler et al. (CMU, CASE)
GRAYER 74 NP B75 189 G. Grayer et al. (CERN, MPIM)
KLIGER 74 SJNP 19 428 G.K. Kliger et al. (ITEP)
Translated from YAF 19 839.
OREN 74 NP B71 189 Y. Oren et al. (ANL, OXF)
THOMPSON 74 NP B69 220 G. Thompson et al. (PURD)
CASON 73 PR D7 1971 N.M. Cason et al. (NDAM)
BOWEN 72 PRL 29 890 D.R. Bowen et al. (NEAS, STON)
HOLMES 72 PR D6 3336 R. Holmes et al. (ROCH)
BALLAM 71B PR D3 2606 J. Ballam et al. (SLAC)
MATTHEWS 71C NP B33 1 J.A.J. Matthews et al. (TNTO, WISC) JP
ARMENISE 70 LNC 4 199 N. Armenise et al. (BARI, BGNA, FIRZ)
BARNHAM 70 PRL 24 1083 K.W.J. Barnham et al. (BIRM)
BARTSCH 70B NP B22 109 J. Bartsch et al. (AACH, BERL, CERN)
CASO 70 LNC 3 707 C. Caso et al. (GENO, HAMB, MILA, SACL)
STUNTEBECK 70 PL 32B 391 P.H. Stuntebeck et al. (NDAM)
ADERHOLZ 69 NP B11 259 M. Aderholz et al. (AACH3, BERL, CERN+)
ANDERSON 69 PRL 22 1390 E.W. Anderson et al. (BNL, CMU)
ARMENISE 68 NC 54A 999 N. Armenise et al. (BARI, BGNA, FIRZ+) I
BALTAY 68 PRL 20 887 C. Baltay et al. (COLU, ROCH, RUTG, YALE) I
CASO 68 NC 54A 983 C. Caso et al. (GENO, HAMB, MILA, SACL)
CRENNELL 68B PL 28B 136 D.J. Crennell et al. (BNL)
JOHNSTON 68 PRL 20 1414 T.F. Johnston et al. (TNTO, WISC) IJP
FOCACCI 66 PRL 17 890 M.N. Focacci et al. (CERN)
GOLDBERG 65 PL 17 354 M. Goldberg et al. (CERN, EPOL, ORSAY+)

$\rho(1700)$

$I^G(J^{PC}) = 1^+(1^{--})$

$\rho(1700)$ MASS

$\eta\rho^0$ AND $\pi^+\pi^-$ MODES

VALUE (MeV)	DOCUMENT ID
1720±20 OUR ESTIMATE	

$\eta\rho^0$ MODE

VALUE (MeV)	EVTS	DOCUMENT ID		TECN	COMMENT
The data in this block is included in the average printed for a previous datablock.					
• • • We do not use the following data for averages, fits, limits, etc. • • •					
1834±12	13.4k	[1] GRIBANOV	20	CMD3	1.1–2.0 $e^+e^- \to \eta\pi^+\pi^-$
1840±10	7.4k	[2] ACHASOV	18	SND	1.22–2.00 $e^+e^- \to \eta\pi^+\pi^-$
1740±20		ANTONELLI	88	DM2	$e^+e^- \to \eta\pi^+\pi^-$
1701±15		[3] FUKUI	88	SPEC	8.95 $\pi^- p \to \eta\pi^+\pi^- n$

[1] Mass and width of the $\rho(770)$ fixed at 775 and 149 MeV, respectively; solution 2 of model 2, $\eta \to \gamma\gamma$ decays used.

[2] From the combined fit of AULCHENKO 15 and ACHASOV 18 in the model with the interfering $\rho(1450)$, $\rho(1700)$ and $\rho(2150)$ with the parameters of the $\rho(1450)$ and $\rho(1700)$ floating and the mass and width of the $\rho(2150)$ fixed at 2155 MeV and 320 MeV, respectively. The phases of the resonances are π, 0 and π, respectively.

[3] Assuming $\rho^+ f_0(1370)$ decay mode interferes with $a_1(1260)^+\pi$ background. From a two Breit-Wigner fit.

$\pi\pi$ MODE

VALUE (MeV)	EVTS	DOCUMENT ID		TECN	COMMENT
The data in this block is included in the average printed for a previous datablock.					
• • • We do not use the following data for averages, fits, limits, etc. • • •					
1770.54± 5.49		[1] BARTOS	17	RVUE	$e^+e^- \to \pi^+\pi^-$
1718.50±65.44		[2] BARTOS	17A	RVUE	$e^+e^- \to \pi^+\pi^-$
1766.80±52.36		[3] BARTOS	17A	RVUE	$\tau^- \to \pi^-\pi^0\nu_\tau$
1644 ±36	20k	[4] LEES	17C	BABR	$J/\psi \to \pi^+\pi^-\pi^0$
1780 ±20 $^{+15}_{-20}$	63.5k	[5] ABRAMOWICZ	12	ZEUS	$ep \to e\pi^+\pi^- p$
1861 ±17		[6] LEES	12G	BABR	$e^+e^- \to \pi^+\pi^-\gamma$
1728 ±17 ±89	5.4M	[7,8] FUJIKAWA	08	BELL	$\tau^- \to \pi^-\pi^0\nu_\tau$
1780 $^{+37}_{-29}$		[9] ABELE	97	CBAR	$\overline{p}n \to \pi^-\pi^0\pi^0$
1719 ±15		[9] BERTIN	97C	OBLX	0.0 $\overline{p}p \to \pi^+\pi^-\pi^0$
1730 ±30		CLEGG	94	RVUE	$e^+e^- \to \pi^+\pi^-$
1768 ±21		BISELLO	89	DM2	$e^+e^- \to \pi^+\pi^-$
1745.7 ±91.9		DUBNICKA	89	RVUE	$e^+e^- \to \pi^+\pi^-$
1546 ±26		GESHKEN...	89	RVUE	
1650		[10] ERKAL	85	RVUE	20–70 $\gamma p \to \gamma\pi$

Downloaded from https://academic.oup.com/ptep/article/2022/8/083C01/6651666 by KIT Library user on 27 September 2022

1550	±70	ABE	84B	HYBR	20 $\gamma p \to \pi^+\pi^- p$
1590	±20	[11] ASTON	80	OMEG	20–70 $\gamma p \to p 2\pi$
1600	±10	[12] ATIYA	79B	SPEC	50 $\gamma C \to C 2\pi$
1598	$^{+24}_{-22}$	BECKER	79	ASPK	17 $\pi^- p$ polarized
1659	±25	[10] LANG	79	RVUE	
1575		[10] MARTIN	78C	RVUE	17 $\pi^- p \to \pi^+\pi^- n$
1610	±30	[10] FROGGATT	77	RVUE	17 $\pi^- p \to \pi^+\pi^- n$
1590	±20	[13] HYAMS	73	ASPK	17 $\pi^- p \to \pi^+\pi^- n$

[1] Applies the Unitary & Analytic Model of the pion electromagnetic form factor of DUBNICKA 10 to analyze the data of LEES 12G and ABLIKIM 16C.
[2] Applies the Unitary & Analytic Model of the pion electromagnetic form factor of DUBNICKA 10 to analyze the data of ACHASOV 06, AKHMETSHIN 07, AUBERT 09AS, and AMBROSINO 11A.
[3] Applies the Unitary & Analytic Model of the pion electromagnetic form factor of DUBNICKA 10 to analyze the data of FUJIKAWA 08.
[4] From a Dalitz plot analysis in an isobar model with $\rho(1450)$ and $\rho(1700)$ masses and widths floating.
[5] Using the KUHN 90 parametrization of the pion form factor, neglecting $\rho-\omega$ interference.
[6] Using the GOUNARIS 68 parametrization of the pion form factor leaving the masses and widths of the $\rho(1450)$, $\rho(1700)$, and $\rho(2150)$ resonances as free parameters of the fit.
[7] $|F_\pi(0)|^2$ fixed to 1.
[8] From the GOUNARIS 68 parametrization of the pion form factor.
[9] T-matrix pole.
[10] From phase shift analysis of HYAMS 73 data.
[11] Simple relativistic Breit-Wigner fit with constant width.
[12] An additional 40 MeV uncertainty in both the mass and width is present due to the choice of the background shape.
[13] Included in BECKER 79 analysis.

$\pi\omega$ MODE

VALUE (MeV)	EVTS	DOCUMENT ID		TECN	COMMENT
• • • We do not use the following data for averages, fits, limits, etc. • • •					
1708±41	7815	[1] ACHASOV	13	SND	1.05–2.00 $e^+e^- \to \pi^0\pi^0\gamma$
1550 to 1620		[2] ACHASOV	00I	SND	$e^+e^- \to \pi^0\pi^0\gamma$
1580 to 1710		[3] ACHASOV	00I	SND	$e^+e^- \to \pi^0\pi^0\gamma$
1710±90		ACHASOV	97	RVUE	$e^+e^- \to \omega\pi^0$

[1] From a phenomenological model based on vector meson dominance with the interfering $\rho(1450)$ and $\rho(1700)$ and their widths fixed at 400 and 250 MeV, respectively. Systematic uncertainty not estimated.
[2] Taking into account both $\rho(1450)$ and $\rho(1700)$ contributions. Using the data of ACHASOV 00I on $e^+e^- \to \omega\pi^0$ and of EDWARDS 00A on $\tau^- \to \omega\pi^-\nu_\tau$. $\rho(1450)$ mass and width fixed at 1400 MeV and 500 MeV respectively.
[3] Taking into account the $\rho(1700)$ contribution only. Using the data of ACHASOV 00I on $e^+e^- \to \omega\pi^0$ and of EDWARDS 00A on $\tau^- \to \omega\pi^-\nu_\tau$.

$K\overline{K}$ MODE

VALUE (MeV)	EVTS	DOCUMENT ID		TECN	CHG	COMMENT
• • • We do not use the following data for averages, fits, limits, etc. • • •						
1688.7± 3.1$^{+141.1}_{-1.3}$		[1] ALBRECHT	20	RVUE		0.9 $\overline{p}p \to K^+K^-\pi^0$
1541 ±12 ± 33	190k	[2] AAIJ	16N	LHCB		$D^0 \to K^0_S K^\pm\pi^\mp$
1740.8±22.2	27k	[3] ABELE	99D	CBAR	±	0.0 $\overline{p}p \to K^+K^-\pi^0$
1582 ±36	1600	CLELAND	82B	SPEC	±	50 $\pi p \to K^0_S K^\pm p$

[1] T-matrix pole, 2 poles, 3 channels, including $\pi\pi$ scattering data from HYAMS 75.
[2] Using the GOUNARIS 68 parameterization with a fixed width. Value is average using different $K\pi$ S-wave parametrizations in fit.
[3] K-matrix pole. Isospin not determined, could be $\omega(1650)$ or $\phi(1680)$.

2 $(\pi^+\pi^-)$ MODE

VALUE (MeV)	EVTS	DOCUMENT ID		TECN	COMMENT
• • • We do not use the following data for averages, fits, limits, etc. • • •					
1851$^{+27}_{-24}$		ACHASOV	97	RVUE	$e^+e^- \to 2(\pi^+\pi^-)$
1570± 20		[1] CORDIER	82	DM1	$e^+e^- \to 2(\pi^+\pi^-)$
1520± 30		[2] ASTON	81E	OMEG	20–70 $\gamma p \to p 4\pi$
1654± 25		[3] DIBIANCA	81	DBC	$\pi^+ d \to pp 2(\pi^+\pi^-)$
1666± 39		[1] BACCI	80	FRAG	$e^+e^- \to 2(\pi^+\pi^-)$
1780	34	KILLIAN	80	SPEC	11 $e^- p \to 2(\pi^+\pi^-)$
1500		[4] ATIYA	79B	SPEC	50 $\gamma C \to C 4\pi^\pm$
1570± 60	65	[5] ALEXANDER	75	HBC	7.5 $\gamma p \to p 4\pi$
1550± 60		[2] CONVERSI	74	OSPK	$e^+e^- \to 2(\pi^+\pi^-)$
1550± 50	160	SCHACHT	74	STRC	5.5–9 $\gamma p \to p 4\pi$
1450±100	340	SCHACHT	74	STRC	9–18 $\gamma p \to p 4\pi$
1430± 50	400	BINGHAM	72B	HBC	9.3 $\gamma p \to p 4\pi$

[1] Simple relativistic Breit-Wigner fit with model dependent width.
[2] Simple relativistic Breit-Wigner fit with constant width.
[3] One peak fit result.
[4] Parameters roughly estimated, not from a fit.
[5] Skew mass distribution compensated by Ross-Stodolsky factor.

$\pi^+\pi^-\pi^0\pi^0$ MODE

VALUE (MeV)	DOCUMENT ID		TECN	COMMENT
• • • We do not use the following data for averages, fits, limits, etc. • • •				
1660±30	ATKINSON	85B	OMEG	20–70 γp

$3(\pi^+\pi^-)$ AND $2(\pi^+\pi^-\pi^0)$ MODES

VALUE (MeV)	DOCUMENT ID		TECN	COMMENT
• • • We do not use the following data for averages, fits, limits, etc. • • •				
1730±34	[1] FRABETTI	04	E687	$\gamma p \to 3\pi^+ 3\pi^- p$
1783±15	CLEGG	90	RVUE	$e^+e^- \to 3(\pi^+\pi^-)2(\pi^+\pi^-\pi^0)$

[1] From a fit with two resonances with the JACOB 72 continuum.

$m_{\rho(1700)^0} - m_{\rho(1700)^\pm}$

VALUE (MeV)	DOCUMENT ID		TECN	COMMENT
• • • We do not use the following data for averages, fits, limits, etc. • • •				
−48.30±83.81	[1] BARTOS	17A	RVUE	$e^+e^- \to \pi^+\pi^-$, $\tau^- \to \pi^-\pi^0\nu_\tau$

[1] Applies the Unitary & Analytic Model of the pion electromagnetic form factor of DUBNICKA 10 to analyze the data of ACHASOV 06, AKHMETSHIN 07, AUBERT 09AS, AMBROSINO 11A, and FUJIKAWA 08.

$\rho(1700)$ WIDTH

$\eta\rho^0$ AND $\pi^+\pi^-$ MODES

VALUE (MeV)	DOCUMENT ID
250±100 OUR ESTIMATE	

$\eta\rho^0$ MODE

VALUE (MeV)	EVTS	DOCUMENT ID		TECN	COMMENT
The data in this block is included in the average printed for a previous datablock.					
• • • We do not use the following data for averages, fits, limits, etc. • • •					
47±19	13.4k	[1] GRIBANOV	20	CMD3	1.1–2.0 $e^+e^- \to \eta\pi^+\pi^-$
132±40	7.4k	[2] ACHASOV	18	SND	1.22–2.00 $e^+e^- \to \eta\pi^+\pi^-$
150±30		ANTONELLI	88	DM2	$e^+e^- \to \eta\pi^+\pi^-$
282±44		[3] FUKUI	88	SPEC	8.95 $\pi^- p \to \eta\pi^+\pi^- n$

[1] Mass and width of the $\rho(770)$ fixed at 775 and 149 MeV, respectively; solution 2 of model 2, $\eta \to \gamma\gamma$ decays used.
[2] From the combined fit of AULCHENKO 15 and ACHASOV 18 in the model with the interfering $\rho(1450)$, $\rho(1700)$ and $\rho(2150)$ with the parameters of the $\rho(1450)$ and $\rho(1700)$ floating and the mass and width of the $\rho(2150)$ fixed at 2155 MeV and 320 MeV, respectively. The phases of the resonances are π, 0 and π, respectively.
[3] Assuming $\rho^+ f_0(1370)$ decay mode interferes with $a_1(1260)^+\pi$ background. From a two Breit-Wigner fit.

$\pi\pi$ MODE

VALUE (MeV)	EVTS	DOCUMENT ID		TECN	COMMENT
The data in this block is included in the average printed for a previous datablock.					
• • • We do not use the following data for averages, fits, limits, etc. • • •					
268.98± 11.40		[1] BARTOS	17	RVUE	$e^+e^- \to \pi^+\pi^-$
489.58± 16.95		[2] BARTOS	17A	RVUE	$e^+e^- \to \pi^+\pi^-$
414.71±119.48		[3] BARTOS	17A	RVUE	$\tau^- \to \pi^-\pi^0\nu_\tau$
109 ± 19	20k	[4] LEES	17C	BABR	$J/\psi \to \pi^+\pi^-\pi^0$
310 ± 30	$^{+25}_{-35}$ 63.5k	[5] ABRAMOWICZ	12	ZEUS	$ep \to e\pi^+\pi^- p$
316 ± 26		[6] LEES	12G	BABR	$e^+e^- \to \pi^+\pi^-\gamma$
164 ± 21	$^{+89}_{-26}$ 5.4M	[7,8] FUJIKAWA	08	BELL	$\tau^- \to \pi^-\pi^0\nu_\tau$
275 ± 45		[9] ABELE	97	CBAR	$\overline{p}n \to \pi^-\pi^0\pi^0$
310 ± 40		[9] BERTIN	97C	OBLX	0.0 $\overline{p}p \to \pi^+\pi^-\pi^0$
400 ±100		CLEGG	94	RVUE	$e^+e^- \to \pi^+\pi^-$
224 ± 22		BISELLO	89	DM2	$e^+e^- \to \pi^+\pi^-$
242.5 ±163.0		DUBNICKA	89	RVUE	$e^+e^- \to \pi^+\pi^-$
620 ± 60		GESHKEN...	89	RVUE	
<315		[10] ERKAL	85	RVUE	20–70 $\gamma p \to \gamma\pi$
280 $^{+30}_{-80}$		ABE	84B	HYBR	20 $\gamma p \to \pi^+\pi^- p$
230 ± 80		[11] ASTON	80	OMEG	20–70 $\gamma p \to p 2\pi$
283 ± 14		[12] ATIYA	79B	SPEC	50 $\gamma C \to C 2\pi$
175 $^{+98}_{-53}$		BECKER	79	ASPK	17 $\pi^- p$ polarized
232 ± 34		[10] LANG	79	RVUE	
340		[10] MARTIN	78C	RVUE	17 $\pi^- p \to \pi^+\pi^- n$
300 ±100		[10] FROGGATT	77	RVUE	17 $\pi^- p \to \pi^+\pi^- n$
180 ± 50		[13] HYAMS	73	ASPK	17 $\pi^- p \to \pi^+\pi^- n$

[1] Applies the Unitary & Analytic Model of the pion electromagnetic form factor of DUBNICKA 10 to analyze the data of LEES 12G and ABLIKIM 16C.
[2] Applies the Unitary & Analytic Model of the pion electromagnetic form factor of DUBNICKA 10 to analyze the data of ACHASOV 06, AKHMETSHIN 07, AUBERT 09AS, and AMBROSINO 11A.
[3] Applies the Unitary & Analytic Model of the pion electromagnetic form factor of DUBNICKA 10 to analyze the data of FUJIKAWA 08.
[4] From a Dalitz plot analysis in an isobar model with $\rho(1450)$ and $\rho(1700)$ masses and widths floating.
[5] Using the KUHN 90 parametrization of the pion form factor, neglecting $\rho-\omega$ interference.
[6] Using the GOUNARIS 68 parametrization of the pion form factor leaving the masses and widths of the $\rho(1450)$, $\rho(1700)$, and $\rho(2150)$ resonances as free parameters of the fit.
[7] $|F_\pi(0)|^2$ fixed to 1.
[8] From the GOUNARIS 68 parametrization of the pion form factor.
[9] T-matrix pole.
[10] From phase shift analysis of HYAMS 73 data.
[11] Simple relativistic Breit-Wigner fit with constant width.
[12] An additional 40 MeV uncertainty in both the mass and width is present due to the choice of the background shape.
[13] Included in BECKER 79 analysis.

Downloaded from https://academic.oup.com/ptep/article/2022/8/083C01/6651666 by KIT Library user on 27 September 2022

$K\overline{K}$ MODE

VALUE (MeV)	EVTS	DOCUMENT ID		TECN	CHG	COMMENT
• • • We do not use the following data for averages, fits, limits, etc. • • •						
$150.9 \pm 2.5^{+60}_{-10.6}$		[1] ALBRECHT	20	RVUE		$0.9\ \overline{p}p \to K^+K^-\pi^0$
187.2 ± 26.7	27k	[2] ABELE	99D	CBAR	±	$0.0\ \overline{p}p \to K^+K^-\pi^0$
265 ± 120	1600	CLELAND	82B	SPEC	±	$50\ \pi p \to K^0_S K^\pm p$

[1] T-matrix pole, 2 poles, 3 channels, including $\pi\pi$ scattering data from HYAMS 75.
[2] K-matrix pole. Isospin not determined, could be $\omega(1650)$ or $\phi(1680)$.

$2(\pi^+\pi^-)$ MODE

VALUE (MeV)	EVTS	DOCUMENT ID		TECN	COMMENT
• • • We do not use the following data for averages, fits, limits, etc. • • •					
510 ± 40		[1] CORDIER	82	DM1	$e^+e^- \to 2(\pi^+\pi^-)$
400 ± 50		[2] ASTON	81E	OMEG	20–70 $\gamma p \to p4\pi$
400 ± 146		[3] DIBIANCA	81	DBC	$\pi^+ d \to pp2(\pi^+\pi^-)$
700 ± 160		[1] BACCI	80	FRAG	$e^+e^- \to 2(\pi^+\pi^-)$
100	34	KILLIAN	80	SPEC	11 $e^-p \to 2(\pi^+\pi^-)$
600		[4] ATIYA	79B	SPEC	50 γC $\to$ C$4\pi^\pm$
340 ± 160	65	[5] ALEXANDER	75	HBC	7.5 $\gamma p \to p4\pi$
360 ± 100		[2] CONVERSI	74	OSPK	$e^+e^- \to 2(\pi^+\pi^-)$
400 ± 120	160	[6] SCHACHT	74	STRC	5.5–9 $\gamma p \to p4\pi$
850 ± 200	340	[6] SCHACHT	74	STRC	9–18 $\gamma p \to p4\pi$
650 ± 100	400	BINGHAM	72B	HBC	9.3 $\gamma p \to p4\pi$

[1] Simple relativistic Breit-Wigner fit with model-dependent width.
[2] Simple relativistic Breit-Wigner fit with constant width.
[3] One peak fit result.
[4] Parameters roughly estimated, not from a fit.
[5] Skew mass distribution compensated by Ross-Stodolsky factor.
[6] Width errors enlarged by us to $4\Gamma/\sqrt{N}$; see the note with the $K^*(892)$ mass.

$\pi^+\pi^-\pi^0\pi^0$ MODE

VALUE (MeV)	DOCUMENT ID		TECN	COMMENT
• • • We do not use the following data for averages, fits, limits, etc. • • •				
300 ± 50	ATKINSON	85B	OMEG	20–70 γp

$\omega\pi^0$ MODE

VALUE (MeV)	DOCUMENT ID		TECN	COMMENT
• • • We do not use the following data for averages, fits, limits, etc. • • •				
350 to 580	[1] ACHASOV	00I	SND	$e^+e^- \to \pi^0\pi^0\gamma$
490 to 1040	[2] ACHASOV	00I	SND	$e^+e^- \to \pi^0\pi^0\gamma$

[1] Taking into account both $\rho(1450)$ and $\rho(1700)$ contributions. Using the data of ACHASOV 00I on $e^+e^- \to \omega\pi^0$ and of EDWARDS 00A on $\tau^- \to \omega\pi^-\nu_\tau$. $\rho(1450)$ mass and width fixed at 1400 MeV and 500 MeV respectively.
[2] Taking into account the $\rho(1700)$ contribution only. Using the data of ACHASOV 00I on $e^+e^- \to \omega\pi^0$ and of EDWARDS 00A on $\tau^- \to \omega\pi^-\nu_\tau$.

$3(\pi^+\pi^-)$ AND $2(\pi^+\pi^-\pi^0)$ MODES

VALUE (MeV)	DOCUMENT ID		TECN	COMMENT
• • • We do not use the following data for averages, fits, limits, etc. • • •				
315 ± 100	[1] FRABETTI	04	E687	$\gamma p \to 3\pi^+3\pi^-p$
285 ± 20	CLEGG	90	RVUE	$e^+e^- \to 3(\pi^+\pi^-)2(\pi^+\pi^-\pi^0)$

[1] From a fit with two resonances with the JACOB 72 continuum.

$\Gamma_{\rho(1700)^0} - \Gamma_{\rho(1700)^\pm}$

VALUE (MeV)	DOCUMENT ID		TECN	COMMENT
• • • We do not use the following data for averages, fits, limits, etc. • • •				
74.87 ± 120.67	[1] BARTOS	17A	RVUE	$e^+e^- \to \pi^+\pi^-, \tau^- \to \pi^-\pi^0\nu_\tau$

[1] Applies the Unitary & Analytic Model of the pion electromagnetic form factor of DUBNICKA 10 to analyze the data of ACHASOV 06, AKHMETSHIN 07, AUBERT 09AS, AMBROSINO 11A, and FUJIKAWA 08.

$\rho(1700)$ DECAY MODES

	Mode	Fraction (Γ_i/Γ)
Γ_1	4π	
Γ_2	$2(\pi^+\pi^-)$	seen
Γ_3	$\rho\pi\pi$	seen
Γ_4	$\rho^0\pi^+\pi^-$	seen
Γ_5	$\rho^0\pi^0\pi^0$	
Γ_6	$\rho^\pm\pi^\mp\pi^0$	seen
Γ_7	$a_1(1260)\pi$	seen
Γ_8	$h_1(1170)\pi$	seen
Γ_9	$\pi(1300)\pi$	seen
Γ_{10}	$\rho\rho$	seen
Γ_{11}	$\pi^+\pi^-$	seen
Γ_{12}	$\pi\pi$	seen
Γ_{13}	$K\overline{K}^*(892)+$ c.c.	seen
Γ_{14}	$\eta\rho$	seen
Γ_{15}	$a_2(1320)\pi$	not seen
Γ_{16}	$K\overline{K}$	seen
Γ_{17}	e^+e^-	seen
Γ_{18}	$\pi^0\omega$	seen
Γ_{19}	$\pi^0\gamma$	not seen

$\rho(1700)$ $\Gamma(i)\Gamma(e^+e^-)/\Gamma(\text{total})$

This combination of a partial width with the partial width into e^+e^- and with the total width is obtained from the cross-section into channel$_i$ in e^+e^- annihilation.

$\Gamma(2(\pi^+\pi^-)) \times \Gamma(e^+e^-)/\Gamma_{\text{total}}$ — $\Gamma_2\Gamma_{17}/\Gamma$

VALUE (keV)	DOCUMENT ID		TECN	COMMENT
• • • We do not use the following data for averages, fits, limits, etc. • • •				
2.6 ± 0.2	DELCOURT	81B	DM1	$e^+e^- \to 2(\pi^+\pi^-)$
2.83 ± 0.42	BACCI	80	FRAG	$e^+e^- \to 2(\pi^+\pi^-)$

$\Gamma(\pi^+\pi^-) \times \Gamma(e^+e^-)/\Gamma_{\text{total}}$ — $\Gamma_{11}\Gamma_{17}/\Gamma$

VALUE (keV)	DOCUMENT ID		TECN	COMMENT
• • • We do not use the following data for averages, fits, limits, etc. • • •				
0.13	[1] DIEKMAN	88	RVUE	$e^+e^- \to \pi^+\pi^-$
$0.029^{+0.016}_{-0.012}$	KURDADZE	83	OLYA	0.64–1.4 $e^+e^- \to \pi^+\pi^-$

[1] Using total width = 220 MeV.

$\Gamma(K\overline{K}^*(892)+\text{c.c.}) \times \Gamma(e^+e^-)/\Gamma_{\text{total}}$ — $\Gamma_{13}\Gamma_{17}/\Gamma$

VALUE (keV)	DOCUMENT ID		TECN	COMMENT
• • • We do not use the following data for averages, fits, limits, etc. • • •				
0.305 ± 0.071	[1] BIZOT	80	DM1	e^+e^-

[1] Model dependent.

$\Gamma(\eta\rho) \times \Gamma(e^+e^-)/\Gamma_{\text{total}}$ — $\Gamma_{14}\Gamma_{17}/\Gamma$

VALUE (eV)	EVTS	DOCUMENT ID		TECN	COMMENT
• • • We do not use the following data for averages, fits, limits, etc. • • •					
$1.35 \pm 0.53 \pm 0.08$	13.4k	[1] GRIBANOV	20	CMD3	1.1–2.0 $e^+e^- \to \eta\pi^+\pi^-$
$84 \pm 26 \pm 4$		[2] LEES	18	BABR	$e^+e^- \to \eta\pi^+\pi^-$
7 ± 3		ANTONELLI	88	DM2	$e^+e^- \to \eta\pi^+\pi^-$

[1] Mass and width of the $\rho(770)$ fixed at 775 and 149 MeV, respectively; solution 2 of model 2, $\eta \to \gamma\gamma$ decays used.
[2] Includes non-resonant contribution. The selected fit model includes three ρ excited states. Model uncertainty is 80%.

$\Gamma(K\overline{K}) \times \Gamma(e^+e^-)/\Gamma_{\text{total}}$ — $\Gamma_{16}\Gamma_{17}/\Gamma$

VALUE (keV)	DOCUMENT ID		TECN	COMMENT
• • • We do not use the following data for averages, fits, limits, etc. • • •				
0.035 ± 0.029	[1] BIZOT	80	DM1	e^+e^-

[1] Model dependent.

$\Gamma(\rho\pi\pi) \times \Gamma(e^+e^-)/\Gamma_{\text{total}}$ — $\Gamma_3\Gamma_{17}/\Gamma$

VALUE (keV)	DOCUMENT ID		TECN	COMMENT
• • • We do not use the following data for averages, fits, limits, etc. • • •				
3.510 ± 0.090	[1] BIZOT	80	DM1	e^+e^-

[1] Model dependent.

$\rho(1700)$ $\Gamma(i)/\Gamma(\text{total}) \times \Gamma(e^+e^-)/\Gamma(\text{total})$

$\Gamma(\pi^0\omega)/\Gamma_{\text{total}} \times \Gamma(e^+e^-)/\Gamma_{\text{total}}$ — $\Gamma_{18}/\Gamma \times \Gamma_{17}/\Gamma$

VALUE (units 10^{-6})	EVTS	DOCUMENT ID		TECN	COMMENT
• • • We do not use the following data for averages, fits, limits, etc. • • •					
0.09 ± 0.05	10.2k	[1] ACHASOV	16D	SND	1.05–2.00 $e^+e^- \to \pi^0\pi^0\gamma$
1.7 ± 0.4	7815	[2] ACHASOV	13	SND	1.05–2.00 $e^+e^- \to \pi^0\pi^0\gamma$

[1] From a phenomenological model based on vector meson dominance with interfering $\rho(700)$, $\rho(1450)$, and $\rho(1700)$. The $\rho(1700)$ mass and width are fixed at 1720 MeV and 250 MeV, respectively. Systematic uncertainty not estimated. Supersedes ACHASOV 13.
[2] From a phenomenological model based on vector meson dominance with the interfering $\rho(1450)$ and $\rho(1700)$ and their widths fixed at 400 and 250 MeV, respectively. Systematic uncertainty not estimated.

$\Gamma(\eta\rho)/\Gamma_{\text{total}} \times \Gamma(e^+e^-)/\Gamma_{\text{total}}$ — $\Gamma_{14}/\Gamma \times \Gamma_{17}/\Gamma$

VALUE (units 10^{-8})	EVTS	DOCUMENT ID		TECN	COMMENT
• • • We do not use the following data for averages, fits, limits, etc. • • •					
$8.3^{+3.8}_{-3.1}$	7.4k	[1] ACHASOV	18	SND	1.22–2.00 $e^+e^- \to \eta\pi^+\pi^-$

[1] From the combined fit of AULCHENKO 15 and ACHASOV 18 in the model with the interfering $\rho(1450)$, $\rho(1700)$ and $\rho(2150)$ with the parameters of the $\rho(1450)$ and $\rho(1700)$ floating and the mass and width of the $\rho(2150)$ fixed at 2155 MeV and 320 MeV, respectively. The phases of the resonances are π, 0 and π, respectively.

Downloaded from https://academic.oup.com/ptep/article/2022/8/083C01/6651666 by KIT Library user on 27 September 2022

$\rho(1700)$ BRANCHING RATIOS

$\Gamma(\rho\pi\pi)/\Gamma(4\pi)$ — Γ_3/Γ_1

VALUE	DOCUMENT ID		TECN	COMMENT
• • • We do not use the following data for averages, fits, limits, etc. • • •				
0.28±0.06	[1] ABELE	01B	CBAR	$0.0\ \overline{p}n \to 5\pi$

[1] $\omega\pi$ not included.

$\Gamma(\rho^0\pi^+\pi^-)/\Gamma(2(\pi^+\pi^-))$ — Γ_4/Γ_2

VALUE	EVTS	DOCUMENT ID		TECN	COMMENT
• • • We do not use the following data for averages, fits, limits, etc. • • •					
∼ 1.0		DELCOURT	81B	DM1	$e^+e^- \to 2(\pi^+\pi^-)$
0.7 ±0.1	500	SCHACHT	74	STRC	$5.5–18\ \gamma p \to p4\pi$
0.80		[1] BINGHAM	72B	HBC	$9.3\ \gamma p \to p4\pi$

[1] The $\pi\pi$ system is in S-wave.

$\Gamma(\rho^0\pi^0\pi^0)/\Gamma(\rho^\pm\pi^\mp\pi^0)$ — Γ_5/Γ_6

VALUE	DOCUMENT ID		TECN	CHG	COMMENT
• • • We do not use the following data for averages, fits, limits, etc. • • •					
<0.10	ATKINSON	85B	OMEG		$20–70\ \gamma p$
<0.15	ATKINSON	82	OMEG	0	$20–70\ \gamma p \to p4\pi$

$\Gamma(a_1(1260)\pi)/\Gamma(4\pi)$ — Γ_7/Γ_1

VALUE	DOCUMENT ID		TECN	COMMENT
• • • We do not use the following data for averages, fits, limits, etc. • • •				
0.16±0.05	[1] ABELE	01B	CBAR	$0.0\ \overline{p}n \to 5\pi$

[1] $\omega\pi$ not included.

$\Gamma(h_1(1170)\pi)/\Gamma(4\pi)$ — Γ_8/Γ_1

VALUE	DOCUMENT ID		TECN	COMMENT
• • • We do not use the following data for averages, fits, limits, etc. • • •				
0.17±0.06	[1] ABELE	01B	CBAR	$0.0\ \overline{p}n \to 5\pi$

[1] $\omega\pi$ not included.

$\Gamma(\pi(1300)\pi)/\Gamma(4\pi)$ — Γ_9/Γ_1

VALUE	DOCUMENT ID		TECN	COMMENT
• • • We do not use the following data for averages, fits, limits, etc. • • •				
0.30±0.10	[1] ABELE	01B	CBAR	$0.0\ \overline{p}n \to 5\pi$

[1] $\omega\pi$ not included.

$\Gamma(\rho\rho)/\Gamma(4\pi)$ — Γ_{10}/Γ_1

VALUE	DOCUMENT ID		TECN	COMMENT
• • • We do not use the following data for averages, fits, limits, etc. • • •				
0.09±0.03	[1] ABELE	01B	CBAR	$0.0\ \overline{p}n \to 5\pi$

[1] $\omega\pi$ not included.

$\Gamma(\pi^+\pi^-)/\Gamma_{total}$ — Γ_{11}/Γ

VALUE	DOCUMENT ID		TECN	COMMENT
• • • We do not use the following data for averages, fits, limits, etc. • • •				
$0.108\pm0.017^{+0.162}_{-0.004}$	[1] ALBRECHT	20	RVUE	$0.9\ \overline{p}p \to K^+K^-\pi^0$
$0.287^{+0.043}_{-0.042}$	BECKER	79	ASPK	$17\ \pi^-p$ polarized
0.15 to 0.30	[2] MARTIN	78C	RVUE	$17\ \pi^-p \to \pi^+\pi^-n$
<0.20	[3] COSTA...	77B	RVUE	$e^+e^- \to 2\pi, 4\pi$
0.30 ±0.05	[2] FROGGATT	77	RVUE	$17\ \pi^-p \to \pi^+\pi^-n$
<0.15	[4] EISENBERG	73	HBC	$5\ \pi^+p \to \Delta^{++}2\pi$
0.25 ±0.05	[5] HYAMS	73	ASPK	$17\ \pi^-p \to \pi^+\pi^-n$

[1] Residue from T-matrix pole, 2 poles, 3 channels, Chew-Mandelstam functions and simplified analytic continuation for the 4π channel. Includes scattering data from HYAMS 75 and model-independent calculation of GARCIA-MARTIN 11A.
[2] From phase shift analysis of HYAMS 73 data.
[3] Estimate using unitarity, time reversal invariance, Breit-Wigner.
[4] Estimated using one-pion-exchange model.
[5] Included in BECKER 79 analysis.

$\Gamma(K\overline{K})/\Gamma_{total}$ — Γ_{16}/Γ

VALUE	DOCUMENT ID		TECN	COMMENT
• • • We do not use the following data for averages, fits, limits, etc. • • •				
$0.007\pm0.006^{+0.041}_{-0.002}$	[1] ALBRECHT	20	RVUE	$0.9\ \overline{p}p \to K^+K^-\pi^0$

[1] Residue from T-matrix pole, 2 poles, 3 channels, Chew-Mandelstam functions and simplified analytic continuation for the 4π channel. Includes scattering data from HYAMS 75 and model-independent calculation of GARCIA-MARTIN 11A.

$\Gamma(\pi^+\pi^-)/\Gamma(2(\pi^+\pi^-))$ — Γ_{11}/Γ_2

VALUE	DOCUMENT ID		TECN	COMMENT
• • • We do not use the following data for averages, fits, limits, etc. • • •				
0.13±0.05	ASTON	80	OMEG	$20–70\ \gamma p \to p2\pi$
<0.14	[1] DAVIER	73	STRC	$6–18\ \gamma p \to p4\pi$
<0.2	[2] BINGHAM	72B	HBC	$9.3\ \gamma p \to p2\pi$

[1] Upper limit is estimate.
[2] 2σ upper limit.

$\Gamma(\pi\pi)/\Gamma(4\pi)$ — Γ_{12}/Γ_1

VALUE	DOCUMENT ID		TECN	COMMENT
• • • We do not use the following data for averages, fits, limits, etc. • • •				
0.16±0.04	[1,2] ABELE	01B	CBAR	$0.0\ \overline{p}n \to 5\pi$

[1] Using ABELE 97.
[2] $\omega\pi$ not included.

$\Gamma(K\overline{K}^*(892)+\text{c.c.})/\Gamma_{total}$ — Γ_{13}/Γ

VALUE	DOCUMENT ID		TECN	COMMENT
• • • We do not use the following data for averages, fits, limits, etc. • • •				
possibly seen	COAN	04	CLEO	$\tau^- \to K^-\pi^-K^+\nu_\tau$

$\Gamma(K\overline{K}^*(892)+\text{c.c.})/\Gamma(2(\pi^+\pi^-))$ — Γ_{13}/Γ_2

VALUE	DOCUMENT ID		TECN	COMMENT
• • • We do not use the following data for averages, fits, limits, etc. • • •				
0.15±0.03	[1] DELCOURT	81B	DM1	$e^+e^- \to \overline{K}K\pi$

[1] Assuming $\rho(1700)$ and ω radial excitations to be degenerate in mass.

$\Gamma(\eta\rho)/\Gamma_{total}$ — Γ_{14}/Γ

VALUE	CL%	DOCUMENT ID		TECN	COMMENT
• • • We do not use the following data for averages, fits, limits, etc. • • •					
possibly seen		AKHMETSHIN	00D	CMD2	$e^+e^- \to \eta\pi^+\pi^-$
<0.04		DONNACHIE	87B	RVUE	
<0.02	58	ATKINSON	86B	OMEG	$20–70\ \gamma p$

$\Gamma(\eta\rho)/\Gamma(2(\pi^+\pi^-))$ — Γ_{14}/Γ_2

VALUE	DOCUMENT ID		TECN	COMMENT
• • • We do not use the following data for averages, fits, limits, etc. • • •				
0.123±0.027	DELCOURT	82	DM1	$e^+e^- \to \pi^+\pi^-$ MM
∼ 0.1	ASTON	80	OMEG	$20–70\ \gamma p$

$\Gamma(\pi^+\pi^-\text{neutrals})/\Gamma(2(\pi^+\pi^-))$ — $(\Gamma_5+\Gamma_6+0.714\Gamma_{14})/\Gamma_2$

VALUE	DOCUMENT ID		TECN	COMMENT
• • • We do not use the following data for averages, fits, limits, etc. • • •				
2.6±0.4	[1] BALLAM	74	HBC	$9.3\ \gamma p$

[1] Upper limit. Background not subtracted.

$\Gamma(a_2(1320)\pi)/\Gamma_{total}$ — Γ_{15}/Γ

VALUE	DOCUMENT ID		TECN	COMMENT
• • • We do not use the following data for averages, fits, limits, etc. • • •				
not seen	AMELIN	00	VES	$37\ \pi^-p \to \eta\pi^+\pi^-n$

$\Gamma(K\overline{K})/\Gamma(2(\pi^+\pi^-))$ — Γ_{16}/Γ_2

VALUE	CL%	DOCUMENT ID		TECN	CHG	COMMENT
• • • We do not use the following data for averages, fits, limits, etc. • • •						
0.015±0.010		[1] DELCOURT	81B	DM1		$e^+e^- \to \overline{K}K$
<0.04	95	BINGHAM	72B	HBC	0	$9.3\ \gamma p$

[1] Assuming $\rho(1700)$ and ω radial excitations to be degenerate in mass.

$\Gamma(K\overline{K})/\Gamma(K\overline{K}^*(892)+\text{c.c.})$ — Γ_{16}/Γ_{13}

VALUE	DOCUMENT ID		TECN	COMMENT
• • • We do not use the following data for averages, fits, limits, etc. • • •				
0.052±0.026	BUON	82	DM1	$e^+e^- \to$ hadrons

$\Gamma(\pi^0\omega)/\Gamma_{total}$ — Γ_{18}/Γ

VALUE	EVTS	DOCUMENT ID		TECN	COMMENT
• • • We do not use the following data for averages, fits, limits, etc. • • •					
not seen		MATVIENKO	15	BELL	$\overline{B}^0 \to D^{*+}\omega\pi^-$
seen	1.6k	ACHASOV	12	SND	$e^+e^- \to \pi^0\pi^0\gamma$
not seen	2382	AKHMETSHIN	03B	CMD2	$e^+e \to \pi^0\pi^0\gamma$
seen		ACHASOV	97	RVUE	$e^+e^- \to \omega\pi^0$

$\Gamma(\pi^0\gamma)/\Gamma_{total}$ — Γ_{19}/Γ

VALUE	DOCUMENT ID		TECN	COMMENT
not seen	[1] ACHASOV	10D	SND	$1.075–2.0\ e^+e^- \to \pi^0\gamma$

[1] From a fit of a VMD model with two effective resonances with masses of 1450 MeV and 1700 MeV to describe the excited vector states $\omega(1420)$, $\rho(1450)$, $\omega(1650)$, and $\rho(1700)$. The width of the highest mass effective resonance is fixed at 315 MeV.

$\rho(1700)$ REFERENCES

ALBRECHT	20	EPJ C80 453	M. Albrecht *et al.*	(Crystal Barrel Collab.)
GRIBANOV	20	JHEP 2001 112	S.S. Gribanov *et al.*	(CMD-3 Collab.)
ACHASOV	18	PR D97 012008	M.N. Achasov *et al.*	(SND Collab.)
LEES	18	PR D97 052007	J.P. Lees *et al.*	(BABAR Collab.)
BARTOS	17	PR D96 113004	E. Bartos *et al.*	
BARTOS	17A	IJMP A32 1750154	E. Bartos *et al.*	
LEES	17C	PR D95 072007	J.P. Lees *et al.*	(BABAR Collab.)
AAIJ	16N	PR D93 052018	R. Aaij *et al.*	(LHCb Collab.)
ABLIKIM	16C	PL B753 629	M. Ablikim *et al.*	(BESIII Collab.)
ACHASOV	16D	PR D94 112001	M.N. Achasov *et al.*	(SND Collab.)
AULCHENKO	15	PR D91 052013	V.M. Aulchenko *et al.*	(SND Collab.)
MATVIENKO	15	PR D92 012013	D. Matvienko *et al.*	(BELLE Collab.)
ACHASOV	13	PR D88 054013	M.N. Achasov *et al.*	(SND Collab.)
ABRAMOWICZ	12	EPJ C72 1869	H. Abramowicz *et al.*	(ZEUS Collab.)
ACHASOV	12	JETPL 94 734	M.N. Achasov *et al.*	
		Translated from ZETFP 94 796.		

Downloaded from https://academic.oup.com/ptep/article/2022/8/083C01/6651666 by KIT Library user on 27 September 2022

LEES	12G	PR D86 032013	J.P. Lees *et al.*	(BABAR Collab.)
AMBROSINO	11A	PL B700 102	F. Ambrosino *et al.*	(KLOE Collab.)
GARCIA-MAR...	11A	PR D83 074004	R. Garcia-Martin *et al.*	(MADR, CRAC)
ACHASOV	10D	PR D98 112001	M.N. Achasov *et al.*	(SND Collab.)
DUBNICKA	10	APS 60 1	S. Dubnicka, A.Z. Dubnickova	
AUBERT	09AS	PRL 103 231801	B. Aubert *et al.*	(BABAR Collab.)
FUJIKAWA	08	PR D78 072006	M. Fujikawa *et al.*	(BELLE Collab.)
AKHMETSHIN	07	PL B648 28	R.R. Akhmetshin *et al.*	(Novosibirsk CMD-2 Collab.)
ACHASOV	06	JETP 103 380	M.N. Achasov *et al.*	(Novosibirsk SND Collab.)
		Translated from ZETF 130 437.		
COAN	04	PRL 92 232001	T.E. Coan *et al.*	(CLEO Collab.)
FRABETTI	04	PL B578 290	P.L. Frabetti *et al.*	(FNAL E687 Collab.)
AKHMETSHIN	03B	PL B562 173	R.R. Akhmetshin *et al.*	(Novosibirsk CMD-2 Collab.)
ABELE	01B	EPJ C21 261	A. Abele *et al.*	(Crystal Barrel Collab.)
ACHASOV	00I	PL B486 29	M.N. Achasov *et al.*	(Novosibirsk SND Collab.)
AKHMETSHIN	00D	PL B489 125	R.R. Akhmetshin *et al.*	(Novosibirsk CMD-2 Collab.)
AMELIN	00	NP A668 83	D. Amelin *et al.*	(VES Collab.)
EDWARDS	00A	PR D61 072003	K.W. Edwards *et al.*	(CLEO Collab.)
ABELE	99D	PL B468 178	A. Abele *et al.*	(Crystal Barrel Collab.)
ABELE	97	PL B391 191	A. Abele *et al.*	(Crystal Barrel Collab.)
ACHASOV	97	PR D55 2663	N.N. Achasov *et al.*	(NOVM)
BERTIN	97C	PL B408 476	A. Bertin *et al.*	(OBELIX Collab.)
CLEGG	94	ZPHY C62 455	A.B. Clegg, A. Donnachie	(LANC, MCHS)
CLEGG	90	ZPHY C45 677	A.B. Clegg, A. Donnachie	(LANC, MCHS)
KUHN	90	ZPHY C48 445	J.H. Kuhn *et al.*	(MPIM)
BISELLO	89	PL B220 321	D. Bisello *et al.*	(DM2 Collab.)
DUBNICKA	89	JP G15 1349	S. Dubnicka *et al.*	(JINR, SLOV)
GESHKEN...	89	ZPHY C45 351	B.V. Geshkenbein	(ITEP)
ANTONELLI	88	PL B212 133	A. Antonelli *et al.*	(DM2 Collab.)
DIEKMAN	88	PRPL 159 99	B. Diekmann	(BONN)
FUKUI	88	PL B202 441	S. Fukui *et al.*	(SUGI, NAGO, KEK, KYOT+)
DONNACHIE	87B	ZPHY C34 257	A. Donnachie, A.B. Clegg	(MCHS, LANC)
ATKINSON	86B	ZPHY C30 531	M. Atkinson *et al.*	(BONN, CERN, GLAS+)
ATKINSON	85B	ZPHY C26 499	M. Atkinson *et al.*	(BONN, CERN, GLAS+)
ERKAL	85	ZPHY C29 485	C. Erkal, M.G. Olsson	(WISC)
ABE	84B	PRL 53 751	K. Abe *et al.*	(SLAC HFP Collab.)
KURDADZE	83	JETPL 37 733	L.M. Kurdadze *et al.*	(NOVO)
		Translated from ZETFP 37 613.		
ATKINSON	82	PL 108B 55	M. Atkinson *et al.*	(BONN, CERN, GLAS+)
BUON	82	PL 118B 221	J. Buon *et al.*	(LALO, MONP)
CLELAND	82B	NP B208 228	W.E. Cleland *et al.*	(DURH, GEVA, LAUS+)
CORDIER	82	PL 109B 129	A. Cordier *et al.*	(LALO)
DELCOURT	82	PL 113B 93	B. Delcourt *et al.*	(LALO)
ASTON	81E	NP B189 15	D. Aston	(BONN, CERN, EPOL, GLAS, LANC+)
DELCOURT	81B	Bonn Conf. 205	B. Delcourt	(ORSAY)
Also		PL 109B 129	A. Cordier *et al.*	(LALO)
DIBIANCA	81	PR D23 595	F.A. di Bianca *et al.*	(CASE, CMU)
ASTON	80	PL 92B 215	D. Aston	(BONN, CERN, EPOL, GLAS, LANC+)
BACCI	80	PL 95B 139	C. Bacci *et al.*	(ROMA, FRAS)
BIZOT	80	Madison Conf. 546	J.C. Bizot *et al.*	(LALO, MONP)
KILLIAN	80	PR D21 3005	T.J. Killian *et al.*	(CORN)
ATIYA	79B	PRL 43 1691	M.S. Atiya *et al.*	(COLU, ILL, FNAL)
BECKER	79	NP B151 46	H. Becker *et al.*	(MPIM, CERN, ZEEM, CRAC)
LANG	79	PR D19 956	C.B. Lang, A. Mas-Parareda	(GRAZ)
MARTIN	78C	ANP 114 1	A.D. Martin, M.R. Pennington	(CERN)
COSTA...	77B	PL 71B 345	B. Costa de Beauregard, B. Pire, T.N. Truong	(EPOL)
FROGGATT	77	NP B129 89	C.D. Froggatt, J.L. Petersen	(GLAS, NORD)
ALEXANDER	75	PL 57B 487	G. Alexander *et al.*	(TELA)
HYAMS	75	NP B100 205	B.D. Hyams *et al.*	(CERN, MPIM)
BALLAM	74	NP B76 375	J. Ballam *et al.*	(SLAC, LBL, MPIM)
CONVERSI	74	PL 52B 493	M. Conversi *et al.*	(ROMA, FRAS)
SCHACHT	74	NP B81 205	P. Schacht *et al.*	(MPIM)
DAVIER	73	NP B58 31	M. Davier *et al.*	(SLAC)
EISENBERG	73	PL 43B 149	Y. Eisenberg *et al.*	(REHO)
HYAMS	73	NP B64 134	B.D. Hyams *et al.*	(CERN, MPIM)
BINGHAM	72B	PL 41B 635	H.H. Bingham *et al.*	(LBL, UCB, SLAC) IGJP
JACOB	72	PR D5 1847	M. Jacob, R. Slansky	
GOUNARIS	68	PRL 21 244	G.J. Gounaris, J.J. Sakurai	

$a_2(1700)$

$I^G(J^{PC}) = 1^-(2^{++})$

$a_2(1700)$ MASS

VALUE (MeV)	EVTS	DOCUMENT ID		TECN	COMMENT
1698 ±44		[1] AMSLER	02	CBAR	$0.9\,\overline{p}p \to \pi^0\eta\eta$
• • • We do not use the following data for averages, fits, limits, etc. • • •					
1686 ±22 $^{+19}_{-7}$		[2] KOPF	21	RVUE	$0.9\,p\overline{p} \to \pi^0\pi^0\eta$, $\pi^0\eta\eta$, $\pi^0K^+K^-$ and 191 $\pi^-p \to \pi^-\pi^-\pi^+p$
1638.9± 2.3$^{+57.4}_{-0.1}$		[3] ALBRECHT	20	RVUE	$0.9\,\overline{p}p \to \pi^0\pi^0\eta$, $\pi^0\eta\eta$, $\pi^0K^+K^-$
1722 ±15 ±67		[4] RODAS	19	JPAC	191 $\pi^-p \to \eta^{(\prime)}\pi^-p$
1681 $^{+22}_{-35}$	46M	[5,6] AGHASYAN	18B	COMP	190 $\pi^-p \to \pi^-\pi^+\pi^-p$
1720 ±10 ±60		[7] JACKURA	18	JPAC	$\pi^-p \to \eta\pi^-p$
1726 ±12 ±25		[6] ABLIKIM	17K	BES3	$\psi(2S) \to \gamma\eta\pi^+\pi^-$
1675 ±25		ANISOVICH	09	RVUE	$0.0\,\overline{p}p$, πN
1722 ± 9 ±15	18k	[8] SCHEGELSKY	06	RVUE	$\gamma\gamma \to \pi^+\pi^-\pi^0$
1702 ± 7	80k	[9] UMAN	06	E835	$5.2\,\overline{p}p \to \eta\eta\pi^0$
1721 ±13 ±44	145k	LU	05	B852	$18\,\pi^-p \to \omega\pi^-\pi^0p$
1737 ± 5 ± 7		ABE	04	BELL	$10.6\,e^+e^- \to e^+e^-K^+K^-$
1767 ±14	221	[10] ACCIARRI	01H	L3	$\gamma\gamma \to K^0_SK^0_S$, E^{ee}_{cm}= 91, 183–209 GeV
1660 ±40		[6] ABELE	99B	CBAR	$1.94\,\overline{p}p \to \pi^0\eta\eta$
~ 1775		[11] GRYGOREV	99	SPEC	$40\,\pi^-p \to K^0_SK^0_Sn$
1752 ±21 ± 4		ACCIARRI	97T	L3	$\gamma\gamma \to \pi^+\pi^-\pi^0$

[1] T-matrix pole.
[2] From T-matrix pole based on combined fit of Crystal Barrel and $\pi\pi$ scattering data (ALBRECHT 20), and COMPASS data (ADOLPH 15), using a coupled-channel model of $\eta\pi$, $\eta'\pi$ and $K\overline{K}$ systems.
[3] T-matrix pole, 2 poles, 2 channels ($\pi\eta$, $K\overline{K}$).
[4] The coupled-channel analysis of both the $\eta\pi$ and $\eta'\pi$ systems using ADOLPH 15 data. The mass is extracted from the T-matrix pole.
[5] Statistical error negligible.
[6] Breit-Wigner mass.
[7] Superseded by RODAS 19.
[8] From analysis of L3 data at 183–209 GeV.
[9] Statistical error only.
[10] Spin 2 dominant, isospin not determined, could also be I=1.
[11] Possibly two $J^P = 2^+$ resonances with isospins 0 and 1.

$a_2(1700)$ WIDTH

VALUE (MeV)	EVTS	DOCUMENT ID		TECN	COMMENT
265 ± 55		[1] AMSLER	02	CBAR	$0.9\,\overline{p}p \to \pi^0\eta\eta$
• • • We do not use the following data for averages, fits, limits, etc. • • •					
421 ± 75 $^{+64}_{-57}$		[2] KOPF	21	RVUE	$0.9\,p\overline{p} \to \pi^0\pi^0\eta$, $\pi^0\eta\eta$, $\pi^0K^+K^-$ and 191 $\pi^-p \to \pi^-\pi^-\pi^+p$
224.0± 2.5$^{+1.8}_{-48.3}$		[3] ALBRECHT	20	RVUE	$0.9\,\overline{p}p \to \pi^0\pi^0\eta$, $\pi^0\eta\eta$, $\pi^0K^+K^-$
247 ± 17 ±63		[4] RODAS	19	JPAC	191 $\pi^-p \to \eta^{(\prime)}\pi^-p$
436 $^{+20}_{-16}$	46M	[5,6] AGHASYAN	18B	COMP	190 $\pi^-p \to \pi^-\pi^+\pi^-p$
280 ± 10 ±70		[7] JACKURA	18	JPAC	$\pi^-p \to \eta\pi^-p$
190 ± 18 ±30		[6] ABLIKIM	17K	BES3	$\psi(2S) \to \gamma\eta\pi^+\pi^-$
270 $^{+50}_{-20}$		ANISOVICH	09	RVUE	$0.0\,\overline{p}p$, πN
336 ± 20 ±20	18k	[8] SCHEGELSKY	06	RVUE	$\gamma\gamma \to \pi^+\pi^-\pi^0$
417 ± 19	80k	[9] UMAN	06	E835	$5.2\,\overline{p}p \to \eta\eta\pi^0$
279 ± 49 ±66	145k	LU	05	B852	$18\,\pi^-p \to \omega\pi^-\pi^0p$
151 ± 22 ±24		ABE	04	BELL	$10.6\,e^+e^- \to e^+e^-K^+K^-$
187 ± 60	221	[10] ACCIARRI	01H	L3	$\gamma\gamma \to K^0_SK^0_S$, E^{ee}_{cm}= 91, 183–209 GeV
280 ± 70		[6] ABELE	99B	CBAR	$1.94\,\overline{p}p \to \pi^0\eta\eta$
150 ±110 ±34		ACCIARRI	97T	L3	$\gamma\gamma \to \pi^+\pi^-\pi^0$

[1] T-matrix pole.
[2] From T-matrix pole based on combined fit of Crystal Barrel and $\pi\pi$ scattering data (ALBRECHT 20), and COMPASS data (ADOLPH 15), using a coupled-channel model of $\eta\pi$, $\eta'\pi$ and $K\overline{K}$ systems.
[3] T-matrix pole, 2 poles, 2 channels ($\pi\eta$, $K\overline{K}$).
[4] The coupled-channel analysis of both the $\eta\pi$ and $\eta'\pi$ systems using ADOLPH 15 data. The width is extracted from the T-matrix pole.
[5] Statistical error negligible.
[6] Breit-Wigner width.
[7] Superseded by RODAS 19.
[8] From analysis of L3 data at 183–209 GeV.
[9] Statistical error only.
[10] Spin 2 dominant, isospin not determined, could also be I=1.

$a_2(1700)$ DECAY MODES

	Mode	Fraction (Γ_i/Γ)
Γ_1	$\eta\pi$	(3.6 ±1.1) %
Γ_2	$\eta'\pi$	
Γ_3	$\gamma\gamma$	$(1.13\pm0.30)\times10^{-6}$
Γ_4	$\rho\pi$	seen
Γ_5	$f_2(1270)\pi$	seen
Γ_6	$K\overline{K}$	(1.9 ±1.2) %
Γ_7	$\omega\pi^-\pi^0$	seen
Γ_8	$\omega\rho$	seen

$a_2(1700)$ PARTIAL WIDTHS

$\Gamma(\eta\pi)$ — Γ_1

VALUE (MeV)	EVTS	DOCUMENT ID		TECN	COMMENT
9.5±2.0	870	[1] SCHEGELSKY	06A	RVUE	$\gamma\gamma \to K^0_SK^0_S$

[1] From analysis of L3 data at 91 and 183–209 GeV, using $a_2(1700)$ mass of 1730 MeV and width of 340 MeV, and SU(3) relations.

$\Gamma(\gamma\gamma)$ — Γ_3

VALUE (keV)	EVTS	DOCUMENT ID		TECN	COMMENT
0.30±0.05	870	[1] SCHEGELSKY	06A	RVUE	$\gamma\gamma \to K^0_SK^0_S$

[1] From analysis of L3 data at 91 and 183–209 GeV, using $a_2(1700)$ mass of 1730 MeV and width of 340 MeV, and SU(3) relations.

$\Gamma(K\overline{K})$ — Γ_6

VALUE (MeV)	EVTS	DOCUMENT ID		TECN	COMMENT
5.0±3.0	870	[1] SCHEGELSKY	06A	RVUE	$\gamma\gamma \to K^0_SK^0_S$

[1] From analysis of L3 data at 91 and 183–209 GeV, using $a_2(1700)$ mass of 1730 MeV and width of 340 MeV, and SU(3) relations.

Downloaded from https://academic.oup.com/ptep/article/2022/8/083C01/6651666 by KIT Library user on 27 September 2022

$a_2(1700)$ $\Gamma(i)\Gamma(\gamma\gamma)/\Gamma(\text{total})$

$[\Gamma(\rho\pi)+\Gamma(f_2(1270)\pi)] \times \Gamma(\gamma\gamma)/\Gamma_{\text{total}}$ — $(\Gamma_4+\Gamma_5)\Gamma_3/\Gamma$

VALUE (keV)	EVTS	DOCUMENT ID		TECN	COMMENT
0.29±0.04±0.02		ACCIARRI	97T	L3	$\gamma\gamma \to \pi^+\pi^-\pi^0$
• • • We do not use the following data for averages, fits, limits, etc. • • •					
$0.37^{+0.12}_{-0.08}\pm0.10$	18k	[1] SCHEGELSKY	06	RVUE	$\gamma\gamma \to \pi^+\pi^-\pi^0$

[1] From analysis of L3 data at 183–209 GeV.

$\Gamma(K\overline{K}) \times \Gamma(\gamma\gamma)/\Gamma_{\text{total}}$ — $\Gamma_6\Gamma_3/\Gamma$

VALUE (eV)	DOCUMENT ID		TECN	COMMENT
• • • We do not use the following data for averages, fits, limits, etc. • • •				
20.6± 4.2± 4.6	[1] ABE	04	BELL	$10.6\ e^+e^- \to e^+e^-K^+K^-$
49 ±11 ±13	[2] ACCIARRI	01H	L3	$\gamma\gamma \to K^0_S K^0_S$, $E^{ee}_{\text{cm}} = 91$, 183–209 GeV

[1] Assuming spin 2.
[2] Spin 2 dominant, isospin not determined, could also be I=1.

$a_2(1700)$ BRANCHING RATIOS

$\Gamma(\rho\pi)/\Gamma(f_2(1270)\pi)$ — Γ_4/Γ_5

VALUE	EVTS	DOCUMENT ID		TECN	COMMENT
• • • We do not use the following data for averages, fits, limits, etc. • • •					
3.4±0.4±0.1	18k	[1] SCHEGELSKY	06	RVUE	$\gamma\gamma \to \pi^+\pi^-\pi^0$

[1] From analysis of L3 data at 183–209 GeV.

$\Gamma(K\overline{K})/\Gamma(\eta\pi)$ — Γ_6/Γ_1

VALUE	DOCUMENT ID		TECN	COMMENT
• • • We do not use the following data for averages, fits, limits, etc. • • •				
$0.029\pm0.04\ ^{+0.011}_{-0.012}$	[1] KOPF	21	RVUE	$0.9\ p\overline{p} \to \pi^0\pi^0\eta$, $\pi^0\eta\eta$, $\pi^0K^+K^-$ and $191\ \pi^-p \to \pi^-\pi^-\pi^+p$
$4.134\pm0.106^{+4.909}_{-2.988}$	[2] ALBRECHT	20	RVUE	$0.9\ \overline{p}p \to \pi^0\pi^0\eta$, $\pi^0\eta\eta$, $\pi^0K^+K^-$

[1] From T-matrix pole based on combined fit of Crystal Barrel and $\pi\pi$ scattering data (ALBRECHT 20), and COMPASS data (ADOLPH 15), using a coupled-channel model of $\eta\pi$, $\eta'\pi$ and $K\overline{K}$ systems.
[2] Residues from T-matrix pole, 2 poles, 2 channels ($\pi\eta$, $K\overline{K}$).

$\Gamma(\eta'\pi)/\Gamma(\eta\pi)$ — Γ_2/Γ_1

VALUE	DOCUMENT ID		TECN	COMMENT
• • • We do not use the following data for averages, fits, limits, etc. • • •				
$0.035\pm0.044^{+0.069}_{-0.012}$	[1] KOPF	21	RVUE	$0.9\ p\overline{p} \to \pi^0\pi^0\eta$, $\pi^0\eta\eta$, $\pi^0K^+K^-$ and $191\ \pi^-p \to \pi^-\pi^-\pi^+p$

[1] From T-matrix pole based on combined fit of Crystal Barrel and $\pi\pi$ scattering data (ALBRECHT 20), and COMPASS data (ADOLPH 15), using a coupled-channel model of $\eta\pi$, $\eta'\pi$ and $K\overline{K}$ systems.

$a_2(1700)$ REFERENCES

KOPF	21	EPJ C81 1056	B. Kopf *et al.*	(BOCH)
ALBRECHT	20	EPJ C80 453	M. Albrecht *et al.*	(Crystal Barrel Collab.)
RODAS	19	PRL 122 042002	A. Rodas *et al.*	(JPAC Collab.)
AGHASYAN	18B	PR D98 092003	M. Aghasyan *et al.*	(COMPASS Collab.)
JACKURA	18	PL B779 464	A. Jackura *et al.*	(JPAC and COMPASS Collab.)
ABLIKIM	17K	PR D95 032002	M. Ablikim *et al.*	(BESIII Collab.)
ADOLPH	15	PL B740 303	M. Adolph *et al.*	(COMPASS Collab.)
ANISOVICH	09	IJMP A24 2481	V.V. Anisovich, A.V. Sarantsev	
SCHEGELSKY	06	EPJ A27 199	V.A. Schegelsky *et al.*	
SCHEGELSKY	06A	EPJ A27 207	V.A. Schegelsky *et al.*	
UMAN	06	PR D73 052009	I. Uman *et al.*	(FNAL E835)
LU	05	PRL 94 032002	M. Lu *et al.*	(BNL E852 Collab.)
ABE	04	EPJ C32 323	K. Abe *et al.*	(BELLE Collab.)
AMSLER	02	EPJ C23 29	C. Amsler *et al.*	
ACCIARRI	01H	PL B501 173	M. Acciarri *et al.*	(L3 Collab.)
ABELE	99B	EPJ C8 67	A. Abele *et al.*	(Crystal Barrel Collab.)
GRYGOREV	99	PAN 62 470 Translated from YAF 62 513.	V.K. Grygorev *et al.*	
ACCIARRI	97T	PL B413 147	M. Acciarri *et al.*	(L3 Collab.)

$f_0(1710)$

$I^G(J^{PC}) = 0^+(0^{++})$

See the review on "Spectroscopy of Light Meson Resonances."

$f_0(1710)$ MASS

OUR EVALUATION below is based on T-matrix poles from BARBERIS 00E and BARBERIS 99D.

VALUE (MeV)	EVTS	DOCUMENT ID		TECN	COMMENT
1704±12 OUR EVALUATION					
1733^{+8}_{-7} OUR AVERAGE Error includes scale factor of 1.5. See the ideogram below.					
1757±24 ± 9		[1] LEES	21A	BABR	$\eta_c(1S) \to \eta' K^+K^-$
1759± 6 $^{+14}_{-25}$	5.5k	[2] ABLIKIM	13N	BES3	$e^+e^- \to J/\psi \to \gamma\eta\eta$
$1750^{+6}_{-7}\ ^{+29}_{-18}$		[3] UEHARA	13	BELL	$\gamma\gamma \to K^0_S K^0_S$
1701± 5 $^{+9}_{-2}$	4k	[4] CHEKANOV	08	ZEUS	$ep \to K^0_S K^0_S X$
1765^{+4}_{-3} ±13		[1] ABLIKIM	06V	BES2	$e^+e^- \to J/\psi \to \gamma\pi^+\pi^-$
1738±30		ABLIKIM	04E	BES2	$J/\psi \to \omega K^+K^-$
1740± 4 $^{+10}_{-25}$		BAI	03G	BES	$J/\psi \to \gamma K\overline{K}$
1740^{+30}_{-25}		BAI	00A	BES	$J/\psi \to \gamma(\pi^+\pi^-\pi^+\pi^-)$
1710±25		[5] FRENCH	99		$300\ pp \to p_f(K^+K^-)p_s$
• • • We do not use the following data for averages, fits, limits, etc. • • •					
1769± 8		[6] RODAS	22	RVUE	$J/\psi(1S) \to \gamma\ (\pi\pi,\ K\overline{K})$
1814±31	7.2k	[7] KHOLODENK...	21	VES	$29\ \pi^-p \to n\omega\phi$
1700±18		[8,9] SARANTSEV	21	RVUE	$J/\psi(1S) \to \gamma\ (\pi\pi,\ K\overline{K},\ \eta\eta,\ \omega\phi)$
1803± 3.5 $^{+45.5}_{-10.4}$		[10] ALBRECHT	20	RVUE	$0.9\ \overline{p}p \to \pi^0\pi^0\eta$, $\pi^0\eta\eta$, $\pi^0K^+K^-$
1744± 7 ± 5	381	[11,12] DOBBS	15		$J/\psi \to \gamma\pi^+\pi^-$
1705±11 ± 5	237	[11,12] DOBBS	15		$\psi(2S) \to \gamma\pi^+\pi^-$
1706± 4 ± 5	1.0k	[11,12] DOBBS	15		$J/\psi \to \gamma K^+K^-$
1690± 8 ± 3	349	[11,12] DOBBS	15		$\psi(2S) \to \gamma K^+K^-$
1795± 7 $^{+23}_{-20}$		ABLIKIM	13J	BES3	$J/\psi \to \gamma\omega\phi$
1812^{+19}_{-26} ±18		[13] ABLIKIM	06J	BES2	$J/\psi \to \gamma\omega\phi$
1750±13		AMSLER	06	CBAR	$1.64\ \overline{p}p \to K^+K^-\pi^0$
1747± 5	80k	[1,14] UMAN	06	E835	$5.2\ \overline{p}p \to \eta\eta\pi^0$
1776±15		VLADIMIRSK...	06	SPEC	$40\ \pi^-p \to K^0_S K^0_S n$
1790^{+40}_{-30}		[15] ABLIKIM	05	BES2	$J/\psi \to \phi\pi^+\pi^-$
1760±15 $^{+15}_{-10}$		[15] ABLIKIM	05Q	BES2	$\psi(2S) \to \gamma\pi^+\pi^-K^+K^-$
1670±20		[1] BINON	05	GAMS	$33\ \pi^-p \to \eta\eta n$
1732±15		[16] ANISOVICH	03	RVUE	
1682±16		TIKHOMIROV	03	SPEC	$40.0\ \pi^-C \to K^0_S K^0_S K^0_L X$
1670±26	3.6k	[17] NICHITIU	02	OBLX	$0\ \overline{p}p \to K^+K^-\pi^+\pi^-\pi^0$
1698±18		[8] BARBERIS	00E		$450\ pp \to p_f\eta\eta p_s$
1770±12		[18] ANISOVICH	99B	SPEC	0.6–$1.2\ p\overline{p} \to \eta\eta\pi^0$
1730±15		BARBERIS	99	OMEG	$450\ pp \to p_s p_f K^+K^-$
1750±20		BARBERIS	99B	OMEG	$450\ pp \to p_s p_f \pi^+\pi^-$
1710±12 ±11		[19] BARBERIS	99D	OMEG	$450\ pp \to K^+K^-, \pi^+\pi^-$
1750±30		[20] ANISOVICH	98B	RVUE	Compilation
1720±39		BAI	98H	BES	$J/\psi \to \gamma\pi^0\pi^0$
1775± 1.5	57	[21] BARKOV	98		$\pi^-p \to K^0_S K^0_S n$
1690±11		[22] ABREU	96C	DLPH	$Z^0 \to K^+K^- + X$
$1696\pm 5\ ^{+9}_{-34}$		[23] BAI	96C	BES	$J/\psi \to \gamma K^+K^-$
$1781\pm 8\ ^{+10}_{-31}$		BAI	96C	BES	$J/\psi \to \gamma K^+K^-$
1768±14		BALOSHIN	95	SPEC	$40\ \pi^-C \to K^0_S K^0_S X$
1750±15		[24] BUGG	95	MRK3	$J/\psi \to \gamma\pi^+\pi^-\pi^+\pi^-$
1620±16		[23] BUGG	95	MRK3	$J/\psi \to \gamma\pi^+\pi^-\pi^+\pi^-$
1748±10		[25] ARMSTRONG	93C	E760	$\overline{p}p \to \pi^0\eta\eta \to 6\gamma$
~ 1750		BREAKSTONE	93	SFM	$pp \to pp\pi^+\pi^-\pi^+\pi^-$
1744±15		[26] ALDE	92D	GAM2	$38\ \pi^-p \to \eta\eta n$
1713±10		[27] ARMSTRONG	89D	OMEG	$300\ pp \to pp K^+K^-$
1706±10		[27] ARMSTRONG	89D	OMEG	$300\ pp \to pp K^0_S K^0_S$
1707±10		[25] AUGUSTIN	88	DM2	$J/\psi \to \gamma K^+K^-$, $K^0_S K^0_S$
1700±15		[23] BOLONKIN	88	SPEC	$40\ \pi^-p \to K^0_S K^0_S n$
1720±60		BOLONKIN	88	SPEC	$40\ \pi^-p \to K^0_S K^0_S n$
1638±10		[28] FALVARD	88	DM2	$J/\psi \to \phi K^+K^-$, $K^0_S K^0_S$
1690± 4		[29] FALVARD	88	DM2	$J/\psi \to \phi K^+K^-$, $K^0_S K^0_S$
1698±15		[25] AUGUSTIN	87	DM2	$J/\psi \to \gamma\pi^+\pi^-$
1720±10 ±10		[23] BALTRUSAIT...	87	MRK3	$J/\psi \to \gamma K^+K^-$
1755± 8		[30] ALDE	86C	GAM2	$38\ \pi^-p \to n2\eta$
1730^{+2}_{-10}		[31] LONGACRE	86	RVUE	$22\ \pi^-p \to n2K^0_S$
1742±15		[25] WILLIAMS	84	MPSF	$200\ \pi^-N \to 2K^0_S X$
1670±50		BLOOM	83	CBAL	$J/\psi \to \gamma 2\eta$
1650±50		BURKE	82	MRK2	$J/\psi \to \gamma 2\rho$
1640±50		[32,33] EDWARDS	82D	CBAL	$J/\psi \to \gamma 2\eta$
1730±10 ±20		[34] ETKIN	82C	MPS	$23\ \pi^-p \to n2K^0_S$

[1] Breit-Wigner mass.
[2] From partial wave analysis including all possible combinations of 0^{++}, 2^{++}, and 4^{++} resonances.
[3] Spin 0 favored over spin 2.
[4] In the SU(3) based model with a specific interference pattern of the $f_2(1270)$, $a^0_2(1320)$, and $f'_2(1525)$ mesons incoherently added to the $f_0(1710)$ and non-resonant background.
[5] $J^P = 0^+$, supersedes by ARMSTRONG 89D.
[6] T-matrix pole from coupled channel K-matrix fit to data on $J/\psi \to \gamma\pi^0\pi^0$ (ABLIKIM 15AE) and $J/\psi \to \gamma K^0_S K^0_S$ (ABLIKIM 18AA).
[7] From partial wave analysis of $\omega\phi$ invariant mass including 0^{++}, 2^{++}, and 0^{-+} resonances.
[8] T-matrix pole.
[9] Close-by state with mass 1765 ± 15 MeV and width 180 ± 20 MeV.
[10] T-matrix pole, 5 poles, 5 channels, including scattering data from HYAMS 75 ($\pi\pi$), LONGACRE 86 ($K\overline{K}$), BINON 83 ($\eta\eta$), and BINON 84C ($\eta\eta'$).

Downloaded from https://academic.oup.com/ptep/article/2022/8/083C01/6651666 by KIT Library user on 27 September 2022

[11] Using CLEO-c data but not authored by the CLEO Collaboration.
[12] From a fit to a Breit-Wigner line shape with fixed $\Gamma = 135$ MeV.
[13] Not seen by LIU 09 in $B^{\pm} \to K^{\pm}\omega\phi$.
[14] Systematic errors not estimated.
[15] This state may be different from $f_0(1710)$, see CLOSE 05.
[16] K-matrix pole, assuming $J^P = 0^+$, from combined analysis of $\pi^- p \to \pi^0\pi^0 n$, $\pi^- p \to K\overline{K} n$, $\pi^+\pi^- \to \pi^+\pi^-$, $\overline{p}p \to \pi^0\pi^0\pi^0$, $\pi^0\eta\eta$, $\pi^0\pi^0\eta$, $\pi^+\pi^-\pi^0$, $K^+K^-\pi^0$, $K^0_S K^0_S \pi^0$, $K^+K^0_S\pi^-$ at rest, $\overline{p}n \to \pi^-\pi^-\pi^+$, $K^0_S K^-\pi^0$, $K^0_S K^0_S \pi^-$ at rest.
[17] Decaying to $f_0(1370)\pi\pi$.
[18] Not seen by AMSLER 02.
[19] Supersedes BARBERIS 99 and BARBERIS 99B.
[20] T-matrix pole, assuming $J^P = 0^+$
[21] No J^{PC} determination.
[22] No J^{PC} determination, width not determined.
[23] $J^P = 2^+$.
[24] From a fit to the 0^+ partial wave.
[25] No J^{PC} determination.
[26] ALDE 92D combines all the GAMS-2000 data.
[27] $J^P = 2^+$, superseded by FRENCH 99.
[28] From an analysis ignoring interference with $f'_2(1525)$.
[29] From an analysis including interference with $f'_2(1525)$.
[30] Superseded by ALDE 92D.
[31] Uses MRK3 data. From a partial-wave analysis of data using a K-matrix formalism with 5 poles, but assuming spin 2. Fit with constrained inelasticity.
[32] $J^P = 2^+$ preferred.
[33] From fit neglecting nearby $f'_2(1525)$. Replaced by BLOOM 83.
[34] Superseded by LONGACRE 86.

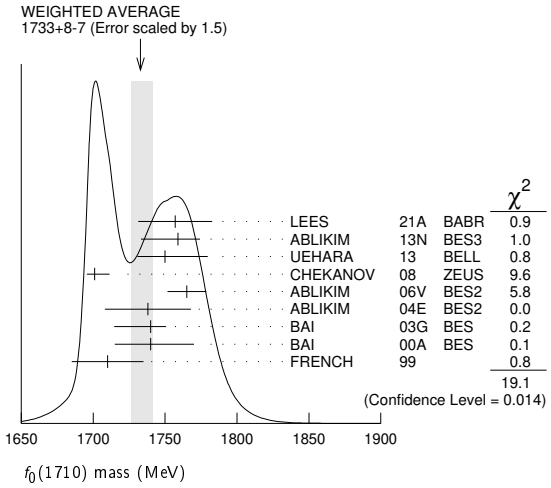

$f_0(1710)$ WIDTH

OUR EVALUATION below is based on T-matrix poles from BARBERIS 00E and BARBERIS 99D.

VALUE (MeV)	EVTS	DOCUMENT ID		TECN	COMMENT
123 ± 18 OUR EVALUATION					
150 $^{+12}_{-10}$ OUR AVERAGE Error includes scale factor of 1.3. See the ideogram below.					
175 ± 23 ± 4		[1] LEES	21A	BABR	$\eta_c(1S) \to \eta' K^+K^-$
172 ± 10 $^{+32}_{-16}$	5.5k	[2] ABLIKIM	13N	BES3	$e^+e^- \to J/\psi \to \gamma\eta\eta$
139 $^{+11}_{-12}$ $^{+96}_{-50}$		[3] UEHARA	13	BELL	$\gamma\gamma \to K^0_S K^0_S$
100 ± 24 $^{+7}_{-22}$	4k	[4] CHEKANOV	08	ZEUS	$ep \to K^0_S K^0_S X$
145 ± 8 ± 69		[1] ABLIKIM	06V	BES2	$e^+e^- \to J/\psi \to \gamma\pi^+\pi^-$
125 ± 20		ABLIKIM	04E	BES2	$J/\psi \to \omega K^+K^-$
166 $^{+5}_{-8}$ $^{+15}_{-10}$		BAI	03G	BES	$J/\psi \to \gamma K\overline{K}$
120 $^{+50}_{-40}$		BAI	00A	BES	$J/\psi \to \gamma(\pi^+\pi^-\pi^+\pi^-)$
105 ± 34		[5] FRENCH	99		$300\ pp \to p_f(K^+K^-)p_s$
• • • We do not use the following data for averages, fits, limits, etc. • • •					
156 ± 12		[6] RODAS	22	RVUE	$J/\psi(1S) \to \gamma(\pi\pi,\ K\overline{K})$
182 ± 19	7.2k	[7] KHOLODENK...	21	VES	$29\ \pi^- p \to n\omega\phi$
255 ± 25		[8,9] SARANTSEV	21	RVUE	$J/\psi(1S) \to \gamma(\pi\pi,\ K\overline{K},\ \eta\eta,\ \omega\phi)$
289.7 ± 5.0 $^{+32.6}_{-19.3}$		[10] ALBRECHT	20	RVUE	$0.9\ \overline{p}p \to \pi^0\pi^0\eta,\ \pi^0\eta\eta,\ \pi^0K^+K^-$
95 ± 10 $^{+78}_{-82}$		ABLIKIM	13J	BES3	$J/\psi \to \gamma\omega\phi$
105 ± 20 ± 28		[11] ABLIKIM	06J	BES2	$J/\psi \to \gamma\omega\phi$
148 $^{+40}_{-30}$		AMSLER	06	CBAR	$1.64\ \overline{p}p \to K^+K^-\pi^0$
188 ± 13	80k	[1,12] UMAN	06	E835	$5.2\ \overline{p}p \to \eta\eta\pi^0$
250 ± 30		VLADIMIRSK...	06	SPEC	$40\ \pi^- p \to K^0_S K^0_S n$
270 $^{+60}_{-30}$		[13] ABLIKIM	05	BES2	$J/\psi \to \phi\pi^+\pi^-$
125 ± 25 $^{+10}_{-15}$		[1] ABLIKIM	05Q	BES2	$\psi(2S) \to \gamma\pi^+\pi^-K^+K^-$
260 ± 50		[1] BINON	05	GAMS	$33\ \pi^- p \to \eta\eta n$
144 ± 30		[14,15] ANISOVICH	03	RVUE	
320 $^{+50}_{-20}$		[15,16] ANISOVICH	03	RVUE	
102 ± 26		TIKHOMIROV	03	SPEC	$40.0\ \pi^- C \to K^0_S K^0_S K^0_L X$
267 ± 44	3651	[17] NICHITIU	02	OBLX	$0\ \overline{p}p \to K^+K^-\pi^+\pi^-\pi^0$
120 ± 26		[9] BARBERIS	00E		$450\ pp \to p_f\eta\eta p_s$
220 ± 40		[18,19] ANISOVICH	99B	SPEC	$0.6\text{–}1.2\ p\overline{p} \to \eta\eta\pi^0$
100 ± 25		BARBERIS	99	OMEG	$450\ pp \to p_s p_f K^+K^-$
160 ± 30		BARBERIS	99B	OMEG	$450\ pp \to p_s p_f \pi^+\pi^-$
126 ± 16 ± 18		[9,20] BARBERIS	99D	OMEG	$450\ pp \to K^+K^-, \pi^+\pi^-$
250 ± 140		[21] ANISOVICH	98B	RVUE	Compilation
30 ± 7	57	[22] BARKOV	98		$\pi^- p \to K^0_S K^0_S n$
103 ± 18 $^{+30}_{-11}$		[23] BAI	96C	BES	$J/\psi \to \gamma K^+K^-$
85 ± 24 $^{+22}_{-19}$		BAI	96C	BES	$J/\psi \to \gamma K^+K^-$
56 ± 19		BALOSHIN	95	SPEC	$40\ \pi^- C \to K^0_S K^0_S X$
160 ± 40		[24] BUGG	95	MRK3	$J/\psi \to \gamma\pi^+\pi^-\pi^+\pi^-$
160 $^{+60}_{-20}$		[23] BUGG	95	MRK3	$J/\psi \to \gamma\pi^+\pi^-\pi^+\pi^-$
264 ± 25		[25] ARMSTRONG	93C	E760	$\overline{p}p \to \pi^0\eta\eta \to 6\gamma$
200 to 300		BREAKSTONE	93	SFM	$pp \to pp\pi^+\pi^-\pi^+\pi^-$
< 80 90% CL		[26] ALDE	92D	GAM2	$38\ \pi^- p \to \eta\eta N^*$
181 ± 30		[27] ARMSTRONG	89D	OMEG	$300\ pp \to ppK^+K^-$
104 ± 30		[27] ARMSTRONG	89D	OMEG	$300\ pp \to ppK^0_S K^0_S$
166.4 ± 33.2		[25] AUGUSTIN	88	DM2	$J/\psi \to \gamma K^+K^-,\ K^0_S K^0_S$
30 ± 20		[23] BOLONKIN	88	SPEC	$40\ \pi^- p \to K^0_S K^0_S n$
350 ± 150		BOLONKIN	88	SPEC	$40\ \pi^- p \to K^0_S K^0_S n$
148 ± 17		[28] FALVARD	88	DM2	$J/\psi \to \phi K^+K^-,\ K^0_S K^0_S$
184 ± 6		[29] FALVARD	88	DM2	$J/\psi \to \phi K^+K^-,\ K^0_S K^0_S$
136 ± 28		[25] AUGUSTIN	87	DM2	$J/\psi \to \gamma\pi^+\pi^-$
130 ± 20		[23] BALTRUSAIT...	87	MRK3	$J/\psi \to \gamma K^+K^-$
122 $^{+74}_{-15}$		[30] LONGACRE	86	RVUE	$22\ \pi^- p \to n2K^0_S$
57 ± 38		[31] WILLIAMS	84	MPSF	$200\ \pi^- N \to 2K^0_S X$
160 ± 80		BLOOM	83	CBAL	$J/\psi \to \gamma 2\eta$
200 ± 100		BURKE	82	MRK2	$J/\psi \to \gamma 2\rho$
220 $^{+100}_{-70}$		[32,33] EDWARDS	82D	CBAL	$J/\psi \to \gamma 2\eta$
200 $^{+156}_{-9}$		[34] ETKIN	82B	MPS	$23\ \pi^- p \to n2K^0_S$

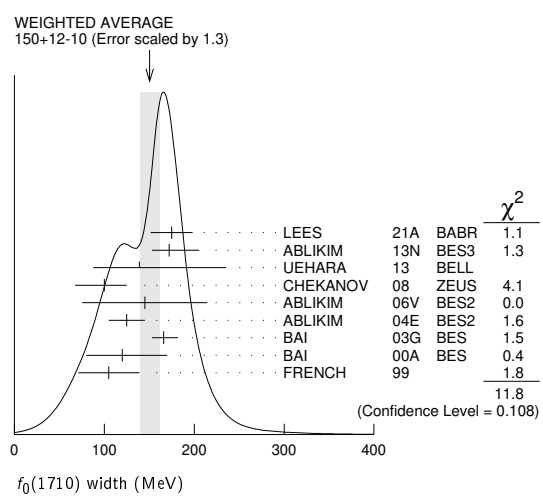

[1] Breit-Wigner width.
[2] From partial wave analysis including all possible combinations of 0^{++}, 2^{++}, and 4^{++} resonances.
[3] Spin 0 favored over spin 2.
[4] In the SU(3) based model with a specific interference pattern of the $f_2(1270)$, $a^0_2(1320)$, and $f'_2(1525)$ mesons incoherently added to the $f_0(1710)$ and non-resonant background.
[5] $J^P = 0^+$, supersedes by ARMSTRONG 89D.

Downloaded from https://academic.oup.com/ptep/article/2022/8/083C01/6651666 by KIT Library user on 27 September 2022

[6] T-matrix pole from coupled channel K-matrix fit to data on $J/\psi \to \gamma\pi^0\pi^0$ (ABLIKIM 15AE) and $J/\psi \to \gamma K^0_S K^0_S$ (ABLIKIM 18AA).
[7] From partial wave analysis of $\omega\phi$ invariant mass including 0^{++}, 2^{++}, and 0^{-+} resonances.
[8] Close-by state with mass 1765 ± 15 MeV and width 180 ± 20 MeV.
[9] T-matrix pole.
[10] T-matrix pole, 5 poles, 5 channels, including scattering data from HYAMS 75 ($\pi\pi$), LONGACRE 86 ($K\overline{K}$), BINON 83 ($\eta\eta$), and BINON 84C ($\eta\eta'$).
[11] Not seen by LIU 09 in $B^\pm \to K^\pm\omega\phi$.
[12] Systematic errors not estimated.
[13] This state may be different from $f_0(1710)$, see CLOSE 05.
[14] (Solution I)
[15] K-matrix pole, assuming $J^P = 0^+$, from combined analysis of $\pi^- p \to \pi^0\pi^0 n$, $\pi^- p \to K\overline{K}n$, $\pi^+\pi^- \to \pi^+\pi^-$, $\overline{p}p \to \pi^0\pi^0\pi^0$, $\pi^0\eta\eta$, $\pi^0\pi^0\eta$, $\pi^+\pi^-\pi^0$, $K^+K^-\pi^0$, $K^0_S K^0_S\pi^0$, $K^+K^0_S\pi^-$ at rest, $\overline{p}n \to \pi^-\pi^-\pi^+$, $K^0_S K^-\pi^0$, $K^0_S K^0_S\pi^-$ at rest.
[16] Solution I.
[17] Decaying to $f_0(1370)\pi\pi$.
[18] $J^P = 0^+$.
[19] Not seen by AMSLER 02.
[20] Supersedes BARBERIS 99 and BARBERIS 99B.
[21] T-matrix pole, assuming $J^P = 0^+$
[22] No J^{PC} determination.
[23] $J^P = 2^+$.
[24] From a fit to the 0^+ partial wave.
[25] No J^{PC} determination.
[26] ALDE 92D combines all the GAMS-2000 data.
[27] $J^P = 2^+$, (0^+ excluded).
[28] From an analysis ignoring interference with $f'_2(1525)$.
[29] From an analysis including interference with $f'_2(1525)$.
[30] Uses MRK3 data. From a partial-wave analysis of data using a K-matrix formalism with 5 poles, but assuming spin 2. Fit with constrained inelasticity.
[31] No J^{PC} determination.
[32] $J^P = 2^+$ preferred.
[33] From fit neglecting nearby $f'_2(1525)$. Replaced by BLOOM 83.
[34] From an amplitude analysis of the $K^0_S K^0_S$ system, superseded by LONGACRE 86.

$f_0(1710)$ DECAY MODES

	Mode	Fraction (Γ_i/Γ)
Γ_1	$K\overline{K}$	seen
Γ_2	$\eta\eta$	seen
Γ_3	$\pi\pi$	seen
Γ_4	$\gamma\gamma$	seen
Γ_5	$\omega\omega$	seen

$f_0(1710)$ $\Gamma(i)\Gamma(\gamma\gamma)/\Gamma(\text{total})$

$\Gamma(K\overline{K}) \times \Gamma(\gamma\gamma)/\Gamma_{\text{total}}$ — $\Gamma_1\Gamma_4/\Gamma$

VALUE (eV)	CL%	DOCUMENT ID		TECN	COMMENT
$12^{+3}_{-2}{}^{+227}_{-8}$		UEHARA	13	BELL	$\gamma\gamma \to K^0_S K^0_S$
• • • We do not use the following data for averages, fits, limits, etc. • • •					
<480	95	ALBRECHT	90G	ARG	$\gamma\gamma \to K^+K^-$
<110	95	[1] BEHREND	89C	CELL	$\gamma\gamma \to K^0_S K^0_S$
<280	95	[1] ALTHOFF	85B	TASS	$\gamma\gamma \to K\overline{K}\pi$

[1] Assuming helicity 2.

$\Gamma(\pi\pi) \times \Gamma(\gamma\gamma)/\Gamma_{\text{total}}$ — $\Gamma_3\Gamma_4/\Gamma$

VALUE (keV)	CL%	DOCUMENT ID		TECN	COMMENT
<0.82	95	[1] BARATE	00E	ALEP	$\gamma\gamma \to \pi^+\pi^-$

[1] Assuming spin 0.

$f_0(1710)$ BRANCHING RATIOS

$\Gamma(K\overline{K})/\Gamma_{\text{total}}$ — Γ_1/Γ

VALUE	EVTS	DOCUMENT ID		TECN	COMMENT
• • • We do not use the following data for averages, fits, limits, etc. • • •					
seen	1004	[1] DOBBS	15		$J/\psi \to \gamma K^+K^-$
seen	349	[1] DOBBS	15		$\psi(2S) \to \gamma K^+K^-$
0.36±0.12		ALBALADEJO	08	RVUE	
$0.38^{+0.09}_{-0.19}$		[2] LONGACRE	86	MPS	$22\ \pi^- p \to n 2K^0_S$

[1] Using CLEO-c data but not authored by the CLEO Collaboration.
[2] From a partial-wave analysis of data using a K-matrix formalism with 5 poles, but assuming spin 2. Fit with constrained inelasticity.

$\Gamma(\eta\eta)/\Gamma_{\text{total}}$ — Γ_2/Γ

VALUE	DOCUMENT ID		TECN
• • • We do not use the following data for averages, fits, limits, etc. • • •			
0.22±0.12	ALBALADEJO	08	RVUE
$0.18^{+0.03}_{-0.13}$	[1] LONGACRE	86	RVUE

[1] From a partial-wave analysis of data using a K-matrix formalism with 5 poles, but assuming spin 2. Fit with constrained inelasticity.

$\Gamma(\pi\pi)/\Gamma_{\text{total}}$ — Γ_3/Γ

VALUE	EVTS	DOCUMENT ID		TECN	COMMENT
• • • We do not use the following data for averages, fits, limits, etc. • • •					
seen	381	[1] DOBBS	15		$J/\psi \to \gamma\pi^+\pi^-$
seen	237	[1] DOBBS	15		$\psi(2S) \to \gamma\pi^+\pi^-$
not seen		AMSLER	02	CBAR	$0.9\ \overline{p}p \to \pi^0\eta\eta$, $\pi^0\pi^0\pi^0$
$0.039^{+0.002}_{-0.024}$		[2] LONGACRE	86	RVUE	

[1] Using CLEO-c data but not authored by the CLEO Collaboration.
[2] From a partial-wave analysis of data using a K-matrix formalism with 5 poles, but assuming spin 2. Fit with constrained inelasticity.

$\Gamma(\pi\pi)/\Gamma(K\overline{K})$ — Γ_3/Γ_1

VALUE	CL%	DOCUMENT ID		TECN	COMMENT
0.23±0.05 OUR AVERAGE		Error includes scale factor of 1.2.			
0.64±0.27 ±0.18		LEES	18A	BABR	$\Upsilon(1S) \to \gamma\pi^+\pi^-$, γK^+K^-
$0.41^{+0.11}_{-0.17}$		ABLIKIM	06V	BES2	$e^+e^- \to J/\psi \to \gamma\pi^+\pi^-$
0.2 ±0.024±0.036		BARBERIS	99D	OMEG	$450\ pp \to K^+K^-, \pi^+\pi^-$
0.39±0.14		ARMSTRONG	91	OMEG	$300\ pp \to pp\pi\pi,\ ppK\overline{K}$
• • • We do not use the following data for averages, fits, limits, etc. • • •					
0.32±0.14		ALBALADEJO	08	RVUE	
< 0.11	95	[1] ABLIKIM	04E	BES2	$J/\psi \to \omega K^+K^-$
$5.8\ ^{+9.1}_{-5.5}$		[2] ANISOVICH	02D	SPEC	Combined fit

[1] Using data from ABLIKIM 04A.
[2] From a combined K-matrix analysis of Crystal Barrel (0. $p\overline{p} \to \pi^0\pi^0\pi^0$, $\pi^0\eta\eta$, $\pi^0\pi^0\eta$), GAMS ($\pi p \to \pi^0\pi^0 n$, $\eta\eta n$, $\eta\eta' n$), and BNL ($\pi p \to K\overline{K}n$) data.

$\Gamma(\eta\eta)/\Gamma(K\overline{K})$ — Γ_2/Γ_1

VALUE	CL%	DOCUMENT ID		TECN	COMMENT
0.48±0.15		BARBERIS	00E		$450\ pp \to p_f\eta\eta p_s$
• • • We do not use the following data for averages, fits, limits, etc. • • •					
$0.46^{+0.70}_{-0.38}$		[1] ANISOVICH	02D	SPEC	Combined fit
<0.02	90	[2] PROKOSHKIN	91	GA24	$300\ \pi^- p \to \pi^- p\eta\eta$

[1] From a combined K-matrix analysis of Crystal Barrel (0. $p\overline{p} \to \pi^0\pi^0\pi^0$, $\pi^0\eta\eta$, $\pi^0\pi^0\eta$), GAMS ($\pi p \to \pi^0\pi^0 n$, $\eta\eta n$, $\eta\eta' n$), and BNL ($\pi p \to K\overline{K}n$) data.
[2] Combining results of GAM4 with those of ARMSTRONG 89D.

$\Gamma(\omega\omega)/\Gamma_{\text{total}}$ — Γ_5/Γ

VALUE	EVTS	DOCUMENT ID		TECN	COMMENT
seen	180	ABLIKIM	06H	BES	$J/\psi \to \gamma\omega\omega$

$f_0(1710)$ REFERENCES

RODAS	22	EPJ C82 80	A. Rodas *et al.*	(JPAC Collab.)
KHOLODENK...	21	PAN 83 1602	M.S. Kholodenko	(VES Collab.)
LEES	21A	PR D104 072002	J.P. Lees *et al.*	(BABAR Collab.)
SARANTSEV	21	PL B816 136227	A.V. Sarantsev *et al.*	(BONN, PNPI)
ALBRECHT	20	EPJ C80 453	M. Albrecht *et al.*	(Crystal Barrel Collab.)
ABLIKIM	18AA	PR D98 072003	M. Ablikim *et al.*	(BESIII Collab.)
LEES	18A	PR D97 112006	J.P. Lees *et al.*	(BABAR Collab.)
ABLIKIM	15AE	PR D92 052003	M. Ablikim *et al.*	(BESIII Collab.)
DOBBS	15	PR D91 052006	S. Dobbs *et al.*	(NWES)
ABLIKIM	13J	PR D87 032008	M. Ablikim *et al.*	(BESIII Collab.)
ABLIKIM	13N	PR D87 092009	M. Ablikim *et al.*	(BESIII Collab.)
UEHARA	13	PTEP 2013 123C01	S. Uehara *et al.*	(BELLE Collab.)
LIU	09	PR D79 071102	C. Liu *et al.*	(BELLE Collab.)
ALBALADEJO	08	PRL 101 252002	M. Albaladejo, J.A. Oller	
CHEKANOV	08	PRL 101 112003	S. Chekanov *et al.*	(ZEUS Collab.)
ABLIKIM	06H	PR D73 112007	M. Ablikim *et al.*	(BES Collab.)
ABLIKIM	06J	PRL 96 162002	M. Ablikim *et al.*	(BES Collab.)
ABLIKIM	06V	PL B642 441	M. Ablikim *et al.*	(BES Collab.)
AMSLER	06	PL B639 165	C. Amsler *et al.*	(Crystal Barrel Collab.)
UMAN	06	PR D73 052009	I. Uman *et al.*	(FNAL E835)
VLADIMIRSK...	06	PAN 69 493 Translated from YAF 69 515.	V.V. Vladimirsky *et al.*	(ITEP, Moscow)
ABLIKIM	05	PL B607 243	M. Ablikim *et al.*	(BES Collab.)
ABLIKIM	05Q	PR D72 092002	M. Ablikim *et al.*	(BES Collab.)
BINON	05	PAN 68 960 Translated from YAF 68 998.	F. Binon *et al.*	
CLOSE	05	PR D71 094022	F.E. Close, Q. Zhao	
ABLIKIM	04A	PL B598 149	M. Ablikim *et al.*	(BES Collab.)
ABLIKIM	04E	PL B603 138	M. Ablikim *et al.*	(BES Collab.)
ANISOVICH	03	EPJ A16 229	V.V. Anisovich *et al.*	
BAI	03G	PR D68 052003	J.Z. Bai *et al.*	(BES Collab.)
TIKHOMIROV	03	PAN 66 828 Translated from YAF 66 860.	G.D. Tikhomirov *et al.*	
AMSLER	02	EPJ C23 29	C. Amsler *et al.*	
ANISOVICH	02D	PAN 65 1545 Translated from YAF 65 1583.	V.V. Anisovich *et al.*	
NICHITIU	02	PL B545 261	F. Nichitiu *et al.*	(OBELIX Collab.)
BAI	00A	PL B472 207	J.Z. Bai *et al.*	(BES Collab.)
BARATE	00E	PL B472 189	R. Barate *et al.*	(ALEPH Collab.)
BARBERIS	00E	PL B479 59	D. Barberis *et al.*	(WA 102 Collab.)
ANISOVICH	99B	PL B449 154	A.V. Anisovich *et al.*	
BARBERIS	99	PL B453 305	D. Barberis *et al.*	(Omega Expt.)
BARBERIS	99B	PL B453 316	D. Barberis *et al.*	(Omega Expt.)
BARBERIS	99D	PL B462 462	D. Barberis *et al.*	(Omega Expt.)
FRENCH	99	PL B460 213	B. French *et al.*	(WA76 Collab.)
ANISOVICH	98B	SPU 41 419 Translated from UFN 168 481.	V.V. Anisovich *et al.*	
BAI	98H	PRL 81 1179	J.Z. Bai *et al.*	(BES Collab.)
BARKOV	98	JETPL 68 764	B.P. Barkov *et al.*	
ABREU	96C	PL B379 309	P. Abreu *et al.*	(DELPHI Collab.)
BAI	96C	PRL 77 3959	J.Z. Bai *et al.*	(BES Collab.)
BALOSHIN	95	PAN 58 46 Translated from YAF 58 50.	O.N. Baloshin *et al.*	(ITEP)

Downloaded from https://academic.oup.com/ptep/article/2022/8/083C01/6651666 by KIT Library user on 27 September 2022

BUGG	95	PL B353 378	D.V. Bugg *et al.*	(LOQM, PNPI, WASH)
ARMSTRONG	93C	PL B307 394	T.A. Armstrong *et al.*	(FNAL, FERR, GENO+)
BREAKSTONE	93	ZPHY C58 251	A.M. Breakstone *et al.*	(IOWA, CERN, DORT+)
ALDE	92D	PL B284 457	D.M. Alde *et al.*	(GAM2 Collab.)
Also		SJNP 54 451	D.M. Alde *et al.*	(GAM2 Collab.)
		Translated from YAF 54 745.		
ARMSTRONG	91	ZPHY C51 351	T.A. Armstrong *et al.*	(ATHU, BARI, BIRM+)
PROKOSHKIN	91	SPD 36 155	Y.D. Prokoshkin	(GAM2 and GAM4 Collab.)
		Translated from DANS 316 900.		
ALBRECHT	90G	ZPHY C48 183	H. Albrecht *et al.*	(ARGUS Collab.)
ARMSTRONG	89D	PL B227 186	T.A. Armstrong, M. Benayoun	(ATHU, BARI, BIRM+)
BEHREND	89C	ZPHY C43 91	H.J. Behrend *et al.*	(CELLO Collab.)
AUGUSTIN	88	PRL 60 2238	J.E. Augustin *et al.*	(DM2 Collab.)
BOLONKIN	88	NP B309 426	B.V. Bolonkin *et al.*	(ITEP, SERP)
FALVARD	88	PR D38 2706	A. Falvard *et al.*	(CLER, FRAS, LALO+)
AUGUSTIN	87	ZPHY C36 369	J.E. Augustin *et al.*	(LALO, CLER, FRAS+)
BALTRUSAIT...	87	PR D35 2077	R.M. Baltrusaitis *et al.*	(Mark III Collab.)
ALDE	86C	PL B182 105	D.M. Alde *et al.*	(SERP, BELG, LANL, LAPP)
LONGACRE	86	PL B177 223	R.S. Longacre *et al.*	(BNL, BRAN, CUNY+)
ALTHOFF	85B	ZPHY C29 189	M. Althoff *et al.*	(TASSO Collab.)
BINON	84C	NC 80A 363	F.G. Binon *et al.*	(BELG, LAPP, SERP+)
WILLIAMS	84	PR D30 877	E.G.H. Williams *et al.*	(VAND, NDAM, TUFTS+)
BINON	83	NC 78A 313	F.G. Binon *et al.*	(BELG, LAPP, SERP+)
BLOOM	83	ARNS 33 143	E.D. Bloom, C. Peck	(SLAC, CIT)
BURKE	82	PRL 49 632	D.L. Burke *et al.*	(LBL, SLAC)
EDWARDS	82D	PRL 48 458	C. Edwards *et al.*	(CIT, HARV, PRIN+)
ETKIN	82B	PR D25 1786	A. Etkin *et al.*	(BNL, CUNY, TUFTS, VAND)
ETKIN	82C	PR D25 2446	A. Etkin *et al.*	(BNL, CUNY, TUFTS, VAND)
HYAMS	75	NP B100 205	B.D. Hyams *et al.*	(CERN, MPIM)

$X(1750)$

$I^G(J^{PC}) = ?^-(1^{--})$

OMITTED FROM SUMMARY TABLE

The $X(1750)$ was separated from the $\phi(1680)$ in the 2022 listings due to its incompatible mass and incompatible pattern of $\overline{K}K$ and $\overline{K}^*(892)K$ branching fractions.

$X(1750)$ MASS

VALUE (MeV)	DOCUMENT ID		TECN	COMMENT
1753.8± 2.7 OUR AVERAGE				
$1784 \pm 12 \; {}^{+0}_{-27}$	ABLIKIM	20F	BES3	$\psi(2S) \to K^+K^-\eta$
$1753.5 \pm 1.5 \pm 2.3$	LINK	02K	FOCS	20–160 $\gamma p \to K^+K^-p$
• • • We do not use the following data for averages, fits, limits, etc. • • •				
1726 ± 22	BUSENITZ	89	TPS	$\gamma p \to K^+K^-X$
1760 ± 20	ATKINSON	85C	OMEG	20–70 $\gamma p \to K\overline{K}X$
1690 ± 10	ASTON	81F	OMEG	25–70 $\gamma p \to K^+K^-X$

$X(1750)$ WIDTH

VALUE (MeV)	DOCUMENT ID		TECN	COMMENT
120 ±10 OUR AVERAGE				
$106 \; {}^{+22}_{-19} \; {}^{+8}_{-36}$	ABLIKIM	20F	BES3	$\psi(2S) \to K^+K^-\eta$
$122.2 \pm 6.2 \pm 8.0$	LINK	02K	FOCS	20–160 $\gamma p \to K^+K^-p$
• • • We do not use the following data for averages, fits, limits, etc. • • •				
121 ± 47	BUSENITZ	89	TPS	$\gamma p \to K^+K^-X$
80 ± 40	ATKINSON	85C	OMEG	20–70 $\gamma p \to K\overline{K}X$
100 ± 40	ASTON	81F	OMEG	25–70 $\gamma p \to K^+K^-X$

$X(1750)$ DECAY MODES

	Mode	Fraction (Γ_i/Γ)
Γ_1	K^+K^-	seen
Γ_2	$\overline{K}^*(892)^0 K^0_S$	not seen
Γ_3	$K^*(892)^\pm K^\mp$	not seen

$\Gamma(\overline{K}^*(892)^0 K^0_S)/\Gamma(K^+K^-)$ — Γ_2/Γ_1

VALUE	CL%	DOCUMENT ID		TECN	COMMENT
<0.065	90	LINK	02K	FOCS	$\gamma p \to K^+K^-p$

$\Gamma(K^*(892)^\pm K^\mp)/\Gamma(K^+K^-)$ — Γ_3/Γ_1

VALUE	CL%	DOCUMENT ID		TECN	COMMENT
<0.183	90	LINK	02K	FOCS	$\gamma p \to K^+K^-p$

$X(1750)$ REFERENCES

ABLIKIM	20F	PR D101 032008	M. Ablikim *et al.*	(BESIII Collab.)
LINK	02K	PL B545 50	J.M. Link *et al.*	(FNAL FOCUS Collab.)
BUSENITZ	89	PR D40 1	J.K. Busenitz *et al.*	(ILL, FNAL)
ATKINSON	85C	ZPHY C27 233	M. Atkinson *et al.*	(BONN, CERN, GLAS+)
ASTON	81F	PL 104B 231	D. Aston	(BONN, CERN, EPOL, GLAS, LANC+)

$\eta(1760)$

$I^G(J^{PC}) = 0^+(0^{-+})$

OMITTED FROM SUMMARY TABLE

Seen by DM2 in the $\rho\rho$ system (BISELLO 89B). Structure in this region has been reported before in the same system (BALTRUSAITIS 86B) and in the $\omega\omega$ system (BALTRUSAITIS 85C, BISELLO 87).

$\eta(1760)$ MASS

VALUE (MeV)	EVTS	DOCUMENT ID		TECN	COMMENT
1751±15 OUR AVERAGE					
$1768 \; {}^{+24}_{-25} \pm 10$	465	[1] ZHANG	12A	BELL	$e^+e^- \to e^+e^-\eta'\pi^+\pi^-$
$1744 \pm 10 \pm 15$	1045	[2] ABLIKIM	06H	BES	$J/\psi \to \gamma\omega\omega$
• • • We do not use the following data for averages, fits, limits, etc. • • •					
$1703 \; {}^{+12}_{-11} \pm 2$		[3] ZHANG	12A	BELL	$e^+e^- \to e^+e^-\eta'\pi^+\pi^-$
1760 ± 11	320	[4] BISELLO	89B	DM2	$J/\psi \to 4\pi\gamma$

[1] From a single-resonance fit.
[2] From a partial wave analysis including $\eta(1760)$, $f_0(1710)$, $f_2(1640)$, and $f_2(1910)$.
[3] From a two-resonance fit.
[4] Estimated by us from various fits. Systematic uncertainties not estimated.

$\eta(1760)$ WIDTH

VALUE (MeV)	EVTS	DOCUMENT ID		TECN	COMMENT
240±30 OUR AVERAGE					
$224 \; {}^{+62}_{-56} \pm 25$	465	[5] ZHANG	12A	BELL	$e^+e^- \to e^+e^-\eta'\pi^+\pi^-$
$244 \; {}^{+24}_{-21} \pm 25$	1045	[6] ABLIKIM	06H	BES	$J/\psi \to \gamma\omega\omega$
• • • We do not use the following data for averages, fits, limits, etc. • • •					
$42 \; {}^{+36}_{-22} \pm 15$		[7] ZHANG	12A	BELL	$e^+e^- \to e^+e^-\eta'\pi^+\pi^-$
60 ± 16	320	[8] BISELLO	89B	DM2	$J/\psi \to 4\pi\gamma$

[5] From a single-resonance fit.
[6] From a partial wave analysis including $\eta(1760)$, $f_0(1710)$, $f_2(1640)$, and $f_2(1910)$.
[7] From a two-resonance fit.
[8] Estimated by us from various fits. Systematic uncertainties not estimated.

$\eta(1760)$ DECAY MODES

	Mode	Fraction (Γ_i/Γ)
Γ_1	4π	
Γ_2	$2\pi^+2\pi^-$	seen
Γ_3	$\pi^+\pi^-2\pi^0$	seen
Γ_4	$\rho^0\rho^0$	seen
Γ_5	$\rho^+\rho^-$	seen
Γ_6	$\omega\omega$	seen
Γ_7	$\eta'\pi^+\pi^-$	seen
Γ_8	$\gamma\gamma$	seen

$\eta(1760)$ $\Gamma(i)\Gamma(\gamma\gamma)/\Gamma(\text{total})$

$\Gamma(\eta'\pi^+\pi^-) \times \Gamma(\gamma\gamma)/\Gamma_{\text{total}}$ — $\Gamma_7\Gamma_8/\Gamma$

VALUE (eV)	EVTS	DOCUMENT ID		TECN	COMMENT
$\mathbf{28.2} \; {}^{+7.9}_{-7.5} \pm 3.7$	465	[9] ZHANG	12A	BELL	$e^+e^- \to e^+e^-\eta'\pi^+\pi^-$
• • • We do not use the following data for averages, fits, limits, etc. • • •					
$3.0 \; {}^{+2.0}_{-1.2} \pm 0.8$	52	[10] ZHANG	12A	BELL	$e^+e^- \to e^+e^-\eta'\pi^+\pi^-$
$18 \; {}^{+13}_{-10} \pm 5$	315	[11] ZHANG	12A	BELL	$e^+e^- \to e^+e^-\eta'\pi^+\pi^-$

[9] From a single-resonance fit.
[10] From a two-resonance fit. For constructive interference with the $X(1835)$.
[11] From a two-resonance fit. For destructive interference with the $X(1835)$.

$\eta(1760)$ BRANCHING RATIOS

$\Gamma(2\pi^+2\pi^-)/\Gamma_{\text{total}}$ — Γ_2/Γ

VALUE	DOCUMENT ID		TECN	COMMENT
seen	BISELLO	89B	DM2	$J/\psi \to \gamma 2\pi^+2\pi^-$

$\Gamma(\pi^+\pi^-2\pi^0)/\Gamma_{\text{total}}$ — Γ_3/Γ

VALUE	DOCUMENT ID		TECN	COMMENT
seen	BISELLO	89B	DM2	$J/\psi \to \gamma\pi^+\pi^-2\pi^0$

Downloaded from https://academic.oup.com/ptep/article/2022/8/083C01/6651666 by KIT Library user on 27 September 2022

$\Gamma(\rho^0\rho^0)/\Gamma_{total}$ — Γ_4/Γ

VALUE	DOCUMENT ID		TECN	COMMENT
seen	BISELLO	89B	DM2	$J/\psi \to \gamma\rho^0\rho^0$
seen	BALTRUSAIT...	86	MRK3	$J/\psi \to \gamma\rho^0\rho^0$

$\Gamma(\rho^+\rho^-)/\Gamma_{total}$ — Γ_5/Γ

VALUE	DOCUMENT ID		TECN	COMMENT
seen	BISELLO	89B	DM2	$J/\psi \to \gamma\rho^+\rho^-$
seen	BALTRUSAIT...	86	MRK3	$J/\psi \to \gamma\rho^+\rho^-$

$\Gamma(\omega\omega)/\Gamma_{total}$ — Γ_6/Γ

VALUE	DOCUMENT ID		TECN	COMMENT
seen	BISELLO	87	DM2	$J/\psi \to \omega\omega$
seen	BALTRUSAIT...	85C	MRK3	$J/\psi \to \gamma\omega\omega$

$\Gamma(\gamma\gamma)/\Gamma(\omega\omega)$ — Γ_8/Γ_6

VALUE	CL%	DOCUMENT ID		TECN	COMMENT
$<2.48\times10^{-3}$	90	[12] ABLIKIM	18O	BES3	$\psi(2S) \to \pi^+\pi^-\gamma\gamma\gamma$

[12] Using results from ABLIKIM 06H.

$\eta(1760)$ REFERENCES

ABLIKIM	18O	PR D97 072014	M. Ablikim *et al.*	(BESIII Collab.)
ZHANG	12A	PR D86 052002	C.C. Zhang *et al.*	(BELLE Collab.)
ABLIKIM	06H	PR D73 112007	M. Ablikim *et al.*	(BES Collab.)
BISELLO	89B	PR D39 701	G. Busetto *et al.*	(DM2 Collab.)
BISELLO	87	PL B192 239	D. Bisello *et al.*	(PADO, CLER, FRAS+)
BALTRUSAIT...	86	PR D33 629	R.M. Baltrusaitis *et al.*	(Mark III Collab.)
BALTRUSAIT...	86B	PR D33 1222	R.M. Baltrusaitis *et al.*	(Mark III Collab.)
BALTRUSAIT...	85C	PRL 55 1723	R.M. Baltrusaitis *et al.*	(CIT, UCSC+)

$\pi(1800)$

$I^G(J^{PC}) = 1^-(0^{-+})$

See the review on "Non-$q\overline{q}$ Mesons."

$\pi(1800)$ MASS

VALUE (MeV)	EVTS	DOCUMENT ID		TECN	CHG	COMMENT
1810^{+9}_{-11} OUR AVERAGE		Error includes scale factor of 2.2. See the ideogram below.				
1804^{+6}_{-9}	46M	[1] AGHASYAN	18B	COMP		$190\ \pi^-p \to \pi^-\pi^+\pi^-p$
$1876\pm18\pm16$	4k	[2] EUGENIO	08	B852	–	$18\ \pi^-p \to \eta\eta\pi^-p$
$1774\pm18\pm20$		[3] CHUNG	02	B852		$18.3\ \pi^-p \to \pi^+\pi^-\pi^-p$
$1863\pm9\pm10$		[4] CHUNG	02	B852		$18.3\ \pi^-p \to \pi^+\pi^-\pi^-p$
$1840\pm10\pm10$	1.2k	AMELIN	96B	VES	–	$37\ \pi^-A \to \eta\eta\pi^-A$
$1775\pm7\pm10$		[5] AMELIN	95B	VES	–	$36\ \pi^-A \to \pi^+\pi^-\pi^-A$
1790 ± 14		[6] BERDNIKOV	94	VES	–	$37\ \pi^-A \to K^+K^-\pi^-A$
$1873\pm33\pm20$		BELADIDZE	92C	VES	–	$36\ \pi^-\mathrm{Be} \to \pi^-\eta'\eta\mathrm{Be}$
$1814\pm10\pm23$	426	BITYUKOV	91	VES	–	$36\ \pi^-\mathrm{C} \to \pi^-\eta\eta\mathrm{C}$
1770 ± 30	1.1k	BELLINI	82	SPEC	–	$40\ \pi^-\mathrm{A} \to 3\pi\mathrm{A}$
• • • We do not use the following data for averages, fits, limits, etc. • • •						
$1785\pm9^{+12}_{-6}$	420k	[7] ALEKSEEV	10	COMP		$190\ \pi^-Pb \to \pi^-\pi^-\pi^+Pb'$
$1737\pm5\pm15$		AMELIN	99	VES		$37\ \pi^-A \to \omega\pi^-\pi^0A^*$

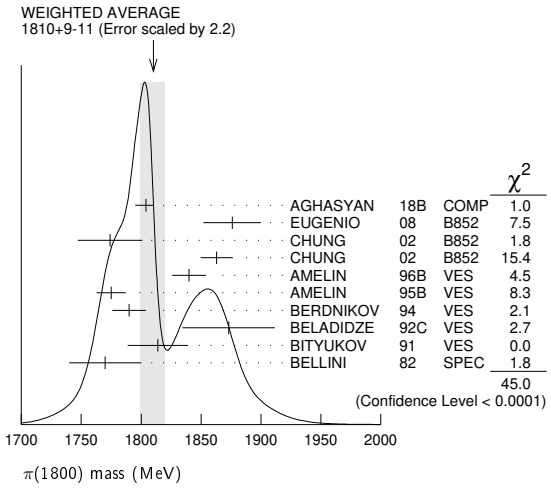

[1] Statistical error negligible.
[2] From a single-pole fit.
[3] In the $f_0(980)\pi$ wave.
[4] In the $f_0(500)\pi$ wave.
[5] From a fit to $J^{PC} = 0^{-+}$ $f_0(980)\pi$, $f_0(1370)\pi$ waves.
[6] From a fit to $J^{PC} = 0^{-+}$ $K_0^*(1430)K^-$ and $f_0(980)\pi^-$ waves.
[7] Superseded by AGHASYAN 2018B.

$\pi(1800)$ WIDTH

VALUE (MeV)	EVTS	DOCUMENT ID		TECN	CHG	COMMENT
215^{+7}_{-8} OUR AVERAGE						
220^{+8}_{-11}	46M	[8] AGHASYAN	18B	COMP		$190\ \pi^-p \to \pi^-\pi^+\pi^-p$
$221\pm26\pm38$	4k	[9] EUGENIO	08	B852	–	$18\ \pi^-p \to \eta\eta\pi^-p$
$223\pm48\pm50$		[10] CHUNG	02	B852		$18.3\ \pi^-p \to \pi^+\pi^-\pi^-p$
$191\pm21\pm20$		[11] CHUNG	02	B852		$18.3\ \pi^-p \to \pi^+\pi^-\pi^-p$
$210\pm30\pm30$	1.2k	AMELIN	96B	VES	–	$37\ \pi^-A \to \eta\eta\pi^-A$
$190\pm15\pm15$		[12] AMELIN	95B	VES	–	$36\ \pi^-A \to \pi^+\pi^-\pi^-A$
210 ± 70		[13] BERDNIKOV	94	VES	–	$37\ \pi^-A \to K^+K^-\pi^-A$
$225\pm35\pm20$		BELADIDZE	92C	VES	–	$36\ \pi^-\mathrm{Be} \to \pi^-\eta'\eta\mathrm{Be}$
$205\pm18\pm32$	426	BITYUKOV	91	VES	–	$36\ \pi^-\mathrm{C} \to \pi^-\eta\eta\mathrm{C}$
310 ± 50	1.1k	BELLINI	82	SPEC	–	$40\ \pi^-\mathrm{A} \to 3\pi\mathrm{A}$
• • • We do not use the following data for averages, fits, limits, etc. • • •						
$208\pm22^{+21}_{-37}$	420k	[14] ALEKSEEV	10	COMP		$190\ \pi^-Pb \to \pi^-\pi^-\pi^+Pb'$
$259\pm19\pm6$		AMELIN	99	VES		$37\ \pi^-A \to \omega\pi^-\pi^0A^*$

[8] Statistical error negligible.
[9] From a single-pole fit.
[10] In the $f_0(980)\pi$ wave.
[11] In the $f_0(500)\pi$ wave.
[12] From a fit to $J^{PC} = 0^{-+}$ $f_0(980)\pi$, $f_0(1370)\pi$ waves.
[13] From a fit to $J^{PC} = 0^{-+}$ $K_0^*(1430)K^-$ and $f_0(980)\pi^-$ waves.
[14] Superseded by AGHASYAN 2018B.

$\pi(1800)$ DECAY MODES

	Mode	Fraction (Γ_i/Γ)
Γ_1	$\pi^+\pi^-\pi^-$	seen
Γ_2	$f_0(500)\pi^-$	seen
Γ_3	$f_0(980)\pi^-$	seen
Γ_4	$f_0(1370)\pi^-$	seen
Γ_5	$f_0(1500)\pi^-$	not seen
Γ_6	$\rho\pi^-$	not seen
Γ_7	$\eta\eta\pi^-$	seen
Γ_8	$a_0(980)\eta$	seen
Γ_9	$a_2(1320)\eta$	not seen
Γ_{10}	$f_2(1270)\pi$	not seen
Γ_{11}	$f_0(1370)\pi^-$	not seen
Γ_{12}	$f_0(1500)\pi^-$	seen
Γ_{13}	$\eta\eta'(958)\pi^-$	seen
Γ_{14}	$K_0^*(1430)K^-$	seen
Γ_{15}	$K^*(892)K^-$	not seen

$\pi(1800)$ BRANCHING RATIOS

$\Gamma(f_0(980)\pi^-)/\Gamma(f_0(500)\pi^-)$ — Γ_3/Γ_2

VALUE	DOCUMENT ID		TECN	COMMENT
$0.44\pm0.08\pm0.38$	[15] CHUNG	02	B852	$18.3\ \pi^-p \to \pi^+\pi^-\pi^-p$

$\Gamma(f_0(980)\pi^-)/\Gamma(f_0(1370)\pi^-)$ — Γ_3/Γ_4

VALUE	DOCUMENT ID		TECN	CHG	COMMENT
• • • We do not use the following data for averages, fits, limits, etc. • • •					
1.7 ± 1.3	[16] AMELIN	95B	VES	–	$36\ \pi^-A \to \pi^+\pi^-\pi^-A$

$\Gamma(f_0(1370)\pi^-)/\Gamma_{total}$ — Γ_4/Γ

VALUE	DOCUMENT ID		TECN	CHG	COMMENT
seen	BELLINI	82	SPEC	–	$40\ \pi^-\mathrm{A} \to 3\pi\mathrm{A}$

$\Gamma(f_0(1500)\pi^-)/\Gamma_{total}$ — Γ_5/Γ

VALUE	DOCUMENT ID		TECN	COMMENT
not seen	CHUNG	02	B852	$18.3\ \pi^-p \to \pi^+\pi^-\pi^-p$

$\Gamma(\rho\pi^-)/\Gamma_{total}$ — Γ_6/Γ

VALUE	DOCUMENT ID		TECN	CHG	COMMENT
not seen	BELLINI	82	SPEC	–	$40\ \pi^-\mathrm{A} \to 3\pi\mathrm{A}$

Downloaded from https://academic.oup.com/ptep/article/2022/8/083C01/6651666 by KIT Library user on 27 September 2022

$\Gamma(\rho\pi^-)/\Gamma(f_0(980)\pi^-)$ — Γ_6/Γ_3

VALUE	CL%	DOCUMENT ID		TECN	CHG	COMMENT
• • • We do not use the following data for averages, fits, limits, etc. • • •						
<0.25		CHUNG	02	B852		$18.3\ \pi^- p \to \pi^+\pi^-\pi^- p$
<0.14	90	AMELIN	95B	VES	–	$36\ \pi^- A \to \pi^+\pi^-\pi^- A$

$\Gamma(\eta\eta\pi^-)/\Gamma(\pi^+\pi^-\pi^-)$ — Γ_7/Γ_1

VALUE	EVTS	DOCUMENT ID		TECN	CHG	COMMENT
• • • We do not use the following data for averages, fits, limits, etc. • • •						
0.5 ± 0.1	1200	[16] AMELIN	96B	VES	–	$37\ \pi^- A \to \eta\eta\pi^- A$

$\Gamma(a_2(1320)\eta)/\Gamma_{total}$ — Γ_9/Γ

VALUE	DOCUMENT ID		TECN	COMMENT
not seen	EUGENIO	08	B852	$18\ \pi^- p \to \eta\eta\pi^- p$

$\Gamma(f_2(1270)\pi)/\Gamma_{total}$ — Γ_{10}/Γ

VALUE	DOCUMENT ID		TECN	COMMENT
not seen	EUGENIO	08	B852	$18\ \pi^- p \to \eta\eta\pi^- p$

$\Gamma(f_0(1370)\pi^-)/\Gamma_{total}$ — Γ_{11}/Γ

VALUE	DOCUMENT ID		TECN	COMMENT
not seen	EUGENIO	08	B852	$18\ \pi^- p \to \eta\eta\pi^- p$

$\Gamma(f_0(1500)\pi^-)/\Gamma(a_0(980)\eta)$ — Γ_{12}/Γ_8

VALUE	EVTS	DOCUMENT ID		TECN	CHG	COMMENT
• • • We do not use the following data for averages, fits, limits, etc. • • •						
0.48 ± 0.17	4k	[16,17] EUGENIO	08	B852	–	$18\ \pi^- p \to \eta\eta\pi^- p$
$0.030^{+0.014}_{-0.011}$		[16] ANISOVICH	01B	SPEC	0	0.6–$1.94\ p\bar{p} \to \eta\eta\pi^0\pi^0$
0.08 ± 0.03	1200	[16,18] AMELIN	96B	VES	–	$37\ \pi^- A \to \eta\eta\pi^- A$

$\Gamma(\eta\eta'(958)\pi^-)/\Gamma(\eta\eta\pi^-)$ — Γ_{13}/Γ_7

VALUE	EVTS	DOCUMENT ID		TECN	CHG	COMMENT
• • • We do not use the following data for averages, fits, limits, etc. • • •						
0.29 ± 0.07		[16] BELADIDZE	92C	VES	–	$36\ \pi^- \mathrm{Be} \to \pi^-\eta'\eta\mathrm{Be}$
0.3 ± 0.1	426 ± 57	[16] BITYUKOV	91	VES	–	$36\ \pi^- \mathrm{C} \to \pi^-\eta\eta\mathrm{C}$

$\Gamma(K_0^*(1430)K^-)/\Gamma_{total}$ — Γ_{14}/Γ

VALUE	DOCUMENT ID		TECN	CHG	COMMENT
seen	BERDNIKOV	94	VES	–	$37\ \pi^- A \to K^+K^-\pi^- A$

$\Gamma(K^*(892)K^-)/\Gamma_{total}$ — Γ_{15}/Γ

VALUE	DOCUMENT ID		TECN	CHG	COMMENT
not seen	BERDNIKOV	94	VES	–	$37\ \pi^- A \to K^+K^-\pi^- A$

[15] Assuming that $f_0(980)$ decays only to $\pi\pi$.
[16] Systematic errors not estimated.
[17] From a single-pole fit.
[18] Assuming that $f_0(1500)$ decays only to $\eta\eta$ and $a_0(980)$ decays only to $\eta\pi$.

$\pi(1800)$ REFERENCES

AGHASYAN	18B	PR D98 092003	M. Aghasyan *et al.*	(COMPASS Collab.)
ALEKSEEV	10	PRL 104 241803	M.G. Alekseev *et al.*	(COMPASS Collab.)
EUGENIO	08	PL B660 466	P. Eugenio *et al.*	(BNL E852 Collab.)
CHUNG	02	PR D65 072001	S.U. Chung *et al.*	(BNL E852 Collab.)
ANISOVICH	01B	PL B500 222	A.V. Anisovich *et al.*	
AMELIN	99	PAN 62 445	D.V. Amelin *et al.*	(VES Collab.)
		Translated from YAF 62 487.		
AMELIN	96B	PAN 59 976	D.V. Amelin *et al.*	(SERP, TBIL) IGJPC
		Translated from YAF 59 1021.		
AMELIN	95B	PL B356 595	D.V. Amelin *et al.*	(SERP, TBIL)
BERDNIKOV	94	PL B337 219	E.B. Berdnikov *et al.*	(SERP, TBIL)
BELADIDZE	92C	SJNP 55 1535	G.M. Beladidze, S.I. Bityukov, G.V. Borisov	(SERP+)
		Translated from YAF 55 2748.		
BITYUKOV	91	PL B268 137	S.I. Bityukov *et al.*	(SERP, TBIL)
BELLINI	82	PRL 48 1697	G. Bellini *et al.*	(MILA, BGNA, JINR)

$f_2(1810)$

$I^G(J^{PC}) = 0^+(2^{++})$

OMITTED FROM SUMMARY TABLE

Needs confirmation.

$f_2(1810)$ MASS

VALUE (MeV)	EVTS	DOCUMENT ID		TECN	COMMENT
1815 ±12 OUR AVERAGE		Error includes scale factor of 1.4. See the ideogram below.			
$1822\ ^{+29}_{-24}\ ^{+66}_{-57}$	5.5k	[1] ABLIKIM	13N	BES3	$e^+e^- \to J/\psi \to \gamma\eta\eta$
$1737 \pm 9\ ^{+198}_{-65}$		[2] UEHARA	10A	BELL	$10.6\ e^+e^- \to e^+e^-\eta\eta$
1800 ± 30	40	ALDE	88D	GAM4	$300\ \pi^- p \to \pi^- p 4\pi^0$
1806 ± 10	1600	ALDE	87	GAM4	$100\ \pi^- p \to 4\pi^0 n$
1870 ± 40		[3] ALDE	86D	GAM4	$100\ \pi^- p \to \eta\eta n$
$1857\ ^{+35}_{-24}$		[4] COSTA	80	OMEG	$10\ \pi^- p \to K^+K^- n$
• • • We do not use the following data for averages, fits, limits, etc. • • •					
$1845.0 \pm 2.2\ ^{+1.6}_{-7.2}$		[5] ALBRECHT	20	RVUE	$0.9\ \bar{p}p \to \pi^0\pi^0\eta$, $\pi^0\eta\eta$, $\pi^0 K^+K^-$
$1858\ ^{+18}_{-71}$		[6] LONGACRE	86	RVUE	Compilation
1799 ± 15		[7] CASON	82	STRC	$8\ \pi^+ p \to \Delta^{++}\pi^0\pi^0$

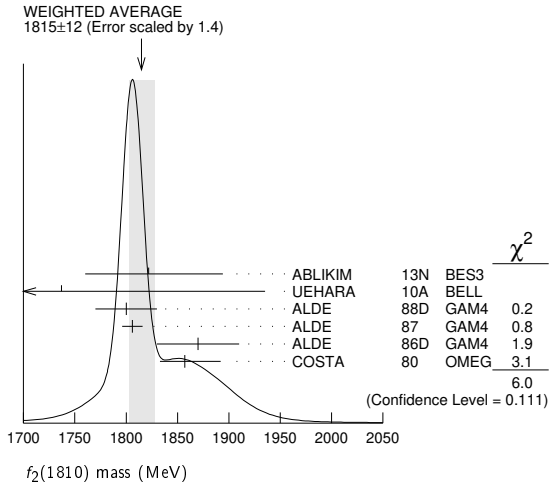

[1] From partial wave analysis including all possible combinations of 0^{++}, 2^{++}, and 4^{++} resonances.
[2] Breit-Wigner mass. Could also be the $f_2(1910)$.
[3] Seen in only one solution.
[4] Error increased by spread of two solutions. Included in LONGACRE 86 global analysis.
[5] T-matrix pole, 4 poles, 4 channels, including scattering data from HYAMS 75 ($\pi\pi$), LONGACRE 86 ($K\bar{K}$), BINON 83 ($\eta\eta$).
[6] From a partial-wave analysis of data using a K-matrix formalism with 5 poles. Includes compilation of several other experiments.
[7] From an amplitude analysis of the reaction $\pi^+\pi^- \to 2\pi^0$. The resonance in the $2\pi^0$ final state is not confirmed by PROKOSHKIN 97.

$f_2(1810)$ WIDTH

VALUE (MeV)	EVTS	DOCUMENT ID		TECN	COMMENT
197 ± 22 OUR AVERAGE		Error includes scale factor of 1.5. See the ideogram below.			
$229\ ^{+52}_{-42}\ ^{+88}_{-155}$	5.5k	[1] ABLIKIM	13N	BES3	$e^+e^- \to J/\psi \to \gamma\eta\eta$
$228\ ^{+21}_{-20}\ ^{+234}_{-153}$		[2] UEHARA	10A	BELL	$10.6\ e^+e^- \to e^+e^-\eta\eta$
160 ± 30	40	ALDE	88D	GAM4	$300\ \pi^- p \to \pi^- p 4\pi^0$
190 ± 20	1600	ALDE	87	GAM4	$100\ \pi^- p \to 4\pi^0 n$
250 ± 30		[3] ALDE	86D	GAM4	$100\ \pi^- p \to \eta\eta n$
$185\ ^{+102}_{-139}$		[4] COSTA	80	OMEG	$10\ \pi^- p \to K^+K^- n$
• • • We do not use the following data for averages, fits, limits, etc. • • •					
$260.9 \pm 3.9\ ^{+199.9}_{-38.2}$		[5] ALBRECHT	20	RVUE	$0.9\ \bar{p}p \to \pi^0\pi^0\eta$, $\pi^0\eta\eta$, $\pi^0 K^+K^-$
$388\ ^{+15}_{-21}$		[6] LONGACRE	86	RVUE	Compilation
$280\ ^{+42}_{-35}$		[7] CASON	82	STRC	$8\ \pi^+ p \to \Delta^{++}\pi^0\pi^0$

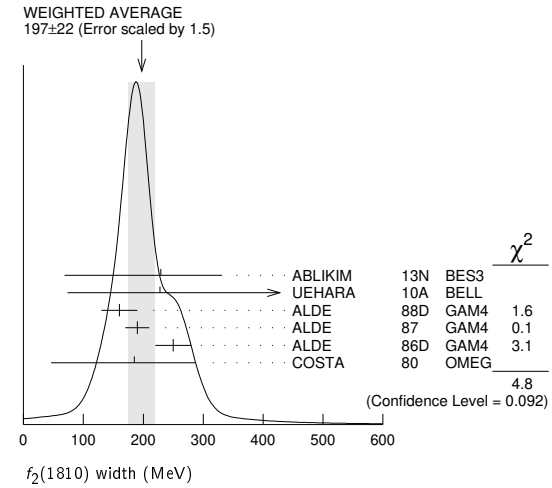

Downloaded from https://academic.oup.com/ptep/article/2022/8/083C01/6651666 by KIT Library user on 27 September 2022

[1] From partial wave analysis including all possible combinations of 0^{++}, 2^{++}, and 4^{++} resonances.
[2] Breit-Wigner width. Could also be the $f_2(1910)$.
[3] Seen in only one solution.
[4] Error increased by spread of two solutions. Included in LONGACRE 86 global analysis.
[5] T-matrix pole, 4 poles, 4 channels, including scattering data from HYAMS 75 ($\pi\pi$), LONGACRE 86 ($K\overline{K}$), BINON 83 ($\eta\eta$).
[6] From a partial-wave analysis of data using a K-matrix formalism with 5 poles. Includes compilation of several other experiments.
[7] From an amplitude analysis of the reaction $\pi^+\pi^- \rightarrow 2\pi^0$. The resonance in the $2\pi^0$ final state is not confirmed by PROKOSHKIN 97.

$f_2(1810)$ DECAY MODES

	Mode	Fraction (Γ_i/Γ)
Γ_1	$\pi\pi$	
Γ_2	$\eta\eta$	seen
Γ_3	$4\pi^0$	seen
Γ_4	K^+K^-	
Γ_5	$\gamma\gamma$	seen

$f_2(1810)$ $\Gamma(i)\Gamma(\gamma\gamma)/\Gamma(\text{total})$

$\Gamma(\eta\eta) \times \Gamma(\gamma\gamma)/\Gamma_{\text{total}}$ — $\Gamma_2\Gamma_5/\Gamma$

VALUE (eV)	DOCUMENT ID		TECN	COMMENT
$5.2^{+0.9+37.3}_{-0.8-4.5}$	[1] UEHARA	10A	BELL	$10.6\ e^+e^- \rightarrow e^+e^-\eta\eta$

[1] Including interference with the $f_2'(1525)$ (parameters fixed to the values from the 2008 edition of this review, PDG 08) and $f_2(1270)$. May also be the $f_0(1500)$.

$f_2(1810)$ BRANCHING RATIOS

$\Gamma(\pi\pi)/\Gamma_{\text{total}}$ — Γ_1/Γ

VALUE	DOCUMENT ID		TECN	COMMENT
• • • We do not use the following data for averages, fits, limits, etc. • • •				
not seen	AMSLER	02	CBAR	$0.9\ \overline{p}p \rightarrow \pi^0\eta\eta, \pi^0\pi^0\pi^0$
not seen	PROKOSHKIN	97	GAM2	$38\ \pi^-p \rightarrow \pi^0\pi^0 n$
$0.21^{+0.02}_{-0.03}$	[1] LONGACRE	86	RVUE	Compilation
0.44 ± 0.03	[2] CASON	82	STRC	$8\ \pi^+p \rightarrow \Delta^{++}\pi^0\pi^0$

[1] From a partial-wave analysis of data using a K-matrix formalism with 5 poles. Includes compilation of several other experiments.
[2] Included in LONGACRE 86 global analysis.

$\Gamma(\eta\eta)/\Gamma_{\text{total}}$ — Γ_2/Γ

VALUE	DOCUMENT ID		TECN	COMMENT
seen	ABLIKIM	13N	BES3	PWA of $J/\psi \rightarrow \gamma\eta\eta$
• • • We do not use the following data for averages, fits, limits, etc. • • •				
$0.008^{+0.028}_{-0.003}$	[1] LONGACRE	86	RVUE	Compilation

[1] From a partial-wave analysis of data using a K-matrix formalism with 5 poles. Includes compilation of several other experiments.

$\Gamma(\pi\pi)/\Gamma(4\pi^0)$ — Γ_1/Γ_3

VALUE	DOCUMENT ID		TECN	COMMENT
• • • We do not use the following data for averages, fits, limits, etc. • • •				
<0.75	ALDE	87	GAM4	$100\ \pi^-p \rightarrow 4\pi^0 n$

$\Gamma(4\pi^0)/\Gamma(\eta\eta)$ — Γ_3/Γ_2

VALUE	DOCUMENT ID		TECN	COMMENT
• • • We do not use the following data for averages, fits, limits, etc. • • •				
0.8 ± 0.3	ALDE	87	GAM4	$100\ \pi^-p \rightarrow 4\pi^0 n$

$\Gamma(K^+K^-)/\Gamma_{\text{total}}$ — Γ_4/Γ

VALUE	DOCUMENT ID		TECN	COMMENT
• • • We do not use the following data for averages, fits, limits, etc. • • •				
$0.003^{+0.019}_{-0.002}$	[1] LONGACRE	86	RVUE	Compilation
seen	COSTA	80	OMEG	$10\ \pi^-p \rightarrow K^+K^-n$

[1] From a partial-wave analysis of data using a K-matrix formalism with 5 poles. Includes compilation of several other experiments.

$f_2(1810)$ REFERENCES

ALBRECHT	20	EPJ C80 453	M. Albrecht *et al.*	(Crystal Barrel Collab.)
ABLIKIM	13N	PR D87 092009	M. Ablikim *et al.*	(BESIII Collab.)
UEHARA	10A	PR D82 114031	S. Uehara *et al.*	(BELLE Collab.)
PDG	08	PL B667 1	C. Amsler *et al.*	(PDG Collab.)
AMSLER	02	EPJ C23 29	C. Amsler *et al.*	
PROKOSHKIN	97	PD 42 117	Y.D. Prokoshkin *et al.*	(SERP)
		Translated from DANS 353 323.		
ALDE	88D	SJNP 47 810	D.M. Alde *et al.*	(SERP, BELG, LANL, LAPP+)
		Translated from YAF 47 1273.		
ALDE	87	PL B198 286	D.M. Alde *et al.*	(LANL, BRUX, SERP, LAPP)
ALDE	86D	NP B269 485	D.M. Alde *et al.*	(BELG, LAPP, SERP, CERN+)
LONGACRE	86	PL B177 223	R.S. Longacre *et al.*	(BNL, BRAN, CUNY+)
BINON	83	NC 78A 313	F.G. Binon *et al.*	(BELG, LAPP, SERP+)
CASON	82	PRL 48 1316	N.M. Cason *et al.*	(NDAM, ANL)
COSTA	80	NP B175 402	G. Costa *et al.*	(BARI, BONN, CERN, GLAS+)
HYAMS	75	NP B100 205	B.D. Hyams *et al.*	(CERN, MPIM)

$X(1835)$

$I^G(J^{PC}) = ?^?(0^{-+})$

OMITTED FROM SUMMARY TABLE

Could be a superposition of two states, one with small width appearing as threshold enhancement in $p\overline{p}$, the other one with a larger width. For the former ABLIKIM 12D determine $J^{PC} = 0^{-+}$.

$X(1835)$ MASS

VALUE (MeV)	EVTS	DOCUMENT ID		TECN	COMMENT
$1826.5^{+13.0}_{-3.4}$ OUR AVERAGE					
$1825.3 \pm 2.4^{+17.3}_{-2.4}$		[1] ABLIKIM	16J	BES3	$J/\psi \rightarrow \gamma\pi^+\pi^-\eta'$
$1844 \pm 9^{+16}_{-25}$		ABLIKIM	15T	BES3	$J/\psi \rightarrow \gamma K^0_S K^0_S \eta$
• • • We do not use the following data for averages, fits, limits, etc. • • •					
$1839 \pm 26 \pm 26$		[2] ABLIKIM	18I	BES3	$J/\psi \rightarrow \gamma\gamma\phi(1020)$
$1909.5 \pm 15.9^{+9.4}_{-27.5}$		[3] ABLIKIM	16J	BES3	$J/\psi \rightarrow \gamma\pi^+\pi^-\eta'$
$1842.2 \pm 4.2^{+7.1}_{-2.6}$	0.6k	ABLIKIM	13U	BES3	$J/\psi \rightarrow \gamma 3(\pi^+\pi^-)$
$1832^{+19}_{-5} \pm 26$		[4] ABLIKIM	12D	BES3	$J/\psi \rightarrow \gamma p\overline{p}$
$1836.5 \pm 3.0^{+5.6}_{-2.1}$	4265	[5] ABLIKIM	11C	BES3	$J/\psi \rightarrow \gamma\pi^+\pi^-\eta'$
$1877.3 \pm 6.3^{+3.4}_{-7.4}$		[6] ABLIKIM	11J	BES3	$J/\psi \rightarrow \omega(\eta\pi^+\pi^-)$
$1837^{+10}_{-12} {}^{+9}_{-7}$	231	[7,8] ALEXANDER	10	CLEO	$J/\psi \rightarrow \gamma p\overline{p}$
$1833.7 \pm 6.1 \pm 2.7$	264	ABLIKIM	05R	BES2	$J/\psi \rightarrow \gamma\pi^+\pi^-\eta'$
1831 ± 7		[8,9] ABLIKIM	05R	BES2	$J/\psi \rightarrow \gamma p\overline{p}$
$1859^{+3}_{-10} {}^{+5}_{-25}$		[8] BAI	03F	BES2	$J/\psi \rightarrow \gamma p\overline{p}$

[1] From a fit of the measured $\pi^+\pi^-\eta'$ lineshape that accounts for the abrupt distortion observed at the $p\overline{p}$ threshold through interference with a second previously unseen narrow resonance near 1870 MeV. The fit uses Breit-Wigner functions for the signal shapes and includes known backgrounds and contributors.
[2] From a fit to $\gamma\phi$ invariant mass. Angular analysis consistent with $J^{PC} = 0^{-+}$. Other J^{PC} not excluded.
[3] Pole mass from a fit of the measured $\pi^+\pi^-\eta'$ lineshape to a Flatte formula that accounts for the abrupt distortion observed at the $p\overline{p}$ threshold; the fit also includes known backgrounds and contributors, as well as an *ad hoc* Breit-Wigner function ($M \approx 1919$ MeV; $\Gamma \approx 51$ MeV) that is required for a good fit.
[4] From the fit including final state interaction effects in isospin 0 *S*-wave according to SIBIRTSEV 05A. Supersedes ABLIKIM 10G.
[5] From a fit of the $\pi^+\pi^-\eta'$ mass distribution to a combination of $\gamma f_1(1510)$, $\gamma X(1835)$, and two states $\gamma X(2120)$ and $\gamma X(2370)$, for $M(\pi^+\pi^-\eta') < 2.8$ GeV,and accounting for backgrounds from non-η' events and $J/\psi \rightarrow \pi^0\pi^+\pi^-\eta'$.
[6] The selected process is $J/\psi \rightarrow \omega a_0(980)\pi$. This state may be due also to $\eta_2(1870)$ or to a combination of $X(1835)$ and $\eta_2(1870)$.
[7] From a fit of the $p\overline{p}$ mass distribution to a combination of $\gamma X(1835)$, γR with $M(R) = 2100$ MeV and $\Gamma(R) = 160$ MeV, and $\gamma p\overline{p}$ phase space, for $M(p\overline{p}) < 2.85$ GeV.
[8] Evidence for a threshold enhancement in the $p\overline{p}$ mass spectrum was also reported by ABE 02K, AUBERT,B 05L, and WANG 05A in $B^+ \rightarrow p\overline{p}K^+$, WANG 05A in $B^0 \rightarrow p\overline{p}K^0_S$, ABE 02W in $\overline{B}^0 \rightarrow p\overline{p}D^0$, DEL-AMO-SANCHEZ 12 in $B \rightarrow D(D^*)p\overline{p}(\pi)$, and WEI 08 in $B^+ \rightarrow p\overline{p}\pi^+$ decays. Not seen by ATHAR 06 in $\Upsilon(1S) \rightarrow p\overline{p}\gamma$.
[9] From the fit including final state interaction effects in isospin 0 *S*-wave according to SIBIRTSEV 05A. Systematic errors not estimated.

$X(1835)$ WIDTH

VALUE (MeV)	CL%	EVTS	DOCUMENT ID		TECN	COMMENT
242^{+14}_{-15} OUR AVERAGE						
$245.2 \pm 13.1^{+4.6}_{-9.6}$			[1] ABLIKIM	16J	BES3	$J/\psi \rightarrow \gamma\pi^+\pi^-\eta'$
$192^{+20}_{-17} {}^{+62}_{-43}$			ABLIKIM	15T	BES3	$J/\psi \rightarrow \gamma K^0_S K^0_S \eta$
• • • We do not use the following data for averages, fits, limits, etc. • • •						
$175 \pm 57 \pm 25$			[2] ABLIKIM	18I	BES3	$J/\psi \rightarrow \gamma\gamma\phi(1020)$
$273.5 \pm 21.4^{+6.1}_{-64.0}$			[3] ABLIKIM	16J	BES3	$J/\psi \rightarrow \gamma\pi^+\pi^-\eta'$
$83 \pm 14 \pm 11$		0.6k	ABLIKIM	13U	BES3	$J/\psi \rightarrow \gamma 3(\pi^+\pi^-)$
< 76	90		[4] ABLIKIM	12D	BES3	$J/\psi \rightarrow \gamma p\overline{p}$
$190 \pm 9^{+38}_{-36}$		4265	[5] ABLIKIM	11C	BES3	$J/\psi \rightarrow \gamma\pi^+\pi^-\eta'$
$57 \pm 12^{+19}_{-4}$			[6] ABLIKIM	11J	BES3	$J/\psi \rightarrow \omega(\eta\pi^+\pi^-)$
0^{+44}_{-0}		231	[7,8] ALEXANDER	10	CLEO	$J/\psi \rightarrow \gamma p\overline{p}$
$67.7 \pm 20.3 \pm 7.7$		264	ABLIKIM	05R	BES2	$J/\psi \rightarrow \gamma\pi^+\pi^-\eta'$
< 153	90		[8,9] ABLIKIM	05R	BES2	$J/\psi \rightarrow \gamma p\overline{p}$
< 30			[8] BAI	03F	BES2	$J/\psi \rightarrow \gamma p\overline{p}$

[1] From a fit of the measured $\pi^+\pi^-\eta'$ lineshape that accounts for the abrupt distortion observed at the $p\overline{p}$ threshold through interference with a second previously unseen narrow resonance near 1870 MeV. The fit uses Breit-Wigner functions for the signal shapes and includes known backgrounds and contributors.
[2] From a fit to $\gamma\phi$ invariant mass. Angular analysis consistent with $J^{PC} = 0^{-+}$. Other J^{PC} not excluded.

Downloaded from https://academic.oup.com/ptep/article/2022/8/083C01/6651666 by KIT Library user on 27 September 2022

[3] Pole width from a fit of the measured $\pi^+\pi^-\eta'$ lineshape to a Flatte formula that accounts for the abrupt distortion observed at the $p\overline{p}$ threshold; the fit also includes known backgrounds and contributors, as well as an *ad hoc* Breit-Wigner function (M $\approx$ 1919 MeV; $\Gamma \approx$ 51 MeV) that is required for a good fit.

[4] From the fit including final state interaction effects in isospin 0 *S*-wave according to SIBIRTSEV 05A. Supersedes ABLIKIM 10G.

[5] From a fit of the $\pi^+\pi^-\eta'$ mass distribution to a combination of $\gamma f_1(1510)$, $\gamma X(1835)$, and two states $\gamma X(2120)$ and $\gamma X(2370)$, for $M(\pi^+\pi^-\eta') < 2.8$ GeV,and accounting for backgrounds from non-η' events and $J/\psi \to \pi^0\pi^+\pi^-\eta'$.

[6] The selected process is $J/\psi \to \omega a_0(980)\pi$. This state may be due also to $\eta_2(1870)$ or to a combination of $X(1835)$ and $\eta_2(1870)$.

[7] From a fit of the $p\overline{p}$ mass distribution to a combination of $\gamma X(1835)$, γR with $M(R) = 2100$ MeV and $\Gamma(R) = 160$ MeV, and $\gamma p\overline{p}$ phase space, for $M(p\overline{p}) < 2.85$ GeV.

[8] Evidence for a threshold enhancement in the $p\overline{p}$ mass spectrum was also reported by ABE 02K, AUBERT,B 05L, and WANG 05A in $B^+ \to p\overline{p}K^+$, WANG 05A in $B^0 \to p\overline{p}K^0_S$, ABE 02W in $\overline{B}^0 \to p\overline{p}D^0$, DEL-AMO-SANCHEZ 12 in $B \to D(D^*)p\overline{p}(\pi)$, and WEI 08 in $B^+ \to p\overline{p}\pi^+$ decays. Not seen by ATHAR 06 in $\Upsilon(1S) \to p\overline{p}\gamma$.

[9] From the fit including final state interaction effects in isospin 0 *S*-wave according to SIBIRTSEV 05A. Systematic errors not estimated.

X(1835) DECAY MODES

	Mode	Fraction (Γ_i/Γ)
Γ_1	$p\overline{p}$	seen
Γ_2	$\eta'\pi^+\pi^-$	seen
Γ_3	$\gamma\gamma$	
Γ_4	$K^0_S K^0_S \eta$	seen
Γ_5	$\gamma\phi(1020)$	possibly seen
Γ_6	$3(\pi^+\pi^-)$	seen

X(1835) Γ(i)Γ(γγ)/Γ(total)

$\Gamma(\eta'\pi^+\pi^-) \times \Gamma(\gamma\gamma)/\Gamma_{total}$ — $\Gamma_2\Gamma_3/\Gamma$

VALUE (eV)	CL%	DOCUMENT ID		TECN	COMMENT
• • • We do not use the following data for averages, fits, limits, etc. • • •					
<35.6	90	[1] ZHANG	12A	BELL	$e^+e^- \to e^+e^-\eta'\pi^+\pi^-$
<83	90	[2] ZHANG	12A	BELL	$e^+e^- \to e^+e^-\eta'\pi^+\pi^-$

[1] From a two-resonance fit and constructive interference of the $\eta(1760)$ and $X(1835)$, a significance of 2.8 σ.

[2] From a two-resonance fit and destructive interference of the $\eta(1760)$ and $X(1835)$, a significance of 2.8 σ.

X(1835) BRANCHING RATIOS

$\Gamma(p\overline{p})/\Gamma(\eta'\pi^+\pi^-)$ — Γ_1/Γ_2

VALUE	DOCUMENT ID		TECN	COMMENT
• • • We do not use the following data for averages, fits, limits, etc. • • •				
0.333	ABLIKIM	05R	BES2	$J/\psi \to \gamma\pi^+\pi^-\eta'$

$\Gamma(\eta'\pi^+\pi^-)/\Gamma(K^0_S K^0_S \eta)$ — Γ_2/Γ_4

VALUE	DOCUMENT ID		TECN	COMMENT
• • • We do not use the following data for averages, fits, limits, etc. • • •				
6.7±1.8	[1] ABLIKIM	15T	BES3	$J/\psi \to \gamma K^0_S K^0_S \eta$

[1] Using resutls from ABLIKIM 05R.

$\Gamma(\eta'\pi^+\pi^-)/\Gamma_{total}$ — Γ_2/Γ

VALUE	DOCUMENT ID		TECN	COMMENT
seen	[1] ABLIKIM	16J	BES3	$J/\psi \to \gamma\pi^+\pi^-\eta'$

[1] ABLIKIM 16J quotes B($J/\psi \to \gamma X(1835)$) × B($X(1835) \to \pi^+\pi^-\eta'$) = (3.93 ± $0.38^{+0.31}_{-0.84}$)×10^{-4} from a fit of the measured $\pi^+\pi^-\eta'$ lineshape that accounts for the abrupt distortion observed at the $p\overline{p}$ threshold with a Flatte formula in addition to known backgrounds and contributors, as well as an *ad hoc* Breit-Wigner (M $\approx$ 1919 MeV; $\Gamma \approx$ 51 MeV) that is required for a good fit. Another explanation for the distortion provided by ABLIKIM 16J is that a second resonance near 1870 MeV interferes with the $X(1835)$; fits to this possibility yield product branching fraction values compatible with that shown within the respective systematic uncertainties.

$\Gamma(\gamma\phi(1020))/\Gamma_{total}$ — Γ_5/Γ

VALUE	DOCUMENT ID		TECN	COMMENT
possibly seen	[1] ABLIKIM	18I	BES3	$J/\psi \to \gamma\gamma\phi(1020)$

[1] Seen as a peak in $\gamma\phi$ invariant mass. Angular analysis consistent with $J^{PC} = 0^{-+}$. Other J^{PC} not excluded.

$\Gamma(\gamma\gamma)/\Gamma(\eta'\pi^+\pi^-)$ — Γ_3/Γ_2

VALUE	CL%	DOCUMENT ID		TECN	COMMENT
<9.80 × 10^{-3}	90	[1] ABLIKIM	18O	BES3	$\psi(2S) \to \pi^+\pi^-\gamma\gamma\gamma$

[1] Using results from ABLIKIM 16J.

$\Gamma(3(\pi^+\pi^-))/\Gamma_{total}$ — Γ_6/Γ

VALUE	EVTS	DOCUMENT ID		TECN	COMMENT
seen	0.6k	ABLIKIM	13U	BES3	$J/\psi \to \gamma 3(\pi^+\pi^-)$

X(1835) REFERENCES

ABLIKIM	18I	PR D97 051101	M. Ablikim *et al.*	(BESIII Collab.)
ABLIKIM	18O	PR D97 072014	M. Ablikim *et al.*	(BESIII Collab.)
ABLIKIM	16J	PRL 117 042002	M. Ablikim *et al.*	(BESIII Collab.)
ABLIKIM	15T	PRL 115 091803	M. Ablikim *et al.*	(BESIII Collab.)
ABLIKIM	13U	PR D88 091502	M. Ablikim *et al.*	(BESIII Collab.)
ABLIKIM	12D	PRL 108 112003	M. Ablikim *et al.*	(BESIII Collab.) JPC
DEL-AMO-SA...	12	PR D85 092017	P. del Amo Sanchez *et al.*	(BABAR Collab.)
ZHANG	12A	PR D86 052002	C.C. Zhang *et al.*	(BELLE Collab.)
ABLIKIM	11C	PRL 106 072002	M. Ablikim *et al.*	(BESIII Collab.)
ABLIKIM	11J	PRL 107 182001	M. Ablikim *et al.*	(BESIII Collab.)
ABLIKIM	10G	CP C34 421	M. Ablikim *et al.*	(BESIII Collab.)
ALEXANDER	10	PR D82 092002	J.P. Alexander *et al.*	(CLEO Collab.)
WEI	08	PL B659 80	J.-T. Wei *et al.*	(BELLE Collab.)
ATHAR	06	PR D73 032001	S.B. Athar *et al.*	(CLEO Collab.)
ABLIKIM	05R	PRL 95 262001	M. Ablikim *et al.*	(BES Collab.)
AUBERT,B	05L	PR D72 051101	B. Aubert *et al.*	(BABAR Collab.)
SIBIRTSEV	05A	PR D71 054010	A. Sibirtsev, J. Haidenbauer	
WANG	05A	PL B617 141	M.-Z. Wang *et al.*	(BELLE Collab.)
BAI	03F	PRL 91 022001	J.Z. Bai *et al.*	(BES II Collab.)
ABE	02K	PRL 88 181803	K. Abe *et al.*	(BELLE Collab.)
ABE	02W	PRL 89 151802	K. Abe *et al.*	(BELLE Collab.)

$\phi_3(1850)$

$I^G(J^{PC}) = 0^-(3^{--})$

$\phi_3(1850)$ MASS

VALUE (MeV)	EVTS	DOCUMENT ID		TECN	COMMENT
1854± 7 OUR AVERAGE					
1855±10		ASTON	88E	LASS	11 $K^-p \to K^-K^+\Lambda$, $K^0_S K^\pm\pi^\mp\Lambda$
1870^{+30}_{-20}	430	ARMSTRONG	82	OMEG	18.5 $K^-p \to K^-K^+\Lambda$
1850±10	123	ALHARRAN	81B	HBC	8.25 $K^-p \to K\overline{K}\Lambda$

$\phi_3(1850)$ WIDTH

VALUE (MeV)	EVTS	DOCUMENT ID		TECN	COMMENT
87^{+28}_{-23} OUR AVERAGE Error includes scale factor of 1.2.					
64±31		ASTON	88E	LASS	11 $K^-p \to K^-K^+\Lambda$, $K^0_S K^\pm\pi^\mp\Lambda$
160^{+90}_{-50}	430	ARMSTRONG	82	OMEG	18.5 $K^-p \to K^-K^+\Lambda$
80^{+40}_{-30}	123	ALHARRAN	81B	HBC	8.25 $K^-p \to K\overline{K}\Lambda$

$\phi_3(1850)$ DECAY MODES

	Mode	Fraction (Γ_i/Γ)
Γ_1	$K\overline{K}$	seen
Γ_2	$K\overline{K}^*(892)+$ c.c.	seen

$\phi_3(1850)$ BRANCHING RATIOS

$\Gamma(K\overline{K}^*(892)+\text{c.c.})/\Gamma(K\overline{K})$ — Γ_2/Γ_1

VALUE	DOCUMENT ID		TECN	COMMENT
$0.55^{+0.85}_{-0.45}$	ASTON	88E	LASS	11 $K^-p \to K^-K^+\Lambda$, $K^0_S K^\pm\pi^\mp\Lambda$
• • • We do not use the following data for averages, fits, limits, etc. • • •				
0.8 ±0.4	ALHARRAN	81B	HBC	8.25 $K^-p \to K\overline{K}\pi\Lambda$

$\phi_3(1850)$ REFERENCES

ASTON	88E	PL B208 324	D. Aston *et al.*	(SLAC, NAGO, CINC, INUS) IGJPC
ARMSTRONG	82	PL 110B 77	T.A. Armstrong *et al.*	(BARI, BIRM, CERN+) JP
ALHARRAN	81B	PL 101B 357	S. Al-Harran *et al.*	(BIRM, CERN, GLAS+)

$\eta_2(1870)$

$I^G(J^{PC}) = 0^+(2^{-+})$

$\eta_2(1870)$ MASS

VALUE (MeV)	EVTS	DOCUMENT ID		TECN	COMMENT
1842± 8 OUR AVERAGE					
1835±12		BARBERIS	00B		450 $pp \to p_f\eta\pi^+\pi^-p_s$
1844±13		BARBERIS	00C		450 $pp \to p_f 4\pi p_s$
1840±25		BARBERIS	97B	OMEG	450 $pp \to pp2(\pi^+\pi^-)$
1875±20±35		ADOMEIT	96	CBAR	1.94 $\overline{p}p \to \eta 3\pi^0$
1881±32±40	26	KARCH	92	CBAL	$e^+e^- \to e^+e^-\eta\pi^0\pi^0$
• • • We do not use the following data for averages, fits, limits, etc. • • •					
1860± 5±15		ANISOVICH	00E	SPEC	0.9–1.94 $\overline{p}p \to \eta 3\pi^0$
1840±15		BAI	99	BES	$J/\psi \to \gamma\eta\pi^+\pi^-$

Downloaded from https://academic.oup.com/ptep/article/2022/8/083C01/6651666 by KIT Library user on 27 September 2022

$\eta_2(1870)$ WIDTH

VALUE (MeV)	EVTS	DOCUMENT ID		TECN	COMMENT
225±14 OUR AVERAGE					
235±22		BARBERIS	00B		450 $pp \to p_f \eta\pi^+\pi^- p_s$
228±23		BARBERIS	00C		450 $pp \to p_f 4\pi p_s$
200±40		BARBERIS	97B	OMEG	450 $pp \to pp2(\pi^+\pi^-)$
200±25±45		ADOMEIT	96	CBAR	1.94 $\overline{p}p \to \eta 3\pi^0$
221±92±44	26	KARCH	92	CBAL	$e^+e^- \to e^+e^-\eta\pi^0\pi^0$
• • • We do not use the following data for averages, fits, limits, etc. • • •					
$250\pm25^{+50}_{-35}$		ANISOVICH	00E	SPEC	0.9–1.94 $\overline{p}p \to \eta 3\pi^0$
170±40		BAI	99	BES	$J/\psi \to \gamma\eta\pi^+\pi^-$

$\eta_2(1870)$ DECAY MODES

	Mode	Fraction (Γ_i/Γ)
Γ_1	$\eta\pi\pi$	seen
Γ_2	$a_2(1320)\pi$	seen
Γ_3	$f_2(1270)\eta$	seen
Γ_4	$a_0(980)\pi$	seen
Γ_5	$\gamma\gamma$	seen

$\eta_2(1870)$ BRANCHING RATIOS

$\Gamma(a_2(1320)\pi)/\Gamma(f_2(1270)\eta)$ — Γ_2/Γ_3

VALUE	DOCUMENT ID		TECN	COMMENT
1.7 ±0.4 OUR AVERAGE				
1.60±0.40	[1] ANISOVICH	11	SPEC	0.9–1.94 $p\overline{p}$
20.4 ±6.6	BARBERIS	00B		450 $pp \to p_f \eta\pi^+\pi^- p_s$
4.1 ±2.3	ADOMEIT	96	CBAR	1.94 $\overline{p}p \to \eta 3\pi^0$

[1] Reanalysis of ADOMEIT 96 and ANISOVICH 00E.

$\Gamma(a_2(1320)\pi)/\Gamma(a_0(980)\pi)$ — Γ_2/Γ_4

VALUE	DOCUMENT ID		COMMENT
32.6±12.6	BARBERIS	00B	450 $pp \to p_f \eta\pi^+\pi^- p_s$

$\Gamma(a_0(980)\pi)/\Gamma(f_2(1270)\eta)$ — Γ_4/Γ_3

VALUE	DOCUMENT ID		TECN	COMMENT
0.48±0.45	[1] ANISOVICH	11	SPEC	0.9–1.94 $p\overline{p}$

[1] Reanalysis of ADOMEIT 96 and ANISOVICH 00E.

$\Gamma(\gamma\gamma)/\Gamma_{total}$ — Γ_5/Γ

VALUE	DOCUMENT ID		TECN	COMMENT
seen	KARCH	92	CBAL	$e^+e^- \to e^+e^-\eta\pi^0\pi^0$

$\eta_2(1870)$ REFERENCES

ANISOVICH	11	EPJ C71 1511	A.V. Anisovich *et al.*	(LOQM, RAL, PNPI)
ANISOVICH	00E	PL B477 19	A.V. Anisovich *et al.*	
BARBERIS	00B	PL B471 435	D. Barberis *et al.*	(WA 102 Collab.)
BARBERIS	00C	PL B471 440	D. Barberis *et al.*	(WA 102 Collab.)
BAI	99	PL B446 356	J.Z. Bai *et al.*	(BES Collab.)
BARBERIS	97B	PL B413 217	D. Barberis *et al.*	(WA 102 Collab.)
ADOMEIT	96	ZPHY C71 227	J. Adomeit *et al.*	(Crystal Barrel Collab.)
KARCH	92	ZPHY C54 33	K. Karch *et al.*	(Crystal Ball Collab.)

$\pi_2(1880)$

$I^G(J^{PC}) = 1^-(2^{-+})$

$\pi_2(1880)$ MASS

VALUE (MeV)	EVTS	DOCUMENT ID		TECN	CHG	COMMENT
1874^{+26}_{-5} OUR AVERAGE Error includes scale factor of 1.6. See the ideogram below.						
1847^{+20}_{-3}	46M	[1] AGHASYAN	18B	COMP		190 $\pi^-p \to \pi^-\pi^+\pi^-p$
1929±24± 18	4k	EUGENIO	08	B852	–	18 $\pi^-p \to \eta\eta\pi^-p$
1876±11± 67	145k	LU	05	B852	–	18 $\pi^-p \to \omega\pi^-\pi^0p$
2003±88±148	69k	KUHN	04	B852	–	18 $\pi^-p \to \eta\pi^+\pi^-\pi^-p$
• • • We do not use the following data for averages, fits, limits, etc. • • •						
1880±20		ANISOVICH	01B	SPEC	0	0.6–1.94 $\overline{p}p \to \eta\eta\pi^0\pi^0$

[1] Statistical error negligible.

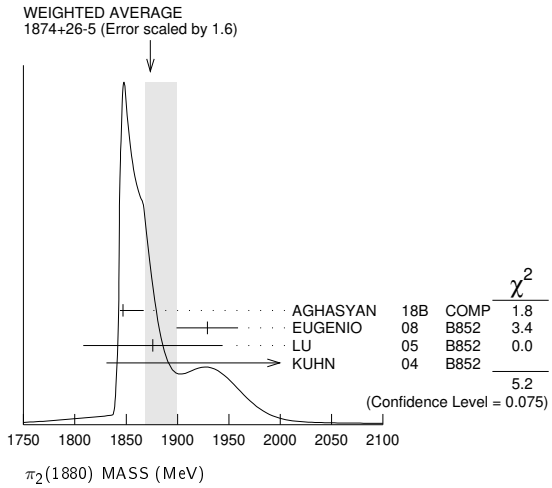

$\pi_2(1880)$ WIDTH

VALUE (MeV)	EVTS	DOCUMENT ID		TECN	CHG	COMMENT
237^{+33}_{-30} OUR AVERAGE Error includes scale factor of 1.2.						
246^{+33}_{-28}	46M	[2] AGHASYAN	18B	COMP		190 $\pi^-p \to \pi^-\pi^+\pi^-p$
323± 87± 43	4k	EUGENIO	08	B852	–	18 $\pi^-p \to \eta\eta\pi^-p$
146± 17± 62	145k	LU	05	B852	–	18 $\pi^-p \to \omega\pi^-\pi^0p$
306±132±121	69k	KUHN	04	B852	–	18 $\pi^-p \to \eta\pi^+\pi^-\pi^-p$
• • • We do not use the following data for averages, fits, limits, etc. • • •						
255± 45		ANISOVICH	01B	SPEC	0	0.6–1.94 $\overline{p}p \to \eta\eta\pi^0\pi^0$

[2] Statistical error negligible.

$\pi_2(1880)$ DECAY MODES

	Mode	Fraction (Γ_i/Γ)
Γ_1	$\eta\eta\pi^-$	seen
Γ_2	$a_0(980)\eta$	seen
Γ_3	$a_2(1320)\eta$	seen
Γ_4	$f_0(1500)\pi$	seen
Γ_5	$f_1(1285)\pi$	seen
Γ_6	$\omega\pi^-\pi^0$	seen

$\Gamma(a_2(1320)\eta)/\Gamma(f_1(1285)\pi)$ — Γ_3/Γ_5

VALUE	EVTS	DOCUMENT ID		TECN	CHG	COMMENT
• • • We do not use the following data for averages, fits, limits, etc. • • •						
22.7±7.3	69k	KUHN	04	B852	–	18 $\pi^-p \to \eta\pi^+\pi^-\pi^-p$

$\Gamma(f_0(1500)\pi)/\Gamma(a_0(980)\eta)$ — Γ_4/Γ_2

VALUE	DOCUMENT ID		TECN	CHG	COMMENT
• • • We do not use the following data for averages, fits, limits, etc. • • •					
$0.28^{+0.20}_{-0.15}$	[3] ANISOVICH	01B	SPEC	0	0.6–1.94 $\overline{p}p \to \eta\eta\pi^0\pi^0$

[3] Systematic errors not estimated.

$\pi_2(1880)$ REFERENCES

AGHASYAN	18B	PR D98 092003	M. Aghasyan *et al.*	(COMPASS Collab.)
EUGENIO	08	PL B660 466	P. Eugenio *et al.*	(BNL E852 Collab.)
LU	05	PRL 94 032002	M. Lu *et al.*	(BNL E852 Collab.)
KUHN	04	PL B595 109	J. Kuhn *et al.*	(BNL E852 Collab.)
ANISOVICH	01B	PL B500 222	A.V. Anisovich *et al.*	

Downloaded from https://academic.oup.com/ptep/article/2022/8/083C01/6651666 by KIT Library user on 27 September 2022

$\rho(1900)$

$I^G(J^{PC}) = 1^+(1^{--})$

OMITTED FROM SUMMARY TABLE

See the review on "Spectroscopy of Light Meson Resonances."

$\rho(1900)$ MASS

VALUE (MeV)	EVTS	DOCUMENT ID		TECN	COMMENT
• • • We do not use the following data for averages, fits, limits, etc. • • •					
1909±17±25	54	[1] AUBERT	08S	BABR	10.6 $e^+e^- \to \phi\pi^0\gamma$
1880±30		AUBERT	06D	BABR	10.6 $e^+e^- \to 3\pi^+3\pi^-\gamma$
1860±20		AUBERT	06D	BABR	10.6 $e^+e^- \to 2(\pi^+\pi^-\pi^0)\gamma$
1910±10		[2,3] FRABETTI	04	E687	$\gamma p \to 3\pi^+3\pi^- p$
1870±10		ANTONELLI	96	SPEC	$e^+e^- \to$ hadrons

[1] From the fit with two resonances.
[2] From a fit with two resonances with the JACOB 72 continuum.
[3] Supersedes FRABETTI 01.

$\rho(1900)$ WIDTH

VALUE (MeV)	EVTS	DOCUMENT ID		TECN	COMMENT
• • • We do not use the following data for averages, fits, limits, etc. • • •					
48±17±2	54	[4] AUBERT	08S	BABR	10.6 $e^+e^- \to \phi\pi^0\gamma$
130±30		AUBERT	06D	BABR	10.6 $e^+e^- \to 3\pi^+3\pi^-\gamma$
160±20		AUBERT	06D	BABR	10.6 $e^+e^- \to 2(\pi^+\pi^-\pi^0)\gamma$
37±13		[5,6] FRABETTI	04	E687	$\gamma p \to 3\pi^+3\pi^- p$
10± 5		ANTONELLI	96	SPEC	$e^+e^- \to$ hadrons

[4] From the fit with two resonances.
[5] From a fit with two resonances with the JACOB 72 continuum.
[6] Supersedes FRABETTI 01.

$\rho(1900)$ $\Gamma(i)\Gamma(e^+e^-)/\Gamma^2(\text{total})$

$\Gamma(\phi\pi)/\Gamma_{\text{total}} \times \Gamma(e^+e^-)/\Gamma_{\text{total}}$ $\qquad \Gamma_4/\Gamma \times \Gamma_6/\Gamma$

VALUE (units 10^{-8})	EVTS	DOCUMENT ID		TECN	COMMENT
• • • We do not use the following data for averages, fits, limits, etc. • • •					
4.2±1.2±0.8	54	[7] AUBERT	08S	BABR	10.6 $e^+e^- \to \phi\pi^0\gamma$

[7] From the fit with two resonances.

$\rho(1900)$ DECAY MODES

	Mode	Fraction (Γ_i/Γ)
Γ_1	6π	seen
Γ_2	$3\pi^+3\pi^-$	seen
Γ_3	$2\pi^+2\pi^-2\pi^0$	
Γ_4	$\phi\pi$	
Γ_5	hadrons	seen
Γ_6	e^+e^-	seen
Γ_7	$\overline{N}N$	not seen

$\rho(1900)$ BRANCHING RATIOS

$\Gamma(6\pi)/\Gamma_{\text{total}}$ $\qquad \Gamma_1/\Gamma$

VALUE	EVTS	DOCUMENT ID		TECN	COMMENT
seen	8k	AKHMETSHIN	13	CMD3	$e^+e^- \to 3\pi^+3\pi^-$
not seen		AGNELLO	02	OBLX	$\overline{n}p \to 3\pi^+2\pi^-\pi^0$
seen		FRABETTI	01	E687	$\gamma p \to 3\pi^+3\pi^- p$
seen		ANTONELLI	96	SPEC	$e^+e^- \to$ hadrons

$\rho(1900)$ REFERENCES

AKHMETSHIN	13	PL B723 82	R.R. Akhmetshin *et al.*	(CMD-3 Collab.)
AUBERT	08S	PR D77 092002	B. Aubert *et al.*	(BABAR Collab.)
AUBERT	06D	PR D73 052003	B. Aubert *et al.*	(BABAR Collab.)
FRABETTI	04	PL B578 290	P.L. Frabetti *et al.*	(FNAL E687 Collab.)
AGNELLO	02	PL B527 39	M. Agnello *et al.*	(OBELIX Collab.)
FRABETTI	01	PL B514 240	P.L. Frabetti *et al.*	(FNAL E687 Collab.)
ANTONELLI	96	PL B365 427	A. Antonelli *et al.*	(FENICE Collab.)
JACOB	72	PR D5 1847	M. Jacob, R. Slansky	

$f_2(1910)$

$I^G(J^{PC}) = 0^+(2^{++})$

OMITTED FROM SUMMARY TABLE

We list here three different peaks with close masses and widths seen in the mass distributions of $\omega\omega$, $\eta\eta'$, and K^+K^- final states. ALDE 91B argues that they are of different nature.

$f_2(1910)$ MASS

$f_2(1910)$ $\omega\omega$ MODE

VALUE (MeV)	DOCUMENT ID		TECN	COMMENT
1900± 9 OUR AVERAGE Error includes scale factor of 1.4. See the ideogram below.				
1890±10	[1] AMELIN	06	VES	36 $\pi^-p \to \omega\omega n$
1897±11	BARBERIS	00F		450 $pp \to p_f\omega\omega p_s$
1924±14	ALDE	90	GAM2	38 $\pi^-p \to \omega\omega n$

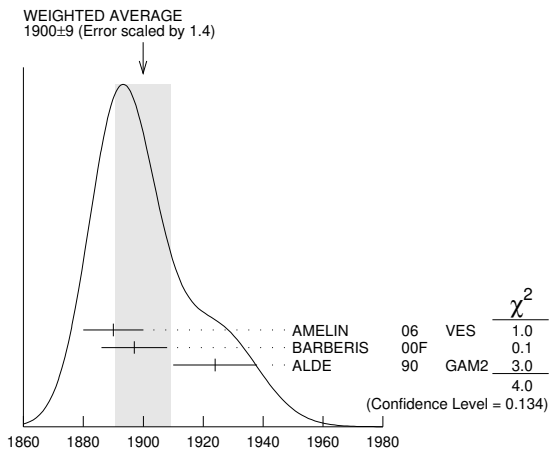

$f_2(1910)$ $\omega\omega$ MODE MASS (MeV)

[1] Supersedes BELADIDZE 92B.

$f_2(1910)$ $\eta\eta'$ MODE

VALUE (MeV)	DOCUMENT ID		TECN	COMMENT
1934±16	[1] BARBERIS	00A		450 $pp \to p_f\eta\eta' p_s$
• • • We do not use the following data for averages, fits, limits, etc. • • •				
1934±20	[2] ANISOVICH	00J	SPEC	
1911±10	ALDE	91B	GAM2	38 $\pi^-p \to \eta\eta' n$

[1] Also compatible with $J^{PC}=1^{-+}$.
[2] Combined fit with $\eta\eta$, $\pi\pi$, and $\eta\pi\pi$.

$f_2(1910)$ K^+K^- MODE

VALUE (MeV)	DOCUMENT ID		TECN	COMMENT
• • • We do not use the following data for averages, fits, limits, etc. • • •				
1941±18	[1] AMSLER	06	CBAR	1.64 $\overline{p}p \to K^+K^-\pi^0$

[1] Tentative, could be $f_2(1950)$.

$f_2(1910)$ WIDTH

$f_2(1910)$ $\omega\omega$ MODE

VALUE (MeV)	DOCUMENT ID		TECN	COMMENT
167±21 OUR AVERAGE Error includes scale factor of 1.3. See the ideogram below.				
165±19	[1] AMELIN	06	VES	36 $\pi^-p \to \omega\omega n$
202±32	BARBERIS	00F		450 $pp \to p_f\omega\omega p_s$
91±50	ALDE	90	GAM2	38 $\pi^-p \to \omega\omega n$

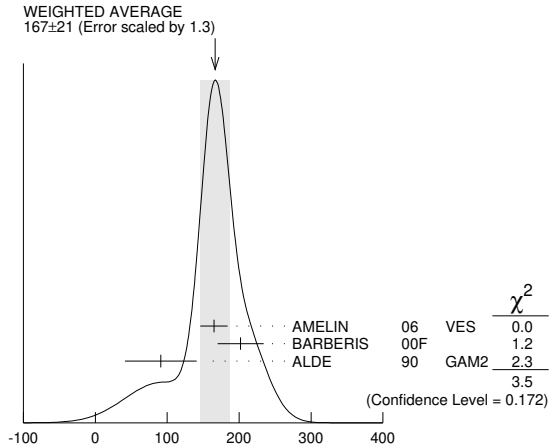

$f_2(1910)$ $\omega\omega$ mode width (MeV)

[1] Supersedes BELADIDZE 92B.

Downloaded from https://academic.oup.com/ptep/article/2022/8/083C01/6651666 by KIT Library user on 27 September 2022

$f_2(1910)$ $\eta\eta'$ MODE

VALUE (MeV)	DOCUMENT ID		TECN	COMMENT
141±41	[1] BARBERIS	00A		450 $pp \to p_f \eta\eta' p_s$
• • • We do not use the following data for averages, fits, limits, etc. • • •				
271±25	[2] ANISOVICH	00J	SPEC	
90±35	ALDE	91B	GAM2	38 $\pi^- p \to \eta\eta' n$

[1] Also compatible with $J^{PC}=1^{-+}$.
[2] Combined fit with $\eta\eta$, $\pi\pi$, and $\eta\pi\pi$.

$f_2(1910)$ K^+K^- MODE

VALUE (MeV)	DOCUMENT ID		TECN	COMMENT
• • • We do not use the following data for averages, fits, limits, etc. • • •				
120±40	AMSLER	06	CBAR	1.64 $\overline{p}p \to K^+K^-\pi^0$

$f_2(1910)$ DECAY MODES

	Mode	Fraction (Γ_i/Γ)
Γ_1	$\pi^0\pi^0$	
Γ_2	K^+K^-	seen
Γ_3	$K^0_S K^0_S$	
Γ_4	$\eta\eta$	seen
Γ_5	$\omega\omega$	seen
Γ_6	$\eta\eta'$	seen
Γ_7	$\eta'\eta'$	
Γ_8	$\rho\rho$	seen
Γ_9	$a_2(1320)\pi$	seen
Γ_{10}	$f_2(1270)\eta$	seen

$f_2(1910)$ BRANCHING RATIOS

$\Gamma(K^+K^-)/\Gamma_{total}$ — Γ_2/Γ

VALUE	DOCUMENT ID		TECN	COMMENT
seen	[1] AMSLER	06	CBAR	1.64 $\overline{p}p \to K^+K^-\pi^0$

[1] Tentative, could be $f_2(1950)$.

$\Gamma(\pi^0\pi^0)/\Gamma(\eta\eta')$ — Γ_1/Γ_6

VALUE	DOCUMENT ID		TECN	COMMENT
• • • We do not use the following data for averages, fits, limits, etc. • • •				
<0.1	ALDE	89	GAM2	38$\pi^- p \to \eta\eta' n$

$\Gamma(K^0_S K^0_S)/\Gamma(\eta\eta')$ — Γ_3/Γ_6

VALUE	CL%	DOCUMENT ID		TECN	COMMENT
• • • We do not use the following data for averages, fits, limits, etc. • • •					
<0.066	90	BALOSHIN	86	SPEC	40$\pi p \to K^0_S K^0_S n$

$\Gamma(\eta\eta)/\Gamma(\eta\eta')$ — Γ_4/Γ_6

VALUE	CL%	DOCUMENT ID		TECN	COMMENT
• • • We do not use the following data for averages, fits, limits, etc. • • •					
<0.05	90	ALDE	91B	GAM2	38 $\pi^- p \to \eta\eta' n$

$\Gamma(\omega\omega)/\Gamma(\eta\eta')$ — Γ_5/Γ_6

VALUE	DOCUMENT ID		COMMENT
• • • We do not use the following data for averages, fits, limits, etc. • • •			
2.6±0.6	BARBERIS	00F	450 $pp \to p_f \omega\omega p_s$

$\Gamma(\eta'\eta')/\Gamma_{total}$ — Γ_7/Γ

VALUE	DOCUMENT ID		TECN	COMMENT
• • • We do not use the following data for averages, fits, limits, etc. • • •				
probably not seen	BARBERIS	00A		450 $pp \to p_f \eta'\eta' p_s$
possibly seen	BELADIDZE	92D	VES	37 $\pi^- p \to \eta'\eta' n$

$\Gamma(\rho\rho)/\Gamma(\omega\omega)$ — Γ_8/Γ_5

VALUE	DOCUMENT ID		COMMENT
• • • We do not use the following data for averages, fits, limits, etc. • • •			
2.6±0.4	BARBERIS	00F	450 $pp \to p_f \omega\omega p_s$

$\Gamma(f_2(1270)\eta)/\Gamma(a_2(1320)\pi)$ — Γ_{10}/Γ_9

VALUE	DOCUMENT ID		TECN	COMMENT
0.09±0.05	[1] ANISOVICH	11	SPEC	0.9–1.94 $p\overline{p}$

[1] Reanalysis of ADOMEIT 96 and ANISOVICH 00E.

$f_2(1910)$ REFERENCES

ANISOVICH 11 EPJ C71 1511 A.V. Anisovich et al. (LOQM, RAL, PNPI)
AMELIN 06 PAN 69 690 D.V. Amelin et al. (VES Collab.)
Translated from YAF 69 715.
AMSLER 06 PL B639 165 C. Amsler et al. (Crystal Barrel Collab.)
ANISOVICH 00E PL B477 19 A.V. Anisovich et al.
ANISOVICH 00J PL B491 47 A.V. Anisovich et al. (RAL, LOQM, PNPI+)
BARBERIS 00A PL B471 429 D. Barberis et al. (WA 102 Collab.)
BARBERIS 00F PL B484 198 D. Barberis et al. (WA 102 Collab.)
ADOMEIT 96 ZPHY C71 227 J. Adomeit et al. (Crystal Barrel Collab.)
BELADIDZE 92B ZPHY C54 367 G.M. Beladidze et al. (VES Collab.)
BELADIDZE 92D ZPHY C57 13 G.M. Beladidze et al. (VES Collab.)
ALDE 91B SJNP 54 455 D.M. Alde et al. (SERP, BELG, LANL, LAPP+)
Translated from YAF 54 751.
Also PL B276 375 D.M. Alde et al. (BELG, SERP, KEK, LANL+)
ALDE 90 PL B241 600 D.M. Alde et al. (SERP, BELG, LANL, LAPP+)
ALDE 89 PL B216 447 D.M. Alde et al. (SERP, BELG, LANL, LAPP)
Also SJNP 48 1035 D.M. Alde et al. (BELG, SERP, LANL, LAPP)
Translated from YAF 48 1724.
BALOSHIN 86 SJNP 43 959 O.N. Baloshin et al. (ITEP)
Translated from YAF 43 1487.

$a_0(1950)$

$I^G(J^{PC}) = 1^-(0^{++})$

OMITTED FROM SUMMARY TABLE

Needs confirmation. Seen in $\gamma\gamma \to \eta_c(1S) \to K\overline{K}\pi$ by LEES 16A with significance 2.5 σ in $K^0_S K^\pm\pi^\mp$ and 4.2 σ in $K^+K^-\pi^0$.

$a_0(1950)$ MASS

VALUE (MeV)	EVTS	DOCUMENT ID		TECN	COMMENT
1931±14±22	12k	[1,2] LEES	16A	BABR	$\gamma\gamma \to \eta_c(1S) \to K\overline{K}\pi$
• • • We do not use the following data for averages, fits, limits, etc. • • •					
1949±32±76	8k	[1] LEES	16A	BABR	$\gamma\gamma \to \eta_c(1S) \to K^0_S K^\pm\pi^\mp$
1927±15±23	4k	[1] LEES	16A	BABR	$\gamma\gamma \to \eta_c(1S) \to K^+K^-\pi^0$

[1] From a model-independent partial wave analysis fit to a relativistic Breit-Wigner function with a floating width.
[2] Weighted average of the $K^0_S K^\pm$ and K^+K^- decay modes.

$a_0(1950)$ WIDTH

VALUE (MeV)	EVTS	DOCUMENT ID		TECN	COMMENT
271±22± 29	12k	[1,2] LEES	16A	BABR	$\gamma\gamma \to \eta_c(1S) \to K\overline{K}\pi$
• • • We do not use the following data for averages, fits, limits, etc. • • •					
265±36±110	8k	[1] LEES	16A	BABR	$\gamma\gamma \to \eta_c(1S) \to K^0_S K^\pm\pi^\mp$
274±28± 30	4k	[1] LEES	16A	BABR	$\gamma\gamma \to \eta_c(1S) \to K^+K^-\pi^0$

[1] From a model-independent partial wave analysis fit to a relativistic Breit-Wigner function with a floating mass.
[2] Weighted average of the $K^0_S K^\pm$ and K^+K^- decay modes.

$a_0(1950)$ DECAY MODES

	Mode	Fraction (Γ_i/Γ)
Γ_1	$K\overline{K}$	seen

$a_0(1950)$ BRANCHING RATIOS

$\Gamma(K\overline{K})/\Gamma_{total}$ — Γ_1/Γ

VALUE	EVTS	DOCUMENT ID		TECN	COMMENT
seen	12k	[1] LEES	16A	BABR	$\gamma\gamma \to \eta_c(1S) \to K\overline{K}\pi$

[1] From a model-independent partial wave analysis.

$a_0(1950)$ REFERENCES

LEES 16A PR D93 012005 J.P. Lees et al. (BABAR Collab.)

$f_2(1950)$

$I^G(J^{PC}) = 0^+(2^{++})$

$f_2(1950)$ MASS

VALUE (MeV)	DOCUMENT ID		TECN	COMMENT
1936 ±12 OUR AVERAGE Error includes scale factor of 1.3. See the ideogram below.				
1940 ±50	BAI	00A	BES	$J/\psi \to \gamma(\pi^+\pi^-\pi^+\pi^-)$
1980 ±22	[1] BARBERIS	00C		450 $pp \to pp4\pi$
1940 ±22	[2] BARBERIS	00C		450 $pp \to pp2\pi2\pi^0$
1960 ±30	BARBERIS	97B	OMEG	450 $pp \to pp2(\pi^+\pi^-)$
1918 ±12	ANTINORI	95	OMEG	300,450 $pp \to pp2(\pi^+\pi^-)$

Downloaded from https://academic.oup.com/ptep/article/2022/8/083C01/6651666 by KIT Library user on 27 September 2022

• • • We do not use the following data for averages, fits, limits, etc. • • •

1955	± 75	[3] RODAS	22	RVUE	$J/\psi(1S) \to \gamma(\pi\pi,\ K\overline{K})$
1978.2	$\pm 1.8^{+28.4}_{-16.9}$	[4] ALBRECHT	20	RVUE	$0.9\ \overline{p}p \to \pi^0\pi^0\eta,\ \pi^0\eta\eta,\ \pi^0K^+K^-$
2038	$^{+13}_{-11}\ ^{+12}_{-73}$	[5] UEHARA	09	BELL	$10.6\ e^+e^- \to e^+e^-\pi^0\pi^0$
1930	± 25	[6] BINON	05	GAMS	$33\ \pi^-p \to \eta\eta n$
1980	$\pm 2\ \pm 14$	ABE	04	BELL	$10.6\ e^+e^- \to e^+e^-K^+K^-$
1867	± 46	[7] AMSLER	02	CBAR	$0.9\ \overline{p}p \to \pi^0\eta\eta,\ \pi^0\pi^0\pi^0$
2010	± 25	ANISOVICH	00J	SPEC	
1980	± 50	ANISOVICH	99B	SPEC	1.35–$1.94\ p\overline{p} \to \eta\eta\pi^0$
~ 1990		[8] OAKDEN	94	RVUE	0.36–$1.55\ \overline{p}p \to \pi\pi$
1950	± 15	[9] ASTON	91	LASS	$11\ K^-p \to \Lambda K\overline{K}\pi\pi$

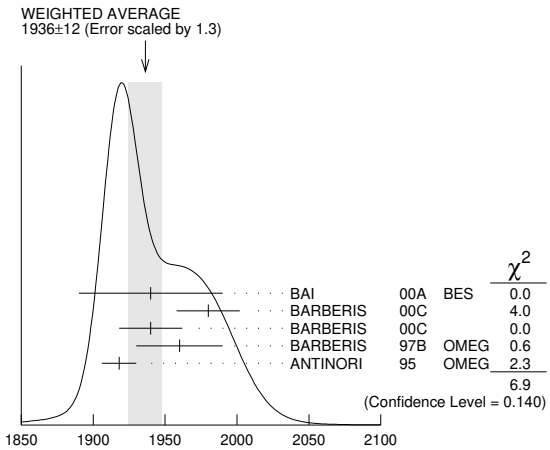

[1] Decaying into $\pi^+\pi^-2\pi^0$.
[2] Decaying into $2(\pi^+\pi^-)$.
[3] T-matrix pole from coupled channel K-matrix fit to data on $J/\psi \to \gamma\pi^0\pi^0$ (ABLIKIM 15AE) and $J/\psi \to \gamma K^0_S K^0_S$ (ABLIKIM 18AA).
[4] T-matrix pole, 4 poles, 4 channels, including scattering data from HYAMS 75 ($\pi\pi$), LONGACRE 86 ($K\overline{K}$), BINON 83 ($\eta\eta$).
[5] Taking into account $f_4(2050)$.
[6] First solution, PWA is ambiguous.
[7] T-matrix pole.
[8] From solution B of amplitude analysis of data on $\overline{p}p \to \pi\pi$. See however KLOET 96 who fit $\pi^+\pi^-$ only and find waves only up to $J = 3$ to be important but not significantly resonant.

$f_2(1950)$ WIDTH

VALUE (MeV)	DOCUMENT ID		TECN	COMMENT
464 ± 24 OUR AVERAGE				
$380\ ^{+120}_{-90}$	BAI	00A	BES	$J/\psi \to \gamma(\pi^+\pi^-\pi^+\pi^-)$
520 ± 50	[1] BARBERIS	00C		$450\ pp \to pp4\pi$
485 ± 55	[2] BARBERIS	00C		$450\ pp \to pp4\pi$
460 ± 40	BARBERIS	97B	OMEG	$450\ pp \to pp2(\pi^+\pi^-)$
390 ± 60	ANTINORI	95	OMEG	$300,450\ pp \to pp2(\pi^+\pi^-)$
• • • We do not use the following data for averages, fits, limits, etc. • • •				
350 ± 113	[3] RODAS	22	RVUE	$J/\psi(1S) \to \gamma(\pi\pi,\ K\overline{K})$
$237.6 \pm 1.6^{+41.6}_{-15.5}$	[4] ALBRECHT	20	RVUE	$0.9\ \overline{p}p \to \pi^0\pi^0\eta,\ \pi^0\eta\eta,\ \pi^0K^+K^-$
$441\ ^{+27}_{-25}\ ^{+28}_{-192}$	[5] UEHARA	09	BELL	$10.6\ e^+e^- \to e^+e^-\pi^0\pi^0$
450 ± 50	[6] BINON	05	GAMS	$33\ \pi^-p \to \eta\eta n$
$297 \pm 12 \pm 6$	ABE	04	BELL	$10.6\ e^+e^- \to e^+e^-K^+K^-$
385 ± 58	[7] AMSLER	02	CBAR	$0.9\ \overline{p}p \to \pi^0\eta\eta,\ \pi^0\pi^0\pi^0$
495 ± 35	ANISOVICH	00J	SPEC	
500 ± 100	ANISOVICH	99B	SPEC	1.35–$1.94\ p\overline{p} \to \eta\eta\pi^0$
~ 100	[8] OAKDEN	94	RVUE	0.36–$1.55\ \overline{p}p \to \pi\pi$
250 ± 50	[9] ASTON	91	LASS	$11\ K^-p \to \Lambda K\overline{K}\pi\pi$

[1] Decaying into $\pi^+\pi^-2\pi^0$.
[2] Decaying into $2(\pi^+\pi^-)$.
[3] T-matrix pole from coupled channel K-matrix fit to data on $J/\psi \to \gamma\pi^0\pi^0$ (ABLIKIM 15AE) and $J/\psi \to \gamma K^0_S K^0_S$ (ABLIKIM 18AA).
[4] T-matrix pole, 4 poles, 4 channels, including scattering data from HYAMS 75 ($\pi\pi$), LONGACRE 86 ($K\overline{K}$), BINON 83 ($\eta\eta$).
[5] Taking into account $f_4(2050)$.
[6] First solution, PWA is ambiguous.
[7] T-matrix pole.
[8] From solution B of amplitude analysis of data on $\overline{p}p \to \pi\pi$. See however KLOET 96 who fit $\pi^+\pi^-$ only and find waves only up to $J = 3$ to be important but not significantly resonant.
[9] Cannot determine spin to be 2.

$f_2(1950)$ DECAY MODES

	Mode	Fraction (Γ_i/Γ)
Γ_1	$K^*(892)\overline{K}^*(892)$	seen
Γ_2	$\pi\pi$	
Γ_3	$\pi^+\pi^-$	seen
Γ_4	$\pi^0\pi^0$	seen
Γ_5	4π	seen
Γ_6	$\pi^+\pi^-\pi^+\pi^-$	
Γ_7	$a_2(1320)\pi$	
Γ_8	$f_2(1270)\pi\pi$	
Γ_9	$\eta\eta$	seen
Γ_{10}	$K\overline{K}$	seen
Γ_{11}	$\gamma\gamma$	seen
Γ_{12}	$p\overline{p}$	seen

$f_2(1950)$ $\Gamma(i)\Gamma(\gamma\gamma)/\Gamma(\text{total})$

$\Gamma(K\overline{K}) \times \Gamma(\gamma\gamma)/\Gamma_{\text{total}}$ — $\Gamma_{10}\Gamma_{11}/\Gamma$

VALUE (eV)	DOCUMENT ID		TECN	COMMENT
• • • We do not use the following data for averages, fits, limits, etc. • • •				
$122 \pm 4 \pm 26$	[1] ABE	04	BELL	$10.6\ e^+e^- \to e^+e^-K^+K^-$

[1] Assuming spin 2.

$\Gamma(\pi\pi) \times \Gamma(\gamma\gamma)/\Gamma_{\text{total}}$ — $\Gamma_2\Gamma_{11}/\Gamma$

VALUE	DOCUMENT ID		TECN	COMMENT
• • • We do not use the following data for averages, fits, limits, etc. • • •				
$162^{+69}_{-42}\ ^{+1137}_{-204}$	[1] UEHARA	09	BELL	$10.6\ e^+e^- \to e^+e^-\pi^0\pi^0$

[1] Taking into account $f_4(2050)$.

$f_2(1950)$ BRANCHING RATIOS

$\Gamma(K^*(892)\overline{K}^*(892))/\Gamma_{\text{total}}$ — Γ_1/Γ

VALUE	DOCUMENT ID		TECN	CHG	COMMENT
seen	ASTON	91	LASS	0	$11\ K^-p \to \Lambda K\overline{K}\pi\pi$

$\Gamma(a_2(1320)\pi)/\Gamma_{\text{total}}$ — Γ_7/Γ

VALUE	DOCUMENT ID		TECN	COMMENT
• • • We do not use the following data for averages, fits, limits, etc. • • •				
not seen	BARBERIS	00B		$450\ pp \to p_f\eta\pi^+\pi^-p_s$
not seen	BARBERIS	00C		$450\ pp \to p_f4\pi p_s$
possibly seen	BARBERIS	97B	OMEG	$450\ pp \to pp2(\pi^+\pi^-)$

$\Gamma(\eta\eta)/\Gamma(4\pi)$ — Γ_9/Γ_5

VALUE	CL%	DOCUMENT ID		COMMENT
• • • We do not use the following data for averages, fits, limits, etc. • • •				
$<5.0 \times 10^{-3}$	90	BARBERIS	00E	$450\ pp \to p_f\eta\eta p_s$

$\Gamma(\eta\eta)/\Gamma(\pi^+\pi^-)$ — Γ_9/Γ_3

VALUE	DOCUMENT ID		TECN	COMMENT
0.14±0.05	AMSLER	02	CBAR	$0.9\ \overline{p}p \to \pi^0\eta\eta,\ \pi^0\pi^0\pi^0$

$\Gamma(p\overline{p})/\Gamma_{\text{total}}$ — Γ_{12}/Γ

VALUE	EVTS	DOCUMENT ID		TECN	COMMENT
seen	111	ALEXANDER	10	CLEO	$\psi(2S) \to \gamma p\overline{p}$

$f_2(1950)$ REFERENCES

RODAS	22	EPJ C82 80	A. Rodas *et al.*	(JPAC Collab.)
ALBRECHT	20	EPJ C80 453	M. Albrecht *et al.*	(Crystal Barrel Collab.)
ABLIKIM	18AA	PR D98 072003	M. Ablikim *et al.*	(BESIII Collab.)
ABLIKIM	15AE	PR D92 052003	M. Ablikim *et al.*	(BESIII Collab.)
ALEXANDER	10	PR D82 092002	J.P. Alexander *et al.*	(CLEO Collab.)
UEHARA	09	PR D79 052009	S. Uehara *et al.*	(BELLE Collab.)
BINON	05	PAN 68 960	F. Binon *et al.*	
		Translated from YAF 68 998.		
ABE	04	EPJ C32 323	K. Abe *et al.*	(BELLE Collab.)
AMSLER	02	EPJ C23 29	C. Amsler *et al.*	
ANISOVICH	00J	PL B491 47	A.V. Anisovich *et al.*	(RAL, LOQM, PNPI+)
BAI	00A	PL B472 207	J.Z. Bai *et al.*	(BES Collab.)
BARBERIS	00B	PL B471 435	D. Barberis *et al.*	(WA 102 Collab.)
BARBERIS	00C	PL B471 440	D. Barberis *et al.*	(WA 102 Collab.)
BARBERIS	00E	PL B479 59	D. Barberis *et al.*	(WA 102 Collab.)
ANISOVICH	99B	PL B449 154	A.V. Anisovich *et al.*	
BARBERIS	97B	PL B413 217	D. Barberis *et al.*	(WA 102 Collab.)
KLOET	96	PR D53 6120	W.M. Kloet, F. Myhrer	(RUTG, NORD)
ANTINORI	95	PL B353 589	F. Antinori *et al.*	(ATHU, BARI, BIRM+) JP
OAKDEN	94	NP A574 731	M.N. Oakden, M.R. Pennington	(DURH)
ASTON	91	NPBPS B21 5	D. Aston *et al.*	(LASS Collab.)
LONGACRE	86	PL B177 223	R.S. Longacre *et al.*	(BNL, BRAN, CUNY+)
BINON	83	NC 78A 313	F.G. Binon *et al.*	(BELG, LAPP, SERP+)
HYAMS	75	NP B100 205	B.D. Hyams *et al.*	(CERN, MPIM)

Downloaded from https://academic.oup.com/ptep/article/2022/8/083C01/6651666 by KIT Library user on 27 September 2022

$a_4(1970)$

$I^G(J^{PC}) = 1^-(4^{++})$

was $a_4(2040)$

$a_4(1970)$ MASS

VALUE (MeV)	EVTS	DOCUMENT ID		TECN	CHG	COMMENT
1967±16 OUR AVERAGE		Error includes scale factor of 2.1. See the ideogram below.				
1935^{+11}_{-13}	46M	[1] AGHASYAN	18B	COMP		$190\ \pi^- p \to \pi^-\pi^+\pi^- p$
1900^{+80}_{-20}		ADOLPH	15	COMP		$191\ \pi^- p \to \eta^{(\prime)}\pi^- p$
$1985\pm10\pm13$	145k	LU	05	B852		$18\ \pi^- p \to \omega\pi^-\pi^0 p$
$1996\pm25\pm43$		CHUNG	02	B852		$18.3\ \pi^- p \to 3\pi p$
$2000\pm40^{+60}_{-20}$		IVANOV	01	B852		$18\ \pi^- p \to \eta'\pi^- p$
2010 ± 20		[2] DONSKOV	96	GAM2	0	$38\ \pi^- p \to \eta\pi^0 n$
2040 ± 30		[3] CLELAND	82B	SPEC	±	$50\ \pi p \to K^0_S K^\pm p$
• • • We do not use the following data for averages, fits, limits, etc. • • •						
$1885\pm13^{+50}_{-2}$	420k	[4] ALEKSEEV	10	COMP		$190\ \pi^- Pb \to \pi^-\pi^-\pi^+ Pb'$
2004 ± 6	80k	[5] UMAN	06	E835		$5.2\ \bar{p}p \to \eta\eta\pi^0$
2005^{+25}_{-45}		[6] ANISOVICH	01F	SPEC		$2.0\ \bar{p}p \to 3\pi^0, \pi^0\eta, \pi^0\eta'$
$1944\pm8\pm50$		[7] AMELIN	99	VES		$37\ \pi^- A \to \omega\pi^-\pi^0 A^*$
1903 ± 10		[8] BALDI	78	SPEC	−	$10\ \pi^- p \to pK^0_S K^-$
2030 ± 50		[9] CORDEN	78C	OMEG	0	$15\ \pi^- p \to 3\pi n$

[1] Statistical error negligible.
[2] From a simultaneous fit to the G_+ and G_0 wave intensities.
[3] From an amplitude analysis.
[4] Superseded by AGHASYAN 2018B.
[5] Statistical error only.
[6] From the combined analysis of ANISOVICH 99C, ANISOVICH 99E, and ANISOVICH 01F.
[7] May be a different state.
[8] From a fit to the Y^0_8 moment. Limited by phase space.
[9] $J^P = 4^+$ is favored, though $J^P = 2^+$ cannot be excluded.

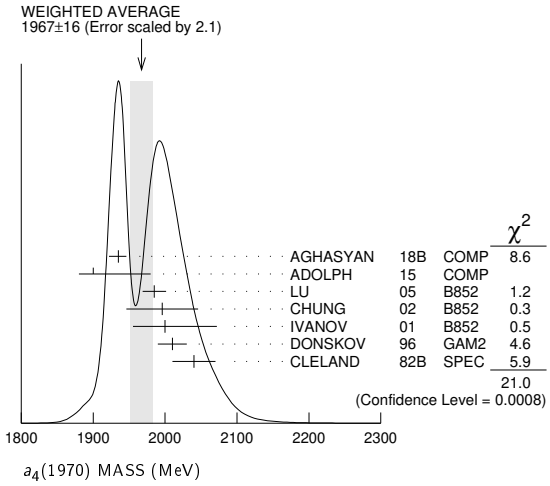

$a_4(1970)$ WIDTH

VALUE (MeV)	EVTS	DOCUMENT ID		TECN	CHG	COMMENT
324^{+15}_{-18} OUR AVERAGE						
333^{+16}_{-21}	46M	[1] AGHASYAN	18B	COMP		$190\ \pi^- p \to \pi^-\pi^+\pi^- p$
300^{+80}_{-100}		ADOLPH	15	COMP		$191\ \pi^- p \to \eta^{(\prime)}\pi^- p$
$231\pm30\pm46$	145k	LU	05	B852		$18\ \pi^- p \to \omega\pi^-\pi^0 p$
$298\pm81\pm85$		CHUNG	02	B852		$18.3\ \pi^- p \to 3\pi p$
$350\pm100^{+70}_{-50}$		IVANOV	01	B852		$18\ \pi^- p \to \eta'\pi^- p$
370 ± 80		[2] DONSKOV	96	GAM2	0	$38\ \pi^- p \to \eta\pi^0 n$
380 ± 150		[3] CLELAND	82B	SPEC	±	$50\ \pi p \to K^0_S K^\pm p$
• • • We do not use the following data for averages, fits, limits, etc. • • •						
$294\pm25^{+46}_{-19}$	420k	[4] ALEKSEEV	10	COMP		$190\ \pi^- Pb \to \pi^-\pi^-\pi^+ Pb'$
401 ± 16	80k	[5] UMAN	06	E835		$5.2\ \bar{p}p \to \eta\eta\pi^0$
180 ± 30		[6] ANISOVICH	01F	SPEC		$2.0\ \bar{p}p \to 3\pi^0, \pi^0\eta, \pi^0\eta'$
$324\pm26\pm75$		[7] AMELIN	99	VES		$37\ \pi^- A \to \omega\pi^-\pi^0 A^*$
166 ± 43		[8] BALDI	78	SPEC	−	$10\ \pi^- p \to pK^0_S K^-$
510 ± 200		[9] CORDEN	78C	OMEG	0	$15\ \pi^- p \to 3\pi n$

[1] Statistical error negligible.
[2] From a simultaneous fit to the G_+ and G_0 wave intensities.
[3] From an amplitude analysis.
[4] Superseded by AGHASYAN 2018B.
[5] Statistical error only.
[6] From the combined analysis of ANISOVICH 99C, ANISOVICH 99E, and ANISOVICH 01F.
[7] May be a different state.
[8] From a fit to the Y^0_8 moment. Limited by phase space.
[9] $J^P = 4^+$ is favored, though $J^P = 2^+$ cannot be excluded.

$a_4(1970)$ DECAY MODES

	Mode	Fraction (Γ_i/Γ)
Γ_1	$K\overline{K}$	seen
Γ_2	$\pi^+\pi^-\pi^0$	seen
Γ_3	$\rho\pi$	seen
Γ_4	$f_2(1270)\pi$	seen
Γ_5	$\omega\pi^-\pi^0$	seen
Γ_6	$\omega\rho$	seen
Γ_7	$\eta\pi$	seen
Γ_8	$\eta'(958)\pi$	seen

$a_4(1970)$ BRANCHING RATIOS

$\Gamma(K\overline{K})/\Gamma_{total}$ — Γ_1/Γ

VALUE	DOCUMENT ID		TECN	CHG	COMMENT
seen	BALDI	78	SPEC	±	$10\ \pi^- p \to K^0_S K^- p$

$\Gamma(\pi^+\pi^-\pi^0)/\Gamma_{total}$ — Γ_2/Γ

VALUE	DOCUMENT ID		TECN	CHG	COMMENT
seen	CORDEN	78C	OMEG	0	$15\ \pi^- p \to 3\pi n$

$\Gamma(\rho\pi)/\Gamma(f_2(1270)\pi)$ — Γ_3/Γ_4

VALUE	EVTS	DOCUMENT ID		TECN	COMMENT
$1.7^{+0.9}_{-0.8}$ OUR AVERAGE		Error includes scale factor of 3.7.			
$2.9^{+0.6}_{-0.4}$	46M	[1] AGHASYAN	18B	COMP	$190\ \pi^- p \to \pi^-\pi^+\pi^- p$
$1.1\pm0.2\pm0.2$		CHUNG	02	B852	$18.3\ \pi^- p \to 3\pi p$

[1] Statistical error negligible.

$\Gamma(\eta\pi)/\Gamma_{total}$ — Γ_7/Γ

VALUE	DOCUMENT ID		TECN	CHG	COMMENT
seen	DONSKOV	96	GAM2	0	$38\ \pi^- p \to \eta\pi^0 n$

$\Gamma(\eta'(958)\pi)/\Gamma(\eta\pi)$ — Γ_8/Γ_7

VALUE	DOCUMENT ID		TECN	COMMENT
0.23±0.07	ADOLPH	15	COMP	$191\ \pi^- p \to \eta^{(\prime)}\pi^- p$

$\Gamma(\omega\rho)/\Gamma_{total}$ — Γ_6/Γ

VALUE	EVTS	DOCUMENT ID		TECN	COMMENT
seen	145k	LU	05	B852	$18\ \pi^- p \to \omega\pi^-\pi^0 p$

$a_4(1970)$ REFERENCES

AGHASYAN	18B	PR D98 092003	M. Aghasyan et al.	(COMPASS Collab.)
ADOLPH	15	PL B740 303	M. Adolph et al.	(COMPASS Collab.)
ALEKSEEV	10	PRL 104 241803	M.G. Alekseev et al.	(COMPASS Collab.)
UMAN	06	PR D73 052009	I. Uman et al.	(FNAL E835)
LU	05	PRL 94 032002	M. Lu et al.	(BNL E852 Collab.)
CHUNG	02	PR D65 072001	S.U. Chung et al.	(BNL E852 Collab.)
ANISOVICH	01F	PL B517 261	A.V. Anisovich et al.	
IVANOV	01	PRL 86 3977	E.I. Ivanov et al.	(BNL E852 Collab.)
AMELIN	99	PAN 62 445 Translated from YAF 62 487.	D.V. Amelin et al.	(VES Collab.)
ANISOVICH	99C	PL B452 173	A.V. Anisovich et al.	
ANISOVICH	99E	PL B452 187	A.V. Anisovich et al.	
DONSKOV	96	PAN 59 982 Translated from YAF 59 1027.	S.V. Donskov et al.	(GAMS Collab.) IGJPC
CLELAND	82B	NP B208 228	W.E. Cleland et al.	(DURH, GEVA, LAUS+)
BALDI	78	PL 74B 413	R. Baldi et al.	(GEVA) JP
CORDEN	78C	NP B136 77	M.J. Corden et al.	(BIRM, RHEL, TELA+) JP

$\rho_3(1990)$

$I^G(J^{PC}) = 1^+(3^{--})$

OMITTED FROM SUMMARY TABLE

$\rho_3(1990)$ MASS

VALUE (MeV)	DOCUMENT ID		TECN	COMMENT
• • • We do not use the following data for averages, fits, limits, etc. • • •				
1982±14	[1] ANISOVICH	02	SPEC	0.6–1.9 $p\overline{p} \to \omega\pi^0, \omega\eta\pi^0, \pi^+\pi^-$
~ 2007	HASAN	94	RVUE	$\overline{p}p \to \pi\pi$

[1] From the combined analysis of ANISOVICH 00J, ANISOVICH 01D, ANISOVICH 01E, and ANISOVICH 02.

Downloaded from https://academic.oup.com/ptep/article/2022/8/083C01/6651666 by KIT Library user on 27 September 2022

$\rho_3(1990)$ WIDTH

VALUE (MeV)	DOCUMENT ID		TECN	COMMENT
• • • We do not use the following data for averages, fits, limits, etc. • • •				
188±24	[2] ANISOVICH	02	SPEC	0.6–1.9 $p\overline{p} \to \omega\pi^0$, $\omega\eta\pi^0$, $\pi^+\pi^-$
∼ 287	HASAN	94	RVUE	$\overline{p}p \to \pi\pi$

[2] From the combined analysis of ANISOVICH 00J, ANISOVICH 01D, ANISOVICH 01E, and ANISOVICH 02.

$\rho_3(1990)$ REFERENCES

ANISOVICH	02	PL B542 8	A.V. Anisovich *et al.*	
ANISOVICH	01D	PL B508 6	A.V. Anisovich *et al.*	
ANISOVICH	01E	PL B513 281	A.V. Anisovich *et al.*	
ANISOVICH	00J	PL B491 47	A.V. Anisovich *et al.*	(RAL, LOQM, PNPI+)
HASAN	94	PL B334 215	A. Hasan, D.V. Bugg	(LOQM)

$\pi_2(2005)$

$I^G(J^{PC}) = 1^-(2^{-+})$

OMITTED FROM SUMMARY TABLE

$\pi_2(2005)$ MASS

VALUE (MeV)	EVTS	DOCUMENT ID		TECN	COMMENT
1963^{+17}_{-27} OUR AVERAGE					
1962^{+17}_{-29}	46M	[1] AGHASYAN	18B	COMP	190 $\pi^-p \to \pi^-\pi^+\pi^-p$
1974±14±83	145k	LU	05	B852	18 $\pi^-p \to \omega\pi^-\pi^0p$
• • • We do not use the following data for averages, fits, limits, etc. • • •					
2005±15		ANISOVICH	01F	SPEC	2.0 $\overline{p}p \to 3\pi^0$, $\pi^0\eta$, $\pi^0\eta'$

[1] Statistical uncertainty negligible.

$\pi_2(2005)$ WIDTH

VALUE (MeV)	EVTS	DOCUMENT ID		TECN	COMMENT
370^{+16}_{-90} OUR AVERAGE					
371^{+16}_{-120}	46M	[1] AGHASYAN	18B	COMP	190 $\pi^-p \to \pi^-\pi^+\pi^-p$
341± 61±139	145k	LU	05	B852	18 $\pi^-p \to \omega\pi^-\pi^0p$
• • • We do not use the following data for averages, fits, limits, etc. • • •					
200± 40		ANISOVICH	01F	SPEC	2.0 $\overline{p}p \to 3\pi^0$, $\pi^0\eta$, $\pi^0\eta'$

[1] Statistical uncertainty negligible.

$\pi_2(2005)$ DECAY MODES

	Mode	Fraction (Γ_i/Γ)
Γ_1	$\pi^-\pi^+\pi^-$	seen
Γ_2	$\omega\pi^0\pi^-$	seen

$\pi_2(2005)$ BRANCHING RATIOS

$\Gamma(\pi^-\pi^+\pi^-)/\Gamma_{total}$ — **Γ_1/Γ**

VALUE	DOCUMENT ID		TECN	COMMENT
seen	AGHASYAN	18B	COMP	190 $\pi^-p \to \pi^-\pi^+\pi^-p$

$\Gamma(\omega\pi^0\pi^-)/\Gamma_{total}$ — **Γ_2/Γ**

VALUE	DOCUMENT ID		TECN	COMMENT
seen	LU	05	B852	18 $\pi^-p \to \omega\pi^-\pi^0p$

$\pi_2(2005)$ REFERENCES

AGHASYAN	18B	PR D98 092003	M. Aghasyan *et al.*	(COMPASS Collab.)
LU	05	PRL 94 032002	M. Lu *et al.*	(BNL E852 Collab.)
ANISOVICH	01F	PL B517 261	A.V. Anisovich *et al.*	

$f_2(2010)$

$I^G(J^{PC}) = 0^+(2^{++})$

$f_2(2010)$ MASS

VALUE (MeV)	DOCUMENT ID		TECN	COMMENT
2011^{+62}_{-76}	[1] ETKIN	88	MPS	22 $\pi^-p \to \phi\phi n$
• • • We do not use the following data for averages, fits, limits, etc. • • •				
2005± 12	VLADIMIRSK...06		SPEC	40 $\pi^-p \to K^0_S K^0_S n$
1980± 20	[2] BOLONKIN	88	SPEC	40 $\pi^-p \to K^0_S K^0_S n$
2050^{+90}_{-50}	ETKIN	85	MPS	22 $\pi^-p \to 2\phi n$
2120^{+20}_{-120}	LINDENBAUM	84	RVUE	
2160± 50	ETKIN	82	MPS	22 $\pi^-p \to 2\phi n$

[1] Includes data of ETKIN 85. The percentage of the resonance going into $\phi\phi$ 2^{++} S_2, D_2, and D_0 is 98^{+1}_{-3}, 0^{+1}_{-0}, and 2^{+2}_{-1}, respectively.

[2] Statistically very weak, only 1.4 s.d.

$f_2(2010)$ WIDTH

VALUE (MeV)	DOCUMENT ID		TECN	COMMENT
202^{+67}_{-62}	[3] ETKIN	88	MPS	22 $\pi^-p \to \phi\phi n$
• • • We do not use the following data for averages, fits, limits, etc. • • •				
209± 32	VLADIMIRSK...06		SPEC	40 $\pi^-p \to K^0_S K^0_S n$
145± 50	[4] BOLONKIN	88	SPEC	40 $\pi^-p \to K^0_S K^0_S n$
200^{+160}_{-50}	ETKIN	85	MPS	22 $\pi^-p \to 2\phi n$
300^{+150}_{-50}	LINDENBAUM	84	RVUE	
310± 70	ETKIN	82	MPS	22 $\pi^-p \to 2\phi n$

[3] Includes data of ETKIN 85.

[4] Statistically very weak, only 1.4 s.d.

$f_2(2010)$ DECAY MODES

	Mode	Fraction (Γ_i/Γ)
Γ_1	$\phi\phi$	seen
Γ_2	$K\overline{K}$	seen

$f_2(2010)$ BRANCHING RATIOS

$\Gamma(K\overline{K})/\Gamma_{total}$ — **Γ_2/Γ**

VALUE	DOCUMENT ID		TECN	COMMENT
seen	VLADIMIRSK...06		SPEC	40 $\pi^-p \to K^0_S K^0_S n$

$f_2(2010)$ REFERENCES

VLADIMIRSK...	06	PAN 69 493 Translated from YAF 69 515.	V.V. Vladimirsky *et al.*	(ITEP, Moscow)
BOLONKIN	88	NP B309 426	B.V. Bolonkin *et al.*	(ITEP, SERP)
ETKIN	88	PL B201 568	A. Etkin *et al.*	(BNL, CUNY)
ETKIN	85	PL 165B 217	A. Etkin *et al.*	(BNL, CUNY)
LINDENBAUM	84	CNPP 13 285	S.J. Lindenbaum	(CUNY)
ETKIN	82	PRL 49 1620	A. Etkin *et al.*	(BNL, CUNY)
Also		Brighton Conf. 351	S.J. Lindenbaum	(BNL, CUNY)

$f_0(2020)$

$I^G(J^{PC}) = 0^+(0^{++})$

OMITTED FROM SUMMARY TABLE

Needs confirmation.

$f_0(2020)$ MASS

VALUE (MeV)	EVTS	DOCUMENT ID		TECN	COMMENT
1992±16		[1,2] BARBERIS	00C		450 $pp \to p_f 4\pi p_s$
• • • We do not use the following data for averages, fits, limits, etc. • • •					
2038±48		[3] RODAS	22	RVUE	$J/\psi(1S) \to \gamma(\pi\pi, K\overline{K})$
1925±25		SARANTSEV	21	RVUE	$J/\psi(1S) \to \gamma(\pi\pi, K\overline{K}, \eta\eta, \omega\phi)$
1910±50		[4] ROPERTZ	18	RVUE	$\overline{B}^0_s \to J/\psi(\pi^+\pi^-/K^+K^-)$
2037± 8	80k	[5] UMAN	06	E835	5.2 $\overline{p}p \to \eta\eta\pi^0$
2040±38		ANISOVICH	00J	SPEC	
2010±60		ALDE	98	GAM4	100 $\pi^-p \to \pi^0\pi^0n$
2020±35		BARBERIS	97B	OMEG	450 $pp \to pp2(\pi^+\pi^-)$

[1] Average between $\pi^+\pi^-2\pi^0$ and $2(\pi^+\pi^-)$.

[2] T-matrix pole.

[3] T-matrix pole from coupled channel K-matrix fit to data on $J/\psi \to \gamma\pi^0\pi^0$ (ABLIKIM 15AE) and $J/\psi \to \gamma K^0_S K^0_S$ (ABLIKIM 18AA).

[4] T-matrix pole of 3 channel unitary model fit to data from AAIJ 14BR and AAIJ 17V extracted using Pade approximants.

[5] Statistical error only.

$f_0(2020)$ WIDTH

VALUE (MeV)	EVTS	DOCUMENT ID		TECN	COMMENT
442± 60		[1,2] BARBERIS	00C		450 $pp \to p_f 4\pi p_s$
• • • We do not use the following data for averages, fits, limits, etc. • • •					
312± 82		[3] RODAS	22	RVUE	$J/\psi(1S) \to \gamma(\pi\pi, K\overline{K})$
320± 35		SARANTSEV	21	RVUE	$J/\psi(1S) \to \gamma(\pi\pi, K\overline{K}, \eta\eta, \omega\phi)$
400± 80		[4] ROPERTZ	18	RVUE	$\overline{B}^0_s \to J/\psi(\pi^+\pi^-/K^+K^-)$

Downloaded from https://academic.oup.com/ptep/article/2022/8/083C01/6651666 by KIT Library user on 27 September 2022

296± 17	80k	[5] UMAN	06	E835	5.2 $\overline{p}p \to \eta\eta\pi^0$
405± 40		ANISOVICH	00J	SPEC	
240±100		ALDE	98	GAM4	100 $\pi^- p \to \pi^0\pi^0 n$
410± 50		BARBERIS	97B	OMEG	450 $pp \to pp2(\pi^+\pi^-)$

[1] Average between $\pi^+\pi^- 2\pi^0$ and $2(\pi^+\pi^-)$.
[2] T-matrix pole.
[3] T-matrix pole from coupled channel K-matrix fit to data on $J/\psi \to \gamma\pi^0\pi^0$ (ABLIKIM 15AE) and $J/\psi \to \gamma K^0_S K^0_S$ (ABLIKIM 18AA).
[4] T-matrix pole of 3 channel unitary model fit to data from AAIJ 14BR and AAIJ 17V extracted using Pade approximants.
[5] Statistical error only.

$f_0(2020)$ DECAY MODES

	Mode	Fraction (Γ_i/Γ)
Γ_1	$\rho\pi\pi$	seen
Γ_2	$\pi^0\pi^0$	seen
Γ_3	$\rho\rho$	seen
Γ_4	$\omega\omega$	seen
Γ_5	$\eta\eta$	seen

$f_0(2020)$ BRANCHING RATIOS

$\Gamma(\rho\rho)/\Gamma(\omega\omega)$ — Γ_3/Γ_4

VALUE	DOCUMENT ID		COMMENT
• • • We do not use the following data for averages, fits, limits, etc. • • •			
~ 3	BARBERIS	00F	450 $pp \to p_f\omega\omega p_s$

$\Gamma(\eta\eta)/\Gamma_{total}$ — Γ_5/Γ

VALUE	DOCUMENT ID		TECN	COMMENT
seen	UMAN	06	E835	5.2 $\overline{p}p \to \eta\eta\pi^0$

$f_0(2020)$ REFERENCES

RODAS	22	EPJ C82 80	A. Rodas *et al.*	(JPAC Collab.)
SARANTSEV	21	PL B816 136227	A.V. Sarantsev *et al.*	(BONN, PNPI)
ABLIKIM	18AA	PR D98 072003	M. Ablikim *et al.*	(BESIII Collab.)
ROPERTZ	18	EPJ C78 1000	S. Ropertz, C. Hanhart, B. Kubis	(BONN, JULI)
AAIJ	17V	JHEP 1708 037	R. Aaij *et al.*	(LHCb Collab.)
ABLIKIM	15AE	PR D92 052003	M. Ablikim *et al.*	(BESIII Collab.)
AAIJ	14BR	PR D89 092006	R. Aaij *et al.*	(LHCb Collab.)
UMAN	06	PR D73 052009	I. Uman *et al.*	(FNAL E835)
ANISOVICH	00J	PL B491 47	A.V. Anisovich *et al.*	(RAL, LOQM, PNPI+)
BARBERIS	00C	PL B471 440	D. Barberis *et al.*	(WA 102 Collab.)
BARBERIS	00F	PL B484 198	D. Barberis *et al.*	(WA 102 Collab.)
ALDE	98	EPJ A3 361	D. Alde *et al.*	(GAM4 Collab.)
Also		PAN 62 405	D. Alde *et al.*	(GAMS Collab.)
		Translated from YAF 62 446.		
BARBERIS	97B	PL B413 217	D. Barberis *et al.*	(WA 102 Collab.)

$f_4(2050)$

$I^G(J^{PC}) = 0^+(4^{++})$

$f_4(2050)$ MASS

VALUE (MeV)	EVTS	DOCUMENT ID		TECN	COMMENT
2018±11 OUR AVERAGE		Error includes scale factor of 2.1. See the ideogram below.			
1960±15		AMELIN	06	VES	36 $\pi^- p \to \omega\omega n$
2005±10		[1] BINON	05	GAMS	33 $\pi^- p \to \eta\eta n$
1998±15		ALDE	98	GAM4	100 $\pi^- p \to \pi^0\pi^0 n$
2060±20		ALDE	90	GAM2	38 $\pi^- p \to \omega\omega n$
2038±30		AUGUSTIN	87	DM2	$J/\psi \to \gamma\pi^+\pi^-$
2086±15		BALTRUSAIT...	87	MRK3	$J/\psi \to \gamma\pi^+\pi^-$
2000±60		ALDE	86D	GAM4	100 $\pi^- p \to n2\eta$
2020±20	40k	[2] BINON	84B	GAM2	38 $\pi^- p \to n2\pi^0$
2015±28		[3] CASON	82	STRC	8 $\pi^+ p \to \Delta^{++}\pi^0\pi^0$
2031^{+25}_{-36}		ETKIN	82B	MPS	23 $\pi^- p \to n2K^0_S$
2020±30	700	APEL	75	NICE	40 $\pi^- p \to n2\pi^0$
2050±25		BLUM	75	ASPK	18.4 $\pi^- p \to nK^+K^-$
• • • We do not use the following data for averages, fits, limits, etc. • • •					
1966±25		[4] ANISOVICH	09	RVUE	0.0 $\overline{p}p$, πN
$1885^{+14}_{-13}{}^{+218}_{-25}$		[5] UEHARA	09	BELL	10.6 $e^+e^- \to e^+e^-\pi^0\pi^0$
2018± 6		ANISOVICH	00J	SPEC	2.0 $\overline{p}p \to \eta\pi^0\pi^0$, $\pi^0\pi^0$, $\eta\eta$, $\eta\eta'$, $\pi\pi$
~ 2000		[6] MARTIN	98	RVUE	$N\overline{N} \to \pi\pi$
~ 2010		[7] MARTIN	97	RVUE	$\overline{N}N \to \pi\pi$
~ 2040		[8] OAKDEN	94	RVUE	0.36–1.55 $\overline{p}p \to \pi\pi$
~ 1990		[9] OAKDEN	94	RVUE	0.36–1.55 $\overline{p}p \to \pi\pi$
1978± 5		[10] ALPER	80	CNTR	62 $\pi^- p \to K^+K^- n$
2040±10		[10] ROZANSKA	80	SPRK	18 $\pi^- p \to p\overline{p}n$
1935±13		[10] CORDEN	79	OMEG	12–15 $\pi^- p \to n2\pi$
1988± 7		EVANGELIS...	79B	OMEG	10 $\pi^- p \to K^+K^- n$
1922±14		[11] ANTIPOV	77	CIBS	25 $\pi^- p \to p3\pi$

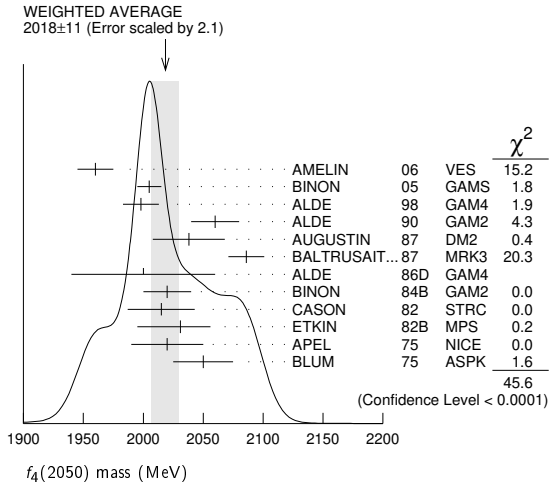

[1] From the first PWA solution.
[2] From a partial-wave analysis of the data.
[3] From an amplitude analysis of the reaction $\pi^+\pi^- \to 2\pi^0$.
[4] K matrix pole.
[5] Taking into account the $f_2(1950)$. Helicity-2 production favored.
[6] Energy-dependent analysis.
[7] Single energy analysis.
[8] From solution A of amplitude analysis of data on $\overline{p}p \to \pi\pi$. See however KLOET 96 who fit $\pi^+\pi^-$ only and find waves only up to $J = 3$ to be important but not significantly resonant.
[9] From solution B of amplitude analysis of data on $\overline{p}p \to \pi\pi$. See however KLOET 96 who fit $\pi^+\pi^-$ only and find waves only up to $J = 3$ to be important but not significantly resonant.
[10] $I(J^P) = 0(4^+)$ from amplitude analysis assuming one-pion exchange.
[11] Width errors enlarged by us to $4\Gamma/\sqrt{N}$; see the note with the $K^*(892)$ mass.

$f_4(2050)$ WIDTH

VALUE (MeV)	EVTS	DOCUMENT ID		TECN	COMMENT
237± 18 OUR AVERAGE		Error includes scale factor of 1.9. See the ideogram below.			
290± 20		AMELIN	06	VES	36 $\pi^- p \to \omega\omega n$
340± 80		[12] BINON	05	GAMS	33 $\pi^- p \to \eta\eta n$
395± 40		ALDE	98	GAM4	100 $\pi^- p \to \pi^0\pi^0 n$
170± 60		ALDE	90	GAM2	38 $\pi^- p \to \omega\omega n$
304± 60		AUGUSTIN	87	DM2	$J/\psi \to \gamma\pi^+\pi^-$
210± 63		BALTRUSAIT...	87	MRK3	$J/\psi \to \gamma\pi^+\pi^-$
400±100		ALDE	86D	GAM4	100 $\pi^- p \to n2\eta$
240± 40	40k	[13] BINON	84B	GAM2	38 $\pi^- p \to n2\pi^0$
190± 14		DENNEY	83	LASS	10 $\pi^+ n/\pi^+ p$
186^{+103}_{-58}		[14] CASON	82	STRC	8 $\pi^+ p \to \Delta^{++}\pi^0\pi^0$
305^{+36}_{-119}		ETKIN	82B	MPS	23 $\pi^- p \to n2K^0_S$
180± 60	700	APEL	75	NICE	40 $\pi^- p \to n2\pi^0$
225^{+120}_{-70}		BLUM	75	ASPK	18.4 $\pi^- p \to nK^+K^-$
• • • We do not use the following data for averages, fits, limits, etc. • • •					
260± 40		[15] ANISOVICH	09	RVUE	0.0 $\overline{p}p$, πN
$453\pm 20^{+31}_{-129}$		[16] UEHARA	09	BELL	10.6 $e^+e^- \to e^+e^-\pi^0\pi^0$
182± 7		ANISOVICH	00J	SPEC	2.0 $\overline{p}p \to \eta\pi^0\pi^0$, $\pi^0\pi^0$, $\eta\eta$, $\eta\eta'$, $\pi\pi$
~ 170		[17] MARTIN	98	RVUE	$N\overline{N} \to \pi\pi$
~ 200		[18] MARTIN	97	RVUE	$\overline{N}N \to \pi\pi$
~ 60		[19] OAKDEN	94	RVUE	0.36–1.55 $\overline{p}p \to \pi\pi$
~ 80		[20] OAKDEN	94	RVUE	0.36–1.55 $\overline{p}p \to \pi\pi$
243± 16		[21] ALPER	80	CNTR	62 $\pi^- p \to K^+K^- n$
140± 15		[21] ROZANSKA	80	SPRK	18 $\pi^- p \to p\overline{p}n$
263± 57		[21] CORDEN	79	OMEG	12–15 $\pi^- p \to n2\pi$
100± 28		EVANGELIS...	79B	OMEG	10 $\pi^- p \to K^+K^- n$
107± 56		[22] ANTIPOV	77	CIBS	25 $\pi^- p \to p3\pi$

[12] From the first PWA solution.
[13] From a partial-wave analysis of the data.
[14] From an amplitude analysis of the reaction $\pi^+\pi^- \to 2\pi^0$.
[15] K matrix pole.
[16] Taking into account the $f_2(1950)$. Helicity-2 production favored.
[17] Energy-dependent analysis.
[18] Single energy analysis.
[19] From solution A of amplitude analysis of data on $\overline{p}p \to \pi\pi$. See however KLOET 96 who fit $\pi^+\pi^-$ only and find waves only up to $J = 3$ to be important but not significantly resonant.
[20] From solution B of amplitude analysis of data on $\overline{p}p \to \pi\pi$. See however KLOET 96 who fit $\pi^+\pi^-$ only and find waves only up to $J = 3$ to be important but not significantly resonant.
[21] $I(J^P) = 0(4^+)$ from amplitude analysis assuming one-pion exchange.

Downloaded from https://academic.oup.com/ptep/article/2022/8/083C01/6651666 by KIT Library user on 27 September 2022

[22] Width errors enlarged by us to $4\Gamma/\sqrt{N}$; see the note with the $K^*(892)$ mass.

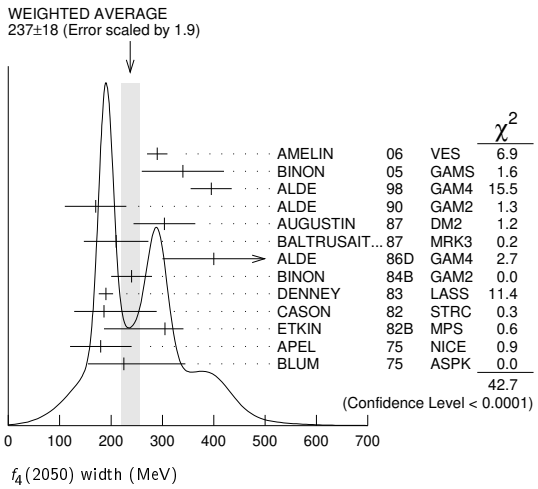

$f_4(2050)$ DECAY MODES

	Mode	Fraction (Γ_i/Γ)
Γ_1	$\omega\omega$	seen
Γ_2	$\pi\pi$	(17.0 ± 1.5) %
Γ_3	$K\overline{K}$	$(6.8^{+3.4}_{-1.8})\times10^{-3}$
Γ_4	$\eta\eta$	$(2.1\pm0.8)\times10^{-3}$
Γ_5	$4\pi^0$	<1.2 %
Γ_6	$\gamma\gamma$	seen
Γ_7	$a_2(1320)\pi$	seen

$f_4(2050)$ $\Gamma(i)\Gamma(\gamma\gamma)/\Gamma(\text{total})$

$\Gamma(K\overline{K})\times\Gamma(\gamma\gamma)/\Gamma_{\text{total}}$ — $\Gamma_3\Gamma_6/\Gamma$

VALUE (keV)	CL%	DOCUMENT ID		TECN	COMMENT
• • • We do not use the following data for averages, fits, limits, etc. • • •					
<0.29	95	ALTHOFF	85B	TASS	$\gamma\gamma\to K\overline{K}\pi$

$\Gamma(\pi\pi)\times\Gamma(\gamma\gamma)/\Gamma_{\text{total}}$ — $\Gamma_2\Gamma_6/\Gamma$

VALUE (eV)	CL%	EVTS	DOCUMENT ID		TECN	COMMENT
• • • We do not use the following data for averages, fits, limits, etc. • • •						
$23.1^{+3.6+70.5}_{-3.3-15.6}$			[23] UEHARA	09	BELL	$10.6\ e^+e^-\to e^+e^-\pi^0\pi^0$
<1100	95	13 ± 4	OEST	90	JADE	$e^+e^-\to e^+e^-\pi^0\pi^0$

[23] Taking into account the $f_2(1950)$. Helicity-2 production favored.

$f_4(2050)$ BRANCHING RATIOS

$\Gamma(\omega\omega)/\Gamma_{\text{total}}$ — Γ_1/Γ

VALUE	DOCUMENT ID		TECN	COMMENT
seen	AMELIN	06	VES	$36\ \pi^-p\to\omega\omega n$
• • • We do not use the following data for averages, fits, limits, etc. • • •				
not seen	BARBERIS	00F		$450\ pp\to p_f\omega\omega p_s$

$\Gamma(\omega\omega)/\Gamma(\pi\pi)$ — Γ_1/Γ_2

VALUE	DOCUMENT ID		TECN	COMMENT
1.5 ± 0.3	ALDE	90	GAM2	$38\ \pi^-p\to\omega\omega n$

$\Gamma(\pi\pi)/\Gamma_{\text{total}}$ — Γ_2/Γ

VALUE	DOCUMENT ID		TECN	COMMENT
0.170 ± 0.015 OUR AVERAGE				
$0.18\ \pm0.03$	[24] BINON	83C	GAM2	$38\ \pi^-p\to n4\gamma$
$0.16\ \pm0.03$	[24] CASON	82	STRC	$8\ \pi^+p\to\Delta^{++}\pi^0\pi^0$
$0.17\ \pm0.02$	[24] CORDEN	79	OMEG	$12\text{–}15\ \pi^-p\to n2\pi$

[24] Assuming one pion exchange.

$\Gamma(K\overline{K})/\Gamma(\pi\pi)$ — Γ_3/Γ_2

VALUE	DOCUMENT ID		TECN	COMMENT
$0.04^{+0.02}_{-0.01}$	ETKIN	82B	MPS	$23\ \pi^-p\to n2K^0_S$

$\Gamma(\eta\eta)/\Gamma_{\text{total}}$ — Γ_4/Γ

VALUE (units 10^{-3})	DOCUMENT ID		TECN	COMMENT
2.1 ± 0.8	ALDE	86D	GAM4	$100\ \pi^-p\to n4\gamma$

$\Gamma(4\pi^0)/\Gamma_{\text{total}}$ — Γ_5/Γ

VALUE	DOCUMENT ID		TECN	COMMENT
<0.012	ALDE	87	GAM4	$100\ \pi^-p\to4\pi^0n$

$\Gamma(a_2(1320)\pi)/\Gamma_{\text{total}}$ — Γ_7/Γ

VALUE	DOCUMENT ID		TECN	COMMENT
seen	AMELIN	00	VES	$37\ \pi^-p\to\eta\pi^+\pi^-n$

$f_4(2050)$ REFERENCES

ANISOVICH 09 IJMP A24 2481 V.V. Anisovich, A.V. Sarantsev
UEHARA 09 PR D79 052009 S. Uehara *et al.* (BELLE Collab.)
AMELIN 06 PAN 69 690 D.V. Amelin *et al.* (VES Collab.)
Translated from YAF 69 715.
BINON 05 PAN 68 960 F. Binon *et al.*
Translated from YAF 68 998.
AMELIN 00 NP A668 83 D. Amelin *et al.* (VES Collab.)
ANISOVICH 00J PL B491 47 A.V. Anisovich *et al.* (RAL, LOQM, PNPI+)
BARBERIS 00F PL B484 198 D. Barberis *et al.* (WA 102 Collab.)
ALDE 98 EPJ A3 361 D. Alde *et al.* (GAM4 Collab.)
Also PAN 62 405 D. Alde *et al.* (GAMS Collab.)
Translated from YAF 62 446.
MARTIN 98 PR C57 3492 B.R. Martin *et al.*
MARTIN 97 PR C56 1114 B.R. Martin, G.C. Oades (LOUC, AARH)
KLOET 96 PR D53 6120 W.M. Kloet, F. Myhrer (RUTG, NORD)
OAKDEN 94 NP A574 731 M.N. Oakden, M.R. Pennington (DURH)
ALDE 90 PL B241 600 D.M. Alde *et al.* (SERP, BELG, LANL, LAPP+)
OEST 90 ZPHY C47 343 T. Oest *et al.* (JADE Collab.)
ALDE 87 PL B198 286 D.M. Alde *et al.* (LANL, BRUX, SERP, LAPP)
AUGUSTIN 87 ZPHY C36 369 J.E. Augustin *et al.* (LALO, CLER, FRAS+)
BALTRUSAIT... 87 PR D35 2077 R.M. Baltrusaitis *et al.* (Mark III Collab.)
ALDE 86D NP B269 485 D.M. Alde *et al.* (BELG, LAPP, SERP, CERN+)
ALTHOFF 85B ZPHY C29 189 M. Althoff *et al.* (TASSO Collab.)
BINON 84B LNC 39 41 F.G. Binon *et al.* (SERP, BELG, LAPP)
BINON 83C SJNP 38 723 F.G. Binon *et al.* (SERP, BRUX+)
Translated from YAF 38 1199.
DENNEY 83 PR D28 2726 D.L. Denney *et al.* (IOWA, MICH)
CASON 82 PRL 48 1316 N.M. Cason *et al.* (NDAM, ANL)
ETKIN 82B PR D25 1786 A. Etkin *et al.* (BNL, CUNY, TUFTS, VAND)
ALPER 80 PL 94B 422 B. Alper *et al.* (AMST, CERN, CRAC, MPIM+)
ROZANSKA 80 NP B162 505 M. Rozanska *et al.* (MPIM, CERN)
CORDEN 79 NP B157 250 M.J. Corden *et al.* (BIRM, RHEL, TELA+) JP
EVANGELIS... 79B NP B154 381 C. Evangelista *et al.* (BARI, BONN, CERN+)
ANTIPOV 77 NP B119 45 Y.M. Antipov *et al.* (SERP, GEVA)
APEL 75 PL 57B 398 W.D. Apel *et al.* (KARLK, KARLE, PISA, SERP+) JP
BLUM 75 PL 57B 403 W. Blum *et al.* (CERN, MPIM) JP

$\pi_2(2100)$

$I^G(J^{PC}) = 1^-(2^{-+})$

OMITTED FROM SUMMARY TABLE

Needs confirmation.

$\pi_2(2100)$ MASS

VALUE (MeV)	DOCUMENT ID		TECN	COMMENT
2090 ± 29 OUR AVERAGE				
2090 ± 30	[1] AMELIN	95B	VES	$36\ \pi^-A\to\pi^+\pi^-\pi^-A$
2100 ± 150	[2] DAUM	81B	CNTR	$63,94\ \pi^-p\to3\pi X$

[1] From a fit to $J^{PC}=2^{-+}$ $f_2(1270)\pi$, $(\pi\pi)_s\pi$ waves.
[2] From a two-resonance fit to four 2^-0^+ waves.

$\pi_2(2100)$ WIDTH

VALUE (MeV)	DOCUMENT ID		TECN	COMMENT
625 ± 50 OUR AVERAGE Error includes scale factor of 1.2.				
520 ± 100	[3] AMELIN	95B	VES	$36\ \pi^-A\to\pi^+\pi^-\pi^-A$
651 ± 50	[4] DAUM	81B	CNTR	$63,94\ \pi^-p\to3\pi X$

[3] From a fit to $J^{PC}=2^{-+}$ $f_2(1270)\pi$, $(\pi\pi)_s\pi$ waves.
[4] From a two-resonance fit to four 2^-0^+ waves.

$\pi_2(2100)$ DECAY MODES

	Mode	Fraction (Γ_i/Γ)
Γ_1	3π	seen
Γ_2	$\rho\pi$	seen
Γ_3	$f_2(1270)\pi$	seen
Γ_4	$(\pi\pi)_s\pi$	seen

$\pi_2(2100)$ BRANCHING RATIOS

$\Gamma(\rho\pi)/\Gamma(3\pi)$ — Γ_2/Γ_1

VALUE	DOCUMENT ID		TECN	COMMENT
0.19 ± 0.05	[5] DAUM	81B	CNTR	$63,94\ \pi^-p$

$\Gamma(f_2(1270)\pi)/\Gamma(3\pi)$ — Γ_3/Γ_1

VALUE	DOCUMENT ID		TECN	COMMENT
0.36 ± 0.09	[5] DAUM	81B	CNTR	$63,94\ \pi^-p$

$\Gamma((\pi\pi)_s\pi)/\Gamma(3\pi)$ — Γ_4/Γ_1

VALUE	DOCUMENT ID		TECN	COMMENT
0.45 ± 0.07	[5] DAUM	81B	CNTR	$63,94\ \pi^-p$

Downloaded from https://academic.oup.com/ptep/article/2022/8/083C01/6651666 by KIT Library user on 27 September 2022

D-wave/S-wave RATIO FOR $\pi_2(2100) \to f_2(1270)\pi$

VALUE	DOCUMENT ID		TECN	COMMENT
0.39±0.23	[5] DAUM	81B	CNTR	63,94 $\pi^- p$

[5] From a two-resonance fit to four 2^-0^+ waves.

$\pi_2(2100)$ REFERENCES

AMELIN	95B	PL B356 595	D.V. Amelin *et al.*	(SERP, TBIL)
DAUM	81B	NP B182 269	C. Daum *et al.*	(AMST, CERN, CRAC, MPIM+)

$f_0(2100)$

$I^G(J^{PC}) = 0^+(0^{++})$

OMITTED FROM SUMMARY TABLE

Needs confirmation.

$f_0(2100)$ MASS

VALUE (MeV)	EVTS	DOCUMENT ID		TECN	COMMENT
2095^{+17}_{-19} OUR AVERAGE					
2116±27±17		LEES	21A	BABR	$\gamma\gamma \to \eta_c(1S) \to \eta'\pi^+\pi^-$
2081±13$^{+24}_{-36}$	5.5k	[1] ABLIKIM	13N	BES3	$e^+e^- \to J/\psi \to \gamma\eta\eta$
2090±30		BAI	00A	BES	$J/\psi \to \gamma(\pi^+\pi^-\pi^+\pi^-)$
• • • We do not use the following data for averages, fits, limits, etc. • • •					
2075±20		SARANTSEV	21	RVUE	$J/\psi(1S) \to \gamma(\pi\pi,\ K\overline{K},\ \eta\eta,\ \omega\phi)$
2090±10± 6	529	[2,3] DOBBS	15		$J/\psi \to \gamma\pi^+\pi^-$
2099±17± 8	283	[2,3] DOBBS	15		$\psi(2S) \to \gamma\pi^+\pi^-$
2105± 8	80k	[4] UMAN	06	E835	5.2 $\overline{p}p \to \eta\eta\pi^0$
2102±13		[5] ANISOVICH	00J	SPEC	2.0 $\overline{p}p \to \eta\pi^0\pi^0$, $\pi^0\pi^0$, $\eta\eta$, $\eta\eta'$, $\pi^+\pi^-$
2105±10		ANISOVICH	99K	SPEC	0.6–1.94 $\overline{p}p \to \eta\eta$, $\eta\eta'$
∼ 2104		BUGG	95		$J/\psi \to \gamma\pi^+\pi^-\pi^+\pi^-$
∼ 2122		HASAN	94	RVUE	$\overline{p}p \to \pi\pi$

[1] From partial wave analysis including all possible combinations of 0^{++}, 2^{++}, and 4^{++} resonances.
[2] Using CLEO-c data but not authored by the CLEO Collaboration.
[3] From a fit to a Breit-Wigner line shape with fixed Γ = 209 MeV.
[4] Statistical error only.
[5] Includes the data of ANISOVICH 00B indicating to exotic decay pattern.

$f_0(2100)$ WIDTH

VALUE (MeV)	EVTS	DOCUMENT ID		TECN	COMMENT
287^{+32}_{-24} OUR AVERAGE					
289± 34±15		LEES	21A	BABR	$\gamma\gamma \to \eta_c(1S) \to \eta'\pi^+\pi^-$
273$^{+27+70}_{-24-23}$	5.5k	[1] ABLIKIM	13N	BES3	$e^+e^- \to J/\psi \to \gamma\eta\eta$
330±100		BAI	00A	BES	$J/\psi \to \gamma(\pi^+\pi^-\pi^+\pi^-)$
• • • We do not use the following data for averages, fits, limits, etc. • • •					
260± 25		SARANTSEV	21	RVUE	$J/\psi(1S) \to \gamma(\pi\pi,\ K\overline{K},\ \eta\eta,\ \omega\phi)$
236± 14	80k	[2] UMAN	06	E835	5.2 $\overline{p}p \to \eta\eta\pi^0$
211± 29		[3] ANISOVICH	00J	SPEC	2.0 $\overline{p}p \to \eta\pi^0\pi^0$, $\pi^0\pi^0$, $\eta\eta$, $\eta\eta'$, $\pi^+\pi^-$
200± 25		ANISOVICH	99K	SPEC	0.6–1.94 $\overline{p}p \to \eta\eta$, $\eta\eta'$
∼ 203		BUGG	95		$J/\psi \to \gamma\pi^+\pi^-\pi^+\pi^-$
∼ 273		HASAN	94	RVUE	$\overline{p}p \to \pi\pi$

[1] From partial wave analysis including all possible combinations of 0^{++}, 2^{++}, and 4^{++} resonances.
[2] Statistical error only.
[3] Includes the data of ANISOVICH 00B indicating to exotic decay pattern.

$f_0(2100)$ REFERENCES

LEES	21A	PR D104 072002	J.P. Lees *et al.*	(BABAR Collab.)
SARANTSEV	21	PL B816 136227	A.V. Sarantsev *et al.*	(BONN, PNPI)
DOBBS	15	PR D91 052006	S. Dobbs *et al.*	(NWES)
ABLIKIM	13N	PR D87 092009	M. Ablikim *et al.*	(BESIII Collab.)
UMAN	06	PR D73 052009	I. Uman *et al.*	(FNAL E835)
ANISOVICH	00B	NP A662 319	A.V. Anisovich *et al.*	
ANISOVICH	00J	PL B491 47	A.V. Anisovich *et al.*	(RAL, LOQM, PNPI+)
BAI	00A	PL B472 207	J.Z. Bai *et al.*	(BES Collab.)
ANISOVICH	99K	PL B468 309	A.V. Anisovich *et al.*	
BUGG	95	PL B353 378	D.V. Bugg *et al.*	(LOQM, PNPI, WASH)
HASAN	94	PL B334 215	A. Hasan, D.V. Bugg	(LOQM)

$f_2(2150)$

$I^G(J^{PC}) = 0^+(2^{++})$

OMITTED FROM SUMMARY TABLE

This entry was previously called T_0.

$f_2(2150)$ MASS

$f_2(2150)$ MASS, COMBINED MODES (MeV)

VALUE (MeV)	EVTS	DOCUMENT ID		TECN	COMMENT
2157±12 OUR AVERAGE Includes data from the datablock that follows this one.					
• • • We do not use the following data for averages, fits, limits, etc. • • •					
2170± 6	80k	[1] UMAN	06	E835	5.2 $\overline{p}p \to \eta\eta\pi^0$

[1] Statistical error only.

$\eta\eta$ MODE

VALUE (MeV)	DOCUMENT ID		TECN	COMMENT
The data in this block is included in the average printed for a previous datablock.				
2157±12 OUR AVERAGE				
2151±16	BARBERIS	00E		450 $pp \to p_f\eta\eta p_s$
2175±20	PROKOSHKIN	95D	GAM4	300 $\pi^- N \to \pi^- N 2\eta$, 450 $pp \to pp2\eta$
2130±35	SINGOVSKI	94	GAM4	450 $pp \to pp2\eta$
• • • We do not use the following data for averages, fits, limits, etc. • • •				
2140±30	[2] ABELE	99B	CBAR	1.94 $\overline{p}p \to \pi^0\eta\eta$
2104±20	[3] ARMSTRONG	93C	E760	$\overline{p}p \to \pi^0\eta\eta \to 6\gamma$

[2] Spin not determined.
[3] No J^{PC} determination.

$\eta\pi\pi$ MODE

VALUE (MeV)	DOCUMENT ID		TECN	CHG	COMMENT
• • • We do not use the following data for averages, fits, limits, etc. • • •					
2135±20±45	[4] ADOMEIT	96	CBAR	0	1.94 $\overline{p}p \to \eta 3\pi^0$

[4] ANISOVICH 00E recommends to withdraw ADOMEIT 96 that assumed a single $J^P = 2^+$ resonance.

$\overline{p}p \to \pi\pi$

VALUE (MeV)	DOCUMENT ID		TECN	COMMENT
• • • We do not use the following data for averages, fits, limits, etc. • • •				
∼ 2090	[5] OAKDEN	94	RVUE	0.36–1.55 $\overline{p}p \to \pi\pi$
∼ 2120	[6] OAKDEN	94	RVUE	0.36–1.55 $\overline{p}p \to \pi\pi$
∼ 2170	[7] MARTIN	80B	RVUE	
∼ 2150	[7] MARTIN	80C	RVUE	
∼ 2150	[8] DULUDE	78B	OSPK	1–2 $\overline{p}p \to \pi^0\pi^0$

[5] OAKDEN 94 makes an amplitude analysis of LEAR data on $\overline{p}p \to \pi\pi$ using a method based on Barrelet zeros. This is solution A. The amplitude analysis of HASAN 94 includes earlier data as well, and assume that the data can be parametrized in terms of towers of nearly degenerate resonances on the leading Regge trajectory. See also KLOET 96 and MARTIN 97 who make related analyses.
[6] From solution B of amplitude analysis of data on $\overline{p}p \to \pi\pi$.
[7] $I(J^P) = 0(2^+)$ from simultaneous analysis of $p\overline{p} \to \pi^-\pi^+$ and $\pi^0\pi^0$.
[8] $I^G(J^P) = 0^+(2^+)$ from partial-wave amplitude analysis.

S-CHANNEL $\overline{p}p$, $\overline{N}N$ or $\overline{K}K$

VALUE (MeV)	DOCUMENT ID		TECN	CHG	COMMENT
• • • We do not use the following data for averages, fits, limits, etc. • • •					
2139$^{+8}_{-9}$	[9] EVANGELIS...	97	SPEC		0.6-2.4 $\overline{p}p \to K^0_S K^0_S$
∼ 2190	[9] CUTTS	78B	CNTR		0.97–3 $\overline{p}p \to \overline{N}N$
2155±15	[9,10] COUPLAND	77	CNTR	0	0.7–2.4 $\overline{p}p \to \overline{p}p$
2193± 2	[9,11] ALSPECTOR	73	CNTR		$\overline{p}p$ S channel

[9] Isospins 0 and 1 not separated.
[10] From a fit to the total elastic cross section.
[11] Referred to as T or T region by ALSPECTOR 73.

$K\overline{K}$ MODE

VALUE (MeV)	DOCUMENT ID		TECN	COMMENT
• • • We do not use the following data for averages, fits, limits, etc. • • •				
2200±13	VLADIMIRSK...	06	SPEC	40 $\pi^- p \to K^0_S K^0_S n$
2150±20	ABLIKIM	04E	BES2	$J/\psi \to \omega K^+K^-$
2130±35	BARBERIS	99	OMEG	450 $pp \to p_s p_f K^+K^-$

Downloaded from https://academic.oup.com/ptep/article/2022/8/083C01/6651666 by KIT Library user on 27 September 2022

$f_2(2150)$ WIDTH

$f_2(2150)$ WIDTH, COMBINED MODES (MeV)

VALUE (MeV)	EVTS	DOCUMENT ID		TECN	COMMENT
152±30 OUR AVERAGE Includes data from the datablock that follows this one. Error includes scale factor of 1.4. See the ideogram below.					
• • • We do not use the following data for averages, fits, limits, etc. • • •					
182±11	80k	[12] UMAN	06	E835	5.2 $\overline{p}p \to \eta\eta\pi^0$

[12] Statistical error only.

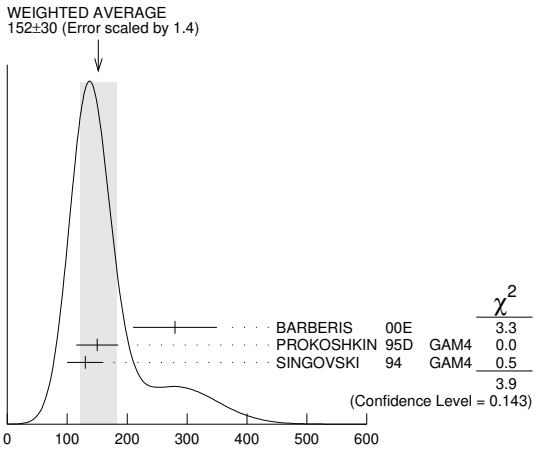

$f_2(2150)$ width, comibined modes (MeV)

$\eta\eta$ MODE

VALUE (MeV)	DOCUMENT ID		TECN	COMMENT
The data in this block is included in the average printed for a previous datablock.				
152±30 OUR AVERAGE Error includes scale factor of 1.4. See the ideogram below.				
280±70	BARBERIS	00E		450 $pp \to p_f \eta\eta p_s$
150±35	PROKOSHKIN	95D	GAM4	300 $\pi^- N \to \pi^- N 2\eta$, 450 $pp \to pp2\eta$
130±30	SINGOVSKI	94	GAM4	450 $pp \to pp2\eta$
• • • We do not use the following data for averages, fits, limits, etc. • • •				
310±50	[13] ABELE	99B	CBAR	1.94 $\overline{p}p \to \pi^0\eta\eta$
203±10	[14] ARMSTRONG	93C	E760	$\overline{p}p \to \pi^0\eta\eta \to 6\gamma$

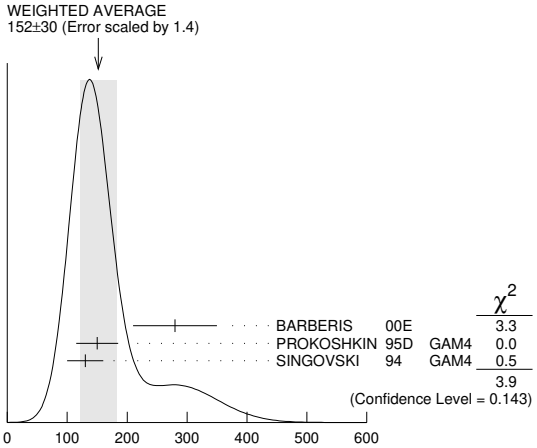

$f_2(2150)$ width, $\eta\eta$ mode (MeV)

[13] Spin not determined.
[14] No J^{PC} determination.

$\eta\pi\pi$ MODE

VALUE (MeV)	DOCUMENT ID		TECN	CHG	COMMENT
• • • We do not use the following data for averages, fits, limits, etc. • • •					
250±25±45	[15] ADOMEIT	96	CBAR	0	1.94 $\overline{p}p \to \eta 3\pi^0$

[15] ANISOVICH 00E recommends to withdraw ADOMEIT 96 that assumed a single $J^P = 2^+$ resonance.

$\overline{p}p \to \pi\pi$

VALUE (MeV)	DOCUMENT ID		TECN	COMMENT
250 OUR ESTIMATE				
• • • We do not use the following data for averages, fits, limits, etc. • • •				
~ 70	[16] OAKDEN	94	RVUE	0.36–1.55 $\overline{p}p \to \pi\pi$
~ 250	[17] MARTIN	80B	RVUE	
~ 250	[17] MARTIN	80C	RVUE	
~ 250	[18] DULUDE	78B	OSPK	1–2 $\overline{p}p \to \pi^0\pi^0$

[16] See however KLOET 96 who fit $\pi^+\pi^-$ only and find waves only up to $J = 3$ to be important but not significantly resonant.
[17] $I(J^P) = 0(2^+)$ from simultaneous analysis of $p\overline{p} \to \pi^-\pi^+$ and $\pi^0\pi^0$.
[18] $I^G(J^P) = 0^+(2^+)$ from partial-wave amplitude analysis.

S-CHANNEL $\overline{p}p$, $\overline{N}N$ or $\overline{K}K$

VALUE (MeV)	DOCUMENT ID		TECN	CHG	COMMENT
• • • We do not use the following data for averages, fits, limits, etc. • • •					
56^{+31}_{-16}	[19] EVANGELIS...	97	SPEC		0.6-2.4 $\overline{p}p \to K^0_S K^0_S$
135±75	[20,21] COUPLAND	77	CNTR	0	0.7–2.4 $\overline{p}p \to \overline{p}p$
98± 8	[21] ALSPECTOR	73	CNTR		$\overline{p}p$ S channel

[19] Isospin 0 and 2 not separated.
[20] From a fit to the total elastic cross section.
[21] Isospins 0 and 1 not separated.

$K\overline{K}$ MODE

VALUE (MeV)	DOCUMENT ID		TECN	COMMENT
• • • We do not use the following data for averages, fits, limits, etc. • • •				
91±62	VLADIMIRSK...06		SPEC	40 $\pi^- p \to K^0_S K^0_S n$
150±30	ABLIKIM	04E	BES2	$J/\psi \to \omega K^+ K^-$
270±50	BARBERIS	99	OMEG	450 $pp \to p_s p_f K^+ K^-$

$f_2(2150)$ DECAY MODES

	Mode	Fraction (Γ_i/Γ)
Γ_1	$\pi\pi$	
Γ_2	$\eta\eta$	seen
Γ_3	$K\overline{K}$	seen
Γ_4	$f_2(1270)\eta$	seen
Γ_5	$a_2(1320)\pi$	seen
Γ_6	$p\overline{p}$	seen

$f_2(2150)$ BRANCHING RATIOS

$\Gamma(K\overline{K})/\Gamma(\eta\eta)$ — Γ_3/Γ_2

VALUE	CL%	DOCUMENT ID		TECN	COMMENT
1.28±0.23		BARBERIS	00E		450 $pp \to p_f \eta\eta p_s$
• • • We do not use the following data for averages, fits, limits, etc. • • •					
<0.1	95	[22] PROKOSHKIN	95D	GAM4	300 $\pi^- N \to \pi^- N 2\eta$, 450 $pp \to pp2\eta$

[22] Using data from ARMSTRONG 89D.

$\Gamma(\pi\pi)/\Gamma(\eta\eta)$ — Γ_1/Γ_2

VALUE	CL%	DOCUMENT ID		TECN	COMMENT
• • • We do not use the following data for averages, fits, limits, etc. • • •					
<0.33	95	[23] PROKOSHKIN	95D	GAM4	300 $\pi^- N \to \pi^- N 2\eta$, 450 $pp \to pp2\eta$

[23] Derived from a $\pi^0\pi^0/\eta\eta$ limit.

$\Gamma(f_2(1270)\eta)/\Gamma(a_2(1320)\pi)$ — Γ_4/Γ_5

VALUE	DOCUMENT ID		TECN	COMMENT
0.79±0.11	[24] ADOMEIT	96	CBAR	1.94 $\overline{p}p \to \eta 3\pi^0$

[24] Using $B(a_2(1320) \to \eta\pi) = 0.145$

$\Gamma(p\overline{p})/\Gamma_{total}$ — Γ_6/Γ

VALUE	EVTS	DOCUMENT ID		TECN	COMMENT
seen	73	ALEXANDER	10	CLEO	$\psi(2S) \to \gamma p\overline{p}$

$f_2(2150)$ REFERENCES

ALEXANDER 10 PR D82 092002 J.P. Alexander *et al.* (CLEO Collab.)
UMAN 06 PR D73 052009 I. Uman *et al.* (FNAL E835)
VLADIMIRSK... 06 PAN 69 493 V.V. Vladimirsky *et al.* (ITEP, Moscow)
Translated from YAF 69 515.
ABLIKIM 04E PL B603 138 M. Ablikim *et al.* (BES Collab.)
ANISOVICH 00E PL B477 19 A.V. Anisovich *et al.*
BARBERIS 00E PL B479 59 D. Barberis *et al.* (WA 102 Collab.)
ABELE 99B EPJ C8 67 A. Abele *et al.* (Crystal Barrel Collab.)
BARBERIS 99 PL B453 305 D. Barberis *et al.* (Omega Expt.)
EVANGELIS... 97 PR D56 3803 C. Evangelista *et al.* (LEAR Collab.)
MARTIN 97 PR C56 1114 B.R. Martin, G.C. Oades (LOUC, AARH)
ADOMEIT 96 ZPHY C71 227 J. Adomeit *et al.* (Crystal Barrel Collab.)
KLOET 96 PR D53 6120 W.M. Kloet, F. Myhrer (RUTG, NORD)
PROKOSHKIN 95D PD 40 495 Y.D. Prokoshkin (SERP) IGJPC
Translated from DANS 344 469.

Downloaded from https://academic.oup.com/ptep/article/2022/8/083C01/6651666 by KIT Library user on 27 September 2022

HASAN	94	PL B334 215	A. Hasan, D.V. Bugg	(LOQM)
OAKDEN	94	NP A574 731	M.N. Oakden, M.R. Pennington	(DURH)
SINGOVSKI	94	NC A107 1911	A.V. Singovsky	(SERP)
ARMSTRONG	93C	PL B307 394	T.A. Armstrong *et al.*	(FNAL, FERR, GENO+)
ARMSTRONG	89D	PL B227 186	T.A. Armstrong, M. Benayoun	(ATHU, BARI, BIRM+)
MARTIN	80B	NP B176 355	B.R. Martin, D. Morgan	(LOUC, RHEL)JP
MARTIN	80C	NP B169 216	A.D. Martin, M.R. Pennington	(DURH)JP
CUTTS	78B	PR D17 16	D. Cutts *et al.*	(STON, WISC)
DULUDE	78B	PL 79B 335	R.S. Dulude *et al.*	(BROW, MIT, BARI)JP
COUPLAND	77	PL 71B 460	M. Coupland *et al.*	(LOQM, RHEL)
ALSPECTOR	73	PRL 30 511	J. Alspector *et al.*	(RUTG, UPNJ)

$\rho(2150)$

$I^G(J^{PC}) = 1^+(1^{--})$

OMITTED FROM SUMMARY TABLE

This entry was previously called $T_1(2190)$. See the review on "Spectroscopy of Light Meson Resonances."

$\rho(2150)$ MASS

e^+e^- PRODUCED

VALUE (MeV)	EVTS	DOCUMENT ID		TECN	COMMENT
• • • We do not use the following data for averages, fits, limits, etc. • • •					
2034 ±13 ± 9		[1] ABLIKIM	21A	BES3	$e^+e^- \to \omega\pi^0$
2111 ±43 ±25		[2] ABLIKIM	21X	BES3	$e^+e^- \to \eta'\pi^+\pi^-$
2255 $^{+17}_{-18}$ $^{+50}_{-41}$	1.8k	[3] ABLIKIM	20F	BES3	$\psi(2S) \to K^+K^-\eta$
2201 ±19		[4] LEES	20	BABR	$e^+e^- \to K^+K^-\gamma$
2227 ± 9 ± 9		[5] LEES	20	RVUE	$e^+e^- \to K^+K^-$
2039 ± 8 $^{+36}_{-18}$		[6] ABLIKIM	19AQ	BES	$J/\psi \to K^+K^-\pi^0$
2239.2± 7.1±11.3		[7] ABLIKIM	19L	BES3	$e^+e^- \to K^+K^-$
2254 ±22		[8] LEES	12G	BABR	$e^+e^- \to \pi^+\pi^-\gamma$
2150 ±40 ±50		AUBERT	07AU	BABR	10.6 $e^+e^- \to f_1(1285)\pi^+\pi^-\gamma$
1990 ±80		AUBERT	07AU	BABR	10.6 $e^+e^- \to \eta'\pi^+\pi^-\gamma$
2153 ±37		BIAGINI	91	RVUE	$e^+e^- \to \pi^+\pi^-$, K^+K^-
2110 ±50		[9] CLEGG	90	RVUE	$e^+e^- \to 3(\pi^+\pi^-)$, $2(\pi^+\pi^-\pi^0)$

[1] From a fit to the cross section between 2.00 and 3.08 GeV with a coherent sum of Breit-Wigner amplitudes, including contributions from $\rho(770)$, $\rho(1450)$ and $\rho(1700)$. Could be another state.
[2] From a Breit-Wigner fit to the Born cross section, including an s-dependent continuum amplitude.
[3] Seen in $\psi(2S)$ decay with branching ratio $\psi(2S) \to X\eta \to K^+K^-\eta = (21.7 \pm 1.9^{+7.7}_{-8.3}) \times 10^{-6}$.
[4] From the fit to the BABAR data of LEES 13Q assuming a coherent sum of a single Breit-Wigner resonance and a nonresonant contribution. The resonance significance is 3.5 σ.
[5] From the fit to the BABAR data of LEES 13Q and BESIII data of ABLIKIM 19L assuming a coherent sum of a single Breit-Wigner resonance and a nonresonant contribution.
[6] Could also be another state. Seen in J/ψ decay with branching ratio $J/\psi \to X\pi^0 \to K^+K^-\pi^0 = (6.7 \pm 1.1^{+2.2}_{-1.8}) \times 10^{-6}$.
[7] The observed structure can be due to both the $\phi(2170)$ and $\rho(2150)$.
[8] Using the GOUNARIS 68 parametrization of the pion form factor leaving the masses and widths of the $\rho(1450)$, $\rho(1700)$, and $\rho(2150)$ resonances as free parameters of the fit.
[9] Includes ATKINSON 85.

$\overline{p}p \to \pi\pi$

VALUE (MeV)	DOCUMENT ID		TECN	COMMENT
• • • We do not use the following data for averages, fits, limits, etc. • • •				
~ 2191	HASAN	94	RVUE	$\overline{p}p \to \pi\pi$
~ 2070	[1] OAKDEN	94	RVUE	0.36–1.55 $\overline{p}p \to \pi\pi$
~ 2170	[2] MARTIN	80B	RVUE	
~ 2100	[2] MARTIN	80C	RVUE	

[1] See however KLOET 96 who fit $\pi^+\pi^-$ only and find waves only up to $J = 3$ to be important but not significantly resonant.
[2] $I(J^P) = 1(1^-)$ from simultaneous analysis of $p\overline{p} \to \pi^-\pi^+$ and $\pi^0\pi^0$.

S-CHANNEL $\overline{N}N$

VALUE (MeV)	DOCUMENT ID		TECN	COMMENT
• • • We do not use the following data for averages, fits, limits, etc. • • •				
2110±35	[1] ANISOVICH	02	SPEC	0.6–1.9 $p\overline{p} \to \omega\pi^0, \omega\eta\pi^0, \pi^+\pi^-$
~ 2190	[2] CUTTS	78B	CNTR	0.97–3 $\overline{p}p \to \overline{N}N$
2155±15	[2,3] COUPLAND	77	CNTR	0.7–2.4 $\overline{p}p \to \overline{p}p$
2193± 2	[2,4] ALSPECTOR	73	CNTR	$\overline{p}p$ S channel
2190±10	[5] ABRAMS	70	CNTR	S channel $\overline{p}N$

[1] From the combined analysis of ANISOVICH 00J, ANISOVICH 01D, ANISOVICH 01E, and ANISOVICH 02.
[2] Isospins 0 and 1 not separated.
[3] From a fit to the total elastic cross section.
[4] Referred to as T or T region by ALSPECTOR 73.
[5] Seen as bump in $I = 1$ state. See also COOPER 68. PEASLEE 75 confirm $\overline{p}p$ results of ABRAMS 70, no narrow structure.

$\pi^-p \to \omega\pi^0 n$

VALUE (MeV)	DOCUMENT ID		TECN	COMMENT
• • • We do not use the following data for averages, fits, limits, etc. • • •				
2140±30	ALDE	95	GAM2	38 $\pi^-p \to \omega\pi^0 n$
2170±30	ALDE	92C	GAM4	100 $\pi^-p \to \omega\pi^0 n$

$\rho(2150)$ WIDTH

e^+e^- PRODUCED

VALUE (MeV)	EVTS	DOCUMENT ID		TECN	COMMENT
• • • We do not use the following data for averages, fits, limits, etc. • • •					
234 ± 30 ± 25		[1] ABLIKIM	21A	BES3	$e^+e^- \to \omega\pi^0$
135 ± 34 ± 30		[2] ABLIKIM	21X	BES3	$e^+e^- \to \eta'\pi^+\pi^-$
460 $^{+54}_{-48}$ $^{+160}_{-90}$	1.8k	[3] ABLIKIM	20F	BES3	$\psi(2S) \to K^+K^-\eta$
70 ± 38		[4] LEES	20	BABR	$e^+e^- \to K^+K^-\gamma$
127 ± 14 ± 4		[5] LEES	20	RVUE	$e^+e^- \to K^+K^-$
196 ± 23 $^{+25}_{-27}$		[6] ABLIKIM	19AQ	BES	$J/\psi \to K^+K^-\pi^0$
139.8± 12.3± 20.6		[7] ABLIKIM	19L	BES3	$e^+e^- \to K^+K^-$
109 ± 76		[8] LEES	12G	BABR	$e^+e^- \to \pi^+\pi^-\gamma$
350 ± 40 ± 50		AUBERT	07AU	BABR	10.6 $e^+e^- \to f_1(1285)\pi^+\pi^-\gamma$
310 ±140		AUBERT	07AU	BABR	10.6 $e^+e^- \to \eta'\pi^+\pi^-\gamma$
389 ± 79		BIAGINI	91	RVUE	$e^+e^- \to \pi^+\pi^-$, K^+K^-
410 ±100		[9] CLEGG	90	RVUE	$e^+e^- \to 3(\pi^+\pi^-)$, $2(\pi^+\pi^-\pi^0)$

[1] From a fit to the cross section between 2.00 and 3.08 GeV with a coherent sum of Breit-Wigner amplitudes, including contributions from $\rho(770)$, $\rho(1450)$ and $\rho(1700)$. Could be another state.
[2] From a Breit-Wigner fit to the Born cross section, including an s-dependent continuum amplitude.
[3] Seen in $\psi(2S)$ decay with branching ratio $\psi(2S) \to X\eta \to K^+K^-\eta = (21.7 \pm 1.9^{+7.7}_{-8.3}) \times 10^{-6}$.
[4] From the fit to the BABAR data of LEES 13Q assuming a coherent sum of a single Breit-Wigner resonance and a nonresonant contribution. The resonance significance is 3.5 σ.
[5] From the fit to the BABAR data of LEES 13Q and BESIII data of ABLIKIM 19L assuming a coherent sum of a single Breit-Wigner resonance and a nonresonant contribution.
[6] Could also be another state. Seen in J/ψ decay with branching ratio $J/\psi \to X\pi^0 \to K^+K^-\pi^0 = (6.7 \pm 1.1^{+2.2}_{-1.8}) \times 10^{-6}$.
[7] The observed structure can be due to both the $\phi(2170)$ and $\rho(2150)$.
[8] Using the GOUNARIS 68 parametrization of the pion form factor leaving the masses and widths of the $\rho(1450)$, $\rho(1700)$, and $\rho(2150)$ resonances as free parameters of the fit.
[9] Includes ATKINSON 85.

$\overline{p}p \to \pi\pi$

VALUE (MeV)	DOCUMENT ID		TECN	COMMENT
• • • We do not use the following data for averages, fits, limits, etc. • • •				
~ 296	HASAN	94	RVUE	$\overline{p}p \to \pi\pi$
~ 40	[1] OAKDEN	94	RVUE	0.36–1.55 $\overline{p}p \to \pi\pi$
~ 250	[2] MARTIN	80B	RVUE	
~ 200	[2] MARTIN	80C	RVUE	

[1] See however KLOET 96 who fit $\pi^+\pi^-$ only and find waves only up to $J = 3$ to be important but not significantly resonant.
[2] $I(J^P) = 1(1^-)$ from simultaneous analysis of $p\overline{p} \to \pi^-\pi^+$ and $\pi^0\pi^0$.

S-CHANNEL $\overline{N}N$

VALUE (MeV)	DOCUMENT ID		TECN	COMMENT
• • • We do not use the following data for averages, fits, limits, etc. • • •				
230±50	[1] ANISOVICH	02	SPEC	0.6–1.9 $p\overline{p} \to \omega\pi^0, \omega\eta\pi^0, \pi^+\pi^-$
135±75	[2,3] COUPLAND	77	CNTR	0.7–2.4 $\overline{p}p \to \overline{p}p$
98± 8	[3] ALSPECTOR	73	CNTR	$\overline{p}p$ S channel
~ 85	[4] ABRAMS	70	CNTR	S channel $\overline{p}N$

[1] From the combined analysis of ANISOVICH 00J, ANISOVICH 01D, ANISOVICH 01E, and ANISOVICH 02.
[2] From a fit to the total elastic cross section.
[3] Isospins 0 and 1 not separated.
[4] Seen as bump in $I = 1$ state. See also COOPER 68. PEASLEE 75 confirm $\overline{p}p$ results of ABRAMS 70, no narrow structure.

$\pi^-p \to \omega\pi^0 n$

VALUE (MeV)	DOCUMENT ID		TECN	COMMENT
• • • We do not use the following data for averages, fits, limits, etc. • • •				
320±70	ALDE	95	GAM2	38 $\pi^-p \to \omega\pi^0 n$
~ 300	ALDE	92C	GAM4	100 $\pi^-p \to \omega\pi^0 n$

$\rho(2150)$ DECAY MODES

	Mode	Fraction (Γ_i/Γ)
Γ_1	e^+e^-	
Γ_2	$\pi^+\pi^-$	seen
Γ_3	K^+K^-	seen

Downloaded from https://academic.oup.com/ptep/article/2022/8/083C01/6651666 by KIT Library user on 27 September 2022

Γ_4	$3(\pi^+\pi^-)$	seen
Γ_5	$2(\pi^+\pi^-\pi^0)$	seen
Γ_6	$\eta'\pi^+\pi^-$	seen
Γ_7	$f_1(1285)\pi^+\pi^-$	seen
Γ_8	$\omega\pi^0$	seen
Γ_9	$\omega\pi^0\eta$	seen
Γ_{10}	$p\overline{p}$	

$\rho(2150)$ $\Gamma(i)\Gamma(e^+e^-)/\Gamma(\text{total})$

$\Gamma(\omega\pi^0) \times \Gamma(e^+e^-)/\Gamma_{\text{total}}$ — $\Gamma_8\Gamma_1/\Gamma$

VALUE (eV)	DOCUMENT ID		TECN	COMMENT
• • • We do not use the following data for averages, fits, limits, etc. • • •				
$34\pm11\pm16$	ABLIKIM	21A	BES3	$e^+e^- \to \omega\pi^0$

$\Gamma(\eta'\pi^+\pi^-) \times \Gamma(e^+e^-)/\Gamma_{\text{total}}$ — $\Gamma_6\Gamma_1/\Gamma$

VALUE (eV)	DOCUMENT ID		TECN	COMMENT
• • • We do not use the following data for averages, fits, limits, etc. • • •				
$23.3\pm5.3\pm3.3$	[1] ABLIKIM	21X	BES3	$e^+e^- \to \eta'\pi^+\pi^-$

[1] From a Breit-Wigner fit to the Born cross section interfering constructively with the continuum. For destructive interference the value is $0.64 \pm 0.49 \pm 0.42$ eV.

$\rho(2150)$ $\Gamma(i)\Gamma(e^+e^-)/\Gamma^2(\text{total})$

$\Gamma(f_1(1285)\pi^+\pi^-)/\Gamma_{\text{total}} \times \Gamma(e^+e^-)/\Gamma_{\text{total}}$ — $\Gamma_7/\Gamma \times \Gamma_1/\Gamma$

VALUE (units 10^{-7})	DOCUMENT ID		TECN	COMMENT
$3.1\pm0.6\pm0.5$	[1] AUBERT	07AU	BABR	$10.6\ e^+e^- \to f_1(1285)\pi^+\pi^-\gamma$

[1] Calculated by us from the reported value of cross section at the peak.

$\Gamma(\eta'\pi^+\pi^-)/\Gamma_{\text{total}} \times \Gamma(e^+e^-)/\Gamma_{\text{total}}$ — $\Gamma_6/\Gamma \times \Gamma_1/\Gamma$

VALUE (units 10^{-8})	DOCUMENT ID		TECN	COMMENT
• • • We do not use the following data for averages, fits, limits, etc. • • •				
4.9 ± 1.9	[1] AUBERT	07AU	BABR	$10.6\ e^+e^- \to \eta'\pi^+\pi^-\gamma$

[1] Calculated by us from the reported value of cross section at the peak.

$\rho(2150)$ REFERENCES

ABLIKIM	21A	PL B813 136059	M. Ablikim *et al.*	(BESIII Collab.)
ABLIKIM	21X	PR D103 072007	M. Ablikim *et al.*	(BESIII Collab.)
ABLIKIM	20F	PR D101 032008	M. Ablikim *et al.*	(BESIII Collab.)
LEES	20	PR D101 012011	J.P. Lees *et al.*	(BESIII Collab.)
ABLIKIM	19AQ	PR D100 032004	M. Ablikim *et al.*	(BESIII Collab.)
ABLIKIM	19L	PR D99 032001	M. Ablikim *et al.*	(BESIII Collab.)
LEES	13Q	PR D88 032013	J.P. Lees *et al.*	(BABAR Collab.)
LEES	12G	PR D86 032013	J.P. Lees *et al.*	(BABAR Collab.)
AUBERT	07AU	PR D76 092005	B. Aubert *et al.*	(BABAR Collab.)
ANISOVICH	02	PL B542 8	A.V. Anisovich *et al.*	
ANISOVICH	01D	PL B508 6	A.V. Anisovich *et al.*	
ANISOVICH	01E	PL B513 281	A.V. Anisovich *et al.*	
ANISOVICH	00J	PL B491 47	A.V. Anisovich *et al.*	(RAL, LOQM, PNPI+)
KLOET	96	PR D53 6120	W.M. Kloet, F. Myhrer	(RUTG, NORD)
ALDE	95	ZPHY C66 379	D.M. Alde *et al.*	(GAMS Collab.) JP
HASAN	94	PL B334 215	A. Hasan, D.V. Bugg	(LOQM)
OAKDEN	94	NP A574 731	M.N. Oakden, M.R. Pennington	(DURH)
ALDE	92C	ZPHY C54 553	D.M. Alde *et al.*	(BELG, SERP, KEK, LANL+)
BIAGINI	91	NC 104A 363	M.E. Biagini *et al.*	(FRAS, PRAG)
CLEGG	90	ZPHY C45 677	A.B. Clegg, A. Donnachie	(LANC, MCHS)
ATKINSON	85	ZPHY C29 333	M. Atkinson *et al.*	(BONN, CERN, GLAS+)
MARTIN	80B	NP B176 355	B.R. Martin, D. Morgan	(LOUC, RHEL) JP
MARTIN	80C	NP B169 216	A.D. Martin, M.R. Pennington	(DURH) JP
CUTTS	78B	PR D17 16	D. Cutts *et al.*	(STON, WISC)
COUPLAND	77	PL 71B 460	M. Coupland *et al.*	(LOQM, RHEL)
PEASLEE	75	PL 57B 189	D.C. Peaslee *et al.*	(CANB, BARI, BROW+)
ALSPECTOR	73	PRL 30 511	J. Alspector *et al.*	(RUTG, UPNJ)
ABRAMS	70	PR D1 1917	R.J. Abrams *et al.*	(BNL)
COOPER	68	PRL 20 1059	W.A. Cooper *et al.*	(ANL)
GOUNARIS	68	PRL 21 244	G.J. Gounaris, J.J. Sakurai	

$\phi(2170)$

$I^G(J^{PC}) = 0^-(1^{--})$

See the review on "Spectroscopy of Light Meson Resonances."

$\phi(2170)$ MASS

VALUE (MeV)	EVTS	DOCUMENT ID		TECN	COMMENT
2162 ± 7 OUR AVERAGE		Error includes scale factor of 1.1.			
$2176 \pm24 \pm 3$		[1] ABLIKIM	21A	BES3	$e^+e^- \to \omega\eta$
$2163.5\pm 6.2\pm 3.0$		[2] ABLIKIM	21T	BES3	$e^+e^- \to \phi\eta$
$2177.5\pm 4.8\pm19.5$		[3] ABLIKIM	20M	BES3	$e^+e^- \to \eta'\phi$
$2126.5\pm16.8\pm12.4$		[4] ABLIKIM	20S	BES3	$e^+e^- \to K^+K^-\pi^0\pi^0$
• • • We do not use the following data for averages, fits, limits, etc. • • •					
$2273.7\pm 5.7\pm19.3$		[5] ABLIKIM	21AP	BES3	$e^+e^- \to K^0_S K^0_L$
$2135 \pm 8 \pm 9$	95	ABLIKIM	19I	BES3	$e^+e^- \to \eta\phi f_0(980)$
$2239.2\pm 7.1\pm11.3$		[6] ABLIKIM	19L	BES3	$e^+e^- \to K^+K^-$
$2200 \pm 6 \pm 5$	471	ABLIKIM	15H	BES3	$J/\psi \to \eta\phi\pi^+\pi^-$
$2180 \pm 8 \pm 8$		[7,8] LEES	12F	BABR	$10.6\ e^+e^- \to \phi\pi^+\pi^-\gamma$
$2079 \pm13 \ {}^{+79}_{-28}$	4.8k	[9] SHEN	09	BELL	$10.6\ e^+e^- \to K^+K^-\pi^+\pi^-\gamma$
$2186 \pm10 \pm 6$	52	ABLIKIM	08F	BES	$J/\psi \to \eta\phi f_0(980)$
$2125 \pm22 \pm10$	483	AUBERT	08S	BABR	$10.6\ e^+e^- \to \phi\eta\gamma$
2192 ± 14	116	[10] AUBERT	07AK	BABR	$10.6\ e^+e^- \to K^+K^-\pi^+\pi^-\gamma$
2169 ± 20	149	[10] AUBERT	07AK	BABR	$10.6\ e^+e^- \to K^+K^-\pi^0\pi^0\gamma$
$2175 \pm10 \pm15$	201	[8,11] AUBERT,BE	06D	BABR	$10.6\ e^+e^- \to K^+K^-\pi\pi\gamma$

[1] From a fit to the cross section between 2.00 and 3.08 GeV with a coherent sum of Breit-Wigner amplitudes, including contributions from $\omega(1420)$ and $\omega(1650)/\phi(1680)$.

[2] From a fit to the cross section below 3.5 GeV measured by BaBar and BESIII with a coherent sum of two modified Breit-Wigner amplitudes ($\phi(1680)$ and $\phi(2170)$) and a nonresonant term.

[3] From a fit using a coherent sum of a phase-space modified Breit-Wigner function and a phase-space term.

[4] By a simultaneous fit of the intermediate channels in a partial-wave analysis, assuming the same structure, modelled with a coherent sum of a nonresonant component and a resonant component by a Breit-Wigner function.

[5] From a fit to the cross section between 2.00 and 3.08 GeV with a sum of Breit-Wigner amplitude and a nonresonant contribution. The observed structure can be also due to $\rho(2150)$.

[6] The observed structure can be due to both the $\phi(2170)$ and $\rho(2150)$.

[7] Fit includes interference with the $\phi(1680)$.

[8] From the $\phi f_0(980)$ component.

[9] From a fit with two incoherent Breit-Wigners.

[10] From the $K^+K^- f_0(980)$ component.

[11] Superseded by LEES 12F.

$\phi(2170)$ WIDTH

VALUE (MeV)	EVTS	DOCUMENT ID		TECN	COMMENT
$100 \ {}^{+31}_{-23}$ OUR AVERAGE		Error includes scale factor of 2.5. See the ideogram below.			
$89 \pm50 \pm 5$		[1] ABLIKIM	21A	BES3	$e^+e^- \to \omega\eta$
$31.1\ {}^{+21.1}_{-11.6}\pm 1.1$		[2] ABLIKIM	21T	BES3	$e^+e^- \to \phi\eta$
$149.0\pm15.6\pm 8.9$		[3] ABLIKIM	20M	BES3	$e^+e^- \to \eta'\phi$
$106.9\pm32.1\pm28.1$		[4] ABLIKIM	20S	BES3	$e^+e^- \to K^+K^-\pi^0\pi^0$
• • • We do not use the following data for averages, fits, limits, etc. • • •					
$86 \pm44 \pm51$		[5] ABLIKIM	21AP	BES3	$e^+e^- \to K^0_S K^0_L$
$104 \pm24 \pm12$	95	ABLIKIM	19I	BES3	$e^+e^- \to \eta\phi f_0(980)$
$139.8\pm12.3\pm20.6$		[6] ABLIKIM	19L	BES3	$e^+e^- \to K^+K^-$
$104 \pm15 \pm15$	471	ABLIKIM	15H	BES3	$J/\psi \to \eta\phi\pi^+\pi^-$
$77 \pm15 \pm10$		[7,8] LEES	12F	BABR	$10.6\ e^+e^- \to \phi\pi^+\pi^-\gamma$
$192 \pm23 \ {}^{+25}_{-61}$	4.8k	[9] SHEN	09	BELL	$10.6\ e^+e^- \to K^+K^-\pi^+\pi^-\gamma$
$65 \pm23 \pm17$	52	ABLIKIM	08F	BES	$J/\psi \to \eta\phi f_0(980)$
$61 \pm50 \pm13$	483	AUBERT	08S	BABR	$10.6\ e^+e^- \to \phi\eta\gamma$
71 ± 21	116	[10] AUBERT	07AK	BABR	$10.6\ e^+e^- \to K^+K^-\pi^+\pi^-\gamma$
102 ± 27	149	[10] AUBERT	07AK	BABR	$10.6\ e^+e^- \to K^+K^-\pi^0\pi^0\gamma$
$58 \pm16 \pm20$	201	[8,11] AUBERT,BE	06D	BABR	$10.6\ e^+e^- \to K^+K^-\pi\pi\gamma$

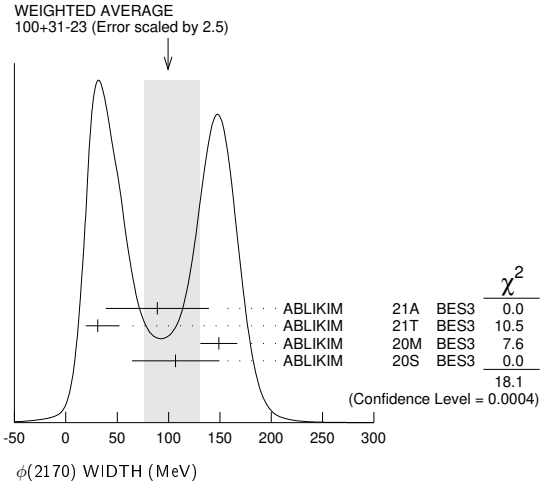

[1] From a fit to the cross section between 2.00 and 3.08 GeV with a coherent sum of Breit-Wigner amplitudes, including contributions from $\omega(1420)$ and $\omega(1650)/\phi(1680)$.

[2] From a fit to the cross section below 3.5 GeV measured by BaBar and BESIII with a coherent sum of two modified Breit-Wigner amplitudes ($\phi(1680)$ and $\phi(2170)$) and a nonresonant term.

[3] From a fit using a coherent sum of a phase-space modified Breit-Wigner function and a phase-space term.

Downloaded from https://academic.oup.com/ptep/article/2022/8/083C01/6651666 by KIT Library user on 27 September 2022

[4] By a simultaneous fit of the intermediate channels in a partial-wave analysis, assuming the same structure, modelled with a coherent sum of a nonresonant component and a resonant component by a Breit-Wigner function.
[5] From a fit to the cross section between 2.00 and 3.08 GeV with a sum of Breit-Wigner amplitude and a nonresonant contribution. The observed structure can be also due to $\rho(2150)$.
[6] The observed structure can be due to both the $\phi(2170)$ and $\rho(2150)$.
[7] Fit includes interference with the $\phi(1680)$.
[8] From the $\phi f_0(980)$ component.
[9] From a fit with two incoherent Breit-Wigners.
[10] From the $K^+ K^- f_0(980)$ component.
[11] Superseded by LEES 12F.

$\phi(2170)$ DECAY MODES

	Mode	Fraction (Γ_i/Γ)
Γ_1	$e^+ e^-$	seen
Γ_2	$\phi\eta$	
Γ_3	$\omega\eta$	
Γ_4	$\phi\eta'$	
Γ_5	$\phi\pi\pi$	
Γ_6	$\phi f_0(980)$	seen
Γ_7	$K^0_S K^0_L$	
Γ_8	$K^+ K^- \pi^+ \pi^-$	
Γ_9	$K^+ K^- f_0(980) \to K^+ K^- \pi^+ \pi^-$	seen
Γ_{10}	$K^+ K^- \pi^0 \pi^0$	
Γ_{11}	$K^+ K^- f_0(980) \to K^+ K^- \pi^0 \pi^0$	seen
Γ_{12}	$K^{*0} K^\pm \pi^\mp$	not seen
Γ_{13}	$K^*(892)^0 \overline{K}^*(892)^0$	not seen
Γ_{14}	$K^*(892)^+ K^*(892)^-$	
Γ_{15}	$K(1460)^+ K^-$ + c.c.	
Γ_{16}	$K_1(1270)^+ K^-$ + c.c.	
Γ_{17}	$K_1(1400)^+ K^-$ + c.c.	

$\phi(2170)$ $\Gamma(i)\Gamma(e^+e^-)/\Gamma(\text{total})$

$\Gamma(\phi\eta) \times \Gamma(e^+e^-)/\Gamma_{\text{total}}$ — $\Gamma_2\Gamma_1/\Gamma$

VALUE (eV)	EVTS	DOCUMENT ID		TECN	COMMENT
• • • We do not use the following data for averages, fits, limits, etc. • • •					
$0.24^{+0.12}_{-0.07}$		[1] ABLIKIM	21T	BES3	$e^+e^- \to \phi\eta$
1.7 ±0.7 ±1.3	483	AUBERT	08S	BABR	10.6 $e^+e^- \to \phi\eta\gamma$

[1] From a solution of the fit to the cross section below 3.5 GeV measured by BaBar and BESIII with a coherent sum of two modified Breit-Wigner amplitudes ($\phi(1680)$ and $\phi(2170)$) and a nonresonant term. The other solution gives $10.11^{+3.87}_{-3.13}$ eV.

$\Gamma(\omega\eta) \times \Gamma(e^+e^-)/\Gamma_{\text{total}}$ — $\Gamma_3\Gamma_1/\Gamma$

VALUE (eV)	DOCUMENT ID		TECN	COMMENT
0.43±0.15±0.04	[1] ABLIKIM	21A	BES3	$e^+e^- \to \omega\eta$

[1] For constructive interference with $\omega(1420)$ and $\omega(1650)/\phi(1680)$. For destructive interference: 1.25 ± 0.48 ± 0.18 eV.

$\Gamma(\phi\eta') \times \Gamma(e^+e^-)/\Gamma_{\text{total}}$ — $\Gamma_4\Gamma_1/\Gamma$

VALUE (eV)	DOCUMENT ID		TECN	COMMENT
7.1±0.7±0.7	[1] ABLIKIM	20M	BES3	$e^+e^- \to \eta'\phi$

[1] From a fit using a coherent sum of a phase-space modified Breit-Wigner function and a phase-space term.

$\Gamma(\phi f_0(980)) \times \Gamma(e^+e^-)/\Gamma_{\text{total}}$ — $\Gamma_6\Gamma_1/\Gamma$

VALUE (eV)	EVTS	DOCUMENT ID		TECN	COMMENT
2.3±0.3±0.3		[1,2] LEES	12F	BABR	10.6 $e^+e^- \to \phi\pi^+\pi^-\gamma$
• • • We do not use the following data for averages, fits, limits, etc. • • •					
2.5±0.8±0.4	201	[2,3] AUBERT,BE	06D	BABR	10.6 $e^+e^- \to K^+K^-\pi\pi\gamma$

[1] From a fit with constructive interference with the $\phi(1680)$. In a fit with destructive interference, the value is larger by a factor of 12.
[2] From the $\phi f_0(980)$ component.
[3] Superseded by LEES 12F.

$\Gamma(K^0_S K^0_L) \times \Gamma(e^+e^-)/\Gamma_{\text{total}}$ — $\Gamma_7\Gamma_1/\Gamma$

VALUE (eV)	DOCUMENT ID		TECN	COMMENT
• • • We do not use the following data for averages, fits, limits, etc. • • •				
0.9±0.6±0.7	[1] ABLIKIM	21AP	BES3	$e^+e^- \to K^0_S K^0_L$

[1] From a fit to the cross section between 2.00 and 3.08 GeV with a sum of Breit-Wigner amplitude and a nonresonant contribution. The observed structure can be also due to $\rho(2150)$.

$\Gamma(K^*(892)^+ K^*(892)^-) \times \Gamma(e^+e^-)/\Gamma_{\text{total}}$ — $\Gamma_{14}\Gamma_1/\Gamma$

VALUE (eV)	CL%	DOCUMENT ID		TECN	COMMENT
<1.9	90	[1] ABLIKIM	20S	BES3	$e^+e^- \to K^+K^-\pi^0\pi^0$

[1] By a simultaneous fit of the intermediate channels in a partial-wave analysis, assuming the same structure, modelled with a coherent sum of a nonresonant component and a resonant component by a Breit-Wigner function.

$\Gamma(K(1460)^+ K^-$ + c.c.$) \times \Gamma(e^+e^-)/\Gamma_{\text{total}}$ — $\Gamma_{15}\Gamma_1/\Gamma$

VALUE (eV)	DOCUMENT ID		TECN	COMMENT
• • • We do not use the following data for averages, fits, limits, etc. • • •				
3.0±3.8	[1] ABLIKIM	20S	BES3	$e^+e^- \to K^+K^-\pi^0\pi^0$

[1] By a simultaneous fit of the intermediate channels in a partial-wave analysis, assuming the same structure, modelled with a coherent sum of a nonresonant component and a resonant component by a Breit-Wigner function.

$\Gamma(K_1(1270)^+ K^-$ + c.c.$) \times \Gamma(e^+e^-)/\Gamma_{\text{total}}$ — $\Gamma_{16}\Gamma_1/\Gamma$

VALUE (eV)	CL%	DOCUMENT ID		TECN	COMMENT
<12.5	90	[1] ABLIKIM	20S	BES3	$e^+e^- \to K^+K^-\pi^0\pi^0$

[1] By a simultaneous fit of the intermediate channels in a partial-wave analysis, assuming the same structure, modelled with a coherent sum of a nonresonant component and a resonant component by a Breit-Wigner function. A second solution of the fit with equal fit quality gives an upper limit value of 297.6 eV.

$\Gamma(K_1(1400)^+ K^-$ + c.c.$) \times \Gamma(e^+e^-)/\Gamma_{\text{total}}$ — $\Gamma_{17}\Gamma_1/\Gamma$

VALUE (eV)	DOCUMENT ID		TECN	COMMENT
• • • We do not use the following data for averages, fits, limits, etc. • • •				
4.7±3.3	[1] ABLIKIM	20S	BES3	$e^+e^- \to K^+K^-\pi^0\pi^0$

[1] By a simultaneous fit of the intermediate channels in a partial-wave analysis, assuming the same structure, modelled with a coherent sum of a nonresonant component and a resonant component by a Breit-Wigner function. A second solution of the fit with equal fit quality gives a value of 98.8 ± 7.8 eV.

$\phi(2170)$ $\Gamma(i)\Gamma(e^+e^-)/\Gamma^2(\text{total})$

$\Gamma(\phi\pi\pi)/\Gamma_{\text{total}} \times \Gamma(e^+e^-)/\Gamma_{\text{total}}$ — $\Gamma_5/\Gamma \times \Gamma_1/\Gamma$

VALUE (units 10^{-7})	EVTS	DOCUMENT ID		TECN	COMMENT
• • • We do not use the following data for averages, fits, limits, etc. • • •					
1.65±0.15±0.18	4.8k	[1] SHEN	09	BELL	10.6 $e^+e^- \to K^+K^-\pi^+\pi^-\gamma$

[1] Multiplied by 3/2 to take into account the $\phi\pi^0\pi^0$ mode. Using B($\phi \to K^+K^-$) = (49.2 ± 0.6)%.

$\phi(2170)$ BRANCHING RATIOS

$\Gamma(K^+K^- f_0(980) \to K^+K^-\pi^+\pi^-)/\Gamma_{\text{total}}$ — Γ_9/Γ

VALUE	DOCUMENT ID		TECN	COMMENT
seen	AUBERT	07AK	BABR	10.6 $e^+e^- \to K^+K^-\pi^+\pi^-\gamma$

$\Gamma(K^+K^- f_0(980) \to K^+K^-\pi^0\pi^0)/\Gamma_{\text{total}}$ — Γ_{11}/Γ

VALUE	DOCUMENT ID		TECN	COMMENT
seen	AUBERT	07AK	BABR	10.6 $e^+e^- \to K^+K^-\pi^0\pi^0\gamma$

$\Gamma(K^{*0} K^\pm \pi^\mp)/\Gamma_{\text{total}}$ — Γ_{12}/Γ

VALUE	DOCUMENT ID		TECN	COMMENT
not seen	AUBERT	07AK	BABR	10.6 GeV e^+e^-

$\Gamma(K^*(892)^0 \overline{K}^*(892)^0)/\Gamma_{\text{total}}$ — Γ_{13}/Γ

VALUE	DOCUMENT ID		TECN	COMMENT
not seen	ABLIKIM	10C	BES2	$J/\psi \to \eta K^+\pi^- K^-\pi^+$

$\phi(2170)$ REFERENCES

ABLIKIM	21A	PL B813 136059	M. Ablikim *et al.*	(BESIII Collab.)
ABLIKIM	21AP	PR D104 092014	M. Ablikim *et al.*	(BESIII Collab.)
ABLIKIM	21T	PR D104 032007	M. Ablikim *et al.*	(BESIII Collab.)
ABLIKIM	20M	PR D102 012008	M. Ablikim *et al.*	(BESIII Collab.)
ABLIKIM	20S	PRL 124 112001	M. Ablikim *et al.*	(BESIII Collab.)
ABLIKIM	19I	PR D99 012014	M. Ablikim *et al.*	(BESIII Collab.)
ABLIKIM	19L	PR D99 032001	M. Ablikim *et al.*	(BESIII Collab.)
ABLIKIM	15H	PR D91 052017	M. Ablikim *et al.*	(BESIII Collab.)
LEES	12F	PR D86 012008	J.P. Lees *et al.*	(BABAR Collab.)
ABLIKIM	10C	PL B685 27	M. Ablikim *et al.*	(BES II Collab.)
SHEN	09	PR D80 031101	C.P. Shen *et al.*	(BELLE Collab.)
ABLIKIM	08F	PRL 100 102003	M. Ablikim *et al.*	(BES Collab.)
AUBERT	08S	PR D77 092002	B. Aubert *et al.*	(BABAR Collab.)
AUBERT	07AK	PR D76 012008	B. Aubert *et al.*	(BABAR Collab.)
AUBERT,BE	06D	PR D74 091103	B. Aubert *et al.*	(BABAR Collab.)

$f_0(2200)$

$I^G(J^{PC}) = 0^+(0^{++})$

OMITTED FROM SUMMARY TABLE

Seen in $K^0_S K^0_S$ (AUGUSTIN 88), K^+K^- (ABLIKIM 05Q) and $\eta\eta$ (BINON 05) system. Not seen in $\Upsilon(1S)$ radiative decays (BARU 89).

$f_0(2200)$ MASS

VALUE (MeV)	EVTS	DOCUMENT ID		TECN	COMMENT
2187±14 OUR AVERAGE					
$2170 \pm 20^{+10}_{-15}$		ABLIKIM	05Q	BES2	$\psi(2S) \to \gamma\pi^+\pi^- K^+K^-$
2197±17		[1] AUGUSTIN	88	DM2	$J/\psi \to \gamma K^0_S K^0_S$

Downloaded from https://academic.oup.com/ptep/article/2022/8/083C01/6651666 by KIT Library user on 27 September 2022

• • • We do not use the following data for averages, fits, limits, etc. • • •					
2200±25		SARANTSEV	21	RVUE	$J/\psi(1S) \to \gamma(\pi\pi, K\overline{K}, \eta\eta, \omega\phi)$
2206±12± 8	381	[2,3] DOBBS	15		$J/\psi \to \gamma K^+ K^-$
2188±17±16	203	[2,3] DOBBS	15		$\psi(2S) \to \gamma K^+ K^-$
2210±50		[4] BINON	05	GAMS	$33\ \pi^- p \to \eta\eta n$
∼ 2122		HASAN	94	RVUE	$\overline{p}p \to \pi\pi$
∼ 2321		HASAN	94	RVUE	$\overline{p}p \to \pi\pi$

[1] Cannot determine spin to be 0.
[2] Using CLEO-c data but not authored by the CLEO Collaboration.
[3] From a fit to a Breit-Wigner line shape with fixed Γ = 238 MeV.
[4] First solution, PWA is ambiguous.

$f_0(2200)$ WIDTH

VALUE (MeV)	DOCUMENT ID		TECN	COMMENT
207±40 OUR AVERAGE				
$220 \pm 60^{+40}_{-45}$	ABLIKIM	05Q	BES2	$\psi(2S) \to \gamma\pi^+\pi^- K^+ K^-$
201±51	[5] AUGUSTIN	88	DM2	$J/\psi \to \gamma K^0_S K^0_S$
• • • We do not use the following data for averages, fits, limits, etc. • • •				
150±30	SARANTSEV	21	RVUE	$J/\psi(1S) \to \gamma(\pi\pi, K\overline{K}, \eta\eta, \omega\phi)$
380±90	[6] BINON	05	GAMS	$33\ \pi^- p \to \eta\eta n$
∼ 273	HASAN	94	RVUE	$\overline{p}p \to \pi\pi$
∼ 223	HASAN	94	RVUE	$\overline{p}p \to \pi\pi$

[5] Cannot determine spin to be 0.
[6] First solution, PWA is ambiguous.

$f_0(2200)$ REFERENCES

SARANTSEV	21	PL B816 136227	A.V. Sarantsev *et al.*	(BONN, PNPI)
DOBBS	15	PR D91 052006	S. Dobbs *et al.*	(NWES)
ABLIKIM	05Q	PR D72 092002	M. Ablikim *et al.*	(BES Collab.)
BINON	05	PAN 68 960	F. Binon *et al.*	
		Translated from YAF 68 998.		
HASAN	94	PL B334 215	A. Hasan, D.V. Bugg	(LOQM)
BARU	89	ZPHY C42 505	S.E. Baru *et al.*	(NOVO)
AUGUSTIN	88	PRL 60 2238	J.E. Augustin *et al.*	(DM2 Collab.)

$f_J(2220)$

$I^G(J^{PC}) = 0^+(2^{++}$ or $4^{++})$

OMITTED FROM SUMMARY TABLE

Needs confirmation. See our mini-review in the 2004 edition of this *Review*, PDG 04.

$f_J(2220)$ MASS

VALUE (MeV)	EVTS	DOCUMENT ID		TECN	COMMENT
2231.1± 3.5 OUR AVERAGE					
2235 ± 4 ± 6	74	BAI	96B	BES	$e^+e^- \to J/\psi \to \gamma\pi^+\pi^-$
$2230\ ^{+6}_{-7} \pm 16$	46	BAI	96B	BES	$e^+e^- \to J/\psi \to \gamma K^+ K^-$
$2232\ ^{+8}_{-7} \pm 15$	23	BAI	96B	BES	$e^+e^- \to J/\psi \to \gamma K^0_S K^0_S$
2235 ± 4 ± 5	32	BAI	96B	BES	$e^+e^- \to J/\psi \to \gamma p\overline{p}$
$2209\ ^{+17}_{-15} \pm 10$		ASTON	88F	LASS	$11\ K^- p \to K^+ K^- \Lambda$
2230 ±20		BOLONKIN	88	SPEC	$40\ \pi^- p \to K^0_S K^0_S n$
2220 ±10	41	[1] ALDE	86B	GA24	$38\text{–}100\ \pi p \to n\eta\eta'$
2230 ± 6 ±14	93	BALTRUSAIT...86D		MRK3	$e^+e^- \to \gamma K^+ K^-$
2232 ± 7 ± 7	23	BALTRUSAIT...86D		MRK3	$e^+e^- \to \gamma K^0_S K^0_S$
• • • We do not use the following data for averages, fits, limits, etc. • • •					
2223.9± 2.5		[2] VLADIMIRSK...08		SPEC	$40\ \pi^- p \to K^0_S K^0_S n + m\pi^0$
2246 ±36		BAI	98H	BES	$J/\psi \to \gamma\pi^0\pi^0$

[1] ALDE 86B uses data from both the GAMS-2000 and GAMS-4000 detectors.
[2] $J^{PC} = 2^{++}$. Systematic uncertainties not evaluated

$f_J(2220)$ WIDTH

VALUE (MeV)	CL%	EVTS	DOCUMENT ID		TECN	COMMENT
23^{+8}_{-7} OUR AVERAGE						
$19\ ^{+13}_{-11} \pm 12$		74	BAI	96B	BES	$e^+e^- \to J/\psi \to \gamma\pi^+\pi^-$
$20\ ^{+20}_{-15} \pm 17$		46	BAI	96B	BES	$e^+e^- \to J/\psi \to \gamma K^+ K^-$
$20\ ^{+25}_{-16} \pm 14$		23	BAI	96B	BES	$e^+e^- \to J/\psi \to \gamma K^0_S K^0_S$
$15\ ^{+12}_{-9} \pm 9$		32	BAI	96B	BES	$e^+e^- \to J/\psi \to \gamma p\overline{p}$
$60\ ^{+107}_{-57}$			ASTON	88F	LASS	$11\ K^- p \to K^+ K^- \Lambda$
80± 30			BOLONKIN	88	SPEC	$40\ \pi^- p \to K^0_S K^0_S n$
$26\ ^{+20}_{-16} \pm 17$		93	BALTRUSAIT...86D		MRK3	$e^+e^- \to \gamma K^+ K^-$
$18\ ^{+23}_{-15} \pm 10$		23	BALTRUSAIT...86D		MRK3	$e^+e^- \to \gamma K^0_S K^0_S$
• • • We do not use the following data for averages, fits, limits, etc. • • •						
8.6 ± 2.5			[1] VLADIMIRSK...08		SPEC	$40\ \pi^- p \to K^0_S K^0_S n$
<80	90		ALDE	87C	GAM2	$38\ \pi^- p \to \eta'\eta n$ $+m\pi^0$

[1] $J^{PC} = 2^{++}$. Systematic uncertainties not evaluated

$f_J(2220)$ DECAY MODES

	Mode	Fraction (Γ_i/Γ)
Γ_1	$\pi\pi$	not seen
Γ_2	$\pi^+\pi^-$	not seen
Γ_3	$K\overline{K}$	not seen
Γ_4	$p\overline{p}$	not seen
Γ_5	$\gamma\gamma$	not seen
Γ_6	$\eta\eta'(958)$	seen
Γ_7	$\phi\phi$	not seen
Γ_8	$\eta\eta$	not seen

$f_J(2220)$ $\Gamma(i)\Gamma(\gamma\gamma)/\Gamma(\text{total})$

$\Gamma(K\overline{K}) \times \Gamma(\gamma\gamma)/\Gamma_{\text{total}}$ — $\Gamma_3\Gamma_5/\Gamma$

VALUE (eV)	CL%	DOCUMENT ID		TECN	COMMENT
< 1.4	95	[1] ACCIARRI	01H	L3	$\gamma\gamma \to K^0_S K^0_S$, E^{ee}_{cm} = 91, 183–209 GeV
• • • We do not use the following data for averages, fits, limits, etc. • • •					
< 5.6	95	[1] GODANG	97	CLE2	$\gamma\gamma \to K^0_S K^0_S$
< 86	95	[1] ALBRECHT	90G	ARG	$\gamma\gamma \to K^+ K^-$
<1000	95	[2] ALTHOFF	85B	TASS	$\gamma\gamma$, $K\overline{K}\pi$

$\Gamma(\pi\pi) \times \Gamma(\gamma\gamma)/\Gamma_{\text{total}}$ — $\Gamma_1\Gamma_5/\Gamma$

VALUE (eV)	CL%	DOCUMENT ID		TECN	COMMENT
<2.5	95	ALAM	98C	CLE2	$\gamma\gamma \to \pi^+\pi^-$

[1] Assuming $J^P = 2^+$.
[2] True for $J^P = 0^+$ and $J^P = 2^+$.

$f_J(2220)$ $\Gamma(i)\Gamma(p\overline{p})/\Gamma^2(\text{total})$

$\Gamma(p\overline{p})/\Gamma_{\text{total}} \times \Gamma(\pi\pi)/\Gamma_{\text{total}}$ — $\Gamma_4/\Gamma \times \Gamma_1/\Gamma$

VALUE (units 10^{-5})	CL%	DOCUMENT ID		TECN	COMMENT
<18	95	[1] AMSLER	01	CBAR	1.4–1.5 $p\overline{p} \to \pi^0\pi^0$
• • • We do not use the following data for averages, fits, limits, etc. • • •					
<(11–42)	99	[2] HASAN	96	SPEC	1.35–1.55 $p\overline{p} \to \pi^+\pi^-$

$\Gamma(p\overline{p})/\Gamma_{\text{total}} \times \Gamma(\phi\phi)/\Gamma_{\text{total}}$ — $\Gamma_4/\Gamma \times \Gamma_7/\Gamma$

VALUE (units 10^{-5})	CL%	DOCUMENT ID		TECN	COMMENT
<6	95	[3] EVANGELIS...	98	SPEC	1.1-2.0 $p\overline{p} \to \phi\phi$

$\Gamma(p\overline{p})/\Gamma_{\text{total}} \times \Gamma(\eta\eta)/\Gamma_{\text{total}}$ — $\Gamma_4/\Gamma \times \Gamma_8/\Gamma$

VALUE (units 10^{-5})	CL%	DOCUMENT ID		TECN	COMMENT
<4	95	[1] AMSLER	01	CBAR	1.4–1.5 $p\overline{p} \to \eta\eta$

[1] For $J^P = 2^+$ in the mass range 2222–2240 MeV and the total width between 10 and 20 MeV.
[2] For $J^P = 2^+$ and $J^P = 4^+$ in the mass range 2220–2245 MeV and the total width of 15 MeV.
[3] For $J^P = 2^+$, the mass of 2235 MeV and the total width of 15 MeV.

$f_J(2220)$ BRANCHING RATIOS

$\Gamma(\pi\pi)/\Gamma_{\text{total}}$ — Γ_1/Γ

VALUE	DOCUMENT ID		COMMENT
not seen	[1] DOBBS	15	$J/\psi \to \gamma\pi\pi$
not seen	[1] DOBBS	15	$\psi(2S) \to \gamma\pi\pi$

[1] Using CLEO-c data but not authored by the CLEO Collaboration.

$\Gamma(K\overline{K})/\Gamma_{\text{total}}$ — Γ_3/Γ

VALUE	DOCUMENT ID		COMMENT
not seen	[1] DOBBS	15	$J/\psi \to \gamma K\overline{K}$
not seen	[1] DOBBS	15	$\psi(2S) \to \gamma K\overline{K}$

[1] Using CLEO-c data but not authored by the CLEO Collaboration.

$\Gamma(\pi\pi)/\Gamma(K\overline{K})$ — Γ_1/Γ_3

VALUE	DOCUMENT ID		TECN	COMMENT
1.0±0.5	BAI	96B	BES	$e^+e^- \to J/\psi \to \gamma 2\pi, K\overline{K}$

Downloaded from https://academic.oup.com/ptep/article/2022/8/083C01/6651666 by KIT Library user on 27 September 2022

$\Gamma(p\overline{p})/\Gamma_{total}$ — Γ_4/Γ

VALUE (units 10^{-4})	CL%	DOCUMENT ID		TECN	COMMENT
• • • We do not use the following data for averages, fits, limits, etc. • • •					
not seen		[1] AUBERT	07AV	BABR	$B \to p\overline{p}K^{(*)}$
not seen		WANG	05A	BELL	$B^+ \to \overline{p}pK^+$
<3.0	95	[2] EVANGELIS...	97	SPEC	1.96-2.40 $\overline{p}p \to K^0_S K^0_S$
<1.1	99.7	[3] BARNES	93	SPEC	1.3-1.57 $\overline{p}p \to K^0_S K^0_S$
<2.6	99.7	[3] BARDIN	87	CNTR	1.3-1.5 $\overline{p}p \to K^+K^-$
<3.6	99.7	[3] SCULLI	87	CNTR	1.29-1.55 $\overline{p}p \to K^+K^-$

[1] Assuming $\Gamma < 30$ MeV.
[2] Assuming $\Gamma \sim 20$ MeV, $J^P = 2^+$ and $B(f_J(2220) \to K\overline{K}) = 100\%$.
[3] Assuming $\Gamma = 30$-35 MeV, $J^P = 2^+$ and $B(f_J(2220) \to K\overline{K}) = 100\%$.

$\Gamma(p\overline{p})/\Gamma(K\overline{K})$ — Γ_4/Γ_3

VALUE	DOCUMENT ID		TECN	COMMENT
0.17±0.09	BAI	96B	BES	$e^+e^- \to J/\psi \to \gamma p\overline{p}, K\overline{K}$

$f_J(2220)$ REFERENCES

DOBBS	15	PR D91 052006	S. Dobbs *et al.*	(NWES)
VLADIMIRSK...	08	PAN 71 2129	V.V. Vladimirsky *et al.*	(ITEP)
		Translated from YAF 71 2166.		
AUBERT	07AV	PR D76 092004	B. Aubert *et al.*	(BABAR Collab.)
WANG	05A	PL B617 141	M.-Z. Wang *et al.*	(BELLE Collab.)
PDG	04	PL B592 1	S. Eidelman *et al.*	(PDG Collab.)
ACCIARRI	01H	PL B501 173	M. Acciarri *et al.*	(L3 Collab.)
AMSLER	01	PL B520 175	C. Amsler *et al.*	(Crystal Barrel Collab.)
ALAM	98C	PRL 81 3328	M.S. Alam *et al.*	(CLEO Collab.)
BAI	98H	PRL 81 1179	J.Z. Bai *et al.*	(BES Collab.)
EVANGELIS...	98	PR D57 5370	C. Evangelista *et al.*	(JETSET Collab.)
EVANGELIS...	97	PR D56 3803	C. Evangelista *et al.*	(LEAR Collab.)
GODANG	97	PRL 79 3829	R. Godang *et al.*	(CLEO Collab.)
BAI	96B	PRL 76 3502	J.Z. Bai *et al.*	(BES Collab.)
HASAN	96	PL B388 376	A. Hasan, D.V. Bugg	(BRUN, LOQM)
BARNES	93	PL B309 469	P.D. Barnes *et al.*	(PS185 Collab.)
ALBRECHT	90G	ZPHY C48 183	H. Albrecht *et al.*	(ARGUS Collab.)
ASTON	88F	PL B215 199	D. Aston *et al.*	(SLAC, NAGO, CINC, INUS) JP
BOLONKIN	88	NP B309 426	B.V. Bolonkin *et al.*	(ITEP, SERP)
ALDE	87C	SJNP 45 255	D. Alde *et al.*	
		Translated from YAF 45 405.		
BARDIN	87	PL B195 292	G. Bardin *et al.*	(SACL, FERR, CERN, PADO+)
SCULLI	87	PRL 58 1715	J. Sculli *et al.*	(NYU, BNL)
ALDE	86B	PL B177 120	D.M. Alde *et al.*	(SERP, BELG, LANL, LAPP)
BALTRUSAIT...	86D	PRL 56 107	R.M. Baltrusaitis	(CIT, UCSC, ILL, SLAC+)
ALTHOFF	85B	ZPHY C29 189	M. Althoff *et al.*	(TASSO Collab.)

OTHER RELATED PAPERS

DEL-AMO-SA...	10O	PRL 105 172001	P. del Amo Sanchez *et al.*	(BABAR Collab.)

$\eta(2225)$

$I^G(J^{PC}) = 0^+(0^{-+})$

OMITTED FROM SUMMARY TABLE

Seen in $J/\psi \to \gamma\phi\phi$. Possibly seen in $B \to \phi\phi K$ by LEES 11A.

$\eta(2225)$ MASS

VALUE (MeV)	EVTS	DOCUMENT ID		TECN	COMMENT
2221^{+13}_{-10} OUR AVERAGE					
2216^{+4+21}_{-5-11}		[1] ABLIKIM	16N	BES3	$J/\psi \to \gamma K^+K^-K^+K^-$
2240^{+30+30}_{-20-20}	196 ± 19	ABLIKIM	08I	BES	$J/\psi \to \gamma K^+K^-K^0_S K^0_L$
2230±25±15		BAI	90B	MRK3	$J/\psi \to \gamma K^+K^-K^+K^-$
2214±20±13		BAI	90B	MRK3	$J/\psi \to \gamma K^+K^-K^0_S K^0_L$
• • • We do not use the following data for averages, fits, limits, etc. • • •					
~ 2220		BISELLO	86B	DM2	$J/\psi \to \gamma K^+K^-K^+K^-$

[1] From a partial wave analysis of $J/\psi \to \gamma\phi\phi$ that also finds significant signals for for $\eta(2100)$, 0^{-+} phase space, $f_0(2100)$, $f_2(2010)$, $f_2(2300)$, $f_2(2340)$, and a previously unseen 0^{-+} state $X(2500)$ ($M = 2470^{+15+101}_{-19-23}$ MeV, $\Gamma = 230^{+64+56}_{-35-33}$ MeV).

$\eta(2225)$ WIDTH

VALUE (MeV)	EVTS	DOCUMENT ID		TECN	COMMENT
185^{+40}_{-20} OUR AVERAGE					
185^{+12+43}_{-14-17}		[1] ABLIKIM	16N	BES3	$J/\psi \to \gamma K^+K^-K^+K^-$
$190 \pm 30^{+60}_{-40}$	196 ± 19	ABLIKIM	08I	BES	$J/\psi \to \gamma K^+K^-K^0_S K^0_L$
$150^{+300}_{-60} \pm 60$		BAI	90B	MRK3	$J/\psi \to \gamma K^+K^-K^+K^-$
• • • We do not use the following data for averages, fits, limits, etc. • • •					
~ 80		BISELLO	86B	DM2	$J/\psi \to \gamma K^+K^-K^+K^-$

[1] From a partial wave analysis of $J/\psi \to \gamma\phi\phi$ that also finds significant signals for for $\eta(2100)$, 0^{-+} phase space, $f_0(2100)$, $f_2(2010)$, $f_2(2300)$, $f_2(2340)$, and a previously unseen 0^{-+} state $X(2500)$ ($M = 2470^{+15+101}_{-19-23}$ MeV, $\Gamma = 230^{+64+56}_{-35-33}$ MeV).

$\eta(2225)$ REFERENCES

ABLIKIM	16N	PR D93 112011	M. Ablikim	(BESIII Collab.)
LEES	11A	PR D84 012001	J.P. Lees *et al.*	(BABAR Collab.)
ABLIKIM	08I	PL B662 330	M. Ablikim *et al.*	(BES Collab.)
BAI	90B	PRL 65 1309	Z. Bai *et al.*	(Mark III Collab.)
BISELLO	86B	PL B179 294	D. Bisello *et al.*	(DM2 Collab.)

$\rho_3(2250)$

$I^G(J^{PC}) = 1^+(3^{--})$

OMITTED FROM SUMMARY TABLE

Contains results mostly from formation experiments. For further production experiments see the Further States entry. See also $\rho(2150)$, $f_2(2150)$, $f_4(2300)$, $\rho_5(2350)$.

$\rho_3(2250)$ MASS

$\overline{p}p \to \pi\pi$ or $K\overline{K}$

VALUE (MeV)	EVTS	DOCUMENT ID		TECN	CHG	COMMENT
• • • We do not use the following data for averages, fits, limits, etc. • • •						
$2248 \pm 17^{+59}_{-5}$	1.8k	[1] ABLIKIM	20F	BES3		$\psi(2S) \to K^+K^-\eta$
~ 2232		HASAN	94	RVUE		$\overline{p}p \to \pi\pi$
~ 2090		[2] OAKDEN	94	RVUE		0.36–1.55 $\overline{p}p \to \pi\pi$
~ 2250		[3] MARTIN	80B	RVUE		
~ 2300		[3] MARTIN	80C	RVUE		
~ 2140		[4] CARTER	78B	CNTR	0	0.7–2.4 $\overline{p}p \to K^-K^+$
~ 2150		[5] CARTER	77	CNTR	0	0.7–2.4 $\overline{p}p \to \pi\pi$

[1] Seen in $\psi(2S)$ decay with branching ratio $\psi(2S) \to X\eta \to K^+K^-\eta = (1.9 \pm 0.4^{+0.5}_{-1.3}) \times 10^{-6}$.
[2] See however KLOET 96 who fit $\pi^+\pi^-$ only and find waves only up to $J = 3$ to be important but not significantly resonant.
[3] $I(J^P) = 1(3^-)$ from simultaneous analysis of $p\overline{p} \to \pi^-\pi^+$ and $\pi^0\pi^0$.
[4] $I = 0, 1$. $J^P = 3^-$ from Barrelet-zero analysis.
[5] $I(J^P) = 1(3^-)$ from amplitude analysis.

S-CHANNEL $\overline{N}N$

VALUE (MeV)	DOCUMENT ID		TECN	CHG	COMMENT
• • • We do not use the following data for averages, fits, limits, etc. • • •					
2260±20	[6] ANISOVICH	02	SPEC		0.6–1.9 $p\overline{p} \to \omega\pi^0$, $\omega\eta\pi^0$, $\pi^+\pi^-$
~ 2190	[7] CUTTS	78B	CNTR		0.97–3 $\overline{p}p \to \overline{N}N$
2155±15	[7,8] COUPLAND	77	CNTR	0	0.7–2.4 $\overline{p}p \to \overline{p}p$
2193± 2	[7,9] ALSPECTOR	73	CNTR		$\overline{p}p$ S channel
2190±10	[10] ABRAMS	70	CNTR		S channel $\overline{p}N$

[6] From the combined analysis of ANISOVICH 00J, ANISOVICH 01D, ANISOVICH 01E, and ANISOVICH 02.
[7] Isospins 0 and 1 not separated.
[8] From a fit to the total elastic cross section.
[9] Referred to as T or T region by ALSPECTOR 73.
[10] Seen as bump in $I = 1$ state. See also COOPER 68. PEASLEE 75 confirm $\overline{p}p$ results of ABRAMS 70, no narrow structure.

Other processes

VALUE (MeV)	DOCUMENT ID		TECN	COMMENT
• • • We do not use the following data for averages, fits, limits, etc. • • •				
2290±20±30	AMELIN	00	VES	37 $\pi^-p \to \eta\pi^+\pi^-n$

$\rho_3(2250)$ WIDTH

$\overline{p}p \to \pi\pi$ or $K\overline{K}$

VALUE (MeV)	EVTS	DOCUMENT ID		TECN	CHG	COMMENT
• • • We do not use the following data for averages, fits, limits, etc. • • •						
$185^{+31+17}_{-26-103}$	1.8k	[11] ABLIKIM	20F	BES3		$\psi(2S) \to K^+K^-\eta$
~ 220		HASAN	94	RVUE		$\overline{p}p \to \pi\pi$
~ 60		[12] OAKDEN	94	RVUE		0.36–1.55 $\overline{p}p \to \pi\pi$
~ 250		[13] MARTIN	80B	RVUE		
~ 200		[13] MARTIN	80C	RVUE		
~ 150		[14] CARTER	78B	CNTR	0	0.7–2.4 $\overline{p}p \to K^-K^+$
~ 200		[15] CARTER	77	CNTR	0	0.7–2.4 $\overline{p}p \to \pi\pi$

[11] Seen in $\psi(2S)$ decay with branching ratio $\psi(2S) \to X\eta \to K^+K^-\eta = (1.9 \pm 0.4^{+0.5}_{-1.3}) \times 10^{-6}$.
[12] See however KLOET 96 who fit $\pi^+\pi^-$ only and find waves only up to $J = 3$ to be important but not significantly resonant.
[13] $I(J^P) = 1(3^-)$ from simultaneous analysis of $p\overline{p} \to \pi^-\pi^+$ and $\pi^0\pi^0$.
[14] $I = 0, 1$. $J^P = 3^-$ from Barrelet-zero analysis.
[15] $I(J^P) = 1(3^-)$ from amplitude analysis.

S-CHANNEL $\overline{N}N$

VALUE (MeV)	DOCUMENT ID		TECN	CHG	COMMENT
• • • We do not use the following data for averages, fits, limits, etc. • • •					
160±25	[16] ANISOVICH	02	SPEC		0.6–1.9 $p\overline{p} \to \omega\pi^0$, $\omega\eta\pi^0$, $\pi^+\pi^-$
135±75	[17,18] COUPLAND	77	CNTR	0	0.7–2.4 $\overline{p}p \to \overline{p}p$

Downloaded from https://academic.oup.com/ptep/article/2022/8/083C01/6651666 by KIT Library user on 27 September 2022

98± 8	[18] ALSPECTOR	73	CNTR	$\overline{p}p$ S channel
~ 85	[19] ABRAMS	70	CNTR	S channel $\overline{p}N$

[16] From the combined analysis of ANISOVICH 00J, ANISOVICH 01D, ANISOVICH 01E, and ANISOVICH 02.
[17] From a fit to the total elastic cross section.
[18] Isospins 0 and 1 not separated.
[19] Seen as bump in $I = 1$ state. See also COOPER 68. PEASLEE 75 confirm $\overline{p}p$ results of ABRAMS 70, no narrow structure.

Other processes

VALUE (MeV)	DOCUMENT ID		TECN	COMMENT
• • • We do not use the following data for averages, fits, limits, etc. • • •				
230±50±80	AMELIN	00	VES	37 $\pi^- p \to \eta\pi^+\pi^- n$

$\rho_3(2250)$ REFERENCES

ABLIKIM	20F	PR D101 032008	M. Ablikim et al.	(BESIII Collab.)
ANISOVICH	02	PL B542 8	A.V. Anisovich et al.	
ANISOVICH	01D	PL B508 6	A.V. Anisovich et al.	
ANISOVICH	01E	PL B513 281	A.V. Anisovich et al.	
AMELIN	00	NP A668 83	D. Amelin et al.	(VES Collab.)
ANISOVICH	00J	PL B491 47	A.V. Anisovich et al.	(RAL, LOQM, PNPI+)
KLOET	96	PR D53 6120	W.M. Kloet, F. Myhrer	(RUTG, NORD)
HASAN	94	PL B334 215	A. Hasan, D.V. Bugg	(LOQM)
OAKDEN	94	NP A574 731	M.N. Oakden, M.R. Pennington	(DURH)
MARTIN	80B	NP B176 355	B.R. Martin, D. Morgan	(LOUC, RHEL) JP
MARTIN	80C	NP B169 216	A.D. Martin, M.R. Pennington	(DURH) JP
CARTER	78B	NP B141 467	A.A. Carter	(LOQM)
CUTTS	78B	PR D17 16	D. Cutts et al.	(STON, WISC)
CARTER	77	PL 67B 117	A.A. Carter et al.	(LOQM, RHEL) JP
COUPLAND	77	PL 71B 460	M. Coupland et al.	(LOQM, RHEL)
PEASLEE	75	PL 57B 189	D.C. Peaslee et al.	(CANB, BARI, BROW+)
ALSPECTOR	73	PRL 30 511	J. Alspector et al.	(RUTG, UPNJ)
ABRAMS	70	PR D1 1917	R.J. Abrams et al.	(BNL)
COOPER	68	PRL 20 1059	W.A. Cooper et al.	(ANL)

$f_2(2300)$

$I^G(J^{PC}) = 0^+(2^{++})$

$f_2(2300)$ MASS

VALUE (MeV)	DOCUMENT ID		TECN	COMMENT
2297±28	[1] ETKIN	88	MPS	22 $\pi^- p \to \phi\phi n$
• • • We do not use the following data for averages, fits, limits, etc. • • •				
2262± 4±28	[2] ABLIKIM	21AI	BES3	3.51–4.60 $e^+e^- \to \phi\Lambda\overline{\Lambda}$
$2243^{+7}_{-6}{}^{+3}_{-29}$	[3] UEHARA	13	BELL	$\gamma\gamma \to K^0_S K^0_S$
2270±12	VLADIMIRSK...06		SPEC	40 $\pi^- p \to K^0_S K^0_S n$
2327± 9± 6	ABE	04	BELL	10.6 $e^+e^- \to e^+e^- K^+K^-$
2231±10	BOOTH	86	OMEG	85 π^-Be $\to 2\phi$Be
2220^{+90}_{-20}	LINDENBAUM	84	RVUE	
2320±40	ETKIN	82	MPS	22 $\pi^- p \to 2\phi n$

[1] Includes data of ETKIN 85. The percentage of the resonance going into $\phi\phi$ 2^{++} S_2, D_2, and D_0 is 6^{+15}_{-5}, 25^{+18}_{-14}, and 69^{+16}_{-27}, respectively.
[2] Threshold enhancement in $\Lambda\overline{\Lambda}$, preferred J^{PC} are 2^{++}, 2^{-+}, or 1^{++}. Could be another state.
[3] Spin 2 preferred, tentatively assigned to $f_2(2300)$.

$f_2(2300)$ WIDTH

VALUE (MeV)	DOCUMENT ID		TECN	COMMENT
149±41	[1] ETKIN	88	MPS	22 $\pi^- p \to \phi\phi n$
• • • We do not use the following data for averages, fits, limits, etc. • • •				
72± 5±43	[2] ABLIKIM	21AI	BES3	3.51–4.60 $e^+e^- \to \phi\Lambda\overline{\Lambda}$
$145\pm12^{+27}_{-34}$	[3] UEHARA	13	BELL	$\gamma\gamma \to K^0_S K^0_S$
90±29	VLADIMIRSK...06		SPEC	40 $\pi^- p \to K^0_S K^0_S n$
275±36±20	ABE	04	BELL	10.6 $e^+e^- \to e^+e^- K^+K^-$
133±50	BOOTH	86	OMEG	85 π^-Be $\to 2\phi$Be
200±50	LINDENBAUM	84	RVUE	
220±70	ETKIN	82	MPS	22 $\pi^- p \to 2\phi n$

[1] Includes data of ETKIN 85.
[2] Threshold enhancement in $\Lambda\overline{\Lambda}$, preferred J^{PC} are 2^{++}, 2^{-+}, or 1^{++}. Could be another state.
[3] Spin 2 preferred, tentatively assigned to $f_2(2300)$.

$f_2(2300)$ DECAY MODES

	Mode	Fraction (Γ_i/Γ)
Γ_1	$\phi\phi$	seen
Γ_2	$K\overline{K}$	seen
Γ_3	$\gamma\gamma$	seen
Γ_4	$\Lambda\overline{\Lambda}$	seen

$f_2(2300)$ $\Gamma(i)\Gamma(\gamma\gamma)/\Gamma(\text{total})$

$\Gamma(K\overline{K}) \times \Gamma(\gamma\gamma)/\Gamma_{\text{total}}$ — $\Gamma_2\Gamma_3/\Gamma$

VALUE (eV)	DOCUMENT ID		TECN	COMMENT
• • • We do not use the following data for averages, fits, limits, etc. • • •				
$3.2^{+0.5}_{-0.4}{}^{+1.3}_{-2.2}$	UEHARA	13	BELL	$\gamma\gamma \to K^0_S K^0_S$
44 ±6 ±12	[1] ABE	04	BELL	10.6 $e^+e^- \to e^+e^- K^+K^-$

[1] Assuming spin 2.

$f_2(2340)$ BRANCHING RATIOS

$\Gamma(\phi\phi)/\Gamma_{\text{total}}$ — Γ_1/Γ

VALUE	DOCUMENT ID		TECN	COMMENT
seen	BOOTH	86	OMEG	85 π^-Be $\to 2\phi$Be
seen	ETKIN	82	MPS	22 $\pi^- p \to 2\phi n$

$\Gamma(K\overline{K})/\Gamma_{\text{total}}$ — Γ_2/Γ

VALUE	DOCUMENT ID		TECN	COMMENT
seen	VLADIMIRSK...06		SPEC	40 $\pi^- p \to K^0_S K^0_S n$
seen	ABE	04	BELL	10.6 $e^+e^- \to e^+e^- K^+K^-$

$\Gamma(\gamma\gamma)/\Gamma_{\text{total}}$ — Γ_3/Γ

VALUE	DOCUMENT ID		TECN	COMMENT
seen	UEHARA	13	BELL	$\gamma\gamma \to K^0_S K^0_S$

$\Gamma(\Lambda\overline{\Lambda})/\Gamma_{\text{total}}$ — Γ_4/Γ

VALUE	DOCUMENT ID		TECN	COMMENT
seen	[1] ABLIKIM	21AI	BES3	3.51–4.60 $e^+e^- \to \phi\Lambda\overline{\Lambda}$

[1] Threshold enhancement in $\Lambda\overline{\Lambda}$, preferred J^{PC} are 2^{++}, 2^{-+}, or 1^{++}. Could be another state.

$f_2(2300)$ REFERENCES

ABLIKIM	21AI	PR D104 052006	M. Ablikim et al.	(BESIII Collab.)
UEHARA	13	PTEP 2013 123C01	S. Uehara et al.	(BELLE Collab.)
VLADIMIRSK...	06	PAN 69 493 Translated from YAF 69 515.	V.V. Vladimirsky et al.	(ITEP, Moscow)
ABE	04	EPJ C32 323	K. Abe et al.	(BELLE Collab.)
ETKIN	88	PL B201 568	A. Etkin et al.	(BNL, CUNY)
BOOTH	86	NP B273 677	P.S.L. Booth et al.	(LIVP, GLAS, CERN)
ETKIN	85	PL 165B 217	A. Etkin et al.	(BNL, CUNY)
LINDENBAUM	84	CNPP 13 285	S.J. Lindenbaum	(CUNY)
ETKIN	82	PRL 49 1620	A. Etkin et al.	(BNL, CUNY)

$f_4(2300)$

$I^G(J^{PC}) = 0^+(4^{++})$

OMITTED FROM SUMMARY TABLE

This entry was previously called $U_0(2350)$. Contains results mostly from formation experiments. For further production experiments see the Further States entry. See also $\rho(2150)$, $f_2(2150)$, $\rho_3(2250)$, $\rho_5(2350)$.

$f_4(2300)$ MASS

$\overline{p}p \to \pi\pi$ or $\overline{K}K$

VALUE (MeV)	DOCUMENT ID		TECN	COMMENT
• • • We do not use the following data for averages, fits, limits, etc. • • •				
~ 2314	HASAN	94	RVUE	$\overline{p}p \to \pi\pi$
~ 2300	[1] MARTIN	80B	RVUE	
~ 2300	[1] MARTIN	80C	RVUE	
~ 2340	[2] CARTER	78B	CNTR	0.7–2.4 $\overline{p}p \to K^-K^+$
~ 2330	DULUDE	78B	OSPK	1–2 $\overline{p}p \to \pi^0\pi^0$
~ 2310	[3] CARTER	77	CNTR	0.7–2.4 $\overline{p}p \to \pi\pi$

[1] $I(J^P) = 0(4^+)$ from simultaneous analysis of $p\overline{p} \to \pi^-\pi^+$ and $\pi^0\pi^0$.
[2] $I(J^P) = 0(4^+)$ from Barrelet-zero analysis.
[3] $I(J^P) = 0(4^+)$ from amplitude analysis.

S-CHANNEL $\overline{p}p$ or $\overline{N}N$

VALUE (MeV)	DOCUMENT ID		TECN	COMMENT
• • • We do not use the following data for averages, fits, limits, etc. • • •				
2283±17	[4] ANISOVICH	00J	SPEC	
~ 2380	[5] CUTTS	78B	CNTR	0.97–3 $\overline{p}p \to \overline{N}N$
2345±15	[5,6] COUPLAND	77	CNTR	0.7–2.4 $\overline{p}p \to \overline{p}p$
2359± 2	[5,7] ALSPECTOR	73	CNTR	$\overline{p}p$ S channel
2375±10	ABRAMS	70	CNTR	S channel $\overline{N}N$

[4] From the combined analysis of ANISOVICH 99C and ANISOVICH 99F on $\overline{p}p \to \eta\pi^0\pi^0$, $\pi^0\pi^0$, $\eta\eta$, $\eta\eta'$, $\pi^+\pi^-$.
[5] Isospins 0 and 1 not separated.
[6] From a fit to the total elastic cross section.
[7] Referred to as U or U region by ALSPECTOR 73.

Downloaded from https://academic.oup.com/ptep/article/2022/8/083C01/6651666 by KIT Library user on 27 September 2022

$\pi^- p \to \eta\pi\pi n$

VALUE (MeV)	DOCUMENT ID		TECN	COMMENT
• • • We do not use the following data for averages, fits, limits, etc. • • •				
$2330 \pm 20 \pm 40$	AMELIN	00	VES	37 $\pi^- p \to \eta\pi^+\pi^- n$

pp CENTRAL PRODUCTION

VALUE (MeV)	DOCUMENT ID		COMMENT
2320±60 OUR ESTIMATE			
• • • We do not use the following data for averages, fits, limits, etc. • • •			
2332 ± 15	BARBERIS	00F	450 $pp \to p_f \omega\omega p_s$

$f_4(2300)$ WIDTH

$\overline{p}p \to \pi\pi$ or $\overline{K}K$

VALUE (MeV)	DOCUMENT ID		TECN	COMMENT
• • • We do not use the following data for averages, fits, limits, etc. • • •				
~ 278	HASAN	94	RVUE	$\overline{p}p \to \pi\pi$
~ 200	[8] MARTIN	80C	RVUE	
~ 150	[9] CARTER	78B	CNTR	0.7–2.4 $\overline{p}p \to K^- K^+$
~ 210	[10] CARTER	77	CNTR	0.7–2.4 $\overline{p}p \to \pi\pi$

[8] $I(J^P) = 0(4^+)$ from simultaneous analysis of $p\overline{p} \to \pi^-\pi^+$ and $\pi^0\pi^0$.
[9] $I(J^P) = 0(4^+)$ from Barrelet-zero analysis.
[10] $I(J^P) = 0(4^+)$ from amplitude analysis.

S-CHANNEL $\overline{p}p$ or $\overline{N}N$

VALUE (MeV)	DOCUMENT ID		TECN	COMMENT
• • • We do not use the following data for averages, fits, limits, etc. • • •				
310 ± 25	[11] ANISOVICH	00J	SPEC	
135^{+150}_{-65}	[12,13] COUPLAND	77	CNTR	0.7–2.4 $\overline{p}p \to \overline{p}p$
165^{+18}_{-8}	[13] ALSPECTOR	73	CNTR	$\overline{p}p$ S channel
~ 190	ABRAMS	70	CNTR	S channel $\overline{N}N$

[11] From the combined analysis of ANISOVICH 99C and ANISOVICH 99F on $\overline{p}p \to \eta\pi^0\pi^0$, $\pi^0\pi^0$, $\eta\eta$, $\eta\eta'$, $\pi^+\pi^-$.
[12] From a fit to the total elastic cross section.
[13] Isospins 0 and 1 not separated.

$\pi^- p \to \eta\pi\pi n$

VALUE (MeV)	DOCUMENT ID		TECN	COMMENT
• • • We do not use the following data for averages, fits, limits, etc. • • •				
$235 \pm 50 \pm 40$	AMELIN	00	VES	37 $\pi^- p \to \eta\pi^+\pi^- n$

pp CENTRAL PRODUCTION

VALUE (MeV)	DOCUMENT ID		COMMENT
250±80 OUR ESTIMATE			
• • • We do not use the following data for averages, fits, limits, etc. • • •			
260 ± 57	BARBERIS	00F	450 $pp \to p_f \omega\omega p_s$

$f_4(2300)$ DECAY MODES

	Mode	Fraction (Γ_i/Γ)
Γ_1	$\rho\rho$	seen
Γ_2	$\omega\omega$	seen
Γ_3	$\eta\pi\pi$	seen
Γ_4	$\pi\pi$	seen
Γ_5	$K\overline{K}$	seen
Γ_6	$N\overline{N}$	seen

$f_4(2300)$ BRANCHING RATIOS

$\Gamma(\rho\rho)/\Gamma(\omega\omega)$ — Γ_1/Γ_2

VALUE	DOCUMENT ID		COMMENT
• • • We do not use the following data for averages, fits, limits, etc. • • •			
2.8 ± 0.5	BARBERIS	00F	450 $pp \to p_f \omega\omega p_s$

$f_4(2300)$ REFERENCES

AMELIN	00	NP A668 83	D. Amelin *et al.*	(VES Collab.)
ANISOVICH	00J	PL B491 47	A.V. Anisovich *et al.*	(RAL, LOQM, PNPI+)
BARBERIS	00F	PL B484 198	D. Barberis *et al.*	(WA 102 Collab.)
ANISOVICH	99C	PL B452 173	A.V. Anisovich *et al.*	
ANISOVICH	99F	NP A651 253	A.V. Anisovich *et al.*	
HASAN	94	PL B334 215	A. Hasan, D.V. Bugg	(LOQM)
MARTIN	80B	NP B176 355	B.R. Martin, D. Morgan	(LOUC, RHEL) JP
MARTIN	80C	NP B169 216	A.D. Martin, M.R. Pennington	(DURH) JP
CARTER	78B	NP B141 467	A.A. Carter	(LOQM)
CUTTS	78B	PR D17 16	D. Cutts *et al.*	(STON, WISC)
DULUDE	78B	PL 79B 335	R.S. Dulude *et al.*	(BROW, MIT, BARI) JP
CARTER	77	PL 67B 117	A.A. Carter *et al.*	(LOQM, RHEL) JP
COUPLAND	77	PL 71B 460	M. Coupland *et al.*	(LOQM, RHEL)
ALSPECTOR	73	PRL 30 511	J. Alspector *et al.*	(RUTG, UPNJ)
ABRAMS	70	PR D1 1917	R.J. Abrams *et al.*	(BNL)

$f_0(2330)$

$I^G(J^{PC}) = 0^+(0^{++})$

OMITTED FROM SUMMARY TABLE

$f_0(2330)$ MASS

VALUE (MeV)	DOCUMENT ID		TECN	COMMENT
• • • We do not use the following data for averages, fits, limits, etc. • • •				
2419 ± 64	[1] RODAS	22	RVUE	$J/\psi(1S) \to \gamma(\pi\pi, K\overline{K})$
2340 ± 20	SARANTSEV	21	RVUE	$J/\psi(1S) \to \gamma(\pi\pi, K\overline{K}, \eta\eta, \omega\phi)$
2314 ± 25	[2] BUGG	04A	RVUE	
2337 ± 14	ANISOVICH	00J	SPEC	2.0 $\overline{p}p \to \pi\pi, \eta\eta$
~ 2321	HASAN	94	RVUE	$\overline{p}p \to \pi\pi$

[1] T-matrix pole from coupled channel K-matrix fit to data on $J/\psi \to \gamma\pi^0\pi^0$ (ABLIKIM 15AE) and $J/\psi \to \gamma K^0_S K^0_S$ (ABLIKIM 18AA).
[2] Partial wave analysis of the data on $p\overline{p} \to \overline{\Lambda}\Lambda$ from BARNES 00.

$f_0(2330)$ WIDTH

VALUE (MeV)	DOCUMENT ID		TECN	COMMENT
• • • We do not use the following data for averages, fits, limits, etc. • • •				
274 ± 94	[1] RODAS	22	RVUE	$J/\psi(1S) \to \gamma(\pi\pi, K\overline{K})$
165 ± 25	SARANTSEV	21	RVUE	$J/\psi(1S) \to \gamma(\pi\pi, K\overline{K}, \eta\eta, \omega\phi)$
144 ± 20	[2] BUGG	04A	RVUE	
217 ± 33	ANISOVICH	00J	SPEC	2.0 $\overline{p}p \to \pi\pi, \eta\eta$
~ 223	HASAN	94	RVUE	$\overline{p}p \to \pi\pi$

[1] T-matrix pole from coupled channel K-matrix fit to data on $J/\psi \to \gamma\pi^0\pi^0$ (ABLIKIM 15AE) and $J/\psi \to \gamma K^0_S K^0_S$ (ABLIKIM 18AA).
[2] Partial wave analysis of the data on $p\overline{p} \to \overline{\Lambda}\Lambda$ from BARNES 00.

$f_0(2330)$ REFERENCES

RODAS	22	EPJ C82 80	A. Rodas *et al.*	(JPAC Collab.)
SARANTSEV	21	PL B816 136227	A.V. Sarantsev *et al.*	(BONN, PNPI)
ABLIKIM	18AA	PR D98 072003	M. Ablikim *et al.*	(BESIII Collab.)
ABLIKIM	15AE	PR D92 052003	M. Ablikim *et al.*	(BESIII Collab.)
BUGG	04A	EPJ C36 161	D.V. Bugg	
ANISOVICH	00J	PL B491 47	A.V. Anisovich *et al.*	(RAL, LOQM, PNPI+)
BARNES	00	PR C62 055203	P.D. Barnes *et al.*	
HASAN	94	PL B334 215	A. Hasan, D.V. Bugg	(LOQM)

$f_2(2340)$

$I^G(J^{PC}) = 0^+(2^{++})$

$f_2(2340)$ MASS

VALUE (MeV)	EVTS	DOCUMENT ID		TECN	COMMENT
2345^{+50}_{-40} OUR AVERAGE					
$2362^{+31}_{-30}{}^{+140}_{-63}$	5.5k	[1] ABLIKIM	13N	BES3	$e^+e^- \to J/\psi \to \gamma\eta\eta$
2339 ± 55		[2] ETKIN	88	MPS	22 $\pi^- p \to \phi\phi n$
• • • We do not use the following data for averages, fits, limits, etc. • • •					
2350 ± 7	80k	[3] UMAN	06	E835	5.2 $\overline{p}p \to \eta\eta\pi^0$
2392 ± 10		BOOTH	86	OMEG	85 π^-Be $\to 2\phi$Be
2360 ± 20		LINDENBAUM	84	RVUE	

[1] From partial wave analysis including all possible combinations of 0^{++}, 2^{++}, and 4^{++} resonances.
[2] Includes data of ETKIN 85. The percentage of the resonance going into $\phi\phi$ 2^{++} S_2, D_2, and D_0 is 37 ± 19, 4^{+12}_{-4}, and 59^{+21}_{-19}, respectively.
[3] Statistical error only.

$f_2(2340)$ WIDTH

VALUE (MeV)	EVTS	DOCUMENT ID		TECN	COMMENT
322^{+70}_{-60} OUR AVERAGE					
$334^{+62}_{-54}{}^{+165}_{-100}$	5.5k	[1] ABLIKIM	13N	BES3	$e^+e^- \to J/\psi \to \gamma\eta\eta$
319^{+81}_{-69}		[2] ETKIN	88	MPS	22 $\pi^- p \to \phi\phi n$
• • • We do not use the following data for averages, fits, limits, etc. • • •					
218 ± 16	80k	[3] UMAN	06	E835	5.2 $\overline{p}p \to \eta\eta\pi^0$
198 ± 50		BOOTH	86	OMEG	85 π^-Be $\to 2\phi$Be
150^{+150}_{-50}		LINDENBAUM	84	RVUE	

[1] From partial wave analysis including all possible combinations of 0^{++}, 2^{++}, and 4^{++} resonances.
[2] Includes data of ETKIN 85.
[3] Statistical error only.

Downloaded from https://academic.oup.com/ptep/article/2022/8/083C01/6651666 by KIT Library user on 27 September 2022

$f_2(2340)$ DECAY MODES

	Mode	Fraction (Γ_i/Γ)
Γ_1	$\phi\phi$	seen
Γ_2	$\eta\eta$	seen

$f_2(2340)$ BRANCHING RATIOS

$\Gamma(\eta\eta)/\Gamma_{total}$ — Γ_2/Γ

VALUE	DOCUMENT ID		TECN	COMMENT
seen	UMAN	06	E835	$5.2\ \overline{p}p \to \eta\eta\pi^0$

$f_2(2340)$ REFERENCES

ABLIKIM	13N	PR D87 092009	M. Ablikim *et al.*	(BESIII Collab.)
UMAN	06	PR D73 052009	I. Uman *et al.*	(FNAL E835)
ETKIN	88	PL B201 568	A. Etkin *et al.*	(BNL, CUNY)
BOOTH	86	NP B273 677	P.S.L. Booth *et al.*	(LIVP, GLAS, CERN)
ETKIN	85	PL 165B 217	A. Etkin *et al.*	(BNL, CUNY)
LINDENBAUM	84	CNPP 13 285	S.J. Lindenbaum	(CUNY)

$\rho_5(2350)$

$I^G(J^{PC}) = 1^+(5^{--})$

OMITTED FROM SUMMARY TABLE

This entry was previously called $U_1(2400)$. See also $\rho(2150)$, $f_2(2150)$, $\rho_3(2250)$, $f_4(2300)$.

$\rho_5(2350)$ MASS

$\pi^- p \to \omega\pi^0 n$

VALUE (MeV)	DOCUMENT ID		TECN	COMMENT
2330±35	ALDE	95	GAM2	$38\ \pi^- p \to \omega\pi^0 n$

$\overline{p}p \to \pi\pi$ or $\overline{K}K$

VALUE (MeV)	DOCUMENT ID		TECN	CHG	COMMENT
• • • We do not use the following data for averages, fits, limits, etc. • • •					
~ 2303	HASAN	94	RVUE		$\overline{p}p \to \pi\pi$
~ 2300	[1] MARTIN	80B	RVUE		
~ 2250	[1] MARTIN	80C	RVUE		
~ 2500	[2] CARTER	78B	CNTR	0	0.7–2.4 $\overline{p}p \to K^-K^+$
~ 2480	[3] CARTER	77	CNTR	0	0.7–2.4 $\overline{p}p \to \pi\pi$

S-CHANNEL $\overline{N}N$

VALUE (MeV)	DOCUMENT ID		TECN	CHG	COMMENT
• • • We do not use the following data for averages, fits, limits, etc. • • •					
2300±45	[4] ANISOVICH	02	SPEC		0.6–1.9 $p\overline{p} \to \omega\pi^0$, $\omega\eta\pi^0$, $\pi^+\pi^-$
2295±30	ANISOVICH	00J	SPEC		
~ 2380	[5] CUTTS	78B	CNTR		0.97–3 $\overline{p}p \to \overline{N}N$
2345±15	[5,6] COUPLAND	77	CNTR	0	0.7–2.4 $\overline{p}p \to \overline{p}p$
2359± 2	[5,7] ALSPECTOR	73	CNTR		$\overline{p}p$ S channel
2350±10	[8] ABRAMS	70	CNTR		S channel $\overline{N}N$
2360±25	[9] OH	70B	HDBC	−0	$\overline{p}(pn)$, $K^*K2\pi$

$\pi^- p \to K^+K^- n$

VALUE (MeV)	DOCUMENT ID		TECN	CHG	COMMENT
• • • We do not use the following data for averages, fits, limits, etc. • • •					
2307±6	ALPER	80	CNTR	0	$62\ \pi^- p \to K^+K^- n$

[1] $I(J^P) = 1(5^-)$ from simultaneous analysis of $p\overline{p} \to \pi^-\pi^+$ and $\pi^0\pi^0$.
[2] $I = 0(1)$; $J^P = 5^-$ from Barrelet-zero analysis.
[3] $I(J^P) = 1(5^-)$ from amplitude analysis.
[4] From the combined analysis of ANISOVICH 00J, ANISOVICH 01D, ANISOVICH 01E, and ANISOVICH 02.
[5] Isospins 0 and 1 not separated.
[6] From a fit to the total elastic cross section.
[7] Referred to as U or U region by ALSPECTOR 73.
[8] For $I = 1$ $\overline{N}N$.
[9] No evidence for this bump seen in the $\overline{p}p$ data of CHAPMAN 71B. Narrow state not confirmed by OH 73 with more data.

$\rho_5(2350)$ WIDTH

$\pi^- p \to \omega\pi^0 n$

VALUE (MeV)	DOCUMENT ID		TECN	COMMENT
400±100	ALDE	95	GAM2	$38\ \pi^- p \to \omega\pi^0 n$

$\overline{p}p \to \pi\pi$ or $\overline{K}K$

VALUE (MeV)	DOCUMENT ID		TECN	CHG	COMMENT
• • • We do not use the following data for averages, fits, limits, etc. • • •					
~ 169	HASAN	94	RVUE		$\overline{p}p \to \pi\pi$
~ 250	[10] MARTIN	80B	RVUE		
~ 300	[10] MARTIN	80C	RVUE		
~ 150	[11] CARTER	78B	CNTR	0	0.7–2.4 $\overline{p}p \to K^-K^+$
~ 210	[12] CARTER	77	CNTR	0	0.7–2.4 $\overline{p}p \to \pi\pi$

S-CHANNEL $\overline{N}N$

VALUE (MeV)	DOCUMENT ID		TECN	CHG	COMMENT
• • • We do not use the following data for averages, fits, limits, etc. • • •					
260± 75	[13] ANISOVICH	02	SPEC		0.6–1.9 $p\overline{p} \to \omega\pi^0$, $\omega\eta\pi^0$, $\pi^+\pi^-$
235^{+65}_{-40}	ANISOVICH	00J	SPEC		
135^{+150}_{-65}	[14,15] COUPLAND	77	CNTR	0	0.7–2.4 $\overline{p}p \to \overline{p}p$
165^{+18}_{-8}	[15] ALSPECTOR	73	CNTR		$\overline{p}p$ S channel
< 60	[16] OH	70B	HDBC	−0	$\overline{p}(pn)$, $K^*K2\pi$
~ 140	ABRAMS	67C	CNTR		S channel $\overline{p}N$

$\pi^- p \to K^+K^- n$

VALUE (MeV)	DOCUMENT ID		TECN	CHG	COMMENT
• • • We do not use the following data for averages, fits, limits, etc. • • •					
245±20	ALPER	80	CNTR	0	$62\ \pi^- p \to K^+K^- n$

[10] $I(J^P) = 1(5^-)$ from simultaneous analysis of $p\overline{p} \to \pi^-\pi^+$ and $\pi^0\pi^0$.
[11] $I = 0(1)$; $J^P = 5^-$ from Barrelet-zero analysis.
[12] $I(J^P) = 1(5^-)$ from amplitude analysis.
[13] From the combined analysis of ANISOVICH 00J, ANISOVICH 01D, ANISOVICH 01E, and ANISOVICH 02.
[14] From a fit to the total elastic cross section.
[15] Isospins 0 and 1 not separated.
[16] No evidence for this bump seen in the $\overline{p}p$ data of CHAPMAN 71B. Narrow state not confirmed by OH 73 with more data.

$\rho_5(2350)$ REFERENCES

ANISOVICH	02	PL B542 8	A.V. Anisovich *et al.*	
ANISOVICH	01D	PL B508 6	A.V. Anisovich *et al.*	
ANISOVICH	01E	PL B513 281	A.V. Anisovich *et al.*	
ANISOVICH	00J	PL B491 47	A.V. Anisovich *et al.*	(RAL, LOQM, PNPI+)
ALDE	95	ZPHY C66 379	D.M. Alde *et al.*	(GAMS Collab.) JP
HASAN	94	PL B334 215	A. Hasan, D.V. Bugg	(LOQM)
ALPER	80	PL 94B 422	B. Alper *et al.*	(AMST, CERN, CRAC, MPIM+)
MARTIN	80B	NP B176 355	B.R. Martin, D. Morgan	(LOUC, RHEL) JP
MARTIN	80C	NP B169 216	A.D. Martin, M.R. Pennington	(DURH) JP
CARTER	78B	NP B141 467	A.A. Carter	(LOQM)
CUTTS	78B	PR D17 16	D. Cutts *et al.*	(STON, WISC)
CARTER	77	PL 67B 117	A.A. Carter *et al.*	(LOQM, RHEL) JP
COUPLAND	77	PL 71B 460	M. Coupland *et al.*	(LOQM, RHEL)
ALSPECTOR	73	PRL 30 511	J. Alspector *et al.*	(RUTG, UPNJ)
OH	73	NP B51 57	B.Y. Oh *et al.*	(MSU)
CHAPMAN	71B	PR D4 1275	J.W. Chapman *et al.*	(MICH)
ABRAMS	70	PR D1 1917	R.J. Abrams *et al.*	(BNL)
OH	70B	PRL 24 1257	B.Y. Oh *et al.*	(MSU)
ABRAMS	67C	PRL 18 1209	R.J. Abrams *et al.*	(BNL)

$X(2370)$

$I^G(J^{PC}) = ?^?(?^{??})$

OMITTED FROM SUMMARY TABLE

$X(2370)$ MASS

VALUE (MeV)	EVTS	DOCUMENT ID		TECN	COMMENT
2341.6±6.5±5.7		[1] ABLIKIM	20Q	BES3	$J/\psi \to \gamma K\overline{K}\eta'$
• • • We do not use the following data for averages, fits, limits, etc. • • •					
$2376.3 \pm 8.7^{+3.2}_{-4.3}$	565	ABLIKIM	11C	BES3	$J/\psi \to \gamma\pi^+\pi^-\eta'$

[1] The state observed by ABLIKIM 11C at 2120 MeV is not observed with 90% CL upper limit of 1.49×10^{-5} for $J/\psi \to \gamma X(2120) \to \gamma K^+K^-\eta'$ and 6.38×10^{-6} for $K^0_S K^0_S \eta'$.

$X(2370)$ WIDTH

VALUE (MeV)	DOCUMENT ID		TECN	COMMENT
117±10± 8	[1] ABLIKIM	20Q	BES3	$J/\psi \to \gamma K\overline{K}\eta'$
• • • We do not use the following data for averages, fits, limits, etc. • • •				
$83 \pm 17^{+44}_{-6}$	ABLIKIM	11C	BES3	$J/\psi \to \gamma\pi^+\pi^-\eta'$

[1] The state observed by ABLIKIM 11C at 2120 MeV is not observed with 90% CL upper limit of 1.49×10^{-5} for $J/\psi \to \gamma X(2120) \to \gamma K^+K^-\eta'$ and 6.38×10^{-6} for $K^0_S K^0_S \eta'$.

$X(2370)$ DECAY MODES

	Mode	Fraction (Γ_i/Γ)
Γ_1	$K^+K^-\eta'$	seen
Γ_2	$K^0_S K^0_S \eta'$	seen
Γ_3	$\pi^+\pi^-\eta'$	seen

Downloaded from https://academic.oup.com/ptep/article/2022/8/083C01/6651666 by KIT Library user on 27 September 2022

$X(2370)$ BRANCHING RATIOS

$\Gamma(K^+K^-\eta')/\Gamma_{total}$ — **Γ_1/Γ**

VALUE	DOCUMENT ID		TECN	COMMENT
seen	ABLIKIM	20Q	BES3	$J/\psi \to \gamma K^+ K^- \eta'$

$\Gamma(K^0_S K^0_S \eta')/\Gamma_{total}$ — **Γ_2/Γ**

VALUE	DOCUMENT ID		TECN	COMMENT
seen	ABLIKIM	20Q	BES3	$J/\psi \to \gamma K^0_S K^0_S \eta'$

$\Gamma(\pi^+\pi^-\eta')/\Gamma_{total}$ — **Γ_3/Γ**

VALUE	DOCUMENT ID		TECN	COMMENT
seen	ABLIKIM	11C	BES3	$J/\psi \to \gamma \pi^+ \pi^- \eta'$

$X(2370)$ REFERENCES

ABLIKIM	20Q	EPJ C80 746	M. Ablikim *et al.*	(BESIII Collab.)
ABLIKIM	11C	PRL 106 072002	M. Ablikim *et al.*	(BESIII Collab.)

$f_6(2510)$

$I^G(J^{PC}) = 0^+(6^{++})$

OMITTED FROM SUMMARY TABLE
Needs confirmation.

$f_6(2510)$ MASS

VALUE (MeV)	DOCUMENT ID		TECN	COMMENT
2465±50 OUR AVERAGE	Error includes scale factor of 2.1.			
2420±30	ALDE	98	GAM4	$100\ \pi^- p \to \pi^0\pi^0 n$
2510±30	BINON	84B	GAM2	$38\ \pi^- p \to n 2\pi^0$
• • • We do not use the following data for averages, fits, limits, etc. • • •				
2485±40	[1] ANISOVICH	00J	SPEC	1.92–2.41 $p\overline{p}$

[1] From the combined analysis of ANISOVICH 99C, ANISOVICH 99F, ANISOVICH 99J, ANISOVICH 99K, and ANISOVICH 00B.

$f_6(2510)$ WIDTH

VALUE (MeV)	DOCUMENT ID		TECN	COMMENT
255±40 OUR AVERAGE				
270±60	ALDE	98	GAM4	$100\ \pi^- p \to \pi^0\pi^0 n$
240±60	BINON	84B	GAM2	$38\ \pi^- p \to n 2\pi^0$
• • • We do not use the following data for averages, fits, limits, etc. • • •				
410±90	[2] ANISOVICH	00J	SPEC	1.92–2.41 $p\overline{p}$

[2] From the combined analysis of ANISOVICH 99C, ANISOVICH 99F, ANISOVICH 99J, ANISOVICH 99K, and ANISOVICH 00B.

$f_6(2510)$ DECAY MODES

	Mode	Fraction (Γ_i/Γ)
Γ_1	$\pi\pi$	(6.0±1.0) %

$f_6(2510)$ BRANCHING RATIOS

$\Gamma(\pi\pi)/\Gamma_{total}$ — **Γ_1/Γ**

VALUE	DOCUMENT ID		TECN	COMMENT
0.06±0.01	[3] BINON	83C	GAM2	$38\ \pi^- p \to n 4\gamma$

[3] Assuming one pion exchange and using data of BOLOTOV 74.

$f_6(2510)$ REFERENCES

ANISOVICH	00B	NP A662 319	A.V. Anisovich *et al.*	
ANISOVICH	00J	PL B491 47	A.V. Anisovich *et al.*	(RAL, LOQM, PNPI+)
ANISOVICH	99C	PL B452 173	A.V. Anisovich *et al.*	
ANISOVICH	99F	NP A651 253	A.V. Anisovich *et al.*	
ANISOVICH	99J	PL B471 271	A.V. Anisovich *et al.*	
ANISOVICH	99K	PL B468 309	A.V. Anisovich *et al.*	
ALDE	98	EPJ A3 361	D. Alde *et al.*	(GAM4 Collab.)
Also		PAN 62 405	D. Alde *et al.*	(GAMS Collab.)
		Translated from YAF 62 446.		
BINON	84B	LNC 39 41	F.G. Binon *et al.*	(SERP, BELG, LAPP) JP
BINON	83C	SJNP 38 723	F.G. Binon *et al.*	(SERP, BRUX+)
		Translated from YAF 38 1199.		
BOLOTOV	74	PL 52B 489	V.N. Bolotov *et al.*	(SERP)

Downloaded from https://academic.oup.com/ptep/article/2022/8/083C01/6651666 by KIT Library user on 27 September 2022

STRANGE MESONS
($S = \pm 1$, $C = B = 0$)

$K^+ = u\overline{s}$, $K^0 = d\overline{s}$, $\overline{K}^0 = \overline{d}s$, $K^- = \overline{u}s$, similarly for K^*'s

$K^{\pm}$

$I(J^P) = \frac{1}{2}(0^-)$

CHARGED KAON MASS

Revised 1994 by T.G. Trippe (LBNL).

The average of the six charged kaon mass measurements which we use in the Particle Listings is

$$m_{K^\pm} = 493.677 \pm 0.013 \text{ MeV (S = 2.4)} , \quad (1)$$

where the error has been increased by the scale factor S. The large scale factor indicates a serious disagreement between different input data. The average before scaling the error is

$$m_{K^\pm} = 493.677 \pm 0.005 \text{ MeV} ,$$
$$\chi^2 = 22.9 \text{ for 5 D.F., Prob. } = 0.04\% , \quad (2)$$

where the high χ^2 and correspondingly low χ^2 probability further quantify the disagreement.

The main disagreement is between the two most recent and precise results,

$$m_{K^\pm} = 493.696 \pm 0.007 \text{ MeV} \quad \text{DENISOV 91}$$
$$m_{K^\pm} = 493.636 \pm 0.011 \text{ MeV (S = 1.5)} \quad \text{GALL 88}$$
$$\text{Average} = 493.679 \pm 0.006 \text{ MeV}$$
$$\chi^2 = 21.2 \text{ for 1 D.F., Prob. } = 0.0004\% , \quad (3)$$

both of which are measurements of x-ray energies from kaonic atoms. Comparing the average in Eq. (3) with the overall average in Eq. (2), it is clear that DENISOV 91 [1] and GALL 88 [2] dominate the overall average, and that their disagreement is responsible for most of the high χ^2.

The GALL 88 measurement was made using four different kaonic atom transitions, K^- Pb ($9 \to 8$), K^- Pb ($11 \to 10$), K^- W ($9 \to 8$), and K^- W ($11 \to 10$). The $m_{K^\pm}$ values they obtain from each of these transitions is shown in the Particle Listings and in Fig. 1. Their K^- Pb ($9 \to 8$) $m_{K^\pm}$is below and somewhat inconsistent with their other three transitions. The average of their four measurements is

$$m_{K^\pm} = 493.636 \pm 0.007 ,$$
$$\chi^2 = 7.0 \text{ for 3 D.F., Prob. } = 7.2\% . \quad (4)$$

This is a low but acceptable χ^2 probability so, to be conservative, GALL 88 scaled up the error on their average by S=1.5 to obtain their published error ±0.011 shown in Eq. (3) above and used in the Particle Listings average.

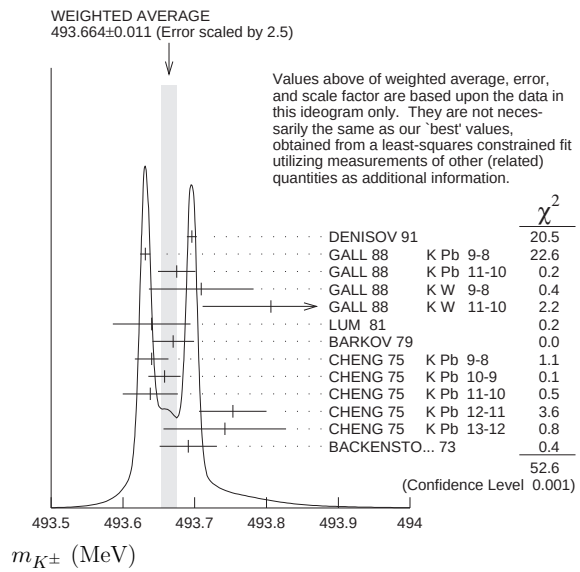

Figure 1: Ideogram of $m_{K^\pm}$ mass measurements. GALL 88 and CHENG 75 measurements are shown separately for each transition they measured.

The ideogram in Fig. 1 shows that the DENISOV 91 measurement and the GALL 88 K^- Pb ($9 \to 8$) measurement yield two well-separated peaks. One might suspect the GALL 88 K^- Pb ($9 \to 8$) measurement since it is responsible both for the internal inconsistency in the GALL 88 measurements and the disagreement with DENISOV 91.

To see if the disagreement could result from a systematic problem with the K^- Pb ($9 \to 8$) transition, we have separated the CHENG 75 [3] data, which also used K^- Pb, into its separate transitions. Figure 1 shows that the CHENG 75 and GALL 88 K^- Pb ($9 \to 8$) values are consistent, suggesting the possibility of a common effect such as contaminant nuclear γ rays near the K^- Pb ($9 \to 8$) transition energy, although the CHENG 75 errors are too large to make a strong conclusion. The average of all 13 measurements has a χ^2 of 52.6 as shown in Fig. 1 and the first line of Table 1, yielding an unacceptable χ^2 probability of 0.00005%. The second line of Table 1 excludes both the GALL 88 and CHENG 75 measurements of the K^- Pb ($9 \to 8$) transition and yields a χ^2 probability of 43%. The third [fourth] line of Table 1 excludes only the GALL 88 K^- Pb ($9 \to 8$) [DENISOV 91] measurement and yields a χ^2 probability of 20% [8.6%]. Table 1 shows that removing both measurements of the K^- Pb ($9 \to 8$) transition produces the most consistent set of data, but that excluding only the GALL 88 K^- Pb ($9 \to 8$) transition or DENISOV 91 also produces acceptable probabilities.

Downloaded from https://academic.oup.com/ptep/article/2022/8/083C01/6651666 by KIT Library user on 27 September 2022

Table 1: $m_{K^{\pm}}$ averages for some combinations of Fig. 1 data.

$m_{K^{\pm}}$ (MeV)	χ^2	D.F.	Prob. (%)	Measurements used
493.664 ± 0.004	52.6	12	0.00005	all 13 measurements
493.690 ± 0.006	10.1	10	43	no K^- Pb(9→8)
493.687 ± 0.006	14.6	11	20	no GALL 88 K^- Pb(9→8)
493.642 ± 0.006	17.8	11	8.6	no DENISOV 91

Yu.M. Ivanov, representing DENISOV 91, has estimated corrections needed for the older experiments because of improved ^{192}Ir and ^{198}Au calibration γ-ray energies. He estimates that CHENG 75 and BACKENSTOSS 73 [4] $m_{K^{\pm}}$ values could be raised by about 15 keV and 22 keV, respectively. With these estimated corrections, Table 1 becomes Table 2. The last line of Table 2 shows that if such corrections are assumed, then GALL 88 K^- Pb (9 → 8) is inconsistent with the rest of the data even when DENISOV 91 is excluded. Yu.M. Ivanov warns that these are rough estimates. Accordingly, we do not use Table 2 to reject the GALL 88 K^- Pb (9 → 8) transition, but we note that a future reanalysis of the CHENG 75 data could be useful because it might provide supporting evidence for such a rejection.

Table 2: $m_{K^{\pm}}$ averages for some combinations of Fig. 1 data after raising CHENG 75 and BACKENSTOSS 73 values by 0.015 and 0.022 MeV respectively.

$m_{K^{\pm}}$ (MeV)	χ^2	D.F.	Prob. (%)	Measurements used
493.666 ± 0.004	53.9	12	0.00003	all 13 measurements
493.693 ± 0.006	9.0	10	53	no K^- Pb(9→8)
493.690 ± 0.006	11.5	11	40	no GALL 88 K^- Pb(9→8)
493.645 ± 0.006	23.0	11	1.8	no DENISOV 91

The GALL 88 measurement uses a Ge semiconductor spectrometer which has a resolution of about 1 keV, so they run the risk of some contaminant nuclear γ rays. Studies of γ rays following stopped π^- and Σ^- absorption in nuclei (unpublished) do not show any evidence for contaminants according to GALL 88 spokesperson, B.L. Roberts. The DENISOV 91 measurement uses a crystal diffraction spectrometer with a resolution of 6.3 eV for radiation at 22.1 keV to measure the 4f-3d transition in K^- ^{12}C. The high resolution and the light nucleus reduce the probability for overlap by contaminant γ rays, compared with the measurement of GALL 88. The DENISOV 91 measurement is supported by their high-precision measurement of the 4d-2p transition energy in π^- ^{12}C, which is good agreement with the calculated energy.

While we suspect that the GALL 88 K^- Pb (9 → 8) measurements could be the problem, we are unable to find clear grounds for rejecting it. Therefore, we retain their measurement in the average and accept the large scale factor until further information can be obtained from new measurements and/or from reanalysis of GALL 88 and CHENG 75 data.

We thank B.L. Roberts (Boston Univ.) and Yu.M. Ivanov (Petersburg Nuclear Physics Inst.) for their extensive help in understanding this problem.

References

1. A.S. Denisov, *et al.* [DENISOV 91], Sov. Phys. JETP Lett. **54**, 558 (1991).
2. K.P. Gall, *et al.* [GALL 88], Phys. Rev. Lett. **60**, 186 (1988).
3. S.C. Cheng, *et al.* [CHENG 75], Nucl. Phys. **A254**, 381 (1975).
4. G. Backenstoss, *et al.* [BACKENSTOSS 73], Phys. Lett. **43B**, 431 (1973).

$K^{\pm}$ MASS

VALUE (MeV)	DOCUMENT ID		TECN	CHG	COMMENT
493.677±0.016 OUR FIT Error includes scale factor of 2.8.					
493.677±0.013 OUR AVERAGE Error includes scale factor of 2.4. See the ideogram below.					
493.696±0.007	[1] DENISOV	91	CNTR	−	Kaonic atoms
493.636±0.011	[2] GALL	88	CNTR	−	Kaonic atoms
493.640±0.054	LUM	81	CNTR	−	Kaonic atoms
493.670±0.029	BARKOV	79	EMUL	±	$e^+ e^- \rightarrow K^+ K^-$
493.657±0.020	[2] CHENG	75	CNTR	−	Kaonic atoms
493.691±0.040	BACKENSTO...	73	CNTR	−	Kaonic atoms
• • • We do not use the following data for averages, fits, limits, etc. • • •					
493.631±0.007	GALL	88	CNTR	−	K^- Pb (9→ 8)
493.675±0.026	GALL	88	CNTR	−	K^- Pb (11→ 10)
493.709±0.073	GALL	88	CNTR	−	K^- W (9→ 8)
493.806±0.095	GALL	88	CNTR	−	K^- W (11→ 10)
493.640±0.022±0.008	[3] CHENG	75	CNTR	−	K^- Pb (9→ 8)
493.658±0.019±0.012	[3] CHENG	75	CNTR	−	K^- Pb (10→ 9)
493.638±0.035±0.016	[3] CHENG	75	CNTR	−	K^- Pb (11→ 10)
493.753±0.042±0.021	[3] CHENG	75	CNTR	−	K^- Pb (12→ 11)
493.742±0.081±0.027	[3] CHENG	75	CNTR	−	K^- Pb (13→ 12)

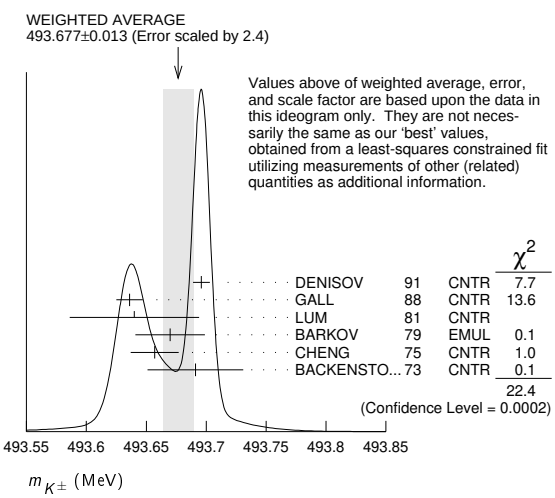

[1] Error increased from 0.0059 based on the error analysis in IVANOV 92.
[2] This value is the authors' combination of all of the separate transitions listed for this paper.
[3] The CHENG 75 values for separate transitions were calculat/ed from their Table 7 transition energies. The first error includes a 20% systematic error in the noncircular contaminant shift. The second error is due to a ±5 eV uncertainty in the theoretical transition energies.

$m_{K^+} - m_{K^-}$

Test of *CPT*.

VALUE (MeV)	EVTS	DOCUMENT ID		TECN	CHG
−0.032±0.090	1.5 M	[1] FORD	72	ASPK	±

[1] FORD 72 uses $m_{\pi^+} - m_{\pi^-} = +28 \pm 70$ keV.

Downloaded from https://academic.oup.com/ptep/article/2022/8/083C01/6651666 by KIT Library user on 27 September 2022

$K^{\pm}$ MEAN LIFE

VALUE (10^{-8} s)	EVTS	DOCUMENT ID		TECN	CHG	COMMENT
1.2380±0.0020 OUR FIT	Error includes scale factor of 1.8.					
1.2379±0.0021 OUR AVERAGE	Error includes scale factor of 1.9. See the ideogram below.					
1.2347±0.0030	15M	[1] AMBROSINO	08	KLOE	±	$\phi \to K^+K^-$
1.2451±0.0030	250k	KOPTEV	95	CNTR		K at rest, U target
1.2368±0.0041	150k	KOPTEV	95	CNTR		K at rest, Cu target
1.2380±0.0016	3M	OTT	71	CNTR	+	K at rest
1.2272±0.0036		LOBKOWICZ	69	CNTR	+	K in flight
1.2443±0.0038		FITCH	65B	CNTR	+	K at rest
• • • We do not use the following data for averages, fits, limits, etc. • • •						
1.2415±0.0024	400k	[2] KOPTEV	95	CNTR		K at rest
1.221 ±0.011		FORD	67	CNTR	±	
1.231 ±0.011		BOYARSKI	62	CNTR	+	

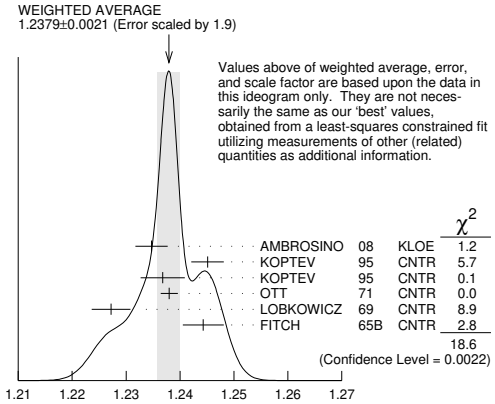

[1] Result obtained by averaging the decay length and decay time analyses taking correlations into account.

[2] KOPTEV 95 report this weighted average of their U-target and Cu-target results, where they have weighted by $1/\sigma$ rather than $1/\sigma^2$.

$(\tau_{K^+} - \tau_{K^-}) / \tau_{average}$

This quantity is a measure of *CPT* invariance in weak interactions.

VALUE (%)	DOCUMENT ID		TECN
0.10 ±0.09 OUR AVERAGE	Error includes scale factor of 1.2.		
−0.4 ±0.4	AMBROSINO	08	KLOE
0.090±0.078	LOBKOWICZ	69	CNTR
0.47 ±0.30	FORD	67	CNTR

See the related review(s):

Rare Kaon Decays

K^+ DECAY MODES

K^- modes are charge conjugates of the modes below.

	Mode		Fraction (Γ_i/Γ)	Scale factor/ Confidence level
	Leptonic and semileptonic modes			
Γ_1	$e^+\nu_e$		$(1.582\pm0.007)\times10^{-5}$	
Γ_2	$\mu^+\nu_\mu$		(63.56 ± 0.11) %	S=1.2
Γ_3	$\pi^0 e^+\nu_e$		(5.07 ± 0.04) %	S=2.1
	Called K^+_{e3}.			
Γ_4	$\pi^0\mu^+\nu_\mu$		(3.352 ± 0.033) %	S=1.9
	Called $K^+_{\mu3}$.			
Γ_5	$\pi^0\pi^0 e^+\nu_e$		$(2.55\pm0.04)\times10^{-5}$	S=1.1
Γ_6	$\pi^+\pi^- e^+\nu_e$		$(4.247\pm0.024)\times10^{-5}$	
Γ_7	$\pi^+\pi^-\mu^+\nu_\mu$		$(1.4\pm0.9)\times10^{-5}$	
Γ_8	$\pi^0\pi^0\pi^0 e^+\nu_e$		$<3.5\times10^{-6}$	CL=90%
	Hadronic modes			
Γ_9	$\pi^+\pi^0$		(20.67 ± 0.08) %	S=1.2
Γ_{10}	$\pi^+\pi^0\pi^0$		(1.760 ± 0.023) %	S=1.1
Γ_{11}	$\pi^+\pi^+\pi^-$		(5.583 ± 0.024) %	
	Leptonic and semileptonic modes with photons			
Γ_{12}	$\mu^+\nu_\mu\gamma$	[a,b]	$(6.2\pm0.8)\times10^{-3}$	
Γ_{13}	$\mu^+\nu_\mu\gamma(\mathrm{SD}^+)$	[c,d]	$(1.33\pm0.22)\times10^{-5}$	
Γ_{14}	$\mu^+\nu_\mu\gamma(\mathrm{SD}^+\mathrm{INT})$	[c,d]	$<2.7\times10^{-5}$	CL=90%
Γ_{15}	$\mu^+\nu_\mu\gamma(\mathrm{SD}^- + \mathrm{SD}^-\mathrm{INT})$	[c,d]	$<2.6\times10^{-4}$	CL=90%
Γ_{16}	$e^+\nu_e\gamma$		$(9.4\pm0.4)\times10^{-6}$	
Γ_{17}	$\pi^0 e^+\nu_e\gamma$	[a,b]	$(2.66\pm0.09)\times10^{-4}$	
Γ_{18}	$\pi^0 e^+\nu_e\gamma(\mathrm{SD})$	[c,d]	$<5.3\times10^{-5}$	CL=90%
Γ_{19}	$\pi^0\mu^+\nu_\mu\gamma$	[a,b]	$(1.25\pm0.25)\times10^{-5}$	
Γ_{20}	$\pi^0\pi^0 e^+\nu_e\gamma$		$<5\times10^{-6}$	CL=90%
	Hadronic modes with photons or $\ell\overline{\ell}$ pairs			
Γ_{21}	$\pi^+\pi^0\gamma(\mathrm{INT})$		$(-4.2\pm0.9)\times10^{-6}$	
Γ_{22}	$\pi^+\pi^0\gamma(\mathrm{DE})$	[a,e]	$(6.0\pm0.4)\times10^{-6}$	
Γ_{23}	$\pi^+\pi^0 e^+e^-$		$(4.24\pm0.14)\times10^{-6}$	
Γ_{24}	$\pi^+\pi^0\pi^0\gamma$	[a,b]	$(7.6\,^{+6.0}_{-3.0})\times10^{-6}$	
Γ_{25}	$\pi^+\pi^+\pi^-\gamma$	[a,b]	$(7.1\pm0.5)\times10^{-6}$	
Γ_{26}	$\pi^+\gamma\gamma$	[a]	$(1.01\pm0.06)\times10^{-6}$	
Γ_{27}	$\pi^+3\gamma$	[a]	$<1.0\times10^{-4}$	CL=90%
Γ_{28}	$\pi^+e^+e^-\gamma$		$(1.19\pm0.13)\times10^{-8}$	
	Leptonic modes with $\ell\overline{\ell}$ pairs			
Γ_{29}	$e^+\nu_e\nu\overline{\nu}$		$<6\times10^{-5}$	CL=90%
Γ_{30}	$\mu^+\nu_\mu\nu\overline{\nu}$		$<1.0\times10^{-6}$	CL=90%
Γ_{31}	$e^+\nu_e e^+e^-$		$(2.48\pm0.20)\times10^{-8}$	
Γ_{32}	$\mu^+\nu_\mu e^+e^-$		$(7.06\pm0.31)\times10^{-8}$	
Γ_{33}	$e^+\nu_e\mu^+\mu^-$		$(1.7\pm0.5)\times10^{-8}$	
Γ_{34}	$\mu^+\nu_\mu\mu^+\mu^-$		$<4.1\times10^{-7}$	CL=90%
	Lepton family number (*LF*), Lepton number (*L*), $\Delta S = \Delta Q$ (*SQ*) violating modes, or $\Delta S = 1$ weak neutral current (*S1*) modes			
Γ_{35}	$\pi^+\pi^+e^-\overline{\nu}_e$	*SQ*	$<1.3\times10^{-8}$	CL=90%
Γ_{36}	$\pi^+\pi^+\mu^-\overline{\nu}_\mu$	*SQ*	$<3.0\times10^{-6}$	CL=95%
Γ_{37}	$\pi^+e^+e^-$	*S1*	$(3.00\pm0.09)\times10^{-7}$	
Γ_{38}	$\pi^+\mu^+\mu^-$	*S1*	$(9.4\pm0.6)\times10^{-8}$	S=2.6
Γ_{39}	$\pi^+\nu\overline{\nu}$	*S1*	$(1.14\,^{+0.40}_{-0.33})\times10^{-10}$	
Γ_{40}	$\pi^+\pi^0\nu\overline{\nu}$	*S1*	$<4.3\times10^{-5}$	CL=90%
Γ_{41}	$\mu^-\nu e^+e^+$	*LF*	$<2.1\times10^{-8}$	CL=90%
Γ_{42}	$\mu^+\nu_e$	*LF* [f]	$<4\times10^{-3}$	CL=90%
Γ_{43}	$\pi^+\mu^+e^-$	*LF*	$<1.3\times10^{-11}$	CL=90%
Γ_{44}	$\pi^+\mu^-e^+$	*LF*	$<6.6\times10^{-11}$	CL=90%
Γ_{45}	$\pi^-\mu^+e^+$	*L*	$<4.2\times10^{-11}$	CL=90%
Γ_{46}	$\pi^-e^+e^+$	*L*	$<2.2\times10^{-10}$	CL=90%
Γ_{47}	$\pi^-\mu^+\mu^+$	*L*	$<4.2\times10^{-11}$	CL=90%
Γ_{48}	$\mu^+\overline{\nu}_e$	*L* [f]	$<3.3\times10^{-3}$	CL=90%
Γ_{49}	$\pi^0e^+\overline{\nu}_e$	*L*	$<3\times10^{-3}$	CL=90%
Γ_{50}	$\pi^+\gamma$	[g]	$<2.3\times10^{-9}$	CL=90%

[a] See the Particle Listings below for the energy limits used in this measurement.

[b] Most of this radiative mode, the low-momentum γ part, is also included in the parent mode listed without γ's.

[c] Structure-dependent part.

[d] See the review on "Form Factors for Radiative Pion and Kaon Decays" for definitions and details.

[e] Direct-emission branching fraction.

[f] Derived from an analysis of neutrino-oscillation experiments.

[g] Violates angular-momentum conservation.

CONSTRAINED FIT INFORMATION

An overall fit to the mean life, a decay rate, and 15 branching ratios uses 35 measurements and one constraint to determine 8 parameters. The overall fit has a $\chi^2 = 53.4$ for 28 degrees of freedom.

The following *off-diagonal* array elements are the correlation coefficients $\langle \delta p_i \delta p_j \rangle / (\delta p_i \cdot \delta p_j)$, in percent, from the fit to parameters p_i, including the branching fractions, $x_i \equiv \Gamma_i/\Gamma_{total}$. The fit constrains the x_i whose labels appear in this array to sum to one.

	x_2	x_3	x_4	x_5	x_9	x_{10}	x_{11}
x_3	−66						
x_4	−64	90					
x_5	−12	−5	−5				
x_9	−67	0	−1	−6			
x_{10}	−13	−6	−5	91	−6		
x_{11}	−14	−6	−6	2	−7	2	
Γ	3	1	1	0	2	0	−24

Downloaded from https://academic.oup.com/ptep/article/2022/8/083C01/6651666 by KIT Library user on 27 September 2022

	Mode	Rate (10^8 s^{-1})	Scale factor
Γ_2	$\mu^+\nu_\mu$	0.5134 ±0.0012	1.5
Γ_3	$\pi^0 e^+\nu_e$ Called K^+_{e3}.	0.0410 ±0.0004	2.1
Γ_4	$\pi^0\mu^+\nu_\mu$ Called $K^+_{\mu3}$.	0.02707±0.00027	1.9
Γ_5	$\pi^0\pi^0 e^+\nu_e$	(2.059 ±0.029) × 10^{-5}	1.1
Γ_9	$\pi^+\pi^0$	0.1670 ±0.0007	1.3
Γ_{10}	$\pi^+\pi^0\pi^0$	0.01421±0.00018	1.1
Γ_{11}	$\pi^+\pi^+\pi^-$	0.04510±0.00019	

$K^{\pm}$ DECAY RATES

$\Gamma(\mu^+\nu_\mu)$ — Γ_2

VALUE (10^6 s^{-1})	DOCUMENT ID		TECN	CHG
51.34±0.12 OUR FIT Error includes scale factor of 1.5.				
• • • We do not use the following data for averages, fits, limits, etc. • • •				
51.2 ±0.8	FORD	67	CNTR	±

$\Gamma(\pi^+\pi^+\pi^-)$ — Γ_{11}

VALUE (10^6 s^{-1})	EVTS	DOCUMENT ID		TECN	CHG
4.510±0.019 OUR FIT					
4.511±0.024		[1] FORD	70	ASPK	
• • • We do not use the following data for averages, fits, limits, etc. • • •					
4.529±0.032	3.2M	[1] FORD	70	ASPK	
4.496±0.030		[1] FORD	67	CNTR	±

[1] First FORD 70 value is second FORD 70 combined with FORD 67.

K^+ BRANCHING RATIOS

Leptonic and semileptonic modes

$\Gamma(e^+\nu_e)/\Gamma(\mu^+\nu_\mu)$ — Γ_1/Γ_2

See the note on "Decay Constants of Charged Pseudoscalar Mesons" in the D^+_s Listings.

VALUE (units 10^{-5})	EVTS	DOCUMENT ID		TECN	CHG
2.488±0.009 OUR AVERAGE					
2.488±0.007±0.007	150k	[1] LAZZERONI	13	NA62	±
2.493±0.025±0.019	13.8k	[2] AMBROSINO	09E	KLOE	±
• • • We do not use the following data for averages, fits, limits, etc. • • •					
2.487±0.011±0.007	60k	[3] LAZZERONI	11	NA62	+
2.51 ±0.15	404	HEINTZE	76	SPEC	+
2.37 ±0.17	534	HEARD	75B	SPEC	+
2.42 ±0.42	112	CLARK	72	OSPK	+

[1] LAZZERONI 13 uses full data sample collected from 2007 to 2008. This ratio is defined to be fully inclusive, including internal-bremsstrahlung.
[2] The ratio is defined to include internal-bremsstrahlung, ignoring direct-emission contributions. AMBROSINO 09E determined the ratio from the measurement of $\Gamma(K \to e\nu(\gamma)$, $E_\gamma < 10$ MeV) / $\Gamma(K \to \mu\nu(\gamma))$. 89.8% of $K \to e\nu(\gamma)$ events had E_γ <10 MeV.
[3] This ratio is defined to be fully inclusive, including internal-bremsstrahlung.

$\Gamma(\mu^+\nu_\mu)/\Gamma_{total}$ — Γ_2/Γ

See the note on "Decay Constants of Charged Pseudoscalar Mesons" in the D^+_s Listings.

VALUE (units 10^{-2})	EVTS	DOCUMENT ID		TECN	CHG	COMMENT
63.56±0.11 OUR FIT Error includes scale factor of 1.2.						
63.60±0.16 OUR AVERAGE						
63.66±0.09±0.15	865k	[1] AMBROSINO	06A	KLOE	+	
63.24±0.44	62k	CHIANG	72	OSPK	+	1.84 GeV/c K^+

[1] Fully inclusive. Used tagged kaons from ϕ decays.

$\Gamma(\pi^0 e^+\nu_e)/\Gamma_{total}$ — Γ_3/Γ

VALUE (units 10^{-2})	EVTS	DOCUMENT ID		TECN	CHG	COMMENT
5.07 ±0.04 OUR FIT Error includes scale factor of 2.1.						
4.94 ±0.05 OUR AVERAGE						
4.965±0.038±0.037		[1] AMBROSINO	08A	KLOE	±	
4.86 ±0.10	3516	CHIANG	72	OSPK	+	1.84 GeV/c K^+
• • • We do not use the following data for averages, fits, limits, etc. • • •						
4.7 ±0.3	429	SHAKLEE	64	HLBC	+	
5.0 ±0.5		ROE	61	HLBC	+	

[1] Depends on K^+ lifetime τ. AMBROSINO 08A uses PDG 06 value of τ = (1.2385 ± 0.0024) × 10^{-8} sec. The correlation between K^+_{e3} and $K^+_{\mu3}$ branching fraction measurements is 62.7%.

$\Gamma(\pi^0 e^+\nu_e)/\Gamma(\mu^+\nu_\mu)$ — Γ_3/Γ_2

VALUE	EVTS	DOCUMENT ID		TECN	CHG
0.0798±0.0008 OUR FIT Error includes scale factor of 1.9.					
• • • We do not use the following data for averages, fits, limits, etc. • • •					
0.069 ±0.006	350	ZELLER	69	ASPK	+
0.0775±0.0033	960	BOTTERILL	68C	ASPK	+
0.069 ±0.006	561	GARLAND	68	OSPK	+
0.0791±0.0054	295	[1] AUERBACH	67	OSPK	+

[1] AUERBACH 67 changed from 0.0797 ± 0.0054. See comment with ratio $\Gamma(\pi^0\mu^+\nu_\mu)/\Gamma(\mu^+\nu_\mu)$. The value 0.0785 ± 0.0025 given in AUERBACH 67 is an average of AUERBACH 67 $\Gamma(\pi^0 e^+\nu_e)/\Gamma(\mu^+\nu_\mu)$ and CESTER 66 $\Gamma(\pi^0 e^+\nu_e)/\left[\Gamma(\mu^+\nu_\mu) + \Gamma(\pi^+\pi^0)\right]$.

$\Gamma(\pi^0 e^+\nu_e)/\left[\Gamma(\mu^+\nu_\mu) + \Gamma(\pi^+\pi^0)\right]$ — $\Gamma_3/(\Gamma_2+\Gamma_9)$

VALUE (units 10^{-2})	EVTS	DOCUMENT ID		TECN	CHG
6.02±0.06 OUR FIT Error includes scale factor of 2.1.					
6.02±0.15 OUR AVERAGE					
6.16±0.22	5110	ESCHSTRUTH	68	OSPK	+
5.89±0.21	1679	CESTER	66	OSPK	+
• • • We do not use the following data for averages, fits, limits, etc. • • •					
5.92±0.65		[1] WEISSENBE...	76	SPEC	+

[1] Value calculated from WEISSENBERG 76 ($\pi^0 e\nu$), ($\mu\nu$), and ($\pi\pi^0$) values to eliminate dependence on our 1974 ($\pi 2\pi^0$) and ($\pi\pi^+\pi^-$) fractions.

$\Gamma(\pi^0 e^+\nu_e)/\left[\Gamma(\pi^0\mu^+\nu_\mu) + \Gamma(\pi^+\pi^0) + \Gamma(\pi^+\pi^0\pi^0)\right]$ — $\Gamma_3/(\Gamma_4+\Gamma_9+\Gamma_{10})$

VALUE	EVTS	DOCUMENT ID		TECN	CHG
0.1967±0.0016 OUR FIT Error includes scale factor of 2.5.					
0.1962±0.0008±0.0035	71k	SHER	03	B865	+

$\Gamma(\pi^0 e^+\nu_e)/\Gamma(\pi^+\pi^0)$ — Γ_3/Γ_9

VALUE	EVTS	DOCUMENT ID		TECN	CHG	COMMENT
0.2454±0.0023 OUR FIT Error includes scale factor of 2.6.						
0.2467±0.0011 OUR AVERAGE Error includes scale factor of 1.1.						
0.2423±0.0015±0.0037	31k	UVAROV	14	ISTR	−	ISTRA+
0.2470±0.0009±0.0004	87k	BATLEY	07A	NA48	±	
• • • We do not use the following data for averages, fits, limits, etc. • • •						
0.221 ±0.012	786	[1] LUCAS	73B	HBC	−	Dalitz pairs only

[1] LUCAS 73B gives N(K_{e3}) = 786 ± 3.1%, N(2π) = 3564 ± 3.1%. We use these values to obtain quoted result.

$\Gamma(\pi^0 e^+\nu_e)/\Gamma(\pi^+\pi^+\pi^-)$ — Γ_3/Γ_{11}

VALUE	EVTS	DOCUMENT ID		TECN	CHG
0.908±0.009 OUR FIT Error includes scale factor of 1.6.					
• • • We do not use the following data for averages, fits, limits, etc. • • •					
0.867±0.027	2768	BARMIN	87	XEBC	+
0.856±0.040	2827	BRAUN	75	HLBC	+
0.850±0.019	4385	[1] HAIDT	71	HLBC	+
0.846±0.021	4385	[1] EICHTEN	68	HLBC	+
0.94 ±0.09	854	BELLOTTI	67B	HLBC	
0.90 ±0.06	230	BORREANI	64	HBC	+

[1] HAIDT 71 is a reanalysis of EICHTEN 68. Not included in average because of large discrepancy in $\Gamma(\pi^0\mu^+\nu)/\Gamma(\pi^0 e^+\nu)$ with more precise results.

$\Gamma(\pi^0\mu^+\nu_\mu)/\Gamma_{total}$ — Γ_4/Γ

VALUE (units 10^{-2})	EVTS	DOCUMENT ID		TECN	CHG	COMMENT
3.352±0.033 OUR FIT Error includes scale factor of 1.9.						
3.24 ±0.04 OUR AVERAGE						
3.233±0.029±0.026		[1] AMBROSINO	08A	KLOE	±	
3.33 ±0.16	2345	CHIANG	72	OSPK	+	1.84 GeV/c K^+
• • • We do not use the following data for averages, fits, limits, etc. • • •						
2.8 ±0.4		[2] TAYLOR	59	EMUL	+	

[1] Depends on K^+ lifetime τ. AMBROSINO 08A uses PDG 06 value of τ = (1.2385 ± 0.0024) × 10^{-8} sec. The correlation between K^+_{e3} and $K^+_{\mu3}$ branching fraction measurements is 62.7%.
[2] Earlier experiments not averaged.

$\Gamma(\pi^0\mu^+\nu_\mu)/\Gamma(\mu^+\nu_\mu)$ — Γ_4/Γ_2

VALUE	EVTS	DOCUMENT ID		TECN	CHG
0.0527±0.0006 OUR FIT Error includes scale factor of 1.8.					
• • • We do not use the following data for averages, fits, limits, etc. • • •					
0.054 ±0.009	240	ZELLER	69	ASPK	+
0.0480±0.0037	424	[1] GARLAND	68	OSPK	+
0.0486±0.0040	307	[2] AUERBACH	67	OSPK	+

[1] GARLAND 68 changed from 0.055 ± 0.004 in agreement with μ-spectrum calculation of GAILLARD 70 appendix B. L.G.Pondrom, (private communication 73).
[2] AUERBACH 67 changed from 0.0602 ± 0.0046 by erratum which brings the μ-spectrum calculation into agreement with GAILLARD 70 appendix B.

Downloaded from https://academic.oup.com/ptep/article/2022/8/083C01/6651666 by KIT Library user on 27 September 2022

$\Gamma(\pi^0\mu^+\nu_\mu)/\Gamma(\pi^0 e^+\nu_e)$ — Γ_4/Γ_3

VALUE	EVTS	DOCUMENT ID		TECN	CHG	COMMENT
0.6608±0.0029 OUR FIT	Error includes scale factor of 1.1.					
0.6618±0.0027 OUR AVERAGE						
0.663 ±0.003 ±0.001	77k	BATLEY	07A	NA48	±	
0.671 ±0.007 ±0.008	24k	HORIE	01	SPEC		
0.670 ±0.014		[1] HEINTZE	77	SPEC	+	
0.667 ±0.017	5601	BOTTERILL	68B	ASPK	+	
• • • We use the following data for averages but not for fits. • • •						
0.6511±0.0064		[2] AMBROSINO	08A	KLOE	±	
• • • We do not use the following data for averages, fits, limits, etc. • • •						
0.608 ±0.014	1585	[3] BRAUN	75	HLBC	+	
0.705 ±0.063	554	[4] LUCAS	73B	HBC	−	Dalitz pairs only
0.698 ±0.025	3480	[5] CHIANG	72	OSPK	+	1.84 GeV/c K^+
0.596 ±0.025		[6] HAIDT	71	HLBC	+	
0.604 ±0.022	1398	[6] EICHTEN	68	HLBC		
0.703 ±0.056	1509	CALLAHAN	66B	HLBC		

[1] HEINTZE 77 value from fit to λ_0. Assumes μ-e universality.
[2] Not used in the fit. This result enters the fit via correlation of K^+_{e3} and $K^+_{\mu3}$ branching fraction measurements of AMBROSINO 08A.
[3] BRAUN 75 value is from form factor fit. Assumes μ-e universality.
[4] LUCAS 73B gives $N(K_{\mu3}) = 554 \pm 7.6\%$, $N(K_{e3}) = 786 \pm 3.1\%$. We divide.
[5] CHIANG 72 $\Gamma(\pi^0\mu^+\nu_\mu)/\Gamma(\pi^0 e^+\nu_e)$ is statistically independent of CHIANG 72 $\Gamma(\pi^0\mu^+\nu_\mu)/\Gamma_{total}$ and $\Gamma(\pi^0 e^+\nu_e)/\Gamma_{total}$.
[6] HAIDT 71 is a reanalysis of EICHTEN 68. Not included in average because of large discrepancy with more precise results.

$[\Gamma(\pi^0\mu^+\nu_\mu) + \Gamma(\pi^+\pi^0)]/\Gamma_{total}$ — $(\Gamma_4+\Gamma_9)/\Gamma$

We combine these two modes for experiments measuring them in xenon bubble chamber because of difficulties of separating them there.

VALUE (units 10^{-2})	EVTS	DOCUMENT ID		TECN	CHG
24.02±0.08 OUR FIT	Error includes scale factor of 1.2.				
• • • We do not use the following data for averages, fits, limits, etc. • • •					
25.4 ±0.9	886	SHAKLEE	64	HLBC	+
23.4 ±1.1		ROE	61	HLBC	+

$\Gamma(\pi^0\mu^+\nu_\mu)/\Gamma(\pi^+\pi^0)$ — Γ_4/Γ_9

VALUE	EVTS	DOCUMENT ID		TECN	CHG
0.1637±0.0006±0.0003	77k	BATLEY	07A	NA48	±

$\Gamma(\pi^0\mu^+\nu_\mu)/\Gamma(\pi^+\pi^+\pi^-)$ — Γ_4/Γ_{11}

VALUE	EVTS	DOCUMENT ID		TECN	CHG	COMMENT
0.600±0.007 OUR FIT	Error includes scale factor of 1.6.					
• • • We do not use the following data for averages, fits, limits, etc. • • •						
0.503±0.019	1505	[1] HAIDT	71	HLBC	+	
0.510±0.017	1505	[1] EICHTEN	68	HLBC	+	
0.63 ±0.07	2845	[2] BISI	65B	BC	+	HBC+HLBC

[1] HAIDT 71 is a reanalysis of EICHTEN 68. Not included in average because of large discrepancy in $\Gamma(\pi^0\mu^+\nu)/\Gamma(\pi^0 e^+\nu)$ with more precise results.
[2] Error enlarged for background problems. See GAILLARD 70.

$\Gamma(\pi^0\pi^0 e^+\nu_e)/\Gamma_{total}$ — Γ_5/Γ

VALUE (units 10^{-5})	EVTS	DOCUMENT ID		TECN	CHG
2.55±0.04 OUR FIT	Error includes scale factor of 1.1.				
2.54±0.89	10	BARMIN	88B	HLBC	+

$\Gamma(\pi^0\pi^0 e^+\nu_e)/\Gamma(\pi^+\pi^0\pi^0)$ — Γ_5/Γ_{10}

VALUE (units 10^{-3})	EVTS	DOCUMENT ID		TECN	CHG
1.449±0.008 OUR FIT					
1.449±0.006±0.006	65.2k	[1] BATLEY	14A	NA48	±

[1] Data collected in 2003–2004. This leads to the scalar form factor $(1+\delta_{EM})\ f_s = 6.079 \pm 0.012 \pm 0.027 \pm 0.046$ where the last error is due to the normalizing decay mode uncertainty.

$\Gamma(\pi^0\pi^0 e^+\nu_e)/\Gamma(\pi^0 e^+\nu_e)$ — Γ_5/Γ_3

VALUE (units 10^{-4})	EVTS	DOCUMENT ID		TECN	CHG
5.03±0.09 OUR FIT	Error includes scale factor of 1.2.				
4.1 $^{+1.0}_{-0.7}$ OUR AVERAGE					
4.2 $^{+1.0}_{-0.9}$	25	BOLOTOV	86B	CALO	−
3.8 $^{+5.0}_{-1.2}$	2	LJUNG	73	HLBC	+

$\Gamma(\pi^+\pi^- e^+\nu_e)/\Gamma(\pi^+\pi^+\pi^-)$ — Γ_6/Γ_{11}

VALUE (units 10^{-4})	EVTS	DOCUMENT ID		TECN	CHG
7.606±0.029 OUR AVERAGE					
7.615±0.008±0.028	1.1M	[1] BATLEY	12	NA48	±
7.35 ±0.01 ±0.19	388k	[2] PISLAK	01	B865	
7.21 ±0.32	30k	ROSSELET	77	SPEC	+
• • • We do not use the following data for averages, fits, limits, etc. • • •					
7.36 ±0.68	500	BOURQUIN	71	ASPK	
7.0 ±0.9	106	SCHWEINB...	71	HLBC	+
5.83 ±0.63	269	ELY	69	HLBC	+

[1] BATLEY 12 uses data collected in 2003–2004. The result is inclusive of $K^\pm \to \pi^+\pi^- e^\pm \nu\gamma$ decays. Using PDG 12 value for $\Gamma(\pi^+\pi^-\pi^+)/\Gamma = (5.59 \pm 0.04)\times 10^{-2}$. BATLEY 12 obtains $B(\pi^+\pi^- e\nu) = (4.257 \pm 0.004 \pm 0.035)\times 10^{-5}$ where the syst. error is dominated by the error on the normalization mode.
[2] PISLAK 01 reports $\Gamma(\pi^+\pi^- e^+\nu_e)/\Gamma_{total} = (4.109 \pm 0.008 \pm 0.110)\times 10^{-5}$ using the PDG 00 value $\Gamma(\pi^+\pi^+\pi^-)/\Gamma_{total} = (5.59 \pm 0.05)\times 10^{-2}$. We divide by the PDG value and unfold its error from the systematic error. PISLAK 03 and PISLAK 10A give additional details on the branching ratio measurement and give improved errors on the S-wave π-π scattering length: $a^0_0 = 0.235 \pm 0.013$ and $a^2_0 = -0.0410 \pm 0.0027$.

$\Gamma(\pi^+\pi^-\mu^+\nu_\mu)/\Gamma_{total}$ — Γ_7/Γ

VALUE (units 10^{-5})	EVTS	DOCUMENT ID		TECN	CHG
• • • We do not use the following data for averages, fits, limits, etc. • • •					
0.77 $^{+0.54}_{-0.50}$	1	CLINE	65	FBC	+

$\Gamma(\pi^+\pi^-\mu^+\nu_\mu)/\Gamma(\pi^+\pi^+\pi^-)$ — Γ_7/Γ_{11}

VALUE (units 10^{-4})	EVTS	DOCUMENT ID		TECN	CHG
2.57±1.55	7	BISI	67	DBC	+
• • • We do not use the following data for averages, fits, limits, etc. • • •					
~ 2.5	1	GREINER	64	EMUL	+

$\Gamma(\pi^0\pi^0\pi^0 e^+\nu_e)/\Gamma_{total}$ — Γ_8/Γ

VALUE (units 10^{-6})	CL%	EVTS	DOCUMENT ID		TECN	CHG
<3.5	90	0	BOLOTOV	88	SPEC	−
• • • We do not use the following data for averages, fits, limits, etc. • • •						
<9	90	0	BARMIN	92	XEBC	+

Hadronic modes

$\Gamma(\pi^+\pi^0)/\Gamma_{total}$ — Γ_9/Γ

VALUE (units 10^{-2})	EVTS	DOCUMENT ID		TECN	CHG	COMMENT
20.67±0.08 OUR FIT	Error includes scale factor of 1.2.					
20.70±0.16 OUR AVERAGE	Error includes scale factor of 1.8.					
20.65±0.05±0.08	1.4M	[1] AMBROSINO	08E	KLOE	+	$\phi \to K^+K^-$
21.18±0.28	16k	CHIANG	72	OSPK	+	1.84 GeV/c K^+
• • • We do not use the following data for averages, fits, limits, etc. • • •						
21.0 ±0.6		CALLAHAN	65	HLBC		See Γ_9/Γ_{11}

[1] Fully inclusive of final-state radiation. The branching ratio is evaluated using K^+ lifetime, $\tau = 12.385$ ns.

$\Gamma(\pi^+\pi^0)/\Gamma(\mu^+\nu_\mu)$ — Γ_9/Γ_2

VALUE	EVTS	DOCUMENT ID		TECN	CHG	COMMENT
0.3252±0.0016 OUR FIT	Error includes scale factor of 1.2.					
0.3325±0.0032 OUR AVERAGE						
0.3329±0.0047±0.0010	45k	USHER	92	SPEC	+	$p\overline{p}$ at rest
0.3355±0.0057		[1] WEISSENBE...	76	SPEC	+	
0.3277±0.0065	4517	[2] AUERBACH	67	OSPK	+	
• • • We do not use the following data for averages, fits, limits, etc. • • •						
0.328 ±0.005	25k	[1] WEISSENBE...	74	STRC	+	
0.305 ±0.018	1600	ZELLER	69	ASPK	+	

[1] WEISSENBERG 76 revises WEISSENBERG 74.
[2] AUERBACH 67 changed from 0.3253 ± 0.0065. See comment with ratio $\Gamma(\pi^0\mu^+\nu_\mu)/\Gamma(\mu^+\nu_\mu)$.

$\Gamma(\pi^+\pi^0)/\Gamma(\pi^+\pi^+\pi^-)$ — Γ_9/Γ_{11}

VALUE	EVTS	DOCUMENT ID		TECN	CHG
3.702±0.022 OUR FIT	Error includes scale factor of 1.1.				
• • • We do not use the following data for averages, fits, limits, etc. • • •					
3.96 ±0.15	1045	CALLAHAN	66	FBC	+

$\Gamma(\pi^+\pi^0\pi^0)/\Gamma_{total}$ — Γ_{10}/Γ

VALUE (units 10^{-2})	EVTS	DOCUMENT ID		TECN	CHG	COMMENT
1.760±0.023 OUR FIT	Error includes scale factor of 1.1.					
1.775±0.028 OUR AVERAGE	Error includes scale factor of 1.2.					
1.763±0.013±0.022		ALOISIO	04A	KLOE	±	
1.84 ±0.06	1307	CHIANG	72	OSPK	+	1.84 GeV/c K^+
• • • We do not use the following data for averages, fits, limits, etc. • • •						
1.53 ±0.11	198	[1] PANDOULAS	70	EMUL	+	
1.8 ±0.2	108	SHAKLEE	64	HLBC	+	
1.7 ±0.2		ROE	61	HLBC	+	
1.5 ±0.2		[2] TAYLOR	59	EMUL	+	

[1] Includes events of TAYLOR 59.
[2] Earlier experiments not averaged.

Downloaded from https://academic.oup.com/ptep/article/2022/8/083C01/6651666 by KIT Library user on 27 September 2022

$\Gamma(\pi^+\pi^0\pi^0)/\Gamma(\pi^+\pi^0)$ — Γ_{10}/Γ_9

VALUE	EVTS	DOCUMENT ID		TECN	CHG	COMMENT
0.0851±0.0012 OUR FIT	Error includes scale factor of 1.1.					
• • • We do not use the following data for averages, fits, limits, etc. • • •						
0.081 ±0.005	574	[1] LUCAS	73B	HBC	−	Dalitz pairs only

[1] LUCAS 73B gives $N(\pi 2\pi^0) = 574 \pm 5.9\%$, $N(2\pi) = 3564 \pm 3.1\%$. We quote $0.5N(\pi 2\pi^0)/N(2\pi)$ where 0.5 is because only Dalitz pair π^0's were used.

$\Gamma(\pi^+\pi^0\pi^0)/\Gamma(\pi^+\pi^+\pi^-)$ — Γ_{10}/Γ_{11}

VALUE	EVTS	DOCUMENT ID		TECN	CHG	COMMENT
0.315±0.004 OUR FIT	Error includes scale factor of 1.1.					
0.303±0.009	2027	BISI	65	BC	+	HBC+HLBC
• • • We do not use the following data for averages, fits, limits, etc. • • •						
0.393±0.099	17	YOUNG	65	EMUL	+	

$\Gamma(\pi^+\pi^+\pi^-)/\Gamma_{total}$ — Γ_{11}/Γ

VALUE (units 10^{-2})	EVTS	DOCUMENT ID		TECN	CHG	COMMENT
5.583±0.024 OUR FIT						
5.565±0.031±0.025	68k	[1] BABUSCI	14B	KLOE	+	
• • • We do not use the following data for averages, fits, limits, etc. • • •						
5.56 ±0.20	2330	[2] CHIANG	72	OSPK	+	1.84 GeV/c K^+
5.34 ±0.21	693	[3] PANDOULAS	70	EMUL	+	
5.71 ±0.15		DEMARCO	65	HBC		
6.0 ±0.4	44	YOUNG	65	EMUL	+	
5.54 ±0.12	2332	CALLAHAN	64	HLBC	+	
5.1 ±0.2	540	SHAKLEE	64	HLBC	+	
5.7 ±0.3		ROE	61	HLBC	+	

[1] Inclusive of final-state radiation. Result obtained from averaging two branching ratios: one from a sample with $K^- \to \mu\nu(\gamma)$ tagging and another with $K^- \to \pi^-\pi^0(\gamma)$ tagging.
[2] Value is not independent of CHIANG 72 $\Gamma(\mu^+\nu_\mu)/\Gamma_{total}$, $\Gamma(\pi^+\pi^0)/\Gamma_{total}$, $\Gamma(\pi^+\pi^0\pi^0)/\Gamma_{total}$, $\Gamma(\pi^0\mu^+\nu_\mu)/\Gamma_{total}$, and $\Gamma(\pi^0 e^+\nu_e)/\Gamma_{total}$.
[3] Includes events of TAYLOR 59.

Leptonic and semileptonic modes with photons

$\Gamma(\mu^+\nu_\mu\gamma)/\Gamma_{total}$ — Γ_{12}/Γ

VALUE (units 10^{-3})	EVTS	DOCUMENT ID		TECN	CHG	COMMENT
6.2±0.8 OUR AVERAGE						
6.6±1.5		[1,2] DEMIDOV	90	XEBC		$P(\mu)$ <231.5 MeV/c
6.0±0.9		BARMIN	88	HLBC	+	$P(\mu)$ <231.5 MeV/c
• • • We do not use the following data for averages, fits, limits, etc. • • •						
3.5±0.8		[2,3] DEMIDOV	90	XEBC		$E(\gamma)$ > 20 MeV
3.2±0.5	57	[4] BARMIN	88	HLBC	+	$E(\gamma)$ >20 MeV
5.4±0.3		[5] AKIBA	85	SPEC		$P(\mu)$ <231.5 MeV/c

[1] $P(\mu)$ cut given in DEMIDOV 90 paper, 235.1 MeV/c, is a misprint according to authors (private communication).
[2] DEMIDOV 90 quotes only inner bremsstrahlung (IB) part.
[3] Not independent of above DEMIDOV 90 value. Cuts differ.
[4] Not independent of above BARMIN 88 value. Cuts differ.
[5] Assumes μ-e universality and uses constraints from $K \to e\nu\gamma$.

$\Gamma(\mu^+\nu_\mu\gamma(SD^+))/\Gamma_{total}$ — Γ_{13}/Γ

Structure-dependent part with $+\gamma$ helicity (SD^+ term). See the "Note on $\pi^\pm \to \ell^\pm\nu\gamma$ and $K^\pm \to \ell^\pm\nu\gamma$ Form Factors" in the $\pi^\pm$ section of the Particle Data Listings above.

VALUE (units 10^{-5})	CL%	EVTS	DOCUMENT ID		TECN
1.33±0.12±0.18		2588	[1] ADLER	00B	B787
• • • We do not use the following data for averages, fits, limits, etc. • • •					
<3.0	90		AKIBA	85	SPEC

[1] ADLER 00B obtains the branching ratio by extrapolating the measurement in the kinematic region $E_\mu > 137$ MeV, $E_\gamma > 90$ MeV to the full SD^+ phase-space. Also reports $|F_V + F_A| = 0.165 \pm 0.007 \pm 0.011$ and $-0.04 < F_V - F_A < 0.24$ at 90% CL.

$\Gamma(\mu^+\nu_\mu\gamma(SD^+INT))/\Gamma_{total}$ — Γ_{14}/Γ

Interference term between internal Bremsstrahlung and SD^+ term. See the "Note on $\pi^\pm \to \ell^\pm\nu\gamma$ and $K^\pm \to \ell^\pm\nu\gamma$ Form Factors" in the $\pi^\pm$ section of the Particle Data Listings above.

VALUE (units 10^{-5})	CL%	DOCUMENT ID		TECN
<2.7	90	AKIBA	85	SPEC

$\Gamma(\mu^+\nu_\mu\gamma(SD^- + SD^-INT))/\Gamma_{total}$ — Γ_{15}/Γ

Sum of structure-dependent part with $-\gamma$ helicity (SD^- term) and interference term between internal Bremsstrahlung and SD^- term. See the "Note on $\pi^\pm \to \ell^\pm\nu\gamma$ and $K^\pm \to \ell^\pm\nu\gamma$ Form Factors" in the $\pi^\pm$ section of the Particle Data Listings above.

VALUE (units 10^{-4})	CL%	DOCUMENT ID		TECN
<2.6	90	[1] AKIBA	85	SPEC

[1] Assumes μ-e universality and uses constraints from $K \to e\nu\gamma$.

$\Gamma(e^+\nu_e\gamma)/\Gamma(\mu^+\nu_\mu)$ — Γ_{16}/Γ_2

VALUE (units 10^{-5})	EVTS	DOCUMENT ID		TECN	CHG	COMMENT
1.483±0.066±0.013	1.4k	[1] AMBROSINO	09E	KLOE	±	E_γ in 10–250 MeV, p_e > 200 MeV/c

[1] AMBROSINO 09E measured the differential width $dR_\gamma/dE_\gamma = (1/\Gamma(K \to \mu\nu))(d\Gamma(K \to e\nu\gamma)/dE_\gamma)$. Result obtained by integrating the differential width over E_γ from 10 to 250 MeV.

$\Gamma(\pi^0 e^+\nu_e\gamma)/\Gamma(\pi^0 e^+\nu_e)$ — Γ_{17}/Γ_3

VALUE (units 10^{-3})	EVTS	DOCUMENT ID		TECN	CHG	COMMENT
5.25±0.17 OUR AVERAGE	Error includes scale factor of 1.3. See the ideogram below.					
5.32±0.10±0.12	7248	[1] POLYARUSH	21	OKA	+	E_γ > 10 MeV, 0.6 < $\cos(\theta_{e\gamma})$ < 0.9
4.7 ±0.2 ±0.3	1456	[2] AKIMENKO	07	ISTR	−	E_γ > 10 MeV, 0.6 < $\cos(\theta_{e\gamma})$ < 0.9
4.6 ±0.8	82	[3] BARMIN	91	XEBC		E_γ > 10 MeV, 0.6 < $\cos(\theta_{e\gamma})$ < 0.9
5.6 ±0.4	192	[4] BOLOTOV	86B	CALO	−	E_γ > 10 MeV
• • • We do not use the following data for averages, fits, limits, etc. • • •						
18.1 ±0.3 ±0.7	4476	[2] AKIMENKO	07	ISTR	−	E_γ>10 MeV, $\theta_{e\gamma}$ >10°
6.3 ±0.2 ±0.3		[2] AKIMENKO	07	ISTR	−	E_γ>30 MeV, $\theta_{e\gamma}$ >20°
15.1 ±2.5	82	[3] BARMIN	91	XEBC		E_γ > 10 MeV, $\cos(\theta_{e\gamma})$ < 0.98
4.8 ±2.0	16	[5] LJUNG	73	HLBC	+	E_γ > 30 MeV
$2.2^{+1.5}_{-1.0}$		[5] LJUNG	73	HLBC	+	E_γ > 30 MeV
7.6 ±2.8	13	[6] ROMANO	71	HLBC		E_γ > 10 MeV
5.3 ±2.2		[6] ROMANO	71	HLBC	+	E_γ > 30 MeV
12 ±8		BELLOTTI	67	HLBC		E_γ > 30 MeV

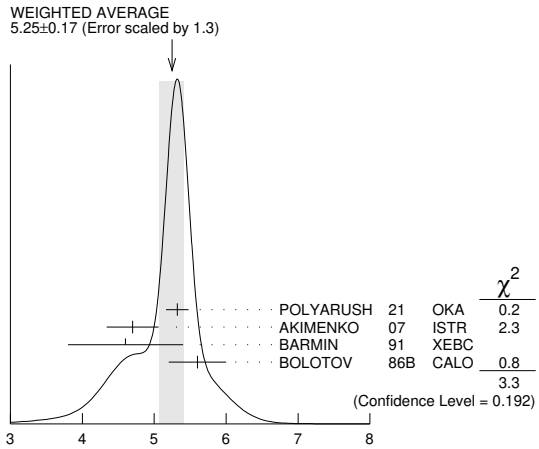

[1] POLYARUSH 21 provides values for three kinematic regions. For averaging, we use value with $E_\gamma > 10$ MeV and $0.6 < \cos(\theta_{e\gamma}) < 0.9$.
[2] AKIMENKO 07 provides values for three kinematic regions. For averaging, we use value with $E_\gamma > 10$ MeV and $0.6 < \cos(\theta_{e\gamma}) < 0.9$.
[3] BARMIN 91 quotes branching ratio $\Gamma(K \to e\pi^0\nu\gamma)/\Gamma_{all}$. The measured normalization is $[\Gamma(K \to e\pi^0\nu) + \Gamma(K \to \pi^+\pi^+\pi^-)]$. For comparison with other experiments we used $\Gamma(K \to e\pi^0\nu)/\Gamma_{all} = 0.0482$ to calculate the values quoted here.
[4] $\cos(\theta_{e\gamma})$ between 0.6 and 0.9.
[5] First LJUNG 73 value is for $\cos(\theta_{e\gamma})$ <0.9, second value is for $\cos(\theta_{e\gamma})$ between 0.6 and 0.9 for comparison with ROMANO 71.
[6] Both ROMANO 71 values are for $\cos(\theta_{e\gamma})$ between 0.6 and 0.9. Second value is for comparison with second LJUNG 73 value. We use lowest E_γ cut for Summary Table value. See ROMANO 71 for E_γ dependence.

$\Gamma(\pi^0 e^+\nu_e\gamma(SD))/\Gamma_{total}$ — Γ_{18}/Γ

Structure-dependent part.

VALUE (units 10^{-5})	CL%	DOCUMENT ID		TECN	CHG
<5.3	90	BOLOTOV	86B	CALO	−

$\Gamma(\pi^0\mu^+\nu_\mu\gamma)/\Gamma_{total}$ — Γ_{19}/Γ

VALUE (units 10^{-5})	CL%	EVTS	DOCUMENT ID		TECN	CHG	COMMENT
1.25±0.25 OUR AVERAGE							
1.10±0.32±0.05		23	[1] ADLER	10	B787		30 < E_γ < 60 MeV
1.46±0.22±0.32		153	[2] TCHIKILEV	07	ISTR	−	30 < E_γ < 60 MeV

Downloaded from https://academic.oup.com/ptep/article/2022/8/083C01/6651666 by KIT Library user on 27 September 2022

• • • We do not use the following data for averages, fits, limits, etc. • • •

2.4 ±0.5 ±0.6		125	SHIMIZU	06	K470	+	E_γ > 30 MeV; $\Theta_{\mu\gamma}$ >20°
<6.1	90	0	LJUNG	73	HLBC	+	$E(\gamma)$ >30 MeV

[1] Value obtained from $B(K^+ \to \pi^0 \mu^+ \nu_\mu \gamma) = (2.51 \pm 0.74 \pm 0.12) \times 10^{-5}$ obtained in the kinematic region $E_\gamma > 20$ MeV, and then theoretical $K_{\mu3\gamma}$ spectrum has been used. Also $B(K^+ \to \pi^0 \mu^+ \nu_\mu \gamma) = (1.58 \pm 0.46 \pm 0.08) \times 10^{-5}$, for $E_\gamma > 30$ MeV and $\theta_{\mu\gamma} > 20°$, was determined.

[2] Obtained from measuring $B(K_{\mu3\gamma}) / B(K_{\mu3})$ and using PDG 02 value $B(K_{\mu3}) = 3.27\%$. $B(K_{\mu3\gamma}) = (8.82 \pm 0.94 \pm 0.86) \times 10^{-5}$ is obtained for 5 MeV < E_γ < 30 MeV.

$\Gamma(\pi^0 \pi^0 e^+ \nu_e \gamma)/\Gamma_{total}$ — Γ_{20}/Γ

VALUE (units 10^{-6})	CL%	EVTS	DOCUMENT ID		TECN	CHG	COMMENT
<5	90	0	BARMIN	92	XEBC	+	E_γ > 10 MeV

Hadronic modes with photons

$\Gamma(\pi^+ \pi^0 \gamma(\text{INT}))/\Gamma_{total}$ — Γ_{21}/Γ

The $K^+ \to \pi^+ \pi^0 \gamma$ differential decay rate can be described in terms of T_{π^+}, the charged pion kinetic energy, and $W^2 = (P_K \cdot P_\gamma)(P_{\pi^+} \cdot P_\gamma) / (m_K\, m_{\pi^+})^2$; then we can write $d^2\Gamma(K^+ \to \pi^+ \pi^0 \gamma) / (dT_{\pi^+}\, dW^2) = d^2\Gamma(K^+ \to \pi^+ \pi^0 \gamma)_{IB} / (dT_{\pi^+}\, dW^2)\, [1 + 2 \cos(\pm\phi + \delta_1^1 - \delta_0^2)\, m_\pi^2\, m_K^2\, W^2\, X_E + m_\pi^4\, m_K^4\, (X_E^2 + X_M^2)\, W^4]$. The IB differential and total branching ratios are expressed in terms of the non-radiative experimental width $\Gamma(K^+ \to \pi^+ \pi^0)$ by Low's theorem. Using PDG 10 $B(K^+ \to \pi^+ \pi^0) = 0.2066 \pm 0.0008$, one obtains respectively $B(K^+ \to \pi^+ \pi^0 \gamma)_{IB}$ (55 < T_{π^+} < 90 MeV)= 2.55×10^{-4} and $B(K^+ \to \pi^+ \pi^0 \gamma)_{IB}$ (0 < T_{π^+} < 80 MeV)= 1.80×10^{-4}. Fitting respectively the piece proportional to W^2 and the piece proportional to W^4, the interference contribution (INT), proportional to X_E, and the direct contribution (DE) proportional to $X_E^2 + X_M^2$ are extracted.

VALUE (units 10^{-6})	EVTS	DOCUMENT ID		TECN	CHG	COMMENT
−4.24±0.63±0.70	600k	[1] BATLEY	10A	NA48	±	T_{π^+} 0–80 MeV

[1] The cut on the photon energy implies $W^2 > 0.2$. BATLEY 10A obtains the INT and DE fractional branchings with respect to IB from a simultaneous kinematical fit of INT and DE and then we use the PDG 10 value for $B(K^+ \to \pi^+ \pi^0) = 20.66 \pm 0.08$ to determine the IB. The INT and DE correlation coefficients −0.83. Assuming a constant electric amplitude, X_E, this INT value implies $X_E = -24 \pm 6$ GeV^{-4}.

$\Gamma(\pi^+ \pi^0 \gamma(\text{DE}))/\Gamma_{total}$ — Γ_{22}/Γ

Direct emission (DE) part of $\Gamma(\pi^+ \pi^0 \gamma)/\Gamma_{total}$, assuming that interference (INT) component is zero.

VALUE (units 10^{-6})	EVTS	DOCUMENT ID		TECN	CHG	COMMENT
5.99±0.27±0.25	600k	[1] BATLEY	10A	NA48	±	T_{π^+} 0–80 MeV

• • • We do not use the following data for averages, fits, limits, etc. • • •

3.8 ±0.8 ±0.7		10k	ALIEV	06	K470	+	T_{π^+} 55–90 MeV
3.7 ±3.9 ±1.0		930	UVAROV	06	ISTR	−	T_{π^-} 55–90 MeV
3.2 ±1.3 ±1.0		4k	ALIEV	03	K470	+	T_{π^+} 55–90 MeV
6.1 ±2.5 ±1.9		4k	ALIEV	03	K470	+	T_{π^+} full range
4.7 ±0.8 ±0.3		20k	[2] ADLER	00C	B787	+	T_{π^+} 55–90 MeV
20.5 ±4.6 $^{+3.9}_{-2.3}$			BOLOTOV	87	WIRE	−	T_{π^-} 55–90 MeV
15.6 ±3.5 ±5.0			ABRAMS	72	ASPK	±	$T_{\pi^\pm}$ 55–90 MeV

[1] The cut on the photon energy implies $W^2 > 0.2$. BATLEY 10A obtains the INT and DE fractional branchings with respect to IB from a simultaneous kinematical fit of INT and DE and then we use the PDG 10 value for $B(K^+ \to \pi^+ \pi^0) = 20.66 \pm 0.08$ to determine the IB. The INT and DE correlation coefficients −0.93. Assuming constant electric and magnetic amplitudes, X_E and X_M, these INTand DE values imply $X_E = -24 \pm 6$ GeV^{-4} and $X_M = -254 \pm 9$ GeV^{-4}.

[2] ADLER 00C measures the INT component to be $(-0.4 \pm 1.6)\%$ of the inner bremsstrahlung (IB) component.

$\Gamma(\pi^+ \pi^0 e^+ e^-)/\Gamma_{total}$ — Γ_{23}/Γ

VALUE (units 10^{-6})	EVTS	DOCUMENT ID		TECN
4.24±0.14	4.9k	[1] BATLEY	19	NA48

[1] BATLEY 19 result is obtained from an exposure of 1.7×10^{11} charged kaon decays recorded in 2003–2004. The study of the kinematic space shows evidence for a structure dependent contribution consistent with predictions from chiral perturbation theory.

$\Gamma(\pi^+ \pi^0 \pi^0 \gamma)/\Gamma(\pi^+ \pi^0 \pi^0)$ — Γ_{24}/Γ_{10}

VALUE (units 10^{-4})	DOCUMENT ID		TECN	CHG	COMMENT
$4.3^{+3.2}_{-1.7}$	BOLOTOV	85	SPEC	−	$E(\gamma)$ > 10 MeV

$\Gamma(\pi^+ \pi^+ \pi^- \gamma)/\Gamma_{total}$ — Γ_{25}/Γ

VALUE (units 10^{-4})	EVTS	DOCUMENT ID		TECN	CHG	COMMENT
0.071±0.005 OUR AVERAGE						
0.071±0.005	450	SHAPKIN	19	OKA	+	$E(\gamma)$ >30 MeV
1.10 ±0.48	7	BARMIN	89	XEBC		$E(\gamma)$ > 5 MeV
1.0 ±0.4		STAMER	65	EMUL	+	$E(\gamma)$ >11 MeV

$\Gamma(\pi^+ \gamma\gamma)/\Gamma_{total}$ — Γ_{26}/Γ

VALUE (units 10^{-7})	CL%	EVTS	DOCUMENT ID		TECN	CHG	COMMENT
10.1 ±0.6 OUR AVERAGE							
10.03±0.51±0.24		215	[1] LAZZERONI	14	NA62	±	
11 ±3 ±1		31	[2] KITCHING	97	B787	+	

• • • We do not use the following data for averages, fits, limits, etc. • • •

9.10±0.72±0.22		149	[3] BATLEY	14	NA48	±	
< 0.083	90		[4] ARTAMONOV	05	B949	+	P_π > 213 MeV/c
< 10	90	0	ATIYA	90B	B787	+	Tπ 117–127 MeV
< 84	90	0	ASANO	82	CNTR	+	Tπ 117–127 MeV
−420 ± 520		0	ABRAMS	77	SPEC	+	Tπ < 92 MeV
< 350	90	0	LJUNG	73	HLBC	+	6–102, 114–127 MeV
< 500	90	0	KLEMS	71	OSPK	+	Tπ < 117 MeV
−100 ± 600			CHEN	68	OSPK	+	Tπ 60–90 MeV

[1] LAZZERONI 14 combines NA62 and NA48/2 results. The result for the full kinematic range is extrapolated from the model-independent branching fraction $(9.65 \pm 0.61 \pm 0.14) \times 10^{-7}$ for $(m_{\gamma\gamma}/m_K)^2 > 0.2$. The measured ChPT parameter $\hat{c} = 1.86 \pm 0.25$.

[2] KITCHING 97 is extrapolated from their model-independent branching fraction $(6.0 \pm 1.5 \pm 0.7) \times 10^{-7}$ for 100 MeV/c<P_{π^+} < 180 MeV/c using Chiral Perturbation Theory.

[3] BATLEY 14 uses data collected in 2003 and 2004. Branching ratio is obtained by determining the parameter $\hat{c} = 1.41 \pm 0.38 \pm 0.11$ and integrating the $\mathcal{O}(p^6)$ chiral spectrum. A model independent value for the branching ratio is also obtained $(8.77 \pm 0.87 \pm 0.17) \times 10^{-7}$ for kinematic range $(m_{\gamma\gamma}/m_K)^2 > 0.2$.

[4] ARTAMONOV 05 limit assumes ChPT with $\hat{c}$= 1.8 with unitarity corrections. With $\hat{c}$= 1.6 and no unitarity corrections they obtain < 2.3×10^{-8} at 90% CL. This partial branching ratio is predicted to be 6.10×10^{-9} and 0.49×10^{-9} for the cases with and without unitarity correction.

$\Gamma(\pi^+ 3\gamma)/\Gamma_{total}$ — Γ_{27}/Γ

Values given here assume a phase space pion energy spectrum.

VALUE (units 10^{-4})	CL%	DOCUMENT ID		TECN	CHG	COMMENT
<1.0	90	ASANO	82	CNTR	+	$T(\pi)$ 117–127 MeV

• • • We do not use the following data for averages, fits, limits, etc. • • •

<3.0	90	KLEMS	71	OSPK	+	$T(\pi)$ >117 MeV

$\Gamma(\pi^+ e^+ e^- \gamma)/\Gamma_{total}$ — Γ_{28}/Γ

VALUE (units 10^{-8})	EVTS	DOCUMENT ID		TECN	COMMENT
1.19±0.12±0.04	113	[1] BATLEY	08	NA48	$m_{ee\gamma}$ > 260 MeV

[1] BATLEY 08 also reports the Chiral Perturbation Theory parameter $\hat{c} = 0.9 \pm 0.45$ obtained using the shape of the $e^+ e^- \gamma$ invariant mass spectrum. By extrapolating the theoretical amplitude to $m_{ee\gamma}$ < 260 MeV, it obtains the inclusive $B(K^+ \to \pi^+ e^+ e^- \gamma) = (1.29 \pm 0.13 \pm 0.03) \times 10^{-8}$, where the first error is the combined statistical and systematic errors and the second error is from the uncertainty in $\hat{c}$.

Leptonic modes with $\ell\bar{\ell}$ pairs

$\Gamma(e^+ \nu_e \nu\bar{\nu})/\Gamma(e^+ \nu_e)$ — Γ_{29}/Γ_1

VALUE	CL%	EVTS	DOCUMENT ID		TECN	CHG
<3.8	90	0	HEINTZE	79	SPEC	+

$\Gamma(\mu^+ \nu_\mu \nu\bar{\nu})/\Gamma_{total}$ — Γ_{30}/Γ

VALUE	CL%	DOCUMENT ID		TECN	CHG
<1.0 × 10^{-6}	90	[1] CORTINA-GIL	21	NA62	+

• • • We do not use the following data for averages, fits, limits, etc. • • •

<2.4 × 10^{-6}	90	[2] ARTAMONOV	16	B949	+
<6.0 × 10^{-6}	90	[3] PANG	73	CNTR	+

[1] CORTINA-GIL 21 assumes Standard Model μ spectrum. The search is performed in the reconstructed missing mass interval m_{miss} > 316 MeV/c^2.

[2] ARTAMONOV 16 assumes Standard model μ spectrum. The search is performed in the muon momentum region between 130 and 175 MeV/c.

[3] PANG 73 assumes μ spectrum from ν-ν interaction of BARDIN 70.

$\Gamma(e^+ \nu_e e^+ e^-)/\Gamma_{total}$ — Γ_{31}/Γ

VALUE (units 10^{-8})	EVTS	DOCUMENT ID		TECN	CHG	COMMENT
2.48± 0.14±0.14	410	POBLAGUEV	02	B865	+	m_{ee} >150 MeV

• • • We do not use the following data for averages, fits, limits, etc. • • •

20 ±20	4	DIAMANT-...	76	SPEC	+	$m_{e^+e^-}$ >140 MeV

$\Gamma(\mu^+ \nu_\mu e^+ e^-)/\Gamma_{total}$ — Γ_{32}/Γ

VALUE (units 10^{-8})	EVTS	DOCUMENT ID		TECN	CHG	COMMENT
7.06± 0.16±0.26	2.7k	POBLAGUEV	02	B865	+	m_{ee} >145 MeV

• • • We do not use the following data for averages, fits, limits, etc. • • •

100 ±30	14	DIAMANT-...	76	SPEC	+	$m_{e^+e^-}$ >140 MeV

$\Gamma(e^+ \nu_e \mu^+ \mu^-)/\Gamma_{total}$ — Γ_{33}/Γ

VALUE (units 10^{-8})	CL%	DOCUMENT ID		TECN
1.72±0.45		MA	06	B865

• • • We do not use the following data for averages, fits, limits, etc. • • •

<50	90	ADLER	98	B787

Downloaded from https://academic.oup.com/ptep/article/2022/8/083C01/6651666 by KIT Library user on 27 September 2022

$\Gamma(\mu^+\nu_\mu\mu^+\mu^-)/\Gamma_{total}$ — Γ_{34}/Γ

VALUE (units 10^{-7})	CL%	DOCUMENT ID		TECN	CHG
<4.1	90	ATIYA	89	B787	+

Lepton Family number (*LF*), Lepton number (*L*), $\Delta S = \Delta Q$ (*SQ*) violating modes, or $\Delta S = 1$ weak neutral current (*S1*) modes

$\Gamma(\pi^+\pi^+e^-\overline{\nu}_e)/\Gamma_{total}$ — Γ_{35}/Γ

Test of $\Delta S = \Delta Q$ rule.

VALUE (units 10^{-7})	CL%	EVTS	DOCUMENT ID		TECN	CHG
• • • We do not use the following data for averages, fits, limits, etc. • • •						
< 9.0	95	0	SCHWEINB...	71	HLBC	+
< 6.9	95	0	ELY	69	HLBC	+
<20.	95		BIRGE	65	FBC	+

$\Gamma(\pi^+\pi^+e^-\overline{\nu}_e)/\Gamma(\pi^+\pi^-e^+\nu_e)$ — Γ_{35}/Γ_6

Test of $\Delta S = \Delta Q$ rule.

VALUE (units 10^{-4})	CL%	EVTS	DOCUMENT ID		TECN
< 3	90	3	[1] BLOCH	76	SPEC
• • • We do not use the following data for averages, fits, limits, etc. • • •					
<130.	95	0	BOURQUIN	71	ASPK

[1] BLOCH 76 quotes 3.6×10^{-4} at CL = 95%, we convert.

$\Gamma(\pi^+\pi^+\mu^-\overline{\nu}_\mu)/\Gamma_{total}$ — Γ_{36}/Γ

Test of $\Delta S = \Delta Q$ rule.

VALUE (units 10^{-6})	CL%	EVTS	DOCUMENT ID		TECN	CHG
<3.0	95	0	BIRGE	65	FBC	+

$\Gamma(\pi^+e^+e^-)/\Gamma_{total}$ — Γ_{37}/Γ

Test for $\Delta S = 1$ weak neutral current. Allowed by combined first-order weak and electromagnetic interactions.

VALUE (units 10^{-7})	EVTS	DOCUMENT ID		TECN	CHG
3.00±0.09 OUR AVERAGE					
3.11±0.04±0.12	7253	[1] BATLEY	09	NA48	±
2.94±0.05±0.14	10300	[2] APPEL	99	SPEC	+
2.75±0.23±0.13	500	[3] ALLIEGRO	92	SPEC	+
2.7 ±0.5	41	[4] BLOCH	75	SPEC	+

[1] Value extrapolated from a measurement in the region $z = (m_{ee}/m_K)^2 > 0.08$. BATLEY 09 also evaluated the shape of the form factor using four different theoretical models.

[2] APPEL 99 establishes vector nature of this decay and determines form factor $f(Z) = f_0(1 + \delta Z)$, $Z = M^2_{ee}/m^2_K$, $\delta = 2.14 \pm 0.13 \pm 0.15$. Also reports constraints on scalar and tensor interactions: $|f_S| < 6.6 \times 10^{-5}$, $|f_T| < 3.7 \times 10^{-4}$ at 90% C.L.

[3] ALLIEGRO 92 assumes a vector interaction with a form factor given by $\lambda = 0.105 \pm 0.035 \pm 0.015$ and a correlation coefficient of -0.82.

[4] BLOCH 75 assumes a vector interaction.

$\Gamma(\pi^+\mu^+\mu^-)/\Gamma_{total}$ — Γ_{38}/Γ

Test for $\Delta S = 1$ weak neutral current. Allowed by higher-order electroweak interactions.

VALUE (units 10^{-8})	CL%	EVTS	DOCUMENT ID		TECN	CHG	COMMENT
9.4 ±0.6 OUR AVERAGE Error includes scale factor of 2.6. See the ideogram below.							
9.62±0.21±0.13		3120	[1] BATLEY	11A	NA48	±	2003-04 data
9.8 ±1.0 ±0.5		110	[2] PARK	02	HYCP	±	
9.22±0.60±0.49		402	[3] MA	00	B865	+	
5.0 ±0.4 ±0.9		207	[4] ADLER	97C	B787	+	
• • • We do not use the following data for averages, fits, limits, etc. • • •							
9.7 ±1.2 ±0.4		65	PARK	02	HYCP	+	
10.0 ±1.9 ±0.7		35	PARK	02	HYCP	−	
<23	90		ATIYA	89	B787	+	

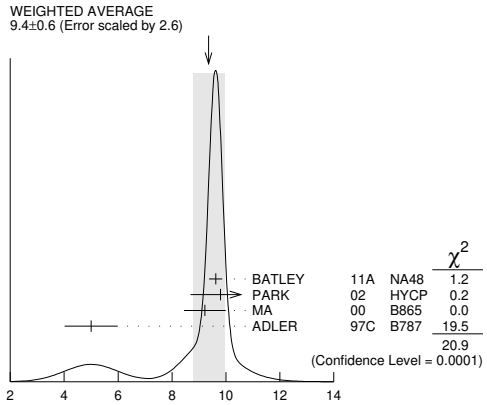

$\Gamma(\pi^+\mu^+\mu^-)/\Gamma_{total}$ — Γ_{38}/Γ

[1] BATLEY 11A also studies the form factor $f(z)$ dependence of the decay, described via single photon exchange: i) assuming a linear form factor, $f(z) = f_0\ (1+\ \delta\ z\ )$, $z = (M_{\mu\mu}/m_K)^2$, finding $f_0 = 0.470 \pm 0.040$ and $\delta = 3.11 \pm 0.57$ and ii) assuming a linear form factor including π-π rescattering , $W_{\pi\pi}$, as in DAMBROSIO 98A, finding $f(z) = G_F\ m^2_K\ (a_+ + b_+\ z) + W_{\pi\pi}(z)$, $a_+ = -0.575 \pm 0.039$, $b_+ = -0.813 \pm 0.145$.

[2] PARK 02 "±" result comes from combining $K^+ \to \pi^+\mu^+\mu^-$ and $K^- \to \pi^-\mu^+\mu^-$, assuming *CP* is conserved.

[3] MA 00 establishes vector nature of this decay and determines form factor $f(z) = f_0\ (1 + \delta\ z)$, $z = (M_{\mu\mu}/m_K)^2$, $\delta = 2.45^{+1.30}_{-0.95}$.

[4] ADLER 97C gives systematic error 0.7×10^{-8} and theoretical uncertainty 0.6×10^{-8}, which we combine in quadrature to obtain our second error.

$\Gamma(\pi^+\nu\overline{\nu})/\Gamma_{total}$ — Γ_{39}/Γ

Test for $\Delta S = 1$ weak neutral current. Allowed by higher-order electroweak interactions. Branching ratio values are extrapolated from the momentum or energy regions shown in the comments assuming Standard Model phase space except for those labeled "Scalar" or "Tensor" to indicate the assumed non-Standard-Model interaction.

VALUE (units 10^{-10})	CL%	EVTS	DOCUMENT ID		TECN	CHG	COMMENT
$1.14^{+0.40}_{-0.33}$ OUR AVERAGE							
$1.06^{+0.41}_{-0.35}$		20	[1] CORTINA-GIL	21B	NA62	+	
$1.73^{+1.15}_{-1.05}$		7	[2] ARTAMONOV	08	B949	+	$140<P_\pi<199$ MeV, $211<P_\pi<229$MeV
• • • We do not use the following data for averages, fits, limits, etc. • • •							
$0.48^{+0.72}_{-0.48}$			[3] CORTINA-GIL	20C	NA62	+	
< 11	90	1	[4] CORTINA-GIL	19B	NA62	+	decay-in-flight
$7.89^{+9.26}_{-5.10}$		3	[5] ARTAMONOV	08	B949	+	$140<P_\pi<199$ MeV
< 22	90	1	[6] ADLER	04	B787	+	$211<P_\pi<229$ MeV
< 27	90		ADLER	04	B787	+	Scalar
< 18	90		ADLER	04	B787	+	Tensor
$1.47^{+1.30}_{-0.89}$		3	[7] ANISIMOVSK...	04	B949	+	$211<P_\pi<229$ MeV
$1.57^{+1.75}_{-0.82}$		2	ADLER	02	B787	+	$P_\pi>211$ MeV/c
< 42	90	1	ADLER	02C	B787	+	$140<P_\pi<195$ MeV
< 47	90		[8] ADLER	02C	B787	+	Scalar
< 25	90		[8] ADLER	02C	B787	+	Tensor
$1.5^{+3.4}_{-1.2}$		1	ADLER	00	B787		In ADLER 02
$4.2^{+9.7}_{-3.5}$		1	ADLER	97	B787		
< 24	90		ADLER	96	B787		
< 75	90		ATIYA	93	B787	+	$T(\pi)$ 115–127 MeV
< 52	90		[9] ATIYA	93	B787	+	
< 170	90	0	ATIYA	93B	B787	+	$T(\pi)$ 60–100 MeV
< 340	90		ATIYA	90	B787	+	
<1400	90		ASANO	81B	CNTR	+	$T(\pi)$ 116–127 MeV

[1] CORTINA-GIL 21B analysis of the NA62 data taken in 2016–2018 observed 20 candidate events with an expected background of 7 events. The achieved single event sensitivity is $(0.839 \pm 0.054) \times 10^{-11}$. The quoted branching ratio includes result from CORTINA-GIL 20C which observed two candidate events. This provides evidence for the very rare $K^+ \to \pi^+\nu\overline{\nu}$ decay, observed with a significance of 3.4 σ. Search for a feebly interacting scalar or pseudo-scalar particle X in the decay $K^+ \to \pi^+X$ was performed and an upper limit from $< 3\times10^{-11}$ to $< 6\times10^{-11}$ at the 90% C.L. was set for an invisible particle with a mass of 0–110 MeV/c^2 and $< 1\times10^{-11}$ for mass of 160–260 MeV/c^2.

[2] Value obtained combining ANISIMOVSKY 04, ADLER 04, and the present ARTAMONOV 08 results.

[3] CORTINA-GIL 20C analysis of the NA62 data taken in 2017 observed two candidate events with an expected background of 1.5 events. The achieved single event sensitivity is $(0.389 \pm 0.024) \times 10^{-10}$. The quoted branching ratio includes result from CORTINA-GIL 19B which observed one candidate event. The corresponding upper limit $B(K^+ \to \pi^+\nu\overline{\nu}) < 1.78 \times 10^{-10}$ at 90% C.L. Superseded by CORTINA-GIL 21B.

[4] Based on a sample of 1.21×10^{11} K^+ decays collected in 2016. One signal candidate is observed while the expected background is 0.152 events. The single-event-sensitivity is estimated to be 3.15×10^{-10}.

[5] Observed 3 events with an estimated background of $0.93 \pm 0.17^{+0.32}_{-0.24}$. Signal-to-background ratio for each of these 3 events is 0.20, 0.42, and 0.47.

[6] Value obtained combining the previous result ADLER 02C with 1 event and the present result with 0 events to obtain an expected background 1.22 ± 0.24 events and 1 event observed.

[7] Value obtained combining the previous E787 result ADLER 02 with 2 events and the present E949 with 1 event. The additional event has a signal-to-background ratio 0.9. Superseded by ARTAMONOV 08.

[8] Superseded by ADLER 04.

[9] Combining ATIYA 93 and ATIYA 93B results. Superseded by ADLER 96.

$\Gamma(\pi^+\pi^0\nu\overline{\nu})/\Gamma_{total}$ — Γ_{40}/Γ

Test for $\Delta S = 1$ weak neutral current. Allowed by higher-order electroweak interactions.

VALUE (units 10^{-5})	CL%	DOCUMENT ID		TECN
<4.3	90	[1] ADLER	01	SPEC

[1] Search region defined by 90 MeV/$c<P_{\pi^+}<188$ MeV/c and 135 MeV$<E_{\pi^0}<180$ MeV.

$\Gamma(\mu^-\nu e^+e^+)/\Gamma(\pi^+\pi^-e^+\nu_e)$ — Γ_{41}/Γ_6

Test of lepton family number conservation.

VALUE (units 10^{-3})	CL%	EVTS	DOCUMENT ID		TECN	CHG
<0.5	90	0	[1] DIAMANT-...	76	SPEC	+

[1] DIAMANT-BERGER 76 quotes this result times our 1975 $\pi^+\pi^-e\nu$ BR ratio.

Downloaded from https://academic.oup.com/ptep/article/2022/8/083C01/6651666 by KIT Library user on 27 September 2022

$\Gamma(\mu^+\nu_e)/\Gamma_{total}$ — Γ_{42}/Γ

Forbidden by lepton family number conservation.

VALUE	CL%	EVTS	DOCUMENT ID		TECN	COMMENT
<0.004	90	0	[1] LYONS	81	HLBC	200 GeV K^+ narrow band ν beam
• • • We do not use the following data for averages, fits, limits, etc. • • •						
<0.012	90		[1] COOPER	82	HLBC	Wideband ν beam

[1] COOPER 82 and LYONS 81 limits on ν_e observation are here interpreted as limits on lepton family number violation in the absence of mixing.

$\Gamma(\pi^+\mu^+e^-)/\Gamma_{total}$ — Γ_{43}/Γ

Test of lepton family number conservation.

VALUE (units 10^{-10})	CL%	DOCUMENT ID		TECN	CHG
<0.13	90	[1] SHER	05	RVUE	+
• • • We do not use the following data for averages, fits, limits, etc. • • •					
<0.21	90	SHER	05	B865	+
<0.39	90	APPEL	00	B865	+
<2.1	90	LEE	90	SPEC	+

[1] This result combines SHER 05 1998 data, APPEL 00 1996 data, and data from BERGMAN 97 and PISLAK 97 theses, all from BNL-E865, with LEE 90 BNL-E777 data.

$\Gamma(\pi^+\mu^-e^+)/\Gamma_{total}$ — Γ_{44}/Γ

Test of lepton family number conservation.

VALUE	CL%	DOCUMENT ID		TECN	CHG
$< 6.6 \times 10^{-11}$	90	ALIBERTI	21	NA62	+
• • • We do not use the following data for averages, fits, limits, etc. • • •					
$< 5.2 \times 10^{-10}$	90	APPEL	00B	B865	+
$<70 \times 10^{-10}$	90	[1] DIAMANT-...	76	SPEC	+

[1] Measurement actually applies to the sum of the $\pi^+\mu^-e^+$ and $\pi^-\mu^+e^+$ modes.

$\Gamma(\pi^-\mu^+e^+)/\Gamma_{total}$ — Γ_{45}/Γ

Test of total lepton number conservation.

VALUE	CL%	DOCUMENT ID		TECN	CHG
$< 4.2 \times 10^{-11}$	90	ALIBERTI	21	NA62	+
• • • We do not use the following data for averages, fits, limits, etc. • • •					
$< 5.0 \times 10^{-10}$	90	APPEL	00B	B865	+
$<70 \times 10^{-10}$	90	[1] DIAMANT-...	76	SPEC	+

[1] Measurement actually applies to the sum of the $\pi^+\mu^-e^+$ and $\pi^-\mu^+e^+$ modes.

$\Gamma(\pi^-e^+e^+)/\Gamma_{total}$ — Γ_{46}/Γ

Test of total lepton number conservation.

VALUE	CL%	DOCUMENT ID		TECN	CHG	COMMENT
$<2.2 \times 10^{-10}$	90	[1] CORTINA-GIL	19A	NA62	+	decay-in-flight
• • • We do not use the following data for averages, fits, limits, etc. • • •						
$<6.4 \times 10^{-10}$	90	APPEL	00B	B865	+	
$<9.2 \times 10^{-9}$	90	DIAMANT-...	76	SPEC	+	
$<1.5 \times 10^{-5}$		CHANG	68	HBC	−	

[1] CORTINA-GIL 19A results are obtained with 2017 data.

$\Gamma(\pi^-\mu^+\mu^+)/\Gamma_{total}$ — Γ_{47}/Γ

Forbidden by total lepton number conservation.

VALUE	CL%	DOCUMENT ID		TECN	CHG	COMMENT
$<4.2 \times 10^{-11}$	90	[1] CORTINA-GIL	19A	NA62	+	decay-in-flight
• • • We do not use the following data for averages, fits, limits, etc. • • •						
$<8.6 \times 10^{-11}$	90	[2] BATLEY	17	NA48	±	
$<1.1 \times 10^{-9}$	90	BATLEY	11A	NA48	±	
$<3.0 \times 10^{-9}$	90	APPEL	00B	B865	+	
$<1.5 \times 10^{-4}$	90	[3] LITTENBERG	92	HBC		

[1] CORTINA-GIL 19A results are obtained with 2017 data.
[2] BATLEY 17 result is based on data taken in 2003 to 2004. Limits for two-body resonance X in $K^{\pm} \to \pi\mu\mu$ decays are also reported.
[3] LITTENBERG 92 is from retroactive data analysis of CHANG 68 bubble chamber data.

$\Gamma(\mu^+\overline{\nu}_e)/\Gamma_{total}$ — Γ_{48}/Γ

Forbidden by total lepton number conservation.

VALUE (units 10^{-3})	CL%	DOCUMENT ID		TECN	COMMENT
<3.3	90	[1] COOPER	82	HLBC	Wideband ν beam

[1] COOPER 82 limit on $\overline{\nu}_e$ observation is here interpreted as a limit on lepton number violation in the absence of mixing.

$\Gamma(\pi^0e^+\overline{\nu}_e)/\Gamma_{total}$ — Γ_{49}/Γ

Forbidden by total lepton number conservation.

VALUE	CL%	DOCUMENT ID		TECN	COMMENT
<0.003	90	[1] COOPER	82	HLBC	Wideband ν beam

[1] COOPER 82 limit on $\overline{\nu}_e$ observation is here interpreted as a limit on lepton number violation in the absence of mixing.

$\Gamma(\pi^+\gamma)/\Gamma_{total}$ — Γ_{50}/Γ

Violates angular momentum conservation and gauge invariance. Current interest in this decay is as a search for non-commutative space-time effects as discussed in ARTAMONOV 05 and for exotic physics such as a vacuum expectation value of a new vector field, non-local Superstring effects, or departures from Lorentz invariance, as discussed in ADLER 02B.

VALUE (units 10^{-9})	CL%	DOCUMENT ID		TECN	CHG
< 2.3	90	ARTAMONOV	05	B949	+
• • • We do not use the following data for averages, fits, limits, etc. • • •					
< 360	90	ADLER	02B	B787	+
<1400	90	ASANO	82	CNTR	+
<4000	90	[1] KLEMS	71	OSPK	+

[1] Test of model of Selleri, Nuovo Cimento **60A** 291 (1969).

CPT VIOLATION TESTS IN $K^{\pm}$ DECAYS

$\Delta = (\Gamma(K^+) - \Gamma(K^-)) / (\Gamma(K^+) + \Gamma(K^-))$

$\Delta(K^{\pm} \to \mu^{\pm}\nu_{\mu})$ RATE DIFFERENCE/SUM

VALUE (%)	DOCUMENT ID		TECN
−0.27±0.21	FORD	67	CNTR

$\Delta(K^{\pm} \to \pi^{\pm}\pi^0)$ RATE DIFFERENCE/SUM

VALUE (%)	DOCUMENT ID		TECN
0.4±0.6	HERZO	69	OSPK

CP VIOLATION TESTS IN $K^{\pm}$ DECAYS

$\Delta = (\Gamma(K^+) - \Gamma(K^-)) / (\Gamma(K^+) + \Gamma(K^-))$

$\Delta(K^{\pm} \to \pi^{\pm}e^+e^-)$ RATE DIFFERENCE/SUM

VALUE (units 10^{-2})	DOCUMENT ID		TECN
−2.2±1.5±0.6	[1] BATLEY	09	NA48

[1] This implies an upper limit of 2.1×10^{-2} at 90% CL.

$\Delta(K^{\pm} \to \pi^{\pm}\mu^+\mu^-)$ RATE DIFFERENCE/SUM

VALUE	DOCUMENT ID		TECN
0.010±0.023 OUR AVERAGE			
0.011±0.023	[1] BATLEY	11A	NA48
−0.02 ±0.11 ±0.04	PARK	02	HYCP

[1] This corresponds to the asymmetry upper limit of $< 2.9 \times 10^{-2}$ at 90% CL.

$\Delta(K^{\pm} \to \pi^{\pm}\pi^0\gamma)$ RATE DIFFERENCE/SUM

VALUE (units 10^{-3})	EVTS	DOCUMENT ID		TECN	CHG	COMMENT
0.0± 1.2 OUR AVERAGE						
0.0± 1.0±0.6	1M	[1] BATLEY	10A	NA48		
4 ±29	2461	SMITH	76	WIRE	±	E_{π} 55–90 MeV
5 ±20	4000	ABRAMS	73B	ASPK	±	E_{π} 51–100 MeV

[1] This value implies the upper bound for this asymmetry 1.5×10^{-3} at 90% CL.

$\Delta(K^{\pm} \to \pi^{\pm}\pi^+\pi^-)$ RATE DIFFERENCE/SUM

VALUE (%)	EVTS	DOCUMENT ID		TECN	CHG
0.04±0.06		[1] FORD	70	ASPK	
• • • We do not use the following data for averages, fits, limits, etc. • • •					
−0.01±0.08		[2] SMITH	73	ASPK	±
0.05±0.07	3.2M	[1] FORD	70	ASPK	
−0.25±0.45		FLETCHER	67	OSPK	
−0.02±0.11		[1] FORD	67	CNTR	

[1] First FORD 70 value is second FORD 70 combined with FORD 67.
[2] SMITH 73 value of $K^{\pm} \to \pi^{\pm}\pi^+\pi^-$ rate difference is derived from SMITH 73 value of $K^{\pm} \to \pi^{\pm}2\pi^0$ rate difference.

$\Delta(K^{\pm} \to \pi^{\pm}\pi^0\pi^0)$ RATE DIFFERENCE/SUM

VALUE (%)	EVTS	DOCUMENT ID		TECN	CHG
−0.02±0.28 OUR AVERAGE					
0.04±0.29		SMITH	73	ASPK	±
−0.6 ±0.9	1802	HERZO	69	OSPK	

T VIOLATION TESTS IN K^+ AND K^- DECAYS

P_T in $K^+ \to \pi^0\mu^+\nu_{\mu}$

T-violating muon polarization. Sensitive to new sources of *CP* violation beyond the Standard Model.

VALUE (units 10^{-3})	EVTS	DOCUMENT ID		TECN	CHG
−1.7±2.3±1.1		[1] ABE	04F	K246	+
• • • We do not use the following data for averages, fits, limits, etc. • • •					
−4.2±4.9±0.9	3.9M	ABE	99S	K246	+

[1] Includes three sets of data: 96-97 (ABE 99S), 98, and 99-00 totaling about three times the ABE 99S data sample. Corresponds to $P_T < 5.0 \times 10^{-3}$ at 90% CL.

Downloaded from https://academic.oup.com/ptep/article/2022/8/083C01/6651666 by KIT Library user on 27 September 2022

P_T in $K^+ \to \mu^+ \nu_\mu \gamma$

T-violating muon polarization. Sensitive to new sources of *CP* violation beyond the Standard Model.

VALUE (units 10^{-2})	EVTS	DOCUMENT ID	TECN	CHG
−0.64±1.85±0.10	114k	[1] ANISIMOVSK...03	K246	+

[1] Muons stopped and polarization measured from decay to positrons.

Im(ξ) in $K^+ \to \pi^0 \mu^+ \nu_\mu$ DECAY (from transverse μ pol.)

Test of *T* reversal invariance.

VALUE	EVTS	DOCUMENT ID		TECN	CHG	COMMENT
−0.006 ±0.008 OUR AVERAGE						
−0.0053±0.0071±0.0036		[1] ABE	04F	K246	+	
−0.016 ±0.025	20M	CAMPBELL	81	CNTR	+	Pol.
• • • We do not use the following data for averages, fits, limits, etc. • • •						
−0.013 ±0.016 ±0.003	3.9M	ABE	99S	CNTR	+	p_T K^+ at rest

[1] Includes three sets of data: 96-97 (ABE 99S), 98, and 99-00 totaling about three times the ABE 99S data sample. Corresponds to Im(ξ) < 0.016 at 90% CL.

DALITZ PLOT PARAMETERS FOR $K \to 3\pi$ DECAYS

Revised 1999 by T.G. Trippe (LBNL).

The Dalitz plot distribution for $K^{\pm} \to \pi^{\pm}\pi^{\pm}\pi^{\mp}$, $K^{\pm} \to \pi^0\pi^0\pi^{\pm}$, and $K^0_L \to \pi^+\pi^-\pi^0$ can be parameterized by a series expansion such as that introduced by Weinberg [1]. We use the form

$$\left|M\right|^2 \propto 1 + g\frac{(s_3 - s_0)}{m^2_{\pi^+}} + h\left[\frac{s_3 - s_0}{m^2_{\pi^+}}\right]^2 + j\,\frac{(s_2 - s_1)}{m^2_{\pi^+}} + k\left[\frac{s_2 - s_1}{m^2_{\pi^+}}\right]^2 + f\,\frac{(s_2 - s_1)}{m^2_{\pi^+}}\frac{(s_3 - s_0)}{m^2_{\pi^+}} + \cdots\ , \qquad (1)$$

where $m^2_{\pi^+}$ has been introduced to make the coefficients g, h, j, and k dimensionless, and

$$s_i = (P_K - P_i)^2 = (m_K - m_i)^2 - 2m_K T_i\ ,\ i = 1, 2, 3,$$
$$s_0 = \frac{1}{3}\sum_i s_i = \frac{1}{3}(m^2_K + m^2_1 + m^2_2 + m^2_3)\quad .$$

Here the P_i are four-vectors, m_i and T_i are the mass and kinetic energy of the ith pion, and the index 3 is used for the odd pion.

The coefficient g is a measure of the slope in the variable s_3 (or T_3) of the Dalitz plot, while h and k measure the quadratic dependence on s_3 and $(s_2 - s_1)$, respectively. The coefficient j is related to the asymmetry of the plot and must be zero if CP invariance holds. Note also that if CP is good, g, h, and k must be the same for $K^+ \to \pi^+\pi^+\pi^-$ as for $K^- \to \pi^-\pi^-\pi^+$.

Since different experiments use different forms for $\left|M\right|^2$, in order to compare the experiments we have converted to g, h, j, and k whatever coefficients have been measured. Where such conversions have been done, the measured coefficient a_y, a_t, a_u, or a_v is given in the comment at the right. For definitions of these coefficients, details of this conversion, and discussion of the data, see the April 1982 version of this note [2].

References

1. S. Weinberg, Phys. Rev. Lett. **4**, 87 (1960).
2. Particle Data Group, Phys. Lett. **111B**, 69 (1982).

ENERGY DEPENDENCE OF $K^{\pm}$ DALITZ PLOT

$|\text{matrix element}|^2 = 1 + gu + hu^2 + kv^2$
where $u = (s_3 - s_0)\ /\ m^2_{\pi}$ and $v = (s_2 - s_1)\ /\ m^2_{\pi}$

LINEAR COEFFICIENT g FOR $K^{\pm} \to \pi^{\pm}\pi^+\pi^-$

Some experiments use Dalitz variables x and y. In the comments we give a_y = coefficient of y term. See note above on "Dalitz Plot Parameters for $K \to 3\pi$ Decays." For discussion of the conversion of a_y to g, see the earlier version of the same note in the *Review* published in Physics Letters **111B** 70 (1982).

VALUE	EVTS	DOCUMENT ID		TECN	CHG	COMMENT
−0.21134±0.00017	471M	[1] BATLEY	07B	NA48	±	
• • • We do not use the following data for averages, fits, limits, etc. • • •						
−0.2221 ±0.0065	225k	DEVAUX	77	SPEC	+	a_y=.2814±.0082
−0.199 ±0.008	81k	[2] LUCAS	73	HBC	−	a_y=0.252±0.011
−0.2157 ±0.0028	750k	FORD	72	ASPK	+	a_y=.2734±.0035
−0.2186 ±0.0028	750k	FORD	72	ASPK	−	a_y=.2770±.0035
−0.200 ±0.009	39819	[3] HOFFMASTER	72	HLBC	+	
−0.196 ±0.012	17898	[4] GRAUMAN	70	HLBC	+	a_y=0.228±0.030
−0.193 ±0.010	50919	MAST	69	HBC	−	a_y=0.244±0.013
−0.218 ±0.016	9994	[5] BUTLER	68	HBC	+	a_y=0.277±0.020
−0.190 ±0.023	5778	[5,6] MOSCOSO	68	HBC	−	a_y=0.242±0.029
−0.22 ±0.024	5428	[5,6] ZINCHENKO	67	HBC	+	a_y=0.28 ± 0.03
−0.220 ±0.035	1347	[7] FERRO-LUZZI	61	HBC	−	a_y=0.28 ± 0.045

[1] Final state strong interaction and radiative corrections not included in the fit.
[2] Quadratic dependence is required by K^0_L experiments.
[3] HOFFMASTER 72 includes GRAUMAN 70 data.
[4] Emulsion data added — all events included by HOFFMASTER 72.
[5] Experiments with large errors not included in average.
[6] Also includes DBC events.
[7] No radiative corrections included.

QUADRATIC COEFFICIENT h FOR $K^{\pm} \to \pi^{\pm}\pi^+\pi^-$

VALUE (units 10^{-2})	EVTS	DOCUMENT ID		TECN	CHG
1.848±0.040	471M	[1] BATLEY	07B	NA48	±
• • • We do not use the following data for averages, fits, limits, etc. • • •					
−0.06 ±1.43	225k	DEVAUX	77	SPEC	+
1.87 ±0.62	750k	FORD	72	ASPK	+
1.25 ±0.62	750k	FORD	72	ASPK	−
−0.9 ±1.4	39819	HOFFMASTER	72	HLBC	+
−0.1 ±1.2	50919	MAST	69	HBC	−

[1] Final state strong interaction and radiative corrections not included in the fit.

QUADRATIC COEFFICIENT k FOR $K^{\pm} \to \pi^{\pm}\pi^+\pi^-$

VALUE (units 10^{-3})	EVTS	DOCUMENT ID		TECN	CHG
− 4.63± 0.14	471M	[1] BATLEY	07B	NA48	±
• • • We do not use the following data for averages, fits, limits, etc. • • •					
−20.5 ± 3.9	225k	DEVAUX	77	SPEC	+
− 7.5 ± 1.9	750k	FORD	72	ASPK	+
− 8.3 ± 1.9	750k	FORD	72	ASPK	−
−10.5 ± 4.5	39819	HOFFMASTER	72	HLBC	+
−14 ±12	50919	MAST	69	HBC	−

[1] Final state strong interaction and radiative corrections not included in the fit.

$(g_+ - g_-)\ /\ (g_+ + g_-)$ FOR $K^{\pm} \to \pi^{\pm}\pi^+\pi^-$

This is a *CP* violating asymmetry between linear coefficients g_+ for $K^+ \to \pi^+\pi^+\pi^-$ decay and g_- for $K^- \to \pi^-\pi^+\pi^-$ decay.

VALUE (units 10^{-4})	EVTS	DOCUMENT ID		TECN
− 1.5± 1.5±1.6	3.1G	[1] BATLEY	07E	NA48
• • • We do not use the following data for averages, fits, limits, etc. • • •				
1.7± 2.1±2.0	1.7G	[2] BATLEY	06	NA48
−70.0±53	3.2M	FORD	70	ASPK

[1] BATLEY 07E includes data from BATLEY 06. Uses quadratic parametrization and value $g_+ + g_- = 2g$ from BATLEY 07B. This measurement neglects any possible charge asymmetries in higher order slope parameters h or k.
[2] This measurement neglects any possible charge asymmetries in higher order slope parameters h or k.

LINEAR COEFFICIENT g FOR $K^{\pm} \to \pi^{\pm}\pi^0\pi^0$

Unless otherwise stated, all experiments include terms quadratic in $(s_3 - s_0)\ /\ m^2_{\pi^+}$. See note above on "Dalitz Plot Parameters for $K \to 3\pi$ Decays."

See BATUSOV 98 for a discussion of the discrepancy between their result and others, especially BOLOTOV 86. At this time we have no way to resolve the discrepancy so we depend on the large scale factor as a warning.

VALUE	EVTS	DOCUMENT ID		TECN	CHG	COMMENT
0.626 ±0.007 OUR AVERAGE						
0.6259±0.0043±0.0093	493k	AKOPDZHAN..	05B	TNF	±	
0.627 ±0.004 ±0.010	252k	[1,2] AJINENKO	03B	ISTR	−	

Downloaded from https://academic.oup.com/ptep/article/2022/8/083C01/6651666 by KIT Library user on 27 September 2022

• • • We do not use the following data for averages, fits, limits, etc. • • •

0.736 ±0.014 ±0.012	33k	BATUSOV	98	SPEC	+	
0.582 ±0.021	43k	BOLOTOV	86	CALO	−	
0.670 ±0.054	3263	BRAUN	76B	HLBC	+	
0.630 ±0.038	5635	SHEAFF	75	HLBC	+	
0.510 ±0.060	27k	SMITH	75	WIRE	+	
0.67 ±0.06	1365	AUBERT	72	HLBC	+	
0.544 ±0.048	4048	DAVISON	69	HLBC	+	Also emulsion

[1] Measured using in-flight decays of the 25 GeV negative secondary beam.

[2] They form new world averages $g_- = (0.617 \pm 0.018)$ and $g_+ = (0.684 \pm 0.033)$ which give $\Delta g_{\tau'} = 0.051 \pm 0.028$.

QUADRATIC COEFFICIENT h FOR $K^{\pm} \to \pi^{\pm}\pi^0\pi^0$

VALUE	EVTS	DOCUMENT ID		TECN	CHG	COMMENT
0.052 ±0.008 OUR AVERAGE						
0.0551±0.0044±0.0086	493k	AKOPDZHAN...05B		TNF	±	
0.046 ±0.004 ±0.012	252k	[1] AJINENKO	03B	ISTR	−	
• • • We do not use the following data for averages, fits, limits, etc. • • •						
0.128 ±0.015 ±0.024	33k	BATUSOV	98	SPEC	+	
0.037 ±0.024	43k	BOLOTOV	86	CALO	−	
0.152 ±0.082	3263	BRAUN	76B	HLBC	+	
0.041 ±0.030	5635	SHEAFF	75	HLBC	+	
0.009 ±0.040	27k	SMITH	75	WIRE	+	
−0.01 ±0.08	1365	AUBERT	72	HLBC	+	
0.026 ±0.050	4048	DAVISON	69	HLBC	+	Also emulsion

[1] Measured using in-flight decays of the 25 GeV negative secondary beam.

QUADRATIC COEFFICIENT k FOR $K^{\pm} \to \pi^{\pm}\pi^0\pi^0$

VALUE	EVTS	DOCUMENT ID		TECN	CHG
0.0054±0.0035 OUR AVERAGE Error includes scale factor of 2.5.					
0.0082±0.0011±0.0014	493k	AKOPDZHAN...05B		TNF	±
0.001 ±0.001 ±0.002	252k	[1] AJINENKO	03B	ISTR	−
• • • We do not use the following data for averages, fits, limits, etc. • • •					
0.0197±0.0045±0.0029	33k	BATUSOV	98	SPEC	+

[1] Measured using in-flight decays of the 25 GeV negative secondary beam.

$(g_+ - g_-)$ / $(g_+ + g_-)$ FOR $K^{\pm} \to \pi^{\pm}\pi^0\pi^0$

A nonzero value for this quantity indicates CP violation.

VALUE (units 10^{-4})	EVTS	DOCUMENT ID		TECN
1.8± 1.8 OUR AVERAGE				
1.8± 1.7±0.6	91.3M	[1] BATLEY	07E	NA48
2 ±18 ±5	619k	[2] AKOPDZHAN...05		TNF
• • • We do not use the following data for averages, fits, limits, etc. • • •				
1.8± 2.2±1.3	47M	[3] BATLEY	06A	NA48

[1] BATLEY 07E includes data from BATLEY 06A. Uses quadratic parametrization and PDG 06 value $g = 0.626 \pm 0.007$ to obtain $g_+ - g_- = (2.2 \pm 2.1 \pm 0.7) \times 10^{-4}$. Neglects any possible charge asymmetries in higher order slope parameters h or k.

[2] Asymmetry obtained assuming that $g_+ + g_- = 2\times 0.652$ (PDG 02) and that asymmetries in h and k are zero.

[3] Linear and quadratic slopes from PDG 04 are used. Any possible charge asymmetries in higher order slope parameters h or k are neglected.

ALTERNATIVE PARAMETRIZATIONS OF $K^{\pm} \to \pi^{\pm}\pi^0\pi^0$ DALITZ PLOT

The following functional form for the matrix element suggested by $\pi\pi$ rescattering in $K^+ \to \pi^+ \text{“}\pi^+\pi^-\text{”} \to \pi^+\pi^0\pi^0$ is used for this fit (CABIBBO 04A, CABIBBO 05): Matrix element $= M_0 + M_1$ where $M_0 = 1 + (1/2)g_0\, u + (1/2)\, h'\, u^2 + (1/2)k_0\, v^2$ with $u = (s_3 - s_0)/(m_{\pi^+})^2$, $v = (s_2 - s_1)/(m_{\pi^+})^2$ and where M_1 takes into account the non-analytic piece due to pi pi rescattering amplitudes a_0 and a_2; The parameters g_0 and h' are related to the parameters g and h of the matrix element squared given in the previous section by the approximations $g_0 \sim g^{PDG}$ and $h' \sim h^{PDG} - (g/2)^2$ and $k_0 \sim k^{PDG}$.

In addition, we also consider the effective field theory framework of COLANGELO 06A and BISSEGGER 09 to extract g_{BB} and h'_{BB}.

LINEAR COEFFICIENT g_0 FOR $K^{\pm} \to \pi^{\pm}\pi^0\pi^0$

VALUE	EVTS	DOCUMENT ID		TECN	CHG
0.6525±0.0009±0.0033	60M	[1] BATLEY	09A	NA48	±
• • • We do not use the following data for averages, fits, limits, etc. • • •					
0.645 ±0.004 ±0.009	23M	[2] BATLEY	06B	NA48	±

[1] This fit is obtained with the CABIBBO 05 matrix element in the $2\pi^0$ invariant mass squared range $0.074094 < m^2_{2\pi^0} < 0.104244$ GeV^2. Electromagnetic corrections and CHPT constraints for $\pi\pi$ phase shifts (a_0 and a_2) have been used. Also measured $(a_0 - a_2)\, m_{\pi^+} = 0.2646 \pm 0.0021 \pm 0.0023$, where k_0 was kept fixed in the fit at -0.0099.

[2] Superseded by BATLEY 09A. This fit is obtained with the CABIBBO 05 matrix element in the $2\pi^0$ invariant mass squared range 0.074 GeV^2 $< m^2_{2\pi^0} < 0.097$ GeV^2, assuming $k = 0$ (no term proportional to $(s_2 - s_1)^2$) and excluding the kinematic region around the cusp ($m^2_{2\pi^0} = (2m_{\pi^+})^2 \pm 0.000525$ GeV^2). Also π-π phase shifts a_0 and a_2 are measured: $(a_0 - a_2)m_{\pi^+} = 0.268 \pm 0.010 \pm 0.004 \pm 0.013$(external) and $a_2\, m_{\pi^+} = -0.041 \pm 0.022 \pm 0.014$.

QUADRATIC COEFFICIENT h' FOR $K^{\pm} \to \pi^{\pm}\pi^0\pi^0$

VALUE	EVTS	DOCUMENT ID		TECN	CHG
−0.0433±0.0008±0.0026	60M	[1] BATLEY	09A	NA48	±
• • • We do not use the following data for averages, fits, limits, etc. • • •					
−0.047 ±0.012 ±0.011	23M	[2] BATLEY	06B	NA48	±

[1] This fit is obtained with the CABIBBO 05 matrix element in the $2\pi^0$ invariant mass squared range $0.074094 < m^2_{2\pi^0} < 0.104244$ GeV^2. Electromagnetic corrections and CHPT constraints for $\pi\pi$ phase shifts (a_0 and a_2) have been used. Also measured $(a_0 - a_2)\, m_{\pi^+} = 0.2646 \pm 0.0021 \pm 0.0023$, where k_0 was kept fixed in the fit at -0.0099.

[2] Superseded by BATLEY 09A. This fit is obtained with the CABIBBO 05 matrix element in the $2\pi^0$ invariant mass squared range 0.074 GeV^2 $< m^2_{2\pi^0} < 0.097$ GeV^2, assuming $k = 0$ (no term proportional to $(s_2 - s_1)^2$) and excluding the kinematic region around the cusp ($m^2_{2\pi^0} = (2m_{\pi^+})^2 \pm 0.000525$ GeV^2). Also π-π phase shifts a_0 and a_2 are measured: $(a_0 - a_2)m_{\pi^+} = 0.268 \pm 0.010 \pm 0.004 \pm 0.013$(external) and $a_2\, m_{\pi^+} = -0.041 \pm 0.022 \pm 0.014$.

QUADRATIC COEFFICIENT k_0 FOR $K^{\pm} \to \pi^{\pm}\pi^0\pi^0$

VALUE	EVTS	DOCUMENT ID		TECN	CHG
0.0095±0.00017±0.00048	60M	[1] BATLEY	09A	NA48	±

[1] Assumed $a_2\, m_{\pi^+} = -0.0044$ in the fit.

LINEAR COEFFICIENT g_{BB} FOR $K^{\pm} \to \pi^{\pm}\pi^0\pi^0$

VALUE	EVTS	DOCUMENT ID		TECN	CHG
0.6219±0.0009±0.0033	60M	[1] BATLEY	09A	NA48	±

[1] This fit is obtained using parametrizations of COLANGELO 06A and BISSEGGER 09 in the $2\pi^0$ invariant mass squared range $0.074094 < m^2_{2\pi^0} < 0.104244$ GeV^2. Electromagnetic corrections and CHPT constraints for $\pi\pi$ phase shifts (a_0 and a_2) have been used. Also measured $(a_0 - a_2)\, m_{\pi^+} = 0.2633 \pm 0.0024 \pm 0.0024$, where k_0 was kept fixed in the fit at 0.0085.

QUADRATIC COEFFICIENT h'_{BB} FOR $K^{\pm} \to \pi^{\pm}\pi^0\pi^0$

VALUE	EVTS	DOCUMENT ID		TECN	CHG
−0.0520±0.0009±0.0026	60M	[1] BATLEY	09A	NA48	±

[1] This fit is obtained using parametrizations of COLANGELO 06A and BISSEGGER 09 in the $2\pi^0$ invariant mass squared range $0.074094 < m^2_{2\pi^0} < 0.104244$ GeV^2. Electromagnetic corrections and CHPT constraints for $\pi\pi$ phase shifts (a_0 and a_2) have been used. Also measured $(a_0 - a_2)\, m_{\pi^+} = 0.2633 \pm 0.0024 \pm 0.0024$, where k_0 was kept fixed in the fit at 0.0085.

$K^{\pm}_{\ell 3}$ FORM FACTORS

In the form factor comments, the following symbols are used.

f_+ and f_- are form factors for the vector matrix element.

f_S and f_T refer to the scalar and tensor term.

$f_0 = f_+ + f_-\, t/(m^2_{K^+} - m^2_{\pi^0})$.

t = momentum transfer to the π.

λ_+ and λ_0 are the linear expansion coefficients of f_+ and f_0:

$f_+(t) = f_+(0)\,(1 + \lambda_+ t\,/m^2_{\pi^+})$

For quadratic expansion

$f_+(t) = f_+(0)\,(1 + \lambda'_+ t\,/m^2_{\pi^+} + \frac{\lambda''_+}{2}\, t^2/m^4_{\pi^+})$

as used by KTeV. If there is a non-vanishing quadratic term, then λ_+ represents an average slope, which is then different from λ'_+.

NA48/2 and OKA quadratic expansion coefficients are converted with

$\lambda'_+{}^{PDG} = \lambda'_+{}^{NA48/2}$ and $\lambda''_+{}^{PDG} = 2\,\lambda''_+{}^{NA48/2}$

$\lambda'_+{}^{PDG} = (\frac{m_{\pi^+}}{m_{\pi^0}})^2\, \lambda'_+{}^{OKA}$ and

$\lambda''_+{}^{PDG} = 2\,(\frac{m_{\pi^+}}{m_{\pi^0}})^4\, \lambda''_+{}^{OKA}$

OKA linear expansion coefficients are converted with

$\lambda_+{}^{PDG} = (\frac{m_{\pi^+}}{m_{\pi^0}})^2\, \lambda_+{}^{OKA}$ and $\lambda_0{}^{PDG} = (\frac{m_{\pi^+}}{m_{\pi^0}})^2\, \lambda_0{}^{OKA}$

The pole parametrization is

$$f_+(t) = f_+(0)\,(\frac{M_V^2}{M_V^2 - t})$$

$$f_0(t) = f_0(0)\,(\frac{M_S^2}{M_S^2 - t})$$

where M_V and M_S are the vector and scalar pole masses.

The following abbreviations are used:

DP = Dalitz plot analysis.

PI = π spectrum analysis.

MU = μ spectrum analysis.

POL= μ polarization analysis.

BR = $K^{\pm}_{\mu 3}/K^{\pm}_{e3}$ branching ratio analysis.

E = positron or electron spectrum analysis.

RC = radiative corrections.

For previous λ'_+ and λ''_+ parametrizations used by NA48 (e.g. LAI 07A) and ISTRA (e.g. YUSHCHENKO 04B) see PDG 18.

Downloaded from https://academic.oup.com/ptep/article/2022/8/083C01/6651666 by KIT Library user on 27 September 2022

λ_+ (LINEAR ENERGY DEPENDENCE OF f_+ IN $K^{\pm}_{e3}$ DECAY)

These results are for a linear expansion only. See the next section for fits including a quadratic term. For radiative correction of the $K^{\pm}_{e3}$ Dalitz plot, see GINSBERG 67, BECHERRAWY 70, CIRIGLIANO 02, CIRIGLIANO 04, and ANDRE 07. Results labeled OUR FIT are discussed in the review "$K^{\pm}_{\ell 3}$ and $K^0_{\ell 3}$ Form Factors" above. For earlier, lower statistics results, see the 2004 edition of this review, Physics Letters **B592** 1 (2004).

VALUE (units 10^{-2})	EVTS	DOCUMENT ID		TECN	CHG	COMMENT
2.959±0.025 OUR FIT		Assuming μ-e universality				
2.956±0.025 OUR AVERAGE						
2.95 ±0.022±0.018	5.25M	YUSHCHENKO	18	OKA	+	
3.044±0.083±0.074	1.1M	AKOPDZANOV	09	TNF	±	
2.966±0.050±0.034	919k	[1] YUSHCHENKO	04B	ISTR	−	DP
2.78 ±0.26 ±0.30	41k	SHIMIZU	00	SPEC	+	DP
2.84 ±0.27 ±0.20	32k	[2] AKIMENKO	91	SPEC		PI, no RC
2.9 ±0.4	62k	[3] BOLOTOV	88	SPEC		PI, no RC
• • • We do not use the following data for averages, fits, limits, etc. • • •						
3.06 ±0.09 ±0.06	550k	[1,4] AJINENKO	03C	ISTR	−	DP
2.93 ±0.15 ±0.2	130k	[4] AJINENKO	02	SPEC		DP

[1] Rescaled to agree with our conventions as noted above.
[2] AKIMENKO 91 state that radiative corrections would raise λ_+ by 0.0013.
[3] BOLOTOV 88 state radiative corrections of GINSBERG 67 would raise λ_+ by 0.002.
[4] Superseded by YUSHCHENKO 04B.

λ_+ (LINEAR ENERGY DEPENDENCE OF f_+ IN $K^{\pm}_{\mu 3}$ DECAY)

Results labeled OUR FIT are discussed in the review "$K^{\pm}_{\ell 3}$ and $K^0_{\ell 3}$ Form Factors" above. For earlier, lower statistics results, see the 2004 edition of this review, Physics Letters **B592** 1 (2004).

VALUE (units 10^{-2})	EVTS	DOCUMENT ID		TECN	CHG	COMMENT
2.959±0.025 OUR FIT		Assuming μ-e universality				
3.09 ±0.25 OUR FIT		Error includes scale factor of 1.5. Not assuming μ-e universality				
2.96 ±0.14 ±0.10	540k	[1] YUSHCHENKO	04	ISTR	−	DP
• • • We do not use the following data for averages, fits, limits, etc. • • •						
3.21 ±0.45	112k	[2] AJINENKO	03	ISTR	−	DP

[1] Rescaled to agree with our conventions as noted above.
[2] Superseded by YUSHCHENKO 04.

λ_0 (LINEAR ENERGY DEPENDENCE OF f_0 IN $K^{\pm}_{\mu 3}$ DECAY)

Results labeled OUR FIT are discussed in the review "$K^{\pm}_{\ell 3}$ and $K^0_{\ell 3}$ Form Factors" above. For earlier, lower statistics results, see the 2004 edition of this review, Physics Letters **B592** 1 (2004).

VALUE (units 10^{-2})	$d\lambda_0/d\lambda_+$	EVTS	DOCUMENT ID		TECN	CHG	COMMENT
1.76 ±0.25 OUR FIT			Error includes scale factor of 2.7. Assuming μ-e universality				
1.73 ±0.27 OUR FIT			Error includes scale factor of 2.6. Not assuming μ-e universality				
1.420±0.114±0.107		2.3M	[1] BATLEY	18	NA48	±	
1.96 ±0.12 ±0.06	−0.348	540k	[2] YUSHCHENKO	04	ISTR	−	DP
• • • We do not use the following data for averages, fits, limits, etc. • • •							
2.09 ±0.45	−0.46	112k	[3] AJINENKO	03	ISTR	−	DP
1.9 ±0.64		24k	[4] HORIE	01	SPEC	+	BR
1.9 ±1.0	+0.03	55k	[5] HEINTZE	77	SPEC	+	BR

[1] Data collected in 2004 by NA48/2. Obtained from a fit with a quadratic vector form factor. Correlation coefficient with linear slope is 0.511, with quadratic slope is −0.513. χ^2/NDF = 409.9/381. BATLEY 18 also performed a combined $K^{\pm}_{e3}$ and $K^{\pm}_{\mu 3}$ fit assuming $\mu - e$ universality and obtained $(14.47 \pm 0.63 \pm 1.17) \times 10^{-3}$.
[2] Rescaled to agree with our conventions as noted above.
[3] Superseded by YUSHCHENKO 04.
[4] HORIE 01 assumes μ-e universality in $K^{\pm}_{\ell 3}$ decay and uses SHIMIZU 00 value λ=0.0278± 0.0040 from $K^{\pm}_{e3}$ decay.
[5] HEINTZE 77 uses $\lambda_+ = 0.029 \pm 0.003$. $d\lambda_0/d\lambda_+$ estimated by us.

λ'_+ (LINEAR $K^{\pm}_{e3}$ FORM FACTOR FROM QUADRATIC FIT)

VALUE (units 10^{-2})	EVTS	DOCUMENT ID		TECN	CHG	COMMENT
2.59 ±0.04 OUR AVERAGE						
2.426±0.078±0.130	4.4M	[1] BATLEY	18	NA48	±	
2.611±0.035±0.028	5.25M	YUSHCHENKO	18	OKA	+	
2.485±0.163±0.034	919k	[2,3] YUSHCHENKO	04B	ISTR	−	DP
• • • We do not use the following data for averages, fits, limits, etc. • • •						
3.07 ±0.21	550k	[2,4] AJINENKO	03C	ISTR	−	DP

[1] Data collected in 2004 by NA48/2. Correlation coefficient with quadratic slope is −0.929. χ^2/NDF = 569.1/687. BATLEY 18 also performed a combined $K^{\pm}_{e3}$ and $K^{\pm}_{\mu 3}$ fit assuming $\mu - e$ universality and obtained $(24.24 \pm 0.75 \pm 1.3) \times 10^{-3}$.
[2] Rescaled to agree with our conventions as noted above.
[3] YUSHCHENKO 04B λ'_+ and λ''_+ are strongly correlated with coefficient $\rho(\lambda'_+, \lambda''_+)$ = −0.95.
[4] Superseded by YUSHCHENKO 04B.

λ''_+(QUADRATIC $K^{\pm}_{e3}$ FORM FACTOR)

VALUE (units 10^{-2})	EVTS	DOCUMENT ID		TECN	CHG	COMMENT
0.186±0.021 OUR AVERAGE						
0.164±0.030±0.039	4.4M	[1] BATLEY	18	NA48	±	
0.191±0.019±0.014	5.25M	YUSHCHENKO	18	OKA	+	
0.192±0.062±0.071	919k	[2,3] YUSHCHENKO	04B	ISTR	−	DP
• • • We do not use the following data for averages, fits, limits, etc. • • •						
−0.5 ±0.7 ±1.5	550k	[2,4] AJINENKO	03C	ISTR	−	DP

[1] Data collected in 2004 by NA48/2. Correlation coefficient with quadratic slope is −0.929. χ^2/NDF = 569.1/687. BATLEY 18 also performed a combined $K^{\pm}_{e3}$ and $K^{\pm}_{\mu 3}$ fit assuming $\mu - e$ universality and obtained $(1.67 \pm 0.29 \pm 0.41) \times 10^{-3}$.
[2] Rescaled to agree with our conventions as noted above.
[3] YUSHCHENKO 04B λ'_+ and λ''_+ are strongly correlated with coefficient $\rho(\lambda'_+, \lambda''_+)$ = −0.95.
[4] Superseded by YUSHCHENKO 04B.

λ'_+ (LINEAR $K^{\pm}_{\mu 3}$ FORM FACTOR FROM QUADRATIC FIT)

VALUE (units 10^{-3})	EVTS	DOCUMENT ID		TECN	CHG
24.27±2.88±2.89	2.3M	[1] BATLEY	18	NA48	±

[1] Data collected in 2004 by NA48/2. Correlation coefficient with quadratic slope is −0.974, with scalar slope is 0.511. χ^2/NDF = 409.9/381. BATLEY 18 also performed a combined $K^{\pm}_{e3}$ and $K^{\pm}_{\mu 3}$ fit assuming $\mu - e$ universality and obtained $(24.24 \pm 0.75 \pm 1.3) \times 10^{-3}$.

λ''_+ (QUADRATIC $K^{\pm}_{\mu 3}$ FORM FACTOR)

VALUE (units 10^{-3})	EVTS	DOCUMENT ID		TECN	CHG
1.83±1.05±1.09	2.3M	[1] BATLEY	18	NA48	±

[1] Data collected in 2004 by NA48/2. Correlation coefficient with linear slope is −0.974, with scalar slope is 0.513. χ^2/NDF = 409.9/381. BATLEY 18 also performed a combined $K^{\pm}_{e3}$ and $K^{\pm}_{\mu 3}$ fit assuming $\mu - e$ universality and obtained $(1.67 \pm 0.29 \pm 0.41) \times 10^{-3}$.

M_V (VECTOR POLE MASS FOR $K^{\pm}_{e3}$ DECAY)

See the review on $K^{\pm}_{l3}$ and K^0_{l3} Form Factors for details.

VALUE (MeV)	EVTS	DOCUMENT ID		TECN	CHG
890.3±2.8 OUR AVERAGE					
885.2±3.3±7.2	4.4M	[1] BATLEY	18	NA48	±
891 ±3	5.25M	[2] YUSHCHENKO	18	OKA	+

[1] Data collected in 2004 by NA48/2. χ^2/NDF = 568.9/688. BATLEY 18 also performed a combined $K^{\pm}_{e3}$ and $K^{\pm}_{\mu 3}$ fit assuming $\mu - e$ universality and obtained 884.4 ± 3.1 ± 6.7 MeV.
[2] Assumed no scalar or tensor contributions to the form factor.

M_V (VECTOR POLE MASS FOR $K^{\pm}_{\mu 3}$ DECAY)

VALUE (MeV)	EVTS	DOCUMENT ID		TECN	CHG
878.4±8.8±8.3	2.3M	[1] BATLEY	18	NA48	±

[1] Data collected in 2004 by NA48/2. χ^2/NDF = 409.9/382. BATLEY 18 also performed a combined $K^{\pm}_{e3}$ and $K^{\pm}_{\mu 3}$ fit assuming $\mu - e$ universality and obtained 884.4 ± 3.1 ± 6.7 MeV.

M_S (SCALAR POLE MASS FOR $K^{\pm}_{\mu 3}$ DECAY)

VALUE (MeV)	EVTS	DOCUMENT ID		TECN	CHG
1214.8±23.5±49.2	2.3M	[1] BATLEY	18	NA48	±

[1] Data collected in 2004 by NA48/2. χ^2/NDF = 409.9/382. BATLEY 18 also performed a combined $K^{\pm}_{e3}$ and $K^{\pm}_{\mu 3}$ fit assuming $\mu - e$ universality and obtained 1208.3±21.2±47.5 MeV.

Λ_+ (DISPERSIVE VECTOR FORM FACTOR IN $K^{\pm}_{e3}$ DECAY)

See the review on $K^{\pm}_{l3}$ and K^0_{l3} Form Factors for details.

VALUE (units 10^{-2})	EVTS	DOCUMENT ID		TECN	CHG
2.460±0.017 OUR AVERAGE					
2.494±0.021±0.064	4.4M	[1] BATLEY	18	NA48	±
2.458±0.018	5.25M	[2] YUSHCHENKO	18	OKA	+

[1] Data collected in 2004 by NA48/2. χ^2/NDF = 569.0/688. BATLEY 18 also performed a combined $K^{\pm}_{e3}$ and $K^{\pm}_{\mu 3}$ fit assuming $\mu - e$ universality and obtained $(24.99 \pm 0.20 \pm 0.62) \times 10^{-3}$.
[2] Assumed no scalar or tensor contributions to the form factor.

Λ_+ (DISPERSIVE VECTOR FORM FACTOR IN $K^{\pm}_{\mu 3}$ DECAY)

VALUE (units 10^{-3})	EVTS	DOCUMENT ID		TECN	CHG
25.36±0.58±0.72	2.3M	[1] BATLEY	18	NA48	±

[1] Data collected in 2004 by NA48/2. χ^2/NDF = 410.3/382. BATLEY 18 also performed a combined $K^{\pm}_{e3}$ and $K^{\pm}_{\mu 3}$ fit assuming $\mu - e$ universality and obtained $(24.99 \pm 0.20 \pm 0.62) \times 10^{-3}$.

Downloaded from https://academic.oup.com/ptep/article/2022/8/083C01/6651666 by KIT Library user on 27 September 2022

ln(C) (DISPERSIVE SCALAR FORM FACTOR in $K^{\pm}_{\mu3}$ decays)

VALUE (units 10^{-3})	EVTS	DOCUMENT ID		TECN	CHG
182.17±6.31±14.45	2.3M	[1] BATLEY	18	NA48	±

[1] Data collected in 2004 by NA48/2. Combined fit with dispersive vector form factor $\Lambda_+ = 25.36 \pm 0.58 \pm 0.72$. Correlation coefficient is 0.104. $\chi^2/NDF = 410.3/382$. BATLEY 18 also performed a combined $K^{\pm}_{e3}$ and $K^{\pm}_{\mu3}$ fit assuming $\mu - e$ universality and obtained $(183.65 \pm 5.92 \pm 14.25) \times 10^{-3}$.

$|f_S/f_+|$ FOR $K^{\pm}_{e3}$ DECAY

Ratio of scalar to f_+ couplings.

VALUE (units 10^{-2})	CL%	EVTS	DOCUMENT ID		TECN	CHG	COMMENT
$-0.08^{+0.34}_{-0.40}$ OUR AVERAGE							
$0.01^{+0.38}_{-0.46}$		5.25M	YUSHCHENKO	18	OKA	+	λ'_+, λ''_+, f_S fit
$-0.37^{+0.66}_{-0.56}\pm0.41$		919k	YUSHCHENKO	04B	ISTR	−	λ'_+, λ''_+, f_S fit
0.2 ±2.6 ±1.4		41k	SHIMIZU	00	SPEC	+	λ_+, f_S, f_T fit
• • • We do not use the following data for averages, fits, limits, etc. • • •							
$0.2\ ^{+2.0}_{-2.2}\ \pm0.3$		550k	[1] AJINENKO	03C	ISTR	−	λ_+, f_S, f_T fit
$-1.9\ ^{+2.5}_{-1.6}$		130k	[1] AJINENKO	02	SPEC		λ_+, f_S fit
7.0 ±1.6 ±1.6		32k	AKIMENKO	91	SPEC		λ_+, f_S, f_T, ϕ fit
0 ± 10		2827	[2] BRAUN	75	HLBC	+	
< 13	90	4017	CHIANG	72	OSPK	+	
14^{+3}_{-4}		2707	[2] STEINER	71	HLBC	+	λ_+, f_S, f_T, ϕ fit
< 23	90		BOTTERILL	68C	ASPK		
< 18	90		BELLOTTI	67B	HLBC		
< 30	95		KALMUS	67	HLBC	+	

[1] Superseded by YUSHCHENKO 04B.
[2] Statistical errors only.

$|f_T/f_+|$ FOR $K^{\pm}_{e3}$ DECAY

Ratio of tensor to f_+ couplings.

VALUE (units 10^{-2})	EVTS	DOCUMENT ID		TECN	CHG	COMMENT
$-1.2\ ^{+1.3}_{-1.1}$ OUR AVERAGE						
$-1.24^{+1.6}_{-1.3}$	5.25M	YUSHCHENKO	18	OKA	+	λ'_+,λ''_+,f_T fit
−1.2 ± 2.1± 1.1	919k	YUSHCHENKO	04B	ISTR	−	λ'_+,λ''_+,f_T fit
1 ±14 ± 9	41k	SHIMIZU	00	SPEC	+	λ_+, f_S, f_T fit
• • • We do not use the following data for averages, fits, limits, etc. • • •						
$2.1\ ^{+6.4}_{-7.5}\pm 2.6$	550k	[1] AJINENKO	03C	ISTR	−	λ_+, f_S, f_T fit
$-4.5\ ^{+6.0}_{-5.7}$	130k	[1] AJINENKO	02	SPEC		λ_+, f_T fit
$53\ ^{+9}_{-10}\ \pm10$	32k	AKIMENKO	91	SPEC		λ_+, f_S, f_T, ϕ fit

[1] Superseded by YUSHCHENKO 04B.

f_S/f_+ FOR $K^{\pm}_{\mu3}$ DECAY

Ratio of scalar to f_+ couplings.

VALUE (units 10^{-2})	EVTS	DOCUMENT ID		TECN	CHG	COMMENT
0.17±0.14±0.54	540k	[1] YUSHCHENKO	04	ISTR	−	DP
• • • We do not use the following data for averages, fits, limits, etc. • • •						
0.4 ±0.5 ±0.5	112k	[2] AJINENKO	03	ISTR	−	DP

[1] The second error is the theoretical error from the uncertainty in the chiral perturbation theory prediction for λ_0, ±0.0053, combined in quadrature with the systematic error ±0.0009.
[2] The second error is the theoretical error from the uncertainty in the chiral perturbation theory prediction for λ_0. Superseded by YUSHCHENKO 04.

f_T/f_+ FOR $K^{\pm}_{\mu3}$ DECAY

Ratio of tensor to f_+ couplings.

VALUE (units 10^{-2})	EVTS	DOCUMENT ID		TECN	CHG	COMMENT
−0.07± 0.71±0.20	540k	YUSHCHENKO	04	ISTR	−	DP
• • • We do not use the following data for averages, fits, limits, etc. • • •						
−2.1 ± 2.8 ±1.4	112k	[1] AJINENKO	03	ISTR	−	DP
2 ±12	1585	BRAUN	75	HLBC		

[1] The second error is the theoretical error from the uncertainty in the chiral perturbation theory prediction for λ_0. Superseded by YUSHCHENKO 04.

$K^{\pm}_{\ell4}$ FORM FACTORS

Based on the parametrizations of AMOROS 99, the $K^{\pm}_{\ell4}$ form factors can be expressed as

$$F_s = f_s + f'_s\, q^2 + f''_s\, q^4 + f'_e\, S_e\, /\, 4m_\pi^2$$
$$F_p = f_p$$
$$G_p = g_p + g'_p\, q^2$$
$$H_p = h_p$$

where $q^2 = (S_\pi\ /\ 4m_\pi^2) - 1$, S_π is the invariant mass squared of the dipion, and S_e is the invariant mass squared of the dilepton.

f_s FOR $K^{\pm} \to \pi^+\pi^- e^{\pm}\nu$ DECAY

VALUE	EVTS	DOCUMENT ID		TECN	CHG
5.712±0.032 OUR AVERAGE					
5.705±0.003±0.035	1.1M	[1] BATLEY	12	NA48	±
5.75 ±0.02 ±0.08	400k	[2] PISLAK	03	B865	+

[1] BATLEY 12 uses data collected in 2003–2004. The result is obtained from a measurement of $\Gamma(\pi^+\pi^- e\nu)/\Gamma(\pi^+\pi^-\pi^+)$ and assumed PDG 12 value of $\Gamma(\pi^+\pi^-\pi^+)/\Gamma = (5.59 \pm 0.04) \times 10^{-2}$.
[2] Radiative corrections included. Using Roy equations and not including isospin breaking, PISLAK 03 obtains the following $\pi\pi$ scattering lengths $a_0^0 = 0.228 \pm 0.012 \pm 0.004\ ^{+0.012}_{-0.016}$(theor.) and $a_0^2 = -0.0365 \pm 0.0023 \pm 0.0008\ ^{+0.0031}_{-0.0026}$(theor.).

f'_s/f_s FOR $K^{\pm} \to \pi^+\pi^- e^{\pm}\nu$ DECAY

VALUE (units 10^{-2})	EVTS	DOCUMENT ID		TECN	CHG
15.2±0.7±0.5	1.13M	[1] BATLEY	10C	NA48	±
• • • We do not use the following data for averages, fits, limits, etc. • • •					
17.2±0.9±0.6	670k	[2] BATLEY	08A	NA48	±

[1] Radiative corrections included. Using Roy equations and including isospin breaking, BATLEY 10C obtains the following scattering lengths $a_0^0 = 0.2220 \pm 0.0128 \pm 0.0050 \pm 0.0037$ (theor.), $a_0^2 = -0.0432 \pm 0.0086 \pm 0.0034 \pm 0.0028$ (theor.). The correlation with $f''_s/f_s = -0.954$ and with $f'_e/f_s = 0.080$. Supersedes BATLEY 08A.
[2] Radiative corrections included. Using Roy equations and not including isospin breaking, BATLEY 08A obtains the following $\pi\pi$ scattering length $a_0^0 = 0.233 \pm 0.016 \pm 0.007$ $a_0^2 = -0.0471 \pm 0.011 \pm 0.004$.

f''_s/f_s FOR $K^{\pm} \to \pi^+\pi^- e^{\pm}\nu$ DECAY

VALUE (units 10^{-2})	EVTS	DOCUMENT ID		TECN	CHG
−7.3±0.7±0.6	1.13M	[1] BATLEY	10C	NA48	±
• • • We do not use the following data for averages, fits, limits, etc. • • •					
−9.0±0.9±0.7	670k	[2] BATLEY	08A	NA48	±

[1] Radiative corrections included. Using Roy equations and including isospin breaking, BATLEY 10C obtains the following scattering lengths $a_0^0 = 0.2220 \pm 0.0128 \pm 0.0050 \pm 0.0037$ (theor.), $a_0^2 = -0.0432 \pm 0.0086 \pm 0.0034 \pm 0.0028$ (theor.). The correlation with $f'_s/f_s = -0.954$ and with $f'_e/f_s = 0.019$. Supersedes BATLEY 08A.
[2] Radiative corrections included. Using Roy equations and not including isospin breaking, BATLEY 08A obtains the following $\pi\pi$ scattering length $a_0^0 = 0.233 \pm 0.016 \pm 0.007$ $a_0^2 = -0.0471 \pm 0.011 \pm 0.004$.

f'_e/f_s FOR $K^{\pm} \to \pi^+\pi^- e^{\pm}\nu$ DECAY

VALUE (units 10^{-2})	EVTS	DOCUMENT ID		TECN	CHG
6.8±0.6±0.7	1.13M	[1] BATLEY	10C	NA48	±
• • • We do not use the following data for averages, fits, limits, etc. • • •					
8.1±0.8±0.9	670k	[2] BATLEY	08A	NA48	±

[1] Radiative corrections included. Using Roy equations and including isospin breaking, BATLEY 10C obtains the following scattering lengths $a_0^0 = 0.2220 \pm 0.0128 \pm 0.0050 \pm 0.0037$ (theor.), $a_0^2 = -0.0432 \pm 0.0086 \pm 0.0034 \pm 0.0028$ (theor.). The correlation with $f'_s/f_s = 0.080$ and with $f''_s/f_s = 0.019$. Supersedes BATLEY 08A.
[2] Radiative corrections included. Using Roy equations and not including isospin breaking, BATLEY 08A obtains the following $\pi\pi$ scattering length $a_0^0 = 0.233 \pm 0.016 \pm 0.007$ $a_0^2 = -0.0471 \pm 0.011 \pm 0.004$.

f_p/f_s FOR $K^{\pm} \to \pi^+\pi^- e^{\pm}\nu$ DECAY

VALUE (units 10^{-2})	EVTS	DOCUMENT ID		TECN	CHG
−4.8±0.3±0.4	1.13M	[1] BATLEY	10C	NA48	±
• • • We do not use the following data for averages, fits, limits, etc. • • •					
−4.8±0.4±0.4	670k	[2] BATLEY	08A	NA48	±

[1] Radiative corrections included. Using Roy equations and including isospin breaking, BATLEY 10C obtains the following scattering lengths $a_0^0 = 0.2220 \pm 0.0128 \pm 0.0050 \pm 0.0037$ (theor.), $a_0^2 = -0.0432 \pm 0.0086 \pm 0.0034 \pm 0.0028$ (theor.). Supersedes BATLEY 08A.
[2] Radiative corrections included. Using Roy equations and not including isospin breaking, BATLEY 08A obtains the following $\pi\pi$ scattering length $a_0^0 = 0.233 \pm 0.016 \pm 0.007$ $a_0^2 = -0.0471 \pm 0.011 \pm 0.004$.

g_p/f_s FOR $K^{\pm} \to \pi^+\pi^- e^{\pm}\nu$ DECAY

VALUE (units 10^{-2})	EVTS	DOCUMENT ID		TECN	CHG
86.8±1.0±1.0	1.13M	[1] BATLEY	10C	NA48	±
• • • We do not use the following data for averages, fits, limits, etc. • • •					
87.3±1.3±1.2	670k	[2] BATLEY	08A	NA48	±
80.9±0.9±1.2	400k	[3] PISLAK	03	B865	±

[1] Radiative corrections included. Using Roy equations and including isospin breaking, BATLEY 10C obtains the following scattering lengths $a_0^0 = 0.2220 \pm 0.0128 \pm 0.0050 \pm 0.0037$ (theor.), $a_0^2 = -0.0432 \pm 0.0086 \pm 0.0034 \pm 0.0028$ (theor.). Supersedes BATLEY 08A. The correlation with $g'_p/f_s = -0.914$. Supersedes BATLEY 08A.
[2] Radiative corrections included. Using Roy equations and not including isospin breaking, BATLEY 08A obtains the following $\pi\pi$ scattering length $a_0^0 = 0.233 \pm 0.016 \pm 0.007$ $a_0^2 = -0.0471 \pm 0.011 \pm 0.004$.
[3] Radiative corrections included. Using Roy equations PISLAK 03 obtains the following scattering lengths $a_0^0 = 0.203 \pm 0.033 \pm 0.004$, $a_0^2 = -0.055 \pm 0.023 \pm 0.003$.

Downloaded from https://academic.oup.com/ptep/article/2022/8/083C01/6651666 by KIT Library user on 27 September 2022

g'_p/f_s FOR $K^{\pm} \to \pi^+\pi^- e^{\pm}\nu$ DECAY

VALUE (units 10^{-2})	EVTS	DOCUMENT ID		TECN	CHG
8.9±1.7±1.3	1.13M	[1] BATLEY	10C	NA48	±
• • • We do not use the following data for averages, fits, limits, etc. • • •					
8.1±2.2±1.5	670k	[2] BATLEY	08A	NA48	±
12.0±1.9±0.7	400k	[3] PISLAK	03	B865	±

[1] Radiative corrections included. Using Roy equations and including isospin breaking, BATLEY 10C obtains the following scattering lengths $a_0^0 = 0.2220 \pm 0.0128 \pm 0.0050 \pm 0.0037$ (theor.), $a_0^2 = -0.0432 \pm 0.0086 \pm 0.0034 \pm 0.0028$ (theor.). The correlation with $g_p/f_s = -0.914$. Supersedes BATLEY 08A.

[2] Radiative corrections included. Using Roy equations and not including isospin breaking, BATLEY 08A obtains the following $\pi\pi$ scattering length $a_0^0 = 0.233 \pm 0.016 \pm 0.007$ $a_0^2 = -0.0471 \pm 0.011 \pm 0.004$.

[3] Radiative corrections included. Using Roy equations PISLAK 03 obtains the following scattering lengths $a_0^0 = 0.203 \pm 0.033 \pm 0.004$, $a_0^2 = -0.055 \pm 0.023 \pm 0.003$.

h_p/f_s FOR $K^{\pm} \to \pi^+\pi^- e^{\pm}\nu$ DECAY

VALUE (units 10^{-2})	EVTS	DOCUMENT ID		TECN	CHG
−39.8±1.5±0.8	1.13M	[1] BATLEY	10C	NA48	±
• • • We do not use the following data for averages, fits, limits, etc. • • •					
−41.1±1.9±0.8	670k	[2] BATLEY	08A	NA48	±
−51.3±3.3±3.5	400k	[3] PISLAK	03	B865	±

[1] Radiative corrections included. Using Roy equations and including isospin breaking, BATLEY 10C obtains the following scattering lengths $a_0^0 = 0.2220 \pm 0.0128 \pm 0.0050 \pm 0.0037$ (theor.), $a_0^2 = -0.0432 \pm 0.0086 \pm 0.0034 \pm 0.0028$ (theor.). Supersedes BATLEY 08A.

[2] Radiative corrections included. Using Roy equations and not including isospin breaking, BATLEY 08A obtains the following $\pi\pi$ scattering length $a_0^0 = 0.233 \pm 0.016 \pm 0.007$ $a_0^2 = -0.0471 \pm 0.011 \pm 0.004$.

[3] Radiative corrections included. Using Roy equations PISLAK 03 obtains the following scattering lengths $a_0^0 = 0.203 \pm 0.033 \pm 0.004$, $a_0^2 = -0.055 \pm 0.023 \pm 0.003$.

DECAY FORM FACTOR FOR $K^{\pm} \to \pi^0\pi^0 e^{\pm}\nu$

Given in BOLOTOV 86B, BARMIN 88B, and SHIMIZU 04.

$K^{\pm} \to \ell^{\pm}\nu\gamma$ FORM FACTORS

For definitions of the axial-vector F_A and vector F_V form factor, see the "Note on $\pi^{\pm} \to \ell^{\pm}\nu\gamma$ and $K^{\pm} \to \ell^{\pm}\nu\gamma$ Form Factors" in the $\pi^{\pm}$ section. In the kaon literature, often different definitions $a_K = F_A/m_K$ and $v_K = F_V/m_K$ are used.

$F_A + F_V$, SUM OF AXIAL-VECTOR AND VECTOR FORM FACTOR FOR $K \to e\nu_e\gamma$

VALUE	EVTS	DOCUMENT ID		TECN	COMMENT
0.133±0.008 OUR AVERAGE		Error includes scale factor of 1.3.			See the ideogram below.
0.125±0.007±0.001	1.4k	[1] AMBROSINO	09E	KLOE	E_γ in 10–250 MeV, $p_e > 200$ MeV/c
0.147±0.011	51	[2] HEINTZE	79	SPEC	
$0.150^{+0.018}_{-0.023}$	56	[3] HEARD	75	SPEC	

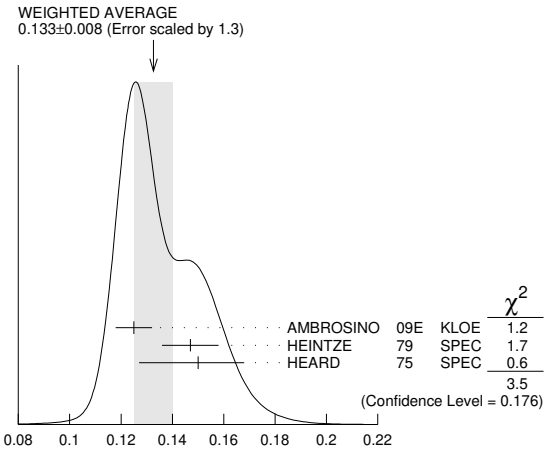

$F_A + F_V$, SUM OF AXIAL-VECTOR AND VECTOR FORM FACTOR FOR $K \to e\nu_e\gamma$

[1] AMBROSINO 09E measures the absolute value $|F_A + F_V|$ which is parametrized as $|F_A + F_V| = F_V\,(1 + \lambda(1-x)) + F_A$, $x = 2E_\gamma/m_K$. $(F_A + F_V)$ and λ are fit parameters. The fitted value of $\lambda = 0.38 \pm 0.20 \pm 0.02$ with a correlation of -0.93 between $(F_A + F_V)$ and λ.

[2] HEINTZE 79 quotes absolute value of $|F_A + F_V| \sin\theta_C$. We use $\sin\theta_C = V_{us} = 0.2205$.

[3] HEARD 75 quotes absolute value of $|F_A + F_V| \sin\theta_C$. We use $\sin\theta_C = V_{us} = 0.2205$.

$F_A + F_V$, SUM OF AXIAL-VECTOR AND VECTOR FORM FACTOR FOR $K \to \mu\nu_\mu\gamma$

VALUE	CL%	EVTS	DOCUMENT ID		TECN	CHG
0.165±0.007±0.011		2588	[1] ADLER	00B	B787	+
• • • We do not use the following data for averages, fits, limits, etc. • • •						
−1.2 to 1.1	90		DEMIDOV	90	XEBC	
< 0.23	90		[1] AKIBA	85	SPEC	

[1] Quotes absolute value. Sign not determined.

$F_A - F_V$, DIFFERENCE OF AXIAL-VECTOR AND VECTOR FORM FACTOR FOR $K \to e\nu_e\gamma$

VALUE	CL%	DOCUMENT ID		TECN
<0.49	90	[1] HEINTZE	79	SPEC

[1] HEINTZE 79 quotes $|F_A - F_V| < \sqrt{11}\,|F_A + F_V|$.

$F_A - F_V$, DIFFERENCE OF AXIAL-VECTOR AND VECTOR FORM FACTOR FOR $K \to \mu\nu_\mu\gamma$

VALUE	CL%	EVTS	DOCUMENT ID		TECN	CHG
−0.153±0.033 OUR AVERAGE	Error includes scale factor of 1.1.					
−0.134±0.021±0.027		95k	KRAVTSOV	19	OKA	+
−0.21 ±0.06		22k	DUK	11	ISTR	−
• • • We do not use the following data for averages, fits, limits, etc. • • •						
−0.24 to 0.04	90	2588	ADLER	00B	B787	+
−2.2 to 0.6	90		DEMIDOV	90	XEBC	
−2.5 to 0.3	90		AKIBA	85	SPEC	

$K^{\pm}$ CHARGE RADIUS

VALUE (fm)	DOCUMENT ID		COMMENT
0.560±0.031 OUR AVERAGE			
0.580±0.040	AMENDOLIA	86B	$Ke \to Ke$
0.530±0.050	DALLY	80	$Ke \to Ke$
• • • We do not use the following data for averages, fits, limits, etc. • • •			
0.620±0.037	BLATNIK	79	VMD + dispersion relations

K^+ LONGITUDINAL POLARIZATION OF EMITTED μ^+

VALUE	CL%	DOCUMENT ID		TECN	CHG	COMMENT
<−0.990	90	[1] AOKI	94	SPEC	+	
• • • We do not use the following data for averages, fits, limits, etc. • • •						
<−0.990	90	IMAZATO	92	SPEC	+	Repl. by AOKI 94
−0.970±0.047		[2] YAMANAKA	86	SPEC	+	
−1.0 ±0.1		[2] CUTTS	69	SPRK	+	
−0.96 ±0.12		[2] COOMBES	57	CNTR	+	

[1] AOKI 94 measures $\xi P_\mu = -0.9996 \pm 0.0030 \pm 0.0048$. The above limit is obtained by summing the statistical and systematic errors in quadrature, normalizing to the physically significant region ($|\xi P_\mu| < 1$) and assuming that ξ=1, its maximum value.

[2] Assumes ξ=1.

FORWARD-BACKWARD ASYMMETRY IN $K^{\pm}$ DECAYS

$$A_{FB}(K^{\pm}_{\pi\mu\mu}) = \frac{\Gamma(\cos(\theta_{K\mu})>0) - \Gamma(\cos(\theta_{K\mu})<0)}{\Gamma(\cos(\theta_{K\mu})>0) + \Gamma(\cos(\theta_{K\mu})<0)}$$

VALUE	CL%	DOCUMENT ID		TECN
<2.3 × 10^{-2}	90	[1] BATLEY	11A	NA48

[1] BATLEY 11A gives a corresponding value of the asymmetry $A_{FB} = (-2.4 \pm 1.8) \times 10^{-2}$.

$K^{\pm}$ REFERENCES

ALIBERTI 21 PRL 127 131802 R. Aliberti et al. (NA62 Collab.)
CORTINA-GIL 21 PL B816 136259 E. Cortina Gil et al. (NA62 Collab.)
CORTINA-GIL 21B JHEP 2106 093 E. Cortina Gil et al. (NA62 Collab.)
POLYARUSH 21 EPJ C81 161 A.Yu. Polyarush et al. (OKA Collab.)
CORTINA-GIL 20C JHEP 2011 042 E. Cortina Gil et al. (NA62 Collab.)
BATLEY 19 PL B788 552 J.R. Batley et al. (NA48/2 Collab.)
CORTINA-GIL 19A PL B797 134794 E. Cortina Gil et al. (NA62 Collab.)
CORTINA-GIL 19B PL B791 156 E. Cortina Gil et al. (NA62 Collab.)
KRAVTSOV 19 EPJ C79 635 V.I. Kravtsov et al. (OKA Collab.)
SHAPKIN 19 EPJ C79 296 M.M. Shapkin et al. (OKA Collab.)
BATLEY 18 JHEP 1810 150 J.R. Batley et al. (NA48/2 Collab.)
PDG 18 PR D98 030001 M. Tanabashi et al. (PDG Collab.)
YUSHCHENKO 18 JETPL 107 139 O.P. Yushchenko et al. (OKA Collab.)
BATLEY 17 PL B769 67 J.R. Batley et al. (NA48/2 Collab.)
ARTAMONOV 16 PR D94 032012 A.V. Artamonov et al. (BNL E949 Collab.)
BABUSCI 14B PL B738 128 D. Babusci et al. (KLOE and KLOE-2 Collab.)
BATLEY 14 PL B730 141 J.R. Batley et al. (CERN NA48/2 Collab.)
BATLEY 14A JHEP 1408 159 J.R. Batley et al. (CERN NA48/2 Collab.)
LAZZERONI 14 PL B732 65 C. Lazzeroni et al. (CERN NA62 Collab.)
UVAROV 14 PAN 77 725 V.A. Uvarov et al. (ISTRA+ Collab.)
Translated from YAF 77 765.
LAZZERONI 13 PL B719 326 C. Lazzeroni et al. (CERN NA62 Collab.)
BATLEY 12 PL B715 105 J.R. Batley et al. (CERN NA48/2 Collab.)
PDG 12 PR D86 010001 J. Beringer et al. (PDG Collab.)
BATLEY 11A PL B697 107 J.R. Batley et al. (CERN NA48/2 Collab.)
DUK 11 PL B695 59 V.A. Duk et al. (ISTRA+ Collab.)
LAZZERONI 11 PL B698 105 C. Lazzeroni et al. (CERN NA62 Collab.)
ADLER 10 PR D81 092001 S. Adler et al. (BNL E787 Collab.)
BATLEY 10A EPJ C68 75 J.R. Batley et al. (CERN NA48/2 Collab.)
BATLEY 10C EPJ C70 635 J.R. Batley et al. (CERN NA48/2 Collab.)
PDG 10 JP G37 075021 K. Nakamura et al. (PDG Collab.)
PISLAK 10A PRL 105 019901E S. Pislak et al. (BNL E865 Collab.)
AKOPDZANOV 09 PAN 71 2074 G.A. Akopdzanov et al. (IHEP)
Translated from YAF 71 2108.

Downloaded from https://academic.oup.com/ptep/article/2022/8/083C01/6651666 by KIT Library user on 27 September 2022

AMBROSINO 09E EPJ C64 627 F. Ambrosino et al. (KLOE Collab.)
Also EPJ C65 703 (errat.) F. Ambrosino et al. (KLOE Collab.)
BATLEY 09 PL B677 246 J.R. Batley et al. (CERN NA48/2 Collab.)
BATLEY 09A EPJ C64 589 J.R. Batley et al. (CERN NA48/2 Collab.)
BISSEGGER 09 NP B806 178 M. Bissegger et al.
AMBROSINO 08 JHEP 0801 073 F. Ambrosino et al. (KLOE Collab.)
AMBROSINO 08A JHEP 0802 098 F. Ambrosino et al. (KLOE Collab.)
AMBROSINO 08E PL B666 305 F. Ambrosino et al. (KLOE Collab.)
ARTAMONOV 08 PRL 101 191802 A.V. Artamonov et al. (BNL E949 Collab.)
Also PR D79 092004 A.V. Artamonov et al. (BNL E949 Collab.)
BATLEY 08 PL B659 493 J.R. Batley et al. (CERN NA48/2 Collab.)
BATLEY 08A EPJ C54 411 J.R. Batley et al. (CERN NA48/2 Collab.)
AKIMENKO 07 PAN 70 702 S.A. Akimenko et al. (ISTRA+ Collab.)
Translated from YAF 70 734.
ANDRE 07 ANP 322 2518 T. Andre (EFI)
BATLEY 07A EPJ C50 329 J.R. Batley et al. (CERN NA48/2 Collab.)
Also EPJ C52 1021 (errat.) J.R. Batley et al. (CERN NA48/2 Collab.)
BATLEY 07B PL B649 349 J.R. Batley et al. (CERN NA48/2 Collab.)
BATLEY 07E EPJ C52 875 J.R. Batley et al. (CERN NA48/2 Collab.)
LAI 07A PL B647 341 A. Lai et al. (CERN NA48 Collab.)
TCHIKILEV 07 PAN 70 29 O.G. Tchikilev et al. (ISTRA+ Collab.)
ALIEV 06 EPJ C46 61 M.A. Aliev et al. (KEK E470 Collab.)
AMBROSINO 06A PL B632 76 F. Ambrosino et al. (KLOE Collab.)
BATLEY 06 PL B634 474 J.R. Batley et al. (CERN NA48/2 Collab.)
BATLEY 06A PL B638 22 J.R. Batley et al. (CERN NA48/2 Collab.)
Also PL B640 297 (errat.) J.R. Batley et al. (CERN NA48/2 Collab.)
BATLEY 06B PL B633 173 J.R. Batley et al. (CERN NA48/2 Collab.)
COLANGELO 06A PL B638 187 G. Colangelo et al.
MA 06 PR D73 037101 H. Ma et al. (BNL E865 Collab.)
PDG 06 JP G33 1 W.-M. Yao et al. (PDG Collab.)
SHIMIZU 06 PL B633 190 S. Shimizu et al. (KEK E470 Collab.)
UVAROV 06 PAN 69 26 V.A. Uvarov et al. (ISTRA+ Collab.)
AKOPDZHAN... 05 EPJ C40 343 G.A. Akopdzhanov et al. (IHEP)
Also PAN 68 948 G.A. Akopdzhanov et al. (IHEP)
Translated from YAF 68 986.
AKOPDZHAN... 05B JETPL 82 675 G.A. Akopdzhanov et al. (IHEP)
Translated from ZETFP 82 771.
ARTAMONOV 05 PL B623 192 A.V. Artamonov et al. (BNL E949 Collab.)
CABIBBO 05 JHEP 0503 021 N. Cabibbo, G. Isidori (CERN, ROMAI, FRAS)
SHER 05 PR D72 012005 A. Sher et al. (BNL E865 Collab.)
ABE 04F PRL 93 131601 M. Abe et al. (KEK E246 Collab.)
Also PR D73 072005 M. Abe et al. (KEK E246 Collab.)
ADLER 04 PR D70 037102 S. Adler et al. (BNL E787 Collab.)
ALOISIO 04A PL B597 139 A. Aloisio et al. (KLOE Collab.)
ANISIMOVSK... 04 PRL 93 031801 V.V. Anisimovsky et al. (BNL E949 Collab.)
Also PR D77 052003 S. Adler et al. (BNL E949 Collab.)
CABIBBO 04A PRL 93 121801 N. Cabibbo (CERN, ROMAI)
CIRIGLIANO 04 EPJ C35 53 V. Cirigliano, H. Neufeld, H. Pichl (CIT, VALE+)
PDG 04 PL B592 1 S. Eidelman et al. (PDG Collab.)
SHIMIZU 04 PR D70 037101 S. Shimizu et al. (KEK E470 Collab.)
YUSHCHENKO 04 PL B581 31 O.P. Yushchenko et al. (INRM, INRM)
YUSHCHENKO 04B PL B589 111 O.P. Yushchenko et al. (INRM)
AJINENKO 03 PAN 66 105 I.V. Ajinenko et al. (IHEP, INRM)
Translated from YAF 66 107.
AJINENKO 03B PL B567 159 I.V. Ajinenko et al. (IHEP, INRM)
AJINENKO 03C PL B574 14 I.V. Ajinenko et al. (IHEP, INRM)
ALIEV 03 PL B554 7 M.A. Aliev et al. (KEK E470 Collab.)
ANISIMOVSK... 03 PL B562 166 V.V. Anisimovsky et al.
PISLAK 03 PR D67 072004 S. Pislak et al. (BNL E865 Collab.)
Also PR D81 119903E S. Pislak et al. (BNL E865 Collab.)
SHER 03 PRL 91 261802 A. Sher et al. (BNL E865 Collab.)
ADLER 02 PRL 88 041803 S. Adler et al. (BNL E787 Collab.)
ADLER 02B PR D65 052009 S. Adler et al. (BNL E787 Collab.)
ADLER 02C PL B537 211 S. Adler et al. (BNL E787 Collab.)
AJINENKO 02 PAN 65 2064 I.V. Ajinenko et al. (IHEP, INRM)
Translated from YAF 65 2125.
CIRIGLIANO 02 EPJ C23 121 V. Cirigliano et al. (VIEN, VALE, MARS)
PARK 02 PRL 88 111801 H.K. Park et al. (FNAL HyperCP Collab.)
PDG 02 PR D66 010001 K. Hagiwara et al. (PDG Collab.)
POBLAGUEV 02 PRL 89 061803 A.A. Poblaguev et al. (BNL 865 Collab.)
ADLER 01 PR D63 032004 S. Adler et al. (BNL E787 Collab.)
HORIE 01 PL B513 311 K. Horie et al. (KEK E426 Collab.)
PISLAK 01 PRL 87 221801 S. Pislak et al. (BNL E865 Collab.)
Also PR D67 072004 S. Pislak et al. (BNL E865 Collab.)
Also PRL 105 019901E S. Pislak et al. (BNL E865 Collab.)
ADLER 00 PRL 84 3768 S. Adler et al. (BNL E787 Collab.)
ADLER 00B PRL 85 2256 S. Adler et al. (BNL E787 Collab.)
ADLER 00C PRL 85 4856 S. Adler et al. (BNL E787 Collab.)
APPEL 00 PRL 85 2450 R. Appel et al. (BNL 865 Collab.)
Also Thesis, Yale Univ. D.R. Bergman
Also Thesis, Univ. Zurich S. Pislak
APPEL 00B PRL 85 2877 R. Appel et al. (BNL 865 Collab.)
MA 00 PRL 84 2580 H. Ma et al. (BNL 865 Collab.)
PDG 00 EPJ C15 1 D.E. Groom et al. (PDG Collab.)
SHIMIZU 00 PL B495 33 S. Shimizu et al. (KEK E246 Collab.)
ABE 99S PRL 83 4253 M. Abe et al. (KEK E246 Collab.)
AMOROS 99 JP G25 1607 G. Amoros, J. Bijnens (LUND, HELS)
APPEL 99 PRL 83 4482 R. Appel et al. (BNL 865 Collab.)
ADLER 98 PR D58 012003 S. Adler et al. (BNL E787 Collab.)
BATUSOV 98 NP B516 3 V.Y. Batusov et al.
DAMBROSIO 98A JHEP 9808 004 G. D'Ambrosio et al.
ADLER 97 PRL 79 2204 S. Adler et al. (BNL E787 Collab.)
ADLER 97C PRL 79 4756 S. Adler et al. (BNL E787 Collab.)
BERGMAN 97 Thesis, Yale Univ. D.R. Bergman
KITCHING 97 PRL 79 4079 P. Kitching et al. (BNL E787 Collab.)
PISLAK 97 Thesis, Univ. Zurich S. Pislak
ADLER 96 PRL 76 1421 S. Adler et al. (BNL E787 Collab.)
KOPTEV 95 JETPL 61 877 V.P. Koptev et al. (PNPI)
Translated from ZETFP 61 865.
AOKI 94 PR D50 69 M. Aoki et al. (INUS, KEK, TOKMS)
ATIYA 93 PRL 70 2521 M.S. Atiya et al. (BNL E787 Collab.)
Also PRL 71 305 (erratum) M.S. Atiya et al. (BNL E787 Collab.)
ATIYA 93B PR D48 1 M.S. Atiya et al. (BNL E787 Collab.)
ALLIEGRO 92 PRL 68 278 C. Alliegro et al. (BNL, FNAL, PSI+)
BARMIN 92 SJNP 55 547 V.V. Barmin et al. (ITEP)
Translated from YAF 55 976.
IMAZATO 92 PRL 69 877 J. Imazato et al. (KEK, INUS, TOKY+)
IVANOV 92 THESIS Yu.M. Ivanov (PNPI)
LITTENBERG 92 PRL 68 443 L.S. Littenberg, R.E. Shrock (BNL, STON)
USHER 92 PR D45 3961 T. Usher et al. (UCI)
AKIMENKO 91 PL B259 225 S.A. Akimenko et al. (SERP, JINR, TBIL+)
BARMIN 91 SJNP 53 606 V.V. Barmin et al. (ITEP)
Translated from YAF 53 981.
DENISOV 91 JETPL 54 558 A.S. Denisov et al. (PNPI)
Translated from ZETFP 54 557.
Also THESIS Yu.M. Ivanov (PNPI)
ATIYA 90 PRL 64 21 M.S. Atiya et al. (BNL E787 Collab.)
ATIYA 90B PRL 65 1188 M.S. Atiya et al. (BNL E787 Collab.)
DEMIDOV 90 SJNP 52 1006 V.S. Demidov et al. (ITEP)
Translated from YAF 52 1595.
LEE 90 PRL 64 165 A.M. Lee et al. (BNL, FNAL, VILL, WASH+)
ATIYA 89 PRL 63 2177 M.S. Atiya et al. (BNL E787 Collab.)
BARMIN 89 SJNP 50 421 V.V. Barmin et al. (ITEP)
Translated from YAF 50 679.
BARMIN 88 SJNP 47 643 V.V. Barmin et al. (ITEP)
Translated from YAF 47 1011.
BARMIN 88B SJNP 48 1032 V.V. Barmin et al. (ITEP)
Translated from YAF 48 1719.
BOLOTOV 88 JETPL 47 7 V.N. Bolotov et al. (ASCI)
Translated from ZETFP 47 8.
GALL 88 PRL 60 186 K.P. Gall et al. (BOST, MIT, WILL, CIT+)
BARMIN 87 SJNP 45 62 V.V. Barmin et al. (ITEP)
Translated from YAF 45 97.
BOLOTOV 87 SJNP 45 1023 V.N. Bolotov et al. (INRM)
Translated from YAF 45 1652.
AMENDOLIA 86B PL B178 435 S.R. Amendolia et al. (CERN NA7 Collab.)
BOLOTOV 86 SJNP 44 73 V.N. Bolotov et al. (INRM)
Translated from YAF 44 117.
BOLOTOV 86B SJNP 44 68 V.N. Bolotov et al. (INRM)
Translated from YAF 44 108.
YAMANAKA 86 PR D34 85 T. Yamanaka et al. (KEK, TOKY)
Also PRL 52 329 R.S. Hayano et al. (TOKY, KEK)
AKIBA 85 PR D32 2911 Y. Akiba et al. (TOKY, TINT, TSUK, KEK)
BOLOTOV 85 JETPL 42 481 V.N. Bolotov et al. (INRM)
Translated from ZETFP 42 390.
ASANO 82 PL 113B 195 Y. Asano et al. (KEK, TOKY, INUS, OSAK)
COOPER 82 PL 112B 97 A.M. Cooper et al. (RL)
PDG 82B PL 111B 70 M. Roos et al. (HELS, CIT, CERN)
ASANO 81B PL 107B 159 Y. Asano et al. (KEK, TOKY, INUS, OSAK)
CAMPBELL 81 PRL 47 1032 M.K. Campbell et al. (YALE, BNL)
Also PR D27 1056 S.R. Blatt et al. (YALE, BNL)
LUM 81 PR D23 2522 G.K. Lum et al. (LBL, NBS+)
LYONS 81 ZPHY C10 215 L. Lyons, C. Albajar, G. Myatt (OXF)
DALLY 80 PRL 45 232 E.B. Dally et al. (UCLA+)
BARKOV 79 NP B148 53 L.M. Barkov et al. (NOVO, KIAE)
BLATNIK 79 LNC 24 39 S. Blatnik, J. Stahov, C.B. Lang (TUZL, GRAZ)
HEINTZE 79 NP B149 365 J. Heintze et al. (HEIDP, CERN)
ABRAMS 77 PR D15 22 R.J. Abrams et al. (BNL)
DEVAUX 77 NP B126 11 B. Devaux et al. (SACL, GEVA)
HEINTZE 77 PL 70B 482 J. Heintze et al. (HEIDP, CERN)
ROSSELET 77 PR D15 574 L. Rosselet et al. (GEVA, SACL)
BLOCH 76 PL 60B 393 P. Bloch et al. (GEVA, SACL)
BRAUN 76B LNC 17 521 H.M. Braun et al. (AACH3, BARI, BELG+)
DIAMANT-... 76 PL 62B 485 A.M. Diamant-Berger et al. (SACL, GEVA)
HEINTZE 76 PL 60B 302 J. Heintze et al. (HEIDP)
SMITH 76 NP B109 173 K.M. Smith et al. (GLAS, LIVP, OXF+)
WEISSENBE... 76 NP B115 55 A.O. Weissenberg et al. (ITEP, LEBD)
BLOCH 75 PL 56B 201 P. Bloch et al. (SACL, GEVA)
BRAUN 75 NP B89 210 H.M. Braun et al. (AACH3, BARI, BRUX+)
CHENG 75 NP A254 381 S.C. Cheng et al. (COLU, YALE)
HEARD 75 PL 55B 324 K.S. Heard et al. (CERN, HEIDH)
HEARD 75B PL 55B 327 K.S. Heard et al. (CERN, HEIDH)
SHEAFF 75 PR D12 2570 M. Sheaff (WISC)
SMITH 75 NP B91 45 K.M. Smith et al. (GLAS, LIVP, OXF+)
WEISSENBE... 74 PL 48B 474 A.O. Weissenberg et al. (ITEP, LEBD)
ABRAMS 73B PRL 30 500 R.J. Abrams et al. (BNL)
BACKENSTO... 73 PL 43B 431 G. Backenstoss et al. (CERN, KARLK, KARLE+)
LJUNG 73 PR D8 1307 D. Ljung, D. Cline (WISC)
Also PRL 28 523 D. Ljung (WISC)
Also PRL 28 1287 D. Cline, D. Ljung (WISC)
Also PRL 23 326 U. Camerini et al. (WISC)
LUCAS 73 PR D8 719 P.W. Lucas, H.D. Taft, W.J. Willis (YALE)
LUCAS 73B PR D8 727 P.W. Lucas, H.D. Taft, W.J. Willis (YALE)
PANG 73 PR D8 1989 C.Y. Pang et al. (EFI, ARIZ, LBL)
Also PL 40B 699 G.D. Cable et al. (EFI, LBL)
SMITH 73 NP B60 411 K.M. Smith et al. (GLAS, LIVP, OXF+)
ABRAMS 72 PRL 29 1118 R.J. Abrams et al. (BNL)
AUBERT 72 NC 12A 509 B. Aubert et al. (ORSAY, BRUX, EPOL)
CHIANG 72 PR D6 1254 I.H. Chiang et al. (ROCH, WISC)
CLARK 72 PRL 29 1274 A.R. Clark et al. (LBL)
FORD 72 PL 38B 335 W.T. Ford et al. (PRIN)
HOFFMASTER 72 NP B36 1 S. Hoffmaster et al. (STEV, SETO, LEHI)
BOURQUIN 71 PL 36B 615 M.H. Bourquin et al. (GEVA, SACL)
HAIDT 71 PR D3 10 D. Haidt (AACH, BARI, CERN, EPOL, NIJM+)
Also PL 29B 691 D. Haidt et al. (AACH, BARI, CERN, EPOL+)
KLEMS 71 PR D4 66 J.H. Klems, R.H. Hildebrand, R. Stiening (CHIC+)
Also PRL 24 1086 J.H. Klems, R.H. Hildebrand, R. Stiening (LRL+)
Also PRL 25 473 J.H. Klems, R.H. Hildebrand, R. Stiening (LRL+)
OTT 71 PR D3 52 R.J. Ott, T.W. Pritchard (LOQM)
ROMANO 71 PL 36B 525 F. Romano et al. (BARI, CERN, ORSAY)
SCHWEINB... 71 PL 36B 246 W. Schweinberger (AACH, BELG, CERN, NIJM+)
STEINER 71 PL 36B 521 H.J. Steiner (AACH, BARI, CERN, EPOL, ORSAY+)
BARDIN 70 PL 32B 121 D.Y. Bardin, S.N. Bilenky, B.M. Pontecorvo (JINR)
BECHERRAWY 70 PR D1 1452 T. Becherrawy (ROCH)
FORD 70 PRL 25 1370 W.T. Ford et al. (PRIN)
GAILLARD 70 CERN 70-14 J.M. Gaillard, L.M. Chounet (CERN, ORSAY)
GRAUMAN 70 PR D1 1277 J. Grauman et al. (STEV, SETO, LEHI)
Also PRL 23 737 J.U. Grauman et al. (STEV, SETO, LEHI)
PANDOULAS 70 PR D2 1205 D. Pandoulas et al. (STEV, SETO)
CUTTS 69 PR 184 1380 D. Cutts et al. (LRL, MIT)
Also PRL 20 955 D. Cutts et al. (LRL, MIT)
DAVISON 69 PR 180 1333 D.C. Davison et al. (UCR)
ELY 69 PR 180 1319 R.P.J. Ely et al. (LOUC, WISC, LRL)
HERZO 69 PR 186 1403 D. Herzo et al. (ILL)
LOBKOWICZ 69 PR 185 1676 F. Lobkowicz et al. (ROCH, BNL)
Also PRL 17 548 F. Lobkowicz et al. (ROCH, BNL)
MAST 69 PR 183 1200 T.S. Mast et al. (LRL)
SELLERI 69 NC 60A 291 F. Selleri
ZELLER 69 PR 182 1420 M.E. Zeller et al. (UCLA, LRL)
BOTTERILL 68B PRL 21 766 D.R. Botterill et al. (OXF)
BOTTERILL 68C PR 174 1661 D.R. Botterill et al. (OXF)
BUTLER 68 UCRL 18420 W.D. Butler et al. (LRL)
CHANG 68 PRL 20 510 C.Y. Chang et al. (UMD, RUTG)
CHEN 68 PRL 20 73 M. Chen et al. (LRL, MIT)
EICHTEN 68 PL 27B 586 T. Eichten (AACH, BARI, CERN, EPOL, ORSAY+)
ESCHSTRUTH 68 PR 165 1487 P.T. Eschstruth et al. (PRIN, PENN)
GARLAND 68 PR 167 1225 R. Garland et al. (COLU, RUTG, WISC)
MOSCOSO 68 Thesis L. Moscoso (ORSAY)
AUERBACH 67 PR 155 1505 L.B. Auerbach et al. (PENN, PRIN)
Also PR D9 3216 L.B. Auerbach
Erratum.
BELLOTTI 67 Heidelberg Conf. E. Bellotti, A. Pullia (MILA)
BELLOTTI 67B NC 52A 1287 E. Bellotti, E. Fiorini, A. Pullia (MILA)
Also PL 20 690 E. Bellotti et al. (MILA)
BISI 67 PL 25B 572 V. Bisi et al. (TORI)
FLETCHER 67 PRL 19 98 C.R. Fletcher et al. (ILL)
FORD 67 PRL 18 1214 W.T. Ford et al. (PRIN)
GINSBERG 67 PR 162 1570 E.S. Ginsberg (MASB)
KALMUS 67 PR 159 1187 G.E. Kalmus, A. Kernan (LRL)
ZINCHENKO 67 Thesis Rutgers A.I. Zinchenko (RUTG)
CALLAHAN 66 NC 44A 90 A.C. Callahan (WISC)
CALLAHAN 66B PR 150 1153 A.C. Callahan et al. (WISC, LRL, UCR+)
CESTER 66 PL 21 343 R. Cester et al. (PPA)
See footnote 1 in AUERBACH 67.
Also PR 155 1505 L.B. Auerbach et al. (PENN, PRIN)
BIRGE 65 PR 139 B1600 R.W. Birge et al. (LRL, WISC)
BISI 65 NC 35 768 V. Bisi et al. (TORI)
BISI 65B PR 139 B1068 V. Bisi et al. (TORI)

Downloaded from https://academic.oup.com/ptep/article/2022/8/083C01/6651666 by KIT Library user on 27 September 2022

CALLAHAN	65	PRL 15 129	A. Callahan, D. Cline	(WISC)
CLINE	65	PL 15 293	D. Cline, W.F. Fry	(WISC)
DEMARCO	65	PR 140 B1430	A. de Marco, C. Grosso, G. Rinaudo	(TORI, CERN)
FITCH	65B	PR 140 B1088	V.L. Fitch, C.A. Quarles, H.C. Wilkins	(PRIN+)
STAMER	65	PR 138 B440	P. Stamer *et al.*	(STEV)
YOUNG	65	Thesis UCRL 16362	P.S. Young	(LRL)
Also		PR 156 1464	P.S. Young, W.Z. Osborne, W.H. Barkas	(LRL)
BORREANI	64	PL 12 123	G. Borreani, G. Rinaudo, A.E. Werbrouck	(TORI)
CALLAHAN	64	PR 136 B1463	A. Callahan, R. March, R. Stark	(WISC)
GREINER	64	PRL 13 284	D.E. Greiner, W.Z. Osborne, W.H. Barkas	(LRL)
SHAKLEE	64	PR 136 B1423	F.S. Shaklee *et al.*	(MICH)
BOYARSKI	62	PR 128 2398	A.M. Boyarski *et al.*	(MIT)
FERRO-LUZZI	61	NC 22 1087	M. Ferro-Luzzi *et al.*	(LRL)
ROE	61	PRL 7 346	B.P. Roe *et al.*	(MICH, LRL)
TAYLOR	59	PR 114 359	S. Taylor *et al.*	(COLU)
COOMBES	57	PR 108 1348	C.A. Coombes *et al.*	(LBL)

OTHER RELATED PAPERS

LITTENBERG	93	ARNPS 43 729	L.S. Littenberg, G. Valencia	(BNL, FNAL)
Rare and Radiative Kaon Decays				
RITCHIE	93	RMP 65 1149	J.L. Ritchie, S.G. Wojcicki	
"Rare K Decays"				
BATTISTON	92	PRPL 214 293	R. Battiston *et al.*	(PGIA, CERN, TRSTT)
Status and Perspectives of K Decay Physics				
BRYMAN	89	IJMP A4 79	D.A. Bryman	(TRIU)
"Rare Kaon Decays"				
CHOUNET	72	PRPL 4C 199	L.M. Chounet, J.M. Gaillard, M.K. Gaillard	(ORSAY+)
FEARING	70	PR D2 542	H.W. Fearing, E. Fischbach, J. Smith	(STON, BOHR)
HAIDT	69B	PL 29B 696	D. Haidt *et al.*	(AACH, BARI, CERN, EPOL+)
CRONIN	68B	Vienna Conf. 241	J.W. Cronin	(PRIN)
Rapporteur talk.				
WILLIS	67	Heidelberg Conf. 273	W.J. Willis	(YALE)
Rapporteur talk.				
CABIBBO	66	Berkeley Conf. 33	N. Cabibbo	(CERN)
ADAIR	64	PL 12 67	R.K. Adair, L.B. Leipuner	(YALE, BNL)
CABIBBO	64	PL 9 352	N. Cabibbo, A. Maksymowicz	(CERN)
Also		PL 11 360	N. Cabibbo, A. Maksymowicz	(CERN)
Also		PL 14 72	N. Cabibbo, A. Maksymowicz	(CERN)
BIRGE	63	PRL 11 35	R.W. Birge *et al.*	(LRL, WISC, BARI)
BLOCK	62B	CERN Conf. 371	M.M. Block, L. Lendinara, L. Monari	(NWES, BGNA)
BRENE	61	NP 22 553	N. Brene, L. Egardt, B. Qvist	(NORD)

K^0

$I(J^P) = \frac{1}{2}(0^-)$

K^0 MASS

VALUE (MeV)	EVTS	DOCUMENT ID		TECN	COMMENT
497.611±0.013 OUR FIT Error includes scale factor of 1.2.					
497.611±0.013 OUR AVERAGE Error includes scale factor of 1.2.					
497.607±0.007±0.015	261k	[1] TOMARADZE	14		$\psi(2S) \to K^0_S X$
497.583±0.005±0.020	35k	AMBROSINO	07B	KLOE	$e^+e^- \to K^0_L K^0_S$
497.625±0.001±0.031	655k	LAI	02	NA48	K^0_L beam
497.661±0.033	3713	BARKOV	87B	CMD	$e^+e^- \to K^0_L K^0_S$
497.742±0.085	780	BARKOV	85B	CMD	$e^+e^- \to K^0_L K^0_S$
• • • We do not use the following data for averages, fits, limits, etc. • • •					
497.44 ±0.50		FITCH	67	OSPK	
498.9 ±0.5	4500	BALTAY	66	HBC	K^0 from $\overline{p}p$
497.44 ±0.33	2223	KIM	65B	HBC	K^0 from $\overline{p}p$
498.1 ±0.4		CHRISTENS...	64	OSPK	

[1] Obtained by analyzing CLEO-c data but not authored by the CLEO Collaboration.

$m_{K^0} - m_{K^\pm}$

VALUE (MeV)	EVTS	DOCUMENT ID		TECN	CHG	COMMENT
3.934±0.020 OUR FIT Error includes scale factor of 1.6.						
• • • We do not use the following data for averages, fits, limits, etc. • • •						
3.95 ±0.21	417	HILL	68B	DBC	+	$K^+d \to K^0pp$
3.90 ±0.25	9	BURNSTEIN	65	HBC	−	
3.71 ±0.35	7	KIM	65B	HBC	−	$K^-p \to n\overline{K}^0$
5.4 ±1.1		CRAWFORD	59	HBC	+	
3.9 ±0.6		ROSENFELD	59	HBC	−	

K^0 MEAN SQUARE CHARGE RADIUS

VALUE (fm^2)	EVTS	DOCUMENT ID		TECN	COMMENT
−0.077±0.010 OUR AVERAGE					
−0.077±0.007±0.011	5037	ABOUZAID	06	KTEV	$K^0_L \to \pi^+\pi^-e^+e^-$
−0.090±0.021		LAI	03C	NA48	$K^0_L \to \pi^+\pi^-e^+e^-$
−0.054±0.026		MOLZON	78		K_S regen. by electrons
• • • We do not use the following data for averages, fits, limits, etc. • • •					
−0.087±0.046		BLATNIK	79		VMD + dispersion relations
−0.050±0.130		FOETH	69B		K_S regen. by electrons

T-VIOLATION PARAMETER IN K^0-$\overline{K}^0$ MIXING

The asymmetry $A_T = \frac{\Gamma(\overline{K}^0 \to K^0) - \Gamma(K^0 \to \overline{K}^0)}{\Gamma(\overline{K}^0 \to K^0) + \Gamma(K^0 \to \overline{K}^0)}$ must vanish if T invariance holds.

ASYMMETRY A_T IN K^0-$\overline{K}^0$ MIXING

VALUE (units 10^{-3})	EVTS	DOCUMENT ID		TECN
6.6±1.3±1.0	640k	[1] ANGELOPO...	98E	CPLR

[1] ANGELOPOULOS 98E measures the asymmetry $A_T = [\Gamma(\overline{K}^0_{t=0} \to e^+\pi^-\nu_{t=\tau}) - \Gamma(K^0_{t=0} \to e^-\pi^+\overline{\nu}_{t=\tau})]/[\Gamma(\overline{K}^0_{t=0} \to e^+\pi^-\nu_{t=\tau}) + \Gamma(K^0_{t=0} \to e^-\pi^+\overline{\nu}_{t=\tau})]$ as a function of the neutral-kaon eigentime τ. The initial strangeness of the neutral kaon is tagged by the charge of the accompanying charged kaon in the reactions $p\overline{p} \to K^-\pi^+K^0$ and $p\overline{p} \to K^+\pi^-\overline{K}^0$. The strangeness at the time of the decay is tagged by the lepton charge. The reported result is the average value of A_T over the interval $1\tau_S < \tau < 20\tau_S$. From this value of A_T ANGELOPOULOS 01B, assuming CPT invariance in the $e\pi\nu$ decay amplitude, determine the T-violating as $\Delta S = \Delta S$ conserving parameter (for its definition, see Review below) $4\mathrm{Re}(\epsilon) = (6.2 \pm 1.4 \pm 1.0) \times 10^{-3}$.

See the related review(s):
CPT Invariance Tests in Neutral Kaon Decay

CP-VIOLATION PARAMETERS

Re(ϵ)

VALUE (units 10^{-3})	DOCUMENT ID		TECN
1.596±0.013	[1] AMBROSINO	06H	KLOE
• • • We do not use the following data for averages, fits, limits, etc. • • •			
1.664±0.010	[2] LAI	05A	NA48

[1] AMBROSINO 06H uses Bell-Steinberger relations with the following measurements: $B(K^0_L \to \pi^+\pi^-)$ in AMBROSINO 06F, $B(K^0_S \to \pi^0\pi^0\pi^0)$ in AMBROSINO 05B, the K^0_S-semileptonic charge asymmetry in AMBROSINO 06E, and K^0-semileptonic results in ANGELOPOULOS 98F.
[2] LAI 05A values are obtained through unitarity (Bell-Steinberger relations), improving determination of η_{000} and combining other data from PDG 04 and APOSTOLAKIS 99B.

CPT-VIOLATION PARAMETERS

In K^0-$\overline{K}^0$ mixing, if CP-violating interactions include a T conserving part then

$$|K_S\rangle = [|K_1\rangle + (\epsilon+\delta)|K_2\rangle]/\sqrt{1+|\epsilon+\delta|^2}$$
$$|K_L\rangle = [|K_2\rangle + (\epsilon-\delta)|K_1\rangle]/\sqrt{1+|\epsilon-\delta|^2}$$

where

$$|K_1\rangle = [|K^0\rangle + |\overline{K}^0\rangle]/\sqrt{2}$$
$$|K_2\rangle = [|K^0\rangle - |\overline{K}^0\rangle]/\sqrt{2}$$

and

$$|\overline{K}^0\rangle = CP|K^0\rangle.$$

The parameter δ specifies the CPT-violating part.

Estimates of δ are given below assuming the validity of the $\Delta S = \Delta Q$ rule. See also THOMSON 95 for a test of CPT-symmetry conservation in K^0 decays using the Bell-Steinberger relation.

REAL PART OF δ

A nonzero value violates CPT invariance.

VALUE (units 10^{-4})	EVTS	DOCUMENT ID		TECN	COMMENT
2.51± 2.25		[1] ABOUZAID	11	KTEV	
• • • We do not use the following data for averages, fits, limits, etc. • • •					
2.3 ± 2.7		[2] AMBROSINO	06H	KLOE	
2.4 ± 2.8		[3] APOSTOLA...	99B	RVUE	
2.9 ± 2.6 ±0.6	1.3M	[4] ANGELOPO...	98F	CPLR	
180 ±200	6481	[5] DEMIDOV	95		$K_{\ell 3}$ reanalysis

[1] ABOUZAID 11 uses Bell-Steinberger relations.
[2] AMBROSINO 06H uses Bell-Steinberger relations with the following measurements: $B(K^0_L \to \pi^+\pi^-)$ in AMBROSINO 06F, $B(K^0_S \to \pi^0\pi^0\pi^0)$ in AMBROSINO 05B, the K^0_S-semileptonic charge asymmetry in AMBROSINO 06E, and K^0-semileptonic results in ANGELOPOULOS 98F.
[3] APOSTOLAKIS 99B assumes only unitarity and combines CPLEAR and other results.
[4] ANGELOPOULOS 98F use $\Delta S = \Delta Q$. If $\Delta S = \Delta Q$ is not assumed, they find $\mathrm{Re}\delta = (3.0 \pm 3.3 \pm 0.6) \times 10^{-4}$.
[5] DEMIDOV 95 reanalyzes data from HART 73 and NIEBERGALL 74.

IMAGINARY PART OF δ

A nonzero value violates CPT invariance.

VALUE (units 10^{-5})	EVTS	DOCUMENT ID		TECN	COMMENT
− 1.5± 1.6		[1] ABOUZAID	11	KTEV	
• • • We do not use the following data for averages, fits, limits, etc. • • •					
0.4± 2.1		[2] AMBROSINO	06H	KLOE	
− 0.2± 2.0		[3] LAI	05A	NA48	
2.4± 5.0		[4] APOSTOLA...	99B	RVUE	
− 90 ± 290 ±100	1.3M	[5] ANGELOPO...	98F	CPLR	
2100 ±3700	6481	[6] DEMIDOV	95		$K_{\ell 3}$ reanalysis

[1] ABOUZAID 11 uses Bell-Steinberger relations.
[2] AMBROSINO 06H uses Bell-Steinberger relations with the following measurements: $B(K^0_L \to \pi^+\pi^-)$ in AMBROSINO 06F, $B(K^0_S \to \pi^0\pi^0\pi^0)$ in AMBROSINO 05B, the K^0_S-semileptonic charge asymmetry in AMBROSINO 06E, and K^0-semileptonic results in ANGELOPOULOS 98F.
[3] LAI 05A values are obtained through unitarity (Bell-Steinberger relations), improving determination of η_{000} and combining other data from PDG 04 and APOSTOLAKIS 99B.
[4] APOSTOLAKIS 99B assumes only unitarity and combines CPLEAR and other results.
[5] If $\Delta S = \Delta Q$ is not assumed, ANGELOPOULOS 98F finds $\mathrm{Im}\delta = (-15 \pm 23 \pm 3) \times 10^{-3}$.
[6] DEMIDOV 95 reanalyzes data from HART 73 and NIEBERGALL 74.

Downloaded from https://academic.oup.com/ptep/article/2022/8/083C01/6651666 by KIT Library user on 27 September 2022

Re(y)

A non-zero value would violate CPT invariance in $\Delta S = \Delta Q$ amplitude. Re(y) is the following combination of K_{e3} decay amplitudes:

$$\mathrm{Re(y)} = \mathrm{Re}\left(\frac{A(\overline{K}^0 \to e^- \pi^+ \overline{\nu}_e)^* - A(K^0 \to e^+ \pi^- \nu_e)}{A(\overline{K}^0 \to e^- \pi^+ \overline{\nu}_e)^* + A(K^0 \to e^+ \pi^- \nu_e)} \right)$$

VALUE (units 10^{-3})	EVTS	DOCUMENT ID	TECN
0.4±2.5	13k	[1] AMBROSINO 06E	KLOE
• • • We do not use the following data for averages, fits, limits, etc. • • •			
0.3±3.1		[2] APOSTOLA... 99B	CPLR

[1] They use the PDG 04 for the K^0_L semileptonic charge asymmetry and PDG 04 (CP review, CPT NOT ASSUMED) for Re(ϵ).

[2] Constrained by Bell-Steinberger (or unitarity) relation.

Re(x_)

A non-zero value would violate CPT invariance in decay amplitudes with $\Delta S \neq \Delta Q$. x_, used here to define Re(x_), and x_+, used below in the $\Delta S = \Delta Q$ section are the following combinations of K_{e3} decay amplitudes:

$$x_\pm = \frac{1}{2}\left(\frac{A(\overline{K}^0 \to \pi^- e^+ \nu_e)}{A(K^0 \to \pi^- e^+ \nu_e)} \pm \frac{A(K^0 \to \pi^+ e^- \overline{\nu}_e)^*}{A(\overline{K}^0 \to \pi^+ e^- \overline{\nu}_e)^*} \right).$$

VALUE (units 10^{-3})	EVTS	DOCUMENT ID	TECN	COMMENT
−2.9± 2.0		[1] AMBROSINO 06H	KLOE	
• • • We do not use the following data for averages, fits, limits, etc. • • •				
−0.8± 2.5	13k	[2] AMBROSINO 06E	KLOE	
−0.5± 3.0		[3] APOSTOLA... 99B	CPLR	Strangeness tagged
2 ±13 ±3	650k	ANGELOPO... 98F	CPLR	Strangeness tagged

[1] AMBROSINO 06H uses Bell-Steinberger relations with the following measurements: B($K^0_L \to \pi^+\pi^-$) in AMBROSINO 06F, B($K^0_S \to \pi^0\pi^0\pi^0$) in AMBROSINO 05B, the K^0_S-semileptonic charge asymmetry in AMBROSINO 06E, and K^0-semileptonic results in ANGELOPOULOS 98F.

[2] Uses PDG 04 for the K^0_L semileptonic charge asymmetry and Re(δ) from CPLEAR, ANGELOPOULOS 98F.

[3] Constrained by Bell-Steinberger (or unitarity) relation.

$|m_{K^0} - m_{\overline{K}^0}| / m_{\text{average}}$

A test of CPT invariance. "Our Evaluation" is described in the "Tests of Conservation Laws" section. It assumes CPT invariance in the decay and neglects some contributions from decay channels other than $\pi\pi$.

VALUE	CL%	DOCUMENT ID	TECN
$<6 \times 10^{-19}$	90	PDG 12	
• • • We do not use the following data for averages, fits, limits, etc. • • •			
$(-3 \pm 4) \times 10^{-18}$		[1] ANGELOPO... 99B	RVUE

[1] ANGELOPOULOS 99B assumes only unitarity and combines CPLEAR and other results.

$(\Gamma_{K^0} - \Gamma_{\overline{K}^0})/m_{\text{average}}$

A test of CPT invariance.

VALUE	DOCUMENT ID	TECN
$(7.8\pm8.4) \times 10^{-18}$	[1] ANGELOPO... 99B	RVUE

[1] ANGELOPOULOS 99B assumes only unitarity and combines CPLEAR with other results. Correlated with $(m_{K^0} - m_{\overline{K}^0}) / m_{\text{average}}$ with a correlation coefficient of −0.95.

TESTS OF $\Delta S = \Delta Q$ RULE

Re(x_+)

A non-zero value would violate the $\Delta S = \Delta Q$ rule in CPT conserving transitions. x_+ is defined above in the Re(x_) section.

VALUE (units 10^{-3})	EVTS	DOCUMENT ID	TECN
−0.9± 3.0 OUR AVERAGE			
−2 ±10		[1] BATLEY 07D	NA48
−0.5± 3.6	13k	[2] AMBROSINO 06E	KLOE
−1.8± 6.1		[3] ANGELOPO... 98D	CPLR

[1] Result obtained from the measurement $\Gamma(K^0_S \to \pi e \nu) / \Gamma(K^0_L \to \pi e \nu) = 0.993 \pm 0.34$, neglecting possible CPT non-invariance and using PDG 06 values of B($K^0_L \to \pi e \nu$) = 0.4053 ± 0.0015, $\tau_L = (5.114 \pm 0.021) \times 10^{-8}$ s and $\tau_S = (0.8958 \pm 0.0005) \times 10^{-10}$ s.

[2] Re(x_+) can be shown to be equal to the following combination of rates:

$$\mathrm{Re}(x_+) = \frac{1}{2} \frac{\Gamma(K^0_S \to \pi e \nu) - \Gamma(K^0_L \to \pi e \nu)}{\Gamma(K^0_S \to \pi e \nu) + \Gamma(K^0_L \to \pi e \nu)}$$

which is valid up to first order in terms violating CPT and/or the $\Delta S = \Delta Q$ rule.

[3] Obtained neglecting CPT violating amplitudes.

K^0 REFERENCES

TOMARADZE	14	PR D89 031501	A. Tomaradze et al.	(NWES, WAYN)
PDG	12	PR D86 010001	J. Beringer et al.	(PDG Collab.)
ABOUZAID	11	PR D83 092001	E. Abouzaid et al.	(FNAL KTeV Collab.)
AMBROSINO	07B	JHEP 0712 073	F. Ambrosino et al.	(KLOE Collab.)
BATLEY	07D	PL B653 145	J.R. Batley et al.	(CERN NA48 Collab.)
ABOUZAID	06	PRL 96 101801	E. Abouzaid et al.	(KTeV Collab.)
AMBROSINO	06E	PL B636 173	F. Ambrosino et al.	(KLOE Collab.)
AMBROSINO	06F	PL B638 140	F. Ambrosino et al.	(KLOE Collab.)
AMBROSINO	06H	JHEP 0612 011	F. Ambrosino et al.	(KLOE Collab.)
PDG	06	JP G33 1	W.-M. Yao et al.	(PDG Collab.)
AMBROSINO	05B	PL B619 61	F. Ambrosino et al.	(KLOE Collab.)
LAI	05A	PL B610 165	A. Lai et al.	(CERN NA48 Collab.)
PDG	04	PL B592 1	S. Eidelman et al.	(PDG Collab.)
LAI	03C	EPJ C30 33	A. Lai et al.	(CERN NA48 Collab.)
LAI	02	PL B533 196	A. Lai et al.	(CERN NA48 Collab.)
ANGELOPO...	01B	EPJ C22 55	A. Angelopoulos et al.	(CPLEAR Collab.)
ANGELOPO...	99B	PL B471 332	A. Angelopoulos et al.	(CPLEAR Collab.)
APOSTOLA...	99B	PL B456 297	A. Apostolakis et al.	(CPLEAR Collab.)
ANGELOPO...	98D	PL B444 38	A. Angelopoulos et al.	(CPLEAR Collab.)
Also		EPJ C22 55	A. Angelopoulos et al.	(CPLEAR Collab.)
ANGELOPO...	98E	PL B444 43	A. Angelopoulos et al.	(CPLEAR Collab.)
ANGELOPO...	98F	PL B444 52	A. Angelopoulos et al.	(CPLEAR Collab.)
Also		EPJ C22 55	A. Angelopoulos et al.	(CPLEAR Collab.)
DEMIDOV	95	PAN 58 968	V. Demidov, K. Gusev, E. Shabalin	(ITEP)
From YAF 58 1041.				
THOMSON	95	PR D51 1412	G.B. Thomson, Y. Zou	(RUTG)
BARKOV	87B	SJNP 46 630	L.M. Barkov et al.	(NOVO)
Translated from YAF 46 1088.				
BARKOV	85B	JETPL 42 138	L.M. Barkov et al.	(NOVO)
Translated from ZETFP 42 113.				
BLATNIK	79	LNC 24 39	S. Blatnik, J. Stahov, C.B. Lang	(TUZL, GRAZ)
MOLZON	78	PRL 41 1213	W.R. Molzon et al.	(EFI+)
NIEBERGALL	74	PL 49B 103	F. Niebergall et al.	(CERN, ORSAY, VIEN)
HART	73	NP B66 317	J.C. Hart et al.	(CAVE, RHEL)
FOETH	69B	PL 30B 276	H. Foeth et al.	(AACH, CERN, TORI)
HILL	68B	PR 168 1534	D.G. Hill et al.	(BNL, CMU)
FITCH	67	PR 164 1711	V.L. Fitch et al.	(PRIN)
BALTAY	66	PR 142 932	C. Baltay et al.	(YALE, BNL)
BURNSTEIN	65	PR 138 B895	R.A. Burnstein, H.A. Rubin	(UMD)
KIM	65B	PR 140 B1334	J.K. Kim, L. Kirsch, D. Miller	(COLU)
CHRISTENS...	64	PRL 13 138	J.H. Christenson et al.	(PRIN)
CRAWFORD	59	PRL 2 112	F.S. Crawford et al.	(LRL)
ROSENFELD	59	PRL 2 110	A.H. Rosenfeld, F.T. Solmitz, R.D. Tripp	(LRL)

K^0_S

$I(J^P) = \frac{1}{2}(0^-)$

K^0_S MEAN LIFE

For earlier measurements, beginning with BOLDT 58B, see our 1986 edition, Physics Letters **170B** 130 (1986).

OUR FIT is described in the note on "CP violation in K_L decays" in the K^0_L Particle Listings. The result labeled "OUR FIT Assuming CPT" ["OUR FIT Not assuming CPT"] includes all measurements except those with the comment "Not assuming CPT" ["Assuming CPT"]. Measurements with neither comment do not assume CPT and enter both fits.

VALUE (10^{-10} s)	EVTS	DOCUMENT ID		TECN	COMMENT
0.8954 ±0.0004 OUR FIT Error includes scale factor of 1.1. Assuming CPT					
0.89564±0.00033 OUR FIT Not assuming CPT					
0.89589±0.00070		[1,2] ABOUZAID	11	KTEV	Not assuming CPT
0.89623±0.00047		[1,3] ABOUZAID	11	KTEV	Assuming CPT
0.89562±0.00029±0.00043	20M	[4] AMBROSINO	11	KLOE	Not assuming CPT
0.89598±0.00048±0.00051	16M	LAI	02C	NA48	
0.8971 ±0.0021		BERTANZA	97	NA31	
0.8941 ±0.0014 ±0.0009		SCHWINGEN...	95	E773	Assuming CPT
0.8929 ±0.0016		GIBBONS	93	E731	Assuming CPT
• • • We do not use the following data for averages, fits, limits, etc. • • •					
0.8965 ±0.0007		[5] ALAVI-HARATI	03	KTEV	Assuming CPT
0.8958 ±0.0013		[6] ALAVI-HARATI	03	KTEV	Not assuming CPT
0.8920 ±0.0044	214k	GROSSMAN	87	SPEC	
0.905 ±0.007		[7] ARONSON	82B	SPEC	
0.881 ±0.009	26k	ARONSON	76	SPEC	
0.8926 ±0.0032 ±0.0002		[8] CARITHERS	75	SPEC	
0.8937 ±0.0048	6M	GEWENIGER	74B	ASPK	
0.8958 ±0.0045	50k	[9] SKJEGGEST...	72	HBC	
0.856 ±0.008	19994	[10] DONALD	68B	HBC	
0.872 ±0.009	20000	[9,10] HILL	68	DBC	

[1] The two ABOUZAID 11 values use the same full KTeV dataset from 1996, 1997, and 1999. The first enters the "assuming CPT" fit and the second enters the "not assuming CPT" fit.

[2] ABOUZAID 11 fit has Δm, τ_S, ϕ_ϵ, Re(ϵ'/ϵ), and Im(ϵ'/ϵ) as free parameters. See Im(ϵ'/ϵ) in the "K^0_L CP violation" section for correlation information.

[3] ABOUZAID 11 fit has Δm and τ_S free but constrains ϕ_ϵ to the Superweak value, i.e. assumes CPT. This τ_S value is correlated with their $\Delta m = m_{K^0_L} - m_{K^0_S}$ measurement in the K^0_L listings. The correlation coefficient $\rho(\tau_S, \Delta m) = -0.670$.

[4] Fit to the proper time distribution.

[5] This ALAVI-HARATI 03 fit has Δm and τ_S free but constrains ϕ_{+-} to the Superweak value, i.e. assumes CPT. This τ_S value is correlated with their $\Delta m = m_{K^0_L} - m_{K^0_S}$ measurement in the K^0_L listings. The correlation coefficient $\rho(\tau_S, \Delta m) = -0.396$. Superseded by ABOUZAID 11.

[6] This ALAVI-HARATI 03 fit has Δm, ϕ_{+-}, and τ_{K_S} free. See ϕ_{+-} in the "K_L CP violation" section for correlation information. Superseded by ABOUZAID 11.

[7] ARONSON 82 find that K^0_S mean life may depend on the kaon energy.

[8] CARITHERS 75 measures the Δm dependence of the total decay rate (inverse mean life) to be $\Gamma(K^0_S) = [(1.122 \pm 0.004) + 0.16(\Delta m - 0.5348)/\Delta m] 10^{10}$/s, or, in terms of mean life, CARITHERS 75 measures $\tau_S = (0.8913 \pm 0.0032) - 0.238\,[\Delta m - 0.5348]$ (10^{-10} s). We have adjusted the measurement to use our best values of ($\Delta m = 0.5293 \pm 0.0009$) ($10^{10}$ $\hbar$ s^{-1}). Our first error is their experiment's error and our second error is the systematic error from using our best values.

Downloaded from https://academic.oup.com/ptep/article/2022/8/083C01/6651666 by KIT Library user on 27 September 2022

[9] HILL 68 has been changed by the authors from the published value (0.865 ± 0.009) because of a correction in the shift due to η_{+-}. SKJEGGESTAD 72 and HILL 68 give detailed discussions of systematics encountered in this type of experiment.
[10] Pre-1971 experiments are excluded from the average because of disagreement with later more precise experiments.

K^0_S DECAY MODES

	Mode		Fraction (Γ_i/Γ)	Scale factor/ Confidence level
	Hadronic modes			
Γ_1	$\pi^0\pi^0$		(30.69 ± 0.05) %	
Γ_2	$\pi^+\pi^-$		(69.20 ± 0.05) %	
Γ_3	$\pi^+\pi^-\pi^0$		$(3.5\ ^{+1.1}_{-0.9})\times10^{-7}$	
	Modes with photons or $\ell\overline{\ell}$ pairs			
Γ_4	$\pi^+\pi^-\gamma$	[a,b]	$(1.79\pm0.05)\times10^{-3}$	
Γ_5	$\pi^+\pi^-e^+e^-$		$(4.79\pm0.15)\times10^{-5}$	
Γ_6	$\pi^0\gamma\gamma$	[a]	$(4.9\ \pm1.8)\times10^{-8}$	
Γ_7	$\gamma\gamma$		$(2.63\pm0.17)\times10^{-6}$	S=3.1
	Semileptonic modes			
Γ_8	$\pi^\pm e^\mp\nu_e$	[c]	$(7.04\pm0.08)\times10^{-4}$	
Γ_9	$\pi^\pm\mu^\mp\nu_\mu$	[c,d]	$(4.56\pm0.20)\times10^{-4}$	
	***CP* violating (*CP*) and $\Delta S=1$ weak neutral current (*S1*) modes**			
Γ_{10}	$3\pi^0$	*CP*	$<2.6\times10^{-8}$	CL=90%
Γ_{11}	$\mu^+\mu^-$	*S1*	$<2.1\times10^{-10}$	CL=90%
Γ_{12}	e^+e^-	*S1*	$<9\times10^{-9}$	CL=90%
Γ_{13}	$\pi^0e^+e^-$	*S1*	[a] $(3.0\ ^{+1.5}_{-1.2})\times10^{-9}$	
Γ_{14}	$\pi^0\mu^+\mu^-$	*S1*	$(2.9\ ^{+1.5}_{-1.2})\times10^{-9}$	

[a] See the Particle Listings below for the energy limits used in this measurement.
[b] Most of this radiative mode, the low-momentum γ part, is also included in the parent mode listed without γ's.
[c] The value is for the sum of the charge states or particle/antiparticle states indicated.
[d] Not a measurement. Calculated as $0.666\cdot B(\pi^\pm e^\mp\nu_e)$.

CONSTRAINED FIT INFORMATION

An overall fit to 4 branching ratios uses 5 measurements and one constraint to determine 4 parameters. The overall fit has a $\chi^2=0.1$ for 2 degrees of freedom.

The following *off-diagonal* array elements are the correlation coefficients $\langle\delta x_i\delta x_j\rangle/(\delta x_i\cdot\delta x_j)$, in percent, from the fit to the branching fractions, $x_i\equiv\Gamma_i/\Gamma_{total}$. The fit constrains the x_i whose labels appear in this array to sum to one.

	x_1	x_2	x_8
x_2	−100		
x_8	−6	4	
x_9	−1	−3	0

K^0_S DECAY RATES

$\Gamma(\pi^\pm e^\mp\nu_e)$ — Γ_8

VALUE (10^6 s^{-1})	EVTS	DOCUMENT ID		TECN	COMMENT
• • • We do not use the following data for averages, fits, limits, etc. • • •					
8.1 ±1.6	75	[1] AKHMETSHIN	99	CMD2	Tagged K^0_S using $\phi\to K^0_LK^0_S$
7.50±0.08		[2] PDG	98		
seen		BURGUN	72	HBC	$K^+p\to K^0p\pi^+$
9.3 ±2.5		AUBERT	65	HLBC	$\Delta S=\Delta Q$, *CP* cons. not assumed

[1] AKHMETSHIN 99 is from a measured branching ratio $B(K^0_S\to\pi e\nu_e)=(7.2\pm1.4)\times10^{-4}$ and $\tau_{K^0_S}=(0.8934\pm0.0008)\times10^{-10}$ s. Not independent of measured branching ratio.
[2] PDG 98 from K^0_L measurements, assuming that $\Delta S=\Delta Q$ in K^0 decay so that $\Gamma(K^0_S\to\pi^\pm e^\mp\nu_e)=\Gamma(K^0_L\to\pi^\pm e^\mp\nu_e)$.

$\Gamma(\pi^\pm\mu^\mp\nu_\mu)$ — Γ_9

VALUE (10^6 s^{-1})	DOCUMENT ID	
• • • We do not use the following data for averages, fits, limits, etc. • • •		
5.25±0.07	[1] PDG	98

[1] PDG 98 from K^0_L measurements, assuming that $\Delta S=\Delta Q$ in K^0 decay so that $\Gamma(K^0_S\to\pi^\pm\mu^\mp\nu_\mu)=\Gamma(K^0_L\to\pi^\pm\mu^\mp\nu_\mu)$.

K^0_S BRANCHING RATIOS

Hadronic modes

$\Gamma(\pi^0\pi^0)/\Gamma_{total}$ — Γ_1/Γ

VALUE	EVTS	DOCUMENT ID		TECN
0.3069±0.0005 OUR FIT				
• • • We do not use the following data for averages, fits, limits, etc. • • •				
0.335 ±0.014	1066	BROWN	63	HLBC
0.288 ±0.021	198	CHRETIEN	63	HLBC
0.30 ±0.035		BROWN	61	HLBC

$\Gamma(\pi^+\pi^-)/\Gamma_{total}$ — Γ_2/Γ

VALUE	EVTS	DOCUMENT ID		TECN	COMMENT
0.6920±0.0005 OUR FIT					
• • • We do not use the following data for averages, fits, limits, etc. • • •					
0.670 ±0.010	3447	DOYLE	69	HBC	$\pi^-p\to\Lambda K^0$

$\Gamma(\pi^+\pi^-)/\Gamma(\pi^0\pi^0)$ — Γ_2/Γ_1

VALUE	EVTS	DOCUMENT ID		TECN	COMMENT
2.255 ±0.005 OUR FIT					
2.2549±0.0054		[1] AMBROSINO	06C	KLOE	
• • • We do not use the following data for averages, fits, limits, etc. • • •					
2.2555±0.0012±0.0054		[2] AMBROSINO	06C	KLOE	
2.236 ±0.003 ±0.015	766k	[2] ALOISIO	02B	KLOE	
2.11 ±0.09	1315	EVERHART	76	WIRE	$\pi^-p\to\Lambda K^0$
2.169 ±0.094	16k	COWELL	74	OSPK	$\pi^-p\to\Lambda K^0$
2.16 ±0.08	4799	HILL	73	DBC	$K^+d\to K^0pp$
2.22 ±0.10	3068	[3] ALITTI	72	HBC	$K^+p\to\pi^+pK^0$
2.22 ±0.08	6380	MORSE	72B	DBC	$K^+n\to K^0p$
2.10 ±0.11	701	[4] NAGY	72	HLBC	$K^+n\to K^0p$
2.22 ±0.095	6150	[5] BALTAY	71	HBC	$Kp\to K^0$neutrals
2.282 ±0.043	7944	[6] MOFFETT	70	OSPK	$K^+n\to K^0p$
2.12 ±0.17	267	[4] BOZOKI	69	HLBC	
2.285 ±0.055	3016	[6] GOBBI	69	OSPK	$K^+n\to K^0p$
2.10 ±0.06	3700	MORFIN	69	HLBC	$K^+n\to K^0p$

[1] This result combines AMBROSINO 06C KLOE 2001-02 data with ALOISIO 02B KLOE 2000 data. $K^0_S\to\pi^+\pi^-$ fully inclusive.
[2] Includes radiative decays $\pi^+\pi^-\gamma$.
[3] The directly measured quantity is $K^0_S\to\pi^+\pi^-/$all $K^0=0.345\pm0.005$.
[4] NAGY 72 is a final result which includes BOZOKI 69.
[5] The directly measured quantity is $K^0_S\to\pi^+\pi^-/$all $\overline{K}^0=0.345\pm0.005$.
[6] MOFFETT 70 is a final result which includes GOBBI 69.

$\Gamma(\pi^+\pi^-\pi^0)/\Gamma_{total}$ — Γ_3/Γ

VALUE (units 10^{-7})	EVTS	DOCUMENT ID		TECN	COMMENT
$3.5^{+1.1}_{-0.9}$ OUR AVERAGE					
$4.7^{+2.2}_{-1.7}\pm^{1.7}_{1.5}$		[1] BATLEY	05	NA48	
$2.5^{+1.3}_{-1.0}\pm^{0.5}_{0.6}$	500k	[2] ADLER	97B	CPLR	
$4.8^{+2.2}_{-1.6}\pm1.1$		[3] ZOU	96	E621	
• • • We do not use the following data for averages, fits, limits, etc. • • •					
$4.1^{+2.5}_{-1.9}\pm^{0.5}_{0.6}$		[4] ADLER	96E	CPLR	Sup. by ADLER 97B
$3.9^{+5.4}_{-1.8}\pm^{0.9}_{0.7}$		[5] THOMSON	94	E621	Sup. by ZOU 96

[1] BATLEY 05 is obtained by measuring the interference parameters in K_S, $K_L\to\pi^+\pi^-\pi^0$: $Re(\lambda)=0.038\pm0.008\pm0.006$ and $Im(\lambda)=-0.013\pm0.005\pm0.004$; the correlation coeff. between $Re(\lambda)$ and $Im(\lambda)$ is 0.66 (statistical only).
[2] ADLER 97B find the *CP*-conserving parameters $Re(\lambda)=(28\pm7\pm3)\times10^{-3}$, $Im(\lambda)=(-10\pm8\pm2)\times10^{-3}$. They estimate $B(K^0_S\to\pi^+\pi^-\pi^0)$ from $Re(\lambda)$ and the K^0_L decay parameters. See also ANGELOPOULOS 98C.
[3] ZOU 96 is from the the measured quantities $|\rho_{+-0}|=0.039^{+0.009}_{-0.006}\pm0.005$ and $\phi_\rho=(-9\pm18)^\circ$.
[4] ADLER 96E is from the measured quantities $Re(\lambda)=0.036\pm0.010^{+0.002}_{-0.003}$ and $Im(\lambda)$ consistent with zero. Note that the quantity λ is the same as ρ_{+-0} used in other footnotes.
[5] THOMSON 94 calculates this branching ratio from their measurements $|\rho_{+-0}|=0.035^{+0.019}_{-0.011}\pm0.004$ and $\phi_\rho=(-59\pm48)^\circ$ where $|\rho_{+-0}|e^{i\phi_\rho}=A(K^0_S\to\pi^+\pi^-\pi^0, l=2)/A(K^0_L\to\pi^+\pi^-\pi^0)$.

Modes with photons or $\ell\overline{\ell}$ pairs

$\Gamma(\pi^+\pi^-\gamma)/\Gamma(\pi^+\pi^-)$ — Γ_4/Γ_2

VALUE (units 10^{-3})	EVTS	DOCUMENT ID		TECN	COMMENT
2.59±0.08 OUR AVERAGE					
2.56±0.09	1286	RAMBERG	93	E731	p_γ >50 MeV/c
2.68±0.15		[1] TAUREG	76	SPEC	p_γ >50 MeV/c

Downloaded from https://academic.oup.com/ptep/article/2022/8/083C01/6651666 by KIT Library user on 27 September 2022

• • • We do not use the following data for averages, fits, limits, etc. • • •

7.10±0.22	3723	RAMBERG	93	E731	p_γ	>20 MeV/c
3.0 ±0.6	29	[2] BOBISUT	74	HLBC	p_γ	>40 MeV/c
2.8 ±0.6		[3] BURGUN	73	HBC	p_γ	>50 MeV/c

[1] TAUREG 76 find direct emission contribution <0.06, CL = 90%.
[2] BOBISUT 74 not included in average because p_γ cut differs. Estimates direct emission contribution to be 0.5 or less, CL = 95%.
[3] BURGUN 73 estimates that direct emission contribution is 0.3 ± 0.6.

$\Gamma(\pi^+\pi^-e^+e^-)/\Gamma_{total}$ — Γ_5/Γ

VALUE (units 10^{-5})	EVTS	DOCUMENT ID		TECN	COMMENT
4.79±0.15 OUR AVERAGE					
4.83±0.11±0.14	23k	[1] BATLEY	11	NA48	2002 data
4.69±0.30	676	[2] LAI	03C	NA48	1998+1999 data
• • • We do not use the following data for averages, fits, limits, etc. • • •					
4.71±0.23±0.22	620	[2,3] LAI	03C	NA48	1999 data
4.5 ±0.7 ±0.4	56	LAI	00B	NA48	1998 data

[1] BATLEY 11 reports $[\Gamma(K^0_S \to \pi^+\pi^-e^+e^-)/\Gamma_{total}]$ / $[B(K^0_L \to \pi^+\pi^-\pi^0)]$ / $[B(\pi^0 \to e^+e^-\gamma)] = (3.28 \pm 0.06 \pm 0.04) \times 10^{-2}$ which we multiply by our best values $B(K^0_L \to \pi^+\pi^-\pi^0) = (12.54 \pm 0.05) \times 10^{-2}$, $B(\pi^0 \to e^+e^-\gamma) = (1.174 \pm 0.035) \times 10^{-2}$. Our first error is their experiment's error and our second error is the systematic error from using our best values. Also a limit on the absolute value of the interference between bremsstrahlung and E1 transition is given : $< 4 \times 10^{-7}$ at 90% C.L.
[2] Uses normalization $BR(K_L \to \pi^+\pi^-\pi^0)*BR(\pi^0 \to e^+e^-) = (1.505 \pm 0.047) \times 10^{-3}$ from our 2000 Edition.
[3] Second error is 0.16(syst) ± 0.15(norm) combined in quadrature.

$\Gamma(\pi^0\gamma\gamma)/\Gamma_{total}$ — Γ_6/Γ

VALUE (units 10^{-8})	CL%	EVTS	DOCUMENT ID		TECN	COMMENT
4.9±1.6±0.9		17	[1] LAI	04	NA48	$m^2_{\gamma\gamma}/m^2_K > 0.2$
• • • We do not use the following data for averages, fits, limits, etc. • • •						
<33	90		LAI	03B	NA48	$m^2_{\gamma\gamma}/m^2_K > 0.2$

[1] Spectrum also measured and found consistent with the one generated by a constant matrix element.

$\Gamma(\gamma\gamma)/\Gamma_{total}$ — Γ_7/Γ

VALUE (units 10^{-6})	CL%	EVTS	DOCUMENT ID		TECN	COMMENT
2.63 ±0.17 OUR AVERAGE			Error includes scale factor of 3.1.			
2.26 ±0.12 ±0.06		711	[1] AMBROSINO	08C	KLOE	$\phi \to K^0_S K^0_L$
2.713±0.063±0.005		7.5k	[2] LAI	03	NA48	
• • • We do not use the following data for averages, fits, limits, etc. • • •						
2.58 ±0.36 ±0.22		149	LAI	00	NA48	
2.2 ±1.1		16	[3] BARR	95B	NA31	
2.4 ±0.9		35	[4] BARR	95B	NA31	
< 13	90		BALATS	89	SPEC	
2.4 ±1.2		19	BURKHARDT	87	NA31	
<133	90		BARMIN	86B	XEBC	

[1] AMBROSINO 08C reports $(2.26 \pm 0.12 \pm 0.06) \times 10^{-6}$ from a measurement of $[\Gamma(K^0_S \to \gamma\gamma)/\Gamma_{total}] \times [B(K^0_S \to \pi^0\pi^0)]$ assuming $B(K^0_S \to \pi^0\pi^0) = (30.69 \pm 0.05) \times 10^{-2}$.
[2] LAI 03 reports $[\Gamma(K^0_S \to \gamma\gamma)/\Gamma_{total}]$ / $[B(K^0_S \to \pi^0\pi^0)] = (8.84 \pm 0.18 \pm 0.10) \times 10^{-6}$ which we multiply by our best value $B(K^0_S \to \pi^0\pi^0) = (30.69 \pm 0.05) \times 10^{-2}$. Our first error is their experiment's error and our second error is the systematic error from using our best value.
[3] BARR 95B result is calculated using $B(K_L \to \gamma\gamma) = (5.86 \pm 0.17) \times 10^{-4}$.
[4] BARR 95B quotes this as the combined BARR 95B + BURKHARDT 87 result after rescaling BURKHARDT 87 to use same branching ratios and lifetimes as BARR 95B.

Semileptonic modes

$\Gamma(\pi^\pm e^\mp \nu_e)/\Gamma_{total}$ — Γ_8/Γ

VALUE (units 10^{-4})	EVTS	DOCUMENT ID		TECN	COMMENT
7.04 ±0.08 OUR FIT					
7.04 ±0.08 OUR AVERAGE					
7.046±0.18±0.16		[1] BATLEY	07D	NA48	$K^0(\overline{K}^0)(t) \to \pi e \nu$
6.91 ±0.34±0.15	624	[2] ALOISIO	02	KLOE	Tagged K^0_S using $\phi \to K^0_L K^0_S$
• • • We use the following data for averages but not for fits. • • •					
7.05 ±0.09	13k	[3] AMBROSINO	06E	KLOE	Not fitted
• • • We do not use the following data for averages, fits, limits, etc. • • •					
7.2 ±1.4	75	AKHMETSHIN	99	CMD2	Tagged K^0_S using $\phi \to K^0_L K^0_S$

[1] Reconstructed from $K^0(\overline{K}^0)(t) \to \pi e \nu$ distributions using PDG values of $B(K^0_L \to \pi e \nu) = 0.4053 \pm 0.0015$, $\tau_L = (5.114 \pm 0.021) \times 10^{-8}$ s and $\tau_S = (0.8958 \pm 0.0005) \times 10^{-10}$ s.
[2] Uses the PDG 00 value for $B(K^0_S \to \pi^+\pi^-)$.
[3] Obtained by imposing $\Sigma_i B(K^0_S \to i) = 1$, where i runs over all the four branching ratios $\pi^+\pi^-$, $\pi^0\pi^0$, $\pi e \nu$, and $\pi \mu \nu$. Input value of $B(K^0_S \to \pi^+\pi^-)$ / $B(K^0_S \to \pi^0\pi^0)$ from AMBROSINO 06C is used. To derive $\Gamma(K^0_S \to \pi^+\mu\nu)$ / $\Gamma(K^0_S \to \pi^+ e \nu)$, lepton universality is assumed, radiative corrections from ANDRE 07 are used, and phase space integrals are taken from KTeV, ALEXOPOULOS 04A. This branching fraction enters our fit via their $\Gamma(\pi^\pm e^\mp \nu_e)$ / $\Gamma(\pi^+\pi^-)$ branching ratio measurement.

$\Gamma(\pi^\pm \mu^\mp \nu_\mu)/\Gamma_{total}$ — Γ_9/Γ

VALUE (units 10^{-4})	EVTS	DOCUMENT ID		TECN	COMMENT
4.56±0.20 OUR FIT					
4.56±0.11±0.17	7223	[1] BABUSCI	20	KLOE	direct measurement

[1] Value obtained by normalizing to the KLOE measurement $B(K^0_S \to \pi^+\pi^-) = (69.196 \pm 0.051)\%$. Also comparison with the PDG 18 based derived value leads to a lepton flavor universality test $|V_{us}\ f_+(0)|^2_{K^0_S \to \pi\mu\nu} / |V_{us}\ f_+(0)|^2_{K^0_S \to \pi e \nu} = 0.975 \pm 0.044$.

$\Gamma(\pi^\pm e^\mp \nu_e)/\Gamma(\pi^+\pi^-)$ — Γ_8/Γ_2

VALUE (units 10^{-4})	EVTS	DOCUMENT ID		TECN
10.18±0.12 OUR FIT				
10.19±0.11±0.07	13k	AMBROSINO	06E	KLOE

CP violating (*CP*) and $\Delta S = 1$ weak neutral current (*S1*) modes

$\Gamma(3\pi^0)/\Gamma_{total}$ — Γ_{10}/Γ

Violates *CP* conservation.

VALUE (units 10^{-7})	CL%	EVTS	DOCUMENT ID		TECN	COMMENT
< 0.26	90	590M	[1] BABUSCI	13C	KLOE	$\phi \to K^0_L K^0_S$
• • • We do not use the following data for averages, fits, limits, etc. • • •						
< 1.2	90	37.8M	AMBROSINO	05B	KLOE	
< 7.4	90	4.9M	[2] LAI	05A	NA48	
<140	90	7M	ACHASOV	99D	SND	
<190	90	17300	[3] ANGELOPO...	98B	CPLR	
<370	90		BARMIN	83	HLBC	

[1] BABUSCI 13C uses 1.7 fb^{-1} of data of $\phi \to K^0_L K^0_S$ decays with K^0_L interaction in the calorimeter, collected from 2004 to 2005. No candidate events were found in the data with an expected background of $0.04^{+0.15}_{-0.03}$ events. Upper limit is obtained by normalizing to $K^0_S \to 2\pi^0$ decays.
[2] LAI 05A value is obtained from their bound on $|\eta_{000}|$ (not assuming *CPT*) and $B(K^0_L \to 3\pi^0) = 0.211 \pm 0.003$, and PDG 04 values for K^0_L and K^0_S lifetimes. If *CPT* is assumed then $B(K^0_S \to 3\pi^0)_{CPT} < 2.3 \times 10^{-7}$ at 90% CL
[3] ANGELOPOULOS 98B is from $Im(\eta_{000}) = -0.05 \pm 0.12 \pm 0.05$, assuming $Re(\eta_{000}) = Re(\epsilon) = 1.635 \times 10^{-3}$ and using the value $B(K^0_L \to \pi^0\pi^0\pi^0) = 0.2112 \pm 0.0027$.

$\Gamma(\mu^+\mu^-)/\Gamma_{total}$ — Γ_{11}/Γ

Test for $\Delta S = 1$ weak neutral current. Allowed by first-order weak interaction combined with electromagnetic interaction.

VALUE	CL%	DOCUMENT ID		TECN
$<2.1 \times 10^{-10}$	90	[1] AAIJ	20AE	LHCB
• • • We do not use the following data for averages, fits, limits, etc. • • •				
$<8 \times 10^{-10}$	90	[2] AAIJ	17BQ	LHCB
$<9 \times 10^{-9}$	90	[3] AAIJ	13G	LHCB
$<3.2 \times 10^{-7}$	90	GJESDAL	73	ASPK
$<7 \times 10^{-6}$	90	HYAMS	69B	OSPK

[1] AAIJ 20AE uses 8.6 fb^{-1} of LHCb data from 2011 to 2012 and 2016 to 2018. The result utilizes the normalization mode branching fraction $B(K^0_S \to \pi^+\pi^-) = (69.20 \pm 0.05) \times 10^{-2}$ from PDG 18. Supersedes AAIJ 17BQ.
[2] AAIJ 17BQ uses 3.0 fb^{-1} of pp collisions at $\sqrt{s} = 7$ and 8 TeV. The result utilizes the normalization mode branching fraction $B(K^0_S \to \pi^+\pi^-) = (69.20 \pm 0.05) \times 10^{-2}$ from PDG 16. Supersedes AAIJ 13G.
[3] AAIJ 13G uses 1.0 fb^{-1} of pp collisions at $\sqrt{s} = 7$ TeV. They obtained $B(K^0_S \to \mu^+\mu^-) < 11 \times 10^{-9}$ at 95% C.L.

$\Gamma(e^+e^-)/\Gamma_{total}$ — Γ_{12}/Γ

Test for $\Delta S = 1$ weak neutral current. Allowed by first-order weak interaction combined with electromagnetic interaction.

VALUE (units 10^{-7})	CL%	DOCUMENT ID		TECN	COMMENT
< 0.09	90	[1] AMBROSINO	09A	KLOE	$e^+e^- \to \phi \to K^0_S K^0_L$
• • • We do not use the following data for averages, fits, limits, etc. • • •					
< 1.4	90	ANGELOPO...	97	CPLR	
< 28	90	BLICK	94	CNTR	Hyperon facility
<100	90	BARMIN	86	XEBC	

[1] AMBROSINO 09A reports $< 0.09 \times 10^{-7}$ from a measurement of $[\Gamma(K^0_S \to e^+e^-)/\Gamma_{total}]$ / $[B(K^0_S \to \pi^+\pi^-)]$ assuming $B(K^0_S \to \pi^+\pi^-) = (69.20 \pm 0.05) \times 10^{-2}$.

$\Gamma(\pi^0 e^+e^-)/\Gamma_{total}$ — Γ_{13}/Γ

Test for $\Delta S = 1$ weak neutral current. Allowed by first-order weak interaction combined with electromagnetic interaction.

VALUE (units 10^{-9})	CL%	EVTS	DOCUMENT ID		TECN	COMMENT
$3.0^{+1.5}_{-1.2} \pm 0.2$		7	[1] BATLEY	03	NA48	m_{ee} >0.165 GeV
• • • We do not use the following data for averages, fits, limits, etc. • • •						
< 140	90		LAI	01	NA48	
< 1100	90	0	BARR	93B	NA31	
<45 000	90		GIBBONS	88	E731	

[1] BATLEY 03 extrapolate also to the full kinematical region using a constant form factor and a vector matrix element. The resulting branching ratio is $(5.8^{+2.9}_{-2.4}) \times 10^{-9}$.

Downloaded from https://academic.oup.com/ptep/article/2022/8/083C01/6651666 by KIT Library user on 27 September 2022

$\Gamma(\pi^0\mu^+\mu^-)/\Gamma_{total}$ — Γ_{14}/Γ

Test for $\Delta S = 1$ weak neutral current. Allowed by first-order weak interaction combined with electromagnetic interaction.

VALUE (units 10^{-9})	EVTS	DOCUMENT ID		TECN	COMMENT
$2.9^{+1.5}_{-1.2}\pm0.2$	6	[1] BATLEY	04A	NA48	NA48/1 K^0_S beam

[1] Background estimate is $0.22^{+0.18}_{-0.11}$ events. Branching ratio assumes a vector matrix element and unit form factor.

K^0_S FORM FACTORS

For discussion, see note on $K_{\ell3}$ form factors in the $K^\pm$ section of the Particle Listings above. Because the semileptonic branching fraction is smaller in K^0_S than K^0_L by the ratio of the mean lives, the K^0_S semileptonic form factor has so far been measured only in the K_{e3} mode using the linear expansion $f_+(t) = f_+(0)\,(1 + \lambda_+ t/m^2_{\pi^+})$, which gives the vector form factor $f_+(t)$ relative to its value at $t = 0$.

λ_+ (LINEAR ENERGY DENSITY OF f_+ IN K^0_{e3} DECAY)

VALUE (units 10^{-2})	EVTS	DOCUMENT ID		TECN
3.39 ± 0.41	15k	AMBROSINO	06E	KLOE

CP VIOLATION IN $K_S \to 3\pi$

Written 1996 by T. Nakada (Paul Scherrer Institute) and L. Wolfenstein (Carnegie-Mellon University).

The possible final states for the decay $K^0 \to \pi^+\pi^-\pi^0$ have isospin $I = 0$, 1, 2, and 3. The $I = 0$ and $I = 2$ states have $CP = +1$ and K_S can decay into them without violating CP symmetry, but they are expected to be strongly suppressed by centrifugal barrier effects. The $I = 1$ and $I = 3$ states, which have no centrifugal barrier, have $CP = -1$ so that the K_S decay to these requires CP violation.

In order to see CP violation in $K_S \to \pi^+\pi^-\pi^0$, it is necessary to observe the interference between K_S and K_L decay, which determines the amplitude ratio

$$\eta_{+-0} = \frac{A(K_S \to \pi^+\pi^-\pi^0)}{A(K_L \to \pi^+\pi^-\pi^0)} \ . \qquad (1)$$

If η_{+-0} is obtained from an integration over the whole Dalitz plot, there is no contribution from the $I = 0$ and $I = 2$ final states and a nonzero value of η_{+-0} is entirely due to CP violation.

Only $I = 1$ and $I = 3$ states, which are $CP = -1$, are allowed for $K^0 \to \pi^0\pi^0\pi^0$ decays and the decay of K_S into $3\pi^0$ is an unambiguous sign of CP violation. Similarly to η_{+-0}, η_{000} is defined as

$$\eta_{000} = \frac{A(K_S \to \pi^0\pi^0\pi^0)}{A(K_L \to \pi^0\pi^0\pi^0)} \ . \qquad (2)$$

If one assumes that CPT invariance holds and that there are no transitions to $I = 3$ (or to nonsymmetric $I = 1$ states), it can be shown that

$$\eta_{+-0} = \eta_{000} = \epsilon + i\frac{\mathrm{Im}\ a_1}{\mathrm{Re}\ a_1} \ . \qquad (3)$$

With the Wu-Yang phase convention, a_1 is the weak decay amplitude for K^0 into $I = 1$ final states; ϵ is determined from CP violation in $K_L \to 2\pi$ decays. The real parts of η_{+-0} and η_{000} are equal to $\mathrm{Re}(\epsilon)$. Since currently-known upper limits on $|\eta_{+-0}|$ and $|\eta_{000}|$ are much larger than $|\epsilon|$, they can be interpreted as upper limits on $\mathrm{Im}(\eta_{+-0})$ and $\mathrm{Im}(\eta_{000})$ and so as limits on the CP-violating phase of the decay amplitude a_1.

CP-VIOLATION PARAMETERS IN K^0_S DECAY

$A_S = [\,\Gamma(K^0_S \to \pi^- e^+ \nu_e) - \Gamma(K^0_S \to \pi^+ e^- \bar{\nu}_e)\,] / \mathrm{SUM}$

Such asymmetry violates CP. If CPT is assumed then $A_S = 2\,\mathrm{Re}(\epsilon)$.

VALUE (units 10^{-3})	EVTS	DOCUMENT ID		TECN
$-3.8\pm5.0\pm2.6$	83k	[1] ANASTASI	18A	KLOE
• • • We do not use the following data for averages, fits, limits, etc. • • •				
$1.5\pm9.6\pm2.9$	13k	AMBROSINO	06E	KLOE

[1] ANASTASI 18A result is a combination of the new measurement and AMBROSINO 06E. The new ANASTASI 18A measurement using data collected from 2004–2005, which corresponds to an integrated luminosity of 1.63 fb^{-1} is $A_S = (-4.9\pm5.7\pm2.6)\times10^{-3}$.

PARAMETERS FOR $K^0_S \to 3\pi$ DECAY

$|\eta_{+-0}|^2 = \Gamma(K^0_S \to \pi^+\pi^-\pi^0,\ CP\text{-violating}) / \Gamma(K^0_L \to \pi^+\pi^-\pi^0)$

CPT assumed valid (i.e. $\mathrm{Re}(\eta_{+-0}) \simeq 0$).

VALUE	CL%	EVTS	DOCUMENT ID		TECN
• • • We do not use the following data for averages, fits, limits, etc. • • •					
<0.23	90	601	[1] BARMIN	85	HLBC
<0.12	90	384	METCALF	72	ASPK

[1] BARMIN 85 find $\mathrm{Re}(\eta_{+-0}) = (0.05\pm0.17)$ and $\mathrm{Im}(\eta_{+-0}) = (0.15\pm0.33)$. Includes events of BALDO-CEOLIN 75.

$\mathrm{Im}(\eta_{+-0}) = \mathrm{Im}(A(K^0_S \to \pi^+\pi^-\pi^0,\ CP\text{-violating}) / A(K^0_L \to \pi^+\pi^-\pi^0))$

VALUE	EVTS	DOCUMENT ID		TECN	COMMENT
$-0.002\pm0.009^{+0.002}_{-0.001}$	500k	[1] ADLER	97B	CPLR	
• • • We do not use the following data for averages, fits, limits, etc. • • •					
$-0.002\pm0.018\pm0.003$	137k	[2] ADLER	96D	CPLR	Sup. by ADLER 97B
$-0.015\pm0.017\pm0.025$	272k	[3] ZOU	94	SPEC	

[1] ADLER 97B also find $\mathrm{Re}(\eta_{+-0}) = -0.002\pm0.007^{+0.004}_{-0.001}$. See also ANGELOPOULOS 98C.
[2] The ADLER 96D fit also yields $\mathrm{Re}(\eta_{+-0}) = 0.006\pm0.013\pm0.001$ with a correlation $+0.66$ between real and imaginary parts. Their results correspond to $|\eta_{+-0}| < 0.037$ with 90% CL.
[3] ZOU 94 use theoretical constraint $\mathrm{Re}(\eta_{+-0}) = \mathrm{Re}(\epsilon) = 0.0016$. Without this constraint they find $\mathrm{Im}(\eta_{+-0}) = 0.019\pm0.061$ and $\mathrm{Re}(\eta_{+-0}) = 0.019\pm0.027$.

$|\eta_{000}|^2 = \Gamma(K^0_S \to 3\pi^0) / \Gamma(K^0_L \to 3\pi^0)$

CPT assumed valid (i.e. $\mathrm{Re}(\eta_{000}) \simeq 0$). This limit determines branching ratio $\Gamma(3\pi^0)/\Gamma_{total}$ above.

VALUE	CL%	EVTS	DOCUMENT ID		TECN	COMMENT
• • • We do not use the following data for averages, fits, limits, etc. • • •						
<0.1	90	632	[1] BARMIN	83	HLBC	
<0.28	90		[2] GJESDAL	74B	SPEC	Indirect meas.

[1] BARMIN 83 find $\mathrm{Re}(\eta_{000}) = (-0.08\pm0.18)$ and $\mathrm{Im}(\eta_{000}) = (-0.05\pm0.27)$. Assuming CPT invariance they obtain the limit quoted above.
[2] GJESDAL 74B uses $K2\pi$, $K_{\mu3}$, and K_{e3} decay results, unitarity, and CPT. Calculates $|(\eta_{000})| = 0.26\pm0.20$. We convert to upper limit.

$\mathrm{Im}(\eta_{000}) = \mathrm{Im}(A(K^0_S \to \pi^0\pi^0\pi^0)/A(K^0_L \to \pi^0\pi^0\pi^0))$

$K^0_S \to \pi^0\pi^0\pi^0$ violates CP conservation, in contrast to $K^0_S \to \pi^+\pi^-\pi^0$ which has a CP-conserving part.

VALUE	EVTS	DOCUMENT ID		TECN	COMMENT
-0.001 ± 0.016 OUR AVERAGE					
$0.000\pm0.009\pm0.013$	4.9M	[1] LAI	05A	NA48	Assumes CPT
$-0.05\ \pm0.12\ \pm0.05$	17300	[2] ANGELOPO...	98B	CPLR	Assumes CPT

[1] LAI 05A assumes $\mathrm{Re}(\eta_{000}) = \mathrm{Re}(\epsilon) = 1.66\times10^{-3}$. The equivalent limit is $|\eta_{000}|_{CPT} < 0.025$ at 90% CL Without assuming CPT invariance, they obtain $\mathrm{Re}(\eta_{000}) = -0.002\pm0.011\pm0.015$ and $\mathrm{Im}(\eta_{000}) = -0.003\pm0.013\pm0.017$ with a statistical correlation coefficient of 0.77 and an overall correlation coefficient of 0.57 between imaginary and real part. The equivalent limit is $|\eta_{000}| < 0.045$ at 90% CL
[2] ANGELOPOULOS 98B assumes $\mathrm{Re}(\eta_{000}) = \mathrm{Re}(\epsilon) = 1.635\times10^{-3}$. Without assuming CPT invariance, they obtain $\mathrm{Re}(\eta_{000}) = 0.18\pm0.14\pm0.06$ and $\mathrm{Im}(\eta_{000}) = 0.15\pm0.20\pm0.03$.

$|\eta_{000}| = |A(K^0_S \to 3\pi^0)/A(K^0_L \to 3\pi^0)|$

A non-zero value violates CP invariance.

VALUE	CL%	EVTS	DOCUMENT ID		TECN
<0.0088	90	590M	BABUSCI	13C	KLOE
• • • We do not use the following data for averages, fits, limits, etc. • • •					
<0.018	90	37.8M	AMBROSINO	05B	KLOE
<0.045	90	4.9M	LAI	05A	NA48

Downloaded from https://academic.oup.com/ptep/article/2022/8/083C01/6651666 by KIT Library user on 27 September 2022

DECAY-PLANE ASYMMETRY IN $\pi^+\pi^-e^+e^-$ DECAYS

This is the *CP*-violating asymmetry

$$A = \frac{N_{\sin\phi\cos\phi>0.0} - N_{\sin\phi\cos\phi<0.0}}{N_{\sin\phi\cos\phi>0.0} + N_{\sin\phi\cos\phi<0.0}}$$

where ϕ is the angle between the e^+e^- and $\pi^+\pi^-$ planes in the K^0_S rest frame.

CP asymmetry A in $K^0_S \to \pi^+\pi^-e^+e^-$

VALUE (%)	DOCUMENT ID		TECN	COMMENT
−0.4±0.8 OUR AVERAGE				
−0.4±0.8	[1] BATLEY	11	NA48	2002 data
−1.1±4.1	LAI	03C	NA48	1998+1999 data
• • • We do not use the following data for averages, fits, limits, etc. • • •				
0.5±4.0±1.6	LAI	03C	NA48	1999 data

[1] The result is used to set the limit $A < 1.5\%$ at 90% C.L.

K^0_S REFERENCES

AAIJ 20AE PRL 125 231801 R. Aaij et al. (LHCb Collab.)
BABUSCI 20 PL B804 135378 D. Babusci et al. (KLOE-2 Collab.)
ANASTASI 18A JHEP 1809 021 A. Anastasi et al. (KLOE-2 Collab.)
PDG 18 PR D98 030001 M. Tanabashi et al. (PDG Collab.)
AAIJ 17BQ EPJ C77 678 R. Aaij et al. (LHCb Collab.)
PDG 16 CP C40 100001 C. Patrignani et al. (PDG Collab.)
AAIJ 13G JHEP 1301 090 R. Aaij et al. (LHCb Collab.)
BABUSCI 13C PL B723 54 D. Babusci et al. (KLOE-2 Collab.)
ABOUZAID 11 PR D83 092001 E. Abouzaid et al. (FNAL KTeV Collab.)
AMBROSINO 11 EPJ C71 1604 F. Ambrosino et al. (KLOE Collab.)
BATLEY 11 PL B694 301 J.R. Batley et al. (CERN NA48/1 Collab.)
AMBROSINO 09A PL B672 203 F. Ambrosino et al. (KLOE Collab.)
AMBROSINO 08C JHEP 0805 051 F. Ambrosino et al. (KLOE Collab.)
ANDRE 07 ANP 322 2518 T. Andre (EFI)
BATLEY 07D PL B653 145 J.R. Batley et al. (CERN NA48 Collab.)
AMBROSINO 06C EPJ C48 767 F. Ambrosino et al. (KLOE Collab.)
AMBROSINO 06E PL B636 173 F. Ambrosino et al. (KLOE Collab.)
AMBROSINO 05B PL B619 61 F. Ambrosino et al. (KLOE Collab.)
BATLEY 05 PL B630 31 J.R. Batley et al. (NA48 Collab.)
LAI 05A PL B610 165 A. Lai et al. (CERN NA48 Collab.)
ALEXOPOU... 04A PR D70 092007 T. Alexopoulos et al. (FNAL KTeV Collab.)
BATLEY 04A PL B599 197 J.R. Batley et al. (NA48 Collab.)
LAI 04 PL B578 276 A. Lai et al. (CERN NA48 Collab.)
PDG 04 PL B592 1 S. Eidelman et al. (PDG Collab.)
ALAVI-HARATI 03 PR D67 012005 A. Alavi-Harati et al. (FNAL KTeV Collab.)
Also PR D70 079904 (errat.) A. Alavi-Harati et al. (FNAL KTeV Collab.)
BATLEY 03 PL B576 43 J.R. Batley et al. (CERN NA48 Collab.)
LAI 03 PL B551 7 A. Lai et al. (CERN NA48 Collab.)
LAI 03B PL B556 105 A. Lai et al. (CERN NA48 Collab.)
LAI 03C EPJ C30 33 A. Lai et al. (CERN NA48 Collab.)
ALOISIO 02 PL B535 37 A. Aloisio et al. (KLOE Collab.)
ALOISIO 02B PL B538 21 A. Aloisio et al. (KLOE Collab.)
LAI 02C PL B537 28 A. Lai et al. (CERN NA48 Collab.)
LAI 01 PL B514 253 A. Lai et al. (CERN NA48 Collab.)
LAI 00 PL B493 29 A. Lai et al. (CERN NA48 Collab.)
LAI 00B PL B496 137 A. Lai et al. (CERN NA48 Collab.)
PDG 00 EPJ C15 1 D.E. Groom et al. (PDG Collab.)
ACHASOV 99D PL B459 674 M.N. Achasov et al.
AKHMETSHIN 99 PL B456 90 R.R. Akhmetshin et al. (Novosibirsk CMD-2 Collab.)
ANGELOPO... 98B PL B425 391 A. Angelopoulos et al. (CPLEAR Collab.)
ANGELOPO... 98C EPJ C5 389 A. Angelopoulos et al. (CPLEAR Collab.)
PDG 98 EPJ C3 1 C. Caso et al. (PDG Collab.)
ADLER 97B PL B407 193 R. Adler et al. (CPLEAR Collab.)
ANGELOPO... 97 PL B413 232 A. Angelopoulos et al. (CPLEAR Collab.)
BERTANZA 97 ZPHY C73 629 L. Bertanza (PISA, CERN, EDIN, MAINZ, ORSAY+)
ADLER 96D PL B370 167 R. Adler et al. (CPLEAR Collab.)
ADLER 96E PL B374 313 R. Adler et al. (CPLEAR Collab.)
ZOU 96 PL B369 362 Y. Zou et al. (RUTG, MINN, MICH)
BARR 95B PL B351 579 G.D. Barr et al. (CERN, EDIN, MAINZ, LALO+)
SCHWINGEN... 95 PRL 74 4376 B. Schwingenheuer et al. (EFI, CHIC+)
BLICK 94 PL B334 234 A.M. Blick et al. (SERP, JINR)
THOMSON 94 PL B337 411 G.B. Thomson et al. (RUTG, MINN, MICH)
ZOU 94 PL B329 519 Y. Zou et al. (RUTG, MINN, MICH)
BARR 93B PL B304 381 G.D. Barr et al. (CERN, EDIN, MAINZ, LALO+)
GIBBONS 93 PRL 70 1199 L.K. Gibbons et al. (FNAL E731 Collab.)
Also PR D55 6625 L.K. Gibbons et al. (FNAL E731 Collab.)
RAMBERG 93 PRL 70 2525 E. Ramberg et al. (FNAL E731 Collab.)
BALATS 89 SJNP 49 828 M.Y. Balats et al. (ITEP)
Translated from YAF 49 1332.
GIBBONS 88 PRL 61 2661 L.K. Gibbons et al. (FNAL E731 Collab.)
BURKHARDT 87 PL B199 139 H. Burkhardt et al. (CERN, EDIN, MAINZ+)
GROSSMAN 87 PRL 59 18 N. Grossman et al. (MINN, MICH, RUTG)
BARMIN 86 SJNP 44 622 V.V. Barmin et al. (ITEP)
Translated from YAF 44 965.
BARMIN 86B NC 96A 159 V.V. Barmin et al. (ITEP, PADO)
PDG 86B PL 170B 130 M. Aguilar-Benitez et al. (CERN, CIT+)
BARMIN 85 NC 85A 67 V.V. Barmin et al. (ITEP, PADO)
Also SJNP 41 759 V.V. Barmin et al. (ITEP)
Translated from YAF 41 1187.
BARMIN 83 PL 128B 129 V.V. Barmin et al. (ITEP, PADO)
Also SJNP 39 269 V.V. Barmin et al. (ITEP, PADO)
Translated from YAF 39 428.
ARONSON 82 PRL 48 1078 S.H. Aronson et al. (BNL, CHIC, STAN+)
ARONSON 82B PRL 48 1306 S.H. Aronson et al. (BNL, CHIC, PURD)
Also PL 116B 73 E. Fischbach et al. (PURD, BNL, CHIC)
Also PR D28 476 S.H. Aronson et al. (BNL, CHIC, PURD)
Also PR D28 495 S.H. Aronson et al. (BNL, CHIC, PURD)
ARONSON 76 NC 32A 236 S.H. Aronson et al. (WISC, EFI, UCSD+)
EVERHART 76 PR D14 661 G.C. Everhart et al. (PENN)
TAUREG 76 PL 65B 92 H. Taureg et al. (HEIDH, CERN, DORT)
BALDO-... 75 NC 25A 688 M. Baldo-Ceolin et al. (PADO, WISC)
CARITHERS 75 PRL 34 1244 W.C.J. Carithers et al. (COLU, NYU)
BOBISUT 74 LNC 11 646 F. Bobisut et al. (PADO)
COWELL 74 PR D10 2083 P.L. Cowell et al. (STON, COLU)
GEWENIGER 74B PL 48B 487 C. Geweniger et al. (CERN, HEIDH)
GJESDAL 74B PL 52B 119 S. Gjesdal et al. (CERN, HEIDH)
BURGUN 73 PL 46B 481 G. Burgun et al. (SACL, CERN)
GJESDAL 73 PL 44B 217 S. Gjesdal et al. (CERN, HEIDH)
HILL 73 PR D8 1290 D.G. Hill et al. (BNL, CMU)
ALITTI 72 PL 39B 568 J. Alitti, E. Lesquoy, A. Muller (SACL)
BURGUN 72 NP B50 194 G. Burgun et al. (SACL, CERN, OSLO)
METCALF 72 PL 40B 703 M. Metcalf et al. (CERN, IPN, WIEN)
MORSE 72B PRL 28 388 R. Morse et al. (COLO, PRIN, UMD)
NAGY 72 NP B47 94 E. Nagy, F. Telbisz, G. Vesztergombi (BUDA)
Also PL 30B 498 G. Bozoki et al. (BUDA)
SKJEGGEST... 72 NP B48 343 O. Skjeggestad et al. (OSLO, CERN, SACL)
BALTAY 71 PRL 27 1678 C. Baltay et al. (COLU)
Also Thesis Nevis 187 W.A. Cooper (COLU)
MOFFETT 70 BAPS 15 512 R. Moffett et al. (ROCH)
BOZOKI 69 PL 30B 498 G. Bozoki et al. (BUDA)
DOYLE 69 Thesis UCRL 18139 J.C. Doyle (LRL)
GOBBI 69 PRL 22 682 B. Gobbi et al. (ROCH)
HYAMS 69B PL 29B 521 B.D. Hyams et al. (CERN, MPIM)
MORFIN 69 PRL 23 660 J.G. Morfin, D. Sinclair (MICH)
DONALD 68B PL 27B 58 R.A. Donald et al. (LIVP, CERN, IPNP+)
HILL 68 PR 171 1418 D.G. Hill et al. (BNL, CMU)
AUBERT 65 PL 17 59 B. Aubert et al. (EPOL, ORSAY)
BROWN 63 PR 130 769 J.L. Brown et al. (LRL, MICH)
CHRETIEN 63 PR 131 2208 M. Chretien et al. (BRAN, BROW, HARV+)
BROWN 61 NC 19 1155 J.L. Brown et al. (MICH)
BOLDT 58B PRL 1 150 E. Boldt, D.O. Caldwell, Y. Pal (MIT)

OTHER RELATED PAPERS

LITTENBERG 93 ARNPS 43 729 L.S. Littenberg, G. Valencia (BNL, FNAL)
Rare and Radiative Kaon Decays
BATTISTON 92 PRPL 214 293 R. Battiston et al. (PGIA, CERN, TRSTT)
Status and Perspectives of K Decay Physics
TRILLING 65B UCRL 16473 G.N. Trilling (LRL)
Updated from 1965 Argonne Conference, page 115.
CRAWFORD 62 CERN Conf. 827 F.S. Crawford (LRL)
FITCH 61 NC 22 1160 V.L. Fitch, P.A. Piroue, R.B. Perkins (PRIN+)
GOOD 61 PR 124 1223 R.H. Good et al. (LRL)
BIRGE 60 Rochester Conf. 601 R.W. Birge et al. (LRL, WISC)
MULLER 60 PRL 4 418 F. Muller et al. (LRL, BNL)

K^0_L

$I(J^P) = \frac{1}{2}(0^-)$

$m_{K^0_L} - m_{K^0_S}$

For earlier measurements, beginning with GOOD 61 and FITCH 61, see our 1986 edition, Physics Letters **170B** 132 (1986).

OUR FIT is described in the note on "*CP* violation in K_L decays" in the K^0_L Particle Listings. The result labeled "OUR FIT Assuming *CPT*" ["OUR FIT Not assuming *CPT*"] includes all measurements except those with the comment "Not assuming *CPT*" ["Assuming *CPT*"]. Measurements with neither comment do not assume *CPT* and enter both fits.

VALUE (10^{10} $\hbar$ s^{-1})		DOCUMENT ID		TECN	COMMENT
0.5293	**±0.0009 OUR FIT**	Error includes scale factor of 1.3. Assuming *CPT*			
0.5289	**±0.0010 OUR FIT**	Not assuming *CPT*			
0.52797±0.00195		[1,2] ABOUZAID	11	KTEV	Not assuming *CPT*
0.52699±0.00123		[1,3] ABOUZAID	11	KTEV	Assuming *CPT*
0.5240	±0.0044 ±0.0033	APOSTOLA...	99C	CPLR	K^0-$\overline{K}^0$ to $\pi^+\pi^-$
0.5297	±0.0030 ±0.0022	[4] SCHWINGEN...	95	E773	20–160 GeV K beams
0.5286	±0.0028	[5] GIBBONS	93	E731	Assuming *CPT*
0.5257	±0.0049 ±0.0021	[4] GIBBONS	93C	E731	Not assuming *CPT*
0.5340	±0.00255±0.0015	[6] GEWENIGER	74C	SPEC	Gap method
0.5334	±0.0040 ±0.0015	[6,7] GJESDAL	74	SPEC	Assuming *CPT*
• • • We do not use the following data for averages, fits, limits, etc. • • •					
0.5261	±0.0015	[8] ALAVI-HARATI	03	KTEV	Assuming *CPT*
0.5288	±0.0043	[9] ALAVI-HARATI	03	KTEV	Not assuming *CPT*
0.5343	±0.0063 ±0.0025	[10] ANGELOPO...	01	CPLR	
0.5295	±0.0020 ±0.0003	[11] ANGELOPO...	98D	CPLR	Assuming *CPT*
0.5307	±0.0013	[12] ADLER	96C	RVUE	
0.5274	±0.0029 ±0.0005	[11] ADLER	95	CPLR	Sup. by ANGELOPOULOS 98D
0.482	±0.014	[13] ARONSON	82B	SPEC	E=30–110 GeV
0.534	±0.007	[14] CARNEGIE	71	ASPK	Gap method
0.542	±0.006	[14] ARONSON	70	ASPK	Gap method
0.542	±0.006	CULLEN	70	CNTR	

[1] The two ABOUZAID 11 values use the same data. The first enters the "assuming *CPT*" fit and the second enters the "not assuming *CPT*" fit.

[2] ABOUZAID 11 fit has Δm, τ_S, ϕ_ϵ, Re(ϵ'/ϵ), and Im(ϵ'/ϵ) as free parameters. See Im(ϵ'/ϵ) in the "K^0_L *CP* violation" section for correlation information.

[3] ABOUZAID 11 fit has Δm and τ_S free but constrains ϕ_ϵ to the Superweak value, i.e. assumes *CPT*. See "K^0_S Mean Life" section for correlation information.

[4] Fits Δm and ϕ_{+-} simultaneously. GIBBONS 93C systematic error is from B. Winstein via private communication. 20–160 GeV K beams.

[5] GIBBONS 93 value assume $\phi_{+-} = \phi_{00} = \phi_{SW} = (43.7 \pm 0.2)^\circ$, i.e. assumes *CPT*. 20–160 GeV K beams.

[6] These two experiments have a common systematic error due to the uncertainty in the momentum scale, as pointed out in WAHL 89.

[7] GJESDAL 74 uses charge asymmetry in $K^0_{\ell 3}$ decays.

[8] ALAVI-HARATI 03 fit Δm and $\tau_{K^0_S}$ simultaneously. ϕ_{+-} is constrained to the Superweak value, i.e. *CPT* is assumed. See "K^0_S Mean Life" section for correlation information. Superseded by ABOUZAID 11.

[9] ALAVI-HARATI 03 fit Δm, ϕ_{+-}, and τ_{K_S} simultaneously. See ϕ_{+-} in the "K_L *CP* violation" section for correlation information. Superseded by ABOUZAID 11.

[10] ANGELOPOULOS 01 uses strong interactions strangeness tagging at two different times.

[11] Uses $\overline{K}^0_{e3}$ and K^0_{e3} strangeness tagging at production and decay. Assumes *CPT* conservation on $\Delta S = -\Delta Q$ transitions.

Downloaded from https://academic.oup.com/ptep/article/2022/8/083C01/6651666 by KIT Library user on 27 September 2022

[12] ADLER 96C is the result of a fit which includes nearly the same data as entered into the "OUR FIT" value above.
[13] ARONSON 82 find that Δm may depend on the kaon energy.
[14] ARONSON 70 and CARNEGIE 71 use K^0_S mean life = $(0.862 \pm 0.006) \times 10^{-10}$ s. We have not attempted to adjust these values for the subsequent change in the K^0_S mean life or in η_{+-}.

K^0_L MEAN LIFE

VALUE (10^{-8} s)	EVTS	DOCUMENT ID		TECN	COMMENT
5.116±0.021 OUR FIT	Error includes scale factor of 1.1.				
5.099±0.021 OUR AVERAGE					
5.072±0.011±0.035	13M	[1] AMBROSINO	06	KLOE	$\sum_i B_i = 1$
5.092±0.017±0.025	15M	AMBROSINO	05C	KLOE	
5.154±0.044	0.4M	VOSBURGH	72	CNTR	
• • • We do not use the following data for averages, fits, limits, etc. • • •					
5.15 ±0.14		DEVLIN	67	CNTR	

[1] AMBROSINO 06 uses $\phi \to K_L K_S$ with K_L tagged by $K_S \to \pi^+\pi^-$. The four major K_l BR's are measured, the small remainder ($\pi^+\pi^-$,$\pi^0\pi^0$,$\gamma\gamma$) is taken from PDG 04. This KLOE K_L lifetime is obtained by imposing $\sum_i B_i = 1$. The correlation matrix among the four measured K_L BR's and this K_L lifetime is

	K_{e3}	$K_{\mu3}$	$3\pi^0$	$\pi^+\pi^-\pi^0$	τ_{K_L}
K_{e3}	1	−0.25	−0.56	−0.07	0.25
$K_{\mu3}$		1	−0.43	−0.20	0.33
$3\pi^0$			1	−0.39	−0.21
$\pi^+\pi^-\pi^0$				1	−0.39
τ_{K_L}					1

These correlations are taken into account in our fit. The average of this KLOE mean life measurement and the independent KLOE measurement in AMBROSINO 05C is $(5.084 \pm 0.023) \times 10^{-8}$ s.

K^0_L DECAY MODES

	Mode			Fraction (Γ_i/Γ)	Scale factor/ Confidence level
	Semileptonic modes				
Γ_1	$\pi^\pm e^\mp \nu_e$ Called K^0_{e3}.		[a]	(40.55 ±0.11) %	S=1.7
Γ_2	$\pi^\pm \mu^\mp \nu_\mu$ Called $K^0_{\mu3}$.		[a]	(27.04 ±0.07) %	S=1.1
Γ_3	$(\pi\mu\text{atom})\nu$			$(1.05 \pm 0.11) \times 10^{-7}$	
Γ_4	$\pi^0\pi^\pm e^\mp \nu$		[a]	$(5.20 \pm 0.11) \times 10^{-5}$	
Γ_5	$\pi^\pm e^\mp \nu e^+ e^-$		[a]	$(1.26 \pm 0.04) \times 10^{-5}$	
	Hadronic modes, including Charge conjugation×Parity Violating (*CPV*) modes				
Γ_6	$3\pi^0$			(19.52 ±0.12) %	S=1.6
Γ_7	$\pi^+\pi^-\pi^0$			(12.54 ±0.05) %	
Γ_8	$\pi^+\pi^-$	CPV	[b]	$(1.967 \pm 0.010) \times 10^{-3}$	S=1.5
Γ_9	$\pi^0\pi^0$	CPV		$(8.64 \pm 0.06) \times 10^{-4}$	S=1.8
	Semileptonic modes with photons				
Γ_{10}	$\pi^\pm e^\mp \nu_e \gamma$		[a,c,d]	$(3.79 \pm 0.06) \times 10^{-3}$	
Γ_{11}	$\pi^\pm \mu^\mp \nu_\mu \gamma$			$(5.65 \pm 0.23) \times 10^{-4}$	
	Hadronic modes with photons or $\ell\bar{\ell}$ pairs				
Γ_{12}	$\pi^0\pi^0\gamma$			$< 2.43 \times 10^{-7}$	CL=90%
Γ_{13}	$\pi^+\pi^-\gamma$		[c,d]	$(4.15 \pm 0.15) \times 10^{-5}$	S=2.8
Γ_{14}	$\pi^+\pi^-\gamma$(DE)			$(2.84 \pm 0.11) \times 10^{-5}$	S=2.0
Γ_{15}	$\pi^0 2\gamma$		[c]	$(1.273 \pm 0.033) \times 10^{-6}$	
Γ_{16}	$\pi^0\gamma e^+ e^-$			$(1.62 \pm 0.17) \times 10^{-8}$	
	Other modes with photons or $\ell\bar{\ell}$ pairs				
Γ_{17}	2γ			$(5.47 \pm 0.04) \times 10^{-4}$	S=1.1
Γ_{18}	3γ			$< 7.4 \times 10^{-8}$	CL=90%
Γ_{19}	$e^+ e^-\gamma$			$(9.4 \pm 0.4) \times 10^{-6}$	S=2.0
Γ_{20}	$\mu^+\mu^-\gamma$			$(3.59 \pm 0.11) \times 10^{-7}$	S=1.3
Γ_{21}	$e^+ e^-\gamma\gamma$		[c]	$(5.95 \pm 0.33) \times 10^{-7}$	
Γ_{22}	$\mu^+\mu^-\gamma\gamma$		[c]	$(1.0 {}^{+0.8}_{-0.6}) \times 10^{-8}$	
	Charge conjugation × Parity (*CP*) or Lepton Family number (*LF*) violating modes, or $\Delta S = 1$ weak neutral current (*S1*) modes				
Γ_{23}	$\mu^+\mu^-$	S1		$(6.84 \pm 0.11) \times 10^{-9}$	
Γ_{24}	$e^+ e^-$	S1		$(9 {}^{+6}_{-4}) \times 10^{-12}$	
Γ_{25}	$\pi^+\pi^- e^+ e^-$	S1	[c]	$(3.11 \pm 0.19) \times 10^{-7}$	
Γ_{26}	$\pi^0\pi^0 e^+ e^-$	S1		$< 6.6 \times 10^{-9}$	CL=90%
Γ_{27}	$\pi^0\pi^0\mu^+\mu^-$	S1		$< 9.2 \times 10^{-11}$	CL=90%
Γ_{28}	$\mu^+\mu^- e^+ e^-$	S1		$(2.69 \pm 0.27) \times 10^{-9}$	
Γ_{29}	$e^+ e^- e^+ e^-$	S1		$(3.56 \pm 0.21) \times 10^{-8}$	
Γ_{30}	$\pi^0\mu^+\mu^-$	CP,S1	[e]	$< 3.8 \times 10^{-10}$	CL=90%
Γ_{31}	$\pi^0 e^+ e^-$	CP,S1	[e]	$< 2.8 \times 10^{-10}$	CL=90%
Γ_{32}	$\pi^0\nu\overline{\nu}$	CP,S1	[f]	$< 3.0 \times 10^{-9}$	CL=90%
Γ_{33}	$\pi^0\pi^0\nu\overline{\nu}$	S1		$< 8.1 \times 10^{-7}$	CL=90%
Γ_{34}	$e^\pm\mu^\mp$	LF	[a]	$< 4.7 \times 10^{-12}$	CL=90%
Γ_{35}	$e^\pm e^\pm\mu^\mp\mu^\mp$	LF	[a]	$< 4.12 \times 10^{-11}$	CL=90%
Γ_{36}	$\pi^0\mu^\pm e^\mp$	LF	[a]	$< 7.6 \times 10^{-11}$	CL=90%
Γ_{37}	$\pi^0\pi^0\mu^\pm e^\mp$	LF		$< 1.7 \times 10^{-10}$	CL=90%
	Lorentz invariance violating modes				
Γ_{38}	$\pi^0\gamma$			$< 1.7 \times 10^{-7}$	CL=90%

[a] The value is for the sum of the charge states or particle/antiparticle states indicated.
[b] This mode includes gammas from inner bremsstrahlung but not the direct emission mode $K^0_L \to \pi^+\pi^-\gamma$(DE).
[c] See the Particle Listings below for the energy limits used in this measurement.
[d] Most of this radiative mode, the low-momentum γ part, is also included in the parent mode listed without γ's.
[e] Allowed by higher-order electroweak interactions.
[f] Violates *CP* in leading order. Test of direct *CP* violation since the indirect *CP*-violating and *CP*-conserving contributions are expected to be suppressed.

CONSTRAINED FIT INFORMATION

An overall fit to the mean life and 15 branching ratios uses 27 measurements and one constraint to determine 11 parameters. The overall fit has a $\chi^2 = 37.4$ for 17 degrees of freedom.

The following *off-diagonal* array elements are the correlation coefficients $\langle \delta p_i \delta p_j \rangle / (\delta p_i \cdot \delta p_j)$, in percent, from the fit to parameters p_i, including the branching fractions, $x_i \equiv \Gamma_i/\Gamma_{\text{total}}$. The fit constrains the x_i whose labels appear in this array to sum to one.

	x_1	x_2	x_6	x_7	x_8	x_9	x_{13}	x_{14}	x_{17}	x_{19}
x_2	−21									
x_6	−77	−29								
x_7	−15	−20	−18							
x_8	53	−11	−47	4						
x_9	30	−23	−11	−12	64					
x_{13}	6	−1	−6	0	12	8				
x_{14}	6	−1	−6	0	11	7	93			
x_{17}	−46	−22	64	−14	−21	8	−3	−3		
x_{19}	−5	−2	7	−1	−3	−1	0	0	4	
Γ	−27	−9	24	15	−13	−6	−2	−2	15	2

	Mode		Rate (10^8 s^{-1})	Scale factor
Γ_1	$\pi^\pm e^\mp \nu_e$ Called K^0_{e3}.	[a]	0.07927±0.00034	1.1
Γ_2	$\pi^\pm \mu^\mp \nu_\mu$ Called $K^0_{\mu3}$.	[a]	0.05286±0.00025	1.1
Γ_6	$3\pi^0$		0.03815±0.00030	1.5
Γ_7	$\pi^+\pi^-\pi^0$		0.02451±0.00015	
Γ_8	$\pi^+\pi^-$	[b]	$(3.844 \pm 0.023) \times 10^{-4}$	1.2
Γ_9	$\pi^0\pi^0$		$(1.690 \pm 0.013) \times 10^{-4}$	1.4
Γ_{13}	$\pi^+\pi^-\gamma$	[c,d]	$(8.11 \pm 0.29) \times 10^{-6}$	2.7
Γ_{14}	$\pi^+\pi^-\gamma$(DE)		$(5.55 \pm 0.21) \times 10^{-6}$	2.0
Γ_{17}	2γ		$(1.069 \pm 0.010) \times 10^{-4}$	1.2
Γ_{19}	$e^+ e^-\gamma$		$(1.84 \pm 0.08) \times 10^{-6}$	1.9

K^0_L DECAY RATES

$\Gamma(\pi^+\pi^-\pi^0)$ — Γ_7

VALUE (10^6 s^{-1})	EVTS	DOCUMENT ID		TECN	COMMENT
2.451±0.015 OUR FIT					
• • • We do not use the following data for averages, fits, limits, etc. • • •					
2.32 ${}^{+0.13}_{-0.15}$	192	BALDO-...	75	HLBC	Assumes *CP*
2.35 ±0.20	180	[1] JAMES	72	HBC	Assumes *CP*
2.71 ±0.28	99	CHO	71	DBC	Assumes *CP*
2.5 ±0.3	98	[1] JAMES	71	HBC	Assumes *CP*
2.12 ±0.33	50	MEISNER	71	HBC	Assumes *CP*
2.20 ±0.35	53	WEBBER	70	HBC	Assumes *CP*
2.62 ${}^{+0.28}_{-0.27}$	136	BEHR	66	HLBC	Assumes *CP*

Downloaded from https://academic.oup.com/ptep/article/2022/8/083C01/6651666 by KIT Library user on 27 September 2022

3.26 ±0.77	18	ANDERSON	65	HBC	
1.4 ±0.4	14	FRANZINI	65	HBC	

[1] JAMES 72 is a final measurement and includes JAMES 71.

$\Gamma(\pi^\pm e^\mp \nu_e)$ — Γ_1

VALUE (10^6 s^{-1})	EVTS	DOCUMENT ID		TECN	COMMENT
7.927±0.034 OUR FIT	Error includes scale factor of 1.1.				
• • • We do not use the following data for averages, fits, limits, etc. • • •					
7.81 ±0.56	620	CHAN	71	HBC	
$7.52^{+0.85}_{-0.72}$		AUBERT	65	HLBC	$\Delta S=\Delta Q$, CP assumed

$\Gamma(\pi^\pm e^\mp \nu_e)+\Gamma(\pi^\pm \mu^\mp \nu_\mu)$ — $(\Gamma_1+\Gamma_2)$

VALUE (10^6 s^{-1})	EVTS	DOCUMENT ID		TECN	COMMENT
13.21±0.05 OUR FIT					
• • • We do not use the following data for averages, fits, limits, etc. • • •					
12.4 ±0.7	410	[1] BURGUN	72	HBC	$K^+ p \to K^0 p \pi^+$
8.47±1.69	126	[1] MANN	72	HBC	$K^- p \to n \overline{K}^0$
13.1 ±1.3	252	[1] WEBBER	71	HBC	$K^- p \to n \overline{K}^0$
11.6 ±0.9	393	[1,2] CHO	70	DBC	$K^+ n \to K^0 p$
10.3 ±0.8	335	[2] HILL	67	DBC	$K^+ n \to K^0 p$
$9.85^{+1.15}_{-1.05}$	109	[1] FRANZINI	65	HBC	

[1] Assumes $\Delta S = \Delta Q$ rule.
[2] CHO 70 includes events of HILL 67.

K^0_L BRANCHING RATIOS

Semileptonic modes

$\Gamma(\pi^\pm e^\mp \nu_e)/\Gamma_{total}$ — Γ_1/Γ

VALUE	EVTS	DOCUMENT ID		TECN
0.4055±0.0011 OUR FIT	Error includes scale factor of 1.7.			
0.4047±0.0028 OUR AVERAGE	Error includes scale factor of 3.1.			
0.4007±0.0005±0.0015	13M	[1] AMBROSINO	06	KLOE
0.4067±0.0011		[2] ALEXOPOU...	04	KTEV

[1] There are correlations between these five KLOE measurements: $B(K_L \to \pi e \nu)$, $B(K_L \to \pi \mu \nu)$, $B(K_L \to 3\pi^0)$, $B(K_L \to \pi^+\pi^-\pi^0)$, and τ_{K_L} measured in AMBROSINO 06. See the footnote for the τ_{K_L} measurement for the correlation matrix.

[2] ALEXOPOULOS 04 constrains $\sum_i B_i = 0.9993$ for the six major K_L branching fractions. The correlations among these branching fractions are taken into account in our fit. The correlation matrix is

	K_{e3}	$K_{\mu3}$	$3\pi^0$	$\pi^+\pi^-\pi^0$	$\pi^+\pi^-$	$\pi^0\pi^0$
K_{e3}	1					
$K_{\mu3}$	0.15	1				
$3\pi^0$	−0.77	−0.62	1			
$\pi^+\pi^-\pi^0$	0.18	0.08	−0.54	1		
$\pi^+\pi^-$	0.28	0.22	−0.48	0.49	1	
$\pi^0\pi^0$	−0.72	−0.54	0.89	−0.46	−0.39	1

$\Gamma(\pi^\pm \mu^\mp \nu_\mu)/\Gamma_{total}$ — Γ_2/Γ

VALUE	EVTS	DOCUMENT ID		TECN
0.2704±0.0007 OUR FIT	Error includes scale factor of 1.1.			
0.2700±0.0008 OUR AVERAGE				
0.2698±0.0005±0.0015	13M	[1] AMBROSINO	06	KLOE
0.2701±0.0009		[2] ALEXOPOU...	04	KTEV

[1] There are correlations between these five KLOE measurements: $B(K_L \to \pi e \nu)$, $B(K_L \to \pi \mu \nu)$, $B(K_L \to 3\pi^0)$, $B(K_L \to \pi^+\pi^-\pi^0)$, and τ_{K_L} measured in AMBROSINO 06. See the footnote for the τ_{K_L} measurement for the correlation matrix.

[2] For correlations with other ALEXOPOULOS 04 measurements, see the footnote with their $B(K_L \to \pi e \nu)$ measurement.

$[\Gamma(\pi^\pm e^\mp \nu_e)+\Gamma(\pi^\pm \mu^\mp \nu_\mu)]/\Gamma_{total}$ — $(\Gamma_1+\Gamma_2)/\Gamma$

VALUE	DOCUMENT ID
0.6760±0.0012 OUR FIT	Error includes scale factor of 1.6.

$\Gamma(\pi^\pm \mu^\mp \nu_\mu)/\Gamma(\pi^\pm e^\mp \nu_e)$ — Γ_2/Γ_1

VALUE	EVTS	DOCUMENT ID		TECN	COMMENT
0.6669±0.0027 OUR FIT	Error includes scale factor of 1.2.				
0.666 ±0.004 OUR AVERAGE	Error includes scale factor of 1.6.				
• • • We use the following data for averages but not for fits. • • •					
0.6740±0.0059	13M	[1] AMBROSINO	06	KLOE	Not in fit
0.6640±0.0014±0.0022	394k	[2] ALEXOPOU...	04	KTEV	Not in fit
• • • We do not use the following data for averages, fits, limits, etc. • • •					
0.702 ±0.011	33k	CHO	80	HBC	
0.662 ±0.037	10k	WILLIAMS	74	ASPK	
0.741 ±0.044	6700	BRANDENB...	73	HBC	
0.662 ±0.030	1309	EVANS	73	HLBC	
0.68 ±0.08	3548	BASILE	70	OSPK	
0.71 ±0.05	770	BUDAGOV	68	HLBC	

[1] AMBROSINO 06 enters the fit via their separate measurements of these two modes.
[2] ALEXOPOULOS 04 enters the fit via their separate measurements of these two modes.

$\Gamma((\pi\mu\text{atom})\nu)/\Gamma(\pi^\pm \mu^\mp \nu_\mu)$ — Γ_3/Γ_2

VALUE (units 10^{-7})	EVTS	DOCUMENT ID		TECN
3.90±0.39	155	[1] ARONSON	86	SPEC
• • • We do not use the following data for averages, fits, limits, etc. • • •				
seen	18	COOMBES	76	WIRE

[1] ARONSON 86 quote theoretical value of (4.31 ± 0.08) × 10^{-7}.

$\Gamma(\pi^0 \pi^\pm e^\mp \nu)/\Gamma_{total}$ — Γ_4/Γ

VALUE (units 10^{-5})	CL%	EVTS	DOCUMENT ID		TECN
5.20±0.11 OUR AVERAGE					
5.21±0.07±0.09		5402	BATLEY	04	NA48
5.16±0.20±0.22		729	MAKOFF	93	E731
• • • We do not use the following data for averages, fits, limits, etc. • • •					
6.2 ±2.0		16	CARROLL	80C	SPEC
< 220	90		[1] DONALDSON	74	SPEC

[1] DONALDSON 74 uses $K^0_L \to \pi^+\pi^-\pi^0$/(all K^0_L) decays = 0.126.

$\Gamma(\pi^\pm e^\mp \nu e^+ e^-)/\Gamma(\pi^+\pi^-\pi^0)$ — Γ_5/Γ_7

VALUE (units 10^{-5})	EVTS	DOCUMENT ID		TECN	COMMENT
10.02±0.17±0.29	19k	[1] ABOUZAID	07C	KTEV	$M_{ee} > 5$ MeV, $E^*_{ee} > 30$ MeV

[1] E^*_{ee} is the energy of the e^+e^- pair in the kaon rest frame. ABOUZAID 07C reports $[\Gamma(K^0_L \to \pi^\pm e^\mp \nu e^+ e^-)/\Gamma(K^0_L \to \pi^+\pi^-\pi^0)]$ / $[B(\pi^0 \to e^+e^-\gamma)]$ = (8.54 ± 0.07 ± 0.13) × 10^{-3} which we multiply by our best value $B(\pi^0 \to e^+e^-\gamma)$ = (1.174 ± 0.035) × 10^{-2}. Our first error is their experiment's error and our second error is the systematic error from using our best value.

Hadronic modes, including Charge conjugation×Parity Violating (CPV) modes

$\Gamma(3\pi^0)/\Gamma_{total}$ — Γ_6/Γ

VALUE	EVTS	DOCUMENT ID		TECN	COMMENT
0.1952±0.0012 OUR FIT	Error includes scale factor of 1.6.				
0.1969±0.0026 OUR AVERAGE	Error includes scale factor of 2.0.				
• • • We use the following data for averages but not for fits. • • •					
0.1997±0.0003±0.0019	13M	[1] AMBROSINO	06	KLOE	Not fitted
0.1945±0.0018		[1] ALEXOPOU...	04	KTEV	Not fitted

[1] We exclude these $B(K_L \to 3\pi^0)$ measurements from our fit because the authors have constrained K_L branching fractions to sum to one. It enters our fit via the other measurements from the experiment and their correlations, along with our constraint that the fitted branching fractions sum to one.

$\Gamma(3\pi^0)/\Gamma(\pi^\pm e^\mp \nu_e)$ — Γ_6/Γ_1

VALUE	EVTS	DOCUMENT ID		TECN	COMMENT
0.481 ±0.004 OUR FIT	Error includes scale factor of 1.8.				
• • • We use the following data for averages but not for fits. • • •					
0.4782±0.0014±0.0053	209k	[1] ALEXOPOU...	04	KTEV	Not in fit
• • • We do not use the following data for averages, fits, limits, etc. • • •					
0.545 ±0.004 ±0.009	38k	KREUTZ	95	NA31	

[1] This measurement enters the fit via their separate measurements of these two modes.

$\Gamma(3\pi^0)/[\Gamma(\pi^\pm e^\mp \nu_e)+\Gamma(\pi^\pm \mu^\mp \nu_\mu)+\Gamma(\pi^+\pi^-\pi^0)]$ — $\Gamma_6/(\Gamma_1+\Gamma_2+\Gamma_7)$

VALUE	EVTS	DOCUMENT ID		TECN	COMMENT
0.2436±0.0018 OUR FIT	Error includes scale factor of 1.6.				
• • • We do not use the following data for averages, fits, limits, etc. • • •					
0.251 ±0.014	549	BUDAGOV	68	HLBC	ORSAY measur.
0.277 ±0.021	444	BUDAGOV	68	HLBC	Ecole polytec.meas
$0.31^{+0.07}_{-0.06}$	29	KULYUKINA	68	CC	
0.24 ±0.08	24	ANIKINA	64	CC	

$\Gamma(3\pi^0)/\Gamma(\pi^+\pi^-\pi^0)$ — Γ_6/Γ_7

VALUE	EVTS	DOCUMENT ID		TECN	COMMENT
1.557±0.012 OUR FIT	Error includes scale factor of 1.3.				
• • • We use the following data for averages but not for fits. • • •					
1.582±0.027	13M	[1] AMBROSINO	06	KLOE	Not in fit
• • • We do not use the following data for averages, fits, limits, etc. • • •					
1.611±0.014±0.034	28k	KREUTZ	95	NA31	
1.65 ±0.07	883	BARMIN	72B	HLBC	Error statistical only
1.80 ±0.13	1010	BUDAGOV	68	HLBC	
2.0 ±0.6	188	ALEKSANYAN	64B	FBC	

[1] AMBROSINO 06 enters the fit via their separate measurements of these two modes.

$\Gamma(\pi^+\pi^-\pi^0)/\Gamma_{total}$ — Γ_7/Γ

VALUE	EVTS	DOCUMENT ID		TECN
0.1254±0.0005 OUR FIT				
0.1255±0.0006 OUR AVERAGE				
0.1263±0.0004±0.0011	13M	[1] AMBROSINO	06	KLOE
0.1252±0.0007		[2] ALEXOPOU...	04	KTEV

[1] There are correlations between these five KLOE measurements: $B(K_L \to \pi e \nu)$, $B(K_L \to \pi \mu \nu)$, $B(K_L \to 3\pi^0)$, $B(K_L \to \pi^+\pi^-\pi^0)$, and τ_{K_L} measured in AMBROSINO 06. See the footnote for the τ_{K_L} measurement for the correlation matrix.

[2] For correlations with other ALEXOPOULOS 04 measurements, see the footnote with their $B(K_L \to \pi e \nu)$ measurement.

Downloaded from https://academic.oup.com/ptep/article/2022/8/083C01/6651666 by KIT Library user on 27 September 2022

$\Gamma(\pi^+\pi^-\pi^0)/\Gamma(\pi^\pm e^\mp \nu_e)$ — Γ_7/Γ_1

VALUE	EVTS	DOCUMENT ID		TECN	COMMENT
0.3092±0.0016 OUR FIT	Error includes scale factor of 1.1.				
• • • We use the following data for averages but not for fits. • • •					
0.3078±0.0005±0.0017	799k	[1] ALEXOPOU...	04	KTEV	Not in fit
• • • We do not use the following data for averages, fits, limits, etc. • • •					
0.336 ±0.003 ±0.007	28k	KREUTZ	95	NA31	

[1] This measurement enters the fit via their separate measurements for the two modes.

$\Gamma(\pi^+\pi^-\pi^0)/[\Gamma(\pi^\pm e^\mp \nu_e)+\Gamma(\pi^\pm \mu^\mp \nu_\mu)+\Gamma(\pi^+\pi^-\pi^0)]$ — $\Gamma_7/(\Gamma_1+\Gamma_2+\Gamma_7)$

VALUE	EVTS	DOCUMENT ID		TECN	COMMENT
0.1565±0.0006 OUR FIT	Error includes scale factor of 1.1.				
• • • We do not use the following data for averages, fits, limits, etc. • • •					
0.163 ±0.003	6499	CHO	77	HBC	
0.1605±0.0038	1590	ALEXANDER	73B	HBC	
0.146 ±0.004	3200	BRANDENB...	73	HBC	
0.159 ±0.010	558	EVANS	73	HLBC	
0.167 ±0.016	1402	KULYUKINA	68	CC	
0.161 ±0.005		HOPKINS	67	HBC	
0.162 ±0.015	126	HAWKINS	66	HBC	
0.159 ±0.015	326	ASTBURY	65B	CC	
0.178 ±0.017	566	GUIDONI	65	HBC	
0.144 ±0.004	1729	HOPKINS	65	HBC	See HOPKINS 67

$\Gamma(\pi^+\pi^-)/\Gamma_{total}$ — Γ_8/Γ

Violates CP conservation.

VALUE (units 10^{-3})	DOCUMENT ID		TECN
1.967±0.010 OUR FIT	Error includes scale factor of 1.5.		
1.975±0.012	[1] ALEXOPOU...	04	KTEV

[1] For correlations with other ALEXOPOULOS 04 measurements, see the footnote with their $B(K_L \to \pi e \nu)$ measurement.

$\Gamma(\pi^+\pi^-)/\Gamma(\pi^\pm e^\mp \nu_e)$ — Γ_8/Γ_1

VALUE (units 10^{-3})	EVTS	DOCUMENT ID		TECN	COMMENT
4.849±0.020 OUR FIT	Error includes scale factor of 1.1.				
4.840±0.020 OUR AVERAGE					
4.826±0.022±0.016	47k	[1] LAI	07	NA48	
• • • We use the following data for averages but not for fits. • • •					
4.856±0.017±0.023	84k	[2] ALEXOPOU...	04	KTEV	Not in fit

[1] The LAI 07 central value of 4.835×10^{-3} has been reduced by 0.19% to 4.826×10^{-3} to subtract the contribution from the direct emission mode $K^0_L \to \pi^+\pi^-\gamma(DE)$.

[2] This measurement enters the fit via their separate measurements for the two modes.

$[\Gamma(\pi^+\pi^-)+\Gamma(\pi^+\pi^-\gamma(DE))]/\Gamma(\pi^\pm\mu^\mp\nu_\mu)$ — $(\Gamma_8+\Gamma_{14})/\Gamma_2$

VALUE (units 10^{-3})	EVTS	DOCUMENT ID		TECN
7.38 ±0.04 OUR FIT	Error includes scale factor of 1.4.			
7.275±0.042±0.054	45k	[1] AMBROSINO	06F	KLOE

[1] Fully inclusive. Taking $B(K^0_L \to \pi\mu\nu)$ from KLOE, AMBROSINO 06, $B(K^0_L \to \pi^+\pi^- + \pi^+\pi^-\gamma(DE)) = (1.963 \pm 0.012 \pm 0.017) \times 10^{-3}$ is obtained.

$\Gamma(\pi^+\pi^-)/[\Gamma(\pi^\pm e^\mp \nu_e)+\Gamma(\pi^\pm \mu^\mp \nu_\mu)]$ — $\Gamma_8/(\Gamma_1+\Gamma_2)$

Violates CP conservation.

VALUE (units 10^{-3})	EVTS	DOCUMENT ID		TECN	COMMENT
2.909±0.013 OUR FIT	Error includes scale factor of 1.3.				
• • • We do not use the following data for averages, fits, limits, etc. • • •					
3.13 ±0.14	1687	COUPAL	85	SPEC	η_{+-}=2.28 ± 0.06
3.04 ±0.14	2703	DEVOE	77	SPEC	η_{+-}=2.25 ± 0.05
2.51 ±0.23	309	[1] DEBOUARD	67	OSPK	η_{+-}=2.00 ± 0.09
2.35 ±0.19	525	[1] FITCH	67	OSPK	η_{+-}=1.94 ± 0.08

[1] Old experiments excluded from fit. See subsection on η_{+-} in section on "PARAMETERS FOR $K^0_L \to 2\pi$ DECAY" below for average η_{+-} of these experiments and for note on discrepancy.

$\Gamma(\pi^\pm e^\mp \nu_e)/\Gamma(2\text{ tracks})$ — $\Gamma_1/(\Gamma_1+\Gamma_2+0.03508\Gamma_6+\Gamma_7+\Gamma_8)$

$\Gamma(2\text{ tracks}) = \Gamma(\pi^\pm e^\mp \nu_e) + \Gamma(\pi^\pm \mu^\mp \nu_\mu) + 0.03508\ \Gamma(3\pi^0) + \Gamma(\pi^+\pi^-\pi^0) + \Gamma(\pi^+\pi^-)$ where 0.03508 is the fraction of $3\pi^0$ events with one Dalitz decay ($\pi^0 \to \gamma e^+ e^-$).

VALUE	EVTS	DOCUMENT ID		TECN
0.5006±0.0009 OUR FIT	Error includes scale factor of 1.3.			
0.4978±0.0035	6.8M	LAI	04B	NA48

$\Gamma(\pi^+\pi^-)/[\Gamma(\pi^\pm e^\mp \nu_e)+\Gamma(\pi^\pm \mu^\mp \nu_\mu)+\Gamma(\pi^+\pi^-\pi^0)]$ — $\Gamma_8/(\Gamma_1+\Gamma_2+\Gamma_7)$

Violates CP conservation.

VALUE (units 10^{-3})	EVTS	DOCUMENT ID		TECN	COMMENT
2.454±0.011 OUR FIT	Error includes scale factor of 1.3.				
• • • We do not use the following data for averages, fits, limits, etc. • • •					
2.60 ±0.07	4200	[1] MESSNER	73	ASPK	η_{+-} = 2.23 ± 0.05

[1] From same data as $\Gamma(\pi^+\pi^-)/\Gamma(\pi^+\pi^-\pi^0)$ MESSNER 73, but with different normalization.

$\Gamma(\pi^+\pi^-)/\Gamma(\pi^+\pi^-\pi^0)$ — Γ_8/Γ_7

Violates CP conservation.

VALUE (units 10^{-2})	EVTS	DOCUMENT ID		TECN	COMMENT
1.568±0.010 OUR FIT	Error includes scale factor of 1.3.				
• • • We do not use the following data for averages, fits, limits, etc. • • •					
1.64 ±0.04	4200	MESSNER	73	ASPK	η_{+-} = 2.23

$\Gamma(\pi^0\pi^0)/\Gamma_{total}$ — Γ_9/Γ

Violates CP conservation.

VALUE (units 10^{-3})	DOCUMENT ID		TECN
0.864±0.006 OUR FIT	Error includes scale factor of 1.8.		
0.865±0.012	[1] ALEXOPOU...	04	KTEV

[1] For correlations with other ALEXOPOULOS 04 measurements, see the footnote with their $B(K_L \to \pi e \nu)$ measurement.

$\Gamma(\pi^0\pi^0)/\Gamma(\pi^+\pi^-)$ — Γ_9/Γ_8

Violates CP conservation.

VALUE	DOCUMENT ID	
0.4395±0.0023 OUR FIT	Error includes scale factor of 2.0.	
0.4390±0.0012	ETAFIT	16

$\Gamma(\pi^0\pi^0)/\Gamma(3\pi^0)$ — Γ_9/Γ_6

Violates CP conservation.

VALUE (units 10^{-2})	EVTS	DOCUMENT ID		TECN	COMMENT
0.443 ±0.004 OUR FIT	Error includes scale factor of 2.1.				
• • • We use the following data for averages but not for fits. • • •					
0.4446±0.0016±0.0019	100k	[1] ALEXOPOU...	04	KTEV	Not in fit
• • • We do not use the following data for averages, fits, limits, etc. • • •					
0.37 ±0.08	29	BARMIN	70	HLBC	η_{00}=2.02 ± 0.23
0.32 ±0.15	30	BUDAGOV	70	HLBC	η_{00}=1.9 ± 0.5
0.46 ±0.11	57	BANNER	69	OSPK	η_{00}=2.2 ± 0.3

[1] This measurement enters the fit via their separate measurements for the two modes.

Semileptonic modes with photons

$\Gamma(\pi^\pm e^\mp \nu_e \gamma)/\Gamma(\pi^\pm e^\mp \nu_e)$ — Γ_{10}/Γ_1

VALUE (units 10^{-2})	EVTS	DOCUMENT ID		TECN	COMMENT
0.935±0.015 OUR AVERAGE	Error includes scale factor of 1.9. See the ideogram below.				
0.924±0.023±0.016	9k	[1] AMBROSINO	08F	KLOE	E^*_γ >30 MeV, $\theta^*_{e\gamma}$ >20°
0.916±0.017	4309	[2] ALEXOPOU...	05	KTEV	E^*_γ >30 MeV, $\theta^*_{e\gamma}$ >20°
$0.964\pm0.008^{+0.011}_{-0.009}$	19k	LAI	05	NA48	E^*_γ >30 MeV, $\theta^*_{e\gamma}$ >20°
$0.908\pm0.008^{+0.013}_{-0.012}$	15k	ALAVI-HARATI	01J	KTEV	$E^*_\gamma \geq 30$ MeV, $\theta^*_{e\gamma} \geq 20°$
$0.934\pm0.036^{+0.055}_{-0.039}$	1384	LEBER	96	NA31	$E^*_\gamma \geq 30$ MeV, $\theta^*_{e\gamma} \geq 20°$

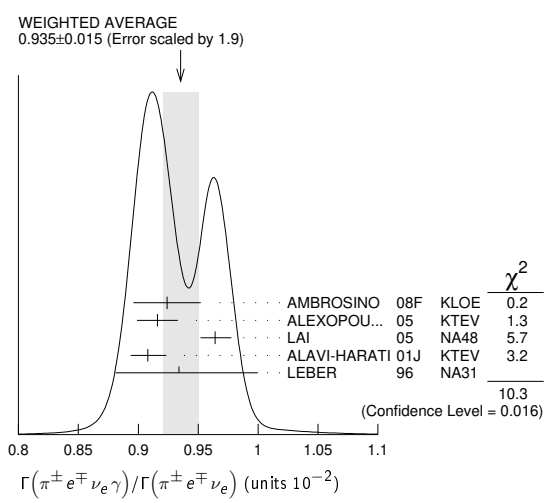

[1] Direct emission contribution measured $\langle X \rangle = -2.3 \pm 1.3 \pm 1.4$.

[2] Also measured cut E^*_γ >10 MeV, $\theta^*_{e\gamma}$ >0° 14221 evts: $\Gamma(\pi^\pm e^\mp \nu_e \gamma) / \Gamma(\pi^\pm e^\mp \nu_e) = (4.942 \pm 0.062)\%$.

$\Gamma(\pi^\pm \mu^\mp \nu_\mu \gamma)/\Gamma(\pi^\pm \mu^\mp \nu_\mu)$ — Γ_{11}/Γ_2

VALUE (units 10^{-3})	EVTS	DOCUMENT ID		TECN	COMMENT
2.09±0.08 OUR AVERAGE					
2.09±0.09		[1] ALEXOPOU...	05	KTEV	E^*_γ > 30 MeV
$2.08\pm0.17^{+0.16}_{-0.21}$	252	BENDER	98	NA48	$E^*_\gamma \geq 30$ MeV

[1] Also measured cut E^*_γ >10 MeV, 1385 evts: $\Gamma(\pi^\pm \mu^\mp \nu_\mu \gamma) / \Gamma(\pi^\pm \mu^\mp \nu_\mu) = (0.530 \pm 0.014 \pm 0.012)\%$.

Downloaded from https://academic.oup.com/ptep/article/2022/8/083C01/6651666 by KIT Library user on 27 September 2022

Hadronic modes with photons or $\ell\bar{\ell}$ pairs

$\Gamma(\pi^0\pi^0\gamma)/\Gamma_{total}$ — Γ_{12}/Γ

VALUE (units 10^{-6})	CL%	DOCUMENT ID		TECN	COMMENT
< 0.243	90	ABOUZAID	08B	KTEV	$K^0_L \to \pi^0\pi^0_D\gamma$, $\pi^0_D \to ee\gamma$
• • • We do not use the following data for averages, fits, limits, etc. • • •					
< 5.6	90	BARR	94	NA31	
<230	90	ROBERTS	94	E799	

$\Gamma(\pi^+\pi^-\gamma)/\Gamma(\pi^+\pi^-\pi^0)$ — Γ_{13}/Γ_7

For earlier limits see our 1992 edition Physical Review **D45** S1 (1992).

VALUE (units 10^{-4})	EVTS	DOCUMENT ID		TECN	COMMENT
• • • We do not use the following data for averages, fits, limits, etc. • • •					
1.23±0.13	516	[1,2] CARROLL	80B	SPEC	E^*_γ > 20 MeV
2.33±0.23	546	[1,3] CARROLL	80B	SPEC	
3.56±0.26	1062	[1,4] CARROLL	80B	SPEC	E^*_γ > 20 MeV

[1] CARROLL 80B quotes $B(\pi^+\pi^-\gamma)$ using normalization $B(\pi^+\pi^-\pi^0) = 0.1239$. We divide by this value to obtain their measured $\Gamma(\pi^+\pi^-\gamma)$ / $\Gamma(\pi^+\pi^-\pi^0)$.
[2] Internal Bremsstrahlung component only.
[3] Direct γ emission component only.
[4] Both IB and DE components.

$\Gamma(\pi^+\pi^-\gamma)/\Gamma(\pi^+\pi^-)$ — Γ_{13}/Γ_8

VALUE (units 10^{-2})	EVTS	DOCUMENT ID		TECN	COMMENT
2.11±0.08 OR FIT Error includes scale factor of 2.9.					
2.11±0.08 OR AVERAGE Error includes scale factor of 2.9.					
2.08±0.02±0.02	8669	[1] ALAVI-HARATI	01B	KTEV	E^*_γ > 20 MeV
2.30±0.07	3136	RAMBERG	93	E731	E^*_γ > 20 MeV

[1] ALAVI-HARATI 01B includes both Direct Emission (DE) and Inner Bremsstrahlung (IB) processes.

$\Gamma(\pi^+\pi^-\gamma(DE))/\Gamma(\pi^+\pi^-\gamma)$ — Γ_{14}/Γ_{13}

These values assume that $\Gamma(K^0_L \to \pi^+\pi^-\gamma) = \Gamma(K^0_L \to \pi^+\pi^-\gamma(DE)) + \Gamma(K^0_L \to \pi^+\pi^-\gamma(IB))$, the sum of widths for the direct emission (DE) and inner bremsstrahlung (IE) processes, with no IB-DE interference. DE assumes a form factor as described in RAMBERG 93.

VALUE	EVTS	DOCUMENT ID		TECN	COMMENT
0.684±0.009 OR FIT					
0.684±0.009 OR AVERAGE					
0.689±0.021	111k	ABOUZAID	06A	KTEV	E^*_γ > 20 MeV
0.683±0.011	8669	ALAVI-HARATI	01B	KTEV	E^*_γ > 20 MeV
0.685±0.041	3136	RAMBERG	93	E731	E^*_γ > 20 MeV

$\Gamma(\pi^0 2\gamma)/\Gamma_{total}$ — Γ_{15}/Γ

VALUE (units 10^{-6})	CL%	EVTS	DOCUMENT ID		TECN	COMMENT
1.273±0.033 OR AVERAGE						
1.28 ±0.06 ±0.01		1.4k	[1] ABOUZAID	08	KTEV	
1.27 ±0.04 ±0.01		2.5k	[2] LAI	02B	NA48	
• • • We do not use the following data for averages, fits, limits, etc. • • •						
1.68 ±0.07 ±0.08		884	[3] ALAVI-HARATI	99B	KTEV	
1.7 ±0.2 ±0.2		63	[4] BARR	92	NA31	
1.86 ±0.60 ±0.60		60	PAPADIMITR...	91	E731	$m_{\gamma\gamma}$ > 280 MeV
<5.1	90		PAPADIMITR...	91	E731	$m_{\gamma\gamma}$ < 264 MeV
2.1 ±0.6		14	[5] BARR	90C	NA31	$m_{\gamma\gamma}$ > 280 MeV

[1] ABOUZAID 08 reports $(1.29 \pm 0.03 \pm 0.05) \times 10^{-6}$ from a measurement of $[\Gamma(K^0_L \to \pi^0 2\gamma)/\Gamma_{total}]$ / $[B(K^0_L \to \pi^0\pi^0)]$ assuming $B(K^0_L \to \pi^0\pi^0) = (8.69 \pm 0.04) \times 10^{-4}$, which we rescale to our best value $B(K^0_L \to \pi^0\pi^0) = (8.64 \pm 0.06) \times 10^{-4}$. Our first error is their experiment's error and our second error is the systematic error from using our best value.
[2] LAI 02B reports $[\Gamma(K^0_L \to \pi^0 2\gamma)/\Gamma_{total}]$ / $[B(K^0_L \to \pi^0\pi^0)] = (1.467 \pm 0.032 \pm 0.032) \times 10^{-3}$ which we multiply by our best value $B(K^0_L \to \pi^0\pi^0) = (8.64 \pm 0.06) \times 10^{-4}$. Our first error is their experiment's error and our second error is the systematic error from using our best value. They also find that $B(\pi^0 2\gamma, m_{\gamma\gamma} < 110 \text{ MeV}) < 0.6 \times 10^{-8}$(90% CL).
[3] ALAVI-HARATI 99B finds that $\Gamma(\pi^0 2\gamma, m_{\gamma\gamma} < 240 \text{ MeV}))$ / $\Gamma(\pi^0 2\gamma) = (17.3 \pm 1.3 \pm 1.5)$%. Superseded by ABOUZAID 08.
[4] BARR 92 find that $\Gamma(\pi^0 2\gamma, m_{\gamma\gamma} < 240 \text{ MeV})/\Gamma(\pi^0 2\gamma) < 0.09$ (90% CL).
[5] BARR 90C superseded by BARR 92.

$\Gamma(\pi^0\gamma e^+e^-)/\Gamma_{total}$ — Γ_{16}/Γ

VALUE (units 10^{-8})	CL%	EVTS	DOCUMENT ID		TECN
1.62±0.14±0.09		125	[1] ABOUZAID	07D	KTEV
• • • We do not use the following data for averages, fits, limits, etc. • • •					
2.34±0.35±0.13		44	ALAVI-HARATI	01E	KTEV
<71	90	0	MURAKAMI	99	SPEC

[1] ABOUZAID 07D includes 1997 (ALAVI-HARATI 01E) and 1999 data. It measures the ratio of $B(K^0_L \to \pi^0\gamma e^+e^-)$ / $B(K^0_L \to \pi^0\pi^0_D)$, where π^0_D is the Dalitz decaying π^0, and uses PDG 06 values $B(K^0_L \to \pi^0\pi^0) = (8.69 \pm 0.04) \times 10^{-4}$, and $B(\pi^0_D \to e^+e^-\gamma) = (1.198 \pm 0.032) \times 10^{-2}$. Supersedes ALAVI-HARATI 01E result.

Other modes with photons or $\ell\bar{\ell}$ pairs

$\Gamma(2\gamma)/\Gamma_{total}$ — Γ_{17}/Γ

VALUE (units 10^{-4})	EVTS	DOCUMENT ID		TECN	COMMENT
5.47±0.04 OR FIT Error includes scale factor of 1.1.					
• • • We do not use the following data for averages, fits, limits, etc. • • •					
4.54±0.84		[1] BANNER	72B	OSPK	
4.5 ±1.0	23	ENSTROM	71	OSPK	K^0_L 1.5–9 GeV/c
5.0 ±1.0		[2] REPELLIN	71	OSPK	
5.5 ±1.1	90	KUNZ	68	OSPK	Norm.to 3 π(C+N)

[1] This value uses $(\eta_{00}/\eta_{+-})^2 = 1.05 \pm 0.14$. In general, $\Gamma(2\gamma)/\Gamma_{total} = [(4.32 \pm 0.55) \times 10^{-4}]\,[(\eta_{00}/\eta_{+-})^2]$.
[2] Assumes regeneration amplitude in copper at 2 GeV is 22 mb. To evaluate for a given regeneration amplitude and error, multiply by (regeneration amplitude/22mb)^2.

$\Gamma(2\gamma)/\Gamma(3\pi^0)$ — Γ_{17}/Γ_6

VALUE (units 10^{-3})	EVTS	DOCUMENT ID		TECN	COMMENT
2.802±0.017 OR FIT					
2.802±0.018 OR AVERAGE					
2.79 ±0.02 ±0.02	27k	ADINOLFI	03	KLOE	
2.81 ±0.01 ±0.02		LAI	03	NA48	
• • • We do not use the following data for averages, fits, limits, etc. • • •					
2.13 ±0.43	28	BARMIN	71	HLBC	
2.24 ±0.28	115	BANNER	69	OSPK	
2.5 ±0.7	16	ARNOLD	68B	HLBC	Vacuum decay

$\Gamma(2\gamma)/\Gamma(\pi^0\pi^0)$ — Γ_{17}/Γ_9

VALUE	EVTS	DOCUMENT ID		TECN
0.633±0.006 OR FIT Error includes scale factor of 1.4.				
0.632±0.004±0.008	110k	BURKHARDT	87	NA31

$\Gamma(3\gamma)/\Gamma_{total}$ — Γ_{18}/Γ

VALUE	CL%	DOCUMENT ID		TECN
<7.4 × 10^{-8}	90	[1] TUNG	11	K391
• • • We do not use the following data for averages, fits, limits, etc. • • •				
<2.4 × 10^{-7}	90	[2] BARR	95C	NA31

[1] TUNG 11 reports the result assuming parity violating interaction and using 2005 data (Run-II and III). Assuming parity conserving or phase space interaction, the 90% upper limits obtained are 7.5×10^{-8} and 8.6×10^{-8}, respectively.
[2] Assumes a phase-space decay distribution.

$\Gamma(e^+e^-\gamma)/\Gamma_{total}$ — Γ_{19}/Γ

VALUE (units 10^{-6})	EVTS	DOCUMENT ID		TECN
9.4±0.4 OR FIT Error includes scale factor of 2.0.				
10.0±0.5 OR AVERAGE Error includes scale factor of 1.5. See the ideogram below.				
10.6±0.2±0.4	6864	[1] FANTI	99B	NA48
9.2±0.5±0.5	1053	BARR	90B	NA31
9.1±0.4$^{+0.6}_{-0.5}$	919	OHL	90B	B845

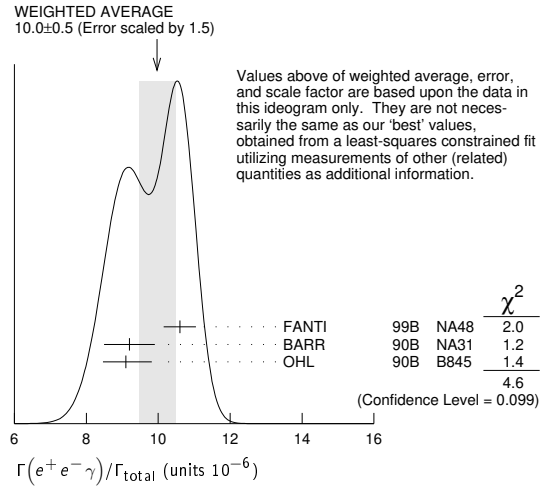

[1] For FANTI 99B, the ±0.4 systematic error includes for uncertainties in the calculation, primarily uncertainties in the $\pi^0 \to e^+e^-\gamma$ and $K^0_L \to \pi^0\pi^0$ branching ratios, evaluated using our 1999 Web edition values.

$\Gamma(e^+e^-\gamma)/\Gamma(3\pi^0)$ — Γ_{19}/Γ_6

VALUE (units 10^{-5})	EVTS	DOCUMENT ID		TECN
4.82±0.21 OR FIT Error includes scale factor of 2.0.				
4.63±0.04±0.13	83k	[1] ABOUZAID	07B	KTEV

[1] ABOUZAID 07B reports $[\Gamma(K^0_L \to e^+e^-\gamma)/\Gamma(K^0_L \to 3\pi^0)]$ / $[3\Gamma(\pi^0 \to 2\gamma)/\Gamma_{total} \times \Gamma(\pi^0 \to e^+e^-\gamma)/\Gamma_{total}] = (1.3302 \pm 0.0046 \pm 0.0103) \times 10^{-3}$ which we multiply by our best value $3\Gamma(\pi^0 \to 2\gamma)/\Gamma_{total} \times \Gamma(\pi^0 \to e^+e^-\gamma)/\Gamma_{total} = 0.0348 \pm 0.0010$. Our first error is their experiment's error and our second error is the systematic error from using our best value.

Downloaded from https://academic.oup.com/ptep/article/2022/8/083C01/6651666 by KIT Library user on 27 September 2022

$\Gamma(\mu^+\mu^-\gamma)/\Gamma_{total}$ — Γ_{20}/Γ

VALUE (units 10^{-7})	EVTS	DOCUMENT ID		TECN
3.59±0.11 OUR AVERAGE Error includes scale factor of 1.3.				
3.62±0.04±0.08	9100	ALAVI-HARATI 01G		KTEV
3.4 ±0.6 ±0.4	45	FANTI	97	NA48
3.23±0.23±0.19	197	SPENCER	95	E799

$\Gamma(e^+e^-\gamma\gamma)/\Gamma_{total}$ — Γ_{21}/Γ

VALUE (units 10^{-7})	EVTS	DOCUMENT ID		TECN	COMMENT
5.95±0.33 OUR AVERAGE					
5.84±0.15±0.32	1543	ALAVI-HARATI 01F		KTEV	$E^*_\gamma > 5$ MeV
8.0 ±1.5 $^{+1.4}_{-1.2}$	40	SETZU	98	NA31	$E^*_\gamma > 5$ MeV
6.5 ±1.2 ±0.6	58	NAKAYA	94	E799	$E^*_\gamma > 5$ MeV
6.6 ±3.2		MORSE	92	B845	$E^*_\gamma > 5$ MeV

$\Gamma(\mu^+\mu^-\gamma\gamma)/\Gamma_{total}$ — Γ_{22}/Γ

VALUE (units 10^{-9})	EVTS	DOCUMENT ID		TECN	COMMENT
$10.4^{+7.5}_{-5.9}\pm0.7$	4	ALAVI-HARATI 00E		KTEV	$m_{\gamma\gamma} \geq 1$ MeV/c^2

Charge conjugation × Parity (*CP*) or Lepton Family number (*LF*) violating modes, or $\Delta S = 1$ weak neutral current (*S1*) modes

$\Gamma(\mu^+\mu^-)/\Gamma(\pi^+\pi^-)$ — Γ_{23}/Γ_8

Test for $\Delta S = 1$ weak neutral current. Allowed by higher-order electroweak interaction.

VALUE (units 10^{-6})	EVTS	DOCUMENT ID		TECN	COMMENT
3.48 ±0.05 OUR AVERAGE					
3.474±0.057	6210	AMBROSE	00	B871	
3.87 ±0.30	179	[1] AKAGI	95	SPEC	
3.38 ±0.17	707	HEINSON	95	B791	
• • • We do not use the following data for averages, fits, limits, etc. • • •					
3.9 ±0.3 ±0.1	178	[2] AKAGI	91B	SPEC	In AKAGI 95
3.45 ±0.18 ±0.13	368	[3] HEINSON	91	SPEC	In HEINSON 95
4.1 ±0.5	54	INAGAKI	89	SPEC	In AKAGI 91B
2.8 ±0.3 ±0.2	87	MATHIAZHA...	89B	SPEC	In HEINSON 91

[1] AKAGI 95 gives this number multiplied by the PDG 1992 average for $\Gamma(K^0_L \to \pi^+\pi^-)/\Gamma(\text{total})$.
[2] AKAGI 91B give this number multiplied by the 1990 PDG average for $\Gamma(K^0_L \to \pi^+\pi^-)/\Gamma(\text{total})$.
[3] HEINSON 91 give $\Gamma(K^0_L \to \mu\mu)/\Gamma_{total}$. We divide out the $\Gamma(K^0_L \to \pi^+\pi^-)/\Gamma_{total}$ PDG average which they used.

$\Gamma(e^+e^-)/\Gamma_{total}$ — Γ_{24}/Γ

Test for $\Delta S = 1$ weak neutral current. Allowed by higher-order electroweak interaction.

VALUE (units 10^{-10})	CL%	EVTS	DOCUMENT ID		TECN
$0.087^{+0.057}_{-0.041}$		4	AMBROSE	98	B871
• • • We do not use the following data for averages, fits, limits, etc. • • •					
<1.6	90	1	AKAGI	95	SPEC
<0.41	90	0	[1] ARISAKA	93B	B791

[1] ARISAKA 93B includes all events with <6 MeV radiated energy.

$\Gamma(\pi^+\pi^-e^+e^-)/\Gamma_{total}$ — Γ_{25}/Γ

Test for $\Delta S = 1$ weak neutral current. Allowed by higher-order electroweak interaction.

VALUE (units 10^{-7})	CL%	EVTS	DOCUMENT ID		TECN	COMMENT
3.11±0.19 OUR AVERAGE						
3.08±0.09±0.18		1125	[1] LAI	03C	NA48	
3.2 ±0.6 ±0.4		37	ADAMS	98	KTEV	
4.4 ±1.3 ±0.5		13	TAKEUCHI	98	SPEC	
• • • We do not use the following data for averages, fits, limits, etc. • • •						
<4.6	90		NOMURA	97	SPEC	$m_{ee} > 4$ MeV

[1] LAI 03C second error is 0.15(syst)±0.10(norm) combined in quadrature. The normalization uses $BR(K_L \to \pi^+\pi^-\pi^0) * BR(\pi^0 \to e^+e^-) = (1.505 \pm 0.047) \times 10^{-3}$ from our 2000 Edition.

$\Gamma(\pi^0\pi^0e^+e^-)/\Gamma_{total}$ — Γ_{26}/Γ

Test for $\Delta S = 1$ weak neutral current. Allowed by higher-order electroweak interaction.

VALUE (units 10^{-9})	CL%	EVTS	DOCUMENT ID	TECN
<6.6	90	1	ALAVI-HARATI 02C	E799

$\Gamma(\pi^0\pi^0\mu^+\mu^-)/\Gamma_{total}$ — Γ_{27}/Γ

Test for $\Delta S = 1$ weak neutral current. Allowed by higher-order electroweak interaction.

VALUE	CL%	DOCUMENT ID		TECN
$<9.2 \times 10^{-11}$	90	[1] ABOUZAID	11A	E799

[1] ABOUZAID 11A also reports $B(K^0_L \to \pi^0\pi^0X^0 \to \pi^0\pi^0\mu^+\mu^-) < 1.0 \times 10^{-10}$ at 90% C.L., where the X^0 is a possible new neutral boson that was reported by PARK 05 with a mass of 214.3 ± 0.5 MeV/c^2.

$\Gamma(\mu^+\mu^-e^+e^-)/\Gamma_{total}$ — Γ_{28}/Γ

Test for $\Delta S = 1$ weak neutral current. Allowed by higher-order electroweak interaction.

VALUE (units 10^{-9})	CL%	EVTS	DOCUMENT ID		TECN	COMMENT
2.69±0.27 OUR AVERAGE						
2.69±0.24±0.12		131	[1] ALAVI-HARATI 03B		KTEV	
2.9 $^{+6.7}_{-2.4}$		1	GU	96	E799	
• • • We do not use the following data for averages, fits, limits, etc. • • •						
2.62±0.40±0.17		43	ALAVI-HARATI 01H		KTEV	Sup. by ALAVI-HARATI 03B
<4900	90		BALATS	83	SPEC	

[1] ALAVI-HARATI 03B also measures the linear slope $\alpha = -1.59 \pm 0.37$.

$\Gamma(e^+e^-e^+e^-)/\Gamma_{total}$ — Γ_{29}/Γ

Test for $\Delta S = 1$ weak neutral current. Allowed by higher-order electroweak interaction.

VALUE (units 10^{-8})	EVTS	DOCUMENT ID		TECN	COMMENT
3.56±0.21 OUR AVERAGE					
3.30±0.24±0.25	200	[1] LAI	05B	NA48	
3.72±0.18±0.23	441	ALAVI-HARATI 01D		KTEV	
3.96±0.78±0.32	27	GU	94	E799	
3.07±1.25±0.26	6	VAGINS	93	B845	
• • • We do not use the following data for averages, fits, limits, etc. • • •					
6 ±2 ±1	18	[2] AKAGI	95	SPEC	m_{ee} >470 MeV
7 ±3 ±2	6	[2] AKAGI	95	SPEC	m_{ee} >470 MeV
10.4 ±3.7 ±1.1	8	[3] BARR	95	NA31	
6 ±2 ±1	18	AKAGI	93	CNTR	Sup. by AKAGI 95
4 ±3	2	BARR	91	NA31	Sup. by BARR 95

[1] LAI 05B uses 1998 and 1999 data. Data are normalized to the observed events of $K^0_L \to \pi^+\pi^-\pi^0$ (π^0 into Dalitz pair) and PDG 04 values are used for $B(K^0_L \to \pi^+\pi^-\pi^0)$ and $B(\pi^0 \to e^+e^-\gamma)$. The systematic error includes a normalization error of ±0.10.
[2] Values are for the total branching fraction, acceptance-corrected for the m_{ee} cuts shown.
[3] Distribution of angles between two e^+e^- pair planes favors *CP*=−1 for K^0_L.

$\Gamma(\pi^0\mu^+\mu^-)/\Gamma_{total}$ — Γ_{30}/Γ

Violates *CP* in leading order. Test for $\Delta S = 1$ weak neutral current. Allowed by higher-order electroweak interaction.

VALUE (units 10^{-9})	CL%	EVTS	DOCUMENT ID		TECN
<0.38	90		ALAVI-HARATI 00D		KTEV
• • • We do not use the following data for averages, fits, limits, etc. • • •					
<5.1	90	0	HARRIS	93	E799

$\Gamma(\pi^0e^+e^-)/\Gamma_{total}$ — Γ_{31}/Γ

Violates *CP* in leading order. Direct and indirect *CP*-violating contributions are expected to be comparable and to dominate the *CP*-conserving part. LAI 02B result suggests that *CP*-violation effects dominate. Test for $\Delta S = 1$ weak neutral current. Allowed by higher-order electroweak interaction.

VALUE (units 10^{-10})	CL%	EVTS	DOCUMENT ID		TECN	COMMENT
< 2.8	90		[1] ALAVI-HARATI 04A		KTEV	combined result
• • • We do not use the following data for averages, fits, limits, etc. • • •						
< 3.5	90		ALAVI-HARATI 04A		KTEV	
0.0047$^{+0.0022}_{-0.0018}$			[2] LAI	02B	NA48	*CP*-conserving part
< 5.1	90	2	ALAVI-HARATI 01		KTEV	
0.01 to 0.02			ALAVI-HARATI 99B		KTEV	*CP*-conserving part
< 43	90	0	HARRIS	93B	E799	
< 75	90	0	BARKER	90	E731	
< 55	90	0	OHL	90	B845	
< 400	90		BARR	88	NA31	
<3200	90		JASTRZEM...	88	SPEC	

[1] Combined result of ALAVI-HARATI 04A 1999-2000 data set and ALAVI-HARATI 01 1997 data set.
[2] LAI 02B uses the absence of a signal in $K^0_L \to \pi^0\gamma\gamma$ with $m(\gamma\gamma)<m(\pi^0)$ and their a_V value to predict this value.

$\Gamma(\pi^0\nu\overline{\nu})/\Gamma_{total}$ — Γ_{32}/Γ

Violates *CP* in leading order. Test of direct *CP* violation since the indirect *CP*-violating and *CP*-conserving contributions are expected to be suppressed. Test of $\Delta S = 1$ weak neutral current.

VALUE (units 10^{-8})	CL%	DOCUMENT ID		TECN
< 0.49	90	[1] AHN	21	KOTO
< 0.30	90	[2] AHN	19	KOTO
• • • We do not use the following data for averages, fits, limits, etc. • • •				
< 5.1	90	[3] AHN	17	KOTO
< 2.6	90	[4] AHN	10	K391
< 6.7	90	[5] AHN	08	K391
<21	90	[6] AHN	06	K391
<59	90	ALAVI-HARATI 00		KTEV

[1] AHN 21 result is based on data collected in 2016, 2017 and 2018, which corresponds to 3.05×10^{19} protons on target. A single event sensitivity of $(7.20 \pm 0.05 \pm 0.66) \times 10^{-10}$ was achieved with 3 candidate events observed and total 1.22 ± 0.26 background events.
[2] AHN 19 result is based on data collected in 2015, which corresponds to 2.2×10^{19} protons on target. A single event sensitivity of $(1.30 \pm 0.01 \pm 0.14) \times 10^{-9}$ was achieved with no candidate events observed. An upper limit of $< 2.4 \times 10^{-9}$ at the 90% C.L. for the $K_L \to \pi^0X^0$ decay was also set, where X^0 is an invisible particle with a mass of 135 MeV/c^2.

Downloaded from https://academic.oup.com/ptep/article/2022/8/083C01/6651666 by KIT Library user on 27 September 2022

[3] AHN 17 result is based on the first 100 hours of physics running in 2013. One candidate event was observed with an expected background of 0.34 ± 0.16 events. An upper limit of $< 3.7 \times 10^{-8}$ at the 90% C.L. for the $K_L \to \pi^0 X^0$ decay was also set, where X^0 is an invisible particle with a mass of 135 MeV/c^2.

[4] Obtained combining Run-2 (AHN 08) and Run-3 data.

[5] Value obtained using data from February to April 2005.

[6] Value obtained analyzing 10% of data of RUN 1 (performed in 2004).

$\Gamma(\pi^0\pi^0\nu\overline{\nu})/\Gamma_{total}$ — Γ_{33}/Γ

VALUE	CL%	DOCUMENT ID		TECN
$<8.1 \times 10^{-7}$	90	[1] OGATA	11	K391
• • • We do not use the following data for averages, fits, limits, etc. • • •				
$<4.7 \times 10^{-5}$	90	[2] NIX	07	K391

[1] Using 2005 Run-I data. OGATA 11 also sets a limit on the $K^0_L \to \pi^0\pi^0 X \to$ invisible particles process: the limit on the branching fraction varied from 7.0×10^{-7} to 4.0×10^{-5} for the mass of X ranging from 50 to 200 MeV/c^2.

[2] Observed 1 event with expected background of 0.43 ± 0.35 events. NIX 07 also measured $B(K^0_L \to \pi^0\pi^0 P) < 1.2\times10^{-6}$ at 90% CL, where P is the pseudoscalar particle and $m_P < 100$ MeV.

$\Gamma(e^\pm\mu^\mp)/\Gamma_{total}$ — Γ_{34}/Γ

Test of lepton family number conservation.

VALUE (units 10^{-11})	CL%	EVTS	DOCUMENT ID		TECN
<0.47	90		AMBROSE	98B	B871
• • • We do not use the following data for averages, fits, limits, etc. • • •					
<9.4	90	0	AKAGI	95	SPEC
<3.9	90	0	ARISAKA	93	B791
<3.3	90	0	[1] ARISAKA	93	B791

[1] This is the combined result of ARISAKA 93 and MATHIAZHAGAN 89.

$\Gamma(e^\pm e^\pm\mu^\mp\mu^\mp)/\Gamma_{total}$ — Γ_{35}/Γ

Test of lepton family number conservation.

VALUE (units 10^{-11})	CL%	EVTS	DOCUMENT ID		TECN	COMMENT
< 4.12	90	0	ALAVI-HARATI	03B	KTEV	
• • • We do not use the following data for averages, fits, limits, etc. • • •						
< 12.3	90	0	[1] ALAVI-HARATI	01H	KTEV	Sup. by ALAVI-HARATI 03B
<610	90	0	[1] GU	96	E799	

[1] Assuming uniform phase space distribution.

$\Gamma(\pi^0\mu^\pm e^\mp)/\Gamma_{total}$ — Γ_{36}/Γ

Test of lepton family number conservation.

VALUE (units 10^{-10})	CL%	DOCUMENT ID		TECN
< 0.76	90	ABOUZAID	08C	KTEV
• • • We do not use the following data for averages, fits, limits, etc. • • •				
<62	90	ARISAKA	98	E799

$\Gamma(\pi^0\pi^0\mu^\pm e^\mp)/\Gamma_{total}$ — Γ_{37}/Γ

Test of lepton family number conservation.

VALUE (units 10^{-10})	CL%	DOCUMENT ID		TECN
<1.7	90	ABOUZAID	08C	KTEV

Lorentz invariance violating modes

$\Gamma(\pi^0\gamma)/\Gamma_{total}$ — Γ_{38}/Γ

VALUE	CL%	DOCUMENT ID		TECN
$<1.7 \times 10^{-7}$	90	[1] SHIMIZU	20	KOTO

[1] SHIMIZU 20 uses data collected from 2016 to 2018 at the J-PARC KOTO experiment. The single event sensitivity is $(7.1 \pm 0.3 \pm 1.6)\times10^{-8}$. No candidate event was observed.

See the related review(s):

V_{ud}, V_{us} the Cabibbo Angle, and CKM Unitarity

ENERGY DEPENDENCE OF K^0_L DALITZ PLOT

For discussion, see note on Dalitz plot parameters in the $K^\pm$ section of the Particle Listings above. For definitions of a_y, a_t, a_u, and a_y, see the earlier version of the same note in the 1982 edition of this *Review* published in Physics Letters **111B** 70 (1982).

$|\text{matrix element}|^2 = 1 + gu + hu^2 + jv + kv^2 + fuv$

where $u = (s_3 - s_0) / m^2_\pi$ and $v = (s_2 - s_1) / m^2_\pi$

LINEAR COEFFICIENT g FOR $K^0_L \to \pi^+\pi^-\pi^0$

VALUE	EVTS	DOCUMENT ID		TECN	COMMENT
0.678 ±0.008 OUR AVERAGE		Error includes scale factor of 1.5. See the ideogram below.			
0.6823±0.0044±0.0044	500k	ANGELOPO...	98C	CPLR	
0.681 ±0.024	6499	CHO	77	HBC	
0.620 ±0.023	4709	PEACH	77	HBC	
0.677 ±0.010	509k	MESSNER	74	ASPK	$a_y = -0.917 \pm 0.013$
• • • We do not use the following data for averages, fits, limits, etc. • • •					
0.69 ±0.07	192	[1] BALDO-...	75	HLBC	
0.590 ±0.022	56k	[1] BUCHANAN	75	SPEC	$a_u = -0.277 \pm 0.010$
0.619 ±0.027	20k	[1,2] BISI	74	ASPK	$a_t = -0.282 \pm 0.011$
0.612 ±0.032		[1] ALEXANDER	73B	HBC	
0.73 ±0.04	3200	[1] BRANDENB...	73	HBC	
0.608 ±0.043	1486	[1] KRENZ	72	HLBC	$a_t = -0.277 \pm 0.018$
0.650 ±0.012	29k	[1] ALBROW	70	ASPK	$a_y = -0.858 \pm 0.015$
0.593 ±0.022	36k	[1,3] BUCHANAN	70	SPEC	$a_u = -0.278 \pm 0.010$
0.664 ±0.056	4400	[1] SMITH	70	OSPK	$a_t = -0.306 \pm 0.024$
0.400 ±0.045	2446	[1] BASILE	68B	OSPK	$a_t = -0.188 \pm 0.020$
0.649 ±0.044	1350	[1] HOPKINS	67	HBC	$a_t = -0.294 \pm 0.018$
0.428 ±0.055	1198	[1] NEFKENS	67	OSPK	$a_u = -0.204 \pm 0.025$

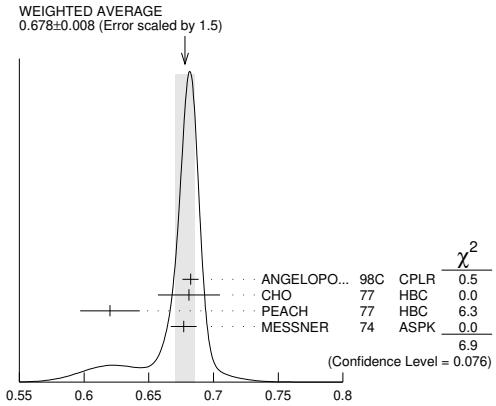

[1] Quadratic dependence required by some experiments. (See sections on "QUADRATIC COEFFICIENT h" and "QUADRATIC COEFFICIENT k" below.) Correlations prevent us from averaging results of fits not including g, h, and k terms.

[2] BISI 74 value comes from quadratic fit with quad. term consistent with zero. g error is thus larger than if linear fit were used.

[3] BUCHANAN 70 result revised by BUCHANAN 75 to include radiative correlations and to use more reliable K^0_L momentum spectrum of second experiment (had same beam).

QUADRATIC COEFFICIENT h FOR $K^0_L \to \pi^+\pi^-\pi^0$

See notes in section "LINEAR COEFFICIENT g FOR $K^0_L \to \pi^+\pi^-\pi^0$ |MATRIX ELEMENT|^2" above.

VALUE	EVTS	DOCUMENT ID		TECN
0.076±0.006 OUR AVERAGE				
0.061±0.004±0.015	500k	ANGELOPO...	98C	CPLR
0.095±0.032	6499	CHO	77	HBC
0.048±0.036	4709	PEACH	77	HBC
0.079±0.007	509k	MESSNER	74	ASPK
• • • We do not use the following data for averages, fits, limits, etc. • • •				
−0.011±0.018	29k	[1] ALBROW	70	ASPK
0.043±0.052	4400	[1] SMITH	70	OSPK

[1] Quadratic coefficients h and k required by some experiments. (See section on "QUADRATIC COEFFICIENT k" below.) Correlations prevent us from averaging results of fits not including g, h, and k terms.

QUADRATIC COEFFICIENT k FOR $K^0_L \to \pi^+\pi^-\pi^0$

VALUE	EVTS	DOCUMENT ID		TECN
0.0099±0.0015 OUR AVERAGE				
0.0104±0.0017±0.0024	500k	ANGELOPO...	98C	CPLR
0.024 ±0.010	6499	CHO	77	HBC
−0.008 ±0.012	4709	PEACH	77	HBC
0.0097±0.0018	509k	MESSNER	74	ASPK

LINEAR COEFFICIENT j FOR $K^0_L \to \pi^+\pi^-\pi^0$ (CP-VIOLATING TERM)

Listed in CP-violation section below.

QUADRATIC COEFFICIENT f FOR $K^0_L \to \pi^+\pi^-\pi^0$ (CP-VIOLATING TERM)

Listed in CP-violation section below.

QUADRATIC COEFFICIENT h FOR $K^0_L \to \pi^0\pi^0\pi^0$

We do not average measurements that do not account for the effect of final state rescattering.

VALUE (units 10^{-3})	EVTS	DOCUMENT ID		TECN
+0.59±0.20±1.16	68M	[1] ABOUZAID	08A	KTEV
• • • We do not use the following data for averages, fits, limits, etc. • • •				
−6.1 ±0.9 ±0.5	14.7M	[2] LAI	01B	NA48
−3.3 ±1.1 ±0.7	5M	[2,3] SOMALWAR	92	E731

[1] Result obtained using Cl3pl model of CABIBBO 05 to include $\pi\pi$ rescattering effects. The systematic error includes an external error of 1.06×10^{-3} from the parametrization input of $(a_0-a_2)\ m_{\pi^+} = 0.268 \pm 0.017$ from BATLEY 06B.

Downloaded from https://academic.oup.com/ptep/article/2022/8/083C01/6651666 by KIT Library user on 27 September 2022

[2] LAI 01B and SOMALWAR 92 results do not include $\pi\pi$ final state rescattering effects.
[3] SOMALWAR 92 chose m_{π^+} as normalization to make it compatible with the Particle Data Group $K^0_L \to \pi^+\pi^-\pi^0$ definitions.

K^0_L FORM FACTORS

For discussion, see note on form factors in the $K^\pm$ section of the Particle Listings above.

In the form factor comments, the following symbols are used.

f_+ and f_- are form factors for the vector matrix element.

f_S and f_T refer to the scalar and tensor term.

$f_0(t) = f_+(t) + f_-(t)\ t/(m^2_{K^0} - m^2_{\pi^+})$.

t = momentum transfer to the π.

λ_+ and λ_0 are the linear expansion coefficients of f_+ and f_0:

$f_+(t) = f_+(0)\ (1 + \lambda_+ t/m^2_{\pi^+})$

For quadratic expansion

$f_+(t) = f_+(0)\ (1 + \lambda'_+ t/m^2_{\pi^+} + \frac{\lambda''_+}{2}\ t^2/m^4_{\pi^+})$

as used by KTeV. If there is a non-vanishing quadratic term, then λ_+ represents an average slope, which is then different from λ'_+.

NA48 (K_{e3}) and ISTRA quadratic expansion coefficients are converted with

$\lambda'_+{}^{PDG} = \lambda_+{}^{NA48}$ and $\lambda''_+{}^{PDG} = 2\ \lambda'_+{}^{NA48}$

$\lambda'_+{}^{PDG} = (\frac{m_{\pi^+}}{m_{\pi^0}})^2\ \lambda_+{}^{ISTRA}$ and

$\lambda''_+{}^{PDG} = 2\ (\frac{m_{\pi^+}}{m_{\pi^0}})^4\ \lambda'_+{}^{ISTRA}$

ISTRA linear expansion coefficients are converted with

$\lambda_+{}^{PDG} = (\frac{m_{\pi^+}}{m_{\pi^0}})^2\ \lambda_+{}^{ISTRA}$ and $\lambda_0{}^{PDG} = (\frac{m_{\pi^+}}{m_{\pi^0}})^2\ \lambda_0{}^{ISTRA}$

The pole parametrization is

$f_+(t) = f_+(0)\ (\frac{M_V^2}{M_V^2 - t})$

$f_0(t) = f_0(0)\ (\frac{M_S^2}{M_S^2 - t})$

where M_V and M_S are the vector and scalar pole masses.

The dispersive parametrization is

$f_+(t) = f_+(0)\ \exp[\ \frac{t}{m^2_\pi}\ (\Lambda_+ + H(t))\ ]$;

$f_0(t) = f_+(0)\ \exp[\ \frac{t}{m^2_K - m^2_\pi}\ (\ln[C] - G(t))\ ]$,

where Λ_+ is the slope parameter and $\ln[C] = \ln[\ f_0\ (m^2_K - m^2_\pi\ )\ ]$ is the logarithm of the scalar form factor at the Callan-Treiman point.

$H(t)$ and $G(t)$ are dispersive integrals.

The following abbreviations are used:

DP = Dalitz plot analysis.
PI = π spectrum analysis.
MU = μ spectrum analysis.
POL= μ polarization analysis.
BR = $K^0_{\mu3}/K^0_{e3}$ branching ratio analysis.
E = positron or electron spectrum analysis.
RC = radiative corrections.

λ_+ (LINEAR ENERGY DEPENDENCE OF f_+ IN K^0_{e3} DECAY)

For radiative correction of K^0_{e3} DP, see GINSBERG 67, BECHERRAWY 70, CIRIGLIANO 02, CIRIGLIANO 04, and ANDRE 07. Results labeled OUR FIT are discussed in the review "$K^\pm_{\ell3}$ and $K^0_{\ell3}$ Form Factors" in the $K^\pm$ Listings. For earlier, lower statistics results, see the 2004 edition of this review, Physics Letters **B592** 1 (2004).

VALUE (units 10^{-2})	EVTS	DOCUMENT ID		TECN	COMMENT
2.82 ±0.04 OUR FIT		Error includes scale factor of 1.1. Assuming μ-e universality			
2.85 ±0.04 OUR AVERAGE					
2.86 ±0.05 ±0.04	2M	AMBROSINO	06D	KLOE	
2.832±0.037±0.043	1.9M	ALEXOPOU...	04A	KTEV	PI, no $\mu = e$
2.88 ±0.04 ±0.11	5.6M	[1] LAI	04C	NA48	DP
• • • We do not use the following data for averages, fits, limits, etc. • • •					
2.84 ±0.07 ±0.13	5.6M	[2] LAI	04C	NA48	DP
2.45 ±0.12 ±0.22	366k	APOSTOLA...	00	CPLR	DP
3.06 ±0.34	74k	BIRULEV	81	SPEC	DP
3.12 ±0.25	500k	GJESDAL	76	SPEC	DP
2.70 ±0.28	25k	BLUMENTHAL	75	SPEC	DP

[1] Results from linear fit and assuming only vector and axial couplings.
[2] Results from linear fit with $|f_S/f_+|$ and $|f_T/f_+|$ free.

λ_+ (LINEAR ENERGY DEPENDENCE OF f_+ IN $K^0_{\mu3}$ DECAY)

Results labeled OUR FIT are discussed in the review "$K^\pm_{\ell3}$ and $K^0_{\ell3}$ Form Factors" in the $K^\pm$ Listings. For earlier, lower statistics results, see the 2004 edition of this review, Physics Letters **B592** 1 (2004).

VALUE (units 10^{-2})	EVTS	DOCUMENT ID		TECN	COMMENT
2.82 ±0.04 OUR FIT		Error includes scale factor of 1.1. Assuming μ-e universality			
2.71 ±0.10 OUR FIT		Error includes scale factor of 1.4. Not assuming μ-e universality			
2.67 ±0.06 ±0.08	2.3M	[1] LAI	07A	NA48	DP
2.745±0.088±0.063	1.5M	ALEXOPOU...	04A	KTEV	DP, no $\mu = e$
2.813±0.051	3.4M	ALEXOPOU...	04A	KTEV	PI, DP, $\mu = e$
3.0 ±0.3	1.6M	DONALDSON	74B	SPEC	DP
• • • We do not use the following data for averages, fits, limits, etc. • • •					
4.27 ±0.44	150k	BIRULEV	81	SPEC	DP

[1] LAI 07A gives a correlation −0.40 between their λ_0 and λ_+ measurements.

λ_0 (LINEAR ENERGY DEPENDENCE OF f_0 IN $K^0_{\mu3}$ DECAY)

Wherever possible, we have converted the above values of $\xi(0)$ into values of λ_0 using the associated λ^μ_+ and $d\xi(0)/d\lambda_+$. Results labeled OUR FIT are discussed in the review "$K^\pm_{\ell3}$ and $K^0_{\ell3}$ Form Factors" in the $K^\pm$ Listings. For earlier, lower statistics results, see the 2004 edition of this review, Physics Letters **B592** 1 (2004).

VALUE (units 10^{-2})	$d\lambda_0/d\lambda_+$	EVTS	DOCUMENT ID		TECN	COMMENT
1.38 ±0.18 OUR FIT			Error includes scale factor of 2.2. Assuming μ-e universality			
1.42 ±0.23 OUR FIT			Error includes scale factor of 2.8. Not assuming μ-e universality			
1.17 ±0.07 ±0.10		2.3M	[1] LAI	07A	NA48	DP
1.657±0.125	−0.44	1.5M	[2] ALEXOPOU...	04A	KTEV	DP, no $\mu = e$
1.635±0.121	−0.85	3.4M	[3] ALEXOPOU...	04A	KTEV	PI, DP, $\mu = e$
+1.9 ±0.4	−0.47	1.6M	[4] DONALDSON	74B	SPEC	DP
• • • We do not use the following data for averages, fits, limits, etc. • • •						
3.41 ±0.67		unknown	150k	[5] BIRULEV	81	SPEC DP

[1] LAI 07A gives a correlation −0.40 between their λ_0 and λ_+ measurements.
[2] ALEXOPOULOS 04A gives a correlation −0.38 between their λ_0 and λ_+ measurements.
[3] ALEXOPOULOS 04A gives a correlation −0.36 between their λ_0 and λ_+ measurements.
[4] DONALDSON 74B $d\lambda_0/d\lambda_+$ obtained from figure 18.
[5] BIRULEV 81 gives $d\lambda_0/d\lambda_+ = -1.5$, giving an unreasonably narrow error ellipse which dominates all other results. We use $d\lambda_0/d\lambda_+ = 0$.

λ'_+(LINEAR K^0_{e3} FORM FACTOR FROM QUADRATIC FIT)

VALUE (units 10^{-2})	EVTS	DOCUMENT ID		TECN	COMMENT
2.40 ±0.12 OUR FIT		Error includes scale factor of 1.2. Assuming μ-e universality			
2.49 ±0.13 OUR FIT		Error includes scale factor of 1.1. Not assuming μ-e universality			
2.48 ±0.17 OUR AVERAGE		Error includes scale factor of 1.5. See the ideogram below.			
2.55 ±0.15 ±0.10	2M	[1] AMBROSINO	06D	KLOE	
2.167±0.137±0.143	1.9M	[2] ALEXOPOU...	04A	KTEV	PI, no $\mu = e$
2.80 ±0.19 ±0.15	5.6M	[3] LAI	04C	NA48	DP

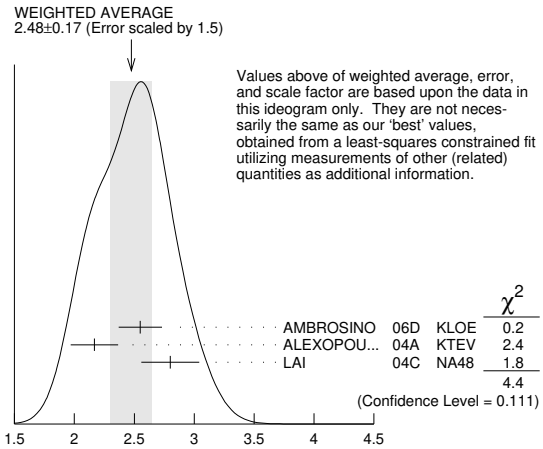

λ'_+(LINEAR K^0_{e3} FORM FACTOR FROM QUADRATIC FIT) (units 10^{-2})

[1] We use AMBROSINO 06D result in the fit not assuming $\mu-e$ universality. This result enters the fit assuming $\mu-e$ universality via AMBROSINO 07C measurement of λ'_+ in $K_{\mu3}$ decays. AMBROSINO 06D gives a correlation −0.95 between their λ'_+ and λ''_+.
[2] ALEXOPOULOS 04A gives a correlation −0.97 between their λ'_+ and λ''_+.
[3] For LAI 04C we calculate a correlation −0.88 between their λ'_+ and λ''_+. /LINEAR00

λ''_+(QUADRATIC K^0_{e3} FORM FACTOR)

VALUE (units 10^{-2})	EVTS	DOCUMENT ID		TECN	COMMENT
0.20 ±0.05 OUR FIT		Error includes scale factor of 1.2. Assuming μ-e universality			
0.16 ±0.05 OUR FIT		Error includes scale factor of 1.1. Not assuming μ-e universality			
0.17 ±0.07 OUR AVERAGE		Error includes scale factor of 1.5. See the ideogram below.			
0.14 ±0.07 ±0.04	2M	[1] AMBROSINO	06D	KLOE	
0.287±0.057±0.053	1.9M	[2] ALEXOPOU...	04A	KTEV	PI, no $\mu = e$
0.04 ±0.08 ±0.04	5.6M	[3,4] LAI	04C	NA48	DP

[1] We use AMBROSINO 06D result in the fit not assuming $\mu-e$ universality. This result enters the fit assuming $\mu-e$ universality via AMBROSINO 07C measurement of λ''_+ in $K_{\mu3}$ decays. AMBROSINO 06D gives a correlation −0.95 between their λ'_+ and λ''_+.
[2] ALEXOPOULOS 04A gives a correlation −0.97 between their λ'_+ and λ''_+.
[3] Values doubled to agree with PDG conventions described above.

Downloaded from https://academic.oup.com/ptep/article/2022/8/083C01/6651666 by KIT Library user on 27 September 2022

[4] LAI 04C gives a correlation −0.88 between their λ'_+ and λ''_+.

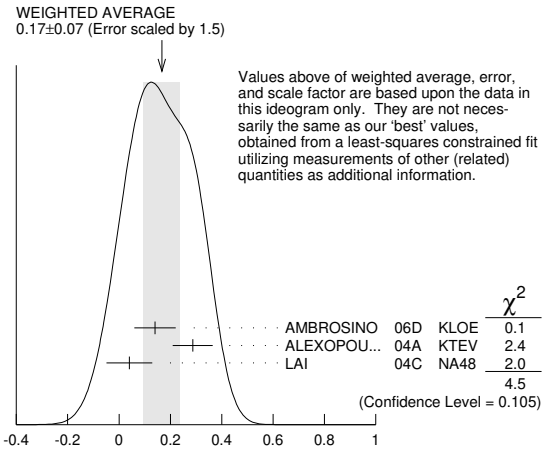

λ''_+(QUADRATIC K^0_{e3} FORM FACTOR) (units 10^{-2})

λ'_+(LINEAR $K^0_{\mu3}$ FORM FACTOR FROM QUADRATIC FIT)

VALUE (units 10^{-2})	EVTS	DOCUMENT ID	TECN	COMMENT
2.40 ±0.12 OUR FIT		Error includes scale factor of 1.2. Assuming μ-e universality		
1.89 ±0.24 OUR FIT		Not assuming μ-e universality		
2.23 ±0.98 ±0.37	1.8M	[1] AMBROSINO 07C	KLOE	no $\mu = e$
2.56 ±0.15 ±0.09	3.8M	[1] AMBROSINO 07C	KLOE	$\mu = e$
2.05 ±0.22 ±0.24	2.3M	[1] LAI 07A	NA48	DP
1.703±0.319±0.177	1.5M	[1] ALEXOPOU... 04A	KTEV	DP, no $\mu = e$
2.064±0.175	3.4M	[1] ALEXOPOU... 04A	KTEV	PI, DP, $\mu = e$

[1] See section λ_0 below for correlations.

λ''_+(QUADRATIC $K^0_{\mu3}$ FORM FACTOR)

VALUE (units 10^{-2})	EVTS	DOCUMENT ID	TECN	COMMENT
0.20 ±0.05 OUR FIT		Error includes scale factor of 1.2. Assuming μ-e universality		
0.37 ±0.12 OUR FIT		Error includes scale factor of 1.3. Not assuming μ-e universality		
0.48 ±0.49 ±0.16	1.8M	[1] AMBROSINO 07C	KLOE	no $\mu = e$
0.15 ±0.07 ±0.04	3.8M	[1] AMBROSINO 07C	KLOE	$\mu = e$
0.26 ±0.09 ±0.10	2.3M	[1] LAI 07A	NA48	DP
0.443±0.131±0.072	1.5M	[1] ALEXOPOU... 04A	KTEV	DP, no $\mu = e$
0.320±0.069	3.4M	[1] ALEXOPOU... 04A	KTEV	PI, DP, $\mu = e$

[1] See section λ_0 below for correlations.

λ_0(LINEAR f_0 $K^0_{\mu3}$ FORM FACTOR FROM QUADRATIC FIT)

VALUE (units 10^{-2})	EVTS	DOCUMENT ID	TECN	COMMENT
1.16 ±0.09 OUR FIT		Error includes scale factor of 1.2. Assuming μ-e universality		
1.07 ±0.14 OUR FIT		Error includes scale factor of 1.3. Not assuming μ-e universality		
0.91 ±0.59 ±0.26	1.8M	[1] AMBROSINO 07C	KLOE	no $\mu = e$
1.54 ±0.18 ±0.13	3.8M	[2] AMBROSINO 07C	KLOE	$\mu = e$
0.95 ±0.11 ±0.08	2.3M	[3] LAI 07A	NA48	DP
1.281±0.136±0.122	1.5M	[4] ALEXOPOU... 04A	KTEV	DP, no $\mu = e$
1.372±0.131	3.4M	[5] ALEXOPOU... 04A	KTEV	PI, DP, $\mu = e$

[1] AMBROSINO 07C, not assuming μ-e universality, gives a correlation matrix

	λ'_+	λ''_+
λ''_+	−0.97	1
λ_0	0.81	−0.91

[2] AMBROSINO 07C, assuming μ-e universality, gives a correlation matrix

	λ'_+	λ''_+
λ''_+	−0.95	1
λ_0	0.29	−0.38

[3] LAI 07A gives a correlation matrix

	λ'_+	λ''_+
λ''_+	−0.96	1
λ_0	0.63	−0.73

[4] ALEXOPOULOS 04A, not assuming μ-e universality, gives a correlation matrix

	λ'_+	λ''_+	λ_0
λ'_+	1		
λ''_+	−0.96	1	
λ_0	0.65	−0.75	1

[5] ALEXOPOULOS 04A, assuming μ-e universality, gives a correlation matrix

	λ'_+	λ''_+	λ_0
λ'_+	1		
λ''_+	−0.97	1	
λ_0	0.34	−0.44	1

M^e_V (POLE MASS FOR K^0_{e3} DECAY)

VALUE (MeV)	EVTS	DOCUMENT ID	TECN	COMMENT
878 ± 6 OUR FIT		Error includes scale factor of 1.1. Assuming μ-e universality		
875 ± 5 OUR AVERAGE				
870 ± 6 ±7	2M	AMBROSINO 06D	KLOE	
881.03± 5.12±4.94	1.9M	ALEXOPOU... 04A	KTEV	PI, no $\mu = e$
859 ±18	5.6M	LAI 04C	NA48	

M^μ_V (POLE MASS FOR $K^0_{\mu3}$ DECAY)

VALUE (MeV)	EVTS	DOCUMENT ID	TECN	COMMENT
878 ± 6 OUR FIT		Error includes scale factor of 1.1. Assuming μ-e universality		
900 ±21 OUR FIT		Error includes scale factor of 1.7. Not assuming μ-e universality		
905 ± 9 ±17	2.3M	[1] LAI 07A	NA48	DP
889.19±12.81± 9.92	1.5M	[1] ALEXOPOU... 04A	KTEV	DP, no $\mu = e$
882.32± 6.54	3.4M	[1] ALEXOPOU... 04A	KTEV	PI, DP, $\mu = e$

[1] See section M^μ_S below for correlations.

M^μ_S (POLE MASS FOR $K^0_{\mu3}$ DECAY)

VALUE (MeV)	EVTS	DOCUMENT ID	TECN	COMMENT
1252 ±90 OUR FIT		Error includes scale factor of 2.6. Assuming μ-e universality		
1222 ±80 OUR FIT		Error includes scale factor of 2.3. Not assuming μ-e universality		
1400 ±46 ±53	2.3M	[1] LAI 07A	NA48	DP
1167.14±28.30±31.04	1.5M	[2] ALEXOPOU... 04A	KTEV	PI, no $\mu = e$
1173.80±39.47	3.4M	[3] ALEXOPOU... 04A	KTEV	PI, DP, $\mu = e$

[1] LAI 07A gives a correlation −0.47 between their M^μ_S and M^μ_V measurements, not assuming μ-e universality.

[2] ALEXOPOULOS 04A gives a correlation −0.46 between their M^μ_S and M^μ_V and measurements, not assuming μ-e universality.

[3] ALEXOPOULOS 04A gives a correlation −0.40 between their M^μ_S and M^μ_V and measurements, assuming μ-e universality.

Λ_+ (DISPERSIVE VECTOR FORM FACTOR FOR $K^0_{\mu3}$ DECAY)

See the review on "$K^\pm_{\ell3}$ and $K^0_{\ell3}$ Form Factors" for details of the dispersive parametrization.

VALUE (units 10^{-2})	EVTS	DOCUMENT ID	TECN	COMMENT
2.51 ±0.06 OUR AVERAGE		Error includes scale factor of 1.5. See the ideogram below.		
2.509±0.035±0.043	3.4M	[1] ABOUZAID 10	KTEV	$\mu = e$
2.57 ±0.04 ±0.04	3.8M	[2] AMBROSINO 07C	KLOE	$\mu = e$
2.33 ±0.05 ±0.08	2.3M	[3] LAI 07A	NA48	DP

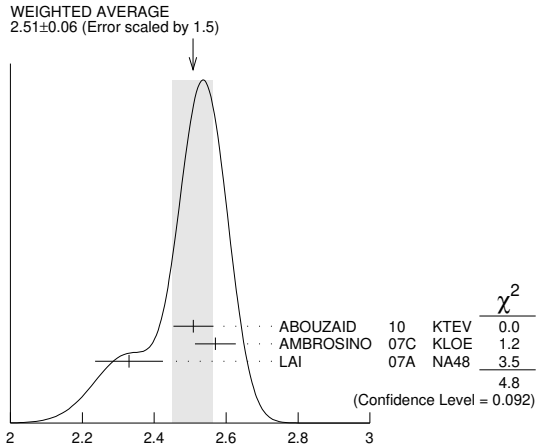

Λ_+ (DISPERSIVE VECTOR FORM FACTOR FOR $K^0_{\mu3}$ DECAY) (units 10^{-2})

[1] Obtained from a sample of 1.9 M K_{e3} and 1.5 M $K_{\mu3}$. The correlation between Λ_+ and ln(C) is −0.269.

[2] AMBROSINO 07C results include 2M K_{e3} events from AMBROSINO 06D. The correlation between Λ_+ and ln(C) is −0.26.

[3] LAI 07A gives a correlation −0.44 between their Λ_+ and ln(C) measurements.

ln(C) (DISPERSIVE SCALAR FORM FACTOR FOR $K^0_{\mu3}$ DECAY)

See the review on "$K^\pm_{\ell3}$ and $K^0_{\ell3}$ Form Factors" for details of the dispersive parametrization.

VALUE (units 10^{-1})	EVTS	DOCUMENT ID	TECN	COMMENT
1.75 ±0.18 OUR AVERAGE		Error includes scale factor of 2.0. See the ideogram below.		
1.915±0.078±0.094	3.4M	[1] ABOUZAID 10	KTEV	$\mu = e$
2.04 ±0.19 ±0.15	3.8M	[2] AMBROSINO 07C	KLOE	$\mu = e$
1.438±0.080±0.112	2.3M	[3] LAI 07A	NA48	DP

[1] Obtained from a sample of 1.9 M K_{e3} and 1.5 M $K_{\mu3}$. The correlation between Λ_+ and ln(C) is −0.269.

[2] AMBROSINO 07C results include 2M K_{e3} events from AMBROSINO 06D. We convert (Λ_+, Λ_0) to (Λ_+, ln(C)) parametrization using ln(C) = (Λ_0 · 11.713 + 0.0398) ±0.0041,

Downloaded from https://academic.oup.com/ptep/article/2022/8/083C01/6651666 by KIT Library user on 27 September 2022

where the error is due to theory parametrization of the form factor. The correlation between Λ_+ and $\ln(C)$ is -0.26.

[3] LAI 07A gives a correlation -0.44 between their Λ_+ and $\ln(C)$ measurements.

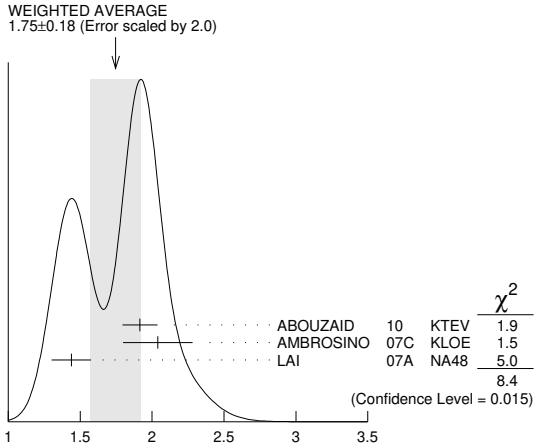

$\ln(C)$ (DISPERSIVE SCALAR FORM FACTOR FOR $K^0_{\mu3}$ DECAY) (units 10^{-1})

$a_1(t_0, Q^2)$ FORM FACTOR PARAMETER

See HILL 06 for a definition of this parameter.

VALUE	EVTS	DOCUMENT ID		TECN
1.023±0.028±0.029	2M	[1] ABOUZAID	06C	KTEV

[1] $Q^2 = 2$ GeV^2, $t_0 = 0.49\,(m_K - m_\pi)^2$. Correlation between a_1 and a_2: $\rho_{12} = -0.064$.

$a_2(t_0, Q^2)$ FORM FACTOR PARAMETER

See HILL 06 for a definition of this parameter.

VALUE	EVTS	DOCUMENT ID		TECN
0.75±1.58±1.47	2M	[1] ABOUZAID	06C	KTEV

[1] $Q^2 = 2$ GeV^2, $t_0 = 0.49\,(m_K - m_\pi)^2$. Correlation between a_1 and a_2: $\rho_{12} = -0.064$.

$|f_S/f_+|$ FOR K^0_{e3} DECAY

Ratio of scalar to f_+ couplings.

VALUE (units 10^{-2})	CL%	EVTS	DOCUMENT ID		TECN	COMMENT
$\mathbf{1.5^{+0.7}_{-1.0}\pm1.2}$		5.6M	[1] LAI	04C	NA48	
• • • We do not use the following data for averages, fits, limits, etc. • • •						
<9.5	95	18k	HILL	78	STRC	
<7.	68	48k	BIRULEV	76	SPEC	See also BIRULEV 81
<4.	68	25k	BLUMENTHAL	75	SPEC	

[1] Results from linear fit with $|f_S/f_+|$ and $|f_T/f_+|$ free.

$|f_T/f_+|$ FOR K^0_{e3} DECAY

Ratio of tensor to f_+ couplings.

VALUE (units 10^{-2})	CL%	EVTS	DOCUMENT ID		TECN	COMMENT
$\mathbf{5^{+3}_{-4}\pm3}$		5.6M	[1] LAI	04C	NA48	
• • • We do not use the following data for averages, fits, limits, etc. • • •						
<40.	95	18k	HILL	78	STRC	
<34.	68	48k	BIRULEV	76	SPEC	See also BIRULEV 81
<23.	68	25k	BLUMENTHAL	75	SPEC	

[1] Results from linear fit with $|f_S/f_+|$ and $|f_T/f_+|$ free.

$|f_T/f_+|$ FOR $K^0_{\mu3}$ DECAY

Ratio of tensor to f_+ couplings.

VALUE (units 10^{-2})	DOCUMENT ID		TECN
12.±12.	BIRULEV	81	SPEC

α_{K^*} DECAY FORM FACTOR FOR $K_L \to \ell^+\ell^-\gamma$, $K^0_L \to \ell^+\ell^-\ell'^+\ell'^-$

Average of all α_{K^*} measurements (from each of three datablocks following this one) assuming lepton universality.

VALUE	DOCUMENT ID
−0.205±0.022 OUR AVERAGE Includes data from the 3 datablocks that follow this one. Error includes scale factor of 1.8. See the ideogram below.	

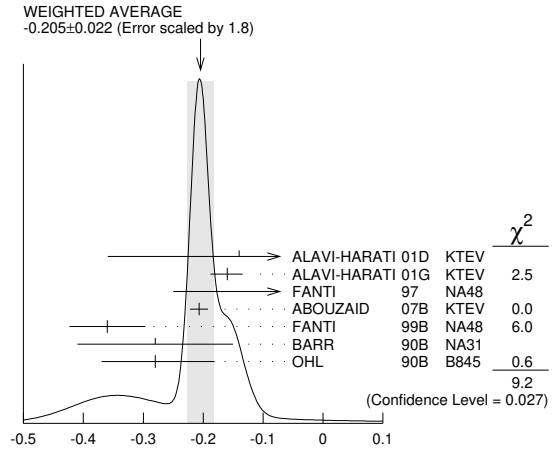

α_{K^*} DECAY FORM FACTOR FOR $K_L \to \ell^+\ell^-\gamma$, $K^0_L \to \ell^+\ell^-\ell'^+\ell'^-$

α_{K^*} DECAY FORM FACTOR FOR $K_L \to e^+e^-\gamma$

α_{K^*} is the constant in the model of BERGSTROM 83 which measures the relative strength of the vector-vector transition $K_L \to K^*\gamma$ with $K^* \to \rho, \omega, \phi \to \gamma^*$ and the pseudoscalar-pseudoscalar transition $K_L \to \pi, \eta, \eta' \to \gamma\gamma^*$.

VALUE	EVTS	DOCUMENT ID		TECN
The data in this block is included in the average printed for a previous datablock.				
−0.217±0.034 OUR AVERAGE Error includes scale factor of 2.4.				
−0.207±0.012±0.009	83k	[1] ABOUZAID	07B	KTEV
−0.36 ±0.06 ±0.02	6864	FANTI	99B	NA48
−0.28 ±0.13		BARR	90B	NA31
$-0.280^{+0.099}_{-0.090}$		OHL	90B	B845

[1] ABOUZAID 07B measures $C\cdot\alpha_{K^*} = -0.517 \pm 0.030 \pm 0.022$. We assume $C = 2.5$, as in all other measurements.

α_{K^*} DECAY FORM FACTOR FOR $K_L \to \mu^+\mu^-\gamma$

α_{K^*} is the constant in the model of BERGSTROM 83 described in the previous section.

VALUE	EVTS	DOCUMENT ID		TECN
The data in this block is included in the average printed for a previous datablock.				
−0.158±0.027 OUR AVERAGE				
$-0.160^{+0.026}_{-0.028}$	9100	ALAVI-HARATI	01G	KTEV
$-0.04\ ^{+0.24}_{-0.21}$		FANTI	97	NA48

$\alpha^{\rm eff}_{K^*}$ DECAY FORM FACTOR FOR $K_L \to e^+e^-e^+e^-$

$\alpha^{\rm eff}_{K^*}$ is the parameter describing the relative strength of an intermediate pseudoscalar decay amplitude and a vector meson decay amplitude in the model of BERGSTROM 83. It takes into account both the radiative effects and the form factor. Since there are two e^+e^- pairs here compared with one in $e^+e^-\gamma$ decays, a factorized expression is used for the $e^+e^-e^+e^-$ decay form factor.

VALUE	EVTS	DOCUMENT ID		TECN
The data in this block is included in the average printed for a previous datablock.				
−0.14±0.16±0.15	441	ALAVI-HARATI	01D	KTEV

α_{DIP} DECAY FORM FACTOR FOR $K^0_L \to \ell^+\ell^-\gamma$, $K^0_L \to \ell^+\ell^-\ell'^+\ell'^-$

Average of all α_{DIP} measurements (from each of three datablocks following this one) assuming lepton universality.

VALUE	DOCUMENT ID
−1.69±0.08 OUR AVERAGE Includes data from the 3 datablocks that follow this one. Error includes scale factor of 1.7.	

α_{DIP} DECAY FORM FACTOR FOR $K^0_L \to e^+e^-\gamma$

α_{DIP} parameter in $K^0_L \to \gamma^*\gamma^*$ form factor by DAMBROSIO 98, motivated by vector meson dominance and a proper short distance behavior.

VALUE	EVTS	DOCUMENT ID		TECN
The data in this block is included in the average printed for a previous datablock.				
−1.729±0.043±0.028	83k	ABOUZAID	07B	KTEV

α_{DIP} DECAY FORM FACTOR FOR $K^0_L \to \mu^+\mu^-\gamma$

α_{DIP} is a constant in the model of DAMBROSIO 98 described in the previous section.

VALUE	EVTS	DOCUMENT ID		TECN
The data in this block is included in the average printed for a previous datablock.				
−1.54±0.10	9100	ALAVI-HARATI	01G	KTEV

α_{DIP} DECAY FORM FACTOR FOR $K^0_L \to e^+e^-\mu^+\mu^-$

α_{DIP} is a constant in the model of DAMBROSIO 98 described in the previous section.

VALUE	EVTS	DOCUMENT ID		TECN
The data in this block is included in the average printed for a previous datablock.				
−1.59±0.37	131	ALAVI-HARATI	03B	KTEV

Downloaded from https://academic.oup.com/ptep/article/2022/8/083C01/6651666 by KIT Library user on 27 September 2022

a_1/a_2 FORM FACTOR FOR M1 DIRECT EMISSION AMPLITUDE

Form factor $= \tilde{g}_{M1}\left[1+\frac{a_1/a_2}{(M_{\bar{D}}^2-M_K^2)+2M_K E_\gamma^*}\right]$ as described in ALAVI-HARATI 00B.

VALUE (GeV^2)	EVTS	DOCUMENT ID		TECN	COMMENT
−0.737±0.014 OUR AVERAGE					
−0.744±0.027±0.032	5241	[1] ABOUZAID	06	KTEV	$\pi^+\pi^-e^+e^-$
−0.738±0.007±0.018	111k	[2] ABOUZAID	06A	KTEV	$\pi^+\pi^+\gamma$
$-0.81\ ^{+0.07}_{-0.13}\ \pm0.02$		[3] LAI	03C	NA48	$\pi^+\pi^-e^+e^-$
−0.737±0.026±0.022		[4] ALAVI-HARATI	01B		$\pi^+\pi^-\gamma$
−0.720±0.028±0.009	1766	[5] ALAVI-HARATI	00B	KTEV	$\pi^+\pi^-e^+e^-$

[1] ABOUZAID 06 also measured $|\tilde{g}_{M1}| = 1.11 \pm 0.14$.
[2] ABOUZAID 06A also measured $|\tilde{g}_{M1}| = 1.198 \pm 0.035 \pm 0.086$.
[3] LAI 03C also measured $\tilde{g}_{M1} = 0.99^{+0.28}_{-0.27} \pm 0.07$.
[4] ALAVI-HARATI 01B fit gives χ^2/DOF = 38.8/27. Linear and quadratic fits give χ^2/DOF = 43.2/27 and 37.6/26 respectively.
[5] ALAVI-HARATI 00B also measured $|\tilde{g}_{M1}| = 1.35^{+0.20}_{-0.17} \pm 0.04$.

$\overline{f}_S$ DECAY FORM FACTOR FOR $K^0_L \to \pi^\pm\pi^0e^\mp\nu_e$

VALUE	DOCUMENT ID		TECN
0.049±0.011 OUR AVERAGE	Error includes scale factor of 1.7.		
0.052±0.006±0.002	BATLEY	04	NA48
0.010±0.016±0.017	MAKOFF	93	E731

$\overline{f}_P$ DECAY FORM FACTOR FOR $K^0_L \to \pi^\pm\pi^0e^\mp\nu_e$

VALUE	DOCUMENT ID		TECN
−0.052±0.012 OUR AVERAGE			
−0.051±0.011±0.005	BATLEY	04	NA48
−0.079±0.049±0.022	MAKOFF	93	E731

λ_g DECAY FORM FACTOR FOR $K^0_L \to \pi^\pm\pi^0e^\mp\nu_e$

VALUE	DOCUMENT ID		TECN
0.085±0.020 OUR AVERAGE			
0.087±0.019±0.006	BATLEY	04	NA48
0.014±0.087±0.070	MAKOFF	93	E731

$\overline{h}$ DECAY FORM FACTOR FOR $K^0_L \to \pi^\pm\pi^0e^\mp\nu_e$

VALUE	DOCUMENT ID		TECN
−0.30±0.13 OUR AVERAGE			
−0.32±0.12±0.07	BATLEY	04	NA48
−0.07±0.31±0.31	MAKOFF	93	E731

L_3 CHIRAL PERT. THEO. PARAM. FOR $K^0_L \to \pi^\pm\pi^0e^\mp\nu_e$

VALUE (units 10^{-3})	DOCUMENT ID		TECN
−3.96±0.28 OUR AVERAGE	Error includes scale factor of 1.6.		
−4.1 ±0.2	BATLEY	04	NA48
−3.4 ±0.4	[1] MAKOFF	93	E731

[1] MAKOFF 93 sign has been changed to negative to agree with the sign convention used in BATLEY 04.

a_V, VECTOR MESON EXCHANGE CONTRIBUTION

VALUE	EVTS	DOCUMENT ID		TECN	COMMENT
−0.43±0.06 OUR AVERAGE		Error includes scale factor of 1.5.			
−0.31±0.05±0.07	1.4k	[1] ABOUZAID	08	KTEV	
−0.46±0.03±0.04		LAI	02B	NA48	$K^0_L \to \pi^0 2\gamma$
−0.67±0.21±0.12		ALAVI-HARATI	01E	KTEV	$K^0_L \to \pi^0e^+e^-\gamma$
• • • We do not use the following data for averages, fits, limits, etc. • • •					
−0.72±0.05±0.06		[2] ALAVI-HARATI	99B	KTEV	$K^0_L \to \pi^0 2\gamma$

[1] Using KTeV dataset collected in 1996, 1997, and 1999.
[2] Superseded by ABOUZAID 08.

See the related review(s):

CP Violation in K^0_L Decays

CP-VIOLATION PARAMETERS IN K^0_L DECAYS

CHARGE ASYMMETRY IN $K^0_{\ell3}$ DECAYS

Such asymmetry violates *CP*. It is related to Re(ϵ).

A_L = weighted average of $A_L(\mu)$ and $A_L(e)$

In previous editions and in the literature the symbol used for this asymmetry was δ_L or δ. We use A_L for consistency with B^0 asymmetry notation and with recent K^0_S notation.

VALUE (%)	EVTS	DOCUMENT ID		TECN	COMMENT
0.332±0.006 OUR AVERAGE		Includes data from the 2 datablocks that follow this one.			
0.333±0.050	33M	WILLIAMS	73	ASPK	$K_{\mu3}+K_{e3}$

$A_L(\mu) = [\Gamma(\pi^-\mu^+\nu_\mu) - \Gamma(\pi^+\mu^-\overline{\nu}_\mu)]$/SUM

Only the combined value below is put into the Meson Summary Table.

VALUE (%)	EVTS	DOCUMENT ID		TECN
The data in this block is included in the average printed for a previous datablock.				
0.304±0.025 OUR AVERAGE				
0.313±0.029	15M	GEWENIGER	74	ASPK
0.278±0.051	7.7M	PICCIONI	72	ASPK
• • • We do not use the following data for averages, fits, limits, etc. • • •				
0.60 ±0.14	4.1M	MCCARTHY	73	CNTR
0.57 ±0.17	1M	[1] PACIOTTI	69	OSPK
0.403±0.134	1M	[1] DORFAN	67	OSPK

[1] PACIOTTI 69 is a reanalysis of DORFAN 67 and is corrected for $\mu^+\mu^-$ range difference in MCCARTHY 72.

$A_L(e) = [\Gamma(\pi^-e^+\nu_e) - \Gamma(\pi^+e^-\overline{\nu}_e)]$/SUM

Only the combined value below is put into the Meson Summary Table.

VALUE (%)	EVTS	DOCUMENT ID		TECN
The data in this block is included in the average printed for a previous datablock.				
0.334 ±0.007 OUR AVERAGE				
0.3322±0.0058±0.0047	298M	ALAVI-HARATI	02	
0.341 ±0.018	34M	GEWENIGER	74	ASPK
0.318 ±0.038	40M	FITCH	73	ASPK
0.346 ±0.033	10M	MARX	70	CNTR
• • • We do not use the following data for averages, fits, limits, etc. • • •				
0.36 ±0.18	600k	ASHFORD	72	ASPK
0.246 ±0.059	10M	[1] SAAL	69	CNTR
0.224 ±0.036	10M	[1] BENNETT	67	CNTR

[1] SAAL 69 is a reanalysis of BENNETT 67.

PARAMETERS FOR $K^0_L \to 2\pi$ DECAY

$\eta_{+-} = A(K^0_L \to \pi^+\pi^-) / A(K^0_S \to \pi^+\pi^-)$
$\eta_{00} = A(K^0_L \to \pi^0\pi^0) / A(K^0_S \to \pi^0\pi^0)$

The fitted values of $|\eta_{+-}|$ and $|\eta_{00}|$ given below are the results of a fit to $|\eta_{+-}|$, $|\eta_{00}|$, $|\eta_{00}/\eta_{+-}|$, and Re(ϵ'/ϵ). Independent information on $|\eta_{+-}|$ and $|\eta_{00}|$ can be obtained from the fitted values of the $K^0_L \to \pi\pi$ and $K^0_S \to \pi\pi$ branching ratios and the K^0_L and K^0_S lifetimes. This information is included as data in the $|\eta_{+-}|$ and $|\eta_{00}|$ sections with a Document ID "BRFIT." See the note "*CP* violation in K_L decays" above for details.

$|\eta_{00}| = |A(K^0_L \to 2\pi^0) / A(K^0_S \to 2\pi^0)|$

VALUE (units 10^{-3})	DOCUMENT ID		TECN	COMMENT
2.220±0.011 OUR FIT	Error includes scale factor of 1.8.			
2.243±0.014	BRFIT	16		
• • • We do not use the following data for averages, fits, limits, etc. • • •				
2.47 ±0.31 ±0.24	ANGELOPO...	98	CPLR	
2.49 ±0.40	[1] ADLER	96B	CPLR	Sup. by ANGELOPOULOS 98
2.33 ±0.18	CHRISTENS...	79	ASPK	
2.71 ±0.37	[2] WOLFF	71	OSPK	Cu reg., 4γ's
2.95 ±0.63	[2] CHOLLET	70	OSPK	Cu reg., 4γ's

[1] Error is statistical only.
[2] CHOLLET 70 gives $|\eta_{00}| = (1.23 \pm 0.24)\times$(regeneration amplitude, 2 GeV/c Cu)/10000mb. WOLFF 71 gives $|\eta_{00}| = (1.13 \pm 0.12)\times$(regeneration amplitude, 2 GeV/c Cu)/10000mb. We compute both $|\eta_{00}|$ values for (regeneration amplitude, 2 GeV/c Cu) = 24 ± 2mb. This regeneration amplitude results from averaging over FAISSNER 69, extrapolated using optical-model calculations of Bohm et al., Physics Letters **27B** 594 (1968) and the data of BALATS 71. (From H. Faissner, private communication).

$|\eta_{+-}| = |A(K^0_L \to \pi^+\pi^-) / A(K^0_S \to \pi^+\pi^-)|$

VALUE (units 10^{-3})	EVTS	DOCUMENT ID		TECN	COMMENT
2.232±0.011 OUR FIT		Error includes scale factor of 1.8.			
2.226±0.007		BRFIT	16		
• • • We do not use the following data for averages, fits, limits, etc. • • •					
2.223±0.012		[1] LAI	07	NA48	
2.219±0.013		[2] AMBROSINO	06F	KLOE	
2.228±0.010		[3] ALEXOPOU...	04	KTEV	
2.286±0.023±0.026	70M	[4] APOSTOLA...	99C	CPLR	K^0-$\overline{K}^0$ asymmetry
2.310±0.043±0.031		[5] ADLER	95B	CPLR	K^0-$\overline{K}^0$ asymmetry
2.32 ±0.14 ±0.03	10^5	ADLER	92B	CPLR	K^0-$\overline{K}^0$ asymmetry
2.30 ±0.035		GEWENIGER	74B	ASPK	

[1] Value obtained from the NA48 measurements of $\Gamma(K^0_L \to \pi^+\pi^-)/\Gamma(K^0_L \to \pi e\nu_e)$ and $\tau_{K^0_S}$ and KLOE measurements of $B(K^0_S \to \pi^+\pi^-)$ and $\tau_{K^0_L}$. $\Gamma(K^0_L \to \pi^+\pi^-)$ is defined to include the inner bremsstrahlung component $\Gamma(K^0_L \to \pi^+\pi^-\gamma(IB))$ but exclude the direct emission component $B(K^0_S \to \pi^+\pi^-(DE))$. Their $|\eta_{+-}|$ value is not directly used in our fit, but enters the fit via their branching ratio and lifetime measurements.
[2] AMBROSINO 06F uses KLOE branching ratios and τ_L together with τ_S from PDG 04. Their $|\eta_{+-}|$ value is not directly used in our fit, but enters the fit via their branching ratio and lifetime measurements.

Downloaded from https://academic.oup.com/ptep/article/2022/8/083C01/6651666 by KIT Library user on 27 September 2022

[3] ALEXOPOULOS 04 $|\eta_{+-}|$ uses their $K^0_L \to \pi\pi$ branching fractions, $\tau_S = (0.8963 \pm 0.0005) \times 10^{-10}$ s from the average of KTeV and NA48 τ_S measurements, and assumes that $\Gamma(K^0_S \to \pi\ell\nu_\ell) = \Gamma(K^0_L \to \pi\ell\nu_\ell)$ giving $B(K^0_S \to \pi\ell\nu_\ell) = 0.118\%$. Their η_{+-} is not directly used in our fit, but enters our fit via their branching ratio measurements.

[4] APOSTOLAKIS 99C report $(2.264 \pm 0.023 \pm 0.026 + 9.1[\tau_s - 0.8934]) \times 10^{-3}$. We evaluate for our 2006 best value $\tau_S = (0.8958 \pm 0.0005) \times 10^{-10}$ s.

[5] ADLER 95B report $(2.312 \pm 0.043 \pm 0.030 - 1[\Delta m - 0.5274] + 9.1[\tau_s - 0.8926]) \times 10^{-3}$. We evaluate for our 1996 best values $\Delta m = (0.5304 \pm 0.0014) \times 10^{-10}$ $\hbar s^{-1}$ and $\tau_s = (0.8927 \pm 0.0009) \times 10^{-10}$ s. Superseded by APOSTOLAKIS 99C.

$|\epsilon| = (2|\eta_{+-}| + |\eta_{00}|)/3$

This expression is a very good approximation, good to about one part in 10^{-4} because of the small measured value of $\phi_{00} - \phi_{+-}$ and small theoretical ambiguities.

VALUE (units 10^{-3})	DOCUMENT ID
2.228±0.011 OUR FIT Error includes scale factor of 1.8.	

$|\eta_{00}/\eta_{+-}|$

VALUE	EVTS	DOCUMENT ID		TECN
0.9950±0.0007 OUR FIT Error includes scale factor of 1.6.				
0.9930±0.0020 OUR AVERAGE				
0.9931±0.0020		[1,2] BARR	93D	NA31
0.9904±0.0084±0.0036		[3] WOODS	88	E731
• • • We do not use the following data for averages, fits, limits, etc. • • •				
0.9939±0.0013±0.0015	1M	[1] BARR	93D	NA31
0.9899±0.0020±0.0025		[1] BURKHARDT	88	NA31

[1] This is the square root of the ratio R given by BURKHARDT 88 and BARR 93D.

[2] This is the combined results from BARR 93D and BURKHARDT 88, taking into account a common systematic uncertainty of 0.0014.

[3] We calculate $|\eta_{00}/\eta_{+-}| = 1 - 3(\epsilon'/\epsilon)$ from WOODS 88 (ϵ'/ϵ) value.

$\mathrm{Re}(\epsilon'/\epsilon) = (1 - |\eta_{00}/\eta_{+-}|)/3$

We have neglected terms of order $\omega \cdot \mathrm{Re}(\epsilon'/\epsilon)$, where $\omega = \mathrm{Re}(A_2)/\mathrm{Re}(A_0) \simeq 1/22$. If included, this correction would lower $\mathrm{Re}(\epsilon'/\epsilon)$ by about 0.04×10^{-3}. See SOZZI 04.

VALUE (units 10^{-3})	DOCUMENT ID		TECN	COMMENT
1.66 ±0.23 OUR FIT Error includes scale factor of 1.6.				
1.68 ±0.20 OUR AVERAGE Error includes scale factor of 1.4. See the ideogram below.				
1.92 ±0.21	[1] ABOUZAID	11	KTEV	Assuming CPT
1.47 ±0.22	BATLEY	02	NA48	
0.74 ±0.52 ±0.29	GIBBONS	93B	E731	
• • • We use the following data for averages but not for fits. • • •				
2.3 ±0.65	[2,3] BARR	93D	NA31	
• • • We do not use the following data for averages, fits, limits, etc. • • •				
2.110±0.343	[1,4] ABOUZAID	11	KTEV	Not assuming CPT
2.07 ±0.28	ALAVI-HARATI	03	KTEV	In ABOUZAID 11
1.53 ±0.26	LAI	01C	NA48	Incl. in BATLEY 02
2.80 ±0.30 ±0.28	ALAVI-HARATI	99D	KTEV	In ALAVI-HARATI 03
1.85 ±0.45 ±0.58	FANTI	99C	NA48	In LAI 01C
2.0 ±0.7	[5] BARR	93D	NA31	
−0.4 ±1.4 ±0.6	PATTERSON	90	E731	in GIBBONS 93B
3.3 ±1.1	[5] BURKHARDT	88	NA31	
3.2 ±2.8 ±1.2	[2] WOODS	88	E731	

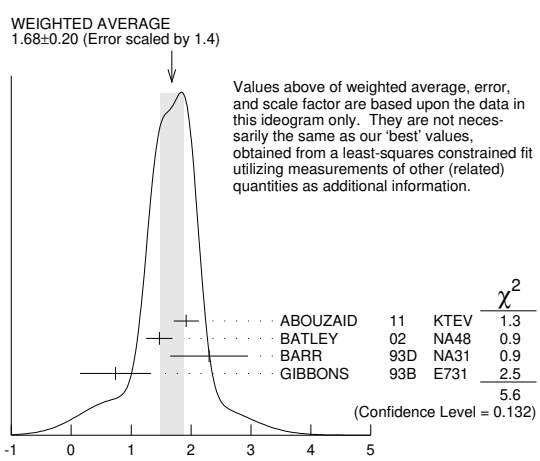

[1] The two ABOUZAID 11 values use the same data. The fits are performed with and without CPT invariance requirement.

[2] These values are derived from $|\eta_{00}/\eta_{+-}|$ measurements. They enter the average in this section but enter the fit via the $|\eta_{00}/\eta_{+-}|$ only.

[3] This is the combined results from BARR 93D and BURKHARDT 88, taking into account their common systematic uncertainty.

[4] We use ABOUZAID 11 $\mathrm{Re}(\epsilon'/\epsilon)$ value with CPT assumption in our fits for $|\eta_{+-}|$, $|\eta_{00}|$, and $\mathrm{Re}(\epsilon'/\epsilon)$.

[5] These values are derived from $|\eta_{00}/\eta_{+-}|$ measurements.

ϕ_{+-}, PHASE of η_{+-}

The dependence of the phase on Δm and τ_S is given for each experiment in the comments below, where Δm is the $K^0_L - K^0_S$ mass difference in units 10^{10} $\hbar s^{-1}$ and τ_S is the K_S mean life in units 10^{-10} s. We also give the regeneration phase ϕ_f in the comments below.

OUR FIT is described in the note on "CP violation in K_L decays" in the K^0_L Particle Listings. Most experiments in this section are included in both the "Not Assuming CPT" and "Assuming CPT" fits. In the latter fit, they have little direct influence on ϕ_{+-} because their errors are large compared to that assuming CPT, but they influence Δm and τ_S through their dependencies on these parameters, which are given in the footnotes.

VALUE (°)	EVTS	DOCUMENT ID		TECN	COMMENT
43.51±0.05 OUR FIT Error includes scale factor of 1.2. Assuming CPT					
43.4 ±0.5 OUR FIT Error includes scale factor of 1.2. Not assuming CPT					
42.9 ±0.6 ±0.3	70M	[1] APOSTOLA...	99C	CPLR	K^0-$\overline{K}^0$ asymmetry
42.9 ±0.8 ±0.2		[2,3] SCHWINGEN...	95	E773	$CH_{1.1}$ regenerator
41.4 ±0.9 ±0.2		[3,4] GIBBONS	93	E731	B_4C regenerator
44.5 ±1.6 ±0.6		[5] CAROSI	90	NA31	Vacuum regen.
43.3 ±1.0 ±0.5		[6] GEWENIGER	74B	ASPK	Vacuum regen.
• • • We do not use the following data for averages, fits, limits, etc. • • •					
43.76±0.64		[7] ABOUZAID	11	KTEV	Not assuming CPT
44.12±0.72±1.20		[8] ALAVI-HARATI	03	KTEV	Not assuming CPT
42.5 ±0.4 ±0.3		[9,10] ADLER	96C	RVUE	
43.4 ±1.1 ±0.3		[11] ADLER	95B	CPLR	K^0-$\overline{K}^0$ asymmetry
42.3 ±4.4 ±1.4	100k	[12] ADLER	92B	CPLR	K^0-$\overline{K}^0$ asymmetry
47.7 ±2.0 ±0.9		[3,13] KARLSSON	90	E731	
44.3 ±2.8 ±0.2		[14] CARITHERS	75	SPEC	C regenerator

[1] APOSTOLAKIS 99C measures $\phi_{+-} = (43.19 \pm 0.53 \pm 0.28) + 300\,[\Delta m - 0.5301]$ (°). We have adjusted the measurement to use our best values of ($\Delta m = 0.5293 \pm 0.0009$) ($10^{10}$ $\hbar$ s^{-1}). Our first error is their experiment's error and our second error is the systematic error from using our best values.

[2] SCHWINGENHEUER 95 measures $\phi_{+-} = (43.53 \pm 0.76) + 173\,[\Delta m - 0.5282] - 275\,[\tau_s - 0.8926]$ (°). We have adjusted the measurement to use our best values of ($\Delta m = 0.5293 \pm 0.0009$) ($10^{10}$ $\hbar$ s^{-1}), ($\tau_s = 0.8954 \pm 0.0004$) ($10^{-10}$ s). Our first error is their experiment's error and our second error is the systematic error from using our best values.

[3] These experiments measure ϕ_{+-}-ϕ_f and calculate the regeneration phase from the power law momentum dependence of the regeneration amplitude using analyticity and dispersion relations. SCHWINGENHEUER 95 [GIBBONS 93] includes a systematic error of 0.35° [0.5°] for uncertainties in their modeling of the regeneration amplitude.

[4] GIBBONS 93 measures $\phi_{+-} = (42.21 \pm 0.9) + 189\,[\Delta m - 0.5257] - 460\,[\tau_s - 0.8922]$ (°). We have adjusted the measurement to use our best values of ($\Delta m = 0.5293 \pm 0.0009$) ($10^{10}$ $\hbar$ s^{-1}), ($\tau_s = 0.8954 \pm 0.0004$) ($10^{-10}$ s). Our first error is their experiment's error and our second error is the systematic error from using our best values. This is actually reported in SCHWINGENHEUER 95, footnote 8. GIBBONS 93 reports ϕ_{+-} (42.2 ± 1.4)°. They measure ϕ_+-ϕ_f and calculate the regeneration phase ϕ_f from the power law momentum dependence of the regeneration amplitude using analyticity. An error of 0.6° is included for possible uncertainties in the regeneration phase.

[5] CAROSI 90 measures $\phi_{+-} = (46.9 \pm 1.4 \pm 0.7) + 579\,[\Delta m - 0.5351] + 303\,[\tau_s - 0.8922]$ (°). We have adjusted the measurement to use our best values of ($\Delta m = 0.5293 \pm 0.0009$) ($10^{10}$ $\hbar$ s^{-1}), ($\tau_s = 0.8954 \pm 0.0004$) ($10^{-10}$ s). Our first error is their experiment's error and our second error is the systematic error from using our best values.

[6] GEWENIGER 74B measures $\phi_{+-} = (49.4 \pm 1.0) + 565\,[\Delta m - 0.540]$ (°). We have adjusted the measurement to use our best values of ($\Delta m = 0.5293 \pm 0.0009$) ($10^{10}$ $\hbar$ s^{-1}). Our first error is their experiment's error and our second error is the systematic error from using our best values.

[7] Not independent of other phase parameters reported in ABOUZAID 11.

[8] ALAVI-HARATI 03 ϕ_{+-} is correlated with their $\Delta m = m_{K^0_L} - m_{K^0_S}$ and τ_{K_S} measurements in the K^0_L and K^0_S sections respectively. The correlation coefficients are $\rho(\phi_{+-},\Delta m) = +0.955$, $\rho(\phi_{+-},\tau_S) = -0.871$, and $\rho(\tau_S,\Delta m) = -0.840$. CPT is not assumed. Uses scintillator Pb regenerator. Superseded by ABOUZAID 11.

[9] ADLER 96C measures $\phi_{+-} = (43.82 \pm 0.41) + 339\,[\Delta m - 0.5307] - 252\,[\tau_s - 0.8922]$ (°). We have adjusted the measurement to use our best values of ($\Delta m = 0.5293 \pm 0.0009$) ($10^{10}$ $\hbar$ s^{-1}), ($\tau_s = 0.8954 \pm 0.0004$) ($10^{-10}$ s). Our first error is their experiment's error and our second error is the systematic error from using our best values.

[10] ADLER 96C is the result of a fit which includes nearly the same data as entered into the "OUR FIT" value in the 1996 edition of this Review (Physical Review **D54** 1 (1996)).

[11] ADLER 95B measures $\phi_{+-} = (42.7 \pm 0.9 \pm 0.6) + 316\,[\Delta m - 0.5274] + 30\,[\tau_s - 0.8926]$ (°). We have adjusted the measurement to use our best values of ($\Delta m = 0.5293 \pm 0.0009$) ($10^{10}$ $\hbar$ s^{-1}), ($\tau_s = 0.8954 \pm 0.0004$) ($10^{-10}$ s). Our first error is their experiment's error and our second error is the systematic error from using our best values.

[12] ADLER 92B quote separately two systematic errors: ±0.4 from their experiment and ±1.0 degrees due to the uncertainty in the value of Δm.

[13] KARLSSON 90 systematic error does not include regeneration phase uncertainty.

[14] CARITHERS 75 measures $\phi_{+-} = (45.5 \pm 2.8) + 224\,[\Delta m - 0.5348]$ (°). We have adjusted the measurement to use our best values of ($\Delta m = 0.5293 \pm 0.0009$) ($10^{10}$ $\hbar$ s^{-1}). Our first error is their experiment's error and our second error is the systematic error from using our best values. $\phi_f = -40.9 \pm 2.6$°.

Downloaded from https://academic.oup.com/ptep/article/2022/8/083C01/6651666 by KIT Library user on 27 September 2022

ϕ_{00}, PHASE OF η_{00}

See comment in ϕ_{+-} header above for treatment of Δm and τ_S dependence, as well as for the inclusion of data in both the "Assuming *CPT*" and "Not Assuming *CPT*" fits.

OUR FIT is described in the note on "*CP* violation in K_L decays" in the K^0_L Particle Listings.

VALUE (°)	DOCUMENT ID		TECN	COMMENT
43.52±0.05 OUR FIT	Error includes scale factor of 1.3. Assuming *CPT*			
43.7 ±0.6 OUR FIT	Error includes scale factor of 1.2. Not assuming *CPT*			
44.5 ±2.3 ±0.5	[1] CAROSI	90	NA31	
• • • We do not use the following data for averages, fits, limits, etc. • • •				
44.06±0.68	[2] ABOUZAID	11	KTEV	Not assuming *CPT*
41.7 ±5.9 ±0.2	[3] ANGELOPO...	98	CPLR	
50.8 ±7.1 ±1.7	[4] ADLER	96B	CPLR	Sup. by ANGELOPOULOS 98
47.4 ±1.4 ±0.9	[5] KARLSSON	90	E731	

[1] CAROSI 90 measures $\phi_{00} = (47.1 \pm 2.1 \pm 1.0) + 579\,[\Delta m - 0.5351] + 252\,[\tau_S - 0.8922]$ (°). We have adjusted the measurement to use our best values of ($\Delta m = 0.5293 \pm 0.0009$) ($10^{10}\ \hbar\ s^{-1}$), ($\tau_S = 0.8954 \pm 0.0004$) ($10^{-10}$ s). Our first error is their experiment's error and our second error is the systematic error from using our best values.

[2] Not independent of other phase parameters reported in ABOUZAID 11.

[3] ANGELOPOULOS 98 measures $\phi_{00} = (42.0 \pm 5.6 \pm 1.9) + 240\,[\Delta m - 0.5307]$ (°). We have adjusted the measurement to use our best values of ($\Delta m = 0.5293 \pm 0.0009$) ($10^{10}\ \hbar\ s^{-1}$). Our first error is their experiment's error and our second error is the systematic error from using our best values. The τ_S dependence is negligible.

[4] ADLER 96B identified initial neutral kaon individually as being a K^0 or a $\overline{K}^0$. The systematic uncertainty is ±1.5° combined in quadrature with ±0.8° due to Δm.

[5] KARLSSON 90 systematic error does not include regeneration phase uncertainty.

$\phi_\epsilon = (2\phi_{+-} + \phi_{00})/3$

This expression is a very good approximation, good to about 10^{-3} degrees because of the small measured values of $\phi_{00} - \phi_{+-}$ and Re ϵ'/ϵ, and small theoretical ambiguities.

VALUE (°)	DOCUMENT ID		TECN	COMMENT
43.52 ±0.05 OUR FIT	Error includes scale factor of 1.2. Assuming *CPT*			
43.5 ±0.5 OUR FIT	Error includes scale factor of 1.3. Not assuming *CPT*			
43.5164±0.0002±0.0518	[1] SUPERWEAK	16		Assuming *CPT*
43.86 ±0.63	[2] ABOUZAID	11	KTEV	Not assuming *CPT*

[1] SUPERWEAK 16 is a fake measurement used to impose the *CPT* or Superweak constraint $\phi_{+-} = \phi_{SW} = \tan^{-1}[2\,\frac{\Delta m}{\hbar}\,(\frac{\tau_S \tau_L}{\tau_L - \tau_S})]$. This "measurement" is linearized using values near the PDG 04 edition values of Δm, τ_S and τ_L, and then adjusted to our current values as described in the following "measurement". SUPERWEAK 16 measures $\phi_\epsilon = (43.50258 \pm 0.00021) + 54.1\,[\Delta m - 0.5289] + 32.0\,[\tau_S - 0.89564]$ (°). We have adjusted the measurement to use our best values of ($\Delta m = 0.5293 \pm 0.0009$) ($10^{10}\ \hbar\ s^{-1}$), ($\tau_S = 0.8954 \pm 0.0004$) ($10^{-10}$ s). Our first error is their experiment's error and our second error is the systematic error from using our best values.

[2] ABOUZAID 11 uses the full KTeV dataset collected in 1996, 1997, and 1999. See Im(ϵ'/ϵ) section for correlation information.

Im(ϵ'/ϵ) = $-(\phi_{00} - \phi_{+-})/3$

For small $|\epsilon'/\epsilon|$, Im(ϵ'/ϵ) is related to the phases of η_{00} and η_{+-} by the above expression.

VALUE (°)	DOCUMENT ID		TECN	COMMENT
−0.002 ±0.005 OUR FIT	Error includes scale factor of 1.7. Assuming *CPT*			
−0.11 ±0.11 OUR FIT	Not assuming *CPT*			
−0.0985±0.1157	[1] ABOUZAID	11	KTEV	Not assuming *CPT*

[1] ABOUZAID 11 uses the full KTeV dataset collected in 1996, 1997, and 1999. The fit has Δm, τ_S, ϕ_ϵ, Re(ϵ'/ϵ), and Im(ϵ'/ϵ) as free parameters. The reported value of Im(ϵ'/ϵ) $= (-17.20 \pm 20.20) \times 10^{-4}$ rad. The correlation coefficients are $\rho(\phi_\epsilon, \Delta m) = 0.828$, $\rho(\phi_\epsilon, \tau_S) = -0.765$, $\rho(\Delta m, \tau_S) = -0.858$, ρ(Im(ϵ'/ϵ), ϕ_ϵ) $= -0.041$, ρ(Im(ϵ'/ϵ), Δm) $= 0.026$, ρ(Im(ϵ'/ϵ), τ_S) $= -0.010$.

DECAY-PLANE ASYMMETRY IN $\pi^+\pi^-e^+e^-$ DECAYS

This is the *CP*-violating asymmetry

$$A = \frac{N_{\sin\phi\cos\phi>0.0} - N_{\sin\phi\cos\phi<0.0}}{N_{\sin\phi\cos\phi>0.0} + N_{\sin\phi\cos\phi<0.0}}$$

where ϕ is the angle between the e^+e^- and $\pi^+\pi^-$ planes in the K^0_L rest frame.

CP ASYMMETRY *A* in $K^0_L \to \pi^+\pi^-e^+e^-$

VALUE (%)	DOCUMENT ID		TECN
13.7±1.5 OUR AVERAGE			
13.6±1.4±1.5	ABOUZAID	06	KTEV
14.2±3.0±1.9	LAI	03C	NA48
13.6±2.5±1.2	ALAVI-HARATI	00B	KTEV

PARAMETERS FOR $e^+e^-e^+e^-$ DECAYS

These are the *CP*-violating parameters in the ϕ distribution, where ϕ is the angle between the planes of the two e^+e^- pairs in the kaon rest frame:

$$d\Gamma/d\phi \propto 1 + \beta_{CP}\cos(2\phi) + \gamma_{CP}\sin(2\phi)$$

where $\beta_{CP} = -0.20$ and $\gamma_{CP} = 0$ values correspond to no *CP* violation.

β_{CP} from $K^0_L \to e^+e^-e^+e^-$

VALUE	EVTS	DOCUMENT ID		TECN	COMMENT
−0.19±0.07 OUR AVERAGE					
−0.13±0.10±0.03	200	[1] LAI	05B	NA48	
−0.23±0.09±0.02	441	ALAVI-HARATI	01D	KTEV	M_{ee} >8 MeV/c^2

[1] LAI 05B obtains $\beta_{CP} = -0.13 \pm 0.10$(stat) if $\gamma_{CP} = 0$ is assumed.

γ_{CP} from $K^0_L \to e^+e^-e^+e^-$

VALUE	EVTS	DOCUMENT ID		TECN	COMMENT
0.01±0.11 OUR AVERAGE	Error includes scale factor of 1.6.				
+0.13±0.10±0.03	200	LAI	05B	NA48	
−0.09±0.09±0.02	441	ALAVI-HARATI	01D	KTEV	M_{ee} >8 MeV/c^2

CHARGE ASYMMETRY IN $\pi^+\pi^-\pi^0$ DECAYS

These are *CP*-violating charge-asymmetry parameters, defined at beginning of section "LINEAR COEFFICIENT *g* FOR $K^0_L \to \pi^+\pi^-\pi^0$ above.

See also note on Dalitz plot parameters in $K^\pm$ section and note on "*CP* violation in K_L decays" above.

LINEAR COEFFICIENT *j* FOR $K^0_L \to \pi^+\pi^-\pi^0$

VALUE	EVTS	DOCUMENT ID		TECN
0.0012±0.0008 OUR AVERAGE				
0.0010±0.0024±0.0030	500k	ANGELOPO...	98C	CPLR
−0.001 ±0.011	6499	CHO	77	
0.001 ±0.003	4709	PEACH	77	
0.0013±0.0009	3M	SCRIBANO	70	
0.0 ±0.017	4400	SMITH	70	OSPK
0.001 ±0.004	238k	BLANPIED	68	

QUADRATIC COEFFICIENT *f* FOR $K^0_L \to \pi^+\pi^-\pi^0$

VALUE	EVTS	DOCUMENT ID		TECN
0.0045±0.0024±0.0059	500k	ANGELOPO...	98C	CPLR

PARAMETERS for $K^0_L \to \pi^+\pi^-\gamma$ DECAY

$|\eta_{+-\gamma}| = |A(K^0_L \to \pi^+\pi^-\gamma,\ CP\ \text{violating})/A(K^0_S \to \pi^+\pi^-\gamma)|$

VALUE (units 10^{-3})	EVTS	DOCUMENT ID		TECN
2.35 ±0.07 OUR AVERAGE				
2.359±0.062±0.040	9045	MATTHEWS	95	E773
2.15 ±0.26 ±0.20	3671	RAMBERG	93B	E731

$\phi_{+-\gamma}$ = phase of $\eta_{+-\gamma}$

VALUE (°)	EVTS	DOCUMENT ID		TECN
44 ± 4 OUR AVERAGE				
43.8± 3.5± 1.9	9045	MATTHEWS	95	E773
72 ±23 ±17	3671	RAMBERG	93B	E731

$|\epsilon'_{+-\gamma}|/\epsilon$ for $K^0_L \to \pi^+\pi^-\gamma$

VALUE	CL%	EVTS	DOCUMENT ID		TECN
<0.3	90	3671	[1] RAMBERG	93B	E731

[1] RAMBERG 93B limit on $|\epsilon'_{+-\gamma}|/\epsilon$ assumes than any difference between η_{+-} and $\eta_{+-\gamma}$ is due to direct *CP* violation.

$|g_{E1}|$ for $K^0_L \to \pi^+\pi^-\gamma$

This parameter is the amplitude of the direct emission of a *CP* violating E1 electric dipole photon.

VALUE	CL%	EVTS	DOCUMENT ID		TECN	COMMENT
<0.21	90	111k	ABOUZAID	06A	KTEV	E^*_γ > 20 MeV

T VIOLATION TESTS IN K^0_L DECAYS

Im(ξ) in $K^0_{\mu3}$ DECAY (from transverse μ pol.)

Test of *T* reversal invariance.

VALUE	EVTS	DOCUMENT ID		TECN	COMMENT
−0.007±0.026 OUR AVERAGE					
0.009±0.030	12M	MORSE	80	CNTR	Polarization
0.35 ±0.30	207k	[1] CLARK	77	SPEC	POL, t=0
−0.085±0.064	2.2M	[2] SANDWEISS	73	CNTR	POL, t=0
−0.02 ±0.08		LONGO	69	CNTR	POL, t=3.3
−0.2 ±0.6		ABRAMS	68B	OSPK	Polarization
• • • We do not use the following data for averages, fits, limits, etc. • • •					
0.012±0.026		SCHMIDT	79	CNTR	Repl. by MORSE 80

[1] CLARK 77 value has additional $\xi(0)$ dependence $+0.21\mathrm{Re}[\xi(0)]$.

[2] SANDWEISS 73 value corrected from value quoted in their paper due to new value of Re(ξ). See footnote 4 of SCHMIDT 79.

CPT-INVARIANCE TESTS IN K^0_L DECAYS

PHASE DIFFERENCE $\phi_{00} - \phi_{+-}$

Test of *CPT*.

OUR FIT is described in the note on "*CP* violation in K_L decays" in the K^0_L Particle Listings.

VALUE (°)	DOCUMENT ID		TECN	COMMENT
0.006±0.014 OUR FIT	Error includes scale factor of 1.7. Assuming *CPT*			
0.34 ±0.32 OUR FIT	Not assuming *CPT*			
0.006±0.008	[1] SUPERWEAK	16		Assuming *CPT*
−0.30 ±0.88	[2] SCHWINGEN...	95		Combined E731, E773

Downloaded from https://academic.oup.com/ptep/article/2022/8/083C01/6651666 by KIT Library user on 27 September 2022

• • • We do not use the following data for averages, fits, limits, etc. • • •

0.30 ±0.35	[3] ABOUZAID	11	KTEV	Not assuming *CPT*
0.39 ±0.22 ±0.45	[4] ALAVI-HARATI	03	KTEV	
0.62 ±0.71 ±0.75	SCHWINGEN...	95	E773	
−1.6 ±1.2	[5] GIBBONS	93	E731	
0.2 ±2.6 ±1.2	[6] CAROSI	90	NA31	
−0.3 ±2.4 ±1.2	KARLSSON	90	E731	

[1] SUPERWEAK 16 is a fake experiment to constrain $\phi_{00} - \phi_{+-}$ to a small value as described in the note "*CP* violation in K_L decays."
[2] This SCHWINGENHEUER 95 values is the combined result of SCHWINGENHEUER 95 and GIBBONS 93, accounting for correlated systematic errors.
[3] Not independent of other phase parameters reported in ABOUZAID 11.
[4] ALAVI-HARATI 03 fit Re(ϵ'/ϵ), Im(ϵ'/ϵ), Δm, τ_S, and ϕ_{+-} simultaneously, not assuming *CPT*. Phase difference is obtained from $\phi_{00} - \phi_{+-} \approx -3\mathrm{Im}(\epsilon'/\epsilon)$ for small $|\epsilon'/\epsilon|$. Superseded by ABOUZAID 11.
[5] GIBBONS 93 give detailed dependence of systematic error on lifetime (see the section on the K^0_S mean life) and mass difference (see the section on $m_{K^0_L} - m_{K^0_S}$).
[6] CAROSI 90 is excluded from the fit because it it is not independent of ϕ_{+-} and ϕ_{00} values.

PHASE DIFFERENCE $\phi_{+-} - \phi_{SW}$

Test of *CPT*. The Superweak phase $\phi_{SW} \equiv \tan^{-1}(2\Delta m/\Delta\Gamma)$ where $\Delta m = m_{K^0_L} - m_{K^0_S}$ and $\Delta\Gamma = \hbar(\tau_L - \tau_S)/(\tau_L\tau_S)$.

VALUE (°)	DOCUMENT ID		TECN
0.61±0.62±1.01	[1] ALAVI-HARATI	03	KTEV

[1] ALAVI-HARATI 03 fit is the same as their ϕ_{+-}, τ_{K_S}, Δm fit, except that the parameter $\phi_{+-} - \phi_{SW}$ is used in place of ϕ.

$\mathrm{Re}(\frac{2}{3}\eta_{+-} + \frac{1}{3}\eta_{00}) - \frac{A_L}{2}$

Test of *CPT*

VALUE (units 10^{-6})	DOCUMENT ID		TECN	COMMENT
−3±35	[1] ALAVI-HARATI	02	E799	Uses A_L from K_{e3} decays

[1] ALAVI-HARATI 02 uses PDG 00 values of η_{+-} and η_{00}.

$\Delta S = \Delta Q$ IN K^0 DECAYS

The relative amount of $\Delta S \neq \Delta Q$ component present is measured by the parameter x, defined as

$$x = A(\overline{K}^0 \to \pi^-\ell^+\nu)/A(K^0 \to \pi^-\ell^+\nu) \ .$$

We list Re{x} and Im{x} for K_{e3} and $K_{\mu3}$ combined.

$x = A(\overline{K}^0 \to \pi^-\ell^+\nu)/A(K^0 \to \pi^-\ell^+\nu) = A(\Delta S{=}{-}\Delta Q)/A(\Delta S{=}\Delta Q)$

REAL PART OF x

VALUE	EVTS	DOCUMENT ID		TECN	COMMENT
−0.0018±0.0041±0.0045		ANGELOPO...	98D	CPLR	K_{e3} from K^0

• • • We do not use the following data for averages, fits, limits, etc. • • •

0.10 $^{+0.18}_{-0.19}$	79	SMITH	75B	WIRE	$\pi^- p \to K^0\Lambda$
0.04 ±0.03	4724	NIEBERGALL	74	ASPK	$K^+ p \to K^0 p\pi^+$
−0.008 ±0.044	1757	FACKLER	73	OSPK	K_{e3} from K^0
−0.03 ±0.07	1367	HART	73	OSPK	K_{e3} from $K^0\Lambda$
−0.070 ±0.036	1079	MALLARY	73	OSPK	K_{e3} from $K^0\Lambda$X
0.03 ±0.06	410	[1] BURGUN	72	HBC	$K^+ p \to K^0 p\pi^+$
0.04 $^{+0.10}_{-0.13}$	100	[2] GRAHAM	72	OSPK	$K_{\mu3}$ from $K^0\Lambda$
−0.05 ±0.09	442	[2] GRAHAM	72	OSPK	$\pi^- p \to K^0\Lambda$
0.26 $^{+0.10}_{-0.14}$	126	MANN	72	HBC	$K^- p \to n\overline{K}^0$
−0.13 ±0.11	342	[2] MANTSCH	72	OSPK	K_{e3} from $K^0\Lambda$
0.04 $^{+0.07}_{-0.08}$	222	[1] BURGUN	71	HBC	$K^+ p \to K^0 p\pi^+$
0.25 $^{+0.07}_{-0.09}$	252	WEBBER	71	HBC	$K^- p \to n\overline{K}^0$
0.12 ±0.09	215	[3] CHO	70	DBC	$K^+ d \to K^0 pp$
−0.020 ±0.025		[4] BENNETT	69	CNTR	Charge asym+ Cu regen.
0.09 $^{+0.14}_{-0.16}$	686	LITTENBERG	69	OSPK	$K^+ n \to K^0 p$
0.03 ±0.03		[4] BENNETT	68	CNTR	
0.09 $^{+0.07}_{-0.09}$	121	JAMES	68	HBC	$\overline{p}p$
0.17 $^{+0.16}_{-0.35}$	116	FELDMAN	67B	OSPK	$\pi^- p \to K^0\Lambda$
0.17 ±0.10	335	[3] HILL	67	DBC	$K^+ d \to K^0 pp$
0.035 $^{+0.11}_{-0.13}$	196	AUBERT	65	HLBC	K^+ charge exch.
0.06 $^{+0.18}_{-0.44}$	152	[5] BALDO-...	65	HLBC	K^+ charge exch.
−0.08 $^{+0.16}_{-0.28}$	109	[6] FRANZINI	65	HBC	$\overline{p}p$

[1] BURGUN 72 is a final result which includes BURGUN 71.
[2] First GRAHAM 72 value is second GRAHAM 72 value combined with MANTSCH 72.
[3] CHO 70 is analysis of unambiguous events in new data and HILL 67.
[4] BENNETT 69 is a reanalysis of BENNETT 68.
[5] BALDO-CEOLIN 65 gives x and θ converted by us to Re(x) and Im(x).
[6] FRANZINI 65 gives x and θ for Re(x) and Im(x). See SCHMIDT 67.

IMAGINARY PART OF x

Assumes $m_{K^0_L} - m_{K^0_S}$ positive. See Listings above.

VALUE	EVTS	DOCUMENT ID		TECN	COMMENT
0.0012±0.0019±0.0009	640k	ANGELOPO...	01B	CPLR	K_{e3} from K^0

• • • We do not use the following data for averages, fits, limits, etc. • • •

0.0012±0.0019	640k	[1] ANGELOPO...	98E	CPLR	K_{e3} from K^0
−0.10 $^{+0.16}_{-0.19}$	79	SMITH	75B	WIRE	$\pi^- p \to K^0\Lambda$
−0.06 ±0.05	4724	NIEBERGALL	74	ASPK	$K^+ p \to K^0 p\pi^+$
−0.017 ±0.060	1757	FACKLER	73	OSPK	K_{e3} from K^0
0.09 ±0.07	1367	HART	73	OSPK	K_{e3} from $K^0\Lambda$
0.107 $^{+0.092}_{-0.074}$	1079	MALLARY	73	OSPK	K_{e3} from $K^0\Lambda$X
0.07 $^{+0.06}_{-0.07}$	410	[2] BURGUN	72	HBC	$K^+ p \to K^0 p\pi^+$
0.12 $^{+0.17}_{-0.16}$	100	[3] GRAHAM	72	OSPK	$K_{\mu3}$ from $K^0\Lambda$
0.05 ±0.13	442	[3] GRAHAM	72	OSPK	$\pi^- p \to K^0\Lambda$
0.21 $^{+0.15}_{-0.12}$	126	MANN	72	HBC	$K^- p \to n\overline{K}^0$
−0.04 ±0.16	342	[3] MANTSCH	72	OSPK	K_{e3} from $K^0\Lambda$
0.12 $^{+0.08}_{-0.09}$	222	[2] BURGUN	71	HBC	$K^+ p \to K^0 p\pi^+$
0.0 ±0.08	252	WEBBER	71	HBC	$K^- p \to n\overline{K}^0$
−0.08 ±0.07	215	[4] CHO	70	DBC	$K^+ d \to K^0 pp$
−0.11 $^{+0.10}_{-0.11}$	686	LITTENBERG	69	OSPK	$K^+ n \to K^0 p$
+0.22 $^{+0.37}_{-0.29}$	121	JAMES	68	HBC	$\overline{p}p$
0.0 ±0.25	116	FELDMAN	67B	OSPK	$\pi^- p \to K^0\Lambda$
−0.20 ±0.10	335	[4] HILL	67	DBC	$K^+ d \to K^0 pp$
−0.21 $^{+0.11}_{-0.15}$	196	AUBERT	65	HLBC	K^+ charge exch.
−0.44 $^{+0.32}_{-0.19}$	152	[5] BALDO-...	65	HLBC	K^+ charge exch.
+0.24 $^{+0.40}_{-0.30}$	109	[6] FRANZINI	65	HBC	$\overline{p}p$

[1] Superseded by ANGELOPOULOS 01B.
[2] BURGUN 72 is a final result which includes BURGUN 71.
[3] First GRAHAM 72 value is second GRAHAM 72 value combined with MANTSCH 72.
[4] Footnote 10 of HILL 67 should read +0.58, not −0.58 (private communication) CHO 70 is analysis of unambiguous events in new data and HILL 67.
[5] BALDO-CEOLIN 65 gives x and θ converted by us to Re(x) and Im(x).
[6] FRANZINI 65 gives x and θ for Re(x) and Im(x). See SCHMIDT 67.

K^0_L REFERENCES

AHN	21	PRL 126 121801	J.K. Ahn *et al.*	(KOTO Collab.)
SHIMIZU	20	PR D102 051103	N. Shimizu *et al.*	(KOTO Collab.)
AHN	19	PRL 122 021802	J.K. Ahn *et al.*	(KOTO Collab.)
AHN	17	PTEP 2017 021C01	J.K. Ahn *et al.*	(KOTO Collab.)
BRFIT	16	RPP 2016 edition	C.-J. Lin	(PDG Collab.)
ETAFIT	16	RPP 2016 edition	C.-J. Lin	(PDG Collab.)
SUPERWEAK	16	RPP 2016 edition	C.-J. Lin	(PDG Collab.)
ABOUZAID	11	PR D83 092001	E. Abouzaid *et al.*	(FNAL KTeV Collab.)
ABOUZAID	11A	PRL 107 201803	E. Abouzaid *et al.*	(KTeV Collab.)
OGATA	11	PR D84 052009	R. Ogata *et al.*	(KEK E391a Collab.)
TUNG	11	PR D83 031101	Y.C. Tung *et al.*	(KEK E391a Collab.)
ABOUZAID	10	PR D81 052001	E. Abouzaid *et al.*	(FNAL KTeV Collab.)
AHN	10	PR D81 072004	J.K. Ahn *et al.*	(KEK E391a Collab.)
ABOUZAID	08	PR D77 112004	E. Abouzaid *et al.*	(FNAL KTeV Collab.)
ABOUZAID	08A	PR D78 032009	E. Abouzaid *et al.*	(FNAL KTeV Collab.)
ABOUZAID	08B	PR D78 032014	E. Abouzaid *et al.*	(FNAL KTeV Collab.)
ABOUZAID	08C	PRL 100 131803	E. Abouzaid *et al.*	(FNAL KTeV Collab.)
AHN	08	PRL 100 201802	J.K. Ahn *et al.*	(KEK E391a Collab.)
AMBROSINO	08F	EPJ C55 539	F. Ambrosino *et al.*	(KLOE Collab.)
ABOUZAID	07B	PRL 99 051804	E. Abouzaid *et al.*	(FNAL KTeV Collab.)
ABOUZAID	07C	PRL 99 081803	E. Abouzaid *et al.*	(FNAL KTeV Collab.)
ABOUZAID	07D	PR D76 052001	E. Abouzaid *et al.*	(FNAL KTeV Collab.)
AMBROSINO	07C	JHEP 0712 105	F. Ambrosino *et al.*	(KLOE Collab.)
ANDRE	07	ANP 322 2518	T. Andre	(EFI)
LAI	07	PL B645 26	A. Lai *et al.*	(CERN NA48 Collab.)
LAI	07A	PL B647 341	A. Lai *et al.*	(CERN NA48 Collab.)
NIX	07	PR D76 011101	J. Nix *et al.*	(KEK E391a Collab.)
ABOUZAID	06	PRL 96 101801	E. Abouzaid *et al.*	(KTeV Collab.)
ABOUZAID	06A	PR D74 032004	E. Abouzaid *et al.*	(KTeV Collab.)
Also		PR D74 039905 (errat.)	E. Abouzaid *et al.*	(KTeV Collab.)
ABOUZAID	06C	PR D74 097101	E. Abouzaid *et al.*	(KTeV Collab.)
AHN	06	PR D74 051105	J.K. Ahn *et al.*	(KEK E391a Collab.)
Also		PR D74 079901 (errat.)	J.K. Ahn *et al.*	(KEK E391a Collab.)
AMBROSINO	06	PL B632 43	F. Ambrosino *et al.*	(KLOE Collab.)
AMBROSINO	06D	PL B636 166	F. Ambrosino *et al.*	(KLOE Collab.)
AMBROSINO	06F	PL B638 140	F. Ambrosino *et al.*	(KLOE Collab.)
BATLEY	06B	PL B633 173	J.R. Batley *et al.*	(CERN NA48/2 Collab.)
HILL	06	PR D74 096006	R.J. Hill	(FNAL)
PDG	06	JP G33 1	W.-M. Yao *et al.*	(PDG Collab.)
ALEXOPOU...	05	PR D71 012001	T. Alexopoulos *et al.*	(FNAL KTeV Collab.)
AMBROSINO	05C	PL B626 15	F. Ambrosino *et al.*	(KLOE Collab.)
CABIBBO	05	JHEP 0503 021	N. Cabibbo, G. Isidori	(CERN, ROMAI, FRAS)
LAI	05	PL B605 247	A. Lai *et al.*	(CERN NA48 Collab.)
LAI	05B	PL B615 31	A. Lai *et al.*	(CERN NA48 Collab.)
PARK	05	PRL 94 021801	H.K. Park *et al.*	(FNAL HyperCP Collab.)
ALAVI-HARATI	04A	PRL 93 021805	A. Alavi-Harati *et al.*	(FNAL KTeV/E799 Collab.)
ALEXOPOU...	04	PR D70 092006	T. Alexopoulos *et al.*	(FNAL KTeV Collab.)
ALEXOPOU...	04A	PR D70 092007	T. Alexopoulos *et al.*	(FNAL KTeV Collab.)
BATLEY	04	PL B595 75	J.R. Batley *et al.*	(CERN NA48 Collab.)
CIRIGLIANO	04	EPJ C35 53	V. Cirigliano, H. Neufeld, H. Pichl	(CIT, VALE+)

Downloaded from https://academic.oup.com/ptep/article/2022/8/083C01/6651666 by KIT Library user on 27 September 2022

LAI	04B	PL B602 41	A. Lai *et al.*	(CERN NA48 Collab.)
LAI	04C	PL B604 1	A. Lai *et al.*	(CERN NA48 Collab.)
PDG	04	PL B592 1	S. Eidelman *et al.*	(PDG Collab.)
SOZZI	04	EPJ C36 37	M. Sozzi	(PISA)
ADINOLFI	03	PL B566 61	M. Adinolfi *et al.*	(KLOE Collab.)
ALAVI-HARATI	03	PR D67 012005	A. Alavi-Harati *et al.*	(FNAL KTeV Collab.)
Also		PR D70 079904 (errat.)	A. Alavi-Harati *et al.*	(FNAL KTeV Collab.)
ALAVI-HARATI	03B	PRL 90 141801	A. ALavi-Harati *et al.*	(FNAL KTeV Collab.)
LAI	03	PL B551 7	A. Lai *et al.*	(CERN NA48 Collab.)
LAI	03C	EPJ C30 33	A. Lai *et al.*	(CERN NA48 Collab.)
ALAVI-HARATI	02	PRL 88 181601	A. Alavi-Harati *et al.*	(FNAL KTeV Collab.)
ALAVI-HARATI	02C	PRL 89 211801	A. Alavi-Harati *et al.*	(FNAL KTeV Collab.)
BATLEY	02	PL B544 97	J.R. Batley *et al.*	(CERN NA48 Collab.)
CIRIGLIANO	02	EPJ C23 121	V. Cirigliano *et al.*	(VIEN, VALE, MARS)
LAI	02B	PL B536 229	A. Lai *et al.*	(CERN NA48 Collab.)
ALAVI-HARATI	01	PRL 86 397	A. Alavi-Harati *et al.*	(FNAL KTeV Collab.)
ALAVI-HARATI	01B	PRL 86 761	A. Alavi-Harati *et al.*	(FNAL KTeV Collab.)
ALAVI-HARATI	01D	PRL 86 5425	A. Alavi-Harati *et al.*	(FNAL KTeV Collab.)
ALAVI-HARATI	01E	PRL 87 021801	A. Alavi-Harati *et al.*	(FNAL KTeV Collab.)
ALAVI-HARATI	01F	PR D64 012003	A. Alavi-Harati *et al.*	(FNAL KTeV Collab.)
ALAVI-HARATI	01G	PRL 87 071801	A. Alavi-Harati *et al.*	(FNAL KTeV Collab.)
ALAVI-HARATI	01H	PRL 87 111802	A. Alavi-Harati *et al.*	(FNAL KTeV Collab.)
ALAVI-HARATI	01J	PR D64 112004	A. Alavi-Harati *et al.*	(FNAL KTeV Collab.)
ANGELOPO...	01	PL B503 49	A. Angelopoulos *et al.*	(CPLEAR Collab.)
ANGELOPO...	01B	EPJ C22 55	A. Angelopoulos *et al.*	(CPLEAR Collab.)
LAI	01B	PL B515 261	A. Lai *et al.*	(CERN NA48 Collab.)
LAI	01C	EPJ C22 231	A. Lai *et al.*	(CERN NA48 Collab.)
ALAVI-HARATI	00	PR D61 072006	A. Alavi-Harati *et al.*	(FNAL KTeV Collab.)
ALAVI-HARATI	00B	PRL 84 408	A. Alavi-Harati *et al.*	(FNAL KTeV Collab.)
ALAVI-HARATI	00D	PRL 84 5279	A. Alavi-Harati *et al.*	(FNAL KTeV Collab.)
ALAVI-HARATI	00E	PR D62 112001	A. Alavi-Harati *et al.*	(FNAL KTeV Collab.)
AMBROSE	00	PRL 84 1389	D. Ambrose *et al.*	(BNL E871 Collab.)
APOSTOLA...	00	PL B473 186	A. Apostolakis *et al.*	(CPLEAR Collab.)
PDG	00	EPJ C15 1	D.E. Groom *et al.*	(PDG Collab.)
ALAVI-HARATI	99B	PRL 83 917	A. Alavi-Harati *et al.*	(FNAL KTeV Collab.)
ALAVI-HARATI	99D	PRL 83 22	A. Alavi-Harati *et al.*	(FNAL KTeV Collab.)
APOSTOLA...	99C	PL B458 545	A. Apostolakis *et al.*	(CPLEAR Collab.)
Also		EPJ C18 41	A. Apostolakis *et al.*	(CPLEAR Collab.)
FANTI	99B	PL B458 553	V. Fanti *et al.*	(CERN NA48 Collab.)
FANTI	99C	PL B465 335	V. Fanti *et al.*	(CERN NA48 Collab.)
MURAKAMI	99	PL B463 333	K. Murakami *et al.*	(KEK E162 Collab.)
ADAMS	98	PRL 80 4123	J. Adams *et al.*	(FNAL KTeV Collab.)
AMBROSE	98	PRL 81 4309	D. Ambrose *et al.*	(BNL E871 Collab.)
AMBROSE	98B	PRL 81 5734	D. Ambrose *et al.*	(BNL E871 Collab.)
ANGELOPO...	98	PL B420 191	A. Angelopoulos *et al.*	(CPLEAR Collab.)
ANGELOPO...	98C	EPJ C5 389	A. Angelopoulos *et al.*	(CPLEAR Collab.)
ANGELOPO...	98D	PL B444 38	A. Angelopoulos *et al.*	(CPLEAR Collab.)
Also		EPJ C22 55	A. Angelopoulos *et al.*	(CPLEAR Collab.)
ANGELOPO...	98E	PL B444 43	A. Angelopoulos *et al.*	(CPLEAR Collab.)
ARISAKA	98	PL B432 230	K. Arisaka *et al.*	(FNAL E799 Collab.)
BENDER	98	PL B418 411	M. Bender *et al.*	(CERN NA48 Collab.)
DAMBROSIO	98	PL B423 385	G. D'Ambrosio, G. Isidori, J. Portoles	
SETZU	98	PL B420 205	M.G. Setzu *et al.*	
TAKEUCHI	98	PL B443 409	Y. Takeuchi *et al.*	(KYOT, KEK, HIRO)
FANTI	97	ZPHY C76 653	V. Fanti *et al.*	(CERN NA48 Collab.)
NOMURA	97	PL B408 445	T. Nomura *et al.*	(KYOT, KEK, HIRO)
ADLER	96B	ZPHY C70 211	R. Adler *et al.*	(CPLEAR Collab.)
ADLER	96C	PL B369 367	R. Adler *et al.*	(CPLEAR Collab.)
GU	96	PRL 76 4312	P. Gu *et al.*	(RUTG, UCLA, EFI, COLO+)
LEBER	96	PL B369 69	F. Leber *et al.*	(MAINZ, CERN, EDIN, ORSAY+)
PDG	96	PR D54 1	R. M. Barnett *et al.*	(PDG Collab.)
ADLER	95	PL B363 237	R. Adler *et al.*	(CPLEAR Collab.)
ADLER	95B	PL B363 243	R. Adler *et al.*	(CPLEAR Collab.)
AKAGI	95	PR D51 2061	T. Akagi *et al.*	(TOHOK, TOKY, KYOT, KEK)
BARR	95	ZPHY C65 361	G.D. Barr *et al.*	(CERN, EDIN, MAINZ, LALO+)
BARR	95C	PL B358 399	G.D. Barr *et al.*	(CERN, EDIN, MAINZ, LALO+)
HEINSON	95	PR D51 985	A.P. Heinson *et al.*	(BNL E791 Collab.)
KREUTZ	95	ZPHY C65 67	A. Kreutz *et al.*	(SIEG, EDIN, MAINZ, ORSAY+)
MATTHEWS	95	PRL 75 2803	J.N. Matthews *et al.*	(RUTG, EFI, ELMT+)
SCHWINGEN...	95	PRL 74 4376	B. Schwingenheuer *et al.*	(EFI, CHIC+)
SPENCER	95	PRL 74 3323	M.B. Spencer *et al.*	(UCLA, EFI, COLO+)
BARR	94	PL B328 528	G.D. Barr *et al.*	(CERN, EDIN, MAINZ, LALO+)
GU	94	PRL 72 3000	P. Gu *et al.*	(RUTG, UCLA, EFI, COLO+)
NAKAYA	94	PRL 73 2169	T. Nakaya *et al.*	(OSAK, UCLA, EFI, COLU+)
ROBERTS	94	PR D50 1874	D. Roberts *et al.*	(UCLA, EFI, COLU+)
AKAGI	93	PR D47 2644	T. Akagi *et al.*	(TOHOK, TOKY, KYOT, KEK)
ARISAKA	93	PRL 70 1049	K. Arisaka *et al.*	(BNL E791 Collab.)
ARISAKA	93B	PRL 71 3910	K. Arisaka *et al.*	(BNL E791 Collab.)
BARR	93D	PL B317 233	G.D. Barr *et al.*	(CERN, EDIN, MAINZ, LALO+)
GIBBONS	93	PRL 70 1199	L.K. Gibbons *et al.*	(FNAL E731 Collab.)
Also		PR D55 6625	L.K. Gibbons *et al.*	(FNAL E731 Collab.)
GIBBONS	93B	PRL 70 1203	L.K. Gibbons *et al.*	(FNAL E731 Collab.)
GIBBONS	93C	Thesis RX-1487	L.K. Gibbons	(CHIC)
Also		PR D55 6625	L.K. Gibbons *et al.*	(FNAL E731 Collab.)
HARRIS	93	PRL 71 3914	D.A. Harris *et al.*	(EFI, UCLA, COLO+)
HARRIS	93B	PRL 71 3918	D.A. Harris *et al.*	(EFI, UCLA, COLO+)
MAKOFF	93	PRL 70 1591	G. Makoff *et al.*	(FNAL E731 Collab.)
Also		PRL 75 2069 (erratum)	G. Makoff *et al.*	
RAMBERG	93	PRL 70 2525	E. Ramberg *et al.*	(FNAL E731 Collab.)
RAMBERG	93B	PRL 70 2529	E.J. Ramberg *et al.*	(FNAL E731 Collab.)
VAGINS	93	PRL 71 35	M.R. Vagins *et al.*	(BNL E845 Collab.)
ADLER	92B	PL B286 180	R. Adler *et al.*	(CPLEAR Collab.)
Also		SJNP 55 840	R. Adler *et al.*	(CPLEAR Collab.)
BARR	92	PL B284 440	G.D. Barr *et al.*	(CERN, EDIN, MAINZ, LALO+)
MORSE	92	PR D45 36	W.M. Morse *et al.*	(BNL, YALE, VASS)
PDG	92	PR D45 S1	K. Hikasa *et al.*	(KEK, LBL, BOST+)
SOMALWAR	92	PRL 68 2580	S.V. Somalwar *et al.*	(FNAL E731 Collab.)
AKAGI	91B	PRL 67 2618	T. Akagi *et al.*	(TOHOK, TOKY, KYOT, KEK)
BARR	91	PL B259 389	G.D. Barr *et al.*	(CERN, EDIN, MAINZ, LALO+)
HEINSON	91	PR D44 1	A.P. Heinson *et al.*	(UCI, UCLA, LANL+)
PAPADIMITR...	91	PR D44 573	V. Papadimitriou *et al.*	(FNAL E731 Collab.)
BARKER	90	PR D41 3546	A.R. Barker *et al.*	(FNAL E731 Collab.)
Also		PRL 61 2661	L.K. Gibbons *et al.*	(FNAL E731 Collab.)
BARR	90B	PL B240 283	G.D. Barr *et al.*	(CERN, EDIN, MAINZ, LALO+)
BARR	90C	PL B242 523	G.D. Barr *et al.*	(CERN, EDIN, MAINZ, LALO+)
CAROSI	90	PL B237 303	R. Carosi *et al.*	(CERN, EDIN, MAINZ, LALO+)
KARLSSON	90	PRL 64 2976	M. Karlsson *et al.*	(FNAL E731 Collab.)
OHL	90	PRL 64 2755	K.E. Ohl *et al.*	(BNL E845 Collab.)
OHL	90B	PRL 65 1407	K.E. Ohl *et al.*	(BNL E845 Collab.)
PATTERSON	90	PRL 64 1491	J.R. Patterson *et al.*	(FNAL E731 Collab.)
INAGAKI	89	PR D40 1712	T. Inagaki *et al.*	(KEK, TOKY, KYOT)
MATHIAZHA...	89	PRL 63 2181	C. Mathiazhagan *et al.*	(UCI, UCLA, LANL+)
MATHIAZHA...	89B	PRL 63 2185	C. Mathiazhagan *et al.*	(UCI, UCLA, LANL+)
WAHL	89	CERN-EP/89-86	H. Wahl	(CERN)
BARR	88	PL B214 303	G.D. Barr *et al.*	(CERN, EDIN, MAINZ, LALO+)
BURKHARDT	88	PL B206 169	H. Burkhardt *et al.*	(CERN, EDIN, MAINZ+)
JASTRZEM...	88	PRL 61 2300	E. Jastrzembski *et al.*	(BNL, YALE)
WOODS	88	PRL 60 1695	M. Woods *et al.*	(FNAL E731 Collab.)
BURKHARDT	87	PL B199 139	H. Burkhardt *et al.*	(CERN, EDIN, MAINZ+)
ARONSON	86	PR D33 3180	S.H. Aronson *et al.*	(BNL, CHIC, STAN+)
Also		PRL 48 1078	S.H. Aronson *et al.*	(BNL, CHIC, STAN+)
PDG	86C	PL 170B 132	M. Aguilar-Benitez *et al.*	(CERN, CIT+)
COUPAL	85	PRL 55 566	D.P. Coupal *et al.*	(CHIC, SACL)
BALATS	83	SJNP 38 556	M.Y. Balats *et al.*	(ITEP)
		Translated from YAF 38 927.		
BERGSTROM	83	PL 131B 229	L. Bergstrom, E. Masso, P. Singer	(CERN)
ARONSON	82	PRL 48 1078	S.H. Aronson *et al.*	(BNL, CHIC, STAN+)
ARONSON	82B	PRL 48 1306	S.H. Aronson *et al.*	(BNL, CHIC, PURD)
Also		PL 116B 73	E. Fischbach *et al.*	(PURD, BNL, CHIC)
Also		PR D28 476	S.H. Aronson *et al.*	(BNL, CHIC, PURD)
Also		PR D28 495	S.H. Aronson *et al.*	(BNL, CHIC, PURD)
PDG	82B	PL 111B 70	M. Roos *et al.*	(HELS, CIT, CERN)
BIRULEV	81	NP B182 1	V.K. Birulev *et al.*	(JINR)
Also		SJNP 31 622	V.K. Birulev *et al.*	(JINR)
		Translated from YAF 31 1204.		
CARROLL	80B	PRL 44 529	A.S. Carroll *et al.*	(BNL, ROCH)
CARROLL	80C	PL 96B 407	A.S. Carroll *et al.*	(BNL, ROCH)
CHO	80	PR D22 2688	Y. Cho *et al.*	(ANL, CMU)
MORSE	80	PR D21 1750	W.M. Morse *et al.*	(BNL, YALE)
CHRISTENS...	79	PRL 43 1209	J.H. Christenson *et al.*	(NYU)
SCHMIDT	79	PRL 43 556	M.P. Schmidt *et al.*	(YALE, BNL)
HILL	78	PL 73B 483	D.G. Hill *et al.*	(BNL, SLAC, SBER)
CHO	77	PR D15 587	Y. Cho *et al.*	(ANL, CMU)
CLARK	77	PR D15 553	A.R. Clark *et al.*	(LBL)
Also		Thesis LBL-4275	G. Shen	(LBL)
DEVOE	77	PR D16 565	R. Devoe *et al.*	(EFI, ANL)
PEACH	77	NP B127 399	K.J. Peach *et al.*	(BGNA, EDIN, GLAS+)
BIRULEV	76	SJNP 24 178	V.K. Birulev *et al.*	(JINR)
		Translated from YAF 24 340.		
COOMBES	76	PRL 37 249	R.W. Coombes *et al.*	(STAN, NYU)
GJESDAL	76	NP B109 118	G. Gjesdal *et al.*	(CERN, HEIDH)
BALDO-...	75	NC 25A 688	M. Baldo-Ceolin *et al.*	(PADO, WISC)
BLUMENTHAL	75	PRL 34 164	R.B. Blumenthal *et al.*	(PENN, CHIC, TEMP)
BUCHANAN	75	PR D11 457	C.D. Buchanan *et al.*	(UCLA, SLAC, JHU)
CARITHERS	75	PRL 34 1244	W.C.J. Carithers *et al.*	(COLU, NYU)
SMITH	75B	Thesis UCSD unpub.	J.G. Smith	(UCSD)
BISI	74	PL 50B 504	V. Bisi, M.I. Ferrero	(TORI)
DONALDSON	74	Thesis SLAC-0184	G. Donaldson	(SLAC)
Also		PR D14 2839	G. Donaldson *et al.*	(SLAC)
DONALDSON	74B	PR D9 2960	G. Donaldson *et al.*	(SLAC, UCSC)
Also		PRL 31 337	G. Donaldson *et al.*	(SLAC, UCSC)
GEWENIGER	74	PL 48B 483	C. Geweniger *et al.*	(CERN, HEIDH)
Also		Thesis CERN Int. 74-4	V. Luth	(CERN)
GEWENIGER	74B	PL 48B 487	C. Geweniger *et al.*	(CERN, HEIDH)
Also		PL 52B 119	S. Gjesdal *et al.*	(CERN, HEIDH)
GEWENIGER	74C	PL 52B 108	C. Geweniger *et al.*	(CERN, HEIDH)
GJESDAL	74	PL 52B 113	S. Gjesdal *et al.*	(CERN, HEIDH)
MESSNER	74	PRL 33 1458	R. Messner *et al.*	(COLO, SLAC, UCSC)
NIEBERGALL	74	PL 49B 103	F. Niebergall *et al.*	(CERN, ORSAY, VIEN)
WILLIAMS	74	PRL 33 240	H.H. Williams *et al.*	(BNL, YALE)
ALEXANDER	73B	NP B65 301	G. Alexander *et al.*	(TELA, HEID)
BRANDENB...	73	PR D8 1978	G.W. Brandenburg *et al.*	(SLAC)
EVANS	73	PR D7 36	G.R. Evans *et al.*	(EDIN, CERN)
Also		PRL 23 427	G.R. Evans *et al.*	(EDIN, CERN)
FACKLER	73	PRL 31 847	O. Fackler *et al.*	(MIT)
FITCH	73	PRL 31 1524	V.L. Fitch *et al.*	(PRIN)
Also		Thesis COO-3072-13	R.C. Webb	(PRIN)
HART	73	NP B66 317	J.C. Hart *et al.*	(CAVE, RHEL)
MALLARY	73	PR D7 1953	M.L. Mallary *et al.*	(CIT)
Also		PRL 25 1214	F.J. Sciulli *et al.*	(CIT)
MCCARTHY	73	PR D7 687	R.L. McCarthy *et al.*	(LBL)
Also		PL 42B 291	R.L. McCarthy *et al.*	(LBL)
Also		Thesis LBL-550	R.L. McCarthy	(LBL)
MESSNER	73	PRL 30 876	R. Messner *et al.*	(COLO, SLAC, UCSC)
SANDWEISS	73	PRL 30 1002	J. Sandweiss *et al.*	(YALE, ANL)
WILLIAMS	73	PRL 31 1521	H.H. Williams *et al.*	(BNL, YALE)
ASHFORD	72	PL 38B 47	V.A. Ashford *et al.*	(UCSD)
BANNER	72B	PRL 29 237	M. Banner *et al.*	(PRIN)
BARMIN	72B	SJNP 15 638	V.V. Barmin *et al.*	(ITEP)
		Translated from YAF 15 1152.		
BURGUN	72	NP B50 194	G. Burgun *et al.*	(SACL, CERN, OSLO)
GRAHAM	72	NC 9A 166	M.F. Graham *et al.*	(ILL, NEAS)
JAMES	72	NP B49 1	F. James *et al.*	(CERN, SACL, OSLO)
KRENZ	72	LNC 4 213	W. Krenz *et al.*	(AACH, CERN, EDIN)
MANN	72	PR D6 137	W.A. Mann *et al.*	(MASA, BNL, YALE)
MANTSCH	72	NC 9A 160	P.M. Mantsch *et al.*	(ILL, NEAS)
MCCARTHY	72	PL 42B 291	R.L. McCarthy *et al.*	(LBL)
PICCIONI	72	PRL 29 1412	R. Piccioni *et al.*	(SLAC)
Also		PR D9 2939	R. Piccioni *et al.*	(SLAC, UCSC, COLO)
VOSBURGH	72	PR D6 1834	K.G. Vosburgh *et al.*	(RUTG, MASA)
Also		PRL 26 866	K.G. Vosburgh *et al.*	(RUTG, MASA)
BALATS	71	SJNP 13 53	M.Y. Balats *et al.*	(ITEP)
		Translated from YAF 13 93.		
BARMIN	71	PL 35B 604	V.V. Barmin *et al.*	(ITEP)
BURGUN	71	LNC 2 1169	G. Burgun *et al.*	(SACL, CERN, OSLO)
CARNEGIE	71	PR D4 1	R.K. Carnegie *et al.*	(PRIN)
CHAN	71	Thesis LBL-350	J.H.S. Chan	(LBL)
CHO	71	PR D3 1557	Y. Cho *et al.*	(CMU, BNL, CASE)
ENSTROM	71	PR D4 2629	J. Enstrom *et al.*	(SLAC, STAN)
Also		Thesis SLAC-0125	J.E. Enstrom	(STAN)
JAMES	71	PL 35B 265	F. James *et al.*	(CERN, SACL, OSLO)
MEISNER	71	PR D3 59	G.W. Meisner *et al.*	(MASA, BNL, YALE)
REPELLIN	71	PL 36B 603	J.P. Repellin *et al.*	(ORSAY, CERN)
WEBBER	71	PR D3 64	B.R. Webber *et al.*	(LRL)
Also		PRL 21 498	B.R. Webber *et al.*	(LRL)
Also		Thesis UCRL 19226	B.R. Webber	(LRL)
WOLFF	71	PL 36B 517	B. Wolff *et al.*	(ORSAY, CERN)
ALBROW	70	PL 33B 516	M.G. Albrow *et al.*	(MCHS, DARE)
ARONSON	70	PRL 25 1057	S.H. Aronson *et al.*	(EFI, ILLC, SLAC)
BARMIN	70	PL 33B 377	V.V. Barmin *et al.*	(ITEP, JINR)
BASILE	70	PR D2 78	P. Basile *et al.*	(SACL)
BECHERRAWY	70	PR D1 1452	T. Becherrawy	(ROCH)
BUCHANAN	70	PL 33B 623	C.D. Buchanan *et al.*	(SLAC, JHU, UCLA)
Also		Private Comm.	A.J. Cox	
BUDAGOV	70	PR D2 815	I.A. Budagov *et al.*	(CERN, ORSAY, EPOL)
Also		PL 28B 215	I.A. Budagov *et al.*	(CERN, ORSAY, EPOL)
CHO	70	PR D1 3031	Y. Cho *et al.*	(CMU, BNL, CASE)
Also		PRL 19 668	D.G. Hill *et al.*	(BNL, CMU)
CHOLLET	70	PL 31B 658	J.C. Chollet *et al.*	(CERN)
CULLEN	70	PL 32B 523	M. Cullen *et al.*	(AACH, CERN, TORI)
MARX	70	PL 32B 219	J. Marx *et al.*	(COLU, HARV, CERN)
Also		Thesis Nevis 179	J. Marx	(COLU)
SCRIBANO	70	PL 32B 224	A. Scribano *et al.*	(PISA, COLU, HARV)
SMITH	70	PL 32B 133	R.C. Smith *et al.*	(UMD, BNL)
WEBBER	70	PR D1 1967	B.R. Webber *et al.*	(LRL)
Also		Thesis UCRL 19226	B.R. Webber	(LRL)
BANNER	69	PR 188 2033	M. Banner *et al.*	(PRIN)
Also		PRL 21 1103	M. Banner *et al.*	(PRIN)
Also		PRL 21 1107	J.W. Cronin, J.K. Liu, J.E. Pilcher	(PRIN)
BENNETT	69	PL 29B 317	S. Bennett *et al.*	(COLU, BNL)
FAISSNER	69	PL 30B 204	H. Faissner *et al.*	(AACH3, CERN, TORI)
LITTENBERG	69	PRL 22 654	L.S. Littenberg *et al.*	(UCSD)
LONGO	69	PR 181 1808	M.J. Longo, K.K. Young, J.A. Helland	(MICH, UCLA)
PACIOTTI	69	Thesis UCRL 19446	M.A. Paciotti	(LRL)
SAAL	69	Thesis	H.J. Saal	(COLU)

Downloaded from https://academic.oup.com/ptep/article/2022/8/083C01/6651666 by KIT Library user on 27 September 2022

ABRAMS	68B	PR 176 1603	R.J. Abrams *et al.*	(ILL)
ARNOLD	68B	PL 28B 56	R.G. Arnold *et al.*	(CERN, ORSAY)
BASILE	68B	PL 28B 58	P. Basile *et al.*	(SACL)
BENNETT	68	PL 27B 244	S. Bennett *et al.*	(COLU, CERN)
BLANPIED	68	PRL 21 1650	W.A. Blanpied *et al.*	(CASE, HARV, MCGI)
BOHM	68B	PL 27B 594	A. Bohm *et al.*	
BUDAGOV	68	NC 57A 182	I.A. Budagov *et al.*	(CERN, ORSAY, IPNP)
Also		PL 28B 215	I.A. Budagov *et al.*	(CERN, ORSAY, EPOL)
JAMES	68	NP B8 365	F. James, H. Briand	(IPNP, CERN)
Also		PRL 21 257	J.A. Helland, M.J. Longo, K.K. Young	(UCLA, MICH)
KULYUKINA	68	JETP 26 20	L.A. Kulyukina *et al.*	(JINR)
		Translated from ZETF 53 29.		
KUNZ	68	Thesis PU-68-46	P.F. Kunz	(PRIN)
BENNETT	67	PRL 19 993	S. Bennett *et al.*	(COLU)
DEBOUARD	67	NC 52A 662	X. de Bouard *et al.*	(CERN)
Also		PL 15 58	X. de Bouard *et al.*	(CERN, ORSAY, MPIM)
DEVLIN	67	PRL 18 54	T.J. Devlin *et al.*	(PRIN, UMD)
Also		PR 169 1045	G.A. Sayer *et al.*	(UMD, PPA, PRIN)
DORFAN	67	PRL 19 987	D.E. Dorfan *et al.*	(SLAC, LRL)
FELDMAN	67B	PR 155 1611	L. Feldman *et al.*	(PENN)
FITCH	67	PR 164 1711	V.L. Fitch *et al.*	(PRIN)
GINSBERG	67	PR 162 1570	E.S. Ginsberg	(MASB)
HILL	67	PRL 19 668	D.G. Hill *et al.*	(BNL, CMU)
HOPKINS	67	PRL 19 185	H.W.K. Hopkins, T.C. Bacon, F.R. Eisler	(BNL)
NEFKENS	67	PR 157 1233	B.M.K. Nefkens *et al.*	(ILL)
SCHMIDT	67	Thesis Nevis 160	P. Schmidt	(COLU)
BEHR	66	PL 22 540	L. Behr *et al.*	(EPOL, MILA, PADO, ORSAY)
HAWKINS	66	PL 21 238	C.J.B. Hawkins	(YALE)
Also		PR 156 1444	C.J.B. Hawkins	(YALE)
ANDERSON	65	PRL 14 475	J.A. Anderson *et al.*	(LRL, WISC)
ASTBURY	65B	PL 18 175	P. Astbury *et al.*	(CERN, ZURI)
AUBERT	65	PL 17 59	B. Aubert *et al.*	(EPOL, ORSAY)
Also		PL 24B 75	J.P. Lowys *et al.*	(EPOL, ORSAY)
BALDO-...	65	NC 38 684	M. Baldo-Ceolin *et al.*	(PADO)
FRANZINI	65	PR 140 B127	P. Franzini *et al.*	(COLU, RUTG)
GUIDONI	65	Argonne Conf. 49	P. Guidoni *et al.*	(BNL, YALE)
HOPKINS	65	Argonne Conf. 67	H.W.K. Hopkins, T.C. Bacon, F. Eisler	(VAND+)
ALEKSANYAN	64B	Dubna Conf. 2 102	A.S. Aleksanyan *et al.*	(YERE)
Also		JETP 19 1019	A.S. Aleksanyan *et al.*	(LEBD, MPEI, YERE)
		Translated from ZETF 46 1504.		
ANIKINA	64	JETP 19 42	M.K. Anikina *et al.*	(GEOR, JINR)
		Translated from ZETF 46 59.		
FITCH	61	NC 22 1160	V.L. Fitch, P.A. Piroue, R.B. Perkins	(PRIN+)
GOOD	61	PR 124 1223	R.H. Good *et al.*	(LRL)

OTHER RELATED PAPERS

HAYAKAWA	93	PR D48 1150	M. Hayakawa, A.I. Sanda	(NAGO)
"Searching for T, CP, CPT, $\Delta S = \Delta Q$ Rule Violations in the Neutral K Meson System: A Guide"				
LITTENBERG	93	ARNPS 43 729	L.S. Littenberg, G. Valencia	(BNL, FNAL)
Rare and Radiative Kaon Decays				
RITCHIE	93	RMP 65 1149	J.L. Ritchie, S.G. Wojcicki	
"Rare K Decays"				
WINSTEIN	93	RMP 65 1113	B. Winstein, L. Wolfenstein	
"The Search for Direct CP Violation"				
BATTISTON	92	PRPL 214 293	R. Battiston *et al.*	(PGIA, CERN, TRSTT)
Status and Perspectives of K Decay Physics				
DIB	92	PR D46 2265	C.O. Dib, R.D. Peccei	(UCLA)
Tests of CPT conservation in the neutral kaon system.				
KLEINKNECHT	92	CNPP 20 281	K. Kleinknecht	(MAINZ)
New Results on CP Violation in Decays of Neutral K Mesons.				
KLEINKNECHT	90	ZPHY C46 S57	K. Kleinknecht	(MAINZ)
PEACH	90	JP G16 131	K.J. Peach	(EDIN)
BRYMAN	89	IJMP A4 79	D.A. Bryman	(TRIU)
"Rare Kaon Decays"				
KLEINKNECHT	76	ARNS 26 1	K. Kleinknecht	(DORT)
GINSBERG	73	PR D8 3887	E.S. Ginsberg, J. Smith	(MIT, STON)
GINSBERG	70	PR D1 229	E.S. Ginsberg	(HAIF)
HEUSSE	70	LNC 3 449	P. Heusse *et al.*	(ORSAY)
CRONIN	68C	Vienna Conf. 281	J.W. Cronin	(PRIN)
RUBBIA	67	PL 24B 531	C. Rubbia, J. Steinberger	(CERN, COLU)
Also		PL 23 167	C. Rubbia, J. Steinberger	(CERN, COLU)
Also		PL 20 207	C. Alff-Steinberger *et al.*	(CERN)
Also		PL 21 595	C. Alff-Steinberger *et al.*	(CERN)
AUERBACH	66	PR 149 1052	L.B. Auerbach *et al.*	(PENN)
Also		PRL 14 192	L.B. Auerbach *et al.*	(PENN)
FIRESTONE	66B	PRL 17 116	A. Firestone *et al.*	(YALE, BNL)
BEHR	65	Argonne Conf. 59	L. Behr *et al.*	(EPOL, MILA, PADO)
MESTVIRISH...	65	JINR P 2449	A.N. Mestvirishvili *et al.*	(JINR)
TRILLING	65B	UCRL 16473	G.N. Trilling	(LRL)
Updated from 1965 Argonne Conference, page 115.				
JOVANOV...	63	BNL Conf. 42	J.V. Jovanovich *et al.*	(BNL, UMD)

$K^*_0(700)$

$I(J^P) = \frac{1}{2}(0^+)$

also known as κ; was $K^*_0(800)$

See the related review(s):

Scalar Mesons below 1 GeV

$K^*_0(700)$ T-Matrix Pole $\sqrt{s}$

VALUE (MeV)	DOCUMENT ID		TECN	COMMENT
(630–730) − i (260–340) OUR ESTIMATE (see Fig. 64.1 in the review)				
• • • We do not use the following data for averages, fits, limits, etc. • • •				
$(648 \pm 7) - i\,(280 \pm 16)$	[1] PELAEZ	20	RVUE	$\pi K \to \pi K$
$(670 \pm 18) - i\,(295 \pm 28)$	[2] PELAEZ	17	RVUE	$\pi K \to \pi K$
$(764 \pm 63^{+71}_{-54}) - i\,(306 \pm 149^{+143}_{-85})$	[3] ABLIKIM	11B	BES2	1.3k $J/\psi \to K^0_S K^0_S \pi^+\pi^-$
$(665 \pm 9) - i\,(268^{+21}_{-6})$	[4] GUO	11B	RVUE	
$(849 \pm 77^{+18}_{-14}) - i\,(256 \pm 40^{+46}_{-22})$	[3] ABLIKIM	10E	BES2	1.4k $J/\psi \to K^\pm K^0_S \pi^\mp \pi^0$
$(663 \pm 8 \pm 34) - i\,(329 \pm 5 \pm 22)$	[5] BUGG	10	RVUE	S-matrix pole
$(706.0 \pm 1.8 \pm 22.8) - i\,(319.4 \pm 2.2 \pm 20.2)$	[6] BONVICINI	08A	CLEO	141k $D^+ \to K^-\pi^+\pi^+$
$(841 \pm 30^{+81}_{-73}) - i\,(309 \pm 45^{+48}_{-72})$	[3] ABLIKIM	06C	BES2	25k $J/\psi \to \overline{K}^*(892)^0 K^+\pi^-$
$(750^{+30}_{-55}) - i\,(342 \pm 60)$	[7] BUGG	06	RVUE	
$(658 \pm 13) - i\,(279 \pm 12)$	[8] DESCOTES-G...	06	RVUE	$\pi K \to \pi K$
$(757 \pm 33) - i\,(279 \pm 41)$	[9] GUO	06	RVUE	
$(694 \pm 53) - i\,(303 \pm 30)$	[10] ZHOU	06	RVUE	$K p \to K^-\pi^+ n$
$(594 \pm 79) - i\,(362 \pm 166)$	[10] ZHENG	04	RVUE	$K^- p \to K^-\pi^+ n$
$(722 \pm 60) - i\,(386 \pm 50)$	[10] BUGG	03	RVUE	11 $K^- p \to K^-\pi^+ n$
$(875 \pm 75) - i\,(335 \pm 110)$	[11] ISHIDA	97B	RVUE	11 $K^- p \to K^-\pi^+ n$
$727 - i\,263$	[12] VANBEVEREN	86	RVUE	

[1] Extracted employing πK partial wave analysis from ESTABROOKS 78 and ASTON 88, Roy-Steiner equations and once subtracted forward dispersion relations.
[2] Reanalysis of ESTABROOKS 78 and ASTON 88 satisfying Forward Dispersion Relations and using sequences of Pade approximants.
[3] Extracted from Breit-Wigner parameters.
[4] Fit to scattering phase shifts using UChPT amplitudes with explicit resonances.
[5] Supersedes BUGG 06. Combined analysis of ASTON 88, ABLIKIM 06C, AITALA 06, and LINK 09 using an s-dependent width with couplings to $K\pi$ and $K\eta'$, and the Adler zero near thresholds.
[6] From a complex pole included in the fit. Using parameters from the model that fits data best.
[7] Reanalysis of ASTON 88, AITALA 02, and ABLIKIM 06C using for the κ an s-dependent width with an Adler zero near threshold.
[8] Using Roy-Steiner equations (ROY 71) consistent with unitarity, analyticity and crossing symmetry constraints.
[9] From UChPT fitted to MERCER 71, BINGHAM 72 and ESTABROOKS 78. Amplitude shown to be consistent with data of ABLIKIM 06C.
[10] Reanalysis of ASTON 88 data.
[11] Reanalysis of ASTON 88 using interfering Breit-Wigner amplitudes. Extracted from Breit-Wigner parameters.
[12] Unitarized Quark Model.

$K^*_0(700)$ Breit-Wigner Mass

VALUE (MeV)	EVTS	DOCUMENT ID		TECN	COMMENT
845 ±17 OUR AVERAGE					
$826 \pm 49^{+49}_{-34}$	1.3k	[1] ABLIKIM	11B	BES2	$J/\psi \to K^0_S K^0_S \pi^+\pi^-$
$810 \pm 68^{+15}_{-24}$	1.4k	[2] ABLIKIM	10E	BES2	$J/\psi \to K^\pm K^0_S \pi^\mp \pi^0$
$856 \pm 17 \pm 13$	54k	LINK	07B	FOCS	$D^+ \to K^-\pi^+\pi^+$
$878 \pm 23^{+64}_{-55}$	25k	[3] ABLIKIM	06C	BES2	$J/\psi \to \overline{K}^*(892)^0 K^+\pi^-$
$797 \pm 19 \pm 43$	15k	[4,5] AITALA	02	E791	$D^+ \to K^-\pi^+\pi^+$
• • • We do not use the following data for averages, fits, limits, etc. • • •					
888.0 ± 1.9	141k	[6] BONVICINI	08A	CLEO	$D^+ \to K^-\pi^+\pi^+$
855 ± 15	0.6k	[7] CAWLFIELD	06A	CLEO	$D^0 \to K^+K^-\pi^0$
905^{+65}_{-30}		[8] ISHIDA	97B	RVUE	11 $K^- p \to K^-\pi^+ n$

[1] The Breit-Wigner parameters from a fit with seven intermediate resonances. The S-matrix pole position is $(764 \pm 63^{+71}_{-54}) - i\,(306 \pm 149^{+143}_{-85})$ MeV.
[2] From a fit including ten additional resonances and energy-independent Breit-Wigner width.
[3] A fit in the $K^*_0(700) + K^*(892) + K^*(1410)$ model with mass and width of the $K^*_0(700)$ from ABLIKIM 06C well describes the left slope of the $K^0_S\pi^-$ invariant mass spectrum in $\tau^- \to K^0_S\pi^-\nu_\tau$ decay studied by EPIFANOV 07. Averaged value from different parameterizations.
[4] Not seen by KOPP 01 using 7070 events of $D^0 \to K^-\pi^+\pi^0$. LINK 02E and LINK 05I show clear evidence for a constant non-resonant scalar amplitude rather than $K^*_0(700)$ in their high statistics analysis of $D^+ \to K^-\pi^+\mu^+\nu_\mu$.
[5] AUBERT 07T does not find evidence for the charged $K^*_0(700)$ using 11k events of $D^0 \to K^-K^+\pi^0$.
[6] Using parameters from the model that fits data best.
[7] Breit-Wigner parameters. A significant S-wave can be also modeled as a non-resonant contribution.
[8] Reanalysis of ASTON 88 using interfering Breit-Wigner amplitudes.

$K^*_0(700)$ Breit-Wigner Width

VALUE (MeV)	EVTS	DOCUMENT ID		TECN	COMMENT
468 ± 30 OUR AVERAGE					
$449 \pm 156^{+144}_{-81}$	1.3k	[1] ABLIKIM	11B	BES2	$J/\psi \to K^0_S K^0_S \pi^+\pi^-$
$536 \pm 87^{+106}_{-47}$	1.4k	[2] ABLIKIM	10E	BES2	$J/\psi \to K^\pm K^0_S \pi^\mp \pi^0$
$464 \pm 28 \pm 22$	54k	LINK	07B	FOCS	$D^+ \to K^-\pi^+\pi^+$
$499 \pm 52^{+55}_{-87}$	25k	[3] ABLIKIM	06C	BES2	$J/\psi \to \overline{K}^*(892)^0 K^+\pi^-$
$410 \pm 43 \pm 87$	15k	[4,5] AITALA	02	E791	$D^+ \to K^-\pi^+\pi^+$
• • • We do not use the following data for averages, fits, limits, etc. • • •					
550.4 ± 11.8	141k	[6] BONVICINI	08A	CLEO	$D^+ \to K^-\pi^+\pi^+$
251 ± 48	0.6k	[7] CAWLFIELD	06A	CLEO	$D^0 \to K^+K^-\pi^0$
545^{+235}_{-110}		[8] ISHIDA	97B	RVUE	11 $K^- p \to K^-\pi^+ n$

[1] The Breit-Wigner parameters from a fit with seven intermediate resonances. The S-matrix pole position is $(764 \pm 63^{+71}_{-54}) - i\,(306 \pm 149^{+143}_{-85})$ MeV.
[2] From a fit including ten additional resonances and energy-independent Breit-Wigner width.
[3] A fit in the $K^*_0(700) + K^*(892) + K^*(1410)$ model with mass and width of the $K^*_0(700)$ from ABLIKIM 06C well describes the left slope of the $K^0_S\pi^-$ invariant mass spectrum

Downloaded from https://academic.oup.com/ptep/article/2022/8/083C01/6651666 by KIT Library user on 27 September 2022

in $\tau^- \to K_S^0 \pi^- \nu_\tau$ decay studied by EPIFANOV 07. Averaged value from different parameterizations.

[4] Not seen by KOPP 01 using 7070 events of $D^0 \to K^- \pi^+ \pi^0$. LINK 02E and LINK 05I show clear evidence for a constant non-resonant scalar amplitude rather than $K_0^*(700)$ in their high statistics analysis of $D^+ \to K^- \pi^+ \mu^+ \nu_\mu$.

[5] AUBERT 07T does not find evidence for the charged $K_0^*(700)$ using 11k events of $D^0 \to K^- K^+ \pi^0$.

[6] Using parameters from the model that fits data best.

[7] Statistical error only. A fit to the Dalitz plot including the $K_0^*(700)^\pm$, $K^*(892)^\pm$, and ϕ resonances modeled as Breit-Wigners. A significant S-wave can be also modeled as a non-resonant contribution.

[8] Reanalysis of ASTON 88 using interfering Breit-Wigner amplitudes.

$K_0^*(700)$ DECAY MODES

	Mode	Fraction (Γ_i/Γ)
Γ_1	$K\pi$	100 %

$K_0^*(700)$ REFERENCES

PELAEZ	20	PRL 124 172001	J.R. Pelaez *et al.*	
PELAEZ	17	EPJ C77 91	J.R. Pelaez, A.Rodas, J.R. de Elvira	
ABLIKIM	11B	PL B698 183	M. Ablikim *et al.*	(BES II Collab.)
GUO	11B	PR D84 034005	Z.-H. Guo, J.A. Oller	
ABLIKIM	10E	PL B693 88	M. Ablikim *et al.*	(BES II Collab.)
BUGG	10	PR D81 014002	D.V. Bugg	(LOQM)
LINK	09	PL B681 14	J.M. Link *et al.*	(FNAL FOCUS Collab.)
BONVICINI	08A	PR D78 052001	G. Bonvicini *et al.*	(CLEO Collab.)
AUBERT	07T	PR D76 011102	B. Aubert *et al.*	(BABAR Collab.)
EPIFANOV	07	PL B654 65	D. Epifanov *et al.*	(BELLE Collab.)
LINK	07B	PL B653 1	J.M. Link *et al.*	(FNAL FOCUS Collab.)
ABLIKIM	06C	PL B633 681	M. Ablikim *et al.*	(BES Collab.)
AITALA	06	PR D73 032004	E.M. Aitala *et al.*	(FNAL E791 Collab.)
Also		PR D74 059901 (errat.)	E.M. Aitala *et al.*	(FNAL E791 Collab.)
BUGG	06	PL B632 471	D.V. Bugg	(LOQM)
CAWLFIELD	06A	PR D74 031108	C. Cawlfield *et al.*	(CLEO Collab.)
DESCOTES-G...	06	EPJ C48 553	S. Descotes-Genon, B. Moussallam	
GUO	06	NP A773 78	F.K. Guo *et al.*	
ZHOU	06	NP A775 212	Z.Y. Zhou, H.Q. Zheng	
LINK	05I	PL B621 72	J.M. Link *et al.*	(FNAL FOCUS Collab.)
ZHENG	04	NP A733 235	H.Q. Zheng *et al.*	
BUGG	03	PL B572 1	D.V. Bugg	
AITALA	02	PRL 89 121801	E.M. Aitala *et al.*	(FNAL E791 Collab.)
LINK	02E	PL B535 43	J.M. Link *et al.*	(FNAL FOCUS Collab.)
KOPP	01	PR D63 092001	S. Kopp *et al.*	(CLEO Collab.)
ISHIDA	97B	PTP 98 621	S. Ishida *et al.*	
ASTON	88	NP B296 493	D. Aston *et al.*	(SLAC, NAGO, CINC, INUS)
VANBEVEREN	86	ZPHY C30 615	E. van Beveren *et al.*	(NIJM, BIEL)
ESTABROOKS	78	NP B133 490	P.G. Estabrooks *et al.*	(MCGI, CARL, DURH+)
BINGHAM	72	NP B41 1	H.H. Bingham *et al.*	(International K^+ Collab.)
MERCER	71	NP B32 381	R. Mercer *et al.*	(JHU)
ROY	71	PL 36B 353	S.M. Roy	

$K^*(892)$

$I(J^P) = \frac{1}{2}(1^-)$

$K^*(892)$ T-Matrix Pole $\sqrt{s}$

VALUE (MeV)	DOCUMENT ID		TECN	COMMENT
$(890 \pm 14) - i\,(26 \pm 6)$ OUR ESTIMATE				
• • • We do not use the following data for averages, fits, limits, etc. • • •				
$(890 \pm 2) - i\,(25.6 \pm 1.2)$	[1] PELAEZ	20	RVUE	$\pi K \to \pi K$
$(892 \pm 1) - i\,(29 \pm 1)$	[2] PELAEZ	17	RVUE	$\pi K \to \pi K$
$(889 \pm 13) - i\,(24 \pm 4)$	[3] PELAEZ	04A	RVUE	$\pi K \to \pi K$

[1] Extracted employing πK partial wave analysis from ESTABROOKS 78 and ASTON 88, Roy-Steiner equations and once subtracted forward dispersion relations.

[2] Reanalysis of ESTABROOKS 78 and ASTON 88 satisfying Forward Dispersion Relations and using sequences of Pade approximants.

[3] Reanalysis of data from ESTABROOKS 78 and ASTON 88 in the unitarized ChPT model.

$K^*(892)$ MASS

CHARGED ONLY, HADROPRODUCED

VALUE (MeV)	EVTS	DOCUMENT ID		TECN	CHG	COMMENT
891.67±0.26 OUR AVERAGE						
892.2 ±0.5 ±1.7		ALBRECHT	20	CBAR		$0.9\,\overline{p}p \to K^+K^-\pi^0$
892.6 ±0.5	5840	BAUBILLIER	84B	HBC	−	$8.25\,K^-p \to \overline{K}^0\pi^-p$
888 ±3		NAPIER	84	SPEC	+	$200\,\pi^-p \to 2K_S^0 X$
891 ±1		NAPIER	84	SPEC	−	$200\,\pi^-p \to 2K_S^0 X$
891.7 ±2.1	3700	BARTH	83	HBC	+	$70\,K^+p \to K^0\pi^+ X$
891 ±1	4100	TOAFF	81	HBC	−	$6.5\,K^-p \to \overline{K}^0\pi^-p$
892.8 ±1.6		AJINENKO	80	HBC	+	$32\,K^+p \to K^0\pi^+ X$
890.7 ±0.9	1800	AGUILAR-...	78B	HBC	±	$0.76\,\overline{p}p \to K^\mp K_S^0\pi^\pm$
886.6 ±2.4	1225	BALAND	78	HBC	±	$12\,\overline{p}p \to (K\pi)^\pm X$
891.7 ±0.6	6706	COOPER	78	HBC	±	$0.76\,\overline{p}p \to (K\pi)^\pm X$
891.9 ±0.7	9000	[1] PALER	75	HBC	−	$14.3\,K^-p \to (K\pi)^- X$
892.2 ±1.5	4404	AGUILAR-...	71B	HBC	−	$3.9,4.6\,K^-p \to (K\pi)^-p$
891 ±2	1000	CRENNELL	69D	DBC	−	$3.9\,K^-N \to K^0\pi^- X$
890 ±3.0	720	BARLOW	67	HBC	±	$1.2\,\overline{p}p \to (K^0\pi)^\pm K^\mp$
889 ±3.0	600	BARLOW	67	HBC	±	$1.2\,\overline{p}p \to (K^0\pi)^\pm K\pi$
891 ±2.3	620	[2] DEBAERE	67B	HBC	+	$3.5\,K^+p \to K^0\pi^+p$
891.0 ±1.2	1700	[3] WOJCICKI	64	HBC	−	$1.7\,K^-p \to \overline{K}^0\pi^-p$
• • • We do not use the following data for averages, fits, limits, etc. • • •						
893.6 $\pm 0.1\,^{+0.2}_{-0.3}$	183k	ABLIKIM	19AQ	BES	±	$J/\psi \to K^+K^-\pi^0$
895.6 ±0.8	4k	[4] LEES	17C	BABR		$J/\psi \to K_S^0 K^\pm\pi^\mp$
893.2 ±0.1 ±1.0	190k	[5] AAIJ	16N	LHCB		$D^0 \to K_S^0 K^\pm\pi^\mp$
893.5 ±1.1	27k	[6] ABELE	99D	CBAR	±	$0.0\,\overline{p}p \to K^+K^-\pi^0$
890.4 ±0.2 ±0.5	80k	[7] BIRD	89	LASS	−	$11\,K^-p \to \overline{K}^0\pi^-p$
890.0 ±2.3	800	[2,3] CLELAND	82	SPEC	+	$30\,K^+p \to K_S^0\pi^+p$
896.0 ±1.1	3200	[2,3] CLELAND	82	SPEC	+	$50\,K^+p \to K_S^0\pi^+p$
893 ±1	3600	[2,3] CLELAND	82	SPEC	−	$50\,K^+p \to K_S^0\pi^-p$
896.0 ±1.9	380	DELFOSSE	81	SPEC	+	$50\,K^\pm p \to K^\pm\pi^0 p$
886.0 ±2.3	187	DELFOSSE	81	SPEC	−	$50\,K^\pm p \to K^\pm\pi^0 p$
894.2 ±2.0	765	[2] CLARK	73	HBC	−	$3.13\,K^-p \to \overline{K}^0\pi^-p$
894.3 ±1.5	1150	[2,3] CLARK	73	HBC	−	$3.3\,K^-p \to \overline{K}^0\pi^-p$
892.0 ±2.6	341	[2] SCHWEING...	68	HBC	−	$5.5\,K^-p \to \overline{K}^0\pi^-p$

[1] Inclusive reaction. Complicated background and phase-space effects.

[2] Mass errors enlarged by us to $\Gamma/\sqrt{N}$. See note.

[3] Number of events in peak reevaluated by us.

[4] From a Dalitz plot analysis in an isobar model with charged and neutral $K^*(892)$ masses and widths floating.

[5] Average of fit results with different parametrizations for the $K\pi$ S-wave.

[6] K-matrix pole.

[7] From a partial wave amplitude analysis.

CHARGED ONLY, PRODUCED IN τ LEPTON DECAYS

VALUE (MeV)	EVTS	DOCUMENT ID		TECN	COMMENT
895.47±0.20±0.74	53k	[1] EPIFANOV	07	BELL	$\tau^- \to K_S^0\pi^-\nu_\tau$
• • • We do not use the following data for averages, fits, limits, etc. • • •					
892.0 ±0.5		[2] BOITO	10	RVUE	$\tau^- \to K_S^0\pi^-\nu_\tau$
892.0 ±0.9		[3,4] BOITO	09	RVUE	$\tau^- \to K_S^0\pi^-\nu_\tau$
895.3 ±0.2		[4,5] JAMIN	08	RVUE	$\tau^- \to K_S^0\pi^-\nu_\tau$
896.4 ±0.9	12k	[6] BONVICINI	02	CLEO	$\tau^- \to K^-\pi^0\nu_\tau$
895 ±2		[7] BARATE	99R	ALEP	$\tau^- \to K^-\pi^0\nu_\tau$

[1] From a fit in the $K_0^*(700) + K^*(892) + K^*(1410)$ model.

[2] From the pole position of the $K\pi$ vector form factor using EPIFANOV 07 and constraints from K_{l3} decays in ANTONELLI 10.

[3] From the pole position of the $K\pi$ vector form factor in the complex s-plane and using EPIFANOV 07 data.

[4] Systematic uncertainties not estimated.

[5] Reanalysis of EPIFANOV 07 using resonance chiral theory.

[6] Calculated by us from the shift by 4.7 ± 0.9 MeV (statistical uncertainty only) reported in BONVICINI 02 with respect to the world average value from PDG 00.

[7] With mass and width of the $K^*(1410)$ fixed at 1412 MeV and 227 MeV, respectively.

NEUTRAL ONLY

VALUE (MeV)	EVTS	DOCUMENT ID		TECN	COMMENT
895.55±0.20 OUR AVERAGE		Error includes scale factor of 1.7. See the ideogram below.			
894.68±0.25±0.05		[1] ABLIKIM	16F	BES3	$D^+ \to K^-\pi^+e^+\nu_e$
895.4 ±0.2 ±0.2	243k	[2] DEL-AMO-SA...	11I	BABR	$D^+ \to K^-\pi^+e^+\nu_e$
895.7 ±0.2 ±0.3	141k	[3] BONVICINI	08A	CLEO	$D^+ \to K^-\pi^+\pi^+$
895.41±0.32$^{+0.35}_{-0.43}$	18k	[4] LINK	05I	FOCS	$D^+ \to K^-\pi^+\mu^+\nu_\mu$
896 ±2		BARBERIS	98E	OMEG	$450\,pp \to p_f p_s K^*\overline{K}^*$
895.9 ±0.5 ±0.2		ASTON	88	LASS	$11\,K^-p \to K^-\pi^+n$
894.52±0.63	25k	[5] ATKINSON	86	OMEG	20–70 γp
894.63±0.76	20k	[5] ATKINSON	86	OMEG	20–70 γp
897 ±1	28k	EVANGELIS...	80	OMEG	$10\,\pi^-p \to K^+\pi^-(\Lambda,\Sigma)$
898.4 ±1.4	1180	AGUILAR-...	78B	HBC	$0.76\,\overline{p}p \to K^\mp K_S^0\pi^\pm$
894.9 ±1.6		WICKLUND	78	ASPK	$3,4,6\,K^\pm N \to (K\pi)^0 N$
897.6 ±0.9		BOWLER	77	DBC	$5.4\,K^+d \to K^+\pi^-pp$
895.5 ±1.0	3600	MCCUBBIN	75	HBC	$3.6\,K^-p \to K^-\pi^+n$
897.1 ±0.7	22k	[5] PALER	75	HBC	$14.3\,K^-p \to (K\pi)^0 X$
896.0 ±0.6	10k	FOX	74	RVUE	$2\,K^-p \to K^-\pi^+n$
896.0 ±0.6		FOX	74	RVUE	$2\,K^+n \to K^+\pi^-p$
896 ±2		[6] MATISON	74	HBC	$12\,K^+p \to K^+\pi^-\Delta$
896 ±1	3186	LEWIS	73	HBC	2.1–$2.7\,K^+p \to K\pi\pi p$
894.0 ±1.3		[6] LINGLIN	73	HBC	2–$13\,K^+p \to K^+\pi^-\pi^+p$
898.4 ±1.3	1700	[7] BUCHNER	72	DBC	$4.6\,K^+n \to K^+\pi^-p$
897.9 ±1.1	2934	[7] AGUILAR-...	71B	HBC	$3.9,4.6\,K^-p \to K^-\pi^+n$
898.0 ±0.7	5362	[7] AGUILAR-...	71B	HBC	$3.9,4.6\,K^-p \to K^-\pi^+\pi^-p$
895 ±1	4300	[8] HABER	70	DBC	$3\,K^-N \to K^-\pi^+ X$
893.7 ±2.0	10k	DAVIS	69	HBC	$12\,K^+p \to K^+\pi^-\pi^+p$
894.7 ±1.4	1040	[7] DAUBER	67B	HBC	$2.0\,K^-p \to K^-\pi^+\pi^-p$

Downloaded from https://academic.oup.com/ptep/article/2022/8/083C01/6651666 by KIT Library user on 27 September 2022

• • • We do not use the following data for averages, fits, limits, etc. • • •

895.50±0.92±2.6		[9] ADUSZKIEW...	20A	NA61	158 pp
898.1 ±1.0	4k	[10] LEES	17C	BABR	$J/\psi \to K^0_S K^\pm \pi^\mp$
895.53±0.17		LEES	13F	BABR	$D^+ \to K^+ K^- \pi^+$
894.9 ±0.5 ±0.7	14.4k	[11] MITCHELL	09A	CLEO	$D^+_s \to K^+ K^- \pi^+$
896.2 ±0.3	20k	[12] AUBERT	07AK	BABR	10.6 $e^+ e^- \to K^{*0} K^\pm \pi^\mp \gamma$
900.7 ±1.1	5900	BARTH	83	HBC	70 $K^+ p \to K^+ \pi^- X$

[1] Taking also into account the $K^*_0(1430)^0$ and $K^*_2(1430)^0$.
[2] Taking into account the $K^*(892)^0$, S-wave and P-wave ($K^*(1410)^0$).
[3] From the isobar model with a complex pole for the κ.
[4] Fit to $K\pi$ mass spectrum includes a non-resonant scalar component.
[5] Inclusive reaction. Complicated background and phase-space effects.
[6] From pole extrapolation.
[7] Mass errors enlarged by us to $\Gamma/\sqrt{N}$. See note.
[8] Number of events in peak reevaluated by us.
[9] For transverse momenta between 0.6 and 0.8 GeV/c and rapidity $0 < y < 0.5$.
[10] From a Dalitz plot analysis in an isobar model with charged and neutral $K^*(892)$ masses and widths floating.
[11] This value comes from a fit with χ^2 of 178/117.
[12] Systematic uncertainties not estimated.

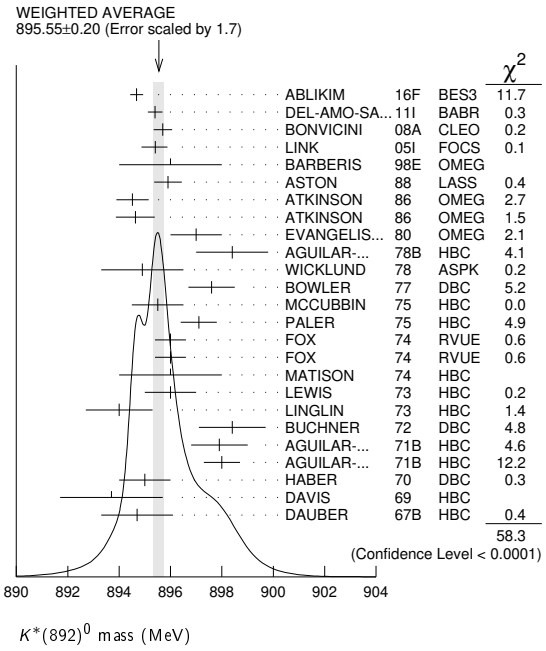

$K^*(892)$ MASSES AND MASS DIFFERENCES

Unrealistically small errors have been reported by some experiments. We use simple "realistic" tests for the minimum errors on the determination of a mass and width from a sample of N events:

$$\delta_{\min}(m) = \frac{\Gamma}{\sqrt{N}}, \quad \delta_{\min}(\Gamma) = 4\frac{\Gamma}{\sqrt{N}} \ . \qquad (1)$$

We consistently increase unrealistic errors before averaging. For a detailed discussion, see the 1971 edition of this Note.

$m_{K^*(892)^0} - m_{K^*(892)^\pm}$

VALUE (MeV)	EVTS	DOCUMENT ID		TECN	CHG	COMMENT
6.7±1.2 OUR AVERAGE						
7.7±1.7	2980	AGUILAR-...	78B	HBC	±0	0.76 $\overline{p}p \to K^\mp K^0_S \pi^\pm$
5.7±1.7	7338	AGUILAR-...	71B	HBC	−0	3.9,4.6 $K^- p$
6.3±4.1	283	[1] BARASH	67B	HBC		0.0 $\overline{p}p$

[1] Number of events in peak reevaluated by us.

$K^*(892)$ RANGE PARAMETER

All from partial wave amplitude analyses.

VALUE (GeV^{-1})	EVTS	DOCUMENT ID		TECN	CHG	COMMENT
2.1 ±0.5 ±0.5	243k	[1] DEL-AMO-SA...	11I	BABR	0	$D^+ \to K^- \pi^+ e^+ \nu_e$
$3.96 \pm 0.54^{+1.31}_{-0.90}$	18k	[2] LINK	05I	FOCS	0	$D^+ \to K^- \pi^+ \mu^+ \nu_\mu$
3.4 ±0.7		ASTON	88	LASS	0	11 $K^- p \to K^- \pi^+ n$
• • • We do not use the following data for averages, fits, limits, etc. • • •						
12.1 ±3.2 ±3.0		BIRD	89	LASS	−	11 $K^- p \to \overline{K}^0 \pi^- p$

[1] Taking into account the $K^*(892)^0$, S-wave and P-wave ($K^*(1410)^0$).
[2] Fit to $K\pi$ mass spectrum includes a non-resonant scalar component.

$K^*(892)$ WIDTH

CHARGED ONLY, HADROPRODUCED

VALUE (MeV)	EVTS	DOCUMENT ID		TECN	CHG	COMMENT
51.4±0.8 OUR FIT						
51.4±0.8 OUR AVERAGE						
54.4±0.9±1.7		ALBRECHT	20	CBAR		0.9 $\overline{p}p \to K^+ K^- \pi^0$
49 ±2	5840	BAUBILLIER	84B	HBC	−	8.25 $K^- p \to \overline{K}^0 \pi^- p$
56 ±4		NAPIER	84	SPEC	−	200 $\pi^- p \to 2K^0_S X$
51 ±2	4100	TOAFF	81	HBC	−	6.5 $K^- p \to \overline{K}^0 \pi^- p$
50.5±5.6		AJINENKO	80	HBC	+	32 $K^+ p \to K^0 \pi^+ X$
45.8±3.6	1800	AGUILAR-...	78B	HBC	±	0.76 $\overline{p}p \to K^\mp K^0_S \pi^\pm$
52.0±2.5	6706	[1] COOPER	78	HBC	±	0.76 $\overline{p}p \to (K\pi)^\pm X$
52.1±2.2	9000	[2] PALER	75	HBC	−	14.3 $K^- p \to (K\pi)^- X$
46.3±6.7	765	[1] CLARK	73	HBC	−	3.13 $K^- p \to \overline{K}^0 \pi^- p$
48.2±5.7	1150	[1,3] CLARK	73	HBC	−	3.3 $K^- p \to \overline{K}^0 \pi^- p$
54.3±3.3	4404	[1] AGUILAR-...	71B	HBC	−	3.9,4.6 $K^- p \to (K\pi)^- p$
46 ±5	1700	[1,3] WOJCICKI	64	HBC	−	1.7 $K^- p \to \overline{K}^0 \pi^- p$
• • • We do not use the following data for averages, fits, limits, etc. • • •						
$46.7 \pm 0.2^{+0.1}_{-0.2}$	183k	ABLIKIM	19AQ	BES	±	$J/\psi \to K^+ K^- \pi^0$
43.6±1.3	4k	[4] LEES	17C	BABR		$J/\psi \to K^0_S K^\pm \pi^\mp$
47.2±0.3±2.3	190k	[5] AAIJ	16N	LHCB		$D^0 \to K^0_S K^\pm \pi^\mp$
54.8±1.7	27k	[6] ABELE	99D	CBAR	±	0.0 $\overline{p}p \to K^+ K^- \pi^0$
45.2±1 ±2	80k	[7] BIRD	89	LASS	−	11 $K^- p \to \overline{K}^0 \pi^- p$
42.8±7.1	3700	BARTH	83	HBC	+	70 $K^+ p \to K^0 \pi^+ X$
64.0±9.2	800	[1,3] CLELAND	82	SPEC	+	30 $K^+ p \to K^0_S \pi^+ p$
62.0±4.4	3200	[1,3] CLELAND	82	SPEC	+	50 $K^+ p \to K^0_S \pi^+ p$
55 ±4	3600	[1,3] CLELAND	82	SPEC	−	50 $K^+ p \to K^0_S \pi^- p$
62.6±3.8	380	DELFOSSE	81	SPEC	+	50 $K^\pm p \to K^\pm \pi^0 p$
50.5±3.9	187	DELFOSSE	81	SPEC	−	50 $K^\pm p \to K^\pm \pi^0 p$

[1] Width errors enlarged by us to $4 \times \Gamma/\sqrt{N}$; see note.
[2] Inclusive reaction. Complicated background and phase-space effects.
[3] Number of events in peak reevaluated by us.
[4] From a Dalitz plot analysis in an isobar model with charged and neutral $K^*(892)$ masses and widths floating.
[5] Average of fit results with different parametrizations for the $K\pi$ S-wave.
[6] K-matrix pole.
[7] From a partial wave amplitude analysis.

CHARGED ONLY, PRODUCED IN τ LEPTON DECAYS

VALUE (MeV)	EVTS	DOCUMENT ID		TECN	COMMENT
46.2±0.6±1.2	53k	[1] EPIFANOV	07	BELL	$\tau^- \to K^0_S \pi^- \nu_\tau$
• • • We do not use the following data for averages, fits, limits, etc. • • •					
46.5±1.1		[2] BOITO	10	RVUE	$\tau^- \to K^0_S \pi^- \nu_\tau$
46.2±0.4		[3,4] BOITO	09	RVUE	$\tau^- \to K^0_S \pi^- \nu_\tau$
47.5±0.4		[4,5] JAMIN	08	RVUE	$\tau^- \to K^0_S \pi^- \nu_\tau$
55 ±8		[6] BARATE	99R	ALEP	$\tau^- \to K^- \pi^0 \nu_\tau$

[1] From a fit in the $K^*_0(700) + K^*(892) + K^*(1410)$ model.
[2] From the pole position of the $K\pi$ vector form factor using EPIFANOV 07 and constraints from K_{l3} decays in ANTONELLI 10.
[3] From the pole position of the $K\pi$ vector form factor in the complex s-plane and using EPIFANOV 07 data.
[4] Systematic uncertainties not estimated.
[5] Reanalysis of EPIFANOV 07 using resonance chiral theory.
[6] With mass and width of the $K^*(1410)$ fixed at 1412 MeV and 227 MeV, respectively.

NEUTRAL ONLY

VALUE (MeV)	EVTS	DOCUMENT ID		TECN	COMMENT
47.3 ±0.5 OUR FIT Error includes scale factor of 1.9.					
47.3 ±0.5 OUR AVERAGE Error includes scale factor of 2.0. See the ideogram below.					
46.53±0.56±0.31		[1] ABLIKIM	16F	BES3	$D^+ \to K^- \pi^+ e^+ \nu_e$
46.5 ±0.3 ±0.2	243k	[2] DEL-AMO-SA...	11I	BABR	$D^+ \to K^- \pi^+ e^+ \nu_e$
45.3 ±0.5 ±0.6	141k	[3] BONVICINI	08A	CLEO	$D^+ \to K^- \pi^+ \pi^+$
$47.79 \pm 0.86^{+1.32}_{-1.06}$	18k	[4] LINK	05I	FOCS	$D^+ \to K^- \pi^+ \mu^+ \nu_\mu$
54 ±3		BARBERIS	98E	OMEG	450 $pp \to p_f p_s K^* \overline{K}^*$
50.8 ±0.8 ±0.9		ASTON	88	LASS	11 $K^- p \to K^- \pi^+ n$
46.5 ±4.3	5900	BARTH	83	HBC	70 $K^+ p \to K^+ \pi^- X$
54 ±2	28k	EVANGELIS...	80	OMEG	10 $\pi^- p \to K^+ \pi^- (\Lambda, \Sigma)$

Downloaded from https://academic.oup.com/ptep/article/2022/8/083C01/6651666 by KIT Library user on 27 September 2022

45.9 ±4.8	1180	AGUILAR-...	78B	HBC	0.76 $\bar{p}p \to K^{\mp} K^0_S \pi^{\pm}$
51.2 ±1.7		WICKLUND	78	ASPK	3,4,6 $K^{\pm} N \to (K\pi)^0 N$
48.9 ±2.5		BOWLER	77	DBC	5.4 $K^+ d \to K^+ \pi^- p p$
48 $^{+3}_{-2}$	3600	MCCUBBIN	75	HBC	3.6 $K^- p \to K^- \pi^+ n$
50.6 ±2.5	22k	[5] PALER	75	HBC	14.3 $K^- p \to (K\pi)^0$ X
47 ±2	10k	FOX	74	RVUE	2 $K^- p \to K^- \pi^+ n$
51 ±2		FOX	74	RVUE	2 $K^+ n \to K^+ \pi^- p$
46.0 ±3.3	3186	[6] LEWIS	73	HBC	2.1–2.7 $K^+ p \to K \pi \pi p$
51.4 ±5.0	1700	[6] BUCHNER	72	DBC	4.6 $K^+ n \to K^+ \pi^- p$
55.8 $^{+4.2}_{-3.4}$	2934	[6] AGUILAR-...	71B	HBC	3.9,4.6 $K^- p \to K^- \pi^+ n$
48.5 ±2.7	5362	AGUILAR-...	71B	HBC	3.9,4.6 $K^- p \to K^- \pi^+ \pi^- p$
54.0 ±3.3	4300	[6,7] HABER	70	DBC	3 $K^- N \to K^- \pi^+$ X
53.2 ±2.1	10k	[6] DAVIS	69	HBC	12 $K^+ p \to K^+ \pi^- \pi^+ p$
44 ±5.5	1040	[6] DAUBER	67B	HBC	2.0 $K^- p \to K^- \pi^+ \pi^- p$
• • • We do not use the following data for averages, fits, limits, etc. • • •					
48.8 ±1.8 ±2.0		[8] ADUSZKIEW...	20A	NA61	158 $p p$
52.6 ±1.7	4k	[9] LEES	17C	BABR	$J/\psi \to K^0_S K^{\pm} \pi^{\mp}$
44.90±0.30		LEES	13F	BABR	$D^+ \to K^+ K^- \pi^+$
45.7 ±1.1 ±0.5	14.4k	[10] MITCHELL	09A	CLEO	$D^+_s \to K^+ K^- \pi^+$
50.6 ±0.9	20k	[11] AUBERT	07AK	BABR	10.6 $e^+ e^- \to K^{*0} K^{\pm} \pi^{\mp} \gamma$

[1] Taking also into account the $K^*_0(1430)^0$ and $K^*_2(1430)^0$.
[2] Taking into account the $K^*(892)^0$, S-wave and P-wave ($K^*(1410)^0$).
[3] From the isobar model with a complex pole for the κ.
[4] Fit to $K\pi$ mass spectrum includes a non-resonant scalar component.
[5] Inclusive reaction. Complicated background and phase-space effects.
[6] Width errors enlarged by us to $4 \times \Gamma/\sqrt{N}$; see note.
[7] Number of events in peak reevaluated by us.
[8] For transverse momenta between 0.6 and 0.8 GeV/c and rapidity $0 < y < 0.5$.
[9] From a Dalitz plot analysis in an isobar model with charged and neutral $K^*(892)$ masses and widths floating.
[10] This value comes from a fit with χ^2 of 178/117.
[11] Systematic uncertainties not estimated.

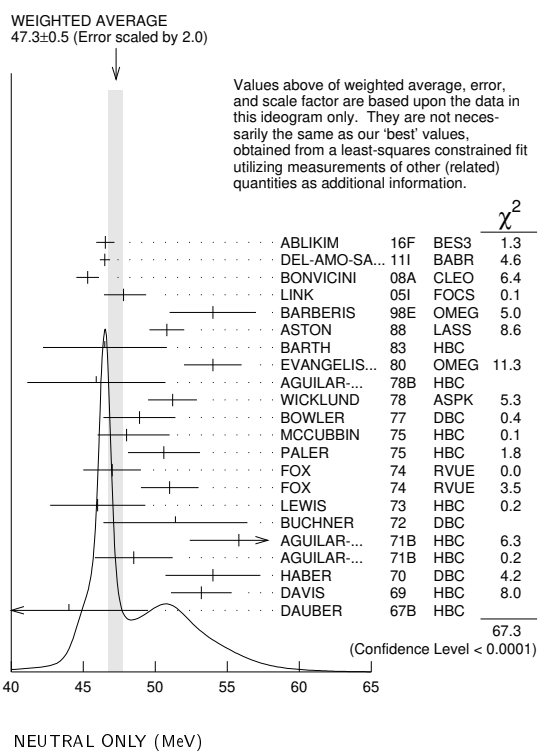

$K^*(892)$ DECAY MODES

	Mode	Fraction (Γ_i/Γ)	Confidence level
Γ_1	$K\pi$	~ 100 %	
Γ_2	$(K\pi)^{\pm}$	(99.902 ± 0.009) %	
Γ_3	$(K\pi)^0$	(99.754 ± 0.021) %	
Γ_4	$K^0\gamma$	$(2.46 \pm 0.21) \times 10^{-3}$	
Γ_5	$K^{\pm}\gamma$	$(9.8 \pm 0.9) \times 10^{-4}$	
Γ_6	$K\pi\pi$	$< 7 \times 10^{-4}$	95%

CONSTRAINED FIT INFORMATION

An overall fit to the total width and a partial width uses 14 measurements and one constraint to determine 3 parameters. The overall fit has a $\chi^2 = 10.7$ for 12 degrees of freedom.

The following *off-diagonal* array elements are the correlation coefficients $\langle \delta p_i \delta p_j \rangle / (\delta p_i \cdot \delta p_j)$, in percent, from the fit to parameters p_i, including the branching fractions, $x_i \equiv \Gamma_i/\Gamma_{total}$. The fit constrains the x_i whose labels appear in this array to sum to one.

	x_2	x_5
x_5	−100	
Γ	17	−17

	Mode	Rate (MeV)
Γ_2	$(K\pi)^{\pm}$	51.4 ±0.8
Γ_5	$K^{\pm}\gamma$	0.050±0.005

CONSTRAINED FIT INFORMATION

An overall fit to the total width and a partial width uses 23 measurements and one constraint to determine 3 parameters. The overall fit has a $\chi^2 = 68.4$ for 21 degrees of freedom.

The following *off-diagonal* array elements are the correlation coefficients $\langle \delta p_i \delta p_j \rangle / (\delta p_i \cdot \delta p_j)$, in percent, from the fit to parameters p_i, including the branching fractions, $x_i \equiv \Gamma_i/\Gamma_{total}$. The fit constrains the x_i whose labels appear in this array to sum to one.

	x_3	x_4
x_4	−100	
Γ	12	−12

	Mode	Rate (MeV)	Scale factor
Γ_3	$(K\pi)^0$	47.2 ±0.5	1.9
Γ_4	$K^0\gamma$	0.117±0.010	

$K^*(892)$ PARTIAL WIDTHS

$\Gamma(K^0\gamma)$ — Γ_4

VALUE (keV)	EVTS	DOCUMENT ID		TECN	CHG	COMMENT
116 ±10 OUR FIT						
116.5± 9.9	584	CARLSMITH	86	SPEC	0	$K^0_L A \to K^0_S \pi^0 A$

$\Gamma(K^{\pm}\gamma)$ — Γ_5

VALUE (keV)	DOCUMENT ID		TECN	CHG	COMMENT
50± 5 OUR FIT					
50± 5 OUR AVERAGE					
48±11	BERG	83	SPEC	−	156 $K^- A \to \overline{K} \pi A$
51± 5	CHANDLEE	83	SPEC	+	200 $K^+ A \to K \pi A$

$K^*(892)$ BRANCHING RATIOS

$\Gamma(K^0\gamma)/\Gamma_{total}$ — Γ_4/Γ

VALUE (units 10^{-3})	DOCUMENT ID		TECN	CHG	COMMENT
2.46±0.21 OUR FIT					
• • • We do not use the following data for averages, fits, limits, etc. • • •					
1.5 ±0.7	CARITHERS	75B	CNTR	0	8–16 $\overline{K}^0 A$

$\Gamma(K^{\pm}\gamma)/\Gamma_{total}$ — Γ_5/Γ

VALUE (units 10^{-3})	CL%	DOCUMENT ID		TECN	CHG	COMMENT
0.98±0.09 OUR FIT						
• • • We do not use the following data for averages, fits, limits, etc. • • •						
<1.6	95	BEMPORAD	73	CNTR	+	10–16 $K^+ A$

$\Gamma(K\pi\pi)/\Gamma((K\pi)^{\pm})$ — Γ_6/Γ_2

VALUE	CL%	DOCUMENT ID		TECN	CHG	COMMENT
$< 7 \times 10^{-4}$	95	JONGEJANS	78	HBC		4 $K^- p \to p \overline{K}^0 2\pi$
• • • We do not use the following data for averages, fits, limits, etc. • • •						
$<20 \times 10^{-4}$		WOJCICKI	64	HBC	−	1.7 $K^- p \to \overline{K}^0 \pi^- p$

$K^*(892)$ REFERENCES

ADUSZKIEW... 20A EPJ C80 460 A. Aduszkiewicz *et al.* (CERN NA61 Collab.)
ALBRECHT 20 EPJ C80 453 M. Albrecht *et al.* (Crystal Barrel Collab.)
PELAEZ 20 PRL 124 172001 J.R. Pelaez *et al.*
ABLIKIM 19AQ PR D100 032004 M. Ablikim *et al.* (BESIII Collab.)
LEES 17C PR D95 072007 J.P. Lees *et al.* (BABAR Collab.)
PELAEZ 17 EPJ C77 91 J.R. Pelaez, A.Rodas, J.R. de Elvira
AAIJ 16N PR D93 052018 R. Aaij *et al.* (LHCb Collab.)
ABLIKIM 16F PR D94 032001 M. Ablikim *et al.* (BESIII Collab.)
LEES 13F PR D87 052010 J.P. Lees *et al.* (BABAR Collab.)

Downloaded from https://academic.oup.com/ptep/article/2022/8/083C01/6651666 by KIT Library user on 27 September 2022

DEL-AMO-SA...	11I	PR D83 072001	P. del Amo Sanchez *et al.*	(BABAR Collab.)
ANTONELLI	10	EPJ C69 399	M. Antonelli *et al.*	(FlaviaNet Working Group)
BOITO	10	JHEP 1009 031	D.R. Boito, R. Escribano, M. Jamin	(BARC)
BOITO	09	EPJ C59 821	D.R. Boito, R. Escribano, M. Jamin	
MITCHELL	09A	PR D79 072008	R.E. Mitchell *et al.*	(CLEO Collab.)
BONVICINI	08A	PR D78 052001	G. Bonvicini *et al.*	(CLEO Collab.)
JAMIN	08	PL B664 78	M. Jamin, A. Pich, J. Portoles	
AUBERT	07AK	PR D76 012008	B. Aubert *et al.*	(BABAR Collab.)
EPIFANOV	07	PL B654 65	D. Epifanov *et al.*	(BELLE Collab.)
LINK	05I	PL B621 72	J.M. Link *et al.*	(FNAL FOCUS Collab.)
PELAEZ	04A	MPL A19 2879	J.R. Pelaez	(MADU)
BONVICINI	02	PRL 88 111803	G. Bonvicini *et al.*	(CLEO Collab.)
PDG	00	EPJ C15 1	D.E. Groom *et al.*	(PDG Collab.)
ABELE	99D	PL B468 178	A. Abele *et al.*	(Crystal Barrel Collab.)
BARATE	99R	EPJ C11 599	R. Barate *et al.*	(ALEPH Collab.)
BARBERIS	98E	PL B436 204	D. Barberis *et al.*	(Omega Expt.)
BIRD	89	SLAC-332	P.F. Bird	(SLAC)
ASTON	88	NP B296 493	D. Aston *et al.*	(SLAC, NAGO, CINC, INUS)
ATKINSON	86	ZPHY C30 521	M. Atkinson *et al.*	(BONN, CERN, GLAS+)
CARLSMITH	86	PRL 56 18	D. Carlsmith *et al.*	(EFI, SACL)
BAUBILLIER	84B	ZPHY C26 37	M. Baubillier *et al.*	(BIRM, CERN, GLAS+)
NAPIER	84	PL 149B 514	A. Napier *et al.*	(TUFTS, ARIZ, FNAL, FLOR+)
BARTH	83	NP B223 296	M. Barth *et al.*	(BRUX, CERN, GENO, MONS+)
BERG	83	Thesis UMI 83-21652	D.M. Berg	(ROCH)
CHANDLEE	83	PRL 51 168	C. Chandlee *et al.*	(ROCH, FNAL, MINN)
CLELAND	82	NP B208 189	W.E. Cleland *et al.*	(DURH, GEVA, LAUS+)
DELFOSSE	81	NP B183 349	A. Delfosse *et al.*	(GEVA, LAUS)
TOAFF	81	PR D23 1500	S. Toaff *et al.*	(ANL, KANS)
AJINENKO	80	ZPHY C5 177	I.V. Ajinenko *et al.*	(SERP, BRUX, MONS+)
EVANGELIS...	80	NP B165 383	C. Evangelista *et al.*	(BARI, BONN, CERN+)
AGUILAR-...	78B	NP B141 101	M. Aguilar-Benitez *et al.*	(MADR, TATA+)
BALAND	78	NP B140 220	J.F. Baland *et al.*	(MONS, BELG, CERN+)
COOPER	78	NP B136 365	A.M. Cooper *et al.*	(TATA, CERN, CDEF+)
ESTABROOKS	78	NP B133 490	P.G. Estabrooks *et al.*	(MCGI, CARL, DURH+)
Also		PR D17 658	P.G. Estabrooks *et al.*	(MCGI, CARL, DURH+)
JONGEJANS	78	NP B139 383	B. Jongejans *et al.*	(ZEEM, CERN, NIJM+)
WICKLUND	78	PR D17 1197	A.B. Wicklund *et al.*	(ANL)
BOWLER	77	NP B126 31	M.G. Bowler *et al.*	(OXF)
CARITHERS	75B	PRL 35 349	W.C.J. Carithers *et al.*	(ROCH, MCGI)
MCCUBBIN	75	NP B86 13	N.A. McCubbin, L. Lyons	(OXF)
PALER	75	NP B96 1	K. Paler *et al.*	(RHEL, SACL, EPOL)
FOX	74	NP B80 403	G.C. Fox, M.L. Griss	(CIT)
MATISON	74	PR D9 1872	M.J. Matison *et al.*	(LBL)
BEMPORAD	73	NP B51 1	C. Bemporad *et al.*	(CERN, ETH, LOIC)
CLARK	73	NP B54 432	A.G. Clark, L. Lyons, D. Radojicic	(OXF)
LEWIS	73	NP B60 283	P.H. Lewis *et al.*	(LOWC, LOIC, CDEF)
LINGLIN	73	NP B55 408	D. Linglin	(CERN)
BUCHNER	72	NP B45 333	K. Buchner *et al.*	(MPIM, CERN, BRUX)
AGUILAR-...	71B	PR D4 2583	M. Aguilar-Benitez, R.L. Eisner, J.B. Kinson	(BNL)
HABER	70	NP B17 289	B. Haber *et al.*	(REHO, SACL, BGNA, EPOL)
CRENNELL	69D	PRL 22 487	D.J. Crennell *et al.*	(BNL)
DAVIS	69	PRL 23 1071	P.J. Davis *et al.*	(LRL)
SCHWEING...	68	PR 166 1317	F. Schweingruber *et al.*	(ANL, NWES)
BARASH	67B	PR 156 1399	N. Barash *et al.*	(COLU)
BARLOW	67	NC 50A 701	J. Barlow *et al.*	(CERN, CDEF, IRAD, LIVP)
DAUBER	67B	PR 153 1403	P.M. Dauber *et al.*	(UCLA)
DEBAERE	67B	NC 51A 401	W. de Baere *et al.*	(BRUX, CERN)
WOJCICKI	64	PR 135 B484	S.G. Wojcicki	(LRL)

$K_1(1270)$

$I(J^P) = \frac{1}{2}(1^+)$

$K_1(1270)$ MASS

VALUE (MeV)	DOCUMENT ID
1253±7 OUR AVERAGE	Includes data from the 4 datablocks that follow this one. Error includes scale factor of 2.2. See the ideogram below.

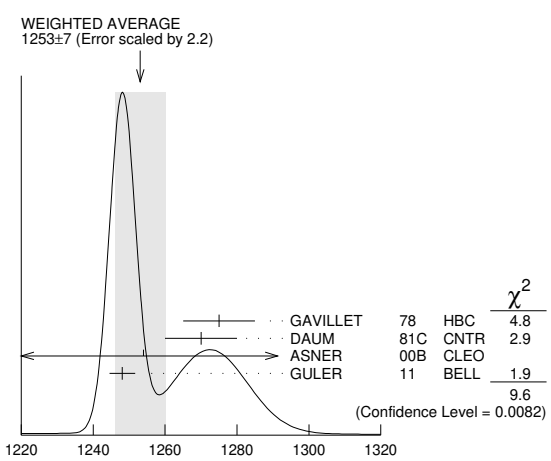

PRODUCED BY K^-, BACKWARD SCATTERING, HYPERON EXCHANGE

VALUE (MeV)	EVTS	DOCUMENT ID	TECN	CHG	COMMENT
The data in this block is included in the average printed for a previous datablock.					
1275±10	700	GAVILLET	78 HBC	+	4.2 $K^- p \to \Xi^- (K\pi\pi)^+$

PRODUCED BY K BEAMS

VALUE (MeV)	DOCUMENT ID	TECN	CHG	COMMENT
The data in this block is included in the average printed for a previous datablock.				
1270±10	[1] DAUM 81C	CNTR	−	63 $K^- p \to K^- 2\pi p$
• • • We do not use the following data for averages, fits, limits, etc. • • •				
∼ 1276	[2] TORNQVIST 82B	RVUE		
∼ 1300	VERGEEST 79	HBC	−	4.2 $K^- p \to (\overline{K}\pi\pi)^- p$
1289±25	[3] CARNEGIE 77	ASPK	±	13 $K^\pm p \to (K\pi\pi)^\pm p$
∼ 1300	BRANDENB... 76	ASPK	±	13 $K^\pm p \to (K\pi\pi)^\pm p$
∼ 1270	OTTER 76	HBC	−	10,14,16 $K^- p \to (\overline{K}\pi\pi)^- p$
1260	DAVIS 72	HBC	+	12 $K^+ p$
1234±12	FIRESTONE 72B	DBC	+	12 $K^+ d$

[1] Well described in the chiral unitary approach of GENG 07 with two poles at 1195 and 1284 MeV and widths of 246 and 146 MeV, respectively.
[2] From a unitarized quark-model calculation.
[3] From a model-dependent fit with Gaussian background to BRANDENBURG 76 data.

PRODUCED BY BEAMS OTHER THAN K MESONS

VALUE (MeV)	EVTS	DOCUMENT ID	TECN	COMMENT
The data in this block is included in the average printed for a previous datablock.				
1248.1 ± 3.3 ±1.4		GULER 11	BELL	$B^+ \to J/\psi K^+ \pi^+ \pi^-$
• • • We do not use the following data for averages, fits, limits, etc. • • •				
1289.81± 0.56±1.66	894k	AAIJ 18AI	LHCB	$D^0 \to K^\mp \pi^\pm \pi^\pm \pi^\mp$
1279 ±10	25k	[1] ABLIKIM 06C	BES2	$J/\psi \to \overline{K}^*(892)^0 K^+ \pi^-$
1294 ±10	310	RODEBACK 81	HBC	4 $\pi^- p \to \Lambda K 2\pi$
1300	40	CRENNELL 72	HBC	4.5 $\pi^- p \to \Lambda K 2\pi$
1242 $^{+9}_{-10}$		[2] ASTIER 69	HBC	$\overline{p}p$
1300	45	CRENNELL 67	HBC	6 $\pi^- p \to \Lambda K 2\pi$

[1] Systematic errors not estimated.
[2] This was called the C meson.

PRODUCED IN τ LEPTON DECAYS

VALUE (MeV)	EVTS	DOCUMENT ID	TECN	CHG	COMMENT
The data in this block is included in the average printed for a previous datablock.					
1254±33±34	7k	ASNER 00B	CLEO	±	$\tau^- \to K^- \pi^+ \pi^- \nu_\tau$

$K_1(1270)$ WIDTH

VALUE (MeV)	DOCUMENT ID
90±20 OUR ESTIMATE	This is only an educated guess; the error given is larger than the error on the average of the published values.
101±12 OUR AVERAGE	Includes data from the 4 datablocks that follow this one. Error includes scale factor of 2.2. See the ideogram below.

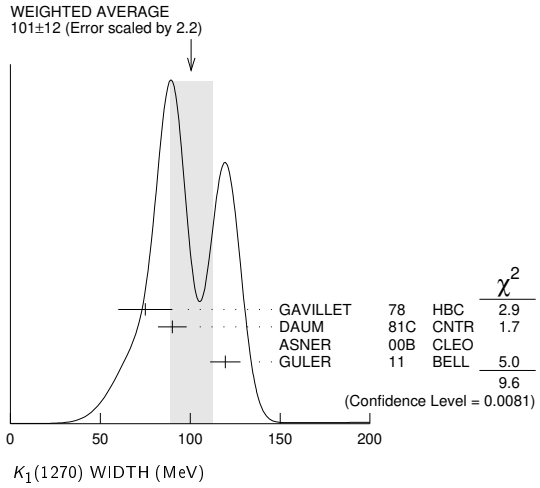

PRODUCED BY K^-, BACKWARD SCATTERING, HYPERON EXCHANGE

VALUE (MeV)	EVTS	DOCUMENT ID	TECN	CHG	COMMENT
The data in this block is included in the average printed for a previous datablock.					
75±15	700	GAVILLET 78	HBC	+	4.2 $K^- p \to \Xi^- K\pi\pi$

PRODUCED BY K BEAMS

VALUE (MeV)	DOCUMENT ID	TECN	CHG	COMMENT
The data in this block is included in the average printed for a previous datablock.				
90± 8	[1] DAUM 81C	CNTR	−	63 $K^- p \to K^- 2\pi p$

Downloaded from https://academic.oup.com/ptep/article/2022/8/083C01/6651666 by KIT Library user on 27 September 2022

• • • We do not use the following data for averages, fits, limits, etc. • • •

~ 150	VERGEEST	79	HBC	−	4.2 $K^- p \to (\overline{K}\pi\pi)^- p$
150±71	[2] CARNEGIE	77	ASPK	±	13 $K^\pm p \to (K\pi\pi)^\pm p$
~ 200	BRANDENB...	76	ASPK	±	13 $K^\pm p \to (K\pi\pi)^\pm p$
120	DAVIS	72	HBC	+	12 $K^+ p$
188±21	FIRESTONE	72B	DBC	+	12 $K^+ d$

[1] Well described in the chiral unitary approach of GENG 07 with two poles at 1195 and 1284 MeV and widths of 246 and 146 MeV, respectively.
[2] From a model-dependent fit with Gaussian background to BRANDENBURG 76 data.

PRODUCED BY BEAMS OTHER THAN K MESONS

VALUE (MeV)	EVTS	DOCUMENT ID		TECN	COMMENT
The data in this block is included in the average printed for a previous datablock.					
119.5 ± 5.2 ±6.7		GULER	11	BELL	$B^+ \to J/\psi K^+\pi^+\pi^-$
• • • We do not use the following data for averages, fits, limits, etc. • • •					
116.11± 1.65±2.96	894k	AAIJ	18AI	LHCB	$D^0 \to K^\mp\pi^\pm\pi^\pm\pi^\mp$
131 ±21	25k	[1] ABLIKIM	06C	BES2	$J/\psi \to \overline{K}^*(892)^0 K^+\pi^-$
66 ±15	310	RODEBACK	81	HBC	$4\pi^- p \to \Lambda K 2\pi$
60	40	CRENNELL	72	HBC	$4.5\pi^- p \to \Lambda K 2\pi$
127 $^{+7}_{-25}$		ASTIER	69	HBC	$\overline{p}p$
60	45	CRENNELL	67	HBC	$6\pi^- p \to \Lambda K 2\pi$

[1] Systematic errors not estimated.

PRODUCED IN τ LEPTON DECAYS

VALUE (MeV)	EVTS	DOCUMENT ID		TECN	CHG	COMMENT
The data in this block is included in the average printed for a previous datablock.						
$260^{+90}_{-70}\pm80$	7k	ASNER	00B	CLEO	±	$\tau^- \to K^-\pi^+\pi^-\nu_\tau$

$K_1(1270)$ DECAY MODES

	Mode	Fraction (Γ_i/Γ)	Scale factor
Γ_1	$K\rho$	(38 ±13) %	2.2
Γ_2	$K_0^*(1430)\pi$	(28 ± 4) %	
Γ_3	$K^*(892)\pi$	(21 ±10) %	2.2
Γ_4	$K\omega$	(11.0± 2.0) %	
Γ_5	$K f_0(1370)$	(3.0± 2.0) %	
Γ_6	γK^0	seen	

$K_1(1270)$ PARTIAL WIDTHS

$\Gamma(K\rho)$ — Γ_1

VALUE (MeV)	DOCUMENT ID		TECN	CHG	COMMENT
• • • We do not use the following data for averages, fits, limits, etc. • • •					
57±5	MAZZUCATO	79	HBC	+	4.2 $K^- p \to \Xi^-(K\pi\pi)^+$
75±6	CARNEGIE	77B	ASPK	±	13 $K^\pm p \to (K\pi\pi)^\pm p$

$\Gamma(K_0^*(1430)\pi)$ — Γ_2

VALUE (MeV)	DOCUMENT ID		TECN	CHG	COMMENT
• • • We do not use the following data for averages, fits, limits, etc. • • •					
26±6	CARNEGIE	77B	ASPK	±	13 $K^\pm p \to (K\pi\pi)^\pm p$

$\Gamma(K^*(892)\pi)$ — Γ_3

VALUE (MeV)	DOCUMENT ID		TECN	CHG	COMMENT
• • • We do not use the following data for averages, fits, limits, etc. • • •					
14±11	MAZZUCATO	79	HBC	+	4.2 $K^- p \to \Xi^-(K\pi\pi)^+$
2± 2	CARNEGIE	77B	ASPK	±	13 $K^\pm p \to (K\pi\pi)^\pm p$

$\Gamma(K\omega)$ — Γ_4

VALUE (MeV)	DOCUMENT ID		TECN	CHG	COMMENT
• • • We do not use the following data for averages, fits, limits, etc. • • •					
4±4	MAZZUCATO	79	HBC	+	4.2 $K^- p \to \Xi^-(K\pi\pi)^+$
24±3	CARNEGIE	77B	ASPK	±	13 $K^\pm p \to (K\pi\pi)^\pm p$

$\Gamma(K f_0(1370))$ — Γ_5

VALUE (MeV)	DOCUMENT ID		TECN	CHG	COMMENT
• • • We do not use the following data for averages, fits, limits, etc. • • •					
22±5	CARNEGIE	77B	ASPK	±	13 $K^\pm p \to (K\pi\pi)^\pm p$

$\Gamma(\gamma K^0)$ — Γ_6

VALUE (keV)	DOCUMENT ID		TECN	COMMENT
73.2±6.1±28.3	ALAVI-HARATI	02B	KTEV	$K + A \to K^* + A$

$K_1(1270)$ BRANCHING RATIOS

$\Gamma(K\rho)/\Gamma_{total}$ — Γ_1/Γ

VALUE	DOCUMENT ID		TECN	COMMENT
0.38 ±0.13 OUR FIT	Error includes scale factor of 2.2.			
0.42 ±0.06	[1] DAUM	81C	CNTR	63 $K^- p \to K^- 2\pi p$
• • • We do not use the following data for averages, fits, limits, etc. • • •				
0.584±0.043	[2] GULER	11	BELL	$B^+ \to J/\psi K^+\pi^+\pi^-$
dominant	RODEBACK	81	HBC	$4\pi^- p \to \Lambda K 2\pi$

$\Gamma(K_0^*(1430)\pi)/\Gamma_{total}$ — Γ_2/Γ

VALUE	DOCUMENT ID		TECN	COMMENT
0.28 ±0.04	[1] DAUM	81C	CNTR	63 $K^- p \to K^- 2\pi p$
• • • We do not use the following data for averages, fits, limits, etc. • • •				
0.0201±0.0064	[2] GULER	11	BELL	$B^+ \to J/\psi K^+\pi^+\pi^-$

$\Gamma(K^*(892)\pi)/\Gamma_{total}$ — Γ_3/Γ

VALUE	DOCUMENT ID		TECN	COMMENT
0.21 ±0.10 OUR FIT	Error includes scale factor of 2.2.			
0.16 ±0.05	[1] DAUM	81C	CNTR	63 $K^- p \to K^- 2\pi p$
• • • We do not use the following data for averages, fits, limits, etc. • • •				
0.171±0.023	[2] GULER	11	BELL	$B^+ \to J/\psi K^+\pi^+\pi^-$

$\Gamma(K^*(892)\pi)/\Gamma(K\rho)$ — Γ_3/Γ_1

VALUE	DOCUMENT ID		TECN	COMMENT
0.56±0.29 OUR FIT	Error includes scale factor of 2.2.			
0.99±0.15±0.18	ABLIKIM	21U	BES3	$D_s^+ \to \overline{K}_1(1270)^0 K^+$

$\Gamma(K\omega)/\Gamma_{total}$ — Γ_4/Γ

VALUE	DOCUMENT ID		TECN	COMMENT
0.11 ±0.02	[1] DAUM	81C	CNTR	63 $K^- p \to K^- 2\pi p$
• • • We do not use the following data for averages, fits, limits, etc. • • •				
0.225±0.052	[2] GULER	11	BELL	$B^+ \to J/\psi K^+\pi^+\pi^-$

$\Gamma(K\omega)/\Gamma(K\rho)$ — Γ_4/Γ_1

VALUE	CL%	DOCUMENT ID		TECN	COMMENT
• • • We do not use the following data for averages, fits, limits, etc. • • •					
<0.30	95	RODEBACK	81	HBC	$4\pi^- p \to \Lambda K 2\pi$

$\Gamma(K f_0(1370))/\Gamma_{total}$ — Γ_5/Γ

VALUE	DOCUMENT ID		TECN	COMMENT
0.03±0.02	[1] DAUM	81C	CNTR	63 $K^- p \to K^- 2\pi p$

D-wave/S-wave RATIO FOR $K_1(1270) \to K^*(892)\pi$

VALUE	DOCUMENT ID		TECN	COMMENT
1.0±0.7	[1] DAUM	81C	CNTR	63 $K^- p \to K^- 2\pi p$

[1] Average from low and high t data.
[2] Assuming that decays are saturated by the $K\rho$, $K_0^*(1430)\pi$, $K^*(892)\pi$, $K\omega$ decay modes and neglecting interference between them. The values $B(\omega \to \pi^+\pi^-) = (1.53^{+0.11}_{-0.13})\%$ and $B(K_0^*(1430) \to K\pi) = (93 \pm 10)\%$ are used. Systematic uncertainties not estimated.

$K_1(1270)$ REFERENCES

ABLIKIM	21U	PR D104 032011	M. Ablikim et al.	(BESIII Collab.)
AAIJ	18AI	EPJ C78 443	R. Aaij et al.	(LHCb Collab.)
GULER	11	PR D83 032005	H. Guler et al.	(BELLE Collab.)
GENG	07	PR D75 014017	L.S. Geng et al.	
ABLIKIM	06C	PL B633 681	M. Ablikim et al.	(BES Collab.)
ALAVI-HARATI	02B	PRL 89 072001	A. Alavi-Harati et al.	(FNAL KTeV Collab.)
ASNER	00B	PR D62 072006	D.M. Asner et al.	(CLEO Collab.)
TORNQVIST	82B	NP B203 268	N.A. Tornqvist	(HELS)
DAUM	81C	NP B187 1	C. Daum et al.	(AMST, CERN, CRAC, MPIM+)
RODEBACK	81	ZPHY C9 9	S. Rodeback et al.	(CERN, CDEF, MADR+)
MAZZUCATO	79	NP B156 532	M. Mazzucato et al.	(CERN, ZEEM, NIJM+)
VERGEEST	79	NP B158 265	J.S.M. Vergeest et al.	(NIJM, AMST, CERN+)
GAVILLET	78	PL 76B 517	P. Gavillet et al.	(AMST, CERN, NIJM+) JP
CARNEGIE	77	NP B127 509	R.K. Carnegie et al.	(SLAC)
CARNEGIE	77B	PL 68B 287	R.K. Carnegie et al.	(SLAC)
BRANDENB...	76	PRL 36 703	G.W. Brandenburg et al.	(SLAC) JP
OTTER	76	NP B106 77	G. Otter et al.	(AACH3, BERL, CERN, LOIC+) JP
CRENNELL	72	PR D6 1220	D.J. Crennell et al.	(BNL)
DAVIS	72	PR D5 2688	P.J. Davis et al.	(LBL)
FIRESTONE	72B	PR D5 505	A. Firestone et al.	(LBL)
ASTIER	69	NP B10 65	A. Astier et al.	(CDEF, CERN, IPNP, LIVP) IJP
CRENNELL	67	PRL 19 44	D.J. Crennell et al.	(BNL) I

$K_1(1400)$

$I(J^P) = \frac{1}{2}(1^+)$

$K_1(1400)$ MASS

VALUE (MeV)	EVTS	DOCUMENT ID		TECN	CHG	COMMENT
1403± 7 OUR AVERAGE						
1463±64±68	7k	ASNER	00B	CLEO	±	$\tau^- \to K^-\pi^+\pi^-\nu_\tau$
1373±14±18		[1] ASTON	87	LASS	0	$11 K^- p \to \overline{K}^0\pi^+\pi^- n$
1392±18		BAUBILLIER	82B	HBC	0	$8.25 K^- p \to K_S^0\pi^+\pi^- n$
1410±25		DAUM	81C	CNTR	−	$63 K^- p \to K^- 2\pi p$
1415±15		ETKIN	80	MPS	0	$6 K^- p \to \overline{K}^0\pi^+\pi^- n$
1404±10		[2] CARNEGIE	77	ASPK	±	$13 K^\pm p \to (K\pi\pi)^\pm p$
• • • We do not use the following data for averages, fits, limits, etc. • • •						
1418± 8	25k	[3] ABLIKIM	06C	BES2		$J/\psi \to \overline{K}^*(892)^0 K^+\pi^-$
~ 1350		[4] TORNQVIST	82B	RVUE		
~ 1400		VERGEEST	79	HBC	−	$4.2 K^- p \to (\overline{K}\pi\pi)^- p$
~ 1400		BRANDENB...	76	ASPK	±	$13 K^\pm p \to (K\pi\pi)^\pm p$

Downloaded from https://academic.oup.com/ptep/article/2022/8/083C01/6651666 by KIT Library user on 27 September 2022

1420	DAVIS	72	HBC	+	12 $K^+ p$
1368±18	FIRESTONE	72B	DBC	+	12 $K^+ d$

[1] From partial-wave analysis of $K^0 \pi^+ \pi^-$ system.
[2] From a model-dependent fit with Gaussian background to BRANDENBURG 76 data.
[3] Systematic errors not estimated.
[4] From a unitarized quark-model calculation.

$K_1(1400)$ WIDTH

VALUE (MeV)	EVTS	DOCUMENT ID		TECN	CHG	COMMENT
174± 13 OUR AVERAGE		Error includes scale factor of 1.6.				See the ideogram below.
$300^{+370}_{-110}\pm140$	7k	ASNER	00B	CLEO	±	$\tau^- \to K^- \pi^+ \pi^- \nu_\tau$
188± 54± 60		[1] ASTON	87	LASS	0	11 $K^- p \to \overline{K}^0 \pi^+ \pi^- n$
276± 65		BAUBILLIER	82B	HBC	0	8.25 $K^- p \to K^0_S \pi^+ \pi^- n$
195± 25		DAUM	81C	CNTR	−	63 $K^- p \to K^- 2\pi p$
180± 10		ETKIN	80	MPS	0	6 $K^- p \to \overline{K}^0 \pi^+ \pi^- n$
142± 16		[2] CARNEGIE	77	ASPK	±	13 $K^\pm p \to (K\pi\pi)^\pm p$
• • • We do not use the following data for averages, fits, limits, etc. • • •						
152± 16	25k	[3] ABLIKIM	06C	BES2		$J/\psi \to \overline{K}^*(892)^0 K^+ \pi^-$
∼ 200		VERGEEST	79	HBC	−	4.2 $K^- p \to (\overline{K}\pi\pi)^- p$
∼ 160		BRANDENB...	76	ASPK	±	13 $K^\pm p \to (K\pi\pi)^\pm p$
80		DAVIS	72	HBC	+	12 $K^+ p$
241± 30		FIRESTONE	72B	DBC	+	12 $K^+ d$

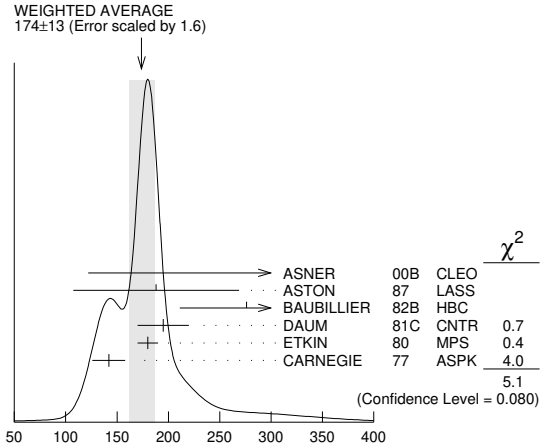

[1] From partial-wave analysis of $K^0 \pi^+ \pi^-$ system.
[2] From a model-dependent fit with Gaussian background to BRANDENBURG 76 data.
[3] Systematic errors not estimated.

$K_1(1400)$ DECAY MODES

	Mode	Fraction (Γ_i/Γ)
Γ_1	$K^*(892)\pi$	(94 ±6) %
Γ_2	$K\rho$	(3.0±3.0) %
Γ_3	$K f_0(1370)$	(2.0±2.0) %
Γ_4	$K\omega$	(1.0±1.0) %
Γ_5	$K_0^*(1430)\pi$	not seen
Γ_6	γK^0	seen
Γ_7	$K\phi$	seen

$K_1(1400)$ PARTIAL WIDTHS

$\Gamma(K^*(892)\pi)$ — Γ_1

VALUE (MeV)	DOCUMENT ID		TECN	CHG	COMMENT
117±10	CARNEGIE	77	ASPK	±	13 $K^\pm p \to (K\pi\pi)^\pm p$

$\Gamma(K\rho)$ — Γ_2

VALUE (MeV)	DOCUMENT ID		TECN	CHG	COMMENT
2±1	CARNEGIE	77	ASPK	±	13 $K^\pm p \to (K\pi\pi)^\pm p$

$\Gamma(K\omega)$ — Γ_4

VALUE (MeV)	DOCUMENT ID		TECN	CHG	COMMENT
23±12	CARNEGIE	77	ASPK	±	13 $K^\pm p \to (K\pi\pi)^\pm p$

$\Gamma(\gamma K^0)$ — Γ_6

VALUE (keV)	DOCUMENT ID		TECN	COMMENT
280.8±23.2±40.4	ALAVI-HARATI	02B	KTEV	$K + A \to K^* + A$

$K_1(1400)$ BRANCHING RATIOS

$\Gamma(K^*(892)\pi)/\Gamma_{total}$ — Γ_1/Γ

VALUE	DOCUMENT ID		TECN	COMMENT
0.94±0.06	[1] DAUM	81C	CNTR	63 $K^- p \to K^- 2\pi p$

[1] Average from low and high t data.

$\Gamma(K\rho)/\Gamma_{total}$ — Γ_2/Γ

VALUE	DOCUMENT ID		TECN	COMMENT
0.03±0.03	[1] DAUM	81C	CNTR	63 $K^- p \to K^- 2\pi p$

[1] Average from low and high t data.

$\Gamma(K f_0(1370))/\Gamma_{total}$ — Γ_3/Γ

VALUE	DOCUMENT ID		TECN	COMMENT
0.02±0.02	[1] DAUM	81C	CNTR	63 $K^- p \to K^- 2\pi p$

[1] Average from low and high t data.

$\Gamma(K\omega)/\Gamma_{total}$ — Γ_4/Γ

VALUE	DOCUMENT ID		TECN	COMMENT
0.01±0.01	[1] DAUM	81C	CNTR	63 $K^- p \to K^- 2\pi p$

[1] Average from low and high t data.

$\Gamma(K\phi)/\Gamma_{total}$ — Γ_7/Γ

VALUE	EVTS	DOCUMENT ID		TECN	COMMENT
seen	24k	[1] AAIJ	21E	LHCB	$B^+ \to J/\psi\phi K^+$

[1] From an amplitude analysis of the decay $B^+ \to J/\psi\phi K^+$ with a significance of 9.2 σ.

$\Gamma(K_0^*(1430)\pi)/\Gamma_{total}$ — Γ_5/Γ

VALUE	DOCUMENT ID		TECN	COMMENT
not seen	[1] DAUM	81C	CNTR	63 $K^- p \to K^- 2\pi p$

[1] Average from low and high t data.

D-wave/S-wave RATIO FOR $K_1(1400) \to K^*(892)\pi$

VALUE	DOCUMENT ID		TECN	COMMENT
0.04±0.01	[1] DAUM	81C	CNTR	63 $K^- p \to K^- 2\pi p$

[1] Average from low and high t data.

$K_1(1400)$ REFERENCES

AAIJ	21E	PRL 127 082001	R. Aaij et al.	(LHCb Collab.)
ABLIKIM	06C	PL B633 681	M. Ablikim et al.	(BES Collab.)
ALAVI-HARATI	02B	PRL 89 072001	A. Alavi-Harati et al.	(FNAL KTeV Collab.)
ASNER	00B	PR D62 072006	D.M. Asner et al.	(CLEO Collab.)
ASTON	87	NP B292 693	D. Aston et al.	(SLAC, NAGO, CINC, INUS)
BAUBILLIER	82B	NP B202 21	M. Baubillier et al.	(BIRM, CERN, GLAS+)
TORNQVIST	82B	NP B203 268	N.A. Tornqvist	(HELS)
DAUM	81C	NP B187 1	C. Daum et al.	(AMST, CERN, CRAC, MPIM+)
ETKIN	80	PR D22 42	A. Etkin et al.	(BNL, CUNY) JP
VERGEEST	79	NP B158 265	J.S.M. Vergeest et al.	(NIJM, AMST, CERN+)
CARNEGIE	77	NP B127 509	R.K. Carnegie et al.	(SLAC)
BRANDENB...	76	PRL 36 703	G.W. Brandenburg et al.	(SLAC) JP
DAVIS	72	PR D5 2688	P.J. Davis et al.	(LBL)
FIRESTONE	72B	PR D5 505	A. Firestone et al.	(LBL)

$K^*(1410)$

$I(J^P) = \frac{1}{2}(1^-)$

$K^*(1410)$ T-MATRIX POLE $\sqrt{s}$

VALUE (MeV)	DOCUMENT ID		TECN	COMMENT
• • • We do not use the following data for averages, fits, limits, etc. • • •				
$(1368 \pm 38) - i\,(106^{+48}_{-59})$	[1] PELAEZ	17	RVUE	$\pi K \to \pi K$

[1] Reanalysis of ESTABROOKS 78 and ASTON 88 satisfying Forward Dispersion Relations and using sequences of Pade approximants.

$K^*(1410)$ MASS

VALUE (MeV)	EVTS	DOCUMENT ID		TECN	CHG	COMMENT
1414±15 OUR AVERAGE		Error includes scale factor of 1.3.				
1380±21±19		ASTON	88	LASS	0	11 $K^- p \to K^- \pi^+ n$
1420± 7±10		ASTON	87	LASS	0	11 $K^- p \to \overline{K}^0 \pi^+ \pi^- n$
• • • We do not use the following data for averages, fits, limits, etc. • • •						
1437± 8±16	190k	[1] AAIJ	16N	LHCB		$D^0 \to (K^0_S \pi^\mp) K^\pm$
1426± 8±24	190k	[2] AAIJ	16N	LHCB		$D^0 \to K^0_S (K^\pm \pi^\mp)$
1276^{+72}_{-77}		[3,4] BOITO	09	RVUE		$\tau^- \to K^0_S \pi^- \nu_\tau$
1367±54		BIRD	89	LASS	−	11 $K^- p \to \overline{K}^0 \pi^- p$
1474±25		BAUBILLIER	82B	HBC	0	8.25 $K^- p \to \overline{K}^0 2\pi n$
1500±30		ETKIN	80	MPS	0	6 $K^- p \to \overline{K}^0 \pi^+ \pi^- n$

[1] Using a parametrization for the $K\pi$ S-wave similar to ASTON 88 with fixed resonance width.
[2] Using a $K\pi$ S-wave parametrization with resonant and non-resonant contributions.
[3] From the pole position of the $K\pi$ vector form factor in the complex s-plane and using EPIFANOV 07 data.

Downloaded from https://academic.oup.com/ptep/article/2022/8/083C01/6651666 by KIT Library user on 27 September 2022

[4] Systematic uncertainties not estimated.

$K^*(1410)$ WIDTH

VALUE (MeV)	EVTS	DOCUMENT ID		TECN	CHG	COMMENT
232± 21 OUR AVERAGE		Error includes scale factor of 1.1.				
176± 52±22		ASTON	88	LASS	0	11 $K^- p \to K^- \pi^+ n$
240± 18±12		ASTON	87	LASS	0	11 $K^- p \to \overline{K}^0 \pi^+ \pi^- n$
• • • We do not use the following data for averages, fits, limits, etc. • • •						
210± 20±60	190k	[1] AAIJ	16N	LHCB		$D^0 \to (K_S^0 \pi^\mp) K^\pm$
270± 20±40	190k	[1] AAIJ	16N	LHCB		$D^0 \to K_S^0 (K^\pm \pi^\mp)$
198^{+61}_{-87}		[2,3] BOITO	09	RVUE		$\tau^- \to K_S^0 \pi^- \nu_\tau$
114±101		BIRD	89	LASS	–	11 $K^- p \to \overline{K}^0 \pi^- p$
275± 65		BAUBILLIER	82B	HBC	0	8.25 $K^- p \to \overline{K}^0 2\pi n$
500±100		ETKIN	80	MPS	0	6 $K^- p \to \overline{K}^0 \pi^+ \pi^- n$

[1] Using a $K\pi$ S-wave parametrization with resonant and non-resonant contributions.
[2] From the pole position of the $K\pi$ vector form factor in the complex s-plane and using EPIFANOV 07 data.
[3] Systematic uncertainties not estimated.

$K^*(1410)$ DECAY MODES

	Mode	Fraction (Γ_i/Γ)	Confidence level
Γ_1	$K^*(892)\pi$	> 40 %	95%
Γ_2	$K\pi$	(6.6±1.3) %	
Γ_3	$K\rho$	< 7 %	95%
Γ_4	γK^0	< 2.3 $\times 10^{-4}$	90%
Γ_5	$K\phi$	seen	

$K^*(1410)$ PARTIAL WIDTHS

$\Gamma(\gamma K^0)$ — Γ_4

VALUE (keV)	CL%	DOCUMENT ID	TECN	COMMENT
<52.9	90	ALAVI-HARATI 02B	KTEV	$K + A \to K^* + A$

$K^*(1410)$ BRANCHING RATIOS

$\Gamma(K\rho)/\Gamma(K^*(892)\pi)$ — Γ_3/Γ_1

VALUE	CL%	DOCUMENT ID		TECN	CHG	COMMENT
<0.17	95	ASTON	84	LASS	0	11 $K^- p \to \overline{K}^0 2\pi n$

$\Gamma(K\pi)/\Gamma(K^*(892)\pi)$ — Γ_2/Γ_1

VALUE	CL%	DOCUMENT ID		TECN	CHG	COMMENT
<0.16	95	ASTON	84	LASS	0	11 $K^- p \to \overline{K}^0 2\pi n$

$\Gamma(K\pi)/\Gamma_{total}$ — Γ_2/Γ

VALUE	DOCUMENT ID		TECN	CHG	COMMENT
0.066±0.010±0.008	ASTON	88	LASS	0	11 $K^- p \to K^- \pi^+ n$

$\Gamma(K\phi)/\Gamma_{total}$ — Γ_5/Γ

VALUE	EVTS	DOCUMENT ID		TECN	COMMENT
seen	24k	[1] AAIJ	21E	LHCB	$B^+ \to J/\psi\phi K^+$

[1] From an amplitude analysis of the decay $B^+ \to J/\psi\phi K^+$ with a significance of 7.7 σ.

$K^*(1410)$ REFERENCES

AAIJ	21E	PRL 127 082001	R. Aaij *et al.*	(LHCb Collab.)
PELAEZ	17	EPJ C77 91	J.R. Pelaez, A.Rodas, J.R. de Elvira	
AAIJ	16N	PR D93 052018	R. Aaij *et al.*	(LHCb Collab.)
BOITO	09	EPJ C59 821	D.R. Boito, R. Escribano, M. Jamin	
EPIFANOV	07	PL B654 65	D. Epifanov *et al.*	(BELLE Collab.)
ALAVI-HARATI	02B	PRL 89 072001	A. Alavi-Harati *et al.*	(FNAL KTeV Collab.)
BIRD	89	SLAC-332	P.F. Bird	(SLAC)
ASTON	88	NP B296 493	D. Aston *et al.*	(SLAC, NAGO, CINC, INUS)
ASTON	87	NP B292 693	D. Aston *et al.*	(SLAC, NAGO, CINC, INUS)
ASTON	84	PL 149B 258	D. Aston *et al.*	(SLAC, CARL, OTTA) JP
BAUBILLIER	82B	NP B202 21	M. Baubillier *et al.*	(BIRM, CERN, GLAS+)
ETKIN	80	PR D22 42	A. Etkin *et al.*	(BNL, CUNY) JP
ESTABROOKS	78	NP B133 490	P.G. Estabrooks *et al.*	(MCGI, CARL, DURH+)

$K_0^*(1430)$

$I(J^P) = \frac{1}{2}(0^+)$

$K_0^*(1430)$ T-MATRIX POLE $\sqrt{s}$

VALUE (MeV)	DOCUMENT ID		TECN	COMMENT
• • • We do not use the following data for averages, fits, limits, etc. • • •				
$(1431 \pm 6) - i\,(110 \pm 19)$	[1] PELAEZ	17	RVUE	$\pi K \to \pi K$

[1] Reanalysis of ESTABROOKS 78 and ASTON 88 satisfying Forward Dispersion Relations and using sequences of Pade approximants.

$K_0^*(1430)$ MASS

VALUE (MeV)	EVTS	DOCUMENT ID		TECN	COMMENT
1425 ±50 OUR ESTIMATE					
• • • We do not use the following data for averages, fits, limits, etc. • • •					
1449 ±17 ± 2		[1] LEES	21A	BABR	$\eta_c(1S) \to \eta' K^+ K^-$
1438 ± 8 ± 4	5.4k	[2] LEES	14E	BABR	$\eta_c(1S) \to K^+ K^- \eta/\pi^0$
1427 ± 4 ±13		[3] BUGG	10	RVUE	S-matrix pole
1466.6± 0.7± 3.4	141k	[4] BONVICINI	08A	CLEO	$D^+ \to K^- \pi^+ \pi^+$
~ 1412		[5] LINK	07	FOCS	$D^+ \to K^- K^+ \pi^+$
1461.0± 4.0± 2.1	54k	[6] LINK	07B	FOCS	$D^+ \to K^- \pi^+ \pi^+$
1406 ±29		[7] BUGG	06	RVUE	
1435 ± 6		[8] ZHOU	06	RVUE	$Kp \to K^- \pi^+ n$
1455 ±20 ±15		ABLIKIM	05Q	BES2	$\psi(2S) \to \gamma\pi^+\pi^- K^+ K^-$
1456 ± 8		[9] ZHENG	04	RVUE	$K^- p \to K^- \pi^+ n$
~ 1419		[10] BUGG	03	RVUE	11 $K^- p \to K^- \pi^+ n$
~ 1440		[11] LI	03	RVUE	11 $K^- p \to K^- \pi^+ n$
1459 ± 9	15k	[12] AITALA	02	E791	$D^+ \to K^- \pi^+ \pi^+$
~ 1440		[13] JAMIN	00	RVUE	$Kp \to Kp$
1436 ± 8		[14] BARBERIS	98E	OMEG	450 $pp \to p_f p_s K^+ K^- \pi^+ \pi^-$
1415 ±25		[10] ANISOVICH	97C	RVUE	11 $K^- p \to K^- \pi^+ n$
~ 1450		[15] TORNQVIST	96	RVUE	$\pi\pi \to \pi\pi$, $K\overline{K}$, $K\pi$
1412 ± 6		[16] ASTON	88	LASS	11 $K^- p \to K^- \pi^+ n$
~ 1430		BAUBILLIER	84B	HBC	8.25 $K^- p \to \overline{K}^0 \pi^- p$
~ 1425		[17] ESTABROOKS	78	ASPK	13 $K^\pm p \to K^\pm \pi^\pm (n, \Delta)$
~ 1450.0		MARTIN	78	SPEC	10 $K^\pm p \to K_S^0 \pi p$

[1] Using a $K\pi - K\eta'$ coupled channel Breit-Wigner function.
[2] Using both $\eta \to \gamma\gamma$ and $\eta \to \pi^+\pi^-\pi^0$. From a likelihood scan in the presence of several interfering scalar-meson resonances with fixed width $\Gamma(K_0^*(1430)) = 210$ MeV.
[3] S-Matrix pole. Supersedes BUGG 06. Combined analysis of ASTON 88, ABLIKIM 06C, AITALA 06, and LINK 09 using an s-dependent width with couplings to $K\pi$ and $K\eta'$, and the Adler zero near thresholds.
[4] From the isobar model with a complex pole for the κ.
[5] From a non-parametric analysis.
[6] A Breit-Wigner mass and width.
[7] S-matrix pole. Reanalysis of ASTON 88, AITALA 02, and ABLIKIM 06C including the κ with an s-dependent width and an Adler zero near threshold.
[8] S-matrix pole. Using ASTON 88 and assuming $K_0^*(700)$, $K_0^*(1950)$.
[9] Using ASTON 88 and assuming $K_0^*(700)$.
[10] T-matrix pole. Reanalysis of ASTON 88 data.
[11] Breit-Wigner fit. Using ASTON 88.
[12] Assuming a low-mass scalar $K\pi$ resonance, $\kappa(700)$.
[13] T-matrix pole. Using data from ESTABROOKS 78 and ASTON 88.
[14] J^P not determined, could be $K_2^*(1430)$.
[15] T-matrix pole.
[16] Uses a model for the background, without this background they get a mass 1340 MeV, where the phase shift passes 90°.
[17] Mass defined by pole position. From elastic $K\pi$ partial-wave analysis.

$K_0^*(1430)$ WIDTH

VALUE (MeV)	EVTS	DOCUMENT ID		TECN	COMMENT
270 ±80 OUR ESTIMATE					
• • • We do not use the following data for averages, fits, limits, etc. • • •					
210 ±20 ±12	5.4k	[1] LEES	14E	BABR	$\eta_c(1S) \to K^+ K^- \eta/\pi^0$
270 ±10 ±40		[2] BUGG	10	RVUE	S-matrix pole
174.2± 1.9± 3.2	141k	[3] BONVICINI	08A	CLEO	$D^+ \to K^- \pi^+ \pi^+$
~ 500		[4] LINK	07	FOCS	$D^+ \to K^- K^+ \pi^+$
177.0± 8.0± 3.4	54k	[5] LINK	07B	FOCS	$D^+ \to K^- \pi^+ \pi^+$
350 ±40		[6] BUGG	06	RVUE	
288 ±22		[7] ZHOU	06	RVUE	$Kp \to K^- \pi^+ n$
$270 \pm 45 \; {}^{+30}_{-35}$		ABLIKIM	05Q	BES2	$\psi(2S) \to \gamma\pi^+\pi^- K^+ K^-$
217 ±31		[8] ZHENG	04	RVUE	$K^- p \to K^- \pi^+ n$
~ 316		[9] BUGG	03	RVUE	11 $K^- p \to K^- \pi^+ n$
~ 350		[10] LI	03	RVUE	11 $K^- p \to K^- \pi^+ n$
175 ±17	15k	[11] AITALA	02	E791	$D^+ \to K^- \pi^+ \pi^+$
~ 300		[12] JAMIN	00	RVUE	$Kp \to Kp$
196 ±45		[13] BARBERIS	98E	OMEG	450 $pp \to p_f p_s K^+ K^- \pi^+ \pi^-$
330 ±50		[9] ANISOVICH	97C	RVUE	11 $K^- p \to K^- \pi^+ n$
~ 320		[14] TORNQVIST	96	RVUE	$\pi\pi \to \pi\pi$, $K\overline{K}$, $K\pi$
294 ±23		ASTON	88	LASS	11 $K^- p \to K^- \pi^+ n$
~ 200		BAUBILLIER	84B	HBC	8.25 $K^- p \to \overline{K}^0 \pi^- p$
200 to 300		[15] ESTABROOKS	78	ASPK	13 $K^\pm p \to K^\pm \pi^\pm (n, \Delta)$

[1] Using both $\eta \to \gamma\gamma$ and $\eta \to \pi^+\pi^-\pi^0$. From a likelihood scan in the presence of several interfering scalar-meson resonances with fixed mass $M(K_0^*(1430)) = 1435$ MeV.
[2] S-Matrix pole. Supersedes BUGG 06. Combined analysis of ASTON 88, ABLIKIM 06C, AITALA 06, and LINK 09 using an s-dependent width with couplings to $K\pi$ and $K\eta'$, and the Adler zero near thresholds.
[3] From the isobar model with a complex pole for the κ.
[4] From a non-parametric analysis.

Downloaded from https://academic.oup.com/ptep/article/2022/8/083C01/6651666 by KIT Library user on 27 September 2022

[5] A Breit-Wigner mass and width.
[6] S-matrix pole. Reanalysis of ASTON 88, AITALA 02, and ABLIKIM 06C including the κ with an s-dependent width and an Adler zero near threshold.
[7] S-matrix pole. Using ASTON 88 and assuming $K_0^*(700)$, $K_0^*(1950)$.
[8] Using ASTON 88 and assuming $K_0^*(700)$.
[9] T-matrix pole. Reanalysis of ASTON 88 data.
[10] Breit-Wigner fit. Using ASTON 88.
[11] Assuming a low-mass scalar $K\pi$ resonance, $\kappa(700)$.
[12] T-matrix pole. Using data from ESTABROOKS 78 and ASTON 88.
[13] J^P not determined, could be $K_2^*(1430)$.
[14] T-matrix pole.
[15] From elastic $K\pi$ partial-wave analysis.

$K_0^*(1430)$ DECAY MODES

	Mode	Fraction (Γ_i/Γ)
Γ_1	$K\pi$	(93 ±10) %
Γ_2	$K\eta$	($8.6^{+2.7}_{-3.4}$) %
Γ_3	$K\eta'(958)$	seen

$K_0^*(1430)$ BRANCHING RATIOS

$\Gamma(K\pi)/\Gamma_{total}$ — Γ_1/Γ

VALUE	DOCUMENT ID		TECN	CHG	COMMENT
0.93±0.04±0.09	ASTON	88	LASS	0	11 $K^-p \to K^-\pi^+n$

$\Gamma(K\eta)/\Gamma(K\pi)$ — Γ_2/Γ_1

VALUE (%)	EVTS	DOCUMENT ID		TECN	COMMENT
$9.2\pm2.5^{+1.0}_{-2.5}$	5.4k	[1] LEES	14E	BABR	$\eta_c(1S) \to K^+K^-\eta/\pi^0$

[1] Using both $\eta \to \gamma\gamma$ and $\eta \to \pi^+\pi^-\pi^0$. From a Dalitz analysis in the presence of several interfering scalar-meson resonances.

$\Gamma(K\eta'(958))/\Gamma_{total}$ — Γ_3/Γ

VALUE	DOCUMENT ID		TECN	COMMENT
seen	ABLIKIM	14J	BES3	$\psi(2S) \to \gamma K^+K^-\eta'(958)$

$\Gamma(K\eta'(958))/\Gamma(K\pi)$ — Γ_3/Γ_1

VALUE	DOCUMENT ID		TECN	COMMENT
0.397±0.064±0.054	[1] LEES	21A	BABR	$\eta_c(1S) \to \eta' K^+K^-$

[1] Using $K\pi$ data from LEES 14E.

$K_0^*(1430)$ REFERENCES

LEES	21A	PR D104 072002	J.P. Lees *et al.*	(BABAR Collab.)
PELAEZ	17	EPJ C77 91	J.R. Pelaez, A.Rodas, J.R. de Elvira	
ABLIKIM	14J	PR D89 074030	M. Ablikim *et al.*	(BESIII Collab.)
LEES	14E	PR D89 112004	J.P. Lees *et al.*	(BABAR Collab.)
BUGG	10	PR D81 014002	D.V. Bugg	(LOQM)
LINK	09	PL B681 14	J.M. Link *et al.*	(FNAL FOCUS Collab.)
BONVICINI	08A	PR D78 052001	G. Bonvicini *et al.*	(CLEO Collab.)
LINK	07	PL B648 156	J.M. Link *et al.*	(FNAL FOCUS Collab.)
LINK	07B	PL B653 1	J.M. Link *et al.*	(FNAL FOCUS Collab.)
ABLIKIM	06C	PL B633 681	M. Ablikim *et al.*	(BES Collab.)
AITALA	06	PR D73 032004	E.M. Aitala *et al.*	(FNAL E791 Collab.)
Also		PR D74 059901 (errat.)	E.M. Aitala *et al.*	(FNAL E791 Collab.)
BUGG	06	PL B632 471	D.V. Bugg	(LOQM)
ZHOU	06	NP A775 212	Z.Y. Zhou, H.Q. Zheng	
ABLIKIM	05Q	PR D72 092002	M. Ablikim *et al.*	(BES Collab.)
ZHENG	04	NP A733 235	H.Q. Zheng *et al.*	
BUGG	03	PL B572 1	D.V. Bugg	
LI	03	PR D67 034025	L. Li, B. Zou, G. Li	
AITALA	02	PRL 89 121801	E.M. Aitala *et al.*	(FNAL E791 Collab.)
JAMIN	00	NP B587 331	M. Jamin *et al.*	
BARBERIS	98E	PL B436 204	D. Barberis *et al.*	(Omega Expt.)
ANISOVICH	97C	PL B413 137	A.V. Anisovich, A.V. Sarantsev	
TORNQVIST	96	PRL 76 1575	N.A. Tornqvist, M. Roos	(HELS)
ASTON	88	NP B296 493	D. Aston *et al.*	(SLAC, NAGO, CINC, INUS)
BAUBILLIER	84B	ZPHY C26 37	M. Baubillier *et al.*	(BIRM, CERN, GLAS+)
ESTABROOKS	78	NP B133 490	P.G. Estabrooks *et al.*	(MCGI, CARL, DURH+)
MARTIN	78	NP B134 392	A.D. Martin *et al.*	(DURH, GEVA)

$K_2^*(1430)$

$I(J^P) = \frac{1}{2}(2^+)$

We consider that phase-shift analyses provide more reliable determinations of the mass and width.

$K_2^*(1430)$ T-MATRIX POLE $\sqrt{s}$

VALUE (MeV)	DOCUMENT ID		TECN	COMMENT
• • • We do not use the following data for averages, fits, limits, etc. • • •				
$(1424 \pm 4) - i\,(66 \pm 2)$	[1] PELAEZ	17	RVUE	$\pi K \to \pi K$

[1] Reanalysis of ESTABROOKS 78 and ASTON 88 satisfying Forward Dispersion Relations and using sequences of Pade approximants.

$K_2^*(1430)$ MASS

CHARGED ONLY, WITH FINAL STATE $K\pi$

VALUE (MeV)	EVTS	DOCUMENT ID		TECN	CHG	COMMENT
1427.3± 1.5 OUR AVERAGE		Error includes scale factor of 1.3. See the ideogram below.				
$1432.7\pm 0.7^{+2.2}_{-2.3}$	183k	ABLIKIM	19AQ	BES	±	$J/\psi \to K^+K^-\pi^0$
1420 ± 4	1587	BAUBILLIER	84B	HBC	−	8.25 $K^-p \to \overline{K}^0\pi^-p$
1436 ± 5.5	400	[2,3] CLELAND	82	SPEC	+	30 $K^+p \to K^0_S\pi^+p$
1430 ± 3.2	1500	[2,3] CLELAND	82	SPEC	+	50 $K^+p \to K^0_S\pi^+p$
1430 ± 3.2	1200	[2,3] CLELAND	82	SPEC	−	50 $K^+p \to K^0_S\pi^-p$
1423 ± 5	935	TOAFF	81	HBC	−	6.5 $K^-p \to \overline{K}^0\pi^-p$
1428.0± 4.6		[4] MARTIN	78	SPEC	+	10 $K^\pm p \to K^0_S\pi p$
1423.8± 4.6		[4] MARTIN	78	SPEC	−	10 $K^\pm p \to K^0_S\pi p$
1420.0± 3.1	1400	AGUILAR-...	71B	HBC	−	3.9,4.6 K^-p
1425 ± 8.0	225	[2,3] BARNHAM	71C	HBC	+	$K^+p \to K^0\pi^+p$
1416 ±10	220	CRENNELL	69D	DBC	−	3.9 $K^-N \to \overline{K}^0\pi^-N$
1414 ±13.0	60	[2] LIND	69	HBC	+	9 $K^+p \to K^0\pi^+p$
1427 ±12	63	[2] SCHWEING...	68	HBC	−	5.5 $K^-p \to \overline{K}\pi N$
1423 ±11.0	39	[2] BASSANO	67	HBC	−	4.6–5.0 $K^-p \to \overline{K}^0\pi^-p$
• • • We do not use the following data for averages, fits, limits, etc. • • •						
1423.4± 2 ±3	24809± 820	[5] BIRD	89	LASS	−	11 $K^-p \to \overline{K}^0\pi^-p$

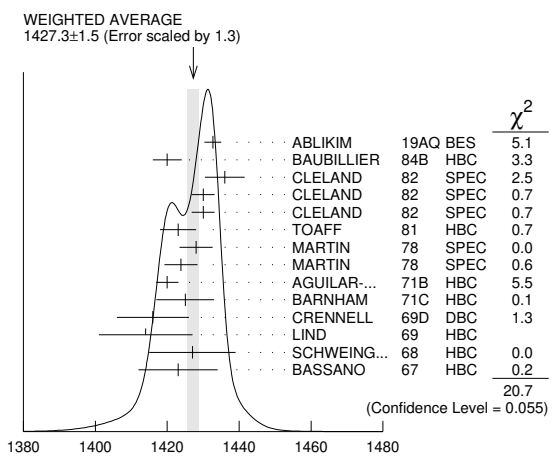

$K_2^*(1430)$ mass, combined neutral and charged (MeV)

NEUTRAL ONLY

VALUE (MeV)	EVTS	DOCUMENT ID		TECN	COMMENT
1432.4± 1.3 OUR AVERAGE					
1431.2± 1.8± 0.7		[6] ASTON	88	LASS	11 $K^-p \to K^-\pi^+n$
1434 ± 4 ± 6		[6] ASTON	87	LASS	11 $K^-p \to \overline{K}^0\pi^+\pi^-n$
1433 ± 6 ±10		[6] ASTON	84B	LASS	11 $K^-p \to \overline{K}^0 2\pi n$
1471 ±12		[6] BAUBILLIER	82B	HBC	8.25 $K^-p \to NK^0_S\pi\pi$
1428 ± 3		[6] ASTON	81C	LASS	11 $K^-p \to K^-\pi^+n$
1434 ± 2		[6] ESTABROOKS	78	ASPK	13 $K^\pm p \to pK\pi$
1440 ±10		[6] BOWLER	77	DBC	5.5 $K^+d \to K\pi pp$
• • • We do not use the following data for averages, fits, limits, etc. • • •					
1428.5± 3.9	1786± 127	[7] AUBERT	07AK	BABR	10.6 $e^+e^- \to K^{*0}K^\pm\pi^\mp\gamma$
1420 ± 7	300	HENDRICK	76	DBC	8.25 $K^+N \to K^+\pi N$
1421.6± 4.2	800	MCCUBBIN	75	HBC	3.6 $K^-p \to K^-\pi^+n$
1420.1± 4.3		[8] LINGLIN	73	HBC	2–13 $K^+p \to K^+\pi^-X$
1419.1± 3.7	1800	AGUILAR-...	71B	HBC	3.9,4.6 K^-p
1416 ± 6	600	CORDS	71	DBC	9 $K^+n \to K^+\pi^-p$
1421.1± 2.6	2200	DAVIS	69	HBC	12 $K^+p \to K^+\pi^-X$

[2] Errors enlarged by us to $\Gamma/\sqrt{N}$; see the note with the $K^*(892)$ mass.
[3] Number of events in peak re-evaluated by us.
[4] Systematic error added by us.
[5] From a partial wave amplitude analysis.
[6] From phase shift or partial-wave analysis.
[7] Systematic errors not estimated.
[8] From pole extrapolation, using world K^+p data summary tape.

Downloaded from https://academic.oup.com/ptep/article/2022/8/083C01/6651666 by KIT Library user on 27 September 2022

$K_2^*(1430)$ WIDTH

CHARGED ONLY, WITH FINAL STATE $K\pi$

VALUE (MeV)	EVTS	DOCUMENT ID		TECN	CHG	COMMENT
100.0± 2.1 OUR FIT						
100.0± 2.2 OUR AVERAGE		Error includes scale factor of 1.1.				
$102.5\pm 1.6^{+3.1}_{-2.8}$	183k	ABLIKIM	19AQ	BES	±	$J/\psi \to K^+K^-\pi^0$
109 ±22	400	[9,10] CLELAND	82	SPEC	+	30 $K^+p \to K^0_S\pi^+p$
124 ±12.8	1500	[9,10] CLELAND	82	SPEC	+	50 $K^+p \to K^0_S\pi^+p$
113 ±12.8	1200	[9,10] CLELAND	82	SPEC	−	50 $K^+p \to K^0_S\pi^-p$
85 ±16	935	TOAFF	81	HBC	−	6.5 $K^-p \to \overline{K}^0\pi^-p$
96.5± 3.8		MARTIN	78	SPEC	+	10 $K^\pm p \to K^0_S\pi p$
97.7± 4.0		MARTIN	78	SPEC	−	10 $K^\pm p \to K^0_S\pi p$
$94.7^{+15.1}_{-12.5}$	1400	AGUILAR-...	71B	HBC	−	3.9,4.6 K^-p
• • • We do not use the following data for averages, fits, limits, etc. • • •						
98 ± 4 ±4	25k	[11] BIRD	89	LASS	−	11 $K^-p \to \overline{K}^0\pi^-p$

NEUTRAL ONLY

VALUE (MeV)	EVTS	DOCUMENT ID		TECN	COMMENT
109 ± 5 OUR AVERAGE		Error includes scale factor of 1.9. See the ideogram below.			
116.5± 3.6± 1.7		[12] ASTON	88	LASS	11 $K^-p \to K^-\pi^+n$
129 ±15 ±15		[12] ASTON	87	LASS	11 $K^-p \to \overline{K}^0\pi^+\pi^-n$
131 ±24 ±20		[12] ASTON	84B	LASS	11 $K^-p \to \overline{K}^0 2\pi n$
143 ±34		[12] BAUBILLIER	82B	HBC	8.25 $K^-p \to N K^0_S\pi\pi$
98 ± 8		[12] ASTON	81C	LASS	11 $K^-p \to K^-\pi^+n$
140 ±30		[12] ETKIN	80	SPEC	6 $K^-p \to \overline{K}^0\pi^+\pi^-n$
98 ± 5		[12] ESTABROOKS	78	ASPK	13 $K^\pm p \to pK\pi$
• • • We do not use the following data for averages, fits, limits, etc. • • •					
113.7± 9.2	1786± 127	[13] AUBERT	07AK	BABR	10.6 $e^+e^- \to K^{*0}K^\pm\pi^\mp\gamma$
125 ±29	300	[9] HENDRICK	76	DBC	8.25 $K^+N \to K^+\pi N$
116 ±18	800	MCCUBBIN	75	HBC	3.6 $K^-p \to K^-\pi^+n$
61 ±14		[14] LINGLIN	73	HBC	2–13 $K^+p \to K^+\pi^-X$
$116.6^{+10.3}_{-15.5}$	1800	AGUILAR-...	71B	HBC	3.9,4.6 K^-p
144 ±24.0	600	[9] CORDS	71	DBC	9 $K^+n \to K^+\pi^-p$
101 ±10	2200	DAVIS	69	HBC	12 $K^+p \to K^+\pi^-\pi^+p$

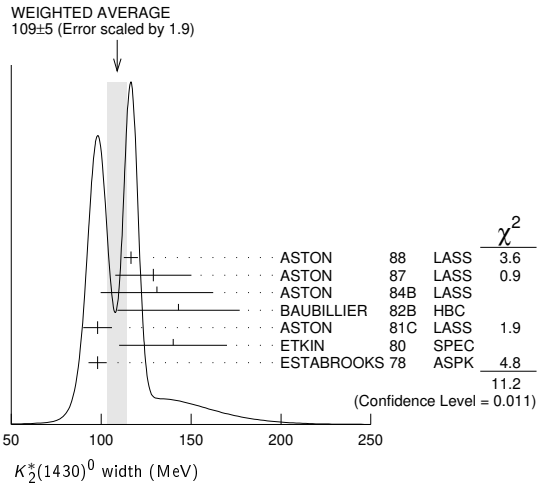

[9] Errors enlarged by us to $4\Gamma/\sqrt{N}$; see the note with the $K^*(892)$ mass.
[10] Number of events in peak re-evaluated by us.
[11] From a partial wave amplitude analysis.
[12] From phase shift or partial-wave analysis.
[13] Systematic errors not estimated.
[14] From pole extrapolation, using world K^+p data summary tape.

$K_2^*(1430)$ DECAY MODES

	Mode	Fraction (Γ_i/Γ)	Scale factor/ Confidence level
Γ_1	$K\pi$	(49.9±1.2) %	
Γ_2	$K^*(892)\pi$	(24.7±1.5) %	
Γ_3	$K^*(892)\pi\pi$	(13.4±2.2) %	
Γ_4	$K\rho$	(8.7±0.8) %	S=1.2
Γ_5	$K\omega$	(2.9±0.8) %	
Γ_6	$K^+\gamma$	$(2.4\pm0.5)\times10^{-3}$	S=1.1
Γ_7	$K\eta$	$(1.5^{+3.4}_{-1.0})\times10^{-3}$	S=1.3
Γ_8	$K\omega\pi$	$< 7.2 \times10^{-4}$	CL=95%
Γ_9	$K^0\gamma$	$< 9 \times10^{-4}$	CL=90%

CONSTRAINED FIT INFORMATION

An overall fit to the total width, a partial width, and 10 branching ratios uses 32 measurements and one constraint to determine 8 parameters. The overall fit has a $\chi^2 = 21.1$ for 25 degrees of freedom.

The following *off-diagonal* array elements are the correlation coefficients $\langle\delta p_i\delta p_j\rangle/(\delta p_i\cdot\delta p_j)$, in percent, from the fit to parameters p_i, including the branching fractions, $x_i \equiv \Gamma_i/\Gamma_{total}$. The fit constrains the x_i whose labels appear in this array to sum to one.

	x_1	x_2	x_3	x_4	x_5	x_6	x_7
x_2	−9						
x_3	−40	−73					
x_4	−8	36	−52				
x_5	−11	−3	−26	−7			
x_6	−1	−1	−1	−1	0		
x_7	−4	−7	−5	−5	−2	0	
Γ	0	0	0	0	0	−10	0

	Mode	Rate (MeV)	Scale factor
Γ_1	$K\pi$	49.9 ±1.6	
Γ_2	$K^*(892)\pi$	24.7 ±1.6	
Γ_3	$K^*(892)\pi\pi$	13.5 ±2.3	
Γ_4	$K\rho$	8.7 ±0.8	1.2
Γ_5	$K\omega$	2.9 ±0.8	
Γ_6	$K^+\gamma$	0.24±0.05	1.1
Γ_7	$K\eta$	$0.15^{+0.34}_{-0.10}$	1.3

$K_2^*(1430)$ PARTIAL WIDTHS

$\Gamma(K^+\gamma)$ — Γ_6

VALUE (keV)	DOCUMENT ID		TECN	CHG	COMMENT
241±50 OUR FIT	Error includes scale factor of 1.1.				
240±45	CIHANGIR	82	SPEC	+	200 $K^+Z \to Z K^+\pi^0$, $Z K^0_S\pi^+$

$\Gamma(K^0\gamma)$ — Γ_9

VALUE (keV)	CL%	DOCUMENT ID		TECN	CHG	COMMENT
< 5.4	90	ALAVI-HARATI	02B	KTEV		$K + A \to K^* + A$
• • • We do not use the following data for averages, fits, limits, etc. • • •						
<84	90	CARLSMITH	87	SPEC	0	60–200 $K^0_L A \to K^0_S\pi^0 A$

$K_2^*(1430)$ BRANCHING RATIOS

$\Gamma(K\pi)/\Gamma_{total}$ — Γ_1/Γ

VALUE	DOCUMENT ID		TECN	CHG	COMMENT
0.499±0.012 OUR FIT					
0.488±0.014 OUR AVERAGE					
0.485±0.006±0.020	[15] ASTON	88	LASS	0	11 $K^-p \to K^-\pi^+n$
0.49 ±0.02	[15] ESTABROOKS	78	ASPK	±	13 $K^\pm p \to pK\pi$

$\Gamma(K^*(892)\pi)/\Gamma(K\pi)$ — Γ_2/Γ_1

VALUE	DOCUMENT ID		TECN	CHG	COMMENT
0.496±0.034 OUR FIT					
0.47 ±0.04 OUR AVERAGE					
0.44 ±0.09	ASTON	84B	LASS	0	11 $K^-p \to \overline{K}^0 2\pi n$
0.62 ±0.19	LAUSCHER	75	HBC	0	10,16 $K^-p \to K^-\pi^+n$
0.54 ±0.16	DEHM	74	DBC	0	4.6 K^+N
0.47 ±0.08	AGUILAR-...	71B	HBC		3.9,4.6 K^-p
0.47 ±0.10	BASSANO	67	HBC	−0	4.6,5.0 K^-p
0.45 ±0.13	BADIER	65C	HBC	−	3 K^-p

$\Gamma(K\omega)/\Gamma(K\pi)$ — Γ_5/Γ_1

VALUE	DOCUMENT ID		TECN	CHG	COMMENT
0.059±0.017 OUR FIT					
0.070±0.035 OUR AVERAGE					
0.05 ±0.04	AGUILAR-...	71B	HBC		3.9,4.6 K^-p
0.13 ±0.07	BASSOMPIE...	69	HBC	0	5 K^+p

$\Gamma(K\rho)/\Gamma(K\pi)$ — Γ_4/Γ_1

VALUE	DOCUMENT ID		TECN	CHG	COMMENT
0.174±0.017 OUR FIT	Error includes scale factor of 1.2.				
$0.150^{+0.029}_{-0.017}$ OUR AVERAGE					
0.18 ±0.05	ASTON	84B	LASS	0	11 $K^-p \to \overline{K}^0 2\pi n$
$0.02^{+0.10}_{-0.02}$	DEHM	74	DBC	0	4.6 K^+N
0.16 ±0.05	AGUILAR-...	71B	HBC		3.9,4.6 K^-p
0.14 ±0.10	BASSANO	67	HBC	−0	4.6,5.0 K^-p
0.14 ±0.07	BADIER	65C	HBC	−	3 K^-p

Downloaded from https://academic.oup.com/ptep/article/2022/8/083C01/6651666 by KIT Library user on 27 September 2022

$\Gamma(K\rho)/\Gamma(K^*(892)\pi)$ — Γ_4/Γ_2

VALUE	DOCUMENT ID		TECN	CHG	COMMENT
0.350±0.031 OUR FIT	Error includes scale factor of 1.4.				
0.354±0.033 OUR AVERAGE	Error includes scale factor of 1.4. See the ideogram below.				
0.293±0.032±0.020	ASTON	87	LASS	0	11 $K^- p \to \overline{K}^0 \pi^+ \pi^- n$
0.38 ±0.09	BAUBILLIER	82B	HBC	0	8.25 $K^- p \to N K^0_S \pi\pi$
0.39 ±0.03	DAUM	81C	CNTR		63 $K^- p \to K^- 2\pi p$

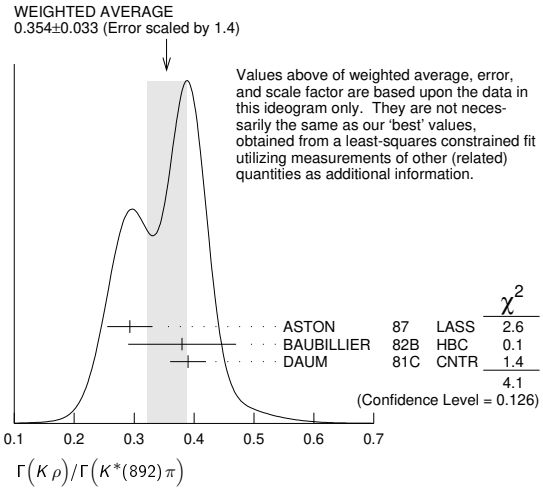

$\Gamma(K\omega)/\Gamma(K^*(892)\pi)$ — Γ_5/Γ_2

VALUE	DOCUMENT ID		TECN	CHG	COMMENT
0.118±0.034 OUR FIT					
0.10 ±0.04	FIELD	67	HBC	–	3.8 $K^- p$

$\Gamma(K\eta)/\Gamma(K^*(892)\pi)$ — Γ_7/Γ_2

VALUE	DOCUMENT ID		TECN	CHG	COMMENT
$0.006^{+0.014}_{-0.004}$ OUR FIT	Error includes scale factor of 1.2.				
0.07 ±0.04	FIELD	67	HBC	–	3.8 $K^- p$

$\Gamma(K\eta)/\Gamma(K\pi)$ — Γ_7/Γ_1

VALUE	CL%	DOCUMENT ID		TECN	CHG	COMMENT
$0.0030^{+0.0070}_{-0.0020}$ OUR FIT		Error includes scale factor of 1.3.				
0 ±0.0056		[16] ASTON	88B	LASS	–	11 $K^- p \to K^- \eta p$
• • • We do not use the following data for averages, fits, limits, etc. • • •						
<0.04	95	AGUILAR-...	71B	HBC		3.9,4.6 $K^- p$
<0.065		[17] BASSOMPIE...	69	HBC		5.0 $K^+ p$
<0.02		BISHOP	69	HBC		3.5 $K^+ p$

$\Gamma(K^*(892)\pi\pi)/\Gamma_{total}$ — Γ_3/Γ

VALUE	DOCUMENT ID		TECN	CHG	COMMENT
0.134±0.022 OUR FIT					
0.12 ±0.04	[18] GOLDBERG	76	HBC	–	3 $K^- p \to p \overline{K}^0 \pi\pi\pi$

$\Gamma(K^*(892)\pi\pi)/\Gamma(K\pi)$ — Γ_3/Γ_1

VALUE	DOCUMENT ID		TECN	CHG	COMMENT
0.27±0.05 OUR FIT					
0.21±0.08	[17,18] JONGEJANS	78	HBC	–	4 $K^- p \to p \overline{K}^0 \pi\pi\pi$

$\Gamma(K\omega\pi)/\Gamma_{total}$ — Γ_8/Γ

VALUE (units 10^{-3})	CL%	EVTS	DOCUMENT ID		TECN	COMMENT
<0.72	95	0	JONGEJANS	78	HBC	4 $K^- p \to p \overline{K}^0 4\pi$

[15] From phase shift analysis.
[16] ASTON 88B quote < 0.0092 at CL=95%. We convert this to a central value and 1 sigma error in order to be able to use it in our constrained fit.
[17] Restated by us.
[18] Assuming $\pi\pi$ system has isospin 1, which is supported by the data.

$K_2^*(1430)$ REFERENCES

ABLIKIM	19AQ	PR D100 032004	M. Ablikim *et al.*	(BESIII Collab.)
PELAEZ	17	EPJ C77 91	J.R. Pelaez, A.Rodas, J.R. de Elvira	
AUBERT	07AK	PR D76 012008	B. Aubert *et al.*	(BABAR Collab.)
ALAVI-HARATI	02B	PRL 89 072001	A. Alavi-Harati *et al.*	(FNAL KTeV Collab.)
BIRD	89	SLAC-332	P.F. Bird	(SLAC)
ASTON	88	NP B296 493	D. Aston *et al.*	(SLAC, NAGO, CINC, INUS)
ASTON	88B	PL B201 169	D. Aston *et al.*	(SLAC, NAGO, CINC, INUS)
ASTON	87	NP B292 693	D. Aston *et al.*	(SLAC, NAGO, CINC, INUS)
CARLSMITH	87	PR D36 3502	D. Carlsmith *et al.*	(EFI, SACL)
ASTON	84B	NP B247 261	D. Aston *et al.*	(SLAC, CARL, OTTA)
BAUBILLIER	84B	ZPHY C26 37	M. Baubillier *et al.*	(BIRM, CERN, GLAS+)
BAUBILLIER	82B	NP B202 21	M. Baubillier *et al.*	(BIRM, CERN, GLAS+)
CIHANGIR	82	PL 117B 123	S. Cihangir *et al.*	(FNAL, MINN, ROCH)
CLELAND	82	NP B208 189	W.E. Cleland *et al.*	(DURH, GEVA, LAUS+)
ASTON	81C	PL 106B 235	D. Aston *et al.*	(SLAC, CARL, OTTA) JP
DAUM	81C	NP B187 1	C. Daum *et al.*	(AMST, CERN, CRAC, MPIM+)
TOAFF	81	PR D23 1500	S. Toaff *et al.*	(ANL, KANS)
ETKIN	80	PR D22 42	A. Etkin *et al.*	(BNL, CUNY) JP
ESTABROOKS	78	NP B133 490	P.G. Estabrooks *et al.*	(MCGI, CARL, DURH+)
Also		PR D17 658	P.G. Estabrooks *et al.*	(MCGI, CARL, DURH+)
JONGEJANS	78	NP B139 383	B. Jongejans *et al.*	(ZEEM, CERN, NIJM+)
MARTIN	78	NP B134 392	A.D. Martin *et al.*	(DURH, GEVA)
BOWLER	77	NP B126 31	M.G. Bowler *et al.*	(OXF)
GOLDBERG	76	LNC 17 253	J. Goldberg	(HAIF)
HENDRICK	76	NP B112 189	K. Hendrickx *et al.*	(MONS, SACL, PARIS+)
LAUSCHER	75	NP B86 189	P. Lauscher *et al.*	(ABCLV Collab.) JP
MCCUBBIN	75	NP B86 13	N.A. McCubbin, L. Lyons	(OXF)
DEHM	74	NP B75 47	G. Dehm *et al.*	(MPIM, BRUX, MONS, CERN)
LINGLIN	73	NP B55 408	D. Linglin	(CERN)
AGUILAR-...	71B	PR D4 2583	M. Aguilar-Benitez, R.L. Eisner, J.B. Kinson	(BNL)
BARNHAM	71C	NP B28 171	K.W.J. Barnham *et al.*	(BIRM, GLAS)
CORDS	71	PR D4 1974	D. Cords *et al.*	(PURD, UCD, IUPU)
BASSOMPIE...	69	NP B13 189	G. Bassompierre *et al.*	(CERN, BRUX) JP
BISHOP	69	NP B9 403	J.M. Bishop *et al.*	(WISC)
CRENNELL	69D	PRL 22 487	D.J. Crennell *et al.*	(BNL)
DAVIS	69	PRL 23 1071	P.J. Davis *et al.*	(LRL)
LIND	69	NP B14 1	V.G. Lind *et al.*	(LRL) JP
SCHWEING...	68	PR 166 1317	F. Schweingruber *et al.*	(ANL, NWES)
Also		Thesis	F.L. Schweingruber	(NWES, NWES)
BASSANO	67	PRL 19 968	D. Bassano *et al.*	(BNL, SYRA)
FIELD	67	PL 24B 638	J.H. Field *et al.*	(UCSD)
BADIER	65C	PL 19 612	J. Badier *et al.*	(EPOL, SACL, AMST)

$K(1460)$

$I(J^P) = \frac{1}{2}(0^-)$

Observed in $K\pi\pi$ partial-wave analysis.

$K(1460)$ MASS

VALUE (MeV)	EVTS	DOCUMENT ID		TECN	CHG	COMMENT
• • • We do not use the following data for averages, fits, limits, etc. • • •						
1482.40±3.58±15.22	894k	AAIJ	18AI	LHCB		$D^0 \to K^\mp 2\pi^\pm \pi^\mp$
~ 1460	63	DAUM	81C	CNTR	–	$K^- p \to K^- 2\pi p$
~ 1400	13	[1] BRANDENB...	76B	ASPK	±	$K^\pm p \to K^+ 2\pi p$

[1] Coupled mainly to $K f_0(1370)$. Decay into $K^*(892)\pi$ seen.

$K(1460)$ WIDTH

VALUE (MeV)	EVTS	DOCUMENT ID		TECN	CHG	COMMENT
• • • We do not use the following data for averages, fits, limits, etc. • • •						
335.60±6.20±8.65	894k	AAIJ	18AI	LHCB		$D^0 \to K^\mp 2\pi^\pm \pi^\mp$
~ 260	63	DAUM	81C	CNTR	–	$K^- p \to K^- 2\pi p$
~ 250	15	[1] BRANDENB...	76B	ASPK	±	$K^\pm p \to K^+ 2\pi p$

[1] Coupled mainly to $K f_0(1370)$. Decay into $K^*(892)\pi$ seen.

$K(1460)$ DECAY MODES

	Mode	Fraction (Γ_i/Γ)
Γ_1	$K^*(892)\pi$	seen
Γ_2	$K\rho$	seen
Γ_3	$K_0^*(1430)\pi$	seen
Γ_4	$K\phi$	seen

$K(1460)$ PARTIAL WIDTHS

$\Gamma(K^*(892)\pi)$ — Γ_1

VALUE (MeV)	DOCUMENT ID		TECN	COMMENT
• • • We do not use the following data for averages, fits, limits, etc. • • •				
~ 109	DAUM	81C	CNTR	63 $K^- p \to K^- 2\pi p$

$\Gamma(K\rho)$ — Γ_2

VALUE (MeV)	DOCUMENT ID		TECN	COMMENT
• • • We do not use the following data for averages, fits, limits, etc. • • •				
~ 34	DAUM	81C	CNTR	63 $K^- p \to K^- 2\pi p$

$\Gamma(K_0^*(1430)\pi)$ — Γ_3

VALUE (MeV)	DOCUMENT ID		TECN	COMMENT
• • • We do not use the following data for averages, fits, limits, etc. • • •				
~ 117	DAUM	81C	CNTR	63 $K^- p \to K^- 2\pi p$

$\Gamma(K\phi)/\Gamma_{total}$ — Γ_4/Γ

VALUE	EVTS	DOCUMENT ID		TECN	COMMENT
seen	24k	[1] AAIJ	21E	LHCB	$B^+ \to J/\psi\phi K^+$

[1] From an amplitude analysis of the decay $B^+ \to J/\psi\phi K^+$ with a significance of 12 σ.

$K(1460)$ REFERENCES

AAIJ	21E	PRL 127 082001	R. Aaij *et al.*	(LHCb Collab.)
AAIJ	18AI	EPJ C78 443	R. Aaij *et al.*	(LHCb Collab.)
DAUM	81C	NP B187 1	C. Daum *et al.*	(AMST, CERN, CRAC, MPIM+)
BRANDENB...	76B	PRL 36 1239	G.W. Brandenburg *et al.*	(SLAC) JP

Downloaded from https://academic.oup.com/ptep/article/2022/8/083C01/6651666 by KIT Library user on 27 September 2022

$K_2(1580)$

$I(J^P) = \frac{1}{2}(2^-)$

OMITTED FROM SUMMARY TABLE

Seen in partial-wave analysis of the $K^-\pi^+\pi^-$ system. Needs confirmation.

$K_2(1580)$ MASS

VALUE (MeV)	DOCUMENT ID		CHG	COMMENT
• • • We do not use the following data for averages, fits, limits, etc. • • •				
~ 1580	OTTER	79	–	10,14,16 K^-p

$K_2(1580)$ WIDTH

VALUE (MeV)	DOCUMENT ID		CHG	COMMENT
• • • We do not use the following data for averages, fits, limits, etc. • • •				
~ 110	OTTER	79	–	10,14,16 K^-p

$K_2(1580)$ DECAY MODES

	Mode	Fraction (Γ_i/Γ)
Γ_1	$K^*(892)\pi$	seen
Γ_2	$K_2^*(1430)\pi$	possibly seen

$K_2(1580)$ BRANCHING RATIOS

$\Gamma(K^*(892)\pi)/\Gamma_{total}$ — **Γ_1/Γ**

VALUE	DOCUMENT ID		TECN	CHG	COMMENT
seen	OTTER	79	HBC	–	10,14,16 K^-p
• • • We do not use the following data for averages, fits, limits, etc. • • •					
possibly seen	GULER	11	BELL		$B^+ \to J/\psi K^+\pi^+\pi^-$

$\Gamma(K_2^*(1430)\pi)/\Gamma_{total}$ — **Γ_2/Γ**

VALUE	DOCUMENT ID		TECN	CHG	COMMENT
possibly seen	OTTER	79	HBC	–	10,14,16 K^-p

$K_2(1580)$ REFERENCES

GULER 11 PR D83 032005 H. Guler et al. (BELLE Collab.)
OTTER 79 NP B147 1 G. Otter et al. (AACH3, BERL, CERN, LOIC+) JP

$K(1630)$

$I(J^P) = \frac{1}{2}(?^?)$

OMITTED FROM SUMMARY TABLE

Seen as a narrow peak, compatible with the experimental resolution, in the invariant mass of the $K_S^0\pi^+\pi^-$ system produced in π^-p interactions at high momentum transfers.

$K(1630)$ MASS

VALUE (MeV)	EVTS	DOCUMENT ID	TECN	COMMENT
1629±7	~ 75	KARNAUKHOV98	BC	16.0 $\pi^-p \to (K_S^0\pi^+\pi^-)X^+\pi^-X^0$

$K(1630)$ WIDTH

VALUE (MeV)	EVTS	DOCUMENT ID	TECN	COMMENT
16^{+19}_{-16}	~ 75	[1] KARNAUKHOV98	BC	16.0 $\pi^-p \to (K_S^0\pi^+\pi^-)X^+\pi^-X^0$

[1] Compatible with an experimental resolution of 14 ± 1 MeV.

$K(1630)$ DECAY MODES

	Mode
Γ_1	$K_S^0\pi^+\pi^-$

$K(1630)$ REFERENCES

KARNAUKHOV 98 PAN 61 203 V.M. Karnaukhov, C. Coca, V.I. Moroz
Translated from YAF 61 252.

$K_1(1650)$

$I(J^P) = \frac{1}{2}(1^+)$

This entry contains various peaks in strange meson systems ($K^+\phi$, $K\pi\pi$) reported in partial-wave analysis in the 1600–1900 mass region.

$K_1(1650)$ MASS

VALUE (MeV)	EVTS	DOCUMENT ID		TECN	CHG	COMMENT
1650±50		FRAME	86	OMEG	+	13 $K^+p \to \phi K^+p$
• • • We do not use the following data for averages, fits, limits, etc. • • •						
$1861\pm10^{+16}_{-46}$	24k	[1] AAIJ	21E	LHCB		$B^+ \to J/\psi\phi K^+$
$1911\pm37^{+124}_{-48}$	24k	[1] AAIJ	21E	LHCB		$B^+ \to J/\psi\phi K^+$
$1793\pm59^{+153}_{-101}$	4289	[2,3] AAIJ	17C	LHCB		$B^+ \to J/\psi\phi K^+$
~ 1840		ARMSTRONG	83	OMEG	–	18.5 $K^-p \to 3Kp$
~ 1800		DAUM	81C	CNTR	–	63 $K^-p \to K^-2\pi p$

[1] One of two K_1 states reported by AAIJ 21E. From an amplitude analysis of the decay $B^+ \to J/\psi\phi K^+$ with a significance of 4.5 σ.
[2] From an amplitude analysis of the decay $B^+ \to J/\psi\phi K^+$ with a significance of 7.6 σ.
[3] Superseded by AAIJ 21E.

$K_1(1650)$ WIDTH

VALUE (MeV)	EVTS	DOCUMENT ID		TECN	CHG	COMMENT
150± 50		FRAME	86	OMEG	+	13 $K^+p \to \phi K^+p$
• • • We do not use the following data for averages, fits, limits, etc. • • •						
$149\pm41^{+231}_{-23}$	24k	[1] AAIJ	21E	LHCB		$B^+ \to J/\psi\phi K^+$
$276\pm50^{+319}_{-159}$	24k	[1] AAIJ	21E	LHCB		$B^+ \to J/\psi\phi K^+$
$365\pm157^{+138}_{-215}$	4289	[2,3] AAIJ	17C	LHCB		$B^+ \to J/\psi\phi K^+$
~ 250		DAUM	81C	CNTR	–	63 $K^-p \to K^-2\pi p$

[1] One of two K_1 states reported by AAIJ 21E. From an amplitude analysis of the decay $B^+ \to J/\psi\phi K^+$ with a significance of 4.5 σ.
[2] From an amplitude analysis of the decay $B^+ \to J/\psi\phi K^+$ with a significance of 7.6 σ.
[3] Superseded by AAIJ 21E.

$K_1(1650)$ DECAY MODES

	Mode
Γ_1	$K\pi\pi$
Γ_2	$K\phi$

$K_1(1650)$ REFERENCES

AAIJ 21E PRL 127 082001 R. Aaij et al. (LHCb Collab.)
AAIJ 17C PRL 118 022003 R. Aaij et al. (LHCb Collab.)
Also PR D95 012002 R. Aaij et al. (LHCb Collab.)
FRAME 86 NP B276 667 D. Frame et al. (GLAS)
ARMSTRONG 83 NP B221 1 T.A. Armstrong et al. (BARI, BIRM, CERN+)
DAUM 81C NP B187 1 C. Daum et al. (AMST, CERN, CRAC, MPIM+)

$K^*(1680)$

$I(J^P) = \frac{1}{2}(1^-)$

$K^*(1680)$ MASS

VALUE (MeV)	EVTS	DOCUMENT ID		TECN	CHG	COMMENT
1718±18 OUR AVERAGE						
$1722\pm20^{+33}_{-109}$	4289	[1] AAIJ	17C	LHCB		$B^+ \to J/\psi\phi K^+$
1677±10± 32		ASTON	88	LASS	0	11 $K^-p \to K^-\pi^+n$
1735±10± 20		ASTON	87	LASS	0	11 $K^-p \to \overline{K}^0\pi^+\pi^-n$
• • • We do not use the following data for averages, fits, limits, etc. • • •						
1678±64		BIRD	89	LASS	–	11 $K^-p \to \overline{K}^0\pi^-p$
1800±70		ETKIN	80	MPS	0	6 $K^-p \to \overline{K}^0\pi^+\pi^-n$
~ 1650		ESTABROOKS	78	ASPK	0	13 $K^\pm p \to K^\pm\pi^\pm n$

[1] From an amplitude analysis of the decay $B^+ \to J/\psi\phi K^+$ with a significance of 8.5 σ.

$K^*(1680)$ WIDTH

VALUE (MeV)	EVTS	DOCUMENT ID		TECN	CHG	COMMENT
322±110 OUR AVERAGE	Error includes scale factor of 4.2.					
$354\pm75^{+140}_{-181}$	4289	[2] AAIJ	17C	LHCB		$B^+ \to J/\psi\phi K^+$
205± 16± 34		ASTON	88	LASS	0	11 $K^-p \to K^-\pi^+n$
423± 18± 30		ASTON	87	LASS	0	11 $K^-p \to \overline{K}^0\pi^+\pi^-n$

Downloaded from https://academic.oup.com/ptep/article/2022/8/083C01/6651666 by KIT Library user on 27 September 2022

• • • We do not use the following data for averages, fits, limits, etc. • • •

454±270	BIRD	89	LASS	−	11	$K^- p \to \overline{K}^0 \pi^- p$
170± 30	ETKIN	80	MPS	0	6	$K^- p \to \overline{K}^0 \pi^+ \pi^- n$
250 to 300	ESTABROOKS	78	ASPK	0	13	$K^\pm p \to K^\pm \pi^\pm n$

[2] From an amplitude analysis of the decay $B^+ \to J/\psi\phi K^+$ with a significance of 8.5 σ.

$K^*(1680)$ DECAY MODES

	Mode	Fraction (Γ_i/Γ)
Γ_1	$K\pi$	(38.7±2.5) %
Γ_2	$K\rho$	$(31.4^{+5.0}_{-2.1})$ %
Γ_3	$K^*(892)\pi$	$(29.9^{+2.2}_{-5.0})$ %
Γ_4	$K\phi$	seen
Γ_5	$K\eta$	$(1.4^{+1.0}_{-0.8})$ %

CONSTRAINED FIT INFORMATION

An overall fit to 4 branching ratios uses 4 measurements and one constraint to determine 3 parameters. The overall fit has a $\chi^2 = 2.9$ for 2 degrees of freedom.

The following *off-diagonal* array elements are the correlation coefficients $\langle \delta x_i \delta x_j \rangle / (\delta x_i \cdot \delta x_j)$, in percent, from the fit to the branching fractions, $x_i \equiv \Gamma_i/\Gamma_{total}$. The fit constrains the x_i whose labels appear in this array to sum to one.

	x_1	x_2
x_2	−36	
x_3	−39	−72

$K^*(1680)$ BRANCHING RATIOS

$\Gamma(K\pi)/\Gamma_{total}$ — Γ_1/Γ

VALUE	DOCUMENT ID		TECN	CHG	COMMENT
0.387±0.026 OUR FIT					
0.388±0.014±0.022	ASTON	88	LASS	0	11 $K^- p \to K^- \pi^+ n$

$\Gamma(K\pi)/\Gamma(K^*(892)\pi)$ — Γ_1/Γ_3

VALUE	DOCUMENT ID		TECN	CHG	COMMENT
$\mathbf{1.30^{+0.23}_{-0.14}}$ **OUR FIT**					
2.8 ±1.1	ASTON	84	LASS	0	11 $K^- p \to \overline{K}^0 2\pi n$

$\Gamma(K\rho)/\Gamma(K\pi)$ — Γ_2/Γ_1

VALUE	DOCUMENT ID		TECN	CHG	COMMENT
$\mathbf{0.81^{+0.14}_{-0.09}}$ **OUR FIT**					
1.2 ±0.4	ASTON	84	LASS	0	11 $K^- p \to \overline{K}^0 2\pi n$

$\Gamma(K\rho)/\Gamma(K^*(892)\pi)$ — Γ_2/Γ_3

VALUE	DOCUMENT ID		TECN	CHG	COMMENT
$\mathbf{1.05^{+0.27}_{-0.11}}$ **OUR FIT**					
$\mathbf{0.97 \pm 0.09^{+0.30}_{-0.10}}$	ASTON	87	LASS	0	11 $K^- p \to \overline{K}^0 \pi^+ \pi^- n$

$\Gamma(K\phi)/\Gamma_{total}$ — Γ_4/Γ

VALUE	EVTS	DOCUMENT ID		TECN	COMMENT
seen	24k	[3] AAIJ	21E	LHCB	$B^+ \to J/\psi\phi K^+$

• • • We do not use the following data for averages, fits, limits, etc. • • •

seen	4289	[4,5] AAIJ	17C	LHCB	$B^+ \to J/\psi\phi K^+$

[3] From an amplitude analysis of the decay $B^+ \to J/\psi\phi K^+$ with a significance of 4.7 σ.
[4] From an amplitude analysis of the decay $B^+ \to J/\psi\phi K^+$ with a significance of 8.5 σ.
[5] Superseded by AAIJ 21E.

$\Gamma(K\eta)/\Gamma(K\pi)$ — Γ_5/Γ_1

VALUE	EVTS	DOCUMENT ID		TECN	COMMENT
$\mathbf{0.037 \pm 0.007^{+0.024}_{-0.018}}$	116k	[6] CHEN	20A	BELL	$D^0 \to K^- \pi^+ \eta$

[6] CHEN 20A quotes the ratio $\Gamma(K^*(1680)^- \to K^-\eta)/\Gamma(K^*(1680)^- \to K^-\pi^0) = 0.11 \pm 0.02^{+0.06}_{-0.04} \pm 0.04(B_{PDG})$ where the last uncertainty comes from $B(\eta \to \gamma\gamma) = (39.41 \pm 0.20)$%. We divide it by 3 taking into account that $\Gamma(K^*(1680)^- \to K^-\pi^0)/\Gamma(K^*(1680)^- \to (K\pi)^-) = 1/3$.

$\Gamma(K\eta)/\Gamma_{total}$ — Γ_5/Γ

VALUE (units 10^{-2})	EVTS	DOCUMENT ID		TECN	COMMENT
• • • We do not use the following data for averages, fits, limits, etc. • • •					
$1.44 \pm 0.21^{+0.96}_{-0.73}$	116k	[7] CHEN	20A	BELL	$D^0 \to K^- \pi^+ \eta$

[7] From an amplitude analysis of the decay $D^0 \to K^- \pi^+ \eta$ with a significance of 16 σ. Not independent of the CHEN 20A measurement of $\Gamma(K^*(1680) \to K\eta)/\Gamma(K^*(1680) \to K\pi)$.

$K^*(1680)$ REFERENCES

AAIJ	21E	PRL 127 082001	R. Aaij *et al.*	(LHCb Collab.)
CHEN	20A	PR D102 012002	Y.Q. Chen *et al.*	(BELLE Collab.)
AAIJ	17C	PRL 118 022003	R. Aaij *et al.*	(LHCb Collab.)
Also		PR D95 012002	R. Aaij *et al.*	(LHCb Collab.)
BIRD	89	SLAC-332	P.F. Bird	(SLAC)
ASTON	88	NP B296 493	D. Aston *et al.*	(SLAC, NAGO, CINC, INUS)
ASTON	87	NP B292 693	D. Aston *et al.*	(SLAC, NAGO, CINC, INUS)
ASTON	84	PL 149B 258	D. Aston *et al.*	(SLAC, CARL, OTTA) JP
ETKIN	80	PR D22 42	A. Etkin *et al.*	(BNL, CUNY) JP
ESTABROOKS	78	NP B133 490	P.G. Estabrooks *et al.*	(MCGI, CARL, DURH+) JP

$K_2(1770)$

$I(J^P) = \frac{1}{2}(2^-)$

See our mini-review in the 2004 edition of this *Review*, PDG 04.

$K_2(1770)$ MASS

VALUE (MeV)	EVTS	DOCUMENT ID		TECN	CHG	COMMENT
1773± 8 OUR AVERAGE						
$1777 \pm 35^{+122}_{-77}$	4289	[1] AAIJ	17C	LHCB		$B^+ \to J/\psi\phi K^+$
1773± 8		[2] ASTON	93	LASS		$11 K^- p \to K^- \omega p$
• • • We do not use the following data for averages, fits, limits, etc. • • •						
1743±15		TIKHOMIROV	03	SPEC		40.0 π^-C → $K^0_S K^0_S K^0_L$ X
1810±20		FRAME	86	OMEG	+	13 $K^+ p \to \phi K^+ p$
~ 1730		ARMSTRONG	83	OMEG	−	18.5 $K^- p \to 3Kp$
~ 1780		[3] DAUM	81C	CNTR	−	63 $K^- p \to K^- 2\pi p$
1710±15	60	CHUNG	74	HBC	−	7.3 $K^- p \to K^- \omega p$
1767± 6		BLIEDEN	72	MMS	−	11–16 $K^- p$
1730±20	306	[4] FIRESTONE	72B	DBC	+	12 $K^+ d$
1765±40		[5] COLLEY	71	HBC	+	10 $K^+ p \to K 2\pi N$
1740		DENEGRI	71	DBC	−	12.6 $K^- d \to \overline{K} 2\pi d$
1745±20		AGUILAR-...	70C	HBC	−	4.6 $K^- p$
1780±15		BARTSCH	70C	HBC	−	10.1 $K^- p$
1760±15		LUDLAM	70	HBC	−	12.6 $K^- p$

[1] From an amplitude analysis of the decay $B^+ \to J/\psi\phi K^+$ with a significance of 5.0 σ.
[2] From a partial wave analysis of the $K^-\omega$ system.
[3] From a partial wave analysis of the $K^- 2\pi$ system.
[4] Produced in conjunction with excited deuteron.
[5] Systematic errors added correspond to spread of different fits.

$K_2(1770)$ WIDTH

VALUE (MeV)	EVTS	DOCUMENT ID		TECN	CHG	COMMENT
186± 14 OUR AVERAGE						
$217 \pm 116^{+221}_{-154}$	4289	[6] AAIJ	17C	LHCB		$B^+ \to J/\psi\phi K^+$
186± 14		[7] ASTON	93	LASS		$11 K^- p \to K^- \omega p$
• • • We do not use the following data for averages, fits, limits, etc. • • •						
147± 70		TIKHOMIROV	03	SPEC		40.0 π^-C → $K^0_S K^0_S K^0_L$ X
140± 40		FRAME	86	OMEG	+	13 $K^+ p \to \phi K^+ p$
~ 220		ARMSTRONG	83	OMEG	−	18.5 $K^- p \to 3Kp$
~ 210		[8] DAUM	81C	CNTR	−	63 $K^- p \to K^- 2\pi p$
110± 50	60	CHUNG	74	HBC	−	7.3 $K^- p \to K^- \omega p$
100± 26		BLIEDEN	72	MMS	−	11–16 $K^- p$
210± 30	306	[9] FIRESTONE	72B	DBC	+	12 $K^+ d$
90± 70		[10] COLLEY	71	HBC	+	10 $K^+ p \to K 2\pi N$
130		DENEGRI	71	DBC	−	12.6 $K^- d \to \overline{K} 2\pi d$
100± 50		AGUILAR-...	70C	HBC	−	4.6 $K^- p$
138± 40		BARTSCH	70C	HBC	−	10.1 $K^- p$
50^{+40}_{-20}		LUDLAM	70	HBC	−	12.6 $K^- p$

[6] From an amplitude analysis of the decay $B^+ \to J/\psi\phi K^+$ with a significance of 5.0 σ.
[7] From a partial wave analysis of the $K^-\omega$ system.
[8] From a partial wave analysis of the $K^- 2\pi$ system.
[9] Produced in conjunction with excited deuteron.
[10] Systematic errors added correspond to spread of different fits.

Downloaded from https://academic.oup.com/ptep/article/2022/8/083C01/6651666 by KIT Library user on 27 September 2022

$K_2(1770)$ DECAY MODES

	Mode	Fraction (Γ_i/Γ)
Γ_1	$K\pi\pi$	
Γ_2	$K_2^*(1430)\pi$	seen
Γ_3	$K^*(892)\pi$	seen
Γ_4	$K f_2(1270)$	seen
Γ_5	$K f_0(980)$	
Γ_6	$K\phi$	seen
Γ_7	$K\omega$	seen

$K_2(1770)$ BRANCHING RATIOS

$\Gamma(K_2^*(1430)\pi)/\Gamma(K\pi\pi)$ — Γ_2/Γ_1

($K_2^*(1430) \to K\pi$)

VALUE	DOCUMENT ID		TECN	CHG	COMMENT
• • • We do not use the following data for averages, fits, limits, etc. • • •					
~ 0.03	DAUM	81C	CNTR		63 $K^-p \to K^-2\pi p$
~ 1.0	[11] FIRESTONE	72B	DBC	+	12 K^+d
<1.0	COLLEY	71	HBC		10 K^+p
0.2 ± 0.2	AGUILAR-...	70C	HBC	−	4.6 K^-p
<1.0	BARTSCH	70C	HBC	−	10.1 K^-p
1.0	BARBARO-...	69	HBC	+	12.0 K^+p

[11] Produced in conjunction with excited deuteron.

$\Gamma(K^*(892)\pi)/\Gamma(K\pi\pi)$ — Γ_3/Γ_1

VALUE	DOCUMENT ID	TECN	COMMENT
• • • We do not use the following data for averages, fits, limits, etc. • • •			
~ 0.23	DAUM	81C CNTR	63 $K^-p \to K^-2\pi p$

$\Gamma(K f_2(1270))/\Gamma(K\pi\pi)$ — Γ_4/Γ_1

($f_2(1270) \to \pi\pi$)

VALUE	DOCUMENT ID	TECN	COMMENT
• • • We do not use the following data for averages, fits, limits, etc. • • •			
~ 0.74	DAUM	81C CNTR	63 $K^-p \to K^-2\pi p$

$\Gamma(K f_0(980))/\Gamma_{total}$ — Γ_5/Γ

VALUE	DOCUMENT ID	TECN	COMMENT
• • • We do not use the following data for averages, fits, limits, etc. • • •			
possibly seen	TIKHOMIROV 03	SPEC	40.0 $\pi^- C \to K_S^0 K_S^0 K_L^0 X$

$\Gamma(K\phi)/\Gamma_{total}$ — Γ_6/Γ

VALUE	EVTS	DOCUMENT ID		TECN	CHG	COMMENT
seen	24k	[12] AAIJ	21E	LHCB		$B^+ \to J/\psi\phi K^+$
seen		ARMSTRONG	83	OMEG	−	18.5 $K^-p \to K^-\phi N$
• • • We do not use the following data for averages, fits, limits, etc. • • •						
seen	4289	[13,14] AAIJ	17C	LHCB		$B^+ \to J/\psi\phi K^+$

[12] From an amplitude analysis of the decay $B^+ \to J/\psi\phi K^+$ with a significance of 7.9 σ.
[13] From an amplitude analysis of the decay $B^+ \to J/\psi\phi K^+$ with a significance of 5.0 σ.
[14] Superseded by AAIJ 21E.

$\Gamma(K\omega)/\Gamma_{total}$ — Γ_7/Γ

VALUE	DOCUMENT ID	TECN	CHG	COMMENT
seen	OTTER 81	HBC	±	8.25,10,16 $K^\pm p$
seen	CHUNG 74	HBC	−	7.3 $K^-p \to K^-\omega p$

$K_2(1770)$ REFERENCES

AAIJ	21E	PRL 127 082001	R. Aaij *et al.*	(LHCb Collab.)
AAIJ	17C	PRL 118 022003	R. Aaij *et al.*	(LHCb Collab.)
Also		PR D95 012002	R. Aaij *et al.*	(LHCb Collab.)
PDG	04	PL B592 1	S. Eidelman *et al.*	(PDG Collab.)
TIKHOMIROV	03	PAN 66 828	G.D. Tikhomirov *et al.*	
		Translated from YAF 66 860.		
ASTON	93	PL B308 186	D. Aston *et al.*	(SLAC, NAGO, CINC, INUS)
FRAME	86	NP B276 667	D. Frame *et al.*	(GLAS)
ARMSTRONG	83	NP B221 1	T.A. Armstrong *et al.*	(BARI, BIRM, CERN+)
DAUM	81C	NP B187 1	C. Daum *et al.*	(AMST, CERN, CRAC, MPIM+)
OTTER	81	NP B181 1	G. Otter	(AACH3, BERL, LOIC, VIEN, BIRM+)
CHUNG	74	PL 51B 413	S.U. Chung *et al.*	(BNL)
BLIEDEN	72	PL 39B 668	H.R. Blieden *et al.*	(STON, NEAS)
FIRESTONE	72B	PR D5 505	A. Firestone *et al.*	(LBL)
COLLEY	71	NP B26 71	D.C. Colley *et al.*	(BIRM, GLAS)
DENEGRI	71	NP B28 13	D. Denegri *et al.*	(JHU) JP
AGUILAR-...	70C	PRL 25 54	M. Aguilar-Benitez *et al.*	(BNL)
BARTSCH	70C	PL 33B 186	J. Bartsch *et al.*	(AACH, BERL, CERN+)
LUDLAM	70	PR D2 1234	T. Ludlam, J. Sandweiss, A.J. Slaughter	(YALE)
BARBARO-...	69	PRL 22 1207	A. Barbaro-Galtieri *et al.*	(LRL)

$K_3^*(1780)$

$I(J^P) = \frac{1}{2}(3^-)$

$K_3^*(1780)$ T-MATRIX POLE $\sqrt{s}$

VALUE (MeV)	DOCUMENT ID		TECN	COMMENT
• • • We do not use the following data for averages, fits, limits, etc. • • •				
$(1754 \pm 13) - i(119 \pm 14)$	[1] PELAEZ	17	RVUE	$\pi K \to \pi K$

[1] Reanalysis of ESTABROOKS 78 and ASTON 88 satisfying Forward Dispersion Relations and using sequences of Pade approximants.

$K_3^*(1780)$ MASS

VALUE (MeV)	EVTS	DOCUMENT ID		TECN	CHG	COMMENT
1779± 8 OUR AVERAGE		Error includes scale factor of 1.2.				
$1813 \pm 15 {}^{+65}_{-16}$	18k	[1] ABLIKIM	20F	BES3		$\psi(2S) \to K^+K^-\eta$
$1781 \pm 8 \pm 4$		[2] ASTON	88	LASS	0	11 $K^-p \to K^-\pi^+n$
$1740 \pm 14 \pm 15$		[2] ASTON	87	LASS	0	11 $K^-p \to \overline{K}^0\pi^+\pi^-n$
1779 ± 11		[3] BALDI	76	SPEC	+	10 $K^+p \to K^0\pi^+p$
1776 ± 26		[4] BRANDENB...	76D	ASPK	0	13 $K^\pm p \to K^\pm\pi^\mp N$
• • • We do not use the following data for averages, fits, limits, etc. • • •						
$1720 \pm 10 \pm 15$	6111	[5] BIRD	89	LASS	−	11 $K^-p \to \overline{K}^0\pi^-p$
1749 ± 10		ASTON	88B	LASS	−	11 $K^-p \to K^-\eta p$
1780 ± 9	300	BAUBILLIER	84B	HBC	−	8.25 $K^-p \to \overline{K}^0\pi^-p$
1790 ± 15		BAUBILLIER	82B	HBC	0	8.25 $K^-p \to K_S^0 2\pi N$
1784 ± 9	2060	CLELAND	82	SPEC	±	50 $K^+p \to K_S^0\pi^\pm p$
1786 ± 15		[6] ASTON	81D	LASS	0	11 $K^-p \to K^-\pi^+n$
1762 ± 9	190	TOAFF	81	HBC	−	6.5 $K^-p \to \overline{K}^0\pi^-p$
1850 ± 50		ETKIN	80	MPS	0	6 $K^-p \to \overline{K}^0\pi^+\pi^-$
1812 ± 28		BEUSCH	78	OMEG		10 $K^-p \to \overline{K}^0\pi^+\pi^-n$
1786 ± 8		CHUNG	78	MPS	0	6 $K^-p \to K^-\pi^+n$

[1] Seen in $\psi(2S)$ decay with branching ratio $\psi(2S) \to K^\pm X \to K^+K^-\eta = (2.0 \pm 0.4 {}^{+1.9}_{-0.4}) \times 10^{-6}$.
[2] From energy-independent partial-wave analysis.
[3] From a fit to Y_6^2 moment. $J^P = 3^-$ found.
[4] Confirmed by phase shift analysis of ESTABROOKS 78, yields $J^P = 3^-$.
[5] From a partial wave amplitude analysis.
[6] From a fit to the Y_6^0 moment.

$K_3^*(1780)$ WIDTH

VALUE (MeV)	EVTS	DOCUMENT ID		TECN	CHG	COMMENT
161±17 OUR AVERAGE		Error includes scale factor of 1.1.				
$191 {}^{+43}_{-37} {}^{+3}_{-81}$	1.8k	[1] ABLIKIM	20F	BES3		$\psi(2S) \to K^+K^-\eta$
$203 \pm 30 \pm 8$		[2] ASTON	88	LASS	0	11 $K^-p \to K^-\pi^+n$
$171 \pm 42 \pm 20$		[2] ASTON	87	LASS	0	11 $K^-p \to \overline{K}^0\pi^+\pi^-n$
135 ± 22		[3] BALDI	76	SPEC	+	10 $K^+p \to K^0\pi^+p$
• • • We do not use the following data for averages, fits, limits, etc. • • •						
$187 \pm 31 \pm 20$	6111	[4] BIRD	89	LASS	−	11 $K^-p \to \overline{K}^0\pi^-p$
$193 {}^{+51}_{-37}$		ASTON	88B	LASS	−	11 $K^-p \to K^-\eta p$
99 ± 30	300	BAUBILLIER	84B	HBC	−	8.25 $K^-p \to \overline{K}^0\pi^-p$
~ 130		BAUBILLIER	82B	HBC	0	8.25 $K^-p \to K_S^0 2\pi N$
191 ± 24	2060	CLELAND	82	SPEC	±	50 $K^+p \to K_S^0\pi^\pm p$
225 ± 60		[5] ASTON	81D	LASS	0	11 $K^-p \to K^-\pi^+n$
~ 80	190	TOAFF	81	HBC	−	6.5 $K^-p \to \overline{K}^0\pi^-p$
240 ± 50		ETKIN	80	MPS	0	6 $K^-p \to \overline{K}^0\pi^+\pi^-$
181 ± 44		[6] BEUSCH	78	OMEG		10 $K^-p \to \overline{K}^0\pi^+\pi^-n$
96 ± 31		CHUNG	78	MPS	0	6 $K^-p \to K^-\pi^+n$
270 ± 70		[7] BRANDENB...	76D	ASPK	0	13 $K^\pm p \to K^\pm\pi^\mp N$

[1] Seen in $\psi(2S)$ decay with branching ratio $\psi(2S) \to K^\pm X \to K^+K^-\eta = (2.0 \pm 0.4 {}^{+1.9}_{-0.4}) \times 10^{-6}$.
[2] From energy-independent partial-wave analysis.
[3] From a fit to Y_6^2 moment. $J^P = 3^-$ found.
[4] From a partial wave amplitude analysis.
[5] From a fit to Y_6^0 moment.
[6] Errors enlarged by us to $4\Gamma/\sqrt{N}$; see the note with the $K^*(892)$ mass.
[7] ESTABROOKS 78 find that BRANDENBURG 76D data are consistent with 175 MeV width. Not averaged.

Downloaded from https://academic.oup.com/ptep/article/2022/8/083C01/6651666 by KIT Library user on 27 September 2022

$K_3^*(1780)$ DECAY MODES

	Mode	Fraction (Γ_i/Γ)	Confidence level
Γ_1	$K\rho$	(31 ± 9) %	
Γ_2	$K^*(892)\pi$	(20 ± 5) %	
Γ_3	$K\pi$	(18.8± 1.0) %	
Γ_4	$K\eta$	(30 ±13) %	
Γ_5	$K_2^*(1430)\pi$	< 16 %	95%

CONSTRAINED FIT INFORMATION

An overall fit to 3 branching ratios uses 4 measurements and one constraint to determine 4 parameters. The overall fit has a $\chi^2 =$ 0.0 for 1 degrees of freedom.

The following *off-diagonal* array elements are the correlation coefficients $\langle \delta x_i \delta x_j \rangle / (\delta x_i \cdot \delta x_j)$, in percent, from the fit to the branching fractions, $x_i \equiv \Gamma_i/\Gamma_{total}$. The fit constrains the x_i whose labels appear in this array to sum to one.

x_2	85		
x_3	18	21	
x_4	−98	−94	−27
	x_1	x_2	x_3

$K_3^*(1780)$ BRANCHING RATIOS

$\Gamma(K\rho)/\Gamma(K^*(892)\pi)$ — Γ_1/Γ_2

VALUE	DOCUMENT ID		TECN	CHG	COMMENT
1.52±0.23 OUR FIT					
1.52±0.21±0.10	ASTON	87	LASS	0	11 $K^-p \to \overline{K}^0\pi^+\pi^-n$

$\Gamma(K^*(892)\pi)/\Gamma(K\pi)$ — Γ_2/Γ_3

VALUE	DOCUMENT ID		TECN	CHG	COMMENT
1.09±0.26 OUR FIT					
1.09±0.26	ASTON	84B	LASS	0	11 $K^-p \to \overline{K}^0 2\pi n$

$\Gamma(K\pi)/\Gamma_{total}$ — Γ_3/Γ

VALUE	DOCUMENT ID		TECN	CHG	COMMENT
0.188±0.010 OUR FIT					
0.188±0.010 OUR AVERAGE					
0.187±0.008±0.008	ASTON	88	LASS	0	11 $K^-p \to K^-\pi^+n$
0.19 ±0.02	ESTABROOKS	78	ASPK	0	13 $K^\pm p \to K\pi N$

$\Gamma(K\eta)/\Gamma(K\pi)$ — Γ_4/Γ_3

VALUE	DOCUMENT ID		TECN	CHG	COMMENT
1.6 ±0.7 OUR FIT					
• • • We do not use the following data for averages, fits, limits, etc. • • •					
0.41±0.050	[1] BIRD	89	LASS	−	11 $K^-p \to \overline{K}^0\pi^-p$
0.50±0.18	ASTON	88B	LASS	−	11 $K^-p \to K^-\eta p$

[1] This result supersedes ASTON 88B.

$\Gamma(K_2^*(1430)\pi)/\Gamma(K^*(892)\pi)$ — Γ_5/Γ_2

VALUE	CL%	DOCUMENT ID		TECN	CHG	COMMENT
<0.78	95	ASTON	87	LASS	0	11 $K^-p \to \overline{K}^0\pi^+\pi^-n$

$K_3^*(1780)$ REFERENCES

ABLIKIM	20F	PR D101 032008	M. Ablikim *et al.*	(BESIII Collab.)
PELAEZ	17	EPJ C77 91	J.R. Pelaez, A.Rodas, J.R. de Elvira	
BIRD	89	SLAC-332	P.F. Bird	(SLAC)
ASTON	88	NP B296 493	D. Aston *et al.*	(SLAC, NAGO, CINC, INUS)
ASTON	88B	PL B201 169	D. Aston *et al.*	(SLAC, NAGO, CINC, INUS) JP
ASTON	87	NP B292 693	D. Aston *et al.*	(SLAC, NAGO, CINC, INUS)
ASTON	84B	NP B247 261	D. Aston *et al.*	(SLAC, CARL, OTTA)
BAUBILLIER	84B	ZPHY C26 37	M. Baubillier *et al.*	(BIRM, CERN, GLAS+)
BAUBILLIER	82B	NP B202 21	M. Baubillier *et al.*	(BIRM, CERN, GLAS+)
CLELAND	82	NP B208 189	W.E. Cleland *et al.*	(DURH, GEVA, LAUS+)
ASTON	81D	PL 99B 502	D. Aston *et al.*	(SLAC, CARL, OTTA) JP
TOAFF	81	PR D23 1500	S. Toaff *et al.*	(ANL, KANS)
ETKIN	80	PR D22 42	A. Etkin *et al.*	(BNL, CUNY) JP
BEUSCH	78	PL 74B 282	W. Beusch *et al.*	(CERN, AACH3, ETH) JP
CHUNG	78	PRL 40 355	S.U. Chung *et al.*	(BNL, BRAN, CUNY+) JP
ESTABROOKS	78	NP B133 490	P.G. Estabrooks *et al.*	(MCGI, CARL, DURH+) JP
Also		PR D17 658	P.G. Estabrooks *et al.*	(MCGI, CARL, DURH+)
BALDI	76	PL 63B 344	R. Baldi *et al.*	(GEVA) JP
BRANDENB...	76D	PL 60B 478	G.W. Brandenburg *et al.*	(SLAC) JP

$K_2(1820)$

$I(J^P) = \frac{1}{2}(2^-)$

See our mini-review in the 2004 edition of this *Review* (PDG 04) under $K_2(1770)$.

$K_2(1820)$ MASS

VALUE (MeV)	EVTS	DOCUMENT ID		TECN	COMMENT
1819±12 OUR AVERAGE					
$1853\pm27^{+18}_{-35}$	4289	[1] AAIJ	17C	LHCB	$B^+ \to J/\psi\phi K^+$
1816±13		[2] ASTON	93	LASS	11 $K^-p \to K^-\omega p$
• • • We do not use the following data for averages, fits, limits, etc. • • •					
~ 1840		[3] DAUM	81C	CNTR	63 $K^-p \to K^-2\pi p$

[1] From an amplitude analysis of the decay $B^+ \to J/\psi\phi K^+$ with a significance of 3.0 σ.
[2] From a partial wave analysis of the $K^-\omega$ system.
[3] From a partial wave analysis of the $K^-2\pi$ system.

$K_2(1820)$ WIDTH

VALUE (MeV)	EVTS	DOCUMENT ID		TECN	COMMENT
264±34 OUR AVERAGE					
$167\pm58^{+82}_{-72}$	4289	[1] AAIJ	17C	LHCB	$B^+ \to J/\psi\phi K^+$
276±35		[2] ASTON	93	LASS	11 $K^-p \to K^-\omega p$
• • • We do not use the following data for averages, fits, limits, etc. • • •					
~ 230		[3] DAUM	81C	CNTR	63 $K^-p \to K^-2\pi p$

[1] From an amplitude analysis of the decay $B^+ \to J/\psi\phi K^+$ with a significance of 3.0 σ.
[2] From a partial wave analysis of the $K^-\omega$ system.
[3] From a partial wave analysis of the $K^-2\pi$ system.

$K_2(1820)$ DECAY MODES

	Mode	Fraction (Γ_i/Γ)
Γ_1	$K\pi\pi$	seen
Γ_2	$K_2^*(1430)\pi$	seen
Γ_3	$K^*(892)\pi$	seen
Γ_4	$Kf_2(1270)$	seen
Γ_5	$K\omega$	seen
Γ_6	$K\phi$	seen

$K_2(1820)$ BRANCHING RATIOS

$\Gamma(K_2^*(1430)\pi)/\Gamma(K\pi\pi)$ — Γ_2/Γ_1

VALUE	DOCUMENT ID		TECN	COMMENT
• • • We do not use the following data for averages, fits, limits, etc. • • •				
~ 0.77	DAUM	81C	CNTR	63 $K^-p \to \overline{K}2\pi p$

$\Gamma(K^*(892)\pi)/\Gamma(K\pi\pi)$ — Γ_3/Γ_1

VALUE	DOCUMENT ID		TECN	COMMENT
• • • We do not use the following data for averages, fits, limits, etc. • • •				
~ 0.05	DAUM	81C	CNTR	63 $K^-p \to \overline{K}2\pi p$

$\Gamma(Kf_2(1270))/\Gamma(K\pi\pi)$ — Γ_4/Γ_1

VALUE	DOCUMENT ID		TECN	COMMENT
• • • We do not use the following data for averages, fits, limits, etc. • • •				
~ 0.18	DAUM	81C	CNTR	63 $K^-p \to \overline{K}2\pi p$

$\Gamma(K\phi)/\Gamma_{total}$ — Γ_6/Γ

VALUE	EVTS	DOCUMENT ID		TECN	COMMENT
seen	24k	[1] AAIJ	21E	LHCB	$B^+ \to J/\psi\phi K^+$
• • • We do not use the following data for averages, fits, limits, etc. • • •					
seen	4289	[2,3] AAIJ	17C	LHCB	$B^+ \to J/\psi\phi K^+$

[1] From an amplitude analysis of the decay $B^+ \to J/\psi\phi K^+$ with a significance of 5.8 σ.
[2] From an amplitude analysis of the decay $B^+ \to J/\psi\phi K^+$ with a significance of 3.0 σ.
[3] Superseded by AAIJ 21E.

$K_2(1820)$ REFERENCES

AAIJ	21E	PRL 127 082001	R. Aaij *et al.*	(LHCb Collab.)
AAIJ	17C	PRL 118 022003	R. Aaij *et al.*	(LHCb Collab.)
Also		PR D95 012002	R. Aaij *et al.*	(LHCb Collab.)
PDG	04	PL B592 1	S. Eidelman *et al.*	(PDG Collab.)
ASTON	93	PL B308 186	D. Aston *et al.*	(SLAC, NAGO, CINC, INUS)
DAUM	81C	NP B187 1	C. Daum *et al.*	(AMST, CERN, CRAC, MPIM+)

Downloaded from https://academic.oup.com/ptep/article/2022/8/083C01/6651666 by KIT Library user on 27 September 2022

$K(1830)$

$I(J^P) = \frac{1}{2}(0^-)$

OMITTED FROM SUMMARY TABLE

Seen in partial-wave analysis of $K\phi$ system. Needs confirmation.

$K(1830)$ MASS

VALUE (MeV)	EVTS	DOCUMENT ID		TECN	CHG	COMMENT
• • • We do not use the following data for averages, fits, limits, etc. • • •						
$1874 \pm 43^{+59}_{-115}$	4289	[1,2] AAIJ	17C	LHCB		$B^+ \to J/\psi\phi K^+$
~ 1830		ARMSTRONG	83	OMEG	−	18.5 $K^- p \to 3Kp$

[1] From an amplitude analysis of the decay $B^+ \to J/\psi\phi K^+$ with a significance of 3.5 σ.

[2] A subsequent amplitude analysis of $B^+ \to J/\psi\phi K^+$ by AAIJ 21E did not confirm this measurement.

$K(1830)$ WIDTH

VALUE (MeV)	EVTS	DOCUMENT ID		TECN	CHG	COMMENT
• • • We do not use the following data for averages, fits, limits, etc. • • •						
$168 \pm 90^{+280}_{-104}$	4289	[3,4] AAIJ	17C	LHCB		$B^+ \to J/\psi\phi K^+$
~ 250		ARMSTRONG	83	OMEG	−	18.5 $K^- p \to 3Kp$

[3] From an amplitude analysis of the decay $B^+ \to J/\psi\phi K^+$ with a significance of 3.5 σ.

[4] A subsequent amplitude analysis of $B^+ \to J/\psi\phi K^+$ by AAIJ 21E did not confirm this measurement.

$K(1830)$ DECAY MODES

	Mode
Γ_1	$K\phi$

$K(1830)$ REFERENCES

AAIJ	21E	PRL 127 082001	R. Aaij *et al.*	(LHCb Collab.)
AAIJ	17C	PRL 118 022003	R. Aaij *et al.*	(LHCb Collab.)
Also		PR D95 012002	R. Aaij *et al.*	(LHCb Collab.)
ARMSTRONG	83	NP B221 1	T.A. Armstrong *et al.*	(BARI, BIRM, CERN+) JP

$K_0^*(1950)$

$I(J^P) = \frac{1}{2}(0^+)$

OMITTED FROM SUMMARY TABLE

Seen in partial-wave analysis of the $K^-\pi^+$ system. Needs confirmation.

$K_0^*(1950)$ MASS

VALUE (MeV)	DOCUMENT ID		TECN	CHG	COMMENT
1944 ± 18 OUR AVERAGE					
$1942 \pm 22 \pm 21$	LEES	21A	BABR		$\gamma\gamma \to \eta_c(1S) \to \eta' K^+ K^-$
$1945 \pm 10 \pm 20$	[1] ASTON	88	LASS	0	11 $K^- p \to K^- \pi^+ n$
• • • We do not use the following data for averages, fits, limits, etc. • • •					
1917 ± 12	[2] ZHOU	06	RVUE		$Kp \to K^- \pi^+ n$
1820 ± 40	[3] ANISOVICH	97C	RVUE		11 $K^- p \to K^- \pi^+ n$

[1] We take the central value of the two solutions and the larger error given.

[2] S-matrix pole. Using ASTON 88 and assuming $K_0^*(700)$, $K_0^*(1430)$.

[3] T-matrix pole. Reanalysis of ASTON 88 data.

$K_0^*(1950)$ WIDTH

VALUE (MeV)	DOCUMENT ID		TECN	CHG	COMMENT
100 ± 40 OUR AVERAGE Error includes scale factor of 1.3.					
$80 \pm 32 \pm 20$	LEES	21A	BABR		$\gamma\gamma \to \eta_c(1S) \to \eta' K^+ K^-$
$201 \pm 34 \pm 79$	[4] ASTON	88	LASS	0	11 $K^- p \to K^- \pi^+ n$
• • • We do not use the following data for averages, fits, limits, etc. • • •					
145 ± 38	[5] ZHOU	06	RVUE		$Kp \to K^- \pi^+ n$
250 ± 100	[6] ANISOVICH	97C	RVUE		11 $K^- p \to K^- \pi^+ n$

[4] We take the central value of the two solutions and the larger error given.

[5] S-matrix pole. Using ASTON 88 and assuming $K_0^*(700)$, $K_0^*(1430)$.

[6] T-matrix pole. Reanalysis of ASTON 88 data.

$K_0^*(1950)$ DECAY MODES

	Mode	Fraction (Γ_i/Γ)
Γ_1	$K^-\pi^+$	(52 ± 14) %

$K_0^*(1950)$ BRANCHING RATIOS

$\Gamma(K^-\pi^+)/\Gamma_{total}$ — Γ_1/Γ

VALUE	DOCUMENT ID		TECN	CHG	COMMENT
0.52 ± 0.08 ± 0.12	[7] ASTON	88	LASS	0	11 $K^- p \to K^- \pi^+ n$
• • • We do not use the following data for averages, fits, limits, etc. • • •					
~ 0.60	[8] ZHOU	06	RVUE		$Kp \to K^- \pi^+ n$

[7] We take the central value of the two solutions and the larger error given.

[8] S-matrix pole. Using ASTON 88 and assuming $K_0^*(700)$, $K_0^*(1430)$.

$K_0^*(1950)$ REFERENCES

LEES	21A	PR D104 072002	J.P. Lees *et al.*	(BABAR Collab.)
ZHOU	06	NP A775 212	Z.Y. Zhou, H.Q. Zheng	
ANISOVICH	97C	PL B413 137	A.V. Anisovich, A.V. Sarantsev	
ASTON	88	NP B296 493	D. Aston *et al.*	(SLAC, NAGO, CINC, INUS)

$K_2^*(1980)$

$I(J^P) = \frac{1}{2}(2^+)$

Needs confirmation.

$K_2^*(1980)$ MASS

VALUE (MeV)	EVTS	DOCUMENT ID		TECN	CHG	COMMENT
1994^{+60}_{-50} OUR AVERAGE Error includes scale factor of 2.8. See the ideogram below.						
$2046^{+17}_{-16} \pm 67 \pm 15$	1.8k	[1] ABLIKIM	20F	BES3		$\psi(2S) \to K^+ K^- \eta$
$1868 \pm 8^{+40}_{-57}$	183k	ABLIKIM	19AQ	BES	±	$J/\psi \to K^+ K^- \pi^0$
$1973 \pm 8 \pm 25$		ASTON	87	LASS	0	11 $K^- p \to \overline{K}^0 \pi^+ \pi^- n$
• • • We do not use the following data for averages, fits, limits, etc. • • •						
$2073 \pm 94^{+245}_{-240}$	4289	[2,3] AAIJ	17C	LHCB		$B^+ \to J/\psi\phi K^+$
2020 ± 20		TIKHOMIROV	03	SPEC		40.0 $\pi^- C \to K^0_S K^0_S K^0_L X$
1978 ± 40	241	BIRD	89	LASS	−	11 $K^- p \to \overline{K}^0 \pi^- p$

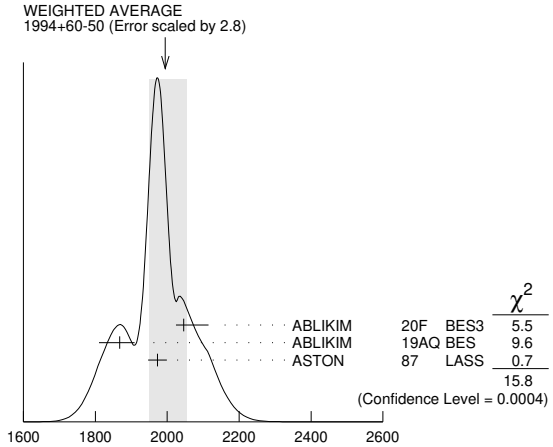

[1] Seen in $\psi(2S)$ decay with branching ratio $\psi(2S) \to K^\pm X \to K^+ K^- \eta = (7.0 \pm 0.5^{+3.7}_{-0.6}) \times 10^{-6}$.

[2] From an amplitude analysis of the decay $B^+ \to J/\psi\phi K^+$ with a significance of 5.4 σ.

[3] A reanalysis by AAIJ 21E using a larger data sample did not confirm this measurement, the new result having a significance of only 1.6 σ.

$K_2^*(1980)$ WIDTH

VALUE (MeV)	EVTS	DOCUMENT ID		TECN	CHG	COMMENT
348^{+50}_{-30} OUR AVERAGE Error includes scale factor of 1.3. See the ideogram below.						
$408^{+38}_{-34} + 72 - 44$	1.8k	[1] ABLIKIM	20F	BES3		$\psi(2S) \to K^+ K^- \eta$
$272 \pm 24^{+50}_{-15}$	183k	ABLIKIM	19AQ	BES	±	$J/\psi \to K^+ K^- \pi^0$
$373 \pm 33 \pm 60$		ASTON	87	LASS	0	11 $K^- p \to \overline{K}^0 \pi^+ \pi^- n$
• • • We do not use the following data for averages, fits, limits, etc. • • •						
$678 \pm 311^{+1153}_{-559}$	4289	[2,3] AAIJ	17C	LHCB		$B^+ \to J/\psi\phi K^+$
180 ± 70		TIKHOMIROV	03	SPEC		40.0 $\pi^- C \to K^0_S K^0_S K^0_L X$
398 ± 47	241	BIRD	89	LASS	−	11 $K^- p \to \overline{K}^0 \pi^- p$

Downloaded from https://academic.oup.com/ptep/article/2022/8/083C01/6651666 by KIT Library user on 27 September 2022

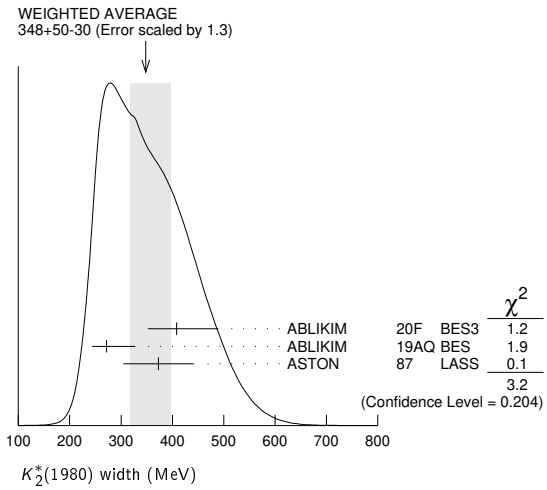

[1] Seen in $\psi(2S)$ decay with branching ratio $\psi(2S) \to K^\pm X \to K^+K^-\eta = (7.0 \pm 0.5^{+3.7}_{-0.6}) \times 10^{-6}$.

[2] From an amplitude analysis of the decay $B^+ \to J/\psi\phi K^+$ with a significance of 5.4 σ.

[3] A reanalysis by AAIJ 21E using a larger data sample did not confirm this measurement, the new result having a significance of only 1.6 σ.

$K_2^*(1980)$ DECAY MODES

	Mode	Fraction (Γ_i/Γ)
Γ_1	$K^*(892)\pi$	possibly seen
Γ_2	$K\rho$	possibly seen
Γ_3	$Kf_2(1270)$	possibly seen
Γ_4	$K\phi$	seen
Γ_5	$K\eta$	seen

$K_2^*(1980)$ BRANCHING RATIOS

$\Gamma(K^*(892)\pi)/\Gamma_{total}$ — Γ_1/Γ

VALUE	DOCUMENT ID		TECN	COMMENT
possibly seen	GULER	11	BELL	$B^+ \to J/\psi K^+\pi^+\pi^-$

$\Gamma(K\rho)/\Gamma_{total}$ — Γ_2/Γ

VALUE	DOCUMENT ID		TECN	COMMENT
possibly seen	GULER	11	BELL	$B^+ \to J/\psi K^+\pi^+\pi^-$

$\Gamma(K\rho)/\Gamma(K^*(892)\pi)$ — Γ_2/Γ_1

VALUE	DOCUMENT ID		TECN	CHG	COMMENT
1.49±0.24±0.09	ASTON	87	LASS	0	11 $K^-p \to \overline{K}^0\pi^+\pi^-n$

$\Gamma(Kf_2(1270))/\Gamma_{total}$ — Γ_3/Γ

VALUE	DOCUMENT ID	TECN	COMMENT
possibly seen	TIKHOMIROV 03	SPEC	40.0 π^-C $\to K^0_S K^0_S K^0_L$X

$\Gamma(K\phi)/\Gamma_{total}$ — Γ_4/Γ

VALUE	EVTS	DOCUMENT ID		TECN	COMMENT
seen	4289	[1,2] AAIJ	17C	LHCB	$B^+ \to J/\psi\phi K^+$

[1] From an amplitude analysis of the decay $B^+ \to J/\psi\phi K^+$ with a significance of 5.4 σ.

[2] A reanalysis by AAIJ 21E using a larger data sample did not confirm this measurement, the new result having a significance of only 1.6 σ.

$\Gamma(K\eta)/\Gamma_{total}$ — Γ_5/Γ

VALUE	EVTS	DOCUMENT ID		TECN	COMMENT
seen	1.8k	[1] ABLIKIM	20F	BES3	$\psi(2S) \to K^+K^-\eta$
seen	116k	[2] CHEN	20A	BELL	$D^0 \to K^-\pi^+\eta$

[1] Seen decaying to $K\eta$ in an amplitude analysis of $\psi(2S) \to K^+K^-\eta$.

[2] From an amplitude analysis of the decay $D^0 \to K^-\pi^+\eta$ with a significance of 17 σ.

$K_2^*(1980)$ REFERENCES

AAIJ	21E	PRL 127 082001	R. Aaij *et al.*	(LHCb Collab.)
ABLIKIM	20F	PR D101 032008	M. Ablikim *et al.*	(BESIII Collab.)
CHEN	20A	PR D102 012002	Y.Q. Chen *et al.*	(BELLE Collab.)
ABLIKIM	19AQ	PR D100 032004	M. Ablikim *et al.*	(BESIII Collab.)
AAIJ	17C	PRL 118 022003	R. Aaij *et al.*	(LHCb Collab.)
Also		PR D95 012002	R. Aaij *et al.*	(LHCb Collab.)
GULER	11	PR D83 032005	H. Guler *et al.*	(BELLE Collab.)
TIKHOMIROV	03	PAN 66 828 Translated from YAF 66 860.	G.D. Tikhomirov *et al.*	
BIRD	89	SLAC-332	P.F. Bird	(SLAC)
ASTON	87	NP B292 693	D. Aston *et al.*	(SLAC, NAGO, CINC, INUS)

$K_4^*(2045)$

$I(J^P) = \frac{1}{2}(4^+)$

$K_4^*(2045)$ MASS

VALUE (MeV)	EVTS	DOCUMENT ID		TECN	CHG	COMMENT
2048^{+8}_{-9} OUR AVERAGE Error includes scale factor of 1.1.						
$2090 \pm 9^{+11}_{-29}$	183k	ABLIKIM	19AQ	BES	±	$J/\psi \to K^+K^-\pi^0$
$2062 \pm 14 \pm 13$		[1] ASTON	86	LASS	0	11 $K^-p \to K^-\pi^+n$
2039 ± 10	400	[2,3] CLELAND	82	SPEC	±	50 $K^+p \to K^0_S\pi^\pm p$
2070^{+100}_{-40}		[4] ASTON	81C	LASS	0	11 $K^-p \to K^-\pi^+n$
• • • We do not use the following data for averages, fits, limits, etc. • • •						
2079 ± 7	431	TORRES	86	MPSF		400 pA $\to 4K$X
2088 ± 20	650	BAUBILLIER	82	HBC	–	8.25 $K^-p \to K^0_S\pi^-p$
2115 ± 46	488	CARMONY	77	HBC	0	9 $K^+d \to K^+\pi$'s X

[1] From a fit to all moments.
[2] From a fit to 8 moments.
[3] Number of events evaluated by us.
[4] From energy-independent partial-wave analysis.

$K_4^*(2045)$ WIDTH

VALUE (MeV)	EVTS	DOCUMENT ID		TECN	CHG	COMMENT
199^{+27}_{-19} OUR AVERAGE						
$201 \pm 19^{+57}_{-17}$	183k	ABLIKIM	19AQ	BES	±	$J/\psi \to K^+K^-\pi^0$
$221 \pm 48 \pm 27$		[5] ASTON	86	LASS	0	11 $K^-p \to K^-\pi^+n$
189 ± 35	400	[6,7] CLELAND	82	SPEC	±	50 $K^+p \to K^0_S\pi^\pm p$
• • • We do not use the following data for averages, fits, limits, etc. • • •						
61 ± 58	431	TORRES	86	MPSF		400 pA $\to 4K$X
170^{+100}_{-50}	650	BAUBILLIER	82	HBC	–	8.25 $K^-p \to K^0_S\pi^-p$
240^{+500}_{-100}		[8] ASTON	81C	LASS	0	11 $K^-p \to K^-\pi^+n$
300 ± 200		CARMONY	77	HBC	0	9 $K^+d \to K^+\pi$'s X

[5] From a fit to all moments.
[6] From a fit to 8 moments.
[7] Number of events evaluated by us.
[8] From energy-independent partial-wave analysis.

$K_4^*(2045)$ DECAY MODES

	Mode	Fraction (Γ_i/Γ)
Γ_1	$K\pi$	(9.9±1.2) %
Γ_2	$K^*(892)\pi\pi$	(9 ±5) %
Γ_3	$K^*(892)\pi\pi\pi$	(7 ±5) %
Γ_4	$\rho K\pi$	(5.7±3.2) %
Γ_5	$\omega K\pi$	(5.0±3.0) %
Γ_6	$\phi K\pi$	(2.8±1.4) %
Γ_7	$\phi K^*(892)$	(1.4±0.7) %

$K_4^*(2045)$ BRANCHING RATIOS

$\Gamma(K\pi)/\Gamma_{total}$ — Γ_1/Γ

VALUE	DOCUMENT ID		TECN	CHG	COMMENT
0.099±0.012	ASTON	88	LASS	0	11 $K^-p \to K^-\pi^+n$

$\Gamma(K^*(892)\pi\pi)/\Gamma(K\pi)$ — Γ_2/Γ_1

VALUE	DOCUMENT ID		TECN	CHG	COMMENT
0.89±0.53	BAUBILLIER	82	HBC	–	8.25 $K^-p \to pK^0_S3\pi$

$\Gamma(K^*(892)\pi\pi\pi)/\Gamma(K\pi)$ — Γ_3/Γ_1

VALUE	DOCUMENT ID		TECN	CHG	COMMENT
0.75±0.49	BAUBILLIER	82	HBC	–	8.25 $K^-p \to pK^0_S3\pi$

$\Gamma(\rho K\pi)/\Gamma(K\pi)$ — Γ_4/Γ_1

VALUE	DOCUMENT ID		TECN	CHG	COMMENT
0.58±0.32	BAUBILLIER	82	HBC	–	8.25 $K^-p \to pK^0_S3\pi$

$\Gamma(\omega K\pi)/\Gamma(K\pi)$ — Γ_5/Γ_1

VALUE	DOCUMENT ID		TECN	CHG	COMMENT
0.50±0.30	BAUBILLIER	82	HBC	–	8.25 $K^-p \to pK^0_S3\pi$

$\Gamma(\phi K\pi)/\Gamma_{total}$ — Γ_6/Γ

VALUE	DOCUMENT ID		TECN	COMMENT
0.028±0.014	[9] TORRES	86	MPSF	400 pA $\to 4K$X

Downloaded from https://academic.oup.com/ptep/article/2022/8/083C01/6651666 by KIT Library user on 27 September 2022

$\Gamma(\phi K^*(892))/\Gamma_{total}$ — Γ_7/Γ

VALUE	DOCUMENT ID		TECN	COMMENT
0.014±0.007	[9] TORRES	86	MPSF	400 $pA \to 4KX$

[9] Error determination is model dependent.

$K_4^*(2045)$ REFERENCES

ABLIKIM	19AQ	PR D100 032004	M. Ablikim *et al.*	(BESIII Collab.)
ASTON	88	NP B296 493	D. Aston *et al.*	(SLAC, NAGO, CINC, INUS)
ASTON	86	PL B180 308	D. Aston *et al.*	(SLAC, NAGO, CINC, INUS)
TORRES	86	PR D34 707	S. Torres *et al.*	(VPI, ARIZ, FNAL, FSU+)
BAUBILLIER	82	PL 118B 447	M. Baubillier *et al.*	(BIRM, CERN, GLAS+)
CLELAND	82	NP B208 189	W.E. Cleland *et al.*	(DURH, GEVA, LAUS+)
ASTON	81C	PL 106B 235	D. Aston *et al.*	(SLAC, CARL, OTTA) JP
CARMONY	77	PR D16 1251	D.D. Carmony *et al.*	(PURD, UCD, IUPU)

$K_2(2250)$

$I(J^P) = \frac{1}{2}(2^-)$

OMITTED FROM SUMMARY TABLE

This entry contains various peaks in strange meson systems reported in the 2150–2260 MeV region, as well as enhancements seen in the antihyperon-nucleon system, either in the mass spectra or in the $J^P = 2^-$ wave.

$K_2(2250)$ MASS

VALUE (MeV)	EVTS	DOCUMENT ID		TECN	CHG	COMMENT
2247±17 OUR AVERAGE						
2200±40		[1] ARMSTRONG	83C	OMEG	−	18 $K^-p \to \Lambda\overline{p}X$
2235±50		[1] BAUBILLIER	81	HBC	−	8 $K^-p \to \Lambda\overline{p}X$
2260±20		[1] CLELAND	81	SPEC	±	50 $K^+p \to \Lambda\overline{p}X$
• • • We do not use the following data for averages, fits, limits, etc. • • •						
2280±20		TIKHOMIROV	03	SPEC		40.0 $\pi^-C \to K^0_S K^0_S K^0_L X$
2147± 4	37	CHLIAPNIK...	79	HBC	+	32 $K^+p \to \overline{\Lambda}pX$
2240±20	20	LISSAUER	70	HBC		9 K^+p

[1] $J^P = 2^-$ from moments analysis.

$K_2(2250)$ WIDTH

VALUE (MeV)	EVTS	DOCUMENT ID		TECN	CHG	COMMENT
180±30 OUR AVERAGE		Error includes scale factor of 1.4.				
150±30		[2] ARMSTRONG	83C	OMEG	−	18 $K^-p \to \Lambda\overline{p}X$
210±30		[2] CLELAND	81	SPEC	±	50 $K^+p \to \Lambda\overline{p}X$
• • • We do not use the following data for averages, fits, limits, etc. • • •						
180±60		TIKHOMIROV	03	SPEC		40.0 $\pi^-C \to K^0_S K^0_S K^0_L X$
∼ 200		[2] BAUBILLIER	81	HBC	−	8 $K^-p \to \Lambda\overline{p}X$
∼ 40	37	CHLIAPNIK...	79	HBC	+	32 $K^+p \to \overline{\Lambda}pX$
80±20	20	LISSAUER	70	HBC		9 K^+p

[2] $J^P = 2^-$ from moments analysis.

$K_2(2250)$ DECAY MODES

	Mode
Γ_1	$K\pi\pi$
Γ_2	$K f_2(1270)$
Γ_3	$K^*(892) f_0(980)$
Γ_4	$p\overline{\Lambda}$

$K_2(2250)$ REFERENCES

TIKHOMIROV	03	PAN 66 828 Translated from YAF 66 860.	G.D. Tikhomirov *et al.*	
ARMSTRONG	83C	NP B227 365	T.A. Armstrong *et al.*	(BARI, BIRM, CERN+)
BAUBILLIER	81	NP B183 1	M. Baubillier *et al.*	(BIRM, CERN, GLAS+) JP
CLELAND	81	NP B184 1	W.E. Cleland *et al.*	(PITT, GEVA, LAUS+) JP
CHLIAPNIK...	79	NP B158 253	P.V. Chliapnikov *et al.*	(CERN, BELG, MONS)
LISSAUER	70	NP B18 491	D. Lissauer *et al.*	(LBL)

$K_3(2320)$

$I(J^P) = \frac{1}{2}(3^+)$

OMITTED FROM SUMMARY TABLE

Seen in the $J^P = 3^+$ wave of the antihyperon-nucleon system. Needs confirmation.

$K_3(2320)$ MASS

VALUE (MeV)	DOCUMENT ID		TECN	CHG	COMMENT
2324±24 OUR AVERAGE					
2330±40	[1] ARMSTRONG	83C	OMEG	−	18 $K^-p \to \Lambda\overline{p}X$
2320±30	[1] CLELAND	81	SPEC	±	50 $K^+p \to \Lambda\overline{p}X$

[1] $J^P = 3^+$ from moments analysis.

$K_3(2320)$ WIDTH

VALUE (MeV)	DOCUMENT ID		TECN	CHG	COMMENT
150±30	[2] ARMSTRONG	83C	OMEG	−	18 $K^-p \to \Lambda\overline{p}X$
• • • We do not use the following data for averages, fits, limits, etc. • • •					
∼ 250	[2] CLELAND	81	SPEC	±	50 $K^+p \to \Lambda\overline{p}X$

[2] $J^P = 3^+$ from moments analysis.

$K_3(2320)$ DECAY MODES

	Mode
Γ_1	$p\overline{\Lambda}$

$K_3(2320)$ REFERENCES

ARMSTRONG	83C	NP B227 365	T.A. Armstrong *et al.*	(BARI, BIRM, CERN+)
CLELAND	81	NP B184 1	W.E. Cleland *et al.*	(PITT, GEVA, LAUS+)

$K_5^*(2380)$

$I(J^P) = \frac{1}{2}(5^-)$

OMITTED FROM SUMMARY TABLE

Needs confirmation.

$K_5^*(2380)$ MASS

VALUE (MeV)	DOCUMENT ID		TECN	CHG	COMMENT
2382±14±19	[1] ASTON	86	LASS	0	11 $K^-p \to K^-\pi^+n$

[1] From a fit to all the moments.

$K_5^*(2380)$ WIDTH

VALUE (MeV)	DOCUMENT ID		TECN	CHG	COMMENT
178±37±32	[2] ASTON	86	LASS	0	11 $K^-p \to K^-\pi^+n$

[2] From a fit to all the moments.

$K_5^*(2380)$ DECAY MODES

	Mode	Fraction (Γ_i/Γ)
Γ_1	$K\pi$	(6.1±1.2) %

$K_5^*(2380)$ BRANCHING RATIOS

$\Gamma(K\pi)/\Gamma_{total}$ — Γ_1/Γ

VALUE	DOCUMENT ID		TECN	CHG	COMMENT
0.061±0.012	ASTON	88	LASS	0	11 $K^-p \to K^-\pi^+n$

$K_5^*(2380)$ REFERENCES

ASTON	88	NP B296 493	D. Aston *et al.*	(SLAC, NAGO, CINC, INUS)
ASTON	86	PL B180 308	D. Aston *et al.*	(SLAC, NAGO, CINC, INUS)

$K_4(2500)$

$I(J^P) = \frac{1}{2}(4^-)$

OMITTED FROM SUMMARY TABLE

Needs confirmation.

$K_4(2500)$ MASS

VALUE (MeV)	DOCUMENT ID		TECN	CHG	COMMENT
2490±20	[1] CLELAND	81	SPEC	±	50 $K^+p \to \Lambda\overline{p}$

[1] $J^P = 4^-$ from moments analysis.

$K_4(2500)$ WIDTH

VALUE (MeV)	DOCUMENT ID		TECN	CHG	COMMENT
• • • We do not use the following data for averages, fits, limits, etc. • • •					
∼ 250	[2] CLELAND	81	SPEC	±	50 $K^+p \to \Lambda\overline{p}$

[2] $J^P = 4^-$ from moments analysis.

$K_4(2500)$ DECAY MODES

	Mode
Γ_1	$p\overline{\Lambda}$

$K_4(2500)$ REFERENCES

CLELAND	81	NP B184 1	W.E. Cleland *et al.*	(PITT, GEVA, LAUS+)

Downloaded from https://academic.oup.com/ptep/article/2022/8/083C01/6651666 by KIT Library user on 27 September 2022

$K(3100)$

$I^G(J^{PC}) = ?^?(?^{??})$

OMITTED FROM SUMMARY TABLE

Narrow peak observed in several ($\Lambda\overline{p}$ + pions) and ($\overline{\Lambda}p$ + pions) states in Σ^- Be reactions by BOURQUIN 86 and in np and nA reactions by ALEEV 93. Not seen by BOEHNLEIN 91. If due to strong decays, this state has exotic quantum numbers (B=0,Q=+1,S=−1 for $\Lambda\overline{p}\pi^+\pi^+$ and $I \geq 3/2$ for $\Lambda\overline{p}\pi^-$). Needs confirmation.

$K(3100)$ MASS

VALUE (MeV)	DOCUMENT ID
≈ 3100 OUR ESTIMATE	

3-BODY DECAYS

VALUE (MeV)	DOCUMENT ID		TECN	COMMENT
3054±11 OUR AVERAGE				
3060± 7±20	[1] ALEEV	93	BIS2	$K(3100) \to \Lambda\overline{p}\pi^+$
3056± 7±20	[1] ALEEV	93	BIS2	$K(3100) \to \overline{\Lambda}p\pi^-$
3055± 8±20	[1] ALEEV	93	BIS2	$K(3100) \to \Lambda\overline{p}\pi^-$
3045± 8±20	[1] ALEEV	93	BIS2	$K(3100) \to \overline{\Lambda}p\pi^+$

4-BODY DECAYS

VALUE (MeV)	DOCUMENT ID		TECN	COMMENT
3059±11 OUR AVERAGE				
3067± 6±20	[1] ALEEV	93	BIS2	$K(3100) \to \Lambda\overline{p}\pi^+\pi^+$
3060± 8±20	[1] ALEEV	93	BIS2	$K(3100) \to \Lambda\overline{p}\pi^+\pi^-$
3055± 7±20	[1] ALEEV	93	BIS2	$K(3100) \to \overline{\Lambda}p\pi^-\pi^-$
3052± 8±20	[1] ALEEV	93	BIS2	$K(3100) \to \overline{\Lambda}p\pi^-\pi^+$
• • • We do not use the following data for averages, fits, limits, etc. • • •				
3105±30	BOURQUIN	86	SPEC	$K(3100) \to \Lambda\overline{p}\pi^+\pi^+$
3115±30	BOURQUIN	86	SPEC	$K(3100) \to \Lambda\overline{p}\pi^+\pi^-$

5-BODY DECAYS

VALUE (MeV)	DOCUMENT ID		TECN	COMMENT
• • • We do not use the following data for averages, fits, limits, etc. • • •				
3095±30	BOURQUIN	86	SPEC	$K(3100) \to \Lambda\overline{p}\pi^+\pi^+\pi^-$

[1] Supersedes ALEEV 90.

$K(3100)$ WIDTH

3-BODY DECAYS

VALUE (MeV)	DOCUMENT ID		TECN	COMMENT
• • • We do not use the following data for averages, fits, limits, etc. • • •				
42±16	[2] ALEEV	93	BIS2	$K(3100) \to \Lambda\overline{p}\pi^+$
36±15	[2] ALEEV	93	BIS2	$K(3100) \to \overline{\Lambda}p\pi^-$
50±18	[2] ALEEV	93	BIS2	$K(3100) \to \Lambda\overline{p}\pi^-$
30±15	[2] ALEEV	93	BIS2	$K(3100) \to \overline{\Lambda}p\pi^+$

4-BODY DECAYS

VALUE (MeV)	CL%	DOCUMENT ID		TECN	COMMENT
• • • We do not use the following data for averages, fits, limits, etc. • • •					
22± 8		[2] ALEEV	93	BIS2	$K(3100) \to \Lambda\overline{p}\pi^+\pi^+$
28±12		[2] ALEEV	93	BIS2	$K(3100) \to \Lambda\overline{p}\pi^+\pi^-$
32±15		[2] ALEEV	93	BIS2	$K(3100) \to \overline{\Lambda}p\pi^-\pi^-$
30±15		[2] ALEEV	93	BIS2	$K(3100) \to \overline{\Lambda}p\pi^-\pi^+$
<30	90	BOURQUIN	86	SPEC	$K(3100) \to \Lambda\overline{p}\pi^+\pi^+$
<80	90	BOURQUIN	86	SPEC	$K(3100) \to \Lambda\overline{p}\pi^+\pi^-$

5-BODY DECAYS

VALUE (MeV)	CL%	DOCUMENT ID		TECN	COMMENT
• • • We do not use the following data for averages, fits, limits, etc. • • •					
<30	90	BOURQUIN	86	SPEC	$K(3100) \to \Lambda\overline{p}\pi^+\pi^+\pi^-$

[2] Supersedes ALEEV 90.

$K(3100)$ DECAY MODES

	Mode
Γ_1	$K(3100)^0 \to \Lambda\overline{p}\pi^+$
Γ_2	$K(3100)^{--} \to \Lambda\overline{p}\pi^-$
Γ_3	$K(3100)^- \to \Lambda\overline{p}\pi^+\pi^-$
Γ_4	$K(3100)^+ \to \Lambda\overline{p}\pi^+\pi^+$
Γ_5	$K(3100)^0 \to \Lambda\overline{p}\pi^+\pi^+\pi^-$
Γ_6	$K(3100)^0 \to \Sigma(1385)^+\overline{p}$

$\Gamma(\Sigma(1385)^+\overline{p})/\Gamma(\Lambda\overline{p}\pi^+)$ — Γ_6/Γ_1

VALUE	CL%	DOCUMENT ID		TECN	COMMENT
<0.04	90	ALEEV	93	BIS2	$K(3100)^0 \to \Sigma(1385)^+\overline{p}$

$K(3100)$ REFERENCES

ALEEV	93	PAN 56 1358 Translated from YAF 56 100.	A.N. Aleev *et al.*	(BIS-2 Collab.)
BOEHNLEIN	91	NPBPS B21 174	A. Boehnlein *et al.*	(FLOR, BNL, IND+)
ALEEV	90	ZPHY C47 533	A.N. Aleev *et al.*	(BIS-2 Collab.)
BOURQUIN	86	PL B172 113	M.H. Bourquin *et al.*	(GEVA, RAL, HEIDP+)

Downloaded from https://academic.oup.com/ptep/article/2022/8/083C01/6651666 by KIT Library user on 27 September 2022

CHARMED MESONS
($C = \pm 1$)

$D^+ = c\overline{d}$, $D^0 = c\overline{u}$, $\overline{D}^0 = \overline{c}u$, $D^- = \overline{c}d$, similarly for D^*'s

$D^{\pm}$

$I(J^P) = \frac{1}{2}(0^-)$

$D^{\pm}$ MASS

The fit includes $D^{\pm}$, D^0, $D_s^{\pm}$, $D^{*\pm}$, D^{*0}, $D_s^{*\pm}$, $D_1(2420)^0$, $D_2^*(2460)^0$, and $D_{s1}(2536)^{\pm}$ mass and mass difference measurements.

VALUE (MeV)	EVTS	DOCUMENT ID		TECN	COMMENT
1869.66 ± 0.05 OUR FIT					
1869.5 ± 0.4 OUR AVERAGE					
1869.53 ± 0.49 ± 0.20	110 ± 15	ANASHIN	10A	KEDR	e^+e^- at $\psi(3770)$
1870.0 ± 0.5 ± 1.0	317	BARLAG	90C	ACCM	π^-Cu 230 GeV
1869.4 ± 0.6		[1] TRILLING	81	RVUE	e^+e^- 3.77 GeV
• • • We do not use the following data for averages, fits, limits, etc. • • •					
1875 ± 10	9	ADAMOVICH	87	EMUL	Photoproduction
1860 ± 16	6	ADAMOVICH	84	EMUL	Photoproduction
1863 ± 4		DERRICK	84	HRS	e^+e^- 29 GeV
1868.4 ± 0.5		[1] SCHINDLER	81	MRK2	e^+e^- 3.77 GeV
1874 ± 5		GOLDHABER	77	MRK1	D^0, D^+ recoil spectra
1868.3 ± 0.9		[1] PERUZZI	77	LGW	e^+e^- 3.77 GeV
1874 ± 11		PICCOLO	77	MRK1	e^+e^- 4.03, 4.41 GeV
1876 ± 15	50	PERUZZI	76	MRK1	$K^{\mp}\pi^{\pm}\pi^{\pm}$

[1] PERUZZI 77 and SCHINDLER 81 errors do not include the 0.13% uncertainty in the absolute SPEAR energy calibration. TRILLING 81 uses the high precision $J/\psi(1S)$ and $\psi(2S)$ measurements of ZHOLENTZ 80 to determine this uncertainty and combines the PERUZZI 77 and SCHINDLER 81 results to obtain the value quoted.

$D^{\pm}$ MEAN LIFE

Measurements with an error $> 100 \times 10^{-15}$ s have been omitted from the Listings.

VALUE (10^{-15} s)	EVTS	DOCUMENT ID		TECN	COMMENT
1033 ± 5 OUR AVERAGE					
1030.4 ± 4.7 ± 3.1	171k	[1] ABUDINEN	21A	BEL2	e^+e^- at $\Upsilon(4S)$
1039.4 ± 4.3 ± 7.0	110k	LINK	02F	FOCS	γ nucleus, ≈ 180 GeV
• • • We do not use the following data for averages, fits, limits, etc. • • •					
$1033.6 \pm 22.1 {}^{+9.9}_{-12.7}$	3.7k	BONVICINI	99	CLEO	$e^+e^- \approx \Upsilon(4S)$
1048 ± 15 ± 11	9k	FRABETTI	94D	E687	$D^+ \to K^-\pi^+\pi^+$
1075 ± 40 ± 18	2.4k	FRABETTI	91	E687	γ Be, $D^+ \to K^-\pi^+\pi^+$
1030 ± 80 ± 60	200	ALVAREZ	90	NA14	γ, $D^+ \to K^-\pi^+\pi^+$
$1050 {}^{+77}_{-72}$	317	[2] BARLAG	90C	ACCM	π^-Cu 230 GeV
1050 ± 80 ± 70	363	ALBRECHT	88I	ARG	e^+e^- 10 GeV
1090 ± 30 ± 25	2.9k	RAAB	88	E691	Photoproduction

[1] ABUDINEN 21A determines the lifetime ratio $\tau(D^+)/\tau(D^0) = 2.510 \pm 0.013 \pm 0.007$.
[2] BARLAG 90C estimates the systematic error to be negligible.

D^+ DECAY MODES

Most decay modes (other than the semileptonic modes) that involve a neutral K meson are now given as K^0_S modes, not as $\overline{K}^0$ modes. Nearly always it is a K^0_S that is measured, and interference between Cabibbo-allowed and doubly Cabibbo-suppressed modes can invalidate the assumption that $2\Gamma(K^0_S) = \Gamma(\overline{K}^0)$.

	Mode		Fraction (Γ_i/Γ)	Scale factor/ Confidence level
	Inclusive modes			
Γ_1	e^+ semileptonic		(16.07 ± 0.30) %	
Γ_2	μ^+ anything		(17.6 ± 3.2) %	
Γ_3	K^- anything		(25.7 ± 1.4) %	
Γ_4	$\overline{K}^0$ anything + K^0 anything		(61 ± 5) %	
Γ_5	K^+ anything		(5.9 ± 0.8) %	
Γ_6	$K^*(892)^-$ anything		(6 ± 5) %	
Γ_7	$\overline{K}^*(892)^0$ anything		(23 ± 5) %	
Γ_8	$K^*(892)^0$ anything		< 6.6 %	CL=90%
Γ_9	η anything		(6.3 ± 0.7) %	
Γ_{10}	η' anything		(1.04 ± 0.18) %	
Γ_{11}	ϕ anything		(1.12 ± 0.04) %	
	Leptonic and semileptonic modes			
Γ_{12}	$e^+\nu_e$		< 8.8 $\times 10^{-6}$	CL=90%
Γ_{13}	$\gamma e^+\nu_e$		< 3.0 $\times 10^{-5}$	CL=90%
Γ_{14}	$\mu^+\nu_\mu$		(3.74 ± 0.17) $\times 10^{-4}$	
Γ_{15}	$\tau^+\nu_\tau$		(1.20 ± 0.27) $\times 10^{-3}$	
Γ_{16}	$\overline{K}^0 e^+\nu_e$		(8.72 ± 0.09) %	
Γ_{17}	$\overline{K}^0\mu^+\nu_\mu$		(8.76 ± 0.19) %	
Γ_{18}	$K^-\pi^+e^+\nu_e$		(4.02 ± 0.18) %	S=3.2
Γ_{19}	$\overline{K}^*(892)^0 e^+\nu_e$, $\overline{K}^*(892)^0 \to K^-\pi^+$		(3.77 ± 0.17) %	
Γ_{20}	$(K^-\pi^+)_{[0.8-1.0]\text{GeV}} e^+\nu_e$		(3.39 ± 0.09) %	
Γ_{21}	$(K^-\pi^+)_{S-wave} e^+\nu_e$		(2.28 ± 0.11) $\times 10^{-3}$	
Γ_{22}	$\overline{K}^*(1410)^0 e^+\nu_e$, $\overline{K}^*(1410)^0 \to K^-\pi^+$		< 6 $\times 10^{-3}$	CL=90%
Γ_{23}	$\overline{K}^*_2(1430)^0 e^+\nu_e$, $\overline{K}^*_2(1430)^0 \to K^-\pi^+$		< 5 $\times 10^{-4}$	CL=90%
Γ_{24}	$K^-\pi^+e^+\nu_e$ nonresonant		< 7 $\times 10^{-3}$	CL=90%
Γ_{25}	$\overline{K}^*(892)^0 e^+\nu_e$		(5.40 ± 0.10) %	S=1.1
Γ_{26}	$K^-\pi^+\mu^+\nu_\mu$		(3.65 ± 0.34) %	
Γ_{27}	$\overline{K}^*(892)^0\mu^+\nu_\mu$, $\overline{K}^*(892)^0 \to K^-\pi^+$		(3.52 ± 0.10) %	
Γ_{28}	$K^-\pi^+\mu^+\nu_\mu$ nonresonant		(1.9 ± 0.5) $\times 10^{-3}$	
Γ_{29}	$\overline{K}^*(892)^0\mu^+\nu_\mu$		(5.27 ± 0.15) %	
Γ_{30}	$K^-\pi^+\pi^0\mu^+\nu_\mu$		< 1.5 $\times 10^{-3}$	CL=90%
Γ_{31}	$\overline{K}_1(1270)^0 e^+\nu_e$, $\overline{K}^0_1 \to K^-\pi^+\pi^0$		(1.06 ± 0.15) $\times 10^{-3}$	
Γ_{32}	$\overline{K}^*_0(1430)^0\mu^+\nu_\mu$		< 2.3 $\times 10^{-4}$	CL=90%
Γ_{33}	$\overline{K}^*(1680)^0\mu^+\nu_\mu$		< 1.5 $\times 10^{-3}$	CL=90%
Γ_{34}	$\pi^0 e^+\nu_e$		(3.72 ± 0.17) $\times 10^{-3}$	S=2.0
Γ_{35}	$\pi^0\mu^+\nu_\mu$		(3.50 ± 0.15) $\times 10^{-3}$	
Γ_{36}	$\eta e^+\nu_e$		(1.11 ± 0.07) $\times 10^{-3}$	
Γ_{37}	$\eta\mu^+\nu_\mu$		(1.04 ± 0.11) $\times 10^{-3}$	
Γ_{38}	$\pi^-\pi^+e^+\nu_e$		(2.45 ± 0.10) $\times 10^{-3}$	
Γ_{39}	$f_0(500)^0 e^+\nu_e$, $f_0(500)^0 \to \pi^+\pi^-$		(6.3 ± 0.5) $\times 10^{-4}$	
Γ_{40}	$\rho^0 e^+\nu_e$		$(2.18 {}^{+0.17}_{-0.25}) \times 10^{-3}$	
Γ_{41}	$\rho^0\mu^+\nu_\mu$		(2.4 ± 0.4) $\times 10^{-3}$	
Γ_{42}	$\omega e^+\nu_e$		(1.69 ± 0.11) $\times 10^{-3}$	
Γ_{43}	$\omega\mu^+\nu_\mu$		(1.77 ± 0.21) $\times 10^{-3}$	
Γ_{44}	$\eta'(958) e^+\nu_e$		(2.0 ± 0.4) $\times 10^{-4}$	
Γ_{45}	$a(980)^0 e^+\nu_e$, $a(980)^0 \to \eta\pi^0$		$(1.7 {}^{+0.8}_{-0.7}) \times 10^{-4}$	
Γ_{46}	$b_1(1235)^0 e^+\nu_e$, $b^0_1 \to \omega\pi^0$		< 1.75 $\times 10^{-4}$	CL=90%
Γ_{47}	$\phi e^+\nu_e$		< 1.3 $\times 10^{-5}$	CL=90%
Γ_{48}	$D^0 e^+\nu_e$		< 1.0 $\times 10^{-4}$	CL=90%
	Hadronic modes with a $\overline{K}$ or $\overline{K}K\overline{K}$			
Γ_{49}	$K^0_S\pi^+$		(1.562 ± 0.031) %	S=1.7
Γ_{50}	$K^0_L\pi^+$		(1.46 ± 0.05) %	
Γ_{51}	$K^-2\pi^+$	[a]	(9.38 ± 0.16) %	S=1.6
Γ_{52}	$(K^-\pi^+)_{S-\text{wave}}\pi^+$		(7.52 ± 0.17) %	
Γ_{53}	$\overline{K}^*_0(700)^0\pi^+$, $\overline{K}^*_0(700) \to K^-\pi^+$			
Γ_{54}	$\overline{K}^*_0(1430)^0\pi^+$, $\overline{K}^*_0(1430)^0 \to K^-\pi^+$	[b]	(1.25 ± 0.06) %	
Γ_{55}	$\overline{K}^*(892)^0\pi^+$, $\overline{K}^*(892)^0 \to K^-\pi^+$		(1.04 ± 0.12) %	
Γ_{56}	$\overline{K}^*(1410)^0\pi^+$, $\overline{K}^{*0} \to K^-\pi^+$		not seen	
Γ_{57}	$\overline{K}^*_2(1430)^0\pi^+$, $\overline{K}^*_2(1430)^0 \to K^-\pi^+$	[b]	(2.3 ± 0.7) $\times 10^{-4}$	
Γ_{58}	$\overline{K}^*(1680)^0\pi^+$, $\overline{K}^*(1680)^0 \to K^-\pi^+$	[b]	(2.2 ± 1.1) $\times 10^{-4}$	
Γ_{59}	$K^-(2\pi^+)_{I=2}$		(1.45 ± 0.26) %	
Γ_{60}	$K^-2\pi^+$ nonresonant			
Γ_{61}	$K^0_S\pi^+\pi^0$	[a]	(7.36 ± 0.21) %	
Γ_{62}	$K^0_S\rho^+$		$(6.14 {}^{+0.60}_{-0.35})$ %	
Γ_{63}	$K^0_S\rho(1450)^+$, $\rho^+ \to \pi^+\pi^0$		$(1.5 {}^{+1.2}_{-1.4}) \times 10^{-3}$	
Γ_{64}	$\overline{K}^*(892)^0\pi^+$, $\overline{K}^*(892)^0 \to K^0_S\pi^0$		(2.64 ± 0.32) $\times 10^{-3}$	
Γ_{65}	$\overline{K}^*_0(1430)^0\pi^+$, $\overline{K}^{*0}_0 \to K^0_S\pi^0$		(2.7 ± 0.9) $\times 10^{-3}$	

Downloaded from https://academic.oup.com/ptep/article/2022/8/083C01/6651666 by KIT Library user on 27 September 2022

Γ_{66}	$\overline{K}_0^*(1680)^0\pi^+$, $\overline{K}_0^{*0} \to K_S^0\pi^0$		$(10\ ^{+7}_{-10})\times10^{-4}$	
Γ_{67}	$\overline{\kappa}^0\pi^+$, $\overline{\kappa}^0 \to K_S^0\pi^0$		$(6\ ^{+5}_{-4})\times10^{-3}$	
Γ_{68}	$K_S^0\pi^+\pi^0$ nonresonant		$(3 \pm 4)\times10^{-3}$	
Γ_{69}	$K_S^0\pi^+\pi^0$ nonresonant and $\overline{\kappa}^0\pi^+$		$(1.37\ ^{+0.21}_{-0.40})$ %	
Γ_{70}	$(K_S^0\pi^0)_{S-\text{wave}}\pi^+$		$(1.27\ ^{+0.27}_{-0.33})$ %	
Γ_{71}	$K_S^0\pi^+\eta$		(1.31 ± 0.05) %	
Γ_{72}	$K_S^0\pi^+\eta'(958)$		$(1.90 \pm 0.21)\times10^{-3}$	
Γ_{73}	$K^-2\pi^+\pi^0$	[c]	(6.25 ± 0.18) %	
Γ_{74}	$K_S^0 2\pi^+\pi^-$	[c]	(3.10 ± 0.09) %	
Γ_{75}	$K^-2\pi^+\eta$		$(1.35 \pm 0.12)\times10^{-3}$	
Γ_{76}	$K_S^0\pi^+\pi^0\eta$		$(1.22 \pm 0.25)\times10^{-3}$	
Γ_{77}	$K^-3\pi^+\pi^-$	[a]	$(5.7 \pm 0.5)\times10^{-3}$	S=1.1
Γ_{78}	$\overline{K}^*(892)^0 2\pi^+\pi^-$, $\overline{K}^*(892)^0 \to K^-\pi^+$		$(1.2 \pm 0.4)\times10^{-3}$	
Γ_{79}	$\overline{K}^*(892)^0\rho^0\pi^+$, $\overline{K}^*(892)^0 \to K^-\pi^+$		$(2.3 \pm 0.4)\times10^{-3}$	
Γ_{80}	$\overline{K}^*(892)^0 a_1(1260)^+$	[d]	$(9.3 \pm 1.9)\times10^{-3}$	
Γ_{81}	$\overline{K}^*(892)^0 2\pi^+\pi^-$ no-ρ, $\overline{K}^*(892)^0 \to K^-\pi^+$			
Γ_{82}	$K^-\rho^0 2\pi^+$		$(1.72 \pm 0.28)\times10^{-3}$	
Γ_{83}	$K^-3\pi^+\pi^-$ nonresonant		$(4.0 \pm 2.9)\times10^{-4}$	
Γ_{84}	$K^+2K_S^0$		$(2.54 \pm 0.13)\times10^{-3}$	
Γ_{85}	$K^+K^-K_S^0\pi^+$		$(2.4 \pm 0.5)\times10^{-4}$	

Pionic modes

Γ_{86}	$\pi^+\pi^0$		$(1.247 \pm 0.033)\times10^{-3}$	
Γ_{87}	$2\pi^+\pi^-$		$(3.27 \pm 0.18)\times10^{-3}$	
Γ_{88}	$\rho^0\pi^+$		$(8.3 \pm 1.5)\times10^{-4}$	
Γ_{89}	$\pi^+(\pi^+\pi^-)_{S-\text{wave}}$		$(1.83 \pm 0.16)\times10^{-3}$	
Γ_{90}	$\sigma\pi^+$, $\sigma \to \pi^+\pi^-$		$(1.38 \pm 0.12)\times10^{-3}$	
Γ_{91}	$f_0(980)\pi^+$, $f_0(980) \to \pi^+\pi^-$		$(1.56 \pm 0.33)\times10^{-4}$	
Γ_{92}	$f_0(1370)\pi^+$, $f_0(1370) \to \pi^+\pi^-$		$(8 \pm 4)\times10^{-5}$	
Γ_{93}	$f_2(1270)\pi^+$, $f_2(1270) \to \pi^+\pi^-$		$(5.0 \pm 0.9)\times10^{-4}$	
Γ_{94}	$\rho(1450)^0\pi^+$, $\rho(1450)^0 \to \pi^+\pi^-$		$< 8 \times10^{-5}$	CL=95%
Γ_{95}	$f_0(1500)\pi^+$, $f_0(1500) \to \pi^+\pi^-$		$(1.1 \pm 0.4)\times10^{-4}$	
Γ_{96}	$f_0(1710)\pi^+$, $f_0(1710) \to \pi^+\pi^-$		$< 5 \times10^{-5}$	CL=95%
Γ_{97}	$f_0(1790)\pi^+$, $f_0(1790) \to \pi^+\pi^-$		$< 7 \times10^{-5}$	CL=95%
Γ_{98}	$(\pi^+\pi^+)_{S-\text{wave}}\pi^-$		$< 1.2 \times10^{-4}$	CL=95%
Γ_{99}	$2\pi^+\pi^-$ nonresonant		$< 1.1 \times10^{-4}$	CL=95%
Γ_{100}	$\pi^+2\pi^0$		$(4.7 \pm 0.4)\times10^{-3}$	
Γ_{101}	$2\pi^+\pi^-\pi^0$		(1.16 ± 0.08) %	
Γ_{102}	$3\pi^+2\pi^-$		$(1.66 \pm 0.16)\times10^{-3}$	S=1.1
Γ_{103}	$\eta\pi^+$		$(3.77 \pm 0.09)\times10^{-3}$	
Γ_{104}	$\eta\pi^+\pi^0$		$(2.05 \pm 0.35)\times10^{-3}$	S=2.2
Γ_{105}	$\eta 2\pi^+\pi^-$		$(3.41 \pm 0.20)\times10^{-3}$	
Γ_{106}	$\eta\pi^+2\pi^0$		$(3.20 \pm 0.33)\times10^{-3}$	
Γ_{107}	$\eta\eta\pi^+$		$(2.96 \pm 0.26)\times10^{-3}$	
Γ_{108}	$\omega\pi^+$		$(2.8 \pm 0.6)\times10^{-4}$	
Γ_{109}	$\omega\pi^+\pi^0$		$(3.9 \pm 0.9)\times10^{-3}$	
Γ_{110}	$\eta'(958)\pi^+$		$(4.97 \pm 0.19)\times10^{-3}$	
Γ_{111}	$\eta'(958)\pi^+\pi^0$		$(1.6 \pm 0.5)\times10^{-3}$	

Hadronic modes with a $K\overline{K}$ pair

Γ_{112}	$K_S^0K^+$		$(3.04 \pm 0.09)\times10^{-3}$	S=2.2
Γ_{113}	$K_L^0K^+$		$(3.21 \pm 0.16)\times10^{-3}$	
Γ_{114}	$K_S^0K^+\pi^0$		$(5.07 \pm 0.30)\times10^{-3}$	
Γ_{115}	$K^*(892)^+K_S^0$		$(2.89 \pm 0.30)\times10^{-3}$	
Γ_{116}	$\overline{K}^*(892)^0K^+$		$(5.2 \pm 1.4)\times10^{-4}$	
Γ_{117}	$K_L^0K^+\pi^0$		$(5.24 \pm 0.31)\times10^{-3}$	
Γ_{118}	$K^+K^-\pi^+$	[a]	$(9.68 \pm 0.18)\times10^{-3}$	
Γ_{119}	$K^+\overline{K}^*(892)^0$, $\overline{K}^*(892)^0 \to K^-\pi^+$		$(2.49\ ^{+0.08}_{-0.13})\times10^{-3}$	
Γ_{120}	$K^+\overline{K}_0^*(1430)^0$, $\overline{K}_0^*(1430)^0 \to K^-\pi^+$		$(1.82 \pm 0.35)\times10^{-3}$	
Γ_{121}	$K^+\overline{K}_2^*(1430)^0$, $\overline{K}_2^* \to K^-\pi^+$		$(1.6\ ^{+1.2}_{-0.8})\times10^{-4}$	
Γ_{122}	$K^+\overline{K}_0^*(700)$, $\overline{K}_0^* \to K^-\pi^+$		$(6.8\ ^{+3.5}_{-2.1})\times10^{-4}$	
Γ_{123}	$a_0(1450)^0\pi^+$, $a_0^0 \to K^+K^-$		$(4.5\ ^{+7.0}_{-1.8})\times10^{-4}$	
Γ_{124}	$\phi(1680)\pi^+$, $\phi \to K^+K^-$		$(4.9\ ^{+4.0}_{-1.9})\times10^{-5}$	
Γ_{125}	$\phi\pi^+$, $\phi \to K^+K^-$		$(2.69\ ^{+0.07}_{-0.08})\times10^{-3}$	
Γ_{126}	$\phi\pi^+$		$(5.70 \pm 0.14)\times10^{-3}$	
Γ_{127}	$K^+K^-\pi^+\pi^0$		$(6.62 \pm 0.32)\times10^{-3}$	
Γ_{128}	$K_S^0K_S^0\pi^+$		$(2.70 \pm 0.13)\times10^{-3}$	
Γ_{129}	$K_S^0K_S^0\pi^+\pi^0$		$(1.34 \pm 0.21)\times10^{-3}$	
Γ_{130}	$K_S^0K^+\eta$		$(1.8 \pm 0.5)\times10^{-4}$	
Γ_{131}	$K^+K_S^0\pi^+\pi^-$		$(1.89 \pm 0.13)\times10^{-3}$	
Γ_{132}	$K_S^0K^+\pi^0\pi^0$		$(5.8 \pm 1.3)\times10^{-4}$	
Γ_{133}	$K_S^0K^-2\pi^+$		$(2.27 \pm 0.13)\times10^{-3}$	
Γ_{134}	$K^+K^-2\pi^+\pi^-$		$(2.3 \pm 1.2)\times10^{-4}$	

A few poorly measured branching fractions:

Γ_{135}	$\phi\pi^+\pi^0$		(2.3 ± 1.0) %	
Γ_{136}	$\phi\rho^+$		< 1.5 %	CL=90%
Γ_{137}	$K^+K^-\pi^+\pi^0$ non-ϕ		$(1.5\ ^{+0.7}_{-0.6})$ %	

Doubly Cabibbo-suppressed modes

Γ_{138}	$K^+\pi^0$		$(2.08 \pm 0.21)\times10^{-4}$	S=1.4
Γ_{139}	$K^+\eta$		$(1.25 \pm 0.16)\times10^{-4}$	S=1.1
Γ_{140}	$K^+\eta'(958)$		$(1.85 \pm 0.20)\times10^{-4}$	
Γ_{141}	$K^+\pi^+\pi^-$		$(4.91 \pm 0.09)\times10^{-4}$	
Γ_{142}	$K^+\rho^0$		$(1.9 \pm 0.5)\times10^{-4}$	
Γ_{143}	$K^*(892)^0\pi^+$, $K^*(892)^0 \to K^+\pi^-$		$(2.3 \pm 0.4)\times10^{-4}$	
Γ_{144}	$K^+f_0(980)$, $f_0(980) \to \pi^+\pi^-$		$(4.4 \pm 2.6)\times10^{-5}$	
Γ_{145}	$K_2^*(1430)^0\pi^+$, $K_2^*(1430)^0 \to K^+\pi^-$		$(3.9 \pm 2.7)\times10^{-5}$	
Γ_{146}	$K^+\pi^+\pi^-$ nonresonant		not seen	
Γ_{147}	$K^+\pi^+\pi^-\pi^0$		$(1.21 \pm 0.09)\times10^{-3}$	
Γ_{148}	$K^+\pi^+\pi^-\pi^0$ nonresonant		$(1.10 \pm 0.07)\times10^{-3}$	
Γ_{149}	$K^+\omega$		$(5.7\ ^{+2.5}_{-2.1})\times10^{-5}$	
Γ_{150}	$2K^+K^-$		$(6.14 \pm 0.11)\times10^{-5}$	
Γ_{151}	$\phi(1020)^0K^+$		$< 2.1 \times10^{-5}$	CL=90%
Γ_{152}	$K^+\phi(1020)$, $\phi \to K^+K^-$		$(4.4 \pm 0.6)\times10^{-6}$	
Γ_{153}	$K^+(K^+K^-)_{S-wave}$		$(5.77 \pm 0.12)\times10^{-5}$	

$\Delta C = 1$ weak neutral current ($C1$) modes, or Lepton Family number (LF), or Lepton number (L), or Baryon number (B) violating modes

Γ_{154}	$\pi^+e^+e^-$	$C1$		$< 1.1 \times10^{-6}$	CL=90%
Γ_{155}	$\pi^+\pi^0e^+e^-$			$< 1.4 \times10^{-5}$	CL=90%
Γ_{156}	$\pi^+\phi$, $\phi \to e^+e^-$		[e]	$(1.7\ ^{+1.4}_{-0.9})\times10^{-6}$	
Γ_{157}	$\pi^+\mu^+\mu^-$	$C1$		$< 6.7 \times10^{-8}$	CL=90%
Γ_{158}	$\pi^+\phi$, $\phi \to \mu^+\mu^-$		[e]	$(1.8 \pm 0.8)\times10^{-6}$	
Γ_{159}	$\rho^+\mu^+\mu^-$	$C1$		$< 5.6 \times10^{-4}$	CL=90%
Γ_{160}	$K^+e^+e^-$		[f]	$< 8.5 \times10^{-7}$	CL=90%
Γ_{161}	$K^+\pi^0e^+e^-$			$< 1.5 \times10^{-5}$	CL=90%
Γ_{162}	$K_S^0\pi^+e^+e^-$			$< 2.6 \times10^{-5}$	CL=90%
Γ_{163}	$K_S^0K^+e^+e^-$			$< 1.1 \times10^{-5}$	CL=90%
Γ_{164}	$K^+\mu^+\mu^-$		[f]	$< 5.4 \times10^{-8}$	CL=90%
Γ_{165}	$\pi^+e^+\mu^-$	LF		$< 2.1 \times10^{-7}$	CL=90%
Γ_{166}	$\pi^+e^-\mu^+$	LF		$< 2.2 \times10^{-7}$	CL=90%
Γ_{167}	$K^+e^+\mu^-$	LF		$< 7.5 \times10^{-8}$	CL=90%
Γ_{168}	$K^+e^-\mu^+$	LF		$< 1.0 \times10^{-7}$	CL=90%
Γ_{169}	π^-2e^+	L		$< 5.3 \times10^{-7}$	CL=90%
Γ_{170}	$\pi^-2\mu^+$	L		$< 1.4 \times10^{-8}$	CL=90%
Γ_{171}	$\pi^-e^+\mu^+$	L		$< 1.3 \times10^{-7}$	CL=90%
Γ_{172}	$\rho^-2\mu^+$	L		$< 5.6 \times10^{-4}$	CL=90%
Γ_{173}	K^-2e^+	L		$< 9 \times10^{-7}$	CL=90%
Γ_{174}	$K_S^0\pi^-2e^+$			$< 3.3 \times10^{-6}$	CL=90%
Γ_{175}	$K^-\pi^02e^+$			$< 8.5 \times10^{-6}$	CL=90%
Γ_{176}	$K^-2\mu^+$	L		$< 1.0 \times10^{-5}$	CL=90%
Γ_{177}	$K^-e^+\mu^+$	L		$< 1.9 \times10^{-6}$	CL=90%
Γ_{178}	$K^*(892)^-2\mu^+$	L		$< 8.5 \times10^{-4}$	CL=90%
Γ_{179}	Λe^+	L,B		$< 1.1 \times10^{-6}$	CL=90%

Downloaded from https://academic.oup.com/ptep/article/2022/8/083C01/6651666 by KIT Library user on 27 September 2022

Γ_{180}	$\overline{\Lambda} e^+$	L,B	< 6.5	$\times 10^{-7}$	CL=90%
Γ_{181}	$\Sigma^0 e^+$	L,B	< 1.7	$\times 10^{-6}$	CL=90%
Γ_{182}	$\overline{\Sigma}^0 e^+$	L,B	< 1.3	$\times 10^{-6}$	CL=90%
Γ_{183}	Unaccounted decay modes		(63.3 ± 0.4) %		S=1.3

[a] The branching fraction for this mode may differ from the sum of the submodes that contribute to it, due to interference effects. See the relevant papers.

[b] These subfractions of the $K^- 2\pi^+$ mode are uncertain: see the Particle Listings.

[c] Submodes of the $D^+ \to K^- 2\pi^+ \pi^0$ and $K^0_S 2\pi^+ \pi^-$ modes were studied by ANJOS 92C and COFFMAN 92B, but with at most 142 events for the first mode and 229 for the second – not enough for precise results. With nothing new for 18 years, we refer to our 2008 edition, Physics Letters **B667** 1 (2008), for those results.

[d] The unseen decay modes of the resonances are included.

[e] This is *not* a test for the ΔC=1 weak neutral current, but leads to the $\pi^+ \ell^+ \ell^-$ final state.

[f] This mode is not a useful test for a ΔC=1 weak neutral current because both quarks must change flavor in this decay.

CONSTRAINED FIT INFORMATION

An overall fit to 31 branching ratios uses 41 measurements and one constraint to determine 17 parameters. The overall fit has a χ^2 = 62.8 for 25 degrees of freedom.

The following *off-diagonal* array elements are the correlation coefficients $\langle \delta x_i \delta x_j \rangle / (\delta x_i \cdot \delta x_j)$, in percent, from the fit to the branching fractions, $x_i \equiv \Gamma_i / \Gamma_{total}$. The fit constrains the x_i whose labels appear in this array to sum to one.

	x_{17}	x_{18}	x_{25}	x_{29}	x_{40}	x_{49}	x_{51}	x_{77}	x_{86}	x_{102}
x_{18}	0									
x_{25}	0	0								
x_{29}	8	0	0							
x_{40}	0	0	0	0						
x_{49}	0	5	0	0	0					
x_{51}	0	28	0	0	0	19				
x_{77}	0	5	0	0	0	4	19			
x_{86}	0	6	0	0	0	4	22	4		
x_{102}	0	5	0	0	0	3	17	75	4	
x_{103}	0	4	0	0	0	3	14	3	3	2
x_{110}	0	5	0	0	0	4	19	4	4	3
x_{112}	0	9	0	0	0	29	31	6	7	5
x_{138}	0	1	0	0	0	1	5	1	1	1
x_{139}	0	1	0	0	0	0	2	0	0	0
x_{140}	0	2	0	0	0	1	6	1	1	1
x_{183}	−49	−57	−26	−41	−5	−19	−58	−26	−14	−23

	x_{103}	x_{110}	x_{112}	x_{138}	x_{139}	x_{140}
x_{110}	3					
x_{112}	4	6				
x_{138}	1	1	1			
x_{139}	14	0	1	0		
x_{140}	1	32	2	0	0	
x_{183}	−10	−16	−22	−3	−2	−5

D^+ BRANCHING RATIOS

Some now-obsolete measurements have been omitted from these Listings.

c-quark decays

$\Gamma(c \to e^+ \text{anything})/\Gamma(c \to \text{anything})$

For the Summary Table, we only use the average of e^+ and μ^+ measurements from $Z^0 \to c\overline{c}$ decays; see the second data block below.

VALUE	EVTS	DOCUMENT ID		TECN	COMMENT
$0.103 \pm 0.009^{+0.009}_{-0.008}$	378	[1] ABBIENDI	99K	OPAL	$Z^0 \to c\overline{c}$

[1] ABBIENDI 99K uses the excess of right-sign over wrong-sign leptons opposite reconstructed $D^*(2010)^+ \to D^0 \pi^+$ decays in $Z^0 \to c\overline{c}$.

$\Gamma(c \to \mu^+ \text{anything})/\Gamma(c \to \text{anything})$

For the Summary Table, we only use the average of e^+ and μ^+ measurements from $Z^0 \to c\overline{c}$ decays; see the next data block.

VALUE	EVTS	DOCUMENT ID		TECN	COMMENT
0.082±0.005 OUR AVERAGE					
0.073±0.008±0.002	73	KAYIS-TOPAK.	05	CHRS	ν_μ emulsion
$0.095 \pm 0.007^{+0.014}_{-0.013}$	2829	ASTIER	00D	NOMD	$\nu_\mu \text{Fe} \to \mu^- \mu^+ X$
$0.090 \pm 0.007^{+0.007}_{-0.006}$	476	[1] ABBIENDI	99K	OPAL	$Z^0 \to c\overline{c}$
$0.086 \pm 0.017^{+0.008}_{-0.007}$	69	[2] ALBRECHT	92F	ARG	$e^+e^- \approx 10$ GeV
0.078±0.009±0.012		ONG	88	MRK2	e^+e^- 29 GeV
0.078±0.015±0.02		BARTEL	87	JADE	e^+e^- 34.6 GeV
$0.082 \pm 0.012^{+0.02}_{-0.01}$		ALTHOFF	84G	TASS	e^+e^- 34.5 GeV
• • • We do not use the following data for averages, fits, limits, etc. • • •					
0.093±0.009±0.009	88	KAYIS-TOPAK.	02	CHRS	See KAYIS-TOPAKSU 05
0.089±0.018±0.025		BARTEL	85J	JADE	See BARTEL 87

[1] ABBIENDI 99K uses the excess of right-sign over wrong-sign leptons opposite reconstructed $D^*(2010)^+ \to D^0 \pi^+$ decays in $Z^0 \to c\overline{c}$.

[2] ALBRECHT 92F uses the excess of right-sign over wrong-sign leptons in a sample of events tagged by fully reconstructed $D^*(2010)^+ \to D^0 \pi^+$ decays.

$\Gamma(c \to \ell^+ \text{anything})/\Gamma(c \to \text{anything})$

This is an average (not a sum) of e^+ and μ^+ measurements.

VALUE	EVTS	DOCUMENT ID		TECN	COMMENT
0.096 ±0.004 OUR AVERAGE					
0.0958±0.0042±0.0028	1828	[1] ABREU	00O	DLPH	$Z^0 \to c\overline{c}$
$0.095 \pm 0.006 \pm^{+0.007}_{-0.006}$	854	[2] ABBIENDI	99K	OPAL	$Z^0 \to c\overline{c}$

[1] ABREU 00O uses leptons opposite fully reconstructed $D^*(2010)^+$, D^+, or D^0 mesons.

[2] ABBIENDI 99K uses the excess of right-sign over wrong-sign leptons opposite reconstructed $D^*(2010)^+ \to D^0 \pi^+$ decays in $Z^0 \to c\overline{c}$.

$\Gamma(c \to D^*(2010)^+ \text{anything})/\Gamma(c \to \text{anything})$

VALUE	EVTS	DOCUMENT ID		TECN	COMMENT
0.255±0.015±0.008	2371	[1] ABREU	00O	DLPH	$Z^0 \to c\overline{c}$

[1] ABREU 00O uses slow pions opposite fully reconstructed $D^*(2010)^+$, D^+, or D^0 mesons as a signal of $D^*(2010)^-$ production.

Inclusive modes

$\Gamma(e^+ \text{semileptonic})/\Gamma_{total}$ — Γ_1/Γ

The sum of our $\overline{K}^0 e^+ \nu_e$, $\overline{K}^*(892)^0 e^+ \nu_e$, $\pi^0 e^+ \nu_e$, $\eta e^+ \nu_e$, $\rho^0 e^+ \nu_e$, and $\omega e^+ \nu_e$ branching fractions is 15.3 ± 0.3%.

VALUE (%)	EVTS	DOCUMENT ID		TECN	COMMENT
16.07±0.30 OUR AVERAGE					
16.13±0.10±0.29	26.2±0.2k	[1] ASNER	10	CLEO	e^+e^- at 3774 MeV
15.2 ±0.9 ±0.8	521 ± 32	ABLIKIM	07G	BES2	$e^+e^- \approx \psi(3770)$
• • • We do not use the following data for averages, fits, limits, etc. • • •					
16.13±0.20±0.33	8798±105	[2] ADAM	06A	CLEO	See ASNER 10
17.0 ±1.9 ±0.7	158	BALTRUSAIT...	85B	MRK3	e^+e^- 3.77 GeV

[1] Using the D^+ and D^0 lifetimes, ASNER 10 finds that the ratio of the D^+ and D^0 semileptonic widths is 0.985 ± 0.015 ± 0.024.

[2] Using the D^+ and D^0 lifetimes, ADAM 06A finds that the ratio of the D^+ and D^0 inclusive e^+ widths is 0.985 ± 0.028 ± 0.015, consistent with the isospin-invariance prediction of 1.

$\Gamma(\mu^+ \text{anything})/\Gamma_{total}$ — Γ_2/Γ

VALUE (%)	EVTS	DOCUMENT ID		TECN	COMMENT
17.6±2.7±1.8	100 ± 12	[1] ABLIKIM	08L	BES2	$e^+e^- \approx \psi(3772)$

[1] ABLIKIM 08L finds the ratio of $D^+ \to \mu^+ X$ and $D^0 \to \mu^+ X$ branching fractions to be 2.59 ± 0.70 ± 0.25, in accord with the ratio of D^+ and D^0 lifetimes, 2.54 ± 0.02.

$\Gamma(K^- \text{anything})/\Gamma_{total}$ — Γ_3/Γ

VALUE (%)	EVTS	DOCUMENT ID		TECN	COMMENT
25.7±1.4 OUR AVERAGE					
24.7±1.3±1.2	631 ± 33	ABLIKIM	07G	BES2	$e^+e^- \approx \psi(3770)$
$27.8^{+3.6}_{-3.1}$		BARLAG	92C	ACCM	π^- Cu 230 GeV
27.1±2.3±2.4		COFFMAN	91	MRK3	e^+e^- 3.77 GeV

$[\Gamma(\overline{K}^0 \text{anything}) + \Gamma(K^0 \text{anything})]/\Gamma_{total}$ — Γ_4/Γ

VALUE (%)	EVTS	DOCUMENT ID		TECN	COMMENT
61 ±5 OUR AVERAGE					
60.5±5.5±3.3	244 ± 22	ABLIKIM	06U	BES2	e^+e^- at 3773 MeV
61.2±6.5±4.3		COFFMAN	91	MRK3	e^+e^- 3.77 GeV

$\Gamma(K^+ \text{anything})/\Gamma_{total}$ — Γ_5/Γ

VALUE (%)	EVTS	DOCUMENT ID		TECN	COMMENT
5.9±0.8 OUR AVERAGE					
6.1±0.9±0.4	189 ± 27	ABLIKIM	07G	BES2	$e^+e^- \approx \psi(3770)$
5.5±1.3±0.9		COFFMAN	91	MRK3	e^+e^- 3.77 GeV

Downloaded from https://academic.oup.com/ptep/article/2022/8/083C01/6651666 by KIT Library user on 27 September 2022

$\Gamma(K^*(892)^- \text{anything})/\Gamma_{total}$ — Γ_6/Γ

VALUE (%)	EVTS	DOCUMENT ID		TECN	COMMENT
5.7±5.2±0.7	7.2 ± 6.5	ABLIKIM	06U	BES2	e^+e^- at 3773 MeV

$\Gamma(\overline{K}^*(892)^0 \text{anything})/\Gamma_{total}$ — Γ_7/Γ

VALUE (%)	EVTS	DOCUMENT ID		TECN	COMMENT
23.2±4.5±3.0	189 ± 36	ABLIKIM	05P	BES	$e^+e^- \approx$ 3773 MeV

$\Gamma(K^*(892)^0 \text{anything})/\Gamma_{total}$ — Γ_8/Γ

VALUE (%)	CL%	DOCUMENT ID		TECN	COMMENT
<6.6	90	ABLIKIM	05P	BES	$e^+e^- \approx$ 3773 MeV

$\Gamma(\eta \text{ anything})/\Gamma_{total}$ — Γ_9/Γ

This ratio includes η particles from η' decays.

VALUE (%)	EVTS	DOCUMENT ID		TECN	COMMENT
6.3±0.5±0.5	1972±142	HUANG	06B	CLEO	e^+e^- at $\psi(3770)$

$\Gamma(\eta' \text{ anything})/\Gamma_{total}$ — Γ_{10}/Γ

VALUE (%)	EVTS	DOCUMENT ID		TECN	COMMENT
1.04±0.16±0.09	82 ± 13	HUANG	06B	CLEO	e^+e^- at $\psi(3770)$

$\Gamma(\phi \text{ anything})/\Gamma_{total}$ — Γ_{11}/Γ

VALUE (%)	EVTS	DOCUMENT ID		TECN	COMMENT
1.12 ±0.04 OUR AVERAGE					
1.135±0.034±0.031	2.7k	ABLIKIM	19AY	BES3	e^+e^- at 3773 MeV
1.03 ±0.10 ±0.07	248 ± 21	HUANG	06B	CLEO	e^+e^- at $\psi(3770)$

Leptonic and semileptonic modes

$\Gamma(e^+\nu_e)/\Gamma_{total}$ — Γ_{12}/Γ

VALUE	CL%	DOCUMENT ID		TECN	COMMENT
$<8.8\times10^{-6}$	90	EISENSTEIN	08	CLEO	e^+e^- at $\psi(3770)$
• • • We do not use the following data for averages, fits, limits, etc. • • •					
$<2.4\times10^{-5}$	90	ARTUSO	05A	CLEO	See EISENSTEIN 08

$\Gamma(\gamma e^+\nu_e)/\Gamma_{total}$ — Γ_{13}/Γ

VALUE	CL%	DOCUMENT ID		TECN	COMMENT
$<3.0\times10^{-5}$	90	[1] ABLIKIM	17M	BES3	e^+e^- at 3.773 GeV

[1] This ABLIKIM 17M limit is for photons with energies greater than 10 MeV.

$\Gamma(\mu^+\nu_\mu)/\Gamma_{total}$ — Γ_{14}/Γ

See the note on "Decay Constants of Charged Pseudoscalar Mesons" in the D_s^+ Listings.

VALUE (units 10^{-4})	EVTS	DOCUMENT ID		TECN	COMMENT
3.74± 0.17 OUR AVERAGE					
3.71± 0.19±0.06	409 ± 21	[1] ABLIKIM	14F	BES3	e^+e^- at $\psi(3770)$
3.82± 0.32±0.09	150 ± 12	[2] EISENSTEIN	08	CLEO	e^+e^- at $\psi(3770)$
• • • We do not use the following data for averages, fits, limits, etc. • • •					
$12.2\ ^{+11.1}_{-5.3}\ \pm1.0$	3	[3] ABLIKIM	05D	BES	$e^+e^- \approx$ 3.773 GeV
$4.40\pm\ 0.66^{+0.09}_{-0.12}$	47 ± 7	[4] ARTUSO	05A	CLEO	See EISENSTEIN 08
3.5 ± 1.4 ±0.6	7	[5] BONVICINI	04A	CLEO	Incl. in ARTUSO 05A
$8\ ^{+16}_{-5}\ ^{+5}_{-2}$	1	[6] BAI	98B	BES	$e^+e^- \to D^{*+}D^-$

[1] ABLIKIM 14F obtain $|V_{cd}|\cdot f_{D^+} = (45.75 \pm 1.20 \pm 0.39)$ MeV, and using $|V_{cd}| = 0.22520 \pm 0.00065$ gets $f_{D^+} = (203.2 \pm 5.3 \pm 1.8)$ MeV.

[2] EISENSTEIN 08, using the D^+ lifetime and assuming $|V_{cd}| = |V_{us}|$, gets $f_{D^+} = (205.8 \pm 8.5 \pm 2.5)$ MeV from this measurement.

[3] ABLIKIM 05D finds a background-subtracted 2.67 ± 1.74 $D^+ \to \mu^+\nu_\mu$ events, and from this obtains $f_{D^+} = 371^{+129}_{-119} \pm 25$ MeV.

[4] ARTUSO 05A obtains $f_{D^+} = 222.6 \pm 16.7^{+2.8}_{-3.4}$ MeV from this measurement.

[5] BONVICINI 04A finds eight events with an estimated background of one, and from the branching fraction obtains $f_{D^+} = 202 \pm 41 \pm 17$ MeV.

[6] BAI 98B obtains $f_{D^+} = (300^{+180+80}_{-150-40})$ MeV from this measurement.

$\Gamma(\tau^+\nu_\tau)/\Gamma_{total}$ — Γ_{15}/Γ

VALUE (units 10^{-3})	CL%	EVTS	DOCUMENT ID		TECN	COMMENT
1.20±0.24±0.12		137	[1] ABLIKIM	19BG	BES3	e^+e^- at 3773 MeV
• • • We do not use the following data for averages, fits, limits, etc. • • •						
<1.2	90		EISENSTEIN	08	CLEO	e^+e^- at $\psi(3770)$
<2.1	90		RUBIN	06A	CLEO	See EISENSTEIN 08

[1] ABLIKIM 19BG observe this mode with a significance of 5.1 σ.

$\Gamma(\overline{K}^0 e^+\nu_e)/\Gamma_{total}$ — Γ_{16}/Γ

VALUE (%)	EVTS	DOCUMENT ID		TECN	COMMENT
8.72 ±0.09 OUR AVERAGE					
8.68 ±0.14 ±0.16	1172	ABLIKIM	21BA	BES3	e^+e^- at 3.773 GeV
8.60 ±0.06 ±0.15	26k	ABLIKIM	17S	BES3	Using $\overline{K}^0 \to \pi^+\pi^-$
8.59 ±0.14 ±0.21	5013	ABLIKIM	16V	BES3	Using $\overline{K}^0 \to 2\pi^0$
8.962±0.054±0.206	40k	[1] ABLIKIM	15AF	BES3	from $D^+ \to K_L e^+\nu_e$
8.83 ±0.10 ±0.20	8.5k	[2] BESSON	09	CLEO	from $D^+ \to K_S e^+\nu_e$
8.95 ±1.59 ±0.67	34	[3] ABLIKIM	05A	BES	from $D^+ \to K_S e^+\nu_e$
• • • We do not use the following data for averages, fits, limits, etc. • • •					
8.53 ±0.13 ±0.23		[4] DOBBS	08	CLEO	See BESSON 09
8.71 ±0.38 ±0.37	545	HUANG	05B	CLEO	See DOBBS 08

[1] ABLIKIM 15AF report $\Gamma(D^+ \to K_L e^+\nu_e)/\Gamma_{total} = (4.481 \pm 0.027 \pm 0.103)\%$. See also the form-factor parameters near the end of this D^+ Listing.

[2] See the form-factor parameters near the end of this D^+ Listing.

[3] The ABLIKIM 05A result together with the $D^0 \to K^-e^+\nu_e$ branching fraction of ABLIKIM 04C and Particle Data Group lifetimes gives $\Gamma(D^0 \to K^-e^+\nu_e)\ /\ \Gamma(D^+ \to \overline{K}^0 e^+\nu_e) = 1.08 \pm 0.22 \pm 0.07$; isospin invariance predicts the ratio is 1.0.

[4] DOBBS 08 establishes $\left|\frac{V_{cd}}{V_{cs}}\cdot\frac{f_+^\pi(0)}{f_+^K(0)}\right| = 0.188 \pm 0.008 \pm 0.002$ from the D^+ and D^0 decays to $\overline{K}e^+\nu_e$ and $\pi e^+\nu_e$. It also finds $\Gamma(D^0 \to K^-e^+\nu_e)\ /\ \Gamma(D^+ \to \overline{K}^0 e^+\nu_e) = 1.06 \pm 0.02 \pm 0.03$; isospin invariance predicts the ratio is 1.0.

$\Gamma(\overline{K}^0\mu^+\nu_\mu)/\Gamma_{total}$ — Γ_{17}/Γ

VALUE (units 10^{-2})	EVTS	DOCUMENT ID		TECN	COMMENT
8.76±0.19 OUR FIT					
8.72±0.07±0.18	21k	ABLIKIM	16G	BES3	e^+e^- at 3773 MeV
• • • We do not use the following data for averages, fits, limits, etc. • • •					
10.3 ±2.3 ±0.8	29 ± 6	ABLIKIM	07	BES2	e^+e^- at 3773 MeV

$\Gamma(\overline{K}^0\mu^+\nu_\mu)/\Gamma(K^-2\pi^+)$ — Γ_{17}/Γ_{51}

VALUE	EVTS	DOCUMENT ID		TECN	COMMENT
0.934±0.025 OUR FIT	Error includes scale factor of 1.2.				
1.019±0.076±0.065	555 ± 39	LINK	04E	FOCS	γ nucleus, $\overline{E}_\gamma \approx$ 180 GeV

$\Gamma(K^-\pi^+e^+\nu_e)/\Gamma_{total}$ — Γ_{18}/Γ

VALUE (units 10^{-2})	EVTS	DOCUMENT ID		TECN	COMMENT
4.02±0.18 OUR FIT	Error includes scale factor of 3.2.				
3.77±0.03±0.08	18.3k	ABLIKIM	16F	BES3	e^+e^- at $\psi(3770)$
• • • We do not use the following data for averages, fits, limits, etc. • • •					
3.50±0.75±0.27	29	ABLIKIM	06O	BES2	e^+e^- at 3773 MeV
$3.5\ ^{+1.2}_{-0.7}\ \pm0.4$	14	BAI	91	MRK3	$e^+e^- \approx$ 3.77 GeV

$\Gamma(K^-\pi^+e^+\nu_e)/\Gamma(K^-2\pi^+)$ — Γ_{18}/Γ_{51}

VALUE	EVTS	DOCUMENT ID		TECN	COMMENT
0.428 ±0.018 OUR FIT	Error includes scale factor of 3.7.				
0.4380±0.0036±0.0042	70k±363	DEL-AMO-SA...11I		BABR	$e^+e^- \approx$ 10.6 GeV

$\Gamma(\overline{K}^*(892)^0 e^+\nu_e, \overline{K}^*(892)^0 \to K^-\pi^+)/\Gamma(K^-\pi^+e^+\nu_e)$ — Γ_{19}/Γ_{18}

VALUE (%)	DOCUMENT ID		TECN	COMMENT
93.94±0.27 OUR AVERAGE				
93.93±0.22±0.18	ABLIKIM	16F	BES3	e^+e^- at $\psi(3770)$
94.11±0.74±0.75	DEL-AMO-SA...11I		BABR	$e^+e^- \approx$ 10.6 GeV

$\Gamma((K^-\pi^+)_{[0.8-1.0]\text{GeV}} e^+\nu_e)/\Gamma_{total}$ — Γ_{20}/Γ

VALUE (units 10^{-2})	EVTS	DOCUMENT ID		TECN	COMMENT
3.39±0.03±0.08	16.2k	ABLIKIM	16F	BES3	e^+e^- at $\psi(3770)$

$\Gamma((K^-\pi^+)_{S-wave} e^+\nu_e)/\Gamma_{total}$ — Γ_{21}/Γ

VALUE (units 10^{-3})	DOCUMENT ID		TECN	COMMENT
2.28±0.08±0.08	ABLIKIM	16F	BES3	e^+e^- at $\psi(3770)$

$\Gamma((K^-\pi^+)_{S-wave} e^+\nu_e)/\Gamma(K^-\pi^+e^+\nu_e)$ — Γ_{21}/Γ_{18}

VALUE (%)	DOCUMENT ID		TECN	COMMENT
5.89±0.17 OUR AVERAGE				
6.05±0.22±0.18	ABLIKIM	16F	BES3	e^+e^- at $\psi(3770)$
5.79±0.16±0.15	DEL-AMO-SA...11I		BABR	$e^+e^- \approx$ 10.6 GeV

$\Gamma(\overline{K}^*(1410)^0 e^+\nu_e, \overline{K}^*(1410)^0 \to K^-\pi^+)/\Gamma_{total}$ — Γ_{22}/Γ

VALUE	CL%	DOCUMENT ID		TECN	COMMENT
$<6\times10^{-3}$	90	DEL-AMO-SA...11I		BABR	$e^+e^- \approx$ 10.6 GeV

$\Gamma(\overline{K}_2^*(1430)^0 e^+\nu_e, \overline{K}_2^*(1430)^0 \to K^-\pi^+)/\Gamma_{total}$ — Γ_{23}/Γ

VALUE	CL%	DOCUMENT ID		TECN	COMMENT
$<5\times10^{-4}$	90	DEL-AMO-SA...11I		BABR	$e^+e^- \approx$ 10.6 GeV

$\Gamma(K^-\pi^+e^+\nu_e \text{ nonresonant})/\Gamma_{total}$ — Γ_{24}/Γ

VALUE	CL%	DOCUMENT ID		TECN	COMMENT
<0.007	90	ANJOS	89B	E691	Photoproduction

$\Gamma(\overline{K}^*(892)^0 e^+\nu_e)/\Gamma_{total}$ — Γ_{25}/Γ

Unseen decay modes of $\overline{K}^*(892)^0$ are included. See the end of the D^+ Listings for measurements of $D^+ \to \overline{K}^*(892)^0\ell^+\nu_\ell$ form-factor ratios.

VALUE (units 10^{-2})	EVTS	DOCUMENT ID		TECN	COMMENT
5.40±0.10 OUR FIT	Error includes scale factor of 1.1.				
5.40±0.10 OUR AVERAGE	Error includes scale factor of 1.1.				
5.31±0.05±0.12	16.2k	ABLIKIM	16F	BES3	e^+e^- at $\psi(3770)$
5.52±0.07±0.13	≈5k	BRIERE	10	CLEO	e^+e^- at $\psi(3770)$
• • • We do not use the following data for averages, fits, limits, etc. • • •					
5.06±1.21±0.40	28 ± 7	ABLIKIM	06O	BES2	e^+e^- at 3773 MeV
5.56±0.27±0.23	422 ± 21	[1] HUANG	05B	CLEO	e^+e^- at $\psi(3770)$

[1] HUANG 05B finds $\Gamma(D^0 \to K^{*-}e^+\nu_e)\ /\ \Gamma(D^+ \to \overline{K}^{*0}e^+\nu_e) = 0.98 \pm 0.08 \pm 0.04$; isospin invariance predicts the ratio is 1.0.

Downloaded from https://academic.oup.com/ptep/article/2022/8/083C01/6651666 by KIT Library user on 27 September 2022

$\Gamma(\overline{K}^*(892)^0 e^+ \nu_e)/\Gamma(K^- 2\pi^+)$ — Γ_{25}/Γ_{51}

Unseen decay modes of the $\overline{K}^*(892)^0$ are included. See the end of the D^+ Listings for measurements of $D^+ \to \overline{K}^*(892)^0 \ell^+ \nu_\ell$ form-factor ratios.

VALUE	EVTS	DOCUMENT ID		TECN	COMMENT
• • • We do not use the following data for averages, fits, limits, etc. • • •					
$0.74 \pm 0.04 \pm 0.05$		BRANDENB...	02	CLEO	$e^+ e^- \approx \Upsilon(4S)$
$0.62 \pm 0.15 \pm 0.09$	35	ADAMOVICH	91	OMEG	π^- 340 GeV
$0.55 \pm 0.08 \pm 0.10$	880	ALBRECHT	91	ARG	$e^+ e^- \approx$ 10.4 GeV
$0.49 \pm 0.04 \pm 0.05$		ANJOS	89B	E691	Photoproduction

$\Gamma(K^- \pi^+ \mu^+ \nu_\mu)/\Gamma(\overline{K}^0 \mu^+ \nu_\mu)$ — Γ_{26}/Γ_{17}

VALUE	EVTS	DOCUMENT ID		TECN	COMMENT
$0.417 \pm 0.030 \pm 0.023$	555 ± 39	LINK	04E	FOCS	γ nucleus, $\overline{E}_\gamma \approx 180$ GeV

$\Gamma(K^- \pi^+ \mu^+ \nu_\mu \text{ nonresonant})/\Gamma(K^- \pi^+ \mu^+ \nu_\mu)$ — Γ_{28}/Γ_{26}

VALUE	EVTS	DOCUMENT ID		TECN	COMMENT
$0.0530 \pm 0.0074^{+0.0099}_{-0.0096}$	14k	LINK	05I	FOCS	γ nucleus, $\overline{E}_\gamma \approx 180$ GeV

$\Gamma(\overline{K}^*(892)^0 \mu^+ \nu_\mu)/\Gamma_{\text{total}}$ — Γ_{29}/Γ

Unseen decay modes of the $\overline{K}^*(892)^0$ are included. See the end of the D^+ Listings for measurements of $D^+ \to \overline{K}^*(892)^0 \ell^+ \nu_\ell$ form-factor ratios.

VALUE (units 10^{-2})	EVTS	DOCUMENT ID		TECN	COMMENT
5.27 ± 0.15 OUR FIT					
$5.27 \pm 0.07 \pm 0.14$	≈ 5k	BRIERE	10	CLEO	$e^+ e^-$ at $\psi(3770)$

$\Gamma(\overline{K}^*(892)^0 \mu^+ \nu_\mu)/\Gamma(\overline{K}^0 \mu^+ \nu_\mu)$ — Γ_{29}/Γ_{17}

Unseen decay modes of the $\overline{K}^*(892)^0$ are included. See the end of the D^+ Listings for measurements of $D^+ \to \overline{K}^*(892)^0 \ell^+ \nu_\ell$ form-factor ratios.

VALUE	EVTS	DOCUMENT ID		TECN	COMMENT
0.602 ± 0.021 OUR FIT					
$0.594 \pm 0.043 \pm 0.033$	555 ± 39	LINK	04E	FOCS	γ nucleus, $\overline{E}_\gamma \approx 180$ GeV

$\Gamma(\overline{K}^*(892)^0 \mu^+ \nu_\mu)/\Gamma(K^- 2\pi^+)$ — Γ_{29}/Γ_{51}

Unseen decay modes of the $\overline{K}^*(892)^0$ are included. See the end of the D^+ Listings for measurements of $D^+ \to \overline{K}^*(892)^0 \ell^+ \nu_\ell$ form-factor ratios.

VALUE	EVTS	DOCUMENT ID		TECN	COMMENT
0.562 ± 0.018 OUR FIT Error includes scale factor of 1.1.					
0.57 ± 0.06 OUR AVERAGE Error includes scale factor of 1.2.					
$0.72 \pm 0.10 \pm 0.05$		BRANDENB...	02	CLEO	$e^+ e^- \approx \Upsilon(4S)$
$0.56 \pm 0.04 \pm 0.06$	875	FRABETTI	93E	E687	γBe $\overline{E}_\gamma \approx 200$ GeV
$0.46 \pm 0.07 \pm 0.08$	224	KODAMA	92C	E653	π^- emulsion 600 GeV
• • • We do not use the following data for averages, fits, limits, etc. • • •					
$0.602 \pm 0.010 \pm 0.021$	12k	[1] LINK	02J	FOCS	γ nucleus, ≈ 180 GeV

[1] This LINK 02J result includes the effects of an interference of a small S-wave $K^- \pi^+$ amplitude with the dominant $\overline{K}^{*0}$ amplitude. (The interference effect is reported in LINK 02E.) This result is redundant with results of LINK 04E elsewhere in these Listings.

$\Gamma(K^- \pi^+ \pi^0 \mu^+ \nu_\mu)/\Gamma(K^- \pi^+ \mu^+ \nu_\mu)$ — Γ_{30}/Γ_{26}

VALUE	CL%	DOCUMENT ID		TECN	COMMENT
<0.042	90	FRABETTI	93E	E687	γBe $\overline{E}_\gamma \approx 200$ GeV

$\Gamma(\overline{K}_1(1270)^0 e^+ \nu_e, \overline{K}_1^0 \to K^- \pi^+ \pi^0)/\Gamma_{\text{total}}$ — Γ_{31}/Γ

VALUE (units 10^{-3})	EVTS	DOCUMENT ID		TECN	COMMENT
$1.06 \pm 0.12^{+0.08}_{-0.10}$	120	[1] ABLIKIM	19BH	BES3	$e^+ e^-$ at 3773 MeV

[1] ABLIKIM 19BH quotes $B(D^+ \to \overline{K}_1(1270)^0 e^+ \nu_e) = (2.30 \pm 0.26^{+0.18}_{-0.21} \pm 0.25) \times 10^{-3}$, where the last uncertainty is due to $B(\overline{K}_1(1270)^0 \to K^- \pi^+ \pi^0) = 0.467 \pm 0.050$.

$\Gamma(\overline{K}_0^*(1430)^0 \mu^+ \nu_\mu)/\Gamma(K^- \pi^+ \mu^+ \nu_\mu)$ — Γ_{32}/Γ_{26}

Unseen decay modes of the $\overline{K}_0^*(1430)^0$ are included.

VALUE	CL%	DOCUMENT ID		TECN	COMMENT
<0.0064	90	LINK	05I	FOCS	γ A, $\overline{E}_\gamma \approx 180$ GeV

$\Gamma(\overline{K}^*(1680)^0 \mu^+ \nu_\mu)/\Gamma(K^- \pi^+ \mu^+ \nu_\mu)$ — Γ_{33}/Γ_{26}

Unseen decay modes of the $\overline{K}^*(1680)^0$ are included.

VALUE	CL%	DOCUMENT ID		TECN	COMMENT
<0.04	90	LINK	05I	FOCS	γ A, $\overline{E}_\gamma \approx 180$ GeV

$\Gamma(\pi^0 e^+ \nu_e)/\Gamma_{\text{total}}$ — Γ_{34}/Γ

VALUE (%)	EVTS	DOCUMENT ID		TECN	COMMENT
0.372 ± 0.017 OUR AVERAGE Error includes scale factor of 2.0.					
$0.363 \pm 0.008 \pm 0.005$	3.4k	ABLIKIM	17S	BES3	Using $\pi^0 \to 2\gamma$
$0.405 \pm 0.016 \pm 0.009$	838	[1] BESSON	09	CLEO	$e^+ e^-$ at $\psi(3770)$
• • • We do not use the following data for averages, fits, limits, etc. • • •					
$0.373 \pm 0.022 \pm 0.013$		[2] DOBBS	08	CLEO	See BESSON 09
$0.44 \pm 0.06 \pm 0.03$	63 ± 9	HUANG	05B	CLEO	See DOBBS 08

[1] See the form-factor parameters near the end of this D^+ Listing.

[2] DOBBS 08 establishes $\left|\frac{V_{cd}}{V_{cs}} \cdot \frac{f_+^\pi(0)}{f_+^K(0)}\right| = 0.188 \pm 0.008 \pm 0.002$ from the D^+ and D^0 decays to $\overline{K} e^+ \nu_e$ and $\pi e^+ \nu_e$. It finds $\Gamma(D^0 \to \pi^- e^+ \nu_e) / \Gamma(D^+ \to \pi^0 e^+ \nu_e) = 2.03 \pm 0.14 \pm 0.08$; isospin invariance predicts the ratio is 2.0.

$\Gamma(\pi^0 \mu^+ \nu_\mu)/\Gamma_{\text{total}}$ — Γ_{35}/Γ

VALUE (%)	EVTS	DOCUMENT ID		TECN	COMMENT
$0.350 \pm 0.011 \pm 0.010$	1.3k	ABLIKIM	18AE	BES3	$e^+ e^-$, 3773 MeV

$\Gamma(\eta e^+ \nu_e)/\Gamma_{\text{total}}$ — Γ_{36}/Γ

VALUE (units 10^{-4})	EVTS	DOCUMENT ID		TECN	COMMENT
11.1 ± 0.7 OUR AVERAGE					
$10.74 \pm 0.81 \pm 0.51$	373	ABLIKIM	18R	BES3	$e^+ e^-$, 3773 MeV
$11.4 \pm 0.9 \pm 0.4$		YELTON	11	CLEO	$e^+ e^-$ at $\psi(3770)$
• • • We do not use the following data for averages, fits, limits, etc. • • •					
$13.3 \pm 2.0 \pm 0.6$	46	MITCHELL	09B	CLEO	See YELTON 11

$\Gamma(\eta \mu^+ \nu_\mu)/\Gamma_{\text{total}}$ — Γ_{37}/Γ

VALUE (units 10^{-4})	EVTS	DOCUMENT ID		TECN	COMMENT
$10.41 \pm 1.12 \pm 0.05$	234	[1] ABLIKIM	20T	BES3	$e^+ e^-$, 3773 MeV

[1] ABLIKIM 20T reports $(10.4 \pm 1.0 \pm 0.5) \times 10^{-4}$ from a measurement of $[\Gamma(D^+ \to \eta \mu^+ \nu_\mu)/\Gamma_{\text{total}}] \times [B(\eta \to 2\gamma)]$ assuming $B(\eta \to 2\gamma) = (39.41 \pm 0.20) \times 10^{-2}$, which we rescale to our best value $B(\eta \to 2\gamma) = (39.36 \pm 0.18) \times 10^{-2}$. Our first error is their experiment's error and our second error is the systematic error from using our best value.

$\Gamma(\pi^- \pi^+ e^+ \nu_e)/\Gamma_{\text{total}}$ — Γ_{38}/Γ

VALUE (units 10^{-3})	EVTS	DOCUMENT ID		TECN	COMMENT
$2.449 \pm 0.074 \pm 0.073$	1.7k	ABLIKIM	19C	BES3	$e^+ e^-$ at 3773 MeV

$\Gamma(f_0(500)^0 e^+ \nu_e, f_0(500)^0 \to \pi^+ \pi^-)/\Gamma(\pi^- \pi^+ e^+ \nu_e)$ — Γ_{39}/Γ_{38}

VALUE (units 10^{-2})	EVTS	DOCUMENT ID		TECN	COMMENT
$25.7 \pm 1.6 \pm 1.1$	1.5k	ABLIKIM	19C	BES3	$\pi^- \pi^+ e^+ \nu_e$ events

$\Gamma(\rho^0 e^+ \nu_e)/\Gamma_{\text{total}}$ — Γ_{40}/Γ

VALUE (units 10^{-3})	EVTS	DOCUMENT ID		TECN	COMMENT
$2.18^{+0.17}_{-0.25}$ OUR FIT					
$2.17 \pm 0.12^{+0.12}_{-0.22}$	447 ± 25	[1] DOBBS	13	CLEO	$e^+ e^-$ at $\psi(3770)$
• • • We do not use the following data for averages, fits, limits, etc. • • •					
$2.1 \pm 0.4 \pm 0.1$	27 ± 6	[2] HUANG	05B	CLEO	See DOBBS 13

[1] DOBBS 13 finds $\Gamma(D^0 \to \rho^- e^+ \nu_e) / 2\,\Gamma(D^+ \to \rho^0 e^+ \nu_e) = 1.03 \pm 0.09^{+0.08}_{-0.02}$; isospin invariance predicts the ratio is 1.0.

[2] HUANG 05B finds $\Gamma(D^0 \to \rho^- e^+ \nu_e) / 2\,\Gamma(D^+ \to \rho^0 e^+ \nu_e) = 1.2^{+0.4}_{-0.3} \pm 0.1$; isospin invariance predicts the ratio is 1.0.

$\Gamma(\rho^0 e^+ \nu_e)/\Gamma(\pi^- \pi^+ e^+ \nu_e)$ — Γ_{40}/Γ_{38}

VALUE (units 10^{-2})	EVTS	DOCUMENT ID		TECN	COMMENT
$76.0 \pm 1.7 \pm 1.1$	1.5k	ABLIKIM	19C	BES3	$\pi^- \pi^+ e^+ \nu_e$ events

$\Gamma(\rho^0 e^+ \nu_e)/\Gamma(\overline{K}^*(892)^0 e^+ \nu_e)$ — Γ_{40}/Γ_{25}

VALUE	EVTS	DOCUMENT ID		TECN	COMMENT
$0.0404^{+0.0033}_{-0.0050}$ OUR FIT					
$0.045 \pm 0.014 \pm 0.009$	49	[1] AITALA	97	E791	π^- nucleus, 500 GeV

[1] AITALA 97 explicitly subtracts $D^+ \to \eta' e^+ \nu_e$ and other backgrounds to get this result.

$\Gamma(\rho^0 \mu^+ \nu_\mu)/\Gamma(\overline{K}^*(892)^0 \mu^+ \nu_\mu)$ — Γ_{41}/Γ_{29}

VALUE	EVTS	DOCUMENT ID		TECN	COMMENT
0.045 ± 0.007 OUR AVERAGE Error includes scale factor of 1.1.					
$0.041 \pm 0.006 \pm 0.004$	320 ± 44	LINK	06B	FOCS	γ A, $\overline{E}_\gamma \approx 180$ GeV
$0.051 \pm 0.015 \pm 0.009$	54	[1] AITALA	97	E791	π^- nucleus, 500 GeV
$0.079 \pm 0.019 \pm 0.013$	39	[2] FRABETTI	97	E687	γ Be, $\overline{E}_\gamma \approx 220$ GeV

[1] AITALA 97 explicitly subtracts $D^+ \to \eta' \mu^+ \nu_\mu$ and other backgrounds to get this result.

[2] Because the reconstruction efficiency for photons is low, this FRABETTI 97 result also includes any $D^+ \to \eta' \mu^+ \nu_\mu \to \gamma \rho^0 \mu^+ \nu_\mu$ events in the numerator.

$\Gamma(\omega e^+ \nu_e)/\Gamma_{\text{total}}$ — Γ_{42}/Γ

VALUE (units 10^{-3})	EVTS	DOCUMENT ID		TECN	COMMENT
1.69 ± 0.11 OUR AVERAGE					
$1.63 \pm 0.11 \pm 0.08$	491 ± 32	ABLIKIM	15W	BES3	292 fb^{-1}, 3773 MeV
$1.82 \pm 0.18 \pm 0.07$	129 ± 13	DOBBS	13	CLEO	$e^+ e^-$ at $\psi(3770)$
• • • We do not use the following data for averages, fits, limits, etc. • • •					
$1.6\ ^{+0.7}_{-0.6} \pm 0.1$	$7.6^{+3.3}_{-2.7}$	HUANG	05B	CLEO	See DOBBS 13

Downloaded from https://academic.oup.com/ptep/article/2022/8/083C01/6651666 by KIT Library user on 27 September 2022

$\Gamma(\omega e^+\nu_e)/\Gamma(\pi^-\pi^+e^+\nu_e)$ — Γ_{42}/Γ_{38}

VALUE (units 10^{-2})	EVTS	DOCUMENT ID		TECN	COMMENT
1.28±0.41±0.15	1.5k	ABLIKIM	19C	BES3	$\pi^-\pi^+e^+\nu_e$ events

$\Gamma(\omega\mu^+\nu_\mu)/\Gamma_{total}$ — Γ_{43}/Γ

VALUE (units 10^{-4})	EVTS	DOCUMENT ID		TECN	COMMENT
17.7±2.1±0.1	194	[1] ABLIKIM	20H	BES3	e^+e^-, 3773 MeV

[1] ABLIKIM 20H reports $(17.7 \pm 1.8 \pm 1.1) \times 10^{-4}$ from a measurement of $[\Gamma(D^+ \to \omega\mu^+\nu_\mu)/\Gamma_{total}] \times [B(\omega(782) \to \pi^+\pi^-\pi^0)]$ assuming $B(\omega(782) \to \pi^+\pi^-\pi^0) = (89.3 \pm 0.6) \times 10^{-2}$, which we rescale to our best value $B(\omega(782) \to \pi^+\pi^-\pi^0) = (89.2 \pm 0.7) \times 10^{-2}$. Our first error is their experiment's error and our second error is the systematic error from using our best value.

$\Gamma(\eta'(958)e^+\nu_e)/\Gamma_{total}$ — Γ_{44}/Γ

VALUE (units 10^{-4})	CL%	EVTS	DOCUMENT ID		TECN	COMMENT
2.0 ±0.4 OUR AVERAGE						
1.91±0.51±0.13		32	ABLIKIM	18R	BES3	e^+e^-, 3773 MeV
2.16±0.53±0.07			YELTON	11	CLEO	e^+e^- at $\psi(3770)$
• • • We do not use the following data for averages, fits, limits, etc. • • •						
<3.5	90		MITCHELL	09B	CLEO	See YELTON 11

$\Gamma(a(980)^0e^+\nu_e,\ a(980)^0 \to \eta\pi^0)/\Gamma_{total}$ — Γ_{45}/Γ

VALUE (units 10^{-4})	EVTS	DOCUMENT ID		TECN	COMMENT
$\mathbf{1.66^{+0.81}_{-0.66}\pm0.11}$	10^{+5}_{-4}	[1] ABLIKIM	18F	BES3	e^+e^- at 3773 MeV

[1] Signal observed at 2.9 σ C.L.

$\Gamma(b_1(1235)^0e^+\nu_e,\ b_1^0 \to \omega\pi^0)/\Gamma_{total}$ — Γ_{46}/Γ

VALUE	CL%	DOCUMENT ID		TECN	COMMENT
<1.75 × 10^{-4}	90	ABLIKIM	20AF	BES3	e^+e^-, 3773 MeV

$\Gamma(\phi e^+\nu_e)/\Gamma_{total}$ — Γ_{47}/Γ

Unseen decay modes of the ϕ are included.

VALUE	CL%	DOCUMENT ID		TECN	COMMENT
<1.3 × 10^{-5}	90	ABLIKIM	15W	BES3	292 fb^{-1}, 3773 MeV
• • • We do not use the following data for averages, fits, limits, etc. • • •					
<0.9 × 10^{-4}	90	YELTON	11	CLEO	e^+e^- at $\psi(3770)$
<1.6 × 10^{-4}	90	MITCHELL	09B	CLEO	See YELTON 11
<0.0201	90	ABLIKIM	06P	BES2	e^+e^- at 3773 MeV
<0.0209	90	BAI	91	MRK3	e^+e^- ≈ 3.77 GeV

$\Gamma(D^0e^+\nu_e)/\Gamma_{total}$ — Γ_{48}/Γ

VALUE	CL%	DOCUMENT ID		TECN	COMMENT
<1.0 × 10^{-4}	90	ABLIKIM	17AD	BES3	e^+e^- at 3.773 GeV

Hadronic modes with a $\overline{K}$ or $\overline{K}K\overline{K}$

$\Gamma(K^0_S\pi^+)/\Gamma_{total}$ — Γ_{49}/Γ

VALUE (units 10^{-2})	EVTS	DOCUMENT ID		TECN	COMMENT
1.562±0.031 OUR FIT	Error includes scale factor of 1.7.				
1.591±0.006±0.030	94k	ABLIKIM	18W	BES3	e^+e^-, 3773 MeV
• • • We do not use the following data for averages, fits, limits, etc. • • •					
1.526±0.022±0.038		[1] DOBBS	07	CLEO	See MENDEZ 10
1.55 ±0.05 ±0.06	2.2k	[1] HE	05	CLEO	See DOBBS 07
1.6 ±0.3 ±0.1	161	ADLER	88C	MRK3	e^+e^- 3.77 GeV

[1] DOBBS 07 and HE 05 use single- and double-tagged events in an overall fit. DOBBS 07 supersedes HE 05.

$\Gamma(K^0_S\pi^+)/\Gamma(K^-2\pi^+)$ — Γ_{49}/Γ_{51}

VALUE	EVTS	DOCUMENT ID		TECN	COMMENT
0.167 ±0.004 OUR FIT	Error includes scale factor of 2.4.				
0.162 ±0.009 OUR AVERAGE	Error includes scale factor of 4.5.				
0.171 ±0.002 ±0.002		BONVICINI	14	CLEO	All CLEO-c runs
0.1530±0.0023±0.0016	10.6k	LINK	02B	FOCS	γ nucleus, $\overline{E}_\gamma \approx 180$ GeV
• • • We do not use the following data for averages, fits, limits, etc. • • •					
0.1682±0.0012±0.0037	30k	MENDEZ	10	CLEO	See BONVICINI 14
0.174 ±0.012 ±0.011	473	[1] BISHAI	97	CLEO	$e^+e^- \approx \Upsilon(4S)$
0.137 ±0.015 ±0.016	264	ANJOS	90C	E691	Photoproduction

[1] See BISHAI 97 for an isospin analysis of $D^+ \to \overline{K}\pi$ amplitudes.

$\Gamma(K^0_L\pi^+)/\Gamma_{total}$ — Γ_{50}/Γ

VALUE (units 10^{-2})	EVTS	DOCUMENT ID		TECN	COMMENT
1.460±0.040±0.035	2023 ± 54	[1] HE	08	CLEO	e^+e^- at $\psi(3770)$

[1] The difference of CLEO $D^+ \to K^0_S\pi^+$ and $K^0_L\pi^+$ branching fractions over the sum (DOBBS 07 and HE 08) is +0.022 ± 0.016 ± 0.018.

$\Gamma(K^-2\pi^+)/\Gamma_{total}$ — Γ_{51}/Γ

VALUE (units 10^{-2})	EVTS	DOCUMENT ID		TECN	COMMENT
9.38 ±0.16 OUR FIT	Error includes scale factor of 1.6.				
9.224±0.059±0.157		BONVICINI	14	CLEO	All CLEO-c runs
• • • We do not use the following data for averages, fits, limits, etc. • • •					
9.14 ±0.10 ±0.17		[1] DOBBS	07	CLEO	See BONVICINI 14
9.5 ±0.2 ±0.3	15.1k	[1] HE	05	CLEO	See DOBBS 07
9.3 ±0.6 ±0.8	1502	[2] BALEST	94	CLEO	$e^+e^- \approx \Upsilon(4S)$
$6.4\ ^{+1.5}_{-1.4}$		[3] BARLAG	92C	ACCM	π^- Cu 230 GeV
9.1 ±1.3 ±0.4	1164	ADLER	88C	MRK3	e^+e^- 3.77 GeV
9.1 ±1.9	239	[4] SCHINDLER	81	MRK2	e^+e^- 3.771 GeV

[1] DOBBS 07 and HE 05 use single- and double-tagged events in an overall fit. DOBBS 07 supersedes HE 05.

[2] BALEST 94 measures the ratio of $D^+ \to K^-\pi^+\pi^+$ and $D^0 \to K^-\pi^+$ branching fractions to be 2.35 ± 0.16 ± 0.16 and uses their absolute measurement of the $D^0 \to K^-\pi^+$ fraction (AKERIB 93).

[3] BARLAG 92C computes the branching fraction by topological normalization.

[4] SCHINDLER 81 (MARK-2) measures $\sigma(e^+e^- \to \psi(3770)) \times$ branching fraction to be 0.38 ± 0.05 nb. We use the MARK-3 (ADLER 88C) value of σ = 4.2 ± 0.6 ± 0.3 nb.

See the related review(s):

Review of Multibody Charm Analyses

$\Gamma((K^-\pi^+)_{S\text{-wave}}\pi^+)/\Gamma(K^-2\pi^+)$ — Γ_{52}/Γ_{51}

This is the "fit fraction" from the Dalitz-plot analysis. The $K^-\pi^+$ S-wave includes a broad scalar κ ($\overline{K}^*_0(700)$), the $\overline{K}^*_0(1430)^0$, and non-resonant background.

VALUE	DOCUMENT ID		TECN	COMMENT
0.801 ±0.012 OUR AVERAGE				
0.8024±0.0138±0.0043	[1] LINK	09	FOCS	MIPWA fit, 53k evts
0.838 ±0.038	[2] BONVICINI	08A	CLEO	QMIPWA fit, 141k evts
0.786 ±0.014 ±0.018	AITALA	06	E791	Dalitz fit, 15.1k events
• • • We do not use the following data for averages, fits, limits, etc. • • •				
0.8323±0.0150±0.0008	[3] LINK	07B	FOCS	See LINK 09

[1] This LINK 09 model-independent partial-wave analysis of the $K^-\pi^+$ S-wave slices the $K^-\pi^+$ mass range into 39 bins.

[2] The BONVICINI 08A QMIPWA (quasi-model-independent partial-wave analysis) of the $K^-\pi^+$ S-wave amplitude slices the $K^-\pi^+$ mass range into 26 bins but keeps the Breit-Wigner $\overline{K}^*_0(1430)^0$.

[3] This LINK 07B fit uses a K matrix. The $K^-\pi^+$ S-wave fit fraction given above breaks down into (207.3 ± 25.5 ± 12.4)% isospin-1/2 and (40.5 ± 9.6 ± 3.2)% isospin-3/2 — with large interference between the two. The isospin-1/2 component includes the κ (or $\overline{K}^*_0(700)^0$) and $\overline{K}^*_0(1430)^0$.

$\Gamma(\overline{K}^*_0(700)^0\pi^+,\overline{K}^*_0(700) \to K^-\pi^+)/\Gamma(K^-2\pi^+)$ — Γ_{53}/Γ_{51}

This is the "fit fraction" from the Dalitz-plot analysis.

VALUE	DOCUMENT ID		TECN	COMMENT
• • • We do not use the following data for averages, fits, limits, etc. • • •				
0.478±0.121±0.053	AITALA	02	E791	See AITALA 06

$\Gamma(\overline{K}^*_0(1430)^0\pi^+,\overline{K}^*_0(1430)^0 \to K^-\pi^+)/\Gamma(K^-2\pi^+)$ — Γ_{54}/Γ_{51}

This is the "fit fraction" from the Dalitz-plot analysis.

VALUE	DOCUMENT ID		TECN	COMMENT
0.1330±0.0062	BONVICINI	08A	CLEO	QMIPWA fit, 141k evts
• • • We do not use the following data for averages, fits, limits, etc. • • •				
0.125 ±0.014 ±0.005	AITALA	02	E791	See AITALA 06
0.284 ±0.022 ±0.059	FRABETTI	94G	E687	Dalitz fit, 8800 evts
0.248 ±0.019 ±0.017	ANJOS	93	E691	γBe 90–260 GeV

$\Gamma(\overline{K}^*(892)^0\pi^+,\overline{K}^*(892)^0 \to K^-\pi^+)/\Gamma(K^-2\pi^+)$ — Γ_{55}/Γ_{51}

This is the "fit fraction" from the Dalitz-plot analysis.

VALUE	DOCUMENT ID		TECN	COMMENT
0.111 ±0.012 OUR AVERAGE	Error includes scale factor of 3.7.			
0.1236±0.0034±0.0034	LINK	09	FOCS	MIPWA fit, 53k evts
0.0988±0.0046	BONVICINI	08A	CLEO	QMIPWA fit, 141k evts
0.119 ±0.002 ±0.020	AITALA	06	E791	Dalitz fit, 15.1k events
• • • We do not use the following data for averages, fits, limits, etc. • • •				
0.1361±0.0041±0.0030	[1] LINK	07B	FOCS	See LINK 09
0.123 ±0.010 ±0.009	AITALA	02	E791	See AITALA 06
0.137 ±0.006 ±0.009	FRABETTI	94G	E687	Dalitz fit, 8800 evts
0.170 ±0.009 ±0.034	ANJOS	93	E691	γBe 90–260 GeV
0.14 ±0.04 ±0.04	ALVAREZ	91B	NA14	Photoproduction
0.13 ±0.01 ±0.07	ADLER	87	MRK3	e^+e^- 3.77 GeV

[1] The statistical error on this LINK 07B value is corrected in LINK 09.

$\Gamma(\overline{K}^*(1410)^0\pi^+,\overline{K}^{*0} \to K^-\pi^+)/\Gamma(K^-2\pi^+)$ — Γ_{56}/Γ_{51}

VALUE (units 10^{-3})	DOCUMENT ID		TECN	COMMENT
not seen	LINK	09	FOCS	MIPWA fit, 53k evts
not seen	BONVICINI	08A	CLEO	QMIPWA fit, 141k evts
• • • We do not use the following data for averages, fits, limits, etc. • • •				
4.8±2.1±1.7	LINK	07B	FOCS	See LINK 09

$\Gamma(\overline{K}^*_2(1430)^0\pi^+,\overline{K}^*_2(1430)^0 \to K^-\pi^+)/\Gamma(K^-2\pi^+)$ — Γ_{57}/Γ_{51}

This is the "fit fraction" from the Dalitz-plot analysis.

VALUE (units 10^{-2})	DOCUMENT ID		TECN	COMMENT
0.24 ±0.08 OUR AVERAGE	Error includes scale factor of 2.2. See the ideogram below.			
0.58 ±0.10 ±0.06	LINK	09	FOCS	MIPWA fit, 53k evts
0.204±0.040	BONVICINI	08A	CLEO	QMIPWA fit, 141k evts
0.2 ±0.1 ±0.1	AITALA	06	E791	Dalitz fit, 15.1k events

Downloaded from https://academic.oup.com/ptep/article/2022/8/083C01/6651666 by KIT Library user on 27 September 2022

• • • We do not use the following data for averages, fits, limits, etc. • • •

0.39 ±0.09 ±0.05	LINK	07B	FOCS	See LINK 09
0.5 ±0.1 ±0.2	AITALA	02	E791	See AITALA 06

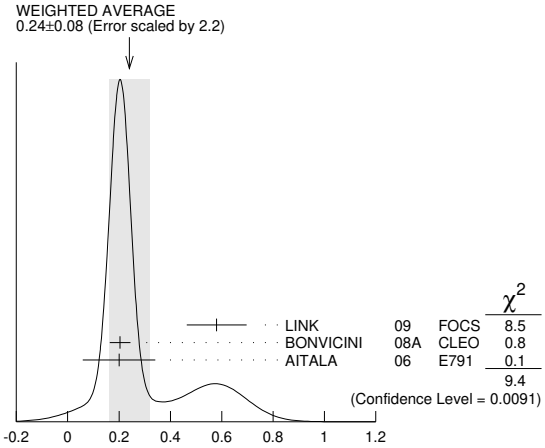

$\Gamma(\overline{K}_2^*(1430)^0\pi^+, \overline{K}_2^*(1430)^0 \to K^-\pi^+)/\Gamma(K^-2\pi^+)$ (units 10^{-2}) — Γ_{57}/Γ_{51}

$\Gamma(\overline{K}^*(1680)^0\pi^+, \overline{K}^*(1680)^0 \to K^-\pi^+)/\Gamma(K^-2\pi^+)$ — Γ_{58}/Γ_{51}

This is the "fit fraction" from the Dalitz-plot analysis.

VALUE (units 10^{-2})	DOCUMENT ID		TECN	COMMENT
0.23 ±0.12 OUR AVERAGE				
1.75 ±0.62 ±0.54	LINK	09	FOCS	MIPWA fit, 53k evts
0.196±0.118	BONVICINI	08A	CLEO	QMIPWA fit, 141k evts
1.2 ±0.6 ±1.2	AITALA	06	E791	Dalitz fit, 15.1k events
• • • We do not use the following data for averages, fits, limits, etc. • • •				
1.90 ±0.63 ±0.43	LINK	07B	FOCS	See LINK 09
2.5 ±0.7 ±0.3	AITALA	02	E791	See AITALA 06
4.7 ±0.6 ±0.7	FRABETTI	94G	E687	Dalitz fit, 8800 evts
3.0 ±0.4 ±1.3	ANJOS	93	E691	γBe 90–260 GeV

$\Gamma(K^-(2\pi^+)_{I=2})/\Gamma(K^-2\pi^+)$ — Γ_{59}/Γ_{51}

VALUE	DOCUMENT ID		TECN	COMMENT
0.155±0.028	BONVICINI	08A	CLEO	QMIPWA fit, 141k evts

$\Gamma(K^-2\pi^+ \text{ nonresonant})/\Gamma(K^-2\pi^+)$ — Γ_{60}/Γ_{51}

This is the "fit fraction" from the Dalitz-plot analysis. Later analyses find little need for this decay mode.

VALUE	DOCUMENT ID		TECN	COMMENT
• • • We do not use the following data for averages, fits, limits, etc. • • •				
0.130±0.058±0.044	AITALA	02	E791	See AITALA 06
0.998±0.037±0.072	FRABETTI	94G	E687	Dalitz fit, 8800 evts
0.838±0.088±0.275	ANJOS	93	E691	γBe 90–260 GeV
0.79 ±0.07 ±0.15	ADLER	87	MRK3	e^+e^- 3.77 GeV

$\Gamma(K^0_S\pi^+\pi^0)/\Gamma_{total}$ — Γ_{61}/Γ

VALUE (units 10^{-2})	EVTS	DOCUMENT ID		TECN	COMMENT
• • • We do not use the following data for averages, fits, limits, etc. • • •					
6.99±0.09±0.25		[1] DOBBS	07	CLEO	See BONVICINI 14
7.2 ±0.2 ±0.4	5.1k	[1] HE	05	CLEO	See DOBBS 07
5.1 ±1.3 ±0.8	159	ADLER	88C	MRK3	e^+e^- 3.77 GeV

[1] DOBBS 07 and HE 05 use single- and double-tagged events in an overall fit. DOBBS 07 supersedes HE 05.

$\Gamma(K^0_S\pi^+\pi^0)/\Gamma(K^-2\pi^+)$ — Γ_{61}/Γ_{51}

VALUE	DOCUMENT ID		TECN	COMMENT
0.785±0.007±0.016	BONVICINI	14	CLEO	All CLEO-c runs

$\Gamma(K^0_S\rho^+)/\Gamma(K^0_S\pi^+\pi^0)$ — Γ_{62}/Γ_{61}

This is the "fit fraction" from the Dalitz-plot analysis.

VALUE (units 10^{-2})	DOCUMENT ID		TECN	COMMENT
83.4±2.2$^{+7.1}_{-3.6}$	[1] ABLIKIM	14E	BES3	e^+e^- at $\psi(3770)$

[1] Fit fraction from Dalitz plot analysis of 142k $D^+ \to K^0_S\pi^+\pi^0$ events.

$\Gamma(K^0_S\rho(1450)^+, \rho^+ \to \pi^+\pi^0)/\Gamma(K^0_S\pi^+\pi^0)$ — Γ_{63}/Γ_{61}

This is the "fit fraction" from the Dalitz-plot analysis.

VALUE (%)	DOCUMENT ID		TECN	COMMENT
2.1±0.3$^{+1.6}_{-1.9}$	ABLIKIM	14E	BES3	e^+e^- at $\psi(3770)$

$\Gamma(\overline{K}^*(892)^0\pi^+, \overline{K}^*(892)^0 \to K^0_S\pi^0)/\Gamma(K^0_S\pi^+\pi^0)$ — Γ_{64}/Γ_{61}

This is the "fit fraction" from the Dalitz-plot analysis.

VALUE (units 10^{-2})	DOCUMENT ID		TECN	COMMENT
3.58±0.17$^{+0.39}_{-0.38}$	[1] ABLIKIM	14E	BES3	e^+e^- at $\psi(3770)$

[1] Fit fraction from Dalitz plot analysis of 142k $D^+ \to K^0_S\pi^+\pi^0$ events.

$\Gamma(\overline{K}_0^*(1430)^0\pi^+, \overline{K}_0^{*0} \to K^0_S\pi^0)/\Gamma(K^0_S\pi^+\pi^0)$ — Γ_{65}/Γ_{61}

This is the "fit fraction" from the Dalitz-plot analysis.

VALUE (%)	DOCUMENT ID		TECN	COMMENT
3.7±0.6±1.1	ABLIKIM	14E	BES3	e^+e^- at $\psi(3770)$

$\Gamma(\overline{K}_0^*(1680)^0\pi^+, \overline{K}_0^{*0} \to K^0_S\pi^0)/\Gamma(K^0_S\pi^+\pi^0)$ — Γ_{66}/Γ_{61}

This is the "fit fraction" from the Dalitz-plot analysis.

VALUE (%)	DOCUMENT ID		TECN	COMMENT
1.3±0.2$^{+0.9}_{-1.3}$	ABLIKIM	14E	BES3	e^+e^- at $\psi(3770)$

$\Gamma(\overline{\kappa}^0\pi^+, \overline{\kappa}^0 \to K^0_S\pi^0)/\Gamma(K^0_S\pi^+\pi^0)$ — Γ_{67}/Γ_{61}

This is the "fit fraction" from the Dalitz-plot analysis.

VALUE (%)	DOCUMENT ID		TECN	COMMENT
7.7±1.2$^{+6.5}_{-4.8}$	ABLIKIM	14E	BES3	e^+e^- at $\psi(3770)$

$\Gamma(K^0_S\pi^+\pi^0 \text{ nonresonant})/\Gamma(K^0_S\pi^+\pi^0)$ — Γ_{68}/Γ_{61}

This is the "fit fraction" from the Dalitz-plot analysis.

VALUE (units 10^{-2})	DOCUMENT ID		TECN	COMMENT
4.6±0.7$^{+5.4}_{-5.1}$	[1] ABLIKIM	14E	BES3	e^+e^- at $\psi(3770)$

[1] Fit fraction from Dalitz plot analysis of 142k $D^+ \to K^0_S\pi^+\pi^0$ events.

$\Gamma(K^0_S\pi^+\pi^0 \text{ nonresonant and } \overline{\kappa}^0\pi^+)/\Gamma(K^0_S\pi^+\pi^0)$ — Γ_{69}/Γ_{61}

This is the "fit fraction" from the Dalitz-plot analysis.

VALUE (%)	DOCUMENT ID		TECN	COMMENT
18.6±1.7$^{+2.3}_{-4.6}$	ABLIKIM	14E	BES3	e^+e^- at $\psi(3770)$

$\Gamma((K^0_S\pi^0)_{S-\text{wave}}\pi^+)/\Gamma(K^0_S\pi^+\pi^0)$ — Γ_{70}/Γ_{61}

The numerator here is the coherent sum of the $\overline{K}_0^*(1430)^0\pi^+$, $\overline{\kappa}^0\pi^+$, and nonresonant contributions.

VALUE (%)	DOCUMENT ID		TECN	COMMENT
17.3±1.4$^{+3.4}_{-4.3}$	ABLIKIM	14E	BES3	e^+e^- at $\psi(3770)$

$\Gamma(K^0_S\pi^+\eta)/\Gamma_{total}$ — Γ_{71}/Γ

VALUE (units 10^{-3})	EVTS	DOCUMENT ID		TECN	COMMENT
13.09±0.37±0.31	1.3k	ABLIKIM	20V	BES3	e^+e^-, 3773 MeV

$\Gamma(K^0_S\pi^+\eta'(958))/\Gamma_{total}$ — Γ_{72}/Γ

VALUE (units 10^{-3})	EVTS	DOCUMENT ID		TECN	COMMENT
1.90±0.17±0.13	267	ABLIKIM	18AC	BES3	e^+e^-, 3773 MeV

$\Gamma(K^-2\pi^+\pi^0)/\Gamma_{total}$ — Γ_{73}/Γ

See our 2008 Review (Physics Letters **B667** 1 (2008)) for measurements of submodes of this mode. There is nothing new since 1992, and the two papers, ANJOS 92C, with 91 ± 12 events above background, and COFFMAN 92B, with 142 ± 20 such events, could not determine submode fractions with much accuracy.

VALUE (units 10^{-2})	EVTS	DOCUMENT ID		TECN	COMMENT
• • • We do not use the following data for averages, fits, limits, etc. • • •					
5.98±0.08±0.16		[1] DOBBS	07	CLEO	See BONVICINI 14
6.0 ±0.2 ±0.2	4.8k	[1] HE	05	CLEO	See DOBBS 07
5.8 ±1.2 ±1.2	142	COFFMAN	92B	MRK3	e^+e^- 3.77 GeV
6.3 $^{+1.4}_{-1.3}$ ±1.2	175	BALTRUSAIT...86E		MRK3	See COFFMAN 92B

[1] DOBBS 07 and HE 05 use single- and double-tagged events in an overall fit. DOBBS 07 supersedes HE 05.

$\Gamma(K^-2\pi^+\pi^0)/\Gamma(K^-2\pi^+)$ — Γ_{73}/Γ_{51}

VALUE	DOCUMENT ID		TECN	COMMENT
0.666±0.006±0.014	BONVICINI	14	CLEO	All CLEO-c runs

$\Gamma(K^0_S2\pi^+\pi^-)/\Gamma_{total}$ — Γ_{74}/Γ

See our 2008 Review (Physics Letters **B667** 1 (2008)) for measurements of submodes of this mode. There is nothing new since 1992, and the two papers, ANJOS 92C, with 229 ± 17 events above background, and COFFMAN 92B, with 209 ± 20 such events, could not determine submode fractions with much accuracy.

VALUE (units 10^{-2})	EVTS	DOCUMENT ID		TECN	COMMENT
• • • We do not use the following data for averages, fits, limits, etc. • • •					
3.122±0.046±0.096		[1] DOBBS	07	CLEO	See BONVICINI 14
3.2 ±0.1 ±0.2	3.2k	[1] HE	05	CLEO	See DOBBS 07
2.1 $^{+1.0}_{-0.9}$		[2] BARLAG	92C	ACCM	π^- Cu 230 GeV
3.3 ±0.8 ±0.2	168	ADLER	88C	MRK3	e^+e^- 3.77 GeV

[1] DOBBS 07 and HE 05 use single- and double-tagged events in an overall fit. DOBBS 07 supersedes HE 05.
[2] BARLAG 92C computes the branching fraction by topological normalization.

Downloaded from https://academic.oup.com/ptep/article/2022/8/083C01/6651666 by KIT Library user on 27 September 2022

$\Gamma(K^- 2\pi^+ \eta)/\Gamma_{total}$ — Γ_{75}/Γ

VALUE (units 10^{-3})	EVTS	DOCUMENT ID		TECN	COMMENT
1.35±0.11±0.04	190	ABLIKIM	20V	BES3	e^+e^-, 3773 MeV

$\Gamma(K^0_S \pi^+ \pi^0 \eta)/\Gamma_{total}$ — Γ_{76}/Γ

VALUE (units 10^{-3})	EVTS	DOCUMENT ID		TECN	COMMENT
1.22±0.24±0.06	50	ABLIKIM	20V	BES3	e^+e^-, 3773 MeV

$\Gamma(K^0_S 2\pi^+ \pi^-)/\Gamma(K^- 2\pi^+)$ — Γ_{74}/Γ_{51}

VALUE	DOCUMENT ID		TECN	COMMENT
0.331±0.004±0.006	BONVICINI	14	CLEO	All CLEO-c runs

$\Gamma(K^- 3\pi^+ \pi^-)/\Gamma(K^- 2\pi^+)$ — Γ_{77}/Γ_{51}

VALUE	EVTS	DOCUMENT ID		TECN	COMMENT
0.061±0.005 OUR FIT	Error includes scale factor of 1.1.				
0.062±0.008 OUR AVERAGE	Error includes scale factor of 1.3.				
0.058±0.002±0.006	2923	LINK	03D	FOCS	γ A, $\overline{E}_\gamma \approx$ 180 GeV
0.077±0.008±0.010	239	FRABETTI	97C	E687	γBe, $\overline{E}_\gamma \approx$ 200 GeV
• • • We do not use the following data for averages, fits, limits, etc. • • •					
0.09 ±0.01 ±0.01	113	ANJOS	90D	E691	Photoproduction

$\Gamma(\overline{K}^*(892)^0 2\pi^+\pi^-, \overline{K}^*(892)^0 \to K^-\pi^+)/\Gamma(K^- 3\pi^+\pi^-)$ — Γ_{78}/Γ_{77}

VALUE	DOCUMENT ID		TECN	COMMENT
0.21±0.04±0.06	LINK	03D	FOCS	γ A, $\overline{E}_\gamma \approx$ 180 GeV

$\Gamma(\overline{K}^*(892)^0 \rho^0 \pi^+, \overline{K}^*(892)^0 \to K^-\pi^+)/\Gamma(K^- 2\pi^+)$ — Γ_{79}/Γ_{51}

VALUE	DOCUMENT ID		TECN	COMMENT
• • • We do not use the following data for averages, fits, limits, etc. • • •				
0.016±0.007±0.004	FRABETTI	97C	E687	γBe, $\overline{E}_\gamma \approx$ 200 GeV

$\Gamma(\overline{K}^*(892)^0 \rho^0 \pi^+, \overline{K}^*(892)^0 \to K^-\pi^+)/\Gamma(K^- 3\pi^+\pi^-)$ — Γ_{79}/Γ_{77}

VALUE	DOCUMENT ID		TECN	COMMENT
0.40±0.03±0.06	LINK	03D	FOCS	γ A, $\overline{E}_\gamma \approx$ 180 GeV

$\Gamma(\overline{K}^*(892)^0 a_1(1260)^+)/\Gamma(K^- 2\pi^+)$ — Γ_{80}/Γ_{51}

Unseen decay modes of the $\overline{K}^*(892)^0$ and $a_1(1260)^+$ are included.

VALUE	DOCUMENT ID		TECN	COMMENT
0.099±0.008±0.018	LINK	03D	FOCS	γ A, $\overline{E}_\gamma \approx$ 180 GeV

$\Gamma(\overline{K}^*(892)^0 2\pi^+\pi^- \text{no-}\rho, \overline{K}^*(892)^0 \to K^-\pi^+)/\Gamma(K^- 2\pi^+)$ — Γ_{81}/Γ_{51}

VALUE	DOCUMENT ID		TECN	COMMENT
• • • We do not use the following data for averages, fits, limits, etc. • • •				
0.032±0.010±0.008	FRABETTI	97C	E687	γBe, $\overline{E}_\gamma \approx$ 200 GeV

$\Gamma(K^- \rho^0 2\pi^+)/\Gamma(K^- 2\pi^+)$ — Γ_{82}/Γ_{51}

VALUE	DOCUMENT ID		TECN	COMMENT
• • • We do not use the following data for averages, fits, limits, etc. • • •				
0.034±0.009±0.005	FRABETTI	97C	E687	γBe, $\overline{E}_\gamma \approx$ 200 GeV

$\Gamma(K^- \rho^0 2\pi^+)/\Gamma(K^- 3\pi^+\pi^-)$ — Γ_{82}/Γ_{77}

VALUE	DOCUMENT ID		TECN	COMMENT
0.30±0.04±0.01	LINK	03D	FOCS	γ A, $\overline{E}_\gamma \approx$ 180 GeV

$\Gamma(K^- 3\pi^+\pi^- \text{ nonresonant})/\Gamma(K^- 3\pi^+\pi^-)$ — Γ_{83}/Γ_{77}

VALUE	CL%	DOCUMENT ID		TECN	COMMENT
0.07 ±0.05±0.01		LINK	03D	FOCS	γ A, $\overline{E}_\gamma \approx$ 180 GeV
• • • We do not use the following data for averages, fits, limits, etc. • • •					
<0.026	90	FRABETTI	97C	E687	γBe, $\overline{E}_\gamma \approx$ 200 GeV

$\Gamma(K^+ 2K^0_S)/\Gamma_{total}$ — Γ_{84}/Γ

VALUE (units 10^{-4})	EVTS	DOCUMENT ID		TECN	COMMENT
25.4±0.5±1.2	3551	ABLIKIM	17A	BES3	$e^+e^- \to \psi(3770)$

$\Gamma(K^+ 2K^0_S)/\Gamma(K^- 2\pi^+)$ — Γ_{84}/Γ_{51}

VALUE	EVTS	DOCUMENT ID		TECN	COMMENT
• • • We do not use the following data for averages, fits, limits, etc. • • •					
0.035±0.010±0.005	39 ± 9	ALBRECHT	94I	ARG	$e^+e^- \approx$ 10 GeV
0.085±0.018	70 ± 12	AMMAR	91	CLEO	$e^+e^- \approx$ 10.5 GeV

$\Gamma(\phi(1020)^0 K^+)/\Gamma_{total}$ — Γ_{151}/Γ

VALUE	CL%	DOCUMENT ID		TECN	COMMENT
<2.1 × 10^{-5}	90	ABLIKIM	19BI	BES3	e^+e^- at 3773 MeV

$\Gamma(K^+ K^- K^0_S \pi^+)/\Gamma(K^0_S 2\pi^+\pi^-)$ — Γ_{85}/Γ_{74}

VALUE (units 10^{-3})	EVTS	DOCUMENT ID		TECN	COMMENT
7.7±1.5±0.9	35 ± 7	LINK	01C	FOCS	γ nucleus, $\overline{E}_\gamma \approx$ 180 GeV

Pionic modes

$\Gamma(\pi^+\pi^0)/\Gamma_{total}$ — Γ_{86}/Γ

VALUE (units 10^{-3})	EVTS	DOCUMENT ID		TECN	COMMENT
1.247±0.033 OUR FIT					
1.259±0.033±0.023	10k	ABLIKIM	18W	BES3	e^+e^-, 3773 MeV

$\Gamma(\pi^+\pi^0)/\Gamma(K^- 2\pi^+)$ — Γ_{86}/Γ_{51}

VALUE (units 10^{-2})	EVTS	DOCUMENT ID		TECN	COMMENT
1.33±0.04 OUR FIT	Error includes scale factor of 1.1.				
1.31±0.06 OUR AVERAGE					
1.29±0.04±0.05	2649 ± 76	MENDEZ	10	CLEO	e^+e^- at 3774 MeV
1.33±0.11±0.09	1229 ± 99	AUBERT,B	06F	BABR	$e^+e^- \approx \Upsilon(4S)$
1.44±0.19±0.10	171 ± 22	ARMS	04	CLEO	$e^+e^- \approx$ 10 GeV
• • • We do not use the following data for averages, fits, limits, etc. • • •					
1.33±0.07±0.06	914 ± 46	RUBIN	06	CLEO	See MENDEZ 10

$\Gamma(2\pi^+\pi^-)/\Gamma(K^- 2\pi^+)$ — Γ_{87}/Γ_{51}

VALUE (units 10^{-2})	EVTS	DOCUMENT ID		TECN	COMMENT
3.48±0.19 OUR AVERAGE	Error includes scale factor of 1.4. See the ideogram below.				
3.52±0.11±0.12	3303 ± 95	RUBIN	06	CLEO	e^+e^- at $\psi(3770)$
4.1 ±1.1 ±0.3	85 ± 22	ABLIKIM	05F	BES	$e^+e^- \approx \psi(3770)$
$3.11 \pm 0.18^{+0.16}_{-0.26}$	1172	AITALA	01B	E791	π^- nucleus, 500 GeV
4.3 ±0.3 ±0.3	236	FRABETTI	97D	E687	γ Be $\approx$ 200 GeV
3.5 ±0.7 ±0.3	83	ANJOS	89	E691	Photoproduction

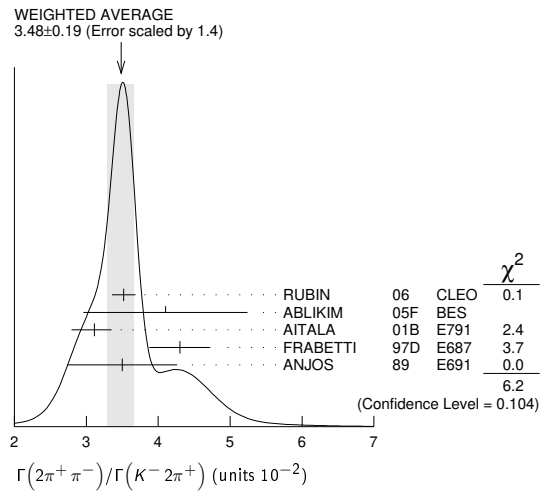

$\Gamma(\rho^0\pi^+)/\Gamma(2\pi^+\pi^-)$ — Γ_{88}/Γ_{87}

This is the "fit fraction" from the Dalitz-plot analysis.

VALUE	DOCUMENT ID		TECN	COMMENT
0.25 ±0.04 OUR AVERAGE	Error includes scale factor of 2.4. See the ideogram below.			
0.200 ±0.023 ±0.009	BONVICINI	07	CLEO	Dalitz fit, $\approx$ 2240 evts
0.3082±0.0314±0.0230	LINK	04	FOCS	Dalitz fit, 1527 ± 51 evts
0.336 ±0.032 ±0.022	AITALA	01B	E791	Dalitz fit, 1172 evts

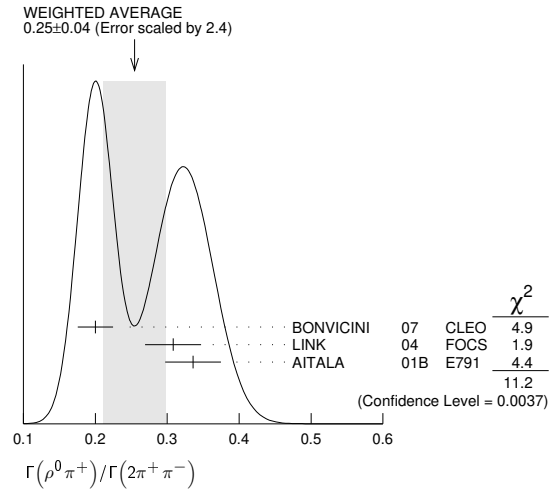

Downloaded from https://academic.oup.com/ptep/article/2022/8/083C01/6651666 by KIT Library user on 27 September 2022

$\Gamma(\pi^+(\pi^+\pi^-)_{S-\text{wave}})/\Gamma(2\pi^+\pi^-)$ — Γ_{89}/Γ_{87}

This is the "fit fraction" from the Dalitz-plot analysis. See also the next three data blocks.

VALUE	DOCUMENT ID		TECN	COMMENT
0.5600±0.0324±0.0214	[1] LINK	04	FOCS	Dalitz fit, 1527 ± 51 evts

[1] LINK 04 borrows a K-matrix parametrization from ANISOVICH 03 of the full π-π S-wave isoscalar scattering amplitude to describe the $\pi^+\pi^-$ S-wave component of the $\pi^+\pi^+\pi^-$ state. The fit fraction given above is a sum over five f_0 mesons, the $f_0(980)$, $f_0(1300)$, $f_0(1200$–$1600)$, $f_0(1500)$, and $f_0(1750)$. See LINK 04 for details and discussion.

$\Gamma(\sigma\pi^+, \sigma\to\pi^+\pi^-)/\Gamma(2\pi^+\pi^-)$ — Γ_{90}/Γ_{87}

This is the "fit fraction" from the Dalitz-plot analysis.

VALUE	DOCUMENT ID		TECN	COMMENT
0.422±0.027 OUR AVERAGE				
0.418±0.014±0.025	BONVICINI	07	CLEO	Dalitz fit, ≈ 2240 evts
0.463±0.090±0.021	AITALA	01B	E791	Dalitz fit, 1172 evts

$\Gamma(f_0(980)\pi^+, f_0(980)\to\pi^+\pi^-)/\Gamma(2\pi^+\pi^-)$ — Γ_{91}/Γ_{87}

This is the "fit fraction" from the Dalitz-plot analysis.

VALUE	DOCUMENT ID		TECN	COMMENT
0.048±0.010 OUR AVERAGE Error includes scale factor of 1.3.				
0.041±0.009±0.003	BONVICINI	07	CLEO	Dalitz fit, ≈ 2240 evts
0.062±0.013±0.004	AITALA	01B	E791	Dalitz fit, 1172 evts

$\Gamma(f_0(1370)\pi^+, f_0(1370)\to\pi^+\pi^-)/\Gamma(2\pi^+\pi^-)$ — Γ_{92}/Γ_{87}

This is the "fit fraction" from the Dalitz-plot analysis.

VALUE	DOCUMENT ID		TECN	COMMENT
0.024±0.013 OUR AVERAGE				
0.026±0.018±0.006	BONVICINI	07	CLEO	Dalitz fit, ≈ 2240 evts
0.023±0.015±0.008	AITALA	01B	E791	Dalitz fit, 1172 evts

$\Gamma(f_2(1270)\pi^+, f_2(1270)\to\pi^+\pi^-)/\Gamma(2\pi^+\pi^-)$ — Γ_{93}/Γ_{87}

This is the "fit fraction" from the Dalitz-plot analysis.

VALUE	DOCUMENT ID		TECN	COMMENT
0.154 ±0.025 OUR AVERAGE Error includes scale factor of 1.9. See the ideogram below.				
0.182 ±0.026 ±0.007	BONVICINI	07	CLEO	Dalitz fit, ≈ 2240 evts
0.1174±0.0190±0.0029	LINK	04	FOCS	Dalitz fit, 1527 ± 51 evts
0.194 ±0.025 ±0.004	AITALA	01B	E791	Dalitz fit, 1172 evts

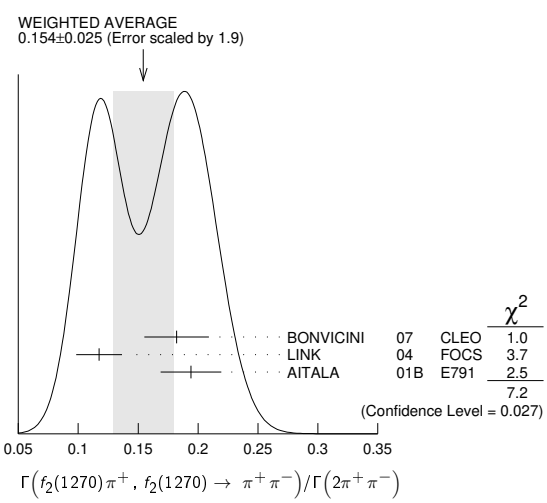

$\Gamma(\rho(1450)^0\pi^+, \rho(1450)^0\to\pi^+\pi^-)/\Gamma(2\pi^+\pi^-)$ — Γ_{94}/Γ_{87}

This is the "fit fraction" from the Dalitz-plot analysis.

VALUE	CL%	DOCUMENT ID		TECN	COMMENT
<0.024	95	BONVICINI	07	CLEO	Dalitz fit, ≈ 2240 evts
• • • We do not use the following data for averages, fits, limits, etc. • • •					
0.007±0.007±0.003		AITALA	01B	E791	Dalitz fit, 1172 evts

$\Gamma(f_0(1500)\pi^+, f_0(1500)\to\pi^+\pi^-)/\Gamma(2\pi^+\pi^-)$ — Γ_{95}/Γ_{87}

This is the "fit fraction" from the Dalitz-plot analysis.

VALUE	DOCUMENT ID		TECN	COMMENT
0.034±0.010±0.008	BONVICINI	07	CLEO	Dalitz fit, ≈ 2240 evts

$\Gamma(f_0(1710)\pi^+, f_0(1710)\to\pi^+\pi^-)/\Gamma(2\pi^+\pi^-)$ — Γ_{96}/Γ_{87}

This is the "fit fraction" from the Dalitz-plot analysis.

VALUE	CL%	DOCUMENT ID		TECN	COMMENT
<0.016	95	BONVICINI	07	CLEO	Dalitz fit, ≈ 2240 evts

$\Gamma(f_0(1790)\pi^+, f_0(1790)\to\pi^+\pi^-)/\Gamma(2\pi^+\pi^-)$ — Γ_{97}/Γ_{87}

This is the "fit fraction" from the Dalitz-plot analysis.

VALUE	CL%	DOCUMENT ID		TECN	COMMENT
<0.02	95	BONVICINI	07	CLEO	Dalitz fit, ≈ 2240 evts

$\Gamma((\pi^+\pi^+)_{S-\text{wave}}\pi^-)/\Gamma(2\pi^+\pi^-)$ — Γ_{98}/Γ_{87}

This is the "fit fraction" from the Dalitz-plot analysis.

VALUE	CL%	DOCUMENT ID		TECN	COMMENT
<0.037	95	BONVICINI	07	CLEO	Dalitz fit, ≈ 2240 evts

$\Gamma(2\pi^+\pi^-$ nonresonant$)/\Gamma(2\pi^+\pi^-)$ — Γ_{99}/Γ_{87}

This is the "fit fraction" from the Dalitz-plot analysis.

VALUE	CL%	DOCUMENT ID		TECN	COMMENT
<0.035	95	BONVICINI	07	CLEO	Dalitz fit, ≈ 2240 evts
• • • We do not use the following data for averages, fits, limits, etc. • • •					
0.078±0.060±0.027		AITALA	01B	E791	Dalitz fit, 1172 evts

$\Gamma(\pi^+2\pi^0)/\Gamma(K^-2\pi^+)$ — Γ_{100}/Γ_{51}

VALUE (units 10^{-2})	EVTS	DOCUMENT ID		TECN	COMMENT
5.0±0.3±0.3	1535 ± 89	RUBIN	06	CLEO	e^+e^- at $\psi(3770)$

$\Gamma(2\pi^+\pi^-\pi^0)/\Gamma(K^-2\pi^+)$ — Γ_{101}/Γ_{51}

VALUE (units 10^{-2})	EVTS	DOCUMENT ID		TECN	COMMENT
12.4±0.5±0.6	5701 ± 205	RUBIN	06	CLEO	e^+e^- at $\psi(3770)$

$\Gamma(3\pi^+2\pi^-)/\Gamma(K^-2\pi^+)$ — Γ_{102}/Γ_{51}

VALUE (units 10^{-2})	EVTS	DOCUMENT ID		TECN	COMMENT
1.77±0.17 OUR FIT					
1.73±0.20±0.17	732 ± 77	RUBIN	06	CLEO	e^+e^- at $\psi(3770)$
• • • We do not use the following data for averages, fits, limits, etc. • • •					
2.3 ±0.4 ±0.2	58	FRABETTI	97C	E687	γBe, $\overline{E}_\gamma \approx$ 200 GeV

$\Gamma(3\pi^+2\pi^-)/\Gamma(K^-3\pi^+\pi^-)$ — Γ_{102}/Γ_{77}

VALUE	EVTS	DOCUMENT ID		TECN	COMMENT
0.289±0.019 OUR FIT					
0.290±0.017±0.011	835	LINK	03D	FOCS	γ A, $\overline{E}_\gamma \approx$ 180 GeV

$\Gamma(\eta\pi^+)/\Gamma_{\text{total}}$ — Γ_{103}/Γ

Unseen decay modes of the η are included.

VALUE (units 10^{-4})	EVTS	DOCUMENT ID		TECN	COMMENT
37.7 ±0.9 OUR FIT					
37.90±0.70±0.68	12k	ABLIKIM	18W	BES3	e^+e^-, 3773 MeV
• • • We do not use the following data for averages, fits, limits, etc. • • •					
30.7 ±2.2 ±1.3	258	ABLIKIM	16D	BES3	e^+e^- at 3773 MeV
34.3 ±1.4 ±1.7	1033±42	ARTUSO	08	CLEO	See MENDEZ 10

$\Gamma(\eta\pi^+)/\Gamma(K^-2\pi^+)$ — Γ_{103}/Γ_{51}

Unseen decay modes of the η are included.

VALUE (units 10^{-2})	EVTS	DOCUMENT ID		TECN	COMMENT
4.02±0.11 OUR FIT Error includes scale factor of 1.1.					
3.87±0.09±0.19	2940 ± 68	MENDEZ	10	CLEO	e^+e^- at 3774 MeV
• • • We do not use the following data for averages, fits, limits, etc. • • •					
3.81±0.26±0.21	377 ± 26	RUBIN	06	CLEO	See ARTUSO 08

$\Gamma(\eta\pi^+\pi^0)/\Gamma_{\text{total}}$ — Γ_{104}/Γ

VALUE (units 10^{-4})	EVTS	DOCUMENT ID		TECN	COMMENT
20.5±3.5 OUR AVERAGE Error includes scale factor of 2.2.					
22.3±1.5±1.0	381	ABLIKIM	20G	BES3	e^+e^-, 3773 MeV
13.8±3.1±1.6	149 ± 34	ARTUSO	08	CLEO	e^+e^- at $\psi(3770)$
• • • We do not use the following data for averages, fits, limits, etc. • • •					
24.7±9.3±1.6	42	ABLIKIM	20AA	BES3	e^+e^-, 3773 MeV

$\Gamma(\eta 2\pi^+\pi^-)/\Gamma_{\text{total}}$ — Γ_{105}/Γ

VALUE (units 10^{-3})	EVTS	DOCUMENT ID		TECN	COMMENT
3.41±0.17±0.10	515	ABLIKIM	20V	BES3	e^+e^-, 3773 MeV

$\Gamma(\eta\pi^+2\pi^0)/\Gamma_{\text{total}}$ — Γ_{106}/Γ

VALUE (units 10^{-3})	EVTS	DOCUMENT ID		TECN	COMMENT
3.20±0.28±0.17	190	ABLIKIM	20V	BES3	e^+e^-, 3773 MeV

$\Gamma(\eta\eta\pi^+)/\Gamma_{\text{total}}$ — Γ_{107}/Γ

VALUE (units 10^{-4})	EVTS	DOCUMENT ID		TECN	COMMENT
29.6±2.4±1.0	179	ABLIKIM	20G	BES3	e^+e^-, 3773 MeV

$\Gamma(\omega\pi^+)/\Gamma_{\text{total}}$ — Γ_{108}/Γ

Unseen decay modes of the ω are included.

VALUE (units 10^{-4})	CL%	EVTS	DOCUMENT ID		TECN	COMMENT
2.79±0.57±0.16		79	ABLIKIM	16D	BES3	e^+e^- at 3773 MeV
• • • We do not use the following data for averages, fits, limits, etc. • • •						
<3.4	90		RUBIN	06	CLEO	e^+e^- at $\psi(3770)$

$\Gamma(\omega\pi^+\pi^0)/\Gamma_{\text{total}}$ — Γ_{109}/Γ

VALUE (units 10^{-3})	EVTS	DOCUMENT ID		TECN	COMMENT
3.87±0.83±0.25	233	[1] ABLIKIM	20AA	BES3	e^+e^-, 3773 MeV

[1] ABLIKIM 20AA reports a statistical significance of 7.7 σ for this measurement.

Downloaded from https://academic.oup.com/ptep/article/2022/8/083C01/6651666 by KIT Library user on 27 September 2022

$\Gamma(\eta'(958)\pi^+)/\Gamma_{total}$ — Γ_{110}/Γ

Unseen decay modes of the $\eta'(958)$ are included.

VALUE (units 10^{-4})	EVTS	DOCUMENT ID		TECN	COMMENT
49.7±1.9 OUR FIT					
51.2±1.4±2.1	3.1k	ABLIKIM	18W	BES3	e^+e^-, 3773 MeV
• • • We do not use the following data for averages, fits, limits, etc. • • •					
44.2±2.5±2.9	352 ± 20	ARTUSO	08	CLEO	See MENDEZ 10

$\Gamma(\eta'(958)\pi^+)/\Gamma(K^-2\pi^+)$ — Γ_{110}/Γ_{51}

Unseen decay modes of the $\eta'(958)$ are included.

VALUE (units 10^{-2})	EVTS	DOCUMENT ID		TECN	COMMENT
5.30±0.21 OUR FIT					
5.12±0.17±0.25	1037 ± 35	MENDEZ	10	CLEO	e^+e^- at 3774 MeV

$\Gamma(\eta'(958)\pi^+\pi^0)/\Gamma_{total}$ — Γ_{111}/Γ

Unseen decay modes of the $\eta'(958)$ are included.

VALUE (units 10^{-4})	EVTS	DOCUMENT ID		TECN	COMMENT
15.7±4.3±2.5	33 ± 9	ARTUSO	08	CLEO	e^+e^- at $\psi(3770)$

Hadronic modes with a $K\overline{K}$ pair

$\Gamma(K^0_S K^+)/\Gamma_{total}$ — Γ_{112}/Γ

VALUE (units 10^{-3})	EVTS	DOCUMENT ID		TECN	COMMENT
3.04 ±0.09 OUR FIT Error includes scale factor of 2.2.					
3.183±0.029±0.060	18k	ABLIKIM	18W	BES3	e^+e^-, 3773 MeV
• • • We do not use the following data for averages, fits, limits, etc. • • •					
3.02 ±0.09 ±0.08	780	ABLIKIM	19M	BES3	See ABLIKIM 18W.
3.14 ±0.09 ±0.08	1971 ±51	BONVICINI	08	CLEO	See MENDEZ 10

$\Gamma(K^0_S K^+)/\Gamma(K^0_S\pi^+)$ — Γ_{112}/Γ_{49}

VALUE	EVTS	DOCUMENT ID		TECN	COMMENT
0.194 ±0.006 OUR FIT Error includes scale factor of 2.8.					
0.1901±0.0024 OUR AVERAGE					
0.1899±0.0011±0.0022	101k±561	WON	09	BELL	e^+e^- at $\Upsilon(4S)$
0.1892±0.0155±0.0073	278 ± 21	ARMS	04	CLEO	$e^+e^-\approx$ 10 GeV
0.1996±0.0119±0.0096	949	LINK	02B	FOCS	γ A, $\overline{E}_\gamma\approx$ 180 GeV
• • • We do not use the following data for averages, fits, limits, etc. • • •					
0.222 ±0.037 ±0.013	63 ± 10	ABLIKIM	05F	BES	$e^+e^-\approx\psi(3770)$
0.222 ±0.041 ±0.019	70	BISHAI	97	CLEO	See ARMS 04
0.25 ±0.04 ±0.02	129	FRABETTI	95	E687	γBe $\overline{E}_\gamma\approx$ 200 GeV
0.271 ±0.065 ±0.039	69	ANJOS	90C	E691	γBe
0.317 ±0.086 ±0.048	31	BALTRUSAIT...	85E	MRK3	e^+e^- 3.77 GeV
0.25 ±0.15	6	SCHINDLER	81	MRK2	e^+e^- 3.771 GeV

$\Gamma(K^0_S K^+)/\Gamma(K^-2\pi^+)$ — Γ_{112}/Γ_{51}

VALUE (units 10^{-2})	EVTS	DOCUMENT ID		TECN	COMMENT
3.24±0.09 OUR FIT Error includes scale factor of 2.3.					
3.35±0.06±0.07	5161 ± 86	MENDEZ	10	CLEO	e^+e^- at 3774 MeV
• • • We do not use the following data for averages, fits, limits, etc. • • •					
3.02±0.18±0.15	949	[1] LINK	02B	FOCS	γ nucleus, $\overline{E}_\gamma\approx$ 180 GeV

[1] This LINK 02B result is redundant with a result in the previous datablock.

$\Gamma(K^0_L K^+)/\Gamma_{total}$ — Γ_{113}/Γ

VALUE (units 10^{-3})	EVTS	DOCUMENT ID		TECN	COMMENT
3.21±0.11±0.11	650	ABLIKIM	19M	BES3	e^+e^- at 3773 MeV

$\Gamma(K^0_S K^+\pi^0)/\Gamma_{total}$ — Γ_{114}/Γ

VALUE (units 10^{-3})	EVTS	DOCUMENT ID		TECN	COMMENT
5.07±0.19±0.23	470	ABLIKIM	19M	BES3	e^+e^- at 3773 MeV

$\Gamma(K^*(892)^+K^0_S)/\Gamma(K^0_S\pi^+)$ — Γ_{115}/Γ_{49}

Unseen decay modes of the $K^*(892)^+$ are included.

VALUE	EVTS	DOCUMENT ID		TECN	COMMENT
• • • We do not use the following data for averages, fits, limits, etc. • • •					
1.1±0.3±0.4	67	FRABETTI	95	E687	γBe $\overline{E}_\gamma\approx$ 200 GeV

$\Gamma(K^*(892)^+K^0_S)/\Gamma(K^0_S K^+\pi^0)$ — $\Gamma_{115}/\Gamma_{114}$

VALUE	EVTS	DOCUMENT ID		TECN	COMMENT
0.571±0.026±0.042	692	[1] ABLIKIM	21AD	BES3	e^+e^- at 3.773 GeV

[1] ABLIKIM 21AD value is a fit fraction from an amplitude analysis of $D^+\to K^+K^0_S\pi^0$ with four components. Reconstructs the $K^*(892)^+$ from its $K^+\pi^0$ final state.

$\Gamma(\overline{K}^*(892)^0K^+)/\Gamma(K^0_S K^+\pi^0)$ — $\Gamma_{116}/\Gamma_{114}$

VALUE	EVTS	DOCUMENT ID		TECN	COMMENT
0.102±0.015±0.022	692	[1] ABLIKIM	21AD	BES3	e^+e^- at 3.773 GeV

[1] ABLIKIM 21AD value is a fit fraction from an amplitude analysis of $D^+\to K^+K^0_S\pi^0$ with four components. Reconstructs the $\overline{K}^*(892)^0$ from its $K^0_S\pi^0$ final state.

$\Gamma(K^0_L K^+\pi^0)/\Gamma_{total}$ — Γ_{117}/Γ

VALUE (units 10^{-3})	EVTS	DOCUMENT ID		TECN	COMMENT
5.24±0.22±0.22	410	ABLIKIM	19M	BES3	e^+e^- at 3773 MeV

$\Gamma(K^+K^-\pi^+)/\Gamma_{total}$ — Γ_{118}/Γ

VALUE (units 10^{-2})	EVTS	DOCUMENT ID		TECN	COMMENT
• • • We do not use the following data for averages, fits, limits, etc. • • •					
0.935±0.017±0.024		[1] DOBBS	07	CLEO	See BONVICINI 14
0.97 ±0.04 ±0.04	1250 ± 40	[1] HE	05	CLEO	See DOBBS 07

[1] DOBBS 07 and HE 05 use single- and double-tagged events in an overall fit. DOBBS 07 supersedes HE 05.

$\Gamma(K^+K^-\pi^+)/\Gamma(K^-2\pi^+)$ — Γ_{118}/Γ_{51}

VALUE (units 10^{-2})	EVTS	DOCUMENT ID		TECN	COMMENT
10.32 ±0.09 OUR AVERAGE Error includes scale factor of 1.4. See the ideogram below.					
10.282±0.002±0.068	23M	AAIJ	19G	LHCB	pp at 8 TeV
10.6 ±0.2 ±0.3		BONVICINI	14	CLEO	All CLEO-c runs
11.7 ±1.3 ±0.7	181 ± 20	ABLIKIM	05F	BES	$e^+e^-\approx\psi(3770)$
10.7 ±0.1 ±0.2	43k	AUBERT	05S	BABR	$e^+e^-\approx\Upsilon(4S)$
9.3 ±1.0 $^{+0.8}_{-0.6}$		JUN	00	SELX	Σ^- nucleus, 600 GeV
9.76 ±0.42 ±0.46		FRABETTI	95B	E687	γ Be, $\overline{E}_\gamma\approx$ 200 GeV

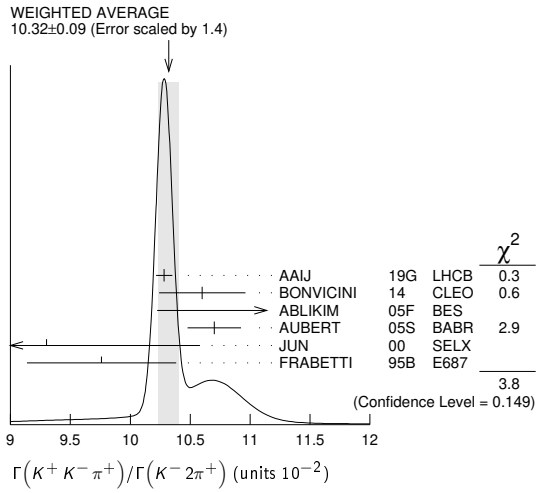

$\Gamma(K^+K^-\pi^+\pi^0)/\Gamma_{total}$ — Γ_{127}/Γ

VALUE (units 10^{-3})	EVTS	DOCUMENT ID		TECN	COMMENT
6.62±0.20±0.25	1.3k	ABLIKIM	20AC	BES3	e^+e^- at 3.773 GeV

$\Gamma(\phi\pi^+)/\Gamma_{total}$ — Γ_{126}/Γ

VALUE (units 10^{-3})	EVTS	DOCUMENT ID		TECN	COMMENT
5.70±0.05±0.13	18k	ABLIKIM	19BI	BES3	e^+e^- at 3773 MeV

$\Gamma(\phi\pi^+,\phi\to K^+K^-)/\Gamma(K^+K^-\pi^+)$ — $\Gamma_{125}/\Gamma_{118}$

This is the "fit fraction" from the Dalitz-plot analysis.

VALUE (%)	DOCUMENT ID		TECN	COMMENT
27.8±0.4 $^{+0.2}_{-0.5}$	RUBIN	08	CLEO	Dalitz fit, 19,458±163 evts
• • • We do not use the following data for averages, fits, limits, etc. • • •				
29.2±3.1±3.0	FRABETTI	95B	E687	Dalitz fit, 915 evts

$\Gamma(K^+\overline{K}^*(892)^0,\overline{K}^*(892)^0\to K^-\pi^+)/\Gamma(K^+K^-\pi^+)$ — $\Gamma_{119}/\Gamma_{118}$

This is the "fit fraction" from the Dalitz-plot analysis.

VALUE (%)	DOCUMENT ID		TECN	COMMENT
25.7±0.5 $^{+0.4}_{-1.2}$	RUBIN	08	CLEO	Dalitz fit, 19,458±163 evts
• • • We do not use the following data for averages, fits, limits, etc. • • •				
30.1±2.0±2.5	FRABETTI	95B	E687	Dalitz fit, 915 evts

$\Gamma(K^+\overline{K}^*_0(1430)^0,\overline{K}^*_0(1430)^0\to K^-\pi^+)/\Gamma(K^+K^-\pi^+)$ — $\Gamma_{120}/\Gamma_{118}$

This is the "fit fraction" from the Dalitz-plot analysis.

VALUE (%)	DOCUMENT ID		TECN	COMMENT
18.8±1.2 $^{+3.3}_{-3.4}$	RUBIN	08	CLEO	Dalitz fit, 19,458±163 evts
• • • We do not use the following data for averages, fits, limits, etc. • • •				
37.0±3.5±1.8	FRABETTI	95B	E687	Dalitz fit, 915 evts

$\Gamma(K^+\overline{K}^*_2(1430)^0,\overline{K}^*_2\to K^-\pi^+)/\Gamma(K^+K^-\pi^+)$ — $\Gamma_{121}/\Gamma_{118}$

This is the "fit fraction" from the Dalitz-plot analysis.

VALUE (%)	DOCUMENT ID		TECN	COMMENT
1.7±0.4 $^{+1.2}_{-0.7}$	RUBIN	08	CLEO	Dalitz fit, 19,458±163 evts

Downloaded from https://academic.oup.com/ptep/article/2022/8/083C01/6651666 by KIT Library user on 27 September 2022

$\Gamma(K^+\overline{K}_0^*(700), \overline{K}_0^* \to K^-\pi^+)/\Gamma(K^+K^-\pi^+)$ — $\Gamma_{122}/\Gamma_{118}$

This is the "fit fraction" from the Dalitz-plot analysis.

VALUE (%)	DOCUMENT ID		TECN	COMMENT
$7.0\pm0.8^{+3.5}_{-2.0}$	RUBIN	08	CLEO	Dalitz fit, 19,458±163 evts

$\Gamma(a_0(1450)^0\pi^+, a_0^0 \to K^+K^-)/\Gamma(K^+K^-\pi^+)$ — $\Gamma_{123}/\Gamma_{118}$

This is the "fit fraction" from the Dalitz-plot analysis.

VALUE (%)	DOCUMENT ID		TECN	COMMENT
$4.6\pm0.6^{+7.2}_{-1.8}$	RUBIN	08	CLEO	Dalitz fit, 19,458±163 evts

$\Gamma(\phi(1680)\pi^+, \phi \to K^+K^-)/\Gamma(K^+K^-\pi^+)$ — $\Gamma_{124}/\Gamma_{118}$

This is the "fit fraction" from the Dalitz-plot analysis.

VALUE (%)	DOCUMENT ID		TECN	COMMENT
$0.51\pm0.11^{+0.37}_{-0.16}$	RUBIN	08	CLEO	Dalitz fit, 19,458±163 evts

$\Gamma(K_S^0K_S^0\pi^+)/\Gamma_{total}$ — Γ_{128}/Γ

VALUE (units 10^{-4})	EVTS	DOCUMENT ID		TECN	COMMENT
27.0±0.5±1.2	4897	ABLIKIM	17A	BES3	$e^+e^- \to \psi(3770)$

$\Gamma(K_S^0K_S^0\pi^+\pi^0)/\Gamma_{total}$ — Γ_{129}/Γ

VALUE (units 10^{-3})	EVTS	DOCUMENT ID		TECN	COMMENT
1.34±0.20±0.06	80	ABLIKIM	20AC	BES3	e^+e^- at 3.773 GeV

$\Gamma(K_S^0K^+\eta)/\Gamma_{total}$ — Γ_{130}/Γ

VALUE (units 10^{-4})	EVTS	DOCUMENT ID		TECN	COMMENT
1.85±0.52±0.08	14	ABLIKIM	20V	BES3	e^+e^-, 3773 MeV

$\Gamma(K^+K_S^0\pi^+\pi^-)/\Gamma(K_S^02\pi^+\pi^-)$ — Γ_{131}/Γ_{74}

VALUE (units 10^{-2})	EVTS	DOCUMENT ID		TECN	COMMENT
5.62±0.39±0.40	469 ± 32	LINK	01C	FOCS	γ nucleus, $\overline{E}_\gamma \approx$ 180 GeV

$\Gamma(K^+K_S^0\pi^+\pi^-)/\Gamma_{total}$ — Γ_{131}/Γ

VALUE (units 10^{-3})	EVTS	DOCUMENT ID		TECN	COMMENT
1.89±0.12±0.05	277	ABLIKIM	20AC	BES3	e^+e^- at 3.773 GeV

$\Gamma(K_S^0K^+\pi^0\pi^0)/\Gamma_{total}$ — Γ_{132}/Γ

VALUE (units 10^{-4})	EVTS	DOCUMENT ID		TECN	COMMENT
5.8±1.2±0.4	34	ABLIKIM	20AC	BES3	e^+e^- at 3.773 GeV

$\Gamma(K_S^0K^-2\pi^+)/\Gamma_{total}$ — Γ_{133}/Γ

VALUE (units 10^{-3})	EVTS	DOCUMENT ID		TECN	COMMENT
2.27±0.12±0.06	467	ABLIKIM	20AC	BES3	e^+e^- at 3.773 GeV

$\Gamma(K_S^0K^-2\pi^+)/\Gamma(K_S^02\pi^+\pi^-)$ — Γ_{133}/Γ_{74}

VALUE (units 10^{-2})	EVTS	DOCUMENT ID		TECN	COMMENT
7.68±0.41±0.32	670 ± 35	LINK	01C	FOCS	γ nucleus, $\overline{E}_\gamma \approx$ 180 GeV

$\Gamma(K^+K^-2\pi^+\pi^-)/\Gamma(K^-3\pi^+\pi^-)$ — Γ_{134}/Γ_{77}

VALUE	EVTS	DOCUMENT ID		TECN	COMMENT
0.040±0.009±0.019	38	LINK	03D	FOCS	γ A, $\overline{E}_\gamma \approx$ 180 GeV

$\Gamma(\phi\pi^+\pi^0)/\Gamma_{total}$ — Γ_{135}/Γ

Unseen decay modes of the ϕ are included.

VALUE	DOCUMENT ID		TECN	COMMENT
0.023±0.010	[1] BARLAG	92C	ACCM	π^- Cu 230 GeV

[1] BARLAG 92C computes the branching fraction using topological normalization.

$\Gamma(\phi\rho^+)/\Gamma(K^-2\pi^+)$ — Γ_{136}/Γ_{51}

Unseen decay modes of the ϕ are included.

VALUE	CL%	DOCUMENT ID		TECN	COMMENT
<0.16	90	DAOUDI	92	CLEO	$e^+e^- \approx$ 10.5 GeV

$\Gamma(K^+K^-\pi^+\pi^0$ non-$\phi)/\Gamma_{total}$ — Γ_{137}/Γ

VALUE	DOCUMENT ID		TECN	COMMENT
$0.015^{+0.007}_{-0.006}$	[1] BARLAG	92C	ACCM	π^- Cu 230 GeV

[1] BARLAG 92C computes the branching fraction using topological normalization.

$\Gamma(K^+K^-\pi^+\pi^0$ non-$\phi)/\Gamma(K^-2\pi^+)$ — Γ_{137}/Γ_{51}

VALUE	CL%	DOCUMENT ID		TECN	COMMENT
• • • We do not use the following data for averages, fits, limits, etc. • • •					
<0.25	90	ANJOS	89E	E691	Photoproduction

Doubly Cabibbo-suppressed modes

$\Gamma(K^+\pi^0)/\Gamma_{total}$ — Γ_{138}/Γ

VALUE (units 10^{-4})	EVTS	DOCUMENT ID		TECN	COMMENT
2.08±0.21 OUR FIT Error includes scale factor of 1.4.					
2.35±0.20 OUR AVERAGE					
2.32±0.21±0.06	1.8k	ABLIKIM	18W	BES3	e^+e^-, 3773 MeV
2.52±0.47±0.26	189 ± 37	AUBERT,B	06F	BABR	$e^+e^- \approx \Upsilon(4S)$
• • • We do not use the following data for averages, fits, limits, etc. • • •					
2.28±0.36±0.17	148 ± 23	DYTMAN	06	CLEO	See MENDEZ 10

$\Gamma(K^+\pi^0)/\Gamma(K^-2\pi^+)$ — Γ_{138}/Γ_{51}

VALUE (units 10^{-3})	EVTS	DOCUMENT ID		TECN	COMMENT
2.21±0.23 OUR FIT Error includes scale factor of 1.5.					
1.9 ±0.2 ±0.1	343 ± 37	MENDEZ	10	CLEO	e^+e^- at 3774 MeV

$\Gamma(K^+\eta)/\Gamma_{total}$ — Γ_{139}/Γ

VALUE (units 10^{-3})	EVTS	DOCUMENT ID		TECN	COMMENT
0.125±0.016 OUR FIT Error includes scale factor of 1.1.					
0.151±0.025±0.014	439	ABLIKIM	18W	BES3	e^+e^-, 3773 MeV

$\Gamma(K^+\eta)/\Gamma(\eta\pi^+)$ — $\Gamma_{139}/\Gamma_{103}$

VALUE (%)	EVTS	DOCUMENT ID		TECN	COMMENT
3.3 ±0.4 OUR FIT Error includes scale factor of 1.1.					
3.06±0.43±0.14	166 ± 23	WON	11	BELL	$e^+e^- \approx \Upsilon(4S)$

$\Gamma(K^+\eta'(958))/\Gamma_{total}$ — Γ_{140}/Γ

VALUE (units 10^{-3})	EVTS	DOCUMENT ID		TECN	COMMENT
0.185±0.020 OUR FIT					
0.164±0.051±0.024	87	ABLIKIM	18W	BES3	e^+e^-, 3773 MeV

$\Gamma(K^+\eta'(958))/\Gamma(\eta'(958)\pi^+)$ — $\Gamma_{140}/\Gamma_{110}$

VALUE (%)	EVTS	DOCUMENT ID		TECN	COMMENT
3.7 ±0.4 OUR FIT					
3.77±0.39±0.10	180 ± 19	WON	11	BELL	$e^+e^- \approx \Upsilon(4S)$

$\Gamma(K^+\pi^+\pi^-)/\Gamma(K^-2\pi^+)$ — Γ_{141}/Γ_{51}

VALUE (units 10^{-3})	EVTS	DOCUMENT ID		TECN	COMMENT
5.238±0.025 OUR AVERAGE					
5.231±0.009±0.023	795k	AAIJ	19G	LHCB	pp at 8 TeV
5.69 ±0.18 ±0.14	2638 ± 84	KO	09	BELL	e^+e^- at $\Upsilon(4S)$
6.5 ±0.8 ±0.4	189 ± 24	LINK	04F	FOCS	γ A, $\overline{E}_\gamma \approx$ 180 GeV
7.7 ±1.7 ±0.8	59 ± 13	AITALA	97C	E791	π^- A, 500 GeV
7.2 ±2.3 ±1.7	21	FRABETTI	95E	E687	γBe, $\overline{E}_\gamma$= 220 GeV

$\Gamma(K^+\rho^0)/\Gamma(K^+\pi^+\pi^-)$ — $\Gamma_{142}/\Gamma_{141}$

This is the "fit fraction" from the Dalitz-plot analysis.

VALUE	DOCUMENT ID		TECN	COMMENT
0.39 ±0.09 OUR AVERAGE				
0.3943±0.0787±0.0815	LINK	04F	FOCS	Dalitz fit, 189 evts
0.37 ±0.14 ±0.07	AITALA	97C	E791	Dalitz fit, 59 evts

$\Gamma(K^*(892)^0\pi^+, K^*(892)^0 \to K^+\pi^-)/\Gamma(K^+\pi^+\pi^-)$ — $\Gamma_{143}/\Gamma_{141}$

This is the "fit fraction" from the Dalitz-plot analysis.

VALUE	DOCUMENT ID		TECN	COMMENT
0.47 ±0.08 OUR AVERAGE				
0.5220±0.0684±0.0638	LINK	04F	FOCS	Dalitz fit, 189 evts
0.35 ±0.14 ±0.01	AITALA	97C	E791	Dalitz fit, 59 evts

$\Gamma(K^+f_0(980), f_0(980) \to \pi^+\pi^-)/\Gamma(K^+\pi^+\pi^-)$ — $\Gamma_{144}/\Gamma_{141}$

This is the "fit fraction" from the Dalitz-plot analysis.

VALUE	DOCUMENT ID		TECN	COMMENT
0.0892±0.0333±0.0412	LINK	04F	FOCS	Dalitz fit, 189 evts

$\Gamma(K_2^*(1430)^0\pi^+, K_2^*(1430)^0 \to K^+\pi^-)/\Gamma(K^+\pi^+\pi^-)$ — $\Gamma_{145}/\Gamma_{141}$

This is the "fit fraction" from the Dalitz-plot analysis.

VALUE	DOCUMENT ID		TECN	COMMENT
0.0803±0.0372±0.0391	LINK	04F	FOCS	Dalitz fit, 189 evts

$\Gamma(K^+\pi^+\pi^-$ nonresonant$)/\Gamma(K^+\pi^+\pi^-)$ — $\Gamma_{146}/\Gamma_{141}$

This is the "fit fraction" from the Dalitz-plot analysis.

VALUE	DOCUMENT ID		TECN	COMMENT
• • • We do not use the following data for averages, fits, limits, etc. • • •				
0.36±0.14±0.07	[1] AITALA	97C	E791	Dalitz fit, 59 evts

[1] LINK 04F, with three times as many events, finds no need for a nonresonant amplitude.

$\Gamma(K^+\pi^+\pi^-\pi^0)/\Gamma_{total}$ — Γ_{147}/Γ

VALUE (units 10^{-3})	EVTS	DOCUMENT ID		TECN	COMMENT
1.21±0.08±0.03	350	[1] ABLIKIM	20Z	BES3	e^+e^- at 3773 MeV

[1] ABLIKIM 20Z subtracted the known branching fractions of $D^+ \to K^+\eta$, $D^+ \to K^+\phi$, and $D^+ \to K^+\omega$ to obtain an estimate of the non-resonant component (ignoring interference effects and possible additional resonant contributions) $B(D^+ \to K^+\pi^+\pi^-\pi^0$ non-resonant$) = (1.13 \pm 0.08 \pm 0.03) \times 10^{-3}$.

$\Gamma(K^+\pi^+\pi^-\pi^0$ nonresonant$)/\Gamma_{total}$ — Γ_{148}/Γ

VALUE (units 10^{-3})	EVTS	DOCUMENT ID		TECN	COMMENT
1.10±0.07 OUR AVERAGE					
1.03±0.12±0.06	112	[1] ABLIKIM	21BB	BES3	e^+e^- at 3.773 GeV
1.13±0.08±0.03	350	[2] ABLIKIM	20Z	BES3	e^+e^- at 3.773 GeV

[1] ABLIKIM 21BB result has subtracted the known branching fractions of $D^+ \to K^+\eta$, $D^+ \to K^+\phi$, and $D^+ \to K^+\omega$ resonances (ignoring interference effects). The result including these components is measured to be $B(D^+ \to K^+\pi^+\pi^-\pi^0) = (1.11 \pm 0.12) \times 10^{-3}$, where the uncertainty is statistical only.

[2] ABLIKIM 20Z result has subtracted the known branching fractions of $D^+ \to K^+\eta$, $D^+ \to K^+\phi$, and $D^+ \to K^+\omega$, ignoring interference effects. The result including these components is measured to be $(1.21 \pm 0.08 \pm 0.03) \times 10^{-3}$.

Downloaded from https://academic.oup.com/ptep/article/2022/8/083C01/6651666 by KIT Library user on 27 September 2022

$\Gamma(K^+\omega)/\Gamma_{total}$ — Γ_{149}/Γ

VALUE (units 10^{-5})	EVTS	DOCUMENT ID		TECN	COMMENT
$5.7^{+2.5}_{-2.1}\pm0.2$	9	ABLIKIM	20Z	BES3	e^+e^-, 3773 MeV

$\Gamma(2K^+K^-)/\Gamma(K^-2\pi^+)$ — Γ_{150}/Γ_{51}

VALUE (units 10^{-4})	EVTS	DOCUMENT ID		TECN	COMMENT
6.54 ±0.05 OUR AVERAGE					
$6.541\pm0.025\pm0.042$	134k	AAIJ	19G	LHCB	pp at 8 TeV
$9.49\pm2.17\pm0.22$	65	[1] LINK	02I	FOCS	γ nucleus, $\approx$ 180 GeV

[1] LINK 02I finds little evidence for ϕK^+ or $f_0(980)\,K^+$ submodes.

$\Gamma(K^+\phi(1020),\ \phi\to K^+K^-)/\Gamma(2K^+K^-)$ — $\Gamma_{152}/\Gamma_{150}$

VALUE (%)	DOCUMENT ID		TECN	COMMENT
7.1±0.9	[1] AAIJ	19H	LHCB	pp at 8TeV

[1] Fit fraction from a Dalitz plot analysis of $D^+\to K^+K^+K^-$ decays. The last uncertainty is due to the amplitude model.

$\Gamma(K^+(K^+K^-)_{S-wave})/\Gamma(2K^+K^-)$ — $\Gamma_{153}/\Gamma_{150}$

VALUE	DOCUMENT ID		TECN	COMMENT
0.94±0.01	[1] AAIJ	19H	LHCB	pp at 8TeV

[1] Fit fraction from a Dalitz plot analysis of $D^+\to K^+K^+K^-$ decays. The last uncertainty is due to the amplitude model.

Rare or forbidden modes

$\Gamma(\pi^+e^+e^-)/\Gamma_{total}$ — Γ_{154}/Γ

A test for the $\Delta C=1$ weak neutral current. Allowed by higher-order electroweak interactions.

VALUE	CL%	DOCUMENT ID		TECN	COMMENT
$<1.1\times10^{-6}$	90	LEES	11G	BABR	$e^+e^-\approx\Upsilon(4S)$
• • • We do not use the following data for averages, fits, limits, etc. • • •					
$<1.6\times10^{-6}$	90	AAIJ	21T	LHCB	1.6 fb^{-1} pp
$<5.9\times10^{-6}$	90	[1] RUBIN	10	CLEO	e^+e^- at $\psi(3770)$
$<7.4\times10^{-6}$	90	HE	05A	CLEO	See RUBIN 10
$<5.2\times10^{-5}$	90	AITALA	99G	E791	π^-N 500 GeV
$<1.1\times10^{-4}$	90	FRABETTI	97B	E687	γ Be, $\overline{E}_\gamma\approx$ 220 GeV
$<6.6\times10^{-5}$	90	AITALA	96	E791	π^-N 500 GeV
$<2.5\times10^{-3}$	90	WEIR	90B	MRK2	e^+e^- 29 GeV
$<2.6\times10^{-3}$	90	HAAS	88	CLEO	e^+e^- 10 GeV

[1] This RUBIN 10 limit is for the e^+e^- mass in the continuum away from the $\phi(1020)$. See the next data block.

$\Gamma(\pi^+\pi^0e^+e^-)/\Gamma_{total}$ — Γ_{155}/Γ

VALUE	CL%	DOCUMENT ID		TECN	COMMENT
$<1.4\times10^{-5}$	90	ABLIKIM	18P	BES3	e^+e^-, 3773 MeV

$\Gamma(\pi^+\phi,\phi\to e^+e^-)/\Gamma_{total}$ — Γ_{156}/Γ

This is *not* a test for the $\Delta C=1$ weak neutral current, but leads to the $\pi^+e^+e^-$ final state.

VALUE	EVTS	DOCUMENT ID		TECN	COMMENT
$(1.7^{+1.4}_{-0.9}\pm0.1)\times10^{-6}$	4	[1] RUBIN	10	CLEO	e^+e^- at $\psi(3770)$
• • • We do not use the following data for averages, fits, limits, etc. • • •					
$(2.7^{+3.6}_{-1.8}\pm0.2)\times10^{-6}$	2	HE	05A	CLEO	See RUBIN 10

[1] This RUBIN 10 result is consistent with the known $D^+\to\phi\pi^+$ and $\phi\to e^+e^-$ fractions.

$\Gamma(\pi^+\mu^+\mu^-)/\Gamma_{total}$ — Γ_{157}/Γ

A test for the $\Delta C=1$ weak neutral current. Allowed by higher-order electroweak interactions.

VALUE	CL%	DOCUMENT ID		TECN	COMMENT
$<6.7\times10^{-8}$	90	AAIJ	21T	LHCB	1.6 fb^{-1} pp
• • • We do not use the following data for averages, fits, limits, etc. • • •					
$<7.3\times10^{-8}$	90	AAIJ	13AF	LHCB	pp at 7 TeV
$<6.5\times10^{-6}$	90	LEES	11G	BABR	$e^+e^-\approx\Upsilon(4S)$
$<3.9\times10^{-6}$	90	[1] ABAZOV	08D	D0	$p\overline{p}$, $E_{cm}=1.96$ TeV
$<8.8\times10^{-6}$	90	LINK	03F	FOCS	γ A, $\overline{E}_\gamma\approx$ 180 GeV
$<1.5\times10^{-5}$	90	AITALA	99G	E791	π^-N 500 GeV
$<8.9\times10^{-5}$	90	FRABETTI	97B	E687	γ Be, $\overline{E}_\gamma\approx$ 220 GeV
$<1.8\times10^{-5}$	90	AITALA	96	E791	π^-N 500 GeV
$<2.2\times10^{-4}$	90	KODAMA	95	E653	π^- emulsion 600 GeV
$<5.9\times10^{-3}$	90	WEIR	90B	MRK2	e^+e^- 29 GeV
$<2.9\times10^{-3}$	90	HAAS	88	CLEO	e^+e^- 10 GeV

[1] This ABAZOV 08D limit is for the $\mu^+\mu^-$ mass in the continuum away from the $\phi(1020)$. See the next data block.

$\Gamma(\pi^+\phi,\ \phi\to\mu^+\mu^-)/\Gamma_{total}$ — Γ_{158}/Γ

This is *not* a test for the $\Delta C=1$ weak neutral current, but leads to the $\pi^+\mu^+\mu^-$ final state.

VALUE	DOCUMENT ID		TECN	COMMENT
$(1.8\pm0.5\pm0.6)\times10^{-6}$	[1] ABAZOV	08D	D0	$p\overline{p}$, $E_{cm}=1.96$ TeV

[1] This ABAZOV 08D value is consistent with the known $D^+\to\phi\pi^+$ and $\phi\to\mu^+\mu^-$ fractions.

$\Gamma(\rho^+\mu^+\mu^-)/\Gamma_{total}$ — Γ_{159}/Γ

A test for the $\Delta C=1$ weak neutral current. Allowed by higher-order electroweak interactions.

VALUE	CL%	DOCUMENT ID		TECN	COMMENT
$<5.6\times10^{-4}$	90	KODAMA	95	E653	π^- emulsion 600 GeV

$\Gamma(K^+e^+e^-)/\Gamma_{total}$ — Γ_{160}/Γ

Both quarks would have to change flavor for this decay to occur.

VALUE	CL%	DOCUMENT ID		TECN	COMMENT
$<8.5\times10^{-7}$	90	AAIJ	21T	LHCB	1.6 fb^{-1} pp
• • • We do not use the following data for averages, fits, limits, etc. • • •					
$<1.0\times10^{-6}$	90	LEES	11G	BABR	$e^+e^-\approx\Upsilon(4S)$
$<3.0\times10^{-6}$	90	RUBIN	10	CLEO	e^+e^- at $\psi(3770)$
$<6.2\times10^{-6}$	90	HE	05A	CLEO	See RUBIN 10
$<2.0\times10^{-4}$	90	AITALA	99G	E791	π^-N 500 GeV
$<2.0\times10^{-4}$	90	FRABETTI	97B	E687	γ Be, $\overline{E}_\gamma\approx$ 220 GeV
$<4.8\times10^{-3}$	90	WEIR	90B	MRK2	e^+e^- 29 GeV

$\Gamma(K^+\pi^0e^+e^-)/\Gamma_{total}$ — Γ_{161}/Γ

VALUE	CL%	DOCUMENT ID		TECN	COMMENT
$<1.5\times10^{-5}$	90	ABLIKIM	18P	BES3	e^+e^-, 3773 MeV

$\Gamma(K^0_S\pi^+e^+e^-)/\Gamma_{total}$ — Γ_{162}/Γ

VALUE	CL%	DOCUMENT ID		TECN	COMMENT
$<2.6\times10^{-5}$	90	ABLIKIM	18P	BES3	e^+e^-, 3773 MeV

$\Gamma(K^0_SK^+e^+e^-)/\Gamma_{total}$ — Γ_{163}/Γ

VALUE	CL%	DOCUMENT ID		TECN	COMMENT
$<1.1\times10^{-5}$	90	ABLIKIM	18P	BES3	e^+e^-, 3773 MeV

$\Gamma(K^+\mu^+\mu^-)/\Gamma_{total}$ — Γ_{164}/Γ

Both quarks would have to change flavor for this decay to occur.

VALUE	CL%	DOCUMENT ID		TECN	COMMENT
$<5.4\times10^{-8}$	90	AAIJ	21T	LHCB	1.6 fb^{-1} pp
• • • We do not use the following data for averages, fits, limits, etc. • • •					
$<4.3\times10^{-6}$	90	LEES	11G	BABR	$e^+e^-\approx\Upsilon(4S)$
$<9.2\times10^{-6}$	90	LINK	03F	FOCS	γ A, $\overline{E}_\gamma\approx$ 180 GeV
$<4.4\times10^{-5}$	90	AITALA	99G	E791	π^-N 500 GeV
$<9.7\times10^{-5}$	90	FRABETTI	97B	E687	γ Be, $\overline{E}_\gamma\approx$ 220 GeV
$<3.2\times10^{-4}$	90	KODAMA	95	E653	π^- emulsion 600 GeV
$<9.2\times10^{-3}$	90	WEIR	90B	MRK2	e^+e^- 29 GeV

$\Gamma(\pi^+e^+\mu^-)/\Gamma_{total}$ — Γ_{165}/Γ

A test of lepton-family-number conservation.

VALUE	CL%	DOCUMENT ID		TECN	COMMENT
$<2.1\times10^{-7}$	90	AAIJ	21T	LHCB	1.6 fb^{-1} pp
• • • We do not use the following data for averages, fits, limits, etc. • • •					
$<2.9\times10^{-6}$	90	LEES	11G	BABR	$e^+e^-\approx\Upsilon(4S)$
$<1.1\times10^{-4}$	90	FRABETTI	97B	E687	γ Be, $\overline{E}_\gamma\approx$ 220 GeV
$<3.3\times10^{-3}$	90	WEIR	90B	MRK2	e^+e^- 29 GeV

$\Gamma(\pi^+e^-\mu^+)/\Gamma_{total}$ — Γ_{166}/Γ

A test of lepton-family-number conservation.

VALUE	CL%	DOCUMENT ID		TECN	COMMENT
$<2.2\times10^{-7}$	90	AAIJ	21T	LHCB	1.6 fb^{-1} pp
• • • We do not use the following data for averages, fits, limits, etc. • • •					
$<3.6\times10^{-6}$	90	LEES	11G	BABR	$e^+e^-\approx\Upsilon(4S)$
$<1.3\times10^{-4}$	90	FRABETTI	97B	E687	γ Be, $\overline{E}_\gamma\approx$ 220 GeV
$<3.3\times10^{-3}$	90	WEIR	90B	MRK2	e^+e^- 29 GeV

$\Gamma(K^+e^+\mu^-)/\Gamma_{total}$ — Γ_{167}/Γ

A test of lepton-family-number conservation.

VALUE	CL%	DOCUMENT ID		TECN	COMMENT
$<7.5\times10^{-8}$	90	AAIJ	21T	LHCB	1.6 fb^{-1} pp
• • • We do not use the following data for averages, fits, limits, etc. • • •					
$<1.2\times10^{-6}$	90	LEES	11G	BABR	$e^+e^-\approx\Upsilon(4S)$
$<1.3\times10^{-4}$	90	FRABETTI	97B	E687	γ Be, $\overline{E}_\gamma\approx$ 220 GeV
$<3.4\times10^{-3}$	90	WEIR	90B	MRK2	e^+e^- 29 GeV

$\Gamma(K^+e^-\mu^+)/\Gamma_{total}$ — Γ_{168}/Γ

A test of lepton-family-number conservation.

VALUE	CL%	DOCUMENT ID		TECN	COMMENT
$<1.0\times10^{-7}$	90	AAIJ	21T	LHCB	1.6 fb^{-1} pp
• • • We do not use the following data for averages, fits, limits, etc. • • •					
$<2.8\times10^{-6}$	90	LEES	11G	BABR	$e^+e^-\approx\Upsilon(4S)$
$<1.2\times10^{-4}$	90	FRABETTI	97B	E687	γ Be, $\overline{E}_\gamma\approx$ 220 GeV
$<3.4\times10^{-3}$	90	WEIR	90B	MRK2	e^+e^- 29 GeV

$\Gamma(\pi^-2e^+)/\Gamma_{total}$ — Γ_{169}/Γ

A test of lepton-number conservation.

VALUE	CL%	DOCUMENT ID		TECN	COMMENT
$<5.3\times10^{-7}$	90	AAIJ	21T	LHCB	1.6 fb^{-1} pp

Downloaded from https://academic.oup.com/ptep/article/2022/8/083C01/6651666 by KIT Library user on 27 September 2022

• • • We do not use the following data for averages, fits, limits, etc. • • •

$<1.9\times10^{-6}$	90	LEES	11G	BABR	$e^+e^-\approx\Upsilon(4S)$
$<1.1\times10^{-6}$	90	RUBIN	10	CLEO	e^+e^- at $\psi(3770)$
$<3.6\times10^{-6}$	90	HE	05A	CLEO	See RUBIN 10
$<9.6\times10^{-5}$	90	AITALA	99G	E791	π^-N 500 GeV
$<1.1\times10^{-4}$	90	FRABETTI	97B	E687	γ Be, $\overline{E}_\gamma\approx$ 220 GeV
$<4.8\times10^{-3}$	90	WEIR	90B	MRK2	e^+e^- 29 GeV

$\Gamma(\pi^-2\mu^+)/\Gamma_{total}$ — Γ_{170}/Γ

A test of lepton-number conservation.

VALUE	CL%	DOCUMENT ID		TECN	COMMENT
$<1.4\times10^{-8}$	90	AAIJ	21T	LHCB	1.6 fb^{-1} pp

• • • We do not use the following data for averages, fits, limits, etc. • • •

$<2.2\times10^{-8}$	90	AAIJ	13AF	LHCB	pp at 7 TeV
$<2.0\times10^{-6}$	90	LEES	11G	BABR	$e^+e^-\approx\Upsilon(4S)$
$<4.8\times10^{-6}$	90	LINK	03F	FOCS	γ A, $\overline{E}_\gamma\approx$ 180 GeV
$<1.7\times10^{-5}$	90	AITALA	99G	E791	π^-N 500 GeV
$<8.7\times10^{-5}$	90	FRABETTI	97B	E687	γ Be, $\overline{E}_\gamma\approx$ 220 GeV
$<2.2\times10^{-4}$	90	KODAMA	95	E653	π^- emulsion 600 GeV
$<6.8\times10^{-3}$	90	WEIR	90B	MRK2	e^+e^- 29 GeV

$\Gamma(\pi^-e^+\mu^+)/\Gamma_{total}$ — Γ_{171}/Γ

A test of lepton-number conservation.

VALUE	CL%	DOCUMENT ID		TECN	COMMENT
$<1.3\times10^{-7}$	90	AAIJ	21T	LHCB	1.6 fb^{-1} pp

• • • We do not use the following data for averages, fits, limits, etc. • • •

$<2.0\times10^{-6}$	90	LEES	11G	BABR	$e^+e^-\approx\Upsilon(4S)$
$<5.0\times10^{-5}$	90	AITALA	99G	E791	π^-N 500 GeV
$<1.1\times10^{-4}$	90	FRABETTI	97B	E687	γ Be, $\overline{E}_\gamma\approx$ 220 GeV
$<3.7\times10^{-3}$	90	WEIR	90B	MRK2	e^+e^- 29 GeV

$\Gamma(\rho^-2\mu^+)/\Gamma_{total}$ — Γ_{172}/Γ

A test of lepton-number conservation.

VALUE	CL%	DOCUMENT ID		TECN	COMMENT
$<5.6\times10^{-4}$	90	KODAMA	95	E653	π^- emulsion 600 GeV

$\Gamma(K^-2e^+)/\Gamma_{total}$ — Γ_{173}/Γ

A test of lepton-number conservation.

VALUE	CL%	DOCUMENT ID		TECN	COMMENT
$<0.9\times10^{-6}$	90	LEES	11G	BABR	$e^+e^-\approx\Upsilon(4S)$

• • • We do not use the following data for averages, fits, limits, etc. • • •

$<3.5\times10^{-6}$	90	RUBIN	10	CLEO	e^+e^- at $\psi(3770)$
$<4.5\times10^{-6}$	90	HE	05A	CLEO	See RUBIN 10
$<1.2\times10^{-4}$	90	FRABETTI	97B	E687	γ Be, $\overline{E}_\gamma\approx$ 220 GeV
$<9.1\times10^{-3}$	90	WEIR	90B	MRK2	e^+e^- 29 GeV

$\Gamma(K^0_S\pi^-2e^+)/\Gamma_{total}$ — Γ_{174}/Γ

VALUE	CL%	DOCUMENT ID		TECN	COMMENT
$<3.3\times10^{-6}$	90	ABLIKIM	19AL	BES3	e^+e^- at 3773 MeV

$\Gamma(K^-\pi^02e^+)/\Gamma_{total}$ — Γ_{175}/Γ

VALUE	CL%	DOCUMENT ID		TECN	COMMENT
$<8.5\times10^{-6}$	90	ABLIKIM	19AL	BES3	e^+e^- at 3773 MeV

$\Gamma(K^-2\mu^+)/\Gamma_{total}$ — Γ_{176}/Γ

A test of lepton-number conservation.

VALUE	CL%	DOCUMENT ID		TECN	COMMENT
$<10\times10^{-6}$	90	LEES	11G	BABR	$e^+e^-\approx\Upsilon(4S)$

• • • We do not use the following data for averages, fits, limits, etc. • • •

$<1.3\times10^{-5}$	90	LINK	03F	FOCS	γ A, $\overline{E}_\gamma\approx$ 180 GeV
$<1.2\times10^{-4}$	90	FRABETTI	97B	E687	γ Be, $\overline{E}_\gamma\approx$ 220 GeV
$<3.2\times10^{-4}$	90	KODAMA	95	E653	π^- emulsion 600 GeV
$<4.3\times10^{-3}$	90	WEIR	90B	MRK2	e^+e^- 29 GeV

$\Gamma(K^-e^+\mu^+)/\Gamma_{total}$ — Γ_{177}/Γ

A test of lepton-number conservation.

VALUE	CL%	DOCUMENT ID		TECN	COMMENT
$<1.9\times10^{-6}$	90	LEES	11G	BABR	$e^+e^-\approx\Upsilon(4S)$

• • • We do not use the following data for averages, fits, limits, etc. • • •

$<1.3\times10^{-4}$	90	FRABETTI	97B	E687	γ Be, $\overline{E}_\gamma\approx$ 220 GeV
$<4.0\times10^{-3}$	90	WEIR	90B	MRK2	e^+e^- 29 GeV

$\Gamma(K^*(892)^-2\mu^+)/\Gamma_{total}$ — Γ_{178}/Γ

A test of lepton-number conservation.

VALUE	CL%	DOCUMENT ID		TECN	COMMENT
$<8.5\times10^{-4}$	90	KODAMA	95	E653	π^- emulsion 600 GeV

$\Gamma(\Lambda e^+)/\Gamma_{total}$ — Γ_{179}/Γ

VALUE	CL%	DOCUMENT ID		TECN	COMMENT
$<1.1\times10^{-6}$	90	ABLIKIM	20D	BES3	e^+e^-, 3773 MeV

$\Gamma(\overline{\Lambda}e^+)/\Gamma_{total}$ — Γ_{180}/Γ

VALUE	CL%	DOCUMENT ID		TECN	COMMENT
$<6.5\times10^{-7}$	90	ABLIKIM	20D	BES3	e^+e^-, 3773 MeV

$\Gamma(\Sigma^0e^+)/\Gamma_{total}$ — Γ_{181}/Γ

VALUE	CL%	DOCUMENT ID		TECN	COMMENT
$<1.7\times10^{-6}$	90	ABLIKIM	20D	BES3	e^+e^-, 3773 MeV

$\Gamma(\overline{\Sigma}^0e^+)/\Gamma_{total}$ — Γ_{182}/Γ

VALUE	CL%	DOCUMENT ID		TECN	COMMENT
$<1.3\times10^{-6}$	90	ABLIKIM	20D	BES3	e^+e^-, 3773 MeV

$D^{\pm}$ CP-VIOLATING DECAY-RATE ASYMMETRIES

This is the difference between D^+ and D^- partial widths for the decay to state f, divided by the sum of the widths:
$A_{CP}(f)=[\Gamma(D^+\to f)-\Gamma(D^-\to\overline{f})]/[\Gamma(D^+\to f)+\Gamma(D^-\to\overline{f})]$.

$A_{CP}(\mu^{\pm}\nu)$ in $D^+\to\mu^+\nu_\mu$, $D^-\to\mu^-\overline{\nu}_\mu$

VALUE (%)	DOCUMENT ID		TECN	COMMENT
$+8\pm8$	EISENSTEIN	08	CLEO	e^+e^- at $\psi(3770)$

$A_{CP}(K^0_Le^{\pm}\nu)$ in $D^+\to K^0_Le^+\nu_e$, $D^-\to K^0_Le^-\overline{\nu}_e$

VALUE (%)	DOCUMENT ID		TECN	COMMENT
$-0.59\pm0.60\pm1.48$	ABLIKIM	15AF	BES3	e^+e^- 3773 MeV

$A_{CP}(K^0_S\pi^{\pm})$ in $D^{\pm}\to K^0_S\pi^{\pm}$

VALUE (%)	EVTS	DOCUMENT ID		TECN	COMMENT
-0.41 ± 0.09 OUR AVERAGE					
$-1.1\pm0.6\pm0.2$		BONVICINI	14	CLEO	All CLEO-c runs
$-0.363\pm0.094\pm0.067$	1738k	[1] KO	12A	BELL	$e^+e^-\approx\Upsilon(nS)$
$-0.44\pm0.13\pm0.10$	807k	DEL-AMO-SA..	11H	BABR	$e^+e^-\approx\Upsilon(4S)$
$-1.6\pm1.5\pm0.9$	10.6k	[2] LINK	02B	FOCS	γ nucleus, $\overline{E}_\gamma\approx$ 180 GeV

• • • We do not use the following data for averages, fits, limits, etc. • • •

$-0.71\pm0.19\pm0.20$		KO	10	BELL	See KO 12A
$-1.3\pm0.7\pm0.3$	30k	MENDEZ	10	CLEO	See BONVICINI 14
$-0.6\pm1.0\pm0.3$		DOBBS	07	CLEO	See MENDEZ 10

[1] KO 12A finds that after subtracting the contribution due to $K^0-\overline{K}^0$ mixing, the CP asymmetry due to the change of charm is $(-0.024\pm0.094\pm0.067)$%, consistent with zero.

[2] LINK 02B measures $N(D^+\to K^0_S\pi^+)/N(D^+\to K^-\pi^+\pi^+)$, the ratio of numbers of events observed, and similarly for the D^-.

$A_{CP}(K^0_LK^{\pm})$ in $D^{\pm}\to K^0_LK^{\pm}$

VALUE (units 10^{-2})	EVTS	DOCUMENT ID		TECN	COMMENT
$-4.2\pm3.2\pm1.2$	650	ABLIKIM	19M	BES3	e^+e^- at 3773 MeV

$A_{CP}(K^{\mp}2\pi^{\pm})$ in $D^+\to K^-2\pi^+$, $D^-\to K^+2\pi^-$

VALUE (%)	EVTS	DOCUMENT ID		TECN	COMMENT
-0.18 ± 0.16 OUR AVERAGE					
$-0.16\pm0.15\pm0.09$	2.3M	ABAZOV	14L	D0	$p\overline{p}$, $\sqrt{s}=1.96$ TeV
$-0.3\pm0.2\pm0.4$		BONVICINI	14	CLEO	All CLEO-c runs

• • • We do not use the following data for averages, fits, limits, etc. • • •

$-0.1\pm0.4\pm0.9$	231k	MENDEZ	10	CLEO	See BONVICINI 14
$-0.5\pm0.4\pm0.9$		DOBBS	07	CLEO	See MENDEZ 10

$A_{CP}(K^{\mp}\pi^{\pm}\pi^{\pm}\pi^0)$ in $D^+\to K^-\pi^+\pi^+\pi^0$, $D^-\to K^+\pi^-\pi^-\pi^0$

VALUE (%)	DOCUMENT ID		TECN	COMMENT
$-0.3\pm0.6\pm0.4$	BONVICINI	14	CLEO	All CLEO-c runs

• • • We do not use the following data for averages, fits, limits, etc. • • •

$1.0\pm0.9\pm0.9$	DOBBS	07	CLEO	See BONVICINI 14

$A_{CP}(K^0_S\pi^{\pm}\pi^0)$ in $D^+\to K^0_S\pi^+\pi^0$, $D^-\to K^0_S\pi^-\pi^0$

VALUE (%)	DOCUMENT ID		TECN	COMMENT
$-0.1\pm0.7\pm0.2$	BONVICINI	14	CLEO	All CLEO-c runs

• • • We do not use the following data for averages, fits, limits, etc. • • •

$0.3\pm0.9\pm0.3$	DOBBS	07	CLEO	See BONVICINI 14

$A_{CP}(K^0_S\pi^{\pm}\eta)$ in $D^{\pm}\to K^0_S\pi^{\pm}\eta$

VALUE (units 10^{-2})	EVTS	DOCUMENT ID		TECN	COMMENT
$-0.9\pm2.9\pm1.0$	1.3k	ABLIKIM	20V	BES3	e^+e^-, 3773 MeV

$A_{CP}(K^0_S\pi^{\pm}\pi^+\pi^-)$ in $D^+\to K^0_S\pi^+\pi^+\pi^-$, $D^-\to K^0_S\pi^-\pi^-\pi^+$

VALUE (%)	DOCUMENT ID		TECN	COMMENT
$0.0\pm1.2\pm0.3$	BONVICINI	14	CLEO	All CLEO-c runs

• • • We do not use the following data for averages, fits, limits, etc. • • •

$0.1\pm1.1\pm0.6$	DOBBS	07	CLEO	See BONVICINI 14

$A_{CP}(K^{\pm}\pi^+\pi^-\pi^0)$ in $D^{\pm}\to K^{\pm}\pi^+\pi^-\pi^0$

VALUE	EVTS	DOCUMENT ID		TECN	COMMENT
$-0.04\pm0.06\pm0.01$	350	ABLIKIM	20Z	BES3	e^+e^-, 3773 MeV

Downloaded from https://academic.oup.com/ptep/article/2022/8/083C01/6651666 by KIT Library user on 27 September 2022

$A_{CP}(\pi^{\pm}\pi^{0})$ in $D^{\pm} \to \pi^{\pm}\pi^{0}$

VALUE (%)	EVTS	DOCUMENT ID		TECN	COMMENT
0.4 ±1.3 OUR AVERAGE		Error includes scale factor of 1.7. See the ideogram below.			
−1.3 ±0.9 ±0.6	28.7k	AAIJ	21U	LHCB	pp at 7, 8, 13 TeV
2.31±1.24±0.23	108k	BABU	18	BELL	At/near $\Upsilon(4S)$, $\Upsilon(5S)$
2.9 ±2.9 ±0.3	2.6k	MENDEZ	10	CLEO	e^+e^- at 3774 MeV

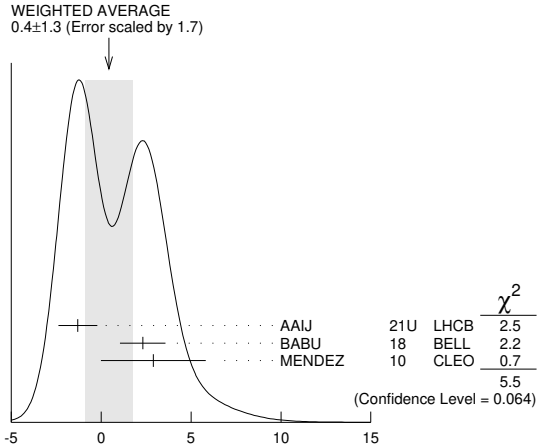

$A_{CP}(\pi^{\pm}\eta)$ in $D^{\pm} \to \pi^{\pm}\eta$

VALUE (%)	EVTS	DOCUMENT ID		TECN	COMMENT
0.3 ±0.8 OUR AVERAGE		Error includes scale factor of 1.2.			
−0.2 ±0.8 ±0.4	32.7k	AAIJ	21U	LHCB	pp at 13 TeV
+1.74±1.13±0.19		WON	11	BELL	$e^+e^- \approx \Upsilon(4S)$
−2.0 ±2.3 ±0.3	2.9k	MENDEZ	10	CLEO	e^+e^- at 3774 MeV

$A_{CP}(\pi^{\pm}\pi^{0}\eta)$ in $D^{\pm} \to \pi^{\pm}\pi^{0}\eta$

VALUE (units 10^{-2})	EVTS	DOCUMENT ID		TECN	COMMENT
−5.8±6.6±1.8	381	ABLIKIM	20G	BES3	e^+e^- at 3.773 GeV

$A_{CP}(\pi^{\pm}\eta\eta)$ in $D^{\pm} \to \pi^{\pm}\eta\eta$

VALUE (units 10^{-2})	EVTS	DOCUMENT ID		TECN	COMMENT
8.0±8.3±1.9	179	ABLIKIM	20G	BES3	e^+e^- at 3.773 GeV

$A_{CP}(\pi^{\pm}\eta'(958))$ in $D^{\pm} \to \pi^{\pm}\eta'(958)$

VALUE (%)	EVTS	DOCUMENT ID		TECN	COMMENT
−0.6 ±0.7 OUR AVERAGE					
−0.61±0.72±0.54	63k	AAIJ	17AF	LHCB	pp at 7, 8 TeV
−0.12±1.12±0.17		WON	11	BELL	$e^+e^- \approx \Upsilon(4S)$
−4.0 ±3.4 ±0.3	1.0k	MENDEZ	10	CLEO	e^+e^- at 3774 MeV

$A_{CP}(\overline{K}^0/K^0K^{\pm})$ in $D^+ \to \overline{K}^0K^+$, $D^- \to K^0K^-$

VALUE (%)	EVTS	DOCUMENT ID		TECN	COMMENT
0.11±0.17 OUR AVERAGE					
0.03±0.17±0.14	1.0M	[1] AAIJ	14BD	LHCB	pp at 7, 8 TeV
0.08±0.28±0.14	277k	KO	13	BELL	e^+e^- at $\Upsilon(4S)$
0.46±0.36±0.25	159k	LEES	13E	BABR	e^+e^- at $\Upsilon(4S)$

[1] AAIJ 14BD reports its result as $A_{CP}(D^{\pm} \to K^0_S\pi^{\pm})$ with CP-violation effects in the $K^0 - \overline{K}^0$ system subtracted. It also measures $A_{CP}(D^{\pm} \to \overline{K}^0/K^0K^{\pm}) + A_{CP}(D^{\pm}_s \to \overline{K}^0/K^0\pi^{\pm}) = (0.41 \pm 0.49 \pm 0.26)\%$.

$A_{CP}(K^0_SK^{\pm})$ in $D^{\pm} \to K^0_SK^{\pm}$

VALUE (%)	EVTS	DOCUMENT ID		TECN	COMMENT
−0.01 ±0.07 OUR AVERAGE					
−0.004±0.061±0.045	6M	AAIJ	19T	LHCB	pp at 7, 8, 13 TeV
−1.8 ±2.7 ±1.6	780	ABLIKIM	19M	BES3	e^+e^- at 3773 MeV
−0.25 ±0.28 ±0.14	277k	KO	13	BELL	e^+e^- at Υ(nS)
0.13 ±0.36 ±0.25	159k	LEES	13E	BABR	e^+e^- at $\Upsilon(4S)$
−0.2 ±1.5 ±0.9	5.2k	MENDEZ	10	CLEO	e^+e^- at 3774 MeV
7.1 ±6.1 ±1.2	949	[1] LINK	02B	FOCS	γ nucleus, $\overline{E}_\gamma \approx 180$ GeV
• • • We do not use the following data for averages, fits, limits, etc. • • •					
−0.16 ±0.58 ±0.25		KO	10	BELL	$e^+e^- \approx \Upsilon(4S)$
6.9 ±6.0 ±1.5	949	[2] LINK	02B	FOCS	γ nucleus, $\overline{E}_\gamma \approx 180$ GeV

[1] LINK 02B measures $N(D^+ \to K^0_SK^+)/N(D^+ \to K^0_S\pi^+)$, the ratio of numbers of events observed, and similarly for the D^-.

[2] LINK 02B measures $N(D^+ \to K^0_SK^+)/N(D^+ \to K^-\pi^+\pi^+)$, the ratio of numbers of events observed, and similarly for the D^-.

$A_{CP}(K^0_SK^{\pm}\pi^{0})$ in $D^{\pm} \to K^0_SK^{\pm}\pi^{0}$

VALUE (units 10^{-2})	EVTS	DOCUMENT ID		TECN	COMMENT
1.4±3.7±2.4	470	ABLIKIM	19M	BES3	e^+e^- at 3773 MeV

$A_{CP}(K^0_LK^{\pm}\pi^{0})$ in $D^{\pm} \to K^0_LK^{\pm}\pi^{0}$

VALUE (units 10^{-2})	EVTS	DOCUMENT ID		TECN	COMMENT
−0.6±4.1±1.7	410	ABLIKIM	19M	BES3	e^+e^- at 3773 MeV

$A_{CP}(K^+K^-\pi^{\pm})$ in $D^{\pm} \to K^+K^-\pi^{\pm}$

See also AAIJ 11G for a search for CP asymmetry in the $D^{\pm} \to K^+K^-\pi^{\pm}$ Dalitz plots using 370k decays and four different binning schemes. No evidence for CP asymmetry was found.

VALUE (%)	EVTS	DOCUMENT ID		TECN	COMMENT
0.37±0.29 OUR AVERAGE					
0.37±0.30±0.15	224k	[1] LEES	13F	BABR	e^+e^- at $\Upsilon(4S)$
−0.03±0.84±0.29		RUBIN	08	CLEO	e^+e^- at 3774 MeV
1.4 ±1.0 ±0.8	43k	[2] AUBERT	05S	BABR	e^+e^- at $\Upsilon(4S)$
0.6 ±1.1 ±0.5	14k	[3] LINK	00B	FOCS	
−1.4 ±2.9		[3] AITALA	97B	E791	$-0.062 < A_{CP} < +0.034$ (90% CL)
−3.1 ±6.8		[3] FRABETTI	94I	E687	$-0.14 < A_{CP} < +0.081$ (90% CL)
• • • We do not use the following data for averages, fits, limits, etc. • • •					
−0.1 ±0.9 ±0.4		[4] BONVICINI	14	CLEO	See RUBIN 08
−0.1 ±1.5 ±0.8		DOBBS	07	CLEO	See BONVICINI 14 and RUBIN 08

[1] This is the integrated CP asymmetry. LEES 13F also searches for CP asymmetries in four regions of the Dalitz plots (two of which are listed below); in comparisons of binned D^+ and D^- Dalitz plots; in parametrized fits to those plots, including 2-body submodes; and in comparisons of Legendre-polynomial distributions for the K^+K^- and $K^-\pi^+$ systems.

[2] AUBERT 05S measures $N(D^+ \to K^+K^-\pi^+)/N(D^+_s \to K^+K^-\pi^+)$, the ratio of the numbers of events observed, and similarly for the D^-.

[3] FRABETTI 94I, AITALA 98C, and LINK 00B measure $N(D^+ \to K^-K^+\pi^+)/N(D^+ \to K^-\pi^+\pi^+)$, the ratio of numbers of events observed, and similarly for the D^-.

[4] RUBIN 08 performs a dedicated analysis of this decay mode on the same dataset, with slightly better precision. We therefore take it that BONVICINI 14 does not supersede RUBIN 08's A_{CP} result.

$A_{CP}(K^{\pm}K^{*0})$ in $D^+ \to K^+\overline{K}^{*0}$, $D^- \to K^-K^{*0}$

VALUE (%)	EVTS	DOCUMENT ID		TECN	COMMENT
− 0.3± 0.4 OUR AVERAGE					
− 0.3± 0.4±0.2	73k	[1] LEES	13F	BABR	e^+e^- at $\Upsilon(4S)$
− 0.4± 2.0±0.6		RUBIN	08	CLEO	Fit-fraction asymmetry
+ 0.9± 1.7±0.7	11k	[2] AUBERT	05S	BABR	e^+e^- at $\Upsilon(4S)$
− 1.0± 5.0		[3] AITALA	97B	E791	$-0.092 < A_{CP} < +0.072$ (90% CL)
−12 ±13		[3] FRABETTI	94I	E687	$-0.33 < A_{CP} < +0.094$ (90% CL)

[1] This LEES 13F result is for the $K^{\mp}\pi^{\pm}$ mass-squared between 0.4 and 1.0 GeV^2, and does not actually separate out the K^*.

[2] AUBERT 05S measures $N(D^+ \to K^+\overline{K}^{*0})/N(D^+_s \to K^+K^-\pi^+)$, the ratio of the numbers of events observed, and similarly for the D^-.

[3] FRABETTI 94I and AITALA 97B measure $N(D^+ \to K^+\overline{K}^*(892)^0)/N(D^+ \to K^-\pi^+\pi^+)$, the ratio of numbers of events observed, and similarly for the D^-.

$A_{CP}(\phi\pi^{\pm})$ in $D^{\pm} \to \phi\pi^{\pm}$

VALUE (%)	EVTS	DOCUMENT ID		TECN	COMMENT
0.01 ±0.09 OUR AVERAGE		Error includes scale factor of 1.8.			
0.003±0.040±0.029	55M	AAIJ	19T	LHCB	pp at 7, 8, 13 TeV
−0.3 ±0.3 ±0.5	97k	[1] LEES	13F	BABR	e^+e^- at $\Upsilon(4S)$
+0.51 ±0.28 ±0.05	237k	STARIC	12	BELL	Mainly at $\Upsilon(4S)$
−1.8 ±1.6 $^{+0.2}_{-0.4}$		RUBIN	08	CLEO	Fit-fraction asymmetry
+0.2 ±1.5 ±0.6	10k	[2] AUBERT	05S	BABR	e^+e^- at $\Upsilon(4S)$
−2.8 ±3.6		[3] AITALA	97B	E791	$-0.087 < A_{CP} < +0.031$ (90% CL)
+6.6 ±8.6		[3] FRABETTI	94I	E687	$-0.075 < A_{CP} < +0.21$ (90% CL)
• • • We do not use the following data for averages, fits, limits, etc. • • •					
−0.04 ±0.14 ±0.14	1.58M	[4] AAIJ	13W	LHCB	pp at 7 TeV

[1] This LEES 13F result is for the K^+K^- mass-squared less than 1.3 GeV^2 and the $K^{\mp}\pi^{\pm}$ mass-squared above 1.0 GeV^2, and does not actually separate out the ϕ.

[2] AUBERT 05S measures $N(D^+ \to \phi\pi^+)/N(D^+_s \to K^+K^-\pi^+)$, the ratio of the numbers of events observed, and similarly for the D^-.

[3] FRABETTI 94I and AITALA 97B measure $N(D^+ \to \phi\pi^+)/N(D^+ \to K^-\pi^+\pi^+)$, the ratio of numbers of events observed, and similarly for the D^-.

[4] See AAIJ 19T.

$A_{CP}(K^{\pm}K^*_0(1430)^0)$ in $D^+ \to K^+\overline{K}^*_0(1430)^0$, $D^- \to K^-K^*_0(1430)^0$

VALUE (%)	DOCUMENT ID		TECN	COMMENT
$+8\pm6^{+4}_{-2}$	RUBIN	08	CLEO	Fit-fraction asymmetry

$A_{CP}(K^{\pm}K^*_2(1430)^0)$ in $D^+ \to K^+\overline{K}^*_2(1430)^0$, $D^- \to K^-K^*_2(1430)^0$

VALUE (%)	DOCUMENT ID		TECN	COMMENT
$+43\pm19^{+5}_{-18}$	RUBIN	08	CLEO	Fit-fraction asymmetry

Downloaded from https://academic.oup.com/ptep/article/2022/8/083C01/6651666 by KIT Library user on 27 September 2022

$A_{CP}(K^{\pm}K_0^*(700))$ in $D^+ \to K^+\overline{K}_0^*(700)$, $D^- \to K^-K_0^*(700)$

VALUE (%)	DOCUMENT ID		TECN	COMMENT
$-12\pm11^{+14}_{-6}$	RUBIN	08	CLEO	Fit-fraction asymmetry

$A_{CP}(a_0(1450)^0\pi^{\pm})$ in $D^{\pm} \to a_0(1450)^0\pi^{\pm}$

VALUE (%)	DOCUMENT ID		TECN	COMMENT
$-19\pm12^{+8}_{-11}$	RUBIN	08	CLEO	Fit-fraction asymmetry

$A_{CP}(\phi(1680)\pi^{\pm})$ in $D^{\pm} \to \phi(1680)\pi^{\pm}$

VALUE (%)	DOCUMENT ID		TECN	COMMENT
$-9\pm22\pm14$	RUBIN	08	CLEO	Fit-fraction asymmetry

$A_{CP}(\pi^+\pi^-\pi^{\pm})$ in $D^{\pm} \to \pi^+\pi^-\pi^{\pm}$

See also AAIJ 14C for a search for CP violation in $D^{\pm} \to \pi^+\pi^-\pi^{\pm}$ Dalitz plots using model-independent binned and unbinned methods. No evidence was found.

VALUE (%)	DOCUMENT ID		TECN	COMMENT
-1.7 ± 4.2	[1] AITALA	97B	E791	$-0.086 < A_{CP} < +0.052$ (90% CL)

[1] AITALA 97B measure $N(D^+ \to \pi^+\pi^-\pi^+)/N(D^+ \to K^-\pi^+\pi^+)$, the ratio of numbers of events observed, and similarly for the D^-.

$A_{CP}(\pi^+\pi^-\pi^{\pm}\eta)$ in $D^{\pm} \to \pi^+\pi^-\pi^{\pm}\eta$

VALUE (units 10^{-2})	EVTS	DOCUMENT ID		TECN	COMMENT
$2.5\pm5.0\pm1.6$	510	ABLIKIM	20V	BES3	e^+e^-, 3773 MeV

$A_{CP}(K_S^0K^{\pm}\pi^+\pi^-)$ in $D^{\pm} \to K_S^0K^{\pm}\pi^+\pi^-$

VALUE (%)	EVTS	DOCUMENT ID		TECN	COMMENT
$-4.2\pm6.4\pm2.2$	523 ± 32	LINK	05E	FOCS	γ A, $\overline{E}_{\gamma}\approx180$ GeV

$A_{CP}(K^{\pm}\pi^0)$ in $D^{\pm} \to K^{\pm}\pi^0$

VALUE (%)	EVTS	DOCUMENT ID		TECN	COMMENT
-3 ± 5 OUR AVERAGE					
$-3.2\pm4.7\pm2.1$	2.5k	AAIJ	21U	LHCB	pp at 7, 8, 13 TeV
$-3.5\pm10.7\pm0.9$	343	MENDEZ	10	CLEO	e^+e^- at 3774 MeV

$A_{CP}(K^{\pm}\eta)$ in $D^{\pm} \to K^{\pm}\eta$

VALUE (units 10^{-2})	EVTS	DOCUMENT ID		TECN	COMMENT
$-6\pm10\pm4$	880	AAIJ	21U	LHCB	pp at 13 TeV

$D^{\pm}$ χ^2 TESTS OF CP-VIOLATION (CPV)

We list model-independent searches for local CP violation in phase-space distributions of multi-body decays.

Most of these searches divide phase space (Dalitz plot for 3-body decays, five-dimensional equivalent for 4-body decays) into bins, and perform a χ^2 test comparing normalised yields N_i, $\overline{N}_i$ in CP-conjugate bin pairs i: $\chi^2 = \Sigma_i(N_i - \alpha\,\overline{N}_i)/\sigma(N_i - \alpha\,\overline{N}_i)$. The factor $\alpha = (\Sigma_i N_i)/(\Sigma_i \overline{N}_i)$ removes the dependence on phase-space-integrated rate asymmetries. The result is used to obtain the probability (p-value) to obtain the measured χ^2 or larger under the assumption of CP conservation [AUBERT 08AO, BEDIAGA 09]. Alternative methods obtain p-values from other test variables based on unbinned analyses [WILLIAMS 11, AAIJ 14C]. Results can be combined using Fisher's method [MOSTELLER 48].

Local CPV in $D^{\pm} \to \pi^+\pi^-\pi^{\pm}$

p-value (%)	EVTS	DOCUMENT ID		TECN	COMMENT
78.1	3.1M	[1] AAIJ	14C	LHCB	χ^2

[1] AAIJ 14C uses binned and unbinned methods, and finds slightly better sensitivity with the former. We took the first value in the table of results for the binned method.

Local CPV in $D^{\pm} \to K^+K^-\pi^{\pm}$

p-value (%)	EVTS	DOCUMENT ID		TECN	COMMENT
31 OUR EVALUATION					
72	224k	LEES	13F	BABR	χ^2
12.7	370k	[1] AAIJ	11G	LHCB	χ^2

[1] AAIJ 11G publishes results for several binning schemes. We picked the first value in their table of results.

CP VIOLATING ASYMMETRIES OF P-ODD (T-ODD) MOMENTS

$A_{Tviol}(K_S^0K^{\pm}\pi^+\pi^-)$ in $D^{\pm} \to K_S^0K^{\pm}\pi^+\pi^-$

$C_T \equiv \vec{p}_{K^+}\cdot(\vec{p}_{\pi^+}\times\vec{p}_{\pi^-})$ is a parity-odd correlation of the K^+, π^+, and π^- momenta for the D^+. $\overline{C}_T \equiv \vec{p}_{K^-}\cdot(\vec{p}_{\pi^-}\times\vec{p}_{\pi^+})$ is the corresponding quantity for the D^-. Then

$A_T \equiv [\Gamma(C_T>0)-\Gamma(C_T<0)]\,/\,[\Gamma(C_T>0)+\Gamma(C_T<0)]$, and

$\overline{A}_T \equiv [\Gamma(-\overline{C}_T>0)-\Gamma(-\overline{C}_T<0)]\,/\,[\Gamma(-\overline{C}_T>0)+\Gamma(-\overline{C}_T<0)]$, and

$A_{Tviol} \equiv \frac{1}{2}(A_T - \overline{A}_T)$. C_T and $\overline{C}_T$ are commonly referred to as T-odd moments, because they are odd under T reversal. However, the T-conjugate process $K_S^0K^{\pm}\pi^+\pi^- \to D^{\pm}$ is not accessible, while the P-conjugate process is.

VALUE (units 10^{-3})	EVTS	DOCUMENT ID		TECN	COMMENT
$-12.0\pm10.0\pm4.6$	21.2 ± 0.4k	LEES	11E	BABR	$e^+e^-\approx\Upsilon(4S)$
• • • We do not use the following data for averages, fits, limits, etc. • • •					
$23\pm62\pm22$	523 ± 32	LINK	05E	FOCS	γ A, $\overline{E}_{\gamma}\approx180$ GeV

SEMILEPTONIC FORM FACTORS

$f_+(0)|V_{cs}|$ in $D^+ \to \overline{K}^0\ell^+\nu_\ell$

VALUE	DOCUMENT ID		TECN	COMMENT
0.719 ±0.011 OUR AVERAGE Error includes scale factor of 1.6. See the ideogram below.				
$0.7053\pm0.0040\pm0.0112$	ABLIKIM	17S	BES3	$K_S^0e^+\nu_e$ 2-parameter fit
$0.737\pm0.006\pm0.009$	[1] ABLIKIM	15AF	BES3	$K_Le^+\nu_e$ 3-parameter fit
$0.707\pm0.010\pm0.009$	[2] BESSON	09	CLEO	$K_Se^+\nu_e$ 3-parameter fit

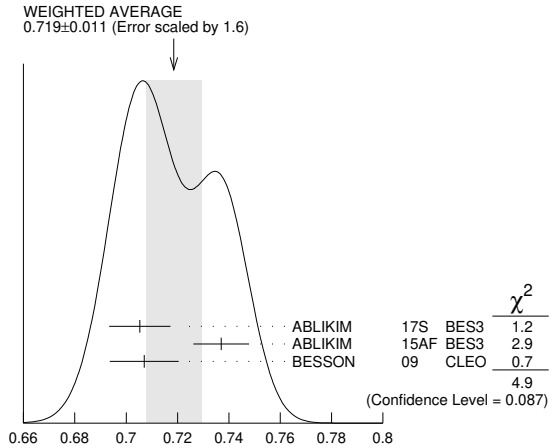

[1] ABLIKIM 15AF finds $0.728\pm0.006\pm0.011$ for a 2-parameter fit.
[2] BESSON 09 finds $0.716\pm0.007\pm0.009$ for a 2-parameter fit.

$r_1 \equiv a_1/a_0$ in $D^+ \to \overline{K}^0\ell^+\nu_\ell$

VALUE	EVTS	DOCUMENT ID		TECN	COMMENT
-2.13 ± 0.14 OUR AVERAGE					
$-2.18\pm0.14\pm0.05$		ABLIKIM	17S	BES3	$K_S^0e^+\nu_e$ 2-parameter fit
$-2.23\pm0.42\pm0.53$	40k	[1] ABLIKIM	15AF	BES3	$K_Le^+\nu_e$ 3-parameter fit
$-1.66\pm0.44\pm0.10$		[2] BESSON	09	CLEO	$K_Se^+\nu_e$ 3-parameter fit

[1] ABLIKIM 15AF finds $r_1 = -1.91\pm0.33\pm0.28$ for a 2-parameter fit.
[2] BESSON 09 finds $r_1 = -2.10\pm0.25\pm0.08$ for 2-parameter fit.

$r_2 \equiv a_2/a_0$ in $D^+ \to \overline{K}^0\ell^+\nu_\ell$

VALUE	EVTS	DOCUMENT ID		TECN	COMMENT
-3 ± 12 OUR AVERAGE Error includes scale factor of 1.5.					
$+11\pm9\pm9$	40k	ABLIKIM	15AF	BES3	$K_Le^+\nu_e$ 3-parameter fit
$-14\pm11\pm1$		BESSON	09	CLEO	$K_Se^+\nu_e$ 3-parameter fit

$f_+(0)|V_{cd}|$ in $D^+ \to \pi^0\ell^+\nu_\ell$

VALUE	DOCUMENT ID		TECN	COMMENT
0.1407±0.0025 OUR AVERAGE				
$0.1400\pm0.0026\pm0.0007$	ABLIKIM	17S	BES3	$\pi^0e^+\nu_e$ 2-parameter fit
$0.146\pm0.007\pm0.002$	BESSON	09	CLEO	$\pi^0e^+\nu_e$ 3-parameter fit

$r_1 \equiv a_1/a_0$ in $D^+ \to \pi^0\ell^+\nu_\ell$

VALUE	DOCUMENT ID		TECN	COMMENT
-2.00 ± 0.13 OUR AVERAGE				
$-2.01\pm0.13\pm0.02$	ABLIKIM	17S	BES3	$\pi^0e^+\nu_e$ 2-parameter fit
$-1.37\pm0.88\pm0.24$	BESSON	09	CLEO	$\pi^0e^+\nu_e$ 3-parameter fit

$r_2 \equiv a_2/a_0$ in $D^+ \to \pi^0\ell^+\nu_\ell$

VALUE	DOCUMENT ID		TECN	COMMENT
$-4\pm5\pm1$	BESSON	09	CLEO	$\pi^0e^+\nu_e$ 3-parameter fit

$f_+(0)|V_{cd}|$ in $D^+ \to \eta\ell^+\nu_\ell$ ($\ell = e$ or ν)

VALUE (units 10^{-2})	EVTS	DOCUMENT ID		TECN	COMMENT
8.4 ±0.4 OUR AVERAGE					
$8.7\pm0.8\pm0.2$	234	ABLIKIM	20T	BES3	$\eta\mu^+\nu_\mu$, z expansion
$7.86\pm0.64\pm0.21$	373	ABLIKIM	18R	BES3	$\eta e^+\nu_e$, z expansion
$8.6\pm0.6\pm0.1$		YELTON	11	CLEO	$\eta e^+\nu_e$, z expansion

$r_1 \equiv a_1/a_0$ in $D^+ \to \eta e^+\nu_e$

VALUE	EVTS	DOCUMENT ID		TECN	COMMENT
-5.3 ± 2.7 OUR AVERAGE Error includes scale factor of 1.9.					
$-7.33\pm1.69\pm0.40$	373	ABLIKIM	18R	BES3	z expansion
$-1.83\pm2.23\pm0.28$		YELTON	11	CLEO	z expansion

$r_V \equiv V(0)/A_1(0)$ in $D^+ \to \omega e^+\nu_e$

VALUE	DOCUMENT ID		TECN	COMMENT
$1.24\pm0.09\pm0.06$	ABLIKIM	15W	BES3	292 fb^{-1}, 3773 MeV

Downloaded from https://academic.oup.com/ptep/article/2022/8/083C01/6651666 by KIT Library user on 27 September 2022

$r_2 \equiv A_2(0)/A_1(0)$ in $D^+ \to \omega e^+ \nu_e$

VALUE	DOCUMENT ID		TECN	COMMENT
1.06±0.15±0.05	ABLIKIM	15W	BES3	292 fb^{-1}, 3773 MeV

$r_V \equiv V(0)/A_1(0)$ in $D^+, D^0 \to \rho e^+ \nu_e$

VALUE	EVTS	DOCUMENT ID		TECN	COMMENT
1.64 ±0.10 OUR AVERAGE		Error includes scale factor of 1.2.			
1.695±0.083±0.051	2.5k	[1] ABLIKIM	19C	BES3	e^+e^- at 3773 MeV
1.48 ±0.15 ±0.05		[1,2] DOBBS	13	CLEO	e^+e^- at $\psi(3770)$

[1] Uses both D^+ and D^0 events.
[2] Using PDG 10 values of V_{cd} and lifetimes, DOBBS 13 gets $A_1(0) = 0.56 \pm 0.01^{+0.02}_{-0.03}$, $A_2(0) = 0.47 \pm 0.06 \pm 0.04$, and $V(0) = 0.84 \pm 0.09^{+0.05}_{-0.06}$.

$r_2 \equiv A_2(0)/A_1(0)$ in $D^+, D^0 \to \rho e^+ \nu_e$

VALUE	EVTS	DOCUMENT ID		TECN	COMMENT
0.84 ±0.06 OUR AVERAGE					
0.845±0.056±0.039	2.5k	[1] ABLIKIM	19C	BES3	e^+e^- at 3773 MeV
0.83 ±0.11 ±0.04		[1,2] DOBBS	13	CLEO	e^+e^- at $\psi(3770)$

[1] Uses both D^+ and D^0 events.
[2] Using PDG 10 values of V_{cd} and lifetimes, DOBBS 13 gets $A_1(0) = 0.56 \pm 0.01^{+0.02}_{-0.03}$, $A_2(0) = 0.47 \pm 0.06 \pm 0.04$, and $V(0) = 0.84 \pm 0.09^{+0.05}_{-0.06}$.

$r_V \equiv V(0)/A_1(0)$ in $D^+ \to \overline{K}^*(892)^0 \ell^+ \nu_\ell$

See also BRIERE 10 for $\overline{K}^* \ell^+ \nu_\ell$ helicity-basis form-factor measurements.

VALUE	EVTS	DOCUMENT ID		TECN	COMMENT
1.49 ±0.05 OUR AVERAGE		Error includes scale factor of 2.1.			See the ideogram below.
1.411±0.058±0.007	16.2k	ABLIKIM	16F	BES3	$\overline{K}^*(892)^0 e^+ \nu_e$
1.463±0.017±0.031		[1] DEL-AMO-SA...	11I	BABR	
1.504±0.057±0.039	15k	[2] LINK	02L	FOCS	$\overline{K}^*(892)^0 \mu^+ \nu_\mu$
1.45 ±0.23 ±0.07	763	ADAMOVICH	99	BEAT	$\overline{K}^*(892)^0 \mu^+ \nu_\mu$
1.90 ±0.11 ±0.09	3000	[3] AITALA	98B	E791	$\overline{K}^*(892)^0 e^+ \nu_e$
1.84 ±0.11 ±0.09	3034	AITALA	98F	E791	$\overline{K}^*(892)^0 \mu^+ \nu_\mu$
1.74 ±0.27 ±0.28	874	FRABETTI	93E	E687	$\overline{K}^*(892)^0 \mu^+ \nu_\mu$
2.00 $^{+0.34}_{-0.32}$ ±0.16	305	KODAMA	92	E653	$\overline{K}^*(892)^0 \mu^+ \nu_\mu$
• • • We do not use the following data for averages, fits, limits, etc. • • •					
2.0 ±0.6 ±0.3	183	ANJOS	90E	E691	$\overline{K}^*(892)^0 e^+ \nu_e$

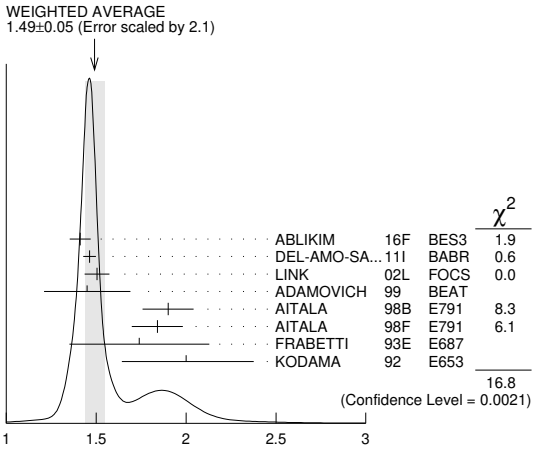

$r_V \equiv V(0)/A_1(0)$ in $D^+ \to \overline{K}^*(892)^0 \ell^+ \nu_\ell$

[1] DEL-AMO-SANCHEZ 11I finds the pole mass $m_A = (2.63 \pm 0.10 \pm 0.13)$ GeV (m_V is fixed at 2 GeV).
[2] LINK 02L includes the effects of interference with an S-wave background. This much improves the goodness of fit, but does not much shift the values of the form factors.
[3] This is slightly different from the AITALA 98B value: see ref. [5] in AITALA 98F.

$r_2 \equiv A_2(0)/A_1(0)$ in $D^+ \to \overline{K}^*(892)^0 \ell^+ \nu_\ell$

See also BRIERE 10 for $\overline{K}^* \ell^+ \nu_\ell$ helicity-basis form-factor measurements.

VALUE	EVTS	DOCUMENT ID		TECN	COMMENT
0.802±0.021 OUR AVERAGE					
0.788±0.042±0.008	16.2k	ABLIKIM	16F	BES3	$\overline{K}^*(892)^0 e^+ \nu_e$
0.801±0.020±0.020		[1] DEL-AMO-SA...	11I	BABR	
0.875±0.049±0.064	15k	[2] LINK	02L	FOCS	$\overline{K}^*(892)^0 \mu^+ \nu_\mu$
1.00 ±0.15 ±0.03	763	ADAMOVICH	99	BEAT	$\overline{K}^*(892)^0 \mu^+ \nu_\mu$
0.71 ±0.08 ±0.09	3000	AITALA	98B	E791	$\overline{K}^*(892)^0 e^+ \nu_e$
0.75 ±0.08 ±0.09	3034	AITALA	98F	E791	$\overline{K}^*(892)^0 \mu^+ \nu_\mu$
0.78 ±0.18 ±0.10	874	FRABETTI	93E	E687	$\overline{K}^*(892)^0 \mu^+ \nu_\mu$
0.82 $^{+0.22}_{-0.23}$ ±0.11	305	KODAMA	92	E653	$\overline{K}^*(892)^0 \mu^+ \nu_\mu$
• • • We do not use the following data for averages, fits, limits, etc. • • •					
0.0 ±0.5 ±0.2	183	ANJOS	90E	E691	$\overline{K}^*(892)^0 e^+ \nu_e$

[1] DEL-AMO-SANCHEZ 11I finds the pole mass $m_A = (2.63 \pm 0.10 \pm 0.13)$ GeV (m_V is fixed at 2 GeV).
[2] LINK 02L includes the effects of interference with an S-wave background. This much improves the goodness of fit, but does not much shift the values of the form factors.

$r_3 \equiv A_3(0)/A_1(0)$ in $D^+ \to \overline{K}^*(892)^0 \ell^+ \nu_\ell$

See also BRIERE 10 for $\overline{K}^* \ell^+ \nu_\ell$ helicity-basis form-factor measurements.

VALUE	EVTS	DOCUMENT ID		TECN	COMMENT
0.04±0.33±0.29	3034	AITALA	98F	E791	$\overline{K}^*(892)^0 \mu^+ \nu_\mu$

Γ_L/Γ_T in $D^+ \to \overline{K}^*(892)^0 \ell^+ \nu_\ell$

See also BRIERE 10 for $\overline{K}^* \ell^+ \nu_\ell$ helicity-basis form-factor measurements.

VALUE	EVTS	DOCUMENT ID		TECN	COMMENT
1.13±0.08 OUR AVERAGE					
1.09±0.10±0.02	763	ADAMOVICH	99	BEAT	$\overline{K}^*(892)^0 \mu^+ \nu_\mu$
1.20±0.13±0.13	874	FRABETTI	93E	E687	$\overline{K}^*(892)^0 \mu^+ \nu_\mu$
1.18±0.18±0.08	305	KODAMA	92	E653	$\overline{K}^*(892)^0 \mu^+ \nu_\mu$
• • • We do not use the following data for averages, fits, limits, etc. • • •					
1.8 $^{+0.6}_{-0.4}$ ±0.3	183	ANJOS	90E	E691	$\overline{K}^*(892)^0 e^+ \nu_e$

Γ_+/Γ_- in $D^+ \to \overline{K}^*(892)^0 \ell^+ \nu_\ell$

See also BRIERE 10 for $\overline{K}^* \ell^+ \nu_\ell$ helicity-basis form-factor measurements.

VALUE	EVTS	DOCUMENT ID		TECN	COMMENT
0.22±0.06 OUR AVERAGE		Error includes scale factor of 1.6.			
0.28±0.05±0.02	763	ADAMOVICH	99	BEAT	$\overline{K}^*(892)^0 \mu^+ \nu_\mu$
0.16±0.05±0.02	305	KODAMA	92	E653	$\overline{K}^*(892)^0 \mu^+ \nu_\mu$
• • • We do not use the following data for averages, fits, limits, etc. • • •					
0.15 $^{+0.07}_{-0.05}$ ±0.03	183	ANJOS	90E	E691	$\overline{K}^*(892)^0 e^+ \nu_e$

Amplitude analyses

$D \to K\pi\pi\pi$ partial wave analyses

Amplitude analyses of D^+ decays to a variety of 4-body kaon or pion final states, fitting simultaneously different partial wave components.

VALUE	DOCUMENT ID		TECN	COMMENT
	ABLIKIM	19AZ	BES3	$D^+ \to K^0_S \pi^+ \pi^+ \pi^-$

$D^{\pm}$ REFERENCES

AAIJ 21T JHEP 2106 044 R. Aaij et al. (LHCb Collab.)
AAIJ 21U JHEP 2106 019 R. Aaij et al. (LHCb Collab.)
ABLIKIM 21AD PR D104 012006 M. Ablikim et al. (BESIII Collab.)
ABLIKIM 21BA PR D104 052008 M. Ablikim et al. (BESIII Collab.)
ABLIKIM 21BB PR D104 072005 M. Ablikim et al. (BESIII Collab.)
ABUDINEN 21A PRL 127 211801 F. Abudinen et al. (BELLE II Collab.)
ABLIKIM 20AA PR D102 052003 M. Ablikim et al. (BESIII Collab.)
ABLIKIM 20AC PR D102 052006 M. Ablikim et al. (BESIII Collab.)
ABLIKIM 20AF PR D102 112005 M. Ablikim et al. (BESIII Collab.)
ABLIKIM 20D PR D101 031102 M. Ablikim et al. (BESIII Collab.)
ABLIKIM 20G PR D101 052009 M. Ablikim et al. (BESIII Collab.)
ABLIKIM 20H PR D101 072005 M. Ablikim et al. (BESIII Collab.)
ABLIKIM 20T PRL 124 231801 M. Ablikim et al. (BESIII Collab.)
ABLIKIM 20V PRL 124 241803 M. Ablikim et al. (BESIII Collab.)
ABLIKIM 20Z PRL 125 141802 M. Ablikim et al. (BESIII Collab.)
AAIJ 19G JHEP 1903 176 R. Aaij et al. (LHCb Collab.)
AAIJ 19H JHEP 1904 063 R. Aaij et al. (LHCb Collab.)
AAIJ 19T PRL 122 191803 R. Aaij et al. (LHCb Collab.)
ABLIKIM 19AL PR D99 112002 M. Ablikim et al. (BESIII Collab.)
ABLIKIM 19AY PR D100 072006 M. Ablikim et al. (BESIII Collab.)
ABLIKIM 19AZ PR D100 072008 M. Ablikim et al. (BESIII Collab.)
ABLIKIM 19BG PRL 123 211802 M. Ablikim et al. (BESIII Collab.)
ABLIKIM 19BH PRL 123 231801 M. Ablikim et al. (BESIII Collab.)
ABLIKIM 19BI PL B798 135017 M. Ablikim et al. (BESIII Collab.)
ABLIKIM 19C PRL 122 062001 M. Ablikim et al. (BESIII Collab.)
ABLIKIM 19M PR D99 032002 M. Ablikim et al. (BESIII Collab.)
ABLIKIM 18AC PR D98 092009 M. Ablikim et al. (BESIII Collab.)
ABLIKIM 18AE PRL 121 171803 M. Ablikim et al. (BESIII Collab.)
ABLIKIM 18F PRL 121 081802 M. Ablikim et al. (BESIII Collab.)
ABLIKIM 18P PR D97 072015 M. Ablikim et al. (BESIII Collab.)
ABLIKIM 18R PR D97 092009 M. Ablikim et al. (BESIII Collab.)
ABLIKIM 18W PR D97 072004 M. Ablikim et al. (BESIII Collab.)
BABU 18 PR D97 011101 V. Babu et al. (BELLE Collab.)
AAIJ 17AF PL B771 21 R. Aaij et al. (LHCb Collab.)
ABLIKIM 17A PL B765 231 M. Ablikim et al. (BESIII Collab.)
ABLIKIM 17AD PR D96 092002 M. Ablikim et al. (BESIII Collab.)
ABLIKIM 17M PR D95 071102 M. Ablikim et al. (BESIII Collab.)
ABLIKIM 17S PR D96 012002 M. Ablikim et al. (BESIII Collab.)
ABLIKIM 16D PRL 116 082001 M. Ablikim et al. (BESIII Collab.)
ABLIKIM 16F PR D94 032001 M. Ablikim et al. (BESIII Collab.)
ABLIKIM 16G EPJ C76 369 M. Ablikim et al. (BESIII Collab.)
ABLIKIM 16V CP C40 113001 M. Ablikim et al. (BESIII Collab.)
ABLIKIM 15AF PR D92 112008 M. Ablikim et al. (BESIII Collab.)
ABLIKIM 15W PR D92 071101 M. Ablikiim et al. (BESIII Collab.)
AAIJ 14BD JHEP 1410 025 R. Aaij et al. (LHCb Collab.)
AAIJ 14C PL B728 585 R. Aaij et al. (LHCb Collab.)
ABAZOV 14L PR D90 111102 V.M. Abazov et al. (D0 Collab.)
ABLIKIM 14E PR D89 052001 M. Ablikim et al. (BESIII Collab.)
ABLIKIM 14F PR D89 051104 M. Ablikim et al. (BESIII Collab.)
BONVICINI 14 PR D89 072002 G. Bonvicini et al. (CLEO Collab.)
AAIJ 13AF PL B724 203 R. Aaij et al. (LHCb Collab.)
AAIJ 13W JHEP 1306 112 R. Aaij et al. (LHCb Collab.)
DOBBS 13 PRL 110 131802 S. Dobbs et al. (CLEO Collab.)
KO 13 JHEP 1302 098 B.R. Ko et al. (BELLE Collab.)
LEES 13E PR D87 052012 J.P. Lees et al. (BABAR Collab.)
LEES 13F PR D87 052010 J.P. Lees et al. (BABAR Collab.)
KO 12A PRL 109 119903 (errat.) B.R. Ko et al. (BELLE Collab.)
Also PRL 109 021601 B.R. Ko et al. (BELLE Collab.)
STARIC 12 PRL 108 071801 M. Staric et al. (BELLE Collab.)
AAIJ 11G PR D84 112008 R. Aaij et al. (LHCb Collab.)
DEL-AMO-SA... 11H PR D83 071103 P. del Amo Sanchez et al. (BABAR Collab.)
DEL-AMO-SA... 11I PR D83 072001 P. del Amo Sanchez et al. (BABAR Collab.)
LEES 11E PR D84 031103 J.P. Lees et al. (BABAR Collab.)
LEES 11G PR D84 072006 J.P. Lees et al. (BABAR Collab.)
WILLIAMS 11 PR D84 054015 M. Williams (LOIC)
WON 11 PRL 107 221801 E. Won et al. (BELLE Collab.)
YELTON 11 PR D84 032001 J. Yelton et al. (CLEO Collab.)
ANASHIN 10A PL B686 84 V.V. Anashin et al. (VEPP-4M KEDR Collab.)
ASNER 10 PR D81 052007 D.M. Asner et al. (CLEO Collab.)

Downloaded from https://academic.oup.com/ptep/article/2022/8/083C01/6651666 by KIT Library user on 27 September 2022

BRIERE	10	PR D81 112001	R.A. Briere et al.	(CLEO Collab.)
KO	10	PRL 104 181602	B.R. Ko et al.	(BELLE Collab.)
MENDEZ	10	PR D81 052013	H. Mendez et al.	(CLEO Collab.)
PDG	10	JP G37 075021	K. Nakamura et al.	(PDG Collab.)
RUBIN	10	PR D82 092007	P. Rubin et al.	(CLEO Collab.)
BEDIAGA	09	PR D80 096006	I. Bediaga et al.	(CBPF, NDAM)
BESSON	09	PR D80 032005	D. Besson et al.	(CLEO Collab.)
Also		PR D79 052010	J.Y. Ge et al.	(CLEO Collab.)
KO	09	PRL 102 221802	B.R. Ko et al.	(BELLE Collab.)
LINK	09	PL B681 14	J.M. Link et al.	(FNAL FOCUS Collab.)
MITCHELL	09B	PRL 102 081801	R.E. Mitchell et al.	(CLEO Collab.)
WON	09	PR D80 111101	E. Won et al.	(BELLE Collab.)
ABAZOV	08D	PRL 100 101801	V.M. Abazov et al.	(D0 Collab.)
ABLIKIM	08L	PL B665 16	M. Ablikim et al.	(BES Collab.)
ARTUSO	08	PR D77 092003	M. Artuso et al.	(CLEO Collab.)
AUBERT	08AO	PR D78 051102	B. Aubert et al.	(BABAR Collab.)
BONVICINI	08	PR D77 091106	G. Bonvicini et al.	(CLEO Collab.)
BONVICINI	08A	PR D78 052001	G. Bonvicini et al.	(CLEO Collab.)
DOBBS	08	PR D77 112005	S. Dobbs et al.	(CLEO Collab.)
Also		PRL 100 251802	D. Cronin-Hennessy et al.	(CLEO Collab.)
EISENSTEIN	08	PR D78 052003	B.I. Eisenstein et al.	(CLEO Collab.)
HE	08	PRL 100 091801	Q. He et al.	(CLEO Collab.)
PDG	08	PL B667 1	C. Amsler et al.	(PDG Collab.)
RUBIN	08	PR D78 072003	P. Rubin et al.	(CLEO Collab.)
ABLIKIM	07	PL B644 20	M. Ablikim et al.	(BES Collab.)
ABLIKIM	07G	PL B658 1	M. Ablikim et al.	(BES Collab.)
BONVICINI	07	PR D76 012001	G. Bonvicini et al.	(CLEO Collab.)
DOBBS	07	PR D76 112001	S. Dobbs et al.	(CLEO Collab.)
LINK	07B	PL B653 1	J.M. Link et al.	(FNAL FOCUS Collab.)
ABLIKIM	06O	EPJ C47 31	M. Ablikim et al.	(BES Collab.)
ABLIKIM	06P	EPJ C47 39	M. Ablikim et al.	(BES Collab.)
ABLIKIM	06U	PL B643 246	M. Ablikim et al.	(BES Collab.)
ADAM	06A	PRL 97 251801	N.E. Adam et al.	(CLEO Collab.)
AITALA	06	PR D73 032004	E.M. Aitala et al.	(FNAL E791 Collab.)
Also		PR D74 059901 (errat.)	E.M. Aitala et al.	(FNAL E791 Collab.)
AUBERT,B	06F	PR D74 011107	B. Aubert et al.	(BABAR Colla.b)
DYTMAN	06	PR D74 071102	S.A. Dytman et al.	(CLEO Collab.)
HUANG	06B	PR D74 112005	G.S. Huang et al.	(CLEO Collab.)
LINK	06B	PL B637 32	J.M. Link et al.	(FNAL FOCUS Collab.)
RUBIN	06	PRL 96 081802	P. Rubin et al.	(CLEO Collab.)
RUBIN	06A	PR D73 112005	P. Rubin et al.	(CLEO Collab.)
ABLIKIM	05A	PL B608 24	M. Ablikim et al.	(BES Collab.)
ABLIKIM	05D	PL B610 183	M. Ablikim et al.	(BES Collab.)
ABLIKIM	05F	PL B622 6	M. Ablikim et al.	(BES Collab.)
ABLIKIM	05P	PL B625 196	M. Ablikim et al.	(BES Collab.)
ARTUSO	05A	PRL 95 251801	M. Artuso et al.	(CLEO Collab.)
AUBERT	05S	PR D71 091101	B. Aubert et al.	(BABAR Collab.)
HE	05	PRL 95 121801	Q. He et al.	(CLEO Collab.)
Also		PRL 96 199903 (errat.)	Q. He et al.	(CLEO Collab.)
HE	05A	PRL 95 221802	Q. He et al.	(CLEO Collab.)
HUANG	05B	PRL 95 181801	G.S. Huang et al.	(CLEO Collab.)
KAYIS-TOPAK...	05	PL B626 24	A. Kayis-Topaksu et al.	(CERN CHORUS Collab.)
LINK	05E	PL B622 239	J.M. Link et al.	(FNAL FOCUS Collab.)
LINK	05I	PL B621 72	J.M. Link et al.	(FNAL FOCUS Collab.)
ABLIKIM	04C	PL B597 39	M. Ablikim et al.	(BEPC BES Collab.)
ARMS	04	PR D69 071102	K. Arms et al.	(CLEO Collab.)
BONVICINI	04A	PR D70 112004	G. Bonvicini et al.	(CLEO Collab.)
LINK	04	PL B585 200	J.M. Link et al.	(FNAL FOCUS Collab.)
LINK	04E	PL B598 33	J.M. Link et al.	(FNAL FOCUS Collab.)
LINK	04F	PL B601 10	J.M. Link et al.	(FNAL FOCUS Collab.)
ANISOVICH	03	EPJ A16 229	V.V. Anisovich et al.	
LINK	03D	PL B561 225	J.M. Link et al.	(FNAL FOCUS Collab.)
LINK	03F	PL B572 21	J.M. Link et al.	(FNAL FOCUS Collab.)
AITALA	02	PRL 89 121801	E.M. Aitala et al.	(FNAL E791 Collab.)
BRANDENB...	02	PRL 89 222001	G. Brandenburg et al.	(CLEO Collab.)
KAYIS-TOPAK...	02	PL B549 48	A. Kayis-Topaksu et al.	(CERN CHORUS Collab.)
LINK	02B	PRL 88 041602	J.M. Link et al.	(FNAL FOCUS Collab.)
Also		PRL 88 159903 (errat.)	J.M. Link et al.	(FNAL FOCUS Collab.)
LINK	02E	PL B535 43	J.M. Link et al.	(FNAL FOCUS Collab.)
LINK	02F	PL B537 192	J.M. Link et al.	(FNAL FOCUS Collab.)
LINK	02I	PL B541 227	J.M. Link et al.	(FNAL FOCUS Collab.)
LINK	02J	PL B541 243	J.M. Link et al.	(FNAL FOCUS Collab.)
LINK	02L	PL B544 89	J.M. Link et al.	(FNAL FOCUS Collab.)
AITALA	01B	PRL 86 770	E.M. Aitala et al.	(FNAL E791 Collab.)
LINK	01C	PRL 87 162001	J.M. Link et al.	(FNAL FOCUS Collab.)
ABREU	00O	EPJ C12 209	P. Abreu et al.	(DELPHI Collab.)
ASTIER	00D	PL B486 35	P. Astier et al.	(CERN NOMAD Collab.)
JUN	00	PRL 84 1857	S.Y. Jun et al.	(FNAL SELEX Collab.)
LINK	00B	PL B491 232	J.M. Link et al.	(FNAL FOCUS Collab.)
Also		PL B495 443 (errat.)	J.M. Link et al.	(FNAL FOCUS Collab.)
ABBIENDI	99K	EPJ C8 573	G. Abbiendi et al.	(OPAL Collab.)
ADAMOVICH	99	EPJ C6 35	M. Adamovich et al.	(CERN BEATRICE Collab.)
AITALA	99G	PL B462 401	E.M. Aitala et al.	(FNAL E791 Collab.)
BONVICINI	99	PRL 82 4586	G. Bonvicini et al.	(CLEO Collab.)
AITALA	98B	PRL 80 1393	E.M. Aitala et al.	(FNAL E791 Collab.)
AITALA	98C	PL B421 405	E.M. Aitala et al.	(FNAL E791 Collab.)
AITALA	98F	PL B440 435	E.M. Aitala et al.	(FNAL E791 Collab.)
BAI	98B	PL B429 188	J.Z. Bai et al.	(BEPC BES Collab.)
AITALA	97	PL B397 325	E.M. Aitala et al.	(FNAL E791 Collab.)
AITALA	97B	PL B403 377	E.M. Aitala et al.	(FNAL E791 Collab.)
AITALA	97C	PL B404 187	E.M. Aitala et al.	(FNAL E791 Collab.)
BISHAI	97	PRL 78 3261	M. Bishai et al.	(CLEO Collab.)
FRABETTI	97	PL B391 235	P.L. Frabetti et al.	(FNAL E687 Collab.)
FRABETTI	97B	PL B398 239	P.L. Frabetti et al.	(FNAL E687 Collab.)
FRABETTI	97C	PL B401 131	P.L. Frabetti et al.	(FNAL E687 Collab.)
FRABETTI	97D	PL B407 79	P.L. Frabetti et al.	(FNAL E687 Collab.)
AITALA	96	PRL 76 364	E.M. Aitala et al.	(FNAL E791 Collab.)
FRABETTI	95	PL B346 199	P.L. Frabetti et al.	(FNAL E687 Collab.)
FRABETTI	95B	PL B351 591	P.L. Frabetti et al.	(FNAL E687 Collab.)
FRABETTI	95E	PL B359 403	P.L. Frabetti et al.	(FNAL E687 Collab.)
KODAMA	95	PL B345 85	K. Kodama et al.	(FNAL E653 Collab.)
ALBRECHT	94I	ZPHY C64 375	H. Albrecht et al.	(ARGUS Collab.)
BALEST	94	PRL 72 2328	R. Balest et al.	(CLEO Collab.)
FRABETTI	94D	PL B323 459	P.L. Frabetti et al.	(FNAL E687 Collab.)
FRABETTI	94G	PL B331 217	P.L. Frabetti et al.	(FNAL E687 Collab.)
FRABETTI	94I	PR D50 2953	P.L. Frabetti et al.	(FNAL E687 Collab.)
AKERIB	93	PRL 71 3070	D.S. Akerib et al.	(CLEO Collab.)
ANJOS	93	PR D48 56	J.C. Anjos et al.	(FNAL E691 Collab.)
FRABETTI	93E	PL B307 262	P.L. Frabetti et al.	(FNAL E687 Collab.)
ALBRECHT	92F	PL B278 202	H. Albrecht et al.	(ARGUS Collab.)
ANJOS	92C	PR D46 1941	J.C. Anjos et al.	(FNAL E691 Collab.)
BARLAG	92C	ZPHY C55 383	S. Barlag et al.	(ACCMOR Collab.)
Also		ZPHY C48 29	S. Barlag et al.	(ACCMOR Collab.)
COFFMAN	92B	PR D45 2196	D.M. Coffman et al.	(Mark III Collab.)
DAOUDI	92	PR D45 3965	M. Daoudi et al.	(CLEO Collab.)
KODAMA	92	PL B274 246	K. Kodama et al.	(FNAL E653 Collab.)
KODAMA	92C	PL B286 187	K. Kodama et al.	(FNAL E653 Collab.)
ADAMOVICH	91	PL B268 142	M.I. Adamovich et al.	(WA82 Collab.)
ALBRECHT	91	PL B255 634	H. Albrecht et al.	(ARGUS Collab.)
ALVAREZ	91B	ZPHY C50 11	M.P. Alvarez et al.	(CERN NA14/2 Collab.)
AMMAR	91	PR D44 3383	R. Ammar et al.	(CLEO Collab.)
BAI	91	PRL 66 1011	Z. Bai et al.	(Mark III Collab.)
COFFMAN	91	PL B263 135	D.M. Coffman et al.	(Mark III Collab.)
FRABETTI	91	PL B263 584	P.L. Frabetti et al.	(FNAL E687 Collab.)
ALVAREZ	90	ZPHY C47 539	M.P. Alvarez et al.	(CERN NA14/2 Collab.)
ANJOS	90C	PR D41 2705	J.C. Anjos et al.	(FNAL E691 Collab.)
ANJOS	90D	PR D42 2414	J.C. Anjos et al.	(FNAL E691 Collab.)
ANJOS	90E	PRL 65 2630	J.C. Anjos et al.	(FNAL E691 Collab.)
BARLAG	90C	ZPHY C46 563	S. Barlag et al.	(ACCMOR Collab.)
WEIR	90B	PR D41 1384	A.J. Weir et al.	(Mark II Collab.)
ANJOS	89	PRL 62 125	J.C. Anjos et al.	(FNAL E691 Collab.)
ANJOS	89B	PRL 62 722	J.C. Anjos et al.	(FNAL E691 Collab.)
ANJOS	89E	PL B223 267	J.C. Anjos et al.	(FNAL E691 Collab.)
ADLER	88C	PRL 60 89	J. Adler et al.	(Mark III Collab.)
ALBRECHT	88I	PL B210 267	H. Albrecht et al.	(ARGUS Collab.)
HAAS	88	PRL 60 1614	P. Haas et al.	(CLEO Collab.)
ONG	88	PRL 60 2587	R.A. Ong et al.	(Mark II Collab.)
RAAB	88	PR D37 2391	J.R. Raab et al.	(FNAL E691 Collab.)
ADAMOVICH	87	EPL 4 887	M.I. Adamovich et al.	(Photon Emulsion Collab.)
ADLER	87	PL B196 107	J. Adler et al.	(Mark III Collab.)
BARTEL	87	ZPHY C33 339	W. Bartel et al.	(JADE Collab.)
BALTRUSAIT...	86E	PRL 56 2140	R.M. Baltrusaitis et al.	(Mark III Collab.)
BALTRUSAIT...	85B	PRL 54 1976	R.M. Baltrusaitis et al.	(Mark III Collab.)
BALTRUSAIT...	85E	PRL 55 150	R.M. Baltrusaitis et al.	(Mark III Collab.)
BARTEL	85J	PL 163B 277	W. Bartel et al.	(JADE Collab.)
ADAMOVICH	84	PL 140B 119	M.I. Adamovich et al.	(CERN WA58 Collab.)
ALTHOFF	84G	ZPHY C22 219	M. Althoff et al.	(TASSO Collab.)
DERRICK	84	PRL 53 1971	M. Derrick et al.	(HRS Collab.)
SCHINDLER	81	PR D24 78	R.H. Schindler et al.	(Mark II Collab.)
TRILLING	81	PRPL 75 57	G.H. Trilling	(LBL, UCB) J
ZHOLENTZ	80	PL 96B 214	A.A. Zholents et al.	(NOVO)
Also		SJNP 34 814 Translated from YAF 34 1471.	A.A. Zholents et al.	(NOVO)
GOLDHABER	77	PL 69B 503	G. Goldhaber et al.	(Mark I Collab.)
PERUZZI	77	PRL 39 1301	I. Peruzzi et al.	(LGW Collab.)
PICCOLO	77	PL 70B 260	M. Piccolo et al.	(Mark I Collab.)
PERUZZI	76	PRL 37 569	I. Peruzzi et al.	(Mark I Collab.)
MOSTELLER	48	Am.Stat.3 No.5 30	R.A. Fisher, F. Mosteller	

OTHER RELATED PAPERS

RICHMAN	95	RMP 67 893	J.D. Richman, P.R. Burchat	(UCSB, STAN)
ROSNER	95	CNPP 21 369	J. Rosner	(CHIC)

D^0

$I(J^P) = \frac{1}{2}(0^-)$

D^0 MASS

The fit includes $D^{\pm}$, D^0, $D_s^{\pm}$, $D^{*\pm}$, D^{*0}, $D_s^{*\pm}$, $D_1(2420)^0$, $D_2^*(2460)^0$, and $D_{s1}(2536)^{\pm}$ mass and mass difference measurements.

Given the recent addition of much more precise measurements, we have omitted all those masses published up through 1990. See any Review before 2015 for those earlier results.

VALUE (MeV)	EVTS	DOCUMENT ID		TECN	COMMENT
1864.84 ±0.05 OUR FIT					
1864.84 ±0.05 OUR AVERAGE					
1864.845±0.025±0.057	63k	[1] TOMARADZE	14		$D^0 \to K^- 2\pi^+ \pi^-$
1864.75 ±0.15 ±0.11		AAIJ	13V	LHCB	$D^0 \to K^+ 2K^- \pi^+$
1864.841±0.048±0.063	4.3k	[2] LEES	13S	BABR	$e^+ e^-$ at $\Upsilon(4S)$
1865.30 ±0.33 ±0.23	0.1k	ANASHIN	10A	KEDR	$e^+ e^-$ at $\psi(3770)$
1864.847±0.150±0.095	0.3k	CAWLFIELD	07	CLEO	$D^0 \to K_S^0 \phi$

[1] Obtained by analyzing CLEO-c data but not authored by the CLEO Collaboration. The largest source of error in the TOMARADZE 14 value is from the uncertainties in the K^- and K_S^0 masses. The systematic error given above is the addition in quadrature of $\pm 0.022 \pm 0.053$ MeV, where the second error is from those mass uncertainties.

[2] The largest source of error in the LEES 13s value is from the uncertainty of the K^+ mass. The quoted systematic error is in fact $\pm 0.043 + 3\,(m_{K^+} - 493.677)$, in MeV.

$m_{D^{\pm}} - m_{D^0}$

The fit includes $D^{\pm}$, D^0, $D_s^{\pm}$, $D^{*\pm}$, D^{*0}, $D_s^{*\pm}$, $D_1(2420)^0$, $D_2^*(2460)^0$, and $D_{s1}(2536)^{\pm}$ mass and mass difference measurements.

VALUE (MeV)	DOCUMENT ID		TECN	COMMENT
4.822±0.015 OUR FIT				
4.76 ±0.12 ±0.07	AAIJ	13V	LHCB	$D^+ \to K^+ K^- \pi^+$

D^0 MEAN LIFE

Measurements with an error $> 10 \times 10^{-15}$ s have been omitted from the average.

VALUE (10^{-15} s)	EVTS	DOCUMENT ID		TECN	COMMENT
410.3± 1.0 OUR AVERAGE					
410.5± 1.1± 0.8	171k	[1] ABUDINEN	21A	BEL2	$e^+ e^-$ at $\Upsilon(4S)$
409.6± 1.1± 1.5	210k	LINK	02F	FOCS	γ nucleus, ≈ 180 GeV
407.9± 6.0± 4.3	10k	KUSHNIR...	01	SELX	$K^- \pi^+$, $K^- \pi^+ \pi^+ \pi^-$
413 ± 3 ± 4	35k	AITALA	99E	E791	$K^- \pi^+$
408.5± 4.1$^{+3.5}_{-3.4}$	25k	BONVICINI	99	CLE2	$e^+ e^- \approx \Upsilon(4S)$
413 ± 4 ± 3	16k	FRABETTI	94D	E687	$K^- \pi^+$, $K^- \pi^+ \pi^+ \pi^-$

Downloaded from https://academic.oup.com/ptep/article/2022/8/083C01/6651666 by KIT Library user on 27 September 2022

• • • We do not use the following data for averages, fits, limits, etc. • • •

424 ±11 ± 7	5118	FRABETTI	91	E687	$K^-\pi^+$, $K^-\pi^+\pi^+\pi^-$
417 ±18 ±15	890	ALVAREZ	90	NA14	$K^-\pi^+$, $K^-\pi^+\pi^+\pi^-$
388 $^{+23}_{-21}$	641	[2] BARLAG	90C	ACCM	π^- Cu 230 GeV
480 ±40 ±30	776	ALBRECHT	88I	ARG	e^+e^- 10 GeV
422 ± 8 ±10	4212	RAAB	88	E691	Photoproduction
420 ±50	90	BARLAG	87B	ACCM	K^- and π^- 200 GeV

[1] ABUDINEN 21A determines the lifetime ratio $\tau(D^+)/\tau(D^0) = 2.510 \pm 0.013 \pm 0.007$.
[2] BARLAG 90C estimate systematic error to be negligible.

See the related review(s):

D^0 — $\overline{D}^0$ Mixing

$|m_{D^0_1} - m_{D^0_2}| = x\,\Gamma$

The D^0_1 and D^0_2 are the mass eigenstates of the D^0 meson, as described in the note on "D^0-$\overline{D}^0$ Mixing," above. The experiments usually present $x \equiv \Delta m/\Gamma$. Then $\Delta m = x\,\Gamma = x\,\hbar/\tau$.

"OUR EVALUATION" comes from CPV allowing averages provided by the Heavy Flavor Averaging Group, see the note on "D^0-$\overline{D}^0$ Mixing."

VALUE (10^{10} $\hbar$ s^{-1})	CL%	DOCUMENT ID		TECN	COMMENT
0.997±0.116 OUR EVALUATION					
0.92 ±0.12 OUR AVERAGE					
0.97 $^{+0.14}_{-0.13}$		[1] AAIJ	21AB	LHCB	pp at 13 TeV, $D^0 \to K^0_S\pi^+\pi^-$
0.66 $^{+0.41}_{-0.37}$		[2] AAIJ	19X	LHCB	pp at 7, 8 TeV, $D^0 \to K^0_S\pi^+\pi^-$
		[3] AAIJ	18K	LHCB	pp at 7, 8, 13 TeV
− 2.10 ±1.29 ±0.41		[4] AAIJ	16V	LHCB	pp at 7 TeV
3.7 ±2.9 ±1.5		[5] LEES	16D	BABR	e^+e^-, 10.6 GeV
		[6] KO	14	BELL	$e^+e^- \to \Upsilon(nS)$
1.37 ±0.46 $^{+0.18}_{-0.28}$		[7] PENG	14	BELL	$e^+e^- \to \Upsilon(nS)$
		[8] AALTONEN	13AE	CDF	$p\overline{p}$ at 1.96 TeV
0.39 ±0.56 ±0.35		[9] DEL-AMO-SA...	10D	BABR	e^+e^-, 10.6 GeV
• • • We do not use the following data for averages, fits, limits, etc. • • •					
		[10] AAIJ	17AO	LHCB	Repl. by AAIJ 18K
		[11] AAIJ	13CE	LHCB	Repl. by AAIJ 17AO
		[12] AAIJ	13N	LHCB	Repl. by AAIJ 13CE
6.4 $^{+1.4}_{-1.7}$ ±1.0		[13] AUBERT	09AN	BABR	e^+e^- at 10.58 GeV
− 2 $^{+7}_{-6}$		[14] LOWREY	09	CLEO	e^+e^- at $\psi(3770)$
1.98 ±0.73 $^{+0.32}_{-0.41}$		[15] ZHANG	07B	BELL	Repl. by PENG 14
< 7	95	[16] ZHANG	06	BELL	e^+e^-
−11 to +22		[15] ASNER	05	CLEO	$e^+e^- \approx$ 10 GeV
< 11	90	BITENC	05	BELL	
< 30	90	CAWLFIELD	05	CLEO	
< 7	95	[16] LI	05A	BELL	See ZHANG 06
< 22	95	[17] LINK	05H	FOCS	γ nucleus
< 23	95	AUBERT	04Q	BABR	
< 11	95	[16] AUBERT	03Z	BABR	e^+e^-, 10.6 GeV
< 7	95	[18] GODANG	00	CLE2	e^+e^-
< 32	90	[19,20] AITALA	98	E791	π^- nucleus, 500 GeV
< 24	90	[21] AITALA	96C	E791	π^- nucleus, 500 GeV
< 21	90	[20,22] ANJOS	88C	E691	Photoproduction

[1] AAIJ 21AB measurement allows for CP violation (none seen).
[2] AAIJ 19X D^0 come from D^{*+} and $\overline{B} \to D^0\mu^-X$ decays (and c.c.). Measurement allows for CP violation (none seen).
[3] The result was established with D^0 from prompt and secondary D^*. Based on 5 fb^{-1} of data collected at $\sqrt{s}$ = 7, 8, 13 TeV. Assumes no CP violation. Reported $x'^2 = (3.9 \pm 2.7) \times 10^{-5}$ and $y' = (5.28 \pm 0.52) \times 10^{-3}$, where $x' = x\cos(\delta) + y\sin(\delta)$, $y' = y$
[4] Model-independent measurement of the charm mixing parameters in the decay $D^0 \to K^0_S\pi^+\pi^-$ using 1.0 fb^{-1} of LHCb data at $\sqrt{s}$ = 7 TeV.
[5] Time-dependent amplitude analysis of $D^0 \to \pi^+\pi^-\pi^0$.
[6] Based on 976 fb^{-1} of data collected at $\Upsilon(nS)$ resonances. Assumes no CP violation. Reported $x'^2 = (0.09 \pm 0.22) \times 10^{-3}$ and $y' = (4.6 \pm 3.4) \times 10^{-3}$, where $x' = x\cos(\delta) + y\sin(\delta)$, $y' = y\cos(\delta) - x\sin(\delta)$ and δ is the strong phase between $D^0 \to K^+\pi^-$ and $\overline{D}^0 \to K^+\pi^-$.
[7] The time-dependent Dalitz-plot analysis of $D^0 \to K^0_S\pi^+\pi^-$ is emplored. Decay-time information and interference on the Dalitz plot are used to distinguish doubly Cabibbo-suppressed decays from mixing and to measure the relative phase between $D^0 \to K^{*+}\pi^-$ and $\overline{D}^0 \to K^{*+}\pi^-$. This value allows CP violation and is sensitive to the sign of Δm.
[8] Based on 9.6 fb^{-1} of data collected at the Tevatron. Assumes no CP violation. Reported $x'^2 = (0.08 \pm 0.18) \times 10^{-3}$ and $y' = (4.3 \pm 4.3) \times 10^{-3}$, where $x' = x\cos(\delta) + y\sin(\delta)$, $y' = y\cos(\delta) - x\sin(\delta)$ and δ is the strong phase between the $D^0 \to K^+\pi^-$ and $\overline{D}^0 \to K^+\pi^-$.
[9] DEL-AMO-SANCHEZ 10D uses 540,800±800 $K^0_S\pi^+\pi^-$ and 79,900±300 $K^0_S K^+K^-$ events in a time-dependent amplitude analysis of the D^0 and $\overline{D}^0$ Dalitz plots. No evidence was found for CP violation, and the values here assume no such violation.
[10] The result was established with D^0 from prompt and secondary D^*. Based on 3 fb^{-1} of data collected at $\sqrt{s}$ = 7, 8 TeV. Assumes no CP violation. Reported $x'^2 = (3.6 \pm 4.3) \times 10^{-5}$ and $y' = (5.23 \pm 0.84) \times 10^{-3}$, where $x' = x\cos(\delta) + y\sin(\delta)$, $y' = y\cos(\delta) - x\sin(\delta)$ and δ is the strong phase between the $D^0 \to K^+\pi^-$ and $\overline{D}^0 \to K^+\pi^-$.
[11] Based on 3 fb^{-1} of data collected at $\sqrt{s}$ = 7, 8 TeV. Assumes no CP violation. Reported $x'^2 = (5.5 \pm 4.9) \times 10^{-4}$ and $y' = (4.8 \pm 1.0) \times 10^{-3}$, where $x' = x\cos(\delta) + y\sin(\delta)$, $y' = y\cos(\delta) - x\sin(\delta)$ and δ is the strong phase between the $D^0 \to K^+\pi^-$ and $\overline{D}^0 \to K^+\pi^-$.
[12] Based on 1 fb^{-1} of data collected at $\sqrt{s}$ = 7 TeV in 2011. Assumes no CP violation. Reported $x'^2 = (-0.9 \pm 1.3) \times 10^{-4}$ and $y' = (7.2 \pm 2.4) \times 10^{-3}$, where $x' = x\cos(\delta) + y\sin(\delta)$, $y' = y\cos(\delta) - x\sin(\delta)$ and δ is the strong phase between the $D^0 \to K^+\pi^-$ and $\overline{D}^0 \to K^+\pi^-$.
[13] The AUBERT 09AN values are inferred from the branching ratio $\Gamma(D^0 \to K^+\pi^-\pi^0$ via $\overline{D}^0)/\Gamma(D^0 \to K^-\pi^+\pi^0)$ given near the end of this Listings. Mixing is distinguished from DCS decays using decay-time information. Interference between mixing and DCS is allowed. The phase between $D^0 \to K^+\pi^-\pi^0$ and $\overline{D}^0 \to K^+\pi^-\pi^0$ is assumed to be small. The width difference here is y'', which is not the same as y_{CP} in the note on D^0–$\overline{D}^0$ mixing.
[14] LOWREY 09 uses quantum correlations in $e^+e^- \to D^0\overline{D}^0$ at the $\psi(3770)$. See below for coherence factors and average relative strong phases for both $D^0 \to K^-\pi^+\pi^0$ and $D^0 \to K^-\pi^-2\pi^+$. A fit that includes external measurements of charm mixing parameters gets $\Delta m = (2.34 \pm 0.61) \times 10^{10}$ $\hbar$ s^{-1}.
[15] The ASNER 05 and ZHANG 07B values are from the time-dependent Dalitz-plot analysis of $D^0 \to K^0_S\pi^+\pi^-$. Decay-time information and interference on the Dalitz plot are used to distinguish doubly Cabibbo-suppressed decays from mixing and to measure the relative phase between $D^0 \to K^{*+}\pi^-$ and $\overline{D}^0 \to K^{*+}\pi^-$. This value allows CP violation and is sensitive to the sign of Δm.
[16] The AUBERT 03Z, LI 05A, and ZHANG 06 limits are inferred from the D^0-$\overline{D}^0$ mixing ratio $\Gamma(K^+\pi^-$ (via $\overline{D}^0$))/$\Gamma(K^-\pi^+)$ given near the end of this D^0 Listings. Decay-time information is used to distinguish DCS decays from D^0-$\overline{D}^0$ mixing. The limit allows interference between the DCS and mixing ratios, and also allows CP violation. AUBERT 03Z assumes the strong phase between $D^0 \to K^+\pi^-$ and $\overline{D}^0 \to K^+\pi^-$ amplitudes is small; if an arbitrary phase is allowed, the limit degrades by 20%. The LI 05A and ZHANG 06 limits are valid for an arbitrary strong phase.
[17] This LINK 05H limit is inferred from the D^0-$\overline{D}^0$ mixing ratio $\Gamma(K^+\pi^-$ (via $\overline{D}^0$))/$\Gamma(K^-\pi^+)$ given near the end of this D^0 Listings. Decay-time information is used to distinguish DCS decays from D^0-$\overline{D}^0$ mixing. The limit allows interference between the DCS and mixing ratios, and also allows CP violation. The strong phase between $D^0 \to K^+\pi^-$ and $\overline{D}^0 \to K^+\pi^-$ is assumed to be small. If an arbitrary relative strong phase is allowed, the limit degrades by 25%.
[18] This GODANG 00 limit is inferred from the D^0-$\overline{D}^0$ mixing ratio $\Gamma(K^+\pi^-$ (via $\overline{D}^0$))/$\Gamma(K^-\pi^+)$ given near the end of this D^0 Listings. Decay-time information is used to distinguish DCS decays from D^0-$\overline{D}^0$ mixing. The limit allows interference between the DCS and mixing ratios, and also allows CP violation. The strong phase between $D^0 \to K^+\pi^-$ and $\overline{D}^0 \to K^+\pi^-$ is assumed to be small. If an arbitrary relative strong phase is allowed, the limit degrades by a factor of two.
[19] AITALA 98 allows interference between the doubly Cabibbo-suppressed and mixing amplitudes, and also allows CP violation in this term, but assumes that $A_D = A_R = 0$. See the note on "D^0-$\overline{D}^0$ Mixing," above.
[20] This limit is inferred from R_M for $f = K^+\pi^-$ and $f = K^+\pi^-\pi^+\pi^-$. See the note on "D^0-$\overline{D}^0$ Mixing," above. Decay-time information is used to distinguish doubly Cabibbo-suppressed decays from D^0-$\overline{D}^0$ mixing.
[21] This limit is inferred from R_M for $f = K^+\ell^-\overline{\nu}_\ell$. See the note on "$D^0$-$\overline{D}^0$ Mixing," above.
[22] ANJOS 88C assumes that $y = 0$. See the note on "D^0-$\overline{D}^0$ Mixing," above. Without this assumption, the limit degrades by about a factor of two.

$(\Gamma_{D^0_1} - \Gamma_{D^0_2})/\Gamma = 2y$

The D^0_1 and D^0_2 are the mass eigenstates of the D^0 meson, as described in the note on "D^0-$\overline{D}^0$ Mixing," above.

Due to the strong phase difference between $D^0 \to K^+\pi^-$ and $\overline{D}^0 \to K^+\pi^-$, we exclude from the average those measurements of y' that are inferred from the D^0-$\overline{D}^0$ mixing ratio $\Gamma(K^+\pi^-$ via $\overline{D}^0$) / $\Gamma(K^+\pi^-)$ given near the end of this D^0 Listings.

Some early results have been omitted. See our 2006 *Review* (Journal of Physics **G33** 1 (2006)).

"OUR EVALUATION" comes from CPV allowing averages provided by the Heavy Flavor Averaging Group, see the note on "D^0-$\overline{D}^0$ Mixing."

VALUE (units 10^{-2})	EVTS	DOCUMENT ID		TECN	COMMENT
1.23± 0.11 OUR EVALUATION					
1.06± 0.16 OUR AVERAGE Error includes scale factor of 1.1.					
0.92 $^{+0.30}_{-0.28}$	30.6M	[1] AAIJ	21AB	LHCB	pp at 13 TeV
1.92± 1.82 $^{+1.29}_{-1.24}$	91k	[2] NAYAK	20	BELL	$D^0 \to K^0_S\omega$
1.14± 0.26±0.18		[3] AAIJ	19	LHCB	pp at 7, 8 TeV
1.48± 0.74	2.3M	[4] AAIJ	19X	LHCB	$D^0 \to K^0_S\pi^+\pi^-$
		[5] AAIJ	18K	LHCB	pp at 7, 8, 13 TeV
0.06± 0.92±0.26		[6] AAIJ	16V	LHCB	pp at 7 TeV
0.4 ± 1.8 ±1.0		[7] LEES	16D	BABR	e^+e^-, 10.6 GeV

Downloaded from https://academic.oup.com/ptep/article/2022/8/083C01/6651666 by KIT Library user on 27 September 2022

$2.22 \pm 0.44 \pm 0.18$		[8] STARIC	16	BELL	$e^+e^- \to \Upsilon(nS)$
$-4.0 \pm 2.6 \pm 1.4$		[9] ABLIKIM	15D	BES3	e^+e^- at $\psi(3770)$
		[10] KO	14	BELL	$e^+e^- \to \Upsilon(nS)$
$0.60 \pm 0.30^{+0.10}_{-0.17}$		[11] PENG	14	BELL	$e^+e^- \to \Upsilon(nS)$
		[12] AALTONEN	13AE	CDF	$p\overline{p}$ at 1.96 TeV
$1.44 \pm 0.36 \pm 0.24$		[13] LEES	13	BABR	$e^+e^- \to \Upsilon(4S)$
$0.55 \pm 0.63 \pm 0.41$		[14] AAIJ	12K	LHCB	pp at 7 TeV
$1.14 \pm 0.40 \pm 0.30$		[15] DEL-AMO-SA..	10D	BABR	e^+e^-, 10.6 GeV
$0.22 \pm 1.22 \pm 1.04$		[16] ZUPANC	09	BELL	$e^+e^- \approx \Upsilon(4S)$
$-1.0 \pm 2.0\ ^{+1.4}_{-1.6}$	18k	[17] ABE	02I	BELL	$e^+e^- \approx \Upsilon(4S)$
$-2.4 \pm 5.0 \pm 2.8$	3393	[18] CSORNA	02	CLE2	$e^+e^- \approx \Upsilon(4S)$
$6.84 \pm 2.78 \pm 1.48$	10k	[17] LINK	00	FOCS	γ nucleus
$+1.6 \pm 5.8 \pm 2.1$		[17] AITALA	99E	E791	$K^-\pi^+$, K^+K^-
• • • We do not use the following data for averages, fits, limits, etc. • • •					
		[19] AAIJ	17AO	LHCB	Repl. by AAIJ 18K
		[20] AAIJ	13CE	LHCB	Repl. by AAIJ 17AO
		[21] AAIJ	13N	LHCB	Repl. by AAIJ 13CE
$2.32 \pm 0.44 \pm 0.36$		[22] AUBERT	09AI	BABR	See LEES 13
$-0.12^{+1.10}_{-1.28} \pm 0.68$		[23] AUBERT	09AN	BABR	e^+e^- at 10.58 GeV
$1.4\ ^{+4.8}_{-5.4}$		[24] LOWREY	09	CLEO	e^+e^- at $\psi(3770)$
1.70 ± 1.52	12.7 ± 0.3k	[25] AALTONEN	08E	CDF	$p\overline{p}$, $\sqrt{s} = 1.96$ TeV
$2.06 \pm 0.66 \pm 0.38$		[26] AUBERT	08U	BABR	See AUBERT 09AI
$1.94 \pm 0.88 \pm 0.62$	4030 ± 90	[25] AUBERT	07W	BABR	$e^+e^- \approx 10.6$ GeV
$2.62 \pm 0.64 \pm 0.50$	160k	[27] STARIC	07	BELL	Repl. by STARIC 16
$0.74 \pm 0.50^{+0.20}_{-0.31}$	534k	[28] ZHANG	07B	BELL	Repl. by PENG 14
-0.7 ± 4.9	$4k \pm 88$	[25,29] ZHANG	06	BELL	e^+e^-
$-3.0\ ^{+5.0}_{-4.8}\ ^{+1.6}_{-0.8}$		[28] ASNER	05	CLEO	$e^+e^- \approx 10$ GeV
-0.3 ± 5.7		[25,29] LI	05A	BELL	See ZHANG 06
$-5.2\ ^{+18.4}_{-16.8}$		[25,29] LINK	05H	FOCS	γ nucleus
$1.6 \pm 0.8\ ^{+1.0}_{-0.8}$	450k	[30] AUBERT	03P	BABR	See AUBERT 08U
$1.6\ ^{+6.2}_{-12.8}$		[25,29] AUBERT	03Z	BABR	e^+e^-, 10.6 GeV
$-5.0\ ^{+2.8}_{-3.2} \pm 0.6$		[25] GODANG	00	CLE2	e^+e^-

[1] AAIJ 21AB analysis of $D^0 \to K^0_S\pi^+\pi^-$ events allows for CP violation (none seen).

[2] NAYAK 20 reports $(1.92 \pm 1.82 \pm 1.24^{+0.34}_{-0.00}) \times 10^{-2}$ where the last uncertainty is due to possible presence of CP-even decays in the data sample. Extracts $y_{CP}=(\Gamma_{CP+} - \Gamma_{CP-}) / (\Gamma_{CP+} + \Gamma_{CP-})$ in $D^0 \to K^0_S\omega$ versus $\overline{D}^0 \to K^0_S\omega$, by measuring the decay lifetime of $D^0 \to K^0_S\omega$ with $\omega \to \pi^+\pi^-\pi^0$ versus $D^0 \to K^-\pi^+$. We list $2y_{CP} = 2y\ (= \Delta\Gamma/\Gamma)$ in the absence of CP violation.

[3] Based on 3 fb^{-1} of data collected at $\sqrt{s} = 7$, 8 TeV. Measures the lifetime difference between $D^0 \to K^-K^+$ and $D^0 \to \pi^-\pi^+$ (CP even) decays and $D^0 \to K^-\pi^+$ (CP mixed) decays, or $y_{CP}=(\Gamma_{CP+} - \Gamma_{CP-}) / (\Gamma_{CP+} + \Gamma_{CP-})$. The D^0 mesons are required to originate from semimuonic decays of B mesons. We list $2y_{CP} = \Delta\Gamma/\Gamma$.

[4] AAIJ 19X D^0 come from D^{*+} and $\overline{B} \to D^0\mu^-X$ decays (and c.c.) in pp collisions at 7 and 8 TeV. Measurement allows for CP violation (none seen).

[5] The result was established with D^0 from prompt and secondary D^*. Based on 5 fb^{-1} of data collected at $\sqrt{s} = 7$, 8, 13 TeV. Assumes no CP violation. Reported $x'^2 = (3.9 \pm 2.7) \times 10^{-5}$ and $y' = (5.28 \pm 0.52) \times 10^{-3}$, where $x' = x\cos(\delta) + y\sin(\delta)$, $y' = y\cos(\delta) - x\sin(\delta)$ and δ is the strong phase between the $D^0 \to K^+\pi^-$ and $\overline{D}^0 \to K^+\pi^-$.

[6] Model-independent measurement of the charm mixing parameters in the decay $D^0 \to K^0_S\pi^+\pi^-$ using 1.0 fb^{-1} of LHCb data at $\sqrt{s} = 7$ TeV.

[7] Time-dependent amplitude analysis of $D^0 \to \pi^+\pi^-\pi^0$.

[8] An improved measurement of $\overline{D}^0 - D^0$ mixing and a search for CP violation in D^0 decays to CP-even final states K^+K^- and $\pi^+\pi^-$ using the final Belle data sample of 976 fb^{-1}.

[9] ABLIKIM 15D uses quantum correlations in $e^+e^- \to D^0\overline{D}^0$ at the $\psi(3770)$.

[10] Based on 976 fb^{-1} of data collected at $\Upsilon(nS)$ resonances. Assumes no CP violation. Reported $x'^2 = (0.09 \pm 0.22) \times 10^{-3}$ and $y' = (4.6 \pm 3.4) \times 10^{-3}$, where $x' = x\cos(\delta) + y\sin(\delta)$, $y' = y\cos(\delta) - x\sin(\delta)$ and δ is the strong phase between $D^0 \to K^+\pi^-$ and $\overline{D}^0 \to K^+\pi^-$.

[11] The time-dependent Dalitz-plot analysis of $D^0 \to K^0_S\pi^+\pi^-$ is emplored. Decay-time information and interference on the Dalitz plot are used to distinguish doubly Cabibbo-suppressed decays from mixing and to measure the relative phase between $D^0 \to K^{*+}\pi^-$ and $\overline{D}^0 \to K^{*+}\pi^-$. This value allows CP violation and is sensitive to the sign of Δm.

[12] Based on 9.6 fb^{-1} of data collected at the Tevatron. Assumes no CP violation. Reported $x'^2 = (0.08 \pm 0.18) \times 10^{-3}$ and $y' = (4.3 \pm 4.3) \times 10^{-3}$, where $x' = x\cos(\delta) + y\sin(\delta)$, $y' = y\cos(\delta) - x\sin(\delta)$ and δ is the strong phase between the $D^0 \to K^+\pi^-$ and $\overline{D}^0 \to K^+\pi^-$.

[13] Obtained $y_{CP} = (0.72 \pm 0.18 \pm 0.12)\%$ based on three effective D^0 lifetimes measured in $K^{\mp}\pi^{\pm}$, K^-K^+, and $\pi^-\pi^+$. We list $2y_{CP} = \Delta\Gamma/\Gamma$.

[14] Compared the lifetimes of D^0 decay to the CP eigenstate K^+K^- with D^0 decay to π^+K^-. The values here assume no CP violation.

[15] DEL-AMO-SANCHEZ 10D uses $540{,}800 \pm 800$ $K^0_S\pi^+\pi^-$ and $79{,}900 \pm 300$ $K^0_S K^+K^-$ events in a time-dependent amplitude analyses of the D^0 and $\overline{D}^0$ Dalitz plots. No evidence was found for CP violation, and the values here assume no such violation.

[16] ZUPANC 09 uses a method based on measuring the mean decay time of $D^0 \to K^0_S K^+K^-$ events for different K^+K^- mass intervals.

[17] LINK 00, AITALA 99E, and ABE 02I measure the lifetime difference between $D^0 \to K^-K^+$ (CP even) decays and $D^0 \to K^-\pi^+$ (CP mixed) decays, or $y_{CP}=[\Gamma(CP+)-\Gamma(CP-)]/[\Gamma(CP+)+\Gamma(CP-)]$. We list $2y_{CP}=\Delta\Gamma/\Gamma$.

[18] CSORNA 02 measures the lifetime difference between $D^0 \to K^-K^+$ and $\pi^-\pi^+$ (CP even) decays and $D^0 \to K^-\pi^+$ (CP mixed) decays, or $y_{CP}=[\Gamma(CP+)-\Gamma(CP-)]/[\Gamma(CP+)+\Gamma(CP-)]$. We list $2y_{CP}=\Delta\Gamma/\Gamma$.

[19] The result was established with D^0 from prompt and secondary D^*. Based on 3 fb^{-1} of data collected at $\sqrt{s} = 7$, 8 TeV. Assumes no CP violation. Reported $x'^2 = (3.6 \pm 4.3) \times 10^{-5}$ and $y' = (5.23 \pm 0.84) \times 10^{-3}$, where $x' = x\cos(\delta) + y\sin(\delta)$, $y' = y\cos(\delta) - x\sin(\delta)$ and δ is the strong phase between the $D^0 \to K^+\pi^-$ and $\overline{D}^0 \to K^+\pi^-$.

[20] Based on 3 fb^{-1} of data collected at $\sqrt{s} = 7$, 8 TeV. Assumes no CP violation. Reported $x'^2 = (5.5 \pm 4.9) \times 10^{-4}$ and $y' = (4.8 \pm 1.0) \times 10^{-3}$, where $x' = x\cos(\delta) + y\sin(\delta)$, $y' = y\cos(\delta) - x\sin(\delta)$ and δ is the strong phase between the $D^0 \to K^+\pi^-$ and $\overline{D}^0 \to K^+\pi^-$.

[21] Based on 1 fb^{-1} of data collected at $\sqrt{s} = 7$ TeV in 2011. Assumes no CP violation. Reported $x'^2 = (-0.9 \pm 1.3) \times 10^{-4}$ and $y' = (7.2 \pm 2.4) \times 10^{-3}$, where $x' = x\cos(\delta) + y\sin(\delta)$, $y' = y\cos(\delta) - x\sin(\delta)$ and δ is the strong phase between the $D^0 \to K^+\pi^-$ and $\overline{D}^0 \to K^+\pi^-$.

[22] This combines the $y_{CP} = (\tau_{K\pi}/\tau_{KK})-1$ using untagged $K^-\pi^+$ and K^-K^+ events of AUBERT 09AI with the disjoint y_{CP} using tagged $K^-\pi^+$, K^-K^+, and $\pi^-\pi^+$ events of AUBERT 08U.

[23] The AUBERT 09AN values are inferred from the branching ratio $\Gamma(D^0 \to K^+\pi^-\pi^0$ via $\overline{D}^0)/\Gamma(D^0 \to K^-\pi^+\pi^0)$ given near the end of this Listings. Mixing is distinguished from DCS decays using decay-time information. Interference between mixing and DCS is allowed. The phase between $D^0 \to K^+\pi^-\pi^0$ and $\overline{D}^0 \to K^+\pi^-\pi^0$ is assumed to be small. The width difference here is y'', which is not the same as y_{CP} in the note on D^0-$\overline{D}^0$ mixing.

[24] LOWREY 09 uses quantum correlations in $e^+e^- \to D^0\overline{D}^0$ at the $\psi(3770)$. See below for coherence factors and average relative strong phases for both $D^0 \to K^-\pi^+\pi^0$ and $D^0 \to K^-\pi^-2\pi^+$. A fit that includes external measurements of charm mixing parameters gets $2y = (1.62 \pm 0.32) \times 10^{-2}$.

[25] The GODANG 00, AUBERT 03Z, LINK 05H, LI 05A, ZHANG 06, AUBERT 07W, and AALTONEN 08E limits are inferred from the D^0-$\overline{D}^0$ mixing ratio $\Gamma(K^+\pi^-$ (via $\overline{D}^0))/\Gamma(K^-\pi^+)$ given near the end of this D^0 Listings. Decay-time information is used to distinguish DCS decays from D^0-$\overline{D}^0$ mixing. The limits allow interference between the DCS and mixing ratios, and all except AUBERT 07W and AALTONEN 08E also allow CP violation. The phase between $D^0 \to K^+\pi^-$ and $\overline{D}^0 \to K^+\pi^-$ is assumed to be small. This is a measurement of y' and is not the same as the y_{CP} of our note above on "D^0-$\overline{D}^0$ Mixing."

[26] This value combines the results of AUBERT 08U and AUBERT 03P.

[27] STARIC 07 compares the lifetimes of D^0 decay to the CP eigenstates K^+K^- and $\pi^+\pi^-$ with D^0 decay to $K^-\pi^+$.

[28] The ASNER 05 and ZHANG 07B values are from the time-dependent Dalitz-plot analysis of $D^0 \to K^0_S\pi^+\pi^-$. Decay-time information and interference on the Dalitz plot are used to distinguish doubly Cabibbo-suppressed decays from mixing and to measure the relative phase between $D^0 \to K^{*+}\pi^-$ and $\overline{D}^0 \to K^{*+}\pi^-$. This limit allows CP violation.

[29] The ranges of AUBERT 03Z, LINK 05H, LI 05A, and ZHANG 06 measurements are for 95% confidence level.

[30] AUBERT 03P measures $Y \equiv 2\tau^0 / (\tau^+ + \tau^-) - 1$, where τ^0 is the $D^0 \to K^-\pi^+$ (and $\overline{D}^0 \to K^+\pi^-$) lifetime, and τ^+ and τ^- are the D^0 and $\overline{D}^0$ lifetimes to CP-even states (here K^-K^+ and $\pi^-\pi^+$). In the limit of CP conservation, $Y = y \equiv \Delta\Gamma / 2\Gamma$ (we list $2y = \Delta\Gamma/\Gamma$). AUBERT 03P also uses $\tau^+ - \tau^-$ to get $\Delta Y = -0.008 \pm 0.006 \pm 0.002$.

|q/p|

The mass eigenstates D^0_1 and D^0_2 are related to the $C = \pm 1$ states by $|D_{1,2}> = p\,|D^0> + q\,|\overline{D}^0>$. See the note on "$D^0$-$\overline{D}^0$ Mixing" above.

"OUR EVALUATION" comes from CPV allowing averages provided by the Heavy Flavor Averaging Group. This would include as-yet-unpublished results, see the note on "D^0-$\overline{D}^0$ Mixing."

VALUE	EVTS	DOCUMENT ID		TECN	COMMENT
0.995 ± 0.016 OUR EVALUATION		HFLAV fit; see the note on "D^0-$\overline{D}^0$ Mixing."			
0.99 ± 0.05 OUR AVERAGE					
0.996 ± 0.052	30.6M	[1] AAIJ	21AB	LHCB	pp at 13 TeV
$1.05\ ^{+0.22}_{-0.17}$	2.3M	[2] AAIJ	19X	LHCB	pp at 7, 8 TeV
		[3] AAIJ	18K	LHCB	pp at 7, 8, 13 TeV
$0.90\ ^{+0.16}_{-0.15}\ ^{+0.08}_{-0.06}$		[4] PENG	14	BELL	$e^+e^- \to \Upsilon(nS)$
• • • We do not use the following data for averages, fits, limits, etc. • • •					
		[5] AAIJ	13CE	LHCB	Repl. by AAIJ 18K
$0.86\ ^{+0.30}_{-0.29}\ ^{+0.10}_{-0.08}$		[6] ZHANG	07B	BELL	Repl. by PENG 14

[1] AAIJ 21AB result comes form analysis of $D^0 \to K^0_S\pi^+\pi^-$ events.

[2] AAIJ 19X measurement comes form analysis of $D^0 \to K^0_S\pi^+\pi^-$ decays. D^0 come from D^{*+} and $\overline{B} \to D^0\mu^-X$ decays (and c.c.) in pp collisions at 7 and 8 TeV.

[3] Based on 5 fb^{-1} of data collected at $\sqrt{s} = 7$, 8, 13 TeV. Allowing for CP violation, the direct CP violation in mixing is reported $1.00 < |q/p| < 1.35$ at the 68.3% CL for the $D^0 \to K^+\pi^-$ and $\overline{D}^0 \to K^+\pi^-$.

[4] The time-dependent Dalitz-plot analysis of $D^0 \to K^0_S\pi^+\pi^-$ is employed. Decay-time information and interference on the Dalitz plot are used to distinguish doubly Cabibbo-suppressed decays from mixing and to measure the relative phase between $D^0 \to K^{*+}\pi^-$ and $\overline{D}^0 \to K^{*+}\pi^-$. This value allows CP violation and is sensitive to the sign of Δm.

Downloaded from https://academic.oup.com/ptep/article/2022/8/083C01/6651666 by KIT Library user on 27 September 2022

[5] Based on 3 fb^{-1} of data collected at $\sqrt{s}$ = 7, 8 TeV. Allowing for *CP* violation, the direct *CP* violation in mixing is reported $0.75 < |q/p| < 1.24$ at the 68.3% CL for the $D^0 \to K^+\pi^-$ and $\overline{D}^0 \to K^+\pi^-$.

[6] The phase of p/q is $(-14^{+16}_{-18} \pm 5)^\circ$. The ZHANG 07B value is from the time-dependent Dalitz-plot analysis of $D^0 \to K^0_S\pi^+\pi^-$. Decay-time information and interference on the Dalitz plot are used to distinguish doubly Cabibbo-suppressed decays from mixing and to measure the relative phase between $D^0 \to K^{*+}\pi^-$ and $\overline{D}^0 \to K^{*+}\pi^-$. This value allows *CP* violation.

A_Γ

A_Γ is the decay-rate asymmetry for *CP*-even final states $A_\Gamma = (\overline{\tau}_+ - \tau_+) / (\overline{\tau}_+ + \tau_+)$.

See the note on "D^0–$\overline{D}^0$ Mixing" above.

VALUE (units 10^{-3})	EVTS	DOCUMENT ID		TECN	COMMENT
0.089±0.113 OUR EVALUATION					
0.09 ±0.17 OUR AVERAGE Error includes scale factor of 1.5. See the ideogram below.					
0.23 ±0.15 ±0.03		[1] AAIJ	21AI	LHCB	$D^0 \to K^+K^-$
0.40 ±0.28 ±0.04		[1] AAIJ	21AI	LHCB	$D^0 \to \pi^+\pi^-$
−0.44 ±0.23 ±0.06	21M	[2] AAIJ	20	LHCB	$D^0 \to K^+K^-$
0.25 ±0.43 ±0.07	7M	[3] AAIJ	20	LHCB	$D^0 \to \pi^+\pi^-$
−0.3 ±2.0 ±0.7		[4] STARIC	16	BELL	$e^+e^- \to \Upsilon(nS)$
−1.2 ±1.2	1.8M	[5] AALTONEN	14Q	CDF	$p\overline{p}$, $\sqrt{s}$ = 1.96 TeV
0.9 ±2.6 ±0.6	0.7M	LEES	13	BABR	$e^+e^- \to \Upsilon(4S)$
−5.9 ±5.9 ±2.1		[6] AAIJ	12K	LHCB	pp at 7 TeV, 2010 data.
• • • We do not use the following data for averages, fits, limits, etc. • • •					
−0.30 ±0.32 ±0.10	9.6M	[6] AAIJ	17AK	LHCB	Repl. by AAIJ 20
0.46 ±0.58 ±0.12	3.0M	[7] AAIJ	17AK	LHCB	Repl. by AAIJ 20
−1.34 ±0.77 $^{+0.26}_{-0.34}$	2.3M	[8] AAIJ	15AA	LHCB	Repl. by AAIJ 20
−0.92 ±1.45 $^{+0.25}_{-0.33}$	0.8M	[9] AAIJ	15AA	LHCB	Repl. by AAIJ 20
−0.35 ±0.62 ±0.12		[6] AAIJ	14AL	LHCB	Repl. by AAIJ 17AK
0.33 ±1.06 ±0.14		[7] AAIJ	14AL	LHCB	Repl. by AAIJ 17AK
2.6 ±3.6 ±0.8		AUBERT	08U	BABR	See LEES 13
0.1 ±3.0 ±2.5		STARIC	07	BELL	Repl. by STARIC 16
8 ±6 ±2		AUBERT	03P	BABR	$e^+e^- \approx \Upsilon(4S)$

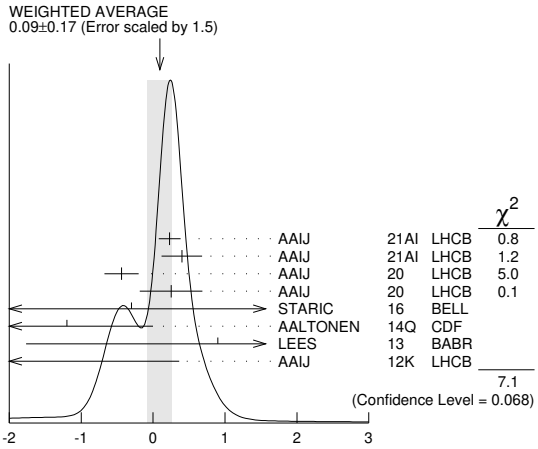

[1] Requires D^0 to originate from $D^*(2010)^+ \to D^0\pi^+$. AAIJ 21AI measures the parameter $\Delta Y_f \simeq -A^f_\Gamma$ up to 1% corrections from y^f_{CP}.

[2] Measured using $D^0 \to K^+K^-$ decays, combines measurements with D^0 either from partially reconstructed semileptonic B hadron decays or from $D^{*+} \to D^0\pi^+$.

[3] Measured using $D^0 \to \pi^+\pi^-$ decays, combines measurements with D^0 either from partially reconstructed semileptonic B hadron decays or from $D^{*+} \to D^0\pi^+$.

[4] An improved measurement of $\overline{D}^0 - D^0$ mixing and a search for *CP* violation in D^0 decays to *CP*-even final states K^+K^- and $\pi^+\pi^-$ using the final Belle data sample of 976 fb^{-1}.

[5] Combined result from $D^0 \to K^+K^-$ and $D^0 \to \pi^+\pi^-$, with D^0 from $D^{*+} \to D^0\pi^+$ (and cc).

[6] Measured using $D^{*+} \to D^0\pi^+$, $D^0 \to K^+K^-$ decays (and cc).

[7] Measured using $D^{*+} \to D^0\pi^+$, $D^0 \to \pi^+\pi^-$ decays (and cc).

[8] Measured using $D^0 \to K^+K^-$ decays, with D^0 from partially reconstructed semileptonic B hadron decays.

[9] Measured using $D^0 \to \pi^+\pi^-$ decays, with D^0 from partially reconstructed semileptonic B hadron decays.

$\phi^{K^0_S\pi\pi}$

Parametrizes *CP* violation in the interference between D^0 mixing and decay. The mass eigenstates D^0_1 and D^0_2 are related to the $C = \pm 1$ states by $|D_{1,2}> = p\,|D^0> + q\,|\overline{D}^0>$. In the absence of *CP* violation in the decay, and using the usual phase convention where *CP* conservation implies q/p is real, $\phi^{K^0_S\pi\pi}$ is identical to the decay-mode-independent parameter $\phi = \arg(q/p)$.

VALUE	EVTS	DOCUMENT ID		TECN	COMMENT
0.02 $^{+0.04}_{-0.05}$ OUR AVERAGE					
0.056 $^{+0.047}_{-0.051}$	30.6M	[1] AAIJ	21AB	LHCB	pp at 13 TeV
−0.09 $^{+0.11}_{-0.16}$	2.3M	[2] AAIJ	19X	LHCB	pp at 7, 8 TeV
−0.10 ±0.19 $^{+0.07}_{-0.09}$	1.2M	[3] PENG	14	BELL	e^+e^- at $\Upsilon(4S,5S)$

[1] AAIJ 21AB result comes form analysis of $D^0 \to K^0_S\pi^+\pi^-$ events.

[2] AAIJ 19X result comes form analysis of $D^0 \to K^0_S\pi^+\pi^-$ events. D^0 come from D^{*+} and $\overline{B} \to D^0\mu^-X$ decays (and c.c.) in pp collisions at 7 and 8 TeV.

[3] PENG 14 reports $-0.10 \pm 0.19 \pm 0.05^{+0.05}_{-0.07}$ value where the last uncertainty is due to the amplitude model. We have added the systematic uncertainties in quadrature.

cos δ

δ is the $D^0 \to K^+\pi^-$ relative strong phase.

VALUE	DOCUMENT ID		TECN	COMMENT
0.97±0.11 OUR AVERAGE				
1.02±0.11±0.06	[1] ABLIKIM	14C	BES3	$e^+e^- \to D^0\overline{D}^0$, 3.77 GeV
0.81 $^{+0.22}_{-0.18}$ $^{+0.07}_{-0.05}$	[2] ASNER	12	CLEO	$e^+e^- \to D^0\overline{D}^0$, 3.77 GeV
• • • We do not use the following data for averages, fits, limits, etc. • • •				
1.03 $^{+0.31}_{-0.17}$ ±0.06	[3] ASNER	08	CLEO	Repl. by ASNER 12

[1] Uses quantum correlations in $e^+e^- \to D^0\overline{D}^0$ at the $\psi(3770)$ to measure the asymmetry of the branching fraction of $D^0 \to K^-\pi^+$ in *CP*-odd and *CP*-even eigenstates to be (12.7 ± 1.3 ± 0.7)%. A fit that includes external measurements of charm mixing parameters finds the value quoted above.

[2] Uses quantum correlations in $e^+e^- \to D^0\overline{D}^0$ at the $\psi(3770)$, where decay rates of *CP*-tagged $K\pi$ final states depend on the strong phases between the decays of $D^0 \to K^+\pi^-$ and $\overline{D}^0 \to K^+\pi^-$. The measurements obtained $\sin(\delta) = -0.01 \pm 0.41 \pm 0.04$ and $|\delta| = (10^{+28}_{-53}{}^{+13}_{-00})^\circ$ as well. A fit that includes external measurements of charm mixing parameters finds $\cos(\delta) = 1.15^{+0.19}_{-0.17}{}^{+0.00}_{-0.08}$, $\sin(\delta) = 0.56^{+0.32}_{-0.31}{}^{+0.21}_{-0.20}$, and $|\delta| = (18^{+11}_{-17})^\circ$.

[3] ASNER 08 uses quantum correlations in $e^+e^- \to D^0\overline{D}^0$ at the $\psi(3770)$, where decay rates of *CP*-tagged $K\pi$ final states depend on cos δ because of interfering amplitudes. The above measurement implies $|\delta| < 75^\circ$ with a confidence level of 95%. A fit that includes external measurements of charm mixing parameters finds cos δ = 1.10 ± 0.35 ± 0.07. See also the note on "D^0– $\overline{D}^0$ Mixing" p. 783 in our 2008 Review (PDG 08).

$D^0 \to K^-\pi^+\pi^0$ COHERENCE FACTOR $R_{K\pi\pi^0}$

See the note on 'D^0-$\overline{D}^0$ Mixing' for the definition. $R_{K\pi\pi^0}$ can have any value between 0 and 1. A value near 1 indicates the decay is dominated by a few intermediate states with limited interference.

VALUE	EVTS	DOCUMENT ID		TECN	COMMENT
0.792±0.033 OUR AVERAGE					
0.78 ±0.04	62.4k	[1] ABLIKIM	21AA	BES3	$e^+e^- \to D^0\overline{D}^0$ at $\psi(3770)$
0.82 ±0.06		[1,2,3] EVANS	16		$e^+e^- \to D^0\overline{D}^0$ at $\psi(3770)$
• • • We do not use the following data for averages, fits, limits, etc. • • •					
0.82 ±0.07		[1,3] LIBBY	14		Repl. by EVANS 16
0.78 $^{+0.11}_{-0.25}$		[4] LOWREY	09	CLEO	Repl. by LIBBY 14

[1] Uses quantum correlations in $e^+e^- \to D^0\overline{D}^0$ at the $\psi(3770)$, where the decay rates of *CP*-tagged $K^-\pi^+\pi^0$ final states depend on $R_{K\pi\pi^0}$ and $\delta^{K\pi\pi^0}$.

[2] A combined fit with a recent LHCb $D^0\overline{D}^0$ mixing results in AAIJ 16F is also reported to be 0.81 ± 0.06.

[3] Obtained by analyzing CLEO-c data but not authored by the CLEO Collaboration.

[4] LOWREY 09 uses quantum correlations in $e^+e^- \to D^0\overline{D}^0$ at the $\psi(3770)$, where the decay rates of *CP*-tagged $K^-\pi^+\pi^0$ final states depend on $R_{K\pi\pi^0}$ and $\delta^{K\pi\pi^0}$. A fit that includes external measurements of charm mixing parameters gets $R_{K\pi\pi^0}$ = 0.84 ± 0.07.

$D^0 \to K^-\pi^+\pi^0$ AVERAGE RELATIVE STRONG PHASE $\delta^{K\pi\pi^0}$

The quoted value of δ is based on the same sign *CP* phase of D^0 and $\overline{D}^0$ convention.

VALUE (°)	EVTS	DOCUMENT ID		TECN	COMMENT
198±10 OUR AVERAGE					
196^{+14}_{-15}	62.4k	[1] ABLIKIM	21AA	BES3	$e^+e^- \to D^0\overline{D}^0$ at $\psi(3770)$
199^{+13}_{-14}		[1,2,3] EVANS	16		$e^+e^- \to D^0\overline{D}^0$ at $\psi(3770)$
• • • We do not use the following data for averages, fits, limits, etc. • • •					
164^{+20}_{-14}		[1,3] LIBBY	14		Repl. by EVANS 16
239^{+32}_{-28}		[4] LOWREY	09	CLEO	Repl. by LIBBY 14

[1] Uses quantum correlations in $e^+e^- \to D^0\overline{D}^0$ at the $\psi(3770)$, where the decay rates of *CP*-tagged $K^-\pi^+\pi^0$ final states depend on $R_{K\pi\pi^0}$ and $\delta^{K\pi\pi^0}$.

[2] A combined fit with a recent LHCB $D^0\overline{D}^0$ mixing results in AAIJ 16F is also reported to be 198^{+14}_{-15} degree.

[3] Obtained by analyzing CLEO-c data but not authored by the CLEO Collaboration.

[4] LOWREY 09 uses quantum correlations in $e^+e^- \to D^0\overline{D}^0$ at the $\psi(3770)$, where the decay rates of *CP*-tagged $K^-\pi^+\pi^0$ final states depend on $R_{K\pi\pi^0}$ and $\delta^{K\pi\pi^0}$. A fit that includes external measurements of charm mixing parameters gets $\delta^{K\pi\pi^0} = (227^{+14}_{-17})^\circ$.

Downloaded from https://academic.oup.com/ptep/article/2022/8/083C01/6651666 by KIT Library user on 27 September 2022

$D^0 \to K^-\pi^-2\pi^+$ COHERENCE FACTOR $R_{K3\pi}$

See the note on 'D^0-$\overline{D}^0$ Mixing' for the definition. $R_{K3\pi}$ can have any value between 0 and 1. A value near 1 indicates the decay is dominated by a few intermediate states with limited interference.

VALUE	EVTS	DOCUMENT ID		TECN	COMMENT
$0.52^{+0.10}_{-0.09}$ OUR AVERAGE					
$0.52^{+0.12}_{-0.10}$	8.6k	[1] ABLIKIM	21AA	BES3	$e^+e^- \to D^0\overline{D}^0$ at $\psi(3770)$
$0.53^{+0.18}_{-0.21}$		[1,2,3] EVANS	16		$e^+e^- \to D^0\overline{D}^0$ at $\psi(3770)$, pp at 7,8 TeV
• • • We do not use the following data for averages, fits, limits, etc. • • •					
$0.458 \pm 0.010 \pm 0.023$	0.9M,3k	[4] AAIJ	18AI	LHCB	amplitude models
$0.32^{+0.20}_{-0.28}$		[1,3] LIBBY	14		Repl. by EVANS 16
$0.36^{+0.24}_{-0.30}$		[5] LOWREY	09	CLEO	Repl. by LIBBY 14

[1] Uses quantum correlations in $e^+e^- \to D^0\overline{D}^0$ at the $\psi(3770)$, where the decay rates of CP-tagged $K^-\pi^-2\pi^+$ final states depend on $R_{K3\pi}$ and $\delta^{K3\pi}$.

[2] A combined fit with a recent LHCB $D^0\overline{D}^0$ mixing results in AAIJ 16F is also reported, to be $0.43^{+0.17}_{-0.13}$.

[3] Obtained by analyzing CLEO-c data but not authored by the CLEO Collaboration.

[4] Calculated from amplitude models to $D^0 \to K^-\pi^-2\pi^+$ and $D^0 \to K^+\pi^+2\pi^-$ and cc. Reports $0.458 \pm 0.010 \pm 0.012 \pm 0.020$ value where the 3rd uncertainty is the model uncertainty. We combined both systematic uncertainties in quadrature. Because of the importance of model independence in the practical use of the coherence factor, we do not include model-derived results in the average.

[5] LOWREY 09 uses quantum correlations in $e^+e^- \to D^0\overline{D}^0$ at the $\psi(3770)$, where the decay rates of CP-tagged $K^-\pi^-2\pi^+$ final states depend on $R_{K3\pi}$ and $\delta^{K3\pi}$. A fit that includes external measurements of charm mixing parameters gets $R_{K3\pi} = 0.33^{+0.26}_{-0.23}$.

$D^0 \to K^-\pi^-2\pi^+$ AVERAGE RELATIVE STRONG PHASE $\delta^{K3\pi}$

The quoted value of δ is based on the same sign CP phase of D^0 and $\overline{D}^0$ convention.

VALUE (°)	EVTS	DOCUMENT ID		TECN	COMMENT
149^{+26}_{-16} OUR AVERAGE Error includes scale factor of 1.4.					
167^{+31}_{-19}	8.6k	[1] ABLIKIM	21AA	BES3	$e^+e^- \to D^0\overline{D}^0$ at $\psi(3770)$
125^{+22}_{-14}		[1,2,3] EVANS	16		$e^+e^- \to D^0\overline{D}^0$ at $\psi(3770)$
• • • We do not use the following data for averages, fits, limits, etc. • • •					
255^{+21}_{-78}		[1,3] LIBBY	14		Repl. by EVANS 16
118^{+62}_{-53}		[4] LOWREY	09	CLEO	Repl. by LIBBY 14

[1] Uses quantum correlations in $e^+e^- \to D^0\overline{D}^0$ at the $\psi(3770)$, where the decay rates of CP-tagged $K^-\pi^-2\pi^+$ final states depend on $R_{K3\pi}$ and $\delta^{K3\pi}$.

[2] A combined fit with a recent LHCb $D^0\overline{D}^0$ mixing results in AAIJ 16F is also reported to be $(128^{+28}_{-17})^\circ$.

[3] Obtained by analyzing CLEO-c data but not authored by the CLEO Collaboration.

[4] LOWREY 09 uses quantum correlations in $e^+e^- \to D^0\overline{D}^0$ at the $\psi(3770)$, where the decay rates of CP-tagged $K^-\pi^-2\pi^+$ final states depend on $R_{K3\pi}$ and $\delta^{K3\pi}$. A fit that includes external measurements of charm mixing parameters gets $\delta^{K3\pi} = (114^{+26}_{-23})^\circ$.

$D^0 \to K^-\pi^-2\pi^+$, $R_{K3\pi}$ ($y \cos\delta^{K3\pi} - x \sin\delta^{K3\pi}$)

VALUE (10^{-3} TeV^{-1})	EVTS	DOCUMENT ID		TECN	COMMENT
-3.0 ± 0.7	42.5k	[1] AAIJ	16F	LHCB	pp at 7, 8 TeV

[1] From a time-dependent analysis of D mixing in $D^0 \to K^+\pi^-\pi^+\pi^-$. This result uses external constraints on $R_M = 1/2\,(x^2 + y^2)$. Without such constraints, AAIJ 16F measure $(0.3 \pm 1.8) \times 10^{-3}$, with a large correlation coefficient to R_M.

$D^0 \to K^0_S K^+\pi^-$ COHERENCE FACTOR $R_{K^0_S K\pi}$

VALUE	DOCUMENT ID		TECN	COMMENT
0.70±0.08	[1] INSLER	12	CLEO	$e^+e^- \to D^0\overline{D}^0$ at 3.77 GeV

[1] Uses quantum correlations in $e^+e^- \to D^0\overline{D}^0$ at the $\psi(3770)$, where the signal side D decays to $K^0_S K\pi$ and the tag-side D decays to $K\pi$, $K\pi\pi\pi$, $K\pi\pi^0$, and 10 additional CP-even, CP-odd, and mixed CP modes involving K^0_S or K^0_L.

$D^0 \to K^0_S K^+\pi^-$ AVERAGE RELATIVE STRONG PHASE $\delta^{K^0_S K\pi}$

The quoted value of δ is based on the same sign CP phase of D^0 and $\overline{D}^0$ convention.

VALUE (°)	DOCUMENT ID		TECN	COMMENT
0.1±15.7	[1] INSLER	12	CLEO	$e^+e^- \to D^0\overline{D}^0$ at 3.77 GeV

[1] Uses quantum correlations in $e^+e^- \to D^0\overline{D}^0$ at the $\psi(3770)$, where the signal side D decays to $K^0_S K\pi$ and the tag-side D decays to $K\pi$, $K\pi\pi\pi$, $K\pi\pi^0$, and 10 additional CP-even, CP-odd, and mixed CP modes involving K^0_S or K^0_L.

$D^0 \to K^*K$ COHERENCE FACTOR R_{K^*K}

VALUE	DOCUMENT ID		TECN	COMMENT
0.94±0.12	[1] INSLER	12	CLEO	$e^+e^- \to D^0\overline{D}^0$ at 3.77 GeV

[1] Uses quantum correlations in $e^+e^- \to D^0\overline{D}^0$ at the $\psi(3770)$, where the signal side D decays to $K^0_S K\pi$ and the tag-side D decays to $K\pi$, $K\pi\pi\pi$, $K\pi\pi^0$., and 10 additional CP-even, CP-odd, and mixed CP modes involving K^0_S or K^0_L.

$D^0 \to K^*K$ AVERAGE RELATIVE STRONG PHASE δ^{K^*K}

The quoted value of δ is based on the same sign CP phase of D^0 and $\overline{D}^0$ convention.

VALUE (°)	DOCUMENT ID		TECN	COMMENT
−16.6±18.4	[1] INSLER	12	CLEO	$e^+e^- \to D^0\overline{D}^0$ at 3.77 GeV

[1] Uses quantum correlations in $e^+e^- \to D^0\overline{D}^0$ at the $\psi(3770)$, where the signal side D decays to $K^0_S K\pi$ and the tag-side D decays to $K\pi$, $K\pi\pi\pi$, $K\pi\pi^0$, and 10 additional CP-even, CP-odd, and mixed CP modes involving K^0_S or K^0_L.

D^0 DECAY MODES

Most decay modes (other than the semileptonic modes) that involve a neutral K meson are now given as K^0_S modes, not as $\overline{K}^0$ modes. Nearly always it is a K^0_S that is measured, and interference between Cabibbo-allowed and doubly Cabibbo-suppressed modes can invalidate the assumption that $2\,\Gamma(K^0_S) = \Gamma(\overline{K}^0)$.

	Mode		Fraction (Γ_i/Γ)	Scale factor/ Confidence level
	Topological modes			
Γ_1	0-prongs	[a]	(15 ± 6) %	
Γ_2	2-prongs		(71 ± 6) %	
Γ_3	4-prongs	[b]	(14.6 ± 0.5) %	
Γ_4	6-prongs	[c]	$(6.5 \pm 1.3) \times 10^{-4}$	
	Inclusive modes			
Γ_5	e^+ anything	[d]	(6.49 ± 0.11) %	
Γ_6	μ^+ anything		(6.8 ± 0.6) %	
Γ_7	K^- anything		(54.7 ± 2.8) %	S=1.3
Γ_8	$\overline{K}^0$ anything + K^0 anything		(47 ± 4) %	
Γ_9	K^+ anything		(3.4 ± 0.4) %	
Γ_{10}	$K^*(892)^-$ anything		(15 ± 9) %	
Γ_{11}	$\overline{K}^*(892)^0$ anything		(9 ± 4) %	
Γ_{12}	$K^*(892)^+$ anything		< 3.6 %	CL=90%
Γ_{13}	$K^*(892)^0$ anything		(2.8 ± 1.3) %	
Γ_{14}	η anything		(9.5 ± 0.9) %	
Γ_{15}	η' anything		(2.48 ± 0.27) %	
Γ_{16}	ϕ anything		(1.08 ± 0.04) %	
Γ_{17}	invisibles		$< 9.4 \times 10^{-5}$	CL=90%
	Semileptonic modes			
Γ_{18}	$K^-\ell^+\nu_\ell$			
Γ_{19}	$K^-e^+\nu_e$		(3.549 ± 0.026) %	S=1.2
Γ_{20}	$K^-\mu^+\nu_\mu$		(3.41 ± 0.04) %	
Γ_{21}	$K^*(892)^-e^+\nu_e$		(2.15 ± 0.16) %	
Γ_{22}	$K^*(892)^-\mu^+\nu_\mu$		(1.89 ± 0.24) %	
Γ_{23}	$K^-\pi^0e^+\nu_e$		$(1.6 {}^{+1.3}_{-0.5})$ %	
Γ_{24}	$\overline{K}^0\pi^-e^+\nu_e$		(1.44 ± 0.04) %	
Γ_{25}	$(\overline{K}^0\pi^-)_{S-wave}\,e^+\nu_e$		$(7.9 \pm 1.7) \times 10^{-4}$	
Γ_{26}	$K^-\pi^+\pi^-e^+\nu_e$		$(2.8 {}^{+1.4}_{-1.1}) \times 10^{-4}$	
Γ_{27}	$K_1(1270)^-e^+\nu_e$		$(1.01 \pm 0.18) \times 10^{-3}$	
Γ_{28}	$K^-\pi^+\pi^-\mu^+\nu_\mu$		$< 1.3 \times 10^{-3}$	CL=90%
Γ_{29}	$(\overline{K}^*(892)\pi)^-\mu^+\nu_\mu$		$< 1.5 \times 10^{-3}$	CL=90%
Γ_{30}	$\pi^-e^+\nu_e$		$(2.91 \pm 0.04) \times 10^{-3}$	
Γ_{31}	$\pi^-\mu^+\nu_\mu$		$(2.67 \pm 0.12) \times 10^{-3}$	S=1.3
Γ_{32}	$\pi^-\pi^0e^+\nu_e$		$(1.45 \pm 0.07) \times 10^{-3}$	
Γ_{33}	$\rho^-e^+\nu_e$		$(1.50 \pm 0.12) \times 10^{-3}$	S=1.9
Γ_{34}	$\rho^-\mu^+\nu_\mu$		$(1.35 \pm 0.13) \times 10^{-3}$	
Γ_{35}	$a(980)^-e^+\nu_e$, $a^- \to \eta\pi^-$		$(1.33 {}^{+0.34}_{-0.30}) \times 10^{-4}$	
Γ_{36}	$b_1(1235)^-e^+\nu_e$, $b_1^- \to \omega\pi^-$		$< 1.12 \times 10^{-4}$	CL=90%
	Hadronic modes with one $\overline{K}$			
Γ_{37}	$K^-\pi^+$		(3.947 ± 0.030) %	S=1.2
Γ_{38}	$K^0_S\pi^0$		(1.240 ± 0.022) %	
Γ_{39}	$K^0_L\pi^0$		$(10.0 \pm 0.7) \times 10^{-3}$	
Γ_{40}	$K^0_S\pi^+\pi^-$	[e]	(2.80 ± 0.18) %	S=1.1
Γ_{41}	$K^0_S\rho^0$		$(6.3 {}^{+0.6}_{-0.8}) \times 10^{-3}$	

Downloaded from https://academic.oup.com/ptep/article/2022/8/083C01/6651666 by KIT Library user on 27 September 2022

Γ_{42}	$K^0_S\omega,\ \omega\to\pi^+\pi^-$		$(2.0\pm0.6)\times10^{-4}$	
Γ_{43}	$K^0_S(\pi^+\pi^-)_{S-wave}$		$(3.3\pm0.8)\times10^{-3}$	
Γ_{44}	$K^0_S f_0(980),\ f_0\to\pi^+\pi^-$		$(1.20^{+0.40}_{-0.23})\times10^{-3}$	
Γ_{45}	$K^0_S f_0(1370),\ f_0\to\pi^+\pi^-$		$(2.8^{+0.9}_{-1.3})\times10^{-3}$	
Γ_{46}	$K^0_S f_2(1270),\ f_2\to\pi^+\pi^-$		$(9^{+10}_{-6})\times10^{-5}$	
Γ_{47}	$K^*(892)^-\pi^+,\ K^{*-}\to K^0_S\pi^-$		$(1.64^{+0.14}_{-0.17})$ %	
Γ_{48}	$K^*_0(1430)^-\pi^+,\ K^{*-}_0\to K^0_S\pi^-$		$(2.67^{+0.40}_{-0.33})\times10^{-3}$	
Γ_{49}	$K^*_2(1430)^-\pi^+,\ K^{*-}_2\to K^0_S\pi^-$		$(3.4^{+1.9}_{-1.0})\times10^{-4}$	
Γ_{50}	$K^*(1680)^-\pi^+,\ K^{*-}\to K^0_S\pi^-$		$(4.4\pm3.5)\times10^{-4}$	
Γ_{51}	$K^*(892)^+\pi^-,\ K^{*+}\to K^0_S\pi^+$	[f]	$(1.13^{+0.60}_{-0.34})\times10^{-4}$	
Γ_{52}	$K^*_0(1430)^+\pi^-,\ K^{*+}_0\to K^0_S\pi^+$	[f]	$<1.4\times10^{-5}$	CL=95%
Γ_{53}	$K^*_2(1430)^+\pi^-,\ K^{*+}_2\to K^0_S\pi^+$	[f]	$<3.4\times10^{-5}$	CL=95%
Γ_{54}	$K^0_S\pi^+\pi^-$ nonresonant		$(2.5^{+6.0}_{-1.6})\times10^{-4}$	
Γ_{55}	$K^-\pi^+\pi^0$	[e]	(14.4 ± 0.5) %	S=2.0
Γ_{56}	$K^-\rho^+$		(11.2 ± 0.7) %	
Γ_{57}	$K^-\rho(1700)^+,\ \rho^+\to\pi^+\pi^0$		$(8.2\pm1.8)\times10^{-3}$	
Γ_{58}	$K^*(892)^-\pi^+,\ K^*(892)^-\to K^-\pi^0$		$(2.31^{+0.40}_{-0.20})$ %	
Γ_{59}	$\overline{K}^*(892)^0\pi^0,\ \overline{K}^*(892)^0\to K^-\pi^+$		(1.95 ± 0.24) %	
Γ_{60}	$K^*_0(1430)^-\pi^+,\ K^{*-}_0\to K^-\pi^0$		$(4.8\pm2.2)\times10^{-3}$	
Γ_{61}	$\overline{K}^*_0(1430)^0\pi^0,\ \overline{K}^{*0}_0\to K^-\pi^+$		$(5.9^{+5.0}_{-1.6})\times10^{-3}$	
Γ_{62}	$K^*(1680)^-\pi^+,\ K^{*-}\to K^-\pi^0$		$(1.9\pm0.7)\times10^{-3}$	
Γ_{63}	$K^-\pi^+\pi^0$ nonresonant		$(1.15^{+0.60}_{-0.20})$ %	
Γ_{64}	$K^0_S2\pi^0$		$(9.1\pm1.1)\times10^{-3}$	S=2.2
Γ_{65}	$K^0_S(2\pi^0)_{S-wave}$		$(2.6\pm0.7)\times10^{-3}$	
Γ_{66}	$\overline{K}^*(892)^0\pi^0,\ \overline{K}^{*0}\to K^0_S\pi^0$		$(8.1\pm0.7)\times10^{-3}$	
Γ_{67}	$\overline{K}^*(1430)^0\pi^0,\ \overline{K}^{*0}\to K^0_S\pi^0$		$(4\pm23)\times10^{-5}$	
Γ_{68}	$\overline{K}^*(1680)^0\pi^0,\ \overline{K}^{*0}\to K^0_S\pi^0$		$(1.0\pm0.4)\times10^{-3}$	
Γ_{69}	$K^0_S f_2(1270),\ f_2\to2\pi^0$		$(2.3\pm1.1)\times10^{-4}$	
Γ_{70}	$2K^0_S$, one $K^0_S\to2\pi^0$		$(3.2\pm1.1)\times10^{-4}$	
Γ_{71}	$K^0_S2\pi^0$ nonresonant			
Γ_{72}	$K^-2\pi^+\pi^-$	[e]	(8.22 ± 0.14) %	S=1.1
Γ_{73}	$K^-\pi^+\rho^0$ total		(6.87 ± 0.31) %	
Γ_{74}	$K^-\pi^+\rho^0$ 3-body		$(6.1\pm1.6)\times10^{-3}$	
Γ_{75}	$\overline{K}^*(892)^0\rho^0,\ \overline{K}^{*0}\to K^-\pi^+$		(1.01 ± 0.05) %	
Γ_{76}	$\overline{K}^*(892)^0\rho^0$ transverse, $\overline{K}^{*0}\to K^-\pi^+$		(1.2 ± 0.4) %	
Γ_{77}	$K^-a_1(1260)^+,\ a_1^+\to\rho^0\pi^+$		(4.32 ± 0.32) %	
Γ_{78}	$K_1(1270)^-\pi^+,\ K_1^-\to K^-\pi^+\pi^-$ total		$(3.9\pm0.4)\times10^{-3}$	
Γ_{79}	$\overline{K}^*(892)^0\pi^+\pi^-$ total, $\overline{K}^*(892)^0\to K^-\pi^+$			
Γ_{80}	$\overline{K}^*(892)^0\pi^+\pi^-$ 3-body, $\overline{K}^{*0}\to K^-\pi^+$			
Γ_{81}	$K_1(1270)^-\pi^+,\ K_1^-\to\overline{K}^*(892)^0\pi^-,\ \overline{K}^{*0}\to K^-\pi^+$		$(6.6\pm2.3)\times10^{-4}$	
Γ_{82}	$K^-2\pi^+\pi^-$ nonresonant		(1.81 ± 0.07) %	
Γ_{83}	$K^0_S\pi^+\pi^-\pi^0$	[g]	(5.2 ± 0.6) %	
Γ_{84}	$K^0_S\eta,\ \eta\to\pi^+\pi^-\pi^0$		$(1.17\pm0.03)\times10^{-3}$	
Γ_{85}	$K^0_S\omega,\ \omega\to\pi^+\pi^-\pi^0$		$(9.9\pm0.6)\times10^{-3}$	
Γ_{86}	$K^-\pi^+2\pi^0$		(8.86 ± 0.23) %	
Γ_{87}	$K^-2\pi^+\pi^-\pi^0$		(4.3 ± 0.4) %	
Γ_{88}	$\overline{K}^*(892)^0\pi^+\pi^-\pi^0,\ \overline{K}^{*0}\to K^-\pi^+$		(1.3 ± 0.6) %	
Γ_{89}	$K^-\pi^+\omega,\ \omega\to\pi^+\pi^-\pi^0$		(2.8 ± 0.5) %	
Γ_{90}	$\overline{K}^*(892)^0\omega,\ \overline{K}^{*0}\to K^-\pi^+,\ \omega\to\pi^+\pi^-\pi^0$		$(6.5\pm3.0)\times10^{-3}$	
Γ_{91}	$K^0_S\eta\pi^0$		(1.01 ± 0.05) %	
Γ_{92}	$K^0_S a_0(980),\ a_0\to\eta\pi^0$		(1.20 ± 0.28) %	
Γ_{93}	$\overline{K}^*(892)^0\eta,\ \overline{K}^{*0}\to K^0_S\pi^0$		$(2.9\pm0.7)\times10^{-3}$	
Γ_{94}	$K^-\pi^+\eta$		(1.88 ± 0.05) %	S=1.4
Γ_{95}	$K^*(892)^0\eta,\ K^{*0}\to K^-\pi^+$		$(8.9^{+0.8}_{-0.6})\times10^{-3}$	
Γ_{96}	$a_0(980)^+K^-,\ a_0^+\to\eta\pi^+$		$(7.4^{+0.9}_{-0.7})\times10^{-3}$	
Γ_{97}	$K^*_2(1980)^-\pi^+,\ K^{*-}_2\to K^-\eta$		$(2.2^{+1.7}_{-1.9})\times10^{-4}$	
Γ_{98}	$K^-\pi^+\pi^0\eta$		$(4.49\pm0.27)\times10^{-3}$	
Γ_{99}	$K^0_S\pi^+\pi^-\eta$		$(2.80\pm0.21)\times10^{-3}$	
Γ_{100}	$K^0_S2\pi^0\eta$		$(1.76\pm0.26)\times10^{-3}$	
Γ_{101}	$K^0_S2\pi^+2\pi^-$		$(2.66\pm0.30)\times10^{-3}$	
Γ_{102}	$K^0_S\rho^0\pi^+\pi^-$, no $K^*(892)^-$		$(1.1\pm0.7)\times10^{-3}$	
Γ_{103}	$K^*(892)^-2\pi^+\pi^-$, $K^*(892)^-\to K^0_S\pi^-$, no ρ^0		$(5\pm7)\times10^{-4}$	
Γ_{104}	$K^*(892)^-\rho^0\pi^+$, $K^*(892)^-\to K^0_S\pi^-$		$(1.6\pm0.6)\times10^{-3}$	
Γ_{105}	$K^0_S2\pi^+2\pi^-$ nonresonant		$<1.2\times10^{-3}$	CL=90%
Γ_{106}	$\overline{K}^0\pi^+\pi^-2\pi^0\,(\pi^0)$			
Γ_{107}	$K^-3\pi^+2\pi^-$		$(2.2\pm0.6)\times10^{-4}$	

Fractions of some of the following modes with resonances have already appeared above as submodes of particular charged-particle modes. These nine modes below are all corrected for unseen decays of the resonances.

Γ_{108}	$K^0_S\eta$	$(5.09\pm0.13)\times10^{-3}$	
Γ_{109}	$K^0_S\omega$	(1.11 ± 0.06) %	
Γ_{110}	$K^0_S\eta'(958)$	$(9.49\pm0.32)\times10^{-3}$	
Γ_{111}	$\overline{K}^*(892)^0\pi^+\pi^-\pi^0$	(1.9 ± 0.9) %	
Γ_{112}	$\overline{K}^*(892)^0\eta$	(1.41 ± 0.12) %	
Γ_{113}	$K^-\pi^+\omega$	(3.1 ± 0.6) %	
Γ_{114}	$\overline{K}^*(892)^0\omega$	(1.1 ± 0.5) %	
Γ_{115}	$K^-\pi^+\eta'(958)$	$(6.43\pm0.34)\times10^{-3}$	
Γ_{116}	$K^0_S\eta'(958)\pi^0$	$(2.52\pm0.27)\times10^{-3}$	
Γ_{117}	$\overline{K}^*(892)^0\eta'(958)$	$<1.0\times10^{-3}$	CL=90%

Hadronic modes with three K's

Γ_{118}	$K^0_S K^+K^-$	$(4.42\pm0.32)\times10^{-3}$	
Γ_{119}	$K^0_S a_0(980)^0,\ a_0^0\to K^+K^-$	$(2.9\pm0.4)\times10^{-3}$	
Γ_{120}	$K^-a_0(980)^+,\ a_0^+\to K^+K^0_S$	$(5.9\pm1.8)\times10^{-4}$	
Γ_{121}	$K^+a_0(980)^-,\ a_0^-\to K^-K^0_S$	$<1.1\times10^{-4}$	CL=95%
Γ_{122}	$K^0_S f_0(980),\ f_0\to K^+K^-$	$<9\times10^{-5}$	CL=95%
Γ_{123}	$K^0_S\phi,\ \phi\to K^+K^-$	$(2.03\pm0.15)\times10^{-3}$	
Γ_{124}	$K^0_S f_0(1370),\ f_0\to K^+K^-$	$(1.7\pm1.1)\times10^{-4}$	
Γ_{125}	$3K^0_S$	$(7.5\pm0.7)\times10^{-4}$	S=1.4
Γ_{126}	$K^+2K^-\pi^+$	$(2.25\pm0.32)\times10^{-4}$	
Γ_{127}	$K^+K^-\overline{K}^*(892)^0,\ \overline{K}^{*0}\to K^-\pi^+$	$(4.5\pm1.8)\times10^{-5}$	
Γ_{128}	$K^-\pi^+\phi,\ \phi\to K^+K^-$	$(4.0\pm1.7)\times10^{-5}$	
Γ_{129}	$\phi\overline{K}^*(892)^0,\ \phi\to K^+K^-,\ \overline{K}^{*0}\to K^-\pi^+$	$(1.08\pm0.21)\times10^{-4}$	
Γ_{130}	$K^+2K^-\pi^+$ nonresonant	$(3.4\pm1.5)\times10^{-5}$	
Γ_{131}	$2K^0_S K^\pm\pi^\mp$	$(5.9\pm1.3)\times10^{-4}$	

Pionic modes

Γ_{132}	$\pi^+\pi^-$	$(1.454\pm0.024)\times10^{-3}$	S=1.4
Γ_{133}	$2\pi^0$	$(8.26\pm0.25)\times10^{-4}$	
Γ_{134}	$\pi^+\pi^-\pi^0$	(1.49 ± 0.06) %	S=2.1
Γ_{135}	$\rho^+\pi^-$	(1.01 ± 0.04) %	
Γ_{136}	$\rho^0\pi^0$	$(3.86\pm0.23)\times10^{-3}$	
Γ_{137}	$\rho^-\pi^+$	$(5.15\pm0.25)\times10^{-3}$	
Γ_{138}	$\rho(1450)^+\pi^-,\ \rho^+\to\pi^+\pi^0$	$(1.6\pm2.1)\times10^{-5}$	
Γ_{139}	$\rho(1450)^0\pi^0,\ \rho^0\to\pi^+\pi^-$	$(4.5\pm2.0)\times10^{-5}$	
Γ_{140}	$\rho(1450)^-\pi^+,\ \rho^-\to\pi^-\pi^0$	$(2.7\pm0.4)\times10^{-4}$	
Γ_{141}	$\rho(1700)^+\pi^-,\ \rho^+\to\pi^+\pi^0$	$(6.1\pm1.5)\times10^{-4}$	
Γ_{142}	$\rho(1700)^0\pi^0,\ \rho^0\to\pi^+\pi^-$	$(7.4\pm1.8)\times10^{-4}$	
Γ_{143}	$\rho(1700)^-\pi^+,\ \rho^-\to\pi^-\pi^0$	$(4.8\pm1.1)\times10^{-4}$	
Γ_{144}	$f_0(980)\pi^0,\ f_0\to\pi^+\pi^-$	$(3.7\pm0.9)\times10^{-5}$	
Γ_{145}	$f_0(500)\pi^0,\ f_0\to\pi^+\pi^-$	$(1.22\pm0.22)\times10^{-4}$	
Γ_{146}	$f_0(1370)\pi^0,\ f_0\to\pi^+\pi^-$	$(5.5\pm2.1)\times10^{-5}$	
Γ_{147}	$f_0(1500)\pi^0,\ f_0\to\pi^+\pi^-$	$(5.8\pm1.6)\times10^{-5}$	
Γ_{148}	$f_0(1710)\pi^0,\ f_0\to\pi^+\pi^-$	$(4.6\pm1.6)\times10^{-5}$	

Downloaded from https://academic.oup.com/ptep/article/2022/8/083C01/6651666 by KIT Library user on 27 September 2022

Γ_{149}	$f_2(1270)\pi^0$, $f_2 \to \pi^+\pi^-$	$(1.97 \pm 0.21) \times 10^{-4}$	
Γ_{150}	$\pi^+\pi^-\pi^0$ nonresonant	$(1.3 \pm 0.4) \times 10^{-4}$	
Γ_{151}	$3\pi^0$	$(2.0 \pm 0.5) \times 10^{-4}$	
Γ_{152}	$2\pi^+2\pi^-$	$(7.56 \pm 0.20) \times 10^{-3}$	
Γ_{153}	$a_1(1260)^+\pi^-$, $a_1^+ \to 2\pi^+\pi^-$ total	$(4.53 \pm 0.31) \times 10^{-3}$	
Γ_{154}	$a_1(1260)^+\pi^-$, $a_1^+ \to \rho^0\pi^+$ S-wave	$(3.13 \pm 0.21) \times 10^{-3}$	
Γ_{155}	$a_1(1260)^+\pi^-$, $a_1^+ \to \rho^0\pi^+$ D-wave	$(1.9 \pm 0.5) \times 10^{-4}$	
Γ_{156}	$a_1(1260)^+\pi^-$, $a_1^+ \to \sigma\pi^+$	$(6.4 \pm 0.7) \times 10^{-4}$	
Γ_{157}	$a_1(1260)^-\pi^+$, $a_1^- \to \rho^0\pi^-$ S-wave	$(2.3 \pm 0.9) \times 10^{-4}$	
Γ_{158}	$a_1(1260)^-\pi^+$, $a_1^- \to \sigma\pi^-$	$(6.0 \pm 3.4) \times 10^{-5}$	
Γ_{159}	$\pi(1300)^+\pi^-$, $\pi(1300)^+ \to \sigma\pi^+$	$(5.1 \pm 2.7) \times 10^{-4}$	
Γ_{160}	$\pi(1300)^-\pi^+$, $\pi(1300)^- \to \sigma\pi^-$	$(2.3 \pm 2.2) \times 10^{-4}$	
Γ_{161}	$a_1(1640)^+\pi^-$, $a_1^+ \to \rho^0\pi^+$ D-wave	$(3.2 \pm 1.6) \times 10^{-4}$	
Γ_{162}	$a_1(1640)^+\pi^-$, $a_1^+ \to \sigma\pi^+$	$(1.8 \pm 1.4) \times 10^{-4}$	
Γ_{163}	$\pi_2(1670)^+\pi^-$, $\pi_2^+ \to f_2(1270)^0\pi^+$, $f_2^0 \to \pi^+\pi^-$	$(2.0 \pm 0.9) \times 10^{-4}$	
Γ_{164}	$\pi_2(1670)^+\pi^-$, $\pi_2^+ \to \sigma\pi^+$	$(2.6 \pm 1.0) \times 10^{-4}$	
Γ_{165}	$2\rho^0$ total	$(1.85 \pm 0.13) \times 10^{-3}$	
Γ_{166}	$2\rho^0$, parallel helicities	$(8.3 \pm 3.2) \times 10^{-5}$	
Γ_{167}	$2\rho^0$, perpendicular helicities	$(4.8 \pm 0.6) \times 10^{-4}$	
Γ_{168}	$2\rho^0$, longitudinal helicities	$(1.27 \pm 0.10) \times 10^{-3}$	
Γ_{169}	$2\rho(770)^0$, S-wave	$(1.8 \pm 1.3) \times 10^{-4}$	
Γ_{170}	$2\rho(770)^0$, P-wave	$(5.3 \pm 1.3) \times 10^{-4}$	
Γ_{171}	$2\rho(770)^0$, D-wave	$(6.2 \pm 3.0) \times 10^{-4}$	
Γ_{172}	Resonant $(\pi^+\pi^-)\pi^+\pi^-$ 3-body total	$(1.51 \pm 0.12) \times 10^{-3}$	
Γ_{173}	$\sigma\pi^+\pi^-$	$(6.2 \pm 0.9) \times 10^{-4}$	
Γ_{174}	$\sigma\rho(770)^0$	$(5.0 \pm 2.5) \times 10^{-4}$	
Γ_{175}	$f_0(980)\pi^+\pi^-$, $f_0 \to \pi^+\pi^-$	$(1.8 \pm 0.5) \times 10^{-4}$	
Γ_{176}	$f_2(1270)\pi^+\pi^-$, $f_2 \to \pi^+\pi^-$	$(3.7 \pm 0.6) \times 10^{-4}$	
Γ_{177}	$2f_2(1270)$, $f_2 \to \pi^+\pi^-$	$(1.6 \pm 1.8) \times 10^{-4}$	
Γ_{178}	$f_0(1370)\sigma$, $f_0 \to \pi^+\pi^-$	$(1.6 \pm 0.5) \times 10^{-3}$	
Γ_{179}	$\pi^+\pi^-2\pi^0$	(1.02 ± 0.09) %	
Γ_{180}	$\eta\pi^0$	[h] $(6.3 \pm 0.6) \times 10^{-4}$	S=1.1
Γ_{181}	$\omega\pi^0$	[h] $(1.17 \pm 0.35) \times 10^{-4}$	
Γ_{182}	$\omega\eta$	$(1.98 \pm 0.18) \times 10^{-3}$	S=1.1
Γ_{183}	$2\pi^+2\pi^-\pi^0$	$(4.2 \pm 0.5) \times 10^{-3}$	
Γ_{184}	$\eta\pi^+\pi^-$	[h] $(1.16 \pm 0.07) \times 10^{-3}$	
Γ_{185}	$\omega\pi^+\pi^-$	[h] $(1.33 \pm 0.20) \times 10^{-3}$	
Γ_{186}	$\omega\pi^0\pi^0$	$< 1.10 \times 10^{-3}$	CL=90%
Γ_{187}	$\eta 2\pi^0$	$(3.8 \pm 1.3) \times 10^{-4}$	
Γ_{188}	$\pi^+\pi^-\pi^0\eta$	$(3.23 \pm 0.22) \times 10^{-3}$	
Γ_{189}	$3\pi^+3\pi^-$	$(4.3 \pm 1.2) \times 10^{-4}$	
Γ_{190}	$\eta'(958)\pi^0$	$(9.2 \pm 1.0) \times 10^{-4}$	
Γ_{191}	$\eta'(958)\pi^+\pi^-$	$(4.5 \pm 1.7) \times 10^{-4}$	
Γ_{192}	2η	$(2.11 \pm 0.19) \times 10^{-3}$	S=2.2
Γ_{193}	$2\eta\pi^0$	$(7.3 \pm 2.2) \times 10^{-4}$	
Γ_{194}	3η	$< 1.3 \times 10^{-4}$	CL=90%
Γ_{195}	$\eta\eta'(958)$	$(1.01 \pm 0.19) \times 10^{-3}$	

Hadronic modes with a $K\overline{K}$ pair

Γ_{196}	K^+K^-	$(4.08 \pm 0.06) \times 10^{-3}$	S=1.6
Γ_{197}	$2K^0_S$	$(1.41 \pm 0.05) \times 10^{-4}$	S=1.1
Γ_{198}	$K^0_S K^-\pi^+$	$(3.3 \pm 0.5) \times 10^{-3}$	S=1.1
Γ_{199}	$\overline{K}^*(892)^0 K^0_S$, $\overline{K}^{*0} \to K^-\pi^+$	$(8.2 \pm 1.6) \times 10^{-5}$	
Γ_{200}	$K^*(892)^+K^-$, $K^{*+} \to K^0_S\pi^+$	$(1.89 \pm 0.30) \times 10^{-3}$	
Γ_{201}	$\overline{K}^*(1410)^0 K^0_S$, $\overline{K}^{*0} \to K^-\pi^+$	$(1.3 \pm 1.9) \times 10^{-4}$	
Γ_{202}	$K^*(1410)^+K^-$, $K^{*+} \to K^0_S\pi^+$	$(3.2 \pm 1.9) \times 10^{-4}$	
Γ_{203}	$(K^-\pi^+)_{S-wave}K^0_S$	$(6.0 \pm 2.9) \times 10^{-4}$	
Γ_{204}	$(K^0_S\pi^+)_{S-wave}K^-$	$(3.9 \pm 1.0) \times 10^{-4}$	
Γ_{205}	$a_0(980)^-\pi^+$, $a_0^- \to K^0_S K^-$	$(1.3 \pm 1.4) \times 10^{-4}$	
Γ_{206}	$a_0(1450)^-\pi^+$, $a_0^- \to K^0_S K^-$	$(2.5 \pm 2.0) \times 10^{-5}$	
Γ_{207}	$a_2(1320)^-\pi^+$, $a_2^- \to K^0_S K^-$	$(5 \pm 5) \times 10^{-6}$	
Γ_{208}	$\rho(1450)^-\pi^+$, $\rho^- \to K^0_S K^-$	$(4.6 \pm 2.5) \times 10^{-5}$	
Γ_{209}	$K^0_S K^+\pi^-$	$(2.17 \pm 0.34) \times 10^{-3}$	S=1.1
Γ_{210}	$K^*(892)^0 K^0_S$, $K^{*0} \to K^+\pi^-$	$(1.12 \pm 0.21) \times 10^{-4}$	
Γ_{211}	$K^*(892)^-K^+$, $K^{*-} \to K^0_S\pi^-$	$(6.2 \pm 1.0) \times 10^{-4}$	
Γ_{212}	$K^*(1410)^0 K^0_S$, $K^{*0} \to K^+\pi^+$	$(5 \pm 8) \times 10^{-5}$	
Γ_{213}	$K^*(1410)^-K^+$, $K^{*-} \to K^0_S\pi^-$	$(2.6 \pm 2.0) \times 10^{-4}$	
Γ_{214}	$(K^+\pi^-)_{S-wave}K^0_S$	$(3.7 \pm 1.9) \times 10^{-4}$	
Γ_{215}	$(K^0_S\pi^-)_{S-wave}K^+$	$(1.4 \pm 0.6) \times 10^{-4}$	
Γ_{216}	$a_0(980)^+\pi^-$, $a_0^+ \to K^0_S K^+$	$(6 \pm 4) \times 10^{-4}$	
Γ_{217}	$a_0(1450)^+\pi^-$, $a_0^+ \to K^0_S K^+$	$(3.2 \pm 2.5) \times 10^{-5}$	
Γ_{218}	$\rho(1700)^+\pi^-$, $\rho^+ \to K^0_S K^+$	$(1.1 \pm 0.6) \times 10^{-5}$	
Γ_{219}	$K^+K^-\pi^0$	$(3.42 \pm 0.14) \times 10^{-3}$	
Γ_{220}	$K^*(892)^+K^-$, $K^*(892)^+ \to K^+\pi^0$	$(1.52 \pm 0.07) \times 10^{-3}$	
Γ_{221}	$K^*(892)^-K^+$, $K^*(892)^- \to K^-\pi^0$	$(5.4 \pm 0.4) \times 10^{-4}$	
Γ_{222}	$(K^+\pi^0)_{S-wave}K^-$	$(2.43 \pm 0.18) \times 10^{-3}$	
Γ_{223}	$(K^-\pi^0)_{S-wave}K^+$	$(1.3 \pm 0.5) \times 10^{-4}$	
Γ_{224}	$f_0(980)\pi^0$, $f_0 \to K^+K^-$	$(3.6 \pm 0.6) \times 10^{-4}$	
Γ_{225}	$\phi\pi^0$, $\phi \to K^+K^-$	$(6.6 \pm 0.4) \times 10^{-4}$	
Γ_{226}	$K^+K^-\pi^0$ nonresonant		
Γ_{227}	$2K^0_S\pi^0$	$< 5.9 \times 10^{-4}$	
Γ_{228}	$K^+K^-\eta$	$(5.9 \pm 1.9) \times 10^{-5}$	
Γ_{229}	$\phi(1020)\eta$	$(1.84 \pm 0.12) \times 10^{-4}$	
Γ_{230}	$K^+K^-\eta$ nonresonant	$(9.9 {}^{+0.9}_{-0.8}) \times 10^{-5}$	
Γ_{231}	$2K^0_S\eta$	$(1.3 \pm 0.6) \times 10^{-4}$	
Γ_{232}	$K^+K^-\pi^0\pi^0$	$(6.9 \pm 0.8) \times 10^{-4}$	
Γ_{233}	$K^+K^-\pi^+\pi^-$	$(2.47 \pm 0.11) \times 10^{-3}$	
Γ_{234}	$\phi(\pi^+\pi^-)_{S-wave}$, $\phi \to K^+K^-$	$(10 \pm 5) \times 10^{-5}$	
Γ_{235}	$(\phi\rho^0)_{S-wave}$, $\phi \to K^+K^-$	$(6.9 \pm 0.6) \times 10^{-4}$	
Γ_{236}	$(\phi\rho^0)_{P-wave}$, $\phi \to K^+K^-$	$(4.0 \pm 1.9) \times 10^{-5}$	
Γ_{237}	$(\phi\rho^0)_{D-wave}$, $\phi \to K^+K^-$	$(4.2 \pm 1.4) \times 10^{-5}$	
Γ_{238}	$K^*(892)^0\overline{K}^*(892)^0$, $K^{*0} \to K^\pm\pi^\mp$		
Γ_{239}	$K^+K^-\rho^0$ 3-body		
Γ_{240}	$f_0(980)\pi^+\pi^-$, $f_0 \to K^+K^-$		
Γ_{241}	$(K^*(892)^0\overline{K}^*(892)^0)_{S-wave}$, $K^{*0} \to K^\pm\pi^\mp$	$(2.24 \pm 0.13) \times 10^{-4}$	
Γ_{242}	$(K^*(892)^0\overline{K}^*(892)^0)_{P-wave}$, $K^* \to K^\pm\pi^\mp$	$(1.20 \pm 0.08) \times 10^{-4}$	
Γ_{243}	$(K^*(892)^0\overline{K}^*(892)^0)_{D-wave}$, $K^* \to K^\pm\pi^\mp$	$(4.7 \pm 0.4) \times 10^{-5}$	
Γ_{244}	$K^*(892)^0K^\mp\pi^\pm$ 3-body, $K^{*0} \to K^\pm\pi^\mp$		
Γ_{245}	$K^*(892)^0(K^-\pi^+)_{S-wave}$ 3-body, $K^{*0} \to K^+\pi^-$	$(1.4 \pm 0.6) \times 10^{-4}$	
Γ_{246}	$(K^-\pi^+)_{P-wave}$, $(K^+\pi^-)_{S-wave}$		
Γ_{247}	$K_1(1270)^\pm K^\mp$, $K_1^\pm \to K^\pm\pi^+\pi^-$		
Γ_{248}	$K_1(1270)^+K^-$, $K_1^+ \to K^{*0}\pi^+$	$(1.4 \pm 0.9) \times 10^{-4}$	
Γ_{249}	$K_1(1270)^+K^-$, $K_1^+ \to K^*(1430)^0\pi^+$, $K^{*0} \to K^+\pi^-$	$(1.5 \pm 0.5) \times 10^{-4}$	
Γ_{250}	$K_1(1270)^+K^-$, $K_1^+ \to \rho^0K^+$	$(2.2 \pm 0.6) \times 10^{-4}$	
Γ_{251}	$K_1(1270)^+K^-$, $K_1^+ \to \omega(782)K^+$, $\omega \to \pi^+\pi^-$	$(1.5 \pm 1.2) \times 10^{-5}$	
Γ_{252}	$K_1(1270)^-K^+$, $K_1^- \to \overline{K}^{*0}\pi^-$		
Γ_{253}	$K_1(1270)^-K^+$, $K_1^- \to \rho^0K^-$	$(1.3 \pm 0.4) \times 10^{-4}$	

Downloaded from https://academic.oup.com/ptep/article/2022/8/083C01/6651666 by KIT Library user on 27 September 2022

Γ_{254}	$K_1(1400)^\pm K^\mp$, $K_1^\pm \to K^\pm \pi^+ \pi^-$				
Γ_{255}	$K_1(1400)^+ K^-$, $K_1^+ \to K^*(892)^0 \pi^+$, $K^{*0} \to K^+ \pi^-$		$(4.6 \pm 0.4) \times 10^{-4}$		
Γ_{256}	$K^*(1410)^+ K^-$, $K^{*+} \to K^{*0} \pi^+$				
Γ_{257}	$K^*(1410)^- K^+$, $K^{*-} \to \overline{K}^{*0} \pi^-$		$(7.0 \pm 1.1) \times 10^{-5}$		
Γ_{258}	$K_1(1680)^+ K^-$, $K_1^+ \to K^{*0} \pi^+$, $K^{*0} \to K^+ \pi^-$		$(8.9 \pm 3.2) \times 10^{-5}$		
Γ_{259}	$K^+ K^- \pi^+ \pi^-$ non-resonant		$(2.7 \pm 0.6) \times 10^{-4}$		
Γ_{260}	$2K^0_S \pi^+ \pi^-$		$(5.3 \pm 0.9) \times 10^{-4}$		
Γ_{261}	$K^0_S K^- \pi^+ \pi^0$		$(1.32 \pm 0.16) \times 10^{-3}$		
Γ_{262}	$K^0_S K^+ \pi^- \pi^0$		$(6.5 \pm 0.7) \times 10^{-4}$		
Γ_{263}	$K^0_S K^- 2\pi^+ \pi^-$		$< 1.4 \times 10^{-4}$	CL=90%	
Γ_{264}	$K^+ K^- \pi^+ \pi^- \pi^0$		$(3.1 \pm 2.0) \times 10^{-3}$		

Other $K\overline{K}X$ modes. They include all decay modes of the ϕ, η, and ω.

Γ_{265}	$\phi \pi^0$		$(1.17 \pm 0.04) \times 10^{-3}$		
Γ_{266}	$\phi \eta$		$(1.8 \pm 0.5) \times 10^{-4}$		
Γ_{267}	$\phi \omega$		$(6.5 \pm 1.0) \times 10^{-4}$		

Radiative modes

Γ_{268}	$\rho^0 \gamma$		$(1.82 \pm 0.32) \times 10^{-5}$		
Γ_{269}	$\omega \gamma$		$< 2.4 \times 10^{-4}$	CL=90%	
Γ_{270}	$\phi \gamma$		$(2.81 \pm 0.19) \times 10^{-5}$		
Γ_{271}	$\overline{K}^*(892)^0 \gamma$		$(4.1 \pm 0.7) \times 10^{-4}$		

Doubly Cabibbo suppressed (DC) modes or $\Delta C = 2$ forbidden via mixing ($C2M$) modes

Γ_{272}	$K^+ \ell^- \overline{\nu}_\ell$ via $\overline{D}^0$		$< 2.2 \times 10^{-5}$	CL=90%	
Γ_{273}	K^+ or $K^*(892)^+ e^- \overline{\nu}_e$ via $\overline{D}^0$		$< 6 \times 10^{-5}$	CL=90%	
Γ_{274}	$K^+ \pi^-$	DC	$(1.50 \pm 0.07) \times 10^{-4}$	S=3.0	
Γ_{275}	$K^+ \pi^-$ via DCS		$(1.363 \pm 0.025) \times 10^{-4}$		
Γ_{276}	$K^+ \pi^-$ via $\overline{D}^0$		$< 1.6 \times 10^{-5}$	CL=95%	
Γ_{277}	$K^0_S \pi^+ \pi^-$ in $D^0 \to \overline{D}^0$		$< 1.8 \times 10^{-4}$	CL=95%	
Γ_{278}	$K^*(892)^+ \pi^-$, $K^{*+} \to K^0_S \pi^+$	DC	$(1.13 {}^{+0.60}_{-0.34}) \times 10^{-4}$		
Γ_{279}	$K_0^*(1430)^+ \pi^-$, $K_0^{*+} \to K^0_S \pi^+$	DC	$< 1.4 \times 10^{-5}$		
Γ_{280}	$K_2^*(1430)^+ \pi^-$, $K_2^{*+} \to K^0_S \pi^+$	DC	$< 3.4 \times 10^{-5}$		
Γ_{281}	$K^+ \pi^- \pi^0$	DC	$(3.05 \pm 0.15) \times 10^{-4}$		
Γ_{282}	$K^+ \pi^- \pi^0$ via $\overline{D}^0$		$(7.6 {}^{+0.5}_{-0.6}) \times 10^{-4}$		
Γ_{283}	$K^+ \pi^+ 2\pi^-$ via DCS		$(2.49 \pm 0.07) \times 10^{-4}$		
Γ_{284}	$K^+ \pi^+ 2\pi^-$	DC	$(2.65 \pm 0.06) \times 10^{-4}$		
Γ_{285}	$K^+ \pi^+ 2\pi^-$ via $\overline{D}^0$		$(7.9 \pm 3.0) \times 10^{-6}$		
Γ_{286}	$K^+ \pi^-$ or $K^+ \pi^+ 2\pi^-$ via $\overline{D}^0$				
Γ_{287}	μ^- anything via $\overline{D}^0$		$< 4 \times 10^{-4}$	CL=90%	

$\Delta C = 1$ weak neutral current ($C1$) modes, Lepton Family number (LF) violating modes, Lepton (L) or Baryon (B) number violating modes

Γ_{288}	$\gamma\gamma$	$C1$	$< 8.5 \times 10^{-7}$	CL=90%	
Γ_{289}	$e^+ e^-$	$C1$	$< 7.9 \times 10^{-8}$	CL=90%	
Γ_{290}	$\mu^+ \mu^-$	$C1$	$< 6.2 \times 10^{-9}$	CL=90%	
Γ_{291}	$\pi^0 e^+ e^-$	$C1$	$< 4 \times 10^{-6}$	CL=90%	
Γ_{292}	$\pi^0 \mu^+ \mu^-$	$C1$	$< 1.8 \times 10^{-4}$	CL=90%	
Γ_{293}	$\eta e^+ e^-$	$C1$	$< 3 \times 10^{-6}$	CL=90%	
Γ_{294}	$\eta \mu^+ \mu^-$	$C1$	$< 5.3 \times 10^{-4}$	CL=90%	
Γ_{295}	$\pi^+ \pi^- e^+ e^-$	$C1$	$< 7 \times 10^{-6}$	CL=90%	
Γ_{296}	$\rho^0 e^+ e^-$	$C1$	$< 1.0 \times 10^{-4}$	CL=90%	
Γ_{297}	$\pi^+ \pi^- \mu^+ \mu^-$	$C1$	$(9.6 \pm 1.2) \times 10^{-7}$		
Γ_{298}	$\pi^+ \pi^- \mu^+ \mu^-$ (non-res)		$< 5.5 \times 10^{-7}$	CL=90%	
Γ_{299}	$\rho^0 \mu^+ \mu^-$	$C1$	$< 2.2 \times 10^{-5}$	CL=90%	
Γ_{300}	$\omega e^+ e^-$	$C1$	$< 6 \times 10^{-6}$	CL=90%	
Γ_{301}	$\omega \mu^+ \mu^-$	$C1$	$< 8.3 \times 10^{-4}$	CL=90%	
Γ_{302}	$K^- K^+ e^+ e^-$	$C1$	$< 1.1 \times 10^{-5}$	CL=90%	
Γ_{303}	$\phi e^+ e^-$	$C1$	$< 5.2 \times 10^{-5}$	CL=90%	
Γ_{304}	$K^- K^+ \mu^+ \mu^-$	$C1$	$(1.54 \pm 0.32) \times 10^{-7}$		
Γ_{305}	$K^- K^+ \mu^+ \mu^-$ (non-res)		$< 3.3 \times 10^{-5}$	CL=90%	
Γ_{306}	$\phi \mu^+ \mu^-$	$C1$	$< 3.1 \times 10^{-5}$	CL=90%	
Γ_{307}	$\overline{K}^0 e^+ e^-$	[i]	$< 2.4 \times 10^{-5}$	CL=90%	
Γ_{308}	$\overline{K}^0 \mu^+ \mu^-$	[i]	$< 2.6 \times 10^{-4}$	CL=90%	
Γ_{309}	$K^- \pi^+ e^+ e^-$				
Γ_{310}	$K^- \pi^+ e^+ e^-$, $675 < m_{ee} < 875$ MeV		$(4.0 \pm 0.5) \times 10^{-6}$		
Γ_{311}	$K^- \pi^+ e^+ e^-$, $1.005 < m_{ee} < 1.035$ GeV		$< 5 \times 10^{-7}$	CL=90%	
Γ_{312}	$\overline{K}^*(892)^0 e^+ e^-$	[i]	$< 4.7 \times 10^{-5}$	CL=90%	
Γ_{313}	$K^- \pi^+ \mu^+ \mu^-$	$C1$	$< 3.59 \times 10^{-4}$	CL=90%	
Γ_{314}	$K^- \pi^+ \mu^+ \mu^-$, $675 < m_{\mu\mu} < 875$ MeV		$(4.2 \pm 0.4) \times 10^{-6}$		
Γ_{315}	$\overline{K}^*(892)^0 \mu^+ \mu^-$	[i]	$< 2.4 \times 10^{-5}$	CL=90%	
Γ_{316}	$\pi^+ \pi^- \pi^0 \mu^+ \mu^-$	$C1$	$< 8.1 \times 10^{-4}$	CL=90%	
Γ_{317}	$\mu^\pm e^\mp$	LF	[j] $< 1.3 \times 10^{-8}$	CL=90%	
Γ_{318}	$\pi^0 e^\pm \mu^\mp$	LF	[j] $< 8.0 \times 10^{-7}$	CL=90%	
Γ_{319}	$\eta e^\pm \mu^\mp$	LF	[j] $< 2.25 \times 10^{-6}$	CL=90%	
Γ_{320}	$\pi^+ \pi^- e^\pm \mu^\mp$	LF	[j] $< 1.71 \times 10^{-6}$	CL=90%	
Γ_{321}	$\rho^0 e^\pm \mu^\mp$	LF	[j] $< 5.0 \times 10^{-7}$	CL=90%	
Γ_{322}	$\omega e^\pm \mu^\mp$	LF	[j] $< 1.71 \times 10^{-6}$	CL=90%	
Γ_{323}	$K^- K^+ e^\pm \mu^\mp$	LF	[j] $< 1.00 \times 10^{-6}$	CL=90%	
Γ_{324}	$\phi e^\pm \mu^\mp$	LF	[j] $< 5.1 \times 10^{-7}$	CL=90%	
Γ_{325}	$\overline{K}^0 e^\pm \mu^\mp$	LF	[j] $< 1.74 \times 10^{-6}$	CL=90%	
Γ_{326}	$K^- \pi^+ e^\pm \mu^\mp$	LF	[j] $< 1.90 \times 10^{-6}$	CL=90%	
Γ_{327}	$\overline{K}^*(892)^0 e^\pm \mu^\mp$	LF	[j] $< 1.25 \times 10^{-6}$	CL=90%	
Γ_{328}	$2\pi^- 2e^+$	L	$< 9.1 \times 10^{-7}$	CL=90%	
Γ_{329}	$2\pi^- 2\mu^+$	L	$< 1.52 \times 10^{-6}$	CL=90%	
Γ_{330}	$K^- \pi^- 2e^+$	L	$< 5.0 \times 10^{-7}$	CL=90%	
Γ_{331}	$K^- \pi^- 2\mu^+$	L	$< 5.3 \times 10^{-7}$	CL=90%	
Γ_{332}	$2K^- 2e^+$	L	$< 3.4 \times 10^{-7}$	CL=90%	
Γ_{333}	$2K^- 2\mu^+$	L	$< 1.0 \times 10^{-7}$	CL=90%	
Γ_{334}	$\pi^- \pi^- e^+ \mu^+$	L	$< 3.06 \times 10^{-6}$	CL=90%	
Γ_{335}	$K^- \pi^- e^+ \mu^+$	L	$< 2.10 \times 10^{-6}$	CL=90%	
Γ_{336}	$2K^- e^+ \mu^+$	L	$< 5.8 \times 10^{-7}$	CL=90%	
Γ_{337}	$p e^-$	L,B	[k] $< 1.0 \times 10^{-5}$	CL=90%	
Γ_{338}	$\overline{p} e^+$	L,B	[l] $< 1.1 \times 10^{-5}$	CL=90%	
Γ_{339}	Unaccounted decay modes		(35.0 ± 1.2) %	S=1.1	

[a] This value is obtained by subtracting the branching fractions for 2-, 4- and 6-prongs from unity.

[b] This is the sum of our $K^- 2\pi^+ \pi^-$, $K^- 2\pi^+ \pi^- \pi^0$, $\overline{K}^0 2\pi^+ 2\pi^-$, $K^+ 2K^- \pi^+$, $2\pi^+ 2\pi^-$, $2\pi^+ 2\pi^- \pi^0$, $K^+ K^- \pi^+ \pi^-$, and $K^+ K^- \pi^+ \pi^- \pi^0$, branching fractions.

[c] This is the sum of our $K^- 3\pi^+ 2\pi^-$ and $3\pi^+ 3\pi^-$ branching fractions.

[d] The branching fractions for the $K^- e^+ \nu_e$, $K^*(892)^- e^+ \nu_e$, $\pi^- e^+ \nu_e$, and $\rho^- e^+ \nu_e$ modes add up to 6.17 ± 0.17 %.

[e] The branching fraction for this mode may differ from the sum of the submodes that contribute to it, due to interference effects. See the relevant papers.

[f] This is a doubly Cabibbo-suppressed mode.

[g] Submodes of the $D^0 \to K^0_S \pi^+ \pi^- \pi^0$ mode with a K^* and/or ρ were studied by COFFMAN 92B, but with only 140 events. With nothing new for 18 years, we refer to our 2008 edition, Physics Letters **B667** 1 (2008), for those results.

[h] This branching fraction includes all the decay modes of the resonance in the final state.

[i] This mode is not a useful test for a ΔC=1 weak neutral current because both quarks must change flavor in this decay.

[j] The value is for the sum of the charge states or particle/antiparticle states indicated.

[k] This limit is for either D^0 or $\overline{D}^0$ to $p e^-$.

[l] This limit is for either D^0 or $\overline{D}^0$ to $\overline{p} e^+$.

Downloaded from https://academic.oup.com/ptep/article/2022/8/083C01/6651666 by KIT Library user on 27 September 2022

CONSTRAINED FIT INFORMATION

An overall fit to 66 branching ratios uses 129 measurements and one constraint to determine 33 parameters. The overall fit has a $\chi^2 = 144.1$ for 97 degrees of freedom.

The following *off-diagonal* array elements are the correlation coefficients $\langle \delta x_i \delta x_j \rangle / (\delta x_i \cdot \delta x_j)$, in percent, from the fit to the branching fractions, $x_i \equiv \Gamma_i/\Gamma_{total}$. The fit constrains the x_i whose labels appear in this array to sum to one.

x_{19}	0									
x_{20}	6	0								
x_{21}	0	0	0							
x_{30}	0	0	0	0						
x_{31}	0	0	0	0	0					
x_{37}	0	4	0	1	4	0				
x_{38}	0	1	0	1	1	0	15			
x_{40}	0	0	0	14	0	0	5	8		
x_{55}	0	1	0	0	1	0	22	3	1	
x_{72}	0	2	0	0	2	0	46	7	2	10
x_{83}	0	0	0	5	0	0	2	3	37	0
x_{87}	0	0	0	0	0	0	8	1	0	2
x_{94}	0	0	0	0	0	0	6	1	0	1
x_{108}	0	0	0	0	0	0	5	1	0	1
x_{109}	0	0	0	1	0	0	0	0	4	0
x_{110}	0	0	0	2	0	0	9	2	12	2
x_{125}	0	0	0	3	0	0	1	2	21	0
x_{132}	0	1	0	0	2	0	42	6	2	9
x_{133}	0	0	0	0	0	0	7	1	0	1
x_{134}	0	1	0	0	1	0	19	3	1	81
x_{152}	0	1	0	0	1	0	30	4	2	6
x_{180}	0	0	0	0	0	0	4	1	0	1
x_{190}	0	0	0	0	0	0	4	1	0	1
x_{192}	0	0	0	0	0	0	2	0	0	0
x_{195}	0	0	0	0	0	0	2	0	0	0
x_{196}	0	2	0	0	2	0	49	7	3	11
x_{197}	0	0	0	1	0	0	7	47	4	2
x_{198}	0	0	0	5	0	0	3	3	34	1
x_{209}	0	0	0	5	0	0	3	3	34	1
x_{270}	0	0	0	0	0	0	11	2	1	2
x_{274}	0	1	0	0	1	0	16	3	1	3
x_{339}	−48	−3	−6	−18	−1	−1	−24	−8	−39	−50
	x_6	x_{19}	x_{20}	x_{21}	x_{30}	x_{31}	x_{37}	x_{38}	x_{40}	x_{55}

x_{83}	1									
x_{87}	12	0								
x_{94}	3	0	0							
x_{108}	2	0	0	0						
x_{109}	0	12	0	0	0					
x_{110}	4	4	1	0	0	1				
x_{125}	1	8	0	0	0	1	2			
x_{132}	19	1	3	2	2	0	4	0		
x_{133}	3	0	1	0	0	0	1	0	3	
x_{134}	8	0	2	1	1	0	2	0	8	1
x_{152}	46	1	6	2	2	0	3	0	12	2
x_{180}	2	0	0	0	0	0	0	0	2	0
x_{190}	2	0	0	0	0	0	0	0	1	0
x_{192}	1	0	0	0	0	0	0	0	1	0
x_{195}	1	0	0	0	0	0	0	0	1	0
x_{196}	22	1	4	3	3	0	4	1	20	3
x_{197}	3	1	1	0	0	0	1	1	3	0
x_{198}	1	13	0	0	0	2	4	7	1	0
x_{209}	1	13	0	0	0	2	4	7	1	0
x_{270}	5	0	1	1	1	0	1	0	4	1
x_{274}	7	0	1	1	1	0	2	0	7	1
x_{339}	−23	−57	−36	−5	−2	−12	−9	−9	−10	−2
	x_{72}	x_{83}	x_{87}	x_{94}	x_{108}	x_{109}	x_{110}	x_{125}	x_{132}	x_{133}

x_{152}	6									
x_{180}	1	1								
x_{190}	1	1	0							
x_{192}	0	0	0	0						
x_{195}	0	1	0	0	0					
x_{196}	9	14	2	2	1	1				
x_{197}	1	2	0	0	0	0	3			
x_{198}	0	1	0	0	0	0	1	1		
x_{209}	0	1	0	0	0	0	1	1	100	
x_{270}	2	3	0	0	0	0	18	1	0	0
x_{274}	3	5	1	1	0	0	8	1	0	0
x_{339}	−42	−13	−1	−2	−2	−2	−12	−4	−19	−19
	x_{134}	x_{152}	x_{180}	x_{190}	x_{192}	x_{195}	x_{196}	x_{197}	x_{198}	x_{209}

x_{274}	2	
x_{339}	−3	−4
	x_{270}	x_{274}

CONSTRAINED FIT INFORMATION

An overall fit to 3 branching ratios uses 3 measurements and one constraint to determine 4 parameters. The overall fit has a $\chi^2 = 0.0$ for 0 degrees of freedom.

The following *off-diagonal* array elements are the correlation coefficients $\langle \delta x_i \delta x_j \rangle / (\delta x_i \cdot \delta x_j)$, in percent, from the fit to the branching fractions, $x_i \equiv \Gamma_i/\Gamma_{total}$. The fit constrains the x_i whose labels appear in this array to sum to one.

x_2	−100		
x_3	−46	39	
x_4	0	0	0
	x_1	x_2	x_3

D^0 BRANCHING RATIOS

Some older now obsolete results have been omitted from these Listings.

Topological modes

$\Gamma(0\text{-prongs})/\Gamma_{total}$ — **Γ_1/Γ**

This value is obtained by subtracting the branching fractions for 2-, 4-, and 6-prongs from unity.

VALUE	DOCUMENT ID
0.15±0.06 OUR FIT	

$\Gamma(4\text{-prongs})/\Gamma(2\text{-prongs})$ — **Γ_3/Γ_2**

VALUE	EVTS	DOCUMENT ID		TECN	COMMENT
0.207±0.016 OUR FIT					
0.207±0.016±0.004	226	ONENGUT	05	CHRS	ν_μ emulsion, $\overline{E}_\nu \approx 27$ GeV

$\Gamma(4\text{-prongs})/\Gamma_{total}$ — **Γ_3/Γ**

This is the sum of our $K^- 2\pi^+ \pi^-$, $K^- 2\pi^+ \pi^- \pi^0$, $\overline{K}^0 2\pi^+ 2\pi^-$, $K^+ 2K^- \pi^+$, $2\pi^+ 2\pi^-$, $2\pi^+ 2\pi^- \pi^0$, $K^+ K^- \pi^+ \pi^-$, and $K^+ K^- \pi^+ \pi^- \pi^0$ branching fractions.

VALUE	DOCUMENT ID	
0.146±0.005 OUR FIT		
0.146±0.005	PDG	19

$\Gamma(6\text{-prongs})/\Gamma_{total}$ — **Γ_4/Γ**

This is the sum of our $K^- 3\pi^+ 2\pi^-$ and $3\pi^+ 3\pi^-$ branching fractions.

VALUE (units 10^{-4})	DOCUMENT ID	
6.5±1.3 OUR FIT		
6.5±1.3	PDG	19

Inclusive modes

$\Gamma(e^+ \text{anything})/\Gamma_{total}$ — **Γ_5/Γ**

The branching fractions for the $K^- e^+ \nu_e$, $K^*(892)^- e^+ \nu_e$, $\pi^- e^+ \nu_e$, and $\rho^- e^+ \nu_e$ modes add up to 6.17 ± 0.17 %.

VALUE (%)	EVTS	DOCUMENT ID		TECN	COMMENT
6.49±0.11 OUR AVERAGE					
6.46±0.09±0.11	6584 ± 96	[1] ASNER	10	CLEO	$e^+ e^-$ at 3774 MeV
6.3 ±0.7 ±0.4	290 ± 32	ABLIKIM	07G	BES2	$e^+ e^- \approx \psi(3770)$
6.46±0.17±0.13	2246 ± 57	ADAM	06A	CLEO	See ASNER 10
6.9 ±0.3 ±0.5	1670	ALBRECHT	96C	ARG	$e^+ e^- \approx$ 10 GeV
6.64±0.18±0.29	4609	KUBOTA	96B	CLE2	$e^+ e^- \approx \Upsilon(4S)$

[1] Using the D^+ and D^0 lifetimes, ASNER 10 finds that the ratio of the D^+ and D^0 semileptonic widths is 0.985 ± 0.015 ± 0.024.

Downloaded from https://academic.oup.com/ptep/article/2022/8/083C01/6651666 by KIT Library user on 27 September 2022

$\Gamma(\mu^+ \text{anything})/\Gamma_{\text{total}}$ — Γ_6/Γ

VALUE (%)	EVTS	DOCUMENT ID		TECN	COMMENT
6.8±0.6 OUR FIT					
6.4±0.8 OUR AVERAGE					
6.8±1.5±0.8	79 ± 10	[1] ABLIKIM	08L	BES2	$e^+e^- \approx \psi(3772)$
6.5±1.2±0.3	36	KAYIS-TOPAK.	05	CHRS	ν_μ emulsion
6.0±0.7±1.2	310	ALBRECHT	96C	ARG	$e^+e^- \approx$ 10 GeV

[1] ABLIKIM 08L finds the ratio of $D^+ \to \mu^+ X$ and $D^0 \to \mu^+ X$ branching fractions to be 2.59 ± 0.70 ± 0.25, in accord with the ratio of D^+ and D^0 lifetimes, 2.54 ± 0.02.

$\Gamma(K^- \text{anything})/\Gamma_{\text{total}}$ — Γ_7/Γ

VALUE	EVTS	DOCUMENT ID		TECN	COMMENT
0.547±0.028 OUR AVERAGE	Error includes scale factor of 1.3. See the ideogram below.				
0.578±0.016±0.032	2098 ± 59	ABLIKIM	07G	BES2	$e^+e^- \approx \psi(3770)$
$0.546^{+0.039}_{-0.038}$		[1] BARLAG	92C	ACCM	π^- Cu 230 GeV
0.609±0.032±0.052		COFFMAN	91	MRK3	e^+e^- 3.77 GeV
0.42 ±0.08		AGUILAR-...	87E	HYBR	πp, pp 360, 400 GeV
0.55 ±0.11	121	SCHINDLER	81	MRK2	e^+e^- 3.771 GeV
0.35 ±0.10	19	VUILLEMIN	78	LGW	e^+e^- 3.772 GeV

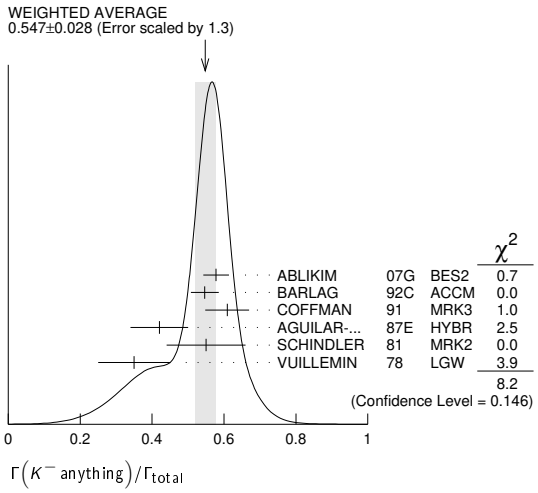

[1] BARLAG 92C computes the branching fraction using topological normalization.

$[\Gamma(\overline{K}^0 \text{anything}) + \Gamma(K^0 \text{anything})]/\Gamma_{\text{total}}$ — Γ_8/Γ

VALUE	EVTS	DOCUMENT ID		TECN	COMMENT
0.47 ±0.04 OUR AVERAGE					
0.476±0.048±0.030	250 ± 25	ABLIKIM	06U	BES2	e^+e^- at 3773 MeV
0.455±0.050±0.032		COFFMAN	91	MRK3	e^+e^- 3.77 GeV

$\Gamma(K^+ \text{anything})/\Gamma_{\text{total}}$ — Γ_9/Γ

VALUE	EVTS	DOCUMENT ID		TECN	COMMENT
0.034±0.004 OUR AVERAGE					
0.035±0.007±0.003	119 ± 23	ABLIKIM	07G	BES2	$e^+e^- \approx \psi(3770)$
$0.034^{+0.007}_{-0.005}$		[1] BARLAG	92C	ACCM	π^- Cu 230 GeV
0.028±0.009±0.004		COFFMAN	91	MRK3	e^+e^- 3.77 GeV
$0.03^{+0.05}_{-0.02}$		AGUILAR-...	87E	HYBR	πp, pp 360, 400 GeV
0.08 ±0.03	25	SCHINDLER	81	MRK2	e^+e^- 3.771 GeV

[1] BARLAG 92C computes the branching fraction using topological normalization.

$\Gamma(K^*(892)^- \text{anything})/\Gamma_{\text{total}}$ — Γ_{10}/Γ

VALUE	EVTS	DOCUMENT ID		TECN	COMMENT
0.153±0.083±0.019	28 ± 15	ABLIKIM	06U	BES2	e^+e^- at 3773 MeV

$\Gamma(\overline{K}^*(892)^0 \text{anything})/\Gamma_{\text{total}}$ — Γ_{11}/Γ

VALUE	EVTS	DOCUMENT ID		TECN	COMMENT
0.087±0.040±0.012	96 ± 44	ABLIKIM	05P	BES	$e^+e^- \approx$ 3773 MeV

$\Gamma(K^*(892)^+ \text{anything})/\Gamma_{\text{total}}$ — Γ_{12}/Γ

VALUE	CL%	DOCUMENT ID		TECN	COMMENT
<0.036	90	ABLIKIM	06U	BES2	e^+e^- at 3773 MeV

$\Gamma(K^*(892)^0 \text{anything})/\Gamma_{\text{total}}$ — Γ_{13}/Γ

VALUE	EVTS	DOCUMENT ID		TECN	COMMENT
0.028±0.012±0.004	31 ± 12	ABLIKIM	05P	BES	$e^+e^- \approx$ 3773 MeV

$\Gamma(\eta \text{ anything})/\Gamma_{\text{total}}$ — Γ_{14}/Γ

This ratio includes η particles from η' decays.

VALUE (%)	EVTS	DOCUMENT ID		TECN	COMMENT
9.5±0.4±0.8	4463±197	HUANG	06B	CLEO	e^+e^- at $\psi(3770)$

$\Gamma(\eta' \text{ anything})/\Gamma_{\text{total}}$ — Γ_{15}/Γ

VALUE (%)	EVTS	DOCUMENT ID		TECN	COMMENT
2.48±0.17±0.21	299 ± 21	HUANG	06B	CLEO	e^+e^- at $\psi(3770)$

$\Gamma(\phi \text{ anything})/\Gamma_{\text{total}}$ — Γ_{16}/Γ

VALUE (%)	EVTS	DOCUMENT ID		TECN	COMMENT
1.08 ±0.04 OUR AVERAGE					
1.091±0.027±0.035	4.1k	ABLIKIM	19AY	BES3	e^+e^- at 3773 MeV
1.05 ±0.08 ±0.07	368 ± 24	HUANG	06B	CLEO	e^+e^- at $\psi(3770)$
• • • We do not use the following data for averages, fits, limits, etc. • • •					
$1.71\ ^{+0.76}_{-0.71}$ ±0.17	9	BAI	00C	BES	$e^+e^- \to D\overline{D}^*, D^*\overline{D}^*$

$\Gamma(\text{invisibles})/\Gamma_{\text{total}}$ — Γ_{17}/Γ

VALUE	CL%	DOCUMENT ID		TECN	COMMENT
$<9.4 \times 10^{-5}$	90	LAI	17	BELL	e^+e^- at $\Upsilon(nS)$, n=4,5

Semileptonic modes

$\Gamma(K^- e^+ \nu_e)/\Gamma_{\text{total}}$ — Γ_{19}/Γ

VALUE (%)	EVTS	DOCUMENT ID		TECN	COMMENT
3.549±0.026 OUR FIT	Error includes scale factor of 1.2.				
3.525±0.023 OUR AVERAGE					
3.567±0.031±0.025	4040	ABLIKIM	21BA	BES3	e^+e^- at 3.773 GeV
3.505±0.014±0.033	71k	[1] ABLIKIM	15X	BES3	2.92 fb^{-1}, 3.773 GeV
3.50 ±0.03 ±0.04	14.1k	[1] BESSON	09	CLEO	e^+e^- at $\psi(3770)$
3.45 ±0.10 ±0.19	1.3k	[2] WIDHALM	06	BELL	$e^+e^- \approx \Upsilon(4S)$
3.82 ±0.40 ±0.27	104	ABLIKIM	04C	BES	e^+e^-, 3.773 GeV
3.4 ±0.5 ±0.4	55	ADLER	89	MRK3	e^+e^- 3.77 GeV
• • • We do not use the following data for averages, fits, limits, etc. • • •					
3.56 ±0.03 ±0.09		[3] DOBBS	08	CLEO	See BESSON 09
3.44 ±0.10 ±0.10	1.3k	COAN	05	CLEO	See DOBBS 08

[1] See the form-factor parameters near the end of this D^0 Listing.

[2] The $\pi^- e^+ \nu_e$ and $K^- e^+ \nu_e$ results of WIDHALM 06 give $|\frac{V_{cd}}{V_{cs}} \cdot \frac{f_+^\pi(0)}{f_+^K(0)}|^2 = 0.042 \pm 0.003 \pm 0.003$.

[3] DOBBS 08 establishes $|\frac{V_{cd}}{V_{cs}} \cdot \frac{f_+^\pi(0)}{f_+^K(0)}| = 0.188 \pm 0.008 \pm 0.002$ from the D^+ and D^0 decays to $\overline{K} e^+ \nu_e$ and $\pi e^+ \nu_e$.

$\Gamma(K^- e^+ \nu_e)/\Gamma(K^- \pi^+)$ — Γ_{19}/Γ_{37}

VALUE	EVTS	DOCUMENT ID		TECN	COMMENT
0.899±0.009 OUR FIT	Error includes scale factor of 1.3.				
0.930±0.013 OUR AVERAGE					
0.927±0.007±0.012	76k±323	[1] AUBERT	07BG	BABR	$e^+e^- \approx \Upsilon(4S)$
0.978±0.027±0.044	2510	[2] BEAN	93C	CLE2	$e^+e^- \approx \Upsilon(4S)$
0.90 ±0.06 ±0.06	584	[3] CRAWFORD	91B	CLEO	$e^+e^- \approx$ 10.5 GeV
0.91 ±0.07 ±0.11	250	[4] ANJOS	89F	E691	Photoproduction

[1] The event samples in this AUBERT 07BG result include radiative photons. The $D^0 \to K^- e^+ \nu_e$ form factor at $q^2 = 0$ is $f_+(0) = 0.727 \pm 0.007 \pm 0.005 \pm 0.007$.

[2] BEAN 93C uses $K^- \mu^+ \nu_\mu$ as well as $K^- e^+ \nu_e$ events and makes a small phase-space adjustment to the number of the μ^+ events to use them as e^+ events. A pole mass of 2.00 ± 0.12 ± 0.18 GeV/c^2 is obtained from the q^2 dependence of the decay rate.

[3] CRAWFORD 91B uses $K^- e^+ \nu_e$ and $K^- \mu^+ \nu_\mu$ candidates to measure a pole mass of $2.1\ ^{+0.4}_{-0.2}\ ^{+0.3}_{-0.2}$ GeV/c^2 from the q^2 dependence of the decay rate.

[4] ANJOS 89F measures a pole mass of $2.1\ ^{+0.4}_{-0.2}$ ± 0.2 GeV/c^2 from the q^2 dependence of the decay rate.

$\Gamma(K^- \mu^+ \nu_\mu)/\Gamma_{\text{total}}$ — Γ_{20}/Γ

VALUE (%)	EVTS	DOCUMENT ID		TECN	COMMENT
3.41 ±0.04 OUR FIT					
3.41 ±0.04 OUR AVERAGE					
3.413±0.019±0.035	47k	ABLIKIM	19B	BES3	e^+e^-, 3773 MeV
3.45 ±0.10 ±0.21	1249 ± 43	WIDHALM	06	BELL	$e^+e^- \approx \Upsilon(4S)$

$\Gamma(K^- \mu^+ \nu_\mu)/\Gamma(\mu^+ \text{anything})$ — Γ_{20}/Γ_6

VALUE	EVTS	DOCUMENT ID		TECN	COMMENT
0.50 ±0.04 OUR FIT					
0.472±0.051±0.040	232	KODAMA	94	E653	π^- emulsion 600 GeV
• • • We do not use the following data for averages, fits, limits, etc. • • •					
0.32 ±0.05 ±0.05	124	KODAMA	91	EMUL	pA 800 GeV

$\Gamma(K^- \mu^+ \nu_\mu)/\Gamma(K^- \pi^+)$ — Γ_{20}/Γ_{37}

VALUE	EVTS	DOCUMENT ID		TECN	COMMENT
0.864±0.012 OUR FIT	Error includes scale factor of 1.1.				
0.84 ±0.04 OUR AVERAGE					
0.852±0.034±0.028	1897	[1] FRABETTI	95G	E687	γBe $\overline{E}_\gamma$= 220 GeV
0.82 ±0.13 ±0.13	338	[2] FRABETTI	93I	E687	γBe $\overline{E}_\gamma$= 221 GeV
0.79 ±0.08 ±0.09	231	[3] CRAWFORD	91B	CLEO	$e^+e^- \approx$ 10.5 GeV

[1] FRABETTI 95G extracts the ratio of form factors $f_-(0)/f_+(0) = -1.3\ ^{+3.6}_{-3.4}$ ± 0.6, and measures a pole mass of $1.87\ ^{+0.11}_{-0.08}\ ^{+0.07}_{-0.06}$ GeV/c^2 from the q^2 dependence of the decay rate.

[2] FRABETTI 93I measures a pole mass of $2.1\ ^{+0.7}_{-0.3}\ ^{+0.7}_{-0.3}$ GeV/c^2 from the q^2 dependence of the decay rate.

[3] CRAWFORD 91B measures a pole mass of 2.00 ± 0.12 ± 0.18 GeV/c^2 from the q^2 dependence of the decay rate.

Downloaded from https://academic.oup.com/ptep/article/2022/8/083C01/6651666 by KIT Library user on 27 September 2022

$\Gamma(K^*(892)^- e^+ \nu_e)/\Gamma_{total}$ — Γ_{21}/Γ

Both decay modes of the $K^*(892)^-$ are included.

VALUE (%)	EVTS	DOCUMENT ID		TECN	COMMENT
2.15±0.16 OUR FIT					
2.16±0.15±0.08	219 ± 16	[1] COAN	05	CLEO	e^+e^- at $\psi(3770)$

[1] COAN 05 uses both $K^-\pi^0$ and $K^0_S\pi^-$ events.

$\Gamma(K^*(892)^- e^+ \nu_e)/\Gamma(\overline{K}^0\pi^- e^+ \nu_e)$ — Γ_{21}/Γ_{24}

VALUE (units 10^{-2})	EVTS	DOCUMENT ID		TECN	COMMENT
94.52±0.97±0.62	3.1k	ABLIKIM	19G	BES3	$K^0_S\pi^- e^+\nu_e$ events

$\Gamma(K^*(892)^- e^+ \nu_e)/\Gamma(K^0_S\pi^+\pi^-)$ — Γ_{21}/Γ_{40}

Unseen decay modes of the $K^*(892)^-$ are included.

VALUE	EVTS	DOCUMENT ID		TECN	COMMENT
0.77±0.07 OUR FIT					
0.76±0.12±0.06	152	[1] BEAN	93C	CLE2	$e^+e^- \approx \Upsilon(4S)$

[1] BEAN 93C uses $K^{*-}\mu^+\nu_\mu$ as well as $K^{*-}e^+\nu_e$ events and makes a small phase-space adjustment to the number of the μ^+ events to use them as e^+ events.

$\Gamma(K^*(892)^- \mu^+ \nu_\mu)/\Gamma(K^0_S\pi^+\pi^-)$ — Γ_{22}/Γ_{40}

Unseen decay modes of the $K^*(892)^-$ are included.

VALUE	EVTS	DOCUMENT ID		TECN	COMMENT
0.674±0.068±0.026	175 ± 17	[1] LINK	05B	FOCS	γ A, $\overline{E}_\gamma \approx$ 180 GeV

[1] LINK 05B finds that in $D^0 \to \overline{K}^0\pi^-\mu^+\nu_\mu$ the $\overline{K}^0\pi^-$ system is 6% in S-wave.

$\Gamma(K^-\pi^0 e^+ \nu_e)/\Gamma_{total}$ — Γ_{23}/Γ

VALUE	EVTS	DOCUMENT ID		TECN	COMMENT
$\mathbf{0.016^{+0.013}_{-0.005}\pm0.002}$	4	[1] BAI	91	MRK3	$e^+e^- \approx$ 3.77 GeV

[1] BAI 91 finds that a fraction $0.79^{+0.15+0.09}_{-0.17-0.03}$ of combined D^+ and D^0 decays to $\overline{K}\pi e^+\nu_e$ (24 events) are $\overline{K}^*(892)e^+\nu_e$. BAI 91 uses 56 $K^-e^+\nu_e$ events to measure a pole mass of 1.8 ± 0.3 ± 0.2 GeV/c^2 from the q^2 dependence of the decay rate.

$\Gamma(\overline{K}^0\pi^- e^+ \nu_e)/\Gamma_{total}$ — Γ_{24}/Γ

VALUE (%)	EVTS	DOCUMENT ID		TECN	COMMENT
1.44 ±0.04 OUR AVERAGE					
1.434±0.029±0.032	3.1k	ABLIKIM	19G	BES3	e^+e^- at 3773 MeV
2.61 ±1.04 ±0.28	9 ± 3	ABLIKIM	06O	BES2	e^+e^- at 3773 MeV
$2.8\ ^{+1.7}_{-0.8}\pm0.3$	6	[1] BAI	91	MRK3	$e^+e^- \approx$ 3.77 GeV

[1] BAI 91 finds that a fraction $0.79^{+0.15+0.09}_{-0.17-0.03}$ of combined D^+ and D^0 decays to $\overline{K}\pi e^+\nu_e$ (24 events) are $\overline{K}^*(892)e^+\nu_e$.

$\Gamma((\overline{K}^0\pi^-)_{S-wave} e^+ \nu_e)/\Gamma(\overline{K}^0\pi^- e^+ \nu_e)$ — Γ_{25}/Γ_{24}

VALUE (units 10^{-2})	EVTS	DOCUMENT ID		TECN	COMMENT
5.51±0.97±0.62	3.1k	ABLIKIM	19G	BES3	$K^0_S\pi^- e^+\nu_e$ events

$\Gamma(K^-\pi^+\pi^- e^+ \nu_e)/\Gamma_{total}$ — Γ_{26}/Γ

VALUE (units 10^{-4})	EVTS	DOCUMENT ID		TECN	COMMENT
$\mathbf{2.8^{+1.4}_{-1.1}\pm0.3}$	8	ARTUSO	07A	CLEO	e^+e^- at $\Upsilon(3770)$

$\Gamma(K_1(1270)^- e^+ \nu_e)/\Gamma_{total}$ — Γ_{27}/Γ

VALUE (units 10^{-4})	EVTS	DOCUMENT ID		TECN	COMMENT
10.1±1.8 OUR AVERAGE					
$10.9\pm1.3^{+0.9}_{-1.6}\pm1.2$	109	[1] ABLIKIM	21AY	BES3	e^+e^- at 3.773 GeV
$7.6^{+4.1}_{-3.0}\pm0.9$	8	[2] ARTUSO	07A	CLEO	e^+e^- at $\Upsilon(3770)$

[1] Uses $B(K_1(1270)^- \to K^-\pi^+\pi^-)$ = (32.9 ± 3.6)%, which is the source of the third uncertainty.

[2] This ARTUSO 07A result is corrected for all decay modes of the $K_1(1270)^-$.

$\Gamma(K^-\pi^+\pi^-\mu^+\nu_\mu)/\Gamma(K^-\mu^+\nu_\mu)$ — Γ_{28}/Γ_{20}

VALUE	CL%	DOCUMENT ID		TECN	COMMENT
<0.037	90	KODAMA	93B	E653	π^- emulsion 600 GeV

$\Gamma((\overline{K}^*(892)\pi)^-\mu^+\nu_\mu)/\Gamma(K^-\mu^+\nu_\mu)$ — Γ_{29}/Γ_{20}

VALUE	CL%	DOCUMENT ID		TECN	COMMENT
<0.043	90	[1] KODAMA	93B	E653	π^- emulsion 600 GeV

[1] KODAMA 93B searched in $K^-\pi^+\pi^-\mu^+\nu_\mu$, but the limit includes other $(\overline{K}^*(892)\pi)^-$ charge states.

$\Gamma(\pi^- e^+ \nu_e)/\Gamma_{total}$ — Γ_{30}/Γ

VALUE (%)	EVTS	DOCUMENT ID		TECN	COMMENT
0.291±0.004 OUR FIT					
0.293±0.004 OUR AVERAGE					
0.295±0.004±0.003	6.3k	[1] ABLIKIM	15X	BES3	2.92 fb^{-1}, 3.773 GeV
0.288±0.008±0.003	1.3k	[1] BESSON	09	CLEO	e^+e^- at $\psi(3770)$
0.279±0.027±0.016	126	[2] WIDHALM	06	BELL	$e^+e^- \approx \Upsilon(4S)$
• • • We do not use the following data for averages, fits, limits, etc. • • •					
0.299±0.011±0.009		[3] DOBBS	08	CLEO	See BESSON 09
0.262±0.025±0.008	117	COAN	05	CLEO	See DOBBS 08

[1] See the form-factor parameters near the end of this D^0 Listing.

[2] The $\pi^-e^+\nu_e$ and $K^-e^+\nu_e$ results of WIDHALM 06 give $|\frac{V_{cd}}{V_{cs}}\cdot\frac{f_+^\pi(0)}{f_+^K(0)}|^2 = 0.042 \pm 0.003 \pm 0.003$.

[3] DOBBS 08 establishes $|\frac{V_{cd}}{V_{cs}}\cdot\frac{f_+^\pi(0)}{f_+^K(0)}| = 0.188 \pm 0.008 \pm 0.002$ from the D^+ and D^0 decays to $\overline{K}e^+\nu_e$ and $\pi e^+\nu_e$.

$\Gamma(\pi^- e^+ \nu_e)/\Gamma(K^- e^+ \nu_e)$ — Γ_{30}/Γ_{19}

VALUE	EVTS	DOCUMENT ID		TECN	COMMENT
0.0821±0.0013 OUR FIT Error includes scale factor of 1.1.					
0.085 ±0.007 OUR AVERAGE					
0.082 ±0.006 ±0.005		[1] HUANG	05	CLEO	$e^+e^- \approx \Upsilon(4S)$
0.101 ±0.020 ±0.003	91	[2] FRABETTI	96B	E687	γ Be, $\overline{E}_\gamma \approx$ 200 GeV
0.103 ±0.039 ±0.013	87	[3] BUTLER	95	CLE2	< 0.156 (90% CL)

[1] HUANG 05 uses both e and μ events, and makes a small correction to the μ events to make them effectively e events. This result gives $|\frac{V_{cd}}{V_{cs}}\cdot\frac{f_+^\pi(0)}{f_+^K(0)}|^2 = 0.038^{+0.006+0.005}_{-0.007-0.003}$.

[2] FRABETTI 96B uses both e and μ events, and makes a small correction to the μ events to make them effectively e events. This result gives $|\frac{V_{cd}}{V_{cs}}\cdot\frac{f_+^\pi(0)}{f_+^K(0)}|^2 = 0.050\pm0.011\pm0.002$.

[3] BUTLER 95 has 87 ± 33 $\pi^-e^+\nu_e$ events. The result gives $|\frac{V_{cd}}{V_{cs}}\cdot\frac{f_+^\pi(0)}{f_+^K(0)}|^2 = 0.052 \pm 0.020 \pm 0.007$.

$\Gamma(\pi^- e^+ \nu_e)/\Gamma(K^-\pi^+)$ — Γ_{30}/Γ_{37}

VALUE (units 10^{-2})	EVTS	DOCUMENT ID		TECN	COMMENT
7.38±0.12 OUR FIT Error includes scale factor of 1.1.					
7.02±0.17±0.23	375k	[1] LEES	15F	BABR	347 fb^{-1}, 10.58 GeV

[1] See the form-factor parameters near the end of the D^0 Listing.

$\Gamma(\pi^-\mu^+\nu_\mu)/\Gamma_{total}$ — Γ_{31}/Γ

VALUE (%)	EVTS	DOCUMENT ID		TECN	COMMENT
0.267±0.012 OUR FIT Error includes scale factor of 1.3.					
0.268±0.012 OUR AVERAGE Error includes scale factor of 1.2.					
0.272±0.008±0.006	2.3k	ABLIKIM	18AE	BES3	e^+e^-, 3773 MeV
0.231±0.026±0.019	106 ± 13	WIDHALM	06	BELL	$e^+e^- \approx \Upsilon(4S)$

$\Gamma(\pi^-\mu^+\nu_\mu)/\Gamma(K^-\mu^+\nu_\mu)$ — Γ_{31}/Γ_{20}

VALUE	EVTS	DOCUMENT ID		TECN	COMMENT
0.0784±0.0035 OUR FIT Error includes scale factor of 1.2.					
0.074 ±0.008 ±0.007	288 ± 29	[1] LINK	05	FOCS	γ A, $\overline{E}_\gamma \approx$ 180 GeV

[1] LINK 05 finds the form-factor ratio $|f_0^\pi(0)/f_0^K(0)|$ to be 0.85 ± 0.04 ± 0.04 ± 0.01.

$\Gamma(\pi^-\pi^0 e^+ \nu_e)/\Gamma_{total}$ — Γ_{32}/Γ

VALUE (units 10^{-3})	EVTS	DOCUMENT ID		TECN	COMMENT
1.445±0.058±0.039	1.1k	[1] ABLIKIM	19C	BES3	e^+e^- at 3773 MeV

[1] Seen 100% via $D^0 \to \rho(770)^-e^+\nu_e$, and also reported as the branching fraction for $D^0 \to \rho(770)^-e^+\nu_e$.

$\Gamma(\rho^- e^+ \nu_e)/\Gamma_{total}$ — Γ_{33}/Γ

VALUE (units 10^{-3})	EVTS	DOCUMENT ID		TECN	COMMENT
1.50 ±0.12 OUR AVERAGE Error includes scale factor of 1.9.					
1.445±0.058±0.039	1.1k	[1] ABLIKIM	19C	BES3	e^+e^- at 3773 MeV
1.77 ±0.12 ±0.10	305 ± 21	[2,3] DOBBS	13	CLEO	e^+e^- at $\psi(3770)$
• • • We do not use the following data for averages, fits, limits, etc. • • •					
1.94 ±0.39 ±0.13	31 ± 6	COAN	05	CLEO	See DOBBS 13

[1] This result is the same as the one reported for $D^0 \to \pi^-\pi^0e^+\nu_e$ which ABLIKIM 19C found to proceed 100% via $D^0 \to \rho(770)^-e^+\nu_e$.

[2] DOBBS 13 finds $\Gamma(D^0 \to \rho^-e^+\nu_e)$ / 2 $\Gamma(D^+ \to \rho^0e^+\nu_e) = 1.03 \pm 0.09^{+0.08}_{-0.02}$; isospin invariance predicts the ratio is 1.0.

[3] See the D^+ Listings for $D \to \rho e^+\nu_e$ form factors.

$\Gamma(\rho^-\mu^+\nu_\mu)/\Gamma_{total}$ — Γ_{34}/Γ

VALUE (units 10^{-3})	EVTS	DOCUMENT ID		TECN	COMMENT
1.35±0.09±0.09	570	ABLIKIM	21BC	BES3	e^+e^- at 3.773 GeV

$\Gamma(a(980)^- e^+ \nu_e,\ a^- \to \eta\pi^-)/\Gamma_{total}$ — Γ_{35}/Γ

VALUE (units 10^{-4})	EVTS	DOCUMENT ID		TECN	COMMENT
$\mathbf{1.33^{+0.33}_{-0.29}\pm0.09}$	26	[1] ABLIKIM	18F	BES3	e^+e^- at 3773 MeV

[1] Signal observed at 6.4 σ C.L.

$\Gamma(b_1(1235)^- e^+ \nu_e,\ b_1^- \to \omega\pi^-)/\Gamma_{total}$ — Γ_{36}/Γ

VALUE	CL%	DOCUMENT ID		TECN	COMMENT
<1.12 × 10^{-4}	90	ABLIKIM	20AF	BES3	e^+e^-, 3773 MeV

Downloaded from https://academic.oup.com/ptep/article/2022/8/083C01/6651666 by KIT Library user on 27 September 2022

Hadronic modes with a single $\overline{K}$

$\Gamma(K^-\pi^+)/\Gamma_{total}$ — Γ_{37}/Γ

VALUE (%)	EVTS	DOCUMENT ID		TECN	COMMENT
3.947±0.030 OUR FIT		Error includes scale factor of 1.2.			
3.909±0.034 OUR AVERAGE					
3.883±0.006±0.051	0.5 M	[1] ABLIKIM	18W	BES3	e^+e^-, 3773 MeV
3.934±0.021±0.061		BONVICINI	14	CLEO	All CLEO-c runs
4.007±0.037±0.072	33.8k	AUBERT	08L	BABR	e^+e^- at $\Upsilon(4S)$
3.82 ±0.07 ±0.12		[2] ARTUSO	98	CLE2	CLEO average
3.90 ±0.09 ±0.12	5.4k	[3] BARATE	97C	ALEP	From Z decays
3.41 ±0.12 ±0.28	1.2k	[3] ALBRECHT	94F	ARG	$e^+e^- \approx \Upsilon(4S)$
3.62 ±0.34 ±0.44		[3] DECAMP	91J	ALEP	From Z decays
• • • We do not use the following data for averages, fits, limits, etc. • • •					
3.891±0.035±0.069		[4] DOBBS	07	CLEO	See BONVICINI 14
3.91 ±0.08 ±0.09	10.3k	[4] HE	05	CLEO	See DOBBS 07
3.81 ±0.15 ±0.16	1.2k	[5] ARTUSO	98	CLE2	e^+e^- at $\Upsilon(4S)$
3.69 ±0.11 ±0.16		[6] COAN	98	CLE2	See ARTUSO 98
4.5 ±0.6 ±0.4		[7] ALBRECHT	94	ARG	$e^+e^- \approx \Upsilon(4S)$
3.95 ±0.08 ±0.17	4.2k	[3,8] AKERIB	93	CLE2	See ARTUSO 98
4.5 ±0.8 ±0.5	56	[3] ABACHI	88	HRS	e^+e^- 29 GeV
4.2 ±0.4 ±0.4	0.9k	ADLER	88C	MRK3	e^+e^- 3.77 GeV
4.1 ±0.6	0.3k	[9] SCHINDLER	81	MRK2	e^+e^- 3.771 GeV
4.3 ±1.0	130	[10] PERUZZI	77	LGW	e^+e^- 3.77 GeV

[1] ABLIKIM 18W measured the combined $K^{\mp}\pi^{\pm}$ branching fraction to be 3.898%. We have subtracted off the doubly Cabibbo-suppressed branching fraction $B(D^0 \to K^+\pi^-) = (1.50 \pm 0.07) \times 10^{-4}$, even though it is less than one-third of the uncertainty of the combined measurement, in order to treat this as a measurement of $B(D^0 \to K^-\pi^+)$.

[2] This combines the CLEO results of ARTUSO 98, COAN 98, and AKERIB 93.

[3] ABACHI 88, DECAMP 91J, AKERIB 93, ALBRECHT 94F, and BARATE 97C use $D^*(2010)^+ \to D^0\pi^+$ decays. The π^+ is both slow and of low p_T with respect to the event thrust axis or nearest jet ($\approx D^{*+}$ direction). The excess number of such π^+'s over background gives the number of $D^*(2010)^+ \to D^0\pi^+$ events, and the fraction with $D^0 \to K^-\pi^+$ gives the $D^0 \to K^-\pi^+$ branching fraction.

[4] DOBBS 07 and HE 05 use single- and double-tagged events in an overall fit. DOBBS 07 supersedes HE 05.

[5] ARTUSO 98, following ALBRECHT 94, uses D^0 mesons from $\overline{B}^0 \to D^*(2010)^+ X \ell^- \overline{\nu}_\ell$ decays. Our average uses the CLEO average of this value with the values of COAN 98 and AKERIB 93.

[6] COAN 98 assumes that $\Gamma(B \to \overline{D} X \ell^+\nu)/\Gamma(B \to X\ell^+\nu) = 1.0 - 3|V_{ub}/V_{cb}|^2 - 0.010 \pm 0.005$, the last term accounting for $\overline{B} \to D_s^+ K X \ell^- \overline{\nu}$. COAN 98 is included in the CLEO average in ARTUSO 98.

[7] ALBRECHT 94 uses D^0 mesons from $\overline{B}^0 \to D^{*+}\ell^-\overline{\nu}_\ell$ decays. This is a different set of events than used by ALBRECHT 94F.

[8] This AKERIB 93 value includes radiative corrections; without them, the value is 0.0391 ± 0.0008 ± 0.0017. AKERIB 93 is included in the CLEO average in ARTUSO 98.

[9] SCHINDLER 81 (MARK-2) measures $\sigma(e^+e^- \to \psi(3770)) \times$ branching fraction to be 0.24 ± 0.02 nb. We use the MARK-3 (ADLER 88C) value of $\sigma = 5.8 \pm 0.5 \pm 0.6$ nb.

[10] PERUZZI 77 (MARK-1) measures $\sigma(e^+e^- \to \psi(3770)) \times$ branching fraction to be 0.25 ± 0.05 nb. We use the MARK-3 (ADLER 88C) value of $\sigma = 5.8 \pm 0.5 \pm 0.6$ nb.

$\Gamma(K^0_S\pi^0)/\Gamma_{total}$ — Γ_{38}/Γ

VALUE (%)	EVTS	DOCUMENT ID		TECN	COMMENT
1.240±0.022 OUR FIT					
1.239±0.006±0.027	67k	ABLIKIM	18W	BES3	e^+e^-, 3773 MeV
• • • We do not use the following data for averages, fits, limits, etc. • • •					
1.240±0.017±0.056	614	HE	08	CLEO	See MENDEZ 10

$\Gamma(K^0_S\pi^0)/[\Gamma(K^-\pi^+)+\Gamma(K^+\pi^-)]$ — $\Gamma_{38}/(\Gamma_{37}+\Gamma_{274})$

VALUE (units 10^{-2})	EVTS	DOCUMENT ID		TECN	COMMENT
31.3±0.6 OUR FIT					
30.4±0.3±0.9	20k	MENDEZ	10	CLEO	e^+e^- at 3774 MeV

$\Gamma(K^0_S\pi^0)/\Gamma(K^0_S\pi^+\pi^-)$ — Γ_{38}/Γ_{40}

VALUE	EVTS	DOCUMENT ID		TECN	COMMENT
0.443±0.028 OUR FIT					
0.44 ±0.02 ±0.05	1942 ± 64	PROCARIO	93B	CLE2	e^+e^- 10.36–10.7 GeV
• • • We do not use the following data for averages, fits, limits, etc. • • •					
0.34 ±0.04 ±0.02	92	[1] ALBRECHT	92P	ARG	$e^+e^- \approx$ 10 GeV
0.36 ±0.04 ±0.08	104	KINOSHITA	91	CLEO	$e^+e^- \sim$ 10.7 GeV

[1] This value is calculated from numbers in Table 1 of ALBRECHT 92P.

$\Gamma(K^0_L\pi^0)/\Gamma_{total}$ — Γ_{39}/Γ

VALUE (%)	EVTS	DOCUMENT ID		TECN	COMMENT
0.998±0.049±0.048	1116	[1] HE	08	CLEO	e^+e^- at $\psi(3770)$

[1] The difference of HE 08 $D^0 \to K^0_S\pi^0$ and $K^0_L\pi^0$ branching fractions over the sum is 0.108 ± 0.025 ± 0.024. This is consistent with U-spin symmetry and the Cabibbo angle.

$\Gamma(K^0_S\pi^+\pi^-)/\Gamma_{total}$ — Γ_{40}/Γ

VALUE (%)	EVTS	DOCUMENT ID		TECN	COMMENT
• • • We do not use the following data for averages, fits, limits, etc. • • •					
2.52±0.20±0.25	284 ± 22	[1] ALBRECHT	94F	ARG	$e^+e^- \approx \Upsilon(4S)$
3.2 ±0.3 ±0.5		ADLER	87	MRK3	e^+e^- 3.77 GeV
2.6 ±0.8	32 ± 8	[2] SCHINDLER	81	MRK2	e^+e^- 3.771 GeV
4.0 ±1.2	28	[3] PERUZZI	77	LGW	e^+e^- 3.77 GeV

[1] See the footnote on the ALBRECHT 94F measurement of $\Gamma(K^-\pi^+)/\Gamma_{total}$ for the method used.

[2] SCHINDLER 81 (MARK-2) measures $\sigma(e^+e^- \to \psi(3770)) \times$ branching fraction to be 0.30 ± 0.08 nb. We use the MARK-3 (ADLER 88C) value of $\sigma = 5.8 \pm 0.5 \pm 0.6$ nb.

[3] PERUZZI 77 (MARK-1) measures $\sigma(e^+e^- \to \psi(3770)) \times$ branching fraction to be 0.46 ± 0.12 nb. We use the MARK-3 (ADLER 88C) value of $\sigma = 5.8 \pm 0.5 \pm 0.6$ nb.

$\Gamma(K^0_S\pi^+\pi^-)/\Gamma(K^-\pi^+)$ — Γ_{40}/Γ_{37}

VALUE	EVTS	DOCUMENT ID		TECN	COMMENT
0.71±0.05 OUR FIT		Error includes scale factor of 1.1.			
0.81±0.05±0.08	856 ± 35	FRABETTI	94J	E687	γBe $\overline{E}_\gamma$=220 GeV
• • • We do not use the following data for averages, fits, limits, etc. • • •					
0.85±0.40	35	AVERY	80	SPEC	$\gamma N \to D^{*+}$
1.4 ±0.5	116	PICCOLO	77	MRK1	e^+e^- 4.03, 4.41 GeV

$\Gamma(K^0_S\rho^0)/\Gamma(K^0_S\pi^+\pi^-)$ — Γ_{41}/Γ_{40}

This is the "fit fraction" from the Dalitz-plot analysis.

VALUE	DOCUMENT ID		TECN	COMMENT
$0.224^{+0.017}_{-0.023}$ OUR AVERAGE	Error includes scale factor of 1.7.			
0.210±0.016	[1] AUBERT	08AL	BABR	Dalitz fit, ≈ 487 k evts
$0.264\pm0.009^{+0.010}_{-0.026}$	MURAMATSU	02	CLE2	Dalitz fit, 5299 evts
• • • We do not use the following data for averages, fits, limits, etc. • • •				
$0.267\pm0.011^{+0.009}_{-0.028}$	ASNER	04A	CLEO	See MURAMATSU 02
0.350±0.028±0.067	FRABETTI	94G	E687	Dalitz fit, 597 evts
0.227±0.032±0.009	ALBRECHT	93D	ARG	Dalitz fit, 440 evts
0.215±0.051±0.037	ANJOS	93	E691	γBe 90–260 GeV
0.20 ±0.06 ±0.03	FRABETTI	92B	E687	γ Be, $\overline{E}_\gamma$= 221 GeV
0.12 ±0.01 ±0.07	ADLER	87	MRK3	e^+e^- 3.77 GeV

[1] The error on this AUBERT 08AL value includes both statistical and systematic uncertainties; the latter dominates.

$\Gamma(K^0_S\omega,\ \omega \to \pi^+\pi^-)/\Gamma(K^0_S\pi^+\pi^-)$ — Γ_{42}/Γ_{40}

This is the "fit fraction" from the Dalitz-plot analysis.

VALUE	DOCUMENT ID		TECN	COMMENT
0.0073±0.0020 OUR AVERAGE				
0.009 ±0.010	[1] AUBERT	08AL	BABR	Dalitz fit, ≈ 487 k evts
$0.0072\pm0.0018^{+0.0010}_{-0.0009}$	MURAMATSU	02	CLE2	Dalitz fit, 5299 evts
• • • We do not use the following data for averages, fits, limits, etc. • • •				
$0.0081\pm0.0019^{+0.0018}_{-0.0010}$	ASNER	04A	CLEO	See MURAMATSU 02

[1] The error on this AUBERT 08AL value includes both statistical and systematic uncertainties; the latter dominates.

$\Gamma(K^0_S(\pi^+\pi^-)_{S-wave})/\Gamma(K^0_S\pi^+\pi^-)$ — Γ_{43}/Γ_{40}

This is the "fit fraction" from the Dalitz-plot analysis. The $(\pi^+\pi^-)_{S-wave}$ includes what in isobar models are the $f_0(980)$ and $f_0(1370)$; see the following two data blocks.

VALUE	DOCUMENT ID		TECN	COMMENT
0.119±0.026	[1] AUBERT	08AL	BABR	Dalitz fit, ≈ 487 k evts

[1] The error on this AUBERT 08AL value includes both statistical and systematic uncertainties; the latter dominates.

$\Gamma(K^0_S f_0(980),\ f_0 \to \pi^+\pi^-)/\Gamma(K^0_S\pi^+\pi^-)$ — Γ_{44}/Γ_{40}

Fit fraction from the Dalitz plot analyses.

VALUE	DOCUMENT ID		TECN	COMMENT
$0.043\pm0.005^{+0.012}_{-0.006}$	MURAMATSU	02	CLE2	Dalitz fit, 5299 evts
• • • We do not use the following data for averages, fits, limits, etc. • • •				
$0.042\pm0.005^{+0.011}_{-0.005}$	ASNER	04A	CLEO	See MURAMATSU 02
0.068±0.016±0.018	FRABETTI	94G	E687	Dalitz fit, 597 evts
0.046±0.018±0.006	ALBRECHT	93D	ARG	Dalitz fit, 440 evts

$\Gamma(K^0_S f_0(1370),\ f_0 \to \pi^+\pi^-)/\Gamma(K^0_S\pi^+\pi^-)$ — Γ_{45}/Γ_{40}

This is the "fit fraction" from the Dalitz-plot analysis.

VALUE	DOCUMENT ID		TECN	COMMENT
$0.099\pm0.011^{+0.028}_{-0.044}$	MURAMATSU	02	CLE2	Dalitz fit, 5299 evts
• • • We do not use the following data for averages, fits, limits, etc. • • •				
$0.098\pm0.014^{+0.026}_{-0.036}$	ASNER	04A	CLEO	See MURAMATSU 02
0.077±0.022±0.031	FRABETTI	94G	E687	Dalitz fit, 597 evts
0.082±0.028±0.013	ALBRECHT	93D	ARG	Dalitz fit, 440 evts

Downloaded from https://academic.oup.com/ptep/article/2022/8/083C01/6651666 by KIT Library user on 27 September 2022

$\Gamma(K^0_S f_2(1270),\ f_2 \to \pi^+\pi^-)/\Gamma(K^0_S\pi^+\pi^-)$ — Γ_{46}/Γ_{40}

This is the "fit fraction" from the Dalitz-plot analysis.

VALUE	DOCUMENT ID		TECN	COMMENT
$0.0032^{+0.0035}_{-0.0022}$ OUR AVERAGE				
0.006 ±0.007	[1] AUBERT	08AL	BABR	Dalitz fit, ≈ 487 k evts
$0.0027\pm0.0015^{+0.0037}_{-0.0017}$	MURAMATSU	02	CLE2	Dalitz fit, 5299 evts
• • • We do not use the following data for averages, fits, limits, etc. • • •				
$0.0036\pm0.0022^{+0.0032}_{-0.0019}$	ASNER	04A	CLEO	See MURAMATSU 02
0.037 ±0.014 ±0.017	FRABETTI	94G	E687	Dalitz fit, 597 evts
0.050 ±0.021 ±0.008	ALBRECHT	93D	ARG	Dalitz fit, 440 evts

[1] The error on this AUBERT 08AL value includes both statistical and systematic uncertainties; the latter dominates.

$\Gamma(K^*(892)^-\pi^+,\ K^{*-} \to K^0_S\pi^-)/\Gamma(K^0_S\pi^+\pi^-)$ — Γ_{47}/Γ_{40}

This is the "fit fraction" from the Dalitz-plot analysis.

VALUE	DOCUMENT ID		TECN	COMMENT
$0.588^{+0.034}_{-0.050}$ OUR AVERAGE Error includes scale factor of 2.0.				
0.557±0.028	[1] AUBERT	08AL	BABR	Dalitz fit, ≈ 487 k evts
$0.657\pm0.013^{+0.018}_{-0.040}$	MURAMATSU	02	CLE2	Dalitz fit, 5299 evts
• • • We do not use the following data for averages, fits, limits, etc. • • •				
$0.663\pm0.013^{+0.024}_{-0.043}$	ASNER	04A	CLEO	See MURAMATSU 02
0.625±0.036±0.026	FRABETTI	94G	E687	Dalitz fit, 597 evts
0.718±0.042±0.030	ALBRECHT	93D	ARG	Dalitz fit, 440 evts
0.480±0.097	ANJOS	93	E691	γBe 90–260 GeV
0.56 ±0.04 ±0.05	ADLER	87	MRK3	e^+e^- 3.77 GeV

[1] The error on this AUBERT 08AL value includes both statistical and systematic uncertainties; the latter dominates.

$\Gamma(K^*_0(1430)^-\pi^+,\ K^{*-}_0 \to K^0_S\pi^-)/\Gamma(K^0_S\pi^+\pi^-)$ — Γ_{48}/Γ_{40}

This is the "fit fraction" from the Dalitz-plot analysis.

VALUE	DOCUMENT ID		TECN	COMMENT
$0.095^{+0.014}_{-0.010}$ OUR AVERAGE				
0.102±0.015	[1] AUBERT	08AL	BABR	Dalitz fit, ≈ 487 k evts
$0.073\pm0.007^{+0.031}_{-0.011}$	MURAMATSU	02	CLE2	Dalitz fit, 5299 evts
• • • We do not use the following data for averages, fits, limits, etc. • • •				
$0.072\pm0.007^{+0.014}_{-0.013}$	ASNER	04A	CLEO	See MURAMATSU 02
0.109±0.027±0.029	FRABETTI	94G	E687	Dalitz fit, 597 evts
0.129±0.034±0.021	ALBRECHT	93D	ARG	Dalitz fit, 440 evts

[1] The error on this AUBERT 08AL value includes both statistical and systematic uncertainties; the latter dominates.

$\Gamma(K^*_2(1430)^-\pi^+,\ K^{*-}_2 \to K^0_S\pi^-)/\Gamma(K^0_S\pi^+\pi^-)$ — Γ_{49}/Γ_{40}

This is the "fit fraction" from the Dalitz-plot analysis.

VALUE	DOCUMENT ID		TECN	COMMENT
$0.0120^{+0.0070}_{-0.0035}$ OUR AVERAGE				
0.022 ±0.016	[1] AUBERT	08AL	BABR	Dalitz fit, ≈ 487 k evts
$0.011\ \pm0.002\ ^{+0.007}_{-0.003}$	MURAMATSU	02	CLE2	Dalitz fit, 5299 evts
• • • We do not use the following data for averages, fits, limits, etc. • • •				
$0.011\ \pm0.002\ ^{+0.005}_{-0.003}$	ASNER	04A	CLEO	See MURAMATSU 02

[1] The error on this AUBERT 08AL value includes both statistical and systematic uncertainties; the latter dominates.

$\Gamma(K^*(1680)^-\pi^+,\ K^{*-} \to K^0_S\pi^-)/\Gamma(K^0_S\pi^+\pi^-)$ — Γ_{50}/Γ_{40}

This is the "fit fraction" from the Dalitz-plot analysis.

VALUE	DOCUMENT ID		TECN	COMMENT
0.016±0.013 OUR AVERAGE				
0.007±0.019	[1] AUBERT	08AL	BABR	Dalitz fit, ≈ 487 k evts
$0.022\pm0.004^{+0.018}_{-0.015}$	MURAMATSU	02	CLE2	Dalitz fit, 5299 evts
• • • We do not use the following data for averages, fits, limits, etc. • • •				
$0.023\pm0.005^{+0.007}_{-0.014}$	ASNER	04A	CLEO	See MURAMATSU 02

[1] The error on this AUBERT 08AL value includes both statistical and systematic uncertainties; the latter dominates.

$\Gamma(K^*(892)^+\pi^-,\ K^{*+} \to K^0_S\pi^+)/\Gamma(K^0_S\pi^+\pi^-)$ — Γ_{51}/Γ_{40}

This is the "fit fraction" from the Dalitz-plot analysis. This is a doubly Cabibbo-suppressed mode.

VALUE (units 10^{-3})	DOCUMENT ID		TECN	COMMENT
$4.0^{+2.0}_{-1.2}$ OUR AVERAGE				
4.6±2.3	[1] AUBERT	08AL	BABR	Dalitz fit, ≈ 487 k evts
$3.4\pm1.3^{+4.1}_{-0.4}$	MURAMATSU	02	CLE2	Dalitz fit, 5299 evts
• • • We do not use the following data for averages, fits, limits, etc. • • •				
$3.4\pm1.3^{+3.6}_{-0.5}$	ASNER	04A	CLEO	See MURAMATSU 02

[1] The error on this AUBERT 08AL value includes both statistical and systematic uncertainties; the latter dominates.

$\Gamma(K^*_0(1430)^+\pi^-,\ K^{*+}_0 \to K^0_S\pi^+)/\Gamma(K^0_S\pi^+\pi^-)$ — Γ_{52}/Γ_{40}

This is the "fit fraction" from the Dalitz-plot analysis. This is a doubly Cabibbo-suppressed mode.

VALUE	CL%	DOCUMENT ID		TECN	COMMENT
$<5\times10^{-4}$	95	AUBERT	08AL	BABR	Dalitz fit, ≈ 487 k evts

$\Gamma(K^*_2(1430)^+\pi^-,\ K^{*+}_2 \to K^0_S\pi^+)/\Gamma(K^0_S\pi^+\pi^-)$ — Γ_{53}/Γ_{40}

This is the "fit fraction" from the Dalitz-plot analysis. This is a doubly Cabibbo-suppressed mode.

VALUE	CL%	DOCUMENT ID		TECN	COMMENT
$<1.2\times10^{-3}$	95	AUBERT	08AL	BABR	Dalitz fit, ≈ 487 k evts

$\Gamma(K^0_S\pi^+\pi^-$ nonresonant$)/\Gamma(K^0_S\pi^+\pi^-)$ — Γ_{54}/Γ_{40}

This is the "fit fraction" from the Dalitz-plot analysis. Neither FRABETTI 94G nor ALBRECHT 93D (quoted in many of the earlier submodes of $K^0_S\pi^+\pi^-$) sees evidence for a nonresonant component.

VALUE	DOCUMENT ID		TECN	COMMENT
$0.009\pm0.004^{+0.020}_{-0.004}$	MURAMATSU	02	CLE2	Dalitz fit, 5299 evts
• • • We do not use the following data for averages, fits, limits, etc. • • •				
$0.007\pm0.007^{+0.021}_{-0.006}$	ASNER	04A	CLEO	See MURAMATSU 02
0.263±0.024±0.041	ANJOS	93	E691	γBe 90–260 GeV
0.26 ±0.08 ±0.05	FRABETTI	92B	E687	γ Be, $\overline{E}_\gamma$ = 221 GeV
0.33 ±0.05 ±0.10	ADLER	87	MRK3	e^+e^- 3.77 GeV

$\Gamma(K^-\pi^+\pi^0)/\Gamma_{total}$ — Γ_{55}/Γ

VALUE (%)	EVTS	DOCUMENT ID		TECN	COMMENT
• • • We do not use the following data for averages, fits, limits, etc. • • •					
14.57±0.12±0.38		[1] DOBBS	07	CLEO	See BONVICINI 14
14.9 ±0.3 ±0.5	19k ±150	[1] HE	05	CLEO	See DOBBS 07
13.3 ±1.2 ±1.3	931	ADLER	88C	MRK3	e^+e^- 3.77 GeV
11.7 ±4.3	37	[2] SCHINDLER	81	MRK2	e^+e^- 3.771 GeV

[1] DOBBS 07 and HE 05 use single- and double-tagged events in an overall fit. DOBBS 07 supersedes HE 05.

[2] SCHINDLER 81 (MARK-2) measures $\sigma(e^+e^- \to \psi(3770)) \times$ branching fraction to be 0.68 ± 0.23 nb. We use the MARK-3 (ADLER 88C) value of σ = 5.8 ± 0.5 ± 0.6 nb.

$\Gamma(K^-\pi^+\pi^0)/\Gamma(K^-\pi^+)$ — Γ_{55}/Γ_{37}

VALUE	EVTS	DOCUMENT ID		TECN	COMMENT
3.65 ±0.13 OUR FIT Error includes scale factor of 2.1.					
3.76 ±0.10 OUR AVERAGE Error includes scale factor of 1.4. See the ideogram below.					
3.802±0.022±0.073		BONVICINI	14	CLEO	All CLEO-c runs
3.81 ±0.07 ±0.26	10k	BARISH	96	CLE2	$e^+e^- \approx \Upsilon(4S)$
3.04 ±0.16 ±0.34	931	[1] ALBRECHT	92P	ARG	$e^+e^- \approx$ 10 GeV
2.8 ±0.14 ±0.52	1050	KINOSHITA	91	CLEO	$e^+e^- \sim$ 10.7 GeV

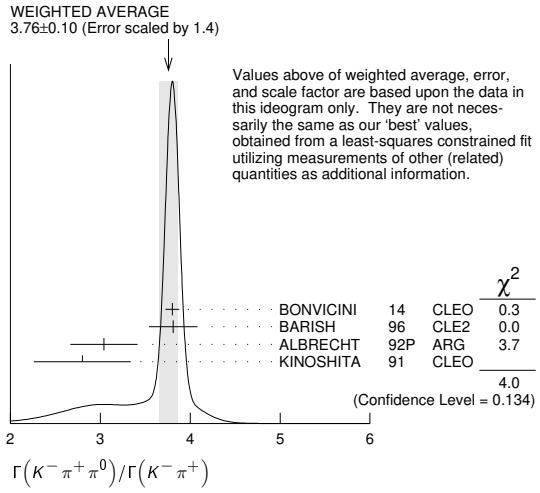

[1] This value is calculated from numbers in Table 1 of ALBRECHT 92P.

$\Gamma(K^-\rho^+)/\Gamma(K^-\pi^+\pi^0)$ — Γ_{56}/Γ_{55}

This is the "fit fraction" from the Dalitz-plot analysis.

VALUE	DOCUMENT ID		TECN	COMMENT
0.78 ±0.04 OUR AVERAGE				
0.788±0.019±0.048	KOPP	01	CLE2	Dalitz fit, ≈ 7,000 evts
0.765±0.041±0.054	FRABETTI	94G	E687	Dalitz fit, 530 evts
• • • We do not use the following data for averages, fits, limits, etc. • • •				
0.647±0.039±0.150	ANJOS	93	E691	γBe 90–260 GeV
0.81 ±0.03 ±0.06	ADLER	87	MRK3	e^+e^- 3.77 GeV

$\Gamma(K^-\rho(1700)^+,\ \rho^+ \to \pi^+\pi^0)/\Gamma(K^-\pi^+\pi^0)$ — Γ_{57}/Γ_{55}

This is the "fit fraction" from the Dalitz-plot analysis.

VALUE	DOCUMENT ID		TECN	COMMENT
0.057±0.008±0.009	KOPP	01	CLE2	Dalitz fit, ≈ 7,000 evts

Downloaded from https://academic.oup.com/ptep/article/2022/8/083C01/6651666 by KIT Library user on 27 September 2022

$\Gamma(K^*(892)^-\pi^+,\ K^*(892)^- \to K^-\pi^0)/\Gamma(K^-\pi^+\pi^0)$ — Γ_{58}/Γ_{55}

This is the "fit fraction" from the Dalitz-plot analysis.

VALUE	DOCUMENT ID		TECN	COMMENT
$0.160^{+0.025}_{-0.013}$ OUR AVERAGE				
$0.161\pm0.007^{+0.027}_{-0.011}$	KOPP	01	CLE2	Dalitz fit, $\approx$ 7,000 evts
$0.148\pm0.028\pm0.049$	FRABETTI	94G	E687	Dalitz fit, 530 evts
• • • We do not use the following data for averages, fits, limits, etc. • • •				
$0.084\pm0.011\pm0.012$	ANJOS	93	E691	γBe 90–260 GeV
$0.12\ \pm0.02\ \pm0.03$	ADLER	87	MRK3	e^+e^- 3.77 GeV

$\Gamma(\overline{K}^*(892)^0\pi^0,\ \overline{K}^*(892)^0 \to K^-\pi^+)/\Gamma(K^-\pi^+\pi^0)$ — Γ_{59}/Γ_{55}

This is the "fit fraction" from the Dalitz-plot analysis.

VALUE	DOCUMENT ID		TECN	COMMENT
0.135 ± 0.016 OUR AVERAGE				
$0.127\pm0.009\pm0.016$	KOPP	01	CLE2	Dalitz fit, $\approx$ 7,000 evts
$0.165\pm0.031\pm0.015$	FRABETTI	94G	E687	Dalitz fit, 530 evts
• • • We do not use the following data for averages, fits, limits, etc. • • •				
$0.142\pm0.018\pm0.024$	ANJOS	93	E691	γBe 90–260 GeV
$0.13\ \pm0.02\ \pm0.03$	ADLER	87	MRK3	e^+e^- 3.77 GeV

$\Gamma(K_0^*(1430)^-\pi^+,\ K_0^{*-} \to K^-\pi^0)/\Gamma(K^-\pi^+\pi^0)$ — Γ_{60}/Γ_{55}

This is the "fit fraction" from the Dalitz-plot analysis.

VALUE	DOCUMENT ID		TECN	COMMENT
$0.033\pm0.006\pm0.014$	KOPP	01	CLE2	Dalitz fit, $\approx$ 7,000 evts

$\Gamma(\overline{K}_0^*(1430)^0\pi^0,\ \overline{K}_0^{*0} \to K^-\pi^+)/\Gamma(K^-\pi^+\pi^0)$ — Γ_{61}/Γ_{55}

This is the "fit fraction" from the Dalitz-plot analysis.

VALUE	DOCUMENT ID		TECN	COMMENT
$0.041\pm0.006^{+0.032}_{-0.009}$	KOPP	01	CLE2	Dalitz fit, $\approx$ 7,000 evts

$\Gamma(K^*(1680)^-\pi^+,\ K^{*-} \to K^-\pi^0)/\Gamma(K^-\pi^+\pi^0)$ — Γ_{62}/Γ_{55}

This is the "fit fraction" from the Dalitz-plot analysis.

VALUE	DOCUMENT ID		TECN	COMMENT
$0.013\pm0.003\pm0.004$	KOPP	01	CLE2	Dalitz fit, $\approx$ 7,000 evts

$\Gamma(K^-\pi^+\pi^0$ nonresonant$)/\Gamma(K^-\pi^+\pi^0)$ — Γ_{63}/Γ_{55}

This is the "fit fraction" from the Dalitz-plot analysis.

VALUE	EVTS	DOCUMENT ID		TECN	COMMENT
$0.080^{+0.040}_{-0.014}$ OUR AVERAGE					
$0.075\pm0.009^{+0.056}_{-0.011}$		KOPP	01	CLE2	Dalitz fit, $\approx$ 7,000 evts
$0.101\pm0.033\pm0.040$		FRABETTI	94G	E687	Dalitz fit, 530 evts
• • • We do not use the following data for averages, fits, limits, etc. • • •					
$0.036\pm0.004\pm0.018$		ANJOS	93	E691	γBe 90–260 GeV
$0.09\ \pm0.02\ \pm0.04$		ADLER	87	MRK3	e^+e^- 3.77 GeV
$0.51\ \pm0.22$	21	SUMMERS	84	E691	Photoproduction

$\Gamma(K_S^0 2\pi^0)/\Gamma_{total}$ — Γ_{64}/Γ

VALUE (units 10^{-3})	EVTS	DOCUMENT ID		TECN	COMMENT
$9.1\ \pm1.1$ OUR AVERAGE Error includes scale factor of 2.2.					
$10.58\pm0.38\pm0.73$	1259	LOWREY	11	CLEO	$e^+e^-\approx$ 3.77 GeV
$8.34\pm0.45\pm0.42$		ASNER	08	CLEO	$e^+e^-\to D^0\overline{D}^0$, 3.77 GeV

$\Gamma(K_S^0(2\pi^0)_{S-wave})/\Gamma(K_S^0 2\pi^0)$ — Γ_{65}/Γ_{64}

This is the "fit fraction" from the Dalitz-plot analysis.

VALUE (units 10^{-2})	DOCUMENT ID		TECN	COMMENT
$28.9\pm6.3\pm3.1$	LOWREY	11	CLEO	Dalitz analysis, 1259 evts

$\Gamma(\overline{K}^*(892)^0\pi^0,\ \overline{K}^{*0} \to K_S^0\pi^0)/\Gamma(K_S^0\pi^0)$ — Γ_{66}/Γ_{38}

This is the "fit fraction" from the Dalitz-plot analysis.

VALUE (units 10^{-2})	DOCUMENT ID		TECN	COMMENT
$65.6\pm\ 5.3\pm2.5$	LOWREY	11	CLEO	Dalitz analysis, 1259 evts
• • • We do not use the following data for averages, fits, limits, etc. • • •				
$55\ ^{+13}_{-10}\ \pm7$	PROCARIO	93B	CLE2	Dalitz plot fit, 122 evts

$\Gamma(\overline{K}^*(1430)^0\pi^0,\ \overline{K}^{*0} \to K_S^0\pi^0)/\Gamma(K_S^0 2\pi^0)$ — Γ_{67}/Γ_{64}

This is the "fit fraction" from the Dalitz-plot analysis.

VALUE (units 10^{-2})	DOCUMENT ID		TECN	COMMENT
$0.49\pm0.45\pm2.51$	LOWREY	11	CLEO	Dalitz analysis, 1259 evts

$\Gamma(\overline{K}^*(1680)^0\pi^0,\ \overline{K}^{*0} \to K_S^0\pi^0)/\Gamma(K_S^0 2\pi^0)$ — Γ_{68}/Γ_{64}

This is the "fit fraction" from the Dalitz-plot analysis.

VALUE (units 10^{-2})	DOCUMENT ID		TECN	COMMENT
$11.2\pm2.7\pm2.5$	LOWREY	11	CLEO	Dalitz analysis, 1259 evts

$\Gamma(K_S^0 f_2(1270),\ f_2 \to 2\pi^0)/\Gamma(K_S^0 2\pi^0)$ — Γ_{69}/Γ_{64}

This is the "fit fraction" from the Dalitz-plot analysis.

VALUE (units 10^{-2})	DOCUMENT ID		TECN	COMMENT
$2.48\pm0.91\pm0.78$	LOWREY	11	CLEO	Dalitz analysis, 1259 evts

$\Gamma(2K_S^0$, one $K_S^0 \to 2\pi^0)/\Gamma(K_S^0 2\pi^0)$ — Γ_{70}/Γ_{64}

This is the "fit fraction" from the Dalitz-plot analysis.

VALUE (units 10^{-2})	DOCUMENT ID		TECN	COMMENT
$3.46\pm0.92\pm0.66$	LOWREY	11	CLEO	Dalitz analysis, 1259 evts

$\Gamma(K_S^0 2\pi^0$ nonresonant$)/\Gamma(K_S^0\pi^0)$ — Γ_{71}/Γ_{38}

This is the "fit fraction" from the Dalitz-plot analysis.

VALUE	DOCUMENT ID		TECN	COMMENT
• • • We do not use the following data for averages, fits, limits, etc. • • •				
$0.37\pm0.08\pm0.04$	PROCARIO	93B	CLE2	Dalitz plot fit, 122 evts

$\Gamma(K^-2\pi^+\pi^-)/\Gamma_{total}$ — Γ_{72}/Γ

VALUE (%)	EVTS	DOCUMENT ID		TECN	COMMENT
• • • We do not use the following data for averages, fits, limits, etc. • • •					
$8.30\pm0.07\pm0.20$		[1] DOBBS	07	CLEO	See BONVICINI 14
$8.3\ \pm0.2\ \pm0.3$	15k	[1] HE	05	CLEO	See DOBBS 07
$7.9\ \pm1.5\ \pm0.9$		[2] ALBRECHT	94	ARG	$e^+e^-\approx\Upsilon(4S)$
$6.80\pm0.27\pm0.57$	1.4k	[3] ALBRECHT	94F	ARG	$e^+e^-\approx\Upsilon(4S)$
$9.1\ \pm0.8\ \pm0.8$	992	ADLER	88C	MRK3	e^+e^- 3.77 GeV
$11.7\ \pm2.5$	185	[4] SCHINDLER	81	MRK2	e^+e^- 3.771 GeV
$6.2\ \pm1.9$	44	[5] PERUZZI	77	LGW	e^+e^- 3.77 GeV

[1] DOBBS 07 and HE 05 use single- and double-tagged events in an overall fit. DOBBS 07 supersedes HE 05.

[2] ALBRECHT 94 uses D^0 mesons from $\overline{B}^0 \to D^{*+}\ell^-\overline{\nu}_\ell$ decays. This is a different set of events than used by ALBRECHT 94F.

[3] See the footnote on the ALBRECHT 94F measurement of $\Gamma(K^-\pi^+)/\Gamma_{total}$ for the method used.

[4] SCHINDLER 81 (MARK-2) measures $\sigma(e^+e^-\to\psi(3770))\times$ branching fraction to be 0.68 ± 0.11 nb. We use the MARK-3 (ADLER 88C) value of $\sigma=5.8\pm0.5\pm0.6$ nb.

[5] PERUZZI 77 (MARK-1) measures $\sigma(e^+e^-\to\psi(3770))\times$ branching fraction to be 0.36 ± 0.10 nb. We use the MARK-3 (ADLER 88C) value of $\sigma=5.8\pm0.5\pm0.6$ nb.

$\Gamma(K^-2\pi^+\pi^-)/\Gamma(K^-\pi^+)$ — Γ_{72}/Γ_{37}

VALUE	EVTS	DOCUMENT ID		TECN	COMMENT
2.083 ± 0.031 OUR FIT					
2.087 ± 0.032 OUR AVERAGE					
$2.106\pm0.013\pm0.032$		BONVICINI	14	CLEO	All CLEO-c runs
$1.94\ \pm0.07\ ^{+0.09}_{-0.11}$		JUN	00	SELX	Σ^- nucleus, 600 GeV
$1.7\ \pm0.2\ \pm0.2$	1745	ANJOS	92C	E691	γBe 90–260 GeV
$1.90\ \pm0.25\ \pm0.20$	337	ALVAREZ	91B	NA14	Photoproduction
$2.12\ \pm0.16\ \pm0.09$		BORTOLETTO	88	CLEO	e^+e^- 10.55 GeV
$2.17\ \pm0.28\ \pm0.23$		ALBRECHT	85F	ARG	e^+e^- 10 GeV
• • • We do not use the following data for averages, fits, limits, etc. • • •					
$2.0\ \pm0.9$	48	BAILEY	86	ACCM	π^-Be fixed target
$2.0\ \pm1.0$	10	BAILEY	83B	SPEC	$\pi^-\text{Be}\to D^0$
$2.2\ \pm0.8$	214	PICCOLO	77	MRK1	e^+e^- 4.03, 4.41 GeV

$\Gamma(K^-\pi^+\rho^0$total$)/\Gamma(K^-2\pi^+\pi^-)$ — Γ_{73}/Γ_{72}

VALUE (units 10^{-2})	DOCUMENT ID		TECN	COMMENT
83.5 ± 3.5 OUR AVERAGE				
$80\ \pm3\ \pm5$	ANJOS	92C	E691	1745 $K^-2\pi^+\pi^-$ evts
$85.5\pm3.2\pm3.0$	COFFMAN	92B	MRK3	1281 $\pm$ 45 $K^-2\pi^+\pi^-$ evts

$\Gamma(K^-\pi^+\rho^0$3-body$)/\Gamma(K^-2\pi^+\pi^-)$ — Γ_{74}/Γ_{72}

VALUE (units 10^{-2})	EVTS	DOCUMENT ID		TECN	COMMENT
7.4 ± 2.0 OUR AVERAGE					
$8.4\pm1.1\pm2.5$	16k	ABLIKIM	17O	BES3	$D^0\to K^-2\pi^+\pi^-$
$5\ \pm3\ \pm2$		ANJOS	92C	E691	1745 $K^-2\pi^+\pi^-$ evts
$8.4\pm2.2\pm4.0$		COFFMAN	92B	MRK3	1281 $\pm$ 45 $K^-2\pi^+\pi^-$ evts

$\Gamma(\overline{K}^*(892)^0\rho^0,\ \overline{K}^{*0} \to K^-\pi^+)/\Gamma(K^-2\pi^+\pi^-)$ — Γ_{75}/Γ_{72}

VALUE (units 10^{-2})	EVTS	DOCUMENT ID		TECN	COMMENT
12.3 ± 0.6 OUR AVERAGE					
$12.3\pm0.4\pm0.5$	16k	ABLIKIM	17O	BES3	$D^0\to K^-2\pi^+\pi^-$
$13\ \pm2\ \pm2$		ANJOS	92C	E691	1745 $K^-2\pi^+\pi^-$ evts

$\Gamma(\overline{K}^*(892)^0\rho^0$transverse, $\overline{K}^{*0} \to K^-\pi^+)/\Gamma(K^-2\pi^+\pi^-)$ — Γ_{76}/Γ_{72}

VALUE	EVTS	DOCUMENT ID		TECN	COMMENT
$0.142\pm0.016\pm0.05$	1281	COFFMAN	92B	MRK3	$K^-2\pi^+\pi^-$ evts

$\Gamma(K^-a_1(1260)^+,\ a_1^+ \to \rho^0\pi^+)/\Gamma(K^-2\pi^+\pi^-)$ — Γ_{77}/Γ_{72}

VALUE (units 10^{-2})	EVTS	DOCUMENT ID		TECN	COMMENT
$53\ \pm4$ OUR AVERAGE					
$54.6\pm2.8\pm\ 3.7$	16k	ABLIKIM	17O	BES3	$D^0\to K^-2\pi^+\pi^-$
$47\ \pm5\ \pm10$	1745	ANJOS	92C	E691	$K^-2\pi^+\pi^-$ evts
$49.2\pm2.4\pm\ 8.0$	1281	COFFMAN	92B	MRK3	$K^-2\pi^+\pi^-$ evts

$\Gamma(K_1(1270)^-\pi^+,\ K_1^- \to K^-\pi^+\pi^-$total$)/\Gamma(K^-2\pi^+\pi^-)$ — Γ_{78}/Γ_{72}

VALUE (units 10^{-2})	EVTS	DOCUMENT ID		TECN	COMMENT
$4.8\ \pm0.4$ OUR AVERAGE					
$4.66\pm0.05\pm0.39\pm0.24$	891k	[1] AAIJ	18AI	LHCB	$D^0\to K^-2\pi^+\pi^-$
$6.6\ \pm1.9\ \pm0.3$	1281	COFFMAN	92B	MRK3	$K^-2\pi^+\pi^-$ evts

[1] The 3rd error is due to the uncertainty in the amplitude model composition.

Downloaded from https://academic.oup.com/ptep/article/2022/8/083C01/6651666 by KIT Library user on 27 September 2022

$\Gamma(K_1(1270)^-\pi^+,\ K_1^- \to \overline{K}^*(892)^0\pi^-,\ \overline{K}^{*0} \to K^-\pi^+)/\Gamma(K^-2\pi^+\pi^-)$ — Γ_{81}/Γ_{72}

VALUE (units 10^{-2})	EVTS	DOCUMENT ID		TECN	COMMENT
0.8±0.2±0.2	16k	ABLIKIM	17O	BES3	$D^0 \to K^-2\pi^+\pi^-$

$\Gamma(K^-2\pi^+\pi^-\text{nonresonant})/\Gamma(K^-2\pi^+\pi^-)$ — Γ_{82}/Γ_{72}

VALUE (units 10^{-2})	EVTS	DOCUMENT ID		TECN	COMMENT
22.0 ±0.8 OUR AVERAGE					
22.04±0.28±2.09±1.51	891k	[1] AAIJ	18AI	LHCB	$D^0 \to K^-2\pi^+\pi^-$
21.9 ±0.6 ±0.6	16k	[2] ABLIKIM	17O	BES3	$D^0 \to K^-2\pi^+\pi^-$
23 ±2 ±3	1.7k	ANJOS	92C	E691	$D^0 \to K^-2\pi^+\pi^-$
24.2 ±2.5 ±6.0	1.2k	COFFMAN	92B	MRK3	$D^0 \to K^-2\pi^+\pi^-$

[1] The 3rd error is due to the uncertainty in the amplitude model composition.
[2] In addition to the 14 ABLIKIM 17O branching ratios we have listed, the paper gives 15 more ratios for mostly non-resonant modes. Four of the 15 have less than 2-standard-deviation significance. Here are some of the omitted modes, with S, P, V, A, and T for scalar, pseudo-scalar, vector, axial-vector, and tensor spin sub-structures: $\pi^+(K^-\rho^0)_P$, $\pi^+(K^-\rho^0)_V$, $\pi^+(\overline{K}^{*0}\pi^-)_P$, $\pi^+(\overline{K}^{*0}\pi^-)_V$, $\pi^+(\pi^-(K^-\pi^+)_{S-wave})_A$, $(K^-\pi^+)_V\,(\pi^+\pi^-)_S$, $(K^-\pi^+)_T\,(\pi^+\pi^-)_S\cdots$

$\Gamma(K_S^0\pi^+\pi^-\pi^0)/\Gamma_{\text{total}}$ — Γ_{83}/Γ

VALUE (%)	EVTS	DOCUMENT ID		TECN	COMMENT
5.2±0.6 OUR FIT					
5.2±1.1±1.2	140	COFFMAN	92B	MRK3	e^+e^- 3.77 GeV
• • • We do not use the following data for averages, fits, limits, etc. • • •					
$6.7^{+1.6}_{-1.7}$		[1] BARLAG	92C	ACCM	π^- Cu 230 GeV

[1] BARLAG 92C computes the branching fraction using topological normalization.

$\Gamma(K_S^0\pi^+\pi^-\pi^0)/\Gamma(K_S^0\pi^+\pi^-)$ — Γ_{83}/Γ_{40}

Branching fractions for submodes of this mode with narrow resonances (the η, ω, η') are fairly well determined (see below). COFFMAN 92B gives fractions of K^* and ρ submodes, but with only 140 ± 28 events above background could not determine them with much accuracy. We omit those measurements here; they are in our 2008 Review (Physics Letters **B667** 1 (2008)).

VALUE	EVTS	DOCUMENT ID		TECN	COMMENT
1.85±0.20 OUR FIT					
1.86±0.23 OUR AVERAGE					
1.80±0.20±0.21	190	[1] ALBRECHT	92P	ARG	$e^+e^- \approx$ 10 GeV
2.8 ±0.8 ±0.8	46	ANJOS	92C	E691	γBe 90–260 GeV
1.85±0.26±0.30	158	KINOSHITA	91	CLEO	$e^+e^- \sim$ 10.7 GeV

[1] This value is calculated from numbers in Table 1 of ALBRECHT 92P.

$\Gamma(K^-\pi^+2\pi^0)/\Gamma_{\text{total}}$ — Γ_{86}/Γ

VALUE (%)	EVTS	DOCUMENT ID		TECN	COMMENT
8.86±0.13±0.19	6.1k	ABLIKIM	19AK	BES3	e^+e^- at 3773 MeV
• • • We do not use the following data for averages, fits, limits, etc. • • •					
17.7 ±2.9		[1] BARLAG	92C	ACCM	π^- Cu 230 GeV
14.9 ±3.7 ±3.0	24	[2] ADLER	88C	MRK3	e^+e^- 3.77 GeV
20.9 $^{+7.4}_{-4.3}$ ±1.2	9	[1] AGUILAR-...	87F	HYBR	πp, pp 360, 400 GeV

[1] AGUILAR-BENITEZ 87F and BARLAG 92C compute the branching fraction using topological normalization. They do not distinguish the presence of a third π^0, and thus are not included in the average.
[2] ADLER 88C uses an absolute normalization method finding this decay channel opposite a detected $\overline{D}^0 \to K^+\pi^-$ in pure $D\overline{D}$ events.

$\Gamma(K^-2\pi^+\pi^-\pi^0)/\Gamma(K^-\pi^+)$ — Γ_{87}/Γ_{37}

VALUE	EVTS	DOCUMENT ID		TECN	COMMENT
1.09±0.10 OUR FIT					
0.98±0.11±0.11	225	[1] ALBRECHT	92P	ARG	$e^+e^- \approx$ 10 GeV

[1] This value is calculated from numbers in Table 1 of ALBRECHT 92P.

$\Gamma(K^-2\pi^+\pi^-\pi^0)/\Gamma(K^-2\pi^+\pi^-)$ — Γ_{87}/Γ_{72}

VALUE	EVTS	DOCUMENT ID		TECN	COMMENT
0.52±0.05 OUR FIT					
0.56±0.07 OUR AVERAGE					
0.55±0.07$^{+0.12}_{-0.09}$	167	KINOSHITA	91	CLEO	$e^+e^- \sim$ 10.7 GeV
0.57±0.06±0.05	180	ANJOS	90D	E691	Photoproduction

$\Gamma(K_S^0\eta\pi^0)/\Gamma_{\text{total}}$ — Γ_{91}/Γ

VALUE (units 10^{-3})	EVTS	DOCUMENT ID		TECN	COMMENT
10.06±0.34±0.30	1.1k	ABLIKIM	20V	BES3	e^+e^-, 3773 MeV

$\Gamma(K_S^0\eta\pi^0)/\Gamma(K_S^0\pi^0)$ — Γ_{91}/Γ_{38}

VALUE	EVTS	DOCUMENT ID		TECN	COMMENT
0.46±0.07±0.06	155 ± 22	[1] RUBIN	04	CLEO	$e^+e^- \approx$ 10 GeV

[1] The η here is detected in its $\gamma\gamma$ mode, but other η modes are included in the value given.

$\Gamma(K_S^0a_0(980),\ a_0 \to \eta\pi^0)/\Gamma(K_S^0\eta\pi^0)$ — Γ_{92}/Γ_{91}

This is the "fit fraction" from the Dalitz-plot analysis, with interference.

VALUE	DOCUMENT ID		TECN	COMMENT
1.19±0.09±0.26	[1] RUBIN	04	CLEO	Dalitz fit, 155 evts

[1] In addition to $K_S^0a_0(980)$ and $\overline{K}^*(892)^0\eta$ modes, RUBIN 04 finds a fit fraction of 0.246 ± 0.092 ± 0.091 for other, undetermined modes.

$\Gamma(\overline{K}^*(892)^0\eta,\ \overline{K}^{*0} \to K_S^0\pi^0)/\Gamma(K_S^0\eta\pi^0)$ — Γ_{93}/Γ_{91}

This is the "fit fraction" from the Dalitz-plot analysis, with interference.

VALUE	DOCUMENT ID		TECN	COMMENT
0.293±0.062±0.035	[1] RUBIN	04	CLEO	Dalitz fit, 155 evts

[1] See the note on RUBIN 04 in the preceding data block.

$\Gamma(K^-\pi^+\eta)/\Gamma_{\text{total}}$ — Γ_{94}/Γ

VALUE (units 10^{-2})	EVTS	DOCUMENT ID		TECN	COMMENT
1.88 ±0.05 OUR FIT Error includes scale factor of 1.4.					
1.853±0.025±0.031	6.1k	ABLIKIM	20V	BES3	e^+e^-, 3773 MeV

$\Gamma(K^-\pi^+\eta)/\Gamma(K^-\pi^+)$ — Γ_{94}/Γ_{37}

VALUE (units 10^{-2})	EVTS	DOCUMENT ID		TECN	COMMENT
47.6±1.3 OUR FIT Error includes scale factor of 1.4.					
50.1±2.0±0.2	116k	[1] CHEN	20A	BELL	e^+e^- at $\Upsilon(4S)$

[1] CHEN 20A reports 0.500 ± 0.002 ± 0.020 ± 0.003 from a measurement of $[\Gamma(D^0 \to K^-\pi^+\eta)/\Gamma(D^0 \to K^-\pi^+)] \times [B(\eta \to 2\gamma)]$ assuming $B(\eta \to 2\gamma) = (39.41 \pm 0.20)\times 10^{-2}$, which we rescale to our best value $B(\eta \to 2\gamma) = (39.36 \pm 0.18)\times 10^{-2}$. Our first error is their experiment's error and our second error is the systematic error from using our best value. The third reported uncertainty is the uncertainty from $B(\eta \to \gamma\gamma)$.

$\Gamma(K^*(892)^0\eta,\ K^{*0} \to K^-\pi^+)/\Gamma(K^-\pi^+\eta)$ — Γ_{95}/Γ_{94}

VALUE (units 10^{-2})	DOCUMENT ID		TECN	COMMENT
47.61±1.32$^{+0.24}_{-0.49}$$^{+3.64}_{-2.71}$	[1] CHEN	20A	BELL	e^+e^- at $\Upsilon(4S)$

[1] The third uncertainty is due to the uncertainty from the Dalitz model .

$\Gamma(a_0(980)^+K^-,\ a_0^+ \to \eta\pi^+)/\Gamma(K^-\pi^+\eta)$ — Γ_{96}/Γ_{94}

VALUE (units 10^{-2})	DOCUMENT ID		TECN	COMMENT
39.28±1.50$^{+1.58}_{-0.51}$$^{+4.38}_{-3.30}$	[1] CHEN	20A	BELL	e^+e^- at $\Upsilon(4S)$

[1] The third uncertainty is due to the uncertainty from the Dalitz model .

$\Gamma(K_2^*(1980)^-\pi^+,\ K_2^{*-} \to K^-\eta)/\Gamma_{\text{total}}$ — Γ_{97}/Γ

VALUE (units 10^{-4})	DOCUMENT ID		TECN	COMMENT
2.2$^{+1.7}_{-1.9}$	CHEN	20A	BELL	e^+e^- at $\Upsilon(4S)$

$\Gamma(K^-\pi^+\pi^0\eta)/\Gamma_{\text{total}}$ — Γ_{98}/Γ

VALUE (units 10^{-3})	EVTS	DOCUMENT ID		TECN	COMMENT
4.49±0.22±0.15	580	ABLIKIM	20V	BES3	e^+e^-, 3773 MeV

$\Gamma(K_S^0\pi^+\pi^-\eta)/\Gamma_{\text{total}}$ — Γ_{99}/Γ

VALUE (units 10^{-3})	EVTS	DOCUMENT ID		TECN	COMMENT
2.80±0.19±0.10	250	ABLIKIM	20V	BES3	e^+e^-, 3773 MeV

$\Gamma(K_S^0 2\pi^0\eta)/\Gamma_{\text{total}}$ — Γ_{100}/Γ

VALUE (units 10^{-3})	EVTS	DOCUMENT ID		TECN	COMMENT
1.76±0.23±0.13	65	ABLIKIM	20V	BES3	e^+e^-, 3773 MeV

$\Gamma(K_S^0 2\pi^+2\pi^-)/\Gamma(K_S^0\pi^+\pi^-)$ — Γ_{101}/Γ_{40}

VALUE	EVTS	DOCUMENT ID		TECN	COMMENT
0.095±0.005±0.007	1283 ± 57	LINK	04D	FOCS	γ A, $\overline{E}_\gamma \approx$ 180 GeV
• • • We do not use the following data for averages, fits, limits, etc. • • •					
0.07 ±0.02 ±0.01	11	[1] ALBRECHT	92P	ARG	$e^+e^- \approx$ 10 GeV
0.149±0.026	56	AMMAR	91	CLEO	$e^+e^- \approx$ 10.5 GeV
0.18 ±0.07 ±0.04	6	ANJOS	90D	E691	Photoproduction

[1] This value is calculated from numbers in Table 1 of ALBRECHT 92P.

$\Gamma(K_S^0\rho^0\pi^+\pi^-,\ \text{no}\,K^*(892)^-)/\Gamma(K_S^0 2\pi^+2\pi^-)$ — $\Gamma_{102}/\Gamma_{101}$

VALUE	DOCUMENT ID		TECN	COMMENT
0.40±0.24±0.07	LINK	04D	FOCS	γ A, $\overline{E}_\gamma \approx$ 180 GeV

$\Gamma(K^*(892)^-2\pi^+\pi^-,\ K^*(892)^- \to K_S^0\pi^-,\ \text{no}\,\rho^0)/\Gamma(K_S^0 2\pi^+2\pi^-)$ — $\Gamma_{103}/\Gamma_{101}$

VALUE	DOCUMENT ID		TECN	COMMENT
0.17±0.28±0.02	LINK	04D	FOCS	γ A, $\overline{E}_\gamma \approx$ 180 GeV

$\Gamma(K^*(892)^-\rho^0\pi^+,\ K^*(892)^- \to K_S^0\pi^-)/\Gamma(K_S^0 2\pi^+2\pi^-)$ — $\Gamma_{104}/\Gamma_{101}$

VALUE	DOCUMENT ID		TECN	COMMENT
0.60±0.21±0.09	LINK	04D	FOCS	γ A, $\overline{E}_\gamma \approx$ 180 GeV

$\Gamma(K_S^0 2\pi^+2\pi^-\text{nonresonant})/\Gamma(K_S^0 2\pi^+2\pi^-)$ — $\Gamma_{105}/\Gamma_{101}$

VALUE	CL%	DOCUMENT ID		TECN	COMMENT
<0.46	90	LINK	04D	FOCS	γ A, $\overline{E}_\gamma \approx$ 180 GeV

$\Gamma(K^-3\pi^+2\pi^-)/\Gamma(K^-2\pi^+\pi^-)$ — Γ_{107}/Γ_{72}

VALUE (units 10^{-3})	EVTS	DOCUMENT ID		TECN	COMMENT
2.70±0.58±0.38	48 ± 10	LINK	04B	FOCS	γA, $\overline{E}_\gamma \approx$ 180 GeV

Downloaded from https://academic.oup.com/ptep/article/2022/8/083C01/6651666 by KIT Library user on 27 September 2022

$\Gamma(K^0_S\eta)/\Gamma_{total}$ — Γ_{108}/Γ

Unseen decay modes of the η are included.

VALUE (units 10^{-3})	EVTS	DOCUMENT ID		TECN	COMMENT
5.09±0.13 OUR FIT					
5.13±0.07±0.12	9.5k	ABLIKIM	18W	BES3	e^+e^-, 3773 MeV
• • • We do not use the following data for averages, fits, limits, etc. • • •					
4.42±0.15±0.28		ASNER	08	CLEO	See MENDEZ 10

$\Gamma(K^0_S\eta)/[\Gamma(K^-\pi^+)+\Gamma(K^+\pi^-)]$ — $\Gamma_{108}/(\Gamma_{37}+\Gamma_{274})$

Unseen decay modes of the η are included.

VALUE (units 10^{-2})	EVTS	DOCUMENT ID		TECN	COMMENT
12.83±0.33 OUR FIT					
12.3 ±0.3 ±0.7	2864±65	MENDEZ	10	CLEO	e^+e^- at 3774 MeV

$\Gamma(K^0_S\eta)/\Gamma(K^0_S\pi^0)$ — Γ_{108}/Γ_{38}

Unseen decay modes of the η are included.

VALUE	EVTS	DOCUMENT ID		TECN	COMMENT
• • • We do not use the following data for averages, fits, limits, etc. • • •					
0.32±0.04±0.03	225 ± 30	PROCARIO	93B	CLE2	$\eta\to\gamma\gamma$

$\Gamma(K^0_S\eta)/\Gamma(K^0_S\pi^+\pi^-)$ — Γ_{108}/Γ_{40}

Unseen decay modes of the η are included.

VALUE	EVTS	DOCUMENT ID		TECN	COMMENT
• • • We do not use the following data for averages, fits, limits, etc. • • •					
0.14±0.02±0.02	80 ± 12	PROCARIO	93B	CLE2	$\eta\to\pi^+\pi^-\pi^0$

$\Gamma(K^0_S\omega)/\Gamma_{total}$ — Γ_{109}/Γ

Unseen decay modes of the ω are included.

VALUE (%)	DOCUMENT ID		TECN	COMMENT
1.11±0.06 OUR FIT				
1.12±0.04±0.05	ASNER	08	CLEO	$e^+e^-\to D^0\overline{D}^0$, 3.77 GeV

$\Gamma(K^0_S\omega)/\Gamma(K^-\pi^+)$ — Γ_{109}/Γ_{37}

Unseen decay modes of the ω are included.

VALUE	DOCUMENT ID		TECN	COMMENT
• • • We do not use the following data for averages, fits, limits, etc. • • •				
0.50±0.18±0.10	ALBRECHT	89D	ARG	e^+e^- 10 GeV

$\Gamma(K^0_S\omega)/\Gamma(K^0_S\pi^+\pi^-)$ — Γ_{109}/Γ_{40}

Unseen decay modes of the ω are included.

VALUE	EVTS	DOCUMENT ID		TECN	COMMENT
0.396±0.032 OUR FIT	Error includes scale factor of 1.1.				
0.33 ±0.09 OUR AVERAGE	Error includes scale factor of 1.1.				
0.29 ±0.08 ±0.05	16	[1] ALBRECHT	92P	ARG	$e^+e^-\approx$ 10 GeV
0.54 ±0.14 ±0.16	40	KINOSHITA	91	CLEO	$e^+e^-\sim$ 10.7 GeV

[1] This value is calculated from numbers in Table 1 of ALBRECHT 92P.

$\Gamma(K^0_S\omega)/\Gamma(K^0_S\pi^+\pi^-\pi^0)$ — Γ_{109}/Γ_{83}

Unseen decay modes of the ω are included.

VALUE	DOCUMENT ID		TECN	COMMENT
0.215±0.026 OUR FIT				
0.220±0.048±0.0116	COFFMAN	92B	MRK3	1281 ± 45 $K^-2\pi^+\pi^-$ evts

$\Gamma(K^0_S\eta'(958))/\Gamma_{total}$ — Γ_{110}/Γ

VALUE (units 10^{-3})	EVTS	DOCUMENT ID		TECN	COMMENT
9.49±0.32 OUR FIT					
9.49±0.20±0.36	3k	ABLIKIM	18W	BES3	e^+e^-, 3773 MeV

$\Gamma(K^0_S\eta'(958))/[\Gamma(K^-\pi^+)+\Gamma(K^+\pi^-)]$ — $\Gamma_{110}/(\Gamma_{37}+\Gamma_{274})$

Unseen decay modes of the $\eta'(958)$ are included.

VALUE (units 10^{-2})	EVTS	DOCUMENT ID		TECN	COMMENT
24.0±0.8 OUR FIT					
24.3±0.8±1.1	1321±42	MENDEZ	10	CLEO	e^+e^- at 3774 MeV

$\Gamma(K^0_S\eta'(958))/\Gamma(K^0_S\pi^+\pi^-)$ — Γ_{110}/Γ_{40}

Unseen decay modes of the $\eta'(958)$ are included.

VALUE	EVTS	DOCUMENT ID		TECN	COMMENT
0.339±0.023 OUR FIT					
0.32 ±0.04 OUR AVERAGE					
0.31 ±0.02 ±0.04	594	PROCARIO	93B	CLE2	$\eta'\to\eta\pi^+\pi^-,\rho^0\gamma$
0.37 ±0.13 ±0.06	18	[1] ALBRECHT	92P	ARG	$e^+e^-\approx$ 10 GeV

[1] This value is calculated from numbers in Table 1 of ALBRECHT 92P.

$\Gamma(\overline{K}^*(892)^0\pi^+\pi^-\pi^0)/\Gamma(K^-2\pi^+\pi^-\pi^0)$ — Γ_{111}/Γ_{87}

Unseen decay modes of the $\overline{K}^*(892)^0$ are included.

VALUE	DOCUMENT ID		TECN	COMMENT
0.45±0.15±0.15	ANJOS	90D	E691	Photoproduction

$\Gamma(\overline{K}^*(892)^0\eta)/\Gamma_{total}$ — Γ_{112}/Γ

VALUE (units 10^{-2})	DOCUMENT ID		TECN	COMMENT
$1.41^{+0.13}_{-0.12}\pm0.01$	[1] CHEN	20A	BELL	e^+e^- at $\Upsilon(4S)$

[1] CHEN 20A reports $(1.41\pm0.04^{+0.12}_{-0.11}\pm0.01)\times10^{-2}$ from a measurement of $[\Gamma(D^0\to\overline{K}^*(892)^0\eta)/\Gamma_{total}]\times[B(\eta\to2\gamma)]$ assuming $B(\eta\to2\gamma)=(39.41\pm0.20)\times10^{-2}$, which we rescale to our best value $B(\eta\to2\gamma)=(39.36\pm0.18)\times10^{-2}$. Our first error is their experiment's error and our second error is the systematic error from using our best value. The third reported uncertainty is the uncertainty from $B(\eta\to\gamma\gamma)$.

$\Gamma(\overline{K}^*(892)^0\eta)/\Gamma(K^-\pi^+)$ — Γ_{112}/Γ_{37}

Unseen decay modes of the $\overline{K}^*(892)^0$ and η are included.

VALUE	EVTS	DOCUMENT ID		TECN	COMMENT
• • • We do not use the following data for averages, fits, limits, etc. • • •					
$0.58\pm0.19^{+0.24}_{-0.28}$	46	KINOSHITA	91	CLEO	$e^+e^-\sim$ 10.7 GeV

$\Gamma(\overline{K}^*(892)^0\eta)/\Gamma(K^-\pi^+\pi^0)$ — Γ_{112}/Γ_{55}

Unseen decay modes of the $\overline{K}^*(892)^0$ and η are included.

VALUE	EVTS	DOCUMENT ID		TECN	COMMENT
• • • We do not use the following data for averages, fits, limits, etc. • • •					
0.13±0.02±0.03	214	PROCARIO	93B	CLE2	$\overline{K}^{*0}\eta\to K^-\pi^+/\gamma\gamma$

$\Gamma(K^-\pi^+\omega)/\Gamma(K^-\pi^+)$ — Γ_{113}/Γ_{37}

Unseen decay modes of the ω are included.

VALUE	EVTS	DOCUMENT ID		TECN	COMMENT
0.78±0.12±0.10	99	[1] ALBRECHT	92P	ARG	$e^+e^-\approx$ 10 GeV

[1] This value is calculated from numbers in Table 1 of ALBRECHT 92P.

$\Gamma(\overline{K}^*(892)^0\omega)/\Gamma(K^-\pi^+)$ — Γ_{114}/Γ_{37}

Unseen decay modes of the $\overline{K}^*(892)^0$ and ω are included.

VALUE	EVTS	DOCUMENT ID		TECN	COMMENT
0.28±0.11±0.04	17	[1] ALBRECHT	92P	ARG	$e^+e^-\approx$ 10 GeV

[1] This value is calculated from numbers in Table 1 of ALBRECHT 92P.

$\Gamma(K^-\pi^+\eta'(958))/\Gamma_{total}$ — Γ_{115}/Γ

VALUE (units 10^{-3})	EVTS	DOCUMENT ID		TECN	COMMENT
6.43±0.15±0.31	2.5k	ABLIKIM	18AC	BES3	e^+e^-, 3773 MeV

$\Gamma(K^-\pi^+\eta'(958))/\Gamma(K^-2\pi^+\pi^-)$ — Γ_{115}/Γ_{72}

Unseen decay modes of the $\eta'(958)$ are included.

VALUE	EVTS	DOCUMENT ID		TECN	COMMENT
0.093±0.014±0.019	286	PROCARIO	93B	CLE2	$\eta'\to\eta\pi^+\pi^-,\rho^0\gamma$

$\Gamma(K^0_S\eta'(958)\pi^0)/\Gamma_{total}$ — Γ_{116}/Γ

VALUE (units 10^{-3})	EVTS	DOCUMENT ID		TECN	COMMENT
2.52±0.22±0.15	289	ABLIKIM	18AC	BES3	e^+e^-, 3773 MeV

$\Gamma(\overline{K}^*(892)^0\eta'(958))/\Gamma(K^-\pi^+\eta'(958))$ — $\Gamma_{117}/\Gamma_{115}$

Unseen decay modes of the $\overline{K}^*(892)^0$ are included.

VALUE	CL%	DOCUMENT ID		TECN
<0.15	90	PROCARIO	93B	CLE2

Hadronic modes with three K's

$\Gamma(K^0_SK^+K^-)/\Gamma(K^0_S\pi^+\pi^-)$ — Γ_{118}/Γ_{40}

VALUE	EVTS	DOCUMENT ID		TECN	COMMENT
0.158±0.001±0.005	14k±116	AUBERT,B	05J	BABR	$e^+e^-\approx\Upsilon(4S)$
• • • We do not use the following data for averages, fits, limits, etc. • • •					
0.20 ±0.05 ±0.04	47	FRABETTI	92B	E687	γ Be, $\overline{E}_\gamma$= 221 GeV
0.170±0.022	136	AMMAR	91	CLEO	$e^+e^-\approx$ 10.5 GeV
0.24 ±0.08		BEBEK	86	CLEO	e^+e^- near $\Upsilon(4S)$
0.185±0.055	52	ALBRECHT	85B	ARG	e^+e^- 10 GeV

$\Gamma(K^0_Sa_0(980)^0,\ a_0^0\to K^+K^-)/\Gamma(K^0_SK^+K^-)$ — $\Gamma_{119}/\Gamma_{118}$

This is the "fit fraction" from the Dalitz-plot analysis, with interference.

VALUE	DOCUMENT ID		TECN	COMMENT
0.664±0.016±0.070	AUBERT,B	05J	BABR	Dalitz fit, 12540±112 evts

$\Gamma(K^-a_0(980)^+,\ a_0^+\to K^+K^0_S)/\Gamma(K^0_SK^+K^-)$ — $\Gamma_{120}/\Gamma_{118}$

This is the "fit fraction" from the Dalitz-plot analysis, with interference.

VALUE	DOCUMENT ID		TECN	COMMENT
0.134±0.011±0.037	AUBERT,B	05J	BABR	Dalitz fit, 12540±112 evts

$\Gamma(K^+a_0(980)^-,\ a_0^-\to K^-K^0_S)/\Gamma(K^0_SK^+K^-)$ — $\Gamma_{121}/\Gamma_{118}$

This is a doubly Cabibbo-suppressed mode.

VALUE	CL%	DOCUMENT ID		TECN	COMMENT
<0.025	95	AUBERT,B	05J	BABR	Dalitz fit, 12540 ± 112 evts

$\Gamma(K^0_Sf_0(980),\ f_0\to K^+K^-)/\Gamma(K^0_SK^+K^-)$ — $\Gamma_{122}/\Gamma_{118}$

VALUE	CL%	DOCUMENT ID		TECN	COMMENT
<0.021	95	AUBERT,B	05J	BABR	Dalitz fit, 12540 ± 112 evts

$\Gamma(K^0_S\phi,\ \phi\to K^+K^-)/\Gamma(K^0_SK^+K^-)$ — $\Gamma_{123}/\Gamma_{118}$

This is the "fit fraction" from the Dalitz-plot analysis, with interference.

VALUE	DOCUMENT ID		TECN	COMMENT
0.459±0.007±0.007	AUBERT,B	05J	BABR	Dalitz fit, 12540±112 evts

$\Gamma(K^0_Sf_0(1370),\ f_0\to K^+K^-)/\Gamma(K^0_SK^+K^-)$ — $\Gamma_{124}/\Gamma_{118}$

This is the "fit fraction" from the Dalitz-plot analysis, with interference.

VALUE	DOCUMENT ID		TECN	COMMENT
0.038±0.007±0.023	[1] AUBERT,B	05J	BABR	Dalitz fit, 12540±112 evts

[1] AUBERT,B 05J calls the mode $K^0_Sf_0(1400)$, but insofar as it is seen here at all, it is certainly the same as $f_0(1370)$.

Downloaded from https://academic.oup.com/ptep/article/2022/8/083C01/6651666 by KIT Library user on 27 September 2022

$\Gamma(3K^0_S)/\Gamma_{total}$ — Γ_{125}/Γ

VALUE (units 10^{-4})	EVTS	DOCUMENT ID		TECN	COMMENT
7.5 ±0.7 OUR FIT	Error includes scale factor of 1.4.				
7.21±0.33±0.44	597	ABLIKIM	17A	BES3	$e^+e^- \to \psi(3770)$

$\Gamma(3K^0_S)/\Gamma(K^0_S\pi^+\pi^-)$ — Γ_{125}/Γ_{40}

VALUE (units 10^{-2})	EVTS	DOCUMENT ID		TECN	COMMENT
2.70±0.26 OUR FIT	Error includes scale factor of 1.2.				
3.2 ±0.4 OUR AVERAGE					
3.58±0.54±0.52	170 ± 26	LINK	05A	FOCS	γBe, $\overline{E}_\gamma \approx 180$ GeV
2.78±0.38±0.48	61	ASNER	96B	CLE2	$e^+e^- \approx \Upsilon(4S)$
7.0 ±2.4 ±1.2	10 ± 3	FRABETTI	94J	E687	γBe, $\overline{E}_\gamma$=220 GeV
3.2 ±1.0	22	AMMAR	91	CLEO	$e^+e^- \approx$ 10.5 GeV
3.4 ±1.4 ±1.0	5	ALBRECHT	90C	ARG	$e^+e^- \approx$ 10 GeV

$\Gamma(K^+2K^-\pi^+)/\Gamma(K^-2\pi^+\pi^-)$ — Γ_{126}/Γ_{72}

VALUE	EVTS	DOCUMENT ID		TECN	COMMENT
0.0027 ±0.0004 OUR AVERAGE	Error includes scale factor of 1.1.				
0.00257±0.00034±0.00024	143	LINK	03G	FOCS	γ A, $\overline{E}_\gamma \approx 180$ GeV
0.0054 ±0.0016 ±0.0008	18	AITALA	01D	E791	π^- A, 500 GeV
0.0028 ±0.0007 ±0.0001	20	FRABETTI	95C	E687	γ Be, $\overline{E}_\gamma \approx 200$ GeV

$\Gamma(K^+K^-\overline{K}^*(892)^0,\ \overline{K}^{*0} \to K^-\pi^+)/\Gamma(K^+2K^-\pi^+)$ — $\Gamma_{127}/\Gamma_{126}$

VALUE	DOCUMENT ID		TECN	COMMENT
0.20±0.07±0.02	LINK	03G	FOCS	γ A, $\overline{E}_\gamma \approx 180$ GeV

$\Gamma(K^-\pi^+\phi,\ \phi \to K^+K^-)/\Gamma(K^+2K^-\pi^+)$ — $\Gamma_{128}/\Gamma_{126}$

VALUE	DOCUMENT ID		TECN	COMMENT
0.18±0.06±0.04	LINK	03G	FOCS	γ A, $\overline{E}_\gamma \approx 180$ GeV

$\Gamma(\phi\overline{K}^*(892)^0,\ \phi \to K^+K^-,\ \overline{K}^{*0} \to K^-\pi^+)/\Gamma(K^+2K^-\pi^+)$ — $\Gamma_{129}/\Gamma_{126}$

VALUE	DOCUMENT ID		TECN	COMMENT
0.48±0.06±0.01	LINK	03G	FOCS	γ A, $\overline{E}_\gamma \approx 180$ GeV

$\Gamma(K^+2K^-\pi^+ \text{nonresonant})/\Gamma(K^+2K^-\pi^+)$ — $\Gamma_{130}/\Gamma_{126}$

VALUE	DOCUMENT ID		TECN	COMMENT
0.15±0.06±0.02	LINK	03G	FOCS	γ A, $\overline{E}_\gamma \approx 180$ GeV

$\Gamma(2K^0_S K^\pm\pi^\mp)/\Gamma(K^0_S\pi^+\pi^-)$ — Γ_{131}/Γ_{40}

VALUE (units 10^{-2})	EVTS	DOCUMENT ID		TECN	COMMENT
2.12±0.38±0.20	57 ± 10	LINK	05A	FOCS	γ Be, $\overline{E}_\gamma \approx$ 180 GeV

Pionic modes

$\Gamma(\pi^+\pi^-)/\Gamma_{total}$ — Γ_{132}/Γ

VALUE (units 10^{-3})	EVTS	DOCUMENT ID		TECN	COMMENT
1.454±0.024 OUR FIT	Error includes scale factor of 1.4.				
1.508±0.018±0.022	21k	ABLIKIM	18W	BES3	e^+e^-, 3773 MeV

$\Gamma(\pi^+\pi^-)/\Gamma(K^-\pi^+)$ — Γ_{132}/Γ_{37}

VALUE (units 10^{-2})	EVTS	DOCUMENT ID		TECN	COMMENT
3.68 ±0.05 OUR FIT	Error includes scale factor of 1.3.				
3.59 ±0.06 OUR AVERAGE					
3.594±0.054±0.040	7334 ± 97	ACOSTA	05C	CDF	$p\overline{p}$, $\sqrt{s}$ = 1.96 TeV
3.53 ±0.12 ±0.06	3453	LINK	03	FOCS	γ A, $\overline{E}_\gamma \approx$ 180 GeV
3.51 ±0.16 ±0.17	710	CSORNA	02	CLE2	$e^+e^- \approx \Upsilon(4S)$
4.0 ±0.2 ±0.3	2043	AITALA	98C	E791	π^- A, 500 GeV
• • • We do not use the following data for averages, fits, limits, etc. • • •					
3.62 ±0.10 ±0.08	2085 ± 54	RUBIN	06	CLEO	See MENDEZ 10
3.4 ±0.7 ±0.1	76 ± 15	ABLIKIM	05F	BES	$e^+e^- \approx \psi(3770)$
4.3 ±0.7 ±0.3	177	FRABETTI	94C	E687	γBe $\overline{E}_\gamma$= 220 GeV
3.48 ±0.30 ±0.23	227	SELEN	93	CLE2	$e^+e^- \approx \Upsilon(4S)$
5.5 ±0.8 ±0.5	120	ANJOS	91D	E691	Photoproduction
5.0 ±0.7 ±0.5	110	ALEXANDER	90	CLEO	e^+e^- 10.5–11 GeV

$\Gamma(\pi^+\pi^-)/[\Gamma(K^-\pi^+)+\Gamma(K^+\pi^-)]$ — $\Gamma_{132}/(\Gamma_{37}+\Gamma_{274})$

VALUE (units 10^{-2})	EVTS	DOCUMENT ID		TECN	COMMENT
3.67±0.05 OUR FIT	Error includes scale factor of 1.3.				
3.70±0.06±0.09	6210 ± 93	MENDEZ	10	CLEO	e^+e^- at 3774 MeV

$\Gamma(2\pi^0)/\Gamma_{total}$ — Γ_{133}/Γ

VALUE (units 10^{-4})	EVTS	DOCUMENT ID		TECN	COMMENT
8.26±0.25 OUR FIT					
8.29±0.30 OUR AVERAGE					
8.24±0.21±0.30	6k	ABLIKIM	15F	BES3	e^+e^- at 3.773GeV
8.4 ±0.1 ±0.5	26k	LEES	12L	BABR	$e^+e^- \approx$ 10.58 GeV

$\Gamma(2\pi^0)/\Gamma(K^-\pi^+)$ — Γ_{133}/Γ_{37}

VALUE (units 10^{-2})	EVTS	DOCUMENT ID		TECN	COMMENT
• • • We do not use the following data for averages, fits, limits, etc. • • •					
2.05±0.13±0.16	499 ± 32	RUBIN	06	CLEO	See MENDEZ 10
2.2 ±0.4 ±0.4	40	SELEN	93	CLE2	$e^+e^- \to \Upsilon(4S)$

$\Gamma(2\pi^0)/[\Gamma(K^-\pi^+)+\Gamma(K^+\pi^-)]$ — $\Gamma_{133}/(\Gamma_{37}+\Gamma_{274})$

VALUE (units 10^{-2})	EVTS	DOCUMENT ID		TECN	COMMENT
2.08±0.07 OUR FIT					
2.06±0.07±0.10	1567 ± 54	MENDEZ	10	CLEO	e^+e^- at 3774 MeV

$\Gamma(\pi^+\pi^-\pi^0)/\Gamma(K^-\pi^+)$ — Γ_{134}/Γ_{37}

VALUE (units 10^{-2})	EVTS	DOCUMENT ID		TECN	COMMENT
37.7±1.6 OUR FIT	Error includes scale factor of 2.2.				
34.4±0.5±1.2	11k±164	RUBIN	06	CLEO	e^+e^- at $\psi(3770)$

$\Gamma(\pi^+\pi^-\pi^0)/\Gamma(K^-\pi^+\pi^0)$ — Γ_{134}/Γ_{55}

VALUE (units 10^{-2})	EVTS	DOCUMENT ID		TECN	COMMENT
10.32±0.25 OUR FIT	Error includes scale factor of 2.3.				
10.41±0.23 OUR AVERAGE	Error includes scale factor of 2.0.				
10.12±0.04±0.18	123k±490	ARINSTEIN	08	BELL	$e^+e^- \approx \Upsilon(4S)$
10.59±0.06±0.13	60k±343	AUBERT,B	06X	BABR	$e^+e^- \approx \Upsilon(4S)$

$\Gamma(\rho^+\pi^-)/\Gamma(\pi^+\pi^-\pi^0)$ — $\Gamma_{135}/\Gamma_{134}$

This is the "fit fraction" from the Dalitz-plot analysis, with interference. See GASPERO 08 and BHATTACHARYA 10A for isospin decompositions of the $D^0 \to \pi^+\pi^0\pi^-$ Dalitz plot, both based on the amplitudes of AUBERT 07BJ. They quantify the conclusion that the final state is dominantly isospin 0.

VALUE (units 10^{-2})	DOCUMENT ID		TECN	COMMENT
68.1±0.6 OUR AVERAGE				
67.8±0.0±0.6	AUBERT	07BJ	BABR	Dalitz fit, 45k events
76.3±1.9±2.5	CRONIN-HEN...	05	CLEO	$e^+e^- \approx$ 10 GeV

$\Gamma(\rho^0\pi^0)/\Gamma(\pi^+\pi^-\pi^0)$ — $\Gamma_{136}/\Gamma_{134}$

This is the "fit fraction" from the Dalitz-plot analysis, with interference.

VALUE (units 10^{-2})	DOCUMENT ID		TECN	COMMENT
25.9±1.1 OUR AVERAGE				
26.2±0.5±1.1	AUBERT	07BJ	BABR	Dalitz fit, 45k events
24.4±2.0±2.1	CRONIN-HEN...	05	CLEO	$e^+e^- \approx$ 10 GeV

$\Gamma(\rho^-\pi^+)/\Gamma(\pi^+\pi^-\pi^0)$ — $\Gamma_{137}/\Gamma_{134}$

This is the "fit fraction" from the Dalitz-plot analysis, with interference.

VALUE (units 10^{-2})	DOCUMENT ID		TECN	COMMENT
34.6±0.8 OUR AVERAGE				
34.6±0.8±0.3	AUBERT	07BJ	BABR	Dalitz fit, 45k events
34.5±2.4±1.3	CRONIN-HEN...	05	CLEO	$e^+e^- \approx$ 10 GeV

$\Gamma(\rho(1450)^+\pi^-,\ \rho^+ \to \pi^+\pi^0)/\Gamma(\pi^+\pi^-\pi^0)$ — $\Gamma_{138}/\Gamma_{134}$

This is the "fit fraction" from the Dalitz-plot analysis.

VALUE (units 10^{-2})	DOCUMENT ID		TECN	COMMENT
0.11±0.07±0.12	AUBERT	07BJ	BABR	Dalitz fit, 45k events

$\Gamma(\rho(1450)^0\pi^0,\ \rho^0 \to \pi^+\pi^-)/\Gamma(\pi^+\pi^-\pi^0)$ — $\Gamma_{139}/\Gamma_{134}$

This is the "fit fraction" from the Dalitz-plot analysis.

VALUE (units 10^{-2})	DOCUMENT ID		TECN	COMMENT
0.30±0.11±0.07	AUBERT	07BJ	BABR	Dalitz fit, 45k events

$\Gamma(\rho(1450)^-\pi^+,\ \rho^- \to \pi^-\pi^0)/\Gamma(\pi^+\pi^-\pi^0)$ — $\Gamma_{140}/\Gamma_{134}$

This is the "fit fraction" from the Dalitz-plot analysis.

VALUE (units 10^{-2})	DOCUMENT ID		TECN	COMMENT
1.79±0.22±0.12	AUBERT	07BJ	BABR	Dalitz fit, 45k events

$\Gamma(\rho(1700)^+\pi^-,\ \rho^+ \to \pi^+\pi^0)/\Gamma(\pi^+\pi^-\pi^0)$ — $\Gamma_{141}/\Gamma_{134}$

This is the "fit fraction" from the Dalitz-plot analysis.

VALUE (units 10^{-2})	DOCUMENT ID		TECN	COMMENT
4.1±0.7±0.7	AUBERT	07BJ	BABR	Dalitz fit, 45k events

$\Gamma(\rho(1700)^0\pi^0,\ \rho^0 \to \pi^+\pi^-)/\Gamma(\pi^+\pi^-\pi^0)$ — $\Gamma_{142}/\Gamma_{134}$

This is the "fit fraction" from the Dalitz-plot analysis.

VALUE (units 10^{-2})	DOCUMENT ID		TECN	COMMENT
5.0±0.6±1.0	AUBERT	07BJ	BABR	Dalitz fit, 45k events

$\Gamma(\rho(1700)^-\pi^+,\ \rho^- \to \pi^-\pi^0)/\Gamma(\pi^+\pi^-\pi^0)$ — $\Gamma_{143}/\Gamma_{134}$

This is the "fit fraction" from the Dalitz-plot analysis.

VALUE (units 10^{-2})	DOCUMENT ID		TECN	COMMENT
3.2±0.4±0.6	AUBERT	07BJ	BABR	Dalitz fit, 45k events

$\Gamma(f_0(980)\pi^0,\ f_0 \to \pi^+\pi^-)/\Gamma(\pi^+\pi^-\pi^0)$ — $\Gamma_{144}/\Gamma_{134}$

This is the "fit fraction" from the Dalitz-plot analysis.

VALUE (units 10^{-2})	DOCUMENT ID		TECN	COMMENT
0.25±0.04±0.04	AUBERT	07BJ	BABR	Dalitz fit, 45k events

$\Gamma(f_0(500)\pi^0,\ f_0 \to \pi^+\pi^-)/\Gamma(\pi^+\pi^-\pi^0)$ — $\Gamma_{145}/\Gamma_{134}$

The $f_0(500)$ is the σ. This is the "fit fraction" from the Dalitz-plot analysis.

VALUE (units 10^{-2})	DOCUMENT ID		TECN	COMMENT
0.82±0.10±0.10	AUBERT	07BJ	BABR	Dalitz fit, 45k events

$\Gamma(f_0(1370)\pi^0,\ f_0 \to \pi^+\pi^-)/\Gamma(\pi^+\pi^-\pi^0)$ — $\Gamma_{146}/\Gamma_{134}$

This is the "fit fraction" from the Dalitz-plot analysis.

VALUE (units 10^{-2})	DOCUMENT ID		TECN	COMMENT
0.37±0.11±0.09	AUBERT	07BJ	BABR	Dalitz fit, 45k events

Downloaded from https://academic.oup.com/ptep/article/2022/8/083C01/6651666 by KIT Library user on 27 September 2022

$\Gamma(f_0(1500)\pi^0,\ f_0\to\pi^+\pi^-)/\Gamma(\pi^+\pi^-\pi^0)$ — $\Gamma_{147}/\Gamma_{134}$

This is the "fit fraction" from the Dalitz-plot analysis.

VALUE (units 10^{-2})	DOCUMENT ID		TECN	COMMENT
0.39±0.08±0.07	AUBERT	07BJ	BABR	Dalitz fit, 45k events

$\Gamma(f_0(1710)\pi^0,\ f_0\to\pi^+\pi^-)/\Gamma(\pi^+\pi^-\pi^0)$ — $\Gamma_{148}/\Gamma_{134}$

This is the "fit fraction" from the Dalitz-plot analysis.

VALUE (units 10^{-2})	DOCUMENT ID		TECN	COMMENT
0.31±0.07±0.08	AUBERT	07BJ	BABR	Dalitz fit, 45k events

$\Gamma(f_2(1270)\pi^0,\ f_2\to\pi^+\pi^-)/\Gamma(\pi^+\pi^-\pi^0)$ — $\Gamma_{149}/\Gamma_{134}$

This is the "fit fraction" from the Dalitz-plot analysis.

VALUE (units 10^{-2})	DOCUMENT ID		TECN	COMMENT
1.32±0.08±0.10	AUBERT	07BJ	BABR	Dalitz fit, 45k events

$\Gamma(\pi^+\pi^-\pi^0\text{nonresonant})/\Gamma(\pi^+\pi^-\pi^0)$ — $\Gamma_{150}/\Gamma_{134}$

This is the "fit fraction" from the Dalitz-plot analysis.

VALUE (units 10^{-2})	DOCUMENT ID		TECN	COMMENT
0.84±0.21±0.12	AUBERT	07BJ	BABR	Dalitz fit, 45k events

$\Gamma(3\pi^0)/\Gamma_{\text{total}}$ — Γ_{151}/Γ

VALUE (units 10^{-4})	CL%	EVTS	DOCUMENT ID		TECN	COMMENT
2.0±0.4±0.3		60	[1] ABLIKIM	18X	BES3	e^+e^-, 3773 MeV
• • • We do not use the following data for averages, fits, limits, etc. • • •						
<3.5		90	RUBIN	06	CLEO	e^+e^- at $\psi(3770)$

[1] Significance of signal reported by ABLIKIM 18X is 4.8σ.

$\Gamma(2\pi^+2\pi^-)/\Gamma(K^-\pi^+)$ — Γ_{152}/Γ_{37}

VALUE (units 10^{-2})	EVTS	DOCUMENT ID		TECN	COMMENT
19.1±0.5 OUR FIT					
19.1±0.4±0.6	7331 ± 130	RUBIN	06	CLEO	e^+e^- at $\psi(3770)$

$\Gamma(2\pi^+2\pi^-)/\Gamma(K^-2\pi^+\pi^-)$ — Γ_{152}/Γ_{72}

VALUE (units 10^{-2})	EVTS	DOCUMENT ID		TECN	COMMENT
9.19±0.22 OUR FIT					
9.20±0.26 OUR AVERAGE					
9.14±0.18±0.22	6360±115	LINK	07A	FOCS	γBe, $\overline{E}_\gamma\approx$ 180 GeV
7.9 ±1.8 ±0.5	162	ABLIKIM	05F	BES	$e^+e^-\approx\psi(3770)$
9.5 ±0.7 ±0.2	814	FRABETTI	95C	E687	γBe, $\overline{E}_\gamma\approx$ 200 GeV
10.2 ±1.3	345	AMMAR	91	CLEO	$e^+e^-\approx$ 10.5 GeV
• • • We do not use the following data for averages, fits, limits, etc. • • •					
11.5 ±2.3 ±1.6	64	ADAMOVICH	92	OMEG	π^- 340 GeV
10.8 ±2.4 ±0.8	79	FRABETTI	92	E687	γBe
9.6 ±1.8 ±0.7	66	ANJOS	91	E691	γBe 80–240 GeV

$\Gamma(a_1(1260)^+\pi^-,\ a_1^+\to 2\pi^+\pi^-\text{total})/\Gamma(2\pi^+2\pi^-)$ — $\Gamma_{153}/\Gamma_{152}$

This is the fit fraction from the coherent amplitude analysis.

VALUE (units 10^{-2})	DOCUMENT ID		TECN	COMMENT
60.0±3.0±2.4	LINK	07A	FOCS	4-body fit, ≈ 5.7k evts

$\Gamma(a_1(1260)^+\pi^-,\ a_1^+\to\rho^0\pi^+\ S\text{-wave})/\Gamma(2\pi^+2\pi^-)$ — $\Gamma_{154}/\Gamma_{152}$

This is the fit fraction from the coherent amplitude analysis.

VALUE (units 10^{-2})	DOCUMENT ID		TECN	COMMENT
41.5±2.5 OUR AVERAGE				
38.1±2.3±3.6	[1] DARGENT	17		4-body fit, 7.3k 4π evts
43.3±2.5±1.9	LINK	07A	FOCS	4-body fit, ≈ 5.7k evts

[1] Obtained by analyzing CLEO-c data but not authored by the CLEO Collaboration.

$\Gamma(a_1(1260)^+\pi^-,\ a_1^+\to\rho^0\pi^+\ D\text{-wave})/\Gamma(2\pi^+2\pi^-)$ — $\Gamma_{155}/\Gamma_{152}$

This is the fit fraction from the coherent amplitude analysis.

VALUE (units 10^{-2})	DOCUMENT ID		TECN	COMMENT
2.5±0.5±0.4	[1] LINK	07A	FOCS	4-body fit, ≈ 5.7k evts

[1] DARGENT 17 using 7.3k events find this contribution negligible.

$\Gamma(a_1(1260)^+\pi^-,\ a_1^+\to\sigma\pi^+)/\Gamma(2\pi^+2\pi^-)$ — $\Gamma_{156}/\Gamma_{152}$

This is the fit fraction from the coherent amplitude analysis.

VALUE (units 10^{-2})	DOCUMENT ID		TECN	COMMENT
8.4±0.9 OUR AVERAGE				
10.2±1.4±3.3	[1] DARGENT	17		7.3k 4-body fit, 4π evts
8.3±0.7±0.6	LINK	07A	FOCS	4-body fit, ≈ 5.7k evts

[1] Obtained by analyzing CLEO-c data but not authored by the CLEO Collaboration.

$\Gamma(a_1(1260)^-\pi^+,\ a_1^-\to\rho^0\pi^-\ S\text{-wave})/\Gamma(2\pi^+2\pi^-)$ — $\Gamma_{157}/\Gamma_{152}$

This is the fit fraction from a coherent amplitude analysis.

VALUE (units 10^{-2})	EVTS	DOCUMENT ID		COMMENT
3.1±0.6±1.0	7.3k	[1] DARGENT	17	4-body fit, 4π evts

[1] Obtained by analyzing CLEO-c data but not authored by the CLEO Collaboration.

$\Gamma(a_1(1260)^-\pi^+,\ a_1^-\to\sigma\pi^-)/\Gamma(2\pi^+2\pi^-)$ — $\Gamma_{158}/\Gamma_{152}$

This is the fit fraction from a coherent amplitude analysis.

VALUE (units 10^{-2})	EVTS	DOCUMENT ID		COMMENT
0.8±0.2±0.4	7.3k	[1] DARGENT	17	4-body fit, 4π evts

[1] Obtained by analyzing CLEO-c data but not authored by the CLEO Collaboration.

$\Gamma(\pi(1300)^+\pi^-,\ \pi(1300)^+\to\sigma\pi^+)/\Gamma(2\pi^+2\pi^-)$ — $\Gamma_{159}/\Gamma_{152}$

This is the fit fraction from a coherent amplitude analysis.

VALUE (units 10^{-2})	EVTS	DOCUMENT ID		COMMENT
6.8±0.9±3.4	7.3k	[1] DARGENT	17	4-body fit, 4π evts

[1] Obtained by analyzing CLEO-c data but not authored by the CLEO Collaboration.

$\Gamma(\pi(1300)^-\pi^+,\ \pi(1300)^-\to\sigma\pi^-)/\Gamma(2\pi^+2\pi^-)$ — $\Gamma_{160}/\Gamma_{152}$

This is the fit fraction from a coherent amplitude analysis.

VALUE (units 10^{-2})	EVTS	DOCUMENT ID		COMMENT
3.0±0.6±2.8	7.3k	[1] DARGENT	17	4-body fit, 4π evts

[1] Obtained by analyzing CLEO-c data but not authored by the CLEO Collaboration.

$\Gamma(a_1(1640)^+\pi^-,\ a_1^+\to\rho^0\pi^+\ D\text{-wave})/\Gamma(2\pi^+2\pi^-)$ — $\Gamma_{161}/\Gamma_{152}$

This is the fit fraction from a coherent amplitude analysis.

VALUE (units 10^{-2})	EVTS	DOCUMENT ID		COMMENT
4.2±0.6±2.0	7.3k	[1,2] DARGENT	17	4-body fit, 4π evts

[1] Obtained by analyzing CLEO-c data but not authored by the CLEO Collaboration.
[2] 4-body fit, 4π evts

$\Gamma(a_1(1640)^+\pi^-,\ a_1^+\to\sigma\pi^+)/\Gamma(2\pi^+2\pi^-)$ — $\Gamma_{162}/\Gamma_{152}$

This is the fit fraction from a coherent amplitude analysis.

VALUE (units 10^{-2})	EVTS	DOCUMENT ID		COMMENT
2.4±0.7±1.7	7.3k	[1] DARGENT	17	4-body fit, 4π evts

[1] Obtained by analyzing CLEO-c data but not authored by the CLEO Collaboration.

$\Gamma(\pi_2(1670)^+\pi^-,\ \pi_2^+\to f_2(1270)^0\pi^+,\ f_2^0\to\pi^+\pi^-)/\Gamma(2\pi^+2\pi^-)$ — $\Gamma_{163}/\Gamma_{152}$

This is the fit fraction from a coherent amplitude analysis.

VALUE (units 10^{-2})	EVTS	DOCUMENT ID		COMMENT
2.7±0.6±1.1	7.3k	[1] DARGENT	17	4-body fit, 4π evts

[1] Obtained by analyzing CLEO-c data but not authored by the CLEO Collaboration.

$\Gamma(\pi_2(1670)^+\pi^-,\ \pi_2^+\to\sigma\pi^+)/\Gamma(2\pi^+2\pi^-)$ — $\Gamma_{164}/\Gamma_{152}$

This is the fit fraction from a coherent amplitude analysis.

VALUE (units 10^{-2})	EVTS	DOCUMENT ID		COMMENT
3.5±0.6±1.2	7.3k	[1] DARGENT	17	4-body fit, 4π evts

[1] Obtained by analyzing CLEO-c data but not authored by the CLEO Collaboration.

$\Gamma(2\rho^0\text{total})/\Gamma(2\pi^+2\pi^-)$ — $\Gamma_{165}/\Gamma_{152}$

This is the fit fraction from the coherent amplitude analysis.

VALUE (units 10^{-2})	DOCUMENT ID		TECN	COMMENT
24.5±1.3±1.0	LINK	07A	FOCS	4-body fit, ≈ 5.7k evts

$\Gamma(2\rho^0,\text{parallel helicities})/\Gamma(2\pi^+2\pi^-)$ — $\Gamma_{166}/\Gamma_{152}$

This is the fit fraction from the coherent amplitude analysis.

VALUE (units 10^{-2})	DOCUMENT ID		TECN	COMMENT
1.1±0.3±0.3	LINK	07A	FOCS	4-body fit, ≈ 5.7k evts

$\Gamma(2\rho^0,\text{perpendicular helicities})/\Gamma(2\pi^+2\pi^-)$ — $\Gamma_{167}/\Gamma_{152}$

This is the fit fraction from the coherent amplitude analysis.

VALUE (units 10^{-2})	DOCUMENT ID		TECN	COMMENT
6.4±0.6±0.5	LINK	07A	FOCS	4-body fit, ≈ 5.7k evts

$\Gamma(2\rho^0,\text{longitudinal helicities})/\Gamma(2\pi^+2\pi^-)$ — $\Gamma_{168}/\Gamma_{152}$

This is the fit fraction from the coherent amplitude analysis.

VALUE (units 10^{-2})	DOCUMENT ID		TECN	COMMENT
16.8±1.0±0.8	LINK	07A	FOCS	4-body fit, ≈ 5.7k evts

$\Gamma(2\rho(770)^0,\ S\text{-wave})/\Gamma(2\pi^+2\pi^-)$ — $\Gamma_{169}/\Gamma_{152}$

This is the fit fraction from a coherent amplitude analysis.

VALUE (units 10^{-2})	EVTS	DOCUMENT ID		COMMENT
2.4±0.7±1.5	7.3k	[1] DARGENT	17	4-body fit, 4π evts

[1] Obtained by analyzing CLEO-c data but not authored by the CLEO Collaboration.

$\Gamma(2\rho(770)^0,\ P\text{-wave})/\Gamma(2\pi^+2\pi^-)$ — $\Gamma_{170}/\Gamma_{152}$

This is the fit fraction from a coherent amplitude analysis.

VALUE (units 10^{-2})	EVTS	DOCUMENT ID		COMMENT
7.0±0.5±1.6	7.3k	[1] DARGENT	17	4-body fit, 4π evts

[1] Obtained by analyzing CLEO-c data but not authored by the CLEO Collaboration.

$\Gamma(2\rho(770)^0,\ D\text{-wave})/\Gamma(2\pi^+2\pi^-)$ — $\Gamma_{171}/\Gamma_{152}$

This is the fit fraction from a coherent amplitude analysis.

VALUE (units 10^{-2})	EVTS	DOCUMENT ID		COMMENT
8.2±1.0±3.9	7.3k	[1] DARGENT	17	4-body fit, 4π evts

[1] Obtained by analyzing CLEO-c data but not authored by the CLEO Collaboration.

$\Gamma(\text{Resonant }(\pi^+\pi^-)\pi^+\pi^-\text{ 3-body total})/\Gamma(2\pi^+2\pi^-)$ — $\Gamma_{172}/\Gamma_{152}$

This is the fit fraction from the coherent amplitude analysis.

VALUE (units 10^{-2})	DOCUMENT ID		TECN	COMMENT
20.0±1.2±1.0	LINK	07A	FOCS	4-body fit, ≈ 5.7k evts

Downloaded from https://academic.oup.com/ptep/article/2022/8/083C01/6651666 by KIT Library user on 27 September 2022

$\Gamma(\sigma\pi^+\pi^-)/\Gamma(2\pi^+2\pi^-)$ — $\Gamma_{173}/\Gamma_{152}$

This is the fit fraction from the coherent amplitude analysis.

VALUE (units 10^{-2})	DOCUMENT ID		TECN	COMMENT
8.2±0.9±0.7	LINK	07A	FOCS	4-body fit, ≈ 5.7k evts

$\Gamma(\sigma\rho(770)^0)/\Gamma(2\pi^+2\pi^-)$ — $\Gamma_{174}/\Gamma_{152}$

This is the fit fraction from a coherent amplitude analysis.

VALUE (units 10^{-2})	EVTS	DOCUMENT ID		COMMENT
6.6±1.0±3.2	7.3k	[1] DARGENT	17	4-body fit, 4π evts

[1] Obtained by analyzing CLEO-c data but not authored by the CLEO Collaboration.

$\Gamma(f_0(1370)\sigma,\ f_0\to\pi^+\pi^-)/\Gamma(2\pi^+2\pi^-)$ — $\Gamma_{178}/\Gamma_{152}$

This is the fit fraction from a coherent amplitude analysis.

VALUE (units 10^{-2})	EVTS	DOCUMENT ID		COMMENT
21.2±1.8±6.7	7.3k	[1] DARGENT	17	4-body fit, 4π evts

[1] Obtained by analyzing CLEO-c data but not authored by the CLEO Collaboration.

$\Gamma(f_0(980)\pi^+\pi^-,\ f_0\to\pi^+\pi^-)/\Gamma(2\pi^+2\pi^-)$ — $\Gamma_{175}/\Gamma_{152}$

This is the fit fraction from the coherent amplitude analysis.

VALUE (units 10^{-2})	DOCUMENT ID		TECN	COMMENT
2.4±0.5±0.4	LINK	07A	FOCS	4-body fit, ≈ 5.7k evts

$\Gamma(f_2(1270)\pi^+\pi^-,\ f_2\to\pi^+\pi^-)/\Gamma(2\pi^+2\pi^-)$ — $\Gamma_{176}/\Gamma_{152}$

This is the fit fraction from the coherent amplitude analysis.

VALUE (units 10^{-2})	DOCUMENT ID		TECN	COMMENT
4.9±0.6±0.5	LINK	07A	FOCS	4-body fit, ≈ 5.7k evts

$\Gamma(2f_2(1270),\ f_2\to\pi^+\pi^-)/\Gamma(2\pi^+2\pi^-)$ — $\Gamma_{177}/\Gamma_{152}$

This is the fit fraction from a coherent amplitude analysis.

VALUE (units 10^{-2})	EVTS	DOCUMENT ID		COMMENT
2.1±0.5±2.3	7.3k	[1] DARGENT	17	4-body fit, 4π evts

[1] Obtained by analyzing CLEO-c data but not authored by the CLEO Collaboration.

$\Gamma(\pi^+\pi^-2\pi^0)/\Gamma(K^-\pi^+)$ — Γ_{179}/Γ_{37}

VALUE (units 10^{-2})	EVTS	DOCUMENT ID		TECN	COMMENT
25.8±1.5±1.8	2724 ± 166	RUBIN	06	CLEO	e^+e^- at $\psi(3770)$

$\Gamma(\eta\pi^0)/\Gamma_{total}$ — Γ_{180}/Γ

Unseen decay modes of the η are included.

VALUE (units 10^{-4})	EVTS	DOCUMENT ID		TECN	COMMENT
6.3±0.6 OUR FIT	Error includes scale factor of 1.1.				
5.8±0.5±0.5	1.7k	ABLIKIM	18L	BES3	e^+e^-, 3773 MeV
• • • We do not use the following data for averages, fits, limits, etc. • • •					
6.5±0.9±0.4	75	ABLIKIM	16D	BES3	See ABLIKIM 18L
6.4±1.0±0.4	156 ± 24	ARTUSO	08	CLEO	See MENDEZ 10

$\Gamma(\eta\pi^0)/\Gamma(K^-\pi^+)$ — Γ_{180}/Γ_{37}

Unseen decay modes of the η are included.

VALUE (units 10^{-2})	EVTS	DOCUMENT ID		TECN	COMMENT
• • • We do not use the following data for averages, fits, limits, etc. • • •					
1.47±0.34±0.11	62 ± 14	RUBIN	06	CLEO	See ARTUSO 08

$\Gamma(\eta\pi^0)/[\Gamma(K^-\pi^+)+\Gamma(K^+\pi^-)]$ — $\Gamma_{180}/(\Gamma_{37}+\Gamma_{274})$

Unseen decay modes of the η are included.

VALUE (units 10^{-2})	EVTS	DOCUMENT ID		TECN	COMMENT
1.60±0.14 OUR FIT	Error includes scale factor of 1.1.				
1.74±0.15±0.11	481 ± 40	MENDEZ	10	CLEO	e^+e^- at 3774 MeV

$\Gamma(\omega\pi^0)/\Gamma_{total}$ — Γ_{181}/Γ

Unseen decay modes of the ω are included.

VALUE (units 10^{-4})	EVTS	DOCUMENT ID		TECN	COMMENT
1.17±0.34±0.07	45	ABLIKIM	16D	BES3	e^+e^-, 3773 MeV

$\Gamma(2\pi^+2\pi^-\pi^0)/\Gamma(K^-\pi^+)$ — Γ_{183}/Γ_{37}

VALUE (units 10^{-2})	EVTS	DOCUMENT ID		TECN	COMMENT
10.7±1.2±0.5	1614 ± 171	RUBIN	06	CLEO	e^+e^- at $\psi(3770)$

$\Gamma(\eta\pi^+\pi^-)/\Gamma_{total}$ — Γ_{184}/Γ

Unseen decay modes of the η are included.

VALUE (units 10^{-4})	EVTS	DOCUMENT ID		TECN	COMMENT
11.6±0.7 OUR AVERAGE					
10.6±1.8±0.7	96	ABLIKIM	20AA	BES3	e^+e^-, 3773 MeV
12.0±0.7±0.4	450	ABLIKIM	20G	BES3	e^+e^-, 3773 MeV
10.9±1.3±0.9	257	ARTUSO	08	CLEO	e^+e^- at $\psi(3770)$

$\Gamma(\eta\pi^+\pi^-)/\Gamma(K^-\pi^+\eta)$ — Γ_{184}/Γ_{94}

VALUE (units 10^{-2})	EVTS	DOCUMENT ID		TECN	COMMENT
6.49±0.09±0.12	13k	LI	21G	BELL	e^+e^- at $\Upsilon(nS)$

$\Gamma(\eta2\pi^0)/\Gamma_{total}$ — Γ_{187}/Γ

VALUE (units 10^{-4})	CL%	EVTS	DOCUMENT ID		TECN	COMMENT
3.8±1.1±0.7		42	[1] ABLIKIM	18X	BES3	e^+e^-, 3773 MeV
• • • We do not use the following data for averages, fits, limits, etc. • • •						
<23.8	90		ABLIKIM	20AA	BES3	e^+e^-, 3773 MeV

[1] Significance of signal reported by ABLIKIM 18X is 3.8σ.

$\Gamma(\pi^+\pi^-\pi^0\eta)/\Gamma_{total}$ — Γ_{188}/Γ

VALUE (units 10^{-3})	EVTS	DOCUMENT ID		TECN	COMMENT
3.23±0.17±0.14	510	ABLIKIM	20V	BES3	e^+e^-, 3773 MeV

$\Gamma(\omega\eta)/\Gamma_{total}$ — Γ_{182}/Γ

VALUE (units 10^{-3})	EVTS	DOCUMENT ID		TECN	COMMENT
1.98±0.18 OUR AVERAGE	Error includes scale factor of 1.1.				
2.15±0.17±0.15	2.2k	ABLIKIM	18L	BES3	e^+e^-, 3773 MeV
1.78±0.19±0.15	600	[1] SMITH	18		e^+e^-, 3773 MeV

[1] Obtained by analyzing CLEO-c data but not authored by the CLEO Collaboration.

$\Gamma(\omega\pi^+\pi^-)/\Gamma_{total}$ — Γ_{185}/Γ

VALUE (units 10^{-3})	EVTS	DOCUMENT ID		TECN	COMMENT
1.33±0.16±0.12	411	ABLIKIM	20AA	BES3	e^+e^-, 3773 MeV

$\Gamma(\omega\pi^+\pi^-)/\Gamma(K^-\pi^+)$ — Γ_{185}/Γ_{37}

Unseen decay modes of the ω are included.

VALUE (units 10^{-2})	EVTS	DOCUMENT ID		TECN	COMMENT
4.1±1.2±0.4	472 ± 132	RUBIN	06	CLEO	e^+e^- at $\psi(3770)$

$\Gamma(\omega\pi^0\pi^0)/\Gamma_{total}$ — Γ_{186}/Γ

VALUE	CL%	DOCUMENT ID		TECN	COMMENT
<1.10 × 10^{-3}	90	ABLIKIM	20AA	BES3	e^+e^-, 3773 MeV

$\Gamma(3\pi^+3\pi^-)/\Gamma(K^-2\pi^+\pi^-)$ — Γ_{189}/Γ_{72}

VALUE (units 10^{-3})	EVTS	DOCUMENT ID		TECN	COMMENT
5.23±0.59±1.35	149 ± 17	LINK	04B	FOCS	γA, $\overline{E}_\gamma \approx$ 180 GeV

$\Gamma(3\pi^+3\pi^-)/\Gamma(K^-3\pi^+2\pi^-)$ — $\Gamma_{189}/\Gamma_{107}$

VALUE	DOCUMENT ID		TECN	COMMENT
• • • We do not use the following data for averages, fits, limits, etc. • • •				
1.93±047±0.48	[1] LINK	04B	FOCS	γA, $\overline{E}_\gamma \approx$ 180 GeV

[1] This LINK 04B result is not independent of other results in these Listings.

$\Gamma(\eta'(958)\pi^0)/\Gamma_{total}$ — Γ_{190}/Γ

Unseen decay modes of the $\eta'(958)$ are included.

VALUE (units 10^{-4})	EVTS	DOCUMENT ID		TECN	COMMENT
9.2±1.0 OUR FIT					
9.3±1.1±0.9	469 ± 56	ABLIKIM	18L	BES3	e^+e^-, 3773 MeV
• • • We do not use the following data for averages, fits, limits, etc. • • •					
8.1±1.5±0.6	50 ± 9	ARTUSO	08	CLEO	See MENDEZ 10

$\Gamma(\eta'(958)\pi^0)/[\Gamma(K^-\pi^+)+\Gamma(K^+\pi^-)]$ — $\Gamma_{190}/(\Gamma_{37}+\Gamma_{274})$

Unseen decay modes of the $\eta'(958)$ are included.

VALUE (units 10^{-2})	EVTS	DOCUMENT ID		TECN	COMMENT
2.32±0.25 OUR FIT					
2.3 ±0.3 ±0.2	159 ± 19	MENDEZ	10	CLEO	e^+e^- at 3774 MeV

$\Gamma(\eta'(958)\pi^+\pi^-)/\Gamma_{total}$ — Γ_{191}/Γ

Unseen decay modes of the $\eta'(958)$ are included.

VALUE (units 10^{-4})	EVTS	DOCUMENT ID		TECN	COMMENT
4.5±1.6±0.5	21 ± 8	ARTUSO	08	CLEO	e^+e^- at $\psi(3770)$

$\Gamma(2\eta)/\Gamma_{total}$ — Γ_{192}/Γ

Unseen decay modes of the η are included.

VALUE (units 10^{-4})	EVTS	DOCUMENT ID		TECN	COMMENT
21.1±1.9 OUR FIT	Error includes scale factor of 2.2.				
22.0±0.7±0.6	3.4k	ABLIKIM	18L	BES3	e^+e^-, 3773 MeV
• • • We do not use the following data for averages, fits, limits, etc. • • •					
16.7±1.4±1.3	255 ± 22	ARTUSO	08	CLEO	See MENDEZ 10

$\Gamma(2\eta)/[\Gamma(K^-\pi^+)+\Gamma(K^+\pi^-)]$ — $\Gamma_{192}/(\Gamma_{37}+\Gamma_{274})$

Unseen decay modes of the η are included.

VALUE (units 10^{-2})	EVTS	DOCUMENT ID		TECN	COMMENT
5.3±0.5 OUR FIT	Error includes scale factor of 2.2.				
4.3±0.3±0.4	430 ± 29	MENDEZ	10	CLEO	e^+e^- at 3774 MeV

$\Gamma(2\eta\pi^0)/\Gamma_{total}$ — Γ_{193}/Γ

VALUE (units 10^{-4})	EVTS	DOCUMENT ID		TECN	COMMENT
7.3±1.6±1.5	27	[1] ABLIKIM	18X	BES3	e^+e^-, 3773 MeV

[1] Significance of signal reported by ABLIKIM 18X is 5.5σ.

Downloaded from https://academic.oup.com/ptep/article/2022/8/083C01/6651666 by KIT Library user on 27 September 2022

$\Gamma(3\eta)/\Gamma_{total}$ — Γ_{194}/Γ

VALUE	CL%	DOCUMENT ID		TECN	COMMENT
$<1.3\times10^{-4}$	90	ABLIKIM	18X	BES3	e^+e^-, 3773 MeV

$\Gamma(\eta\eta'(958))/\Gamma_{total}$ — Γ_{195}/Γ

Unseen decay modes of the η and $\eta'(958)$ are included.

VALUE (units 10^{-4})	EVTS	DOCUMENT ID		TECN	COMMENT
10.1±1.9 OUR FIT					
9.4±2.5±1.1	158 ± 41	ABLIKIM	18L	BES3	e^+e^-, 3773 MeV
• • • We do not use the following data for averages, fits, limits, etc. • • •					
12.6±2.5±1.1	46 ± 9	ARTUSO	08	CLEO	See MENDEZ 10

$\Gamma(\eta\eta'(958))/[\Gamma(K^-\pi^+)+\Gamma(K^+\pi^-)]$ — $\Gamma_{195}/(\Gamma_{37}+\Gamma_{274})$

Unseen decay modes of the η and $\eta'(958)$ are included.

VALUE (units 10^{-2})	EVTS	DOCUMENT ID		TECN	COMMENT
2.5±0.5 OUR FIT					
2.7±0.6±0.3	66 ± 15	MENDEZ	10	CLEO	e^+e^- at 3774 MeV

Hadronic modes with a $K\overline{K}$ pair

$\Gamma(K^+K^-)/\Gamma_{total}$ — Γ_{196}/Γ

VALUE (units 10^{-3})	EVTS	DOCUMENT ID		TECN	COMMENT
4.08 ±0.06 OUR FIT	Error includes scale factor of 1.6.				
4.233±0.021±0.064	56k	ABLIKIM	18W	BES3	e^+e^-, 3773 MeV
• • • We do not use the following data for averages, fits, limits, etc. • • •					
4.08 ±0.08 ±0.09	4.7k	BONVICINI	08	CLEO	See MENDEZ 10

$\Gamma(K^+K^-)/\Gamma(K^-\pi^+)$ — Γ_{196}/Γ_{37}

VALUE	EVTS	DOCUMENT ID		TECN	COMMENT
0.1033±0.0013 OUR FIT	Error includes scale factor of 1.6.				
0.1010±0.0016 OUR AVERAGE	Error includes scale factor of 1.4. See the ideogram below.				
0.122 ±0.011 ±0.004	242 ± 20	ABLIKIM	05F	BES	$e^+e^-\approx\psi(3770)$
0.0992±0.0011±0.0012	16k±200	ACOSTA	05C	CDF	$p\overline{p}$, $\sqrt{s}$=1.96 TeV
0.0993±0.0014±0.0014	11k	LINK	03	FOCS	γ nucleus, $\overline{E}_\gamma\approx$ 180 GeV
0.1040±0.0033±0.0027	1900	CSORNA	02	CLE2	$e^+e^-\approx\Upsilon(4S)$
0.109 ±0.003 ±0.003	3317	AITALA	98C	E791	π^- nucleus, 500 GeV
0.116 ±0.007 ±0.007	1102	ASNER	96B	CLE2	$e^+e^-\approx\Upsilon(4S)$
0.109 ±0.007 ±0.009	581	FRABETTI	94C	E687	γBe $\overline{E}_\gamma$= 220 GeV
0.107 ±0.010 ±0.009	193	ANJOS	91D	E691	Photoproduction
0.117 ±0.010 ±0.007	249	ALEXANDER	90	CLEO	e^+e^- 10.5–11 GeV
• • • We do not use the following data for averages, fits, limits, etc. • • •					
0.107 ±0.029 ±0.015	103	ADAMOVICH	92	OMEG	π^- 340 GeV
0.138 ±0.027 ±0.010	155	FRABETTI	92	E687	γBe
0.16 ±0.05	34	ALVAREZ	91B	NA14	Photoproduction
0.10 ±0.02 ±0.01	131	ALBRECHT	90C	ARG	$e^+e^-\approx$ 10 GeV
0.122 ±0.018 ±0.012	118	BALTRUSAIT...	85E	MRK3	e^+e^- 3.77 GeV
0.113 ±0.030		ABRAMS	79D	MRK2	e^+e^- 3.77 GeV

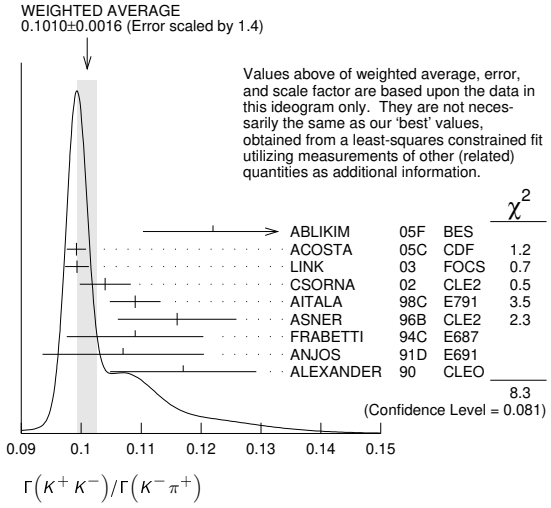

$\Gamma(K^+K^-)/[\Gamma(K^-\pi^+)+\Gamma(K^+\pi^-)]$ — $\Gamma_{196}/(\Gamma_{37}+\Gamma_{274})$

VALUE (units 10^{-2})	EVTS	DOCUMENT ID		TECN	COMMENT
10.29±0.13 OUR FIT	Error includes scale factor of 1.6.				
10.41±0.11±0.12	13.8k	MENDEZ	10	CLEO	e^+e^- at 3774 MeV

$\Gamma(K^+K^-)/\Gamma(\pi^+\pi^-)$ — $\Gamma_{196}/\Gamma_{132}$

The unused results here are redundant with $\Gamma(K^+K^-)/\Gamma(K^-\pi^+)$ and $\Gamma(\pi^+\pi^-)/\Gamma(K^-\pi^+)$ measurements by the same experiments.

VALUE	EVTS	DOCUMENT ID		TECN	COMMENT
• • • We do not use the following data for averages, fits, limits, etc. • • •					
2.760±0.040±0.034	7334	ACOSTA	05C	CDF	$p\overline{p}$, $\sqrt{s}$=1.96 TeV
2.81 ±0.10 ±0.06		LINK	03	FOCS	γ nucleus, $\overline{E}_\gamma\approx$ 180 GeV
2.96 ±0.16 ±0.15	710	CSORNA	02	CLE2	$e^+e^-\approx\Upsilon(4S)$
2.75 ±0.15 ±0.16		AITALA	98C	E791	π^- nucleus, 500 GeV
2.53 ±0.46 ±0.19		FRABETTI	94C	E687	γBe $\overline{E}_\gamma$= 220 GeV
2.23 ±0.81 ±0.46		ADAMOVICH	92	OMEG	π^- 340 GeV
1.95 ±0.34 ±0.22		ANJOS	91D	E691	Photoproduction
2.5 ±0.7		ALBRECHT	90C	ARG	$e^+e^-\approx$ 10 GeV
2.35 ±0.37 ±0.28		ALEXANDER	90	CLEO	e^+e^- 10.5–11 GeV

$\Gamma(2K^0_S)/\Gamma_{total}$ — Γ_{197}/Γ

VALUE (units 10^{-4})	EVTS	DOCUMENT ID		TECN	COMMENT
1.41±0.05 OUR FIT	Error includes scale factor of 1.1.				
1.67±0.11±0.11	576	ABLIKIM	17A	BES3	$e^+e^-\to\psi(3770)$
• • • We do not use the following data for averages, fits, limits, etc. • • •					
1.46±0.32±0.09	68 ± 15	BONVICINI	08	CLEO	See MENDEZ 10

$\Gamma(2K^0_S)/[\Gamma(K^-\pi^+)+\Gamma(K^+\pi^-)]$ — $\Gamma_{197}/(\Gamma_{37}+\Gamma_{274})$

VALUE (units 10^{-2})	EVTS	DOCUMENT ID		TECN	COMMENT
0.357±0.013 OUR FIT	Error includes scale factor of 1.1.				
0.41 ±0.04 ±0.02	215 ± 23	MENDEZ	10	CLEO	e^+e^- at 3774 MeV

$\Gamma(2K^0_S)/\Gamma(K^0_S\pi^+\pi^-)$ — Γ_{197}/Γ_{40}

This is the same as $\Gamma(K^0\overline{K}^0)/\Gamma(\overline{K}^0\pi^+\pi^-)$ because $D^0\to K^0_S K^0_L$ is forbidden by CP conservation.

VALUE (units 10^{-2})	EVTS	DOCUMENT ID		TECN	COMMENT
0.506±0.034 OUR FIT					
1.20 ±0.22 OUR AVERAGE					
1.44 ±0.32 ±0.16	79 ± 17	LINK	05A	FOCS	γ Be, $\overline{E}_\gamma\approx$ 180 GeV
1.01 ±0.22 ±0.16	26	ASNER	96B	CLE2	$e^+e^-\approx\Upsilon(4S)$
3.9 ±1.3 ±1.3	20 ± 7	FRABETTI	94J	E687	γBe $\overline{E}_\gamma$=220 GeV
• • • We do not use the following data for averages, fits, limits, etc. • • •					
$2.1\ ^{+1.1}_{-0.8}$ ±0.2	5	ALEXANDER	90	CLEO	e^+e^- 10.5–11 GeV

$\Gamma(2K^0_S)/\Gamma(K^0_S\pi^0)$ — Γ_{197}/Γ_{38}

VALUE (units 10^{-2})	EVTS	DOCUMENT ID		TECN	COMMENT
1.14 ±0.04 OUR FIT	Error includes scale factor of 1.1.				
1.101±0.023±0.030	4.8k	DASH	17	BELL	At/near $\Upsilon(4S)$, $\Upsilon(5S)$

$\Gamma(K^0_S K^-\pi^+)/\Gamma(K^-\pi^+)$ — Γ_{198}/Γ_{37}

VALUE	DOCUMENT ID		TECN	COMMENT
0.084±0.013 OUR FIT	Error includes scale factor of 1.1.			
0.08 ±0.03	[1] ANJOS	91	E691	γBe 80–240 GeV

[1] The factor 100 at the top of column 2 of Table I of ANJOS 91 should be omitted.

$\Gamma(\phi\pi^0)/\Gamma_{total}$ — Γ_{265}/Γ

VALUE (units 10^{-3})	EVTS	DOCUMENT ID		TECN	COMMENT
1.168±0.028±0.028	3.3k	ABLIKIM	19BI	BES3	e^+e^- at 3773 MeV

$\Gamma(\phi\eta)/\Gamma_{total}$ — Γ_{266}/Γ

VALUE (units 10^{-4})	EVTS	DOCUMENT ID		TECN	COMMENT
1.81±0.46±0.06	102	ABLIKIM	19BI	BES3	e^+e^- at 3773 MeV

$\Gamma(K^0_S K^-\pi^+)/\Gamma(K^0_S\pi^+\pi^-)$ — Γ_{198}/Γ_{40}

VALUE	EVTS	DOCUMENT ID		TECN	COMMENT
0.118±0.017 OUR FIT	Error includes scale factor of 1.1.				
0.119±0.021 OUR AVERAGE	Error includes scale factor of 1.3.				
0.108±0.019	61	AMMAR	91	CLEO	$e^+e^-\approx$ 10.5 GeV
0.16 ±0.03 ±0.02	39	ALBRECHT	90C	ARG	$e^+e^-\approx$ 10 GeV

$\Gamma(\overline{K}^*(892)^0 K^0_S,\ \overline{K}^{*0}\to K^-\pi^+)/\Gamma(K^0_S K^-\pi^+)$ — $\Gamma_{199}/\Gamma_{198}$

Fit fraction from Dalitz plot analyses. The fraction for the $K^0_S\pi^+$ mass between 792 and 992 MeV is 0.370 ± 0.003 ± 0.012.

VALUE (units 10^{-2})	EVTS	DOCUMENT ID		TECN	COMMENT
2.47±0.15±0.23	113k	[1] AAIJ	16N	LHCB	Dalitz plot fit

[1] AAIJ 16N gives results for two S-wave parameterisations. We take the values from the model with LASS parametrization, and the difference as a systematic uncertainty.

$\Gamma(K^*(892)^+K^-,\ K^{*+}\to K^0_S\pi^+)/\Gamma(K^0_S K^-\pi^+)$ — $\Gamma_{200}/\Gamma_{198}$

Fit fraction from Dalitz plot analyses.

VALUE (units 10^{-2})	EVTS	DOCUMENT ID		TECN	COMMENT
56.9±0.6±1.1	113k	[1] AAIJ	16N	LHCB	Dalitz plot fit

[1] AAIJ 16N gives results for two S-wave parameterisations. We take the values from the model with LASS parametrization, and the difference as a systematic uncertainty.

Downloaded from https://academic.oup.com/ptep/article/2022/8/083C01/6651666 by KIT Library user on 27 September 2022

$\Gamma(\overline{K}^*(1410)^0 K^0_S, \overline{K}^{*0} \to K^-\pi^+)/\Gamma(K^0_S K^-\pi^+)$ — $\Gamma_{201}/\Gamma_{198}$

Fit fraction from Dalitz plot analyses.

VALUE (units 10^{-2})	EVTS	DOCUMENT ID	TECN	COMMENT
3.8±0.5±5.6	113k	[1] AAIJ 16N	LHCB	Dalitz plot fit

[1] AAIJ 16N gives results for two S-wave parameterisations. We take the values from the model with LASS parametrization, and the difference as a uncertainty (which in this case dominates)

$\Gamma(K^*(1410)^+ K^-, K^{*+} \to K^0_S\pi^+)/\Gamma(K^0_S K^-\pi^+)$ — $\Gamma_{202}/\Gamma_{198}$

Fit fraction from Dalitz plot analyses.

VALUE (units 10^{-2})	EVTS	DOCUMENT ID	TECN	COMMENT
9.6±1.1±5.4	113k	[1] AAIJ 16N	LHCB	Dalitz plot fit

[1] AAIJ 16N gives results for two S-wave parameterisations. We take the values from the model with LASS parametrization, and the difference as a systematic uncertainty (which in this case dominates).

$\Gamma((K^-\pi^+)_{S-wave} K^0_S)/\Gamma(K^0_S K^-\pi^+)$ — $\Gamma_{203}/\Gamma_{198}$

Fit fraction from Dalitz plot analyses.

VALUE (units 10^{-2})	EVTS	DOCUMENT ID	TECN	COMMENT
18±2±8	113k	[1] AAIJ 16N	LHCB	Dalitz plot fit

[1] AAIJ 16N gives results for two S-wave parameterisations. We take the values from the model with LASS parametrization, and the difference as a systematic uncertainty (which in this case dominates).

$\Gamma((K^0_S\pi^+)_{S-wave} K^-)/\Gamma(K^0_S K^-\pi^+)$ — $\Gamma_{204}/\Gamma_{198}$

Fit fraction from Dalitz plot analyses.

VALUE (units 10^{-2})	EVTS	DOCUMENT ID	TECN	COMMENT
11.7±1.0±2.3	113k	[1] AAIJ 16N	LHCB	Dalitz plot fit

[1] AAIJ 16N gives results for two S-wave parameterisations. We take the values from the model with LASS parametrization, and the difference as a systematic uncertainty.

$\Gamma(a_0(980)^-\pi^+, a_0^- \to K^0_S K^-)/\Gamma(K^0_S K^-\pi^+)$ — $\Gamma_{205}/\Gamma_{198}$

Fit fraction from Dalitz plot analyses.

VALUE (units 10^{-2})	EVTS	DOCUMENT ID	TECN	COMMENT
4.0±0.7±4.1	113k	[1] AAIJ 16N	LHCB	Dalitz plot fit

[1] AAIJ 16N gives results for two S-wave parameterisations. We take the values from the model with LASS parametrization, and the difference as a systematic uncertainty (which in this case dominates).

$\Gamma(a_0(1450)^-\pi^+, a_0^- \to K^0_S K^-)/\Gamma(K^0_S K^-\pi^+)$ — $\Gamma_{206}/\Gamma_{198}$

Fit fraction from Dalitz plot analyses.

VALUE (units 10^{-2})	EVTS	DOCUMENT ID	TECN	COMMENT
0.74±0.15±0.57	113k	[1] AAIJ 16N	LHCB	Dalitz plot fit

[1] AAIJ 16N gives results for two S-wave parameterisations. We take the values from the model with LASS parametrization, and the difference as a systematic uncertainty (which in this case dominates).

$\Gamma(a_2(1320)^-\pi^+, a_2^- \to K^0_S K^-)/\Gamma(K^0_S K^-\pi^+)$ — $\Gamma_{207}/\Gamma_{198}$

VALUE (units 10^{-2})	EVTS	DOCUMENT ID	TECN	COMMENT
0.15±0.06±0.14	113k	[1] AAIJ 16N	LHCB	Dalitz plot fit

[1] AAIJ 16N gives results for two S-wave parameterisations. We take the values from the model with LASS parametrization, and the difference as a systematic uncertainty.

$\Gamma(\rho(1450)^-\pi^+, \rho^- \to K^0_S K^-)/\Gamma(K^0_S K^-\pi^+)$ — $\Gamma_{208}/\Gamma_{198}$

Fit fraction from Dalitz plot analyses.

VALUE (units 10^{-2})	EVTS	DOCUMENT ID	TECN	COMMENT
1.4±0.2±0.7	113k	[1] AAIJ 16N	LHCB	Dalitz plot fit

[1] AAIJ 16N gives results for two S-wave parameterisations. We take the values from the model with LASS parametrization, and the difference as a systematic uncertainty.

$\Gamma(K^0_S K^+\pi^-)/\Gamma(K^-\pi^+)$ — Γ_{209}/Γ_{37}

VALUE	DOCUMENT ID	TECN	COMMENT
• • • We do not use the following data for averages, fits, limits, etc. • • •			
0.05 ± 0.025	[1] ANJOS 91	E691	γBe 80–240 GeV

[1] The factor 100 at the top of column 2 of Table I of ANJOS 91 should be omitted.

$\Gamma(K^0_S K^+\pi^-)/\Gamma(K^0_S\pi^+\pi^-)$ — Γ_{209}/Γ_{40}

VALUE	EVTS	DOCUMENT ID	TECN	COMMENT
• • • We do not use the following data for averages, fits, limits, etc. • • •				
0.098 ± 0.020	55	AMMAR 91	CLEO	$e^+e^- \approx$ 10.5 GeV

$\Gamma(K^0_S K^+\pi^-)/\Gamma(K^0_S K^-\pi^+)$ — $\Gamma_{209}/\Gamma_{198}$

VALUE	EVTS	DOCUMENT ID	TECN	COMMENT
0.654±0.007 OUR FIT				
0.654±0.007 OUR AVERAGE				
$0.655\pm0.004\pm0.006$	76k,113k	AAIJ 16N	LHCB	pp at 7, 8 TeV
$0.592\pm0.044\pm0.018$		INSLER 12	CLEO	$e^+e^- \to D^0\overline{D}^0$ at 3.77 GeV

$\Gamma(K^*(892)^0 K^0_S, K^{*0} \to K^+\pi^-)/\Gamma(\overline{K}^*(892)^0 K^0_S, \overline{K}^{*0} \to K^-\pi^+)$ — $\Gamma_{210}/\Gamma_{199}$

VALUE	CL%	DOCUMENT ID	TECN	COMMENT
0.356±0.034±0.007		[1] INSLER 12	CLEO	$e^+e^- \to D^0\overline{D}^0$, 3.77 GeV
• • • We do not use the following data for averages, fits, limits, etc. • • •				
<0.010	90	AMMAR 91	CLEO	$e^+e^- \approx$ 10.5 GeV

[1] Uses quantum correlations in $e^+e^- \to D^0\overline{D}^0$ at the $\psi(3770)$, where the signal side D decays to $K^0_S K\pi$ and the tag-side D decays to $K\pi$, $K\pi\pi\pi$, $K\pi\pi^0$, and 10 additional CP-even, CP-odd, and mixed CP modes involving K^0_S or K^0_L.

$\Gamma(K^*(892)^0 K^0_S, K^{*0} \to K^+\pi^-)/\Gamma(K^0_S K^+\pi^-)$ — $\Gamma_{210}/\Gamma_{209}$

Fit fraction from Dalitz plot analyses.

VALUE (units 10^{-2})	EVTS	DOCUMENT ID	TECN	COMMENT
5.17±0.21±0.47	76k	[1] AAIJ 16N	LHCB	Dalitz plot fit

[1] AAIJ 16N gives results for two S-wave parameterisations. We take the values from the model with LASS parametrization, and the difference as a systematic uncertainty.

$\Gamma(K^*(892)^- K^+, K^{*-} \to K^0_S\pi^-)/\Gamma(K^0_S K^+\pi^-)$ — $\Gamma_{211}/\Gamma_{209}$

Fit fraction from Dalitz plot analyses.

VALUE (units 10^{-2})	EVTS	DOCUMENT ID	TECN	COMMENT
28.8±0.4±1.5	76k	[1] AAIJ 16N	LHCB	Dalitz plot fit

[1] AAIJ 16N gives results for two S-wave parameterisations. We take the values from the model with LASS parametrization, and the difference as a systematic uncertainty.

$\Gamma(K^*(1410)^0 K^0_S, K^{*0} \to K^+\pi^+)/\Gamma(K^0_S K^+\pi^-)$ — $\Gamma_{212}/\Gamma_{209}$

Fit fraction from Dalitz plot analyses.

VALUE (units 10^{-2})	EVTS	DOCUMENT ID	TECN	COMMENT
2.2±0.6±3.7	76k	[1] AAIJ 16N	LHCB	Dalitz plot fit

[1] AAIJ 16N gives results for two S-wave parameterisations. We take the values from the model with LASS parametrization, and the difference as a systematic uncertainty (which in this case dominates).

$\Gamma(K^*(1410)^- K^+, K^{*-} \to K^0_S\pi^-)/\Gamma(K^0_S K^+\pi^-)$ — $\Gamma_{213}/\Gamma_{209}$

Fit fraction from Dalitz plot analyses.

VALUE (units 10^{-2})	EVTS	DOCUMENT ID	TECN	COMMENT
11.9±1.5±9.1	76k	[1] AAIJ 16N	LHCB	Dalitz plot fit

[1] AAIJ 16N gives results for two S-wave parameterisations. We take the values from the model with LASS parametrization, and the difference as a systematic uncertainty (which in this case dominates).

$\Gamma((K^+\pi^-)_{S-wave} K^0_S)/\Gamma(K^0_S K^+\pi^-)$ — $\Gamma_{214}/\Gamma_{209}$

Fit fraction from Dalitz plot analyses.

VALUE (units 10^{-2})	EVTS	DOCUMENT ID	TECN	COMMENT
17±2±8	76k	[1] AAIJ 16N	LHCB	Dalitz plot fit

[1] AAIJ 16N gives results for two S-wave parameterisations. We take the values from the model with LASS parametrization, and the difference as a systematic uncertainty.

$\Gamma((K^0_S\pi^-)_{S-wave} K^+)/\Gamma(K^0_S K^+\pi^-)$ — $\Gamma_{215}/\Gamma_{209}$

Fit fraction from Dalitz plot analyses.

VALUE (units 10^{-2})	EVTS	DOCUMENT ID	TECN	COMMENT
6.3±0.9±2.3	76k	[1] AAIJ 16N	LHCB	Dalitz plot fit

[1] AAIJ 16N gives results for two S-wave parameterisations. We take the values from the model with LASS parametrization, and the difference as a systematic uncertainty.

$\Gamma(a_0(980)^+\pi^-, a_0^+ \to K^0_S K^+)/\Gamma(K^0_S K^+\pi^-)$ — $\Gamma_{216}/\Gamma_{209}$

Fit fraction from Dalitz plot analyses.

VALUE (units 10^{-2})	EVTS	DOCUMENT ID	TECN	COMMENT
26±2±18	76k	[1] AAIJ 16N	LHCB	Dalitz plot fit

[1] AAIJ 16N gives results for two S-wave parameterisations. We take the values from the model with LASS parametrization, and the difference as a systematic uncertainty (which in this case dominates).

$\Gamma(a_0(1450)^+\pi^-, a_0^+ \to K^0_S K^+)/\Gamma(K^0_S K^+\pi^-)$ — $\Gamma_{217}/\Gamma_{209}$

Fit fraction from Dalitz plot analyses.

VALUE (units 10^{-2})	EVTS	DOCUMENT ID	TECN	COMMENT
1.5±0.3±1.1	76k	[1] AAIJ 16N	LHCB	Dalitz plot fit

[1] AAIJ 16N gives results for two S-wave parameterisations. We take the values from the model with LASS parametrization, and the difference as a systematic uncertainty (which in this case dominates).

$\Gamma(\rho(1700)^+\pi^-, \rho^+ \to K^0_S K^+)/\Gamma(K^0_S K^+\pi^-)$ — $\Gamma_{218}/\Gamma_{209}$

Fit fraction from Dalitz plot analyses.

VALUE (units 10^{-2})	EVTS	DOCUMENT ID	TECN	COMMENT
0.53±0.11±0.23	76k	[1] AAIJ 16N	LHCB	Dalitz plot fit

[1] AAIJ 16N gives results for two S-wave parameterisations. We take the values from the model with LASS parametrization, and the difference as a systematic uncertainty.

$\Gamma(K^+K^-\pi^0)/\Gamma(K^-\pi^+\pi^0)$ — Γ_{219}/Γ_{55}

VALUE (units 10^{-2})	EVTS	DOCUMENT ID	TECN	COMMENT
2.37±0.03±0.04	11k±122	AUBERT,B 06X	BABR	$e^+e^- \approx \Upsilon(4S)$
• • • We do not use the following data for averages, fits, limits, etc. • • •				
0.95 ± 0.26	151	ASNER 96B	CLE2	$e^+e^- \approx \Upsilon(4S)$

Downloaded from https://academic.oup.com/ptep/article/2022/8/083C01/6651666 by KIT Library user on 27 September 2022

$\Gamma(K^*(892)^+ K^-, K^*(892)^+ \to K^+\pi^0)/\Gamma(K^+K^-\pi^0)$ — $\Gamma_{220}/\Gamma_{219}$

This is the "fit fraction" from the Dalitz-plot analysis with interference.

VALUE (units 10^{-2})	DOCUMENT ID		TECN	COMMENT
44.4±0.8±0.6	AUBERT	07T	BABR	Dalitz fit II, 11k evts
• • • We do not use the following data for averages, fits, limits, etc. • • •				
46.1±3.1	[1] CAWLFIELD	06A	CLEO	Dalitz fit, 627 ± 30 evts

[1] The error on this CAWLFIELD 06A result is statistical only.

$\Gamma(K^*(892)^- K^+, K^*(892)^- \to K^-\pi^0)/\Gamma(K^+K^-\pi^0)$ — $\Gamma_{221}/\Gamma_{219}$

This is the "fit fraction" from the Dalitz-plot analysis with interference.

VALUE (units 10^{-2})	DOCUMENT ID		TECN	COMMENT
15.9±0.7±0.6	AUBERT	07T	BABR	Dalitz fit II, 11k evts
• • • We do not use the following data for averages, fits, limits, etc. • • •				
12.3±2.2	[1] CAWLFIELD	06A	CLEO	Dalitz fit, 627 ± 30 evts

[1] The error on this CAWLFIELD 06A result is statistical only.

$\Gamma((K^+\pi^0)_{S-wave} K^-)/\Gamma(K^+K^-\pi^0)$ — $\Gamma_{222}/\Gamma_{219}$

This is the "fit fraction" from the Dalitz-plot analysis with interference.

VALUE (units 10^{-2})	DOCUMENT ID		TECN	COMMENT
71.1±3.7±1.9	[1] AUBERT	07T	BABR	Dalitz fit II, 11k evts

[1] The only major difference between fits I and II in the AUBERT 07T analysis is in this mode, where the fit-I fraction is (16.3 ± 3.4 ± 2.1)%.

$\Gamma((K^-\pi^0)_{S-wave} K^+)/\Gamma(K^+K^-\pi^0)$ — $\Gamma_{223}/\Gamma_{219}$

This is the "fit fraction" from the Dalitz-plot analysis with interference.

VALUE (units 10^{-2})	DOCUMENT ID		TECN	COMMENT
3.9±0.9±1.0	AUBERT	07T	BABR	Dalitz fit II, 11k evts

$\Gamma(f_0(980)\pi^0, f_0 \to K^+K^-)/\Gamma(K^+K^-\pi^0)$ — $\Gamma_{224}/\Gamma_{219}$

This is the "fit fraction" from the Dalitz-plot analysis with interference.

VALUE (units 10^{-2})	DOCUMENT ID		TECN	COMMENT
10.5±1.1±1.2	[1] AUBERT	07T	BABR	Dalitz fit II, 11k evts

[1] When AUBERT 07T replace the $f_0(980)\pi^0$ mode with $a_0(980)\pi^0$, the fit fraction is a negligibly different (11.0 ± 1.5 ± 1.2)%.

$\Gamma(\phi\pi^0, \phi \to K^+K^-)/\Gamma(K^+K^-\pi^0)$ — $\Gamma_{225}/\Gamma_{219}$

This is the "fit fraction" from the Dalitz-plot analysis with interference.

VALUE (units 10^{-2})	DOCUMENT ID		TECN	COMMENT
19.4±0.6±0.5	AUBERT	07T	BABR	Dalitz fit II, 11k evts
• • • We do not use the following data for averages, fits, limits, etc. • • •				
14.9±1.6	[1] CAWLFIELD	06A	CLEO	Dalitz fit, 627 ± 30 evts

[1] The error on this CAWLFIELD 06A result is statistical only.

$\Gamma(K^+K^-\pi^0 \text{nonresonant})/\Gamma(K^+K^-\pi^0)$ — $\Gamma_{226}/\Gamma_{219}$

This is the "fit fraction" from the Dalitz-plot analysis with interference.

VALUE	DOCUMENT ID		TECN	COMMENT
• • • We do not use the following data for averages, fits, limits, etc. • • •				
0.360±0.037	[1] CAWLFIELD	06A	CLEO	Dalitz fit, 627 ± 30 evts

[1] The error is statistical only. CAWLFIELD 06A also fits the Dalitz plot replacing this flat nonresonant background with broad S-wave $\kappa^\pm \to K^\pm\pi^0$ resonances. There is no significant improvement in the fit, and $K^{*\pm}K^\mp$ and $\phi\pi^0$ results are not much changed.

$\Gamma(2K^0_S\pi^0)/\Gamma_{total}$ — Γ_{227}/Γ

VALUE	DOCUMENT ID		TECN	COMMENT
<0.00059	ASNER	96B	CLE2	$e^+e^- \approx \Upsilon(4S)$

$\Gamma(K^+K^-\eta)/\Gamma_{total}$ — Γ_{228}/Γ

VALUE (units 10^{-4})	EVTS	DOCUMENT ID		TECN	COMMENT
0.59±0.18±0.05	13	ABLIKIM	20V	BES3	e^+e^-, 3773 MeV

$\Gamma(K^+K^-\eta)/\Gamma(K^-\pi^+\eta)$ — Γ_{228}/Γ_{94}

VALUE (units 10^{-3})	EVTS	DOCUMENT ID		TECN	COMMENT
$9.57^{+0.36}_{-0.33}\pm0.20$	1.4k	LI	21G	BELL	e^+e^- at $\Upsilon(nS)$

$\Gamma(\phi(1020)\eta)/\Gamma(K^-\pi^+\eta)$ — Γ_{229}/Γ_{94}

VALUE (units 10^{-3})	EVTS	DOCUMENT ID		TECN	COMMENT
9.8±0.6±0.1	1.4k	[1] LI	21G	BELL	e^+e^- at $\Upsilon(nS)$

[1] LI 21G reports $[\Gamma(D^0 \to \phi(1020)\eta)/\Gamma(D^0 \to K^-\pi^+\eta)] \times [B(\phi(1020) \to K^+K^-)] = (4.82 \pm 0.23 \pm 0.16) \times 10^{-3}$ which we divide by our best value $B(\phi(1020) \to K^+K^-) = (49.1 \pm 0.5) \times 10^{-2}$. Our first error is their experiment's error and our second error is the systematic error from using our best value.

$\Gamma(K^+K^-\eta \text{nonresonant})/\Gamma(K^-\pi^+\eta)$ — Γ_{230}/Γ_{94}

VALUE (units 10^{-3})	EVTS	DOCUMENT ID		TECN	COMMENT
$5.26^{+0.45}_{-0.38}\pm0.11$	1.4k	LI	21G	BELL	e^+e^- at $\Upsilon(nS)$

$\Gamma(2K^0_S\eta)/\Gamma_{total}$ — Γ_{231}/Γ

VALUE (units 10^{-4})	EVTS	DOCUMENT ID		TECN	COMMENT
1.33±0.59±0.18	7	ABLIKIM	20V	BES3	e^+e^-, 3773 MeV

$\Gamma(K^+K^-\pi^0\pi^0)/\Gamma_{total}$ — Γ_{232}/Γ

VALUE (units 10^{-4})	EVTS	DOCUMENT ID		TECN	COMMENT
6.9±0.7±0.4	132	ABLIKIM	20AC	BES3	e^+e^- at 3.773 GeV

$\Gamma(K^+K^-\pi^+\pi^-)/\Gamma(K^-2\pi^+\pi^-)$ — Γ_{233}/Γ_{72}

VALUE (units 10^{-2})	EVTS	DOCUMENT ID		TECN	COMMENT
3.00±0.13 OUR AVERAGE					
2.95±0.11±0.08	2669 ± 101	[1] LINK	05G	FOCS	γBe, $\overline{E}_\gamma \approx 180$ GeV
3.13±0.37±0.36	136 ± 15	AITALA	98D	E791	π^- nucleus, 500 GeV
3.5 ±0.4 ±0.2	244 ± 26	FRABETTI	95C	E687	γBe, $\overline{E}_\gamma \approx 200$ GeV
• • • We do not use the following data for averages, fits, limits, etc. • • •					
4.4 ±1.8 ±0.5	19 ± 8	ABLIKIM	05F	BES	$e^+e^- \approx \psi(3770)$
4.1 ±0.7 ±0.5	114 ± 20	ALBRECHT	94I	ARG	$e^+e^- \approx 10$ GeV
3.14±1.0	89 ± 29	AMMAR	91	CLEO	$e^+e^- \approx 10.5$ GeV
$2.8\ ^{+0.8}_{-0.7}$		ANJOS	91	E691	γBe 80–240 GeV

[1] LINK 05G uses a smaller, cleaner subset of 1279 ± 48 events for the amplitude analysis that gives the results in the next data blocks.

$\Gamma(\phi(\pi^+\pi^-)_{S-wave}, \phi \to K^+K^-)/\Gamma(K^+K^-\pi^+\pi^-)$ — $\Gamma_{234}/\Gamma_{233}$

This is the fraction from a coherent amplitude analysis.

VALUE (units 10^{-2})	EVTS	DOCUMENT ID		TECN	COMMENT
4.0±0.6±2.1	3k	[1] DARGENT	17		4-body fit, $KK\pi\pi$ events
• • • We do not use the following data for averages, fits, limits, etc. • • •					
10.3±1.0±0.8	3k	[2] ARTUSO	12	CLEO	4-body fit, $KK\pi\pi$ events
1 ±1	1.3k	LINK	05G	FOCS	4-body fit, $KK\pi\pi$ events

[1] Obtained by analyzing CLEO data but not authored by the CLEO Collaboration.
[2] See DARGENT 17

$\Gamma((\phi\rho^0)_{S-wave}, \phi \to K^+K^-)/\Gamma(K^+K^-\pi^+\pi^-)$ — $\Gamma_{235}/\Gamma_{233}$

This is the fraction from a coherent amplitude analysis.

VALUE (units 10^{-2})	EVTS	DOCUMENT ID		TECN	COMMENT
28.1±1.3±1.7	2.9k	[1,2] DARGENT	17		4-body fit, $KK\pi\pi$ evts
• • • We do not use the following data for averages, fits, limits, etc. • • •					
38.3±2.5±3.8		[1,3] ARTUSO	12	CLEO	Fitting 2959 evts.
29 ±2 ±1		LINK	05G	FOCS	Fits 1279 ± 48 evts.

[1] ARTUSO 12 and DARGENT 17 use the same dataset, but ARTUSO 12 uses a formulation for the D-wave component that is in fact a mix of S- and D-wave, while DARGENT 17 uses a pure D-wave. This explains the discrepancy in their $\rho\phi$ S- and D-wave components.
[2] Obtained by analyzing CLEO data but not authored by the CLEO Collaboration.
[3] See DARGENT 17

$\Gamma((\phi\rho^0)_{P-wave}, \phi \to K^+K^-)/\Gamma(K^+K^-\pi^+\pi^-)$ — $\Gamma_{236}/\Gamma_{233}$

This is the fit fraction from a coherent amplitude analysis.

VALUE (units 10^{-2})	EVTS	DOCUMENT ID		COMMENT
1.6±0.3±0.7	2.9k	[1] DARGENT	17	4-body fit, $KK\pi\pi$ evts

[1] Obtained by analyzing CLEO data but not authored by the CLEO Collaboration.

$\Gamma((\phi\rho^0)_{D-wave}, \phi \to K^+K^-)/\Gamma(K^+K^-\pi^+\pi^-)$ — $\Gamma_{237}/\Gamma_{233}$

VALUE (units 10^{-2})	EVTS	DOCUMENT ID		TECN	COMMENT
1.7±0.4±0.4	2.9k	[1,2] DARGENT	17		4-body fit, $KK\pi\pi$ evts
• • • We do not use the following data for averages, fits, limits, etc. • • •					
3.4±0.7±0.6		[1,3] ARTUSO	12	CLEO	Fitting 2959 evts.

[1] ARTUSO 12 use a formulation for the D-wave component that is in fact a mix of S- and D-wave, while DARGENT 17 uses a pure D-wave.
[2] Obtained by analyzing CLEO data but not authored by the CLEO Collaboration.
[3] See DARGENT 17

$\Gamma(K^*(892)^0\overline{K}^*(892)^0, K^{*0} \to K^\pm\pi^\mp)/\Gamma(K^+K^-\pi^+\pi^-)$ — $\Gamma_{238}/\Gamma_{233}$

This is the fraction from a coherent amplitude analysis.

VALUE (units 10^{-2})	DOCUMENT ID		TECN	COMMENT
• • • We do not use the following data for averages, fits, limits, etc. • • •				
3±2±1	LINK	05G	FOCS	Fits 1279 ± 48 evts.

$\Gamma(K^+K^-\rho^0 \text{3-body})/\Gamma(K^+K^-\pi^+\pi^-)$ — $\Gamma_{239}/\Gamma_{233}$

This is the fraction from a coherent amplitude analysis.

VALUE (units 10^{-2})	DOCUMENT ID		TECN	COMMENT
• • • We do not use the following data for averages, fits, limits, etc. • • •				
2±2±2	LINK	05G	FOCS	Fits 1279 ± 48 evts.

$\Gamma(f_0(980)\pi^+\pi^-, f_0 \to K^+K^-)/\Gamma(K^+K^-\pi^+\pi^-)$ — $\Gamma_{240}/\Gamma_{233}$

This is the fraction from a coherent amplitude analysis.

VALUE (units 10^{-2})	DOCUMENT ID		TECN	COMMENT
• • • We do not use the following data for averages, fits, limits, etc. • • •				
15±3±2	LINK	05G	FOCS	Fits 1279 ± 48 evts.

Downloaded from https://academic.oup.com/ptep/article/2022/8/083C01/6651666 by KIT Library user on 27 September 2022

$\Gamma((K^*(892)^0\overline{K}^*(892)^0)_{S-wave}, K^{*0} \to K^\pm\pi^\mp)/\Gamma(K^+K^-\pi^+\pi^-)$ — $\Gamma_{241}/\Gamma_{233}$

VALUE (units 10^{-2})	EVTS	DOCUMENT ID		TECN	COMMENT
9.06±0.35 OUR AVERAGE					
9.18±0.21±0.28	163k	AAIJ	19C	LHCB	4-body fit, $KK\pi\pi$ evts
4.5 ±0.8 ±2.0	3k	[1] DARGENT	17		4-body fit, $KK\pi\pi$ evts
• • • We do not use the following data for averages, fits, limits, etc. • • •					
6.1 ±0.8 ±0.9	3k	[2] ARTUSO	12	CLEO	4-body fit, $KK\pi\pi$ evts

[1] Obtained by analyzing CLEO data but not authored by the CLEO Collaboration.
[2] See DARGENT 17

$\Gamma((K^*(892)^0\overline{K}^*(892)^0)_{P-wave}, K^* \to K^\pm\pi^\mp)/\Gamma(K^+K^-\pi^+\pi^-)$ — $\Gamma_{242}/\Gamma_{233}$

This is the fit fraction from a coherent amplitude analysis.

VALUE (units 10^{-2})	EVTS	DOCUMENT ID		TECN	COMMENT
4.87±0.24 OUR AVERAGE					
4.90±0.16±0.18	163k	AAIJ	19C	LHCB	4-body fit, $KK\pi\pi$ evts
3.6 ±0.7 ±1.5	2.9k	[1] DARGENT	17		4-body fit, $KK\pi\pi$ evts

[1] Obtained by analyzing CLEO data but not authored by the CLEO Collaboration.

$\Gamma((K^*(892)^0\overline{K}^*(892)^0)_{D-wave}, K^* \to K^\pm\pi^\mp)/\Gamma(K^+K^-\pi^+\pi^-)$ — $\Gamma_{243}/\Gamma_{233}$

This is the fit fraction from a coherent amplitude analysis.

VALUE (units 10^{-2})	EVTS	DOCUMENT ID		TECN	COMMENT
1.89±0.13 OUR AVERAGE					
1.85±0.09±0.10	163k	AAIJ	19C	LHCB	4-body fit, $KK\pi\pi$ evts
4.0 ±0.6 ±0.7	2.9k	[1] DARGENT	17		4-body fit, $KK\pi\pi$ evts

[1] Obtained by analyzing CLEO data but not authored by the CLEO Collaboration.

$\Gamma(K^*(892)^0K^\mp\pi^\pm$ 3-body, $K^{*0} \to K^\pm\pi^\mp)/\Gamma(K^+K^-\pi^+\pi^-)$ — $\Gamma_{244}/\Gamma_{233}$

This is the fraction from a coherent amplitude analysis.

VALUE (units 10^{-2})	DOCUMENT ID		TECN	COMMENT
• • • We do not use the following data for averages, fits, limits, etc. • • •				
11±2±1	LINK	05G	FOCS	Fits 1279 ± 48 evts.

$\Gamma(K^*(892)^0(K^-\pi^+)_{S-wave}$ 3-body, $K^{*0} \to K^+\pi^-)/\Gamma(K^+K^-\pi^+\pi^-)$ — $\Gamma_{245}/\Gamma_{233}$

This is the fit fraction from a coherent amplitude analysis.

VALUE (units 10^{-2})	EVTS	DOCUMENT ID		COMMENT
5.8±1.2±2.1	2.9k	[1] DARGENT	17	4-body fit, $KK\pi\pi$ evts

[1] Obtained by analyzing CLEO data but not authored by the CLEO Collaboration.

$\Gamma((K^-\pi^+)_{P-wave}, (K^+\pi^-)_{S-wave})/\Gamma(K^+K^-\pi^+\pi^-)$ — $\Gamma_{246}/\Gamma_{233}$

VALUE (units 10^{-2})	DOCUMENT ID		TECN	COMMENT
• • • We do not use the following data for averages, fits, limits, etc. • • •				
10.9±1.2±1.7	[1] ARTUSO	12	CLEO	Fitting 2959 evts.

[1] See DARGENT 17

$\Gamma(K_1(1270)^\pm K^\mp, K_1^\pm \to K^\pm\pi^+\pi^-)/\Gamma(K^+K^-\pi^+\pi^-)$ — $\Gamma_{247}/\Gamma_{233}$

This is the fraction from a coherent amplitude analysis.

VALUE (units 10^{-2})	DOCUMENT ID		TECN	COMMENT
• • • We do not use the following data for averages, fits, limits, etc. • • •				
33±6±4	[1] LINK	05G	FOCS	Fits 1279 ± 48 evts.

[1] This LINK 05G value includes $K_1(1270)^\pm \to \rho^0K^\pm$, $\to K_0^*(1430)^0\pi^\pm$, and $K^*(892)^0\pi^\pm$.

$\Gamma(K_1(1270)^+K^-, K_1^+ \to K^{*0}\pi^+)/\Gamma(K^+K^-\pi^+\pi^-)$ — $\Gamma_{248}/\Gamma_{233}$

VALUE (units 10^{-2})	EVTS	DOCUMENT ID		TECN	COMMENT
5.5±1.4±3.4	3k	[1] DARGENT	17		4-body fit, $KK\pi\pi$ evts
• • • We do not use the following data for averages, fits, limits, etc. • • •					
7.3±0.8±1.9	3k	[2] ARTUSO	12	CLEO	4-body fit, $KK\pi\pi$ events

[1] Obtained by analyzing CLEO data but not authored by the CLEO Collaboration.
[2] See DARGENT 17

$\Gamma(K_1(1270)^+K^-, K_1^+ \to K^*(1430)^0\pi^+, K^{*0} \to K^+\pi^-)/\Gamma(K^+K^-\pi^+\pi^-)$ — $\Gamma_{249}/\Gamma_{233}$

This is the fit fraction from a coherent amplitude analysis.

VALUE (units 10^{-2})	EVTS	DOCUMENT ID		COMMENT
6.1±1.2±1.8	2.9k	[1] DARGENT	17	4-body fit, $KK\pi\pi$ evts

[1] Obtained by analyzing CLEO data but not authored by the CLEO Collaboration.

$\Gamma(K_1(1270)^+K^-, K_1^+ \to \rho^0K^+)/\Gamma(K^+K^-\pi^+\pi^-)$ — $\Gamma_{250}/\Gamma_{233}$

VALUE (units 10^{-2})	EVTS	DOCUMENT ID		TECN	COMMENT
9.1±1.5±1.9	2.9k	[1] DARGENT	17		4-body fit, $KK\pi\pi$ evts
• • • We do not use the following data for averages, fits, limits, etc. • • •					
4.7±0.7±0.8		[2] ARTUSO	12	CLEO	Fitting 2959 evts.

[1] Obtained by analyzing CLEO data but not authored by the CLEO Collaboration.
[2] see DARGENT 17

$\Gamma(K_1(1270)^+K^-, K_1^+ \to \omega(782)K^+, \omega \to \pi^+\pi^-)/\Gamma(K^+K^-\pi^+\pi^-)$ — $\Gamma_{251}/\Gamma_{233}$

This is the fit fraction from a coherent amplitude analysis.

VALUE (units 10^{-2})	EVTS	DOCUMENT ID		COMMENT
0.6±0.3±0.4	2.9k	[1] DARGENT	17	4-body fit, $KK\pi\pi$ evts

[1] Obtained by analyzing CLEO data but not authored by the CLEO Collaboration.

$\Gamma(K_1(1270)^-K^+, K_1^- \to \overline{K}^{*0}\pi^-)/\Gamma(K^+K^-\pi^+\pi^-)$ — $\Gamma_{252}/\Gamma_{233}$

VALUE (units 10^{-2})	DOCUMENT ID		TECN	COMMENT
• • • We do not use the following data for averages, fits, limits, etc. • • •				
0.9±0.3±0.4	[1] ARTUSO	12	CLEO	Fitting 2959 evts.

[1] See DARGENT 17

$\Gamma(K_1(1270)^-K^+, K_1^- \to \rho^0K^-)/\Gamma(K^+K^-\pi^+\pi^-)$ — $\Gamma_{253}/\Gamma_{233}$

VALUE (units 10^{-2})	EVTS	DOCUMENT ID		TECN	COMMENT
5.4±0.7±1.3	2.9k	[1] DARGENT	17		4-body fit, $KK\pi\pi$ evts
• • • We do not use the following data for averages, fits, limits, etc. • • •					
6.0±0.8±0.6		[2] ARTUSO	12	CLEO	Fitting 2959 evts.

[1] Obtained by analyzing CLEO data but not authored by the CLEO Collaboration.
[2] See DARGENT 17

$\Gamma(K_1(1400)^\pm K^\mp, K_1^\pm \to K^\pm\pi^+\pi^-)/\Gamma(K^+K^-\pi^+\pi^-)$ — $\Gamma_{254}/\Gamma_{233}$

This is the fraction from a coherent amplitude analysis.

VALUE (units 10^{-2})	DOCUMENT ID		TECN	COMMENT
• • • We do not use the following data for averages, fits, limits, etc. • • •				
22±3±4	LINK	05G	FOCS	Fits 1279 ± 48 evts.

$\Gamma(K_1(1400)^+K^-, K_1^+ \to K^*(892)^0\pi^+, K^{*0} \to K^+\pi^-)/\Gamma(K^+K^-\pi^+\pi^-)$ — $\Gamma_{255}/\Gamma_{233}$

This is the fit fraction from a coherent amplitude analysis.

VALUE (units 10^{-2})	EVTS	DOCUMENT ID		TECN	COMMENT
18.7 ±1.5 OUR AVERAGE					
19.08±0.60±1.46	163k	AAIJ	19C	LHCB	4-body fit, $KK\pi\pi$ evts
12.4 ±2.6 ±6.3	2.9k	[1] DARGENT	17		4-body fit, $KK\pi\pi$ evts

[1] Obtained by analyzing CLEO data but not authored by the CLEO Collaboration.

$\Gamma(K^*(1410)^+K^-, K^{*+} \to K^{*0}\pi^+)/\Gamma(K^+K^-\pi^+\pi^-)$ — $\Gamma_{256}/\Gamma_{233}$

VALUE (units 10^{-2})	DOCUMENT ID		TECN	COMMENT
• • • We do not use the following data for averages, fits, limits, etc. • • •				
4.2±0.7±0.8	[1,2] ARTUSO	12	CLEO	Fitting 2959 evts.

[1] DARGENT 17 find $K^*(1410)^+\pi^-$ and $K^*(1680)^+\pi^-$, which both peak outside the $D^0 \to KK\pi\pi$ kinematic range, effectively indistinguishable; we list their result under $K^*(1680)^+\pi^-$.
[2] See DARGENT 17

$\Gamma(K^*(1410)^-K^+, K^{*-} \to \overline{K}^{*0}\pi^-)/\Gamma(K^+K^-\pi^+\pi^-)$ — $\Gamma_{257}/\Gamma_{233}$

VALUE (units 10^{-2})	EVTS	DOCUMENT ID		TECN	COMMENT
2.82±0.19±0.39	163k	AAIJ	19C	LHCB	4-body fit, $KK\pi\pi$ evts
• • • We do not use the following data for averages, fits, limits, etc. • • •					
4.7 ±0.7 ±0.7	3k	[1] ARTUSO	12	CLEO	4-body fit, $KK\pi\pi$ evts

[1] See DARGENT 17.

$\Gamma(K_1(1680)^+K^-, K_1^+ \to K^{*0}\pi^+, K^{*0} \to K^+\pi^-)/\Gamma(K^+K^-\pi^+\pi^-)$ — $\Gamma_{258}/\Gamma_{233}$

This is the fit fraction from a coherent amplitude analysis.

VALUE (units 10^{-2})	EVTS	DOCUMENT ID		COMMENT
3.6±0.8±1.0	2.9k	[1,2] DARGENT	17	4-body fit, $KK\pi\pi$ evts

[1] DARGENT 17 find $K^*(1410)^+\pi^-$ and $K^*(1680)^+\pi^-$, which both peak outside the $D^0 \to KK\pi\pi$ kinematic range, effectively indistinguishable.
[2] Obtained by analyzing CLEO data but not authored by the CLEO Collaboration.

$\Gamma(K^+K^-\pi^+\pi^-$ non-resonant$)/\Gamma(K^+K^-\pi^+\pi^-)$ — $\Gamma_{259}/\Gamma_{233}$

This is the fit fraction from a coherent amplitude analysis.

VALUE (units 10^{-2})	EVTS	DOCUMENT ID		COMMENT
11.1±1.2±2.2	2.9k	[1] DARGENT	17	4-body fit, $KK\pi\pi$ evts

[1] Obtained by analyzing CLEO data but not authored by the CLEO Collaboration.

$\Gamma(2K_S^0\pi^+\pi^-)/\Gamma_{total}$ — Γ_{260}/Γ

VALUE (units 10^{-4})	EVTS	DOCUMENT ID		TECN	COMMENT
5.3±0.9±0.3	63	ABLIKIM	20AC	BES3	e^+e^- at 3.773 GeV

$\Gamma(2K_S^0\pi^+\pi^-)/\Gamma(K_S^0\pi^+\pi^-)$ — Γ_{260}/Γ_{40}

VALUE (units 10^{-2})	EVTS	DOCUMENT ID		TECN	COMMENT
4.3 ±0.8 OUR AVERAGE					
4.16±0.70±0.42	113 ± 21	LINK	05A	FOCS	γ Be, $\overline{E}_\gamma \approx$ 180 GeV
6.2 ±2.0 ±1.6	25	ALBRECHT	94I	ARG	$e^+e^- \approx$ 10 GeV

$\Gamma(K_S^0K^-\pi^+\pi^0)/\Gamma_{total}$ — Γ_{261}/Γ

VALUE (units 10^{-3})	EVTS	DOCUMENT ID		TECN	COMMENT
1.32±0.14±0.07	195	ABLIKIM	20AC	BES3	e^+e^- at 3.773 GeV

Downloaded from https://academic.oup.com/ptep/article/2022/8/083C01/6651666 by KIT Library user on 27 September 2022

$\Gamma(K^0_S K^+ \pi^- \pi^0)/\Gamma_{total}$ — Γ_{262}/Γ

VALUE (units 10^{-4})	EVTS	DOCUMENT ID		TECN	COMMENT
6.5±0.7±0.2	119	ABLIKIM	20AC	BES3	e^+e^- at 3.773 GeV

$\Gamma(K^0_S K^- 2\pi^+ \pi^-)/\Gamma(K^0_S 2\pi^+ 2\pi^-)$ — $\Gamma_{263}/\Gamma_{101}$

VALUE	CL%	DOCUMENT ID		TECN	COMMENT
<0.054	90	LINK	04D	FOCS	γ A, $\overline{E}_\gamma \approx 180$ GeV

$\Gamma(K^+ K^- \pi^+ \pi^- \pi^0)/\Gamma_{total}$ — Γ_{264}/Γ

VALUE	DOCUMENT ID		TECN	COMMENT
0.0031±0.0020	[1] BARLAG	92C	ACCM	π^- Cu 230 GeV

[1] BARLAG 92C computes the branching fraction using topological normalization.

$\Gamma(\phi\pi^0)/\Gamma(K^+ K^-)$ — $\Gamma_{265}/\Gamma_{196}$

VALUE	EVTS	DOCUMENT ID		TECN	COMMENT
• • • We do not use the following data for averages, fits, limits, etc. • • •					
0.194±0.006±0.009	1254	TAJIMA	04	BELL	e^+e^- at $\Upsilon(4S)$

$\Gamma(\phi\eta)/\Gamma(K^+ K^-)$ — $\Gamma_{266}/\Gamma_{196}$

VALUE (units 10^{-2})	EVTS	DOCUMENT ID		TECN	COMMENT
3.59±1.14±0.18	31	TAJIMA	04	BELL	e^+e^- at $\Upsilon(4S)$

$\Gamma(\phi\omega)/\Gamma_{total}$ — Γ_{267}/Γ

VALUE (units 10^{-4})	CL%	EVTS	DOCUMENT ID		TECN	COMMENT
6.48±0.96±0.40		196	[1] ABLIKIM	22	BES3	e^+e^- at 3.773 GeV
• • • We do not use the following data for averages, fits, limits, etc. • • •						
<21	90		ALBRECHT	94I	ARG	$e^+e^- \approx 10$ GeV

[1] ABLIKIM 22 determines the longitudinal polarization fraction of the ϕ and ω, $f_L = 0.00 \pm 0.10 \pm 0.08$, corresponding to $f_L < 0.24$ at 95% CL.

Radiative modes

$\Gamma(\rho^0\gamma)/\Gamma(\pi^+\pi^-)$ — $\Gamma_{268}/\Gamma_{132}$

VALUE (units 10^{-2})	EVTS	DOCUMENT ID		TECN	COMMENT
1.25±0.21±0.05	500	NANUT	17	BELL	e^+e^- at Υ(nS), n=2,3,4,5

$\Gamma(\omega\gamma)/\Gamma_{total}$ — Γ_{269}/Γ

VALUE	CL%	DOCUMENT ID		TECN
<2.4 × 10^{-4}	90	ASNER	98	CLE2

$\Gamma(\phi\gamma)/\Gamma(K^-\pi^+)$ — Γ_{270}/Γ_{37}

VALUE (units 10^{-4})	EVTS	DOCUMENT ID		TECN	COMMENT
7.1 ±0.5 OUR FIT					
7.15±0.78±0.69	243 ± 25	AUBERT	08AZ	BABR	$e^+e^- \approx 10.6$ GeV

$\Gamma(\phi\gamma)/\Gamma(K^+ K^-)$ — $\Gamma_{270}/\Gamma_{196}$

VALUE (units 10^{-3})	EVTS	DOCUMENT ID		TECN	COMMENT
6.9 ±0.5 OUR FIT					
6.88±0.47±0.21	524	NANUT	17	BELL	e^+e^- at Υ(nS), n=2,3,4,5
• • • We do not use the following data for averages, fits, limits, etc. • • •					
$6.31^{+1.70}_{-1.48}{}^{+0.30}_{-0.36}$	28	TAJIMA	04	BELL	See NANUT 17

$\Gamma(\overline{K}^*(892)^0\gamma)/\Gamma(K^-\pi^+)$ — Γ_{271}/Γ_{37}

VALUE (units 10^{-3})	EVTS	DOCUMENT ID		TECN	COMMENT
10.5 ±1.7 OUR AVERAGE	Error includes scale factor of 3.1.				
11.9 ±0.5 ±0.5	9.1k	NANUT	17	BELL	e^+e^- at Υ(nS), n=2,3,4,5
8.43±0.51±0.70	2.2k	AUBERT	08AZ	BABR	$e^+e^- \approx 10.6$ GeV

Doubly Cabibbo-suppressed / Mixing modes

$\Gamma(K^+\ell^-\overline{\nu}_\ell \text{ via } \overline{D}^0)/\Gamma(K^-\ell^+\nu_\ell)$ — Γ_{272}/Γ_{18}

This is a limit on R_M without the complications of possible doubly Cabibbo-suppressed decays that occur when using hadronic modes. For the limits on $|m_1 - m_2|$ and $(\Gamma_1 - \Gamma_2)/\Gamma$ that come from the best mixing limit, see near the beginning of these D^0 Listings.

VALUE	CL%	DOCUMENT ID		TECN	COMMENT
< 6.1 × 10^{-4}	90	[1] BITENC	08	BELL	e^+e^-, 10.58 GeV
• • • We do not use the following data for averages, fits, limits, etc. • • •					
<50 × 10^{-4}	90	[2] AITALA	96C	E791	π^- nucleus, 500 GeV

[1] The BITENC 08 right-sign sample includes about 15% of $D^0 \to K^-\pi^0\ell^+\nu_\ell$ and other decays.

[2] AITALA 96C uses $D^{*+} \to D^0\pi^+$ (and charge conjugate) decays to identify the charm at production and $D^0 \to K^-\ell^+\nu_\ell$ (and charge conjugate) decays to identify the charm at decay.

$\Gamma(K^+ \text{ or } K^*(892)^+ e^-\overline{\nu}_e \text{ via } \overline{D}^0)/[\Gamma(K^- e^+\nu_e) + \Gamma(K^*(892)^- e^+\nu_e)]$ — $\Gamma_{273}/(\Gamma_{19}+\Gamma_{21})$

This is a limit on R_M without the complications of possible doubly Cabibbo-suppressed decays that occur when using hadronic modes. The experiments use $D^{*+} \to D^0\pi^+$ (and charge conjugate) decays to identify the charm at production and the charge of the e to identify the charm at decay. These limits do not allow CP violation. For the limits on $|m_1 - m_2|$ and $(\Gamma_1 - \Gamma_2)/\Gamma$ that come from the best mixing limit, see near the beginning of these D^0 Listings.

VALUE	CL%	DOCUMENT ID		TECN	COMMENT
<0.001	90	BITENC	05	BELL	$e^+e^- \approx 10.6$ GeV
• • • We do not use the following data for averages, fits, limits, etc. • • •					
−0.0013 <R< +0.0012	90	AUBERT	07AB	BABR	$e^+e^- \approx 10.58$ GeV
<0.0078	90	CAWLFIELD	05	CLEO	$e^+e^- \approx 10.6$ GeV
<0.0042	90	AUBERT,B	04Q	BABR	See AUBERT 07AB

$\Gamma(K^+\pi^-)/\Gamma(K^-\pi^+)$ — Γ_{274}/Γ_{37}

This is R, the time-integrated wrong-sign rate compared to the right-sign rate. See the note on "D^0-$\overline{D}^0$ Mixing," near the start of the D^0 Listings.

The experiments here use the charge of the pion in $D^*(2010)^\pm \to (D^0 \text{ or } \overline{D}^0)\,\pi^\pm$ decay to tell whether a D^0 or a $\overline{D}^0$ was born. The $D^0 \to K^+\pi^-$ decay can occur directly by doubly Cabibbo-suppressed (DCS) decay, or indirectly by $D^0 \to \overline{D}^0$ mixing followed by $\overline{D}^0 \to K^+\pi^-$ decay. Some of the experiments can use the decay-time information to disentangle the two mechanisms. Here, we list the experimental branching ratio, which if there is no mixing is the DCS ratio. See the next data block for values of the DCS ratio R_D, and the following data block for limits on the mixing ratio R_M. See the section on CP-violating asymmetries near the end of this D^0 Listing for values of A_D, and the note on "D^0-$\overline{D}^0$ Mixing" for limits on x' and y'.

Some early limits have been omitted from this Listing; see our 1998 edition (The European Physical Journal **C3** 1 (1998)) and our 2006 edition (Journal of Physics **G33** 1 (2006)).

VALUE (units 10^{-3})	EVTS	DOCUMENT ID		TECN	COMMENT
3.79±0.18 OUR FIT	Error includes scale factor of 3.3.				
3.79±0.18 OUR AVERAGE	Error includes scale factor of 3.3. See the ideogram below.				
4.15±0.10	12.7±0.3k	[1] AALTONEN	08E	CDF	$p\overline{p}$, $\sqrt{s} = 1.96$ TeV
3.53±0.08±0.04	4030 ± 90	[2] AUBERT	07W	BABR	$e^+e^- \approx 10.6$ GeV
3.77±0.08±0.05	4024 ± 88	[1] ZHANG	06	BELL	e^+e^-
• • • We do not use the following data for averages, fits, limits, etc. • • •					
4.05±0.21±0.11	2.0 ± 0.1k	[3] ABULENCIA	06X	CDF	See AALTONEN 08E
$3.81 \pm 0.17^{+0.08}_{-0.16}$	845 ± 40	[2] LI	05A	BELL	See ZHANG 06
$4.29^{+0.63}_{-0.61} \pm 0.27$	234	[4] LINK	05H	FOCS	γ nucleus
3.57±0.22±0.27		[5] AUBERT	03Z	BABR	See AUBERT 07W
4.04±0.85±0.25	149	[6] LINK	01	FOCS	γ nucleus
$3.32^{+0.63}_{-0.65} \pm 0.40$	45	[1] GODANG	00	CLE2	e^+e^-
$6.8\ ^{+3.4}_{-3.3}\ \pm 0.7$	34	[2] AITALA	98	E791	π^- nucl., 500 GeV

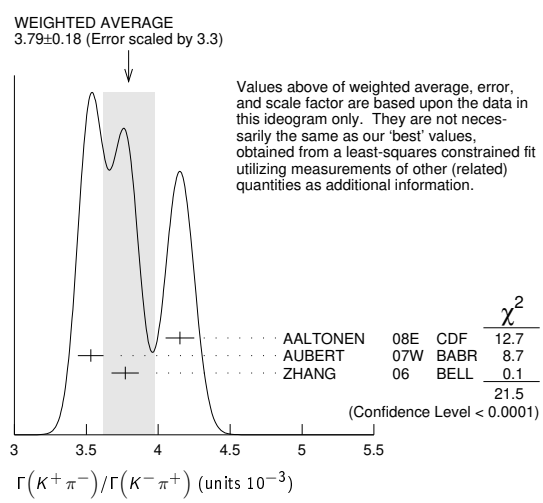

[1] GODANG 00, ZHANG 06, and AALTONEN 08E allow CP violation.

[2] AITALA 98, LI 05A, and AUBERT 07W assume no CP violation.

[3] This ABULENCIA 06X result assumes no mixing.

[4] This LINK 05H result assumes no mixing but allows CP violation. If neither mixing nor CP violation is allowed, $R = (4.29 \pm 0.63 \pm 0.28) \times 10^{-3}$.

[5] This AUBERT 03Z result allows CP violation. If CP violation is not allowed, $R = 0.00359 \pm 0.00020 \pm 0.00027$.

[6] This LINK 01 result assumes no mixing or CP violation.

Downloaded from https://academic.oup.com/ptep/article/2022/8/083C01/6651666 by KIT Library user on 27 September 2022

$\Gamma(K^+\pi^-$ via DCS$)/\Gamma(K^-\pi^+)$ — Γ_{275}/Γ_{37}

This is R_D, the doubly Cabibbo-suppressed ratio when mixing is allowed.

VALUE (units 10^{-3})	EVTS	DOCUMENT ID		TECN	COMMENT
3.45 ±0.06 OUR AVERAGE		Error includes scale factor of 1.5. See the ideogram below.			
3.454±0.040±0.020	722k	[1] AAIJ	18K	LHCB	pp at 7, 8, 13 TeV
3.53 ±0.13		[2] KO	14	BELL	$e^+e^- \to \Upsilon(nS)$
3.51 ±0.35		[3] AALTONEN	13AE	CDF	$p\overline{p}$ at 1.96 TeV
3.04 ±0.55	13k	AALTONEN	08E	CDF	$p\overline{p}$, $\sqrt{s}$ =1.96 TeV
3.03 ±0.16 ±0.10	4.0k	[4] AUBERT	07W	BABR	$e^+e^- \approx$ 10.6 GeV
3.64 ±0.17	4.0k	[5] ZHANG	06	BELL	e^+e^-
5.17 $^{+1.47}_{-1.58}$ ±0.76	234	[6] LINK	05H	FOCS	γ nucleus
4.8 ±1.2 ±0.4	45	[7] GODANG	00	CLE2	e^+e^-
• • • We do not use the following data for averages, fits, limits, etc. • • •					
3.533±0.054	236k	[8] AAIJ	17AO	LHCB	See AAIJ 18K
3.568±0.066		[9] AAIJ	13CE	LHCB	pp at 7, 8 TeV
3.52 ±0.15		[10] AAIJ	13N	LHCB	Repl. by AAIJ 13CE
2.87 ±0.37	0.8k	LI	05A	BELL	See ZHANG 06

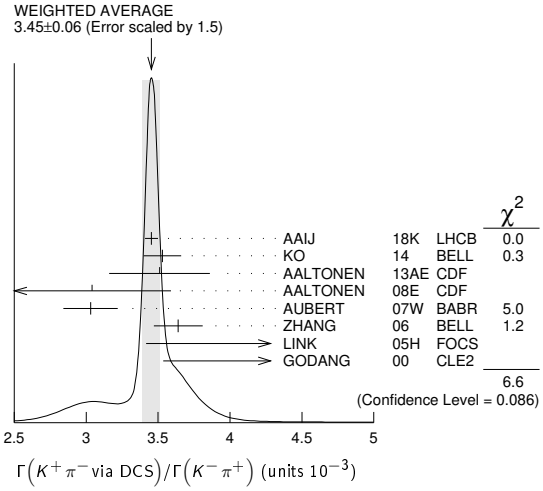

[1] This AAIJ 18K value is for direct and indirect CP violation allowed. The value is the same if either one or the other is not allowed, but in each case the error then is $(0.028 \pm 0.014) \times 10^{-3}$.
[2] Based on 976 fb^{-1} of data collected at $\Upsilon(nS)$ resonances. Assumes no CP violation.
[3] Based on 9.6 fb^{-1} of data collected at the Tevatron. Assumes no CP violation.
[4] Result is the same whether or not CP violation is allowed.
[5] This ZHANG 06 assumes no CP violation.
[6] This LINK 05H result allows CP violation. Allowing mixing but not CP violation, $R_D = (3.81 \,^{+1.67}_{-1.63} \pm 0.92) \times 10^{-3}$.
[7] This GODANG 00 result allows CP violation.
[8] The result was established with D^0 from prompt and secondary D^* assuming no CPV or no direct CPV.
[9] Based on 3 fb^{-1} of data collected at $\sqrt{s}$ = 7, 8 TeV. Assumes no CP violation.
[10] Based on 1 fb^{-1} of data collected at $\sqrt{s}$ = 7 TeV in 2011. Assumes no CP violation.

$\Gamma(K^+\pi^-$ via $\overline{D}^0)/\Gamma(K^-\pi^+)$ — Γ_{276}/Γ_{37}

This is R_M in the note on "D^0-$\overline{D}^0$ Mixing" near the start of the D^0 Listings. The experiments here (1) use the charge of the pion in $D^*(2010)^\pm \to (D^0$ or $\overline{D}^0)\ \pi^\pm$ decay to tell whether a D^0 or a $\overline{D}^0$ was born; and (2) use the decay-time distribution to disentangle doubly Cabibbo-suppressed decay and mixing. For the limits on $|m_1 - m_2|$ and $(\Gamma_1 - \Gamma_2)/\Gamma$ that come from the best mixing limit, see near the beginning of these D^0 Listings.

VALUE	CL%	DOCUMENT ID		TECN	COMMENT
<0.00040	95	[1] ZHANG	06	BELL	e^+e^-
• • • We do not use the following data for averages, fits, limits, etc. • • •					
<0.00046	95	[2] LI	05A	BELL	See ZHANG 06
<0.0063	95	[3] LINK	05H	FOCS	γ nucleus
<0.0013	95	[4] AUBERT	03Z	BABR	e^+e^-, 10.6 GeV
<0.00041	95	[5] GODANG	00	CLE2	e^+e^-
<0.0092	95	[6] BARATE	98W	ALEP	e^+e^- at Z^0
<0.005	90	[7] ANJOS	88C	E691	Photoproduction

[1] This ZHANG 06 result allows CP violation, but the result does not change if CP violation is not allowed.
[2] This LI 05A result allows CP violation. The limit becomes < 0.00042 (95% CL) if CP violation is not allowed.
[3] LINK 05H obtains the same result whether or not CP violation is allowed.
[4] This AUBERT 03Z result allows CP violation and assumes that the strong phase between $D^0 \to K^+\pi^-$ and $\overline{D}^0 \to K^+\pi^-$ is small, and limits only $D^0 \to \overline{D}^0$ transitions via off-shell intermediate states. The limit on transitions via on-shell intermediate states is 0.0016.
[5] This GODANG 00 result allows CP violation and assumes that the strong phase between $D^0 \to K^+\pi^-$ and $\overline{D}^0 \to K^+\pi^-$ is small, and limits only $D^0 \to \overline{D}^0$ transitions via off-shell intermediate states. The limit on transitions via on-shell intermediate states is 0.0017.
[6] This BARATE 98W result assumes no interference between the DCS and mixing amplitudes ($y' = 0$ in the note on "D^0-$\overline{D}^0$ Mixing" near the start of the D^0 Listings). When interference is allowed, the limit degrades to 0.036 (95%CL).
[7] This ANJOS 88C result assumes no interference between the DCS and mixing amplitudes ($y' = 0$ in the note on "D^0-$\overline{D}^0$ Mixing" near the start of the D^0 Listings). When interference is allowed, the limit degrades to 0.019.

$\Gamma(K^0_S\pi^+\pi^-$ in $D^0 \to \overline{D}^0)/\Gamma(K^0_S\pi^+\pi^-)$ — Γ_{277}/Γ_{40}

This is R_M in the note on "D^0-$\overline{D}^0$ Mixing" near the start of the D^0 Listings. The experiments here (1) use the charge of the pion in $D^*(2010)^\pm \to (D^0$ or $\overline{D}^0)\ \pi^\pm$ decay to tell whether a D^0 or a $\overline{D}^0$ was born; and (2) use the decay-time distribution to disentangle doubly Cabibbo-suppressed decay and mixing. For the limits on $|m_1 - m_2|$ and $(\Gamma_1 - \Gamma_2)/\Gamma$ that come from the best mixing limit, see near the beginning of these D^0 Listings.

VALUE	CL%	DOCUMENT ID		TECN	COMMENT
<0.0063	95	[1] ASNER	05	CLEO	$e^+e^- \approx$ 10 GeV

[1] This ASNER 05 limit allows CP violation. If CP violation is not allowed, the limit is 0.0042 at 95% CL.

$\Gamma(K^+\pi^-\pi^0)/\Gamma(K^-\pi^+\pi^0)$ — Γ_{281}/Γ_{55}

The experiments here use the charge of the pion in $D^*(2010)^\pm \to (D^0$ or $\overline{D}^0)\ \pi^\pm$ decay to tell whether a D^0 or a $\overline{D}^0$ was born. The $D^0 \to K^+\pi^-\pi^0$ decay can occur directly by doubly Cabibbo-suppressed (DCS) decay, or indirectly by $D^0 \to \overline{D}^0$ mixing followed by $\overline{D}^0 \to K^+\pi^-\pi^0$ decay.

VALUE (units 10^{-3})	EVTS	DOCUMENT ID		TECN	COMMENT
2.12±0.07 OUR AVERAGE					
2.01±0.11		[1] EVANS	16	CLEO	$e^+e^- \to D^0\overline{D}^0$ at $\psi(3770)$
2.14±0.08±0.08	763	[2] AUBERT,B	06N	BABR	$e^+e^- \approx \Upsilon(4S)$
2.29±0.15 $^{+0.13}_{-0.09}$	1.9k	TIAN	05	BELL	$e^+e^- \approx \Upsilon(4S)$
4.3 $^{+1.1}_{-1.0}$ ±0.7	38	BRANDENB...	01	CLE2	$e^+e^- \approx \Upsilon(4S)$

[1] A combined fit with a recent LHCb $D^0\overline{D}^0$ mixing results in AAIJ 16F is also reported to be $(2.00 \pm 0.11) \times 10^{-3}$.
[2] This AUBERT,B 06N result assumes no mixing.

$\Gamma(K^+\pi^-\pi^0$ via $\overline{D}^0)/\Gamma(K^-\pi^+\pi^0)$ — Γ_{282}/Γ_{55}

This is R_M in the note on "D^0-$\overline{D}^0$ Mixing" near the start of the D^0 Listings. The experiments here (1) use the charge of the pion in $D^*(2010)^\pm \to (D^0$ or $\overline{D}^0)\ \pi^\pm$ decay to tell whether a D^0 or a $\overline{D}^0$ was born; and (2) use the decay-time distribution to disentangle doubly Cabibbo-suppressed decay and mixing. For the limits on $|m_1 - m_2|$ and $(\Gamma_1 - \Gamma_2)/\Gamma$ that come from the best mixing limit, see near the beginning of these D^0 Listings.

VALUE (units 10^{-3})	CL%	DOCUMENT ID		TECN	COMMENT
5.25 $^{+0.25}_{-0.31}$ ±0.12		AUBERT	09AN	BABR	e^+e^- at 10.58 GeV
• • • We do not use the following data for averages, fits, limits, etc. • • •					
<0.54	95	[1] AUBERT,B	06N	BABR	$e^+e^- \approx \Upsilon(4S)$

[1] This AUBERT,B 06N limit assumes no CP violation. The measured value corresponding to the limit is $(2.3 \,^{+1.8}_{-1.4} \pm 0.4) \times 10^{-4}$. If CP violation is allowed, this becomes $(1.0 \,^{+2.2}_{-0.7} \pm 0.3) \times 10^{-4}$.

$\Gamma(K^+\pi^+2\pi^-$ via DCS$)/\Gamma(K^-2\pi^+\pi^-)$ — Γ_{283}/Γ_{72}

VALUE (units 10^{-3})	EVTS	DOCUMENT ID		TECN	COMMENT
3.03 ±0.07 OUR AVERAGE					
3.025±0.077	42k,11M	[1] AAIJ	16F	LHCB	pp at 7, 8 TeV
3.03 ±0.13		[2] EVANS	16	CLEO	$e^+e^- \to D^0\overline{D}^0$ at $\psi(3770)$

[1] This result uses external input on the mixing parameters x, y. Without this input, the result is $(3.215 \pm 0.136) \times 10^{-3}$.
[2] A combined fit with a recent LHCb $D^0\overline{D}^0$ mixing results in AAIJ 16F is also reported to be $(3.01 \pm 0.07) \times 10^{-3}$.

$\Gamma(K^+\pi^+2\pi^-)/\Gamma(K^-2\pi^+\pi^-)$ — Γ_{284}/Γ_{72}

The experiments here use the charge of the pion in $D^*(2010)^\pm \to (D^0$ or $\overline{D}^0)\ \pi^\pm$ decay to tell whether a D^0 or a $\overline{D}^0$ was born. The $D^0 \to K^+\pi^-\pi^+\pi^-$ decay can occur directly by doubly Cabibbo-suppressed (DCS) decay, or indirectly by $D^0 \to \overline{D}^0$ mixing followed by $\overline{D}^0 \to K^+\pi^-\pi^+\pi^-$ decay. Some of the experiments can use the decay-time information to disentangle the two mechanisms. Here, we list the experimental branching ratio, which if there is no mixing is the DCS ratio; in the next data block we give the limits on the mixing ratio.

Some early limits have been omitted from this Listing; see our 1998 edition (EPJ **C3** 1).

VALUE (units 10^{-3})	CL%	EVTS	DOCUMENT ID		TECN	COMMENT
3.22±0.05 OUR AVERAGE						
3.22±0.05		42k,11M	[1] AAIJ	16F	LHCB	pp at 7, 8 TeV
3.24±0.08±0.07		3.3k	[2] WHITE	13	BELL	$e^+e^- \approx \Upsilon(4S)$
4.4 $^{+1.3}_{-1.2}$ ±0.4		54	[2] DYTMAN	01	CLE2	$e^+e^- \approx \Upsilon(4S)$
2.5 $^{+3.6}_{-3.4}$ ±0.3			[3] AITALA	98	E791	π^- nucl., 500 GeV

Downloaded from https://academic.oup.com/ptep/article/2022/8/083C01/6651666 by KIT Library user on 27 September 2022

• • • We do not use the following data for averages, fits, limits, etc. • • •

$3.20 \pm 0.18 ^{+0.18}_{-0.13}$	1.7k	[2] TIAN	05	BELL	See WHITE 13
<18	90	[2] AMMAR	91	CLEO	$e^+e^- \approx$ 10.5 GeV
<18	90	[4] ANJOS	88C	E691	Photoproduction

[1] AAIJ 16F result comes from time-dependent analysis that uses external input on the mixing parameters x, y. Without this input, the result is $(3.29 \pm 0.08) \times 10^{-3}$.

[2] AMMAR 91 cannot and DYTMAN 01, TIAN 05 do not distinguish between doublyCabibbo-suppressed decay and D^0-$\overline{D}^0$ mixing.

[3] This AITALA 98result assumes no D^0-$\overline{D}^0$ mixing (R_M in the note on "D^0-$\overline{D}^0$ Mixing").It becomes $-0.0020 ^{+0.0117}_{-0.0106} \pm 0.0035$ whenmixing is allowed and decay-time information is used todistinguish doubly Cabibbo-suppressed decays from mixing.

[4] ANJOS 88C uses decay-time information to distinguish doubly Cabibbo-suppressed (DCS) decays from D^0-$\overline{D}^0$ mixing. However, the result assumes no interference between the DCS and mixing amplitudes ($y' = 0$ in the note on "D^0-$\overline{D}^0$ Mixing" near the start of the D^0 Listings). When interference is allowed, the limit degrades to 0.033.

$\Gamma(K^+\pi^+2\pi^- \text{via } \overline{D}^0)/\Gamma(K^-2\pi^+\pi^-)$ — Γ_{285}/Γ_{72}

This is a D^0-$\overline{D}^0$ mixing limit. The experiments here (1) use the charge of the pion in $D^*(2010)^\pm \to (D^0 \text{ or } \overline{D}^0)\,\pi^\pm$ decay to tell whether a D^0 or a $\overline{D}^0$ was born; and (2) use the decay-time distribution to disentangle doubly Cabibbo-suppressed decay and mixing. For the limits on $|m_{D^0_1} - m_{D^0_2}|$ and $(\Gamma_{D^0_1} - \Gamma_{D^0_2})/\Gamma_{D^0}$ that come from the best mixing limit, see near the beginning of these D^0 Listings.

VALUE (units 10^{-5})	CL%	DOCUMENT ID		TECN	COMMENT
9.6±3.6		[1] AAIJ	16F	LHCB	pp at 7, 8 TeV
• • • We do not use the following data for averages, fits, limits, etc. • • •					
<500	90	[2] ANJOS	88C	E691	Photoproduction

[1] AAIJ 16F result comes from an unconstrained decay-time dependent fit to the wrong-sign to right-sign decay rates ratio as $(x^2 + y^2)/2$.

[2] ANJOS 88C uses decay-time information to distinguish doubly Cabibbo-suppressed (DCS) decays from D^0-$\overline{D}^0$ mixing. However, the result assumes no interference between the DCS and mixing amplitudes ($y' = 0$ in the note on "D^0-$\overline{D}^0$ Mixing" near the start of the D^0 Listings). When interference is allowed, the limit degrades to 0.007.

$\Gamma(K^+\pi^- \text{or } K^+\pi^+2\pi^- \text{via } \overline{D}^0)/\Gamma(K^-\pi^+ \text{or } K^-2\pi^+\pi^-)$ — Γ_{286}/Γ_0

This is a D^0-$\overline{D}^0$ mixing limit. For the limits on $|m_{D^0_1} - m_{D^0_2}|$ and $(\Gamma_{D^0_1} - \Gamma_{D^0_2})/\Gamma_{D^0}$ that come from the best mixing limit, see near the beginning of these D^0 Listings.

VALUE	CL%	DOCUMENT ID		TECN	COMMENT
• • • We do not use the following data for averages, fits, limits, etc. • • •					
<0.0085	90	[1] AITALA	98	E791	π^- nucleus, 500 GeV
<0.0037	90	[2] ANJOS	88C	E691	Photoproduction

[1] AITALA 98 uses decay-time information to distinguish doubly Cabibbo-suppressed decays from D^0-$\overline{D}^0$ mixing. The fit allows interference between the two amplitudes, and also allows CP violation in this term. The central value obtained is $0.0039 ^{+0.0036}_{-0.0032} \pm 0.0016$. When interference is disallowed, the result becomes $0.0021 \pm 0.0009 \pm 0.0002$.

[2] This combines results of ANJOS 88C on $K^+\pi^-$ and $K^+\pi^-\pi^+\pi^-$ (via $\overline{D}^0$) reported in the data block above (see footnotes there). It assumes no interference.

$\Gamma(\mu^- \text{anything via } \overline{D}^0)/\Gamma(\mu^+ \text{anything})$ — Γ_{287}/Γ_6

This is a D^0-$\overline{D}^0$ mixing limit. See the somewhat better limits above.

VALUE	CL%	DOCUMENT ID		TECN	COMMENT
<0.0056	90	LOUIS	86	SPEC	π^- W 225 GeV
• • • We do not use the following data for averages, fits, limits, etc. • • •					
<0.012	90	BENVENUTI	85	CNTR	μC, 200 GeV
<0.044	90	BODEK	82	SPEC	$\pi^-, p\text{Fe} \to D^0$

Rare or forbidden modes

$\Gamma(\gamma\gamma)/\Gamma_{\text{total}}$ — Γ_{288}/Γ

$D^0 \to \gamma\gamma$ is a flavor-changing neutral-current decay, forbidden in the Standard Model at the tree level.

VALUE	CL%	DOCUMENT ID		TECN	COMMENT
< 8.5 × 10^{-7}	90	NISAR	16	BELL	e^+e^- at $\Upsilon(4S)$, $\Upsilon(5S)$
• • • We do not use the following data for averages, fits, limits, etc. • • •					
< 3.8 × 10^{-6}	90	ABLIKIM	15F	BES3	e^+e^- at 3.773 GeV
< 2.2 × 10^{-6}	90	LEES	12L	BABR	$e^+e^- \approx$ 10.58 GeV
<29 × 10^{-6}	90	COAN	03	CLE2	$e^+e^- \approx \Upsilon(4S)$

$\Gamma(e^+e^-)/\Gamma_{\text{total}}$ — Γ_{289}/Γ

A test for the $\Delta C = 1$ weak neutral current. Allowed by first-order weak interaction combined with electromagnetic interaction.

VALUE	CL%	DOCUMENT ID		TECN	COMMENT
<7.9 × 10^{-8}	90	PETRIC	10	BELL	$e^+e^- \approx \Upsilon(4S)$
• • • We do not use the following data for averages, fits, limits, etc. • • •					
<1.7 × 10^{-7}	90	LEES	12Q	BABR	$e^+e^- \approx$ 10.58 GeV
<1.2 × 10^{-6}	90	AUBERT,B	04Y	BABR	$e^+e^- \approx \Upsilon(4S)$
<8.19 × 10^{-6}	90	PRIPSTEIN	00	E789	p nucleus, 800 GeV
<6.2 × 10^{-6}	90	AITALA	99G	E791	$\pi^- N$ 500 GeV
<1.3 × 10^{-5}	90	FREYBERGER	96	CLE2	$e^+e^- \approx \Upsilon(4S)$
<1.3 × 10^{-4}	90	ADLER	88	MRK3	e^+e^- 3.77 GeV
<1.7 × 10^{-4}	90	ALBRECHT	88G	ARG	e^+e^- 10 GeV
<2.2 × 10^{-4}	90	HAAS	88	CLEO	e^+e^- 10 GeV

$\Gamma(\mu^+\mu^-)/\Gamma_{\text{total}}$ — Γ_{290}/Γ

A test for the $\Delta C = 1$ weak neutral current. Allowed by first-order weak interaction combined with electromagnetic interaction.

VALUE	CL%	DOCUMENT ID		TECN	COMMENT
<6.2 × 10^{-9}	90	AAIJ	13AI	LHCB	pp at 7 TeV
• • • We do not use the following data for averages, fits, limits, etc. • • •					
0.6–8.1 × 10^{-7}	90	[1] LEES	12Q	BABR	$e^+e^- \approx$ 10.58 GeV
<2.1 × 10^{-7}	90	AALTONEN	10X	CDF	$p\overline{p}$, $\sqrt{s}$ = 1.96 TeV
<1.4 × 10^{-7}	90	PETRIC	10	BELL	$e^+e^- \approx \Upsilon(4S)$
<2.0 × 10^{-6}	90	ABT	04	HERB	pA, 920 GeV
<1.3 × 10^{-6}	90	AUBERT,B	04Y	BABR	$e^+e^- \approx \Upsilon(4S)$
<2.5 × 10^{-6}	90	ACOSTA	03F	CDF	See AALTONEN 10X
<1.56 × 10^{-5}	90	PRIPSTEIN	00	E789	p nucleus, 800 GeV
<5.2 × 10^{-6}	90	AITALA	99G	E791	$\pi^- N$ 500 GeV
<4.1 × 10^{-6}	90	ADAMOVICH	97	BEAT	π^- Cu, W 350 GeV
<4.2 × 10^{-6}	90	ALEXOPOU...	96	E771	p Si, 800 GeV
<3.4 × 10^{-5}	90	FREYBERGER	96	CLE2	$e^+e^- \approx \Upsilon(4S)$
<7.6 × 10^{-6}	90	ADAMOVICH	95	BEAT	See ADAMOVICH 97
<4.4 × 10^{-5}	90	KODAMA	95	E653	π^- emulsion 600 GeV
<3.1 × 10^{-5}	90	[2] MISHRA	94	E789	-4.1 ± 4.8 events
<7.0 × 10^{-5}	90	ALBRECHT	88G	ARG	e^+e^- 10 GeV
<1.1 × 10^{-5}	90	LOUIS	86	SPEC	π^- W 225 GeV
<3.4 × 10^{-4}	90	AUBERT	85	EMC	Deep inelast. $\mu^- N$

[1] LEES 12Q gives a 2-sided range.

[2] Here MISHRA 94 uses "the statistical approach advocated by the PDG." For an alternate approach, giving a limit of 9×10^{-6} at 90% confidence level, see the paper.

$\Gamma(\pi^0 e^+e^-)/\Gamma_{\text{total}}$ — Γ_{291}/Γ

A test for the $\Delta C = 1$ weak neutral current. Allowed by higher-order electroweak interactions.

VALUE	CL%	DOCUMENT ID		TECN	COMMENT
<4 × 10^{-6}	90	ABLIKIM	18P	BES3	e^+e^-, 3773 MeV
• • • We do not use the following data for averages, fits, limits, etc. • • •					
<4.5 × 10^{-5}	90	FREYBERGER	96	CLE2	$e^+e^- \approx \Upsilon(4S)$

$\Gamma(\pi^0\mu^+\mu^-)/\Gamma_{\text{total}}$ — Γ_{292}/Γ

A test for the ΔC=1 weak neutral current. Allowed by higher-order electroweak interactions.

VALUE	CL%	DOCUMENT ID		TECN	COMMENT
<1.8 × 10^{-4}	90	KODAMA	95	E653	π^- emulsion 600 GeV
• • • We do not use the following data for averages, fits, limits, etc. • • •					
<5.4 × 10^{-4}	90	FREYBERGER	96	CLE2	$e^+e^- \approx \Upsilon(4S)$

$\Gamma(\eta e^+e^-)/\Gamma_{\text{total}}$ — Γ_{293}/Γ

A test for the $\Delta C = 1$ weak neutral current. Allowed by higher-order electroweak interactions.

VALUE	CL%	DOCUMENT ID		TECN	COMMENT
<3 × 10^{-6}	90	ABLIKIM	18P	BES3	e^+e^-, 3773 MeV
• • • We do not use the following data for averages, fits, limits, etc. • • •					
<1.1 × 10^{-4}	90	FREYBERGER	96	CLE2	$e^+e^- \approx \Upsilon(4S)$

$\Gamma(\eta\mu^+\mu^-)/\Gamma_{\text{total}}$ — Γ_{294}/Γ

A test for the $\Delta C = 1$ weak neutral current. Allowed by higher-order electroweak interactions.

VALUE	CL%	DOCUMENT ID		TECN	COMMENT
<5.3 × 10^{-4}	90	FREYBERGER	96	CLE2	$e^+e^- \approx \Upsilon(4S)$

$\Gamma(\pi^+\pi^-e^+e^-)/\Gamma_{\text{total}}$ — Γ_{295}/Γ

A test for the $\Delta C = 1$ weak neutral current. Allowed by higher-order electroweak interactions.

VALUE	CL%	DOCUMENT ID		TECN	COMMENT
<7 × 10^{-6}	90	ABLIKIM	18P	BES3	e^+e^-, 3773 MeV
• • • We do not use the following data for averages, fits, limits, etc. • • •					
<3.73 × 10^{-4}	90	AITALA	01C	E791	π^- nucleus, 500 GeV

$\Gamma(\rho^0 e^+e^-)/\Gamma_{\text{total}}$ — Γ_{296}/Γ

A test for the $\Delta C = 1$ weak neutral current. Allowed by higher-order electroweak interactions.

VALUE	CL%	DOCUMENT ID		TECN	COMMENT
<1.0 × 10^{-4}	90	[1] FREYBERGER	96	CLE2	$e^+e^- \approx \Upsilon(4S)$
• • • We do not use the following data for averages, fits, limits, etc. • • •					
<1.24 × 10^{-4}	90	AITALA	01C	E791	π^- nucleus, 500 GeV
<4.5 × 10^{-4}	90	HAAS	88	CLEO	e^+e^- 10 GeV

[1] This FREYBERGER 96 limit is obtained using a phase-space model. The limit changes to $< 1.8 \times 10^{-4}$ using a photon pole amplitude model.

$\Gamma(\pi^+\pi^-\mu^+\mu^-)/\Gamma_{\text{total}}$ — Γ_{297}/Γ

A test for the $\Delta C = 1$ weak neutral current. Allowed by higher-order electroweak interactions.

VALUE (units 10^{-7})	EVTS	DOCUMENT ID		TECN	COMMENT
9.64±0.48±1.10	561	[1] AAIJ	17BG	LHCB	pp at 8 TeV

[1] The second AAIJ 17BG error is the systematic 0.51×10^{-7} and normalization 0.97×10^{-7} mode errors added in quadrature.

Downloaded from https://academic.oup.com/ptep/article/2022/8/083C01/6651666 by KIT Library user on 27 September 2022

$\Gamma(\pi^+\pi^-\mu^+\mu^-(\text{non-res}))/\Gamma_{\text{total}}$ — Γ_{298}/Γ

VALUE	CL%	DOCUMENT ID		TECN	COMMENT
$<5.5\times10^{-7}$	90	[1] AAIJ	14B	LHCB	pp at 7 TeV
• • • We do not use the following data for averages, fits, limits, etc. • • •					
$<3.0\times10^{-5}$	90	AITALA	01C	E791	π^- nucleus, 500 GeV

[1] AAIJ 14B measures this branching-fraction limit relative to the $\pi^+\pi^-\phi$, $\phi\to\mu^+\mu^-$ fraction. The above limit excludes the resonant ϕ, ω, and ρ regions, and then fills those gaps with a phase-space model.

$\Gamma(\rho^0\mu^+\mu^-)/\Gamma_{\text{total}}$ — Γ_{299}/Γ

A test for the $\Delta C=1$ weak neutral current. Allowed by higher-order electroweak interactions.

VALUE	CL%	DOCUMENT ID		TECN	COMMENT
$<2.2\times10^{-5}$	90	AITALA	01C	E791	π^- nucleus, 500 GeV
• • • We do not use the following data for averages, fits, limits, etc. • • •					
$<4.9\times10^{-4}$	90	[1] FREYBERGER	96	CLE2	$e^+e^-\approx\Upsilon(4S)$
$<2.3\times10^{-4}$	90	KODAMA	95	E653	π^- emulsion 600 GeV
$<8.1\times10^{-4}$	90	HAAS	88	CLEO	e^+e^- 10 GeV

[1] This FREYBERGER 96 limit is obtained using a phase-space model. The limit changes to $<4.5\times10^{-4}$ using a photon pole amplitude model.

$\Gamma(\omega e^+e^-)/\Gamma_{\text{total}}$ — Γ_{300}/Γ

A test for the $\Delta C=1$ weak neutral current. Allowed by higher-order electroweak interactions.

VALUE	CL%	DOCUMENT ID		TECN	COMMENT
$<6\times10^{-6}$	90	ABLIKIM	18P	BES3	e^+e^-, 3773 MeV
• • • We do not use the following data for averages, fits, limits, etc. • • •					
$<1.8\times10^{-4}$	90	[1] FREYBERGER	96	CLE2	$e^+e^-\approx\Upsilon(4S)$

[1] This FREYBERGER 96 limit is obtained using a phase-space model. The limit changes to $<2.7\times10^{-4}$ using a photon pole amplitude model.

$\Gamma(\omega\mu^+\mu^-)/\Gamma_{\text{total}}$ — Γ_{301}/Γ

A test for the $\Delta C=1$ weak neutral current. Allowed by higher-order electroweak interactions.

VALUE	CL%	DOCUMENT ID		TECN	COMMENT
$<8.3\times10^{-4}$	90	[1] FREYBERGER	96	CLE2	$e^+e^-\approx\Upsilon(4S)$

[1] This FREYBERGER 96 limit is obtained using a phase-space model. The limit changes to $<6.5\times10^{-4}$ using a photon pole amplitude model.

$\Gamma(K^-K^+e^+e^-)/\Gamma_{\text{total}}$ — Γ_{302}/Γ

A test for the $\Delta C=1$ weak neutral current. Allowed by higher-order electroweak interactions.

VALUE	CL%	DOCUMENT ID		TECN	COMMENT
$<1.1\times10^{-5}$	90	ABLIKIM	18P	BES3	e^+e^-, 3773 MeV
• • • We do not use the following data for averages, fits, limits, etc. • • •					
$<3.15\times10^{-4}$	90	AITALA	01C	E791	π^- nucleus, 500 GeV

$\Gamma(K^-\pi^+e^+e^-, 675<m_{ee}<875\text{ MeV})/\Gamma_{\text{total}}$ — Γ_{310}/Γ

VALUE (units 10^{-6})	EVTS	DOCUMENT ID		TECN	COMMENT
$4.0\pm0.5\pm0.2\pm0.1$	68	[1,2] LEES	19A	BABR	e^+e^- near $\Upsilon(4S)$

[1] Observation with 9.7 σ significance. The last uncertainty is due to the uncertainty on the branching fraction of the normalization mode, $D^0\to K^-\pi^+\pi^+\pi^-$. The second uncertainty is other systematic and is dominated by the model parameterization.

[2] LEES 19A also sets an upper limit for non-resonant regions, where long-distance effects are expected to be small: $<3.1\times10^{-6}$ at 90% CL.

$\Gamma(K^-\pi^+e^+e^-, 1.005<m_{ee}<1.035\text{ GeV})/\Gamma_{\text{total}}$ — Γ_{311}/Γ

VALUE	CL%	DOCUMENT ID		TECN	COMMENT
$<5\times10^{-7}$	90	[1] LEES	19A	BABR	e^+e^- near $\Upsilon(4S)$

[1] LEES 19A also sets an upper limit for non-resonant regions, where long-distance effects are expected to be small: $<3.1\times10^{-6}$ at 90% CL.

$\Gamma(\phi e^+e^-)/\Gamma_{\text{total}}$ — Γ_{303}/Γ

A test for the $\Delta C=1$ weak neutral current. Allowed by higher-order electroweak interactions.

VALUE	CL%	DOCUMENT ID		TECN	COMMENT
$<5.2\times10^{-5}$	90	[1] FREYBERGER	96	CLE2	$e^+e^-\approx\Upsilon(4S)$
• • • We do not use the following data for averages, fits, limits, etc. • • •					
$<5.9\times10^{-5}$	90	AITALA	01C	E791	π^- nucleus, 500 GeV

[1] This FREYBERGER 96 limit is obtained using a phase-space model. The limit changes to $<7.6\times10^{-5}$ using a photon pole amplitude model.

$\Gamma(K^-K^+\mu^+\mu^-)/\Gamma_{\text{total}}$ — Γ_{304}/Γ

A test for the $\Delta C=1$ weak neutral current. Allowed by higher-order electroweak interactions.

VALUE (units 10^{-7})	EVTS	DOCUMENT ID		TECN	COMMENT
$1.54\pm0.27\pm0.18$	34	[1] AAIJ	17BG	LHCB	pp at 8 TeV

[1] The second AAIJ 17BG error is the systematic 0.09×10^{-7} and normalization 0.16×10^{-7} mode errors added in quadrature.

$\Gamma(K^-K^+\mu^+\mu^-(\text{non-res}))/\Gamma_{\text{total}}$ — Γ_{305}/Γ

VALUE	CL%	DOCUMENT ID		TECN	COMMENT
$<3.3\times10^{-5}$	90	AITALA	01C	E791	π^- nucleus, 500 GeV

$\Gamma(\phi\mu^+\mu^-)/\Gamma_{\text{total}}$ — Γ_{306}/Γ

A test for the $\Delta C=1$ weak neutral current. Allowed by higher-order electroweak interactions.

VALUE	CL%	DOCUMENT ID		TECN	COMMENT
$<3.1\times10^{-5}$	90	AITALA	01C	E791	π^- nucleus, 500 GeV
• • • We do not use the following data for averages, fits, limits, etc. • • •					
$<4.1\times10^{-4}$	90	[1] FREYBERGER	96	CLE2	$e^+e^-\approx\Upsilon(4S)$

[1] This FREYBERGER 96 limit is obtained using a phase-space model. The limit changes to $<2.4\times10^{-4}$ using a photon pole amplitude model.

$\Gamma(\overline{K}^0e^+e^-)/\Gamma_{\text{total}}$ — Γ_{307}/Γ

Not a useful test for $\Delta C=1$ weak neutral current because both quarks must change flavor.

VALUE	CL%	DOCUMENT ID		TECN	COMMENT
$<2.4\times10^{-5}$	90	[1] ABLIKIM	18P	BES3	e^+e^-, 3773 MeV
• • • We do not use the following data for averages, fits, limits, etc. • • •					
$<1.1\times10^{-4}$	90	FREYBERGER	96	CLE2	$e^+e^-\approx\Upsilon(4S)$
$<1.7\times10^{-3}$	90	ADLER	89C	MRK3	e^+e^- 3.77 GeV

[1] ABLIKIM 18P report a 90% C.L. limit on $D^0\to K^0_S e^+e^-$ of 1.2×10^{-5} which is here interpreted in terms of $D^0\to\overline{K}^0e^+e^-$.

$\Gamma(\overline{K}^0\mu^+\mu^-)/\Gamma_{\text{total}}$ — Γ_{308}/Γ

Not a useful test for $\Delta C=1$ weak neutral current because both quarks must change flavor.

VALUE	CL%	DOCUMENT ID		TECN	COMMENT
$<2.6\times10^{-4}$	90	KODAMA	95	E653	π^- emulsion 600 GeV
• • • We do not use the following data for averages, fits, limits, etc. • • •					
$<6.7\times10^{-4}$	90	FREYBERGER	96	CLE2	$e^+e^-\approx\Upsilon(4S)$

$\Gamma(K^-\pi^+e^+e^-)/\Gamma_{\text{total}}$ — Γ_{309}/Γ

A test for the $\Delta C=1$ weak neutral current. Allowed by higher-order electroweak interactions.

VALUE	CL%	DOCUMENT ID		TECN	COMMENT
• • • We do not use the following data for averages, fits, limits, etc. • • •					
$<4.1\times10^{-5}$	90	ABLIKIM	18P	BES3	see LEES 19A
$<3.85\times10^{-4}$	90	AITALA	01C	E791	π^- nucleus, 500 GeV

$\Gamma(\overline{K}^*(892)^0e^+e^-)/\Gamma_{\text{total}}$ — Γ_{312}/Γ

Not a useful test for $\Delta C=1$ weak neutral current because both quarks must change flavor.

VALUE	CL%	DOCUMENT ID		TECN	COMMENT
$<4.7\times10^{-5}$	90	AITALA	01C	E791	π^- nucleus, 500 GeV
• • • We do not use the following data for averages, fits, limits, etc. • • •					
$<1.4\times10^{-4}$	90	[1] FREYBERGER	96	CLE2	$e^+e^-\approx\Upsilon(4S)$

[1] This FREYBERGER 96 limit is obtained using a phase-space model. The limit changes to $<2.0\times10^{-4}$ using a photon pole amplitude model.

$\Gamma(K^-\pi^+\mu^+\mu^-)/\Gamma_{\text{total}}$ — Γ_{313}/Γ

A test for the $\Delta C=1$ weak neutral current. Allowed by higher-order electroweak interactions.

VALUE	CL%	DOCUMENT ID		TECN	COMMENT
$<3.59\times10^{-4}$	90	AITALA	01C	E791	π^- nucleus, 500 GeV

$\Gamma(K^-\pi^+\mu^+\mu^-, 675<m_{\mu\mu}<875\text{ MeV})/\Gamma_{\text{total}}$ — Γ_{314}/Γ

VALUE (units 10^{-6})	EVTS	DOCUMENT ID		TECN	COMMENT
$4.17\pm0.12\pm0.40$	2.4k	[1] AAIJ	16I	LHCB	pp at 8 TeV

[1] AAIJ 16I uses $B(D^0\to K^-\pi^+\pi^+\pi^-)=(8.287\pm0.043\pm0.200)\times10^{-2}$ value for the normalization mode.

$\Gamma(\overline{K}^*(892)^0\mu^+\mu^-)/\Gamma_{\text{total}}$ — Γ_{315}/Γ

Not a useful test for $\Delta C=1$ weak neutral current because both quarks must change flavor.

VALUE	CL%	DOCUMENT ID		TECN	COMMENT
$<2.4\times10^{-5}$	90	AITALA	01C	E791	π^- nucleus, 500 GeV
• • • We do not use the following data for averages, fits, limits, etc. • • •					
$<1.18\times10^{-3}$	90	[1] FREYBERGER	96	CLE2	$e^+e^-\approx\Upsilon(4S)$

[1] This FREYBERGER 96 limit is obtained using a phase-space model. The limit changes to $<1.0\times10^{-3}$ using a photon pole amplitude model.

$\Gamma(\pi^+\pi^-\pi^0\mu^+\mu^-)/\Gamma_{\text{total}}$ — Γ_{316}/Γ

A test for the $\Delta C=1$ weak neutral current. Allowed by higher-order electroweak interactions.

VALUE	CL%	DOCUMENT ID		TECN	COMMENT
$<8.1\times10^{-4}$	90	KODAMA	95	E653	π^- emulsion 600 GeV

$\Gamma(\mu^\pm e^\mp)/\Gamma_{\text{total}}$ — Γ_{317}/Γ

A test of lepton family number conservation.

VALUE	CL%	DOCUMENT ID		TECN	COMMENT
$<1.3\times10^{-8}$	90	AAIJ	16H	LHCB	pp at 7, 8 GeV
• • • We do not use the following data for averages, fits, limits, etc. • • •					
$<3.3\times10^{-7}$	90	LEES	12Q	BABR	$e^+e^-\approx$ 10.58 GeV
$<2.6\times10^{-7}$	90	PETRIC	10	BELL	$e^+e^-\approx\Upsilon(4S)$
$<8.1\times10^{-7}$	90	AUBERT,B	04Y	BABR	$e^+e^-\approx\Upsilon(4S)$
$<1.72\times10^{-5}$	90	PRIPSTEIN	00	E789	p nucleus, 800 GeV

Downloaded from https://academic.oup.com/ptep/article/2022/8/083C01/6651666 by KIT Library user on 27 September 2022

$< 8.1 \times 10^{-6}$	90	AITALA	99G	E791	$\pi^- N$ 500 GeV
$< 1.9 \times 10^{-5}$	90	[1] FREYBERGER	96	CLE2	$e^+e^- \approx \Upsilon(4S)$
$< 1.0 \times 10^{-4}$	90	ALBRECHT	88G	ARG	e^+e^- 10 GeV
$< 2.7 \times 10^{-4}$	90	HAAS	88	CLEO	e^+e^- 10 GeV
$< 1.2 \times 10^{-4}$	90	BECKER	87C	MRK3	e^+e^- 3.77 GeV
$< 9 \times 10^{-4}$	90	PALKA	87	SILI	200 GeV πp
$<21 \times 10^{-4}$	90	[2] RILES	87	MRK2	e^+e^- 29 GeV

[1] This is the corrected result given in the erratum to FREYBERGER 96.
[2] RILES 87 assumes $B(D \to K\pi) = 3.0\%$ and has production model dependency.

$\Gamma(\pi^0 e^\pm \mu^\mp)/\Gamma_{total}$ — Γ_{318}/Γ

A test of lepton family number conservation. The value is for the sum of the two charge states.

VALUE	CL%	DOCUMENT ID		TECN	COMMENT
$<8.0 \times 10^{-7}$	90	LEES	20A	BABR	e^+e^- at $\Upsilon(4S)$
• • • We do not use the following data for averages, fits, limits, etc. • • •					
$<8.6 \times 10^{-5}$	90	FREYBERGER	96	CLE2	$e^+e^- \approx \Upsilon(4S)$

$\Gamma(\eta e^\pm \mu^\mp)/\Gamma_{total}$ — Γ_{319}/Γ

A test of lepton family number conservation. The value is for the sum of the two charge states.

VALUE	CL%	DOCUMENT ID		TECN	COMMENT
$<22.5 \times 10^{-7}$	90	[1] LEES	20A	BABR	e^+e^- at $\Upsilon(4S)$
• • • We do not use the following data for averages, fits, limits, etc. • • •					
$< 1.0 \times 10^{-4}$	90	FREYBERGER	96	CLE2	$e^+e^- \approx \Upsilon(4S)$

[1] LEES 20A quotes separate limits $B(D^0 \to \eta e^\pm \mu^\mp,\ \eta \to \gamma\gamma) < 24.0 \times 10^{-7}$ and $B(D^0 \to \eta e^\pm \mu^\mp,\ \eta \to \pi^+\pi^-\pi^0) < 43.0 \times 10^{-7}$.

$\Gamma(\pi^+\pi^- e^\pm \mu^\mp)/\Gamma_{total}$ — Γ_{320}/Γ

A test of lepton family-number conservation.

VALUE	CL%	DOCUMENT ID		TECN	COMMENT
$<1.71 \times 10^{-6}$	90	LEES	20B	BABR	e^+e^- at $\Upsilon(4S)$
• • • We do not use the following data for averages, fits, limits, etc. • • •					
$<1.5 \times 10^{-5}$	90	AITALA	01C	E791	π^- nucleus, 500 GeV

$\Gamma(\rho^0 e^\pm \mu^\mp)/\Gamma_{total}$ — Γ_{321}/Γ

A test of lepton family number conservation. The value is for the sum of the two charge states.

VALUE	CL%	DOCUMENT ID		TECN	COMMENT
$<5.0 \times 10^{-7}$	90	LEES	20A	BABR	e^+e^- at $\Upsilon(4S)$
• • • We do not use the following data for averages, fits, limits, etc. • • •					
$<6.6 \times 10^{-5}$	90	AITALA	01C	E791	π^- nucleus, 500 GeV
$<4.9 \times 10^{-5}$	90	[1] FREYBERGER	96	CLE2	$e^+e^- \approx \Upsilon(4S)$

[1] This FREYBERGER 96 limit is obtained using a phase-space model. The limit changes to $< 5.0 \times 10^{-5}$ using a photon pole amplitude model.

$\Gamma(\omega e^\pm \mu^\mp)/\Gamma_{total}$ — Γ_{322}/Γ

A test of lepton family number conservation. The value is for the sum of the two charge states.

VALUE	CL%	DOCUMENT ID		TECN	COMMENT
$<17.1 \times 10^{-7}$	90	LEES	20A	BABR	e^+e^- at $\Upsilon(4S)$
• • • We do not use the following data for averages, fits, limits, etc. • • •					
$< 1.2 \times 10^{-4}$	90	[1] FREYBERGER	96	CLE2	$e^+e^- \approx \Upsilon(4S)$

[1] This FREYBERGER 96 limit is obtained using a phase-space model. The same limit is obtained using a photon pole amplitude model.

$\Gamma(K^- K^+ e^\pm \mu^\mp)/\Gamma_{total}$ — Γ_{323}/Γ

A test of lepton family-number conservation.

VALUE	CL%	DOCUMENT ID		TECN	COMMENT
$<1.00 \times 10^{-6}$	90	LEES	20B	BABR	e^+e^- at $\Upsilon(4S)$
• • • We do not use the following data for averages, fits, limits, etc. • • •					
$<1.8 \times 10^{-4}$	90	AITALA	01C	E791	π^- nucleus, 500 GeV

$\Gamma(\phi e^\pm \mu^\mp)/\Gamma_{total}$ — Γ_{324}/Γ

A test of lepton family number conservation. The value is for the sum of the two charge states.

VALUE	CL%	DOCUMENT ID		TECN	COMMENT
$<5.1 \times 10^{-7}$	90	LEES	20A	BABR	e^+e^- at $\Upsilon(4S)$
• • • We do not use the following data for averages, fits, limits, etc. • • •					
$<4.7 \times 10^{-5}$	90	AITALA	01C	E791	π^- nucleus, 500 GeV
$<3.4 \times 10^{-5}$	90	[1] FREYBERGER	96	CLE2	$e^+e^- \approx \Upsilon(4S)$

[1] This FREYBERGER 96 limit is obtained using a phase-space model. The limit changes to $< 3.3 \times 10^{-5}$ using a photon pole amplitude model.

$\Gamma(\overline{K}^0 e^\pm \mu^\mp)/\Gamma_{total}$ — Γ_{325}/Γ

A test of lepton family number conservation. The value is for the sum of the two charge states.

VALUE	CL%	DOCUMENT ID		TECN	COMMENT
$<17.4 \times 10^{-7}$	90	[1] LEES	20A	BABR	e^+e^- at $\Upsilon(4S)$
• • • We do not use the following data for averages, fits, limits, etc. • • •					
$< 1.0 \times 10^{-4}$	90	FREYBERGER	96	CLE2	$e^+e^- \approx \Upsilon(4S)$

[1] LEES 20A quotes $B(D^0 \to K^0_S e^\pm \mu^\mp) < 8.7 \times 10^{-7}$ at 90% CL.

$\Gamma(K^- \pi^+ e^\pm \mu^\mp)/\Gamma_{total}$ — Γ_{326}/Γ

A test of lepton family-number conservation.

VALUE	CL%	DOCUMENT ID		TECN	COMMENT
$<1.90 \times 10^{-6}$	90	LEES	20B	BABR	e^+e^- at $\Upsilon(4S)$
• • • We do not use the following data for averages, fits, limits, etc. • • •					
$<5.53 \times 10^{-4}$	90	AITALA	01C	E791	π^- nucleus, 500 GeV

$\Gamma(\overline{K}^*(892)^0 e^\pm \mu^\mp)/\Gamma_{total}$ — Γ_{327}/Γ

A test of lepton family number conservation. The value is for the sum of the two charge states.

VALUE	CL%	DOCUMENT ID		TECN	COMMENT
$<12.5 \times 10^{-7}$	90	LEES	20A	BABR	e^+e^- at $\Upsilon(4S)$
• • • We do not use the following data for averages, fits, limits, etc. • • •					
$< 8.3 \times 10^{-5}$	90	AITALA	01C	E791	π^- nucleus, 500 GeV
$< 1.0 \times 10^{-4}$	90	[1] FREYBERGER	96	CLE2	$e^+e^- \approx \Upsilon(4S)$

[1] This FREYBERGER 96 limit is obtained using a phase-space model. The same limit is obtained using a photon pole amplitude model.

$\Gamma(2\pi^- 2e^+)/\Gamma_{total}$ — Γ_{328}/Γ

A test of lepton-number conservation.

VALUE	CL%	DOCUMENT ID		TECN	COMMENT
$<9.1 \times 10^{-7}$	90	LEES	20B	BABR	e^+e^- at $\Upsilon(4S)$
• • • We do not use the following data for averages, fits, limits, etc. • • •					
$<1.12 \times 10^{-4}$	90	[1] AITALA	01C	E791	π^- nucleus, 500 GeV

[1] Value includes decay to the charge conjugate state.

$\Gamma(2\pi^- 2\mu^+)/\Gamma_{total}$ — Γ_{329}/Γ

A test of lepton-number conservation.

VALUE	CL%	DOCUMENT ID		TECN	COMMENT
$<1.52 \times 10^{-6}$	90	LEES	20B	BABR	e^+e^- at $\Upsilon(4S)$
• • • We do not use the following data for averages, fits, limits, etc. • • •					
$<2.9 \times 10^{-5}$	90	[1] AITALA	01C	E791	π^- nucleus, 500 GeV

[1] Value includes decay to the charge conjugate state.

$\Gamma(K^- \pi^- 2e^+)/\Gamma_{total}$ — Γ_{330}/Γ

A test of lepton-number conservation.

VALUE	CL%	DOCUMENT ID		TECN	COMMENT
$<5.0 \times 10^{-7}$	90	LEES	20B	BABR	e^+e^- at $\Upsilon(4S)$
• • • We do not use the following data for averages, fits, limits, etc. • • •					
$<2.8 \times 10^{-6}$	90	ABLIKIM	19AL	BES3	e^+e^- at 3773 MeV
$<2.06 \times 10^{-4}$	90	[1] AITALA	01C	E791	π^- nucleus, 500 GeV

[1] Value includes decay to the charge conjugate state.

$\Gamma(K^- \pi^- 2\mu^+)/\Gamma_{total}$ — Γ_{331}/Γ

A test of lepton-number conservation.

VALUE	CL%	DOCUMENT ID		TECN	COMMENT
$<5.3 \times 10^{-7}$	90	LEES	20B	BABR	e^+e^- at $\Upsilon(4S)$
• • • We do not use the following data for averages, fits, limits, etc. • • •					
$<3.9 \times 10^{-4}$	90	[1] AITALA	01C	E791	π^- nucleus, 500 GeV

[1] Value includes decay to the charge conjugate state.

$\Gamma(2K^- 2e^+)/\Gamma_{total}$ — Γ_{332}/Γ

A test of lepton-number conservation.

VALUE	CL%	DOCUMENT ID		TECN	COMMENT
$<3.4 \times 10^{-7}$	90	LEES	20B	BABR	e^+e^- at $\Upsilon(4S)$
• • • We do not use the following data for averages, fits, limits, etc. • • •					
$<1.52 \times 10^{-4}$	90	[1] AITALA	01C	E791	π^- nucleus, 500 GeV

[1] Value includes decay to the charge conjugate state.

$\Gamma(2K^- 2\mu^+)/\Gamma_{total}$ — Γ_{333}/Γ

A test of lepton-number conservation.

VALUE	CL%	DOCUMENT ID		TECN	COMMENT
$<1.0 \times 10^{-7}$	90	LEES	20B	BABR	e^+e^- at $\Upsilon(4S)$
• • • We do not use the following data for averages, fits, limits, etc. • • •					
$<9.4 \times 10^{-5}$	90	[1] AITALA	01C	E791	π^- nucleus, 500 GeV

[1] Value includes decay to the charge conjugate state.

$\Gamma(\pi^-\pi^- e^+ \mu^+)/\Gamma_{total}$ — Γ_{334}/Γ

A test of lepton-number conservation.

VALUE	CL%	DOCUMENT ID		TECN	COMMENT
$<3.06 \times 10^{-6}$	90	LEES	20B	BABR	e^+e^- at $\Upsilon(4S)$
• • • We do not use the following data for averages, fits, limits, etc. • • •					
$<7.9 \times 10^{-5}$	90	[1] AITALA	01C	E791	π^- nucleus, 500 GeV

[1] Value includes decay to the charge conjugate state.

$\Gamma(K^- \pi^- e^+ \mu^+)/\Gamma_{total}$ — Γ_{335}/Γ

A test of lepton-number conservation.

VALUE	CL%	DOCUMENT ID		TECN	COMMENT
$<2.10 \times 10^{-6}$	90	LEES	20B	BABR	e^+e^- at $\Upsilon(4S)$
• • • We do not use the following data for averages, fits, limits, etc. • • •					
$<2.18 \times 10^{-4}$	90	[1] AITALA	01C	E791	π^- nucleus, 500 GeV

[1] Value includes decay to the charge conjugate state.

Downloaded from https://academic.oup.com/ptep/article/2022/8/083C01/6651666 by KIT Library user on 27 September 2022

$\Gamma(2K^- e^+ \mu^+)/\Gamma_{total}$ — Γ_{336}/Γ

A test of lepton-number conservation.

VALUE	CL%	DOCUMENT ID		TECN	COMMENT
$<5.8 \times 10^{-7}$	90	LEES	20B	BABR	e^+e^- at $\Upsilon(4S)$
• • • We do not use the following data for averages, fits, limits, etc. • • •					
$<5.7 \times 10^{-5}$	90	[1] AITALA	01C	E791	π^- nucleus, 500 GeV

[1] Value includes decay to the charge conjugate state.

$\Gamma(pe^-)/\Gamma_{total}$ — Γ_{337}/Γ

A test of baryon- and lepton-number conservation.

VALUE	CL%	DOCUMENT ID		TECN	COMMENT
$<1.0 \times 10^{-5}$	90	[1] RUBIN	09	CLEO	e^+e^- at $\psi(3770)$

[1] This RUBIN 09 limit is for either $D^0 \to pe^-$ or $\overline{D}^0 \to pe^-$ decay.

$\Gamma(\overline{p}e^+)/\Gamma_{total}$ — Γ_{338}/Γ

A test of baryon- and lepton-number conservation.

VALUE	CL%	DOCUMENT ID		TECN	COMMENT
$<1.1 \times 10^{-5}$	90	[1] RUBIN	09	CLEO	e^+e^- at $\psi(3770)$

[1] This RUBIN 09 limit is for either $D^0 \to \overline{p}e^+$ or $\overline{D}^0 \to \overline{p}e^+$ decay.

D^0 CP-VIOLATING DECAY-RATE ASYMMETRIES

This is the difference between D^0 and $\overline{D}^0$ partial widths for the decay to state f, divided by the sum of the widths:
$A_{CP}(f) = [\Gamma(D^0 \to f) - \Gamma(\overline{D}^0 \to \overline{f})] / [\Gamma(D^0 \to f) + \Gamma(\overline{D}^0 \to \overline{f})]$.

$A_{CP}(K^+K^-)$ in $D^0, \overline{D}^0 \to K^+K^-$

VALUE (%)	EVTS	DOCUMENT ID		TECN	COMMENT
-0.07 ± 0.11 OUR AVERAGE					
$0.04 \pm 0.12 \pm 0.10$	4.56M	AAIJ	17M	LHCB	pp 7, 8 TeV
$-0.24 \pm 0.22 \pm 0.09$	476k	[1] AALTONEN	12B	CDF	$p\overline{p}$, $\sqrt{s}$=1.96 TeV
$0.00 \pm 0.34 \pm 0.13$	129k	[2] AUBERT	08M	BABR	$e^+e^- \approx$ 10.6 GeV
$-0.43 \pm 0.30 \pm 0.11$	120k	[3] STARIC	08	BELL	$e^+e^- \approx \Upsilon(4S)$
$+2.0 \pm 1.2 \pm 0.6$		[4] ACOSTA	05C	CDF	$p\overline{p}$, $\sqrt{s}$=1.96 TeV
$0.0 \pm 2.2 \pm 0.8$	3023	[4] CSORNA	02	CLE2	$e^+e^- \approx \Upsilon(4S)$
$-0.1 \pm 2.2 \pm 1.5$	3330	[4] LINK	00B	FOCS	
$-1.0 \pm 4.9 \pm 1.2$	609	[4] AITALA	98C	E791	$-0.093 < A_{CP} < +0.073$ (90% CL)
• • • We do not use the following data for averages, fits, limits, etc. • • •					
$-0.06 \pm 0.15 \pm 0.10$	1.8M	[1] AAIJ	14AK	LHCB	See AAIJ 17M

[1] See also "D^0 CP-violating asymmetry differences" at the end of the CP-violating asymmetries.
[2] AUBERT 08M uses corrected numbers of events directly, not ratios with $K^\mp\pi^\pm$ events.
[3] STARIC 08 uses $D^0 \to K^-\pi^+$ and $\overline{D}^0 \to K^+\pi^-$ decays to correct for detector-induced asymmetries.
[4] AITALA 98C, LINK 00B, CSORNA 02, and ACOSTA 05C measure $N(D^0 \to K^+K^-)/N(D^0 \to K^-\pi^+)$, the ratio of numbers of events observed, and similarly for the $\overline{D}^0$.

$A_{CP}(K^0_S K^0_S)$ in $D^0, \overline{D}^0 \to K^0_S K^0_S$

VALUE (%)	EVTS	DOCUMENT ID		TECN	COMMENT
-1.9 ± 1.1 OUR AVERAGE	Error includes scale factor of 1.1.				
$-3.1 \pm 1.2 \pm 0.5$	8.1k	[1] AAIJ	21X	LHCB	pp at 13 TeV
$-0.02 \pm 1.53 \pm 0.17$	5.4k	[2] DASH	17	BELL	At/near $\Upsilon(4S)$, $\Upsilon(5S)$
$-2.9 \pm 5.2 \pm 2.2$	630	AAIJ	15AT	LHCB	pp at 7, 8 TeV
-23 ± 19	65	BONVICINI	01	CLE2	$e^+e^- \approx$ 10.6 GeV
• • • We do not use the following data for averages, fits, limits, etc. • • •					
$2.3 \pm 2.8 \pm 0.9$	1.7k	AAIJ	18AV	LHCB	see AAIJ 21X

[1] AAIJ 21X reports a value of $(-3.1 \pm 1.2 \pm 0.4 \pm 0.2) \times 10^{-2}$ where the third uncertainty is from $A_{CP}(K^+K^-) = 0.04 \pm 0.12 \pm 0.10\%$, as measured by LHCb. We have added the systematic uncertainties in quadrature. Supersedes AAIJ 18AV.
[2] The systematic uncertainty is dominated by the uncertainty on A_{CP} in the control channel $D^0 \to K^0_S\pi^0$.

$A_{CP}(\pi^+\pi^-)$ in $D^0, \overline{D}^0 \to \pi^+\pi^-$

VALUE (%)	EVTS	DOCUMENT ID		TECN	COMMENT
0.13 ± 0.14 OUR AVERAGE					
$0.07 \pm 0.14 \pm 0.11$		[1] AAIJ	17M	LHCB	pp 7, 8 TeV
$0.22 \pm 0.24 \pm 0.11$	215k	[2] AALTONEN	12B	CDF	$p\overline{p}$, $\sqrt{s}$=1.96 TeV
$-0.24 \pm 0.52 \pm 0.22$	63.7k	[3] AUBERT	08M	BABR	$e^+e^- \approx$ 10.6 GeV
$0.43 \pm 0.52 \pm 0.12$	51k	[4] STARIC	08	BELL	$e^+e^- \approx \Upsilon(4S)$
$1.0 \pm 1.3 \pm 0.6$		[5] ACOSTA	05C	CDF	$p\overline{p}$, $\sqrt{s}$=1.96 TeV
$1.9 \pm 3.2 \pm 0.8$	1136	[5] CSORNA	02	CLE2	$e^+e^- \approx \Upsilon(4S)$
$4.8 \pm 3.9 \pm 2.5$	1177	[5] LINK	00B	FOCS	
$-4.9 \pm 7.8 \pm 3.0$	343	[5] AITALA	98C	E791	$-0.186 < A_{CP} < +0.088$ (90% CL)
• • • We do not use the following data for averages, fits, limits, etc. • • •					
$-0.20 \pm 0.19 \pm 0.10$	774k	[2,6] AAIJ	14AK	LHCB	See AAIJ 17M

[1] AAIJ 17M value combines $\Delta A_{CP}(\pi\pi, KK)$ from AAIJ 16D, $A_{CP}(KK)$ from AAIJ 17M, and $A_{CP}(\pi\pi)$ from AAIJ 14AK.
[2] See also "D^0 CP-violating asymmetry differences" at the end of the CP-violating asymmetries.
[3] AUBERT 08M uses corrected numbers of events directly, not ratios with $K^\mp\pi^\pm$ events.
[4] STARIC 08 uses $D^0 \to K^-\pi^+$ and $\overline{D}^0 \to K^+\pi^-$ decays to correct for detector-induced asymmetries.
[5] AITALA 98C, LINK 00B, CSORNA 02, and ACOSTA 05C measure $N(D^0 \to \pi^+\pi^-)/N(D^0 \to K^-\pi^+)$, the ratio of numbers of events observed, and similarly for the $\overline{D}^0$.
[6] AAIJ 14AK uses $\Delta A_{CP}(\pi\pi, KK)$ and $A_{CP}(KK)$ reported in the same paper.

$A_{CP}(\pi^0\pi^0)$ in $D^0, \overline{D}^0 \to \pi^0\pi^0$

VALUE (%)	EVTS	DOCUMENT ID		TECN	COMMENT
0.0 ± 0.6 OUR AVERAGE					
$-0.03 \pm 0.64 \pm 0.10$	34k	NISAR	14	BELL	e^+e^- at/near Υ's
0.1 ± 4.8	810	BONVICINI	01	CLE2	$e^+e^- \approx$ 10.6 GeV

$A_{CP}(\rho\gamma)$ in $D^0, \overline{D}^0 \to \rho\gamma$

VALUE (units 10^{-2})	DOCUMENT ID		TECN	COMMENT
$5.6 \pm 15.2 \pm 0.6$	NANUT	17	BELL	e^+e^- at Υ(nS), n=2,3,4,5

$A_{CP}(\phi\gamma)$ in $D^0, \overline{D}^0 \to \phi\gamma$

VALUE (units 10^{-2})	DOCUMENT ID		TECN	COMMENT
$-9.4 \pm 6.6 \pm 0.1$	NANUT	17	BELL	e^+e^- at Υ(nS), n=2,3,4,5

$A_{CP}(\overline{K}^*(892)^0\gamma)$ in $D^0, \overline{D}^0 \to \overline{K}^*(892)^0\gamma$

VALUE (units 10^{-2})	DOCUMENT ID		TECN	COMMENT
$-0.3 \pm 2.0 \pm 0.0$	NANUT	17	BELL	e^+e^- at Υ(nS), n=2,3,4,5

$A_{CP}(\pi^+\pi^-\pi^0)$ in $D^0, \overline{D}^0 \to \pi^+\pi^-\pi^0$

VALUE (%)	EVTS	DOCUMENT ID		TECN	COMMENT
0.3 ± 0.4 OUR AVERAGE					
0.43 ± 1.30	$123k \pm 490$	ARINSTEIN	08	BELL	$e^+e^- \approx \Upsilon(4S)$
$0.31 \pm 0.41 \pm 0.17$	$80 \pm .3k$	[1] AUBERT	08AO	BABR	$e^+e^- \approx$ 10.6 GeV
$1\ ^{+9}_{-7}\ \pm 5$		CRONIN-HEN...	05	CLEO	$e^+e^- \approx$ 10 GeV

[1] AUBERT 08AO report their result using a different sign convention.

$A_{CP}(\eta\pi^+\pi^-)$ in $D^0, \overline{D}^0 \to \eta\pi^+\pi^-$

VALUE (units 10^{-2})	EVTS	DOCUMENT ID		TECN	COMMENT
$0.9 \pm 1.2 \pm 0.5$	13k	LI	21G	BELL	e^+e^- at Υ(nS)
• • • We do not use the following data for averages, fits, limits, etc. • • •					
$9.6 \pm 5.4 \pm 1.8$	450	ABLIKIM	20G	BES3	e^+e^- at 3.773 GeV

$A_{CP}(\rho(770)^+\pi^- \to \pi^+\pi^-\pi^0)$ in $D^0 \to \rho^+\pi^-$, $\overline{D}^0 \to \rho^-\pi^+$

VALUE (%)	DOCUMENT ID		TECN	COMMENT
$+1.2 \pm 0.8 \pm 0.3$	AUBERT	08AO	BABR	Table 1, $-$Col.5/2$\times$Col.2

$A_{CP}(\rho(770)^0\pi^0 \to \pi^+\pi^-\pi^0)$ in $D^0, \overline{D}^0 \to \rho^0\pi^0$

VALUE (%)	DOCUMENT ID		TECN	COMMENT
$-3.1 \pm 2.7 \pm 1.2$	AUBERT	08AO	BABR	Table 1, $-$Col.5/2$\times$Col.2

$A_{CP}(\rho(770)^-\pi^+ \to \pi^+\pi^-\pi^0)$ in $D^0 \to \rho^-\pi^+$, $\overline{D}^0 \to \rho^+\pi^-$

VALUE (%)	DOCUMENT ID		TECN	COMMENT
$-1.0 \pm 1.6 \pm 0.7$	AUBERT	08AO	BABR	Table 1, $-$Col.5/2$\times$Col.2

$A_{CP}(\rho(1450)^+\pi^- \to \pi^+\pi^-\pi^0)$ in $D^0 \to \rho(1450)^+\pi^-$, $\overline{D}^0 \to$ c.c.

VALUE (%)	DOCUMENT ID		TECN	COMMENT
$0 \pm 50 \pm 50$	AUBERT	08AO	BABR	Table 1, $-$Col.5/2$\times$Col.2

$A_{CP}(\rho(1450)^0\pi^0 \to \pi^+\pi^-\pi^0)$ in $D^0, \overline{D}^0 \to \rho(1450)^0\pi^0$

VALUE (%)	DOCUMENT ID		TECN	COMMENT
$-17 \pm 33 \pm 17$	AUBERT	08AO	BABR	Table 1, $-$Col.5/2$\times$Col.2

$A_{CP}(\rho(1450)^-\pi^+ \to \pi^+\pi^-\pi^0)$ in $D^0 \to \rho(1450)^-\pi^+$, $\overline{D}^0 \to$ c.c.

VALUE (%)	DOCUMENT ID		TECN	COMMENT
$+6 \pm 8 \pm 3$	AUBERT	08AO	BABR	Table 1, $-$Col.5/2$\times$Col.2

$A_{CP}(\rho(1700)^+\pi^- \to \pi^+\pi^-\pi^0)$ in $D^0 \to \rho(1700)^+\pi^-$, $\overline{D}^0 \to$ c.c.

VALUE (%)	DOCUMENT ID		TECN	COMMENT
$-5 \pm 13 \pm 5$	AUBERT	08AO	BABR	Table 1, $-$Col.5/2$\times$Col.2

$A_{CP}(\rho(1700)^0\pi^0 \to \pi^+\pi^-\pi^0)$ in $D^0, \overline{D}^0 \to \rho(1700)^0\pi^0$

VALUE (%)	DOCUMENT ID		TECN	COMMENT
$+13 \pm 8 \pm 3$	AUBERT	08AO	BABR	Table 1, $-$Col.5/2$\times$Col.2

$A_{CP}(\rho(1700)^-\pi^+ \to \pi^+\pi^-\pi^0)$ in $D^0 \to \rho(1700)^-\pi^+$, $\overline{D}^0 \to$ c.c.

VALUE (%)	DOCUMENT ID		TECN	COMMENT
$+8 \pm 10 \pm 5$	AUBERT	08AO	BABR	Table 1, $-$Col.5/2$\times$Col.2

$A_{CP}(f_0(980)\pi^0 \to \pi^+\pi^-\pi^0)$ in $D^0, \overline{D}^0 \to f_0(980)\pi^0$

VALUE (%)	DOCUMENT ID		TECN	COMMENT
$0 \pm 25 \pm 25$	AUBERT	08AO	BABR	Table 1, $-$Col.5/2$\times$Col.2

$A_{CP}(f_0(1370)\pi^0 \to \pi^+\pi^-\pi^0)$ in $D^0, \overline{D}^0 \to f_0(1370)\pi^0$

VALUE (%)	DOCUMENT ID		TECN	COMMENT
$+25 \pm 13 \pm 13$	AUBERT	08AO	BABR	Table 1, $-$Col.5/2$\times$Col.2

$A_{CP}(f_0(1500)\pi^0 \to \pi^+\pi^-\pi^0)$ in $D^0, \overline{D}^0 \to f_0(1500)\pi^0$

VALUE (%)	DOCUMENT ID		TECN	COMMENT
$0 \pm 13 \pm 13$	AUBERT	08AO	BABR	Table 1, $-$Col.5/2$\times$Col.2

$A_{CP}(f_0(1710)\pi^0 \to \pi^+\pi^-\pi^0)$ in $D^0, \overline{D}^0 \to f_0(1710)\pi^0$

VALUE (%)	DOCUMENT ID		TECN	COMMENT
$0 \pm 17 \pm 17$	AUBERT	08AO	BABR	Table 1, $-$Col.5/2$\times$Col.2

Downloaded from https://academic.oup.com/ptep/article/2022/8/083C01/6651666 by KIT Library user on 27 September 2022

$A_{CP}(f_2(1270)\pi^0 \to \pi^+\pi^-\pi^0)$ in $D^0, \overline{D}^0 \to f_2(1270)\pi^0$

VALUE (%)	DOCUMENT ID		TECN	COMMENT
−4±4±4	AUBERT	08AO	BABR	Table 1, −Col.5/2×Col.2

$A_{CP}(\sigma(400)\pi^0 \to \pi^+\pi^-\pi^0)$ in $D^0, \overline{D}^0 \to \sigma(400)\pi^0$

VALUE (%)	DOCUMENT ID		TECN	COMMENT
+6±6±6	AUBERT	08AO	BABR	Table 1, −Col.5/2×Col.2

A_{CP}(nonresonant $\pi^+\pi^-\pi^0$) in $D^0, \overline{D}^0 \to$ nonresonant $\pi^+\pi^-\pi^0$

VALUE (%)	DOCUMENT ID		TECN	COMMENT
−13±19±13	AUBERT	08AO	BABR	Table 1, −Col.5/2×Col.2

$A_{CP}(2\pi^+2\pi^-)$ in $D^0, \overline{D}^0 \to 2\pi^+2\pi^-$

VALUE (%)	EVTS	DOCUMENT ID		COMMENT
0.54±1.04±0.51	7.3k	[1,2] DARGENT	17	e^+e^- at $\psi(3770)$

[1] Decay rate asymmetry integrated in decay time and across full 4π phase space.
[2] Obtained by analyzing CLEO-c data but not authored by the CLEO Collaboration.

$A_{CP}(a_1(1260)^+\pi^- \to 2\pi^+2\pi^-)$ in $D^0 \to a_1(1260)^+\pi^-, \overline{D}^0 \to$ c.c.

VALUE (%)	EVTS	DOCUMENT ID		COMMENT
4.7±2.6±4.9	7.3k	[1] DARGENT	17	4-body fit, 4π evts

[1] Obtained by analyzing CLEO-c data but not authored by the CLEO Collaboration.

$A_{CP}(a_1(1260)^-\pi^+ \to 2\pi^+2\pi^-)$ in $D^0 \to a_1(1260)^-\pi^+, \overline{D}^0 \to$ c.c.

VALUE (%)	EVTS	DOCUMENT ID		COMMENT
13.7±13.8±11.4	7.3k	[1] DARGENT	17	4-body fit, 4π evts

[1] Obtained by analyzing CLEO-c data but not authored by the CLEO Collaboration.

$A_{CP}(\pi(1300)^+\pi^- \to 2\pi^+2\pi^-)$ in $D^0 \to \pi(1300)^+\pi^-, \overline{D}^0 \to$ c.c.

VALUE (%)	EVTS	DOCUMENT ID		COMMENT
−1.6±12.9±6.7	7.3k	[1] DARGENT	17	4-body fit, 4π evts

[1] Obtained by analyzing CLEO-c data but not authored by the CLEO Collaboration.

$A_{CP}(\pi(1300)^-\pi^+ \to 2\pi^+2\pi^-)$ in $D^0 \to \pi(1300)^-\pi^+, \overline{D}^0 \to$ c.c.

VALUE (%)	EVTS	DOCUMENT ID		COMMENT
−5.6±11.9±27.7	7.3k	[1] DARGENT	17	4-body fit, 4π evts

[1] Obtained by analyzing CLEO-c data but not authored by the CLEO Collaboration.

$A_{CP}(a_1(1640)^+\pi^- \to 2\pi^+2\pi^-)$ in $D^0 \to a_1(1640)^+\pi^-, \overline{D}^0 \to$ c.c.

VALUE (%)	EVTS	DOCUMENT ID		COMMENT
8.6±17.8±19.3	7.3k	[1] DARGENT	17	4-body fit, 4π evts

[1] Obtained by analyzing CLEO-c data but not authored by the CLEO Collaboration.

$A_{CP}(\pi_2(1670)^+\pi^- \to 2\pi^+2\pi^-)$ in $D^0 \to \pi_2(1670)^+\pi^-, \overline{D}^0 \to$ c.c.

VALUE (%)	EVTS	DOCUMENT ID		COMMENT
7.3±15.1±10.4	7.3k	[1] DARGENT	17	4-body fit, 4π evts

[1] Obtained by analyzing CLEO-c data but not authored by the CLEO Collaboration.

$A_{CP}(\sigma f_0(1370) \to 2\pi^+2\pi^-)$ in $D^0, \overline{D}^0 \to \sigma f_0(1370)$

VALUE (%)	EVTS	DOCUMENT ID		COMMENT
−14.6±16.5±9.4	7.3k	[1] DARGENT	17	4-body fit, 4π evts

[1] Obtained by analyzing CLEO-c data but not authored by the CLEO Collaboration.

$A_{CP}(\sigma\rho(770)^0 \to 2\pi^+2\pi^-)$ in $D^0, \overline{D}^0 \to \sigma\rho(770)^0$

VALUE (%)	EVTS	DOCUMENT ID		COMMENT
2.5±16.8±20.8	7.3k	[1] DARGENT	17	4-body fit, 4π evts

[1] Obtained by analyzing CLEO-c data but not authored by the CLEO Collaboration.

$A_{CP}(2\rho(770)^0 \to 2\pi^+2\pi^-)$ in $D^0, \overline{D}^0 \to 2\rho(770)^0$

VALUE (%)	EVTS	DOCUMENT ID		COMMENT
−5.6±5.0±2.9	7.3k	[1] DARGENT	17	4-body fit, 4π evts

[1] Obtained by analyzing CLEO-c data but not authored by the CLEO Collaboration.

$A_{CP}(2f_2(1270) \to 2\pi^+2\pi^-)$ in $D^0, \overline{D}^0 \to 2f_2(1270)$

VALUE (%)	EVTS	DOCUMENT ID		COMMENT
−28.3±12.3±20.9	7.3k	[1] DARGENT	17	4-body fit, 4π evts

[1] Obtained by analyzing CLEO-c data but not authored by the CLEO Collaboration.

$A_{CP}(\pi^+\pi^-\pi^0\eta)$ in $D^0, \overline{D}^0 \to \pi^+\pi^-\pi^0\eta$

VALUE (units 10^{-2})	EVTS	DOCUMENT ID		TECN	COMMENT
−5.5±5.2±2.4	510	ABLIKIM	20V	BES3	e^+e^-, 3773 MeV

$A_{CP}(K^+K^-\pi^0)$ in $D^0, \overline{D}^0 \to K^+K^-\pi^0$

VALUE (%)	EVTS	DOCUMENT ID		TECN	COMMENT
−1.00±1.67±0.25	11 ± 0.11k	AUBERT	08AO	BABR	$e^+e^- \approx$ 10.6 GeV

$A_{CP}(K^*(892)^+K^- \to K^+K^-\pi^0)$ in $D^0 \to K^*(892)^+K^-, \overline{D}^0 \to$ c.c.

VALUE (%)	DOCUMENT ID		TECN	COMMENT
−0.9±1.2±0.4	[1] AUBERT	08AO	BABR	Table 1, −Col.5/2×Col.2

[1] AUBERT 08AO report their result using a different sign convention.

$A_{CP}(K^*(1410)^+K^- \to K^+K^-\pi^0)$ in $D^0 \to K^*(1410)^+K^-, \overline{D}^0 \to$ c.c.

VALUE (%)	DOCUMENT ID		TECN	COMMENT
−21±23±8	AUBERT	08AO	BABR	Table 1, −Col.5/2×Col.2

$A_{CP}((K^+\pi^0)_{S-wave}K^- \to K^+K^-\pi^0)$ in $D^0 \to (K^+\pi^0)_S K^-, \overline{D}^0 \to$ c.c.

VALUE (%)	DOCUMENT ID		TECN	COMMENT
+7±15±3	AUBERT	08AO	BABR	Table 1, −Col.5/2×Col.2

$A_{CP}(\phi(1020)\pi^0 \to K^+K^-\pi^0)$ in $D^0, \overline{D}^0 \to \phi(1020)\pi^0$

VALUE (%)	DOCUMENT ID		TECN	COMMENT
+1.1±2.1±0.5	AUBERT	08AO	BABR	Table 1, −Col.5/2×Col.2

$A_{CP}(f_0(980)\pi^0 \to K^+K^-\pi^0)$ in $D^0, \overline{D}^0 \to f_0(980)\pi^0$

VALUE (%)	DOCUMENT ID		TECN	COMMENT
−3±19±1	AUBERT	08AO	BABR	Table 1, −Col.5/2×Col.2

$A_{CP}(a_0(980)^0\pi^0 \to K^+K^-\pi^0)$ in $D^0, \overline{D}^0 \to a_0(980)^0\pi^0$

VALUE (%)	DOCUMENT ID		TECN	COMMENT
−5±16±2	[1] AUBERT	08AO	BABR	Table 1, −Col.5/2×Col.2

[1] This AUBERT 08AO value is obtained when the $a_0(980)^0$ replaces the $f_0(980)$ in the fit.

$A_{CP}(f'_2(1525)\pi^0 \to K^+K^-\pi^0)$ in $D^0, \overline{D}^0 \to f'_2(1525)\pi^0$

VALUE (%)	DOCUMENT ID		TECN	COMMENT
0±50±150	AUBERT	08AO	BABR	Table 1, −Col.5/2×Col.2

$A_{CP}(K^*(892)^-K^+ \to K^+K^-\pi^0)$ in $D^0 \to K^*(892)^-K^+, \overline{D}^0 \to$ c.c.

VALUE (%)	DOCUMENT ID		TECN	COMMENT
−5±4±1	AUBERT	08AO	BABR	Table 1, −Col.5/2×Col.2

$A_{CP}(K^*(1410)^-K^+ \to K^+K^-\pi^0)$ in $D^0 \to K^*(1410)^-K^+, \overline{D}^0 \to$ c.c.

VALUE (%)	DOCUMENT ID		TECN	COMMENT
−17±28±7	AUBERT	08AO	BABR	Table 1, −Col.5/2×Col.2

$A_{CP}((K^-\pi^0)_{S-wave}K^+ \to K^+K^-\pi^0)$ in $D^0 \to (K^-\pi^0)_S K^+, \overline{D}^0 \to$ c.c.

VALUE (%)	DOCUMENT ID		TECN	COMMENT
−7±40±8	AUBERT	08AO	BABR	Table 1, −Col.5/2×Col.2

$A_{CP}(K^+K^-\eta)$ in $D^0, \overline{D}^0 \to K^+K^-\eta$

VALUE (units 10^{-2})	EVTS	DOCUMENT ID		TECN	COMMENT
−1.4±3.3±1.1	1.4k	LI	21G	BELL	e^+e^- at Υ(nS)

$A_{CP}(\phi(1020)\eta \to K^+K^-\eta)$ in $D^0, \overline{D}^0 \to \phi(1020)\eta$

VALUE (units 10^{-2})	EVTS	DOCUMENT ID		TECN	COMMENT
−1.9±4.4±0.6	1.4k	LI	21G	BELL	e^+e^- at Υ(nS)

$A_{CP}(K^0_S\pi^0)$ in $D^0, \overline{D}^0 \to K^0_S\pi^0$

VALUE (%)	EVTS	DOCUMENT ID		TECN	COMMENT
−0.20±0.17 OUR AVERAGE					
−0.21±0.16±0.07	467k	[1] NISAR	14	BELL	e^+e^- at/near Υ's
0.1 ±1.3	9099	BONVICINI	01	CLE2	$e^+e^- \approx$ 10.6 GeV
• • • We do not use the following data for averages, fits, limits, etc. • • •					
−0.28±0.19±0.10	326k	KO	11	BELL	See NISAR 14
−1.8 ±3.0		BARTELT	95	CLE2	See BONVICINI 01

[1] After subtracting CPV in $K^0 - \overline{K}^0$ mixing, NISAR 14 gets $A_{CP} = (+0.12 \pm 0.16 \pm 0.07)$%.

$A_{CP}(K^0_S\eta)$ in $D^0, \overline{D}^0 \to K^0_S\eta$

VALUE (%)	EVTS	DOCUMENT ID		TECN	COMMENT
+0.54±0.51±0.16	46k	KO	11	BELL	$e^+e^- \approx \Upsilon(4S)$

$A_{CP}(K^0_S\eta')$ in $D^0, \overline{D}^0 \to K^0_S\eta'$

VALUE (%)	EVTS	DOCUMENT ID		TECN	COMMENT
+0.98±0.67±0.14	27k	KO	11	BELL	$e^+e^- \approx \Upsilon(4S)$

$A_{CP}(K^0_S\phi)$ in $D^0, \overline{D}^0 \to K^0_S\phi$

VALUE (%)	DOCUMENT ID		TECN	COMMENT
−2.8±9.4	BARTELT	95	CLE2	$-18.2 < A_{CP} < +12.6\%$ (90%CL)

$A_{CP}(K^\mp\pi^\pm)$ in $D^0 \to K^-\pi^+, \overline{D}^0 \to K^+\pi^-$

VALUE (%)	EVTS	DOCUMENT ID		TECN	COMMENT
0.2 ±0.5 OUR AVERAGE					
−0.01±0.91		AAIJ	18K	LHCB	pp at 7, 8, 13 TeV
0.3 ±0.3 ±0.6		BONVICINI	14	CLEO	All CLEO-c runs
• • • We do not use the following data for averages, fits, limits, etc. • • •					
+0.5 ±0.4 ±0.9	150k	MENDEZ	10	CLEO	See BONVICINI 14
−0.4 ±0.5 ±0.9		DOBBS	07	CLEO	See BONVICINI 14

Downloaded from https://academic.oup.com/ptep/article/2022/8/083C01/6651666 by KIT Library user on 27 September 2022

$A_{CP}(K^{\pm}\pi^{\mp})$ in $D^0 \to K^+\pi^-$, $\overline{D}^0 \to K^-\pi^+$

VALUE (%)	EVTS	DOCUMENT ID		TECN	COMMENT
− 0.9± 1.4 OUR AVERAGE					
− 1.7± 1.6		[1,2] AAIJ	17AO	LHCB	pp at 7,8 TeV
− 2.1± 5.2±1.5	4.0k	AUBERT	07W	BABR	$e^+e^- \approx$ 10.6 GeV
+ 2.3± 4.7	4.0k	[3] ZHANG	06	BELL	e^+e^-
+18 ±14 ±4		[4] LINK	05H	FOCS	γ nucleus
+ 9.5± 6.1±8.3		[5] AUBERT	03Z	BABR	e^+e^-, 10.6 GeV
+ 2 $^{+19}_{-20}$ ±1	45	[6] GODANG	00	CLE2	e^+e^-
• • • We do not use the following data for averages, fits, limits, etc. • • •					
− 0.7± 1.9		[1] AAIJ	13CE	LHCB	Repl. by AAIJ 17AO
− 8.0± 7.7	0.8k	[7] LI	05A	BELL	See ZHANG 06

[1] Based on 3 fb^{-1} of data collected at $\sqrt{s}$ = 7, 8 TeV. Allowing for CP violation, the direct CP-violation in mixing is reported for the $D^0 \to K^+\pi^-$ and $\overline{D}^0 \to K^+\pi^-$.
[2] The CPV is derived from $A_{CP} = (R_D^+ - R_D^-)/(R_D^+ + R_D^-)$.
[3] This ZHANG 06 result allows mixing.
[4] This LINK 05H result assumes no mixing. If mixing is allowed, it becomes $0.13^{+0.33}_{-0.25} \pm 0.10$.
[5] This AUBERT 03Z limit assumes no mixing. If mixing is allowed, the 95% confidence-level interval is $(-2.8 < A_D < 4.9)\times10^{-3}$.
[6] This GODANG 00 result assumes no D^0-$\overline{D}^0$ mixing and becomes $-0.43 < A_{CP} < +0.34$ at 95% CL. If mixing is allowd $A_{CP} = -0.01^{+0.16}_{-0.17} \pm 0.01$.
[7] This LI 05A result allows mixing.

$A_{CP}(K^-\pi^+)$ in $D_{CP(\pm1)} \to K^{\mp}\pi^{\pm}$

$A_{CP}(K^-\pi^+) = [B(D_{CP(-)} \to K^-\pi^+ + c.c.) - B(D_{CP(+)} \to K^-\pi^+ + c.c.)]$ / Sum

VALUE (%)	DOCUMENT ID		TECN	COMMENT
12.7±1.3±0.7	[1] ABLIKIM	14C	BES3	$e^+e^- \to D^0\overline{D}^0$, 3.77 GeV

[1] ABLIKIM 14C uses quantum correlations in $e^+e^- \to D^0\overline{D}^0$ at the $\psi(3770)$ to measure the asymmetry of the branching fraction of $D^0 \to K^-\pi^+$ in CP-odd and CP-even eigenstates. It then extracts the strong-phase difference $\delta_{K\pi}$.

$A_{CP}(K^{\mp}\pi^{\pm}\pi^0)$ in $D^0 \to K^-\pi^+\pi^0$, $\overline{D}^0 \to K^+\pi^-\pi^0$

VALUE (%)	DOCUMENT ID		TECN	COMMENT
0.1±0.5 OUR AVERAGE				
0.1±0.3±0.4	BONVICINI	14	CLEO	All CLEO-c runs
−3.1±8.6	[1] KOPP	01	CLE2	$e^+e^- \approx$ 10.6 GeV
• • • We do not use the following data for averages, fits, limits, etc. • • •				
0.2±0.4±0.8	DOBBS	07	CLEO	See BONVICINI 14

[1] KOPP 01 fits separately the D^0 and $\overline{D}^0$ Dalitz plots and then calculates the integrated difference of normalized densities divided by the integrated sum.

$A_{CP}(K^{\pm}\pi^{\mp}\pi^0)$ in $D^0 \to K^+\pi^-\pi^0$, $\overline{D}^0 \to K^-\pi^+\pi^0$

VALUE (%)	EVTS	DOCUMENT ID		TECN	COMMENT
0 ± 5 OUR AVERAGE					
−0.6± 5.3	1978 ± 104	TIAN	05	BELL	$e^+e^- \approx \Upsilon(4S)$
+9 $^{+25}_{-22}$	38	BRANDENB...	01	CLE2	$e^+e^- \approx \Upsilon(4S)$

$A_{CP}(K^0_S\pi^+\pi^-)$ in $D^0, \overline{D}^0 \to K^0_S\pi^+\pi^-$

VALUE (%)	EVTS	DOCUMENT ID		TECN	COMMENT
−0.1 ±0.8 OUR AVERAGE					
−0.05±0.57±0.54	350k	[1] AALTONEN	12AD	CDF	
−0.9 ±2.1 $^{+1.6}_{-5.7}$	4854	[2] ASNER	04A	CLEO	$e^+e^- \approx$ 10 GeV

[1] This is the overall result of AALTONEN 12AD. Following are the 15 CP fit-fraction asymmetries from the amplitude analysis of the D^0 and $\overline{D}^0 \to K^0_S\pi^+\pi^-$ Dalitz plots.
[2] This is the overall result of ASNER 04A; CP-violating limits are also given below for each of the 10 resonant submodes found in an amplitude analysis of the D^0 and $\overline{D}^0 \to K^0_S\pi^+\pi^-$ Dalitz plots.

$A_{CP}(K^{\mp}\pi^{\pm}\eta)$ in $D^0, \overline{D}^0 \to K^{\mp}\pi^{\pm}\eta$

VALUE (units 10^{-2})	EVTS	DOCUMENT ID		TECN	COMMENT
−1.9±1.3±1.0	6.1k	ABLIKIM	20V	BES3	e^+e^-, 3773 MeV

$A_{CP}(K^0_S\pi^0\eta)$ in $D^0, \overline{D}^0 \to K^0_S\pi^0\eta$

VALUE (units 10^{-2})	EVTS	DOCUMENT ID		TECN	COMMENT
−3.9±3.2±0.8	1.1k	ABLIKIM	20V	BES3	e^+e^-, 3773 MeV

$A_{CP}(K^{\mp}\pi^{\pm}\pi^0\eta)$ in $D^0, \overline{D}^0 \to K^{\mp}\pi^{\pm}\pi^0\eta$

VALUE (units 10^{-2})	EVTS	DOCUMENT ID		TECN	COMMENT
−7.9±4.8±2.5	580	ABLIKIM	20V	BES3	e^+e^-, 3773 MeV

$A_{CP}(K^*(892)^{\mp}\pi^{\pm} \to K^0_S\pi^+\pi^-)$ in $D^0 \to K^{*-}\pi^+$, $\overline{D}^0 \to K^{*+}\pi^-$

VALUE (%)	DOCUMENT ID		TECN	COMMENT
+0.36±0.33±0.40	AALTONEN	12AD	CDF	Dalitz fit, ∼ 350k evts
• • • We do not use the following data for averages, fits, limits, etc. • • •				
+2.5 ±1.9 $^{+3.3}_{-0.8}$	ASNER	04A	CLEO	Dalitz fit, 4854 evts

$A_{CP}(K^*(892)^{\pm}\pi^{\mp} \to K^0_S\pi^+\pi^-)$ in $D^0 \to K^{*+}\pi^-$, $\overline{D}^0 \to K^{*-}\pi^+$

This is a doubly Cabibbo-suppressed mode.

VALUE (%)	DOCUMENT ID		TECN	COMMENT
+ 1.0± 5.7± 2.1	AALTONEN	12AD	CDF	Dalitz fit, ∼ 350k evts
• • • We do not use the following data for averages, fits, limits, etc. • • •				
−21 ±42 ±28	ASNER	04A	CLEO	Dalitz fit, 4854 evts

$A_{CP}(K^0_S\rho^0 \to K^0_S\pi^+\pi^-)$ in $D^0 \to \overline{K}^0\rho^0$, $\overline{D}^0 \to K^0\rho^0$

VALUE (%)	DOCUMENT ID		TECN	COMMENT
−0.05±0.50±0.08	AALTONEN	12AD	CDF	Dalitz fit, ∼ 350k evts
• • • We do not use the following data for averages, fits, limits, etc. • • •				
+3.1 ±3.8 $^{+2.7}_{-2.2}$	ASNER	04A	CLEO	Dalitz fit, 4854 evts

$A_{CP}(K^0_S\omega \to K^0_S\pi^+\pi^-)$ in $D^0 \to \overline{K}^0\omega$, $\overline{D}^0 \to K^0\omega$

VALUE (%)	DOCUMENT ID		TECN	COMMENT
−12.6± 6.0± 2.6	AALTONEN	12AD	CDF	Dalitz fit, ∼ 350k evts
• • • We do not use the following data for averages, fits, limits, etc. • • •				
−26 ±24 $^{+22}_{-4}$	ASNER	04A	CLEO	Dalitz fit, 4854 evts

$A_{CP}(K^0_S f_0(980) \to K^0_S\pi^+\pi^-)$ in $D^0 \to \overline{K}^0 f_0(980)$, $\overline{D}^0 \to K^0 f_0(980)$

VALUE (%)	DOCUMENT ID		TECN	COMMENT
−0.4± 2.2± 1.6	AALTONEN	12AD	CDF	Dalitz fit, ∼ 350k evts
• • • We do not use the following data for averages, fits, limits, etc. • • •				
−4.7±11.0$^{+24.9}_{-8.8}$	ASNER	04A	CLEO	Dalitz fit, 4854 evts

$A_{CP}(K^0_S f_2(1270) \to K^0_S\pi^+\pi^-)$ in $D^0 \to \overline{K}^0 f_2(1270)$, $\overline{D}^0 \to K^0 f_2(1270)$

VALUE (%)	DOCUMENT ID		TECN	COMMENT
− 4.0± 3.4± 3.0	AALTONEN	12AD	CDF	Dalitz fit, ∼ 350k evts
• • • We do not use the following data for averages, fits, limits, etc. • • •				
+34 ±51 $^{+33}_{-79}$	ASNER	04A	CLEO	Dalitz fit, 4854 evts

$A_{CP}(K^0_S f_0(1370) \to K^0_S\pi^+\pi^-)$ in $D^0 \to \overline{K}^0 f_0(1370)$, $\overline{D}^0 \to K^0 f_0(1370)$

VALUE (%)	DOCUMENT ID		TECN	COMMENT
− 0.5± 4.6± 7.7	AALTONEN	12AD	CDF	Dalitz fit, ∼ 350k evts
• • • We do not use the following data for averages, fits, limits, etc. • • •				
+18 ±10 $^{+13}_{-22}$	ASNER	04A	CLEO	Dalitz fit, 4854 evts

$A_{CP}(K^0_S\rho^0(1450))$ in $D^0 \to \overline{K}^0\rho^0(1450)$, $\overline{D}^0 \to K^0\rho^0(1450)$

VALUE (%)	DOCUMENT ID		TECN	COMMENT
−4.1±5.2±8.1	AALTONEN	12AD	CDF	Dalitz fit, ∼ 350k evts

$A_{CP}(K^0_S f_0(600))$ in $D^0 \to \overline{K}^0 f_0(600)$, $\overline{D}^0 \to K^0 f_0(600)$

VALUE (%)	DOCUMENT ID		TECN	COMMENT
−2.7±2.7±3.6	AALTONEN	12AD	CDF	Dalitz fit, ∼ 350k evts

$A_{CP}(K^*(1410)^{\mp}\pi^{\pm})$ in $D^0 \to K^*(1410)^-\pi^+$, $\overline{D}^0 \to K^*(1410)^+\pi^-$

VALUE (%)	DOCUMENT ID		TECN	COMMENT
−2.3±5.7±6.4	AALTONEN	12AD	CDF	Dalitz fit, ∼ 350k evts

$A_{CP}(K^*_0(1430)^{\mp}\pi^{\pm} \to K^0_S\pi^+\pi^-)$ in $D^0 \to K^*_0(1430)^-\pi^+$, $\overline{D}^0 \to$ c.c.

VALUE (%)	DOCUMENT ID		TECN	COMMENT
4.0± 2.4±3.8	AALTONEN	12AD	CDF	Dalitz fit, ∼ 350k evts
• • • We do not use the following data for averages, fits, limits, etc. • • •				
−0.2±11.3$^{+8.8}_{-5.0}$	ASNER	04A	CLEO	Dalitz fit, 4854 evts

$A_{CP}(K^*_0(1430)^{\pm}\pi^{\mp})$ in $D^0 \to K^*_0(1430)^+\pi^-$, $\overline{D}^0 \to K^*_0(1430)^-\pi^+$

This is a doubly Cabibbo-suppressed mode.

VALUE (%)	DOCUMENT ID		TECN	COMMENT
+12±11±10	AALTONEN	12AD	CDF	Dalitz fit, ∼ 350k evts

$A_{CP}(K^*_2(1430)^{\mp}\pi^{\pm} \to K^0_S\pi^+\pi^-)$ in $D^0 \to K^*_2(1430)^-\pi^+$, $\overline{D}^0 \to$ c.c.

VALUE (%)	DOCUMENT ID		TECN	COMMENT
+2.9± 4.0± 4.1	AALTONEN	12AD	CDF	Dalitz fit, ∼ 350k evts
• • • We do not use the following data for averages, fits, limits, etc. • • •				
−7 ±25 $^{+13}_{-26}$	ASNER	04A	CLEO	Dalitz fit, 4854 evts

$A_{CP}(K^*_2(1430)^{\pm}\pi^{\mp})$ in $D^0 \to K^*_2(1430)^+\pi^-$, $\overline{D}^0 \to K^*_2(1430)^-\pi^+$

This is a doubly Cabibbo-suppressed mode.

VALUE (%)	DOCUMENT ID		TECN	COMMENT
−10±14±29	AALTONEN	12AD	CDF	Dalitz fit, ∼ 350k evts

$A_{CP}(K^*(1680)^{\mp}\pi^{\pm} \to K^0_S\pi^+\pi^-)$ in $D^0 \to K^*(1680)^-\pi^+$, $\overline{D}^0 \to$ c.c.

VALUE (%)	DOCUMENT ID		TECN	COMMENT
• • • We do not use the following data for averages, fits, limits, etc. • • •				
−36±19$^{+10}_{-35}$	ASNER	04A	CLEO	Dalitz fit, 4854 evts

Downloaded from https://academic.oup.com/ptep/article/2022/8/083C01/6651666 by KIT Library user on 27 September 2022

$A_{CP}(K^-\pi^+\pi^+\pi^-)$ in $D^0 \to K^-\pi^+\pi^+\pi^-$, $\overline{D}^0 \to K^+\pi^-\pi^-\pi^+$

VALUE (%)	DOCUMENT ID		TECN	COMMENT
0.2±0.3±0.4	BONVICINI	14	CLEO	All CLEO-c runs
• • • We do not use the following data for averages, fits, limits, etc. • • •				
+0.7±0.5±0.9	DOBBS	07	CLEO	See BONVICINI 14

$A_{CP}(K^\pm\pi^\mp\pi^+\pi^-)$ in $D^0 \to K^+\pi^-\pi^+\pi^-$, $\overline{D}^0 \to K^-\pi^+\pi^+\pi^-$

VALUE (%)	EVTS	DOCUMENT ID		TECN	COMMENT
−1.8±4.4	1721 ± 75	TIAN	05	BELL	$e^+e^- \approx \Upsilon(4S)$

$A_{CP}(K^+K^-\pi^+\pi^-)$ in D^0, $\overline{D}^0 \to K^+K^-\pi^+\pi^-$

See also AAIJ 13BR for a search for CP violation in $D^0 \to K^+K^-\pi^+\pi^-$ in binned phase space. No evidence of CP violation was found.

VALUE (%)	EVTS	DOCUMENT ID		TECN	COMMENT
1.3 ±1.7 OUR AVERAGE					
1.84±1.74±0.3	2.9k	[1] DARGENT	17		e^+e^-
−8.2 ±5.6 ±4.7	828 ± 46	LINK	05E	FOCS	γ A, $\overline{E}_\gamma \approx$ 180 GeV

[1] Obtained by analyzing CLEO data but not authored by the CLEO Collaboration.

$A_{CP}(K_1^*(1270)^+K^- \to K^+K^-\pi^+\pi^-)$ in $D^0 \to K_1^*(1270)^+K^-$, $\overline{D}^0 \to$ c.c.

Including the full $K_1^*(1270)^+$ phase space accessible in this decay chain, with its various resonance contributions.

VALUE (%)	EVTS	DOCUMENT ID		TECN	COMMENT
− 2.3±1.7 OUR AVERAGE					
− 2.6±1.7± 0.2	163k	AAIJ	19C	LHCB	4-body fit, $KK\pi\pi$ evts
25.3±9.7±12.7	2.9k	[1] DARGENT	17		4-body fit, $KK\pi\pi$ evts

[1] Obtained by analyzing CLEO data but not authored by the CLEO Collaboration.

$A_{CP}(K_1^*(1270)^+K^- \to K^{*0}\pi^+K^-)$ in $D^0 \to K_1^*(1270)^+K^-$, $\overline{D}^0 \to$ c.c.

VALUE (%)	DOCUMENT ID		TECN	COMMENT
−0.7±10.4	ARTUSO	12	CLEO	Amplitude fit, 2959 evts.

$A_{CP}(K_1^*(1270)^-K^+ \to \overline{K}^{*0}\pi^-K^+)$ in $D^0 \to K_1^*(1270)^-K^+$, $\overline{D}^0 \to$ c.c.

VALUE (%)	DOCUMENT ID		TECN	COMMENT
−10.0±31.5	ARTUSO	12	CLEO	Amplitude fit, 2959 evts.

$A_{CP}(K_1^*(1270)^-K^+ \to K^+K^-\pi^+\pi^-)$ in $D^0 \to K_1^*(1270)^-K^+$, $\overline{D}^0 \to$ c.c.

Including the full $K_1^*(1270)^-$ phase space accessible in this decay chain, with its various resonance contributions.

VALUE (%)	EVTS	DOCUMENT ID		TECN	COMMENT
1.7± 3.5 OUR AVERAGE					
3.3± 3.5± 0.5	163k	AAIJ	19C	LHCB	4-body fit, $KK\pi\pi$ evts
−50.4±12.0±16.1	2.9k	[1] DARGENT	17		4-body fit, $KK\pi\pi$ evts

[1] Obtained by analyzing CLEO data but not authored by the CLEO Collaboration.

$A_{CP}(K_1^*(1270)^+K^- \to \rho^0K^+K^-)$ in $D^0 \to K_1^*(1270)^+K^-$, $\overline{D}^0 \to$ c.c.

VALUE (%)	DOCUMENT ID		TECN	COMMENT
−6.5±16.9	ARTUSO	12	CLEO	Amplitude fit, 2959 evts.

$A_{CP}(K_1^*(1270)^-K^+ \to \rho^0K^-K^+)$ in $D^0 \to K_1^*(1270)^-K^+$, $\overline{D}^0 \to$ c.c.

VALUE (%)	DOCUMENT ID		TECN	COMMENT
+9.6±12.9	ARTUSO	12	CLEO	Amplitude fit, 2959 evts.

$A_{CP}(K_1(1400)^+K^- \to K^+K^-\pi^+\pi^-)$ in $D^0 \to K_1(1400)^+K^-$, $\overline{D}^0 \to$ c.c.

Including the full $K_1(1400)^+$ phase space accessible in this decay chain, with its various resonance contributions.

VALUE (%)	EVTS	DOCUMENT ID		TECN	COMMENT
−4.4± 2.1 OUR AVERAGE					
−4.5± 2.1± 0.3	163k	AAIJ	19C	LHCB	4-body fit, $KK\pi\pi$ evts
9.2±15.2±20.3	2.9k	[1] DARGENT	17		4-body fit, $KK\pi\pi$ evts

[1] Obtained by analyzing CLEO data but not authored by the CLEO Collaboration.

$A_{CP}(K^*(1410)^+K^- \to K^{*0}\pi^+K^-)$ in $D^0 \to K^*(1410)^+K^-$, $\overline{D}^0 \to$ c.c.

VALUE (%)	DOCUMENT ID		TECN	COMMENT
−20.0±16.8	ARTUSO	12	CLEO	Amplitude fit, 2959 evts.

$A_{CP}(K^*(1410)^-K^+ \to \overline{K}^{*0}\pi^-K^+)$ in $D^0 \to K^*(1410)^-K^+$, $\overline{D}^0 \to$ c.c.

VALUE (%)	DOCUMENT ID		TECN	COMMENT
−1.1±13.7	ARTUSO	12	CLEO	Amplitude fit, 2959 evts.

$A_{CP}(K^*(1680)^+K^- \to K^+K^-\pi^+\pi^-)$ in $D^0 \to K^*(1680)^+K^-$, $\overline{D}^0 \to$ c.c.

Including the full $K^*(1680)^+$ phase space accessible in this decay chain, with its various resonance contributions.

VALUE (%)	EVTS	DOCUMENT ID		COMMENT
−17.1±21.8±18.5	2.9k	[1] DARGENT	17	4-body fit, $KK\pi\pi$ evts

[1] Obtained by analyzing CLEO data but not authored by the CLEO Collaboration.

$A_{CP}(K^{*0}\overline{K}^{*0})$ in D^0, $\overline{D}^0 \to K^{*0}\overline{K}^{*0}$

Including S, P, D wave

VALUE (%)	EVTS	DOCUMENT ID		COMMENT
−4.6±9.0±11.3	2.9k	[1] DARGENT	17	4-body fit, $KK\pi\pi$ evts

[1] Obtained by analyzing CLEO data but not authored by the CLEO Collaboration.

$A_{CP}(K^{*0}\overline{K}^{*0}$ S-wave) in D^0, $\overline{D}^0 \to K^{*0}\overline{K}^{*0}$ S-wave

VALUE (%)	EVTS	DOCUMENT ID		TECN	COMMENT
−3.9± 2.2 OUR AVERAGE					
−4.3± 2.2±0.5	163k	AAIJ	19C	LHCB	4-body fit, $KK\pi\pi$ evts
+9.5±13.5	3k	ARTUSO	12	CLEO	4-body fit, $KK\pi\pi$ evts

$A_{CP}(\phi\rho^0)$ in D^0, $\overline{D}^0 \to \phi\rho^0$

Including S, P, D wave

VALUE (%)	EVTS	DOCUMENT ID		COMMENT
1.5±4.6±8.0	2.9k	[1] DARGENT	17	4-body fit, $K\pi\pi$ evts

[1] Obtained by analyzing CLEO data but not authored by the CLEO Collaboration.

$A_{CP}(\phi\rho^0$ S-wave) in D^0, $\overline{D}^0 \to \phi\rho^0$ S-wave

VALUE (%)	DOCUMENT ID		TECN	COMMENT
−2.7±5.3	ARTUSO	12	CLEO	Amplitude fit, 2959 evts.

$A_{CP}(\phi\rho^0$ D-wave) in D^0, $\overline{D}^0 \to \phi\rho^0$ D-wave

VALUE (%)	DOCUMENT ID		TECN	COMMENT
−37.1±19.0	ARTUSO	12	CLEO	Amplitude fit, 2959 evts.

$A_{CP}(\phi(\pi^+\pi^-)_{S-wave})$ in D^0, $\overline{D}^0 \to \phi(\pi^+\pi^-)_{S-wave}$

VALUE (%)	EVTS	DOCUMENT ID		TECN	COMMENT
6 ± 6 OUR AVERAGE					
5.8± 6.1± 0.8	163k	AAIJ	19C	LHCB	4-body fit, $KK\pi\pi$ evts
−4.0±18.0±44.6	3k	[1] DARGENT	17		4-body fit, $KK\pi\pi$ evts
• • • We do not use the following data for averages, fits, limits, etc. • • •					
−8.6±10.4	3k	[2] ARTUSO	12	CLEO	4-body fit, $KK\pi\pi$ evts

[1] Obtained by analyzing CLEO data but not authored by the CLEO Collaboration.
[2] see DARGENT 17

$A_{CP}(K^*(892)^0(K^-\pi^+)_{S-wave})$ in D^0, $\overline{D}^0 \to K^*(892)^0(K^-\pi^+)_{S-wave}$

VALUE (%)	EVTS	DOCUMENT ID		COMMENT
−13.1±17.9±31.2	2.9k	[1] DARGENT	17	4-body fit, $KK\pi\pi$ evts

[1] Obtained by analyzing CLEO data but not authored by the CLEO Collaboration.

$A_{CP}(K^+K^-\pi^+\pi^-$ non-resonant) in D^0, $\overline{D}^0 \to K^+K^-\pi^+\pi^-$ non-resonant

VALUE (%)	DOCUMENT ID		COMMENT
+8.2±10.9±17.1	[1] DARGENT	17	4-body fit, 2.9k $KK\pi\pi$ evts

[1] Obtained by analyzing CLEO data but not authored by the CLEO Collaboration.

$A_{CP}((K^-\pi^+)_{P-wave}(K^+\pi^-)_{S-wave})$ in $D^0 \to (K^-\pi^+)_{P-wave}(K^+\pi^-)_{S-wave}$, $\overline{D}^0 \to$ c.c.

VALUE (%)	DOCUMENT ID		TECN	COMMENT
+2.7±10.6	ARTUSO	12	CLEO	Amplitude fit, 2959 evts.

$A_{CP}(K^+K^-\mu^+\mu^-)$ in D^0, $\overline{D}^0 \to K^+K^-\mu^+\mu^-$

VALUE (%)	EVTS	DOCUMENT ID		TECN	COMMENT
0±11±2	110	AAIJ	18I	LHCB	pp at 7, 8, 13TeV

$A_{CP}(\pi^+\pi^-\mu^+\mu^-)$ in D^0, $\overline{D}^0 \to \pi^+\pi^-\mu^+\mu^-$

VALUE (%)	EVTS	DOCUMENT ID		TECN	COMMENT
4.9±3.8±0.7	1.1k	AAIJ	18I	LHCB	pp at 7, 8, 13TeV

D^0 CP-EVEN FRACTIONS

The CP-even fraction F_+, defined for self-conjugate final states, like the coherence factor is useful for measuring the unitary triangle angle γ in $B \to DK$ decays. A purely CP-even state has $F_+ = 1$, a CP-odd one has $F_+ = 0$. For details, see NAYAK 15.

CP-even fraction in $D^0 \to \pi^+\pi^-\pi^0$ decays

VALUE (%)	DOCUMENT ID		COMMENT
97.3±1.7	MALDE	15	Uses CLEO data
• • • We do not use the following data for averages, fits, limits, etc. • • •			
96.8±1.7±0.6	NAYAK	15	see MALDE 15

CP-even fraction in $D^0 \to K^+K^-\pi^0$ decays

VALUE (%)	DOCUMENT ID		COMMENT
73.2±5.5	MALDE	15	Uses CLEO data
• • • We do not use the following data for averages, fits, limits, etc. • • •			
73.1±5.8±2.1	NAYAK	15	see MALDE 15

CP-even fraction in $D^0 \to \pi^+\pi^-\pi^+\pi^-$ decays

VALUE (%)	DOCUMENT ID		TECN	COMMENT
76.9±2.1±1.0	[1] HARNEW	18		Uses CLEO-c data
• • • We do not use the following data for averages, fits, limits, etc. • • •				
72.9±0.9±1.8	[1,2] DARGENT	17		from amplitude model
73.7±2.8	MALDE	15	CLEO	amplitude model independent

[1] Obtained by analyzing CLEO-c data but not authored by the CLEO Collaboration.
[2] MALDE 15 and DARGENT 17 use different CLEO data sets, so in principle their results could be averaged. However, given the importance that model-independence has in the use of this value, we exclude the amplitude model-derived result from the average.

Downloaded from https://academic.oup.com/ptep/article/2022/8/083C01/6651666 by KIT Library user on 27 September 2022

CP-even fraction in $D^0 \to K^0_S \pi^+ \pi^- \pi^0$ decays

VALUE (%)	DOCUMENT ID		COMMENT
23.8±1.2±1.2	[1] RESMI	18	Uses CLEO-c data

[1] Obtained by analyzing CLEO-c data but not authored by the CLEO Collaboration.

CP-even fraction in $D^0 \to K^+ K^- \pi^+ \pi^-$ decays

VALUE (%)	DOCUMENT ID		COMMENT
75.3±1.8±3.9	[1] DARGENT	17	from amplitude model

[1] Obtained by analyzing CLEO data but not authored by the CLEO Collaboration.

D^0 CP-VIOLATING ASYMMETRY DIFFERENCES

$\Delta A_{CP} = A_{CP}(K^+K^-) - A_{CP}(\pi^+\pi^-)$

CP violation in these modes can come from the decay amplitudes (direct) and/or from mixing or interference of mixing and decay (indirect). The difference ΔA_{CP} is primarily sensitive to the direct component, and only retains a second-order dependence on the indirect component for measurements where the mean decay time of the K^+K^- and $\pi^+\pi^-$ samples are not identical. The results below are averaged assuming the indirect component can be neglected.

VALUE (%)	EVTS	DOCUMENT ID		TECN	COMMENT
−0.154±0.029	53M,17M	AAIJ	19D	LHCB	Time-integrated
• • • We do not use the following data for averages, fits, limits, etc. • • •					
−0.10 ±0.08 ±0.03	6.5M,2.2M	AAIJ	16D	LHCB	See AAIJ 19D
0.14 ±0.16 ±0.08	2.2M,0.8M	AAIJ	14AK	LHCB	See AAIJ 19D
0.49 ±0.30 ±0.14	0.56M,0.22M	AAIJ	13AD	LHCB	See AAIJ 14AK
−0.82 ±0.21 ±0.11	1.4M,0.4M	AAIJ	12G	LHCB	See AAIJ 16D
−0.46 ±0.31 ±0.12		AALTONEN	12B	CDF	See AALTONEN 12O
−0.62 ±0.21 ±0.10		AALTONEN	12O	CDF	Time-integrated
0.24 ±0.62 ±0.26		[1] AUBERT	08M	BABR	Time-integrated
−0.86 ±0.60 ±0.07	120k	STARIC	08	BELL	Time-integrated

[1] Calculated from the AUBERT 08M values of $A_{CP}(K^+K^-)$ and $A_{CP}(\pi^+\pi^-)$. The systematic error here combines the systematic errors in quadrature, and therefore somewhat over-estimates it.

D^0 TESTS OF LOCAL CP-VIOLATION (CPV)

We list model-independent searches for local CP violation in phase-space distributions of multi-body decays.

Most of these searches divide phase space (Dalitz plot for 3-body decays, five-dimensional equivalent for 4-body decays) into bins, and perform a χ^2 test comparing normalised yields N_i, $\overline{N}_i$ in CP-conjugate bin pairs i: $\chi^2 = \Sigma_i (N_i - \alpha\, \overline{N}_i)/\sigma(N_i - \alpha\, \overline{N}_i)$. The factor $\alpha = (\Sigma_i N_i)/(\Sigma_i \overline{N}_i)$ removes the dependence on phase-space-integrated rate asymmetries. The result is used to obtain the probability (p-value) to obtain the measured χ^2 or larger under the assumption of CP conservation [AUBERT 08AO, BEDIAGA 09]. Alternative methods obtain p-values from other test variables based on unbinned analyses [WILLIAMS 11, AAIJ 14C]. Results can be combined using Fisher's method [MOSTELLER 48].

Local CPV in $D^0, \overline{D}^0 \to \pi^+\pi^-\pi^0$

p-value (%)	EVTS	DOCUMENT ID		TECN	COMMENT
4.9 OUR EVALUATION					
2.6	566k	[1] AAIJ	15A	LHCB	unbinned method
32.8	82k	AUBERT	08AO	BABR	χ^2

[1] Unusually, AAIJ 15A assigns an uncertainty on the p value of ±0.5%. This results from limited test statistics.

Local CPV in $D^0, \overline{D}^0 \to \pi^+\pi^-\pi^+\pi^-$

p-value (%)	EVTS	DOCUMENT ID		TECN	COMMENT
0.6±0.2	1.0M	[1] AAIJ	17AE	LHCB	unbinned, P-odd
• • • We do not use the following data for averages, fits, limits, etc. • • •					
4.6±0.5	1.0M	[2,3] AAIJ	17AE	LHCB	unbinned, P-even
41	330k	[2,4] AAIJ	13BR	LHCB	χ^2, P-even

[1] This AAIJ 17AE value tests CP Violation in P-odd variables.
[2] This value tests CP Violation in P-even variables.
[3] Not included in average as correlation to P-odd measurement using the same data is unclear.
[4] See AAIJ 17AE.

Local CPV in $D^0, \overline{D}^0 \to K^0_S \pi^+\pi^-$

p-value (%)	EVTS	DOCUMENT ID		TECN	COMMENT
96	350k	AALTONEN	12AD	CDF	χ^2

Local CPV in $D^0, \overline{D}^0 \to K^+K^-\pi^0$

p-value (%)	EVTS	DOCUMENT ID		TECN	COMMENT
16.6	11k	AUBERT	08AO	BABR	χ^2

Local CPV in $D^0, \overline{D}^0 \to K^+K^-\pi^+\pi^-$

p-value (%)	EVTS	DOCUMENT ID		TECN	COMMENT
9.1	57k	AAIJ	13BR	LHCB	χ^2

CP VIOLATING ASYMMETRIES OF P-ODD (T-ODD) MOMENTS

The CP-sensitive P-odd (T-odd) correlation in D^0, $\overline{D}^0$ decays. The D^0 and $\overline{D}^0$ are distinguished by the charge of the parent D^*: $D^{*+} \to D^0\pi^+$ and $D^{*-} \to \overline{D}^0\pi^-$.

$A_{Tviol}(K^+K^-\pi^+\pi^-)$ in $D^0, \overline{D}^0 \to K^+K^-\pi^+\pi^-$

$C_T \equiv \vec{p}_{K^+} \cdot (\vec{p}_{\pi^+} \times \vec{p}_{\pi^-})$ is a parity-odd correlation of the K^+, π^+, and π^- momenta (evaluated in the D^0 rest frame) for the D^0. $\overline{C}_T \equiv \vec{p}_{K^-} \cdot (\vec{p}_{\pi^-} \times \vec{p}_{\pi^+})$ is the corresponding quantity for the $\overline{D}^0$. Then
$A_T \equiv [\Gamma(C_T > 0) - \Gamma(C_T < 0)] / [\Gamma(C_T > 0) + \Gamma(C_T < 0)]$, and
$\overline{A}_T \equiv [\Gamma(-\overline{C}_T > 0) - \Gamma(-\overline{C}_T < 0)] / [\Gamma(-\overline{C}_T > 0) + \Gamma(-\overline{C}_T < 0)]$, and
$A_{Tviol} \equiv \frac{1}{2}(A_T - \overline{A}_T)$. C_T and $\overline{C}_T$ are commonly referred to as T-odd moments, because they are odd under T reversal. However, the T-conjugate process $K^+K^-\pi^+\pi^- \to D^0$ is not accessible, while the P-conjugate process is.

VALUE (units 10^{-3})	EVTS	DOCUMENT ID		TECN	COMMENT
2.9± 2.2 OUR AVERAGE					
5.2± 3.7± 0.7	110k	[1] KIM	19	BELL	e^+e^- at $\Upsilon(1S)-\Upsilon(6S)$
1.8± 2.9± 0.4	171k	AAIJ	14BC	LHCB	$B \to D^0\mu^-X$
1.0± 5.1± 4.4	47k	DEL-AMO-SA...10		BABR	$e^+e^- \approx$ 10.6 GeV
• • • We do not use the following data for averages, fits, limits, etc. • • •					
10 ±57 ±37	0.8k	LINK	05E	FOCS	γ A, $\overline{E}_\gamma \approx$ 180 GeV

[1] KIM 19 also study CP-violating asymmetries in several other kinematic variables. No evidence for CP violation is found in any of them.

$A_{Tviol}(K_S\pi^+\pi^-\pi^0)$ in $D^0, \overline{D}^0 \to K_S\pi^+\pi^-\pi^0$

VALUE (units 10^{-3})	EVTS	DOCUMENT ID		TECN	COMMENT
$-0.28\pm1.38^{+0.23}_{-0.76}$	745k	[1] PRASANTH	17	BELL	e^+e^- at Υ(nS)'s

[1] PRASANTH 17 also measures A_{Tviol} in sub-regions of the $D^0 \to K_S\pi^+\pi^-\pi^0$ phase-space. No evidence of T violation is found.

D^0 CPT-VIOLATING DECAY-RATE ASYMMETRIES

$A_{CPT}(K^\mp\pi^\pm)$ in $D^0 \to K^-\pi^+$, $\overline{D}^0 \to K^+\pi^-$

$A_{CPT}(t)$ is defined in terms of the time-dependent decay probabilities $P(D^0 \to K^-\pi^+)$ and $\overline{P}(\overline{D}^0 \to K^+\pi^-)$ by $A_{CPT}(t) = (\overline{P} - P)/(\overline{P} + P)$. For small mixing parameters $x \equiv \Delta m/\Gamma$ and $y \equiv \Delta\Gamma/2\Gamma$ (as is the case), and times t, $A_{CPT}(t)$ reduces to [y $Re\,\xi$ - x $Im\,\xi$] Γt, where ξ is the CPT-violating parameter.

The following is actually y $Re\,\xi$ - x $Im\,\xi$.

VALUE	DOCUMENT ID		TECN	COMMENT
0.0083±0.0065±0.0041	LINK	03B	FOCS	γ nucleus, $\overline{E}_\gamma \approx$ 180 GeV

$D^0 \to K^*(892)^-\ell^+\nu_\ell$ FORM FACTORS

$r_V \equiv V(0)/A_1(0)$ in $D^0 \to K^*(892)^-\ell^+\nu_\ell$

VALUE	EVTS	DOCUMENT ID		TECN	COMMENT
1.46±0.07 OUR AVERAGE					
1.46±0.07±0.02	3k	ABLIKIM	19G	BES3	$K^*(892)^-e^+\nu_e$
1.71±0.68±0.34		LINK	05B	FOCS	$K^*(892)^-\mu^+\nu_\mu$

$r_2 \equiv A_2(0)/A_1(0)$ in $D^0 \to K^*(892)^-\ell^+\nu_\ell$

VALUE	EVTS	DOCUMENT ID		TECN	COMMENT
0.68±0.06 OUR AVERAGE					
0.67±0.06±0.01	3k	ABLIKIM	19G	BES3	$K^*(892)^-e^+\nu_e$
0.91±0.37±0.10		LINK	05B	FOCS	$K^*(892)^-\mu^+\nu_\mu$

$D^0 \to K^-/\pi^-\ell^+\nu_\ell$ FORM FACTORS

$f_+(0)$ in $D^0 \to K^-\ell^+\nu_\ell$

VALUE	EVTS	DOCUMENT ID		TECN	COMMENT
0.736 ±0.004 OUR AVERAGE					
0.7368±0.0026±0.0036	71k	ABLIKIM	15X	BES3	$\ell=e$, 2-parameter fit
0.727 ±0.007 ±0.009		AUBERT	07BG	BABR	$\ell=e$, 2-parameter fit

$f_+(0)|V_{cs}|$ in $D^0 \to K^-\ell^+\nu_\ell$

VALUE	EVTS	DOCUMENT ID		TECN	COMMENT
0.7166±0.0030 OUR AVERAGE					
0.7133±0.0038±0.0029	47k	ABLIKIM	19B	BES3	$\ell=\mu$, 2-parameter fit
0.7172±0.0025±0.0035	71k	[1] ABLIKIM	15X	BES3	$\ell=e$, 2-parameter fit
0.726 ±0.008 ±0.004		BESSON	09	CLEO	$\ell=e$, 3-parameter fit

[1] The 3-parameter fit yields 0.7195 ± 0.0035 ± 0.0041.

$r_1 \equiv a_1/a_0$ in $D^0 \to K^-\ell^+\nu_\ell$

VALUE	EVTS	DOCUMENT ID		TECN	COMMENT
−2.40±0.16 OUR AVERAGE					
−2.33±0.16±0.08	71k	[1] ABLIKIM	15X	BES3	$\ell=e$, 3-parameter fit
−2.65±0.34±0.08		BESSON	09	CLEO	$\ell=e$, 3-parameter fit

[1] The 2-parameter fit yields −2.23 ± 0.09 ± 0.06.

Downloaded from https://academic.oup.com/ptep/article/2022/8/083C01/6651666 by KIT Library user on 27 September 2022

$r_2 \equiv a_2/a_0$ in $D^0 \to K^- \ell^+ \nu_\ell$

VALUE	EVTS	DOCUMENT ID		TECN	COMMENT
5 ±4 OUR AVERAGE					
3.4±3.9±2.4	71k	ABLIKIM	15X	BES3	$\ell=e$, 3-parameter fit
13 ±9 ±1		BESSON	09	CLEO	$\ell=e$, 3-parameter fit

$f_+(0)$ in $D^0 \to \pi^- \ell^+ \nu_\ell$

VALUE	EVTS	DOCUMENT ID		TECN	COMMENT
0.6372±0.0080±0.0044	6.3k	ABLIKIM	15X	BES3	$\ell=e$, 2-parameter fit

$f_+(0)|V_{cd}|$ in $D^0 \to \pi^- \ell^+ \nu_\ell$

VALUE	EVTS	DOCUMENT ID		TECN	COMMENT
0.1436±0.0026 OUR AVERAGE Error includes scale factor of 1.5. See the ideogram below.					
0.1435±0.0018±0.0009	6.3k	[1] ABLIKIM	15X	BES3	$\ell=e$, 2-parameter fit
0.1374±0.0038±0.0024	5.3k	[2] LEES	15F	BABR	$\ell=e$, 3-parameter fit
0.152 ±0.005 ±0.001		BESSON	09	CLEO	$\ell=e$, 3-parameter fit

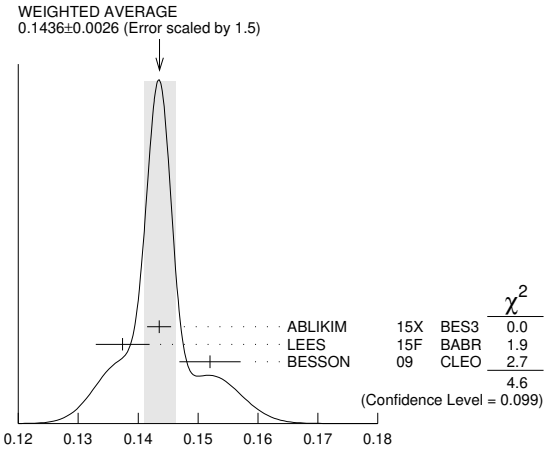

[1] The 3-parameter fit yields 0.1420 ± 0.0024 ± 0.0010.

[2] LEES 15F reports a value 0.1374 ± 0.0038 ± 0.0022 ± 0.0009, where the last uncertainty is due to the uncertainties of the $D^0 \to K^- \pi^+$ branching fraction.

$r_1 \equiv a_1/a_0$ in $D^0 \to \pi^- \ell^+ \nu_\ell$

VALUE	EVTS	DOCUMENT ID		TECN	COMMENT
−1.97±0.28 OUR AVERAGE Error includes scale factor of 1.4. See the ideogram below.					
−1.84±0.22±0.07	6.3k	[1] ABLIKIM	15X	BES3	$\ell=e$, 3-parameter fit
−1.31±0.70±0.43	5.3k	LEES	15F	BABR	$\ell=e$, 3-parameter fit
−2.80±0.49±0.04		BESSON	09	CLEO	$\ell=e$, 3-parameter fit

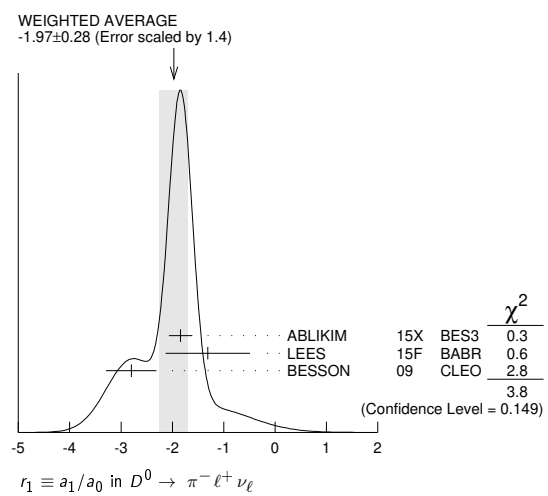

[1] The 2-parameter fit yields −2.04 ± 0.08 ± 0.03.

$r_2 \equiv a_1/a_0$ in $D^0 \to \pi^- \ell^+ \nu_\ell$

VALUE	EVTS	DOCUMENT ID		TECN	COMMENT
−0.2±2.2 OUR AVERAGE Error includes scale factor of 1.7. See the ideogram below.					
−1.4±1.5±0.5	6.3k	ABLIKIM	15X	BES3	$\ell=e$, 3-parameter fit
−4.2±4.0±1.9	5.3k	LEES	15F	BABR	$\ell=e$, 3-parameter fit
6 ±3 ±0		BESSON	09	CLEO	$\ell=e$, 3-parameter fit

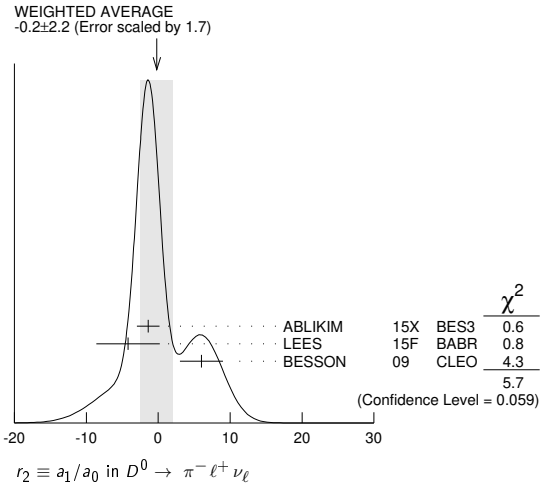

Amplitude analyses

$D \to K\pi\pi\pi$, $D \to KK\pi\pi$ partial wave analyses

Amplitude analyses of D^0 decays to a variety of 4-body kaon or pion final states, fitting simultaneously different partial wave components.

VALUE	DOCUMENT ID		TECN	COMMENT
	[1] AAIJ	19C	LHCB	$D^0 \to K^+ K^- \pi^+ \pi^-$
	ABLIKIM	19AK	BES3	$D^0 \to K^- \pi^+ \pi^0 \pi^0$
	AAIJ	18AI	LHCB	$D^0 \to K^- \pi^+ \pi^+ \pi^-$
	ABLIKIM	17O	BES3	$D^0 \to K^- \pi^+ \pi^+ \pi^-$

[1] AAIJ 19C also provides measurements of CP violation in $D^0 \to K^+ K^- \pi^+ \pi^-$, with results compatible with CP symmetry.

D^0 REFERENCES

ABLIKIM	22	PRL 128 011803	M. Ablikim et al.	(BESIII Collab.)
AAIJ	21AB	PRL 127 111801	R. Aaij et al.	(LHCb Collab.)
AAIJ	21AI	PR D104 072010	R. Aaij et al.	(LHCb Collab.)
AAIJ	21X	PR D104 L031102	R. Aaij et al.	(LHCb Collab.)
ABLIKIM	21AA	JHEP 2105 164	M. Ablikim et al.	(BESIII Collab.)
ABLIKIM	21AY	PRL 127 131801	M. Ablikim et al.	(BESIII Collab.)
ABLIKIM	21BA	PR D104 052008	M. Ablikim et al.	(BESIII Collab.)
ABLIKIM	21BC	PR D104 L091103	M. Ablikim et al.	(BESIII Collab.)
ABUDINEN	21A	PRL 127 211801	F. Abudinen et al.	(BELLE II Collab.)
LI	21G	JHEP 2109 075	L.K. Li et al.	(BELLE Collab.)
AAIJ	20	PR D101 012005	R. Aaij et al.	(LHCb Collab.)
ABLIKIM	20AA	PR D102 052003	M. Ablikim et al.	(BESIII Collab.)
ABLIKIM	20AC	PR D102 052006	M. Ablikim et al.	(BESIII Collab.)
ABLIKIM	20AF	PR D102 112005	M. Ablikim et al.	(BESIII Collab.)
ABLIKIM	20G	PR D101 052009	M. Ablikim et al.	(BESIII Collab.)
ABLIKIM	20V	PRL 124 241803	M. Ablikim et al.	(BESIII Collab.)
CHEN	20A	PR D102 012002	Y.Q. Chen et al.	(BELLE Collab.)
LEES	20A	PR D101 112003	J.P. Lees et al.	(BABAR Collab.)
LEES	20B	PRL 124 071802	J.P. Lees et al.	(BABAR Collab.)
NAYAK	20	PR D102 071102	M. Nayak et al.	(BELLE Collab.)
AAIJ	19	PRL 122 011802	R. Aaij et al.	(LHCb Collab.)
AAIJ	19C	JHEP 1902 126	R. Aaij et al.	(LHCb Collab.)
AAIJ	19D	PRL 122 211803	R. Aaij et al.	(LHCb Collab.)
AAIJ	19X	PRL 122 231802	R. Aaij et al.	(LHCb Collab.)
ABLIKIM	19AK	PR D99 092008	M. Ablikim et al.	(BESIII Collab.)
ABLIKIM	19AL	PR D99 112002	M. Ablikim et al.	(BESIII Collab.)
ABLIKIM	19AY	PR D100 072006	M. Ablikim et al.	(BESIII Collab.)
ABLIKIM	19B	PRL 122 011804	M. Ablikim et al.	(BESIII Collab.)
ABLIKIM	19BI	PL B798 135017	M. Ablikim et al.	(BESIII Collab.)
ABLIKIM	19C	PRL 122 062001	M. Ablikim et al.	(BESIII Collab.)
ABLIKIM	19G	PR D99 011103	M. Ablikim et al.	(BESIII Collab.)
KIM	19	PR D99 011104	J.B. Kim et al.	(BELLE Collab.)
LEES	19A	PRL 122 081802	J.P. Lees et al.	(BABAR Collab.)
PDG	19	RPP 2019 at pdg.lbl.gov	M. Tanabashi et al.	(PDG Collab.)
AAIJ	18AI	EPJ C78 443	R. Aaij et al.	(LHCb Collab.)
AAIJ	18AV	JHEP 1811 048	R. Aaij et al.	(LHCb Collab.)
AAIJ	18I	PRL 121 091801	R. Aaij et al.	(LHCb Collab.)
AAIJ	18K	PR D97 031101	R. Aaij et al.	(LHCb Collab.)
ABLIKIM	18AC	PR D98 092009	M. Ablikim et al.	(BESIII Collab.)
ABLIKIM	18AE	PRL 121 171803	M. Ablikim et al.	(BESIII Collab.)
ABLIKIM	18F	PRL 121 081802	M. Ablikim et al.	(BESIII Collab.)
ABLIKIM	18L	PR D97 052005	M. Ablikim et al.	(BESIII Collab.)
ABLIKIM	18P	PR D97 072015	M. Ablikim et al.	(BESIII Collab.)
ABLIKIM	18W	PR D97 072004	M. Ablikim et al.	(BESIII Collab.)
ABLIKIM	18X	PL B781 368	M. Ablikim et al.	(BESIII Collab.)
HARNEW	18	JHEP 1801 144	S. Harnew et al.	(BRIS, PNNL)
RESMI	18	JHEP 1801 082	P.K. Resmi et al.	
SMITH	18	PR D98 051101	M.J. Smith, D. Cinabro, P. Naik	(LTU, WAYN+)
AAIJ	17AE	PL B769 345	R. Aaij et al.	(LHCb Collab.)
AAIJ	17AK	PRL 118 261803	R. Aaij et al.	(LHCb Collab.)
AAIJ	17AO	PR D95 052004	R. Aaij et al.	(LHCb Collab.)
Also		PR D96 099907 (errat.)	R. Aaij et al.	(LHCb Collab.)
AAIJ	17BG	PRL 119 181805	R. Aaij et al.	(LHCb Collab.)
AAIJ	17M	PL B767 177	R. Aaij et al.	(LHCb Collab.)
ABLIKIM	17A	PL B765 231	M. Ablikim et al.	(BESIII Collab.)
ABLIKIM	17O	PR D95 072010	M. Ablikim et al.	(BESIII Collab.)
DARGENT	17	JHEP 1705 143	P. dArgent et al.	(HEID, BRIS)
DASH	17	PRL 119 171801	N. Dash et al.	(BELLE Collab.)
LAI	17	PR D95 011102	Y.-T. Lai et al.	(BELLE Collab.)
NANUT	17	PRL 118 051801	T. Nanut et al.	(BELLE Collab.)
PRASANTH	17	PR D95 091101	K. Prasanth et al.	(BELLE Collab.)
AAIJ	16D	PRL 116 191601	R. Aaij et al.	(LHCb Collab.)
AAIJ	16F	PRL 116 241801	R. Aaij et al.	(LHCb Collab.)
AAIJ	16H	PL B754 167	R. Aaij et al.	(LHCb Collab.)
AAIJ	16I	PL B757 558	R. Aaij et al.	(LHCb Collab.)
AAIJ	16N	PR D93 052018	R. Aaij et al.	(LHCb Collab.)

Downloaded from https://academic.oup.com/ptep/article/2022/8/083C01/6651666 by KIT Library user on 27 September 2022

AAIJ	16V	JHEP 1604 033	R. Aaij *et al.*	(LHCb Collab.)
ABLIKIM	16D	PRL 116 082001	M. Ablikim *et al.*	(BESIII Collab.)
EVANS	16	PL B757 520	T. Evans *et al.*	(OXF, BRIS, MDRA)
Also		PL B765 402 (errat.)	T. Evans *et al.*	(OXF, BRIS, MDRA)
LEES	16D	PR D93 112014	J.P. Lees *et al.*	(BABAR Collab.)
NISAR	16	PR D93 051102	N.K. Nisar *et al.*	(BELLE Collab.)
STARIC	16	PL B753 412	M. Staric *et al.*	(BELLE Collab.)
AAIJ	15A	PL B740 158	R. Aaij *et al.*	(LHCb Collab.)
AAIJ	15AA	JHEP 1504 043	R. Aaij *et al.*	(LHCb Collab.)
AAIJ	15AT	JHEP 1510 055	R. Aaij *et al.*	(LHCb Collab.)
ABLIKIM	15D	PL B744 339	M. Ablikim *et al.*	(BESIII Collab.)
ABLIKIM	15F	PR D91 112015	M. Ablikim *et al.*	(BESIII Collab.)
ABLIKIM	15X	PR D92 072012	M. Ablikim *et al.*	(BESIII Collab.)
LEES	15F	PR D91 052022	J.P. Lees *et al.*	(BABAR Collab.)
MALDE	15	PL B747 9	S. Malde *et al.*	(BRIS, CERN, MDRA, OXF+)
NAYAK	15	PL B740 1	M. Nayak *et al.*	(MDRA, OXF, CERN, CMU+)
AAIJ	14AK	JHEP 1407 041	R. Aaij *et al.*	(LHCb Collab.)
AAIJ	14AL	PRL 112 041801	R. Aaij *et al.*	(LHCb Collab.)
AAIJ	14B	PL B728 234	R. Aaij *et al.*	(LHCb Collab.)
AAIJ	14BC	JHEP 1410 005	R. Aaij *et al.*	(LHCb Collab.)
AAIJ	14C	PL B728 585	R. Aaij *et al.*	(LHCb Collab.)
AALTONEN	14Q	PR D90 111103	T. Aaltonen *et al.*	(CDF Collab.)
ABLIKIM	14C	PL B734 227	M. Ablikim *et al.*	(BESIII Collab.)
BONVICINI	14	PR D89 072002	G. Bonvicini *et al.*	(CLEO Collab.)
KO	14	PRL 112 111801	B.R. Ko *et al.*	(BELLE Collab.)
LIBBY	14	PL B731 197	J. Libby *et al.*	(MDRA, OXF, PNL, +)
NISAR	14	PRL 112 211601	N.K. Nisar *et al.*	(BELLE Collab.)
PENG	14	PR D89 091103	T. Peng *et al.*	(BELLE Collab.)
TOMARADZE	14	PR D89 031501	A. Tomaradze *et al.*	(NWES, WAYN)
AAIJ	13AD	PL B723 33	R. Aaij *et al.*	(LHCb Collab.)
AAIJ	13AI	PL B725 15	R. Aaij *et al.*	(LHCb Collab.)
AAIJ	13BR	PL B726 623	R. Aaij *et al.*	(LHCb Collab.)
AAIJ	13CE	PRL 111 251801	R. Aaij *et al.*	(LHCb Collab.)
AAIJ	13N	PRL 110 101802	R. Aaij *et al.*	(LHCb Collab.)
AAIJ	13V	JHEP 1306 065	R. Aaij *et al.*	(LHCb Collab.)
AALTONEN	13AE	PRL 111 231802	T. Aaltonen *et al.*	(CDF Collab.)
DOBBS	13	PRL 110 131802	S. Dobbs *et al.*	(CLEO Collab.)
LEES	13	PR D87 012004	J.P. Lees *et al.*	(BABAR Collab.)
LEES	13S	PR D88 071104	J.P. Lees *et al.*	(BABAR Collab.)
WHITE	13	PR D88 051101	E. White *et al.*	(BELLE Collab.)
AAIJ	12G	PRL 108 111602	R. Aaij *et al.*	(LHCb Collab.)
AAIJ	12K	JHEP 1204 129	R. Aaij *et al.*	(LHCb Collab.)
AALTONEN	12AD	PR D86 032007	T. Aaltonen *et al.*	(CDF Collab.)
AALTONEN	12B	PR D85 012009	T. Aaltonen *et al.*	(CDF Collab.)
AALTONEN	12O	PRL 109 111801	T. Aaltonen *et al.*	(CDF Collab.)
ARTUSO	12	PR D85 122002	M. Artuso *et al.*	(CLEO Collab.)
ASNER	12	PR D86 112001	D.M. Asner	(CLEO Collab.)
INSLER	12	PR D85 092016	J. Insler *et al.*	(CLEO Collab.)
Also		PR D94 099905 (errat.)	J. Insler *et al.*	(CLEO Collab.)
LEES	12L	PR D85 091107	J.P. Lees *et al.*	(BABAR Collab.)
LEES	12Q	PR D86 032001	J.P. Lees *et al.*	(BABAR Collab.)
KO	11	PRL 106 211801	B.R. Ko *et al.*	(BELLE Collab.)
LOWREY	11	PR D84 092005	N. Lowrey *et al.*	(CLEO Collab.)
WILLIAMS	11	PR D84 054015	M. Williams	(LOIC)
AALTONEN	10X	PR D82 091105	T. Aaltonen *et al.*	(CDF Collab.)
ANASHIN	10A	PL B686 84	V.V. Anashin *et al.*	(VEPP-4M KEDR Collab.)
ASNER	10	PR D81 052007	D.M. Asner *et al.*	(CLEO Collab.)
BHATTACHAR...	10A	PR D81 096008	B. Bhattacharya, C.-W. Chiang, J.L. Rosner	(CHIC+)
DEL-AMO-SA...	10	PR D81 111103	P. del Amo Sanchez *et al.*	(BABAR Collab.)
DEL-AMO-SA...	10D	PRL 105 081803	P. del Amo Sanchez *et al.*	(BABAR Collab.)
MENDEZ	10	PR D81 052013	H. Mendez *et al.*	(CLEO Collab.)
PETRIC	10	PR D81 091102	M. Petric *et al.*	(BELLE Collab.)
AUBERT	09AI	PR D80 071103	B. Aubert *et al.*	(BABAR Collab.)
AUBERT	09AN	PRL 103 211801	B. Aubert *et al.*	(BABAR Collab.)
BEDIAGA	09	PR D80 096006	I. Bediaga *et al.*	(CBPF, NDAM)
BESSON	09	PR D80 032005	D. Besson *et al.*	(CLEO Collab.)
Also		PR D79 052010	J.Y. Ge *et al.*	(CLEO Collab.)
LOWREY	09	PR D80 031105	N. Lowrey *et al.*	(CLEO Collab.)
RUBIN	09	PR D79 097101	P. Rubin *et al.*	(CLEO Collab.)
ZUPANC	09	PR D80 052006	A. Zupanc *et al.*	(BELLE Collab.)
AALTONEN	08E	PRL 100 121802	T. Aaltonen *et al.*	(CDF Collab.)
ABLIKIM	08L	PL B665 16	M. Ablikim *et al.*	(BES Collab.)
ARINSTEIN	08	PL B662 102	K. Arinstein *et al.*	(BELLE Collab.)
ARTUSO	08	PR D77 092003	M. Artuso *et al.*	(CLEO Collab.)
ASNER	08	PR D78 012001	D.M. Asner *et al.*	(CLEO Collab.)
AUBERT	08AL	PR D78 034023	B. Aubert *et al.*	(BABAR Collab.)
AUBERT	08AO	PR D78 051102	B. Aubert *et al.*	(BABAR Collab.)
AUBERT	08AZ	PR D78 071101	B. Aubert *et al.*	(BABAR Collab.)
AUBERT	08L	PRL 100 051802	B. Aubert *et al.*	(BABAR Collab.)
AUBERT	08M	PRL 100 061803	B. Aubert *et al.*	(BABAR Collab.)
AUBERT	08U	PR D78 011105	B. Aubert *et al.*	(BABAR Collab.)
BITENC	08	PR D77 112003	U. Bitenc *et al.*	(BELLE Collab.)
BONVICINI	08	PR D77 091106	G. Bonvicini *et al.*	(CLEO Collab.)
DOBBS	08	PR D77 112005	S. Dobbs *et al.*	(CLEO Collab.)
Also		PRL 100 251802	D. Cronin-Hennessy *et al.*	(CLEO Collab.)
GASPERO	08	PR D78 014015	M. Gaspero *et al.*	(ROMA, CINN, TELA)
HE	08	PRL 100 091801	Q. He *et al.*	(CLEO Collab.)
PDG	08	PL B667 1	C. Amsler *et al.*	(PDG Collab.)
STARIC	08	PL B670 190	M. Staric *et al.*	(BELLE Collab.)
ABLIKIM	07G	PL B658 1	M. Ablikim *et al.*	(BES Collab.)
ARTUSO	07A	PRL 99 191801	M. Artuso *et al.*	(CLEO Collab.)
AUBERT	07AB	PR D76 014018	B. Aubert *et al.*	(BABAR Collab.)
AUBERT	07BG	PR D76 052005	B. Aubert *et al.*	(BABAR Collab.)
AUBERT	07BJ	PRL 99 251801	B. Aubert *et al.*	(BABAR Collab.)
AUBERT	07T	PR D76 011102	B. Aubert *et al.*	(BABAR Collab.)
AUBERT	07W	PRL 98 211802	B. Aubert *et al.*	(BABAR Collab.)
CAWLFIELD	07	PRL 98 092002	C. Cawlfield *et al.*	(CLEO Collab.)
DOBBS	07	PR D76 112001	S. Dobbs *et al.*	(CLEO Collab.)
LINK	07A	PR D75 052003	J.M. Link *et al.*	(FNAL FOCUS Collab.)
STARIC	07	PRL 98 211803	M. Staric *et al.*	(BELLE Collab.)
ZHANG	07B	PRL 99 131803	L.M. Zhang *et al.*	(BELLE Collab.)
ABLIKIM	06O	EPJ C47 31	M. Ablikim *et al.*	(BES Collab.)
ABLIKIM	06U	PL B643 246	M. Ablikim *et al.*	(BES Collab.)
ABULENCIA	06X	PR D74 031109	A. Abulencia *et al.*	(CDF Collab.)
ADAM	06A	PRL 97 251801	N.E. Adam *et al.*	(CLEO Collab.)
AUBERT,B	06N	PRL 97 221803	B. Aubert *et al.*	(BABAR Collab.)
AUBERT,B	06X	PR D74 091102	B. Aubert *et al.*	(BABAR Collab.)
CAWLFIELD	06A	PR D74 031108	C. Cawlfield *et al.*	(CLEO Collab.)
HUANG	06B	PR D74 112005	G.S. Huang *et al.*	(CLEO Collab.)
PDG	06	JP G33 1	W.-M. Yao *et al.*	(PDG Collab.)
RUBIN	06	PRL 96 081802	P. Rubin *et al.*	(CLEO Collab.)
WIDHALM	06	PRL 97 061804	L. Widhalm *et al.*	(BELLE Collab.)
ZHANG	06	PRL 96 151801	L.M. Zhang *et al.*	(BELLE Collab.)
ABLIKIM	05F	PL B622 6	M. Ablikim *et al.*	(BES Collab.)
ABLIKIM	05P	PL B625 196	M. Ablikim *et al.*	(BES Collab.)
ACOSTA	05C	PRL 94 122001	D. Acosta *et al.*	(FNAL CDF Collab.)
ASNER	05	PR D72 012001	D.M. Asner *et al.*	(CLEO Collab.)
AUBERT,B	05J	PR D72 052008	B. Aubert *et al.*	(BABAR Collab.)
BITENC	05	PR D72 071101	U. Bitenc *et al.*	(BELLE Collab.)
CAWLFIELD	05	PR D71 077101	C. Cawlfield *et al.*	(CLEO Collab.)
COAN	05	PRL 95 181802	T.E. Coan *et al.*	(CLEO Collab.)
CRONIN-HEN...	05	PR D72 031102	D. Cronin-Hennessy *et al.*	(CLEO Collab.)
HE	05	PRL 95 121801	Q. He *et al.*	(CLEO Collab.)
Also		PRL 96 199903 (errat.)	Q. He *et al.*	(CLEO Collab.)
HUANG	05	PRL 94 011802	G.S. Huang *et al.*	(CLEO Collab.)
KAYIS-TOPAK...	05	PL B626 24	A. Kayis-Topaksu *et al.*	(CERN CHORUS Collab.)
LI	05A	PRL 94 071801	J. Li *et al.*	(BELLE Collab.)
LINK	05	PL B607 51	J.M. Link *et al.*	(FNAL FOCUS Collab.)
LINK	05A	PL B607 59	J.M. Link *et al.*	(FNAL FOCUS Collab.)
LINK	05B	PL B607 67	J.M. Link *et al.*	(FNAL FOCUS Collab.)
LINK	05E	PL B622 239	J.M. Link *et al.*	(FNAL FOCUS Collab.)
LINK	05G	PL B610 225	J.M. Link *et al.*	(FNAL FOCUS Collab.)
LINK	05H	PL B618 23	J.M. Link *et al.*	(FNAL FOCUS Collab.)
ONENGUT	05	PL B613 105	G. Onengut *et al.*	(CERN CHORUS Collab.)
TIAN	05	PRL 95 231801	X.C. Tian *et al.*	(BELLE Collab.)
ABLIKIM	04C	PL B597 39	M. Ablikim *et al.*	(BEPC BES Collab.)
ABT	04	PL B596 173	I. Abt *et al.*	(HERA B Collab.)
ASNER	04A	PR D70 091101	D.M. Asner *et al.*	(CLEO Collab.)
AUBERT	04Q	PR D69 051101	B. Aubert *et al.*	(BABAR Collab.)
AUBERT,B	04Q	PR D70 091102	B. Aubert *et al.*	(BABAR Collab.)
AUBERT,B	04Y	PRL 93 191801	B. Aubert *et al.*	(BABAR Collab.)
LINK	04B	PL B586 21	J.M. Link *et al.*	(FNAL FOCUS Collab.)
LINK	04D	PL B586 191	J.M. Link *et al.*	(FNAL FOCUS Collab.)
RUBIN	04	PRL 93 111801	P. Rubin *et al.*	(CLEO Collab.)
TAJIMA	04	PRL 92 101803	O. Tajima *et al.*	(BELLE Collab.)
ACOSTA	03F	PR D68 091101	D. Acosta *et al.*	(CDF Collab.)
AUBERT	03P	PRL 91 121801	B. Aubert *et al.*	(BABAR Collab.)
AUBERT	03Z	PRL 91 171801	B. Aubert *et al.*	(BABAR Collab.)
COAN	03	PRL 90 101801	T.E. Coan *et al.*	(CLEO Collab.)
LINK	03	PL B555 167	J.M. Link *et al.*	(FNAL FOCUS Collab.)
LINK	03B	PL B556 7	J.M. Link *et al.*	(FNAL FOCUS Collab.)
LINK	03G	PL B575 190	J.M. Link *et al.*	(FNAL FOCUS Collab.)
ABE	02I	PRL 88 162001	K. Abe *et al.*	(KEK BELLE Collab.)
CSORNA	02	PR D65 092001	S.E. Csorna *et al.*	(CLEO Collab.)
LINK	02F	PL B537 192	J.M. Link *et al.*	(FNAL FOCUS Collab.)
MURAMATSU	02	PRL 89 251802	H. Muramatsu *et al.*	(CLEO Collab.)
Also		PRL 90 059901 (errat.)	H. Muramatsu *et al.*	(CLEO Collab.)
AITALA	01C	PRL 86 3969	E.M. Aitala *et al.*	(FNAL E791 Collab.)
AITALA	01D	PR D64 112003	E.M. Aitala *et al.*	(FNAL E791 Collab.)
BONVICINI	01	PR D63 071101	G. Bonvicini *et al.*	(CLEO Collab.)
BRANDENB...	01	PRL 87 071802	G. Brandenburg *et al.*	(CLEO Collab.)
DYTMAN	01	PR D64 111101	S.A. Dytman *et al.*	(CLEO Collab.)
KOPP	01	PR D63 092001	S. Kopp *et al.*	(CLEO Collab.)
KUSHNIR...	01	PRL 86 5243	A. Kushnirenko *et al.*	(FNAL SELEX Collab.)
LINK	01	PRL 86 2955	J.M. Link *et al.*	(FNAL FOCUS Collab.)
BAI	00C	PR D62 052001	J.Z. Bai *et al.*	(BEPC BES Collab.)
GODANG	00	PRL 84 5038	R. Godang *et al.*	(CLEO Collab.)
JUN	00	PRL 84 1857	S.Y. Jun *et al.*	(FNAL SELEX Collab.)
LINK	00	PL B485 62	J.M. Link *et al.*	(FNAL FOCUS Collab.)
LINK	00B	PL B491 232	J.M. Link *et al.*	(FNAL FOCUS Collab.)
Also		PL B495 443 (errat.)	J.M. Link *et al.*	(FNAL FOCUS Collab.)
PRIPSTEIN	00	PR D61 032005	D. Pripstein *et al.*	(FNAL E789 Collab.)
AITALA	99E	PRL 83 32	E.M. Aitala *et al.*	(FNAL E791 Collab.)
AITALA	99G	PL B462 401	E.M. Aitala *et al.*	(FNAL E791 Collab.)
BONVICINI	99	PRL 82 4586	G. Bonvicini *et al.*	(CLEO Collab.)
AITALA	98	PR D57 13	E.M. Aitala *et al.*	(FNAL E791 Collab.)
AITALA	98C	PL B421 405	E.M. Aitala *et al.*	(FNAL E791 Collab.)
AITALA	98D	PL B423 185	E.M. Aitala *et al.*	(FNAL E791 Collab.)
ARTUSO	98	PRL 80 3193	M. Artuso *et al.*	(CLEO Collab.)
ASNER	98	PR D58 092001	D.M. Asner *et al.*	(CLEO Collab.)
BARATE	98W	PL B436 211	R. Barate *et al.*	(ALEPH Collab.)
COAN	98	PRL 80 1150	T.E. Coan *et al.*	(CLEO Collab.)
PDG	98	EPJ C3 1	C. Caso *et al.*	(PDG Collab.)
ADAMOVICH	97	PL B408 469	M.I. Adamovich *et al.*	(CERN BEATRICE Collab.)
BARATE	97C	PL B403 367	R. Barate *et al.*	(ALEPH Collab.)
AITALA	96C	PRL 77 2384	E.M. Aitala *et al.*	(FNAL E791 Collab.)
ALBRECHT	96C	PL B374 249	H. Albrecht *et al.*	(ARGUS Collab.)
ALEXOPOU...	96	PRL 77 2380	T. Alexopoulos *et al.*	(FNAL E771 Collab.)
ASNER	96B	PR D54 4211	D.M. Asner *et al.*	(CLEO Collab.)
BARISH	96	PL B373 334	B.C. Barish *et al.*	(CLEO Collab.)
FRABETTI	96B	PL B382 312	P.L. Frabetti *et al.*	(FNAL E687 Collab.)
FREYBERGER	96	PRL 76 3065	A. Freyberger *et al.*	(CLEO Collab.)
Also		PRL 77 2147 (erratum)	A. Freyberger *et al.*	(CLEO Collab.)
KUBOTA	96B	PR D54 2994	Y. Kubota *et al.*	(CLEO Collab.)
ADAMOVICH	95	PL B353 563	M.I. Adamovich *et al.*	(CERN BEATRICE Collab.)
BARTELT	95	PR D52 4860	J.E. Bartelt *et al.*	(CLEO Collab.)
BUTLER	95	PR D52 2656	F. Butler *et al.*	(CLEO Collab.)
FRABETTI	95C	PL B354 486	P.L. Frabetti *et al.*	(FNAL E687 Collab.)
FRABETTI	95G	PL B364 127	P.L. Frabetti *et al.*	(FNAL E687 Collab.)
KODAMA	95	PL B345 85	K. Kodama *et al.*	(FNAL E653 Collab.)
ALBRECHT	94	PL B324 249	H. Albrecht *et al.*	(ARGUS Collab.)
ALBRECHT	94F	PL B340 125	H. Albrecht *et al.*	(ARGUS Collab.)
ALBRECHT	94I	ZPHY C64 375	H. Albrecht *et al.*	(ARGUS Collab.)
FRABETTI	94C	PL B321 295	P.L. Frabetti *et al.*	(FNAL E687 Collab.)
FRABETTI	94D	PL B323 459	P.L. Frabetti *et al.*	(FNAL E687 Collab.)
FRABETTI	94G	PL B331 217	P.L. Frabetti *et al.*	(FNAL E687 Collab.)
FRABETTI	94J	PL B340 254	P.L. Frabetti *et al.*	(FNAL E687 Collab.)
KODAMA	94	PL B336 605	K. Kodama *et al.*	(FNAL E653 Collab.)
MISHRA	94	PR D50 9	C.S. Mishra *et al.*	(FNAL E789 Collab.)
AKERIB	93	PRL 71 3070	D.S. Akerib *et al.*	(CLEO Collab.)
ALBRECHT	93D	PL B308 435	H. Albrecht *et al.*	(ARGUS Collab.)
ANJOS	93	PR D48 56	J.C. Anjos *et al.*	(FNAL E691 Collab.)
BEAN	93C	PL B317 647	A. Bean *et al.*	(CLEO Collab.)
FRABETTI	93I	PL B315 203	P.L. Frabetti *et al.*	(FNAL E687 Collab.)
KODAMA	93B	PL B313 260	K. Kodama *et al.*	(FNAL E653 Collab.)
PROCARIO	93B	PR D48 4007	M. Procario *et al.*	(CLEO Collab.)
SELEN	93	PRL 71 1973	M.A. Selen *et al.*	(CLEO Collab.)
ADAMOVICH	92	PL B280 163	M.I. Adamovich *et al.*	(CERN WA82 Collab.)
ALBRECHT	92P	ZPHY C56 7	H. Albrecht *et al.*	(ARGUS Collab.)
ANJOS	92C	PR D46 1941	J.C. Anjos *et al.*	(FNAL E691 Collab.)
BARLAG	92C	ZPHY C55 383	S. Barlag *et al.*	(ACCMOR Collab.)
Also		ZPHY C48 29	S. Barlag *et al.*	(ACCMOR Collab.)
COFFMAN	92B	PR D45 2196	D.M. Coffman *et al.*	(Mark III Collab.)
Also		PRL 64 2615	J. Adler *et al.*	(Mark III Collab.)
FRABETTI	92	PL B281 167	P.L. Frabetti *et al.*	(FNAL E687 Collab.)
FRABETTI	92B	PL B286 195	P.L. Frabetti *et al.*	(FNAL E687 Collab.)
ALVAREZ	91B	ZPHY C50 11	M.P. Alvarez *et al.*	(CERN NA14/2 Collab.)
AMMAR	91	PR D44 3383	R. Ammar *et al.*	(CLEO Collab.)
ANJOS	91	PR D43 635	J.C. Anjos *et al.*	(FNAL-TPS Collab.)
ANJOS	91D	PR D44 3371	J.C. Anjos *et al.*	(FNAL-TPS Collab.)
BAI	91	PRL 66 1011	Z. Bai *et al.*	(Mark III Collab.)
COFFMAN	91	PL B263 135	D.M. Coffman *et al.*	(Mark III Collab.)
CRAWFORD	91B	PR D44 3394	G. Crawford *et al.*	(CLEO Collab.)
DECAMP	91J	PL B266 218	D. Decamp *et al.*	(ALEPH Collab.)
FRABETTI	91	PL B263 584	P.L. Frabetti *et al.*	(FNAL E687 Collab.)
KINOSHITA	91	PR D43 2836	K. Kinoshita *et al.*	(CLEO Collab.)
KODAMA	91	PRL 66 1819	K. Kodama *et al.*	(FNAL E653 Collab.)
ALBRECHT	90C	ZPHY C46 9	H. Albrecht *et al.*	(ARGUS Collab.)
ALEXANDER	90	PRL 65 1184	J. Alexander *et al.*	(CLEO Collab.)
ALVAREZ	90	ZPHY C47 539	M.P. Alvarez *et al.*	(CERN NA14/2 Collab.)
ANJOS	90D	PR D42 2414	J.C. Anjos *et al.*	(FNAL E691 Collab.)
BARLAG	90C	ZPHY C46 563	S. Barlag *et al.*	(ACCMOR Collab.)
ADLER	89	PRL 62 1821	J. Adler *et al.*	(Mark III Collab.)
ADLER	89C	PR D40 906	J. Adler *et al.*	(Mark III Collab.)

Downloaded from https://academic.oup.com/ptep/article/2022/8/083C01/6651666 by KIT Library user on 27 September 2022

ALBRECHT	89D	ZPHY C43 181	H. Albrecht *et al.*	(ARGUS Collab.)
ANJOS	89F	PRL 62 1587	J.C. Anjos *et al.*	(FNAL E691 Collab.)
ABACHI	88	PL B205 411	S. Abachi *et al.*	(HRS Collab.)
ADLER	88	PR D37 2023	J. Adler *et al.*	(Mark III Collab.)
ADLER	88C	PRL 60 89	J. Adler *et al.*	(Mark III Collab.)
ALBRECHT	88G	PL B209 380	H. Albrecht *et al.*	(ARGUS Collab.)
ALBRECHT	88I	PL B210 267	H. Albrecht *et al.*	(ARGUS Collab.)
ANJOS	88C	PRL 60 1239	J.C. Anjos *et al.*	(FNAL E691 Collab.)
BORTOLETTO	88	PR D37 1719	D. Bortoletto *et al.*	(CLEO Collab.)
Also		PR D39 1471 (erratum)	D. Bortoletto *et al.*	(CLEO Collab.)
HAAS	88	PRL 60 1614	P. Haas *et al.*	(CLEO Collab.)
RAAB	88	PR D37 2391	J.R. Raab *et al.*	(FNAL E691 Collab.)
ADLER	87	PL B196 107	J. Adler *et al.*	(Mark III Collab.)
AGUILAR-...	87E	ZPHY C36 551	M. Aguilar-Benitez *et al.*	(LEBC-EHS Collab.)
Also		ZPHY C40 321	M. Aguilar-Benitez *et al.*	(LEBC-EHS Collab.)
AGUILAR-...	87F	ZPHY C36 559	M. Aguilar-Benitez *et al.*	(LEBC-EHS Collab.)
Also		ZPHY C38 520 (erratum)	M. Aguilar-Benitez *et al.*	(LEBC-EHS Collab.)
BARLAG	87B	ZPHY C37 17	S. Barlag *et al.*	(ACCMOR Collab.)
BECKER	87C	PL B193 147	J.J. Becker *et al.*	(Mark III Collab.)
Also		PL B198 590 (erratum)	J.J. Becker *et al.*	(Mark III Collab.)
PALKA	87	PL B189 238	H. Palka *et al.*	(ACCMOR Collab.)
RILES	87	PR D35 2914	K. Riles *et al.*	(Mark II Collab.)
BAILEY	86	ZPHY C30 51	R. Bailey *et al.*	(ACCMOR Collab.)
BEBEK	86	PRL 56 1893	C. Bebek *et al.*	(CLEO Collab.)
LOUIS	86	PRL 56 1027	W.C. Louis *et al.*	(PRIN, CHIC, ISU)
ALBRECHT	85B	PL 158B 525	H. Albrecht *et al.*	(ARGUS Collab.)
ALBRECHT	85F	PL 150B 235	H. Albrecht *et al.*	(ARGUS Collab.)
AUBERT	85	PL 155B 461	J.J. Aubert *et al.*	(EMC Collab.)
BALTRUSAIT...	85E	PRL 55 150	R.M. Baltrusaitis *et al.*	(Mark III Collab.)
BENVENUTI	85	PL 158B 531	A.C. Benvenuti *et al.*	(BCDMS Collab.)
SUMMERS	84	PRL 52 410	D.J. Summers *et al.*	(UCSB, CARL, COLO+)
BAILEY	83B	PL 132B 237	R. Bailey *et al.*	(ACCMOR Collab.)
BODEK	82	PL 113B 82	A. Bodek *et al.*	(ROCH, CIT, CHIC, FNAL+)
SCHINDLER	81	PR D24 78	R.H. Schindler *et al.*	(Mark II Collab.)
AVERY	80	PRL 44 1309	P. Avery *et al.*	(ILL, FNAL, COLU)
ABRAMS	79D	PRL 43 481	G.S. Abrams *et al.*	(Mark II Collab.)
VUILLEMIN	78	PRL 41 1149	V. Vuillemin *et al.*	(LGW Collab.)
PERUZZI	77	PRL 39 1301	I. Peruzzi *et al.*	(LGW Collab.)
PICCOLO	77	PL 70B 260	M. Piccolo *et al.*	(Mark I Collab.)
MOSTELLER	48	Am.Stat.3 No.5 30	R.A. Fisher, F. Mosteller	

OTHER RELATED PAPERS

RICHMAN	95	RMP 67 893	J.D. Richman, P.R. Burchat	(UCSB, STAN)
ROSNER	95	CNPP 21 369	J. Rosner	(CHIC)

$D^*(2007)^0$

$I(J^P) = \frac{1}{2}(1^-)$
I, J, P need confirmation.

J consistent with 1, value 0 ruled out (NGUYEN 77).

$D^*(2007)^0$ MASS

The fit includes $D^\pm$, D^0, $D_s^\pm$, $D^{*\pm}$, D^{*0}, $D_s^{*\pm}$, $D_1(2420)^0$, $D_2^*(2460)^0$, and $D_{s1}(2536)^\pm$ mass and mass difference measurements.

VALUE (MeV)	DOCUMENT ID	TECN	COMMENT
2006.85±0.05 OUR FIT Error includes scale factor of 1.1.			
• • • We do not use the following data for averages, fits, limits, etc. • • •			
2006 ±1.5	[1] GOLDHABER 77	MRK1	e^+e^-

[1] From simultaneous fit to $D^*(2010)^+$, $D^*(2007)^0$, D^+, and D^0.

$m_{D^*(2007)^0} - m_{D^0}$

The fit includes $D^\pm$, D^0, $D_s^\pm$, $D^{*\pm}$, D^{*0}, $D_s^{*\pm}$, $D_1(2420)^0$, $D_2^*(2460)^0$, and $D_{s1}(2536)^\pm$ mass and mass difference measurements.

VALUE (MeV)	EVTS	DOCUMENT ID	TECN	COMMENT
142.014±0.030 OUR FIT Error includes scale factor of 1.5.				
142.016±0.030 OUR AVERAGE Error includes scale factor of 1.5.				
142.007±0.015±0.014	10k	[2] TOMARADZE 15	CLEO	$e^+e^- \to$ hadrons
142.2 ±0.3 ±0.2	145	ALBRECHT 95F	ARG	$e^+e^- \to$ hadrons
142.12 ±0.05 ±0.05	1176	BORTOLETTO 92B	CLE2	$e^+e^- \to$ hadrons
• • • We do not use the following data for averages, fits, limits, etc. • • •				
142.2 ±2.0		SADROZINSKI 80	CBAL	$D^{*0} \to D^0\pi^0$
142.7 ±1.7		[3] GOLDHABER 77	MRK1	e^+e^-

[2] Obtained by analyzing CLEO-c data but not authored by the CLEO Collaboration . This value comes from the average of the results for two decay modes, $D^0 \to K^-\pi^+$ and $D^0 \to K^-\pi^+\pi^-\pi^+$.
[3] From simultaneous fit to $D^*(2010)^+$, $D^*(2007)^0$, D^+, and D^0.

$D^*(2007)^0$ WIDTH

VALUE (MeV)	CL%	DOCUMENT ID	TECN	COMMENT
<2.1	90	[4] ABACHI 88B	HRS	$D^{*0} \to D^+\pi^-$

[4] Assuming $m_{D^{*0}} = 2007.2 \pm 2.1$ MeV/c^2.

$D^*(2007)^0$ DECAY MODES

$\overline{D}^*(2007)^0$ modes are charge conjugates of modes below.

	Mode	Fraction (Γ_i/Γ)
Γ_1	$D^0\pi^0$	(64.7 ±0.9) %
Γ_2	$D^0\gamma$	(35.3 ±0.9) %
Γ_3	$D^0e^+e^-$	(3.91±0.33) × 10^{-3}

CONSTRAINED FIT INFORMATION

An overall fit to 2 branching ratios uses 5 measurements and one constraint to determine 2 parameters. The overall fit has a χ^2 = 2.5 for 4 degrees of freedom.

The following *off-diagonal* array elements are the correlation coefficients $\langle \delta x_i \delta x_j \rangle / (\delta x_i \cdot \delta x_j)$, in percent, from the fit to the branching fractions, $x_i \equiv \Gamma_i/\Gamma_{total}$. The fit constrains the x_i whose labels appear in this array to sum to one.

	x_1
x_2	−100

$D^*(2007)^0$ BRANCHING RATIOS

$\Gamma(D^0\pi^0)/\Gamma(D^0\gamma)$ — Γ_1/Γ_2

VALUE	EVTS	DOCUMENT ID		TECN	COMMENT
1.83±0.07 OUR FIT Error includes scale factor of 1.1.					
1.85±0.07 OUR AVERAGE					
1.90±0.07±0.05	4.9k	ABLIKIM	15B	BES3	10.6 $e^+e^- \to$ hadrons
1.74±0.02±0.13		AUBERT,BE	05G	BABR	10.6 $e^+e^- \to$ hadrons

$\Gamma(D^0e^+e^-)/\Gamma(D^0\gamma)$ — Γ_3/Γ_2

VALUE (units 10^{-3})	EVTS	DOCUMENT ID		TECN	COMMENT
11.08±0.76±0.49	421	ABLIKIM	21BD	BES3	4.178 GeV e^+e^-

$\Gamma(D^0\pi^0)/\Gamma_{total}$ — Γ_1/Γ

VALUE	EVTS	DOCUMENT ID		TECN	COMMENT
0.647±0.009 OUR FIT					
• • • We do not use the following data for averages, fits, limits, etc. • • •					
0.655±0.008±0.005	3.2k	[5] ABLIKIM	15B	BES3	$e^+e^- \to$ hadrons
0.635±0.003±0.017	69k	[5] AUBERT,BE	05G	BABR	10.6 $e^+e^- \to$ hadrons
0.596±0.035±0.028	858	[6] ALBRECHT	95F	ARG	$e^+e^- \to$ hadrons
0.636±0.023±0.033	1097	[6] BUTLER	92	CLE2	$e^+e^- \to$ hadrons

$\Gamma(D^0\gamma)/\Gamma_{total}$ — Γ_2/Γ

VALUE	EVTS	DOCUMENT ID		TECN	COMMENT
0.353±0.009 OUR FIT					
0.381±0.029 OUR AVERAGE					
0.404±0.035±0.028	456	[6] ALBRECHT	95F	ARG	$e^+e^- \to$ hadrons
0.364±0.023±0.033	621	[6] BUTLER	92	CLE2	$e^+e^- \to$ hadrons
0.37 ±0.08 ±0.08		ADLER	88D	MRK3	e^+e^-
• • • We do not use the following data for averages, fits, limits, etc. • • •					
0.345±0.008±0.005	1.8k	[5] ABLIKIM	15B	BES3	$e^+e^- \to$ hadrons
0.365±0.003±0.017	68k	[5] AUBERT,BE	05G	BABR	10.6 $e^+e^- \to$ hadrons
0.47 ±0.23		LOW	87	HRS	29 GeV e^+e^-
0.53 ±0.13		BARTEL	85G	JADE	e^+e^-, hadrons
0.47 ±0.12		COLES	82	MRK2	e^+e^-
0.45 ±0.15		GOLDHABER	77	MRK1	e^+e^-

[5] Derived from the ratio $\Gamma(D^0\pi^0)$ / $\Gamma(D^0\gamma)$ assuming that the branching fractions of $D^{*0} \to D^0\pi^0$ and $D^{*0} \to D^0\gamma$ decays sum to 100%
[6] The BUTLER 92 and ALBRECHT 95F branching ratios are not independent, they have been constrained by the authors to sum to 100%.

$D^*(2007)^0$ REFERENCES

ABLIKIM	21BD	PR D104 112012	M. Ablikim *et al.*	(BESIII Collab.)
ABLIKIM	15B	PR D91 031101	M. Ablikim *et al.*	(BESIII Collab.)
TOMARADZE	15	PR D91 011102	A. Tomaradze *et al.*	(NWES)
AUBERT,BE	05G	PR D72 091101	B. Aubert *et al.*	(BABAR Collab.)
ALBRECHT	95F	ZPHY C66 63	H. Albrecht *et al.*	(ARGUS Collab.)
BORTOLETTO	92B	PRL 69 2046	D. Bortoletto *et al.*	(CLEO Collab.)
BUTLER	92	PRL 69 2041	F. Butler *et al.*	(CLEO Collab.)
ABACHI	88B	PL B212 533	S. Abachi *et al.*	(ANL, IND, MICH, PURD+)
ADLER	88D	PL B208 152	J. Adler *et al.*	(Mark III Collab.)
LOW	87	PL B183 232	E.H. Low *et al.*	(HRS Collab.)
BARTEL	85G	PL 161B 197	W. Bartel *et al.*	(JADE Collab.)
COLES	82	PR D26 2190	M.W. Coles *et al.*	(LBL, SLAC)
SADROZINSKI	80	Madison Conf. 681	H.F.W. Sadrozinski *et al.*	(PRIN, CIT+)
GOLDHABER	77	PL 69B 503	G. Goldhaber *et al.*	(Mark I Collab.)
NGUYEN	77	PRL 39 262	H.K. Nguyen *et al.*	(LBL, SLAC) J

$D^*(2010)^\pm$

$I(J^P) = \frac{1}{2}(1^-)$
I, J, P need confirmation.

$D^*(2010)^\pm$ MASS

The fit includes $D^\pm$, D^0, $D_s^\pm$, $D^{*\pm}$, D^{*0}, $D_s^{*\pm}$, $D_1(2420)^0$, $D_2^*(2460)^0$, and $D_{s1}(2536)^\pm$ mass and mass difference measurements.

VALUE (MeV)	DOCUMENT ID	TECN	CHG	COMMENT
2010.26±0.05 OUR FIT				

Downloaded from https://academic.oup.com/ptep/article/2022/8/083C01/6651666 by KIT Library user on 27 September 2022

• • • We do not use the following data for averages, fits, limits, etc. • • •

2008	±3	[1] GOLDHABER	77	MRK1	±	e^+e^-
2008.6	±1.0	[2] PERUZZI	77	LGW	±	e^+e^-

[1] From simultaneous fit to $D^*(2010)^+$, $D^*(2007)^0$, D^+, and D^0; not independent of FELDMAN 77B mass difference below.
[2] PERUZZI 77 mass not independent of FELDMAN 77B mass difference below and PERUZZI 77 D^0 mass value.

$m_{D^*(2010)^+} - m_{D^+}$

The fit includes $D^\pm$, D^0, $D_s^\pm$, $D^{*\pm}$, D^{*0}, $D_s^{*\pm}$, $D_1(2420)^0$, $D_2^*(2460)^0$, and $D_{s1}(2536)^\pm$ mass and mass difference measurements.

VALUE (MeV)	EVTS	DOCUMENT ID		TECN	COMMENT
140.603 ±0.015 OUR FIT					
140.602 ±0.014 OUR AVERAGE					
140.6010±0.0068±0.0129	151k	LEES	17F	BABR	$e^+e^- \to$ hadrons
140.64 ±0.08 ±0.06	620	BORTOLETTO	92B	CLE2	$e^+e^- \to$ hadrons

$m_{D^*(2010)^+} - m_{D^0}$

The fit includes $D^\pm$, D^0, $D_s^\pm$, $D^{*\pm}$, D^{*0}, $D_s^{*\pm}$, $D_1(2420)^0$, $D_2^*(2460)^0$, and $D_{s1}(2536)^\pm$ mass and mass difference measurements.

VALUE (MeV)	EVTS	DOCUMENT ID		TECN	COMMENT
145.4258±0.0017 OUR FIT					
145.4258±0.0020 OUR AVERAGE		Error includes scale factor of 1.2.			
145.4259±0.0004±0.0017	312.8k	LEES	13X	BABR	$D^{*\pm} \to D^0\pi^\pm \to (K\pi, K3\pi)\pi^\pm$
145.412 ±0.002 ±0.012		ANASTASSOV	02	CLE2	$D^{*\pm} \to D^0\pi^\pm \to (K\pi)\pi^\pm$
145.54 ±0.08	611	[3] ADINOLFI	99	BEAT	$D^{*\pm} \to D^0\pi^\pm$
145.45 ±0.02		[3] BREITWEG	99	ZEUS	$D^{*\pm} \to D^0\pi^\pm \to (K\pi)\pi^\pm$
145.42 ±0.05		[3] BREITWEG	99	ZEUS	$D^{*\pm} \to D^0\pi^\pm \to (K^-3\pi)\pi^\pm$
145.5 ±0.15	103	[4] ADLOFF	97B	H1	$D^{*\pm} \to D^0\pi^\pm$
145.44 ±0.08	152	[4] BREITWEG	97	ZEUS	$D^{*\pm} \to D^0\pi^\pm$, $D^0 \to K^-3\pi$
145.42 ±0.11	199	[4] BREITWEG	97	ZEUS	$D^{*\pm} \to D^0\pi^\pm$, $D^0 \to K^-\pi^+$
145.4 ±0.2	48	[4] DERRICK	95	ZEUS	$D^{*\pm} \to D^0\pi^\pm$
145.39 ±0.06 ±0.03		BARLAG	92B	ACCM	π^- 230 GeV
145.5 ±0.2	115	[4] ALEXANDER	91B	OPAL	$D^{*\pm} \to D^0\pi^\pm$
145.30 ±0.06		[4] DECAMP	91J	ALEP	$D^{*\pm} \to D^0\pi^\pm$
145.40 ±0.05 ±0.10		ABACHI	88B	HRS	$D^{*\pm} \to D^0\pi^\pm$
145.46 ±0.07 ±0.03		ALBRECHT	85F	ARG	$D^{*\pm} \to D^0\pi^+$
145.5 ±0.3	28	BAILEY	83	SPEC	$D^{*\pm} \to D^0\pi^\pm$
145.5 ±0.3	60	FITCH	81	SPEC	π^-A
145.3 ±0.5	30	FELDMAN	77B	MRK1	$D^{*+} \to D^0\pi^+$
• • • We do not use the following data for averages, fits, limits, etc. • • •					
145.4256±0.0006±0.0017	138.5k	LEES	13X	BABR	$D^{*\pm} \to D^0\pi^\pm \to (K^-\pi^+)\pi^\pm$
145.4266±0.0005±0.0019	174.3k	LEES	13X	BABR	$D^{*\pm} \to D^0\pi^\pm \to (K^-2\pi^+\pi^-)\pi^\pm$
145.44 ±0.09	122	[4] BREITWEG	97B	ZEUS	$D^{*\pm} \to D^0\pi^\pm$, $D^0 \to K^-\pi^+$
145.8 ±1.5	16	AHLEN	83	HRS	$D^{*+} \to D^0\pi^+$
145.1 ±1.8	12	BAILEY	83	SPEC	$D^{*\pm} \to D^0\pi^\pm$
145.1 ±0.5	14	BAILEY	83	SPEC	$D^{*\pm} \to D^0\pi^\pm$
145.5 ±0.5	14	YELTON	82	MRK2	29 $e^+e^- \to K^-\pi^+$
~ 145.5		AVERY	80	SPEC	γA
145.2 ±0.6	2	BLIETSCHAU	79	BEBC	νp

[3] Statistical errors only.
[4] Systematic error not evaluated.

$m_{D^*(2010)^+} - m_{D^*(2007)^0}$

VALUE (MeV)	DOCUMENT ID		TECN	COMMENT
• • • We do not use the following data for averages, fits, limits, etc. • • •				
2.6±1.8	[5] PERUZZI	77	LGW	e^+e^-

[5] Not independent of FELDMAN 77B mass difference above, PERUZZI 77 D^0 mass, and GOLDHABER 77 $D^*(2007)^0$ mass.

$D^*(2010)^\pm$ WIDTH

VALUE (keV)	CL%	EVTS	DOCUMENT ID		TECN	COMMENT
83.4±1.8 OUR AVERAGE						
83.3±1.2± 1.4		312.8k	[6] LEES	13X	BABR	$D^{*\pm} \to D^0\pi^\pm \to (K\pi, K3\pi)\pi^\pm$
96 ±4 ±22			[6] ANASTASSOV	02	CLE2	$D^{*\pm} \to D^0\pi^\pm \to (K\pi)\pi^\pm$
• • • We do not use the following data for averages, fits, limits, etc. • • •						
83.4±1.7± 1.5		138.5k	[6] LEES	13X	BABR	$D^{*\pm} \to D^0\pi^\pm \to (K^-\pi^+)\pi^\pm$
83.2±1.5± 2.6		174.3k	[6] LEES	13X	BABR	$D^{*\pm} \to D^0\pi^\pm \to (K^-2\pi^+\pi^-)\pi^\pm$
<131	90	110	BARLAG	92B	ACCM	π^- 230 GeV

[6] Ignoring the electromagnetic contribution from $D^{*\pm} \to D^\pm\gamma$.

$D^*(2010)^\pm$ DECAY MODES

$D^*(2010)^-$ modes are charge conjugates of the modes below.

	Mode	Fraction (Γ_i/Γ)
Γ_1	$D^0\pi^+$	(67.7±0.5) %
Γ_2	$D^+\pi^0$	(30.7±0.5) %
Γ_3	$D^+\gamma$	(1.6±0.4) %

CONSTRAINED FIT INFORMATION

An overall fit to 3 branching ratios uses 6 measurements and one constraint to determine 3 parameters. The overall fit has a χ^2 = 0.3 for 4 degrees of freedom.

The following *off-diagonal* array elements are the correlation coefficients $\langle \delta x_i \delta x_j \rangle / (\delta x_i \cdot \delta x_j)$, in percent, from the fit to the branching fractions, $x_i \equiv \Gamma_i/\Gamma_{total}$. The fit constrains the x_i whose labels appear in this array to sum to one.

	x_1	x_2
x_2	−62	
x_3	−43	−44

$D^*(2010)^+$ BRANCHING RATIOS

$\Gamma(D^0\pi^+)/\Gamma_{total}$ — Γ_1/Γ

VALUE	DOCUMENT ID		TECN	COMMENT
0.677 ±0.005 OUR FIT				
0.677 ±0.006 OUR AVERAGE				
0.6759±0.0029±0.0064	[7,8,9] BARTELT	98	CLE2	e^+e^-
0.688 ±0.024 ±0.013	ALBRECHT	95F	ARG	$e^+e^- \to$ hadrons
0.681 ±0.010 ±0.013	[7] BUTLER	92	CLE2	$e^+e^- \to$ hadrons
• • • We do not use the following data for averages, fits, limits, etc. • • •				
0.57 ±0.04 ±0.04	ADLER	88D	MRK3	e^+e^-
0.44 ±0.10	COLES	82	MRK2	e^+e^-
0.6 ±0.15	[9] GOLDHABER	77	MRK1	e^+e^-

$\Gamma(D^+\pi^0)/\Gamma_{total}$ — Γ_2/Γ

VALUE	EVTS	DOCUMENT ID		TECN	COMMENT
0.307 ±0.005 OUR FIT					
0.3073±0.0013±0.0062		[7,8,9] BARTELT	98	CLE2	e^+e^-
• • • We do not use the following data for averages, fits, limits, etc. • • •					
0.312 ±0.011 ±0.008	1404	ALBRECHT	95F	ARG	$e^+e^- \to$ hadrons
0.308 ±0.004 ±0.008	410	[7] BUTLER	92	CLE2	$e^+e^- \to$ hadrons
0.26 ±0.02 ±0.02		ADLER	88D	MRK3	e^+e^-
0.34 ±0.07		COLES	82	MRK2	e^+e^-

$\Gamma(D^+\gamma)/\Gamma_{total}$ — Γ_3/Γ

VALUE	CL%	EVTS	DOCUMENT ID		TECN	COMMENT
0.016 ±0.004 OUR FIT						
0.016 ±0.005 OUR AVERAGE						
0.0168±0.0042±0.0029			[7,8] BARTELT	98	CLE2	e^+e^-
0.011 ±0.014 ±0.016		12	[7] BUTLER	92	CLE2	$e^+e^- \to$ hadrons
• • • We do not use the following data for averages, fits, limits, etc. • • •						
<0.052		90	ALBRECHT	95F	ARG	$e^+e^- \to$ hadrons
0.17 ±0.05 ±0.05			ADLER	88D	MRK3	e^+e^-
0.22 ±0.12			[10] COLES	82	MRK2	e^+e^-

[7] The branching ratios are not independent, they have been constrained by the authors to sum to 100%.
[8] Systematic error includes theoretical error on the prediction of the ratio of hadronic modes.
[9] Assuming that isospin is conserved in the decay.
[10] Not independent of $\Gamma(D^0\pi^+)/\Gamma_{total}$ and $\Gamma(D^+\pi^0)/\Gamma_{total}$ measurement.

$D^*(2010)^\pm$ REFERENCES

LEES	17F	PRL 119 202003	J.P. Lees *et al.*	(BABAR Collab.)
LEES	13X	PRL 111 111801	J.P. Lees *et al.*	(BABAR Collab.)
Also		PR D88 052003	J.P. Lees *et al.*	(BABAR Collab.)
Also		PR D88 079902 (errat.)	J.P. Lees *et al.*	(BABAR Collab.)
ANASTASSOV	02	PR D65 032003	A. Anastassov *et al.*	(CLEO Collab.)
ADINOLFI	99	NP B547 3	M. Adinolfi *et al.*	(Beatrice Collab.)
BREITWEG	99	EPJ C6 67	J. Breitweg *et al.*	(ZEUS Collab.)
BARTELT	98	PRL 80 3919	J. Bartelt *et al.*	(CLEO Collab.)
ADLOFF	97B	ZPHY C72 593	C. Adloff *et al.*	(H1 Collab.)
BREITWEG	97	PL B401 192	J. Breitweg *et al.*	(ZEUS Collab.)

Downloaded from https://academic.oup.com/ptep/article/2022/8/083C01/6651666 by KIT Library user on 27 September 2022

BREITWEG	97B	PL B407 402	J. Breitweg *et al.*	(ZEUS Collab.)
ALBRECHT	95F	ZPHY C66 63	H. Albrecht *et al.*	(ARGUS Collab.)
DERRICK	95	PL B349 225	M. Derrick *et al.*	(ZEUS Collab.)
BARLAG	92B	PL B278 480	S. Barlag *et al.*	(ACCMOR Collab.)
BORTOLETTO	92B	PRL 69 2046	D. Bortoletto *et al.*	(CLEO Collab.)
BUTLER	92	PRL 69 2041	F. Butler *et al.*	(CLEO Collab.)
ALEXANDER	91B	PL B262 341	G. Alexander *et al.*	(OPAL Collab.)
DECAMP	91J	PL B266 218	D. Decamp *et al.*	(ALEPH Collab.)
ABACHI	88B	PL B212 533	S. Abachi *et al.*	(ANL, IND, MICH, PURD+)
ADLER	88D	PL B208 152	J. Adler *et al.*	(Mark III Collab.)
ALBRECHT	85F	PL 150B 235	H. Albrecht *et al.*	(ARGUS Collab.)
AHLEN	83	PRL 51 1147	S.P. Ahlen *et al.*	(ANL, IND, LBL+)
BAILEY	83	PL 132B 230	R. Bailey *et al.*	(AMST, BRIS, CERN, CRAC+)
COLES	82	PR D26 2190	M.W. Coles *et al.*	(LBL, SLAC)
YELTON	82	PRL 49 430	J.M. Yelton *et al.*	(SLAC, LBL, UCB+)
FITCH	81	PRL 46 761	V.L. Fitch *et al.*	(PRIN, SACL, TORI+)
AVERY	80	PRL 44 1309	P. Avery *et al.*	(ILL, FNAL, COLU)
BLIETSCHAU	79	PL 86B 108	J. Blietschau *et al.*	(AACH3, BONN, CERN+)
FELDMAN	77B	PRL 38 1313	G.J. Feldman *et al.*	(Mark I Collab.)
GOLDHABER	77	PL 69B 503	G. Goldhaber *et al.*	(Mark I Collab.)
PERUZZI	77	PRL 39 1301	I. Peruzzi *et al.*	(LGW Collab.)

$D_0^*(2300)$

$I(J^P) = \frac{1}{2}(0^+)$

was $D_0^*(2400)$

There is a strong evidence that recent data on $B \to D\pi\pi$ (AAIJ 15Y, AAIJ 16AH) and $B \to D\pi K$ (AAIJ 14BH, AAIJ 15V, AAIJ 15X) call for two poles in the scalar $I = 1/2$ πD amplitude in this mass range. The data are consistent with a lower pole at $(2105^{+6}_{-8}) - i(102^{+10}_{-11})$ MeV and a higher pole at $(2451^{+35}_{-26}) - i(134^{+7}_{-8})$ MeV (DU 18A, DU 19, DU 21). For details see review on "Heavy Non-$q\overline{q}$ Mesons."

$D_0^*(2300)$ MASS

VALUE (MeV)	EVTS	DOCUMENT ID		TECN	CHG	COMMENT
2343±10 OUR AVERAGE		Error includes scale factor of 1.5. See the ideogram below.				
2360±15±30		[1] AAIJ	15X	LHCB	+	$B^0 \to \overline{D}^0 K^+ \pi^-$
2349± 6± 4		[2] AAIJ	15Y	LHCB	+	$B^0 \to \overline{D}^0 \pi^+ \pi^-$
2297± 8±20	3.4k	AUBERT	09AB	BABR	0	$B^- \to D^+ \pi^- \pi^-$
2308±17±32		ABE	04D	BELL	0	$B^- \to D^+ \pi^- \pi^-$
• • • We do not use the following data for averages, fits, limits, etc. • • •						
2354± 7±11		[3] AAIJ	15Y	LHCB	+	$B^0 \to \overline{D}^0 \pi^+ \pi^-$
2403±14±35	18.8k	[4] LINK	04A	FOCS	+	γ A
2407±21±35	9.8k	[4] LINK	04A	FOCS	0	γ A

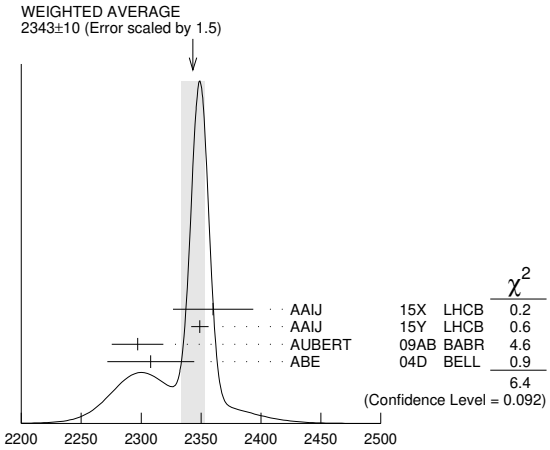

[1] From the Dalitz plot analysis including various K^* and D^{**} mesons as well as broad structures in the $K\pi$ S-wave and the $D\pi$ S- and P-waves.
[2] Modeling the $\pi^+\pi^-$ S-wave with the Isobar formalism.
[3] Modeling the $\pi^+\pi^-$ S-wave with the K-matrix formalism.

$D_0^*(2300)$ WIDTH

VALUE (MeV)	EVTS	DOCUMENT ID		TECN	CHG	COMMENT
229±16 OUR AVERAGE						
255±26±51		[1] AAIJ	15X	LHCB	+	$B^0 \to \overline{D}^0 K^+ \pi^-$
217±13±13		[2] AAIJ	15Y	LHCB	+	$B^0 \to \overline{D}^0 \pi^+ \pi^-$
273±12±48	3.4k	AUBERT	09AB	BABR	0	$B^- \to D^+ \pi^- \pi^-$
276±21±63		ABE	04D	BELL	0	$B^- \to D^+ \pi^- \pi^-$
• • • We do not use the following data for averages, fits, limits, etc. • • •						
230±15±21		[3] AAIJ	15Y	LHCB	+	$B^0 \to \overline{D}^0 \pi^+ \pi^-$
283±24±34	18.8k	[4] LINK	04A	FOCS	+	γ A
240±55±59	9.8k	[4] LINK	04A	FOCS	0	γ A

[1] From the Dalitz plot analysis including various K^* and D^{**} mesons as well as broad structures in the $K\pi$ S-wave and the $D\pi$ S- and P-waves.
[2] Modeling the $\pi^+\pi^-$ S-wave with the Isobar formalism.
[3] Modeling the $\pi^+\pi^-$ S-wave with the K-matrix formalism.
[4] Possibly the feed-down from another state.

$D_0^*(2300)$ DECAY MODES

	Mode	Fraction (Γ_i/Γ)
Γ_1	$D\pi^\pm$	seen

$\Gamma(D\pi^\pm)/\Gamma_{total}$ — Γ_1/Γ

VALUE	EVTS	DOCUMENT ID		TECN	CHG	COMMENT
seen		AAIJ	15X	LHCB	+	$D^*(2300)^+ \to D^0\pi^+$
seen		AAIJ	15Y	LHCB	+	$D^*(2300)^+ \to D^0\pi^+$
seen	3.4k	AUBERT	09AB	BABR	0	$D^*(2300)^0 \to D^+\pi^-$
seen		ABE	04D	BELL	0	$D^*(2300)^0 \to D^+\pi^-$
seen	18.8k	LINK	04A	FOCS	+	$D^*(2300)^+ \to D^0\pi^+$

$D_0^*(2300)$ REFERENCES

DU	21	PRL 126 192001	M.-L. Du *et al.*	
DU	19	PR D99 114002	M.-L. Du, F.-K. Guo, U.-G. Meissner	
DU	18A	PR D98 094018	M.-L. Du *et al.*	
AAIJ	16AH	PR D94 072001	R. Aaij *et al.*	(LHCb Collab.)
AAIJ	15V	PR D91 092002	R. Aaij *et al.*	(LHCb Collab.)
Also		PR D93 119901 (errat.)	R. Aaij *et al.*	(LHCb Collab.)
AAIJ	15X	PR D92 012012	R. Aaij *et al.*	(LHCb Collab.)
AAIJ	15Y	PR D92 032002	R. Aaij *et al.*	(LHCb Collab.)
AAIJ	14BH	PR D90 072003	R. Aaij *et al.*	(LHCb Collab.)
AUBERT	09AB	PR D79 112004	B. Aubert *et al.*	(BABAR Collab.)
ABE	04D	PR D69 112002	K. Abe *et al.*	(BELLE Collab.)
LINK	04A	PL B586 11	J.M. Link *et al.*	(FOCUS Collab.)

$D_1(2420)$

$I(J^P) = \frac{1}{2}(1^+)$

$D_1(2420)$ MASS

The fit includes $D^\pm$, D^0, $D_s^\pm$, $D^{*\pm}$, D^{*0}, $D_s^{*\pm}$, $D_1(2420)^0$, $D_2^*(2460)^0$, and $D_{s1}(2536)^\pm$ mass and mass difference measurements.

VALUE (MeV)	EVTS	DOCUMENT ID		TECN	CHG	COMMENT
2422.1±0.6 OUR FIT		Error includes scale factor of 1.7.				
2422.1±0.8 OUR AVERAGE		Error includes scale factor of 2.1. See the ideogram below.				
2424.8±0.1±0.7	79k	[1] AAIJ	20D	LHCB	0	$B^- \to D^{*+}\pi^-\pi^-$
2427.2±1.0±1.2	4207	ABLIKIM	20P	BES3	+	$e^+e^- \to D^+D^-\pi^+\pi^-$
2419.6±0.1±0.7	210k	AAIJ	13CC	LHCB	0	$pp \to D^{*+}\pi^- X$
2423.1±1.5$^{+0.4}_{-1.0}$	2.7k	[2] ABRAMOWICZ13		ZEUS	0	$e^\pm p \to D^{(*)+}\pi^- X$
2421.9±4.7$^{+3.4}_{-1.2}$	759	[3] ABRAMOWICZ13		ZEUS	+	$e^\pm p \to D^{(*)0}\pi^+ X$
2420.1±0.1±0.8	103k	DEL-AMO-SA...	10P	BABR	0	$e^+e^- \to D^{*+}\pi^- X$
2426 ±3 ±1	151	ABE	05A	BELL	0	$B^- \to D^0\pi^+\pi^-\pi^-$
2421 ±2 ±1	124	ABE	05A	BELL	+	$\overline{B}^0 \to D^+\pi^+\pi^-\pi^-$
2421.4±1.5±0.9		[4] ABE	04D	BELL	0	$B^- \to D^{*+}\pi^-\pi^-$
2421 $^{+1}_{-2}$ ±2	286	AVERY	94C	CLE2	0	$e^+e^- \to D^{*+}\pi^- X$
2425 ±2 ±2	146	BERGFELD	94B	CLE2	+	$e^+e^- \to D^{*0}\pi^+ X$
2422 ±2 ±2	51	FRABETTI	94B	E687	0	γBe $\to D^{*+}\pi^- X$
2428 ±3 ±2	279	AVERY	90	CLEO	0	$e^+e^- \to D^{*+}\pi^- X$
2414 ±2 ±5	171	ALBRECHT	89H	ARG	0	$e^+e^- \to D^{*+}\pi^- X$
2428 ±8 ±5	171	ANJOS	89C	TPS	0	$\gamma N \to D^{*+}\pi^- X$
2443 ±7 ±5	190	ANJOS	89C	TPS	+	$\gamma N \to D^0\pi^+ X^0$
• • • We do not use the following data for averages, fits, limits, etc. • • •						
2420.5±2.1±0.9	3.1k	[5] CHEKANOV	09	ZEUS	0	$e^\pm p \to D^{*+}\pi^- X$
2421.7±0.7±0.6	7.5k	ABULENCIA	06A	CDF	0	1900 $p\overline{p} \to D^{*+}\pi^- X$
2425 ±3	235	[6] ABREU	98M	DLPH	0	e^+e^-

[1] From a full four-body amplitude analysis of the $B^- \to D^{*+}\pi^-\pi^-$ decay.
[2] From the combined fit of the $M(D^+\pi^-)$ and $M(D^{*+}\pi^-)$ distributions. and A_{D_2} fixed to the theoretical prediction of -1.
[3] From the fit of the $M(D^0\pi^+)$ distribution. The widths of the D_1^+ and D_2^{*+} are fixed to 25 MeV and 37 MeV, and A_{D_1} and A_{D_2} are fixed to the theoretical predictions of 3 and -1, respectively.
[4] Fit includes the contribution from $D_1^*(2430)^0$.
[5] Calculated using the mass difference $m(D_1^0) - m(D^{*+})_{PDG}$ reported below and $m(D^{*+})_{PDG} = 2010.27 \pm 0.17$ MeV. The 0.17 MeV uncertainty of the PDG mass value should be added to the experimental uncertainty of 0.9 MeV.

Downloaded from https://academic.oup.com/ptep/article/2022/8/083C01/6651666 by KIT Library user on 27 September 2022

[6] No systematic error given.

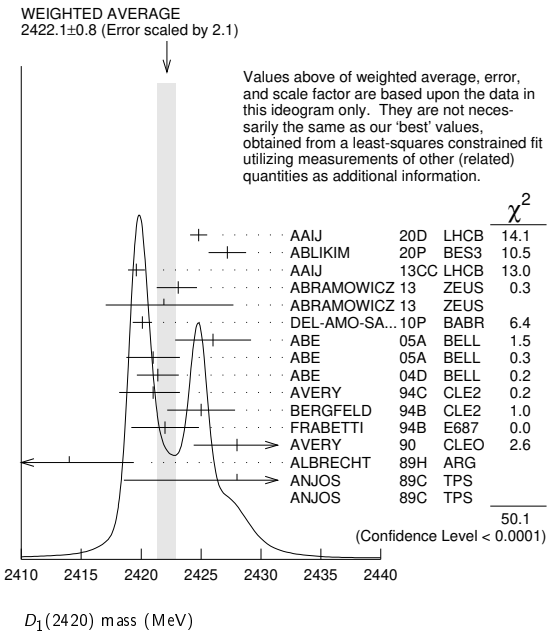

$m_{D_1(2420)^0} - m_{D^{*+}}$

The fit includes $D^{\pm}$, D^0, $D_s^{\pm}$, $D^{*\pm}$, D^{*0}, $D_s^{*\pm}$, $D_1(2420)^0$, $D_2^*(2460)^0$, and $D_{s1}(2536)^{\pm}$ mass and mass difference measurements.

VALUE (MeV)	EVTS	DOCUMENT ID		TECN	COMMENT
411.8±0.6 OUR FIT	Error includes scale factor of 1.7.				
411.5±0.8 OUR AVERAGE					
410.2±2.1±0.9	3.1k	CHEKANOV	09	ZEUS	$e^{\pm}p \to D^{*+}\pi^-X$
411.7±0.7±0.4	7.5k	ABULENCIA	06A	CDF	1900 $p\overline{p} \to D^{*+}\pi^-X$

$m_{D_1(2420)^{\pm}} - m_{D_1(2420)^0}$

VALUE (MeV)	DOCUMENT ID		TECN	COMMENT
$4^{+2}_{-3}\pm3$	BERGFELD	94B	CLE2	$e^+e^- \to$ hadrons

$D_1(2420)$ WIDTH

VALUE (MeV)	EVTS	DOCUMENT ID		TECN	CHG	COMMENT
31.3± 1.9 OUR AVERAGE	Error includes scale factor of 2.8. See the ideogram below.					
33.6± 0.3± 2.7	79k	[1] AAIJ	20D	LHCB	0	$B^- \to D^{*+}\pi^-\pi^-$
23.2± 2.3± 2.3	4207	ABLIKIM	20P	BES3	+	$e^+e^- \to D^+D^-\pi^+\pi^-$
35.2± 0.4± 0.9	210k	AAIJ	13CC	LHCB	0	$pp \to D^{*+}\pi^-X$
38.8± $5.0^{+1.9}_{-5.4}$	2.7k	[2] ABRAMOWICZ	13	ZEUS	0	$e^{\pm}p \to D^{(*)+}\pi^-X$
31.4± 0.5± 1.3	103k	DEL-AMO-SA...	10P	BABR	0	$e^+e^- \to D^{*+}\pi^-X$
20.0± 1.7± 1.3	7.5k	ABULENCIA	06A	CDF	0	1900 $p\overline{p} \to D^{*+}\pi^-X$
24 ± 7 ± 8	151	ABE	05A	BELL	0	$B^- \to D^0\pi^+\pi^-\pi^-$
21 ± 5 ± 8	124	ABE	05A	BELL	+	$\overline{B}^0 \to D^+\pi^+\pi^-\pi^-$
23.7± 2.7± 4.0		[3] ABE	04D	BELL	0	$B^- \to D^{*+}\pi^-\pi^-$
20 $^{+6}_{-5}$ ± 3	286	AVERY	94C	CLE2	0	$e^+e^- \to D^{*+}\pi^-X$
26 $^{+8}_{-7}$ ± 4	146	BERGFELD	94B	CLE2	+	$e^+e^- \to D^0\pi^+X$
15 ± 8 ± 4	51	FRABETTI	94B	E687	0	γBe $\to D^{*+}\pi^-X$
23 $^{+8}_{-6}$ $^{+10}_{-3}$	279	AVERY	90	CLEO	0	$e^+e^- \to D^{*+}\pi^-X$
13 ± 6 $^{+10}_{-5}$	171	ALBRECHT	89H	ARG	0	$e^+e^- \to D^{*+}\pi^-X$
41 ±19 ± 8	190	ANJOS	89C	TPS	+	$\gamma N \to D^0\pi^+X^0$
• • • We do not use the following data for averages, fits, limits, etc. • • •						
53.2± $7.2^{+3.3}_{-4.9}$	3.1k	CHEKANOV	09	ZEUS	0	$e^{\pm}p \to D^{*+}\pi^-X$
58 ±14 ±10	171	ANJOS	89C	TPS	0	$\gamma N \to D^{*+}\pi^-X$

[1] From a full four-body amplitude analysis of the $B^- \to D^{*+}\pi^-\pi^-$ decay.
[2] From the combined fit of the $M(D^+\pi^-)$ and $M(D^{*+}\pi^-)$ distributions. and A_{D_2} fixed to the theoretical prediction of −1.
[3] Fit includes the contribution from $D_1^*(2430)^0$.

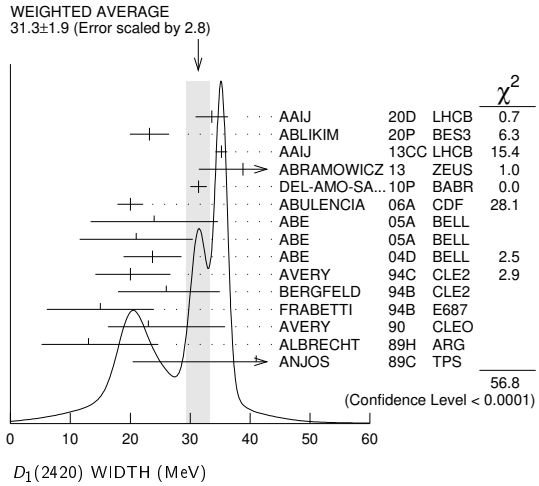

$D_1(2420)$ DECAY MODES

$\overline{D}_1(2420)$ modes are charge conjugates of modes below.

	Mode	Fraction (Γ_i/Γ)
Γ_1	$D^*(2007)^0\pi$	seen
Γ_2	$D\pi^+\pi^-$	
Γ_3	$D\rho^0$	
Γ_4	$Df_0(500)$	
Γ_5	$D_0^*(2300)^0\pi$	
Γ_6	$D^0\pi$	
Γ_7	$D^*\pi^+\pi^-$	

$D_1(2420)$ BRANCHING RATIOS

$\Gamma(D^*(2007)^0\pi)/\Gamma_{total}$ — Γ_1/Γ

VALUE	DOCUMENT ID		TECN	CHG	COMMENT
seen	ACKERSTAFF	97W	OPAL	0	$e^+e^- \to D^{*+}\pi^-X$
seen	AVERY	90	CLEO	0	$e^+e^- \to D^{*+}\pi^-X$
seen	ALBRECHT	89H	ARG	0	$e^+e^- \to D^{*}\pi^-X$
seen	ANJOS	89C	TPS	0	$\gamma N \to D^{*+}\pi^-X$
seen	ANJOS	89C	TPS	+	$\gamma N \to D^0\pi^+X^0$

$\Gamma(D^0\pi)/\Gamma(D^*(2007)^0\pi)$ — Γ_6/Γ_1

VALUE	CL%	DOCUMENT ID		TECN	CHG	COMMENT
<0.18	90	BERGFELD	94B	CLE2	+	$e^+e^- \to$ hadrons
• • • We do not use the following data for averages, fits, limits, etc. • • •						
<0.24	90	AVERY	90	CLEO	0	$e^+e^- \to D^+\pi^-X$

$D_1(2420)$ POLARIZATION AMPLITUDE A_{D_1}

A polarization amplitude A_{D_1} is a parameter that depends on the initial polarization of the D_1 and is sensitive to a possible S-wave contribution to its decay. For D_1 decays the helicity angle, θ_h, distribution varies like $1 + A_{D_1}\cos^2\theta_h$, where θ_h is the angle in the D^* rest frame between the two pions emitted by the $D_1 \to D^*\pi$ and the $D^* \to D\pi$.

Unpolarized D_1 decaying purely via D-wave is predicted to give $A_{D_1} = 3$.

VALUE	EVTS	DOCUMENT ID		TECN	CHG	COMMENT
5.73±0.25 OUR AVERAGE						
7.8 $^{+6.7}_{-2.7}$ $^{+4.6}_{-1.8}$	2.7k	[1] ABRAMOWICZ	13	ZEUS	0	$e^{\pm}p \to D^{(*)+}\pi^-X$
5.72±0.25	103k	DEL-AMO-SA...	10P	BABR	0	$e^+e^- \to D^{*+}\pi^-X$
5.9 $^{+3.0}_{-1.7}$ $^{+2.4}_{-1.0}$		CHEKANOV	09	ZEUS	0	$e^{\pm}p \to D^{*+}\pi^-X$
• • • We do not use the following data for averages, fits, limits, etc. • • •						
3.30±0.48	210k	[2] AAIJ	13CC	LHCB	0	$pp \to D^{*+}\pi^-X$
3.8 ±0.6 ±0.8		[3] AUBERT	09Y	BABR	0	$B^+ \to D_1^0\ell^+\nu_\ell$
3.8 ±0.6 ±0.8		[3] AUBERT	09Y	BABR	+	$B^0 \to D_1^-\ell^+\nu_\ell$
2.74 $^{+1.40}_{-0.93}$		[4] AVERY	94C	CLE2	0	$e^+e^- \to D^{*+}\pi^-X$

[1] From the combined fit of the $M(D^+\pi^-)$ and $M(D^{*+}\pi^-)$ distributions. and A_{D_2} fixed to the theoretical prediction of −1. A pure D-wave not excluded although some S-wave mixing possible.
[2] Systematic uncertainty not estimated. Resonance parameters fixed.
[3] Assuming $\Gamma(\Upsilon(4S) \to B^+B^-) / \Gamma(\Upsilon(4S) \to B^0\overline{B}^0) = 1.065 \pm 0.026$ and equal partial widths and helicity angle distributions for charged and neutral D_1 mesons.
[4] Systematic uncertainties not estimated.

Downloaded from https://academic.oup.com/ptep/article/2022/8/083C01/6651666 by KIT Library user on 27 September 2022

$D_1(2420)$ REFERENCES

AAIJ	20D	PR D101 032005	R. Aaij *et al.*	(LHCb Collab.)
ABLIKIM	20P	PL B804 135395	M. Ablikim *et al.*	(BESIII Collab.)
AAIJ	13CC	JHEP 1309 145	R. Aaij *et al.*	(LHCb Collab.)
ABRAMOWICZ	13	NP B866 229	H. Abramowicz *et al.*	(ZEUS Collab.)
DEL-AMO-SA...	10P	PR D82 111101	P. del Amo Sanchez *et al.*	(BABAR Collab.)
AUBERT	09Y	PRL 103 051803	B. Aubert *et al.*	(BABAR Collab.)
CHEKANOV	09	EPJ C60 25	S. Chekanov *et al.*	(ZEUS Collab.)
ABULENCIA	06A	PR D73 051104	A. Abulencia *et al.*	(CDF Collab.)
ABE	05A	PRL 94 221805	K. Abe *et al.*	(BELLE Collab.)
ABE	04D	PR D69 112002	K. Abe *et al.*	(BELLE Collab.)
ABREU	98M	PL B426 231	P. Abreu *et al.*	(DELPHI Collab.)
ACKERSTAFF	97W	ZPHY C76 425	K. Ackerstaff *et al.*	(OPAL Collab.)
AVERY	94C	PL B331 236	P. Avery *et al.*	(CLEO Collab.)
BERGFELD	94B	PL B340 194	T. Bergfeld *et al.*	(CLEO Collab.)
FRABETTI	94B	PRL 72 324	P.L. Frabetti *et al.*	(FNAL E687 Collab.)
AVERY	90	PR D41 774	P. Avery, D. Besson	(CLEO Collab.)
ALBRECHT	89H	PL B232 398	H. Albrecht *et al.*	(ARGUS Collab.) JP
ANJOS	89C	PRL 62 1717	J.C. Anjos *et al.*	(FNAL E691 Collab.)

$D_1(2430)^0$

$I(J^P) = \frac{1}{2}(1^+)$

$J^P = 1^+$ determined by AAIJ 20D.

$D_1(2430)^0$ MASS

VALUE (MeV)	EVTS	DOCUMENT ID		TECN	COMMENT
2412± 9 OUR AVERAGE					
2411± 3± 9	79k	[1] AAIJ	20D	LHCB	$B^- \to D^{*+}\pi^-\pi^-$
2427±26±25		ABE	04D	BELL	$B^- \to D^{*+}\pi^-\pi^-$
• • • We do not use the following data for averages, fits, limits, etc. • • •					
2477±28		[2] AUBERT	06L	BABR	$\overline{B}^0 \to D^{*+}\omega\pi^-$

[1] From a full four-body amplitude analysis of the $B^- \to D^{*+}\pi^-\pi^-$ decay.
[2] Systematic errors not estimated.

$D_1(2430)^0$ WIDTH

VALUE (MeV)	EVTS	DOCUMENT ID		TECN	COMMENT
314± 29 OUR AVERAGE					
309± 9±28	79k	[1] AAIJ	20D	LHCB	$B^- \to D^{*+}\pi^-\pi^-$
$384^{+107}_{-75}\pm74$		ABE	04D	BELL	$B^- \to D^{*+}\pi^-\pi^-$
• • • We do not use the following data for averages, fits, limits, etc. • • •					
266± 97		[2] AUBERT	06L	BABR	$\overline{B}^0 \to D^{*+}\omega\pi^-$

[1] From a full four-body amplitude analysis of the $B^- \to D^{*+}\pi^-\pi^-$ decay.
[2] Systematic errors not estimated.

$D_1(2430)^0$ DECAY MODES

	Mode	Fraction (Γ_i/Γ)
Γ_1	$D^*(2010)^+\pi^-$	seen

$D_1(2430)^0$ REFERENCES

AAIJ	20D	PR D101 032005	R. Aaij *et al.*	(LHCb Collab.) JP
AUBERT	06L	PR D74 012001	B. Aubert *et al.*	(BABAR Collab.)
ABE	04D	PR D69 112002	K. Abe *et al.*	(BELLE Collab.)

$D_2^*(2460)$

$I(J^P) = \frac{1}{2}(2^+)$

$D_2^*(2460)$ MASS

The fit includes $D^\pm$, D^0, $D_s^\pm$, $D^{*\pm}$, D^{*0}, $D_s^{*\pm}$, $D_1(2420)^0$, $D_2^*(2460)^0$, and $D_{s1}(2536)^\pm$ mass and mass difference measurements.

VALUE (MeV)	EVTS	DOCUMENT ID		TECN	CHG	COMMENT
$2461.1^{+0.7}_{-0.8}$ OUR FIT Error includes scale factor of 6.2.						
2461.1±0.7 OUR AVERAGE Error includes scale factor of 5.2. See the ideogram below.						
2463.7±0.4±0.7	28k	[1] AAIJ	16AH	LHCB	0	$B^- \to D^+\pi^-\pi^-$
2464.0±1.4±0.5	2k	[2] AAIJ	15V	LHCB	0	$B^- \to D^+K^-\pi^-$
2465.6±1.8±1.3		[3] AAIJ	15X	LHCB	+	$B^0 \to \overline{D}^0K^+\pi^-$
2468.6±0.6±0.3		[4] AAIJ	15Y	LHCB	+	$B^0 \to \overline{D}^0\pi^+\pi^-$
2460.4±0.4±1.2	82k	AAIJ	13CC	LHCB	0	$pp \to D^{*+}\pi^-X$
2460.4±0.1±0.1	675k	AAIJ	13CC	LHCB	0	$pp \to D^+\pi^-X$
2463.1±0.2±0.6	342k	AAIJ	13CC	LHCB	+	$pp \to D^0\pi^+X$
$2462.5\pm2.4^{+1.3}_{-1.1}$	2.3k	[5] ABRAMOWICZ	13	ZEUS	0	$e^\pm p \to D^{(*)+}\pi^-X$
$2460.6\pm4.4^{+3.6}_{-0.8}$	1371	[6] ABRAMOWICZ	13	ZEUS	+	$e^\pm p \to D^{(*)0}\pi^+X$
2462.2±0.1±0.8	243k	DEL-AMO-SA...	10P	BABR	0	$e^+e^- \to D^+\pi^-X$
2465.4±0.2±1.1	111k	[7] DEL-AMO-SA...	10P	BABR	+	$e^+e^- \to D^0\pi^+X$
2460.4±1.2±2.2	3.4k	AUBERT	09AB	BABR	0	$B^- \to D^+\pi^-\pi^-$
$2465.7\pm1.8^{+1.4}_{-4.8}$	2909	KUZMIN	07	BELL	+	$e^+e^- \to$ hadrons
2461.6±2.1±3.3		[8] ABE	04D	BELL	0	$B^- \to D^+\pi^-\pi^-$
2464.5±1.1±1.9	5.8k	[8] LINK	04A	FOCS	0	γ A
2465 ±3 ±3	486	AVERY	94C	CLE2	0	$e^+e^- \to D^+\pi^-X$
2463 ±3 ±3	310	BERGFELD	94B	CLE2	+	$e^+e^- \to D^0\pi^+X$
2453 ±3 ±2	128	FRABETTI	94B	E687	0	γBe $\to D^+\pi^-X$
2453 ±3 ±2	185	FRABETTI	94B	E687	+	γBe $\to D^0\pi^+X$
2461 ±3 ±1	440	AVERY	90	CLEO	0	$e^+e^- \to D^{*+}\pi^-X$
2455 ±3 ±5	337	ALBRECHT	89B	ARG	0	$e^+e^- \to D^+\pi^-X$
2469 ±4 ±6		ALBRECHT	89F	ARG	+	$e^+e^- \to D^0\pi^+X$
2459 ±3 ±2	153	ANJOS	89C	TPS	0	$\gamma N \to D^+\pi^-X$
• • • We do not use the following data for averages, fits, limits, etc. • • •						
2468.1±0.6±0.5		[9] AAIJ	15Y	LHCB	+	$B^0 \to \overline{D}^0\pi^+\pi^-$
$2469.1\pm3.7^{+1.2}_{-1.3}$	1.5k	[10] CHEKANOV	09	ZEUS	0	$e^\pm p \to D^{(*)+}\pi^-X$
2463.3±0.6±0.8	20k	ABULENCIA	06A	CDF	0	1900 $p\overline{p} \to D^+\pi^-X$
2467.6±1.5±0.8	3.5k	[11] LINK	04A	FOCS	+	γ A
2461 ±6	126	[12] ABREU	98M	DLPH	0	e^+e^-
2466 ±7	1	ASRATYAN	95	BEBC	0	53,40 $\nu(\overline{\nu}) \to pX,dX$

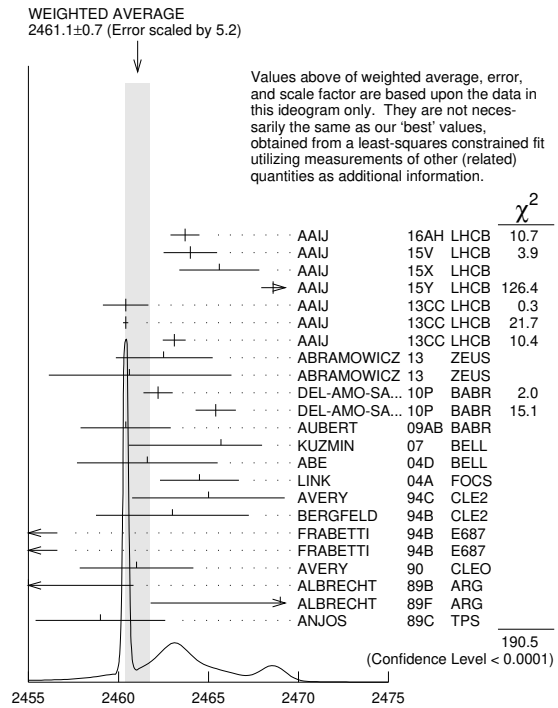

[1] From the amplitude analysis in the model describing the $D^+\pi^-$ wave together with virtual contributions from the $D^*(2007)^0$ and B^{*0} states, and components corresponding to the $D_2^*(2460)^0$, $D_1^*(2680)^0$, $D_3^*(2760)^0$, and $D_2^*(3000)^0$ resonances.
[2] From the amplitude analysis in the model describing the $D^+\pi^-$ wave together with virtual contributions from the $D^*(2007)^0$ and B^{*0} states, nonresonant spin-0 and spin-1 components as well as the $D_0^*(2400)^0$, $D_2^*(2460)^0$ and $D_1^*(2760)^0$ resonances.
[3] From the Dalitz plot analysis including various K^* and D^{**} mesons as well as broad structures in the $K\pi$ S-wave and the $D\pi$ S- and P-waves.
[4] Modeling the $\pi^+\pi^-$ S-wave with the Isobar formalism.
[5] From the combined fit of the $M(D^+\pi^-)$ and $M(D^{*+}\pi^-)$ distributions. and A_{D_2} fixed to the theoretical prediction of -1.
[6] From the fit of the $M(D^0\pi^+)$ distribution. The widths of the D_1^+ and D_2^{*+} are fixed to 25 MeV and 37 MeV, and A_{D_1} and A_{D_2} are fixed to the theoretical predictions of 3 and -1, respectively.
[7] At a fixed width of 50.5 MeV.
[8] Fit includes the contribution from $D_0^*(2400)^0$.
[9] Modeling the $\pi^+\pi^-$ S-wave with the K-matrix formalism.
[10] Calculated using the mass difference $m(D_2^{*0}) - m(D^{*+})_{PDG}$ reported below and $m(D^{*+})_{PDG} = 2010.27 \pm 0.17$ MeV. The 0.17 MeV uncertainty of the PDG mass value should be added to the experimental uncertainty of $^{+1.2}_{-1.3}$ MeV.
[11] Fit includes the contribution from $D_0^*(2400)^\pm$. Not independent of the corresponding mass difference measurement, $(m_{D_2^*(2460)^\pm}) - (m_{D_2^*(2460)^0})$.
[12] No systematic error given.

Downloaded from https://academic.oup.com/ptep/article/2022/8/083C01/6651666 by KIT Library user on 27 September 2022

$m_{D_2^*(2460)^0} - m_{D^+}$

The fit includes $D^\pm$, D^0, $D_s^\pm$, $D^{*\pm}$, D^{*0}, $D_s^{*\pm}$, $D_1(2420)^0$, $D_2^*(2460)^0$, and $D_{s1}(2536)^\pm$ mass and mass difference measurements.

VALUE (MeV)	EVTS	DOCUMENT ID		TECN	COMMENT
$591.5^{+0.7}_{-0.8}$ OUR FIT	Error includes scale factor of 5.9.				
$593.9\pm0.6\pm0.5$	20k	ABULENCIA	06A	CDF	1900 $p\overline{p} \to D^+\pi^- X$

$m_{D_2^*(2460)^0} - m_{D^{*+}}$

The fit includes $D^\pm$, D^0, $D_s^\pm$, $D^{*\pm}$, D^{*0}, $D_s^{*\pm}$, $D_1(2420)^0$, $D_2^*(2460)^0$, and $D_{s1}(2536)^\pm$ mass and mass difference measurements.

VALUE (MeV)	EVTS	DOCUMENT ID		TECN	COMMENT
$450.9^{+0.7}_{-0.8}$ OUR FIT	Error includes scale factor of 5.9.				
$458.8\pm3.7^{+1.2}_{-1.3}$	1.5k	CHEKANOV	09	ZEUS	$e^\pm p \to D^{(*)+}\pi^- X$

$m_{D_2^*(2460)^\pm} - m_{D_2^*(2460)^0}$

VALUE (MeV)	DOCUMENT ID		TECN	COMMENT
2.4 ± 1.7 OUR AVERAGE				
$3.1\pm1.9\pm0.9$	LINK	04A	FOCS	γ A
$-2\ \pm4\ \pm4$	BERGFELD	94B	CLE2	$e^+e^- \to$ hadrons
$0\ \pm4$	FRABETTI	94B	E687	γBe $\to D\pi$X
$14\ \pm5\ \pm8$	ALBRECHT	89F	ARG	$e^+e^- \to D^0\pi^+$X

$D_2^*(2460)$ WIDTH

VALUE (MeV)	EVTS	DOCUMENT ID		TECN	CHG	COMMENT
47.3± 0.8 OUR AVERAGE	Error includes scale factor of 1.5. See the ideogram below.					
$47.0\pm0.8\pm1.0$	28k	[1] AAIJ	16AH	LHCB	0	$B^- \to D^+\pi^-\pi^-$
$43.8\pm2.9\pm1.8$	2k	[2] AAIJ	15V	LHCB	0	$B^- \to D^+K^-\pi^-$
$46.0\pm3.4\pm3.2$		[3] AAIJ	15X	LHCB	+	$B^0 \to \overline{D}^0K^+\pi^-$
$47.3\pm1.5\pm0.7$		[4] AAIJ	15Y	LHCB	+	$B^0 \to \overline{D}^0\pi^+\pi^-$
$43.2\pm1.2\pm3.0$	82k	AAIJ	13CC	LHCB	0	$pp \to D^{*+}\pi^- X$
$45.6\pm0.4\pm1.1$	675k	AAIJ	13CC	LHCB	0	$pp \to D^+\pi^- X$
$48.6\pm1.3\pm1.9$	342k	AAIJ	13CC	LHCB	+	$pp \to D^0\pi^+ X$
$46.6\pm8.1^{+5.9}_{-3.8}$	2.3k	[5] ABRAMOWICZ	13	ZEUS	0	$e^\pm p \to D^{(*)+}\pi^- X$
$50.5\pm0.6\pm0.7$	243k	DEL-AMO-SA...	10P	BABR	0	$e^+e^- \to D^+\pi^- X$
$41.8\pm2.5\pm2.9$	3.4k	AUBERT	09AB	BABR	0	$B^- \to D^+\pi^-\pi^-$
$49.7\pm3.8\pm6.4$	2909	KUZMIN	07	BELL	+	$e^+e^- \to$ hadrons
$49.2\pm2.3\pm1.3$	20k	ABULENCIA	06A	CDF	0	1900 $p\overline{p} \to D^+\pi^- X$
$45.6\pm4.4\pm6.7$		[6] ABE	04D	BELL	0	$B^- \to D^+\pi^-\pi^-$
$38.7\pm5.3\pm2.9$	5.8k	[6] LINK	04A	FOCS	0	γ A
$34.1\pm6.5\pm4.2$	3.5k	[7] LINK	04A	FOCS	+	γ A
$28\ ^{+8}_{-7}\ \pm6$	486	AVERY	94C	CLE2	0	$e^+e^- \to D^+\pi^- X$
$27\ ^{+11}_{-8}\ \pm5$	310	BERGFELD	94B	CLE2	+	$e^+e^- \to D^0\pi^+ X$
$25\ \pm10\ \pm5$	128	FRABETTI	94B	E687	0	γBe $\to D^+\pi^- X$
$23\ \pm9\ \pm5$	185	FRABETTI	94B	E687	+	γBe $\to D^0\pi^+ X$
$20\ ^{+9}_{-12}\ ^{+9}_{-10}$	440	AVERY	90	CLEO	0	$e^+e^- \to D^{*+}\pi^- X$
$15\ ^{+13}_{-10}\ ^{+5}_{-10}$	337	ALBRECHT	89B	ARG	0	$e^+e^- \to D^+\pi^- X$
$20\ \pm10\ \pm5$	153	ANJOS	89C	TPS	0	$\gamma N \to D^+\pi^- X$
• • • We do not use the following data for averages, fits, limits, etc. • • •						
$46.0\pm1.4\pm1.8$		[8] AAIJ	15Y	LHCB	+	$B^0 \to \overline{D}^0\pi^+\pi^-$

[1] From the amplitude analysis in the model describing the $D^+\pi^-$ wave together with virtual contributions from the $D^*(2007)^0$ and B^{*0} states, and components corresponding to the $D_2^*(2460)^0$, $D_1^*(2680)^0$, $D_3^*(2760)^0$, and $D_2^*(3000)^0$ resonances.

[2] From the amplitude analysis in the model describing the $D^+\pi^-$ wave together with virtual contributions from the $D^*(2007)^0$ and B^{*0} states, nonresonant spin-0 and spin-1 components as well as the $D_0^*(2400)^0$, $D_2^*(2460)^0$ and $D_1^*(2760)^0$ resonances.

[3] From the Dalitz plot analysis including various K^* and D^{**} mesons as well as broad structures in the $K\pi$ S-wave and the $D\pi$ S- and P-waves.

[4] Modeling the $\pi^+\pi^-$ S-wave with the Isobar formalism.

[5] From the combined fit of the $M(D^+\pi^-)$ and $M(D^{*+}\pi^-)$ distributions. and A_{D_2} fixed to the theoretical prediction of -1.

[6] Fit includes the contribution from $D_0^*(2400)^0$.

[7] Fit includes the contribution from $D_0^*(2400)^\pm$.

[8] Modeling the $\pi^+\pi^-$ S-wave with the K-matrix formalism.

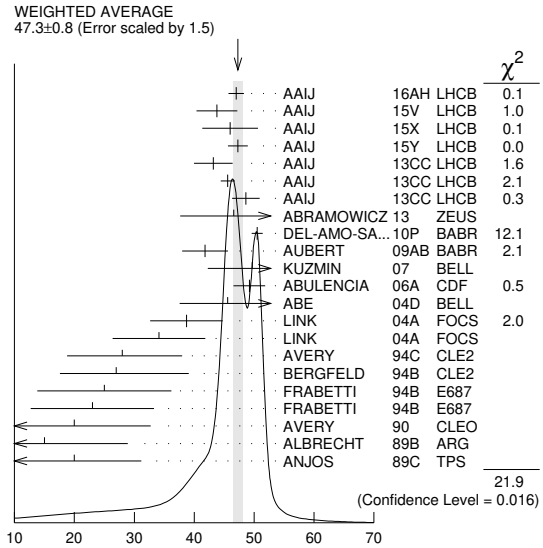

$D_2^*(2460)$ DECAY MODES

$\overline{D}_2^*(2460)$ modes are charge conjugates of modes below.

	Mode	Fraction (Γ_i/Γ)
Γ_1	$D\pi^-$	seen
Γ_2	$D^*(2010)\pi^-$	seen
Γ_3	$D\pi^+\pi^-$	
Γ_4	$D^*\pi^+\pi^-$	

$D_2^*(2460)$ BRANCHING RATIOS

$\Gamma(D\pi^-)/\Gamma_{total}$ — Γ_1/Γ

VALUE	EVTS	DOCUMENT ID		TECN	CHG	COMMENT
seen	3.4k	AUBERT	09AB	BABR	0	$B^- \to D^+\pi^-\pi^-$
seen	337	ALBRECHT	89B	ARG	0	$e^+e^- \to D^+\pi^-$X
seen		ALBRECHT	89F	ARG	+	$e^+e^- \to D^0\pi^+$X
seen		ANJOS	89C	TPS	0	$\gamma N \to D^+\pi^- X$

$\Gamma(D^*(2010)\pi^-)/\Gamma_{total}$ — Γ_2/Γ

VALUE	DOCUMENT ID		TECN	CHG	COMMENT
seen	ACKERSTAFF	97W	OPAL	0	$e^+e^- \to D^{*+}\pi^-$X
seen	AVERY	90	CLEO	0	$e^+e^- \to D^{*+}\pi^-$X
seen	ALBRECHT	89H	ARG	0	$e^+e^- \to D^*\pi^-$X

$\Gamma(D\pi^-)/\Gamma(D^*(2010)\pi^-)$ — Γ_1/Γ_2

VALUE	EVTS	DOCUMENT ID		TECN	CHG	COMMENT
1.52 ± 0.14 OUR AVERAGE						
$1.4\ \pm0.3\ \pm0.3$	2.3k	[1] ABRAMOWICZ	13	ZEUS	0	$e^\pm p \to D^{(*)+}\pi^- X$
$1.1\ \pm0.4\ ^{+0.3}_{-0.2}$	1371	[2] ABRAMOWICZ	13	ZEUS	+	$e^\pm p \to D^{(*)0}\pi^+ X$
$1.47\pm0.03\pm0.16$	379k	DEL-AMO-SA...	10P	BABR	0	$e^+e^- \to D^{(*)+}\pi^- X$
$2.8\ \pm0.8\ ^{+0.5}_{-0.6}$	1.5k	CHEKANOV	09	ZEUS	0	$e^\pm p \to D^{(*)+}\pi^- X$
$2.2\ \pm0.7\ \pm0.6$		AVERY	94C	CLE2	0	$e^+e^- \to D^{*+}\pi^-$X
$1.9\ \pm1.1\ \pm0.3$		BERGFELD	94B	CLE2	+	$e^+e^- \to$ hadrons
$2.3\ \pm0.8$		AVERY	90	CLEO	0	e^+e^-
$3.0\ \pm1.1\ \pm1.5$		ALBRECHT	89H	ARG	0	$e^+e^- \to D^*\pi^-$X
• • • We do not use the following data for averages, fits, limits, etc. • • •						
$1.9\ \pm0.5$		ABE	04D	BELL	0	$B^- \to D^{(*)+}\pi^-\pi^-$

[1] From the combined fit of the $M(D^+\pi^-)$ and $M(D^{*+}\pi^-)$ distributions. and A_{D_2} fixed to the theoretical prediction of -1.

[2] From the fit of the $M(D^0\pi^+)$ distribution. The widths of the D_1^+ and D_2^{*+} are fixed to 25 MeV and 37 MeV, and A_{D_1} and A_{D_2} are fixed to the theoretical predictions of 3 and -1, respectively.

Downloaded from https://academic.oup.com/ptep/article/2022/8/083C01/6651666 by KIT Library user on 27 September 2022

$\Gamma(D\pi^-)/[\Gamma(D\pi^-)+\Gamma(D^*(2010)\pi^-)]$ — $\Gamma_1/(\Gamma_1+\Gamma_2)$

VALUE	EVTS	DOCUMENT ID		TECN	CHG	COMMENT
• • • We do not use the following data for averages, fits, limits, etc. • • •						
$0.62\pm0.03\pm0.02$	8414	[1] AUBERT	09Y	BABR	0	$B^+ \to D_2^{*0}\ell^+\nu_\ell$
$0.62\pm0.03\pm0.02$	3361	[1] AUBERT	09Y	BABR	+	$\overline{B}^0 \to D_2^{*+}\ell^-\nu_\ell$

[1] Assuming $\Gamma(\Upsilon(4S) \to B^+B^-) / \Gamma(\Upsilon(4S) \to B^0\overline{B}^0) = 1.065 \pm 0.026$ and equal partial widths for charged and neutral D_2^* mesons.

$D_2^*(2460)$ POLARIZATION AMPLITUDE A_{D_2}

A polarization amplitude A_{D_2} is a parameter that depends on the initial polarization of the D_2. For D_2 decays the helicity angle, θ_H, distribution varies like $1 + A_{D_2}\cos^2(\theta_H)$, where θ_H is the angle in the D^* rest frame between the two pions emitted by the $D_2 \to D^*\pi$ and $D^* \to D\pi$.

VALUE	EVTS	DOCUMENT ID		TECN	CHG	COMMENT
• • • We do not use the following data for averages, fits, limits, etc. • • •						
-1.16 ± 0.35	2.3k	[1] ABRAMOWICZ	13	ZEUS	0	$e^\pm p \to D^{(*)+}\pi^- X$
consistent with -1	243k	DEL-AMO-SA...	10P	BABR	0	$e^+e^- \to D^+\pi^- X$
$-0.74^{+0.49}_{-0.38}$		[2] AVERY	94C	CLE2	0	$e^+e^- \to D^{*+}\pi^- X$

[1] From the combined fit of the $M(D^+\pi^-)$ and $M(D^{*+}\pi^-)$ distributions.
[2] Systematic uncertainties not estimated.

$D_2^*(2460)$ REFERENCES

AAIJ	16AH	PR D94 072001	R. Aaij et al.	(LHCb Collab.)
AAIJ	15V	PR D91 092002	R. Aaij et al.	(LHCb Collab.)
Also		PR D93 119901 (errat.)	R. Aaij et al.	(LHCb Collab.)
AAIJ	15X	PR D92 012012	R. Aaij et al.	(LHCb Collab.)
AAIJ	15Y	PR D92 032002	R. Aaij et al.	(LHCb Collab.)
AAIJ	13CC	JHEP 1309 145	R. Aaij et al.	(LHCb Collab.)
ABRAMOWICZ	13	NP B866 229	H. Abramowicz et al.	(ZEUS Collab.)
DEL-AMO-SA...	10P	PR D82 111101	P. del Amo Sanchez et al.	(BABAR Collab.)
AUBERT	09AB	PR D79 112004	B. Aubert et al.	(BABAR Collab.)
AUBERT	09Y	PRL 103 051803	B. Aubert et al.	(BABAR Collab.)
CHEKANOV	09	EPJ C60 25	S. Chekanov et al.	(ZEUS Collab.)
KUZMIN	07	PR D76 012006	A. Kuzmin et al.	(BELLE Collab.)
ABULENCIA	06A	PR D73 051104	A. Abulencia et al.	(CDF Collab.)
ABE	04D	PR D69 112002	K. Abe et al.	(BELLE Collab.)
LINK	04A	PL B586 11	J.M. Link et al.	(FOCUS Collab.)
ABREU	98M	PL B426 231	P. Abreu et al.	(DELPHI Collab.)
ACKERSTAFF	97W	ZPHY C76 425	K. Ackerstaff et al.	(OPAL Collab.)
ASRATYAN	95	ZPHY C68 43	A.E. Asratyan et al.	(BIRM, BELG, CERN+)
AVERY	94C	PL B331 236	P. Avery et al.	(CLEO Collab.)
BERGFELD	94B	PL B340 194	T. Bergfeld et al.	(CLEO Collab.)
FRABETTI	94B	PRL 72 324	P.L. Frabetti et al.	(FNAL E687 Collab.)
AVERY	90	PR D41 774	P. Avery, D. Besson	(CLEO Collab.)
ALBRECHT	89B	PL B221 422	H. Albrecht et al.	(ARGUS Collab.) JP
ALBRECHT	89F	PL B231 208	H. Albrecht et al.	(ARGUS Collab.)
ALBRECHT	89H	PL B232 398	H. Albrecht et al.	(ARGUS Collab.) JP
ANJOS	89C	PRL 62 1717	J.C. Anjos et al.	(FNAL E691 Collab.)

$D_0(2550)^0$

$I(J^P) = \frac{1}{2}(0^-)$

OMITTED FROM SUMMARY TABLE
$J^P = 0^-$ determined by AAIJ 20D.

$D_0(2550)^0$ MASS

VALUE (MeV)	EVTS	DOCUMENT ID		TECN	COMMENT
2549 ±19 OUR AVERAGE		Error includes scale factor of 4.6.			See the ideogram below.
$2518 \pm 2 \pm 7$	79k	[1] AAIJ	20D	LHCB	$B^- \to D^{*+}\pi^-\pi^-$
$2579.5 \pm 3.4 \pm 5.5$	60k	AAIJ	13CC	LHCB	$pp \to D^{*+}\pi^- X$
$2539.4 \pm 4.5 \pm 6.8$	34k	DEL-AMO-SA...	10P	BABR	$e^+e^- \to D^{*+}\pi^- X$

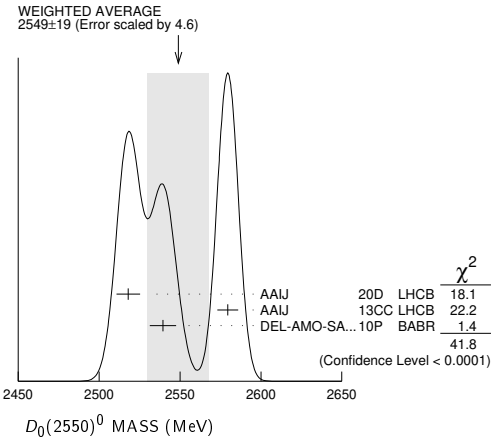

[1] From a full four-body amplitude analysis of the $B^- \to D^{*+}\pi^-\pi^-$ decay.

$D_0(2550)^0$ WIDTH

VALUE (MeV)	EVTS	DOCUMENT ID		TECN	COMMENT
165 ±24 OUR AVERAGE		Error includes scale factor of 2.0.			See the ideogram below.
$199 \pm 5 \pm 17$	79k	[1] AAIJ	20D	LHCB	$B^- \to D^{*+}\pi^-\pi^-$
$177.5 \pm 17.8 \pm 46.0$	60k	AAIJ	13CC	LHCB	$pp \to D^{*+}\pi^- X$
$130 \pm 12 \pm 13$	34k	DEL-AMO-SA...	10P	BABR	$e^+e^- \to D^{*+}\pi^- X$

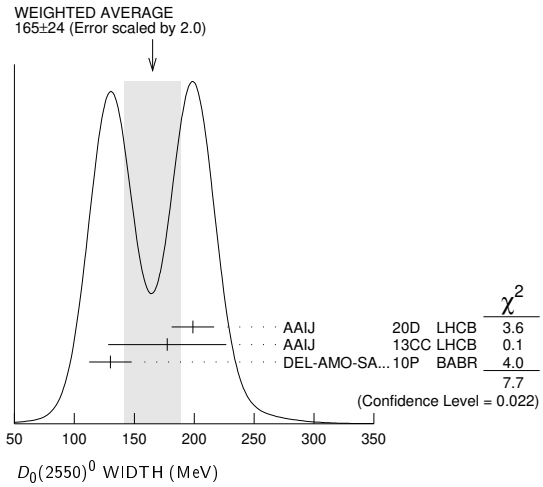

[1] From a full four-body amplitude analysis of the $B^- \to D^{*+}\pi^-\pi^-$ decay.

$D_0(2550)^0$ DECAY MODES

	Mode	Fraction (Γ_i/Γ)
Γ_1	$D^{*+}\pi^-$	seen

$D_0(2550)^0$ POLARIZATION AMPLITUDE A_{D_J}

A polarization amplitude A_{D_J} is a parameter that depends on the initial polarization of the D_J. For D_J decays the helicity angle, θ_H, distribution varies like $1 + A_{D_J}\cos^2(\theta_H)$, where θ_H is the angle in the D_J rest frame between the two pions emitted in the $D_J \to D^*\pi$ and $D^* \to D\pi$ decays.

VALUE	EVTS	DOCUMENT ID		TECN	COMMENT
• • • We do not use the following data for averages, fits, limits, etc. • • •					
4.2 ± 1.3	60k	[1] AAIJ	13CC	LHCB	$pp \to D^{*+}\pi^- X$

[1] Systematic uncertainty not estimated.

$D_0(2550)^0$ REFERENCES

AAIJ	20D	PR D101 032005	R. Aaij et al.	(LHCb Collab.) JP
AAIJ	13CC	JHEP 1309 145	R. Aaij et al.	(LHCb Collab.)
DEL-AMO-SA...	10P	PR D82 111101	P. del Amo Sanchez et al.	(BABAR Collab.)

$D_1^*(2600)^0$

$I(J^P) = \frac{1}{2}(1^-)$

OMITTED FROM SUMMARY TABLE
was $D_J^*(2600)$
$J^P = 1^-$ determined by AAIJ 20D.

$D_1^*(2600)^0$ MASS

VALUE (MeV)	EVTS	DOCUMENT ID		TECN	CHG	COMMENT
2627 ±10 OUR AVERAGE		Error includes scale factor of 4.4.				See the ideogram below.
$2641.9 \pm 1.8 \pm 4.5$	79k	[1] AAIJ	20D	LHCB		$B^- \to D^{*+}\pi^-\pi^-$
$2681.1 \pm 5.6 \pm 14.0$	28k	[2] AAIJ	16AH	LHCB		$B^- \to D^+\pi^-\pi^-$
$2649.2 \pm 3.5 \pm 3.5$	51k	AAIJ	13CC	LHCB		$pp \to D^{*+}\pi^- X$
$2608.7 \pm 2.4 \pm 2.5$	26k	DEL-AMO-SA...	10P	BABR	0	$e^+e^- \to D^+\pi^- X$
$2621.3 \pm 3.7 \pm 4.2$	13k	[3] DEL-AMO-SA...	10P	BABR	+	$e^+e^- \to D^0\pi^+ X$

[1] From a full four-body amplitude analysis of the $B^- \to D^{*+}\pi^-\pi^-$ decay.
[2] From the amplitude analysis in the model describing the $D^+\pi^-$ wave together with virtual contributions from the $D^*(2007)^0$ and B^{*0} states, and components corresponding to the $D_2^*(2460)^0$, $D_1^*(2680)^0$, $D_3^*(2760)^0$, and $D_2^*(3000)^0$ resonances.
[3] At a fixed width of 93 MeV.

Downloaded from https://academic.oup.com/ptep/article/2022/8/083C01/6651666 by KIT Library user on 27 September 2022

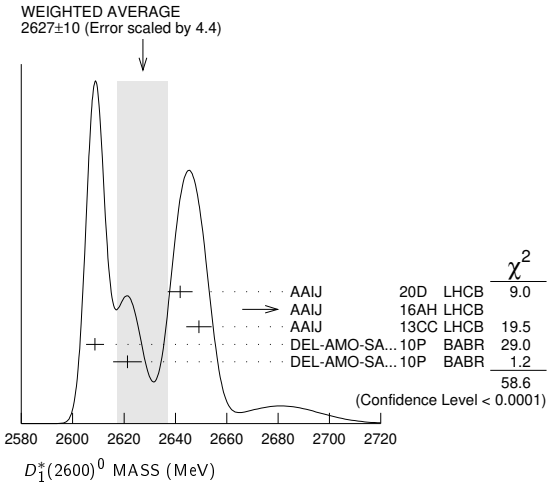

$D_1^*(2600)^0$ WIDTH

VALUE (MeV)	EVTS	DOCUMENT ID		TECN	COMMENT
141 ±23 OUR AVERAGE		Error includes scale factor of 2.7. See the ideogram below.			
149 ± 4 ±20	79k	[1] AAIJ	20D	LHCB	$B^- \to D^{*+}\pi^-\pi^-$
186.7± 8.5 ±11.9	28k	[2] AAIJ	16AH	LHCB	$B^- \to D^+\pi^-\pi^-$
140.2±17.1 ±18.6	51k	AAIJ	13CC	LHCB	$pp \to D^{*+}\pi^- X$
93 ± 6 ±13	26k	DEL-AMO-SA..	10P	BABR	$e^+e^- \to D^+\pi^- X$

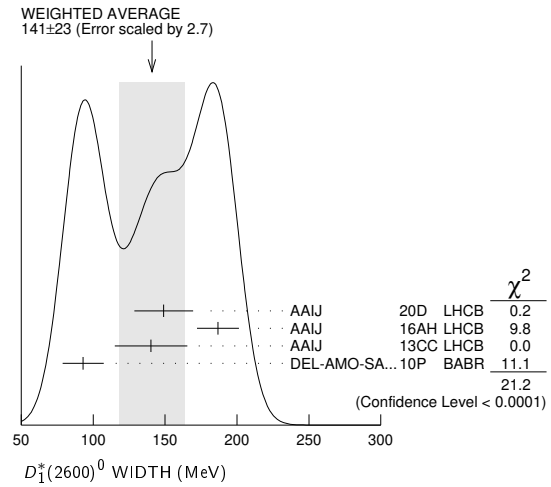

[1] From a full four-body amplitude analysis of the $B^- \to D^{*+}\pi^-\pi^-$ decay.

[2] From the amplitude analysis in the model describing the $D^+\pi^-$ wave together with virtual contributions from the $D^*(2007)^0$ and B^{*0} states, and components corresponding to the $D_2^*(2460)^0$, $D_1^*(2680)^0$, $D_3^*(2760)^0$, and $D_2^*(3000)^0$ resonances.

$D_1^*(2600)^0$ DECAY MODES

	Mode	Fraction (Γ_i/Γ)
Γ_1	$D\pi$	seen
Γ_2	$D^+\pi^-$	seen
Γ_3	$D^0\pi^\pm$	seen
Γ_4	$D^*\pi$	seen
Γ_5	$D^{*+}\pi^-$	seen

$D_1^*(2600)^0$ BRANCHING RATIOS

$\Gamma(D^+\pi^-)/\Gamma(D^{*+}\pi^-)$ — Γ_2/Γ_5

VALUE	EVTS	DOCUMENT ID		TECN	COMMENT
0.32±0.02±0.09	76k	DEL-AMO-SA...	10P	BABR	$e^+e^- \to D^{(*)+}\pi^- X$

$D_1^*(2600)^0$ REFERENCES

AAIJ	20D	PR D101 032005	R. Aaij *et al.*	(LHCb Collab.) JP
AAIJ	16AH	PR D94 072001	R. Aaij *et al.*	(LHCb Collab.)
AAIJ	13CC	JHEP 1309 145	R. Aaij *et al.*	(LHCb Collab.)
DEL-AMO-SA...	10P	PR D82 111101	P. del Amo Sanchez *et al.*	(BABAR Collab.)

$D^*(2640)^\pm$

$I(J^P) = \frac{1}{2}(?^?)$

OMITTED FROM SUMMARY TABLE

Seen in Z decays by ABREU 98M. Not seen by ABBIENDI 01N and CHEKANOV 09. Needs confirmation.

$D^*(2640)^\pm$ MASS

VALUE (MeV)	EVTS	DOCUMENT ID		TECN	COMMENT
2637±2±6	66 ± 14	ABREU	98M	DLPH	$e^+e^- \to D^{*+}\pi^+\pi^- X$

$D^*(2640)^\pm$ WIDTH

VALUE (MeV)	CL%	DOCUMENT ID		TECN	COMMENT
<15	95	ABREU	98M	DLPH	$e^+e^- \to D^{*+}\pi^+\pi^- X$

$D^*(2640)^+$ DECAY MODES

$D^*(2640)^-$ modes are charge conjugates of modes below.

	Mode	Fraction (Γ_i/Γ)
Γ_1	$D^*(2010)^+\pi^+\pi^-$	seen

$D^*(2640)^\pm$ REFERENCES

CHEKANOV	09	EPJ C60 25	S. Chekanov *et al.*	(ZEUS Collab.)
ABBIENDI	01N	EPJ C20 445	G. Abbiendi *et al.*	(OPAL Collab.)
ABREU	98M	PL B426 231	P. Abreu *et al.*	(DELPHI Collab.)

$D_2(2740)^0$

$I(J^P) = \frac{1}{2}(2^-)$

OMITTED FROM SUMMARY TABLE

was $D(2740)^0$

$J^P = 2^-$ determined by (AAIJ 20D).

$D_2(2740)^0$ MASS

VALUE (MeV)	EVTS	DOCUMENT ID		TECN	COMMENT
2747 ±6 OUR AVERAGE					
2751 ±3 ± 7	79k	[1] AAIJ	20D	LHCB	$B^- \to D^{*+}\pi^-\pi^-$
2737.0±3.5±11.2	7.7k	AAIJ	13CC	LHCB	$pp \to D^{*+}\pi^- X$

[1] From a full four-body amplitude analysis of the $B^- \to D^{*+}\pi^-\pi^-$ decay.

$D_2(2740)^0$ WIDTH

VALUE (MeV)	EVTS	DOCUMENT ID		TECN	COMMENT
88 ±19 OUR AVERAGE					
102 ± 6 ±26	79k	[1] AAIJ	20D	LHCB	$B^- \to D^{*+}\pi^-\pi^-$
73.2±13.4±25.0	7.7k	AAIJ	13CC	LHCB	$pp \to D^{*+}\pi^- X$

[1] From a full four-body amplitude analysis of the $B^- \to D^{*+}\pi^-\pi^-$ decay.

$D_2(2740)^0$ DECAY MODES

	Mode	Fraction (Γ_i/Γ)
Γ_1	$D^{*+}\pi^-$	seen

$D_2(2740)^0$ POLARIZATION AMPLITUDE A_{D_J}

A polarization amplitude A_{D_J} is a parameter that depends on the initial polarization of the D_J. For D_J decays the helicity angle, θ_H, distribution varies like $1 + A_{D_J}\cos^2(\theta_H)$, where θ_H is the angle in the D_J rest frame between the two pions emitted in the $D_J \to D^*\pi$ and $D^* \to D\pi$ decays.

VALUE	EVTS	DOCUMENT ID		TECN	COMMENT
• • • We do not use the following data for averages, fits, limits, etc. • • •					
3.1±2.2	7.7k	[1] AAIJ	13CC	LHCB	$pp \to D^{*+}\pi^- X$

[1] Systematic uncertainty not estimated.

$D_2(2740)^0$ REFERENCES

AAIJ	20D	PR D101 032005	R. Aaij *et al.*	(LHCb Collab.) JP
AAIJ	13CC	JHEP 1309 145	R. Aaij *et al.*	(LHCb Collab.)

Downloaded from https://academic.oup.com/ptep/article/2022/8/083C01/6651666 by KIT Library user on 27 September 2022

$D_3^*(2750)$

$I(J^P) = \frac{1}{2}(3^-)$

J^P determined by AAIJ 15Y from the Dalitz plot analysis of $B^0 \to \overline{D}^0 \pi^+ \pi^-$ decays.

$D_3^*(2750)$ MASS

VALUE (MeV)	EVTS	DOCUMENT ID		TECN	CHG	COMMENT
2763.1± 3.2 OUR AVERAGE		Error includes scale factor of 2.1. See the ideogram below.				
2753 ± 4 ± 6	79k	[1] AAIJ	20D	LHCB		$B^- \to D^{*+}\pi^-\pi^-$
2775.5± 4.5± 6.5	28k	[2] AAIJ	16AH	LHCB		$B^- \to D^+\pi^-\pi^-$
2798 ± 7 ± 7		[3] AAIJ	15Y	LHCB		$B^0 \to \overline{D}^0\pi^+\pi^-$
2761.1± 5.1± 6.5	14k	AAIJ	13CC	LHCB	0	$pp \to D^{*+}\pi^-X$
2760.1± 1.1± 3.7	56k	AAIJ	13CC	LHCB	0	$pp \to D^+\pi^-X$
2771.7± 1.7± 3.8	20k	AAIJ	13CC	LHCB	+	$pp \to D^0\pi^+X$
2752.4± 1.7± 2.7	23.5k	[4] DEL-AMO-SA...	10P	BABR	0	$e^+e^- \to D^{*+}\pi^-X$
2763.3± 2.3± 2.3	11.3k	[4] DEL-AMO-SA...	10P	BABR	0	$e^+e^- \to D^+\pi^-X$
2769.7± 3.8± 1.5	5.7k	[4,5] DEL-AMO-SA...	10P	BABR	+	$e^+e^- \to D^0\pi^+X$
• • • We do not use the following data for averages, fits, limits, etc. • • •						
2802 ±11 ±10		[6] AAIJ	15Y	LHCB		$B^0 \to \overline{D}^0\pi^+\pi^-$

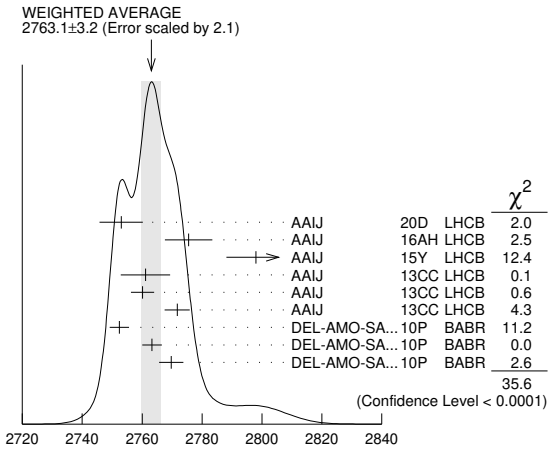

[1] From a full four-body amplitude analysis of the $B^- \to D^{*+}\pi^-\pi^-$ decay.
[2] From the amplitude analysis in the model describing the $D^+\pi^-$ wave together with virtual contributions from the $D^*(2007)^0$ and B^{*0} states, and components corresponding to the $D_2^*(2460)^0$, $D_1^*(2680)^0$, $D_3^*(2760)^0$, and $D_2^*(3000)^0$ resonances.
[3] Modeling the $\pi^+\pi^-$ S-wave with the Isobar formalism.
[4] The states observed in the $D^*\pi$ and $D\pi$ final states are not necessarily the same.
[5] At a fixed width of 60.9 MeV.
[6] Modeling the $\pi^+\pi^-$ S-wave with the K-matrix formalism.

$D_3^*(2750)$ WIDTH

VALUE (MeV)	EVTS	DOCUMENT ID		TECN	CHG	COMMENT
66 ± 5 OUR AVERAGE						
66 ±10 ±14	79k	[1] AAIJ	20D	LHCB		$B^- \to D^{*+}\pi^-\pi^-$
95.3± 9.6±34.0	28k	[2] AAIJ	16AH	LHCB		$B^- \to D^+\pi^-\pi^-$
105 ±18 ±24		[3] AAIJ	15Y	LHCB		$B^0 \to \overline{D}^0\pi^+\pi^-$
74.4± 3.4±37.0	14k	AAIJ	13CC	LHCB	0	$pp \to D^{*+}\pi^-X$
74.4± 3.4±19.1	56k	AAIJ	13CC	LHCB	0	$pp \to D^+\pi^-X$
66.7± 6.6±10.5	20k	AAIJ	13CC	LHCB	+	$pp \to D^0\pi^+X$
71 ± 6 ±11	23.5k	[4] DEL-AMO-SA...	10P	BABR		$e^+e^- \to D^{*+}\pi^-X$
60.9± 5.1± 3.6	11.3k	[4] DEL-AMO-SA...	10P	BABR		$e^+e^- \to D^+\pi^-X$
• • • We do not use the following data for averages, fits, limits, etc. • • •						
154 ±27 ±16		[5] AAIJ	15Y	LHCB		$B^0 \to \overline{D}^0\pi^+\pi^-$

[1] From a full four-body amplitude analysis of the $B^- \to D^{*+}\pi^-\pi^-$ decay.
[2] From the amplitude analysis in the model describing the $D^+\pi^-$ wave together with virtual contributions from the $D^*(2007)^0$ and B^{*0} states, and components corresponding to the $D_2^*(2460)^0$, $D_1^*(2680)^0$, $D_3^*(2760)^0$, and $D_2^*(3000)^0$ resonances.
[3] Modeling the $\pi^+\pi^-$ S-wave with the Isobar formalism.
[4] The states observed in the $D^*\pi$ and $D\pi$ final states are not necessarily the same.
[5] Modeling the $\pi^+\pi^-$ S-wave with the K-matrix formalism.

$D_3^*(2750)$ DECAY MODES

	Mode	Fraction (Γ_i/Γ)
Γ_1	$D\pi$	seen
Γ_2	$D^+\pi^-$	seen
Γ_3	$D^0\pi^\pm$	seen
Γ_4	$D^*\pi$	seen
Γ_5	$D^{*+}\pi^-$	seen

$D_3^*(2750)$ BRANCHING RATIOS

$\Gamma(D^+\pi^-)/\Gamma(D^{*+}\pi^-)$ — **Γ_2/Γ_5**

VALUE	EVTS	DOCUMENT ID		TECN	COMMENT
0.42±0.05±0.11	34.8k	[1] DEL-AMO-SA...	10P	BABR	$e^+e^- \to D^{(*)+}\pi^-X$

[1] The states observed in the $D^*\pi$ and $D\pi$ final states are not necessarily the same.

$D_3^*(2750)$ POLARIZATION AMPLITUDE A_D

A polarization amplitude A_D is a parameter that depends on the initial polarization of the $D_3^*(2750)$. For $D_3^*(2750)$ decays the helicity angle, θ_H, distribution varies like $1 + A_D \cos(\theta_H)$, where θ_H is the angle in the D^* rest frame between the two pions emitted by the $D_3^*(2750) \to D^*\pi$ and $D^* \to D\pi$.

VALUE	EVTS	DOCUMENT ID		TECN	COMMENT
• • • We do not use the following data for averages, fits, limits, etc. • • •					
−0.33±0.28	23.5k	[1] DEL-AMO-SA...	10P	BABR	$e^+e^- \to D^{*+}\pi^-X$

[1] Systematic uncertainties not estimated. The states observed in the $D^*\pi$ and $D\pi$ final states are not necessarily the same.

$D_3^*(2750)$ REFERENCES

AAIJ 20D PR D101 032005 R. Aaij et al. (LHCb Collab.)
AAIJ 16AH PR D94 072001 R. Aaij et al. (LHCb Collab.)
AAIJ 15Y PR D92 032002 R. Aaij et al. (LHCb Collab.) JP
AAIJ 13CC JHEP 1309 145 R. Aaij et al. (LHCb Collab.)
DEL-AMO-SA... 10P PR D82 111101 P. del Amo Sanchez et al. (BABAR Collab.)

$D_1^*(2760)^0$

$I(J^P) = \frac{1}{2}(1^-)$

OMITTED FROM SUMMARY TABLE

J^P determined by AAIJ 15V from the Dalitz plot analysis of $B^- \to D^+K^-\pi^-$ decays.

$D_1^*(2760)^0$ MASS

VALUE (MeV)	EVTS	DOCUMENT ID		TECN	COMMENT
2781±18±13	2k	[1] AAIJ	15V	LHCB	$B^- \to D^+K^-\pi^-$

[1] From the amplitude analysis in the model describing the $D^+\pi^-$ wave together with virtual contributions from the $D^*(2007)^0$ and B^{*0} states, nonresonant spin-0 and spin-1 components as well as the $D_0^*(2400)^0$, $D_2^*(2460)^0$ and $D_1^*(2760)^0$ resonances.

$D_1^*(2760)^0$ WIDTH

VALUE (MeV)	EVTS	DOCUMENT ID		TECN	COMMENT
177±32±21	2k	[1] AAIJ	15V	LHCB	$B^- \to D^+K^-\pi^-$

[1] From the amplitude analysis in the model describing the $D^+\pi^-$ wave together with virtual contributions from the $D^*(2007)^0$ and B^{*0} states, nonresonant spin-0 and spin-1 components as well as the $D_0^*(2400)^0$, $D_2^*(2460)^0$ and $D_1^*(2760)^0$ resonances.

$D_1^*(2760)^0$ DECAY MODES

	Mode	Fraction (Γ_i/Γ)
Γ_1	D^+K^-	seen

$D_1^*(2760)^0$ BRANCHING RATIOS

$\Gamma(D^+K^-)/\Gamma_{total}$ — **Γ_1/Γ**

VALUE	DOCUMENT ID		TECN	COMMENT
seen	[1] AAIJ	15V	LHCB	$B^- \to D^+K^-\pi^-$

[1] From the amplitude analysis in the model describing the $D^+\pi^-$ wave together with virtual contributions from the $D^*(2007)^0$ and B^{*0} states, nonresonant spin-0 and spin-1 components as well as the $D_0^*(2400)^0$, $D_2^*(2460)^0$ and $D_1^*(2760)^0$ resonances.

Downloaded from https://academic.oup.com/ptep/article/2022/8/083C01/6651666 by KIT Library user on 27 September 2022

$D_1^*(2760)^0$ REFERENCES

AAIJ	15V	PR D91 092002	R. Aaij *et al.*	(LHCb Collab.) JP
Also		PR D93 119901 (errat.)	R. Aaij *et al.*	(LHCb Collab.)

$D(3000)^0$

$I(J^P) = \frac{1}{2}(?^?)$

OMITTED FROM SUMMARY TABLE

Both natural- and unnatural-parity components observed depending on the decay mode (AAIJ 13CC).

$D(3000)^0$ MASS

VALUE (MeV)	EVTS	DOCUMENT ID		TECN	COMMENT
3214 ±29 ±49	28k	[1] AAIJ	16AH	LHCB	$B^- \to D^+\pi^-\pi^-$
• • • We do not use the following data for averages, fits, limits, etc. • • •					
2971.8± 8.7	9.5k	[2,3] AAIJ	13CC	LHCB	$pp \to D^{*+}\pi^- X$
3008.1± 4.0	17.6k	[2,4] AAIJ	13CC	LHCB	$pp \to D^+\pi^- X$

[1] From the amplitude analysis in the model describing the $D^+\pi^-$ wave together with virtual contributions from the $D^*(2007)^0$ and B^{*0} states, and components corresponding to the $D_2^*(2460)^0$, $D_1^*(2680)^0$, $D_3^*(2760)^0$, and $D_2^*(3000)^0$ resonances.

[2] Systematic uncertainty not estimated.

[3] Unnatural parity preferred.

[4] Natural parity state. A state $D(3000)^+$ is possibly seen in $D^0\pi^+$ final state.

$D(3000)^0$ WIDTH

VALUE (MeV)	EVTS	DOCUMENT ID		TECN	COMMENT
186 ±38 ±72	28k	[5] AAIJ	16AH	LHCB	$B^- \to D^+\pi^-\pi^-$
• • • We do not use the following data for averages, fits, limits, etc. • • •					
188.1±44.8	9.5k	[6,7] AAIJ	13CC	LHCB	$pp \to D^{*+}\pi^- X$
110.5±11.5	17.6k	[6,8] AAIJ	13CC	LHCB	$pp \to D^+\pi^- X$

[5] From the amplitude analysis in the model describing the $D^+\pi^-$ wave together with virtual contributions from the $D^*(2007)^0$ and B^{*0} states, and components corresponding to the $D_2^*(2460)^0$, $D_1^*(2680)^0$, $D_3^*(2760)^0$, and $D_2^*(3000)^0$ resonances.

[6] Systematic uncertainty not estimated.

[7] Unnatural parity preferred.

[8] Natural parity state. A state $D(3000)^+$ is possibly seen in $D^0\pi^+$ final state.

$D(3000)^0$ DECAY MODES

	Mode	Fraction (Γ_i/Γ)
Γ_1	$D^{*+}\pi^-$	seen

$D(3000)^0$ POLARIZATION AMPLITUDE A_{D_J}

A polarization amplitude A_{D_J} is a parameter that depends on the initial polarization of the D_J. For D_J decays the helicity angle, θ_H, distribution varies like $1 + A_{D_J}\cos^2(\theta_H)$, where θ_H is the angle in the D_J rest frame between the two pions emitted in the $D_J \to D^*\pi$ and $D^* \to D\pi$ decays.

VALUE	EVTS	DOCUMENT ID		TECN	COMMENT
• • • We do not use the following data for averages, fits, limits, etc. • • •					
1.5±0.9	9.5k	[9] AAIJ	13CC	LHCB	$pp \to D^{*+}\pi^- X$

[9] Systematic uncertainty not estimated.

$D(3000)^0$ REFERENCES

AAIJ	16AH	PR D94 072001	R. Aaij *et al.*	(LHCb Collab.)
AAIJ	13CC	JHEP 1309 145	R. Aaij *et al.*	(LHCb Collab.)

Downloaded from https://academic.oup.com/ptep/article/2022/8/083C01/6651666 by KIT Library user on 27 September 2022

CHARMED, STRANGE MESONS ($C = \pm1$, $S = \pm1$) (including possibly non-$q\overline{q}$ states)

$D_s^+ = c\overline{s}$, $D_s^- = \overline{c}s$, similarly for D_s^*'s

$D_s^\pm$

$I(J^P) = 0(0^-)$

The angular distributions of the decays of the ϕ and $\overline{K}^*(892)^0$ in the $\phi\pi^+$ and $K^+\overline{K}^*(892)^0$ modes strongly indicate that the spin is zero. The parity given is that expected of a $c\overline{s}$ ground state.

$D_s^\pm$ MASS

The fit includes $D^\pm$, D^0, $D_s^\pm$, $D^{*\pm}$, D^{*0}, $D_s^{*\pm}$, $D_1(2420)^0$, $D_2^*(2460)^0$, and $D_{s1}(2536)^\pm$ mass and mass difference measurements. Measurements of the $D_s^\pm$ mass with an error greater than 10 MeV are omitted from the fit and average. A number of early measurements have been omitted altogether.

VALUE (MeV)	EVTS	DOCUMENT ID		TECN	COMMENT
1968.35 ± 0.07 OUR FIT					
1969.0 ± 1.4 OUR AVERAGE Error includes scale factor of 1.5. See the ideogram below.					
1967.0 ± 1.0 ± 1.0	54	BARLAG	90C	ACCM	π^- Cu 230 GeV
1969.3 ± 1.4 ± 1.4		ALBRECHT	88	ARG	e^+e^- 9.4–10.6 GeV
1972.7 ± 1.5 ± 1.0	21	BECKER	87B	SILI	200 GeV π, K, p
1972.4 ± 3.7 ± 3.7	27	BLAYLOCK	87	MRK3	e^+e^- 4.14 GeV
1963 ± 3 ± 3	30	DERRICK	85B	HRS	e^+e^- 29 GeV
1970 ± 5 ± 5	104	CHEN	83C	CLEO	e^+e^- 10.5 GeV
• • • We do not use the following data for averages, fits, limits, etc. • • •					
1968.3 ± 0.7 ± 0.7	290	[1] ANJOS	88	E691	Photoproduction
1980 ±15	6	USHIDA	86	EMUL	ν wideband
1973.6 ± 2.6 ± 3.0	163	ALBRECHT	85D	ARG	e^+e^- 10 GeV
1948 ±28 ±10	65	AIHARA	84D	TPC	e^+e^- 29 GeV
1975 ± 9 ±10	49	ALTHOFF	84	TASS	e^+e^- 14–25 GeV
1975 ± 4	3	BAILEY	84	ACCM	hadron$^+$ Be $\to \phi\pi^+$ X

[1] ANJOS 88 enters the fit via $m_{D_s^\pm} - m_{D^\pm}$ (see below).

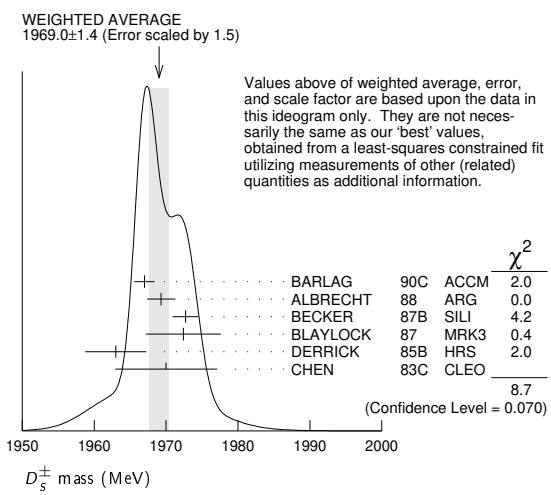

$m_{D_s^\pm} - m_{D^\pm}$

The fit includes $D^\pm$, D^0, $D_s^\pm$, $D^{*\pm}$, D^{*0}, $D_s^{*\pm}$, $D_1(2420)^0$, $D_2^*(2460)^0$, and $D_{s1}(2536)^\pm$ mass and mass difference measurements.

VALUE (MeV)	EVTS	DOCUMENT ID		TECN	COMMENT
98.69±0.05 OUR FIT					
98.69±0.05 OUR AVERAGE					
98.68±0.03±0.04		AAIJ	13V	LHCB	$D_s^+ \to K^+K^-\pi^+$
99.41±0.38±0.21		ACOSTA	03D	CDF2	$\overline{p}p$, $\sqrt{s}$= 1.96 TeV
98.4 ±0.1 ±0.3	48k	AUBERT	02G	BABR	$e^+e^- \approx \Upsilon(4S)$
99.5 ±0.6 ±0.3		BROWN	94	CLE2	$e^+e^- \approx \Upsilon(4S)$
98.5 ±1.5	555	CHEN	89	CLEO	e^+e^- 10.5 GeV
99.0 ±0.8	290	ANJOS	88	E691	Photoproduction

$D_s^\pm$ MEAN LIFE

Measurements with an error greater than 100×10^{-15} s or with fewer than 100 events have been omitted from the Listings.

VALUE (10^{-15} s)	EVTS	DOCUMENT ID		TECN	COMMENT
504 ± 4 OUR AVERAGE Error includes scale factor of 1.2.					
506.4± 3.0± 1.7±1.7		[1] AAIJ	17AN	LHCB	pp at 7, 8 TeV
507.4± 5.5± 5.1	13.6k	LINK	05J	FOCS	$\Phi\pi^+$ and $\overline{K}^{*0}K^+$
472.5±17.2± 6.6	760	IORI	01	SELX	600 GeV Σ^-, π^-, p
518 ±14 ± 7	1662	AITALA	99	E791	π^- nucleus, 500 GeV
$486.3 \pm 15.0^{+4.9}_{-5.1}$	2167	[2] BONVICINI	99	CLE2	$e^+e^- \approx \Upsilon(4S)$
475 ±20 ± 7	900	FRABETTI	93F	E687	γBe, $\phi\pi^+$
500 ±60 ±30	104	FRABETTI	90	E687	γBe, $\phi\pi^+$
470 ±40 ±20	228	RAAB	88	E691	Photoproduction

[1] This AAIJ 17AN value is derived from the difference between the D_s^- and D^- widths. The 3rd uncertainty, $\pm1.7 \times 10^{-15}$ s, arises from the uncertainty of the D^- width.
[2] BONVICINI 99 obtains 1.19 ± 0.04 for the ratio of D_s^+ to D^0 lifetimes.

D_s^+ DECAY MODES

Unless otherwise noted, the branching fractions for modes with a resonance in the final state include all the decay modes of the resonance. D_s^- modes are charge conjugates of the modes below.

	Mode		Fraction (Γ_i/Γ)	Scale factor/ Confidence level
	Inclusive modes			
Γ_1	e^+ semileptonic	[a]	(6.33 ±0.15) %	
Γ_2	π^+ anything		(119.3 ±1.4) %	
Γ_3	π^- anything		(43.2 ±0.9) %	
Γ_4	π^0 anything		(123 ±7) %	
Γ_5	K^- anything		(18.7 ±0.5) %	
Γ_6	K^+ anything		(28.9 ±0.7) %	
Γ_7	K_S^0 anything		(19.0 ±1.1) %	
Γ_8	η anything	[b]	(29.9 ±2.8) %	
Γ_9	ω anything		(6.1 ±1.4) %	
Γ_{10}	η' anything	[c]	(10.3 ±1.4) %	S=1.1
Γ_{11}	$f_0(980)$ anything, $f_0 \to \pi^+\pi^-$		< 1.3 %	CL=90%
Γ_{12}	ϕ anything		(15.7 ±1.0) %	
Γ_{13}	K^+K^- anything		(15.8 ±0.7) %	
Γ_{14}	$K_S^0K^+$ anything		(5.8 ±0.5) %	
Γ_{15}	$K_S^0K^-$ anything		(1.9 ±0.4) %	
Γ_{16}	$2K_S^0$ anything		(1.70 ±0.32) %	
Γ_{17}	$2K^+$ anything		< 2.6 $\times 10^{-3}$	CL=90%
Γ_{18}	$2K^-$ anything		< 6 $\times 10^{-4}$	CL=90%
	Leptonic and semileptonic modes			
Γ_{19}	$e^+\nu_e$		< 8.3 $\times 10^{-5}$	CL=90%
Γ_{20}	$\mu^+\nu_\mu$		(5.43 ±0.15) $\times 10^{-3}$	
Γ_{21}	$\tau^+\nu_\tau$		(5.32 ±0.11) %	
Γ_{22}	$\gamma e^+\nu_e$		< 1.3 $\times 10^{-4}$	CL=90%
Γ_{23}	$K^+K^-e^+\nu_e$		—	
Γ_{24}	$\phi e^+\nu_e$	[d]	(2.39 ±0.16) %	S=1.3
Γ_{25}	$\phi\mu^+\nu_\mu$		(1.9 ±0.5) %	
Γ_{26}	$\eta e^+\nu_e + \eta'(958)e^+\nu_e$	[d]	(3.03 ±0.24) %	
Γ_{27}	$\eta e^+\nu_e$	[d]	(2.32 ±0.08) %	
Γ_{28}	$\eta'(958)e^+\nu_e$	[d]	(8.0 ±0.7) $\times 10^{-3}$	
Γ_{29}	$\eta\mu^+\nu_\mu$		(2.4 ±0.5) %	
Γ_{30}	$\eta'(958)\mu^+\nu_\mu$		(1.1 ±0.5) %	
Γ_{31}	$\omega e^+\nu_e$	[e]	< 2.0 $\times 10^{-3}$	CL=90%
Γ_{32}	$K^0e^+\nu_e$		(3.4 ±0.4) $\times 10^{-3}$	
Γ_{33}	$K^*(892)^0e^+\nu_e$	[d]	(2.15 ±0.28) $\times 10^{-3}$	S=1.1
Γ_{34}	$f_0(980)e^+\nu_e$, $f_0 \to \pi^+\pi^-$			
Γ_{35}	$a_0(980)^0e^+\nu_e$, $a_0(980)^0 \to \pi^0\eta$		< 1.2 $\times 10^{-4}$	CL=90%
	Hadronic modes with a $K\overline{K}$ pair			
Γ_{36}	$K^+K_S^0$		(1.453±0.035) %	
Γ_{37}	$K^+K_L^0$		(1.49 ±0.06) %	
Γ_{38}	$K^+\overline{K}^0$		(2.95 ±0.14) %	
Γ_{39}	$K^+K^-\pi^+$	[f]	(5.38 ±0.10) %	S=1.1
Γ_{40}	$\phi\pi^+$	[d,g]	(4.5 ±0.4) %	
Γ_{41}	$\phi\pi^+$, $\phi \to K^+K^-$	[g]	(2.22 ±0.06) %	
Γ_{42}	$K^+\overline{K}^*(892)^0$, $\overline{K}^{*0} \to K^-\pi^+$		(2.58 ±0.06) %	
Γ_{43}	$f_0(980)\pi^+$, $f_0 \to K^+K^-$		(1.11 ±0.19) %	

Downloaded from https://academic.oup.com/ptep/article/2022/8/083C01/6651666 by KIT Library user on 27 September 2022

Γ_{44}	$f_0(1370)\pi^+$, $f_0 \to K^+K^-$		$(7.1 \pm 2.9) \times 10^{-4}$		
Γ_{45}	$f_0(1710)\pi^+$, $f_0 \to K^+K^-$		$(6.7 \pm 2.8) \times 10^{-4}$		
Γ_{46}	$K^+\overline{K}_0^*(1430)^0$, $\overline{K}_0^* \to K^-\pi^+$		$(1.76 \pm 0.25) \times 10^{-3}$		
Γ_{47}	$K^+K_S^0\pi^0$		(1.52 ± 0.22) %		
Γ_{48}	$2K_S^0\pi^+$		$(7.7 \pm 0.6) \times 10^{-3}$		
Γ_{49}	$K^0\overline{K}^0\pi^+$		—		
Γ_{50}	$K^*(892)^+\overline{K}^0$	[d]	(5.4 ± 1.2) %		
Γ_{51}	$K^+K^-\pi^+\pi^0$		(5.50 ± 0.24) %		S=1.3
Γ_{52}	$\phi\rho^+$	[d]	(5.59 ± 0.34) %		
Γ_{53}	$\overline{K}_1(1270)^0K^+$, $\overline{K}_1(1270)^0 \to K^-\rho^+$		$(5.7 \pm 0.6) \times 10^{-3}$		
Γ_{54}	$\overline{K}_1(1270)^0K^+$, $\overline{K}_1(1270)^0 \to K^*(892)\pi$		(1.31 ± 0.25) %		
Γ_{55}	$\overline{K}_1(1400)^0K^+$, $\overline{K}_1(1400)^0 \to K^*(892)\pi$		(2.0 ± 0.4) %		
Γ_{56}	$a_0(980)^0\rho^+$, $a_0(980)^0 \to K^+K^-$		$(1.9 \pm 0.4) \times 10^{-3}$		
Γ_{57}	$f_1(1420)^0\pi^+$, $f_1(1420)^0 \to K^*(892)^\mp K^\pm$		$(3.9 \pm 0.7) \times 10^{-3}$		
Γ_{58}	$f_1(1420)^0\pi^+$, $f_1(1420)^0 \to a_0(980)^0\pi^0$, $a_0(980)^0 \to K^+K^-$		$(4.0 \pm 1.4) \times 10^{-4}$		
Γ_{59}	$\eta(1475)\pi^+$, $\eta(1475) \to a_0(980)^0\pi^0$, $a_0(980)^0 \to K^+K^-$		$(7.0 \pm 2.8) \times 10^{-4}$		
Γ_{60}	$K_S^0K^-2\pi^+$		(1.53 ± 0.08) %		S=1.5
Γ_{61}	$K^*(892)^+\overline{K}^*(892)^0$	[d]	(5.64 ± 0.35) %		
Γ_{62}	$\eta(1475)K_S^0$, $\eta \to K^*(892)^0\pi^+$, $K^{*0} \to K^-\pi^+$		$(3.4 \pm 1.0) \times 10^{-4}$		
Γ_{63}	$\eta(1475)\pi^+$, $\eta \to \overline{K}^*(892)^+K^-$, $\overline{K}^{*+} \to K_S^0\pi^+$		$(3.4 \pm 1.0) \times 10^{-4}$		
Γ_{64}	$\eta(1475)\pi^+$, $\eta \to a_0(980)^-\pi^+$, $a_0^- \to K_S^0K^-$		$(1.7 \pm 0.9) \times 10^{-3}$		
Γ_{65}	$f_1(1285)\pi^+$, $f_1 \to a_0(980)^-\pi^+$, $a_0^- \to K_S^0K^-$		$(3.4 \pm 0.8) \times 10^{-4}$		
Γ_{66}	$K^+K_S^0\pi^+\pi^-$		$(9.5 \pm 0.8) \times 10^{-3}$		S=1.1
Γ_{67}	$K^+K^-2\pi^+\pi^-$		$(8.6 \pm 1.5) \times 10^{-3}$		
Γ_{68}	$\phi 2\pi^+\pi^-$	[d]	(1.21 ± 0.16) %		
Γ_{69}	$\phi\rho^0\pi^+$, $\phi \to K^+K^-$		$(6.4 \pm 1.3) \times 10^{-3}$		
Γ_{70}	$\phi a_1(1260)^+$, $\phi \to K^+K^-$, $a_1^+ \to \rho^0\pi^+$		$(7.4 \pm 1.2) \times 10^{-3}$		
Γ_{71}	$\phi 2\pi^+\pi^-$ non-ρ, $\phi \to K^+K^-$		$(1.8 \pm 0.7) \times 10^{-3}$		
Γ_{72}	$K^+K^-\rho^0\pi^+$ non-ϕ	<	2.6×10^{-4}		CL=90%
Γ_{73}	$K^+K^-2\pi^+\pi^-$ nonresonant		$(9 \pm 7) \times 10^{-4}$		
Γ_{74}	$2K_S^0 2\pi^+\pi^-$		$(7.8 \pm 3.3) \times 10^{-4}$		

Hadronic modes without K's

Γ_{75}	$\pi^+\pi^0$	<	1.2×10^{-4}		CL=90%
Γ_{76}	$2\pi^+\pi^-$		(1.08 ± 0.04) %		
Γ_{77}	$\rho^0\pi^+$		$(1.9 \pm 1.2) \times 10^{-4}$		
Γ_{78}	$\pi^+(\pi^+\pi^-)_{S-\text{wave}}$	[h]	$(9.0 \pm 0.4) \times 10^{-3}$		
Γ_{79}	$f_0(980)\pi^+$, $f_0 \to \pi^+\pi^-$				
Γ_{80}	$f_0(1370)\pi^+$, $f_0 \to \pi^+\pi^-$				
Γ_{81}	$f_0(1500)\pi^+$, $f_0 \to \pi^+\pi^-$				
Γ_{82}	$f_2(1270)\pi^+$, $f_2 \to \pi^+\pi^-$		$(1.09 \pm 0.19) \times 10^{-3}$		
Γ_{83}	$\rho(1450)^0\pi^+$, $\rho^0 \to \pi^+\pi^-$		$(2.9 \pm 1.9) \times 10^{-4}$		
Γ_{84}	$\pi^+2\pi^0$		$(6.5 \pm 1.3) \times 10^{-3}$		
Γ_{85}	$2\pi^+\pi^-\pi^0$		—		
Γ_{86}	$\eta\pi^+$	[d]	(1.68 ± 0.09) %		S=1.1
Γ_{87}	$\omega\pi^+$	[d]	$(1.92 \pm 0.30) \times 10^{-3}$		
Γ_{88}	$3\pi^+2\pi^-$		$(7.9 \pm 0.8) \times 10^{-3}$		
Γ_{89}	$2\pi^+\pi^-2\pi^0$		—		
Γ_{90}	$\eta\rho^+$	[d]	(8.9 ± 0.8) %		
Γ_{91}	$\eta\pi^+\pi^0$		(9.5 ± 0.5) %		
Γ_{92}	$\eta(\pi^+\pi^0)_{P-wave}$		$(5.1 \pm 3.1) \times 10^{-3}$		
Γ_{93}	$2\pi^+\pi^-\eta$		(3.12 ± 0.16) %		
Γ_{94}	$a_1(1260)^+\eta$, $a_1^+ \to \rho(770)^0\pi^+$, $\rho^0 \to \pi^+\pi^-$		(1.73 ± 0.16) %		
Γ_{95}	$a_1(1260)^+\eta$, $a_1^+ \to f_0(500)\pi^+$, $f_0 \to \pi^+\pi^-$		$(2.5 \pm 0.9) \times 10^{-3}$		
Γ_{96}	$a_0(980)^+\pi^{0+}$, $a_0(980)^+ \to \eta\pi^+$		(2.2 ± 0.4) %		
Γ_{97}	$a_0(980)^+\rho(770)^0$, $a_0^+ \to \eta\pi^+$		$(2.1 \pm 0.9) \times 10^{-3}$		
Γ_{98}	$\eta(1405)\pi^+$, $\eta(1405) \to a_0(980)^-\pi^+$, $a_0^- \to \eta\pi^-$		$(2.2 \pm 0.7) \times 10^{-4}$		
Γ_{99}	$\eta(1405)\pi^+$, $\eta(1405) \to a_0(980)^+\pi^-$, $a_0^+ \to \eta\pi^+$		$(2.2 \pm 0.7) \times 10^{-4}$		
Γ_{100}	$f_1(1420)\pi^+$, $f_1 \to a_0(980)^-\pi^+$, $a_0^- \to \eta\pi^-$		$(5.9 \pm 1.8) \times 10^{-4}$		
Γ_{101}	$f_1(1420)\pi^+$, $f_1 \to a_0(980)^+\pi^-$, $a_0^+ \to \eta\pi^+$		$(5.3 \pm 1.8) \times 10^{-4}$		
Γ_{102}	$\omega\pi^+\pi^0$	[d]	(2.8 ± 0.7) %		
Γ_{103}	$3\pi^+2\pi^-\pi^0$		(4.9 ± 3.2) %		
Γ_{104}	$\omega 2\pi^+\pi^-$	[d]	(1.6 ± 0.5) %		
Γ_{105}	$\eta'(958)\pi^+$	[c,d]	(3.94 ± 0.25) %		
Γ_{106}	$3\pi^+2\pi^-2\pi^0$		—		
Γ_{107}	$\omega\eta\pi^+$	[d]	< 2.13 %		CL=90%
Γ_{108}	$\eta'(958)\rho^+$	[c,d]	(5.8 ± 1.5) %		
Γ_{109}	$\eta'(958)\pi^+\pi^0$		(5.6 ± 0.8) %		
Γ_{110}	$\eta'(958)\pi^+\pi^0$ nonresonant		< 5.1 %		CL=90%

Modes with one or three K's

Γ_{111}	$K^+\pi^0$		$(7.4 \pm 0.5) \times 10^{-4}$		
Γ_{112}	$K_S^0\pi^+$		$(1.10 \pm 0.05) \times 10^{-3}$		
Γ_{113}	$K^+\eta$	[d]	$(1.73 \pm 0.08) \times 10^{-3}$		
Γ_{114}	$K^+\omega$	[d]	$(8.7 \pm 2.5) \times 10^{-4}$		
Γ_{115}	$K^+\eta'(958)$	[d]	$(2.64 \pm 0.24) \times 10^{-3}$		
Γ_{116}	$K^+\pi^+\pi^-$		$(6.5 \pm 0.4) \times 10^{-3}$		
Γ_{117}	$K^+\rho^0$		$(2.5 \pm 0.4) \times 10^{-3}$		
Γ_{118}	$K^+\rho(1450)^0$, $\rho^0 \to \pi^+\pi^-$		$(6.9 \pm 2.4) \times 10^{-4}$		
Γ_{119}	$K^*(892)^0\pi^+$, $K^{*0} \to K^+\pi^-$		$(1.40 \pm 0.24) \times 10^{-3}$		
Γ_{120}	$K^*(1410)^0\pi^+$, $K^{*0} \to K^+\pi^-$		$(1.22 \pm 0.28) \times 10^{-3}$		
Γ_{121}	$K^*(1430)^0\pi^+$, $K^{*0} \to K^+\pi^-$		$(5.0 \pm 3.4) \times 10^{-4}$		
Γ_{122}	$K^+\pi^+\pi^-$ nonresonant		$(1.03 \pm 0.34) \times 10^{-3}$		
Γ_{123}	$K^0\pi^+\pi^0$		(1.08 ± 0.06) %		
Γ_{124}	$K_S^0 2\pi^+\pi^-$		$(2.8 \pm 1.0) \times 10^{-3}$		
Γ_{125}	$K^+\omega\pi^0$	[d]	< 8.2×10^{-3}		CL=90%
Γ_{126}	$K^+\omega\pi^+\pi^-$	[d]	< 5.4×10^{-3}		CL=90%
Γ_{127}	$K^+\omega\eta$	[d]	< 7.9×10^{-3}		CL=90%
Γ_{128}	$2K^+K^-$		$(2.15 \pm 0.20) \times 10^{-4}$		
Γ_{129}	ϕK^+, $\phi \to K^+K^-$		$(8.8 \pm 2.0) \times 10^{-5}$		

Doubly Cabibbo-suppressed modes

Γ_{130}	$2K^+\pi^-$		$(1.276 \pm 0.031) \times 10^{-4}$		
Γ_{131}	$K^+K^*(892)^0$, $K^{*0} \to K^+\pi^-$		$(6.0 \pm 3.4) \times 10^{-5}$		

Baryon-antibaryon mode

Γ_{132}	$p\overline{n}$		$(1.22 \pm 0.11) \times 10^{-3}$		
Γ_{133}	$p\overline{p}e^+\nu_e$	<	2.0×10^{-4}		CL=90%

$\Delta C = 1$ weak neutral current ($C1$) modes, Lepton family number (LF), or Lepton number (L) violating modes

Γ_{134}	$\pi^+e^+e^-$	[i]	< 5.5×10^{-6}		CL=90%
Γ_{135}	$\pi^+\phi$, $\phi \to e^+e^-$	[j]	$(6 {}^{+8}_{-4}) \times 10^{-6}$		
Γ_{136}	$\pi^+\mu^+\mu^-$	[i]	< 1.8×10^{-7}		CL=90%
Γ_{137}	$K^+e^+e^-$	$C1$	< 3.7×10^{-6}		CL=90%
Γ_{138}	$K^+\mu^+\mu^-$	$C1$	< 1.4×10^{-7}		CL=90%
Γ_{139}	$K^*(892)^+\mu^+\mu^-$	$C1$	< 1.4×10^{-3}		CL=90%
Γ_{140}	$\pi^+e^+\mu^-$	LF	< 1.1×10^{-6}		CL=90%
Γ_{141}	$\pi^+e^-\mu^+$	LF	< 9.4×10^{-7}		CL=90%
Γ_{142}	$K^+e^+\mu^-$	LF	< 7.9×10^{-7}		CL=90%
Γ_{143}	$K^+e^-\mu^+$	LF	< 5.6×10^{-7}		CL=90%
Γ_{144}	π^-2e^+	L	< 1.4×10^{-6}		CL=90%
Γ_{145}	$\pi^-2\mu^+$	L	< 8.6×10^{-8}		CL=90%
Γ_{146}	$\pi^-e^+\mu^+$	L	< 6.3×10^{-7}		CL=90%
Γ_{147}	K^-2e^+	L	< 7.7×10^{-7}		CL=90%
Γ_{148}	$K^-2\mu^+$	L	< 2.6×10^{-8}		CL=90%
Γ_{149}	$K^-e^+\mu^+$	L	< 2.6×10^{-7}		CL=90%
Γ_{150}	$K^*(892)^-2\mu^+$	L	< 1.4×10^{-3}		CL=90%

Downloaded from https://academic.oup.com/ptep/article/2022/8/083C01/6651666 by KIT Library user on 27 September 2022

[a] This is the purely e^+ semileptonic branching fraction: the e^+ fraction from τ^+ decays has been subtracted off. The sum of our (non-τ) e^+ exclusive fractions — an $e^+\nu_e$ with an η, η', ϕ, K^0, or K^{*0} — is 5.99 ± 0.31 %.

[b] This fraction includes η from η' decays.

[c] The sum of our exclusive η' fractions — $\eta' e^+\nu_e$, $\eta'\mu^+\nu_\mu$, $\eta'\pi^+$, $\eta'\rho^+$, and $\eta' K^+$ — is 11.8 ± 1.6%.

[d] This branching fraction includes all the decay modes of the final-state resonance.

[e] A test for $u\overline{u}$ or $d\overline{d}$ content in the D_s^+. Neither Cabibbo-favored nor Cabibbo-suppressed decays can contribute, and $\omega-\phi$ mixing is an unlikely explanation for any fraction above about 2×10^{-4}.

[f] The branching fraction for this mode may differ from the sum of the submodes that contribute to it, due to interference effects. See the relevant papers.

[g] We decouple the $D_s^+ \to \phi\pi^+$ branching fraction obtained from mass projections (and used to get some of the other branching fractions) from the $D_s^+ \to \phi\pi^+$, $\phi \to K^+K^-$ branching fraction obtained from the Dalitz-plot analysis of $D_s^+ \to K^+K^-\pi^+$. That is, the ratio of these two branching fractions is not exactly the $\phi \to K^+K^-$ branching fraction 0.491.

[h] This is the average of a model-independent and a K-matrix parametrization of the $\pi^+\pi^-$ S-wave and is a sum over several f_0 mesons.

[i] This mode is not a useful test for a ΔC=1 weak neutral current because both quarks must change flavor in this decay.

[j] This is *not* a test for the ΔC=1 weak neutral current, but leads to the $\pi^+\ell^+\ell^-$ final state.

CONSTRAINED FIT INFORMATION

An overall fit to 13 branching ratios uses 21 measurements and one constraint to determine 10 parameters. The overall fit has a χ^2 = 11.6 for 12 degrees of freedom.

The following *off-diagonal* array elements are the correlation coefficients $\langle\delta x_i\delta x_j\rangle/(\delta x_i\cdot\delta x_j)$, in percent, from the fit to the branching fractions, $x_i \equiv \Gamma_i/\Gamma_{total}$. The fit constrains the x_i whose labels appear in this array to sum to one.

x_{39}	27							
x_{51}	8	1						
x_{60}	25	6	15					
x_{66}	20	4	12	46				
x_{76}	17	33	2	7	5			
x_{86}	1	14	−9	−15	−12	6		
x_{87}	0	1	0	−1	0	0	4	
x_{116}	3	20	−6	−9	−7	7	12	0
	x_{36}	x_{39}	x_{51}	x_{60}	x_{66}	x_{76}	x_{86}	x_{87}

See the related review(s):

D_s^+ Branching Fractions

D_s^+ BRANCHING RATIOS

A number of older, now obsolete results have been omitted. They may be found in earlier editions.

Inclusive modes

$\Gamma(e^+\text{semileptonic})/\Gamma_{total}$ — Γ_1/Γ

This is the purely e^+ semileptonic branching fraction: the e^+ fraction from τ^+ decays has been subtracted off.

VALUE (%)	EVTS	DOCUMENT ID		TECN	COMMENT
6.33±0.15 OUR AVERAGE					
6.30±0.13±0.10	17k	[1,2] ABLIKIM	21AC	BES3	e^+e^- at 4.178–4.230 GeV
6.52±0.39±0.15	0.5k	[3] ASNER	10	CLEO	e^+e^- at 3774 MeV

[1] ABLIKIM 21AC finds that the ratio of the D_s^+ and D^0 semielectronic widths is 0.790 ± 0.016 ± 0.020.

[2] ABLIKIM 21AC reports a value of (6.30 ± 0.13 ± 0.09 ± 0.04) × 10^{-2}, where the last uncertainty is an external systematic from B($D_s^+ \to \tau\nu$). We have added the systematic uncertainties in quadrature.

[3] Using the D_s^+ and D^0 lifetimes, ASNER 10 finds that the ratio of the D_s^+ and D^0 semileptonic widths is 0.828 ± 0.051 ± 0.025.

$\Gamma(\pi^+\text{anything})/\Gamma_{total}$ — Γ_2/Γ

Events with two π^+'s count twice, etc. But π^+'s from $K_S^0 \to \pi^+\pi^-$ are not included.

VALUE (%)	DOCUMENT ID		TECN	COMMENT
119.3±1.2±0.7	DOBBS	09	CLEO	e^+e^- at 4170 MeV

$\Gamma(\pi^-\text{anything})/\Gamma_{total}$ — Γ_3/Γ

Events with two π^-'s count twice, etc. But π^-'s from $K_S^0 \to \pi^+\pi^-$ are not included.

VALUE (%)	DOCUMENT ID		TECN	COMMENT
43.2±0.9±0.3	DOBBS	09	CLEO	e^+e^- at 4170 MeV

$\Gamma(\pi^0\text{anything})/\Gamma_{total}$ — Γ_4/Γ

Events with two π^0's count twice, etc. But π^0's from $K_S^0 \to 2\pi^0$ are not included.

VALUE (%)	DOCUMENT ID		TECN	COMMENT
123.4±3.8±5.3	DOBBS	09	CLEO	e^+e^- at 4170 MeV

$\Gamma(K^-\text{anything})/\Gamma_{total}$ — Γ_5/Γ

VALUE (%)	DOCUMENT ID		TECN	COMMENT
18.7±0.5±0.2	DOBBS	09	CLEO	e^+e^- at 4170 MeV

$\Gamma(K^+\text{anything})/\Gamma_{total}$ — Γ_6/Γ

VALUE (%)	DOCUMENT ID		TECN	COMMENT
28.9±0.6±0.3	DOBBS	09	CLEO	e^+e^- at 4170 MeV

$\Gamma(K_S^0\text{anything})/\Gamma_{total}$ — Γ_7/Γ

VALUE (%)	DOCUMENT ID		TECN	COMMENT
19.0±1.0±0.4	DOBBS	09	CLEO	e^+e^- at 4170 MeV

$\Gamma(\eta\text{anything})/\Gamma_{total}$ — Γ_8/Γ

This ratio includes η particles from η' decays.

VALUE (%)	EVTS	DOCUMENT ID		TECN	COMMENT
29.9±2.2±1.7		DOBBS	09	CLEO	e^+e^- at 4170 MeV
• • • We do not use the following data for averages, fits, limits, etc. • • •					
23.5±3.1±2.0	674 ± 91	HUANG	06B	CLEO	See DOBBS 09

$\Gamma(\omega\text{anything})/\Gamma_{total}$ — Γ_9/Γ

VALUE (%)	DOCUMENT ID		TECN	COMMENT
6.1±1.4±0.3	DOBBS	09	CLEO	e^+e^- at 4170 MeV

$\Gamma(\eta'\text{anything})/\Gamma_{total}$ — Γ_{10}/Γ

VALUE (%)	EVTS	DOCUMENT ID		TECN	COMMENT
10.3±1.4 OUR AVERAGE Error includes scale factor of 1.1.					
8.8±1.8±0.5	68	ABLIKIM	15Z	BES3	482 pb^{-1}, 4009 MeV
11.7±1.7±0.7		DOBBS	09	CLEO	e^+e^- at 4170 MeV
• • • We do not use the following data for averages, fits, limits, etc. • • •					
8.7±1.9±0.8	68	HUANG	06B	CLEO	See DOBBS 09

$\Gamma(f_0(980)\text{anything}, f_0 \to \pi^+\pi^-)/\Gamma_{total}$ — Γ_{11}/Γ

VALUE (%)	CL%	DOCUMENT ID		TECN	COMMENT
<1.3	90	DOBBS	09	CLEO	e^+e^- at 4170 MeV

$\Gamma(\phi\text{anything})/\Gamma_{total}$ — Γ_{12}/Γ

VALUE (%)	EVTS	DOCUMENT ID		TECN	COMMENT
15.7±0.8±0.6		DOBBS	09	CLEO	e^+e^- at 4170 MeV
• • • We do not use the following data for averages, fits, limits, etc. • • •					
16.1±1.2±1.1	398 ± 27	HUANG	06B	CLEO	See DOBBS 09

$\Gamma(K^+K^-\text{anything})/\Gamma_{total}$ — Γ_{13}/Γ

VALUE (%)	DOCUMENT ID		TECN	COMMENT
15.8±0.6±0.3	DOBBS	09	CLEO	e^+e^- at 4170 MeV

$\Gamma(K_S^0K^+\text{anything})/\Gamma_{total}$ — Γ_{14}/Γ

VALUE (%)	DOCUMENT ID		TECN	COMMENT
5.8±0.5±0.1	DOBBS	09	CLEO	e^+e^- at 4170 MeV

$\Gamma(K_S^0K^-\text{anything})/\Gamma_{total}$ — Γ_{15}/Γ

VALUE (%)	DOCUMENT ID		TECN	COMMENT
1.9±0.4±0.1	DOBBS	09	CLEO	e^+e^- at 4170 MeV

$\Gamma(2K_S^0\text{anything})/\Gamma_{total}$ — Γ_{16}/Γ

VALUE (%)	DOCUMENT ID		TECN	COMMENT
1.7±0.3±0.1	DOBBS	09	CLEO	e^+e^- at 4170 MeV

$\Gamma(2K^+\text{anything})/\Gamma_{total}$ — Γ_{17}/Γ

VALUE (%)	CL%	DOCUMENT ID		TECN	COMMENT
<0.26	90	DOBBS	09	CLEO	e^+e^- at 4170 MeV

$\Gamma(2K^-\text{anything})/\Gamma_{total}$ — Γ_{18}/Γ

VALUE (%)	CL%	DOCUMENT ID		TECN	COMMENT
<0.06	90	DOBBS	09	CLEO	e^+e^- at 4170 MeV

Downloaded from https://academic.oup.com/ptep/article/2022/8/083C01/6651666 by KIT Library user on 27 September 2022

Leptonic and semileptonic modes

See the related review(s):

Leptonic Decays of Charged Pseudoscalar Mesons

$\Gamma(e^+\nu_e)/\Gamma_{total}$ — Γ_{19}/Γ

VALUE	CL%	DOCUMENT ID		TECN	COMMENT
$<0.83\times10^{-4}$	90	[1] ZUPANC	13	BELL	e^+e^- at $\Upsilon(4S),\Upsilon(5S)$
• • • We do not use the following data for averages, fits, limits, etc. • • •					
$<2.3\ \times10^{-4}$	90	DEL-AMO-SA...	10J	BABR	e^+e^-, 10.58 GeV
$<1.2\ \times10^{-4}$	90	ALEXANDER	09	CLEO	e^+e^- at 4170 MeV
$<1.3\ \times10^{-4}$	90	PEDLAR	07A	CLEO	See ALEXANDER 09

[1] ZUPANC 13 also gives the limit as $<1.0\times10^{-4}$ at 95% CL.

$\Gamma(\mu^+\nu_\mu)/\Gamma_{total}$ — Γ_{20}/Γ

See the note on "Decay Constants of Charged Pseudoscalar Mesons."

VALUE (units 10^{-3})	EVTS	DOCUMENT ID		TECN	COMMENT
5.43±0.15 OUR AVERAGE					
5.35±0.13±0.16	2.2k	ABLIKIM	21BE	BES3	e^+e^-,4.178,4.226 GeV
5.17±0.75±0.21	69	[1] ABLIKIM	16O	BES3	e^+e^- at 4.009 GeV
5.31±0.28±0.20	492 ± 26	[2] ZUPANC	13	BELL	e^+e^- at $\Upsilon(4S),\Upsilon(5S)$
6.02±0.38±0.34	275 ± 17	[3] DEL-AMO-SA...	10J	BABR	e^+e^-, 10.58 GeV
5.65±0.45±0.17	235 ± 14	ALEXANDER	09	CLEO	e^+e^- at 4170 MeV
• • • We do not use the following data for averages, fits, limits, etc. • • •					
5.49±0.16±0.15	1.1k	ABLIKIM	19E	BES3	e^+e^- at 4178 MeV
6.44±0.76±0.57	169 ± 18	[4] WIDHALM	08	BELL	See ZUPANC 13
5.94±0.66±0.31	88	[5] PEDLAR	07A	CLEO	See ALEXANDER 09
6.8 ±1.1 ±1.8	553	[6] HEISTER	02I	ALEP	Z decays

[1] ABLIKIM 16O also reports that when constrained by the Standard Model ratio of $\Gamma(D_s^+\to\tau^+\nu_\tau)/\Gamma(D_s^+\to\mu^+\nu_\mu)=9.76$, the branching fraction is found to be $(0.495\pm0.067\pm0.026)$%. The constrained value is used to obtain the decay constant, $f_{D_s^+}=(241.0\pm16.3\pm6.6)$ MeV.

[2] ZUPANC 13 uses both $\mu^+\nu$ and $\tau^+\nu$ events to get $f_{D_s}=(255.5\pm4.2\pm5.1)$ MeV.

[3] DEL-AMO-SANCHEZ 10J uses $\mu^+\nu_\mu$ and $\tau^+\nu_\tau$ events together to get $f_{D_s}=(258.6\pm6.4\pm7.5)$ MeV.

[4] WIDHALM 08 gets $f_{D_s}=(275\pm16\pm12)$ MeV from the branching fraction.

[5] PEDLAR 07A also fits μ^+ and τ^+ events together and gets an effective $\mu^+\nu_\mu$ branching fraction of $(6.38\pm0.59\pm0.33)\times10^{-3}$

[6] This HEISTER 02I result is not actually an independent measurement of the absolute $\mu^+\nu_\mu$ branching fraction, but is in fact based on our $\phi\pi^+$ branching fraction of 3.6 ± 0.9%, so it cannot be included in our overall fit. HEISTER 02I combines its $D_s^+\to\tau^+\nu_\tau$ and $\mu^+\nu_\mu$ branching fractions to get $f_{D_s}=(285\pm19\pm40)$ MeV.

$\Gamma(\mu^+\nu_\mu)/\Gamma(\phi\pi^+)$ — Γ_{20}/Γ_{40}

See the note on "Decay Constants of Charged Pseudoscalar Mesons" above.

VALUE	EVTS	DOCUMENT ID		TECN	COMMENT
• • • We do not use the following data for averages, fits, limits, etc. • • •					
0.143±0.018±0.006	489 ± 55	[1] AUBERT	07V	BABR	$e^+e^-\approx\Upsilon(4S)$
0.23 ±0.06 ±0.04	18	[2] ALEXANDROV	00	BEAT	π^- nucleus, 350 GeV
0.173±0.023±0.035	182	[3] CHADHA	98	CLE2	$e^+e^-\approx\Upsilon(4S)$
0.245±0.052±0.074	39	[4] ACOSTA	94	CLE2	See CHADHA 98

[1] AUBERT 07V gets $f_{D_s^+}=(283\pm17\pm16)$ MeV, using $\Gamma(D_s^+\to\phi\pi^+)/\Gamma(\text{total})=(4.71\pm0.46)$%.

[2] ALEXANDROV 00 uses $f_D^2/f_{D_s}^2=0.82\pm0.09$ from a lattice-gauge-theory calculation to get the relative numbers of $D^+\to\mu^+\nu_\mu$ and $D_s^+\to\mu^+\nu_\mu$ events. The present result leads to $f_{D_s}=(323\pm44\pm36)$ MeV.

[3] CHADHA 98 obtains $f_{D_s}=(280\pm19\pm28\pm34)$ MeV from this measurement, using $\Gamma(D_s^+\to\phi\pi^+)/\Gamma(\text{total})=0.036\pm0.009$.

[4] ACOSTA 94 obtains $f_{D_s}=(344\pm37\pm52\pm42)$ MeV from this measurement, using $\Gamma(D_s^+\to\phi\pi^+)/\Gamma(\text{total})=0.037\pm0.009$.

$\Gamma(\tau^+\nu_\tau)/\Gamma_{total}$ — Γ_{21}/Γ

See the note on "Decay Constants of Charged Pseudoscalar Mesons" above.

VALUE (%)	EVTS	DOCUMENT ID		TECN	COMMENT
5.32±0.11 OUR AVERAGE					
5.29±0.25±0.20	1.7k	[1] ABLIKIM	21AF	BES3	e^+e^- at 4.178, 4.226 GeV
5.27±0.10±0.12	4.9k	[2] ABLIKIM	21AZ	BES3	e^+e^- at 4.178, 4.226 GeV
5.21±0.25±0.17	950	[3] ABLIKIM	21BE	BES3	e^+e^- at 4.178, 4.226 GeV
3.28±1.83±0.37	33	[4] ABLIKIM	16O	BES3	e^+e^- at 4.009 GeV
$5.70\pm0.21^{+0.31}_{-0.30}$	2.2k	[5] ZUPANC	13	BELL	e^+e^- at $\Upsilon(4S)$, $\Upsilon(5S)$
4.96±0.37±0.57	748	[6] DEL-AMO-SA...	10J	BABR	$e^-\overline{\nu}_e\nu_\tau$, $\mu^-\overline{\nu}_\mu\nu_\tau$
6.42±0.81±0.18	126	[7] ALEXANDER	09	CLEO	$\tau^+\to\pi^+\overline{\nu}_\tau$
5.52±0.57±0.21	155	[7] NAIK	09A	CLEO	$\tau^+\to\rho^+\overline{\nu}_\tau$
5.30±0.47±0.22	181	[7] ONYISI	09	CLEO	$\tau^+\to e^+\nu_e\overline{\nu}_\tau$
• • • We do not use the following data for averages, fits, limits, etc. • • •					
6.17±0.71±0.34	102	[8] ECKLUND	08	CLEO	See ONYISI 09
8.0 ±1.3 ±0.4	47	[8] PEDLAR	07A	CLEO	See ALEXANDER 09
5.79±0.77±1.84	881	[9] HEISTER	02I	ALEP	Z decays
7.0 ±2.1 ±2.0	22	[10] ABBIENDI	01L	OPAL	$D_s^{*+}\to\gamma D_s^+$ from Z's
7.4 ±2.8 ±2.4	16	[11] ACCIARRI	97F	L3	$D_s^{*+}\to\gamma D_s^+$ from Z's

[1] ABLIKIM 21F uses $\tau^+\to\pi^+\pi^0\overline{\nu}$ decays.

[2] ABLIKIM 21AZ uses $\tau^+\to e^+\nu_e\overline{\nu}_\tau$ decays.

[3] ABLIKIM 21BE uses $\tau^+\to e^+\nu_e\overline{\nu}_\tau$ decays. When constrained by the Standard Model ratio of $\Gamma(D_s^+\to\tau^+\nu_\tau)/\Gamma(D_s^+\to\mu^+\nu_\mu)=9.75$, the branching fraction is found to be $(5.22\pm0.10\pm0.14)$%.

[4] ABLIKIM 16O also reports that when constrained by the Standard Model ratio of $\Gamma(D_s^+\to\tau^+\nu_\tau)/\Gamma(D_s^+\to\mu^+\nu_\mu)=9.76$; the branching fraction is found to be $(4.83\pm0.65\pm0.26)$%.

[5] ZUPANC 13 uses both $\mu^+\nu$ and $\tau^+\nu$ events to get $f_{D_s}=(255.5\pm4.2\pm5.1)$ MeV.

[6] DEL-AMO-SANCHEZ 10J (with a small correction; see LEES 15D) uses $\mu^+\nu_\mu$ and $\tau^+\nu_\tau$ events together to get $f_{D_s}=(259.9\pm6.6\pm7.6)$ MeV.

[7] ALEXANDER 09, NAIK 09A, and ONYISI 09 use different τ decay modes and are independent. The three papers combined give $f_{D_s}=(259.7\pm7.8\pm3.4)$ MeV.

[8] ECKLUND 08 and PEDLAR 07A are independent: ECKLUND 08 uses $\tau^+\to e^+\nu_e\overline{\nu}_\tau$ events, PEDLAR 07A uses $\tau^+\to\pi^+\overline{\nu}_\tau$ events.

[9] HEISTER 02I combines its $D_s^+\to\tau^+\nu_\tau$ and $\mu^+\nu_\mu$ branching fractions to get $f_{D_s}=(285\pm19\pm40)$ MeV.

[10] This ABBIENDI 01L value gives a decay constant f_{D_s} of $(286\pm44\pm41)$ MeV.

[11] The second ACCIARRI 97F error here combines in quadrature systematic (0.016) and normalization (0.018) errors. The branching fraction gives $f_{D_s}=(309\pm58\pm33\pm38)$ MeV.

$\Gamma(\tau^+\nu_\tau)/\Gamma(\mu^+\nu_\mu)$ — Γ_{21}/Γ_{20}

VALUE	EVTS	DOCUMENT ID		TECN	COMMENT
• • • We do not use the following data for averages, fits, limits, etc. • • •					
$10.73\pm0.69^{+0.56}_{-0.53}$	2.2k/492	[1] ZUPANC	13	BELL	e^+e^- at $\Upsilon(4S),\Upsilon(5S)$
11.0 ±1.4 ±0.6	102	[2] ECKLUND	08	CLEO	See ONYISI 09

[1] This ZUPANC 13 ratio is not independent of the separate $\tau\nu$ and $\mu\nu$ fractions listed above.

[2] This ECKLUND 08 value also uses results from PEDLAR 07A, and it is not independent of other results in these Listings. Combined with earlier CLEO results, the decay constant f_{D_s} is 274 ± 10 ± 5 MeV.

$\Gamma(\gamma e^+\nu_e)/\Gamma_{total}$ — Γ_{22}/Γ

VALUE	CL%	DOCUMENT ID		TECN	COMMENT
$<1.3\times10^{-4}$	90	ABLIKIM	19AD	BES3	for $E_\gamma>10$ MeV

$\Gamma(K^+K^-e^+\nu_e)/\Gamma(K^+K^-\pi^+)$ — Γ_{23}/Γ_{39}

VALUE	DOCUMENT ID		TECN	COMMENT
• • • We do not use the following data for averages, fits, limits, etc. • • •				
0.558±0.007±0.016	[1] AUBERT	08AN	BABR	e^+e^- at $\Upsilon(4S)$

[1] This AUBERT 08AN ratio is only for the K^+K^- mass in the range 1.01–to–1.03 GeV in the numerator and 1.0095–to–1.0295 GeV in the denominator.

$\Gamma(\phi e^+\nu_e)/\Gamma_{total}$ — Γ_{24}/Γ

See the end of the D_s^+ Listings for measurements of $D_s^+\to\phi e^+\nu_e$ form factors. Unseen decay modes of the ϕ are included.

VALUE (%)	EVTS	DOCUMENT ID		TECN	COMMENT
2.39±0.16 OUR AVERAGE Error includes scale factor of 1.3. See the ideogram below.					
2.26±0.45±0.09	26	ABLIKIM	18A	BES3	e^+e^- at 4.009 GeV
2.14±0.17±0.08	207	HIETALA	15		Uses CLEO data
2.61±0.03±0.17	25k	AUBERT	08AN	BABR	e^+e^- at $\Upsilon(4S)$
• • • We do not use the following data for averages, fits, limits, etc. • • •					
2.36±0.23±0.13	106	ECKLUND	09	CLEO	See HIETALA 15
2.29±0.37±0.11	45	YELTON	09	CLEO	See ECKLUND 09

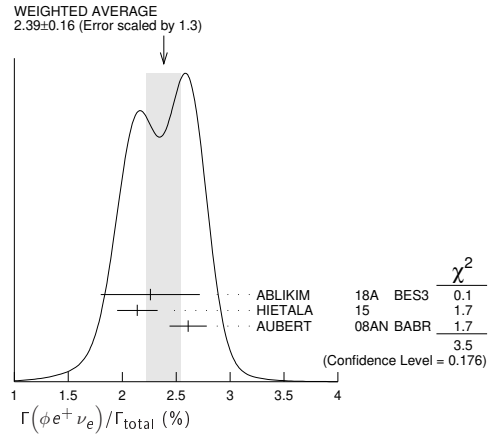

Downloaded from https://academic.oup.com/ptep/article/2022/8/083C01/6651666 by KIT Library user on 27 September 2022

$\Gamma(\phi e^+\nu_e)/\Gamma(\phi\pi^+)$ — Γ_{24}/Γ_{40}

As noted in the comment column, most of these measurements use $\phi\mu^+\nu_\mu$ events in addition to or instead of $\phi e^+\nu_e$ events.

VALUE	EVTS	DOCUMENT ID		TECN	COMMENT
• • • We do not use the following data for averages, fits, limits, etc. • • •					
$0.540\pm0.033\pm0.048$	793	LINK	02J	FOCS	Uses $\phi\mu^+\nu_\mu$
$0.54\ \pm0.05\ \pm0.04$	367	BUTLER	94	CLE2	Uses $\phi e^+\nu_e$ and $\phi\mu^+\nu_\mu$
$0.58\ \pm0.17\ \pm0.07$	97	FRABETTI	93G	E687	Uses $\phi\mu^+\nu_\mu$
$0.57\ \pm0.15\ \pm0.15$	104	ALBRECHT	91	ARG	Uses $\phi e^+\nu_e$
$0.49\ \pm0.10\ ^{+0.10}_{-0.14}$	54	ALEXANDER	90B	CLEO	Uses $\phi e^+\nu_e$ and $\phi\mu^+\nu_\mu$

$\Gamma(\phi\mu^+\nu_\mu)/\Gamma_{total}$ — Γ_{25}/Γ

VALUE (%)	EVTS	DOCUMENT ID		TECN	COMMENT
$1.94\pm0.53\pm0.09$	22	ABLIKIM	18A	BES3	e^+e^- at 4.009 GeV

$\Gamma(\eta e^+\nu_e)/\Gamma_{total}$ — Γ_{27}/Γ

Unseen decay modes of the η are included.

VALUE (%)	EVTS	DOCUMENT ID		TECN	COMMENT
$2.32\ \pm0.08$ OUR AVERAGE					
$2.323\pm0.063\pm0.063$	1.8k	ABLIKIM	19S	BES3	e^+e^- at 4178 MeV
$2.30\ \pm0.31\ \pm0.08$	63	ABLIKIM	16T	BES3	e^+e^- at 4.009 GeV
$2.28\ \pm0.14\ \pm0.19$	358	[1] HIETALA	15		Uses CLEO data
• • • We do not use the following data for averages, fits, limits, etc. • • •					
$2.48\ \pm0.29\ \pm0.13$	82	YELTON	09	CLEO	See HIETALA 15

[1] Obtained by analyzing CLEO-c data but not authored by the CLEO Collaboration.

$\Gamma(\eta e^+\nu_e)/\Gamma(\phi e^+\nu_e)$ — Γ_{27}/Γ_{24}

Unseen decay modes of the η and the ϕ are included.

VALUE	EVTS	DOCUMENT ID		TECN	COMMENT
• • • We do not use the following data for averages, fits, limits, etc. • • •					
$1.24\pm0.12\pm0.15$	440	[1] BRANDENB...	95	CLE2	See HIETALA 15

[1] BRANDENBURG 95 uses both e^+ and μ^+ events and makes a phase-space adjustment to use the μ^+ events as e^+ events.

$\Gamma(\eta'(958)e^+\nu_e)/\Gamma_{total}$ — Γ_{28}/Γ

Unseen decay modes of the $\eta'(958)$ are included.

VALUE (%)	EVTS	DOCUMENT ID		TECN	COMMENT
$0.80\ \pm0.07$ OUR AVERAGE					
$0.824\pm0.073\pm0.027$	261	ABLIKIM	19S	BES3	e^+e^- at 4178 MeV
$0.93\ \pm0.30\ \pm0.05$	14	ABLIKIM	16T	BES3	e^+e^- at 4009 MeV
$0.68\ \pm0.15\ \pm0.06$	20	[1] HIETALA	15		Uses CLEO data
• • • We do not use the following data for averages, fits, limits, etc. • • •					
$0.91\ \pm0.33\ \pm0.05$	7.5	YELTON	09	CLEO	See HIETALA 15

[1] Obtained by analyzing CLEO-c data but not authored by the CLEO Collaboration.

$\Gamma(\eta'(958)e^+\nu_e)/\Gamma(\phi e^+\nu_e)$ — Γ_{28}/Γ_{24}

Unseen decay modes of the resonances are included.

VALUE	EVTS	DOCUMENT ID		TECN	COMMENT
• • • We do not use the following data for averages, fits, limits, etc. • • •					
$0.43\pm0.11\pm0.07$	29	[1] BRANDENB...	95	CLE2	See HIETALA 15

[1] BRANDENBURG 95 uses both e^+ and μ^+ events and makes a phase-space adjustment to use the μ^+ events as e^+ events.

$[\Gamma(\eta e^+\nu_e)+\Gamma(\eta'(958)e^+\nu_e)]/\Gamma(\phi e^+\nu_e)$ — $\Gamma_{26}/\Gamma_{24}=(\Gamma_{27}+\Gamma_{28})/\Gamma_{24}$

Unseen decay modes of the resonances are included.

VALUE	DOCUMENT ID		TECN	COMMENT
• • • We do not use the following data for averages, fits, limits, etc. • • •				
$1.67\pm0.17\pm0.17$	[1] BRANDENB...	95	CLE2	See HIETALA 15

[1] This BRANDENBURG 95 data is redundant with data in previous blocks.

$\Gamma(\eta\mu^+\nu_\mu)/\Gamma_{total}$ — Γ_{29}/Γ

VALUE (%)	EVTS	DOCUMENT ID		TECN	COMMENT
$2.42\pm0.46\pm0.11$	44	ABLIKIM	18A	BES3	e^+e^- at 4.009 GeV

$\Gamma(\eta'(958)\mu^+\nu_\mu)/\Gamma_{total}$ — Γ_{30}/Γ

VALUE (%)	EVTS	DOCUMENT ID		TECN	COMMENT
$1.06\pm0.54\pm0.07$	10	ABLIKIM	18A	BES3	e^+e^- at 4.009 GeV

$\Gamma(\omega e^+\nu_e)/\Gamma_{total}$ — Γ_{31}/Γ

A test for $u\overline{u}$ or $d\overline{d}$ content in the D_s^+. Neither Cabibbo-favored nor Cabibbo-suppressed decays can contribute, and $\omega-\phi$ mixing is an unlikely explanation for any fraction above about 2×10^{-4}.

VALUE (%)	CL%	DOCUMENT ID		TECN	COMMENT
<0.20	90	MARTIN	11	CLEO	e^+e^- at 4170 MeV

$\Gamma(K^0e^+\nu_e)/\Gamma_{total}$ — Γ_{32}/Γ

VALUE (%)	EVTS	DOCUMENT ID		TECN	COMMENT
$0.34\ \pm0.04$ OUR AVERAGE					
$0.325\pm0.038\pm0.016$	117	[1] ABLIKIM	19D	BES3	e^+e^- at 4178 MeV
$0.39\ \pm0.08\ \pm0.03$	42	HIETALA	15		Uses CLEO data
• • • We do not use the following data for averages, fits, limits, etc. • • •					
$0.37\ \pm0.10\ \pm0.02$	14	YELTON	09	CLEO	See HIETALA 15

[1] K^0 reconstructed via $K^0\to K^0_S\to\pi^+\pi^-$ decays.

$\Gamma(K^*(892)^0e^+\nu_e)/\Gamma_{total}$ — Γ_{33}/Γ

Unseen decay modes of the $K^*(892)^0$ are included.

VALUE (%)	EVTS	DOCUMENT ID		TECN	COMMENT
0.215 ± 0.028 OUR AVERAGE Error includes scale factor of 1.1.					
$0.237\pm0.026\pm0.020$	155	ABLIKIM	19D	BES3	e^+e^- at 4178 MeV
$0.18\ \pm0.04\ \pm0.01$	32	[1] HIETALA	15		e^+e^- at 4.170 GeV
• • • We do not use the following data for averages, fits, limits, etc. • • •					
$0.18\ \pm0.07\ \pm0.01$	7.5	YELTON	09	CLEO	See HIETALA 15

[1] Uses CLEO data, but not authored by the CLEO collaboration

$\Gamma(f_0(980)e^+\nu_e, f_0\to\pi^+\pi^-)/\Gamma_{total}$ — Γ_{34}/Γ

VALUE (%)	EVTS	DOCUMENT ID		TECN	COMMENT
• • • We do not use the following data for averages, fits, limits, etc. • • •					
$0.13\pm0.03\pm0.01$	42	[1] HIETALA	15		Uses CLEO data
$0.20\pm0.03\pm0.01$	44	ECKLUND	09	CLEO	See HIETALA 15
$0.13\pm0.04\pm0.01$	13	YELTON	09	CLEO	See ECKLUND 09

[1] HIETALA 15 uses a tighter cut on the reconstructed $\pi^+\pi^-$ mass (±60 MeV around the f^0) than ECKLUND 09. It finds that applying the same tight cut to both analyses gives consistent results.

$\Gamma(a_0(980)^0e^+\nu_e, a_0(980)^0\to\pi^0\eta)/\Gamma_{total}$ — Γ_{35}/Γ

VALUE	CL%	DOCUMENT ID		TECN	COMMENT
$<1.2\times10^{-4}$	90	ABLIKIM	21Y	BES3	e^+e^- at 4.178–4.226 GeV

Hadronic modes with a $K\overline{K}$ pair

$\Gamma(K^+K^0_S)/\Gamma_{total}$ — Γ_{36}/Γ

VALUE (%)	EVTS	DOCUMENT ID		TECN	COMMENT
1.453 ± 0.035 OUR FIT					
$1.46\ \pm0.05$ OUR AVERAGE Error includes scale factor of 1.2.					
$1.425\pm0.038\pm0.031$	1.8k	ABLIKIM	19AM	BES3	e^+e^- at 4178 MeV
$1.52\ \pm0.05\ \pm0.03$		ONYISI	13	CLEO	e^+e^- at 4.17 GeV
• • • We do not use the following data for averages, fits, limits, etc. • • •					
$1.49\ \pm0.07\ \pm0.05$		[1] ALEXANDER	08	CLEO	See ONYISI 13

[1] ALEXANDER 08 uses single- and double-tagged events in an overall fit.

$\Gamma(K^+K^0_S)/\Gamma(K^+K^-\pi^+)$ — Γ_{36}/Γ_{39}

VALUE (units 10^{-2})	EVTS	DOCUMENT ID		TECN	COMMENT
$27.55\pm0.18\pm0.50$	40k	ABLIKIM	20R	BES3	e^+e^-, 4178 $\sim$ 4226 MeV

$\Gamma(K^+K^0_L)/\Gamma_{total}$ — Γ_{37}/Γ

VALUE (%)	EVTS	DOCUMENT ID		TECN	COMMENT
$1.485\pm0.039\pm0.046$	2.3k	ABLIKIM	19AM	BES3	e^+e^- at 4178 MeV

$\Gamma(K^+\overline{K}^0)/\Gamma_{total}$ — Γ_{38}/Γ

VALUE (%)	EVTS	DOCUMENT ID		TECN	COMMENT
$2.95\pm0.11\pm0.09$	2.0k	[1] ZUPANC	13	BELL	e^+e^- at $\Upsilon(4S),\Upsilon(5S)$

[1] ZUPANC 13 finds the $\overline{K}^0$ from its missing-mass squared, not from $K^0_S\to\pi^+\pi^-$. The DCS ($D_s^+\to K^+K^0$) contribution to this fraction is estimated to be an order of magnitude below the statistical uncertainty.

$\Gamma(K^+K^-\pi^+)/\Gamma_{total}$ — Γ_{39}/Γ

VALUE (%)	EVTS	DOCUMENT ID		TECN	COMMENT
5.38 ± 0.10 OUR FIT Error includes scale factor of 1.1.					
5.45 ± 0.11 OUR AVERAGE Error includes scale factor of 1.1.					
$5.47\pm0.08\pm0.13$	5.1k	ABLIKIM	21AE	BES3	e^+e^- at 4.178 GeV
$5.55\pm0.14\pm0.13$		ONYISI	13	CLEO	e^+e^- at 4.17 GeV
$5.06\pm0.15\pm0.21$	4.1k	ZUPANC	13	BELL	e^+e^- at $\Upsilon(4S),\Upsilon(5S)$
$5.78\pm0.20\pm0.30$		DEL-AMO-SA...	10J	BABR	e^+e^-, 10.58 GeV
• • • We do not use the following data for averages, fits, limits, etc. • • •					
$5.50\pm0.23\pm0.16$		[1] ALEXANDER	08	CLEO	See ONYISI 13

[1] ALEXANDER 08 uses single- and double-tagged events in an overall fit.

$\Gamma(\phi\pi^+)/\Gamma_{total}$ — Γ_{40}/Γ

The results here are model-independent. For earlier, model-dependent results, see our PDG 06 edition. We decouple the $D_s^+\to\phi\pi^+$ branching fraction obtained from mass projections (and used to get some of the other branching fractions) from the $D_s^+\to\phi\pi^+$, $\phi\to K^+K^-$ branching fraction obtained from the Dalitz-plot analysis of $D_s^+\to K^+K^-\pi^+$. That is, the ratio of these two branching fractions is not exactly the $\phi\to K^+K^-$ branching fraction 0.491.

VALUE (%)	EVTS	DOCUMENT ID		TECN	COMMENT
$4.5\ \pm0.4$ OUR AVERAGE					
$4.62\pm0.36\pm0.51$		[1] AUBERT	06N	BABR	e^+e^- at $\Upsilon(4S)$
$4.81\pm0.52\pm0.38$	212 ± 19	[2] AUBERT	05V	BABR	$e^+e^-\approx\Upsilon(4S)$
$3.59\pm0.77\pm0.48$		[3] ARTUSO	96	CLE2	e^+e^- at $\Upsilon(4S)$
• • • We do not use the following data for averages, fits, limits, etc. • • •					
$3.9\ ^{+5.1}_{-1.9}\ ^{+1.8}_{-1.1}$		[4] BAI	95C	BES	e^+e^- 4.03 GeV

[1] This AUBERT 06N measurement uses $\overline{B}^0\to D_s^{(*)-}D^{(*)+}$ and $B^-\to D_s^{(*)-}D^{(*)0}$ decays, including some from other papers. However, the result is independent of AUBERT 05V.

Downloaded from https://academic.oup.com/ptep/article/2022/8/083C01/6651666 by KIT Library user on 27 September 2022

[2] AUBERT 05V uses the ratio of $B^0 \to D^{*-} D_s^{*+}$ events seen in two different ways, in both of which the $D^{*-} \to \overline{D}^0 \pi^-$ decay is fully reconstructed: (1) The $D_s^{*+} \to D_s^+ \gamma$, $D_s^+ \to \phi\pi^+$ decay is fully reconstructed. (2) The number of events in the D_s^+ peak in the missing mass spectrum against the $D^{*-}\gamma$ is measured.

[3] ARTUSO 96 uses partially reconstructed $\overline{B}^0 \to D^{*+} D_s^{*-}$ decays to get a model-independent value for $\Gamma(D_s^- \to \phi\pi^-)/\Gamma(D^0 \to K^-\pi^+)$ of 0.92 ± 0.20 ± 0.11.

[4] BAI 95C uses $e^+e^- \to D_s^+ D_s^-$ events in which one or both of the $D_s^\pm$ are observed to obtain the first model-independent measurement of the $D_s^+ \to \phi\pi^+$ branching fraction, without assumptions about $\sigma(D_s^\pm)$. However, with only two "doubly-tagged" events, the statistical error is very large.

$\Gamma(\phi\pi^+, \phi \to K^+K^-)/\Gamma(K^+K^-\pi^+)$ — Γ_{41}/Γ_{39}

This is the "fit fraction" from the Dalitz-plot analysis. We decouple the $D_s^+ \to \phi\pi^+$ branching fraction obtained from mass projections (and used to get some of the other branching fractions) from the $D_s^+ \to \phi\pi^+$, $\phi \to K^+K^-$ branching fraction obtained from the Dalitz-plot analysis of $D_s^+ \to K^+K^-\pi^+$. That is, the ratio of these two branching fractions is not exactly the $\phi \to K^+K^-$ branching fraction 0.491.

VALUE (units 10^{-2})	EVTS	DOCUMENT ID		TECN	COMMENT
41.2±0.7 OUR AVERAGE					
40.5±0.7±0.9	18.6k	ABLIKIM	21AE	BES3	e^+e^- at 4.178 GeV
41.4±0.8±0.5		DEL-AMO-SA...	11G	BABR	Dalitz fit, 96k evts
42.2±1.6±0.3		MITCHELL	09A	CLEO	Dalitz fit, 12k evts
• • • We do not use the following data for averages, fits, limits, etc. • • •					
39.6±3.3±4.7		FRABETTI	95B	E687	Dalitz fit, 701 evts

$\Gamma(K^+\overline{K}^*(892)^0, \overline{K}^{*0} \to K^-\pi^+)/\Gamma(K^+K^-\pi^+)$ — Γ_{42}/Γ_{39}

This is the "fit fraction" from the Dalitz-plot analysis.

VALUE (units 10^{-2})	EVTS	DOCUMENT ID		TECN	COMMENT
47.9±0.6 OUR AVERAGE					
48.3±0.9±0.6	18.6k	ABLIKIM	21AE	BES3	e^+e^- at 4.178 GeV
47.9±0.5±0.5		DEL-AMO-SA...	11G	BABR	Dalitz fit, 96k evts
47.4±1.5±0.4		MITCHELL	09A	CLEO	Dalitz fit, 12k evts
• • • We do not use the following data for averages, fits, limits, etc. • • •					
47.8±4.6±4.0		FRABETTI	95B	E687	Dalitz fit, 701 evts

$\Gamma(f_0(980)\pi^+, f_0 \to K^+K^-)/\Gamma(K^+K^-\pi^+)$ — Γ_{43}/Γ_{39}

This is the "fit fraction" from the Dalitz-plot analysis. This is likely a superposition of $D_s^+ \to f_0(980)\pi$ and $D_s^+ \to a_0(980)\pi$ which are indistinguishable in such an analysis.

VALUE (units 10^{-2})	EVTS	DOCUMENT ID		TECN	COMMENT
20.6±3.5 OUR AVERAGE Error includes scale factor of 2.5. See the ideogram below.					
19.3±1.7±2.0	18.6k	ABLIKIM	21AE	BES3	e^+e^- at 4.178 GeV
16.4±0.7±2.0		DEL-AMO-SA...	11G	BABR	Dalitz fit, 96k evts
28.2±1.9±1.8		MITCHELL	09A	CLEO	Dalitz fit, 12k evts
• • • We do not use the following data for averages, fits, limits, etc. • • •					
11.0±3.5±2.6		FRABETTI	95B	E687	Dalitz fit, 701 evts

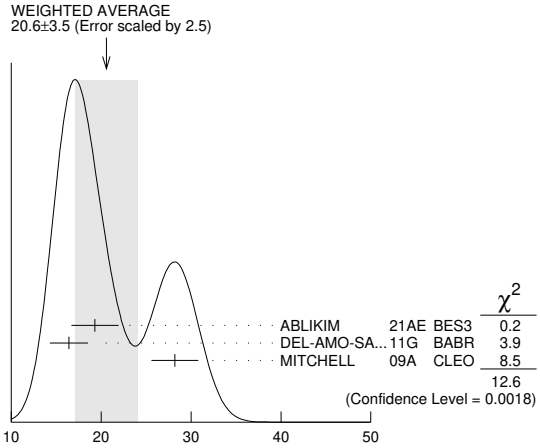

$\Gamma(f_0(1370)\pi^+, f_0 \to K^+K^-)/\Gamma(K^+K^-\pi^+)$ — Γ_{44}/Γ_{39}

This is the "fit fraction" from the Dalitz-plot analysis.

VALUE (units 10^{-2})	EVTS	DOCUMENT ID		TECN	COMMENT
1.3±0.5 OUR AVERAGE Error includes scale factor of 2.8. See the ideogram below.					
1.2±0.4±0.2	18.6k	ABLIKIM	21AE	BES3	e^+e^- at 4.178 GeV
1.1±0.1±0.2		DEL-AMO-SA...	11G	BABR	Dalitz fit, 96k evts
4.3±0.6±0.5		MITCHELL	09A	CLEO	Dalitz fit, 12k evts

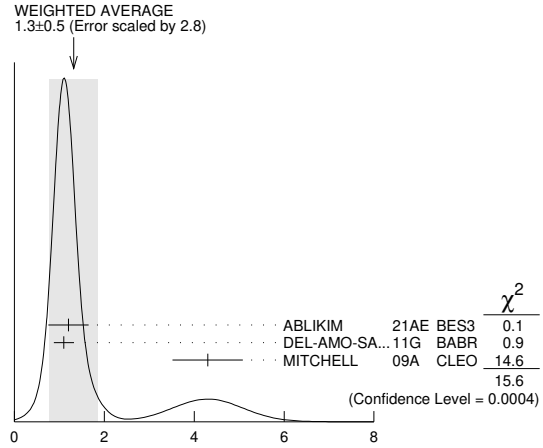

$\Gamma(f_0(1710)\pi^+, f_0 \to K^+K^-)/\Gamma(K^+K^-\pi^+)$ — Γ_{45}/Γ_{39}

This is the "fit fraction" from the Dalitz-plot analysis.

VALUE (units 10^{-2})	EVTS	DOCUMENT ID		TECN	COMMENT
1.3±0.5 OUR AVERAGE Error includes scale factor of 3.8.					
1.9±0.4±0.6	18.6k	ABLIKIM	21AE	BES3	e^+e^- at 4.178 GeV
1.1±0.1±0.1		DEL-AMO-SA...	11G	BABR	Dalitz fit, 96k evts
3.4±0.5±0.3		MITCHELL	09A	CLEO	Dalitz fit, 12k evts
• • • We do not use the following data for averages, fits, limits, etc. • • •					
3.4±2.3±3.5		FRABETTI	95B	E687	Dalitz fit, 701 evts

$\Gamma(K^+\overline{K}_0^*(1430)^0, \overline{K}_0^* \to K^-\pi^+)/\Gamma(K^+K^-\pi^+)$ — Γ_{46}/Γ_{39}

This is the "fit fraction" from the Dalitz-plot analysis.

VALUE (units 10^{-2})	EVTS	DOCUMENT ID		TECN	COMMENT
3.3±0.5 OUR AVERAGE					
3.0±0.6±0.5	18.6k	ABLIKIM	21AE	BES3	e^+e^- at 4.178 GeV
2.4±0.3±1.0		DEL-AMO-SA...	11G	BABR	Dalitz fit, 96k evts
3.9±0.5±0.5		MITCHELL	09A	CLEO	Dalitz fit, 12k evts
• • • We do not use the following data for averages, fits, limits, etc. • • •					
9.3±3.2±3.2		FRABETTI	95B	E687	Dalitz fit, 701 evts

$\Gamma(K^+K_S^0\pi^0)/\Gamma_{total}$ — Γ_{47}/Γ

VALUE (%)	DOCUMENT ID		TECN	COMMENT
1.52±0.09±0.20	ONYISI	13	CLEO	e^+e^- at 4.17 GeV

$\Gamma(2K_S^0\pi^+)/\Gamma_{total}$ — Γ_{48}/Γ

VALUE (%)	DOCUMENT ID		TECN	COMMENT
0.77±0.05±0.03	ONYISI	13	CLEO	e^+e^- at 4.17 GeV

$\Gamma(K^*(892)^+\overline{K}^0)/\Gamma(\phi\pi^+)$ — Γ_{50}/Γ_{40}

Unseen decay modes of the resonances are included.

VALUE	DOCUMENT ID		TECN	COMMENT
1.20±0.21±0.13	CHEN	89	CLEO	e^+e^- 10 GeV

$\Gamma(K^+K^-\pi^+\pi^0)/\Gamma_{total}$ — Γ_{51}/Γ

VALUE (%)	EVTS	DOCUMENT ID		TECN	COMMENT
5.50±0.24 OUR FIT Error includes scale factor of 1.3.					
5.51±0.28 OUR AVERAGE Error includes scale factor of 1.5.					
5.42±0.10±0.17	3k	[1] ABLIKIM	21U	BES3	e^+e^- at 4.178–4.226 GeV
6.37±0.21±0.56		ONYISI	13	CLEO	e^+e^- at 4.17 GeV
• • • We do not use the following data for averages, fits, limits, etc. • • •					
5.65±0.29±0.40		[2] ALEXANDER	08	CLEO	See ONYISI 13

[1] ABLIKIM 21U uses an amplitude analysis of $D_s^+ \to K^+K^-\pi^+\pi^0$ with 9 components.

[2] ALEXANDER 08 uses single- and double-tagged events in an overall fit.

$\Gamma(\phi\rho^+)/\Gamma_{total}$ — Γ_{52}/Γ

VALUE (units 10^{-2})	EVTS	DOCUMENT ID		TECN	COMMENT
5.59±0.15±0.30	3k	[1] ABLIKIM	21U	BES3	e^+e^- at 4.178–4.226 GeV

[1] ABLIKIM 21U uses an amplitude analysis of $D_s^+ \to K^+K^-\pi^+\pi^0$ with 9 components.

$\Gamma(\overline{K}_1(1270)^0 K^+, \overline{K}_1(1270)^0 \to K^-\rho^+)/\Gamma_{total}$ — Γ_{53}/Γ

VALUE (units 10^{-2})	EVTS	DOCUMENT ID		TECN	COMMENT
0.57±0.05±0.04	3k	[1] ABLIKIM	21U	BES3	e^+e^- at 4.178–4.226 GeV

[1] ABLIKIM 21U uses an amplitude analysis of $D_s^+ \to K^+K^-\pi^+\pi^0$ with 9 components.

Downloaded from https://academic.oup.com/ptep/article/2022/8/083C01/6651666 by KIT Library user on 27 September 2022

$\Gamma(\overline{K}_1(1270)^0 K^+, \overline{K}_1(1270)^0 \to K^*(892)\pi)/\Gamma_{total}$ — Γ_{54}/Γ

VALUE (units 10^{-2})	EVTS	DOCUMENT ID		TECN	COMMENT
1.31±0.18±0.18	3k	[1,2] ABLIKIM	21U	BES3	e^+e^- at 4.178–4.226 GeV

[1] ABLIKIM 21U uses an amplitude analysis of $D_s^+ \to K^+K^-\pi^+\pi^0$ with 9 components.
[2] $\overline{K}_1(1270)^0 \to K^*(892)\pi$ denotes a sum over $\overline{K}(892)^0\pi^0$ and $K(892)^-\pi^+$ final states, which are assumed to have relative branching ratio 1/2, as per isospin.

$\Gamma(\overline{K}_1(1400)^0 K^+, \overline{K}_1(1400)^0 \to K^*(892)\pi)/\Gamma_{total}$ — Γ_{55}/Γ

VALUE (units 10^{-2})	EVTS	DOCUMENT ID		TECN	COMMENT
1.98±0.27±0.32	3k	[1] ABLIKIM	21U	BES3	e^+e^- at 4.178–4.226 GeV

[1] $\overline{K}_1(1400)^0 \to K^*(892)\pi$ denotes a sum over $\overline{K}(892)^0\pi^0$ and $K(892)^-\pi^+$ final states, which are assumed to have relative branching ratio 1/2, as per isospin.

$\Gamma(a_0(980)^0\rho^+, a_0(980)^0 \to K^+K^-)/\Gamma_{total}$ — Γ_{56}/Γ

VALUE (units 10^{-2})	EVTS	DOCUMENT ID		TECN	COMMENT
0.19±0.03±0.03	3k	[1] ABLIKIM	21U	BES3	e^+e^- at 4.178–4.226 GeV

[1] ABLIKIM 21U uses an amplitude analysis of $D_s^+ \to K^+K^-\pi^+\pi^0$ with 9 components.

$\Gamma(f_1(1420)^0\pi^+, f_1(1420)^0 \to K^*(892)^\mp K^\pm)/\Gamma_{total}$ — Γ_{57}/Γ

VALUE (units 10^{-2})	EVTS	DOCUMENT ID		TECN	COMMENT
0.39±0.06±0.03	3k	[1] ABLIKIM	21U	BES3	e^+e^- at 4.178–4.226 GeV

[1] ABLIKIM 21U uses an amplitude analysis of $D_s^+ \to K^+K^-\pi^+\pi^0$ with 9 components.

$\Gamma(f_1(1420)^0\pi^+, f_1(1420)^0 \to a_0(980)^0\pi^0, a_0(980)^0 \to K^+K^-)/\Gamma_{total}$ — Γ_{58}/Γ

VALUE (units 10^{-2})	EVTS	DOCUMENT ID		TECN	COMMENT
0.04±0.01±0.01	3k	[1] ABLIKIM	21U	BES3	e^+e^- at 4.178–4.226 GeV

[1] ABLIKIM 21U uses an amplitude analysis of $D_s^+ \to K^+K^-\pi^+\pi^0$ with 9 components.

$\Gamma(\eta(1475)\pi^+, \eta(1475) \to a_0(980)^0\pi^0, a_0(980)^0 \to K^+K^-)/\Gamma_{total}$ — Γ_{59}/Γ

VALUE (units 10^{-2})	EVTS	DOCUMENT ID		TECN	COMMENT
0.07±0.02±0.02	3k	[1] ABLIKIM	21U	BES3	e^+e^- at 4.178–4.226 GeV

[1] ABLIKIM 21U uses an amplitude analysis of $D_s^+ \to K^+K^-\pi^+\pi^0$ with 9 components.

$\Gamma(\phi\rho^+)/\Gamma(\phi\pi^+)$ — Γ_{52}/Γ_{40}

VALUE	EVTS	DOCUMENT ID		TECN	COMMENT
$\mathbf{1.86\pm0.26^{+0.29}_{-0.40}}$	253	AVERY	92	CLE2	$e^+e^- \simeq$ 10.5 GeV

$\Gamma(K^0_S K^-2\pi^+)/\Gamma_{total}$ — Γ_{60}/Γ

VALUE (%)	EVTS	DOCUMENT ID		TECN	COMMENT
1.53±0.08 OUR FIT	Error includes scale factor of 1.5.				
1.53±0.11 OUR AVERAGE	Error includes scale factor of 1.8.				
1.46±0.05±0.05	1.3k	ABLIKIM	21K	BES3	e^+e^- at 4.178–4.226 GeV
1.69±0.07±0.08		ONYISI	13	CLEO	e^+e^- at 4.17 GeV
• • • We do not use the following data for averages, fits, limits, etc. • • •					
1.64±0.10±0.07		[1] ALEXANDER	08	CLEO	See ONYISI 13

[1] ALEXANDER 08 uses single- and double-tagged events in an overall fit.

$\Gamma(K^*(892)^+\overline{K}^*(892)^0)/\Gamma(K^0_S K^-2\pi^+)$ — Γ_{61}/Γ_{60}

VALUE (units 10^{-2})	EVTS	DOCUMENT ID		TECN	COMMENT
40.6±2.9±4.9	1.3k	[1,2] ABLIKIM	21K	BES3	e^+e^- at 4.178–4.226 GeV

[1] Predominantly S-wave, with a significant D-wave component.
[2] $D_s^+ \to K^0_S K^-2\pi^+$ amplitude analysis with 13 components.

$\Gamma(\eta(1475)\pi^+, \eta \to a_0(980)^-\pi^+, a_0^- \to K^0_S K^-)/\Gamma(K^0_S K^-2\pi^+)$ — Γ_{64}/Γ_{60}

VALUE (units 10^{-2})	EVTS	DOCUMENT ID		TECN	COMMENT
10.8±2.6±5.2	1.3k	[1] ABLIKIM	21K	BES3	e^+e^- at 4.178–4.226 GeV

[1] $D_s^+ \to K^0_S K^-2\pi^+$ amplitude analysis with 13 components.

$\Gamma(\eta(1475)K^0_S, \eta \to K^*(892)^0\pi^+, K^{*0} \to K^-\pi^+)/\Gamma(K^0_S K^-2\pi^+)$ — Γ_{62}/Γ_{60}

VALUE (units 10^{-2})	EVTS	DOCUMENT ID		TECN	COMMENT
2.2±0.6±0.2	1.3k	[1] ABLIKIM	21K	BES3	e^+e^- at 4.178–4.226 GeV

[1] $D_s^+ \to K^0_S K^-2\pi^+$ amplitude analysis with 13 components.

$\Gamma(\eta(1475)\pi^+, \eta \to \overline{K}^*(892)^+K^-, \overline{K}^{*+} \to K^0_S\pi^+)/\Gamma(K^0_S K^-2\pi^+)$ — Γ_{63}/Γ_{60}

VALUE (units 10^{-2})	EVTS	DOCUMENT ID		TECN	COMMENT
2.2±0.6±0.2	1.3k	[1] ABLIKIM	21K	BES3	e^+e^- at 4.178–4.226 GeV

[1] $D_s^+ \to K^0_S K^-2\pi^+$ amplitude analysis with 13 components.

$\Gamma(f_1(1285)\pi^+, f_1 \to a_0(980)^-\pi^+, a_0^- \to K^0_S K^-)/\Gamma(K^0_S K^-2\pi^+)$ — Γ_{65}/Γ_{60}

VALUE (units 10^{-2})	EVTS	DOCUMENT ID		TECN	COMMENT
2.2±0.5±0.2	1.3k	[1] ABLIKIM	21K	BES3	e^+e^- at 4.178–4.226 GeV

[1] $D_s^+ \to K^0_S K^-2\pi^+$ amplitude analysis with 13 components.

$\Gamma(K^*(892)^+\overline{K}^*(892)^0)/\Gamma_{total}$ — Γ_{61}/Γ

VALUE (units 10^{-2})	EVTS	DOCUMENT ID		TECN	COMMENT
5.64±0.23±0.27	3k	[1] ABLIKIM	21U	BES3	e^+e^- at 4.178–4.226 GeV

[1] ABLIKIM 21U uses an amplitude analysis of $D_s^+ \to K^+K^-\pi^+\pi^0$ with 9 components.

$\Gamma(K^*(892)^+\overline{K}^*(892)^0)/\Gamma(\phi\pi^+)$ — Γ_{61}/Γ_{40}

Unseen decay modes of the resonances are included.

VALUE	DOCUMENT ID		TECN	COMMENT
1.6±0.4±0.4	ALBRECHT	92B	ARG	$e^+e^- \simeq$ 10.4 GeV

$\Gamma(K^+K^0_S\pi^+\pi^-)/\Gamma_{total}$ — Γ_{66}/Γ

VALUE (%)	DOCUMENT ID		TECN	COMMENT
0.95±0.08 OUR FIT Error includes scale factor of 1.1.				
1.03±0.06±0.08	ONYISI	13	CLEO	e^+e^- at 4.17 GeV

$\Gamma(K^+K^0_S\pi^+\pi^-)/\Gamma(K^0_S K^-2\pi^+)$ — Γ_{66}/Γ_{60}

VALUE	EVTS	DOCUMENT ID		TECN	COMMENT
0.62 ±0.05 OUR FIT					
0.586±0.052±0.043	476	LINK	01C	FOCS	γ A, $\overline{E}_\gamma \approx$ 180 GeV

$\Gamma(K^+K^-2\pi^+\pi^-)/\Gamma(K^+K^-\pi^+)$ — Γ_{67}/Γ_{39}

VALUE	EVTS	DOCUMENT ID		TECN	COMMENT
0.160±0.027 OUR AVERAGE					
0.150±0.019±0.025	240	LINK	03D	FOCS	γ A, $\overline{E}_\gamma \approx$ 180 GeV
0.188±0.036±0.040	75	FRABETTI	97C	E687	γBe, $\overline{E}_\gamma \approx$ 200 GeV

$\Gamma(\phi 2\pi^+\pi^-)/\Gamma(\phi\pi^+)$ — Γ_{68}/Γ_{40}

VALUE	EVTS	DOCUMENT ID		TECN	COMMENT
0.269±0.027 OUR AVERAGE					
0.249±0.024±0.021	136	LINK	03D	FOCS	γ A, $\overline{E}_\gamma \approx$ 180 GeV
0.28 ±0.06 ±0.01	40	FRABETTI	97C	E687	γBe, $\overline{E}_\gamma \approx$ 200 GeV
0.58 ±0.21 ±0.10	21	FRABETTI	92	E687	γBe
0.42 ±0.13 ±0.07	19	ANJOS	88	E691	Photoproduction
1.11 ±0.37 ±0.28	62	ALBRECHT	85D	ARG	e^+e^- 10 GeV

$\Gamma(K^+K^-\rho^0\pi^+ \text{non-}\phi)/\Gamma(K^+K^-2\pi^+\pi^-)$ — Γ_{72}/Γ_{67}

VALUE	CL%	DOCUMENT ID		TECN	COMMENT
<0.03	90	LINK	03D	FOCS	γ A, $\overline{E}_\gamma \approx$ 180 GeV

$\Gamma(\phi\rho^0\pi^+, \phi \to K^+K^-)/\Gamma(K^+K^-2\pi^+\pi^-)$ — Γ_{69}/Γ_{67}

VALUE	DOCUMENT ID		TECN	COMMENT
0.75±0.06±0.04	LINK	03D	FOCS	γ A, $\overline{E}_\gamma \approx$ 180 GeV

$\Gamma(\phi a_1(1260)^+, \phi \to K^+K^-, a_1^+ \to \rho^0\pi^+)/\Gamma(K^+K^-\pi^+)$ — Γ_{70}/Γ_{39}

VALUE	DOCUMENT ID		TECN	COMMENT
0.137±0.019±0.011	LINK	03D	FOCS	γ A, $\overline{E}_\gamma \approx$ 180 GeV

$\Gamma(K^+K^-2\pi^+\pi^- \text{nonresonant})/\Gamma(K^+K^-2\pi^+\pi^-)$ — Γ_{73}/Γ_{67}

VALUE	DOCUMENT ID		TECN	COMMENT
0.10±0.06±0.05	LINK	03D	FOCS	γ A, $\overline{E}_\gamma \approx$ 180 GeV

$\Gamma(\phi 2\pi^+\pi^- \text{non-}\rho, \phi \to K^+K^-)/\Gamma(K^+K^-2\pi^+\pi^-)$ — Γ_{71}/Γ_{67}

VALUE	DOCUMENT ID		TECN	COMMENT
0.21±0.05±0.06	LINK	03D	FOCS	γ A, $\overline{E}_\gamma \approx$ 180 GeV

$\Gamma(2K^0_S 2\pi^+\pi^-)/\Gamma(K^0_S K^-2\pi^+)$ — Γ_{74}/Γ_{60}

VALUE	EVTS	DOCUMENT ID		TECN	COMMENT
0.051±0.015±0.015	37 ± 10	LINK	04D	FOCS	γ A, $\overline{E}_\gamma \approx$ 180 GeV

Pionic modes

$\Gamma(\pi^+\pi^0)/\Gamma(K^+K^0_S)$ — Γ_{75}/Γ_{36}

VALUE (units 10^{-2})	CL%	DOCUMENT ID		TECN	COMMENT
<2.3	90	MENDEZ	10	CLEO	e^+e^- at 4170 MeV
• • • We do not use the following data for averages, fits, limits, etc. • • •					
<4.1	90	ADAMS	07A	CLEO	See MENDEZ 10

$\Gamma(\pi^+\pi^0)/\Gamma_{total}$ — Γ_{75}/Γ

VALUE	CL%	DOCUMENT ID		TECN	COMMENT
$<1.2\times10^{-4}$	90	[1] GUAN	21	BELL	$e^+e^- \approx \Upsilon(4,5S)$

[1] Uses $B(D_s^+ \to \pi^+\phi,\ \phi \to K^+K^-) = (2.24 \pm 0.08)\%$.

$\Gamma(2\pi^+\pi^-)/\Gamma_{total}$ — Γ_{76}/Γ

VALUE (%)	DOCUMENT ID		TECN	COMMENT
1.08±0.04 OUR FIT				
1.11±0.04±0.04	ONYISI	13	CLEO	e^+e^- at 4.17 GeV
• • • We do not use the following data for averages, fits, limits, etc. • • •				
1.11±0.07±0.04	[1] ALEXANDER	08	CLEO	See ONYISI 13

[1] ALEXANDER 08 uses single- and double-tagged events in an overall fit.

Downloaded from https://academic.oup.com/ptep/article/2022/8/083C01/6651666 by KIT Library user on 27 September 2022

$\Gamma(2\pi^+\pi^-)/\Gamma(K^+K^-\pi^+)$ — Γ_{76}/Γ_{39}

VALUE	EVTS	DOCUMENT ID		TECN	COMMENT
0.200±0.007 OUR FIT					
0.199±0.004±0.009	≈ 10.5k	AUBERT	09O	BABR	e^+e^- ≈ 10.6 GeV
• • • We do not use the following data for averages, fits, limits, etc. • • •					
0.265±0.041±0.031	98	FRABETTI	97D	E687	γ Be ≈ 200 GeV

$\Gamma(\rho^0\pi^+)/\Gamma(2\pi^+\pi^-)$ — Γ_{77}/Γ_{76}

VALUE	CL%	DOCUMENT ID		TECN	COMMENT
0.018±0.005±0.010		AUBERT	09O	BABR	Dalitz fit, ≈ 10.5k evts
• • • We do not use the following data for averages, fits, limits, etc. • • •					
not seen		LINK	04	FOCS	Dalitz fit, 1475 ± 50 evts
0.058±0.023±0.037		AITALA	01A	E791	Dalitz fit, 848 evts
<0.073	90	FRABETTI	97D	E687	γ Be ≈ 200 GeV

$\Gamma(\pi^+(\pi^+\pi^-)_{S-\text{wave}})/\Gamma(2\pi^+\pi^-)$ — Γ_{78}/Γ_{76}

This is the "fit fraction" from the Dalitz-plot analysis. See also KLEMPT 08, which uses 568 $D_s^+ \to 3\pi$ decays (over 280 background events) from FNAL E791 to study various parametrizations of the decay amplitudes. The emphasis there is more on S-wave $\pi\pi$ decay products — 20 different solutions are given — than on D_s^+ fit fractions.

VALUE	DOCUMENT ID		TECN	COMMENT
0.833 ±0.020 OUR AVERAGE				
0.830 ±0.009 ±0.019	[1] AUBERT	09O	BABR	Dalitz fit, ≈ 10.5k evts
0.8704±0.0560±0.0438	[2] LINK	04	FOCS	Dalitz fit, 1475 ± 50 evts

[1] AUBERT 09O gives the amplitude and phase of the $\pi^+\pi^-$ S-wave in 29 $\pi^+\pi^-$ invariant-mass bins.

[2] LINK 04 borrows a K-matrix parametrization from ANISOVICH 03 of the full π-π S-wave isoscalar scattering amplitude to describe the $\pi^+\pi^-$ S-wave component of the $\pi^+\pi^+\pi^-$ state. The fit fraction given above is a sum over five f_0 mesons, the $f_0(980)$, $f_0(1300)$, $f_0(1200–1600)$, $f_0(1500)$, and $f_0(1750)$. See LINK 04 for details and discussion.

$\Gamma(f_0(980)\pi^+, f_0 \to \pi^+\pi^-)/\Gamma(2\pi^+\pi^-)$ — Γ_{79}/Γ_{76}

This is the "fit fraction" from the Dalitz-plot analysis. See above for the full $\pi^+(\pi^+\pi^-)_{S-wave}$ fit fraction.

VALUE	DOCUMENT ID		TECN	COMMENT
• • • We do not use the following data for averages, fits, limits, etc. • • •				
0.565±0.043±0.047	AITALA	01A	E791	Dalitz fit, 848 evts
1.074±0.140±0.043	FRABETTI	97D	E687	γ Be ≈ 200 GeV

$\Gamma(f_0(1370)\pi^+, f_0 \to \pi^+\pi^-)/\Gamma(2\pi^+\pi^-)$ — Γ_{80}/Γ_{76}

This is the "fit fraction" from the Dalitz-plot analysis. See above for the full $\pi^+(\pi^+\pi^-)_{S-wave}$ fit fraction.

VALUE	DOCUMENT ID		TECN	COMMENT
• • • We do not use the following data for averages, fits, limits, etc. • • •				
0.324±0.077±0.017	AITALA	01A	E791	Dalitz fit, 848 evts

$\Gamma(f_0(1500)\pi^+, f_0 \to \pi^+\pi^-)/\Gamma(2\pi^+\pi^-)$ — Γ_{81}/Γ_{76}

This is the "fit fraction" from the Dalitz-plot analysis. See above for the full $\pi^+(\pi^+\pi^-)_{S-wave}$ fit fraction.

VALUE	DOCUMENT ID		TECN	COMMENT
• • • We do not use the following data for averages, fits, limits, etc. • • •				
0.274±0.114±0.019	[1] FRABETTI	97D	E687	γ Be ≈ 200 GeV

[1] FRABETTI 97D calls this mode $S(1475)\pi^+$, but finds the mass and width of this $S(1475)$ to be in excellent agreement with those of the $f_0(1500)$.

$\Gamma(f_2(1270)\pi^+, f_2 \to \pi^+\pi^-)/\Gamma(2\pi^+\pi^-)$ — Γ_{82}/Γ_{76}

This is the "fit fraction" from the Dalitz-plot analysis.

VALUE	DOCUMENT ID		TECN	COMMENT
0.101 ±0.018 OUR AVERAGE				
0.101 ±0.015 ±0.011	AUBERT	09O	BABR	Dalitz fit, ≈ 10.5k evts
0.0974±0.0449±0.0294	LINK	04	FOCS	Dalitz fit, 1475 ± 50 evts
• • • We do not use the following data for averages, fits, limits, etc. • • •				
0.197 ±0.033 ±0.006	AITALA	01A	E791	Dalitz fit, 848 evts
0.123 ±0.056 ±0.018	FRABETTI	97D	E687	γ Be ≈ 200 GeV

$\Gamma(\rho(1450)^0\pi^+, \rho^0 \to \pi^+\pi^-)/\Gamma(2\pi^+\pi^-)$ — Γ_{83}/Γ_{76}

This is the "fit fraction" from the Dalitz-plot analysis.

VALUE	DOCUMENT ID		TECN	COMMENT
0.027 ±0.018 OUR AVERAGE				
0.023 ±0.008 ±0.017	AUBERT	09O	BABR	Dalitz fit, ≈ 10.5k evts
0.0656±0.0343±0.0440	LINK	04	FOCS	Dalitz fit, 1475 ± 50 evts
• • • We do not use the following data for averages, fits, limits, etc. • • •				
0.044 ±0.021 ±0.002	AITALA	01A	E791	Dalitz fit, 848 evts

$\Gamma(\pi^+2\pi^0)/\Gamma_{\text{total}}$ — Γ_{84}/Γ

VALUE (%)	EVTS	DOCUMENT ID		TECN	COMMENT
0.65±0.13±0.03	72 ± 16	NAIK	09A	CLEO	e^+e^- at 4170 MeV

$\Gamma(2\pi^+\pi^-\pi^0)/\Gamma(\phi\pi^+)$ — Γ_{85}/Γ_{40}

VALUE	CL%	DOCUMENT ID		TECN	COMMENT
• • • We do not use the following data for averages, fits, limits, etc. • • •					
<3.3	90	ANJOS	89E	E691	Photoproduction

$\Gamma(\eta\pi^+)/\Gamma_{\text{total}}$ — Γ_{86}/Γ

Unseen decay modes of the η are included.

VALUE (%)	EVTS	DOCUMENT ID		TECN	COMMENT
1.68±0.09 OUR FIT Error includes scale factor of 1.1.					
1.71±0.08 OUR AVERAGE					
1.67±0.08±0.06		ONYISI	13	CLEO	e^+e^- at 4.17 GeV
1.82±0.14±0.07	0.8k	ZUPANC	13	BELL	e^+e^- at $\Upsilon(4S), \Upsilon(5S)$
• • • We do not use the following data for averages, fits, limits, etc. • • •					
1.58±0.11±0.18		[1] ALEXANDER	08	CLEO	See ONYISI 13

[1] ALEXANDER 08 uses single- and double-tagged events in an overall fit.

$\Gamma(\eta\pi^+)/\Gamma(K^+K^0_S)$ — Γ_{86}/Γ_{36}

Unseen decay modes of the η are included.

VALUE	EVTS	DOCUMENT ID		TECN	COMMENT
1.15 ±0.07 OUR FIT Error includes scale factor of 1.1.					
• • • We do not use the following data for averages, fits, limits, etc. • • •					
1.236±0.043±0.063	2587 ± 89	MENDEZ	10	CLEO	See ONYISI 13

$\Gamma(\eta\pi^+)/\Gamma(\phi\pi^+)$ — Γ_{86}/Γ_{40}

Unseen decay modes of the resonances are included.

VALUE	EVTS	DOCUMENT ID		TECN	COMMENT
• • • We do not use the following data for averages, fits, limits, etc. • • •					
0.48±0.03±0.04	920	JESSOP	98	CLE2	$e^+e^- \approx \Upsilon(4S)$
0.54±0.09±0.06	165	ALEXANDER	92	CLE2	See JESSOP 98

$\Gamma(\eta\pi^+)/\Gamma(\phi\pi^+, \phi \to K^+K^-)$ — Γ_{86}/Γ_{41}

VALUE (%)	EVTS	DOCUMENT ID		TECN	COMMENT
84.80±0.47±2.64	22k	GUAN	21	BELL	$e^+e^- \approx \Upsilon(4,5S)$

$\Gamma(\eta\pi^+)/\Gamma(K^+K^-\pi^+)$ — Γ_{86}/Γ_{39}

VALUE (units 10^{-2})	EVTS	DOCUMENT ID		TECN	COMMENT
31.94±0.33±0.49	19.5k	ABLIKIM	20R	BES3	e^+e^-, 4178 ∼ 4226 MeV

$\Gamma(2\pi^+\pi^-\eta)/\Gamma_{\text{total}}$ — Γ_{93}/Γ

VALUE (units 10^{-2})	EVTS	DOCUMENT ID		TECN	COMMENT
3.12±0.13±0.09	2.1k	ABLIKIM	21AR	BES3	e^+e^- at 4.178–4.226 GeV

$\Gamma(a_1(1260)^+\eta, a_1^+ \to \rho(770)^0\pi^+, \rho^0 \to \pi^+\pi^-)/\Gamma(2\pi^+\pi^-\eta)$ — Γ_{94}/Γ_{93}

VALUE (units 10^{-2})	DOCUMENT ID		TECN	COMMENT
55.4±3.9±2.0	[1] ABLIKIM	21AR	BES3	e^+e^- at 4.178–4.226 GeV

[1] $D_s^+ \to 2\pi^+\pi^-\eta$ amplitude analysis with 11 components.

$\Gamma(a_1(1260)^+\eta, a_1^+ \to f_0(500)\pi^+, f_0 \to \pi^+\pi^-)/\Gamma(2\pi^+\pi^-\eta)$ — Γ_{95}/Γ_{93}

VALUE (units 10^{-2})	DOCUMENT ID		TECN	COMMENT
8.1±1.9±2.1	[1] ABLIKIM	21AR	BES3	e^+e^- at 4.178–4.226 GeV

[1] $D_s^+ \to 2\pi^+\pi^-\eta$ amplitude analysis with 11 components.

$\Gamma(a_0(980)^+\rho(770)^0, a_0^+ \to \eta\pi^+)/\Gamma(2\pi^+\pi^-\eta)$ — Γ_{97}/Γ_{93}

VALUE (units 10^{-2})	DOCUMENT ID		TECN	COMMENT
6.7±2.5±1.5	[1] ABLIKIM	21AR	BES3	e^+e^- at 4.178–4.226 GeV

[1] $D_s^+ \to 2\pi^+\pi^-\eta$ amplitude analysis with 11 components.

$\Gamma(\eta(1405)\pi^+, \eta(1405) \to a_0(980)^-\pi^+, a_0^- \to \eta\pi^-)/\Gamma(2\pi^+\pi^-\eta)$ — Γ_{98}/Γ_{93}

VALUE (units 10^{-2})	DOCUMENT ID		TECN	COMMENT
0.7±0.2±0.1	[1] ABLIKIM	21AR	BES3	e^+e^- at 4.178–4.226 GeV

[1] $D_s^+ \to 2\pi^+\pi^-\eta$ amplitude analysis with 11 components.

$\Gamma(\eta(1405)\pi^+, \eta(1405) \to a_0(980)^+\pi^-, a_0^+ \to \eta\pi^+)/\Gamma(2\pi^+\pi^-\eta)$ — Γ_{99}/Γ_{93}

VALUE (units 10^{-2})	DOCUMENT ID		TECN	COMMENT
0.7±0.2±0.1	[1] ABLIKIM	21AR	BES3	e^+e^- at 4.178–4.226 GeV

[1] $D_s^+ \to 2\pi^+\pi^-\eta$ amplitude analysis with 11 components.

$\Gamma(f_1(1420)\pi^+, f_1 \to a_0(980)^-\pi^+, a_0^- \to \eta\pi^-)/\Gamma(2\pi^+\pi^-\eta)$ — Γ_{100}/Γ_{93}

VALUE (units 10^{-2})	DOCUMENT ID		TECN	COMMENT
1.9±0.5±0.3	[1] ABLIKIM	21AR	BES3	e^+e^- at 4.178–4.226 GeV

[1] $D_s^+ \to 2\pi^+\pi^-\eta$ amplitude analysis with 11 components.

$\Gamma(f_1(1420)\pi^+, f_1 \to a_0(980)^+\pi^-, a_0^+ \to \eta\pi^+)/\Gamma(2\pi^+\pi^-\eta)$ — Γ_{101}/Γ_{93}

VALUE (units 10^{-2})	DOCUMENT ID		TECN	COMMENT
1.7±0.5±0.3	[1] ABLIKIM	21AR	BES3	e^+e^- at 4.178–4.226 GeV

[1] $D_s^+ \to 2\pi^+\pi^-\eta$ amplitude analysis with 11 components.

$\Gamma(\omega\pi^+)/\Gamma_{\text{total}}$ — Γ_{87}/Γ

Unseen decay modes of the ω are included.

VALUE (%)	EVTS	DOCUMENT ID		TECN	COMMENT
0.192±0.030 OUR FIT					
0.181±0.032 OUR AVERAGE					
0.177±0.032±0.013	65 ± 12	ABLIKIM	19AH	BES3	e^+e^- at 4.178 GeV
0.21 ±0.09 ±0.01	6 ± 2.4	GE	09A	CLEO	e^+e^- at 4170 MeV

Downloaded from https://academic.oup.com/ptep/article/2022/8/083C01/6651666 by KIT Library user on 27 September 2022

$\Gamma(\omega\pi^+)/\Gamma(\eta\pi^+)$ — Γ_{87}/Γ_{86}

Unseen decay modes of the resonances are included.

VALUE	DOCUMENT ID		TECN	COMMENT
0.115±0.018 OUR FIT				
0.16 ±0.04 ±0.03	BALEST	97	CLE2	$e^+e^- \approx \Upsilon(4S)$

$\Gamma(3\pi^+2\pi^-)/\Gamma(K^+K^-\pi^+)$ — Γ_{88}/Γ_{39}

VALUE	EVTS	DOCUMENT ID		TECN	COMMENT
0.146±0.014 OUR AVERAGE					
0.145±0.011±0.010	671	LINK	03D	FOCS	γ A, $\overline{E}_\gamma \approx$ 180 GeV
0.158±0.042±0.031	37	FRABETTI	97C	E687	γBe, $\overline{E}_\gamma \approx$ 200 GeV

$\Gamma(\eta\rho^+)/\Gamma_{total}$ — Γ_{90}/Γ

Unseen decay modes of the η are included.

VALUE (%)	EVTS	DOCUMENT ID		TECN	COMMENT
8.9±0.6±0.5	328 ± 22	NAIK	09A	CLEO	$\eta \to 2\gamma$

$\Gamma(\eta\rho^+)/\Gamma(\phi\pi^+)$ — Γ_{90}/Γ_{40}

Unseen decay modes of the resonances are included.

VALUE	EVTS	DOCUMENT ID		TECN	COMMENT
• • • We do not use the following data for averages, fits, limits, etc. • • •					
2.98±0.20±0.39	447	JESSOP	98	CLE2	$e^+e^- \approx \Upsilon(4S)$
$2.86\pm0.38^{+0.36}_{-0.38}$	217	AVERY	92	CLE2	See JESSOP 98

$\Gamma(\eta\rho^+)/\Gamma(\eta\pi^+\pi^0)$ — Γ_{90}/Γ_{91}

VALUE (units 10^{-2})	EVTS	DOCUMENT ID		TECN	COMMENT
78.3±5.0±2.1	1.2k	ABLIKIM	19BE	BES3	$\eta\pi^+\pi^0$ amplitude analysis

$\Gamma(\eta\pi^+\pi^0)/\Gamma_{total}$ — Γ_{91}/Γ

VALUE (%)	EVTS	DOCUMENT ID		TECN	COMMENT
9.5 ±0.5 OUR AVERAGE					
9.50±0.28±0.41	2.6k	ABLIKIM	19BE	BES3	e^+e^- at 4.178 GeV
9.2 ±0.4 ±1.1		ONYISI	13	CLEO	e^+e^- at 4.17 GeV

$\Gamma(\eta(\pi^+\pi^0)_{P-wave})/\Gamma(\eta\pi^+\pi^0)$ — Γ_{92}/Γ_{91}

VALUE (units 10^{-2})	EVTS	DOCUMENT ID		TECN	COMMENT
5.4±2.1±2.5	1.2k	ABLIKIM	19BE	BES3	$\eta\pi^+\pi^0$ amplitude analysis

$\Gamma(a_0(980)^{+0}\pi^{0+},\ a_0(980)^{+0} \to \eta\pi^{+0})/\Gamma(\eta\pi^+\pi^0)$ — Γ_{96}/Γ_{91}

VALUE (units 10^{-2})	EVTS	DOCUMENT ID		TECN	COMMENT
23.2±2.3±3.3	1.2k	[1] ABLIKIM	19BE	BES3	$\eta\pi^+\pi^0$ amplitude analysis

[1] Coherent sum of $D_s^+ \to a_0^+\pi^0 \to \eta\pi^+\pi^0$ and $D_s^+ \to a_0^0\pi^+ \to \eta\pi^+\pi^0$. ABLIKIM 19BE find $a_0(980)^0 - f(980)$ mixing effects negligibly small in this $D_s^+ \to \eta\pi^+\pi^0$ Dalitz plot analysis.

$\Gamma(\omega\pi^+\pi^0)/\Gamma_{total}$ — Γ_{102}/Γ

Unseen decay modes of the ω are included.

VALUE (%)	EVTS	DOCUMENT ID		TECN	COMMENT
2.78±0.65±0.25	34 ± 7.9	GE	09A	CLEO	e^+e^- at 4170 MeV

$\Gamma(3\pi^+2\pi^-\pi^0)/\Gamma_{total}$ — Γ_{103}/Γ

VALUE	DOCUMENT ID		TECN	COMMENT
$\mathbf{0.049^{+0.033}_{-0.030}}$	BARLAG	92C	ACCM	π^- 230 GeV

$\Gamma(\omega 2\pi^+\pi^-)/\Gamma_{total}$ — Γ_{104}/Γ

Unseen decay modes of the ω are included.

VALUE (%)	EVTS	DOCUMENT ID		TECN	COMMENT
1.58±0.45±0.09	29 ± 8.2	GE	09A	CLEO	e^+e^- at 4170 MeV

$\Gamma(\eta'(958)\pi^+)/\Gamma_{total}$ — Γ_{105}/Γ

Unseen decay modes of the $\eta'(958)$ are included.

VALUE (%)	DOCUMENT ID		TECN	COMMENT
3.94±0.15±0.20	ONYISI	13	CLEO	e^+e^- at 4.17 GeV
• • • We do not use the following data for averages, fits, limits, etc. • • •				
3.77±0.25±0.30	[1] ALEXANDER	08	CLEO	See ONYISI 13

[1] ALEXANDER 08 uses single- and double-tagged events in an overall fit.

$\Gamma(\eta'(958)\pi^+)/\Gamma(K^+K^0_S)$ — Γ_{105}/Γ_{36}

Unseen decay modes of the $\eta'(958)$ are included.

VALUE	EVTS	DOCUMENT ID		TECN	COMMENT
• • • We do not use the following data for averages, fits, limits, etc. • • •					
2.654±0.088±0.139	1436 ± 47	MENDEZ	10	CLEO	See ONYISI 13

$\Gamma(\eta'(958)\pi^+)/\Gamma(\phi\pi^+)$ — Γ_{105}/Γ_{40}

Unseen decay modes of the resonances are included.

VALUE	EVTS	DOCUMENT ID		TECN	COMMENT
• • • We do not use the following data for averages, fits, limits, etc. • • •					
1.03±0.06±0.07	537	JESSOP	98	CLE2	$e^+e^- \approx \Upsilon(4S)$
1.20±0.15±0.11	281	ALEXANDER	92	CLE2	See JESSOP 98
$2.5\ \pm1.0\ ^{+1.5}_{-0.4}$	22	ALVAREZ	91	NA14	Photoproduction
2.5 ±0.5 ±0.3	215	ALBRECHT	90D	ARG	$e^+e^- \approx 10.4$ GeV

$\Gamma(\eta'(958)\pi^+)/\Gamma(K^+K^-\pi^+)$ — Γ_{105}/Γ_{39}

VALUE (units 10^{-2})	EVTS	DOCUMENT ID		TECN	COMMENT
69.4±0.8±3.8	9.9k	ABLIKIM	20R	BES3	e^+e^-, 4178 ∼ 4226 MeV

$\Gamma(\omega\eta\pi^+)/\Gamma_{total}$ — Γ_{107}/Γ

Unseen decay modes of the ω and η are included.

VALUE	CL%	DOCUMENT ID		TECN	COMMENT
<2.13 × 10^{-2}	90	GE	09A	CLEO	e^+e^- at 4170 MeV

$\Gamma(\eta'(958)\rho^+)/\Gamma_{total}$ — Γ_{108}/Γ

VALUE (%)	DOCUMENT ID		TECN	COMMENT
5.8±1.4±0.4	ABLIKIM	15Z	BES3	482 pb^{-1}, 4009 MeV

$\Gamma(\eta'(958)\rho^+)/\Gamma(\phi\pi^+)$ — Γ_{108}/Γ_{40}

Unseen decay modes of the resonances are included.

VALUE	EVTS	DOCUMENT ID		TECN	COMMENT
• • • We do not use the following data for averages, fits, limits, etc. • • •					
2.78±0.28±0.30	137	[1] JESSOP	98	CLE2	$e^+e^- \approx \Upsilon(4S)$
$3.44\pm0.62^{+0.44}_{-0.46}$	68	AVERY	92	CLE2	See JESSOP 98

[1] This JESSOP 98 fraction, when combined with other η' fractions, greatly overshoots the inclusive η' fraction. See the measurement just above, which fits nicely.

$\Gamma(\eta'(958)\pi^+\pi^0)/\Gamma_{total}$ — Γ_{109}/Γ

VALUE (%)	DOCUMENT ID		TECN	COMMENT
5.6±0.5±0.6	ONYISI	13	CLEO	e^+e^- at 4.17 GeV

$\Gamma(\eta'(958)\pi^+\pi^0\text{nonresonant})/\Gamma_{total}$ — Γ_{110}/Γ

VALUE	CL%	DOCUMENT ID		TECN	COMMENT
<5.1 × 10^{-2}	90	ABLIKIM	15Z	BES3	482 pb^{-1}, 4009 MeV

Modes with one or three K's

$\Gamma(K^+\pi^0)/\Gamma(K^+K^0_S)$ — Γ_{111}/Γ_{36}

VALUE (units 10^{-2})	EVTS	DOCUMENT ID		TECN	COMMENT
4.2±1.4±0.2	202 ± 70	MENDEZ	10	CLEO	e^+e^- at 4170 MeV
• • • We do not use the following data for averages, fits, limits, etc. • • •					
5.5±1.3±0.7	141 ± 34	ADAMS	07A	CLEO	See MENDEZ 10

$\Gamma(K^+\pi^0)/\Gamma(K^+K^-\pi^+)$ — Γ_{111}/Γ_{39}

VALUE (units 10^{-3})	EVTS	DOCUMENT ID		TECN	COMMENT
13.73±0.90±0.33	2.3k	ABLIKIM	20R	BES3	e^+e^-, 4178 ∼ 4226 MeV

$\Gamma(K^+\pi^0)/\Gamma(\phi\pi^+,\ \phi \to K^+K^-)$ — Γ_{111}/Γ_{41}

VALUE (%)	EVTS	DOCUMENT ID		TECN	COMMENT
3.28±0.23±0.13	12k	GUAN	21	BELL	$e^+e^- \approx \Upsilon(4,5S)$

$\Gamma(K^0_S\pi^+)/\Gamma(K^+K^0_S)$ — Γ_{112}/Γ_{36}

VALUE (units 10^{-2})	EVTS	DOCUMENT ID		TECN	COMMENT
8.12±0.28 OUR AVERAGE					
8.5 ±0.7 ±0.2	393 ± 33	MENDEZ	10	CLEO	e^+e^- at 4170 MeV
8.03±0.24±0.19	17.6k±481	WON	09	BELL	e^+e^- at $\Upsilon(4S)$
10.4 ±2.4 ±1.4	113 ± 26	LINK	08	FOCS	γ A, $\overline{E}_\gamma \approx$ 180 GeV
• • • We do not use the following data for averages, fits, limits, etc. • • •					
8.2 ±0.9 ±0.2	206 ± 22	ADAMS	07A	CLEO	See MENDEZ 10

$\Gamma(K^0_S\pi^+)/\Gamma(K^+K^-\pi^+)$ — Γ_{112}/Γ_{39}

VALUE (units 10^{-3})	EVTS	DOCUMENT ID		TECN	COMMENT
20.35±0.62±0.42	2.7k	ABLIKIM	20R	BES3	e^+e^-, 4178 ∼ 4226 MeV

$\Gamma(K^+\eta)/\Gamma(K^+K^0_S)$ — Γ_{113}/Γ_{36}

Unseen decay modes of the η are included.

VALUE (units 10^{-2})	EVTS	DOCUMENT ID		TECN	COMMENT
11.8±2.2±0.6	222 ± 41	MENDEZ	10	CLEO	e^+e^- at 4170 MeV

$\Gamma(K^+\eta)/\Gamma(\eta\pi^+)$ — Γ_{113}/Γ_{86}

VALUE (units 10^{-2})	EVTS	DOCUMENT ID		TECN	COMMENT
• • • We do not use the following data for averages, fits, limits, etc. • • •					
8.9±1.5±0.4	113 ± 18	ADAMS	07A	CLEO	See MENDEZ 10

$\Gamma(K^+\eta)/\Gamma(K^+K^-\pi^+)$ — Γ_{113}/Γ_{39}

VALUE (units 10^{-2})	EVTS	DOCUMENT ID		TECN	COMMENT
2.97±0.18±0.06	1.8k	ABLIKIM	20R	BES3	e^+e^-, 4178 ∼ 4226 MeV

$\Gamma(K^+\eta)/\Gamma(\phi\pi^+,\ \phi \to K^+K^-)$ — Γ_{113}/Γ_{41}

VALUE (%)	EVTS	DOCUMENT ID		TECN	COMMENT
7.81±0.22±0.24	14k	GUAN	21	BELL	$e^+e^- \approx \Upsilon(4,5S)$

Downloaded from https://academic.oup.com/ptep/article/2022/8/083C01/6651666 by KIT Library user on 27 September 2022

$\Gamma(K^+\omega)/\Gamma_{total}$ — Γ_{114}/Γ

Unseen decay modes of the ω are included.

VALUE (units 10^{-4})	CL%	EVTS	DOCUMENT ID		TECN	COMMENT
8.7±2.4±0.8		29	[1] ABLIKIM	19AH	BES3	e^+e^- at 4.178 GeV
• • • We do not use the following data for averages, fits, limits, etc. • • •						
<24	90		GE	09A	CLEO	e^+e^- at 4170 MeV

[1] Evidence for mode at 4.4σ.

$\Gamma(K^+\eta'(958))/\Gamma(K^+K^0_S)$ — Γ_{115}/Γ_{36}

Unseen decay modes of the $\eta'(958)$ are included.

VALUE (units 10^{-2})	EVTS	DOCUMENT ID		TECN	COMMENT
11.8±3.6±0.7	56 ± 17	MENDEZ	10	CLEO	e^+e^- at 4170 MeV

$\Gamma(K^+\eta'(958))/\Gamma(\eta'(958)\pi^+)$ — $\Gamma_{115}/\Gamma_{105}$

VALUE (units 10^{-2})	EVTS	DOCUMENT ID		TECN	COMMENT
• • • We do not use the following data for averages, fits, limits, etc. • • •					
4.2±1.3±0.3	28 ± 9	ADAMS	07A	CLEO	See MENDEZ 10

$\Gamma(K^+\eta'(958))/\Gamma(K^+K^-\pi^+)$ — Γ_{115}/Γ_{39}

VALUE (units 10^{-2})	EVTS	DOCUMENT ID		TECN	COMMENT
4.91±0.31±0.31	675	ABLIKIM	20R	BES3	e^+e^-, 4178 ∼ 4226 MeV

$\Gamma(K^+\pi^+\pi^-)/\Gamma_{total}$ — Γ_{116}/Γ

VALUE (%)	DOCUMENT ID		TECN	COMMENT
0.65 ±0.04 OUR FIT				
0.654±0.033±0.025	ONYISI	13	CLEO	e^+e^- at 4.17 GeV
• • • We do not use the following data for averages, fits, limits, etc. • • •				
0.69 ±0.05 ±0.03	[1] ALEXANDER	08	CLEO	See ONYISI 13

[1] ALEXANDER 08 uses single- and double-tagged events in an overall fit.

$\Gamma(K^+\pi^+\pi^-)/\Gamma(K^+K^-\pi^+)$ — Γ_{116}/Γ_{39}

VALUE	EVTS	DOCUMENT ID		TECN	COMMENT
0.120±0.007 OUR FIT					
0.127±0.007±0.014	567 ± 31	LINK	04F	FOCS	γ A, $\overline{E}_\gamma \approx 180$ GeV

$\Gamma(K^+\rho^0)/\Gamma(K^+\pi^+\pi^-)$ — $\Gamma_{117}/\Gamma_{116}$

This is the "fit fraction" from the Dalitz-plot analysis.

VALUE	DOCUMENT ID		TECN	COMMENT
0.3883±0.0531±0.0261	LINK	04F	FOCS	Dalitz fit, 567 evts

$\Gamma(K^+\rho(1450)^0, \rho^0 \to \pi^+\pi^-)/\Gamma(K^+\pi^+\pi^-)$ — $\Gamma_{118}/\Gamma_{116}$

This is the "fit fraction" from the Dalitz-plot analysis.

VALUE	DOCUMENT ID		TECN	COMMENT
0.1062±0.0351±0.0104	LINK	04F	FOCS	Dalitz fit, 567 evts

$\Gamma(K^*(892)^0\pi^+, K^{*0} \to K^+\pi^-)/\Gamma(K^+\pi^+\pi^-)$ — $\Gamma_{119}/\Gamma_{116}$

This is the "fit fraction" from the Dalitz-plot analysis.

VALUE	DOCUMENT ID		TECN	COMMENT
0.2164±0.0321±0.0114	LINK	04F	FOCS	Dalitz fit, 567 evts

$\Gamma(K^*(1410)^0\pi^+, K^{*0} \to K^+\pi^-)/\Gamma(K^+\pi^+\pi^-)$ — $\Gamma_{120}/\Gamma_{116}$

This is the "fit fraction" from the Dalitz-plot analysis.

VALUE	DOCUMENT ID		TECN	COMMENT
0.1882±0.0403±0.0122	LINK	04F	FOCS	Dalitz fit, 567 evts

$\Gamma(K^*(1430)^0\pi^+, K^{*0} \to K^+\pi^-)/\Gamma(K^+\pi^+\pi^-)$ — $\Gamma_{121}/\Gamma_{116}$

This is the "fit fraction" from the Dalitz-plot analysis.

VALUE	DOCUMENT ID		TECN	COMMENT
0.0765±0.0500±0.0170	LINK	04F	FOCS	Dalitz fit, 567 evts

$\Gamma(K^+\pi^+\pi^-\text{nonresonant})/\Gamma(K^+\pi^+\pi^-)$ — $\Gamma_{122}/\Gamma_{116}$

This is the "fit fraction" from the Dalitz-plot analysis.

VALUE	DOCUMENT ID		TECN	COMMENT
0.1588±0.0492±0.0153	LINK	04F	FOCS	Dalitz fit, 567 evts

$\Gamma(K^0\pi^+\pi^0)/\Gamma_{total}$ — Γ_{123}/Γ

VALUE (%)	EVTS	DOCUMENT ID		TECN	COMMENT
1.08 ±0.06 OUR AVERAGE					
1.086±0.060±0.030	666	[1] ABLIKIM	21AB	BES3	e^+e^- at 4.178–4.226 GeV
1.00 ±0.18 ±0.04	44	NAIK	09A	CLEO	e^+e^- at 4170 MeV

[1] ABLIKIM 21AB uses an amplitude analysis with 5 resonant modes plus one background component, and measures $B(D_s^+ \to K^0_S\pi^+\pi^0) = (5.43 \pm 0.30 \pm 0.15) \times 10^{-3}$.

$\Gamma(K^0_S 2\pi^+\pi^-)/\Gamma(K^0_S K^- 2\pi^+)$ — Γ_{124}/Γ_{60}

VALUE	EVTS	DOCUMENT ID		TECN	COMMENT
0.18±0.04±0.05	179 ± 36	LINK	08	FOCS	γ A, $\overline{E}_\gamma \approx 180$ GeV

$\Gamma(K^+\omega\pi^0)/\Gamma_{total}$ — Γ_{125}/Γ

Unseen decay modes of the ω are included.

VALUE (%)	CL%	DOCUMENT ID		TECN	COMMENT
<0.82	90	GE	09A	CLEO	e^+e^- at 4170 MeV

$\Gamma(K^+\omega\pi^+\pi^-)/\Gamma_{total}$ — Γ_{126}/Γ

Unseen decay modes of the ω are included.

VALUE (%)	CL%	DOCUMENT ID		TECN	COMMENT
<0.54	90	GE	09A	CLEO	e^+e^- at 4170 MeV

$\Gamma(K^+\omega\eta)/\Gamma_{total}$ — Γ_{127}/Γ

Unseen decay modes of the ω and η are included.

VALUE (%)	CL%	DOCUMENT ID		TECN	COMMENT
<0.79	90	GE	09A	CLEO	e^+e^- at 4170 MeV

$\Gamma(2K^+K^-)/\Gamma(K^+K^-\pi^+)$ — Γ_{128}/Γ_{39}

VALUE (units 10^{-3})	EVTS	DOCUMENT ID		TECN	COMMENT
4.0 ±0.3 ±0.2	748 ± 60	DEL-AMO-SA...	11G	BABR	$e^+e^- \approx \Upsilon(4S)$
• • • We do not use the following data for averages, fits, limits, etc. • • •					
$8.95 \pm 2.12^{+2.24}_{-2.31}$	31	LINK	02I	FOCS	γ A, ≈ 180 GeV

$\Gamma(\phi K^+, \phi \to K^+K^-)/\Gamma(2K^+K^-)$ — $\Gamma_{129}/\Gamma_{128}$

VALUE	DOCUMENT ID		TECN	COMMENT
0.41±0.08±0.03	DEL-AMO-SA...	11G	BABR	$e^+e^- \approx \Upsilon(4S)$

Doubly Cabibbo-suppressed modes

$\Gamma(2K^+\pi^-)/\Gamma(K^+K^-\pi^+)$ — Γ_{130}/Γ_{39}

VALUE (units 10^{-3})	EVTS	DOCUMENT ID		TECN	COMMENT
2.371±0.034 OUR AVERAGE					
2.372±0.024±0.025	67k	AAIJ	19G	LHCB	pp at 8 TeV
2.3 ±0.3 ±0.2	356 ± 52	DEL-AMO-SA...	11G	BABR	$e^+e^- \approx \Upsilon(4S)$
2.29 ±0.28 ±0.12	281 ± 34	KO	09	BELL	e^+e^- at $\Upsilon(4S)$
5.2 ±1.7 ±1.1	27 ± 9	LINK	05K	FOCS	<0.78%, CL = 90%

$\Gamma(K^+K^*(892)^0, K^{*0} \to K^+\pi^-)/\Gamma(2K^+\pi^-)$ — $\Gamma_{131}/\Gamma_{130}$

VALUE	DOCUMENT ID		TECN	COMMENT
0.47±0.22±0.15	DEL-AMO-SA...	11G	BABR	$e^+e^- \approx \Upsilon(4S)$

Baryon-antibaryon mode

$\Gamma(p\overline{n})/\Gamma_{total}$ — Γ_{132}/Γ

This is the only baryonic mode allowed kinematically.

VALUE (units 10^{-3})	EVTS	DOCUMENT ID		TECN	COMMENT
1.22±0.11 OUR AVERAGE					
1.21±0.10±0.05	193 ± 17	ABLIKIM	19O	BES3	e^+e^-, E_{cm} = 4178 MeV
$1.30 \pm 0.36^{+0.12}_{-0.16}$	13.0 ± 3.6	ATHAR	08	CLEO	e^+e^-, $E_{cm} \approx 4170$ MeV

$\Gamma(p\overline{p}e^+\nu_e)/\Gamma_{total}$ — Γ_{133}/Γ

VALUE	CL%	DOCUMENT ID		TECN	COMMENT
<2.0 × 10^{-4}	90	ABLIKIM	19BD	BES3	e^+e^- at 4178 MeV

Rare or forbidden modes

$\Gamma(\pi^+e^+e^-)/\Gamma_{total}$ — Γ_{134}/Γ

This mode is not a useful test for a ΔC=1 weak neutral current because both quarks must change flavor in this decay.

VALUE	CL%	DOCUMENT ID		TECN	COMMENT
< 5.5 × 10^{-6}	90	AAIJ	21T	LHCB	1.6 fb^{-1} pp
• • • We do not use the following data for averages, fits, limits, etc. • • •					
<13 × 10^{-6}	90	LEES	11G	BABR	$e^+e^- \approx \Upsilon(4S)$
< 2.2 × 10^{-5}	90	[1] RUBIN	10	CLEO	e^+e^- at 4170 MeV
<27 × 10^{-5}	90	AITALA	99G	E791	$\pi^- N$ 500 GeV

[1] This RUBIN 10 limit is for the e^+e^- mass in the continuum away from the $\phi(1020)$. See the next data block.

$\Gamma(\pi^+\phi, \phi \to e^+e^-)/\Gamma_{total}$ — Γ_{135}/Γ

This is *not* a test for the $\Delta C = 1$ weak neutral current, but leads to the $\pi^+e^+e^-$ final state.

VALUE	EVTS	DOCUMENT ID		TECN	COMMENT
$(6^{+8}_{-4} \pm 1) \times 10^{-6}$	3	RUBIN	10	CLEO	e^+e^- at 4170 MeV

$\Gamma(\pi^+\mu^+\mu^-)/\Gamma_{total}$ — Γ_{136}/Γ

This mode is not a useful test for a ΔC=1 weak neutral current because both quarks must change flavor in this decay.

VALUE	CL%	DOCUMENT ID		TECN	COMMENT
<1.8 × 10^{-7}	90	AAIJ	21T	LHCB	1.6 fb^{-1} pp
• • • We do not use the following data for averages, fits, limits, etc. • • •					
<4.1 × 10^{-7}	90	AAIJ	13AF	LHCB	pp at 7 TeV
<4.3 × 10^{-5}	90	LEES	11G	BABR	$e^+e^- \approx \Upsilon(4S)$
<2.6 × 10^{-5}	90	LINK	03F	FOCS	γ A, $\overline{E}_\gamma \approx 180$ GeV
<1.4 × 10^{-4}	90	AITALA	99G	E791	$\pi^- N$ 500 GeV
<4.3 × 10^{-4}	90	KODAMA	95	E653	π^- emulsion 600 GeV

Downloaded from https://academic.oup.com/ptep/article/2022/8/083C01/6651666 by KIT Library user on 27 September 2022

$\Gamma(K^+ e^+ e^-)/\Gamma_{total}$ — Γ_{137}/Γ

A test for the ΔC=1 weak neutral current. Allowed by higher-order electroweak interactions.

VALUE	CL%	DOCUMENT ID		TECN	COMMENT
$<3.7\times10^{-6}$	90	LEES	11G	BABR	$e^+e^-\approx\Upsilon(4S)$
• • • We do not use the following data for averages, fits, limits, etc. • • •					
$<4.9\times10^{-6}$	90	AAIJ	21T	LHCB	1.6 fb^{-1} pp
$<5.2\times10^{-5}$	90	RUBIN	10	CLEO	e^+e^- at 4170 MeV
$<1.6\times10^{-3}$	90	AITALA	99G	E791	π^-N 500 GeV

$\Gamma(K^+\mu^+\mu^-)/\Gamma_{total}$ — Γ_{138}/Γ

A test for the ΔC=1 weak neutral current. Allowed by higher-order electroweak interactions.

VALUE	CL%	DOCUMENT ID		TECN	COMMENT
$<1.4\times10^{-7}$	90	AAIJ	21T	LHCB	1.6 fb^{-1} pp
• • • We do not use the following data for averages, fits, limits, etc. • • •					
$<21\times10^{-6}$	90	LEES	11G	BABR	$e^+e^-\approx\Upsilon(4S)$
$<3.6\times10^{-5}$	90	LINK	03F	FOCS	γ A, $\overline{E}_\gamma\approx$ 180 GeV
$<1.4\times10^{-4}$	90	AITALA	99G	E791	π^-N 500 GeV
$<5.9\times10^{-4}$	90	KODAMA	95	E653	π^- emulsion 600 GeV

$\Gamma(K^*(892)^+\mu^+\mu^-)/\Gamma_{total}$ — Γ_{139}/Γ

A test for the ΔC=1 weak neutral current. Allowed by higher-order electroweak interactions.

VALUE	CL%	DOCUMENT ID		TECN	COMMENT
$<1.4\times10^{-3}$	90	KODAMA	95	E653	π^- emulsion 600 GeV

$\Gamma(\pi^+ e^+\mu^-)/\Gamma_{total}$ — Γ_{140}/Γ

A test of lepton-family-number conservation.

VALUE	CL%	DOCUMENT ID		TECN	COMMENT
$<1.1\times10^{-6}$	90	AAIJ	21T	LHCB	1.6 fb^{-1} pp
• • • We do not use the following data for averages, fits, limits, etc. • • •					
$<12\times10^{-6}$	90	LEES	11G	BABR	$e^+e^-\approx\Upsilon(4S)$

$\Gamma(\pi^+ e^-\mu^+)/\Gamma_{total}$ — Γ_{141}/Γ

A test of lepton-family-number conservation.

VALUE	CL%	DOCUMENT ID		TECN	COMMENT
$<9.4\times10^{-7}$	90	AAIJ	21T	LHCB	1.6 fb^{-1} pp
• • • We do not use the following data for averages, fits, limits, etc. • • •					
$<20\times10^{-6}$	90	LEES	11G	BABR	$e^+e^-\approx\Upsilon(4S)$

$\Gamma(K^+ e^+\mu^-)/\Gamma_{total}$ — Γ_{142}/Γ

A test of lepton-family-number conservation.

VALUE	CL%	DOCUMENT ID		TECN	COMMENT
$<7.9\times10^{-7}$	90	AAIJ	21T	LHCB	1.6 fb^{-1} pp
• • • We do not use the following data for averages, fits, limits, etc. • • •					
$<14\times10^{-6}$	90	LEES	11G	BABR	$e^+e^-\approx\Upsilon(4S)$

$\Gamma(K^+ e^-\mu^+)/\Gamma_{total}$ — Γ_{143}/Γ

A test of lepton-family-number conservation.

VALUE	CL%	DOCUMENT ID		TECN	COMMENT
$<5.6\times10^{-7}$	90	AAIJ	21T	LHCB	1.6 fb^{-1} pp
• • • We do not use the following data for averages, fits, limits, etc. • • •					
$<9.7\times10^{-6}$	90	LEES	11G	BABR	$e^+e^-\approx\Upsilon(4S)$

$\Gamma(\pi^- 2e^+)/\Gamma_{total}$ — Γ_{144}/Γ

A test of lepton-number conservation.

VALUE	CL%	DOCUMENT ID		TECN	COMMENT
$<1.4\times10^{-6}$	90	AAIJ	21T	LHCB	1.6 fb^{-1} pp
• • • We do not use the following data for averages, fits, limits, etc. • • •					
$<4.1\times10^{-6}$	90	LEES	11G	BABR	$e^+e^-\approx\Upsilon(4S)$
$<1.8\times10^{-5}$	90	RUBIN	10	CLEO	e^+e^- at 4170 MeV
$<69\times10^{-5}$	90	AITALA	99G	E791	π^-N 500 GeV

$\Gamma(\pi^- 2\mu^+)/\Gamma_{total}$ — Γ_{145}/Γ

A test of lepton-number conservation.

VALUE	CL%	DOCUMENT ID		TECN	COMMENT
$<8.6\times10^{-8}$	90	AAIJ	21T	LHCB	1.6 fb^{-1} pp
• • • We do not use the following data for averages, fits, limits, etc. • • •					
$<1.2\times10^{-7}$	90	AAIJ	13AF	LHCB	pp at 7 TeV
$<1.4\times10^{-5}$	90	LEES	11G	BABR	$e^+e^-\approx\Upsilon(4S)$
$<2.9\times10^{-5}$	90	LINK	03F	FOCS	γ A, $\overline{E}_\gamma\approx$ 180 GeV
$<8.2\times10^{-5}$	90	AITALA	99G	E791	π^-N 500 GeV
$<4.3\times10^{-4}$	90	KODAMA	95	E653	π^- emulsion 600 GeV

$\Gamma(\pi^- e^+\mu^+)/\Gamma_{total}$ — Γ_{146}/Γ

A test of lepton-number conservation.

VALUE	CL%	DOCUMENT ID		TECN	COMMENT
$<6.3\times10^{-7}$	90	AAIJ	21T	LHCB	1.6 fb^{-1} pp
• • • We do not use the following data for averages, fits, limits, etc. • • •					
$<8.4\times10^{-6}$	90	LEES	11G	BABR	$e^+e^-\approx\Upsilon(4S)$
$<7.3\times10^{-4}$	90	AITALA	99G	E791	π^-N 500 GeV

$\Gamma(K^- 2e^+)/\Gamma_{total}$ — Γ_{147}/Γ

A test of lepton-number conservation.

VALUE	CL%	DOCUMENT ID		TECN	COMMENT
$<7.7\times10^{-7}$	90	AAIJ	21T	LHCB	1.6 fb^{-1} pp
• • • We do not use the following data for averages, fits, limits, etc. • • •					
$<5.2\times10^{-6}$	90	LEES	11G	BABR	$e^+e^-\approx\Upsilon(4S)$
$<1.7\times10^{-5}$	90	RUBIN	10	CLEO	e^+e^- at 4170 MeV
$<63\times10^{-5}$	90	AITALA	99G	E791	π^-N 500 GeV

$\Gamma(K^- 2\mu^+)/\Gamma_{total}$ — Γ_{148}/Γ

A test of lepton-number conservation.

VALUE	CL%	DOCUMENT ID		TECN	COMMENT
$<2.6\times10^{-8}$	90	AAIJ	21T	LHCB	1.6 fb^{-1} pp
• • • We do not use the following data for averages, fits, limits, etc. • • •					
$<1.3\times10^{-5}$	90	LEES	11G	BABR	$e^+e^-\approx\Upsilon(4S)$
$<1.3\times10^{-5}$	90	LINK	03F	FOCS	γ A, $\overline{E}_\gamma\approx$ 180 GeV
$<1.8\times10^{-4}$	90	AITALA	99G	E791	π^-N 500 GeV
$<5.9\times10^{-4}$	90	KODAMA	95	E653	π^- emulsion 600 GeV

$\Gamma(K^- e^+\mu^+)/\Gamma_{total}$ — Γ_{149}/Γ

A test of lepton-number conservation.

VALUE	CL%	DOCUMENT ID		TECN	COMMENT
$<2.6\times10^{-7}$	90	AAIJ	21T	LHCB	1.6 fb^{-1} pp
• • • We do not use the following data for averages, fits, limits, etc. • • •					
$<6.1\times10^{-6}$	90	LEES	11G	BABR	$e^+e^-\approx\Upsilon(4S)$
$<6.8\times10^{-4}$	90	AITALA	99G	E791	π^-N 500 GeV

$\Gamma(K^*(892)^- 2\mu^+)/\Gamma_{total}$ — Γ_{150}/Γ

A test of lepton-number conservation.

VALUE	CL%	DOCUMENT ID		TECN	COMMENT
$<1.4\times10^{-3}$	90	KODAMA	95	E653	π^- emulsion 600 GeV

$D_s^\pm$ Amplitude analyses

$D_s^+ \to K^+K^-\pi^+$ partial wave analyses

Amplitude analyses of D_s^+ decays to the $K^+K^-\pi^+$ final state, fitting simultaneously different partial wave components.

VALUE	EVTS	DOCUMENT ID		TECN	COMMENT
seen	18.6k	[1] ABLIKIM	21AE	BES3	e^+e^- at 4.178 GeV
seen	96k	[1] DEL-AMO-SA...	11G	BABR	e^+e^- at $\Upsilon(4S)$
seen	12k	[1] MITCHELL	09A	CLEO	e^+e^- at 4.17 GeV
seen	701	[2] FRABETTI	95B	E687	

[1] Amplitude analysis with 6 components.
[2] Amplitude analysis with 5 components.

$D_s^+ \to 2\pi^+\pi^-\eta$ partial wave analyses

Amplitude analyses of D_s^+ decays to the $\pi^+\pi^+\pi^-\eta$ final state, fitting simultaneously different partial wave components.

VALUE	EVTS	DOCUMENT ID		TECN	COMMENT
seen	2.1k	[1] ABLIKIM	21AR	BES3	e^+e^- at 4.178–4.226 GeV

[1] Amplitude analysis with 11 components.

$D_s^+ \to (KS)^0 K^- 2\pi^+$ partial wave analyses

Amplitude analyses of D_s^+ decays to the $K_S^0 K^- 2\pi^+$ final state, fitting simultaneously different partial wave components.

VALUE	EVTS	DOCUMENT ID		TECN	COMMENT
seen	1.3k	[1] ABLIKIM	21K	BES3	e^+e^- at 4.178–4.226 GeV

[1] Amplitude analysis with 13 components.

$D_s^+ \to K^-K^+\pi^+\pi^0$ partial wave analyses

Amplitude analyses of D_s^+ decays to the $K^-K^+\pi^+\pi^0$ final state, fitting simultaneously different partial wave components.

VALUE	EVTS	DOCUMENT ID		TECN	COMMENT
seen	3k	[1] ABLIKIM	21U	BES3	e^+e^- at 4.178–4.226 GeV

[1] ABLIKIM 21U uses an amplitude analysis with 9 components.

$D_s^+ - D_s^-$ CP-VIOLATING DECAY-RATE ASYMMETRIES

This is the difference between D_s^+ and D_s^- partial widths for the decay to state f, divided by the sum of the widths:
$A_{CP}(f)=[\Gamma(D_s^+\to f)-\Gamma(D_s^-\to \overline{f})]\,/\,[\Gamma(D_s^+\to f)+\Gamma(D_s^-\to \overline{f})]$.

$A_{CP}(\mu^\pm\nu)$ in $D_s^+ \to \mu^+\nu$, $D_s^- \to \mu^-\overline{\nu}_\mu$

VALUE (%)	EVTS	DOCUMENT ID		TECN	COMMENT
-0.2 ± 2.5 OUR AVERAGE					
$-1.2\pm2.5\pm1.0$	2.2k	ABLIKIM	21BE	BES3	e^+e^- at 4.178, 4.226 GeV
4.8 ± 6.1		ALEXANDER	09	CLEO	e^+e^- at 4170 MeV

Downloaded from https://academic.oup.com/ptep/article/2022/8/083C01/6651666 by KIT Library user on 27 September 2022

$A_{CP}(\tau^\pm\nu)$ in $D_s^+ \to \tau^+\nu_\tau$, $D_s^- \to \tau^-\overline{\nu}_\tau$

VALUE (%)	EVTS	DOCUMENT ID		TECN	COMMENT
2.9±4.8±1.0	950	[1] ABLIKIM	21BE	BES3	e^+e^- at 4.178, 4.226 GeV

[1] ABLIKIM 21BE also reports that when constrained by the Standard Model ratio of $\Gamma(D_s^+ \to \tau^+\nu_\tau)/\Gamma(D_s^+ \to \mu^+\nu_\mu) = 9.75$, the result is $(-0.1 \pm 1.9 \pm 1.0)$%.

$A_{CP}(K^\pm K_S^0)$ in $D_s^\pm \to K^\pm K_S^0$

VALUE (%)	EVTS	DOCUMENT ID		TECN	COMMENT
0.09±0.26 OUR AVERAGE					
0.6 ±2.8 ±0.6	1.8k	ABLIKIM	19AM	BES3	e^+e^- at 4178 MeV
−0.05±0.23±0.24	288k	[1] LEES	13E	BABR	e^+e^- at $\Upsilon(4S)$
2.6 ±1.5 ±0.6		ONYISI	13	CLEO	e^+e^- at 4.17 GeV
0.12±0.36±0.22		KO	10	BELL	$e^+e^- \approx \Upsilon(4S)$
• • • We do not use the following data for averages, fits, limits, etc. • • •					
4.7 ±1.8 ±0.9	4.0k	MENDEZ	10	CLEO	See ONYISI 13
4.9 ±2.1 ±0.9		ALEXANDER	08	CLEO	See MENDEZ 10

[1] LEES 13E finds that after subtracting the contribution due to $K^0 - \overline{K}^0$ mixing, the CP asymmetry is $(+0.28 \pm 0.23 \pm 0.24)$%.

$A_{CP}(K^\pm K_L^0)$ in $D_s^\pm \to K^\pm K_L^0$

VALUE (units 10^{-2})	EVTS	DOCUMENT ID		TECN	COMMENT
−1.1±2.6±0.6	2.3k	ABLIKIM	19AM	BES3	e^+e^- at 4178 MeV

$A_{CP}(K^+K^-\pi^\pm)$ in $D_s^\pm \to K^+K^-\pi^\pm$

VALUE (%)	DOCUMENT ID		TECN	COMMENT
−0.5±0.8±0.4	ONYISI	13	CLEO	e^+e^- at 4.17 GeV
• • • We do not use the following data for averages, fits, limits, etc. • • •				
0.3±1.1±0.8	ALEXANDER	08	CLEO	See ONYISI 13

$A_{CP}(\phi\pi^\pm)$ in $D_s^\pm \to \phi\pi^\pm$

VALUE (%)	DOCUMENT ID		TECN	COMMENT
−0.38±0.26±0.08	ABAZOV	14B	D0	$p\overline{p}$ at 1.96 TeV

$A_{CP}(K^\pm K_S^0\pi^0)$ in $D_s^\pm \to K^\pm K_S^0\pi^0$

VALUE (%)	DOCUMENT ID		TECN	COMMENT
−1.6±6.0±1.1	ONYISI	13	CLEO	e^+e^- at 4.17 GeV

$A_{CP}(2K_S^0\pi^\pm)$ in $D_s^\pm \to 2K_S^0\pi^\pm$

VALUE (%)	DOCUMENT ID		TECN	COMMENT
3.1±5.2±0.6	ONYISI	13	CLEO	e^+e^- at 4.17 GeV

$A_{CP}(K^+K^-\pi^\pm\pi^0)$ in $D_s^\pm \to K^+K^-\pi^\pm\pi^0$

VALUE (%)	DOCUMENT ID		TECN	COMMENT
0.0±2.7±1.2	ONYISI	13	CLEO	e^+e^- at 4.17 GeV
• • • We do not use the following data for averages, fits, limits, etc. • • •				
−5.9±4.2±1.2	ALEXANDER	08	CLEO	See ONYISI 13

$A_{CP}(K^\pm K_S^0\pi^+\pi^-)$ in $D_s^\pm \to K^\pm K_S^0\pi^+\pi^-$

VALUE (%)	DOCUMENT ID		TECN	COMMENT
−5.7±5.3±0.9	ONYISI	13	CLEO	e^+e^- at 4.17 GeV

$A_{CP}(K_S^0K^\mp 2\pi^\pm)$ in $D_s^+ \to K_S^0K^\mp 2\pi^\pm$

VALUE (%)	DOCUMENT ID		TECN	COMMENT
4.1±2.7±0.9	ONYISI	13	CLEO	e^+e^- at 4.17 GeV
• • • We do not use the following data for averages, fits, limits, etc. • • •				
−0.7±3.6±1.1	ALEXANDER	08	CLEO	See ONYISI 13

$A_{CP}(\pi^+\pi^-\pi^\pm)$ in $D_s^\pm \to \pi^+\pi^-\pi^\pm$

VALUE (%)	DOCUMENT ID		TECN	COMMENT
−0.7±3.0±0.6	ONYISI	13	CLEO	e^+e^- at 4.17 GeV
• • • We do not use the following data for averages, fits, limits, etc. • • •				
2.0±4.6±0.7	ALEXANDER	08	CLEO	See ONYISI 13

$A_{CP}(\pi^\pm\eta)$ in $D_s^\pm \to \pi^\pm\eta$

VALUE (%)	EVTS	DOCUMENT ID		TECN	COMMENT
0.3±0.4 OUR AVERAGE					
0.8±0.7±0.5	38k	AAIJ	21U	LHCB	pp at 13 TeV
0.2±0.3±0.3	22k	GUAN	21	BELL	$e^+e^- \approx \Upsilon(4,5S)$
• • • We do not use the following data for averages, fits, limits, etc. • • •					
1.1±3.0±0.8		ONYISI	13	CLEO	e^+e^- at 4.17 GeV
−4.6±2.9±0.3	2.5k	MENDEZ	10	CLEO	See ONYISI 13
−8.2±5.2±0.8		ALEXANDER	08	CLEO	See MENDEZ 10

$A_{CP}(\pi^\pm\eta')$ in $D_s^\pm \to \pi^\pm\eta'$

VALUE (%)	EVTS	DOCUMENT ID		TECN	COMMENT
−0.9 ±0.5 OUR AVERAGE					
−0.82±0.36±0.35	152k	AAIJ	17AF	LHCB	pp at 7, 8 TeV
−2.2 ±2.2 ±0.6		ONYISI	13	CLEO	e^+e^- at 4.17 GeV
• • • We do not use the following data for averages, fits, limits, etc. • • •					
−6.1 ±3.0 ±0.3	1.4k	MENDEZ	10	CLEO	See ONYISI 13
−5.5 ±3.7 ±1.2		ALEXANDER	08	CLEO	See MENDEZ 10

$A_{CP}(\eta\pi^\pm\pi^0)$ in $D_s^\pm \to \eta\pi^\pm\pi^0$

VALUE (%)	DOCUMENT ID		TECN	COMMENT
−0.5±3.9±2.0	ONYISI	13	CLEO	e^+e^- at 4.17 GeV

$A_{CP}(\eta'\pi^\pm\pi^0)$ in $D_s^\pm \to \eta'\pi^\pm\pi^0$

VALUE (%)	DOCUMENT ID		TECN	COMMENT
−0.4±7.4±1.9	ONYISI	13	CLEO	e^+e^- at 4.17 GeV

$A_{CP}(K^\pm\pi^0)$ in $D_s^\pm \to K^\pm\pi^0$

VALUE (%)	EVTS	DOCUMENT ID		TECN	COMMENT
2 ± 4 OUR AVERAGE Error includes scale factor of 1.2.					
− 0.8± 3.9±1.2	2.8k	AAIJ	21U	LHCB	pp at 7, 8, 13 TeV
6.4± 4.4±1.1	12k	GUAN	21	BELL	$e^+e^- \approx \Upsilon(4,5S)$
• • • We do not use the following data for averages, fits, limits, etc. • • •					
−26.6±23.8±0.9	202	MENDEZ	10	CLEO	e^+e^- at 4170 MeV
2 ±29		ADAMS	07A	CLEO	See MENDEZ 10

$A_{CP}(\overline{K}^0/K^0\pi^\pm)$ in $D_s^+ \to \overline{K}^0\pi^+$, $D_s^- \to K^0\pi^-$

VALUE (%)	EVTS	DOCUMENT ID		TECN	COMMENT
0.4 ±0.5 OUR AVERAGE					
0.38±0.46±0.17	121k	[1] AAIJ	14BD	LHCB	pp at 7, 8 TeV
0.3 ±2.0 ±0.3	14k	LEES	13E	BABR	e^+e^- at $\Upsilon(4S)$
• • • We do not use the following data for averages, fits, limits, etc. • • •					
0.61±0.83±0.14	26k	AAIJ	13W	LHCB	See AAIJ 14BD

[1] AAIJ 14BD reports its result as $A_{CP}(D_s^\pm \to K_S^0K^\pm)$ with CP-violation effects in the $K^0 - \overline{K}^0$ system subtracted. It also measures $A_{CP}(D^\pm \to \overline{K}^0/K^0K^\pm) + A_{CP}(D_s^\pm \to \overline{K}^0/K^0\pi^\pm) = (0.41 \pm 0.49 \pm 0.26)$%.

$A_{CP}(K_S^0\pi^\pm)$ in $D_s^\pm \to K_S^0\pi^\pm$

VALUE (%)	EVTS	DOCUMENT ID		TECN	COMMENT
0.20± 0.18 OUR AVERAGE					
0.16± 0.17±0.05	721k	AAIJ	19T	LHCB	pp at 7, 8, 13 TeV
0.6 ± 2.0 ±0.3	14k	LEES	13E	BABR	e^+e^- at $\Upsilon(4S)$
5.45± 2.50±0.33		KO	10	BELL	$e^+e^- \approx \Upsilon(4S)$
16.3 ± 7.3 ±0.3	0.4k	MENDEZ	10	CLEO	e^+e^- at 4170 MeV
• • • We do not use the following data for averages, fits, limits, etc. • • •					
27 ±11		ADAMS	07A	CLEO	See MENDEZ 10

$A_{CP}(K^\pm\pi^+\pi^-)$ in $D_s^\pm \to K^\pm\pi^+\pi^-$

VALUE (%)	DOCUMENT ID		TECN	COMMENT
4.5±4.8±0.6	ONYISI	13	CLEO	e^+e^- at 4.17 GeV
• • • We do not use the following data for averages, fits, limits, etc. • • •				
11.2±7.0±0.9	ALEXANDER	08	CLEO	See ONYISI 13

$A_{CP}(K_S^0\pi^+\pi^0)$ in $D_s^\pm \to K_S^0\pi^+\pi^0$

VALUE (%)	EVTS	DOCUMENT ID		TECN	COMMENT
2.7±5.5±0.9	666	[1] ABLIKIM	21AB	BES3	e^+e^- at 4.178–4.226 GeV

[1] ABLIKIM 21AB uses an amplitude analysis with 5 resonant modes plus one background component.

$A_{CP}(K^\pm\eta)$ in $D_s^\pm \to K^\pm\eta$

VALUE (%)	EVTS	DOCUMENT ID		TECN	COMMENT
1.8± 1.9 OUR AVERAGE					
0.9± 3.7±1.1	2.5k	AAIJ	21U	LHCB	pp at 13 TeV
2.1± 2.1±0.4	14k	GUAN	21	BELL	$e^+e^- \approx \Upsilon(4,5S)$
• • • We do not use the following data for averages, fits, limits, etc. • • •					
9.3±15.2±0.9	222	MENDEZ	10	CLEO	e^+e^- at 4170 MeV
−20 ±18		ADAMS	07A	CLEO	See MENDEZ 10

$A_{CP}(K^\pm\eta'(958))$ in $D_s^\pm \to K^\pm\eta'(958)$

VALUE (%)	EVTS	DOCUMENT ID		TECN	COMMENT
6.0±18.9±0.9	56 ± 17	MENDEZ	10	CLEO	e^+e^- at 4170 MeV
• • • We do not use the following data for averages, fits, limits, etc. • • •					
−17 ±37		ADAMS	07A	CLEO	See MENDEZ 10

CP VIOLATING ASYMMETRIES OF P-ODD (T-ODD) MOMENTS

$A_{Tviol}(K_S^0K^\pm\pi^+\pi^-)$ in $D_s^\pm \to K_S^0K^\pm\pi^+\pi^-$

$C_T \equiv \vec{p}_{K^+} \cdot (\vec{p}_{\pi^+} \times \vec{p}_{\pi^-})$ is a parity-odd correlation of the K^+, π^+, and π^- momenta for the D_s^+. $\overline{C}_T \equiv \vec{p}_{K^-} \cdot (\vec{p}_{\pi^-} \times \vec{p}_{\pi^+})$ is the corresponding quantity for the D_s^-. Then

$A_T \equiv [\Gamma(C_T > 0) - \Gamma(C_T < 0)] / [\Gamma(C_T > 0) + \Gamma(C_T < 0)]$, and

$\overline{A}_T \equiv [\Gamma(-\overline{C}_T > 0) - \Gamma(-\overline{C}_T < 0)] / [\Gamma(-\overline{C}_T > 0) + \Gamma(-\overline{C}_T < 0)]$, and

$A_{Tviol} \equiv \frac{1}{2}(A_T - \overline{A}_T)$. C_T and $\overline{C}_T$ are commonly referred to as T-odd moments, because they are odd under T reversal. However, the T-conjugate process $K_S^0K^\pm\pi^+\pi^- \to D_s^\pm$ is not accessible, while the P-conjugate process is.

VALUE (units 10^{-3})	EVTS	DOCUMENT ID		TECN	COMMENT
−13.6± 7.7± 3.4	29.8±0.3k	LEES	11E	BABR	$e^+e^- \approx \Upsilon(4S)$
• • • We do not use the following data for averages, fits, limits, etc. • • •					
−36 ±67 ±23	508 ± 34	LINK	05E	FOCS	γ A, $\overline{E}_\gamma \approx 180$ GeV

Downloaded from https://academic.oup.com/ptep/article/2022/8/083C01/6651666 by KIT Library user on 27 September 2022

D_s^+ Semileptonic Form Factors and Decay Constants

$r_2 \equiv A_2(0)/A_1(0)$ in $D_s^+ \to \phi \ell^+ \nu_\ell$

VALUE	EVTS	DOCUMENT ID		TECN	COMMENT
0.84 ±0.11 OUR AVERAGE Error includes scale factor of 2.4.					
0.816±0.036±0.030	25±0.5k	[1] AUBERT	08AN	BABR	$\phi e^+ \nu_e$
0.713±0.202±0.284	793	LINK	04C	FOCS	$\phi \mu^+ \nu_\mu$
1.57 ±0.25 ±0.19	271	AITALA	99D	E791	$\phi e^+ \nu_e$, $\phi \mu^+ \nu_\mu$
1.4 ±0.5 ±0.3	308	AVERY	94B	CLE2	$\phi e^+ \nu_e$
1.1 ±0.8 ±0.1	90	FRABETTI	94F	E687	$\phi \mu^+ \nu_\mu$
2.1 $^{+0.6}_{-0.5}$ ±0.2	19	KODAMA	93	E653	$\phi \mu^+ \nu_\mu$

[1] To compare with previous measurements, this AUBERT 08AN value is from a fit that fixes the pole masses at $m_A = 2.5$ GeV/c^2 and $m_V = 2.1$ GeV/c^2. A simultaneous fit to r_2, r_V, r_0 (a significant s-wave contribution) and m_A, gives $r_2 = 0.763 \pm 0.071 \pm 0.065$.

$r_V \equiv V(0)/A_1(0)$ in $D_s^+ \to \phi \ell^+ \nu_\ell$

VALUE	EVTS	DOCUMENT ID		TECN	COMMENT
1.80 ±0.08 OUR AVERAGE					
1.807±0.046±0.065	25±0.5k	[1] AUBERT	08AN	BABR	$\phi e^+ \nu_e$
1.549±0.250±0.148	793	LINK	04C	FOCS	$\phi \mu^+ \nu_\mu$
2.27 ±0.35 ±0.22	271	AITALA	99D	E791	$\phi e^+ \nu_e$, $\phi \mu^+ \nu_\mu$
0.9 ±0.6 ±0.3	308	AVERY	94B	CLE2	$\phi e^+ \nu_e$
1.8 ±0.9 ±0.2	90	FRABETTI	94F	E687	$\phi \mu^+ \nu_\mu$
2.3 $^{+1.1}_{-0.9}$ ±0.4	19	KODAMA	93	E653	$\phi \mu^+ \nu_\mu$

[1] To compare with previous measurements, this AUBERT 08AN value is from a fit that fixes the pole masses at $m_A = 2.5$ GeV/c^2 and $m_V = 2.1$ GeV/c^2. A simultaneous fit to r_2, r_V, r_0 (a significant s-wave contribution) and m_A, gives $r_V = 1.849 \pm 0.060 \pm 0.095$.

Γ_L/Γ_T in $D_s^+ \to \phi \ell^+ \nu_\ell$

VALUE	EVTS	DOCUMENT ID		TECN	COMMENT
0.72±0.18 OUR AVERAGE					
1.0 ±0.3 ±0.2	308	AVERY	94B	CLE2	$\phi e^+ \nu_e$
1.0 ±0.5 ±0.1	90	[1] FRABETTI	94F	E687	$\phi \mu^+ \nu_\mu$
0.54±0.21±0.10	19	[1] KODAMA	93	E653	$\phi \mu^+ \nu_\mu$

[1] FRABETTI 94F and KODAMA 93 evaluate Γ_L/Γ_T for a lepton mass of zero.

$f_+(0)\,|V_{cs}|$ in $D_s^+ \to \eta e^+ \nu_e$

VALUE	EVTS	DOCUMENT ID		TECN	COMMENT
0.4455±0.0053±0.0044	1.8k	ABLIKIM	19S	BES3	e^+e^- at 4178 MeV

$f_+(0)\,|V_{cs}|$ in $D_s^+ \to \eta' e^+ \nu_e$

VALUE	EVTS	DOCUMENT ID		TECN	COMMENT
0.477±0.049±0.011	261	ABLIKIM	19S	BES3	e^+e^- at 4178 MeV

$f_+(0)|V_{cd}|$ in $D_s^+ \to K^0 e^+ \nu_e$

VALUE	EVTS	DOCUMENT ID		TECN	COMMENT
0.162±0.019±0.003	117	[1] ABLIKIM	19D	BES3	$K_S^0 e^+ \nu_e$

[1] Using a two parameter fit in the z expansion.

$r_V \equiv V(0)/A_1(0)$ in $D_s^+ \to K^*(892)^0 e^+ \nu_e$

VALUE	EVTS	DOCUMENT ID		TECN	COMMENT
1.67±0.34±0.16	155	ABLIKIM	19D	BES3	e^+e^- at 4178 MeV

$r_2 \equiv A_2(0)/A_1(0)$ in $D_s^+ \to K^*(892)^0 e^+ \nu_e$

VALUE	EVTS	DOCUMENT ID		TECN	COMMENT
0.77±0.28±0.07	155	ABLIKIM	19D	BES3	e^+e^- at 4178 MeV

$f_{D_s^+}\,|V_{cs}|$ in $D_s^+ \to \mu^+ \nu_\mu$

VALUE (MeV)	EVTS	DOCUMENT ID		TECN	COMMENT
243.1±3.0±3.6±1.0	2.2K	[1] ABLIKIM	21BE	BES3	e^+e^- at 4.178, 4.226 GeV
• • • We do not use the following data for averages, fits, limits, etc. • • •					
246.2±3.6±3.5	1.1k	ABLIKIM	19E	BES3	e^+e^- at 4178 MeV

[1] The third uncertainty is dominated by the uncertainty of the D_s^+ lifetime.

$f_{D_s^+}\,|V_{cs}|$ in $D_s^+ \to \tau^+ \nu_\tau$

VALUE (MeV)	EVTS	DOCUMENT ID		TECN	COMMENT
245.3±3.0 OUR AVERAGE					
251.6±5.9±4.9	1.7k	[1] ABLIKIM	21AF	BES3	e^+e^- at 4.178, 4.226 GeV
244.4±2.3±2.9	4.9k	[2] ABLIKIM	21AZ	BES3	e^+e^- at 4.178, 4.226 GeV
243.0±5.8±4.0±1.0	950	[3,4] ABLIKIM	21BE	BES3	e^+e^- at 4.178, 4.226 GeV

[1] ABLIKIM 21F uses $\tau^+ \to \pi^+\pi^0\overline{\nu}$ decays.
[2] ABLIKIM 21AZ uses $\tau^+ \to e^+\nu_e\overline{\nu}_\tau$ decays.
[3] ABLIKIM 21BE uses $\tau^+ \to e^+\nu_e\overline{\nu}_\tau$ decays. When constrained by the Standard Model ratio of $\Gamma(D_s^+ \to \tau^+\nu_\tau)/\Gamma(D_s^+ \to \mu^+\nu_\mu) = 9.75$, the result is $243.2 \pm 2.3 \pm 3.3 \pm 1.0$.
[4] The third uncertainty is dominated by the uncertainty of the D_s^+ lifetime.

$D_s^\pm$ REFERENCES

AAIJ	21T	JHEP 2106 044	R. Aaij et al.	(LHCb Collab.)
AAIJ	21U	JHEP 2106 019	R. Aaij et al.	(LHCb Collab.)
ABLIKIM	21AB	JHEP 2106 181	M. Ablikim et al.	(BESIII Collab.)
ABLIKIM	21AC	PR D104 012003	M. Ablikim et al.	(BESIII Collab.)
ABLIKIM	21AE	PR D104 012016	M. Ablikim et al.	(BESIII Collab.)
ABLIKIM	21AF	PR D104 032001	M. Ablikim et al.	(BESIII Collab.)
ABLIKIM	21AR	PR D104 L071101	M. Ablikim et al.	(BESIII Collab.)
ABLIKIM	21AZ	PRL 127 171801	M. Ablikim et al.	(BESIII Collab.)
ABLIKIM	21BE	PR D104 052009	M. Ablikim et al.	(BESIII Collab.)
ABLIKIM	21F	PR D103 052011	M. Ablikim et al.	(BESIII Collab.)
ABLIKIM	21K	PR D103 092006	M. Ablikim et al.	(BESIII Collab.)
ABLIKIM	21U	PR D104 032011	M. Ablikim et al.	(BESIII Collab.)
ABLIKIM	21Y	PR D103 092004	M. Ablikim et al.	(BESIII Collab.)
GUAN	21	PR D103 112005	Y. Guan et al.	(BELLE Collab.)
ABLIKIM	20R	JHEP 2008 146	M. Ablikim et al.	(BESIII Collab.)
AAIJ	19G	JHEP 1903 176	R. Aaij et al.	(LHCb Collab.)
AAIJ	19T	PRL 122 191803	R. Aaij et al.	(LHCb Collab.)
ABLIKIM	19AD	PR D99 072002	M. Ablikim et al.	(BESIII Collab.)
ABLIKIM	19AH	PR D99 091101	M. Ablikim et al.	(BESIII Collab.)
ABLIKIM	19AM	PR D99 112005	M. Ablikim et al.	(BESIII Collab.)
ABLIKIM	19BD	PR D100 112008	M. Ablikim et al.	(BESIII Collab.)
ABLIKIM	19BE	PRL 123 112001	M. Ablikim et al.	(BESIII Collab.)
ABLIKIM	19D	PRL 122 061801	M. Ablikim et al.	(BESIII Collab.)
ABLIKIM	19E	PRL 122 071802	M. Ablikim et al.	(BESIII Collab.)
ABLIKIM	19O	PR D99 031101	M. Ablikim et al.	(BESIII Collab.)
ABLIKIM	19S	PRL 122 121801	M. Ablikim et al.	(BESIII Collab.)
ABLIKIM	18A	PR D97 012006	M. Ablikim et al.	(BESIII Collab.)
AAIJ	17AF	PL B771 21	R. Aaij et al.	(LHCb Collab.)
AAIJ	17AN	PRL 119 101801	R. Aaij et al.	(LHCb Collab.)
ABLIKIM	16O	PR D94 072004	M. Ablikim et al.	(BESIII Collab.)
ABLIKIM	16T	PR D94 112003	M. Ablikim et al.	(BESIII Collab.)
ABLIKIM	15Z	PL B750 466	M. Ablikim et al.	(BESIII Collab.)
HIETALA	15	PR D92 012009	J. Hietala et al.	(MINN, LUTH, OXF)
LEES	15D	PR D91 019901 (errat.)	J.P. Lees et al.	(BABAR Collab.)
AAIJ	14BD	JHEP 1410 025	R. Aaij et al.	(LHCb Collab.)
ABAZOV	14B	PRL 112 111804	V.M. Abazov et al.	(D0 Collab.)
AAIJ	13AF	PL B724 203	R. Aaij et al.	(LHCb Collab.)
AAIJ	13V	JHEP 1306 065	R. Aaij et al.	(LHCb Collab.)
AAIJ	13W	JHEP 1306 112	R. Aaij et al.	(LHCb Collab.)
LEES	13E	PR D87 052012	J.P. Lees et al.	(BABAR Collab.)
ONYISI	13	PR D88 032009	P.U.E. Onyisi et al.	(CLEO Collab.)
ZUPANC	13	JHEP 1309 139	A. Zupanc et al.	(BELLE Collab.)
DEL-AMO-SA...	11G	PR D83 052001	P. del Amo Sanchez et al.	(BABAR Collab.)
LEES	11E	PR D84 031103	J.P. Lees et al.	(BABAR Collab.)
LEES	11G	PR D84 072006	J.P. Lees et al.	(BABAR Collab.)
MARTIN	11	PR D84 012005	L. Martin et al.	(CLEO Collab.)
ASNER	10	PR D81 052007	D.M. Asner et al.	(CLEO Collab.)
DEL-AMO-SA...	10J	PR D82 091103	P. del Amo Sanchez et al.	(BABAR Collab.)
Also		PR D91 019901 (errat.)	J.P. Lees et al.	(BABAR Collab.)
KO	10	PRL 104 181602	B.R. Ko et al.	(BELLE Collab.)
MENDEZ	10	PR D81 052013	H. Mendez et al.	(CLEO Collab.)
RUBIN	10	PR D82 092007	P. Rubin et al.	(CLEO Collab.)
ALEXANDER	09	PR D79 052001	J.P. Alexander et al.	(CLEO Collab.)
AUBERT	09O	PR D79 032003	B. Aubert et al.	(BABAR Collab.)
DOBBS	09	PR D79 112008	S. Dobbs et al.	(CLEO Collab.)
ECKLUND	09	PR D80 052009	K.M. Ecklund et al.	(CLEO Collab.)
GE	09A	PR D80 051102	J.Y. Ge et al.	(CLEO Collab.)
KO	09	PRL 102 221802	B.R. Ko et al.	(BELLE Collab.)
MITCHELL	09A	PR D79 072008	R.E. Mitchell et al.	(CLEO Collab.)
NAIK	09A	PR D80 112004	P. Naik et al.	(CLEO Collab.)
ONYISI	09	PR D79 052002	P.U.E. Onyisi et al.	(CLEO Collab.)
WON	09	PR D80 111101	E. Won et al.	(BELLE Collab.)
YELTON	09	PR D80 052007	J. Yelton et al.	(CLEO Collab.)
ALEXANDER	08	PRL 100 161804	J.P. Alexander et al.	(CLEO Collab.)
ATHAR	08	PRL 100 181802	S.B. Athar et al.	(CLEO Collab.)
AUBERT	08AN	PR D78 051101	B. Aubert et al.	(BABAR Collab.)
ECKLUND	08	PRL 100 161801	K.M. Ecklund et al.	(CLEO Collab.)
KLEMPT	08	EPJ C55 39	E. Klempt, M. Matveev, A.V. Sarantsev	(BONN+)
LINK	08	PL B660 147	J.M. Link et al.	(FNAL FOCUS Collab.)
WIDHALM	08	PRL 100 241801	L. Widhalm et al.	(BELLE Collab.)
ADAMS	07A	PRL 99 191805	G.S. Adams et al.	(CLEO Collab.)
AUBERT	07V	PRL 98 141801	B. Aubert et al.	(BABAR Collab.)
PEDLAR	07A	PR D76 072002	T.K. Pedlar et al.	(CLEO Collab.)
Also		PRL 99 071802	M. Artuso et al.	(CLEO Collab.)
AUBERT	06N	PR D74 031103	B. Aubert et al.	(BABAR Collab.)
HUANG	06B	PR D74 112005	G.S. Huang et al.	(CLEO Collab.)
PDG	06	JP G33 1	W.-M. Yao et al.	(PDG Collab.)
AUBERT	05V	PR D71 091104	B. Aubert et al.	(BABAR Collab.)
LINK	05E	PL B622 239	J.M. Link et al.	(FNAL FOCUS Collab.)
LINK	05J	PRL 95 052003	J.M. Link et al.	(FNAL FOCUS Collab.)
LINK	05K	PL B624 166	J.M. Link et al.	(FNAL FOCUS Collab.)
LINK	04	PL B585 200	J.M. Link et al.	(FNAL FOCUS Collab.)
LINK	04C	PL B586 183	J.M. Link et al.	(FNAL FOCUS Collab.)
LINK	04D	PL B586 191	J.M. Link et al.	(FNAL FOCUS Collab.)
LINK	04F	PL B601 10	J.M. Link et al.	(FNAL FOCUS Collab.)
ACOSTA	03D	PR D68 072004	D. Acosta et al.	(FNAL CDF-II Collab.)
ANISOVICH	03	EPJ A16 229	V.V. Anisovich et al.	
LINK	03D	PL B561 225	J.M. Link et al.	(FNAL FOCUS Collab.)
LINK	03F	PL B572 21	J.M. Link et al.	(FNAL FOCUS Collab.)
AUBERT	02G	PR D65 091104	B. Aubert et al.	(BABAR Collab.)
HEISTER	02I	PL B528 1	A. Heister et al.	(ALEPH Collab.)
LINK	02I	PL B541 227	J.M. Link et al.	(FNAL FOCUS Collab.)
LINK	02J	PL B541 243	J.M. Link et al.	(FNAL FOCUS Collab.)
ABBIENDI	01L	PL B516 236	G. Abbiendi et al.	(OPAL Collab.)
AITALA	01A	PRL 86 765	E.M. Aitala et al.	(FNAL E791 Collab.)
IORI	01	PL B523 22	M. Iori et al.	(FNAL SELEX Collab.)
LINK	01C	PRL 87 162001	J.M. Link et al.	(FNAL FOCUS Collab.)
ALEXANDROV	00	PL B478 31	Y. Alexandrov et al.	(CERN BEATRICE Collab.)
AITALA	99	PL B445 449	E.M. Aitala et al.	(FNAL E791 Collab.)
AITALA	99D	PL B450 294	E.M. Aitala et al.	(FNAL E791 Collab.)
AITALA	99G	PL B462 401	E.M. Aitala et al.	(FNAL E791 Collab.)
BONVICINI	99	PRL 82 4586	G. Bonvicini et al.	(CLEO Collab.)
CHADHA	98	PR D58 032002	M. Chada et al.	(CLEO Collab.)
JESSOP	98	PR D58 052002	C.P. Jessop et al.	(CLEO Collab.)
ACCIARRI	97F	PL B396 327	M. Acciarri et al.	(L3 Collab.)
BALEST	97	PRL 79 1436	R. Balest et al.	(CLEO Collab.)
FRABETTI	97C	PL B401 131	P.L. Frabetti et al.	(FNAL E687 Collab.)
FRABETTI	97D	PL B407 79	P.L. Frabetti et al.	(FNAL E687 Collab.)
ARTUSO	96	PL B378 364	M. Artuso et al.	(CLEO Collab.)
BAI	95C	PR D52 3781	J.Z. Bai et al.	(BES Collab.)
BRANDENB...	95	PRL 75 3804	G.W. Brandenburg et al.	(CLEO Collab.)
FRABETTI	95B	PL B351 591	P.L. Frabetti et al.	(FNAL E687 Collab.)
KODAMA	95	PL B345 85	K. Kodama et al.	(FNAL E653 Collab.)
ACOSTA	94	PR D49 5690	D. Acosta et al.	(CLEO Collab.)
AVERY	94B	PL B337 405	P. Avery et al.	(CLEO Collab.)
BROWN	94	PR D50 1884	D. Brown et al.	(CLEO Collab.)
BUTLER	94	PL B324 255	F. Butler et al.	(CLEO Collab.)
FRABETTI	94F	PL B328 187	P.L. Frabetti et al.	(FNAL E687 Collab.)
FRABETTI	93F	PRL 71 827	P.L. Frabetti et al.	(FNAL E687 Collab.)

Downloaded from https://academic.oup.com/ptep/article/2022/8/083C01/6651666 by KIT Library user on 27 September 2022

FRABETTI	93G	PL B313 253	P.L. Frabetti *et al.*	(FNAL E687 Collab.)
KODAMA	93	PL B309 483	K. Kodama *et al.*	(FNAL E653 Collab.)
ALBRECHT	92B	ZPHY C53 361	H. Albrecht *et al.*	(ARGUS Collab.)
ALEXANDER	92	PRL 68 1275	J. Alexander *et al.*	(CLEO Collab.)
AVERY	92	PRL 68 1279	P. Avery *et al.*	(CLEO Collab.)
BARLAG	92C	ZPHY C55 383	S. Barlag *et al.*	(ACCMOR Collab.)
Also		ZPHY C48 29	S. Barlag *et al.*	(ACCMOR Collab.)
FRABETTI	92	PL B281 167	P.L. Frabetti *et al.*	(FNAL E687 Collab.)
ALBRECHT	91	PL B255 634	H. Albrecht *et al.*	(ARGUS Collab.)
ALVAREZ	91	PL B255 639	M.P. Alvarez *et al.*	(CERN NA14/2 Collab.)
ALBRECHT	90D	PL B245 315	H. Albrecht *et al.*	(ARGUS Collab.)
ALEXANDER	90B	PRL 65 1531	J. Alexander *et al.*	(CLEO Collab.)
BARLAG	90C	ZPHY C46 563	S. Barlag *et al.*	(ACCMOR Collab.)
FRABETTI	90	PL B251 639	P.L. Frabetti *et al.*	(FNAL E687 Collab.)
ANJOS	89E	PL B223 267	J.C. Anjos *et al.*	(FNAL E691 Collab.)
CHEN	89	PL B226 192	W.Y. Chen *et al.*	(CLEO Collab.)
ALBRECHT	88	PL B207 349	H. Albrecht *et al.*	(ARGUS Collab.)
ANJOS	88	PRL 60 897	J.C. Anjos *et al.*	(FNAL E691 Collab.)
RAAB	88	PR D37 2391	J.R. Raab *et al.*	(FNAL E691 Collab.)
BECKER	87B	PL B184 277	H. Becker *et al.*	(NA11 and NA32 Collabs.)
BLAYLOCK	87	PRL 58 2171	G.T. Blaylock *et al.*	(Mark III Collab.)
USHIDA	86	PRL 56 1767	N. Ushida *et al.*	(FNAL E531 Collab.)
ALBRECHT	85D	PL 153B 343	H. Albrecht *et al.*	(ARGUS Collab.)
DERRICK	85B	PRL 54 2568	M. Derrick *et al.*	(HRS Collab.)
AIHARA	84D	PRL 53 2465	H. Aihara *et al.*	(TPC Collab.)
ALTHOFF	84	PL 136B 130	M. Althoff *et al.*	(TASSO Collab.)
BAILEY	84	PL 139B 320	R. Bailey *et al.*	(ACCMOR Collab.)
CHEN	83C	PRL 51 634	A. Chen *et al.*	(CLEO Collab.)

OTHER RELATED PAPERS

RICHMAN	95	RMP 67 893	J.D. Richman, P.R. Burchat	(UCSB, STAN)

$D_s^{*\pm}$

$I(J^P) = 0(?^?)$

J^P is natural, width and decay modes consistent with 1^-.

$D_s^{*\pm}$ MASS

The fit includes $D^{\pm}$, D^0, $D_s^{\pm}$, $D^{*\pm}$, D^{*0}, $D_s^{*\pm}$, $D_1(2420)^0$, $D_2^*(2460)^0$, and $D_{s1}(2536)^{\pm}$ mass and mass difference measurements.

VALUE (MeV)	DOCUMENT ID		TECN	COMMENT
2112.2±0.4 OUR FIT				
2106.6±2.1±2.7	[1] BLAYLOCK	87	MRK3	$e^+e^- \to D_s^{\pm}\gamma X$

[1] Assuming $D_s^{\pm}$ mass = 1968.7 ± 0.9 MeV.

$m_{D_s^{*\pm}} - m_{D_s^{\pm}}$

The fit includes $D^{\pm}$, D^0, $D_s^{\pm}$, $D^{*\pm}$, D^{*0}, $D_s^{*\pm}$, $D_1(2420)^0$, $D_2^*(2460)^0$, and $D_{s1}(2536)^{\pm}$ mass and mass difference measurements.

VALUE (MeV)	EVTS	DOCUMENT ID		TECN	COMMENT
143.8 ± 0.4 OUR FIT					
143.9 ± 0.4 OUR AVERAGE					
143.76± 0.39±0.40		GRONBERG	95	CLE2	e^+e^-
144.22± 0.47±0.37		BROWN	94	CLE2	e^+e^-
142.5 ± 0.8 ±1.5		[2] ALBRECHT	88	ARG	$e^+e^- \to D_s^{\pm}\gamma X$
139.5 ± 8.3 ±9.7	60	AIHARA	84D	TPC	$e^+e^- \to$ hadrons
• • • We do not use the following data for averages, fits, limits, etc. • • •					
143.0 ±18.0	8	ASRATYAN	85	HLBC	FNAL 15-ft, ν-^{2}H
110 ±46		BRANDELIK	79	DASP	$e^+e^- \to D_s^{\pm}\gamma X$

[2] Result includes data of ALBRECHT 84B.

$D_s^{*\pm}$ WIDTH

VALUE (MeV)	CL%	DOCUMENT ID		TECN	COMMENT
< 1.9	90	GRONBERG	95	CLE2	e^+e^-
< 4.5	90	ALBRECHT	88	ARG	$E_{cm}^{ee} = 10.2$ GeV
• • • We do not use the following data for averages, fits, limits, etc. • • •					
< 4.9	90	BROWN	94	CLE2	e^+e^-
<22	90	BLAYLOCK	87	MRK3	$e^+e^- \to D_s^{\pm}\gamma X$

D_s^{*+} DECAY MODES

D_s^{*-} modes are charge conjugates of the modes below.

	Mode	Fraction (Γ_i/Γ)
Γ_1	$D_s^+\gamma$	(93.5±0.7) %
Γ_2	$D_s^+\pi^0$	(5.8±0.7) %
Γ_3	$D_s^+e^+e^-$	(6.7±1.6) × 10^{-3}

CONSTRAINED FIT INFORMATION

An overall fit to 2 branching ratios uses 3 measurements and one constraint to determine 3 parameters. The overall fit has a χ^2 = 0.0 for 1 degrees of freedom.

The following *off-diagonal* array elements are the correlation coefficients $\langle \delta x_i \delta x_j \rangle / (\delta x_i \cdot \delta x_j)$, in percent, from the fit to the branching fractions, $x_i \equiv \Gamma_i/\Gamma_{total}$. The fit constrains the x_i whose labels appear in this array to sum to one.

	x_1	x_2
x_2	−97	
x_3	−19	−4

D_s^{*+} BRANCHING RATIOS

$\Gamma(D_s^+\gamma)/\Gamma_{total}$ — Γ_1/Γ

VALUE	DOCUMENT ID		TECN	COMMENT
0.935±0.007 OUR FIT				
• • • We do not use the following data for averages, fits, limits, etc. • • •				
seen	ASRATYAN	91	HLBC	$\bar{\nu}_\mu$ Ne
seen	ALBRECHT	88	ARG	$e^+e^- \to D_s^{\pm}\gamma X$
seen	AIHARA	84D		
seen	ALBRECHT	84B		
seen	BRANDELIK	79		

$\Gamma(D_s^+\pi^0)/\Gamma(D_s^+\gamma)$ — Γ_2/Γ_1

VALUE	DOCUMENT ID		TECN	COMMENT
0.062±0.008 OUR FIT				
0.062±0.008 OUR AVERAGE				
0.062±0.005±0.006	AUBERT,BE	05G	BABR	10.6 $e^+e^- \to$ hadrons
$0.062^{+0.020}_{-0.018}$±0.022	GRONBERG	95	CLE2	e^+e^-

$\Gamma(D_s^+e^+e^-)/\Gamma(D_s^+\gamma)$ — Γ_3/Γ_1

VALUE (units 10^{-3})	EVTS	DOCUMENT ID		TECN	COMMENT
7.2±1.7 OUR FIT					
$7.2^{+1.5}_{-1.3}$±1.0	38	CRONIN-HEN	12	CLEO	4.17 $e^+e^- \to$ hadrons

$D_s^{*\pm}$ REFERENCES

CRONIN-HEN	12	PR D86 072005	D. Cronin-Hennessey *et al.*	(CLEO Collab.)
AUBERT,BE	05G	PR D72 091101	B. Aubert *et al.*	(BABAR Collab.)
GRONBERG	95	PRL 75 3232	J. Gronberg *et al.*	(CLEO Collab.)
BROWN	94	PR D50 1884	D. Brown *et al.*	(CLEO Collab.)
ASRATYAN	91	PL B257 525	A.E. Asratyan *et al.*	(ITEP, BELG, SACL+)
ALBRECHT	88	PL B207 349	H. Albrecht *et al.*	(ARGUS Collab.)
BLAYLOCK	87	PRL 58 2171	G.T. Blaylock *et al.*	(Mark III Collab.)
ASRATYAN	85	PL 156B 441	A.E. Asratyan *et al.*	(ITEP, SERP)
AIHARA	84D	PRL 53 2465	H. Aihara *et al.*	(TPC Collab.)
ALBRECHT	84B	PL 146B 111	H. Albrecht *et al.*	(ARGUS Collab.)
BRANDELIK	79	PL 80B 412	R. Brandelik *et al.*	(DASP Collab.)

$D_{s0}^*(2317)^{\pm}$

$I(J^P) = 0(0^+)$

J, P need confirmation.

AUBERT 06P and CHOI 15A do not observe neutral and doubly charged partners of the $D_{s0}^*(2317)^+$. See the review on "Heavy Non-$q\bar{q}$ Mesons."

$D_{s0}^*(2317)^{\pm}$ MASS

The fit includes $D^{\pm}$, D^0, $D_s^{\pm}$, $D^{*\pm}$, D^{*0}, $D_s^{*\pm}$, $D_1(2420)^0$, $D_2^*(2460)^0$, and $D_{s1}(2536)^{\pm}$ mass and mass difference measurements.

VALUE (MeV)	EVTS	DOCUMENT ID		TECN	COMMENT
2317.8±0.5 OUR FIT					
2318.0±0.7 OUR AVERAGE					
2318.3±1.2±1.2	115	[1] ABLIKIM	18J	BES3	4.6 $e^+e^- \to D_s^{*\pm}D_{s0}^*(2317)^{\mp}$
2319.6±0.2±1.4	3.1k	AUBERT	06P	BABR	10.6 $e^+e^- \to D_s^+\pi^0 X$
2317.3±0.4±0.8	1.0k	[2] AUBERT	04E	BABR	10.6 e^+e^-
• • • We do not use the following data for averages, fits, limits, etc. • • •					
2317.2±1.3	88	[3] AUBERT,B	04S	BABR	$B \to D_{s0}^{(*)}(2317)^+\overline{D}^{(*)}$
2317.2±0.5±0.9	761	[4] MIKAMI	04	BELL	10.6 e^+e^-
2316.8±0.4±3.0	1.2k	[4,5] AUBERT	03G	BABR	10.6 e^+e^-
2317.6±1.3	273	[4,6] AUBERT	03G	BABR	10.6 e^+e^-
2319.8±2.1±2.0	24	[4] KROKOVNY	03B	BELL	10.6 e^+e^-

[1] From a fit of the D_s^* recoil mass where the $D_{s0}^*(2317)$ signal is described with a Crystal Ball function convolved with a Gaussian function.
[2] Supersedes AUBERT 03G.
[3] Systematic errors not evaluated.

Downloaded from https://academic.oup.com/ptep/article/2022/8/083C01/6651666 by KIT Library user on 27 September 2022

[4] Not independent of the corresponding $m_{D^*_{s0}(2317)} - m_{D_s}$.
[5] From $D^+_s \to K^+K^-\pi^+$ decay.
[6] From $D^+_s \to K^+K^-\pi^+\pi^0$ decay.

$m_{D^*_{s0}(2317)^\pm} - m_{D^\pm_s}$

The fit includes $D^\pm$, D^0, $D^\pm_s$, $D^{*\pm}$, D^{*0}, $D^{*\pm}_s$, $D_1(2420)^0$, $D^*_2(2460)^0$, and $D_{s1}(2536)^\pm$ mass and mass difference measurements.

VALUE (MeV)	EVTS	DOCUMENT ID		TECN	COMMENT
349.4±0.5 OUR FIT					
349.2±0.7 OUR AVERAGE					
348.7±0.5±0.7	761	MIKAMI	04	BELL	10.6 e^+e^-
350.0±1.2±1.0	135	BESSON	03	CLE2	10.6 e^+e^-
351.3±2.1±1.9	24	[7] KROKOVNY	03B	BELL	10.6 e^+e^-
• • • We do not use the following data for averages, fits, limits, etc. • • •					
349.6±0.4±3.0	1267	[8,9] AUBERT	03G	BABR	10.6 e^+e^-
350.2±1.3	273	[10,11] AUBERT	03G	BABR	10.6 e^+e^-

[7] Recalculated by us using $m_{D^+_s} = 1968.5 \pm 0.6$ MeV.
[8] From $D^+_s \to K^+K^-\pi^+$ decay.
[9] Recalculated by us using $m_{D^+_s} = 1967.20 \pm 0.03$ MeV.
[10] From $D^+_s \to K^+K^-\pi^+\pi^0$ decay.
[11] Recalculated by us using $m_{D^+_s} = 1967.4 \pm 0.2$ MeV. Systematic errors not estimated.

$D^*_{s0}(2317)^\pm$ WIDTH

VALUE (MeV)	CL%	EVTS	DOCUMENT ID		TECN	COMMENT
< 3.8	95	3180	AUBERT	06P	BABR	10.6 $e^+e^- \to D^+_s\pi^0 X$
• • • We do not use the following data for averages, fits, limits, etc. • • •						
< 4.6	90	761	MIKAMI	04	BELL	10.6 e^+e^-
<10			AUBERT	03G	BABR	10.6 e^+e^-
< 7	90	135	BESSON	03	CLE2	10.6 e^+e^-

$D^*_{s0}(2317)^\pm$ DECAY MODES

$D^*_{s0}(2317)^-$ modes are charge conjugates of modes below.

	Mode	Fraction (Γ_i/Γ)	Confidence level
Γ_1	$D^+_s\pi^0$	(100^{+0}_{-20}) %	
Γ_2	$D^+_s\gamma$	< 5 %	90%
Γ_3	$D^*_s(2112)^+\gamma$	< 6 %	90%
Γ_4	$D^+_s\gamma\gamma$	< 18 %	95%
Γ_5	$D^*_s(2112)^+\pi^0$	< 11 %	90%
Γ_6	$D^+_s\pi^+\pi^-$	< 4 $\times 10^{-3}$	90%
Γ_7	$D^+_s\pi^0\pi^0$	not seen	

$D^*_{s0}(2317)^\pm$ BRANCHING RATIOS

$\Gamma(D^+_s\pi^0)/\Gamma_{total}$ — Γ_1/Γ

VALUE	EVTS	DOCUMENT ID		TECN	COMMENT
$\mathbf{1.00^{+0.00}_{-0.14}{}^{+0.00}_{-0.14}}$	47	ABLIKIM	18J	BES3	4.6 $e^+e^- \to D^{*\pm}_s D^*_{s0}(2317)^\mp$
• • • We do not use the following data for averages, fits, limits, etc. • • •					
seen	1.5k	AUBERT	03G	BABR	10.6 e^+e^-

$\Gamma(D^+_s\gamma)/\Gamma(D^+_s\pi^0)$ — Γ_2/Γ_1

VALUE	CL%	DOCUMENT ID		TECN	COMMENT
<0.05	90	MIKAMI	04	BELL	10.6 e^+e^-
• • • We do not use the following data for averages, fits, limits, etc. • • •					
<0.14	95	AUBERT	06P	BABR	10.6 e^+e^-
<0.052	90	BESSON	03	CLE2	10.6 e^+e^-

$\Gamma(D^*_s(2112)^+\gamma)/\Gamma(D^+_s\pi^0)$ — Γ_3/Γ_1

VALUE	CL%	DOCUMENT ID		TECN	COMMENT
<0.059	90	BESSON	03	CLE2	10.6 e^+e^-
• • • We do not use the following data for averages, fits, limits, etc. • • •					
<0.16	95	AUBERT	06P	BABR	10.6 e^+e^-
<0.18	90	MIKAMI	04	BELL	10.6 e^+e^-

$\Gamma(D^+_s\gamma\gamma)/\Gamma(D^+_s\pi^0)$ — Γ_4/Γ_1

VALUE	CL%	DOCUMENT ID		TECN	COMMENT
<0.18	95	AUBERT	06P	BABR	10.6 e^+e^-
• • • We do not use the following data for averages, fits, limits, etc. • • •					
not seen		AUBERT	03G	BABR	10.6 e^+e^-

$\Gamma(D^*_s(2112)^+\pi^0)/\Gamma(D^+_s\pi^0)$ — Γ_5/Γ_1

VALUE	CL%	DOCUMENT ID		TECN	COMMENT
<0.11	90	BESSON	03	CLE2	10.6 e^+e^-

$\Gamma(D^+_s\pi^+\pi^-)/\Gamma(D^+_s\pi^0)$ — Γ_6/Γ_1

VALUE	CL%	DOCUMENT ID		TECN	COMMENT
<0.004	90	MIKAMI	04	BELL	10.6 e^+e^-
• • • We do not use the following data for averages, fits, limits, etc. • • •					
<0.005	95	AUBERT	06P	BABR	10.6 e^+e^-
<0.019	90	BESSON	03	CLE2	10.6 e^+e^-

$\Gamma(D^+_s\pi^0\pi^0)/\Gamma(D^+_s\pi^0)$ — Γ_7/Γ_1

VALUE	CL%	DOCUMENT ID		TECN	COMMENT
<0.25	95	AUBERT	06P	BABR	10.6 e^+e^-

$D^*_{s0}(2317)^\pm$ REFERENCES

ABLIKIM	18J	PR D97 051103	M. Ablikim *et al.*	(BESIII Collab.)
CHOI	15A	PR D91 092011	S.-K. Choi *et al.*	(BELLE Collab.)
AUBERT	06P	PR D74 032007	B. Aubert *et al.*	(BABAR Collab.)
AUBERT	04E	PR D69 031101	B. Aubert *et al.*	(BABAR Collab.)
AUBERT,B	04S	PRL 93 181801	B. Aubert *et al.*	(BABAR Collab.)
MIKAMI	04	PRL 92 012002	Y. Mikami *et al.*	(BELLE Collab.)
AUBERT	03G	PRL 90 242001	B. Aubert *et al.*	(BABAR Collab.)
BESSON	03	PR D68 032002	D. Besson *et al.*	(CLEO Collab.)
KROKOVNY	03B	PRL 91 262002	P. Krokovny *et al.*	(BELLE Collab.)

$D_{s1}(2460)^\pm$

$I(J^P) = 0(1^+)$

See the review on "Heavy Non-$q\overline{q}$ Mesons."

$D_{s1}(2460)^\pm$ MASS

The fit includes $D^\pm$, D^0, $D^\pm_s$, $D^{*\pm}$, D^{*0}, $D^{*\pm}_s$, $D_1(2420)^0$, $D^*_2(2460)^0$, and $D_{s1}(2536)^\pm$ mass and mass difference measurements.

VALUE (MeV)	EVTS	DOCUMENT ID		TECN	COMMENT
2459.5±0.6 OUR FIT Error includes scale factor of 1.1.					
2459.6±0.9 OUR AVERAGE Error includes scale factor of 1.3.					
2460.1±0.2±0.8		[1] AUBERT	06P	BABR	10.6 e^+e^-
2458.0±1.0±1.0	195	AUBERT	04E	BABR	10.6 e^+e^-
• • • We do not use the following data for averages, fits, limits, etc. • • •					
2459.5±1.2±3.7	920	AUBERT	06P	BABR	10.6 $e^+e^- \to D^+_s\gamma X$
2458.6±1.0±2.5	560	AUBERT	06P	BABR	10.6 $e^+e^- \to D^+_s\pi^0\gamma X$
2460.2±0.2±0.8	123	AUBERT	06P	BABR	10.6 $e^+e^- \to D^+_s\pi^+\pi^- X$
2458.9±1.5	112	[2] AUBERT,B	04S	BABR	$B \to D_{s1}(2460)^+\overline{D}^{(*)}$
2461.1±1.6	139	[3] AUBERT,B	04S	BABR	$B \to D_{s1}(2460)^+\overline{D}^{(*)}$
2456.5±1.3±1.3	126	[4,5] MIKAMI	04	BELL	10.6 e^+e^-
2459.5±1.3±2.0	152	[6,7] MIKAMI	04	BELL	10.6 e^+e^-
2459.9±0.9±1.6	60	[6,7] MIKAMI	04	BELL	10.6 e^+e^-
2459.2±1.6±2.0	57	KROKOVNY	03B	BELL	10.6 e^+e^-

[1] The average of the values obtained from the $D^+_s\gamma$, $D^+_s\pi^0\gamma$, $D^+_s\pi^+\pi^-$ final state.
[2] Systematic errors not evaluated. From the decay to $D^{*+}_s\pi^0$.
[3] Systematic errors not evaluated. From the decay to $D^+_s\gamma$.
[4] Not independent of the corresponding $m_{D_{s1}(2460)^\pm} - m_{D^{*\pm}_s}$.
[5] Using $m_{D^{*+}_s} = 2112.4 \pm 0.7$ MeV.
[6] Not independent of the corresponding $m_{D_{s1}(2460)^\pm} - m_{D^\pm_s}$.
[7] Using $m_{D^+_s} = 1968.5 \pm 0.6$ MeV.

$m_{D_{s1}(2460)^\pm} - m_{D^{*\pm}_s}$

The fit includes $D^\pm$, D^0, $D^\pm_s$, $D^{*\pm}$, D^{*0}, $D^{*\pm}_s$, $D_1(2420)^0$, $D^*_2(2460)^0$, and $D_{s1}(2536)^\pm$ mass and mass difference measurements.

VALUE (MeV)	EVTS	DOCUMENT ID		TECN	COMMENT
347.3±0.7 OUR FIT Error includes scale factor of 1.2.					
347.1±2.2 OUR AVERAGE Error includes scale factor of 1.9. See the ideogram below.					
344.1±1.3±1.1	126	MIKAMI	04	BELL	10.6 e^+e^-
351.2±1.7±1.0	41	BESSON	03	CLE2	10.6 e^+e^-
346.8±1.6±1.9	57	[8] KROKOVNY	03B	BELL	10.6 e^+e^-

[8] Recalculated by us using $m_{D^{*+}_s} = 2112.4 \pm 0.7$ MeV.

Downloaded from https://academic.oup.com/ptep/article/2022/8/083C01/6651666 by KIT Library user on 27 September 2022

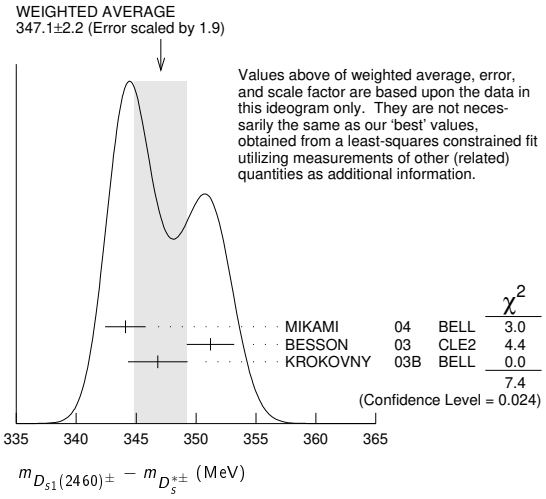

$m_{D_{s1}(2460)^{\pm}} - m_{D_s^{\pm}}$

The fit includes $D^{\pm}$, D^0, $D_s^{\pm}$, $D^{*\pm}$, D^{*0}, $D_s^{*\pm}$, $D_1(2420)^0$, $D_2^*(2460)^0$, and $D_{s1}(2536)^{\pm}$ mass and mass difference measurements.

VALUE (MeV)	EVTS	DOCUMENT ID		TECN	COMMENT
491.1±0.6 OUR FIT Error includes scale factor of 1.1.					
491.3±1.4 OUR AVERAGE					
491.0±1.3±1.9	152	[9] MIKAMI	04	BELL	10.6 e^+e^-
491.4±0.9±1.5	60	[10] MIKAMI	04	BELL	10.6 e^+e^-

[9] From the decay to $D_s^{\pm}\gamma$.
[10] From the decay to $D_s^{\pm}\pi^+\pi^-$.

$D_{s1}(2460)^{\pm}$ WIDTH

VALUE (MeV)	CL%	EVTS	DOCUMENT ID		TECN	COMMENT
< 3.5	95	123	AUBERT	06P	BABR	10.6 $e^+e^- \to D_s^+\pi^+\pi^- X$
• • • We do not use the following data for averages, fits, limits, etc. • • •						
< 6.3	95	560	AUBERT	06P	BABR	10.6 $e^+e^- \to D_s^+\pi^0\gamma X$
<10		195	AUBERT	04E	BABR	10.6 e^+e^-
< 5.5	90	126	MIKAMI	04	BELL	10.6 e^+e^-
< 7	90	41	BESSON	03	CLE2	10.6 e^+e^-

$D_{s1}(2460)^+$ DECAY MODES

$D_{s1}(2460)^-$ modes are charge conjugates of the modes below.

	Mode	Fraction (Γ_i/Γ)	Scale factor/ Confidence level
Γ_1	$D_s^{*+}\pi^0$	(48 ±11) %	
Γ_2	$D_s^+\gamma$	(18 ± 4) %	
Γ_3	$D_s^+\pi^+\pi^-$	(4.3± 1.3) %	S=1.1
Γ_4	$D_s^{*+}\gamma$	< 8 %	CL=90%
Γ_5	$D_{s0}^*(2317)^+\gamma$	($3.7^{+5.0}_{-2.4}$) %	
Γ_6	$D_s^+\pi^0$		
Γ_7	$D_s^+\pi^0\pi^0$		
Γ_8	$D_s^+\gamma\gamma$		

CONSTRAINED FIT INFORMATION

An overall fit to 7 branching ratios uses 8 measurements and one constraint to determine 5 parameters. The overall fit has a χ^2 = 3.4 for 4 degrees of freedom.

The following *off-diagonal* array elements are the correlation coefficients $\langle \delta x_i \delta x_j \rangle / (\delta x_i \cdot \delta x_j)$, in percent, from the fit to the branching fractions, $x_i \equiv \Gamma_i/\Gamma_{total}$. The fit constrains the x_i whose labels appear in this array to sum to one.

	x_1	x_2	x_3
x_2	80		
x_3	68	62	
x_5	−3	25	26

$D_{s1}(2460)^{\pm}$ BRANCHING RATIOS

$\Gamma(D_s^{*+}\pi^0)/\Gamma_{total}$ — Γ_1/Γ

VALUE	EVTS	DOCUMENT ID		TECN	COMMENT
0.48±0.11 OUR FIT					
0.56±0.13±0.09		[11] AUBERT	06N	BABR	$B \to D_{s1}(2460)^- \overline{D}^{(*)}$
• • • We do not use the following data for averages, fits, limits, etc. • • •					
seen	41	BESSON	03	CLE2	10.6 e^+e^-

[11] Evaluated in AUBERT 06N including measurements from AUBERT,B 04S.

$\Gamma(D_s^+\gamma)/\Gamma_{total}$ — Γ_2/Γ

VALUE	DOCUMENT ID		TECN	COMMENT
0.18±0.04 OUR FIT				
0.16±0.04±0.03	[12] AUBERT	06N	BABR	$B \to D_{s1}(2460)^- \overline{D}^{(*)}$

[12] Evaluated in AUBERT 06N including measurements from AUBERT,B 04S.

$\Gamma(D_s^+\gamma)/\Gamma(D_s^{*+}\pi^0)$ — Γ_2/Γ_1

VALUE	CL%	EVTS	DOCUMENT ID		TECN	COMMENT
0.38 ±0.05 OUR FIT						
0.44 ±0.09 OUR AVERAGE						
0.55 ±0.13 ±0.08		152	MIKAMI	04	BELL	10.6 e^+e^-
0.38 ±0.11 ±0.04		38	KROKOVNY	03B	BELL	10.6 e^+e^-
• • • We do not use the following data for averages, fits, limits, etc. • • •						
0.274±0.045±0.020		251	[13] AUBERT,B	04S	BABR	$B \to D_{s1}(2460)^+ \overline{D}^{(*)}$
< 0.49	90		BESSON	03	CLE2	10.6 e^+e^-

[13] Used by AUBERT 06N in their measurement of $B(D_s^{*-}\pi^0)$ and $B(D_s^-\gamma)$.

$\Gamma(D_s^+\pi^+\pi^-)/\Gamma(D_s^{*+}\pi^0)$ — Γ_3/Γ_1

VALUE	CL%	EVTS	DOCUMENT ID		TECN	COMMENT
0.090±0.020 OUR FIT Error includes scale factor of 1.2.						
0.14 ±0.04 ±0.02		60	MIKAMI	04	BELL	10.6 e^+e^-
• • • We do not use the following data for averages, fits, limits, etc. • • •						
<0.08		90	BESSON	03	CLE2	10.6 e^+e^-

$\Gamma(D_s^{*+}\gamma)/\Gamma(D_s^{*+}\pi^0)$ — Γ_4/Γ_1

VALUE	CL%	DOCUMENT ID		TECN	COMMENT
<0.16	90	BESSON	03	CLE2	10.6 e^+e^-
• • • We do not use the following data for averages, fits, limits, etc. • • •					
<0.31	90	MIKAMI	04	BELL	10.6 e^+e^-

$\Gamma(D_{s0}^*(2317)^+\gamma)/\Gamma(D_s^{*+}\pi^0)$ — Γ_5/Γ_1

VALUE	CL%	DOCUMENT ID		TECN	COMMENT
<0.22	95	AUBERT	04E	BABR	10.6 e^+e^-
• • • We do not use the following data for averages, fits, limits, etc. • • •					
<0.58	90	BESSON	03	CLE2	10.6 e^+e^-

$\Gamma(D_s^{*+}\pi^0)/[\Gamma(D_s^{*+}\pi^0)+\Gamma(D_{s0}^*(2317)^+\gamma)]$ — $\Gamma_1/(\Gamma_1+\Gamma_5)$

VALUE	DOCUMENT ID		TECN	COMMENT
0.93±0.09 OUR FIT				
0.97±0.09±0.05	AUBERT	06P	BABR	10.6 e^+e^-

$\Gamma(D_s^+\gamma)/[\Gamma(D_s^{*+}\pi^0)+\Gamma(D_{s0}^*(2317)^+\gamma)]$ — $\Gamma_2/(\Gamma_1+\Gamma_5)$

VALUE	DOCUMENT ID		TECN	COMMENT
0.35 ±0.04 OUR FIT				
0.337±0.036±0.038	AUBERT	06P	BABR	10.6 e^+e^-

$\Gamma(D_s^+\pi^+\pi^-)/[\Gamma(D_s^{*+}\pi^0)+\Gamma(D_{s0}^*(2317)^+\gamma)]$ — $\Gamma_3/(\Gamma_1+\Gamma_5)$

VALUE	DOCUMENT ID		TECN	COMMENT
0.083±0.017 OUR FIT Error includes scale factor of 1.2.				
0.077±0.013±0.008	AUBERT	06P	BABR	10.6 e^+e^-

$\Gamma(D_s^{*+}\gamma)/[\Gamma(D_s^{*+}\pi^0)+\Gamma(D_{s0}^*(2317)^+\gamma)]$ — $\Gamma_4/(\Gamma_1+\Gamma_5)$

VALUE	CL%	DOCUMENT ID		TECN	COMMENT
<0.24	95	AUBERT	06P	BABR	10.6 e^+e^-

$\Gamma(D_{s0}^*(2317)^+\gamma)/[\Gamma(D_s^{*+}\pi^0)+\Gamma(D_{s0}^*(2317)^+\gamma)]$ — $\Gamma_5/(\Gamma_1+\Gamma_5)$

VALUE	CL%	DOCUMENT ID		TECN	COMMENT
<0.25	95	AUBERT	06P	BABR	10.6 e^+e^-

$\Gamma(D_s^+\pi^0)/[\Gamma(D_s^{*+}\pi^0)+\Gamma(D_{s0}^*(2317)^+\gamma)]$ — $\Gamma_6/(\Gamma_1+\Gamma_5)$

VALUE	CL%	DOCUMENT ID		TECN	COMMENT
<0.042	95	AUBERT	06P	BABR	10.6 e^+e^-

$\Gamma(D_s^+\pi^0\pi^0)/[\Gamma(D_s^{*+}\pi^0)+\Gamma(D_{s0}^*(2317)^+\gamma)]$ — $\Gamma_7/(\Gamma_1+\Gamma_5)$

VALUE	CL%	DOCUMENT ID		TECN	COMMENT
<0.68	95	AUBERT	06P	BABR	10.6 e^+e^-

$\Gamma(D_s^+\gamma\gamma)/[\Gamma(D_s^{*+}\pi^0)+\Gamma(D_{s0}^*(2317)^+\gamma)]$ — $\Gamma_8/(\Gamma_1+\Gamma_5)$

VALUE	CL%	DOCUMENT ID		TECN	COMMENT
<0.33	95	AUBERT	06P	BABR	10.6 e^+e^-

Downloaded from https://academic.oup.com/ptep/article/2022/8/083C01/6651666 by KIT Library user on 27 September 2022

$D_{s1}(2460)^{\pm}$ REFERENCES

AUBERT	06N	PR D74 031103	B. Aubert *et al.*	(BABAR Collab.)
AUBERT	06P	PR D74 032007	B. Aubert *et al.*	(BABAR Collab.)
AUBERT	04E	PR D69 031101	B. Aubert *et al.*	(BABAR Collab.)
AUBERT,B	04S	PRL 93 181801	B. Aubert *et al.*	(BABAR Collab.)
MIKAMI	04	PRL 92 012002	Y. Mikami *et al.*	(BELLE Collab.)
BESSON	03	PR D68 032002	D. Besson *et al.*	(CLEO Collab.)
KROKOVNY	03B	PRL 91 262002	P. Krokovny *et al.*	(BELLE Collab.)

$D_{s1}(2536)^{\pm}$

$I(J^P) = 0(1^+)$
J, P need confirmation.

Seen in $D^*(2010)^+ K^0$, $D^*(2007)^0 K^+$, and $D_s^+ \pi^+ \pi^-$. Not seen in $D^+ K^0$ or $D^0 K^+$. $J^P = 1^+$ assignment strongly favored.

$D_{s1}(2536)^{\pm}$ MASS

The fit includes $D^{\pm}$, D^0, $D_s^{\pm}$, $D^{*\pm}$, D^{*0}, $D_s^{*\pm}$, $D_1(2420)^0$, $D_2^*(2460)^0$, and $D_{s1}(2536)^{\pm}$ mass and mass difference measurements.

VALUE (MeV)	EVTS	DOCUMENT ID		TECN	COMMENT
2535.11±0.06 OUR FIT					
2535.21±0.28 OUR AVERAGE					
2537.7 ±0.5 ±3.1	24	[1] ABLIKIM	19P	BES3	4.6 $e^+e^- \to D_s^+ \overline{D}^0 K^-$
2535.7 ±0.6 ±0.5	46	[2] ABAZOV	09G	D0	$B_s^0 \to D_{s1}^- \mu^+ \nu_\mu X$
2534.78±0.31±0.40	182	AUBERT	08B	BABR	$B \to \overline{D}^{(*)} D^* K$
2534.6 ±0.3 ±0.7	193	AUBERT	06P	BABR	10.6 $e^+e^- \to D_s^+ \pi^+ \pi^- X$
2535.3 ±0.7	92	[3] HEISTER	02B	ALEP	$e^+e^- \to D^{*+} K^0 X$, $D^{*0} K^+ X$
2534.2 ±1.2	9	ASRATYAN	94	BEBC	$\nu N \to D^* K^0 X, D^{*0} K^{\pm} X$
2535 ±0.6 ±1	75	FRABETTI	94B	E687	γBe $\to D^{*+} K^0 X$, $D^{*0} K^+ X$
2535.2 ±0.5 ±1.5	28	ALBRECHT	92R	ARG	10.4 $e^+e^- \to D^{*0} K^+ X$
2536.6 ±0.7 ±0.4		AVERY	90	CLEO	$e^+e^- \to D^{*+} K^0 X$
2535.9 ±0.6 ±2.0		ALBRECHT	89E	ARG	$D_{s1}^* \to D^*(2010) K^0$
• • • We do not use the following data for averages, fits, limits, etc. • • •					
2534.1 ±0.6	116	[4] AUSHEV	11	BELL	$B \to D_{s1}(2536)^+ D^{(*)}$
2535.08±0.01±0.15	8038	[5] LEES	11B	BABR	10.6 $e^+e^- \to D^{*+} K_S^0 X$
2535.57$^{+0.44}_{-0.41}$±0.10	236	[6] CHEKANOV	09	ZEUS	$e^{\pm} p \to D^{*+} K_S^0 X$, $D^{*0} K^+ X$
2535.3 ±0.2 ±0.5	134	[7] ALEXANDER	93	CLE2	$e^+e^- \to D^{*0} K^+ X$
2534.8 ±0.6 ±0.6	44	[8] ALEXANDER	93	CLE2	$e^+e^- \to D^{*+} K^0 X$
2535 ± 28		[9] ASRATYAN	88	HLBC	$\nu N \to D_s \gamma\gamma X$

[1] From a fit of the D_s^+ recoil mass distribution with an incoherent sum of the S-wave and D-wave Breit-Wigner line shapes.
[2] Using the $D^*(2010)^{\pm}$ mass of 2010.0 ± 0.4 MeV from PDG 06.
[3] Calculated using $m(D^*(2010)^{\pm}) = 2010.0 \pm 0.5$ MeV, $m(D^*(2007)^0) = 2006.7 \pm 0.5$ MeV, and the mass difference below.
[4] Systematic uncertainties not evaluated.
[5] Calculated using the mass difference $m(D_{s1}^+) - m(D^{*+})_{PDG}$ below and $m(D^{*+})_{PDG} = 2010.25 \pm 0.14$ MeV. Assuming S-wave decay of the $D_{s1}(2536)$ to $D^{*+} K_S^0$, using a Breit-Wigner line shape corresponding to L=0.
[6] Calculated using the mass difference $m(D_{s1}^+) - m(D^{*+})_{PDG}$ reported below and $m(D^{*+})_{PDG} = 2010.27 \pm 0.17$ MeV.
[7] Calculated using $m(D^*(2007)^0)$=2006.6 ± 0.5 MeV and the mass difference below.
[8] Calculated using $m(D^*(2010)^{\pm})$=2010.1 ± 0.6 MeV and the mass difference below.
[9] Not seen in $D^* K$.

$m_{D_{s1}(2536)^{\pm}} - m_{D_s^*(2111)}$

The fit includes $D^{\pm}$, D^0, $D_s^{\pm}$, $D^{*\pm}$, D^{*0}, $D_s^{*\pm}$, $D_1(2420)^0$, $D_2^*(2460)^0$, and $D_{s1}(2536)^{\pm}$ mass and mass difference measurements.

VALUE (MeV)	DOCUMENT ID		TECN	COMMENT
422.9± 0.4 OUR FIT				
424 ±28	ASRATYAN	88	HLBC	$D_s^{*\pm}\gamma$

$m_{D_{s1}(2536)^{\pm}} - m_{D^*(2010)^{\pm}}$

The fit includes $D^{\pm}$, D^0, $D_s^{\pm}$, $D^{*\pm}$, D^{*0}, $D_s^{*\pm}$, $D_1(2420)^0$, $D_2^*(2460)^0$, and $D_{s1}(2536)^{\pm}$ mass and mass difference measurements.

VALUE (MeV)	EVTS	DOCUMENT ID		TECN	COMMENT
524.85±0.04 OUR FIT					
524.84±0.04 OUR AVERAGE					
524.83±0.01±0.04	8038	[10] LEES	11B	BABR	10.6 $e^+e^- \to D^{*+} K_S^0 X$
525.30$^{+0.44}_{-0.41}$±0.10	236 ± 30	CHEKANOV	09	ZEUS	$e^{\pm} p \to D^{*+} K_S^0 X$, $D^{*0} K^+ X$
525.3 ±0.6 ±0.1	41	HEISTER	02B	ALEP	$e^+e^- \to D^{*+} K^0 X$
524.7 ±0.6 ±0.2	44	ALEXANDER	93	CLE2	$e^+e^- \to D^{*+} K_S^0 X$

[10] Assuming S-wave decay of the $D_{s1}(2536)$ to $D^{*+} K_S^0$, using a Breit-Wigner line shape corresponding to L=0.

$m_{D_{s1}(2536)^{\pm}} - m_{D^*(2007)^0}$

The fit includes $D^{\pm}$, D^0, $D_s^{\pm}$, $D^{*\pm}$, D^{*0}, $D_s^{*\pm}$, $D_1(2420)^0$, $D_2^*(2460)^0$, and $D_{s1}(2536)^{\pm}$ mass and mass difference measurements.

VALUE (MeV)	EVTS	DOCUMENT ID		TECN	COMMENT
528.26±0.05 OUR FIT Error includes scale factor of 1.2.					
528.68±0.28 OUR AVERAGE					
528.7 ±1.9 ±0.5	51	HEISTER	02B	ALEP	$e^+e^- \to D^{*0} K^+ X$
527.3 ±2.2	29	ACKERSTAFF	97W	OPAL	$e^+e^- \to D^{*0} K^+ X$
528.7 ±0.2 ±0.2	134	ALEXANDER	93	CLE2	$e^+e^- \to D^{*0} K^+ X$

$D_{s1}(2536)^{\pm}$ WIDTH

VALUE (MeV)	CL%	EVTS	DOCUMENT ID		TECN	COMMENT
0.92±0.05 OUR AVERAGE						
1.7 ±1.2 ±0.6		24	[11] ABLIKIM	19P	BES3	4.6 $e^+e^- \to D_s^+ \overline{D}^0 K^-$
0.92±0.03±0.04		8038	[12] LEES	11B	BABR	10.6 $e^+e^- \to D^{*+} K_S^0 X$
• • • We do not use the following data for averages, fits, limits, etc. • • •						
0.75±0.23		116	[13] AUSHEV	11	BELL	$B \to D_{s1}(2536)^+ D^{(*)}$
< 2.5	95	193	AUBERT	06P	BABR	10.6 $e^+e^- \to D_s^+ \pi^+ \pi^- X$
< 3.2	90	75	FRABETTI	94B	E687	γBe $\to D^{*+} K^0 X$, $D^{*0} K^+ X$
< 2.3	90		ALEXANDER	93	CLEO	$e^+e^- \to D^{*0} K^+ X$
< 3.9	90		ALBRECHT	92R	ARG	10.4 $e^+e^- \to D^{*0} K^+ X$
< 5.44	90		AVERY	90	CLEO	$e^+e^- \to D^{*+} K^0 X$
< 4.6	90		ALBRECHT	89E	ARG	$D_{s1}^* \to D^*(2010) K^0$

[11] From a fit of the D_s^+ recoil mass distribution with an incoherent sum of the S-wave and S-wave Breit-Wigner line shapes.
[12] Assuming S-wave decay of the $D_{s1}(2536)$ to $D^{*+} K_S^0$, using a Breit-Wigner line shape corresponding to L=0.
[13] Systematic uncertainties not evaluated.

$D_{s1}(2536)^+$ DECAY MODES

Branching fractions are given relative to the one **DEFINED AS 1**. $D_{s1}(2536)^-$ modes are charge conjugates of the modes below.

	Mode	Fraction (Γ_i/Γ)	Confidence level
Γ_1	$D^*(2010)^+ K^0$	0.85 ±0.12	
Γ_2	$(D^*(2010)^+ K^0)_{S-wave}$	0.61 ±0.09	
Γ_3	$(D^*(2010)^+ K^0)_{D-wave}$		
Γ_4	$D^+ \pi^- K^+$	0.028±0.005	
Γ_5	$D^*(2007)^0 K^+$	**DEFINED AS 1**	
Γ_6	$D^+ K^0$	<0.34	90%
Γ_7	$D^0 K^+$	<0.12	90%
Γ_8	$D_s^{*+} \gamma$	possibly seen	
Γ_9	$D_s^+ \pi^+ \pi^-$	seen	

$D_{s1}(2536)^+$ BRANCHING RATIOS

$\Gamma(D^*(2007)^0 K^+)/\Gamma(D^*(2010)^+ K^0)$ — Γ_5/Γ_1

VALUE	EVTS	DOCUMENT ID		TECN	COMMENT
1.18±0.16 OUR AVERAGE					
0.88±0.24±0.08	116	AUSHEV	11	BELL	$B \to D_{s1}(2536)^+ D^{(*)}$
2.3 ±0.6 ±0.3	236 ± 30	CHEKANOV	09	ZEUS	$e^{\pm} p \to D^{*+} K_S^0 X$, $D^{*0} K^+ X$
1.32±0.47±0.23	92	[14] HEISTER	02B	ALEP	$e^+e^- \to D^{*+} K^0 X$, $D^{*0} K^+ X$
1.9 $^{+1.1}_{-0.9}$ ±0.4	35	[14] ACKERSTAFF	97W	OPAL	$e^+e^- \to D^{*0} K^+ X$, $D^{*+} K^0 X$
1.1 ±0.3		ALEXANDER	93	CLEO	$e^+e^- \to D^{*0} K^+ X, D^{*+} K^0 X$
1.4 ±0.3 ±0.2		[15] ALBRECHT	92R	ARG	10.4 $e^+e^- \to D^{*0} K^+ X, D^{*+} K^0 X$

[14] Ratio of the production rates measured in Z^0 decays.
[15] Evaluated by us from published inclusive cross-sections.

$\Gamma((D^*(2010)^+ K^0)_{S-wave})/\Gamma(D^*(2010)^+ K^0)$ — Γ_2/Γ_1

VALUE	EVTS	DOCUMENT ID		TECN	COMMENT
0.72±0.05±0.01	5485	BALAGURA	08	BELL	10.6 $e^+e^- \to D^{*+} K^0 X$

$\Gamma(D^+ \pi^- K^+)/\Gamma(D^*(2010)^+ K^0)$ — Γ_4/Γ_1

VALUE (units 10^{-2})	EVTS	DOCUMENT ID		TECN	COMMENT
3.27±0.18±0.37	1264	BALAGURA	08	BELL	10.6 $e^+e^- \to D^+ \pi^- K^+ X$

Downloaded from https://academic.oup.com/ptep/article/2022/8/083C01/6651666 by KIT Library user on 27 September 2022

$\Gamma(D^+K^0)/\Gamma(D^*(2010)^+K^0)$ — Γ_6/Γ_1

VALUE	CL%	DOCUMENT ID		TECN	COMMENT
<0.40	90	ALEXANDER	93	CLEO	$e^+e^- \to D^{*+}K^0X$
• • • We do not use the following data for averages, fits, limits, etc. • • •					
<0.43	90	ALBRECHT	89E	ARG	$D^*_{s1} \to D^*(2010)K^0$

$\Gamma(D^0K^+)/\Gamma(D^*(2007)^0K^+)$ — Γ_7/Γ_5

VALUE	CL%	DOCUMENT ID		TECN	COMMENT
<0.12	90	ALEXANDER	93	CLEO	$e^+e^- \to D^{*0}K^+X$

$\Gamma(D^{*+}_s\gamma)/\Gamma_{total}$ — Γ_8/Γ

VALUE	DOCUMENT ID		TECN	COMMENT
possibly seen	ASRATYAN	88	HLBC	$\nu N \to D_s\gamma\gamma X$

$\Gamma(D^{*+}_s\gamma)/\Gamma(D^*(2007)^0K^+)$ — Γ_8/Γ_5

VALUE	CL%	DOCUMENT ID		TECN	COMMENT
<0.42	90	ALEXANDER	93	CLEO	$e^+e^- \to D^{*0}K^+X$

$\Gamma(D^+_s\pi^+\pi^-)/\Gamma_{total}$ — Γ_9/Γ

VALUE	DOCUMENT ID		TECN	COMMENT
seen	AUBERT	06P	BABR	10.6 $e^+e^- \to D^+_s\pi^+\pi^-X$

$D_{s1}(2536)^{\pm}$ REFERENCES

ABLIKIM	19P	CP C43 031001	M. Ablikim *et al.*	(BESIII Collab.)
AUSHEV	11	PR D83 051102	T. Aushev *et al.*	(BELLE Collab.)
LEES	11B	PR D83 072003	J.P. Lees *et al.*	(BABAR Collab.)
ABAZOV	09G	PRL 102 051801	V.M. Abazov *et al.*	(D0 Collab.)
CHEKANOV	09	EPJ C60 25	S. Chekanov *et al.*	(ZEUS Collab.)
AUBERT	08B	PR D77 011102	B. Aubert *et al.*	(BABAR Collab.)
BALAGURA	08	PR D77 032001	V. Balagura *et al.*	(BELLE Collab.)
AUBERT	06P	PR D74 032007	B. Aubert *et al.*	(BABAR Collab.)
PDG	06	JP G33 1	W.-M. Yao *et al.*	(PDG Collab.)
HEISTER	02B	PL B526 34	A. Heister *et al.*	(ALEPH Collab.)
ACKERSTAFF	97W	ZPHY C76 425	K. Ackerstaff *et al.*	(OPAL Collab.)
ASRATYAN	94	ZPHY C61 563	A.E. Asratyan *et al.*	(BIRM, BELG, CERN+)
FRABETTI	94B	PRL 72 324	P.L. Frabetti *et al.*	(FNAL E687 Collab.)
ALEXANDER	93	PL B303 377	J. Alexander *et al.*	(CLEO Collab.)
ALBRECHT	92R	PL B297 425	H. Albrecht *et al.*	(ARGUS Collab.)
AVERY	90	PR D41 774	P. Avery, D. Besson	(CLEO Collab.)
ALBRECHT	89E	PL B230 162	H. Albrecht *et al.*	(ARGUS Collab.)
ASRATYAN	88	ZPHY C40 483	A.E. Asratyan *et al.*	(ITEP, SERP)

$D^*_{s2}(2573)$

$I(J^P) = 0(2^+)$

$D^*_{s2}(2573)$ MASS

VALUE (MeV)	EVTS	DOCUMENT ID		TECN	COMMENT
2569.1 ±0.8 OUR AVERAGE		Error includes scale factor of 2.4. See the ideogram below.			
2570.7 ±2.0 ±1.7	62	[1] ABLIKIM	19P	BES3	4.6 $e^+e^- \to D^+_s\overline{D}^0K^-$
2568.39±0.29±0.26		AAIJ	14AW	LHCB	$B^0_s \to \overline{D}^0K^-\pi^+$
2569.4 ±1.6 ±0.5	82	AAIJ	11A	LHCB	$B_s \to D^*_{s2}(2573)\mu\overline{\nu}X$
2572.2 ±0.3 ±1.0		AUBERT,BE	06E	BABR	$e^+e^- \to DKX$
2574.5 ±3.3 ±1.6		ALBRECHT	96	ARG	$e^+e^- \to D^0K^+X$
2573.2 $^{+1.7}_{-1.6}$ ±0.9	217	KUBOTA	94	CLE2	$e^+e^- \sim$ 10.5 GeV
• • • We do not use the following data for averages, fits, limits, etc. • • •					
2570.0 ±4.3	25	[2] EVDOKIMOV	04	SELX	600 $\Sigma^-A \to D^0K^+X$
2568.6 ±3.2	64	[3] HEISTER	02B	ALEP	$e^+e^- \to D^0K^+X$

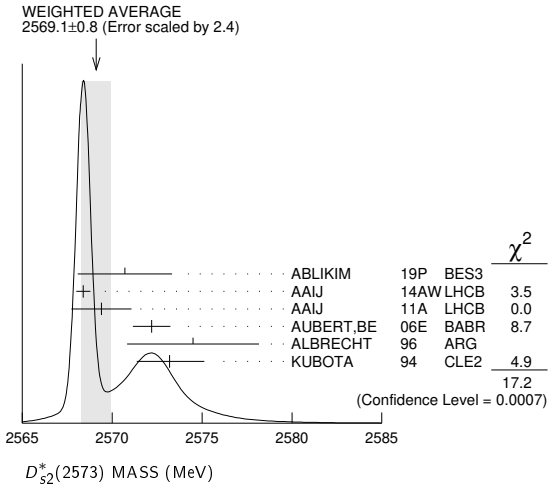

[1] From a fit of the D^+_s recoil mass distribution .
[2] Not independent of the mass difference below.
[3] Calculated using $m_{D^0} = 1864.5 \pm 0.5$ MeV and the mass difference below.

$m_{D^*_{s2}(2573)} - m_{D^0}$

VALUE (MeV)	EVTS	DOCUMENT ID		TECN	COMMENT
704 ±3 ±1	64	HEISTER	02B	ALEP	$e^+e^- \to D^0K^+X$
• • • We do not use the following data for averages, fits, limits, etc. • • •					
705.4±4.3	25	[1] EVDOKIMOV	04	SELX	600 $\Sigma^-A \to D^0K^+X$

[1] Systematic errors not estimated.

$D^*_{s2}(2573)$ WIDTH

VALUE (MeV)	EVTS	DOCUMENT ID		TECN	COMMENT
16.9±0.7 OUR AVERAGE					
17.2±3.6±1.1	62	[1] ABLIKIM	19P	BES3	4.6 $e^+e^- \to D^+_s\overline{D}^0K^-$
16.9±0.5±0.6		AAIJ	14AW	LHCB	$B^0_s \to \overline{D}^0K^-\pi^+$
12.1±4.5±1.6	82	AAIJ	11A	LHCB	$B_s \to D^*_{s2}(2573)\mu\overline{\nu}X$
27.1±0.6±5.6		AUBERT,BE	06E	BABR	$e^+e^- \to DKX$
10.4±8.3±3.0		ALBRECHT	96	ARG	$e^+e^- \to D^0K^+X$
16 $^{+5}_{-4}$ ±3	217	KUBOTA	94	CLE2	$e^+e^- \sim$ 10.5 GeV
• • • We do not use the following data for averages, fits, limits, etc. • • •					
14 $^{+9}_{-6}$	25	[2] EVDOKIMOV	04	SELX	600 $\Sigma^-A \to D^0K^+X$

[1] From a fit of the D^+_s recoil mass distribution .
[2] Systematic errors not estimated.

$D^*_{s2}(2573)^+$ DECAY MODES

$D^*_{s2}(2573)^-$ modes are charge conjugates of the modes below.

	Mode	Fraction (Γ_i/Γ)
Γ_1	D^0K^+	seen
Γ_2	$D^*(2007)^0K^+$	not seen
Γ_3	$D^+K^0_S$	seen
Γ_4	$D^{*+}K^0_S$	seen

$D^*_{s2}(2573)^+$ BRANCHING RATIOS

$\Gamma(D^0K^+)/\Gamma_{total}$ — Γ_1/Γ

VALUE	EVTS	DOCUMENT ID		TECN	CHG	COMMENT
seen	217	KUBOTA	94	CLE2	±	$e^+e^- \sim$ 10.5 GeV

$\Gamma(D^*(2007)^0K^+)/\Gamma(D^0K^+)$ — Γ_2/Γ_1

VALUE	CL%	DOCUMENT ID		TECN	CHG	COMMENT
<0.33	90	KUBOTA	94	CLE2	+	$e^+e^- \sim$ 10.5 GeV

$\Gamma(D^{*+}K^0_S)/\Gamma(D^+K^0_S)$ — Γ_4/Γ_3

VALUE	EVTS	DOCUMENT ID		TECN	COMMENT
0.044±0.005±0.011	2000	[1] AAIJ	16AW	LHCB	$pp \to D^{*+}K^0_SX$ at 7, 8 TeV

[1] First observation of the $D^*_{s2}(2573)^+ \to D^{*+}K^0_S$ decay with a significance of 6.9 σ.

$D^*_{s2}(2573)$ REFERENCES

ABLIKIM	19P	CP C43 031001	M. Ablikim *et al.*	(BESIII Collab.)
AAIJ	16AW	JHEP 1602 133	R. Aaij *et al.*	(LHCb Collab.)
AAIJ	14AW	PRL 113 162001	R. Aaij *et al.*	(LHCb Collab.) JP
AAIJ	11A	PL B698 14	R. Aaij *et al.*	(LHCb Collab.)
AUBERT,BE	06E	PRL 97 222001	B. Aubert *et al.*	(BABAR Collab.)
EVDOKIMOV	04	PRL 93 242001	A.V. Evdokimov *et al.*	(SELEX Collab.)
HEISTER	02B	PL B526 34	A. Heister *et al.*	(ALEPH Collab.)
ALBRECHT	96	ZPHY C69 405	H. Albrecht *et al.*	(ARGUS Collab.)
KUBOTA	94	PRL 72 1972	Y. Kubota *et al.*	(CLEO Collab.)

$D_{s0}(2590)^+$

$I(J^P) = 0(0^-)$

OMITTED FROM SUMMARY TABLE

$D_{s0}(2590)^+$ MASS

VALUE (MeV)	EVTS	DOCUMENT ID		TECN	COMMENT
2591±6±7	444	[1] AAIJ	21A	LHCB	$B^0 \to D^-(D^+K^+\pi^-)$

[1] The mass is calculated from the position of the T-matrix pole

$D_{s0}(2590)^+$ WIDTH

VALUE (MeV)	EVTS	DOCUMENT ID		TECN	COMMENT
89±16±12	444	[1] AAIJ	21A	LHCB	$B^0 \to D^-(D^+K^+\pi^-)$

[1] The width is calculated from the position of the T-matrix pole

Downloaded from https://academic.oup.com/ptep/article/2022/8/083C01/6651666 by KIT Library user on 27 September 2022

$D_{s0}(2590)^+$ DECAY MODES

	Mode	Fraction (Γ_i/Γ)
Γ_1	$D^+ K^+ \pi^-$	seen

$\Gamma(D^+ K^+ \pi^-)/\Gamma_{total}$ — **Γ_1/Γ**

VALUE	EVTS	DOCUMENT ID		TECN	COMMENT
seen	444	AAIJ	21A	LHCB	$B^0 \to D^-(D^+ K^+ \pi^-)$

$D_{s0}(2590)^+$ REFERENCES

AAIJ 21A PRL 126 122002 R. Aaij et al. (LHCb Collab.)

$D_{s1}^*(2700)^\pm$

$I(J^P) = 0(1^-)$

$D_{s1}^*(2700)^+$ MASS

VALUE (MeV)	EVTS	DOCUMENT ID		TECN	COMMENT
2714 ± 5 OUR AVERAGE		Error includes scale factor of 1.5. See the ideogram below.			
2732.3± 4.3± 5.8	15.7k	AAIJ	16AW	LHCB	$pp \to D^{*+} K_S^0 X$ at 7, 8 TeV
$2699\ ^{+14}_{-7}$		[1] LEES	15C	BABR	$B \to D D^0 K^+$
2709.2± 1.9± 4.5	52k	[2] AAIJ	12AU	LHCB	$pp \to (D K)^+ X$ at 7 TeV
$2710 \pm 2\ ^{+12}_{-7}$	10.4k	[3] AUBERT	09AR	BABR	$e^+ e^- \to D^{(*)} K X$
$2708 \pm 9\ ^{+11}_{-10}$	182	BRODZICKA	08	BELL	$B^+ \to D^0 \overline{D}^0 K^+$
• • • We do not use the following data for averages, fits, limits, etc. • • •					
$2694 \pm 8\ ^{+13}_{-3}$		LEES	15C	BABR	$B^0 \to D^- D^0 K^+$
2707 ± 8 ± 8		LEES	15C	BABR	$B^+ \to \overline{D}^0 D^0 K^+$
2688 ± 4 ± 3		[4] AUBERT,BE	06E	BABR	10.6 $e^+ e^- \to D K X$

[1] From a combined analysis of $B^0 \to D^- D^0 K^+$ and $B^+ \to \overline{D}^0 D^0 K^+$.
[2] From the combined fit of the $D^+ K_S^0$ and $D^0 K^+$ modes in the model including the $D_{s2}^*(2573)^+$, $D_{s1}^*(2700)^+$ and spin-0 $D_{sJ}^*(2860)^+$.
[3] From simultaneous fits to the two $D K$ mass spectra and to the total $D^* K$ mass spectrum.
[4] Superseded by AUBERT 09AR.

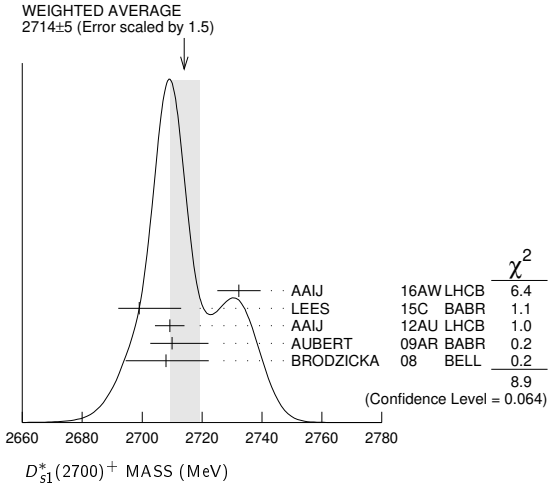

$D_{s1}^*(2700)^+$ WIDTH

VALUE (MeV)	EVTS	DOCUMENT ID		TECN	COMMENT
122 ±10 OUR AVERAGE					
136 ±19 ±24	15.7k	AAIJ	16AW	LHCB	$pp \to D^{*+} K_S^0 X$ at 7, 8 TeV
$127\ ^{+24}_{-19}$		[1] LEES	15C	BABR	$B \to D D^0 K^+$
115.8± 7.3±12.1	52k	[2] AAIJ	12AU	LHCB	$pp \to (D K)^+ X$ at 7 TeV
$149 \pm 7\ ^{+39}_{-52}$	10.4k	[3] AUBERT	09AR	BABR	$e^+ e^- \to D^{(*)} K X$
$108 \pm 23\ ^{+36}_{-31}$	182	BRODZICKA	08	BELL	$B^+ \to D^0 \overline{D}^0 K^+$
• • • We do not use the following data for averages, fits, limits, etc. • • •					
$145 \pm 24\ ^{+22}_{-14}$		LEES	15C	BABR	$B^0 \to D^- D^0 K^+$
$113 \pm 21\ ^{+20}_{-16}$		LEES	15C	BABR	$B^+ \to \overline{D}^0 D^0 K^+$
112 ± 7 ±36		[4] AUBERT,BE	06E	BABR	10.6 $e^+ e^- \to D K X$

[1] From a combined analysis of $B^0 \to D^- D^0 K^+$ and $B^+ \to \overline{D}^0 D^0 K^+$.
[2] From the combined fit of the $D^+ K_S^0$ and $D^0 K^+$ modes in the model including the $D_{s2}^*(2573)^+$, $D_{s1}^*(2700)^+$ and spin-0 $D_{sJ}^*(2860)^+$.
[3] From simultaneous fits to the two $D K$ mass spectra and to the total $D^* K$ mass spectrum.
[4] Superseded by AUBERT 09AR.

$D_{s1}^*(2700)^\pm$ DECAY MODES

	Mode	Fraction (Γ_i/Γ)
Γ_1	$D K$	
Γ_2	$D^0 K^+$	seen
Γ_3	$D^+ K_S^0$	seen
Γ_4	$D^* K$	
Γ_5	$D^{*0} K^+$	seen
Γ_6	$D^{*+} K_S^0$	seen

$D_{s1}^*(2700)^\pm$ BRANCHING RATIOS

$\Gamma(D^* K)/\Gamma(D K)$ — **Γ_4/Γ_1**

VALUE	EVTS	DOCUMENT ID		TECN	COMMENT
0.91±0.13±0.12	10.4k	[1] AUBERT	09AR	BABR	$e^+ e^- \to D^{(*)} K X$

[1] From the average of the corresponding ratios with $D^{(*)0} K^+$ and $D^{(*)+} K_S^0$.

$\Gamma(D^{*0} K^+)/\Gamma(D^0 K^+)$ — **Γ_5/Γ_2**

VALUE	EVTS	DOCUMENT ID		TECN	COMMENT
0.88±0.14±0.14	7716	[1] AUBERT	09AR	BABR	$e^+ e^- \to D^{(*)} K X$

[1] From the $D^{*0} K^+$ and $D^0 K^+$, where $D^{*0} \to D^0 \pi^0$.

$\Gamma(D^{*+} K_S^0)/\Gamma(D^+ K_S^0)$ — **Γ_6/Γ_3**

VALUE	EVTS	DOCUMENT ID		TECN	COMMENT
1.14±0.39±0.23	2700	[1] AUBERT	09AR	BABR	$e^+ e^- \to D^{(*)} K X$

[1] From the $D^{*+} K_S^0$ and $D^+ K_S^0$, where $D^{*+} \to D^+ \pi^0$.

$D_{s1}^*(2700)^\pm$ REFERENCES

AAIJ 16AW JHEP 1602 133 R. Aaij et al. (LHCb Collab.)
LEES 15C PR D91 052002 J.P. Lees et al. (BABAR Collab.)
AAIJ 12AU JHEP 1210 151 R. Aaij et al. (LHCb Collab.)
AUBERT 09AR PR D80 092003 B. Aubert et al. (BABAR Collab.)
BRODZICKA 08 PRL 100 092001 J. Brodzicka et al. (BELLE Collab.)
AUBERT,BE 06E PRL 97 222001 B. Aubert et al. (BABAR Collab.)

$D_{s1}^*(2860)^\pm$

$I(J^P) = 0(1^-)$

OMITTED FROM SUMMARY TABLE
J^P consistent with 1^- from angular analysis of AAIJ 14AW.

$D_{s1}^*(2860)^+$ MASS

VALUE (MeV)	DOCUMENT ID		TECN	COMMENT
2859±12±24	[1] AAIJ	14AW	LHCB	$B_s^0 \to \overline{D}^0 K^- \pi^+$

[1] Separated from the spin-3 component $D_{s3}^*(2860)^-$ by a fit of the helicity angle of the $\overline{D}^0 K^-$ system, with a statistical significance of the spin-3 and spin-1 components in excess of 10 σ.

$D_{s1}^*(2860)^+$ WIDTH

VALUE (MeV)	DOCUMENT ID		TECN	COMMENT
159±23±77	[1] AAIJ	14AW	LHCB	$B_s^0 \to \overline{D}^0 K^- \pi^+$

[1] Separated from the spin-3 component $D_{s3}^*(2860)^-$ by a fit of the helicity angle of the $\overline{D}^0 K^-$ system, with a statistical significance of the spin-3 and spin-1 components in excess of 10 σ.

$D_{s1}^*(2860)^\pm$ REFERENCES

AAIJ 14AW PRL 113 162001 R. Aaij et al. (LHCb Collab.) JP

Downloaded from https://academic.oup.com/ptep/article/2022/8/083C01/6651666 by KIT Library user on 27 September 2022

$D_{s3}^*(2860)^\pm$

$I(J^P) = 0(3^-)$

J^P consistent with 3^- from angular analysis of AAIJ 14AW. Observed by AUBERT,BE 06E and AUBERT 09AR in inclusive production of DK and D^*K in e^+e^- annihilation.

$D_{s3}^*(2860)^+$ MASS

VALUE (MeV)	EVTS	DOCUMENT ID		TECN	COMMENT
2860.5±2.6±6.5		[1] AAIJ	14AW	LHCB	$B_s^0 \to \overline{D}^0 K^- \pi^+$
• • • We do not use the following data for averages, fits, limits, etc. • • •					
2867.1±4.3±1.9	3.1k	AAIJ	16AW	LHCB	$pp \to D^{*+} K_S^0 X$ at 7, 8 TeV
2866.1±1.0±6.3	36k	[2,3] AAIJ	12AU	LHCB	$pp \to (DK)^+ X$ at 7 TeV
2862 ±2 $^{+5}_{-2}$	3122	[2,4] AUBERT	09AR	BABR	$e^+e^- \to D^{(*)} KX$
2856.6±1.5±5.0		[5] AUBERT,BE	06E	BABR	$e^+e^- \to DKX$

[1] Separated from the spin-1 component $D_{s1}^*(2860)^-$ by a fit of the helicity angle of the $\overline{D}^0 K^-$ system, with a statistical significance of the spin-3 and spin-1 components in excess of 10 σ.
[2] Possible contribution from the $D_{s1}^*(2860)$ state.
[3] From the combined fit of the $D^+ K_S^0$ and $D^0 K^+$ modes in the model including the $D_{s2}^*(2573)^+$, $D_{s1}^*(2700)^+$ and spin-0 $D_{sJ}^*(2860)^+$.
[4] From simultaneous fits to the two DK mass spectra and to the total D^*K mass spectrum.
[5] Superseded by AUBERT 09AR.

$D_{s3}^*(2860)^+$ WIDTH

VALUE (MeV)	EVTS	DOCUMENT ID		TECN	COMMENT
53 ± 7 ± 7		[1] AAIJ	14AW	LHCB	$B_s^0 \to \overline{D}^0 K^- \pi^+$
• • • We do not use the following data for averages, fits, limits, etc. • • •					
50 ±11 ±13	3.1k	AAIJ	16AW	LHCB	$pp \to D^{*+} K_S^0 X$ at 7, 8 TeV
69.9± 3.2± 6.6	36k	[2,3] AAIJ	12AU	LHCB	$pp \to (DK)^+ X$ at 7 TeV
48 ± 3 ± 6	3122	[2,4] AUBERT	09AR	BABR	$e^+e^- \to D^{(*)} KX$
47 ± 7 ±10		[5] AUBERT,BE	06E	BABR	$e^+e^- \to DKX$

[1] Separated from the spin-1 component $D_{s1}^*(2860)^-$ by a fit of the helicity angle of the $\overline{D}^0 K^-$ system, with a statistical significance of the spin-3 and spin-1 components in excess of 10 σ.
[2] Possible contribution from the $D_{s1}^*(2860)$ state.
[3] From the combined fit of the $D^+ K_S^0$ and $D^0 K^+$ modes in the model including the $D_{s2}^*(2573)^+$, $D_{s1}^*(2700)^+$ and spin-0 $D_{sJ}^*(2860)^+$.
[4] From simultaneous fits to the two DK mass spectra and to the total D^*K mass spectrum.
[5] Superseded by AUBERT 09AR.

$D_{s3}^*(2860)^\pm$ DECAY MODES

	Mode	Fraction (Γ_i/Γ)
Γ_1	DK	
Γ_2	$D^0 K^+$	seen
Γ_3	$D^+ K_S^0$	seen
Γ_4	D^*K	
Γ_5	$D^{*0} K^+$	seen
Γ_6	$D^{*+} K_S^0$	seen

$D_{s3}^*(2860)^\pm$ BRANCHING RATIOS

$\Gamma(D^*K)/\Gamma(DK)$ — Γ_4/Γ_1

VALUE	EVTS	DOCUMENT ID		TECN	COMMENT
1.10±0.15±0.19	3122	[1] AUBERT	09AR	BABR	$e^+e^- \to D^{(*)} KX$

[1] From the average of the corresponding ratios with $D^{(*)0} K^+$ and $D^{(*)+} K_S^0$.

$\Gamma(D^{*0} K^+)/\Gamma(D^0 K^+)$ — Γ_5/Γ_2

VALUE	EVTS	DOCUMENT ID		TECN	COMMENT
1.04±0.17±0.20	2241	[1] AUBERT	09AR	BABR	$e^+e^- \to D^{(*)} KX$

[1] From the $D^{*0} K^+$ and $D^0 K^+$, where $D^{*0} \to D^0 \pi^0$.

$\Gamma(D^{*+} K_S^0)/\Gamma(D^+ K_S^0)$ — Γ_6/Γ_3

VALUE	EVTS	DOCUMENT ID		TECN	COMMENT
1.38±0.35±0.49	881	[1] AUBERT	09AR	BABR	$e^+e^- \to D^{(*)} KX$

[1] From the $D^{*+} K_S^0$ and $D^+ K_S^0$, where $D^{*+} \to D^+ \pi^0$.

$D_{s3}^*(2860)^\pm$ REFERENCES

AAIJ	16AW JHEP 1602 133	R. Aaij *et al.*	(LHCb Collab.)
AAIJ	14AW PRL 113 162001	R. Aaij *et al.*	(LHCb Collab.) JP
AAIJ	12AU JHEP 1210 151	R. Aaij *et al.*	(LHCb Collab.)
AUBERT	09AR PR D80 092003	B. Aubert *et al.*	(BABAR Collab.)
AUBERT,BE	06E PRL 97 222001	B. Aubert *et al.*	(BABAR Collab.)

$X_0(2900)$

$I(J^P) = ?(0^+)$

OMITTED FROM SUMMARY TABLE

An exotic state with minimal quark content $\overline{c}d\overline{s}u$. Observed by AAIJ 20AI using full amplitude analysis of $B^+ \to D^+D^-K^+$ decays.

$X_0(2900)$ MASS

VALUE (MeV)	EVTS	DOCUMENT ID		TECN	COMMENT
2866±7±2	1.2k	[1] AAIJ	20AI	LHCB	$B^+ \to D^+D^-K^+$

[1] Obtained from the full amplitude analysis. Parameterized with the relativistic Breit-Wigner line shape. Also confirmed by the model-independent analysis of AAIJ 20AF.

$X_0(2900)$ WIDTH

VALUE (MeV)	EVTS	DOCUMENT ID		TECN	COMMENT
57±12±4	1.2k	[1] AAIJ	20AI	LHCB	$B^+ \to D^+D^-K^+$

[1] Obtained from the full amplitude analysis. Parameterized with the relativistic Breit-Wigner line shape. Also confirmed by the model-independent analysis of AAIJ 20AF.

$X_0(2900)$ DECAY MODES

	Mode	Fraction (Γ_i/Γ)
Γ_1	D^-K^+	seen

$X_0(2900)$ BRANCHING RATIOS

$\Gamma(D^-K^+)/\Gamma_{total}$ — Γ_1/Γ

VALUE	DOCUMENT ID		TECN	COMMENT
seen	AAIJ	20AI	LHCB	$B^+ \to D^+D^-K^+$

$X_0(2900)$ REFERENCES

AAIJ	20AF PRL 125 242001	R. Aaij *et al.*	(LHCb Collab.)
AAIJ	20AI PR D102 112003	R. Aaij *et al.*	(LHCb Collab.)

$X_1(2900)$

$I(J^P) = ?(1^-)$

OMITTED FROM SUMMARY TABLE

An exotic state with minimal quark content $\overline{c}d\overline{s}u$. Observed by AAIJ 20AI using full amplitude analysis of $B^+ \to D^+D^-K^+$ decays.

$X_1(2900)$ MASS

VALUE (MeV)	EVTS	DOCUMENT ID		TECN	COMMENT
2904±5±1	1.2k	[1] AAIJ	20AI	LHCB	$B^+ \to D^+D^-K^+$

[1] Obtained from the full amplitude analysis. Parameterized with the relativistic Breit-Wigner line shape. Also confirmed by the model-independent analysis of AAIJ 20AF.

$X_1(2900)$ WIDTH

VALUE (MeV)	EVTS	DOCUMENT ID		TECN	COMMENT
110±11±4	1.2k	[1] AAIJ	20AI	LHCB	$B^+ \to D^+D^-K^+$

[1] Obtained from the full amplitude analysis. Parameterized with the relativistic Breit-Wigner line shape. Also confirmed by the model-independent analysis of AAIJ 20AF.

$X_1(2900)$ DECAY MODES

	Mode	Fraction (Γ_i/Γ)
Γ_1	D^-K^+	seen

$X_1(2900)$ BRANCHING RATIOS

$\Gamma(D^-K^+)/\Gamma_{total}$ — Γ_1/Γ

VALUE	DOCUMENT ID		TECN	COMMENT
seen	AAIJ	20AI	LHCB	$B^+ \to D^+D^-K^+$

$X_1(2900)$ REFERENCES

AAIJ	20AF PRL 125 242001	R. Aaij *et al.*	(LHCb Collab.)
AAIJ	20AI PR D102 112003	R. Aaij *et al.*	(LHCb Collab.)

Downloaded from https://academic.oup.com/ptep/article/2022/8/083C01/6651666 by KIT Library user on 27 September 2022

$D_{sJ}(3040)^{\pm}$

$I(J^P) = 0(?^?)$

OMITTED FROM SUMMARY TABLE

Observed by AUBERT 09AR in inclusive production of $D^* K$ in $e^+ e^-$ annihilation.

$D_{sJ}(3040)^+$ MASS

VALUE (MeV)	DOCUMENT ID		TECN	COMMENT
$3044 \pm 8^{+30}_{-5}$	AUBERT	09AR	BABR	$e^+ e^- \to D^* K X$

$D_{sJ}(3040)^+$ WIDTH

VALUE (MeV)	DOCUMENT ID		TECN	COMMENT
$239 \pm 35^{+46}_{-42}$	AUBERT	09AR	BABR	$e^+ e^- \to D^* K X$

$D_{sJ}(3040)^{\pm}$ DECAY MODES

	Mode
Γ_1	$D^* K$
Γ_2	$D^{*0} K^+$
Γ_3	$D^{*+} K^0_S$

$D_{sJ}(3040)^{\pm}$ REFERENCES

AUBERT 09AR PR D80 092003 B. Aubert *et al.* (BABAR Collab.)

Downloaded from https://academic.oup.com/ptep/article/2022/8/083C01/6651666 by KIT Library user on 27 September 2022

BOTTOM MESONS
($B = \pm 1$)

$B^+ = u\overline{b}$, $B^0 = d\overline{b}$, $\overline{B}^0 = \overline{d}b$, $B^- = \overline{u}b$, similarly for B^*'s

B-particle organization

Many measurements of B decays involve admixtures of B hadrons. Previously we arbitrarily included such admixtures in the $B^\pm$ section, but because of their importance we have created two new sections: "$B^\pm/B^0$ Admixture" for $\Upsilon(4S)$ results and "$B^\pm/B^0/B^0_s$/b-baryon Admixture" for results at higher energies. Most inclusive decay branching fractions and χ_b at high energy are found in the Admixture sections. B^0-$\overline{B}^0$ mixing data are found in the B^0 section, while B^0_s-$\overline{B}^0_s$ mixing data and B-$\overline{B}$ mixing data for a B^0/B^0_s admixture are found in the B^0_s section. CP-violation data are found in the $B^\pm$, B^0, and $B^\pm$ B^0 Admixture sections. b-baryons are found near the end of the Baryon section. Recently, we also created a new section: "V_{cb} and V_{ub} CKM Matrix Elements."

The organization of the B sections is now as follows, where bullets indicate particle sections and brackets indicate reviews.

[Production and Decay of b-flavored Hadrons]
[A Short Note on HFLAV Activities]
- $B^\pm$
  - mass, mean life
  - branching fractions
  - polarization in $B^\pm$ decay
  - CP violation
- B^0
  - mass, mean life
  - branching fractions
  - [Polarization in B decay]
  - polarization in B^0 decay
  - [B-$\overline{B}$ Mixing]
  - B^0-$\overline{B}^0$ mixing
  - CP violation
- $B^\pm$ B^0 Admixture
  - branching fractions, CP violation
  - CP violation
- $B^\pm/B^0/B^0_s$/b-baryon Admixture
  - mean life
  - production fractions
  - branching fractions
  - χ_b at high energy
  - production fractions in hadronic Z decay
- V_{cb} and V_{ub} CKM Matrix Elements
  - [Determination of V_{cb} and V_{ub}]

- B^*
  - mass
- $B_1(5721)^0$
  - mass
- $B^*_J(5732)$
  - mass, width
- $B_2(5747)^0$
  - mass
- B^0_s
  - mass, mean life
  - branching fractions
  - polarization in B^0_s decay
  - B^0_s-$\overline{B}^0_s$ mixing
- B^*_s
  - mass
- $B^*_{sJ}(5850)$
  - mass, width
- $B^\pm_c$
  - mass, mean life
  - branching fractions

At the end of Baryon Listings:
- Λ_b
  - mass, mean life
  - branching fractions
- Σ_b, Σ^*_b
  - mass
- Ξ^0_b, Ξ^-_b
  - mean life
- Ω^-_b
  - mass, mean life
  - branching fractions
- b-baryon Admixture
  - mean life
  - branching fractions

See the related review(s):
Production and Decay of b-flavored Hadrons

HEAVY FLAVOR AVERAGING GROUP

Revised June 2021 by U. Egede (Monash University) and A. Soffer (Tel Aviv University)

The Heavy Flavor Averaging Group (HFLAV) is an international collaboration of physicists from experiments measuring properties of heavy flavored particles, *i.e.*, hadrons containing b and c quarks, and τ leptons. HFLAV calculates and publishes [1] world average values of quantities such as lifetimes, branching fractions, form factors, mixing parameters, and CP-violating asymmetries. Most parameters concern decays of B and D mesons, and many are related to elements of the Cabibbo-Kobayashi-Maskawa (CKM) quark mixing matrix [2], [3].

HFLAV was originally formed in 2002 to continue the activities of the LEP Heavy Flavor Steering group. Since its inception, a wide range of results have become available from increasingly larger data sets. Consequently, HFLAV has expanded to include eight subgroups:

- b-hadron lifetimes and oscillations, including parameters of CP violation in b mixing;
- decay-time-dependent CP violation in B decays, and angles of the CKM Unitarity Triangle;
- semileptonic decays of b-hadrons ($B \to X\ell\nu$, $\ell = e, \mu, \tau$), including determinations of the CKM matrix elements $|V_{cb}|$ and $|V_{ub}|$;
- b-hadron decays to hadronic final states containing c-quarks (open charm and charmonium);
- (rarer) b-hadron decays to final states not containing c-quarks, including fully hadronic, semileptonic ($B \to X\ell\ell, X\nu\bar{\nu}$), leptonic, and radiative decays;
- CP- and T-violating asymmetries of D mesons and D^0–$\bar{D}^0$ mixing;
- c-hadron decays (hadronic, semileptonic, leptonic), properties of excited D states and charm baryons and determination of $|V_{cs}|$ and $|V_{cd}|$;
- τ-lepton physics including branching fractions, tests of lepton universality, determination of $|V_{us}|$, and searches for lepton flavor violation.

Downloaded from https://academic.oup.com/ptep/article/2022/8/083C01/6651666 by KIT Library user on 27 September 2022

Each subgroup has one or two conveners and typically a half-dozen members representing experiments that conduct measurements in that area. Most groups contain representatives from the Belle II and LHCb experiments, and some groups have representatives from the ATLAS, BABAR, Belle, BESIII and CMS experiments. Members of HFLAV are appointed by their respective experimental collaborations. HFLAV has two co-leaders, who are appointed by the managements of Belle II and LHCb.

The averaging procedures used by HFLAV are similar to those of the PDG [4]. When sufficient information is available in publications when calculating world averages, common parameters used for different input measurements are adjusted (rescaled) to common values. The p-value of the fit is provided to indicate the consistency of the measurements included in the average. However, unlike the PDG, when obtaining a world average with a low p-value (*i.e.*, a large χ^2 per degree of freedom), HFLAV does not usually scale the resulting uncertainty. Rather, the systematic uncertainties of the measurements are reviewed with experts from the experiments to understand the discrepancy. Unless inconsistencies among measurements are found, no correction is made to the calculated uncertainty. Close communication between representatives of the experiments and HFLAV members who perform averages helps ensure that measurement uncertainties, known correlations, and systematic effects are properly accounted for. If a special treatment is needed to calculate an average, or if an approximation used in an average calculation might not be sufficiently accurate (*e.g.*, assuming Gaussian uncertainties when the likelihood function is non-Gaussian), a note is included in the HFLAV publication and online documentation to describe this.

In general, HFLAV uses all publicly available results that have written documentation such as a journal publication, preprint, or conference note. These include preliminary results presented at conferences and workshops. However, preliminary results that remain unpublished for an extended period of time, or for which no publication is planned, are not included. A special subset of HFLAV averages are included in the PDG listings; for these averages, only measurements that are published or accepted for publication are used. The averages provided by HFLAV are listed by the PDG as "OUR EVALUATION" with a corresponding note.

All HFLAV averages and input measurements are documented in an approximately biennial journal paper or preprint; the most recent version is Ref. [1]. The latest results and plots are posted on an extensive set of webpages that are updated several times per year; these are available at

`https://hflav.web.cern.ch`.

References:

1. Y. Amhis *et al.* (Heavy Flavor Averaging Group), Eur. Phys. J. **C81**, 226 (2021), [arXiv:1909.12524], updated results and plots available at `https://hflav.web.cern.ch/`.
2. N. Cabibbo, Phys. Rev. Lett. **10**, 531 (1963).
3. M. Kobayashi and T. Maskawa, Prog. Theor. Phys. **49**, 652 (1973).
4. See Section 5 of the "Introduction" to this *Review*.

$B^{\pm}$

$I(J^P) = \frac{1}{2}(0^-)$

Quantum numbers not measured. Values shown are quark-model predictions.

See also the $B^{\pm}/B^0$ ADMIXTURE and $B^{\pm}/B^0/B^0_s/b$-baryon ADMIXTURE sections.

$B^{\pm}$ MASS

The fit uses m_{B^+}, $(m_{B^0} - m_{B^+})$, and m_{B^0} to determine m_{B^+}, m_{B^0}, and the mass difference.

VALUE (MeV)	EVTS	DOCUMENT ID		TECN	COMMENT
5279.34±0.12 OUR FIT					
5279.25±0.26 OUR AVERAGE					
5279.38±0.11±0.33		[1] AAIJ	12E	LHCB	pp at 7 TeV
5279.10±0.41±0.36		[2] ACOSTA	06	CDF	$p\overline{p}$ at 1.96 TeV
5279.1 ±0.4 ±0.4	526	[3] CSORNA	00	CLE2	$e^+e^- \to \Upsilon(4S)$
5279.1 ±1.7 ±1.4	147	ABE	96B	CDF	$p\overline{p}$ at 1.8 TeV
• • • We do not use the following data for averages, fits, limits, etc. • • •					
5278.8 ±0.54±2.0	362	ALAM	94	CLE2	$e^+e^- \to \Upsilon(4S)$
5278.3 ±0.4 ±2.0		BORTOLETTO	92	CLEO	$e^+e^- \to \Upsilon(4S)$
5280.5 ±1.0 ±2.0		[4] ALBRECHT	90J	ARG	$e^+e^- \to \Upsilon(4S)$
5275.8 ±1.3 ±3.0	32	ALBRECHT	87C	ARG	$e^+e^- \to \Upsilon(4S)$
5278.2 ±1.8 ±3.0	12	[5] ALBRECHT	87D	ARG	$e^+e^- \to \Upsilon(4S)$
5278.6 ±0.8 ±2.0		BEBEK	87	CLEO	$e^+e^- \to \Upsilon(4S)$

[1] Uses $B^+ \to J/\psi K^+$ fully reconstructed decays.
[2] Uses exclusively reconstructed final states containing a $J/\psi \to \mu^+\mu^-$ decays.
[3] CSORNA 00 uses fully reconstructed 526 $B^+ \to J/\psi^{(\prime)} K^+$ events and invariant masses without beam constraint.
[4] ALBRECHT 90J assumes 10580 for $\Upsilon(4S)$ mass. Supersedes ALBRECHT 87C and ALBRECHT 87D.
[5] Found using fully reconstructed decays with $J/\psi(1S)$. ALBRECHT 87D assume $m_{\Upsilon(4S)}$ = 10577 MeV.

$B^{\pm}$ MEAN LIFE

See $B^{\pm}/B^0/B^0_s/b$-baryon ADMIXTURE section for data on B-hadron mean life averaged over species of bottom particles.

"OUR EVALUATION" is an average using rescaled values of the data listed below. The average and rescaling were performed by the Heavy Flavor Averaging Group (HFLAV) and are described at https://hflav.web.cern.ch/. The averaging/rescaling procedure takes into account correlations between the measurements and asymmetric lifetime errors.

VALUE (10^{-12} s)	EVTS	DOCUMENT ID		TECN	COMMENT
1.638±0.004 OUR EVALUATION					
1.637±0.004±0.003		AAIJ	14E	LHCB	pp at 7 TeV
1.639±0.009±0.009		[1] AALTONEN	11	CDF	$p\overline{p}$ at 1.96 TeV
1.663±0.023±0.015		[2] AALTONEN	11B	CDF	$p\overline{p}$ at 1.96 TeV
1.635±0.011±0.011		[3] ABE	05B	BELL	$e^+e^- \to \Upsilon(4S)$
1.624±0.014±0.018		[4] ABDALLAH	04E	DLPH	$e^+e^- \to Z$
1.636±0.058±0.025		[5] ACOSTA	02C	CDF	$p\overline{p}$ at 1.8 TeV
1.673±0.032±0.023		[6] AUBERT	01F	BABR	$e^+e^- \to \Upsilon(4S)$
1.648±0.049±0.035		[7] BARATE	00R	ALEP	$e^+e^- \to Z$
1.643±0.037±0.025		[8] ABBIENDI	99J	OPAL	$e^+e^- \to Z$
$1.637\pm0.058^{+0.045}_{-0.043}$		[7] ABE	98Q	CDF	$p\overline{p}$ at 1.8 TeV
1.66 ±0.06 ±0.03		[8] ACCIARRI	98S	L3	$e^+e^- \to Z$
1.66 ±0.06 ±0.05		[8] ABE	97J	SLD	$e^+e^- \to Z$
$1.58\ ^{+0.21}_{-0.18}\ ^{+0.04}_{-0.03}$	94	[5] BUSKULIC	96J	ALEP	$e^+e^- \to Z$
1.61 ±0.16 ±0.12		[7,9] ABREU	95Q	DLPH	$e^+e^- \to Z$
1.72 ±0.08 ±0.06		[10] ADAM	95	DLPH	$e^+e^- \to Z$
1.52 ±0.14 ±0.09		[7] AKERS	95T	OPAL	$e^+e^- \to Z$
• • • We do not use the following data for averages, fits, limits, etc. • • •					
1.695±0.026±0.015		[6] ABE	02H	BELL	Repl. by ABE 05B
1.68 ±0.07 ±0.02		[5] ABE	98B	CDF	Repl. by ACOSTA 02C
1.56 ±0.13 ±0.06		[7] ABE	96C	CDF	Repl. by ABE 98Q
1.58 ±0.09 ±0.03		[11] BUSKULIC	96J	ALEP	$e^+e^- \to Z$
1.58 ±0.09 ±0.04		[7] BUSKULIC	96J	ALEP	Repl. by BARATE 00R
1.70 ±0.09		[12] ADAM	95	DLPH	$e^+e^- \to Z$
1.61 ±0.16 ±0.05	148	[5] ABE	94D	CDF	Repl. by ABE 98B
$1.30\ ^{+0.33}_{-0.29}$ ±0.16	92	[7] ABREU	93D	DLPH	Sup. by ABREU 95Q
1.56 ±0.19 ±0.13	134	[10] ABREU	93G	DLPH	Sup. by ADAM 95
$1.51\ ^{+0.30}_{-0.28}\ ^{+0.12}_{-0.14}$	59	[7] ACTON	93C	OPAL	Sup. by AKERS 95T
$1.47\ ^{+0.22}_{-0.19}\ ^{+0.15}_{-0.14}$	77	[7] BUSKULIC	93D	ALEP	Sup. by BUSKULIC 96J

[1] Measured mean life using fully reconstructed decays ($J/\psi K^{(*)}$).

Downloaded from https://academic.oup.com/ptep/article/2022/8/083C01/6651666 by KIT Library user on 27 September 2022

[2] Measured using $B^- \to D^0 \pi^-$ with $D^0 \to K^- \pi^+$ events that were selected using a silicon vertex trigger.
[3] Measurement performed using a combined fit of *CP*-violation, mixing and lifetimes.
[4] Measurement performed using an inclusive reconstruction and B flavor identification technique.
[5] Measured mean life using fully reconstructed decays.
[6] Events are selected in which one B meson is fully reconstructed while the second B meson is reconstructed inclusively.
[7] Data analyzed using $D/D^* \ell X$ event vertices.
[8] Data analyzed using charge of secondary vertex.
[9] ABREU 95Q assumes $B(B^0 \to D^{**-} \ell^+ \nu_\ell) = 3.2 \pm 1.7\%$.
[10] Data analyzed using vertex-charge technique to tag B charge.
[11] Combined result of $D/D^* \ell X$ analysis and fully reconstructed B analysis.
[12] Combined ABREU 95Q and ADAM 95 result.

τ_{B^+}/τ_{B^-}

VALUE	DOCUMENT ID		TECN	COMMENT
1.002±0.004±0.002	[1] AAIJ	14E	LHCB	pp at 7 TeV

[1] Measured using $B^{\pm} \to J/\psi K^{\pm}$ decays.

B^+ DECAY MODES

B^- modes are charge conjugates of the modes below. Modes which do not identify the charge state of the B are listed in the $B^{\pm}/B^0$ ADMIXTURE section.

The branching fractions listed below assume 50% $B^0\overline{B}^0$ and 50% B^+B^- production at the $\Upsilon(4S)$. We have attempted to bring older measurements up to date by rescaling their assumed $\Upsilon(4S)$ production ratio to 50:50 and their assumed D, D_s, D^*, and ψ branching ratios to current values whenever this would affect our averages and best limits significantly.

Indentation is used to indicate a subchannel of a previous reaction. All resonant subchannels have been corrected for resonance branching fractions to the final state so the sum of the subchannel branching fractions can exceed that of the final state.

For inclusive branching fractions, *e.g.*, $B \to D^{\pm} X$, the values usually are multiplicities, not branching fractions. They can be greater than one.

	Mode		Fraction (Γ_i/Γ)	Scale factor/ Confidence level
	Semileptonic and leptonic modes			
Γ_1	$\ell^+ \nu_\ell X$	[a]	(10.99 ± 0.28) %	
Γ_2	$e^+ \nu_e X_c$		(10.8 ± 0.4) %	
Γ_3	$\ell^+ \nu_\ell X_u$		$(1.65 \pm 0.21) \times 10^{-3}$	
Γ_4	$D \ell^+ \nu_\ell X$		(9.6 ± 0.7) %	
Γ_5	$\overline{D}^0 \ell^+ \nu_\ell$	[a]	(2.30 ± 0.09) %	
Γ_6	$\overline{D}^0 \tau^+ \nu_\tau$		$(7.7 \pm 2.5) \times 10^{-3}$	
Γ_7	$\overline{D}^*(2007)^0 \ell^+ \nu_\ell$	[a]	(5.58 ± 0.22) %	
Γ_8	$\overline{D}^*(2007)^0 \tau^+ \nu_\tau$		(1.88 ± 0.20) %	
Γ_9	$D^- \pi^+ \ell^+ \nu_\ell$		$(4.4 \pm 0.4) \times 10^{-3}$	
Γ_{10}	$\overline{D}_0^*(2420)^0 \ell^+ \nu_\ell$, $\overline{D}_0^{*0} \to D^- \pi^+$		$(2.5 \pm 0.5) \times 10^{-3}$	
Γ_{11}	$\overline{D}_2^*(2460)^0 \ell^+ \nu_\ell$, $\overline{D}_2^{*0} \to D^- \pi^+$		$(1.53 \pm 0.16) \times 10^{-3}$	
Γ_{12}	$D^{(*)} n \pi \ell^+ \nu_\ell$ (n $\geq$ 1)		(1.85 ± 0.25) %	
Γ_{13}	$D^{*-} \pi^+ \ell^+ \nu_\ell$		$(6.0 \pm 0.4) \times 10^{-3}$	
Γ_{14}	$\overline{D}_1(2420)^0 \ell^+ \nu_\ell$, $\overline{D}_1^0 \to D^{*-} \pi^+$		$(3.03 \pm 0.20) \times 10^{-3}$	
Γ_{15}	$\overline{D}_1'(2430)^0 \ell^+ \nu_\ell$, $\overline{D}_1'^0 \to D^{*-} \pi^+$		$(2.7 \pm 0.6) \times 10^{-3}$	
Γ_{16}	$\overline{D}_2^*(2460)^0 \ell^+ \nu_\ell$, $\overline{D}_2^{*0} \to D^{*-} \pi^+$		$(1.01 \pm 0.24) \times 10^{-3}$	S=2.0
Γ_{17}	$\overline{D}^0 \pi^+ \pi^- \ell^+ \nu_\ell$		$(1.6 \pm 0.4) \times 10^{-3}$	
Γ_{18}	$\overline{D}^{*0} \pi^+ \pi^- \ell^+ \nu_\ell$		$(8 \pm 5) \times 10^{-4}$	
Γ_{19}	$D_s^{(*)-} K^+ \ell^+ \nu_\ell$		$(6.1 \pm 1.0) \times 10^{-4}$	
Γ_{20}	$D_s^- K^+ \ell^+ \nu_\ell$		$(3.0 \pm^{1.4}_{1.2}) \times 10^{-4}$	
Γ_{21}	$D_s^{*-} K^+ \ell^+ \nu_\ell$		$(2.9 \pm 1.9) \times 10^{-4}$	
Γ_{22}	$\pi^0 \ell^+ \nu_\ell$		$(7.80 \pm 0.27) \times 10^{-5}$	
Γ_{23}	$\pi^0 e^+ \nu_e$			
Γ_{24}	$\eta \ell^+ \nu_\ell$		$(3.9 \pm 0.5) \times 10^{-5}$	
Γ_{25}	$\eta' \ell^+ \nu_\ell$		$(2.3 \pm 0.8) \times 10^{-5}$	
Γ_{26}	$\omega \ell^+ \nu_\ell$	[a]	$(1.19 \pm 0.09) \times 10^{-4}$	
Γ_{27}	$\omega \mu^+ \nu_\mu$			
Γ_{28}	$\rho^0 \ell^+ \nu_\ell$	[a]	$(1.58 \pm 0.11) \times 10^{-4}$	
Γ_{29}	$\pi^+ \pi^- \ell^+ \nu_\ell$		$(2.3 \pm 0.4) \times 10^{-4}$	
Γ_{30}	$p \overline{p} \ell^+ \nu_\ell$		$(5.8 \pm^{2.6}_{2.3}) \times 10^{-6}$	
Γ_{31}	$p \overline{p} \mu^+ \nu_\mu$		$(5.32 \pm 0.34) \times 10^{-6}$	
Γ_{32}	$p \overline{p} e^+ \nu_e$		$(8.2 \pm^{4.0}_{3.3}) \times 10^{-6}$	
Γ_{33}	$e^+ \nu_e$		$< 9.8 \times 10^{-7}$	CL=90%
Γ_{34}	$\mu^+ \nu_\mu$		$< 8.6 \times 10^{-7}$	CL=90%
Γ_{35}	$\tau^+ \nu_\tau$		$(1.09 \pm 0.24) \times 10^{-4}$	S=1.2
Γ_{36}	$\ell^+ \nu_\ell \gamma$		$< 3.0 \times 10^{-6}$	CL=90%
Γ_{37}	$e^+ \nu_e \gamma$		$< 4.3 \times 10^{-6}$	CL=90%
Γ_{38}	$\mu^+ \nu_\mu \gamma$		$< 3.4 \times 10^{-6}$	CL=90%
Γ_{39}	$\mu^+ \mu^- \mu^+ \nu_\mu$		$< 1.6 \times 10^{-8}$	CL=95%
	Inclusive modes			
Γ_{40}	$D^0 X$		(8.6 ± 0.7) %	
Γ_{41}	$\overline{D}^0 X$		(79 ± 4) %	
Γ_{42}	$D^+ X$		(2.5 ± 0.5) %	
Γ_{43}	$D^- X$		(9.9 ± 1.2) %	
Γ_{44}	$D_s^+ X$		$(7.9 \pm^{1.4}_{1.3})$ %	
Γ_{45}	$D_s^- X$		$(1.10 \pm^{0.40}_{0.32})$ %	
Γ_{46}	$\Lambda_c^+ X$		$(2.1 \pm^{0.9}_{0.6})$ %	
Γ_{47}	$\overline{\Lambda}_c^- X$		$(2.8 \pm^{1.1}_{0.9})$ %	
Γ_{48}	$\overline{c} X$		(97 ± 4) %	
Γ_{49}	$c X$		$(23.4 \pm^{2.2}_{1.8})$ %	
Γ_{50}	$c/\overline{c} X$		(120 ± 6) %	
	D, D^*, or D_s modes			
Γ_{51}	$\overline{D}^0 \pi^+$		$(4.68 \pm 0.13) \times 10^{-3}$	
Γ_{52}	$D_{CP(+1)} \pi^+$	[b]	$(2.05 \pm 0.20) \times 10^{-3}$	
Γ_{53}	$D_{CP(-1)} \pi^+$	[b]	$(2.1 \pm 0.4) \times 10^{-3}$	
Γ_{54}	$\overline{D}^0 \rho^+$		(1.34 ± 0.18) %	
Γ_{55}	$\overline{D}^0 K^+$		$(3.69 \pm 0.16) \times 10^{-4}$	
Γ_{56}	$D_{CP(+1)} K^+$	[b]	$(1.83 \pm 0.08) \times 10^{-4}$	
Γ_{57}	$D_{CP(-1)} K^+$	[b]	$(1.99 \pm 0.19) \times 10^{-4}$	
Γ_{58}	$D^0 K^+$		$(3.64 \pm 0.25) \times 10^{-6}$	
Γ_{59}	$[K^- \pi^+]_D K^+$	[c]	$< 2.8 \times 10^{-7}$	CL=90%
Γ_{60}	$[K^+ \pi^-]_D K^+$	[c]	$< 2.0 \times 10^{-5}$	CL=90%
Γ_{61}	$[K^- \pi^+ \pi^0]_D K^+$		seen	
Γ_{62}	$[K^+ \pi^- \pi^0]_D K^+$		seen	
Γ_{63}	$[K^- \pi^+ \pi^+ \pi^-]_D K^+$		seen	
Γ_{64}	$[K^+ \pi^- \pi^+ \pi^-]_D K^+$		seen	
Γ_{65}	$[\pi^+ \pi^+ \pi^- \pi^-] K^+$			
Γ_{66}	$[\pi^+ \pi^- \pi^+ \pi^-]_D K^*(892)^+$			
Γ_{67}	$[K^- \pi^+]_D K^*(892)^+$	[c]		
Γ_{68}	$[K^+ \pi^-]_D K^*(892)^+$	[c]		
Γ_{69}	$[K^- \pi^+ \pi^- \pi^+]_D K^*(892)^+$			
Γ_{70}	$[K^+ \pi^- \pi^+ \pi^-]_D K^*(892)^+$			
Γ_{71}	$[K^- \pi^+]_D \pi^+$	[c]	$(6.3 \pm 1.1) \times 10^{-7}$	
Γ_{72}	$[K^+ \pi^-]_D \pi^+$		$(1.7 \pm 0.4) \times 10^{-4}$	
Γ_{73}	$[K^- \pi^+ \pi^0]_D \pi^+$		seen	
Γ_{74}	$[K^+ \pi^- \pi^0]_D \pi^+$		seen	
Γ_{75}	$[K^- \pi^+ \pi^+ \pi^-]_D \pi^+$		seen	
Γ_{76}	$[K^+ \pi^- \pi^+ \pi^-]_D \pi^+$		seen	
Γ_{77}	$[K^- \pi^+]_{(D\pi)} \pi^+$			
Γ_{78}	$[K^+ \pi^-]_{(D\pi)} \pi^+$			
Γ_{79}	$[K^- \pi^+]_{(D\gamma)} \pi^+$			
Γ_{80}	$[K^+ \pi^-]_{(D\gamma)} \pi^+$			
Γ_{81}	$[K^- \pi^+]_{(D\pi)} K^+$			
Γ_{82}	$[K^+ \pi^-]_{(D\pi)} K^+$			
Γ_{83}	$[K^- \pi^+]_{(D\gamma)} K^+$			
Γ_{84}	$[K^+ \pi^-]_{(D\gamma)} K^+$			
Γ_{85}	$[\pi^+ \pi^- \pi^0]_D K^-$		$(4.6 \pm 0.9) \times 10^{-6}$	
Γ_{86}	$[K_S^0 K^+ \pi^-]_D K^+$		seen	
Γ_{87}	$[K^*(892)^- K^+]_D K^+$			
Γ_{88}	$[K_S^0 K^- \pi^+]_D K^+$		seen	
Γ_{89}	$[K^*(892)^+ K^-]_D K^+$		seen	
Γ_{90}	$[K_S^0 K^- \pi^+]_D \pi^+$		seen	
Γ_{91}	$[K^*(892)^+ K^-]_D \pi^+$		seen	
Γ_{92}	$[K_S^0 K^+ \pi^-]_D \pi^+$		seen	
Γ_{93}	$[K^*(892)^- K^+]_D \pi^+$		seen	
Γ_{94}	$[K^+ K^- \pi^0]_D K^+$			
Γ_{95}	$[K^+ K^- \pi^0]_D \pi^+$			
Γ_{96}	$[\pi^+ \pi^- \pi^0]_D K^+$			

Downloaded from https://academic.oup.com/ptep/article/2022/8/083C01/6651666 by KIT Library user on 27 September 2022

Γ_{97}	$[\pi^+\pi^-\pi^0]_D\,\pi^+$				
Γ_{98}	$\overline{D}^0 K^*(892)^+$		$(5.3 \pm 0.4)\times10^{-4}$		
Γ_{99}	$D_{CP(-1)}\,K^*(892)^+$	[b]	$(2.7 \pm 0.8)\times10^{-4}$		
Γ_{100}	$D_{CP(+1)}\,K^*(892)^+$	[b]	$(6.2 \pm 0.7)\times10^{-4}$		
Γ_{101}	$D^0 K^*(892)^+$		$(5.4 {}^{+1.8}_{-4.0})\times10^{-6}$		
Γ_{102}	$\overline{D}^0 K^+\pi^+\pi^-$		$(5.2 \pm 2.1)\times10^{-4}$		
Γ_{103}	$[K^+\pi^-]_D\,K^+\pi^-\pi^+$				
Γ_{104}	$[K^-\pi^+]_D\,K^+\pi^-\pi^+$				
Γ_{105}	$D_{CP(+1)}\,K^+\pi^-\pi^+$				
Γ_{106}	$\overline{D}^0 K^+\overline{K}^0$		$(5.5 \pm 1.6)\times10^{-4}$		
Γ_{107}	$\overline{D}^0 K^+\overline{K}^*(892)^0$		$(7.5 \pm 1.7)\times10^{-4}$		
Γ_{108}	$\overline{D}^0\pi^+\pi^+\pi^-$		$(5.6 \pm 2.1)\times10^{-3}$	S=3.6	
Γ_{109}	$[K^-\pi^+]_D\,\pi^+\pi^-\pi^+$				
Γ_{110}	$\overline{D}^0\pi^+\pi^+\pi^-$ nonresonant		$(5 \pm 4)\times10^{-3}$		
Γ_{111}	$\overline{D}^0\pi^+\rho^0$		$(4.2 \pm 3.0)\times10^{-3}$		
Γ_{112}	$\overline{D}^0 a_1(1260)^+$		$(4 \pm 4)\times10^{-3}$		
Γ_{113}	$\overline{D}^0\omega\pi^+$		$(4.1 \pm 0.9)\times10^{-3}$		
Γ_{114}	$D^*(2010)^-\pi^+\pi^+$		$(1.35 \pm 0.22)\times10^{-3}$		
Γ_{115}	$D^*(2010)^-K^+\pi^+$		$(8.2 \pm 1.4)\times10^{-5}$		
Γ_{116}	$\overline{D}_1(2420)^0\pi^+,\ \overline{D}_1^0 \to D^*(2010)^-\pi^+$		$(8.4 \pm 1.5)\times10^{-4}$		
Γ_{117}	$D^-\pi^+\pi^+$		$(1.07 \pm 0.05)\times10^{-3}$		
Γ_{118}	$D^-K^+\pi^+$		$(7.7 \pm 0.5)\times10^{-5}$		
Γ_{119}	$D_0^*(2300)^0 K^+,\ D_0^{*0} \to D^-\pi^+$		$(6.1 \pm 2.4)\times10^{-6}$		
Γ_{120}	$D_2^*(2460)^0 K^+,\ D_2^{*0} \to D^-\pi^+$		$(2.32 \pm 0.23)\times10^{-5}$		
Γ_{121}	$D_1^*(2760)^0 K^+,\ D_1^{*0} \to D^-\pi^+$		$(3.6 \pm 1.2)\times10^{-6}$		
Γ_{122}	D^+K^0		$< 2.9 \times10^{-6}$	CL=90%	
Γ_{123}	$D^+K^+\pi^-$		$(5.6 \pm 1.1)\times10^{-6}$		
Γ_{124}	$D_2^*(2460)^0 K^+,\ D_2^{*0} \to D^+\pi^-$		$< 6.3 \times10^{-7}$	CL=90%	
Γ_{125}	D^+K^{*0}		$< 4.9 \times10^{-7}$	CL=90%	
Γ_{126}	$D^+\overline{K}^{*0}$		$< 1.4 \times10^{-6}$	CL=90%	
Γ_{127}	$\overline{D}^*(2007)^0\pi^+$		$(5.18 \pm 0.15)\times10^{-3}$		
Γ_{128}	$\overline{D}^{*0}_{CP(+1)}\pi^+$	[d]	$(2.9 \pm 0.6)\times10^{-3}$		
Γ_{129}	$D^{*0}_{CP(-1)}\pi^+$	[d]	$(2.6 \pm 1.0)\times10^{-3}$		
Γ_{130}	$\overline{D}^*(2007)^0\omega\pi^+$		$(4.5 \pm 1.2)\times10^{-3}$		
Γ_{131}	$\overline{D}^*(2007)^0\rho^+$		$(9.8 \pm 1.7)\times10^{-3}$		
Γ_{132}	$\overline{D}^*(2007)^0 K^+$		$(4.20 {}^{+0.31}_{-0.28})\times10^{-4}$		
Γ_{133}	$\overline{D}^{*0}_{CP(+1)}K^+$	[d]	$(2.75 \pm 0.35)\times10^{-4}$		
Γ_{134}	$\overline{D}^{*0}_{CP(-1)}K^+$	[d]	$(2.31 \pm 0.31)\times10^{-4}$		
Γ_{135}	$D^*(2007)^0 K^+$		$(4.5 \pm 1.2)\times10^{-6}$		
Γ_{136}	$\overline{D}^*(2007)^0 K^*(892)^+$		$(8.1 \pm 1.4)\times10^{-4}$		
Γ_{137}	$\overline{D}^*(2007)^0 K^+\overline{K}^0$		$< 1.06 \times10^{-3}$	CL=90%	
Γ_{138}	$\overline{D}^*(2007)^0 K^+\overline{K}^*(892)^0$		$(1.5 \pm 0.4)\times10^{-3}$		
Γ_{139}	$\overline{D}^*(2007)^0\pi^+\pi^+\pi^-$		(1.03 ± 0.12) %		
Γ_{140}	$\overline{D}^*(2007)^0 a_1(1260)^+$		(1.9 ± 0.5) %		
Γ_{141}	$\overline{D}^*(2007)^0\pi^-\pi^+\pi^+\pi^0$		(1.8 ± 0.4) %		
Γ_{142}	$\overline{D}^{*0}3\pi^+2\pi^-$		$(5.7 \pm 1.2)\times10^{-3}$		
Γ_{143}	$D^*(2010)^+\pi^0$		$< 3.6 \times10^{-6}$		
Γ_{144}	$D^*(2010)^+K^0$		$< 9.0 \times10^{-6}$	CL=90%	
Γ_{145}	$D^*(2010)^-\pi^+\pi^+\pi^0$		(1.5 ± 0.7) %		
Γ_{146}	$D^*(2010)^-\pi^+\pi^+\pi^+\pi^-$		$(2.6 \pm 0.4)\times10^{-3}$		
Γ_{147}	$\overline{D}^{**0}\pi^+$	[e]	$(5.7 \pm 1.2)\times10^{-3}$		
Γ_{148}	$\overline{D}_1^*(2420)^0\pi^+$		$(1.5 \pm 0.6)\times10^{-3}$	S=1.3	
Γ_{149}	$\overline{D}_1(2420)^0\pi^+\times B(\overline{D}_1^0 \to \overline{D}^0\pi^+\pi^-)$		$(2.5 {}^{+1.6}_{-1.4})\times10^{-4}$	S=3.9	
Γ_{150}	$\overline{D}_1(2420)^0\pi^+\times B(\overline{D}_1^0 \to \overline{D}^0\pi^+\pi^-$ (nonresonant))		$(2.2 \pm 1.0)\times10^{-4}$		
Γ_{151}	$\overline{D}_1(2430)^0\pi^+,\ \overline{D}_1^0 \to D^*(2010)^-\pi^+$		$(3.5 \pm 0.6)\times10^{-4}$		
Γ_{152}	$\overline{D}(2550)^0\pi^+,\ \overline{D}^0 \to D^*(2010)^-\pi^+$		$(7.2 \pm 1.4)\times10^{-5}$		
Γ_{153}	$\overline{D}_J^*(2600)^0\pi^+,\ \overline{D}_J^{*0} \to D^*(2010)^-\pi^+$		$(6.8 \pm 1.3)\times10^{-5}$		
Γ_{154}	$\overline{D}_2^*(2462)^0\pi^+,\ \overline{D}_2^{*0} \to D^-\pi^+$		$(3.56 \pm 0.24)\times10^{-4}$		
Γ_{155}	$\overline{D}_2^*(2462)^0\pi^+,\ \overline{D}_2^{*0} \to \overline{D}^0\pi^-\pi^+$		$(2.2 \pm 1.0)\times10^{-4}$		
Γ_{156}	$\overline{D}_2^*(2462)^0\pi^+,\ \overline{D}_2^{*0} \to \overline{D}^0\pi^-\pi^+$ (nonresonant)		$< 1.7 \times10^{-4}$	CL=90%	
Γ_{157}	$\overline{D}_2^*(2462)^0\pi^+,\ \overline{D}_2^{*0} \to D^*(2010)^-\pi^+$		$(2.2 \pm 1.1)\times10^{-4}$		
Γ_{158}	$\overline{D}_0^*(2400)^0\pi^+ \times B(\overline{D}_0^*(2400)^0 \to D^-\pi^+)$		$(6.4 \pm 1.4)\times10^{-4}$		
Γ_{159}	$\overline{D}_1(2421)^0\pi^+,\ \overline{D}_1^0 \to D^{*-}\pi^+$		$(7.4 \pm 1.0)\times10^{-4}$		
Γ_{160}	$\overline{D}_2^*(2462)^0\pi^+,\ \overline{D}_2^{*0} \to D^{*-}\pi^+$		$(1.98 \pm 0.30)\times10^{-4}$		
Γ_{161}	$\overline{D}_1'(2427)^0\pi^+,\ \overline{D}_1'^0 \to D^{*-}\pi^+$		$(3.5 \pm 0.9)\times10^{-4}$	S=1.5	
Γ_{162}	$\overline{D}_1(2420)^0\pi^+\times B(\overline{D}_1^0 \to \overline{D}^{*0}\pi^+\pi^-)$		$< 6 \times10^{-6}$	CL=90%	
Γ_{163}	$\overline{D}_1^*(2420)^0\rho^+$		$< 1.4 \times10^{-3}$	CL=90%	
Γ_{164}	$\overline{D}_2^*(2460)^0\pi^+$		$< 1.3 \times10^{-3}$	CL=90%	
Γ_{165}	$\overline{D}_2^*(2460)^0\pi^+\times B(\overline{D}_2^{*0} \to \overline{D}^{*0}\pi^+\pi^-)$		$< 2.2 \times10^{-5}$	CL=90%	
Γ_{166}	$\overline{D}_1^*(2680)^0\pi^+,\ \overline{D}_1^*(2680)^0 \to D^-\pi^+$		$(8.4 \pm 2.1)\times10^{-5}$		
Γ_{167}	$\overline{D}(2740)^0\pi^+,\ \overline{D}^0 \to D^*(2010)^-\pi^+$		$(3.3 \pm 1.5)\times10^{-5}$		
Γ_{168}	$\overline{D}_3^*(2750)^0\pi^+,\ \overline{D}_3^{*0} \to D^*(2010)^-\pi^+$		$(1.10 \pm 0.32)\times10^{-5}$		
Γ_{169}	$\overline{D}_3^*(2760)^0\pi^+,\ \overline{D}_3^*(2760)^0\pi^+ \to D^-\pi^+$		$(1.00 \pm 0.22)\times10^{-5}$		
Γ_{170}	$\overline{D}_2^*(3000)^0\pi^+,\ \overline{D}_2^*(3000)^0\pi^+ \to D^-\pi^+$		$(2.0 \pm 1.4)\times10^{-6}$		
Γ_{171}	$\overline{D}_2^*(2460)^0\rho^+$		$< 4.7 \times10^{-3}$	CL=90%	
Γ_{172}	$\overline{D}^0 D_s^+$		$(9.0 \pm 0.9)\times10^{-3}$		
Γ_{173}	$D_{s0}^*(2317)^+\overline{D}^0,\ D_{s0}^{*+} \to D_s^+\pi^0$		$(8.0 {}^{+1.6}_{-1.3})\times10^{-4}$		
Γ_{174}	$D_{s0}(2317)^+\overline{D}^0\times B(D_{s0}(2317)^+ \to D_s^{*+}\gamma)$		$< 7.6 \times10^{-4}$	CL=90%	
Γ_{175}	$D_{s0}(2317)^+\overline{D}^*(2007)^0\times B(D_{s0}(2317)^+ \to D_s^+\pi^0)$		$(9 \pm 7)\times10^{-4}$		
Γ_{176}	$D_{sJ}(2457)^+\overline{D}^0$		$(3.1 {}^{+1.0}_{-0.9})\times10^{-3}$		
Γ_{177}	$D_{sJ}(2457)^+\overline{D}^0\times B(D_{sJ}(2457)^+ \to D_s^+\gamma)$		$(4.6 {}^{+1.3}_{-1.1})\times10^{-4}$		
Γ_{178}	$D_{sJ}(2457)^+\overline{D}^0\times B(D_{sJ}(2457)^+ \to D_s^+\pi^+\pi^-)$		$< 2.2 \times10^{-4}$	CL=90%	
Γ_{179}	$D_{sJ}(2457)^+\overline{D}^0\times B(D_{sJ}(2457)^+ \to D_s^+\pi^0)$		$< 2.7 \times10^{-4}$	CL=90%	
Γ_{180}	$D_{sJ}(2457)^+\overline{D}^0\times B(D_{sJ}(2457)^+ \to D_s^{*+}\gamma)$		$< 9.8 \times10^{-4}$	CL=90%	
Γ_{181}	$D_{sJ}(2457)^+\overline{D}^*(2007)^0$		(1.20 ± 0.30) %		
Γ_{182}	$D_{sJ}(2457)^+\overline{D}^*(2007)^0\times B(D_{sJ}(2457)^+ \to D_s^+\gamma)$		$(1.4 {}^{+0.7}_{-0.6})\times10^{-3}$		
Γ_{183}	$\overline{D}^0 D_{s1}(2536)^+\times B(D_{s1}(2536)^+ \to D^*(2007)^0K^+ + D^*(2010)^+K^0)$		$(4.0 \pm 1.0)\times10^{-4}$		
Γ_{184}	$\overline{D}^0 D_{s1}(2536)^+\times B(D_{s1}(2536)^+ \to D^*(2007)^0K^+)$		$(2.2 \pm 0.7)\times10^{-4}$		
Γ_{185}	$\overline{D}^*(2007)^0 D_{s1}(2536)^+\times B(D_{s1}(2536)^+ \to D^*(2007)^0K^+)$		$(5.5 \pm 1.6)\times10^{-4}$		
Γ_{186}	$\overline{D}^0 D_{s1}(2536)^+\times B(D_{s1}(2536)^+ \to D^{*+}K^0)$		$(2.3 \pm 1.1)\times10^{-4}$		
Γ_{187}	$\overline{D}^0 D_{sJ}(2700)^+\times B(D_{sJ}(2700)^+ \to D^0K^+)$		$(5.6 \pm 1.8)\times10^{-4}$	S=1.7	
Γ_{188}	$\overline{D}^{*0} D_{s1}(2536)^+,\ D_{s1}^+ \to D^{*+}K^0$		$(3.9 \pm 2.6)\times10^{-4}$		
Γ_{189}	$\overline{D}^0 D_{sJ}(2573)^+,\ D_{sJ}^+ \to D^0K^+$		$(8 \pm 15)\times10^{-6}$		
Γ_{190}	$\overline{D}^{*0} D_{sJ}(2573),\ D_{sJ}^+ \to D^0K^+$		$< 2 \times10^{-4}$	CL=90%	
Γ_{191}	$\overline{D}^*(2007)^0 D_{sJ}(2573),\ D_{sJ}^+ \to D^0K^+$		$< 5 \times10^{-4}$	CL=90%	
Γ_{192}	$\overline{D}^0 D_s^{*+}$		$(7.6 \pm 1.6)\times10^{-3}$		
Γ_{193}	$\overline{D}^*(2007)^0 D_s^+$		$(8.2 \pm 1.7)\times10^{-3}$		
Γ_{194}	$\overline{D}^*(2007)^0 D_s^{*+}$		(1.71 ± 0.24) %		
Γ_{195}	$D_s^{(*)+}\overline{D}^{**0}$		(2.7 ± 1.2) %		
Γ_{196}	$\overline{D}^*(2007)^0 D^*(2010)^+$		$(8.1 \pm 1.7)\times10^{-4}$		

Downloaded from https://academic.oup.com/ptep/article/2022/8/083C01/6651666 by KIT Library user on 27 September 2022

Γ_{197}	$\overline{D}^0 D^*(2010)^+ + \overline{D}^*(2007)^0 D^+$	<	1.30	%	CL=90%
Γ_{198}	$\overline{D}^0 D^*(2010)^+$	(	3.9 ± 0.5)	$\times 10^{-4}$	
Γ_{199}	$\overline{D}^0 D^+$	(	3.8 ± 0.4)	$\times 10^{-4}$	
Γ_{200}	$\overline{D}^0 D^+ K^0$	(	1.55 ± 0.21)	$\times 10^{-3}$	
Γ_{201}	$D^+ \overline{D}^*(2007)^0$	(	6.3 ± 1.7)	$\times 10^{-4}$	
Γ_{202}	$\overline{D}^*(2007)^0 D^+ K^0$	(	2.1 ± 0.5)	$\times 10^{-3}$	
Γ_{203}	$\overline{D}^0 D^*(2010)^+ K^0$	(	3.8 ± 0.4)	$\times 10^{-3}$	
Γ_{204}	$\overline{D}^*(2007)^0 D^*(2010)^+ K^0$	(	9.2 ± 1.2)	$\times 10^{-3}$	
Γ_{205}	$\overline{D}^0 D^0 K^+$	(	1.45 ± 0.33)	$\times 10^{-3}$	S=2.6
Γ_{206}	$\overline{D}^*(2007)^0 D^0 K^+$	(	2.26 ± 0.23)	$\times 10^{-3}$	
Γ_{207}	$\overline{D}^0 D^*(2007)^0 K^+$	(	6.3 ± 0.5)	$\times 10^{-3}$	
Γ_{208}	$\overline{D}^*(2007)^0 D^*(2007)^0 K^+$	(	1.12 ± 0.13)	%	
Γ_{209}	$D^- D^+ K^+$	(	2.2 ± 0.7)	$\times 10^{-4}$	
Γ_{210}	$X_0(2900) D^+,\ X_0 \to D^- K^+$	(	1.2 ± 0.5)	$\times 10^{-5}$	
Γ_{211}	$X_1(2900) D^+,\ X_1 \to D^- K^+$	(	6.7 ± 2.3)	$\times 10^{-5}$	
Γ_{212}	$D^- D^+ K^+$ nonresonant	(	5.3 ± 1.8)	$\times 10^{-5}$	
Γ_{213}	$D^- D^*(2010)^+ K^+$	(	6.3 ± 1.1)	$\times 10^{-4}$	
Γ_{214}	$D^*(2010)^- D^+ K^+$	(	6.0 ± 1.3)	$\times 10^{-4}$	
Γ_{215}	$D^*(2010)^- D^*(2010)^+ K^+$	(	1.32 ± 0.18)	$\times 10^{-3}$	
Γ_{216}	$(\overline{D}+\overline{D}^*)(D+D^*)K$	(	4.05 ± 0.30)	%	
Γ_{217}	$D_s^+ \pi^0$	(	1.6 ± 0.5)	$\times 10^{-5}$	
Γ_{218}	$D_s^{*+} \pi^0$	<	2.6	$\times 10^{-4}$	CL=90%
Γ_{219}	$D_s^+ \eta$	<	4	$\times 10^{-4}$	CL=90%
Γ_{220}	$D_s^{*+} \eta$	<	6	$\times 10^{-4}$	CL=90%
Γ_{221}	$D_s^+ \rho^0$	<	3.0	$\times 10^{-4}$	CL=90%
Γ_{222}	$D_s^{*+} \rho^0$	<	4	$\times 10^{-4}$	CL=90%
Γ_{223}	$D_s^+ \omega$	<	4	$\times 10^{-4}$	CL=90%
Γ_{224}	$D_s^{*+} \omega$	<	6	$\times 10^{-4}$	CL=90%
Γ_{225}	$D_s^+ a_1(1260)^0$	<	1.8	$\times 10^{-3}$	CL=90%
Γ_{226}	$D_s^{*+} a_1(1260)^0$	<	1.3	$\times 10^{-3}$	CL=90%
Γ_{227}	$D_s^+ K^+ K^-$	(	7.2 ± 1.1)	$\times 10^{-6}$	
Γ_{228}	$D_s^+ \phi$	<	4.2	$\times 10^{-7}$	CL=90%
Γ_{229}	$D_s^{*+} \phi$	<	1.2	$\times 10^{-5}$	CL=90%
Γ_{230}	$D_s^+ \overline{K}^0$	<	8	$\times 10^{-4}$	CL=90%
Γ_{231}	$D_s^{*+} \overline{K}^0$	<	9	$\times 10^{-4}$	CL=90%
Γ_{232}	$D_s^+ \overline{K}^*(892)^0$	<	4.4	$\times 10^{-6}$	CL=90%
Γ_{233}	$D_s^+ K^{*0}$	<	3.5	$\times 10^{-6}$	CL=90%
Γ_{234}	$D_s^{*+} \overline{K}^*(892)^0$	<	3.5	$\times 10^{-4}$	CL=90%
Γ_{235}	$D_s^- \pi^+ K^+$	(	1.80 ± 0.22)	$\times 10^{-4}$	
Γ_{236}	$D_s^{*-} \pi^+ K^+$	(	1.45 ± 0.24)	$\times 10^{-4}$	
Γ_{237}	$D_s^- \pi^+ K^*(892)^+$	<	5	$\times 10^{-3}$	CL=90%
Γ_{238}	$D_s^{*-} \pi^+ K^*(892)^+$	<	7	$\times 10^{-3}$	CL=90%
Γ_{239}	$D_s^- K^+ K^+$	(	9.7 ± 2.1)	$\times 10^{-6}$	
Γ_{240}	$D_s^{*-} K^+ K^+$	<	1.5	$\times 10^{-5}$	CL=90%

Charmonium modes

Γ_{241}	$\eta_c K^+$	(	1.09 ± 0.08)	$\times 10^{-3}$	
Γ_{242}	$\eta_c K^+,\ \eta_c \to K_S^0 K^{\mp}\pi^{\pm}$	(	2.7 ± 0.6)	$\times 10^{-5}$	
Γ_{243}	$\eta_c K^*(892)^+$	(	$1.1\ ^{+0.5}_{-0.4}$)	$\times 10^{-3}$	
Γ_{244}	$\eta_c K^+ \pi^+ \pi^-$	<	3.9	$\times 10^{-4}$	CL=90%
Γ_{245}	$\eta_c K^+ \omega(782)$	<	5.3	$\times 10^{-4}$	CL=90%
Γ_{246}	$\eta_c K^+ \eta$	<	2.2	$\times 10^{-4}$	CL=90%
Γ_{247}	$\eta_c K^+ \pi^0$	<	6.2	$\times 10^{-5}$	CL=90%
Γ_{248}	$\eta_c(2S) K^+$	(	4.4 ± 1.0)	$\times 10^{-4}$	
Γ_{249}	$\eta_c(2S) K^+,\ \eta_c \to p\overline{p}$	(	3.5 ± 0.8)	$\times 10^{-8}$	
Γ_{250}	$\eta_c(2S) K^+,\ \eta_c \to K_S^0 K^{\mp}\pi^{\pm}$	(	$3.4\ ^{+2.3}_{-1.6}$)	$\times 10^{-6}$	
Γ_{251}	$\eta_c(2S) K^+,\ \eta_c \to p\overline{p}\pi^+\pi^-$	(	1.12 ± 0.18)	$\times 10^{-6}$	
Γ_{252}	$h_c(1P) K^+,\ h_c \to J/\psi\pi^+\pi^-$	<	3.4	$\times 10^{-6}$	CL=90%
Γ_{253}	$X(3730)^0 K^+,\ X^0 \to \eta_c \eta$	<	4.6	$\times 10^{-5}$	CL=90%
Γ_{254}	$X(3730)^0 K^+,\ X^0 \to \eta_c \pi^0$	<	5.7	$\times 10^{-6}$	CL=90%
Γ_{255}	$\eta_{c2}(1D) K^+,\ \eta_{c2} \to h_c \gamma$	<	3.7	$\times 10^{-5}$	CL=90%
Γ_{256}	$\eta_{c2}(1D) \pi^+ K_S^0,\ \eta_{c2} \to h_c \gamma$	<	1.1	$\times 10^{-4}$	CL=90%
Γ_{257}	$\psi_2(3823) K^+,\ \psi_2 \to J/\psi\pi^+\pi^-$	(	2.8 ± 0.6)	$\times 10^{-7}$	
Γ_{258}	$\chi_{c1}(3872) K^+$	(	2.1 ± 0.7)	$\times 10^{-4}$	
Γ_{259}	$\chi_{c0}(3915) K^+$	<	2.8	$\times 10^{-4}$	CL=90%
Γ_{260}	$\chi_{c0}(3915) K^+,\ \chi_{c0} \to D^+ D^-$	(	8.1 ± 3.3)	$\times 10^{-6}$	
Γ_{261}	$\chi_{c0}(3915) K^+,\ \chi_{c0} \to \eta_c \eta$	<	4.7	$\times 10^{-5}$	CL=90%
Γ_{262}	$(Xchi)_{c0}(3915) K^+,\ \chi_{c0} \to \eta_c \pi^0$	<	1.7	$\times 10^{-5}$	CL=90%
Γ_{263}	$X(4014)^0 K^+,\ X^0 \to \eta_c \eta$	<	3.9	$\times 10^{-5}$	CL=90%
Γ_{264}	$X(4014)^0 K^+,\ X^0 \to \eta_c \pi^0$	<	1.2	$\times 10^{-5}$	CL=90%
Γ_{265}	$Z_c(3900)^0 K^+,\ Z_c^0 \to \eta_c \pi^+\pi^-$	<	4.7	$\times 10^{-5}$	CL=90%
Γ_{266}	$X(4020)^0 K^+,\ X^0 \to \eta_c \pi^+\pi^-$	<	1.6	$\times 10^{-5}$	CL=90%
Γ_{267}	$\chi_{c1}(3872) K^*(892)^+$	<	6	$\times 10^{-4}$	CL=90%
Γ_{268}	$\chi_{c1}(3872)^+ K^0,\ \chi_{c1}^+ \to J/\psi(1S)\pi^+\pi^0$ [f]	<	6.1	$\times 10^{-6}$	CL=90%
Γ_{269}	$\chi_{c1}(3872) K^0 \pi^+$	(	2.8 ± 1.2)	$\times 10^{-4}$	
Γ_{270}	$Z_c(4430)^+ K^0,\ Z_c^+ \to J/\psi\pi^+$	<	1.5	$\times 10^{-5}$	CL=95%
Γ_{271}	$Z_c(4430)^+ K^0,\ Z_c^+ \to \psi(2S)\pi^+$	<	4.7	$\times 10^{-5}$	CL=95%
Γ_{272}	$\psi(4230)^0 K^+,\ \psi^0 \to J/\psi\pi^+\pi^-$	<	1.56	$\times 10^{-5}$	CL=95%
Γ_{273}	$\chi_{c0}(3915) K^+,\ \chi_{c0} \to J/\psi\gamma$	<	1.4	$\times 10^{-5}$	CL=90%
Γ_{274}	$\chi_{c0}(3915) K^+,\ \chi_{c0} \to \chi_{c1}(1P)\pi^0$	<	3.8	$\times 10^{-5}$	CL=90%
Γ_{275}	$X(3930)^0 K^+,\ X^0 \to J/\psi\gamma$	<	2.5	$\times 10^{-6}$	CL=90%
Γ_{276}	$J/\psi(1S) K^+$	(	1.020 ± 0.019)	$\times 10^{-3}$	
Γ_{277}	$J/\psi(1S) K^0 \pi^+$	(	1.14 ± 0.11)	$\times 10^{-3}$	
Γ_{278}	$J/\psi(1S) K^+ \pi^+ \pi^-$	(	8.1 ± 1.3)	$\times 10^{-4}$	S=2.5
Γ_{279}	$J/\psi(1S) K^+ K^- K^+$	(	3.37 ± 0.29)	$\times 10^{-5}$	
Γ_{280}	$\chi_{c0}(3915) K^+,\ \chi_{c0} \to p\overline{p}$	<	7.1	$\times 10^{-8}$	CL=95%
Γ_{281}	$J/\psi(1S) K^*(892)^+$	(	1.43 ± 0.08)	$\times 10^{-3}$	
Γ_{282}	$J/\psi(1S) K(1270)^+$	(	1.8 ± 0.5)	$\times 10^{-3}$	
Γ_{283}	$J/\psi(1S) K(1400)^+$	<	5	$\times 10^{-4}$	CL=90%
Γ_{284}	$J/\psi(1S) \eta K^+$	(	1.24 ± 0.14)	$\times 10^{-4}$	
Γ_{285}	$\chi_{c1-odd}(3872) K^+,\ \chi_{c1-odd} \to J/\psi\eta$	<	3.8	$\times 10^{-6}$	CL=90%
Γ_{286}	$\psi(4160) K^+,\ \psi \to J/\psi\eta$	<	7.4	$\times 10^{-6}$	CL=90%
Γ_{287}	$J/\psi(1S) \eta' K^+$	<	8.8	$\times 10^{-5}$	CL=90%
Γ_{288}	$J/\psi(1S) \phi K^+$	(	5.0 ± 0.4)	$\times 10^{-5}$	
Γ_{289}	$J/\psi(1S) K_1(1650),\ K_1 \to \phi K^+$	(	$6\ ^{+10}_{-6}$)	$\times 10^{-6}$	
Γ_{290}	$J/\psi(1S) K^*(1680)^+,\ K^* \to \phi K^+$	(	$3.4\ ^{+1.9}_{-2.2}$)	$\times 10^{-6}$	
Γ_{291}	$J/\psi(1S) K_2^*(1980),\ K_2^* \to \phi K^+$	(	$1.5\ ^{+0.9}_{-0.5}$)	$\times 10^{-6}$	
Γ_{292}	$J/\psi(1S) K(1830)^+,\ K(1830)^+ \to \phi K^+$	(	$1.3\ ^{+1.3}_{-1.1}$)	$\times 10^{-6}$	
Γ_{293}	$\chi_{c1}(4140) K^+,\ \chi_{c1} \to J/\psi(1S)\phi$	(	10 ± 4)	$\times 10^{-6}$	
Γ_{294}	$\chi_{c1}(4274) K^+,\ \chi_{c1} \to J/\psi(1S)\phi$	(	$3.6\ ^{+2.2}_{-1.8}$)	$\times 10^{-6}$	
Γ_{295}	$\chi_{c0}(4500) K^+,\ \chi_c^0 \to J/\psi(1S)\phi$	(	$3.3\ ^{+2.1}_{-1.7}$)	$\times 10^{-6}$	
Γ_{296}	$\chi_{c0}(4700) K^+,\ \chi_{c0} \to J/\psi(1S)\phi$	(	$6\ ^{+5}_{-4}$)	$\times 10^{-6}$	
Γ_{297}	$J/\psi(1S)\omega K^+$	(	$3.20\ ^{+0.60}_{-0.32}$)	$\times 10^{-4}$	
Γ_{298}	$\chi_{c0}(3915) K^+,\ \chi_{c0} \to J/\psi\omega$	(	$3.0\ ^{+0.9}_{-0.7}$)	$\times 10^{-5}$	
Γ_{299}	$J/\psi(1S)\pi^+$	(	3.92 ± 0.08)	$\times 10^{-5}$	
Γ_{300}	$J/\psi(1S)\pi^+\pi^+\pi^+\pi^-\pi^-$	(	1.17 ± 0.13)	$\times 10^{-5}$	
Γ_{301}	$\psi(2S)\pi^+\pi^+\pi^-$	(	1.9 ± 0.4)	$\times 10^{-5}$	
Γ_{302}	$J/\psi(1S)\rho^+$	(	4.1 ± 0.5)	$\times 10^{-5}$	S=1.4
Γ_{303}	$J/\psi(1S)\pi^+\pi^0$ nonresonant	<	7.3	$\times 10^{-6}$	CL=90%
Γ_{304}	$J/\psi(1S) a_1(1260)^+$	<	1.2	$\times 10^{-3}$	CL=90%
Γ_{305}	$J/\psi(1S) p\overline{p}\pi^+$	<	5.0	$\times 10^{-7}$	CL=90%
Γ_{306}	$J/\psi(1S) p\overline{\Lambda}$	(	1.46 ± 0.12)	$\times 10^{-5}$	
Γ_{307}	$J/\psi(1S)\overline{\Sigma}^0 p$	<	1.1	$\times 10^{-5}$	CL=90%
Γ_{308}	$J/\psi(1S) D^+$	<	1.2	$\times 10^{-4}$	CL=90%
Γ_{309}	$J/\psi(1S)\overline{D}^0\pi^+$	<	2.5	$\times 10^{-5}$	CL=90%
Γ_{310}	$\psi(2S)\pi^+$	(	2.44 ± 0.30)	$\times 10^{-5}$	
Γ_{311}	$\psi(2S) K^+$	(	6.24 ± 0.20)	$\times 10^{-4}$	
Γ_{312}	$\psi(2S) K^*(892)^+$	(	6.7 ± 1.4)	$\times 10^{-4}$	S=1.3
Γ_{313}	$\psi(2S) K^0 \pi^+$				
Γ_{314}	$\psi(2S) K^+ \pi^+ \pi^-$	(	4.3 ± 0.5)	$\times 10^{-4}$	
Γ_{315}	$\psi(2S)\phi(1020) K^+$	(	4.0 ± 0.7)	$\times 10^{-6}$	
Γ_{316}	$\psi(3770) K^+$	(	4.3 ± 1.1)	$\times 10^{-4}$	
Γ_{317}	$\psi(3770) K+,\psi \to D^0\overline{D}^0$	(	1.5 ± 0.5)	$\times 10^{-4}$	S=1.4
Γ_{318}	$\psi(3770) K+,\psi \to D^+ D^-$	(	9.4 ± 3.5)	$\times 10^{-5}$	
Γ_{319}	$\psi(3770) K^+,\ \psi \to p\overline{p}$	<	2	$\times 10^{-7}$	CL=95%
Γ_{320}	$\psi(4040) K^+$	<	1.3	$\times 10^{-4}$	CL=90%

Downloaded from https://academic.oup.com/ptep/article/2022/8/083C01/6651666 by KIT Library user on 27 September 2022

Γ_{321}	$\psi(4040)K^+,\ \psi \to D^+D^-$	$(1.1 \pm 0.5)\times10^{-5}$		
Γ_{322}	$\psi(4160)K^+$	$(5.1 \pm 2.7)\times10^{-4}$		
Γ_{323}	$\psi(4160)K^+,\ \psi \to \overline{D}^0D^0$	$(8 \pm 5)\times10^{-5}$		
Γ_{324}	$\psi(4160)K^+,\ \psi \to D^+D^-$	$(1.5 \pm 0.6)\times10^{-5}$		
Γ_{325}	$\psi(4415)K^+,\ \psi \to D^+D^-$	$(2.0 \pm 0.8)\times10^{-5}$		
Γ_{326}	$\chi_{c0}\pi^+,\ \chi_{c0} \to \pi^+\pi^-$	$< 1 \times10^{-7}$	CL=90%	
Γ_{327}	$\chi_{c0}K^+$	$(1.51 {}^{+0.15}_{-0.13})\times10^{-4}$		
Γ_{328}	$\chi_{c0}K^*(892)^+$	$< 2.1 \times10^{-4}$	CL=90%	
Γ_{329}	$\chi_{c1}(1P)\pi^+$	$(2.2 \pm 0.5)\times10^{-5}$		
Γ_{330}	$\chi_{c1}(1P)K^+$	$(4.74 \pm 0.22)\times10^{-4}$		
Γ_{331}	$\chi_{c1}(1P)K^*(892)^+$	$(3.0 \pm 0.6)\times10^{-4}$		S=1.1
Γ_{332}	$\chi_{c1}(1P)K^0\pi^+$	$(5.8 \pm 0.4)\times10^{-4}$		
Γ_{333}	$\chi_{c1}(1P)K^+\pi^0$	$(3.29 \pm 0.35)\times10^{-4}$		
Γ_{334}	$\chi_{c1}(1P)K^+\pi^+\pi^-$	$(3.74 \pm 0.30)\times10^{-4}$		
Γ_{335}	$\chi_{c1}(2P)K^+,\ \chi_{c1}(2P) \to \pi^+\pi^-\chi_{c1}(1P)$	$< 1.1 \times10^{-5}$	CL=90%	
Γ_{336}	$\chi_{c2}K^+$	$(1.1 \pm 0.4)\times10^{-5}$		
Γ_{337}	$\chi_{c2}K^+,\ \chi_{c2} \to p\overline{p}\pi^+\pi^-$	$< 1.9 \times10^{-7}$		
Γ_{338}	$\chi_{c2}K^*(892)^+$	$< 1.2 \times10^{-4}$	CL=90%	
Γ_{339}	$\chi_{c2}K^0\pi^+$	$(1.16 \pm 0.25)\times10^{-4}$		
Γ_{340}	$\chi_{c2}K^+\pi^0$	$< 6.2 \times10^{-5}$	CL=90%	
Γ_{341}	$\chi_{c2}K^+\pi^+\pi^-$	$(1.34 \pm 0.19)\times10^{-4}$		
Γ_{342}	$\chi_{c2}(3930)K^+,\ \chi_{c2} \to D^+D^-$	$(1.6 \pm 0.6)\times10^{-5}$		
Γ_{343}	$\chi_{c2}(3930)\pi^+,\ \chi_{c2} \to \pi^+\pi^-$	$< 1 \times10^{-7}$	CL=90%	
Γ_{344}	$h_c(1P)K^+$	$(3.7 \pm 1.2)\times10^{-5}$		
Γ_{345}	$h_c(1P)K^+,\ h_c \to p\overline{p}$	$< 6.4 \times10^{-8}$	CL=95%	

K or K^* modes

Γ_{346}	$K^0\pi^+$	$(2.37 \pm 0.08)\times10^{-5}$		
Γ_{347}	$K^+\pi^0$	$(1.29 \pm 0.05)\times10^{-5}$		
Γ_{348}	$\eta' K^+$	$(7.04 \pm 0.25)\times10^{-5}$		
Γ_{349}	$\eta' K^*(892)^+$	$(4.8 {}^{+1.8}_{-1.6})\times10^{-6}$		
Γ_{350}	$\eta' K_0^*(1430)^+$	$(5.2 \pm 2.1)\times10^{-6}$		
Γ_{351}	$\eta' K_2^*(1430)^+$	$(2.8 \pm 0.5)\times10^{-5}$		
Γ_{352}	ηK^+	$(2.4 \pm 0.4)\times10^{-6}$		S=1.7
Γ_{353}	$\eta K^*(892)^+$	$(1.93 \pm 0.16)\times10^{-5}$		
Γ_{354}	$\eta K_0^*(1430)^+$	$(1.8 \pm 0.4)\times10^{-5}$		
Γ_{355}	$\eta K_2^*(1430)^+$	$(9.1 \pm 3.0)\times10^{-6}$		
Γ_{356}	$\eta(1295)K^+ \times B(\eta(1295) \to \eta\pi\pi)$	$(2.9 {}^{+0.8}_{-0.7})\times10^{-6}$		
Γ_{357}	$\eta(1405)K^+ \times B(\eta(1405) \to \eta\pi\pi)$	$< 1.3 \times10^{-6}$	CL=90%	
Γ_{358}	$\eta(1405)K^+ \times B(\eta(1405) \to K^*K)$	$< 1.2 \times10^{-6}$	CL=90%	
Γ_{359}	$\eta(1475)K^+ \times B(\eta(1475) \to K^*K)$	$(1.38 {}^{+0.21}_{-0.18})\times10^{-5}$		
Γ_{360}	$f_1(1285)K^+$	$< 2.0 \times10^{-6}$	CL=90%	
Γ_{361}	$f_1(1420)K^+ \times B(f_1(1420) \to \eta\pi\pi)$	$< 2.9 \times10^{-6}$	CL=90%	
Γ_{362}	$f_1(1420)K^+ \times B(f_1(1420) \to K^*K)$	$< 4.1 \times10^{-6}$	CL=90%	
Γ_{363}	$\phi(1680)K^+ \times B(\phi(1680) \to K^*K)$	$< 3.4 \times10^{-6}$	CL=90%	
Γ_{364}	$f_0(1500)K^+$	$(3.7 \pm 2.2)\times10^{-6}$		
Γ_{365}	ωK^+	$(6.5 \pm 0.4)\times10^{-6}$		
Γ_{366}	$\omega K^*(892)^+$	$< 7.4 \times10^{-6}$	CL=90%	
Γ_{367}	$\omega(K\pi)_0^{*+}$	$(2.8 \pm 0.4)\times10^{-5}$		
Γ_{368}	$\omega K_0^*(1430)^+$	$(2.4 \pm 0.5)\times10^{-5}$		
Γ_{369}	$\omega K_2^*(1430)^+$	$(2.1 \pm 0.4)\times10^{-5}$		
Γ_{370}	$a_0(980)^+K^0 \times B(a_0(980)^+ \to \eta\pi^+)$	$< 3.9 \times10^{-6}$	CL=90%	
Γ_{371}	$a_0(980)^0K^+ \times B(a_0(980)^0 \to \eta\pi^0)$	$< 2.5 \times10^{-6}$	CL=90%	
Γ_{372}	$K^*(892)^0\pi^+$	$(1.01 \pm 0.08)\times10^{-5}$		
Γ_{373}	$K^*(892)^+\pi^0$	$(6.8 \pm 0.9)\times10^{-6}$		
Γ_{374}	$K^+\pi^-\pi^+$	$(5.10 \pm 0.29)\times10^{-5}$		
Γ_{375}	$K^+\pi^-\pi^+$ nonresonant	$(1.63 {}^{+0.21}_{-0.15})\times10^{-5}$		
Γ_{376}	$\omega(782)K^+$	$(6 \pm 9)\times10^{-6}$		
Γ_{377}	$K^+f_0(980) \times B(f_0(980) \to \pi^+\pi^-)$	$(9.4 {}^{+1.0}_{-1.2})\times10^{-6}$		
Γ_{378}	$f_2(1270)^0K^+$	$(1.07 \pm 0.27)\times10^{-6}$		
Γ_{379}	$f_0(1370)^0K^+ \times B(f_0(1370)^0 \to \pi^+\pi^-)$	$< 1.07 \times10^{-5}$	CL=90%	
Γ_{380}	$\rho^0(1450)K^+ \times B(\rho^0(1450) \to \pi^+\pi^-)$	$< 1.17 \times10^{-5}$	CL=90%	
Γ_{381}	$f_2'(1525)K^+ \times B(f_2'(1525) \to \pi^+\pi^-)$	$< 3.4 \times10^{-6}$	CL=90%	
Γ_{382}	$K^+\rho^0$	$(3.7 \pm 0.5)\times10^{-6}$		
Γ_{383}	$K_0^*(1430)^0\pi^+$	$(3.9 {}^{+0.6}_{-0.5})\times10^{-5}$		S=1.4
Γ_{384}	$K_2^*(1430)^0\pi^+$	$(5.6 {}^{+2.2}_{-1.5})\times10^{-6}$		
Γ_{385}	$K^*(1410)^0\pi^+$	$< 4.5 \times10^{-5}$	CL=90%	
Γ_{386}	$K^*(1680)^0\pi^+$	$< 1.2 \times10^{-5}$	CL=90%	
Γ_{387}	$K^+\pi^0\pi^0$	$(1.62 \pm 0.19)\times10^{-5}$		
Γ_{388}	$f_0(980)K^+ \times B(f_0 \to \pi^0\pi^0)$	$(2.8 \pm 0.8)\times10^{-6}$		
Γ_{389}	$K^-\pi^+\pi^+$	$< 4.6 \times10^{-8}$	CL=90%	
Γ_{390}	$K^-\pi^+\pi^+$ nonresonant	$< 5.6 \times10^{-5}$	CL=90%	
Γ_{391}	$K_1(1270)^0\pi^+$	$< 4.0 \times10^{-5}$	CL=90%	
Γ_{392}	$K_1(1400)^0\pi^+$	$< 3.9 \times10^{-5}$	CL=90%	
Γ_{393}	$K^0\pi^+\pi^0$	$< 6.6 \times10^{-5}$	CL=90%	
Γ_{394}	$K_0^*(1430)^+\pi^0$	$(1.19 {}^{+0.20}_{-0.23})\times10^{-5}$		
Γ_{395}	$K^0\rho^+$	$(7.3 {}^{+1.0}_{-1.2})\times10^{-6}$		
Γ_{396}	$K^*(892)^+\pi^+\pi^-$	$(7.5 \pm 1.0)\times10^{-5}$		
Γ_{397}	$K^*(892)^+\rho^0$	$(4.6 \pm 1.1)\times10^{-6}$		
Γ_{398}	$K^*(892)^+f_0(980)$	$(4.2 \pm 0.7)\times10^{-6}$		
Γ_{399}	$a_1^+K^0$	$(3.5 \pm 0.7)\times10^{-5}$		
Γ_{400}	$b_1^+K^0 \times B(b_1^+ \to \omega\pi^+)$	$(9.6 \pm 1.9)\times10^{-6}$		
Γ_{401}	$K^*(892)^0\rho^+$	$(9.2 \pm 1.5)\times10^{-6}$		
Γ_{402}	$K_1(1400)^+\rho^0$	$< 7.8 \times10^{-4}$	CL=90%	
Γ_{403}	$K_2^*(1430)^+\rho^0$	$< 1.5 \times10^{-3}$	CL=90%	
Γ_{404}	$b_1^0K^+ \times B(b_1^0 \to \omega\pi^0)$	$(9.1 \pm 2.0)\times10^{-6}$		
Γ_{405}	$b_1^+K^{*0} \times B(b_1^+ \to \omega\pi^+)$	$< 5.9 \times10^{-6}$	CL=90%	
Γ_{406}	$b_1^0K^{*+} \times B(b_1^0 \to \omega\pi^0)$	$< 6.7 \times10^{-6}$	CL=90%	
Γ_{407}	$K^+\overline{K}^0$	$(1.31 \pm 0.17)\times10^{-6}$		S=1.2
Γ_{408}	$\overline{K}^0K^+\pi^0$	$< 2.4 \times10^{-5}$	CL=90%	
Γ_{409}	$K^+K_S^0K_S^0$	$(1.05 \pm 0.04)\times10^{-5}$		
Γ_{410}	$f_0(980)K^+,\ f_0 \to K_S^0K_S^0$	$(1.47 \pm 0.33)\times10^{-5}$		
Γ_{411}	$f_0(1710)K^+,\ f_0 \to K_S^0K_S^0$	$(4.8 {}^{+4.0}_{-2.6})\times10^{-7}$		
Γ_{412}	$K^+K_S^0K_S^0$ nonresonant	$(2.0 \pm 0.4)\times10^{-5}$		
Γ_{413}	$K_S^0K_S^0\pi^+$	$< 5.1 \times10^{-7}$	CL=90%	
Γ_{414}	$K^+K^-\pi^+$	$(5.2 \pm 0.4)\times10^{-6}$		
Γ_{415}	$K^+K^-\pi^+$ nonresonant	$(1.68 \pm 0.26)\times10^{-6}$		
Γ_{416}	$K^+\overline{K}^*(892)^0$	$(5.9 \pm 0.8)\times10^{-7}$		
Γ_{417}	$K^+\overline{K}_0^*(1430)^0$	$(3.8 \pm 1.3)\times10^{-7}$		
Γ_{418}	$\pi^+(K^+K^-)_{S-wave}$	$(8.5 \pm 0.9)\times10^{-7}$		
Γ_{419}	$K^+K^+\pi^-$	$< 1.1 \times10^{-8}$	CL=90%	
Γ_{420}	$K^+K^+\pi^-$ nonresonant	$< 8.79 \times10^{-5}$	CL=90%	
Γ_{421}	$f_2'(1525)K^+$	$(1.8 \pm 0.5)\times10^{-6}$		S=1.1
Γ_{422}	$K^+f_J(2220)$			
Γ_{423}	$K^{*+}\pi^+K^-$	$< 1.18 \times10^{-5}$	CL=90%	
Γ_{424}	$K^*(892)^+K^*(892)^0$	$(9.1 \pm 2.9)\times10^{-7}$		
Γ_{425}	$K^{*+}K^+\pi^-$	$< 6.1 \times10^{-6}$	CL=90%	
Γ_{426}	$K^+K^-K^+$	$(3.40 \pm 0.14)\times10^{-5}$		S=1.4
Γ_{427}	$K^+\phi$	$(8.8 {}^{+0.7}_{-0.6})\times10^{-6}$		S=1.1
Γ_{428}	$f_0(980)K^+ \times B(f_0(980) \to K^+K^-)$	$(9.4 \pm 3.2)\times10^{-6}$		
Γ_{429}	$a_2(1320)K^+ \times B(a_2(1320) \to K^+K^-)$	$< 1.1 \times10^{-6}$	CL=90%	
Γ_{430}	$X_0(1550)K^+ \times B(X_0(1550) \to K^+K^-)$	$(4.3 \pm 0.7)\times10^{-6}$		
Γ_{431}	$\phi(1680)K^+ \times B(\phi(1680) \to K^+K^-)$	$< 8 \times10^{-7}$	CL=90%	
Γ_{432}	$f_0(1710)K^+ \times B(f_0(1710) \to K^+K^-)$	$(1.1 \pm 0.6)\times10^{-6}$		
Γ_{433}	$K^+K^-K^+$ nonresonant	$(2.38 {}^{+0.28}_{-0.50})\times10^{-5}$		
Γ_{434}	$K^*(892)^+K^+K^-$	$(3.6 \pm 0.5)\times10^{-5}$		
Γ_{435}	$K^*(892)^+\phi$	$(10.0 \pm 2.0)\times10^{-6}$		S=1.7
Γ_{436}	$\phi(K\pi)_0^{*+}$	$(8.3 \pm 1.6)\times10^{-6}$		
Γ_{437}	$\phi K_1(1270)^+$	$(6.1 \pm 1.9)\times10^{-6}$		
Γ_{438}	$\phi K_1(1400)^+$	$< 3.2 \times10^{-6}$	CL=90%	
Γ_{439}	$\phi K^*(1410)^+$	$< 4.3 \times10^{-6}$	CL=90%	
Γ_{440}	$\phi K_0^*(1430)^+$	$(7.0 \pm 1.6)\times10^{-6}$		
Γ_{441}	$\phi K_2^*(1430)^+$	$(8.4 \pm 2.1)\times10^{-6}$		
Γ_{442}	$\phi K_2^*(1770)^+$	$< 1.50 \times10^{-5}$	CL=90%	

Downloaded from https://academic.oup.com/ptep/article/2022/8/083C01/6651666 by KIT Library user on 27 September 2022

Γ_{443}	$\phi K_2^*(1820)^+$	< 1.63	$\times 10^{-5}$	CL=90%
Γ_{444}	$a_1^+ K^{*0}$	< 3.6	$\times 10^{-6}$	CL=90%
Γ_{445}	$K^+ \phi\phi$	(4.2 ± 0.8)	$\times 10^{-6}$	S=2.2
Γ_{446}	$\eta' \eta' K^+$	< 2.5	$\times 10^{-5}$	CL=90%
Γ_{447}	$\omega \phi K^+$	< 1.9	$\times 10^{-6}$	CL=90%
Γ_{448}	$X(1812) K^+ \times B(X \to \omega\phi)$	< 3.2	$\times 10^{-7}$	CL=90%
Γ_{449}	$K^*(892)^+ \gamma$	(3.92 ± 0.22)	$\times 10^{-5}$	S=1.7
Γ_{450}	$K_1(1270)^+ \gamma$	$(4.4 {}^{+0.7}_{-0.6})$	$\times 10^{-5}$	
Γ_{451}	$\eta K^+ \gamma$	(7.9 ± 0.9)	$\times 10^{-6}$	
Γ_{452}	$\eta' K^+ \gamma$	$(2.9 {}^{+1.0}_{-0.9})$	$\times 10^{-6}$	
Γ_{453}	$\phi K^+ \gamma$	(2.7 ± 0.4)	$\times 10^{-6}$	S=1.2
Γ_{454}	$K^+ \pi^- \pi^+ \gamma$	(2.58 ± 0.15)	$\times 10^{-5}$	S=1.3
Γ_{455}	$K^*(892)^0 \pi^+ \gamma$	(2.33 ± 0.12)	$\times 10^{-5}$	
Γ_{456}	$K^+ \rho^0 \gamma$	(8.2 ± 0.9)	$\times 10^{-6}$	
Γ_{457}	$(K^+ \pi^-)_{NR} \pi^+ \gamma$	$(9.9 {}^{+1.7}_{-2.0})$	$\times 10^{-6}$	
Γ_{458}	$K^0 \pi^+ \pi^0 \gamma$	(4.6 ± 0.5)	$\times 10^{-5}$	
Γ_{459}	$K_1(1400)^+ \gamma$	$(10 {}^{+5}_{-4})$	$\times 10^{-6}$	
Γ_{460}	$K^*(1410)^+ \gamma$	$(2.7 {}^{+0.8}_{-0.6})$	$\times 10^{-5}$	
Γ_{461}	$K_0^*(1430)^0 \pi^+ \gamma$	$(1.32 {}^{+0.26}_{-0.32})$	$\times 10^{-6}$	
Γ_{462}	$K_2^*(1430)^+ \gamma$	(1.4 ± 0.4)	$\times 10^{-5}$	
Γ_{463}	$K^*(1680)^+ \gamma$	$(6.7 {}^{+1.7}_{-1.4})$	$\times 10^{-5}$	
Γ_{464}	$K_3^*(1780)^+ \gamma$	< 3.9	$\times 10^{-5}$	CL=90%
Γ_{465}	$K_4^*(2045)^+ \gamma$	< 9.9	$\times 10^{-3}$	CL=90%

Light unflavored meson modes

Γ_{466}	$\rho^+ \gamma$	(9.8 ± 2.5)	$\times 10^{-7}$	
Γ_{467}	$\pi^+ \pi^0$	(5.5 ± 0.4)	$\times 10^{-6}$	S=1.2
Γ_{468}	$\pi^+ \pi^+ \pi^-$	(1.52 ± 0.14)	$\times 10^{-5}$	
Γ_{469}	$\rho^0 \pi^+$	(8.3 ± 1.2)	$\times 10^{-6}$	
Γ_{470}	$\pi^+ f_0(980),\ f_0 \to \pi^+ \pi^-$	< 1.5	$\times 10^{-6}$	CL=90%
Γ_{471}	$\pi^+ f_2(1270)$	$(2.2 {}^{+0.7}_{-0.4})$	$\times 10^{-6}$	
Γ_{472}	$\rho(1450)^0 \pi^+,\ \rho^0 \to \pi^+ \pi^-$	$(1.4 {}^{+0.6}_{-0.9})$	$\times 10^{-6}$	
Γ_{473}	$\rho(1450)^0 \pi^+,\ \rho^0 \to K^+ K^-$	(1.60 ± 0.14)	$\times 10^{-6}$	
Γ_{474}	$f_0(1370) \pi^+,\ f_0 \to \pi^+ \pi^-$	< 4.0	$\times 10^{-6}$	CL=90%
Γ_{475}	$f_0(500) \pi^+,\ f_0 \to \pi^+ \pi^-$	< 4.1	$\times 10^{-6}$	CL=90%
Γ_{476}	$\pi^+ \pi^- \pi^+$ nonresonant	$(5.3 {}^{+1.5}_{-1.1})$	$\times 10^{-6}$	
Γ_{477}	$\pi^+ \pi^0 \pi^0$	< 8.9	$\times 10^{-4}$	CL=90%
Γ_{478}	$\rho^+ \pi^0$	(1.09 ± 0.14)	$\times 10^{-5}$	
Γ_{479}	$\pi^+ \pi^- \pi^+ \pi^0$	< 4.0	$\times 10^{-3}$	CL=90%
Γ_{480}	$\rho^+ \rho^0$	(2.40 ± 0.19)	$\times 10^{-5}$	
Γ_{481}	$\rho^+ f_0(980),\ f_0 \to \pi^+ \pi^-$	< 2.0	$\times 10^{-6}$	CL=90%
Γ_{482}	$a_1(1260)^+ \pi^0$	(2.6 ± 0.7)	$\times 10^{-5}$	
Γ_{483}	$a_1(1260)^0 \pi^+$	(2.0 ± 0.6)	$\times 10^{-5}$	
Γ_{484}	$\omega \pi^+$	(6.9 ± 0.5)	$\times 10^{-6}$	
Γ_{485}	$\omega \rho^+$	(1.59 ± 0.21)	$\times 10^{-5}$	
Γ_{486}	$\eta \pi^+$	(4.02 ± 0.27)	$\times 10^{-6}$	
Γ_{487}	$\eta \rho^+$	(7.0 ± 2.9)	$\times 10^{-6}$	S=2.8
Γ_{488}	$\eta' \pi^+$	(2.7 ± 0.9)	$\times 10^{-6}$	S=1.9
Γ_{489}	$\eta' \rho^+$	(9.7 ± 2.2)	$\times 10^{-6}$	
Γ_{490}	$\phi \pi^+$	(3.2 ± 1.5)	$\times 10^{-8}$	
Γ_{491}	$\phi \rho^+$	< 3.0	$\times 10^{-6}$	CL=90%
Γ_{492}	$a_0(980)^0 \pi^+,\ a_0^0 \to \eta \pi^0$	< 5.8	$\times 10^{-6}$	CL=90%
Γ_{493}	$a_0(980)^+ \pi^0,\ a_0^+ \to \eta \pi^+$	< 1.4	$\times 10^{-6}$	CL=90%
Γ_{494}	$\pi^+ \pi^+ \pi^+ \pi^- \pi^-$	< 8.6	$\times 10^{-4}$	CL=90%
Γ_{495}	$\rho^0 a_1(1260)^+$	< 6.2	$\times 10^{-4}$	CL=90%
Γ_{496}	$\rho^0 a_2(1320)^+$	< 7.2	$\times 10^{-4}$	CL=90%
Γ_{497}	$b_1^0 \pi^+,\ b_1^0 \to \omega \pi^0$	(6.7 ± 2.0)	$\times 10^{-6}$	
Γ_{498}	$b_1^+ \pi^0,\ b_1^+ \to \omega \pi^+$	< 3.3	$\times 10^{-6}$	CL=90%
Γ_{499}	$\pi^+ \pi^+ \pi^+ \pi^- \pi^- \pi^0$	< 6.3	$\times 10^{-3}$	CL=90%
Γ_{500}	$b_1^+ \rho^0,\ b_1^+ \to \omega \pi^+$	< 5.2	$\times 10^{-6}$	CL=90%
Γ_{501}	$a_1(1260)^+ a_1(1260)^0$	< 1.3	%	CL=90%
Γ_{502}	$b_1^0 \rho^+,\ b_1^0 \to \omega \pi^0$	< 3.3	$\times 10^{-6}$	CL=90%

Charged particle ($h^{\pm}$) modes

$h^{\pm} = K^{\pm}$ or $\pi^{\pm}$

Γ_{503}	$h^+ \pi^0$	$(1.6 {}^{+0.7}_{-0.6})$	$\times 10^{-5}$	
Γ_{504}	ωh^+	$(1.38 {}^{+0.27}_{-0.24})$	$\times 10^{-5}$	
Γ_{505}	$h^+ X^0$ (Familon)	< 4.9	$\times 10^{-5}$	CL=90%
Γ_{506}	$K^+ X^0,\ X^0 \to \mu^+ \mu^-$	< 1	$\times 10^{-7}$	CL=95%

Baryon modes

Γ_{507}	$p \overline{p} \pi^+$	(1.62 ± 0.20)	$\times 10^{-6}$	
Γ_{508}	$p \overline{p} \pi^+$ nonresonant	< 5.3	$\times 10^{-5}$	CL=90%
Γ_{509}	$p \overline{p} \pi^+ \pi^0$	(4.6 ± 1.3)	$\times 10^{-6}$	
Γ_{510}	$p \overline{p} \pi^+ \pi^+ \pi^-$			
Γ_{511}	$p \overline{p} K^+$	(5.9 ± 0.5)	$\times 10^{-6}$	S=1.5
Γ_{512}	$\Theta(1710)^{++} \overline{p},\ \Theta^{++} \to p K^+$ [g]	< 9.1	$\times 10^{-8}$	CL=90%
Γ_{513}	$f_J(2220) K^+,\ f_J \to p \overline{p}$ [g]	< 4.1	$\times 10^{-7}$	CL=90%
Γ_{514}	$p \overline{\Lambda}(1520)$	(3.1 ± 0.6)	$\times 10^{-7}$	
Γ_{515}	$p \overline{p} K^+$ nonresonant	< 8.9	$\times 10^{-5}$	CL=90%
Γ_{516}	$p \overline{p} K^*(892)^+$	$(3.6 {}^{+0.8}_{-0.7})$	$\times 10^{-6}$	
Γ_{517}	$f_J(2220) K^{*+},\ f_J \to p \overline{p}$	< 7.7	$\times 10^{-7}$	CL=90%
Γ_{518}	$p \overline{\Lambda}$	$(2.4 {}^{+1.0}_{-0.9})$	$\times 10^{-7}$	
Γ_{519}	$p \overline{\Lambda} \gamma$	$(2.4 {}^{+0.5}_{-0.4})$	$\times 10^{-6}$	
Γ_{520}	$p \overline{\Lambda} \pi^0$	$(3.0 {}^{+0.7}_{-0.6})$	$\times 10^{-6}$	
Γ_{521}	$p \overline{\Sigma}(1385)^0$	< 4.7	$\times 10^{-7}$	CL=90%
Γ_{522}	$\Delta^+ \overline{\Lambda}$	< 8.2	$\times 10^{-7}$	CL=90%
Γ_{523}	$p \overline{\Sigma} \gamma$	< 4.6	$\times 10^{-6}$	CL=90%
Γ_{524}	$p \overline{\Lambda} \pi^+ \pi^-$	(1.13 ± 0.13)	$\times 10^{-5}$	
Γ_{525}	$p \overline{\Lambda} \pi^+ \pi^-$ nonresonant	(5.9 ± 1.1)	$\times 10^{-6}$	
Γ_{526}	$p \overline{\Lambda} \rho^0,\ \rho^0 \to \pi^+ \pi^-$	(4.8 ± 0.9)	$\times 10^{-6}$	
Γ_{527}	$p \overline{\Lambda} f_2(1270),\ f_2 \to \pi^+ \pi^-$	(2.0 ± 0.8)	$\times 10^{-6}$	
Γ_{528}	$p \overline{\Lambda} K^+ K^-$	(4.1 ± 0.7)	$\times 10^{-6}$	
Γ_{529}	$p \overline{\Lambda} \phi$	(8.0 ± 2.2)	$\times 10^{-7}$	
Γ_{530}	$\overline{p} \Lambda K^+ K^-$	(3.7 ± 0.6)	$\times 10^{-6}$	
Γ_{531}	$\Lambda \overline{\Lambda} \pi^+$	< 9.4	$\times 10^{-7}$	CL=90%
Γ_{532}	$\Lambda \overline{\Lambda} K^+$	(3.4 ± 0.6)	$\times 10^{-6}$	
Γ_{533}	$\Lambda \overline{\Lambda} K^{*+}$	$(2.2 {}^{+1.2}_{-0.9})$	$\times 10^{-6}$	
Γ_{534}	$\Lambda(1520) \overline{\Lambda} K^+$	(2.2 ± 0.7)	$\times 10^{-6}$	
Γ_{535}	$\Lambda \overline{\Lambda}(1520) K^+$	< 2.08	$\times 10^{-6}$	
Γ_{536}	$\overline{\Delta}^0 p$	< 1.38	$\times 10^{-6}$	CL=90%
Γ_{537}	$\Delta^{++} \overline{p}$	< 1.4	$\times 10^{-7}$	CL=90%
Γ_{538}	$D^+ p \overline{p}$	< 1.5	$\times 10^{-5}$	CL=90%
Γ_{539}	$D^*(2010)^+ p \overline{p}$	< 1.5	$\times 10^{-5}$	CL=90%
Γ_{540}	$\overline{D}^0 p \overline{p} \pi^+$	(3.72 ± 0.27)	$\times 10^{-4}$	
Γ_{541}	$\overline{D}^{*0} p \overline{p} \pi^+$	(3.73 ± 0.32)	$\times 10^{-4}$	
Γ_{542}	$D^- p \overline{p} \pi^+ \pi^-$	(1.66 ± 0.30)	$\times 10^{-4}$	
Γ_{543}	$D^{*-} p \overline{p} \pi^+ \pi^-$	(1.86 ± 0.25)	$\times 10^{-4}$	
Γ_{544}	$p \overline{\Lambda}^0 \overline{D}^0$	(1.43 ± 0.32)	$\times 10^{-5}$	
Γ_{545}	$p \overline{\Lambda}^0 \overline{D}^*(2007)^0$	< 5	$\times 10^{-5}$	CL=90%
Γ_{546}	$\overline{\Lambda}_c^- p \pi^+$	(2.3 ± 0.4)	$\times 10^{-4}$	S=2.2
Γ_{547}	$\overline{\Lambda}_c^- \Delta(1232)^{++}$	< 1.9	$\times 10^{-5}$	CL=90%
Γ_{548}	$\overline{\Lambda}_c^- \Delta_X(1600)^{++}$	(4.7 ± 1.0)	$\times 10^{-5}$	
Γ_{549}	$\overline{\Lambda}_c^- \Delta_X(2420)^{++}$	(3.7 ± 0.8)	$\times 10^{-5}$	
Γ_{550}	$(\overline{\Lambda}_c^- p)_s \pi^+$ [h]	(3.1 ± 0.7)	$\times 10^{-5}$	
Γ_{551}	$\overline{\Sigma}_c(2520)^0 p$	< 3	$\times 10^{-6}$	CL=90%
Γ_{552}	$\overline{\Sigma}_c(2800)^0 p$	(2.6 ± 0.9)	$\times 10^{-5}$	
Γ_{553}	$\overline{\Lambda}_c^- p \pi^+ \pi^0$	(1.8 ± 0.6)	$\times 10^{-3}$	
Γ_{554}	$\overline{\Lambda}_c^- p \pi^+ \pi^+ \pi^-$	(2.2 ± 0.7)	$\times 10^{-3}$	
Γ_{555}	$\overline{\Lambda}_c^- p \pi^+ \pi^+ \pi^- \pi^0$	< 1.34	%	CL=90%
Γ_{556}	$\Lambda_c^+ \Lambda_c^- K^+$	(4.9 ± 0.7)	$\times 10^{-4}$	
Γ_{557}	$\Xi_c(2930) \Lambda_c^+,\ \Xi_c \to K^+ \Lambda_c^-$	(1.7 ± 0.5)	$\times 10^{-4}$	
Γ_{558}	$\overline{\Sigma}_c(2455)^0 p$	(2.9 ± 0.7)	$\times 10^{-5}$	
Γ_{559}	$\overline{\Sigma}_c(2455)^0 p \pi^0$	(3.5 ± 1.1)	$\times 10^{-4}$	
Γ_{560}	$\overline{\Sigma}_c(2455)^0 p \pi^- \pi^+$	(3.5 ± 1.1)	$\times 10^{-4}$	
Γ_{561}	$\overline{\Sigma}_c(2455)^{--} p \pi^+ \pi^+$	(2.37 ± 0.20)	$\times 10^{-4}$	
Γ_{562}	$\overline{\Lambda}_c(2593)^- / \overline{\Lambda}_c(2625)^- p \pi^+$	< 1.9	$\times 10^{-4}$	CL=90%
Γ_{563}	$\overline{\Xi}_c^0 \Lambda_c^+$	(9.5 ± 2.3)	$\times 10^{-4}$	
Γ_{564}	$\overline{\Xi}_c^0 \Lambda_c^+,\ \overline{\Xi}_c^0 \to \overline{\Xi}^+ \pi^-$	(1.76 ± 0.29)	$\times 10^{-5}$	
Γ_{565}	$\overline{\Xi}_c^0 \Lambda_c^+,\ \overline{\Xi}_c^0 \to \Lambda K^+ \pi^-$	(1.14 ± 0.26)	$\times 10^{-5}$	
Γ_{566}	$\overline{\Xi}_c^0 \Lambda_c^+,\ \overline{\Xi}_c^0 \to p K^- K^- \pi^+$	(5.5 ± 1.9)	$\times 10^{-6}$	
Γ_{567}	$\Lambda_c^+ \overline{\Xi}_c^{\prime 0}$	< 6.5	$\times 10^{-4}$	CL=90%
Γ_{568}	$\Lambda_c^+ \overline{\Xi}_c(2645)^0$	< 7.9	$\times 10^{-4}$	CL=90%
Γ_{569}	$\Lambda_c^+ \overline{\Xi}_c(2790)^0$	(1.1 ± 0.4)	$\times 10^{-3}$	

Downloaded from https://academic.oup.com/ptep/article/2022/8/083C01/6651666 by KIT Library user on 27 September 2022

Lepton Family number (*LF*) or Lepton number (*L*) or Baryon number (*B*) violating modes, or/and $\Delta B = 1$ weak neutral current (*B1*) modes

Γ_{570}	$\pi^+ \ell^+ \ell^-$	*B1*		< 4.9	$\times 10^{-8}$	CL=90%
Γ_{571}	$\pi^+ e^+ e^-$	*B1*		< 8.0	$\times 10^{-8}$	CL=90%
Γ_{572}	$\pi^+ \mu^+ \mu^-$	*B1*		(1.78 ± 0.23)	$\times 10^{-8}$	
Γ_{573}	$\pi^+ \nu \overline{\nu}$	*B1*		< 1.4	$\times 10^{-5}$	CL=90%
Γ_{574}	$K^+ \ell^+ \ell^-$	*B1*	[a]	(4.7 ± 0.5)	$\times 10^{-7}$	S=2.3
Γ_{575}	$K^+ e^+ e^-$	*B1*		(5.6 ± 0.6)	$\times 10^{-7}$	
Γ_{576}	$K^+ \mu^+ \mu^-$	*B1*		(4.53 ± 0.35)	$\times 10^{-7}$	S=1.8
Γ_{577}	$K^+ \mu^+ \mu^-$ nonresonant	*B1*		(4.37 ± 0.27)	$\times 10^{-7}$	
Γ_{578}	$K^+ \tau^+ \tau^-$	*B1*		< 2.25	$\times 10^{-3}$	CL=90%
Γ_{579}	$K^+ \overline{\nu} \nu$	*B1*		< 1.6	$\times 10^{-5}$	CL=90%
Γ_{580}	$\rho^+ \nu \overline{\nu}$	*B1*		< 3.0	$\times 10^{-5}$	CL=90%
Γ_{581}	$K^*(892)^+ \ell^+ \ell^-$	*B1*	[a]	(1.01 ± 0.11)	$\times 10^{-6}$	S=1.1
Γ_{582}	$K^*(892)^+ e^+ e^-$	*B1*		(1.55 $^{+0.40}_{-0.31}$)	$\times 10^{-6}$	
Γ_{583}	$K^*(892)^+ \mu^+ \mu^-$	*B1*		(9.6 ± 1.0)	$\times 10^{-7}$	
Γ_{584}	$K^*(892)^+ \nu \overline{\nu}$	*B1*		< 4.0	$\times 10^{-5}$	CL=90%
Γ_{585}	$K^+ \pi^+ \pi^- \mu^+ \mu^-$	*B1*		(4.3 ± 0.4)	$\times 10^{-7}$	
Γ_{586}	$\phi K^+ \mu^+ \mu^-$	*B1*		(7.9 $^{+2.1}_{-1.7}$)	$\times 10^{-8}$	
Γ_{587}	$\overline{\Lambda} p \nu \overline{\nu}$			< 3.0	$\times 10^{-5}$	CL=90%
Γ_{588}	$\pi^+ e^+ \mu^-$	*LF*		< 6.4	$\times 10^{-3}$	CL=90%
Γ_{589}	$\pi^+ e^- \mu^+$	*LF*		< 6.4	$\times 10^{-3}$	CL=90%
Γ_{590}	$\pi^+ e^\pm \mu^\mp$	*LF*		< 1.7	$\times 10^{-7}$	CL=90%
Γ_{591}	$\pi^+ e^+ \tau^-$	*LF*		< 7.4	$\times 10^{-5}$	CL=90%
Γ_{592}	$\pi^+ e^- \tau^+$	*LF*		< 2.0	$\times 10^{-5}$	CL=90%
Γ_{593}	$\pi^+ e^\pm \tau^\mp$	*LF*		< 7.5	$\times 10^{-5}$	CL=90%
Γ_{594}	$\pi^+ \mu^+ \tau^-$	*LF*		< 6.2	$\times 10^{-5}$	CL=90%
Γ_{595}	$\pi^+ \mu^- \tau^+$	*LF*		< 4.5	$\times 10^{-5}$	CL=90%
Γ_{596}	$\pi^+ \mu^\pm \tau^\mp$	*LF*		< 7.2	$\times 10^{-5}$	CL=90%
Γ_{597}	$K^+ e^+ \mu^-$	*LF*		< 7.0	$\times 10^{-9}$	CL=90%
Γ_{598}	$K^+ e^- \mu^+$	*LF*		< 6.4	$\times 10^{-9}$	CL=90%
Γ_{599}	$K^+ e^\pm \mu^\mp$	*LF*		< 9.1	$\times 10^{-8}$	CL=90%
Γ_{600}	$K^+ e^+ \tau^-$	*LF*		< 4.3	$\times 10^{-5}$	CL=90%
Γ_{601}	$K^+ e^- \tau^+$	*LF*		< 1.5	$\times 10^{-5}$	CL=90%
Γ_{602}	$K^+ e^\pm \tau^\mp$	*LF*		< 3.0	$\times 10^{-5}$	CL=90%
Γ_{603}	$K^+ \mu^+ \tau^-$	*LF*		< 4.5	$\times 10^{-5}$	CL=90%
Γ_{604}	$K^+ \mu^- \tau^+$	*LF*		< 2.8	$\times 10^{-5}$	CL=90%
Γ_{605}	$K^+ \mu^\pm \tau^\mp$	*LF*		< 4.8	$\times 10^{-5}$	CL=90%
Γ_{606}	$K^*(892)^+ e^+ \mu^-$	*LF*		< 1.3	$\times 10^{-6}$	CL=90%
Γ_{607}	$K^*(892)^+ e^- \mu^+$	*LF*		< 9.9	$\times 10^{-7}$	CL=90%
Γ_{608}	$K^*(892)^+ e^\pm \mu^\mp$	*LF*		< 1.4	$\times 10^{-6}$	CL=90%
Γ_{609}	$\pi^- e^+ e^+$	*L*		< 2.3	$\times 10^{-8}$	CL=90%
Γ_{610}	$\pi^- \mu^+ \mu^+$	*L*		< 4.0	$\times 10^{-9}$	CL=95%
Γ_{611}	$\pi^- e^+ \mu^+$	*L*		< 1.5	$\times 10^{-7}$	CL=90%
Γ_{612}	$\rho^- e^+ e^+$	*L*		< 1.7	$\times 10^{-7}$	CL=90%
Γ_{613}	$\rho^- \mu^+ \mu^+$	*L*		< 4.2	$\times 10^{-7}$	CL=90%
Γ_{614}	$\rho^- e^+ \mu^+$	*L*		< 4.7	$\times 10^{-7}$	CL=90%
Γ_{615}	$K^- e^+ e^+$	*L*		< 3.0	$\times 10^{-8}$	CL=90%
Γ_{616}	$K^- \mu^+ \mu^+$	*L*		< 4.1	$\times 10^{-8}$	CL=90%
Γ_{617}	$K^- e^+ \mu^+$	*L*		< 1.6	$\times 10^{-7}$	CL=90%
Γ_{618}	$K^*(892)^- e^+ e^+$	*L*		< 4.0	$\times 10^{-7}$	CL=90%
Γ_{619}	$K^*(892)^- \mu^+ \mu^+$	*L*		< 5.9	$\times 10^{-7}$	CL=90%
Γ_{620}	$K^*(892)^- e^+ \mu^+$	*L*		< 3.0	$\times 10^{-7}$	CL=90%
Γ_{621}	$D^- e^+ e^+$	*L*		< 2.6	$\times 10^{-6}$	CL=90%
Γ_{622}	$D^- e^+ \mu^+$	*L*		< 1.8	$\times 10^{-6}$	CL=90%
Γ_{623}	$D^- \mu^+ \mu^+$	*L*		< 6.9	$\times 10^{-7}$	CL=95%
Γ_{624}	$D^{*-} \mu^+ \mu^+$	*L*		< 2.4	$\times 10^{-6}$	CL=95%
Γ_{625}	$D_s^- \mu^+ \mu^+$	*L*		< 5.8	$\times 10^{-7}$	CL=95%
Γ_{626}	$\overline{D}^0 \pi^- \mu^+ \mu^+$	*L*		< 1.5	$\times 10^{-6}$	CL=95%
Γ_{627}	$\Lambda^0 \mu^+$	*L,B*		< 6	$\times 10^{-8}$	CL=90%
Γ_{628}	$\Lambda^0 e^+$	*L,B*		< 3.2	$\times 10^{-8}$	CL=90%
Γ_{629}	$\overline{\Lambda}^0 \mu^+$	*L,B*		< 6	$\times 10^{-8}$	CL=90%
Γ_{630}	$\overline{\Lambda}^0 e^+$	*L,B*		< 8	$\times 10^{-8}$	CL=90%

[a] An ℓ indicates an e or a μ mode, not a sum over these modes.

[b] An $CP(\pm 1)$ indicates the CP=+1 and CP=−1 eigenstates of the D^0-$\overline{D}^0$ system.

[c] D denotes D^0 or $\overline{D}^0$.

[d] D^0_{CP+} decays into $D^0 \pi^0$ with the D^0 reconstructed in CP-even eigenstates $K^+ K^-$ and $\pi^+ \pi^-$.

[e] $\overline{D}^{**}$ represents an excited state with mass $2.2 < M < 2.8$ GeV/c^2.

[f] $\chi_{c1}(3872)^+$ is a hypothetical charged partner of the $\chi_{c1}(3872)$.

[g] $\Theta(1710)^{++}$ is a possible narrow pentaquark state and $G(2220)$ is a possible glueball resonance.

[h] $(\overline{\Lambda}_c^- p)_s$ denotes a low-mass enhancement near 3.35 GeV/c^2.

CONSTRAINED FIT INFORMATION

An overall fit to 3 branching ratios uses 6 measurements and one constraint to determine 3 parameters. The overall fit has a $\chi^2 =$ 3.7 for 4 degrees of freedom.

The following *off-diagonal* array elements are the correlation coefficients $\langle \delta x_i \delta x_j \rangle / (\delta x_i \cdot \delta x_j)$, in percent, from the fit to the branching fractions, $x_i \equiv \Gamma_i / \Gamma_{total}$. The fit constrains the x_i whose labels appear in this array to sum to one.

x_{407}	10	
	x_{346}	

CONSTRAINED FIT INFORMATION

An overall fit to 18 branching ratios uses 58 measurements and one constraint to determine 12 parameters. The overall fit has a $\chi^2 = 64.2$ for 47 degrees of freedom.

The following *off-diagonal* array elements are the correlation coefficients $\langle \delta x_i \delta x_j \rangle / (\delta x_i \cdot \delta x_j)$, in percent, from the fit to the branching fractions, $x_i \equiv \Gamma_i / \Gamma_{total}$. The fit constrains the x_i whose labels appear in this array to sum to one.

x_8	33									
x_{51}	0	0								
x_{108}	0	0	7							
x_{149}	0	0	1	13						
x_{276}	0	0	0	0	0					
x_{281}	0	0	0	0	0	0				
x_{299}	0	0	0	0	0	86	0			
x_{311}	0	0	0	0	0	40	0	35		
x_{576}	0	0	0	0	0	14	0	12	6	
x_{583}	0	0	0	0	0	0	5	0	0	0
	x_7	x_8	x_{51}	x_{108}	x_{149}	x_{276}	x_{281}	x_{299}	x_{311}	x_{576}

B^+ BRANCHING RATIOS

$\Gamma(\ell^+ \nu_\ell X)/\Gamma_{total}$ — Γ_1/Γ

"OUR EVALUATION" is an average using rescaled values of the data listed below. The average and rescaling were performed by the Heavy Flavor Averaging Group (HFLAV) and are described at https://hflav.web.cern.ch/. The averaging/rescaling procedure takes into account correlations between the measurements.

VALUE (units 10^{-2})	DOCUMENT ID		TECN	COMMENT
10.99±0.28 OUR EVALUATION				
10.76±0.32 OUR AVERAGE Error includes scale factor of 1.1.				
11.17±0.25±0.28	[1] URQUIJO	07	BELL	$e^+e^- \to \Upsilon(4S)$
10.28±0.26±0.39	[2] AUBERT,B	06Y	BABR	$e^+e^- \to \Upsilon(4S)$
10.25±0.57±0.65	[3] ARTUSO	97	CLE2	$e^+e^- \to \Upsilon(4S)$
• • • We do not use the following data for averages, fits, limits, etc. • • •				
11.15±0.26±0.41	[4] OKABE	05	BELL	Repl. by URQUIJO 07
10.1 ±1.8 ±1.5	ATHANAS	94	CLE2	Sup. by ARTUSO 97

[1] URQUIJO 07 report a measurement of (10.34 ± 023 ± 0.25)% for the partial branching fraction of $B^+ \to e^+ \nu_e X_c$ decay with electron energy above 0.6 GeV. We converted the result to $B^+ \to e^+ \nu_e X$ branching fraction.

[2] The measurements are obtained for charged and neutral B mesons partial rates of semileptonic decay to electrons with momentum above 0.6 GeV/c in the B rest frame. The best precision on the ratio is achieved for a momentum threshold of 1.0 GeV: B($B^+ \to e^+ \nu_e X$) / B($B^0 \to e^+ \nu_e X$) = 1.074 ± 0.041 ± 0.026.

[3] ARTUSO 97 uses partial reconstruction of $B \to D^* \ell \nu_\ell$ and inclusive semileptonic branching ratio from BARISH 96B (0.1049 ± 0.0017 ± 0.0043).

[4] The measurements are obtained for charged and neutral B mesons partial rates of semileptonic decay to electrons with momentum above 0.6 GeV/c in the B rest frame, and their ratio of B($B^+ \to e^+ \nu_e X$)/B($B^0 \to e^+ \nu_e X$) = 1.08 ± 0.05 ± 0.02.

$\Gamma(e^+ \nu_e X_c)/\Gamma_{total}$ — Γ_2/Γ

VALUE (units 10^{-2})	DOCUMENT ID		TECN	COMMENT
10.79±0.25±0.27	[1] URQUIJO	07	BELL	$e^+e^- \to \Upsilon(4S)$

[1] Measure the independent B^+ and B^0 partial branching fractions with electron threshold energies of 0.4 GeV.

$\Gamma(\ell^+ \nu_\ell X_u)/\Gamma_{total}$ — Γ_3/Γ

Requires $E^*_\ell > 1$ GeV, where E^*_ℓ is letpon energy in B rest frame.

VALUE (units 10^{-3})	DOCUMENT ID		TECN	COMMENT
1.65±0.10±0.18	[1] CAO	21A	BELL	$e^+e^- \to \Upsilon(4S)$

[1] The correlation of 50% with B($B^0 \to \ell^+ \nu_\ell X_u$)(letpon energy in B rest frame $E^*_\ell >$ 1 GeV) was reported.

Downloaded from https://academic.oup.com/ptep/article/2022/8/083C01/6651666 by KIT Library user on 27 September 2022

$\Gamma(\overline{D}^0 \ell^+ \nu_\ell)/\Gamma_{total}$ — Γ_5/Γ

"OUR EVALUATION" is an average using rescaled values of the data listed below. The average and rescaling were performed by the Heavy Flavor Averaging Group (HFLAV) and are described at https://hflav.web.cern.ch/. The averaging/rescaling procedure takes into account correlations between the measurements. $\ell = e$ or μ, not sum over e and μ modes.

VALUE (%)	DOCUMENT ID		TECN	COMMENT
2.30±0.09 OUR EVALUATION				
2.29±0.08 OUR AVERAGE				
2.29±0.08±0.09	[1] AUBERT	10	BABR	$e^+e^- \to \Upsilon(4S)$
2.34±0.03±0.13	AUBERT	09A	BABR	$e^+e^- \to \Upsilon(4S)$
2.21±0.13±0.19	[2] BARTELT	99	CLE2	$e^+e^- \to \Upsilon(4S)$
1.6 ±0.6 ±0.3	[3] FULTON	91	CLEO	$e^+e^- \to \Upsilon(4S)$
• • • We do not use the following data for averages, fits, limits, etc. • • •				
2.33±0.09±0.09	[1] AUBERT	08Q	BABR	Repl. by AUBERT 09A
1.94±0.15±0.34	[4] ATHANAS	97	CLE2	Repl. by BARTELT 99

[1] Uses a fully reconstructed B meson as a tag on the recoil side.
[2] Assumes equal production of B^+ and B^0 at the $\Upsilon(4S)$.
[3] FULTON 91 assumes equal production of $B^0\overline{B}^0$ and B^+B^- at the $\Upsilon(4S)$.
[4] ATHANAS 97 uses missing energy and missing momentum to reconstruct neutrino.

$\Gamma(\overline{D}^0 \ell^+ \nu_\ell)/\Gamma(\ell^+ \nu_\ell X)$ — Γ_5/Γ_1

VALUE	DOCUMENT ID		TECN	COMMENT
0.255±0.009±0.009	[1] AUBERT	10	BABR	$e^+e^- \to \Upsilon(4S)$

[1] Uses a fully reconstructed B meson on the recoil side.

$\Gamma(\overline{D}^0 \ell^+ \nu_\ell)/\Gamma(D \ell^+ \nu_\ell X)$ — Γ_5/Γ_4

VALUE	DOCUMENT ID		TECN	COMMENT
0.230±0.020 OUR AVERAGE				
0.25 ±0.06	[1] AAIJ	19AC	LHCB	pp at 7 and 8 TeV
0.227±0.014±0.016	[2] AUBERT	07AN	BABR	$e^+e^- \to \Upsilon(4S)$

[1] The relative branching fractions of $B^- \to D^0$, D^{*0}, D^{**0} in the $B^- \to D^0 X \mu^- \overline{\nu}$ channel are determined by fitting the distribution of the missing mass in $\overline{B}^{*0}_{s2} \to B^- K^+$ decays.
[2] Uses a fully reconstructed B meson on the recoil side.

$\Gamma(\overline{D}^0 \tau^+ \nu_\tau)/\Gamma_{total}$ — Γ_6/Γ

VALUE (units 10^{-2})	DOCUMENT ID		TECN	COMMENT
0.77±0.22±0.12	[1] BOZEK	10	BELL	$e^+e^- \to \Upsilon(4S)$
• • • We do not use the following data for averages, fits, limits, etc. • • •				
0.67±0.37±0.13	[2] AUBERT	08N	BABR	Repl. by AUBERT 09S

[1] Assumes equal production of B^+ and B^0 at the $\Upsilon(4S)$.
[2] Uses a fully reconstructed B meson as a tag on the recoil side.

$\Gamma(\overline{D}^0 \tau^+ \nu_\tau)/\Gamma(\overline{D}^0 \ell^+ \nu_\ell)$ — Γ_6/Γ_5

VALUE	DOCUMENT ID		TECN	COMMENT
0.429±0.082±0.052	[1,2] LEES	12D	BABR	$e^+e^- \to \Upsilon(4S)$
• • • We do not use the following data for averages, fits, limits, etc. • • •				
0.314±0.170±0.049	[1] AUBERT	09S	BABR	Repl. by LEES 12D

[1] Uses a fully reconstructed B meson as a tag on the recoil side.
[2] Uses $\tau^+ \to e^+\nu_e\overline{\nu}_\tau$ and $\tau^+ \to \mu^+\nu_\mu\overline{\nu}_\tau$ and e^+ or μ^+ as ℓ^+.

$\Gamma(\overline{D}^*(2007)^0 \ell^+ \nu_\ell)/\Gamma_{total}$ — Γ_7/Γ

"OUR EVALUATION" is an average using rescaled values of the data listed below. The average and rescaling were performed by the Heavy Flavor Averaging Group (HFLAV) and are described at https://hflav.web.cern.ch/. The averaging/rescaling procedure takes into account correlations between the measurements. $\ell = e$ or μ, not sum over e and μ modes.

VALUE (%)	EVTS	DOCUMENT ID		TECN	COMMENT
5.58±0.22 OUR EVALUATION					
5.60±0.26 OUR FIT Error includes scale factor of 1.5.					
5.58±0.26 OUR AVERAGE Error includes scale factor of 1.5. See the ideogram below.					
5.40±0.02±0.21		AUBERT	09A	BABR	$e^+e^- \to \Upsilon(4S)$
5.56±0.08±0.41		[1] AUBERT	08AT	BABR	$e^+e^- \to \Upsilon(4S)$
6.50±0.20±0.43		[2] ADAM	03	CLE2	$e^+e^- \to \Upsilon(4S)$
6.6 ±1.6 ±1.5		[3] ALBRECHT	92C	ARG	$e^+e^- \to \Upsilon(4S)$
• • • We do not use the following data for averages, fits, limits, etc. • • •					
5.83±0.15±0.30		[4] AUBERT	08Q	BABR	Repl. by AUBERT 09A
6.50±0.20±0.43		[5] BRIERE	02	CLE2	$e^+e^- \to \Upsilon(4S)$
5.13±0.54±0.64	302	[6] BARISH	95	CLE2	Repl. by ADAM 03
seen	398	[7] SANGHERA	93	CLE2	$e^+e^- \to \Upsilon(4S)$
4.1 $^{+0.8}_{-0.9}$ ±0.8		[8] FULTON	91	CLEO	$e^+e^- \to \Upsilon(4S)$
7.0 ±1.8 ±1.4		[9] ANTREASYAN	90B	CBAL	$e^+e^- \to \Upsilon(4S)$

[1] Measured using the dependence of $B^- \to D^{*0}e^-\overline{\nu}_e$ decay differential rate and the form factor description by CAPRINI 98.
[2] Simultaneous measurements of both $B^0 \to D^*(2010)^-\ell\nu$ and $B^+ \to \overline{D}(2007)^0\ell\nu$.
[3] ALBRECHT 92C reports 0.058±0.014±0.013. We rescale using the method described in STONE 94 but with the updated PDG 94 $B(D^0 \to K^-\pi^+)$. Assumes equal production of $B^0\overline{B}^0$ and B^+B^- at the $\Upsilon(4S)$.
[4] Uses a fully reconstructed B meson as a tag on the recoil side.
[5] The results are based on the same analysis and data sample reported in ADAM 03.
[6] BARISH 95 use $B(D^0 \to K^-\pi^+)$ = (3.91 ± 0.08 ± 0.17)% and $B(D^{*0} \to D^0\pi^0)$ = (63.6 ± 2.3 ± 3.3)%.
[7] Combining $\overline{D}^{*0}\ell^+\nu_\ell$ and $\overline{D}^{*-}\ell^+\nu_\ell$ SANGHERA 93 test $V-A$ structure and fit the decay angular distributions to obtain $A_{FB} = 3/4*(\Gamma^- - \Gamma^+)/\Gamma = 0.14 \pm 0.06 \pm 0.03$. Assuming a value of V_{cb}, they measure V, A_1, and A_2, the three form factors for the $D^*\ell\nu_\ell$ decay, where results are slightly dependent on model assumptions.
[8] Assumes equal production of $B^0\overline{B}^0$ and B^+B^- at the $\Upsilon(4S)$. Uncorrected for D and D^* branching ratio assumptions.
[9] ANTREASYAN 90B is average over B and $\overline{D}^*(2010)$ charge states.

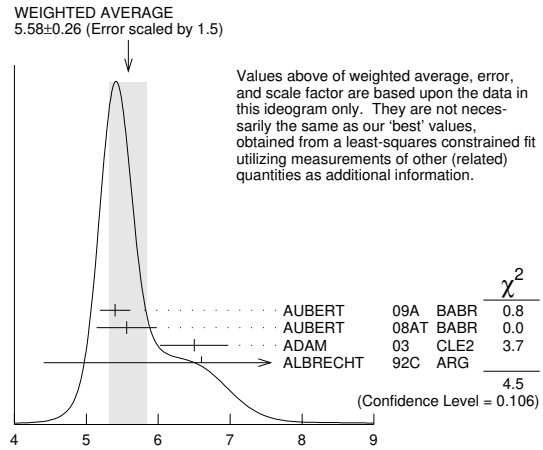

$\Gamma(\overline{D}^*(2007)^0 \ell^+ \nu_\ell)/\Gamma_{total}$ — Γ_7/Γ

$\Gamma(\overline{D}^*(2007)^0 \ell^+ \nu_\ell)/\Gamma(D \ell^+ \nu_\ell X)$ — Γ_7/Γ_4

VALUE	DOCUMENT ID		TECN	COMMENT
0.582±0.018±0.030	[1] AUBERT	07AN	BABR	$e^+e^- \to \Upsilon(4S)$

[1] Uses a fully reconstructed B meson on the recoil side.

$\Gamma(\overline{D}^*(2007)^0 \tau^+ \nu_\tau)/\Gamma_{total}$ — Γ_8/Γ

VALUE (units 10^{-2})	DOCUMENT ID		TECN	COMMENT
1.88±0.20 OUR FIT				
$2.12^{+0.28}_{-0.27}$±0.29	[1] BOZEK	10	BELL	$e^+e^- \to \Upsilon(4S)$
• • • We do not use the following data for averages, fits, limits, etc. • • •				
2.25±0.48±0.28	[2] AUBERT	08N	BABR	Repl. by AUBERT 09S

[1] Assumes equal production of B^+ and B^0 at the $\Upsilon(4S)$.
[2] Uses a fully reconstructed B meson as a tag on the recoil side.

$\Gamma(\overline{D}^*(2007)^0 \tau^+ \nu_\tau)/\Gamma(\overline{D}^*(2007)^0 \ell^+ \nu_\ell)$ — Γ_8/Γ_7

VALUE	DOCUMENT ID		TECN	COMMENT
0.335±0.034 OUR FIT				
0.322±0.032±0.022	[1,2] LEES	12D	BABR	$e^+e^- \to \Upsilon(4S)$
• • • We do not use the following data for averages, fits, limits, etc. • • •				
0.346±0.073±0.034	[1] AUBERT	09S	BABR	Repl. by LEES 12D

[1] Uses a fully reconstructed B meson as a tag on the recoil side.
[2] Uses $\tau^+ \to e^+\nu_e\overline{\nu}_\tau$ and $\tau^+ \to \mu^+\nu_\mu\overline{\nu}_\tau$ and e^+ or μ^+ as ℓ^+.

$\Gamma(D^-\pi^+\ell^+\nu_\ell)/\Gamma_{total}$ — Γ_9/Γ

VALUE (units 10^{-3})	DOCUMENT ID		TECN	COMMENT
4.4 ±0.4 OUR AVERAGE				
4.55±0.27±0.39	VOSSEN	18	BELL	$e^+e^- \to \Upsilon(4S)$
4.2 ±0.6 ±0.3	[1] AUBERT	08Q	BABR	$e^+e^- \to \Upsilon(4S)$
• • • We do not use the following data for averages, fits, limits, etc. • • •				
4.3 ±0.6 ±0.2	[1,2] LIVENTSEV	08	BELL	Repl. by VOSSEN 18
5.6 ±1.0 ±0.2	[3] LIVENTSEV	05	BELL	Repl. by LIVENTSEV 08

[1] Uses a fully reconstructed B meson as a tag on the recoil side.
[2] LIVENTSEV 08 reports $(4.0 \pm 0.4 \pm 0.6) \times 10^{-3}$ from a measurement of $[\Gamma(B^+ \to D^-\pi^+\ell^+\nu_\ell)/\Gamma_{total}]$ / $[B(B^+ \to \overline{D}^0\ell^+\nu_\ell)]$ assuming $B(B^+ \to \overline{D}^0\ell^+\nu_\ell) = (2.15 \pm 0.22) \times 10^{-2}$, which we rescale to our best value $B(B^+ \to \overline{D}^0\ell^+\nu_\ell) = (2.30 \pm 0.09) \times 10^{-2}$. Our first error is their experiment's error and our second error is the systematic error from using our best value.
[3] LIVENTSEV 05 reports $[\Gamma(B^+ \to D^-\pi^+\ell^+\nu_\ell)/\Gamma_{total}]$ / $[B(B^0 \to D^-\ell^+\nu_\ell)]$ = 0.25 ± 0.03 ± 0.03 which we multiply by our best value $B(B^0 \to D^-\ell^+\nu_\ell) = (2.24 \pm 0.09) \times 10^{-2}$. Our first error is their experiment's error and our second error is the systematic error from using our best value.

$\Gamma(\overline{D}^*_0(2420)^0 \ell^+ \nu_\ell, \overline{D}^{*0}_0 \to D^-\pi^+)/\Gamma_{total}$ — Γ_{10}/Γ

VALUE (units 10^{-3})	DOCUMENT ID		TECN	COMMENT
2.5±0.5 OUR AVERAGE				
2.6±0.5±0.4	[1] AUBERT	08BL	BABR	$e^+e^- \to \Upsilon(4S)$
2.4±0.4±0.6	[1] LIVENTSEV	08	BELL	$e^+e^- \to \Upsilon(4S)$

[1] Uses a fully reconstructed B meson as a tag on the recoil side.

Downloaded from https://academic.oup.com/ptep/article/2022/8/083C01/6651666 by KIT Library user on 27 September 2022

$\Gamma(\overline{D}_2^*(2460)^0 \ell^+ \nu_\ell, \overline{D}_2^{*0} \to D^- \pi^+)/\Gamma_{total}$ — Γ_{11}/Γ

VALUE (units 10^{-3})	DOCUMENT ID		TECN	COMMENT
1.53±0.16 OUR AVERAGE				
1.42±0.15±0.15	[1] AUBERT	09Y	BABR	$e^+e^- \to \Upsilon(4S)$
1.5 ±0.2 ±0.2	[2] AUBERT	08BL	BABR	$e^+e^- \to \Upsilon(4S)$
2.2 ±0.3 ±0.4	[2] LIVENTSEV	08	BELL	$e^+e^- \to \Upsilon(4S)$

[1] Uses a simultaneous fit of all B semileptonic decays without full reconstruction of events. AUBERT 09Y reports $B(B^+ \to \overline{D}_2^*(2460)^0 \ell^+ \nu_\ell) \cdot B(\overline{D}_2^*(2460)^0 \to D^{(*)-}\pi^+) = (2.29 \pm 0.23 \pm 0.21) \times 10^{-3}$ and the authors have provided us the individual measurement.
[2] Uses a fully reconstructed B meson as a tag on the recoil side.

$\Gamma(D^{(*)} n\pi \ell^+ \nu_\ell (n \geq 1))/\Gamma(D \ell^+ \nu_\ell X)$ — Γ_{12}/Γ_4

VALUE	DOCUMENT ID		TECN	COMMENT
0.193±0.022 OUR AVERAGE				
0.21 ±0.07	[1,2] AAIJ	19AC	LHCB	pp at 7 and 8 TeV
0.191±0.013±0.019	[3] AUBERT	07AN	BABR	$e^+e^- \to \Upsilon(4S)$

[1] The relative branching fractions of $B^- \to D^0$, D^{*0}, D^{**0} in the $B^- \to D^0 X \mu^- \overline{\nu}$ channel are determined by fitting the distribution of the missing mass in $\overline{B}_{s2}^{*0} \to B^- K^+$ decays.
[2] In this measurement of $f_{D^{**0}} = B(B^- \to (D^{**0} \to D^0 X)\mu^- \overline{\nu})/B(B^- \to D^0 X \mu^- \overline{\nu})$, D^{**0} refers collectively to L = 1 states $D_0^*(2400)$, $D_1(2420)$, $D_1(2430)$, and $D_2^*(2460)$, as well as other resonances such as radially excited D mesons, and to nonresonant contributions with additional pions.
[3] Uses a fully reconstructed B meson on the recoil side.

$\Gamma(D^{*-} \pi^+ \ell^+ \nu_\ell)/\Gamma_{total}$ — Γ_{13}/Γ

VALUE (units 10^{-3})	DOCUMENT ID		TECN	COMMENT
6.0 ±0.4 OUR AVERAGE				
6.03±0.43±0.38	VOSSEN	18	BELL	$e^+e^- \to \Upsilon(4S)$
5.9 ±0.5 ±0.4	[1] AUBERT	08Q	BABR	$e^+e^- \to \Upsilon(4S)$
• • • We do not use the following data for averages, fits, limits, etc. • • •				
6.8 ±1.1 ±0.3	[1,2] LIVENTSEV	08	BELL	Repl. by VOSSEN 18
6.0 ±1.4 ±0.1	[3,4] LIVENTSEV	05	BELL	Repl. by LIVENTSEV 08

[1] Uses a fully reconstructed B meson as a tag on the recoil side.
[2] LIVENTSEV 08 reports $(6.4 \pm 0.8 \pm 0.9) \times 10^{-3}$ from a measurement of $[\Gamma(B^+ \to D^{*-}\pi^+\ell^+\nu_\ell)/\Gamma_{total}]$ / $[B(B^+ \to \overline{D}^0 \ell^+ \nu_\ell)]$ assuming $B(B^+ \to \overline{D}^0 \ell^+ \nu_\ell) = (2.15 \pm 0.22) \times 10^{-2}$, which we rescale to our best value $B(B^+ \to \overline{D}^0 \ell^+ \nu_\ell) = (2.30 \pm 0.09) \times 10^{-2}$. Our first error is their experiment's error and our second error is the systematic error from using our best value.
[3] Excludes D^{*+} contribution to $D\pi$ modes.
[4] LIVENTSEV 05 reports $[\Gamma(B^+ \to D^{*-}\pi^+\ell^+\nu_\ell)/\Gamma_{total}]$ / $[B(B^0 \to D^*(2010)^-\ell^+\nu_\ell)] = 0.12 \pm 0.02 \pm 0.02$ which we multiply by our best value $B(B^0 \to D^*(2010)^-\ell^+\nu_\ell) = (4.97 \pm 0.12) \times 10^{-2}$. Our first error is their experiment's error and our second error is the systematic error from using our best value.

$\Gamma(\overline{D}_1(2420)^0 \ell^+ \nu_\ell, \overline{D}_1^0 \to D^{*-}\pi^+)/\Gamma_{total}$ — Γ_{14}/Γ

VALUE (units 10^{-3})	DOCUMENT ID		TECN	COMMENT
3.03±0.20 OUR AVERAGE				
2.97±0.17±0.17	[1] AUBERT	09Y	BABR	$e^+e^- \to \Upsilon(4S)$
2.9 ±0.3 ±0.3	[2] AUBERT	08BL	BABR	$e^+e^- \to \Upsilon(4S)$
4.2 ±0.7 ±0.7	[2] LIVENTSEV	08	BELL	$e^+e^- \to \Upsilon(4S)$
3.73±0.85±0.57	[3] ANASTASSOV	98	CLE2	$e^+e^- \to \Upsilon(4S)$

[1] Uses a simultaneous measurement of all B semileptonic decays without full reconstruction of events.
[2] Uses a fully reconstructed B meson as a tag on the recoil side.
[3] Assumes equal production of B^+ and B^0 at the $\Upsilon(4S)$.

$\Gamma(\overline{D}_1'(2430)^0 \ell^+ \nu_\ell, \overline{D}_1'^0 \to D^{*-}\pi^+)/\Gamma_{total}$ — Γ_{15}/Γ

VALUE (units 10^{-3})	CL%	DOCUMENT ID		TECN	COMMENT
2.7±0.4±0.5		[1] AUBERT	08BL	BABR	$e^+e^- \to \Upsilon(4S)$
• • • We do not use the following data for averages, fits, limits, etc. • • •					
<0.7	90	[1] LIVENTSEV	08	BELL	$e^+e^- \to \Upsilon(4S)$

[1] Uses a fully reconstructed B meson as a tag on the recoil side.

$\Gamma(\overline{D}_2^*(2460)^0 \ell^+ \nu_\ell, \overline{D}_2^{*0} \to D^{*-}\pi^+)/\Gamma_{total}$ — Γ_{16}/Γ

VALUE (units 10^{-3})	CL%	DOCUMENT ID		TECN	COMMENT
1.01±0.24 OUR AVERAGE		Error includes scale factor of 2.0.			
0.87±0.11±0.07		[1] AUBERT	09Y	BABR	$e^+e^- \to \Upsilon(4S)$
1.5 ±0.2 ±0.2		[2] AUBERT	08BL	BABR	$e^+e^- \to \Upsilon(4S)$
1.8 ±0.6 ±0.3		[2] LIVENTSEV	08	BELL	$e^+e^- \to \Upsilon(4S)$
• • • We do not use the following data for averages, fits, limits, etc. • • •					
<1.6	90	[3] ANASTASSOV	98	CLE2	$e^+e^- \to \Upsilon(4S)$

[1] Uses a simultaneous fit of all B semileptonic decays without full reconstruction of events. AUBERT 09Y reports $B(B^+ \to \overline{D}_2^*(2460)^0 \ell^+ \nu_\ell) \cdot B(\overline{D}_2^*(2460)^0 \to D^{(*)-}\pi^+) = (2.29 \pm 0.23 \pm 0.21) \times 10^{-3}$ and the authors have provided us the individual measurement.
[2] Uses a fully reconstructed B meson as a tag on the recoil side.
[3] Assumes equal production of B^+ and B^0 at the $\Upsilon(4S)$.

$\Gamma(\overline{D}^0 \pi^+ \pi^- \ell^+ \nu_\ell)/\Gamma(\overline{D}^0 \ell^+ \nu_\ell)$ — Γ_{17}/Γ_5

VALUE (units 10^{-2})	DOCUMENT ID		TECN	COMMENT
7.1±1.3±0.8	[1] LEES	16	BABR	$e^+e^- \to \Upsilon(4S)$

[1] Measurement used electrons and muons as leptons.

$\Gamma(\overline{D}^{*0} \pi^+ \pi^- \ell^+ \nu_\ell)/\Gamma(\overline{D}^*(2007)^0 \ell^+ \nu_\ell)$ — Γ_{18}/Γ_7

VALUE (units 10^{-2})	DOCUMENT ID		TECN	COMMENT
1.4±0.7±0.4	[1] LEES	16	BABR	$e^+e^- \to \Upsilon(4S)$

[1] Measurement used electrons and muons as leptons.

$\Gamma(D_s^{(*)-} K^+ \ell^+ \nu_\ell)/\Gamma_{total}$ — Γ_{19}/Γ

VALUE (units 10^{-4})	DOCUMENT ID		TECN	COMMENT
6.1 ±1.0 OUR AVERAGE				
5.9 ±1.2 ±1.5	[1] STYPULA	12	BELL	$e^+e^- \to \Upsilon(4S)$
$6.13^{+1.04}_{-1.03} \pm 0.67$	[1] DEL-AMO-SA...	11L	BABR	$e^+e^- \to \Upsilon(4S)$

[1] Assumes equal production of B^+ and B^0 at the $\Upsilon(4S)$.

$\Gamma(D_s^- K^+ \ell^+ \nu_\ell)/\Gamma_{total}$ — Γ_{20}/Γ

VALUE (units 10^{-4})	DOCUMENT ID		TECN	COMMENT
$\mathbf{3.0 \pm 0.9^{+1.1}_{-0.8}}$	[1] STYPULA	12	BELL	$e^+e^- \to \Upsilon(4S)$

[1] Assumes equal production of B^+ and B^0 at the $\Upsilon(4S)$.

$\Gamma(D_s^{*-} K^+ \ell^+ \nu_\ell)/\Gamma_{total}$ — Γ_{21}/Γ

VALUE (units 10^{-4})	DOCUMENT ID		TECN	COMMENT
$\mathbf{2.9 \pm 1.6^{+1.1}_{-1.0}}$	[1,2] STYPULA	12	BELL	$e^+e^- \to \Upsilon(4S)$

[1] Assumes equal production of B^+ and B^0 at the $\Upsilon(4S)$.
[2] STYPULA 12 provides also an upper limit of 0.56×10^{-3} at 90% CL for the same data. Also measures branching fraction of the combined modes of $D_s^- K^+ \ell^+ \nu_\ell$ and $D_s^{*-} K^+ \ell^+ \nu_\ell$ as $B(B^+ \to D_s^{(*)-} K^+ \ell^+ \nu_\ell) = (5.9 \pm 1.2 \pm 1.5) \times 10^{-4}$.

$\Gamma(\pi^0 \ell^+ \nu_\ell)/\Gamma_{total}$ — Γ_{22}/Γ

"OUR EVALUATION" is an average using rescaled values of the data listed below. The average and rescaling were performed by the Heavy Flavor Averaging Group (HFLAV) and are described at https://hflav.web.cern.ch/. The averaging/rescaling procedure takes into account correlations between the measurements.

VALUE (units 10^{-4})	DOCUMENT ID		TECN	COMMENT
0.780±0.027 OUR EVALUATION				
0.748±0.029 OUR AVERAGE				
0.80 ±0.08 ±0.04	[1] SIBIDANOV	13	BELL	$e^+e^- \to \Upsilon(4S)$
0.77 ±0.04 ±0.03	[2] LEES	12AA	BABR	$e^+e^- \to \Upsilon(4S)$
0.705±0.025±0.035	[3] DEL-AMO-SA...	11C	BABR	$e^+e^- \to \Upsilon(4S)$
0.82 ±0.09 ±0.05	[3] AUBERT	08AV	BABR	$e^+e^- \to \Upsilon(4S)$
0.77 ±0.14 ±0.08	[4] HOKUUE	07	BELL	$e^+e^- \to \Upsilon(4S)$
• • • We do not use the following data for averages, fits, limits, etc. • • •				
0.74 ±0.05 ±0.10	[5] AUBERT,B	05O	BABR	Repl. by DEL-AMO-SANCHEZ 11C

[1] The signal events are tagged by a second B meson reconstructed in the fully hadronic decays.
[2] Uses loose neutrino reconstruction technique. Assumes $B(\Upsilon(4S) \to B^+B^-) = (51.6 \pm 0.6)\%$ and $B(\Upsilon(4S) \to B^0\overline{B}^0) = (48.4 \pm 0.6)\%$.
[3] Using the isospin symmetry relation, B^+ and B^0 branching fractions are combined.
[4] The signal events are tagged by a second B meson reconstructed in the semileptonic mode $B \to D^{(*)}\ell\nu_\ell$.
[5] B^+ and B^0 decays combined assuming isospin symmetry. Systematic errors include both experimental and form-factor uncertainties.

$\Gamma(\pi^0 e^+ \nu_e)/\Gamma_{total}$ — Γ_{23}/Γ

VALUE (units 10^{-4})	CL%	DOCUMENT ID		TECN	COMMENT
• • • We do not use the following data for averages, fits, limits, etc. • • •					
0.9±0.2±0.2		[1] ALEXANDER	96T	CLE2	$e^+e^- \to \Upsilon(4S)$
<22	90	ANTREASYAN	90B	CBAL	$e^+e^- \to \Upsilon(4S)$

[1] Derived based in the reported B^0 result by assuming isospin symmetry: $\Gamma(B^0 \to \pi^-\ell^+\nu) = 2\Gamma(B^+ \to \pi^0\ell^+\nu)$.

$\Gamma(\eta \ell^+ \nu_\ell)/\Gamma_{total}$ — Γ_{24}/Γ

VALUE (units 10^{-4})	CL%	DOCUMENT ID		TECN	COMMENT
0.39±0.05 OUR AVERAGE					
0.42±0.11±0.03		[1] BELENO	17	BELL	$e^+e^- \to \Upsilon(4S)$
0.38±0.05±0.05		[2] LEES	12AA	BABR	$e^+e^- \to \Upsilon(4S)$
0.31±0.06±0.08		[2] AUBERT	09Q	BABR	$e^+e^- \to \Upsilon(4S)$
0.64±0.20±0.03		[3] AUBERT	08AV	BABR	$e^+e^- \to \Upsilon(4S)$
• • • We do not use the following data for averages, fits, limits, etc. • • •					
0.36±0.05±0.04		[2] DEL-AMO-SA...	11F	BABR	Repl. by LEES 12AA
<1.01	90	[4] ADAM	07	CLE2	$e^+e^- \to \Upsilon(4S)$
0.84±0.31±0.18		[5] ATHAR	03	CLE2	Repl. by ADAM 07

[1] Uses missing-mass technique by fully reconstructing the hadronic decay chain of the accompanying B.
[2] Uses loose neutrino reconstruction technique. Assumes $B(\Upsilon(4S) \to B^+B^-) = (51.6 \pm 0.6)\%$ and $B(\Upsilon(4S) \to B^0\overline{B}^0) = (48.4 \pm 0.6)\%$.

Downloaded from https://academic.oup.com/ptep/article/2022/8/083C01/6651666 by KIT Library user on 27 September 2022

[3] Assumes equal production of B^+ and B^0 at the $\Upsilon(4S)$.
[4] The B^0 and B^+ results are combined assuming the isospin, B lifetimes, and relative charged/neutral B production at the $\Upsilon(4S)$.
[5] ATHAR 03 reports systematic errors 0.16 ± 0.09, which are experimental systematic and systematic due to model dependence. We combine these in quadrature.

$\Gamma(\eta' \ell^+ \nu_\ell)/\Gamma_{total}$ — Γ_{25}/Γ

VALUE (units 10^{-4})	CL%	DOCUMENT ID		TECN	COMMENT
0.23±0.08 OUR AVERAGE					
$0.24 \pm 0.08 \pm 0.03$		[1] LEES	12AA	BABR	$e^+e^- \to \Upsilon(4S)$
$0.04 \pm 0.22 {}^{+0.05}_{-0.02}$		[2] AUBERT	08AV	BABR	$e^+e^- \to \Upsilon(4S)$
$2.66 \pm 0.80 \pm 0.56$		[3] ADAM	07	CLE2	$e^+e^- \to \Upsilon(4S)$
• • • We do not use the following data for averages, fits, limits, etc. • • •					
<0.72	90	[4] BELENO	17	BELL	$e^+e^- \to \Upsilon(4S)$
$0.24 \pm 0.08 \pm 0.03$		[1] DEL-AMO-SA...	11F	BABR	Repl. by LEES 12AA

[1] Uses loose neutrino reconstruction technique. Assumes $B(\Upsilon(4S) \to B^+B^-) = (51.6 \pm 0.6)\%$ and $B(\Upsilon(4S) \to B^0\overline{B}^0) = (48.4 \pm 0.6)\%$.
[2] Assumes equal production of B^+ and B^0 at the $\Upsilon(4S)$.
[3] The B^0 and B^+ results are combined assuming the isospin, B lifetimes, and relative charged/neutral B production at the $\Upsilon(4S)$. Corresponds to 90% CL interval $(1.20\text{–}4.46) \times 10^{-4}$.
[4] Uses missing-mass technique by fully reconstructing the hadronic decay chain of the accompanying B.

$\Gamma(\omega \ell^+ \nu_\ell)/\Gamma_{total}$ — Γ_{26}/Γ

$\ell = e$ or μ, not sum over e and μ modes.

VALUE (units 10^{-4})	CL%	DOCUMENT ID		TECN	COMMENT
1.19±0.09 OUR AVERAGE					
$1.21 \pm 0.14 \pm 0.08$		[1,2] LEES	13A	BABR	$e^+e^- \to \Upsilon(4S)$
$1.35 \pm 0.21 \pm 0.11$		[3] LEES	13T	BABR	$e^+e^- \to \Upsilon(4S)$
$1.07 \pm 0.16 \pm 0.07$		[4] SIBIDANOV	13	BELL	$e^+e^- \to \Upsilon(4S)$
$1.19 \pm 0.16 \pm 0.09$		[2,5] LEES	12AA	BABR	$e^+e^- \to \Upsilon(4S)$
$1.3 \pm 0.4 \pm 0.4$		[6] SCHWANDA	04	BELL	$e^+e^- \to \Upsilon(4S)$
• • • We do not use the following data for averages, fits, limits, etc. • • •					
$1.14 \pm 0.16 \pm 0.08$		[2] AUBERT	09Q	BABR	Repl. by LEES 13A
<2.1	90	[7] BEAN	93B	CLE2	$e^+e^- \to \Upsilon(4S)$

[1] LEES 13A reports $(1.21 \pm 0.14 \pm 0.08) \times 10^{-4}$ from a measurement of $[\Gamma(B^+ \to \omega\ell^+\nu_\ell)/\Gamma_{total}] \times [B(\omega(782) \to \pi^+\pi^-\pi^0)]$ assuming $B(\omega(782) \to \pi^+\pi^-\pi^0) = (89.2 \pm 0.7) \times 10^{-2}$.
[2] Uses $B(\Upsilon(4S) \to B^+B^-) = (51.6 \pm 0.6)\%$ and $B(\Upsilon(4S) \to B^0\overline{B}^0) = (48.4 \pm 0.6)\%$.
[3] Uses semileptonic tagging. Assumes $B(\omega \to \pi^+\pi^-\pi^0) = (89.2 \pm 0.7)\%$ and that the production ratio of B^+B^- to $B^0\overline{B}^0$ from $\Upsilon(4S)$ is 1.056 ± 0.028. The partial branching fractions in three bins of q^2 are also reported.
[4] The signal events are tagged by a second B meson reconstructed in the fully hadronic decays.
[5] Uses loose neutrino reconstruction technique.
[6] Assumes equal production of B^+ and B^0 at the $\Upsilon(4S)$.
[7] BEAN 93B limit set using ISGW Model. Using isospin and the quark model to combine $\Gamma(\rho^0\ell^+\nu_\ell)$ and $\Gamma(\rho^-\ell^+\nu_\ell)$ with this result, they obtain a limit $<(1.6\text{–}2.7) \times 10^{-4}$ at 90% CL for $B^+ \to \omega\ell^+\nu_\ell$. The range corresponds to the ISGW, WSB, and KS models. An upper limit on $|V_{ub}/V_{cb}| < 0.8\text{–}0.13$ at 90% CL is derived as well.

$\Gamma(\omega \mu^+ \nu_\mu)/\Gamma_{total}$ — Γ_{27}/Γ

VALUE	DOCUMENT ID		TECN
• • • We do not use the following data for averages, fits, limits, etc. • • •			
seen	[1] ALBRECHT	91C	ARG

[1] In ALBRECHT 91C, one event is fully reconstructed providing evidence for the $b \to u$ transition.

$\Gamma(\rho^0 \ell^+ \nu_\ell)/\Gamma_{total}$ — Γ_{28}/Γ

$\ell = e$ or μ, not sum over e and μ modes.

"OUR EVALUATION" is an average using rescaled values of the data listed below. The average and rescaling were performed by the Heavy Flavor Averaging Group (HFLAV) and are described at https://hflav.web.cern.ch/. The averaging/rescaling procedure takes into account correlations between the measurements and asymmetric lifetime errors.

VALUE (units 10^{-4})	CL%	DOCUMENT ID		TECN	COMMENT
1.58±0.11 OUR EVALUATION					
1.42±0.23 OUR AVERAGE		Error includes scale factor of 2.4. See the ideogram below.			
$1.83 \pm 0.10 \pm 0.10$		[1] SIBIDANOV	13	BELL	$e^+e^- \to \Upsilon(4S)$
$0.94 \pm 0.08 \pm 0.14$		[2] DEL-AMO-SA...	11C	BABR	$e^+e^- \to \Upsilon(4S)$
$1.33 \pm 0.23 \pm 0.18$		[3] HOKUUE	07	BELL	$e^+e^- \to \Upsilon(4S)$
$1.34 \pm 0.15 {}^{+0.28}_{-0.32}$		[4] BEHRENS	00	CLE2	$e^+e^- \to \Upsilon(4S)$
• • • We do not use the following data for averages, fits, limits, etc. • • •					
$1.16 \pm 0.11 \pm 0.30$		[2] AUBERT,B	05O	BABR	Repl. by DEL-AMO-SANCHEZ 11C
$1.40 \pm 0.21 {}^{+0.32}_{-0.33}$		[4] BEHRENS	00	CLE2	$e^+e^- \to \Upsilon(4S)$
$1.2 \pm 0.2 {}^{+0.3}_{-0.4}$		[4] ALEXANDER	96T	CLE2	$e^+e^- \to \Upsilon(4S)$
<2.1	90	[5] BEAN	93B	CLE2	$e^+e^- \to \Upsilon(4S)$

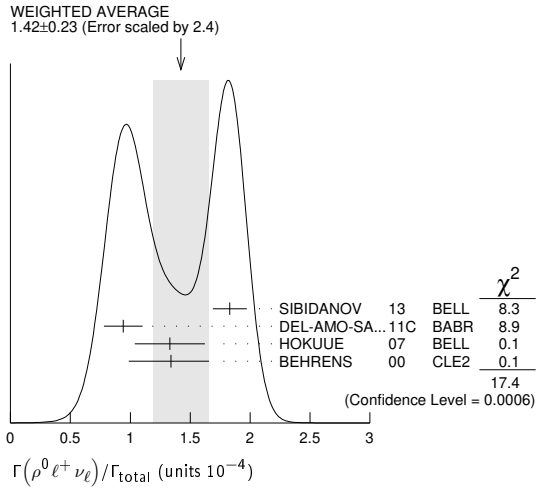

[1] The signal events are tagged by a second B meson reconstructed in the fully hadronic decays.
[2] B^+ and B^0 decays combined assuming isospin symmetry. Systematic errors include both experimental and form-factor uncertainties.
[3] The signal events are tagged by a second B meson reconstructed in the semileptonic mode $B \to D^{(*)}\ell\nu_\ell$.
[4] Derived based in the reported B^0 result by assuming isospin symmetry: $\Gamma(B^0 \to \rho^-\ell^+\nu) = 2\Gamma(B^+ \to \rho^0\ell^+\nu) \approx 2\Gamma(B^+ \to \omega\ell^+\nu)$.
[5] BEAN 93B limit set using ISGW Model. Using isospin and the quark model to combine $\Gamma(\omega^0\ell^+\nu_\ell)$ and $\Gamma(\rho^-\ell^+\nu_\ell)$ with this result, they obtain a limit $<(1.6\text{–}2.7) \times 10^{-4}$ at 90% CL for $B^+ \to \rho^0\ell^+\nu_\ell$. The range corresponds to the ISGW, WSB, and KS models. An upper limit on $|V_{ub}/V_{cb}| < 0.8\text{–}0.13$ at 90% CL is derived as well.

$\Gamma(\pi^+\pi^-\ell^+\nu_\ell)/\Gamma_{total}$ — Γ_{29}/Γ

VALUE (units 10^{-5})	DOCUMENT ID		TECN	COMMENT
$\mathbf{22.7 {}^{+1.9}_{-1.6} \pm 3.5}$	BELENO	21	BELL	$e^+e^- \to \Upsilon(4S)$

$\Gamma(p\overline{p}\ell^+\nu_\ell)/\Gamma_{total}$ — Γ_{30}/Γ

VALUE (units 10^{-6})	DOCUMENT ID		TECN	COMMENT
$\mathbf{5.8 {}^{+2.4}_{-2.1} \pm 0.9}$	[1] TIEN	14	BELL	$e^+e^- \to \Upsilon(4S)$

[1] Assumes equal production of B^+ and B^0 at the $\Upsilon(4S)$.

$\Gamma(p\overline{p}\mu^+\nu_\mu)/\Gamma_{total}$ — Γ_{31}/Γ

VALUE (units 10^{-6})	CL%	DOCUMENT ID		TECN	COMMENT
• • • We do not use the following data for averages, fits, limits, etc. • • •					
<8.5	90	[1] TIEN	14	BELL	$e^+e^- \to \Upsilon(4S)$

[1] Assumes equal production of B^+ and B^0 at the $\Upsilon(4S)$.

$\Gamma(p\overline{p}\mu^+\nu_\mu)/\Gamma(J/\psi(1S)K^+)$ — Γ_{31}/Γ_{276}

VALUE (units 10^{-3})	DOCUMENT ID		TECN	COMMENT
5.22±0.31±0.03	[1] AAIJ	20K	LHCB	pp at 7, 8 and 13 TeV

[1] AAIJ 20K reports $[\Gamma(B^+ \to p\overline{p}\mu^+\nu_\mu)/\Gamma(B^+ \to J/\psi(1S)K^+)] / [B(J/\psi(1S) \to \mu^+\mu^-)] = (8.75 \pm 0.39 \pm 0.35) \times 10^{-2}$ which we multiply by our best value $B(J/\psi(1S) \to \mu^+\mu^-) = (5.961 \pm 0.033) \times 10^{-2}$. Our first error is their experiment's error and our second error is the systematic error from using our best value.

$\Gamma(p\overline{p}e^+\nu_e)/\Gamma_{total}$ — Γ_{32}/Γ

VALUE (units 10^{-6})	CL%	DOCUMENT ID		TECN	COMMENT
$\mathbf{8.2 {}^{+3.7}_{-3.2} \pm 0.6}$		[1] TIEN	14	BELL	$e^+e^- \to \Upsilon(4S)$
• • • We do not use the following data for averages, fits, limits, etc. • • •					
<5200	90	[2] ADAM	03B	CLE2	$e^+e^- \to \Upsilon(4S)$

[1] Assumes equal production of B^+ and B^0 at the $\Upsilon(4S)$.
[2] Based on phase-space model; if V–A model is used, the 90% CL upper limit becomes $< 1.2 \times 10^{-3}$.

$\Gamma(e^+\nu_e)/\Gamma_{total}$ — Γ_{33}/Γ

VALUE (units 10^{-6})	CL%	DOCUMENT ID		TECN	COMMENT
< 0.98	90	[1] SATOYAMA	07	BELL	$e^+e^- \to \Upsilon(4S)$
• • • We do not use the following data for averages, fits, limits, etc. • • •					
< 3.5	90	[2] YOOK	15	BELL	$e^+e^- \to \Upsilon(4S)$
< 8	90	[1] AUBERT	10E	BABR	$e^+e^- \to \Upsilon(4S)$
< 1.9	90	[1] AUBERT	09V	BABR	$e^+e^- \to \Upsilon(4S)$
< 5.2	90	[1] AUBERT	08AD	BABR	$e^+e^- \to \Upsilon(4S)$
<15	90	ARTUSO	95	CLE2	$e^+e^- \to \Upsilon(4S)$

[1] Assumes equal production of B^+ and B^0 at the $\Upsilon(4S)$.
[2] Assumes $B(\Upsilon(4S) \to B^+B^-) = 0.513 \pm 0.006$.

Downloaded from https://academic.oup.com/ptep/article/2022/8/083C01/6651666 by KIT Library user on 27 September 2022

$\Gamma(\mu^+\nu_\mu)/\Gamma_{total}$ — Γ_{34}/Γ

VALUE (units 10^{-6})	CL%	DOCUMENT ID		TECN	COMMENT
< 0.86	90	[1] PRIM	20	BELL	$e^+e^- \to \Upsilon(4S)$
• • • We do not use the following data for averages, fits, limits, etc. • • •					
0.29 to 1.07	90	[2] SIBIDANOV	18	BELL	$e^+e^- \to \Upsilon(4S)$
< 2.7	90	[3] YOOK	15	BELL	$e^+e^- \to \Upsilon(4S)$
<11	90	[4] AUBERT	10E	BABR	$e^+e^- \to \Upsilon(4S)$
< 1.0	90	[4] AUBERT	09V	BABR	$e^+e^- \to \Upsilon(4S)$
< 5.6	90	[4] AUBERT	08AD	BABR	$e^+e^- \to \Upsilon(4S)$
< 1.7	90	[4,5] SATOYAMA	07	BELL	$e^+e^- \to \Upsilon(4S)$
< 6.6	90	AUBERT	04O	BABR	Repl. by AUBERT 09V
<21	90	ARTUSO	95	CLE2	$e^+e^- \to \Upsilon(4S)$

[1] This is a 90% C.L. upper limit in the frequentist approach. The corresponding upper limit in the Bayesian approach is $< 8.9 \times 10^{-7}$. A 2.8 standard deviation signal above the background is found, with a measured branching fraction $(5.3 \pm 2.0 \pm 0.9) \times 10^{-7}$.
[2] This is a 90% confidence interval in the frequentist approach. A 2.4 standard deviation signal above the background is found, with a measured branching fraction $(6.46 \pm 2.22 \pm 1.60) \times 10^{-7}$.
[3] Assumes $B(\Upsilon(4S) \to B^+B^-) = 0.513 \pm 0.006$.
[4] Assumes equal production of B^+ and B^0 at the $\Upsilon(4S)$.
[5] Superseded by SIBIDANOV 18.

$\Gamma(\tau^+\nu_\tau)/\Gamma_{total}$ — Γ_{35}/Γ

See the note on "Decay Constants of Charged Pseudoscalar Mesons" in the D_s^+ Listings.

VALUE (units 10^{-4})	CL%	DOCUMENT ID		TECN	COMMENT
1.09±0.24 OUR AVERAGE		Error includes scale factor of 1.2.			
$1.25 \pm 0.28 \pm 0.27$		[1,2] KRONENBIT...	15	BELL	$e^+e^- \to \Upsilon(4S)$
$0.72^{+0.27}_{-0.25} \pm 0.11$		[3] HARA	13	BELL	$e^+e^- \to \Upsilon(4S)$
$1.83^{+0.53}_{-0.49} \pm 0.24$		[2,4] LEES	13K	BABR	$e^+e^- \to \Upsilon(4S)$
$1.7 \pm 0.8 \pm 0.2$		[2,5] AUBERT	10E	BABR	$e^+e^- \to \Upsilon(4S)$
• • • We do not use the following data for averages, fits, limits, etc. • • •					
$1.54^{+0.38}_{-0.37}{}^{+0.29}_{-0.31}$		[2,6] HARA	10	BELL	Repl. by KRONENBIT-TER 15
$1.8^{+0.9}_{-0.8} \pm 0.45$		[2,7] AUBERT	08D	BABR	Repl. by LEES 13K
$0.9 \pm 0.6 \pm 0.1$		[2,5] AUBERT	07AL	BABR	Repl. by AUBERT 10E
< 2.6	90	[2] AUBERT	06K	BABR	$e^+e^- \to \Upsilon(4S)$
$1.79^{+0.56}_{-0.49}{}^{+0.46}_{-0.51}$		[2,7] IKADO	06	BELL	Repl. by HARA 13
< 4.2	90	[2] AUBERT,B	05B	BABR	Repl. by AUBERT 06K
< 8.3	90	[8] BARATE	01E	ALEP	$e^+e^- \to Z$
< 8.4	90	[2] BROWDER	01	CLE2	$e^+e^- \to \Upsilon(4S)$
< 5.7	90	[9] ACCIARRI	97F	L3	$e^+e^- \to Z$
<104	90	[10] ALBRECHT	95D	ARG	$e^+e^- \to \Upsilon(4S)$
< 22	90	ARTUSO	95	CLE2	$e^+e^- \to \Upsilon(4S)$
< 18	90	[11] BUSKULIC	95	ALEP	$e^+e^- \to Z$

[1] Requires one reconstructed semileptonic B decay $B^- \to D^{(*)0}\ell^-\overline{\nu}_\ell$ in the recoil.
[2] Assumes equal production of B^+ and B^0 at the $\Upsilon(4S)$.
[3] The authors combine their result with that from HARA 10 obtaining $B(B^- \to \tau^-\overline{\nu}_\tau) = (0.96 \pm 0.26) \times 10^{-4}$ and deriving $f_B\,|V_{ub}| = (7.4 \pm 0.8 \pm 0.5) \times 10^{-4}$ GeV.
[4] Requires a fully reconstructed hadronic B-decay in the recoil. Reports that this result combined with AUBERT 10E value gives $B(B^- \to \tau^-\overline{\nu}_\tau) = (1.79 \pm 0.48) \times 10^{-4}$.
[5] Requires one reconstructed semileptonic B decay $B^- \to D^0\ell^-\overline{\nu}_\ell X$ in the recoil.
[6] Requires one reconstructed semileptonic B decay $B^- \to D^{(*)0}\ell^-\overline{\nu}_\ell X$ in the recoil.
[7] The analysis is based on a sample of events with one fully reconstructed tag B in a hadronic decay mode $B^- \to D^{(*)0}X^-$.
[8] The energy-flow and b-tagging algorithms were used.
[9] ACCIARRI 97F uses missing-energy technique and $f(b \to B^-) = (38.2 \pm 2.5)\%$.
[10] ALBRECHT 95D uses full reconstruction of one B decay as tag.
[11] BUSKULIC 95 uses same missing-energy technique as in $\overline{b} \to \tau^+\nu_\tau X$, but analysis is restricted to endpoint region of missing-energy distribution.

$\Gamma(\ell^+\nu_\ell\gamma)/\Gamma_{total}$ — Γ_{36}/Γ

VALUE	CL%	DOCUMENT ID		TECN	COMMENT
$< 3.0 \times 10^{-6}$	90	[1,2] GELB	18	BELL	$e^+e^- \to \Upsilon(4S)$
• • • We do not use the following data for averages, fits, limits, etc. • • •					
$< 3.5 \times 10^{-6}$	90	[2,3] HELLER	15	BELL	$e^+e^- \to \Upsilon(4S)$
$<15.6 \times 10^{-6}$	90	[2] AUBERT	09AT	BABR	$e^+e^- \to \Upsilon(4S)$

[1] Supersedes HELLER 15.
[2] Assumes equal production of B^+ and B^0 at the $\Upsilon(4S)$.
[3] Superseded by GELB 18.

$\Gamma(e^+\nu_e\gamma)/\Gamma_{total}$ — Γ_{37}/Γ

VALUE	CL%	DOCUMENT ID		TECN	COMMENT
$< 4.3 \times 10^{-6}$	90	[1,2] GELB	18	BELL	$e^+e^- \to \Upsilon(4S)$
• • • We do not use the following data for averages, fits, limits, etc. • • •					
$< 6.1 \times 10^{-6}$	90	[2,3] HELLER	15	BELL	$e^+e^- \to \Upsilon(4S)$
$< 17 \times 10^{-6}$	90	[2] AUBERT	09AT	BABR	$e^+e^- \to \Upsilon(4S)$
$<200 \times 10^{-6}$	90	[4] BROWDER	97	CLE2	$e^+e^- \to \Upsilon(4S)$

[1] Supersedes HELLER 15.
[2] Assumes equal production of B^+ and B^0 at the $\Upsilon(4S)$.
[3] Superseded by GELB 18.
[4] BROWDER 97 uses the hermiticity of the CLEOII detector to reconstruct the neutrino energy and momentum.

$\Gamma(\mu^+\nu_\mu\gamma)/\Gamma_{total}$ — Γ_{38}/Γ

VALUE	CL%	DOCUMENT ID		TECN	COMMENT
$< 3.4 \times 10^{-6}$	90	[1,2] GELB	18	BELL	$e^+e^- \to \Upsilon(4S)$
• • • We do not use the following data for averages, fits, limits, etc. • • •					
$< 3.4 \times 10^{-6}$	90	[2,3] HELLER	15	BELL	$e^+e^- \to \Upsilon(4S)$
$<24 \times 10^{-6}$	90	[2,4] AUBERT	09AT	BABR	$e^+e^- \to \Upsilon(4S)$
$<52 \times 10^{-6}$	90	[5] BROWDER	97	CLE2	$e^+e^- \to \Upsilon(4S)$

[1] Supersedes HELLER 15.
[2] Assumes equal production of B^+ and B^0 at the $\Upsilon(4S)$.
[3] Superseded by GELB 18.
[4] Note that the value given by AUBERT 09AT is 24×10^{-6} in the paper abstract, and 26×10^{-6} in the paper itself (Table I).
[5] BROWDER 97 uses the hermiticity of the CLEOII detector to reconstruct the neutrino energy and momentum.

$\Gamma(\mu^+\mu^-\mu^+\nu_\mu)/\Gamma_{total}$ — Γ_{39}/Γ

VALUE	CL%	DOCUMENT ID		TECN	COMMENT
$<1.6 \times 10^{-8}$	95	[1] AAIJ	19P	LHCB	pp at 7, 8, 13 TeV

[1] AAIJ 19P limit established for the kinematic region where the lower of the two $M(\mu^+\mu^-)$ is less than 980 MeV/c^2.

$\Gamma(D^0X)/\Gamma_{total}$ — Γ_{40}/Γ

VALUE	DOCUMENT ID		TECN	COMMENT
0.086±0.006±0.004	[1] AUBERT	07N	BABR	$e^+e^- \to \Upsilon(4S)$
• • • We do not use the following data for averages, fits, limits, etc. • • •				
$0.098 \pm 0.009 \pm 0.006$	[1] AUBERT,BE	04B	BABR	Repl. by AUBERT 07N

[1] Events are selected by completely reconstructing one B and searching for a reconstructed charmed particle in the rest of the event. The last error includes systematic and charm branching ratio uncertainties.

$\Gamma(\overline{D}^0X)/\Gamma_{total}$ — Γ_{41}/Γ

VALUE	DOCUMENT ID		TECN	COMMENT
$0.786 \pm 0.016^{+0.034}_{-0.033}$	[1] AUBERT	07N	BABR	$e^+e^- \to \Upsilon(4S)$
• • • We do not use the following data for averages, fits, limits, etc. • • •				
$0.793 \pm 0.025^{+0.045}_{-0.044}$	[1] AUBERT,BE	04B	BABR	Repl. by AUBERT 07N

[1] Events are selected by completely reconstructing one B and searching for a reconstructed charmed particle in the rest of the event. The last error includes systematic and charm branching ratio uncertainties.

$\Gamma(D^0X)/[\Gamma(D^0X)+\Gamma(\overline{D}^0X)]$ — $\Gamma_{40}/(\Gamma_{40}+\Gamma_{41})$

VALUE	DOCUMENT ID		TECN	COMMENT
0.098±0.007±0.001	AUBERT	07N	BABR	$e^+e^- \to \Upsilon(4S)$
• • • We do not use the following data for averages, fits, limits, etc. • • •				
$0.110 \pm 0.010 \pm 0.003$	AUBERT,BE	04B	BABR	Repl. by AUBERT 07N

$\Gamma(D^+X)/\Gamma_{total}$ — Γ_{42}/Γ

VALUE	DOCUMENT ID		TECN	COMMENT
0.025±0.005±0.002	[1] AUBERT	07N	BABR	$e^+e^- \to \Upsilon(4S)$
• • • We do not use the following data for averages, fits, limits, etc. • • •				
$0.038 \pm 0.009 \pm 0.005$	[1] AUBERT,BE	04B	BABR	Repl. by AUBERT 07N

[1] Events are selected by completely reconstructing one B and searching for a reconstructed charmed particle in the rest of the event. The last error includes systematic and charm branching ratio uncertainties.

$\Gamma(D^-X)/\Gamma_{total}$ — Γ_{43}/Γ

VALUE	DOCUMENT ID		TECN	COMMENT
0.099±0.008±0.009	[1] AUBERT	07N	BABR	$e^+e^- \to \Upsilon(4S)$
• • • We do not use the following data for averages, fits, limits, etc. • • •				
$0.098 \pm 0.012 \pm 0.014$	[1] AUBERT,BE	04B	BABR	Repl. by AUBERT 07N

[1] Events are selected by completely reconstructing one B and searching for a reconstructed charmed particle in the rest of the event. The last error includes systematic and charm branching ratio uncertainties.

$\Gamma(D^+X)/[\Gamma(D^+X)+\Gamma(D^-X)]$ — $\Gamma_{42}/(\Gamma_{42}+\Gamma_{43})$

VALUE	DOCUMENT ID		TECN	COMMENT
0.204±0.035±0.001	AUBERT	07N	BABR	$e^+e^- \to \Upsilon(4S)$
• • • We do not use the following data for averages, fits, limits, etc. • • •				
$0.278 \pm 0.052 \pm 0.009$	AUBERT,BE	04B	BABR	Repl. by AUBERT 07N

$\Gamma(D_s^+X)/\Gamma_{total}$ — Γ_{44}/Γ

VALUE	DOCUMENT ID		TECN	COMMENT
$0.079 \pm 0.006^{+0.013}_{-0.011}$	[1] AUBERT	07N	BABR	$e^+e^- \to \Upsilon(4S)$
• • • We do not use the following data for averages, fits, limits, etc. • • •				
$0.143 \pm 0.016^{+0.051}_{-0.034}$	[1] AUBERT,BE	04B	BABR	Repl. by AUBERT 07N

[1] Events are selected by completely reconstructing one B and searching for a reconstructed charmed particle in the rest of the event. The last error includes systematic and charm branching ratio uncertainties.

Downloaded from https://academic.oup.com/ptep/article/2022/8/083C01/6651666 by KIT Library user on 27 September 2022

$\Gamma(D_s^- X)/\Gamma_{total}$ — Γ_{45}/Γ

VALUE	CL%	DOCUMENT ID		TECN	COMMENT
$\mathbf{0.011^{+0.004}_{-0.003}{}^{+0.002}_{-0.001}}$		[1] AUBERT	07N	BABR	$e^+e^- \to \Upsilon(4S)$
• • • We do not use the following data for averages, fits, limits, etc. • • •					
<0.022	90	[1] AUBERT,BE	04B	BABR	Repl. by AUBERT 07N

[1] Events are selected by completely reconstructing one B and searching for a reconstructed charmed particle in the rest of the event. The last error includes systematic and charm branching ratio uncertainties.

$\Gamma(D_s^+ X)/[\Gamma(D_s^+ X)+\Gamma(D_s^- X)]$ — $\Gamma_{44}/(\Gamma_{44}+\Gamma_{45})$

VALUE	DOCUMENT ID		TECN	COMMENT
$\mathbf{0.884\pm0.038\pm0.002}$	AUBERT	07N	BABR	$e^+e^- \to \Upsilon(4S)$
• • • We do not use the following data for averages, fits, limits, etc. • • •				
$0.966\pm0.039\pm0.012$	AUBERT,BE	04B	BABR	Repl. by AUBERT 07N

$\Gamma(D_s^- X)/[\Gamma(D_s^+ X)+\Gamma(D_s^- X)]$ — $\Gamma_{45}/(\Gamma_{44}+\Gamma_{45})$

VALUE	CL%	DOCUMENT ID		TECN	COMMENT
$\mathbf{<0.126}$	90	AUBERT,BE	04B	BABR	$e^+e^- \to \Upsilon(4S)$

$\Gamma(\Lambda_c^+ X)/\Gamma_{total}$ — Γ_{46}/Γ

VALUE	DOCUMENT ID		TECN	COMMENT
$\mathbf{0.021\pm0.005^{+0.008}_{-0.004}}$	[1] AUBERT	07N	BABR	$e^+e^- \to \Upsilon(4S)$
• • • We do not use the following data for averages, fits, limits, etc. • • •				
$0.029\pm0.008^{+0.011}_{-0.007}$	[1] AUBERT,BE	04B	BABR	Repl. by AUBERT 07N

[1] Events are selected by completely reconstructing one B and searching for a reconstructed charmed particle in the rest of the event. The last error includes systematic and charm branching ratio uncertainties.

$\Gamma(\overline{\Lambda}_c^- X)/\Gamma_{total}$ — Γ_{47}/Γ

VALUE	DOCUMENT ID		TECN	COMMENT
$\mathbf{0.028\pm0.005^{+0.010}_{-0.007}}$	[1] AUBERT	07N	BABR	$e^+e^- \to \Upsilon(4S)$
• • • We do not use the following data for averages, fits, limits, etc. • • •				
$0.035\pm0.008^{+0.013}_{-0.009}$	[1] AUBERT,BE	04B	BABR	Repl. by AUBERT 07N

[1] Events are selected by completely reconstructing one B and searching for a reconstructed charmed particle in the rest of the event. The last error includes systematic and charm branching ratio uncertainties.

$\Gamma(\Lambda_c^+ X)/[\Gamma(\Lambda_c^+ X)+\Gamma(\overline{\Lambda}_c^- X)]$ — $\Gamma_{46}/(\Gamma_{46}+\Gamma_{47})$

VALUE	DOCUMENT ID		TECN	COMMENT
$\mathbf{0.427\pm0.071\pm0.001}$	AUBERT	07N	BABR	$e^+e^- \to \Upsilon(4S)$
• • • We do not use the following data for averages, fits, limits, etc. • • •				
$0.452\pm0.090\pm0.003$	AUBERT,BE	04B	BABR	Repl. by AUBERT 07N

$\Gamma(\overline{c}X)/\Gamma_{total}$ — Γ_{48}/Γ

VALUE	DOCUMENT ID		TECN	COMMENT
$\mathbf{0.968\pm0.019^{+0.041}_{-0.039}}$	[1] AUBERT	07N	BABR	$e^+e^- \to \Upsilon(4S)$
• • • We do not use the following data for averages, fits, limits, etc. • • •				
$0.983\pm0.030^{+0.054}_{-0.051}$	[1] AUBERT,BE	04B	BABR	Repl. by AUBERT 07N

[1] Events are selected by completely reconstructing one B and searching for a reconstructed charmed particle in the rest of the event. The last error includes systematic and charm branching ratio uncertainties.

$\Gamma(cX)/\Gamma_{total}$ — Γ_{49}/Γ

VALUE	DOCUMENT ID		TECN	COMMENT
$\mathbf{0.234\pm0.012^{+0.018}_{-0.014}}$	[1] AUBERT	07N	BABR	$e^+e^- \to \Upsilon(4S)$
• • • We do not use the following data for averages, fits, limits, etc. • • •				
$0.330\pm0.022^{+0.055}_{-0.037}$	[1] AUBERT,BE	04B	BABR	Repl. by AUBERT 07N

[1] Events are selected by completely reconstructing one B and searching for a reconstructed charmed particle in the rest of the event. The last error includes systematic and charm branching ratio uncertainties.

$\Gamma(c/\overline{c}X)/\Gamma_{total}$ — Γ_{50}/Γ

VALUE	DOCUMENT ID		TECN	COMMENT
$\mathbf{1.202\pm0.023^{+0.053}_{-0.049}}$	[1] AUBERT	07N	BABR	$e^+e^- \to \Upsilon(4S)$
• • • We do not use the following data for averages, fits, limits, etc. • • •				
$1.313\pm0.037^{+0.088}_{-0.075}$	[1] AUBERT,BE	04B	BABR	Repl. by AUBERT 07N

[1] Events are selected by completely reconstructing one B and searching for a reconstructed charmed particle in the rest of the event. The last error includes systematic and charm branching ratio uncertainties.

$\Gamma(\overline{D}^0\pi^+)/\Gamma_{total}$ — Γ_{51}/Γ

VALUE (units 10^{-3})	EVTS	DOCUMENT ID		TECN	COMMENT
4.68±0.13 OUR FIT					
4.70±0.13 OUR AVERAGE					
$4.34\pm0.10\pm0.23$		[1] KATO	18	BELL	$e^+e^- \to \Upsilon(4S)$
$4.90\pm0.07\pm0.22$		[2] AUBERT	07H	BABR	$e^+e^- \to \Upsilon(4S)$
$4.9\ \pm0.6\ \pm0.2$		[3] ABULENCIA	06J	CDF	$p\overline{p}$ at 1.96 TeV
$4.49\pm0.21\pm0.23$		[4] AUBERT,BE	06J	BABR	$e^+e^- \to \Upsilon(4S)$
$4.97\pm0.12\pm0.29$		[2,5] AHMED	02B	CLE2	$e^+e^- \to \Upsilon(4S)$
$5.0\ \pm0.7\ \pm0.6$	54	[6] BORTOLETTO	92	CLEO	$e^+e^- \to \Upsilon(4S)$
$5.4\ ^{+1.8}_{-1.5}\ ^{+1.2}_{-0.9}$	14	[7] BEBEK	87	CLEO	$e^+e^- \to \Upsilon(4S)$
• • • We do not use the following data for averages, fits, limits, etc. • • •					
$4.68\pm0.26\pm0.04$		[8] AUBERT,B	04P	BABR	Repl. by AUBERT 07H
$5.5\ \pm0.4\ \pm0.5$	304	[9] ALAM	94	CLE2	Repl. by AHMED 02B
$2.0\ \pm0.8\ \pm0.6$	12	[6] ALBRECHT	90J	ARG	$e^+e^- \to \Upsilon(4S)$
$1.9\ \pm1.0\ \pm0.6$	7	[10] ALBRECHT	88K	ARG	$e^+e^- \to \Upsilon(4S)$

[1] Measures absolute branching fractions using a missing-mass technique.
[2] Assumes equal production of B^+ and B^0 at the $\Upsilon(4S)$.
[3] ABULENCIA 06J reports $[\Gamma(B^+ \to \overline{D}^0\pi^+)/\Gamma_{total}]$ / $[B(B^0 \to D^-\pi^+)] = 1.97 \pm 0.10 \pm 0.21$ which we multiply by our best value $B(B^0 \to D^-\pi^+) = (2.51 \pm 0.08) \times 10^{-3}$. Our first error is their experiment's error and our second error is the systematic error from using our best value.
[4] Uses a missing-mass method. Does not depend on D branching fractions or B^+/B^0 production rates.
[5] AHMED 02B reports an additional uncertainty on the branching ratios to account for 4.5% uncertainty on relative production of B^0 and B^+, which is not included here.
[6] Assumes equal production of B^+ and B^0 at the $\Upsilon(4S)$ and uses the Mark III branching fractions for the D.
[7] BEBEK 87 value has been updated in BERKELMAN 91 to use same assumptions as noted for BORTOLETTO 92.
[8] AUBERT,B 04P reports $[\Gamma(B^+ \to \overline{D}^0\pi^+)/\Gamma_{total}] \times [B(D^0 \to K^-\pi^+)] = (1.846 \pm 0.032 \pm 0.097) \times 10^{-4}$ which we divide by our best value $B(D^0 \to K^-\pi^+) = (3.947 \pm 0.030) \times 10^{-2}$. Our first error is their experiment's error and our second error is the systematic error from using our best value.
[9] ALAM 94 assume equal production of B^+ and B^0 at the $\Upsilon(4S)$ and use the CLEO II absolute $B(D^0 \to K^-\pi^+)$ and the PDG 1992 $B(D^0 \to K^-\pi^+\pi^0)/B(D^0 \to K^-\pi^+)$ and $B(D^0 \to K^-2\pi^+\pi^-)/B(D^0 \to K^-\pi^+)$.
[10] ALBRECHT 88K assumes $B^0\overline{B}^0$:B^+B^- ratio is 45:55. Superseded by ALBRECHT 90J.

$\Gamma(\overline{D}^0\rho^+)/\Gamma_{total}$ — Γ_{54}/Γ

VALUE	EVTS	DOCUMENT ID		TECN	COMMENT
0.0134±0.0018 OUR AVERAGE					
$0.0135\pm0.0012\pm0.0015$	212	[1] ALAM	94	CLE2	$e^+e^- \to \Upsilon(4S)$
$0.013\ \pm0.004\ \pm0.004$	19	[2] ALBRECHT	90J	ARG	$e^+e^- \to \Upsilon(4S)$
• • • We do not use the following data for averages, fits, limits, etc. • • •					
$0.021\ \pm0.008\ \pm0.009$	10	[3] ALBRECHT	88K	ARG	$e^+e^- \to \Upsilon(4S)$

[1] ALAM 94 assume equal production of B^+ and B^0 at the $\Upsilon(4S)$ and use the CLEO II absolute $B(D^0 \to K^-\pi^+)$ and the PDG 1992 $B(D^0 \to K^-\pi^+\pi^0)/B(D^0 \to K^-\pi^+)$ and $B(D^0 \to K^-2\pi^+\pi^-)/B(D^0 \to K^-\pi^+)$.
[2] Assumes equal production of B^+ and B^0 at the $\Upsilon(4S)$ and uses the Mark III branching fractions for the D.
[3] ALBRECHT 88K assumes $B^0\overline{B}^0$:B^+B^- ratio is 45:55.

$\Gamma(\overline{D}^0K^+)/\Gamma(\overline{D}^0\pi^+)$ — Γ_{55}/Γ_{51}

VALUE (units 10^{-2})	DOCUMENT ID		TECN	COMMENT
7.89 ±0.27 OUR AVERAGE	Error includes scale factor of 2.3. See the ideogram below.			
$7.96\ \pm0.03\ \pm0.13$	AAIJ	21Q	LHCB	pp at 7, 8, 13 TeV
$6.77\ \pm0.23\ \pm0.30$	HORII	08	BELL	$e^+e^- \to \Upsilon(4S)$
$8.31\ \pm0.35\ \pm0.20$	AUBERT	04N	BABR	$e^+e^- \to \Upsilon(4S)$
$9.9\ ^{+1.4}_{-1.2}\ ^{+0.7}_{-0.6}$	BORNHEIM	03	CLE2	$e^+e^- \to \Upsilon(4S)$
• • • We do not use the following data for averages, fits, limits, etc. • • •				
$7.768\pm0.038\pm0.066$	[1,2] AAIJ	18A	LHCB	pp at 7, 8, 13 TeV
$7.79\ \pm0.06\ \pm0.19$	AAIJ	16L	LHCB	pp at 7, 8 TeV
$7.93\ \pm0.10\ \pm0.18$	[3] AAIJ	16L	LHCB	pp at 7, 8 TeV
$7.71\ \pm0.17\ \pm0.26$	[3] AAIJ	13AE	LHCB	Repl. by AAIJ 16L
$7.74\ \pm0.12\ \pm0.19$	AAIJ	12M	LHCB	Repl. by AAIJ 16L
$9.4\ \pm0.9\ \pm0.7$	ABE	03D	BELL	Repl. by SWAIN 03
$7.7\ \pm0.5\ \pm0.6$	SWAIN	03	BELL	Repl. by HORII 08
$7.9\ \pm0.9\ \pm0.6$	ABE	01I	BELL	Repl. by ABE 03D
$5.5\ \pm1.4\ \pm0.5$	ATHANAS	98	CLE2	Repl. by BORNHEIM 03

[1] Supersedes AAIJ 16L.
[2] Superseded by AAIJ 21Q.
[3] Uses $B^{\pm} \to [K^{\pm}\pi^{\mp}\pi^+\pi^-]_D h^{\pm}$ mode.

Downloaded from https://academic.oup.com/ptep/article/2022/8/083C01/6651666 by KIT Library user on 27 September 2022

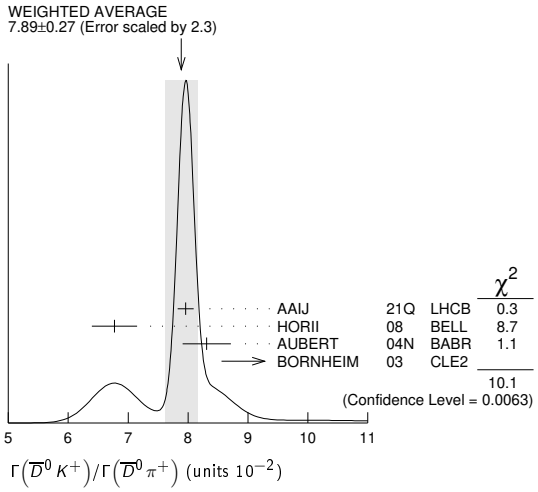

$\Gamma(D_{CP(+1)}K^+)/\Gamma(D_{CP(+1)}\pi^+)$ — Γ_{56}/Γ_{52}

VALUE	DOCUMENT ID		TECN	COMMENT
0.089±0.008 OUR AVERAGE				
0.089±0.008±0.003	[1,2] ABE	06	BELL	$e^+e^- \to \Upsilon(4S)$
0.088±0.016±0.005	[3] AUBERT	04N	BABR	$e^+e^- \to \Upsilon(4S)$
• • • We do not use the following data for averages, fits, limits, etc. • • •				
0.125±0.036±0.010	[3] ABE	03D	BELL	Repl. by SWAIN 03
0.093±0.018±0.008	[3] SWAIN	03	BELL	Repl. by ABE 06

[1] Reports a double ratio of $B(B^+ \to D_{CP(+1)}K^+)/B(B^+ \to D_{CP(+1)}\pi^+)$ and $B(B^+ \to \overline{D}^0K^+)/B(B^+ \to \overline{D}^0\pi^+)$, 1.13 ± 0.16 ± 0.08. We multiply by our best value $B(B^+ \to \overline{D}^0K^+)/B(B^+ \to \overline{D}^0\pi^+) = 0.083 \pm 0.006$. Our first error is their experiment's error and the second error is systematic error from using our best value.

[2] ABE 06 reports $[\Gamma(B^+ \to D_{CP(+1)}K^+)/\Gamma(B^+ \to D_{CP(+1)}\pi^+)] / [\Gamma(B^+ \to \overline{D}^0K^+)/\Gamma(B^+ \to \overline{D}^0\pi^+)] = 1.13 \pm 0.06 \pm 0.08$ which we multiply by our best value $\Gamma(B^+ \to \overline{D}^0K^+)/\Gamma(B^+ \to \overline{D}^0\pi^+) = 0.0789 \pm 0.0027$. Our first error is their experiment's error and our second error is the systematic error from using our best value.

[3] CP=+1 eigenstate of $D^0\overline{D}^0$ system is reconstructed via K^+K^- and $\pi^+\pi^-$.

$\Gamma(D_{CP(+1)}K^+)/\Gamma(\overline{D}^0K^+)$ — Γ_{56}/Γ_{55}

VALUE	DOCUMENT ID		TECN	COMMENT
0.495±0.007 OUR AVERAGE				
0.494±0.008±0.006	[1] AAIJ	18A	LHCB	pp at 7, 8, 13 TeV
0.496±0.014±0.008	[2] AAIJ	18A	LHCB	pp at 7, 8, 13 TeV
0.489±0.010±0.009	[3] AAIJ	16L	LHCB	pp at 7, 8 TeV
0.65 ±0.12 ±0.06	[4] AALTONEN	10A	CDF	$p\overline{p}$ at 1.96 TeV
0.590±0.045±0.025	[5] DEL-AMO-SA...10G		BABR	$e^+e^- \to \Upsilon(4S)$
• • • We do not use the following data for averages, fits, limits, etc. • • •				
0.504±0.019±0.006	[6] AAIJ	12M	LHCB	Repl. by AAIJ 16L
0.53 ±0.05 ±0.025	AUBERT	08AA	BABR	Repl. by DEL-AMO-SANCHEZ 10G
0.45 ±0.06 ±0.02	AUBERT	06J	BABR	Repl. by AUBERT 08AA

[1] Uses $D \to K^+K^-$ decay mode and reports $R_{CP+} = 0.988 \pm 0.015 \pm 0.011$ which we have divided by 2.

[2] Uses $D \to \pi^+\pi^-$ decay mode and reports $R_{CP+} = 0.992 \pm 0.027 \pm 0.015$ which we have divided by 2.

[3] AAIJ 16L reports $R_{CP+} = 0.978 \pm 0.019 \pm 0.018$ which we have divided by 2.

[4] Reports $R_{CP+} = 2\,(B(B^- \to D_{CP(+1)}K^-) + B(B^+ \to D_{CP(+1)}K^+)) / (B(B^- \to D^0K^-) + B(B^+ \to \overline{D}^0K^+)) = 1.30 \pm 0.24 \pm 0.12$ that we have divided by 2.

[5] Reports $R_{CP+} = 1.18 \pm 0.09 \pm 0.05$ that we have divided by 2.

[6] AAIJ 12M reports $R_{CP+} = 1.007 \pm 0.038 \pm 0.012$ which we have divided by 2.

$\Gamma(D_{CP(-1)}K^+)/\Gamma(D_{CP(-1)}\pi^+)$ — Γ_{57}/Γ_{53}

VALUE	DOCUMENT ID		TECN	COMMENT
0.097±0.016±0.007	[1] ABE	06	BELL	$e^+e^- \to \Upsilon(4S)$
• • • We do not use the following data for averages, fits, limits, etc. • • •				
0.119±0.028±0.006	[2] ABE	03D	BELL	Repl. by SWAIN 03
0.108±0.019±0.007	[2] SWAIN	03	BELL	Repl. by ABE 06

[1] Reports a double ratio of $B(B^+ \to D_{CP(-1)}K^+)/B(B^+ \to D_{CP(-1)}\pi^+)$ and $B(B^+ \to \overline{D}^0K^+)/B(B^+ \to \overline{D}^0\pi^+)$, 1.17 ± 0.14 ± 0.14. We multiply by our best value of $B(B^+ \to \overline{D}^0K^+)/B(B^+ \to \overline{D}^0\pi^+) = 0.083 \pm 0.006$. Our first error is their experiment's error and the second error is systematic error from using our best value.

[2] CP=−1 eigenstate of $D^0\overline{D}^0$ system is reconstructed via $K^0_S\pi^0$, $K^0_S\omega$, $K^0_S\phi$, $K^0_S\eta$, and $K^0_S\eta'$.

$\Gamma(D_{CP(-1)}K^+)/\Gamma(\overline{D}^0K^+)$ — Γ_{57}/Γ_{55}

VALUE	DOCUMENT ID		TECN	COMMENT
0.54 ±0.04±0.02	[1] DEL-AMO-SA...10G		BABR	$e^+e^- \to \Upsilon(4S)$
• • • We do not use the following data for averages, fits, limits, etc. • • •				
0.515±0.05±0.025	AUBERT	08AA	BABR	Repl. by DEL-AMO-SANCHEZ 10G
0.43 ±0.05±0.02	AUBERT	06J	BABR	Repl. by AUBERT 08AA

[1] Reports $R_{CP+} = 1.07 \pm 0.08 \pm 0.04$ that we have divided by 2.

$\Gamma(D^0K^+)/\Gamma(\overline{D}^0K^+)$ — Γ_{58}/Γ_{55}

"OUR EVALUATION" is derived from $r_B(B^+ \to D^0K^+)$ data block listed in "CP vilation parameters" section.

VALUE (units 10^{-3})	DOCUMENT ID
9.88±0.52 OUR EVALUATION	

$\Gamma([K^-\pi^+]_D K^+)/\Gamma_{total}$ — Γ_{59}/Γ

VALUE	CL%	DOCUMENT ID		TECN	COMMENT
<2.8 × 10⁻⁷	90	HORII	08	BELL	$e^+e^- \to \Upsilon(4S)$
• • • We do not use the following data for averages, fits, limits, etc. • • •					
<6.3 × 10⁻⁷	90	SAIGO	05	BELL	$e^+e^- \to \Upsilon(4S)$

$\Gamma([K^-\pi^+]_D K^+)/\Gamma([K^+\pi^-]_D K^+)$ — Γ_{59}/Γ_{60}

VALUE (units 10^{-3})	CL%	DOCUMENT ID		TECN	COMMENT
14 ±7 OUR AVERAGE Error includes scale factor of 14.7.					
9.5±0.5±0.3		[1] AAIJ	21Q	LHCB	pp at 7, 8, 13 TeV
25.2±0.8±0.4		[2] AAIJ	21Q	LHCB	pp at 7, 8, 13 TeV
22.0±8.6±2.6		[3] AALTONEN	11AJ	CDF	$p\overline{p}$ at 1.96 TeV
$16.3^{+4.4+0.7}_{-4.1-1.3}$		HORII	11	BELL	$e^+e^- \to \Upsilon(4S)$
11 ±6 ±2		DEL-AMO-SA...10H		BABR	$e^+e^- \to \Upsilon(4S)$
• • • We do not use the following data for averages, fits, limits, etc. • • •					
18.8±1.1±1.0		[4] AAIJ	16L	LHCB	pp at 7, 8 TeV
15.2±2.0±0.4		AAIJ	12M	LHCB	Repl. by AAIJ 16L
$7.8^{+6.2+2.0}_{-5.7-2.8}$		HORII	08	BELL	Repl. by HORII 11
<29	90	[5] AUBERT	05G	BABR	Repl. by DEL-AMO-SANCHEZ 10H
<44	90	[6] SAIGO	05	BELL	$e^+e^- \to \Upsilon(4S)$
<26	90	[7] AUBERT,B	04L	BABR	Repl. by AUBERT 05G

[1] Uses the ratio of $B^- \to [K^+\pi^-]_D K^-$ and $B^- \to [K^-\pi^+]_D K^-$. AAIJ 21Q gives the charge-averaged rate as 0.0173 ± 0.0006, where the statistical and systematic uncertainties have been combined according to the correlations between the observables.

[2] Uses the ratio of $B^+ \to [K^-\pi^+]_D K^+$ and $B^+ \to [K^+\pi^-]_D K^+$. AAIJ 21Q gives the charge-averaged rate as 0.0173 ± 0.0006, where the statistical and systematic uncertainties have been combined according to the correlations between the observables.

[3] AALTONEN 11AJ also measures the ratio separately for B^+ ($R^+(K)$) and B^- ($R^-(K)$) and obtains: $R^+(K) = (42.6 \pm 13.7 \pm 2.8) \times 10^{-3}$, $R^-(K) = (3.8 \pm 10.3 \pm 2.7) \times 10^{-3}$.

[4] Superseded by AAIJ 21Q.

[5] AUBERT 05G extract a constraint on the magnitude of the ratio of amplitudes $|A(B^+ \to D^0K^+) / A(B^+ \to \overline{D}^0K^+)| < 0.23$ at 90% CL (Bayesian). Similar measurements from $B^+ \to D^{*0}K^+$ are also reported.

[6] SAIGO 05 extract a constraint on the magnitude of the ratio of amplitudes $|A(B^+ \to D^0K^+) / A(B^+ \to \overline{D}^0K^+)| < 0.27$ at 90% CL.

[7] AUBERT,B 04L extract a constraint on the magnitude of the ratio of amplitudes $|A(B^+ \to D^0K^+)/A(B^+ \to \overline{D}^0K^+)| < 0.22$ at 90% CL.

$\Gamma([K^-\pi^+\pi^0]_D K^+)/\Gamma([K^+\pi^-\pi^0]_D K^+)$ — Γ_{61}/Γ_{62}

VALUE (units 10^{-3})	CL%	DOCUMENT ID		TECN	COMMENT
16 ±4 OUR AVERAGE					
14.0±4.7±2.1		[1] AAIJ	15W	LHCB	pp at 7, 8 TeV
19.8±6.2±2.4		NAYAK	13	BELL	$e^+e^- \to \Upsilon(4S)$
• • • We do not use the following data for averages, fits, limits, etc. • • •					
<21	90	[2] LEES	11D	BABR	$e^+e^- \to \Upsilon(4S)$
<39	95	[3] AUBERT	07BN	BABR	Repl. by LEES 11D

[1] Uses $D^0 \to K^-\pi^+\pi^0$ for the favored mode, and $D^0 \to K^+\pi^-\pi^0$ for the suppressed mode.

[2] Extracts a constraint on the magnitude of the ratio of amplitudes $|A(B^+ \to D^0K^+)/A(B^+ \to \overline{D}^0K^+)| < 0.13$ at 95% CL.

[3] Extracts a constraint on the magnitude of the ratio of amplitudes $|A(B^+ \to D^0K^+)/A(B^+ \to \overline{D}^0K^+)| < 0.19$ at 95% CL.

$\Gamma([K^-\pi^+\pi^+\pi^-]_D K^+)/\Gamma([K^+\pi^-\pi^+\pi^-]_D K^+)$ — Γ_{63}/Γ_{64}

VALUE (units 10^{-2})	DOCUMENT ID		TECN	COMMENT
1.40±0.15±0.06	AAIJ	16L	LHCB	pp at 7, 8 TeV
• • • We do not use the following data for averages, fits, limits, etc. • • •				
1.24±0.27	AAIJ	13AE	LHCB	Repl. by AAIJ 16L

$\Gamma([\pi^+\pi^+\pi^-\pi^-]K^+)/\Gamma([K^+\pi^-\pi^+\pi^-]_D K^+)$ — Γ_{65}/Γ_{64}

VALUE	DOCUMENT ID		TECN	COMMENT
0.975±0.037±0.019	AAIJ	16L	LHCB	pp at 7, 8 TeV

Downloaded from https://academic.oup.com/ptep/article/2022/8/083C01/6651666 by KIT Library user on 27 September 2022

$\Gamma([K^-\pi^+]_D K^*(892)^+)/\Gamma([K^+\pi^-]_D K^*(892)^+)$ — Γ_{67}/Γ_{68}

VALUE	DOCUMENT ID		TECN	COMMENT
0.012±0.004 OUR AVERAGE				
0.011±0.004±0.001	AAIJ	17BO	LHCB	pp at 7, 8, 13 TeV
0.066±0.031±0.010	AUBERT	09AJ	BABR	$e^+e^- \to \Upsilon(4S)$
• • • We do not use the following data for averages, fits, limits, etc. • • •				
0.046±0.031±0.008	AUBERT,B	05V	BABR	Repl. by AUBERT 09AJ

$\Gamma([K^-\pi^+\pi^-\pi^+]_D K^*(892)^+)/\Gamma([K^+\pi^-\pi^+\pi^-]_D K^*(892)^+)$ — Γ_{69}/Γ_{70}

VALUE	DOCUMENT ID		TECN	COMMENT
0.011±0.005±0.003	AAIJ	17BO	LHCB	pp at 7, 8, 13 TeV

$\Gamma([\pi^+\pi^-\pi^+\pi^-]_D K^*(892)^+)/\Gamma([K^+\pi^-\pi^+\pi^-]_D K^*(892)^+)$ — Γ_{66}/Γ_{70}

VALUE	DOCUMENT ID		TECN	COMMENT
1.08±0.13±0.03	AAIJ	17BO	LHCB	pp at 7, 8, 13 TeV

$\Gamma([K^-\pi^+]_D\pi^+)/\Gamma_{total}$ — Γ_{71}/Γ

VALUE (units 10^{-7})	DOCUMENT ID		TECN	COMMENT
$6.29^{+1.02+0.37}_{-0.98-0.48}$	HORII	08	BELL	$e^+e^- \to \Upsilon(4S)$
• • • We do not use the following data for averages, fits, limits, etc. • • •				
$6.6\ ^{+1.9}_{-1.7}\ \pm0.5$	SAIGO	05	BELL	Repl. by HORII 08

$\Gamma([K^-\pi^+]_D\pi^+)/\Gamma([K^+\pi^-]_D\pi^+)$ — Γ_{71}/Γ_{72}

VALUE (units 10^{-3})	DOCUMENT ID		TECN	COMMENT
3.6 ±0.5 OUR AVERAGE Error includes scale factor of 7.9.				
4.15±0.08±0.04	[1] AAIJ	21Q	LHCB	pp at 7, 8, 13 TeV
3.20±0.07±0.04	[2] AAIJ	21Q	LHCB	pp at 7, 8, 13 TeV
2.8 ±0.7 ±0.4	[3] AALTONEN	11AJ	CDF	$p\overline{p}$ at 1.96 TeV
$3.28^{+0.38+0.12}_{-0.36-0.18}$	HORII	11	BELL	$e^+e^- \to \Upsilon(4S)$
3.3 ±0.6 ±0.4	DEL-AMO-SA...	10H	BABR	$e^+e^- \to \Upsilon(4S)$
• • • We do not use the following data for averages, fits, limits, etc. • • •				
3.60±0.12±0.09	[4] AAIJ	16L	LHCB	pp at 7, 8 TeV
4.10±0.25±0.05	AAIJ	12M	LHCB	Repl. by AAIJ 16L
$3.40^{+0.55+0.15}_{-0.53-0.22}$	HORII	08	BELL	Repl. by HORII 11
$3.5\ ^{+1.0}_{-0.9}\ \pm0.2$	SAIGO	05	BELL	Repl. by HORII 08

[1] Uses the ratio of $B^- \to [K^+\pi^-]_D K^-$ and $B^- \to [K^-\pi^+]_D K^-$. AAIJ 21Q gives the charge-averaged rate as 0.00368 ± 0.00007, where the statistical and systematic uncertainties have been combined according to the correlations between the observables.

[2] Uses the ratio of $B^+ \to [K^-\pi^+]_D\pi^+$ and $B^+ \to [K^+\pi^-]_D\pi^+$. AAIJ 21Q gives the charge-averaged rate as 0.00368 ± 0.00007, where the statistical and systematic uncertainties have been combined according to the correlations between the observables.

[3] AALTONEN 11AJ also measures the ratio separately for B^+ ($R^+(\pi)$) and B^- ($R^-(\pi)$) and obtains: $R^+(\pi) = (2.4 \pm 1.0 \pm 0.4) \times 10^{-3}$, $R^-(K) = (3.1 \pm 1.1 \pm 0.4) \times 10^{-3}$.

[4] Superseded by AAIJ 21Q.

$\Gamma([K^-\pi^+\pi^0]_D\pi^+)/\Gamma([K^+\pi^-\pi^0]_D\pi^+)$ — Γ_{73}/Γ_{74}

VALUE (units 10^{-3})	DOCUMENT ID		TECN	COMMENT
2.2 ±0.4 OUR AVERAGE				
2.35±0.49±0.06	[1] AAIJ	15W	LHCB	pp at 7, 8 TeV
$1.89\pm0.54^{+0.22}_{-0.25}$	NAYAK	13	BELL	$e^+e^- \to \Upsilon(4S)$

[1] Uses $D^0 \to K^-\pi^+\pi^0$ for the favored mode, and $D^0 \to K^+\pi^-\pi^0$ for the suppressed mode.

$\Gamma([K^-\pi^+\pi^+\pi^-]_D\pi^+)/\Gamma([K^+\pi^-\pi^+\pi^-]_D\pi^+)$ — Γ_{75}/Γ_{76}

VALUE (units 10^{-3})	DOCUMENT ID		TECN	COMMENT
3.77±0.18±0.06	AAIJ	16L	LHCB	pp at 7, 8 TeV
• • • We do not use the following data for averages, fits, limits, etc. • • •				
3.7 ±0.4	AAIJ	13AE	LHCB	Repl. by AAIJ 16L

$\Gamma([K^-\pi^+]_{(D\pi)}\pi^+)/\Gamma([K^+\pi^-]_{(D\pi)}\pi^+)$ — Γ_{77}/Γ_{78}

VALUE (units 10^{-3})	DOCUMENT ID		TECN	COMMENT
4.4 ±0.6 OUR AVERAGE Error includes scale factor of 1.1.				
4.05±0.56±0.59	[1] AAIJ	21Q	LHCB	pp at 7, 8, 13 TeV
5.36±0.56±0.58	[2] AAIJ	21Q	LHCB	pp at 7, 8, 13 TeV
3.2 ±0.9 ±0.8	DEL-AMO-SA...	10H	BABR	$e^+e^- \to \Upsilon(4S)$

[1] Uses the ratio of $B^- \to ([K^+\pi^-]_D\pi^0)_{D^*}\pi^-$ and $B^- \to ([K^-\pi^+]_D\pi^0)_{D^*}\pi^-$, without inclusion of the neutral pion in the reconstruction. AAIJ 21Q gives the charge-averaged rate as 0.00471 ± 0.00077, where the statistical and systematic uncertainties have been combined according to the correlations between the observables.

[2] Uses the ratio of $B^+ \to ([K^+\pi^-]_D\pi^0)_{D^*}\pi^+$ and $B^+ \to ([K^-\pi^+]_D\pi^0)_{D^*}\pi^+$, without inclusion of the neutral pion in the reconstruction. AAIJ 21Q gives the charge-averaged rate as 0.00471 ± 0.00077, where the statistical and systematic uncertainties have been combined according to the correlations between the observables.

$\Gamma([K^-\pi^+]_{(D\gamma)}\pi^+)/\Gamma([K^+\pi^-]_{(D\gamma)}\pi^+)$ — Γ_{79}/Γ_{80}

VALUE (units 10^{-3})	DOCUMENT ID		TECN	COMMENT
4.1 ±1.0 OUR AVERAGE				
4.72±0.92±1.18	[1] AAIJ	21Q	LHCB	pp at 7, 8, 13 TeV
4.03±0.91±1.14	[2] AAIJ	21Q	LHCB	pp at 7, 8, 13 TeV
2.7 ±1.4 ±2.2	DEL-AMO-SA...	10H	BABR	$e^+e^- \to \Upsilon(4S)$

[1] Uses the ratio of $B^- \to ([K^+\pi^-]_D\gamma)_{D^*}\pi^-$ and $B^- \to ([K^-\pi^+]_D\gamma)_{D^*}\pi^-$, without inclusion of the photon in the reconstruction. AAIJ 21Q gives the charge-averaged rate as 0.00420 ± 0.00138, where the statistical and systematic uncertainties have been combined according to the correlations between the observables.

[2] Uses the ratio of $B^+ \to ([K^-\pi^+]_D\gamma)_{D^*}\pi^+$ and $B^- \to ([K^+\pi^-]_D\gamma)_{D^*}\pi^+$, without inclusion of the photon in the reconstruction. AAIJ 21Q gives the charge-averaged rate as 0.00420 ± 0.00138, where the statistical and systematic uncertainties have been combined according to the correlations between the observables.

$\Gamma([K^-\pi^+]_{(D\pi)}K^+)/\Gamma([K^+\pi^-]_{(D\pi)}K^+)$ — Γ_{81}/Γ_{82}

VALUE (units 10^{-3})	DOCUMENT ID		TECN	COMMENT
2.8±2.8 OUR AVERAGE Error includes scale factor of 3.0. See the ideogram below.				
20.2±3.5±2.3	[1] AAIJ	21Q	LHCB	pp at 7, 8, 13 TeV
3.3±3.5±2.2	[2] AAIJ	21Q	LHCB	pp at 7, 8, 13 TeV
1.8±0.9±0.4	DEL-AMO-SA...	10H	BABR	$e^+e^- \to \Upsilon(4S)$

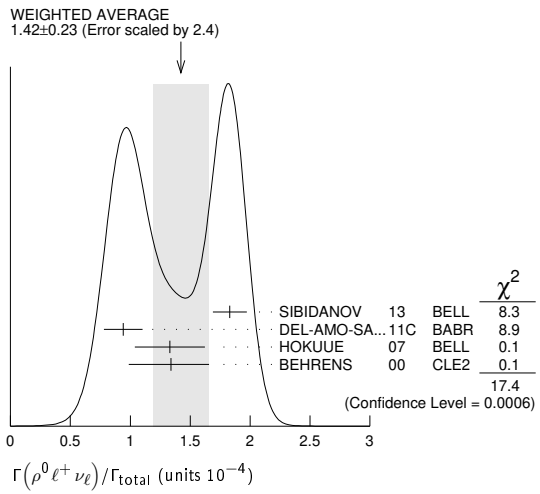

[1] Uses the ratio of $B^- \to ([K^+\pi^-]_D\pi^0)_{D^*}K^-$ and $B^- \to ([K^-\pi^+]_D\pi^0)_{D^*}K^-$, without inclusion of the neutral pion in the reconstruction. AAIJ 21Q gives the charge-averaged rate as 0.0118 ± 0.0034, where the statistical and systematic uncertainties have been combined according to the correlations between the observables.

[2] Uses the ratio of $B^+ \to ([K^+\pi^-]_D\pi^0)_{D^*}\pi^+$ and $B^+ \to ([K^-\pi^+]_D\pi^0)_{D^*}\pi^+$, without inclusion of the neutral pion in the reconstruction. AAIJ 21Q gives the charge-averaged rate as 0.0118 ± 0.0034, where the statistical and systematic uncertainties have been combined according to the correlations between the observables.

$\Gamma([K^-\pi^+]_{(D\gamma)}K^+)/\Gamma([K^+\pi^-]_{(D\gamma)}K^+)$ — Γ_{83}/Γ_{84}

VALUE (units 10^{-3})	DOCUMENT ID		TECN	COMMENT
1.4± 1.6 OUR AVERAGE				
11.7±21.5±31.3	[1] AAIJ	21Q	LHCB	pp at 7, 8, 13 TeV
29.2±21.4±31.2	[2] AAIJ	21Q	LHCB	pp at 7, 8, 13 TeV
1.3± 1.4± 0.8	DEL-AMO-SA...	10H	BABR	$e^+e^- \to \Upsilon(4S)$

[1] Uses the ratio of $B^- \to ([K^+\pi^-]_D\gamma)_{D^*}K^-$ and $B^- \to ([K^-\pi^+]_D\gamma)_{D^*}K^-$, without inclusion of the photon in the reconstruction. AAIJ 21Q gives the charge-averaged rate as 0.0163 ± 0.0373, where the statistical and systematic uncertainties have been combined according to the correlations between the observables.

[2] Uses the ratio of $B^+ \to ([K^-\pi^+]_D\gamma)_{D^*}K^+$ and $B^+ \to ([K^+\pi^-]_D\gamma)_{D^*}K^+$, without inclusion of the photon in the reconstruction. AAIJ 21Q gives the charge-averaged rate as 0.0163 ± 0.0373, where the statistical and systematic uncertainties have been combined according to the correlations between the observables.

$\Gamma([\pi^+\pi^-\pi^0]_D K^-)/\Gamma_{total}$ — Γ_{85}/Γ

VALUE (units 10^{-6})	DOCUMENT ID		TECN	COMMENT
4.6±0.8±0.4	[1] AUBERT	07BJ	BABR	$e^+e^- \to \Upsilon(4S)$
• • • We do not use the following data for averages, fits, limits, etc. • • •				
5.5±1.0±0.7	[1] AUBERT,B	05T	BABR	Repl. by AUBERT 07BJ

[1] Assumes equal production of B^+ and B^0 at the $\Upsilon(4S)$.

Downloaded from https://academic.oup.com/ptep/article/2022/8/083C01/6651666 by KIT Library user on 27 September 2022

$\Gamma([K^0_S K^+\pi^-]_D K^+)/\Gamma([K^0_S K^+\pi^-]_D \pi^+)$ — Γ_{86}/Γ_{92}

VALUE	DOCUMENT ID		TECN	COMMENT
0.092±0.009±0.004	[1] AAIJ	14V	LHCB	pp at 7, 8 TeV
• • • We do not use the following data for averages, fits, limits, etc. • • •				
0.081±0.008±0.004	[2] AAIJ	20N	LHCB	pp at 7, 8, 13 TeV

[1] The anaysis uses all of $D \to K^0_S K\pi$ Dalitz decays.
[2] The analysis uses $D \to K^0_S K\pi$ Dalitz decays with $K^{*-}K^+$ region excluded.

$\Gamma([K^0_S K^-\pi^+]_D K^+)/\Gamma([K^0_S K^-\pi^+]_D \pi^+)$ — Γ_{88}/Γ_{90}

VALUE	DOCUMENT ID		TECN	COMMENT
0.066±0.009±0.002	[1] AAIJ	14V	LHCB	pp at 7, 8 TeV
• • • We do not use the following data for averages, fits, limits, etc. • • •				
0.073±0.006±0.002	[2] AAIJ	20N	LHCB	pp at 7, 8, 13 TeV

[1] The anaysis uses all of $D \to K^0_S K\pi$ Dalitz decays.
[2] The analysis uses $D \to K^0_S K\pi$ Dalitz decays with $K^{*-}K^+$ region excluded.

$\Gamma([K^*(892)^- K^+]_D K^+)/\Gamma([K^*(892)^- K^+]_D \pi^+)$ — Γ_{87}/Γ_{93}

VALUE	DOCUMENT ID		TECN	COMMENT
0.079±0.004±0.002	[1] AAIJ	20N	LHCB	pp at 7, 8, 13 TeV
• • • We do not use the following data for averages, fits, limits, etc. • • •				
0.084±0.011±0.003	[1] AAIJ	14V	LHCB	Repl. by AAIJ 20N

[1] The Analysis uses $D \to K^*(892)\,K \to K^0_S K\pi$ decays.

$\Gamma([K^*(892)^+ K^-]_D K^+)/\Gamma([K^*(892)^+ K^-]_D \pi^+)$ — Γ_{89}/Γ_{91}

VALUE	DOCUMENT ID		TECN	COMMENT
0.062±0.006±0.003	[1] AAIJ	20N	LHCB	pp at 7, 8, 13 TeV
• • • We do not use the following data for averages, fits, limits, etc. • • •				
0.056±0.013±0.002	[1] AAIJ	14V	LHCB	Repl. by AAIJ 20N

[1] The Analysis uses $D \to K^*(892)\,K \to K^0_S K\pi$ decays.

$\Gamma([K^+K^-\pi^0]_D K^+)/\Gamma([K^+K^-\pi^0]_D \pi^+)$ — Γ_{94}/Γ_{95}

VALUE	DOCUMENT ID		TECN	COMMENT
0.95±0.22±0.05	[1] AAIJ	15W	LHCB	pp at 7, 8 TeV

[1] Uses $D \to K^+K^-\pi^0$ mode.

$\Gamma([\pi^+\pi^-\pi^0]_D K^+)/\Gamma([\pi^+\pi^-\pi^0]_D \pi^+)$ — Γ_{96}/Γ_{97}

VALUE	DOCUMENT ID		TECN	COMMENT
0.98±0.11±0.05	[1] AAIJ	15W	LHCB	pp at 7, 8 TeV

[1] Uses $D \to \pi^+\pi^-\pi^0$ mode.

$\Gamma([K^0_S K^+\pi^-]_D \pi^+)/\Gamma([K^0_S K^-\pi^+]_D \pi^+)$ — Γ_{92}/Γ_{90}

VALUE	DOCUMENT ID		TECN	COMMENT
1.528±0.058±0.025	[1] AAIJ	14V	LHCB	pp at 7, 8 TeV
• • • We do not use the following data for averages, fits, limits, etc. • • •				
0.706±0.019±0.009	[2] AAIJ	20N	LHCB	pp at 7, 8, 13 TeV

[1] The anaysis uses all of $D \to K^0_S K\pi$ Dalitz decays.
[2] The analysis uses $D \to K^0_S K\pi$ Dalitz decays with $K^{*-}K^+$ region excluded.

$\Gamma([K^*(892)^- K^+]_D \pi^+)/\Gamma([K^*(892)^+ K^-]_D \pi^+)$ — Γ_{93}/Γ_{91}

VALUE	DOCUMENT ID		TECN	COMMENT
2.585±0.057±0.019	[1] AAIJ	20N	LHCB	pp at 7, 8, 13 TeV
• • • We do not use the following data for averages, fits, limits, etc. • • •				
2.57 ±0.13 ±0.06	[1] AAIJ	14V	LHCB	Repl. by AAIJ 20N

[1] The Analysis uses $D \to K^*(892)\,K \to K^0_S K\pi$ decays.

$\Gamma(\overline{D}^0 K^*(892)^+)/\Gamma_{total}$ — Γ_{98}/Γ

VALUE (units 10^{-4})	DOCUMENT ID		TECN	COMMENT
5.3 ±0.4 OUR AVERAGE				
5.29±0.30±0.34	[1] AUBERT	06Z	BABR	$e^+e^- \to \Upsilon(4S)$
6.1 ±1.6 ±1.7	[1] MAHAPATRA	02	CLE2	$e^+e^- \to \Upsilon(4S)$
• • • We do not use the following data for averages, fits, limits, etc. • • •				
6.3 ±0.7 ±0.5	[1] AUBERT	04Q	BABR	Repl. by AUBERT 06Z

[1] Assumes equal production of B^+ and B^0 at the $\Upsilon(4S)$.

$\Gamma(D_{CP(-1)} K^*(892)^+)/\Gamma(\overline{D}^0 K^*(892)^+)$ — Γ_{99}/Γ_{98}

VALUE	DOCUMENT ID		TECN	COMMENT
0.515±0.135±0.065	[1] AUBERT	09AJ	BABR	$e^+e^- \to \Upsilon(4S)$
• • • We do not use the following data for averages, fits, limits, etc. • • •				
0.325±0.13 ±0.04	[2] AUBERT,B	05U	BABR	Repl. by AUBERT 09AJ

[1] The authors report $R_{CP-} = 1.03 \pm 0.27 \pm 0.13$ which is, assuming CP conservation, twice the value of the quoted above branching ratio,
[2] The authors report $R_{CP-} = 0.65 \pm 0.26 \pm 0.08$ which is, assuming CP conservation, twice the value of the quoted above branching ratio.

$\Gamma(D_{CP(+1)} K^*(892)^+)/\Gamma(\overline{D}^0 K^*(892)^+)$ — Γ_{100}/Γ_{98}

VALUE	DOCUMENT ID		TECN	COMMENT
1.16 ±0.08 OUR AVERAGE				
1.18 ±0.08 ±0.02	[1] AAIJ	18X	LHCB	pp at 7, 8, 13 TeV
1.085±0.175±0.045	[2] AUBERT	09AJ	BABR	$e^+e^- \to \Upsilon(4S)$
• • • We do not use the following data for averages, fits, limits, etc. • • •				
1.18 ±0.08 ±0.01	[3] AAIJ	17BO	LHCB	Repl. by AAIJ 18X
0.98 ±0.20 ±0.055	[4] AUBERT,B	05U	BABR	Repl. by AUBERT 09AJ

[1] Measures the ratio separately for K^+K^- and $\pi^+\pi^-$ final states, $R_{KK} = 1.22 \pm 0.09 \pm 0.02$ and $R_{\pi\pi} = 1.08 \pm 0.14 \pm 0.03$, and combines the two results.
[2] The authors report $R_{CP+} = 2.17 \pm 0.35 \pm 0.09$ which is, assuming CP conservation, twice the value of the quoted above branching ratio,
[3] Measures the ratio separately for K^+K^- and $\pi^+\pi^-$ final states, $R_{KK} = 1.22 \pm 0.09 \pm 0.01$ and $R_{\pi\pi} = 1.08 \pm 0.14 \pm 0.03$, and combines the two results.
[4] The authors report $R_{CP+} = 1.96 \pm 0.40 \pm 0.11$ which is, assuming CP conservation, twice the value of the quoted above branching ratio.

$\Gamma(D^0 K^*(892)^+)/\Gamma(\overline{D}^0 K^*(892)^+)$ — Γ_{101}/Γ_{98}

"OUR EVALUATION" is derived from $r_B(B^+ \to D^0 K^{*+})$ data block listed in "CP vilation parameters" section.

VALUE (units 10^{-3})	DOCUMENT ID
$10.2^{+3.2}_{-6.9}$ OUR EVALUATION	

$\Gamma(\overline{D}^0 K^+\pi^+\pi^-)/\Gamma(\overline{D}^0\pi^+\pi^+\pi^-)$ — $\Gamma_{102}/\Gamma_{108}$

VALUE (units 10^{-2})	DOCUMENT ID		TECN	COMMENT
9.4±1.3±0.9	AAIJ	12T	LHCB	pp at 7 TeV

$\Gamma(D_{CP(+1)} K^+\pi^-\pi^+)/\Gamma([K^+\pi^-]_D K^+\pi^-\pi^+)$ — $\Gamma_{105}/\Gamma_{103}$

VALUE	DOCUMENT ID		TECN	COMMENT
1.040±0.064	AAIJ	15BC	LHCB	pp at 7, 8 TeV

$\Gamma([K^-\pi^+]_D K^+\pi^-\pi^+)/\Gamma([K^+\pi^-]_D K^+\pi^-\pi^+)$ — $\Gamma_{104}/\Gamma_{103}$

VALUE (units 10^{-4})	DOCUMENT ID		TECN	COMMENT
85^{+36}_{-33}	AAIJ	15BC	LHCB	pp at 7, 8 TeV

$\Gamma(\overline{D}^0 K^+\overline{K}^0)/\Gamma_{total}$ — Γ_{106}/Γ

VALUE (units 10^{-4})	DOCUMENT ID		TECN	COMMENT
5.5±1.4±0.8	[1] DRUTSKOY	02	BELL	$e^+e^- \to \Upsilon(4S)$

[1] Assumes equal production of B^+ and B^0 at the $\Upsilon(4S)$.

$\Gamma(\overline{D}^0 K^+\overline{K}^*(892)^0)/\Gamma_{total}$ — Γ_{107}/Γ

VALUE (units 10^{-4})	DOCUMENT ID		TECN	COMMENT
7.5±1.3±1.1	[1] DRUTSKOY	02	BELL	$e^+e^- \to \Upsilon(4S)$

[1] Assumes equal production of B^+ and B^0 at the $\Upsilon(4S)$.

$\Gamma(\overline{D}^0\pi^+\pi^+\pi^-)/\Gamma_{total}$ — Γ_{108}/Γ

VALUE	DOCUMENT ID		TECN	COMMENT
0.0056±0.0021 OUR FIT Error includes scale factor of 3.6.				
0.0115±0.0029±0.0021	[1] BORTOLETTO92		CLEO	$e^+e^- \to \Upsilon(4S)$

[1] BORTOLETTO 92 assumes equal production of B^+ and B^0 at the $\Upsilon(4S)$ and uses Mark III branching fractions for the D.

$\Gamma(\overline{D}^0\pi^+\pi^+\pi^-)/\Gamma(\overline{D}^0\pi^+)$ — Γ_{108}/Γ_{51}

VALUE	DOCUMENT ID		TECN	COMMENT
1.2 ±0.4 OUR FIT Error includes scale factor of 3.7.				
1.27±0.06±0.11	AAIJ	11E	LHCB	pp at 7 TeV

$\Gamma([K^-\pi^+]_D\pi^+\pi^-\pi^+)/\Gamma([K^+\pi^-]_D K^+\pi^-\pi^+)$ — $\Gamma_{109}/\Gamma_{103}$

VALUE (units 10^{-4})	DOCUMENT ID		TECN	COMMENT
42.7±5.6	AAIJ	15BC	LHCB	pp at 7, 8 TeV

$\Gamma(\overline{D}^0\pi^+\pi^+\pi^-$ nonresonant$)/\Gamma_{total}$ — Γ_{110}/Γ

VALUE	DOCUMENT ID		TECN	COMMENT
0.0051±0.0034±0.0023	[1] BORTOLETTO92		CLEO	$e^+e^- \to \Upsilon(4S)$

[1] BORTOLETTO 92 assumes equal production of B^+ and B^0 at the $\Upsilon(4S)$ and uses Mark III branching fractions for the D.

$\Gamma(\overline{D}^0\pi^+\rho^0)/\Gamma_{total}$ — Γ_{111}/Γ

VALUE	DOCUMENT ID		TECN	COMMENT
0.0042±0.0023±0.0020	[1] BORTOLETTO92		CLEO	$e^+e^- \to \Upsilon(4S)$

[1] BORTOLETTO 92 assumes equal production of B^+ and B^0 at the $\Upsilon(4S)$ and uses Mark III branching fractions for the D.

$\Gamma(\overline{D}^0 a_1(1260)^+)/\Gamma_{total}$ — Γ_{112}/Γ

VALUE	DOCUMENT ID		TECN	COMMENT
0.0045±0.0019±0.0031	[1] BORTOLETTO92		CLEO	$e^+e^- \to \Upsilon(4S)$

[1] BORTOLETTO 92 assumes equal production of B^+ and B^0 at the $\Upsilon(4S)$ and uses Mark III branching fractions for the D.

Downloaded from https://academic.oup.com/ptep/article/2022/8/083C01/6651666 by KIT Library user on 27 September 2022

$\Gamma(\overline{D}^0\omega\pi^+)/\Gamma_{total}$ — Γ_{113}/Γ

VALUE	DOCUMENT ID		TECN	COMMENT
0.0041±0.0007±0.0006	[1] ALEXANDER	01B	CLE2	$e^+e^- \to \Upsilon(4S)$

[1] Assumes equal production of B^+ and B^0 at the $\Upsilon(4S)$. The signal is consistent with all observed $\omega\pi^+$ having proceeded through the ρ'^+ resonance at mass $1349 \pm 25^{+10}_{-5}$ MeV and width $547 \pm 86^{+46}_{-45}$ MeV.

$\Gamma(D^*(2010)^-\pi^+\pi^+)/\Gamma_{total}$ — Γ_{114}/Γ

VALUE (units 10^{-3})	CL%	EVTS	DOCUMENT ID		TECN	COMMENT
1.35±0.22 OUR AVERAGE						
1.25±0.08±0.22			[1] ABE	04D	BELL	$e^+e^- \to \Upsilon(4S)$
1.9 ±0.7 ±0.3		14	[2] ALAM	94	CLE2	$e^+e^- \to \Upsilon(4S)$
2.6 ±1.4 ±0.7		11	[3] ALBRECHT	90J	ARG	$e^+e^- \to \Upsilon(4S)$
$2.4\ ^{+1.7}_{-1.6}\ ^{+1.0}_{-0.6}$		3	[4] BEBEK	87	CLEO	$e^+e^- \to \Upsilon(4S)$
• • • We do not use the following data for averages, fits, limits, etc. • • •						
<4.	90		[5] BORTOLETTO	92	CLEO	$e^+e^- \to \Upsilon(4S)$
5. ±2. ±3.		7	[6] ALBRECHT	87C	ARG	$e^+e^- \to \Upsilon(4S)$

[1] Assumes equal production of B^+ and B^0 at the $\Upsilon(4S)$.
[2] ALAM 94 assume equal production of B^+ and B^0 at the $\Upsilon(4S)$ and use the CLEO II $B(D^*(2010)^+ \to D^0\pi^+)$ and absolute $B(D^0 \to K^-\pi^+)$ and the PDG 1992 $B(D^0 \to K^-\pi^+\pi^0)/B(D^0 \to K^-\pi^+)$ and $B(D^0 \to K^-2\pi^+\pi^-)/B(D^0 \to K^-\pi^+)$.
[3] Assumes equal production of B^+ and B^0 at the $\Upsilon(4S)$ and uses the Mark III branching fractions for the D.
[4] BEBEK 87 value has been updated in BERKELMAN 91 to use same assumptions as noted for BORTOLETTO 92.
[5] BORTOLETTO 92 assumes equal production of B^+ and B^0 at the $\Upsilon(4S)$ and uses Mark III branching fractions for the D and $D^*(2010)$. The authors also find the product branching fraction into $D^{**}\pi$ followed by $D^{**} \to D^*(2010)\pi$ to be $0.0014^{+0.0008}_{-0.0006} \pm 0.0003$ where D^{**} represents all orbitally excited D mesons.
[6] ALBRECHT 87C use PDG 86 branching ratios for D and $D^*(2010)$ and assume $B(\Upsilon(4S) \to B^+B^-) = 55\%$ and $B(\Upsilon(4S) \to B^0\overline{B}^0) = 45\%$. Superseded by ALBRECHT 90J.

$\Gamma(D^*(2010)^-K^+\pi^+)/\Gamma_{total}$ — Γ_{115}/Γ

VALUE (units 10^{-5})	DOCUMENT ID		TECN	COMMENT
8.2±0.3±1.4	[1] AAIJ	17AR	LHCB	pp at 7 , 8 TeV

[1] The branching fraction of the normalization mode $B^+ \to D^{*-}\pi^+\pi^+$ is rescaled to the updated ratio of $\Upsilon(4S) \to B^+B^-$ to $\Upsilon(4S) \to B^0\overline{B}^0$ decay rates of 1.058 ± 0.024.

$\Gamma(D^*(2010)^-K^+\pi^+)/\Gamma(D^*(2010)^-\pi^+\pi^+)$ — $\Gamma_{115}/\Gamma_{114}$

VALUE (units 10^{-2})	DOCUMENT ID		TECN	COMMENT
6.39±0.27±0.48	[1] AAIJ	17AR	LHCB	pp at 7, 8 TeV

[1] Uses $D^{*-} \to \overline{D}^0\pi^-$ and $\overline{D}^0 \to K^+\pi^-$ decays.

$\Gamma(\overline{D}_1(2420)^0\pi^+, \overline{D}_1^0 \to D^*(2010)^-\pi^+)/\Gamma_{total}$ — Γ_{116}/Γ

VALUE (units 10^{-4})	DOCUMENT ID		TECN	COMMENT
8.42±0.08±1.46	[1] AAIJ	20D	LHCB	pp at 7, 8, 13 TeV

[1] AAIJ 20D used a 4-body amplitude analysis of $B^- \to D^{*+}\pi^-\pi^-$ decays.

$\Gamma(\overline{D}_1(2420)^0\pi^+, \overline{D}_1^0 \to D^*(2010)^-\pi^+)/\Gamma(\overline{D}^0\pi^+\pi^+\pi^-)$ — $\Gamma_{116}/\Gamma_{108}$

VALUE (units 10^{-2})	DOCUMENT ID		TECN	COMMENT
9.3±1.6±0.9	[1] AAIJ	11E	LHCB	pp at 7 TeV

[1] AAIJ 11E reports $(9.3 \pm 1.6 \pm 0.9) \times 10^{-2}$ from a measurement of $[\Gamma(B^+ \to \overline{D}_1(2420)^0\pi^+, \overline{D}_1^0 \to D^*(2010)^-\pi^+)/\Gamma(B^+ \to \overline{D}^0\pi^+\pi^+\pi^-)] \times [B(D^*(2010)^+ \to D^0\pi^+)]$ assuming $B(D^*(2010)^+ \to D^0\pi^+) = (67.7\pm0.5)\times10^{-2}$.

$\Gamma(D^-\pi^+\pi^+)/\Gamma_{total}$ — Γ_{117}/Γ

VALUE (units 10^{-3})	CL%	EVTS	DOCUMENT ID		TECN	COMMENT
1.07±0.05 OUR AVERAGE						
1.08±0.03±0.05			[1] AUBERT	09AB	BABR	$e^+e^- \to \Upsilon(4S)$
1.02±0.04±0.15			[1] ABE	04D	BELL	$e^+e^- \to \Upsilon(4S)$
• • • We do not use the following data for averages, fits, limits, etc. • • •						
<1.4	90		[2] ALAM	94	CLE2	$e^+e^- \to \Upsilon(4S)$
<7	90		[3] BORTOLETTO	92	CLEO	$e^+e^- \to \Upsilon(4S)$
$2.5\ ^{+4.1}_{-2.3}\ ^{+2.4}_{-0.8}$		1	[4] BEBEK	87	CLEO	$e^+e^- \to \Upsilon(4S)$

[1] Assumes equal production of B^+ and B^0 at the $\Upsilon(4S)$.
[2] ALAM 94 assume equal production of B^+ and B^0 at the $\Upsilon(4S)$ and use the Mark III $B(D^+ \to K^-2\pi^+)$.
[3] BORTOLETTO 92 assumes equal production of B^+ and B^0 at the $\Upsilon(4S)$ and uses Mark III branching fractions for the D. The product branching fraction into $D_0^*(2340)\pi$ followed by $D_0^*(2340) \to D\pi$ is < 0.005 at 90%CL and into $D_2^*(2460)$ followed by $D_2^*(2460) \to D\pi$ is < 0.004 at 90%CL.
[4] BEBEK 87 assume the $\Upsilon(4S)$ decays 43% to $B^0\overline{B}^0$. $B(D^- \to K^+\pi^-\pi^-) = (9.1 \pm 1.3 \pm 0.4)\%$ is assumed.

$\Gamma(D^-K^+\pi^+)/\Gamma(D^-\pi^+\pi^+)$ — $\Gamma_{118}/\Gamma_{117}$

VALUE (units 10^{-2})	DOCUMENT ID		TECN	COMMENT
7.20±0.19±0.21	AAIJ	15V	LHCB	pp at 7, 8 TeV

$\Gamma(D_0^*(2300)^0K^+, D_0^{*0} \to D^-\pi^+)/\Gamma_{total}$ — Γ_{119}/Γ

VALUE (units 10^{-6})	DOCUMENT ID		TECN	COMMENT
6.1±1.9±1.5	[1] AAIJ	15V	LHCB	pp at 7, 8 TeV

[1] Performs the amplitude analysis by fitting the square-Dalitz-plot distribution.

$\Gamma(D_2^*(2460)^0K^+, D_2^{*0} \to D^-\pi^+)/\Gamma_{total}$ — Γ_{120}/Γ

VALUE (units 10^{-6})	DOCUMENT ID		TECN	COMMENT
23.2±1.1±2.0	[1] AAIJ	15V	LHCB	pp at 7, 8 TeV

[1] Performs the amplitude analysis by fitting the square-Dalitz-plot distribution.

$\Gamma(D_1^*(2760)^0K^+, D_1^{*0} \to D^-\pi^+)/\Gamma_{total}$ — Γ_{121}/Γ

VALUE (units 10^{-6})	DOCUMENT ID		TECN	COMMENT
3.6±0.9±0.8	[1] AAIJ	15V	LHCB	pp at 7, 8 TeV

[1] Performs the amplitude analysis by fitting the square-Dalitz-plot distribution.

$\Gamma(D^+K^0)/\Gamma_{total}$ — Γ_{122}/Γ

VALUE (units 10^{-6})	CL%	DOCUMENT ID		TECN	COMMENT
<2.9	90	[1] DEL-AMO-SA...	10K	BABR	$e^+e^- \to \Upsilon(4S)$
• • • We do not use the following data for averages, fits, limits, etc. • • •					
<5.0	90	[1] AUBERT,B	05E	BABR	Repl. by DEL-AMO-SANCHEZ 10K

[1] Assumes equal production of B^+ and B^0 at the $\Upsilon(4S)$.

$\Gamma(D^+K^+\pi^-)/\Gamma(D^-K^+\pi^+)$ — $\Gamma_{123}/\Gamma_{118}$

VALUE (units 10^{-2})	DOCUMENT ID		TECN	COMMENT
7.3±1.2±0.7	AAIJ	16M	LHCB	pp at 7, 8 TeV

$\Gamma(D_2^*(2460)^0K^+, D_2^{*0} \to D^+\pi^-)/\Gamma_{total}$ — Γ_{124}/Γ

VALUE	CL%	DOCUMENT ID		TECN	COMMENT
<6.3 × 10^{-7}	90	AAIJ	16R	LHCB	pp at 7, 8 TeV

$\Gamma(D^+K^{*0})/\Gamma_{total}$ — Γ_{125}/Γ

VALUE	CL%	DOCUMENT ID		TECN	COMMENT
<4.9 × 10^{-7}	90	AAIJ	16M	LHCB	pp at 7, 8 TeV
• • • We do not use the following data for averages, fits, limits, etc. • • •					
<1.8 × 10^{-6}	90	AAIJ	13R	LHCB	Repl. by AAIJ 16M
<3.0 × 10^{-6}	90	[1] DEL-AMO-SA...	10K	BABR	$e^+e^- \to \Upsilon(4S)$

[1] Assumes equal production of B^+ and B^0 at the $\Upsilon(4S)$.

$\Gamma(D^+\overline{K}^{*0})/\Gamma_{total}$ — Γ_{126}/Γ

VALUE (units 10^{-6})	CL%	DOCUMENT ID		TECN	COMMENT
<1.4	90	AAIJ	13R	LHCB	pp at 7 TeV

$\Gamma(\overline{D}^*(2007)^0\pi^+)/\Gamma_{total}$ — Γ_{127}/Γ

VALUE (units 10^{-3})	EVTS	DOCUMENT ID		TECN	COMMENT
5.18 ±0.15 OUR AVERAGE					
5.35 ±0.04 ±0.22		AAIJ	21Q	LHCB	pp at 7, 8, 13 TeV
4.82 ±0.12 ±0.35		[1] KATO	18	BELL	$e^+e^- \to \Upsilon(4S)$
5.52 ±0.17 ±0.42		[2] AUBERT	07H	BABR	$e^+e^- \to \Upsilon(4S)$
5.3 ±0.4 ±0.1		[3,4] AUBERT,BE	06J	BABR	$e^+e^- \to \Upsilon(4S)$
4.34 ±0.47 ±0.18		[5] BRANDENB...	98	CLE2	$e^+e^- \to \Upsilon(4S)$
5.2 ±0.7 ±0.7	71	[6] ALAM	94	CLE2	$e^+e^- \to \Upsilon(4S)$
7.2 ±1.8 ±1.6		[7] BORTOLETTO	92	CLEO	$e^+e^- \to \Upsilon(4S)$
4.0 ±1.4 ±1.2	9	[7] ALBRECHT	90J	ARG	$e^+e^- \to \Upsilon(4S)$
• • • We do not use the following data for averages, fits, limits, etc. • • •					
4.664±0.029±0.268		[8] AAIJ	18A	LHCB	pp at 7, 8, 13 TeV
2.7 ±4.4		[9] BEBEK	87	CLEO	$e^+e^- \to \Upsilon(4S)$

[1] Measures absolute branching fractions using a missing-mass technique.
[2] Assumes equal production of B^+ and B^0 at the $\Upsilon(4S)$.
[3] AUBERT,BE 06J reports $[\Gamma(B^+ \to \overline{D}^*(2007)^0\pi^+)/\Gamma_{total}]$ / $[B(B^+ \to \overline{D}^0\pi^+)] = 1.14 \pm 0.07 \pm 0.04$ which we multiply by our best value $B(B^+ \to \overline{D}^0\pi^+) = (4.68 \pm 0.13) \times 10^{-3}$. Our first error is their experiment's error and our second error is the systematic error from using our best value.
[4] Uses a missing-mass method. Does not depend on D branching fractions or B^+/B^0 production rates.
[5] BRANDENBURG 98 assume equal production of B^+ and B^0 at $\Upsilon(4S)$ and use the D^* reconstruction technique. The first error is their experiment's error and the second error is the systematic error from the PDG 96 value of $B(D^* \to D\pi)$.
[6] ALAM 94 assume equal production of B^+ and B^0 at the $\Upsilon(4S)$ and use the CLEO II $B(D^*(2007)^0 \to D^0\pi^0)$ and absolute $B(D^0 \to K^-\pi^+)$ and the PDG 1992 $B(D^0 \to K^-\pi^+\pi^0)/B(D^0 \to K^-\pi^+)$ and $B(D^0 \to K^-2\pi^+\pi^-)/B(D^0 \to K^-\pi^+)$.
[7] Assumes equal production of B^+ and B^0 at the $\Upsilon(4S)$ and uses Mark III branching fractions for the D and $D^*(2010)$.
[8] Superseded by AAIJ 21Q.
[9] This is a derived branching ratio, using the inclusive pion spectrum and other two-body B decays. BEBEK 87 assume the $\Upsilon(4S)$ decays 43% to $B^0\overline{B}^0$.

$\Gamma(\overline{D}^*(2007)^0\omega\pi^+)/\Gamma_{total}$ — Γ_{130}/Γ

VALUE	DOCUMENT ID		TECN	COMMENT
0.0045±0.0010±0.0007	[1] ALEXANDER	01B	CLE2	$e^+e^- \to \Upsilon(4S)$

[1] Assumes equal production of B^+ and B^0 at the $\Upsilon(4S)$. The signal is consistent with all observed $\omega\pi^+$ having proceeded through the ρ'^+ resonance at mass $1349 \pm 25^{+10}_{-5}$ MeV and width $547 \pm 86^{+46}_{-45}$ MeV.

Downloaded from https://academic.oup.com/ptep/article/2022/8/083C01/6651666 by KIT Library user on 27 September 2022

$\Gamma(\overline{D}^*(2007)^0\rho^+)/\Gamma_{total}$ — Γ_{131}/Γ

VALUE	EVTS	DOCUMENT ID		TECN	COMMENT
0.0098±0.0017 OUR AVERAGE					
0.0098±0.0006±0.0017		[1] CSORNA	03	CLE2	$e^+e^- \to \Upsilon(4S)$
0.010 ±0.006 ±0.004	7	[2] ALBRECHT	90J	ARG	$e^+e^- \to \Upsilon(4S)$
• • • We do not use the following data for averages, fits, limits, etc. • • •					
0.0168±0.0021±0.0028	86	[3] ALAM	94	CLE2	$e^+e^- \to \Upsilon(4S)$

[1] Assumes equal production of B^0 and B^+ at the $\Upsilon(4S)$ resonance. The second error combines the systematic and theoretical uncertainties in quadrature. CSORNA 03 includes data used in ALAM 94. A full angular fit to three complex helicity amplitudes is performed.
[2] Assumes equal production of B^+ and B^0 at the $\Upsilon(4S)$ and uses Mark III branching fractions for the D and $D^*(2010)$.
[3] ALAM 94 assume equal production of B^+ and B^0 at the $\Upsilon(4S)$ and use the CLEO II $B(D^*(2007)^0 \to D^0\pi^0)$ and absolute $B(D^0 \to K^-\pi^+)$ and the PDG 1992 $B(D^0 \to K^-\pi^+\pi^0)/B(D^0 \to K^-\pi^+)$ and $B(D^0 \to K^-2\pi^+\pi^-)/B(D^0 \to K^-\pi^+)$. The nonresonant $\pi^+\pi^0$ contribution under the ρ^+ is negligible.

$\Gamma(\overline{D}^*(2007)^0K^+)/\Gamma_{total}$ — Γ_{132}/Γ

VALUE (units 10^{-4})	DOCUMENT ID		TECN	COMMENT
$4.20^{+0.31}_{-0.28}$ OUR AVERAGE				
$4.21^{+0.30}_{-0.26}\pm0.12$	[1] AUBERT	05N	BABR	$e^+e^- \to \Upsilon(4S)$
4.0 ±1.1 ±0.1	[2] ABE	01I	BELL	$e^+e^- \to \Upsilon(4S)$

[1] AUBERT 05N reports $[\Gamma(B^+ \to \overline{D}^*(2007)^0K^+)/\Gamma_{total}] / [B(B^+ \to \overline{D}^*(2007)^0\pi^+)] = 0.0813 \pm 0.0040^{+0.0042}_{-0.0031}$ which we multiply by our best value $B(B^+ \to \overline{D}^*(2007)^0\pi^+) = (5.18 \pm 0.15) \times 10^{-3}$. Our first error is their experiment's error and our second error is the systematic error from using our best value.
[2] ABE 01I reports $[\Gamma(B^+ \to \overline{D}^*(2007)^0K^+)/\Gamma_{total}] / [B(B^+ \to \overline{D}^*(2007)^0\pi^+)] = 0.078 \pm 0.019 \pm 0.009$ which we multiply by our best value $B(B^+ \to \overline{D}^*(2007)^0\pi^+) = (5.18 \pm 0.15) \times 10^{-3}$. Our first error is their experiment's error and our second error is the systematic error from using our best value.

$\Gamma(\overline{D}^{*0}_{CP(+1)}K^+)/\Gamma_{total}$ — Γ_{133}/Γ

VALUE (units 10^{-4})	DOCUMENT ID		TECN	COMMENT
$2.75\pm0.29^{+0.21}_{-0.19}$	[1] AUBERT	08BF	BABR	$e^+e^- \to \Upsilon(4S)$

[1] AUBERT 08BF reports $[\Gamma(B^+ \to \overline{D}^{*0}_{CP(+1)}K^+)/\Gamma_{total}] / [B(B^+ \to \overline{D}^*(2007)^0K^+)] = 0.655 \pm 0.065 \pm 0.020$ which we multiply by our best value $B(B^+ \to \overline{D}^*(2007)^0K^+) = (4.20^{+0.31}_{-0.28}) \times 10^{-4}$. Our first error is their experiment's error and our second error is the systematic error from using our best value.

$\Gamma(\overline{D}^*(2007)^0K^+)/\Gamma(\overline{D}^*(2007)^0\pi^+)$ — $\Gamma_{132}/\Gamma_{127}$

VALUE (units 10^{-2})	DOCUMENT ID		TECN	COMMENT
8.51 ±0.12 ±0.48	[1] AAIJ	21Q	LHCB	pp at 7, 8, 13 TeV
• • • We do not use the following data for averages, fits, limits, etc. • • •				
7.930±0.110±0.560	[2] AAIJ	18A	LHCB	pp at 7, 8, 13 TeV

[1] Uses semi-inclusive reconstruction of $B^+ \to ([K^+\pi^-]_{D\gamma/\pi^0})_{D^*}K^+/\pi^+$. Decays of $D^* \to D\gamma/\pi^0$ are reconstructed without inclusion of π^0 or γ.
[2] Superseded by AAIJ 21Q.

$\Gamma(\overline{D}^{*0}_{CP(+1)}K^+)/\Gamma(\overline{D}^{*0}_{CP(+1)}\pi^+)$ — $\Gamma_{133}/\Gamma_{128}$

VALUE	DOCUMENT ID		TECN	COMMENT
0.095±0.017 OUR AVERAGE				
0.11 ±0.02 ±0.02	[1] ABE	06	BELL	$e^+e^- \to \Upsilon(4S)$
0.086±0.021±0.007	[2] AUBERT	05N	BABR	$e^+e^- \to \Upsilon(4S)$

[1] Reports a double ratio of $B(B^+ \to D^{*0}_{CP(+1)}K^+)/B(B^+ \to D^{*0}_{CP(+1)}\pi^+)$ and $B(B^+ \to \overline{D}^{*0}K^+)/B(B^+ \to \overline{D}^{*0}\pi^+)$, 1.41 ± 0.25 ± 0.06. We multiply by our best value of $B(B^+ \to \overline{D}^{*0}K^+)/B(B^+ \to \overline{D}^{*0}\pi^+) = 0.080 \pm 0.011$. Our first error is their experiment's error and the second error is systematic error from using our best value.
[2] Uses $D^{*0} \to D^0\pi^0$ with D^0 reconstructed in the CP-even eigenstates K^+K^- and $\pi^+\pi^-$.

$\Gamma(\overline{D}^{*0}_{CP(-1)}K^+)/\Gamma_{total}$ — Γ_{134}/Γ

VALUE (units 10^{-4})	DOCUMENT ID		TECN	COMMENT
$2.31\pm0.27^{+0.17}_{-0.16}$	[1] AUBERT	08BF	BABR	$e^+e^- \to \Upsilon(4S)$

[1] AUBERT 08BF reports $[\Gamma(B^+ \to \overline{D}^{*0}_{CP(-1)}K^+)/\Gamma_{total}] / [B(B^+ \to \overline{D}^*(2007)^0K^+)] = 0.55 \pm 0.06 \pm 0.02$ which we multiply by our best value $B(B^+ \to \overline{D}^*(2007)^0K^+) = (4.20^{+0.31}_{-0.28}) \times 10^{-4}$. Our first error is their experiment's error and our second error is the systematic error from using our best value.

$\Gamma(\overline{D}^{*0}_{CP(-1)}K^+)/\Gamma(D^{*0}_{CP(-1)}\pi^+)$ — $\Gamma_{134}/\Gamma_{129}$

VALUE	DOCUMENT ID		TECN	COMMENT
0.09±0.03±0.01	[1] ABE	06	BELL	$e^+e^- \to \Upsilon(4S)$

[1] Reports a double ratio of $B(B^+ \to (D^*_{CP(-1)})^0K^+)/B(B^+ \to (D^*_{CP(-1)})^0\pi^+)$ and $B(B^+ \to \overline{D}^{*0}K^+)/B(B^+ \to \overline{D}^{*0}\pi^+)$, 1.15 ± 0.31 ± 0.12. We multiply by our best value of $B(B^+ \to \overline{D}^{*0}K^+)/B(B^+ \to \overline{D}^{*0}\pi^+) = 0.080 \pm 0.011$. Our first error is their experiment's error and the second error is systematic error from using our best value.

$\Gamma(D^*(2007)^0K^+)/\Gamma(\overline{D}^*(2007)^0K^+)$ — $\Gamma_{135}/\Gamma_{132}$

"OUR EVALUATION" is derived from $r_B(B^+ \to D^{*0}K^+)$ data block listed in "CP vilation parameters" section.

VALUE (units 10^{-2})	DOCUMENT ID
$1.08^{+0.27}_{-0.29}$ OUR EVALUATION	

$\Gamma(\overline{D}^*(2007)^0K^*(892)^+)/\Gamma_{total}$ — Γ_{136}/Γ

VALUE (units 10^{-4})	DOCUMENT ID		TECN	COMMENT
8.1±1.4 OUR AVERAGE				
8.3±1.1±1.0	[1] AUBERT	04K	BABR	$e^+e^- \to \Upsilon(4S)$
7.2±2.2±2.6	[2] MAHAPATRA	02	CLE2	$e^+e^- \to \Upsilon(4S)$

[1] Assumes equal production of B^+ and B^0 at the $\Upsilon(4S)$.
[2] Assumes equal production of B^+ and B^0 at the $\Upsilon(4S)$ and an unpolarized final state.

$\Gamma(\overline{D}^*(2007)^0K^+\overline{K}^0)/\Gamma_{total}$ — Γ_{137}/Γ

VALUE (units 10^{-4})	CL%	DOCUMENT ID		TECN	COMMENT
<10.6	90	[1] DRUTSKOY	02	BELL	$e^+e^- \to \Upsilon(4S)$

[1] Assumes equal production of B^+ and B^0 at the $\Upsilon(4S)$.

$\Gamma(\overline{D}^*(2007)^0K^+\overline{K}^*(892)^0)/\Gamma_{total}$ — Γ_{138}/Γ

VALUE (units 10^{-4})	DOCUMENT ID		TECN	COMMENT
15.3±3.1±2.9	[1] DRUTSKOY	02	BELL	$e^+e^- \to \Upsilon(4S)$

[1] Assumes equal production of B^+ and B^0 at the $\Upsilon(4S)$.

$\Gamma(\overline{D}^*(2007)^0\pi^+\pi^+\pi^-)/\Gamma_{total}$ — Γ_{139}/Γ

VALUE (units 10^{-2})	EVTS	DOCUMENT ID		TECN	COMMENT
1.03 ±0.12 OUR AVERAGE					
1.055±0.047±0.129		[1] MAJUMDER	04	BELL	$e^+e^- \to \Upsilon(4S)$
0.94 ±0.20 ±0.17	48	[2,3] ALAM	94	CLE2	$e^+e^- \to \Upsilon(4S)$

[1] Assumes equal production of B^+ and B^0 at the $\Upsilon(4S)$.
[2] ALAM 94 assume equal production of B^+ and B^0 at the $\Upsilon(4S)$ and use the CLEO II $B(D^*(2007)^0 \to D^0\pi^0)$ and absolute $B(D^0 \to K^-\pi^+)$ and the PDG 1992 $B(D^0 \to K^-\pi^+\pi^0)/B(D^0 \to K^-\pi^+)$ and $B(D^0 \to K^-2\pi^+\pi^-)/B(D^0 \to K^-\pi^+)$.
[3] The three pion mass is required to be between 1.0 and 1.6 GeV consistent with an a_1 meson. (If this channel is dominated by a_1^+, the branching ratio for $\overline{D}^{*0}a_1^+$ is twice that for $\overline{D}^{*0}\pi^+\pi^+\pi^-$.)

$\Gamma(\overline{D}^*(2007)^0a_1(1260)^+)/\Gamma_{total}$ — Γ_{140}/Γ

VALUE	DOCUMENT ID		TECN	COMMENT
0.0188±0.0040±0.0034	[1,2] ALAM	94	CLE2	$e^+e^- \to \Upsilon(4S)$

[1] ALAM 94 value is twice their $\Gamma(\overline{D}^*(2007)^0\pi^+\pi^+\pi^-)/\Gamma_{total}$ value based on their observation that the three pions are dominantly in the $a_1(1260)$ mass range 1.0 to 1.6 GeV.
[2] ALAM 94 assume equal production of B^+ and B^0 at the $\Upsilon(4S)$ and use the CLEO II $B(D^*(2007)^0 \to D^0\pi^0)$ and absolute $B(D^0 \to K^-\pi^+)$ and the PDG 1992 $B(D^0 \to K^-\pi^+\pi^0)/B(D^0 \to K^-\pi^+)$ and $B(D^0 \to K^-2\pi^+\pi^-)/B(D^0 \to K^-\pi^+)$.

$\Gamma(\overline{D}^*(2007)^0\pi^-\pi^+\pi^+\pi^0)/\Gamma_{total}$ — Γ_{141}/Γ

VALUE	DOCUMENT ID		TECN	COMMENT
0.0180±0.0024±0.0027	[1] ALEXANDER	01B	CLE2	$e^+e^- \to \Upsilon(4S)$

[1] Assumes equal production of B^+ and B^0 at the $\Upsilon(4S)$. The signal is consistent with all observed $\omega\pi^+$ having proceeded through the ρ'^+ resonance at mass $1349 \pm 25^{+10}_{-5}$ MeV and width $547 \pm 86^{+46}_{-45}$ MeV.

$\Gamma(\overline{D}^{*0}3\pi^+2\pi^-)/\Gamma_{total}$ — Γ_{142}/Γ

VALUE (units 10^{-3})	DOCUMENT ID		TECN	COMMENT
5.67±0.91±0.85	[1] MAJUMDER	04	BELL	$e^+e^- \to \Upsilon(4S)$

[1] Assumes equal production of B^+ and B^0 at the $\Upsilon(4S)$.

$\Gamma(D^*(2010)^+\pi^0)/\Gamma_{total}$ — Γ_{143}/Γ

VALUE	CL%	DOCUMENT ID		TECN	COMMENT
$<3.6 \times 10^{-6}$		[1] IWABUCHI	08	BELL	$e^+e^- \to \Upsilon(4S)$
• • • We do not use the following data for averages, fits, limits, etc. • • •					
$<1.7 \times 10^{-4}$	90	[2] BRANDENB...	98	CLE2	$e^+e^- \to \Upsilon(4S)$

[1] Assumes equal production of B^+ and B^0 at the $\Upsilon(4S)$.
[2] BRANDENBURG 98 assume equal production of B^+ and B^0 at $\Upsilon(4S)$ and use the D^* partial reconstruction technique. The first error is their experiment's error and the second error is the systematic error from the PDG 96 value of $B(D^* \to D\pi)$.

$\Gamma(D^*(2010)^+K^0)/\Gamma_{total}$ — Γ_{144}/Γ

VALUE	CL%	DOCUMENT ID		TECN	COMMENT
$<9.0 \times 10^{-6}$	90	[1] AUBERT,B	05E	BABR	$e^+e^- \to \Upsilon(4S)$
• • • We do not use the following data for averages, fits, limits, etc. • • •					
$<9.5 \times 10^{-5}$	90	[1] GRITSAN	01	CLE2	$e^+e^- \to \Upsilon(4S)$

[1] Assumes equal production of B^+ and B^0 at the $\Upsilon(4S)$.

Downloaded from https://academic.oup.com/ptep/article/2022/8/083C01/6651666 by KIT Library user on 27 September 2022

$\Gamma(D^*(2010)^-\pi^+\pi^+\pi^0)/\Gamma_{total}$ — Γ_{145}/Γ

VALUE	EVTS	DOCUMENT ID		TECN	COMMENT
0.0152±0.0071±0.0001	26	[1] ALBRECHT	90J	ARG	$e^+e^- \to \Upsilon(4S)$
• • • We do not use the following data for averages, fits, limits, etc. • • •					
0.043 ±0.013 ±0.026	24	[2] ALBRECHT	87C	ARG	$e^+e^- \to \Upsilon(4S)$

[1] ALBRECHT 90J reports 0.018 ± 0.007 ± 0.005 from a measurement of $[\Gamma(B^+ \to D^*(2010)^-\pi^+\pi^+\pi^0)/\Gamma_{total}] \times [B(D^*(2010)^+ \to D^0\pi^+)]$ assuming $B(D^*(2010)^+ \to D^0\pi^+) = 0.57 \pm 0.06$, which we rescale to our best value $B(D^*(2010)^+ \to D^0\pi^+) = (67.7 \pm 0.5) \times 10^{-2}$. Our first error is their experiment's error and our second error is the systematic error from using our best value. Assumes equal production of B^+ and B^0 at the $\Upsilon(4S)$ and uses MarkIII branching fractions for the D.

[2] ALBRECHT 87C use PDG 86 branching ratios for D and $D^*(2010)$ and assume $B(\Upsilon(4S) \to B^+B^-) = 55\%$ and $B(\Upsilon(4S) \to B^0\overline{B}^0) = 45\%$. Superseded by ALBRECHT 90J.

$\Gamma(D^*(2010)^-\pi^+\pi^+\pi^+\pi^-)/\Gamma_{total}$ — Γ_{146}/Γ

VALUE (units 10^{-3})	CL%	DOCUMENT ID		TECN	COMMENT
2.56±0.26±0.33		[1] MAJUMDER	04	BELL	$e^+e^- \to \Upsilon(4S)$
• • • We do not use the following data for averages, fits, limits, etc. • • •					
<10	90	[2] ALBRECHT	90J	ARG	$e^+e^- \to \Upsilon(4S)$

[1] Assumes equal production of B^+ and B^0 at the $\Upsilon(4S)$.

[2] Assumes equal production of B^+ and B^0 at the $\Upsilon(4S)$ and uses MarkIII branching fractions for the D and $D^*(2010)$.

$\Gamma(\overline{D}^{**0}\pi^+)/\Gamma_{total}$ — Γ_{147}/Γ

D^{**0} represents an excited state with mass $2.2 < M < 2.8$ GeV/c^2.

VALUE (units 10^{-3})	DOCUMENT ID		TECN	COMMENT
5.7±1.2±0.2	[1,2] AUBERT,BE	06J	BABR	$e^+e^- \to \Upsilon(4S)$

[1] AUBERT,BE 06J reports $[\Gamma(B^+ \to \overline{D}^{**0}\pi^+)/\Gamma_{total}] / [B(B^+ \to \overline{D}^0\pi^+)] = 1.22 \pm 0.13 \pm 0.23$ which we multiply by our best value $B(B^+ \to \overline{D}^0\pi^+) = (4.68 \pm 0.13) \times 10^{-3}$. Our first error is their experiment's error and our second error is the systematic error from using our best value.

[2] Uses a missing-mass method. Does not depend on D branching fractions or B^+/B^0 production rates.

$\Gamma(\overline{D}_1^*(2420)^0\pi^+)/\Gamma_{total}$ — Γ_{148}/Γ

VALUE	EVTS	DOCUMENT ID		TECN	COMMENT
0.0015±0.0006 OUR AVERAGE	Error includes scale factor of 1.3.				
0.0011±0.0005±0.0002	8	[1] ALAM	94	CLE2	$e^+e^- \to \Upsilon(4S)$
0.0025±0.0007±0.0006		[2] ALBRECHT	94D	ARG	$e^+e^- \to \Upsilon(4S)$

[1] ALAM 94 assume equal production of B^+ and B^0 at the $\Upsilon(4S)$ and use the CLEO II $B(D^*(2010)^+ \to D^0\pi^+)$ and absolute $B(D^0 \to K^-\pi^+)$ and the PDG 1992 $B(D^0 \to K^-\pi^+\pi^0)/B(D^0 \to K^-\pi^+)$ and assuming $B(D_1(2420)^0 \to D^*(2010)^+\pi^-) = 67\%$.

[2] ALBRECHT 94D assume equal production of B^+ and B^0 at the $\Upsilon(4S)$ and use the CLEO II $B(D^*(2010)^+ \to D^0\pi^+)$ assuming $B(D_1(2420)^0 \to D^*(2010)^+\pi^-) = 67\%$.

$\Gamma(\overline{D}_1(2420)^0\pi^+ \times B(\overline{D}_1^0 \to \overline{D}^0\pi^+\pi^-))/\Gamma_{total}$ — Γ_{149}/Γ

VALUE (units 10^{-4})	DOCUMENT ID		TECN	COMMENT
$2.5\ ^{+1.6}_{-1.4}$ OUR FIT	Error includes scale factor of 3.9.			
$1.85\pm0.29\ ^{+0.35}_{-0.55}$	[1] ABE	05A	BELL	$e^+e^- \to \Upsilon(4S)$

[1] Assumes equal production of B^+ and B^0 at the $\Upsilon(4S)$.

$\Gamma(\overline{D}_1(2420)^0\pi^+ \times B(\overline{D}_1^0 \to \overline{D}^0\pi^+\pi^-))/\Gamma(\overline{D}^0\pi^+\pi^+\pi^-)$ — $\Gamma_{149}/\Gamma_{108}$

VALUE (units 10^{-2})	DOCUMENT ID		TECN	COMMENT
$4.6\ ^{+3.3}_{-2.7}$ OUR FIT	Error includes scale factor of 3.9.			
10.3±1.5±0.9	AAIJ	11E	LHCB	pp at 7 TeV

$\Gamma(\overline{D}_1(2420)^0\pi^+ \times B(\overline{D}_1^0 \to \overline{D}^0\pi^+\pi^- \text{(nonresonant)}))/\Gamma(\overline{D}^0\pi^+\pi^+\pi^-)$ — $\Gamma_{150}/\Gamma_{108}$

VALUE (units 10^{-2})	DOCUMENT ID		TECN	COMMENT
4.0±0.7±0.5	[1] AAIJ	11E	LHCB	pp at 7 TeV

[1] Excludes decays where $\overline{D}_1(2420)^0 \to D*(2010)^-\pi^+$.

$\Gamma(\overline{D}_1(2430)^0\pi^+, \overline{D}_1^0 \to D^*(2010)^-\pi^+)/\Gamma_{total}$ — Γ_{151}/Γ

VALUE (units 10^{-4})	DOCUMENT ID		TECN	COMMENT
3.51±0.06±0.61	[1] AAIJ	20D	LHCB	pp at 7, 8, 13 TeV

[1] AAIJ 20D used a 4-body amplitude analysis of $B^- \to D^{*+}\pi^-\pi^-$ decays.

$\Gamma(\overline{D}_2^*(2462)^0\pi^+, \overline{D}_2^{*0} \to D^-\pi^+)/\Gamma_{total}$ — Γ_{154}/Γ

VALUE (units 10^{-4})	DOCUMENT ID		TECN	COMMENT
3.56±0.24 OUR AVERAGE				
3.62±0.06±0.30	[1] AAIJ	16AH	LHCB	pp at 7, 8 TeV
3.5 ±0.2 ±0.4	[2] AUBERT	09AB	BABR	$e^+e^- \to \Upsilon(4S)$
3.4 ±0.3 ±0.72	[2] ABE	04D	BELL	$e^+e^- \to \Upsilon(4S)$

[1] Measured using a Dalitz plot analysis of $B^- \to D^+\pi^-\pi^-$ decays.

[2] Assumes equal production of B^+ and B^0 at the $\Upsilon(4S)$.

$\Gamma(\overline{D}_2^*(2462)^0\pi^+, \overline{D}_2^{*0} \to \overline{D}^0\pi^-\pi^+)/\Gamma(\overline{D}^0\pi^+\pi^+\pi^-)$ — $\Gamma_{155}/\Gamma_{108}$

VALUE (units 10^{-2})	DOCUMENT ID		TECN	COMMENT
4.0±1.0±0.4	AAIJ	11E	LHCB	pp at 7 TeV

$\Gamma(\overline{D}_2^*(2462)^0\pi^+, \overline{D}_2^{*0} \to \overline{D}^0\pi^-\pi^+ \text{(nonresonant)})/\Gamma(\overline{D}^0\pi^+\pi^+\pi^-)$ — $\Gamma_{156}/\Gamma_{108}$

VALUE	CL%	DOCUMENT ID		TECN	COMMENT
<3.0 × 10^{-2}	90	[1] AAIJ	11E	LHCB	pp at 7 TeV

[1] Excludes decays where $\overline{D}_2^*(2462)^0 \to D^*(2010)^-\pi^+$.

$\Gamma(\overline{D}_2^*(2462)^0\pi^+, \overline{D}_2^{*0} \to D^*(2010)^-\pi^+)/\Gamma(\overline{D}^0\pi^+\pi^+\pi^-)$ — $\Gamma_{157}/\Gamma_{108}$

VALUE (units 10^{-2})	DOCUMENT ID		TECN	COMMENT
3.9±1.2±0.4	[1] AAIJ	11E	LHCB	pp at 7 TeV

[1] Uses $B(D^*(2010)^+ \to D^0\pi^+) = (67.7 +- 0.5)\%$.

$\Gamma(\overline{D}_0^*(2400)^0\pi^+ \times B(\overline{D}_0^*(2400)^0 \to D^-\pi^+))/\Gamma_{total}$ — Γ_{158}/Γ

VALUE (units 10^{-4})	DOCUMENT ID		TECN	COMMENT
6.4±1.4 OUR AVERAGE				
6.8±0.3±2.0	[1] AUBERT	09AB	BABR	$e^+e^- \to \Upsilon(4S)$
6.1±0.6±1.8	[1] ABE	04D	BELL	$e^+e^- \to \Upsilon(4S)$

[1] Assumes equal production of B^+ and B^0 at the $\Upsilon(4S)$.

$\Gamma(\overline{D}_1(2421)^0\pi^+, \overline{D}_1^0 \to D^{*-}\pi^+)/\Gamma_{total}$ — Γ_{159}/Γ

VALUE (units 10^{-4})	DOCUMENT ID		TECN	COMMENT
7.4 ±1.0 OUR AVERAGE				
7.95±0.09±1.34	[1] AAIJ	20D	LHCB	pp at 7, 8, 13 TeV
6.8 ±0.7 ±1.3	[2] ABE	04D	BELL	$e^+e^- \to \Upsilon(4S)$

[1] AAIJ 20D used a 4-body amplitude analysis of $B^- \to D^{*+}\pi^-\pi^-$ decays.

[2] Assumes equal production of B^+ and B^0 at the $\Upsilon(4S)$.

$\Gamma(\overline{D}_2^*(2462)^0\pi^+, \overline{D}_2^{*0} \to D^{*-}\pi^+)/\Gamma_{total}$ — Γ_{160}/Γ

VALUE (units 10^{-4})	DOCUMENT ID		TECN	COMMENT
1.98±0.30 OUR AVERAGE				
2.08±0.03±0.37	[1] AAIJ	20D	LHCB	pp at 7, 8, 13 TeV
1.8 ±0.3 ±0.4	[2] ABE	04D	BELL	$e^+e^- \to \Upsilon(4S)$

[1] AAIJ 20D used a 4-body amplitude analysis of $B^- \to D^{*+}\pi^-\pi^-$ decays.

[2] Assumes equal production of B^+ and B^0 at the $\Upsilon(4S)$.

$\Gamma(\overline{D}_1'(2427)^0\pi^+, \overline{D}_1^0 \to D^{*-}\pi^+)/\Gamma_{total}$ — Γ_{161}/Γ

VALUE (units 10^{-4})	DOCUMENT ID		TECN	COMMENT
3.5 ±0.9 OUR AVERAGE	Error includes scale factor of 1.5.			
2.96±0.30±0.63	[1] AAIJ	20D	LHCB	pp at 7, 8, 13 TeV
5.0 ±0.4 ±1.1	[2] ABE	04D	BELL	$e^+e^- \to \Upsilon(4S)$

[1] AAIJ 20D used a 4-body amplitude analysis of $B^- \to D^{*+}\pi^-\pi^-$ decays.

[2] Assumes equal production of B^+ and B^0 at the $\Upsilon(4S)$.

$\Gamma(\overline{D}_1(2420)^0\pi^+ \times B(\overline{D}_1^0 \to \overline{D}^{*0}\pi^+\pi^-))/\Gamma_{total}$ — Γ_{162}/Γ

VALUE (units 10^{-4})	CL%	DOCUMENT ID		TECN	COMMENT
<0.06	90	[1] ABE	05A	BELL	$e^+e^- \to \Upsilon(4S)$

[1] Assumes equal production of B^+ and B^0 at the $\Upsilon(4S)$.

$\Gamma(\overline{D}_1^*(2420)^0\rho^+)/\Gamma_{total}$ — Γ_{163}/Γ

VALUE	CL%	DOCUMENT ID		TECN	COMMENT
<0.0014	90	[1] ALAM	94	CLE2	$e^+e^- \to \Upsilon(4S)$

[1] ALAM 94 assume equal production of B^+ and B^0 at the $\Upsilon(4S)$ and use the CLEO II $B(D^*(2010)^+ \to D^0\pi^+)$ assuming $B(D_1(2420)^0 \to D^*(2010)^+\pi^-) = 67\%$.

$\Gamma(\overline{D}_2^*(2460)^0\pi^+)/\Gamma_{total}$ — Γ_{164}/Γ

VALUE	CL%	DOCUMENT ID		TECN	COMMENT
<0.0013	90	[1] ALAM	94	CLE2	$e^+e^- \to \Upsilon(4S)$
• • • We do not use the following data for averages, fits, limits, etc. • • •					
<0.0028	90	[2] ALAM	94	CLE2	$e^+e^- \to \Upsilon(4S)$
<0.0023	90	[3] ALBRECHT	94D	ARG	$e^+e^- \to \Upsilon(4S)$

[1] ALAM 94 assume equal production of B^+ and B^0 at the $\Upsilon(4S)$ and use the MarkIII $B(D^+ \to K^-2\pi^+)$ and $B(D_2^*(2460)^0 \to D^+\pi^-) = 30\%$.

[2] ALAM 94 assume equal production of B^+ and B^0 at the $\Upsilon(4S)$ and use the MarkIII $B(D^+ \to K^-2\pi^+)$, the CLEO II $B(D^*(2010)^+ \to D^0\pi^+)$ and $B(D_2^*(2460)^0 \to D^*(2010)^+\pi^-) = 20\%$.

[3] ALBRECHT 94D assume equal production of B^+ and B^0 at the $\Upsilon(4S)$ and use the CLEO II $B(D^*(2010)^+ \to D^0\pi^+)$ and $B(D_2^*(2460)^0 \to D^*(2010)^+\pi^-) = 30\%$.

$\Gamma(\overline{D}_2^*(2460)^0\pi^+ \times B(\overline{D}_2^{*0} \to \overline{D}^{*0}\pi^+\pi^-))/\Gamma_{total}$ — Γ_{165}/Γ

VALUE (units 10^{-4})	CL%	DOCUMENT ID		TECN	COMMENT
<0.22	90	[1] ABE	05A	BELL	$e^+e^- \to \Upsilon(4S)$

[1] Assumes equal production of B^+ and B^0 at the $\Upsilon(4S)$.

Downloaded from https://academic.oup.com/ptep/article/2022/8/083C01/6651666 by KIT Library user on 27 September 2022

$\Gamma(\overline{D}_2^*(2460)^0\rho^+)/\Gamma_{total}$ — Γ_{171}/Γ

VALUE	CL%	DOCUMENT ID		TECN	COMMENT
<0.0047	90	[1] ALAM	94	CLE2	$e^+e^- \to \Upsilon(4S)$
<0.005	90	[2] ALAM	94	CLE2	$e^+e^- \to \Upsilon(4S)$

[1] ALAM 94 assume equal production of B^+ and B^0 at the $\Upsilon(4S)$ and use the Mark III $B(D^+ \to K^-2\pi^+)$ and $B(D_2^*(2460)^0 \to D^+\pi^-) = 30\%$.

[2] ALAM 94 assume equal production of B^+ and B^0 at the $\Upsilon(4S)$ and use the Mark III $B(D^+ \to K^-2\pi^+)$, the CLEO II $B(D^*(2010)^+ \to D^0\pi^+)$ and $B(D_2^*(2460)^0 \to D^*(2010)^+\pi^-) = 20\%$.

$\Gamma(\overline{D}(2550)^0\pi^+, \overline{D}^0 \to D^*(2010)^-\pi^+)/\Gamma_{total}$ — Γ_{152}/Γ

VALUE (units 10^{-4})	DOCUMENT ID		TECN	COMMENT
0.72±0.01±0.14	[1] AAIJ	20D	LHCB	pp at 7, 8, 13 TeV

[1] AAIJ 20D used a 4-body amplitude analysis of $B^- \to D^{*+}\pi^-\pi^-$ decays.

$\Gamma(\overline{D}_J^*(2600)^0\pi^+, \overline{D}_J^{*0} \to D^*(2010)^-\pi^+)/\Gamma_{total}$ — Γ_{153}/Γ

VALUE (units 10^{-4})	DOCUMENT ID		TECN	COMMENT
0.68±0.01±0.13	[1] AAIJ	20D	LHCB	pp at 7, 8, 13 TeV

[1] AAIJ 20D used a 4-body amplitude analysis of $B^- \to D^{*+}\pi^-\pi^-$ decays.

$\Gamma(\overline{D}_1^*(2680)^0\pi^+, \overline{D}_1^*(2680)^0 \to D^-\pi^+)/\Gamma_{total}$ — Γ_{166}/Γ

VALUE (units 10^{-4})	DOCUMENT ID		TECN	COMMENT
0.84±0.06±0.20	[1] AAIJ	16AH	LHCB	pp at 7, 8 TeV

[1] Measured using a Dalitz plot analysis of $B^+ \to D^-\pi^+\pi^+$ decays.

$\Gamma(\overline{D}(2740)^0\pi^+, \overline{D}^0 \to D^*(2010)^-\pi^+)/\Gamma_{total}$ — Γ_{167}/Γ

VALUE (units 10^{-4})	DOCUMENT ID		TECN	COMMENT
0.33±0.02±0.15	[1] AAIJ	20D	LHCB	pp at 7, 8, 13 TeV

[1] AAIJ 20D used a 4-body amplitude analysis of $B^- \to D^{*+}\pi^-\pi^-$ decays.

$\Gamma(\overline{D}_3^*(2750)^0\pi^+, \overline{D}_3^{*0} \to D^*(2010)^-\pi^+)/\Gamma_{total}$ — Γ_{168}/Γ

VALUE (units 10^{-4})	DOCUMENT ID		TECN	COMMENT
0.11±0.01±0.03	[1] AAIJ	20D	LHCB	pp at 7, 8, 13 TeV

[1] AAIJ 20D used a 4-body amplitude analysis of $B^- \to D^{*+}\pi^-\pi^-$ decays.

$\Gamma(\overline{D}_3^*(2760)^0\pi^+, \overline{D}_3^*(2760)^0\pi^+ \to D^-\pi^+)/\Gamma_{total}$ — Γ_{169}/Γ

VALUE (units 10^{-5})	DOCUMENT ID		TECN	COMMENT
1.0±0.1±0.2	[1] AAIJ	16AH	LHCB	pp at 7, 8 TeV

[1] Measured using a Dalitz plot analysis of $B^+ \to D^-\pi^+\pi^+$ decays.

$\Gamma(\overline{D}_2^*(3000)^0\pi^+, \overline{D}_2^*(3000)^0\pi^+ \to D^-\pi^+)/\Gamma_{total}$ — Γ_{170}/Γ

VALUE (units 10^{-6})	DOCUMENT ID		TECN	COMMENT
2±1±1	[1] AAIJ	16AH	LHCB	pp at 7, 8 TeV

[1] Measured using a Dalitz plot analysis of $B^+ \to D^-\pi^+\pi^+$ decays.

$\Gamma(\overline{D}^0 D_s^+)/\Gamma_{total}$ — Γ_{172}/Γ

VALUE (units 10^{-3})	DOCUMENT ID		TECN	COMMENT
9.0±0.9 OUR AVERAGE				
8.6±0.2±1.1	[1] AAIJ	13AP	LHCB	pp at 7 TeV
9.5±2.0±0.8	[2] AUBERT	06N	BABR	$e^+e^- \to \Upsilon(4S)$
9.8±2.6±0.9	[3] GIBAUT	96	CLE2	$e^+e^- \to \Upsilon(4S)$
14 ±8 ±1	[4] ALBRECHT	92G	ARG	$e^+e^- \to \Upsilon(4S)$
13 ±6 ±1	[5] BORTOLETTO	90	CLEO	$e^+e^- \to \Upsilon(4S)$

[1] Uses $B(B^0 \to D^-D_s^+) = (7.2 \pm 0.8) \times 10^{-3}$.

[2] AUBERT 06N reports $(0.92 \pm 0.14 \pm 0.18) \times 10^{-2}$ from a measurement of $[\Gamma(B^+ \to \overline{D}^0 D_s^+)/\Gamma_{total}] \times [B(D_s^+ \to \phi\pi^+)]$ assuming $B(D_s^+ \to \phi\pi^+) = 0.0462 \pm 0.0062$, which we rescale to our best value $B(D_s^+ \to \phi\pi^+) = (4.5 \pm 0.4) \times 10^{-2}$. Our first error is their experiment's error and our second error is the systematic error from using our best value.

[3] GIBAUT 96 reports $0.0126 \pm 0.0022 \pm 0.0025$ from a measurement of $[\Gamma(B^+ \to \overline{D}^0 D_s^+)/\Gamma_{total}] \times [B(D_s^+ \to \phi\pi^+)]$ assuming $B(D_s^+ \to \phi\pi^+) = 0.035$, which we rescale to our best value $B(D_s^+ \to \phi\pi^+) = (4.5 \pm 0.4) \times 10^{-2}$. Our first error is their experiment's error and our second error is the systematic error from using our best value.

[4] ALBRECHT 92G reports $0.024 \pm 0.012 \pm 0.004$ from a measurement of $[\Gamma(B^+ \to \overline{D}^0 D_s^+)/\Gamma_{total}] \times [B(D_s^+ \to \phi\pi^+)]$ assuming $B(D_s^+ \to \phi\pi^+) = 0.027$, which we rescale to our best value $B(D_s^+ \to \phi\pi^+) = (4.5 \pm 0.4) \times 10^{-2}$. Our first error is their experiment's error and our second error is the systematic error from using our best value. Assumes PDG 1990 D^0 branching ratios, e.g., $B(D^0 \to K^-\pi^+) = 3.71 \pm 0.25\%$.

[5] BORTOLETTO 90 reports 0.029 ± 0.013 from a measurement of $[\Gamma(B^+ \to \overline{D}^0 D_s^+)/\Gamma_{total}] \times [B(D_s^+ \to \phi\pi^+)]$ assuming $B(D_s^+ \to \phi\pi^+) = 0.02$, which we rescale to our best value $B(D_s^+ \to \phi\pi^+) = (4.5 \pm 0.4) \times 10^{-2}$. Our first error is their experiment's error and our second error is the systematic error from using our best value.

$\Gamma(D_{s0}^*(2317)^+\overline{D}^0, D_{s0}^{*+} \to D_s^+\pi^0)/\Gamma_{total}$ — Γ_{173}/Γ

VALUE (units 10^{-3})	DOCUMENT ID		TECN	COMMENT
$0.80^{+0.16}_{-0.13}$ OUR AVERAGE				
$0.80^{+0.17}_{-0.16} \pm 0.02$	[1,2] CHOI	15A	BELL	$e^+e^- \to \Upsilon(4S)$
$0.80^{+0.35}_{-0.21} \pm 0.07$	[2,3] AUBERT,B	04S	BABR	$e^+e^- \to \Upsilon(4S)$
• • • We do not use the following data for averages, fits, limits, etc. • • •				
$0.65^{+0.26}_{-0.24} \pm 0.06$	[2,4] KROKOVNY	03B	BELL	Repl. by CHOI 15A

[1] CHOI 15A reports $(8.0^{+1.3}_{-1.2} \pm 1.1 \pm 0.4) \times 10^{-4}$ from a measurement of $[\Gamma(B^+ \to D_{s0}^*(2317)^+\overline{D}^0, D_{s0}^{*+} \to D_s^+\pi^0)/\Gamma_{total}] \times [B(D_s^+ \to K^+K^-\pi^+)]$ assuming $B(D_s^+ \to K^+K^-\pi^+) = (5.39 \pm 0.21) \times 10^{-2}$, which we rescale to our best value $B(D_s^+ \to K^+K^-\pi^+) = (5.38 \pm 0.10) \times 10^{-2}$. Our first error is their experiment's error and our second error is the systematic error from using our best value.

[2] Assumes equal production of B^+ and B^0 at the $\Upsilon(4S)$.

[3] AUBERT,B 04S reports $(1.0 \pm 0.3^{+0.4}_{-0.2}) \times 10^{-3}$ from a measurement of $[\Gamma(B^+ \to D_{s0}^*(2317)^+\overline{D}^0, D_{s0}^{*+} \to D_s^+\pi^0)/\Gamma_{total}] \times [B(D_s^+ \to \phi\pi^+)]$ assuming $B(D_s^+ \to \phi\pi^+) = 0.036 \pm 0.009$, which we rescale to our best value $B(D_s^+ \to \phi\pi^+) = (4.5 \pm 0.4) \times 10^{-2}$. Our first error is their experiment's error and our second error is the systematic error from using our best value.

[4] KROKOVNY 03B reports $(0.81^{+0.30}_{-0.27} \pm 0.24) \times 10^{-3}$ from a measurement of $[\Gamma(B^+ \to D_{s0}^*(2317)^+\overline{D}^0, D_{s0}^{*+} \to D_s^+\pi^0)/\Gamma_{total}] \times [B(D_s^+ \to \phi\pi^+)]$ assuming $B(D_s^+ \to \phi\pi^+) = 0.036 \pm 0.009$, which we rescale to our best value $B(D_s^+ \to \phi\pi^+) = (4.5 \pm 0.4) \times 10^{-2}$. Our first error is their experiment's error and our second error is the systematic error from using our best value.

$\Gamma(D_{s0}(2317)^+\overline{D}^0 \times B(D_{s0}(2317)^+ \to D_s^{*+}\gamma))/\Gamma_{total}$ — Γ_{174}/Γ

VALUE (units 10^{-3})	CL%	DOCUMENT ID		TECN	COMMENT
<0.76	90	[1] KROKOVNY	03B	BELL	$e^+e^- \to \Upsilon(4S)$

[1] Assumes equal production of B^+ and B^0 at the $\Upsilon(4S)$.

$\Gamma(D_{s0}(2317)^+\overline{D}^*(2007)^0 \times B(D_{s0}(2317)^+ \to D_s^+\pi^0))/\Gamma_{total}$ — Γ_{175}/Γ

VALUE (units 10^{-3})	DOCUMENT ID		TECN	COMMENT
$0.9 \pm 0.6^{+0.4}_{-0.3}$	[1] AUBERT,B	04S	BABR	$e^+e^- \to \Upsilon(4S)$

[1] Assumes equal production of B^+ and B^0 at the $\Upsilon(4S)$.

$\Gamma(D_{sJ}(2457)^+\overline{D}^0)/\Gamma_{total}$ — Γ_{176}/Γ

VALUE (units 10^{-3})	DOCUMENT ID		TECN	COMMENT
$3.1^{+1.0}_{-0.9}$ OUR AVERAGE				
4.3±1.6±1.3	[1] AUBERT	06N	BABR	$e^+e^- \to \Upsilon(4S)$
$4.6^{+1.8}_{-1.6} \pm 1.0$	[2,3] AUBERT,B	04S	BABR	$e^+e^- \to \Upsilon(4S)$
$2.1^{+1.1}_{-0.9} \pm 0.5$	[2,4] KROKOVNY	03B	BELL	$e^+e^- \to \Upsilon(4S)$

[1] Uses a missing-mass method in the events that one of the B mesons is fully reconstructed.

[2] Assumes equal production of B^+ and B^0 at the $\Upsilon(4S)$.

[3] AUBERT,B 04S reports $[\Gamma(B^+ \to D_{sJ}(2457)^+\overline{D}^0)/\Gamma_{total}] \times [B(D_{s1}(2460)^+ \to D_s^{*+}\pi^0)] = (2.2^{+0.8}_{-0.7} \pm 0.3) \times 10^{-3}$ which we divide by our best value $B(D_{s1}(2460)^+ \to D_s^{*+}\pi^0) = (48 \pm 11) \times 10^{-2}$. Our first error is their experiment's error and our second error is the systematic error from using our best value.

[4] KROKOVNY 03B reports $[\Gamma(B^+ \to D_{sJ}(2457)^+\overline{D}^0)/\Gamma_{total}] \times [B(D_{s1}(2460)^+ \to D_s^{*+}\pi^0)] = (1.0^{+0.5}_{-0.4} \pm 0.1) \times 10^{-3}$ which we divide by our best value $B(D_{s1}(2460)^+ \to D_s^{*+}\pi^0) = (48 \pm 11) \times 10^{-2}$. Our first error is their experiment's error and our second error is the systematic error from using our best value.

$\Gamma(D_{sJ}(2457)^+\overline{D}^0 \times B(D_{sJ}(2457)^+ \to D_s^+\gamma))/\Gamma_{total}$ — Γ_{177}/Γ

VALUE (units 10^{-3})	DOCUMENT ID		TECN	COMMENT
$0.46^{+0.13}_{-0.11}$ OUR AVERAGE				
$0.48^{+0.19}_{-0.13} \pm 0.04$	[1,2] AUBERT,B	04S	BABR	$e^+e^- \to \Upsilon(4S)$
$0.45^{+0.15}_{-0.14} \pm 0.04$	[1,3] KROKOVNY	03B	BELL	$e^+e^- \to \Upsilon(4S)$

[1] Assumes equal production of B^+ and B^0 at the $\Upsilon(4S)$.

[2] AUBERT,B 04S reports $(0.6 \pm 0.2^{+0.2}_{-0.1}) \times 10^{-3}$ from a measurement of $[\Gamma(B^+ \to D_{sJ}(2457)^+\overline{D}^0 \times B(D_{sJ}(2457)^+ \to D_s^+\gamma))/\Gamma_{total}] \times [B(D_s^+ \to \phi\pi^+)]$ assuming $B(D_s^+ \to \phi\pi^+) = 0.036 \pm 0.009$, which we rescale to our best value $B(D_s^+ \to \phi\pi^+) = (4.5 \pm 0.4) \times 10^{-2}$. Our first error is their experiment's error and our second error is the systematic error from using our best value.

[3] KROKOVNY 03B reports $(0.56^{+0.16}_{-0.15} \pm 0.17) \times 10^{-3}$ from a measurement of $[\Gamma(B^+ \to D_{sJ}(2457)^+\overline{D}^0 \times B(D_{sJ}(2457)^+ \to D_s^+\gamma))/\Gamma_{total}] \times [B(D_s^+ \to \phi\pi^+)]$ assuming $B(D_s^+ \to \phi\pi^+) = 0.036 \pm 0.009$, which we rescale to our best value $B(D_s^+ \to \phi\pi^+) = (4.5 \pm 0.4) \times 10^{-2}$. Our first error is their experiment's error and our second error is the systematic error from using our best value.

Downloaded from https://academic.oup.com/ptep/article/2022/8/083C01/6651666 by KIT Library user on 27 September 2022

$\Gamma(D_{sJ}(2457)^+ \overline{D}^0 \times B(D_{sJ}(2457)^+ \to D_s^+ \pi^+ \pi^-))/\Gamma_{total}$ — Γ_{178}/Γ

VALUE (units 10^{-3})	CL%	DOCUMENT ID		TECN	COMMENT
<0.22	90	[1] KROKOVNY	03B	BELL	$e^+e^- \to \Upsilon(4S)$

[1] Assumes equal production of B^+ and B^0 at the $\Upsilon(4S)$.

$\Gamma(D_{sJ}(2457)^+ \overline{D}^0 \times B(D_{sJ}(2457)^+ \to D_s^+ \pi^0))/\Gamma_{total}$ — Γ_{179}/Γ

VALUE (units 10^{-3})	CL%	DOCUMENT ID		TECN	COMMENT
<0.27	90	[1] KROKOVNY	03B	BELL	$e^+e^- \to \Upsilon(4S)$

[1] Assumes equal production of B^+ and B^0 at the $\Upsilon(4S)$.

$\Gamma(D_{sJ}(2457)^+ \overline{D}^0 \times B(D_{sJ}(2457)^+ \to D_s^{*+} \gamma))/\Gamma_{total}$ — Γ_{180}/Γ

VALUE (units 10^{-3})	CL%	DOCUMENT ID		TECN	COMMENT
<0.98	90	[1] KROKOVNY	03B	BELL	$e^+e^- \to \Upsilon(4S)$

[1] Assumes equal production of B^+ and B^0 at the $\Upsilon(4S)$.

$\Gamma(D_{sJ}(2457)^+ \overline{D}^*(2007)^0)/\Gamma_{total}$ — Γ_{181}/Γ

VALUE (units 10^{-3})	DOCUMENT ID		TECN	COMMENT
12.0±3.0 OUR AVERAGE				
$11.2 \pm 2.6 \pm 2.0$	[1] AUBERT	06N	BABR	$e^+e^- \to \Upsilon(4S)$
$16\ ^{+8}_{-6}\ \pm 4$	[2,3] AUBERT,B	04S	BABR	$e^+e^- \to \Upsilon(4S)$

[1] Uses a missing-mass method in the events that one of the B mesons is fully reconstructed.
[2] AUBERT,B 04S reports $[\Gamma(B^+ \to D_{sJ}(2457)^+ \overline{D}^*(2007)^0)/\Gamma_{total}] \times [B(D_{s1}(2460)^+ \to D_s^{*+}\pi^0)] = (7.6 \pm 1.7^{+3.2}_{-2.4}) \times 10^{-3}$ which we divide by our best value $B(D_{s1}(2460)^+ \to D_s^{*+}\pi^0) = (48 \pm 11) \times 10^{-2}$. Our first error is their experiment's error and our second error is the systematic error from using our best value.
[3] Assumes equal production of B^+ and B^0 at the $\Upsilon(4S)$.

$\Gamma(D_{sJ}(2457)^+ \overline{D}^*(2007)^0 \times B(D_{sJ}(2457)^+ \to D_s^+ \gamma))/\Gamma_{total}$ — Γ_{182}/Γ

VALUE (units 10^{-3})	DOCUMENT ID		TECN	COMMENT
$\mathbf{1.4 \pm 0.4^{+0.6}_{-0.4}}$	[1] AUBERT,B	04S	BABR	$e^+e^- \to \Upsilon(4S)$

[1] Assumes equal production of B^+ and B^0 at the $\Upsilon(4S)$.

$\Gamma(\overline{D}^0 D_{s1}(2536)^+ \times B(D_{s1}(2536)^+ \to D^*(2007)^0 K^+))/\Gamma_{total}$ — Γ_{184}/Γ

VALUE (units 10^{-4})	CL%	DOCUMENT ID		TECN	COMMENT
2.16±0.52±0.45		[1] AUBERT	08B	BABR	$e^+e^- \to \Upsilon(4S)$
• • • We do not use the following data for averages, fits, limits, etc. • • •					
<2	90	AUBERT	03X	BABR	Repl. by AUBERT 08B

[1] Assumes equal production of B^+ and B^0 at the $\Upsilon(4S)$.

$\Gamma(\overline{D}^0 D_{s1}(2536)^+ \times B(D_{s1}(2536)^+ \to D^*(2007)^0 K^+ + D^*(2010)^+ K^0))/\Gamma_{total}$ — Γ_{183}/Γ

VALUE (units 10^{-4})	DOCUMENT ID		TECN	COMMENT
3.97±0.85±0.56	[1,2] AUSHEV	11	BELL	$e^+e^- \to \Upsilon(4S)$

[1] Uses $\Gamma(D^*(2007)^0 \to D^0\pi^0)$ / $\Gamma(D^*(2007)^0 \to D^0\gamma) = 1.74 \pm 0.13$ and $\Gamma(D_{s1}(2536)^+ \to D^*(2007)^0 K^+)$ / $\Gamma(D_{s1}(2536)^+ \to D^*(2010)^+ K^0) = 1.36 \pm 0.2$.
[2] Assumes equal production of B^+ and B^0 at the $\Upsilon(4S)$.

$\Gamma(\overline{D}^*(2007)^0 D_{s1}(2536)^+ \times B(D_{s1}(2536)^+ \to D^*(2007)^0 K^+))/\Gamma_{total}$ — Γ_{185}/Γ

VALUE (units 10^{-4})	CL%	DOCUMENT ID		TECN	COMMENT
5.46±1.17±1.04		[1] AUBERT	08B	BABR	$e^+e^- \to \Upsilon(4S)$
• • • We do not use the following data for averages, fits, limits, etc. • • •					
<7	90	AUBERT	03X	BABR	Repl. by AUBERT 08B

[1] Assumes equal production of B^+ and B^0 at the $\Upsilon(4S)$.

$\Gamma(\overline{D}^0 D_{s1}(2536)^+ \times B(D_{s1}(2536)^+ \to D^{*+} K^0))/\Gamma_{total}$ — Γ_{186}/Γ

VALUE (units 10^{-4})	DOCUMENT ID		TECN	COMMENT
2.30±0.98±0.43	[1] AUBERT	08B	BABR	$e^+e^- \to \Upsilon(4S)$

[1] Assumes equal production of B^+ and B^0 at the $\Upsilon(4S)$.

$\Gamma(\overline{D}^0 D_{sJ}(2700)^+ \times B(D_{sJ}(2700)^+ \to D^0 K^+))/\Gamma_{total}$ — Γ_{187}/Γ

VALUE (units 10^{-4})	DOCUMENT ID		TECN	COMMENT
5.6 ±1.8 OUR AVERAGE Error includes scale factor of 1.7.				
$5.02 \pm 0.71 \pm 0.93$	[1] LEES	15C	BABR	$e^+e^- \to \Upsilon(4S)$
$11.3\ \pm 2.2\ ^{+1.4}_{-2.8}$	[1] BRODZICKA	08	BELL	$e^+e^- \to \Upsilon(4S)$

[1] Assumes equal production of B^+ and B^0 at the $\Upsilon(4S)$.

$\Gamma(\overline{D}^{*0} D_{s1}(2536)^+,\ D_{s1}^+ \to D^{*+} K^0)/\Gamma_{total}$ — Γ_{188}/Γ

VALUE (units 10^{-4})	DOCUMENT ID		TECN	COMMENT
3.92±2.46±0.83	[1] AUBERT	08B	BABR	$e^+e^- \to \Upsilon(4S)$

[1] Assumes equal production of B^+ and B^0 at the $\Upsilon(4S)$.

$\Gamma(\overline{D}^0 D_{sJ}(2573)^+,\ D_{sJ}^+ \to D^0 K^+)/\Gamma_{total}$ — Γ_{189}/Γ

VALUE (units 10^{-4})	DOCUMENT ID		TECN	COMMENT
0.08±0.14±0.05	[1] LEES	15C	BABR	$e^+e^- \to \Upsilon(4S)$

[1] Assumes equal production of B^+ and B^0 at the $\Upsilon(4S)$.

$\Gamma(\overline{D}^{*0} D_{sJ}(2573),\ D_{sJ}^+ \to D^0 K^+)/\Gamma_{total}$ — Γ_{190}/Γ

VALUE (units 10^{-4})	CL%	DOCUMENT ID		TECN	COMMENT
<2	90	AUBERT	03X	BABR	$e^+e^- \to \Upsilon(4S)$

$\Gamma(\overline{D}^*(2007)^0 D_{sJ}(2573),\ D_{sJ}^+ \to D^0 K^+)/\Gamma_{total}$ — Γ_{191}/Γ

VALUE (units 10^{-4})	CL%	DOCUMENT ID		TECN	COMMENT
<5	90	AUBERT	03X	BABR	$e^+e^- \to \Upsilon(4S)$

$\Gamma(\overline{D}^0 D_s^{*+})/\Gamma_{total}$ — Γ_{192}/Γ

VALUE	DOCUMENT ID		TECN	COMMENT
0.0076±0.0016 OUR AVERAGE				
$0.0079 \pm 0.0017 \pm 0.0007$	[1] AUBERT	06N	BABR	$e^+e^- \to \Upsilon(4S)$
$0.0068 \pm 0.0025 \pm 0.0006$	[2] GIBAUT	96	CLE2	$e^+e^- \to \Upsilon(4S)$
$0.010\ \pm 0.007\ \pm 0.001$	[3] ALBRECHT	92G	ARG	$e^+e^- \to \Upsilon(4S)$

[1] AUBERT 06N reports $(0.77 \pm 0.15 \pm 0.13) \times 10^{-2}$ from a measurement of $[\Gamma(B^+ \to \overline{D}^0 D_s^{*+})/\Gamma_{total}] \times [B(D_s^+ \to \phi\pi^+)]$ assuming $B(D_s^+ \to \phi\pi^+) = 0.0462 \pm 0.0062$, which we rescale to our best value $B(D_s^+ \to \phi\pi^+) = (4.5 \pm 0.4) \times 10^{-2}$. Our first error is their experiment's error and our second error is the systematic error from using our best value.
[2] GIBAUT 96 reports $0.0087 \pm 0.0027 \pm 0.0017$ from a measurement of $[\Gamma(B^+ \to \overline{D}^0 D_s^{*+})/\Gamma_{total}] \times [B(D_s^+ \to \phi\pi^+)]$ assuming $B(D_s^+ \to \phi\pi^+) = 0.035$, which we rescale to our best value $B(D_s^+ \to \phi\pi^+) = (4.5 \pm 0.4) \times 10^{-2}$. Our first error is their experiment's error and our second error is the systematic error from using our best value.
[3] ALBRECHT 92G reports $0.016 \pm 0.012 \pm 0.003$ from a measurement of $[\Gamma(B^+ \to \overline{D}^0 D_s^{*+})/\Gamma_{total}] \times [B(D_s^+ \to \phi\pi^+)]$ assuming $B(D_s^+ \to \phi\pi^+) = 0.027$, which we rescale to our best value $B(D_s^+ \to \phi\pi^+) = (4.5 \pm 0.4) \times 10^{-2}$. Our first error is their experiment's error and our second error is the systematic error from using our best value. Assumes PDG 1990 D^0 branching ratios, e.g., $B(D^0 \to K^-\pi^+) = 3.71 \pm 0.25\%$.

$\Gamma(\overline{D}^*(2007)^0 D_s^+)/\Gamma_{total}$ — Γ_{193}/Γ

VALUE	DOCUMENT ID		TECN	COMMENT
0.0082±0.0017 OUR AVERAGE				
$0.0078 \pm 0.0018 \pm 0.0007$	[1] AUBERT	06N	BABR	$e^+e^- \to \Upsilon(4S)$
$0.011\ \pm 0.004\ \pm 0.001$	[2] GIBAUT	96	CLE2	$e^+e^- \to \Upsilon(4S)$
$0.008\ \pm 0.006\ \pm 0.001$	[3] ALBRECHT	92G	ARG	$e^+e^- \to \Upsilon(4S)$

[1] AUBERT 06N reports $(0.76 \pm 0.15 \pm 0.13) \times 10^{-2}$ from a measurement of $[\Gamma(B^+ \to \overline{D}^*(2007)^0 D_s^+)/\Gamma_{total}] \times [B(D_s^+ \to \phi\pi^+)]$ assuming $B(D_s^+ \to \phi\pi^+) = 0.0462 \pm 0.0062$, which we rescale to our best value $B(D_s^+ \to \phi\pi^+) = (4.5 \pm 0.4) \times 10^{-2}$. Our first error is their experiment's error and our second error is the systematic error from using our best value.
[2] GIBAUT 96 reports $0.0140 \pm 0.0043 \pm 0.0035$ from a measurement of $[\Gamma(B^+ \to \overline{D}^*(2007)^0 D_s^+)/\Gamma_{total}] \times [B(D_s^+ \to \phi\pi^+)]$ assuming $B(D_s^+ \to \phi\pi^+) = 0.035$, which we rescale to our best value $B(D_s^+ \to \phi\pi^+) = (4.5 \pm 0.4) \times 10^{-2}$. Our first error is their experiment's error and our second error is the systematic error from using our best value.
[3] ALBRECHT 92G reports $0.013 \pm 0.009 \pm 0.002$ from a measurement of $[\Gamma(B^+ \to \overline{D}^*(2007)^0 D_s^+)/\Gamma_{total}] \times [B(D_s^+ \to \phi\pi^+)]$ assuming $B(D_s^+ \to \phi\pi^+) = 0.027$, which we rescale to our best value $B(D_s^+ \to \phi\pi^+) = (4.5 \pm 0.4) \times 10^{-2}$. Our first error is their experiment's error and our second error is the systematic error from using our best value. Assumes PDG 1990 D^0 and $D^*(2007)^0$ branching ratios, e.g., $B(D^0 \to K^-\pi^+) = 3.71 \pm 0.25\%$ and $B(D^*(2007)^0 \to D^0\pi^0) = 55 \pm 6\%$.

$\Gamma(\overline{D}^*(2007)^0 D_s^{*+})/\Gamma_{total}$ — Γ_{194}/Γ

VALUE	DOCUMENT ID		TECN	COMMENT
0.0171±0.0024 OUR AVERAGE				
$0.0167 \pm 0.0019 \pm 0.0015$	[1] AUBERT	06N	BABR	$e^+e^- \to \Upsilon(4S)$
$0.024\ \pm 0.009\ \pm 0.002$	[2] GIBAUT	96	CLE2	$e^+e^- \to \Upsilon(4S)$
$0.019\ \pm 0.010\ \pm 0.002$	[3] ALBRECHT	92G	ARG	$e^+e^- \to \Upsilon(4S)$

[1] AUBERT 06N reports $(1.62 \pm 0.22 \pm 0.18) \times 10^{-2}$ from a measurement of $[\Gamma(B^+ \to \overline{D}^*(2007)^0 D_s^{*+})/\Gamma_{total}] \times [B(D_s^+ \to \phi\pi^+)]$ assuming $B(D_s^+ \to \phi\pi^+) = 0.0462 \pm 0.0062$, which we rescale to our best value $B(D_s^+ \to \phi\pi^+) = (4.5 \pm 0.4) \times 10^{-2}$. Our first error is their experiment's error and our second error is the systematic error from using our best value.
[2] GIBAUT 96 reports $0.0310 \pm 0.0088 \pm 0.0065$ from a measurement of $[\Gamma(B^+ \to \overline{D}^*(2007)^0 D_s^{*+})/\Gamma_{total}] \times [B(D_s^+ \to \phi\pi^+)]$ assuming $B(D_s^+ \to \phi\pi^+) = 0.035$, which we rescale to our best value $B(D_s^+ \to \phi\pi^+) = (4.5 \pm 0.4) \times 10^{-2}$. Our first error is their experiment's error and our second error is the systematic error from using our best value.
[3] ALBRECHT 92G reports $0.031 \pm 0.016 \pm 0.005$ from a measurement of $[\Gamma(B^+ \to \overline{D}^*(2007)^0 D_s^{*+})/\Gamma_{total}] \times [B(D_s^+ \to \phi\pi^+)]$ assuming $B(D_s^+ \to \phi\pi^+) = 0.027$, which we rescale to our best value $B(D_s^+ \to \phi\pi^+) = (4.5 \pm 0.4) \times 10^{-2}$. Our first error is their experiment's error and our second error is the systematic error from using our best value. Assumes PDG 1990 D^0 and $D^*(2007)^0$ branching ratios, e.g., $B(D^0 \to K^-\pi^+) = 3.71 \pm 0.25\%$ and $B(D^*(2007)^0 \to D^0\pi^0) = 55 \pm 6\%$.

$\Gamma(D_s^{(*)+} \overline{D}^{**0})/\Gamma_{total}$ — Γ_{195}/Γ

VALUE	DOCUMENT ID		TECN	COMMENT
$\mathbf{(2.73 \pm 0.93 \pm 0.68) \times 10^{-2}}$	[1] AHMED	00B	CLE2	$e^+e^- \to \Upsilon(4S)$

[1] AHMED 00B reports their experiment's uncertainties $(\pm 0.78 \pm 0.48 \pm 0.68)\%$, where the first error is statistical, the second is systematic, and the third is the uncertainty in the $D_s \to \phi\pi$ branching fraction. We combine the first two in quadrature.

Downloaded from https://academic.oup.com/ptep/article/2022/8/083C01/6651666 by KIT Library user on 27 September 2022

$\Gamma(\overline{D}^*(2007)^0 D^*(2010)^+)/\Gamma_{total}$ — Γ_{196}/Γ

VALUE (units 10^{-4})	CL%	DOCUMENT ID		TECN	COMMENT
8.1±1.2±1.2		[1] AUBERT,B	06A	BABR	$e^+e^- \to \Upsilon(4S)$
• • • We do not use the following data for averages, fits, limits, etc. • • •					
<110	90	BARATE	98Q	ALEP	$e^+e^- \to Z$

[1] Assumes equal production of B^+ and B^0 at the $\Upsilon(4S)$.

$[\Gamma(\overline{D}^0 D^*(2010)^+) + \Gamma(\overline{D}^*(2007)^0 D^+)]/\Gamma_{total}$ — Γ_{197}/Γ

VALUE (units 10^{-4})	CL%	DOCUMENT ID		TECN	COMMENT
<130	90	BARATE	98Q	ALEP	$e^+e^- \to Z$

$\Gamma(\overline{D}^0 D^*(2010)^+)/\Gamma_{total}$ — Γ_{198}/Γ

VALUE (units 10^{-4})	DOCUMENT ID		TECN	COMMENT
3.9 ±0.5 OUR AVERAGE				
3.6 ±0.5 ±0.4	[1] AUBERT,B	06A	BABR	$e^+e^- \to \Upsilon(4S)$
4.57±0.71±0.56	[1] MAJUMDER	05	BELL	$e^+e^- \to \Upsilon(4S)$

[1] Assumes equal production of B^+ and B^0 at the $\Upsilon(4S)$.

$\Gamma(\overline{D}^0 D^+)/\Gamma_{total}$ — Γ_{199}/Γ

VALUE (units 10^{-4})	CL%	DOCUMENT ID		TECN	COMMENT
3.8 ±0.4 OUR AVERAGE					
3.85±0.31±0.38		[1] ADACHI	08	BELL	$e^+e^- \to \Upsilon(4S)$
3.8 ±0.6 ±0.5		[1] AUBERT,B	06A	BABR	$e^+e^- \to \Upsilon(4S)$
• • • We do not use the following data for averages, fits, limits, etc. • • •					
4.83±0.78±0.58		[1] MAJUMDER	05	BELL	Repl. by ADACHI 08
<67	90	BARATE	98Q	ALEP	$e^+e^- \to Z$

[1] Assumes equal production of B^+ and B^0 at the $\Upsilon(4S)$.

$\Gamma(\overline{D}^0 D^+ K^0)/\Gamma_{total}$ — Γ_{200}/Γ

VALUE (units 10^{-3})	CL%	DOCUMENT ID		TECN	COMMENT
1.55±0.17±0.13		[1] DEL-AMO-SA...	11B	BABR	$e^+e^- \to \Upsilon(4S)$
• • • We do not use the following data for averages, fits, limits, etc. • • •					
<2.8	90	[1] AUBERT	03X	BABR	Repl. by DEL-AMO-SANCHEZ 11B

[1] Assumes equal production of B^+ and B^0 at the $\Upsilon(4S)$.

$\Gamma(D^+ \overline{D}^*(2007)^0)/\Gamma_{total}$ — Γ_{201}/Γ

VALUE (units 10^{-4})	DOCUMENT ID		TECN	COMMENT
6.3±1.4±1.0	[1] AUBERT,B	06A	BABR	$e^+e^- \to \Upsilon(4S)$

[1] Assumes equal production of B^+ and B^0 at the $\Upsilon(4S)$.

$\Gamma(\overline{D}^*(2007)^0 D^+ K^0)/\Gamma_{total}$ — Γ_{202}/Γ

VALUE (units 10^{-3})	CL%	DOCUMENT ID		TECN	COMMENT
2.06±0.38±0.30		[1] DEL-AMO-SA...	11B	BABR	$e^+e^- \to \Upsilon(4S)$
• • • We do not use the following data for averages, fits, limits, etc. • • •					
<6.1	90	[1] AUBERT	03X	BABR	Repl. by DEL-AMO-SANCHEZ 11B

[1] Assumes equal production of B^+ and B^0 at the $\Upsilon(4S)$.

$\Gamma(\overline{D}^0 D^*(2010)^+ K^0)/\Gamma_{total}$ — Γ_{203}/Γ

VALUE (units 10^{-3})	DOCUMENT ID		TECN	COMMENT
3.81±0.31±0.23	[1] DEL-AMO-SA...	11B	BABR	$e^+e^- \to \Upsilon(4S)$
• • • We do not use the following data for averages, fits, limits, etc. • • •				
$5.2\ ^{+1.0}_{-0.9}$ ±0.7	[1] AUBERT	03X	BABR	Repl. by DEL-AMO-SANCHEZ 11B

[1] Assumes equal production of B^+ and B^0 at the $\Upsilon(4S)$.

$\Gamma(\overline{D}^*(2007)^0 D^*(2010)^+ K^0)/\Gamma_{total}$ — Γ_{204}/Γ

VALUE (units 10^{-3})	DOCUMENT ID		TECN	COMMENT
9.17±0.83±0.90	[1] DEL-AMO-SA...	11B	BABR	$e^+e^- \to \Upsilon(4S)$
• • • We do not use the following data for averages, fits, limits, etc. • • •				
$7.8\ ^{+2.3}_{-2.1}$ ±1.4	[1] AUBERT	03X	BABR	Repl. by DEL-AMO-SANCHEZ 11B

[1] Assumes equal production of B^+ and B^0 at the $\Upsilon(4S)$.

$\Gamma(\overline{D}^0 D^0 K^+)/\Gamma_{total}$ — Γ_{205}/Γ

VALUE (units 10^{-3})	DOCUMENT ID		TECN	COMMENT
1.45±0.33 OUR AVERAGE	Error includes scale factor of 2.6.			
1.31±0.07±0.12	[1] DEL-AMO-SA...	11B	BABR	$e^+e^- \to \Upsilon(4S)$
$2.22\pm0.22\ ^{+0.26}_{-0.24}$	[1] BRODZICKA	08	BELL	$e^+e^- \to \Upsilon(4S)$
• • • We do not use the following data for averages, fits, limits, etc. • • •				
1.17±0.21±0.15	[1] CHISTOV	04	BELL	Repl. by BRODZICKA 08
1.9 ±0.3 ±0.3	[1] AUBERT	03X	BABR	Repl. by DEL-AMO-SANCHEZ 11B

[1] Assumes equal production of B^+ and B^0 at the $\Upsilon(4S)$.

$\Gamma(\overline{D}^*(2007)^0 D^0 K^+)/\Gamma_{total}$ — Γ_{206}/Γ

VALUE (units 10^{-3})	CL%	DOCUMENT ID		TECN	COMMENT
2.26±0.16±0.17		[1] DEL-AMO-SA...	11B	BABR	$e^+e^- \to \Upsilon(4S)$
• • • We do not use the following data for averages, fits, limits, etc. • • •					
<3.8	90	[1] AUBERT	03X	BABR	Repl. by DEL-AMO-SANCHEZ 11B

[1] Assumes equal production of B^+ and B^0 at the $\Upsilon(4S)$.

$\Gamma(\overline{D}^0 D^*(2007)^0 K^+)/\Gamma_{total}$ — Γ_{207}/Γ

VALUE (units 10^{-3})	DOCUMENT ID		TECN	COMMENT
6.32±0.19±0.45	[1] DEL-AMO-SA...	11B	BABR	$e^+e^- \to \Upsilon(4S)$
• • • We do not use the following data for averages, fits, limits, etc. • • •				
4.7 ±0.7 ±0.7	[1] AUBERT	03X	BABR	Repl. by DEL-AMO-SANCHEZ 11B

[1] Assumes equal production of B^+ and B^0 at the $\Upsilon(4S)$.

$\Gamma(\overline{D}^*(2007)^0 D^*(2007)^0 K^+)/\Gamma_{total}$ — Γ_{208}/Γ

VALUE (units 10^{-3})	DOCUMENT ID		TECN	COMMENT
11.23±0.36±1.26	[1] DEL-AMO-SA...	11B	BABR	$e^+e^- \to \Upsilon(4S)$
• • • We do not use the following data for averages, fits, limits, etc. • • •				
$5.3\ ^{+1.1}_{-1.0}$ ±1.2	[1] AUBERT	03X	BABR	Repl. by DEL-AMO-SANCHEZ 11B

[1] Assumes equal production of B^+ and B^0 at the $\Upsilon(4S)$.

$\Gamma(D^- D^+ K^+)/\Gamma_{total}$ — Γ_{209}/Γ

VALUE (units 10^{-3})	CL%	DOCUMENT ID		TECN	COMMENT
0.22±0.05±0.05		[1] DEL-AMO-SA...	11B	BABR	$e^+e^- \to \Upsilon(4S)$
• • • We do not use the following data for averages, fits, limits, etc. • • •					
<0.90	90	[1] CHISTOV	04	BELL	$e^+e^- \to \Upsilon(4S)$
<0.4	90	[1] AUBERT	03X	BABR	Repl. by DEL-AMO-SANCHEZ 11B

[1] Assumes equal production of B^+ and B^0 at the $\Upsilon(4S)$.

$\Gamma(X_0(2900) D^+, X_0 \to D^- K^+)/\Gamma(D^- D^+ K^+)$ — $\Gamma_{210}/\Gamma_{209}$

VALUE (units 10^{-2})	DOCUMENT ID		TECN	COMMENT
5.6±1.4±0.5	[1] AAIJ	20AI	LHCB	pp at 7, 8, 13 TeV

[1] Measured in Dalitz plot analysis of $B^+ \to D^- D^+ K^+$ decays.

$\Gamma(X_1(2900) D^+, X_1 \to D^- K^+)/\Gamma(D^- D^+ K^+)$ — $\Gamma_{211}/\Gamma_{209}$

VALUE (units 10^{-2})	DOCUMENT ID		TECN	COMMENT
30.6±2.4±2.1	[1] AAIJ	20AI	LHCB	pp at 7, 8, 13 TeV

[1] Measured in Dalitz plot analysis of $B^+ \to D^- D^+ K^+$ decays.

$\Gamma(D^- D^+ K^+ \text{nonresonant})/\Gamma(D^- D^+ K^+)$ — $\Gamma_{212}/\Gamma_{209}$

VALUE (units 10^{-2})	DOCUMENT ID		TECN	COMMENT
24.2±2.2±0.5	[1] AAIJ	20AI	LHCB	pp at 7, 8, 13 TeV

[1] Measured in Dalitz plot analysis of $B^+ \to D^- D^+ K^+$ decays.

$\Gamma(D^- D^*(2010)^+ K^+)/\Gamma_{total}$ — Γ_{213}/Γ

VALUE (units 10^{-3})	CL%	DOCUMENT ID		TECN	COMMENT
0.63±0.09±0.06		[1] DEL-AMO-SA...	11B	BABR	$e^+e^- \to \Upsilon(4S)$
• • • We do not use the following data for averages, fits, limits, etc. • • •					
<0.7	90	[1] AUBERT	03X	BABR	Repl. by DEL-AMO-SANCHEZ 11B

[1] Assumes equal production of B^+ and B^0 at the $\Upsilon(4S)$.

$\Gamma(D^- D^*(2010)^+ K^+)/\Gamma(\overline{D}^0 D^0 K^+)$ — $\Gamma_{213}/\Gamma_{205}$

VALUE	DOCUMENT ID		TECN	COMMENT
0.517±0.015±0.017	[1] AAIJ	20AN	LHCB	pp at 7, 8, 13 TeV

[1] Uses $D^+ \to K^-\pi^+\pi^+$, $D^0 \to K^-\pi^+$ and $D^0 \to K^-\pi^+\pi^+\pi^-$ decays.

$\Gamma(D^*(2010)^- D^+ K^+)/\Gamma_{total}$ — Γ_{214}/Γ

VALUE (units 10^{-3})	DOCUMENT ID		TECN	COMMENT
0.60±0.10±0.08	[1] DEL-AMO-SA...	11B	BABR	$e^+e^- \to \Upsilon(4S)$
• • • We do not use the following data for averages, fits, limits, etc. • • •				
1.5 ±0.3 ±0.2	[1] AUBERT	03X	BABR	Repl. by DEL-AMO-SANCHEZ 11B

[1] Assumes equal production of B^+ and B^0 at the $\Upsilon(4S)$.

$\Gamma(D^*(2010)^- D^+ K^+)/\Gamma(\overline{D}^0 D^0 K^+)$ — $\Gamma_{214}/\Gamma_{205}$

VALUE	DOCUMENT ID		TECN	COMMENT
0.577±0.016±0.018	[1] AAIJ	20AN	LHCB	pp at 7, 8, 13 TeV

[1] Uses $D^+ \to K^-\pi^+\pi^+$, $D^0 \to K^-\pi^+$ and $D^0 \to K^-\pi^+\pi^+\pi^-$ decays.

$\Gamma(D^- D^*(2010)^+ K^+)/\Gamma(D^*(2010)^- D^+ K^+)$ — $\Gamma_{213}/\Gamma_{214}$

VALUE	DOCUMENT ID		TECN	COMMENT
0.907±0.033±0.014	[1] AAIJ	20AN	LHCB	pp at 7, 8, 13 TeV

[1] Uses $D^+ \to K^-\pi^+\pi^+$, $D^0 \to K^-\pi^+$ and $D^0 \to K^-\pi^+\pi^+\pi^-$ decays.

Downloaded from https://academic.oup.com/ptep/article/2022/8/083C01/6651666 by KIT Library user on 27 September 2022

$\Gamma(D^*(2010)^- D^*(2010)^+ K^+)/\Gamma_{total}$ — Γ_{215}/Γ

VALUE (units 10^{-3})	CL%	DOCUMENT ID	TECN	COMMENT
1.32±0.13±0.12		[1] DEL-AMO-SA...11B	BABR	$e^+e^- \to \Upsilon(4S)$
• • • We do not use the following data for averages, fits, limits, etc. • • •				
<1.8	90	[1] AUBERT 03X	BABR	Repl. by DEL-AMO-SANCHEZ 11B

[1] Assumes equal production of B^+ and B^0 at the $\Upsilon(4S)$.

$\Gamma((\overline{D}+\overline{D}^*)(D+D^*)K)/\Gamma_{total}$ — Γ_{216}/Γ

VALUE (units 10^{-2})	DOCUMENT ID	TECN	COMMENT
4.05±0.11±0.28	[1] DEL-AMO-SA...11B	BABR	$e^+e^- \to \Upsilon(4S)$
• • • We do not use the following data for averages, fits, limits, etc. • • •			
3.5 ±0.3 ±0.5	[1] AUBERT 03X	BABR	Repl. by DEL-AMO-SANCHEZ 11B

[1] Assumes equal production of B^+ and B^0 at the $\Upsilon(4S)$.

$\Gamma(D_s^+\pi^0)/\Gamma_{total}$ — Γ_{217}/Γ

VALUE (units 10^{-5})	CL%	DOCUMENT ID	TECN	COMMENT
$1.6^{+0.6}_{-0.5}\pm0.1$		[1] AUBERT 07M	BABR	$e^+e^- \to \Upsilon(4S)$
• • • We do not use the following data for averages, fits, limits, etc. • • •				
<16	90	[2] ALEXANDER 93B	CLE2	$e^+e^- \to \Upsilon(4S)$

[1] AUBERT 07M reports $[\Gamma(B^+ \to D_s^+\pi^0)/\Gamma_{total}] \times [B(D_s^+ \to \phi\pi^+)] = (7.0^{+2.4}_{-2.1}{}^{+0.6}_{-0.8}) \times 10^{-7}$ which we divide by our best value $B(D_s^+ \to \phi\pi^+) = (4.5 \pm 0.4) \times 10^{-2}$. Our first error is their experiment's error and our second error is the systematic error from using our best value.

[2] ALEXANDER 93B reports $< 2.0 \times 10^{-4}$ from a measurement of $[\Gamma(B^+ \to D_s^+\pi^0)/\Gamma_{total}] \times [B(D_s^+ \to \phi\pi^+)]$ assuming $B(D_s^+ \to \phi\pi^+) = 0.037$, which we rescale to our best value $B(D_s^+ \to \phi\pi^+) = 4.5 \times 10^{-2}$.

$[\Gamma(D_s^+\pi^0)+\Gamma(D_s^{*+}\pi^0)]/\Gamma_{total}$ — $(\Gamma_{217}+\Gamma_{218})/\Gamma$

VALUE	CL%	DOCUMENT ID	TECN	COMMENT
$<5\times10^{-4}$	90	[1] ALBRECHT 93E	ARG	$e^+e^- \to \Upsilon(4S)$

[1] ALBRECHT 93E reports $< 0.9 \times 10^{-3}$ from a measurement of $[\left[\Gamma(B^+ \to D_s^+\pi^0) + \Gamma(B^+ \to D_s^{*+}\pi^0)\right]/\Gamma_{total}] \times [B(D_s^+ \to \phi\pi^+)]$ assuming $B(D_s^+ \to \phi\pi^+) = 0.027$, which we rescale to our best value $B(D_s^+ \to \phi\pi^+) = 4.5 \times 10^{-2}$.

$\Gamma(D_s^{*+}\pi^0)/\Gamma_{total}$ — Γ_{218}/Γ

VALUE	CL%	DOCUMENT ID	TECN	COMMENT
$<2.6\times10^{-4}$	90	[1] ALEXANDER 93B	CLE2	$e^+e^- \to \Upsilon(4S)$

[1] ALEXANDER 93B reports $< 3.2 \times 10^{-4}$ from a measurement of $[\Gamma(B^+ \to D_s^{*+}\pi^0)/\Gamma_{total}] \times [B(D_s^+ \to \phi\pi^+)]$ assuming $B(D_s^+ \to \phi\pi^+) = 0.037$, which we rescale to our best value $B(D_s^+ \to \phi\pi^+) = 4.5 \times 10^{-2}$.

$\Gamma(D_s^+\eta)/\Gamma_{total}$ — Γ_{219}/Γ

VALUE	CL%	DOCUMENT ID	TECN	COMMENT
$<4\times10^{-4}$	90	[1] ALEXANDER 93B	CLE2	$e^+e^- \to \Upsilon(4S)$

[1] ALEXANDER 93B reports $< 4.6 \times 10^{-4}$ from a measurement of $[\Gamma(B^+ \to D_s^+\eta)/\Gamma_{total}] \times [B(D_s^+ \to \phi\pi^+)]$ assuming $B(D_s^+ \to \phi\pi^+) = 0.037$, which we rescale to our best value $B(D_s^+ \to \phi\pi^+) = 4.5 \times 10^{-2}$.

$\Gamma(D_s^{*+}\eta)/\Gamma_{total}$ — Γ_{220}/Γ

VALUE	CL%	DOCUMENT ID	TECN	COMMENT
$<6\times10^{-4}$	90	[1] ALEXANDER 93B	CLE2	$e^+e^- \to \Upsilon(4S)$

[1] ALEXANDER 93B reports $< 7.5 \times 10^{-4}$ from a measurement of $[\Gamma(B^+ \to D_s^{*+}\eta)/\Gamma_{total}] \times [B(D_s^+ \to \phi\pi^+)]$ assuming $B(D_s^+ \to \phi\pi^+) = 0.037$, which we rescale to our best value $B(D_s^+ \to \phi\pi^+) = 4.5 \times 10^{-2}$.

$\Gamma(D_s^+\rho^0)/\Gamma_{total}$ — Γ_{221}/Γ

VALUE	CL%	DOCUMENT ID	TECN	COMMENT
$<3.0\times10^{-4}$	90	[1] ALEXANDER 93B	CLE2	$e^+e^- \to \Upsilon(4S)$

[1] ALEXANDER 93B reports $< 3.7 \times 10^{-4}$ from a measurement of $[\Gamma(B^+ \to D_s^+\rho^0)/\Gamma_{total}] \times [B(D_s^+ \to \phi\pi^+)]$ assuming $B(D_s^+ \to \phi\pi^+) = 0.037$, which we rescale to our best value $B(D_s^+ \to \phi\pi^+) = 4.5 \times 10^{-2}$.

$[\Gamma(D_s^+\rho^0)+\Gamma(D_s^+\overline{K}^*(892)^0)]/\Gamma_{total}$ — $(\Gamma_{221}+\Gamma_{232})/\Gamma$

VALUE	CL%	DOCUMENT ID	TECN	COMMENT
$<2.0\times10^{-3}$	90	[1] ALBRECHT 93E	ARG	$e^+e^- \to \Upsilon(4S)$

[1] ALBRECHT 93E reports $< 3.4 \times 10^{-3}$ from a measurement of $[\left[\Gamma(B^+ \to D_s^+\rho^0) + \Gamma(B^+ \to D_s^+\overline{K}^*(892)^0)\right]/\Gamma_{total}] \times [B(D_s^+ \to \phi\pi^+)]$ assuming $B(D_s^+ \to \phi\pi^+) = 0.027$, which we rescale to our best value $B(D_s^+ \to \phi\pi^+) = 4.5 \times 10^{-2}$.

$\Gamma(D_s^{*+}\rho^0)/\Gamma_{total}$ — Γ_{222}/Γ

VALUE	CL%	DOCUMENT ID	TECN	COMMENT
$<4\times10^{-4}$	90	[1] ALEXANDER 93B	CLE2	$e^+e^- \to \Upsilon(4S)$

[1] ALEXANDER 93B reports $< 4.8 \times 10^{-4}$ from a measurement of $[\Gamma(B^+ \to D_s^{*+}\rho^0)/\Gamma_{total}] \times [B(D_s^+ \to \phi\pi^+)]$ assuming $B(D_s^+ \to \phi\pi^+) = 0.037$, which we rescale to our best value $B(D_s^+ \to \phi\pi^+) = 4.5 \times 10^{-2}$.

$[\Gamma(D_s^{*+}\rho^0)+\Gamma(D_s^{*+}\overline{K}^*(892)^0)]/\Gamma_{total}$ — $(\Gamma_{222}+\Gamma_{234})/\Gamma$

VALUE	CL%	DOCUMENT ID	TECN	COMMENT
$<1.2\times10^{-3}$	90	[1] ALBRECHT 93E	ARG	$e^+e^- \to \Upsilon(4S)$

[1] ALBRECHT 93E reports $< 2.0 \times 10^{-3}$ from a measurement of $[\left[\Gamma(B^+ \to D_s^{*+}\rho^0) + \Gamma(B^+ \to D_s^{*+}\overline{K}^*(892)^0)\right]/\Gamma_{total}] \times [B(D_s^+ \to \phi\pi^+)]$ assuming $B(D_s^+ \to \phi\pi^+) = 0.027$, which we rescale to our best value $B(D_s^+ \to \phi\pi^+) = 4.5 \times 10^{-2}$.

$\Gamma(D_s^+\omega)/\Gamma_{total}$ — Γ_{223}/Γ

VALUE	CL%	DOCUMENT ID	TECN	COMMENT
$<4\times10^{-4}$	90	[1] ALEXANDER 93B	CLE2	$e^+e^- \to \Upsilon(4S)$
• • • We do not use the following data for averages, fits, limits, etc. • • •				
$<2.0\times10^{-3}$	90	[2] ALBRECHT 93E	ARG	$e^+e^- \to \Upsilon(4S)$

[1] ALEXANDER 93B reports $< 4.8 \times 10^{-4}$ from a measurement of $[\Gamma(B^+ \to D_s^+\omega)/\Gamma_{total}] \times [B(D_s^+ \to \phi\pi^+)]$ assuming $B(D_s^+ \to \phi\pi^+) = 0.037$, which we rescale to our best value $B(D_s^+ \to \phi\pi^+) = 4.5 \times 10^{-2}$.

[2] ALBRECHT 93E reports $< 3.4 \times 10^{-3}$ from a measurement of $[\Gamma(B^+ \to D_s^+\omega)/\Gamma_{total}] \times [B(D_s^+ \to \phi\pi^+)]$ assuming $B(D_s^+ \to \phi\pi^+) = 0.027$, which we rescale to our best value $B(D_s^+ \to \phi\pi^+) = 4.5 \times 10^{-2}$.

$\Gamma(D_s^{*+}\omega)/\Gamma_{total}$ — Γ_{224}/Γ

VALUE	CL%	DOCUMENT ID	TECN	COMMENT
$<6\times10^{-4}$	90	[1] ALEXANDER 93B	CLE2	$e^+e^- \to \Upsilon(4S)$
• • • We do not use the following data for averages, fits, limits, etc. • • •				
$<1.1\times10^{-3}$	90	[2] ALBRECHT 93E	ARG	$e^+e^- \to \Upsilon(4S)$

[1] ALEXANDER 93B reports $< 6.8 \times 10^{-4}$ from a measurement of $[\Gamma(B^+ \to D_s^{*+}\omega)/\Gamma_{total}] \times [B(D_s^+ \to \phi\pi^+)]$ assuming $B(D_s^+ \to \phi\pi^+) = 0.037$, which we rescale to our best value $B(D_s^+ \to \phi\pi^+) = 4.5 \times 10^{-2}$.

[2] ALBRECHT 93E reports $< 1.9 \times 10^{-3}$ from a measurement of $[\Gamma(B^+ \to D_s^{*+}\omega)/\Gamma_{total}] \times [B(D_s^+ \to \phi\pi^+)]$ assuming $B(D_s^+ \to \phi\pi^+) = 0.027$, which we rescale to our best value $B(D_s^+ \to \phi\pi^+) = 4.5 \times 10^{-2}$.

$\Gamma(D_s^+ a_1(1260)^0)/\Gamma_{total}$ — Γ_{225}/Γ

VALUE	CL%	DOCUMENT ID	TECN	COMMENT
$<1.8\times10^{-3}$	90	[1] ALBRECHT 93E	ARG	$e^+e^- \to \Upsilon(4S)$

[1] ALBRECHT 93E reports $< 3.0 \times 10^{-3}$ from a measurement of $[\Gamma(B^+ \to D_s^+ a_1(1260)^0)/\Gamma_{total}] \times [B(D_s^+ \to \phi\pi^+)]$ assuming $B(D_s^+ \to \phi\pi^+) = 0.027$, which we rescale to our best value $B(D_s^+ \to \phi\pi^+) = 4.5 \times 10^{-2}$.

$\Gamma(D_s^{*+} a_1(1260)^0)/\Gamma_{total}$ — Γ_{226}/Γ

VALUE	CL%	DOCUMENT ID	TECN	COMMENT
$<1.3\times10^{-3}$	90	[1] ALBRECHT 93E	ARG	$e^+e^- \to \Upsilon(4S)$

[1] ALBRECHT 93E reports $< 2.2 \times 10^{-3}$ from a measurement of $[\Gamma(B^+ \to D_s^{*+} a_1(1260)^0)/\Gamma_{total}] \times [B(D_s^+ \to \phi\pi^+)]$ assuming $B(D_s^+ \to \phi\pi^+) = 0.027$, which we rescale to our best value $B(D_s^+ \to \phi\pi^+) = 4.5 \times 10^{-2}$.

$\Gamma(D_s^+ K^+ K^-)/\Gamma(\overline{D}^0 D_s^+)$ — $\Gamma_{227}/\Gamma_{172}$

VALUE (units 10^{-4})	DOCUMENT ID	TECN	COMMENT
8.0±0.9±0.1	[1] AAIJ 18B	LHCB	pp at 7, 8, 13 TeV

[1] AAIJ 18B reports $[\Gamma(B^+ \to D_s^+ K^+ K^-)/\Gamma(B^+ \to \overline{D}^0 D_s^+)] / [B(D^0 \to K^+ K^-)] = 0.197 \pm 0.015 \pm 0.017$ which we multiply by our best value $B(D^0 \to K^+ K^-) = (4.08 \pm 0.06) \times 10^{-3}$. Our first error is their experiment's error and our second error is the systematic error from using our best value.

$\Gamma(D_s^+\phi)/\Gamma_{total}$ — Γ_{228}/Γ

VALUE (units 10^{-6})	CL%	DOCUMENT ID	TECN	COMMENT
< 0.42	90	[1] AAIJ 18B	LHCB	pp at 7, 8, 13 TeV
• • • We do not use the following data for averages, fits, limits, etc. • • •				
$1.7\ ^{+1.1}_{-0.7}\pm0.2$		[2] AAIJ 13R	LHCB	Repl. by AAIJ 18B
< 1.9	90	[3] AUBERT 06F	BABR	$e^+e^- \to \Upsilon(4S)$
<1000	90	[4] ALBRECHT 93E	ARG	$e^+e^- \to \Upsilon(4S)$
< 260	90	[5] ALEXANDER 93B	CLE2	$e^+e^- \to \Upsilon(4S)$

[1] AAIJ 18B uses $B^+ \to D_s^+\overline{D}^0$ decays for normalization.

[2] AAIJ 13R reports $(1.87^{+1.25}_{-0.73} \pm 0.19 \pm 0.32) \times 10^{-6}$ from a measurement of $[\Gamma(B^+ \to D_s^+\phi)/\Gamma_{total}] / [B(B^+ \to \overline{D}^0 D_s^+)]$ assuming $B(B^+ \to \overline{D}^0 D_s^+) = (10.0 \pm 1.7) \times 10^{-3}$, which we rescale to our best value $B(B^+ \to \overline{D}^0 D_s^+) = (9.0 \pm 0.9) \times 10^{-3}$.

Downloaded from https://academic.oup.com/ptep/article/2022/8/083C01/6651666 by KIT Library user on 27 September 2022

Our first error is their experiment's error and our second error is the systematic error from using our best value.

[3] Assumes equal production of B^+ and B^0 at the $\Upsilon(4S)$.

[4] ALBRECHT 93E reports $< 1.7\times10^{-3}$ from a measurement of $[\Gamma(B^+ \to D_s^+\phi)/\Gamma_{total}] \times [B(D_s^+ \to \phi\pi^+)]$ assuming $B(D_s^+ \to \phi\pi^+) = 0.027$, which we rescale to our best value $B(D_s^+ \to \phi\pi^+) = 4.5 \times 10^{-2}$.

[5] ALEXANDER 93B reports $< 3.1 \times 10^{-4}$ from a measurement of $[\Gamma(B^+ \to D_s^+\phi)/\Gamma_{total}] \times [B(D_s^+ \to \phi\pi^+)]$ assuming $B(D_s^+ \to \phi\pi^+) = 0.037$, which we rescale to our best value $B(D_s^+ \to \phi\pi^+) = 4.5 \times 10^{-2}$.

$\Gamma(D_s^{*+}\phi)/\Gamma_{total}$ — Γ_{229}/Γ

VALUE	CL%	DOCUMENT ID		TECN	COMMENT
$<1.2\times10^{-5}$	90	[1] AUBERT	06F	BABR	$e^+e^- \to \Upsilon(4S)$
• • • We do not use the following data for averages, fits, limits, etc. • • •					
$<1.3\times10^{-3}$	90	[2] ALBRECHT	93E	ARG	$e^+e^- \to \Upsilon(4S)$
$<3.5\times10^{-4}$	90	[3] ALEXANDER	93B	CLE2	$e^+e^- \to \Upsilon(4S)$

[1] Assumes equal production of B^+ and B^0 at the $\Upsilon(4S)$.

[2] ALBRECHT 93E reports $< 2.1 \times 10^{-3}$ from a measurement of $[\Gamma(B^+ \to D_s^{*+}\phi)/\Gamma_{total}] \times [B(D_s^+ \to \phi\pi^+)]$ assuming $B(D_s^+ \to \phi\pi^+) = 0.027$, which we rescale to our best value $B(D_s^+ \to \phi\pi^+) = 4.5 \times 10^{-2}$.

[3] ALEXANDER 93B reports $< 4.2 \times 10^{-4}$ from a measurement of $[\Gamma(B^+ \to D_s^{*+}\phi)/\Gamma_{total}] \times [B(D_s^+ \to \phi\pi^+)]$ assuming $B(D_s^+ \to \phi\pi^+) = 0.037$, which we rescale to our best value $B(D_s^+ \to \phi\pi^+) = 4.5 \times 10^{-2}$.

$\Gamma(D_s^+\overline{K}^0)/\Gamma_{total}$ — Γ_{230}/Γ

VALUE	CL%	DOCUMENT ID		TECN	COMMENT
$<8 \times 10^{-4}$	90	[1] ALEXANDER	93B	CLE2	$e^+e^- \to \Upsilon(4S)$
• • • We do not use the following data for averages, fits, limits, etc. • • •					
$<1.5\times10^{-3}$	90	[2] ALBRECHT	93E	ARG	$e^+e^- \to \Upsilon(4S)$

[1] ALEXANDER 93B reports $< 10.3\times10^{-4}$ from a measurement of $[\Gamma(B^+ \to D_s^+\overline{K}^0)/\Gamma_{total}] \times [B(D_s^+ \to \phi\pi^+)]$ assuming $B(D_s^+ \to \phi\pi^+) = 0.037$, which we rescale to our best value $B(D_s^+ \to \phi\pi^+) = 4.5 \times 10^{-2}$.

[2] ALBRECHT 93E reports $< 2.5 \times 10^{-3}$ from a measurement of $[\Gamma(B^+ \to D_s^+\overline{K}^0)/\Gamma_{total}] \times [B(D_s^+ \to \phi\pi^+)]$ assuming $B(D_s^+ \to \phi\pi^+) = 0.027$, which we rescale to our best value $B(D_s^+ \to \phi\pi^+) = 4.5 \times 10^{-2}$.

$\Gamma(D_s^{*+}\overline{K}^0)/\Gamma_{total}$ — Γ_{231}/Γ

VALUE	CL%	DOCUMENT ID		TECN	COMMENT
$<9 \times 10^{-4}$	90	[1] ALEXANDER	93B	CLE2	$e^+e^- \to \Upsilon(4S)$
• • • We do not use the following data for averages, fits, limits, etc. • • •					
$<1.9\times10^{-3}$	90	[2] ALBRECHT	93E	ARG	$e^+e^- \to \Upsilon(4S)$

[1] ALEXANDER 93B reports $< 10.9\times10^{-4}$ from a measurement of $[\Gamma(B^+ \to D_s^{*+}\overline{K}^0)/\Gamma_{total}] \times [B(D_s^+ \to \phi\pi^+)]$ assuming $B(D_s^+ \to \phi\pi^+) = 0.037$, which we rescale to our best value $B(D_s^+ \to \phi\pi^+) = 4.5 \times 10^{-2}$.

[2] ALBRECHT 93E reports $< 3.1 \times 10^{-3}$ from a measurement of $[\Gamma(B^+ \to D_s^{*+}\overline{K}^0)/\Gamma_{total}] \times [B(D_s^+ \to \phi\pi^+)]$ assuming $B(D_s^+ \to \phi\pi^+) = 0.027$, which we rescale to our best value $B(D_s^+ \to \phi\pi^+) = 4.5 \times 10^{-2}$.

$\Gamma(D_s^+\overline{K}^*(892)^0)/\Gamma_{total}$ — Γ_{232}/Γ

VALUE	CL%	DOCUMENT ID		TECN	COMMENT
$<4.4\times10^{-6}$	90	AAIJ	13R	LHCB	pp at 7 TeV
• • • We do not use the following data for averages, fits, limits, etc. • • •					
$<4 \times 10^{-4}$	90	[1] ALEXANDER	93B	CLE2	$e^+e^- \to \Upsilon(4S)$

[1] ALEXANDER 93B reports $< 4.4 \times 10^{-4}$ from a measurement of $[\Gamma(B^+ \to D_s^+\overline{K}^*(892)^0)/\Gamma_{total}] \times [B(D_s^+ \to \phi\pi^+)]$ assuming $B(D_s^+ \to \phi\pi^+) = 0.037$, which we rescale to our best value $B(D_s^+ \to \phi\pi^+) = 4.5 \times 10^{-2}$.

$\Gamma(D_s^+K^{*0})/\Gamma_{total}$ — Γ_{233}/Γ

VALUE (units 10^{-6})	CL%	DOCUMENT ID		TECN	COMMENT
<3.5	90	AAIJ	13R	LHCB	pp at 7 TeV

$\Gamma(D_s^{*+}\overline{K}^*(892)^0)/\Gamma_{total}$ — Γ_{234}/Γ

VALUE	CL%	DOCUMENT ID		TECN	COMMENT
$<3.5\times10^{-4}$	90	[1] ALEXANDER	93B	CLE2	$e^+e^- \to \Upsilon(4S)$

[1] ALEXANDER 93B reports $< 4.3 \times 10^{-4}$ from a measurement of $[\Gamma(B^+ \to D_s^{*+}\overline{K}^*(892)^0)/\Gamma_{total}] \times [B(D_s^+ \to \phi\pi^+)]$ assuming $B(D_s^+ \to \phi\pi^+) = 0.037$, which we rescale to our best value $B(D_s^+ \to \phi\pi^+) = 4.5 \times 10^{-2}$.

$\Gamma(D_s^-\pi^+K^+)/\Gamma_{total}$ — Γ_{235}/Γ

VALUE (units 10^{-4})	CL%	DOCUMENT ID		TECN	COMMENT
1.80±0.22 OUR AVERAGE					
$1.71^{+0.08}_{-0.07}\pm0.25$		[1] WIECHCZYN...	09	BELL	$e^+e^- \to \Upsilon(4S)$
$2.02\pm0.13\pm0.38$		[1] AUBERT	08G	BABR	$e^+e^- \to \Upsilon(4S)$
• • • We do not use the following data for averages, fits, limits, etc. • • •					
<7	90	[2] ALBRECHT	93E	ARG	$e^+e^- \to \Upsilon(4S)$

[1] Assumes equal production of B^+ and B^0 at the $\Upsilon(4S)$.

[2] ALBRECHT 93E reports $< 1.1\times10^{-3}$ from a measurement of $[\Gamma(B^+ \to D_s^-\pi^+K^+)/\Gamma_{total}] \times [B(D_s^+ \to \phi\pi^+)]$ assuming $B(D_s^+ \to \phi\pi^+) = 0.027$, which we rescale to our best value $B(D_s^+ \to \phi\pi^+) = 4.5 \times 10^{-2}$.

$\Gamma(D_s^{*-}\pi^+K^+)/\Gamma_{total}$ — Γ_{236}/Γ

VALUE (units 10^{-4})	CL%	DOCUMENT ID		TECN	COMMENT
1.45±0.24 OUR AVERAGE					
$1.31^{+0.13}_{-0.12}\pm0.28$		[1] WIECHCZYN...	09	BELL	$e^+e^- \to \Upsilon(4S)$
$1.67\pm0.16\pm0.35$		[1] AUBERT	08G	BABR	$e^+e^- \to \Upsilon(4S)$
• • • We do not use the following data for averages, fits, limits, etc. • • •					
<10	90	[2] ALBRECHT	93E	ARG	$e^+e^- \to \Upsilon(4S)$

[1] Assumes equal production of B^+ and B^0 at the $\Upsilon(4S)$.

[2] ALBRECHT 93E reports $< 1.6\times10^{-3}$ from a measurement of $[\Gamma(B^+ \to D_s^{*-}\pi^+K^+)/\Gamma_{total}] \times [B(D_s^+ \to \phi\pi^+)]$ assuming $B(D_s^+ \to \phi\pi^+) = 0.027$, which we rescale to our best value $B(D_s^+ \to \phi\pi^+) = 4.5 \times 10^{-2}$.

$\Gamma(D_s^-\pi^+K^*(892)^+)/\Gamma_{total}$ — Γ_{237}/Γ

VALUE	CL%	DOCUMENT ID		TECN	COMMENT
$<5\times10^{-3}$	90	[1] ALBRECHT	93E	ARG	$e^+e^- \to \Upsilon(4S)$

[1] ALBRECHT 93E reports $< 8.6 \times 10^{-3}$ from a measurement of $[\Gamma(B^+ \to D_s^-\pi^+K^*(892)^+)/\Gamma_{total}] \times [B(D_s^+ \to \phi\pi^+)]$ assuming $B(D_s^+ \to \phi\pi^+) = 0.027$, which we rescale to our best value $B(D_s^+ \to \phi\pi^+) = 4.5 \times 10^{-2}$.

$\Gamma(D_s^{*-}\pi^+K^*(892)^+)/\Gamma_{total}$ — Γ_{238}/Γ

VALUE	CL%	DOCUMENT ID		TECN	COMMENT
$<7\times10^{-3}$	90	[1] ALBRECHT	93E	ARG	$e^+e^- \to \Upsilon(4S)$

[1] ALBRECHT 93E reports $< 1.1 \times 10^{-2}$ from a measurement of $[\Gamma(B^+ \to D_s^{*-}\pi^+K^*(892)^+)/\Gamma_{total}] \times [B(D_s^+ \to \phi\pi^+)]$ assuming $B(D_s^+ \to \phi\pi^+) = 0.027$, which we rescale to our best value $B(D_s^+ \to \phi\pi^+) = 4.5 \times 10^{-2}$.

$\Gamma(D_s^-K^+K^+)/\Gamma_{total}$ — Γ_{239}/Γ

VALUE (units 10^{-5})	DOCUMENT ID		TECN	COMMENT
0.97±0.21 OUR AVERAGE				
$0.93\pm0.22\pm0.10$	[1] WIECHCZYN...	15	BELL	$e^+e^- \to \Upsilon(4S)$
$1.1 \pm0.4 \pm0.2$	[1] AUBERT	08G	BABR	$e^+e^- \to \Upsilon(4S)$

[1] Assumes equal production of B^+ and B^0 at the $\Upsilon(4S)$.

$\Gamma(D_s^-K^+K^+)/\Gamma(D_s^-\pi^+K^+)$ — $\Gamma_{239}/\Gamma_{235}$

VALUE	DOCUMENT ID		TECN	COMMENT
0.054±0.013±0.006	WIECHCZYN...	15	BELL	$e^+e^- \to \Upsilon(4S)$

$\Gamma(D_s^{*-}K^+K^+)/\Gamma_{total}$ — Γ_{240}/Γ

VALUE (units 10^{-4})	CL%	DOCUMENT ID		TECN	COMMENT
<0.15	90	[1] AUBERT	08G	BABR	$e^+e^- \to \Upsilon(4S)$

[1] Assumes equal production of B^+ and B^0 at the $\Upsilon(4S)$.

$\Gamma(\eta_c K^+)/\Gamma_{total}$ — Γ_{241}/Γ

VALUE (units 10^{-3})	DOCUMENT ID		TECN	COMMENT
1.09±0.08 OUR AVERAGE				
$0.96\pm0.12\pm0.06\pm0.03$	[1,2] LEES	20C	BABR	$e^+e^- \to \Upsilon(4S)$
$0.74^{+0.09}_{-0.08}\pm0.29$	[3] CHILIKIN	19	BELL	$e^+e^- \to \Upsilon(4S)$
$1.20\pm0.08\pm0.07$	[1] KATO	18	BELL	$e^+e^- \to \Upsilon(4S)$
$1.25^{+0.25}_{-0.20}\pm0.12$	[4] AUBERT,B	05L	BABR	$e^+e^- \to \Upsilon(4S)$
$1.25\pm0.14^{+0.39}_{-0.40}$	[5] FANG	03	BELL	$e^+e^- \to \Upsilon(4S)$
$0.69^{+0.26}_{-0.21}\pm0.22$	[6] EDWARDS	01	CLE2	$e^+e^- \to \Upsilon(4S)$
• • • We do not use the following data for averages, fits, limits, etc. • • •				
0.87 ± 0.15	[1,7] AUBERT	06E	BABR	Repl. by LEES 20C
$1.02\pm0.12\pm0.06$	[7,8] AUBERT,B	04B	BABR	$e^+e^- \to \Upsilon(4S)$

[1] Measures absolute branching fractions using a missing-mass technique.

[2] LEES 20C measurement's last uncertainty is due to the used $B(B^\pm \to K^\pm J/\psi)$ value.

[3] CHILIKIN 19 reports $[\Gamma(B^+ \to \eta_c K^+)/\Gamma_{total}] \times [B(\eta_c(1S) \to \pi^+\pi^-p\overline{p})] = (39.4^{+4.1+2.2}_{-3.9-1.8}) \times 10^{-7}$ which we divide by our best value $B(\eta_c(1S) \to \pi^+\pi^-p\overline{p}) = (5.3 \pm 2.1) \times 10^{-3}$. Our first error is their experiment's error and our second error is the systematic error from using our best value.

[4] AUBERT,B 05L reports $[\Gamma(B^+ \to \eta_c K^+)/\Gamma_{total}] \times [B(\eta_c(1S) \to p\overline{p})] = (1.8^{+0.3}_{-0.2} \pm 0.2)\times10^{-6}$ which we divide by our best value $B(\eta_c(1S) \to p\overline{p}) = (1.44 \pm 0.14) \times 10^{-3}$. Our first error is their experiment's error and our second error is the systematic error from using our best value.

[5] Assumes equal production of B^+ and B^0 at the $\Upsilon(4S)$.

[6] EDWARDS 01 assumes equal production of B^0 and B^+ at the $\Upsilon(4S)$. The correlated uncertainties (28.3)% from $B(J/\psi(1S) \to \gamma\eta_c)$ in those modes have been accounted for.

Downloaded from https://academic.oup.com/ptep/article/2022/8/083C01/6651666 by KIT Library user on 27 September 2022

[7] The ratio of $B(B^{\pm} \to K^{\pm}\eta_c)\ B(\eta_c \to K\overline{K}\pi) = (7.4 \pm 0.5 \pm 0.7) \times 10^{-5}$ reported in AUBERT,B 04B and $B(B^{\pm} \to K^{\pm}\eta_c) = (8.7 \pm 1.5) \times 10^{-3}$ reported in AUBERT 06E contribute to the determination of $B(\eta_c \to K\overline{K}\pi)$, which is used by others for normalization.

[8] AUBERT,B 04B reports $[\Gamma(B^+ \to \eta_c K^+)/\Gamma_{total}] \times [B(\eta_c(1S) \to K\overline{K}\pi)] = (0.074 \pm 0.005 \pm 0.007) \times 10^{-3}$ which we divide by our best value $B(\eta_c(1S) \to K\overline{K}\pi) = (7.3 \pm 0.4) \times 10^{-2}$. Our first error is their experiment's error and our second error is the systematic error from using our best value.

$\Gamma(B^+ \to \eta_c K^+)/\Gamma_{total} \times \Gamma(\eta_c(1S) \to \gamma\gamma)/\Gamma_{total}$ — $\Gamma_{241}/\Gamma \times \Gamma_{56}^{\eta_c(1S)}/\Gamma^{\eta_c(1S)}$

VALUE (units 10^{-6})	DOCUMENT ID		TECN	COMMENT
$0.22^{+0.09+0.04}_{-0.07-0.02}$	[1] WICHT	08	BELL	$e^+e^- \to \Upsilon(4S)$

[1] Assumes equal production of B^+ and B^0 at the $\Upsilon(4S)$.

$\Gamma(\eta_c K^+, \eta_c \to K^0_S K^{\mp}\pi^{\pm})/\Gamma_{total}$ — Γ_{242}/Γ

VALUE (units 10^{-6})	DOCUMENT ID		TECN	COMMENT
$26.7 \pm 1.4^{+5.7}_{-5.5}$	[1,2] VINOKUROVA	11	BELL	$e^+e^- \to \Upsilon(4S)$

[1] Assumes equal production of B^0 and B^+ from Upsilon(4S) decays.

[2] VINOKUROVA 11 reports $(26.7 \pm 1.4^{+2.9}_{-2.6} \pm 4.9) \times 10^{-6}$, where the first uncertainty is statistical, the second is due to systematics, and the third comes from interference of $\eta_c(1S) \to K^0_S K^{\pm}\pi^{\mp}$ with nonresonant $K^0_S K^{\pm}\pi^{\mp}$. We combined both systematic uncertainties to single values.

$\Gamma(\eta_c K^*(892)^+)/\Gamma_{total}$ — Γ_{243}/Γ

VALUE (units 10^{-3})	DOCUMENT ID		TECN	COMMENT
$1.1^{+0.5}_{-0.4} \pm 0.1$	[1,2] AUBERT	07AV	BABR	$e^+e^- \to \Upsilon(4S)$

[1] AUBERT 07AV reports $[\Gamma(B^+ \to \eta_c K^*(892)^+)/\Gamma_{total}] \times [B(\eta_c(1S) \to p\overline{p})] = (1.57^{+0.56+0.45}_{-0.46-0.36}) \times 10^{-6}$ which we divide by our best value $B(\eta_c(1S) \to p\overline{p}) = (1.44 \pm 0.14) \times 10^{-3}$. Our first error is their experiment's error and our second error is the systematic error from using our best value.

[2] Assumes equal production of B^+ and B^0 at the $\Upsilon(4S)$.

$\Gamma(\eta_c K^+\pi^+\pi^-)/\Gamma_{total}$ — Γ_{244}/Γ

VALUE	CL%	DOCUMENT ID		TECN	COMMENT
$<3.9 \times 10^{-4}$	90	VINOKUROVA	15	BELL	$e^+e^- \to \Upsilon(4S)$

$\Gamma(\eta_c K^+\omega(782))/\Gamma_{total}$ — Γ_{245}/Γ

VALUE	CL%	DOCUMENT ID		TECN	COMMENT
$<5.3 \times 10^{-4}$	90	VINOKUROVA	15	BELL	$e^+e^- \to \Upsilon(4S)$

$\Gamma(\eta_c K^+\eta)/\Gamma_{total}$ — Γ_{246}/Γ

VALUE	CL%	DOCUMENT ID		TECN	COMMENT
$<2.2 \times 10^{-4}$	90	VINOKUROVA	15	BELL	$e^+e^- \to \Upsilon(4S)$

$\Gamma(\eta_c K^+\pi^0)/\Gamma_{total}$ — Γ_{247}/Γ

VALUE	CL%	DOCUMENT ID		TECN	COMMENT
$<6.2 \times 10^{-5}$	90	VINOKUROVA	15	BELL	$e^+e^- \to \Upsilon(4S)$

$\Gamma(\eta_c(2S) K^+)/\Gamma_{total}$ — Γ_{248}/Γ

VALUE (units 10^{-4})	DOCUMENT ID		TECN	COMMENT
4.4±1.0 OUR AVERAGE				
$3.5 \pm 1.7 \pm 0.5 \pm 0.1$	[1,2] LEES	20C	BABR	$e^+e^- \to \Upsilon(4S)$
$4.8 \pm 1.1 \pm 0.3$	[2] KATO	18	BELL	$e^+e^- \to \Upsilon(4S)$
• • • We do not use the following data for averages, fits, limits, etc. • • •				
$3.4 \pm 1.8 \pm 0.3$	[2] AUBERT	06E	BABR	Repl. by LEES 20C

[1] LEES 20C measurement's last uncertainty is due to the used $B(B^{\pm} \to K^{\pm}J/\psi)$ value.

[2] Measures absolute branching fractions using a missing-mass technique.

$\Gamma(\eta_c(2S) K^+, \eta_c \to p\overline{p})/\Gamma_{total}$ — Γ_{249}/Γ

VALUE (units 10^{-8})	CL%	DOCUMENT ID		TECN	COMMENT
$3.47 \pm 0.72 \pm 0.26$		[1] AAIJ	17AD	LHCB	pp at 7 and 8 TeV
• • • We do not use the following data for averages, fits, limits, etc. • • •					
<10.6	95	[2] AAIJ	13S	LHCB	Repl. by AAIJ 17AD

[1] Measured relative to $B^+ \to J/\psi K^+$ decay with charmonia reconstructed in $p\overline{p}$ final state and using $B(B^+ \to J/\psi K^+) \times B(J/\psi \to p\overline{p}) = (2.17 \pm 0.08) \times 10^{-6}$. The last uncertainty includes the uncertainty of $B(B^+ \to J/\psi K^+) \times B(J/\psi \to p\overline{p})$.

[2] Measured relative to $B^+ \to J/\psi K^+$ decay with charmonia reconstructed in $p\overline{p}$ final state and using $B(B^+ \to J/\psi K^+) = (1.013 \pm 0.034) \times 10^{-3}$ and $B(J/\psi \to p\overline{p}) = (2.17 \pm 0.07) \times 10^{-3}$.

$\Gamma(\eta_c(2S) K^+, \eta_c \to p\overline{p}\pi^+\pi^-)/\Gamma_{total}$ — Γ_{251}/Γ

VALUE (units 10^{-7})	DOCUMENT ID		TECN	COMMENT
$11.2^{+1.8+0.5}_{-1.6-0.7}$	CHILIKIN	19	BELL	$e^+e^- \to \Upsilon(4S)$

$\Gamma(B^+ \to h_c(1P) K^+)/\Gamma_{total} \times \Gamma(h_c(1P) \to \gamma\eta_c(1S))/\Gamma_{total}$ — $\Gamma_{344}/\Gamma \times \Gamma_{22}^{h_c(1P)}/\Gamma^{h_c(1P)}$

VALUE (units 10^{-4})	CL%	DOCUMENT ID		TECN	COMMENT
<0.48	90	[1] AUBERT	08AB	BABR	$e^+e^- \to \Upsilon(4S)$

[1] Uses the production ratio of $(B^+B^-)/(B^0\overline{B}^0) = 1.026 \pm 0.032$ at $\Upsilon(4S)$.

$\Gamma(B^+ \to \eta_c(2S) K^+)/\Gamma_{total} \times \Gamma(\eta_c(2S) \to \gamma\gamma)/\Gamma_{total}$ — $\Gamma_{248}/\Gamma \times \Gamma_{16}^{\eta_c(2S)}/\Gamma^{\eta_c(2S)}$

VALUE (units 10^{-6})	CL%	DOCUMENT ID		TECN	COMMENT
<0.18	90	[1] WICHT	08	BELL	$e^+e^- \to \Upsilon(4S)$

[1] Assumes equal production of B^+ and B^0 at the $\Upsilon(4S)$.

$\Gamma(\eta_c(2S) K^+, \eta_c \to K^0_S K^{\mp}\pi^{\pm})/\Gamma_{total}$ — Γ_{250}/Γ

VALUE (units 10^{-6})	DOCUMENT ID		TECN	COMMENT
$3.4^{+2.2+0.5}_{-1.5-0.4}$	[1,2] VINOKUROVA	11	BELL	$e^+e^- \to \Upsilon(4S)$

[1] Assumes equal production of B^0 and B^+ from Upsilon(4S) decays.

[2] The first uncertainty includes both statistical and interference effects while the second is due to systematics.

$\Gamma(J/\psi(1S) K^+)/\Gamma_{total}$ — Γ_{276}/Γ

VALUE (units 10^{-4})	EVTS	DOCUMENT ID		TECN	COMMENT
10.20± 0.19 OUR FIT					
10.18± 0.20 OUR AVERAGE					
$10.32 \pm 0.07 \pm 0.24$		[1] CHOUDHURY	21	BELL	$e^+e^- \to \Upsilon(4S)$
$9.4 \pm 0.7 \pm 0.8$		[2] CHILIKIN	19	BELL	$e^+e^- \to \Upsilon(4S)$
$8.9 \pm 0.6 \pm 0.5$		[3] KATO	18	BELL	$e^+e^- \to \Upsilon(4S)$
$8.1 \pm 1.3 \pm 0.7$		[3] AUBERT	06E	BABR	$e^+e^- \to \Upsilon(4S)$
$10.61 \pm 0.15 \pm 0.48$		[4] AUBERT	05J	BABR	$e^+e^- \to \Upsilon(4S)$
$10.4 \pm 1.1 \pm 0.1$		[5] AUBERT,B	05L	BABR	$e^+e^- \to \Upsilon(4S)$
$10.2 \pm 0.8 \pm 0.7$		[4] JESSOP	97	CLE2	$e^+e^- \to \Upsilon(4S)$
$9.24 \pm 3.04 \pm 0.05$		[6] BORTOLETTO	92	CLEO	$e^+e^- \to \Upsilon(4S)$
$8.09 \pm 3.50 \pm 0.04$	6	[7] ALBRECHT	90J	ARG	$e^+e^- \to \Upsilon(4S)$
• • • We do not use the following data for averages, fits, limits, etc. • • •					
$10.1 \pm 0.2 \pm 0.7$		[4] ABE	03B	BELL	Repl. by CHOUDHURY 21
$10.1 \pm 0.3 \pm 0.5$		[4] AUBERT	02	BABR	Repl. by AUBERT 05J
$11.0 \pm 1.5 \pm 0.9$	59	[4] ALAM	94	CLE2	Repl. by JESSOP 97
$22 \pm 10 \pm 2$		BUSKULIC	92G	ALEP	$e^+e^- \to Z$
7 ± 4	3	[8] ALBRECHT	87D	ARG	$e^+e^- \to \Upsilon(4S)$
$10 \pm 7 \pm 2$	3	[9] BEBEK	87	CLEO	$e^+e^- \to \Upsilon(4S)$
9 ± 5	3	[10] ALAM	86	CLEO	$e^+e^- \to \Upsilon(4S)$

[1] CHOUDHURY 21 uses the relative production fraction of charged (f^{+-}) to neutral (f^{00}) B mesons at $\Upsilon(4S)$ value of $f^{+-}/f^{00} = 1.058 \pm 0.024$.

[2] CHILIKIN 19 reports $[\Gamma(B^+ \to J/\psi(1S) K^+)/\Gamma_{total}] \times [B(J/\psi(1S) \to p\overline{p}\pi^+\pi^-)] = (56.4^{+3.3+2.7}_{-3.2-2.5}) \times 10^{-7}$ which we divide by our best value $B(J/\psi(1S) \to p\overline{p}\pi^+\pi^-) = (6.0 \pm 0.5) \times 10^{-3}$. Our first error is their experiment's error and our second error is the systematic error from using our best value.

[3] Measures absolute branching fractions using a missing-mass technique.

[4] Assumes equal production of B^+ and B^0 at the $\Upsilon(4S)$.

[5] AUBERT,B 05L reports $[\Gamma(B^+ \to J/\psi(1S) K^+)/\Gamma_{total}] \times [B(J/\psi(1S) \to p\overline{p})] = (2.2 \pm 0.2 \pm 0.1) \times 10^{-6}$ which we divide by our best value $B(J/\psi(1S) \to p\overline{p}) = (2.120 \pm 0.029) \times 10^{-3}$. Our first error is their experiment's error and our second error is the systematic error from using our best value.

[6] BORTOLETTO 92 reports $(8 \pm 2 \pm 2) \times 10^{-4}$ from a measurement of $[\Gamma(B^+ \to J/\psi(1S) K^+)/\Gamma_{total}] \times [B(J/\psi(1S) \to e^+e^-)]$ assuming $B(J/\psi(1S) \to e^+e^-) = 0.069 \pm 0.009$, which we rescale to our best value $B(J/\psi(1S) \to e^+e^-) = (5.971 \pm 0.032) \times 10^{-2}$. Our first error is their experiment's error and our second error is the systematic error from using our best value. Assumes equal production of B^+ and B^0 at the $\Upsilon(4S)$.

[7] ALBRECHT 90J reports $(7 \pm 3 \pm 1) \times 10^{-4}$ from a measurement of $[\Gamma(B^+ \to J/\psi(1S) K^+)/\Gamma_{total}] \times [B(J/\psi(1S) \to e^+e^-)]$ assuming $B(J/\psi(1S) \to e^+e^-) = 0.069 \pm 0.009$, which we rescale to our best value $B(J/\psi(1S) \to e^+e^-) = (5.971 \pm 0.032) \times 10^{-2}$. Our first error is their experiment's error and our second error is the systematic error from using our best value. Assumes equal production of B^+ and B^0 at the $\Upsilon(4S)$.

[8] ALBRECHT 87D assume $B^+B^-/B^0\overline{B}^0$ ratio is 55/45. Superseded by ALBRECHT 90J.

[9] BEBEK 87 value has been updated in BERKELMAN 91 to use same assumptions as noted for BORTOLETTO 92.

[10] ALAM 86 assumes $B^{\pm}/B^0$ ratio is 60/40.

$\Gamma(\eta_c K^+)/\Gamma(J/\psi(1S) K^+)$ — $\Gamma_{241}/\Gamma_{276}$

VALUE	DOCUMENT ID		TECN	COMMENT
0.88±0.10 OUR AVERAGE				
$0.85 \pm 0.06 \pm 0.08$	[1] AAIJ	13S	LHCB	pp at 7 TeV
$1.33 \pm 0.10 \pm 0.43$	[2] AUBERT,B	04B	BABR	$e^+e^- \to \Upsilon(4S)$

[1] AAIJ 13S reports $[\Gamma(B^+ \to \eta_c K^+)/\Gamma(B^+ \to J/\psi(1S) K^+)] \times [B(\eta_c(1S) \to p\overline{p})] / [B(J/\psi(1S) \to p\overline{p})] = 0.578 \pm 0.035 \pm 0.026$ which we multiply or divide by our best values $B(\eta_c(1S) \to p\overline{p}) = (1.44 \pm 0.14) \times 10^{-3}$, $B(J/\psi(1S) \to p\overline{p}) = (2.120 \pm 0.029) \times 10^{-3}$. Our first error is their experiment's error and our second error is the systematic error from using our best values.

[2] Uses BABAR measurement of $B(B^+ \to J/\psi K^+) = (10.1 \pm 0.3 \pm 0.5) \times 10^{-4}$.

Downloaded from https://academic.oup.com/ptep/article/2022/8/083C01/6651666 by KIT Library user on 27 September 2022

$\Gamma(B^+ \to J/\psi(1S)K^+)/\Gamma_{total} \times \Gamma(J/\psi(1S) \to \gamma\gamma)/\Gamma_{total}$ — $\Gamma_{276}/\Gamma \times \Gamma_{334}^{J/\psi(1S)}/\Gamma^{J/\psi(1S)}$

VALUE (units 10^{-6})	CL%	DOCUMENT ID		TECN	COMMENT
<0.16	90	[1] WICHT	08	BELL	$e^+e^- \to \Upsilon(4S)$

[1] Assumes equal production of B^+ and B^0 at the $\Upsilon(4S)$.

$\Gamma(J/\psi(1S)K^+\pi^+\pi^-)/\Gamma_{total}$ — Γ_{278}/Γ

VALUE (units 10^{-3})	CL%	EVTS	DOCUMENT ID		TECN	COMMENT
0.81 ±0.13 OUR AVERAGE Error includes scale factor of 2.5. See the ideogram below.						
0.716±0.010±0.060			[1] GULER	11	BELL	$e^+e^- \to \Upsilon(4S)$
1.16 ±0.07 ±0.09			[1] AUBERT	05R	BABR	$e^+e^- \to \Upsilon(4S)$
0.69 ±0.18 ±0.12			[2] ACOSTA	02F	CDF	$p\overline{p}$ 1.8 TeV
1.39 ±0.81 ±0.01			[3] BORTOLETTO	92	CLEO	$e^+e^- \to \Upsilon(4S)$
1.39 ±0.91 ±0.01		6	[4] ALBRECHT	87D	ARG	$e^+e^- \to \Upsilon(4S)$
• • • We do not use the following data for averages, fits, limits, etc. • • •						
<1.8	90		[5] ALBRECHT	90J	ARG	$e^+e^- \to \Upsilon(4S)$

[1] Assumes equal production of B^+ and B^0 at the $\Upsilon(4S)$.
[2] ACOSTA 02F uses as reference of $B(B \to J/\psi(1S)K^+) = (10.1 \pm 0.6) \times 10^{-4}$. The second error includes the systematic error and the uncertainties of the branching ratio.
[3] BORTOLETTO 92 reports $(1.2 \pm 0.6 \pm 0.4) \times 10^{-3}$ from a measurement of $[\Gamma(B^+ \to J/\psi(1S)K^+\pi^+\pi^-)/\Gamma_{total}] \times [B(J/\psi(1S) \to e^+e^-)]$ assuming $B(J/\psi(1S) \to e^+e^-) = 0.069 \pm 0.009$, which we rescale to our best value $B(J/\psi(1S) \to e^+e^-) = (5.971 \pm 0.032) \times 10^{-2}$. Our first error is their experiment's error and our second error is the systematic error from using our best value. Assumes equal production of B^+ and B^0 at the $\Upsilon(4S)$.
[4] ALBRECHT 87D reports $(1.2 \pm 0.8) \times 10^{-3}$ from a measurement of $[\Gamma(B^+ \to J/\psi(1S)K^+\pi^+\pi^-)/\Gamma_{total}] \times [B(J/\psi(1S) \to e^+e^-)]$ assuming $B(J/\psi(1S) \to e^+e^-) = 0.069 \pm 0.009$, which we rescale to our best value $B(J/\psi(1S) \to e^+e^-) = (5.971 \pm 0.032) \times 10^{-2}$. Our first error is their experiment's error and our second error is the systematic error from using our best value. They actually report 0.0011 ± 0.0007 assuming $B^+B^-/B^0\overline{B}^0$ ratio is 55/45. We rescale to 50/50. Analysis explicitly removes $B^+ \to \psi(2S)K^+$.
[5] ALBRECHT 90J reports $< 1.6 \times 10^{-3}$ from a measurement of $[\Gamma(B^+ \to J/\psi(1S)K^+\pi^+\pi^-)/\Gamma_{total}] \times [B(J/\psi(1S) \to e^+e^-)]$ assuming $B(J/\psi(1S) \to e^+e^-) = 0.069$, which we rescale to our best value $B(J/\psi(1S) \to e^+e^-) = 5.971 \times 10^{-2}$. Assumes equal production of B^+ and B^0 at the $\Upsilon(4S)$.

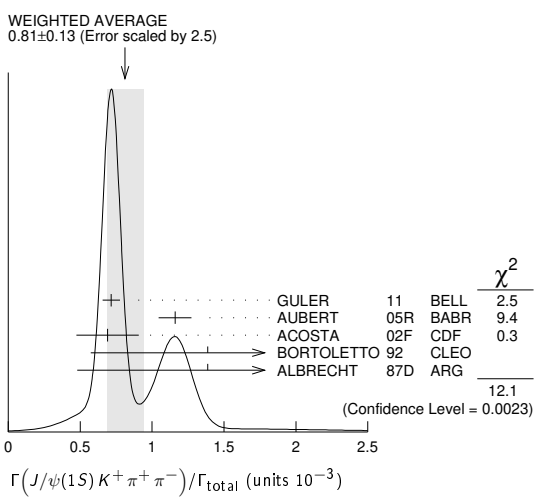

$\Gamma(J/\psi(1S)K^+K^-K^+)/\Gamma_{total}$ — Γ_{279}/Γ

VALUE (units 10^{-6})	DOCUMENT ID		TECN	COMMENT
33.7±2.5±1.4	LEES	15	BABR	$e^+e^- \to \Upsilon(4S)$

$\Gamma(h_c(1P)K^+,\ h_c \to J/\psi\pi^+\pi^-)/\Gamma_{total}$ — Γ_{252}/Γ

VALUE	CL%	DOCUMENT ID		TECN	COMMENT
<3.4 × 10^{-6}	90	[1] AUBERT	05R	BABR	$e^+e^- \to \Upsilon(4S)$

[1] Assumes equal production of B^+ and B^0 at the $\Upsilon(4S)$.

$\Gamma(X(3730)^0K^+,\ X^0 \to \eta_c\eta)/\Gamma_{total}$ — Γ_{253}/Γ

VALUE	CL%	DOCUMENT ID		TECN	COMMENT
<4.6 × 10^{-5}	90	VINOKUROVA	15	BELL	$e^+e^- \to \Upsilon(4S)$

$\Gamma(X(3730)^0K^+,\ X^0 \to \eta_c\pi^0)/\Gamma_{total}$ — Γ_{254}/Γ

VALUE	CL%	DOCUMENT ID		TECN	COMMENT
<5.7 × 10^{-6}	90	VINOKUROVA	15	BELL	$e^+e^- \to \Upsilon(4S)$

$\Gamma(\eta_{c2}(1D)K^+,\ \eta_{c2} \to h_c\gamma)/\Gamma_{total}$ — Γ_{255}/Γ

VALUE	CL%	DOCUMENT ID		TECN	COMMENT
<3.7 × 10^{-5}	90	CHILIKIN	20	BELL	$e^+e^- \to \Upsilon(4S)$

$\Gamma(\eta_{c2}(1D)\pi^+K^0_S,\ \eta_{c2} \to h_c\gamma)/\Gamma_{total}$ — Γ_{256}/Γ

VALUE	CL%	DOCUMENT ID		TECN	COMMENT
<1.1 × 10^{-4}	90	CHILIKIN	20	BELL	$e^+e^- \to \Upsilon(4S)$

$\Gamma(\psi_2(3823)K^+,\ \psi_2 \to J/\psi\pi^+\pi^-)/\Gamma_{total}$ — Γ_{257}/Γ

VALUE (units 10^{-7})	DOCUMENT ID		TECN	COMMENT
2.82±0.54±0.13	[1] AAIJ	20S	LHCB	pp at 7, 8, 13 TeV

[1] The first error is statistic; the second error is the total systematic error.

$\Gamma(\chi_{c1}(3872)K^+)/\Gamma_{total}$ — Γ_{258}/Γ

VALUE (units 10^{-4})	CL%	DOCUMENT ID		TECN	COMMENT
2.1±0.6±0.3±0.1		[1,2] LEES	20C	BABR	$e^+e^- \to \Upsilon(4S)$
• • • We do not use the following data for averages, fits, limits, etc. • • •					
<2.6	90	[1] KATO	18	BELL	$e^+e^- \to \Upsilon(4S)$
2.6±0.7±0.9		[3,4] AUBERT	06	BABR	Repl. by AUBERT 08Y
<3.2	90	[1] AUBERT	06E	BABR	$e^+e^- \to \Upsilon(4S)$
3.3±1.1±1.1		[3,5] AUBERT	05R	BABR	Repl. by AUBERT 06
3.5±0.8±1.2		[6] CHOI	03	BELL	Repl. by CHOI 11

[1] Measures absolute branching fractions using a missing-mass technique.
[2] LEES 20C measurement's last uncertainty is due to the used $B(B^{\pm} \to K^{\pm}J/\psi)$ value.
[3] Assumes equal production of B^+ and B^0 at the $\Upsilon(4S)$.
[4] AUBERT 06 reports $[\Gamma(B^+ \to \chi_{c1}(3872)K^+)/\Gamma_{total}] \times [B(\chi_{c1}(3872) \to \pi^+\pi^-J/\psi(1S))] = (10.1 \pm 2.5 \pm 1.0) \times 10^{-6}$ which we divide by our best value $B(\chi_{c1}(3872) \to \pi^+\pi^-J/\psi(1S)) = (3.8 \pm 1.2) \times 10^{-2}$. Our first error is their experiment's error and our second error is the systematic error from using our best value.
[5] AUBERT 05R reports $[\Gamma(B^+ \to \chi_{c1}(3872)K^+)/\Gamma_{total}] \times [B(\chi_{c1}(3872) \to \pi^+\pi^-J/\psi(1S))] = (12.8 \pm 4.1) \times 10^{-6}$ which we divide by our best value $B(\chi_{c1}(3872) \to \pi^+\pi^-J/\psi(1S)) = (3.8 \pm 1.2) \times 10^{-2}$. Our first error is their experiment's error and our second error is the systematic error from using our best value.
[6] CHOI 03 reports $[\Gamma(B^+ \to \chi_{c1}(3872)K^+)/\Gamma_{total}] \times [B(\chi_{c1}(3872) \to \pi^+\pi^-J/\psi(1S))] = (13.6 \pm 3.0 \pm 0.5) \times 10^{-6}$ which we divide by our best value $B(\chi_{c1}(3872) \to \pi^+\pi^-J/\psi(1S)) = (3.8 \pm 1.2) \times 10^{-2}$. Our first error is their experiment's error and our second error is the systematic error from using our best value.

$\Gamma(\chi_{c1}(3872)K^*(892)^+)/\Gamma_{total}$ — Γ_{267}/Γ

VALUE	CL%	DOCUMENT ID		TECN	COMMENT
<6 × 10^{-4}	90	[1,2] AUBERT	09B	BABR	$e^+e^- \to \Upsilon(4S)$
• • • We do not use the following data for averages, fits, limits, etc. • • •					
<6 × 10^{-4}	90	[2,3] AUBERT	09B	BABR	$e^+e^- \to \Upsilon(4S)$

[1] AUBERT 09B reports $[\Gamma(B^+ \to \chi_{c1}(3872)K^*(892)^+)/\Gamma_{total}] \times [B(\chi_{c1}(3872) \to \gamma J/\psi)] < 4.8 \times 10^{-6}$ which we divide by our best value $B(\chi_{c1}(3872) \to \gamma J/\psi) = 8 \times 10^{-3}$.
[2] Uses $B(\Upsilon(4S) \to B^+B^-) = (51.6 \pm 0.6)\%$ and $B(\Upsilon(4S) \to B^0\overline{B}^0) = (48.4 \pm 0.6)\%$.
[3] AUBERT 09B reports $[\Gamma(B^+ \to \chi_{c1}(3872)K^*(892)^+)/\Gamma_{total}] \times [B(\chi_{c1}(3872) \to \gamma\psi(2S))] < 28 \times 10^{-6}$ which we divide by our best value $B(\chi_{c1}(3872) \to \gamma\psi(2S)) = 4.5 \times 10^{-2}$.

$\Gamma(\chi_{c0}(3915)K^+)/\Gamma_{total}$ — Γ_{259}/Γ

VALUE	CL%	DOCUMENT ID		TECN	COMMENT
<2.8 × 10^{-4}	90	[1] KATO	18	BELL	$e^+e^- \to \Upsilon(4S)$

[1] Measures absolute branching fractions using a missing-mass technique.

$\Gamma(\chi_{c0}(3915)K^+,\ \chi_{c0} \to D^+D^-)/\Gamma(D^-D^+K^+)$ — $\Gamma_{260}/\Gamma_{209}$

VALUE (units 10^{-2})	DOCUMENT ID		TECN	COMMENT
3.7±0.9±0.2	[1] AAIJ	20AI	LHCB	pp at 7, 8, 13 TeV

[1] Measured in Dalitz plot analysis of $B^+ \to D^-D^+K^+$ decays.

$\Gamma(\chi_{c0}(3915)K^+,\ \chi_{c0} \to \eta_c\eta)/\Gamma_{total}$ — Γ_{261}/Γ

VALUE	CL%	DOCUMENT ID		TECN	COMMENT
<4.7 × 10^{-5}	90	[1] VINOKUROVA	15	BELL	$e^+e^- \to \Upsilon(4S)$

[1] Upper limit is corrected in the Erratum.

$\Gamma((Xchi)_{c0}(3915)K^+,\ \chi_{c0} \to \eta_c\pi^0)/\Gamma_{total}$ — Γ_{262}/Γ

VALUE	CL%	DOCUMENT ID		TECN	COMMENT
<1.7 × 10^{-5}	90	[1] VINOKUROVA	15	BELL	$e^+e^- \to \Upsilon(4S)$

[1] Upper limit is corrected in the Erratum.

$\Gamma(X(4014)^0K^+,\ X^0 \to \eta_c\eta)/\Gamma_{total}$ — Γ_{263}/Γ

VALUE	CL%	DOCUMENT ID		TECN	COMMENT
<3.9 × 10^{-5}	90	VINOKUROVA	15	BELL	$e^+e^- \to \Upsilon(4S)$

$\Gamma(X(4014)^0K^+,\ X^0 \to \eta_c\pi^0)/\Gamma_{total}$ — Γ_{264}/Γ

VALUE	CL%	DOCUMENT ID		TECN	COMMENT
<1.2 × 10^{-5}	90	VINOKUROVA	15	BELL	$e^+e^- \to \Upsilon(4S)$

Downloaded from https://academic.oup.com/ptep/article/2022/8/083C01/6651666 by KIT Library user on 27 September 2022

$\Gamma(Z_c(3900)^0 K^+, Z_c^0 \to \eta_c \pi^+ \pi^-)/\Gamma_{total}$ — Γ_{265}/Γ

VALUE	CL%	DOCUMENT ID		TECN	COMMENT
$<4.7 \times 10^{-5}$	90	VINOKUROVA	15	BELL	$e^+e^- \to \Upsilon(4S)$

$\Gamma(X(4020)^0 K^+, X^0 \to \eta_c \pi^+ \pi^-)/\Gamma_{total}$ — Γ_{266}/Γ

VALUE	CL%	DOCUMENT ID		TECN	COMMENT
$<1.6 \times 10^{-5}$	90	VINOKUROVA	15	BELL	$e^+e^- \to \Upsilon(4S)$

$\Gamma(\chi_{c1}(3872)^+ K^0, \chi_{c1}^+ \to J/\psi(1S)\pi^+\pi^0)/\Gamma_{total}$ — Γ_{268}/Γ

VALUE (units 10^{-6})	CL%	DOCUMENT ID		TECN	COMMENT
< 6.1	90	[1,2] CHOI	11	BELL	$e^+e^- \to \Upsilon(4S)$
• • • We do not use the following data for averages, fits, limits, etc. • • •					
<22	90	[3] AUBERT	05B	BABR	$e^+e^- \to \Upsilon(4S)$

[1] Assumes $\pi^+\pi^0$ originates from ρ^+.
[2] Assumes equal production of B^+ and B^0 at the $\Upsilon(4S)$.
[3] Assumes equal production of B^+ and B^0 at the $\Upsilon(4S)$. The isovector-X hypothesis is excluded with a likelihood test at 1×10^{-4} level.

$\Gamma(\chi_{c1}(3872) K^0 \pi^+)/\Gamma_{total}$ — Γ_{269}/Γ

VALUE (units 10^{-4})	DOCUMENT ID		TECN	COMMENT
2.8±0.8±0.9	[1] BALA	15	BELL	$e^+e^- \to \Upsilon(4S)$

[1] BALA 15 reports $[\Gamma(B^+ \to \chi_{c1}(3872) K^0\pi^+)/\Gamma_{total}] \times [B(\chi_{c1}(3872) \to \pi^+\pi^- J/\psi(1S))] = (10.6 \pm 3.0 \pm 0.9) \times 10^{-6}$ which we divide by our best value $B(\chi_{c1}(3872) \to \pi^+\pi^- J/\psi(1S)) = (3.8 \pm 1.2) \times 10^{-2}$. Our first error is their experiment's error and our second error is the systematic error from using our best value.

$\Gamma(Z_c(4430)^+ K^0, Z_c^+ \to J/\psi\pi^+)/\Gamma_{total}$ — Γ_{270}/Γ

VALUE (units 10^{-5})	CL%	DOCUMENT ID		TECN	COMMENT
<1.5	95	[1] AUBERT	09AA	BABR	$e^+e^- \to \Upsilon(4S)$

[1] Assumes equal production of B^+ and B^0 at the $\Upsilon(4S)$.

$\Gamma(Z_c(4430)^+ K^0, Z_c^+ \to \psi(2S)\pi^+)/\Gamma_{total}$ — Γ_{271}/Γ

VALUE (units 10^{-5})	CL%	DOCUMENT ID		TECN	COMMENT
<4.7	95	[1] AUBERT	09AA	BABR	$e^+e^- \to \Upsilon(4S)$

[1] Assumes equal production of B^+ and B^0 at the $\Upsilon(4S)$.

$\Gamma(\psi(4230)^0 K^+, \psi^0 \to J/\psi\pi^+\pi^-)/\Gamma_{total}$ — Γ_{272}/Γ

VALUE (units 10^{-6})	CL%	DOCUMENT ID		TECN	COMMENT
<15.6	95	[1,2] GARG	19	BELL	$e^+e^- \to \Upsilon(4S)$
• • • We do not use the following data for averages, fits, limits, etc. • • •					
<29	95	[2] AUBERT	06	BABR	$e^+e^- \to \Upsilon(4S)$

[1] Corresponds to a 90% CL upper limit of $< 14 \times 10^{-6}$.
[2] Assumes equal production of B^+ and B^0 at the $\Upsilon(4S)$.

$\Gamma(\chi_{c0}(3915) K^+, \chi_{c0} \to J/\psi\gamma)/\Gamma_{total}$ — Γ_{273}/Γ

VALUE (units 10^{-6})	CL%	DOCUMENT ID		TECN	COMMENT
<14	90	[1] AUBERT,BE	06M	BABR	$e^+e^- \to \Upsilon(4S)$

[1] Assumes equal production of B^+ and B^0 at the $\Upsilon(4S)$.

$\Gamma(\chi_{c0}(3915) K^+, \chi_{c0} \to \chi_{c1}(1P)\pi^0)/\Gamma_{total}$ — Γ_{274}/Γ

VALUE	CL%	DOCUMENT ID		TECN	COMMENT
$<3.8 \times 10^{-5}$	90	[1] BHARDWAJ	19	BELL	$e^+e^- \to \Upsilon(4S)$

[1] Assumes equal production of B^+ and B^0 at the $\Upsilon(4S)$.

$\Gamma(X(3930)^0 K^+, X^0 \to J/\psi\gamma)/\Gamma_{total}$ — Γ_{275}/Γ

VALUE (units 10^{-6})	CL%	DOCUMENT ID		TECN	COMMENT
<2.5	90	[1] AUBERT,BE	06M	BABR	$e^+e^- \to \Upsilon(4S)$

[1] Assumes equal production of B^+ and B^0 at the $\Upsilon(4S)$.

$\Gamma(J/\psi(1S) K^0 \pi^+)/\Gamma_{total}$ — Γ_{277}/Γ

VALUE (units 10^{-3})	DOCUMENT ID		TECN	COMMENT
• • • We do not use the following data for averages, fits, limits, etc. • • •				
1.101±0.021	[1] AUBERT	09AA	BABR	$e^+e^- \to \Upsilon(4S)$

[1] Does not report systematic uncertainties.

$\Gamma(J/\psi(1S) K^*(892)^+)/\Gamma_{total}$ — Γ_{281}/Γ

For polarization information see the Listings at the end of the "B^0 Branching Ratios" section.

VALUE (units 10^{-3})	EVTS	DOCUMENT ID		TECN	COMMENT
1.43 ±0.08 OUR FIT					
1.43 ±0.08 OUR AVERAGE					
$1.78\ ^{+0.36}_{-0.32} \pm 0.02$		[1,2] AUBERT	07AV	BABR	$e^+e^- \to \Upsilon(4S)$
1.454±0.047±0.097		[2] AUBERT	05J	BABR	$e^+e^- \to \Upsilon(4S)$
1.28 ±0.07 ±0.14		[2] ABE	02N	BELL	$e^+e^- \to \Upsilon(4S)$
1.41 ±0.23 ±0.24		[2] JESSOP	97	CLE2	$e^+e^- \to \Upsilon(4S)$
1.58 ±0.47 ±0.27		[3] ABE	96H	CDF	$p\overline{p}$ at 1.8 TeV
1.50 ±1.08 ±0.01		[4] BORTOLETTO	92	CLEO	$e^+e^- \to \Upsilon(4S)$
1.85 ±1.30 ±0.01	2	[5] ALBRECHT	90J	ARG	$e^+e^- \to \Upsilon(4S)$
• • • We do not use the following data for averages, fits, limits, etc. • • •					
1.37 ±0.09 ±0.11		[2] AUBERT	02	BABR	Repl. by AUBERT 05J
1.78 ±0.51 ±0.23	13	[2] ALAM	94	CLE2	Sup. by JESSOP 97

[1] AUBERT 07AV reports $[\Gamma(B^+ \to J/\psi(1S) K^*(892)^+)/\Gamma_{total}] \times [B(J/\psi(1S) \to p\overline{p})] = (3.78\ ^{+0.72}_{-0.64}\ ^{+0.28}_{-0.23}) \times 10^{-6}$ which we divide by our best value $B(J/\psi(1S) \to p\overline{p}) = (2.120 \pm 0.029) \times 10^{-3}$. Our first error is their experiment's error and our second error is the systematic error from using our best value.
[2] Assumes equal production of B^+ and B^0 at the $\Upsilon(4S)$.
[3] ABE 96H assumes that $B(B^+ \to J/\psi K^+) = (1.02 \pm 0.14) \times 10^{-3}$.
[4] BORTOLETTO 92 reports $(1.3 \pm 0.9 \pm 0.3) \times 10^{-3}$ from a measurement of $[\Gamma(B^+ \to J/\psi(1S) K^*(892)^+)/\Gamma_{total}] \times [B(J/\psi(1S) \to e^+e^-)]$ assuming $B(J/\psi(1S) \to e^+e^-) = 0.069 \pm 0.009$, which we rescale to our best value $B(J/\psi(1S) \to e^+e^-) = (5.971 \pm 0.032) \times 10^{-2}$. Our first error is their experiment's error and our second error is the systematic error from using our best value. Assumes equal production of B^+ and B^0 at the $\Upsilon(4S)$.
[5] ALBRECHT 90J reports $(1.6 \pm 1.1 \pm 0.3) \times 10^{-3}$ from a measurement of $[\Gamma(B^+ \to J/\psi(1S) K^*(892)^+)/\Gamma_{total}] \times [B(J/\psi(1S) \to e^+e^-)]$ assuming $B(J/\psi(1S) \to e^+e^-) = 0.069 \pm 0.009$, which we rescale to our best value $B(J/\psi(1S) \to e^+e^-) = (5.971 \pm 0.032) \times 10^{-2}$. Our first error is their experiment's error and our second error is the systematic error from using our best value. Assumes equal production of B^+ and B^0 at the $\Upsilon(4S)$.

$\Gamma(J/\psi(1S) K^*(892)^+)/\Gamma(J/\psi(1S) K^+)$ — $\Gamma_{281}/\Gamma_{276}$

VALUE	DOCUMENT ID		TECN	COMMENT
1.39±0.09 OUR AVERAGE				
1.37±0.05±0.08	AUBERT	05J	BABR	$e^+e^- \to \Upsilon(4S)$
1.45±0.20±0.17	[1] JESSOP	97	CLE2	$e^+e^- \to \Upsilon(4S)$
1.92±0.60±0.17	ABE	96Q	CDF	$p\overline{p}$
• • • We do not use the following data for averages, fits, limits, etc. • • •				
1.37±0.10±0.08	[2] AUBERT	02	BABR	Repl. by AUBERT 05J

[1] JESSOP 97 assumes equal production of B^+ and B^0 at the $\Upsilon(4S)$. The measurement is actually measured as an average over kaon charged and neutral states.
[2] Assumes equal production of B^+ and B^0 at the $\Upsilon(4S)$.

$\Gamma(J/\psi(1S) K(1270)^+)/\Gamma_{total}$ — Γ_{282}/Γ

VALUE (units 10^{-3})	DOCUMENT ID		TECN	COMMENT
1.80±0.34±0.39	[1] ABE	01L	BELL	$e^+e^- \to \Upsilon(4S)$

[1] Uses the PDG value of $B(B^+ \to J/\psi(1S) K^+) = (1.00 \pm 0.10) \times 10^{-3}$.

$\Gamma(J/\psi(1S) K(1400)^+)/\Gamma(J/\psi(1S) K(1270)^+)$ — $\Gamma_{283}/\Gamma_{282}$

VALUE	CL%	DOCUMENT ID		TECN	COMMENT
<0.30	90	ABE	01L	BELL	$e^+e^- \to \Upsilon(4S)$

$\Gamma(J/\psi(1S)\eta K^+)/\Gamma_{total}$ — Γ_{284}/Γ

VALUE (units 10^{-5})	DOCUMENT ID		TECN	COMMENT
12.4±1.4 OUR AVERAGE				
12.7±1.1±1.1	[1] IWASHITA	14	BELL	$e^+e^- \to \Upsilon(4S)$
10.8±2.3±2.4	[1] AUBERT	04Y	BABR	$e^+e^- \to \Upsilon(4S)$

[1] Assumes equal production of B^+ and B^0 at the $\Upsilon(4S)$.

$\Gamma(\chi_{c1-odd}(3872) K^+, \chi_{c1-odd} \to J/\psi\eta)/\Gamma_{total}$ — Γ_{285}/Γ

VALUE	CL%	DOCUMENT ID		TECN	COMMENT
$<3.8 \times 10^{-6}$	90	IWASHITA	14	BELL	$e^+e^- \to \Upsilon(4S)$

$\Gamma(\psi(4160) K^+, \psi \to J/\psi\eta)/\Gamma_{total}$ — Γ_{286}/Γ

VALUE	CL%	DOCUMENT ID		TECN	COMMENT
$<7.4 \times 10^{-6}$	90	IWASHITA	14	BELL	$e^+e^- \to \Upsilon(4S)$

$\Gamma(J/\psi(1S)\eta' K^+)/\Gamma_{total}$ — Γ_{287}/Γ

VALUE (units 10^{-5})	CL%	DOCUMENT ID		TECN	COMMENT
<8.8	90	[1] XIE	07	BELL	$e^+e^- \to \Upsilon(4S)$

[1] Assumes equal production of B^+ and B^0 at the $\Upsilon(4S)$.

$\Gamma(J/\psi(1S)\phi K^+)/\Gamma_{total}$ — Γ_{288}/Γ

VALUE (units 10^{-5})	DOCUMENT ID		TECN	COMMENT
5.0 ±0.4 OUR AVERAGE				
5.00±0.37±0.15	LEES	15	BABR	$e^+e^- \to \Upsilon(4S)$
4.4 ±1.4 ±0.5	[1] AUBERT	03O	BABR	$e^+e^- \to \Upsilon(4S)$
$8.8\ ^{+3.5}_{-3.0} \pm 1.3$	[2] ANASTASSOV	00	CLE2	$e^+e^- \to \Upsilon(4S)$

[1] Assumes equal production of B^+ and B^0 at the $\Upsilon(4S)$.
[2] ANASTASSOV 00 finds 10 events on a background of 0.5 ± 0.2. Assumes equal production of B^0 and B^+ at the $\Upsilon(4S)$, a uniform Dalitz plot distribution, isotropic $J/\psi(1S)$ and ϕ decays, and $B(B^+ \to J/\psi(1S)\phi K^+) = B(B^0 \to J/\psi(1S)\phi K^0)$.

$\Gamma(J/\psi(1S) K_1(1650), K_1 \to \phi K^+)/\Gamma(J/\psi(1S)\phi K^+)$ — $\Gamma_{289}/\Gamma_{288}$

VALUE	DOCUMENT ID		TECN	COMMENT
$0.12 \pm 0.10\ ^{+0.17}_{-0.06}$	[1] AAIJ	17	LHCB	pp at 7, 8 TeV

[1] Measured in amplitude analysis of $B^+ \to J/\psi(1S)\phi K^+$.

Downloaded from https://academic.oup.com/ptep/article/2022/8/083C01/6651666 by KIT Library user on 27 September 2022

$\Gamma(J/\psi(1S)K^*(1680)^+,\ K^*\to\phi K^+)/\Gamma(J/\psi(1S)\phi K^+)$ — $\Gamma_{290}/\Gamma_{288}$

VALUE (units 10^{-2})	DOCUMENT ID		TECN	COMMENT
$6.7\pm1.9^{+3.2}_{-3.9}$	[1] AAIJ	17	LHCB	pp at 7, 8 TeV

[1] Measured in amplitude analysis of $B^+\to J/\psi(1S)\phi K^+$.

$\Gamma(J/\psi(1S)K_2^*(1980),\ K_2^*\to\phi K^+)/\Gamma(J/\psi(1S)\phi K^+)$ — $\Gamma_{291}/\Gamma_{288}$

VALUE (units 10^{-2})	DOCUMENT ID		TECN	COMMENT
$2.9\pm0.8^{+1.7}_{-0.7}$	[1] AAIJ	17	LHCB	pp at 7, 8 TeV

[1] Measured in amplitude analysis of $B^+\to J/\psi(1S)\phi K^+$.

$\Gamma(J/\psi(1S)K(1830)^+,\ K(1830)^+\to\phi K^+)/\Gamma(J/\psi(1S)\phi K^+)$ — $\Gamma_{292}/\Gamma_{288}$

VALUE (units 10^{-2})	DOCUMENT ID		TECN	COMMENT
$2.6\pm1.1^{+2.3}_{-1.8}$	[1] AAIJ	17	LHCB	pp at 7, 8 TeV

[1] Measured in amplitude analysis of $B^+\to J/\psi(1S)\phi K^+$.

$\Gamma(\chi_{c1}(4140)K^+,\ \chi_{c1}\to J/\psi(1S)\phi)/\Gamma(J/\psi(1S)\phi K^+)$ — $\Gamma_{293}/\Gamma_{288}$

VALUE	CL%	DOCUMENT ID		TECN	COMMENT
0.19 ±0.08 OUR AVERAGE					
$0.13\ \pm0.032^{+4.8}_{-2.0}$		[1] AAIJ	17	LHCB	pp at 7, 8 TeV
$0.19\ \pm0.07\ \pm0.04$		[2] ABAZOV	14A	D0	$p\overline{p}$ at 1.96 TeV
• • • We do not use the following data for averages, fits, limits, etc. • • •					
<0.133	90	LEES	15	BABR	$e^+e^-\to\Upsilon(4S)$
<0.07	90	[3] AAIJ	12AA	LHCB	pp at 7 TeV

[1] Measured in amplitude analysis of $B^+\to J/\psi(1S)\phi K^+$.
[2] Reported a threshold enhancement in the $J/\psi\phi$ mass distribution consistent with the $\chi_{c1}(4140)$ state with a statistical significance of 3.1 standard deviations.
[3] Branching fractions are normalized to 382 ± 22 events of $B^+\to J/\psi\phi K^+$.

$\Gamma(\chi_{c1}(4274)K^+,\ \chi_{c1}\to J/\psi(1S)\phi)/\Gamma(J/\psi(1S)\phi K^+)$ — $\Gamma_{294}/\Gamma_{288}$

VALUE (units 10^{-2})	CL%	DOCUMENT ID		TECN	COMMENT
$7.1\pm2.5^{+3.5}_{-2.4}$		[1] AAIJ	17	LHCB	pp at 7, 8 TeV
• • • We do not use the following data for averages, fits, limits, etc. • • •					
<18.1	90	LEES	15	BABR	$e^+e^-\to\Upsilon(4S)$
<8	90	[2] AAIJ	12AA	LHCB	Repl. by AAIJ 17

[1] Measured in amplitude analysis of $B^+\to J/\psi(1S)\phi K^+$.
[2] Branching fractions are normalized to 382 ± 22 events of $B^+\to J/\psi\phi K^+$.

$\Gamma(\chi_{c0}(4500)K^+,\ \chi_c^0\to J/\psi(1S)\phi)/\Gamma(J/\psi(1S)\phi K^+)$ — $\Gamma_{295}/\Gamma_{288}$

VALUE (units 10^{-2})	DOCUMENT ID		TECN	COMMENT
$6.6\pm2.4^{+3.5}_{-2.3}$	[1] AAIJ	17	LHCB	pp at 7, 8 TeV

[1] Measured in amplitude analysis of $B^+\to J/\psi(1S)\phi K^+$.

$\Gamma(\chi_{c0}(4700)K^+,\ \chi_{c0}\to J/\psi(1S)\phi)/\Gamma(J/\psi(1S)\phi K^+)$ — $\Gamma_{296}/\Gamma_{288}$

VALUE	DOCUMENT ID		TECN	COMMENT
$0.12\pm0.05^{+0.09}_{-0.05}$	[1] AAIJ	17	LHCB	pp at 7, 8 TeV

[1] Measured in amplitude analysis of $B^+\to J/\psi(1S)\phi K^+$.

$\Gamma(J/\psi(1S)\omega K^+)/\Gamma_{total}$ — Γ_{297}/Γ

VALUE (units 10^{-4})	DOCUMENT ID		TECN	COMMENT
$3.2\pm0.1^{+0.6}_{-0.3}$	[1] DEL-AMO-SA...10B		BABR	$e^+e^-\to\Upsilon(4S)$
• • • We do not use the following data for averages, fits, limits, etc. • • •				
$3.5\pm0.2\pm0.4$	[1] AUBERT	08W	BABR	Repl. by DEL-AMO-SANCHEZ 10B

[1] Assumes equal production of B^+ and B^0 at the $\Upsilon(4S)$.

$\Gamma(\chi_{c0}(3915)K^+,\ \chi_{c0}\to J/\psi\omega)/\Gamma_{total}$ — Γ_{298}/Γ

VALUE (units 10^{-5})	DOCUMENT ID		TECN	COMMENT
$3.0^{+0.7+0.5}_{-0.6-0.3}$	[1] DEL-AMO-SA...10B		BABR	$e^+e^-\to\Upsilon(4S)$
• • • We do not use the following data for averages, fits, limits, etc. • • •				
$4.9^{+1.0}_{-0.9}\pm0.5$	[1] AUBERT	08W	BABR	Repl. by DEL-AMO-SANCHEZ 10B

[1] Assumes equal production of B^+ and B^0 at the $\Upsilon(4S)$.

$\Gamma(\chi_{c0}(3915)K^+,\ \chi_{c0}\to p\overline{p})/\Gamma_{total}$ — Γ_{280}/Γ

VALUE	CL%	DOCUMENT ID		TECN	COMMENT
$<7.1\times10^{-8}$	95	[1] AAIJ	13S	LHCB	pp at 7 TeV

[1] Measured relative to $B^+\to J/\psi K^+$ decay with charmonia reconstructed in $p\overline{p}$ final state and using $B(B^+\to J/\psi K^+)=(1.013\pm0.034)\times10^{-3}$ and $B(J/\psi\to p\overline{p})=(2.17\pm0.07)\times10^{-3}$.

$\Gamma(J/\psi(1S)\pi^+)/\Gamma_{total}$ — Γ_{299}/Γ

VALUE	DOCUMENT ID		TECN	COMMENT
$(3.92\pm0.08\ \ )\times10^{-5}$ OUR FIT				
$(3.8\ \pm0.6\ \pm0.3)\times10^{-5}$	[1] ABE	03B	BELL	$e^+e^-\to\Upsilon(4S)$

[1] Assumes equal production of B^+ and B^0 at the $\Upsilon(4S)$.

$\Gamma(J/\psi(1S)\pi^+)/\Gamma(J/\psi(1S)K^+)$ — $\Gamma_{299}/\Gamma_{276}$

VALUE (units 10^{-2})	EVTS	DOCUMENT ID		TECN	COMMENT
3.85 ± 0.04 OUR FIT					
3.85 ± 0.04 OUR AVERAGE					
$3.83\pm0.03\pm0.03$		AAIJ	17O	LHCB	pp at 7, 8 TeV
$3.5\ \pm0.3\ \pm1.2$		AABOUD	16L	ATLS	pp at 7, 8 TeV
$4.86\pm0.82\pm0.15$		ABULENCIA	09	CDF	$p\overline{p}$ at 1.96 TeV
$5.37\pm0.45\pm0.11$		AUBERT	04P	BABR	$e^+e^-\to\Upsilon(4S)$
$5.0\ ^{+1.9}_{-1.7}\ \pm0.1$		ABE	96R	CDF	$p\overline{p}$ 1.8 TeV
$5.2\ \pm2.4$		BISHAI	96	CLE2	$e^+e^-\to\Upsilon(4S)$
• • • We do not use the following data for averages, fits, limits, etc. • • •					
$3.83\pm0.11\pm0.07$		AAIJ	12AC	LHCB	Repl. by AAIJ 17O
$3.91\pm0.78\pm0.19$		AUBERT	02F	BABR	Repl. by AUBERT 04P
$4.3\ \pm2.3$	5	[1] ALEXANDER	95	CLE2	Sup. by BISHAI 96

[1] Assumes equal production of B^+B^- and $B^0\overline{B}^0$ on $\Upsilon(4S)$.

$\Gamma(J/\psi(1S)\pi^+\pi^+\pi^+\pi^-\pi^-)/\Gamma(\psi(2S)K^+)$ — $\Gamma_{300}/\Gamma_{311}$

VALUE (units 10^{-2})	DOCUMENT ID		TECN	COMMENT
$1.88\pm0.17\pm0.09$	[1] AAIJ	17K	LHCB	pp at 7 and 8 TeV

[1] Contains also the contribution from $B^+\to\psi(2S)[\to J/\psi\pi^+\pi^-]\pi^+\pi^+\pi^-$ decays.

$\Gamma(\psi(2S)\pi^+\pi^+\pi^-)/\Gamma(\psi(2S)K^+)$ — $\Gamma_{301}/\Gamma_{311}$

VALUE (units 10^{-2})	DOCUMENT ID		TECN	COMMENT
$3.04\pm0.50\pm0.26$	AAIJ	17K	LHCB	pp at 7 and 8 TeV

$\Gamma(J/\psi(1S)\rho^+)/\Gamma_{total}$ — Γ_{302}/Γ

VALUE (units 10^{-5})	CL%	DOCUMENT ID		TECN	COMMENT
4.1 ±0.5 OUR AVERAGE Error includes scale factor of 1.4.					
$3.81^{+0.25}_{-0.24}\pm0.35$		AAIJ	19O	LHCB	pp at 7 and 8 TeV
$5.0\ \pm0.7\ \pm0.3$		[1] AUBERT	07AC	BABR	$e^+e^-\to\Upsilon(4S)$
• • • We do not use the following data for averages, fits, limits, etc. • • •					
<77	90	BISHAI	96	CLE2	$e^+e^-\to\Upsilon(4S)$

[1] Assumes equal production of B^+ and B^0 at the $\Upsilon(4S)$.

$\Gamma(J/\psi(1S)\pi^+\pi^0\text{nonresonant})/\Gamma_{total}$ — Γ_{303}/Γ

VALUE (units 10^{-5})	CL%	DOCUMENT ID		TECN	COMMENT
<0.73	90	[1] AUBERT	07AC	BABR	$e^+e^-\to\Upsilon(4S)$

[1] Assumes equal production of B^+ and B^0 at the $\Upsilon(4S)$.

$\Gamma(J/\psi(1S)a_1(1260)^+)/\Gamma_{total}$ — Γ_{304}/Γ

VALUE	CL%	DOCUMENT ID		TECN	COMMENT
$<1.2\times10^{-3}$	90	BISHAI	96	CLE2	$e^+e^-\to\Upsilon(4S)$

$\Gamma(J/\psi(1S)p\overline{p}\pi^+)/\Gamma_{total}$ — Γ_{305}/Γ

VALUE	CL%	DOCUMENT ID		TECN	COMMENT
$<5.0\times10^{-7}$	90	[1] AAIJ	13Z	LHCB	pp at 7 TeV

[1] Uses $B(B_s^0\to J/\psi(1S)\pi^+\pi^-)=(1.98\pm0.20)\times10^{-4}$.

$\Gamma(J/\psi(1S)p\overline{\Lambda})/\Gamma_{total}$ — Γ_{306}/Γ

VALUE (units 10^{-6})	CL%	DOCUMENT ID		TECN	COMMENT
14.6 ± 1.2 OUR AVERAGE					
$15.1\pm0.8\pm1.0$		[1] SIRUNYAN	19CM	CMS	pp at 8 TeV
$11.7\pm2.8^{+1.8}_{-2.3}$		[2] XIE	05	BELL	$e^+e^-\to\Upsilon(4S)$
$12\ ^{+9}_{-6}$		[2] AUBERT	03K	BABR	$e^+e^-\to\Upsilon(4S)$
• • • We do not use the following data for averages, fits, limits, etc. • • •					
<41	90	ZANG	04	BELL	$e^+e^-\to\Upsilon(4S)$

[1] SIRUNYAN 19CM reports $B(B^+\to J/\psi\overline{\Lambda}p)/B(B^+\to J/\psi K^*(892))=(1.054\pm0.057\pm0.035\pm0.011)\times10^{-2}$ and rescaled with the best value of $B(B^+\to J/\psi K^*(892))=(1.43\pm0.08)\times10^{-3}$, where the last uncertainty is the uncertainty from the branching fractions of $\overline{\Lambda}$ and $K^*(892)$ to reconstructed final states.
[2] Assumes equal production of B^+ and B^0 at the $\Upsilon(4S)$.

$\Gamma(J/\psi(1S)\overline{\Sigma}^0p)/\Gamma_{total}$ — Γ_{307}/Γ

VALUE	CL%	DOCUMENT ID		TECN	COMMENT
$<1.1\times10^{-5}$	90	[1] XIE	05	BELL	$e^+e^-\to\Upsilon(4S)$

[1] Assumes equal production of B^+ and B^0 at the $\Upsilon(4S)$.

$\Gamma(J/\psi(1S)D^+)/\Gamma_{total}$ — Γ_{308}/Γ

VALUE (units 10^{-5})	CL%	DOCUMENT ID		TECN	COMMENT
<12	90	[1] AUBERT	05U	BABR	$e^+e^-\to\Upsilon(4S)$

[1] Assumes equal production of B^+ and B^0 at the $\Upsilon(4S)$.

$\Gamma(J/\psi(1S)\overline{D}^0\pi^+)/\Gamma_{total}$ — Γ_{309}/Γ

VALUE (units 10^{-5})	CL%	DOCUMENT ID		TECN	COMMENT
<2.5	90	[1] ZHANG	05B	BELL	$e^+e^-\to\Upsilon(4S)$
• • • We do not use the following data for averages, fits, limits, etc. • • •					
<5.2	90	[1] AUBERT	05R	BABR	$e^+e^-\to\Upsilon(4S)$

[1] Assumes equal production of B^+ and B^0 at the $\Upsilon(4S)$.

Downloaded from https://academic.oup.com/ptep/article/2022/8/083C01/6651666 by KIT Library user on 27 September 2022

$\Gamma(\psi(2S)\pi^+)/\Gamma_{total}$ — Γ_{310}/Γ

VALUE (units 10^{-5})	DOCUMENT ID		TECN	COMMENT
2.44±0.22±0.20	[1] BHARDWAJ	08	BELL	$e^+e^- \to \Upsilon(4S)$

[1] Assumes equal production of B^+ and B^0 at the $\Upsilon(4S)$.

$\Gamma(\psi(2S)\pi^+)/\Gamma(\psi(2S)K^+)$ — $\Gamma_{310}/\Gamma_{311}$

VALUE (units 10^{-2})	DOCUMENT ID		TECN	COMMENT
3.97±0.29 OUR AVERAGE				
3.95±0.40±0.12	AAIJ	12AC	LHCB	pp at 7 TeV
3.99±0.36±0.17	BHARDWAJ	08	BELL	$e^+e^- \to \Upsilon(4S)$

$\Gamma(\psi(2S)K^+)/\Gamma_{total}$ — Γ_{311}/Γ

VALUE (units 10^{-4})	EVTS	DOCUMENT ID		TECN	COMMENT
6.24± 0.20 OUR FIT					
6.40± 0.34 OUR AVERAGE					
4.6 ± 1.0 ±0.7		[1] LEES	20C	BABR	$e^+e^- \to \Upsilon(4S)$
6.4 ± 1.0 ±0.4		[1] KATO	18	BELL	$e^+e^- \to \Upsilon(4S)$
6.65± 0.17±0.55		[2] GULER	11	BELL	$e^+e^- \to \Upsilon(4S)$
6.17± 0.32±0.44		[2] AUBERT	05J	BABR	$e^+e^- \to \Upsilon(4S)$
7.8 ± 0.7 ±0.9		[2] RICHICHI	01	CLE2	$e^+e^- \to \Upsilon(4S)$
18 ± 8 ±4	5	[2] ALBRECHT	90J	ARG	$e^+e^- \to \Upsilon(4S)$
• • • We do not use the following data for averages, fits, limits, etc. • • •					
4.9 ± 1.6 ±0.4		[1] AUBERT	06E	BABR	Repl. by LEES 20C
6.9 ± 0.6		[2] ABE	03B	BELL	Repl. by GULER 11
6.4 ± 0.5 ±0.8		[2] AUBERT	02	BABR	Repl. by AUBERT 05J
6.1 ± 2.3 ±0.9	7	[2] ALAM	94	CLE2	Repl. by RICHICHI 01
<5 at 90% CL		[2] BORTOLETTO	92	CLEO	$e^+e^- \to \Upsilon(4S)$
22 ±17	3	[3] ALBRECHT	87D	ARG	$e^+e^- \to \Upsilon(4S)$

[1] Measures absolute branching fractions using a missing-mass technique.
[2] Assumes equal production of B^+ and B^0 at the $\Upsilon(4S)$.
[3] ALBRECHT 87D assume $B^+B^-/B^0\overline{B}^0$ ratio is 55/45. Superseded by ALBRECHT 90J.

$\Gamma(\psi(2S)K^+)/\Gamma(J/\psi(1S)K^+)$ — $\Gamma_{311}/\Gamma_{276}$

VALUE	DOCUMENT ID		TECN	COMMENT
0.611±0.019 OUR FIT				
0.605±0.021 OUR AVERAGE				
0.58 ±0.11 ±0.02	[1] AAIJ	13S	LHCB	pp at 7 TeV
0.607±0.018±0.013	[2,3] AAIJ	12L	LHCB	pp at 7 TeV
0.63 ±0.05 ±0.08	ABAZOV	09Y	D0	$p\overline{p}$ at 1.96 TeV
0.558±0.082±0.056	ABE	98O	CDF	$p\overline{p}$ 1.8 TeV
• • • We do not use the following data for averages, fits, limits, etc. • • •				
0.64 ±0.06 ±0.07	[4] AUBERT	02	BABR	$e^+e^- \to \Upsilon(4S)$

[1] AAIJ 13S reports $[\Gamma(B^+ \to \psi(2S)K^+)/\Gamma(B^+ \to J/\psi(1S)K^+)] \times [B(\psi(2S) \to p\overline{p})] / [B(J/\psi(1S) \to p\overline{p})] = 0.080 \pm 0.012 \pm 0.009$ which we multiply or divide by our best values $B(\psi(2S) \to p\overline{p}) = (2.94 \pm 0.08) \times 10^{-4}$, $B(J/\psi(1S) \to p\overline{p}) = (2.120 \pm 0.029) \times 10^{-3}$. Our first error is their experiment's error and our second error is the systematic error from using our best values.
[2] AAIJ 12L reports $0.594 \pm 0.006 \pm 0.016 \pm 0.015$ from a measurement of $[\Gamma(B^+ \to \psi(2S)K^+)/\Gamma(B^+ \to J/\psi(1S)K^+)] \times [B(J/\psi(1S) \to e^+e^-)] / [B(\psi(2S) \to e^+e^-)]$ assuming $B(J/\psi(1S) \to e^+e^-) = (5.94 \pm 0.06) \times 10^{-2}$, $B(\psi(2S) \to e^+e^-) = (7.72 \pm 0.17) \times 10^{-3}$, which we rescale to our best values $B(J/\psi(1S) \to e^+e^-) = (5.971 \pm 0.032) \times 10^{-2}$, $B(\psi(2S) \to e^+e^-) = (7.93 \pm 0.17) \times 10^{-3}$. Our first error is their experiment's error and our second error is the systematic error from using our best values.
[3] Assumes $B(J/\psi \to \mu^+\mu^-) / B(\psi(2S) \to \mu^+\mu^-) = B(J/\psi \to e^+e^-) / B(\psi(2S) \to e^+e^-) = 7.69 \pm 0.19$.
[4] Assumes equal production of B^+ and B^0 at the $\Upsilon(4S)$.

$\Gamma(\psi(2S)K^*(892)^+)/\Gamma_{total}$ — Γ_{312}/Γ

VALUE (units 10^{-4})	CL%	DOCUMENT ID		TECN	COMMENT
6.7 ±1.4 OUR AVERAGE		Error includes scale factor of 1.3.			
5.92±0.85±0.89		[1] AUBERT	05J	BABR	$e^+e^- \to \Upsilon(4S)$
9.2 ±1.9 ±1.2		[1] RICHICHI	01	CLE2	$e^+e^- \to \Upsilon(4S)$
• • • We do not use the following data for averages, fits, limits, etc. • • •					
<30	90	[1] ALAM	94	CLE2	Repl. by RICHICHI 01
<35	90	[1] BORTOLETTO	92	CLEO	$e^+e^- \to \Upsilon(4S)$
<49	90	[1] ALBRECHT	90J	ARG	$e^+e^- \to \Upsilon(4S)$

[1] Assumes equal production of B^+ and B^0 at the $\Upsilon(4S)$.

$\Gamma(\psi(2S)K^*(892)^+)/\Gamma(\psi(2S)K^+)$ — $\Gamma_{312}/\Gamma_{311}$

VALUE	DOCUMENT ID		TECN	COMMENT
0.96±0.15±0.09	AUBERT	05J	BABR	$e^+e^- \to \Upsilon(4S)$

$\Gamma(\psi(2S)K^0\pi^+)/\Gamma_{total}$ — Γ_{313}/Γ

VALUE (units 10^{-3})	DOCUMENT ID		TECN	COMMENT
• • • We do not use the following data for averages, fits, limits, etc. • • •				
0.588±0.034	[1] AUBERT	09AA	BABR	$e^+e^- \to \Upsilon(4S)$

[1] Does not report systematic uncertainties.

$\Gamma(\psi(2S)K^+\pi^+\pi^-)/\Gamma_{total}$ — Γ_{314}/Γ

VALUE (units 10^{-4})	EVTS	DOCUMENT ID		TECN	COMMENT
4.3 ± 0.5 OUR AVERAGE					
4.31± 0.20±0.50		[1] GULER	11	BELL	$e^+e^- \to \Upsilon(4S)$
19 ±11 ±4	3	[1] ALBRECHT	90J	ARG	$e^+e^- \to \Upsilon(4S)$

[1] Assumes equal production of B^+ and B^0 at the $\Upsilon(4S)$.

$\Gamma(\psi(2S)\phi(1020)K^+)/\Gamma_{total}$ — Γ_{315}/Γ

VALUE (units 10^{-6})	DOCUMENT ID		TECN	COMMENT
4.0±0.4±0.6	[1,2] KHACHATRY...17C		CMS	pp at 8 TeV

[1] Measured using $B^+ \to \psi(2S)K^+$ as a normalization channel. The second error represents total systematic uncertainties including those from branching fractions which were taken from PDG 16 as $B(\phi \to K^+K^-) = 0.489 \pm 0.005$ and $B(B^+ \to \psi(2S)K^+) = (6.26 \pm 0.24) \times 10^{-4}$.
[2] An upper limit on the fraction of the non-ϕ component in $B^+ \to \psi(2S)K^+K^-K^+$ decays is set as 0.26 at the 95% confidence level.

$\Gamma(\psi(3770)K^+)/\Gamma_{total}$ — Γ_{316}/Γ

VALUE (units 10^{-3})	CL%	DOCUMENT ID		TECN	COMMENT
0.43±0.11 OUR AVERAGE					
0.32±0.20±0.05±0.01		[1,2] LEES	20C	BABR	$e^+e^- \to \Upsilon(4S)$
0.48±0.11±0.07		[3] CHISTOV	04	BELL	$e^+e^- \to \Upsilon(4S)$
• • • We do not use the following data for averages, fits, limits, etc. • • •					
<0.23	90	[2] KATO	18	BELL	$e^+e^- \to \Upsilon(4S)$
3.5 ±2.5 ±0.3		[2] AUBERT	06E	BABR	Repl. by LEES 20C

[1] LEES 20C measurement's last uncertainty is due to the used $B(B^{\pm} \to K^{\pm}J/\psi)$ value.
[2] Measures absolute branching fractions using a missing-mass technique.
[3] Assumes equal production of B^+ and B^0 at the $\Upsilon(4S)$.

$\Gamma(\psi(3770)K^+)/\Gamma(D^-D^+K^+)$ — $\Gamma_{316}/\Gamma_{209}$

VALUE	DOCUMENT ID		TECN	COMMENT
$0.352\pm0.035^{+0.034}_{-0.031}$	[1,2] AAIJ	20AI	LHCB	pp at 7, 8, 13 TeV

[1] AAIJ 20AI reports $[\Gamma(B^+ \to \psi(3770)K^+)/\Gamma(B^+ \to D^-D^+K^+)] \times [B(\psi(3770) \to D^+D^-)] = (14.5 \pm 1.2 \pm 0.8) \times 10^{-2}$ which we divide by our best value $B(\psi(3770) \to D^+D^-) = (41 \pm 4) \times 10^{-2}$. Our first error is their experiment's error and our second error is the systematic error from using our best value.
[2] Measured in Dalitz plot analysis of $B^+ \to D^-D^+K^+$ decays.

$\Gamma(\psi(3770)K^+, \psi \to D^0\overline{D}^0)/\Gamma_{total}$ — Γ_{317}/Γ

VALUE (units 10^{-4})	DOCUMENT ID		TECN	COMMENT
1.5 ±0.5 OUR AVERAGE	Error includes scale factor of 1.4.			
1.18±0.41±0.15	[1] LEES	15C	BABR	$e^+e^- \to \Upsilon(4S)$
2.2 ±0.5 ±0.3	[1] BRODZICKA	08	BELL	$e^+e^- \to \Upsilon(4S)$
• • • We do not use the following data for averages, fits, limits, etc. • • •				
1.41±0.30±0.22	[1] AUBERT	08B	BABR	Repl. by LEES 15C
3.4 ±0.8 ±0.5	[1] CHISTOV	04	BELL	Repl. by BRODZICKA 08

[1] Assumes equal production of B^+ and B^0 at the $\Upsilon(4S)$.

$\Gamma(\psi(3770)K^+, \psi \to D^+D^-)/\Gamma_{total}$ — Γ_{318}/Γ

VALUE (units 10^{-4})	DOCUMENT ID		TECN	COMMENT
0.94±0.35 OUR AVERAGE				
0.84±0.32±0.21	[1] AUBERT	08B	BABR	$e^+e^- \to \Upsilon(4S)$
1.4 ±0.8 ±0.2	[1] CHISTOV	04	BELL	$e^+e^- \to \Upsilon(4S)$

[1] Assumes equal production of B^+ and B^0 at the $\Upsilon(4S)$.

$\Gamma(\psi(3770)K^+, \psi \to p\overline{p})/\Gamma_{total}$ — Γ_{319}/Γ

VALUE	CL%	DOCUMENT ID		TECN	COMMENT
$<2\times10^{-7}$	95	[1] AAIJ	17AD	LHCB	pp at 7 and 8 TeV

[1] Measured relative to $B^+ \to J/\psi K^+$ decay with charmonia reconstructed in $p\overline{p}$ final state and using $B(B^+ \to J/\psi K^+) \times B(J/\psi \to p\overline{p}) = (2.17 \pm 0.08) \times 10^{-6}$.

$\Gamma(\psi(4040)K^+)/\Gamma_{total}$ — Γ_{320}/Γ

VALUE	CL%	DOCUMENT ID		TECN	COMMENT
$<1.3\times10^{-4}$	90	AAIJ	13BC	LHCB	pp at 7, 8 TeV
• • • We do not use the following data for averages, fits, limits, etc. • • •					
$<3.0\times10^{-3}$	90	[1] IWASHITA	14	BELL	$e^+e^- \to \Upsilon(4S)$

[1] IWASHITA 14 reports $[\Gamma(B^+ \to \psi(4040)K^+)/\Gamma_{total}] \times [B(\psi(4040) \to J/\psi\eta)] < 15.5 \times 10^{-6}$ which we divide by our best value $B(\psi(4040) \to J/\psi\eta) = 5.2 \times 10^{-3}$.

$\Gamma(\psi(4040)K^+, \psi \to D^+D^-)/\Gamma(D^-D^+K^+)$ — $\Gamma_{321}/\Gamma_{209}$

VALUE (units 10^{-2})	DOCUMENT ID		TECN	COMMENT
5.0±1.3±0.4	[1] AAIJ	20AI	LHCB	pp at 7, 8, 13 TeV

[1] Measured in Dalitz plot analysis of $B^+ \to D^-D^+K^+$ decays.

$\Gamma(\psi(4160)K^+)/\Gamma_{total}$ — Γ_{322}/Γ

VALUE (units 10^{-4})	DOCUMENT ID		TECN	COMMENT
$5.1^{+1.3+2.5}_{-1.2-2.4}$	[1] AAIJ	13BC	LHCB	pp at 7, 8 TeV

[1] AAIJ 13BC reports $[\Gamma(B^+ \to \psi(4160)K^+)/\Gamma_{total}] \times B(\psi(4160) \to \mu^+\mu^-) = (3.5^{+0.9}_{-0.8}) \times 10^{-9}$ which we devide by our best value $B(\psi(4160) \to e^+e^-) = (6.9 \pm 3.3) \times 10^{-6}$ assuming lepton universality. Our first error is their experiment's error and our second error is the systematic error from using our best value.

$\Gamma(\psi(4160)K^+, \psi \to \overline{D}^0D^0)/\Gamma_{total}$ — Γ_{323}/Γ

VALUE (units 10^{-4})	DOCUMENT ID		TECN	COMMENT
0.84±0.41±0.33	[1] LEES	15C	BABR	$e^+e^- \to \Upsilon(4S)$

[1] Assumes equal production of B^+ and B^0 at the $\Upsilon(4S)$.

Downloaded from https://academic.oup.com/ptep/article/2022/8/083C01/6651666 by KIT Library user on 27 September 2022

$\Gamma(\psi(4160)K^+, \psi \to D^+D^-)/\Gamma(D^-D^+K^+)$ — $\Gamma_{324}/\Gamma_{209}$

VALUE (units 10^{-2})	DOCUMENT ID		TECN	COMMENT
6.6±1.5±1.2	[1] AAIJ	20AI	LHCB	pp at 7, 8, 13 TeV

[1] Measured in Dalitz plot analysis of $B^+ \to D^-D^+K^+$ decays.

$\Gamma(\psi(4415)K^+, \psi \to D^+D^-)/\Gamma(D^-D^+K^+)$ — $\Gamma_{325}/\Gamma_{209}$

VALUE (units 10^{-2})	DOCUMENT ID		TECN	COMMENT
9.2±1.4±1.5	[1] AAIJ	20AI	LHCB	pp at 7, 8, 13 TeV

[1] Measured in Dalitz plot analysis of $B^+ \to D^-D^+K^+$ decays.

$\Gamma(\chi_{c0}\pi^+, \chi_{c0} \to \pi^+\pi^-)/\Gamma_{total}$ — Γ_{326}/Γ

VALUE (units 10^{-6})	CL%	DOCUMENT ID		TECN	COMMENT
<0.1	90	[1] AUBERT	09L	BABR	$e^+e^- \to \Upsilon(4S)$
• • • We do not use the following data for averages, fits, limits, etc. • • •					
<0.3	90	[1] AUBERT,B	05G	BABR	Repl. by AUBERT 09L

[1] Assumes equal production of B^+ and B^0 at the $\Upsilon(4S)$.

$\Gamma(\chi_{c0}K^+)/\Gamma_{total}$ — Γ_{327}/Γ

VALUE (units 10^{-4})	CL%	DOCUMENT ID		TECN	COMMENT
$1.51^{+0.15}_{-0.13}$ OUR AVERAGE					
$2.0 \pm 1.3 \pm 0.3 \pm 0.1$		[1,2] LEES	20C	BABR	$e^+e^- \to \Upsilon(4S)$
$1.8^{+0.6}_{-0.5} \pm 0.6$		[3] CHILIKIN	19	BELL	$e^+e^- \to \Upsilon(4S)$
$1.84 \pm 0.25 \pm 0.14$		[4,5] LEES	12O	BABR	$e^+e^- \to \Upsilon(4S)$
$1.68 \pm 0.32 \pm 0.16$		[4,6] LEES	12O	BABR	$e^+e^- \to \Upsilon(4S)$
$1.8 \pm 0.8 \pm 0.1$		[7] LEES	11I	BABR	$e^+e^- \to \Upsilon(4S)$
$1.23^{+0.28}_{-0.25} \pm 0.05$		[4,8] AUBERT	08AI	BABR	$e^+e^- \to \Upsilon(4S)$
$4.3 \pm 2.0 \pm 0.2$		[9] AUBERT,BE	06M	BABR	$e^+e^- \to \Upsilon(4S)$
$1.12 \pm 0.12^{+0.30}_{-0.20}$		[4] GARMASH	06	BELL	$e^+e^- \to \Upsilon(4S)$
• • • We do not use the following data for averages, fits, limits, etc. • • •					
<3.3	90	[2] KATO	18	BELL	$e^+e^- \to \Upsilon(4S)$
<2.7	95	[10] AAIJ	13S	LHCB	pp at 7 TeV
<5	90	[4,11] WICHT	08	BELL	$e^+e^- \to \Upsilon(4S)$
<1.8	90	[2] AUBERT	06E	BABR	$e^+e^- \to \Upsilon(4S)$
$1.84 \pm 0.32 \pm 0.31$		[4,12] AUBERT	06O	BABR	Repl. by LEES 12O
<8.9	90	[4] AUBERT	05K	BABR	$e^+e^- \to \Upsilon(4S)$
$1.39 \pm 0.49 \pm 0.11$		[13] AUBERT,B	05N	BABR	Repl. by AUBERT 08AI
$1.96 \pm 0.35^{+2.00}_{-0.42}$		[4] GARMASH	05	BELL	Repl. by GARMASH 06
2.7 ± 0.7		[14] AUBERT	04T	BABR	Repl. by AUBERT,B 04P
$3.0 \pm 0.8 \pm 0.3$		[15] AUBERT,B	04P	BABR	Repl. by AUBERT,B 05N
$6.0^{+2.1}_{-1.8} \pm 1.1$		[16] ABE	02B	BELL	Repl. by GARMASH 05
<4.8	90	[17] EDWARDS	01	CLE2	$e^+e^- \to \Upsilon(4S)$

[1] LEES 20C measurement's last uncertainty is due to the used $B(B^{\pm} \to K^{\pm}J/\psi)$ value.
[2] Measures absolute branching fractions using a missing-mass technique.
[3] CHILIKIN 19 reports $[\Gamma(B^+ \to \chi_{c0}K^+)/\Gamma_{total}] \times [B(\chi_{c0}(1P) \to p\overline{p}\pi^+\pi^-)] = (3.7^{+1.2}_{-1.0}{}^{+0.2}_{-0.3}) \times 10^{-7}$ which we divide by our best value $B(\chi_{c0}(1P) \to p\overline{p}\pi^+\pi^-) = (2.1 \pm 0.7) \times 10^{-3}$. Our first error is their experiment's error and our second error is the systematic error from using our best value.
[4] Assumes equal production of B^+ and B^0 at the $\Upsilon(4S)$.
[5] Measured in the $B^+ \to K^+K^-K^+$ decay.
[6] Measured in the $B^+ \to K^+K^0_SK^0_S$ decay.
[7] LEES 11I reports $[\Gamma(B^+ \to \chi_{c0}K^+)/\Gamma_{total}] \times [B(\chi_{c0}(1P) \to \pi\pi)] = (1.53 \pm 0.66 \pm 0.27) \times 10^{-6}$ which we divide by our best value $B(\chi_{c0}(1P) \to \pi\pi) = (8.51 \pm 0.33) \times 10^{-3}$. Our first error is their experiment's error and our second error is the systematic error from using our best value.
[8] AUBERT 08AI reports $(0.70 \pm 0.10^{+0.12}_{-0.10}) \times 10^{-6}$ for $B(B^+ \to \chi_{c0}K^+) \times B(\chi_{c0} \to \pi^+\pi^-)$. We compute $B(B^+ \to \chi_{c0}K^+)$ using the PDG value $B(\chi_{c0} \to \pi\pi)=(8.51 \pm 0.33) \times 10^{-3}$ and 2/3 for the $\pi^+\pi^-$ fraction. Our first error is their experiment's error and the second error is systematic error from using our best value.
[9] AUBERT,BE 06M reports $[\Gamma(B^+ \to \chi_{c0}K^+)/\Gamma_{total}] \times [B(\chi_{c0}(1P) \to \gamma J/\psi(1S))] = (6.1 \pm 2.6 \pm 1.1) \times 10^{-6}$ which we divide by our best value $B(\chi_{c0}(1P) \to \gamma J/\psi(1S)) = (1.40 \pm 0.05) \times 10^{-2}$. Our first error is their experiment's error and our second error is the systematic error from using our best value. The significance of the observed signal is 2.4 σ.
[10] AAIJ 13S reports $[\Gamma(B^+ \to \chi_{c0}K^+)/\Gamma_{total}] \times [B(\chi_{c0}(1P) \to p\overline{p})] < 6 \times 10^{-8}$ which we divide by our best value $B(\chi_{c0}(1P) \to p\overline{p}) = 2.21 \times 10^{-4}$.
[11] WICHT 08 reports $[\Gamma(B^+ \to \chi_{c0}K^+)/\Gamma_{total}] \times [B(\chi_{c0}(1P) \to \gamma\gamma)] < 0.11 \times 10^{-6}$ which we divide by our best value $B(\chi_{c0}(1P) \to \gamma\gamma) = 2.04 \times 10^{-4}$.
[12] Measured in the $B^+ \to K^+K^-K^+$ decay.
[13] AUBERT,B 05N reports $(0.66 \pm 0.22 \pm 0.08) \times 10^{-6}$ for $B(B^+ \to \chi^0_cK^+) \times B(\chi^0_c \to \pi^+\pi^-)$. We compute $B(B^+ \to \chi^0_cK^+)$ using the PDG value $B(\chi^0_c \to \pi^+\pi^-) = (7.1 \pm 0.6) \times 10^{-3}$ and 2/3 for the $\pi^+\pi^-$ fraction.
[14] The measurement performed using decay channels $\chi_{c0} \to \pi^+\pi^-$ and $\chi_{c0} \to K^+K^-$. The ratio of the branching ratios for these channels is found to be consistent with world average.
[15] AUBERT 04P reports $B(B^+ \to \chi_{c0}K^+) \times B(\chi_{c0} \to \pi^+\pi^-) = (1.5 \pm 0.4 \pm 0.1) \times 10^{-6}$ and used PDG value of $B(\chi_{c0} \to \pi\pi) = (7.4 \pm 0.8) \times 10^{-3}$ and Clebsh-Gordan coefficient to compute $B(B^{\pm} -> \chi_{c0}K^+)$.
[16] ABE 02B measures the ratio of $B(B^+ \to \chi_{c0}K^+)/B(B^+ \to J/\psi(1S)K^+) = 0.60 + 0.21 - 0.18 \pm 0.05 \pm 0.08$, where the third error is due to the uncertainty in the $B(\chi_{c0} \to \pi^+\pi^-)$, and uses $B(B^+ \to J/\psi(1S)K^+) = (10.0 \pm 1.0) \times 10^{-4}$ to obtain the result.
[17] EDWARDS 01 assumes equal production of B^0 and B^+ at the $\Upsilon(4S)$. The correlated uncertainties (28.3)% from $B(J/\psi(1S) \to \gamma\eta_c)$ in those modes have been accounted for.

$\Gamma(\chi_{c0}K^*(892)^+)/\Gamma_{total}$ — Γ_{328}/Γ

VALUE (units 10^{-4})	CL%	DOCUMENT ID		TECN	COMMENT
< 2.1	90	[1] AUBERT	08BD	BABR	$e^+e^- \to \Upsilon(4S)$
• • • We do not use the following data for averages, fits, limits, etc. • • •					
<28.6	90	[1] AUBERT	05K	BABR	Repl. by AUBERT 08BD

[1] Assumes equal production of B^+ and B^0 at the $\Upsilon(4S)$.

$\Gamma(\chi_{c1}(1P)\pi^+)/\Gamma_{total}$ — Γ_{329}/Γ

VALUE (units 10^{-5})	DOCUMENT ID		TECN	COMMENT
2.2±0.4±0.3	[1] KUMAR	06	BELL	$e^+e^- \to \Upsilon(4S)$

[1] Assumes equal production of B^+ and B^0 at the $\Upsilon(4S)$.

$\Gamma(\chi_{c1}(1P)K^+)/\Gamma_{total}$ — Γ_{330}/Γ

VALUE (units 10^{-4})	DOCUMENT ID		TECN	COMMENT
4.74± 0.22 OUR AVERAGE				
$4.0 \pm 0.8 \pm 0.6 \pm 0.1$	[1,2] LEES	20C	BABR	$e^+e^- \to \Upsilon(4S)$
$9^{+3}_{-2} \pm 4$	[3] CHILIKIN	19	BELL	$e^+e^- \to \Upsilon(4S)$
$5.8 \pm 0.9 \pm 0.5$	[1] KATO	18	BELL	$e^+e^- \to \Upsilon(4S)$
$4.94 \pm 0.11 \pm 0.33$	[4] BHARDWAJ	11	BELL	$e^+e^- \to \Upsilon(4S)$
$4.5 \pm 0.1 \pm 0.3$	[5] AUBERT	09B	BABR	$e^+e^- \to \Upsilon(4S)$
$15.5 \pm 5.4 \pm 2.0$	[6] ACOSTA	02F	CDF	$p\overline{p}$ 1.8 TeV
• • • We do not use the following data for averages, fits, limits, etc. • • •				
$8.1 \pm 1.4 \pm 0.7$	[1] AUBERT	06E	BABR	Repl. by LEES 20C
$5.1 \pm 0.4 \pm 0.1$	[7] AUBERT,BE	06M	BABR	Repl. by AUBERT 09B
$4.49 \pm 0.19 \pm 0.53$	[4] SONI	06	BELL	Repl. by BHARDWAJ 11
$5.79 \pm 0.26 \pm 0.65$	[4] AUBERT	05J	BABR	Repl. by AUBERT,BE 06M
$6.0 \pm 0.9 \pm 0.2$	[8] AUBERT	02	BABR	Repl. by AUBERT 05J
$9.7 \pm 4.0 \pm 0.9$	[4] ALAM	94	CLE2	$e^+e^- \to \Upsilon(4S)$
$19 \pm 13 \pm 6$	[9] ALBRECHT	92E	ARG	$e^+e^- \to \Upsilon(4S)$

[1] Measures absolute branching fractions using a missing-mass technique.
[2] LEES 20C measurement's last uncertainty is due to the used $B(B^{\pm} \to K^{\pm}J/\psi)$ value.
[3] CHILIKIN 19 reports $[\Gamma(B^+ \to \chi_{c1}(1P)K^+)/\Gamma_{total}] \times [B(\chi_{c1}(1P) \to p\overline{p}\pi^+\pi^-)] = (4.7^{+1.3}_{-1.2}{}^{+0.4}_{-0.2}) \times 10^{-7}$ which we divide by our best value $B(\chi_{c1}(1P) \to p\overline{p}\pi^+\pi^-) = (5.0 \pm 1.9) \times 10^{-4}$. Our first error is their experiment's error and our second error is the systematic error from using our best value.
[4] Assumes equal production of B^+ and B^0 at the $\Upsilon(4S)$.
[5] Uses $\chi_{c1,2} \to J/\psi\gamma$. Assumes $B(\Upsilon(4S) \to B^+B^-) = (51.6 \pm 0.6)$% and $B(\Upsilon(4S) \to B^0\overline{B}^0) = (48.4 \pm 0.6)$%.
[6] ACOSTA 02F uses as reference of $B(B \to J/\psi(1S)K^+) = (10.1 \pm 0.6) \times 10^{-4}$. The second error includes the systematic error and the uncertainties of the branching ratio.
[7] AUBERT,BE 06M reports $[\Gamma(B^+ \to \chi_{c1}(1P)K^+)/\Gamma_{total}] \times [B(\chi_{c1}(1P) \to \gamma J/\psi(1S))] = (1.76 \pm 0.07 \pm 0.12) \times 10^{-4}$ which we divide by our best value $B(\chi_{c1}(1P) \to \gamma J/\psi(1S)) = (34.3 \pm 1.0) \times 10^{-2}$. Our first error is their experiment's error and our second error is the systematic error from using our best value.
[8] AUBERT 02 reports $(7.5 \pm 0.9 \pm 0.8) \times 10^{-4}$ from a measurement of $[\Gamma(B^+ \to \chi_{c1}(1P)K^+)/\Gamma_{total}] \times [B(\chi_{c1}(1P) \to \gamma J/\psi(1S))]$ assuming $B(\chi_{c1}(1P) \to \gamma J/\psi(1S)) = 0.273 \pm 0.016$, which we rescale to our best value $B(\chi_{c1}(1P) \to \gamma J/\psi(1S)) = (34.3 \pm 1.0) \times 10^{-2}$. Our first error is their experiment's error and our second error is the systematic error from using our best value. Assumes equal production of B^+ and B^0 at the $\Upsilon(4S)$.
[9] ALBRECHT 92E assumes no $\chi_{c2}(1P)$ production and $B(\Upsilon(4S) \to B^+B^-) = 50$%.

$\Gamma(\chi_{c1}(1P)K^+)/\Gamma(J/\psi(1S)K^+)$ — $\Gamma_{330}/\Gamma_{276}$

VALUE	DOCUMENT ID		TECN	COMMENT
0.60±0.07±0.02	[1] AUBERT	02	BABR	$e^+e^- \to \Upsilon(4S)$

[1] AUBERT 02 reports $0.75 \pm 0.08 \pm 0.05$ from a measurement of $[\Gamma(B^+ \to \chi_{c1}(1P)K^+)/\Gamma(B^+ \to J/\psi(1S)K^+)] \times [B(\chi_{c1}(1P) \to \gamma J/\psi(1S))]$ assuming $B(\chi_{c1}(1P) \to \gamma J/\psi(1S)) = 0.273 \pm 0.016$, which we rescale to our best value $B(\chi_{c1}(1P) \to \gamma J/\psi(1S)) = (34.3 \pm 1.0) \times 10^{-2}$. Our first error is their experiment's error and our second error is the systematic error from using our best value. Assumes equal production of B^+ and B^0 at the $\Upsilon(4S)$.

$\Gamma(\chi_{c1}(1P)\pi^+)/\Gamma(\chi_{c1}(1P)K^+)$ — $\Gamma_{329}/\Gamma_{330}$

VALUE	DOCUMENT ID		TECN	COMMENT
0.043±0.008±0.003	[1] KUMAR	06	BELL	$e^+e^- \to \Upsilon(4S)$

[1] Assumes equal production of B^+ and B^0 at the $\Upsilon(4S)$.

$\Gamma(\chi_{c1}(1P)K^*(892)^+)/\Gamma_{total}$ — Γ_{331}/Γ

VALUE (units 10^{-4})	CL%	DOCUMENT ID		TECN	COMMENT
3.0 ±0.6 OUR AVERAGE		Error includes scale factor of 1.1.			
$2.6 \pm 0.5 \pm 0.4$		[1] AUBERT	09B	BABR	$e^+e^- \to \Upsilon(4S)$
$4.05 \pm 0.59 \pm 0.95$		[2] SONI	06	BELL	$e^+e^- \to \Upsilon(4S)$
• • • We do not use the following data for averages, fits, limits, etc. • • •					
$2.94 \pm 0.95 \pm 0.98$		[2] AUBERT	05J	BABR	Repl. by AUBERT 09B
<21	90	[2] ALAM	94	CLE2	$e^+e^- \to \Upsilon(4S)$

[1] Uses $\chi_{c1,2} \to J/\psi\gamma$. Assumes $B(\Upsilon(4S) \to B^+B^-) = (51.6 \pm 0.6)$% and $B(\Upsilon(4S) \to B^0\overline{B}^0) = (48.4 \pm 0.6)$%.
[2] Assumes equal production of B^+ and B^0 at the $\Upsilon(4S)$.

Downloaded from https://academic.oup.com/ptep/article/2022/8/083C01/6651666 by KIT Library user on 27 September 2022

$\Gamma(\chi_{c1}(1P)K^*(892)^+)/\Gamma(\chi_{c1}(1P)K^+)$ — $\Gamma_{331}/\Gamma_{330}$

VALUE	DOCUMENT ID		TECN	COMMENT
0.51±0.17±0.16	AUBERT	05J	BABR	$e^+e^- \to \Upsilon(4S)$

$\Gamma(\chi_{c1}(1P)K^0\pi^+)/\Gamma_{total}$ — Γ_{332}/Γ

VALUE (units 10^{-4})	DOCUMENT ID		TECN	COMMENT
5.75±0.26±0.32	[1] BHARDWAJ	16	BELL	$e^+e^- \to \Upsilon(4S)$

[1] Assumes equal production of B^+ and B^0 at the $\Upsilon(4S)$.

$\Gamma(\chi_{c1}(1P)K^0\pi^+)/\Gamma(J/\psi(1S)K^0\pi^+)$ — $\Gamma_{332}/\Gamma_{277}$

VALUE	DOCUMENT ID		TECN	COMMENT
0.503±0.030±0.014	[1] LEES	12B	BABR	$e^+e^- \to \Upsilon(4S)$

[1] LEES 12B reports 0.501 ± 0.024 ± 0.028 from a measurement of $[\Gamma(B^+ \to \chi_{c1}(1P)K^0\pi^+)/\Gamma(B^+ \to J/\psi(1S)K^0\pi^+)] \times [B(\chi_{c1}(1P) \to \gamma J/\psi(1S))]$ assuming $B(\chi_{c1}(1P) \to \gamma J/\psi(1S)) = (34.4 \pm 1.5) \times 10^{-2}$, which we rescale to our best value $B(\chi_{c1}(1P) \to \gamma J/\psi(1S)) = (34.3 \pm 1.0) \times 10^{-2}$. Our first error is their experiment's error and our second error is the systematic error from using our best value.

$\Gamma(\chi_{c1}(1P)K^+\pi^0)/\Gamma_{total}$ — Γ_{333}/Γ

VALUE (units 10^{-4})	DOCUMENT ID		TECN	COMMENT
3.29±0.29±0.19	[1] BHARDWAJ	16	BELL	$e^+e^- \to \Upsilon(4S)$

[1] Assumes equal production of B^+ and B^0 at the $\Upsilon(4S)$.

$\Gamma(\chi_{c1}(1P)K^+\pi^+\pi^-)/\Gamma_{total}$ — Γ_{334}/Γ

VALUE (units 10^{-4})	DOCUMENT ID		TECN	COMMENT
3.74±0.18±0.24	[1] BHARDWAJ	16	BELL	$e^+e^- \to \Upsilon(4S)$

[1] Assumes equal production of B^+ and B^0 at the $\Upsilon(4S)$.

$\Gamma(\chi_{c1}(2P)K^+, \chi_{c1}(2P) \to \pi^+\pi^-\chi_{c1}(1P))/\Gamma_{total}$ — Γ_{335}/Γ

VALUE	CL%	DOCUMENT ID		TECN	COMMENT
$<1.1 \times 10^{-5}$	90	[1,2] BHARDWAJ	16	BELL	$e^+e^- \to \Upsilon(4S)$

[1] BHARDWAJ 16 analysis fixes mass and width of the $\chi_{c1}(2P)$ state to 3920 MeV and 20 MeV.
[2] Assumes equal production of B^+ and B^0 at the $\Upsilon(4S)$.

$\Gamma(\chi_{c2}K^+)/\Gamma_{total}$ — Γ_{336}/Γ

VALUE (units 10^{-5})	CL%	DOCUMENT ID		TECN	COMMENT
$1.11^{+0.36}_{-0.34}\pm0.09$		[1] BHARDWAJ	11	BELL	$e^+e^- \to \Upsilon(4S)$
• • • We do not use the following data for averages, fits, limits, etc. • • •					
<1.8	90	[2] AUBERT	09B	BABR	$e^+e^- \to \Upsilon(4S)$
<20	90	[3] AUBERT	06E	BABR	$e^+e^- \to \Upsilon(4S)$
<2.9	90	[1] SONI	06	BELL	Repl. by BHARDWAJ 11
<3.0	90	[1] AUBERT	05K	BABR	Repl. by AUBERT 06E

[1] Assumes equal production of B^+ and B^0 at the $\Upsilon(4S)$.
[2] Uses $\chi_{c1,2} \to J/\psi\gamma$. Assumes $B(\Upsilon(4S) \to B^+B^-) = (51.6 \pm 0.6)\%$ and $B(\Upsilon(4S) \to B^0\overline{B}^0) = (48.4 \pm 0.6)\%$.
[3] Perform measurements of absolute branching fractions using a missing mass technique.

$\Gamma(\chi_{c2}K^+, \chi_{c2} \to p\overline{p}\pi^+\pi^-)/\Gamma_{total}$ — Γ_{337}/Γ

VALUE	DOCUMENT ID		TECN	COMMENT
$<1.9 \times 10^{-7}$	CHILIKIN	19	BELL	$e^+e^- \to \Upsilon(4S)$

$\Gamma(B^+ \to \chi_{c2}K^+)/\Gamma_{total} \times \Gamma(\chi_{c2}(1P) \to \gamma\gamma)/\Gamma_{total}$ — $\Gamma_{336}/\Gamma \times \Gamma_{96}^{\chi_{c2}(1P)}/\Gamma^{\chi_{c2}(1P)}$

VALUE (units 10^{-6})	CL%	DOCUMENT ID		TECN	COMMENT
<0.09	90	[1] WICHT	08	BELL	$e^+e^- \to \Upsilon(4S)$

[1] Assumes equal production of B^+ and B^0 at the $\Upsilon(4S)$.

$\Gamma(\chi_{c2}K^*(892)^+)/\Gamma_{total}$ — Γ_{338}/Γ

VALUE	CL%	DOCUMENT ID		TECN	COMMENT
$<12 \times 10^{-5}$	90	[1] AUBERT	09B	BABR	$e^+e^- \to \Upsilon(4S)$
• • • We do not use the following data for averages, fits, limits, etc. • • •					
$<12.7 \times 10^{-5}$	90	[2] SONI	06	BELL	$e^+e^- \to \Upsilon(4S)$
$<1.2 \times 10^{-5}$	90	[2] AUBERT	05K	BABR	Repl. by AUBERT 09B

[1] Uses $\chi_{c1,2} \to J/\psi\gamma$. Assumes $B(\Upsilon(4S) \to B^+B^-) = (51.6 \pm 0.6)\%$ and $B(\Upsilon(4S) \to B^0\overline{B}^0) = (48.4 \pm 0.6)\%$.
[2] Assumes equal production of B^+ and B^0 at the $\Upsilon(4S)$.

$\Gamma(\chi_{c2}K^0\pi^+)/\Gamma_{total}$ — Γ_{339}/Γ

VALUE (units 10^{-4})	DOCUMENT ID		TECN	COMMENT
1.16±0.22±0.12	[1] BHARDWAJ	16	BELL	$e^+e^- \to \Upsilon(4S)$

[1] Assumes equal production of B^+ and B^0 at the $\Upsilon(4S)$.

$\Gamma(\chi_{c2}K^+\pi^0)/\Gamma_{total}$ — Γ_{340}/Γ

VALUE	CL%	DOCUMENT ID		TECN	COMMENT
$<0.62 \times 10^{-4}$	90	[1] BHARDWAJ	16	BELL	$e^+e^- \to \Upsilon(4S)$

[1] Assumes equal production of B^+ and B^0 at the $\Upsilon(4S)$.

$\Gamma(\chi_{c2}K^+\pi^+\pi^-)/\Gamma_{total}$ — Γ_{341}/Γ

VALUE (units 10^{-4})	DOCUMENT ID		TECN	COMMENT
1.34±0.17±0.09	[1] BHARDWAJ	16	BELL	$e^+e^- \to \Upsilon(4S)$

[1] Assumes equal production of B^+ and B^0 at the $\Upsilon(4S)$.

$\Gamma(\chi_{c2}(3930)K^+, \chi_{c2} \to D^+D^-)/\Gamma(D^-D^+K^+)$ — $\Gamma_{342}/\Gamma_{209}$

VALUE (units 10^{-2})	DOCUMENT ID		TECN	COMMENT
7.2±1.2±0.3	[1] AAIJ	20AI	LHCB	pp at 7, 8, 13 TeV

[1] Measured in Dalitz plot analysis of $B^+ \to D^-D^+K^+$ decays.

$\Gamma(\chi_{c2}(3930)\pi^+, \chi_{c2} \to \pi^+\pi^-)/\Gamma_{total}$ — Γ_{343}/Γ

VALUE (units 10^{-6})	CL%	DOCUMENT ID		TECN	COMMENT
<0.1	90	[1] AUBERT	09L	BABR	$e^+e^- \to \Upsilon(4S)$

[1] Assumes equal production of B^+ and B^0 at the $\Upsilon(4S)$.

$\Gamma(h_c(1P)K^+)/\Gamma_{total}$ — Γ_{344}/Γ

VALUE (units 10^{-5})	CL%	DOCUMENT ID		TECN	COMMENT
$3.7^{+1.0+0.8}_{-0.9-0.8}$		CHILIKIN	19	BELL	$e^+e^- \to \Upsilon(4S)$
• • • We do not use the following data for averages, fits, limits, etc. • • •					
<3.8	90	[1] FANG	06	BELL	$e^+e^- \to \Upsilon(4S)$

[1] Assumes equal production of B^+ and B^0 at the $\Upsilon(4S)$ and $B(h_c \to \eta_c\gamma) = 50\%$.

$\Gamma(h_c(1P)K^+, h_c \to p\overline{p})/\Gamma_{total}$ — Γ_{345}/Γ

VALUE	CL%	DOCUMENT ID		TECN	COMMENT
$<6.4 \times 10^{-8}$	95	[1] AAIJ	13S	LHCB	pp at 7 TeV

[1] Measured relative to $B^+ \to J/\psi K^+$ decay with charmonia reconstructed in $p\overline{p}$ final state and using $B(B^+ \to J/\psi K^+) = (1.013 \pm 0.034) \times 10^{-3}$ and $B(J/\psi \to p\overline{p}) = (2.17 \pm 0.07) \times 10^{-3}$.

$\Gamma(K^0\pi^+)/\Gamma_{total}$ — Γ_{346}/Γ

VALUE (units 10^{-6})	CL%	DOCUMENT ID		TECN	COMMENT
23.7 ± 0.8 OUR FIT					
23.8 ± 0.7 OUR AVERAGE					
23.97± 0.53±0.71		[1] DUH	13	BELL	$e^+e^- \to \Upsilon(4S)$
23.9 ± 1.1 ±1.0		[1] AUBERT,BE	06C	BABR	$e^+e^- \to \Upsilon(4S)$
$18.8^{+3.7}_{-3.3}{}^{+2.1}_{-1.8}$		[1] BORNHEIM	03	CLE2	$e^+e^- \to \Upsilon(4S)$
• • • We do not use the following data for averages, fits, limits, etc. • • •					
$22.8^{+0.8}_{-0.7}$ ±1.3		[1] LIN	07	BELL	Repl. by DUH 13
26.0 ± 1.3 ±1.0		[1] AUBERT,BE	05E	BABR	Repl. by AUBERT,BE 06C
22.3 ± 1.7 ±1.1		[1] AUBERT	04M	BABR	Repl. by AUBERT,BE 05E
22.0 ± 1.9 ±1.1		[1] CHAO	04	BELL	Repl. by LIN 07
$19.4^{+3.1}_{-3.0}$ ±1.6		[1] CASEY	02	BELL	Repl. by CHAO 04
$13.7^{+5.7}_{-4.8}{}^{+1.9}_{-1.8}$		[1] ABE	01H	BELL	Repl. by CASEY 02
$18.2^{+3.3}_{-3.0}$ ±2.0		[1] AUBERT	01E	BABR	Repl. by AUBERT 04M
$18.2^{+4.6}_{-4.0}$ ±1.6		[1] CRONIN-HEN..	00	CLE2	Repl. by BORNHEIM 03
23 $^{+11}_{-10}$ ±3.6		GODANG	98	CLE2	Repl. by CRONIN-HENNESSY 00
<48	90	ASNER	96	CLE2	Repl. by GODANG 98
<190	90	ALBRECHT	91B	ARG	$e^+e^- \to \Upsilon(4S)$
<100	90	[2] AVERY	89B	CLEO	$e^+e^- \to \Upsilon(4S)$
<680	90	AVERY	87	CLEO	$e^+e^- \to \Upsilon(4S)$

[1] Assumes equal production of B^+ and B^0 at the $\Upsilon(4S)$.
[2] AVERY 89B reports $< 9 \times 10^{-5}$ assuming the $\Upsilon(4S)$ decays 43% to $B^0\overline{B}^0$. We rescale to 50%.

$\Gamma(K^+\pi^0)/\Gamma_{total}$ — Γ_{347}/Γ

VALUE (units 10^{-6})	CL%	DOCUMENT ID		TECN	COMMENT
12.9 ±0.5 OUR AVERAGE					
12.62±0.31±0.56		[1] DUH	13	BELL	$e^+e^- \to \Upsilon(4S)$
13.6 ±0.6 ±0.7		[1] AUBERT	07BC	BABR	$e^+e^- \to \Upsilon(4S)$
$12.9^{+2.4}_{-2.2}{}^{+1.2}_{-1.1}$		[1] BORNHEIM	03	CLE2	$e^+e^- \to \Upsilon(4S)$
• • • We do not use the following data for averages, fits, limits, etc. • • •					
12.4 ±0.5 ±0.6		[1] LIN	07A	BELL	Repl. by DUH 13
12.0 ±0.7 ±0.6		[1] AUBERT	05L	BABR	Repl. by AUBERT 07BC
$12.0 \pm 1.3^{+1.3}_{-0.9}$		[1] CHAO	04	BELL	Repl. by LIN 07A
$12.8^{+1.2}_{-1.1}$ ±1.0		[1] AUBERT	03L	BABR	Repl. by AUBERT 05L
$13.0^{+2.5}_{-2.4}$ ±1.3		[1] CASEY	02	BELL	Repl. by CHAO 04
$16.3^{+3.5}_{-3.3}{}^{+1.6}_{-1.8}$		[1] ABE	01H	BELL	Repl. by CASEY 02
$10.8^{+2.1}_{-1.9}$ ±1.0		[1] AUBERT	01E	BABR	Repl. by AUBERT 03L
$11.6^{+3.0}_{-2.7}{}^{+1.4}_{-1.3}$		[1] CRONIN-HEN..	00	CLE2	Repl. by BORNHEIM 03
<16	90	GODANG	98	CLE2	Repl. by CRONIN-HENNESSY 00
<14	90	ASNER	96	CLE2	Repl. by GODANG 98

[1] Assumes equal production of B^+ and B^0 at the $\Upsilon(4S)$.

Downloaded from https://academic.oup.com/ptep/article/2022/8/083C01/6651666 by KIT Library user on 27 September 2022

$\Gamma(K^+\pi^0)/\Gamma(K^0\pi^+)$ — $\Gamma_{347}/\Gamma_{346}$

VALUE	DOCUMENT ID		TECN	COMMENT
0.54±0.03±0.04	LIN	07A	BELL	$e^+e^- \to \Upsilon(4S)$
• • • We do not use the following data for averages, fits, limits, etc. • • •				
$2.38^{+0.98}_{-1.10}{}^{+0.39}_{-0.26}$	ABE	01H	BELL	Repl. by LIN 07A

$\Gamma(\eta' K^+)/\Gamma_{total}$ — Γ_{348}/Γ

VALUE (units 10^{-6})	DOCUMENT ID		TECN	COMMENT
70.4± 2.5 OUR AVERAGE				
71.5± 1.3±3.2	[1] AUBERT	09AV	BABR	$e^+e^- \to \Upsilon(4S)$
$61\ ^{+10}_{-8}\ \pm1$	[1,2] WICHT	08	BELL	$e^+e^- \to \Upsilon(4S)$
69.2± 2.2±3.7	[1] SCHUEMANN	06	BELL	$e^+e^- \to \Upsilon(4S)$
$80\ ^{+10}_{-9}\ \pm7$	[1] RICHICHI	00	CLE2	$e^+e^- \to \Upsilon(4S)$
• • • We do not use the following data for averages, fits, limits, etc. • • •				
70.0± 1.5±2.8	[1] AUBERT	07AE	BABR	Repl. by AUBERT 09AV
68.9± 2.0±3.2	[1] AUBERT	05M	BABR	Repl. by AUBERT 07AE
76.9± 3.5±4.4	[1] AUBERT	03W	BABR	Repl. by AUBERT 05M
$79\ ^{+12}_{-11}\ \pm9$	[1] ABE	01M	BELL	Repl. by SCHUEMANN 06
70 ± 8 ±5	[1] AUBERT	01G	BABR	Repl. by AUBERT 03W
$65\ ^{+15}_{-14}\ \pm9$	BEHRENS	98	CLE2	Repl. by RICHICHI 00

[1] Assumes equal production of B^+ and B^0 at the $\Upsilon(4S)$.
[2] WICHT 08 reports $[\Gamma(B^+ \to \eta' K^+)/\Gamma_{total}] \times [B(\eta'(958) \to \gamma\gamma)] = (1.40^{+0.16}_{-0.15}{}^{+0.15}_{-0.12}) \times 10^{-6}$ which we divide by our best value $B(\eta'(958) \to \gamma\gamma) = (2.307 \pm 0.033) \times 10^{-2}$. Our first error is their experiment's error and our second error is the systematic error from using our best value.

$\Gamma(\eta' K^*(892)^+)/\Gamma_{total}$ — Γ_{349}/Γ

VALUE (units 10^{-6})	CL%	DOCUMENT ID		TECN	COMMENT
$\mathbf{4.8^{+1.6}_{-1.4}\pm0.8}$		[1] DEL-AMO-SA...	10A	BABR	$e^+e^- \to \Upsilon(4S)$
• • • We do not use the following data for averages, fits, limits, etc. • • •					
$4.9^{+1.9}_{-1.7}\pm0.8$		[1] AUBERT	07E	BABR	Repl. by DEL-AMO-SANCHEZ 10A
< 2.9	90	[1] SCHUEMANN	07	BELL	$e^+e^- \to \Upsilon(4S)$
<14	90	[1] AUBERT,B	04D	BABR	Repl. by AUBERT 07E
<35	90	[1] RICHICHI	00	CLE2	$e^+e^- \to \Upsilon(4S)$
<13	90	BEHRENS	98	CLE2	Repl. by RICHICHI 00

[1] Assumes equal production of B^+ and B^0 at the $\Upsilon(4S)$.

$\Gamma(\eta' K_0^*(1430)^+)/\Gamma_{total}$ — Γ_{350}/Γ

VALUE (units 10^{-6})	DOCUMENT ID		TECN	COMMENT
5.2±1.9±1.0	[1] DEL-AMO-SA...	10A	BABR	$e^+e^- \to \Upsilon(4S)$

[1] Assumes equal production of B^+ and B^0 at the $\Upsilon(4S)$.

$\Gamma(\eta' K_2^*(1430)^+)/\Gamma_{total}$ — Γ_{351}/Γ

VALUE (units 10^{-6})	DOCUMENT ID		TECN	COMMENT
$\mathbf{28.0^{+4.6}_{-4.3}\pm2.6}$	[1] DEL-AMO-SA...	10A	BABR	$e^+e^- \to \Upsilon(4S)$

[1] Assumes equal production of B^+ and B^0 at the $\Upsilon(4S)$.

$\Gamma(\eta K^+)/\Gamma_{total}$ — Γ_{352}/Γ

VALUE (units 10^{-6})	CL%	DOCUMENT ID		TECN	COMMENT
2.4 ±0.4 OUR AVERAGE		Error includes scale factor of 1.7.			
2.12±0.23±0.11		[1] HOI	12	BELL	$e^+e^- \to \Upsilon(4S)$
$2.94^{+0.39}_{-0.34}\pm0.21$		[1] AUBERT	09AV	BABR	$e^+e^- \to \Upsilon(4S)$
$2.2\ ^{+2.8}_{-2.2}$		[1] RICHICHI	00	CLE2	$e^+e^- \to \Upsilon(4S)$
• • • We do not use the following data for averages, fits, limits, etc. • • •					
$2.21^{+0.48}_{-0.42}\pm0.01$		[1,2] WICHT	08	BELL	Repl. by HOI 12
3.7 ±0.4 ±0.1		[1] AUBERT	07AE	BABR	Repl. by AUBERT 09AV
$1.9\ \pm0.3\ ^{+0.2}_{-0.1}$		[1] CHANG	07B	BELL	Repl. by HOI 12
3.3 ±0.6 ±0.3		[1] AUBERT,B	05K	BABR	Repl. by AUBERT 07AE
2.1 ±0.6 ±0.2		[1] CHANG	05A	BELL	Repl. by CHANG 07B
3.4 ±0.8 ±0.2		[1] AUBERT	04H	BABR	Repl. by AUBERT,B 05K
<14	90	BEHRENS	98	CLE2	Repl. by RICHICHI 00

[1] Assumes equal production of B^+ and B^0 at the $\Upsilon(4S)$.
[2] WICHT 08 reports $[\Gamma(B^+ \to \eta K^+)/\Gamma_{total}] \times [B(\eta \to 2\gamma)] = (0.87^{+0.16}_{-0.15}{}^{+0.10}_{-0.07}) \times 10^{-6}$ which we divide by our best value $B(\eta \to 2\gamma) = (39.36 \pm 0.18) \times 10^{-2}$. Our first error is their experiment's error and our second error is the systematic error from using our best value.

$\Gamma(\eta K^*(892)^+)/\Gamma_{total}$ — Γ_{353}/Γ

VALUE (units 10^{-6})	CL%	DOCUMENT ID		TECN	COMMENT
19.3±1.6 OUR AVERAGE					
$19.3^{+2.0}_{-1.9}\pm1.5$		[1] WANG	07B	BELL	$e^+e^- \to \Upsilon(4S)$
18.9±1.8±1.3		[1] AUBERT,B	06H	BABR	$e^+e^- \to \Upsilon(4S)$
$26.4^{+9.6}_{-8.2}\pm3.3$		[1] RICHICHI	00	CLE2	$e^+e^- \to \Upsilon(4S)$
• • • We do not use the following data for averages, fits, limits, etc. • • •					
25.6±4.0±2.4		[1] AUBERT,B	04D	BABR	Repl. by AUBERT,B 06H
<30	90	BEHRENS	98	CLE2	Repl. by RICHICHI 00

[1] Assumes equal production of B^+ and B^0 at the $\Upsilon(4S)$.

$\Gamma(\eta K_0^*(1430)^+)/\Gamma_{total}$ — Γ_{354}/Γ

VALUE (units 10^{-6})	DOCUMENT ID		TECN	COMMENT
18.2±2.6±2.6	[1] AUBERT,B	06H	BABR	$e^+e^- \to \Upsilon(4S)$

[1] Assumes equal production of B^+ and B^0 at the $\Upsilon(4S)$.

$\Gamma(\eta K_2^*(1430)^+)/\Gamma_{total}$ — Γ_{355}/Γ

VALUE (units 10^{-6})	DOCUMENT ID		TECN	COMMENT
9.1±2.7±1.4	[1] AUBERT,B	06H	BABR	$e^+e^- \to \Upsilon(4S)$

[1] Assumes equal production of B^+ and B^0 at the $\Upsilon(4S)$.

$\Gamma(\eta(1295) K^+ \times B(\eta(1295) \to \eta\pi\pi))/\Gamma_{total}$ — Γ_{356}/Γ

VALUE (units 10^{-6})	DOCUMENT ID		TECN	COMMENT
$\mathbf{2.9^{+0.8}_{-0.7}\pm0.2}$	[1] AUBERT	08X	BABR	$e^+e^- \to \Upsilon(4S)$

[1] Assumes equal production of B^+ and B^0 at the $\Upsilon(4S)$.

$\Gamma(\eta(1405) K^+ \times B(\eta(1405) \to \eta\pi\pi))/\Gamma_{total}$ — Γ_{357}/Γ

VALUE (units 10^{-6})	CL%	DOCUMENT ID		TECN	COMMENT
<1.3	90	[1] AUBERT	08X	BABR	$e^+e^- \to \Upsilon(4S)$

[1] Assumes equal production of B^+ and B^0 at the $\Upsilon(4S)$.

$\Gamma(\eta(1405) K^+ \times B(\eta(1405) \to K^* K))/\Gamma_{total}$ — Γ_{358}/Γ

VALUE (units 10^{-6})	CL%	DOCUMENT ID		TECN	COMMENT
<1.2	90	[1] AUBERT	08X	BABR	$e^+e^- \to \Upsilon(4S)$

[1] Assumes equal production of B^+ and B^0 at the $\Upsilon(4S)$.

$\Gamma(\eta(1475) K^+ \times B(\eta(1475) \to K^* K))/\Gamma_{total}$ — Γ_{359}/Γ

VALUE (units 10^{-6})	DOCUMENT ID		TECN	COMMENT
$\mathbf{13.8^{+1.8}_{-1.7}{}^{+1.0}_{-0.6}}$	[1] AUBERT	08X	BABR	$e^+e^- \to \Upsilon(4S)$

[1] Assumes equal production of B^+ and B^0 at the $\Upsilon(4S)$.

$\Gamma(f_1(1285) K^+)/\Gamma_{total}$ — Γ_{360}/Γ

VALUE (units 10^{-6})	CL%	DOCUMENT ID		TECN	COMMENT
<2.0	90	[1] AUBERT	08X	BABR	$e^+e^- \to \Upsilon(4S)$

[1] Assumes equal production of B^+ and B^0 at the $\Upsilon(4S)$.

$\Gamma(f_1(1420) K^+ \times B(f_1(1420) \to \eta\pi\pi))/\Gamma_{total}$ — Γ_{361}/Γ

VALUE (units 10^{-6})	CL%	DOCUMENT ID		TECN	COMMENT
<2.9	90	[1] AUBERT	08X	BABR	$e^+e^- \to \Upsilon(4S)$

[1] Assumes equal production of B^+ and B^0 at the $\Upsilon(4S)$.

$\Gamma(f_1(1420) K^+ \times B(f_1(1420) \to K^* K))/\Gamma_{total}$ — Γ_{362}/Γ

VALUE (units 10^{-6})	CL%	DOCUMENT ID		TECN	COMMENT
<4.1	90	[1] AUBERT	08X	BABR	$e^+e^- \to \Upsilon(4S)$

[1] Assumes equal production of B^+ and B^0 at the $\Upsilon(4S)$.

$\Gamma(\phi(1680) K^+ \times B(\phi(1680) \to K^* K))/\Gamma_{total}$ — Γ_{363}/Γ

VALUE (units 10^{-6})	CL%	DOCUMENT ID		TECN	COMMENT
<3.4	90	[1] AUBERT	08X	BABR	$e^+e^- \to \Upsilon(4S)$

[1] Assumes equal production of B^+ and B^0 at the $\Upsilon(4S)$.

$\Gamma(f_0(1500) K^+)/\Gamma_{total}$ — Γ_{364}/Γ

VALUE (units 10^{-6})	CL%	DOCUMENT ID		TECN	COMMENT
3.7± 2.2 OUR AVERAGE					
17 ± 4 ±12		[1] LEES	12O	BABR	$e^+e^- \to \Upsilon(4S)$
20 ±10 ±27		[2] LEES	12O	BABR	$e^+e^- \to \Upsilon(4S)$
$3.2^{+2.2}_{-2.3}\pm0.2$		[3,4] AUBERT	08AI	BABR	$e^+e^- \to \Upsilon(4S)$
• • • We do not use the following data for averages, fits, limits, etc. • • •					
<19	90	[4,5] AUBERT,B	05N	BABR	Repl. by AUBERT 08AI

[1] Measured in the $B^+ \to K^+K^-K^+$ decay.
[2] Measured in the $B^+ \to K^+K^0_SK^0_S$ decay.
[3] AUBERT 08AI reports $B(B^+ \to f_0(1500)K^+) \cdot B(f_0(1500) \to \pi^+\pi^-) = (0.73 \pm 0.21^{+0.47}_{-0.48}) \times 10^{-6}$. We divide this result by our best value of $B(f_0(1500) \to \pi\pi) = (34.5 \pm 2.2) \times 10^{-2}$ multiplied by 2/3 to account for the $\pi^+\pi^-$ fraction. Our first quoted uncertainty is the combined experiment's uncertainty and our second is the systematic uncertainty from using out best value.
[4] Assumes equal production of B^+ and B^0 at the $\Upsilon(4S)$.
[5] AUBERT,B 05N reports $B(B^+ \to f_0(1500)K^+) \cdot B(f_0(1500) \to \pi^+\pi^-) < 4.4 \times 10^{-6}$. We divide this result by our best value of $B(f_0(1500) \to \pi\pi) = (34.5 \pm 2.2) \times 10^{-2}$ multiplied by 2/3 to account for the $\pi^+\pi^-$ fraction. Our first quoted uncertainty is the combined experiment's uncertainty and our second is the systematic uncertainty from using out best value.

Downloaded from https://academic.oup.com/ptep/article/2022/8/083C01/6651666 by KIT Library user on 27 September 2022

$\Gamma(\omega K^+)/\Gamma_{total}$ — Γ_{365}/Γ

VALUE (units 10^{-6})	CL%	DOCUMENT ID		TECN	COMMENT
6.5±0.4 OUR AVERAGE					
6.8±0.4±0.4		[1] CHOBANOVA	14	BELL	$e^+e^- \to \Upsilon(4S)$
6.3±0.5±0.3		[1] AUBERT	07AE	BABR	$e^+e^- \to \Upsilon(4S)$
$3.2^{+2.4}_{-1.9}\pm0.8$		[1] JESSOP	00	CLE2	$e^+e^- \to \Upsilon(4S)$
• • • We do not use the following data for averages, fits, limits, etc. • • •					
6.1±0.6±0.4		[1] AUBERT,B	06E	BABR	AUBERT 07AE
8.1±0.6±0.6		[1] JEN	06	BELL	Repl. by CHOBANOVA 14
4.8±0.8±0.4		[1] AUBERT	04H	BABR	Repl. by AUBERT,B 06E
$6.5^{+1.3}_{-1.2}\pm0.6$		[1] WANG	04A	BELL	Repl. by JEN 06
$9.2^{+2.6}_{-2.3}\pm1.0$		[1] LU	02	BELL	Repl. by WANG 04A
<4	90	[1] AUBERT	01G	BABR	$e^+e^- \to \Upsilon(4S)$
$1.5^{+7}_{-6}\pm2$		[1] BERGFELD	98	CLE2	Repl. by JESSOP 00

[1] Assumes equal production of B^+ and B^0 at the $\Upsilon(4S)$.

$\Gamma(\omega K^*(892)^+)/\Gamma_{total}$ — Γ_{366}/Γ

VALUE (units 10^{-6})	CL%	DOCUMENT ID		TECN	COMMENT
< 7.4	90	[1] AUBERT	09H	BABR	$e^+e^- \to \Upsilon(4S)$
• • • We do not use the following data for averages, fits, limits, etc. • • •					
< 3.4	90	[1] AUBERT,B	06T	BABR	Repl. by AUBERT 09H
< 7.4	90	[1] AUBERT	05O	BABR	Repl. by AUBERT,B 06T
<87	90	[1] BERGFELD	98	CLE2	

[1] Assumes equal production of B^+ and B^0 at the $\Upsilon(4S)$.

$\Gamma(\omega(K\pi)_0^{*+})/\Gamma_{total}$ — Γ_{367}/Γ

$(K\pi)_0^{*+}$ is the total S-wave composed of $K_0^*(1430)$ and nonresonant that are described using LASS shape.

VALUE (units 10^{-6})	DOCUMENT ID		TECN	COMMENT
27.5±3.0±2.6	[1] AUBERT	09H	BABR	$e^+e^- \to \Upsilon(4S)$

[1] Assumes equal production of B^+ and B^0 at the $\Upsilon(4S)$.

$\Gamma(\omega K_0^*(1430)^+)/\Gamma_{total}$ — Γ_{368}/Γ

VALUE (units 10^{-6})	DOCUMENT ID		TECN	COMMENT
24.0±2.6±4.4	[1] AUBERT	09H	BABR	$e^+e^- \to \Upsilon(4S)$

[1] Assumes equal production of B^+ and B^0 at the $\Upsilon(4S)$.

$\Gamma(\omega K_2^*(1430)^+)/\Gamma_{total}$ — Γ_{369}/Γ

VALUE (units 10^{-6})	DOCUMENT ID		TECN	COMMENT
21.5±3.6±2.4	[1] AUBERT	09H	BABR	$e^+e^- \to \Upsilon(4S)$

[1] Assumes equal production of B^+ and B^0 at the $\Upsilon(4S)$.

$\Gamma(a_0(980)^0 K^+ \times B(a_0(980)^0 \to \eta\pi^0))/\Gamma_{total}$ — Γ_{371}/Γ

VALUE (units 10^{-6})	CL%	DOCUMENT ID		TECN	COMMENT
<2.5	90	[1] AUBERT,BE	04	BABR	$e^+e^- \to \Upsilon(4S)$

[1] Assumes equal production of charged and neutral B mesons from $\Upsilon(4S)$ decays.

$\Gamma(a_0(980)^+ K^0 \times B(a_0(980)^+ \to \eta\pi^+))/\Gamma_{total}$ — Γ_{370}/Γ

VALUE (units 10^{-6})	CL%	DOCUMENT ID		TECN	COMMENT
<3.9	90	[1] AUBERT,BE	04	BABR	$e^+e^- \to \Upsilon(4S)$

[1] Assumes equal production of charged and neutral B mesons from $\Upsilon(4S)$ decays.

$\Gamma(K^*(892)^0\pi^+)/\Gamma_{total}$ — Γ_{372}/Γ

VALUE (units 10^{-6})	CL%	DOCUMENT ID		TECN	COMMENT
10.1 ±0.8 OUR AVERAGE					
10.1 ±1.7 ±1.0		[1] LEES	17G	BABR	$e^+e^- \to \Upsilon(4S)$
$10.8 \pm0.6 ^{+1.2}_{-1.4}$		[2] AUBERT	08AI	BABR	$e^+e^- \to \Upsilon(4S)$
$9.67\pm0.64^{+0.81}_{-0.89}$		[2] GARMASH	06	BELL	$e^+e^- \to \Upsilon(4S)$
• • • We do not use the following data for averages, fits, limits, etc. • • •					
$13.5 \pm1.2 ^{+0.8}_{-0.9}$		[2] AUBERT,B	05N	BABR	Repl. by AUBERT 08AI
$9.8 \pm0.9 ^{+1.1}_{-1.2}$		[2] GARMASH	05	BELL	Repl. by GARMASH 06
$15.5 \pm1.8 ^{+1.5}_{-4.0}$		[2,3] AUBERT,B	04P	BABR	Repl. by AUBERT,B 05N
$19.4 ^{+4.2}_{-3.9} ^{+4.1}_{-7.1}$		[4] GARMASH	02	BELL	Repl. by GARMASH 05
<119	90	[5] ABE	00C	SLD	$e^+e^- \to Z$
< 16	90	[2] JESSOP	00	CLE2	$e^+e^- \to \Upsilon(4S)$
<390	90	[6] ADAM	96D	DLPH	$e^+e^- \to Z$
< 41	90	ASNER	96	CLE2	Repl. by JESSOP 00
<480	90	[6] ABREU	95N	DLPH	Sup. by ADAM 96D
<170	90	ALBRECHT	91B	ARG	$e^+e^- \to \Upsilon(4S)$
<150	90	[7] AVERY	89B	CLEO	$e^+e^- \to \Upsilon(4S)$
<260	90	AVERY	87	CLEO	$e^+e^- \to \Upsilon(4S)$

[1] Obtains the result from a Dalitz analysis of $B^+ \to K_S^0\pi^+\pi^0$ decays. The first error is statistical, the second combines all the systematic uncertainties reported in the paper, including signal modelling.

[2] Assumes equal production of B^+ and B^0 at the $\Upsilon(4S)$.

[3] AUBERT 04P also report a branching ratio for $B^+ \to$ "higher K^* resonances" π^+, $K^* \to K^+\pi^-$, $(25.1 \pm 2.0^{+11.0}_{-5.7}) \times 10^{-6}$.

[4] Uses a reference decay mode $B^+ \to \overline{D}^0\pi^+$ and $\overline{D}^0 \to K^+\pi^-$ with $B(B^+ \to \overline{D}^0\pi^+)\cdot B(\overline{D}^0 \to K^+\pi^-) = (20.3 \pm 2.0) \times 10^{-5}$.

[5] ABE 00C assumes $B(Z \to b\overline{b})=(21.7 \pm 0.1)\%$ and the B fractions $f_{B^0}=f_{B^+}=(39.7^{+1.8}_{-2.2})\%$ and $f_{B_s}=(10.5^{+1.8}_{-2.2})\%$.

[6] Assumes a B^0, B^- production fraction of 0.39 and a B_s production fraction of 0.12.

[7] AVERY 89B reports $< 1.3 \times 10^{-4}$ assuming the $\Upsilon(4S)$ decays 43% to $B^0\overline{B}^0$. We rescale to 50%.

$\Gamma(K^*(892)^+\pi^0)/\Gamma_{total}$ — Γ_{373}/Γ

VALUE (units 10^{-6})	CL%	DOCUMENT ID		TECN	COMMENT
6.8±0.9 OUR AVERAGE					
$6.4\pm0.9^{+0.4}_{-0.5}$		[1] LEES	17G	BABR	$e^+e^- \to \Upsilon(4S)$
8.2±1.5±1.1		[2] LEES	11I	BABR	$e^+e^- \to \Upsilon(4S)$
• • • We do not use the following data for averages, fits, limits, etc. • • •					
6.9±2.0±1.3		[2] AUBERT	05X	BABR	Repl. by LEES 11I
<31	90	[2] JESSOP	00	CLE2	$e^+e^- \to \Upsilon(4S)$
<99	90	ASNER	96	CLE2	Repl. by JESSOP 00

[1] Obtains the result from a Dalitz analysis of $B^+ \to K_S^0\pi^+\pi^0$ decays. The first error is statistical, the second combines all the systematic uncertainties reported in the paper, including signal modelling.

[2] Assumes equal production of B^+ and B^0 at the $\Upsilon(4S)$.

$\Gamma(K^+\pi^-\pi^+)/\Gamma(K^+K^-K^+)$ — $\Gamma_{374}/\Gamma_{426}$

VALUE	DOCUMENT ID		TECN	COMMENT
1.703±0.011±0.022	AAIJ	20AJ	LHCB	pp at 7 and 8 TeV

$\Gamma(K^+\pi^-\pi^+)/\Gamma_{total}$ — Γ_{374}/Γ

VALUE (units 10^{-6})	DOCUMENT ID		TECN	COMMENT
51.0±2.9 OUR AVERAGE				
54.4±1.1±4.6	[1] AUBERT	08AI	BABR	$e^+e^- \to \Upsilon(4S)$
48.8±1.1±3.6	[1] GARMASH	06	BELL	$e^+e^- \to \Upsilon(4S)$
• • • We do not use the following data for averages, fits, limits, etc. • • •				
64.1±2.4±4.0	[1] AUBERT,B	05N	BABR	Repl. by AUBERT 08AI
46.6±2.1±4.3	[1] GARMASH	05	BELL	Repl. by GARMASH 06
53.6±3.1±5.1	[1] GARMASH	04	BELL	Repl. by GARMASH 05
59.1±3.8±3.2	[2] AUBERT	03M	BABR	Repl. by AUBERT,B 05N
55.6±5.8±7.7	[3] GARMASH	02	BELL	Repl. by GARMASH 04

[1] Assumes equal production of B^+ and B^0 at the $\Upsilon(4S)$.

[2] Assumes equal production of B^0 and B^+ at the $\Upsilon(4S)$; charm and charmonium contributions are subtracted, otherwise no assumptions about intermediate resonances.

[3] Uses a reference decay mode $B^+ \to \overline{D}^0\pi^+$ and $\overline{D}^0 \to K^+\pi^-$ with $B(B^+ \to \overline{D}^0\pi^+)\cdot B(\overline{D}^0 \to K^+\pi^-) = (20.3 \pm 2.0) \times 10^{-5}$.

$\Gamma(K^+\pi^-\pi^+ \text{nonresonant})/\Gamma_{total}$ — Γ_{375}/Γ

VALUE (units 10^{-6})	CL%	DOCUMENT ID		TECN	COMMENT
$16.3^{+2.1}_{-1.5}$ OUR AVERAGE					
$9.3\pm1.0^{+6.9}_{-1.7}$		[1,2] AUBERT	08AI	BABR	$e^+e^- \to \Upsilon(4S)$
$16.9\pm1.3^{+1.7}_{-1.6}$		[1] GARMASH	06	BELL	$e^+e^- \to \Upsilon(4S)$
• • • We do not use the following data for averages, fits, limits, etc. • • •					
$2.9\pm0.6^{+0.8}_{-0.5}$		[1] AUBERT,B	05N	BABR	Repl. by AUBERT 08AI
$17.3\pm1.7^{+17.2}_{-8.0}$		[1] GARMASH	05	BELL	Repl. by GARMASH 06
< 17	90	[1] AUBERT,B	04P	BABR	Repl. by AUBERT,B 05N
<330	90	[3] ADAM	96D	DLPH	$e^+e^- \to Z$
< 28	90	BERGFELD	96B	CLE2	$e^+e^- \to \Upsilon(4S)$
<400	90	[3] ABREU	95N	DLPH	Sup. by ADAM 96D
<330	90	ALBRECHT	91E	ARG	$e^+e^- \to \Upsilon(4S)$
<190	90	[4] AVERY	89B	CLEO	$e^+e^- \to \Upsilon(4S)$

[1] Assumes equal production of B^+ and B^0 at the $\Upsilon(4S)$.

[2] Calculate the total nonresonant contribution by combining the S-wave composed of $K_0^*(1430)$ and nonresonant that are described using LASS shape.

[3] Assumes a B^0, B^- production fraction of 0.39 and a B_s production fraction of 0.12.

[4] AVERY 89B reports $< 1.7 \times 10^{-4}$ assuming the $\Upsilon(4S)$ decays 43% to $B^0\overline{B}^0$. We rescale to 50%.

$\Gamma(\omega(782)K^+)/\Gamma_{total}$ — Γ_{376}/Γ

VALUE (units 10^{-6})	DOCUMENT ID		TECN	COMMENT
$5.9^{+8.8+0.5}_{-9.0-0.4}$	[1,2] AUBERT	08AI	BABR	$e^+e^- \to \Upsilon(4S)$

[1] Assumes equal production of B^+ and B^0 at the $\Upsilon(4S)$.

[2] AUBERT 08AI reports $[\Gamma(B^+ \to \omega(782)K^+)/\Gamma_{total}] \times [B(\omega(782) \to \pi^+\pi^-)] = (0.09 \pm 0.13^{+0.036}_{-0.045}) \times 10^{-6}$ which we divide by our best value $B(\omega(782) \to \pi^+\pi^-) = (1.53^{+0.11}_{-0.13}) \times 10^{-2}$. Our first error is their experiment's error and our second error is the systematic error from using our best value.

Downloaded from https://academic.oup.com/ptep/article/2022/8/083C01/6651666 by KIT Library user on 27 September 2022

$\Gamma(K^+ f_0(980) \times B(f_0(980) \to \pi^+\pi^-))/\Gamma_{total}$ — Γ_{377}/Γ

VALUE (units 10^{-6})	CL%	DOCUMENT ID		TECN	COMMENT
$9.4\ ^{+1.0}_{-1.2}$ OUR AVERAGE					
$10.3 \pm 0.5\ ^{+2.0}_{-1.4}$		[1] AUBERT	08AI	BABR	$e^+e^- \to \Upsilon(4S)$
$8.78 \pm 0.82\ ^{+0.85}_{-1.76}$		[1] GARMASH	06	BELL	$e^+e^- \to \Upsilon(4S)$
• • • We do not use the following data for averages, fits, limits, etc. • • •					
$9.47 \pm 0.97\ ^{+0.62}_{-0.88}$		[1] AUBERT,B	05N	BABR	Repl. by AUBERT 08AI
$7.55 \pm 1.24\ ^{+1.63}_{-1.18}$		[1] GARMASH	05	BELL	Repl. by GARMASH 06
$9.2 \pm 1.2\ ^{+2.1}_{-2.6}$		[2] AUBERT,B	04P	BABR	Repl. by AUBERT,B 05N
$9.6\ ^{+2.5}_{-2.3}\ ^{+3.7}_{-1.7}$		[3] GARMASH	02	BELL	Repl. by GARMASH 05
<80	90	[4] AVERY	89B	CLEO	$e^+e^- \to \Upsilon(4S)$

[1] Assumes equal production of B^+ and B^0 at the $\Upsilon(4S)$.
[2] AUBERT,B 04P also reports $B(B^+ \to$ "higher f^0 resonances" $\pi^+, f(980)^0 \to \pi^+\pi^-) = (3.2 \pm 1.2\ ^{+6.0}_{-2.9}) \times 10^{-6}$.
[3] Uses a reference decay mode $B^+ \to \overline{D}^0\pi^+$ and $\overline{D}^0 \to K^+\pi^-$ with $B(B^+ \to \overline{D}^0\pi^+) \times B(\overline{D}^0 \to K^+\pi^-) = (20.3 \pm 2.0) \times 10^{-5}$. Only charged pions from the $f_0(980)$ are used.
[4] AVERY 89B reports $< 7 \times 10^{-5}$ assuming the $\Upsilon(4S)$ decays 43% to $B^0\overline{B}^0$. We rescale to 50%.

$\Gamma(f_2(1270)^0 K^+)/\Gamma_{total}$ — Γ_{378}/Γ

VALUE (units 10^{-6})	CL%	DOCUMENT ID		TECN	COMMENT
1.07 ± 0.27 OUR AVERAGE					
$0.89\ ^{+0.38}_{-0.33}\ ^{+0.01}_{-0.03}$		[1,2] AUBERT	08AI	BABR	$e^+e^- \to \Upsilon(4S)$
$1.33 \pm 0.30\ ^{+0.23}_{-0.34}$		[1] GARMASH	06	BELL	$e^+e^- \to \Upsilon(4S)$
• • • We do not use the following data for averages, fits, limits, etc. • • •					
<16	90	[3] AUBERT,B	05N	BABR	Repl. by AUBERT 08AI
< 2.3	90	[4] GARMASH	05	BELL	Repl. by GARMASH 06

[1] Assumes equal production of B^+ and B^0 at the $\Upsilon(4S)$.
[2] AUBERT 08AI reports $(0.50 \pm 0.15\ ^{+0.15}_{-0.11}) \times 10^{-6}$ for $B(B^+ \to f_2(1270) K^+) \times B(f_2 \to \pi^+\pi^-)$. We compute $B(B^+ \to f_2(1270) K^+)$ using the PDG value $B(f_2(1270) \to \pi\pi) = (84.2\ ^{+2.9}_{-0.9}) \times 10^{-2}$ and 2/3 for the $\pi^+\pi^-$ fraction. Our first error is their experiment's error and the second error is systematic error from using our best value.
[3] AUBERT,B 05N reports 8.9×10^{-6} at 90% CL for $B(B^+ \to f_2(1270) K^+) \times B(f_2(1270) \to \pi^+\pi^-)$. We rescaled it using the PDG value $B(f_2(1270) \to \pi\pi) = 84.7\%$ and 2/3 for the $\pi^+\pi^-$ fraction.
[4] GARMASH 05 reports 1.3×10^{-6} at 90% CL for $B(B^+ \to f_2(1270) K^+) \times B(f_2(1270) \to \pi^+\pi^-)$. We rescaled it using the PDG value $B(f_2(1270) \to \pi\pi) = 84.7\%$ and 2/3 for the $\pi^+\pi^-$ fraction.

$\Gamma(f_0(1370)^0 K^+ \times B(f_0(1370)^0 \to \pi^+\pi^-))/\Gamma_{total}$ — Γ_{379}/Γ

VALUE	CL%	DOCUMENT ID		TECN	COMMENT
$<10.7 \times 10^{-6}$	90	[1] AUBERT,B	05N	BABR	$e^+e^- \to \Upsilon(4S)$

[1] Assumes equal production of B^+ and B^0 at the $\Upsilon(4S)$.

$\Gamma(\rho^0(1450) K^+ \times B(\rho^0(1450) \to \pi^+\pi^-))/\Gamma_{total}$ — Γ_{380}/Γ

VALUE	CL%	DOCUMENT ID		TECN	COMMENT
$<11.7 \times 10^{-6}$	90	[1] AUBERT,B	05N	BABR	$e^+e^- \to \Upsilon(4S)$

[1] Assumes equal production of B^+ and B^0 at the $\Upsilon(4S)$.

$\Gamma(f_2'(1525) K^+ \times B(f_2'(1525) \to \pi^+\pi^-))/\Gamma_{total}$ — Γ_{381}/Γ

VALUE	CL%	DOCUMENT ID		TECN	COMMENT
$<3.4 \times 10^{-6}$	90	[1] AUBERT,B	05N	BABR	$e^+e^- \to \Upsilon(4S)$

[1] Assumes equal production of B^+ and B^0 at the $\Upsilon(4S)$.

$\Gamma(K^+\rho^0)/\Gamma_{total}$ — Γ_{382}/Γ

VALUE (units 10^{-6})	CL%	DOCUMENT ID		TECN	COMMENT
3.7 ± 0.5 OUR AVERAGE					
$3.56 \pm 0.45\ ^{+0.57}_{-0.46}$		[1] AUBERT	08AI	BABR	$e^+e^- \to \Upsilon(4S)$
$3.89 \pm 0.47\ ^{+0.43}_{-0.41}$		[1] GARMASH	06	BELL	$e^+e^- \to \Upsilon(4S)$
• • • We do not use the following data for averages, fits, limits, etc. • • •					
$5.07 \pm 0.75\ ^{+0.55}_{-0.88}$		[1] AUBERT,B	05N	BABR	Repl. by AUBERT 08AI
$4.78 \pm 0.75\ ^{+1.01}_{-0.97}$		[1] GARMASH	05	BELL	Repl. by GARMASH 06
< 6.2	90	[2] AUBERT,B	04P	BABR	Repl. by AUBERT,B 05N
< 12	90	[3] GARMASH	02	BELL	$e^+e^- \to \Upsilon(4S)$
< 86	90	[4] ABE	00C	SLD	$e^+e^- \to Z$
< 17	90	[1] JESSOP	00	CLE2	$e^+e^- \to \Upsilon(4S)$
<120	90	[5] ADAM	96D	DLPH	$e^+e^- \to Z$
< 19	90	ASNER	96	CLE2	Repl. by JESSOP 00
<190	90	[5] ABREU	95N	DLPH	Sup. by ADAM 96D
<180	90	ALBRECHT	91B	ARG	$e^+e^- \to \Upsilon(4S)$
< 80	90	[6] AVERY	89B	CLEO	$e^+e^- \to \Upsilon(4S)$
<260	90	AVERY	87	CLEO	$e^+e^- \to \Upsilon(4S)$

[1] Assumes equal production of B^+ and B^0 at the $\Upsilon(4S)$.
[2] AUBERT 04P reports a central value of $(3.9 \pm 1.2\ ^{+1.3}_{-3.5}) \times 10^{-6}$ for this branching ratio.
[3] Uses a reference decay mode $B^+ \to \overline{D}^0\pi^+$ and $\overline{D}^0 \to K^+\pi^-$ with $B(B^+ \to \overline{D}^0\pi^+) \cdot B(\overline{D}^0 \to K^+\pi^-) = (20.3 \pm 2.0) \times 10^{-5}$.
[4] ABE 00C assumes $B(Z \to b\overline{b}) = (21.7 \pm 0.1)\%$ and the B fractions $f_{B^0} = f_{B^+} = (39.7\ ^{+1.8}_{-2.2})\%$ and $f_{B_s} = (10.5\ ^{+1.8}_{-2.2})\%$.
[5] Assumes production fractions $f_{B^0} = f_{B^-} = 0.39$ and $f_{B_s} = 0.12$.
[6] AVERY 89B reports $< 7 \times 10^{-5}$ assuming the $\Upsilon(4S)$ decays 43% to $B^0\overline{B}^0$. We rescale to 50%.

$\Gamma(K_0^*(1430)^0\pi^+)/\Gamma_{total}$ — Γ_{383}/Γ

VALUE (units 10^{-6})	DOCUMENT ID		TECN	COMMENT
$39\ ^{+6}_{-5}$ OUR AVERAGE Error includes scale factor of 1.4. See the ideogram below.				
$34.6 \pm 3.3 \pm 4.6$	[1] LEES	17G	BABR	$e^+e^- \to \Upsilon(4S)$
$32.0 \pm 1.2\ ^{+10.8}_{-6.0}$	[2] AUBERT	08AI	BABR	$e^+e^- \to \Upsilon(4S)$
$51.6 \pm 1.7\ ^{+7.0}_{-7.5}$	[2] GARMASH	06	BELL	$e^+e^- \to \Upsilon(4S)$
• • • We do not use the following data for averages, fits, limits, etc. • • •				
$44.4 \pm 2.2 \pm 5.3$	[2,3] AUBERT,B	05N	BABR	Repl. by AUBERT 08AI
$45.0 \pm 2.9\ ^{+15.0}_{-10.7}$	[2] GARMASH	05	BELL	Repl. by GARMASH 06

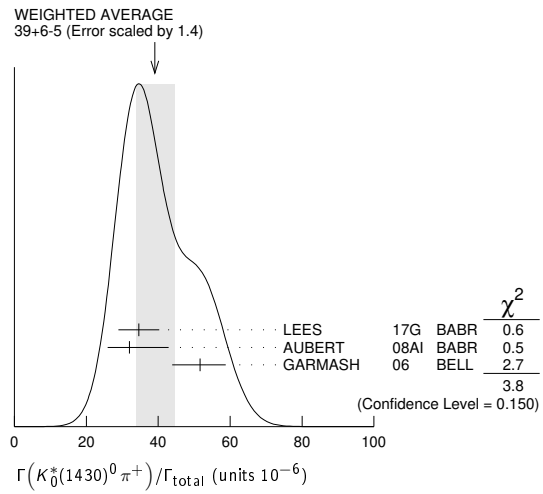

[1] Obtains the result from a Dalitz analysis of $B^+ \to K_S^0\pi^+\pi^0$ decays. The first error is statistical, the second combines all the systematic uncertainties reported in the paper, including signal modelling.
[2] Assumes equal production of B^+ and B^0 at the $\Upsilon(4S)$.
[3] See erratum: AUBERT,BE 06A.

$\Gamma(K_2^*(1430)^0\pi^+)/\Gamma_{total}$ — Γ_{384}/Γ

VALUE (units 10^{-6})	CL%	DOCUMENT ID		TECN	COMMENT
$5.6\ ^{+2.2}_{-1.5} \pm 0.1$		[1,2] AUBERT	08AI	BABR	$e^+e^- \to \Upsilon(4S)$
• • • We do not use the following data for averages, fits, limits, etc. • • •					
< 23	90	[3] AUBERT,B	05N	BABR	Repl. by AUBERT 08AI
< 6.9	90	[4] GARMASH	05	BELL	$e^+e^- \to \Upsilon(4S)$
<680	90	ALBRECHT	91B	ARG	$e^+e^- \to \Upsilon(4S)$

[1] Assumes equal production of B^+ and B^0 at the $\Upsilon(4S)$.
[2] AUBERT 08AI reports $(1.85 \pm 0.41\ ^{+0.61}_{-0.29}) \times 10^{-6}$ for $B(B^+ \to K_2^*(1430)^0\pi^+) \times B(K_2^*(1430)^0 \to K^+\pi^-)$. We compute $B(B^+ \to K_2^*(1430)^0\pi^+)$ using the PDG value $B(K_2^*(1430)^0 \to K\pi) = (49.9 \pm 1.2) \times 10^{-2}$ and 2/3 for the $K^+\pi^-$ fraction. Our first error is their experiment's error and the second error is systematic error from using our best value.
[3] AUBERT,B 05N reports 7.7×10^{-6} at 90% CL for $B(B^+ \to K_2^*(1430)^0\pi^+) \times B(K_2^*(1430)^0 \to K^+\pi^-)$. We rescaled it using the PDG value $B(K_2^*(1430)^0 \to K\pi) = 49.9\%$ and 2/3 for the $K^+\pi^-$ fraction.
[4] GARMASH 05 reports 2.3×10^{-6} at 90% CL for $B(B^+ \to K_2^*(1430)^0\pi^+) \times B(K_2^*(1430)^0 \to K^+\pi^-)$. We rescaled it using the PDG value $B(K_2^*(1430)^0 \to K\pi) = 49.9\%$ and 2/3 for the $K^+\pi^-$ mode.

$\Gamma(K^*(1410)^0\pi^+)/\Gamma_{total}$ — Γ_{385}/Γ

VALUE (units 10^{-6})	CL%	DOCUMENT ID		TECN	COMMENT
<45	90	[1] GARMASH	05	BELL	$e^+e^- \to \Upsilon(4S)$

[1] GARMASH 05 reports 2.0×10^{-6} at 90% CL for $B(B^+ \to K^*(1410)^0\pi^+) \times B(K^*(1410)^0 \to K^+\pi^-)$. We rescaled it using the PDG value $B(K^*(1410)^0 \to K\pi) = 6.6\%$ and 2/3 for the $K^+\pi^-$ mode.

Downloaded from https://academic.oup.com/ptep/article/2022/8/083C01/6651666 by KIT Library user on 27 September 2022

$\Gamma(K^*(1680)^0\pi^+)/\Gamma_{total}$ — Γ_{386}/Γ

VALUE (units 10^{-6})	CL%	DOCUMENT ID		TECN	COMMENT
<12	90	[1] GARMASH	05	BELL	$e^+e^- \to \Upsilon(4S)$
• • • We do not use the following data for averages, fits, limits, etc. • • •					
<15	90	[2] AUBERT,B	05N	BABR	$e^+e^- \to \Upsilon(4S)$

[1] GARMASH 05 reports 3.1×10^{-6} at 90% CL for $B(B^+ \to K^*(1680)^0\pi^+) \times B(K^*(1680)^0 \to K^+\pi^-)$. We rescaled it using the PDG value $B(K^*(1680)^0 \to K\pi) = 38.7\%$ and 2/3 for the $K^+\pi^-$ mode.
[2] AUBERT,B 05N reports 3.8×10^{-6} at 90% CL for $B(B^+ \to K^*(1680)^0\pi^+) \times B(K^*(1680)^0 \to K^+\pi^-)$. We rescaled it using the PDG value $B(K^*(1680)^0 \to K\pi) = 38.7\%$ and 2/3 for the $K^+\pi^-$ fraction.

$\Gamma(K^+\pi^0\pi^0)/\Gamma_{total}$ — Γ_{387}/Γ

VALUE (units 10^{-6})	DOCUMENT ID		TECN	COMMENT
16.2±1.2±1.5	[1] LEES	11I	BABR	$e^+e^- \to \Upsilon(4S)$

[1] Assumes equal production of B^+ and B^0 at the $\Upsilon(4S)$.

$\Gamma(f_0(980)K^+ \times B(f_0 \to \pi^0\pi^0))/\Gamma_{total}$ — Γ_{388}/Γ

VALUE (units 10^{-6})	DOCUMENT ID		TECN	COMMENT
2.8±0.6±0.5	[1] LEES	11I	BABR	$e^+e^- \to \Upsilon(4S)$

[1] Assumes equal production of B^+ and B^0 at the $\Upsilon(4S)$.

$\Gamma(K^-\pi^+\pi^+)/\Gamma_{total}$ — Γ_{389}/Γ

VALUE	CL%	DOCUMENT ID		TECN	COMMENT
$<4.6 \times 10^{-8}$	90	AAIJ	17E	LHCB	pp at 7, 8 TeV
• • • We do not use the following data for averages, fits, limits, etc. • • •					
$<9.5 \times 10^{-7}$	90	[1] AUBERT	08BE	BABR	$e^+e^- \to \Upsilon(4S)$
$<4.5 \times 10^{-6}$	90	[1] GARMASH	04	BELL	$e^+e^- \to \Upsilon(4S)$
$<1.8 \times 10^{-6}$	90	[2] AUBERT	03M	BABR	Repl. by AUBERT 08BE
$<7.0 \times 10^{-6}$	90	[3] GARMASH	02	BELL	$e^+e^- \to \Upsilon(4S)$

[1] Assumes equal production of B^+ and B^0 at the $\Upsilon(4S)$.
[2] Assumes equal production of B^0 and B^+ at the $\Upsilon(4S)$; charm and charmonium contributions are subtracted, otherwise no assumptions about intermediate resonances.
[3] Uses a reference decay mode $B^+ \to \overline{D}^0\pi^+$ and $\overline{D}^0 \to K^+\pi^-$ with $B(B^+ \to \overline{D}^0\pi^+)\cdot B(\overline{D}^0 \to K^+\pi^-) = (20.3 \pm 2.0) \times 10^{-5}$.

$\Gamma(K^-\pi^+\pi^+ \text{nonresonant})/\Gamma_{total}$ — Γ_{390}/Γ

VALUE (units 10^{-6})	CL%	DOCUMENT ID		TECN	COMMENT
<56	90	BERGFELD	96B	CLE2	$e^+e^- \to \Upsilon(4S)$

$\Gamma(K_1(1270)^0\pi^+)/\Gamma_{total}$ — Γ_{391}/Γ

VALUE	CL%	DOCUMENT ID		TECN	COMMENT
$<4.0 \times 10^{-5}$	90	[1] AUBERT	10D	BABR	$e^+e^- \to \Upsilon(4S)$

[1] Assumes equal production of B^+ and B^0 at the $\Upsilon(4S)$.

$\Gamma(K_1(1400)^0\pi^+)/\Gamma_{total}$ — Γ_{392}/Γ

VALUE	CL%	DOCUMENT ID		TECN	COMMENT
$<3.9 \times 10^{-5}$	90	[1] AUBERT	10D	BABR	$e^+e^- \to \Upsilon(4S)$
• • • We do not use the following data for averages, fits, limits, etc. • • •					
$<2.6 \times 10^{-3}$	90	ALBRECHT	91B	ARG	$e^+e^- \to \Upsilon(4S)$

[1] Assumes equal production of B^+ and B^0 at the $\Upsilon(4S)$.

$\Gamma(K^0\pi^+\pi^0)/\Gamma_{total}$ — Γ_{393}/Γ

VALUE (units 10^{-6})	CL%	DOCUMENT ID		TECN	COMMENT
$31.8 \pm 1.8^{+6.3}_{-2.1}$		[1] LEES	17G	BABR	$e^+e^- \to \Upsilon(4S)$
<66	90	[2] ECKHART	02	CLE2	$e^+e^- \to \Upsilon(4S)$

[1] Obtains the result from a Dalitz analysis of $B^+ \to K^0_S\pi^+\pi^0$ decays. The first error is statistical, the second combines all the systematic uncertainties reported in the paper, including signal modelling.
[2] Assumes equal production of B^+ and B^0 at the $\Upsilon(4S)$.

$\Gamma(K^0\rho^+)/\Gamma_{total}$ — Γ_{395}/Γ

VALUE (units 10^{-6})	CL%	DOCUMENT ID		TECN	COMMENT
$7.3^{+1.0}_{-1.2}$ OUR AVERAGE					
$6.5 \pm 1.1^{+0.8}_{-1.9}$		[1] LEES	17G	BABR	$e^+e^- \to \Upsilon(4S)$
$8.0^{+1.4}_{-1.3} \pm 0.6$		AUBERT	07Z	BABR	$e^+e^- \to \Upsilon(4S)$
• • • We do not use the following data for averages, fits, limits, etc. • • •					
<48	90	ASNER	96	CLE2	$e^+e^- \to \Upsilon(4S)$

[1] Obtains the result from a Dalitz analysis of $B^+ \to K^0_S\pi^+\pi^0$ decays. The first error is statistical, the second combines all the systematic uncertainties reported in the paper, including signal modelling.

$\Gamma(K^*_0(1430)^+\pi^0)/\Gamma_{total}$ — Γ_{394}/Γ

VALUE (units 10^{-6})	DOCUMENT ID		TECN	COMMENT
$11.9 \pm 1.7^{+1.0}_{-1.6}$	[1] LEES	17G	BABR	$e^+e^- \to \Upsilon(4S)$

[1] Obtains the result from a Dalitz analysis of $B^+ \to K^0_S\pi^+\pi^0$ decays. The first error is statistical, the second combines all the systematic uncertainties reported in the paper, including signal modelling.

$\Gamma(K^*(892)^+\pi^+\pi^-)/\Gamma_{total}$ — Γ_{396}/Γ

VALUE (units 10^{-6})	CL%	DOCUMENT ID		TECN	COMMENT
75.3±6.0±8.1		[1] AUBERT,B	06U	BABR	$e^+e^- \to \Upsilon(4S)$
• • • We do not use the following data for averages, fits, limits, etc. • • •					
<1100	90	ALBRECHT	91E	ARG	$e^+e^- \to \Upsilon(4S)$

[1] Assumes equal production of B^+ and B^0 at the $\Upsilon(4S)$.

$\Gamma(K^*(892)^+\rho^0)/\Gamma_{total}$ — Γ_{397}/Γ

VALUE (units 10^{-6})	CL%	DOCUMENT ID		TECN	COMMENT
4.6±1.0±0.4		[1] DEL-AMO-SA...11D		BABR	$e^+e^- \to \Upsilon(4S)$
• • • We do not use the following data for averages, fits, limits, etc. • • •					
< 6.1	90	[1] AUBERT,B	06G	BABR	Repl. by DEL-AMO-SANCHEZ 11D
$10.6^{+3.0}_{-2.6} \pm 2.4$		[1] AUBERT	03V	BABR	Repl. by AUBERT,B 06G
< 74	90	[2] GODANG	02	CLE2	$e^+e^- \to \Upsilon(4S)$
<900	90	ALBRECHT	91B	ARG	$e^+e^- \to \Upsilon(4S)$

[1] Assumes equal production of B^+ and B^0 at the $\Upsilon(4S)$.
[2] Assumes a helicity 00 configuration. For a helicity 11 configuration, the limit decreases to 4.9×10^{-5}.

$\Gamma(K^*(892)^+f_0(980))/\Gamma_{total}$ — Γ_{398}/Γ

VALUE (units 10^{-6})	DOCUMENT ID		TECN	COMMENT
4.2±0.6±0.3	[1] DEL-AMO-SA...11D		BABR	$e^+e^- \to \Upsilon(4S)$
• • • We do not use the following data for averages, fits, limits, etc. • • •				
5.2±1.2±0.5	[1] AUBERT,B	06G	BABR	Repl. by DEL-AMO-SANCHEZ 11D

[1] Assumes equal production of B^+ and B^0 at the $\Upsilon(4S)$.

$\Gamma(a_1^+K^0)/\Gamma_{total}$ — Γ_{399}/Γ

VALUE (units 10^{-6})	DOCUMENT ID		TECN	COMMENT
34.9±5.0±4.4	[1,2] AUBERT	08F	BABR	$e^+e^- \to \Upsilon(4S)$

[1] Assumes equal production of B^+ and B^0 at the $\Upsilon(4S)$.
[2] Assumes $a_1^\pm$ decays only to 3π and $B(a_1^\pm \to \pi^\pm\pi^\mp\pi^\pm) = 0.5$.

$\Gamma(b_1^+K^0 \times B(b_1^+ \to \omega\pi^+))/\Gamma_{total}$ — Γ_{400}/Γ

VALUE (units 10^{-6})	DOCUMENT ID		TECN	COMMENT
9.6±1.7±0.9	[1] AUBERT	08AG	BABR	$e^+e^- \to \Upsilon(4S)$

[1] Assumes equal production of B^+ and B^0 at the $\Upsilon(4S)$.

$\Gamma(K^*(892)^0\rho^+)/\Gamma_{total}$ — Γ_{401}/Γ

VALUE (units 10^{-6})	DOCUMENT ID		TECN	COMMENT
9.2±1.5 OUR AVERAGE				
9.6±1.7±1.5	[1] AUBERT,B	06G	BABR	$e^+e^- \to \Upsilon(4S)$
8.9±1.7±1.2	[1] ZHANG	05D	BELL	$e^+e^- \to \Upsilon(4S)$

[1] Assumes equal production of B^+ and B^0 at the $\Upsilon(4S)$.

$\Gamma(K_1(1400)^+\rho^0)/\Gamma_{total}$ — Γ_{402}/Γ

VALUE	CL%	DOCUMENT ID		TECN	COMMENT
$<7.8 \times 10^{-4}$	90	ALBRECHT	91B	ARG	$e^+e^- \to \Upsilon(4S)$

$\Gamma(K^*_2(1430)^+\rho^0)/\Gamma_{total}$ — Γ_{403}/Γ

VALUE	CL%	DOCUMENT ID		TECN	COMMENT
$<1.5 \times 10^{-3}$	90	ALBRECHT	91B	ARG	$e^+e^- \to \Upsilon(4S)$

$\Gamma(b_1^0K^+ \times B(b_1^0 \to \omega\pi^0))/\Gamma_{total}$ — Γ_{404}/Γ

VALUE (units 10^{-6})	DOCUMENT ID		TECN	COMMENT
9.1±1.7±1.0	[1] AUBERT	07BI	BABR	$e^+e^- \to \Upsilon(4S)$

[1] Assumes equal production of B^+ and B^0 at the $\Upsilon(4S)$.

$\Gamma(b_1^+K^{*0} \times B(b_1^+ \to \omega\pi^+))/\Gamma_{total}$ — Γ_{405}/Γ

VALUE	CL%	DOCUMENT ID		TECN	COMMENT
$<5.9 \times 10^{-6}$	90	[1] AUBERT	09AF	BABR	$e^+e^- \to \Upsilon(4S)$

[1] Assumes equal production of B^+ and B^0 at the $\Upsilon(4S)$.

$\Gamma(b_1^0K^{*+} \times B(b_1^0 \to \omega\pi^0))/\Gamma_{total}$ — Γ_{406}/Γ

VALUE	CL%	DOCUMENT ID		TECN	COMMENT
$<6.7 \times 10^{-6}$	90	[1] AUBERT	09AF	BABR	$e^+e^- \to \Upsilon(4S)$

[1] Assumes equal production of B^+ and B^0 at the $\Upsilon(4S)$.

$\Gamma(K^+\overline{K}^0)/\Gamma_{total}$ — Γ_{407}/Γ

VALUE (units 10^{-6})	CL%	DOCUMENT ID		TECN	COMMENT
1.31±0.17 OUR FIT Error includes scale factor of 1.2.					
1.19±0.18 OUR AVERAGE					
1.11±0.19±0.05		[1] DUH	13	BELL	$e^+e^- \to \Upsilon(4S)$
1.61±0.44±0.09		[1] AUBERT,BE	06C	BABR	$e^+e^- \to \Upsilon(4S)$
• • • We do not use the following data for averages, fits, limits, etc. • • •					
$1.22^{+0.32+0.13}_{-0.28-0.16}$		[1] LIN	07	BELL	Repl. by DUH 13
1.0 ±0.4 ±0.1		[1] ABE	05G	BELL	Repl. by LIN 07
1.5 ±0.5 ±0.1		[1] AUBERT,BE	05E	BABR	Repl. by AUBERT,BE 06C

Downloaded from https://academic.oup.com/ptep/article/2022/8/083C01/6651666 by KIT Library user on 27 September 2022

< 2.5	90	[1] AUBERT	04M	BABR	Repl. by AUBERT,BE 05E
< 3.3	90	[1] CHAO	04	BELL	$e^+e^- \to \Upsilon(4S)$
< 3.3	90	[1] BORNHEIM	03	CLE2	$e^+e^- \to \Upsilon(4S)$
< 2.0	90	[1] CASEY	02	BELL	Repl. by CHAO 04
< 5.0	90	[1] ABE	01H	BELL	$e^+e^- \to \Upsilon(4S)$
< 2.4	90	[1] AUBERT	01E	BABR	$e^+e^- \to \Upsilon(4S)$
< 5.1	90	[1] CRONIN-HEN..00		CLE2	$e^+e^- \to \Upsilon(4S)$
<21	90	GODANG	98	CLE2	Repl. by CRONIN-HENNESSY 00

[1] Assumes equal production of B^+ and B^0 at the $\Upsilon(4S)$.

$\Gamma(K^+\overline{K}^0)/\Gamma(K^0\pi^+)$ — $\Gamma_{407}/\Gamma_{346}$

VALUE	DOCUMENT ID	TECN	COMMENT
0.055±0.007 OUR FIT Error includes scale factor of 1.2.			
0.064±0.009±0.004	AAIJ	13BS LHCB	pp at 7 TeV

$\Gamma(\overline{K}^0K^+\pi^0)/\Gamma_{total}$ — Γ_{408}/Γ

VALUE	CL%	DOCUMENT ID	TECN	COMMENT
$<24\times10^{-6}$	90	[1] ECKHART 02	CLE2	$e^+e^- \to \Upsilon(4S)$

[1] Assumes equal production of B^+ and B^0 at the $\Upsilon(4S)$.

$\Gamma(K^+K^0_SK^0_S)/\Gamma_{total}$ — Γ_{409}/Γ

VALUE (units 10^{-6})	DOCUMENT ID	TECN	COMMENT
10.5 ±0.4 OUR AVERAGE			
10.42±0.43±0.22	[1] KALIYAR 19	BELL	$e^+e^- \to \Upsilon(4S)$
10.6 ±0.5 ±0.3	[1,2] LEES 12O	BABR	$e^+e^- \to \Upsilon(4S)$
• • • We do not use the following data for averages, fits, limits, etc. • • •			
10.7 ±1.2 ±1.0	[1] AUBERT,B 04V	BABR	Repl. by LEES 12O
13.4 ±1.9 ±1.5	[1] GARMASH 04	BELL	Repl. by KALIYAR 19

[1] Assumes equal production of B^+ and B^0 at the $\Upsilon(4S)$.
[2] All intermediate charmonium and charm resonances are removed, except of χ_{c0}.

$\Gamma(f_0(980)K^+,\ f_0\to K^0_SK^0_S)/\Gamma_{total}$ — Γ_{410}/Γ

VALUE (units 10^{-6})	DOCUMENT ID	TECN	COMMENT
14.7±2.8±1.8	[1] LEES 12O	BABR	$e^+e^- \to \Upsilon(4S)$

[1] Assumes equal production of B^+ and B^0 at the $\Upsilon(4S)$.

$\Gamma(f_0(1710)K^+,\ f_0\to K^0_SK^0_S)/\Gamma_{total}$ — Γ_{411}/Γ

VALUE (units 10^{-6})	DOCUMENT ID	TECN	COMMENT
$0.48^{+0.40}_{-0.24}\pm0.11$	[1] LEES 12O	BABR	$e^+e^- \to \Upsilon(4S)$

[1] Assumes equal production of B^+ and B^0 at the $\Upsilon(4S)$.

$\Gamma(K^+K^0_SK^0_S\,\text{nonresonant})/\Gamma_{total}$ — Γ_{412}/Γ

VALUE (units 10^{-6})	DOCUMENT ID	TECN	COMMENT
19.8±3.7±2.5	[1] LEES 12O	BABR	$e^+e^- \to \Upsilon(4S)$

[1] Assumes equal production of B^+ and B^0 at the $\Upsilon(4S)$.

$\Gamma(K^0_SK^0_S\pi^+)/\Gamma_{total}$ — Γ_{413}/Γ

VALUE	CL%	DOCUMENT ID	TECN	COMMENT
$<5.1\times10^{-7}$	90	[1] AUBERT 09J	BABR	$e^+e^- \to \Upsilon(4S)$
• • • We do not use the following data for averages, fits, limits, etc. • • •				
$<8.7\times10^{-7}$		[1] KALIYAR 19	BELL	$e^+e^- \to \Upsilon(4S)$
$<3.2\times10^{-6}$	90	[1] GARMASH 04	BELL	$e^+e^- \to \Upsilon(4S)$

[1] Assumes equal production of B^+ and B^0 at the $\Upsilon(4S)$.

$\Gamma(K^+K^-\pi^+)/\Gamma(K^+K^-K^+)$ — $\Gamma_{414}/\Gamma_{426}$

VALUE	DOCUMENT ID	TECN	COMMENT
0.151±0.004±0.008	AAIJ 20AJ	LHCB	pp at 7 and 8 TeV

$\Gamma(K^+K^-\pi^+)/\Gamma_{total}$ — Γ_{414}/Γ

VALUE (units 10^{-6})	CL%	DOCUMENT ID	TECN	COMMENT
5.2 ±0.4 OUR AVERAGE				
5.38±0.40±0.35		[1,2] HSU 17	BELL	$e^+e^- \to \Upsilon(4S)$
5.0 ±0.5 ±0.5		[2] AUBERT 07BB	BABR	$e^+e^- \to \Upsilon(4S)$
• • • We do not use the following data for averages, fits, limits, etc. • • •				
<13	90	[2] GARMASH 04	BELL	$e^+e^- \to \Upsilon(4S)$
< 6.3	90	[2,3] AUBERT 03M	BABR	Repl. by AUBERT 07BB
<12	90	[4] GARMASH 02	BELL	$e^+e^- \to \Upsilon(4S)$

[1] HSU 17 provides also measurement as a function of K^+K^- invariant mass.
[2] Assumes equal production of B^+ and B^0 at the $\Upsilon(4S)$.
[3] Charm and charmonium contributions are subtracted, otherwise no assumptions about intermediate resonances.
[4] Uses a reference decay mode $B^+ \to \overline{D}^0\pi^+$ and $\overline{D}^0 \to K^+\pi^-$ with $B(B^+ \to \overline{D}^0\pi^+)\cdot B(\overline{D}^0 \to K^+\pi^-) = (20.3 \pm 2.0)\times10^{-5}$.

$\Gamma(K^+K^-\pi^+\,\text{nonresonant})/\Gamma_{total}$ — Γ_{415}/Γ

VALUE (units 10^{-6})	CL%	DOCUMENT ID	TECN	COMMENT
1.68±0.23±0.13		[1] AAIJ 19AL	LHCB	pp at 7, 8 TeV
• • • We do not use the following data for averages, fits, limits, etc. • • •				
<75	90	BERGFELD 96B	CLE2	$e^+e^- \to \Upsilon(4S)$

[1] AAIJ 19AL reports $0.323 \pm 0.015 \pm 0.041$ fit fraction for $B^+ \to K^+K^-\pi^+$ nonresonant from the amplitude analysis of $B^\pm \to \pi^\pm K^+K^-$ decays. We use the PDG 19 value $B(B^+ \to K^+K^-\pi^+) = (5.2 \pm 0.4)\times10^{-6}$ to obtain $B(B^+ \to K^+K^-\pi^+$ nonresonant). Our first error is the experiment's error and the second error is systematic error from using our best value.

$\Gamma(K^+\overline{K}^*(892)^0)/\Gamma_{total}$ — Γ_{416}/Γ

VALUE (units 10^{-7})	CL%	DOCUMENT ID	TECN	COMMENT
5.9±0.6±0.5		[1] AAIJ 19AL	LHCB	pp at 7, 8 TeV
• • • We do not use the following data for averages, fits, limits, etc. • • •				
< 11	90	[2] AUBERT 07AR	BABR	$e^+e^- \to \Upsilon(4S)$
<1290	90	ABBIENDI 00B	OPAL	$e^+e^- \to Z$
<1380	90	[3] ABE 00C	SLD	$e^+e^- \to Z$
< 53	90	[2] JESSOP 00	CLE2	$e^+e^- \to \Upsilon(4S)$

[1] AAIJ 19AL reports $(7.5 \pm 0.6 \pm 0.5)\times10^{-2}$ fit fraction for $B^+ \to K^+\overline{K}^*(892)^0$ from the amplitude analysis of $B^\pm \to \pi^\pm K^+K^-$ decays. We use the PDG 19 value $B(B^+ \to K^+K^-\pi^+) = (5.2 \pm 0.4)\times10^{-6}$ to obtain $B(B^+ \to K^+\overline{K}^*(892)^0,\ \overline{K}^*(892)^0 \to K^+\pi^-)$. We compute $B(B^+ \to K^+\overline{K}^*(892)^0)$ using 2/3 of $B(\overline{K}^*(892)^0 \to (K\pi)^0) = (99.754 \pm 0.021)\%$ for the $K^+\pi^-$ fraction. Our first error is the experiment's error and the second error is systematic error from using our best value.
[2] Assumes equal production of B^+ and B^0 at the $\Upsilon(4S)$.
[3] ABE 00C assumes $B(Z \to b\overline{b}) = (21.7 \pm 0.1)\%$ and the B fractions $f_{B^0} = f_{B^+} = (39.7^{+1.8}_{-2.2})\%$ and $f_{B_s} = (10.5^{+1.8}_{-2.2})\%$.

$\Gamma(K^+\overline{K}^*_0(1430)^0)/\Gamma_{total}$ — Γ_{417}/Γ

VALUE (units 10^{-6})	CL%	DOCUMENT ID	TECN	COMMENT
0.38±0.12±0.05		[1] AAIJ 19AL	LHCB	pp at 7, 8 TeV
• • • We do not use the following data for averages, fits, limits, etc. • • •				
<2.2	90	[2] AUBERT 07AR	BABR	$e^+e^- \to \Upsilon(4S)$

[1] AAIJ 19AL reports $(4.5 \pm 0.7 \pm 1.2)\times10^{-2}$ for fit fraction for $B^+ \to K^+\overline{K}^*_0(1430)^0$ from the amplitude analysis of $B^\pm \to \pi^\pm K^+K^-$ decays. We use the PDG 19 value $B(B^+ \to K^+K^-\pi^+) = (5.2 \pm 0.4)\times10^{-6}$ to obtain $B(B^+ \to K^+\overline{K}^*_0(1430)^0,\ \overline{K}^*_0(1430)^0 \to K^+\pi^-)$. We compute $B(B^+ \to K^+\overline{K}^*_0(1430)^0)$ using 2/3 of PDG 19 value $B(K^*_0(1430)^0 \to K\pi) = (93 \pm 10)\%$ for the $K^+\pi^-$ fraction. Our first error is the experiment's error and the second error is systematic error from using our best value.
[2] Assumes equal production of B^+ and B^0 at the $\Upsilon(4S)$.

$\Gamma(\rho(1450)^0\pi^+,\ \rho^0\to K^+K^-)/\Gamma_{total}$ — Γ_{473}/Γ

VALUE (units 10^{-6})	DOCUMENT ID	TECN	COMMENT
1.60±0.08±0.12	[1] AAIJ 19AL	LHCB	pp at 7, 8 TeV

[1] AAIJ 19AL reports $0.307 \pm 0.012 \pm 0.009$ fit fraction for $B^+ \to \rho(1450)\pi^+$ from the amplitude analysis of $B^\pm \to \pi^\pm K^+K^-$ decays. We use the PDG 19 value $B(B^+ \to K^+K^-\pi^+) = (5.2 \pm 0.4)\times10^{-6}$ to obtain $B(B^+ \to \rho(1450)\pi^+,\ \rho(1450) \to K^+K^-)$. Our first error is the experiment's error and the second error is systematic error from using our best value.

$\Gamma(\pi^+(K^+K^-)_{S-wave})/\Gamma_{total}$ — Γ_{418}/Γ

VALUE (units 10^{-7})	DOCUMENT ID	TECN	COMMENT
8.53±0.67±0.66	[1] AAIJ 19AL	LHCB	pp at 7, 8 TeV

[1] AAIJ 19AL reports $0.164 \pm 0.008 \pm 0.01$ fit fraction for $B^+ \to \pi^+(K^+K^-)_{S-wave}$ in the region of $0.95 < m(K^+K^-) < 1.42$ GeV/c^2 from the amplitude analysis of $B^\pm \to \pi^\pm K^+K^-$ decays. We use the PDG 19 value $B(B^+ \to K^+K^-\pi^+) = (5.2 \pm 0.4)\times10^{-6}$ to obtain $B(B^+ \to \pi^+(K^+K^-)_{S-wave})$. Our first error is the experiment's error and the second error is systematic error from using our best value.

$\Gamma(K^+K^+\pi^-)/\Gamma_{total}$ — Γ_{419}/Γ

VALUE	CL%	DOCUMENT ID	TECN	COMMENT
$<1.1\times10^{-8}$	90	AAIJ 17E	LHCB	pp at 7, 8 TeV
• • • We do not use the following data for averages, fits, limits, etc. • • •				
$<1.6\times10^{-7}$	90	[1] AUBERT 08BE	BABR	$e^+e^- \to \Upsilon(4S)$
$<2.4\times10^{-6}$	90	[1] GARMASH 04	BELL	$e^+e^- \to \Upsilon(4S)$
$<1.3\times10^{-6}$	90	[2] AUBERT 03M	BABR	Repl. by AUBERT 08BE
$<3.2\times10^{-6}$	90	[3] GARMASH 02	BELL	$e^+e^- \to \Upsilon(4S)$

[1] Assumes equal production of B^+ and B^0 at the $\Upsilon(4S)$.
[2] Assumes equal production of B^0 and B^+ at the $\Upsilon(4S)$; charm and charmonium contributions are subtracted, otherwise no assumptions about intermediate resonances.
[3] Uses a reference decay mode $B^+ \to \overline{D}^0\pi^+$ and $\overline{D}^0 \to K^+\pi^-$ with $B(B^+ \to \overline{D}^0\pi^+)\cdot B(\overline{D}^0 \to K^+\pi^-) = (20.3 \pm 2.0)\times10^{-5}$.

Downloaded from https://academic.oup.com/ptep/article/2022/8/083C01/6651666 by KIT Library user on 27 September 2022

$\Gamma(K^+K^+\pi^-$ nonresonant$)/\Gamma_{total}$ — Γ_{420}/Γ

VALUE (units 10^{-6})	CL%	DOCUMENT ID		TECN	COMMENT
<87.9	90	ABBIENDI	00B	OPAL	$e^+e^- \to Z$

$\Gamma(f_2'(1525)K^+)/\Gamma_{total}$ — Γ_{421}/Γ

VALUE (units 10^{-6})	CL%	DOCUMENT ID		TECN	COMMENT
1.8 ±0.5 OUR AVERAGE		Error includes scale factor of 1.1.			
$1.56\pm0.36\pm0.30$		[1,2] LEES	12O	BABR	$e^+e^- \to \Upsilon(4S)$
$2.8 \pm0.9 {}^{+0.5}_{-0.4}$		[1,3] LEES	12O	BABR	$e^+e^- \to \Upsilon(4S)$
• • • We do not use the following data for averages, fits, limits, etc. • • •					
<8	90	[1,4] GARMASH	05	BELL	$e^+e^- \to \Upsilon(4S)$

[1] Assumes equal production of B^+ and B^0 at the $\Upsilon(4S)$.
[2] Measured in the $B^+ \to K^+K^-K^+$ decay.
[3] Measured in the $B^+ \to K^+K^0_SK^0_S$ decay.
[4] GARMASH 05 reports $B(B^+ \to f_2'(1525)K^+)\cdot B(f_2'(1525) \to K^+K^-) < 4.9\times10^{-6}$ at 90% CL. We divide this result by our best value of $B(f_2'(1525) \to K\overline{K}) = 87.6\times10^{-2}$ multiplied by 2/3 to account for the K^+K^- fraction.

$\Gamma(K^+f_J(2220))/\Gamma_{total}$ — Γ_{422}/Γ

VALUE (units 10^{-6})	DOCUMENT ID		TECN	COMMENT
not seen	[1] HUANG	03	BELL	$e^+e^- \to \Upsilon(4S)$

[1] No evidence is found for such decay and set a limit on $B(B^+ \to f_J(2220))\times B(f_J(2220) \to \phi\phi) < 1.2\times10^{-6}$ at 90%CL where the $f_J(2220)$ is a possible glueball state.

$\Gamma(K^{*+}\pi^+K^-)/\Gamma_{total}$ — Γ_{423}/Γ

VALUE (units 10^{-6})	CL%	DOCUMENT ID		TECN	COMMENT
<11.8	90	[1] AUBERT,B	06U	BABR	$e^+e^- \to \Upsilon(4S)$

[1] Assumes equal production of B^+ and B^0 at the $\Upsilon(4S)$.

$\Gamma(K^*(892)^+K^*(892)^0)/\Gamma_{total}$ — Γ_{424}/Γ

VALUE (units 10^{-6})	CL%	DOCUMENT ID		TECN	COMMENT
0.91±0.29 OUR AVERAGE					
$0.77^{+0.35}_{-0.30}\pm0.12$		[1] GOH	15	BELL	$e^+e^- \to \Upsilon(4S)$
$1.2 \pm0.5 \pm0.1$		[2] AUBERT	09F	BABR	$e^+e^- \to \Upsilon(4S)$
• • • We do not use the following data for averages, fits, limits, etc. • • •					
<71	90	[3] GODANG	02	CLE2	$e^+e^- \to \Upsilon(4S)$

[1] Signal significance is 2.7 standard deviations. This measurement corresponds to an upper limit of $< 1.31\times10^{-6}$ at 90% CL.
[2] Signal signicance is 3.7 standard deviations.
[3] Assumes a helicity 00 configuration. For a helicity 11 configuration, the limit decreases to 4.8×10^{-5}.

$\Gamma(K^{*+}K^+\pi^-)/\Gamma_{total}$ — Γ_{425}/Γ

VALUE (units 10^{-6})	CL%	DOCUMENT ID		TECN	COMMENT
<6.1	90	[1] AUBERT,B	06U	BABR	$e^+e^- \to \Upsilon(4S)$

[1] Assumes equal production of B^+ and B^0 at the $\Upsilon(4S)$.

$\Gamma(K^+K^-K^+)/\Gamma_{total}$ — Γ_{426}/Γ

VALUE (units 10^{-6})	CL%	DOCUMENT ID		TECN	COMMENT
34.0±1.4 OUR AVERAGE		Error includes scale factor of 1.4.			
$34.6\pm0.6\pm0.9$		[1,2] LEES	12O	BABR	$e^+e^- \to \Upsilon(4S)$
$30.6\pm1.2\pm2.3$		[1] GARMASH	05	BELL	$e^+e^- \to \Upsilon(4S)$
• • • We do not use the following data for averages, fits, limits, etc. • • •					
$35.2\pm0.9\pm1.6$		[1] AUBERT	06O	BABR	Repl. by LEES 12O
$32.8\pm1.8\pm2.8$		[1] GARMASH	04	BELL	Repl. by GARMASH 05
$29.6\pm2.1\pm1.6$		[3] AUBERT	03M	BABR	Repl. by AUBERT 06O
$35.3\pm3.7\pm4.5$		[4] GARMASH	02	BELL	Repl. by GARMASH 04
<200	90	[5] ADAM	96D	DLPH	$e^+e^- \to Z$
<320	90	[5] ABREU	95N	DLPH	Sup. by ADAM 96D
<350	90	ALBRECHT	91E	ARG	$e^+e^- \to \Upsilon(4S)$

[1] Assumes equal production of B^+ and B^0 at the $\Upsilon(4S)$.
[2] All intermediate charmonium and charm resonances are removed, except of χ_{c0}.
[3] Assumes equal production of B^0 and B^+ at the $\Upsilon(4S)$; charm and charmonium contributions are subtracted, otherwise no assumptions about intermediate resonances.
[4] Uses a reference decay mode $B^+ \to \overline{D}^0\pi^+$ and $\overline{D}^0 \to K^+\pi^-$ with $B(B^+ \to \overline{D}^0\pi^+)\cdot B(\overline{D}^0 \to K^+\pi^-) = (20.3\pm2.0)\times10^{-5}$.
[5] Assumes B^0 and B^- production fractions of 0.39, and B_s production fraction of 0.12.

$\Gamma(K^+\phi)/\Gamma_{total}$ — Γ_{427}/Γ

VALUE (units 10^{-6})	CL%	DOCUMENT ID		TECN	COMMENT
$8.8 {}^{+0.7}_{-0.6}$ OUR AVERAGE		Error includes scale factor of 1.1.			
$9.2 \pm0.4 {}^{+0.7}_{-0.5}$		[1] LEES	12O	BABR	$e^+e^- \to \Upsilon(4S)$
$7.6 \pm1.3 \pm0.6$		[2] ACOSTA	05J	CDF	$p\overline{p}$ at 1.96 TeV
$9.60\pm0.92^{+1.05}_{-0.85}$		[1] GARMASH	05	BELL	$e^+e^- \to \Upsilon(4S)$
$5.5 {}^{+2.1}_{-1.8} \pm0.6$		[1] BRIERE	01	CLE2	$e^+e^- \to \Upsilon(4S)$
• • • We do not use the following data for averages, fits, limits, etc. • • •					
$8.4 \pm0.7 \pm0.7$		[1] AUBERT	06O	BABR	Repl. by LEES 12O
$10.0 {}^{+0.9}_{-0.8} \pm0.5$		[1] AUBERT	04A	BABR	Repl. by AUBERT 06O
$9.4 \pm1.1 \pm0.7$		[1] CHEN	03B	BELL	Repl. by GARMASH 05
$14.6 {}^{+3.0}_{-2.8} \pm2.0$		[3] GARMASH	02	BELL	Repl. by CHEN 03B
$7.7 {}^{+1.6}_{-1.4} \pm0.8$		[1] AUBERT	01D	BABR	$e^+e^- \to \Upsilon(4S)$
<144	90	[4] ABE	00C	SLD	$e^+e^- \to Z$
< 5	90	[1] BERGFELD	98	CLE2	
<280	90	[5] ADAM	96D	DLPH	$e^+e^- \to Z$
< 12	90	ASNER	96	CLE2	$e^+e^- \to \Upsilon(4S)$
<440	90	[6] ABREU	95N	DLPH	Sup. by ADAM 96D
<180	90	ALBRECHT	91B	ARG	$e^+e^- \to \Upsilon(4S)$
< 90	90	[7] AVERY	89B	CLEO	$e^+e^- \to \Upsilon(4S)$
<210	90	AVERY	87	CLEO	$e^+e^- \to \Upsilon(4S)$

[1] Assumes equal production of B^+ and B^0 at the $\Upsilon(4S)$.
[2] Uses $B(B^+ \to J/\psi K^+) = (1.00\pm0.04)\times10^{-3}$ and $B(J/\psi \to \mu^+\mu^-) = 0.0588\pm0.0010$.
[3] Uses a reference decay mode $B^+ \to \overline{D}^0\pi^+$ and $\overline{D}^0 \to K^+\pi^-$ with $B(B^+ \to \overline{D}^0\pi^+)\cdot B(\overline{D}^0 \to K^+\pi^-) = (20.3\pm2.0)\times10^{-5}$.
[4] ABE 00C assumes $B(Z \to b\overline{b})=(21.7\pm0.1)\%$ and the B fractions $f_{B^0}=f_{B^+}=(39.7^{+1.8}_{-2.2})\%$ and $f_{B_s}=(10.5^{+1.8}_{-2.2})\%$.
[5] ADAM 96D assumes $f_{B^0} = f_{B^-} = 0.39$ and $f_{B_s} = 0.12$.
[6] Assumes a B^0, B^- production fraction of 0.39 and a B_s production fraction of 0.12.
[7] AVERY 89B reports $< 8\times10^{-5}$ assuming the $\Upsilon(4S)$ decays 43% to $B^0\overline{B}^0$. We rescale to 50%.

$\Gamma(f_0(980)K^+\times B(f_0(980)\to K^+K^-))/\Gamma_{total}$ — Γ_{428}/Γ

VALUE (units 10^{-6})	CL%	DOCUMENT ID		TECN	COMMENT
9.4±1.6±2.8		[1] LEES	12O	BABR	$e^+e^- \to \Upsilon(4S)$
• • • We do not use the following data for averages, fits, limits, etc. • • •					
$6.5\pm2.5\pm1.6$		[1] AUBERT	06O	BABR	$e^+e^- \to \Upsilon(4S)$
<2.9	90	[1] GARMASH	05	BELL	$e^+e^- \to \Upsilon(4S)$

[1] Assumes equal production of B^+ and B^0 at the $\Upsilon(4S)$.

$\Gamma(a_2(1320)K^+\times B(a_2(1320)\to K^+K^-))/\Gamma_{total}$ — Γ_{429}/Γ

VALUE	CL%	DOCUMENT ID		TECN	COMMENT
$<1.1\times10^{-6}$	90	[1] GARMASH	05	BELL	$e^+e^- \to \Upsilon(4S)$

[1] Assumes equal production of B^+ and B^0 at the $\Upsilon(4S)$.

$\Gamma(X_0(1550)K^+\times B(X_0(1550)\to K^+K^-))/\Gamma_{total}$ — Γ_{430}/Γ

$X_0(1550)$ is a possible spin zero state near 1.55 GeV/c^2 invariant mass of K^+K^-.

VALUE (units 10^{-6})	DOCUMENT ID		TECN	COMMENT
4.3±0.6±0.3	[1] AUBERT	06O	BABR	$e^+e^- \to \Upsilon(4S)$

[1] Assumes equal production of B^+ and B^0 at the $\Upsilon(4S)$.

$\Gamma(\phi(1680)K^+\times B(\phi(1680)\to K^+K^-))/\Gamma_{total}$ — Γ_{431}/Γ

VALUE	CL%	DOCUMENT ID		TECN	COMMENT
$<0.8\times10^{-6}$	90	[1] GARMASH	05	BELL	$e^+e^- \to \Upsilon(4S)$

[1] Assumes equal production of B^+ and B^0 at the $\Upsilon(4S)$.

$\Gamma(f_0(1710)K^+\times B(f_0(1710)\to K^+K^-))/\Gamma_{total}$ — Γ_{432}/Γ

VALUE (units 10^{-6})	DOCUMENT ID		TECN	COMMENT
1.12±0.25±0.50	[1] LEES	12O	BABR	$e^+e^- \to \Upsilon(4S)$
• • • We do not use the following data for averages, fits, limits, etc. • • •				
$1.7 \pm1.0 \pm0.3$	[1] AUBERT	06O	BABR	Repl. by LEES 12O

[1] Assumes equal production of B^+ and B^0 at the $\Upsilon(4S)$.

$\Gamma(K^+K^-K^+$ nonresonant$)/\Gamma_{total}$ — Γ_{433}/Γ

VALUE (units 10^{-6})	CL%	DOCUMENT ID		TECN	COMMENT
$23.8^{+2.8}_{-5.0}$ OUR AVERAGE					
$22.8\pm2.7\pm7.6$		[1] LEES	12O	BABR	$e^+e^- \to \Upsilon(4S)$
$24.0\pm1.5^{+2.6}_{-6.0}$		[1] GARMASH	05	BELL	$e^+e^- \to \Upsilon(4S)$
• • • We do not use the following data for averages, fits, limits, etc. • • •					
$50.0\pm6.0\pm4.0$		[1] AUBERT	06O	BABR	Repl. by LEES 12O
<38	90	BERGFELD	96B	CLE2	$e^+e^- \to \Upsilon(4S)$

[1] Assumes equal production of B^+ and B^0 at the $\Upsilon(4S)$.

$\Gamma(K^*(892)^+K^+K^-)/\Gamma_{total}$ — Γ_{434}/Γ

VALUE (units 10^{-6})	CL%	DOCUMENT ID		TECN	COMMENT
36.2±3.3±3.6		[1] AUBERT,B	06U	BABR	$e^+e^- \to \Upsilon(4S)$
• • • We do not use the following data for averages, fits, limits, etc. • • •					
<1600	90	ALBRECHT	91E	ARG	$e^+e^- \to \Upsilon(4S)$

[1] Assumes equal production of B^+ and B^0 at the $\Upsilon(4S)$.

Downloaded from https://academic.oup.com/ptep/article/2022/8/083C01/6651666 by KIT Library user on 27 September 2022

$\Gamma(K^*(892)^+\phi)/\Gamma_{total}$ — Γ_{435}/Γ

VALUE (units 10^{-6})	CL%	DOCUMENT ID		TECN	COMMENT
10.0±2.0 OUR AVERAGE		Error includes scale factor of 1.7.			
$11.2\pm1.0\pm0.9$		[1] AUBERT	07BA	BABR	$e^+e^-\to\Upsilon(4S)$
$6.7^{+2.1}_{-1.9}{}^{+0.7}_{-1.0}$		[1] CHEN	03B	BELL	$e^+e^-\to\Upsilon(4S)$
• • • We do not use the following data for averages, fits, limits, etc. • • •					
$12.7^{+2.2}_{-2.0}\pm1.1$		[1] AUBERT	03V	BABR	Repl. by AUBERT 07BA
$9.7^{+4.2}_{-3.4}\pm1.7$		[1] AUBERT	01D	BABR	Repl. by AUBERT 03V
$<$ 22.5	90	[1] BRIERE	01	CLE2	$e^+e^-\to\Upsilon(4S)$
$<$ 41	90	[1] BERGFELD	98	CLE2	
$<$ 70	90	ASNER	96	CLE2	$e^+e^-\to\Upsilon(4S)$
$<$1300	90	ALBRECHT	91B	ARG	$e^+e^-\to\Upsilon(4S)$

[1] Assumes equal production of B^+ and B^0 at the $\Upsilon(4S)$.

$\Gamma(\phi(K\pi)_0^{*+})/\Gamma_{total}$ — Γ_{436}/Γ

$(K\pi)_0^{*+}$ is the total S-wave composed of $K_0^*(1430)$ and nonresonant that are described using LASS shape.

VALUE (units 10^{-6})	DOCUMENT ID		TECN	COMMENT
8.3±1.4±0.8	[1] AUBERT	08BI	BABR	$e^+e^-\to\Upsilon(4S)$

[1] Assumes equal production of B^+ and B^0 at the $\Upsilon(4S)$.

$\Gamma(\phi K_1(1270)^+)/\Gamma_{total}$ — Γ_{437}/Γ

VALUE (units 10^{-6})	DOCUMENT ID		TECN	COMMENT
6.1±1.6±1.1	[1] AUBERT	08BI	BABR	$e^+e^-\to\Upsilon(4S)$

[1] Assumes equal production of B^+ and B^0 at the $\Upsilon(4S)$.

$\Gamma(\phi K_1(1400)^+)/\Gamma_{total}$ — Γ_{438}/Γ

VALUE (units 10^{-6})	CL%	DOCUMENT ID		TECN	COMMENT
$<$ 3.2	90	[1] AUBERT	08BI	BABR	$e^+e^-\to\Upsilon(4S)$
• • • We do not use the following data for averages, fits, limits, etc. • • •					
$<$1100	90	ALBRECHT	91B	ARG	$e^+e^-\to\Upsilon(4S)$

[1] Assumes equal production of B^+ and B^0 at the $\Upsilon(4S)$.

$\Gamma(\phi K^*(1410)^+)/\Gamma_{total}$ — Γ_{439}/Γ

VALUE (units 10^{-6})	CL%	DOCUMENT ID		TECN	COMMENT
$<$4.3	90	[1] AUBERT	08BI	BABR	$e^+e^-\to\Upsilon(4S)$

[1] Assumes equal production of B^+ and B^0 at the $\Upsilon(4S)$.

$\Gamma(\phi K_0^*(1430)^+)/\Gamma_{total}$ — Γ_{440}/Γ

VALUE (units 10^{-6})	DOCUMENT ID		TECN	COMMENT
7.0±1.3±0.9	[1] AUBERT	08BI	BABR	$e^+e^-\to\Upsilon(4S)$

[1] Assumes equal production of B^+ and B^0 at the $\Upsilon(4S)$.

$\Gamma(\phi K_2^*(1430)^+)/\Gamma_{total}$ — Γ_{441}/Γ

VALUE (units 10^{-6})	CL%	DOCUMENT ID		TECN	COMMENT
8.4±1.8±1.0		[1] AUBERT	08BI	BABR	$e^+e^-\to\Upsilon(4S)$
• • • We do not use the following data for averages, fits, limits, etc. • • •					
$<$3400	90	ALBRECHT	91B	ARG	$e^+e^-\to\Upsilon(4S)$

[1] Assumes equal production of B^+ and B^0 at the $\Upsilon(4S)$.

$\Gamma(\phi K_2^*(1770)^+)/\Gamma_{total}$ — Γ_{442}/Γ

VALUE (units 10^{-6})	CL%	DOCUMENT ID		TECN	COMMENT
$<$15.0	90	[1] AUBERT	08BI	BABR	$e^+e^-\to\Upsilon(4S)$

[1] Assumes equal production of B^+ and B^0 at the $\Upsilon(4S)$.

$\Gamma(\phi K_2^*(1820)^+)/\Gamma_{total}$ — Γ_{443}/Γ

VALUE (units 10^{-6})	CL%	DOCUMENT ID		TECN	COMMENT
$<$16.3	90	[1] AUBERT	08BI	BABR	$e^+e^-\to\Upsilon(4S)$

[1] Assumes equal production of B^+ and B^0 at the $\Upsilon(4S)$.

$\Gamma(a_1^+ K^{*0})/\Gamma_{total}$ — Γ_{444}/Γ

VALUE (units 10^{-6})	CL%	DOCUMENT ID		TECN	COMMENT
$<$3.6	90	[1,2] DEL-AMO-SA...10I		BABR	$e^+e^-\to\Upsilon(4S)$

[1] Assumes $B(a_1^\pm\to\pi^\pm\pi^\mp\pi^\pm)=0.5$
[2] Assumes equal production of B^+ and B^0 at the $\Upsilon(4S)$.

$\Gamma(K^+\phi\phi)/\Gamma_{total}$ — Γ_{445}/Γ

VALUE (units 10^{-6})	DOCUMENT ID		TECN	COMMENT
4.2 ±0.8 OUR AVERAGE	Error includes scale factor of 2.2. See the ideogram below.			
$3.43^{+0.48}_{-0.46}\pm0.22$	[1] MOHANTY	21	BELL	$e^+e^-\to\Upsilon(4S)$
$5.6\ \pm0.5\ \pm0.3$	[1] LEES	11A	BABR	$e^+e^-\to\Upsilon(4S)$
$2.6\ ^{+1.1}_{-0.9}\ \pm0.3$	[1] HUANG	03	BELL	$e^+e^-\to\Upsilon(4S)$
• • • We do not use the following data for averages, fits, limits, etc. • • •				
$7.5\ \pm1.0\ \pm0.7$	[1] AUBERT,BE	06H	BABR	Repl. by LEES 11A

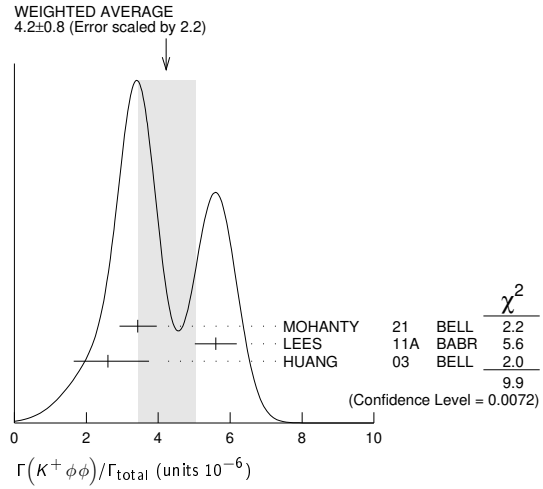

[1] Assumes equal production of B^0 and B^+ at the $\Upsilon(4S)$ and the $\phi\phi$ invariant mass below 2.85 GeV/c^2.

$\Gamma(\eta'\eta' K^+)/\Gamma_{total}$ — Γ_{446}/Γ

VALUE (units 10^{-6})	CL%	DOCUMENT ID		TECN	COMMENT
$<$25	90	[1] AUBERT,B	06P	BABR	$e^+e^-\to\Upsilon(4S)$

[1] Assumes equal production of B^+ and B^0 at the $\Upsilon(4S)$.

$\Gamma(\omega\phi K^+)/\Gamma_{total}$ — Γ_{447}/Γ

VALUE (units 10^{-6})	CL%	DOCUMENT ID		TECN	COMMENT
$<$1.9	90	[1] LIU	09	BELL	$e^+e^-\to\Upsilon(4S)$

[1] Assumes equal production of B^+ and B^0 at the $\Upsilon(4S)$.

$\Gamma(X(1812)K^+\times B(X\to\omega\phi))/\Gamma_{total}$ — Γ_{448}/Γ

VALUE (units 10^{-6})	CL%	DOCUMENT ID		TECN	COMMENT
$<$0.32	90	[1] LIU	09	BELL	$e^+e^-\to\Upsilon(4S)$

[1] Assumes equal production of B^+ and B^0 at the $\Upsilon(4S)$.

$\Gamma(K^*(892)^+\gamma)/\Gamma_{total}$ — Γ_{449}/Γ

VALUE (units 10^{-5})	CL%	DOCUMENT ID		TECN	COMMENT
3.92±0.22 OUR AVERAGE		Error includes scale factor of 1.7.			
$3.76\pm0.10\pm0.12$		[1] HORIGUCHI	17	BELL	$e^+e^-\to\Upsilon(4S)$
$4.22\pm0.14\pm0.16$		[2] AUBERT	09AO	BABR	$e^+e^-\to\Upsilon(4S)$
$3.76^{+0.89}_{-0.83}\pm0.28$		[3] COAN	00	CLE2	$e^+e^-\to\Upsilon(4S)$
• • • We do not use the following data for averages, fits, limits, etc. • • •					
$3.87\pm0.28\pm0.26$		[4] AUBERT,BE	04A	BABR	Repl. by AUBERT 09AO
$4.25\pm0.31\pm0.24$		[3] NAKAO	04	BELL	Repl. by HORIGUCHI 17
$3.83\pm0.62\pm0.22$		[3] AUBERT	02C	BABR	Repl. by AUBERT,BE 04A
$5.7\ \pm3.1\ \pm1.1$		[5] AMMAR	93	CLE2	Repl. by COAN 00
$<$ 55	90	[6] ALBRECHT	89G	ARG	$e^+e^-\to\Upsilon(4S)$
$<$ 55	90	[6] AVERY	89B	CLEO	$e^+e^-\to\Upsilon(4S)$
$<$180	90	AVERY	87	CLEO	$e^+e^-\to\Upsilon(4S)$

[1] Uses $B(\Upsilon(4S)\to B^+B^-)=(51.4\pm0.6)\%$ and $B(\Upsilon(4S)\to B^0\overline{B}^0)=(48.6\pm0.6)\%$.
[2] Uses $B(\Upsilon(4S)\to B^+B^-)=(51.6\pm0.6)\%$ and $B(\Upsilon(4S)\to B^0\overline{B}^0)=(48.4\pm0.6)\%$.
[3] Assumes equal production of B^+ and B^0 at the $\Upsilon(4S)$.
[4] Uses the production ratio of charged and neutral B from $\Upsilon(4S)$ decays $R^{+/0}=1.006\pm0.048$.
[5] AMMAR 93 observed 4.1 ± 2.3 events above background.
[6] Assumes the $\Upsilon(4S)$ decays 43% to $B^0\overline{B}^0$.

$\Gamma(K_1(1270)^+\gamma)/\Gamma_{total}$ — Γ_{450}/Γ

VALUE (units 10^{-5})	CL%	DOCUMENT ID		TECN	COMMENT
4.4 $^{+0.7}_{-0.6}$ OUR AVERAGE					
$4.41^{+0.63}_{-0.44}\pm0.58$		[1,2] DEL-AMO-SA...16		BABR	$e^+e^-\to\Upsilon(4S)$
$4.3\ \pm0.9\ \pm0.9$		[3] YANG	05	BELL	$e^+e^-\to\Upsilon(4S)$
• • • We do not use the following data for averages, fits, limits, etc. • • •					
$<$ 9.9	90	[3] NISHIDA	02	BELL	Repl. by YANG 05
$<$730	90	[4] ALBRECHT	89G	ARG	$e^+e^-\to\Upsilon(4S)$

[1] Requires $M_{K\pi\pi}<1.8$ GeV/c^2.
[2] Uses $B(\Upsilon(4S)\to B^+B^-)=0.513\pm0.006$.
[3] Assumes equal production of B^+ and B^0 at the $\Upsilon(4S)$.
[4] ALBRECHT 89G reports <0.0066 assuming the $\Upsilon(4S)$ decays 45% to $B^0\overline{B}^0$. We rescale to 50%.

$\Gamma(\eta K^+\gamma)/\Gamma_{total}$ — Γ_{451}/Γ

VALUE (units 10^{-6})	DOCUMENT ID		TECN	COMMENT
7.9±0.9 OUR AVERAGE				
$7.7\pm1.0\pm0.4$	[1,2] AUBERT	09	BABR	$e^+e^-\to\Upsilon(4S)$
$8.4\pm1.5^{+1.2}_{-0.9}$	[2,3] NISHIDA	05	BELL	$e^+e^-\to\Upsilon(4S)$

Downloaded from https://academic.oup.com/ptep/article/2022/8/083C01/6651666 by KIT Library user on 27 September 2022

• • • We do not use the following data for averages, fits, limits, etc. • • •

$10.0 \pm 1.3 \pm 0.5$	[1,2] AUBERT,B	06M	BABR	Repl. by AUBERT 09

[1] $m_{\eta K} < 3.25$ GeV/c^2.
[2] Assumes equal production of B^+ and B^0 at the $\Upsilon(4S)$.
[3] $m_{\eta K} < 2.4$ GeV/c^2

$\Gamma(\eta' K^+\gamma)/\Gamma_{total}$ — Γ_{452}/Γ

VALUE (units 10^{-6})	DOCUMENT ID		TECN	COMMENT
$2.9^{+1.0}_{-0.9}$ OUR AVERAGE				
$3.6 \pm 1.2 \pm 0.4$	[1,2] WEDD	10	BELL	$e^+e^- \to \Upsilon(4S)$
$1.9^{+1.5}_{-1.2} \pm 0.1$	[1,3] AUBERT,B	06M	BABR	$e^+e^- \to \Upsilon(4S)$

[1] Assumes equal production of B^+ and B^0 at the $\Upsilon(4S)$.
[2] $m_{\eta' K} < 3.4$ GeV/c^2.
[3] Set the upper limit of 4.2×10^{-6} at 90% CL with $m_{\eta' K} < 3.25$ GeV/c^2.

$\Gamma(\phi K^+\gamma)/\Gamma_{total}$ — Γ_{453}/Γ

VALUE (units 10^{-6})	DOCUMENT ID		TECN	COMMENT
2.7 ± 0.4 OUR AVERAGE Error includes scale factor of 1.2.				
$2.48 \pm 0.30 \pm 0.24$	[1] SAHOO	11A	BELL	$e^+e^- \to \Upsilon(4S)$
$3.5 \pm 0.6 \pm 0.4$	[1] AUBERT	07Q	BABR	$e^+e^- \to \Upsilon(4S)$
• • • We do not use the following data for averages, fits, limits, etc. • • •				
$3.4 \pm 0.9 \pm 0.4$	[1] DRUTSKOY	04	BELL	Repl. by SAHOO 11A

[1] Assumes equal production of B^+ and B^0 at $\Upsilon(4S)$.

$\Gamma(K^+\pi^-\pi^+\gamma)/\Gamma_{total}$ — Γ_{454}/Γ

VALUE (units 10^{-5})	DOCUMENT ID		TECN	COMMENT
2.58 ± 0.15 OUR AVERAGE Error includes scale factor of 1.3. See the ideogram below.				
$2.45 \pm 0.09 \pm 0.12$	[1,2] DEL-AMO-SA...16		BABR	$e^+e^- \to \Upsilon(4S)$
$2.95 \pm 0.13 \pm 0.20$	[1,3] AUBERT	07R	BABR	$e^+e^- \to \Upsilon(4S)$
$2.50 \pm 0.18 \pm 0.22$	[3,4] YANG	05	BELL	$e^+e^- \to \Upsilon(4S)$
• • • We do not use the following data for averages, fits, limits, etc. • • •				
$2.4 \pm 0.5 \; ^{+0.4}_{-0.2}$	[3,5] NISHIDA	02	BELL	Repl. by YANG 05

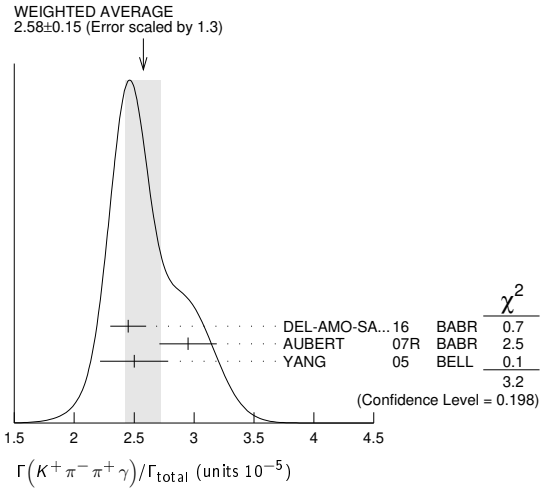

[1] $M_{K\pi\pi} < 1.8$ GeV/c^2.
[2] Uses B($\Upsilon(4S) \to B^+B^-$) = 0.513 ± 0.006.
[3] Assumes equal production of B^+ and B^0 at the $\Upsilon(4S)$.
[4] $M_{K\pi\pi} < 2.0$ GeV/c^2.
[5] $M_{K\pi\pi} < 2.4$ GeV/c^2.

$\Gamma(K^*(892)^0\pi^+\gamma)/\Gamma_{total}$ — Γ_{455}/Γ

VALUE (units 10^{-5})	DOCUMENT ID		TECN	COMMENT
2.33 ± 0.12 OUR AVERAGE				
$2.34 \pm 0.09 \; ^{+0.08}_{-0.07}$	[1,2] DEL-AMO-SA...16		BABR	$e^+e^- \to \Upsilon(4S)$
$2.0 \; ^{+0.7}_{-0.6} \pm 0.2$	[3,4] NISHIDA	02	BELL	$e^+e^- \to \Upsilon(4S)$

[1] Requires $M_{K\pi\pi} < 1.8$ GeV/c^2.
[2] Uses B($\Upsilon(4S) \to B^+B^-$) = 0.513 ± 0.006.
[3] Assumes equal production of B^+ and B^0 at the $\Upsilon(4S)$.
[4] $M_{K\pi\pi} < 2.4$ GeV/c^2.

$\Gamma(K^+\rho^0\gamma)/\Gamma_{total}$ — Γ_{456}/Γ

VALUE (units 10^{-6})	CL%	DOCUMENT ID		TECN	COMMENT
$8.2 \pm 0.4 \pm 0.8$		[1,2] DEL-AMO-SA...16		BABR	$e^+e^- \to \Upsilon(4S)$
• • • We do not use the following data for averages, fits, limits, etc. • • •					
<20	90	[3,4] NISHIDA	02	BELL	$e^+e^- \to \Upsilon(4S)$

[1] Requires $M_{K\pi\pi} < 1.8$ GeV/c^2.
[2] Uses B($\Upsilon(4S) \to B^+B^-$) = 0.513 ± 0.006.
[3] Assumes equal production of B^+ and B^0 at the $\Upsilon(4S)$.
[4] $M_{K\pi\pi} < 2.4$ GeV/c^2.

$\Gamma((K^+\pi^-)_{NR}\pi^+\gamma)/\Gamma_{total}$ — Γ_{457}/Γ

VALUE (units 10^{-6})	CL%	DOCUMENT ID		TECN	COMMENT
$9.9 \pm 0.7^{+1.5}_{-1.9}$		[1,2] DEL-AMO-SA...16		BABR	$e^+e^- \to \Upsilon(4S)$
• • • We do not use the following data for averages, fits, limits, etc. • • •					
<9.2	90	[3,4] NISHIDA	02	BELL	$e^+e^- \to \Upsilon(4S)$

[1] Requires $M_{K\pi\pi} < 1.8$ GeV/c^2.
[2] Uses B($\Upsilon(4S) \to B^+B^-$) = 0.513 ± 0.006.
[3] Assumes equal production of B^+ and B^0 at the $\Upsilon(4S)$.
[4] $M_{K\pi\pi} < 2.4$ GeV/c^2.

$\Gamma(K^0\pi^+\pi^0\gamma)/\Gamma_{total}$ — Γ_{458}/Γ

VALUE (units 10^{-5})	DOCUMENT ID		TECN	COMMENT
$4.56 \pm 0.42 \pm 0.31$	[1,2] AUBERT	07R	BABR	$e^+e^- \to \Upsilon(4S)$

[1] $M_{K\pi\pi} < 1.8$ GeV/c^2.
[2] Assumes equal production of B^+ and B^0 at the $\Upsilon(4S)$.

$\Gamma(K_1(1400)^+\gamma)/\Gamma_{total}$ — Γ_{459}/Γ

VALUE (units 10^{-6})	CL%	DOCUMENT ID		TECN	COMMENT
$9.7^{+4.6+2.9}_{-2.9-2.4}$		[1,2] DEL-AMO-SA...16		BABR	$e^+e^- \to \Upsilon(4S)$
• • • We do not use the following data for averages, fits, limits, etc. • • •					
<15	90	[3] YANG	05	BELL	$e^+e^- \to \Upsilon(4S)$
<50	90	[3] NISHIDA	02	BELL	Repl. by YANG 05
<2200	90	[4] ALBRECHT	89G	ARG	$e^+e^- \to \Upsilon(4S)$

[1] Requires $M_{K\pi\pi} < 1.8$ GeV/c^2.
[2] Uses B($\Upsilon(4S) \to B^+B^-$) = 0.513 ± 0.006.
[3] Assumes equal production of B^+ and B^0 at the $\Upsilon(4S)$.
[4] ALBRECHT 89G reports < 0.0020 assuming the $\Upsilon(4S)$ decays 45% to $B^0\overline{B}^0$. We rescale to 50%.

$\Gamma(K^*(1410)^+\gamma)/\Gamma_{total}$ — Γ_{460}/Γ

VALUE (units 10^{-5})	DOCUMENT ID		TECN	COMMENT
$2.71^{+0.54+0.59}_{-0.48-0.37}$	[1,2] DEL-AMO-SA...16		BABR	$e^+e^- \to \Upsilon(4S)$

[1] Requires $M_{K\pi\pi} < 1.8$ GeV/c^2.
[2] Uses B($\Upsilon(4S) \to B^+B^-$) = 0.513 ± 0.006.

$\Gamma(K_0^*(1430)^0\pi^+\gamma)/\Gamma_{total}$ — Γ_{461}/Γ

VALUE (units 10^{-6})	DOCUMENT ID		TECN	COMMENT
$1.32^{+0.09+0.24}_{-0.10-0.30}$	[1,2] DEL-AMO-SA...16		BABR	$e^+e^- \to \Upsilon(4S)$

[1] Requires $M_{K\pi\pi} < 1.8$ GeV/c^2.
[2] Uses B($\Upsilon(4S) \to B^+B^-$) = 0.513 ± 0.006.

$\Gamma(K_2^*(1430)^+\gamma)/\Gamma_{total}$ — Γ_{462}/Γ

VALUE (units 10^{-5})	CL%	DOCUMENT ID		TECN	COMMENT
1.4 ± 0.4 OUR AVERAGE					
$0.87^{+0.70+0.87}_{-0.53-1.04}$		[1,2] DEL-AMO-SA...16		BABR	$e^+e^- \to \Upsilon(4S)$
$1.45 \pm 0.40 \pm 0.15$		[3] AUBERT,B	04U	BABR	$e^+e^- \to \Upsilon(4S)$
• • • We do not use the following data for averages, fits, limits, etc. • • •					
<140	90	[4] ALBRECHT	89G	ARG	$e^+e^- \to \Upsilon(4S)$

[1] Requires $M_{K\pi\pi} < 1.8$ GeV/c^2.
[2] Uses B($\Upsilon(4S) \to B^+B^-$) = 0.513 ± 0.006.
[3] Assumes equal production of B^+ and B^0 at the $\Upsilon(4S)$.
[4] ALBRECHT 89G reports < 0.0013 assuming the $\Upsilon(4S)$ decays 45% to $B^0\overline{B}^0$. We rescale to 50%.

$\Gamma(K^*(1680)^+\gamma)/\Gamma_{total}$ — Γ_{463}/Γ

VALUE (units 10^{-5})	CL%	DOCUMENT ID		TECN	COMMENT
$6.67^{+0.93+1.44}_{-0.78-1.14}$		[1,2] DEL-AMO-SA...16		BABR	$e^+e^- \to \Upsilon(4S)$
• • • We do not use the following data for averages, fits, limits, etc. • • •					
<190	90	[3] ALBRECHT	89G	ARG	$e^+e^- \to \Upsilon(4S)$

[1] Requires $M_{K\pi\pi} < 1.8$ GeV/c^2.
[2] Uses B($\Upsilon(4S) \to B^+B^-$) = 0.513 ± 0.006.
[3] ALBRECHT 89G reports < 0.0017 assuming the $\Upsilon(4S)$ decays 45% to $B^0\overline{B}^0$. We rescale to 50%.

Downloaded from https://academic.oup.com/ptep/article/2022/8/083C01/6651666 by KIT Library user on 27 September 2022

$\Gamma(K_3^*(1780)^+\gamma)/\Gamma_{total}$ — Γ_{464}/Γ

VALUE (units 10^{-6})	CL%	DOCUMENT ID		TECN	COMMENT
< 39	90	[1,2] NISHIDA	05	BELL	$e^+e^- \to \Upsilon(4S)$
• • • We do not use the following data for averages, fits, limits, etc. • • •					
<5500	90	[3] ALBRECHT	89G	ARG	$e^+e^- \to \Upsilon(4S)$

[1] Assumes equal production of B^+ and B^0 at the $\Upsilon(4S)$.
[2] Uses $B(K_3^*(1780) \to \eta K) = 0.11^{+0.05}_{-0.04}$.
[3] ALBRECHT 89G reports < 0.005 assuming the $\Upsilon(4S)$ decays 45% to $B^0\overline{B}^0$. We rescale to 50%.

$\Gamma(K_4^*(2045)^+\gamma)/\Gamma_{total}$ — Γ_{465}/Γ

VALUE	CL%	DOCUMENT ID		TECN	COMMENT
<0.0099	90	[1] ALBRECHT	89G	ARG	$e^+e^- \to \Upsilon(4S)$

[1] ALBRECHT 89G reports < 0.0090 assuming the $\Upsilon(4S)$ decays 45% to $B^0\overline{B}^0$. We rescale to 50%.

$\Gamma(\rho^+\gamma)/\Gamma_{total}$ — Γ_{466}/Γ

VALUE (units 10^{-6})	CL%	DOCUMENT ID		TECN	COMMENT
0.98±0.25 OUR AVERAGE					
$1.20^{+0.42}_{-0.37}\pm0.20$		[1] AUBERT	08BH	BABR	$e^+e^- \to \Upsilon(4S)$
$0.87^{+0.29}_{-0.27}{}^{+0.09}_{-0.11}$		[1] TANIGUCHI	08	BELL	$e^+e^- \to \Upsilon(4S)$
• • • We do not use the following data for averages, fits, limits, etc. • • •					
$1.10^{+0.37}_{-0.33}\pm0.09$		[1] AUBERT	07L	BABR	Repl. by AUBERT 08BH
$0.55^{+0.42}_{-0.36}{}^{+0.09}_{-0.08}$		[1] MOHAPATRA	06	BELL	Repl. by TANIGUCHI 08
$0.9\ ^{+0.6}_{-0.5}\ \pm0.1$	90	[1] AUBERT	05	BABR	Repl. by AUBERT 07L
< 2.2	90	[1] MOHAPATRA	05	BELL	$e^+e^- \to \Upsilon(4S)$
< 2.1	90	[1] AUBERT	04C	BABR	$e^+e^- \to \Upsilon(4S)$
<13	90	[1,2] COAN	00	CLE2	$e^+e^- \to \Upsilon(4S)$

[1] Assumes equal production of B^+ and B^0 at $\Upsilon(4S)$.
[2] No evidence for a nonresonant $K\pi\gamma$ contamination was seen; the central value assumes no contamination.

$\Gamma(\pi^+\pi^0)/\Gamma_{total}$ — Γ_{467}/Γ

VALUE (units 10^{-6})	CL%	DOCUMENT ID		TECN	COMMENT
5.5 ±0.4 OUR AVERAGE		Error includes scale factor of 1.2.			
5.86±0.26±0.38		[1] DUH	13	BELL	$e^+e^- \to \Upsilon(4S)$
5.02±0.46±0.29		[1] AUBERT	07BC	BABR	$e^+e^- \to \Upsilon(4S)$
$4.6\ ^{+1.8}_{-1.6}\ ^{+0.6}_{-0.7}$		[1] BORNHEIM	03	CLE2	$e^+e^- \to \Upsilon(4S)$
• • • We do not use the following data for averages, fits, limits, etc. • • •					
6.5 ±0.4 ±0.4		[1] LIN	07A	BELL	Repl. by DUH 13
5.8 ±0.6 ±0.4		[1] AUBERT	05L	BABR	Repl. by AUBERT 07BC
5.0 ±1.2 ±0.5		[1] CHAO	04	BELL	Repl. by LIN 07A
$5.5\ ^{+1.0}_{-1.9}\ \pm0.6$		[1] AUBERT	03L	BABR	Repl. by AUBERT 05L
$7.4\ ^{+2.3}_{-2.2}\ \pm0.9$		[1] CASEY	02	BELL	Repl. by CHAO 04
< 13.4	90	[1] ABE	01H	BELL	$e^+e^- \to \Upsilon(4S)$
< 9.6	90	[1] AUBERT	01E	BABR	$e^+e^- \to \Upsilon(4S)$
< 12.7	90	[1] CRONIN-HEN...	00	CLE2	$e^+e^- \to \Upsilon(4S)$
< 20	90	GODANG	98	CLE2	Repl. by CRONIN-HENNESSY 00
< 17	90	ASNER	96	CLE2	Repl. by GODANG 98
< 240	90	[1] ALBRECHT	90B	ARG	$e^+e^- \to \Upsilon(4S)$
<2300	90	[2] BEBEK	87	CLEO	$e^+e^- \to \Upsilon(4S)$

[1] Assumes equal production of B^+ and B^0 at the $\Upsilon(4S)$.
[2] BEBEK 87 assume the $\Upsilon(4S)$ decays 43% to $B^0\overline{B}^0$.

$\Gamma(\pi^+\pi^0)/\Gamma(K^0\pi^+)$ — $\Gamma_{467}/\Gamma_{346}$

VALUE	DOCUMENT ID		TECN	COMMENT
0.285±0.02±0.02	LIN	07A	BELL	$e^+e^- \to \Upsilon(4S)$

$\Gamma(\pi^+\pi^+\pi^-)/\Gamma(K^+K^-K^+)$ — $\Gamma_{468}/\Gamma_{426}$

VALUE	DOCUMENT ID		TECN	COMMENT
0.488±0.005±0.009	AAIJ	20AJ	LHCB	pp at 7 and 8 TeV

$\Gamma(\pi^+\pi^+\pi^-)/\Gamma_{total}$ — Γ_{468}/Γ

VALUE (units 10^{-6})	CL%	DOCUMENT ID		TECN	COMMENT
$\mathbf{15.2\pm0.6^{+1.3}_{-1.2}}$		[1] AUBERT	09L	BABR	$e^+e^- \to \Upsilon(4S)$
• • • We do not use the following data for averages, fits, limits, etc. • • •					
16.2±1.2±0.9		[1] AUBERT,B	05G	BABR	Repl. by AUBERT 09L
10.9±3.3±1.6		[1] AUBERT	03M	BABR	Repl. by AUBERT 05G
<130	90	[2] ADAM	96D	DLPH	$e^+e^- \to Z$
<220	90	[3] ABREU	95N	DLPH	Sup. by ADAM 96D
<450	90	[4] ALBRECHT	90B	ARG	$e^+e^- \to \Upsilon(4S)$
<190	90	[5] BORTOLETTO	89	CLEO	$e^+e^- \to \Upsilon(4S)$

[1] Assumes equal production of B^0 and B^+ at the $\Upsilon(4S)$; charm and charmonium contributions are subtracted, otherwise no assumptions about intermediate resonances.
[2] ADAM 96D assumes $f_{B^0} = f_{B^-} = 0.39$ and $f_{B_s} = 0.12$.
[3] Assumes a B^0, B^- production fraction of 0.39 and a B_s production fraction of 0.12.
[4] ALBRECHT 90B limit assumes equal production of $B^0\overline{B}^0$ and B^+B^- at $\Upsilon(4S)$.
[5] BORTOLETTO 89 reports $< 1.7\times10^{-4}$ assuming the $\Upsilon(4S)$ decays 43% to $B^0\overline{B}^0$. We rescale to 50%.

$\Gamma(\rho^0\pi^+)/\Gamma_{total}$ — Γ_{469}/Γ

VALUE (units 10^{-6})	CL%	DOCUMENT ID		TECN	COMMENT
8.3±1.2 OUR AVERAGE					
$8.1\pm0.7^{+1.3}_{-1.6}$		[1] AUBERT	09L	BABR	$e^+e^- \to \Upsilon(4S)$
$8.0^{+2.3}_{-2.0}\pm0.7$		[1] GORDON	02	BELL	$e^+e^- \to \Upsilon(4S)$
$10.4^{+3.3}_{-3.4}\pm2.1$		[1] JESSOP	00	CLE2	$e^+e^- \to \Upsilon(4S)$
• • • We do not use the following data for averages, fits, limits, etc. • • •					
$8.8\pm1.0^{+0.6}_{-0.9}$		[1] AUBERT,B	05G	BABR	Repl. by AUBERT 09L
9.5±1.1±0.9		[1] AUBERT	04Z	BABR	Repl. by AUBERT 05G
< 83	90	[2] ABE	00C	SLD	$e^+e^- \to Z$
<160	90	[3] ADAM	96D	DLPH	$e^+e^- \to Z$
< 43	90	ASNER	96	CLE2	Repl. by JESSOP 00
<260	90	[4] ABREU	95N	DLPH	Sup. by ADAM 96D
<150	90	[1] ALBRECHT	90B	ARG	$e^+e^- \to \Upsilon(4S)$
<170	90	[5] BORTOLETTO	89	CLEO	$e^+e^- \to \Upsilon(4S)$
<230	90	[5] BEBEK	87	CLEO	$e^+e^- \to \Upsilon(4S)$
<600	90	GILES	84	CLEO	Repl. by BEBEK 87

[1] Assumes equal production of B^+ and B^0 at the $\Upsilon(4S)$.
[2] ABE 00C assumes $B(Z \to b\overline{b})=(21.7 \pm 0.1)\%$ and the B fractions $f_{B^0}=f_{B^+}=(39.7^{+1.8}_{-2.2})\%$ and $f_{B_s}=(10.5^{+1.8}_{-2.2})\%$.
[3] ADAM 96D assumes $f_{B^0} = f_{B^-} = 0.39$ and $f_{B_s} = 0.12$.
[4] Assumes a B^0, B^- production fraction of 0.39 and a B_s production fraction of 0.12.
[5] Papers assume the $\Upsilon(4S)$ decays 43% to $B^0\overline{B}^0$. We rescale to 50%.

$[\Gamma(K^*(892)^0\pi^+) + \Gamma(\rho^0\pi^+)]/\Gamma_{total}$ — $(\Gamma_{372}+\Gamma_{469})/\Gamma$

VALUE (units 10^{-6})	DOCUMENT ID		TECN	COMMENT
$\mathbf{170^{+120}_{-\ 80}\pm20}$	[1] ADAM	96D	DLPH	$e^+e^- \to Z$

[1] ADAM 96D assumes $f_{B^0} = f_{B^-} = 0.39$ and $f_{B_s} = 0.12$.

$\Gamma(\pi^+ f_0(980),\ f_0 \to \pi^+\pi^-)/\Gamma_{total}$ — Γ_{470}/Γ

VALUE (units 10^{-6})	CL%	DOCUMENT ID		TECN	COMMENT
< 1.5	90	[1] AUBERT	09L	BABR	$e^+e^- \to \Upsilon(4S)$
• • • We do not use the following data for averages, fits, limits, etc. • • •					
< 3.0	90	[1] AUBERT,B	05G	BABR	Repl. by AUBERT 09L
<140	90	[2] BORTOLETTO	89	CLEO	$e^+e^- \to \Upsilon(4S)$

[1] Assumes equal production of B^+ and B^0 at the $\Upsilon(4S)$.
[2] BORTOLETTO 89 reports $< 1.2\times10^{-4}$ assuming the $\Upsilon(4S)$ decays 43% to $B^0\overline{B}^0$. We rescale to 50%.

$\Gamma(\pi^+ f_2(1270))/\Gamma_{total}$ — Γ_{471}/Γ

VALUE (units 10^{-6})	CL%	DOCUMENT ID		TECN	COMMENT
$\mathbf{2.2\ ^{+0.7}_{-0.4}}$ **OUR AVERAGE**					
17.0 ±2.4 ±2.1		[1] AAIJ	19AL	LHCB	pp at 7, 8 TeV
$1.60^{+0.67}_{-0.44}{}^{+0.02}_{-0.06}$		[2,3] AUBERT	09L	BABR	$e^+e^- \to \Upsilon(4S)$
• • • We do not use the following data for averages, fits, limits, etc. • • •					
$4.10\pm1.28^{+0.04}_{-0.14}$		[3,4] AUBERT,B	05G	BABR	Repl. by AUBERT 09L
<240	90	[5] BORTOLETTO	89	CLEO	$e^+e^- \to \Upsilon(4S)$

[1] AAIJ 19AL reports 0.075 ± 0.008 ± 0.007 fit fraction for $B^+ \to f_2(1270)\pi^+$ from the amplitude analysis of $B^\pm \to \pi^\pm K^+K^-$ decays. We use the PDG 19 value $B(B^+ \to K^+K^-\pi^+) = (5.2 \pm 0.4)\times10^{-6}$ to obtain $B(B^+ \to f_2(1270)\pi^+, f_2(1270) \to K^+K^-)$. We compute $B(B^+ \to f_2(1270)\pi^+)$ using 1/2 of PDG 19 value of $B(f_2(1270) \to K\overline{K}) = (4.6^{+0.5}_{-0.4})\%$ for K^+K^- fraction. Our first error is the experiment's error and the second error is systematic error from using our best value.
[2] AUBERT 09L reports $[\Gamma(B^+ \to \pi^+ f_2(1270))/\Gamma_{total}] \times [B(f_2(1270) \to \pi^+\pi^-)] = (0.9 \pm 0.2 \pm 0.1^{+0.3}_{-0.1})\times10^{-6}$ which we divide by our best value $B(f_2(1270) \to \pi^+\pi^-) = (56.2^{+1.9}_{-0.6})\times10^{-2}$. Our first error is their experiment's error and our second error is the systematic error from using our best value.
[3] Assumes equal production of B^+ and B^0 at the $\Upsilon(4S)$.
[4] AUBERT,B 05G reports $[\Gamma(B^+ \to \pi^+ f_2(1270))/\Gamma_{total}] \times [B(f_2(1270) \to \pi^+\pi^-)] = (2.3 \pm 0.6 \pm 0.4)\times10^{-6}$ which we divide by our best value $B(f_2(1270) \to \pi^+\pi^-) = (56.2^{+1.9}_{-0.6})\times10^{-2}$. Our first error is their experiment's error and our second error is the systematic error from using our best value.
[5] BORTOLETTO 89 reports $< 2.1\times10^{-4}$ assuming the $\Upsilon(4S)$ decays 43% to $B^0\overline{B}^0$. We rescale to 50%.

$\Gamma(\rho(1450)^0\pi^+,\ \rho^0 \to \pi^+\pi^-)/\Gamma_{total}$ — Γ_{472}/Γ

VALUE (units 10^{-6})	CL%	DOCUMENT ID		TECN	COMMENT
$\mathbf{1.4\pm0.4^{+0.5}_{-0.8}}$		[1] AUBERT	09L	BABR	$e^+e^- \to \Upsilon(4S)$
• • • We do not use the following data for averages, fits, limits, etc. • • •					
<2.3	90	[1] AUBERT,B	05G	BABR	Repl. by AUBERT 09L

[1] Assumes equal production of B^+ and B^0 at the $\Upsilon(4S)$.

Downloaded from https://academic.oup.com/ptep/article/2022/8/083C01/6651666 by KIT Library user on 27 September 2022

$\Gamma(f_0(1370)\pi^+,\ f_0 \to \pi^+\pi^-)/\Gamma_{total}$ — Γ_{474}/Γ

VALUE (units 10^{-6})	CL%	DOCUMENT ID		TECN	COMMENT
<4.0	90	[1] AUBERT	09L	BABR	$e^+e^- \to \Upsilon(4S)$
• • • We do not use the following data for averages, fits, limits, etc. • • •					
<3.0	90	[1] AUBERT,B	05G	BABR	Repl. by AUBERT 09L

[1] Assumes equal production of B^+ and B^0 at the $\Upsilon(4S)$.

$\Gamma(f_0(500)\pi^+,\ f_0 \to \pi^+\pi^-)/\Gamma_{total}$ — Γ_{475}/Γ

VALUE (units 10^{-6})	CL%	DOCUMENT ID		TECN	COMMENT
<4.1	90	[1] AUBERT,B	05G	BABR	$e^+e^- \to \Upsilon(4S)$

[1] Assumes equal production of B^+ and B^0 at the $\Upsilon(4S)$.

$\Gamma(\pi^+\pi^-\pi^+ \text{nonresonant})/\Gamma_{total}$ — Γ_{476}/Γ

VALUE (units 10^{-6})	CL%	DOCUMENT ID		TECN	COMMENT
$5.3\pm0.7^{+1.3}_{-0.8}$		[1] AUBERT	09L	BABR	$e^+e^- \to \Upsilon(4S)$
• • • We do not use the following data for averages, fits, limits, etc. • • •					
< 4.6	90	[1] AUBERT,B	05G	BABR	Repl. by AUBERT 09L
<41	90	BERGFELD	96B	CLE2	$e^+e^- \to \Upsilon(4S)$

[1] Assumes equal production of B^+ and B^0 at the $\Upsilon(4S)$.

$\Gamma(\pi^+\pi^0\pi^0)/\Gamma_{total}$ — Γ_{477}/Γ

VALUE	CL%	DOCUMENT ID		TECN	COMMENT
$<8.9\times10^{-4}$	90	[1] ALBRECHT	90B	ARG	$e^+e^- \to \Upsilon(4S)$

[1] ALBRECHT 90B limit assumes equal production of $B^0\overline{B}^0$ and B^+B^- at $\Upsilon(4S)$.

$\Gamma(\rho^+\pi^0)/\Gamma_{total}$ — Γ_{478}/Γ

VALUE (units 10^{-6})	CL%	DOCUMENT ID		TECN	COMMENT
10.9±1.4 OUR AVERAGE					
10.2±1.4±0.9		[1] AUBERT	07X	BABR	$e^+e^- \to \Upsilon(4S)$
$13.2\pm2.3^{+1.4}_{-1.9}$		[1] ZHANG	05A	BELL	$e^+e^- \to \Upsilon(4S)$
• • • We do not use the following data for averages, fits, limits, etc. • • •					
10.9±1.9±1.9		[1] AUBERT	04Z	BABR	Repl. by AUBERT 07X
< 43	90	[1,2] JESSOP	00	CLE2	$e^+e^- \to \Upsilon(4S)$
< 77	90	ASNER	96	CLE2	Repl. by JESSOP 00
<550	90	[1] ALBRECHT	90B	ARG	$e^+e^- \to \Upsilon(4S)$

[1] Assumes equal production of B^+ and B^0 at the $\Upsilon(4S)$.
[2] Assumes no nonresonant contributions of $B^+ \to \pi^+\pi^0\pi^0$.

$\Gamma(\pi^+\pi^-\pi^+\pi^0)/\Gamma_{total}$ — Γ_{479}/Γ

VALUE	CL%	DOCUMENT ID		TECN	COMMENT
$<4.0\times10^{-3}$	90	[1] ALBRECHT	90B	ARG	$e^+e^- \to \Upsilon(4S)$

[1] ALBRECHT 90B limit assumes equal production of $B^0\overline{B}^0$ and B^+B^- at $\Upsilon(4S)$.

$\Gamma(\rho^+\rho^0)/\Gamma_{total}$ — Γ_{480}/Γ

VALUE (units 10^{-6})	CL%	DOCUMENT ID		TECN	COMMENT
24.0±1.9 OUR AVERAGE					
23.7±1.4±1.4		[1] AUBERT	09G	BABR	$e^+e^- \to \Upsilon(4S)$
$31.7\pm7.1^{+3.8}_{-6.7}$		[1,2] ZHANG	03B	BELL	$e^+e^- \to \Upsilon(4S)$
• • • We do not use the following data for averages, fits, limits, etc. • • •					
16.8±2.2±2.3		[1] AUBERT,BE	06G	BABR	Repl. by AUBERT 09G
$22.5^{+5.7}_{-5.4}\pm5.8$		[1] AUBERT	03V	BABR	Repl. by AUBERT,BE 06G
< 1000	90	[1] ALBRECHT	90B	ARG	$e^+e^- \to \Upsilon(4S)$

[1] Assumes equal production of B^+ and B^0 at the $\Upsilon(4S)$.
[2] The systematic error includes the error associated with the helicity-mix uncertainty.

$\Gamma(\rho^+ f_0(980),\ f_0 \to \pi^+\pi^-)/\Gamma_{total}$ — Γ_{481}/Γ

VALUE (units 10^{-6})	CL%	DOCUMENT ID		TECN	COMMENT
<2.0	90	[1] AUBERT	09G	BABR	$e^+e^- \to \Upsilon(4S)$
• • • We do not use the following data for averages, fits, limits, etc. • • •					
<1.9	90	[1] AUBERT,BE	06G	BABR	Repl. by AUBERT 09G

[1] Assumes equal production of B^+ and B^0 at the $\Upsilon(4S)$.

$\Gamma(a_1(1260)^+\pi^0)/\Gamma_{total}$ — Γ_{482}/Γ

VALUE (units 10^{-6})	CL%	DOCUMENT ID		TECN	COMMENT
26.4±5.4±4.1		[1,2] AUBERT	07BL	BABR	$e^+e^- \to \Upsilon(4S)$
• • • We do not use the following data for averages, fits, limits, etc. • • •					
<1700	90	[1] ALBRECHT	90B	ARG	$e^+e^- \to \Upsilon(4S)$

[1] Assumes equal production of B^+ and B^0 at the $\Upsilon(4S)$.
[2] Assumes a_1^+ decays only to 3π and $B(a_1^+ \to \pi^\pm\pi^\mp\pi^+) = 0.5$.

$\Gamma(a_1(1260)^0\pi^+)/\Gamma_{total}$ — Γ_{483}/Γ

VALUE (units 10^{-6})	CL%	DOCUMENT ID		TECN	COMMENT
20.4±4.7±3.4		[1,2] AUBERT	07BL	BABR	$e^+e^- \to \Upsilon(4S)$
• • • We do not use the following data for averages, fits, limits, etc. • • •					
<900	90	[1] ALBRECHT	90B	ARG	$e^+e^- \to \Upsilon(4S)$

[1] Assumes equal production of B^+ and B^0 at the $\Upsilon(4S)$.
[2] Assumes a_1^0 decays only to 3π and $B(a_1^+ \to \pi^\pm\pi^\mp\pi^0) = 1.0$.

$\Gamma(\omega\pi^+)/\Gamma_{total}$ — Γ_{484}/Γ

VALUE (units 10^{-6})	CL%	DOCUMENT ID		TECN	COMMENT
6.9±0.5 OUR AVERAGE					
6.7±0.5±0.4		[1] AUBERT	07AE	BABR	$e^+e^- \to \Upsilon(4S)$
6.9±0.6±0.5		[1] JEN	06	BELL	$e^+e^- \to \Upsilon(4S)$
$11.3^{+3.3}_{-2.9}\pm1.4$		[1] JESSOP	00	CLE2	$e^+e^- \to \Upsilon(4S)$
• • • We do not use the following data for averages, fits, limits, etc. • • •					
6.1±0.7±0.4		[1] AUBERT,B	06E	BABR	Repl. by AUBERT 07AE
5.5±0.9±0.5		[1] AUBERT	04H	BABR	Repl. by AUBERT,B 06E
$5.7^{+1.4}_{-1.3}\pm0.6$		[1] WANG	04A	BELL	Repl. by JEN 06
$4.2^{+2.0}_{-1.8}\pm0.5$		[1] LU	02	BELL	Repl. by WANG 04A
$6.6^{+2.1}_{-1.8}\pm0.7$		[1] AUBERT	01G	BABR	Repl. by AUBERT 04H
< 23	90	[1] BERGFELD	98	CLE2	Repl. by JESSOP 00
<400	90	[1] ALBRECHT	90B	ARG	$e^+e^- \to \Upsilon(4S)$

[1] Assumes equal production of B^+ and B^0 at the $\Upsilon(4S)$.

$\Gamma(\omega\rho^+)/\Gamma_{total}$ — Γ_{485}/Γ

VALUE (units 10^{-6})	CL%	DOCUMENT ID		TECN	COMMENT
15.9±1.6±1.4		[1] AUBERT	09H	BABR	$e^+e^- \to \Upsilon(4S)$
• • • We do not use the following data for averages, fits, limits, etc. • • •					
$10.6\pm2.1^{+1.6}_{-1.0}$		[1] AUBERT,B	06T	BABR	Repl. by AUBERT 09H
$12.6^{+3.7}_{-3.3}\pm1.6$		[1] AUBERT	05O	BABR	Repl. by AUBERT,B 06T
<61	90	[1] BERGFELD	98	CLE2	

[1] Assumes equal production of B^+ and B^0 at the $\Upsilon(4S)$.

$\Gamma(\eta\pi^+)/\Gamma_{total}$ — Γ_{486}/Γ

VALUE (units 10^{-6})	CL%	DOCUMENT ID		TECN	COMMENT
4.02±0.27 OUR AVERAGE					
4.07±0.26±0.21		[1] HOI	12	BELL	$e^+e^- \to \Upsilon(4S)$
4.00±0.40±0.24		[1] AUBERT	09AV	BABR	$e^+e^- \to \Upsilon(4S)$
$1.2\ ^{+2.8}_{-1.2}$		[1] RICHICHI	00	CLE2	$e^+e^- \to \Upsilon(4S)$
• • • We do not use the following data for averages, fits, limits, etc. • • •					
5.0 ±0.5 ±0.3		[1] AUBERT	07AE	BABR	Repl. by AUBERT 09AV
4.2 ±0.4 ±0.2		[1] CHANG	07B	BELL	Repl. by HOI 12
5.1 ±0.6 ±0.3		[1] AUBERT,B	05K	BABR	Repl. by AUBERT 07AE
4.8 ±0.7 ±0.3		[1] CHANG	05A	BELL	Repl. by CHANG 07B
5.3 ±1.0 ±0.3		[1] AUBERT	04H	BABR	Repl. by AUBERT,B 05K
< 15	90	BEHRENS	98	CLE2	Repl. by RICHICHI 00
<700	90	[1] ALBRECHT	90B	ARG	$e^+e^- \to \Upsilon(4S)$

[1] Assumes equal production of B^+ and B^0 at the $\Upsilon(4S)$.

$\Gamma(\eta\rho^+)/\Gamma_{total}$ — Γ_{487}/Γ

VALUE (units 10^{-6})	CL%	DOCUMENT ID		TECN	COMMENT
7.0±2.9 OUR AVERAGE Error includes scale factor of 2.8.					
9.9±1.2±0.8		[1] AUBERT	08AH	BABR	$e^+e^- \to \Upsilon(4S)$
$4.1^{+1.4}_{-1.3}\pm0.4$		[1] WANG	07B	BELL	$e^+e^- \to \Upsilon(4S)$
• • • We do not use the following data for averages, fits, limits, etc. • • •					
8.4±1.9±1.1		[1] AUBERT,B	05K	BABR	Repl. by AUBERT 08AH
<14	90	[1] AUBERT,B	04D	BABR	Repl. by AUBERT,B 05K
<15	90	[1] RICHICHI	00	CLE2	$e^+e^- \to \Upsilon(4S)$
<32	90	BEHRENS	98	CLE2	Repl. by RICHICHI 00

[1] Assumes equal production of B^+ and B^0 at the $\Upsilon(4S)$.

$\Gamma(\eta'\pi^+)/\Gamma_{total}$ — Γ_{488}/Γ

VALUE (units 10^{-6})	CL%	DOCUMENT ID		TECN	COMMENT
2.7 ±0.9 OUR AVERAGE Error includes scale factor of 1.9.					
3.5 ±0.6 ±0.2		[1] AUBERT	09AV	BABR	$e^+e^- \to \Upsilon(4S)$
$1.76^{+0.67+0.15}_{-0.62-0.14}$		[1] SCHUEMANN	06	BELL	$e^+e^- \to \Upsilon(4S)$
• • • We do not use the following data for averages, fits, limits, etc. • • •					
3.9 ±0.7 ±0.3		[1] AUBERT	07AE	BABR	Repl. by AUBERT 09AV
4.0 ±0.8 ±0.4		[1] AUBERT,B	05K	BABR	Repl. by AUBERT 07AE
< 4.5	90	[1] AUBERT	04H	BABR	Repl. by AUBERT,B 05K
< 7.0	90	[1] ABE	01M	BELL	$e^+e^- \to \Upsilon(4S)$
<12	90	[1] AUBERT	01G	BABR	$e^+e^- \to \Upsilon(4S)$
<12	90	[1] RICHICHI	00	CLE2	$e^+e^- \to \Upsilon(4S)$
<31	90	BEHRENS	98	CLE2	Repl. by RICHICHI 00

[1] Assumes equal production of B^+ and B^0 at the $\Upsilon(4S)$.

$\Gamma(\eta'\rho^+)/\Gamma_{total}$ — Γ_{489}/Γ

VALUE (units 10^{-6})	CL%	DOCUMENT ID		TECN	COMMENT
$9.7^{+1.9}_{-1.8}\pm1.1$		[1] DEL-AMO-SA...10A		BABR	$e^+e^- \to \Upsilon(4S)$

Downloaded from https://academic.oup.com/ptep/article/2022/8/083C01/6651666 by KIT Library user on 27 September 2022

• • • We do not use the following data for averages, fits, limits, etc. • • •

$8.7^{+3.1+2.3}_{-2.8-1.3}$		[1] AUBERT	07E	BABR	Repl. by DEL-AMO-SANCHEZ 10A
<5.8	90	[1] SCHUEMANN	07	BELL	$e^+e^- \to \Upsilon(4S)$
<22	90	[1] AUBERT,B	04D	BABR	Repl. by AUBERT 07E
<33	90	[1] RICHICHI	00	CLE2	$e^+e^- \to \Upsilon(4S)$
<47	90	BEHRENS	98	CLE2	Repl. by RICHICHI 00

[1] Assumes equal production of B^+ and B^0 at the $\Upsilon(4S)$.

$\Gamma(\phi\pi^+)/\Gamma_{total}$ — Γ_{490}/Γ

VALUE (units 10^{-8})	CL%	DOCUMENT ID		TECN	COMMENT
$3.2\pm1.5\pm0.3$		[1] AAIJ	19AL	LHCB	pp at 7, 8 TeV

• • • We do not use the following data for averages, fits, limits, etc. • • •

<15	90	[2] AAIJ	14A	LHCB	Repl. by AAIJ 19AL
<33	90	[3] KIM	12A	BELL	$e^+e^- \to \Upsilon(4S)$
<24	90	[3] AUBERT,B	06C	BABR	$e^+e^- \to \Upsilon(4S)$
<41	90	[3] AUBERT	04A	BABR	Repl. by AUBERT,B 06C
<140	90	[3] AUBERT	01D	BABR	$e^+e^- \to \Upsilon(4S)$
<15300	90	[4] ABE	00C	SLD	$e^+e^- \to Z$
<500	90	[3] BERGFELD	98	CLE2	

[1] AAIJ 19AL reports $(0.3\pm0.1\pm0.1)\times10^{-2}$ fit fraction for $B^+ \to \phi(1020)\pi^+$ from the amplitude analysis of $B^\pm \to \pi^\pm K^+K^-$ decays. We use the PDG 19 value $B(B^+ \to K^+K^-\pi^+) = (5.2\pm0.4)\times10^{-6}$ to obtain $B(B^+ \to \phi(1020)\pi^+,\ \phi(1020) \to K^+K^-)$. We compute $B(B^+ \to \phi(1020)\pi^+)$ using the PDG 19 value of $B(\phi(1020) \to K^+K^-) = (49.2\pm0.5)\%$. Our first error is the experiment's error and the second error is systematic error from using our best value.

[2] Measures $B(B^+ \to \phi\pi^+)/B(B^+ \to \phi K^+) < 0.018$ at 90% C.L. and assumes $B(B^+ \to \phi K^+) = (8.8^{+0.7}_{-0.6})\times10^{-6}$.

[3] Assumes equal production of B^+ and B^0 at the $\Upsilon(4S)$.

[4] ABE 00C assumes $B(Z \to b\overline{b}) = (21.7\pm0.1)\%$ and the B fractions $f_{B^0} = f_{B^+} = (39.7^{+1.8}_{-2.2})\%$ and $f_{B_s} = (10.5^{+1.8}_{-2.2})\%$.

$\Gamma(\phi\rho^+)/\Gamma_{total}$ — Γ_{491}/Γ

VALUE (units 10^{-6})	CL%	DOCUMENT ID		TECN	COMMENT
<3.0	90	[1] AUBERT	08BK	BABR	$e^+e^- \to \Upsilon(4S)$

• • • We do not use the following data for averages, fits, limits, etc. • • •

<16		[1] BERGFELD	98	CLE2	

[1] Assumes equal production of B^+ and B^0 at the $\Upsilon(4S)$.

$\Gamma(a_0(980)^0\pi^+,\ a_0^0 \to \eta\pi^0)/\Gamma_{total}$ — Γ_{492}/Γ

VALUE (units 10^{-6})	CL%	DOCUMENT ID		TECN	COMMENT
<5.8	90	[1] AUBERT,BE	04	BABR	$e^+e^- \to \Upsilon(4S)$

[1] Assumes equal production of charged and neutral B mesons from $\Upsilon(4S)$ decays.

$\Gamma(a_0(980)^+\pi^0,\ a_0^+ \to \eta\pi^+)/\Gamma_{total}$ — Γ_{493}/Γ

VALUE (units 10^{-6})	CL%	DOCUMENT ID		TECN	COMMENT
<1.4	90	[1] AUBERT	08A	BABR	$e^+e^- \to \Upsilon(4S)$

[1] Assumes equal production of B^+ and B^0 at the $\Upsilon(4S)$.

$\Gamma(\pi^+\pi^+\pi^+\pi^-\pi^-)/\Gamma_{total}$ — Γ_{494}/Γ

VALUE	CL%	DOCUMENT ID		TECN	COMMENT
$<8.6\times10^{-4}$	90	[1] ALBRECHT	90B	ARG	$e^+e^- \to \Upsilon(4S)$

[1] ALBRECHT 90B limit assumes equal production of $B^0\overline{B}^0$ and B^+B^- at $\Upsilon(4S)$.

$\Gamma(\rho^0 a_1(1260)^+)/\Gamma_{total}$ — Γ_{495}/Γ

VALUE	CL%	DOCUMENT ID		TECN	COMMENT
$<6.2\times10^{-4}$	90	[1] BORTOLETTO	89	CLEO	$e^+e^- \to \Upsilon(4S)$

• • • We do not use the following data for averages, fits, limits, etc. • • •

$<6.0\times10^{-4}$	90	[2] ALBRECHT	90B	ARG	$e^+e^- \to \Upsilon(4S)$
$<3.2\times10^{-3}$	90	[1] BEBEK	87	CLEO	$e^+e^- \to \Upsilon(4S)$

[1] BORTOLETTO 89 reports $<5.4\times10^{-4}$ assuming the $\Upsilon(4S)$ decays 43% to $B^0\overline{B}^0$. We rescale to 50%.

[2] ALBRECHT 90B limit assumes equal production of $B^0\overline{B}^0$ and B^+B^- at $\Upsilon(4S)$.

$\Gamma(\rho^0 a_2(1320)^+)/\Gamma_{total}$ — Γ_{496}/Γ

VALUE	CL%	DOCUMENT ID		TECN	COMMENT
$<7.2\times10^{-4}$	90	[1] BORTOLETTO	89	CLEO	$e^+e^- \to \Upsilon(4S)$

• • • We do not use the following data for averages, fits, limits, etc. • • •

$<2.6\times10^{-3}$	90	[2] BEBEK	87	CLEO	$e^+e^- \to \Upsilon(4S)$

[1] BORTOLETTO 89 reports $<6.3\times10^{-4}$ assuming the $\Upsilon(4S)$ decays 43% to $B^0\overline{B}^0$. We rescale to 50%.

[2] BEBEK 87reports $<2.3\times10^{-3}$ assuming the $\Upsilon(4S)$ decays 43% to $B^0\overline{B}^0$. We rescale to 50%.

$\Gamma(b_1^0\pi^+,\ b_1^0 \to \omega\pi^0)/\Gamma_{total}$ — Γ_{497}/Γ

VALUE (units 10^{-6})	DOCUMENT ID		TECN	COMMENT
$6.7\pm1.7\pm1.0$	[1] AUBERT	07BI	BABR	$e^+e^- \to \Upsilon(4S)$

[1] Assumes equal production of B^+ and B^0 at the $\Upsilon(4S)$.

$\Gamma(b_1^+\pi^0,\ b_1^+ \to \omega\pi^+)/\Gamma_{total}$ — Γ_{498}/Γ

VALUE (units 10^{-6})	CL%	DOCUMENT ID		TECN	COMMENT
<3.3	90	[1] AUBERT	08AG	BABR	$e^+e^- \to \Upsilon(4S)$

[1] Assumes equal production of B^+ and B^0 at the $\Upsilon(4S)$.

$\Gamma(\pi^+\pi^+\pi^+\pi^-\pi^-\pi^0)/\Gamma_{total}$ — Γ_{499}/Γ

VALUE	CL%	DOCUMENT ID		TECN	COMMENT
$<6.3\times10^{-3}$	90	[1] ALBRECHT	90B	ARG	$e^+e^- \to \Upsilon(4S)$

[1] ALBRECHT 90B limit assumes equal production of $B^0\overline{B}^0$ and B^+B^- at $\Upsilon(4S)$.

$\Gamma(b_1^+\rho^0,\ b_1^+ \to \omega\pi^+)/\Gamma_{total}$ — Γ_{500}/Γ

VALUE	CL%	DOCUMENT ID		TECN	COMMENT
$<5.2\times10^{-6}$	90	[1] AUBERT	09AF	BABR	$e^+e^- \to \Upsilon(4S)$

[1] Assumes equal production of B^+ and B^0 at the $\Upsilon(4S)$.

$\Gamma(b_1^0\rho^+,\ b_1^0 \to \omega\pi^0)/\Gamma_{total}$ — Γ_{502}/Γ

VALUE	CL%	DOCUMENT ID		TECN	COMMENT
$<3.3\times10^{-6}$	90	[1] AUBERT	09AF	BABR	$e^+e^- \to \Upsilon(4S)$

[1] Assumes equal production of B^+ and B^0 at the $\Upsilon(4S)$.

$\Gamma(a_1(1260)^+a_1(1260)^0)/\Gamma_{total}$ — Γ_{501}/Γ

VALUE	CL%	DOCUMENT ID		TECN	COMMENT
$<1.3\times10^{-2}$	90	[1] ALBRECHT	90B	ARG	$e^+e^- \to \Upsilon(4S)$

[1] ALBRECHT 90B limit assumes equal production of $B^0\overline{B}^0$ and B^+B^- at $\Upsilon(4S)$.

$\Gamma(h^+\pi^0)/\Gamma_{total}$ — Γ_{503}/Γ

$h^+ = K^+$ or π^+

VALUE (units 10^{-6})	DOCUMENT ID		TECN	COMMENT
$16^{+6}_{-5}\pm3.6$	GODANG	98	CLE2	$e^+e^- \to \Upsilon(4S)$

$\Gamma(\omega h^+)/\Gamma_{total}$ — Γ_{504}/Γ

$h^+ = K^+$ or π^+

VALUE (units 10^{-6})	DOCUMENT ID		TECN	COMMENT
$13.8^{+2.7}_{-2.4}$ OUR AVERAGE				
$13.4^{+3.3}_{-2.9}\pm1.1$	[1] LU	02	BELL	$e^+e^- \to \Upsilon(4S)$
$14.3^{+3.6}_{-3.2}\pm2.0$	[1] JESSOP	00	CLE2	$e^+e^- \to \Upsilon(4S)$

• • • We do not use the following data for averages, fits, limits, etc. • • •

$25^{+8}_{-7}\pm3$	[1] BERGFELD	98	CLE2	Repl. by JESSOP 00

[1] Assumes equal production of B^+ and B^0 at the $\Upsilon(4S)$.

$\Gamma(h^+X^0(\text{Familon}))/\Gamma_{total}$ — Γ_{505}/Γ

VALUE (units 10^{-6})	CL%	DOCUMENT ID		TECN	COMMENT
<49	90	[1] AMMAR	01B	CLE2	$e^+e^- \to \Upsilon(4S)$

[1] AMMAR 01B searched for the two-body decay of the B meson to a massless neutral feebly-interacting particle X^0 such as the familon, the Nambu-Goldstone boson associated with a spontaneously broken global family symmetry.

$\Gamma(K^+X^0,\ X^0 \to \mu^+\mu^-)/\Gamma_{total}$ — Γ_{506}/Γ

X^0 stands here for a long-lived scalar particle.

VALUE	CL%	DOCUMENT ID		TECN	COMMENT
$<1\times10^{-7}$	95	[1] AAIJ	17AQ	LHCB	pp at 7, 8 TeV

[1] AAIJ 17AQ searched for a long-lived scalar particle $X^0 \to \mu^+\mu^-$ in the mass range 250–4700 MeV and lifetime range 0.1–1000 ps. The limit is between 10^{-7} and 2×10^{-10} in these ranges except in vetoed mass regions around K_S^0, J/ψ, $\psi(2S)$, and $\psi(3770)$.

$\Gamma(p\overline{p}\pi^+)/\Gamma_{total}$ — Γ_{507}/Γ

VALUE (units 10^{-6})	CL%	DOCUMENT ID		TECN	COMMENT
1.62 ± 0.20 OUR AVERAGE					
$1.60^{+0.22}_{-0.19}\pm0.12$		[1,2,3] WEI	08	BELL	$e^+e^- \to \Upsilon(4S)$
$1.69\pm0.29\pm0.26$		[1] AUBERT	07AV	BABR	$e^+e^- \to \Upsilon(4S)$

• • • We do not use the following data for averages, fits, limits, etc. • • •

$1.07\pm0.11\pm0.11$		[4] AAIJ	14AF	LHCB	pp at 7, 8 TeV
$3.06^{+0.73}_{-0.62}\pm0.37$		[1,3] WANG	04	BELL	Repl. by WEI 08
<3.7	90	[1,2] ABE	02K	BELL	Repl. by WANG 04
<500	90	[5] ABREU	95N	DLPH	Repl. by ADAM 96D
<160	90	[6] BEBEK	89	CLEO	$e^+e^- \to \Upsilon(4S)$
$570\pm150\pm210$		[7] ALBRECHT	88F	ARG	$e^+e^- \to \Upsilon(4S)$

[1] Assumes equal production of B^+ and B^0 at the $\Upsilon(4S)$.

[2] Explicitly vetoes resonant production of $p\overline{p}$ from Charmonium states.

[3] Also provides results with $m_{p\overline{p}} < 2.85$ GeV/c^2 and angular asymmetry of $p\overline{p}$ system.

[4] Requires $m_{p\overline{p}} < 2.85$ GeV/c^2.

[5] Assumes a B^0, B^- production fraction of 0.39 and a B_s production fraction of 0.12.

[6] BEBEK 89 reports $<1.4\times10^{-4}$ assuming the $\Upsilon(4S)$ decays 43% to $B^0\overline{B}^0$. We rescale to 50%.

[7] ALBRECHT 88F reports $(5.2\pm1.4\pm1.9)\times10^{-4}$ assuming the $\Upsilon(4S)$ decays 45% to $B^0\overline{B}^0$. We rescale to 50%.

Downloaded from https://academic.oup.com/ptep/article/2022/8/083C01/6651666 by KIT Library user on 27 September 2022

$\Gamma(p\overline{p}\pi^+ \text{nonresonant})/\Gamma_{\text{total}}$ — Γ_{508}/Γ

VALUE (units 10^{-6})	CL%	DOCUMENT ID		TECN	COMMENT
<53	90	BERGFELD	96B	CLE2	$e^+e^- \to \Upsilon(4S)$

$\Gamma(p\overline{p}\pi^+\pi^0)/\Gamma_{\text{total}}$ — Γ_{509}/Γ

VALUE (units 10^{-6})	DOCUMENT ID		TECN	COMMENT
4.58±1.17±0.67	[1] CHU	20	BELL	$e^+e^- \to \Upsilon(4S)$

[1] Assumes equal production of B^0 and B^+ from $\Upsilon(4S)$ decays. This measurement is quoted for $M(\pi^+\pi^0) < 1.3$ GeV.

$\Gamma(p\overline{p}\pi^+\pi^+\pi^-)/\Gamma_{\text{total}}$ — Γ_{510}/Γ

VALUE	CL%	DOCUMENT ID		TECN	COMMENT
• • • We do not use the following data for averages, fits, limits, etc. • • •					
$<5.2\times10^{-4}$	90	[1] ALBRECHT	88F	ARG	$e^+e^- \to \Upsilon(4S)$

[1] ALBRECHT 88F reports $< 4.7\times10^{-4}$ assuming the $\Upsilon(4S)$ decays 45% to $B^0\overline{B}^0$. We rescale to 50%.

$\Gamma(p\overline{p}K^+)/\Gamma_{\text{total}}$ — Γ_{511}/Γ

VALUE (units 10^{-6})	DOCUMENT ID		TECN	COMMENT
5.9 ±0.5 OUR AVERAGE Error includes scale factor of 1.5.				
$5.54^{+0.27}_{-0.25}\pm0.36$	[1,2,3] WEI	08	BELL	$e^+e^- \to \Upsilon(4S)$
6.7 ±0.5 ±0.4	[1,3] AUBERT,B	05L	BABR	$e^+e^- \to \Upsilon(4S)$
• • • We do not use the following data for averages, fits, limits, etc. • • •				
$4.59^{+0.38}_{-0.34}\pm0.50$	[1,2,3] WANG	05A	BELL	Repl. by WEI 08
$5.66^{+0.67}_{-0.57}\pm0.62$	[1,2,3] WANG	04	BELL	Repl. by WANG 05A
$4.3\ ^{+1.1}_{-0.9}\pm0.5$	[1,2] ABE	02K	BELL	Repl. by WANG 04

[1] Assumes equal production of B^+ and B^0 at the $\Upsilon(4S)$.
[2] Explicitly vetoes resonant production of $p\overline{p}$ from Charmonium states.
[3] Provides also results with $m_{p\overline{p}} < 2.85$ GeV/c^2 and angular asymmetry of $p\overline{p}$ system.

$\Gamma(p\overline{p}K^+)/\Gamma(J/\psi(1S)K^+)$ — $\Gamma_{511}/\Gamma_{276}$

VALUE	DOCUMENT ID		TECN	COMMENT
0.0104±0.0005±0.0001	[1,2] AAIJ	13S	LHCB	pp at 7 TeV

[1] AAIJ 13S reports $[\Gamma(B^+ \to p\overline{p}K^+)/\Gamma(B^+ \to J/\psi(1S)K^+)]$ / $[B(J/\psi(1S) \to p\overline{p})] = 4.91 \pm 0.19 \pm 0.14$ which we multiply by our best value $B(J/\psi(1S) \to p\overline{p}) = (2.120 \pm 0.029)\times10^{-3}$. Our first error is their experiment's error and our second error is the systematic error from using our best value.
[2] Measurement includes contribution where $p\overline{p}$ is produced in charmonia decays.

$\Gamma(\Theta(1710)^{++}\overline{p},\ \Theta^{++} \to pK^+)/\Gamma_{\text{total}}$ — Γ_{512}/Γ

VALUE (units 10^{-6})	CL%	DOCUMENT ID		TECN	COMMENT
<0.091	90	[1] WANG	05A	BELL	$e^+e^- \to \Upsilon(4S)$
• • • We do not use the following data for averages, fits, limits, etc. • • •					
<0.1	90	[1,2] AUBERT,B	05L	BABR	$e^+e^- \to \Upsilon(4S)$

[1] Assumes equal production of B^+ and B^0 at the $\Upsilon(4S)$.
[2] Provides upper limits depending on the pentaquark masses between 1.43 to 2.0 GeV/c^2.

$\Gamma(f_J(2220)K^+,\ f_J \to p\overline{p})/\Gamma_{\text{total}}$ — Γ_{513}/Γ

VALUE (units 10^{-6})	CL%	DOCUMENT ID		TECN	COMMENT
<0.41	90	[1] WANG	05A	BELL	$e^+e^- \to \Upsilon(4S)$

[1] Assumes equal production of B^+ and B^0 at the $\Upsilon(4S)$.

$\Gamma(p\overline{\Lambda}(1520))/\Gamma_{\text{total}}$ — Γ_{514}/Γ

VALUE (units 10^{-7})	CL%	DOCUMENT ID		TECN	COMMENT
3.15±0.48±0.27		[1] AAIJ	14AF	LHCB	pp at 7, 8 TeV
• • • We do not use the following data for averages, fits, limits, etc. • • •					
$3.9\ ^{+1.0}_{-0.9}\pm0.3$		[1] AAIJ	13AU	LHCB	Repl. by AAIJ 14AF
<15	90	[2] AUBERT,B	05L	BABR	$e^+e^- \to \Upsilon(4S)$

[1] Uses $B(B^+ \to J/\psi K^+) = (1.016 \pm 0.033)\times10^{-3}$, $B(J/\psi \to p\overline{p}) = (2.17 \pm 0.07)\times10^{-3}$ and $B(\Lambda(1520) \to K^-p) = 0.234 \pm 0.016$.
[2] Assumes equal production of B^+ and B^0 at the $\Upsilon(4S)$.

$\Gamma(p\overline{p}K^+ \text{nonresonant})/\Gamma_{\text{total}}$ — Γ_{515}/Γ

VALUE (units 10^{-6})	CL%	DOCUMENT ID		TECN	COMMENT
<89	90	BERGFELD	96B	CLE2	$e^+e^- \to \Upsilon(4S)$

$\Gamma(p\overline{p}K^*(892)^+)/\Gamma_{\text{total}}$ — Γ_{516}/Γ

VALUE (units 10^{-6})	DOCUMENT ID		TECN	COMMENT
$3.6\ ^{+0.8}_{-0.7}$ OUR AVERAGE				
$3.38^{+0.73}_{-0.60}\pm0.39$	[1,2] CHEN	08C	BELL	$e^+e^- \to \Upsilon(4S)$
5.3 ±1.5 ±1.3	[2] AUBERT	07AV	BABR	$e^+e^- \to \Upsilon(4S)$
• • • We do not use the following data for averages, fits, limits, etc. • • •				
$10.3\ ^{+3.6}_{-2.8}\ ^{+1.3}_{-1.7}$	[2,3] WANG	04	BELL	Repl. by CHEN 08C

[1] Explicitly vetoes resonant production of $p\overline{p}$ from charmonium states.
[2] Assumes equal production of B^+ and B^0 at the $\Upsilon(4S)$.
[3] Explicitly vetoes resonant production of $p\overline{p}$ from charmonium states. The branching fraction for $M_{p\overline{p}} < 2.85$ GeV/c^2 is also reported.

$\Gamma(f_J(2220)K^{*+},\ f_J \to p\overline{p})/\Gamma_{\text{total}}$ — Γ_{517}/Γ

VALUE (units 10^{-6})	CL%	DOCUMENT ID		TECN	COMMENT
<0.77	90	[1] AUBERT	07AV	BABR	$e^+e^- \to \Upsilon(4S)$

[1] Assumes equal production of B^+ and B^0 at the $\Upsilon(4S)$.

$\Gamma(p\overline{\Lambda})/\Gamma_{\text{total}}$ — Γ_{518}/Γ

VALUE (units 10^{-6})	CL%	DOCUMENT ID		TECN	COMMENT
$0.24^{+0.10}_{-0.08}\pm0.03$		[1] AAIJ	17R	LHCB	pp at 7, 8 TeV
• • • We do not use the following data for averages, fits, limits, etc. • • •					
< 0.32	90	[2] TSAI	07	BELL	$e^+e^- \to \Upsilon(4S)$
< 0.49	90	[2] CHANG	05	BELL	Repl. by TSAI 07
< 1.5	90	[2] BORNHEIM	03	CLE2	$e^+e^- \to \Upsilon(4S)$
< 2.2	90	[2] ABE	02O	BELL	$e^+e^- \to \Upsilon(4S)$
< 2.6	90	[2] COAN	99	CLE2	$e^+e^- \to \Upsilon(4S)$
<60	90	[3] AVERY	89B	CLEO	$e^+e^- \to \Upsilon(4S)$
<93	90	[4] ALBRECHT	88F	ARG	$e^+e^- \to \Upsilon(4S)$

[1] Statistical significance of the signal is 4.1 standard deviations where the the normalisation is based on $B(B^+ \to K^0_S\pi^+) = (11.895 \pm 0.375)\times10^{-06}$.
[2] Assumes equal production of B^+ and B^0 at the $\Upsilon(4S)$.
[3] AVERY 89B reports $< 5\times10^{-5}$ assuming the $\Upsilon(4S)$ decays 43% to $B^0\overline{B}^0$. We rescale to 50%.
[4] ALBRECHT 88F reports $< 8.5\times10^{-5}$ assuming the $\Upsilon(4S)$ decays 45% to $B^0\overline{B}^0$. We rescale to 50%.

$\Gamma(p\overline{\Lambda}\gamma)/\Gamma_{\text{total}}$ — Γ_{519}/Γ

VALUE (units 10^{-6})	CL%	DOCUMENT ID		TECN	COMMENT
$2.45^{+0.44}_{-0.38}\pm0.22$		[1] WANG	07C	BELL	$e^+e^- \to \Upsilon(4S)$
• • • We do not use the following data for averages, fits, limits, etc. • • •					
$2.16^{+0.58}_{-0.53}\pm0.20$		[1] LEE	05	BELL	Repl. by WANG 07C
<3.9	90	[2] EDWARDS	03	CLE2	$e^+e^- \to \Upsilon(4S)$

[1] Assumes equal production of B^+ and B^0 at the $\Upsilon(4S)$.
[2] Corresponds to $E_\gamma > 1.5$ GeV. The limit changes to 3.3×10^{-6} for $E_\gamma > 2.0$ GeV.

$\Gamma(p\overline{\Lambda}\pi^0)/\Gamma_{\text{total}}$ — Γ_{520}/Γ

VALUE (units 10^{-6})	DOCUMENT ID		TECN	COMMENT
$3.00^{+0.61}_{-0.53}\pm0.33$	[1] WANG	07C	BELL	$e^+e^- \to \Upsilon(4S)$

[1] Assumes equal production of B^+ and B^0 at the $\Upsilon(4S)$.

$\Gamma(p\overline{\Sigma}(1385)^0)/\Gamma_{\text{total}}$ — Γ_{521}/Γ

VALUE (units 10^{-6})	CL%	DOCUMENT ID		TECN	COMMENT
<0.47	90	[1] WANG	07C	BELL	$e^+e^- \to \Upsilon(4S)$

[1] Assumes equal production of B^+ and B^0 at the $\Upsilon(4S)$.

$\Gamma(\Delta^+\overline{\Lambda})/\Gamma_{\text{total}}$ — Γ_{522}/Γ

VALUE (units 10^{-6})	CL%	DOCUMENT ID		TECN	COMMENT
<0.82	90	[1] WANG	07C	BELL	$e^+e^- \to \Upsilon(4S)$

[1] Assumes equal production of B^+ and B^0 at the $\Upsilon(4S)$.

$\Gamma(p\overline{\Sigma}\gamma)/\Gamma_{\text{total}}$ — Γ_{523}/Γ

VALUE (units 10^{-6})	CL%	DOCUMENT ID		TECN	COMMENT
<4.6	90	[1] LEE	05	BELL	$e^+e^- \to \Upsilon(4S)$
• • • We do not use the following data for averages, fits, limits, etc. • • •					
<7.9	90	[2] EDWARDS	03	CLE2	$e^+e^- \to \Upsilon(4S)$

[1] Assumes equal production of B^+ and B^0 at the $\Upsilon(4S)$.
[2] Corresponds to $E_\gamma > 1.5$ GeV. The limit changes to 6.4×10^{-6} for $E_\gamma > 2.0$ GeV.

$\Gamma(p\overline{\Lambda}\pi^+\pi^-)/\Gamma_{\text{total}}$ — Γ_{524}/Γ

VALUE (units 10^{-6})	CL%	DOCUMENT ID		TECN	COMMENT
$11.28^{+0.91}_{-0.72}\pm1.03$		[1] CHEN	09C	BELL	$e^+e^- \to \Upsilon(4S)$
• • • We do not use the following data for averages, fits, limits, etc. • • •					
<200	90	[2] ALBRECHT	88F	ARG	$e^+e^- \to \Upsilon(4S)$

[1] Assumes equal production of B^+ and B^0 at the $\Upsilon(4S)$.
[2] ALBRECHT 88F reports $< 1.8\times10^{-4}$ assuming the $\Upsilon(4S)$ decays 45% to $B^0\overline{B}^0$. We rescale to 50%.

$\Gamma(p\overline{\Lambda}\pi^+\pi^- \text{nonresonant})/\Gamma_{\text{total}}$ — Γ_{525}/Γ

VALUE (units 10^{-6})	DOCUMENT ID		TECN	COMMENT
$5.92^{+0.88}_{-0.84}\pm0.69$	[1] CHEN	09C	BELL	$e^+e^- \to \Upsilon(4S)$

[1] Assumes equal production of B^+ and B^0 at the $\Upsilon(4S)$.

$\Gamma(p\overline{\Lambda}\rho^0,\ \rho^0 \to \pi^+\pi^-)/\Gamma_{\text{total}}$ — Γ_{526}/Γ

VALUE (units 10^{-6})	DOCUMENT ID		TECN	COMMENT
$4.78^{+0.67}_{-0.64}\pm0.60$	[1] CHEN	09C	BELL	$e^+e^- \to \Upsilon(4S)$

[1] Assumes equal production of B^+ and B^0 at the $\Upsilon(4S)$.

Downloaded from https://academic.oup.com/ptep/article/2022/8/083C01/6651666 by KIT Library user on 27 September 2022

$\Gamma(p\overline{\Lambda}f_2(1270),\ f_2\to\pi^+\pi^-)/\Gamma_{total}$ — Γ_{527}/Γ

VALUE (units 10^{-6})	DOCUMENT ID		TECN	COMMENT
$2.03^{+0.77}_{-0.72}\pm0.27$	[1] CHEN	09C	BELL	$e^+e^-\to\Upsilon(4S)$

[1] Assumes equal production of B^+ and B^0 at the $\Upsilon(4S)$.

$\Gamma(p\overline{\Lambda}K^+K^-)/\Gamma_{total}$ — Γ_{528}/Γ

VALUE (units 10^{-6})	DOCUMENT ID		TECN	COMMENT
$4.10^{+0.45}_{-0.43}\pm0.50$	[1] LU	19	BELL	$e^+e^-\to\Upsilon(4S)$

[1] Assumes equal production of B^+ and B^0 at the $\Upsilon(4S)$.

$\Gamma(p\overline{\Lambda}\phi)/\Gamma_{total}$ — Γ_{529}/Γ

VALUE (units 10^{-6})	DOCUMENT ID		TECN	COMMENT
$0.795\pm0.209\pm0.077$	[1] LU	19	BELL	$e^+e^-\to\Upsilon(4S)$

[1] Assumes equal production of B^+ and B^0 at the $\Upsilon(4S)$.

$\Gamma(\overline{p}\Lambda K^+K^-)/\Gamma_{total}$ — Γ_{530}/Γ

VALUE (units 10^{-6})	DOCUMENT ID		TECN	COMMENT
$3.70^{+0.39}_{-0.37}\pm0.44$	[1] LU	19	BELL	$e^+e^-\to\Upsilon(4S)$

[1] Assumes equal production of B^+ and B^0 at the $\Upsilon(4S)$.

$\Gamma(\Lambda\overline{\Lambda}\pi^+)/\Gamma_{total}$ — Γ_{531}/Γ

VALUE (units 10^{-6})	CL%	DOCUMENT ID		TECN	COMMENT
<0.94	90	[1,2] CHANG	09	BELL	Repl. by CHANG 09
• • • We do not use the following data for averages, fits, limits, etc. • • •					
<2.8	90	[2] LEE	04	BELL	$e^+e^-\to\Upsilon(4S)$

[1] For $m_{\Lambda\overline{\Lambda}}<2.85$ GeV/c^2.
[2] Assumes equal production of B^+ and B^0 at the $\Upsilon(4S)$.

$\Gamma(\Lambda\overline{\Lambda}K^+)/\Gamma_{total}$ — Γ_{532}/Γ

VALUE (units 10^{-6})	DOCUMENT ID		TECN	COMMENT
$3.38^{+0.41}_{-0.36}\pm0.41$	[1,2] CHANG	09	BELL	$e^+e^-\to\Upsilon(4S)$
• • • We do not use the following data for averages, fits, limits, etc. • • •				
$2.91^{+0.9}_{-0.70}\pm0.38$	[2] LEE	04	BELL	Repl. by CHANG 09

[1] Excluding charmonium events in $2.85<m_{\Lambda\overline{\Lambda}}<3.128$ GeV/c^2 and $3.315<m_{\Lambda\overline{\Lambda}}<3.735$ GeV/c^2. Measurements in various $m_{\Lambda\overline{\Lambda}}$ bins are also reported.
[2] Assumes equal production of B^+ and B^0 at the $\Upsilon(4S)$.

$\Gamma(\Lambda\overline{\Lambda}K^{*+})/\Gamma_{total}$ — Γ_{533}/Γ

VALUE (units 10^{-6})	DOCUMENT ID		TECN	COMMENT
$2.19^{+1.13}_{-0.88}\pm0.33$	[1,2] CHANG	09	BELL	$e^+e^-\to\Upsilon(4S)$

[1] For $m_{\Lambda\overline{\Lambda}}<2.85$ GeV/c^2.
[2] Assumes equal production of B^+ and B^0 at the $\Upsilon(4S)$.

$\Gamma(\Lambda(1520)\overline{\Lambda}K^+)/\Gamma_{total}$ — Γ_{534}/Γ

VALUE (units 10^{-6})	DOCUMENT ID		TECN	COMMENT
$2.23\pm0.63\pm0.25$	[1] LU	19	BELL	$e^+e^-\to\Upsilon(4S)$

[1] Assumes equal production of B^+ and B^0 at the $\Upsilon(4S)$.

$\Gamma(\Lambda\overline{\Lambda}(1520)K^+)/\Gamma_{total}$ — Γ_{535}/Γ

VALUE	DOCUMENT ID		TECN	COMMENT
$<2.08\times10^{-6}$	[1] LU	19	BELL	$e^+e^-\to\Upsilon(4S)$

[1] Assumes equal production of B^+ and B^0 at the $\Upsilon(4S)$.

$\Gamma(\overline{\Delta}^0p)/\Gamma_{total}$ — Γ_{536}/Γ

VALUE (units 10^{-6})	CL%	DOCUMENT ID		TECN	COMMENT
< 1.38	90	[1] WEI	08	BELL	$e^+e^-\to\Upsilon(4S)$
• • • We do not use the following data for averages, fits, limits, etc. • • •					
<380	90	[2] BORTOLETTO	89	CLEO	$e^+e^-\to\Upsilon(4S)$

[1] Assumes equal production of B^+ and B^0 at the $\Upsilon(4S)$.
[2] BORTOLETTO 89 reports $<3.3\times10^{-4}$ assuming the $\Upsilon(4S)$ decays 43% to $B^0\overline{B}^0$. We rescale to 50%.

$\Gamma(\Delta^{++}\overline{p})/\Gamma_{total}$ — Γ_{537}/Γ

VALUE (units 10^{-6})	CL%	DOCUMENT ID		TECN	COMMENT
< 0.14	90	[1] WEI	08	BELL	$e^+e^-\to\Upsilon(4S)$
• • • We do not use the following data for averages, fits, limits, etc. • • •					
<150	90	[2] BORTOLETTO	89	CLEO	$e^+e^-\to\Upsilon(4S)$

[1] Assumes equal production of B^+ and B^0 at the $\Upsilon(4S)$.
[2] BORTOLETTO 89 reports $<1.3\times10^{-4}$ assuming the $\Upsilon(4S)$ decays 43% to $B^0\overline{B}^0$. We rescale to 50%.

$\Gamma(D^+p\overline{p})/\Gamma_{total}$ — Γ_{538}/Γ

VALUE	CL%	DOCUMENT ID		TECN	COMMENT
$<1.5\times10^{-5}$	90	[1] ABE	02W	BELL	$e^+e^-\to\Upsilon(4S)$

[1] Assumes equal production of B^+ and B^0 at the $\Upsilon(4S)$.

$\Gamma(D^*(2010)^+p\overline{p})/\Gamma_{total}$ — Γ_{539}/Γ

VALUE	CL%	DOCUMENT ID		TECN	COMMENT
$<1.5\times10^{-5}$	90	[1] ABE	02W	BELL	$e^+e^-\to\Upsilon(4S)$

[1] Assumes equal production of B^+ and B^0 at the $\Upsilon(4S)$.

$\Gamma(\overline{D}^0p\overline{p}\pi^+)/\Gamma_{total}$ — Γ_{540}/Γ

VALUE (units 10^{-4})	DOCUMENT ID		TECN	COMMENT
$3.72\pm0.11\pm0.25$	[1,2] DEL-AMO-SA...12		BABR	$e^+e^-\to\Upsilon(4S)$

[1] Uses the values of D and D^* branching fractions from PDG 08.
[2] Assumes equal production of B^+ and B^0 at the $\Upsilon(4S)$.

$\Gamma(\overline{D}^{*0}p\overline{p}\pi^+)/\Gamma_{total}$ — Γ_{541}/Γ

VALUE (units 10^{-4})	DOCUMENT ID		TECN	COMMENT
$3.73\pm0.17\pm0.27$	[1,2] DEL-AMO-SA...12		BABR	$e^+e^-\to\Upsilon(4S)$

[1] Uses the values of D and D^* branching fractions from PDG 08.
[2] Assumes equal production of B^+ and B^0 at the $\Upsilon(4S)$.

$\Gamma(D^-p\overline{p}\pi^+\pi^-)/\Gamma_{total}$ — Γ_{542}/Γ

VALUE (units 10^{-4})	DOCUMENT ID		TECN	COMMENT
$1.66\pm0.13\pm0.27$	[1,2] DEL-AMO-SA...12		BABR	$e^+e^-\to\Upsilon(4S)$

[1] Uses the values of D and D^* branching fractions from PDG 08.
[2] Assumes equal production of B^+ and B^0 at the $\Upsilon(4S)$.

$\Gamma(D^{*-}p\overline{p}\pi^+\pi^-)/\Gamma_{total}$ — Γ_{543}/Γ

VALUE (units 10^{-4})	DOCUMENT ID		TECN	COMMENT
$1.86\pm0.16\pm0.19$	[1,2] DEL-AMO-SA...12		BABR	$e^+e^-\to\Upsilon(4S)$

[1] Uses the values of D and D^* branching fractions from PDG 08.
[2] Assumes equal production of B^+ and B^0 at the $\Upsilon(4S)$.

$\Gamma(p\overline{\Lambda}^0\overline{D}^0)/\Gamma_{total}$ — Γ_{544}/Γ

VALUE (units 10^{-5})	DOCUMENT ID		TECN	COMMENT
$1.43^{+0.28}_{-0.25}\pm0.18$	[1,2] CHEN	11F	BELL	$e^+e^-\to\Upsilon(4S)$

[1] Uses $B(\Lambda\to p\pi^-)=63.9\pm0.5\%$, $B(D^0\to K^-\pi^+)=3.89\pm0.05\%$, and $B(D^0\to K^-\pi^+\pi^0)=13.9\pm0.5\%$.
[2] Assumes equal production of B^0 and B^+ from Upsilon(4S) decays.

$\Gamma(p\overline{\Lambda}^0\overline{D}^*(2007)^0)/\Gamma_{total}$ — Γ_{545}/Γ

VALUE (units 10^{-5})	CL%	DOCUMENT ID		TECN	COMMENT
<5	90	[1,2,3] CHEN	11F	BELL	$e^+e^-\to\Upsilon(4S)$

[1] CHEN 11F reports $<4.8\times10^{-5}$ from a measurement of $[\Gamma(B^+\to p\overline{\Lambda}^0\overline{D}^*(2007)^0)/\Gamma_{total}]/[B(D^*(2007)^0\to D^0\pi^0)]$ assuming $B(D^*(2007)^0\to D^0\pi^0)=(61.9\pm2.9)\times10^{-2}$, which we rescale to our best value $B(D^*(2007)^0\to D^0\pi^0)=64.7\times10^{-2}$.
[2] Uses $B(\Lambda\to p\pi^-)=63.9\pm0.5\%$ and $B(D^0\to K^-\pi^+)=3.89\pm0.05\%$.
[3] Assumes equal production of B^0 and B^+ from Upsilon(4S) decays.

$\Gamma(\overline{\Lambda}_c^-p\pi^+)/\Gamma_{total}$ — Γ_{546}/Γ

VALUE (units 10^{-4})	DOCUMENT ID		TECN	COMMENT
2.3 ±0.4 OUR AVERAGE	Error includes scale factor of 2.2. See the ideogram below.			
$2.71\pm0.16\pm0.14$	[1,2] AUBERT	08BN	BABR	$e^+e^-\to\Upsilon(4S)$
$1.60\pm0.20\pm0.08$	[1,3] GABYSHEV	06A	BELL	$e^+e^-\to\Upsilon(4S)$
$1.9\ \pm0.5\ \pm0.1$	[1,4] DYTMAN	02	CLE2	$e^+e^-\to\Upsilon(4S)$
• • • We do not use the following data for averages, fits, limits, etc. • • •				
$1.5\ \pm0.4\ \pm0.1$	[1,5] GABYSHEV	02	BELL	Repl. by GABYSHEV 06A
$6.2\ ^{+2.3}_{-2.0}\ \pm1.6$	[1,6] FU	97	CLE2	Repl. by DYTMAN 02

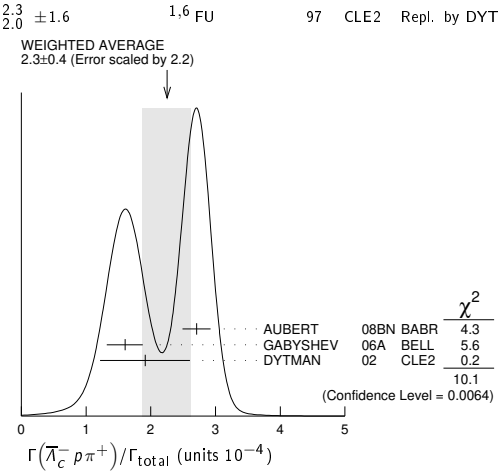

Downloaded from https://academic.oup.com/ptep/article/2022/8/083C01/6651666 by KIT Library user on 27 September 2022

[1] Assumes equal production of B^+ and B^0 at the $\Upsilon(4S)$.

[2] AUBERT 08BN reports $(3.4 \pm 0.1 \pm 0.9) \times 10^{-4}$ from a measurement of $[\Gamma(B^+ \to \overline{\Lambda}_c^- p\pi^+)/\Gamma_{total}] \times [B(\Lambda_c^+ \to pK^-\pi^+)]$ assuming $B(\Lambda_c^+ \to pK^-\pi^+) = (5.0 \pm 1.3) \times 10^{-2}$, which we rescale to our best value $B(\Lambda_c^+ \to pK^-\pi^+) = (6.28 \pm 0.32) \times 10^{-2}$. Our first error is their experiment's error and our second error is the systematic error from using our best value.

[3] GABYSHEV 06A reports $(2.01 \pm 0.15 \pm 0.20) \times 10^{-4}$ from a measurement of $[\Gamma(B^+ \to \overline{\Lambda}_c^- p\pi^+)/\Gamma_{total}] \times [B(\Lambda_c^+ \to pK^-\pi^+)]$ assuming $B(\Lambda_c^+ \to pK^-\pi^+) = 0.05$, which we rescale to our best value $B(\Lambda_c^+ \to pK^-\pi^+) = (6.28 \pm 0.32) \times 10^{-2}$. Our first error is their experiment's error and our second error is the systematic error from using our best value.

[4] DYTMAN 02 reports $(2.4^{+0.63}_{-0.62}) \times 10^{-4}$ from a measurement of $[\Gamma(B^+ \to \overline{\Lambda}_c^- p\pi^+)/\Gamma_{total}] \times [B(\Lambda_c^+ \to pK^-\pi^+)]$ assuming $B(\Lambda_c^+ \to pK^-\pi^+) = 0.05$, which we rescale to our best value $B(\Lambda_c^+ \to pK^-\pi^+) = (6.28 \pm 0.32) \times 10^{-2}$. Our first error is their experiment's error and our second error is the systematic error from using our best value.

[5] GABYSHEV 02 reports $(1.87^{+0.51}_{-0.49}) \times 10^{-4}$ from a measurement of $[\Gamma(B^+ \to \overline{\Lambda}_c^- p\pi^+)/\Gamma_{total}] \times [B(\Lambda_c^+ \to pK^-\pi^+)]$ assuming $B(\Lambda_c^+ \to pK^-\pi^+) = 0.05$, which we rescale to our best value $B(\Lambda_c^+ \to pK^-\pi^+) = (6.28 \pm 0.32) \times 10^{-2}$. Our first error is their experiment's error and our second error is the systematic error from using our best value.

[6] FU 97 uses PDG 96 values of Λ_c branching fraction.

$\Gamma(\overline{\Lambda}_c^- \Delta(1232)^{++})/\Gamma_{total}$ — Γ_{547}/Γ

VALUE (units 10^{-5})	CL%	DOCUMENT ID		TECN	COMMENT
<1.9	90	GABYSHEV	06A	BELL	$e^+e^- \to \Upsilon(4S)$

$\Gamma(\overline{\Lambda}_c^- \Delta_X(1600)^{++})/\Gamma_{total}$ — Γ_{548}/Γ

VALUE (units 10^{-5})	DOCUMENT ID		TECN	COMMENT
4.7±0.9±0.2	[1] GABYSHEV	06A	BELL	$e^+e^- \to \Upsilon(4S)$

[1] GABYSHEV 06A reports $(5.9 \pm 1.0 \pm 0.6) \times 10^{-5}$ from a measurement of $[\Gamma(B^+ \to \overline{\Lambda}_c^- \Delta_X(1600)^{++})/\Gamma_{total}] \times [B(\Lambda_c^+ \to pK^-\pi^+)]$ assuming $B(\Lambda_c^+ \to pK^-\pi^+) = 0.05$, which we rescale to our best value $B(\Lambda_c^+ \to pK^-\pi^+) = (6.28 \pm 0.32) \times 10^{-2}$. Our first error is their experiment's error and our second error is the systematic error from using our best value.

$\Gamma(\overline{\Lambda}_c^- \Delta_X(2420)^{++})/\Gamma_{total}$ — Γ_{549}/Γ

VALUE (units 10^{-5})	DOCUMENT ID		TECN	COMMENT
$3.7^{+0.9}_{-0.8}$±0.2	[1] GABYSHEV	06A	BELL	$e^+e^- \to \Upsilon(4S)$

[1] GABYSHEV 06A reports $(4.7^{+1.0}_{-0.9} \pm 0.4) \times 10^{-5}$ from a measurement of $[\Gamma(B^+ \to \overline{\Lambda}_c^- \Delta_X(2420)^{++})/\Gamma_{total}] \times [B(\Lambda_c^+ \to pK^-\pi^+)]$ assuming $B(\Lambda_c^+ \to pK^-\pi^+) = 0.05$, which we rescale to our best value $B(\Lambda_c^+ \to pK^-\pi^+) = (6.28 \pm 0.32) \times 10^{-2}$. Our first error is their experiment's error and our second error is the systematic error from using our best value.

$\Gamma((\overline{\Lambda}_c^- p)_s \pi^+)/\Gamma_{total}$ — Γ_{550}/Γ

$(\overline{\Lambda}_c^- p)_s$ denotes a low-mass enhancement near 3.35 GeV/c^2.

VALUE (units 10^{-5})	DOCUMENT ID		TECN	COMMENT
$3.1^{+0.7}_{-0.6}$±0.2	[1] GABYSHEV	06A	BELL	$e^+e^- \to \Upsilon(4S)$

[1] GABYSHEV 06A reports $(3.9^{+0.8}_{-0.7} \pm 0.4) \times 10^{-5}$ from a measurement of $[\Gamma(B^+ \to (\overline{\Lambda}_c^- p)_s \pi^+)/\Gamma_{total}] \times [B(\Lambda_c^+ \to pK^-\pi^+)]$ assuming $B(\Lambda_c^+ \to pK^-\pi^+) = 0.05$, which we rescale to our best value $B(\Lambda_c^+ \to pK^-\pi^+) = (6.28 \pm 0.32) \times 10^{-2}$. Our first error is their experiment's error and our second error is the systematic error from using our best value.

$\Gamma(\overline{\Sigma}_c(2520)^0 p)/\Gamma_{total}$ — Γ_{551}/Γ

VALUE (units 10^{-5})	CL%	DOCUMENT ID		TECN	COMMENT
<0.3	90	[1,2] AUBERT	08BN	BABR	$e^+e^- \to \Upsilon(4S)$
• • • We do not use the following data for averages, fits, limits, etc. • • •					
<2.7	90	[1,2] GABYSHEV	06A	BELL	$e^+e^- \to \Upsilon(4S)$
<4.6	90	[1,2] GABYSHEV	02	BELL	Repl. by GABYSHEV 06A

[1] Assumes equal production of B^+ and B^0 at the $\Upsilon(4S)$.

[2] Uses the value for $\Lambda_c \to pK^-\pi^+$ branching ratio (5.0 ± 1.3)%.

$\Gamma(\overline{\Sigma}_c(2520)^0 p)/\Gamma(\overline{\Lambda}_c^- p\pi^+)$ — $\Gamma_{551}/\Gamma_{546}$

VALUE (units 10^{-3})	CL%	DOCUMENT ID		TECN	COMMENT
<9	90	AUBERT	08BN	BABR	$e^+e^- \to \Upsilon(4S)$

$\Gamma(\overline{\Sigma}_c(2800)^0 p)/\Gamma_{total}$ — Γ_{552}/Γ

VALUE (units 10^{-5})	DOCUMENT ID		TECN	COMMENT
2.6±0.7±0.4	[1] AUBERT	08BN	BABR	$e^+e^- \to \Upsilon(4S)$

[1] AUBERT 08BN reports $[\Gamma(B^+ \to \overline{\Sigma}_c(2800)^0 p)/\Gamma_{total}]$ / $[B(B^+ \to \overline{\Lambda}_c^- p\pi^+)] = 0.117 \pm 0.023 \pm 0.024$ which we multiply by our best value $B(B^+ \to \overline{\Lambda}_c^- p\pi^+) = (2.3 \pm 0.4) \times 10^{-4}$. Our first error is their experiment's error and our second error is the systematic error from using our best value.

$\Gamma(\overline{\Lambda}_c^- p\pi^+\pi^0)/\Gamma_{total}$ — Γ_{553}/Γ

VALUE (units 10^{-3})	CL%	DOCUMENT ID		TECN	COMMENT
$1.81 \pm 0.29^{+0.52}_{-0.50}$		[1,2] DYTMAN	02	CLE2	$e^+e^- \to \Upsilon(4S)$
• • • We do not use the following data for averages, fits, limits, etc. • • •					
<3.12	90	[3] FU	97	CLE2	$e^+e^- \to \Upsilon(4S)$

[1] Assumes equal production of B^+ and B^0 at the $\Upsilon(4S)$.

[2] DYTMAN 02 measurement uses $B(\Lambda_c^- \to \overline{p}K^+\pi^-) = 5.0 \pm 1.3\%$. The second error includes the systematic and the uncertainty of the branching ratio.

[3] FU 97 uses PDG 96 values of Λ_c branching ratio.

$\Gamma(\overline{\Lambda}_c^- p\pi^+\pi^+\pi^-)/\Gamma_{total}$ — Γ_{554}/Γ

VALUE (units 10^{-3})	CL%	DOCUMENT ID		TECN	COMMENT
$2.25 \pm 0.25^{+0.63}_{-0.61}$		[1,2] DYTMAN	02	CLE2	$e^+e^- \to \Upsilon(4S)$
• • • We do not use the following data for averages, fits, limits, etc. • • •					
<1.46	90	[3] FU	97	CLE2	$e^+e^- \to \Upsilon(4S)$

[1] Assumes equal production of B^+ and B^0 at the $\Upsilon(4S)$.

[2] DYTMAN 02 measurement uses $B(\Lambda_c^- \to \overline{p}K^+\pi^-) = 5.0 \pm 1.3\%$. The second error includes the systematic and the uncertainty of the branching ratio.

[3] FU 97 uses PDG 96 values of Λ_c branching ratio.

$\Gamma(\overline{\Lambda}_c^- p\pi^+\pi^+\pi^-\pi^0)/\Gamma_{total}$ — Γ_{555}/Γ

VALUE	CL%	DOCUMENT ID		TECN	COMMENT
$<1.34 \times 10^{-2}$	90	[1] FU	97	CLE2	$e^+e^- \to \Upsilon(4S)$

[1] FU 97 uses PDG 96 values of Λ_c branching ratio.

$\Gamma(\Lambda_c^+ \Lambda_c^- K^+)/\Gamma_{total}$ — Γ_{556}/Γ

VALUE (units 10^{-4})	DOCUMENT ID		TECN	COMMENT
4.9 ±0.7 OUR AVERAGE				
4.80±0.43±0.60	LI	18A	BELL	$e^+e^- \to \Upsilon(4S)$
9.1 ±4.5 ±0.5	[1,2] AUBERT	08H	BABR	$e^+e^- \to \Upsilon(4S)$
• • • We do not use the following data for averages, fits, limits, etc. • • •				
6.3 ±2.5 ±0.3	[2,3] GABYSHEV	06	BELL	Repl. by LI 18A.

[1] AUBERT 08H reports $(1.14 \pm 0.15 \pm 0.62) \times 10^{-3}$ from a measurement of $[\Gamma(B^+ \to \Lambda_c^+ \Lambda_c^- K^+)/\Gamma_{total}] \times [B(\Lambda_c^+ \to pK^-\pi^+)]$ assuming $B(\Lambda_c^+ \to pK^-\pi^+) = (5.0 \pm 1.3) \times 10^{-2}$, which we rescale to our best value $B(\Lambda_c^+ \to pK^-\pi^+) = (6.28 \pm 0.32) \times 10^{-2}$. Our first error is their experiment's error and our second error is the systematic error from using our best value.

[2] Assumes equal production of B^+ and B^0 at the $\Upsilon(4S)$.

[3] GABYSHEV 06 reports $(7.9^{+1.0}_{-0.9} \pm 3.6) \times 10^{-4}$ from a measurement of $[\Gamma(B^+ \to \Lambda_c^+ \Lambda_c^- K^+)/\Gamma_{total}] \times [B(\Lambda_c^+ \to pK^-\pi^+)]$ assuming $B(\Lambda_c^+ \to pK^-\pi^+) = (5.0 \pm 1.3) \times 10^{-2}$, which we rescale to our best value $B(\Lambda_c^+ \to pK^-\pi^+) = (6.28 \pm 0.32) \times 10^{-2}$. Our first error is their experiment's error and our second error is the systematic error from using our best value.

$\Gamma(\Xi_c(2930)\Lambda_c^+, \Xi_c \to K^+\Lambda_c^-)/\Gamma_{total}$ — Γ_{557}/Γ

VALUE (units 10^{-4})	DOCUMENT ID		TECN	COMMENT
1.73±0.45±0.21	[1] LI	18A	BELL	$e^+e^- \to \Upsilon(4S)$

[1] The $\Xi_c(2930)$ is found in its decay to $K^-\Lambda_c^+$ in $B^- \to K^-\Lambda_c^-\Lambda_c^+$ with a significance more than 5 sigma.

$\Gamma(\overline{\Sigma}_c(2455)^0 p)/\Gamma_{total}$ — Γ_{558}/Γ

VALUE (units 10^{-5})	CL%	DOCUMENT ID		TECN	COMMENT
$2.9 \pm 0.6^{+0.2}_{-0.1}$		[1,2] GABYSHEV	06A	BELL	$e^+e^- \to \Upsilon(4S)$
• • • We do not use the following data for averages, fits, limits, etc. • • •					
<8	90	[1,3] DYTMAN	02	CLE2	$e^+e^- \to \Upsilon(4S)$
<9.3	90	[1,4] GABYSHEV	02	BELL	Repl. by GABYSHEV 06A

[1] Assumes equal production of B^+ and B^0 at the $\Upsilon(4S)$.

[2] GABYSHEV 06A reports $(3.7 \pm 0.7 \pm 0.4) \times 10^{-5}$ from a measurement of $[\Gamma(B^+ \to \overline{\Sigma}_c(2455)^0 p)/\Gamma_{total}] \times [B(\Lambda_c^+ \to pK^-\pi^+)]$ assuming $B(\Lambda_c^+ \to pK^-\pi^+) = 0.05$, which we rescale to our best value $B(\Lambda_c^+ \to pK^-\pi^+) = (6.28 \pm 0.32) \times 10^{-2}$. Our first error is their experiment's error and our second error is the systematic error from using our best value.

[3] DYTMAN 02 measurement uses $B(\Lambda_c^- \to \overline{p}K^+\pi^-) = 5.0 \pm 1.3\%$. The second error includes the systematic and the uncertainty of the branching ratio.

[4] Uses the value for $\Lambda_c \to pK^-\pi^+$ branching ratio (5.0 ± 1.3)%.

$\Gamma(\overline{\Sigma}_c(2455)^0 p)/\Gamma(\overline{\Lambda}_c^- p\pi^+)$ — $\Gamma_{558}/\Gamma_{546}$

VALUE	DOCUMENT ID		TECN	COMMENT
0.123±0.012±0.008	[1] AUBERT	08BN	BABR	$e^+e^- \to \Upsilon(4S)$

[1] Assumes equal production of B^+ and B^0 at the $\Upsilon(4S)$.

Downloaded from https://academic.oup.com/ptep/article/2022/8/083C01/6651666 by KIT Library user on 27 September 2022

$\Gamma(\overline{\Sigma}_c(2455)^0 p\pi^0)/\Gamma_{total}$ — Γ_{559}/Γ

VALUE (units 10^{-4})	DOCUMENT ID		TECN	COMMENT
3.5±1.1±0.2	[1,2] DYTMAN	02	CLE2	$e^+e^- \to \Upsilon(4S)$

[1] DYTMAN 02 reports (4.4 ± 1.4) × 10^{-4} from a measurement of $[\Gamma(B^+ \to \overline{\Sigma}_c(2455)^0 p\pi^0)/\Gamma_{total}] \times [B(\Lambda_c^+ \to pK^-\pi^+)]$ assuming $B(\Lambda_c^+ \to pK^-\pi^+) = 0.05$, which we rescale to our best value $B(\Lambda_c^+ \to pK^-\pi^+) = (6.28 \pm 0.32) \times 10^{-2}$. Our first error is their experiment's error and our second error is the systematic error from using our best value.
[2] Assumes equal production of B^+ and B^0 at the $\Upsilon(4S)$.

$\Gamma(\overline{\Sigma}_c(2455)^0 p\pi^-\pi^+)/\Gamma_{total}$ — Γ_{560}/Γ

VALUE (units 10^{-4})	DOCUMENT ID		TECN	COMMENT
3.5±1.0±0.2	[1,2] DYTMAN	02	CLE2	$e^+e^- \to \Upsilon(4S)$

[1] DYTMAN 02 reports (4.4 ± 1.3) × 10^{-4} from a measurement of $[\Gamma(B^+ \to \overline{\Sigma}_c(2455)^0 p\pi^-\pi^+)/\Gamma_{total}] \times [B(\Lambda_c^+ \to pK^-\pi^+)]$ assuming $B(\Lambda_c^+ \to pK^-\pi^+) = 0.05$, which we rescale to our best value $B(\Lambda_c^+ \to pK^-\pi^+) = (6.28 \pm 0.32) \times 10^{-2}$. Our first error is their experiment's error and our second error is the systematic error from using our best value.
[2] Assumes equal production of B^+ and B^0 at the $\Upsilon(4S)$.

$\Gamma(\overline{\Sigma}_c(2455)^{--} p\pi^+\pi^+)/\Gamma_{total}$ — Γ_{561}/Γ

VALUE (units 10^{-4})	DOCUMENT ID		TECN	COMMENT
2.37±0.20 OUR AVERAGE				
$2.37 \pm 0.16 {}^{+0.13}_{-0.12}$	[1,2] LEES	12Z	BABR	$e^+e^- \to \Upsilon(4S)$
2.2 ±0.8 ±0.1	[1,3] DYTMAN	02	CLE2	$e^+e^- \to \Upsilon(4S)$

[1] Assumes equal production of B^+ and B^0 at the $\Upsilon(4S)$.
[2] LEES 12Z reports $(2.98 \pm 0.16 \pm 0.15 \pm 0.77) \times 10^{-4}$ from a measurement of $[\Gamma(B^+ \to \overline{\Sigma}_c(2455)^{--} p\pi^+\pi^+)/\Gamma_{total}] \times [B(\Lambda_c^+ \to pK^-\pi^+)]$ assuming $B(\Lambda_c^+ \to pK^-\pi^+) = (5.0 \pm 1.3) \times 10^{-2}$, which we rescale to our best value $B(\Lambda_c^+ \to pK^-\pi^+) = (6.28 \pm 0.32) \times 10^{-2}$. Our first error is their experiment's error and our second error is the systematic error from using our best value.
[3] DYTMAN 02 reports $(2.8 \pm 0.9 \pm 0.5 \pm 0.7) \times 10^{-4}$ from a measurement of $[\Gamma(B^+ \to \overline{\Sigma}_c(2455)^{--} p\pi^+\pi^+)/\Gamma_{total}] \times [B(\Lambda_c^+ \to pK^-\pi^+)]$ assuming $B(\Lambda_c^+ \to pK^-\pi^+) = (5.0 \pm 1.3) \times 10^{-2}$, which we rescale to our best value $B(\Lambda_c^+ \to pK^-\pi^+) = (6.28 \pm 0.32) \times 10^{-2}$. Our first error is their experiment's error and our second error is the systematic error from using our best value.

$\Gamma(\overline{\Lambda}_c(2593)^-/\overline{\Lambda}_c(2625)^- p\pi^+)/\Gamma_{total}$ — Γ_{562}/Γ

VALUE	CL%	DOCUMENT ID		TECN	COMMENT
<1.9 × 10^{-4}	90	[1,2] DYTMAN	02	CLE2	$e^+e^- \to \Upsilon(4S)$

[1] Assumes equal production of B^+ and B^0 at the $\Upsilon(4S)$.
[2] DYTMAN 02 measurement uses $B(\Lambda_c^- \to \overline{p}K^+\pi^-) = 5.0 \pm 1.3\%$. The second error includes the systematic and the uncertainty of the branching ratio.

$\Gamma(\overline{\Xi}_c^0 \Lambda_c^+)/\Gamma_{total}$ — Γ_{563}/Γ

VALUE (units 10^{-4})	DOCUMENT ID		TECN	COMMENT
9.51±2.10±0.88	[1] LI	19A	BELL	$e^+e^- \to \Upsilon(4S)$

[1] First measured the absolute branching fraction using a missing-mass technique.

$\Gamma(\overline{\Xi}_c^0 \Lambda_c^+, \overline{\Xi}_c^0 \to \overline{\Xi}^+\pi^-)/\Gamma_{total}$ — Γ_{564}/Γ

VALUE (units 10^{-5})	DOCUMENT ID		TECN	COMMENT
1.76±0.29 OUR AVERAGE				
1.71±0.28±0.15	[1] LI	19A	BELL	$e^+e^- \to \Upsilon(4S)$
2.0 ±0.7 ±0.1	[2,3] AUBERT	08H	BABR	$e^+e^- \to \Upsilon(4S)$
• • • We do not use the following data for averages, fits, limits, etc. • • •				
$4.5 {}^{+1.8}_{-1.5}$ ±0.2	[3,4] CHISTOV	06A	BELL	Repl. by LI 19A

[1] Using a hadronic B-tagging method based on a full reconstruction.
[2] AUBERT 08H reports $(2.51 \pm 0.89 \pm 0.61) \times 10^{-5}$ from a measurement of $[\Gamma(B^+ \to \overline{\Xi}_c^0 \Lambda_c^+, \overline{\Xi}_c^0 \to \overline{\Xi}^+\pi^-)/\Gamma_{total}] \times [B(\Lambda_c^+ \to pK^-\pi^+)]$ assuming $B(\Lambda_c^+ \to pK^-\pi^+) = (5.0 \pm 1.3) \times 10^{-2}$, which we rescale to our best value $B(\Lambda_c^+ \to pK^-\pi^+) = (6.28 \pm 0.32) \times 10^{-2}$. Our first error is their experiment's error and our second error is the systematic error from using our best value.
[3] Assumes equal production of B^+ and B^0 at the $\Upsilon(4S)$.
[4] CHISTOV 06A reports $(5.6 {}^{+1.9}_{-1.5} \pm 1.9) \times 10^{-5}$ from a measurement of $[\Gamma(B^+ \to \overline{\Xi}_c^0 \Lambda_c^+, \overline{\Xi}_c^0 \to \overline{\Xi}^+\pi^-)/\Gamma_{total}] \times [B(\Lambda_c^+ \to pK^-\pi^+)]$ assuming $B(\Lambda_c^+ \to pK^-\pi^+) = (5.0 \pm 1.3) \times 10^{-2}$, which we rescale to our best value $B(\Lambda_c^+ \to pK^-\pi^+) = (6.28 \pm 0.32) \times 10^{-2}$. Our first error is their experiment's error and our second error is the systematic error from using our best value.

$\Gamma(\overline{\Xi}_c^0 \Lambda_c^+, \overline{\Xi}_c^0 \to \Lambda K^+\pi^-)/\Gamma_{total}$ — Γ_{565}/Γ

VALUE (units 10^{-5})	DOCUMENT ID		TECN	COMMENT
1.14±0.26 OUR AVERAGE				
1.11±0.26±0.10	[1] LI	19A	BELL	$e^+e^- \to \Upsilon(4S)$
1.4 ±0.8 ±0.1	[2,3] AUBERT	08H	BABR	$e^+e^- \to \Upsilon(4S)$
• • • We do not use the following data for averages, fits, limits, etc. • • •				
$3.2 {}^{+1.1}_{-0.9}$ ±0.2	[3,4] CHISTOV	06A	BELL	Repl. by LI 19A

[1] Using a hadronic B-tagging method based on a full reconstruction.
[2] AUBERT 08H reports $(1.70 \pm 0.93 \pm 0.53) \times 10^{-5}$ from a measurement of $[\Gamma(B^+ \to \overline{\Xi}_c^0 \Lambda_c^+, \overline{\Xi}_c^0 \to \Lambda K^+\pi^-)/\Gamma_{total}] \times [B(\Lambda_c^+ \to pK^-\pi^+)]$ assuming $B(\Lambda_c^+ \to pK^-\pi^+) = (5.0 \pm 1.3) \times 10^{-2}$, which we rescale to our best value $B(\Lambda_c^+ \to pK^-\pi^+) = (6.28 \pm 0.32) \times 10^{-2}$. Our first error is their experiment's error and our second error is the systematic error from using our best value.
[3] Assumes equal production of B^+ and B^0 at the $\Upsilon(4S)$.
[4] CHISTOV 06A reports $(4.0 {}^{+1.1}_{-0.9} \pm 1.3) \times 10^{-5}$ from a measurement of $[\Gamma(B^+ \to \overline{\Xi}_c^0 \Lambda_c^+, \overline{\Xi}_c^0 \to \Lambda K^+\pi^-)/\Gamma_{total}] \times [B(\Lambda_c^+ \to pK^-\pi^+)]$ assuming $B(\Lambda_c^+ \to pK^-\pi^+) = (5.0 \pm 1.3) \times 10^{-2}$, which we rescale to our best value $B(\Lambda_c^+ \to pK^-\pi^+) = (6.28 \pm 0.32) \times 10^{-2}$. Our first error is their experiment's error and our second error is the systematic error from using our best value.

$\Gamma(\overline{\Xi}_c^0 \Lambda_c^+, \overline{\Xi}_c^0 \to pK^-K^-\pi^+)/\Gamma_{total}$ — Γ_{566}/Γ

VALUE (units 10^{-6})	DOCUMENT ID		TECN	COMMENT
5.47±1.78±0.57	[1] LI	19A	BELL	$e^+e^- \to \Upsilon(4S)$

[1] Using a hadronic B-tagging method based on a full reconstruction.

$\Gamma(\Lambda_c^+ \overline{\Xi}_c'^0)/\Gamma_{total}$ — Γ_{567}/Γ

VALUE	CL%	DOCUMENT ID		TECN	COMMENT
<6.5 × 10^{-4}	90	[1] LI	19G	BELL	$e^+e^- \to \Upsilon(4S)$

[1] Uses fully reconstructed B^+ meson on tag side and recoil against Λ_c^+ on signal side.

$\Gamma(\Lambda_c^+ \overline{\Xi}_c(2645)^0)/\Gamma_{total}$ — Γ_{568}/Γ

VALUE	CL%	DOCUMENT ID		TECN	COMMENT
<7.9 × 10^{-4}	90	[1] LI	19G	BELL	$e^+e^- \to \Upsilon(4S)$

[1] Uses fully reconstructed B^+ meson on tag side and recoil against Λ_c^+ on signal side.

$\Gamma(\Lambda_c^+ \overline{\Xi}_c(2790)^0)/\Gamma_{total}$ — Γ_{569}/Γ

VALUE (units 10^{-3})	DOCUMENT ID		TECN	COMMENT
1.1±0.4±0.2	[1] LI	19G	BELL	$e^+e^- \to \Upsilon(4S)$

[1] Uses fully reconstructed B^+ meson on tag side and recoil against Λ_c^+ on signal side.

$\Gamma(\pi^+ \ell^+ \ell^-)/\Gamma_{total}$ — Γ_{570}/Γ

VALUE	CL%	DOCUMENT ID		TECN	COMMENT
<4.9 × 10^{-8}	90	[1] WEI	08A	BELL	$e^+e^- \to \Upsilon(4S)$
• • • We do not use the following data for averages, fits, limits, etc. • • •					
<6.6 × 10^{-8}	90	[1] LEES	13M	BABR	$e^+e^- \to \Upsilon(4S)$
<1.2 × 10^{-7}	90	[1] AUBERT	07AG	BABR	$e^+e^- \to \Upsilon(4S)$

[1] Assumes equal production of B^+ and B^0 at the $\Upsilon(4S)$.

$\Gamma(\pi^+ e^+ e^-)/\Gamma_{total}$ — Γ_{571}/Γ

Test for ΔB=1 weak neutral current. Allowed by higher-order electroweak interactions.

VALUE	CL%	DOCUMENT ID		TECN	COMMENT
< 8.0 × 10^{-8}	90	[1] WEI	08A	BELL	$e^+e^- \to \Upsilon(4S)$
• • • We do not use the following data for averages, fits, limits, etc. • • •					
<12.5 × 10^{-8}	90	[1] LEES	13M	BABR	$e^+e^- \to \Upsilon(4S)$
<18 × 10^{-8}	90	[1] AUBERT	07AG	BABR	$e^+e^- \to \Upsilon(4S)$
< 3.9 × 10^{-3}	90	[2] WEIR	90B	MRK2	e^+e^- 29 GeV

[1] Assumes equal production of B^+ and B^0 at the $\Upsilon(4S)$.
[2] WEIR 90B assumes B^+ production cross section from LUND.

$\Gamma(\pi^+ \mu^+ \mu^-)/\Gamma_{total}$ — Γ_{572}/Γ

Test for ΔB=1 weak neutral current. Allowed by higher-order electroweak interactions.

VALUE (units 10^{-8})	CL%	DOCUMENT ID		TECN	COMMENT
1.78±0.22±0.03		[1] AAIJ	15AR	LHCB	pp at 7, 8 TeV
• • • We do not use the following data for averages, fits, limits, etc. • • •					
< 5.5	90	[2] LEES	13M	BABR	$e^+e^- \to \Upsilon(4S)$
2.3 ±0.6 ±0.1		AAIJ	12AY	LHCB	Repl. by AAIJ 15AR
< 6.9	90	[2] WEI	08A	BELL	$e^+e^- \to \Upsilon(4S)$
<28	90	[2] AUBERT	07AG	BABR	$e^+e^- \to \Upsilon(4S)$

[1] AAIJ 15AR reports $(1.83 \pm 0.24 \pm 0.05) \times 10^{-8}$ from a measurement of $[\Gamma(B^+ \to \pi^+\mu^+\mu^-)/\Gamma_{total}] / [B(B^+ \to J/\psi(1S)K^+)] / [B(J/\psi(1S) \to \mu^+\mu^-)]$ assuming $B(B^+ \to J/\psi(1S)K^+) = (1.05 \pm 0.05) \times 10^{-3}$, $B(J/\psi(1S) \to \mu^+\mu^-) = (5.961 \pm 0.033) \times 10^{-2}$, which we rescale to our best values $B(B^+ \to J/\psi(1S)K^+) = (1.020 \pm 0.019) \times 10^{-3}$, $B(J/\psi(1S) \to \mu^+\mu^-) = (5.961 \pm 0.033) \times 10^{-2}$. Our first error is their experiment's error and our second error is the systematic error from using our best values.
[2] Assumes equal production of B^+ and B^0 at the $\Upsilon(4S)$.

$\Gamma(\pi^+ \mu^+ \mu^-)/\Gamma(K^+ \mu^+ \mu^-)$ — $\Gamma_{572}/\Gamma_{576}$

VALUE	DOCUMENT ID		TECN	COMMENT
• • • We do not use the following data for averages, fits, limits, etc. • • •				
0.053±0.014±0.001	AAIJ	12AY	LHCB	Repl. by AAIJ 15AR

$\Gamma(\pi^+ \nu\overline{\nu})/\Gamma_{total}$ — Γ_{573}/Γ

Test for ΔB=1 weak neutral current. Allowed by higher-order electroweak interactions.

VALUE	CL%	DOCUMENT ID		TECN	COMMENT
<1.4 × 10^{-5}	90	[1] GRYGIER	17	BELL	$e^+e^- \to \Upsilon(4S)$

Downloaded from https://academic.oup.com/ptep/article/2022/8/083C01/6651666 by KIT Library user on 27 September 2022

• • • We do not use the following data for averages, fits, limits, etc. • • •

$<9.8\times10^{-5}$	90	[1] LUTZ	13	BELL	$e^+e^-\to\Upsilon(4S)$
$<1.7\times10^{-4}$	90	[1] CHEN	07D	BELL	$e^+e^-\to\Upsilon(4S)$
$<1.0\times10^{-4}$	90	[1] AUBERT	05H	BABR	$e^+e^-\to\Upsilon(4S)$

[1] Assumes equal production of B^+ and B^0 at the $\Upsilon(4S)$.

$\Gamma(K^+\ell^+\ell^-)/\Gamma_{total}$ — Γ_{574}/Γ

Test for $\Delta B=1$ weak neutral current. Allowed by higher-order electroweak interactions.

VALUE (units 10^{-7})		DOCUMENT ID		TECN	COMMENT
4.7 ±0.5 OUR AVERAGE		Error includes scale factor of 2.3. See the ideogram below.			
$5.99^{+0.45}_{-0.43}\pm0.14$		CHOUDHURY	21	BELL	$e^+e^-\to\Upsilon(4S)$
$4.36\pm0.15\pm0.18$		[1] AAIJ	13H	LHCB	pp at 7 TeV
4.8 ±0.9 ±0.2		[2] AUBERT	09T	BABR	$e^+e^-\to\Upsilon(4S)$
• • • We do not use the following data for averages, fits, limits, etc. • • •					
$5.3\ ^{+0.6}_{-0.5}\pm0.3$		[2,3] WEI	09A	BELL	$e^+e^-\to\Upsilon(4S)$
$3.8\ ^{+0.9}_{-0.8}\pm0.2$		[2] AUBERT,B	06J	BABR	Repl. by AUBERT 09T
$5.3\ ^{+1.1}_{-1.0}\pm0.3$		[2] ISHIKAWA	03	BELL	Repl. by WEI 09A

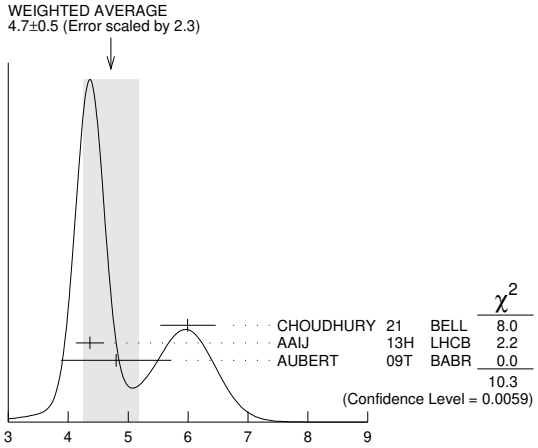

[1] Uses $B(B^+\to J/\psi K^+\to\mu^+\mu^-K^+)=(6.01\pm0.21)\times10^{-5}$.
[2] Assumes equal production of B^+ and B^0 at the $\Upsilon(4S)$.
[3] Superseded by CHOUDHURY 21.

$\Gamma(K^+e^+e^-)/\Gamma_{total}$ — Γ_{575}/Γ

Test for $\Delta B=1$ weak neutral current. Allowed by higher-order electroweak interactions.

VALUE (units 10^{-7})	CL%	DOCUMENT ID		TECN	COMMENT
5.6 ±0.6 OUR AVERAGE					
$5.75^{+0.64}_{-0.61}\pm0.15$		CHOUDHURY	21	BELL	$e^+e^-\to\Upsilon(4S)$
$5.1\ ^{+1.2}_{-1.1}\pm0.2$		[1] AUBERT	09T	BABR	$e^+e^-\to\Upsilon(4S)$
• • • We do not use the following data for averages, fits, limits, etc. • • •					
$5.7\ ^{+0.9}_{-0.8}\pm0.3$		[1,2] WEI	09A	BELL	$e^+e^-\to\Upsilon(4S)$
$4.2\ ^{+1.2}_{-1.1}\pm0.2$		[1] AUBERT,B	06J	BABR	Repl. by AUBERT 09T
$10.5\ ^{+2.5}_{-2.2}\pm0.7$		[1] AUBERT	03U	BABR	Repl. by AUBERT,B 06J
$6.3\ ^{+1.9}_{-1.7}\pm0.3$		[3] ISHIKAWA	03	BELL	Repl. by WEI 09A
<14	90	[1] ABE	02	BELL	$e^+e^-\to\Upsilon(4S)$
< 9	90	[1] AUBERT	02L	BABR	$e^+e^-\to\Upsilon(4S)$
<24	90	[4] ANDERSON	01B	CLE2	$e^+e^-\to\Upsilon(4S)$

[1] Assumes equal production of B^+ and B^0 at the $\Upsilon(4S)$.
[2] Superseded by CHOUDHURY 21.
[3] Assumes equal production of B^0 and B^+ at $\Upsilon(4S)$. The second error is a total of systematic uncertainties including model dependence.
[4] The result is for di-lepton masses above 0.5 GeV.

$\Gamma(K^+\mu^+\mu^-)/\Gamma_{total}$ — Γ_{576}/Γ

Test for $\Delta B=1$ weak neutral current. Allowed by higher-order electroweak interactions.

VALUE (units 10^{-7})	CL%	DOCUMENT ID		TECN	COMMENT
4.53±0.35 OUR FIT		Error includes scale factor of 1.8.			
4.5 ±0.6 OUR AVERAGE		Error includes scale factor of 2.9.			
$6.24^{+0.65}_{-0.61}\pm0.16$		CHOUDHURY	21	BELL	$e^+e^-\to\Upsilon(4S)$
$4.29\pm0.07\pm0.21$		[1] AAIJ	14M	LHCB	pp at 7, 8 TeV
$4.1\ ^{+1.6}_{-1.5}\pm0.2$		[2] AUBERT	09T	BABR	$e^+e^-\to\Upsilon(4S)$
• • • We do not use the following data for averages, fits, limits, etc. • • •					
$4.36\pm0.15\pm0.18$		[3] AAIJ	13H	LHCB	Repl. by AAIJ 14M
$5.3\ ^{+0.8}_{-0.7}\pm0.3$		[2,4] WEI	09A	BELL	$e^+e^-\to\Upsilon(4S)$
$3.1\ ^{+1.5}_{-1.2}\pm0.3$		[2] AUBERT,B	06J	BABR	Repl. by AUBERT 09T
$0.7\ ^{+1.9}_{-1.1}\pm0.2$		[2] AUBERT	03U	BABR	Repl. by AUBERT,B 06J
$4.5\ ^{+1.4}_{-1.2}\pm0.3$		[5] ISHIKAWA	03	BELL	Repl. by WEI 09A
$9.8\ ^{+4.6}_{-3.6}\pm1.6$		[2] ABE	02	BELL	Repl. by ISHIKAWA 03
< 12	90	[2] AUBERT	02L	BABR	$e^+e^-\to\Upsilon(4S)$
< 36.8	90	[6] ANDERSON	01B	CLE2	$e^+e^-\to\Upsilon(4S)$
< 52	90	[7] AFFOLDER	99B	CDF	$p\overline{p}$ at 1.8 TeV
< 100	90	[8] ABE	96L	CDF	Repl. by AFFOLDER 99B
< 2400	90	[9] ALBRECHT	91E	ARG	$e^+e^-\to\Upsilon(4S)$
<64000	90	[10] WEIR	90B	MRK2	e^+e^- 29 GeV
< 1700	90	[11] AVERY	89B	CLEO	$e^+e^-\to\Upsilon(4S)$
< 3800	90	[12] AVERY	87	CLEO	$e^+e^-\to\Upsilon(4S)$

[1] Uses $B(B^+\to J/\psi(1S)K^+)=(0.998\pm0.014\pm0.040)\times10^{-3}$ for normalization.
[2] Assumes equal production of B^+ and B^0 at the $\Upsilon(4S)$.
[3] Uses $B(B^+\to J/\psi K^+\to\mu^+\mu^-K^+)=(6.01\pm0.21)\times10^{-5}$.
[4] Superseded by CHOUDHURY 21.
[5] Assumes equal production of B^0 and B^+ at $\Upsilon(4S)$. The second error is a total of systematic uncertainties including model dependence.
[6] The result is for di-lepton masses above 0.5 GeV.
[7] AFFOLDER 99B measured relative to $B^+\to J/\psi(1S)K^+$.
[8] ABE 96L measured relative to $B^+\to J/\psi(1S)K^+$ using PDG 94 branching ratios.
[9] ALBRECHT 91E reports $<2.2\times10^{-4}$ assuming the $\Upsilon(4S)$ decays 45% to $B^0\overline{B}^0$. We rescale to 50%.
[10] WEIR 90B assumes B^+ production cross section from LUND.
[11] AVERY 89B reports $<1.5\times10^{-4}$ assuming the $\Upsilon(4S)$ decays 43% to $B^0\overline{B}^0$. We rescale to 50%.
[12] AVERY 87 reports $<3.2\times10^{-4}$ assuming the $\Upsilon(4S)$ decays 40% to $B^0\overline{B}^0$. We rescale to 50%.

$\Gamma(K^+\mu^+\mu^-\text{nonresonant})/\Gamma_{total}$ — Γ_{577}/Γ

VALUE (units 10^{-7})	DOCUMENT ID		TECN	COMMENT
4.37±0.15±0.23	[1] AAIJ	17Y	LHCB	pp at 7, 8 TeV

[1] Measured in amplitude analysis using model including short-distance $K^+\mu^+\mu^-$ and $\rho(770)$, $\omega(782)$, $\phi(1020)$, J/ψ, $\psi(2S)$, $\psi(3770)$, $\psi(4040)$, $\psi(4160)$, and $\psi(4415)$ contributions.

$\Gamma(K^+\tau^+\tau^-)/\Gamma_{total}$ — Γ_{578}/Γ

VALUE	CL%	DOCUMENT ID		TECN	COMMENT
$<2.25\times10^{-3}$	90	[1,2] LEES	17	BABR	$e^+e^-\to\Upsilon(4S)$

[1] Uses only leptonic decays of τ and the quoted limit combines the final states $K^+e^+e^-$, $K^+\mu^+\mu^-$, and $K^+e^\pm\mu^\mp$.
[2] If observed events are interpreted as a signal the branching fraction measurement becomes $(1.31\ ^{+0.66}_{-0.61}\ ^{+0.35}_{-0.25})\times10^{-3}$.

$\Gamma(K^+\mu^+\mu^-)/\Gamma(J/\psi(1S)K^+)$ — $\Gamma_{576}/\Gamma_{276}$

VALUE (units 10^{-3})		DOCUMENT ID		TECN	COMMENT
0.444±0.034 OUR FIT		Error includes scale factor of 1.7.			
0.46 ±0.04 ±0.02		AALTONEN	11AI	CDF	$p\overline{p}$ at 1.96 TeV
• • • We do not use the following data for averages, fits, limits, etc. • • •					
0.38 ±0.05 ±0.02		AALTONEN	11L	CDF	Repl. by AALTONEN 11AI
0.59 ±0.15 ±0.03		AALTONEN	09B	CDF	Repl. by AALTONEN 11L

$\Gamma(K^+\overline{\nu}\nu)/\Gamma_{total}$ — Γ_{579}/Γ

Test for $\Delta B=1$ weak neutral current. Allowed by higher-order electroweak interactions.

VALUE	CL%	DOCUMENT ID		TECN	COMMENT
$<1.6\times10^{-5}$	90	[1,2] LEES	13I	BABR	$e^+e^-\to\Upsilon(4S)$
• • • We do not use the following data for averages, fits, limits, etc. • • •					
$<4.1\times10^{-5}$	90	[3] ABUDINEN	21	BEL2	$e^+e^-\to\Upsilon(4S)$
$<1.9\times10^{-5}$	90	[1,4] GRYGIER	17	BELL	$e^+e^-\to\Upsilon(4S)$
$<5.5\times10^{-5}$	90	[1] LUTZ	13	BELL	$e^+e^-\to\Upsilon(4S)$
$<1.3\times10^{-5}$	90	[1] DEL-AMO-SA.10Q		BABR	Repl. by LEES 13I
$<1.4\times10^{-5}$	90	[1] CHEN	07D	BELL	$e^+e^-\to\Upsilon(4S)$
$<5.2\times10^{-5}$	90	[1] AUBERT	05H	BABR	$e^+e^-\to\Upsilon(4S)$
$<2.4\times10^{-4}$	90	[1] BROWDER	01	CLE2	$e^+e^-\to\Upsilon(4S)$

[1] Assumes equal production of B^+ and B^0 at the $\Upsilon(4S)$.
[2] Also reported a limit $<3.7\times10^{-5}$ at 90% CL obtained using a fully reconstructed hadronic B-tag evnets.
[3] Using an inclusive tagging method that exploits not only the properties of the $B^+\to K^+\nu\overline{\nu}$ decay, but also the inclusive properties of the other B meson in the event.
[4] The result was reported in arXiv:1702.03224, but missing from the publication by mistake.

$\Gamma(\rho^+\nu\overline{\nu})/\Gamma_{total}$ — Γ_{580}/Γ

Test for $\Delta B=1$ weak neutral current. Allowed by higher-order electroweak interaction.

VALUE	CL%	DOCUMENT ID		TECN	COMMENT
$<3.0\times10^{-5}$	90	[1] GRYGIER	17	BELL	$e^+e^-\to\Upsilon(4S)$
• • • We do not use the following data for averages, fits, limits, etc. • • •					
$<2.13\times10^{-4}$	90	[1] LUTZ	13	BELL	$e^+e^-\to\Upsilon(4S)$
$<1.5\times10^{-4}$	90	[1] CHEN	07D	BELL	Repl. by LUTZ 13

[1] Assumes equal production of B^+ and B^0 at the $\Upsilon(4S)$.

Downloaded from https://academic.oup.com/ptep/article/2022/8/083C01/6651666 by KIT Library user on 27 September 2022

$\Gamma(K^*(892)^+\ell^+\ell^-)/\Gamma_{total}$ — Γ_{581}/Γ

Test for $\Delta B=1$ weak neutral current. Allowed by higher-order electroweak interactions.

VALUE (units 10^{-7})	CL%	DOCUMENT ID		TECN	COMMENT
10.1 ±1.1 OUR AVERAGE					Error includes scale factor of 1.1.
9.24±0.93±0.67		AAIJ	14M	LHCB	pp at 7, 8 TeV
$14.0\ ^{+4.0}_{-3.7}\pm0.9$		[1] AUBERT	09T	BABR	$e^+e^-\to\Upsilon(4S)$
$12.4\ ^{+2.3}_{-2.1}\pm1.3$		[1] WEI	09A	BELL	$e^+e^-\to\Upsilon(4S)$
• • • We do not use the following data for averages, fits, limits, etc. • • •					
11.6 ±1.9		[2] AAIJ	12AH	LHCB	Repl. by AAIJ 14M
$7.3\ ^{+5.0}_{-4.2}\pm2.1$		[1] AUBERT,B	06J	BABR	Repl. by AUBERT 09T
<22	90	[1] ISHIKAWA	03	BELL	$e^+e^-\to\Upsilon(4S)$

[1] Assumes equal production of B^+ and B^0 at the $\Upsilon(4S)$.
[2] Measured in $B^+\to K^*(892)^+\mu^+\mu^-$ decays.

$\Gamma(K^*(892)^+e^+e^-)/\Gamma_{total}$ — Γ_{582}/Γ

Test for $\Delta B=1$ weak neutral current. Allowed by higher-order electroweak interactions.

VALUE (units 10^{-7})	CL%	DOCUMENT ID		TECN	COMMENT
$15.5\ ^{+4.0}_{-3.1}$ OUR AVERAGE					
$13.8\ ^{+4.7}_{-4.2}\pm0.8$		[1] AUBERT	09T	BABR	$e^+e^-\to\Upsilon(4S)$
$17.3\ ^{+5.0}_{-4.2}\pm2.0$		[1] WEI	09A	BELL	$e^+e^-\to\Upsilon(4S)$
• • • We do not use the following data for averages, fits, limits, etc. • • •					
$7.5\ ^{+7.6}_{-6.5}\pm3.8$		[1] AUBERT,B	06J	BABR	Repl. by AUBERT 09T
$2.0\ ^{+13.4}_{-8.7}\pm2.8$		[1] AUBERT	03U	BABR	$e^+e^-\to\Upsilon(4S)$
< 46	90	[2] ISHIKAWA	03	BELL	$e^+e^-\to\Upsilon(4S)$
< 89	90	[1] ABE	02	BELL	Repl. by ISHIKAWA 03
< 95	90	[1] AUBERT	02L	BABR	$e^+e^-\to\Upsilon(4S)$
<6900	90	[3] ALBRECHT	91E	ARG	$e^+e^-\to\Upsilon(4S)$

[1] Assumes equal production of B^+ and B^0 at the $\Upsilon(4S)$.
[2] Assumes equal production of B^0 and B^+ at $\Upsilon(4S)$. The second error is a total of systematic uncertainties including model dependence.
[3] ALBRECHT 91E reports $<6.3\times10^{-4}$ assuming the $\Upsilon(4S)$ decays 45% to $B^0\overline{B}^0$. We rescale to 50%.

$\Gamma(K^*(892)^+\mu^+\mu^-)/\Gamma_{total}$ — Γ_{583}/Γ

Test for $\Delta B=1$ weak neutral current. Allowed by higher-order electroweak interactions.

VALUE (units 10^{-7})	CL%	DOCUMENT ID		TECN	COMMENT
9.6 ± 1.0 OUR FIT					
9.6 ± 1.1 OUR AVERAGE					
9.24± 0.93±0.67		[1] AAIJ	14M	LHCB	pp at 7, 8 TeV
$14.6\ ^{+7.9}_{-7.5}\pm1.2$		[2] AUBERT	09T	BABR	$e^+e^-\to\Upsilon(4S)$
$11.1\ ^{+3.2}_{-2.7}\pm1.0$		[2] WEI	09A	BELL	$e^+e^-\to\Upsilon(4S)$
• • • We do not use the following data for averages, fits, limits, etc. • • •					
11.6 ± 1.9		AAIJ	12AH	LHCB	Repl. by AAIJ 14M
$9.7\ ^{+9.4}_{-6.9}\pm1.4$		[2] AUBERT,B	06J	BABR	Repl. by AUBERT 09T
$30.7\ ^{+25.8}_{-17.8}\pm4.2$		[2] AUBERT	03U	BABR	$e^+e^-\to\Upsilon(4S)$
$6.5\ ^{+6.9}_{-5.3}\ ^{+1.5}_{-1.6}$		[3] ISHIKAWA	03	BELL	Repl. by WEI 09A
< 39	90	[2] ABE	02	BELL	Repl. by ISHIKAWA 03
<170	90	[2] AUBERT	02L	BABR	$e^+e^-\to\Upsilon(4S)$

[1] Uses $B(B^+\to J/\psi(1S)K^*(892)^+)=(1.431\pm0.027\pm0.090)\times10^{-3}$ for normalization.
[2] Assumes equal production of B^+ and B^0 at the $\Upsilon(4S)$.
[3] Assumes equal production of B^0 and B^+ at $\Upsilon(4S)$. The second error is a total of systematic uncertainties including model dependence. The 90% C.L. upper limit is 2.2×10^{-6}.

$\Gamma(K^*(892)^+\mu^+\mu^-)/\Gamma(J/\psi(1S)K^*(892)^+)$ — $\Gamma_{583}/\Gamma_{281}$

VALUE (units 10^{-3})	DOCUMENT ID		TECN	COMMENT
0.67±0.08 OUR FIT				
0.67±0.22±0.04	AALTONEN	11AI	CDF	$p\overline{p}$ at 1.96 TeV

$\Gamma(K^*(892)^+\nu\overline{\nu})/\Gamma_{total}$ — Γ_{584}/Γ

Test for $\Delta B=1$ weak neutral current. Allowed by higher-order electroweak interaction.

VALUE	CL%	DOCUMENT ID		TECN	COMMENT
$<4.0\times10^{-5}$	90	[1] LUTZ	13	BELL	$e^+e^-\to\Upsilon(4S)$
• • • We do not use the following data for averages, fits, limits, etc. • • •					
$<6.1\times10^{-5}$	90	[1] GRYGIER	17	BELL	$e^+e^-\to\Upsilon(4S)$
$<6.4\times10^{-5}$	90	[1,2] LEES	13I	BABR	$e^+e^-\to\Upsilon(4S)$
$<8\times10^{-5}$	90	AUBERT	08BC	BABR	Repl. by LEES 13I
$<1.4\times10^{-4}$	90	[1] CHEN	07D	BELL	$e^+e^-\to\Upsilon(4S)$

[1] Assumes equal production of B^+ and B^0 at the $\Upsilon(4S)$.
[2] Also reported a limit $<11.6\times10^{-5}$ at 90% CL obtained using a fully reconstructed hadronic B-tag evnets.

$\Gamma(K^+\pi^+\pi^-\mu^+\mu^-)/\Gamma(\psi(2S)K^+)$ — $\Gamma_{585}/\Gamma_{311}$

VALUE (units 10^{-4})	DOCUMENT ID		TECN	COMMENT
$6.95\ ^{+0.46}_{-0.43}\pm0.34$	AAIJ	14AZ	LHCB	pp at 7, 8 TeV

$\Gamma(\phi K^+\mu^+\mu^-)/\Gamma(J/\psi(1S)\phi K^+)$ — $\Gamma_{586}/\Gamma_{288}$

VALUE (units 10^{-3})	DOCUMENT ID		TECN	COMMENT
$1.58\ ^{+0.36}_{-0.32}\ ^{+0.19}_{-0.07}$	AAIJ	14AZ	LHCB	pp at 7, 8 TeV

$\Gamma(\overline{\Lambda}p\nu\overline{\nu})/\Gamma_{total}$ — Γ_{587}/Γ

VALUE	CL%	DOCUMENT ID		TECN	COMMENT
$<3.0\times10^{-5}$	90	[1] LEES	19C	BABR	$e^+e^-\to\Upsilon(4S)$

[1] Signal candidates are identified by first fully reconstructing B^+ in one of many possible exclusive decays to hadronic final states.

$\Gamma(\pi^+e^+\mu^-)/\Gamma_{total}$ — Γ_{588}/Γ

Test of lepton family number conservation.

VALUE	CL%	DOCUMENT ID		TECN	COMMENT
<0.0064	90	[1] WEIR	90B	MRK2	e^+e^- 29 GeV

[1] WEIR 90B assumes B^+ production cross section from LUND.

$\Gamma(\pi^+e^-\mu^+)/\Gamma_{total}$ — Γ_{589}/Γ

Test of lepton family number conservation.

VALUE	CL%	DOCUMENT ID		TECN	COMMENT
<0.0064	90	[1] WEIR	90B	MRK2	e^+e^- 29 GeV

[1] WEIR 90B assumes B^+ production cross section from LUND.

$\Gamma(\pi^+e^\pm\mu^\mp)/\Gamma_{total}$ — Γ_{590}/Γ

VALUE	CL%	DOCUMENT ID		TECN	COMMENT
$<1.7\times10^{-7}$	90	[1] AUBERT	07AG	BABR	$e^+e^-\to\Upsilon(4S)$

[1] Assumes equal production of B^+ and B^0 at the $\Upsilon(4S)$.

$\Gamma(\pi^+e^+\tau^-)/\Gamma_{total}$ — Γ_{591}/Γ

Test of lepton family number conservation.

VALUE (units 10^{-6})	CL%	DOCUMENT ID		TECN	COMMENT
<74	90	[1] LEES	12P	BABR	$e^+e^-\to\Upsilon(4S)$

[1] Uses a fully reconstructed hadronic B decay as a tag on the recoil side.

$\Gamma(\pi^+e^-\tau^+)/\Gamma_{total}$ — Γ_{592}/Γ

Test of lepton family number conservation.

VALUE (units 10^{-6})	CL%	DOCUMENT ID		TECN	COMMENT
<20	90	[1] LEES	12P	BABR	$e^+e^-\to\Upsilon(4S)$

[1] Uses a fully reconstructed hadronic B decay as a tag on the recoil side.

$\Gamma(\pi^+e^\pm\tau^\mp)/\Gamma_{total}$ — Γ_{593}/Γ

Test of lepton family number conservation.

VALUE (units 10^{-6})	CL%	DOCUMENT ID		TECN	COMMENT
<75	90	[1,2] LEES	12P	BABR	$e^+e^-\to\Upsilon(4S)$

[1] Assumes $B(B^+\to h^+\ell^+\tau^-)=B(B^+\to h^+\ell^-\tau^+)$.
[2] Uses a fully reconstructed hadronic B decay as a tag on the recoil side.

$\Gamma(\pi^+\mu^+\tau^-)/\Gamma_{total}$ — Γ_{594}/Γ

Test of lepton family number conservation.

VALUE (units 10^{-6})	CL%	DOCUMENT ID		TECN	COMMENT
<62	90	[1] LEES	12P	BABR	$e^+e^-\to\Upsilon(4S)$

[1] Uses a fully reconstructed hadronic B decay as a tag on the recoil side.

$\Gamma(\pi^+\mu^-\tau^+)/\Gamma_{total}$ — Γ_{595}/Γ

Test of lepton family number conservation.

VALUE (units 10^{-6})	CL%	DOCUMENT ID		TECN	COMMENT
<45	90	[1] LEES	12P	BABR	$e^+e^-\to\Upsilon(4S)$

[1] Uses a fully reconstructed hadronic B decay as a tag on the recoil side.

$\Gamma(\pi^+\mu^\pm\tau^\mp)/\Gamma_{total}$ — Γ_{596}/Γ

Test of lepton family number conservation.

VALUE (units 10^{-6})	CL%	DOCUMENT ID		TECN	COMMENT
<72	90	[1,2] LEES	12P	BABR	$e^+e^-\to\Upsilon(4S)$

[1] Assumes $B(B^+\to h^+\ell^+\tau^-)=B(B^+\to h^+\ell^-\tau^+)$.
[2] Uses a fully reconstructed hadronic B decay as a tag on the recoil side.

$\Gamma(K^+e^+\mu^-)/\Gamma_{total}$ — Γ_{597}/Γ

Test of lepton family number conservation.

VALUE	CL%	DOCUMENT ID		TECN	COMMENT
$<7.0\times10^{-9}$	90	AAIJ	19AM	LHCB	pp at 7, 8 TeV
• • • We do not use the following data for averages, fits, limits, etc. • • •					
$<3.0\times10^{-8}$	90	CHOUDHURY	21	BELL	$e^+e^-\to\Upsilon(4S)$
$<0.91\times10^{-7}$	90	[1] AUBERT,B	06J	BABR	$e^+e^-\to\Upsilon(4S)$
$<8\times10^{-7}$	90	[1] AUBERT	02L	BABR	Repl. by AUBERT,B 06J
$<6.4\times10^{-3}$	90	[2] WEIR	90B	MRK2	e^+e^- 29 GeV

[1] Assumes equal production of B^+ and B^0 at the $\Upsilon(4S)$.
[2] WEIR 90B assumes B^+ production cross section from LUND.

$\Gamma(K^+e^-\mu^+)/\Gamma_{total}$ — Γ_{598}/Γ

Test of lepton family number conservation.

VALUE	CL%	DOCUMENT ID		TECN	COMMENT
$<6.4\times10^{-9}$	90	AAIJ	19AM	LHCB	pp at 7, 8 TeV

Downloaded from https://academic.oup.com/ptep/article/2022/8/083C01/6651666 by KIT Library user on 27 September 2022

• • • We do not use the following data for averages, fits, limits, etc. • • •

$<8.5 \times 10^{-8}$	90	CHOUDHURY	21	BELL	$e^+e^- \to \Upsilon(4S)$
$<1.3 \times 10^{-7}$	90	[1] AUBERT,B	06J	BABR	$e^+e^- \to \Upsilon(4S)$
$<6.4 \times 10^{-3}$	90	[2] WEIR	90B	MRK2	e^+e^- 29 GeV

[1] Assumes equal production of B^+ and B^0 at the $\Upsilon(4S)$.
[2] WEIR 90B assumes B^+ production cross section from LUND.

$\Gamma(K^+ e^{\pm}\mu^{\mp})/\Gamma_{total}$ — Γ_{599}/Γ

VALUE (units 10^{-7})	CL%	DOCUMENT ID		TECN	COMMENT
<0.91	90	[1] AUBERT,B	06J	BABR	$e^+e^- \to \Upsilon(4S)$

[1] Assumes equal production of B^+ and B^0 at the $\Upsilon(4S)$.

$\Gamma(K^+ e^+\tau^-)/\Gamma_{total}$ — Γ_{600}/Γ

Test of lepton family number conservation.

VALUE (units 10^{-6})	CL%	DOCUMENT ID		TECN	COMMENT
<43	90	[1] LEES	12P	BABR	$e^+e^- \to \Upsilon(4S)$

[1] Uses a fully reconstructed hadronic B decay as a tag on the recoil side.

$\Gamma(K^+ e^-\tau^+)/\Gamma_{total}$ — Γ_{601}/Γ

Test of lepton family number conservation.

VALUE (units 10^{-6})	CL%	DOCUMENT ID		TECN	COMMENT
<15	90	[1] LEES	12P	BABR	$e^+e^- \to \Upsilon(4S)$

[1] Uses a fully reconstructed hadronic B decay as a tag on the recoil side.

$\Gamma(K^+ e^{\pm}\tau^{\mp})/\Gamma_{total}$ — Γ_{602}/Γ

Test of lepton family number conservation.

VALUE (units 10^{-6})	CL%	DOCUMENT ID		TECN	COMMENT
<30	90	[1,2] LEES	12P	BABR	$e^+e^- \to \Upsilon(4S)$

[1] Assumes $B(B^+ \to h^+\ell^+\tau^-) = B(B^+ \to h^+\ell^-\tau^+)$.
[2] Uses a fully reconstructed hadronic B decay as a tag on the recoil side.

$\Gamma(K^+ \mu^+\tau^-)/\Gamma_{total}$ — Γ_{603}/Γ

Test of lepton family number conservation.

VALUE (units 10^{-6})	CL%	DOCUMENT ID		TECN	COMMENT
<45	90	[1] LEES	12P	BABR	$e^+e^- \to \Upsilon(4S)$

[1] Uses a fully reconstructed hadronic B decay as a tag on the recoil side.

$\Gamma(K^+ \mu^-\tau^+)/\Gamma_{total}$ — Γ_{604}/Γ

Test of lepton family number conservation.

VALUE	CL%	DOCUMENT ID		TECN	COMMENT
$<2.8 \times 10^{-5}$	90	[1] LEES	12P	BABR	$e^+e^- \to \Upsilon(4S)$

• • • We do not use the following data for averages, fits, limits, etc. • • •

$<3.9 \times 10^{-5}$	90	[2] AAIJ	20P	LHCB	pp at 7, 8, 13 TeV

[1] Uses a fully reconstructed hadronic B decay as a tag on the recoil side.
[2] Uses the $B^*_{s2}{}^0 \to B^+K^-$ decays for kinematic constraints.

$\Gamma(K^+ \mu^{\pm}\tau^{\mp})/\Gamma_{total}$ — Γ_{605}/Γ

Test of lepton family number conservation.

VALUE (units 10^{-6})	CL%	DOCUMENT ID		TECN	COMMENT
<48	90	[1,2] LEES	12P	BABR	$e^+e^- \to \Upsilon(4S)$

• • • We do not use the following data for averages, fits, limits, etc. • • •

<77	90	[1] AUBERT	07AZ	BABR	Repl. by LEES 12P

[1] Uses a fully reconstructed hadronic B decay as a tag on the recoil side.
[2] Assumes $B(B^+ \to h^+\ell^+\tau^-) = B(B^+ \to h^+\ell^-\tau^+)$.

$\Gamma(K^*(892)^+ e^+\mu^-)/\Gamma_{total}$ — Γ_{606}/Γ

VALUE (units 10^{-7})	CL%	DOCUMENT ID		TECN	COMMENT
<13	90	[1] AUBERT,B	06J	BABR	$e^+e^- \to \Upsilon(4S)$

[1] Assumes equal production of B^+ and B^0 at the $\Upsilon(4S)$.

$\Gamma(K^*(892)^+ e^-\mu^+)/\Gamma_{total}$ — Γ_{607}/Γ

VALUE (units 10^{-7})	CL%	DOCUMENT ID		TECN	COMMENT
<9.9	90	[1] AUBERT,B	06J	BABR	$e^+e^- \to \Upsilon(4S)$

[1] Assumes equal production of B^+ and B^0 at the $\Upsilon(4S)$.

$\Gamma(K^*(892)^+ e^{\pm}\mu^{\mp})/\Gamma_{total}$ — Γ_{608}/Γ

Test of lepton family number conservation.

VALUE	CL%	DOCUMENT ID		TECN	COMMENT
$<1.4 \times 10^{-6}$	90	[1] AUBERT,B	06J	BABR	$e^+e^- \to \Upsilon(4S)$

• • • We do not use the following data for averages, fits, limits, etc. • • •

$<7.9 \times 10^{-6}$	90	[1] AUBERT	02L	BABR	Repl. by AUBERT,B 06J

[1] Assumes equal production of B^+ and B^0 at the $\Upsilon(4S)$.

$\Gamma(\pi^- e^+ e^+)/\Gamma_{total}$ — Γ_{609}/Γ

Test of total lepton number conservation.

VALUE	CL%	DOCUMENT ID		TECN	COMMENT
$<2.3 \times 10^{-8}$	90	[1] LEES	12J	BABR	$e^+e^- \to \Upsilon(4S)$

• • • We do not use the following data for averages, fits, limits, etc. • • •

$<1.6 \times 10^{-6}$	90	[1] EDWARDS	02B	CLE2	$e^+e^- \to \Upsilon(4S)$
<0.0039	90	[2] WEIR	90B	MRK2	e^+e^- 29 GeV

[1] Assumes equal production of B^+ and B^0 at the $\Upsilon(4S)$.
[2] WEIR 90B assumes B^+ production cross section from LUND.

$\Gamma(\pi^- \mu^+\mu^+)/\Gamma_{total}$ — Γ_{610}/Γ

Test of total lepton number conservation.

VALUE	CL%	DOCUMENT ID		TECN	COMMENT
$< 4.0 \times 10^{-9}$	95	[1] AAIJ	14AC	LHCB	pp at 7, 8 TeV

• • • We do not use the following data for averages, fits, limits, etc. • • •

$< 1.3 \times 10^{-8}$	95	[2] AAIJ	12AD	LHCB	Repl. by AAIJ 14AC
$< 4.4 \times 10^{-8}$	90	AAIJ	12C	LHCB	pp at 7 TeV
$<10.7 \times 10^{-8}$	90	[3] LEES	12J	BABR	$e^+e^- \to \Upsilon(4S)$
$< 1.4 \times 10^{-6}$	90	[3] EDWARDS	02B	CLE2	$e^+e^- \to \Upsilon(4S)$
$< 9.1 \times 10^{-3}$	90	[4] WEIR	90B	MRK2	e^+e^- 29 GeV

[1] Uses $B^+ \to J/\psi K^+$, $J/\psi \to \mu^+\mu^-$ mode for normalization. Obtains neutrino-mass-dependent upper limits in the range 0.4–4.0 $\times 10^{-9}$. This limit is applicable for Majorana neutrino lifetime < 1 ps.
[2] Uses $B^+ \to J/\psi K^+$, $J/\psi \to \mu^+\mu^-$ mode for normalization. Obtains neutrino-mass-dependent upper limits in the range 0.4–1.0 $\times 10^{-8}$.
[3] Assumes equal production of B^+ and B^0 at the $\Upsilon(4S)$.
[4] WEIR 90B assumes B^+ production cross section from LUND.

$\Gamma(\pi^- e^+\mu^+)/\Gamma_{total}$ — Γ_{611}/Γ

Test of total lepton number conservation.

VALUE	CL%	DOCUMENT ID		TECN	COMMENT
$<1.5 \times 10^{-7}$	90	[1] LEES	14A	BABR	$e^+e^- \to \Upsilon(4S)$

• • • We do not use the following data for averages, fits, limits, etc. • • •

$<1.3 \times 10^{-6}$	90	[1] EDWARDS	02B	CLE2	$e^+e^- \to \Upsilon(4S)$
<0.0064	90	[2] WEIR	90B	MRK2	e^+e^- 29 GeV

[1] Assumes equal production of B^+ and B^0 at the $\Upsilon(4S)$.
[2] WEIR 90B assumes B^+ production cross section from LUND.

$\Gamma(\rho^- e^+ e^+)/\Gamma_{total}$ — Γ_{612}/Γ

Test of total lepton number conservation.

VALUE (units 10^{-6})	CL%	DOCUMENT ID		TECN	COMMENT
<0.17	90	[1] LEES	14A	BABR	$e^+e^- \to \Upsilon(4S)$

• • • We do not use the following data for averages, fits, limits, etc. • • •

<2.6	90	[1] EDWARDS	02B	CLE2	$e^+e^- \to \Upsilon(4S)$

[1] Assumes equal production of B^+ and B^0 at the $\Upsilon(4S)$.

$\Gamma(\rho^- \mu^+\mu^+)/\Gamma_{total}$ — Γ_{613}/Γ

Test of total lepton number conservation.

VALUE (units 10^{-6})	CL%	DOCUMENT ID		TECN	COMMENT
<0.42	90	LEES	14A	BABR	$e^+e^- \to \Upsilon(4S)$

• • • We do not use the following data for averages, fits, limits, etc. • • •

<5.0	90	[1] EDWARDS	02B	CLE2	$e^+e^- \to \Upsilon(4S)$

[1] Assumes equal production of B^+ and B^0 at the $\Upsilon(4S)$.

$\Gamma(\rho^- e^+\mu^+)/\Gamma_{total}$ — Γ_{614}/Γ

Test of total lepton number conservation.

VALUE (units 10^{-6})	CL%	DOCUMENT ID		TECN	COMMENT
<0.47	90	[1] LEES	14A	BABR	$e^+e^- \to \Upsilon(4S)$

• • • We do not use the following data for averages, fits, limits, etc. • • •

<3.3	90	[1] EDWARDS	02B	CLE2	$e^+e^- \to \Upsilon(4S)$

[1] Assumes equal production of B^+ and B^0 at the $\Upsilon(4S)$.

$\Gamma(K^- e^+ e^+)/\Gamma_{total}$ — Γ_{615}/Γ

Test of total lepton number conservation.

VALUE	CL%	DOCUMENT ID		TECN	COMMENT
$<3.0 \times 10^{-8}$	90	[1] LEES	12J	BABR	$e^+e^- \to \Upsilon(4S)$

• • • We do not use the following data for averages, fits, limits, etc. • • •

$<1.0 \times 10^{-6}$	90	[1] EDWARDS	02B	CLE2	$e^+e^- \to \Upsilon(4S)$
<0.0039	90	[2] WEIR	90B	MRK2	e^+e^- 29 GeV

[1] Assumes equal production of B^+ and B^0 at the $\Upsilon(4S)$.
[2] WEIR 90B assumes B^+ production cross section from LUND.

$\Gamma(K^- \mu^+\mu^+)/\Gamma_{total}$ — Γ_{616}/Γ

Test of total lepton number conservation.

VALUE	CL%	DOCUMENT ID		TECN	COMMENT
$<4.1 \times 10^{-8}$	90	AAIJ	12C	LHCB	pp at 7 TeV

• • • We do not use the following data for averages, fits, limits, etc. • • •

$<6.7 \times 10^{-8}$	90	[1] LEES	12J	BABR	$e^+e^- \to \Upsilon(4S)$
$<1.8 \times 10^{-6}$	90	[1] EDWARDS	02B	CLE2	$e^+e^- \to \Upsilon(4S)$
$<9.1 \times 10^{-3}$	90	[2] WEIR	90B	MRK2	e^+e^- 29 GeV

[1] Assumes equal production of B^+ and B^0 at the $\Upsilon(4S)$.
[2] WEIR 90B assumes B^+ production cross section from LUND.

$\Gamma(K^- e^+\mu^+)/\Gamma_{total}$ — Γ_{617}/Γ

Test of total lepton number conservation.

VALUE	CL%	DOCUMENT ID		TECN	COMMENT
$<1.6 \times 10^{-7}$	90	[1] LEES	14A	BABR	$e^+e^- \to \Upsilon(4S)$

• • • We do not use the following data for averages, fits, limits, etc. • • •

$<2.0 \times 10^{-6}$	90	[1] EDWARDS	02B	CLE2	$e^+e^- \to \Upsilon(4S)$
<0.0064	90	[2] WEIR	90B	MRK2	e^+e^- 29 GeV

[1] Assumes equal production of B^+ and B^0 at the $\Upsilon(4S)$.
[2] WEIR 90B assumes B^+ production cross section from LUND.

Downloaded from https://academic.oup.com/ptep/article/2022/8/083C01/6651666 by KIT Library user on 27 September 2022

$\Gamma(K^*(892)^- e^+ e^+)/\Gamma_{total}$ — Γ_{618}/Γ

Test of total lepton number conservation.

VALUE (units 10^{-6})	CL%	DOCUMENT ID		TECN	COMMENT
<0.40	90	[1] LEES	14A	BABR	$e^+e^- \to \Upsilon(4S)$
• • • We do not use the following data for averages, fits, limits, etc. • • •					
<2.8	90	[1] EDWARDS	02B	CLE2	$e^+e^- \to \Upsilon(4S)$

[1] Assumes equal production of B^+ and B^0 at the $\Upsilon(4S)$.

$\Gamma(K^*(892)^- \mu^+ \mu^+)/\Gamma_{total}$ — Γ_{619}/Γ

Test of total lepton number conservation.

VALUE (units 10^{-6})	CL%	DOCUMENT ID		TECN	COMMENT
<0.59	90	[1] LEES	14A	BABR	$e^+e^- \to \Upsilon(4S)$
• • • We do not use the following data for averages, fits, limits, etc. • • •					
<8.3	90	[1] EDWARDS	02B	CLE2	$e^+e^- \to \Upsilon(4S)$

[1] Assumes equal production of B^+ and B^0 at the $\Upsilon(4S)$.

$\Gamma(K^*(892)^- e^+ \mu^+)/\Gamma_{total}$ — Γ_{620}/Γ

Test of total lepton number conservation.

VALUE (units 10^{-6})	CL%	DOCUMENT ID		TECN	COMMENT
<0.30	90	[1] LEES	14A	BABR	$e^+e^- \to \Upsilon(4S)$
• • • We do not use the following data for averages, fits, limits, etc. • • •					
<4.4	90	[1] EDWARDS	02B	CLE2	$e^+e^- \to \Upsilon(4S)$

[1] Assumes equal production of B^+ and B^0 at the $\Upsilon(4S)$.

$\Gamma(D^- e^+ e^+)/\Gamma_{total}$ — Γ_{621}/Γ

VALUE	CL%	DOCUMENT ID		TECN	COMMENT
$<2.6 \times 10^{-6}$	90	[1] LEES	14A	BABR	$e^+e^- \to \Upsilon(4S)$
$<2.6 \times 10^{-6}$	90	[1,2] SEON	11	BELL	$e^+e^- \to \Upsilon(4S)$

[1] Assumes equal production of B^0 and B^+ from Upsilon(4S) decays.
[2] Uses $D^- \to K^+\pi^-\pi^-$ mode and 3-body phase-space hypothesis for the signal decays.

$\Gamma(D^- e^+ \mu^+)/\Gamma_{total}$ — Γ_{622}/Γ

VALUE	CL%	DOCUMENT ID		TECN	COMMENT
$<1.8 \times 10^{-6}$	90	[1,2] SEON	11	BELL	$e^+e^- \to \Upsilon(4S)$
• • • We do not use the following data for averages, fits, limits, etc. • • •					
$<2.1 \times 10^{-6}$	90	[1] LEES	14A	BABR	$e^+e^- \to \Upsilon(4S)$

[1] Assumes equal production of B^0 and B^+ from Upsilon(4S) decays.
[2] Uses $D^- \to K^+\pi^-\pi^-$ mode and 3-body phase-space hypothesis for the signal decays.

$\Gamma(D^- \mu^+ \mu^+)/\Gamma_{total}$ — Γ_{623}/Γ

VALUE	CL%	DOCUMENT ID		TECN	COMMENT
$< 6.9 \times 10^{-7}$	95	[1] AAIJ	12AD	LHCB	pp at 7 TeV
• • • We do not use the following data for averages, fits, limits, etc. • • •					
$<17 \times 10^{-7}$	90	[2] LEES	14A	BABR	$e^+e^- \to \Upsilon(4S)$
$< 1.1 \times 10^{-6}$	90	[2,3] SEON	11	BELL	$e^+e^- \to \Upsilon(4S)$

[1] Uses $B^+ \to \psi(2S)K^+$, $\psi(2S) \to J/\psi\pi^+\pi^-$ mode for normalization.
[2] Assumes equal production of B^0 and B^+ from Upsilon(4S) decays.
[3] Uses $D^- \to K^+\pi^-\pi^-$ mode and 3-body phase-space hypothesis for the signal decays.

$\Gamma(D^{*-} \mu^+ \mu^+)/\Gamma_{total}$ — Γ_{624}/Γ

VALUE	CL%	DOCUMENT ID		TECN	COMMENT
$<2.4 \times 10^{-6}$	95	[1] AAIJ	12AD	LHCB	pp at 7 TeV

[1] Uses $B^+ \to \psi(2S)K^+$, $\psi(2S) \to J/\psi\pi^+\pi^-$ mode for normalization.

$\Gamma(D_s^- \mu^+ \mu^+)/\Gamma_{total}$ — Γ_{625}/Γ

VALUE	CL%	DOCUMENT ID		TECN	COMMENT
$<5.8 \times 10^{-7}$	95	[1] AAIJ	12AD	LHCB	pp at 7 TeV

[1] Uses $B^+ \to \psi(2S)K^+$, $\psi(2S) \to J/\psi\pi^+\pi^-$ mode for normalization. Obtains neutrino-mass-dependent upper limits in the range 1.5–8.0 $\times 10^{-7}$.

$\Gamma(\overline{D}^0 \pi^- \mu^+ \mu^+)/\Gamma_{total}$ — Γ_{626}/Γ

VALUE	CL%	DOCUMENT ID		TECN	COMMENT
$<1.5 \times 10^{-6}$	95	[1] AAIJ	12AD	LHCB	pp at 7 TeV

[1] Uses $B^+ \to \psi(2S)K^+$, $\psi(2S) \to J/\psi\pi^+\pi^-$ mode for normalization. Obtains neutrino-mass-dependent upper limits in the range 0.3–1.5 $\times 10^{-6}$.

$\Gamma(\Lambda^0 \mu^+)/\Gamma_{total}$ — Γ_{627}/Γ

VALUE	CL%	DOCUMENT ID		TECN	COMMENT
$<6 \times 10^{-8}$	90	[1,2] DEL-AMO-SA...	11K	BABR	$e^+e^- \to \Upsilon(4S)$

[1] DEL-AMO-SANCHEZ 11K reports $< 6.1 \times 10^{-8}$ from a measurement of $[\Gamma(B^+ \to \Lambda^0\mu^+)/\Gamma_{total}] \times [B(\Lambda \to p\pi^-)]$ assuming $B(\Lambda \to p\pi^-) = (63.9 \pm 0.5) \times 10^{-2}$.
[2] Uses $B(\Upsilon(4S) \to B^0\overline{B}^0) = (51.6 \pm 0.6)\%$ and $B(\Upsilon(4S) \to B^+B^-) = (48.4 \pm 0.6)\%$.

$\Gamma(\Lambda^0 e^+)/\Gamma_{total}$ — Γ_{628}/Γ

VALUE	CL%	DOCUMENT ID		TECN	COMMENT
$<3.2 \times 10^{-8}$	90	[1,2] DEL-AMO-SA...	11K	BABR	$e^+e^- \to \Upsilon(4S)$

[1] DEL-AMO-SANCHEZ 11K reports $< 3.2 \times 10^{-8}$ from a measurement of $[\Gamma(B^+ \to \Lambda^0 e^+)/\Gamma_{total}] \times [B(\Lambda \to p\pi^-)]$ assuming $B(\Lambda \to p\pi^-) = (63.9 \pm 0.5) \times 10^{-2}$.
[2] Uses $B(\Upsilon(4S) \to B^0\overline{B}^0) = (51.6 \pm 0.6)\%$ and $B(\Upsilon(4S) \to B^+B^-) = (48.4 \pm 0.6)\%$.

$\Gamma(\overline{\Lambda}^0 \mu^+)/\Gamma_{total}$ — Γ_{629}/Γ

VALUE	CL%	DOCUMENT ID		TECN	COMMENT
$<6 \times 10^{-8}$	90	[1,2] DEL-AMO-SA...	11K	BABR	$e^+e^- \to \Upsilon(4S)$

[1] DEL-AMO-SANCHEZ 11K reports $< 6.2 \times 10^{-8}$ from a measurement of $[\Gamma(B^+ \to \overline{\Lambda}^0\mu^+)/\Gamma_{total}] \times [B(\Lambda \to p\pi^-)]$ assuming $B(\Lambda \to p\pi^-) = (63.9 \pm 0.5) \times 10^{-2}$.
[2] Uses $B(\Upsilon(4S) \to B^0\overline{B}^0) = (51.6 \pm 0.6)\%$ and $B(\Upsilon(4S) \to B^+B^-) = (48.4 \pm 0.6)\%$.

$\Gamma(\overline{\Lambda}^0 e^+)/\Gamma_{total}$ — Γ_{630}/Γ

VALUE	CL%	DOCUMENT ID		TECN	COMMENT
$<8 \times 10^{-8}$	90	[1,2] DEL-AMO-SA...	11K	BABR	$e^+e^- \to \Upsilon(4S)$

[1] DEL-AMO-SANCHEZ 11K reports $< 8.1 \times 10^{-8}$ from a measurement of $[\Gamma(B^+ \to \overline{\Lambda}^0 e^+)/\Gamma_{total}] \times [B(\Lambda \to p\pi^-)]$ assuming $B(\Lambda \to p\pi^-) = (63.9 \pm 0.5) \times 10^{-2}$.
[2] Uses $B(\Upsilon(4S) \to B^0\overline{B}^0) = (51.6 \pm 0.6)\%$ and $B(\Upsilon(4S) \to B^+B^-) = (48.4 \pm 0.6)\%$.

POLARIZATION IN B^+ DECAY

In decays involving two vector mesons, one can distinguish among the states in which meson polarizations are both longitudinal (L) or both are transverse and parallel ($\|$) or perpendicular ($\perp$) to each other with the parameters Γ_L/Γ, $\Gamma_\perp/\Gamma$, and the relative phases $\phi_\|$ and $\phi_\perp$. See the definitions in the note on "Polarization in B Decays" review in the B^0 Particle Listings.

Γ_L/Γ in $B^+ \to \overline{D}^{*0}\rho^+$

VALUE	DOCUMENT ID		TECN	COMMENT
0.892±0.018±0.016	CSORNA	03	CLE2	$e^+e^- \to \Upsilon(4S)$

Γ_L/Γ in $B^+ \to \overline{D}^{*0}K^{*+}$

VALUE	DOCUMENT ID		TECN	COMMENT
0.86±0.06±0.03	AUBERT	04K	BABR	$e^+e^- \to \Upsilon(4S)$

Γ_L/Γ in $B^+ \to J/\psi K^{*+}$

VALUE	DOCUMENT ID		TECN	COMMENT
0.604±0.015±0.018	ITOH	05	BELL	$e^+e^- \to \Upsilon(4S)$

$\Gamma_\perp/\Gamma$ in $B^+ \to J/\psi K^{*+}$

VALUE	DOCUMENT ID		TECN	COMMENT
0.180±0.014±0.010	ITOH	05	BELL	$e^+e^- \to \Upsilon(4S)$

Γ_L/Γ in $B^+ \to \omega K^{*+}$

VALUE	DOCUMENT ID		TECN	COMMENT
0.41±0.18±0.05	AUBERT	09H	BABR	$e^+e^- \to \Upsilon(4S)$

Γ_L/Γ in $B^+ \to \omega K_2^*(1430)^+$

VALUE	DOCUMENT ID		TECN	COMMENT
0.56±0.10±0.04	AUBERT	09H	BABR	$e^+e^- \to \Upsilon(4S)$

Γ_L/Γ in $B^+ \to K^{*+}\overline{K}^{*0}$

VALUE	DOCUMENT ID		TECN	COMMENT
$0.82^{+0.15}_{-0.21}$ OUR AVERAGE				
$1.06 \pm 0.30 \pm 0.14$	[1] GOH	15	BELL	$e^+e^- \to \Upsilon(4S)$
$0.75^{+0.16}_{-0.26} \pm 0.03$	[2,3] AUBERT	09F	BABR	$e^+e^- \to \Upsilon(4S)$

[1] Signal significance 2.7 standard deviations.
[2] Signal significance 3.7 standard deviations.
[3] Assumes equal production of B^+ and B^0 at the $\Upsilon(4S)$.

Γ_L/Γ in $B^+ \to \phi K^*(892)^+$

VALUE	DOCUMENT ID		TECN	COMMENT
0.50±0.05 OUR AVERAGE				
0.49±0.05±0.03	AUBERT	07BA	BABR	$e^+e^- \to \Upsilon(4S)$
0.52±0.08±0.03	CHEN	05A	BELL	$e^+e^- \to \Upsilon(4S)$
• • • We do not use the following data for averages, fits, limits, etc. • • •				
0.46±0.12±0.03	AUBERT	03V	BABR	Repl. by AUBERT 07BA

$\Gamma_\perp/\Gamma$ in $B^+ \to \phi K^{*+}$

VALUE	DOCUMENT ID		TECN	COMMENT
0.20±0.05 OUR AVERAGE				
0.21±0.05±0.02	AUBERT	07BA	BABR	$e^+e^- \to \Upsilon(4S)$
0.19±0.08±0.02	CHEN	05A	BELL	$e^+e^- \to \Upsilon(4S)$

$\phi_\|$ in $B^+ \to \phi K^{*+}$

VALUE (°)	DOCUMENT ID		TECN	COMMENT
2.34±0.18 OUR AVERAGE				
2.47±0.20±0.07	AUBERT	07BA	BABR	$e^+e^- \to \Upsilon(4S)$
2.10±0.28±0.04	CHEN	05A	BELL	$e^+e^- \to \Upsilon(4S)$

$\phi_\perp$ in $B^+ \to \phi K^{*+}$

VALUE (°)	DOCUMENT ID		TECN	COMMENT
2.58±0.17 OUR AVERAGE				
2.69±0.20±0.03	AUBERT	07BA	BABR	$e^+e^- \to \Upsilon(4S)$
2.31±0.30±0.07	CHEN	05A	BELL	$e^+e^- \to \Upsilon(4S)$

Downloaded from https://academic.oup.com/ptep/article/2022/8/083C01/6651666 by KIT Library user on 27 September 2022

$\delta_0(B^+ \to \phi K^{*+})$

VALUE (rad)	DOCUMENT ID		TECN	COMMENT
3.07±0.18±0.06	AUBERT	07BA	BABR	$e^+e^- \to \Upsilon(4S)$

$A^0_{CP}(B^+ \to \phi K^{*+})$

VALUE	DOCUMENT ID		TECN	COMMENT
0.17±0.11±0.02	AUBERT	07BA	BABR	$e^+e^- \to \Upsilon(4S)$

$A^{\perp}_{CP}(B^+ \to \phi K^{*+})$

VALUE	DOCUMENT ID		TECN	COMMENT
0.22±0.24±0.08	AUBERT	07BA	BABR	$e^+e^- \to \Upsilon(4S)$

$\Delta\phi_{\parallel}(B^+ \to \phi K^{*+})$

VALUE (rad)	DOCUMENT ID		TECN	COMMENT
0.07±0.20±0.05	AUBERT	07BA	BABR	$e^+e^- \to \Upsilon(4S)$

$\Delta\phi_{\perp}(B^+ \to \phi K^{*+})$

VALUE (rad)	DOCUMENT ID		TECN	COMMENT
0.19±0.20±0.07	AUBERT	07BA	BABR	$e^+e^- \to \Upsilon(4S)$

$\Delta\delta_0(B^+ \to \phi K^{*+})$

VALUE (rad)	DOCUMENT ID		TECN	COMMENT
0.20±0.18±0.03	AUBERT	07BA	BABR	$e^+e^- \to \Upsilon(4S)$

Γ_L/Γ in $B^+ \to \phi K_1(1270)^+$

VALUE	DOCUMENT ID		TECN	COMMENT
$0.46^{+0.12}_{-0.13}{}^{+0.06}_{-0.07}$	AUBERT	08BI	BABR	$e^+e^- \to \Upsilon(4S)$

Γ_L/Γ in $B^+ \to \phi K^*_2(1430)^+$

VALUE	DOCUMENT ID		TECN	COMMENT
$0.80^{+0.09}_{-0.10}$±0.03	AUBERT	08BI	BABR	$e^+e^- \to \Upsilon(4S)$

$\delta_0(B^+ \to \phi K^*_2(1430)^+)$

VALUE (rad)	DOCUMENT ID		TECN	COMMENT
3.59±0.19±0.12	AUBERT	08BI	BABR	$e^+e^- \to \Upsilon(4S)$

$\Delta\delta_0(B^+ \to \phi K^*_2(1430)^+)$

VALUE (rad)	DOCUMENT ID		TECN	COMMENT
−0.05±0.19±0.06	AUBERT	08BI	BABR	$e^+e^- \to \Upsilon(4S)$

Γ_L/Γ in $B^+ \to \rho^0 K^*(892)^+$

VALUE	DOCUMENT ID		TECN	COMMENT
0.78±0.12±0.03	DEL-AMO-SA...11D		BABR	$e^+e^- \to \Upsilon(4S)$
• • • We do not use the following data for averages, fits, limits, etc. • • •				
$0.96^{+0.04}_{-0.15}$±0.04	AUBERT	03V	BABR	Repl. by DEL-AMO-SANCHEZ 11D

$\Gamma_L/\Gamma(B^+ \to K^*(892)^0\rho^+)$

VALUE	DOCUMENT ID		TECN	COMMENT
0.48±0.08 OUR AVERAGE				
0.52±0.10±0.04	AUBERT,B	06G	BABR	$e^+e^- \to \Upsilon(4S)$
0.43±0.11$^{+0.05}_{-0.02}$	ZHANG	05D	BELL	$e^+e^- \to \Upsilon(4S)$

Γ_L/Γ in $B^+ \to \mu^+\mu^- K^*(892)^+$ ($1.0 < q^2 < 8.68$ GeV$^2/c^4$)

VALUE	DOCUMENT ID		TECN	COMMENT
$0.60^{+0.31}_{-0.25}$±0.13	[1] SIRUNYAN	21AC	CMS	pp at 8 TeV

[1] SIRUNYAN 21AC measurement is performed in $1.0 < q^2 < 8.68$ GeV$^2/c^4$. Reports also measurements in several other q^2 intervals.

Γ_L/Γ in $B^+ \to \mu^+\mu^- K^*(892)^+$ ($1.1 < q^2 < 6.0$ GeV$^2/c^4$)

VALUE	DOCUMENT ID		TECN	COMMENT
0.59±0.09±0.03	[1] AAIJ	21J	LHCB	pp at 7, 8, 13 TeV

[1] The full set of CP-averaged angular observables is measured as a function of the q^2. The measured Γ_L is related to the polarisation of the $K^*(892)^+$.

Γ_L/Γ in $B^+ \to \mu^+\mu^- K^*(892)^+$ ($10.09 < q^2 < 12.86$ GeV$^2/c^4$)

VALUE	DOCUMENT ID		TECN	COMMENT
$0.88^{+0.10}_{-0.13}$±0.05	[1] SIRUNYAN	21AC	CMS	pp at 8 TeV

[1] SIRUNYAN 21AC measurement is performed in $10.09 < q^2 < 12.86$ GeV$^2/c^4$. Reports also measurements in several other q^2 intervals.

Γ_L/Γ in $B^+ \to \mu^+\mu^- K^*(892)^+$ ($14.18 < q^2 < 19.0$ GeV$^2/c^4$)

VALUE	DOCUMENT ID		TECN	COMMENT
$0.55^{+0.13}_{-0.10}$±0.06	[1] SIRUNYAN	21AC	CMS	pp at 8 TeV

[1] SIRUNYAN 21AC measurement is performed in $14.18 < q^2 < 19.0$ GeV$^2/c^4$. Reports also measurements in several other q^2 intervals.

Γ_L/Γ in $B^+ \to \mu^+\mu^- K^*(892)^+$ ($15.0 < q^2 < 19.0$ GeV$^2/c^4$)

VALUE	DOCUMENT ID		TECN	COMMENT
$0.40^{+0.13}_{-0.11}$±0.03	[1] AAIJ	21J	LHCB	pp at 7, 8, 13 TeV

[1] The full set of CP-averaged angular observables is measured as a function of the q^2. The measured Γ_L is related to the polarisation of the $K^*(892)^+$.

Γ_L/Γ in $B^+ \to \rho^+\rho^0$

VALUE	DOCUMENT ID		TECN	COMMENT
0.950±0.016 OUR AVERAGE				
0.950±0.015±0.006	AUBERT	09G	BABR	$e^+e^- \to \Upsilon(4S)$
0.948±0.106±0.021	ZHANG	03B	BELL	$e^+e^- \to \Upsilon(4S)$
• • • We do not use the following data for averages, fits, limits, etc. • • •				
0.905±0.042$^{+0.023}_{-0.027}$	AUBERT,BE	06G	BABR	Repl. by AUBERT 09G
0.97 $^{+0.03}_{-0.07}$ ±0.04	AUBERT	03V	BABR	Repl. by AUBERT,BE 06G

Γ_L/Γ in $B^+ \to \omega\rho^+$

VALUE	DOCUMENT ID		TECN	COMMENT
0.90±0.05±0.03	AUBERT	09H	BABR	$e^+e^- \to \Upsilon(4S)$
• • • We do not use the following data for averages, fits, limits, etc. • • •				
0.82±0.11±0.02	AUBERT,B	06T	BABR	Repl. by AUBERT 09H
0.88$^{+0.12}_{-0.15}$±0.03	AUBERT	05O	BABR	Repl. by AUBERT,B 06T

Γ_L/Γ in $B^+ \to p\overline{p}K^*(892)^+$

VALUE	DOCUMENT ID		TECN	COMMENT
0.32±0.17±0.09	CHEN	08C	BELL	$e^+e^- \to \Upsilon(4S)$

CP VIOLATION

A_{CP} is defined as

$$\frac{B(B^- \to \overline{f}) - B(B^+ \to f)}{B(B^- \to \overline{f}) + B(B^+ \to f)},$$

the *CP*-violation charge asymmetry of exclusive B^- and B^+ decay.

$A_{CP}(B^+ \to J/\psi(1S)K^+)$

VALUE (units 10^{-3})	DOCUMENT ID		TECN	COMMENT
1.8± 3.0 OUR AVERAGE	Error includes scale factor of 1.5. See the ideogram below.			
0.9± 2.7± 0.7	AAIJ	17AP	LHCB	pp at 7, 8 TeV
5.9± 3.6± 0.7	ABAZOV	13M	D0	$p\overline{p}$ at 1.96 TeV
− 7.6± 5.0± 2.2	SAKAI	10	BELL	$e^+e^- \to \Upsilon(4S)$
90 ±70 ±20	[1] WEI	08	BELL	$e^+e^- \to \Upsilon(4S)$
30 ±14 ±10	[2] AUBERT	05J	BABR	$e^+e^- \to \Upsilon(4S)$
18 ±43 ± 4	[3] BONVICINI	00	CLE2	$e^+e^- \to \Upsilon(4S)$
• • • We do not use the following data for averages, fits, limits, etc. • • •				
7.5± 6.1± 3.0	[4] ABAZOV	08O	D0	Repl. by ABAZOV 13M
30 ±15 ± 6	AUBERT	04P	BABR	Repl. by AUBERT 05J
−26 ±22 ±17	ABE	03B	BELL	Repl. by SAKAI 10
3 ±30 ± 4	AUBERT	02F	BABR	Repl. by AUBERT 04P

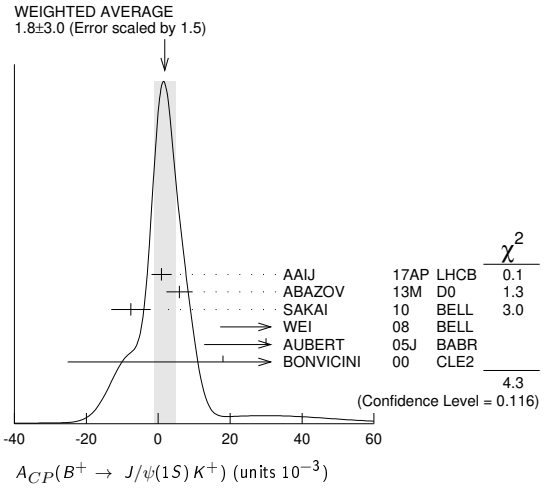

[1] Uses $B^+ \to J/\psi K^+$, where $J/\psi \to p\overline{p}$.
[2] The result reported corresponds to $-A_{CP}$.
[3] A +0.3% correction is applied due to a slightly higher reconstruction efficiency for the positive kaons.
[4] Uses $J/\psi \to \mu^+\mu^-$ decay.

Downloaded from https://academic.oup.com/ptep/article/2022/8/083C01/6651666 by KIT Library user on 27 September 2022

$A_{CP}(B^+ \to J/\psi(1S)\pi^+)$

VALUE (units 10^{-2})	DOCUMENT ID		TECN	COMMENT
1.8 ± 1.2 OUR AVERAGE	Error includes scale factor of 1.3.			
1.91 ± 0.89 ± 0.16	[1] AAIJ	17O	LHCB	pp at 7, 8 TeV
− 4.2 ± 4.4 ± 0.9	ABAZOV	13M	D0	$p\overline{p}$ at 1.96 TeV
12.3 ± 8.5 ± 0.4	AUBERT	04P	BABR	$e^+e^- \to \Upsilon(4S)$
− 2.3 ± 16.4 ± 1.5	ABE	03B	BELL	$e^+e^- \to \Upsilon(4S)$
• • • We do not use the following data for averages, fits, limits, etc. • • •				
0.5 ± 2.7 ± 1.1	[2] AAIJ	12AC	LHCB	Repl. by AAIJ 17O
− 9 ± 8 ± 3	[3] ABAZOV	08O	D0	Repl. by ABAZOV 13M
1 ± 22 ± 1	AUBERT	02F	BABR	Repl. by AUBERT 04P

[1] Obtained by using LHCb measurement of $A_{CP}(B^+ \to J/\psi K^+) = (0.09 \pm 0.27 \pm 0.07) \times 10^{-2}$ of AAIJ 17AP.
[2] Uses $A_{CP}(B^+ \to J/\psi K^+) = 0.001 \pm 0.007$ to extract production asymmetry.
[3] Uses $J/\psi \to \mu^+\mu^-$ decay.

$A_{CP}(B^+ \to J/\psi\rho^+)$

VALUE	DOCUMENT ID		TECN	COMMENT
−0.05 ± 0.05 OUR AVERAGE				
$-0.045^{+0.056}_{-0.057} \pm 0.008$	AAIJ	19O	LHCB	pp at 7 and 8 TeV
−0.11 ± 0.12 ± 0.08	AUBERT	07AC	BABR	$e^+e^- \to \Upsilon(4S)$

$A_{CP}(B^+ \to J/\psi K^*(892)^+)$

VALUE	DOCUMENT ID		TECN	COMMENT
−0.048 ± 0.029 ± 0.016	[1] AUBERT	05J	BABR	$e^+e^- \to \Upsilon(4S)$

[1] The result reported corresponds to $-A_{CP}$.

$A_{CP}(B^+ \to \eta_c K^+)$

VALUE	DOCUMENT ID		TECN	COMMENT
0.01 ± 0.07 OUR AVERAGE	Error includes scale factor of 2.2.			
0.040 ± 0.034 ± 0.004	[1] AAIJ	14AF	LHCB	pp at 7, 8 TeV
−0.16 ± 0.08 ± 0.02	[1] WEI	08	BELL	$e^+e^- \to \Upsilon(4S)$
• • • We do not use the following data for averages, fits, limits, etc. • • •				
0.046 ± 0.057 ± 0.007	[1] AAIJ	13AU	LHCB	Repl. by AAIJ 14AF

[1] Uses $B^+ \to \eta_c K^+$, where $\eta_c \to p\overline{p}$.

$A_{CP}(B^+ \to \psi(2S)\pi^+)$

VALUE	DOCUMENT ID		TECN	COMMENT
0.03 ± 0.06 OUR AVERAGE				
0.048 ± 0.090 ± 0.011	[1] AAIJ	12AC	LHCB	pp at 7 TeV
0.022 ± 0.085 ± 0.016	BHARDWAJ	08	BELL	$e^+e^- \to \Upsilon(4S)$

[1] Uses $A_{CP}(B^+ \to J/\psi K^+) = 0.001 \pm 0.007$ to extract production asymmetry.

$A_{CP}(B^+ \to \psi(2S)K^+)$

VALUE	DOCUMENT ID		TECN	COMMENT
0.012 ± 0.020 OUR AVERAGE	Error includes scale factor of 1.5. See the ideogram below.			
0.092 ± 0.058 ± 0.004	[1] AAIJ	14AF	LHCB	pp at 7, 8 TeV
0.024 ± 0.014 ± 0.008	[2] AAIJ	12AC	LHCB	pp at 7 TeV
0.052 ± 0.059 ± 0.020	AUBERT	05J	BABR	$e^+e^- \to \Upsilon(4S)$
−0.042 ± 0.020 ± 0.017	ABE	03B	BELL	$e^+e^- \to \Upsilon(4S)$
0.02 ± 0.091 ± 0.01	[3] BONVICINI	00	CLE2	$e^+e^- \to \Upsilon(4S)$
• • • We do not use the following data for averages, fits, limits, etc. • • •				
−0.002 ± 0.123 ± 0.012	[1,2] AAIJ	13AU	LHCB	Repl. by AAIJ 14AF

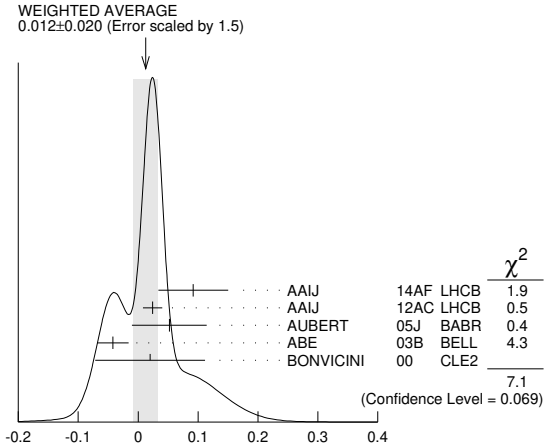

[1] Uses $\psi(2S) \to p\overline{p}$ decays.
[2] Uses $A_{CP}(B^+ \to J/\psi K^+) = 0.001 \pm 0.007$ to extract production asymmetry.
[3] A +0.3% correction is applied due to a slightly higher reconstruction efficiency for the positive kaons.

$A_{CP}(B^+ \to \psi(2S)K^*(892)^+)$

VALUE	DOCUMENT ID		TECN	COMMENT
0.077 ± 0.207 ± 0.051	[1] AUBERT	05J	BABR	$e^+e^- \to \Upsilon(4S)$

[1] The result reported corresponds to $-A_{CP}$.

$A_{CP}(B^+ \to \chi_{c1}(1P)\pi^+)$

VALUE	DOCUMENT ID		TECN	COMMENT
0.07 ± 0.18 ± 0.02	KUMAR	06	BELL	$e^+e^- \to \Upsilon(4S)$

$A_{CP}(B^+ \to \chi_{c0}K^+)$

VALUE	DOCUMENT ID		TECN	COMMENT
−0.20 ± 0.18 OUR AVERAGE	Error includes scale factor of 1.5. See the ideogram below.			
−0.96 ± 0.37 ± 0.04	LEES	11I	BABR	$e^+e^- \to \Upsilon(4S)$
$-0.14 \pm 0.15^{+0.03}_{-0.06}$	AUBERT	08AI	BABR	$e^+e^- \to \Upsilon(4S)$
$-0.065 \pm 0.20^{+0.035}_{-0.024}$	GARMASH	06	BELL	$e^+e^- \to \Upsilon(4S)$

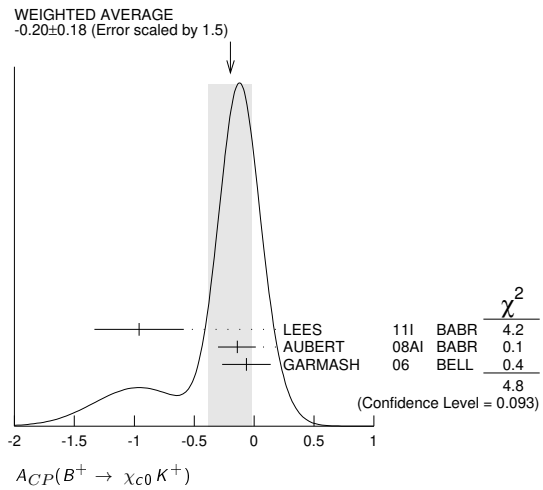

$A_{CP}(B^+ \to \chi_{c1}K^+)$

VALUE	DOCUMENT ID		TECN	COMMENT
−0.009 ± 0.033 OUR AVERAGE				
−0.01 ± 0.03 ± 0.02	KUMAR	06	BELL	$e^+e^- \to \Upsilon(4S)$
−0.003 ± 0.076 ± 0.017	[1] AUBERT	05J	BABR	$e^+e^- \to \Upsilon(4S)$

[1] The result reported corresponds to $-A_{CP}$.

$A_{CP}(B^+ \to \chi_{c1}K^*(892)^+)$

VALUE	DOCUMENT ID		TECN	COMMENT
0.471 ± 0.378 ± 0.268	[1] AUBERT	05J	BABR	$e^+e^- \to \Upsilon(4S)$

[1] The result reported corresponds to $-A_{CP}$.

$A_{CP}(B^+ \to D^0\ell^+\nu_\ell)$

VALUE (units 10^{-2})	DOCUMENT ID		TECN	COMMENT
−0.14 ± 0.14 ± 0.14	[1] ABAZOV	17A	D0	$p\overline{p}$ at 1.96 TeV

[1] Uses $D^0 \to K^-\pi^+$ decays and $f(B^+) = 0.56 \pm 0.01$ from 10.4 fb^{-1} of Run II data.

$A_{CP}(B^+ \to \overline{D^0}\pi^+)$

VALUE	DOCUMENT ID		TECN	COMMENT
−0.007 ± 0.007 OUR AVERAGE				
−0.006 ± 0.005 ± 0.010	[1] AAIJ	13AE	LHCB	pp at 7 TeV
−0.008 ± 0.008	ABE	06	BELL	$e^+e^- \to \Upsilon(4S)$

[1] Uses $B^\pm \to [K^\pm\pi^\mp\pi^+\pi^-]_D h^\pm$ mode.

$A_{CP}(B^+ \to D_{CP(+1)}\pi^+)$

VALUE	DOCUMENT ID		TECN	COMMENT
−0.0080 ± 0.0024 OUR AVERAGE				
−0.008 ± 0.002 ± 0.002	[1] AAIJ	21Q	LHCB	pp at 7, 8, 13 TeV
−0.0098 ± 0.0043 ± 0.0021	AAIJ	16L	LHCB	pp at 7, 8 TeV
0.035 ± 0.024	ABE	06	BELL	$e^+e^- \to \Upsilon(4S)$
• • • We do not use the following data for averages, fits, limits, etc. • • •				
−0.008 ± 0.003 ± 0.002	[2,3] AAIJ	18A	LHCB	pp at 7, 8, 13 TeV
−0.008 ± 0.006 ± 0.002	[3,4] AAIJ	18A	LHCB	pp at 7, 8, 13 TeV

[1] Uses $D \to K^+K^-$ and $D \to \pi^+\pi^-$ decay modes.
[2] Uses $D \to K^+K^-$ decay mode.
[3] Superseded by AAIJ 21Q.
[4] Uses $D \to \pi^+\pi^-$ decay mode.

$A_{CP}(B^+ \to D_{CP(-1)}\pi^+)$

VALUE	DOCUMENT ID		TECN	COMMENT
0.017 ± 0.026	ABE	06	BELL	$e^+e^- \to \Upsilon(4S)$

$A_{CP}([K^\mp\pi^\pm\pi^+\pi^-]_D\pi^+)$

VALUE	DOCUMENT ID		TECN	COMMENT
0.023 ± 0.048 ± 0.005	AAIJ	16L	LHCB	pp at 7, 8 TeV
• • • We do not use the following data for averages, fits, limits, etc. • • •				
0.13 ± 0.10	AAIJ	13AE	LHCB	Repl. by AAIJ 16L

Downloaded from https://academic.oup.com/ptep/article/2022/8/083C01/6651666 by KIT Library user on 27 September 2022

$A_{CP}(B^+ \to [\pi^+\pi^+\pi^-\pi^-]_D K^+)$

VALUE	DOCUMENT ID		TECN	COMMENT
0.100±0.034±0.018	AAIJ	16L	LHCB	pp at 7, 8 TeV

$A_{CP}(B^+ \to [\pi^+\pi^-\pi^+\pi^-]_D K^*(892)^+)$

VALUE	DOCUMENT ID		TECN	COMMENT
0.02±0.11±0.01	AAIJ	17BO	LHCB	pp at 7, 8, 13 TeV

$A_{CP}(B^+ \to \overline{D}^0 K^+)$

VALUE	DOCUMENT ID		TECN	COMMENT
−0.017 ±0.005 OUR AVERAGE				
−0.019 ±0.005 ±0.002	[1] AAIJ	18A	LHCB	pp at 7, 8, 13 TeV
−0.0194±0.0072±0.0060	AAIJ	16L	LHCB	pp at 7, 8 TeV
0.010 ±0.026 ±0.005	[2] AAIJ	15W	LHCB	pp at 7, 8 TeV
0.066 ±0.036	ABE	06	BELL	$e^+e^- \to \Upsilon(4S)$
• • • We do not use the following data for averages, fits, limits, etc. • • •				
0.000 ±0.012 ±0.002	[3] AAIJ	16L	LHCB	pp at 7, 8 TeV
−0.029 ±0.020 ±0.018	[3] AAIJ	13AE	LHCB	Repl. by AAIJ 16L
0.003 ±0.080 ±0.037	[4] ABE	03D	BELL	Repl. by SWAIN 03
0.04 ±0.06 ±0.03	[5] SWAIN	03	BELL	Repl. by ABE 06

[1] Supersedes AAIJ 16L.
[2] Uses $D^0 \to K^-\pi^+\pi^0$ for the favored mode, and $D^0 \to K^+\pi^-\pi^0$ for the suppressed mode.
[3] Uses $B^{\pm} \to [K^{\pm}\pi^{\mp}\pi^+\pi^-]_D h^{\pm}$ mode.
[4] Corresponds to 90% confidence range $-0.15 < A_{CP} < 0.16$.
[5] Corresponds to 90% confidence range $-0.07 < A_{CP} < 0.15$.

$A_{CP}([K^{\mp}\pi^{\pm}\pi^+\pi^-]_D K^+)$

VALUE	DOCUMENT ID		TECN	COMMENT
−0.313±0.102±0.038	AAIJ	16L	LHCB	pp at 7, 8 TeV
• • • We do not use the following data for averages, fits, limits, etc. • • •				
−0.42 ±0.22	AAIJ	13AE	LHCB	Repl. by AAIJ 16L

$A_{CP}(B^+ \to [\pi^+\pi^+\pi^-\pi^-]_D \pi^+)$

VALUE (units 10^{-3})	DOCUMENT ID		TECN	COMMENT
−4.1±7.9±2.4	AAIJ	16L	LHCB	pp at 7, 8 TeV

$A_{CP}(B^+ \to [K^-\pi^+]_D K^+)$

VALUE	DOCUMENT ID		TECN	COMMENT
−0.58±0.21 OUR AVERAGE				
−0.82±0.44±0.09	AALTONEN	11AJ	CDF	$p\overline{p}$ at 1.96 TeV
$-0.39^{+0.26}_{-0.28}{}^{+0.04}_{-0.03}$	HORII	11	BELL	$e^+e^- \to \Upsilon(4S)$
$-0.86\pm0.47^{+0.12}_{-0.16}$	DEL-AMO-SA...	10H	BABR	$e^+e^- \to \Upsilon(4S)$
• • • We do not use the following data for averages, fits, limits, etc. • • •				
$-0.1\ ^{+0.8}_{-1.0}\ \pm0.4$	HORII	08	BELL	Repl. by HORII 11
$+0.88^{+0.77}_{-0.62}\pm0.06$	SAIGO	05	BELL	Repl. by HORII 08

$A_{CP}(B^+ \to [K^-\pi^+\pi^0]_D K^+)$

VALUE	DOCUMENT ID		TECN	COMMENT
0.07±0.30 OUR AVERAGE Error includes scale factor of 1.5.				
−0.20±0.27±0.04	[1] AAIJ	15W	LHCB	pp at 7, 8 TeV
0.41±0.30±0.05	NAYAK	13	BELL	$e^+e^- \to \Upsilon(4S)$

[1] Uses $D^0 \to K^-\pi^+\pi^0$ for the favored mode, and $D^0 \to K^+\pi^-\pi^0$ for the suppressed mode.

$A_{CP}(B^+ \to [K^+K^-\pi^0]_D K^+)$

VALUE	DOCUMENT ID		TECN	COMMENT
0.30±0.20±0.02	[1] AAIJ	15W	LHCB	pp at 7, 8 TeV

[1] Uses $D \to K^+K^-\pi^0$ mode.

$A_{CP}(B^+ \to [\pi^+\pi^-\pi^0]_D K^+)$

VALUE	DOCUMENT ID		TECN	COMMENT
0.054±0.091±0.011	[1] AAIJ	15W	LHCB	pp at 7, 8 TeV

[1] Uses $D \to \pi^+\pi^-\pi^0$ mode.

$A_{CP}(B^+ \to \overline{D}^0 K^*(892)^+)$

VALUE	DOCUMENT ID		TECN	COMMENT
−0.007±0.019 OUR AVERAGE				
−0.004±0.023±0.008	[1] AAIJ	17BO	LHCB	pp at 7, 8, 13 TeV
−0.013±0.031±0.009	[2] AAIJ	17BO	LHCB	pp at 7, 8, 13 TeV

[1] Uses $B^{\pm} \to [K^{\pm}\pi^{\mp}]_D K^*(892)^{\pm}$ decay mode .
[2] Uses $B^{\pm} \to [K^{\pm}\pi^{\mp}\pi^+\pi^-]_D K^*(892)^{\pm}$ decay mode .

$A_{CP}(B^+ \to [K^-\pi^+]_{\overline{D}} K^*(892)^+)$

VALUE	DOCUMENT ID		TECN	COMMENT
−0.75±0.16 OUR AVERAGE				
−0.81±0.17±0.04	AAIJ	17BO	LHCB	pp at 7, 8, 13 TeV
−0.34±0.43±0.16	AUBERT	09AJ	BABR	$e^+e^- \to \Upsilon(4S)$
• • • We do not use the following data for averages, fits, limits, etc. • • •				
−0.22±0.61±0.17	AUBERT,B	05V	BABR	Repl. by AUBERT 09AJ

$A_{CP}(B^+ \to [K^-\pi^+\pi^-\pi^+]_{\overline{D}} K^*(892)^+)$

VALUE	DOCUMENT ID		TECN	COMMENT
−0.45±0.21±0.14	AAIJ	17BO	LHCB	pp at 7, 8, 13 TeV

$A_{CP}(B^+ \to [K^-\pi^+]_D \pi^+)$

VALUE	DOCUMENT ID		TECN	COMMENT
0.00±0.09 OUR AVERAGE				
0.13±0.25±0.02	AALTONEN	11AJ	CDF	$p\overline{p}$ at 1.96 TeV
$-0.04\pm0.11^{+0.02}_{-0.01}$	HORII	11	BELL	$e^+e^- \to \Upsilon(4S)$
0.03±0.17±0.04	DEL-AMO-SA...	10H	BABR	$e^+e^- \to \Upsilon(4S)$
• • • We do not use the following data for averages, fits, limits, etc. • • •				
$-0.02^{+0.15}_{-0.16}\pm0.04$	HORII	08	BELL	Repl. by HORII 11
$+0.30^{+0.29}_{-0.25}\pm0.06$	SAIGO	05	BELL	Repl. by HORII 08

$A_{CP}(B^+ \to [K^-\pi^+\pi^0]_D \pi^+)$

VALUE	DOCUMENT ID		TECN	COMMENT
0.35 ±0.16 OUR AVERAGE				
0.438±0.190±0.011	[1] AAIJ	15W	LHCB	pp at 7, 8 TeV
$0.16\ \pm0.27\ ^{+0.03}_{-0.04}$	NAYAK	13	BELL	$e^+e^- \to \Upsilon(4S)$

[1] Uses $D^0 \to K^-\pi^+\pi^0$ for the favored mode, and $D^0 \to K^+\pi^-\pi^0$ for the suppressed mode.

$A_{CP}(B^+ \to [K^+K^-\pi^0]_D \pi^+)$

VALUE	DOCUMENT ID		TECN	COMMENT
−0.030±0.040±0.005	[1] AAIJ	15W	LHCB	pp at 7, 8 TeV

[1] Uses $D \to K^+K^-$ mode.

$A_{CP}(B^+ \to [\pi^+\pi^-\pi^0]_D \pi^+)$

VALUE	DOCUMENT ID		TECN	COMMENT
−0.016±0.020±0.004	[1] AAIJ	15W	LHCB	pp at 7, 8 TeV

[1] Uses $D \to \pi^+\pi^-$ mode.

$A_{CP}(B^+ \to [K^-\pi^+]_{(D\pi)} \pi^+)$

VALUE	DOCUMENT ID		TECN	COMMENT
−0.09±0.27±0.05	DEL-AMO-SA...	10H	BABR	$e^+e^- \to \Upsilon(4S)$

$A_{CP}(B^+ \to [K^-\pi^+]_{(D\gamma)} \pi^+)$

VALUE	DOCUMENT ID		TECN	COMMENT
−0.65±0.55±0.22	DEL-AMO-SA...	10H	BABR	$e^+e^- \to \Upsilon(4S)$

$A_{CP}(B^+ \to [K^-\pi^+]_{(D\pi)} K^+)$

VALUE	DOCUMENT ID		TECN	COMMENT
0.77±0.35±0.12	DEL-AMO-SA...	10H	BABR	$e^+e^- \to \Upsilon(4S)$

$A_{CP}(B^+ \to [K^-\pi^+]_{(D\gamma)} K^+)$

VALUE	DOCUMENT ID		TECN	COMMENT
$\mathbf{0.36\pm0.94^{+0.25}_{-0.41}}$	DEL-AMO-SA...	10H	BABR	$e^+e^- \to \Upsilon(4S)$

$A_{CP}(B^+ \to [\pi^+\pi^-\pi^0]_D K^+)$

VALUE	DOCUMENT ID		TECN	COMMENT
−0.02±0.15±0.03	[1] AUBERT	07BJ	BABR	$e^+e^- \to \Upsilon(4S)$
• • • We do not use the following data for averages, fits, limits, etc. • • •				
−0.02±0.16±0.03	AUBERT,B	05T	BABR	Repl. by AUBERT 07BJ

[1] Uses a Dalitz plot analysis of $D^0 \to \pi^+\pi^-\pi^0$. Also reports the one-sigma regions: $0.06 < r_B < 0.78$, $-30^\circ < \gamma < 76^\circ$, and $-27^\circ < \delta < 78^\circ$.

$A_{CP}(B^+ \to [K^0_S K^+\pi^-]_D K^+)$

VALUE	DOCUMENT ID		TECN	COMMENT
0.095±0.089±0.018	[1] AAIJ	20N	LHCB	pp at 7, 8, 13 TeV
• • • We do not use the following data for averages, fits, limits, etc. • • •				
0.040±0.091±0.018	[2] AAIJ	14V	LHCB	Repl. by AAIJ 20N

[1] The analysis uses $D \to K^0_S K\pi$ Dalitz decays with $K^{*-}K^+$ region excluded.
[2] The anaysis uses all of $D \to K^0_S K\pi$ Dalitz decays.

$A_{CP}(B^+ \to [K^0_S K^-\pi^+]_D K^+)$

VALUE	DOCUMENT ID		TECN	COMMENT
−0.038±0.075±0.011	[1] AAIJ	20N	LHCB	pp at 7, 8, 13 TeV
• • • We do not use the following data for averages, fits, limits, etc. • • •				
0.233±0.129±0.024	[2] AAIJ	14V	LHCB	Repl. by AAIJ 20N

[1] The analysis uses $D \to K^0_S K\pi$ Dalitz decays with $K^{*-}K^+$ region excluded.
[2] The anaysis uses all of $D \to K^0_S K\pi$ Dalitz decays.

$A_{CP}(B^+ \to [K^0_S K^-\pi^+]_D \pi^+)$

VALUE	DOCUMENT ID		TECN	COMMENT
0.003±0.015±0.003	[1] AAIJ	20N	LHCB	pp at 7, 8, 13 TeV
• • • We do not use the following data for averages, fits, limits, etc. • • •				
−0.052±0.029±0.017	[2] AAIJ	14V	LHCB	Repl. by AAIJ 20N

[1] The analysis uses $D \to K^0_S K\pi$ Dalitz decays with $K^{*-}K^+$ region excluded.
[2] The anaysis uses all of $D \to K^0_S K\pi$ Dalitz decays.

Downloaded from https://academic.oup.com/ptep/article/2022/8/083C01/6651666 by KIT Library user on 27 September 2022

$A_{CP}(B^+ \to [K^0_S K^+ \pi^-]_D \pi^+)$

VALUE	DOCUMENT ID		TECN	COMMENT
−0.034±0.020±0.003	[1] AAIJ	20N	LHCB	pp at 7, 8, 13 TeV
• • • We do not use the following data for averages, fits, limits, etc. • • •				
−0.025±0.024±0.010	[2] AAIJ	14V	LHCB	Repl. by AAIJ 20N

[1] The analysis uses $D \to K^0_S K\pi$ Dalitz decays with $K^{*-} K^+$ region excluded.
[2] The anaysis uses all of $D \to K^0_S K\pi$ Dalitz decays.

$A_{CP}(B^+ \to [K^*(892)^- K^+]_D K^+)$

VALUE	DOCUMENT ID		TECN	COMMENT
0.084±0.049±0.008	[1] AAIJ	20N	LHCB	pp at 7, 8, 13 TeV
• • • We do not use the following data for averages, fits, limits, etc. • • •				
0.026±0.109±0.029	[1] AAIJ	14V	LHCB	Repl. by AAIJ 20N

[1] The Analysis uses $D \to K^*(892) K \to K^0_S K\pi$ decays.

$A_{CP}(B^+ \to [K^*(892)^+ K^-]_D K^+)$

VALUE	DOCUMENT ID		TECN	COMMENT
0.021±0.094±0.017	[1] AAIJ	20N	LHCB	pp at 7, 8, 13 TeV
• • • We do not use the following data for averages, fits, limits, etc. • • •				
0.336±0.208±0.026	[1] AAIJ	14V	LHCB	Repl. by AAIJ 20N

[1] The Analysis uses $D \to K^*(892) K \to K^0_S K\pi$ decays.

$A_{CP}(B^+ \to [K^*(892)^+ K^-]_D \pi^+)$

VALUE	DOCUMENT ID		TECN	COMMENT
0.007±0.017±0.003	[1] AAIJ	20N	LHCB	pp at 7, 8, 13 TeV
• • • We do not use the following data for averages, fits, limits, etc. • • •				
−0.054±0.043±0.017	[1] AAIJ	14V	LHCB	Repl. by AAIJ 20N

[1] The Analysis uses $D \to K^*(892) K \to K^0_S K\pi$ decays.

$A_{CP}(B^+ \to [K^*(892)^- K^+]_D \pi^+)$

VALUE	DOCUMENT ID		TECN	COMMENT
−0.020±0.011±0.003	[1] AAIJ	20N	LHCB	pp at 7, 8, 13 TeV
• • • We do not use the following data for averages, fits, limits, etc. • • •				
−0.012±0.028±0.010	[1] AAIJ	14V	LHCB	Repl. by AAIJ 20N

[1] The Analysis uses $D \to K^*(892) K \to K^0_S K\pi$ decays.

$A_{CP}(B^+ \to D_{CP(+1)} K^+)$

VALUE	DOCUMENT ID		TECN	COMMENT
0.132±0.015 OUR AVERAGE	Error includes scale factor of 1.8.			
0.136±0.009±0.001	[1] AAIJ	21Q	LHCB	pp at 7, 8, 13 TeV
0.097±0.018±0.009	AAIJ	16L	LHCB	pp at 7, 8 TeV
0.39 ±0.17 ±0.04	AALTONEN	10A	CDF	$p\overline{p}$ at 1.96 TeV
0.25 ±0.06 ±0.02	[2] DEL-AMO-SA...	10G	BABR	$e^+e^- \to \Upsilon(4S)$
0.06 ±0.14 ±0.05	ABE	06	BELL	$e^+e^- \to \Upsilon(4S)$
• • • We do not use the following data for averages, fits, limits, etc. • • •				
0.126±0.014±0.002	[3,4] AAIJ	18A	LHCB	pp at 7, 8, 13 TeV
0.115±0.025±0.007	[4,5] AAIJ	18A	LHCB	pp at 7, 8, 13 TeV
0.145±0.032±0.010	[6] AAIJ	12M	LHCB	Repl. by AAIJ 16L
0.27 ±0.09 ±0.04	AUBERT	08AA	BABR	Repl. by DEL-AMO-SANCHEZ 10G
0.35 ±0.13 ±0.04	AUBERT	06J	BABR	Repl. by AUBERT 08AA
0.07 ±0.17 ±0.06	AUBERT	04N	BABR	Repl. by AUBERT 06J
0.29 ±0.26 ±0.05	[7] ABE	03D	BELL	Repl. by SWAIN 03
0.06 ±0.19 ±0.04	[8] SWAIN	03	BELL	Repl. by ABE 06

[1] Uses $D \to K^+K^-$ and $D \to \pi^+\pi^-$ decay modes.
[2] Reports the first evidence for direct CP violation in $B \to DK$ decays with 3.6 standard deviations.
[3] Uses $D \to K^+K^-$ decay mode.
[4] Superseded by AAIJ 21Q.
[5] Uses $D \to \pi^+\pi^-$ decay mode.
[6] AAIJ 12M reports an evidence of direct CP violation in $B^\pm \to DK^\pm$ decays with a total significance of 5.8 σ.
[7] Corresponds to 90% confidence range $-0.14 < A_{CP} < 0.73$.
[8] Corresponds to 90% confidence range $-0.26 < A_{CP} < 0.38$.

$A_{ADS}(B^+ \to DK^+)$

$A_{ADS}(B^+ \to DK^+) = \frac{(R^-_K - R^+_K)}{(R^-_K + R^+_K)}$ where

$R^-_K = \Gamma(B^- \to [K^+\pi^-]_D K^-) / \Gamma(B^- \to [K^-\pi^+]_D K^-)$ and

$R^+_K = \Gamma(B^+ \to [K^-\pi^+]_D K^+) / \Gamma(B^+ \to [K^+\pi^-]_D K^+)$

VALUE	DOCUMENT ID		TECN	COMMENT
−0.451±0.026	[1] AAIJ	21Q	LHCB	pp at 7, 8, 13 TeV
• • • We do not use the following data for averages, fits, limits, etc. • • •				
−0.403±0.056±0.011	[2] AAIJ	16L	LHCB	pp at 7, 8 TeV
−0.52 ±0.15 ±0.02	AAIJ	12M	LHCB	Repl. by AAIJ 16L

[1] The statistical and systematic uncertainties have been combined according to the correlations between the R^-_K and R^+_K observables.
[2] Superseded by AAIJ 21Q.

$A_{ADS}(B^+ \to D\pi^+)$

$A_{ADS}(B^+ \to D\pi^+) = \frac{(R^-_\pi - R^+_\pi)}{(R^-_\pi + R^+_\pi)}$ where

$R^-_\pi = \Gamma(B^- \to [K^+\pi^-]_D \pi^-) / \Gamma(B^- \to [K^-\pi^+]_D \pi^-)$ and

$R^+_\pi = \Gamma(B^+ \to [K^-\pi^+]_D \pi^+) / \Gamma(B^+ \to [K^+\pi^-]_D \pi^+)$

VALUE	DOCUMENT ID		TECN	COMMENT
0.129±0.014	[1] AAIJ	21Q	LHCB	pp at 7, 8, 13 TeV
• • • We do not use the following data for averages, fits, limits, etc. • • •				
0.100±0.031±0.009	[2] AAIJ	16L	LHCB	pp at 7, 8 TeV
0.143±0.062±0.011	AAIJ	12M	LHCB	Repl. by AAIJ 16L

[1] The statistical and systematic uncertainties have been combined according to the correlations between the R^-_π and R^+_π observables.
[2] Superseded by AAIJ 21Q.

$A_{ADS}(B^+ \to D^*(D\gamma) K^+)$

$A_{ADS}(B^+ \to D^*(D\gamma) K^+) = (R^-_K - R^+_K) / (R^-_K + R^+_K)$, where

$R^-_K = \Gamma(B^- \to (\gamma[K^+\pi^-]_D)_{D^*} K^-) / \Gamma(B^- \to (\gamma[K^-\pi^+]_D)_{D^*} K^-)$ and

$R^+_K = \Gamma(B^+ \to (\gamma[K^-\pi^+]_D)_{D^*} K^+) / \Gamma(B^+ \to (\gamma[K^+\pi^-]_D)_{D^*} K^+)$

VALUE	DOCUMENT ID		TECN	COMMENT
−0.558±1.349	[1] AAIJ	21Q	LHCB	pp at 7, 8, 13 TeV

[1] The statistical and systematic uncertainties have been combined according to the correlations between the R^-_K and R^+_K observables.

$A_{ADS}(B^+ \to D^*(D\pi^0) K^+)$

$A_{ADS}(B^+ \to D^*(D\pi^0) K^+) = (R^-_K - R^+_K) / (R^-_K + R^+_K)$, where

$R^-_K = \Gamma(B^- \to ([K^+\pi^-]_D \pi^0)_{D^*} K^-) / \Gamma(B^- \to ([K^-\pi^+]_D \pi^0)_{D^*} K^-)$ and

$R^+_K = \Gamma(B^+ \to ([K^-\pi^+]_D \pi^0)_{D^*} K^+) / \Gamma(B^+ \to ([K^+\pi^-]_D \pi^0)_{D^*} K^+)$

VALUE	DOCUMENT ID		TECN	COMMENT
0.717±0.286	[1] AAIJ	21Q	LHCB	pp at 7, 8, 13 TeV

[1] The statistical and systematic uncertainties have been combined according to the correlations between the R^-_K and R^+_K observables.

$A_{ADS}(B^+ \to D^*(D\gamma)\pi^+)$

$A_{ADS}(B^+ \to D^*(D\gamma)\pi^+) = (R^-_\pi - R^+_\pi) / (R^-_\pi + R^+_\pi)$, where

$R^-_\pi = \Gamma(B^- \to (\gamma[K^+\pi^-]_D)_{D^*} \pi^-) / \Gamma(B^- \to (\gamma[K^-\pi^+]_D)_{D^*} \pi^-)$ and

$R^+_\pi = \Gamma(B^+ \to (\gamma[K^-\pi^+]_D)_{D^*} \pi^+) / \Gamma(B^+ \to (\gamma[K^+\pi^-]_D)_{D^*} \pi^+)$

VALUE	DOCUMENT ID		TECN	COMMENT
0.079±0.128	[1] AAIJ	21Q	LHCB	pp at 7, 8, 13 TeV

[1] The statistical and systematic uncertainties have been combined according to the correlations between the R^-_π and R^+_π observables.

$A_{ADS}(B^+ \to D^*(D\pi^0)\pi^+)$

$A_{ADS}(B^+ \to D^*(D\pi^0)\pi^+) = (R^-_\pi - R^+_\pi) / (R^-_\pi + R^+_\pi)$, where

$R^-_\pi = \Gamma(B^- \to ([K^+\pi^-]_D \pi^0)_{D^*} \pi^-) / \Gamma(B^- \to ([K^-\pi^+]_D \pi^0)_{D^*} \pi^-)$ and

$R^+_\pi = \Gamma(B^+ \to ([K^-\pi^+]_D \pi^0)_{D^*} \pi^+) / \Gamma(B^+ \to ([K^+\pi^-]_D \pi^0)_{D^*} \pi^+)$

VALUE	DOCUMENT ID		TECN	COMMENT
−0.140±0.059	[1] AAIJ	21Q	LHCB	pp at 7, 8, 13 TeV

[1] The statistical and systematic uncertainties have been combined according to the correlations between the R^-_π and R^+_π observables.

$A_{ADS}(B^+ \to [K^-\pi^+]_D K^+\pi^-\pi^+)$

VALUE	DOCUMENT ID		TECN	COMMENT
$-0.33^{+0.36}_{-0.34}$	AAIJ	15BC	LHCB	pp at 7, 8 TeV

$A_{ADS}(B^+ \to [K^-\pi^+]_D \pi^+\pi^-\pi^+)$

VALUE	DOCUMENT ID		TECN	COMMENT
−0.013±0.087	AAIJ	15BC	LHCB	pp at 7, 8 TeV

$A_{CP}(B^+ \to D_{CP(-1)} K^+)$

VALUE	DOCUMENT ID		TECN	COMMENT
−0.10±0.07 OUR AVERAGE				
−0.09±0.07±0.02	DEL-AMO-SA...	10G	BABR	$e^+e^- \to \Upsilon(4S)$
−0.12±0.14±0.05	ABE	06	BELL	$e^+e^- \to \Upsilon(4S)$
• • • We do not use the following data for averages, fits, limits, etc. • • •				
−0.09±0.09±0.02	AUBERT	08AA	BABR	Repl. by DEL-AMO-SANCHEZ 10G
−0.06±0.13±0.04	AUBERT	06J	BABR	Repl. by AUBERT 08AA
−0.22±0.24±0.04	[1] ABE	03D	BELL	Repl. by SWAIN 03
−0.19±0.17±0.05	[2] SWAIN	03	BELL	Repl. by ABE 06

[1] Corresponds to 90% confidence range $-0.62 < A_{CP} < 0.18$.
[2] Corresponds to 90% confidence range $-0.47 < A_{CP} < 0.11$.

$A_{CP}(B^+ \to [K^+K^-]_D K^+\pi^-\pi^+)$

VALUE	DOCUMENT ID		TECN	COMMENT
−0.045±0.064±0.011	AAIJ	15BC	LHCB	pp at 7, 8 TeV

Downloaded from https://academic.oup.com/ptep/article/2022/8/083C01/6651666 by KIT Library user on 27 September 2022

$A_{CP}(B^+ \to [\pi^+\pi^-]_D K^+\pi^-\pi^+)$

VALUE	DOCUMENT ID		TECN	COMMENT
$-0.054\pm0.101\pm0.011$	AAIJ	15BC	LHCB	pp at 7, 8 TeV

$A_{CP}(B^+ \to [K^-\pi^+]_D K^+\pi^-\pi^+)$

VALUE	DOCUMENT ID		TECN	COMMENT
$0.013\pm0.019\pm0.013$	AAIJ	15BC	LHCB	pp at 7, 8 TeV

$A_{CP}(B^+ \to [K^+K^-]_D \pi^+\pi^-\pi^+)$

VALUE	DOCUMENT ID		TECN	COMMENT
$-0.019\pm0.011\pm0.010$	AAIJ	15BC	LHCB	pp at 7, 8 TeV

$A_{CP}(B^+ \to [\pi^+\pi^-]_D \pi^+\pi^-\pi^+)$

VALUE	DOCUMENT ID		TECN	COMMENT
$-0.013\pm0.016\pm0.010$	AAIJ	15BC	LHCB	pp at 7, 8 TeV

$A_{CP}(B^+ \to [K^-\pi^+]_D \pi^+\pi^-\pi^+)$

VALUE	DOCUMENT ID		TECN	COMMENT
$-0.002\pm0.003\pm0.011$	AAIJ	15BC	LHCB	pp at 7, 8 TeV

$A_{CP}(B^+ \to \overline{D}^{*0}\pi^+)$

VALUE	DOCUMENT ID		TECN	COMMENT
-0.0004 ± 0.0021 OUR AVERAGE	Error includes scale factor of 1.1.			
$-0.004\ \pm0.004\ \pm0.001$	[1] AAIJ	21Q	LHCB	pp at 7, 8, 13 TeV
$0.001\ \pm0.002\ \pm0.001$	[2] AAIJ	21Q	LHCB	pp at 7, 8, 13 TeV
$-0.014\ \pm0.015$	ABE	06	BELL	$e^+e^- \to \Upsilon(4S)$
• • • We do not use the following data for averages, fits, limits, etc. • • •				
$0.000\ \pm0.006\ \pm0.001$	[1,3] AAIJ	18A	LHCB	pp at 7, 8, 13 TeV
$0.002\ \pm0.003\ \pm0.001$	[2,3] AAIJ	18A	LHCB	pp at 7, 8, 13 TeV

[1] Uses $D^{*0} \to D^0\gamma$ decay mode.
[2] Uses $D^{*0} \to D^0\pi^0$ decay mode.
[3] Superseded by AAIJ 21Q.

$A_{CP}(B^+ \to (D^*_{CP(+1)})^0\pi^+)$

VALUE	DOCUMENT ID		TECN	COMMENT
0.010 ± 0.007 OUR AVERAGE				
$0.000\pm0.014\pm0.006$	[1] AAIJ	21Q	LHCB	pp at 7, 8, 13 TeV
$0.013\pm0.007\pm0.003$	[2] AAIJ	21Q	LHCB	pp at 7, 8, 13 TeV
-0.021 ± 0.045	ABE	06	BELL	$e^+e^- \to \Upsilon(4S)$
• • • We do not use the following data for averages, fits, limits, etc. • • •				
$-0.003\pm0.017\pm0.002$	[1,3] AAIJ	18A	LHCB	pp at 7, 8, 13 TeV
$0.025\pm0.010\pm0.003$	[2,3] AAIJ	18A	LHCB	pp at 7, 8, 13 TeV

[1] Uses $D^{*0} \to D^0\gamma$ decay mode.
[2] Uses $D^{*0} \to D^0\pi^0$ decay mode.
[3] Superseded by AAIJ 21Q.

$A_{CP}(B^+ \to (D^*_{CP(-1)})^0\pi^+)$

VALUE	DOCUMENT ID		TECN	COMMENT
-0.090 ± 0.051	ABE	06	BELL	$e^+e^- \to \Upsilon(4S)$

$A_{CP}(B^+ \to D^{*0}K^+)$

VALUE	DOCUMENT ID		TECN	COMMENT
0.012 ± 0.010 OUR AVERAGE	Error includes scale factor of 1.5.			
$-0.004\pm0.014\pm0.003$	[1] AAIJ	21Q	LHCB	pp at 7, 8, 13 TeV
$0.020\pm0.007\pm0.003$	[2] AAIJ	21Q	LHCB	pp at 7, 8, 13 TeV
$-0.06\ \pm0.04\ \pm0.01$	AUBERT	08BF	BABR	$e^+e^- \to \Upsilon(4S)$
-0.089 ± 0.086	ABE	06	BELL	$e^+e^- \to \Upsilon(4S)$
• • • We do not use the following data for averages, fits, limits, etc. • • •				
$0.001\pm0.021\pm0.007$	[1,3] AAIJ	18A	LHCB	pp at 7, 8, 13 TeV
$0.006\pm0.012\pm0.004$	[2,3] AAIJ	18A	LHCB	pp at 7, 8, 13 TeV

[1] Uses $D^{*0} \to D^0\gamma$ decay mode.
[2] Uses $D^{*0} \to D^0\pi^0$ decay mode.
[3] Superseded by AAIJ 21Q.

$A_{CP}(B^+ \to D^{*0}_{CP(+1)}K^+)$

VALUE	DOCUMENT ID		TECN	COMMENT
$-0.09\ \pm0.05$ OUR AVERAGE	Error includes scale factor of 2.6. See the ideogram below.			
$0.123\pm0.054\pm0.031$	[1] AAIJ	21Q	LHCB	pp at 7, 8, 13 TeV
$-0.115\pm0.019\pm0.009$	[2] AAIJ	21Q	LHCB	pp at 7, 8, 13 TeV
$-0.11\ \pm0.09\ \pm0.01$	AUBERT	08BF	BABR	$e^+e^- \to \Upsilon(4S)$
$-0.20\ \pm0.22\ \pm0.04$	ABE	06	BELL	$e^+e^- \to \Upsilon(4S)$
• • • We do not use the following data for averages, fits, limits, etc. • • •				
$0.276\pm0.094\pm0.047$	[1,3] AAIJ	18A	LHCB	pp at 7, 8, 13 TeV
$-0.151\pm0.033\pm0.011$	[2,3] AAIJ	18A	LHCB	pp at 7, 8, 13 TeV
$-0.10\ \pm0.23\ ^{+0.03}_{-0.04}$	AUBERT	05N	BABR	Repl. by AUBERT 08BF

[1] Uses $D^{*0} \to D^0\gamma$ decay mode.
[2] Uses $D^{*0} \to D^0\pi^0$ decay mode.
[3] Superseded by AAIJ 21Q.

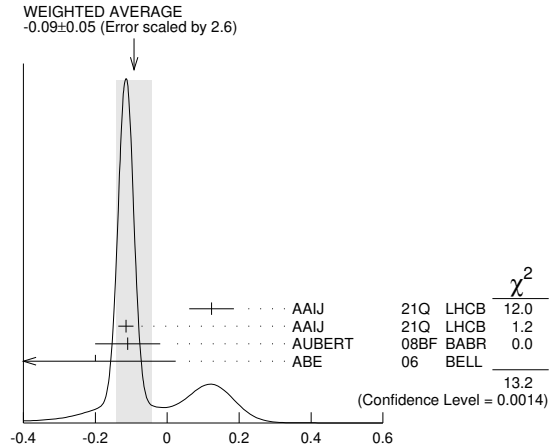

$A_{CP}(B^+ \to D^{*0}_{CP(+1)}K^+)$

$A_{CP}(B^+ \to D^*_{CP(-1)}K^+)$

VALUE	DOCUMENT ID		TECN	COMMENT
0.07 ± 0.10 OUR AVERAGE				
$+0.06\pm0.10\pm0.02$	AUBERT	08BF	BABR	$e^+e^- \to \Upsilon(4S)$
$+0.13\pm0.30\pm0.08$	ABE	06	BELL	$e^+e^- \to \Upsilon(4S)$

$A_{CP}(B^+ \to D_{CP(+1)}K^*(892)^+)$

VALUE	DOCUMENT ID		TECN	COMMENT
0.08 ± 0.06 OUR AVERAGE				
$0.08\pm0.06\pm0.01$	[1] AAIJ	17BO	LHCB	pp at 7, 8, 13 TeV
$0.09\pm0.13\pm0.06$	AUBERT	09AJ	BABR	$e^+e^- \to \Upsilon(4S)$
• • • We do not use the following data for averages, fits, limits, etc. • • •				
$-0.08\pm0.19\pm0.08$	AUBERT,B	05U	BABR	Repl. by AUBERT 09AJ

[1] Measures the asymmetry separately for K^+K^- and $\pi^+\pi^-$ final states, $A(KK) = 0.06\pm0.07\pm0.01$and $A(\pi\pi) = 0.15\pm0.13\pm0.01$, and combines the two results. The value of $A(\pi\pi)$ was updated in AAIJ 18X.

$A_{CP}(B^+ \to D_{CP(-1)}K^*(892)^+)$

VALUE	DOCUMENT ID		TECN	COMMENT
$-0.23\pm0.21\pm0.07$	AUBERT	09AJ	BABR	$e^+e^- \to \Upsilon(4S)$
• • • We do not use the following data for averages, fits, limits, etc. • • •				
$-0.26\pm0.40\pm0.12$	AUBERT,B	05U	BABR	Repl. by AUBERT 09AJ

$A_{CP}(B^+ \to D_s^+\phi)$

VALUE	DOCUMENT ID		TECN	COMMENT
$-0.01\pm0.41\pm0.03$	AAIJ	13R	LHCB	pp at 7 TeV

$A_{CP}(B^+ \to D_s^+\overline{D}^0)$

VALUE (%)	DOCUMENT ID		TECN	COMMENT
$-0.4\pm0.5\pm0.5$	AAIJ	18W	LHCB	pp at 7, 8 TeV

$A_{CP}(B^+ \to D^{*+}\overline{D}^{*0})$

VALUE	DOCUMENT ID		TECN	COMMENT
$-0.15\pm0.11\pm0.02$	AUBERT,B	06A	BABR	$e^+e^- \to \Upsilon(4S)$

$A_{CP}(B^+ \to D^{*+}\overline{D}^0)$

VALUE	DOCUMENT ID		TECN	COMMENT
$-0.06\pm0.13\pm0.02$	AUBERT,B	06A	BABR	$e^+e^- \to \Upsilon(4S)$

$A_{CP}(B^+ \to D^+\overline{D}^{*0})$

VALUE	DOCUMENT ID		TECN	COMMENT
$0.13\pm0.18\pm0.04$	AUBERT,B	06A	BABR	$e^+e^- \to \Upsilon(4S)$

$A_{CP}(B^+ \to D^+\overline{D}^0)$

VALUE	DOCUMENT ID		TECN	COMMENT
0.016 ± 0.025 OUR AVERAGE				
$0.023\pm0.027\pm0.004$	AAIJ	18W	LHCB	pp at 7, 8 TeV
$0.00\ \pm0.08\ \pm0.02$	ADACHI	08	BELL	$e^+e^- \to \Upsilon(4S)$
$-0.13\ \pm0.14\ \pm0.02$	AUBERT,B	06A	BABR	$e^+e^- \to \Upsilon(4S)$

$A_{CP}(B^+ \to K_S^0\pi^+)$

VALUE	DOCUMENT ID		TECN	COMMENT
-0.017 ± 0.016 OUR AVERAGE				
$-0.022\pm0.025\pm0.010$	AAIJ	13BS	LHCB	pp at 7 TeV
$-0.011\pm0.021\pm0.006$	DUH	13	BELL	$e^+e^- \to \Upsilon(4S)$
$-0.029\pm0.039\pm0.010$	[1] AUBERT,BE	06C	BABR	$e^+e^- \to \Upsilon(4S)$
$0.18\ \pm0.24$	[2] CHEN	00	CLE2	$e^+e^- \to \Upsilon(4S)$

Downloaded from https://academic.oup.com/ptep/article/2022/8/083C01/6651666 by KIT Library user on 27 September 2022

• • • We do not use the following data for averages, fits, limits, etc. • • •

$0.03 \pm 0.03 \pm 0.01$	LIN	07	BELL	Repl. by DUH 13
$-0.09 \pm 0.05 \pm 0.01$	[3] AUBERT,BE	05E	BABR	Repl. by AUBERT,BE 06C
$0.05 \pm 0.05 \pm 0.01$	[4] CHAO	05A	BELL	Repl. by LIN 07
$-0.05 \pm 0.08 \pm 0.01$	[5] AUBERT	04M	BABR	Repl. by AUBERT,BE 05E
$0.07 {}^{+0.09}_{-0.08} {}^{+0.01}_{-0.03}$	[6] UNNO	03	BELL	Repl. by CHAO 05A
$0.46 \pm 0.15 \pm 0.02$	[7] CASEY	02	BELL	Repl. by UNNO 03
$0.098 {}^{+0.430}_{-0.343} {}^{+0.020}_{-0.063}$	[8] ABE	01K	BELL	Repl. by CASEY 02
$-0.21 \pm 0.18 \pm 0.03$	[9] AUBERT	01E	BABR	Repl. by AUBERT 04M

[1] Corresponds to 90% confidence range $-0.092 < A_{CP} < 0.036$.
[2] Corresponds to 90% confidence range $-0.22 < A_{CP} < 0.56$.
[3] Corresponds to 90% confidence range $-0.16 < A_{CP} < -0.02$.
[4] Corresponds to 90% confidence range $-0.04 < A_{CP} < 0.13$.
[5] Corresponds to 90% confidence range $-0.18 < A_{CP} < 0.08$.
[6] Corresponds to 90% confidence range $-0.10 < A_{CP} < +0.22$.
[7] Corresponds to 90% confidence range $+0.19 < A_{CP} < +0.72$.
[8] Corresponds to 90% confidence range $-0.53 < A_{CP} < 0.82$.
[9] Corresponds to 90% confidence range $-0.51 < A_{CP} < 0.09$.

$A_{CP}(B^+ \to K^+\pi^0)$

VALUE	DOCUMENT ID		TECN	COMMENT
0.030±0.013 OUR AVERAGE				
$0.025 \pm 0.015 \pm 0.007$	AAIJ	21H	LHCB	pp at 13 TeV
$0.043 \pm 0.024 \pm 0.002$	DUH	13	BELL	$e^+e^- \to \Upsilon(4S)$
$0.030 \pm 0.039 \pm 0.010$	AUBERT	07BC	BABR	$e^+e^- \to \Upsilon(4S)$
-0.29 ± 0.23	[1] CHEN	00	CLE2	$e^+e^- \to \Upsilon(4S)$
• • • We do not use the following data for averages, fits, limits, etc. • • •				
$0.07 \pm 0.03 \pm 0.01$	LIN	08	BELL	Repl. by DUH 13
$0.06 \pm 0.06 \pm 0.01$	[2] AUBERT	05L	BABR	Repl. by AUBERT 07BC
$0.06 \pm 0.06 \pm 0.02$	[2] CHAO	05A	BELL	Repl. by CHAO 04B
$0.04 \pm 0.05 \pm 0.02$	[3] CHAO	04B	BELL	Repl. by LIN 08
$-0.09 \pm 0.09 \pm 0.01$	[4] AUBERT	03L	BABR	Repl. by AUBERT 05L
$-0.02 \pm 0.19 \pm 0.02$	[5] CASEY	02	BELL	Repl. by CHAO 04B
$-0.059 {}^{+0.222}_{-0.196} {}^{+0.055}_{-0.017}$	[6] ABE	01K	BELL	Repl. by CASEY 02
$0.00 \pm 0.18 \pm 0.04$	[7] AUBERT	01E	BABR	Repl. by AUBERT 03L

[1] Corresponds to 90% confidence range $-0.67 < A_{CP} < 0.09$.
[2] Corresponds to a 90% CL interval of $-0.06 < A_{CP} < 0.18$.
[3] Corresponds to 90% CL interval of $-0.05 < A_{CP} < 0.13$.
[4] Corresponds to 90% confidence range $-0.24 < A_{CP} < 0.06$.
[5] Corresponds to 90% confidence range $-0.35 < A_{CP} < +0.30$.
[6] Corresponds to 90% confidence range $-0.40 < A_{CP} < 0.36$.
[7] Corresponds to 90% confidence range $-0.30 < A_{CP} < +0.30$.

$A_{CP}(B^+ \to \eta' K^+)$

VALUE	DOCUMENT ID		TECN	COMMENT
0.004±0.011 OUR AVERAGE				
$-0.002 \pm 0.012 \pm 0.006$	[1] AAIJ	15O	LHCB	pp at 7, 8 TeV
$0.008 {}^{+0.017}_{-0.018} \pm 0.009$	AUBERT	09AV	BABR	$e^+e^- \to \Upsilon(4S)$
$0.028 \pm 0.028 \pm 0.021$	SCHUEMANN	06	BELL	$e^+e^- \to \Upsilon(4S)$
0.03 ± 0.12	[2] CHEN	00	CLE2	$e^+e^- \to \Upsilon(4S)$
• • • We do not use the following data for averages, fits, limits, etc. • • •				
$0.010 \pm 0.022 \pm 0.006$	AUBERT	07AE	BABR	Repl. by AUBERT 09AV
$0.033 \pm 0.028 \pm 0.005$	[3] AUBERT	05M	BABR	Repl. by AUBERT 07AE
$0.037 \pm 0.045 \pm 0.011$	[4] AUBERT	03W	BABR	Repl. by AUBERT 05M
$-0.11 \pm 0.11 \pm 0.02$	[5] AUBERT	02E	BABR	Repl. by AUBERT 05M
$-0.015 \pm 0.070 \pm 0.009$	[6] CHEN	02B	BELL	Repl. by SCHUEMANN 06
$0.06 \pm 0.15 \pm 0.01$	[7] ABE	01M	BELL	Repl. by CHEN 02B

[1] Obtained using $A_{CP}(B^{\pm} \to J/\psi K^{\pm}) = (0.3 \pm 0.6) \times 10^{-2}$.
[2] Corresponds to 90% confidence range $-0.17 < A_{CP} < 0.23$.
[3] Corresponds to 90% confidence range $-0.012 < A_{CP} < 0.078$.
[4] Corresponds to 90% confidence range $-0.04 < A_{CP} < 0.11$.
[5] Corresponds to 90% confidence range $-0.28 < A_{CP} < 0.07$.
[6] Corresponds to 90% confidence range $-0.13 < A_{CP} < 0.10$.
[7] Corresponds to 90% confidence range $-0.20 < A_{CP} < 0.32$.

$A_{CP}(B^+ \to \eta' K^*(892)^+)$

VALUE	DOCUMENT ID		TECN	COMMENT
−0.26±0.27±0.02	DEL-AMO-SA...	10A	BABR	$e^+e^- \to \Upsilon(4S)$
• • • We do not use the following data for averages, fits, limits, etc. • • •				
$-0.30 {}^{+0.33}_{-0.37} \pm 0.02$	[1] AUBERT	07E	BABR	Repl. by DEL-AMO-SANCHEZ 10A

[1] Reports A_{CP} with the opposite sign convention.

$A_{CP}(B^+ \to \eta' K_0^*(1430)^+)$

VALUE	DOCUMENT ID		TECN	COMMENT
0.06±0.20±0.02	DEL-AMO-SA...	10A	BABR	$e^+e^- \to \Upsilon(4S)$

$A_{CP}(B^+ \to \eta' K_2^*(1430)^+)$

VALUE	DOCUMENT ID		TECN	COMMENT
0.15±0.13±0.02	DEL-AMO-SA...	10A	BABR	$e^+e^- \to \Upsilon(4S)$

$A_{CP}(B^+ \to \eta K^+)$

VALUE	DOCUMENT ID		TECN	COMMENT
−0.37±0.08 OUR AVERAGE				
$-0.38 \pm 0.11 \pm 0.01$	HOI	12	BELL	$e^+e^- \to \Upsilon(4S)$
$-0.36 \pm 0.11 \pm 0.03$	AUBERT	09AV	BABR	$e^+e^- \to \Upsilon(4S)$
• • • We do not use the following data for averages, fits, limits, etc. • • •				
$-0.22 \pm 0.11 \pm 0.01$	AUBERT	07AE	BABR	Repl. by AUBERT 09AV
$-0.39 \pm 0.16 \pm 0.03$	CHANG	07B	BELL	Repl. by HOI 12
$-0.20 \pm 0.15 \pm 0.01$	AUBERT,B	05K	BABR	Repl. by AUBERT 07AE
$-0.49 \pm 0.31 \pm 0.07$	CHANG	05A	BELL	Repl. by CHANG 07B
$-0.52 \pm 0.24 \pm 0.01$	AUBERT	04H	BABR	Repl. by AUBERT,B 05K

$A_{CP}(B^+ \to \eta K^*(892)^+)$

VALUE	DOCUMENT ID		TECN	COMMENT
0.02±0.06 OUR AVERAGE				
$0.03 \pm 0.10 \pm 0.01$	WANG	07B	BELL	$e^+e^- \to \Upsilon(4S)$
$0.01 \pm 0.08 \pm 0.02$	AUBERT,B	06H	BABR	$e^+e^- \to \Upsilon(4S)$
• • • We do not use the following data for averages, fits, limits, etc. • • •				
$0.13 \pm 0.14 \pm 0.02$	AUBERT,B	04D	BABR	Repl. by AUBERT,B 06H

$A_{CP}(B^+ \to \eta K_0^*(1430)^+)$

VALUE	DOCUMENT ID		TECN	COMMENT
0.05±0.13±0.02	AUBERT,B	06H	BABR	$e^+e^- \to \Upsilon(4S)$

$A_{CP}(B^+ \to \eta K_2^*(1430)^+)$

VALUE	DOCUMENT ID		TECN	COMMENT
−0.45±0.30±0.02	AUBERT,B	06H	BABR	$e^+e^- \to \Upsilon(4S)$

$A_{CP}(B^+ \to \omega K^+)$

VALUE	DOCUMENT ID		TECN	COMMENT
−0.02±0.04 OUR AVERAGE				
$-0.03 \pm 0.04 \pm 0.01$	CHOBANOVA	14	BELL	$e^+e^- \to \Upsilon(4S)$
$-0.01 \pm 0.07 \pm 0.01$	AUBERT	07AE	BABR	$e^+e^- \to \Upsilon(4S)$
• • • We do not use the following data for averages, fits, limits, etc. • • •				
$0.05 \pm 0.09 \pm 0.01$	AUBERT,B	06E	BABR	Repl. by AUBERT 07AE
$0.05 {}^{+0.08}_{-0.07} \pm 0.01$	JEN	06	BELL	Repl. by CHOBANOVA 14
$-0.09 \pm 0.17 \pm 0.01$	AUBERT	04H	BABR	Repl. by AUBERT,B 06E
$0.06 {}^{+0.21}_{-0.18} \pm 0.01$	[1] WANG	04A	BELL	Repl. by JEN 06
$-0.21 \pm 0.28 \pm 0.03$	[2] LU	02	BELL	Repl. by WANG 04A

[1] Corresponds to 90% CL interval $0.15 < A_{CP} < 0.90$
[2] Corresponds to 90% confidence range $-0.70 < A_{CP} < +0.38$.

$A_{CP}(B^+ \to \omega K^{*+})$

VALUE	DOCUMENT ID		TECN	COMMENT
+0.29±0.35±0.02	AUBERT	09H	BABR	$e^+e^- \to \Upsilon(4S)$

$A_{CP}(B^+ \to \omega(K\pi)_0^{*+})$

VALUE	DOCUMENT ID		TECN	COMMENT
−0.10±0.09±0.02	AUBERT	09H	BABR	$e^+e^- \to \Upsilon(4S)$

$A_{CP}(B^+ \to \omega K_2^*(1430)^+)$

VALUE	DOCUMENT ID		TECN	COMMENT
+0.14±0.15±0.02	AUBERT	09H	BABR	$e^+e^- \to \Upsilon(4S)$

$A_{CP}(B^+ \to K^{*0}\pi^+)$

VALUE	DOCUMENT ID		TECN	COMMENT
−0.04 ±0.09 OUR AVERAGE Error includes scale factor of 2.1.				
$-0.12 \pm 0.21 {}^{+0.08}_{-0.14}$	[1] LEES	17G	BABR	$e^+e^- \to \Upsilon(4S)$
$0.032 \pm 0.052 {}^{+0.016}_{-0.013}$	AUBERT	08AI	BABR	$e^+e^- \to \Upsilon(4S)$
$-0.149 \pm 0.064 \pm 0.022$	GARMASH	06	BELL	$e^+e^- \to \Upsilon(4S)$
• • • We do not use the following data for averages, fits, limits, etc. • • •				
$0.068 \pm 0.078 {}^{+0.070}_{-0.067}$	AUBERT,B	05N	BABR	Repl. by AUBERT 08AI

[1] Obtains the result from a Dalitz analysis of $B^+ \to K_S^0\pi^+\pi^0$ decays. The first error is statistical, the second combines all the systematic uncertainties reported in the paper, including signal modelling.

$A_{CP}(B^+ \to K^*(892)^+\pi^0)$

VALUE	DOCUMENT ID		TECN	COMMENT
−0.39±0.21 OUR AVERAGE Error includes scale factor of 1.6.				
$-0.52 \pm 0.14 {}^{+0.06}_{-0.05}$	[1] LEES	17G	BABR	$e^+e^- \to \Upsilon(4S)$
$-0.06 \pm 0.24 \pm 0.04$	LEES	11I	BABR	$e^+e^- \to \Upsilon(4S)$
• • • We do not use the following data for averages, fits, limits, etc. • • •				
$0.04 \pm 0.29 \pm 0.05$	AUBERT	05X	BABR	Repl. by LEES 11I

[1] Obtains the result from a Dalitz analysis of $B^+ \to K_S^0\pi^+\pi^0$ decays. The first error is statistical, the second combines all the systematic uncertainties reported in the paper, including signal modelling.

$A_{CP}(B^+ \to K^+\pi^-\pi^+)$

VALUE	DOCUMENT ID		TECN	COMMENT
0.027±0.008 OUR AVERAGE				
$0.025 \pm 0.004 \pm 0.008$	[1] AAIJ	14BO	LHCB	pp at 7, 8 TeV
$0.028 \pm 0.020 \pm 0.023$	AUBERT	08AI	BABR	$e^+e^- \to \Upsilon(4S)$
$0.049 \pm 0.026 \pm 0.020$	GARMASH	06	BELL	$e^+e^- \to \Upsilon(4S)$

Downloaded from https://academic.oup.com/ptep/article/2022/8/083C01/6651666 by KIT Library user on 27 September 2022

• • • We do not use the following data for averages, fits, limits, etc. • • •

$0.032 \pm 0.008 \pm 0.008$	AAIJ	13AZ	LHCB	Repl. by AAIJ 14BO
$-0.013 \pm 0.037 \pm 0.011$	AUBERT,B	05N	BABR	Repl. by AUBERT 08AI
$0.01 \pm 0.07 \pm 0.03$	AUBERT	03M	BABR	Repl. by AUBERT,B 05N

[1] AAIJ 14BO reports also *CP* asymmetries in restricted regions of phase space.

$A_{CP}(B^+ \to K^+ K^- K^+$ nonresonant)

VALUE	DOCUMENT ID		TECN	COMMENT
$0.060 \pm 0.044 \pm 0.019$	LEES	12O	BABR	$e^+e^- \to \Upsilon(4S)$

$A_{CP}(B^+ \to f(980)^0 K^+)$

VALUE	DOCUMENT ID		TECN	COMMENT
$-0.08 \pm 0.08 \pm 0.04$	[1] LEES	12O	BABR	$e^+e^- \to \Upsilon(4S)$

[1] Measured in the $B^+ \to K^+ K^- K^+$ decay.

$A_{CP}(B^+ \to f_2(1270) K^+)$

VALUE	DOCUMENT ID		TECN	COMMENT
$-0.68^{+0.19}_{-0.17}$ OUR AVERAGE				
$-0.85 \pm 0.22^{+0.26}_{-0.13}$	AUBERT	08AI	BABR	$e^+e^- \to \Upsilon(4S)$
$-0.59 \pm 0.22 \pm 0.036$	GARMASH	06	BELL	$e^+e^- \to \Upsilon(4S)$

$A_{CP}(B^+ \to f_0(1500) K^+)$

VALUE	DOCUMENT ID		TECN	COMMENT
$0.28 \pm 0.26^{+0.15}_{-0.14}$	AUBERT	08AI	BABR	$e^+e^- \to \Upsilon(4S)$

$A_{CP}(B^+ \to f'_2(1525)^0 K^+)$

VALUE	DOCUMENT ID		TECN	COMMENT
$-0.08^{+0.05}_{-0.04}$ OUR AVERAGE				
$0.18 \pm 0.18 \pm 0.04$	[1] LEES	11I	BABR	$e^+e^- \to \Upsilon(4S)$
$-0.106 \pm 0.050^{+0.036}_{-0.015}$	AUBERT	08AI	BABR	$e^+e^- \to \Upsilon(4S)$
$-0.077 \pm 0.065^{+0.046}_{-0.026}$	GARMASH	06	BELL	$e^+e^- \to \Upsilon(4S)$

• • • We do not use the following data for averages, fits, limits, etc. • • •

$0.14 \pm 0.10 \pm 0.04$	[2] LEES	12O	BABR	$e^+e^- \to \Upsilon(4S)$
$-0.31 \pm 0.25 \pm 0.08$	[3] AUBERT	06O	BABR	Repl. by LEES 12O
$0.088 \pm 0.095^{+0.097}_{-0.056}$	AUBERT,B	05N	BABR	Repl. by AUBERT 08AI

[1] Measured in $B^+ \to f_0 K^+$ with $f_0 \to \pi^0\pi^0$ decay.
[2] Measured in the $B^+ \to K^+ K^- K^+$ decay assuming $A_{CP}(B^+ \to f'_2(1525)^0 K^+) = A_{CP}(B^+ \to f_0(1500)^0 K^+) = A_{CP}(B^+ \to f_0(1710)^0 K^+)$
[3] Measured in the $B^+ \to K^+ K^- K^+$ decay.

$A_{CP}(B^+ \to \rho^0 K^+)$

VALUE	DOCUMENT ID		TECN	COMMENT
0.37 ± 0.10 OUR AVERAGE				
$0.44 \pm 0.10^{+0.06}_{-0.14}$	AUBERT	08AI	BABR	$e^+e^- \to \Upsilon(4S)$
$0.30 \pm 0.11^{+0.11}_{-0.04}$	GARMASH	06	BELL	$e^+e^- \to \Upsilon(4S)$

• • • We do not use the following data for averages, fits, limits, etc. • • •

$0.32 \pm 0.13^{+0.10}_{-0.08}$	AUBERT,B	05N	BABR	Repl. by AUBERT 08AI

$A_{CP}(B^+ \to K^0 \pi^+ \pi^0)$

VALUE	DOCUMENT ID		TECN	COMMENT
$0.07 \pm 0.05 \pm 0.04$	[1] LEES	17G	BABR	$e^+e^- \to \Upsilon(4S)$

[1] Obtains the result from a Dalitz analysis of $B^+ \to K^0_S \pi^+ \pi^0$ decays. The first error is statistical, the second combines all the systematic uncertainties reported in the paper, including signal modelling.

$A_{CP}(B^+ \to K^*_0(1430)^0 \pi^+)$

VALUE	DOCUMENT ID		TECN	COMMENT
0.061 ± 0.032 OUR AVERAGE				
$0.14 \pm 0.10^{+0.14}_{-0.06}$	[1] LEES	17G	BABR	$e^+e^- \to \Upsilon(4S)$
$0.032 \pm 0.035^{+0.034}_{-0.028}$	AUBERT	08AI	BABR	$e^+e^- \to \Upsilon(4S)$
$0.076 \pm 0.038^{+0.028}_{-0.022}$	GARMASH	06	BELL	$e^+e^- \to \Upsilon(4S)$

• • • We do not use the following data for averages, fits, limits, etc. • • •

$-0.064 \pm 0.032^{+0.023}_{-0.026}$	AUBERT,B	05N	BABR	Repl. by AUBERT 08AI

[1] Obtains the result from a Dalitz analysis of $B^+ \to K^0_S \pi^+ \pi^0$ decays. The first error is statistical, the second combines all the systematic uncertainties reported in the paper, including signal modelling.

$A_{CP}(B^+ \to K^*_0(1430)^+ \pi^0)$

VALUE	DOCUMENT ID		TECN	COMMENT
$0.26 \pm 0.12^{+0.14}_{-0.08}$	[1] LEES	17G	BABR	$e^+e^- \to \Upsilon(4S)$

[1] Obtains the result from a Dalitz analysis of $B^+ \to K^0_S \pi^+ \pi^0$ decays. The first error is statistical, the second combines all the systematic uncertainties reported in the paper, including signal modelling.

$A_{CP}(B^+ \to K^*_2(1430)^0 \pi^+)$

VALUE	DOCUMENT ID		TECN	COMMENT
$0.05 \pm 0.23^{+0.18}_{-0.08}$	AUBERT	08AI	BABR	$e^+e^- \to \Upsilon(4S)$

$A_{CP}(B^+ \to K^+ \pi^0 \pi^0)$

VALUE	DOCUMENT ID		TECN	COMMENT
$-0.06 \pm 0.06 \pm 0.04$	LEES	11I	BABR	$e^+e^- \to \Upsilon(4S)$

$A_{CP}(B^+ \to K^0 \rho^+)$

VALUE	DOCUMENT ID		TECN	COMMENT
-0.03 ± 0.15 OUR AVERAGE				
$0.21 \pm 0.19^{+0.24}_{-0.20}$	[1] LEES	17G	BABR	$e^+e^- \to \Upsilon(4S)$
$-0.12 \pm 0.17 \pm 0.02$	AUBERT	07Z	BABR	$e^+e^- \to \Upsilon(4S)$

[1] Obtains the result from a Dalitz analysis of $B^+ \to K^0_S \pi^+ \pi^0$ decays. The first error is statistical, the second combines all the systematic uncertainties reported in the paper, including signal modelling.

$A_{CP}(B^+ \to K^{*+} \pi^+ \pi^-)$

VALUE	DOCUMENT ID		TECN	COMMENT
$0.07 \pm 0.07 \pm 0.04$	AUBERT,B	06U	BABR	$e^+e^- \to \Upsilon(4S)$

$A_{CP}(B^+ \to \rho^0 K^*(892)^+)$

VALUE	DOCUMENT ID		TECN	COMMENT
$0.31 \pm 0.13 \pm 0.03$	DEL-AMO-SA...11D		BABR	$e^+e^- \to \Upsilon(4S)$

• • • We do not use the following data for averages, fits, limits, etc. • • •

$0.20^{+0.32}_{-0.29} \pm 0.04$	AUBERT	03V	BABR	Repl. by DEL-AMO-SANCHEZ 11D

$A_{CP}(B^+ \to K^*(892)^+ f_0(980))$

VALUE	DOCUMENT ID		TECN	COMMENT
$-0.15 \pm 0.12 \pm 0.03$	DEL-AMO-SA...11D		BABR	$e^+e^- \to \Upsilon(4S)$

• • • We do not use the following data for averages, fits, limits, etc. • • •

$-0.34 \pm 0.21 \pm 0.03$	AUBERT,B	06G	BABR	Repl. by DEL-AMO-SANCHEZ 11D

$A_{CP}(B^+ \to a_1^+ K^0)$

VALUE	DOCUMENT ID		TECN	COMMENT
$+0.12 \pm 0.11 \pm 0.02$	AUBERT	08F	BABR	$e^+e^- \to \Upsilon(4S)$

$A_{CP}(B^+ \to b_1^+ K^0)$

VALUE	DOCUMENT ID		TECN	COMMENT
$-0.03 \pm 0.15 \pm 0.02$	AUBERT	08AG	BABR	$e^+e^- \to \Upsilon(4S)$

$A_{CP}(B^+ \to K^*(892)^0 \rho^+)$

VALUE	DOCUMENT ID		TECN	COMMENT
$-0.01 \pm 0.16 \pm 0.02$	AUBERT,B	06G	BABR	$e^+e^- \to \Upsilon(4S)$

$A_{CP}(B^+ \to b_1^0 K^+)$

VALUE	DOCUMENT ID		TECN	COMMENT
$-0.46 \pm 0.20 \pm 0.02$	AUBERT	07BI	BABR	$e^+e^- \to \Upsilon(4S)$

$A_{CP}(B^+ \to K^0 K^+)$

VALUE	DOCUMENT ID		TECN	COMMENT
0.04 ± 0.14 OUR AVERAGE				
$0.014 \pm 0.168 \pm 0.002$	DUH	13	BELL	$e^+e^- \to \Upsilon(4S)$
$0.10 \pm 0.26 \pm 0.03$	[1] AUBERT,BE	06C	BABR	$e^+e^- \to \Upsilon(4S)$

• • • We do not use the following data for averages, fits, limits, etc. • • •

$0.13^{+0.23}_{-0.24} \pm 0.02$	LIN	07	BELL	Repl. by DUH 13
$0.15 \pm 0.33 \pm 0.03$	[2] AUBERT,BE	05E	BABR	Repl. by AUBERT,BE 06C

[1] Corresponds to 90% confidence range $-0.31 < A_{CP} < 0.54$.
[2] Corresponds to 90% confidence range $-0.43 < A_{CP} < 0.68$.

$A_{CP}(B^+ \to K^0_S K^+)$

VALUE	DOCUMENT ID		TECN	COMMENT
$-0.21 \pm 0.14 \pm 0.01$	AAIJ	13BS	LHCB	pp at 7 TeV

$A_{CP}(B^+ \to K^+ K^0_S K^0_S)$

VALUE	DOCUMENT ID		TECN	COMMENT
0.025 ± 0.031 OUR AVERAGE				
$0.016 \pm 0.039 \pm 0.009$	KALIYAR	19	BELL	$e^+e^- \to \Upsilon(4S)$
$0.04^{+0.04}_{-0.05} \pm 0.02$	LEES	12O	BABR	$e^+e^- \to \Upsilon(4S)$

• • • We do not use the following data for averages, fits, limits, etc. • • •

$-0.04 \pm 0.11 \pm 0.02$	[1] AUBERT,B	04V	BABR	Repl. by LEES 12O

[1] Corresponds to 90% confidence range $-0.23 < A_{CP} < 0.15$.

$A_{CP}(B^+ \to K^+ K^- \pi^+)$

VALUE	DOCUMENT ID		TECN	COMMENT
-0.122 ± 0.021 OUR AVERAGE				
$-0.170 \pm 0.073 \pm 0.017$	[1] HSU	17	BELL	$e^+e^- \to \Upsilon(4S)$
$-0.123 \pm 0.017 \pm 0.014$	[2] AAIJ	14BO	LHCB	pp at 7, 8 TeV
$0.00 \pm 0.10 \pm 0.03$	AUBERT	07BB	BABR	$e^+e^- \to \Upsilon(4S)$

Downloaded from https://academic.oup.com/ptep/article/2022/8/083C01/6651666 by KIT Library user on 27 September 2022

• • • We do not use the following data for averages, fits, limits, etc. • • •

$-0.141 \pm 0.040 \pm 0.019$	[3] AAIJ	14	LHCB	Repl. by AAIJ 14BO

[1] HSU 17 provides also measurement as a function of K^+K^- invariant mass.
[2] AAIJ 14BO reports also *CP* asymmetries in restricted regions of phase space.
[3] AAIJ 14 reports $A_{CP}(B^+ \to K^+K^-\pi^+) = -0.648 \pm 0.070 \pm 0.013 \pm 0.007$ in the Dalitz plot region of $m^2_{K^+K^-} < 1.5$ GeV^2/c^4. The third uncertainty is due to the *CP* asymmetry of the $B^{\pm} \to J/\psi K^{\pm}$ reference mode uncertainty.

$A_{CP}(B^+ \to K^+K^-\pi^+$ nonresonant$)$

VALUE	DOCUMENT ID		TECN	COMMENT
$-0.107 \pm 0.053 \pm 0.035$	[1] AAIJ	19AL	LHCB	pp at 7, 8 TeV

[1] Uses amplitude analysis of $B^{\pm} \to \pi^{\pm}K^+K^-$ decays.

$A_{CP}(B^+ \to K^+\overline{K}^*(892)^0)$

VALUE	DOCUMENT ID		TECN	COMMENT
$0.123 \pm 0.087 \pm 0.045$	[1] AAIJ	19AL	LHCB	pp at 7, 8 TeV

[1] Uses amplitude analysis of $B^{\pm} \to \pi^{\pm}K^+K^-$ decays.

$A_{CP}(B^+ \to K^+\overline{K}^*_0(1430)^0)$

VALUE	DOCUMENT ID		TECN	COMMENT
$0.104 \pm 0.149 \pm 0.088$	[1] AAIJ	19AL	LHCB	pp at 7, 8 TeV

[1] Uses amplitude analysis of $B^{\pm} \to \pi^{\pm}K^+K^-$ decays.

$A_{CP}(B^+ \to \phi\pi^+)$

VALUE	DOCUMENT ID		TECN	COMMENT
$0.098 \pm 0.436 \pm 0.266$	[1] AAIJ	19AL	LHCB	pp at 7, 8 TeV

[1] Uses amplitude analysis of $B^{\pm} \to \pi^{\pm}K^+K^-$ decays.

$A_{CP}(B^+ \to \pi^+(K^+K^-)_{S-wave})$

VALUE	DOCUMENT ID		TECN	COMMENT
$-0.664 \pm 0.038 \pm 0.019$	[1] AAIJ	19AL	LHCB	pp at 7, 8 TeV

[1] Uses amplitude analysis of $B^{\pm} \to \pi^{\pm}K^+K^-$ decays in the $\pi\pi - KK$ rescattering mass region of $0.95 < m(K^+K^-) < 1.42$ GeV/c^2.

$A_{CP}(B^+ \to K^+K^-K^+)$

VALUE	DOCUMENT ID		TECN	COMMENT
-0.033 ± 0.008 OUR AVERAGE				
$-0.036 \pm 0.004 \pm 0.007$	[1] AAIJ	14BO	LHCB	pp at 7, 8 TeV
$-0.017^{+0.019}_{-0.014} \pm 0.014$	[2] LEES	12O	BABR	$e^+e^- \to \Upsilon(4S)$
• • • We do not use the following data for averages, fits, limits, etc. • • •				
$-0.043 \pm 0.009 \pm 0.008$	AAIJ	13AZ	LHCB	Repl. by AAIJ 14BO
$-0.017 \pm 0.026 \pm 0.015$	AUBERT	06O	BABR	Repl. by LEES 12O
$0.02 \pm 0.07 \pm 0.03$	AUBERT	03M	BABR	Repl. by AUBERT 06O

[1] AAIJ 14BO reports also *CP* asymmetries in restricted regions of phase space.
[2] All intermediate charmonium and charm resonances are removed, except of χ_{c0}.

$A_{CP}(B^+ \to \phi K^+)$

VALUE	DOCUMENT ID		TECN	COMMENT
0.024 ± 0.028 OUR AVERAGE	Error includes scale factor of 2.3.			
$0.017 \pm 0.011 \pm 0.006$	[1] AAIJ	15O	LHCB	pp at 7, 8 TeV
$0.128 \pm 0.044 \pm 0.013$	LEES	12O	BABR	$e^+e^- \to \Upsilon(4S)$
$-0.07 \pm 0.17^{+0.03}_{-0.02}$	ACOSTA	05J	CDF	$p\overline{p}$ at 1.96 TeV
$0.01 \pm 0.12 \pm 0.05$	[2] CHEN	03B	BELL	$e^+e^- \to \Upsilon(4S)$
• • • We do not use the following data for averages, fits, limits, etc. • • •				
$0.022 \pm 0.021 \pm 0.009$	AAIJ	14A	LHCB	Repl. by AAIJ 15O
$0.00 \pm 0.08 \pm 0.02$	AUBERT	06O	BABR	Repl. by LEES 12O
$0.04 \pm 0.09 \pm 0.01$	[3] AUBERT	04A	BABR	Repl. by AUBERT 06O
$-0.05 \pm 0.20 \pm 0.03$	[4] AUBERT	02E	BABR	$e^+e^- \to \Upsilon(4S)$

[1] Obtained using $A_{CP}(B^{\pm} \to J/\psi K^{\pm}) = (0.3 \pm 0.6) \times 10^{-2}$.
[2] Corresponds to 90% confidence range $-0.20 < A_{CP} < 0.22$.
[3] Corresponds to 90% confidence range $-0.10 < A_{CP} < 0.18$.
[4] Corresponds to 90% confidence range $-0.37 < A_{CP} < 0.28$.

$A_{CP}(B^+ \to X_0(1550)K^+)$

VALUE	DOCUMENT ID		TECN	COMMENT
$-0.04 \pm 0.07 \pm 0.02$	[1] AUBERT	06O	BABR	$e^+e^- \to \Upsilon(4S)$

[1] Measured in the $B^+ \to K^+K^-K^+$ decay.

$A_{CP}(B^+ \to K^{*+}K^+K^-)$

VALUE	DOCUMENT ID		TECN	COMMENT
$0.11 \pm 0.08 \pm 0.03$	AUBERT,B	06U	BABR	$e^+e^- \to \Upsilon(4S)$

$A_{CP}(B^+ \to \phi K^*(892)^+)$

VALUE	DOCUMENT ID		TECN	COMMENT
-0.01 ± 0.08 OUR AVERAGE				
$0.00 \pm 0.09 \pm 0.04$	AUBERT	07BA	BABR	$e^+e^- \to \Upsilon(4S)$
$-0.02 \pm 0.14 \pm 0.03$	[1] CHEN	05A	BELL	$e^+e^- \to \Upsilon(4S)$
• • • We do not use the following data for averages, fits, limits, etc. • • •				
$0.16 \pm 0.17 \pm 0.03$	AUBERT	03V	BABR	Repl. by AUBERT 07BA
$-0.13 \pm 0.29^{+0.08}_{-0.11}$	[2] CHEN	03B	BELL	Repl. by CHEN 05A
$-0.43^{+0.36}_{-0.30} \pm 0.06$	[3] AUBERT	02E	BABR	Repl. by AUBERT 03V

[1] Corresponds to 90% confidence range $-0.25 < A_{CP} < 0.22$.
[2] Corresponds to 90% confidence range $-0.64 < A_{CP} < 0.36$.
[3] Corresponds to 90% confidence range $-0.88 < A_{CP} < 0.18$.

$A_{CP}(B^+ \to \phi(K\pi)^{*+}_0)$

VALUE	DOCUMENT ID		TECN	COMMENT
$0.04 \pm 0.15 \pm 0.04$	AUBERT	08BI	BABR	$e^+e^- \to \Upsilon(4S)$

$A_{CP}(B^+ \to \phi K_1(1270)^+)$

VALUE	DOCUMENT ID		TECN	COMMENT
$0.15 \pm 0.19 \pm 0.05$	AUBERT	08BI	BABR	$e^+e^- \to \Upsilon(4S)$

$A_{CP}(B^+ \to \phi K^*_2(1430)^+)$

VALUE	DOCUMENT ID		TECN	COMMENT
$-0.23 \pm 0.19 \pm 0.06$	AUBERT	08BI	BABR	$e^+e^- \to \Upsilon(4S)$

$A_{CP}(B^+ \to K^+\phi\phi)$

VALUE	DOCUMENT ID		TECN	COMMENT
-0.08 ± 0.07 OUR AVERAGE				
$-0.02 \pm 0.11 \pm 0.11$	[1] MOHANTY	21	BELL	$e^+e^- \to \Upsilon(4S)$
$-0.10 \pm 0.08 \pm 0.02$	[1] LEES	11A	BABR	$e^+e^- \to \Upsilon(4S)$

[1] Assumes $m_{\phi\phi} < 2.85$ GeV/c^2.

$A_{CP}(B^+ \to K^+[\phi\phi]_{\eta_c})$

VALUE	DOCUMENT ID		TECN	COMMENT
0.10 ± 0.08 OUR AVERAGE				
$0.12 \pm 0.12 \pm 0.01$	[1] MOHANTY	21	BELL	$e^+e^- \to \Upsilon(4S)$
$0.09 \pm 0.10 \pm 0.02$	[1] LEES	11A	BABR	$e^+e^- \to \Upsilon(4S)$

[1] $m_{\phi\phi}$ is consistent with η_c mass in [2.94, 3.02] GeV/c^2.

$A_{CP}(B^+ \to K^*(892)^+\gamma)$

VALUE	DOCUMENT ID		TECN	COMMENT
0.014 ± 0.018 OUR AVERAGE				
$0.011 \pm 0.023 \pm 0.003$	[1] HORIGUCHI	17	BELL	$e^+e^- \to \Upsilon(4S)$
$0.018 \pm 0.028 \pm 0.007$	AUBERT	09AO	BABR	$e^+e^- \to \Upsilon(4S)$

[1] Uses B($\Upsilon(4S) \to B^+B^-$) = (51.4 ± 0.6)% and B($\Upsilon(4S) \to B^0\overline{B}^0$) = (48.6 ± 0.6)%.

$A_{CP}(B^+ \to X_s\gamma)$

VALUE	DOCUMENT ID		TECN	COMMENT
$0.0275 \pm 0.0184 \pm 0.0032$	[1] WATANUKI	19	BELL	$e^+e^- \to \Upsilon(4S)$

[1] Using a sum-of-exclusive technique with $m_{X_s} < 2.8$ GeV/c^2.

$A_{CP}(B^+ \to \eta K^+\gamma)$

VALUE	DOCUMENT ID		TECN	COMMENT
-0.12 ± 0.07 OUR AVERAGE				
$-0.09 \pm 0.10 \pm 0.01$	[1] AUBERT	09	BABR	$e^+e^- \to \Upsilon(4S)$
$-0.16 \pm 0.09 \pm 0.06$	[2] NISHIDA	05	BELL	$e^+e^- \to \Upsilon(4S)$
• • • We do not use the following data for averages, fits, limits, etc. • • •				
$-0.09 \pm 0.12 \pm 0.01$	[1] AUBERT,B	06M	BABR	Repl. by AUBERT 09

[1] $m_{\eta K} < 3.25$ GeV/c^2.
[2] $m_{\eta K} < 2.4$ GeV/c^2

$A_{CP}(B^+ \to \phi K^+\gamma)$

VALUE	DOCUMENT ID		TECN	COMMENT
-0.13 ± 0.11 OUR AVERAGE	Error includes scale factor of 1.1.			
$-0.03 \pm 0.11 \pm 0.08$	SAHOO	11A	BELL	$e^+e^- \to \Upsilon(4S)$
$-0.26 \pm 0.14 \pm 0.05$	AUBERT	07Q	BABR	$e^+e^- \to \Upsilon(4S)$

$A_{CP}(B^+ \to \rho^+\gamma)$

VALUE	DOCUMENT ID		TECN	COMMENT
$-0.11 \pm 0.32 \pm 0.09$	TANIGUCHI	08	BELL	$e^+e^- \to \Upsilon(4S)$

$A_{CP}(B^+ \to \pi^+\pi^0)$

VALUE	DOCUMENT ID		TECN	COMMENT
0.03 ± 0.04 OUR AVERAGE				
$0.025 \pm 0.043 \pm 0.007$	DUH	13	BELL	$e^+e^- \to \Upsilon(4S)$
$0.03 \pm 0.08 \pm 0.01$	AUBERT	07BC	BABR	$e^+e^- \to \Upsilon(4S)$
• • • We do not use the following data for averages, fits, limits, etc. • • •				
$0.07 \pm 0.06 \pm 0.01$	LIN	08	BELL	Repl. by DUH 13
$-0.01 \pm 0.10 \pm 0.02$	[1] AUBERT	05L	BABR	Repl. by AUBERT 07BC
$0.00 \pm 0.10 \pm 0.02$	[2] CHAO	05A	BELL	Repl. by CHAO 04B
$-0.02 \pm 0.10 \pm 0.01$	[3] CHAO	04B	BELL	Repl. by LIN 08
$-0.03^{+0.18}_{-0.17} \pm 0.02$	[4] AUBERT	03L	BABR	Repl. by AUBERT 05L
$0.30 \pm 0.30^{+0.06}_{-0.04}$	[5] CASEY	02	BELL	Repl. by CHAO 04B

[1] Corresponds to a 90% CL interval of $-0.19 < A_{CP} < 0.21$.
[2] Corresponds to a 90% CL interval of $-0.17 < A_{CP} < 0.16$.
[3] This corresponds to 90% CL interval of $-0.18 < A_{CP} < 0.14$.
[4] Corresponds to 90% confidence range $-0.32 < A_{CP} < 0.27$.
[5] Corresponds to 90% confidence range $-0.23 < A_{CP} < +0.86$.

$A_{CP}(B^+ \to \pi^+\pi^-\pi^+)$

VALUE	DOCUMENT ID		TECN	COMMENT
0.057 ± 0.013 OUR AVERAGE				
$0.058 \pm 0.008 \pm 0.011$	[1] AAIJ	14BO	LHCB	pp at 7, 8 TeV
$0.032 \pm 0.044^{+0.040}_{-0.037}$	AUBERT	09L	BABR	$e^+e^- \to \Upsilon(4S)$

Downloaded from https://academic.oup.com/ptep/article/2022/8/083C01/6651666 by KIT Library user on 27 September 2022

• • • We do not use the following data for averages, fits, limits, etc. • • •

$0.117 \pm 0.021 \pm 0.011$	[2] AAIJ	14	LHCB	Repl. by AAIJ 14BO
$-0.007 \pm 0.077 \pm 0.025$	AUBERT,B	05G	BABR	Repl. by AUBERT 09L
$-0.39 \pm 0.33 \pm 0.12$	AUBERT	03M	BABR	Repl. by AUBERT 05G

[1] AAIJ 14BO reports also CP asymmetries in restricted regions of phase space.
[2] AAIJ 14 reports $A_{CP}(B^+ \to \pi^+\pi^-\pi^+) = 0.584 \pm 0.082 \pm 0.027 \pm 0.007$ in the Dalitz plot region of $m^2_{\pi^+\pi^-} > 15$ GeV^2/c^4 or $m^2_{\pi^+\pi^-} < 0.4$ GeV^2/c^4. The third uncertainty is due to the CP asymmetry of the $B^{\pm} \to J/\psi K^{\pm}$ reference mode uncertainty.

$A_{CP}(B^+ \to \rho^0\pi^+)$

VALUE	DOCUMENT ID		TECN	COMMENT
0.009±0.019 OUR AVERAGE				
$0.007 \pm 0.011 \pm 0.016$	[1] AAIJ	20A	LHCB	pp at 7, 8 TeV
$0.18 \pm 0.07 \,^{+0.05}_{-0.15}$	AUBERT	09L	BABR	$e^+e^- \to \Upsilon(4S)$
• • • We do not use the following data for averages, fits, limits, etc. • • •				
$-0.074 \pm 0.120 \,^{+0.035}_{-0.055}$	AUBERT,B	05G	BABR	Repl. by AUBERT 09L
$-0.19 \pm 0.11 \pm 0.02$	AUBERT	04Z	BABR	Repl. by AUBERT,B 05G

[1] This result is obtained with an amplitude analysis of $B^+ \to \pi^+\pi^+\pi^-$ decays, using the isobar model within the mass range $1.0 < m(\pi^+\pi^-) < 1.5$ GeV to describe the $\pi^+\pi^-$ S-wave contribution.

$A_{CP}(B^+ \to f_2(1270)\pi^+)$

VALUE	DOCUMENT ID		TECN	COMMENT
0.40 ±0.06 OUR AVERAGE				
$0.468 \pm 0.061 \pm 0.046$	[1] AAIJ	20A	LHCB	pp at 7, 8 TeV
$0.267 \pm 0.102 \pm 0.048$	[2] AAIJ	19AL	LHCB	pp at 7, 8 TeV
$0.41 \pm 0.25 \,^{+0.18}_{-0.15}$	AUBERT	09L	BABR	$e^+e^- \to \Upsilon(4S)$
• • • We do not use the following data for averages, fits, limits, etc. • • •				
$-0.004 \pm 0.247 \,^{+0.028}_{-0.032}$	AUBERT,B	05G	BABR	Repl. by AUBERT 09L

[1] This result is obtained with an amplitude analysis of $B^+ \to \pi^+\pi^+\pi^-$ decays, using the isobar model within the mass range $1.0 < m(\pi^+\pi^-) < 1.5$ GeV to describe the $\pi^+\pi^-$ S-wave contribution.
[2] Uses amplitude analysis of $B^{\pm} \to \pi^{\pm}K^+K^-$ decays.

$A_{CP}(B^+ \to \rho^0(1450)\pi^+)$

VALUE	DOCUMENT ID		TECN	COMMENT
−0.11 ±0.05 OUR AVERAGE				
$-0.129 \pm 0.033 \pm 0.359$	[1] AAIJ	20A	LHCB	pp at 7, 8 TeV
$-0.109 \pm 0.044 \pm 0.024$	[2] AAIJ	19AL	LHCB	pp at 7, 8 TeV
$-0.06 \pm 0.28 \,^{+0.23}_{-0.40}$	AUBERT	09L	BABR	$e^+e^- \to \Upsilon(4S)$

[1] This result is obtained with an amplitude analysis of $B^+ \to \pi^+\pi^+\pi^-$ decays, using the isobar model within the mass range $1.0 < m(\pi^+\pi^-) < 1.5$ GeV to describe the $\pi^+\pi^-$ S-wave contribution.
[2] Uses amplitude analysis of $B^{\pm} \to \pi^{\pm}K^+K^-$ decays.

$A_{CP}(B^+ \to \rho_3(1690)\pi^+)$

VALUE	DOCUMENT ID		TECN	COMMENT
−0.801±0.114±0.253	[1] AAIJ	20A	LHCB	pp at 7, 8 TeV

[1] This result is obtained with an amplitude analysis of $B^+ \to \pi^+\pi^+\pi^-$ decays, using the isobar model within the mass range $1.0 < m(\pi^+\pi^-) < 1.5$ GeV to describe the $\pi^+\pi^-$ S-wave contribution.

$A_{CP}(B^+ \to f_0(1370)\pi^+)$

VALUE	DOCUMENT ID		TECN	COMMENT
0.72±0.15±0.16	AUBERT	09L	BABR	$e^+e^- \to \Upsilon(4S)$

$A_{CP}(B^+ \to \pi^+\pi^-\pi^+$ nonresonant)

VALUE	DOCUMENT ID		TECN	COMMENT
$\mathbf{-0.14 \pm 0.14 \,^{+0.18}_{-0.08}}$	AUBERT	09L	BABR	$e^+e^- \to \Upsilon(4S)$

$A_{CP}(B^+ \to \rho^+\pi^0)$

VALUE	DOCUMENT ID		TECN	COMMENT
0.02±0.11 OUR AVERAGE				
$-0.01 \pm 0.13 \pm 0.02$	AUBERT	07X	BABR	$e^+e^- \to \Upsilon(4S)$
$0.06 \pm 0.17 \,^{+0.04}_{-0.05}$	ZHANG	05A	BELL	$e^+e^- \to \Upsilon(4S)$
• • • We do not use the following data for averages, fits, limits, etc. • • •				
$0.24 \pm 0.16 \pm 0.06$	AUBERT	04Z	BABR	Repl. by AUBERT 07X

$A_{CP}(B^+ \to \rho^+\rho^0)$

VALUE	DOCUMENT ID		TECN	COMMENT
−0.05 ±0.05 OUR AVERAGE				
$-0.054 \pm 0.055 \pm 0.010$	AUBERT	09G	BABR	$e^+e^- \to \Upsilon(4S)$
$0.00 \pm 0.22 \pm 0.03$	ZHANG	03B	BELL	$e^+e^- \to \Upsilon(4S)$
• • • We do not use the following data for averages, fits, limits, etc. • • •				
$-0.12 \pm 0.13 \pm 0.10$	AUBERT,BE	06G	BABR	Repl. by AUBERT 09G
$-0.19 \pm 0.23 \pm 0.03$	AUBERT	03V	BABR	Repl. by AUBERT,BE 06G

$A_{CP}(B^+ \to \omega\pi^+)$

VALUE	DOCUMENT ID		TECN	COMMENT
−0.04 ±0.05 OUR AVERAGE				
$-0.048 \pm 0.065 \pm 0.038$	[1] AAIJ	20A	LHCB	pp at 7, 8 TeV
$-0.02 \pm 0.08 \pm 0.01$	AUBERT	07AE	BABR	$e^+e^- \to \Upsilon(4S)$
$-0.02 \pm 0.09 \pm 0.01$	JEN	06	BELL	$e^+e^- \to \Upsilon(4S)$
-0.34 ± 0.25	[2] CHEN	00	CLE2	$e^+e^- \to \Upsilon(4S)$
• • • We do not use the following data for averages, fits, limits, etc. • • •				
$-0.01 \pm 0.10 \pm 0.01$	AUBERT,B	06E	BABR	Repl. by AUBERT 07AE
$0.03 \pm 0.16 \pm 0.01$	AUBERT	04H	BABR	Repl. by AUBERT,B 06E
$0.50 \,^{+0.23}_{-0.20} \pm 0.02$	[3] WANG	04A	BELL	Repl. by JEN 06
$-0.01 \,^{+0.29}_{-0.31} \pm 0.03$	[4] AUBERT	02E	BABR	Repl. by AUBERT 04H

[1] This result is obtained with an amplitude analysis of $B^+ \to \pi^+\pi^+\pi^-$ decays, using the isobar model within the mass range $1.0 < m(\pi^+\pi^-) < 1.5$ GeV to describe the $\pi^+\pi^-$ S-wave contribution.
[2] Corresponds to 90% confidence range $-0.75 < A_{CP} < 0.07$.
[3] Corresponds to 90% CL interval $-0.25 < A_{CP} < 0.41$
[4] Corresponds to 90% confidence range $-0.50 < A_{CP} < 0.46$.

$A_{CP}(B^+ \to \omega\rho^+)$

VALUE	DOCUMENT ID		TECN	COMMENT
−0.20±0.09±0.02	AUBERT	09H	BABR	$e^+e^- \to \Upsilon(4S)$
• • • We do not use the following data for averages, fits, limits, etc. • • •				
$0.04 \pm 0.18 \pm 0.02$	AUBERT,B	06T	BABR	Repl. by AUBERT 09H
$0.05 \pm 0.26 \pm 0.02$	AUBERT	05O	BABR	Repl. by AUBERT,B 06T

$A_{CP}(B^+ \to \eta\pi^+)$

VALUE	DOCUMENT ID		TECN	COMMENT
−0.14±0.07 OUR AVERAGE Error includes scale factor of 1.4.				
$-0.19 \pm 0.06 \pm 0.01$	HOI	12	BELL	$e^+e^- \to \Upsilon(4S)$
$-0.03 \pm 0.09 \pm 0.03$	AUBERT	09AV	BABR	$e^+e^- \to \Upsilon(4S)$
• • • We do not use the following data for averages, fits, limits, etc. • • •				
$-0.08 \pm 0.10 \pm 0.01$	AUBERT	07AE	BABR	Repl. by AUBERT 09AV
$-0.23 \pm 0.09 \pm 0.02$	CHANG	07B	BELL	Repl. by HOI 12
$-0.13 \pm 0.12 \pm 0.01$	AUBERT,B	05K	BABR	Repl. by AUBERT 07AE
$0.07 \pm 0.15 \pm 0.03$	CHANG	05A	BELL	Repl. by CHANG 07B
$-0.44 \pm 0.18 \pm 0.01$	AUBERT	04H	BABR	Repl. by AUBERT,B 05K

$A_{CP}(B^+ \to \eta\rho^+)$

VALUE	DOCUMENT ID		TECN	COMMENT
0.11±0.11 OUR AVERAGE				
$0.13 \pm 0.11 \pm 0.02$	AUBERT	08AH	BABR	$e^+e^- \to \Upsilon(4S)$
$-0.04 \,^{+0.34}_{-0.32} \pm 0.01$	WANG	07B	BELL	$e^+e^- \to \Upsilon(4S)$
• • • We do not use the following data for averages, fits, limits, etc. • • •				
$0.02 \pm 0.18 \pm 0.02$	AUBERT,B	05K	BABR	Repl. by AUBERT 08AH

$A_{CP}(B^+ \to \eta'\pi^+)$

VALUE	DOCUMENT ID		TECN	COMMENT
0.06±0.16 OUR AVERAGE				
$0.03 \pm 0.17 \pm 0.02$	AUBERT	09AV	BABR	$e^+e^- \to \Upsilon(4S)$
$0.20 \,^{+0.37}_{-0.36} \pm 0.04$	SCHUEMANN	06	BELL	$e^+e^- \to \Upsilon(4S)$
• • • We do not use the following data for averages, fits, limits, etc. • • •				
$0.21 \pm 0.17 \pm 0.01$	AUBERT	07AE	BABR	Repl. by AUBERT 09AV
$0.14 \pm 0.16 \pm 0.01$	AUBERT,B	05K	BABR	Repl. by AUBERT 07AE

$A_{CP}(B^+ \to \eta'\rho^+)$

VALUE	DOCUMENT ID		TECN	COMMENT
0.26±0.17±0.02	DEL-AMO-SA...10A		BABR	$e^+e^- \to \Upsilon(4S)$
• • • We do not use the following data for averages, fits, limits, etc. • • •				
$0.04 \pm 0.28 \pm 0.02$	[1] AUBERT	07E	BABR	Repl. by DEL-AMO-SANCHEZ 10A

[1] Reports A_{CP} with the opposite sign convention.

$A_{CP}(B^+ \to b_1^0\pi^+)$

VALUE	DOCUMENT ID		TECN	COMMENT
+0.05±0.16±0.02	AUBERT	07BI	BABR	$e^+e^- \to \Upsilon(4S)$

$A_{CP}(B^+ \to p\overline{p}\pi^+)$

VALUE	DOCUMENT ID		TECN	COMMENT
0.00±0.04 OUR AVERAGE				
$-0.02 \pm 0.05 \pm 0.02$	[1] WEI	08	BELL	$e^+e^- \to \Upsilon(4S)$
$+0.04 \pm 0.07 \pm 0.04$	AUBERT	07AV	BABR	$e^+e^- \to \Upsilon(4S)$
• • • We do not use the following data for averages, fits, limits, etc. • • •				
$-0.16 \pm 0.22 \pm 0.01$	WANG	04	BELL	Repl. by WEI 08

[1] Requires $m_{p\overline{p}} < 2.85$ GeV/c^2.

$A_{CP}(B^+ \to p\overline{p}K^+)$

VALUE	DOCUMENT ID		TECN	COMMENT
0.00 ±0.04 OUR AVERAGE Error includes scale factor of 2.2.				
$0.021 \pm 0.020 \pm 0.004$	[1] AAIJ	14AF	LHCB	pp at 7, 8 TeV
$-0.17 \pm 0.10 \pm 0.02$	[1] WEI	08	BELL	$e^+e^- \to \Upsilon(4S)$
$-0.16 \,^{+0.07}_{-0.08} \pm 0.04$	[1] AUBERT,B	05L	BABR	$e^+e^- \to \Upsilon(4S)$

Downloaded from https://academic.oup.com/ptep/article/2022/8/083C01/6651666 by KIT Library user on 27 September 2022

• • • We do not use the following data for averages, fits, limits, etc. • • •

$-0.047 \pm 0.036 \pm 0.007$	[1] AAIJ	13AU	LHCB	Repl. by AAIJ 14AF
$-0.05 \pm 0.11 \pm 0.01$	WANG	04	BELL	Repl. by WEI 08

[1] Requires $m_{p\overline{p}} < 2.85$ GeV/c^2.

$A_{CP}(B^+ \to p\overline{p}K^*(892)^+)$

VALUE	DOCUMENT ID		TECN	COMMENT
0.21±0.16 OUR AVERAGE	Error includes scale factor of 1.4.			
$-0.01 \pm 0.19 \pm 0.02$	CHEN	08C	BELL	$e^+e^- \to \Upsilon(4S)$
$+0.32 \pm 0.13 \pm 0.05$	AUBERT	07AV	BABR	$e^+e^- \to \Upsilon(4S)$

$A_{CP}(B^+ \to p\overline{\Lambda}\gamma)$

VALUE	DOCUMENT ID		TECN	COMMENT
+0.17±0.16±0.05	WANG	07C	BELL	$e^+e^- \to \Upsilon(4S)$

$A_{CP}(B^+ \to p\overline{\Lambda}\pi^0)$

VALUE	DOCUMENT ID		TECN	COMMENT
+0.01±0.17±0.04	WANG	07C	BELL	$e^+e^- \to \Upsilon(4S)$

$A_{CP}(B^+ \to K^+\ell^+\ell^-)$

VALUE	DOCUMENT ID		TECN	COMMENT
−0.02±0.08 OUR AVERAGE				
$-0.03 \pm 0.14 \pm 0.01$	[1] LEES	12S	BABR	$e^+e^- \to \Upsilon(4S)$
$-0.18 \pm 0.18 \pm 0.01$	AUBERT	09T	BABR	$e^+e^- \to \Upsilon(4S)$
$+0.04 \pm 0.10 \pm 0.02$	WEI	09A	BELL	$e^+e^- \to \Upsilon(4S)$
• • • We do not use the following data for averages, fits, limits, etc. • • •				
$-0.07 \pm 0.22 \pm 0.02$	AUBERT,B	06J	BABR	Repl. by AUBERT 09T

[1] Measured in the union of $0.10 < q^2 < 8.12$ GeV^2/c^4 and $q^2 > 10.11$ GeV^2/c^4. LEES 12S reports also individual measurements $A_{CP}(B^+ \to K^+\ell^+\ell^-) = 0.02 \pm 0.18 \pm 0.01$ for $0.10 < q^2 < 8.12$ GeV^2/c^4 and $A_{CP}(B^+ \to K^+\ell^+\ell^-) = -0.06^{+0.22}_{-0.21} \pm 0.01$ for $q^2 > 10.11$ GeV^2/c^4.

$A_{CP}(B^+ \to K^+e^+e^-)$

VALUE	DOCUMENT ID		TECN	COMMENT
+0.14±0.14±0.03	WEI	09A	BELL	$e^+e^- \to \Upsilon(4S)$

$A_{CP}(B^+ \to K^+\mu^+\mu^-)$

VALUE	DOCUMENT ID		TECN	COMMENT
0.011±0.017 OUR AVERAGE				
$0.012 \pm 0.017 \pm 0.001$	AAIJ	14AN	LHCB	pp at 7, 8 TeV
$-0.05 \pm 0.13 \pm 0.03$	WEI	09A	BELL	$e^+e^- \to \Upsilon(4S)$
• • • We do not use the following data for averages, fits, limits, etc. • • •				
$0.000 \pm 0.033 \pm 0.009$	AAIJ	13BN	LHCB	Repl. by AAIJ 14AN

$A_{CP}(B^+ \to \pi^+\mu^+\mu^-)$

VALUE	DOCUMENT ID		TECN	COMMENT
−0.11±0.12±0.01	AAIJ	15AR	LHCB	pp at 7, 8 TeV

$A_{CP}(B^+ \to K^{*+}\ell^+\ell^-)$

VALUE	DOCUMENT ID		TECN	COMMENT
−0.09±0.14 OUR AVERAGE				
$0.01^{+0.26}_{-0.24} \pm 0.02$	AUBERT	09T	BABR	$e^+e^- \to \Upsilon(4S)$
$-0.13^{+0.17}_{-0.16} \pm 0.01$	WEI	09A	BELL	$e^+e^- \to \Upsilon(4S)$
• • • We do not use the following data for averages, fits, limits, etc. • • •				
$0.03 \pm 0.23 \pm 0.03$	AUBERT,B	06J	BABR	Repl. by AUBERT 09T

$A_{CP}(B^+ \to K^*e^+e^-)$

VALUE	DOCUMENT ID		TECN	COMMENT
$-0.14^{+0.23}_{-0.22} \pm 0.02$	WEI	09A	BELL	$e^+e^- \to \Upsilon(4S)$

$A_{CP}(B^+ \to K^*\mu^+\mu^-)$

VALUE	DOCUMENT ID		TECN	COMMENT
−0.12±0.24±0.02	WEI	09A	BELL	$e^+e^- \to \Upsilon(4S)$

CP VIOLATION PARAMETERS IN $B^+ \to DK^+$ AND SIMILAR DECAYS

The parameters r_{B^+} and δ_{B^+} are the magnitude ratio and strong phase difference between the amplitudes of $A(B^+ \to \overline{D}^{(*)0}K^{(*)+})$ and $A(B^- \to D^{(*)0}K^{(*)-})$. The measured observables are defined as $x_\pm = r_{B^+}\cos(\delta_{B^+} \pm \gamma)$ and $y_\pm = r_{B^+}\sin(\delta_{B^+} \pm \gamma)$, and can be used to measure the CKM angle γ.

"OUR EVALUATION" is provided by the Heavy Flavor Averaging Group (HFLAV). It is derived from combinations of their results on $B^+ \to DK^+$ and related processes.

γ

For angle $\gamma(\phi_3)$ of the CKM unitarity triangle, see the review on "*CP* Violation" in the Reviews section.

"OUR EVALUATION" is provided by the Heavy Flavor Averaging Group (HFLAV).

VALUE (°)	CL%	DOCUMENT ID		TECN	COMMENT
$65.9^{+3.3}_{-3.5}$ OUR EVALUATION					
• • • We do not use the following data for averages, fits, limits, etc. • • •					
$65.4^{+3.8}_{-4.2}$		[1] AAIJ	21AM	LHCB	pp at 7, 8, 13 TeV
$68.7^{+5.2}_{-5.1}$		[2] AAIJ	21L	LHCB	pp at 7, 8, 13 TeV
44 ± 12		[3,4] AAIJ	21M	LHCB	pp at 7, 8, 13 TeV
$5.7^{+10.2}_{-8.8} \pm 6.7$		[5] RESMI	19	BELL	$e^+e^- \to \Upsilon(4S)$
87^{+11}_{-12}		[6] AAIJ	18AD	LHCB	Repl. by AAIJ 21L
128^{+17}_{-22}		[7] AAIJ	18U	LHCB	pp at 7, 8 TeV
5–86 or 185–266		[8] AAIJ	18Z	LHCB	pp at 7, 8 TeV
80^{+21}_{-22}		[9] AAIJ	16AA	LHCB	Repl. by AAIJ 16Z
$72.2^{+6.8}_{-7.3}$		[10] AAIJ	16AQ	LHCB	Repl. by AAIJ 21AM
71 ± 20		[11,12] AAIJ	16Z	LHCB	pp at 7, 8 TeV
74^{+20}_{-19}		AAIJ	15BC	LHCB	pp at 7, 8 TeV
$63.5^{+7.2}_{-6.7}$		[13,14] AAIJ	15K	LHCB	pp at 7, 8 TeV
62^{+15}_{-14}		[15] AAIJ	14BA	LHCB	Repl. by AAIJ 21L
84^{+49}_{-42}		[16] AAIJ	14BE	LHCB	Repl. by AAIJ 14BA
115^{+28}_{-43}		[17] AAIJ	14BF	LHCB	Repl. by AAIJ 18U
$72.6^{+9.7}_{-17.2}$		[18] AAIJ	13AK	LHCB	Repl. by AAIJ 21AM
69^{+17}_{-16}		[19] LEES	13B	BABR	$e^+e^- \to \Upsilon(4S)$
44^{+43}_{-38}		[20,21] AAIJ	12AQ	LHCB	Repl. by AAIJ 13AK
$77.3^{+15.1}_{-14.9} \pm 5.9$		[21,22] AIHARA	12	BELL	$e^+e^- \to \Upsilon(4S)$
$68 \pm 14 \pm 5$		[23] DEL-AMO-SA...	10F	BABR	Repl. by LEES 13B
7 to 173	95	[24] DEL-AMO-SA...	10G	BABR	$e^+e^- \to \Upsilon(4S)$
$78.4^{+10.8}_{-11.6} \pm 9.6$		[25] POLUEKTOV	10	BELL	$e^+e^- \to \Upsilon(4S)$
162 ± 56		[26] AUBERT	09R	BABR	$e^+e^- \to \Upsilon(4S)$
$76^{+22}_{-23} \pm 7.1$		[27] AUBERT	08AL	BABR	Repl. by DEL-AMO-SANCHEZ 10F
$53^{+15}_{-18} \pm 10$		[28] POLUEKTOV	06	BELL	Repl. by POLUEKTOV 10
$70 \pm 31^{+18}_{-15}$		[29] AUBERT,B	05Y	BABR	Repl. by AUBERT 08AL
$77^{+17}_{-19} \pm 17$		[30] POLUEKTOV	04	BELL	Repl. by POLUEKTOV 06

[1] AAIJ 21AM presents a combination of existing measurements from LHCb collaboration. It includes also charm mixing parameters.

[2] Uses binned Dalitz plot analysis of $D \to K^0_S\pi^+\pi^-$ and $K^0_S K^+K^-$ from $B^\pm \to DK^\pm$ modes. Strong phase measurements from CLEO-c and BES-III of the D decay over the Dalitz plot are used as input. Value is modulo 180°.

[3] Measured in $B^0_s \to D^\pm_s K^\mp\pi^\pm\pi^\mp$ decays in restricted phase space with $m(K^+\pi^+\pi^-) < 1950$ MeV, $m(K^+\pi^-) < 1200$ MeV and $m(\pi^+\pi^-) < 1200$ MeV. The value is modulo 180°.

[4] A model-independent coherence factor for the decay $B_s \to D_s K\pi\pi$ (in the restricted phase space region) is also reported.

[5] Uses binned analysis of $D \to K^0_S\pi^+\pi^-\pi^0$ from $B^\pm \to DK^\pm$ modes over the phase space. Strong phase measurements from RESMI 18 analysis of CLEO-c data of the D decay over the phase space binning are used as input.

[6] Uses binned Dalitz plot analysis of $D \to K^0_S\pi^+\pi^-$ and $K^0_S K^+K^-$ from $B^\pm \to DK^\pm$ modes. Strong phase measurements from CLEO-c of the D decay over the Dalitz plot are used as input.

[7] Measured in $B^0_s \to D^\mp_s K^\pm$ decays, constraining $-2\beta_s$ by the measurement of $\phi_s = 0.030 \pm 0.033$ from HFLAV. The value is modulo 180°.

[8] AAIJ 18Z reports the intervals (5–86)° or (185–266)° at 68% C.L. The extraction uses the time dependent CP violation measurement in $B^0 \to D^\mp\pi^\pm$ decays with external input and some theoretical assumptions.

[9] Uses Dalitz plot analysis of $D \to K^0_S\pi^+\pi^-$ decays coming from $B^0 \to DK^*(892)^0$ modes. Measures $r_{B^0} = 0.39 \pm 0.13$, and $\delta_{B^0} = 197^{+24}_{-20}$ degrees.

[10] A combination of measurements from analyses of time-integrated $B^+ \to DK^+$, $B^0 \to DK^{(*)0}$, $B^0 \to DK^+\pi^-$, and $B^+ \to DK^+\pi^+\pi^-$ tree-level decays. In addition, results from a time-dependent analysis of $B^0_s \to D_s K$ decays are included.

[11] A model-independent binned Dalitz plot analysis of the decays $B^0 \to DK^{*0}$, with $D \to K^0_S\pi^+\pi^-$ and $D \to K^0_S K^+K^-$. The results cannot be combined with the model-dependent analysis of the same dataset reported in AAIJ 16AA.

[12] Angle γ required to satisfy $0 < \gamma < 180$ degrees.

[13] Obtained by measuring time-dependent *CP* asymmetry in $B^0_s \to K^+K^-$ and using a U-spin relation between $B^0_s \to K^+K^-$ and $B^0 \to \pi^+\pi^-$.

[14] Results are also presented using additional inputs on $B^0 \to \pi^0\pi^0$ and $B^+ \to \pi^+\pi^0$ decays from other experiments and isospin symmetry assumptions. The dependence of the results on the maximum allowed amount of U-spin breaking up to 50% is also included.

[15] Uses binned Dalitz plot analysis of $B^+ \to DK^+$ decays, with $D \to K^0_S\pi^+\pi^-$ and $D \to K^0_S K^+K^-$. Strong phase measurements from CLEO-c (LIBBY 10) of the D

Downloaded from https://academic.oup.com/ptep/article/2022/8/083C01/6651666 by KIT Library user on 27 September 2022

decay over the Dalitz plot are used as input. Solution that satisfies $0 < \gamma < 180$ is chosen.

[16] AAIJ 14BE uses model-dependent analysis of $D \to K^0_S \pi^+ \pi^-$ amplitudes. The model is the same as in DEL-AMO-SANCHEZ 10F.

[17] Measured in $B^0_s \to D^{\mp}_s K^{\pm}$ decays, constraining $-2\beta_s$ by the measurement of $\phi_s = 0.01 \pm 0.07 \pm 0.0$ from AAIJ 13AR. The value is modulo 180° at 68% CL.

[18] Presents a confidence region $55.4° < \gamma < 82.3°$ at 68% CL with best fit value 72.6° and includes both statistical and systematic uncertainties. The corresponding 95% CL is $40.2° < \gamma < 92.7°$. The value is determined from combination of measuremets using D meson decaying to K^+K^-, $\pi^+\pi^-$, $K^{\pm}\pi^{\mp}$, $K^0_S\pi^+\pi^-$, $K^0_S K^+K^-$, and $K^{\pm}\pi^{\mp}\pi^{\pm}\pi^{\mp}$. Combines $B^{\pm} \to D K^{\pm}$ and $B^{\pm} \to D\pi^{\pm}$.

[19] Reports combination of published measurements using GGSZ, GLW, and ADS methods. Reports also 2σ range of 41–102° and a 5.9σ significance for $\gamma(B^+ \to D^{(*)0} K^{(*)+}) \neq 0$ hypothesis.

[20] Reports combined statistical and systematic uncertainties.

[21] Uses binned Dalitz plot of $\overline{D}^0 \to K^0_S \pi^+\pi^-$ decays from $B^+ \to \overline{D}^0 K^+$. Measurement of strong phases in $\overline{D}^0 \to K^0_S \pi^+\pi^-$ Dalitz plot from LIBBY 10 is used as input.

[22] We combined the systematics in quadrature. The authors report separately the contribution to the systematic uncertainty due to the uncertainty on the bin-averaged strong phase difference between D^0 and $\overline{D}^0$ amplitudes.

[23] Uses Dalitz plot analysis of $\overline{D}^0 \to K^0_S \pi^+\pi^-$, $K^0_S K^+K^-$ decays from $B^+ \to D^{(*)} K^+$, $D K^{*+}$ modes. The corresponding two standard deviation interval for γ is $39° < \gamma < 98°$. CP conservation in the combined result is ruled out with a significance of 3.5 standard deviations.

[24] Reports confidence intervals for the CKM angle γ from the measured values of the GLW parameters using $B^{\pm} \to D K^{\pm}$ decays with D mesons decaying to non-$CP(K\pi)$, CP-even (K^+K^-, $\pi^+\pi^-$), and CP-odd ($K^0_S\pi^0$, $K^0_S\omega$) states.

[25] Uses Dalitz plot analysis of $\overline{D}^0 \to K^0_S \pi^+\pi^-$ decays from $B^+ \to D^{(*)} K^+$ modes. The corresponding two standard deviation interval for γ is $54.2° < \gamma < 100.5°$. CP conservation in the combined result is ruled out with a significance of 3.5 standard deviations.

[26] Uses Dalitz plot analysis of $D^0 \to K^0_S \pi^+\pi^-$ decays coming from $B^0 \to D^0 K^{*0}$ modes. The corresponding 95% CL interval is $77° < \gamma < 247°$. A 180 degree ambiguity is implied.

[27] Uses Dalitz plot analysis of $\overline{D}^0 \to K^0_S \pi^+\pi^-$ and $\overline{D}^0 \to K^0_S K^+K^-$ decays coming from $B^{\pm} \to D^{(*)} K^{(*)\pm}$ modes. The corresponding two standard deviation interval is $29° < \gamma < 122°$.

[28] Uses a Dalitz plot analysis of the $\overline{D}^0 \to K^0_S \pi^+\pi^-$ decays; Combines the $D K^+$, $D^* K^+$ and $D K^{*+}$ modes. The corresponding two standard deviations interval for gamma is $8° < \gamma < 111°$.

[29] Uses a Dalitz plot analysis of neutral $D \to K^0_S \pi^+\pi^-$ decays coming from $B^{\pm} \to D K^{\pm}$ and $B^{\pm} \to D^{*0} K^{\pm}$ followed by $D^{*0} \to D\pi^0$, $D\gamma$. The corresponding two standard deviations interval for gamma is $12° < \gamma < 137°$. AUBERT,B 05Y also reports the amplitude ratios and the strong phases.

[30] Uses a Dalitz plot analysis of the 3-body $D \to K^0_S \pi^+\pi^-$ decays coming from $B^{\pm} \to D K^{\pm}$ and $B^{\pm} \to D^* K^{\pm}$ followed by $D^* \to D\pi^0$; here we use D to denote that the neutral D meson produced in the decay is an admixture of D^0 and $\overline{D}^0$. The corresponding two standard deviations interval for γ is $26° < \gamma < 126°$. POLUEKTOV 04 also reports the amplitude ratios and the strong phases.

$r_B(B^+ \to D^0 K^+)$

r_B and δ_B are the amplitude ratio and relative strong phase between the amplitudes of $A(B^+ \to D^0 K^+)$ and $A(B^+ \to \overline{D}^0 K^+)$,

"OUR EVALUATION" is provided by the Heavy Flavor Averaging Group (HFLAV).

VALUE	CL%	DOCUMENT ID		TECN	COMMENT
0.0994±0.0026 OUR EVALUATION					
• • • We do not use the following data for averages, fits, limits, etc. • • •					
$0.0904^{+0.0077}_{-0.0075}$		[1] AAIJ	21L	LHCB	pp at 7, 8, 13 TeV
$0.323 \pm 0.147 \pm 0.056$		[2] RESMI	19	BELL	$e^+e^- \to \Upsilon(4S)$
$0.086^{+0.013}_{-0.014}$		[3] AAIJ	18AD	LHCB	Repl. by AAIJ 21L
$0.080^{+0.019}_{-0.021}$		[4] AAIJ	14BA	LHCB	Repl. by AAIJ 21L
0.06 ± 0.04		[5] AAIJ	14BE	LHCB	Repl. by AAIJ 14BA
0.097 ± 0.011		[6] AAIJ	13AE	LHCB	pp at 7 TeV
$0.092^{+0.013}_{-0.012}$		[7] LEES	13B	BABR	$e^+e^- \to \Upsilon(4S)$
0.07 ± 0.04		[8,9] AAIJ	12AQ	LHCB	pp at 7 TeV
$0.145 \pm 0.030 \pm 0.015$		[9,10] AIHARA	12	BELL	$e^+e^- \to \Upsilon(4S)$
<0.13	90	[11] LEES	11D	BABR	$e^+e^- \to \Upsilon(4S)$
$0.096 \pm 0.029 \pm 0.006$		[12] DEL-AMO-SA...10F		BABR	Repl. by LEES 13B
$0.095^{+0.051}_{-0.041}$		[13] DEL-AMO-SA...10H		BABR	Repl. by LEES 13B
$0.160^{+0.040}_{-0.038}{}^{+0.051}_{-0.015}$		[14] POLUEKTOV	10	BELL	$e^+e^- \to \Upsilon(4S)$
$0.086 \pm 0.032 \pm 0.015$		[15] AUBERT	08AL	BABR	Repl. by DEL-AMO-SANCHEZ 10F
<0.19	90	HORII	08	BELL	$e^+e^- \to \Upsilon(4S)$
$0.159^{+0.054}_{-0.050} \pm 0.050$		[16] POLUEKTOV	06	BELL	Repl. by POLUEKTOV 10
$0.12 \pm 0.08 \pm 0.05$		[17] AUBERT,B	05Y	BABR	Repl. by AUBERT 08AL

[1] Uses binned analysis of $D \to K^0_S \pi^+\pi^-\pi^0$ from $B^{\pm} \to D K^{\pm}$ modes over the phase space. Strong phase measurements from CLEO-c and BES-III data of the D decay over the phase space binning are used as input.

[2] Uses binned analysis of $D \to K^0_S \pi^+\pi^-\pi^0$ from $B^{\pm} \to D K^{\pm}$ modes over the phase space. Strong phase measurements from RESMI 18 analysis of CLEO-c data of the D decay over the phase space binning are used as input.

[3] Uses binned Dalitz plot analysis of $D \to K^0_S \pi^+\pi^-$ and $K^0_S K^+K^-$ from $B^{\pm} \to D K^{\pm}$ modes. Strong phase measurements from CLEO-c of the D decay over the Dalitz plot are used as input.

[4] Uses binned Dalitz plot analysis of $B^+ \to D K^+$ decays, with $D \to K^0_S \pi^+\pi^-$ and $D \to K^0_S K^+K^-$. Strong phase measurements from CLEO-c (LIBBY 10) of the D decay over the Dalitz plot are used as input.

[5] AAIJ 14BE uses model-dependent analysis of $D \to K^0_S \pi^+\pi^-$ amplitudes. The model is the same as in DEL-AMO-SANCHEZ 10F.

[6] Uses $B^{\pm} \to [K^{\pm}\pi^{\mp}\pi^+\pi^-]_D h^{\pm}$ mode.

[7] Reports combination of published measurements using GGSZ, GLW, and ADS methods.

[8] Reports combined statistical and systematic uncertainties.

[9] Uses binned Dalitz plot of $\overline{D}^0 \to K^0_S \pi^+\pi^-$ decays from $B^+ \to \overline{D}^0 K^+$. Measurement of strong phases in $\overline{D}^0 \to K^0_S \pi^+\pi^-$ Dalitz plot from LIBBY 10 is used as input.

[10] We combined the systematics in quadrature. The authors report separately the contribution to the systematic uncertainty due to the uncertainty on the bin-averaged strong phase difference between D^0 and $\overline{D}^0$ amplitudes.

[11] Uses decays of neutral D to $K^-\pi^+\pi^0$.

[12] Uses Dalitz plot analysis of $\overline{D}^0 \to K^0_S \pi^+\pi^-$, $K^0_S K^+K^-$ decays from $B^+ \to D^{(*)} K^{(*)+}$ modes. The corresponding two standard deviation interval is $0.037 < r_B < 0.155$.

[13] Uses the Cabibbo suppressed decay of $B^+ \to \overline{D} K^+$ followed by $\overline{D} \to K^-\pi^+$.

[14] Uses Dalitz plot analysis of $\overline{D}^0 \to K^0_S \pi^+\pi^-$ decays from $B^+ \to D^0 K^+$ modes. The corresponding two standard deviation interval is $0.084 < r_B < 0.239$.

[15] Uses Dalitz plot analysis of $\overline{D}^0 \to K^0_S \pi^+\pi^-$ and $\overline{D}^0 \to K^0_S K^+K^-$ decays coming from $B^{\pm} \to D^{(*)} K^{(*)\pm}$ modes.

[16] Uses a Dalitz plot analysis of the $\overline{D}^0 \to K^0_S \pi^+\pi^-$ decays; Combines the $D K^+$, $D^* K^+$ and $D K^{*+}$ modes.

[17] Uses a Dalitz analysis of neutral D decays to $K^0_S \pi^+\pi^-$ in the processes $B^{\pm} \to D^{(*)} K^{\pm}$, $D^* \to D\pi^0$, $D\gamma$.

$\delta_B(B^+ \to D^0 K^+)$

"OUR EVALUATION" is provided by the Heavy Flavor Averaging Group (HFLAV).

VALUE (°)	DOCUMENT ID		TECN	COMMENT
$127.7^{+3.6}_{-3.9}$ OUR EVALUATION				
• • • We do not use the following data for averages, fits, limits, etc. • • •				
$118.3^{+5.5}_{-5.6}$	[1] AAIJ	21L	LHCB	pp at 7, 8, 13 TeV
$83.4^{+18.3}_{-16.6} \pm 5.1$	[2] RESMI	19	BELL	$e^+e^- \to \Upsilon(4S)$
101 ± 11	[3] AAIJ	18AD	LHCB	Repl. by AAIJ 21L
134^{+14}_{-15}	[4] AAIJ	14BA	LHCB	Repl. by AAIJ 21L
115^{+41}_{-51}	[5] AAIJ	14BE	LHCB	Repl. by AAIJ 14BA
105^{+16}_{-17}	[6] LEES	13B	BABR	$e^+e^- \to \Upsilon(4S)$
137^{+35}_{-46}	[7,8] AAIJ	12AQ	LHCB	pp at 7 TeV
$129.9 \pm 15.0 \pm 6.0$	[8,9] AIHARA	12	BELL	$e^+e^- \to \Upsilon(4S)$
$119^{+19}_{-20} \pm 4$	[10] DEL-AMO-SA...10F		BABR	Repl. by LEES 13B
$136.7^{+13.0}_{-15.8} \pm 23.2$	[11] POLUEKTOV	10	BELL	$e^+e^- \to \Upsilon(4S)$
$109^{+27}_{-30} \pm 8$	[12] AUBERT	08AL	BABR	Repl. by DEL-AMO-SANCHEZ 10F
$145.7^{+19.0}_{-19.7} \pm 23.1$	[13] POLUEKTOV	06	BELL	Repl. by POLUEKTOV 10
$104 \pm 45^{+23}_{-32}$	[14] AUBERT,B	05Y	BABR	Repl. by AUBERT 08AL

[1] Uses binned Dalitz plot analysis of $D \to K^0_S \pi^+\pi^-$ and $K^0_S K^+K^-$ from $B^{\pm} \to D K^{\pm}$ modes. Strong phase measurements from CLEO-c and BES-III of the D decay over the Dalitz plot are used as input. Value is modulo 180°.

[2] Uses binned analysis of $D \to K^0_S \pi^+\pi^-\pi^0$ from $B^{\pm} \to D K^{\pm}$ modes over the phase space. Strong phase measurements from RESMI 18 analysis of CLEO-c data of the D decay over the phase space binning are used as input.

[3] Uses binned Dalitz plot analysis of $D \to K^0_S \pi^+\pi^-$ and $K^0_S K^+K^-$ from $B^{\pm} \to D K^{\pm}$ modes. Strong phase measurements from CLEO-c of the D decay over the Dalitz plot are used as input.

[4] Uses binned Dalitz plot analysis of $B^+ \to D K^+$ decays, with $D \to K^0_S \pi^+\pi^-$ and $D \to K^0_S K^+K^-$. Strong phase measurements from CLEO-c (LIBBY 10) of the D decay over the Dalitz plot are used as input.

[5] AAIJ 14BE uses model-dependent analysis of $D \to K^0_S \pi^+\pi^-$ amplitudes. The model is the same as in DEL-AMO-SANCHEZ 10F.

[6] Reports combination of published measurements using GGSZ, GLW, and ADS methods.

[7] Reports combined statistical and systematic uncertainties.

[8] Uses binned Dalitz plot of $\overline{D}^0 \to K^0_S \pi^+\pi^-$ decays from $B^+ \to \overline{D}^0 K^+$. Measurement of strong phases in $\overline{D}^0 \to K^0_S \pi^+\pi^-$ Dalitz plot from LIBBY 10 is used as input.

[9] We combined the systematics in quadrature. The authors report separately the contribution to the systematic uncertainty due to the uncertainty on the bin-averaged strong phase difference between D^0 and $\overline{D}^0$ amplitudes.

[10] Uses Dalitz plot analysis of $\overline{D}^0 \to K^0_S \pi^+\pi^-$, $K^0_S K^+K^-$ decays from $B^+ \to D^{(*)} K^{(*)+}$ modes. The corresponding two standard deviation interval is $75° < \delta_B < 157°$.

[11] Uses Dalitz plot analysis of $\overline{D}^0 \to K^0_S \pi^+\pi^-$ decays from $B^+ \to \overline{D}^0 K^+$ modes. The corresponding two standard deviation interval is $102.2° < \delta_B < 162.3°$.

Downloaded from https://academic.oup.com/ptep/article/2022/8/083C01/6651666 by KIT Library user on 27 September 2022

[12] Uses Dalitz plot analysis of $\overline{D}^0 \to K^0_S \pi^+ \pi^-$ and $\overline{D}^0 \to K^0_S K^+ K^-$ decays coming from $B^{\pm} \to D^{(*)} K^{(*)\pm}$ modes.
[13] Uses a Dalitz plot analysis of the $\overline{D}^0 \to K^0_S \pi^+ \pi^-$ decays; Combines the $D K^+$, $D^* K^+$ and $D K^{*+}$ modes.
[14] Uses a Dalitz analysis of neutral D decays to $K^0_S \pi^+ \pi^-$ in the processes $B^{\pm} \to D^{(*)} K^{\pm}$, $D^* \to D \pi^0$, $D \gamma$.

$r_B(B^+ \to D^0 \pi^+)$

VALUE (units 10^{-3})	DOCUMENT ID		TECN	COMMENT
• • • We do not use the following data for averages, fits, limits, etc. • • •				
5.0 ± 1.7	[1] AAIJ	21L	LHCB	pp at 7, 8, 13 TeV

[1] Uses binned Dalitz plot analysis of $D \to K^0_S \pi^+ \pi^-$ and $K^0_S K^+ K^-$ from $B^{\pm} \to D \pi^{\pm}$ modes. Strong phase measurements from CLEO-c and BES-III of the D decay over the Dalitz plot are used as input.

$\delta_B(B^+ \to D^0 \pi^+)$

VALUE (°)	DOCUMENT ID		TECN	COMMENT
• • • We do not use the following data for averages, fits, limits, etc. • • •				
291^{+24}_{-26}	[1] AAIJ	21L	LHCB	pp at 7, 8, 13 TeV

[1] Uses binned Dalitz plot analysis of $D \to K^0_S \pi^+ \pi^-$ and $K^0_S K^+ K^-$ from $B^{\pm} \to D \pi^{\pm}$ modes. Strong phase measurements from CLEO-c and BES-III of the D decay over the Dalitz plot are used as input. Value is modulo 180°.

$r_B(B^+ \to D^0 K^{*+})$

r_B and δ_B are the amplitude ratio and relative strong phase between the amplitudes of $A_{CP}(B^+ \to D^0 K^{*+})$ and $A_{CP}(B^+ \to \overline{D}^0 K^{*+})$,

"OUR EVALUATION" is provided by the Heavy Flavor Averaging Group (HFLAV).

VALUE	DOCUMENT ID		TECN	COMMENT
$0.101^{+0.016}_{-0.034}$ OUR EVALUATION				
• • • We do not use the following data for averages, fits, limits, etc. • • •				
$0.143^{+0.048}_{-0.049}$	[1] LEES	13B	BABR	$e^+ e^- \to \Upsilon(4S)$
$0.166^{+0.073}_{-0.069}$	[2] DEL-AMO-SA...	10F	BABR	Repl. by LEES 13B
0.31 ± 0.07	[3] AUBERT	09AJ	BABR	Repl. by LEES 13B
$0.181^{+0.088}_{-0.108} \pm 0.042$	[4] AUBERT	08AL	BABR	Repl. by AUBERT 09AJ
$0.564^{+0.216}_{-0.155} \pm 0.093$	[5] POLUEKTOV	06	BELL	$e^+ e^- \to \Upsilon(4S)$

[1] Reports combination of published measurements using GGSZ, GLW, and ADS methods.
[2] DEL-AMO-SANCHEZ 10F reports $r_B \cdot k = 0.149^{+0.066}_{-0.062}$ for k = 0.9.
[3] Obtained by combining the GLW and ADS methods. The 2-sigma range corresponds to [0.17, 0.43].
[4] Uses Dalitz plot analysis of $\overline{D}^0 \to K^0_S \pi^+ \pi^-$ and $\overline{D}^0 \to K^0_S K^+ K^-$ decays coming from $B^{\pm} \to D^{(*)} K^{(*)\pm}$ modes.
[5] Uses a Dalitz plot analysis of the $\overline{D}^0 \to K^0_S \pi^+ \pi^-$ decays; Combines the $D K^+$, $D^* K^+$ and $D K^{*+}$ modes.

$\delta_B(B^+ \to D^0 K^{*+})$

"OUR EVALUATION" is provided by the Heavy Flavor Averaging Group (HFLAV).

VALUE (°)	DOCUMENT ID		TECN	COMMENT
48^{+59}_{-16} OUR EVALUATION				
• • • We do not use the following data for averages, fits, limits, etc. • • •				
101 ± 43	[1] LEES	13B	BABR	$e^+ e^- \to \Upsilon(4S)$
111 ± 32	DEL-AMO-SA...	10F	BABR	Repl. by LEES 13B
$104^{+39}_{-37} \pm 18$	[2] AUBERT	08AL	BABR	Repl. by LEES 13B
$242.6^{+20.2}_{-23.2} \pm 49.4$	[3] POLUEKTOV	06	BELL	$e^+ e^- \to \Upsilon(4S)$

[1] Reports combination of published measurements using GGSZ, GLW, and ADS methods.
[2] Uses Dalitz plot analysis of $\overline{D}^0 \to K^0_S \pi^+ \pi^-$ and $\overline{D}^0 \to K^0_S K^+ K^-$ decays coming from $B^{\pm} \to D^{(*)} K^{(*)\pm}$ modes.
[3] Uses a Dalitz plot analysis of the $\overline{D}^0 \to K^0_S \pi^+ \pi^-$ decays; Combines the $D K^+$, $D^* K^+$ and $D K^{*+}$ modes.

$r_B(B^+ \to D^{*0} K^+)$

r_B and δ_B are the amplitude ratio and relative strong phase between the amplitudes of $A(B^+ \to D^{*0} K^+)$ and $A(B^+ \to \overline{D}^{*0} K^+)$,

"OUR EVALUATION" is provided by the Heavy Flavor Averaging Group (HFLAV).

VALUE	DOCUMENT ID		TECN	COMMENT
$0.104^{+0.013}_{-0.014}$ OUR EVALUATION				
• • • We do not use the following data for averages, fits, limits, etc. • • •				
$0.106^{+0.019}_{-0.036}$	[1] LEES	13B	BABR	$e^+ e^- \to \Upsilon(4S)$
$0.133^{+0.042}_{-0.039} \pm 0.013$	[2] DEL-AMO-SA...	10F	BABR	Repl. by LEES 13B
$0.096^{+0.035}_{-0.051}$	[3] DEL-AMO-SA...	10H	BABR	Repl. by LEES 13B
$0.196^{+0.072}_{-0.069} \pm 0.064$	[4] POLUEKTOV	10	BELL	$e^+ e^- \to \Upsilon(4S)$
$0.135 \pm 0.050 \pm 0.012$	[5] AUBERT	08AL	BABR	Repl. by DEL-AMO-SANCHEZ 10F
$0.175^{+0.108}_{-0.099} \pm 0.050$	[6] POLUEKTOV	06	BELL	Repl. by POLUEKTOV 10
$0.17 \pm 0.10 \pm 0.04$	[7] AUBERT,B	05Y	BABR	Repl. by AUBERT 08AL

[1] Reports combination of published measurements using GGSZ, GLW, and ADS methods.
[2] Uses Dalitz plot analysis of $\overline{D}^0 \to K^0_S \pi^+ \pi^-$, $K^0_S K^+ K^-$ decays from $B^+ \to D^{(*)} K^{(*)+}$ modes. The corresponding two standard deviation interval is $0.049 < r^*_B < 0.215$.
[3] Uses the Cabibbo suppressed decay of $B^+ \to \overline{D}^* K^+$ followed by $\overline{D}^* \to \overline{D} \pi^0$ or $\overline{D} \gamma$, and $\overline{D} \to K^- \pi^+$.
[4] Uses Dalitz plot analysis of $\overline{D}^0 \to K^0_S \pi^+ \pi^-$ decays from $B^+ \to D^{*0} K^+$ modes. The corresponding two standard deviation interval is $0.061 < r^*_B < 0.271$.
[5] Uses Dalitz plot analysis of $\overline{D}^0 \to K^0_S \pi^+ \pi^-$ and $\overline{D}^0 \to K^0_S K^+ K^-$ decays coming from $B^{\pm} \to D^{(*)} K^{(*)\pm}$ modes.
[6] Uses a Dalitz plot analysis of the $\overline{D}^0 \to K^0_S \pi^+ \pi^-$ decays; Combines the $D K^+$, $D^* K^+$ and $D K^{*+}$ modes.
[7] Uses a Dalitz analysis of neutral D decays to $K^0_S \pi^+ \pi^-$ in the processes $B^{\pm} \to D^{(*)} K^{\pm}$, $D^* \to D \pi^0$, $D \gamma$.

$\delta_B(B^+ \to D^{*0} K^+)$

"OUR EVALUATION" is provided by the Heavy Flavor Averaging Group (HFLAV).

VALUE (°)	DOCUMENT ID		TECN	COMMENT
$314.8^{+7.9}_{-9.9}$ OUR EVALUATION				
• • • We do not use the following data for averages, fits, limits, etc. • • •				
294^{+21}_{-31}	[1] LEES	13B	BABR	$e^+ e^- \to \Upsilon(4S)$
$278 \pm 21 \pm 6$	[2] DEL-AMO-SA...	10F	BABR	Repl. by LEES 13B
$341.9^{+18.0}_{-19.6} \pm 23.1$	[3] POLUEKTOV	10	BELL	$e^+ e^- \to \Upsilon(4S)$
$297^{+27}_{-29} \pm 6.4$	[4] AUBERT	08AL	BABR	Repl. by DEL-AMO-SANCHEZ 10F
$302.0^{+33.8}_{-35.1} \pm 23.7$	[5] POLUEKTOV	06	BELL	Repl. by POLUEKTOV 10
$296 \pm 41^{+20}_{-19}$	[6] AUBERT,B	05Y	BABR	Repl. by AUBERT 08AL

[1] Reports combination of published measurements using GGSZ, GLW, and ADS methods. We added 360° to the value of $(-66^{+21}_{-31})°$ quoted by LEES 13B.
[2] Uses Dalitz plot analysis of $\overline{D}^0 \to K^0_S \pi^+ \pi^-$, $K^0_S K^+ K^-$ decays from $B^+ \to D^{(*)} K^{(*)+}$ modes. The corresponding two standard deviation interval is $236° < \delta^*_B < 322°$.
[3] Uses Dalitz plot analysis of $\overline{D}^0 \to K^0_S \pi^+ \pi^-$ decays from $B^+ \to D^* K^+$ modes. The corresponding two standard deviation interval is $296.5° < \delta^*_B < 382.7°$.
[4] Uses Dalitz plot analysis of $\overline{D}^0 \to K^0_S \pi^+ \pi^-$ and $\overline{D}^0 \to K^0_S K^+ K^-$ decays coming from $B^{\pm} \to D^{(*)} K^{(*)\pm}$ modes.
[5] Uses a Dalitz plot analysis of the $\overline{D}^0 \to K^0_S \pi^+ \pi^-$ decays; Combines the $D K^+$, $D^* K^+$ and $D K^{*+}$ modes.
[6] Uses a Dalitz analysis of neutral D decays to $K^0_S \pi^+ \pi^-$ in the processes $B^{\pm} \to D^{(*)} K^{\pm}$, $D^* \to D \pi^0$, $D \gamma$.

PARTIAL BRANCHING FRACTIONS

$B(B^+ \to K^{*+} \ell^+ \ell^-)$ ($q^2 < 2.0$ GeV^2/c^4)

VALUE (units 10^{-7})	DOCUMENT ID		TECN	COMMENT
1.4 ± 0.5 OUR AVERAGE				
$1.37^{+0.60}_{-0.58}$	AAIJ	12AH	LHCB	pp at 7 TeV
$1.30 \pm 0.98 \pm 0.14$	AALTONEN	11AI	CDF	$p\overline{p}$ at 1.96 TeV

$B(B^+ \to K^{*+} \ell^+ \ell^-)$ ($2.0 < q^2 < 4.3$ GeV^2/c^4)

VALUE (units 10^{-7})	DOCUMENT ID		TECN	COMMENT
1.1 ± 0.5 OUR AVERAGE				
$1.24^{+0.60}_{-0.55}$	AAIJ	12AH	LHCB	pp at 7 TeV
$0.71 \pm 1.00 \pm 0.15$	AALTONEN	11AI	CDF	$p\overline{p}$ at 1.96 TeV

$B(B^+ \to K^{*+} \ell^+ \ell^-)$ ($4.3 < q^2 < 8.68$ GeV^2/c^4)

VALUE (units 10^{-7})	DOCUMENT ID		TECN	COMMENT
$2.4^{+0.8}_{-0.7}$ OUR AVERAGE				
$2.50^{+0.88}_{-0.74}$	AAIJ	12AH	LHCB	pp at 7 TeV
$1.71 \pm 1.58 \pm 0.49$	AALTONEN	11AI	CDF	$p\overline{p}$ at 1.96 TeV

$B(B^+ \to K^{*+} \ell^+ \ell^-)$ ($10.09 < q^2 < 12.86$ GeV^2/c^4)

VALUE (units 10^{-7})	DOCUMENT ID		TECN	COMMENT
2.1 ± 0.6 OUR AVERAGE				
$2.13^{+0.72}_{-0.66}$	AAIJ	12AH	LHCB	pp at 7 TeV
$1.97 \pm 0.99 \pm 0.22$	AALTONEN	11AI	CDF	$p\overline{p}$ at 1.96 TeV

Downloaded from https://academic.oup.com/ptep/article/2022/8/083C01/6651666 by KIT Library user on 27 September 2022

$B(B^+ \to K^{*+}\ell^+\ell^-)$ $(14.18 < q^2 < 16.0\ GeV^2/c^4)$

VALUE (units 10^{-7})	DOCUMENT ID		TECN	COMMENT
$0.86^{+0.40}_{-0.32}$ OUR AVERAGE				
$1.00^{+0.47}_{-0.38}$	AAIJ	12AH	LHCB	pp at 7 TeV
$0.52 \pm 0.61 \pm 0.09$	AALTONEN	11AI	CDF	$p\overline{p}$ at 1.96 TeV

$B(B^+ \to K^{*+}\ell^+\ell^-)$ $(15.0 < q^2 < 19.0\ GeV^2/c^4)$

VALUE (units 10^{-7})	DOCUMENT ID		TECN	COMMENT
$1.78^{+0.32}_{-0.29}$ OUR AVERAGE				
$2.9\ ^{+1.0}_{-0.8} \pm 0.3$	[1] WEHLE	21	BELL	$e^+e^- \to \Upsilon(4S)$
$2.1\ ^{+1.2}_{-1.0} \pm 0.2$	[2] WEHLE	21	BELL	$e^+e^- \to \Upsilon(4S)$
$1.58^{+0.32}_{-0.29} \pm 0.11$	[3] AAIJ	14M	LHCB	pp at 7, 8 TeV

[1] Measured with $\mu^+\mu^-$ as lepton pair.
[2] Measured with e^+e^- as lepton pair.
[3] Uses $B(B^+ \to J/\psi(1S)K^*(892)^+) = (1.431 \pm 0.027 \pm 0.090) \times 10^{-3}$ for normalization and $\mu^+\mu^-$ as a lepton pair.

$B(B^+ \to K^{*+}\ell^+\ell^-)$ $(q^2 > 16.0\ GeV^2/c^4)$

VALUE (units 10^{-7})	DOCUMENT ID		TECN	COMMENT
1.3 ± 0.4 OUR AVERAGE				
1.25 ± 0.46	AAIJ	12AH	LHCB	pp at 7 TeV
$1.57 \pm 0.96 \pm 0.17$	AALTONEN	11AI	CDF	$p\overline{p}$ at 1.96 TeV

$B(B^+ \to K^{*+}\ell^+\ell^-)$ $(1.0 < q^2 < 6.0\ GeV^2/c^4)$

VALUE (units 10^{-7})	DOCUMENT ID		TECN	COMMENT
$1.72^{+0.40}_{-0.32}$ OUR AVERAGE				
$1.2\ ^{+0.9}_{-0.7} \pm 0.2$	[1,2] WEHLE	21	BELL	$e^+e^- \to \Upsilon(4S)$
$1.7\ ^{+1.0}_{-1.0} \pm 0.2$	[2,3] WEHLE	21	BELL	$e^+e^- \to \Upsilon(4S)$
$1.79^{+0.41}_{-0.37} \pm 0.13$	[4] AAIJ	14M	LHCB	pp at 7, 8 TeV
$2.57 \pm 1.61 \pm 0.40$	AALTONEN	11AI	CDF	$p\overline{p}$ at 1.96 TeV
• • • We do not use the following data for averages, fits, limits, etc. • • •				
$2.90^{+0.90}_{-0.85}$	AAIJ	12AH	LHCB	Repl. by AAIJ 14M

[1] Measured with $\mu^+\mu^-$ as lepton pair.
[2] Result is determined for the range $1.1 < q^2 < 6.0\ GeV^4/c^2$.
[3] Measured with e^+e^- as lepton pair.
[4] Uses $B(B^+ \to J/\psi(1S)K^*(892)^+) = (1.431 \pm 0.027 \pm 0.090) \times 10^{-3}$ for normalization and $\mu^+\mu^-$ as a lepton pair. Measured in $1.1 < q^2 < 6.0\ GeV^2/c^4$.

$B(B^+ \to K^{*+}\ell^+\ell^-)$ $(0.0 < q^2 < 4.3\ GeV^2/c^4)$

VALUE (units 10^{-7})	DOCUMENT ID		TECN	COMMENT
$2.01 \pm 1.39 \pm 0.27$	AALTONEN	11AI	CDF	$p\overline{p}$ at 1.96 TeV

$B(B^+ \to K^{*+}\mu^+\mu^-)$ / $B(B^+ \to K^{*+}e^+e^-)$ $(0.045 < q^2 < 1.1\ GeV^2/c^4)$

VALUE	DOCUMENT ID		TECN	COMMENT
$0.62^{+0.60}_{-0.36} \pm 0.07$	WEHLE	21	BELL	$e^+e^- \to \Upsilon(4S)$

$B(B^+ \to K^{*+}\mu^+\mu^-)$ / $B(B^+ \to K^{*+}e^+e^-)$ $(1.1 < q^2 < 6.0\ GeV^2/c^4)$

VALUE	DOCUMENT ID		TECN	COMMENT
$0.72^{+0.99}_{-0.44} \pm 0.14$	WEHLE	21	BELL	$e^+e^- \to \Upsilon(4S)$

$B(B^+ \to K^{*+}\mu^+\mu^-)/B(B^+ \to K^{*+}e^+e^-)$ $(15.0 < q^2 < 19.0\ GeV^2/c^4)$

VALUE	DOCUMENT ID		TECN	COMMENT
$1.40^{+1.99}_{-0.68} \pm 0.11$	WEHLE	21	BELL	$e^+e^- \to \Upsilon(4S)$

$B(B^+ \to K^+\ell^+\ell^-)$ $(q^2 < 2.0\ GeV^2/c^4)$

VALUE (units 10^{-7})	DOCUMENT ID		TECN	COMMENT
0.51 ± 0.08 OUR AVERAGE	Error includes scale factor of 1.5.			
$0.556 \pm 0.053 \pm 0.027$	[1] AAIJ	13H	LHCB	pp at 7 TeV
$0.36 \pm 0.11 \pm 0.03$	AALTONEN	11AI	CDF	$p\overline{p}$ at 1.96 TeV

[1] Measured in $0.05 < q^2 < 2.0\ GeV^2/c^4$ range.

$B(B^+ \to K^+\ell^+\ell^-)$ $(2.0 < q^2 < 4.3\ GeV^2/c^4)$

VALUE (units 10^{-7})	DOCUMENT ID		TECN	COMMENT
0.60 ± 0.07 OUR AVERAGE	Error includes scale factor of 1.3.			
$0.573 \pm 0.053 \pm 0.023$	AAIJ	13H	LHCB	pp at 7 TeV
$0.80 \pm 0.15 \pm 0.05$	AALTONEN	11AI	CDF	$p\overline{p}$ at 1.96 TeV

$B(B^+ \to K^+\ell^+\ell^-)$ $(4.3 < q^2 < 8.68\ GeV^2/c^4)$

VALUE (units 10^{-7})	DOCUMENT ID		TECN	COMMENT
1.03 ± 0.07 OUR AVERAGE				
$1.003 \pm 0.070 \pm 0.039$	AAIJ	13H	LHCB	pp at 7 TeV
$1.18 \pm 0.19 \pm 0.09$	AALTONEN	11AI	CDF	$p\overline{p}$ at 1.96 TeV

$B(B^+ \to K^+\ell^+\ell^-)$ $(10.09 < q^2 < 12.86\ GeV^2/c^4)$

VALUE (units 10^{-7})	DOCUMENT ID		TECN	COMMENT
0.58 ± 0.05 OUR AVERAGE				
$0.565 \pm 0.050 \pm 0.022$	AAIJ	13H	LHCB	pp at 7 TeV
$0.68 \pm 0.12 \pm 0.05$	AALTONEN	11AI	CDF	$p\overline{p}$ at 1.96 TeV

$B(B^+ \to K^+\ell^+\ell^-)$ $(14.18 < q^2 < 16.0\ GeV^2/c^4)$

VALUE (units 10^{-7})	DOCUMENT ID		TECN	COMMENT
0.40 ± 0.05 OUR AVERAGE	Error includes scale factor of 1.4.			
$0.377 \pm 0.036 \pm 0.015$	AAIJ	13H	LHCB	pp at 7 TeV
$0.53 \pm 0.10 \pm 0.03$	AALTONEN	11AI	CDF	$p\overline{p}$ at 1.96 TeV

$B(B^+ \to K^+\ell^+\ell^-)$ $(16.0 < q^2 < 18.0\ GeV^2/c^4)$

VALUE (units 10^{-7})	DOCUMENT ID		TECN	COMMENT
$0.354 \pm 0.036 \pm 0.018$	AAIJ	13H	LHCB	pp at 7 TeV

$B(B^+ \to K^+\ell^+\ell^-)$ $(18.0 < q^2 < 22.0\ GeV^2/c^4)$

F_H is a fractional contribution of (pseudo) scalar and tensor amplitudes to the decay width in the massless muon approximation.

VALUE (units 10^{-7})	DOCUMENT ID		TECN	COMMENT
$0.312 \pm 0.040 \pm 0.016$	AAIJ	13H	LHCB	pp at 7 TeV

$B(B^+ \to K^+\ell^+\ell^-)$ $(15.0 < q^2 < 22.0\ GeV^2/c^4)$

VALUE (units 10^{-7})	DOCUMENT ID		TECN	COMMENT
$0.85 \pm 0.03 \pm 0.04$	[1] AAIJ	14M	LHCB	pp at 7, 8 TeV

[1] Uses $B(B^+ \to J/\psi(1S)K^+) = (0.998 \pm 0.014 \pm 0.040) \times 10^{-3}$ for normalization and $\mu^+\mu^-$ as a lepton pair.

$B(B^+ \to K^+\ell^+\ell^-)$ $(16.0 < q^2\ GeV^2/c^4)$

VALUE (units 10^{-7})	DOCUMENT ID		TECN	COMMENT
$0.48 \pm 0.11 \pm 0.03$	AALTONEN	11AI	CDF	$p\overline{p}$ at 1.96 TeV

$B(B^+ \to K^+\ell^+\ell^-)$ $(1.0 < q^2 < 6.0\ GeV^2/c^4)$

VALUE (units 10^{-7})	DOCUMENT ID		TECN	COMMENT
1.26 ± 0.12 OUR AVERAGE	Error includes scale factor of 1.9. See the ideogram below.			
$2.30\ ^{+0.41}_{-0.38} \pm 0.05$	[1] CHOUDHURY	21	BELL	$e^+e^- \to \Upsilon(4S)$
$1.66\ ^{+0.32}_{-0.29} \pm 0.04$	[2] CHOUDHURY	21	BELL	$e^+e^- \to \Upsilon(4S)$
$1.40\ ^{+0.98}_{-0.34} \pm 0.69$	[3] AAIJ	19S	LHCB	pp at 7, 8, 13 TeV
$1.19 \pm 0.034 \pm 0.059$	[4] AAIJ	14M	LHCB	pp at 7, 8 TeV
$1.41 \pm 0.20 \pm 0.10$	AALTONEN	11AI	CDF	$p\overline{p}$ at 1.96 TeV
• • • We do not use the following data for averages, fits, limits, etc. • • •				
$1.56\ ^{+0.19}_{-0.15}\ ^{+0.06}_{-0.04}$	[5] AAIJ	14AR	LHCB	pp at 7, 8 TeV
$1.205 \pm 0.085 \pm 0.070$	AAIJ	13H	LHCB	Repl. by AAIJ 14M

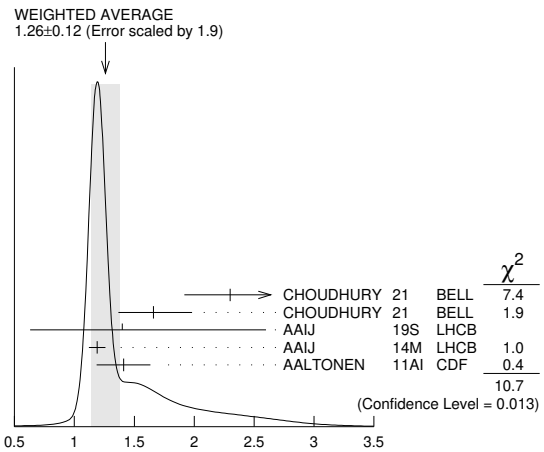

$B(B^+ \to K^+\ell^+\ell^-)$ $(1.0 < q^2 < 6.0\ GeV^2/c^4)$ (units 10^{-7})

[1] Measured for $B^+ \to K^+\mu^+\mu^-$ decays. Measurements in other q^2 bins are also reported.
[2] Measured for $B^+ \to K^+e^+e^-$ decays. Measurements in other q^2 bins are also reported.
[3] Measured by taking the ratio of the branching fraction from $B^+ \to K^+e^+e^-$ and $B^+ \to J/\psi(e^+e^-)K^+$ decays and multiplying it by the measured value of $B^+ \to J/\psi K^+$ and $J/\psi \to e^+e^-$ as in PDG 18. The branching fraction of $B^+ \to K^+e^+e^-$ is determined in the region $1.1 < q^2 < 6\ GeV^2/c^4$.
[4] Uses $B(B^+ \to J/\psi(1S)K^+) = (0.998 \pm 0.014 \pm 0.040) \times 10^{-3}$ for normalization and $\mu^+\mu^-$ for leptons. Measured for $1.1 < q^2 < 6.0\ GeV^2/c^4$.
[5] Measured by taking the ratio of the branching fraction from $B^+ \to K^+e^+e^-$ and $B^+ \to J/\psi(e^+e^-)K^+$decays and multiplying it by the measured value of $B^+ \to J/\psi K^+$ and $J/\psi \to e^+e^-$ as in PDG 12.The branching fraction of $B^+ \to K^+e^+e^-$ is determined in the region $1 < q^2 < 6\ GeV^2/c^4$.

Downloaded from https://academic.oup.com/ptep/article/2022/8/083C01/6651666 by KIT Library user on 27 September 2022

$B(B^+ \to K^+\mu^+\mu^-)$ / $B(B^+ \to K^+e^+e^-)$ ($1.0 < q^2 < 6.0$ GeV^2/c^4)

VALUE	DOCUMENT ID		TECN	COMMENT
0.86 ±0.06 OUR AVERAGE				
$1.39\ ^{+0.36}_{-0.33} \pm 0.02$	[1] CHOUDHURY	21	BELL	$e^+e^- \to \Upsilon(4S)$
$0.846\ ^{+0.060}_{-0.054}\ ^{+0.016}_{-0.014}$	[2] AAIJ	19S	LHCB	pp at 7, 8, 13 TeV
• • • We do not use the following data for averages, fits, limits, etc. • • •				
$0.745\ ^{+0.090}_{-0.074} \pm 0.036$	[3] AAIJ	14AR	LHCB	pp at 7, 8 TeV

[1] Measurements in other q^2 bins are also reported.
[2] The ratio is determined using the relative branching fractions of the decays $B^+ \to K^+\ell^+\ell^-$ and $B^+ \to J/\psi(\to \ell^+\ell^-)K^+$, with $\ell = e, \mu$. Measured for the region $1.1 < q^2 < 6.0$ GeV^2/c^4.
[3] The ratio is determined using the relative branching fractions of the decays $B^+ \to K^+\ell^+\ell^-$ and $B^+ \to J/\psi(\to \ell^+\ell^-)K^+$, with $\ell = e, \mu$.

$B(B^+ \to K^+\ell^+\ell^-)$ ($0.0 < q^2 < 4.3$ GeV^2/c^4)

VALUE (units 10^{-7})	DOCUMENT ID		TECN	COMMENT
1.13±0.19±0.08	AALTONEN	11AI	CDF	$p\overline{p}$ at 1.96 TeV

$B(B^+ \to K^+\pi^+\pi^-\mu^+\mu^-)$ ($1.00 < q^2 < 6.00$ GeV^2/c^4)

VALUE (units 10^{-7})	DOCUMENT ID		TECN	COMMENT
$\mathbf{1.38^{+0.15}_{-0.14} \pm 0.08}$	AAIJ	14AZ	LHCB	pp at 7, 8 TeV

$B(B^+ \to K^+\pi^+\pi^-\mu^+\mu^-)$ ($0.10 < q^2 < 2.00$ GeV^2/c^4)

VALUE (units 10^{-7})	DOCUMENT ID		TECN	COMMENT
$\mathbf{1.33^{+0.13}_{-0.12} \pm 0.09}$	AAIJ	14AZ	LHCB	pp at 7, 8 TeV

$B(B^+ \to K^+\pi^+\pi^-\mu^+\mu^-)$ ($2.00 < q^2 < 4.30$ GeV^2/c^4)

VALUE (units 10^{-8})	DOCUMENT ID		TECN	COMMENT
$\mathbf{5.38^{+0.94}_{-0.87} \pm 0.35}$	AAIJ	14AZ	LHCB	pp at 7, 8 TeV

$B(B^+ \to K^+\pi^+\pi^-\mu^+\mu^-)$ ($4.30 < q^2 < 8.68$ GeV^2/c^4)

VALUE (units 10^{-7})	DOCUMENT ID		TECN	COMMENT
$\mathbf{1.01^{+0.12}_{-0.13} \pm 0.09}$	AAIJ	14AZ	LHCB	pp at 7, 8 TeV

$B(B^+ \to K^+\pi^+\pi^-\mu^+\mu^-)$ ($10.09 < q^2 < 12.86$ GeV^2/c^4)

VALUE (units 10^{-8})	DOCUMENT ID		TECN	COMMENT
$\mathbf{5.07^{+0.94}_{-0.89} \pm 0.47}$	AAIJ	14AZ	LHCB	pp at 7, 8 TeV

$B(B^+ \to K^+\pi^+\pi^-\mu^+\mu^-)$ ($14.18 < q^2 < 19.00$ GeV^2/c^4)

VALUE (units 10^{-8})	DOCUMENT ID		TECN	COMMENT
$\mathbf{0.48^{+0.39}_{-0.29} \pm 0.05}$	AAIJ	14AZ	LHCB	pp at 7, 8 TeV

$B(B^+ \to \pi^+\mu^+\mu^-)/B(B^+ \to K^+\mu^+\mu^-)$ ($1.00 < q^2 < 6.00$ GeV^2/c^4)

VALUE (units 10^{-2})	DOCUMENT ID		TECN	COMMENT
3.8±0.9±0.1	AAIJ	15AR	LHCB	pp at 7, 8 TeV

$B(B^+ \to \pi^+\mu^+\mu^-)$ ($1.00 < q^2 < 6.00$ GeV^2/c^4)

VALUE (units 10^{-9})	DOCUMENT ID		TECN	COMMENT
$\mathbf{4.55^{+1.05}_{-1.00} \pm 0.15}$	AAIJ	15AR	LHCB	pp at 7, 8 TeV

$B(B^+ \to \pi^+\mu^+\mu^-)$ ($15.00 < q^2 < 22.00$ GeV^2/c^4)

VALUE (units 10^{-9})	DOCUMENT ID		TECN	COMMENT
$\mathbf{3.29^{+0.84}_{-0.70} \pm 0.07}$	AAIJ	15AR	LHCB	pp at 7, 8 TeV

$B(B^+ \to \pi^+\mu^+\mu^-)/B(B^+ \to K^+\mu^+\mu^-)$ ($15.0 < q^2 < 22.0$ GeV^2/c^4)

VALUE (units 10^{-2})	DOCUMENT ID		TECN	COMMENT
3.7±0.8±0.1	AAIJ	15AR	LHCB	pp at 7, 8 TeV

$A_{FB}(B^+ \to K^+\mu^+\mu^-)$ ($1.1 < q^2 < 6.0$ GeV^2/c^4)

A_{FB} is the forward-backward angular asymmetry of the lepton pair in $B \to K^{(*)}\ell^+\ell^-$ decay as defined in B^+, B^0 admixture particle listings.

VALUE	DOCUMENT ID		TECN	COMMENT
−0.003±0.017 OUR AVERAGE				
$-0.14\ ^{+0.07}_{-0.06} \pm 0.03$	[1] SIRUNYAN	18DX	CMS	pp at 8 TeV
$0.005 \pm 0.015 \pm 0.010$	[2] AAIJ	14O	LHCB	pp at 7,8 TeV
• • • We do not use the following data for averages, fits, limits, etc. • • •				
$0.02\ ^{+0.05}_{-0.03}\ ^{+0.02}_{-0.01}$	AAIJ	13H	LHCB	Repl. by AAIJ 14O

[1] Measurement is performed in $1.0 < q^2 < 6.0$ GeV^2/c^4. SIRUNYAN 18DX reports also measurements in several other q^2 intervals.
[2] AAIJ 14O reports 68% C.L. interval, which we encode as midpoint with uncertainty as half of the width of interval.

$A_{FB}(B^+ \to K^+\mu^+\mu^-)$ ($15.0 < q^2 < 22.0$ GeV^2/c^4)

VALUE	DOCUMENT ID		TECN	COMMENT
−0.015±0.015±0.01	[1] AAIJ	14O	LHCB	pp at 7, 8 TeV

[1] AAIJ 14O reports 68% C.L. interval, which we encode as midpoint with uncertainty as half of the width of interval.

$F_H(B^+ \to K^+\mu^+\mu^-)$ ($1.1 < q^2 < 6.0$ GeV^2/c^4)

F_H is a fractional contribution of (pseudo) scalar and tensor amplitudes to the decay width in the massless muon approximation.

VALUE	DOCUMENT ID		TECN	COMMENT
0.04±0.04 OUR AVERAGE				
$0.38\ ^{+0.17}_{-0.21} \pm 0.09$	[1] SIRUNYAN	18DX	CMS	pp at 8 TeV
$0.03 \pm 0.03 \pm 0.02$	[2] AAIJ	14O	LHCB	pp at 7, 8 TeV
• • • We do not use the following data for averages, fits, limits, etc. • • •				
$0.05\ ^{+0.08}_{-0.05}\ ^{+0.04}_{-0.02}$	AAIJ	13H	LHCB	Repl. by AAIJ 14O

[1] Measurement is performed in $1.0 < q^2 < 6.0$ GeV^2/c^4. SIRUNYAN 18DX reports also measurements in several other q^2 intervals.
[2] AAIJ 14O reports 68% C.L. interval, which we encode as midpoint with uncertainty as half of the width of interval.

$F_H(B^+ \to K^+\mu^+\mu^-)$ ($15.0 < q^2 < 22.0$ GeV^2/c^4)

F_H is a fractional contribution of (pseudo) scalar and tensor amplitudes to the decay width in the massless muon approximation.

VALUE	DOCUMENT ID		TECN	COMMENT
0.035±0.035±0.02	[1] AAIJ	14O	LHCB	pp at 7, 8 TeV

[1] AAIJ 14O reports 68% C.L. interval, which we encode as midpoint with uncertainty as half of the width of interval.

FORWARD-BACKWARD ASYMMETRIES

The forward-backward assymmetry is defined as $A_{FB} = [\ N(q_{FB} > 0) - N(q_{FB} < 0)]\ /\ [N(q_{FB} > 0) + N(q_{FB} < 0)\ ]$, where $q_{FB} = -q_B \cdot \mathrm{sgn}(\eta_B)$ with q_B as the B hadron electric charge, η_B as its pseudorapidity, and $\mathrm{sgn}(\eta_B)$ as a sign function of η_B.

$A_{FB}(B^{\pm} \to J/\psi K^{\pm})$

VALUE (units 10^{-2})	DOCUMENT ID		TECN	COMMENT
−0.24±0.41±0.19	ABAZOV	15	D0	$p\overline{p}$ at 1.96 TeV

$A_{FB}(B^{\pm} \to K^*(892)^+\mu^+\mu^-)$ ($1.0 < q^2 < 8.68$ GeV^2/c^4)

VALUE	DOCUMENT ID		TECN	COMMENT
$\mathbf{-0.14^{+0.32}_{-0.35} \pm 0.17}$	[1,2] SIRUNYAN	21AC	CMS	pp at 8 TeV

[1] SIRUNYAN 21AC measurement is performed in $1.0 < q^2 < 8.68$ GeV^2/c^4. Reports also measurements in several other q^2 intervals.
[2] A_{FB} is defined with respect to $\mu^+\mu^-$ direction and not the B direction.

$A_{FB}(B^{\pm} \to K^*(892)^+\mu^+\mu^-)$ ($1.1 < q^2 < 6.0$ GeV^2/c^4)

VALUE	DOCUMENT ID		TECN	COMMENT
$\mathbf{-0.08^{+0.07}_{-0.08} \pm 0.02}$	[1] AAIJ	21J	LHCB	pp at 7, 8, 13 TeV

[1] The full set of CP-averaged angular observables is measured as a function of the q^2. The A_{FB} is measured related to the dimuon system.

$A_{FB}(B^{\pm} \to K^*(892)^+\mu^+\mu^-)$ ($10.09 < q^2 < 12.86$ GeV^2/c^4)

VALUE	DOCUMENT ID		TECN	COMMENT
$\mathbf{0.09^{+0.16}_{-0.11} \pm 0.04}$	[1,2] SIRUNYAN	21AC	CMS	pp at 8 TeV

[1] SIRUNYAN 21AC measurement is performed in $10.09 < q^2 < 12.86$ GeV^2/c^4. Reports also measurements in several other q^2 intervals.
[2] A_{FB} is defined with respect to $\mu^+\mu^-$ direction and not the B direction.

$A_{FB}(B^{\pm} \to K^*(892)^+\mu^+\mu^-)$ ($14.18 < q^2 < 19.0$ GeV^2/c^4)

VALUE	DOCUMENT ID		TECN	COMMENT
$\mathbf{0.33^{+0.11}_{-0.07} \pm 0.05}$	[1,2] SIRUNYAN	21AC	CMS	pp at 8 TeV

[1] SIRUNYAN 21AC measurement is performed in $14.18 < q^2 < 19.0$ GeV^2/c^4. Reports also measurements in several other q^2 intervals.
[2] A_{FB} is defined with respect to $\mu^+\mu^-$ direction and not the B direction.

$A_{FB}(B^{\pm} \to K^*(892)^+\mu^+\mu^-)$ ($15.0 < q^2 < 19.0$ GeV^2/c^4)

VALUE	DOCUMENT ID		TECN	COMMENT
0.31±0.06±0.04	[1] AAIJ	21J	LHCB	pp at 7, 8, 13 TeV

[1] The full set of CP-averaged angular observables is measured as a function of the q^2. The A_{FB} is measured related to the dimuon system.

$A_P(B^+) = [\sigma(B^-) - \sigma(B^+)]\ /\ [\sigma(B^-) + \sigma(B^+)]$

Production asymmetries

VALUE (units 10^{-3})	DOCUMENT ID		TECN	COMMENT
−5.2±1.9 OUR AVERAGE				
$-4.1 \pm 4.9 \pm 1.0$	[1] AAIJ	17AP	LHCB	pp at 7 TeV
$-5.3 \pm 3.1 \pm 1.0$	[1] AAIJ	17AP	LHCB	pp at 8 TeV

Downloaded from https://academic.oup.com/ptep/article/2022/8/083C01/6651666 by KIT Library user on 27 September 2022

$-2.3\pm2.4\pm3.7$	[2] AAIJ	17BF LHCB	pp at 7 TeV
$-7.4\pm1.5\pm3.2$	[2] AAIJ	17BF LHCB	pp at 8 TeV

[1] AAIJ 17AP uses $B^+ \to \overline{D}^0\pi^+$ decays with B^+ transverse momenta p_T and rapidities y in the region of $2 < p_T < 30$ GeV/c and $2.1 < y < 4.5$.

[2] AAIJ 17BF uses $B^+ \to J/\psi K^+$ decays with B^+ transverse momenta p_T and rapidities y in the region of $0 < p_T < 30$ GeV/c and $2.1 < y < 4.5$.

$B^{\pm}$ REFERENCES

AAIJ	21AM	JHEP 2112 141	R. Aaij et al.	(LHCb Collab.)
AAIJ	21H	PRL 126 091802	R. Aaij et al.	(LHCb Collab.)
AAIJ	21J	PRL 126 161802	R. Aaij et al.	(LHCb Collab.)
AAIJ	21L	JHEP 2102 169	R. Aaij et al.	(LHCb Collab.)
AAIJ	21M	JHEP 2103 137	R. Aaij et al.	(LHCb Collab.)
AAIJ	21Q	JHEP 2104 081	R. Aaij et al.	(LHCb Collab.)
ABUDINEN	21	PRL 127 181802	F. Abudinen et al.	(BELLE II Collab.)
BELENO	21	PR D103 112001	C. Beleno et al.	(BELLE Collab.)
CAO	21A	PR D104 012008	L. Cao et al.	(BELLE Collab.)
CHOUDHURY	21	JHEP 2103 105	S. Choudhury et al.	(BELLE Collab.)
MOHANTY	21	PR D103 052013	S. Mohanty et al.	(Belle Collab.)
SIRUNYAN	21AC	JHEP 2104 124	A.M. Sirunyan et al.	(CMS Collab.)
WEHLE	21	PRL 126 161801	S. Wehle et al.	(BELLE Collab.)
AAIJ	20A	PRL 124 031801	R. Aaij et al.	(LHCb Collab.)
Also		PR D101 012006	R. Aaij et al.	(LHCb Collab.)
AAIJ	20AI	PR D102 112003	R. Aaij et al.	(LHCb Collab.)
AAIJ	20AJ	PR D102 112010	R. Aaij et al.	(LHCb Collab.)
AAIJ	20AN	JHEP 2012 139	R. Aaij et al.	(LHCb Collab.)
AAIJ	20D	PR D101 032005	R. Aaij et al.	(LHCb Collab.)
AAIJ	20K	JHEP 2003 146	R. Aaij et al.	(LHCb Collab.)
AAIJ	20N	JHEP 2006 058	R. Aaij et al.	(LHCb Collab.)
AAIJ	20P	JHEP 2006 129	R. Aaij et al.	(LHCb Collab.)
AAIJ	20S	JHEP 2008 123	R. Aaij et al.	(LHCb Collab.)
CHILIKIN	20	JHEP 2005 034	K. Chilikin et al.	(BELLE Collab.)
CHU	20	PR D101 052012	K. Chu et al.	(BELLE Collab.)
LEES	20C	PRL 124 152001	J.P. Lees et al.	(BABAR Collab.)
PRIM	20	PR D101 032007	M.T. Prim et al.	(BELLE Collab.)
AAIJ	19AC	PR D99 092009	R. Aaij et al.	(LHCb Collab.)
AAIJ	19AL	PRL 123 231802	R. Aaij et al.	(LHCb Collab.)
AAIJ	19AM	PRL 123 241802	R. Aaij et al.	(LHCb Collab.)
AAIJ	19O	EPJ C79 537	R. Aaij et al.	(LHCb Collab.)
AAIJ	19P	EPJ C79 675	R. Aaij et al.	(LHCb Collab.)
AAIJ	19S	PRL 122 191801	R. Aaij et al.	(LHCb Collab.)
BHARDWAJ	19	PR D99 111101	V. Bhardwaj et al.	(BELLE Collab.)
CHILIKIN	19	PR D100 012001	K. Chilikin et al.	(BELLE Collab.)
GARG	19	PR D99 071102	R. Garg et al.	(BELLE Collab.)
KALIYAR	19	PR D99 031102	A.B. Kaliyar et al.	(BELLE Collab.)
LEES	19C	PR D100 111101	J.P. Lees et al.	(BABAR Collab.)
LI	19A	PRL 122 082001	Y.B. Li et al.	(BELLE Collab.)
LI	19G	PR D100 112010	Y. Li et al.	(BELLE Collab.)
LU	19	PR D99 032003	P.-C. Lu et al.	(BELLE Collab.)
PDG	19	RPP 2019 at pdg.lbl.gov	M. Tanabashi et al.	(PDG Collab.)
RESMI	19	JHEP 1910 178	P.K. Resmi et al.	(BELLE Collab.)
SIRUNYAN	19CM	JHEP 1912 100	A.M. Sirunyan et al.	(CMS Collab.)
WATANUKI	19	PR D99 032012	S. Watanuki et al.	(BELLE Collab.)
AAIJ	18A	PL B777 16	R. Aaij et al.	(LHCb Collab.)
AAIJ	18AD	JHEP 1808 176	R. Aaij et al.	(LHCb Collab.)
Also		JHEP 1810 107 (errat.)	R. Aaij et al.	(LHCb Collab.)
AAIJ	18B	JHEP 1801 131	R. Aaij et al.	(LHCb Collab.)
AAIJ	18U	JHEP 1803 059	R. Aaij et al.	(LHCb Collab.)
AAIJ	18W	JHEP 1805 160	R. Aaij et al.	(LHCb Collab.)
AAIJ	18X	JHEP 1805 067	R. Aaij et al.	(LHCb Collab.)
AAIJ	18Z	JHEP 1806 084	R. Aaij et al.	(LHCb Collab.)
GELB	18	PR D98 112016	M. Gelb et al.	(BELLE Collab.)
KATO	18	PR D97 012005	Y. Kato et al.	(BELLE Collab.)
LI	18A	EPJ C78 252	Y.B. Li et al.	(BELLE Collab.)
PDG	18	PR D98 030001	M. Tanabashi et al.	(PDG Collab.)
RESMI	18	JHEP 1801 082	P.K. Resmi et al.	
SIBIDANOV	18	PRL 121 031801	A. Sibidanov et al.	(BELLE Collab.)
SIRUNYAN	18DX	PR D98 112011	A.M. Sirunyan et al.	(CMS Collab.)
VOSSEN	18	PR D98 012005	A. Vossen et al.	(BELLE Collab.)
AAIJ	17	PR D95 012002	R. Aaij et al.	(LHCb Collab.)
AAIJ	17AD	PL B769 305	R. Aaij et al.	(LHCb Collab.)
AAIJ	17AP	PR D95 052005	R. Aaij et al.	(LHCb Collab.)
AAIJ	17AQ	PR D95 071101	R. Aaij et al.	(LHCb Collab.)
AAIJ	17AR	PR D96 011101	R. Aaij et al.	(LHCb Collab.)
AAIJ	17BF	PL B774 139	R. Aaij et al.	(LHCb Collab.)
AAIJ	17BO	JHEP 1711 156	R. Aaij et al.	(LHCb Collab.)
AAIJ	17E	PL B765 307	R. Aaij et al.	(LHCb Collab.)
AAIJ	17K	EPJ C77 72	R. Aaij et al.	(LHCb Collab.)
AAIJ	17O	JHEP 1703 036	R. Aaij et al.	(LHCb Collab.)
AAIJ	17R	JHEP 1704 162	R. Aaij et al.	(LHCb Collab.)
AAIJ	17Y	EPJ C77 161	R. Aaij et al.	(LHCb Collab.)
ABAZOV	17A	PR D95 031101	V.M. Abazov et al.	(D0 Collab.)
BELENO	17	PR D96 091102	C. Beleno et al.	(BELLE Collab.)
GRYGIER	17	PR D96 091101	J. Grygier et al.	(BELLE Collab.)
HORIGUCHI	17	PRL 119 191802	T. Horiguchi et al.	(BELLE Collab.)
HSU	17	PR D96 031101	C.-L. Hsu et al.	(BELLE Collab.)
KHACHATRY...	17C	PL B764 66	V. Khachatryan et al.	(CMS Collab.)
LEES	17	PRL 118 031802	J.P. Lees et al.	(BABAR Collab.)
LEES	17G	PR D96 072001	J.P. Lees et al.	(BABAR Collab.)
AABOUD	16L	EPJ C76 513	M. Aaboud et al.	(ATLAS Collab.)
AAIJ	16AA	JHEP 1608 137	R. Aaij et al.	(LHCb Collab.)
AAIJ	16AH	PR D94 072001	R. Aaij et al.	(LHCb Collab.)
AAIJ	16AQ	JHEP 1612 087	R. Aaij et al.	(LHCb Collab.)
AAIJ	16L	PL B760 117	R. Aaij et al.	(LHCb Collab.)
AAIJ	16M	PR D93 051101	R. Aaij et al.	(LHCb Collab.)
AAIJ	16R	PR D93 119902	R. Aaij et al.	(LHCb Collab.)
AAIJ	16Z	JHEP 1606 131	R. Aaij et al.	(LHCb Collab.)
BHARDWAJ	16	PR D93 052016	V. Bhardwaj et al.	(BELLE Collab.)
DEL-AMO-SA...	16	PR D93 052013	P. del Amo Sanchez et al.	(BABAR Collab.)
LEES	16	PRL 116 041801	J.P. Lees et al.	(BABAR Collab.)
PDG	16	CP C40 100001	C. Patrignani et al.	(PDG Collab.)
AAIJ	15AR	JHEP 1510 034	R. Aaij et al.	(LHCb Collab.)
AAIJ	15BC	PR D92 112005	R. Aaij et al.	(LHCb Collab.)
AAIJ	15K	PL B741 1	R. Aaij et al.	(LHCb Collab.)
AAIJ	15O	PRL 115 051801	R. Aaij et al.	(LHCb Collab.)
AAIJ	15V	PR D91 092002	R. Aaij et al.	(LHCb Collab.)
Also		PR D93 119901 (errat.)	R. Aaij et al.	(LHCb Collab.)
AAIJ	15W	PR D91 112014	R. Aaij et al.	(LHCb Collab.)
ABAZOV	15	PRL 114 051803	V.M. Abazov et al.	(D0 Collab.)
BALA	15	PR D91 051101	A. Bala et al.	(BELLE Collab.)
CHOI	15A	PR D91 092011	S.-K. Choi et al.	(BELLE Collab.)
GOH	15	PR D91 071101	Y.M. Goh et al.	(BELLE Collab.)
HELLER	15	PR D91 112009	A. Heller et al.	(BELLE Collab.)
KRONENBIT...	15	PR D92 051102	B. Kronenbitter et al.	(BELLE Collab.)
LEES	15	PR D91 012003	J.P. Lees et al.	(BABAR Collab.)
LEES	15C	PR D91 052002	J.P. Lees et al.	(BABAR Collab.)
VINOKUROVA	15	JHEP 1506 132	A. Vinokurova et al.	(BELLE Collab.)
Also		JHEP 1702 088 (errat.)	A. Vinokurava et al.	(BELLE Collab.)
WIECHCZYN...	15	PR D91 032008	J. Wiechczynski et al.	(BELLE Collab.)
YOOK	15	PR D91 052016	Y. Yook et al.	(BELLE Collab.)
AAIJ	14	PRL 112 011801	R. Aaij et al.	(LHCb Collab.)
AAIJ	14A	PL B728 85	R. Aaij et al.	(LHCb Collab.)
AAIJ	14AC	PRL 112 131802	R. Aaij et al.	(LHCb Collab.)
AAIJ	14AF	PRL 113 141801	R. Aaij et al.	(LHCb Collab.)
AAIJ	14AN	JHEP 1409 177	R. Aaij et al.	(LHCb Collab.)
AAIJ	14AR	PRL 113 151601	R. Aaij et al.	(LHCb Collab.)
AAIJ	14AZ	JHEP 1410 064	R. Aaij et al.	(LHCb Collab.)
AAIJ	14BA	JHEP 1410 097	R. Aaij et al.	(LHCb Collab.)
AAIJ	14BE	NP B888 169	R. Aaij et al.	(LHCb Collab.)
AAIJ	14BF	JHEP 1411 060	R. Aaij et al.	(LHCb Collab.)
AAIJ	14BO	PR D90 112004	R. Aaij et al.	(LHCb Collab.)
AAIJ	14E	JHEP 1404 114	R. Aaij et al.	(LHCb Collab.)
AAIJ	14M	JHEP 1406 133	R. Aaij et al.	(LHCb Collab.)
AAIJ	14O	JHEP 1405 082	R. Aaij et al.	(LHCb Collab.)
AAIJ	14V	PL B733 36	R. Aaij et al.	(LHCb Collab.)
ABAZOV	14A	PR D89 012004	V.M. Abazov et al.	(D0 Collab.)
CHOBANOVA	14	PR D90 012002	V. Chobanova et al.	(BELLE Collab.)
IWASHITA	14	PTEP 2014 043C01	T. Iwashita et al.	(BELLE Collab.)
LEES	14A	PR D89 011102	J.P. Lees et al.	(BABAR Collab.)
TIEN	14	PR D89 011101	K.-J. Tien et al.	(BELLE Collab.)
AAIJ	13AE	PL B723 44	R. Aaij et al.	(LHCb Collab.)
AAIJ	13AK	PL B726 151	R. Aaij et al.	(LHCb Collab.)
AAIJ	13AP	PR D87 092007	R. Aaij et al.	(LHCb Collab.)
AAIJ	13AR	PR D87 112010	R. Aaij et al.	(LHCb Collab.)
AAIJ	13AU	PR D88 052015	R. Aaij et al.	(LHCb Collab.)
AAIJ	13AZ	PRL 111 101801	R. Aaij et al.	(LHCb Collab.)
AAIJ	13BC	PRL 111 112003	R. Aaij et al.	(LHCb Collab.)
AAIJ	13BN	PRL 111 151801	R. Aaij et al.	(LHCb Collab.)
AAIJ	13BS	PL B726 646	R. Aaij et al.	(LHCb Collab.)
AAIJ	13H	JHEP 1302 105	R. Aaij et al.	(LHCb Collab.)
AAIJ	13R	JHEP 1302 043	R. Aaij et al.	(LHCb Collab.)
AAIJ	13S	EPJ C73 2462	R. Aaij et al.	(LHCb Collab.)
AAIJ	13Z	JHEP 1309 006	R. Aaij et al.	(LHCb Collab.)
ABAZOV	13M	PRL 110 241801	V.M. Abazov et al.	(D0 Collab.)
DUH	13	PR D87 031103	Y. T. Duh et al.	(BELLE Collab.)
HARA	13	PRL 110 131801	K. Hara et al.	(BELLE Collab.)
LEES	13A	PR D87 032004	J.P. Lees et al.	(BABAR Collab.)
LEES	13B	PR D87 052015	J.P. Lees et al.	(BABAR Collab.)
LEES	13I	PR D87 112005	J.P. Lees et al.	(BABAR Collab.)
LEES	13K	PR D88 031102	J.P. Lees et al.	(BABAR Collab.)
LEES	13M	PR D88 032012	J.P. Lees et al.	(BABAR Collab.)
LEES	13T	PR D88 072006	J.P. Lees et al.	(BABAR Collab.)
LUTZ	13	PR D87 111103	O. Lutz et al.	(BELLE Collab.)
NAYAK	13	PR D88 091104	M. Nayak et al.	(BELLE Collab.)
SIBIDANOV	13	PR D88 032005	A. Sibidanov et al.	(BELLE Collab.)
AAIJ	12AA	PR D85 091103	R. Aaij et al.	(LHCb Collab.)
AAIJ	12AC	PR D85 091105	R. Aaij et al.	(LHCb Collab.)
AAIJ	12AD	PR D85 112004	R. Aaij et al.	(LHCb Collab.)
AAIJ	12AH	JHEP 1207 133	R. Aaij et al.	(LHCb Collab.)
AAIJ	12AQ	PL B718 43	R. Aaij et al.	(LHCb Collab.)
AAIJ	12AY	JHEP 1212 125	R. Aaij et al.	(LHCb Collab.)
AAIJ	12C	PRL 108 101601	R. Aaij et al.	(LHCb Collab.)
AAIJ	12E	PL B708 241	R. Aaij et al.	(LHCb Collab.)
AAIJ	12L	EPJ C72 2118	R. Aaij et al.	(LHCb Collab.)
AAIJ	12M	PL B712 203	R. Aaij et al.	(LHCb Collab.)
Also		PL B713 351 (errat.)	R. Aaij et al.	(LHCb Collab.)
AAIJ	12T	PRL 108 161801	R. Aaij et al.	(LHCb Collab.)
AIHARA	12	PR D85 112014	H. Aihara et al.	(BELLE Collab.)
DEL-AMO-SA...	12	PR D85 092017	P. del Amo Sanchez et al.	(BABAR Collab.)
HOI	12	PRL 108 031801	C.-T. Hoi et al.	(BELLE Collab.)
KIM	12A	PR D86 031101	J.H. Kim et al.	(BELLE Collab.)
LEES	12AA	PR D86 092004	J.P. Lees et al.	(BABAR Collab.)
LEES	12B	PR D85 052003	J.P. Lees et al.	(BABAR Collab.)
LEES	12D	PRL 109 101802	J.P. Lees et al.	(BABAR Collab.)
Also		PR D88 072012	J.P. Lees et al.	(BABAR Collab.)
LEES	12J	PR D85 071103	J.P. Lees et al.	(BABAR Collab.)
LEES	12O	PR D85 112010	J.P. Lees et al.	(BABAR Collab.)
LEES	12P	PR D86 012004	J.P. Lees et al.	(BABAR Collab.)
LEES	12S	PR D86 032012	J.P. Lees et al.	(BABAR Collab.)
LEES	12Z	PR D86 091102	J.P. Lees et al.	(BABAR Collab.)
PDG	12	PR D86 010001	J. Beringer et al.	(PDG Collab.)
STYPULA	12	PR D86 072007	J. Stypula et al.	(BELLE Collab.)
AAIJ	11E	PR D84 092001	R. Aaij et al.	(LHCb Collab.)
Also		PR D85 039904 (errat.)	R. Aaij et al.	(LHCb Collab.)
AALTONEN	11	PRL 106 121804	T. Aaltonen et al.	(CDF Collab.)
AALTONEN	11AI	PRL 107 201802	T. Aaltonen et al.	(CDF Collab.)
AALTONEN	11AJ	PR D84 091504	T. Aaltonen et al.	(CDF Collab.)
AALTONEN	11B	PR D83 032008	T. Aaltonen et al.	(CDF Collab.)
AALTONEN	11L	PRL 106 161801	T. Aaltonen et al.	(CDF Collab.)
AUSHEV	11	PR D83 051102	T. Aushev et al.	(BELLE Collab.)
BHARDWAJ	11	PRL 107 091803	V. Bhardwaj et al.	(BELLE Collab.)
CHEN	11F	PR D84 071501	P. Chen et al.	(BELLE Collab.)
CHOI	11	PR D84 052004	S.-K. Choi et al.	(BELLE Collab.)
DEL-AMO-SA...	11B	PR D83 032004	P. del Amo Sanchez et al.	(BABAR Collab.)
DEL-AMO-SA...	11C	PR D83 032007	P. del Amo Sanchez et al.	(BABAR Collab.)
DEL-AMO-SA...	11D	PR D83 051101	P. del Amo Sanchez et al.	(BABAR Collab.)
DEL-AMO-SA...	11F	PR D83 052011	P. del Amo Sanchez et al.	(BABAR Collab.)
DEL-AMO-SA...	11K	PR D83 091101	P. del Amo Sanchez et al.	(BABAR Collab.)
DEL-AMO-SA...	11L	PRL 107 041804	P. del Amo Sanchez et al.	(BABAR Collab.)
GULER	11	PR D83 032005	H. Guler et al.	(BELLE Collab.)
HORII	11	PRL 106 231803	Y. Horii et al.	(BELLE Collab.)
LEES	11A	PR D84 012001	J.P. Lees et al.	(BABAR Collab.)
LEES	11D	PR D84 012002	J.P. Lees et al.	(BABAR Collab.)
LEES	11I	PR D84 092007	J.P. Lees et al.	(BABAR Collab.)
SAHOO	11A	PR D84 071101	H. Sahoo et al.	(BELLE Collab.)
SEON	11	PR D84 071106	O. Seon et al.	(BELLE Collab.)
VINOKUROVA	11	PL B706 139	A. Vinokurova et al.	(BELLE Collab.)
AALTONEN	10A	PR D81 031105	T. Aaltonen et al.	(CDF Collab.)
AUBERT	10	PRL 104 011802	B. Aubert et al.	(BABAR Collab.)
AUBERT	10D	PR D81 052009	B. Aubert et al.	(BABAR Collab.)
AUBERT	10E	PR D81 051101	B. Aubert et al.	(BABAR Collab.)
BOZEK	10	PR D82 072005	A. BOZEK et al.	(BELLE Collab.)
DEL-AMO-SA...	10A	PR D82 011502	P. del Amo Sanchez et al.	(BABAR Collab.)
DEL-AMO-SA...	10B	PR D82 011101	P. del Amo Sanchez et al.	(BABAR Collab.)
DEL-AMO-SA...	10F	PRL 105 121801	P. del Amo Sanchez et al.	(BABAR Collab.)
DEL-AMO-SA...	10G	PR D82 072004	P. del Amo Sanchez et al.	(BABAR Collab.)
DEL-AMO-SA...	10H	PR D82 072006	P. del Amo Sanchez et al.	(BABAR Collab.)
DEL-AMO-SA...	10I	PR D82 091101	P. del Amo Sanchez et al.	(BABAR Collab.)
DEL-AMO-SA...	10K	PR D82 092006	P. del Amo Sanchez et al.	(BABAR Collab.)
DEL-AMO-SA...	10Q	PR D82 112002	P. del Amo Sanchez et al.	(BABAR Collab.)
HARA	10	PR D82 071101	K. Hara et al.	(BELLE Collab.)
LIBBY	10	PR D82 112006	J. Libby et al.	(CLEO Collab.)
POLUEKTOV	10	PR D81 112002	A. Poluektov et al.	(BELLE Collab.)
SAKAI	10	PR D82 091104	K. Sakai et al.	(BELLE Collab.)
WEDD	10	PR D81 111104	R. Wedd et al.	(BELLE Collab.)
AALTONEN	09B	PR D79 011104	T. Aaltonen et al.	(CDF Collab.)
ABAZOV	09Y	PR D79 111102	V.M. Abazov et al.	(D0 Collab.)
ABULENCIA	09	PR D79 112003	A. Abulencia et al.	(CDF Collab.)

Downloaded from https://academic.oup.com/ptep/article/2022/8/083C01/6651666 by KIT Library user on 27 September 2022

AUBERT 09 PR D79 011102 B. Aubert et al. (BABAR Collab.)
AUBERT 09A PR D79 012002 B. Aubert et al. (BABAR Collab.)
AUBERT 09AA PR D79 112001 B. Aubert et al. (BABAR Collab.)
AUBERT 09AB PR D79 112004 B. Aubert et al. (BABAR Collab.)
AUBERT 09AF PR D80 051101 B. Aubert et al. (BABAR Collab.)
AUBERT 09AJ PR D80 092001 B. Aubert et al. (BABAR Collab.)
AUBERT 09AO PRL 103 211802 B. Aubert et al. (BABAR Collab.)
AUBERT 09AT PR D80 111105 B. Aubert et al. (BABAR Collab.)
AUBERT 09AV PR D80 112002 B. Aubert et al. (BABAR Collab.)
AUBERT 09B PRL 102 132001 B. Aubert et al. (BABAR Collab.)
AUBERT 09F PR D79 051102 B. Aubert et al. (BABAR Collab.)
AUBERT 09G PRL 102 141802 B. Aubert et al. (BABAR Collab.)
AUBERT 09H PR D79 052005 B. Aubert et al. (BABAR Collab.)
AUBERT 09J PR D79 051101 B. Aubert et al. (BABAR Collab.)
AUBERT 09L PR D79 072006 B. Aubert et al. (BABAR Collab.)
AUBERT 09Q PR D79 052011 B. Aubert et al. (BABAR Collab.)
AUBERT 09R PR D79 072003 B. Aubert et al. (BABAR Collab.)
AUBERT 09S PR D79 092002 B. Aubert et al. (BABAR Collab.)
AUBERT 09T PRL 102 091803 B. Aubert et al. (BABAR Collab.)
Also EPAPS Document No. E-PRLTAO-102-060910 (BABAR Collab.)
AUBERT 09V PR D79 091101 B. Aubert et al. (BABAR Collab.)
AUBERT 09Y PRL 103 051803 B. Aubert et al. (BABAR Collab.)
CHANG 09 PR D79 052006 Y.-W. Chang et al. (BELLE Collab.)
CHEN 09C PR D80 111103 P. Chen et al. (BELLE Collab.)
LIU 09 PR D79 071102 C. Liu et al. (BELLE Collab.)
WEI 09A PRL 103 171801 J.-T. Wei et al. (BELLE Collab.)
Also EPAPS Supplement EPAPS_appendix.pdf (BELLE Collab.)
WIECHCZYN... 09 PR D80 052005 J. Wiechczynski et al. (BELLE Collab.)
ABAZOV 08O PRL 100 211802 V.M. Abazov et al. (D0 Collab.)
ADACHI 08 PR D77 091101 I. Adachi et al. (BELLE Collab.)
AUBERT 08A PR D77 011101 B. Aubert et al. (BABAR Collab.)
AUBERT 08AA PR D77 111102 B. Aubert et al. (BABAR Collab.)
AUBERT 08AB PR D78 012006 B. Aubert et al. (BABAR Collab.)
AUBERT 08AD PR D77 091104 B. Aubert et al. (BABAR Collab.)
AUBERT 08AG PR D78 011104 B. Aubert et al. (BABAR Collab.)
AUBERT 08AH PR D78 011107 B. Aubert et al. (BABAR Collab.)
AUBERT 08AI PR D78 012004 B. Aubert et al. (BABAR Collab.)
AUBERT 08AL PR D78 034023 B. Aubert et al. (BABAR Collab.)
AUBERT 08AT PRL 100 231803 B. Aubert et al. (BABAR Collab.)
AUBERT 08AV PRL 101 081801 B. Aubert et al. (BABAR Collab.)
AUBERT 08B PR D77 011102 B. Aubert et al. (BABAR Collab.)
AUBERT 08BC PR D78 072007 B. Aubert et al. (BABAR Collab.)
AUBERT 08BD PR D78 091101 B. Aubert et al. (BABAR Collab.)
AUBERT 08BE PR D78 091102 B. Aubert et al. (BABAR Collab.)
AUBERT 08BF PR D78 092002 B. Aubert et al. (BABAR Collab.)
AUBERT 08BH PR D78 112001 B. Aubert et al. (BABAR Collab.)
AUBERT 08BI PRL 101 161801 B. Aubert et al. (BABAR Collab.)
AUBERT 08BK PRL 101 201801 B. Aubert et al. (BABAR Collab.)
AUBERT 08BL PRL 101 261802 B. Aubert et al. (BABAR Collab.)
AUBERT 08BN PR D78 112003 B. Aubert et al. (BABAR Collab.)
AUBERT 08D PR D77 011107 B. Aubert et al. (BABAR Collab.)
AUBERT 08F PRL 100 051803 B. Aubert et al. (BABAR Collab.)
AUBERT 08G PRL 100 171803 B. Aubert et al. (BABAR Collab.)
AUBERT 08H PR D77 031101 B. Aubert et al. (BABAR Collab.)
AUBERT 08N PRL 100 021801 B. Aubert et al. (BABAR Collab.)
Also PR D79 092002 B. Aubert et al. (BABAR Collab.)
AUBERT 08Q PRL 100 151802 B. Aubert et al. (BABAR Collab.)
AUBERT 08W PRL 101 082001 B. Aubert et al. (BABAR Collab.)
AUBERT 08X PRL 101 091801 B. Aubert et al. (BABAR Collab.)
AUBERT 08Y PR D77 111101 B. Aubert et al. (BABAR Collab.)
BHARDWAJ 08 PR D78 051104 V. Bhardwaj et al. (BELLE Collab.)
BRODZICKA 08 PRL 100 092001 J. Brodzicka et al. (BELLE Collab.)
CHEN 08C PRL 100 251801 J.-H. Chen et al. (BELLE Collab.)
HORII 08 PR D78 071901 Y. Horii et al. (BELLE Collab.)
IWABUCHI 08 PRL 101 041601 M. Iwabuchi et al. (BELLE Collab.)
LIN 08 NAT 452 332 S.-W. Lin et al. (BELLE Collab.)
LIVENTSEV 08 PR D77 091503 D. Liventsev et al. (BELLE Collab.)
PDG 08 PL B667 1 C. Amsler et al. (PDG Collab.)
TANIGUCHI 08 PRL 101 111801 N. Taniguchi et al. (BELLE Collab.)
WEI 08 PL B659 80 J.-T. Wei et al. (BELLE Collab.)
WEI 08A PR D78 011101 J.-T. Wei et al. (BELLE Collab.)
WICHT 08 PL B662 323 J. Wicht et al. (BELLE Collab.)
ADAM 07 PRL 99 041802 N.E. Adam et al. (CLEO Collab.)
Also PR D76 012007 D.M. Asner et al. (CLEO Collab.)
AUBERT 07AC PR D76 031101 B. Aubert et al. (BABAR Collab.)
AUBERT 07AE PR D76 031103 B. Aubert et al. (BABAR Collab.)
AUBERT 07AG PRL 99 051801 B. Aubert et al. (BABAR Collab.)
AUBERT 07AL PR D76 052002 B. Aubert et al. (BABAR Collab.)
AUBERT 07AN PR D76 051101 B. Aubert et al. (BABAR Collab.)
AUBERT 07AR PR D76 071103 B. Aubert et al. (BABAR Collab.)
AUBERT 07AV PR D76 092004 B. Aubert et al. (BABAR Collab.)
AUBERT 07AZ PRL 99 201801 B. Aubert et al. (BABAR Collab.)
AUBERT 07BA PRL 99 201802 B. Aubert et al. (BABAR Collab.)
AUBERT 07BB PRL 99 221801 B. Aubert et al. (BABAR Collab.)
AUBERT 07BC PR D76 091102 B. Aubert et al. (BABAR Collab.)
AUBERT 07BI PRL 99 241803 B. Aubert et al. (BABAR Collab.)
AUBERT 07BJ PRL 99 251801 B. Aubert et al. (BABAR Collab.)
AUBERT 07BL PRL 99 261801 B. Aubert et al. (BABAR Collab.)
AUBERT 07BN PR D76 111101 B. Aubert et al. (BABAR Collab.)
AUBERT 07E PRL 98 051802 B. Aubert et al. (BABAR Collab.)
AUBERT 07H PR D75 031101 B. Aubert et al. (BABAR Collab.)
AUBERT 07L PRL 98 151802 B. Aubert et al. (BABAR Collab.)
AUBERT 07M PRL 98 171801 B. Aubert et al. (BABAR Collab.)
AUBERT 07N PR D75 072002 B. Aubert et al. (BABAR Collab.)
AUBERT 07Q PR D75 051102 B. Aubert et al. (BABAR Collab.)
AUBERT 07R PRL 98 211804 B. Aubert et al. (BABAR Collab.)
Also PRL 100 189903E B. Aubert et al. (BABAR Collab.)
Also PRL 100 199905E B. Aubert et al. (BABAR Collab.)
AUBERT 07X PR D75 091103 B. Aubert et al. (BABAR Collab.)
AUBERT 07Z PR D76 011103 B. Aubert et al. (BABAR Collab.)
CHANG 07B PR D75 071104 P. Chang et al. (BELLE Collab.)
CHEN 07D PRL 99 221802 K.-F. Chen et al. (BELLE Collab.)
HOKUUE 07 PL B648 139 T. Hokuue et al. (BELLE Collab.)
LIN 07 PRL 98 181804 S.-W. Lin et al. (BELLE Collab.)
LIN 07A PRL 99 121601 S.-W. Lin et al. (BELLE Collab.)
SATOYAMA 07 PL B647 67 N. Satoyama et al. (BELLE Collab.)
SCHUEMANN 07 PR D75 092002 J. Schuemann et al. (BELLE Collab.)
TSAI 07 PR D75 111101 Y.-T. Tsai et al. (BELLE Collab.)
URQUIJO 07 PR D75 032001 P. Urquijo et al. (BELLE Collab.)
WANG 07B PR D75 092005 C.H. Wang et al. (BELLE Collab.)
WANG 07C PR D76 052004 M.-Z. Wang et al. (BELLE Collab.)
XIE 07 PR D75 017101 Q.L. Xie et al. (BELLE Collab.)
ABE 06 PR D73 051106 K. Abe et al. (BELLE Collab.)
ABULENCIA 06J PRL 96 191801 A. Abulencia et al. (CDF Collab.)
ACOSTA 06 PRL 96 202001 D. Acosta et al. (CDF Collab.)
AUBERT 06 PR D73 011101 B. Aubert et al. (BABAR Collab.)
AUBERT 06E PRL 96 052002 B. Aubert et al. (BABAR Collab.)
AUBERT 06F PR D73 011103 B. Aubert et al. (BABAR Collab.)
AUBERT 06J PR D73 051105 B. Aubert et al. (BABAR Collab.)
AUBERT 06K PR D73 057101 B. Aubert et al. (BABAR Collab.)
AUBERT 06N PR D74 031103 B. Aubert et al. (BABAR Collab.)
AUBERT 06O PR D74 032003 B. Aubert et al. (BABAR Collab.)
AUBERT 06Z PR D73 111104 B. Aubert et al. (BABAR Collab.)
AUBERT,B 06A PR D73 112004 B. Aubert et al. (BABAR Collab.)
AUBERT,B 06C PR D74 011102 B. Aubert et al. (BABAR Collab.)
AUBERT,B 06E PR D74 011106 B. Aubert et al. (BABAR Collab.)
AUBERT,B 06G PRL 97 201801 B. Aubert et al. (BABAR Collab.)
AUBERT,B 06H PRL 97 201802 B. Aubert et al. (BABAR Collab.)
AUBERT,B 06J PR D73 092001 B. Aubert et al. (BABAR Collab.)
AUBERT,B 06M PR D74 031102 B. Aubert et al. (BABAR Collab.)
AUBERT,B 06P PR D74 031105 B. Aubert et al. (BABAR Collab.)
AUBERT,B 06T PR D74 051102 B. Aubert et al. (BABAR Collab.)
AUBERT,B 06U PR D74 051104 B. Aubert et al. (BABAR Collab.)
AUBERT,B 06Y PR D74 091105 B. Aubert et al. (BABAR Collab.)
AUBERT,BE 06A PR D74 099903 (errat.) B. Aubert et al. (BABAR Collab.)
AUBERT,BE 06C PRL 97 171805 B. Aubert et al. (BABAR Collab.)
AUBERT,BE 06G PRL 97 261801 B. Aubert et al. (BABAR Collab.)
AUBERT,BE 06H PRL 97 261803 B. Aubert et al. (BABAR Collab.)
AUBERT,BE 06J PR D74 111102 B. Aubert et al. (BABAR Collab.)
AUBERT,BE 06M PR D74 071101 B. Aubert et al. (BABAR Collab.)
CHISTOV 06A PR D74 111105 R. Chistov et al. (BELLE Collab.)
FANG 06 PR D74 012007 F. Fang et al. (BELLE Collab.)
GABYSHEV 06 PRL 97 202003 N. Gabyshev et al. (BELLE Collab.)
GABYSHEV 06A PRL 97 242001 N. Gabyshev et al. (BELLE Collab.)
GARMASH 06 PRL 96 251803 A. Garmash et al. (BELLE Collab.)
IKADO 06 PRL 97 251802 K. Ikado et al. (BELLE Collab.)
JEN 06 PR D74 111101 C.-M. Jen et al. (BELLE Collab.)
KUMAR 06 PR D74 051103 R. Kumar et al. (BELLE Collab.)
MOHAPATRA 06 PRL 96 221601 D. Mohapatra et al. (BELLE Collab.)
POLUEKTOV 06 PR D73 112009 A. Poluektov et al. (BELLE Collab.)
SCHUEMANN 06 PRL 97 061802 J. Schuemann et al. (BELLE Collab.)
SONI 06 PL B634 155 N. Soni et al. (BELLE Collab.)
ABE 05A PRL 94 221805 K. Abe et al. (BELLE Collab.)
ABE 05B PR D71 072003 K. Abe et al. (BELLE Collab.)
Also PR D71 079903 (errat.) K. Abe et al. (BELLE Collab.)
ABE 05G PRL 95 231802 K. Abe et al. (BELLE Collab.)
ACOSTA 05J PRL 95 031801 D. Acosta et al. (CDF Collab.)
AUBERT 05 PRL 94 011801 B. Aubert et al. (BABAR Collab.)
AUBERT 05B PR D71 031501 B. Aubert et al. (BABAR Collab.)
AUBERT 05G PR D72 032004 B. Aubert et al. (BABAR Collab.)
AUBERT 05H PRL 94 101801 B. Aubert et al. (BABAR Collab.)
AUBERT 05J PRL 94 141801 B. Aubert et al. (BABAR Collab.)
AUBERT 05K PRL 94 171801 B. Aubert et al. (BABAR Collab.)
AUBERT 05L PRL 94 181802 B. Aubert et al. (BABAR Collab.)
AUBERT 05M PRL 94 191802 B. Aubert et al. (BABAR Collab.)
AUBERT 05N PR D71 031102 B. Aubert et al. (BABAR Collab.)
AUBERT 05O PR D71 031103 B. Aubert et al. (BABAR Collab.)
AUBERT 05R PR D71 071103 B. Aubert et al. (BABAR Collab.)
AUBERT 05U PR D71 091103 B. Aubert et al. (BABAR Collab.)
AUBERT 05X PR D71 111101 B. Aubert et al. (BABAR Collab.)
AUBERT,B 05B PRL 95 041804 B. Aubert et al. (BABAR Collab.)
AUBERT,B 05E PR D72 011102 B. Aubert et al. (BABAR Collab.)
AUBERT,B 05G PR D72 052002 B. Aubert et al. (BABAR Collab.)
AUBERT,B 05K PRL 95 131803 B. Aubert et al. (BABAR Collab.)
AUBERT,B 05L PR D72 051101 B. Aubert et al. (BABAR Collab.)
AUBERT,B 05N PR D72 072003 B. Aubert et al. (BABAR Collab.)
Also PR D74 099903 (errat.) B. Aubert et al. (BABAR Collab.)
AUBERT,B 05O PR D72 051102 B. Aubert et al. (BABAR Collab.)
AUBERT,B 05T PR D72 071102 B. Aubert et al. (BABAR Collab.)
AUBERT,B 05U PR D72 071103 B. Aubert et al. (BABAR Collab.)
AUBERT,B 05V PR D72 071104 B. Aubert et al. (BABAR Collab.)
AUBERT,B 05Y PRL 95 121802 B. Aubert et al. (BABAR Collab.)
AUBERT,BE 05E PRL 95 221801 B. Aubert et al. (BABAR Collab.)
CHANG 05 PR D71 072007 M.-C. Chang et al. (BELLE Collab.)
CHANG 05A PR D71 091106 P. Chang et al. (BELLE Collab.)
CHAO 05A PR D71 031502 Y. Chao et al. (BELLE Collab.)
CHEN 05A PRL 94 221804 K.-F. Chen et al. (BELLE Collab.)
GARMASH 05 PR D71 092003 A. Garmash et al. (BELLE Collab.)
ITOH 05 PRL 95 091601 R. Itoh et al. (BELLE Collab.)
LEE 05 PRL 95 061802 Y.-J. Lee et al. (BELLE Collab.)
LIVENTSEV 05 PR D72 051109 D. Liventsev et al. (BELLE Collab.)
MAJUMDER 05 PRL 95 041803 G. Majumder et al. (BELLE Collab.)
MOHAPATRA 05 PR D72 011101 D. Mohapatra et al. (BELLE Collab.)
NISHIDA 05 PL B610 23 S. Nishida et al. (BELLE Collab.)
OKABE 05 PL B614 27 T. Okabe et al. (BELLE Collab.)
SAIGO 05 PRL 94 091601 M. Saigo et al. (BELLE Collab.)
WANG 05A PL B617 141 M.-Z. Wang et al. (BELLE Collab.)
XIE 05 PR D72 051105 Q.L. Xie et al. (BELLE Collab.)
YANG 05 PRL 94 111802 H. Yang et al. (BELLE Collab.)
ZHANG 05A PRL 94 031801 J. Zhang et al. (BELLE Collab.)
ZHANG 05B PR D71 091107 L.M. Zhang et al. (BELLE Collab.)
ZHANG 05D PRL 95 141801 J. Zhang et al. (BELLE Collab.)
ABDALLAH 04E EPJ C33 307 J. Abdallah et al. (DELPHI Collab.)
ABE 04D PR D69 112002 K. Abe et al. (BELLE Collab.)
AUBERT 04A PR D69 011102 B. Aubert et al. (BABAR Collab.)
AUBERT 04C PRL 92 111801 B. Aubert et al. (BABAR Collab.)
AUBERT 04H PRL 92 061801 B. Aubert et al. (BABAR Collab.)
AUBERT 04K PRL 92 141801 B. Aubert et al. (BABAR Collab.)
AUBERT 04M PRL 92 201802 B. Aubert et al. (BABAR Collab.)
AUBERT 04N PRL 92 202002 B. Aubert et al. (BABAR Collab.)
AUBERT 04O PRL 92 221803 B. Aubert et al. (BABAR Collab.)
AUBERT 04P PRL 92 241802 B. Aubert et al. (BABAR Collab.)
AUBERT 04Q PR D69 051101 B. Aubert et al. (BABAR Collab.)
AUBERT 04T PR D69 071103 B. Aubert et al. (BABAR Collab.)
AUBERT 04Y PRL 93 041801 B. Aubert et al. (BABAR Collab.)
AUBERT 04Z PRL 93 051802 B. Aubert et al. (BABAR Collab.)
AUBERT,B 04B PR D70 011101 B. Aubert et al. (BABAR Collab.)
AUBERT,B 04D PR D70 032006 B. Aubert et al. (BABAR Collab.)
AUBERT,B 04L PRL 93 131804 B. Aubert et al. (BABAR Collab.)
AUBERT,B 04P PR D70 092001 B. Aubert et al. (BABAR Collab.)
AUBERT,B 04S PRL 93 181801 B. Aubert et al. (BABAR Collab.)
AUBERT,B 04U PR D70 091105 B. Aubert et al. (BABAR Collab.)
AUBERT,B 04V PRL 93 181805 B. Aubert et al. (BABAR Collab.)
AUBERT,BE 04 PR D70 111102 B. Aubert et al. (BABAR Collab.)
AUBERT,BE 04A PR D70 112006 B. Aubert et al. (BABAR Collab.)
AUBERT,BE 04B PR D70 091106 B. Aubert et al. (BABAR Collab.)
CHAO 04 PR D69 111102 Y. Chao et al. (BELLE Collab.)
CHAO 04B PRL 93 191802 Y. Chao et al. (BELLE Collab.)
CHISTOV 04 PRL 93 051803 R. Chistov et al. (BELLE Collab.)
DRUTSKOY 04 PRL 92 051801 A. Drutskoy et al. (BELLE Collab.)
GARMASH 04 PR D69 012001 A. Garmash et al. (BELLE Collab.)
LEE 04 PRL 93 211801 Y.-J. Lee et al. (BELLE Collab.)
MAJUMDER 04 PR D70 111103 G. Majumder et al. (BELLE Collab.)
NAKAO 04 PR D69 112001 M. Nakao et al. (BELLE Collab.)
POLUEKTOV 04 PR D70 072003 A. Poluektov et al. (BELLE Collab.)
SCHWANDA 04 PRL 93 131803 C. Schwanda et al. (BELLE Collab.)
WANG 04 PRL 92 131801 M.Z. Wang et al. (BELLE Collab.)
WANG 04A PR D70 012001 C.H. Wang et al. (BELLE Collab.)
ZANG 04 PR D69 017101 S.L. Zang et al. (BELLE Collab.)
ABE 03B PR D67 032003 K. Abe et al. (BELLE Collab.)
ABE 03D PRL 90 131803 K. Abe et al. (BELLE Collab.)
ADAM 03 PR D67 032001 N.E. Adam et al. (CLEO Collab.)
ADAM 03B PR D68 012004 N.E. Adam et al. (CLEO Collab.)
ATHAR 03 PR D68 072003 S.B. Athar et al. (CLEO Collab.)

Downloaded from https://academic.oup.com/ptep/article/2022/8/083C01/6651666 by KIT Library user on 27 September 2022

AUBERT	03K	PRL 90 231801	B. Aubert *et al.*	(BABAR Collab.)
AUBERT	03L	PRL 91 021801	B. Aubert *et al.*	(BABAR Collab.)
AUBERT	03M	PRL 91 051801	B. Aubert *et al.*	(BABAR Collab.)
AUBERT	03O	PRL 91 071801	B. Aubert *et al.*	(BABAR Collab.)
AUBERT	03U	PRL 91 221802	B. Aubert *et al.*	(BABAR Collab.)
AUBERT	03V	PRL 91 171802	B. Aubert *et al.*	(BABAR Collab.)
AUBERT	03W	PRL 91 161801	B. Aubert *et al.*	(BABAR Collab.)
AUBERT	03X	PR D68 092001	B. Aubert *et al.*	(BABAR Collab.)
BORNHEIM	03	PR D68 052002	A. Bornheim *et al.*	(CLEO Collab.)
CHEN	03B	PRL 91 201801	K.-F. Chen *et al.*	(BELLE Collab.)
CHOI	03	PRL 91 262001	S.-K. Choi *et al.*	(BELLE Collab.)
CSORNA	03	PR D67 112002	S.E. Csorna *et al.*	(CLEO Collab.)
EDWARDS	03	PR D68 011102	K.W. Edwards *et al.*	(CLEO Collab.)
FANG	03	PRL 90 071801	F. Fang *et al.*	(BELLE Collab.)
HUANG	03	PRL 91 241802	H.-C. Huang *et al.*	(BELLE Collab.)
ISHIKAWA	03	PRL 91 261601	A. Ishikawa *et al.*	(BELLE Collab.)
KROKOVNY	03B	PRL 91 262002	P. Krokovny *et al.*	(BELLE Collab.)
SWAIN	03	PR D68 051101	S.K. Swain *et al.*	(BELLE Collab.)
UNNO	03	PR D68 011103	Y. Unno *et al.*	(BELLE Collab.)
ZHANG	03B	PRL 91 221801	J. Zhang *et al.*	(BELLE Collab.)
ABE	02	PRL 88 021801	K. Abe *et al.*	(BELLE Collab.)
ABE	02B	PRL 88 031802	K. Abe *et al.*	(BELLE Collab.)
ABE	02H	PRL 88 171801	K. Abe *et al.*	(BELLE Collab.)
ABE	02K	PRL 88 181803	K. Abe *et al.*	(BELLE Collab.)
ABE	02N	PL B538 11	K. Abe *et al.*	(BELLE Collab.)
ABE	02O	PR D65 091103	K. Abe *et al.*	(BELLE Collab.)
ABE	02W	PRL 89 151802	K. Abe *et al.*	(BELLE Collab.)
ACOSTA	02C	PR D65 092009	D. Acosta *et al.*	(CDF Collab.)
ACOSTA	02F	PR D66 052005	D. Acosta *et al.*	(CDF Collab.)
AHMED	02B	PR D66 031101	S. Ahmed *et al.*	(CLEO Collab.)
AUBERT	02	PR D65 032001	B. Aubert *et al.*	(BABAR Collab.)
AUBERT	02C	PRL 88 101805	B. Aubert *et al.*	(BABAR Collab.)
AUBERT	02E	PR D65 051101	B. Aubert *et al.*	(BABAR Collab.)
AUBERT	02F	PR D65 091101	B. Aubert *et al.*	(BABAR Collab.)
AUBERT	02L	PRL 88 241801	B. Aubert *et al.*	(BABAR Collab.)
BRIERE	02	PRL 89 081803	R. Briere *et al.*	(CLEO Collab.)
CASEY	02	PR D66 092002	B.C.K. Casey *et al.*	(BELLE Collab.)
CHEN	02B	PL B546 196	K.-F. Chen *et al.*	(BELLE Collab.)
DRUTSKOY	02	PL B542 171	A. Drutskoy *et al.*	(BELLE Collab.)
DYTMAN	02	PR D66 091101	S.A. Dytman *et al.*	(CLEO Collab.)
ECKHART	02	PRL 89 251801	E. Eckhart *et al.*	(CLEO Collab.)
EDWARDS	02B	PR D65 111102	K.W. Edwards *et al.*	(CLEO Collab.)
GABYSHEV	02	PR D66 091102	N. Gabyshev *et al.*	(BELLE Collab.)
GARMASH	02	PR D65 092005	A. Garmash *et al.*	(BELLE Collab.)
GODANG	02	PRL 88 021802	R. Godang *et al.*	(CLEO Collab.)
GORDON	02	PL B542 183	A. Gordon *et al.*	(BELLE Collab.)
LU	02	PRL 89 191801	R.-S. Lu *et al.*	(BELLE Collab.)
MAHAPATRA	02	PRL 88 101803	R. Mahapatra *et al.*	(CLEO Collab.)
NISHIDA	02	PRL 89 231801	S. Nishida *et al.*	(BELLE Collab.)
ABE	01H	PRL 87 101801	K. Abe *et al.*	(BELLE Collab.)
ABE	01I	PRL 87 111801	K. Abe *et al.*	(BELLE Collab.)
ABE	01K	PR D64 071101	K. Abe *et al.*	(BELLE Collab.)
ABE	01L	PRL 87 161601	K. Abe *et al.*	(BELLE Collab.)
ABE	01M	PL B517 309	K. Abe *et al.*	(BELLE Collab.)
ALEXANDER	01B	PR D64 092001	J.P. Alexander *et al.*	(CLEO Collab.)
AMMAR	01B	PRL 87 271801	R. Ammar *et al.*	(CLEO Collab.)
ANDERSON	01B	PRL 87 181803	S. Anderson *et al.*	(CLEO Collab.)
AUBERT	01D	PRL 87 151801	B. Aubert *et al.*	(BABAR Collab.)
AUBERT	01E	PRL 87 151802	B. Aubert *et al.*	(BABAR Collab.)
AUBERT	01F	PRL 87 201803	B. Aubert *et al.*	(BABAR Collab.)
AUBERT	01G	PRL 87 221802	B. Aubert *et al.*	(BABAR Collab.)
BARATE	01E	EPJ C19 213	R. Barate *et al.*	(ALEPH Collab.)
BRIERE	01	PRL 86 3718	R.A. Biere *et al.*	(CLEO Collab.)
BROWDER	01	PRL 86 2950	T.E. Browder *et al.*	(CLEO Collab.)
EDWARDS	01	PRL 86 30	K.W. Edwards *et al.*	(CLEO Collab.)
GRITSAN	01	PR D64 077501	A. Gritsan *et al.*	(CLEO Collab.)
RICHICHI	01	PR D63 031103	S.J. Richichi *et al.*	(CLEO Collab.)
ABBIENDI	00B	PL B476 233	G. Abbiendi *et al.*	(OPAL Collab.)
ABE	00C	PR D62 071101	K. Abe *et al.*	(SLD Collab.)
AHMED	00B	PR D62 112003	S. Ahmed *et al.*	(CLEO Collab.)
ANASTASSOV	00	PRL 84 1393	A. Anastassov *et al.*	(CLEO Collab.)
BARATE	00R	PL B492 275	R. Barate *et al.*	(ALEPH Collab.)
BEHRENS	00	PR D61 052001	B.H. Behrens *et al.*	(CLEO Collab.)
BONVICINI	00	PRL 84 5940	G. Bonvicini *et al.*	(CLEO Collab.)
CHEN	00	PRL 85 525	S. Chen *et al.*	(CLEO Collab.)
COAN	00	PRL 84 5283	T.E. Coan *et al.*	(CLEO Collab.)
CRONIN-HEN...	00	PRL 85 515	D. Cronin-Hennessy *et al.*	(CLEO Collab.)
CSORNA	00	PR D61 111101	S.E. Csorna *et al.*	(CLEO Collab.)
JESSOP	00	PRL 85 2881	C.P. Jessop *et al.*	(CLEO Collab.)
RICHICHI	00	PRL 85 520	S.J. Richichi *et al.*	(CLEO Collab.)
ABBIENDI	99J	EPJ C12 609	G. Abbiendi *et al.*	(OPAL Collab.)
AFFOLDER	99B	PRL 83 3378	T. Affolder *et al.*	(CDF Collab.)
BARTELT	99	PRL 82 3746	J. Bartelt *et al.*	(CLEO Collab.)
COAN	99	PR D59 111101	T.E. Coan *et al.*	(CLEO Collab.)
ABE	98B	PR D57 5382	F. Abe *et al.*	(CDF Collab.)
ABE	98O	PR D58 072001	F. Abe *et al.*	(CDF Collab.)
ABE	98Q	PR D58 092002	F. Abe *et al.*	(CDF Collab.)
ACCIARRI	98S	PL B438 417	M. Acciarri *et al.*	(L3 Collab.)
ANASTASSOV	98	PRL 80 4127	A. Anastassov *et al.*	(CLEO Collab.)
ATHANAS	98	PRL 80 5493	M. Athanas *et al.*	(CLEO Collab.)
BARATE	98Q	EPJ C4 387	R. Barate *et al.*	(ALEPH Collab.)
BEHRENS	98	PRL 80 3710	B.H. Behrens *et al.*	(CLEO Collab.)
BERGFELD	98	PRL 81 272	T. Bergfeld *et al.*	(CLEO Collab.)
BRANDENB...	98	PRL 80 2762	G. Brandenbrug *et al.*	(CLEO Collab.)
CAPRINI	98	NP B530 153	I. Caprini, L. Lellouch, M. Neubert	(BCIP, CERN)
GODANG	98	PRL 80 3456	R. Godang *et al.*	(CLEO Collab.)
ABE	97J	PRL 79 590	K. Abe *et al.*	(SLD Collab.)
ACCIARRI	97F	PL B396 327	M. Acciarri *et al.*	(L3 Collab.)
ARTUSO	97	PL B399 321	M. Artuso *et al.*	(CLEO Collab.)
ATHANAS	97	PRL 79 2208	M. Athanas *et al.*	(CLEO Collab.)
BROWDER	97	PR D56 11	T. Browder *et al.*	(CLEO Collab.)
FU	97	PRL 79 3125	X. Fu *et al.*	(CLEO Collab.)
JESSOP	97	PRL 79 4533	C.P. Jessop *et al.*	(CLEO Collab.)
ABE	96B	PR D53 3496	F. Abe *et al.*	(CDF Collab.)
ABE	96C	PRL 76 4462	F. Abe *et al.*	(CDF Collab.)
ABE	96H	PRL 76 2015	F. Abe *et al.*	(CDF Collab.)
ABE	96L	PRL 76 4675	F. Abe *et al.*	(CDF Collab.)
ABE	96Q	PR D54 6596	F. Abe *et al.*	(CDF Collab.)
ABE	96R	PRL 77 5176	F. Abe *et al.*	(CDF Collab.)
ADAM	96D	ZPHY C72 207	W. Adam *et al.*	(DELPHI Collab.)
ALEXANDER	96T	PRL 77 5000	J.P. Alexander *et al.*	(CLEO Collab.)
ASNER	96	PR D53 1039	D.M. Asner *et al.*	(CLEO Collab.)
BARISH	96B	PRL 76 1570	B.C. Barish *et al.*	(CLEO Collab.)
BERGFELD	96B	PRL 77 4503	T. Bergfeld *et al.*	(CLEO Collab.)
BISHAI	96	PL B369 186	M. Bishai *et al.*	(CLEO Collab.)
BUSKULIC	96J	ZPHY C71 31	D. Buskulic *et al.*	(ALEPH Collab.)
GIBAUT	96	PR D53 4734	D. Gibaut *et al.*	(CLEO Collab.)
PDG	96	PR D54 1	R. M. Barnett *et al.*	(PDG Collab.)
ABREU	95N	PL B357 255	P. Abreu *et al.*	(DELPHI Collab.)
ABREU	95Q	ZPHY C68 13	P. Abreu *et al.*	(DELPHI Collab.)
ADAM	95	ZPHY C68 363	W. Adam *et al.*	(DELPHI Collab.)
AKERS	95T	ZPHY C67 379	R. Akers *et al.*	(OPAL Collab.)
ALBRECHT	95D	PL B353 554	H. Albrecht *et al.*	(ARGUS Collab.)
ALEXANDER	95	PL B341 435	J. Alexander *et al.*	(CLEO Collab.)
Also		PL B347 469 (erratum)	J. Alexander *et al.*	(CLEO Collab.)
ARTUSO	95	PRL 75 785	M. Artuso *et al.*	(CLEO Collab.)
BARISH	95	PR D51 1014	B.C. Barish *et al.*	(CLEO Collab.)
BUSKULIC	95	PL B343 444	D. Buskulic *et al.*	(ALEPH Collab.)
ABE	94D	PRL 72 3456	F. Abe *et al.*	(CDF Collab.)
ALAM	94	PR D50 43	M.S. Alam *et al.*	(CLEO Collab.)
ALBRECHT	94D	PL B335 526	H. Albrecht *et al.*	(ARGUS Collab.)
ATHANAS	94	PRL 73 3503	M. Athanas *et al.*	(CLEO Collab.)
Also		PRL 74 3090 (erratum)	M. Athanas *et al.*	(CLEO Collab.)
PDG	94	PR D50 1173	L. Montanet *et al.*	(CERN, LBL, BOST+)
STONE	94	HEPSY 93-11	S. Stone	
Published in B Decays, 2nd Edition, World Scientific, Singapore				
ABREU	93D	ZPHY C57 181	P. Abreu *et al.*	(DELPHI Collab.)
ABREU	93G	PL B312 253	P. Abreu *et al.*	(DELPHI Collab.)
ACTON	93C	PL B307 247	P.D. Acton *et al.*	(OPAL Collab.)
ALBRECHT	93E	ZPHY C60 11	H. Albrecht *et al.*	(ARGUS Collab.)
ALEXANDER	93B	PL B319 365	J. Alexander *et al.*	(CLEO Collab.)
AMMAR	93	PRL 71 674	R. Ammar *et al.*	(CLEO Collab.)
BEAN	93B	PRL 70 2681	A. Bean *et al.*	(CLEO Collab.)
BUSKULIC	93D	PL B307 194	D. Buskulic *et al.*	(ALEPH Collab.)
Also		PL B325 537 (erratum)	D. Buskulic *et al.*	(ALEPH Collab.)
SANGHERA	93	PR D47 791	S. Sanghera *et al.*	(CLEO Collab.)
ALBRECHT	92C	PL B275 195	H. Albrecht *et al.*	(ARGUS Collab.)
ALBRECHT	92E	PL B277 209	H. Albrecht *et al.*	(ARGUS Collab.)
ALBRECHT	92G	ZPHY C54 1	H. Albrecht *et al.*	(ARGUS Collab.)
BORTOLETTO	92	PR D45 21	D. Bortoletto *et al.*	(CLEO Collab.)
BUSKULIC	92G	PL B295 396	D. Buskulic *et al.*	(ALEPH Collab.)
ALBRECHT	91B	PL B254 288	H. Albrecht *et al.*	(ARGUS Collab.)
ALBRECHT	91C	PL B255 297	H. Albrecht *et al.*	(ARGUS Collab.)
ALBRECHT	91E	PL B262 148	H. Albrecht *et al.*	(ARGUS Collab.)
BERKELMAN	91	ARNPS 41 1	K. Berkelman, S. Stone	(CORN, SYRA)
"Decays of B Mesons"				
FULTON	91	PR D43 651	R. Fulton *et al.*	(CLEO Collab.)
ALBRECHT	90B	PL B241 278	H. Albrecht *et al.*	(ARGUS Collab.)
ALBRECHT	90J	ZPHY C48 543	H. Albrecht *et al.*	(ARGUS Collab.)
ANTREASYAN	90B	ZPHY C48 553	D. Antreasyan *et al.*	(Crystal Ball Collab.)
BORTOLETTO	90	PRL 64 2117	D. Bortoletto *et al.*	(CLEO Collab.)
Also		PR D45 21	D. Bortoletto *et al.*	(CLEO Collab.)
WEIR	90B	PR D41 1384	A.J. Weir *et al.*	(Mark II Collab.)
ALBRECHT	89G	PL B229 304	H. Albrecht *et al.*	(ARGUS Collab.)
AVERY	89B	PL B223 470	P. Avery *et al.*	(CLEO Collab.)
BEBEK	89	PRL 62 8	C. Bebek *et al.*	(CLEO Collab.)
BORTOLETTO	89	PRL 62 2436	D. Bortoletto *et al.*	(CLEO Collab.)
ALBRECHT	88F	PL B209 119	H. Albrecht *et al.*	(ARGUS Collab.)
ALBRECHT	88K	PL B215 424	H. Albrecht *et al.*	(ARGUS Collab.)
ALBRECHT	87C	PL B185 218	H. Albrecht *et al.*	(ARGUS Collab.)
ALBRECHT	87D	PL B199 451	H. Albrecht *et al.*	(ARGUS Collab.)
AVERY	87	PL B183 429	P. Avery *et al.*	(CLEO Collab.)
BEBEK	87	PR D36 1289	C. Bebek *et al.*	(CLEO Collab.)
ALAM	86	PR D34 3279	M.S. Alam *et al.*	(CLEO Collab.)
PDG	86	PL 170B 1	M. Aguilar-Benitez *et al.*	(CERN, CIT+)
GILES	84	PR D30 2279	R. Giles *et al.*	(CLEO Collab.)

B^0

$I(J^P) = \frac{1}{2}(0^-)$

Quantum numbers not measured. Values shown are quark-model predictions.

See also the $B^{\pm}/B^0$ ADMIXTURE and $B^{\pm}/B^0/B^0_s/b$-baryon ADMIXTURE sections.

See the Note "Production and Decay of b-flavored Hadrons" at the beginning of the $B^{\pm}$ Particle Listings and the Note on "B^0-$\overline{B}^0$ Mixing" near the end of the B^0 Particle Listings.

B^0 MASS

The fit uses m_{B^+}, $(m_{B^0} - m_{B^+})$, and m_{B^0} to determine m_{B^+}, m_{B^0}, and the mass difference.

VALUE (MeV)	EVTS	DOCUMENT ID		TECN	COMMENT
5279.66±0.12 OUR FIT					
5279.63±0.20 OUR AVERAGE					
5279.74±0.30±0.10		[1] AAIJ	19U	LHCB	pp at 7, 8, 13 TeV
5279.6 ±0.2 ±1.0		[2] AAD	13U	ATLS	pp at 7 TeV
5279.58±0.15±0.28		[3] AAIJ	12E	LHCB	pp at 7 TeV
5279.63±0.53±0.33		[4] ACOSTA	06	CDF	$p\overline{p}$ at 1.96 TeV
5279.1 ±0.7 ±0.3	135	[5] CSORNA	00	CLE2	$e^+e^- \rightarrow \Upsilon(4S)$
5281.3 ±2.2 ±1.4	51	ABE	96B	CDF	$p\overline{p}$ at 1.8 TeV
• • • We do not use the following data for averages, fits, limits, etc. • • •					
5279.2 ±0.54±2.0	340	ALAM	94	CLE2	$e^+e^- \rightarrow \Upsilon(4S)$
5278.0 ±0.4 ±2.0		BORTOLETTO	92	CLEO	$e^+e^- \rightarrow \Upsilon(4S)$
5279.6 ±0.7 ±2.0	40	[6] ALBRECHT	90J	ARG	$e^+e^- \rightarrow \Upsilon(4S)$
5278.2 ±1.0 ±3.0	40	ALBRECHT	87C	ARG	$e^+e^- \rightarrow \Upsilon(4S)$
5279.5 ±1.6 ±3.0	7	[7] ALBRECHT	87D	ARG	$e^+e^- \rightarrow \Upsilon(4S)$
5280.6 ±0.8 ±2.0		BEBEK	87	CLEO	$e^+e^- \rightarrow \Upsilon(4S)$

[1] Uses $B^0 \rightarrow J/\psi p\overline{p}$ decays.

[2] Measured with $B^0_d \rightarrow J/\psi(\mu^+\mu^-)\, K^0_S(\pi^+\pi^-)$ decays.

[3] Uses $B^0 \rightarrow J/\psi K^0$ fully reconstructed decays.

[4] Uses exclusively reconstructed final states containing a $J/\psi \rightarrow \mu^+\mu^-$ decays.

[5] CSORNA 00 uses fully reconstructed 135 $B^0 \rightarrow J/\psi^{(\prime)} K^0_S$ events and invariant masses without beam constraint.

[6] ALBRECHT 90J assumes 10580 for $\Upsilon(4S)$ mass. Supersedes ALBRECHT 87C and ALBRECHT 87D.

[7] Found using fully reconstructed decays with J/ψ. ALBRECHT 87D assume $m_{\Upsilon(4S)} =$ 10577 MeV.

Downloaded from https://academic.oup.com/ptep/article/2022/8/083C01/6651666 by KIT Library user on 27 September 2022

$m_{B^0} - m_{B^+}$

VALUE (MeV)	DOCUMENT ID		TECN	COMMENT
0.32±0.05 OUR FIT				
0.33±0.05 OUR AVERAGE				
0.57±0.49±0.10	[1] SIRUNYAN	18DF	CMS	pp at 8 TeV
0.20±0.17±0.11	[1] AAIJ	12E	LHCB	pp at 7 TeV
0.33±0.05±0.03	[2] AUBERT	08AF	BABR	$e^+e^- \to \Upsilon(4S)$
0.53±0.67±0.14	[1] ACOSTA	06	CDF	$p\overline{p}$ at 1.96 TeV
0.41±0.25±0.19	ALAM	94	CLE2	$e^+e^- \to \Upsilon(4S)$
−0.4 ±0.6 ±0.5	BORTOLETTO	92	CLEO	$e^+e^- \to \Upsilon(4S)$
−0.9 ±1.2 ±0.5	ALBRECHT	90J	ARG	$e^+e^- \to \Upsilon(4S)$
2.0 ±1.1 ±0.3	[3] BEBEK	87	CLEO	$e^+e^- \to \Upsilon(4S)$

[1] Uses exclusively reconstructed final states containing a $J/\psi \to \mu^+\mu^-$ decay.
[2] Uses the B-momentum distributions in the e^+e^- rest frame.
[3] BEBEK 87 actually measure the difference between half of E_{cm} and the $B^\pm$ or B^0 mass, so the $m_{B^0} - m_{B^\pm}$ is more accurate. Assume $m_{\Upsilon(4S)} = 10580$ MeV.

$m_{B^0_H} - m_{B^0_L}$

See the B^0-$\overline{B}^0$ MIXING PARAMETERS section near the end of these B^0 Listings.

B^0 MEAN LIFE

See $B^\pm/B^0/B^0_s/b$-baryon ADMIXTURE section for data on B-hadron mean life averaged over species of bottom particles.

"OUR EVALUATION" is an average using rescaled values of the data listed below. The average and rescaling were performed by the Heavy Flavor Averaging Group (HFLAV) and are described at https://hflav.web.cern.ch/. The averaging/rescaling procedure takes into account correlations between the measurements and asymmetric lifetime errors.

VALUE (10^{-12} s)	EVTS	DOCUMENT ID		TECN	COMMENT
1.519±0.004 OUR EVALUATION					
1.515±0.005±0.006		[1] SIRUNYAN	18BY	CMS	pp at 8 TeV
1.534±0.019±0.021		[2] ABAZOV	15A	D0	$p\overline{p}$ at 1.96 TeV
1.499±0.013±0.005		[3] AAIJ	14E	LHCB	pp at 7 TeV
1.524±0.006±0.004		[4] AAIJ	14E	LHCB	pp at 7 TeV
1.524±0.011±0.004		[5] AAIJ	14R	LHCB	pp at 7 TeV
1.509±0.012±0.018		[6] AAD	13U	ATLS	pp at 7 TeV
1.508±0.025±0.043		[3] ABAZOV	12U	D0	$p\overline{p}$ at 1.96 TeV
1.507±0.010±0.008		[7] AALTONEN	11	CDF	$p\overline{p}$ at 1.96 TeV
1.414±0.018±0.034		[8] ABAZOV	09E	D0	$p\overline{p}$ at 1.96 TeV
$1.504\pm0.013^{+0.018}_{-0.013}$		[9] AUBERT	06G	BABR	$e^+e^- \to \Upsilon(4S)$
1.534±0.008±0.010		[10] ABE	05B	BELL	$e^+e^- \to \Upsilon(4S)$
1.531±0.021±0.031		[11] ABDALLAH	04E	DLPH	$e^+e^- \to Z$
$1.523^{+0.024}_{-0.023}\pm0.022$		[12] AUBERT	03C	BABR	$e^+e^- \to \Upsilon(4S)$
1.533±0.034±0.038		[13] AUBERT	03H	BABR	$e^+e^- \to \Upsilon(4S)$
1.497±0.073±0.032		[14] ACOSTA	02C	CDF	$p\overline{p}$ at 1.8 TeV
1.529±0.012±0.029		[15] AUBERT	02H	BABR	$e^+e^- \to \Upsilon(4S)$
1.546±0.032±0.022		[16] AUBERT	01F	BABR	$e^+e^- \to \Upsilon(4S)$
1.541±0.028±0.023		[15] ABBIENDI,G	00B	OPAL	$e^+e^- \to Z$
1.518±0.053±0.034		[17] BARATE	00R	ALEP	$e^+e^- \to Z$
1.523±0.057±0.053		[18] ABBIENDI	99J	OPAL	$e^+e^- \to Z$
$1.474\pm0.039^{+0.052}_{-0.051}$		[17] ABE	98Q	CDF	$p\overline{p}$ at 1.8 TeV
1.52 ±0.06 ±0.04		[18] ACCIARRI	98S	L3	$e^+e^- \to Z$
1.64 ±0.08 ±0.08		[18] ABE	97J	SLD	$e^+e^- \to Z$
1.532±0.041±0.040		[19] ABREU	97F	DLPH	$e^+e^- \to Z$
$1.25\ ^{+0.15}_{-0.13}\pm0.05$	121	[14] BUSKULIC	96J	ALEP	$e^+e^- \to Z$
$1.49\ ^{+0.17}_{-0.15}\ ^{+0.08}_{-0.06}$		[20] BUSKULIC	96J	ALEP	$e^+e^- \to Z$
$1.61\ ^{+0.14}_{-0.13}\pm0.08$		[17,21] ABREU	95Q	DLPH	$e^+e^- \to Z$
1.63 ±0.14 ±0.13		[22] ADAM	95	DLPH	$e^+e^- \to Z$
1.53 ±0.12 ±0.08		[17,23] AKERS	95T	OPAL	$e^+e^- \to Z$
• • • We do not use the following data for averages, fits, limits, etc. • • •					
$1.501\ ^{+0.078}_{-0.074}\pm0.050$		[3] ABAZOV	07S	D0	Repl. by ABAZOV 12U
1.524±0.030±0.016		[3] ABULENCIA	07A	CDF	Repl. by AALTONEN 11
$1.473\ ^{+0.052}_{-0.050}\pm0.023$		[8] ABAZOV	05B	D0	Repl. by ABAZOV 05W
$1.40\ ^{+0.11}_{-0.10}\pm0.03$		[3] ABAZOV	05C	D0	Repl. by ABAZOV 07S
1.530±0.043±0.023		[8] ABAZOV	05W	D0	Repl. by ABAZOV 09E
1.54 ±0.05 ±0.02		[24] ACOSTA	05	CDF	Repl. by AALTONEN 11
1.554±0.030±0.019		[16] ABE	02H	BELL	Repl. by ABE 05B
1.58 ±0.09 ±0.02		[14] ABE	98B	CDF	Repl. by ACOSTA 02C
1.54 ±0.08 ±0.06		[17] ABE	96C	CDF	Repl. by ABE 98Q
1.55 ±0.06 ±0.03		[25] BUSKULIC	96J	ALEP	$e^+e^- \to Z$
1.61 ±0.07 ±0.04		[17] BUSKULIC	96J	ALEP	Repl. by BARATE 00R
1.62 ±0.12		[26] ADAM	95	DLPH	$e^+e^- \to Z$
1.57 ±0.18 ±0.08	121	[14] ABE	94D	CDF	Repl. by ABE 98B
$1.17\ ^{+0.29}_{-0.23}\pm0.16$	96	[17] ABREU	93D	DLPH	Sup. by ABREU 95Q
1.55 ±0.25 ±0.18	76	[22] ABREU	93G	DLPH	Sup. by ADAM 95
$1.51\ ^{+0.24}_{-0.23}\ ^{+0.12}_{-0.14}$	78	[17] ACTON	93C	OPAL	Sup. by AKERS 95T
$1.52\ ^{+0.20}_{-0.18}\ ^{+0.07}_{-0.13}$	77	[17] BUSKULIC	93D	ALEP	Sup. by BUSKULIC 96J
$1.20\ ^{+0.52}_{-0.36}\ ^{+0.16}_{-0.14}$	15	[27] WAGNER	90	MRK2	$E^{ee}_{cm} = 29$ GeV
$0.82\ ^{+0.57}_{-0.37}\pm0.27$		[28] AVERILL	89	HRS	$E^{ee}_{cm} = 29$ GeV

[1] Measured using $B^0 \to J/\psi K^*(892)^0$ and $B^0 \to J/\psi K^0_S$ decays.
[2] Measured using $B^0 \to D^-\mu^+\nu X$ decays.
[3] Measured mean life using $B^0 \to J/\psi K^0_S$ decays.
[4] Measured using $B^0 \to J/\psi K^{*0}$ decays.
[5] Measured using $B^0 \to K^+\pi^-$ decays.
[6] Measured with $B^0_d \to J/\psi(\mu^+\mu^-)\ K^0_S(\pi^+\pi^-)$ decays.
[7] Measured mean life using fully reconstructed decays ($J/\psi K^{(*)}$).
[8] Measured mean life using $B^0 \to J/\psi K^{*0}$ decays.
[9] Measured using a simultaneous fit of the B^0 lifetime and $\overline{B}^0 B^0$ oscillation frequency Δm_d in the partially reconstructed $B^0 \to D^{*-}\ell\nu$ decays.
[10] Measurement performed using a combined fit of CP-violation, mixing and lifetimes.
[11] Measurement performed using an inclusive reconstruction and B flavor identification technique.
[12] AUBERT 03C uses a sample of approximately 14,000 exclusively reconstructed $B^0 \to D^*(2010)^-\ell\nu$ and simultaneously measures the lifetime and oscillation frequency.
[13] Measurement performed with decays $B^0 \to D^{*-}\pi^+$ and $B^0 \to D^{*-}\rho^+$ using a partial reconstruction technique.
[14] Measured mean life using fully reconstructed decays.
[15] Data analyzed using partially reconstructed $\overline{B}^0 \to D^{*+}\ell^-\overline{\nu}$ decays.
[16] Events are selected in which one B meson is fully reconstructed while the second B meson is reconstructed inclusively.
[17] Data analyzed using $D/D^*\ell X$ event vertices.
[18] Data analyzed using charge of secondary vertex.
[19] Data analyzed using inclusive $D/D^*\ell X$.
[20] Measured mean life using partially reconstructed $D^{*-}\pi^+X$ vertices.
[21] ABREU 95Q assumes $B(B^0 \to D^{**-}\ell^+\nu_\ell) = 3.2 \pm 1.7\%$.
[22] Data analyzed using vertex-charge technique to tag B charge.
[23] AKERS 95T assumes $B(B^0 \to D_s^{(*)}D^{0(*)}) = 5.0 \pm 0.9\%$ to find B^+/B^0 yield.
[24] Measured using the time-dependent angular analysis of $B^0_d \to J/\psi K^{*0}$ decays.
[25] Combined result of $D/D^*\ell x$ analysis, fully reconstructed B analysis, and partially reconstructed $D^{*-}\pi^+X$ analysis.
[26] Combined ABREU 95Q and ADAM 95 result.
[27] WAGNER 90 tagged B^0 mesons by their decays into $D^{*-}e^+\nu$ and $D^{*-}\mu^+\nu$ where the D^{*-} is tagged by its decay into $\pi^-\overline{D}^0$.
[28] AVERILL 89 is an estimate of the B^0 mean lifetime assuming that $B^0 \to D^{*+} + X$ always.

$\tau_{B^0}/\tau_{\overline{B}^0}$

VALUE	DOCUMENT ID		TECN	COMMENT
1.000±0.008±0.009	[1] AAIJ	14E	LHCB	pp at 7 TeV

[1] Measured using $B^0 \to J/\psi K^{*0}$ decays.

MEAN LIFE RATIO τ_{B^+}/τ_{B^0}

τ_{B^+}/τ_{B^0} (direct measurements)

"OUR EVALUATION" is an average using rescaled values of the data listed below. The average and rescaling were performed by the Heavy Flavor Averaging Group (HFLAV) and are described at https://hflav.web.cern.ch/. The averaging/rescaling procedure takes into account correlations between the measurements and asymmetric lifetime errors.

VALUE	EVTS	DOCUMENT ID		TECN	COMMENT
1.076±0.004 OUR EVALUATION					
1.074±0.005±0.003		[1] AAIJ	14E	LHCB	pp at 7 TeV
1.088±0.009±0.004		[2] AALTONEN	11	CDF	$p\overline{p}$ at 1.96 TeV
1.080±0.016±0.014		[3] ABAZOV	05D	D0	$p\overline{p}$ at 1.96 TeV
1.066±0.008±0.008		[4] ABE	05B	BELL	$e^+e^- \to \Upsilon(4S)$
1.060±0.021±0.024		[5] ABDALLAH	04E	DLPH	$e^+e^- \to Z$
1.093±0.066±0.028		[6] ACOSTA	02C	CDF	$p\overline{p}$ at 1.8 TeV
1.082±0.026±0.012		[7] AUBERT	01F	BABR	$e^+e^- \to \Upsilon(4S)$
1.085±0.059±0.018		[3] BARATE	00R	ALEP	$e^+e^- \to Z$
1.079±0.064±0.041		[8] ABBIENDI	99J	OPAL	$e^+e^- \to Z$
$1.110\pm0.056^{+0.033}_{-0.030}$		[3] ABE	98Q	CDF	$p\overline{p}$ at 1.8 TeV
1.09 ±0.07 ±0.03		[8] ACCIARRI	98S	L3	$e^+e^- \to Z$
1.01 ±0.07 ±0.06		[8] ABE	97J	SLD	$e^+e^- \to Z$
$1.27\ ^{+0.23}_{-0.19}\ ^{+0.03}_{-0.02}$		[6] BUSKULIC	96J	ALEP	$e^+e^- \to Z$
$1.00\ ^{+0.17}_{-0.15}\pm0.10$		[3,9] ABREU	95Q	DLPH	$e^+e^- \to Z$
$1.06\ ^{+0.13}_{-0.11}\pm0.10$		[10] ADAM	95	DLPH	$e^+e^- \to Z$
$0.99\ \pm0.14\ ^{+0.05}_{-0.04}$		[3,11] AKERS	95T	OPAL	$e^+e^- \to Z$

Downloaded from https://academic.oup.com/ptep/article/2022/8/083C01/6651666 by KIT Library user on 27 September 2022

• • • We do not use the following data for averages, fits, limits, etc. • • •

$1.091 \pm 0.023 \pm 0.014$		[7] ABE	02H	BELL	Repl. by ABE 05B
$1.06 \pm 0.07 \pm 0.02$		[6] ABE	98B	CDF	Repl. by ACOSTA 02C
$1.01 \pm 0.11 \pm 0.02$		[3] ABE	96C	CDF	Repl. by ABE 98Q
$1.03 \pm 0.08 \pm 0.02$		[12] BUSKULIC	96J	ALEP	$e^+e^- \to Z$
$0.98 \pm 0.08 \pm 0.03$		[3] BUSKULIC	96J	ALEP	Repl. by BARATE 00R
$1.02 \pm 0.16 \pm 0.05$	269	[6] ABE	94D	CDF	Repl. by ABE 98B
$1.11 {}^{+0.51}_{-0.39} \pm 0.11$	188	[3] ABREU	93D	DLPH	Sup. by ABREU 95Q
$1.01 {}^{+0.29}_{-0.22} \pm 0.12$	253	[10] ABREU	93G	DLPH	Sup. by ADAM 95
$1.0 {}^{+0.33}_{-0.25} \pm 0.08$	130	ACTON	93C	OPAL	Sup. by AKERS 95T
$0.96 {}^{+0.19}_{-0.15} {}^{+0.18}_{-0.12}$	154	[3] BUSKULIC	93D	ALEP	Sup. by BUSKULIC 96J

[1] Measured using $B \to J/\psi K^{(*)}$ decays.
[2] Measured mean life using fully reconstructed decays ($J/\psi K^{(*)}$).
[3] Data analyzed using $D/D^*\mu X$ vertices.
[4] Measurement performed using a combined fit of *CP*-violation, mixing and lifetimes.
[5] Measurement performed using an inclusive reconstruction and B flavor identification technique.
[6] Measured using fully reconstructed decays.
[7] Events are selected in which one B meson is fully reconstructed while the second B meson is reconstructed inclusively.
[8] Data analyzed using charge of secondary vertex.
[9] ABREU 95Q assumes $B(B^0 \to D^{**-}\ell^+\nu_\ell) = 3.2 \pm 1.7\%$.
[10] Data analyzed using vertex-charge technique to tag B charge.
[11] AKERS 95T assumes $B(B^0 \to D_s^{(*)} D^{0(*)}) = 5.0 \pm 0.9\%$ to find B^+/B^0 yield.
[12] Combined result of $D/D^*\ell X$ analysis and fully reconstructed B analysis.

τ_{B^+}/τ_{B^0} (inferred from branching fractions)

These measurements are inferred from the branching fractions for semileptonic decay or other spectator-dominated decays by assuming that the rates for such decays are equal for B^0 and B^+. We do not use measurements which assume equal production of B^0 and B^+ because of the large uncertainty in the production ratio.

"OUR EVALUATION" has been obtained by the Heavy Flavor Averaging Group (HFLAV) by taking into account correlations between measurements.

VALUE	CL%	EVTS	DOCUMENT ID		TECN	COMMENT
1.076 ± 0.034 OUR EVALUATION						
1.07 ± 0.04 OUR AVERAGE						
$1.07 \pm 0.04 \pm 0.03$			URQUIJO	07	BELL	$e^+e^- \to \Upsilon(4S)$
$1.067 \pm 0.041 \pm 0.033$			AUBERT,B	06Y	BABR	$e^+e^- \to \Upsilon(4S)$
• • • We do not use the following data for averages, fits, limits, etc. • • •						
$0.95 {}^{+0.117}_{-0.080} \pm 0.091$			[1] ARTUSO	97	CLE2	$e^+e^- \to \Upsilon(4S)$
$1.15 \pm 0.17 \pm 0.06$			[2] JESSOP	97	CLE2	$e^+e^- \to \Upsilon(4S)$
$0.93 \pm 0.18 \pm 0.12$			[3] ATHANAS	94	CLE2	Sup. by ARTUSO 97
$0.91 \pm 0.27 \pm 0.21$			[4] ALBRECHT	92C	ARG	$e^+e^- \to \Upsilon(4S)$
1.0 ± 0.4		29	[4,5] ALBRECHT	92G	ARG	$e^+e^- \to \Upsilon(4S)$
$0.89 \pm 0.19 \pm 0.13$			[4] FULTON	91	CLEO	$e^+e^- \to \Upsilon(4S)$
$1.00 \pm 0.23 \pm 0.14$			[4] ALBRECHT	89L	ARG	$e^+e^- \to \Upsilon(4S)$
0.49 to 2.3	90		[6] BEAN	87B	CLEO	$e^+e^- \to \Upsilon(4S)$

[1] ARTUSO 97 uses partial reconstruction of $B \to D^*\ell\nu_\ell$ and independent of B^0 and B^+ production fraction.
[2] Assumes equal production of B^+ and B^0 at the $\Upsilon(4S)$.
[3] ATHANAS 94 uses events tagged by fully reconstructed B^- decays and partially or fully reconstructed B^0 decays.
[4] Assumes equal production of B^0 and B^+.
[5] ALBRECHT 92G data analyzed using $B \to D_s\overline{D}$, $D_s\overline{D}^*$, $D_s^*\overline{D}$, $D_s^*\overline{D}^*$ events.
[6] BEAN 87B assume the fraction of $B^0\overline{B}^0$ events at the $\Upsilon(4S)$ is 0.41.

$\Delta\Gamma_{B^0_d}/\Gamma_{B^0_d}$

$\Gamma_{B^0_d}$ and $\Delta\Gamma_{B^0_d}$ are the decay rate average and difference between two B^0_d *CP* eigenstates (light − heavy). The λ_{CP} characterizes B^0 and $\overline{B}^0$ decays to states of charmonium plus K^0_L, see the review on "*CP* Violation" in the reviews section.

"OUR EVALUATION" has been obtained by the Heavy Flavor Averaging Group (HFLAV) by taking into account correlations between measurements.

VALUE (units 10^{-2})	CL%	DOCUMENT ID		TECN	COMMENT
0.1 ± 1.0 OUR EVALUATION					
0.1 ± 1.0 OUR AVERAGE					
$3.4 \pm 2.3 \pm 2.4$		[1] SIRUNYAN	18BY	CMS	pp at 8 TeV
$-0.1 \pm 1.1 \pm 0.9$		[2] AABOUD	16G	ATLS	pp at 7, 8 TeV
$-4.4 \pm 2.5 \pm 1.1$		[3] AAIJ	14E	LHCB	pp at 7 TeV
$1.7 \pm 1.8 \pm 1.1$		[4] HIGUCHI	12	BELL	$e^+e^- \to \Upsilon(4S)$
$0.8 \pm 3.7 \pm 1.8$		[5] AUBERT,B	04C	BABR	$e^+e^- \to \Upsilon(4S)$
0 ± 9		[6] ABDALLAH	03B	DLPH	$e^+e^- \to Z$
• • • We do not use the following data for averages, fits, limits, etc. • • •					
0.50 ± 1.38		ABAZOV	14	D0	$p\overline{p}$ at 1.96 TeV
< 80	95	[7] BEHRENS	00B	CLE2	$e^+e^- \to \Upsilon(4S)$

[1] Measured using $B^0 \to J/\psi K^*(892)^0$ and $B^0 \to J/\psi K^0_S$ decays, and assuming $\beta = 21.9 \pm 0.7$ degrees.
[2] Measured from the ratio of decay time distributions of $B^0 \to J/\psi K^0_S$ and $B^0 \to J/\psi K^{*0}$ decays.
[3] Measured using the effective lifetimes of $B^0 \to J/\psi K^0_S$ and $B^0 \to J/\psi K^{*0}$ decays.
[4] Reports $-\Delta\Gamma_d/\Gamma_d$ using $B^0 \to J/\psi K^0_S$, $J/\psi K^0_L$, $D^-\pi^+$, $D^{*-}\pi^+$, $D^{*-}\rho^+$, and $D^{*-}\ell^+\nu$ decays.
[5] Corresponds to 90% confidence range [−0.084, 0.068].
[6] Used the measured $\tau_{B^0} = 1.55 \pm 0.03$ ps. Corresponds to an upper limit of < 0.18 at 95% C.L.
[7] BEHRENS 00B uses high-momentum lepton tags and partially reconstructed $\overline{B}^0 \to D^{*+}\pi^-$, ρ^- decays to determine the flavor of the B meson. Assumes Δ_{md}=0.478 ± 0.018 ps^{-1} and τ_{B^0}=1.548 ± 0.032 ps.

B^0 DECAY MODES

$\overline{B}^0$ modes are charge conjugates of the modes below. Reactions indicate the weak decay vertex and do not include mixing. Modes which do not identify the charge state of the B are listed in the $B^\pm/B^0$ ADMIXTURE section.

The branching fractions listed below assume 50% $B^0\overline{B}^0$ and 50% B^+B^- production at the $\Upsilon(4S)$. We have attempted to bring older measurements up to date by rescaling their assumed $\Upsilon(4S)$ production ratio to 50:50 and their assumed D, D_s, D^*, and ψ branching ratios to current values whenever this would affect our averages and best limits significantly.

Indentation is used to indicate a subchannel of a previous reaction. All resonant subchannels have been corrected for resonance branching fractions to the final state so the sum of the subchannel branching fractions can exceed that of the final state.

For inclusive branching fractions, *e.g.*, $B \to D^\pm X$, the values usually are multiplicities, not branching fractions. They can be greater than one.

	Mode		Fraction (Γ_i/Γ)	Scale factor/ Confidence level
Γ_1	$\ell^+\nu_\ell X$	[a]	(10.33 ± 0.28) %	
Γ_2	$e^+\nu_e X_c$		(10.1 ± 0.4) %	
Γ_3	$\ell^+\nu_\ell X_u$		$(1.51 \pm 0.19) \times 10^{-3}$	
Γ_4	$D\ell^+\nu_\ell X$		(9.3 ± 0.8) %	
Γ_5	$D^-\ell^+\nu_\ell$	[a]	(2.24 ± 0.09) %	
Γ_6	$D^-\tau^+\nu_\tau$		(1.05 ± 0.23) %	
Γ_7	$D^*(2010)^-\ell^+\nu_\ell$	[a]	(4.97 ± 0.12) %	
Γ_8	$D^*(2010)^-\tau^+\nu_\tau$		(1.58 ± 0.09) %	S=1.1
Γ_9	$\overline{D}^0\pi^-\ell^+\nu_\ell$		$(4.1 \pm 0.5) \times 10^{-3}$	
Γ_{10}	$D^*_0(2300)^-\ell^+\nu_\ell$, $D^{*-}_0 \to \overline{D}^0\pi^-$		$(3.0 \pm 1.2) \times 10^{-3}$	S=1.8
Γ_{11}	$D^*_2(2460)^-\ell^+\nu_\ell$, $D^{*-}_2 \to \overline{D}^0\pi^-$		$(1.21 \pm 0.33) \times 10^{-3}$	S=1.8
Γ_{12}	$\overline{D}^{(*)}n\pi\ell^+\nu_\ell (n \geq 1)$		(2.3 ± 0.5) %	
Γ_{13}	$\overline{D}^{*0}\pi^-\ell^+\nu_\ell$		$(5.8 \pm 0.8) \times 10^{-3}$	S=1.4
Γ_{14}	$D_1(2420)^-\ell^+\nu_\ell$, $D^-_1 \to \overline{D}^{*0}\pi^-$		$(2.80 \pm 0.28) \times 10^{-3}$	
Γ_{15}	$D'_1(2430)^-\ell^+\nu_\ell$, $D'^-_1 \to \overline{D}^{*0}\pi^-$		$(3.1 \pm 0.9) \times 10^{-3}$	
Γ_{16}	$D^*_2(2460)^-\ell^+\nu_\ell$, $D^{*-}_2 \to \overline{D}^{*0}\pi^-$		$(6.8 \pm 1.2) \times 10^{-4}$	
Γ_{17}	$D^-\pi^+\pi^-\ell^+\nu_\ell$		$(1.3 \pm 0.5) \times 10^{-3}$	
Γ_{18}	$D^{*-}\pi^+\pi^-\ell^+\nu_\ell$		$(1.4 \pm 0.5) \times 10^{-3}$	
Γ_{19}	$\rho^-\ell^+\nu_\ell$	[a]	$(2.94 \pm 0.21) \times 10^{-4}$	
Γ_{20}	$\pi^-\ell^+\nu_\ell$	[a]	$(1.50 \pm 0.06) \times 10^{-4}$	
Γ_{21}	$\pi^-\mu^+\nu_\mu$			
Γ_{22}	$\pi^-\tau^+\nu_\tau$		$< 2.5 \times 10^{-4}$	CL=90%
	Inclusive modes			
Γ_{23}	$K^\pm X$		(78 ± 8) %	
Γ_{24}	D^0X		(8.1 ± 1.5) %	
Γ_{25}	$\overline{D}^0X$		(47.4 ± 2.8) %	
Γ_{26}	D^+X		< 3.9 %	CL=90%
Γ_{27}	D^-X		(36.9 ± 3.3) %	
Γ_{28}	D^+_sX		$(10.3 {}^{+2.1}_{-1.8})$ %	
Γ_{29}	D^-_sX		< 2.6 %	CL=90%
Γ_{30}	Λ^+_cX		< 3.1 %	CL=90%
Γ_{31}	$\overline{\Lambda}^-_cX$		$(5.0 {}^{+2.1}_{-1.5})$ %	
Γ_{32}	$\overline{c}X$		(95 ± 5) %	
Γ_{33}	cX		(24.6 ± 3.1) %	
Γ_{34}	$\overline{c}/cX$		(119 ± 6) %	

Downloaded from https://academic.oup.com/ptep/article/2022/8/083C01/6651666 by KIT Library user on 27 September 2022

D, D^*, or D_s modes

Γ_{35}	$D^- \pi^+$		$(2.51 \pm 0.08) \times 10^{-3}$	
Γ_{36}	$D^- \rho^+$		$(7.6 \pm 1.2) \times 10^{-3}$	
Γ_{37}	$D^- K^0 \pi^+$		$(4.9 \pm 0.9) \times 10^{-4}$	
Γ_{38}	$D^- K^*(892)^+$		$(4.5 \pm 0.7) \times 10^{-4}$	
Γ_{39}	$D^- \omega \pi^+$		$(2.8 \pm 0.6) \times 10^{-3}$	
Γ_{40}	$D^- K^+$		$(2.05 \pm 0.08) \times 10^{-4}$	
Γ_{41}	$D^- K^+ \pi^+ \pi^-$		$(3.5 \pm 0.8) \times 10^{-4}$	
Γ_{42}	$D^- K^+ \overline{K}^0$		$< 3.1 \times 10^{-4}$	CL=90%
Γ_{43}	$D^- K^+ \overline{K}^*(892)^0$		$(8.8 \pm 1.9) \times 10^{-4}$	
Γ_{44}	$\overline{D}^0 \pi^+ \pi^-$		$(8.8 \pm 0.5) \times 10^{-4}$	
Γ_{45}	$D^*(2010)^- \pi^+$		$(2.74 \pm 0.13) \times 10^{-3}$	
Γ_{46}	$\overline{D}^0 K^+ K^-$		$(6.1 \pm 0.5) \times 10^{-5}$	
Γ_{47}	$D^- \pi^+ \pi^+ \pi^-$		$(6.0 \pm 0.6) \times 10^{-3}$	
Γ_{48}	$(D^- \pi^+ \pi^+ \pi^-)$ nonresonant		$(3.9 \pm 1.9) \times 10^{-3}$	
Γ_{49}	$D^- \pi^+ \rho^0$		$(1.1 \pm 1.0) \times 10^{-3}$	
Γ_{50}	$D^- a_1(1260)^+$		$(6.0 \pm 3.3) \times 10^{-3}$	
Γ_{51}	$D^*(2010)^- \pi^+ \pi^0$		(1.5 ± 0.5) %	
Γ_{52}	$D^*(2010)^- \rho^+$		$(6.8 \pm 0.9) \times 10^{-3}$	
Γ_{53}	$D^*(2010)^- K^+$		$(2.12 \pm 0.15) \times 10^{-4}$	
Γ_{54}	$D^*(2010)^- K^0 \pi^+$		$(3.0 \pm 0.8) \times 10^{-4}$	
Γ_{55}	$D^*(2010)^- K^*(892)^+$		$(3.3 \pm 0.6) \times 10^{-4}$	
Γ_{56}	$D^*(2010)^- K^+ \overline{K}^0$		$< 4.7 \times 10^{-4}$	CL=90%
Γ_{57}	$D^*(2010)^- K^+ \overline{K}^*(892)^0$		$(1.29 \pm 0.33) \times 10^{-3}$	
Γ_{58}	$D^*(2010)^- \pi^+ \pi^+ \pi^-$		$(7.21 \pm 0.29) \times 10^{-3}$	
Γ_{59}	$(D^*(2010)^- \pi^+ \pi^+ \pi^-)$ nonresonant		$(0.0 \pm 2.5) \times 10^{-3}$	
Γ_{60}	$D^*(2010)^- \pi^+ \rho^0$		$(5.7 \pm 3.2) \times 10^{-3}$	
Γ_{61}	$D^*(2010)^- a_1(1260)^+$		(1.30 ± 0.27) %	
Γ_{62}	$\overline{D}_1(2420)^0 \pi^- \pi^+$, $\overline{D}_1^0 \to D^{*-} \pi^+$		$(1.47 \pm 0.35) \times 10^{-4}$	
Γ_{63}	$D^*(2010)^- K^+ \pi^- \pi^+$		$(4.7 \pm 0.4) \times 10^{-4}$	
Γ_{64}	$D^*(2010)^- \pi^+ \pi^+ \pi^- \pi^0$		(1.76 ± 0.27) %	
Γ_{65}	$D^{*-} 3\pi^+ 2\pi^-$		$(4.7 \pm 0.9) \times 10^{-3}$	
Γ_{66}	$D^*(2010)^- \omega \pi^+$		$(2.46 \pm 0.18) \times 10^{-3}$	S=1.2
Γ_{67}	$\overline{D}_1(2430)^0 \omega$, $\overline{D}_1^0 \to D^{*-} \pi^+$		$(2.7 {}^{+0.8}_{-0.4}) \times 10^{-4}$	
Γ_{68}	$D^{*-} \rho(1450)^+$, $\rho^+ \to \omega \pi^+$		$(1.07 {}^{+0.40}_{-0.34}) \times 10^{-3}$	
Γ_{69}	$\overline{D}_1(2420)^0 \omega$, $\overline{D}_1^0 \to D^{*-} \pi^+$		$(7.0 \pm 2.2) \times 10^{-5}$	
Γ_{70}	$\overline{D}_2^*(2460)^0 \omega$, $\overline{D}_2^0 \to D^{*-} \pi^+$		$(4.0 \pm 1.4) \times 10^{-5}$	
Γ_{71}	$D^{*-} b_1(1235)^+$, $b_1^+ \to \omega \pi^+$		$< 7 \times 10^{-5}$	CL=90%
Γ_{72}	$\overline{D}^{**-} \pi^+$	[b]	$(1.9 \pm 0.9) \times 10^{-3}$	
Γ_{73}	$D_1(2420)^- \pi^+$, $D_1^- \to D^- \pi^+ \pi^-$		$(9.9 {}^{+2.0}_{-2.5}) \times 10^{-5}$	
Γ_{74}	$D_1(2420)^- \pi^+$, $D_1^- \to D^{*-} \pi^+ \pi^-$		$< 3.3 \times 10^{-5}$	CL=90%
Γ_{75}	$\overline{D}_2^*(2460)^- \pi^+$, $(D_2^*)^- \to D^0 \pi^-$		$(2.38 \pm 0.16) \times 10^{-4}$	
Γ_{76}	$\overline{D}_0^*(2400)^- \pi^+$, $(D_0^*)^- \to D^0 \pi^-$		$(7.6 \pm 0.8) \times 10^{-5}$	
Γ_{77}	$D_2^*(2460)^- \pi^+$, $(D_2^*)^- \to D^{*-} \pi^+ \pi^-$		$< 2.4 \times 10^{-5}$	CL=90%
Γ_{78}	$\overline{D}_2^*(2460)^- \rho^+$		$< 4.9 \times 10^{-3}$	CL=90%
Γ_{79}	$D^0 \overline{D}^0$		$(1.4 \pm 0.7) \times 10^{-5}$	
Γ_{80}	$D^{*0} \overline{D}^0$		$< 2.9 \times 10^{-4}$	CL=90%
Γ_{81}	$D^- D^+$		$(2.11 \pm 0.18) \times 10^{-4}$	
Γ_{82}	$D^\pm D^{*\mp}$ (CP-averaged)		$(6.1 \pm 0.6) \times 10^{-4}$	
Γ_{83}	$D^- D_s^+$		$(7.2 \pm 0.8) \times 10^{-3}$	
Γ_{84}	$D^*(2010)^- D_s^+$		$(8.0 \pm 1.1) \times 10^{-3}$	
Γ_{85}	$D^- D_s^{*+}$		$(7.4 \pm 1.6) \times 10^{-3}$	
Γ_{86}	$D^*(2010)^- D_s^{*+}$		(1.77 ± 0.14) %	
Γ_{87}	$D_{s0}(2317)^- K^+$, $D_{s0}^- \to D_s^- \pi^0$		$(4.2 \pm 1.4) \times 10^{-5}$	
Γ_{88}	$D_{s0}(2317)^- \pi^+$, $D_{s0}^- \to D_s^- \pi^0$		$< 2.5 \times 10^{-5}$	CL=90%
Γ_{89}	$D_{sJ}(2457)^- K^+$, $D_{sJ}^- \to D_s^- \pi^0$		$< 9.4 \times 10^{-6}$	CL=90%
Γ_{90}	$D_{sJ}(2457)^- \pi^+$, $D_{sJ}^- \to D_s^- \pi^0$		$< 4.0 \times 10^{-6}$	CL=90%
Γ_{91}	$D_s^- D_s^+$		$< 3.6 \times 10^{-5}$	CL=90%
Γ_{92}	$D_s^{*-} D_s^+$		$< 1.3 \times 10^{-4}$	CL=90%
Γ_{93}	$D_s^{*-} D_s^{*+}$		$< 2.4 \times 10^{-4}$	CL=90%
Γ_{94}	$D_{s0}^*(2317)^+ D^-$, $D_{s0}^{*+} \to D_s^+ \pi^0$		$(1.06 \pm 0.16) \times 10^{-3}$	S=1.1
Γ_{95}	$D_{s0}(2317)^+ D^-$, $D_{s0}^+ \to D_s^{*+} \gamma$		$< 9.5 \times 10^{-4}$	CL=90%
Γ_{96}	$D_{s0}(2317)^+ D^*(2010)^-$, $D_{s0}^+ \to D_s^+ \pi^0$		$(1.5 \pm 0.6) \times 10^{-3}$	
Γ_{97}	$D_{sJ}(2457)^+ D^-$		$(3.5 \pm 1.1) \times 10^{-3}$	
Γ_{98}	$D_{sJ}(2457)^+ D^-$, $D_{sJ}^+ \to D_s^+ \gamma$		$(6.5 {}^{+1.7}_{-1.4}) \times 10^{-4}$	
Γ_{99}	$D_{sJ}(2457)^+ D^-$, $D_{sJ}^+ \to D_s^{*+} \gamma$		$< 6.0 \times 10^{-4}$	CL=90%
Γ_{100}	$D_{sJ}(2457)^+ D^-$, $D_{sJ}^+ \to D_s^+ \pi^+ \pi^-$		$< 2.0 \times 10^{-4}$	CL=90%
Γ_{101}	$D_{sJ}(2457)^+ D^-$, $D_{sJ}^+ \to D_s^+ \pi^0$		$< 3.6 \times 10^{-4}$	CL=90%
Γ_{102}	$D^*(2010)^- D_{sJ}(2457)^+$		$(9.3 \pm 2.2) \times 10^{-3}$	
Γ_{103}	$D_{sJ}(2457)^+ D^*(2010)$, $D_{sJ}^+ \to D_s^+ \gamma$		$(2.3 {}^{+0.9}_{-0.7}) \times 10^{-3}$	
Γ_{104}	$D^- D_{s1}(2536)^+$, $D_{s1}^+ \to D^{*0} K^+ + D^{*+} K^0$		$(2.8 \pm 0.7) \times 10^{-4}$	
Γ_{105}	$D^- D_{s1}(2536)^+$, $D_{s1}^+ \to D^{*0} K^+$		$(1.7 \pm 0.6) \times 10^{-4}$	
Γ_{106}	$D^- D_{s1}(2536)^+$, $D_{s1}^+ \to D^{*+} K^0$		$(2.6 \pm 1.1) \times 10^{-4}$	
Γ_{107}	$D^*(2010)^- D_{s1}(2536)^+$, $D_{s1}^+ \to D^{*0} K^+ + D^{*+} K^0$		$(5.0 \pm 1.4) \times 10^{-4}$	
Γ_{108}	$D^*(2010)^- D_{s1}(2536)^+$, $D_{s1}^+ \to D^{*0} K^+$		$(3.3 \pm 1.1) \times 10^{-4}$	
Γ_{109}	$D^{*-} D_{s1}(2536)^+$, $D_{s1}^+ \to D^{*+} K^0$		$(5.0 \pm 1.7) \times 10^{-4}$	
Γ_{110}	$D^- D_{sJ}(2573)^+$, $D_{sJ}^+ \to D^0 K^+$		$(3.4 \pm 1.8) \times 10^{-5}$	
Γ_{111}	$D^*(2010)^- D_{sJ}(2573)^+$, $D_{sJ}^+ \to D^0 K^+$		$< 2 \times 10^{-4}$	CL=90%
Γ_{112}	$D^- D_{sJ}(2700)^+$, $D_{sJ}^+ \to D^0 K^+$		$(7.1 \pm 1.2) \times 10^{-4}$	
Γ_{113}	$D^+ \pi^-$		$(7.3 \pm 1.2) \times 10^{-7}$	
Γ_{114}	$D_s^+ \pi^-$		$(2.03 \pm 0.18) \times 10^{-5}$	
Γ_{115}	$D_s^{*+} \pi^-$		$(2.1 \pm 0.4) \times 10^{-5}$	S=1.4
Γ_{116}	$D_s^+ \rho^-$		$< 2.4 \times 10^{-5}$	CL=90%
Γ_{117}	$D_s^{*+} \rho^-$		$(4.1 \pm 1.3) \times 10^{-5}$	
Γ_{118}	$D_s^+ a_0^-$		$< 1.9 \times 10^{-5}$	CL=90%
Γ_{119}	$D_s^{*+} a_0^-$		$< 3.6 \times 10^{-5}$	CL=90%
Γ_{120}	$D_s^+ a_1(1260)^-$		$< 2.1 \times 10^{-3}$	CL=90%
Γ_{121}	$D_s^{*+} a_1(1260)^-$		$< 1.7 \times 10^{-3}$	CL=90%
Γ_{122}	$D_s^+ a_2^-$		$< 1.9 \times 10^{-4}$	CL=90%
Γ_{123}	$D_s^{*+} a_2^-$		$< 2.0 \times 10^{-4}$	CL=90%
Γ_{124}	$D_s^- K^+$		$(2.7 \pm 0.5) \times 10^{-5}$	S=2.7
Γ_{125}	$D_s^{*-} K^+$		$(2.19 \pm 0.30) \times 10^{-5}$	
Γ_{126}	$D_s^- K^*(892)^+$		$(3.5 \pm 1.0) \times 10^{-5}$	
Γ_{127}	$D_s^{*-} K^*(892)^+$		$(3.2 {}^{+1.5}_{-1.3}) \times 10^{-5}$	
Γ_{128}	$D_s^- \pi^+ K^0$		$(9.7 \pm 1.4) \times 10^{-5}$	
Γ_{129}	$D_s^{*-} \pi^+ K^0$		$< 1.10 \times 10^{-4}$	CL=90%
Γ_{130}	$D_s^- K^+ \pi^+ \pi^-$		$(1.7 \pm 0.5) \times 10^{-4}$	
Γ_{131}	$D_s^- \pi^+ K^*(892)^0$		$< 3.0 \times 10^{-3}$	CL=90%
Γ_{132}	$D_s^{*-} \pi^+ K^*(892)^0$		$< 1.6 \times 10^{-3}$	CL=90%
Γ_{133}	$\overline{D}^0 K^0$		$(5.2 \pm 0.7) \times 10^{-5}$	
Γ_{134}	$\overline{D}^0 K^+ \pi^-$		$(8.8 \pm 1.7) \times 10^{-5}$	
Γ_{135}	$\overline{D}^0 K^*(892)^0$		$(4.5 \pm 0.6) \times 10^{-5}$	
Γ_{136}	$\overline{D}^0 K^*(1410)^0$		$< 6.7 \times 10^{-5}$	CL=90%
Γ_{137}	$\overline{D}^0 K_0^*(1430)^0$		$(7 \pm 7) \times 10^{-6}$	
Γ_{138}	$\overline{D}^0 K_2^*(1430)^0$		$(2.1 \pm 0.9) \times 10^{-5}$	
Γ_{139}	$D_0^*(2300)^- K^+$, $D_0^{*-} \to \overline{D}^0 \pi^-$		$(1.9 \pm 0.9) \times 10^{-5}$	
Γ_{140}	$D_2^*(2460)^- K^+$, $D_2^{*-} \to \overline{D}^0 \pi^-$		$(2.03 \pm 0.35) \times 10^{-5}$	
Γ_{141}	$D_3^*(2760)^- K^+$, $D_3^{*-} \to \overline{D}^0 \pi^-$		$< 1.0 \times 10^{-6}$	CL=90%
Γ_{142}	$\overline{D}^0 K^+ \pi^-$ nonresonant		$< 3.7 \times 10^{-5}$	CL=90%
Γ_{143}	$[K^+ K^-]_D K^*(892)^0$		$(4.2 \pm 0.7) \times 10^{-5}$	
Γ_{144}	$[\pi^+ \pi^-]_D K^*(892)^0$		$(6.0 \pm 1.1) \times 10^{-5}$	
Γ_{145}	$[\pi^+ K^-]_D K^*(892)^0$			
Γ_{146}	$[K^+ \pi^-]_D K^*(892)^0$			
Γ_{147}	$[\pi^+ \pi^- \pi^+ \pi^-]_D K^{*0}$		$(4.6 \pm 0.9) \times 10^{-5}$	

Downloaded from https://academic.oup.com/ptep/article/2022/8/083C01/6651666 by KIT Library user on 27 September 2022

Γ_{148}	$[\pi^+ K^- \pi^+ \pi^-]_D K^{*0}$			
Γ_{149}	$[K^+ \pi^- \pi^+ \pi^-]_D K^{*0}$			
Γ_{150}	$\overline{D}^0 \pi^0$	$(2.63 \pm 0.14) \times 10^{-4}$		
Γ_{151}	$\overline{D}^0 \rho^0$	$(3.21 \pm 0.21) \times 10^{-4}$		
Γ_{152}	$\overline{D}^0 f_2$	$(1.56 \pm 0.21) \times 10^{-4}$		
Γ_{153}	$\overline{D}^0 \eta$	$(2.36 \pm 0.32) \times 10^{-4}$	S=2.5	
Γ_{154}	$\overline{D}^0 \eta'$	$(1.38 \pm 0.16) \times 10^{-4}$	S=1.3	
Γ_{155}	$\overline{D}^0 \omega$	$(2.54 \pm 0.16) \times 10^{-4}$		
Γ_{156}	$D^0 \phi$	$< 2.3 \times 10^{-6}$	CL=95%	
Γ_{157}	$D^0 K^+ \pi^-$	$(5.3 \pm 3.2) \times 10^{-6}$		
Γ_{158}	$D^0 K^*(892)^0$	$(3.0 \pm 0.6) \times 10^{-6}$		
Γ_{159}	$\overline{D}^{*0} \gamma$	$< 2.5 \times 10^{-5}$	CL=90%	
Γ_{160}	$\overline{D}^*(2007)^0 \pi^0$	$(2.2 \pm 0.6) \times 10^{-4}$	S=2.6	
Γ_{161}	$\overline{D}^*(2007)^0 \rho^0$	$< 5.1 \times 10^{-4}$	CL=90%	
Γ_{162}	$\overline{D}^*(2007)^0 \eta$	$(2.3 \pm 0.6) \times 10^{-4}$	S=2.8	
Γ_{163}	$\overline{D}^*(2007)^0 \eta'$	$(1.40 \pm 0.22) \times 10^{-4}$		
Γ_{164}	$\overline{D}^*(2007)^0 \pi^+ \pi^-$	$(6.2 \pm 2.2) \times 10^{-4}$		
Γ_{165}	$\overline{D}^*(2007)^0 K^0$	$(3.6 \pm 1.2) \times 10^{-5}$		
Γ_{166}	$\overline{D}^*(2007)^0 K^*(892)^0$	$< 6.9 \times 10^{-5}$	CL=90%	
Γ_{167}	$D^*(2007)^0 K^*(892)^0$	$< 4.0 \times 10^{-5}$	CL=90%	
Γ_{168}	$D^*(2007)^0 \pi^+ \pi^+ \pi^- \pi^-$	$(2.7 \pm 0.5) \times 10^{-3}$		
Γ_{169}	$D^*(2010)^+ D^*(2010)^-$	$(8.0 \pm 0.6) \times 10^{-4}$		
Γ_{170}	$\overline{D}^*(2007)^0 \omega$	$(3.6 \pm 1.1) \times 10^{-4}$	S=3.1	
Γ_{171}	$D^*(2010)^+ D^-$	$(6.1 \pm 1.5) \times 10^{-4}$	S=1.6	
Γ_{172}	$D^*(2007)^0 \overline{D}^*(2007)^0$	$< 9 \times 10^{-5}$	CL=90%	
Γ_{173}	$D^- D^0 K^+$	$(1.07 \pm 0.11) \times 10^{-3}$		
Γ_{174}	$D^- D^*(2007)^0 K^+$	$(3.5 \pm 0.4) \times 10^{-3}$		
Γ_{175}	$D^*(2010)^- D^0 K^+$	$(2.47 \pm 0.21) \times 10^{-3}$		
Γ_{176}	$D^*(2010)^- D^*(2007)^0 K^+$	(1.06 ± 0.09) %		
Γ_{177}	$D^- D^+ K^0$	$(7.5 \pm 1.7) \times 10^{-4}$		
Γ_{178}	$D^*(2010)^- D^+ K^0 + D^- D^*(2010)^+ K^0$	$(6.4 \pm 0.5) \times 10^{-3}$		
Γ_{179}	$D^*(2010)^- D^*(2010)^+ K^0$	$(8.1 \pm 0.7) \times 10^{-3}$		
Γ_{180}	$D^{*-} D_{s1}(2536)^+,\ D_{s1}^+ \to D^{*+} K^0$	$(8.0 \pm 2.4) \times 10^{-4}$		
Γ_{181}	$\overline{D}^0 D^0 K^0$	$(2.7 \pm 1.1) \times 10^{-4}$		
Γ_{182}	$D^0 \overline{D}^0 K^+ \pi^-$	$(3.5 \pm 0.5) \times 10^{-4}$		
Γ_{183}	$\overline{D}^0 D^*(2007)^0 K^0 + \overline{D}^*(2007)^0 D^0 K^0$	$(1.1 \pm 0.5) \times 10^{-3}$		
Γ_{184}	$\overline{D}^*(2007)^0 D^*(2007)^0 K^0$	$(2.4 \pm 0.9) \times 10^{-3}$		
Γ_{185}	$(\overline{D}+\overline{D}^*)(D+D^*)K$	(3.68 ± 0.26) %		

Charmonium modes

Γ_{186}	$\eta_c K^0$	$(8.0 \pm 1.1) \times 10^{-4}$		
Γ_{187}	$\eta_c(1S) K^+ \pi^-$	$(6.0 \pm 0.7) \times 10^{-4}$		
Γ_{188}	$\eta_c(1S) K^+ \pi^-$ (NR)	$(6.2 \pm 1.3) \times 10^{-5}$		
Γ_{189}	$X(4100)^- K^+,\ X^- \to \eta_c \pi^-$	$(2.0 \pm 1.0) \times 10^{-5}$		
Γ_{190}	$\eta_c(1S) K^*(1410)^0$	$(1.9 \pm 1.5) \times 10^{-4}$		
Γ_{191}	$\eta_c(1S) K_0^*(1430)^0$	$(1.6 \pm 0.4) \times 10^{-4}$		
Γ_{192}	$\eta_c(1S) K_2^*(1430)^0$	$(5.0 {}^{+2.3}_{-2.7}) \times 10^{-5}$		
Γ_{193}	$\eta_c(1S) K^*(1680)^0$	$(3 \pm 4) \times 10^{-5}$		
Γ_{194}	$\eta_c(1S) K_0^*(1950)^0$	$(4.4 {}^{+3.0}_{-4.0}) \times 10^{-5}$		
Γ_{195}	$\eta_c K^*(892)^0$	$(5.2 {}^{+0.8}_{-0.9}) \times 10^{-4}$	S=1.6	
Γ_{196}	$\eta_c(2S) K_S^0,\ \eta_c \to p\overline{p}\pi^+\pi^-$	$(4.2 {}^{+1.4}_{-1.2}) \times 10^{-7}$		
Γ_{197}	$\eta_c(2S) K^{*0}$	$< 3.9 \times 10^{-4}$	CL=90%	
Γ_{198}	$h_c(1P) K_S^0$	$< 1.4 \times 10^{-5}$		
Γ_{199}	$h_c(1P) K^{*0}$	$< 4 \times 10^{-4}$	CL=90%	
Γ_{200}	$J/\psi(1S) K^0$	$(8.91 \pm 0.21) \times 10^{-4}$		
Γ_{201}	$J/\psi(1S) K^+ \pi^-$	$(1.15 \pm 0.05) \times 10^{-3}$		
Γ_{202}	$J/\psi(1S) K^*(892)^0$	$(1.27 \pm 0.05) \times 10^{-3}$		
Γ_{203}	$J/\psi(1S) \eta K_S^0$	$(5.4 \pm 0.9) \times 10^{-5}$		
Γ_{204}	$J/\psi(1S) \eta' K_S^0$	$< 2.5 \times 10^{-5}$	CL=90%	
Γ_{205}	$J/\psi(1S) \phi K^0$	$(4.9 \pm 1.0) \times 10^{-5}$	S=1.3	
Γ_{206}	$J/\psi(1S) \omega K^0$	$(2.3 \pm 0.4) \times 10^{-4}$		
Γ_{207}	$\chi_{c0}(3915),\ \chi_{c0} \to J/\psi\omega$	$(2.1 \pm 0.9) \times 10^{-5}$		
Γ_{208}	$J/\psi(1S) K(1270)^0$	$(1.3 \pm 0.5) \times 10^{-3}$		
Γ_{209}	$J/\psi(1S) \pi^0$	$(1.66 \pm 0.10) \times 10^{-5}$		
Γ_{210}	$J/\psi(1S) \eta$	$(1.08 \pm 0.23) \times 10^{-5}$	S=1.5	
Γ_{211}	$J/\psi(1S) \pi^+ \pi^-$	$(4.00 \pm 0.15) \times 10^{-5}$		
Γ_{212}	$J/\psi(1S) \pi^+ \pi^-$ nonresonant	$< 1.2 \times 10^{-5}$	CL=90%	
Γ_{213}	$J/\psi(1S) f_0(500),\ f_0 \to \pi\pi$	$(8.8 {}^{+1.2}_{-1.6}) \times 10^{-6}$		
Γ_{214}	$J/\psi(1S) f_2$	$(3.3 {}^{+0.5}_{-0.6}) \times 10^{-6}$	S=1.5	
Γ_{215}	$J/\psi(1S) \rho^0$	$(2.55 {}^{+0.18}_{-0.16}) \times 10^{-5}$		
Γ_{216}	$J/\psi(1S) f_0(980),\ f_0 \to \pi^+\pi^-$	$< 1.1 \times 10^{-6}$	CL=90%	
Γ_{217}	$J/\psi(1S) \rho(1450)^0,\ \rho^0 \to \pi\pi$	$(2.9 {}^{+1.6}_{-0.7}) \times 10^{-6}$		
Γ_{218}	$J/\psi \rho(1700)^0,\ \rho^0 \to \pi^+\pi^-$	$(2.0 \pm 1.3) \times 10^{-6}$		
Γ_{219}	$J/\psi(1S) \omega$	$(1.8 {}^{+0.7}_{-0.5}) \times 10^{-5}$		
Γ_{220}	$J/\psi(1S) K^+ K^-$	$(2.54 \pm 0.35) \times 10^{-6}$		
Γ_{221}	$J/\psi(1S) a_0(980),\ a_0 \to K^+ K^-$	$(4.7 \pm 3.4) \times 10^{-7}$		
Γ_{222}	$J/\psi(1S) \phi$	$< 1.1 \times 10^{-7}$	CL=90%	
Γ_{223}	$J/\psi(1S) \eta'(958)$	$(7.6 \pm 2.4) \times 10^{-6}$		
Γ_{224}	$J/\psi(1S) K^0 \pi^+ \pi^-$	$(4.5 \pm 0.4) \times 10^{-4}$		
Γ_{225}	$J/\psi(1S) K^0 K^- \pi^+ +$ c.c.	$< 2.1 \times 10^{-5}$	CL=90%	
Γ_{226}	$J/\psi(1S) K^0 K^+ K^-$	$(2.5 \pm 0.7) \times 10^{-5}$	S=1.8	
Γ_{227}	$J/\psi(1S) K^0 K^\pm \pi^\mp$			
Γ_{228}	$J/\psi(1S) K^0 \rho^0$	$(5.4 \pm 3.0) \times 10^{-4}$		
Γ_{229}	$J/\psi(1S) K^*(892)^+ \pi^-$	$(8 \pm 4) \times 10^{-4}$		
Γ_{230}	$J/\psi(1S) \pi^+ \pi^- \pi^+ \pi^-$	$(1.44 \pm 0.12) \times 10^{-5}$		
Γ_{231}	$J/\psi(1S) f_1(1285)$	$(8.4 \pm 2.1) \times 10^{-6}$		
Γ_{232}	$J/\psi(1S) K^*(892)^0 \pi^+ \pi^-$	$(6.6 \pm 2.2) \times 10^{-4}$		
Γ_{233}	$\eta_{c2}(1D) K_S^0,\ \eta_{c2} \to h_c \gamma$	$< 3.5 \times 10^{-5}$	CL=90%	
Γ_{234}	$\eta_{c2}(1D) \pi^- K^+,\ \eta_{c2} \to h_c \gamma$	$< 1.0 \times 10^{-4}$	CL=90%	
Γ_{235}	$\chi_{c1}(3872)^- K^+$	$< 5 \times 10^{-4}$	CL=90%	
Γ_{236}	$\chi_{c1}(3872)^- K^+,\ \chi_{c1}(3872)^- \to J/\psi(1S) \pi^- \pi^0$	[c] $< 4.2 \times 10^{-6}$	CL=90%	
Γ_{237}	$\chi_{c1}(3872) K^0$	$(1.1 \pm 0.4) \times 10^{-4}$		
Γ_{238}	$\chi_{c1}(3872) K^*(892)^0$	$(1.0 \pm 0.5) \times 10^{-4}$		
Γ_{239}	$\chi_{c1}(3872) K^+ \pi^-$	$(2.1 \pm 0.8) \times 10^{-4}$		
Γ_{240}	$\chi_{c1}(3872) \gamma$	$< 1.3 \times 10^{-5}$	CL=90%	
Γ_{241}	$Z_c(4430)^\pm K^\mp,\ Z_c^\pm \to \psi(2S) \pi^\pm$	$(6.0 {}^{+3.0}_{-2.4}) \times 10^{-5}$		
Γ_{242}	$Z_c(4430)^\pm K^\mp,\ Z_c^\pm \to J/\psi \pi^\pm$	$(5.4 {}^{+4.0}_{-1.2}) \times 10^{-6}$		
Γ_{243}	$Z_c(3900)^\pm K^\mp,\ Z_c^\pm \to J/\psi \pi^\pm$	$< 9 \times 10^{-7}$		
Γ_{244}	$Z_c(4200)^\pm K^\mp,\ X^\pm \to J/\psi \pi^\pm$	$(2.2 {}^{+1.3}_{-0.8}) \times 10^{-5}$		
Γ_{245}	$J/\psi(1S) p\overline{p}$	$(4.5 \pm 0.6) \times 10^{-7}$		
Γ_{246}	$J/\psi(1S) \gamma$	$< 1.5 \times 10^{-6}$	CL=90%	
Γ_{247}	$J/\psi(1S) \overline{D}^0$	$< 1.3 \times 10^{-5}$	CL=90%	
Γ_{248}	$\psi(2S) \pi^0$	$(1.17 \pm 0.19) \times 10^{-5}$		
Γ_{249}	$\psi(2S) K^0$	$(5.8 \pm 0.5) \times 10^{-4}$		
Γ_{250}	$\psi(3770) K^0,\ \psi \to \overline{D}^0 D^0$	$< 1.23 \times 10^{-4}$	CL=90%	
Γ_{251}	$\psi(3770) K^0,\ \psi \to D^- D^+$	$< 1.88 \times 10^{-4}$	CL=90%	
Γ_{252}	$\psi(2S) \pi^+ \pi^-$	$(2.24 \pm 0.35) \times 10^{-5}$		
Γ_{253}	$\psi(2S) K^+ \pi^-$	$(5.8 \pm 0.4) \times 10^{-4}$		
Γ_{254}	$\psi(2S) K^*(892)^0$	$(5.9 \pm 0.4) \times 10^{-4}$		
Γ_{255}	$\chi_{c0} K^0$	$(1.9 \pm 0.4) \times 10^{-4}$		
Γ_{256}	$\chi_{c0} K^*(892)^0$	$(1.7 \pm 0.4) \times 10^{-4}$		
Γ_{257}	$\chi_{c1} \pi^0$	$(1.12 \pm 0.28) \times 10^{-5}$		
Γ_{258}	$\chi_{c1} K^0$	$(3.95 \pm 0.27) \times 10^{-4}$		
Γ_{259}	$\chi_{c1} \pi^- K^+$	$(4.97 \pm 0.30) \times 10^{-4}$		
Γ_{260}	$\chi_{c1} K^*(892)^0$	$(2.38 \pm 0.19) \times 10^{-4}$	S=1.2	
Γ_{261}	$X(4051)^- K^+,\ X^- \to \chi_{c1} \pi^-$	$(3.0 {}^{+4.0}_{-1.8}) \times 10^{-5}$		
Γ_{262}	$X(4248)^- K^+,\ X^- \to \chi_{c1} \pi^-$	$(4.0 {}^{+20.0}_{-1.0}) \times 10^{-5}$		
Γ_{263}	$\chi_{c1} \pi^+ \pi^- K^0$	$(3.2 \pm 0.5) \times 10^{-4}$		
Γ_{264}	$\chi_{c1} \pi^- \pi^0 K^+$	$(3.5 \pm 0.6) \times 10^{-4}$		
Γ_{265}	$\chi_{c2} K^0$	$< 1.5 \times 10^{-5}$	CL=90%	
Γ_{266}	$\chi_{c2} K^*(892)^0$	$(4.9 \pm 1.2) \times 10^{-5}$	S=1.1	
Γ_{267}	$\chi_{c2} \pi^- K^+$	$(7.2 \pm 1.0) \times 10^{-5}$		
Γ_{268}	$\chi_{c2} \pi^+ \pi^- K^0$	$< 1.70 \times 10^{-4}$	CL=90%	
Γ_{269}	$\chi_{c2} \pi^- \pi^0 K^+$	$< 7.4 \times 10^{-5}$	CL=90%	
Γ_{270}	$\psi(4660) K^0,\ \psi \to \Lambda_c^+ \Lambda_c^-$	$< 2.3 \times 10^{-4}$	CL=90%	
Γ_{271}	$\psi(4230)^0 K^0,\ \psi^0 \to J/\psi \pi^+ \pi^-$	$< 1.7 \times 10^{-5}$	CL=90%	

K* or *K modes

Γ_{272}	$K^+ \pi^-$	$(1.96 \pm 0.05) \times 10^{-5}$		
Γ_{273}	$K^0 \pi^0$	$(9.9 \pm 0.5) \times 10^{-6}$		
Γ_{274}	$\eta' K^0$	$(6.6 \pm 0.4) \times 10^{-5}$	S=1.4	
Γ_{275}	$\eta' K^*(892)^0$	$(2.8 \pm 0.6) \times 10^{-6}$		
Γ_{276}	$\eta' K_0^*(1430)^0$	$(6.3 \pm 1.6) \times 10^{-6}$		

Downloaded from https://academic.oup.com/ptep/article/2022/8/083C01/6651666 by KIT Library user on 27 September 2022

Γ_{277}	$\eta' K_2^*(1430)^0$		$(1.37 \pm 0.32) \times 10^{-5}$		
Γ_{278}	ηK^0		$(1.23 {}^{+0.27}_{-0.24}) \times 10^{-6}$		
Γ_{279}	$\eta K^*(892)^0$		$(1.59 \pm 0.10) \times 10^{-5}$		
Γ_{280}	$\eta K_0^*(1430)^0$		$(1.10 \pm 0.22) \times 10^{-5}$		
Γ_{281}	$\eta K_2^*(1430)^0$		$(9.6 \pm 2.1) \times 10^{-6}$		
Γ_{282}	ωK^0		$(4.8 \pm 0.4) \times 10^{-6}$		
Γ_{283}	$a_0(980)^0 K^0,\ a_0^0 \to \eta\pi^0$		$< 7.8 \times 10^{-6}$	CL=90%	
Γ_{284}	$b_1^0 K^0,\ b_1^0 \to \omega\pi^0$		$< 7.8 \times 10^{-6}$	CL=90%	
Γ_{285}	$a_0(980)^\pm K^\mp,\ a_0^\pm \to \eta\pi^\pm$		$< 1.9 \times 10^{-6}$	CL=90%	
Γ_{286}	$b_1^- K^+,\ b_1^- \to \omega\pi^-$		$(7.4 \pm 1.4) \times 10^{-6}$		
Γ_{287}	$b_1^0 K^{*0},\ b_1^0 \to \omega\pi^0$		$< 8.0 \times 10^{-6}$	CL=90%	
Γ_{288}	$b_1^- K^{*+},\ b_1^- \to \omega\pi^-$		$< 5.0 \times 10^{-6}$	CL=90%	
Γ_{289}	$a_0(1450)^\pm K^\mp,\ a_0^\pm \to \eta\pi^\pm$		$< 3.1 \times 10^{-6}$	CL=90%	
Γ_{290}	$K_S^0 X^0$ (Familon)		$< 5.3 \times 10^{-5}$	CL=90%	
Γ_{291}	$\omega K^*(892)^0$		$(2.0 \pm 0.5) \times 10^{-6}$		
Γ_{292}	$\omega (K\pi)_0^{*0}$		$(1.84 \pm 0.25) \times 10^{-5}$		
Γ_{293}	$\omega K_0^*(1430)^0$		$(1.60 \pm 0.34) \times 10^{-5}$		
Γ_{294}	$\omega K_2^*(1430)^0$		$(1.01 \pm 0.23) \times 10^{-5}$		
Γ_{295}	$\omega K^+\pi^-$ nonresonant		$(5.1 \pm 1.0) \times 10^{-6}$		
Γ_{296}	$K^+\pi^-\pi^0$		$(3.78 \pm 0.32) \times 10^{-5}$		
Γ_{297}	$K^+\rho^-$		$(7.0 \pm 0.9) \times 10^{-6}$		
Γ_{298}	$K^+\rho(1450)^-$		$(2.4 \pm 1.2) \times 10^{-6}$		
Γ_{299}	$K^+\rho(1700)^-$		$(6 \pm 7) \times 10^{-7}$		
Γ_{300}	$(K^+\pi^-\pi^0)$ nonresonant		$(2.8 \pm 0.6) \times 10^{-6}$		
Γ_{301}	$(K\pi)_0^{*+}\pi^-,\ (K\pi)_0^{*+} \to K^+\pi^0$		$(3.4 \pm 0.5) \times 10^{-5}$		
Γ_{302}	$(K\pi)_0^{*0}\pi^0,\ (K\pi)_0^{*0} \to K^+\pi^-$		$(8.6 \pm 1.7) \times 10^{-6}$		
Γ_{303}	$K_2^*(1430)^0\pi^0$		$< 4.0 \times 10^{-6}$	CL=90%	
Γ_{304}	$K^*(1680)^0\pi^0$		$< 7.5 \times 10^{-6}$	CL=90%	
Γ_{305}	$K_x^{*0}\pi^0$	[d]	$(6.1 \pm 1.6) \times 10^{-6}$		
Γ_{306}	$K^0\pi^+\pi^-$		$(4.97 \pm 0.18) \times 10^{-5}$		
Γ_{307}	$K^0\pi^+\pi^-$ nonresonant		$(1.39 {}^{+0.26}_{-0.18}) \times 10^{-5}$		S=1.6
Γ_{308}	$K^0\rho^0$		$(3.4 \pm 1.1) \times 10^{-6}$		S=2.3
Γ_{309}	$K^*(892)^+\pi^-$		$(7.5 \pm 0.4) \times 10^{-6}$		
Γ_{310}	$K_0^*(1430)^+\pi^-$		$(3.3 \pm 0.7) \times 10^{-5}$		S=2.0
Γ_{311}	$K_x^{*+}\pi^-$	[d]	$(5.1 \pm 1.6) \times 10^{-6}$		
Γ_{312}	$K^*(1410)^+\pi^-,\ K^{*+} \to K^0\pi^+$		$< 3.8 \times 10^{-6}$	CL=90%	
Γ_{313}	$(K\pi)_0^{*+}\pi^-,\ (K\pi)_0^{*+} \to K^0\pi^+$		$(1.62 \pm 0.13) \times 10^{-5}$		
Γ_{314}	$f_0(980) K^0,\ f_0 \to \pi^+\pi^-$		$(8.1 \pm 0.8) \times 10^{-6}$		S=1.3
Γ_{315}	$K^0 f_0(500)$		$(1.6 {}^{+2.5}_{-1.6}) \times 10^{-7}$		
Γ_{316}	$K^0 f_0(1500)$		$(1.3 \pm 0.8) \times 10^{-6}$		
Γ_{317}	$f_2(1270) K^0$		$(2.7 {}^{+1.3}_{-1.2}) \times 10^{-6}$		
Γ_{318}	$f_x(1300) K0, f_x \to \pi^+\pi^-$		$(1.8 \pm 0.7) \times 10^{-6}$		
Γ_{319}	$K^*(892)^0\pi^0$		$(3.3 \pm 0.6) \times 10^{-6}$		
Γ_{320}	$K_2^*(1430)^+\pi^-$		$(3.65 \pm 0.34) \times 10^{-6}$		
Γ_{321}	$K^*(1680)^+\pi^-$		$(1.41 \pm 0.10) \times 10^{-5}$		
Γ_{322}	$K^+\pi^-\pi^+\pi^-$	[e]	$< 2.3 \times 10^{-4}$	CL=90%	
Γ_{323}	$\rho^0 K^+\pi^-$		$(2.8 \pm 0.7) \times 10^{-6}$		
Γ_{324}	$f_0(980) K^+\pi^-,\ f_0 \to \pi\pi$		$(1.4 {}^{+0.5}_{-0.6}) \times 10^{-6}$		
Γ_{325}	$K^+\pi^-\pi^+\pi^-$ nonresonant		$< 2.1 \times 10^{-6}$	CL=90%	
Γ_{326}	$K^*(892)^0\pi^+\pi^-$		$(5.5 \pm 0.5) \times 10^{-5}$		
Γ_{327}	$K^*(892)^0\rho^0$		$(3.9 \pm 1.3) \times 10^{-6}$		S=1.9
Γ_{328}	$K^*(892)^0 f_0(980),\ f_0 \to \pi\pi$		$(3.9 {}^{+2.1}_{-1.8}) \times 10^{-6}$		S=3.9
Γ_{329}	$K_1(1270)^+\pi^-$		$< 3.0 \times 10^{-5}$	CL=90%	
Γ_{330}	$K_1(1400)^+\pi^-$		$< 2.7 \times 10^{-5}$	CL=90%	
Γ_{331}	$a_1(1260)^- K^+$	[e]	$(1.6 \pm 0.4) \times 10^{-5}$		
Γ_{332}	$K^*(892)^+\rho^-$		$(1.03 \pm 0.26) \times 10^{-5}$		
Γ_{333}	$K_0^*(1430)^+\rho^-$		$(2.8 \pm 1.2) \times 10^{-5}$		
Γ_{334}	$K_1(1400)^0\rho^0$		$< 3.0 \times 10^{-3}$	CL=90%	
Γ_{335}	$K_0^*(1430)^0\rho^0$		$(2.7 \pm 0.6) \times 10^{-5}$		
Γ_{336}	$K_0^*(1430)^0 f_0(980),\ f_0 \to \pi\pi$		$(2.7 \pm 0.9) \times 10^{-6}$		
Γ_{337}	$K_2^*(1430)^0 f_0(980),\ f_0 \to \pi\pi$		$(8.6 \pm 2.0) \times 10^{-6}$		
Γ_{338}	K^+K^-		$(7.8 \pm 1.5) \times 10^{-8}$		
Γ_{339}	$K^0\overline{K}^0$		$(1.21 \pm 0.16) \times 10^{-6}$		
Γ_{340}	$K^0K^-\pi^+$		$(6.7 \pm 0.5) \times 10^{-6}$		
Γ_{341}	$K^*(892)^\pm K^\mp$		$< 4 \times 10^{-7}$	CL=90%	
Γ_{342}	$\overline{K}^{*0}K^0 + K^{*0}\overline{K}^0$		$< 9.6 \times 10^{-7}$	CL=90%	
Γ_{343}	$K^+K^-\pi^0$		$(2.2 \pm 0.6) \times 10^{-6}$		
Γ_{344}	$K_S^0K_S^0\pi^0$		$< 9 \times 10^{-7}$	CL=90%	
Γ_{345}	$K_S^0K_S^0\eta$		$< 1.0 \times 10^{-6}$	CL=90%	
Γ_{346}	$K_S^0K_S^0\eta'$		$< 2.0 \times 10^{-6}$	CL=90%	
Γ_{347}	$K^0K^+K^-$		$(2.68 \pm 0.11) \times 10^{-5}$		
Γ_{348}	$K^0\phi$		$(7.3 \pm 0.7) \times 10^{-6}$		
Γ_{349}	$f_0(980) K^0,\ f_0 \to K^+K^-$		$(7.0 {}^{+3.5}_{-3.0}) \times 10^{-6}$		
Γ_{350}	$f_0(1500) K^0$		$(1.3 {}^{+0.7}_{-0.5}) \times 10^{-5}$		
Γ_{351}	$f_2'(1525)^0 K^0$		$(3 {}^{+5}_{-4}) \times 10^{-7}$		
Γ_{352}	$f_0(1710) K^0,\ f_0 \to K^+K^-$		$(4.4 \pm 0.9) \times 10^{-6}$		
Γ_{353}	$K^0K^+K^-$ nonresonant		$(3.3 \pm 1.0) \times 10^{-5}$		
Γ_{354}	$K_S^0K_S^0K_S^0$		$(6.0 \pm 0.5) \times 10^{-6}$		S=1.1
Γ_{355}	$f_0(980) K^0,\ f_0 \to K_S^0K_S^0$		$(2.7 \pm 1.8) \times 10^{-6}$		
Γ_{356}	$f_0(1710) K^0,\ f_0 \to K_S^0K_S^0$		$(5.0 {}^{+5.0}_{-2.6}) \times 10^{-7}$		
Γ_{357}	$f_2(2010) K^0,\ f_2 \to K_S^0K_S^0$		$(5 \pm 6) \times 10^{-7}$		
Γ_{358}	$K_S^0K_S^0K_S^0$ nonresonant		$(1.33 \pm 0.31) \times 10^{-5}$		
Γ_{359}	$K_S^0K_S^0K_L^0$		$< 1.6 \times 10^{-5}$	CL=90%	
Γ_{360}	$K^*(892)^0K^+K^-$		$(2.75 \pm 0.26) \times 10^{-5}$		
Γ_{361}	$K^*(892)^0\phi$		$(1.00 \pm 0.05) \times 10^{-5}$		
Γ_{362}	$K^+K^-\pi^+\pi^-$ nonresonant		$< 7.17 \times 10^{-5}$	CL=90%	
Γ_{363}	$K^*(892)^0K^-\pi^+$		$(4.5 \pm 1.3) \times 10^{-6}$		
Γ_{364}	$K^*(892)^0\overline{K}^*(892)^0$		$(8.3 \pm 2.4) \times 10^{-7}$		S=1.5
Γ_{365}	$K^+K^+\pi^-\pi^-$ nonresonant		$< 6.0 \times 10^{-6}$	CL=90%	
Γ_{366}	$K^*(892)^0K^+\pi^-$		$< 2.2 \times 10^{-6}$	CL=90%	
Γ_{367}	$K^*(892)^0K^*(892)^0$		$< 2 \times 10^{-7}$	CL=90%	
Γ_{368}	$K^*(892)^+K^*(892)^-$		$< 2.0 \times 10^{-6}$	CL=90%	
Γ_{369}	$K_1(1400)^0\phi$		$< 5.0 \times 10^{-3}$	CL=90%	
Γ_{370}	$\phi(K\pi)_0^{*0}$		$(4.3 \pm 0.4) \times 10^{-6}$		
Γ_{371}	$\phi(K\pi)_0^{*0}$ $(1.60 < m_{K\pi} < 2.15)$	[f]	$< 1.7 \times 10^{-6}$	CL=90%	
Γ_{372}	$K_0^*(1430)^0K^-\pi^+$		$< 3.18 \times 10^{-5}$	CL=90%	
Γ_{373}	$K_0^*(1430)^0\overline{K}^*(892)^0$		$< 3.3 \times 10^{-6}$	CL=90%	
Γ_{374}	$K_0^*(1430)^0\overline{K}_0^*(1430)^0$		$< 8.4 \times 10^{-6}$	CL=90%	
Γ_{375}	$K_0^*(1430)^0\phi$		$(3.9 \pm 0.8) \times 10^{-6}$		
Γ_{376}	$K_0^*(1430)^0K^*(892)^0$		$< 1.7 \times 10^{-6}$	CL=90%	
Γ_{377}	$K_0^*(1430)^0K_0^*(1430)^0$		$< 4.7 \times 10^{-6}$	CL=90%	
Γ_{378}	$K^*(1680)^0\phi$		$< 3.5 \times 10^{-6}$	CL=90%	
Γ_{379}	$K^*(1780)^0\phi$		$< 2.7 \times 10^{-6}$	CL=90%	
Γ_{380}	$K^*(2045)^0\phi$		$< 1.53 \times 10^{-5}$	CL=90%	
Γ_{381}	$K_2^*(1430)^0\rho^0$		$< 1.1 \times 10^{-3}$	CL=90%	
Γ_{382}	$K_2^*(1430)^0\phi$		$(6.8 \pm 0.9) \times 10^{-6}$		S=1.2
Γ_{383}	$K^0\phi\phi$		$(3.7 \pm 0.7) \times 10^{-6}$		S=1.3
Γ_{384}	$\eta'\eta'K^0$		$< 3.1 \times 10^{-5}$	CL=90%	
Γ_{385}	$\eta K^0\gamma$		$(7.6 \pm 1.8) \times 10^{-6}$		
Γ_{386}	$\eta' K^0\gamma$		$< 6.4 \times 10^{-6}$	CL=90%	
Γ_{387}	$K^0\phi\gamma$		$(2.7 \pm 0.7) \times 10^{-6}$		
Γ_{388}	$K^+\pi^-\gamma$		$(4.6 \pm 1.4) \times 10^{-6}$		
Γ_{389}	$K^*(892)^0\gamma$		$(4.18 \pm 0.25) \times 10^{-5}$		S=2.1
Γ_{390}	$K^*(1410)\gamma$		$< 1.3 \times 10^{-4}$	CL=90%	
Γ_{391}	$K^+\pi^-\gamma$ nonresonant		$< 2.6 \times 10^{-6}$	CL=90%	
Γ_{392}	$K^*(892)^0X(214),\ X \to \mu^+\mu^-$	[g]	$< 2.26 \times 10^{-8}$	CL=90%	
Γ_{393}	$K^0\pi^+\pi^-\gamma$		$(1.99 \pm 0.18) \times 10^{-5}$		
Γ_{394}	$K^+\pi^-\pi^0\gamma$		$(4.1 \pm 0.4) \times 10^{-5}$		
Γ_{395}	$K_1(1270)^0\gamma$		$< 5.8 \times 10^{-5}$	CL=90%	
Γ_{396}	$K_1(1400)^0\gamma$		$< 1.2 \times 10^{-5}$	CL=90%	
Γ_{397}	$K_2^*(1430)^0\gamma$		$(1.24 \pm 0.24) \times 10^{-5}$		
Γ_{398}	$K^*(1680)^0\gamma$		$< 2.0 \times 10^{-3}$	CL=90%	
Γ_{399}	$K_3^*(1780)^0\gamma$		$< 8.3 \times 10^{-5}$	CL=90%	
Γ_{400}	$K_4^*(2045)^0\gamma$		$< 4.3 \times 10^{-3}$	CL=90%	

Light unflavored meson modes

Γ_{401}	$\rho^0\gamma$		$(8.6 \pm 1.5) \times 10^{-7}$		
Γ_{402}	$\rho^0X(214),\ X \to \mu^+\mu^-$	[g]	$< 1.73 \times 10^{-8}$	CL=90%	
Γ_{403}	$\omega\gamma$		$(4.4 {}^{+1.8}_{-1.6}) \times 10^{-7}$		
Γ_{404}	$\phi\gamma$		$< 1.0 \times 10^{-7}$	CL=90%	
Γ_{405}	$\pi^+\pi^-$		$(5.12 \pm 0.19) \times 10^{-6}$		
Γ_{406}	$\pi^0\pi^0$		$(1.59 \pm 0.26) \times 10^{-6}$		S=1.4
Γ_{407}	$\eta\pi^0$		$(4.1 \pm 1.7) \times 10^{-7}$		
Γ_{408}	$\eta\eta$		$< 1.0 \times 10^{-6}$	CL=90%	
Γ_{409}	$\eta'\pi^0$		$(1.2 \pm 0.6) \times 10^{-6}$		S=1.7
Γ_{410}	$\eta'\eta'$		$< 1.7 \times 10^{-6}$	CL=90%	
Γ_{411}	$\eta'\eta$		$< 1.2 \times 10^{-6}$	CL=90%	

Downloaded from https://academic.oup.com/ptep/article/2022/8/083C01/6651666 by KIT Library user on 27 September 2022

Γ_{412}	$\eta' \rho^0$		< 1.3	$\times 10^{-6}$	CL=90%
Γ_{413}	$\eta' f_0(980),\ f_0 \to \pi^+\pi^-$		< 9	$\times 10^{-7}$	CL=90%
Γ_{414}	$\eta \rho^0$		< 1.5	$\times 10^{-6}$	CL=90%
Γ_{415}	$\eta f_0(980),\ f_0 \to \pi^+\pi^-$		< 4	$\times 10^{-7}$	CL=90%
Γ_{416}	$\omega\eta$		$(9.4 {}^{+4.0}_{-3.1})$	$\times 10^{-7}$	
Γ_{417}	$\omega\eta'$		$(1.0 {}^{+0.5}_{-0.4})$	$\times 10^{-6}$	
Γ_{418}	$\omega\rho^0$		< 1.6	$\times 10^{-6}$	CL=90%
Γ_{419}	$\omega f_0(980),\ f_0 \to \pi^+\pi^-$		< 1.5	$\times 10^{-6}$	CL=90%
Γ_{420}	$\omega\omega$		(1.2 ± 0.4)	$\times 10^{-6}$	
Γ_{421}	$\phi\pi^0$		< 1.5	$\times 10^{-7}$	CL=90%
Γ_{422}	$\phi\eta$		< 5	$\times 10^{-7}$	CL=90%
Γ_{423}	$\phi\eta'$		< 5	$\times 10^{-7}$	CL=90%
Γ_{424}	$\phi\pi^+\pi^-$		(1.8 ± 0.5)	$\times 10^{-7}$	
Γ_{425}	$\phi\rho^0$		< 3.3	$\times 10^{-7}$	CL=90%
Γ_{426}	$\phi f_0(980),\ f_0 \to \pi^+\pi^-$		< 3.8	$\times 10^{-7}$	CL=90%
Γ_{427}	$\phi\omega$		< 7	$\times 10^{-7}$	CL=90%
Γ_{428}	$\phi\phi$		< 2.7	$\times 10^{-8}$	CL=90%
Γ_{429}	$a_0(980)^\pm\pi^\mp,\ a_0^\pm \to \eta\pi^\pm$		< 3.1	$\times 10^{-6}$	CL=90%
Γ_{430}	$a_0(1450)^\pm\pi^\mp,\ a_0^\pm \to \eta\pi^\pm$		< 2.3	$\times 10^{-6}$	CL=90%
Γ_{431}	$\pi^+\pi^-\pi^0$		< 7.2	$\times 10^{-4}$	CL=90%
Γ_{432}	$\rho^0\pi^0$		(2.0 ± 0.5)	$\times 10^{-6}$	
Γ_{433}	$\rho^\mp\pi^\pm$	[h]	(2.30 ± 0.23)	$\times 10^{-5}$	
Γ_{434}	$\pi^+\pi^-\pi^+\pi^-$		< 1.12	$\times 10^{-5}$	CL=90%
Γ_{435}	$\rho^0\pi^+\pi^-$		< 8.8	$\times 10^{-6}$	CL=90%
Γ_{436}	$\rho^0\rho^0$		(9.6 ± 1.5)	$\times 10^{-7}$	
Γ_{437}	$f_0(980)\pi^+\pi^-,\ f_0 \to \pi^+\pi^-$		< 3.0	$\times 10^{-6}$	CL=90%
Γ_{438}	$\rho^0 f_0(980),\ f_0 \to \pi^+\pi^-$		(7.8 ± 2.5)	$\times 10^{-7}$	
Γ_{439}	$f_0(980) f_0(980),\ f_0 \to \pi^+\pi^-,\ f_0 \to \pi^+\pi^-$		< 1.9	$\times 10^{-7}$	CL=90%
Γ_{440}	$f_0(980) f_0(980),\ f_0 \to \pi^+\pi^-,\ f_0 \to K^+K^-$		< 2.3	$\times 10^{-7}$	CL=90%
Γ_{441}	$a_1(1260)^\mp\pi^\pm$	[h]	(2.6 ± 0.5)	$\times 10^{-5}$	S=1.9
Γ_{442}	$a_2(1320)^\mp\pi^\pm$	[h]	< 6.3	$\times 10^{-6}$	CL=90%
Γ_{443}	$\pi^+\pi^-\pi^0\pi^0$		< 3.1	$\times 10^{-3}$	CL=90%
Γ_{444}	$\rho^+\rho^-$		(2.77 ± 0.19)	$\times 10^{-5}$	
Γ_{445}	$a_1(1260)^0\pi^0$		< 1.1	$\times 10^{-3}$	CL=90%
Γ_{446}	$\omega\pi^0$		< 5	$\times 10^{-7}$	CL=90%
Γ_{447}	$\pi^+\pi^+\pi^-\pi^-\pi^0$		< 9.0	$\times 10^{-3}$	CL=90%
Γ_{448}	$a_1(1260)^+\rho^-$		< 6.1	$\times 10^{-5}$	CL=90%
Γ_{449}	$a_1(1260)^0\rho^0$		< 2.4	$\times 10^{-3}$	CL=90%
Γ_{450}	$b_1^\mp\pi^\pm,\ b_1^\mp \to \omega\pi^\mp$		(1.09 ± 0.15)	$\times 10^{-5}$	
Γ_{451}	$b_1^0\pi^0,\ b_1^0 \to \omega\pi^0$		< 1.9	$\times 10^{-6}$	CL=90%
Γ_{452}	$b_1^-\rho^+,\ b_1^- \to \omega\pi^-$		< 1.4	$\times 10^{-6}$	CL=90%
Γ_{453}	$b_1^0\rho^0,\ b_1^0 \to \omega\pi^0$		< 3.4	$\times 10^{-6}$	CL=90%
Γ_{454}	$\pi^+\pi^+\pi^+\pi^-\pi^-\pi^-$		< 3.0	$\times 10^{-3}$	CL=90%
Γ_{455}	$a_1(1260)^+ a_1(1260)^-,\ a_1^+ \to 2\pi^+\pi^-,\ a_1^- \to 2\pi^-\pi^+$		(1.18 ± 0.31)	$\times 10^{-5}$	
Γ_{456}	$\pi^+\pi^+\pi^+\pi^-\pi^-\pi^-\pi^0$		< 1.1	%	CL=90%

Baryon modes

Γ_{457}	$p\overline{p}$		(1.25 ± 0.32)	$\times 10^{-8}$	
Γ_{458}	$p\overline{p}\pi^+\pi^-$		(2.87 ± 0.19)	$\times 10^{-6}$	
Γ_{459}	$p\overline{p}K^+\pi^-$		(6.3 ± 0.5)	$\times 10^{-6}$	
Γ_{460}	$p\overline{p}K^0$		(2.66 ± 0.32)	$\times 10^{-6}$	
Γ_{461}	$\Theta(1540)^+\overline{p},\ \Theta^+ \to pK^0_S$	[i]	< 5	$\times 10^{-8}$	CL=90%
Γ_{462}	$f_J(2220)K^0,\ f_J \to p\overline{p}$		< 4.5	$\times 10^{-7}$	CL=90%
Γ_{463}	$p\overline{p}K^*(892)^0$		$(1.24 {}^{+0.28}_{-0.25})$	$\times 10^{-6}$	
Γ_{464}	$f_J(2220)K^*_0,\ f_J \to p\overline{p}$		< 1.5	$\times 10^{-7}$	CL=90%
Γ_{465}	$p\overline{p}K^+K^-$		(1.21 ± 0.32)	$\times 10^{-7}$	
Γ_{466}	$p\overline{p}\pi^0$		(5.0 ± 1.9)	$\times 10^{-7}$	
Γ_{467}	$pp\overline{p}\overline{p}$		< 2.0	$\times 10^{-7}$	CL=90%
Γ_{468}	$p\overline{\Lambda}\pi^-$		(3.14 ± 0.29)	$\times 10^{-6}$	
Γ_{469}	$p\overline{\Lambda}\pi^-\gamma$		< 6.5	$\times 10^{-7}$	CL=90%
Γ_{470}	$p\overline{\Sigma}(1385)^-$		< 2.6	$\times 10^{-7}$	CL=90%
Γ_{471}	$\Delta(1232)^+\overline{p} + \Delta(1232)^- p$		< 1.6	$\times 10^{-6}$	
Γ_{472}	$\Delta^0\overline{\Lambda}$		< 9.3	$\times 10^{-7}$	CL=90%
Γ_{473}	$p\overline{\Lambda}K^-$		< 8.2	$\times 10^{-7}$	CL=90%
Γ_{474}	$p\overline{\Lambda}D^-$		(2.5 ± 0.4)	$\times 10^{-5}$	
Γ_{475}	$p\overline{\Lambda}D^{*-}$		(3.4 ± 0.8)	$\times 10^{-5}$	
Γ_{476}	$p\overline{\Sigma}^0\pi^-$		< 3.8	$\times 10^{-6}$	CL=90%
Γ_{477}	$\overline{\Lambda}\Lambda$		< 3.2	$\times 10^{-7}$	CL=90%
Γ_{478}	$\overline{\Lambda}\Lambda K^0$		$(4.8 {}^{+1.0}_{-0.9})$	$\times 10^{-6}$	
Γ_{479}	$\overline{\Lambda}\Lambda K^{*0}$		$(2.5 {}^{+0.9}_{-0.8})$	$\times 10^{-6}$	
Γ_{480}	$\overline{\Lambda}\Lambda D^0$		$(1.00 {}^{+0.30}_{-0.26})$	$\times 10^{-5}$	
Γ_{481}	$D^0\Sigma^0\overline{\Lambda}$ + c.c.		< 3.1	$\times 10^{-5}$	CL=90%
Γ_{482}	$\Delta^0\overline{\Delta}^0$		< 1.5	$\times 10^{-3}$	CL=90%
Γ_{483}	$\Delta^{++}\overline{\Delta}^{--}$		< 1.1	$\times 10^{-4}$	CL=90%
Γ_{484}	$\overline{D}^0 p\overline{p}$		(1.04 ± 0.07)	$\times 10^{-4}$	
Γ_{485}	$D_s^-\overline{\Lambda}p$		(2.8 ± 0.9)	$\times 10^{-5}$	
Γ_{486}	$\overline{D}^*(2007)^0 p\overline{p}$		(9.9 ± 1.1)	$\times 10^{-5}$	
Γ_{487}	$D^*(2010)^- p\overline{n}$		(1.4 ± 0.4)	$\times 10^{-3}$	
Γ_{488}	$D^- p\overline{p}\pi^+$		(3.32 ± 0.31)	$\times 10^{-4}$	
Γ_{489}	$D^*(2010)^- p\overline{p}\pi^+$		(4.7 ± 0.5)	$\times 10^{-4}$	S=1.2
Γ_{490}	$\overline{D}^0 p\overline{p}\pi^+\pi^-$		(3.0 ± 0.5)	$\times 10^{-4}$	
Γ_{491}	$\overline{D}^{*0} p\overline{p}\pi^+\pi^-$		(1.9 ± 0.5)	$\times 10^{-4}$	
Γ_{492}	$\Theta_c\overline{p}\pi^+,\ \Theta_c \to D^- p$		< 9	$\times 10^{-6}$	CL=90%
Γ_{493}	$\Theta_c\overline{p}\pi^+,\ \Theta_c \to D^{*-} p$		< 1.4	$\times 10^{-5}$	CL=90%
Γ_{494}	$\overline{\Sigma}_c^{--}\Delta^{++}$		< 8	$\times 10^{-4}$	CL=90%
Γ_{495}	$\overline{\Lambda}_c^- p\pi^+\pi^-$		(1.02 ± 0.14)	$\times 10^{-3}$	S=1.3
Γ_{496}	$\overline{\Lambda}_c^- p$		(1.54 ± 0.18)	$\times 10^{-5}$	
Γ_{497}	$\overline{\Lambda}_c^- p\pi^0$		(1.55 ± 0.19)	$\times 10^{-4}$	
Γ_{498}	$\Sigma_c(2455)^- p$		< 2.4	$\times 10^{-5}$	
Γ_{499}	$\overline{\Lambda}_c^- p\pi^+\pi^-\pi^0$		< 5.07	$\times 10^{-3}$	CL=90%
Γ_{500}	$\overline{\Lambda}_c^- p\pi^+\pi^-\pi^+\pi^-$		< 2.74	$\times 10^{-3}$	CL=90%
Γ_{501}	$\overline{\Lambda}_c^- p\pi^+\pi^-$ (nonresonant)		(5.5 ± 1.0)	$\times 10^{-4}$	S=1.3
Γ_{502}	$\overline{\Sigma}_c(2520)^{--} p\pi^+$		(1.02 ± 0.18)	$\times 10^{-4}$	
Γ_{503}	$\overline{\Sigma}_c(2520)^0 p\pi^-$		< 3.1	$\times 10^{-5}$	CL=90%
Γ_{504}	$\overline{\Sigma}_c(2455)^0 p\pi^-$		(1.08 ± 0.16)	$\times 10^{-4}$	
Γ_{505}	$\overline{\Sigma}_c(2455)^0 N^0,\ N^0 \to p\pi^-$		(6.4 ± 1.7)	$\times 10^{-5}$	
Γ_{506}	$\overline{\Sigma}_c(2455)^{--} p\pi^+$		(1.83 ± 0.24)	$\times 10^{-4}$	
Γ_{507}	$\Lambda_c^- pK^+\pi^-$		(3.4 ± 0.7)	$\times 10^{-5}$	
Γ_{508}	$\overline{\Sigma}_c(2455)^{--} pK^+,\ \overline{\Sigma}_c^{--} \to \overline{\Lambda}_c^-\pi^-$		(8.8 ± 2.5)	$\times 10^{-6}$	
Γ_{509}	$\Lambda_c^- pK^*(892)^0$		< 2.42	$\times 10^{-5}$	CL=90%
Γ_{510}	$\Lambda_c^- pK^+K^-$		(2.0 ± 0.4)	$\times 10^{-5}$	
Γ_{511}	$\Lambda_c^- p\phi$		< 1.0	$\times 10^{-5}$	CL=90%
Γ_{512}	$\Lambda_c^- p\overline{p}p$		< 2.8	$\times 10^{-6}$	
Γ_{513}	$\overline{\Lambda}_c^- \Lambda K^+$		(4.8 ± 1.1)	$\times 10^{-5}$	
Γ_{514}	$\overline{\Lambda}_c^- \Lambda_c^+$		< 1.6	$\times 10^{-5}$	CL=95%
Γ_{515}	$\overline{\Lambda}_c(2593)^- / \overline{\Lambda}_c(2625)^- p$		< 1.1	$\times 10^{-4}$	CL=90%
Γ_{516}	$\overline{\Xi}_c^- \Lambda_c^+$		(1.2 ± 0.8)	$\times 10^{-3}$	
Γ_{517}	$\overline{\Xi}_c^- \Lambda_c^+,\ \overline{\Xi}_c^- \to \overline{\Xi}^+\pi^-\pi^-$		(2.4 ± 1.1)	$\times 10^{-5}$	S=1.8
Γ_{518}	$\overline{\Xi}_c^- \Lambda_c^+,\ \overline{\Xi}_c^- \to \overline{p}K^+\pi^-$		(5.3 ± 1.7)	$\times 10^{-6}$	
Γ_{519}	$\Lambda_c^+\Lambda_c^- K^0$		(4.0 ± 0.9)	$\times 10^{-4}$	
Γ_{520}	$\overline{\Xi}_c(2930)^- \Lambda_c^+,\ \overline{\Xi}_c^- \to \Lambda_c^- K^0$		(2.4 ± 0.6)	$\times 10^{-4}$	

Lepton Family number (*LF*) or Lepton number (*L*) or Baryon number (*B*) violating modes, or/and $\Delta B = 1$ weak neutral current (*B1*) modes

Γ_{521}	$\gamma\gamma$	*B1*		< 3.2	$\times 10^{-7}$	CL=90%
Γ_{522}	e^+e^-	*B1*		< 2.5	$\times 10^{-9}$	CL=90%
Γ_{523}	$e^+e^-\gamma$	*B1*		< 1.2	$\times 10^{-7}$	CL=90%
Γ_{524}	$\mu^+\mu^-$	*B1*		$(7 {}^{+13}_{-11})$	$\times 10^{-11}$	S=1.8
Γ_{525}	$\mu^+\mu^-\gamma$	*B1*		< 2.0	$\times 10^{-9}$	CL=95%
Γ_{526}	$\mu^+\mu^-\mu^+\mu^-$	*B1*		< 6.9	$\times 10^{-10}$	CL=95%
Γ_{527}	$SP,\ S \to \mu^+\mu^-,\ P \to \mu^+\mu^-$	*B1*	[j]	< 6.0	$\times 10^{-10}$	CL=95%
Γ_{528}	$\tau^+\tau^-$	*B1*		< 2.1	$\times 10^{-3}$	CL=95%
Γ_{529}	$\pi^0\ell^+\ell^-$	*B1*		< 5.3	$\times 10^{-8}$	CL=90%
Γ_{530}	$\pi^0 e^+e^-$	*B1*		< 8.4	$\times 10^{-8}$	CL=90%
Γ_{531}	$\pi^0\mu^+\mu^-$	*B1*		< 6.9	$\times 10^{-8}$	CL=90%
Γ_{532}	$\eta\ell^+\ell^-$	*B1*		< 6.4	$\times 10^{-8}$	CL=90%
Γ_{533}	ηe^+e^-	*B1*		< 1.08	$\times 10^{-7}$	CL=90%
Γ_{534}	$\eta\mu^+\mu^-$	*B1*		< 1.12	$\times 10^{-7}$	CL=90%
Γ_{535}	$\pi^0\nu\overline{\nu}$	*B1*		< 9	$\times 10^{-6}$	CL=90%
Γ_{536}	$K^0\ell^+\ell^-$	*B1*	[a]	(3.3 ± 0.6)	$\times 10^{-7}$	
Γ_{537}	$K^0 e^+e^-$	*B1*		$(2.5 {}^{+1.1}_{-0.9})$	$\times 10^{-7}$	S=1.3
Γ_{538}	$K^0\mu^+\mu^-$	*B1*		(3.39 ± 0.35)	$\times 10^{-7}$	S=1.1
Γ_{539}	$K^0\nu\overline{\nu}$	*B1*		< 2.6	$\times 10^{-5}$	CL=90%
Γ_{540}	$\rho^0\nu\overline{\nu}$	*B1*		< 4.0	$\times 10^{-5}$	CL=90%
Γ_{541}	$K^*(892)^0\ell^+\ell^-$	*B1*	[a]	$(9.9 {}^{+1.2}_{-1.1})$	$\times 10^{-7}$	
Γ_{542}	$K^*(892)^0 e^+e^-$	*B1*		$(1.03 {}^{+0.19}_{-0.17})$	$\times 10^{-6}$	

Downloaded from https://academic.oup.com/ptep/article/2022/8/083C01/6651666 by KIT Library user on 27 September 2022

Γ_{543}	$K^*(892)^0\mu^+\mu^-$	$B1$		$(9.4 \pm 0.5) \times 10^{-7}$	
Γ_{544}	$K^*(892)^0\chi$, $\chi \to \mu^+\mu^-$				
Γ_{545}	$\pi^+\pi^-\mu^+\mu^-$	$B1$		$(2.1 \pm 0.5) \times 10^{-8}$	
Γ_{546}	$K^*(892)^0\nu\overline{\nu}$	$B1$	$<$	1.8×10^{-5}	CL=90%
Γ_{547}	invisible	$B1$	$<$	2.4×10^{-5}	CL=90%
Γ_{548}	$\nu\overline{\nu}\gamma$	$B1$	$<$	1.6×10^{-5}	CL=90%
Γ_{549}	$\phi\nu\overline{\nu}$	$B1$	$<$	1.27×10^{-4}	CL=90%
Γ_{550}	$e^\pm\mu^\mp$	LF	[h] $<$	1.0×10^{-9}	CL=90%
Γ_{551}	$\pi^0 e^\pm\mu^\mp$	LF	$<$	1.4×10^{-7}	CL=90%
Γ_{552}	$K^0 e^\pm\mu^\mp$	LF	$<$	3.8×10^{-8}	CL=90%
Γ_{553}	$K^*(892)^0 e^+\mu^-$	LF	$<$	1.6×10^{-7}	CL=90%
Γ_{554}	$K^*(892)^0 e^-\mu^+$	LF	$<$	1.2×10^{-7}	CL=90%
Γ_{555}	$K^*(892)^0 e^\pm\mu^\mp$	LF	$<$	1.8×10^{-7}	CL=90%
Γ_{556}	$e^\pm\tau^\mp$	LF	[h] $<$	1.6×10^{-5}	CL=90%
Γ_{557}	$\mu^\pm\tau^\mp$	LF	[h] $<$	1.4×10^{-5}	CL=95%
Γ_{558}	$\Lambda_c^+\mu^-$	L,B	$<$	1.4×10^{-6}	CL=90%
Γ_{559}	$\Lambda_c^+ e^-$	L,B	$<$	4×10^{-6}	CL=90%

[a] An ℓ indicates an e or a μ mode, not a sum over these modes.

[b] $\overline{D}^{**}$ represents an excited state with mass $2.2 < M < 2.8$ GeV/c^2.

[c] $\chi_{c1}(3872)^+$ is a hypothetical charged partner of the $\chi_{c1}(3872)$.

[d] Stands for the possible candidates of $K^*(1410)$, $K_0^*(1430)$ and $K_2^*(1430)$.

[e] B^0 and B_s^0 contributions not separated. Limit is on weighted average of the two decay rates.

[f] This decay refers to the coherent sum of resonant and nonresonant $J^P = 0^+$ $K\pi$ components with $1.60 < m_{K\pi} < 2.15$ GeV/c^2.

[g] $X(214)$ is a hypothetical particle of mass 214 MeV/c^2 reported by the HyperCP experiment, Physical Review Letters **94** 021801 (2005)

[h] The value is for the sum of the charge states or particle/antiparticle states indicated.

[i] $\Theta(1540)^+$ denotes a possible narrow pentaquark state.

[j] Here S and P are the hypothetical scalar and pseudoscalar particles with masses of 2.5 GeV/c^2 and 214.3 MeV/c^2, respectively.

CONSTRAINED FIT INFORMATION

An overall fit to 36 branching ratios uses 93 measurements and one constraint to determine 23 parameters. The overall fit has a $\chi^2 = 63.5$ for 71 degrees of freedom.

The following *off-diagonal* array elements are the correlation coefficients $\langle \delta x_i \delta x_j \rangle / (\delta x_i \cdot \delta x_j)$, in percent, from the fit to the branching fractions, $x_i \equiv \Gamma_i/\Gamma_{total}$. The fit constrains the x_i whose labels appear in this array to sum to one.

	x_7	x_8	x_{35}	x_{47}	x_{73}	x_{114}	x_{124}	x_{200}	x_{202}	x_{249}
x_8	40									
x_{35}	0	0								
x_{47}	0	0	28							
x_{73}	0	0	4	13						
x_{114}	0	0	19	6	1					
x_{124}	0	0	7	2	0	1				
x_{200}	0	0	0	0	0	0	0			
x_{202}	0	0	0	0	0	0	0	0		
x_{249}	0	0	0	0	0	0	0	0	0	
x_{254}	0	0	0	0	0	0	0	0	0	19
x_{260}	0	0	0	0	0	0	0	0	29	0
x_{266}	0	0	0	0	0	0	0	0	6	0
x_{272}	0	0	0	0	0	0	0	0	0	0
x_{306}	0	0	0	0	0	0	0	0	0	0
x_{340}	0	0	0	0	0	0	0	0	0	0
x_{347}	0	0	0	0	0	0	0	0	0	0
x_{361}	0	0	0	0	0	0	0	0	0	0
x_{405}	0	0	0	0	0	0	0	0	0	0
x_{436}	0	0	0	0	0	0	0	0	0	0
x_{538}	0	0	0	0	0	0	0	0	0	0
x_{543}	0	0	0	0	0	0	0	0	15	0

	x_{254}	x_{260}	x_{266}	x_{272}	x_{306}	x_{340}	x_{347}	x_{361}	x_{405}	x_{436}
x_{260}	0									
x_{266}	0	22								
x_{272}	0	0	0							
x_{306}	0	0	0	0						
x_{340}	0	0	0	0	16					
x_{347}	0	0	0	0	27	4				
x_{361}	0	0	0	0	0	0	0			
x_{405}	0	0	0	27	0	0	0	0		
x_{436}	0	0	0	0	0	0	0	20	0	
x_{538}	0	0	0	0	0	0	0	0	0	0
x_{543}	0	4	1	0	0	0	0	0	0	0

	x_{538}
x_{543}	0

B^0 BRANCHING RATIOS

For branching ratios in which the charge of the decaying B is not determined, see the $B^\pm$ section.

$\Gamma(\ell^+\nu_\ell X)/\Gamma_{total}$ — Γ_1/Γ

"OUR EVALUATION" is an average using rescaled values of the data listed below. The average and rescaling were performed by the Heavy Flavor Averaging Group (HFLAV) and are described at https://hflav.web.cern.ch/. The averaging/rescaling procedure takes into account correlations between the measurements.

VALUE (units 10^{-2})	DOCUMENT ID		TECN	COMMENT
10.33±0.28 OUR EVALUATION				
10.14±0.30 OUR AVERAGE Error includes scale factor of 1.1.				
10.46±0.30±0.23	[1] URQUIJO	07	BELL	$e^+e^- \to \Upsilon(4S)$
9.64±0.27±0.33	[2] AUBERT,B	06Y	BABR	$e^+e^- \to \Upsilon(4S)$
10.78±0.60±0.69	[3] ARTUSO	97	CLE2	$e^+e^- \to \Upsilon(4S)$
9.3 ±1.1 ±1.5	ALBRECHT	94	ARG	$e^+e^- \to \Upsilon(4S)$
9.9 ±3.0 ±0.9	HENDERSON	92	CLEO	$e^+e^- \to \Upsilon(4S)$
• • • We do not use the following data for averages, fits, limits, etc. • • •				
10.32±0.36±0.35	[4] OKABE	05	BELL	Repl. by URQUIJO 07
10.9 ±0.7 ±1.1	ATHANAS	94	CLE2	Sup. by ARTUSO 97

[1] URQUIJO 07 report a measurement of (9.80 ± 0.29 ± 0.21)% for the partial branching fraction of $B \to e\nu_e X_c$ decay with electron energy above 0.6 GeV. We converted the result to $B \to e\nu_e X$ branching fraction.

[2] The measurements are obtained for charged and neutral B mesons partial rates of semileptonic decay to electrons with momentum above 0.6 GeV/c in the B rest frame. The best precision on the ratio is achieved for a momentum threshold of 1.0 GeV: $B(B^+ \to e^+\nu_e X) / B(B^0 \to e^+\nu_e X) = 1.074 \pm 0.041 \pm 0.026$.

[3] ARTUSO 97 uses partial reconstruction of $B \to D^*\ell\nu_\ell$ and inclusive semileptonic branching ratio from BARISH 96B (0.1049 ± 0.0017 ± 0.0043).

[4] The measurements are obtained for charged and neutral B mesons partial rates of semileptonic decay to electrons with momentum above 0.6 GeV/c in the B rest frame, and their ratio of $B(B^+ \to e^+\nu_e X)/B(B^0 \to e^+\nu_e X) = 1.08 \pm 0.05 \pm 0.02$.

$\Gamma(e^+\nu_e X_c)/\Gamma_{total}$ — Γ_2/Γ

VALUE (units 10^{-2})	DOCUMENT ID		TECN	COMMENT
10.08±0.30±0.22	[1] URQUIJO	07	BELL	$e^+e^- \to \Upsilon(4S)$

[1] Measure the independent B^+ and B^0 partial branching fractions with electron threshold energies of 0.4 GeV.

$\Gamma(\ell^+\nu_\ell X_u)/\Gamma_{total}$ — Γ_3/Γ

Requires $E_\ell^* > 1$ GeV, where E_ℓ^* is letpon energy in B rest frame.

VALUE (units 10^{-3})	DOCUMENT ID		TECN	COMMENT
1.51±0.10±0.16	[1] CAO	21A	BELL	$e^+e^- \to \Upsilon(4S)$

[1] The correlation of 50% with $B(B^+ \to \ell^+\nu_\ell X_u)$(letpon energy in B rest frame $E_\ell^* >$ 1 GeV) was reported.

$\Gamma(D^-\ell^+\nu_\ell)/\Gamma_{total}$ — Γ_5/Γ

ℓ denotes e or μ, not the sum.

"OUR EVALUATION" is an average using rescaled values of the data listed below. The average and rescaling were performed by the Heavy Flavor Averaging Group (HFLAV) and are described at https://hflav.web.cern.ch/. The averaging/rescaling procedure takes into account correlations between the measurements.

VALUE (%)	DOCUMENT ID		TECN	COMMENT
2.24±0.09 OUR EVALUATION				
2.25±0.08 OUR AVERAGE				
2.31±0.03±0.11	[1] GLATTAUER	16	BELL	$e^+e^- \to \Upsilon(4S)$
2.21±0.11±0.11	[2] AUBERT	10	BABR	$e^+e^- \to \Upsilon(4S)$
2.09±0.13±0.18	[3] BARTELT	99	CLE2	$e^+e^- \to \Upsilon(4S)$
2.35±0.20±0.44	[4] BUSKULIC	97	ALEP	$e^+e^- \to Z$

Downloaded from https://academic.oup.com/ptep/article/2022/8/083C01/6651666 by KIT Library user on 27 September 2022

• • • We do not use the following data for averages, fits, limits, etc. • • •

2.21±0.11±0.12	[2] AUBERT	08Q	BABR	Repl. by AUBERT 10
2.13±0.12±0.39	ABE	02E	BELL	Repl. by GLATTAUER 16
1.87±0.15±0.32	[5] ATHANAS	97	CLE2	Repl. by BARTELT 99
1.8 ±0.6 ±0.3	[6] FULTON	91	CLEO	$e^+e^- \to \Upsilon(4S)$
2.0 ±0.7 ±0.6	[7] ALBRECHT	89J	ARG	$e^+e^- \to \Upsilon(4S)$

[1] Uses a fully reconstructed B meson as a tag on the recoil side while the other, on the signal side, is partially reconstructed from $B \to D\ell\nu$.
[2] Uses a fully reconstructed B meson as a tag on the recoil side.
[3] Assumes equal production of B^+ and B^0 at the $\Upsilon(4S)$.
[4] BUSKULIC 97 assumes fraction (B^+) = fraction (B^0) = (37.8 ± 2.2)% and PDG 96 values for B lifetime and branching ratio of D^* and D decays.
[5] ATHANAS 97 uses missing energy and missing momentum to reconstruct neutrino.
[6] FULTON 91 assumes assuming equal production of B^0 and B^+ at the $\Upsilon(4S)$ and uses Mark III D and D^* branching ratios.
[7] ALBRECHT 89J reports 0.018 ± 0.006 ± 0.005. We rescale using the method described in STONE 94 but with the updated PDG 94 $B(D^0 \to K^-\pi^+)$.

$\Gamma(D^-\ell^+\nu_\ell)/\Gamma(\ell^+\nu_\ell X)$ — Γ_5/Γ_1

VALUE	DOCUMENT ID		TECN	COMMENT
0.230±0.011±0.011	[1] AUBERT	10	BABR	$e^+e^- \to \Upsilon(4S)$

[1] Uses a fully reconstructed B meson on the recoil side.

$\Gamma(D^-\ell^+\nu_\ell)/\Gamma(D\ell^+\nu_\ell X)$ — Γ_5/Γ_4

VALUE	DOCUMENT ID		TECN	COMMENT
0.215±0.016±0.013	[1] AUBERT	07AN	BABR	$e^+e^- \to \Upsilon(4S)$

[1] Uses a fully reconstructed B meson on the recoil side.

$\Gamma(D^-\tau^+\nu_\tau)/\Gamma_{total}$ — Γ_6/Γ

VALUE (units 10^{-2})	DOCUMENT ID		TECN	COMMENT
• • • We do not use the following data for averages, fits, limits, etc. • • •				
1.04±0.35±0.18	[1] AUBERT	08N	BABR	Repl. by AUBERT 09S

[1] Uses a fully reconstructed B meson as a tag on the recoil side.

$\Gamma(D^-\tau^+\nu_\tau)/\Gamma(D^-\ell^+\nu_\ell)$ — Γ_6/Γ_5

VALUE	DOCUMENT ID		TECN	COMMENT
0.469±0.084±0.053	[1,2] LEES	12D	BABR	$e^+e^- \to \Upsilon(4S)$
• • • We do not use the following data for averages, fits, limits, etc. • • •				
0.489±0.165±0.069	[1] AUBERT	09S	BABR	Repl. by LEES 12D

[1] Uses a fully reconstructed B meson as a tag on the recoil side.
[2] Uses $\tau^+ \to e^+\nu_e\overline{\nu}_\tau$ and $\tau^+ \to \mu^+\nu_\mu\overline{\nu}_\tau$ and e^+ or μ^+ as ℓ^+.

$\Gamma(D^*(2010)^-\ell^+\nu_\ell)/\Gamma_{total}$ — Γ_7/Γ

"OUR EVALUATION" is an average using rescaled values of the data listed below. The average and rescaling were performed by the Heavy Flavor Averaging Group (HFLAV) and are described at https://hflav.web.cern.ch/. The averaging/rescaling procedure takes into account correlations between the measurements.

VALUE (%)	EVTS	DOCUMENT ID		TECN	COMMENT
4.97±0.12 OUR EVALUATION		This value assumes isospin symmetry.			
5.14±0.15 OUR FIT		Error includes scale factor of 1.3.			
5.16±0.16 OUR AVERAGE		Error includes scale factor of 1.4. See the ideogram below.			
5.02±0.02±0.16		[1] WAHEED	21	BELL	$e^+e^- \to \Upsilon(4S)$
5.49±0.16±0.25		[2] AUBERT	08Q	BABR	$e^+e^- \to \Upsilon(4S)$
4.69±0.04±0.34		[3] AUBERT	08R	BABR	$e^+e^- \to \Upsilon(4S)$
5.90±0.22±0.50		[4] ABDALLAH	04D	DLPH	$e^+e^- \to Z^0$
6.09±0.19±0.40		[5] ADAM	03	CLE2	$e^+e^- \to \Upsilon(4S)$
$4.70\pm0.13^{+0.36}_{-0.31}$		[6] ABREU	01H	DLPH	$e^+e^- \to Z$
5.26±0.20±0.46		[7] ABBIENDI	00Q	OPAL	$e^+e^- \to Z$
5.53±0.26±0.52		[8] BUSKULIC	97	ALEP	$e^+e^- \to Z$
• • • We do not use the following data for averages, fits, limits, etc. • • •					
4.90±0.02±0.16		[1] WAHEED	19	BELL	Repl. by WAHEED 21
4.58±0.03±0.26		[1] DUNGEL	10	BELL	Repl. by WAHEED 19
$4.90\pm0.07^{+0.36}_{-0.35}$		[4] AUBERT	05E	BABR	Repl. by AUBERT 08R
5.39±0.11±0.34		[9] ABDALLAH	04D	DLPH	$e^+e^- \to Z^0$
4.59±0.23±0.40		[10] ABE	02F	BELL	Repl. by DUNGEL 10
6.09±0.19±0.40		[11] BRIERE	02	CLE2	$e^+e^- \to \Upsilon(4S)$
5.08±0.21±0.66		[12] ACKERSTAFF	97G	OPAL	Repl. by ABBIENDI 00Q
5.52±0.17±0.68		[13] ABREU	96P	DLPH	Repl. by ABREU 01H
4.49±0.32±0.39	376	[14] BARISH	95	CLE2	Repl. by ADAM 03
5.18±0.30±0.62	410	[15] BUSKULIC	95N	ALEP	Sup. by BUSKULIC 97
4.5 ±0.3 ±0.4		[16] ALBRECHT	94	ARG	$e^+e^- \to \Upsilon(4S)$
4.7 ±0.5 ±0.5	235	[17] ALBRECHT	93	ARG	$e^+e^- \to \Upsilon(4S)$
seen	398	[18] SANGHERA	93	CLE2	$e^+e^- \to \Upsilon(4S)$
7.0 ±1.8 ±1.4		[19] ANTREASYAN	90B	CBAL	$e^+e^- \to \Upsilon(4S)$
		[20] ALBRECHT	89C	ARG	$e^+e^- \to \Upsilon(4S)$
6.0 ±1.0 ±1.4		[21] ALBRECHT	89J	ARG	$e^+e^- \to \Upsilon(4S)$
4.0 ±0.4 ±0.6		[22] BORTOLETTO	89B	CLEO	$e^+e^- \to \Upsilon(4S)$
7.0 ±1.2 ±1.9	47	[23] ALBRECHT	87J	ARG	$e^+e^- \to \Upsilon(4S)$

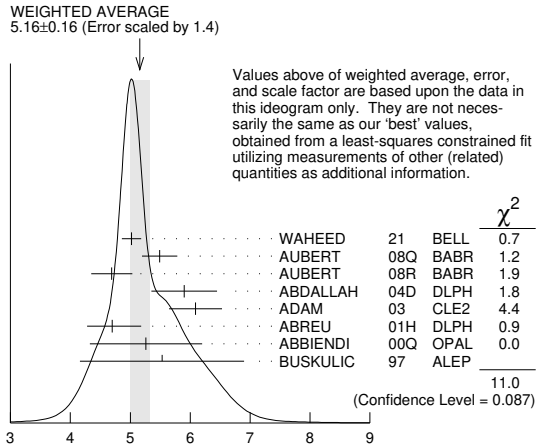

[1] WAHEED 21 uses fully reconstructed $D^{*-}\ell^+\nu$ events ($\ell = e$ or μ).
[2] Uses a fully reconstructed B meson as a tag on the recoil side.
[3] Measured using fully reconstructed D^* sample and a simultaneous fit to the Caprini-Lellouch-Neubert form factor parameters: $\rho^2 = 1.191 \pm 0.048 \pm 0.028$, $R_1(1) = 1.429 \pm 0.061 \pm 0.044$, and $R_2(1) = 0.827 \pm 0.038 \pm 0.022$.
[4] Measured using fully reconstructed D^* sample.
[5] Uses the combined fit of both $B^0 \to D^*(2010)^-\ell\nu$ and $B^+ \to \overline{D}(2007)^0\ell\nu$ samples.
[6] ABREU 01H measured using about 5000 partial reconstructed D^* sample.
[7] ABBIENDI 00Q assumes the fraction $B(b \to B^0) = (39.7^{+1.8}_{-2.2})$%. This result is an average of two methods using exclusive and partial D^* reconstruction.
[8] BUSKULIC 97 assumes fraction (B^+) = fraction (B^0) = (37.8 ± 2.2)% and PDG 96 values for B lifetime and D^* and D branching fractions.
[9] Combines with previous partial reconstructed D^* measurement.
[10] Assumes equal production of B^+ and B^0 at the $\Upsilon(4S)$.
[11] The results are based on the same analysis and data sample reported in ADAM 03.
[12] ACKERSTAFF 97G assumes fraction (B^+) = fraction (B^0) = (37.8±2.2)% and PDG 96 values for B lifetime and branching ratio of D^* and D decays.
[13] ABREU 96P result is the average of two methods using exclusive and partial D^* reconstruction.
[14] BARISH 95 use $B(D^0 \to K^-\pi^+)$ = (3.91 ± 0.08 ± 0.17)% and $B(D^{*+} \to D^0\pi^+)$ = (68.1 ± 1.0 ± 1.3)%.
[15] BUSKULIC 95N assumes fraction (B^+) = fraction (B^0) = 38.2 ± 1.3 ± 2.2% and τ_{B^0} = 1.58 ± 0.06 ps. $\Gamma(D^{*-}\ell^+\nu_\ell)$/total = [5.18 − 0.13(fraction(B^0)−38.2)−1.5(τ_{B^0} − 1.58)]%.
[16] ALBRECHT 94 assumes $B(D^{*+} \to D^0\pi^+)$ = 68.1 ± 1.0 ± 1.3%. Uses partial reconstruction of D^{*+} and is independent of D^0 branching ratios.
[17] ALBRECHT 93 reports 0.052 ± 0.005 ± 0.006. We rescale using the method described in STONE 94 but with the updated PDG 94 $B(D^0 \to K^-\pi^+)$. We have taken their average e and μ value. They also obtain $\alpha = 2*\Gamma^0/(\Gamma^- + \Gamma^+) - 1 = 1.1 \pm 0.4 \pm 0.2$, $A_{AF} = 3/4*(\Gamma^- - \Gamma^+)/\Gamma = 0.2 \pm 0.08 \pm 0.06$ and a value of $|V_{cb}|$ = 0.036–0.045 depending on model assumptions.
[18] Combining $\overline{D}^{*0}\ell^+\nu_\ell$ and $\overline{D}^{*-}\ell^+\nu_\ell$ SANGHERA 93 test $V-A$ structure and fit the decay angular distributions to obtain $A_{FB} = 3/4*(\Gamma^- - \Gamma^+)/\Gamma = 0.14 \pm 0.06 \pm 0.03$. Assuming a value of V_{cb}, they measure V, A_1, and A_2, the three form factors for the $D^*\ell\nu_\ell$ decay, where results are slightly dependent on model assumptions.
[19] ANTREASYAN 90B is average over B and $\overline{D}^*(2010)$ charge states.
[20] The measurement of ALBRECHT 89C suggests a D^* polarization γ_L/γ_T of 0.85 ± 0.45. or α = 0.7 ± 0.9.
[21] ALBRECHT 89J is ALBRECHT 87J value rescaled using $B(D^*(2010)^- \to D^0\pi^-)$ = 0.57 ± 0.04 ± 0.04. Superseded by ALBRECHT 93.
[22] We have taken average of the the BORTOLETTO 89B values for electrons and muons, 0.046 ± 0.005 ± 0.007. We rescale using the method described in STONE 94 but with the updated PDG 94 $B(D^0 \to K^-\pi^+)$. The measurement suggests a D^* polarization parameter value α = 0.65 ± 0.66 ± 0.25.
[23] ALBRECHT 87J assume μ-e universality, the $B(\Upsilon(4S) \to B^0\overline{B}^0)$ = 0.45, the $B(D^0 \to K^-\pi^+)$ = (0.042 ± 0.004 ± 0.004), and the $B(D^*(2010)^- \to D^0\pi^-)$ = 0.49 ± 0.08. Superseded by ALBRECHT 89J.

$\Gamma(D^*(2010)^-\ell^+\nu_\ell)/\Gamma(D\ell^+\nu_\ell X)$ — Γ_7/Γ_4

VALUE	DOCUMENT ID		TECN	COMMENT
0.537±0.031±0.036	[1] AUBERT	07AN	BABR	$e^+e^- \to \Upsilon(4S)$

[1] Uses a fully reconstructed B meson on the recoil side.

$\Gamma(D^*(2010)^-\tau^+\nu_\tau)/\Gamma_{total}$ — Γ_8/Γ

VALUE (units 10^{-2})	DOCUMENT ID		TECN	COMMENT
1.58±0.09 OUR FIT	Error includes scale factor of 1.1.			
1.48±0.18 OUR AVERAGE	Error includes scale factor of 1.1.			
1.42±0.094±0.140	[1] AAIJ	18D	LHCB	pp at 7, 8 TeV
$2.02^{+0.40}_{-0.37}\pm0.37$	[2] MATYJA	07	BELL	$e^+e^- \to \Upsilon(4S)$

Downloaded from https://academic.oup.com/ptep/article/2022/8/083C01/6651666 by KIT Library user on 27 September 2022

• • • We do not use the following data for averages, fits, limits, etc. • • •

1.11±0.51 ±0.06	[3] AUBERT	08N	BABR	Repl. by AUBERT 09S

[1] Noramlizes to $B(B^0 \to D^*(2010)^- \pi^+ \pi^- \pi^+) = (7.214 \pm 0.28) \times 10^{-3}$.
[2] Observed in the recoil of the accompanying B meson.
[3] Uses a fully reconstructed B meson as a tag on the recoil side.

$\Gamma(D^*(2010)^- \tau^+ \nu_\tau)/\Gamma(D^*(2010)^- \ell^+ \nu_\ell)$ — Γ_8/Γ_7

VALUE	DOCUMENT ID		TECN	COMMENT
0.308±0.016 OUR FIT				
0.315±0.018 OUR AVERAGE				
0.291±0.019±0.029	[1] AAIJ	18D	LHCB	pp at 7, 8 TeV
0.302±0.030±0.011	[2] SATO	16B	BELL	$e^+e^- \to \Upsilon(4S)$
0.336±0.027±0.030	[3] AAIJ	15Q	LHCB	pp at 7, 8 TeV
0.355±0.039±0.021	[4,5] LEES	12D	BABR	$e^+e^- \to \Upsilon(4S)$
• • • We do not use the following data for averages, fits, limits, etc. • • •				
0.207±0.095±0.008	[4] AUBERT	09S	BABR	Repl. by LEES 12D

[1] Uses $\tau^+ \to \pi^+\pi^-\pi^+\overline{\nu}_\tau$ and $\tau^+ \to \pi^+\pi^-\pi^+\pi^0\overline{\nu}_\tau$, and μ^+ as ℓ^+.
[2] Uses semileptonic B decay events for tagging and $\tau^+ \to \ell^+\nu_\ell\overline{\nu}_\tau$ mode.
[3] Uses $\tau^+ \to \mu^+\nu_\mu\overline{\nu}_\tau$ and μ^+ as ℓ^+.
[4] Uses a fully reconstructed B meson as a tag on the recoil side.
[5] Uses $\tau^+ \to e^+\nu_e\overline{\nu}_\tau$ and $\tau^+ \to \mu^+\nu_\mu\overline{\nu}_\tau$ and e^+ or μ^+ as ℓ^+.

$\Gamma(D^*(2010)^- \tau^+ \nu_\tau)/\Gamma(D^*(2010)^- \pi^+\pi^+\pi^-)$ — Γ_8/Γ_{58}

VALUE	DOCUMENT ID		TECN	COMMENT
1.97±0.13±0.18	[1] AAIJ	18D	LHCB	pp at 7, 8 TeV

[1] Uses $\tau^+ \to \pi^+\pi^-\pi^+\overline{\nu}_\tau$ and $\tau^+ \to \pi^+\pi^-\pi^+\pi^0\overline{\nu}_\tau$ modes.

$\Gamma(\overline{D}^0 \pi^- \ell^+ \nu_\ell)/\Gamma_{total}$ — Γ_9/Γ

VALUE (units 10^{-3})	DOCUMENT ID		TECN	COMMENT
4.1 ±0.5 OUR AVERAGE				
4.05±0.36±0.41	VOSSEN	18	BELL	$e^+e^- \to \Upsilon(4S)$
4.3 ±0.8 ±0.3	[1] AUBERT	08Q	BABR	$e^+e^- \to \Upsilon(4S)$
• • • We do not use the following data for averages, fits, limits, etc. • • •				
4.4 ±0.9 ±0.2	[1,2] LIVENTSEV	08	BELL	Repl. by VOSSEN 18
3.4 ±1.0 ±0.1	[3] LIVENTSEV	05	BELL	Repl. by LIVENTSEV 08

[1] Uses a fully reconstructed B meson as a tag on the recoil side.
[2] LIVENTSEV 08 reports $(4.2 \pm 0.7 \pm 0.6) \times 10^{-3}$ from a measurement of $[\Gamma(B^0 \to \overline{D}^0\pi^-\ell^+\nu_\ell)/\Gamma_{total}] / [B(B^0 \to D^-\ell^+\nu_\ell)]$ assuming $B(B^0 \to D^-\ell^+\nu_\ell) = (2.12 \pm 0.20) \times 10^{-2}$, which we rescale to our best value $B(B^0 \to D^-\ell^+\nu_\ell) = (2.24 \pm 0.09) \times 10^{-2}$. Our first error is their experiment's error and our second error is the systematic error from using our best value.
[3] LIVENTSEV 05 reports $[\Gamma(B^0 \to \overline{D}^0\pi^-\ell^+\nu_\ell)/\Gamma_{total}] / [B(B^+ \to \overline{D}^0\ell^+\nu_\ell)] = 0.15 \pm 0.03 \pm 0.03$ which we multiply by our best value $B(B^+ \to \overline{D}^0\ell^+\nu_\ell) = (2.30 \pm 0.09) \times 10^{-2}$. Our first error is their experiment's error and our second error is the systematic error from using our best value.

$\Gamma(D_0^*(2300)^- \ell^+ \nu_\ell,\ D_0^{*-} \to \overline{D}^0\pi^-)/\Gamma_{total}$ — Γ_{10}/Γ

VALUE (units 10^{-3})	DOCUMENT ID		TECN	COMMENT
3.0±1.2 OUR AVERAGE Error includes scale factor of 1.8.				
4.4±0.8±0.6	[1] AUBERT	08BL	BABR	$e^+e^- \to \Upsilon(4S)$
2.0±0.7±0.5	[1] LIVENTSEV	08	BELL	$e^+e^- \to \Upsilon(4S)$

[1] Uses a fully reconstructed B meson as a tag on the recoil side.

$\Gamma(D_2^*(2460)^- \ell^+ \nu_\ell,\ D_2^{*-} \to \overline{D}^0\pi^-)/\Gamma_{total}$ — Γ_{11}/Γ

VALUE (units 10^{-3})	DOCUMENT ID		TECN	COMMENT
1.21±0.33 OUR AVERAGE Error includes scale factor of 1.8.				
1.10±0.17±0.08	[1] AUBERT	09Y	BABR	$e^+e^- \to \Upsilon(4S)$
2.2 ±0.4 ±0.4	[2] LIVENTSEV	08	BELL	$e^+e^- \to \Upsilon(4S)$

[1] Uses a simultaneous fit of all B semileptonic decays without full reconstruction of events. AUBERT 09Y reports $B(B^0 \to \overline{D}_2^*(2460)^-\ell^+\nu_\ell) \cdot B(\overline{D}_2^*(2460)^- \to \overline{D}^{(*)0}\pi^-) = (1.77 \pm 0.26 \pm 0.11) \times 10^{-3}$ and the authors have provided us the individual measurement.
[2] Uses a fully reconstructed B meson as a tag on the recoil side.

$\Gamma(\overline{D}^{(*)} n\pi \ell^+ \nu_\ell (n \geq 1))/\Gamma(D\ell^+\nu_\ell X)$ — Γ_{12}/Γ_4

VALUE	DOCUMENT ID		TECN	COMMENT
0.248±0.032±0.030	[1] AUBERT	07AN	BABR	$e^+e^- \to \Upsilon(4S)$

[1] Uses a fully reconstructed B meson on the recoil side.

$\Gamma(\overline{D}^{*0}\pi^-\ell^+\nu_\ell)/\Gamma_{total}$ — Γ_{13}/Γ

VALUE (units 10^{-3})	DOCUMENT ID		TECN	COMMENT
5.8 ±0.8 OUR AVERAGE Error includes scale factor of 1.4.				
6.46±0.53±0.52	VOSSEN	18	BELL	$e^+e^- \to \Upsilon(4S)$
4.8 ±0.8 ±0.4	[1] AUBERT	08Q	BABR	$e^+e^- \to \Upsilon(4S)$
• • • We do not use the following data for averages, fits, limits, etc. • • •				
5.9 ±2.3 ±0.2	[1,2] LIVENTSEV	08	BELL	Repl. by VOSSEN 18
5.6 ±1.2 ±0.2	[3,4] LIVENTSEV	05	BELL	Repl. by LIVENTSEV 08

[1] Uses a fully reconstructed B meson as a tag on the recoil side.
[2] LIVENTSEV 08 reports $(5.6 \pm 2.1 \pm 0.8) \times 10^{-3}$ from a measurement of $[\Gamma(B^0 \to \overline{D}^{*0}\pi^-\ell^+\nu_\ell)/\Gamma_{total}] / [B(B^0 \to D^-\ell^+\nu_\ell)]$ assuming $B(B^0 \to D^-\ell^+\nu_\ell) = (2.12 \pm 0.20) \times 10^{-2}$, which we rescale to our best value $B(B^0 \to D^-\ell^+\nu_\ell) = (2.24 \pm 0.09) \times 10^{-2}$. Our first error is their experiment's error and our second error is the systematic error from using our best value.
[3] Excludes D^{*+} contribution to $D\pi$ modes.
[4] LIVENTSEV 05 reports $[\Gamma(B^0 \to \overline{D}^{*0}\pi^-\ell^+\nu_\ell)/\Gamma_{total}] / [B(B^+ \to \overline{D}^*(2007)^0\ell^+\nu_\ell)] = 0.10 \pm 0.02 \pm 0.01$ which we multiply by our best value $B(B^+ \to \overline{D}^*(2007)^0\ell^+\nu_\ell) = (5.58 \pm 0.22) \times 10^{-2}$. Our first error is their experiment's error and our second error is the systematic error from using our best value.

$\Gamma(D_1(2420)^- \ell^+ \nu_\ell,\ D_1^- \to \overline{D}^{*0}\pi^-)/\Gamma_{total}$ — Γ_{14}/Γ

VALUE (units 10^{-3})	DOCUMENT ID		TECN	COMMENT
2.80±0.28 OUR AVERAGE				
2.78±0.24±0.25	[1] AUBERT	09Y	BABR	$e^+e^- \to \Upsilon(4S)$
2.7 ±0.4 ±0.3	[2] AUBERT	08BL	BABR	$e^+e^- \to \Upsilon(4S)$
5.4 ±1.9 ±0.9	[2] LIVENTSEV	08	BELL	$e^+e^- \to \Upsilon(4S)$

[1] Uses a simultaneous measurement of all B semileptonic decays without full reconstruction of events.
[2] Uses a fully reconstructed B meson as a tag on the recoil side.

$\Gamma(D_1'(2430)^- \ell^+ \nu_\ell,\ D_1'^- \to \overline{D}^{*0}\pi^-)/\Gamma_{total}$ — Γ_{15}/Γ

VALUE (units 10^{-3})	CL%	DOCUMENT ID		TECN	COMMENT
3.1±0.7±0.5		[1] AUBERT	08BL	BABR	$e^+e^- \to \Upsilon(4S)$
• • • We do not use the following data for averages, fits, limits, etc. • • •					
<5.0	90	[1] LIVENTSEV	08	BELL	$e^+e^- \to \Upsilon(4S)$

[1] Uses a fully reconstructed B meson as a tag on the recoil side.

$\Gamma(D_2^*(2460)^- \ell^+ \nu_\ell,\ D_2^{*-} \to \overline{D}^{*0}\pi^-)/\Gamma_{total}$ — Γ_{16}/Γ

VALUE (units 10^{-3})	CL%	DOCUMENT ID		TECN	COMMENT
0.68±0.12 OUR AVERAGE					
0.67±0.12±0.05		[1] AUBERT	09Y	BABR	$e^+e^- \to \Upsilon(4S)$
0.7 ±0.2 ±0.2		[2] AUBERT	08BL	BABR	$e^+e^- \to \Upsilon(4S)$
• • • We do not use the following data for averages, fits, limits, etc. • • •					
<3.0	90	[2] LIVENTSEV	08	BELL	$e^+e^- \to \Upsilon(4S)$

[1] Uses a simultaneous fit of all B semileptonic decays without full reconstruction of events. AUBERT 09Y reports $B(B^0 \to \overline{D}_2^*(2460)^-\ell^+\nu_\ell) \cdot B(\overline{D}_2^*(2460)^- \to \overline{D}^{(*)0}\pi^-) = (1.77 \pm 0.26 \pm 0.11) \times 10^{-3}$ and the authors have provided us the individual measurement.
[2] Uses a fully reconstructed B meson as a tag on the recoil side.

$\Gamma(D^-\pi^+\pi^-\ell^+\nu_\ell)/\Gamma(D^-\ell^+\nu_\ell)$ — Γ_{17}/Γ_5

VALUE (units 10^{-2})	DOCUMENT ID		TECN	COMMENT
5.8±1.8±1.2	[1] LEES	16	BABR	$e^+e^- \to \Upsilon(4S)$

[1] Measurement used electrons and muons as leptons.

$\Gamma(D^{*-}\pi^+\pi^-\ell^+\nu_\ell)/\Gamma(D^*(2010)^-\ell^+\nu_\ell)$ — Γ_{18}/Γ_7

VALUE (units 10^{-2})	DOCUMENT ID		TECN	COMMENT
2.8±0.8±0.6	[1] LEES	16	BABR	$e^+e^- \to \Upsilon(4S)$

[1] Measurement used electrons and muons as leptons.

$\Gamma(\rho^-\ell^+\nu_\ell)/\Gamma_{total}$ — Γ_{19}/Γ

$\ell = e$ or μ, not sum over e and μ modes.

"OUR EVALUATION" has been obtained by the Heavy Flavor Averaging Group (HFLAV) by including both B^0 and B^+ decays. The average assumes equality of the semileptonic decay width for these isospin conjugate states.

VALUE (units 10^{-4})	CL%	DOCUMENT ID		TECN	COMMENT
2.94±0.11±0.18 OUR EVALUATION					
2.45±0.32 OUR AVERAGE Error includes scale factor of 1.6. See the ideogram below.					
3.22±0.27±0.24		[1] SIBIDANOV	13	BELL	$e^+e^- \to \Upsilon(4S)$
1.75±0.15±0.27		[2] DEL-AMO-SA...11C		BABR	$e^+e^- \to \Upsilon(4S)$
2.93±0.37±0.37		[3] ADAM	07	CLE2	$e^+e^- \to \Upsilon(4S)$
2.17±0.54±0.32		[4] HOKUUE	07	BELL	$e^+e^- \to \Upsilon(4S)$
$2.57 \pm 0.29^{+0.53}_{-0.62}$		[5] BEHRENS	00	CLE2	$e^+e^- \to \Upsilon(4S)$
• • • We do not use the following data for averages, fits, limits, etc. • • •					
2.14±0.21±0.56		[2] AUBERT,B	05O	BABR	Repl. by DEL-AMO-SANCHEZ 11C
$2.17 \pm 0.34^{+0.62}_{-0.68}$		[6] ATHAR	03	CLE2	Repl. by ADAM 07
3.29±0.42±0.72		[7] AUBERT	03E	BABR	Repl. by AUBERT,B 05O
$2.69 \pm 0.41^{+0.61}_{-0.64}$		[8] BEHRENS	00	CLE2	$e^+e^- \to \Upsilon(4S)$
$2.5 \pm 0.4^{+0.7}_{-0.9}$		[9] ALEXANDER	96T	CLE2	Repl. by BEHRENS 00
<4.1	90	[10] BEAN	93B	CLE2	$e^+e^- \to \Upsilon(4S)$

[1] The signal events are tagged by a second B meson reconstructed in the fully hadronic decays.
[2] B^+ and B^0 decays combined assuming isospin symmetry. Systematic errors include both experimental and form-factor uncertainties.
[3] The B^0 and B^+ results are combined assuming the isospin, B lifetimes, and relative charged/neutral B production at the $\Upsilon(4S)$.
[4] The signal events are tagged by a second B meson reconstructed in the semileptonic mode $B \to D^{(*)}\ell\nu_\ell$.
[5] Averaging with ALEXANDER 96T results including experimental and theoretical correlations considered, BEHRENS 00 reports systematic errors $^{+0.33}_{-0.46} \pm 0.41$, where the second error is theoretical model dependence. We combine these in quadrature.

Downloaded from https://academic.oup.com/ptep/article/2022/8/083C01/6651666 by KIT Library user on 27 September 2022

[6] ATHAR 03 reports systematic errors $^{+0.47}_{-0.50} \pm 0.41 \pm 0.01$, which are experimental systematic, systematic due to residual form-factor uncertainties in the signal, and systematic due to residual form-factor uncertainties in the cross-feed modes, respectively. We combine these in quadrature.

[7] Uses isospin constraints and extrapolation to all electron energies according to five different form-factor calculations. The second error combines the systematic and theoretical uncertainties in quadrature.

[8] BEHRENS 00 reports $^{+0.35}_{-0.40} \pm 0.50$, where the second error is the theoretical model dependence. We combine these in quadrature. B^+ and B^0 decays combined using isospin symmetry: $\Gamma(B^0 \to \rho^- \ell^+ \nu) = 2\Gamma(B^+ \to \rho^0 \ell^+ \nu) \approx 2\Gamma(B^+ \to \omega \ell^+ \nu)$. No evidence for $\omega \ell \nu$ is reported.

[9] ALEXANDER 96T reports $^{+0.5}_{-0.7} \pm 0.5$ where the second error is the theoretical model dependence. We combine these in quadrature. B^+ and B^0 decays combined using isospin symmetry: $\Gamma(B^0 \to \rho^- \ell^+ \nu) = 2\Gamma(B^+ \to \rho^0 \ell^+ \nu) \approx 2\Gamma(B^+ \to \omega \ell^+ \nu)$. No evidence for $\omega \ell \nu$ is reported.

[10] BEAN 93B limit set using ISGW Model. Using isospin and the quark model to combine $\Gamma(\rho^0 \ell^+ \nu_\ell)$ and $\Gamma(\omega \ell^+ \nu_\ell)$ with this result, they obtain a limit $<(1.6\text{–}2.7) \times 10^{-4}$ at 90% CL for $B^+ \to$ (ω or ρ^0) $\ell^+ \nu_\ell$. The range corresponds to the ISGW, WSB, and KS models. An upper limit on $|V_{ub}/V_{cb}| < 0.08\text{–}0.13$ at 90% CL is derived as well.

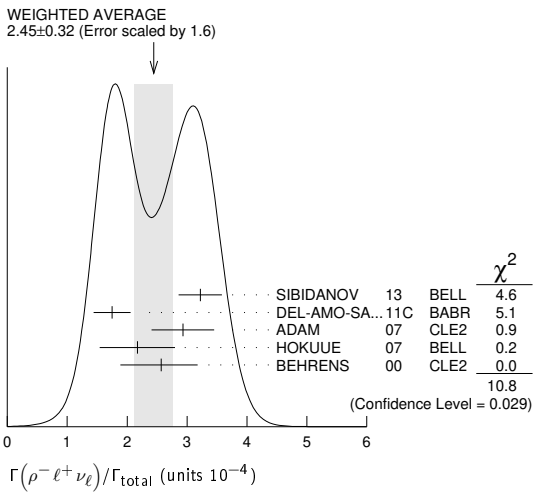

$\Gamma(\pi^- \ell^+ \nu_\ell)/\Gamma_{total}$ — Γ_{20}/Γ

"OUR EVALUATION" is provided by the Heavy Flavor Averaging Group (HFLAV) and the procedure is described at https://hflav.web.cern.ch/.

VALUE (units 10^{-4})	DOCUMENT ID		TECN	COMMENT
1.50±0.06 OUR EVALUATION				
1.46±0.04 OUR AVERAGE				
1.49±0.09±0.07	[1] SIBIDANOV	13	BELL	$e^+e^- \to \Upsilon(4S)$
1.47±0.05±0.06	[2,3] LEES	12AA	BABR	$e^+e^- \to \Upsilon(4S)$
1.41±0.05±0.07	[4] DEL-AMO-SA...	11C	BABR	$e^+e^- \to \Upsilon(4S)$
1.49±0.04±0.07	[2] HA	11	BELL	$e^+e^- \to \Upsilon(4S)$
1.54±0.17±0.09	[4] AUBERT	08AV	BABR	$e^+e^- \to \Upsilon(4S)$
1.37±0.15±0.11	[5,6] ADAM	07	CLE2	$e^+e^- \to \Upsilon(4S)$
1.38±0.19±0.14	[7] HOKUUE	07	BELL	$e^+e^- \to \Upsilon(4S)$
• • • We do not use the following data for averages, fits, limits, etc. • • •				
1.42±0.05±0.08	[2] DEL-AMO-SA...	11F	BABR	Repl. by LEES 12AA
1.46±0.07±0.08	[8] AUBERT	07J	BABR	Repl. by DEL-AMO-SANCHEZ 11F
1.33±0.17±0.11	[9] AUBERT,B	06K	BABR	Repl. by AUBERT 08AV
1.38±0.10±0.18	[10] AUBERT,B	05O	BABR	Repl. by DEL-AMO-SANCHEZ 11C
1.33±0.18±0.13	[11] ATHAR	03	CLE2	Repl. by ADAM 07
1.8 ±0.4 ±0.4	[12] ALEXANDER	96T	CLE2	Repl. by ATHAR 03

[1] The signal events are tagged by a second B meson reconstructed in the fully hadronic decays.

[2] Uses loose neutrino reconstruction technique. Assumes $B(\Upsilon(4S) \to B^+B^-) = (51.6 \pm 0.6)\%$ and $B(\Upsilon(4S) \to B^0\overline{B}^0) = (48.4 \pm 0.6)\%$.

[3] Reports also a branching fraction value $B(B^0 \to \pi^- \ell^+ \nu) = (1.45 \pm 0.04 \pm 0.06) \times 10^{-4}$ from the decays of B^+ and B^0 that are combined using the isospin symmetry relation.

[4] Using the isospin symmetry relation, B^+ and B^0 branching fractions are combined.

[5] The B^0 and B^+ results are combined assuming the isospin, B lifetimes, and relative charged/neutral B production at the $\Upsilon(4S)$.

[6] Also report the rate for $q^2 > 16$ GeV^2 of $(0.41 \pm 0.08 \pm 0.04) \times 10^{-4}$ from which they obtain $|V_{ub}| = 3.6 \pm 0.4 \pm 0.2^{+0.6}_{-0.4}$ (last error is from theory).

[7] The signal events are tagged by a second B meson reconstructed in the semileptonic mode $B \to D^{(*)} \ell \nu_\ell$.

[8] The analysis uses events in which the signal B decays are reconstructed with an innovative loose neutrino reconstruction technique.

[9] The signals are tagged by a second B meson reconstructed in a semileptonic or hadronic decay. The B^0 and B^+ results are combined assuming the isospin symmetry.

[10] B^+ and B^0 decays combined assuming isospin symmetry. Systematic errors include both experimental and form-factor uncertainties.

[11] ATHAR 03 reports systematic errors $0.11 \pm 0.01 \pm 0.07$, which are experimental systematic, systematic due to residual form-factor uncertainties in the signal, and systematic due to residual form-factor uncertainties in the cross-feed modes, respectively. We combine these in quadrature.

[12] ALEXANDER 96T gives systematic errors $\pm 0.3 \pm 0.2$ where the second error reflects the estimated model dependence. We combine these in quadrature. Assumes isospin symmetry: $\Gamma(B^0 \to \pi^- \ell^+ \nu) = 2 \times \Gamma(B^+ \to \pi^0 \ell^+ \nu)$.

$\Gamma(\pi^- \mu^+ \nu_\mu)/\Gamma_{total}$ — Γ_{21}/Γ

VALUE	DOCUMENT ID		TECN
• • • We do not use the following data for averages, fits, limits, etc. • • •			
seen	[1] ALBRECHT	91C	ARG

[1] In ALBRECHT 91C, one event is fully reconstructed providing evidence for the $b \to u$ transition.

$\Gamma(\pi^- \tau^+ \nu_\tau)/\Gamma_{total}$ — Γ_{22}/Γ

VALUE	CL%	DOCUMENT ID		TECN	COMMENT
<2.5 × 10⁻⁴	90	[1] HAMER	16	BELL	$e^+e^- \to \Upsilon(4S)$

[1] Assumes equal production of B^+ and B^0 at the $\Upsilon(4S)$.

$\Gamma(K^\pm X)/\Gamma_{total}$ — Γ_{23}/Γ

VALUE	DOCUMENT ID		TECN	COMMENT
0.78±0.08	[1] ALBRECHT	96D	ARG	$e^+e^- \to \Upsilon(4S)$

[1] Average multiplicity.

$\Gamma(D^0 X)/\Gamma_{total}$ — Γ_{24}/Γ

VALUE	DOCUMENT ID		TECN	COMMENT
0.081±0.014±0.005	[1] AUBERT	07N	BABR	$e^+e^- \to \Upsilon(4S)$
• • • We do not use the following data for averages, fits, limits, etc. • • •				
0.063±0.019±0.005	[1] AUBERT,BE	04B	BABR	Repl. by AUBERT 07N

[1] Events are selected by completely reconstructing one B and searching for a reconstructed charmed particle in the rest of the event. The last error includes systematic and charm branching ratio uncertainties.

$\Gamma(\overline{D}^0 X)/\Gamma_{total}$ — Γ_{25}/Γ

VALUE	DOCUMENT ID		TECN	COMMENT
0.474±0.020$^{+0.020}_{-0.019}$	[1] AUBERT	07N	BABR	$e^+e^- \to \Upsilon(4S)$
• • • We do not use the following data for averages, fits, limits, etc. • • •				
0.511±0.031±0.028	[1] AUBERT,BE	04B	BABR	Repl. by AUBERT 07N

[1] Events are selected by completely reconstructing one B and searching for a reconstructed charmed particle in the rest of the event. The last error includes systematic and charm branching ratio uncertainties.

$\Gamma(D^0 X)/[\Gamma(D^0 X) + \Gamma(\overline{D}^0 X)]$ — $\Gamma_{24}/(\Gamma_{24}+\Gamma_{25})$

VALUE	DOCUMENT ID		TECN	COMMENT
0.146±0.022±0.006	AUBERT	07N	BABR	$e^+e^- \to \Upsilon(4S)$
• • • We do not use the following data for averages, fits, limits, etc. • • •				
0.110±0.031±0.008	AUBERT,BE	04B	BABR	Repl. by AUBERT 07N

$\Gamma(D^+ X)/\Gamma_{total}$ — Γ_{26}/Γ

VALUE	CL%	DOCUMENT ID		TECN	COMMENT
<0.039	90	[1] AUBERT	07N	BABR	$e^+e^- \to \Upsilon(4S)$
• • • We do not use the following data for averages, fits, limits, etc. • • •					
<0.051	90	[1] AUBERT,BE	04B	BABR	Repl. by AUBERT 07N

[1] Events are selected by completely reconstructing one B and searching for a reconstructed charmed particle in the rest of the event. The last error includes systematic and charm branching ratio uncertainties.

$\Gamma(D^- X)/\Gamma_{total}$ — Γ_{27}/Γ

VALUE	DOCUMENT ID		TECN	COMMENT
0.369±0.016$^{+0.030}_{-0.027}$	[1] AUBERT	07N	BABR	$e^+e^- \to \Upsilon(4S)$
• • • We do not use the following data for averages, fits, limits, etc. • • •				
0.397±0.030$^{+0.040}_{-0.038}$	[1] AUBERT,BE	04B	BABR	Repl. by AUBERT 07N

[1] Events are selected by completely reconstructing one B and searching for a reconstructed charmed particle in the rest of the event. The last error includes systematic and charm branching ratio uncertainties.

$\Gamma(D^+ X)/[\Gamma(D^+ X) + \Gamma(D^- X)]$ — $\Gamma_{26}/(\Gamma_{26}+\Gamma_{27})$

VALUE	DOCUMENT ID		TECN	COMMENT
0.058±0.028±0.006	AUBERT	07N	BABR	$e^+e^- \to \Upsilon(4S)$
• • • We do not use the following data for averages, fits, limits, etc. • • •				
0.055±0.040±0.006	AUBERT,BE	04B	BABR	Repl. by AUBERT 07N

$\Gamma(D_s^+ X)/\Gamma_{total}$ — Γ_{28}/Γ

VALUE	DOCUMENT ID		TECN	COMMENT
0.103±0.012$^{+0.017}_{-0.014}$	[1] AUBERT	07N	BABR	$e^+e^- \to \Upsilon(4S)$
• • • We do not use the following data for averages, fits, limits, etc. • • •				
0.109±0.021$^{+0.039}_{-0.024}$	[1] AUBERT,BE	04B	BABR	Repl. by AUBERT 07N

[1] Events are selected by completely reconstructing one B and searching for a reconstructed charmed particle in the rest of the event. The last error includes systematic and charm branching ratio uncertainties.

Downloaded from https://academic.oup.com/ptep/article/2022/8/083C01/6651666 by KIT Library user on 27 September 2022

$\Gamma(D_s^- X)/\Gamma_{total}$ — Γ_{29}/Γ

VALUE	CL%	DOCUMENT ID		TECN	COMMENT
<0.026	90	[1] AUBERT	07N	BABR	$e^+e^- \to \Upsilon(4S)$
• • • We do not use the following data for averages, fits, limits, etc. • • •					
<0.087	90	[1] AUBERT,BE	04B	BABR	Repl. by AUBERT 07N

[1] Events are selected by completely reconstructing one B and searching for a reconstructed charmed particle in the rest of the event. The last error includes systematic and charm branching ratio uncertainties.

$\Gamma(D_s^+ X)/[\Gamma(D_s^+ X)+\Gamma(D_s^- X)]$ — $\Gamma_{28}/(\Gamma_{28}+\Gamma_{29})$

VALUE	DOCUMENT ID		TECN	COMMENT
0.879±0.066±0.005	AUBERT	07N	BABR	$e^+e^- \to \Upsilon(4S)$
• • • We do not use the following data for averages, fits, limits, etc. • • •				
0.733±0.092±0.010	AUBERT,BE	04B	BABR	Repl. by AUBERT 07N

$\Gamma(\Lambda_c^+ X)/\Gamma_{total}$ — Γ_{30}/Γ

VALUE	CL%	DOCUMENT ID		TECN	COMMENT
<0.031	90	[1] AUBERT	07N	BABR	$e^+e^- \to \Upsilon(4S)$
• • • We do not use the following data for averages, fits, limits, etc. • • •					
<0.038	90	[1] AUBERT,BE	04B	BABR	Repl. by AUBERT 07N

[1] Events are selected by completely reconstructing one B and searching for a reconstructed charmed particle in the rest of the event. The last error includes systematic and charm branching ratio uncertainties.

$\Gamma(\overline{\Lambda}_c^- X)/\Gamma_{total}$ — Γ_{31}/Γ

VALUE	DOCUMENT ID		TECN	COMMENT
0.05 $\pm0.010^{+0.019}_{-0.011}$	[1] AUBERT	07N	BABR	$e^+e^- \to \Upsilon(4S)$
• • • We do not use the following data for averages, fits, limits, etc. • • •				
$0.049\pm0.017^{+0.018}_{-0.011}$	[1] AUBERT,BE	04B	BABR	Repl. by AUBERT 07N

[1] Events are selected by completely reconstructing one B and searching for a reconstructed charmed particle in the rest of the event. The last error includes systematic and charm branching ratio uncertainties.

$\Gamma(\Lambda_c^+ X)/[\Gamma(\Lambda_c^+ X)+\Gamma(\overline{\Lambda}_c^- X)]$ — $\Gamma_{30}/(\Gamma_{30}+\Gamma_{31})$

VALUE	DOCUMENT ID		TECN	COMMENT
$0.243^{+0.119}_{-0.121}\pm0.003$	AUBERT	07N	BABR	$e^+e^- \to \Upsilon(4S)$
• • • We do not use the following data for averages, fits, limits, etc. • • •				
0.286±0.142±0.007	AUBERT,BE	04B	BABR	Repl. by AUBERT 07N

$\Gamma(\overline{c}X)/\Gamma_{total}$ — Γ_{32}/Γ

VALUE	DOCUMENT ID		TECN	COMMENT
$0.947\pm0.030^{+0.045}_{-0.040}$	[1] AUBERT	07N	BABR	$e^+e^- \to \Upsilon(4S)$
• • • We do not use the following data for averages, fits, limits, etc. • • •				
$1.039\pm0.051^{+0.063}_{-0.058}$	[1] AUBERT,BE	04B	BABR	Repl. by AUBERT 07N

[1] Events are selected by completely reconstructing one B and searching for a reconstructed charmed particle in the rest of the event. The last error includes systematic and charm branching ratio uncertainties.

$\Gamma(cX)/\Gamma_{total}$ — Γ_{33}/Γ

VALUE	DOCUMENT ID		TECN	COMMENT
$0.246\pm0.024^{+0.021}_{-0.017}$	[1] AUBERT	07N	BABR	$e^+e^- \to \Upsilon(4S)$
• • • We do not use the following data for averages, fits, limits, etc. • • •				
$0.237\pm0.036^{+0.041}_{-0.027}$	[1] AUBERT,BE	04B	BABR	Repl. by AUBERT 07N

[1] Events are selected by completely reconstructing one B and searching for a reconstructed charmed particle in the rest of the event. The last error includes systematic and charm branching ratio uncertainties.

$\Gamma(\overline{c}/cX)/\Gamma_{total}$ — Γ_{34}/Γ

VALUE	DOCUMENT ID		TECN	COMMENT
$1.193\pm0.030^{+0.053}_{-0.049}$	[1] AUBERT	07N	BABR	$e^+e^- \to \Upsilon(4S)$
• • • We do not use the following data for averages, fits, limits, etc. • • •				
$1.276\pm0.062^{+0.088}_{-0.074}$	[1] AUBERT,BE	04B	BABR	Repl. by AUBERT 07N

[1] Events are selected by completely reconstructing one B and searching for a reconstructed charmed particle in the rest of the event. The last error includes systematic and charm branching ratio uncertainties.

$\Gamma(D^-\pi^+)/\Gamma_{total}$ — Γ_{35}/Γ

VALUE (units 10^{-3})	EVTS	DOCUMENT ID		TECN	COMMENT
2.51±0.08 OUR FIT					
2.56±0.08 OUR AVERAGE					
2.48±0.01±0.10		WAHEED	22	BELL	$e^+e^- \to \Upsilon(4S)$
2.55±0.05±0.16		[1] AUBERT	07H	BABR	$e^+e^- \to \Upsilon(4S)$
3.03±0.23±0.23		[2] AUBERT,BE	06J	BABR	$e^+e^- \to \Upsilon(4S)$
2.68±0.12±0.24		[1,3] AHMED	02B	CLE2	$e^+e^- \to \Upsilon(4S)$
2.7 ±0.6 ±0.5		[4] BORTOLETTO	92	CLEO	$e^+e^- \to \Upsilon(4S)$
4.8 ±1.1 ±1.1	22	[5] ALBRECHT	90J	ARG	$e^+e^- \to \Upsilon(4S)$
5.1 $^{+2.8}_{-2.5}$ $^{+1.3}_{-1.2}$	4	[6] BEBEK	87	CLEO	$e^+e^- \to \Upsilon(4S)$
• • • We do not use the following data for averages, fits, limits, etc. • • •					
2.73±0.19±0.05		[1,7] AUBERT,B	04O	BABR	Repl. by AUBERT 07H
2.83±0.42±0.05	81	[8] ALAM	94	CLE2	Repl. by AHMED 02B
3.1 ±1.3 ±1.0	7	[5] ALBRECHT	88K	ARG	$e^+e^- \to \Upsilon(4S)$

[1] Assumes equal production of B^+ and B^0 at the $\Upsilon(4S)$.
[2] Uses a missing-mass method. Does not depend on D branching fractions or B^+/B^0 production rates.
[3] AHMED 02B reports an additional uncertainty on the branching ratios to account for 4.5% uncertainty on relative production of B^0 and B^+, which is not included here.
[4] BORTOLETTO 92 assumes equal production of B^+ and B^0 at the $\Upsilon(4S)$ and uses MarkIII branching fractions for the D.
[5] ALBRECHT 88K assumes $B^0\overline{B}^0$:B^+B^- production ratio is 45:55. Superseded by ALBRECHT 90J which assumes 50:50.
[6] BEBEK 87 value has been updated in BERKELMAN 91 to use same assumptions as noted for BORTOLETTO 92.
[7] AUBERT,B 04O reports $[\Gamma(B^0 \to D^-\pi^+)/\Gamma_{total}] \times [B(D^+ \to K^0_S\pi^+)] = (42.7 \pm 2.1 \pm 2.2) \times 10^{-6}$ which we divide by our best value $B(D^+ \to K^0_S\pi^+) = (1.562 \pm 0.031) \times 10^{-2}$. Our first error is their experiment's error and our second error is the systematic error from using our best value.
[8] ALAM 94 reports $[\Gamma(B^0 \to D^-\pi^+)/\Gamma_{total}] \times [B(D^+ \to K^-2\pi^+)] = (0.265 \pm 0.032 \pm 0.023) \times 10^{-3}$ which we divide by our best value $B(D^+ \to K^-2\pi^+) = (9.38 \pm 0.16) \times 10^{-2}$. Our first error is their experiment's error and our second error is the systematic error from using our best value. Assumes equal production of B^+ and B^0 at the $\Upsilon(4S)$.

$\Gamma(D^-\ell^+\nu_\ell)/\Gamma(D^-\pi^+)$ — Γ_5/Γ_{35}

VALUE	DOCUMENT ID		TECN	COMMENT
9.9±1.0±0.9	AALTONEN	09E	CDF	$p\overline{p}$ at 1.96 TeV

$\Gamma(D^-\rho^+)/\Gamma_{total}$ — Γ_{36}/Γ

VALUE	EVTS	DOCUMENT ID		TECN	COMMENT
0.0076±0.0012 OUR AVERAGE					
0.0075±0.0013±0.0001	79	[1] ALAM	94	CLE2	$e^+e^- \to \Upsilon(4S)$
0.009 ±0.005 ±0.003	9	[2] ALBRECHT	90J	ARG	$e^+e^- \to \Upsilon(4S)$
• • • We do not use the following data for averages, fits, limits, etc. • • •					
0.022 ±0.012 ±0.009	6	[2] ALBRECHT	88K	ARG	$e^+e^- \to \Upsilon(4S)$

[1] ALAM 94 reports $[\Gamma(B^0 \to D^-\rho^+)/\Gamma_{total}] \times [B(D^+ \to K^-2\pi^+)] = 0.000704 \pm 0.000096 \pm 0.000070$ which we divide by our best value $B(D^+ \to K^-2\pi^+) = (9.38 \pm 0.16) \times 10^{-2}$. Our first error is their experiment's error and our second error is the systematic error from using our best value. Assumes equal production of B^+ and B^0 at the $\Upsilon(4S)$.
[2] ALBRECHT 88K assumes $B^0\overline{B}^0$:B^+B^- production ratio is 45:55. Superseded by ALBRECHT 90J which assumes 50:50.

$\Gamma(D^-K^0\pi^+)/\Gamma_{total}$ — Γ_{37}/Γ

VALUE (units 10^{-4})	DOCUMENT ID		TECN	COMMENT
4.9±0.7±0.5	[1] AUBERT,BE	05B	BABR	$e^+e^- \to \Upsilon(4S)$

[1] Assumes equal production of B^+ and B^0 at the $\Upsilon(4S)$.

$\Gamma(D^-K^*(892)^+)/\Gamma_{total}$ — Γ_{38}/Γ

VALUE (units 10^{-4})	DOCUMENT ID		TECN	COMMENT
4.5±0.7 OUR AVERAGE				
4.6±0.6±0.5	[1] AUBERT,BE	05B	BABR	$e^+e^- \to \Upsilon(4S)$
3.7±1.5±1.0	[1] MAHAPATRA	02	CLE2	$e^+e^- \to \Upsilon(4S)$

[1] Assumes equal production of B^+ and B^0 at the $\Upsilon(4S)$.

$\Gamma(D^-\omega\pi^+)/\Gamma_{total}$ — Γ_{39}/Γ

VALUE	DOCUMENT ID		TECN	COMMENT
0.0028±0.0005±0.0004	[1] ALEXANDER	01B	CLE2	$e^+e^- \to \Upsilon(4S)$

[1] Assumes equal production of B^+ and B^0 at the $\Upsilon(4S)$. The signal is consistent with all observed $\omega\pi^+$ having proceeded through the ρ'^+ resonance at mass $1349 \pm 25^{+10}_{-5}$ MeV and width $547 \pm 86^{+46}_{-45}$ MeV.

$\Gamma(D^-K^+)/\Gamma(D^-\pi^+)$ — Γ_{40}/Γ_{35}

VALUE (units 10^{-2})	DOCUMENT ID		TECN	COMMENT
8.19±0.20 OUR AVERAGE				
8.19±0.20±0.23	WAHEED	22	BELL	$e^+e^- \to \Upsilon(4S)$
8.22±0.11±0.25	AAIJ	13P	LHCB	pp at 7 TeV
6.8 ±1.5 ±0.7	ABE	01I	BELL	$e^+e^- \to \Upsilon(4S)$

$\Gamma(D^-K^+\pi^+\pi^-)/\Gamma(D^-\pi^+\pi^+\pi^-)$ — Γ_{41}/Γ_{47}

VALUE (units 10^{-2})	DOCUMENT ID		TECN	COMMENT
5.9±1.1±0.5	AAIJ	12T	LHCB	pp at 7 TeV

$\Gamma(D^-K^+\overline{K}^0)/\Gamma_{total}$ — Γ_{42}/Γ

VALUE (units 10^{-4})	CL%	DOCUMENT ID		TECN	COMMENT
<3.1	90	[1] DRUTSKOY	02	BELL	$e^+e^- \to \Upsilon(4S)$

[1] Assumes equal production of B^+ and B^0 at the $\Upsilon(4S)$.

$\Gamma(D^-K^+\overline{K}^*(892)^0)/\Gamma_{total}$ — Γ_{43}/Γ

VALUE (units 10^{-4})	DOCUMENT ID		TECN	COMMENT
8.8±1.1±1.5	[1] DRUTSKOY	02	BELL	$e^+e^- \to \Upsilon(4S)$

[1] Assumes equal production of B^+ and B^0 at the $\Upsilon(4S)$.

Downloaded from https://academic.oup.com/ptep/article/2022/8/083C01/6651666 by KIT Library user on 27 September 2022

$\Gamma(\overline{D}^0\pi^+\pi^-)/\Gamma_{total}$ — Γ_{44}/Γ

VALUE (units 10^{-4})	CL%	EVTS	DOCUMENT ID		TECN	COMMENT
8.8 ±0.5 OUR AVERAGE						
8.95±0.15±0.52			[1] AAIJ	15Y	LHCB	pp at 7, 8 TeV
8.4 ±0.4 ±0.8			[2] KUZMIN	07	BELL	$e^+e^- \to \Upsilon(4S)$
• • • We do not use the following data for averages, fits, limits, etc. • • •						
8.0 ±0.6 ±1.5			[2,3] SATPATHY	03	BELL	Repl. by KUZMIN 07
< 16	90		[2] ALAM	94	CLE2	$e^+e^- \to \Upsilon(4S)$
< 70	90		[4] BORTOLETTO	92	CLEO	$e^+e^- \to \Upsilon(4S)$
<340	90		[5] BEBEK	87	CLEO	$e^+e^- \to \Upsilon(4S)$
700 ± 500		5	[6] BEHRENDS	83	CLEO	$e^+e^- \to \Upsilon(4S)$

[1] The second uncertainty combines in quadrature all systematic uncertainties quoted in the paper. AAIJ 15Y reports $B(B^0 \to \overline{D}^0\pi^+\pi^-) = (8.46 \pm 0.14 \pm 0.49) \times 10^{-4}$ in the kinematic region $m(\overline{D}^0\pi^\pm) > 2.1$ GeV which we corrected to the full phase-space dividing by 0.945 from Belle.

[2] Assumes equal production of B^+ and B^0 at the $\Upsilon(4S)$.

[3] No assumption about the intermediate mechanism is made in the analysis.

[4] BORTOLETTO 92 assumes equal production of B^+ and B^0 at the $\Upsilon(4S)$ and uses Mark III branching fractions for the D. The product branching fraction into $D_0^*(2340)\pi$ followed by $D_0^*(2340) \to D^0\pi$ is < 0.0001 at 90% CL and into $D_2^*(2460)$ followed by $D_2^*(2460) \to D^0\pi$ is < 0.0004 at 90% CL.

[5] BEBEK 87 assume the $\Upsilon(4S)$ decays 43% to $B^0\overline{B}^0$. We rescale to 50%. $B(D^0 \to K^-\pi^+) = (4.2 \pm 0.4 \pm 0.4)$% and $B(D^0 \to K^-\pi^+\pi^+\pi^-) = (9.1 \pm 0.8 \pm 0.8)$% were used.

[6] Corrected by us using assumptions: $B(D^0 \to K^-\pi^+) = (0.042 \pm 0.006)$ and $B(\Upsilon(4S) \to B^0\overline{B}^0) = 50$%. The product branching ratio is $B(B^0 \to \overline{D}^0\pi^+\pi^-)B(\overline{D}^0 \to K^+\pi^-) = (0.39 \pm 0.26) \times 10^{-2}$.

$\Gamma(D^*(2010)^-\pi^+)/\Gamma_{total}$ — Γ_{45}/Γ

VALUE (units 10^{-3})	EVTS	DOCUMENT ID		TECN	COMMENT
2.74±0.13 OUR AVERAGE					
2.79±0.08±0.17		[1] AUBERT	07H	BABR	$e^+e^- \to \Upsilon(4S)$
2.48±0.34±0.08		[2,3] AUBERT,BE	06J	BABR	$e^+e^- \to \Upsilon(4S)$
2.81±0.24±0.05		[4] BRANDENB...	98	CLE2	$e^+e^- \to \Upsilon(4S)$
2.6 ±0.3 ±0.4	82	[5] ALAM	94	CLE2	$e^+e^- \to \Upsilon(4S)$
3.37±0.96±0.02		[6] BORTOLETTO	92	CLEO	$e^+e^- \to \Upsilon(4S)$
2.36±0.88±0.02	12	[7] ALBRECHT	90J	ARG	$e^+e^- \to \Upsilon(4S)$
$2.36^{+1.50}_{-1.10}$±0.02	5	[8] BEBEK	87	CLEO	$e^+e^- \to \Upsilon(4S)$
• • • We do not use the following data for averages, fits, limits, etc. • • •					
10 ±4 ±1	8	[9] AKERS	94J	OPAL	$e^+e^- \to Z$
2.7 ±1.4 ±1.0	5	[10] ALBRECHT	87C	ARG	$e^+e^- \to \Upsilon(4S)$
3.5 ±2 ±2		[11] ALBRECHT	86F	ARG	$e^+e^- \to \Upsilon(4S)$
17 ±5 ±5	41	[12] GILES	84	CLEO	$e^+e^- \to \Upsilon(4S)$

[1] Assumes equal production of B^+ and B^0 at the $\Upsilon(4S)$.

[2] AUBERT,BE 06J reports $[\Gamma(B^0 \to D^*(2010)^-\pi^+)/\Gamma_{total}] / [B(B^0 \to D^-\pi^+)] = 0.99 \pm 0.11 \pm 0.08$ which we multiply by our best value $B(B^0 \to D^-\pi^+) = (2.51 \pm 0.08) \times 10^{-3}$. Our first error is their experiment's error and our second error is the systematic error from using our best value.

[3] Uses a missing-mass method. Does not depend on D branching fractions or B^+/B^0 production rates.

[4] BRANDENBURG 98 assume equal production of B^+ and B^0 at $\Upsilon(4S)$ and use the D^* reconstruction technique. The first error is their experiment's error and the second error is the systematic error from the PDG 96 value of $B(D^* \to D\pi)$.

[5] ALAM 94 assume equal production of B^+ and B^0 at the $\Upsilon(4S)$ and use the CLEO II $B(D^*(2010)^+ \to D^0\pi^+)$ and absolute $B(D^0 \to K^-\pi^+)$ and the PDG 1992 $B(D^0 \to K^-\pi^+\pi^0)/B(D^0 \to K^-\pi^+)$ and $B(D^0 \to K^-2\pi^+\pi^-)/B(D^0 \to K^-\pi^+)$.

[6] BORTOLETTO 92 reports $(4.0 \pm 1.0 \pm 0.7) \times 10^{-3}$ from a measurement of $[\Gamma(B^0 \to D^*(2010)^-\pi^+)/\Gamma_{total}] \times [B(D^*(2010)^+ \to D^0\pi^+)]$ assuming $B(D^*(2010)^+ \to D^0\pi^+) = 0.57 \pm 0.06$, which we rescale to our best value $B(D^*(2010)^+ \to D^0\pi^+) = (67.7 \pm 0.5) \times 10^{-2}$. Our first error is their experiment's error and our second error is the systematic error from using our best value. Assumes equal production of B^+ and B^0 at the $\Upsilon(4S)$ and uses Mark III branching fractions for the D.

[7] ALBRECHT 90J reports $(2.8 \pm 0.9 \pm 0.6) \times 10^{-3}$ from a measurement of $[\Gamma(B^0 \to D^*(2010)^-\pi^+)/\Gamma_{total}] \times [B(D^*(2010)^+ \to D^0\pi^+)]$ assuming $B(D^*(2010)^+ \to D^0\pi^+) = 0.57 \pm 0.06$, which we rescale to our best value $B(D^*(2010)^+ \to D^0\pi^+) = (67.7 \pm 0.5) \times 10^{-2}$. Our first error is their experiment's error and our second error is the systematic error from using our best value. Assumes equal production of B^+ and B^0 at the $\Upsilon(4S)$ and uses Mark III branching fractions for the D.

[8] BEBEK 87 reports $(2.8^{+1.5}_{-1.2}{}^{+1.0}_{-0.6}) \times 10^{-3}$ from a measurement of $[\Gamma(B^0 \to D^*(2010)^-\pi^+)/\Gamma_{total}] \times [B(D^*(2010)^+ \to D^0\pi^+)]$ assuming $B(D^*(2010)^+ \to D^0\pi^+) = 0.57 \pm 0.06$, which we rescale to our best value $B(D^*(2010)^+ \to D^0\pi^+) = (67.7 \pm 0.5) \times 10^{-2}$. Our first error is their experiment's error and our second error is the systematic error from using our best value. Updated in BERKELMAN 91 to use same assumptions as noted for BORTOLETTO 92 and ALBRECHT 90J.

[9] Assumes $B(Z \to b\overline{b}) = 0.217$ and 38% B_d production fraction.

[10] ALBRECHT 87C use PDG 86 branching ratios for D and $D^*(2010)$ and assume $B(\Upsilon(4S) \to B^+B^-) = 55$% and $B(\Upsilon(4S) \to B^0\overline{B}^0) = 45$%. Superseded by ALBRECHT 90J.

[11] ALBRECHT 86F uses pseudomass that is independent of D^0 and D^+ branching ratios.

[12] Assumes $B(D^*(2010)^+ \to D^0\pi^+) = 0.60^{+0.08}_{-0.15}$. Assumes $B(\Upsilon(4S) \to B^0\overline{B}^0) = 0.40 \pm 0.02$ Does not depend on D branching ratios.

$\Gamma(D^*(2010)^-\ell^+\nu_\ell)/\Gamma(D^*(2010)^-\pi^+)$ — Γ_7/Γ_{45}

VALUE	DOCUMENT ID		TECN	COMMENT
16.5±2.3±1.1	AALTONEN	09E	CDF	$p\overline{p}$ at 1.96 TeV

$\Gamma(\overline{D}^0K^+K^-)/\Gamma(\overline{D}^0\pi^+\pi^-)$ — Γ_{46}/Γ_{44}

VALUE	DOCUMENT ID		TECN	COMMENT
0.069±0.004±0.003	AAIJ	18AZ	LHCB	pp at 7, 8 TeV
• • • We do not use the following data for averages, fits, limits, etc. • • •				
0.056±0.011±0.007	AAIJ	12AM	LHCB	pp at 7 TeV, Repl. by AAIJ 18AZ

$\Gamma(D^-\pi^+\pi^+\pi^-)/\Gamma_{total}$ — Γ_{47}/Γ

VALUE	DOCUMENT ID		TECN	COMMENT
0.0060±0.0006 OUR FIT				
0.0080±0.0021±0.0014	[1] BORTOLETTO	92	CLEO	$e^+e^- \to \Upsilon(4S)$

[1] BORTOLETTO 92 assumes equal production of B^+ and B^0 at the $\Upsilon(4S)$ and uses Mark III branching fractions for the D.

$\Gamma(D^-\pi^+\pi^+\pi^-)/\Gamma(D^-\pi^+)$ — Γ_{47}/Γ_{35}

VALUE	DOCUMENT ID		TECN	COMMENT
2.39±0.23 OUR FIT				
2.38±0.11±0.21	AAIJ	11E	LHCB	pp at 7 TeV

$\Gamma((D^-\pi^+\pi^+\pi^-)\text{ nonresonant})/\Gamma_{total}$ — Γ_{48}/Γ

VALUE	DOCUMENT ID		TECN	COMMENT
0.0039±0.0014±0.0013	[1] BORTOLETTO	92	CLEO	$e^+e^- \to \Upsilon(4S)$

[1] BORTOLETTO 92 assumes equal production of B^+ and B^0 at the $\Upsilon(4S)$ and uses Mark III branching fractions for the D.

$\Gamma(D^-\pi^+\rho^0)/\Gamma_{total}$ — Γ_{49}/Γ

VALUE	DOCUMENT ID		TECN	COMMENT
0.0011±0.0009±0.0004	[1] BORTOLETTO	92	CLEO	$e^+e^- \to \Upsilon(4S)$

[1] BORTOLETTO 92 assumes equal production of B^+ and B^0 at the $\Upsilon(4S)$ and uses Mark III branching fractions for the D.

$\Gamma(D^-a_1(1260)^+)/\Gamma_{total}$ — Γ_{50}/Γ

VALUE	DOCUMENT ID		TECN	COMMENT
0.0060±0.0022±0.0024	[1] BORTOLETTO	92	CLEO	$e^+e^- \to \Upsilon(4S)$

[1] BORTOLETTO 92 assumes equal production of B^+ and B^0 at the $\Upsilon(4S)$ and uses Mark III branching fractions for the D.

$\Gamma(D^*(2010)^-\pi^+\pi^0)/\Gamma_{total}$ — Γ_{51}/Γ

VALUE	EVTS	DOCUMENT ID		TECN	COMMENT
0.0152±0.0052±0.0001	51	[1] ALBRECHT	90J	ARG	$e^+e^- \to \Upsilon(4S)$
• • • We do not use the following data for averages, fits, limits, etc. • • •					
0.015 ±0.008 ±0.008	8	[2] ALBRECHT	87C	ARG	$e^+e^- \to \Upsilon(4S)$

[1] ALBRECHT 90J reports $0.018 \pm 0.004 \pm 0.005$ from a measurement of $[\Gamma(B^0 \to D^*(2010)^-\pi^+\pi^0)/\Gamma_{total}] \times [B(D^*(2010)^+ \to D^0\pi^+)]$ assuming $B(D^*(2010)^+ \to D^0\pi^+) = 0.57 \pm 0.06$, which we rescale to our best value $B(D^*(2010)^+ \to D^0\pi^+) = (67.7 \pm 0.5) \times 10^{-2}$. Our first error is their experiment's error and our second error is the systematic error from using our best value. Assumes equal production of B^+ and B^0 at the $\Upsilon(4S)$ and uses Mark III branching fractions for the D.

[2] ALBRECHT 87C use PDG 86 branching ratios for D and $D^*(2010)$ and assume $B(\Upsilon(4S) \to B^+B^-) = 55$% and $B(\Upsilon(4S) \to B^0\overline{B}^0) = 45$%. Superseded by ALBRECHT 90J.

$\Gamma(D^*(2010)^-\rho^+)/\Gamma_{total}$ — Γ_{52}/Γ

VALUE (units 10^{-3})	EVTS	DOCUMENT ID		TECN	COMMENT
6.8 ± 0.9 OUR AVERAGE					
6.8 ± 0.3 ± 0.9		[1,2] CSORNA	03	CLE2	$e^+e^- \to \Upsilon(4S)$
16.0 ±11.3 ± 0.1		[3] BORTOLETTO	92	CLEO	$e^+e^- \to \Upsilon(4S)$
5.89± 3.52± 0.04	19	[4] ALBRECHT	90J	ARG	$e^+e^- \to \Upsilon(4S)$
• • • We do not use the following data for averages, fits, limits, etc. • • •					
		[2,5] MATVIENKO	15	BELL	$e^+e^- \to \Upsilon(4S)$
7.4 ± 1.0 ± 1.4	76	[6,7] ALAM	94	CLE2	$e^+e^- \to \Upsilon(4S)$
81 ±29 $^{+59}_{-24}$	19	[8] CHEN	85	CLEO	$e^+e^- \to \Upsilon(4S)$

[1] The second error combines the systematic and theoretical uncertainties in quadrature. CSORNA 03 includes data used in ALAM 94. A full angular fit to three complex helicity amplitudes is performed.

[2] Assumes equal production of B^0 and B^+ at the $\Upsilon(4S)$ resonance.

[3] BORTOLETTO 92 reports $0.019 \pm 0.008 \pm 0.011$ from a measurement of $[\Gamma(B^0 \to D^*(2010)^-\rho^+)/\Gamma_{total}] \times [B(D^*(2010)^+ \to D^0\pi^+)]$ assuming $B(D^*(2010)^+ \to D^0\pi^+) = 0.57 \pm 0.06$, which we rescale to our best value $B(D^*(2010)^+ \to D^0\pi^+) = (67.7 \pm 0.5) \times 10^{-2}$. Our first error is their experiment's error and our second error is the systematic error from using our best value. Assumes equal production of B^+ and B^0 at the $\Upsilon(4S)$ and uses Mark III branching fractions for the D.

[4] ALBRECHT 90J reports $0.007 \pm 0.003 \pm 0.003$ from a measurement of $[\Gamma(B^0 \to D^*(2010)^-\rho^+)/\Gamma_{total}] \times [B(D^*(2010)^+ \to D^0\pi^+)]$ assuming $B(D^*(2010)^+ \to D^0\pi^+) = 0.57 \pm 0.06$, which we rescale to our best value $B(D^*(2010)^+ \to D^0\pi^+) = (67.7 \pm 0.5) \times 10^{-2}$. Our first error is their experiment's error and our second error is the systematic error from using our best value. Assumes equal production of B^+ and B^0 at the $\Upsilon(4S)$ and uses Mark III branching fractions for the D.

Downloaded from https://academic.oup.com/ptep/article/2022/8/083C01/6651666 by KIT Library user on 27 September 2022

[5] MATVIENKO 15 reports $B(B^0 \to D^*(2010)^- \rho^+,\ \rho^+ \to \omega\pi^+) = (1.48 \pm 0.27^{+0.15}_{-0.09}{}^{+0.21}_{-0.56}) \times 10^{-3}$. The last uncertainty is a model one.

[6] ALAM 94 assume equal production of B^+ and B^0 at the $\Upsilon(4S)$ and use the CLEO II $B(D^*(2010)^+ \to D^0\pi^+)$ and absolute $B(D^0 \to K^-\pi^+)$ and the PDG 1992 $B(D^0 \to K^-\pi^+\pi^0)/B(D^0 \to K^-\pi^+)$ and $B(D^0 \to K^-2\pi^+\pi^-)/B(D^0 \to K^-\pi^+)$.

[7] This decay is nearly completely longitudinally polarized, $\Gamma_L/\Gamma = (93 \pm 5 \pm 5)\%$, as expected from the factorization hypothesis (ROSNER 90). The nonresonant $\pi^+\pi^0$ contribution under the ρ^+ is less than 9% at 90% CL.

[8] Uses $B(D^* \to D^0\pi^+) = 0.6 \pm 0.15$ and $B(\Upsilon(4S) \to B^0\overline{B}^0) = 0.4$. Does not depend on D branching ratios.

$\Gamma(D^*(2010)^- K^+)/\Gamma_{total}$ — Γ_{53}/Γ

VALUE (units 10^{-4})	DOCUMENT ID		TECN	COMMENT
2.12±0.15 OUR AVERAGE				
2.12±0.12±0.10	[1] AUBERT	06A	BABR	$e^+e^- \to \Upsilon(4S)$
2.0 ±0.4 ±0.1	[2] ABE	01I	BELL	$e^+e^- \to \Upsilon(4S)$

[1] AUBERT 06A reports $[\Gamma(B^0 \to D^*(2010)^- K^+)/\Gamma_{total}] / [B(B^0 \to D^*(2010)^-\pi^+)] = 0.0776 \pm 0.0034 \pm 0.0029$ which we multiply by our best value $B(B^0 \to D^*(2010)^-\pi^+) = (2.74 \pm 0.13) \times 10^{-3}$. Our first error is their experiment's error and our second error is the systematic error from using our best value.

[2] ABE 01I reports $[\Gamma(B^0 \to D^*(2010)^- K^+)/\Gamma_{total}] / [B(B^0 \to D^*(2010)^-\pi^+)] = 0.074 \pm 0.015 \pm 0.006$ which we multiply by our best value $B(B^0 \to D^*(2010)^-\pi^+) = (2.74 \pm 0.13) \times 10^{-3}$. Our first error is their experiment's error and our second error is the systematic error from using our best value.

$\Gamma(D^*(2010)^- K^+)/\Gamma(D^*(2010)^-\pi^+)$ — Γ_{53}/Γ_{45}

VALUE	DOCUMENT ID		TECN	COMMENT
$(7.76\pm0.34\pm0.26) \times 10^{-2}$	AAIJ	13AO	LHCB	pp at 7 TeV

$\Gamma(D^*(2010)^- K^0\pi^+)/\Gamma_{total}$ — Γ_{54}/Γ

VALUE (units 10^{-4})	DOCUMENT ID		TECN	COMMENT
3.0±0.7±0.3	[1] AUBERT,BE	05B	BABR	$e^+e^- \to \Upsilon(4S)$

[1] Assumes equal production of B^+ and B^0 at the $\Upsilon(4S)$.

$\Gamma(D^*(2010)^- K^*(892)^+)/\Gamma_{total}$ — Γ_{55}/Γ

VALUE (units 10^{-4})	DOCUMENT ID		TECN	COMMENT
3.3±0.6 OUR AVERAGE				
3.2±0.6±0.3	[1] AUBERT,BE	05B	BABR	$e^+e^- \to \Upsilon(4S)$
3.8±1.3±0.8	[2] MAHAPATRA	02	CLE2	$e^+e^- \to \Upsilon(4S)$

[1] Assumes equal production of B^+ and B^0 at the $\Upsilon(4S)$.

[2] Assumes equal production of B^+ and B^0 at the $\Upsilon(4S)$ and an unpolarized final state.

$\Gamma(D^*(2010)^- K^+\overline{K}^0)/\Gamma_{total}$ — Γ_{56}/Γ

VALUE (units 10^{-4})	CL%	DOCUMENT ID		TECN	COMMENT
<4.7	90	[1] DRUTSKOY	02	BELL	$e^+e^- \to \Upsilon(4S)$

[1] Assumes equal production of B^+ and B^0 at the $\Upsilon(4S)$.

$\Gamma(D^*(2010)^- K^+\overline{K}^*(892)^0)/\Gamma_{total}$ — Γ_{57}/Γ

VALUE (units 10^{-4})	DOCUMENT ID		TECN	COMMENT
12.9±2.2±2.5	[1] DRUTSKOY	02	BELL	$e^+e^- \to \Upsilon(4S)$

[1] Assumes equal production of B^+ and B^0 at the $\Upsilon(4S)$.

$\Gamma(D^*(2010)^-\pi^+\pi^+\pi^-)/\Gamma_{total}$ — Γ_{58}/Γ

VALUE (units 10^{-3})	CL%	DOCUMENT ID		TECN	COMMENT
7.21±0.29 OUR AVERAGE					
7.26±0.11± 0.31		[1] LEES	16H	BABR	$e^+e^- \to \Upsilon(4S)$
6.81±0.23± 0.72		[2] MAJUMDER	04	BELL	$e^+e^- \to \Upsilon(4S)$
6.3 ±1.0 ± 1.1		[3,4] ALAM	94	CLE2	$e^+e^- \to \Upsilon(4S)$
13.4 ±3.6 ± 0.1		[5] BORTOLETTO	92	CLEO	$e^+e^- \to \Upsilon(4S)$
10.1 ±4.1 ± 0.1		[6] ALBRECHT	90J	ARG	$e^+e^- \to \Upsilon(4S)$
• • • We do not use the following data for averages, fits, limits, etc. • • •					
33 ±9 ±16		[7] ALBRECHT	87C	ARG	$e^+e^- \to \Upsilon(4S)$
<42	90	[8] BEBEK	87	CLEO	$e^+e^- \to \Upsilon(4S)$

[1] Assumes $B(\Upsilon(4S) \to B^0\overline{B}^0) = 0.486 \pm 0.006$.

[2] Assumes equal production of B^+ and B^0 at the $\Upsilon(4S)$.

[3] ALAM 94 assume equal production of B^+ and B^0 at the $\Upsilon(4S)$ and use the CLEO II $B(D^*(2010)^+ \to D^0\pi^+)$ and absolute $B(D^0 \to K^-\pi^+)$ and the PDG 1992 $B(D^0 \to K^-\pi^+\pi^0)/B(D^0 \to K^-\pi^+)$ and $B(D^0 \to K^-2\pi^+\pi^-)/B(D^0 \to K^-\pi^+)$.

[4] The three pion mass is required to be between 1.0 and 1.6 GeV consistent with an a_1 meson. (If this channel is dominated by a_1^+, the branching ratio for $\overline{D}^{*-}a_1^+$ is twice that for $\overline{D}^{*-}\pi^+\pi^+\pi^-$.)

[5] BORTOLETTO 92 reports $0.0159 \pm 0.0028 \pm 0.0037$ from a measurement of $[\Gamma(B^0 \to D^*(2010)^-\pi^+\pi^+\pi^-)/\Gamma_{total}] \times [B(D^*(2010)^+ \to D^0\pi^+)]$ assuming $B(D^*(2010)^+ \to D^0\pi^+) = 0.57 \pm 0.06$, which we rescale to our best value $B(D^*(2010)^+ \to D^0\pi^+) = (67.7 \pm 0.5) \times 10^{-2}$. Our first error is their experiment's error and our second error is the systematic error from using our best value. Assumes equal production of B^+ and B^0 at the $\Upsilon(4S)$ and uses Mark III branching fractions for the D.

[6] ALBRECHT 90J reports $0.012 \pm 0.003 \pm 0.004$ from a measurement of $[\Gamma(B^0 \to D^*(2010)^-\pi^+\pi^+\pi^-)/\Gamma_{total}] \times [B(D^*(2010)^+ \to D^0\pi^+)]$ assuming $B(D^*(2010)^+ \to D^0\pi^+) = 0.57 \pm 0.06$, which we rescale to our best value $B(D^*(2010)^+ \to D^0\pi^+) = (67.7 \pm 0.5) \times 10^{-2}$. Our first error is their experiment's error and our second error is the systematic error from using our best value. Assumes equal production of B^+ and B^0 at the $\Upsilon(4S)$ and uses Mark III branching fractions for the D.

[7] ALBRECHT 87C use PDG 86 branching ratios for D and $D^*(2010)$ and assume $B(\Upsilon(4S) \to B^+B^-) = 55\%$ and $B(\Upsilon(4S) \to B^0\overline{B}^0) = 45\%$. Superseded by ALBRECHT 90J.

[8] BEBEK 87 value has been updated in BERKELMAN 91 to use same assumptions as noted for BORTOLETTO 92.

$\Gamma((D^*(2010)^-\pi^+\pi^+\pi^-)$ nonresonant$)/\Gamma_{total}$ — Γ_{59}/Γ

VALUE	DOCUMENT ID		TECN	COMMENT
0.0000±0.0019±0.0016	[1] BORTOLETTO	92	CLEO	$e^+e^- \to \Upsilon(4S)$

[1] BORTOLETTO 92 assumes equal production of B^+ and B^0 at the $\Upsilon(4S)$ and uses Mark III branching fractions for the D and $D^*(2010)$.

$\Gamma(D^*(2010)^-\pi^+\rho^0)/\Gamma_{total}$ — Γ_{60}/Γ

VALUE	DOCUMENT ID		TECN	COMMENT
0.00573±0.00317±0.00004	[1] BORTOLETTO	92	CLEO	$e^+e^- \to \Upsilon(4S)$

[1] BORTOLETTO 92 reports $0.0068 \pm 0.0032 \pm 0.0021$ from a measurement of $[\Gamma(B^0 \to D^*(2010)^-\pi^+\rho^0)/\Gamma_{total}] \times [B(D^*(2010)^+ \to D^0\pi^+)]$ assuming $B(D^*(2010)^+ \to D^0\pi^+) = 0.57 \pm 0.06$, which we rescale to our best value $B(D^*(2010)^+ \to D^0\pi^+) = (67.7 \pm 0.5) \times 10^{-2}$. Our first error is their experiment's error and our second error is the systematic error from using our best value. Assumes equal production of B^+ and B^0 at the $\Upsilon(4S)$ and uses Mark III branching fractions for the D.

$\Gamma(D^*(2010)^- a_1(1260)^+)/\Gamma_{total}$ — Γ_{61}/Γ

VALUE	DOCUMENT ID		TECN	COMMENT
0.0130±0.0027 OUR AVERAGE				
0.0126±0.0020±0.0022	[1,2] ALAM	94	CLE2	$e^+e^- \to \Upsilon(4S)$
0.0152±0.0070±0.0001	[3] BORTOLETTO	92	CLEO	$e^+e^- \to \Upsilon(4S)$

[1] ALAM 94 value is twice their $\Gamma(D^*(2010)^-\pi^+\pi^+\pi^-)/\Gamma_{total}$ value based on their observation that the three pions are dominantly in the $a_1(1260)$ mass range 1.0 to 1.6 GeV.

[2] ALAM 94 assume equal production of B^+ and B^0 at the $\Upsilon(4S)$ and use the CLEO II $B(D^*(2010)^+ \to D^0\pi^+)$ and absolute $B(D^0 \to K^-\pi^+)$ and the PDG 1992 $B(D^0 \to K^-\pi^+\pi^0)/B(D^0 \to K^-\pi^+)$ and $B(D^0 \to K^-2\pi^+\pi^-)/B(D^0 \to K^-\pi^+)$.

[3] BORTOLETTO 92 reports $0.018 \pm 0.006 \pm 0.006$ from a measurement of $[\Gamma(B^0 \to D^*(2010)^- a_1(1260)^+)/\Gamma_{total}] \times [B(D^*(2010)^+ \to D^0\pi^+)]$ assuming $B(D^*(2010)^+ \to D^0\pi^+) = 0.57 \pm 0.06$, which we rescale to our best value $B(D^*(2010)^+ \to D^0\pi^+) = (67.7 \pm 0.5) \times 10^{-2}$. Our first error is their experiment's error and our second error is the systematic error from using our best value. Assumes equal production of B^+ and B^0 at the $\Upsilon(4S)$ and uses Mark III branching fractions for the D.

$\Gamma(\overline{D}_1(2420)^0\pi^-\pi^+,\ \overline{D}_1^0 \to D^{*-}\pi^+)/\Gamma(D^*(2010)^-\pi^+\pi^+\pi^-)$ — Γ_{62}/Γ_{58}

VALUE	DOCUMENT ID		TECN	COMMENT
$(2.04\pm0.42\pm0.22) \times 10^{-2}$	AAIJ	13AO	LHCB	pp at 7 TeV

$\Gamma(D^*(2010)^- K^+\pi^-\pi^+)/\Gamma(D^*(2010)^-\pi^+\pi^+\pi^-)$ — Γ_{63}/Γ_{58}

VALUE	DOCUMENT ID		TECN	COMMENT
$(6.47\pm0.37\pm0.35) \times 10^{-2}$	AAIJ	13AO	LHCB	pp at 7 TeV

$\Gamma(D^*(2010)^-\pi^+\pi^+\pi^-\pi^0)/\Gamma_{total}$ — Γ_{64}/Γ

VALUE	EVTS	DOCUMENT ID		TECN	COMMENT
0.0176±0.0027 OUR AVERAGE					
0.0172±0.0014±0.0024		[1] ALEXANDER	01B	CLE2	$e^+e^- \to \Upsilon(4S)$
0.0345±0.0181±0.0003	28	[2] ALBRECHT	90J	ARG	$e^+e^- \to \Upsilon(4S)$

[1] Assumes equal production of B^+ and B^0 at the $\Upsilon(4S)$. The signal is consistent with all observed $\omega\pi^+$ having proceeded through the ρ'^+ resonance at mass $1349 \pm 25^{+10}_{-5}$ MeV and width $547 \pm 86^{+46}_{-45}$ MeV.

[2] ALBRECHT 90J reports $0.041 \pm 0.015 \pm 0.016$ from a measurement of $[\Gamma(B^0 \to D^*(2010)^-\pi^+\pi^+\pi^-\pi^0)/\Gamma_{total}] \times [B(D^*(2010)^+ \to D^0\pi^+)]$ assuming $B(D^*(2010)^+ \to D^0\pi^+) = 0.57 \pm 0.06$, which we rescale to our best value $B(D^*(2010)^+ \to D^0\pi^+) = (67.7 \pm 0.5) \times 10^{-2}$. Our first error is their experiment's error and our second error is the systematic error from using our best value. Assumes equal production of B^+ and B^0 at the $\Upsilon(4S)$ and uses Mark III branching fractions for the D.

$\Gamma(D^{*-}3\pi^+2\pi^-)/\Gamma_{total}$ — Γ_{65}/Γ

VALUE (units 10^{-3})	DOCUMENT ID		TECN	COMMENT
4.72±0.59±0.71	[1] MAJUMDER	04	BELL	$e^+e^- \to \Upsilon(4S)$

[1] Assumes equal production of B^+ and B^0 at the $\Upsilon(4S)$.

$\Gamma(D^*(2010)^-\omega\pi^+)/\Gamma_{total}$ — Γ_{66}/Γ

VALUE (units 10^{-3})	DOCUMENT ID		TECN	COMMENT
2.46±0.18 OUR AVERAGE Error includes scale factor of 1.2.				
2.31±0.11±0.14	[1] MATVIENKO	15	BELL	$e^+e^- \to \Upsilon(4S)$
2.88±0.21±0.31	[1] AUBERT	06L	BABR	$e^+e^- \to \Upsilon(4S)$
2.9 ±0.3 ±0.4	[1,2] ALEXANDER	01B	CLE2	$e^+e^- \to \Upsilon(4S)$

[1] Assumes equal production of B^+ and B^0 at the $\Upsilon(4S)$.

[2] The signal is consistent with all observed $\omega\pi^+$ having proceeded through the ρ'^+ resonance at mass $1349 \pm 25^{+10}_{-5}$ MeV and width $547 \pm 86^{+46}_{-45}$ MeV.

Downloaded from https://academic.oup.com/ptep/article/2022/8/083C01/6651666 by KIT Library user on 27 September 2022

$\Gamma(\overline{D}_1(2430)^0\omega,\ \overline{D}_1^0 \to D^{*-}\pi^+)/\Gamma_{total}$ — Γ_{67}/Γ

VALUE (units 10^{-4})	DOCUMENT ID		TECN	COMMENT
$2.7^{+0.8}_{-0.4}$ OUR AVERAGE				
$2.5 \pm 0.4^{+0.8}_{-0.2}$	[1,2] MATVIENKO	15	BELL	$e^+e^- \to \Upsilon(4S)$
$4.1 \pm 1.2 \pm 1.1$	[3] AUBERT	06L	BABR	$e^+e^- \to \Upsilon(4S)$

[1] Assumes equal production of B^+ and B^0.
[2] The measurement is obtained by amplitude analysis of $B^0 \to D^{*-}\omega\pi^+$. The second uncertainty combines in quadrature experimental systematic and model uncertainties.
[3] Obtained by fitting the events with $\cos\theta_{D^*} < 0.5$ and scaling up the result by a factor of 4/3. No interference effects between $B^0 \to D_1'\omega$ and $D^*\omega\pi$ are assumed.

$\Gamma(D^{*-}\rho(1450)^+,\ \rho^+ \to \omega\pi^+)/\Gamma_{total}$ — Γ_{68}/Γ

VALUE (units 10^{-3})	DOCUMENT ID		TECN	COMMENT
$1.07^{+0.15+0.40}_{-0.31-0.13}$	[1,2] MATVIENKO	15	BELL	$e^+e^- \to \Upsilon(4S)$

[1] Obtained by amplitude analysis of $\overline{B}^0 \to D^{*-}\omega\pi^+$. The second uncertainty combines in qudrature experimental systematic and model uncertainties.
[2] Assumes equal production of B^0 and B^+ at $\Upsilon(4S)$.

$\Gamma(\overline{D}_1(2420)^0\omega,\ \overline{D}_1^0 \to D^{*-}\pi^+)/\Gamma_{total}$ — Γ_{69}/Γ

VALUE (units 10^{-4})	DOCUMENT ID		TECN	COMMENT
$0.7 \pm 0.2 \pm 0.1$	[1,2] MATVIENKO	15	BELL	$e^+e^- \to \Upsilon(4S)$

[1] Obtained by amplitude analysis of $\overline{B}^0 \to D^{*-}\omega\pi^+$. The second uncertainty combines in qudrature experimental systematic and model uncertainties.
[2] Assumes equal production of B^0 and B^+ at $\Upsilon(4S)$.

$\Gamma(\overline{D}_2^*(2460)^0\omega,\ \overline{D}_2^0 \to D^{*-}\pi^+)/\Gamma_{total}$ — Γ_{70}/Γ

VALUE (units 10^{-4})	DOCUMENT ID		TECN	COMMENT
$0.4 \pm 0.1 \pm 0.1$	[1,2] MATVIENKO	15	BELL	$e^+e^- \to \Upsilon(4S)$

[1] Obtained by amplitude analysis of $\overline{B}^0 \to D^{*-}\omega\pi^+$. The second uncertainty combines in qudrature experimental systematic and model uncertainties.
[2] Assumes equal production of B^0 and B^+ at $\Upsilon(4S)$.

$\Gamma(D^{*-}b_1(1235)^+,\ b_1^+ \to \omega\pi^+)/\Gamma_{total}$ — Γ_{71}/Γ

VALUE	CL%	DOCUMENT ID		TECN	COMMENT
$<0.7 \times 10^{-4}$	90	[1] MATVIENKO	15	BELL	$e^+e^- \to \Upsilon(4S)$

[1] Assumes equal production of B^0 and B^+ at $\Upsilon(4S)$.

$\Gamma(\overline{D}^{**-}\pi^+)/\Gamma_{total}$ — Γ_{72}/Γ

D^{**-} represents an excited state with mass $2.2 < M < 2.8$ GeV/c^2.

VALUE (units 10^{-3})	DOCUMENT ID		TECN	COMMENT
$1.9 \pm 0.9 \pm 0.1$	[1,2] AUBERT,BE	06J	BABR	$e^+e^- \to \Upsilon(4S)$

[1] AUBERT,BE 06J reports $[\Gamma(B^0 \to \overline{D}^{**-}\pi^+)/\Gamma_{total}] / [B(B^0 \to D^-\pi^+)] = 0.77 \pm 0.22 \pm 0.29$ which we multiply by our best value $B(B^0 \to D^-\pi^+) = (2.51 \pm 0.08) \times 10^{-3}$. Our first error is their experiment's error and our second error is the systematic error from using our best value.
[2] Uses a missing-mass method. Does not depend on D branching fractions or B^+/B^0 production rates.

$\Gamma(D_1(2420)^-\pi^+,\ D_1^- \to D^-\pi^+\pi^-)/\Gamma_{total}$ — Γ_{73}/Γ

VALUE (units 10^{-4})	DOCUMENT ID		TECN	COMMENT
$0.99^{+0.20}_{-0.25}$ OUR FIT				
$0.89 \pm 0.15^{+0.17}_{-0.32}$	[1] ABE	05A	BELL	$e^+e^- \to \Upsilon(4S)$

[1] Assumes equal production of B^+ and B^0 at the $\Upsilon(4S)$.

$\Gamma(D_1(2420)^-\pi^+,\ D_1^- \to D^-\pi^+\pi^-)/\Gamma(D^-\pi^+\pi^+\pi^-)$ — Γ_{73}/Γ_{47}

VALUE (units 10^{-2})	DOCUMENT ID		TECN	COMMENT
1.7 ± 0.4 OUR FIT				
$2.1 \pm 0.5^{+0.3}_{-0.5}$	AAIJ	11E	LHCB	pp at 7 TeV

$\Gamma(D_1(2420)^-\pi^+,\ D_1^- \to D^{*-}\pi^+\pi^-)/\Gamma_{total}$ — Γ_{74}/Γ

VALUE (units 10^{-4})	CL%	DOCUMENT ID		TECN	COMMENT
<0.33	90	[1] ABE	05A	BELL	$e^+e^- \to \Upsilon(4S)$

[1] Assumes equal production of B^+ and B^0 at the $\Upsilon(4S)$.

$\Gamma(D^*(2010)^-\pi^+\pi^+\pi^-)/\Gamma(D^*(2010)^-\pi^+)$ — Γ_{58}/Γ_{45}

VALUE	DOCUMENT ID		TECN	COMMENT
$2.64 \pm 0.04 \pm 0.13$	AAIJ	13AO	LHCB	pp at 7 TeV

$\Gamma(\overline{D}_2^*(2460)^-\pi^+,\ (D_2^*)^- \to D^0\pi^-)/\Gamma_{total}$ — Γ_{75}/Γ

VALUE (units 10^{-4})	CL%	DOCUMENT ID		TECN	COMMENT
2.38 ± 0.16 OUR AVERAGE					
$2.44 \pm 0.07 \pm 0.16$		[1] AAIJ	15Y	LHCB	pp at 7, 8 TeV
$2.15 \pm 0.17 \pm 0.31$		[2,3] KUZMIN	07	BELL	$e^+e^- \to \Upsilon(4S)$
• • • We do not use the following data for averages, fits, limits, etc. • • •					
<14.7	90	[2] ALAM	94	CLE2	$e^+e^- \to \Upsilon(4S)$

[1] Result obtained using the isobar formalism. The second uncertainty combines in quadrature all systematic uncertainties quoted in the paper.
[2] Assumes equal production of B^+ and B^0 at the $\Upsilon(4S)$.
[3] Our second uncertainty combines systematics and model errors quoted in the paper.

$\Gamma(\overline{D}_0^*(2400)^-\pi^+,\ (D_0^*)^- \to D^0\pi^-)/\Gamma_{total}$ — Γ_{76}/Γ

VALUE (units 10^{-4})	DOCUMENT ID		TECN	COMMENT
0.76 ± 0.08 OUR AVERAGE				
$0.77 \pm 0.05 \pm 0.06$	[1] AAIJ	15Y	LHCB	pp at 7, 8 TeV
$0.60 \pm 0.13 \pm 0.27$	[2,3] KUZMIN	07	BELL	$e^+e^- \to \Upsilon(4S)$

[1] Result obtained using the isobar formalism. The second uncertainty combines in quadrature all systematic uncertainties quoted in the paper.
[2] Assumes equal production of B^+ and B^0 at the $\Upsilon(4S)$.
[3] Our second uncertainty combines systematics and model errors quoted in the paper.

$\Gamma(D_2^*(2460)^-\pi^+,\ (D_2^*)^- \to D^{*-}\pi^+\pi^-)/\Gamma_{total}$ — Γ_{77}/Γ

VALUE (units 10^{-4})	CL%	DOCUMENT ID		TECN	COMMENT
<0.24	90	[1] ABE	05A	BELL	$e^+e^- \to \Upsilon(4S)$

[1] Assumes equal production of B^+ and B^0 at the $\Upsilon(4S)$.

$\Gamma(\overline{D}_2^*(2460)^-\rho^+)/\Gamma_{total}$ — Γ_{78}/Γ

VALUE	CL%	DOCUMENT ID		TECN	COMMENT
<0.0049	90	[1] ALAM	94	CLE2	$e^+e^- \to \Upsilon(4S)$

[1] ALAM 94 assumes equal production of B^+ and B^0 at the $\Upsilon(4S)$ and use the CLEO II absolute $B(D^0 \to K^-\pi^+)$ and $B(D_2^*(2460)^+ \to D^0\pi^+) = 30\%$.

$\Gamma(D^0\overline{D}^0)/\Gamma_{total}$ — Γ_{79}/Γ

VALUE (units 10^{-4})	CL%	DOCUMENT ID		TECN	COMMENT
$0.14 \pm 0.06 \pm 0.03$		[1] AAIJ	13AP	LHCB	pp at 7 TeV
• • • We do not use the following data for averages, fits, limits, etc. • • •					
<0.43	90	[2] ADACHI	08	BELL	$e^+e^- \to \Upsilon(4S)$
<0.6	90	[2] AUBERT,B	06A	BABR	$e^+e^- \to \Upsilon(4S)$

[1] Uses $B(B^0 \to D^-D^+) = (2.11 \pm 0.31) \times 10^{-4}$ and $B(B^+ \to \overline{D}^0 D_s^+) = (10.1 \pm 1.7) \times 10^{-3}$.
[2] Assumes equal production of B^+ and B^0 at the $\Upsilon(4S)$.

$\Gamma(D^{*0}\overline{D}^0)/\Gamma_{total}$ — Γ_{80}/Γ

VALUE (units 10^{-4})	CL%	DOCUMENT ID		TECN	COMMENT
<2.9	90	[1] AUBERT,B	06A	BABR	$e^+e^- \to \Upsilon(4S)$

[1] Assumes equal production of B^+ and B^0 at the $\Upsilon(4S)$.

$\Gamma(D^-D^+)/\Gamma_{total}$ — Γ_{81}/Γ

VALUE (units 10^{-4})	CL%	DOCUMENT ID		TECN	COMMENT
2.11 ± 0.18 OUR AVERAGE					
$2.12 \pm 0.16 \pm 0.18$		[1] ROHRKEN	12	BELL	$e^+e^- \to \Upsilon(4S)$
$1.97 \pm 0.20 \pm 0.20$		[1] FRATINA	07	BELL	$e^+e^- \to \Upsilon(4S)$
$2.8 \pm 0.4 \pm 0.5$		[1] AUBERT,B	06A	BABR	$e^+e^- \to \Upsilon(4S)$
• • • We do not use the following data for averages, fits, limits, etc. • • •					
$1.91 \pm 0.51 \pm 0.30$		[1] MAJUMDER	05	BELL	Repl. by FRATINA 07
< 9.4	90	[1] LIPELES	00	CLE2	$e^+e^- \to \Upsilon(4S)$
<59	90	BARATE	98Q	ALEP	$e^+e^- \to Z$
<12	90	ASNER	97	CLE2	$e^+e^- \to \Upsilon(4S)$

[1] Assumes equal production of B^+ and B^0 at the $\Upsilon(4S)$.

$\Gamma(D^\pm D^{*\mp}(CP\text{-averaged}))/\Gamma_{total}$ — Γ_{82}/Γ

VALUE (units 10^{-4})	DOCUMENT ID		TECN	COMMENT
$6.14 \pm 0.29 \pm 0.50$	[1] ROHRKEN	12	BELL	$e^+e^- \to \Upsilon(4S)$

[1] Assumes equal production of B^+ and B^0 at the $\Upsilon(4S)$.

$\Gamma(D^-D_s^+)/\Gamma_{total}$ — Γ_{83}/Γ

VALUE	EVTS	DOCUMENT ID		TECN	COMMENT
0.0072 ± 0.0008 OUR AVERAGE					
$0.0073 \pm 0.0004 \pm 0.0007$		[1] ZUPANC	07	BELL	$e^+e^- \to \Upsilon(4S)$
$0.0066 \pm 0.0014 \pm 0.0006$		[2] AUBERT	06N	BABR	$e^+e^- \to \Upsilon(4S)$
$0.0068 \pm 0.0024 \pm 0.0006$		[3] GIBAUT	96	CLE2	$e^+e^- \to \Upsilon(4S)$
$0.010 \pm 0.009 \pm 0.001$		[4] ALBRECHT	92G	ARG	$e^+e^- \to \Upsilon(4S)$
$0.0053 \pm 0.0030 \pm 0.0005$		[5] BORTOLETTO	92	CLEO	$e^+e^- \to \Upsilon(4S)$
• • • We do not use the following data for averages, fits, limits, etc. • • •					
0.012 ± 0.007	3	[6] BORTOLETTO	90	CLEO	$e^+e^- \to \Upsilon(4S)$

[1] ZUPANC 07 reports $(7.5 \pm 0.2 \pm 1.1) \times 10^{-3}$ from a measurement of $[\Gamma(B^0 \to D^-D_s^+)/\Gamma_{total}] \times [B(D_s^+ \to \phi\pi^+)]$ assuming $B(D_s^+ \to \phi\pi^+) = (4.4 \pm 0.6) \times 10^{-2}$, which we rescale to our best value $B(D_s^+ \to \phi\pi^+) = (4.5 \pm 0.4) \times 10^{-2}$. Our first error is their experiment's error and our second error is the systematic error from using our best value.
[2] AUBERT 06N reports $(0.64 \pm 0.13 \pm 0.10) \times 10^{-2}$ from a measurement of $[\Gamma(B^0 \to D^-D_s^+)/\Gamma_{total}] \times [B(D_s^+ \to \phi\pi^+)]$ assuming $B(D_s^+ \to \phi\pi^+) = 0.0462 \pm 0.0062$, which we rescale to our best value $B(D_s^+ \to \phi\pi^+) = (4.5 \pm 0.4) \times 10^{-2}$. Our first error is their experiment's error and our second error is the systematic error from using our best value.
[3] GIBAUT 96 reports $0.0087 \pm 0.0024 \pm 0.0020$ from a measurement of $[\Gamma(B^0 \to D^-D_s^+)/\Gamma_{total}] \times [B(D_s^+ \to \phi\pi^+)]$ assuming $B(D_s^+ \to \phi\pi^+) = 0.035$, which we rescale to our best value $B(D_s^+ \to \phi\pi^+) = (4.5 \pm 0.4) \times 10^{-2}$. Our first error is their experiment's error and our second error is the systematic error from using our best value.

Downloaded from https://academic.oup.com/ptep/article/2022/8/083C01/6651666 by KIT Library user on 27 September 2022

[4] ALBRECHT 92G reports 0.017 ± 0.013 ± 0.006 from a measurement of $[\Gamma(B^0 \to D^- D_s^+)/\Gamma_{total}] \times [B(D_s^+ \to \phi\pi^+)]$ assuming $B(D_s^+ \to \phi\pi^+) = 0.027$, which we rescale to our best value $B(D_s^+ \to \phi\pi^+) = (4.5 \pm 0.4) \times 10^{-2}$. Our first error is their experiment's error and our second error is the systematic error from using our best value. Assumes PDG 1990 D^+ branching ratios, e.g., $B(D^+ \to K^- 2\pi^+) = 7.7 \pm 1.0\%$.

[5] BORTOLETTO 92 reports 0.0080 ± 0.0045 ± 0.0030 from a measurement of $[\Gamma(B^0 \to D^- D_s^+)/\Gamma_{total}] \times [B(D_s^+ \to \phi\pi^+)]$ assuming $B(D_s^+ \to \phi\pi^+) = 0.030 \pm 0.011$, which we rescale to our best value $B(D_s^+ \to \phi\pi^+) = (4.5 \pm 0.4) \times 10^{-2}$. Our first error is their experiment's error and our second error is the systematic error from using our best value. Assumes equal production of B^+ and B^0 at the $\Upsilon(4S)$ and uses Mark III branching fractions for the D.

[6] BORTOLETTO 90 assume $B(D_s \to \phi\pi^+) = 2\%$. Superseded by BORTOLETTO 92.

$\Gamma(D^*(2010)^- D_s^+)/\Gamma_{total}$ — Γ_{84}/Γ

VALUE	EVTS	DOCUMENT ID		TECN	COMMENT
0.0080±0.0011 OUR AVERAGE					
0.0073±0.0013±0.0007		[1] AUBERT	06N	BABR	$e^+e^- \to \Upsilon(4S)$
0.0083±0.0015±0.0007		[2] AUBERT	03I	BABR	$e^+e^- \to \Upsilon(4S)$
0.0088±0.0017±0.0008		[3] AHMED	00B	CLE2	$e^+e^- \to \Upsilon(4S)$
0.008 ±0.006 ±0.001		[4] ALBRECHT	92G	ARG	$e^+e^- \to \Upsilon(4S)$
0.011 ±0.006 ±0.001		[5] BORTOLETTO	92	CLEO	$e^+e^- \to \Upsilon(4S)$
• • • We do not use the following data for averages, fits, limits, etc. • • •					
0.0072±0.0022±0.0006		[6] GIBAUT	96	CLE2	Repl. by AHMED 00B
0.024 ±0.014	3	[7] BORTOLETTO	90	CLEO	$e^+e^- \to \Upsilon(4S)$

[1] AUBERT 06N reports $(0.71 \pm 0.13 \pm 0.09) \times 10^{-2}$ from a measurement of $[\Gamma(B^0 \to D^*(2010)^- D_s^+)/\Gamma_{total}] \times [B(D_s^+ \to \phi\pi^+)]$ assuming $B(D_s^+ \to \phi\pi^+) = 0.0462 \pm 0.0062$, which we rescale to our best value $B(D_s^+ \to \phi\pi^+) = (4.5 \pm 0.4) \times 10^{-2}$. Our first error is their experiment's error and our second error is the systematic error from using our best value.

[2] AUBERT 03I reports 0.0103 ± 0.0014 ± 0.0013 from a measurement of $[\Gamma(B^0 \to D^*(2010)^- D_s^+)/\Gamma_{total}] \times [B(D_s^+ \to \phi\pi^+)]$ assuming $B(D_s^+ \to \phi\pi^+) = 0.036$, which we rescale to our best value $B(D_s^+ \to \phi\pi^+) = (4.5 \pm 0.4) \times 10^{-2}$. Our first error is their experiment's error and our second error is the systematic error from using our best value.

[3] AHMED 00B reports 0.0110 ± 0.0018 ± 0.0011 from a measurement of $[\Gamma(B^0 \to D^*(2010)^- D_s^+)/\Gamma_{total}] \times [B(D_s^+ \to \phi\pi^+)]$ assuming $B(D_s^+ \to \phi\pi^+) = 0.036$, which we rescale to our best value $B(D_s^+ \to \phi\pi^+) = (4.5 \pm 0.4) \times 10^{-2}$. Our first error is their experiment's error and our second error is the systematic error from using our best value.

[4] ALBRECHT 92G reports 0.014 ± 0.010 ± 0.003 from a measurement of $[\Gamma(B^0 \to D^*(2010)^- D_s^+)/\Gamma_{total}] \times [B(D_s^+ \to \phi\pi^+)]$ assuming $B(D_s^+ \to \phi\pi^+) = 0.027$, which we rescale to our best value $B(D_s^+ \to \phi\pi^+) = (4.5 \pm 0.4) \times 10^{-2}$. Our first error is their experiment's error and our second error is the systematic error from using our best value. Assumes PDG 1990 D^+ and $D^*(2010)^+$ branching ratios, e.g., $B(D^0 \to K^-\pi^+) = 3.71 \pm 0.25\%$, $B(D^+ \to K^- 2\pi^+) = 7.1 \pm 1.0\%$, and $B(D^*(2010)^+ \to D^0\pi^+) = 55 \pm 4\%$.

[5] BORTOLETTO 92 reports 0.016 ± 0.009 ± 0.006 from a measurement of $[\Gamma(B^0 \to D^*(2010)^- D_s^+)/\Gamma_{total}] \times [B(D_s^+ \to \phi\pi^+)]$ assuming $B(D_s^+ \to \phi\pi^+) = 0.030 \pm 0.011$, which we rescale to our best value $B(D_s^+ \to \phi\pi^+) = (4.5 \pm 0.4) \times 10^{-2}$. Our first error is their experiment's error and our second error is the systematic error from using our best value. Assumes equal production of B^+ and B^0 at the $\Upsilon(4S)$ and uses Mark III branching fractions for the D and $D^*(2010)$.

[6] GIBAUT 96 reports 0.0093 ± 0.0023 ± 0.0016 from a measurement of $[\Gamma(B^0 \to D^*(2010)^- D_s^+)/\Gamma_{total}] \times [B(D_s^+ \to \phi\pi^+)]$ assuming $B(D_s^+ \to \phi\pi^+) = 0.035$, which we rescale to our best value $B(D_s^+ \to \phi\pi^+) = (4.5 \pm 0.4) \times 10^{-2}$. Our first error is their experiment's error and our second error is the systematic error from using our best value.

[7] BORTOLETTO 90 assume $B(D_s \to \phi\pi^+) = 2\%$. Superseded by BORTOLETTO 92.

$\Gamma(D^- D_s^{*+})/\Gamma_{total}$ — Γ_{85}/Γ

VALUE	DOCUMENT ID		TECN	COMMENT
0.0074±0.0016 OUR AVERAGE				
0.0071±0.0016±0.0006	[1] AUBERT	06N	BABR	$e^+e^- \to \Upsilon(4S)$
0.0078±0.0032±0.0007	[2] GIBAUT	96	CLE2	$e^+e^- \to \Upsilon(4S)$
0.016 ±0.012 ±0.001	[3] ALBRECHT	92G	ARG	$e^+e^- \to \Upsilon(4S)$

[1] AUBERT 06N reports $(0.69 \pm 0.16 \pm 0.09) \times 10^{-2}$ from a measurement of $[\Gamma(B^0 \to D^- D_s^{*+})/\Gamma_{total}] \times [B(D_s^+ \to \phi\pi^+)]$ assuming $B(D_s^+ \to \phi\pi^+) = 0.0462 \pm 0.0062$, which we rescale to our best value $B(D_s^+ \to \phi\pi^+) = (4.5 \pm 0.4) \times 10^{-2}$. Our first error is their experiment's error and our second error is the systematic error from using our best value.

[2] GIBAUT 96 reports 0.0100 ± 0.0035 ± 0.0022 from a measurement of $[\Gamma(B^0 \to D^- D_s^{*+})/\Gamma_{total}] \times [B(D_s^+ \to \phi\pi^+)]$ assuming $B(D_s^+ \to \phi\pi^+) = 0.035$, which we rescale to our best value $B(D_s^+ \to \phi\pi^+) = (4.5 \pm 0.4) \times 10^{-2}$. Our first error is their experiment's error and our second error is the systematic error from using our best value.

[3] ALBRECHT 92G reports 0.027 ± 0.017 ± 0.009 from a measurement of $[\Gamma(B^0 \to D^- D_s^{*+})/\Gamma_{total}] \times [B(D_s^+ \to \phi\pi^+)]$ assuming $B(D_s^+ \to \phi\pi^+) = 0.027$, which we rescale to our best value $B(D_s^+ \to \phi\pi^+) = (4.5 \pm 0.4) \times 10^{-2}$. Our first error is their experiment's error and our second error is the systematic error from using our best value. Assumes PDG 1990 D^+ branching ratios, e.g., $B(D^+ \to K^- 2\pi^+) = 7.7 \pm 1.0\%$.

$\Gamma(D^*(2010)^- D_s^{*+})/\Gamma_{total}$ — Γ_{86}/Γ

VALUE	DOCUMENT ID		TECN	COMMENT
0.0177±0.0014 OUR AVERAGE				
0.0173±0.0018±0.0015	[1] AUBERT	06N	BABR	$e^+e^- \to \Upsilon(4S)$
0.0188±0.0009±0.0017	[2] AUBERT	05V	BABR	$e^+e^- \to \Upsilon(4S)$
0.0158±0.0027±0.0014	[3] AUBERT	03I	BABR	$e^+e^- \to \Upsilon(4S)$
0.015 ±0.004 ±0.001	[4] AHMED	00B	CLE2	$e^+e^- \to \Upsilon(4S)$
0.016 ±0.009 ±0.001	[5] ALBRECHT	92G	ARG	$e^+e^- \to \Upsilon(4S)$
• • • We do not use the following data for averages, fits, limits, etc. • • •				
0.016 ±0.005 ±0.001	[6] GIBAUT	96	CLE2	Repl. by AHMED 00B

[1] AUBERT 06N reports $(1.68 \pm 0.21 \pm 0.19) \times 10^{-2}$ from a measurement of $[\Gamma(B^0 \to D^*(2010)^- D_s^{*+})/\Gamma_{total}] \times [B(D_s^+ \to \phi\pi^+)]$ assuming $B(D_s^+ \to \phi\pi^+) = 0.0462 \pm 0.0062$, which we rescale to our best value $B(D_s^+ \to \phi\pi^+) = (4.5 \pm 0.4) \times 10^{-2}$. Our first error is their experiment's error and our second error is the systematic error from using our best value.

[2] A partial reconstruction technique is used and the result is independent of the particle decay rate of D_s^+ meson. It also provides a model-independent determination of $B(D_s^+ \to \phi\pi^+) = (4.81 \pm 0.52 \pm 0.38)\%$.

[3] AUBERT 03I reports 0.0197 ± 0.0015 ± 0.0030 from a measurement of $[\Gamma(B^0 \to D^*(2010)^- D_s^{*+})/\Gamma_{total}] \times [B(D_s^+ \to \phi\pi^+)]$ assuming $B(D_s^+ \to \phi\pi^+) = 0.036$, which we rescale to our best value $B(D_s^+ \to \phi\pi^+) = (4.5 \pm 0.4) \times 10^{-2}$. Our first error is their experiment's error and our second error is the systematic error from using our best value.

[4] AHMED 00B reports 0.0182 ± 0.0037 ± 0.0025 from a measurement of $[\Gamma(B^0 \to D^*(2010)^- D_s^{*+})/\Gamma_{total}] \times [B(D_s^+ \to \phi\pi^+)]$ assuming $B(D_s^+ \to \phi\pi^+) = 0.036$, which we rescale to our best value $B(D_s^+ \to \phi\pi^+) = (4.5 \pm 0.4) \times 10^{-2}$. Our first error is their experiment's error and our second error is the systematic error from using our best value.

[5] ALBRECHT 92G reports 0.026 ± 0.014 ± 0.006 from a measurement of $[\Gamma(B^0 \to D^*(2010)^- D_s^{*+})/\Gamma_{total}] \times [B(D_s^+ \to \phi\pi^+)]$ assuming $B(D_s^+ \to \phi\pi^+) = 0.027$, which we rescale to our best value $B(D_s^+ \to \phi\pi^+) = (4.5 \pm 0.4) \times 10^{-2}$. Our first error is their experiment's error and our second error is the systematic error from using our best value. Assumes PDG 1990 D^+ and $D^*(2010)^+$ branching ratios, e.g., $B(D^0 \to K^-\pi^+) = 3.71 \pm 0.25\%$, $B(D^+ \to K^- 2\pi^+) = 7.1 \pm 1.0\%$, and $B(D^*(2010)^+ \to D^0\pi^+) = 55 \pm 4\%$.

[6] GIBAUT 96 reports 0.0203 ± 0.0050 ± 0.0036 from a measurement of $[\Gamma(B^0 \to D^*(2010)^- D_s^{*+})/\Gamma_{total}] \times [B(D_s^+ \to \phi\pi^+)]$ assuming $B(D_s^+ \to \phi\pi^+) = 0.035$, which we rescale to our best value $B(D_s^+ \to \phi\pi^+) = (4.5 \pm 0.4) \times 10^{-2}$. Our first error is their experiment's error and our second error is the systematic error from using our best value.

$\Gamma(D^*(2010)^- D_s^{*+})/\Gamma(D^*(2010)^- D_s^+)$ — Γ_{86}/Γ_{84}

VALUE	DOCUMENT ID		TECN	COMMENT
2.19±0.08±0.02	[1] AAIJ	21S	LHCB	pp at 13 TeV

[1] AAIJ 21S reports $[\Gamma(B^0 \to D^*(2010)^- D_s^{*+})/\Gamma(B^0 \to D^*(2010)^- D_s^+)] \times [B(D_s^{*+} \to D_s^+\gamma)] = 2.045 \pm 0.022 \pm 0.071$ which we divide by our best value $B(D_s^{*+} \to D_s^+\gamma) = (93.5 \pm 0.7) \times 10^{-2}$. Our first error is their experiment's error and our second error is the systematic error from using our best value.

$[\Gamma(D^*(2010)^- D_s^+) + \Gamma(D^*(2010)^- D_s^{*+})]/\Gamma_{total}$ — $(\Gamma_{84}+\Gamma_{86})/\Gamma$

VALUE (units 10^{-2})	EVTS	DOCUMENT ID		TECN	COMMENT
2.5 ±0.4 OUR AVERAGE					
2.40±0.35±0.22		[1] AUBERT	03I	BABR	$e^+e^- \to \Upsilon(4S)$
3.3 ±0.9 ±0.3	22	[2] BORTOLETTO	90	CLEO	$e^+e^- \to \Upsilon(4S)$

[1] AUBERT 03I reports $(3.00 \pm 0.19 \pm 0.39) \times 10^{-2}$ from a measurement of $[\left[\Gamma(B^0 \to D^*(2010)^- D_s^+) + \Gamma(B^0 \to D^*(2010)^- D_s^{*+})\right]/\Gamma_{total}] \times [B(D_s^+ \to \phi\pi^+)]$ assuming $B(D_s^+ \to \phi\pi^+) = 0.036$, which we rescale to our best value $B(D_s^+ \to \phi\pi^+) = (4.5 \pm 0.4) \times 10^{-2}$. Our first error is their experiment's error and our second error is the systematic error from using our best value.

[2] BORTOLETTO 90 reports $(7.5 \pm 2.0) \times 10^{-2}$ from a measurement of $[\left[\Gamma(B^0 \to D^*(2010)^- D_s^+) + \Gamma(B^0 \to D^*(2010)^- D_s^{*+})\right]/\Gamma_{total}] \times [B(D_s^+ \to \phi\pi^+)]$ assuming $B(D_s^+ \to \phi\pi^+) = 0.02$, which we rescale to our best value $B(D_s^+ \to \phi\pi^+) = (4.5 \pm 0.4) \times 10^{-2}$. Our first error is their experiment's error and our second error is the systematic error from using our best value.

$\Gamma(D_{s0}(2317)^- K^+,\ D_{s0}^- \to D_s^- \pi^0)/\Gamma_{total}$ — Γ_{87}/Γ

VALUE (units 10^{-5})	DOCUMENT ID		TECN	COMMENT
$4.2^{+1.4}_{-1.3}$±0.4	[1] DRUTSKOY	05	BELL	$e^+e^- \to \Upsilon(4S)$

[1] DRUTSKOY 05 reports $(5.3^{+1.5}_{-1.3} \pm 1.6) \times 10^{-5}$ from a measurement of $[\Gamma(B^0 \to D_{s0}(2317)^- K^+,\ D_{s0}^- \to D_s^- \pi^0)/\Gamma_{total}] \times [B(D_s^+ \to \phi\pi^+)]$ assuming $B(D_s^+ \to \phi\pi^+) = 0.036 \pm 0.009$, which we rescale to our best value $B(D_s^+ \to \phi\pi^+) = (4.5 \pm 0.4) \times 10^{-2}$. Our first error is their experiment's error and our second error is the systematic error from using our best value.

$\Gamma(D_{s0}(2317)^- \pi^+,\ D_{s0}^- \to D_s^- \pi^0)/\Gamma_{total}$ — Γ_{88}/Γ

VALUE (units 10^{-5})	CL%	DOCUMENT ID		TECN	COMMENT
<2.5	90	[1] DRUTSKOY	05	BELL	$e^+e^- \to \Upsilon(4S)$

[1] Assumes equal production of B^+ and B^0 at the $\Upsilon(4S)$.

Downloaded from https://academic.oup.com/ptep/article/2022/8/083C01/6651666 by KIT Library user on 27 September 2022

$\Gamma(D_{sJ}(2457)^- K^+,\ D_{sJ}^- \to D_s^- \pi^0)/\Gamma_{total}$ — Γ_{89}/Γ

VALUE (units 10^{-5})	CL%	DOCUMENT ID		TECN	COMMENT
<0.94	90	[1] DRUTSKOY	05	BELL	$e^+e^- \to \Upsilon(4S)$

[1] Assumes equal production of B^+ and B^0 at the $\Upsilon(4S)$.

$\Gamma(D_{sJ}(2457)^- \pi^+,\ D_{sJ}^- \to D_s^- \pi^0)/\Gamma_{total}$ — Γ_{90}/Γ

VALUE (units 10^{-5})	CL%	DOCUMENT ID		TECN	COMMENT
<0.40	90	[1] DRUTSKOY	05	BELL	$e^+e^- \to \Upsilon(4S)$

[1] Assumes equal production of B^+ and B^0 at the $\Upsilon(4S)$.

$\Gamma(D_s^- D_s^+)/\Gamma_{total}$ — Γ_{91}/Γ

VALUE	CL%	DOCUMENT ID		TECN	COMMENT
$< 3.6 \times 10^{-5}$	90	[1] ZUPANC	07	BELL	$e^+e^- \to \Upsilon(4S)$
• • • We do not use the following data for averages, fits, limits, etc. • • •					
$<10 \times 10^{-5}$	90	[1] AUBERT,BE	05F	BABR	$e^+e^- \to \Upsilon(4S)$

[1] Assumes equal production of B^+ and B^0 at the $\Upsilon(4S)$.

$\Gamma(D_s^{*-} D_s^+)/\Gamma_{total}$ — Γ_{92}/Γ

VALUE	CL%	DOCUMENT ID		TECN	COMMENT
$<1.3 \times 10^{-4}$	90	[1] AUBERT,BE	05F	BABR	$e^+e^- \to \Upsilon(4S)$

[1] Assumes equal production of B^+ and B^0 at the $\Upsilon(4S)$.

$\Gamma(D_s^{*-} D_s^{*+})/\Gamma_{total}$ — Γ_{93}/Γ

VALUE	CL%	DOCUMENT ID		TECN	COMMENT
$<2.4 \times 10^{-4}$	90	[1] AUBERT,BE	05F	BABR	$e^+e^- \to \Upsilon(4S)$

[1] Assumes equal production of B^+ and B^0 at the $\Upsilon(4S)$.

$\Gamma(D_{s0}^*(2317)^+ D^-,\ D_{s0}^{*+} \to D_s^+ \pi^0)/\Gamma_{total}$ — Γ_{94}/Γ

VALUE (units 10^{-3})	DOCUMENT ID		TECN	COMMENT
1.06±0.16 OUR AVERAGE	Error includes scale factor of 1.1.			
$0.99^{+0.16}_{-0.15} \pm 0.03$	[1,2] CHOI	15A	BELL	$e^+e^- \to \Upsilon(4S)$
$1.4^{+0.5}_{-0.4} \pm 0.1$	[2,3] AUBERT,B	04S	BABR	$e^+e^- \to \Upsilon(4S)$
• • • We do not use the following data for averages, fits, limits, etc. • • •				
$0.69^{+0.29}_{-0.24} \pm 0.06$	[2,4] KROKOVNY	03B	BELL	Repl. by CHOI 15A

[1] CHOI 15A reports $(10.2^{+1.3}_{-1.2} \pm 1.0 \pm 0.4) \times 10^{-4}$ from a measurement of $[\Gamma(B^0 \to D_{s0}^*(2317)^+ D^-,\ D_{s0}^{*+} \to D_s^+ \pi^0)/\Gamma_{total}] \times [B(D_s^+ \to K^+K^-\pi^+)] \times [B(D^+ \to K^-2\pi^+)]$ assuming $B(D_s^+ \to K^+K^-\pi^+) = (5.39 \pm 0.21) \times 10^{-2}$, $B(D^+ \to K^-2\pi^+) = (9.13 \pm 0.19) \times 10^{-2}$, which we rescale to our best values $B(D_s^+ \to K^+K^-\pi^+) = (5.38 \pm 0.10) \times 10^{-2}$, $B(D^+ \to K^-2\pi^+) = (9.38 \pm 0.16) \times 10^{-2}$. Our first error is their experiment's error and our second error is the systematic error from using our best values.

[2] Assumes equal production of B^+ and B^0 at the $\Upsilon(4S)$.

[3] AUBERT,B 04S reports $(1.8 \pm 0.4^{+0.7}_{-0.5}) \times 10^{-3}$ from a measurement of $[\Gamma(B^0 \to D_{s0}^*(2317)^+ D^-,\ D_{s0}^{*+} \to D_s^+ \pi^0)/\Gamma_{total}] \times [B(D_s^+ \to \phi\pi^+)]$ assuming $B(D_s^+ \to \phi\pi^+) = 0.036 \pm 0.009$, which we rescale to our best value $B(D_s^+ \to \phi\pi^+) = (4.5 \pm 0.4) \times 10^{-2}$. Our first error is their experiment's error and our second error is the systematic error from using our best value.

[4] KROKOVNY 03B reports $(0.86^{+0.33}_{-0.26} \pm 0.26) \times 10^{-3}$ from a measurement of $[\Gamma(B^0 \to D_{s0}^*(2317)^+ D^-,\ D_{s0}^{*+} \to D_s^+ \pi^0)/\Gamma_{total}] \times [B(D_s^+ \to \phi\pi^+)]$ assuming $B(D_s^+ \to \phi\pi^+) = 0.036 \pm 0.009$, which we rescale to our best value $B(D_s^+ \to \phi\pi^+) = (4.5 \pm 0.4) \times 10^{-2}$. Our first error is their experiment's error and our second error is the systematic error from using our best value.

$\Gamma(D_{s0}(2317)^+ D^-,\ D_{s0}^+ \to D_s^{*+} \gamma)/\Gamma_{total}$ — Γ_{95}/Γ

VALUE (units 10^{-3})	CL%	DOCUMENT ID		TECN	COMMENT
<0.95	90	[1] KROKOVNY	03B	BELL	$e^+e^- \to \Upsilon(4S)$

[1] Assumes equal production of B^+ and B^0 at the $\Upsilon(4S)$.

$\Gamma(D_{s0}(2317)^+ D^*(2010)^-,\ D_{s0}^+ \to D_s^+ \pi^0)/\Gamma_{total}$ — Γ_{96}/Γ

VALUE (units 10^{-3})	DOCUMENT ID		TECN	COMMENT
$1.5 \pm 0.4^{+0.5}_{-0.4}$	[1] AUBERT,B	04S	BABR	$e^+e^- \to \Upsilon(4S)$

[1] Assumes equal production of B^+ and B^0 at the $\Upsilon(4S)$.

$\Gamma(D_{sJ}(2457)^+ D^-)/\Gamma_{total}$ — Γ_{97}/Γ

VALUE (units 10^{-3})	DOCUMENT ID		TECN	COMMENT
3.5±1.1 OUR AVERAGE				
2.6±1.5±0.7	[1] AUBERT	06N	BABR	$e^+e^- \to \Upsilon(4S)$
$4.8^{+2.2}_{-1.6} \pm 1.1$	[2,3] AUBERT,B	04S	BABR	$e^+e^- \to \Upsilon(4S)$
$3.9^{+1.5}_{-1.3} \pm 0.9$	[2,4] KROKOVNY	03B	BELL	$e^+e^- \to \Upsilon(4S)$

[1] Uses a missing-mass method in the events that one of the B mesons is fully reconstructed.

[2] Assumes equal production of B^+ and B^0 at the $\Upsilon(4S)$.

[3] AUBERT,B 04S reports $[\Gamma(B^0 \to D_{sJ}(2457)^+ D^-)/\Gamma_{total}] \times [B(D_{s1}(2460)^+ \to D_s^{*+}\pi^0)] = (2.3^{+1.0}_{-0.7} \pm 0.3) \times 10^{-3}$ which we divide by our best value $B(D_{s1}(2460)^+ \to D_s^{*+}\pi^0) = (48 \pm 11) \times 10^{-2}$. Our first error is their experiment's error and our second error is the systematic error from using our best value.

[4] KROKOVNY 03B reports $[\Gamma(B^0 \to D_{sJ}(2457)^+ D^-)/\Gamma_{total}] \times [B(D_{s1}(2460)^+ \to D_s^{*+}\pi^0)] = (1.9^{+0.7}_{-0.6} \pm 0.2) \times 10^{-3}$ which we divide by our best value $B(D_{s1}(2460)^+ \to D_s^{*+}\pi^0) = (48 \pm 11) \times 10^{-2}$. Our first error is their experiment's error and our second error is the systematic error from using our best value.

$\Gamma(D_{sJ}(2457)^+ D^-,\ D_{sJ}^+ \to D_s^+ \gamma)/\Gamma_{total}$ — Γ_{98}/Γ

VALUE (units 10^{-3})	DOCUMENT ID		TECN	COMMENT
$0.65^{+0.17}_{-0.14}$ OUR AVERAGE				
$0.64^{+0.24}_{-0.16} \pm 0.06$	[1,2] AUBERT,B	04S	BABR	$e^+e^- \to \Upsilon(4S)$
$0.66^{+0.21}_{-0.19} \pm 0.06$	[1,3] KROKOVNY	03B	BELL	$e^+e^- \to \Upsilon(4S)$

[1] Assumes equal production of B^+ and B^0 at the $\Upsilon(4S)$.

[2] AUBERT,B 04S reports $(0.8 \pm 0.2^{+0.3}_{-0.2}) \times 10^{-3}$ from a measurement of $[\Gamma(B^0 \to D_{sJ}(2457)^+ D^-,\ D_{sJ}^+ \to D_s^+ \gamma)/\Gamma_{total}] \times [B(D_s^+ \to \phi\pi^+)]$ assuming $B(D_s^+ \to \phi\pi^+) = 0.036 \pm 0.009$, which we rescale to our best value $B(D_s^+ \to \phi\pi^+) = (4.5 \pm 0.4) \times 10^{-2}$. Our first error is their experiment's error and our second error is the systematic error from using our best value.

[3] KROKOVNY 03B reports $(0.82^{+0.22}_{-0.19} \pm 0.25) \times 10^{-3}$ from a measurement of $[\Gamma(B^0 \to D_{sJ}(2457)^+ D^-,\ D_{sJ}^+ \to D_s^+ \gamma)/\Gamma_{total}] \times [B(D_s^+ \to \phi\pi^+)]$ assuming $B(D_s^+ \to \phi\pi^+) = 0.036 \pm 0.009$, which we rescale to our best value $B(D_s^+ \to \phi\pi^+) = (4.5 \pm 0.4) \times 10^{-2}$. Our first error is their experiment's error and our second error is the systematic error from using our best value.

$\Gamma(D_{sJ}(2457)^+ D^-,\ D_{sJ}^+ \to D_s^{*+} \gamma)/\Gamma_{total}$ — Γ_{99}/Γ

VALUE (units 10^{-3})	CL%	DOCUMENT ID		TECN	COMMENT
<0.60	90	[1] KROKOVNY	03B	BELL	$e^+e^- \to \Upsilon(4S)$

[1] Assumes equal production of B^+ and B^0 at the $\Upsilon(4S)$.

$\Gamma(D_{sJ}(2457)^+ D^-,\ D_{sJ}^+ \to D_s^+ \pi^+\pi^-)/\Gamma_{total}$ — Γ_{100}/Γ

VALUE (units 10^{-3})	CL%	DOCUMENT ID		TECN	COMMENT
<0.20	90	[1] KROKOVNY	03B	BELL	$e^+e^- \to \Upsilon(4S)$

[1] Assumes equal production of B^+ and B^0 at the $\Upsilon(4S)$.

$\Gamma(D_{sJ}(2457)^+ D^-,\ D_{sJ}^+ \to D_s^+ \pi^0)/\Gamma_{total}$ — Γ_{101}/Γ

VALUE (units 10^{-3})	CL%	DOCUMENT ID		TECN	COMMENT
<0.36	90	[1] KROKOVNY	03B	BELL	$e^+e^- \to \Upsilon(4S)$

[1] Assumes equal production of B^+ and B^0 at the $\Upsilon(4S)$.

$\Gamma(D^*(2010)^- D_{sJ}(2457)^+)/\Gamma_{total}$ — Γ_{102}/Γ

VALUE (units 10^{-3})	DOCUMENT ID		TECN	COMMENT
9.3±2.2 OUR AVERAGE				
8.8±2.0±1.4	[1] AUBERT	06N	BABR	$e^+e^- \to \Upsilon(4S)$
$11^{+5}_{-4} \pm 3$	[2,3] AUBERT,B	04S	BABR	$e^+e^- \to \Upsilon(4S)$

[1] Uses a missing-mass method in the events that one of the B mesons is fully reconstructed.

[2] AUBERT,B 04S reports $[\Gamma(B^0 \to D^*(2010)^- D_{sJ}(2457)^+)/\Gamma_{total}] \times [B(D_{s1}(2460)^+ \to D_s^{*+}\pi^0)] = (5.5 \pm 1.2^{+2.2}_{-1.6}) \times 10^{-3}$ which we divide by our best value $B(D_{s1}(2460)^+ \to D_s^{*+}\pi^0) = (48 \pm 11) \times 10^{-2}$. Our first error is their experiment's error and our second error is the systematic error from using our best value.

[3] Assumes equal production of B^+ and B^0 at the $\Upsilon(4S)$.

$\Gamma(D_{sJ}(2457)^+ D^*(2010),\ D_{sJ}^+ \to D_s^+ \gamma)/\Gamma_{total}$ — Γ_{103}/Γ

VALUE (units 10^{-3})	DOCUMENT ID		TECN	COMMENT
$2.3 \pm 0.3^{+0.9}_{-0.6}$	[1] AUBERT,B	04S	BABR	$e^+e^- \to \Upsilon(4S)$

[1] Assumes equal production of B^+ and B^0 at the $\Upsilon(4S)$.

$[\Gamma(D^- D_{s1}(2536)^+,\ D_{s1}^+ \to D^{*0} K^+) + \Gamma(D^{*+} K^0)]/\Gamma_{total}$ — $\Gamma_{104}/\Gamma = (\Gamma_{105}+\Gamma_{106})/\Gamma$

VALUE (units 10^{-4})	DOCUMENT ID		TECN	COMMENT
2.75±0.62±0.36	[1,2] AUSHEV	11	BELL	$e^+e^- \to \Upsilon(4S)$

[1] Uses $\Gamma(D^*(2007)^0 \to D^0\pi^0)\ /\ \Gamma(D^*(2007)^0 \to D^0\gamma) = 1.74 \pm 0.13$ and $\Gamma(D_{s1}(2536)^+ \to D^*(2007)^0 K^+)\ /\ \Gamma(D_{s1}(2536)^+ \to D^*(2010)^+ K^0) = 1.36 \pm 0.2$.

[2] Assumes equal production of B^+ and B^0 at the $\Upsilon(4S)$.

$\Gamma(D^- D_{s1}(2536)^+,\ D_{s1}^+ \to D^{*0} K^+)/\Gamma_{total}$ — Γ_{105}/Γ

VALUE (units 10^{-4})	CL%	DOCUMENT ID		TECN	COMMENT
1.71±0.48±0.32		[1] AUBERT	08B	BABR	$e^+e^- \to \Upsilon(4S)$
• • • We do not use the following data for averages, fits, limits, etc. • • •					
<5	90	AUBERT	03X	BABR	Repl. by AUBERT 08B

[1] Assumes equal production of B^+ and B^0 at the $\Upsilon(4S)$.

$\Gamma(D^- D_{s1}(2536)^+,\ D_{s1}^+ \to D^{*+} K^0)/\Gamma_{total}$ — Γ_{106}/Γ

VALUE (units 10^{-4})	DOCUMENT ID		TECN	COMMENT
2.61±1.03±0.31	[1] AUBERT	08B	BABR	$e^+e^- \to \Upsilon(4S)$

[1] Assumes equal production of B^+ and B^0 at the $\Upsilon(4S)$.

Downloaded from https://academic.oup.com/ptep/article/2022/8/083C01/6651666 by KIT Library user on 27 September 2022

$[\Gamma(D^*(2010)^- D_{s1}(2536)^+,\ D_{s1}^+ \to D^{*0} K^+) + \Gamma(D^{*+} K^0)]/\Gamma_{total}$ — $\Gamma_{107}/\Gamma = (\Gamma_{108}+\Gamma_{109})/\Gamma$

VALUE (units 10^{-4})	DOCUMENT ID		TECN	COMMENT
5.01±1.21±0.70	[1,2] AUSHEV	11	BELL	$e^+e^- \to \Upsilon(4S)$

[1] Uses $\Gamma(D^*(2007)^0 \to D^0\pi^0)$ / $\Gamma(D^*(2007)^0 \to D^0\gamma)$ = 1.74 ± 0.13 and $\Gamma(D_{s1}(2536)^+ \to D^*(2007)^0 K^+)$ / $\Gamma(D_{s1}(2536)^+ \to D^*(2010)^+ K^0)$ = 1.36 ± 0.2.
[2] Assumes equal production of B^+ and B^0 at the $\Upsilon(4S)$.

$\Gamma(D^*(2010)^- D_{s1}(2536)^+,\ D_{s1}^+ \to D^{*0} K^+)/\Gamma_{total}$ — Γ_{108}/Γ

VALUE (units 10^{-4})	CL%	DOCUMENT ID		TECN	COMMENT
3.32±0.88±0.66		[1] AUBERT	08B	BABR	$e^+e^- \to \Upsilon(4S)$
• • • We do not use the following data for averages, fits, limits, etc. • • •					
<7	90	AUBERT	03X	BABR	Repl. by AUBERT 08B

[1] Assumes equal production of B^+ and B^0 at the $\Upsilon(4S)$.

$\Gamma(D^{*-} D_{s1}(2536)^+,\ D_{s1}^+ \to D^{*+} K^0)/\Gamma_{total}$ — Γ_{109}/Γ

VALUE (units 10^{-4})	DOCUMENT ID		TECN	COMMENT
5.00±1.51±0.67	[1] AUBERT	08B	BABR	$e^+e^- \to \Upsilon(4S)$

[1] Assumes equal production of B^+ and B^0 at the $\Upsilon(4S)$.

$\Gamma(D^- D_{sJ}(2573)^+,\ D_{sJ}^+ \to D^0 K^+)/\Gamma_{total}$ — Γ_{110}/Γ

VALUE (units 10^{-5})	CL%	DOCUMENT ID		TECN	COMMENT
3.4±1.7±0.5		[1] LEES	15C	BABR	$e^+e^- \to \Upsilon(4S)$
• • • We do not use the following data for averages, fits, limits, etc. • • •					
<10	90	AUBERT	03X	BABR	$e^+e^- \to \Upsilon(4S)$

[1] Assumes equal production of B^+ and B^0 at the $\Upsilon(4S)$.

$\Gamma(D^*(2010)^- D_{sJ}(2573)^+,\ D_{sJ}^+ \to D^0 K^+)/\Gamma_{total}$ — Γ_{111}/Γ

VALUE (units 10^{-4})	CL%	DOCUMENT ID		TECN	COMMENT
<2	90	AUBERT	03X	BABR	$e^+e^- \to \Upsilon(4S)$

$\Gamma(D^- D_{sJ}(2700)^+,\ D_{sJ}^+ \to D^0 K^+)/\Gamma_{total}$ — Γ_{112}/Γ

VALUE (units 10^{-4})	DOCUMENT ID		TECN	COMMENT
7.14±0.96±0.69	[1] LEES	15C	BABR	$e^+e^- \to \Upsilon(4S)$

[1] Assumes equal production of B^+ and B^0 at the $\Upsilon(4S)$.

$\Gamma(D^+\pi^-)/\Gamma_{total}$ — Γ_{113}/Γ

VALUE (units 10^{-7})	DOCUMENT ID		TECN	COMMENT
7.3±1.2±0.2	[1,2] DAS	10	BELL	$e^+e^- \to \Upsilon(4S)$

[1] DAS 10 reports $[\Gamma(B^0 \to D^+\pi^-)/\Gamma_{total}]$ / $[B(B^0 \to D^-\pi^+)] = (2.92 \pm 0.38 \pm 0.31) \times 10^{-4}$ which we multiply by our best value $B(B^0 \to D^-\pi^+) = (2.51 \pm 0.08) \times 10^{-3}$. Our first error is their experiment's error and our second error is the systematic error from using our best value.
[2] Derived using $\tan(\theta_C)\ f_D/f_{D_s} \sqrt{B(B^0 \to D_s^+\pi^-)/B(B^0 \to D^-\pi^+)}$ by assuming the flavor SU(3) symmetry, where θ_C is the Cabibbo angle, f_D (f_{D_s}) is the D (D_s) meson decay constant.

$\Gamma(D_s^+\pi^-)/\Gamma_{total}$ — Γ_{114}/Γ

VALUE (units 10^{-6})	CL%	DOCUMENT ID		TECN	COMMENT
20.3±1.8 OUR FIT					
21.6±2.6 OUR AVERAGE					
19.9±2.6±1.8		[1] DAS	10	BELL	$e^+e^- \to \Upsilon(4S)$
25 ±4 ±2		[1] AUBERT	08AJ	BABR	$e^+e^- \to \Upsilon(4S)$
• • • We do not use the following data for averages, fits, limits, etc. • • •					
14.0±3.5±1.3		[2] AUBERT	07K	BABR	Repl. by AUBERT 08AJ
25 ±9 ±2		[3] AUBERT	03D	BABR	Repl. by AUBERT 07K
$19\ ^{+9}_{-7}$ ±2		[4] KROKOVNY	02	BELL	Repl. by DAS 10
< 220	90	[5] ALEXANDER	93B	CLE2	$e^+e^- \to \Upsilon(4S)$
<1300	90	[6] BORTOLETTO	90	CLEO	$e^+e^- \to \Upsilon(4S)$

[1] Assumes equal production of B^+ and B^0 at the $\Upsilon(4S)$.
[2] AUBERT 07K reports $[\Gamma(B^0 \to D_s^+\pi^-)/\Gamma_{total}] \times [B(D_s^+ \to \phi\pi^+)] = (0.63 \pm 0.15 \pm 0.05) \times 10^{-6}$ which we divide by our best value $B(D_s^+ \to \phi\pi^+) = (4.5 \pm 0.4) \times 10^{-2}$. Our first error is their experiment's error and our second error is the systematic error from using our best value.
[3] AUBERT 03D reports $[\Gamma(B^0 \to D_s^+\pi^-)/\Gamma_{total}] \times [B(D_s^+ \to \phi\pi^+)] = (1.13 \pm 0.33 \pm 0.21) \times 10^{-6}$ which we divide by our best value $B(D_s^+ \to \phi\pi^+) = (4.5 \pm 0.4) \times 10^{-2}$. Our first error is their experiment's error and our second error is the systematic error from using our best value.
[4] KROKOVNY 02 reports $[\Gamma(B^0 \to D_s^+\pi^-)/\Gamma_{total}] \times [B(D_s^+ \to \phi\pi^+)] = (0.86\ ^{+0.37}_{-0.30} \pm 0.11) \times 10^{-6}$ which we divide by our best value $B(D_s^+ \to \phi\pi^+) = (4.5 \pm 0.4) \times 10^{-2}$. Our first error is their experiment's error and our second error is the systematic error from using our best value.
[5] ALEXANDER 93B reports $< 270 \times 10^{-6}$ from a measurement of $[\Gamma(B^0 \to D_s^+\pi^-)/\Gamma_{total}] \times [B(D_s^+ \to \phi\pi^+)]$ assuming $B(D_s^+ \to \phi\pi^+) = 0.037$, which we rescale to our best value $B(D_s^+ \to \phi\pi^+) = 4.5 \times 10^{-2}$.
[6] BORTOLETTO 90 assume $B(D_s \to \phi\pi^+) = 2\%$.

$[\Gamma(D_s^+\pi^-) + \Gamma(D_s^- K^+)]/\Gamma_{total}$ — $(\Gamma_{114}+\Gamma_{124})/\Gamma$

VALUE	CL%	DOCUMENT ID		TECN	COMMENT
<1.0 × 10^{-3}	90	[1] ALBRECHT	93E	ARG	$e^+e^- \to \Upsilon(4S)$

[1] ALBRECHT 93E reports $< 1.7 \times 10^{-3}$ from a measurement of $[\left[\Gamma(B^0 \to D_s^+\pi^-) + \Gamma(B^0 \to D_s^- K^+)\right]/\Gamma_{total}] \times [B(D_s^+ \to \phi\pi^+)]$ assuming $B(D_s^+ \to \phi\pi^+) = 0.027$, which we rescale to our best value $B(D_s^+ \to \phi\pi^+) = 4.5 \times 10^{-2}$.

$\Gamma(D_s^+\pi^-)/\Gamma(D^-\pi^+)$ — Γ_{114}/Γ_{35}

VALUE (units 10^{-3})	DOCUMENT ID		TECN	COMMENT
8.1±0.7 OUR FIT				
7.7±0.7±0.6	AAIJ	21W	LHCB	pp at 7, 8, 13 TeV

$\Gamma(D_s^{*+}\pi^-)/\Gamma_{total}$ — Γ_{115}/Γ

VALUE (units 10^{-5})	CL%	DOCUMENT ID		TECN	COMMENT
2.1 ±0.4 OUR AVERAGE		Error includes scale factor of 1.4.			
1.75±0.34±0.20		[1] JOSHI	10	BELL	$e^+e^- \to \Upsilon(4S)$
$2.6\ ^{+0.5}_{-0.4}$ ±0.2		[1] AUBERT	08AJ	BABR	$e^+e^- \to \Upsilon(4S)$
• • • We do not use the following data for averages, fits, limits, etc. • • •					
2.9 ±0.7 ±0.3		[2] AUBERT	07K	BABR	Repl. by AUBERT 08AJ
< 4.1	90	AUBERT	03D	BABR	Repl. by AUBERT 07K
<40	90	[3] ALEXANDER	93B	CLE2	$e^+e^- \to \Upsilon(4S)$

[1] Assumes equal production of B^+ and B^0 at the $\Upsilon(4S)$.
[2] AUBERT 07K reports $[\Gamma(B^0 \to D_s^{*+}\pi^-)/\Gamma_{total}] \times [B(D_s^+ \to \phi\pi^+)] = (1.32 \pm 0.27 \pm 0.15) \times 10^{-6}$ which we divide by our best value $B(D_s^+ \to \phi\pi^+) = (4.5 \pm 0.4) \times 10^{-2}$. Our first error is their experiment's error and our second error is the systematic error from using our best value.
[3] ALEXANDER 93B reports $< 44 \times 10^{-5}$ from a measurement of $[\Gamma(B^0 \to D_s^{*+}\pi^-)/\Gamma_{total}] \times [B(D_s^+ \to \phi\pi^+)]$ assuming $B(D_s^+ \to \phi\pi^+) = 0.037$, which we rescale to our best value $B(D_s^+ \to \phi\pi^+) = 4.5 \times 10^{-2}$.

$[\Gamma(D_s^{*+}\pi^-) + \Gamma(D_s^{*-} K^+)]/\Gamma_{total}$ — $(\Gamma_{115}+\Gamma_{125})/\Gamma$

VALUE	CL%	DOCUMENT ID		TECN	COMMENT
<7 × 10^{-4}	90	[1] ALBRECHT	93E	ARG	$e^+e^- \to \Upsilon(4S)$

[1] ALBRECHT 93E reports $< 1.2 \times 10^{-3}$ from a measurement of $[\left[\Gamma(B^0 \to D_s^{*+}\pi^-) + \Gamma(B^0 \to D_s^{*-} K^+)\right]/\Gamma_{total}] \times [B(D_s^+ \to \phi\pi^+)]$ assuming $B(D_s^+ \to \phi\pi^+) = 0.027$, which we rescale to our best value $B(D_s^+ \to \phi\pi^+) = 4.5 \times 10^{-2}$.

$\Gamma(D_s^+\rho^-)/\Gamma_{total}$ — Γ_{116}/Γ

VALUE (units 10^{-5})	CL%	DOCUMENT ID		TECN	COMMENT
< 2.4	90	[1] AUBERT	08AJ	BABR	$e^+e^- \to \Upsilon(4S)$
• • • We do not use the following data for averages, fits, limits, etc. • • •					
<130	90	[2] ALBRECHT	93E	ARG	$e^+e^- \to \Upsilon(4S)$
< 50	90	[3] ALEXANDER	93B	CLE2	$e^+e^- \to \Upsilon(4S)$

[1] Assumes equal production of B^+ and B^0 at the $\Upsilon(4S)$.
[2] ALBRECHT 93E reports $< 2.2 \times 10^{-3}$ from a measurement of $[\Gamma(B^0 \to D_s^+\rho^-)/\Gamma_{total}] \times [B(D_s^+ \to \phi\pi^+)]$ assuming $B(D_s^+ \to \phi\pi^+) = 0.027$, which we rescale to our best value $B(D_s^+ \to \phi\pi^+) = 4.5 \times 10^{-2}$.
[3] ALEXANDER 93B reports $< 6.6 \times 10^{-4}$ from a measurement of $[\Gamma(B^0 \to D_s^+\rho^-)/\Gamma_{total}] \times [B(D_s^+ \to \phi\pi^+)]$ assuming $B(D_s^+ \to \phi\pi^+) = 0.037$, which we rescale to our best value $B(D_s^+ \to \phi\pi^+) = 4.5 \times 10^{-2}$.

$\Gamma(D_s^{*+}\rho^-)/\Gamma_{total}$ — Γ_{117}/Γ

VALUE (units 10^{-5})	CL%	DOCUMENT ID		TECN	COMMENT
$4.1\ ^{+1.3}_{-1.2}$±0.4		[1] AUBERT	08AJ	BABR	$e^+e^- \to \Upsilon(4S)$
• • • We do not use the following data for averages, fits, limits, etc. • • •					
<150	90	[2] ALBRECHT	93E	ARG	$e^+e^- \to \Upsilon(4S)$
< 60	90	[3] ALEXANDER	93B	CLE2	$e^+e^- \to \Upsilon(4S)$

[1] Assumes equal production of B^+ and B^0 at the $\Upsilon(4S)$.
[2] ALBRECHT 93E reports $< 2.5 \times 10^{-3}$ from a measurement of $[\Gamma(B^0 \to D_s^{*+}\rho^-)/\Gamma_{total}] \times [B(D_s^+ \to \phi\pi^+)]$ assuming $B(D_s^+ \to \phi\pi^+) = 0.027$, which we rescale to our best value $B(D_s^+ \to \phi\pi^+) = 4.5 \times 10^{-2}$.
[3] ALEXANDER 93B reports $< 7.4 \times 10^{-4}$ from a measurement of $[\Gamma(B^0 \to D_s^{*+}\rho^-)/\Gamma_{total}] \times [B(D_s^+ \to \phi\pi^+)]$ assuming $B(D_s^+ \to \phi\pi^+) = 0.037$, which we rescale to our best value $B(D_s^+ \to \phi\pi^+) = 4.5 \times 10^{-2}$.

$\Gamma(D_s^+ a_0^-)/\Gamma_{total}$ — Γ_{118}/Γ

VALUE (units 10^{-5})	CL%	DOCUMENT ID		TECN	COMMENT
<1.9	90	[1] AUBERT	06X	BABR	$e^+e^- \to \Upsilon(4S)$

[1] Assumes equal production of B^+ and B^0 at the $\Upsilon(4S)$.

Downloaded from https://academic.oup.com/ptep/article/2022/8/083C01/6651666 by KIT Library user on 27 September 2022

$\Gamma(D_s^{*+} a_0^-)/\Gamma_{total}$ — Γ_{119}/Γ

VALUE (units 10^{-5})	CL%	DOCUMENT ID		TECN	COMMENT
<3.6	90	[1] AUBERT	06X	BABR	$e^+e^- \to \Upsilon(4S)$

[1] Assumes equal production of B^+ and B^0 at the $\Upsilon(4S)$.

$\Gamma(D_s^+ a_1(1260)^-)/\Gamma_{total}$ — Γ_{120}/Γ

VALUE	CL%	DOCUMENT ID		TECN	COMMENT
$<2.1 \times 10^{-3}$	90	[1] ALBRECHT	93E	ARG	$e^+e^- \to \Upsilon(4S)$

[1] ALBRECHT 93E reports $< 3.5 \times 10^{-3}$ from a measurement of $[\Gamma(B^0 \to D_s^+ a_1(1260)^-)/\Gamma_{total}] \times [B(D_s^+ \to \phi\pi^+)]$ assuming $B(D_s^+ \to \phi\pi^+) = 0.027$, which we rescale to our best value $B(D_s^+ \to \phi\pi^+) = 4.5 \times 10^{-2}$.

$\Gamma(D_s^{*+} a_1(1260)^-)/\Gamma_{total}$ — Γ_{121}/Γ

VALUE	CL%	DOCUMENT ID		TECN	COMMENT
$<1.7 \times 10^{-3}$	90	[1] ALBRECHT	93E	ARG	$e^+e^- \to \Upsilon(4S)$

[1] ALBRECHT 93E reports $< 2.9 \times 10^{-3}$ from a measurement of $[\Gamma(B^0 \to D_s^{*+} a_1(1260)^-)/\Gamma_{total}] \times [B(D_s^+ \to \phi\pi^+)]$ assuming $B(D_s^+ \to \phi\pi^+) = 0.027$, which we rescale to our best value $B(D_s^+ \to \phi\pi^+) = 4.5 \times 10^{-2}$.

$\Gamma(D_s^+ a_2^-)/\Gamma_{total}$ — Γ_{122}/Γ

VALUE (units 10^{-5})	CL%	DOCUMENT ID		TECN	COMMENT
<19	90	[1] AUBERT	06X	BABR	$e^+e^- \to \Upsilon(4S)$

[1] Assumes equal production of B^+ and B^0 at the $\Upsilon(4S)$.

$\Gamma(D_s^{*+} a_2^-)/\Gamma_{total}$ — Γ_{123}/Γ

VALUE (units 10^{-5})	CL%	DOCUMENT ID		TECN	COMMENT
<20	90	[1] AUBERT	06X	BABR	$e^+e^- \to \Upsilon(4S)$

[1] Assumes equal production of B^+ and B^0 at the $\Upsilon(4S)$.

$\Gamma(D_s^- K^+)/\Gamma_{total}$ — Γ_{124}/Γ

VALUE (units 10^{-6})	CL%	DOCUMENT ID		TECN	COMMENT
27 ± 5 OUR FIT Error includes scale factor of 2.7.					
22 ± 5 OUR AVERAGE Error includes scale factor of 1.8.					
19.1 ± 2.4 ± 1.7		[1] DAS	10	BELL	$e^+e^- \to \Upsilon(4S)$
29 ± 4 ± 2		[1] AUBERT	08AJ	BABR	$e^+e^- \to \Upsilon(4S)$
• • • We do not use the following data for averages, fits, limits, etc. • • •					
27 ± 5 ± 2		[2] AUBERT	07K	BABR	Repl. by AUBERT 08AJ
26 ± 10 ± 2		[3] AUBERT	03D	BABR	Repl. by AUBERT 07K
$36^{+11}_{-10} \pm 3$		[4] KROKOVNY	02	BELL	Repl. by DAS 10
< 190	90	[5] ALEXANDER	93B	CLE2	$e^+e^- \to \Upsilon(4S)$
<1300	90	[6] BORTOLETTO	90	CLEO	$e^+e^- \to \Upsilon(4S)$

[1] Assumes equal production of B^+ and B^0 at the $\Upsilon(4S)$.

[2] AUBERT 07K reports $[\Gamma(B^0 \to D_s^- K^+)/\Gamma_{total}] \times [B(D_s^+ \to \phi\pi^+)] = (1.21 \pm 0.17 \pm 0.11) \times 10^{-6}$ which we divide by our best value $B(D_s^+ \to \phi\pi^+) = (4.5 \pm 0.4) \times 10^{-2}$. Our first error is their experiment's error and our second error is the systematic error from using our best value.

[3] AUBERT 03D reports $[\Gamma(B^0 \to D_s^- K^+)/\Gamma_{total}] \times [B(D_s^+ \to \phi\pi^+)] = (1.16 \pm 0.36 \pm 0.24) \times 10^{-6}$ which we divide by our best value $B(D_s^+ \to \phi\pi^+) = (4.5 \pm 0.4) \times 10^{-2}$. Our first error is their experiment's error and our second error is the systematic error from using our best value.

[4] KROKOVNY 02 reports $[\Gamma(B^0 \to D_s^- K^+)/\Gamma_{total}] \times [B(D_s^+ \to \phi\pi^+)] = (1.61^{+0.45}_{-0.38} \pm 0.21) \times 10^{-6}$ which we divide by our best value $B(D_s^+ \to \phi\pi^+) = (4.5 \pm 0.4) \times 10^{-2}$. Our first error is their experiment's error and our second error is the systematic error from using our best value.

[5] ALEXANDER 93B reports $< 230 \times 10^{-6}$ from a measurement of $[\Gamma(B^0 \to D_s^- K^+)/\Gamma_{total}] \times [B(D_s^+ \to \phi\pi^+)]$ assuming $B(D_s^+ \to \phi\pi^+) = 0.037$, which we rescale to our best value $B(D_s^+ \to \phi\pi^+) = 4.5 \times 10^{-2}$.

[6] BORTOLETTO 90 assume $B(D_s \to \phi\pi^+) = 2\%$.

$\Gamma(D_s^{*-} K^+)/\Gamma_{total}$ — Γ_{125}/Γ

VALUE (units 10^{-5})	CL%	DOCUMENT ID		TECN	COMMENT
2.19 ± 0.30 OUR AVERAGE					
2.02 ± 0.33 ± 0.22		[1] JOSHI	10	BELL	$e^+e^- \to \Upsilon(4S)$
2.4 ± 0.4 ± 0.2		[1] AUBERT	08AJ	BABR	$e^+e^- \to \Upsilon(4S)$
• • • We do not use the following data for averages, fits, limits, etc. • • •					
2.2 ± 0.6 ± 0.2		[2] AUBERT	07K	BABR	Repl. by AUBERT 08AJ
< 2.5	90	AUBERT	03D	BABR	Repl. by AUBERT 07K
<14	90	[3] ALEXANDER	93B	CLE2	$e^+e^- \to \Upsilon(4S)$

[1] Assumes equal production of B^+ and B^0 at the $\Upsilon(4S)$.

[2] AUBERT 07K reports $[\Gamma(B^0 \to D_s^{*-} K^+)/\Gamma_{total}] \times [B(D_s^+ \to \phi\pi^+)] = (0.97 \pm 0.24 \pm 0.12) \times 10^{-6}$ which we divide by our best value $B(D_s^+ \to \phi\pi^+) = (4.5 \pm 0.4) \times 10^{-2}$. Our first error is their experiment's error and our second error is the systematic error from using our best value.

[3] ALEXANDER 93B reports $< 17 \times 10^{-5}$ from a measurement of $[\Gamma(B^0 \to D_s^{*-} K^+)/\Gamma_{total}] \times [B(D_s^+ \to \phi\pi^+)]$ assuming $B(D_s^+ \to \phi\pi^+) = 0.037$, which we rescale to our best value $B(D_s^+ \to \phi\pi^+) = 4.5 \times 10^{-2}$.

$\Gamma(D_s^- K^+)/\Gamma(D^-\pi^+)$ — Γ_{124}/Γ_{35}

VALUE (units 10^{-2})	DOCUMENT ID		TECN	COMMENT
1.09 ± 0.19 OUR FIT Error includes scale factor of 2.7.				
1.29 ± 0.05 ± 0.08	AAIJ	15AC	LHCB	pp at 7, 8 TeV

$\Gamma(D_s^- K^*(892)^+)/\Gamma_{total}$ — Γ_{126}/Γ

VALUE (units 10^{-5})	CL%	DOCUMENT ID		TECN	COMMENT
$3.5^{+1.0}_{-0.9} \pm 0.4$		[1] AUBERT	08AJ	BABR	$e^+e^- \to \Upsilon(4S)$
• • • We do not use the following data for averages, fits, limits, etc. • • •					
<280	90	[2] ALBRECHT	93E	ARG	$e^+e^- \to \Upsilon(4S)$
< 80	90	[3] ALEXANDER	93B	CLE2	$e^+e^- \to \Upsilon(4S)$

[1] Assumes equal production of B^+ and B^0 at the $\Upsilon(4S)$.

[2] ALBRECHT 93E reports $< 4.6 \times 10^{-3}$ from a measurement of $[\Gamma(B^0 \to D_s^- K^*(892)^+)/\Gamma_{total}] \times [B(D_s^+ \to \phi\pi^+)]$ assuming $B(D_s^+ \to \phi\pi^+) = 0.027$, which we rescale to our best value $B(D_s^+ \to \phi\pi^+) = 4.5 \times 10^{-2}$.

[3] ALEXANDER 93B reports $< 9.7 \times 10^{-4}$ from a measurement of $[\Gamma(B^0 \to D_s^- K^*(892)^+)/\Gamma_{total}] \times [B(D_s^+ \to \phi\pi^+)]$ assuming $B(D_s^+ \to \phi\pi^+) = 0.037$, which we rescale to our best value $B(D_s^+ \to \phi\pi^+) = 4.5 \times 10^{-2}$.

$\Gamma(D_s^{*-} K^*(892)^+)/\Gamma_{total}$ — Γ_{127}/Γ

VALUE (units 10^{-5})	CL%	DOCUMENT ID		TECN	COMMENT
$3.2^{+1.4}_{-1.2} \pm 0.4$		[1] AUBERT	08AJ	BABR	$e^+e^- \to \Upsilon(4S)$
• • • We do not use the following data for averages, fits, limits, etc. • • •					
<350	90	[2] ALBRECHT	93E	ARG	$e^+e^- \to \Upsilon(4S)$
< 90	90	[3] ALEXANDER	93B	CLE2	$e^+e^- \to \Upsilon(4S)$

[1] Assumes equal production of B^+ and B^0 at the $\Upsilon(4S)$.

[2] ALBRECHT 93E reports $< 5.8 \times 10^{-3}$ from a measurement of $[\Gamma(B^0 \to D_s^{*-} K^*(892)^+)/\Gamma_{total}] \times [B(D_s^+ \to \phi\pi^+)]$ assuming $B(D_s^+ \to \phi\pi^+) = 0.027$, which we rescale to our best value $B(D_s^+ \to \phi\pi^+) = 4.5 \times 10^{-2}$.

[3] ALEXANDER 93B reports $< 11.0 \times 10^{-4}$ from a measurement of $[\Gamma(B^0 \to D_s^{*-} K^*(892)^+)/\Gamma_{total}] \times [B(D_s^+ \to \phi\pi^+)]$ assuming $B(D_s^+ \to \phi\pi^+) = 0.037$, which we rescale to our best value $B(D_s^+ \to \phi\pi^+) = 4.5 \times 10^{-2}$.

$\Gamma(D_s^- \pi^+ K^0)/\Gamma_{total}$ — Γ_{128}/Γ

VALUE (units 10^{-4})	CL%	DOCUMENT ID		TECN	COMMENT
0.97 ± 0.14 OUR AVERAGE					
0.94 ± 0.12 ± 0.10		[1] WIECHCZYN...	15	BELL	$e^+e^- \to \Upsilon(4S)$
1.10 ± 0.26 ± 0.20		[1] AUBERT	08G	BABR	$e^+e^- \to \Upsilon(4S)$
• • • We do not use the following data for averages, fits, limits, etc. • • •					
<40	90	[2] ALBRECHT	93E	ARG	$e^+e^- \to \Upsilon(4S)$

[1] Assumes equal production of B^+ and B^0 at the $\Upsilon(4S)$.

[2] ALBRECHT 93E reports $< 7.3 \times 10^{-3}$ from a measurement of $[\Gamma(B^0 \to D_s^- \pi^+ K^0)/\Gamma_{total}] \times [B(D_s^+ \to \phi\pi^+)]$ assuming $B(D_s^+ \to \phi\pi^+) = 0.027$, which we rescale to our best value $B(D_s^+ \to \phi\pi^+) = 4.5 \times 10^{-2}$.

$\Gamma(D_s^{*-} \pi^+ K^0)/\Gamma_{total}$ — Γ_{129}/Γ

VALUE (units 10^{-4})	CL%	DOCUMENT ID		TECN	COMMENT
< 1.10	90	[1] AUBERT	08G	BABR	$e^+e^- \to \Upsilon(4S)$
• • • We do not use the following data for averages, fits, limits, etc. • • •					
<25	90	[2] ALBRECHT	93E	ARG	$e^+e^- \to \Upsilon(4S)$

[1] Assumes equal production of B^+ and B^0 at the $\Upsilon(4S)$.

[2] ALBRECHT 93E reports $< 4.2 \times 10^{-3}$ from a measurement of $[\Gamma(B^0 \to D_s^{*-} \pi^+ K^0)/\Gamma_{total}] \times [B(D_s^+ \to \phi\pi^+)]$ assuming $B(D_s^+ \to \phi\pi^+) = 0.027$, which we rescale to our best value $B(D_s^+ \to \phi\pi^+) = 4.5 \times 10^{-2}$.

$\Gamma(D_s^- K^+ \pi^+ \pi^-)/\Gamma_{total}$ — Γ_{130}/Γ

VALUE (units 10^{-4})	DOCUMENT ID		TECN	COMMENT
1.71 ± 0.31 ± 0.34	[1] AAIJ	12AX	LHCB	pp at 7 TeV

[1] AAIJ 12AX reports $[\Gamma(B^0 \to D_s^- K^+ \pi^+ \pi^-)/\Gamma_{total}] / [B(B_s^0 \to D_s^- K^+ \pi^+ \pi^-)] = 0.54 \pm 0.07 \pm 0.07$ which we multiply by our best value $B(B_s^0 \to D_s^- K^+ \pi^+ \pi^-) = (3.2 \pm 0.6) \times 10^{-4}$. Our first error is their experiment's error and our second error is the systematic error from using our best value.

$\Gamma(D_s^- \pi^+ K^*(892)^0)/\Gamma_{total}$ — Γ_{131}/Γ

VALUE	CL%	DOCUMENT ID		TECN	COMMENT
$<3.0 \times 10^{-3}$	90	[1] ALBRECHT	93E	ARG	$e^+e^- \to \Upsilon(4S)$

[1] ALBRECHT 93E reports $< 5.0 \times 10^{-3}$ from a measurement of $[\Gamma(B^0 \to D_s^- \pi^+ K^*(892)^0)/\Gamma_{total}] \times [B(D_s^+ \to \phi\pi^+)]$ assuming $B(D_s^+ \to \phi\pi^+) = 0.027$, which we rescale to our best value $B(D_s^+ \to \phi\pi^+) = 4.5 \times 10^{-2}$.

Downloaded from https://academic.oup.com/ptep/article/2022/8/083C01/6651666 by KIT Library user on 27 September 2022

$\Gamma(D_s^{*-}\pi^+ K^*(892)^0)/\Gamma_{total}$ — Γ_{132}/Γ

VALUE	CL%	DOCUMENT ID		TECN	COMMENT
$<1.6\times10^{-3}$	90	[1] ALBRECHT	93E	ARG	$e^+e^-\to\Upsilon(4S)$

[1] ALBRECHT 93E reports $<2.7\times10^{-3}$ from a measurement of $[\Gamma(B^0\to D_s^{*-}\pi^+K^*(892)^0)/\Gamma_{total}]\times[B(D_s^+\to\phi\pi^+)]$ assuming $B(D_s^+\to\phi\pi^+)=0.027$, which we rescale to our best value $B(D_s^+\to\phi\pi^+)=4.5\times10^{-2}$.

$\Gamma(\overline{D}^0 K^0)/\Gamma_{total}$ — Γ_{133}/Γ

VALUE (units 10^{-5})	DOCUMENT ID		TECN	COMMENT
5.2±0.7 OUR AVERAGE				
5.3±0.7±0.3	[1] AUBERT,B	06L	BABR	$e^+e^-\to\Upsilon(4S)$
$5.0^{+1.3}_{-1.2}\pm0.6$	[1] KROKOVNY	03	BELL	$e^+e^-\to\Upsilon(4S)$

[1] Assumes equal production of B^+ and B^0 at the $\Upsilon(4S)$.

$\Gamma(\overline{D}^0 K^+\pi^-)/\Gamma_{total}$ — Γ_{134}/Γ

VALUE (units 10^{-6})	DOCUMENT ID		TECN	COMMENT
88±15±9	[1] AUBERT	06A	BABR	$e^+e^-\to\Upsilon(4S)$

[1] Assumes equal production of B^+ and B^0 at the $\Upsilon(4S)$.

$\Gamma(\overline{D}^0 K^+\pi^-)/\Gamma(\overline{D}^0\pi^+\pi^-)$ — Γ_{134}/Γ_{44}

VALUE	DOCUMENT ID		TECN	COMMENT
0.106±0.007±0.008	AAIJ	13AQ	LHCB	pp at 7 TeV

$\Gamma(\overline{D}^0 K^*(892)^0)/\Gamma_{total}$ — Γ_{135}/Γ

VALUE (units 10^{-5})	DOCUMENT ID		TECN	COMMENT
4.5±0.6 OUR AVERAGE				
5.4±0.3±1.1	[1,2] AAIJ	15X	LHCB	pp at 7, 8 TeV
4.0±0.7±0.3	[3] AUBERT,B	06L	BABR	$e^+e^-\to\Upsilon(4S)$
$4.8^{+1.1}_{-1.0}\pm0.5$	[3] KROKOVNY	03	BELL	$e^+e^-\to\Upsilon(4S)$
• • • We do not use the following data for averages, fits, limits, etc. • • •				
5.7±0.9±0.6	[3] AUBERT	06A	BABR	Repl. by AUBERT,B 06L

[1] AAIJ 15X reports $(5.13\pm0.20\pm0.15\pm0.24\pm0.60)\times10^{-5}$ from a measurement of $[\Gamma(B^0\to\overline{D}^0K^*(892)^0)/\Gamma_{total}]\times[B(B^0\to\overline{D}^0K^+\pi^-)]$ assuming $B(B^0\to\overline{D}^0K^+\pi^-)=(9.2\pm0.6\pm0.7\pm0.6)\times10^{-5}$, which we rescale to our best value $B(B^0\to\overline{D}^0K^+\pi^-)=(8.8\pm1.7)\times10^{-5}$. Our first error is their experiment's error and our second error is the systematic error from using our best value.
[2] Measured via amplitude analysis of $B^0\to\overline{D}^0K^+\pi^-$, which excludes contribution from decay via $D^*(2010)^-$ resonance.
[3] Assumes equal production of B^+ and B^0 at the $\Upsilon(4S)$.

$\Gamma(\overline{D}^0 K^*(1410)^0)/\Gamma_{total}$ — Γ_{136}/Γ

VALUE	CL%	DOCUMENT ID		TECN	COMMENT
$<6.7\times10^{-5}$	90	[1] AAIJ	15X	LHCB	pp at 7, 8 TeV

[1] Measured via amplitude analysis of $B^0\to\overline{D}^0K^+\pi^-$, which excludes contribution from decay via $D^*(2010)^-$ resonance.

$\Gamma(\overline{D}^0 K_0^*(1430)^0)/\Gamma_{total}$ — Γ_{137}/Γ

VALUE (units 10^{-5})	DOCUMENT ID		TECN	COMMENT
0.7±0.7±0.1	[1,2] AAIJ	15X	LHCB	pp at 7, 8 TeV

[1] AAIJ 15X reports $(0.71\pm0.27\pm0.33\pm0.47\pm0.08)\times10^{-5}$ from a measurement of $[\Gamma(B^0\to\overline{D}^0K_0^*(1430)^0)/\Gamma_{total}]\times[B(B^0\to\overline{D}^0K^+\pi^-)]$ assuming $B(B^0\to\overline{D}^0K^+\pi^-)=(9.2\pm0.6\pm0.7\pm0.6)\times10^{-5}$, which we rescale to our best value $B(B^0\to\overline{D}^0K^+\pi^-)=(8.8\pm1.7)\times10^{-5}$. Our first error is their experiment's error and our second error is the systematic error from using our best value.
[2] Measured via amplitude analysis of $B^0\to\overline{D}^0K^+\pi^-$, which excludes contribution from decay via $D^*(2010)^-$ resonance.

$\Gamma(\overline{D}^0 K_2^*(1430)^0)/\Gamma_{total}$ — Γ_{138}/Γ

VALUE (units 10^{-5})	DOCUMENT ID		TECN	COMMENT
2.1±0.8±0.4	[1,2] AAIJ	15X	LHCB	pp at 7, 8 TeV

[1] AAIJ 15X reports $(2.04\pm0.45\pm0.30\pm0.54\pm0.25)\times10^{-5}$ from a measurement of $[\Gamma(B^0\to\overline{D}^0K_2^*(1430)^0)/\Gamma_{total}]\times[B(B^0\to\overline{D}^0K^+\pi^-)]$ assuming $B(B^0\to\overline{D}^0K^+\pi^-)=(9.2\pm0.6\pm0.7\pm0.6)\times10^{-5}$, which we rescale to our best value $B(B^0\to\overline{D}^0K^+\pi^-)=(8.8\pm1.7)\times10^{-5}$. Our first error is their experiment's error and our second error is the systematic error from using our best value.
[2] Measured via amplitude analysis of $B^0\to\overline{D}^0K^+\pi^-$, which excludes contribution from decay via $D^*(2010)^-$ resonance.

$\Gamma(D_0^*(2300)^-K^+,\ D_0^{*-}\to\overline{D}^0\pi^-)/\Gamma_{total}$ — Γ_{139}/Γ

VALUE (units 10^{-5})	DOCUMENT ID		TECN	COMMENT
1.9±0.8±0.4	[1,2] AAIJ	15X	LHCB	pp at 7, 8 TeV

[1] AAIJ 15X reports $(1.77\pm0.26\pm0.19\pm0.67\pm0.20)\times10^{-5}$ from a measurement of $[\Gamma(B^0\to D_0^*(2300)^-K^+,\ D_0^{*-}\to\overline{D}^0\pi^-)/\Gamma_{total}]\times[B(B^0\to\overline{D}^0K^+\pi^-)]$ assuming $B(B^0\to\overline{D}^0K^+\pi^-)=(9.2\pm0.6\pm0.7\pm0.6)\times10^{-5}$, which we rescale to our best value $B(B^0\to\overline{D}^0K^+\pi^-)=(8.8\pm1.7)\times10^{-5}$. Our first error is their experiment's error and our second error is the systematic error from using our best value.
[2] Measured via amplitude analysis of $B^0\to\overline{D}^0K^+\pi^-$, which excludes contribution from decay via $D^*(2010)^-$ resonance.

$\Gamma(D_2^*(2460)^-K^+,\ D_2^{*-}\to\overline{D}^0\pi^-)/\Gamma_{total}$ — Γ_{140}/Γ

VALUE (units 10^{-6})	DOCUMENT ID		TECN	COMMENT
20.3±3.5 OUR AVERAGE				
22 ±2 ±4	[1,2] AAIJ	15X	LHCB	pp at 7, 8 TeV
18.3±4.0±3.1	[3] AUBERT	06A	BABR	$e^+e^-\to\Upsilon(4S)$

[1] AAIJ 15X reports $(2.12\pm0.10\pm0.11\pm0.11\pm0.25)\times10^{-5}$ from a measurement of $[\Gamma(B^0\to D_2^*(2460)^-K^+,\ D_2^{*-}\to\overline{D}^0\pi^-)/\Gamma_{total}]\times[B(B^0\to\overline{D}^0K^+\pi^-)]$ assuming $B(B^0\to\overline{D}^0K^+\pi^-)=(9.2\pm0.6\pm0.7\pm0.6)\times10^{-5}$, which we rescale to our best value $B(B^0\to\overline{D}^0K^+\pi^-)=(8.8\pm1.7)\times10^{-5}$. Our first error is their experiment's error and our second error is the systematic error from using our best value.
[2] Measured via amplitude analysis of $B^0\to\overline{D}^0K^+\pi^-$, which excludes contribution from decay via $D^*(2010)^-$ resonance.
[3] Assumes equal production of B^+ and B^0 at the $\Upsilon(4S)$.

$\Gamma(D_3^*(2760)^-K^+,\ D_3^{*-}\to\overline{D}^0\pi^-)/\Gamma_{total}$ — Γ_{141}/Γ

VALUE	CL%	DOCUMENT ID		TECN	COMMENT
$<0.10\times10^{-5}$	90	[1] AAIJ	15X	LHCB	pp at 7, 8 TeV

[1] Measured via amplitude analysis of $B^0\to\overline{D}^0K^+\pi^-$, which excludes contribution from decay via $D^*(2010)^-$ resonance.

$\Gamma(\overline{D}^0 K^+\pi^-\text{nonresonant})/\Gamma_{total}$ — Γ_{142}/Γ

VALUE (units 10^{-6})	CL%	DOCUMENT ID		TECN	COMMENT
<37	90	[1] AUBERT	06A	BABR	$e^+e^-\to\Upsilon(4S)$

[1] Assumes equal production of B^+ and B^0 at the $\Upsilon(4S)$.

$\Gamma([K^+K^-]_D K^*(892)^0)/\Gamma(\overline{D}^0 K^*(892)^0)$ — $\Gamma_{143}/\Gamma_{135}$

VALUE	DOCUMENT ID		TECN	COMMENT
0.92±0.10±0.02	AAIJ	19N	LHCB	pp at 7, 8, 13 TeV
• • • We do not use the following data for averages, fits, limits, etc. • • •				
$1.05^{+0.17}_{-0.15}\pm0.04$	AAIJ	14BN	LHCB	Repl. by AAIJ 16S
$1.36^{+0.37}_{-0.32}\pm0.07$	AAIJ	13L	LHCB	Repl. by AAIJ 14BN

$\Gamma([\pi^+\pi^-]_D K^*(892)^0)/\Gamma(\overline{D}^0 K^*(892)^0)$ — $\Gamma_{144}/\Gamma_{135}$

VALUE	DOCUMENT ID		TECN	COMMENT
1.32±0.19±0.03	AAIJ	19N	LHCB	pp at 7, 8, 13 TeV
• • • We do not use the following data for averages, fits, limits, etc. • • •				
$1.21^{+0.28}_{-0.25}\pm0.05$	AAIJ	14BN	LHCB	Repl. by AAIJ 16S

$\Gamma([\pi^+K^-]_D K^*(892)^0)/\Gamma([K^+\pi^-]_D K^*(892)^0)$ — $\Gamma_{145}/\Gamma_{146}$

VALUE	DOCUMENT ID		TECN	COMMENT
0.080±0.015±0.002	AAIJ	19N	LHCB	pp at 7, 8, 13 TeV

$\Gamma([\pi^+\pi^-\pi^+\pi^-]_D K^{*0})/\Gamma(\overline{D}^0 K^*(892)^0)$ — $\Gamma_{147}/\Gamma_{135}$

VALUE	DOCUMENT ID		TECN	COMMENT
1.01±0.16±0.04	AAIJ	19N	LHCB	pp at 7, 8, 13 TeV

$\Gamma([\pi^+K^-\pi^+\pi^-]_D K^{*0})/\Gamma([K^+\pi^-\pi^+\pi^-]_D K^{*0})$ — $\Gamma_{148}/\Gamma_{149}$

VALUE	DOCUMENT ID		TECN	COMMENT
0.073±0.018±0.002	AAIJ	19N	LHCB	pp at 7, 8, 13 TeV

$\Gamma(\overline{D}^0\pi^0)/\Gamma_{total}$ — Γ_{150}/Γ

VALUE (units 10^{-4})	CL%	DOCUMENT ID		TECN	COMMENT
2.63±0.14 OUR AVERAGE					
2.69±0.09±0.13		[1] LEES	11M	BABR	$e^+e^-\to\Upsilon(4S)$
2.25±0.14±0.35		[1] BLYTH	06	BELL	$e^+e^-\to\Upsilon(4S)$
$2.74^{+0.36}_{-0.32}\pm0.55$		[1] COAN	02	CLE2	$e^+e^-\to\Upsilon(4S)$
• • • We do not use the following data for averages, fits, limits, etc. • • •					
2.9 ±0.2 ±0.3		[1] AUBERT	04B	BABR	Repl. by LEES 11M
3.1 ±0.4 ±0.5		[1] ABE	02J	BELL	Repl. by BLYTH 06
<1.2	90	[2] NEMATI	98	CLE2	Repl. by COAN 02
<4.8	90	[3] ALAM	94	CLE2	Repl. by NEMATI 98

[1] Assumes equal production of B^+ and B^0 at the $\Upsilon(4S)$.
[2] NEMATI 98 assumes equal production of B^+ and B^0 at the $\Upsilon(4S)$ and use the PDG 96 values for D^0, D^{*0}, η, η', and ω branching fractions.
[3] ALAM 94 assume equal production of B^+ and B^0 at the $\Upsilon(4S)$ and use the CLEO II absolute $B(D^0\to K^-\pi^+)$ and the PDG 1992 $B(D^0\to K^-\pi^+\pi^0)/B(D^0\to K^-\pi^+)$ and $B(D^0\to K^-2\pi^+\pi^-)/B(D^0\to K^-\pi^+)$.

$\Gamma(\overline{D}^0\rho^0)/\Gamma_{total}$ — Γ_{151}/Γ

VALUE (units 10^{-4})	CL%	DOCUMENT ID		TECN	COMMENT
3.21±0.21 OUR AVERAGE					
3.21±0.10±0.21		[1] AAIJ	15Y	LHCB	pp at 7, 8 TeV
3.19±0.20±0.45		[2,3] KUZMIN	07	BELL	$e^+e^-\to\Upsilon(4S)$
• • • We do not use the following data for averages, fits, limits, etc. • • •					
2.9 ±1.0 ±0.4		[2] SATPATHY	03	BELL	Repl. by KUZMIN 07
< 3.9	90	[4] NEMATI	98	CLE2	$e^+e^-\to\Upsilon(4S)$
< 5.5	90	[5] ALAM	94	CLE2	Repl. by NEMATI 98

Downloaded from https://academic.oup.com/ptep/article/2022/8/083C01/6651666 by KIT Library user on 27 September 2022

< 6.0	90	[6] BORTOLETTO92	CLEO	$e^+e^- \to \Upsilon(4S)$	
<27.0	90	[7] ALBRECHT 88K	ARG	$e^+e^- \to \Upsilon(4S)$	

[1] Measured using isobar formalism in the decay chain $B^0 \to \overline{D}^0\rho(770)$, $\rho \to \pi^+\pi^-$ assuming $B(\rho(770) \to \pi^+\pi^-) = 1$. The second uncertainty combines in quadrature all systematic uncertainties quoted in the paper.
[2] Assumes equal production of B^+ and B^0 at the $\Upsilon(4S)$.
[3] Our second uncertainty combines systematics and model errors quoted in the paper.
[4] NEMATI 98 assumes equal production of B^+ and B^0 at the $\Upsilon(4S)$ and use the PDG 96 values for D^0, D^{*0}, η, η', and ω branching fractions.
[5] ALAM 94 assume equal production of B^+ and B^0 at the $\Upsilon(4S)$ and use the CLEO II absolute $B(D^0 \to K^-\pi^+)$ and the PDG 1992 $B(D^0 \to K^-\pi^+\pi^0)/B(D^0 \to K^-\pi^+)$ and $B(D^0 \to K^-2\pi^+\pi^-)/B(D^0 \to K^-\pi^+)$.
[6] BORTOLETTO 92 assumes equal production of B^+ and B^0 at the $\Upsilon(4S)$ and uses Mark III branching fractions for the D.
[7] ALBRECHT 88K reports < 0.003 assuming $B^0\overline{B}^0$:B^+B^- production ratio is 45:55. We rescale to 50%.

$\Gamma(\overline{D}^0 f_2)/\Gamma_{total}$ — Γ_{152}/Γ

VALUE (units 10^{-4})	DOCUMENT ID		TECN	COMMENT
1.56±0.21 OUR AVERAGE				
1.68±0.11±0.21	[1] AAIJ	15Y	LHCB	pp at 7, 8 TeV
1.20±0.18±0.38	[2,3] KUZMIN	07	BELL	$e^+e^- \to \Upsilon(4S)$

[1] Result obtained using the isobar formalism. The second uncertainty combines in quadrature all systematic uncertainties quoted in the paper. Measured in the decay chain $B^0 \to \overline{D}^0 f_2(1270)$, $f_2 \to \pi^+\pi^-$.
[2] Assumes equal production of B^+ and B^0 at the $\Upsilon(4S)$.
[3] Our second uncertainty combines systematics and model errors quoted in the paper.

$\Gamma(\overline{D}^0\eta)/\Gamma_{total}$ — Γ_{153}/Γ

VALUE (units 10^{-4})	CL%	DOCUMENT ID		TECN	COMMENT
2.36±0.32 OUR AVERAGE		Error includes scale factor of 2.5.			
2.53±0.09±0.11		[1] LEES	11M	BABR	$e^+e^- \to \Upsilon(4S)$
1.77±0.16±0.21		[1] BLYTH	06	BELL	$e^+e^- \to \Upsilon(4S)$
• • • We do not use the following data for averages, fits, limits, etc. • • •					
2.5 ±0.2 ±0.3		[1] AUBERT	04B	BABR	Repl. by LEES 11M
$1.4\ ^{+0.5}_{-0.4}$ ±0.3		[1] ABE	02J	BELL	Repl. by BLYTH 06
<1.3	90	[2] NEMATI	98	CLE2	$e^+e^- \to \Upsilon(4S)$
<6.8	90	[3] ALAM	94	CLE2	Repl. by NEMATI 98

[1] Assumes equal production of B^+ and B^0 at the $\Upsilon(4S)$.
[2] NEMATI 98 assumes equal production of B^+ and B^0 at the $\Upsilon(4S)$ and use the PDG 96 values for D^0, D^{*0}, η, η', and ω branching fractions.
[3] ALAM 94 assume equal production of B^+ and B^0 at the $\Upsilon(4S)$ and use the CLEO II absolute $B(D^0 \to K^-\pi^+)$ and the PDG 1992 $B(D^0 \to K^-\pi^+\pi^0)/B(D^0 \to K^-\pi^+)$ and $B(D^0 \to K^-2\pi^+\pi^-)/B(D^0 \to K^-\pi^+)$.

$\Gamma(\overline{D}^0\eta')/\Gamma_{total}$ — Γ_{154}/Γ

VALUE (units 10^{-4})	CL%	DOCUMENT ID		TECN	COMMENT
1.38±0.16 OUR AVERAGE		Error includes scale factor of 1.3.			
1.48±0.13±0.07		[1] LEES	11M	BABR	$e^+e^- \to \Upsilon(4S)$
$1.14\pm0.20\ ^{+0.10}_{-0.13}$		[1] SCHUMANN	05	BELL	$e^+e^- \to \Upsilon(4S)$
• • • We do not use the following data for averages, fits, limits, etc. • • •					
1.7 ±0.4 ±0.2		[1] AUBERT	04B	BABR	Repl. by LEES 11M
<9.4	90	[2] NEMATI	98	CLE2	$e^+e^- \to \Upsilon(4S)$
<8.6	90	[3] ALAM	94	CLE2	Repl. by NEMATI 98

[1] Assumes equal production of B^+ and B^0 at the $\Upsilon(4S)$.
[2] NEMATI 98 assumes equal production of B^+ and B^0 at the $\Upsilon(4S)$ and use the PDG 96 values for D^0, D^{*0}, η, η', and ω branching fractions.
[3] ALAM 94 assume equal production of B^+ and B^0 at the $\Upsilon(4S)$ and use the CLEO II absolute $B(D^0 \to K^-\pi^+)$ and the PDG 1992 $B(D^0 \to K^-\pi^+\pi^0)/B(D^0 \to K^-\pi^+)$ and $B(D^0 \to K^-2\pi^+\pi^-)/B(D^0 \to K^-\pi^+)$.

$\Gamma(\overline{D}^0\eta')/\Gamma(\overline{D}^0\eta)$ — $\Gamma_{154}/\Gamma_{153}$

VALUE	DOCUMENT ID		TECN	COMMENT
0.54±0.07±0.01	LEES	11M	BABR	$e^+e^- \to \Upsilon(4S)$
• • • We do not use the following data for averages, fits, limits, etc. • • •				
0.7 ±0.2 ±0.1	AUBERT	04B	BABR	Repl. by LEES 11M

$\Gamma(\overline{D}^0\omega)/\Gamma_{total}$ — Γ_{155}/Γ

VALUE (units 10^{-4})	CL%	DOCUMENT ID		TECN	COMMENT
2.54±0.16 OUR AVERAGE					
2.75±0.72±0.35		[1] AAIJ	15Y	LHCB	pp at 7, 8 TeV
2.57±0.11±0.14		[2] LEES	11M	BABR	$e^+e^- \to \Upsilon(4S)$
2.37±0.23±0.28		[2] BLYTH	06	BELL	$e^+e^- \to \Upsilon(4S)$
• • • We do not use the following data for averages, fits, limits, etc. • • •					
3.0 ±0.3 ±0.4		[2] AUBERT	04B	BABR	Repl. by LEES 11M
$1.8 \pm 0.5\ ^{+0.4}_{-0.3}$		[2] ABE	02J	BELL	Repl. by BLYTH 06
<5.1	90	[3] NEMATI	98	CLE2	$e^+e^- \to \Upsilon(4S)$
<6.3	90	[4] ALAM	94	CLE2	Repl. by NEMATI 98

[1] Result obtained using the isobar model. The second uncertainty combines in quadrature all systematic uncertainties quoted in the paper.
[2] Assumes equal production of B^+ and B^0 at the $\Upsilon(4S)$.
[3] NEMATI 98 assumes equal production of B^+ and B^0 at the $\Upsilon(4S)$ and use the PDG 96 values for D^0, D^{*0}, η, η', and ω branching fractions.
[4] ALAM 94 assume equal production of B^+ and B^0 at the $\Upsilon(4S)$ and use the CLEO II absolute $B(D^0 \to K^-\pi^+)$ and the PDG 1992 $B(D^0 \to K^-\pi^+\pi^0)/B(D^0 \to K^-\pi^+)$ and $B(D^0 \to K^-2\pi^+\pi^-)/B(D^0 \to K^-\pi^+)$.

$\Gamma(D^0\phi)/\Gamma_{total}$ — Γ_{156}/Γ

VALUE	CL%	DOCUMENT ID		TECN	COMMENT
$< 2.3 \times 10^{-6}$	95	AAIJ	18AY	LHCB	pp at 7 and 8 TeV
• • • We do not use the following data for averages, fits, limits, etc. • • •					
$<11.6 \times 10^{-6}$	90	[1] AUBERT	07AO	BABR	$e^+e^- \to \Upsilon(4S)$

[1] Assumes equal production of B^+ and B^0 at the $\Upsilon(4S)$.

$\Gamma(D^0K^+\pi^-)/\Gamma_{total}$ — Γ_{157}/Γ

VALUE (units 10^{-6})	CL%	DOCUMENT ID		TECN	COMMENT
• • • We do not use the following data for averages, fits, limits, etc. • • •					
<19	90	[1] AUBERT	06A	BABR	Repl. by AUBERT 09AE

[1] Assumes equal production of B^+ and B^0 at the $\Upsilon(4S)$.

$\Gamma(D^0K^+\pi^-)/\Gamma(\overline{D}^0K^+\pi^-)$ — $\Gamma_{157}/\Gamma_{134}$

VALUE	DOCUMENT ID		TECN	COMMENT
0.060±0.034 OUR AVERAGE				
$0.045\ ^{+0.056}_{-0.050}\ ^{+0.028}_{-0.018}$	[1,2] NEGISHI	12	BELL	$e^+e^- \to \Upsilon(4S)$
0.068±0.042	[3] AUBERT	09AE	BABR	$e^+e^- \to \Upsilon(4S)$

[1] Assumes equal production of B^0 and B^+ at $\Upsilon(4S)$.
[2] Uses $D^0 \to K^-\pi^+$ mode. Restricts $K^+\pi^-$ mass within ±50 MeV of the nominal K^{*0} mass. Corresponds to the upper limit, < 0.16 at 95% CL.
[3] Reports a signal at the level of 2.5 standard deviations after combining results from $D^0 \to K^+\pi^-$, $K^+\pi^-\pi^0$, and $K^+\pi^-\pi^+\pi^-$.

$\Gamma(D^0K^*(892)^0)/\Gamma_{total}$ — Γ_{158}/Γ

VALUE (units 10^{-5})	CL%	DOCUMENT ID		TECN	COMMENT
• • • We do not use the following data for averages, fits, limits, etc. • • •					
<1.1	90	[1] AUBERT,B	06L	BABR	$e^+e^- \to \Upsilon(4S)$
<1.8	90	[1] KROKOVNY	03	BELL	$e^+e^- \to \Upsilon(4S)$

[1] Assumes equal production of B^+ and B^0 at the $\Upsilon(4S)$.

$\Gamma(D^0K^*(892)^0)/\Gamma(\overline{D}^0K^*(892)^0)$ — $\Gamma_{158}/\Gamma_{135}$

"OUR EVALUATION" is derived from $r_{B^0}(B^0 \to D K^{*0})$ data block listed in "CP vilation parameters" section.

VALUE (units 10^{-2})	DOCUMENT ID
$6.6\ ^{+1.1}_{-1.2}$ OUR EVALUATION	

$\Gamma(\overline{D}^{*0}\gamma)/\Gamma_{total}$ — Γ_{159}/Γ

VALUE	CL%	DOCUMENT ID		TECN	COMMENT
$<2.5 \times 10^{-5}$	90	[1] AUBERT,B	05Q	BABR	$e^+e^- \to \Upsilon(4S)$
• • • We do not use the following data for averages, fits, limits, etc. • • •					
$<5.0 \times 10^{-5}$	90	[1] ARTUSO	00	CLE2	$e^+e^- \to \Upsilon(4S)$

[1] Assumes equal production of B^+ and B^0 at the $\Upsilon(4S)$.

$\Gamma(\overline{D}^*(2007)^0\pi^0)/\Gamma_{total}$ — Γ_{160}/Γ

VALUE (units 10^{-4})	CL%	DOCUMENT ID		TECN	COMMENT
2.2 ±0.6 OUR AVERAGE		Error includes scale factor of 2.6. See the ideogram below.			
3.05±0.14±0.28		[1] LEES	11M	BABR	$e^+e^- \to \Upsilon(4S)$
1.39±0.18±0.26		[1] BLYTH	06	BELL	$e^+e^- \to \Upsilon(4S)$
$2.20\ ^{+0.59}_{-0.52}$±0.79		[1] COAN	02	CLE2	$e^+e^- \to \Upsilon(4S)$
• • • We do not use the following data for averages, fits, limits, etc. • • •					
2.9 ±0.4 ±0.5		[1] AUBERT	04B	BABR	Repl. by LEES 11M
$2.7\ ^{+0.8}_{-0.7}\ ^{+0.5}_{-0.6}$		[1] ABE	02J	BELL	Repl. by BLYTH 06
<4.4	90	[2] NEMATI	98	CLE2	Repl. by COAN 02
<9.7	90	[3] ALAM	94	CLE2	Repl. by NEMATI 98

[1] Assumes equal production of B^+ and B^0 at the $\Upsilon(4S)$.
[2] NEMATI 98 assumes equal production of B^+ and B^0 at the $\Upsilon(4S)$ and use the PDG 96 values for D^0, D^{*0}, η, η', and ω branching fractions.
[3] ALAM 94 assume equal production of B^+ and B^0 at the $\Upsilon(4S)$ and use the CLEO II $B(D^*(2007)^0 \to D^0\pi^0)$ and absolute $B(D^0 \to K^-\pi^+)$ and the PDG 1992 $B(D^0 \to K^-\pi^+\pi^0)/B(D^0 \to K^-\pi^+)$ and $B(D^0 \to K^-2\pi^+\pi^-)/B(D^0 \to K^-\pi^+)$.

Downloaded from https://academic.oup.com/ptep/article/2022/8/083C01/6651666 by KIT Library user on 27 September 2022

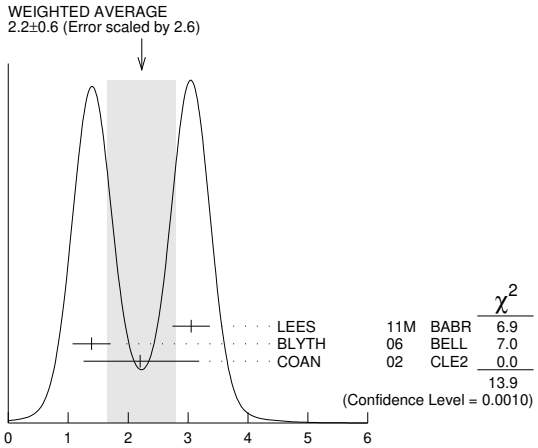

$\Gamma(\overline{D}^0\pi^0)/\Gamma(\overline{D}^*(2007)^0\pi^0)$ — $\Gamma_{150}/\Gamma_{160}$

VALUE	DOCUMENT ID		TECN	COMMENT
0.90±0.08 OUR AVERAGE				
0.88±0.05±0.06	LEES	11M	BABR	$e^+e^- \to \Upsilon(4S)$
1.62±0.23±0.35	BLYTH	06	BELL	$e^+e^- \to \Upsilon(4S)$
• • • We do not use the following data for averages, fits, limits, etc. • • •				
1.0 ±0.1 ±0.2	AUBERT	04B	BABR	Repl. by LEES 11M

$\Gamma(\overline{D}^*(2007)^0\rho^0)/\Gamma_{total}$ — Γ_{161}/Γ

VALUE	CL%	DOCUMENT ID		TECN	COMMENT
<5.1 $\times 10^{-4}$	90	[1] SATPATHY	03	BELL	$e^+e^- \to \Upsilon(4S)$
• • • We do not use the following data for averages, fits, limits, etc. • • •					
<0.00056	90	[2] NEMATI	98	CLE2	$e^+e^- \to \Upsilon(4S)$
<0.00117	90	[3] ALAM	94	CLE2	Repl. by NEMATI 98

[1] Assumes equal production of B^+ and B^0 at the $\Upsilon(4S)$.
[2] NEMATI 98 assumes equal production of B^+ and B^0 at the $\Upsilon(4S)$ and use the PDG 96 values for D^0, D^{*0}, η, η', and ω branching fractions.
[3] ALAM 94 assume equal production of B^+ and B^0 at the $\Upsilon(4S)$ and use the CLEO II $B(D^*(2007)^0 \to D^0\pi^0)$ and absolute $B(D^0 \to K^-\pi^+)$ and the PDG 1992 $B(D^0 \to K^-\pi^+\pi^0)/B(D^0 \to K^-\pi^+)$ and $B(D^0 \to K^-2\pi^+\pi^-)/B(D^0 \to K^-\pi^+)$.

$\Gamma(\overline{D}^*(2007)^0\eta)/\Gamma_{total}$ — Γ_{162}/Γ

VALUE (units 10^{-4})	CL%	DOCUMENT ID		TECN	COMMENT
2.3 ±0.6 OUR AVERAGE		Error includes scale factor of 2.8.			
2.69±0.14±0.23		[1] LEES	11M	BABR	$e^+e^- \to \Upsilon(4S)$
1.40±0.28±0.26		[1] BLYTH	06	BELL	$e^+e^- \to \Upsilon(4S)$
• • • We do not use the following data for averages, fits, limits, etc. • • •					
2.6 ±0.4 ±0.4		[1] AUBERT	04B	BABR	Repl. by LEES 11M
<4.6	90	[1] ABE	02J	BELL	$e^+e^- \to \Upsilon(4S)$
<2.6	90	[2] NEMATI	98	CLE2	$e^+e^- \to \Upsilon(4S)$
<6.9	90	[3] ALAM	94	CLE2	Repl. by NEMATI 98

[1] Assumes equal production of B^+ and B^0 at the $\Upsilon(4S)$.
[2] NEMATI 98 assumes equal production of B^+ and B^0 at the $\Upsilon(4S)$ and use the PDG 96 values for D^0, D^{*0}, η, η', and ω branching fractions.
[3] ALAM 94 assume equal production of B^+ and B^0 at the $\Upsilon(4S)$ and use the CLEO II $B(D^*(2007)^0 \to D^0\pi^0)$ and absolute $B(D^0 \to K^-\pi^+)$ and the PDG 1992 $B(D^0 \to K^-\pi^+\pi^0)/B(D^0 \to K^-\pi^+)$ and $B(D^0 \to K^-2\pi^+\pi^-)/B(D^0 \to K^-\pi^+)$.

$\Gamma(\overline{D}^0\eta)/\Gamma(\overline{D}^*(2007)^0\eta)$ — $\Gamma_{153}/\Gamma_{162}$

VALUE	DOCUMENT ID		TECN	COMMENT
0.99±0.10 OUR AVERAGE				
0.97±0.07±0.07	LEES	11M	BABR	$e^+e^- \to \Upsilon(4S)$
1.27±0.29±0.25	BLYTH	06	BELL	$e^+e^- \to \Upsilon(4S)$
• • • We do not use the following data for averages, fits, limits, etc. • • •				
0.9 ±0.2 ±0.1	AUBERT	04B	BABR	Repl. by LEES 11M

$\Gamma(\overline{D}^*(2007)^0\eta')/\Gamma(\overline{D}^*(2007)^0\eta)$ — $\Gamma_{163}/\Gamma_{162}$

VALUE	DOCUMENT ID		TECN	COMMENT
0.61±0.14±0.02	LEES	11M	BABR	$e^+e^- \to \Upsilon(4S)$
• • • We do not use the following data for averages, fits, limits, etc. • • •				
0.5 ±0.3 ±0.1	AUBERT	04B	BABR	Repl. by LEES 11M

$\Gamma(\overline{D}^*(2007)^0\eta')/\Gamma_{total}$ — Γ_{163}/Γ

VALUE (units 10^{-4})	CL%	DOCUMENT ID		TECN	COMMENT
1.40±0.22 OUR AVERAGE					
1.48±0.22±0.13		[1] LEES	11M	BABR	$e^+e^- \to \Upsilon(4S)$
1.21±0.34±0.22		[1] SCHUMANN	05	BELL	$e^+e^- \to \Upsilon(4S)$
• • • We do not use the following data for averages, fits, limits, etc. • • •					
1.3 ±0.7 ±0.2		[1,2] AUBERT	04B	BABR	Repl. by LEES 11M
<14	90	BRANDENB...	98	CLE2	$e^+e^- \to \Upsilon(4S)$
<19	90	[3] NEMATI	98	CLE2	$e^+e^- \to \Upsilon(4S)$
<27	90	[4] ALAM	94	CLE2	Repl. by NEMATI 98

[1] Assumes equal production of B^+ and B^0 at the $\Upsilon(4S)$.
[2] Reports an upper limit $< 2.6 \times 10^{-4}$ at 90% CL.
[3] NEMATI 98 assumes equal production of B^+ and B^0 at the $\Upsilon(4S)$ and use the PDG 96 values for D^0, D^{*0}, η, η', and ω branching fractions.
[4] ALAM 94 assume equal production of B^+ and B^0 at the $\Upsilon(4S)$ and use the CLEO II $B(D^*(2007)^0 \to D^0\pi^0)$ and absolute $B(D^0 \to K^-\pi^+)$ and the PDG 1992 $B(D^0 \to K^-\pi^+\pi^0)/B(D^0 \to K^-\pi^+)$ and $B(D^0 \to K^-2\pi^+\pi^-)/B(D^0 \to K^-\pi^+)$.

$\Gamma(\overline{D}^0\eta')/\Gamma(\overline{D}^*(2007)^0\eta')$ — $\Gamma_{154}/\Gamma_{163}$

VALUE	DOCUMENT ID		TECN	COMMENT
0.96±0.18±0.06	LEES	11M	BABR	$e^+e^- \to \Upsilon(4S)$
• • • We do not use the following data for averages, fits, limits, etc. • • •				
1.3 ±0.8 ±0.2	AUBERT	04B	BABR	Repl. by LEES 11M

$\Gamma(\overline{D}^*(2007)^0\pi^+\pi^-)/\Gamma_{total}$ — Γ_{164}/Γ

VALUE	DOCUMENT ID		TECN	COMMENT
(6.2±1.2±1.8) $\times 10^{-4}$	[1,2] SATPATHY	03	BELL	$e^+e^- \to \Upsilon(4S)$

[1] Assumes equal production of B^+ and B^0 at the $\Upsilon(4S)$.
[2] No assumption about the intermediate mechanism is made in the analysis.

$\Gamma(\overline{D}^*(2007)^0K^0)/\Gamma_{total}$ — Γ_{165}/Γ

VALUE (units 10^{-5})	CL%	DOCUMENT ID		TECN	COMMENT
3.6±1.2±0.3		[1] AUBERT,B	06L	BABR	$e^+e^- \to \Upsilon(4S)$
• • • We do not use the following data for averages, fits, limits, etc. • • •					
<6.6	90	[1] KROKOVNY	03	BELL	$e^+e^- \to \Upsilon(4S)$

[1] Assumes equal production of B^+ and B^0 at the $\Upsilon(4S)$.

$\Gamma(\overline{D}^*(2007)^0K^*(892)^0)/\Gamma_{total}$ — Γ_{166}/Γ

VALUE	CL%	DOCUMENT ID		TECN	COMMENT
<6.9 $\times 10^{-5}$	90	[1] KROKOVNY	03	BELL	$e^+e^- \to \Upsilon(4S)$

[1] Assumes equal production of B^+ and B^0 at the $\Upsilon(4S)$.

$\Gamma(D^*(2007)^0K^*(892)^0)/\Gamma_{total}$ — Γ_{167}/Γ

VALUE	CL%	DOCUMENT ID		TECN	COMMENT
<4.0 $\times 10^{-5}$	90	[1] KROKOVNY	03	BELL	$e^+e^- \to \Upsilon(4S)$

[1] Assumes equal production of B^+ and B^0 at the $\Upsilon(4S)$.

$\Gamma(D^*(2007)^0\pi^+\pi^+\pi^-\pi^-)/\Gamma_{total}$ — Γ_{168}/Γ

VALUE (units 10^{-3})	DOCUMENT ID		TECN	COMMENT
2.7 ±0.5 OUR AVERAGE				
2.60±0.47±0.37	[1] MAJUMDER	04	BELL	$e^+e^- \to \Upsilon(4S)$
3.0 ±0.7 ±0.6	[1] EDWARDS	02	CLE2	$e^+e^- \to \Upsilon(4S)$

[1] Assumes equal production of B^+ and B^0 at the $\Upsilon(4S)$.

$\Gamma(D^*(2007)^0\pi^+\pi^+\pi^-\pi^-)/\Gamma(D^*(2010)^-\pi^+\pi^+\pi^-\pi^0)$ — Γ_{168}/Γ_{64}

VALUE	DOCUMENT ID		TECN	COMMENT
0.17±0.04±0.02	[1] EDWARDS	02	CLE2	$e^+e^- \to \Upsilon(4S)$

[1] Assumes equal production of B^+ and B^0 at the $\Upsilon(4S)$.

$\Gamma(D^*(2010)^+D^*(2010)^-)/\Gamma_{total}$ — Γ_{169}/Γ

VALUE (units 10^{-4})	CL%	DOCUMENT ID		TECN	COMMENT
8.0 ±0.6 OUR AVERAGE					
7.82±0.38±0.63		[1] KRONENBIT...	12	BELL	$e^+e^- \to \Upsilon(4S)$
8.1 ±0.6 ±1.0		[1] AUBERT,B	06A	BABR	$e^+e^- \to \Upsilon(4S)$
9.9 $^{+4.2}_{-3.3}$ ±1.2		[1] LIPELES	00	CLE2	$e^+e^- \to \Upsilon(4S)$
• • • We do not use the following data for averages, fits, limits, etc. • • •					
8.1 ±0.8 ±1.1		[1] MIYAKE	05	BELL	Repl. by KRONENBIT-TER 12
8.3 ±1.6 ±1.2		[1,2] AUBERT	02M	BABR	Repl. by AUBERT,B 06B
6.2 $^{+4.0}_{-2.9}$ ±1.0		[3] ARTUSO	99	CLE2	Repl. by LIPELES 00
<61	90	[4] BARATE	98Q	ALEP	$e^+e^- \to Z$
<22	90	[5] ASNER	97	CLE2	Repl. by ARTUSO 99

[1] Assumes equal production of B^+ and B^0 at the $\Upsilon(4S)$.
[2] AUBERT 02M also assumes the measured CP-odd fraction of the final states is 0.22 ± 0.18 ± 0.03.
[3] ARTUSO 99 uses $B(\Upsilon(4S) \to B^0\overline{B}^0)$=(48 ± 4)%.
[4] BARATE 98Q (ALEPH) observes 2 events with an expected background of 0.10 ± 0.03 which corresponds to a branching ratio of $(2.3^{+1.9}_{-1.2} \pm 0.4) \times 10^{-3}$.
[5] ASNER 97 at CLEO observes 1 event with an expected background of 0.022 ± 0.011. This corresponds to a branching ratio of $(5.3^{+7.1}_{-3.7} \pm 1.0) \times 10^{-4}$.

Downloaded from https://academic.oup.com/ptep/article/2022/8/083C01/6651666 by KIT Library user on 27 September 2022

$\Gamma(\overline{D}^*(2007)^0\omega)/\Gamma_{total}$ — Γ_{170}/Γ

VALUE (units 10^{-4})	CL%	DOCUMENT ID		TECN	COMMENT
3.6 ±1.1 OUR AVERAGE		Error includes scale factor of 3.1.			
4.55±0.24±0.39		[1] LEES	11M	BABR	$e^+e^- \to \Upsilon(4S)$
2.29±0.39±0.40		[1] BLYTH	06	BELL	$e^+e^- \to \Upsilon(4S)$
• • • We do not use the following data for averages, fits, limits, etc. • • •					
4.2 ±0.7 ±0.9	90	[1] AUBERT	04B	BABR	Repl. by LEES 11M
< 7.9	90	[1] ABE	02J	BELL	$e^+e^- \to \Upsilon(4S)$
< 7.4	90	[2] NEMATI	98	CLE2	$e^+e^- \to \Upsilon(4S)$
<21	90	[3] ALAM	94	CLE2	Repl. by NEMATI 98

[1] Assumes equal production of B^+ and B^0 at the $\Upsilon(4S)$.
[2] NEMATI 98 assumes equal production of B^+ and B^0 at the $\Upsilon(4S)$ and use the PDG 96 values for D^0, D^{*0}, η, η', and ω branching fractions.
[3] ALAM 94 assume equal production of B^+ and B^0 at the $\Upsilon(4S)$ and use the CLEO II $B(D^*(2007)^0 \to D^0\pi^0)$ and absolute $B(D^0 \to K^-\pi^+)$ and the PDG 1992 $B(D^0 \to K^-\pi^+\pi^0)/B(D^0 \to K^-\pi^+)$ and $B(D^0 \to K^-2\pi^+\pi^-)/B(D^0 \to K^-\pi^+)$.

$\Gamma(\overline{D}^0\omega)/\Gamma(\overline{D}^*(2007)^0\omega)$ — $\Gamma_{155}/\Gamma_{170}$

VALUE	DOCUMENT ID		TECN	COMMENT
0.58±0.06 OUR AVERAGE				
0.56±0.04±0.04	LEES	11M	BABR	$e^+e^- \to \Upsilon(4S)$
1.04±0.20±0.17	BLYTH	06	BELL	$e^+e^- \to \Upsilon(4S)$
• • • We do not use the following data for averages, fits, limits, etc. • • •				
0.7 ±0.1 ±0.1	AUBERT	04B	BABR	Repl. by LEES 11M

$\Gamma(D^*(2010)^+D^-)/\Gamma_{total}$ — Γ_{171}/Γ

VALUE (units 10^{-4})	CL%	DOCUMENT ID		TECN	COMMENT
6.1±1.5 OUR AVERAGE		Error includes scale factor of 1.6.			
5.7±0.7±0.7		[1] AUBERT,B	06A	BABR	$e^+e^- \to \Upsilon(4S)$
$11.7\pm2.6^{+2.2}_{-2.5}$		[1,2] ABE	02Q	BELL	$e^+e^- \to \Upsilon(4S)$
• • • We do not use the following data for averages, fits, limits, etc. • • •					
8.8±1.0±1.3		[1] AUBERT	03J	BABR	Repl. by AUBERT,B 06B
$14.8\pm3.8^{+2.8}_{-3.1}$		[1,3] ABE	02Q	BELL	$e^+e^- \to \Upsilon(4S)$
< 6.3	90	[1] LIPELES	00	CLE2	$e^+e^- \to \Upsilon(4S)$
<56	90	BARATE	98Q	ALEP	$e^+e^- \to Z$
<18	90	ASNER	97	CLE2	$e^+e^- \to \Upsilon(4S)$

[1] Assumes equal production of B^+ and B^0 at the $\Upsilon(4S)$.
[2] The measurement is performed using fully reconstructed D^* and D^+ decays.
[3] The measurement is performed using a partial reconstruction technique for the D^* and fully reconstructed D^+ decays as a cross check.

$\Gamma(D^*(2007)^0\overline{D}^*(2007)^0)/\Gamma_{total}$ — Γ_{172}/Γ

VALUE (units 10^{-4})	CL%	DOCUMENT ID		TECN	COMMENT
< 0.9	90	[1] AUBERT,B	06A	BABR	$e^+e^- \to \Upsilon(4S)$
• • • We do not use the following data for averages, fits, limits, etc. • • •					
<270	90	BARATE	98Q	ALEP	$e^+e^- \to Z$

[1] Assumes equal production of B^+ and B^0 at the $\Upsilon(4S)$.

$\Gamma(D^-D^0K^+)/\Gamma_{total}$ — Γ_{173}/Γ

VALUE (units 10^{-3})	DOCUMENT ID		TECN	COMMENT
1.07±0.07±0.09	[1] DEL-AMO-SA...	11B	BABR	$e^+e^- \to \Upsilon(4S)$
• • • We do not use the following data for averages, fits, limits, etc. • • •				
1.7 ±0.3 ±0.3	[1] AUBERT	03X	BABR	Repl. by DEL-AMO-SANCHEZ 11B

[1] Assumes equal production of B^+ and B^0 at the $\Upsilon(4S)$.

$\Gamma(D^-D^*(2007)^0K^+)/\Gamma_{total}$ — Γ_{174}/Γ

VALUE (units 10^{-3})	DOCUMENT ID		TECN	COMMENT
3.46±0.18±0.37	[1] DEL-AMO-SA...	11B	BABR	$e^+e^- \to \Upsilon(4S)$
• • • We do not use the following data for averages, fits, limits, etc. • • •				
4.6 ±0.7 ±0.7	[1] AUBERT	03X	BABR	Repl. by DEL-AMO-SANCHEZ 11B

[1] Assumes equal production of B^+ and B^0 at the $\Upsilon(4S)$.

$\Gamma(D^*(2010)^-D^0K^+)/\Gamma_{total}$ — Γ_{175}/Γ

VALUE (units 10^{-3})	DOCUMENT ID		TECN	COMMENT
2.47±0.10±0.18	[1] DEL-AMO-SA...	11B	BABR	$e^+e^- \to \Upsilon(4S)$
• • • We do not use the following data for averages, fits, limits, etc. • • •				
$3.1\ ^{+0.4}_{-0.3}\ \pm0.4$	[1] AUBERT	03X	BABR	Repl. by DEL-AMO-SANCHEZ 11B

[1] Assumes equal production of B^+ and B^0 at the $\Upsilon(4S)$.

$\Gamma(D^*(2010)^-D^0K^+)/\Gamma(D^-D^0K^+)$ — $\Gamma_{175}/\Gamma_{173}$

VALUE	DOCUMENT ID		TECN	COMMENT
1.754±0.028±0.038	[1] AAIJ	20AN	LHCB	pp at 7, 8, 13 TeV

[1] Uses $D^+ \to K^-\pi^+\pi^+$, $D^0 \to K^-\pi^+$ and $D^0 \to K^-\pi^+\pi^+\pi^-$ decays.

$\Gamma(D^*(2010)^-D^*(2007)^0K^+)/\Gamma_{total}$ — Γ_{176}/Γ

VALUE (units 10^{-3})	DOCUMENT ID		TECN	COMMENT
10.6±0.33±0.86	[1] DEL-AMO-SA...	11B	BABR	$e^+e^- \to \Upsilon(4S)$
• • • We do not use the following data for averages, fits, limits, etc. • • •				
11.8±1.0 ±1.7	[1] AUBERT	03X	BABR	Repl. by DEL-AMO-SANCHEZ 11B

[1] Assumes equal production of B^+ and B^0 at the $\Upsilon(4S)$.

$\Gamma(D^-D^+K^0)/\Gamma_{total}$ — Γ_{177}/Γ

VALUE (units 10^{-3})	CL%	DOCUMENT ID		TECN	COMMENT
0.75±0.12±0.12		[1] DEL-AMO-SA...	11B	BABR	$e^+e^- \to \Upsilon(4S)$
• • • We do not use the following data for averages, fits, limits, etc. • • •					
<1.7	90	[1] AUBERT	03X	BABR	Repl. by DEL-AMO-SANCHEZ 11B

[1] Assumes equal production of B^+ and B^0 at the $\Upsilon(4S)$.

$[\Gamma(D^*(2010)^-D^+K^0)+\Gamma(D^-D^*(2010)^+K^0)]/\Gamma_{total}$ — Γ_{178}/Γ

VALUE (units 10^{-3})	DOCUMENT ID		TECN	COMMENT
6.41±0.36±0.39	[1] DEL-AMO-SA...	11B	BABR	$e^+e^- \to \Upsilon(4S)$
• • • We do not use the following data for averages, fits, limits, etc. • • •				
6.5 ±1.2 ±1.0	[1] AUBERT	03X	BABR	Repl. by DEL-AMO-SANCHEZ 11B

[1] Assumes equal production of B^+ and B^0 at the $\Upsilon(4S)$.

$\Gamma(D^*(2010)^-D^*(2010)^+K^0)/\Gamma_{total}$ — Γ_{179}/Γ

VALUE (units 10^{-3})	DOCUMENT ID		TECN	COMMENT
8.1 ±0.7 OUR AVERAGE				
8.26±0.43±0.67	[1] DEL-AMO-SA...	11B	BABR	$e^+e^- \to \Upsilon(4S)$
6.8 ±0.8 ±1.4	[1,2] DALSENO	07	BELL	$e^+e^- \to \Upsilon(4S)$
8.8 ±0.8 ±1.4	[1,2] AUBERT,B	06Q	BABR	$e^+e^- \to \Upsilon(4S)$
• • • We do not use the following data for averages, fits, limits, etc. • • •				
$8.8\ ^{+1.5}_{-1.4}\ \pm1.3$	[1] AUBERT	03X	BABR	Repl. by AUBERT,B 06Q

[1] Assumes equal production of B^+ and B^0 at the $\Upsilon(4S)$.
[2] The result is rescaled by a factor of 2 to convert from K^0_S to K^0.

$\Gamma(D^{*-}D_{s1}(2536)^+,\ D^+_{s1} \to D^{*+}K^0)/\Gamma_{total}$ — Γ_{180}/Γ

VALUE (units 10^{-4})	DOCUMENT ID		TECN	COMMENT
8.0±2.4 OUR AVERAGE				
$7.6^{+4.8+1.6}_{-4.2-1.4}$	[1,2] DALSENO	07	BELL	$e^+e^- \to \Upsilon(4S)$
8.2±2.6±1.2	[1,2] AUBERT,B	06Q	BABR	$e^+e^- \to \Upsilon(4S)$

[1] Assumes equal production of B^+ and B^0 at the $\Upsilon(4S)$.
[2] The result is rescaled by a factor of 2 to convert from K^0_S to K^0.

$\Gamma(\overline{D}^0D^0K^0)/\Gamma_{total}$ — Γ_{181}/Γ

VALUE (units 10^{-3})	CL%	DOCUMENT ID		TECN	COMMENT
0.27±0.10±0.05		[1] DEL-AMO-SA...	11B	BABR	$e^+e^- \to \Upsilon(4S)$
• • • We do not use the following data for averages, fits, limits, etc. • • •					
<1.4	90	[1] AUBERT	03X	BABR	Repl. by DEL-AMO-SANCHEZ 11B

[1] Assumes equal production of B^+ and B^0 at the $\Upsilon(4S)$.

$\Gamma(D^0\overline{D}^0K^+\pi^-)/\Gamma(D^*(2010)^-D^0K^+)$ — $\Gamma_{182}/\Gamma_{175}$

VALUE (%)	DOCUMENT ID		TECN	COMMENT
14.2±1.1±1.0	[1] AAIJ	20AG	LHCB	pp at 7, 8, and 13 TeV

[1] AAIJ 20AG excluded contributions from $B^0 \to D^{*-}D^0K^+$ transitions with $D^{*-} \to \overline{D}^0\pi^-$.

$[\Gamma(\overline{D}^0D^*(2007)^0K^0)+\Gamma(\overline{D}^*(2007)^0D^0K^0)]/\Gamma_{total}$ — Γ_{183}/Γ

VALUE (units 10^{-3})	CL%	DOCUMENT ID		TECN	COMMENT
1.08±0.32±0.36		[1] DEL-AMO-SA...	11B	BABR	$e^+e^- \to \Upsilon(4S)$
• • • We do not use the following data for averages, fits, limits, etc. • • •					
<3.7	90	[1] AUBERT	03X	BABR	Repl. by DEL-AMO-SANCHEZ 11B

[1] Assumes equal production of B^+ and B^0 at the $\Upsilon(4S)$.

$\Gamma(\overline{D}^*(2007)^0D^*(2007)^0K^0)/\Gamma_{total}$ — Γ_{184}/Γ

VALUE (units 10^{-3})	CL%	DOCUMENT ID		TECN	COMMENT
2.40±0.55±0.67		[1] DEL-AMO-SA...	11B	BABR	$e^+e^- \to \Upsilon(4S)$
• • • We do not use the following data for averages, fits, limits, etc. • • •					
<6.6	90	[1] AUBERT	03X	BABR	Repl. by DEL-AMO-SANCHEZ 11B

[1] Assumes equal production of B^+ and B^0 at the $\Upsilon(4S)$.

$\Gamma((\overline{D}+\overline{D}^*)(D+D^*)K)/\Gamma_{total}$ — Γ_{185}/Γ

VALUE (units 10^{-2})	DOCUMENT ID		TECN	COMMENT
3.68±0.10±0.24	[1] DEL-AMO-SA...	11B	BABR	$e^+e^- \to \Upsilon(4S)$
• • • We do not use the following data for averages, fits, limits, etc. • • •				
4.3 ±0.3 ±0.6	[1] AUBERT	03X	BABR	Repl. by DEL-AMO-SANCHEZ 11B

[1] Assumes equal production of B^+ and B^0 at the $\Upsilon(4S)$.

Downloaded from https://academic.oup.com/ptep/article/2022/8/083C01/6651666 by KIT Library user on 27 September 2022

$\Gamma(\eta_c K^0)/\Gamma_{total}$ — Γ_{186}/Γ

VALUE (units 10^{-3})	DOCUMENT ID		TECN	COMMENT
0.80±0.11 OUR AVERAGE				
$0.71^{+0.12}_{-0.10}\pm0.28$	[1] CHILIKIN	19	BELL	$e^+e^-\to\Upsilon(4S)$
$0.58^{+0.20+0.06}_{-0.18-0.05}$	[2,3] AUBERT	07AV	BABR	$e^+e^-\to\Upsilon(4S)$
$0.89\pm0.15\pm0.05$	[2,4] AUBERT,B	04B	BABR	$e^+e^-\to\Upsilon(4S)$
$1.23\pm0.23^{+0.40}_{-0.41}$	[2] FANG	03	BELL	$e^+e^-\to\Upsilon(4S)$
$1.09^{+0.55}_{-0.42}\pm0.33$	[5] EDWARDS	01	CLE2	$e^+e^-\to\Upsilon(4S)$

[1] CHILIKIN 19 reports $[\Gamma(B^0\to\eta_c K^0)/\Gamma_{total}]\times[B(\eta_c(1S)\to\pi^+\pi^-p\overline{p})]=(38.0^{+6.4+1.3}_{-2.9-4.7})\times10^{-7}$ which we divide by our best value $B(\eta_c(1S)\to\pi^+\pi^-p\overline{p})=(5.3\pm2.1)\times10^{-3}$. Our first error is their experiment's error and our second error is the systematic error from using our best value.
[2] Assumes equal production of B^+ and B^0 at the $\Upsilon(4S)$.
[3] AUBERT 07AV reports $[\Gamma(B^0\to\eta_c K^0)/\Gamma_{total}]\times[B(\eta_c(1S)\to p\overline{p})]=(0.83^{+0.28}_{-0.26}\pm0.05)\times10^{-6}$ which we divide by our best value $B(\eta_c(1S)\to p\overline{p})=(1.44\pm0.14)\times10^{-3}$. Our first error is their experiment's error and our second error is the systematic error from using our best value.
[4] AUBERT,B 04B reports $[\Gamma(B^0\to\eta_c K^0)/\Gamma_{total}]\times[B(\eta_c(1S)\to K\overline{K}\pi)]=(0.0648\pm0.0085\pm0.0071)\times10^{-3}$ which we divide by our best value $B(\eta_c(1S)\to K\overline{K}\pi)=(7.3\pm0.4)\times10^{-2}$. Our first error is their experiment's error and our second error is the systematic error from using our best value.
[5] EDWARDS 01 assumes equal production of B^0 and B^+ at the $\Upsilon(4S)$. The correlated uncertainties (28.3)% from $B(J/\psi(1S)\to\gamma\eta_c)$ in those modes have been accounted for.

$\Gamma(\eta_c K^0)/\Gamma(J/\psi(1S)K^0)$ — $\Gamma_{186}/\Gamma_{200}$

VALUE	DOCUMENT ID		TECN	COMMENT
1.39±0.20±0.45	[1] AUBERT,B	04B	BABR	$e^+e^-\to\Upsilon(4S)$

[1] Uses BABAR measurement of $B(B^0\to J/\psi K^0)=(8.5\pm0.5\pm0.6)\times10^{-4}$.

$\Gamma(\eta_c(1S)K^+\pi^-)/\Gamma(J/\psi(1S)K^+\pi^-)$ — $\Gamma_{187}/\Gamma_{201}$

VALUE	DOCUMENT ID		TECN	COMMENT
0.53±0.03±0.05	[1] AAIJ	18AN	LHCB	pp at 7, 8, 13 TeV

[1] AAIJ 18AN reports $[\Gamma(B^0\to\eta_c(1S)K^+\pi^-)/\Gamma(B^0\to J/\psi(1S)K^+\pi^-)]\times[B(\eta_c(1S)\to p\overline{p})]/[B(J/\psi(1S)\to p\overline{p})]=0.357\pm0.015\pm0.008$ which we multiply or divide by our best values $B(\eta_c(1S)\to p\overline{p})=(1.44\pm0.14)\times10^{-3}$, $B(J/\psi(1S)\to p\overline{p})=(2.120\pm0.029)\times10^{-3}$. Our first error is their experiment's error and our second error is the systematic error from using our best values.

$\Gamma(\eta_c(1S)K^*(1410)^0)/\Gamma(\eta_c(1S)K^+\pi^-)$ — $\Gamma_{190}/\Gamma_{187}$

VALUE (units 10^{-2})	DOCUMENT ID		TECN	COMMENT
32±24±6	[1] AAIJ	18AN	LHCB	pp at 7, 8, 13 TeV

[1] AAIJ 18AN reports $[\Gamma(B^0\to\eta_c(1S)K^*(1410)^0)/\Gamma(B^0\to\eta_c(1S)K^+\pi^-)]\times[B(K^*(1410)\to K\pi)]=0.021\pm0.011\pm0.011$ which we divide by our best value $B(K^*(1410)\to K\pi)=(6.6\pm1.3)\times10^{-2}$. Our first error is their experiment's error and our second error is the systematic error from using our best value.

$\Gamma(\eta_c(1S)K^+\pi^-(NR))/\Gamma(\eta_c(1S)K^+\pi^-)$ — $\Gamma_{188}/\Gamma_{187}$

VALUE (units 10^{-2})	DOCUMENT ID		TECN	COMMENT
$10.3\pm1.4^{+1.0}_{-1.2}$	AAIJ	18AN	LHCB	pp at 7, 8, 13 TeV

$\Gamma(\eta_c(1S)K_0^*(1430)^0)/\Gamma(\eta_c(1S)K^+\pi^-)$ — $\Gamma_{191}/\Gamma_{187}$

VALUE (units 10^{-2})	DOCUMENT ID		TECN	COMMENT
27±5±3	[1] AAIJ	18AN	LHCB	pp at 7, 8, 13 TeV

[1] AAIJ 18AN reports $[\Gamma(B^0\to\eta_c(1S)K_0^*(1430)^0)/\Gamma(B^0\to\eta_c(1S)K^+\pi^-)]\times[B(K_0^*(1430)\to K\pi)]=0.253\pm0.035^{+0.035}_{-0.028}$ which we divide by our best value $B(K_0^*(1430)\to K\pi)=(93\pm10)\times10^{-2}$. Our first error is their experiment's error and our second error is the systematic error from using our best value.

$\Gamma(\eta_c(1S)K_2^*(1430)^0)/\Gamma(\eta_c(1S)K^+\pi^-)$ — $\Gamma_{192}/\Gamma_{187}$

VALUE (units 10^{-2})	DOCUMENT ID		TECN	COMMENT
$8.2^{+3.6}_{-4.4}\pm0.2$	[1] AAIJ	18AN	LHCB	pp at 7, 8, 13 TeV

[1] AAIJ 18AN reports $[\Gamma(B^0\to\eta_c(1S)K_2^*(1430)^0)/\Gamma(B^0\to\eta_c(1S)K^+\pi^-)]\times[B(K_2^*(1430)\to K\pi)]=0.041\pm0.015^{+0.010}_{-0.016}$ which we divide by our best value $B(K_2^*(1430)\to K\pi)=(49.9\pm1.2)\times10^{-2}$. Our first error is their experiment's error and our second error is the systematic error from using our best value.

$\Gamma(\eta_c(1S)K^*(1680)^0)/\Gamma(\eta_c(1S)K^+\pi^-)$ — $\Gamma_{193}/\Gamma_{187}$

VALUE (units 10^{-2})	DOCUMENT ID		TECN	COMMENT
$5.7^{+6.5}_{-6.8}\pm0.4$	[1] AAIJ	18AN	LHCB	pp at 7, 8, 13 TeV

[1] AAIJ 18AN reports $[\Gamma(B^0\to\eta_c(1S)K^*(1680)^0)/\Gamma(B^0\to\eta_c(1S)K^+\pi^-)]\times[B(K^*(1680)\to K\pi)]=0.022\pm0.020^{+0.015}_{-0.017}$ which we divide by our best value $B(K^*(1680)\to K\pi)=(38.7\pm2.5)\times10^{-2}$. Our first error is their experiment's error and our second error is the systematic error from using our best value.

$\Gamma(\eta_c(1S)K_0^*(1950)^0)/\Gamma(\eta_c(1S)K^+\pi^-)$ — $\Gamma_{194}/\Gamma_{187}$

VALUE (units 10^{-2})	DOCUMENT ID		TECN	COMMENT
$7^{+4}_{-6}\pm2$	[1] AAIJ	18AN	LHCB	pp at 7, 8, 13 TeV

[1] AAIJ 18AN reports $[\Gamma(B^0\to\eta_c(1S)K_0^*(1950)^0)/\Gamma(B^0\to\eta_c(1S)K^+\pi^-)]\times[B(K_0^*(1950)\to K^-\pi^+)]=0.038\pm0.018^{+0.014}_{-0.025}$ which we divide by our best value $B(K_0^*(1950)\to K^-\pi^+)=(52\pm14)\times10^{-2}$. Our first error is their experiment's error and our second error is the systematic error from using our best value.

$\Gamma(X(4100)^-K^+,\ X^-\to\eta_c\pi^-)/\Gamma(\eta_c(1S)K^+\pi^-)$ — $\Gamma_{189}/\Gamma_{187}$

VALUE (units 10^{-2})	DOCUMENT ID		TECN	COMMENT
$3.3\pm1.1^{+1.2}_{-1.1}$	AAIJ	18AN	LHCB	pp at 7, 8, 13 TeV

$\Gamma(\eta_c K^*(892)^0)/\Gamma_{total}$ — Γ_{195}/Γ

VALUE (units 10^{-4})	DOCUMENT ID		TECN	COMMENT
$5.2^{+0.8}_{-0.9}$ OUR AVERAGE Error includes scale factor of 1.6. See the ideogram below.				
$4.42\pm0.24^{+0.54}_{-0.66}$	[1] AAIJ	18AN	LHCB	pp at 7, 8, 13 TeV
$6.7\pm0.8\pm0.5$	[2,3] AUBERT	08AB	BABR	$e^+e^-\to\Upsilon(4S)$
$7.2^{+2.2}_{-2.0}\pm0.7$	[4,5] AUBERT	07AV	BABR	$e^+e^-\to\Upsilon(4S)$
$16.2\pm3.2^{+5.5}_{-6.0}$	[5] FANG	03	BELL	$e^+e^-\to\Upsilon(4S)$

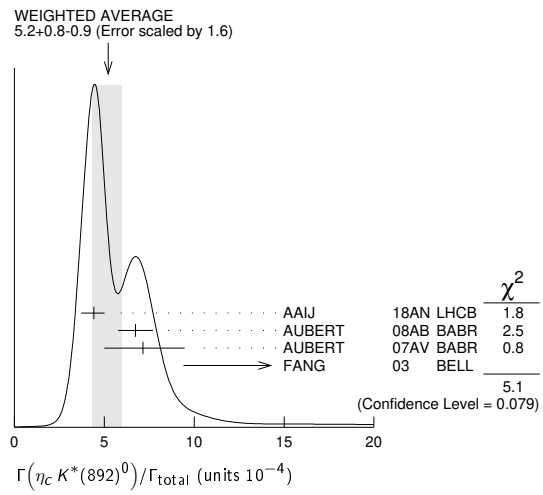

[1] AAIJ 18AN reports $B(B^0\to\eta_c K^*(892)^0,\ K^*(892)^0\to K^+\pi^-)=(2.95\pm0.16^{+0.36}_{-0.44})\times10^{-4}$ using the fitted fraction of $0.514\pm0.019^{+0.017}_{-0.048}$ from Dalitz decay of $B(B^0\to\eta_c K^+\pi^-)=(5.73\pm0.24\pm0.67)\times10^{-4}$ and corrected for $B(K^*(892)^0\to K^+\pi^-)=2/3$.
[2] AUBERT 08AB reports $[\Gamma(B^0\to\eta_c K^*(892)^0)/\Gamma_{total}]/[B(B^+\to\eta_c K^+)]=0.62\pm0.06\pm0.05$ which we multiply by our best value $B(B^+\to\eta_c K^+)=(1.09\pm0.08)\times10^{-3}$. Our first error is their experiment's error and our second error is the systematic error from using our best value.
[3] Uses the production ratio of $(B^+B^-)/(B^0\overline{B}^0)=1.026\pm0.032$ at $\Upsilon(4S)$.
[4] AUBERT 07AV reports $[\Gamma(B^0\to\eta_c K^*(892)^0)/\Gamma_{total}]\times[B(\eta_c(1S)\to p\overline{p})]=(1.03^{+0.27}_{-0.24}\pm0.17)\times10^{-6}$ which we divide by our best value $B(\eta_c(1S)\to p\overline{p})=(1.44\pm0.14)\times10^{-3}$. Our first error is their experiment's error and our second error is the systematic error from using our best value.
[5] Assumes equal production of B^+ and B^0 at the $\Upsilon(4S)$.

$\Gamma(\eta_c(2S)K_S^0,\ \eta_c\to p\overline{p}\pi^+\pi^-)/\Gamma_{total}$ — Γ_{196}/Γ

VALUE (units 10^{-7})	DOCUMENT ID		TECN	COMMENT
$4.2^{+1.4+0.3}_{-1.2-0.3}$	CHILIKIN	19	BELL	$e^+e^-\to\Upsilon(4S)$

$\Gamma(\eta_c(2S)K^{*0})/\Gamma_{total}$ — Γ_{197}/Γ

VALUE (units 10^{-4})	CL%	DOCUMENT ID		TECN	COMMENT
<3.9	90	[1] AUBERT	08AB	BABR	$e^+e^-\to\Upsilon(4S)$

[1] Uses the production ratio of $(B^+B^-)/(B^0\overline{B}^0)=1.026\pm0.032$ at $\Upsilon(4S)$.

$\Gamma(h_c(1P)K_S^0)/\Gamma_{total}$ — Γ_{198}/Γ

VALUE	DOCUMENT ID		TECN	COMMENT
$<1.4\times10^{-5}$	CHILIKIN	19	BELL	$e^+e^-\to\Upsilon(4S)$

$\Gamma(B^0\to h_c(1P)K^{*0})/\Gamma_{total}\times\Gamma(h_c(1P)\to\gamma\eta_c(1S))/\Gamma_{total}$ — $\Gamma_{199}/\Gamma\times\Gamma_{22}^{h_c(1P)}/\Gamma^{h_c(1P)}$

VALUE (units 10^{-4})	CL%	DOCUMENT ID		TECN	COMMENT
<2.2	90	[1] AUBERT	08AB	BABR	$e^+e^-\to\Upsilon(4S)$

[1] Uses the production ratio of $(B^+B^-)/(B^0\overline{B}^0)=1.026\pm0.032$ at $\Upsilon(4S)$.

Downloaded from https://academic.oup.com/ptep/article/2022/8/083C01/6651666 by KIT Library user on 27 September 2022

$\Gamma(\eta_c K^*(892)^0)/\Gamma(\eta_c K^0)$ — $\Gamma_{195}/\Gamma_{186}$

VALUE	DOCUMENT ID		TECN	COMMENT
$1.33 \pm 0.36^{+0.24}_{-0.33}$	FANG	03	BELL	$e^+e^- \to \Upsilon(4S)$

$\Gamma(J/\psi(1S)K^0)/\Gamma_{total}$ — Γ_{200}/Γ

VALUE (units 10^{-4})	CL%	EVTS	DOCUMENT ID		TECN	COMMENT
8.91±0.21 OUR FIT						
8.91±0.21 OUR AVERAGE						
9.02±0.10±0.26			[1] CHOUDHURY	21	BELL	$e^+e^- \to \Upsilon(4S)$
8.1 ±0.9 ±0.6			[2] CHILIKIN	19	BELL	$e^+e^- \to \Upsilon(4S)$
$8.8\ ^{+1.4}_{-1.3}$ ±0.1			[3,4] AUBERT	07AV	BABR	$e^+e^- \to \Upsilon(4S)$
8.69±0.22±0.30			[4] AUBERT	05J	BABR	$e^+e^- \to \Upsilon(4S)$
9.5 ±0.8 ±0.6			[4] AVERY	00	CLE2	$e^+e^- \to \Upsilon(4S)$
11.5 ±2.3 ±1.7			[5] ABE	96H	CDF	$p\overline{p}$ at 1.8 TeV
6.93±4.07±0.04			[6] BORTOLETTO	92	CLEO	$e^+e^- \to \Upsilon(4S)$
9.24±7.21±0.05		2	[7] ALBRECHT	90J	ARG	$e^+e^- \to \Upsilon(4S)$
• • • We do not use the following data for averages, fits, limits, etc. • • •						
7.9 ±0.4 ±0.9			[4] ABE	03B	BELL	Repl. by CHOUDHURY 21
8.3 ±0.4 ±0.5			[4] AUBERT	02	BABR	Repl. by AUBERT 05J
$8.5\ ^{+1.4}_{-1.2}$ ±0.6			[4] JESSOP	97	CLE2	Repl. by AVERY 00
7.5 ±2.4 ±0.8		10	[6] ALAM	94	CLE2	Sup. by JESSOP 97
<50	90		ALAM	86	CLEO	$e^+e^- \to \Upsilon(4S)$

[1] CHOUDHURY 21 uses the relative production fraction of charged (f^{+-}) to neutral (f^{00}) B mesons at $\Upsilon(4S)$ value of $f^{+-}/f^{00} = 1.058 \pm 0.024$.

[2] CHILIKIN 19 reports $[\Gamma(B^0 \to J/\psi(1S)K^0)/\Gamma_{total}] \times [B(J/\psi(1S) \to p\overline{p}\pi^+\pi^-)] = (48.6^{+4.6}_{-4.4}{}^{+2.4}_{-2.6}) \times 10^{-7}$ which we divide by our best value $B(J/\psi(1S) \to p\overline{p}\pi^+\pi^-) = (6.0 \pm 0.5) \times 10^{-3}$. Our first error is their experiment's error and our second error is the systematic error from using our best value.

[3] AUBERT 07AV reports $[\Gamma(B^0 \to J/\psi(1S)K^0)/\Gamma_{total}] \times [B(J/\psi(1S) \to p\overline{p})] = (1.87^{+0.28}_{-0.26} \pm 0.07) \times 10^{-6}$ which we divide by our best value $B(J/\psi(1S) \to p\overline{p}) = (2.120 \pm 0.029) \times 10^{-3}$. Our first error is their experiment's error and our second error is the systematic error from using our best value.

[4] Assumes equal production of B^+ and B^0 at the $\Upsilon(4S)$.

[5] ABE 96H assumes that $B(B^+ \to J/\psi K^+) = (1.02 \pm 0.14) \times 10^{-3}$.

[6] BORTOLETTO 92 reports $(6 \pm 3 \pm 2) \times 10^{-4}$ from a measurement of $[\Gamma(B^0 \to J/\psi(1S)K^0)/\Gamma_{total}] \times [B(J/\psi(1S) \to e^+e^-)]$ assuming $B(J/\psi(1S) \to e^+e^-) = 0.069 \pm 0.009$, which we rescale to our best value $B(J/\psi(1S) \to e^+e^-) = (5.971 \pm 0.032) \times 10^{-2}$. Our first error is their experiment's error and our second error is the systematic error from using our best value. Assumes equal production of B^+ and B^0 at the $\Upsilon(4S)$.

[7] ALBRECHT 90J reports $(8 \pm 6 \pm 2) \times 10^{-4}$ from a measurement of $[\Gamma(B^0 \to J/\psi(1S)K^0)/\Gamma_{total}] \times [B(J/\psi(1S) \to e^+e^-)]$ assuming $B(J/\psi(1S) \to e^+e^-) = 0.069 \pm 0.009$, which we rescale to our best value $B(J/\psi(1S) \to e^+e^-) = (5.971 \pm 0.032) \times 10^{-2}$. Our first error is their experiment's error and our second error is the systematic error from using our best value. Assumes equal production of B^+ and B^0 at the $\Upsilon(4S)$.

$\Gamma(J/\psi(1S)K^+\pi^-)/\Gamma_{total}$ — Γ_{201}/Γ

VALUE (units 10^{-3})	CL%	DOCUMENT ID		TECN	COMMENT
1.15 ±0.05 OUR AVERAGE					
1.15 ±0.01 ±0.05		CHILIKIN	14	BELL	$\overline{B}^0 \to J/\psi K^-\pi^+$
1.16 ±0.56 ±0.01		[1] BORTOLETTO	92	CLEO	$e^+e^- \to \Upsilon(4S)$
• • • We do not use the following data for averages, fits, limits, etc. • • •					
1.079±0.011		[2] AUBERT	09AA	BABR	$e^+e^- \to \Upsilon(4S)$
<1.3	90	[3] ALBRECHT	87D	ARG	$e^+e^- \to \Upsilon(4S)$
<6.3	90	GILES	84	CLEO	$e^+e^- \to \Upsilon(4S)$

[1] BORTOLETTO 92 reports $(1.0 \pm 0.4 \pm 0.3) \times 10^{-3}$ from a measurement of $[\Gamma(B^0 \to J/\psi(1S)K^+\pi^-)/\Gamma_{total}] \times [B(J/\psi(1S) \to e^+e^-)]$ assuming $B(J/\psi(1S) \to e^+e^-) = 0.069 \pm 0.009$, which we rescale to our best value $B(J/\psi(1S) \to e^+e^-) = (5.971 \pm 0.032) \times 10^{-2}$. Our first error is their experiment's error and our second error is the systematic error from using our best value. Assumes equal production of B^+ and B^0 at the $\Upsilon(4S)$.

[2] Does not report systematic uncertainties.

[3] ALBRECHT 87D assume $B^+B^-/B^0\overline{B}^0$ ratio is 55/45. $K\pi$ system is specifically selected as nonresonant.

$\Gamma(J/\psi(1S)K^*(892)^0)/\Gamma_{total}$ — Γ_{202}/Γ

VALUE (units 10^{-3})	EVTS	DOCUMENT ID		TECN	COMMENT
1.27 ±0.05 OUR FIT					
1.28 ±0.05 OUR AVERAGE					
1.19 ±0.01 ±0.08		CHILIKIN	14	BELL	$\overline{B}^0 \to J/\psi K^-\pi^+$
$1.33\ ^{+0.22}_{-0.21}$ ±0.02		[1,2] AUBERT	07AV	BABR	$e^+e^- \to \Upsilon(4S)$
1.309±0.026±0.077		[2] AUBERT	05J	BABR	$e^+e^- \to \Upsilon(4S)$
1.29 ±0.05 ±0.13		[2] ABE	02N	BELL	$e^+e^- \to \Upsilon(4S)$
1.74 ±0.20 ±0.18		[3] ABE	98O	CDF	$p\overline{p}$ 1.8 TeV
1.32 ±0.17 ±0.17		[4] JESSOP	97	CLE2	$e^+e^- \to \Upsilon(4S)$
1.27 ±0.65 ±0.01		[5] BORTOLETTO	92	CLEO	$e^+e^- \to \Upsilon(4S)$
1.27 ±0.60 ±0.01	6	[6] ALBRECHT	90J	ARG	$e^+e^- \to \Upsilon(4S)$
4.04 ±1.81 ±0.02	5	[7] BEBEK	87	CLEO	$e^+e^- \to \Upsilon(4S)$
• • • We do not use the following data for averages, fits, limits, etc. • • •					
1.24 ±0.05 ±0.09		[2] AUBERT	02	BABR	Repl. by AUBERT 05J
1.36 ±0.27 ±0.22		[8] ABE	96H	CDF	Sup. by ABE 98O
1.69 ±0.31 ±0.18	29	[9] ALAM	94	CLE2	Sup. by JESSOP 97
		[10] ALBRECHT	94G	ARG	$e^+e^- \to \Upsilon(4S)$
4.0 ±0.30		[11] ALBAJAR	91E	UA1	$E^{p\overline{p}}_{cm}$= 630 GeV
3.3 ±0.18	5	[12] ALBRECHT	87D	ARG	$e^+e^- \to \Upsilon(4S)$
4.1 ±0.18	5	[13] ALAM	86	CLEO	Repl. by BEBEK 87

[1] AUBERT 07AV reports $[\Gamma(B^0 \to J/\psi(1S)K^*(892)^0)/\Gamma_{total}] \times [B(J/\psi(1S) \to p\overline{p})] = (2.82^{+0.30}_{-0.28}{}^{+0.36}_{-0.35}) \times 10^{-6}$ which we divide by our best value $B(J/\psi(1S) \to p\overline{p}) = (2.120 \pm 0.029) \times 10^{-3}$. Our first error is their experiment's error and our second error is the systematic error from using our best value.

[2] Assumes equal production of B^+ and B^0 at the $\Upsilon(4S)$.

[3] ABE 98O reports $[B(B^0 \to J/\psi(1S)K^*(892)^0)]/[B(B^+ \to J/\psi(1S)K^+)] = 1.76 \pm 0.14 \pm 0.15$. We multiply by our best value $B(B^+ \to J/\psi(1S)K^+) = (9.9 \pm 1.0) \times 10^{-4}$. Our first error is their experiment's error and our second error is the systematic error from using our best value.

[4] Assumes equal production of B^+ and B^0 at the $\Upsilon(4S)$.

[5] BORTOLETTO 92 reports $(1.1 \pm 0.5 \pm 0.3) \times 10^{-3}$ from a measurement of $[\Gamma(B^0 \to J/\psi(1S)K^*(892)^0)/\Gamma_{total}] \times [B(J/\psi(1S) \to e^+e^-)]$ assuming $B(J/\psi(1S) \to e^+e^-) = 0.069 \pm 0.009$, which we rescale to our best value $B(J/\psi(1S) \to e^+e^-) = (5.971 \pm 0.032) \times 10^{-2}$. Our first error is their experiment's error and our second error is the systematic error from using our best value. Assumes equal production of B^+ and B^0 at the $\Upsilon(4S)$.

[6] ALBRECHT 90J reports $(1.1 \pm 0.5 \pm 0.2) \times 10^{-3}$ from a measurement of $[\Gamma(B^0 \to J/\psi(1S)K^*(892)^0)/\Gamma_{total}] \times [B(J/\psi(1S) \to e^+e^-)]$ assuming $B(J/\psi(1S) \to e^+e^-) = 0.069 \pm 0.009$, which we rescale to our best value $B(J/\psi(1S) \to e^+e^-) = (5.971 \pm 0.032) \times 10^{-2}$. Our first error is their experiment's error and our second error is the systematic error from using our best value. Assumes equal production of B^+ and B^0 at the $\Upsilon(4S)$.

[7] BEBEK 87 reports $(3.5 \pm 1.6 \pm 0.3) \times 10^{-3}$ from a measurement of $[\Gamma(B^0 \to J/\psi(1S)K^*(892)^0)/\Gamma_{total}] \times [B(J/\psi(1S) \to e^+e^-)]$ assuming $B(J/\psi(1S) \to e^+e^-) = 0.069 \pm 0.009$, which we rescale to our best value $B(J/\psi(1S) \to e^+e^-) = (5.971 \pm 0.032) \times 10^{-2}$. Our first error is their experiment's error and our second error is the systematic error from using our best value. Updated in BORTOLETTO 92 to use the same assumptions.

[8] ABE 96H assumes that $B(B^+ \to J/\psi K^+) = (1.02 \pm 0.14) \times 10^{-3}$.

[9] The neutral and charged B events together are predominantly longitudinally polarized, $\Gamma_L/\Gamma = 0.080 \pm 0.08 \pm 0.05$. This can be compared with a prediction using HQET, 0.73 (KRAMER 92). This polarization indicates that the $B \to \psi K^*$ decay is dominated by the $CP = -1$ CP eigenstate. Assumes equal production of B^+ and B^0 at the $\Upsilon(4S)$.

[10] ALBRECHT 94G measures the polarization in the vector-vector decay to be predominantly longitudinal, $\Gamma_T/\Gamma = 0.03 \pm 0.16 \pm 0.15$ making the neutral decay a CP eigenstate when the K^{*0} decays through $K^0_S\pi^0$.

[11] ALBAJAR 91E assumes B^0_d production fraction of 36%.

[12] ALBRECHT 87D assume $B^+B^-/B^0\overline{B}^0$ ratio is 55/45. Superseded by ALBRECHT 90J.

[13] ALAM 86 assumes $B^\pm/B^0$ ratio is 60/40. The observation of the decay $B^+ \to J/\psi K^*(892)^+$ (HAAS 85) has been retracted in this paper.

$\Gamma(J/\psi(1S)K^*(892)^0)/\Gamma(J/\psi(1S)K^0)$ — $\Gamma_{202}/\Gamma_{200}$

VALUE	DOCUMENT ID		TECN	COMMENT
1.50±0.09 OUR AVERAGE				
1.51±0.05±0.08	AUBERT	05J	BABR	$e^+e^- \to \Upsilon(4S)$
1.39±0.36±0.10	ABE	96Q	CDF	$p\overline{p}$
• • • We do not use the following data for averages, fits, limits, etc. • • •				
1.49±0.10±0.08	[1] AUBERT	02	BABR	Repl. by AUBERT 05J

[1] Assumes equal production of B^+ and B^0 at the $\Upsilon(4S)$.

$\Gamma(J/\psi(1S)\eta K^0_S)/\Gamma_{total}$ — Γ_{203}/Γ

VALUE (units 10^{-5})	DOCUMENT ID		TECN	COMMENT
5.4 ±0.9 OUR AVERAGE				
5.22±0.78±0.49	[1] IWASHITA	14	BELL	$e^+e^- \to \Upsilon(4S)$
8.4 ±2.6 ±2.7	[1] AUBERT	04Y	BABR	$e^+e^- \to \Upsilon(4S)$

[1] Assumes equal production of B^+ and B^0 at the $\Upsilon(4S)$.

$\Gamma(J/\psi(1S)\eta' K^0_S)/\Gamma_{total}$ — Γ_{204}/Γ

VALUE (units 10^{-5})	CL%	DOCUMENT ID		TECN	COMMENT
<2.5	90	[1] XIE	07	BELL	$e^+e^- \to \Upsilon(4S)$

[1] Assumes equal production of B^+ and B^0 at the $\Upsilon(4S)$.

$\Gamma(J/\psi(1S)\omega K^0)/\Gamma_{total}$ — Γ_{206}/Γ

VALUE (units 10^{-4})	DOCUMENT ID		TECN	COMMENT
2.3±0.3±0.3	[1] DEL-AMO-SA...10B		BABR	$e^+e^- \to \Upsilon(4S)$
• • • We do not use the following data for averages, fits, limits, etc. • • •				
3.1±0.6±0.3	[1] AUBERT	08W	BABR	Repl. by DEL-AMO-SANCHEZ 10B

[1] Assumes equal production of B^+ and B^0 at the $\Upsilon(4S)$.

Downloaded from https://academic.oup.com/ptep/article/2022/8/083C01/6651666 by KIT Library user on 27 September 2022

$\Gamma(\chi_{c0}(3915),\ \chi_{c0} \to J/\psi\omega)/\Gamma_{total}$ — Γ_{207}/Γ

VALUE (units 10^{-5})	DOCUMENT ID	TECN	COMMENT
$2.1 \pm 0.9 \pm 0.3$	[1] DEL-AMO-SA...10B	BABR	$e^+e^- \to \Upsilon(4S)$
• • • We do not use the following data for averages, fits, limits, etc. • • •			
$1.3^{+1.3}_{-1.1} \pm 0.2$	[1,2] AUBERT	08W BABR	Repl. by DEL-AMO-SANCHEZ 10B

[1] Assumes equal production of B^+ and B^0 at the $\Upsilon(4S)$.
[2] Corresponds to upper limit of 3.9×10^{-5} at 90% CL.

$\Gamma(J/\psi(1S)\phi K^0)/\Gamma_{total}$ — Γ_{205}/Γ

VALUE (units 10^{-5})	DOCUMENT ID	TECN	COMMENT
4.9 ±1.0 OUR AVERAGE	Error includes scale factor of 1.3.		
$4.43 \pm 0.76 \pm 0.19$	LEES 15	BABR	$e^+e^- \to \Upsilon(4S)$
$10.2 \pm 3.8 \pm 1.0$	[1] AUBERT 03O	BABR	$e^+e^- \to \Upsilon(4S)$
$8.8\ ^{+3.5}_{-3.0} \pm 1.3$	[2] ANASTASSOV 00	CLE2	$e^+e^- \to \Upsilon(4S)$

[1] Assumes equal production of B^+ and B^0 at the $\Upsilon(4S)$.
[2] ANASTASSOV 00 finds 10 events on a background of 0.5 ± 0.2. Assumes equal production of B^0 and B^+ at the $\Upsilon(4S)$, a uniform Dalitz plot distribution, isotropic $J/\psi(1S)$ and ϕ decays, and $B(B^+ \to J/\psi(1S)\phi K^+) = B(B^0 \to J/\psi(1S)\phi K^0)$.

$\Gamma(J/\psi(1S)K(1270)^0)/\Gamma_{total}$ — Γ_{208}/Γ

VALUE (units 10^{-3})	DOCUMENT ID	TECN	COMMENT
$1.30 \pm 0.34 \pm 0.32$	[1] ABE 01L	BELL	$e^+e^- \to \Upsilon(4S)$

[1] Assumes equal production of B^+ and B^0 at the $\Upsilon(4S)$ and uses the PDG value of $B(B^+ \to J/\psi(1S)K^+) = (1.00 \pm 0.10) \times 10^{-3}$.

$\Gamma(J/\psi(1S)\pi^0)/\Gamma_{total}$ — Γ_{209}/Γ

VALUE (units 10^{-5})	CL%	DOCUMENT ID	TECN	COMMENT
1.66±0.10 OUR AVERAGE				
$1.62 \pm 0.11 \pm 0.06$		[1] PAL 18	BELL	$e^+e^- \to \Upsilon(4S)$
$1.69 \pm 0.14 \pm 0.07$		[1] AUBERT 08AU	BABR	$e^+e^- \to \Upsilon(4S)$
$2.5\ ^{+1.1}_{-0.9} \pm 0.2$		[1] AVERY 00	CLE2	$e^+e^- \to \Upsilon(4S)$
• • • We do not use the following data for averages, fits, limits, etc. • • •				
$1.94 \pm 0.22 \pm 0.17$		[1] AUBERT,B 06B	BABR	Repl. by AUBERT 08AU
$2.3 \pm 0.5 \pm 0.2$		[1] ABE 03B	BELL	Repl. by PAL 18
$2.0 \pm 0.6 \pm 0.2$		[1] AUBERT 02	BABR	Repl. by AUBERT,B 06B
< 32	90	[2] ACCIARRI 97C	L3	
< 5.8	90	BISHAI 96	CLE2	Sup. by AVERY 00
< 690	90	[1] ALEXANDER 95	CLE2	Sup. by BISHAI 96

[1] Assumes equal production of B^+ and B^0 at the $\Upsilon(4S)$.
[2] ACCIARRI 97C assumes B^0 production fraction $(39.5 \pm 4.0)\%$ and B_s $(12.0 \pm 3.0)\%$.

$\Gamma(J/\psi(1S)\eta)/\Gamma_{total}$ — Γ_{210}/Γ

VALUE (units 10^{-6})	CL%	DOCUMENT ID	TECN	COMMENT
10.8±2.3 OUR AVERAGE		Error includes scale factor of 1.5.		
$7.3 \pm 2.5 \pm 1.3$		[1] AAIJ 15D	LHCB	pp at 7, 8 TeV
$12.3^{+1.8}_{-1.7} \pm 0.7$		[2,3] CHANG 12	BELL	$e^+e^- \to \Upsilon(4S)$
• • • We do not use the following data for averages, fits, limits, etc. • • •				
$9.5 \pm 1.7 \pm 0.8$		[3] CHANG 07A	BELL	Repl. by CHANG 12
< 27	90	[3] AUBERT 03O	BABR	$e^+e^- \to \Upsilon(4S)$
< 1200	90	[4] ACCIARRI 97C	L3	

[1] AAIJ 15D reports $[\Gamma(B^0 \to J/\psi(1S)\eta)/\Gamma_{total}]$ / $[B(B^0_s \to J/\psi(1S)\eta)] = (1.85 \pm 0.61 \pm 0.14) \times 10^{-2}$ which we multiply by our best value $B(B^0_s \to J/\psi(1S)\eta) = (4.0 \pm 0.7) \times 10^{-4}$. Our first error is their experiment's error and our second error is the systematic error from using our best value.
[2] Reconstructs η in $\gamma\gamma$ and $\pi^+\pi^-\pi^0$ decays.
[3] Assumes equal production of B^+ and B^0 at the $\Upsilon(4S)$.
[4] ACCIARRI 97C assumes B^0 production fraction $(39.5 \pm 4.0\%)$ and B_s $(12.0 \pm 3.0\%)$.

$\Gamma(J/\psi(1S)\pi^+\pi^-)/\Gamma_{total}$ — Γ_{211}/Γ

VALUE (units 10^{-5})	DOCUMENT ID	TECN	COMMENT
4.00±0.15 OUR AVERAGE			
$3.98 \pm 0.14 \pm 0.07$	[1,2] AAIJ 13M	LHCB	pp at 7 TeV
$4.6 \pm 0.7 \pm 0.6$	[3] AUBERT 03B	BABR	$e^+e^- \to \Upsilon(4S)$

[1] AAIJ 13M reports $(3.97 \pm 0.09 \pm 0.11 \pm 0.16) \times 10^{-5}$ from a measurement of $[\Gamma(B^0 \to J/\psi(1S)\pi^+\pi^-)/\Gamma_{total}]$ / $[B(B^+ \to J/\psi(1S)K^+)]$ assuming $B(B^+ \to J/\psi(1S)K^+) = (1.018 \pm 0.042) \times 10^{-3}$, which we rescale to our best value $B(B^+ \to J/\psi(1S)K^+) = (1.020 \pm 0.019) \times 10^{-3}$. Our first error is their experiment's error and our second error is the systematic error from using our best value.
[2] AAIJ 13M does not report correlations between various measurements of the $J/\psi\pi\pi$ final state.
[3] Assumes equal production of B^+ and B^0 at the $\Upsilon(4S)$.

$\Gamma(J/\psi(1S)\pi^+\pi^-\text{nonresonant})/\Gamma_{total}$ — Γ_{212}/Γ

VALUE (units 10^{-5})	CL%	DOCUMENT ID	TECN	COMMENT
<1.2	90	[1] AUBERT 07AC	BABR	$e^+e^- \to \Upsilon(4S)$

[1] Assumes equal production of B^+ and B^0 at the $\Upsilon(4S)$.

$\Gamma(J/\psi(1S)f_0(500),\ f_0 \to \pi\pi)/\Gamma_{total}$ — Γ_{213}/Γ

VALUE (units 10^{-6})	DOCUMENT ID	TECN	COMMENT
$8.8 \pm 0.5\ ^{+1.1}_{-1.5}$	[1] AAIJ 14X	LHCB	pp at 7, 8 TeV
• • • We do not use the following data for averages, fits, limits, etc. • • •			
$6.4\ ^{+2.5}_{-1.1} \pm 0.2$	[2,3] AAIJ 13M	LHCB	Repl. by AAIJ 14X

[1] AAIJ 14X uses Dalitz plot analysis of $B^0 \to J/\psi\pi^+\pi^-$.
[2] AAIJ 13M reports $(6.4 \pm 0.8\ ^{+2.4}_{-0.8}) \times 10^{-6}$ from a measurement of $[\Gamma(B^0 \to J/\psi(1S)f_0(500),\ f_0 \to \pi\pi)/\Gamma_{total}]$ / $[B(B^0 \to J/\psi(1S)\pi^+\pi^-)]$ assuming $B(B^0 \to J/\psi(1S)\pi^+\pi^-) = (3.97 \pm 0.09 \pm 0.11 \pm 0.16) \times 10^{-5}$, which we rescale to our best value $B(B^0 \to J/\psi(1S)\pi^+\pi^-) = (4.00 \pm 0.15) \times 10^{-5}$. Our first error is their experiment's error and our second error is the systematic error from using our best value.
[3] AAIJ 13M does not report correlations between various measurements of the $J/\psi\pi\pi$ final state. Measured in Dalitz plot like analysis of $B^0 \to J/\psi\pi^+\pi^-$.

$\Gamma(J/\psi(1S)f_2)/\Gamma_{total}$ — Γ_{214}/Γ

VALUE (units 10^{-5})	CL%	DOCUMENT ID	TECN	COMMENT
$0.33^{+0.05}_{-0.06}$ OUR AVERAGE		Error includes scale factor of 1.5.		
$0.30 \pm 0.03\ ^{+0.02}_{-0.03}$		[1] AAIJ 14X	LHCB	pp at 7, 8 TeV
$0.42 \pm 0.06 \pm 0.02$		[2,3] AAIJ 13M	LHCB	pp at 7 TeV
• • • We do not use the following data for averages, fits, limits, etc. • • •				
<0.5	90	[4,5] AUBERT 07AC	BABR	$e^+e^- \to \Upsilon(4S)$

[1] AAIJ 14X uses Dalitz plot analysis of $B^0 \to J/\psi\pi^+\pi^-$.
[2] AAIJ 13M reports $[\Gamma(B^0 \to J/\psi(1S)f_2)/\Gamma_{total}] \times [B(f_2(1270) \to \pi\pi)] = (3.5 \pm 0.4 \pm 0.4) \times 10^{-6}$ from a measurement of $[\Gamma(B^0 \to J/\psi(1S)f_2)/\Gamma_{total}] \times [B(f_2(1270) \to \pi\pi)]$ / $[B(B^0 \to J/\psi(1S)\pi^+\pi^-)]$ assuming $B(B^0 \to J/\psi(1S)\pi^+\pi^-) = (3.97 \pm 0.09 \pm 0.11 \pm 0.16) \times 10^{-5}$, which we rescale to our best values $B(f_2(1270) \to \pi\pi) = (84.2\ ^{+2.9}_{-0.9}) \times 10^{-2}$, $B(B^0 \to J/\psi(1S)\pi^+\pi^-) = (4.00 \pm 0.15) \times 10^{-5}$. Our first error is their experiment's error and our second error is the systematic error from using our best values.
[3] AAIJ 13M does not report correlations between various measurements of the $J/\psi\pi\pi$ final state. Measured in Dalitz plot like analysis of $B^0 \to J/\psi\pi^+\pi^-$.
[4] AUBERT 07AC reports $[\Gamma(B^0 \to J/\psi(1S)f_2)/\Gamma_{total}] \times [B(f_2(1270) \to \pi\pi)] < 0.46 \times 10^{-5}$ which we divide by our best value $B(f_2(1270) \to \pi\pi) = 84.2 \times 10^{-2}$.
[5] Assumes equal production of B^+ and B^0 at the $\Upsilon(4S)$.

$\Gamma(J/\psi(1S)\rho^0)/\Gamma_{total}$ — Γ_{215}/Γ

VALUE (units 10^{-5})	CL%	DOCUMENT ID	TECN	COMMENT
$2.55^{+0.18}_{-0.16}$ OUR AVERAGE				
$2.50 \pm 0.10\ ^{+0.18}_{-0.15}$		[1] AAIJ 14X	LHCB	pp at 7, 8 TeV
$2.7 \pm 0.3 \pm 0.2$		[2] AUBERT 07AC	BABR	$e^+e^- \to \Upsilon(4S)$
• • • We do not use the following data for averages, fits, limits, etc. • • •				
$2.51\ ^{+0.22}_{-0.23} \pm 0.10$		[3,4] AAIJ 13M	LHCB	Repl. by AAIJ 14X
$1.6 \pm 0.6 \pm 0.4$		[2] AUBERT 03B	BABR	Repl. by AUBERT 07AC
<25	90	BISHAI 96	CLE2	$e^+e^- \to \Upsilon(4S)$

[1] AAIJ 14X uses Dalitz plot analysis of $B^0 \to J/\psi\pi^+\pi^-$. We assume $B(\rho(770)^0 \to \pi^+\pi^-) = 100\%$.
[2] Assumes equal production of B^+ and B^0 at the $\Upsilon(4S)$.
[3] AAIJ 13M reports $(2.49\ ^{+0.20}_{-0.13}\ ^{+0.16}_{-0.23}) \times 10^{-5}$ from a measurement of $[\Gamma(B^0 \to J/\psi(1S)\rho^0)/\Gamma_{total}]$ / $[B(B^0 \to J/\psi(1S)\pi^+\pi^-)]$ assuming $B(B^0 \to J/\psi(1S)\pi^+\pi^-) = (3.97 \pm 0.09 \pm 0.11 \pm 0.16) \times 10^{-5}$, which we rescale to our best value $B(B^0 \to J/\psi(1S)\pi^+\pi^-) = (4.00 \pm 0.15) \times 10^{-5}$. Our first error is their experiment's error and our second error is the systematic error from using our best value.
[4] AAIJ 13M does not report correlations between various measurements of the $J/\psi\pi\pi$ final state. Measured in Dalitz plot like analysis of $B^0 \to J/\psi\pi^+\pi^-$. Assumes $B(\rho(770)^0 \to \pi\pi) = 100\%$.

$\Gamma(J/\psi(1S)f_0(980),\ f_0 \to \pi^+\pi^-)/\Gamma_{total}$ — Γ_{216}/Γ

VALUE	CL%	DOCUMENT ID	TECN	COMMENT
$<1.1 \times 10^{-6}$	90	[1] AAIJ 13M	LHCB	pp at 7 TeV

[1] AAIJ 13M does not provide correlations between various measurements of the $J/\psi\pi^+\pi^-$ final state. The measurements were obtained from a Dalitz plot like analysis of $B^0 \to J/\psi\pi^+\pi^-$. Also reports $\Gamma(J/\psi(1S)f_0(980),\ f_0 \to \pi^+\pi^-)/\Gamma_{total} = (6.1\ ^{+3.1}_{-2.0}\ ^{+1.7}_{-1.4}) \times 10^{-6}$.

$\Gamma(J/\psi(1S)\rho(1450)^0,\ \rho^0 \to \pi\pi)/\Gamma_{total}$ — Γ_{217}/Γ

VALUE (units 10^{-6})	DOCUMENT ID	TECN	COMMENT
$2.9^{+1.6}_{-0.7}$ OUR AVERAGE			
$4.6 \pm 1.1 \pm 1.9$	[1] AAIJ 14X	LHCB	pp at 7, 8 TeV
$2.1\ ^{+2.4}_{-0.7} \pm 0.1$	[2,3] AAIJ 13M	LHCB	pp at 7 TeV

[1] AAIJ 14X uses Dalitz plot analysis of $B^0 \to J/\psi\pi^+\pi^-$.
[2] AAIJ 13M reports $(2.1\ ^{+1.0}_{-0.6}\ ^{+2.2}_{-0.4}) \times 10^{-6}$ from a measurement of $[\Gamma(B^0 \to J/\psi(1S)\rho(1450)^0,\ \rho^0 \to \pi\pi)/\Gamma_{total}]$ / $[B(B^0 \to J/\psi(1S)\pi^+\pi^-)]$ assuming $B(B^0 \to J/\psi(1S)\pi^+\pi^-) = (3.97 \pm 0.09 \pm 0.11 \pm 0.16) \times 10^{-5}$, which we rescale

Downloaded from https://academic.oup.com/ptep/article/2022/8/083C01/6651666 by KIT Library user on 27 September 2022

to our best value $B(B^0 \to J/\psi(1S)\pi^+\pi^-) = (4.00 \pm 0.15) \times 10^{-5}$. Our first error is their experiment's error and our second error is the systematic error from using our best value.

[3] AAIJ 13M does not report correlations between various measurements of the $J/\psi\pi\pi$ final state. Measured in Dalitz plot like analysis of $B^0 \to J/\psi\pi^+\pi^-$.

$\Gamma(J/\psi\rho(1700)^0, \rho^0 \to \pi^+\pi^-)/\Gamma_{total}$ — Γ_{218}/Γ

VALUE (units 10^{-6})	DOCUMENT ID		TECN	COMMENT
2.0±0.5±1.2	[1] AAIJ	14X	LHCB	pp at 7, 8 TeV

[1] AAIJ 14X uses Dalitz plot analysis of $B^0 \to J/\psi\pi^+\pi^-$.

$\Gamma(J/\psi(1S)\omega)/\Gamma_{total}$ — Γ_{219}/Γ

VALUE (units 10^{-5})	CL%	DOCUMENT ID		TECN	COMMENT
$\mathbf{1.8^{+0.7}_{-0.5} \pm 0.1}$		[1] AAIJ	14X	LHCB	pp at 7, 8 TeV
• • • We do not use the following data for averages, fits, limits, etc. • • •					
<27	90	BISHAI	96	CLE2	$e^+e^- \to \Upsilon(4S)$

[1] AAIJ 14X reports $[\Gamma(B^0 \to J/\psi(1S)\omega)/\Gamma_{total}] \times [B(\omega(782) \to \pi^+\pi^-)] = (2.7^{+0.8+0.7}_{-0.6-0.5}) \times 10^{-7}$ which we divide by our best value $B(\omega(782) \to \pi^+\pi^-) = (1.53^{+0.11}_{-0.13}) \times 10^{-2}$. Our first error is their experiment's error and our second error is the systematic error from using our best value.

$\Gamma(J/\psi(1S)\omega)/\Gamma(J/\psi(1S)\rho^0)$ — $\Gamma_{219}/\Gamma_{215}$

VALUE	DOCUMENT ID		TECN	COMMENT
$\mathbf{0.61^{+0.24+0.31}_{-0.14-0.16}}$	[1,2] AAIJ	13M	LHCB	pp at 7 TeV

[1] AAIJ 13M reports $0.61^{+0.24+0.31}_{-0.14-0.16}$ from a measurement of $[\Gamma(B^0 \to J/\psi(1S)\omega)/\Gamma(B^0 \to J/\psi(1S)\rho^0)] \times [B(\omega(782) \to \pi^+\pi^-)]$ assuming $B(\omega(782) \to \pi^+\pi^-) = (1.53^{+0.11}_{-0.13}) \times 10^{-2}$.

[2] AAIJ 13M does not report correlations between various measurements of the $J/\psi\pi\pi$ final state. Measured in Dalitz plot like analysis of $B^0 \to J/\psi\pi^+\pi^-$. Assumes $B(\rho(770)^0 \to \pi\pi) = 100\%$.

$\Gamma(J/\psi(1S)\omega)/\Gamma(J/\psi(1S)\rho^0)$ — $\Gamma_{219}/\Gamma_{215}$

VALUE	DOCUMENT ID		TECN	COMMENT
$\mathbf{0.89 \pm 0.19^{+0.07}_{-0.13}}$	AAIJ	13A	LHCB	pp at 7 TeV

$\Gamma(J/\psi(1S)K^+K^-)/\Gamma_{total}$ — Γ_{220}/Γ

VALUE (units 10^{-6})	DOCUMENT ID		TECN	COMMENT
2.54±0.35±0.05	[1] AAIJ	13BT	LHCB	pp at 7 TeV

[1] AAIJ 13BT reports $(2.53 \pm 0.31 \pm 0.19) \times 10^{-6}$ from a measurement of $[\Gamma(B^0 \to J/\psi(1S)K^+K^-)/\Gamma_{total}] / [B(B^+ \to J/\psi(1S)K^+)]$ assuming $B(B^+ \to J/\psi(1S)K^+) = (1.018 \pm 0.042) \times 10^{-3}$, which we rescale to our best value $B(B^+ \to J/\psi(1S)K^+) = (1.020 \pm 0.019) \times 10^{-3}$. Our first error is their experiment's error and our second error is the systematic error from using our best value.

$\Gamma(J/\psi(1S)a_0(980), a_0 \to K^+K^-)/\Gamma_{total}$ — Γ_{221}/Γ

VALUE (units 10^{-6})	DOCUMENT ID		TECN	COMMENT
0.470±0.331±0.072	[1] AAIJ	13BT	LHCB	pp at 7 TeV

[1] AAIJ 13BT uses $B(\overline{B}^0 \to J/\psi K^+K^-) = (2.53 \pm 0.31 \pm 0.19) \times 10^{-6}$ to derive this result. It also reports the equivalent upper limit of $< 9.0 \times 10^{-7}$ at 90% CL.

$\Gamma(J/\psi(1S)\phi)/\Gamma_{total}$ — Γ_{222}/Γ

VALUE	CL%	DOCUMENT ID		TECN	COMMENT
$\mathbf{< 1.1 \times 10^{-7}}$	90	AAIJ	21K	LHCB	pp at 7, 8, 13 TeV
• • • We do not use the following data for averages, fits, limits, etc. • • •					
$< 10.1 \times 10^{-7}$	90	LEES	15	BABR	$e^+e^- \to \Upsilon(4S)$
$< 1.9 \times 10^{-7}$	90	[1] AAIJ	13BT	LHCB	pp at 7 TeV
$< 9.4 \times 10^{-7}$	90	[2] LIU	08I	BELL	$e^+e^- \to \Upsilon(4S)$
$< 9.2 \times 10^{-6}$	90	[2] AUBERT	03O	BABR	$e^+e^- \to \Upsilon(4S)$

[1] AAIJ 13BT uses $B(B^0 \to J/\psi(1S)K^+K^-) = (2.53 \pm 0.31 \pm 0.19) \times 10^{-6}$ and $B(\phi \to K^+K^-) = (48.9 \pm 0.5)\%$ to obtain this result.

[2] Assumes equal production of B^+ and B^0 at the $\Upsilon(4S)$.

$\Gamma(J/\psi(1S)\eta'(958))/\Gamma_{total}$ — Γ_{223}/Γ

VALUE (units 10^{-6})	CL%	DOCUMENT ID		TECN	COMMENT
7.6±2.2±1.0		[1] AAIJ	15D	LHCB	pp at 7, 8 TeV
• • • We do not use the following data for averages, fits, limits, etc. • • •					
< 7.4	90	[2,3] CHANG	12	BELL	$e^+e^- \to \Upsilon(4S)$
<63	90	[3] AUBERT	03O	BABR	$e^+e^- \to \Upsilon(4S)$

[1] AAIJ 15D reports $[\Gamma(B^0 \to J/\psi(1S)\eta'(958))/\Gamma_{total}] / [B(B^0_s \to J/\psi(1S)\eta')] = (2.28 \pm 0.65 \pm 0.16) \times 10^{-2}$ which we multiply by our best value $B(B^0_s \to J/\psi(1S)\eta') = (3.3 \pm 0.4) \times 10^{-4}$. Our first error is their experiment's error and our second error is the systematic error from using our best value.

[2] Reconstructs $\eta'(985)$ in $(etapi + pi)^-$ and $\rho(770)$ decays.

[3] Assumes equal production of B^+ and B^0 at the $\Upsilon(4S)$.

$\Gamma(J/\psi(1S)\eta)/\Gamma(J/\psi(1S)\eta'(958))$ — $\Gamma_{210}/\Gamma_{223}$

VALUE	DOCUMENT ID		TECN	COMMENT
1.111±0.475±0.062	[1] AAIJ	15D	LHCB	pp at 7, 8 TeV

[1] Uses $J/\psi \to \mu^+\mu^-$, $\eta' \to \rho^0\gamma$, and $\eta' \to \eta\pi^+\pi^-$ decays.

$\Gamma(J/\psi(1S)K^0\pi^+\pi^-)/\Gamma(J/\psi(1S)K^0)$ — $\Gamma_{224}/\Gamma_{200}$

VALUE	DOCUMENT ID		TECN	COMMENT
0.50 ±0.04 OUR AVERAGE				
0.493±0.034±0.027	AAIJ	14L	LHCB	pp at 7 TeV
1.24 ±0.40 ±0.15	AFFOLDER	02B	CDF	$p\overline{p}$ 1.8 TeV

$\Gamma(J/\psi(1S)K^0K^+K^-)/\Gamma_{total}$ — Γ_{226}/Γ

VALUE (units 10^{-6})	DOCUMENT ID		TECN	COMMENT
25 ±7 OUR AVERAGE Error includes scale factor of 1.8.				
34.9±6.7±1.5	LEES	15	BABR	$e^+e^- \to \Upsilon(4S)$
20.2±4.3±1.9	[1] AAIJ	14L	LHCB	pp at 7 TeV

[1] Measured with $B(B^0 \to J/\psi K^0_S K^+K^-)$ / $B(B^0 \to J/\psi K^0_S)$ using PDG 12 for the involved branching fractions.

$\Gamma(J/\psi(1S)K^0K^-\pi^+ + c.c.)/\Gamma_{total}$ — Γ_{225}/Γ

VALUE	CL%	DOCUMENT ID		TECN	COMMENT
$\mathbf{<21 \times 10^{-6}}$	90	[1] AAIJ	14L	LHCB	pp at 7 TeV

[1] Measured with $B(B^0 \to J/\psi K^0_S K^\pm\pi^\mp)$ / $B(B^0 \to J/\psi K^0_S\pi^+\pi^-)$ using PDG 12 values for the involved branching fractions.

$\Gamma(J/\psi(1S)K^0\rho^0)/\Gamma_{total}$ — Γ_{228}/Γ

VALUE (units 10^{-4})	DOCUMENT ID		TECN	COMMENT
5.4±2.9±0.9	[1] AFFOLDER	02B	CDF	$p\overline{p}$ 1.8 TeV

[1] Uses $B^0 \to J/\psi(1S)K^0_S$ decay as a reference and $B(B^0 \to J/\psi(1S)K^0) = 8.3 \times 10^{-4}$.

$\Gamma(J/\psi(1S)K^*(892)^+\pi^-)/\Gamma_{total}$ — Γ_{229}/Γ

VALUE (units 10^{-4})	DOCUMENT ID		TECN	COMMENT
7.7±4.1±1.3	[1] AFFOLDER	02B	CDF	$p\overline{p}$ 1.8 TeV

[1] Uses $B^0 \to J/\psi(1S)K^0_S$ decay as a reference and $B(B^0 \to J/\psi(1S)K^0) = 8.3 \times 10^{-4}$.

$\Gamma(J/\psi(1S)\pi^+\pi^-\pi^+\pi^-)/\Gamma(J/\psi(1S)\pi^+\pi^-)$ — $\Gamma_{230}/\Gamma_{211}$

VALUE	DOCUMENT ID		TECN	COMMENT
0.361±0.017±0.021	[1] AAIJ	14Y	LHCB	pp at 7, 8 TeV

[1] Excludes contributions from $\psi(2S)$ and $\chi_{c1}(3872)$ decaying to $J/\psi(1S)\pi^+\pi^-$.

$\Gamma(J/\psi(1S)f_1(1285))/\Gamma_{total}$ — Γ_{231}/Γ

VALUE (units 10^{-6})	DOCUMENT ID		TECN	COMMENT
$\mathbf{8.4^{+2.1}_{-2.0} \pm 0.5}$	[1] AAIJ	14Y	LHCB	pp at 7, 8 TeV

[1] AAIJ 14Y reports $(8.37 \pm 1.95^{+0.71}_{-0.66} \pm 0.35) \times 10^{-6}$ from a measurement of $[\Gamma(B^0 \to J/\psi(1S)f_1(1285))/\Gamma_{total}] \times [B(f_1(1285) \to 2\pi^+2\pi^-)]$ assuming $B(f_1(1285) \to 2\pi^+2\pi^-) = 0.11^{+0.007}_{-0.006}$, which we rescale to our best value $B(f_1(1285) \to 2\pi^+2\pi^-) = (10.9 \pm 0.6) \times 10^{-2}$. Our first error is their experiment's error and our second error is the systematic error from using our best value.

$\Gamma(J/\psi(1S)K^*(892)^0\pi^+\pi^-)/\Gamma_{total}$ — Γ_{232}/Γ

VALUE (units 10^{-4})	DOCUMENT ID		TECN	COMMENT
6.6±1.9±1.1	[1] AFFOLDER	02B	CDF	$p\overline{p}$ 1.8 TeV

[1] Uses $B^0 \to J/\psi(1S)K^*(892)^0$ decay as a reference and $B(B^0 \to J/\psi(1S)K^0) = 12.4 \times 10^{-4}$.

$\Gamma(\eta_{c2}(1D)K^0_S, \eta_{c2} \to h_c\gamma)/\Gamma_{total}$ — Γ_{233}/Γ

VALUE	CL%	DOCUMENT ID		TECN	COMMENT
$\mathbf{<3.5 \times 10^{-5}}$	90	CHILIKIN	20	BELL	$e^+e^- \to \Upsilon(4S)$

$\Gamma(\eta_{c2}(1D)\pi^-K^+, \eta_{c2} \to h_c\gamma)/\Gamma_{total}$ — Γ_{234}/Γ

VALUE	CL%	DOCUMENT ID		TECN	COMMENT
$\mathbf{<1.0 \times 10^{-4}}$	90	CHILIKIN	20	BELL	$e^+e^- \to \Upsilon(4S)$

$\Gamma(\chi_{c1}(3872)K^0)/\Gamma_{total}$ — Γ_{237}/Γ

VALUE (units 10^{-4})	CL%	DOCUMENT ID		TECN	COMMENT
1.1 ±0.4 OUR AVERAGE					
1.05±0.31±0.34		[1] CHOI	11	BELL	$e^+e^- \to \Upsilon(4S)$
1.4 ±0.7 ±0.7		[2] DEL-AMO-SA...10B		BABR	$e^+e^- \to \Upsilon(4S)$
• • • We do not use the following data for averages, fits, limits, etc. • • •					
<2.8	90	[3,4] BHARDWAJ	11	BELL	$e^+e^- \to \Upsilon(4S)$
2.6 ±1.3 ±0.6		[4,5] AUSHEV	10	BELL	$e^+e^- \to \Upsilon(4S)$
<6	90	[6,7] AUBERT	09B	BABR	$e^+e^- \to \Upsilon(4S)$
6.1 ±3.1 ±1.5		[4,6,8] AUBERT	08B	BABR	$e^+e^- \to \Upsilon(4S)$
<1.6	90	[9] AUBERT	08Y	BABR	$e^+e^- \to \Upsilon(4S)$
<2.7	90	[10] AUBERT	06	BABR	Repl. by AUBERT 08Y
3.4 ±1.6 $^{+1.4}_{-1.3}$		[11,12] GOKHROO	06	BELL	$e^+e^- \to \Upsilon(4S)$

[1] CHOI 11 reports $[\Gamma(B^0 \to \chi_{c1}(3872)K^0)/\Gamma_{total}] / [B(B^+ \to \chi_{c1}(3872)K^+)] = 0.50 \pm 0.14 \pm 0.04$ which we multiply by our best value $B(B^+ \to \chi_{c1}(3872)K^+) = (2.1 \pm 0.7) \times 10^{-4}$. Our first error is their experiment's error and our second error is the systematic error from using our best value.

[2] DEL-AMO-SANCHEZ 10B reports $[\Gamma(B^0 \to \chi_{c1}(3872)K^0)/\Gamma_{total}] \times [B(\chi_{c1}(3872) \to \omega J/\psi(1S))] = (6 \pm 3 \pm 1) \times 10^{-6}$ which we divide by our best value $B(\chi_{c1}(3872) \to \omega J/\psi(1S)) = (4.3 \pm 2.1) \times 10^{-2}$. Our first error is their experiment's error and our second error is the systematic error from using our best value.

Downloaded from https://academic.oup.com/ptep/article/2022/8/083C01/6651666 by KIT Library user on 27 September 2022

[3] BHARDWAJ 11 reports $[\Gamma(B^0 \to \chi_{c1}(3872) K^0)/\Gamma_{total}] \times [B(\chi_{c1}(3872) \to \gamma J/\psi)] < 2.4 \times 10^{-6}$ which we divide by our best value $B(\chi_{c1}(3872) \to \gamma J/\psi) = 8 \times 10^{-3}$.

[4] Assumes equal production of B^+ and B^0 at the $\Upsilon(4S)$.

[5] AUSHEV 10 reports $[\Gamma(B^0 \to \chi_{c1}(3872) K^0)/\Gamma_{total}] \times [B(\chi_{c1}(3872) \to \overline{D}^{*0} D^0)] = (0.97 \pm 0.46 \pm 0.13) \times 10^{-4}$ which we divide by our best value $B(\chi_{c1}(3872) \to \overline{D}^{*0} D^0) = (37 \pm 9) \times 10^{-2}$. Our first error is their experiment's error and our second error is the systematic error from using our best value.

[6] Uses $B(\Upsilon(4S) \to B^+ B^-) = (51.6 \pm 0.6)\%$ and $B(\Upsilon(4S) \to B^0 \overline{B}^0) = (48.4 \pm 0.6)\%$.

[7] AUBERT 09B reports $[\Gamma(B^0 \to \chi_{c1}(3872) K^0)/\Gamma_{total}] \times [B(\chi_{c1}(3872) \to \gamma J/\psi)] < 4.9 \times 10^{-6}$ which we divide by our best value $B(\chi_{c1}(3872) \to \gamma J/\psi) = 8 \times 10^{-3}$.

[8] AUBERT 08B reports $[\Gamma(B^0 \to \chi_{c1}(3872) K^0)/\Gamma_{total}] \times [B(\chi_{c1}(3872) \to \overline{D}^{*0} D^0)] = (2.22 \pm 1.05 \pm 0.42) \times 10^{-4}$ which we divide by our best value $B(\chi_{c1}(3872) \to \overline{D}^{*0} D^0) = (37 \pm 9) \times 10^{-2}$. Our first error is their experiment's error and our second error is the systematic error from using our best value.

[9] AUBERT 08Y reports $[\Gamma(B^0 \to \chi_{c1}(3872) K^0)/\Gamma_{total}] \times [B(\chi_{c1}(3872) \to \pi^+\pi^- J/\psi(1S))] < 6.0 \times 10^{-6}$ which we divide by our best value $B(\chi_{c1}(3872) \to \pi^+\pi^- J/\psi(1S)) = 3.8 \times 10^{-2}$.

[10] AUBERT 06 reports $[\Gamma(B^0 \to \chi_{c1}(3872) K^0)/\Gamma_{total}] \times [B(\chi_{c1}(3872) \to \pi^+\pi^- J/\psi(1S))] < 10.3 \times 10^{-6}$ which we divide by our best value $B(\chi_{c1}(3872) \to \pi^+\pi^- J/\psi(1S)) = 3.8 \times 10^{-2}$.

[11] GOKHROO 06 reports $[\Gamma(B^0 \to \chi_{c1}(3872) K^0)/\Gamma_{total}] \times [B(\chi_{c1}(3872) \to D^0\overline{D}^0\pi^0)] = (1.66 \pm 0.70^{+0.32}_{-0.37}) \times 10^{-4}$ which we divide by our best value $B(\chi_{c1}(3872) \to D^0\overline{D}^0\pi^0) = (49^{+18}_{-20}) \times 10^{-2}$. Our first error is their experiment's error and our second error is the systematic error from using our best value.

[12] Measure the near-threshold enhancements in the $(D^0\overline{D}^0\pi^0)$ system at a mass $3875.2 \pm 0.7^{+0.3}_{-1.6} \pm 0.8$ MeV/c^2.

$\Gamma(\chi_{c1}(3872)^- K^+)/\Gamma_{total}$ — Γ_{235}/Γ

VALUE	CL%	DOCUMENT ID		TECN	COMMENT
$<5 \times 10^{-4}$	90	[1] AUBERT	06E	BABR	$e^+e^- \to \Upsilon(4S)$

[1] Perform measurements of absolute branching fractions using a missing mass technique.

$\Gamma(\chi_{c1}(3872)^- K^+, \chi_{c1}(3872)^- \to J/\psi(1S)\pi^-\pi^0)/\Gamma_{total}$ — Γ_{236}/Γ

VALUE (units 10^{-6})	CL%	DOCUMENT ID		TECN	COMMENT
<4.2	90	[1,2] CHOI	11	BELL	$e^+e^- \to \Upsilon(4S)$
• • • We do not use the following data for averages, fits, limits, etc. • • •					
<5.4	90	[2,3] AUBERT	05B	BABR	$e^+e^- \to \Upsilon(4S)$

[1] Assumes $\pi^+\pi^0$ originates from ρ^+.

[2] Assumes equal production of B^+ and B^0 at the $\Upsilon(4S)$.

[3] The isovector-X hypothesis is excluded with a likelihood test at 1×10^{-4} level.

$\Gamma(\chi_{c1}(3872) K^*(892)^0)/\Gamma_{total}$ — Γ_{238}/Γ

VALUE (units 10^{-4})	CL%	DOCUMENT ID		TECN	COMMENT
1.0±0.4±0.3		[1] BALA	15	BELL	$e^+e^- \to \Upsilon(4S)$
• • • We do not use the following data for averages, fits, limits, etc. • • •					
<3.3	90	[2,3] AUBERT	09B	BABR	$e^+e^- \to \Upsilon(4S)$
<1.0	90	[3,4] AUBERT	09B	BABR	$e^+e^- \to \Upsilon(4S)$

[1] BALA 15 reports $[\Gamma(B^0 \to \chi_{c1}(3872) K^*(892)^0)/\Gamma_{total}] \times [B(\chi_{c1}(3872) \to \pi^+\pi^- J/\psi(1S))] = (4.0 \pm 1.5 \pm 0.3) \times 10^{-6}$ which we divide by our best value $B(\chi_{c1}(3872) \to \pi^+\pi^- J/\psi(1S)) = (3.8 \pm 1.2) \times 10^{-2}$. Our first error is their experiment's error and our second error is the systematic error from using our best value.

[2] AUBERT 09B reports $[\Gamma(B^0 \to \chi_{c1}(3872) K^*(892)^0)/\Gamma_{total}] \times [B(\chi_{c1}(3872) \to \gamma J/\psi)] < 2.8 \times 10^{-6}$ which we divide by our best value $B(\chi_{c1}(3872) \to \gamma J/\psi) = 8 \times 10^{-3}$.

[3] Uses $B(\Upsilon(4S) \to B^+ B^-) = (51.6 \pm 0.6)\%$ and $B(\Upsilon(4S) \to B^0 \overline{B}^0) = (48.4 \pm 0.6)\%$.

[4] AUBERT 09B reports $[\Gamma(B^0 \to \chi_{c1}(3872) K^*(892)^0)/\Gamma_{total}] \times [B(\chi_{c1}(3872) \to \gamma\psi(2S))] < 4.4 \times 10^{-6}$ which we divide by our best value $B(\chi_{c1}(3872) \to \gamma\psi(2S)) = 4.5 \times 10^{-2}$.

$\Gamma(\chi_{c1}(3872) K^+\pi^-)/\Gamma_{total}$ — Γ_{239}/Γ

VALUE (units 10^{-4})	DOCUMENT ID		TECN	COMMENT
2.1±0.4±0.7	[1,2] BALA	15	BELL	$e^+e^- \to \Upsilon(4S)$

[1] BALA 15 reports $[\Gamma(B^0 \to \chi_{c1}(3872) K^+\pi^-)/\Gamma_{total}] \times [B(\chi_{c1}(3872) \to \pi^+\pi^- J/\psi(1S))] = (7.9 \pm 1.3 \pm 0.4) \times 10^{-6}$ which we divide by our best value $B(\chi_{c1}(3872) \to \pi^+\pi^- J/\psi(1S)) = (3.8 \pm 1.2) \times 10^{-2}$. Our first error is their experiment's error and our second error is the systematic error from using our best value.

[2] Assumes equal production of B^+ and B^0 at the $\Upsilon(4S)$.

$\Gamma(\chi_{c1}(3872)\gamma)/\Gamma_{total}$ — Γ_{240}/Γ

VALUE	CL%	DOCUMENT ID		TECN	COMMENT
$<1.3 \times 10^{-5}$	90	[1,2] CHOU	19	BELL	$e^+e^- \to \Upsilon(4S)$

[1] Assumes equal production of B^+ and B^0 at $\Upsilon(4S)$.

[2] CHOU 19 reports $[\Gamma(B^0 \to \chi_{c1}(3872)\gamma)/\Gamma_{total}] \times [B(\chi_{c1}(3872) \to \pi^+\pi^- J/\psi(1S))] < 5.1 \times 10^{-7}$ which we divide by our best value $B(\chi_{c1}(3872) \to \pi^+\pi^- J/\psi(1S)) = 3.8 \times 10^{-2}$.

$\Gamma(Z_c(4430)^\pm K^\mp, Z_c^\pm \to \psi(2S)\pi^\pm)/\Gamma_{total}$ — Γ_{241}/Γ

VALUE (units 10^{-5})	CL%	DOCUMENT ID		TECN	COMMENT
$6.0^{+1.7}_{-2.0}{}^{+2.5}_{-1.4}$		CHILIKIN	13	BELL	$e^+e^- \to \Upsilon(4S)$
• • • We do not use the following data for averages, fits, limits, etc. • • •					
<3.1	95	[1] AUBERT	09AA	BABR	$e^+e^- \to \Upsilon(4S)$
$3.2^{+1.8}_{-0.9}{}^{+5.3}_{-1.6}$		[1] MIZUK	09	BELL	$e^+e^- \to \Upsilon(4S)$
$4.1 \pm 1.0 \pm 1.4$		[1,2] CHOI	08	BELL	Repl. by MIZUK 09

[1] Assumes equal production of B^+ and B^0 at the $\Upsilon(4S)$.

[2] Establishes the $(Z_c4430)^+$ with a significance of 6.5 sigma. Needs confirmation.

$\Gamma(Z_c(4430)^\pm K^\mp, Z_c^\pm \to J/\psi\pi^\pm)/\Gamma_{total}$ — Γ_{242}/Γ

VALUE (units 10^{-6})	CL%	DOCUMENT ID		TECN	COMMENT
$5.4^{+4.0}_{-1.0}{}^{+1.1}_{-0.6}$		CHILIKIN	14	BELL	$\overline{B}^0 \to J/\psi K^-\pi^+$
• • • We do not use the following data for averages, fits, limits, etc. • • •					
<4	95	[1] AUBERT	09AA	BABR	$e^+e^- \to \Upsilon(4S)$

[1] Assumes equal production of B^+ and B^0 at the $\Upsilon(4S)$.

$\Gamma(Z_c(3900)^\pm K^\mp, Z_c^\pm \to J/\psi\pi^\pm)/\Gamma_{total}$ — Γ_{243}/Γ

VALUE	DOCUMENT ID		TECN	COMMENT
$<9 \times 10^{-7}$	CHILIKIN	14	BELL	$\overline{B}^0 \to J/\psi K^-\pi^+$

$\Gamma(Z_c(4200)^\pm K^\mp, X^\pm \to J/\psi\pi^\pm)/\Gamma_{total}$ — Γ_{244}/Γ

VALUE (units 10^{-5})	DOCUMENT ID		TECN	COMMENT
$2.2^{+0.7}_{-0.5}{}^{+1.1}_{-0.6}$	CHILIKIN	14	BELL	$\overline{B}^0 \to J/\psi K^-\pi^+$

$\Gamma(Z_c(3900)^\pm K^\mp, Z_c^\pm \to J/\psi\pi^\pm)/\Gamma(J/\psi(1S) K^*(892)^0)$ — $\Gamma_{243}/\Gamma_{202}$

VALUE	CL%	DOCUMENT ID		TECN	COMMENT
$<1.5 \times 10^{-2}$	90	ABAZOV	18B	D0	$p\overline{p}$ at 1.96 TeV

$\Gamma(J/\psi(1S) p\overline{p})/\Gamma_{total}$ — Γ_{245}/Γ

VALUE (units 10^{-7})	CL%	DOCUMENT ID		TECN	COMMENT
4.51±0.40±0.44		[1] AAIJ	19U	LHCB	pp at 7, 8, 13 TeV
• • • We do not use the following data for averages, fits, limits, etc. • • •					
< 5.2	90	[2] AAIJ	13Z	LHCB	Repl. by AAIJ 19U
< 8.3	90	[3] XIE	05	BELL	$e^+e^- \to \Upsilon(4S)$
<19	90	[3] AUBERT	03K	BABR	$e^+e^- \to \Upsilon(4S)$

[1] Measured relative to $B^0_s \to J/\psi\phi$ assuming $B(B^0_s \to J/\psi\phi) = (10.5 \pm 0.13 \pm 0.64) \times 10^{-4}$ and taking into account small K^+K^- S-wave contribution. Measurement assumes $f_s/f_d = 0.259 \pm 0.015$ for 7, 8 TeV data and f_s/f_d multiplied by 1.068 ± 0.046 for 13 TeV data.

[2] Uses $B(B^0_s \to J/\psi(1S)\pi^+\pi^-) = (1.98 \pm 0.20) \times 10^{-4}$.

[3] Assumes equal production of B^+ and B^0 at the $\Upsilon(4S)$.

$\Gamma(J/\psi(1S)\gamma)/\Gamma_{total}$ — Γ_{246}/Γ

VALUE (units 10^{-6})	CL%	DOCUMENT ID		TECN	COMMENT
<1.5	90	[1] AAIJ	15BB	LHCB	pp at 7, 8 TeV
• • • We do not use the following data for averages, fits, limits, etc. • • •					
<1.6	90	[2] AUBERT,B	04T	BABR	$e^+e^- \to \Upsilon(4S)$

[1] Branching fractions of normalization modes $B^0 \to J/\psi\gamma X$ taken from PDG 14. Uses $f_s/f_d = 0.259 \pm 0.015$.

[2] Assumes equal production of B^+ and B^0 at the $\Upsilon(4S)$.

$\Gamma(J/\psi(1S)\overline{D}^0)/\Gamma_{total}$ — Γ_{247}/Γ

VALUE (units 10^{-5})	CL%	DOCUMENT ID		TECN	COMMENT
<1.3	90	[1] AUBERT	05U	BABR	$e^+e^- \to \Upsilon(4S)$
• • • We do not use the following data for averages, fits, limits, etc. • • •					
<2.0	90	[1] ZHANG	05B	BELL	$e^+e^- \to \Upsilon(4S)$

[1] Assumes equal production of B^+ and B^0 at the $\Upsilon(4S)$.

$\Gamma(\psi(2S)\pi^0)/\Gamma_{total}$ — Γ_{248}/Γ

VALUE (units 10^{-5})	DOCUMENT ID		TECN	COMMENT
1.17±0.17±0.08	[1] CHOBANOVA	16	BELL	$e^+e^- \to \Upsilon(4S)$

[1] Assumes equal production of B^+ and B^0 at the $\Upsilon(4S)$.

$\Gamma(\psi(2S) K^0)/\Gamma_{total}$ — Γ_{249}/Γ

VALUE (units 10^{-4})	CL%	DOCUMENT ID		TECN	COMMENT
5.8 ±0.5 OUR FIT					
5.8 ±0.5 OUR AVERAGE					
4.7 ±0.7 ±0.7		[1] AAIJ	14L	LHCB	pp at 7 TeV
6.46±0.65±0.51		[2] AUBERT	05J	BABR	$e^+e^- \to \Upsilon(4S)$
6.7 ±1.1		[2] ABE	03B	BELL	$e^+e^- \to \Upsilon(4S)$
5.0 ±1.1 ±0.6		[2] RICHICHI	01	CLE2	$e^+e^- \to \Upsilon(4S)$
• • • We do not use the following data for averages, fits, limits, etc. • • •					
6.9 ±1.1 ±1.1		[2] AUBERT	02	BABR	Repl. by AUBERT 05J
< 8	90	[2] ALAM	94	CLE2	$e^+e^- \to \Upsilon(4S)$
<15	90	[2] BORTOLETTO	92	CLEO	$e^+e^- \to \Upsilon(4S)$
<28	90	[2] ALBRECHT	90J	ARG	$e^+e^- \to \Upsilon(4S)$

[1] Measured with $B(B^0 \to \psi(2S) K^0_S) \times B(\psi(2S) \to J/\psi\pi^+\pi^-)$ / $B(B^0 \to J/\psi K^0_S)$ using PDG 12 values for the involved branching fractions.

[2] Assumes equal production of B^+ and B^0 at the $\Upsilon(4S)$.

Downloaded from https://academic.oup.com/ptep/article/2022/8/083C01/6651666 by KIT Library user on 27 September 2022

$\Gamma(\psi(2S)K^0)/\Gamma(J/\psi(1S)K^0)$ — $\Gamma_{249}/\Gamma_{200}$

VALUE	DOCUMENT ID		TECN	COMMENT
0.82±0.13±0.12	[1] AUBERT	02	BABR	$e^+e^- \to \Upsilon(4S)$

[1] Assumes equal production of B^+ and B^0 at the $\Upsilon(4S)$.

$\Gamma(\psi(3770)K^0, \psi \to \overline{D}^0 D^0)/\Gamma_{total}$ — Γ_{250}/Γ

VALUE (units 10^{-4})	CL%	DOCUMENT ID		TECN	COMMENT
<1.23	90	[1] AUBERT	08B	BABR	$e^+e^- \to \Upsilon(4S)$

[1] Assumes equal production of B^+ and B^0 at the $\Upsilon(4S)$.

$\Gamma(\psi(3770)K^0, \psi \to D^- D^+)/\Gamma_{total}$ — Γ_{251}/Γ

VALUE (units 10^{-4})	CL%	DOCUMENT ID		TECN	COMMENT
<1.88	90	[1] AUBERT	08B	BABR	$e^+e^- \to \Upsilon(4S)$

[1] Assumes equal production of B^+ and B^0 at the $\Upsilon(4S)$.

$\Gamma(\psi(2S)\pi^+\pi^-)/\Gamma(J/\psi(1S)\pi^+\pi^-)$ — $\Gamma_{252}/\Gamma_{211}$

VALUE	DOCUMENT ID		TECN	COMMENT
0.56±0.07±0.05	[1] AAIJ	13AA	LHCB	pp at 7 TeV

[1] Assuming lepton universality for dimuon decay modes of J/ψ and $\psi(2S)$ mesons, the ratio $B(J/\psi \to \mu^+\mu^-)/B(\psi(2S) \to \mu^+\mu^-) = B(J/\psi \to e^+e^-)/B(\psi(2S) \to e^+e^-) = 7.69 \pm 0.19$ was used.

$\Gamma(\psi(2S)K^+\pi^-)/\Gamma_{total}$ — Γ_{253}/Γ

VALUE (units 10^{-4})	CL%	DOCUMENT ID		TECN	COMMENT
5.80±0.39		[1,2] CHILIKIN	13	BELL	$e^+e^- \to \Upsilon(4S)$
• • • We do not use the following data for averages, fits, limits, etc. • • •					
5.57±0.16		[3] AUBERT	09AA	BABR	$e^+e^- \to \Upsilon(4S)$
5.68±0.13±0.42		[2] MIZUK	09	BELL	$e^+e^- \to \Upsilon(4S)$
<10	90	[2] ALBRECHT	90J	ARG	$e^+e^- \to \Upsilon(4S)$

[1] Combines measurements with $\psi(2S) \to \ell^+\ell^-$ with measurement from MIZUK 09 which uses $\psi(2S) \to J/\psi\pi^+\pi^-$.
[2] Assumes equal production of B^+ and B^0 at the $\Upsilon(4S)$.
[3] Does not report systematic uncertainties.

$\Gamma(\psi(2S)K^*(892)^0)/\Gamma_{total}$ — Γ_{254}/Γ

VALUE (units 10^{-4})	CL%	DOCUMENT ID		TECN	COMMENT
5.9 ±0.4 OUR FIT					
6.0 $^{+0.5}_{-0.7}$ OUR AVERAGE	Error includes scale factor of 1.1.				
$5.55^{+0.22+0.41}_{-0.23-0.84}$		[1] CHILIKIN	13	BELL	$e^+e^- \to \Upsilon(4S)$
6.49±0.59±0.97		[1] AUBERT	05J	BABR	$e^+e^- \to \Upsilon(4S)$
7.6 ±1.1 ±1.0		[1] RICHICHI	01	CLE2	$e^+e^- \to \Upsilon(4S)$
9.0 ±2.2 ±0.9		[2] ABE	98O	CDF	$p\overline{p}$ 1.8 TeV
• • • We do not use the following data for averages, fits, limits, etc. • • •					
$5.52^{+0.35+0.53}_{-0.32-0.58}$		[1] MIZUK	09	BELL	$e^+e^- \to \Upsilon(4S)$
<19	90	[1] ALAM	94	CLE2	Repl. by RICHICHI 01
14 ±8 ±4		[1] BORTOLETTO	92	CLEO	$e^+e^- \to \Upsilon(4S)$
<23	90	[1] ALBRECHT	90J	ARG	$e^+e^- \to \Upsilon(4S)$

[1] Assumes equal production of B^+ and B^0 at the $\Upsilon(4S)$.
[2] ABE 98O reports $[B(B^0 \to \psi(2S)K^*(892)^0)]/[B(B^+ \to J/\psi(1S)K^+)] = 0.908 \pm 0.194 \pm 0.10$. We multiply by our best value $B(B^+ \to J/\psi(1S)K^+) = (9.9 \pm 1.0) \times 10^{-4}$. Our first error is their experiment's error and our second error is the systematic error from using our best value.

$\Gamma(\psi(2S)K^*(892)^0)/\Gamma(J/\psi(1S)K^*(892)^0)$ — $\Gamma_{254}/\Gamma_{202}$

VALUE	DOCUMENT ID		TECN	COMMENT
0.487±0.018±0.011	[1,2] AAIJ	12L	LHCB	pp at 7 TeV

[1] AAIJ 12L reports $0.476 \pm 0.014 \pm 0.010 \pm 0.012$ from a measurement of $[\Gamma(B^0 \to \psi(2S)K^*(892)^0)/\Gamma(B^0 \to J/\psi(1S)K^*(892)^0)] \times [B(J/\psi(1S) \to e^+e^-)] / [B(\psi(2S) \to e^+e^-)]$ assuming $B(J/\psi(1S) \to e^+e^-) = (5.94 \pm 0.06) \times 10^{-2}$, $B(\psi(2S) \to e^+e^-) = (7.72 \pm 0.17) \times 10^{-3}$, which we rescale to our best values $B(J/\psi(1S) \to e^+e^-) = (5.971 \pm 0.032) \times 10^{-2}$, $B(\psi(2S) \to e^+e^-) = (7.93 \pm 0.17) \times 10^{-3}$. Our first error is their experiment's error and our second error is the systematic error from using our best values.
[2] Assumes $B(J/\psi \to \mu^+\mu^-) / B(\psi(2S) \to \mu^+\mu^-) = B(J/\psi \to e^+e^-) / B(\psi(2S) \to e^+e^-) = 7.69 \pm 0.19$.

$\Gamma(\psi(2S)K^*(892)^0)/\Gamma(\psi(2S)K^0)$ — $\Gamma_{254}/\Gamma_{249}$

VALUE	DOCUMENT ID		TECN	COMMENT
1.02±0.10 OUR FIT				
1.00±0.14±0.09	AUBERT	05J	BABR	$e^+e^- \to \Upsilon(4S)$

$\Gamma(\chi_{c0}K^0)/\Gamma_{total}$ — Γ_{255}/Γ

VALUE (units 10^{-6})	CL%	DOCUMENT ID		TECN	COMMENT
195^{+42}_{-36}±11		[1] AAIJ	18F	LHCB	pp at 7, 8 TeV
• • • We do not use the following data for averages, fits, limits, etc. • • •					
145^{+103}_{-85}± 8		[2,3] LEES	12I	BABR	$e^+e^- \to \Upsilon(4S)$
148± 30±13		[2,4] LEES	12O	BABR	$e^+e^- \to \Upsilon(4S)$
142^{+55}_{-44}±22		[2,5] AUBERT	09AU	BABR	$e^+e^- \to \Upsilon(4S)$
< 113	90	[5] GARMASH	07	BELL	$e^+e^- \to \Upsilon(4S)$
<1240	90	[2] AUBERT	05K	BABR	$e^+e^- \to \Upsilon(4S)$
< 500	90	[6] EDWARDS	01	CLE2	$e^+e^- \to \Upsilon(4S)$

[1] AAIJ 18F uses Dalitz plot analysis of the $B^0 \to K^0_S\pi^+\pi^-$ final state decays. For the branching fraction of the reference mode, the PDG 18 average $B(B^0 \to K^0_S\pi^+\pi^-) = (4.96 \pm 0.20) \times 10^{-5}$ is used. We compute $B(B^0 \to \chi_{c0}K^0)$ using the PDG value $B(\chi_{c0} \to \pi\pi) = (8.51 \pm 0.33) \times 10^{-3}$ and 2/3 for the $\pi^+\pi^-$ fraction. Our first error is their experiment's error and the second error is systematic error from using our best value.
[2] Assumes equal production of B^+ and B^0 at the $\Upsilon(4S)$.
[3] LEES 12I reports $[\Gamma(B^0 \to \chi_{c0}K^0)/\Gamma_{total}] \times [B(\chi_{c0}(1P) \to K^0_S K^0_S)] = (0.46^{+0.25}_{-0.17} \pm 0.21) \times 10^{-6}$ which we divide by our best value $B(\chi_{c0}(1P) \to K^0_S K^0_S) = (3.16 \pm 0.17) \times 10^{-3}$. Our first error is their experiment's error and our second error is the systematic error from using our best value.
[4] Measured in the $B^0 \to K^0_S K^+ K^-$ decay.
[5] Uses Dalitz plot analysis of the $B^0 \to K^0\pi^+\pi^-$ final state decays.
[6] EDWARDS 01 assumes equal production of B^0 and B^+ at the $\Upsilon(4S)$. The correlated uncertainties (28.3)% from $B(J/\psi(1S) \to \gamma\eta_c)$ in those modes have been accounted for.

$\Gamma(\chi_{c0}K^*(892)^0)/\Gamma_{total}$ — Γ_{256}/Γ

VALUE (units 10^{-4})	CL%	DOCUMENT ID		TECN	COMMENT
1.7±0.3±0.2		[1] AUBERT	08BD	BABR	$e^+e^- \to \Upsilon(4S)$
• • • We do not use the following data for averages, fits, limits, etc. • • •					
<7.7	90	[1] AUBERT	05K	BABR	Repl. by AUBERT 08BD

[1] Assumes equal production of B^+ and B^0 at the $\Upsilon(4S)$.

$\Gamma(\chi_{c1}\pi^0)/\Gamma_{total}$ — Γ_{257}/Γ

VALUE (units 10^{-5})	DOCUMENT ID		TECN	COMMENT
1.12±0.25±0.12	[1] KUMAR	08	BELL	$e^+e^- \to \Upsilon(4S)$

[1] Assumes equal production of B^+ and B^0 at the $\Upsilon(4S)$.

$\Gamma(\chi_{c1}K^0)/\Gamma_{total}$ — Γ_{258}/Γ

VALUE (units 10^{-4})	CL%	DOCUMENT ID		TECN	COMMENT
3.95±0.27 OUR AVERAGE					
15 $^{+5}_{-4}$ ±6		[1] CHILIKIN	19	BELL	$e^+e^- \to \Upsilon(4S)$
$3.78^{+0.17}_{-0.16}$±0.33		[2] BHARDWAJ	11	BELL	$e^+e^- \to \Upsilon(4S)$
4.2 ±0.3 ±0.3		[3] AUBERT	09B	BABR	$e^+e^- \to \Upsilon(4S)$
3.1 $^{+1.5}_{-1.1}$ ±0.1		[4] AVERY	00	CLE2	$e^+e^- \to \Upsilon(4S)$
• • • We do not use the following data for averages, fits, limits, etc. • • •					
3.51±0.33±0.45		[2] SONI	06	BELL	Repl. by BHARDWAJ 11
4.53±0.41±0.51		[2] AUBERT	05J	BABR	Repl. by AUBERT 09B
4.3 ±1.4 ±0.1		[5] AUBERT	02	BABR	Repl. by AUBERT 05J
<27	90	[2] ALAM	94	CLE2	$e^+e^- \to \Upsilon(4S)$

[1] CHILIKIN 19 reports $[\Gamma(B^0 \to \chi_{c1}K^0)/\Gamma_{total}] \times [B(\chi_{c1}(1P) \to p\overline{p}\pi^+\pi^-)] = (7.4^{+2.4+0.6}_{-2.0-0.4}) \times 10^{-7}$ which we divide by our best value $B(\chi_{c1}(1P) \to p\overline{p}\pi^+\pi^-) = (5.0 \pm 1.9) \times 10^{-4}$. Our first error is their experiment's error and our second error is the systematic error from using our best value.
[2] Assumes equal production of B^+ and B^0 at the $\Upsilon(4S)$.
[3] Uses $\chi_{c1,2} \to J/\psi\gamma$. Assumes $B(\Upsilon(4S) \to B^+B^-) = (51.6 \pm 0.6)\%$ and $B(\Upsilon(4S) \to B^0\overline{B}^0) = (48.4 \pm 0.6)\%$.
[4] AVERY 00 reports $(3.9^{+1.9}_{-1.3} \pm 0.4) \times 10^{-4}$ from a measurement of $[\Gamma(B^0 \to \chi_{c1}K^0)/\Gamma_{total}] \times [B(\chi_{c1}(1P) \to \gamma J/\psi(1S))]$ assuming $B(\chi_{c1}(1P) \to \gamma J/\psi(1S)) = 0.273 \pm 0.016$, which we rescale to our best value $B(\chi_{c1}(1P) \to \gamma J/\psi(1S)) = (34.3 \pm 1.0) \times 10^{-2}$. Our first error is their experiment's error and our second error is the systematic error from using our best value. Assumes equal production of B^+ and B^0 at the $\Upsilon(4S)$.
[5] AUBERT 02 reports $(5.4 \pm 1.4 \pm 1.1) \times 10^{-4}$ from a measurement of $[\Gamma(B^0 \to \chi_{c1}K^0)/\Gamma_{total}] \times [B(\chi_{c1}(1P) \to \gamma J/\psi(1S))]$ assuming $B(\chi_{c1}(1P) \to \gamma J/\psi(1S)) = 0.273 \pm 0.016$, which we rescale to our best value $B(\chi_{c1}(1P) \to \gamma J/\psi(1S)) = (34.3 \pm 1.0) \times 10^{-2}$. Our first error is their experiment's error and our second error is the systematic error from using our best value. Assumes equal production of B^+ and B^0 at the $\Upsilon(4S)$.

$\Gamma(\chi_{c1}K^0)/\Gamma(J/\psi(1S)K^0)$ — $\Gamma_{258}/\Gamma_{200}$

VALUE	DOCUMENT ID		TECN	COMMENT
0.53±0.16±0.01	[1] AUBERT	02	BABR	$e^+e^- \to \Upsilon(4S)$

[1] AUBERT 02 reports 0.66 ± 0.11 ± 0.17 from a measurement of $[\Gamma(B^0 \to \chi_{c1}K^0)/\Gamma(B^0 \to J/\psi(1S)K^0)] \times [B(\chi_{c1}(1P) \to \gamma J/\psi(1S))]$ assuming $B(\chi_{c1}(1P) \to \gamma J/\psi(1S)) = 0.273 \pm 0.016$, which we rescale to our best value $B(\chi_{c1}(1P) \to \gamma J/\psi(1S)) = (34.3 \pm 1.0) \times 10^{-2}$. Our first error is their experiment's error and our second error is the systematic error from using our best value. Assumes equal production of B^+ and B^0 at the $\Upsilon(4S)$.

Downloaded from https://academic.oup.com/ptep/article/2022/8/083C01/6651666 by KIT Library user on 27 September 2022

$\Gamma(\chi_{c1}\pi^- K^+)/\Gamma_{total}$ — Γ_{259}/Γ

VALUE (units 10^{-4})	DOCUMENT ID		TECN	COMMENT
4.97±0.12±0.28	[1] BHARDWAJ	16	BELL	$e^+e^- \to \Upsilon(4S)$
• • • We do not use the following data for averages, fits, limits, etc. • • •				
3.83±0.10±0.39	[1] MIZUK	08	BELL	Repl. by BHARDWAJ 16

[1] Assumes equal production of B^+ and B^0 at the $\Upsilon(4S)$.

$\Gamma(\chi_{c1}\pi^- K^+)/\Gamma(J/\psi(1S)K^+\pi^-)$ — $\Gamma_{259}/\Gamma_{201}$

VALUE	DOCUMENT ID		TECN
0.476±0.021±0.013	[1] LEES	12B	BABR

[1] LEES 12B reports 0.474±0.013±0.026 from a measurement of $[\Gamma(B^0 \to \chi_{c1}\pi^- K^+)/\Gamma(B^0 \to J/\psi(1S)K^+\pi^-)] \times [B(\chi_{c1}(1P) \to \gamma J/\psi(1S))]$ assuming $B(\chi_{c1}(1P) \to \gamma J/\psi(1S)) = (34.4 \pm 1.5) \times 10^{-2}$, which we rescale to our best value $B(\chi_{c1}(1P) \to \gamma J/\psi(1S)) = (34.3 \pm 1.0) \times 10^{-2}$. Our first error is their experiment's error and our second error is the systematic error from using our best value.

$\Gamma(\chi_{c1}K^*(892)^0)/\Gamma_{total}$ — Γ_{260}/Γ

VALUE (units 10^{-4})	CL%	DOCUMENT ID		TECN	COMMENT
2.38±0.19 OUR FIT Error includes scale factor of 1.2.					
$2.22^{+0.40}_{-0.31}$ OUR AVERAGE Error includes scale factor of 1.6.					
2.5 ±0.2 ±0.2		[1] AUBERT	09B	BABR	$e^+e^- \to \Upsilon(4S)$
$1.73^{+0.15+0.34}_{-0.12-0.22}$		[2] MIZUK	08	BELL	$e^+e^- \to \Upsilon(4S)$
• • • We do not use the following data for averages, fits, limits, etc. • • •					
3.14±0.34±0.72		[2] SONI	06	BELL	Repl. by MIZUK 08
3.27±0.42±0.64		[2] AUBERT	05J	BABR	Repl. by AUBERT 09B
3.8 ±1.3 ±0.1		[3] AUBERT	02	BABR	Repl. by AUBERT 05J
<21	90	[4] ALAM	94	CLE2	$e^+e^- \to \Upsilon(4S)$

[1] Uses $\chi_{c1,2} \to J/\psi\gamma$. Assumes $B(\Upsilon(4S) \to B^+B^-) = (51.6 \pm 0.6)\%$ and $B(\Upsilon(4S) \to B^0\overline{B}^0) = (48.4 \pm 0.6)\%$.
[2] Assumes equal production of B^+ and B^0 at the $\Upsilon(4S)$.
[3] AUBERT 02 reports $(4.8 \pm 1.4 \pm 0.9) \times 10^{-4}$ from a measurement of $[\Gamma(B^0 \to \chi_{c1}K^*(892)^0)/\Gamma_{total}] \times [B(\chi_{c1}(1P) \to \gamma J/\psi(1S))]$ assuming $B(\chi_{c1}(1P) \to \gamma J/\psi(1S)) = 0.273 \pm 0.016$, which we rescale to our best value $B(\chi_{c1}(1P) \to \gamma J/\psi(1S)) = (34.3 \pm 1.0) \times 10^{-2}$. Our first error is their experiment's error and our second error is the systematic error from using our best value. Assumes equal production of B^+ and B^0 at the $\Upsilon(4S)$.
[4] BORTOLETTO 92 assumes equal production of B^+ and B^0 at the $\Upsilon(4S)$.

$\Gamma(\chi_{c1}K^*(892)^0)/\Gamma(J/\psi(1S)K^*(892)^0)$ — $\Gamma_{260}/\Gamma_{202}$

VALUE (units 10^{-2})	DOCUMENT ID		TECN	COMMENT
18.8±1.5 OUR FIT Error includes scale factor of 1.1.				
19.8±1.1±1.5	[1] AAIJ	13AC	LHCB	pp at 7 TeV

[1] Uses $B(\chi_{c1} \to J/\psi\gamma) = (34.4 \pm 1.5)\%$.

$\Gamma(\chi_{c1}K^*(892)^0)/\Gamma(\chi_{c1}K^0)$ — $\Gamma_{260}/\Gamma_{258}$

VALUE	DOCUMENT ID		TECN	COMMENT
0.72±0.11±0.12	AUBERT	05J	BABR	$e^+e^- \to \Upsilon(4S)$
• • • We do not use the following data for averages, fits, limits, etc. • • •				
0.89±0.34±0.17	[1] AUBERT	02	BABR	Repl. by AUBERT 05J

[1] Assumes equal production of B^+ and B^0 at the $\Upsilon(4S)$.

$\Gamma(X(4051)^- K^+, X^- \to \chi_{c1}\pi^-)/\Gamma_{total}$ — Γ_{261}/Γ

VALUE (units 10^{-5})	CL%	DOCUMENT ID		TECN	COMMENT
$3.0^{+1.5+3.7}_{-0.8-1.6}$		[1] MIZUK	08	BELL	$e^+e^- \to \Upsilon(4S)$
• • • We do not use the following data for averages, fits, limits, etc. • • •					
<1.8	90	[1,2] LEES	12B	BABR	

[1] Assumes equal production of B^+ and B^0 at the $\Upsilon(4S)$.
[2] Uses $\chi_{c1} \to J/\psi\gamma$ mode. Uses $\chi_{c1} \to J/\psi\gamma$ mode. Finds a good description of the data without this $B^0 \to X(4051)^+K^-$ decay mode in a fit.

$\Gamma(X(4248)^- K^+, X^- \to \chi_{c1}\pi^-)/\Gamma_{total}$ — Γ_{262}/Γ

VALUE (units 10^{-5})	CL%	DOCUMENT ID		TECN	COMMENT
$4.0^{+2.3+19.7}_{-0.9-0.5}$		[1] MIZUK	08	BELL	$e^+e^- \to \Upsilon(4S)$
• • • We do not use the following data for averages, fits, limits, etc. • • •					
<4.0	90	[1,2] LEES	12B	BABR	

[1] Assumes equal production of B^+ and B^0 at the $\Upsilon(4S)$.
[2] Uses $\chi_{c1} \to J/\psi\gamma$ mode. Finds a good description of the data without this $B^0 \to X(4248)^+K^-$ decay mode in a fit.

$\Gamma(\chi_{c1}\pi^+\pi^- K^0)/\Gamma_{total}$ — Γ_{263}/Γ

VALUE (units 10^{-4})	DOCUMENT ID		TECN	COMMENT
3.16±0.35±0.32	[1] BHARDWAJ	16	BELL	$e^+e^- \to \Upsilon(4S)$

[1] Assumes equal production of B^+ and B^0 at the $\Upsilon(4S)$.

$\Gamma(\chi_{c1}\pi^-\pi^0 K^+)/\Gamma_{total}$ — Γ_{264}/Γ

VALUE (units 10^{-4})	DOCUMENT ID		TECN	COMMENT
3.52±0.52±0.24	[1] BHARDWAJ	16	BELL	$e^+e^- \to \Upsilon(4S)$

[1] Assumes equal production of B^+ and B^0 at the $\Upsilon(4S)$.

$\Gamma(\chi_{c2}K^0)/\Gamma_{total}$ — Γ_{265}/Γ

VALUE	CL%	DOCUMENT ID		TECN	COMMENT
$<1.5 \times 10^{-5}$	90	[1] BHARDWAJ	11	BELL	$e^+e^- \to \Upsilon(4S)$
• • • We do not use the following data for averages, fits, limits, etc. • • •					
$<2.8 \times 10^{-5}$	90	[2] AUBERT	09B	BABR	$e^+e^- \to \Upsilon(4S)$
$<2.6 \times 10^{-5}$	90	[1] SONI	06	BELL	Repl. by BHARDWAJ 11
$<4.1 \times 10^{-5}$	90	[1] AUBERT	05K	BABR	$e^+e^- \to \Upsilon(4S)$

[1] Assumes equal production of B^+ and B^0 at the $\Upsilon(4S)$.
[2] Uses $\chi_{c1,2} \to J/\psi\gamma$. Assumes $B(\Upsilon(4S) \to B^+B^-) = (51.6 \pm 0.6)\%$ and $B(\Upsilon(4S) \to B^0\overline{B}^0) = (48.4 \pm 0.6)\%$.

$\Gamma(\chi_{c2}K^*(892)^0)/\Gamma_{total}$ — Γ_{266}/Γ

VALUE (units 10^{-5})	CL%	DOCUMENT ID		TECN	COMMENT
4.9±1.2 OUR FIT Error includes scale factor of 1.1.					
6.6±1.8±0.5		[1] AUBERT	09B	BABR	$e^+e^- \to \Upsilon(4S)$
• • • We do not use the following data for averages, fits, limits, etc. • • •					
<7.1	90	[2] SONI	06	BELL	$e^+e^- \to \Upsilon(4S)$
<3.6	90	[2] AUBERT	05K	BABR	Repl. by AUBERT 09B

[1] Uses $\chi_{c1,2} \to J/\psi\gamma$. Assumes $B(\Upsilon(4S) \to B^+B^-) = (51.6 \pm 0.6)\%$ and $B(\Upsilon(4S) \to B^0\overline{B}^0) = (48.4 \pm 0.6)\%$.
[2] Assumes equal production of B^+ and B^0 at the $\Upsilon(4S)$.

$\Gamma(\chi_{c2}K^*(892)^0)/\Gamma(\chi_{c1}K^*(892)^0)$ — $\Gamma_{266}/\Gamma_{260}$

VALUE (units 10^{-2})	DOCUMENT ID		TECN	COMMENT
20 ±5 OUR FIT Error includes scale factor of 1.1.				
17.1±5.0±2.0	[1] AAIJ	13AC	LHCB	pp at 7 TeV

[1] Uses $B(\chi_{c1} \to J/\psi\gamma)/B(\chi_{c2} \to J/\psi\gamma) = 1.76 \pm 0.11$.

$\Gamma(\chi_{c2}\pi^- K^+)/\Gamma_{total}$ — Γ_{267}/Γ

VALUE (units 10^{-4})	DOCUMENT ID		TECN	COMMENT
0.72±0.09±0.05	[1] BHARDWAJ	16	BELL	$e^+e^- \to \Upsilon(4S)$

[1] Assumes equal production of B^+ and B^0 at the $\Upsilon(4S)$.

$\Gamma(\chi_{c2}\pi^+\pi^- K^0)/\Gamma_{total}$ — Γ_{268}/Γ

VALUE	CL%	DOCUMENT ID		TECN	COMMENT
$<1.70 \times 10^{-4}$	90	[1] BHARDWAJ	16	BELL	$e^+e^- \to \Upsilon(4S)$

[1] Assumes equal production of B^+ and B^0 at the $\Upsilon(4S)$.

$\Gamma(\chi_{c2}\pi^-\pi^0 K^+)/\Gamma_{total}$ — Γ_{269}/Γ

VALUE	CL%	DOCUMENT ID		TECN	COMMENT
$<0.74 \times 10^{-4}$	90	[1] BHARDWAJ	16	BELL	$e^+e^- \to \Upsilon(4S)$

[1] Assumes equal production of B^+ and B^0 at the $\Upsilon(4S)$.

$\Gamma(\psi(4660)K^0, \psi \to \Lambda_c^+\Lambda_c^-)/\Gamma_{total}$ — Γ_{270}/Γ

VALUE	CL%	DOCUMENT ID		TECN	COMMENT
$<2.3 \times 10^{-4}$	90	[1] LI	18D	BELL	$e^+e^- \to \Upsilon(4S)$

[1] Assumes $B(\Upsilon(4S) \to B^0\overline{B}^0) = 48.6 \pm 0.6\%$ and $B(\Lambda_c^+ \to pK^-\pi^+) = 6.23 \pm 0.33\%$.

$\Gamma(\psi(4230)^0 K^0, \psi^0 \to J/\psi\pi^+\pi^-)/\Gamma_{total}$ — Γ_{271}/Γ

VALUE	CL%	DOCUMENT ID		TECN	COMMENT
$<17 \times 10^{-6}$	90	[1] GARG	19	BELL	$e^+e^- \to \Upsilon(4S)$

[1] Assumes equal production of B^0 and B^+ at the $\Upsilon(4S)$.

$\Gamma(K^+\pi^-)/\Gamma_{total}$ — Γ_{272}/Γ

VALUE (units 10^{-6})	CL%	DOCUMENT ID		TECN	COMMENT
19.6 ± 0.5 OUR FIT					
19.6 ± 0.5 OUR AVERAGE					
20.00± 0.34±0.60		[1] DUH	13	BELL	$e^+e^- \to \Upsilon(4S)$
19.1 ± 0.6 ±0.6		[1] AUBERT	07B	BABR	$e^+e^- \to \Upsilon(4S)$
$18.0^{+2.3}_{-2.1} \pm^{1.2}_{0.9}$		[1] BORNHEIM	03	CLE2	$e^+e^- \to \Upsilon(4S)$
• • • We do not use the following data for averages, fits, limits, etc. • • •					
19.9 ± 0.4 ±0.8		[1] LIN	07A	BELL	Repl. by DUH 13
18.5 ± 1.0 ±0.7		[1] CHAO	04	BELL	Repl. by LIN 07A
17.9 ± 0.9 ±0.7		[1] AUBERT	02Q	BABR	Repl. by AUBERT 07B
22.5 ± 1.9 ±1.8		[1] CASEY	02	BELL	Repl. by CHAO 04
$19.3^{+3.4}_{-3.2} \pm^{1.5}_{0.6}$		[1] ABE	01H	BELL	Repl. by CASEY 02
16.7 ± 1.6 ±1.3		[1] AUBERT	01E	BABR	Repl. by AUBERT 02Q
< 66	90	[2] ABE	00C	SLD	$e^+e^- \to Z$
$17.2^{+2.5}_{-2.4} \pm 1.2$		[1] CRONIN-HEN..	00	CLE2	Repl. by BORNHEIM 03
$15^{+5.}_{-4} \pm 1.4$		GODANG	98	CLE2	Repl. by CRONIN-HENNESSY 00
$24^{+17}_{-11} \pm 2$		[3] ADAM	96D	DLPH	$e^+e^- \to Z$
< 17	90	ASNER	96	CLE2	Sup. by ADAM 96D
< 30	90	[4] BUSKULIC	96V	ALEP	$e^+e^- \to Z$
< 90	90	[5] ABREU	95N	DLPH	Sup. by ADAM 96D
< 81	90	[6] AKERS	94L	OPAL	$e^+e^- \to Z$

Downloaded from https://academic.oup.com/ptep/article/2022/8/083C01/6651666 by KIT Library user on 27 September 2022

< 26	90	[7] BATTLE	93	CLE2	$e^+e^- \to \Upsilon(4S)$
<180	90	ALBRECHT	91B	ARG	$e^+e^- \to \Upsilon(4S)$
< 90	90	[8] AVERY	89B	CLEO	$e^+e^- \to \Upsilon(4S)$
<320	90	AVERY	87	CLEO	$e^+e^- \to \Upsilon(4S)$

[1] Assumes equal production of B^+ and B^0 at the $\Upsilon(4S)$.
[2] ABE 00C assumes $B(Z \to b\overline{b})=(21.7 \pm 0.1)\%$ and the B fractions $f_{B^0}=f_{B^+}=(39.7^{+1.8}_{-2.2})\%$ and $f_{B_s}=(10.5^{+1.8}_{-2.2})\%$.
[3] ADAM 96D assumes $f_{B^0} = f_{B^-} = 0.39$ and $f_{B_s} = 0.12$. Contributions from B^0 and B_s decays cannot be separated. Limits are given for the weighted average of the decay rates for the two neutral B mesons.
[4] BUSKULIC 96V assumes PDG 96 production fractions for B^0, B^+, B_s, b baryons.
[5] Assumes a B^0, B^- production fraction of 0.39 and a B_s production fraction of 0.12. Contributions from B^0 and B^0_s decays cannot be separated. Limits are given for the weighted average of the decay rates for the two neutral B mesons.
[6] Assumes $B(Z \to b\overline{b}) = 0.217$ and B^0_d (B^0_s) fraction 39.5% (12%).
[7] BATTLE 93 assumes equal production of $B^0\overline{B}^0$ and B^+B^- at $\Upsilon(4S)$.
[8] Assumes the $\Upsilon(4S)$ decays 43% to $B^0\overline{B}^0$.

$\Gamma(K^+\pi^-)/\Gamma(K^0\pi^0)$ — $\Gamma_{272}/\Gamma_{273}$

VALUE	DOCUMENT ID		TECN	COMMENT
2.16±0.16±0.16	LIN	07A	BELL	$e^+e^- \to \Upsilon(4S)$
• • • We do not use the following data for averages, fits, limits, etc. • • •				
$1.20^{+0.50}_{-0.58}{}^{+0.22}_{-0.32}$	[1] ABE	01H	BELL	Repl. by LIN 07A

[1] Assumes equal production of B^+ and B^0 at the $\Upsilon(4S)$.

$[\Gamma(K^+\pi^-)+\Gamma(\pi^+\pi^-)]/\Gamma_{total}$ — $(\Gamma_{272}+\Gamma_{405})/\Gamma$

VALUE (units 10^{-6})	EVTS	DOCUMENT ID		TECN	COMMENT
19± 6 OUR AVERAGE					
$28^{+15}_{-10}\pm20$		[1] ADAM	96D	DLPH	$e^+e^- \to Z$
$18^{+6}_{-5}{}^{+3}_{-4}$	17.2	ASNER	96	CLE2	$e^+e^- \to \Upsilon(4S)$
• • • We do not use the following data for averages, fits, limits, etc. • • •					
$24^{+8}_{-7}\pm2$		[2] BATTLE	93	CLE2	$e^+e^- \to \Upsilon(4S)$

[1] ADAM 96D assumes $f_{B^0} = f_{B^-} = 0.39$ and $f_{B_s} = 0.12$. Contributions from B^0 and B_s decays cannot be separated. Limits are given for the weighted average of the decay rates for the two neutral B mesons.
[2] BATTLE 93 assumes equal production of $B^0\overline{B}^0$ and B^+B^- at $\Upsilon(4S)$.

$\Gamma(K^0\pi^0)/\Gamma_{total}$ — Γ_{273}/Γ

VALUE (units 10^{-6})	CL%	DOCUMENT ID		TECN	COMMENT
9.9 ±0.5 OUR AVERAGE					
9.68±0.46±0.50		[1] DUH	13	BELL	$e^+e^- \to \Upsilon(4S)$
10.1 ±0.6 ±0.4		[1] LEES	13D	BABR	$e^+e^- \to \Upsilon(4S)$
$12.8^{+4.0}_{-3.3}{}^{+1.7}_{-1.4}$		[1] BORNHEIM	03	CLE2	$e^+e^- \to \Upsilon(4S)$
• • • We do not use the following data for averages, fits, limits, etc. • • •					
8.7 ±0.5 ±0.6		[1] FUJIKAWA	10A	BELL	Repl. by DUH 13
10.3 ±0.7 ±0.6		[1] AUBERT	08E	BABR	Repl. by LEES 13D
9.2 ±0.7 ±0.6		[1] LIN	07A	BELL	Repl. by FUJIKAWA 10A
11.4 ±0.9 ±0.6		[1] AUBERT	05Y	BABR	Repl. by AUBERT 08E
11.4 ±1.7 ±0.8		[1] AUBERT	04M	BABR	Repl. by AUBERT 05Y
11.7 ±2.3 $^{+1.2}_{-1.3}$		[1] CHAO	04	BELL	Repl. by LIN 07A
8.0 $^{+3.3}_{-3.1}$ ±1.6		[1] CASEY	02	BELL	Repl. by CHAO 04
16.0 $^{+7.2}_{-5.9}$ $^{+2.5}_{-2.7}$		[1] ABE	01H	BELL	Repl. by CASEY 02
8.2 $^{+3.1}_{-2.7}$ ±1.2		[1] AUBERT	01E	BABR	Repl. by AUBERT 04M
14.6 $^{+5.9}_{-5.1}$ $^{+2.4}_{-3.3}$		[1] CRONIN-HEN...	00	CLE2	Repl. by BORNHEIM 03
<41	90	GODANG	98	CLE2	Repl. by CRONIN-HENNESSY 00
<40	90	ASNER	96	CLE2	Rep. by GODANG 98

[1] Assumes equal production of B^+ and B^0 at the $\Upsilon(4S)$.

$\Gamma(\eta' K^0)/\Gamma_{total}$ — Γ_{274}/Γ

VALUE (units 10^{-6})	DOCUMENT ID		TECN	COMMENT
66 ± 4 OUR AVERAGE	Error includes scale factor of 1.4.			
68.5± 2.2±3.1	[1] AUBERT	09AV	BABR	$e^+e^- \to \Upsilon(4S)$
$58.9^{+3.6}_{-3.5}\pm4.3$	[1] SCHUEMANN	06	BELL	$e^+e^- \to \Upsilon(4S)$
89 $^{+18}_{-16}$ ±9	[1] RICHICHI	00	CLE2	$e^+e^- \to \Upsilon(4S)$
• • • We do not use the following data for averages, fits, limits, etc. • • •				
66.6± 2.6±2.8	[1] AUBERT	07AE	BABR	Repl. by AUBERT 09AV
67.4± 3.3±3.2	[1] AUBERT	05M	BABR	AUBERT 07AE
60.6± 5.6±4.6	[1] AUBERT	03W	BABR	Repl. by AUBERT 05M
55 $^{+19}_{-16}$ ±8	[1] ABE	01M	BELL	Repl. by SCHUEMANN 06
42 $^{+13}_{-11}$ ±4	[1] AUBERT	01G	BABR	Repl. by AUBERT 03W
47 $^{+27}_{-20}$ ±9	BEHRENS	98	CLE2	Repl. by RICHICHI 00

[1] Assumes equal production of B^+ and B^0 at the $\Upsilon(4S)$.

$\Gamma(\eta' K^*(892)^0)/\Gamma_{total}$ — Γ_{275}/Γ

VALUE (units 10^{-6})	CL%	DOCUMENT ID		TECN	COMMENT
2.8±0.6 OUR AVERAGE					
2.6±0.7±0.2		[1] SATO	14	BELL	$e^+e^- \to \Upsilon(4S)$
$3.1^{+0.9}_{-0.8}\pm0.3$		[1] DEL-AMO-SA...	10A	BABR	$e^+e^- \to \Upsilon(4S)$
• • • We do not use the following data for averages, fits, limits, etc. • • •					
3.8±1.1±0.5		[1] AUBERT	07E	BABR	Repl. by DEL-AMO-SANCHEZ 10A
< 2.6	90	[1] SCHUEMANN	07	BELL	$e^+e^- \to \Upsilon(4S)$
< 7.6	90	[1] AUBERT,B	04D	BABR	Repl. by AUBERT 07E
<24	90	[1] RICHICHI	00	CLE2	$e^+e^- \to \Upsilon(4S)$
<39	90	BEHRENS	98	CLE2	Repl. by RICHICHI 00

[1] Assumes equal production of B^+ and B^0 at the $\Upsilon(4S)$.

$\Gamma(\eta' K_0^*(1430)^0)/\Gamma_{total}$ — Γ_{276}/Γ

VALUE (units 10^{-6})	DOCUMENT ID		TECN	COMMENT
6.3±1.3±0.9	[1] DEL-AMO-SA...	10A	BABR	$e^+e^- \to \Upsilon(4S)$

[1] Assumes equal production of B^+ and B^0 at the $\Upsilon(4S)$.

$\Gamma(\eta' K_2^*(1430)^0)/\Gamma_{total}$ — Γ_{277}/Γ

VALUE (units 10^{-6})	DOCUMENT ID		TECN	COMMENT
$\mathbf{13.7^{+3.0}_{-2.9}\pm1.2}$	[1] DEL-AMO-SA...	10A	BABR	$e^+e^- \to \Upsilon(4S)$

[1] Assumes equal production of B^+ and B^0 at the $\Upsilon(4S)$.

$\Gamma(\eta K^0)/\Gamma_{total}$ — Γ_{278}/Γ

VALUE (units 10^{-6})	CL%	DOCUMENT ID		TECN	COMMENT
$\mathbf{1.23^{+0.27}_{-0.24}}$ **OUR AVERAGE**					
$1.27^{+0.33}_{-0.29}\pm0.08$		[1] HOI	12	BELL	$e^+e^- \to \Upsilon(4S)$
$1.15^{+0.43}_{-0.38}\pm0.09$		[1] AUBERT	09AV	BABR	$e^+e^- \to \Upsilon(4S)$
• • • We do not use the following data for averages, fits, limits, etc. • • •					
< 1.9	90	[1] CHANG	07B	BELL	Repl. by HOI 12
< 2.9	90	[1] AUBERT,B	06V	BABR	$e^+e^- \to \Upsilon(4S)$
< 2.5	90	[1] AUBERT,B	05K	BABR	$e^+e^- \to \Upsilon(4S)$
< 2.0	90	[1] CHANG	05A	BELL	Repl. by CHANG 07B
< 5.2	90	[1] AUBERT	04H	BABR	Repl. by AUBERT,B 05K
< 9.3	90	[1] RICHICHI	00	CLE2	$e^+e^- \to \Upsilon(4S)$
<33	90	BEHRENS	98	CLE2	Repl. by RICHICHI 00

[1] Assumes equal production of B^+ and B^0 at the $\Upsilon(4S)$.

$\Gamma(\eta K^*(892)^0)/\Gamma_{total}$ — Γ_{279}/Γ

VALUE (units 10^{-6})	CL%	DOCUMENT ID		TECN	COMMENT
15.9±1.0 OUR AVERAGE					
15.2±1.2±1.0		[1] WANG	07B	BELL	$e^+e^- \to \Upsilon(4S)$
16.5±1.1±0.8		[1] AUBERT,B	06H	BABR	$e^+e^- \to \Upsilon(4S)$
$13.8^{+5.5}_{-4.6}\pm1.6$		[1] RICHICHI	00	CLE2	$e^+e^- \to \Upsilon(4S)$
• • • We do not use the following data for averages, fits, limits, etc. • • •					
18.6±2.3±1.2		[1] AUBERT,B	04D	BABR	Repl. by AUBERT,B 06H
<30	90	BEHRENS	98	CLE2	Repl. by RICHICHI 00

[1] Assumes equal production of B^+ and B^0 at the $\Upsilon(4S)$.

$\Gamma(\eta K_0^*(1430)^0)/\Gamma_{total}$ — Γ_{280}/Γ

VALUE (units 10^{-6})	DOCUMENT ID		TECN	COMMENT
11.0±1.6±1.5	[1] AUBERT,B	06H	BABR	$e^+e^- \to \Upsilon(4S)$

[1] Assumes equal production of B^+ and B^0 at the $\Upsilon(4S)$.

$\Gamma(\eta K_2^*(1430)^0)/\Gamma_{total}$ — Γ_{281}/Γ

VALUE (units 10^{-6})	DOCUMENT ID		TECN	COMMENT
9.6±1.8±1.1	[1] AUBERT,B	06H	BABR	$e^+e^- \to \Upsilon(4S)$

[1] Assumes equal production of B^+ and B^0 at the $\Upsilon(4S)$.

$\Gamma(\omega K^0)/\Gamma_{total}$ — Γ_{282}/Γ

VALUE (units 10^{-6})	CL%	DOCUMENT ID		TECN	COMMENT
4.8±0.4 OUR AVERAGE					
4.5±0.4±0.3		[1] CHOBANOVA	14	BELL	$e^+e^- \to \Upsilon(4S)$
5.4±0.8±0.3		[1] AUBERT	07AE	BABR	$e^+e^- \to \Upsilon(4S)$
$10.0^{+5.4}_{-4.2}\pm1.4$		[1] JESSOP	00	CLE2	$e^+e^- \to \Upsilon(4S)$
• • • We do not use the following data for averages, fits, limits, etc. • • •					
6.2±1.0±0.4		[1] AUBERT,B	06E	BABR	Repl. by AUBERT 07AE
$4.4^{+0.8}_{-0.7}\pm0.4$		[1] JEN	06	BELL	Repl. by CHOBANOVA 14
$5.9^{+1.6}_{-1.3}\pm0.5$		[1] AUBERT	04H	BABR	Repl. by AUBERT,B 06E
$4.0^{+1.9}_{-1.6}\pm0.5$		[1] WANG	04A	BELL	Repl. by JEN 06
<13	90	[1] AUBERT	01G	BABR	Repl. by AUBERT 04H
<57	90	[1] BERGFELD	98	CLE2	Repl. by JESSOP 00

[1] Assumes equal production of B^+ and B^0 at the $\Upsilon(4S)$.

Downloaded from https://academic.oup.com/ptep/article/2022/8/083C01/6651666 by KIT Library user on 27 September 2022

$\Gamma(a_0(980)^0 K^0,\ a_0^0 \to \eta\pi^0)/\Gamma_{total}$ — Γ_{283}/Γ

VALUE (units 10^{-6})	CL%	DOCUMENT ID		TECN	COMMENT
<7.8	90	[1] AUBERT,BE	04	BABR	$e^+e^- \to \Upsilon(4S)$

[1] Assumes equal production of charged and neutral B mesons at $\Upsilon(4S)$.

$\Gamma(b_1^0 K^0,\ b_1^0 \to \omega\pi^0)/\Gamma_{total}$ — Γ_{284}/Γ

VALUE (units 10^{-6})	CL%	DOCUMENT ID		TECN	COMMENT
<7.8	90	[1] AUBERT	08AG	BABR	$e^+e^- \to \Upsilon(4S)$

[1] Assumes equal production of B^+ and B^0 at the $\Upsilon(4S)$.

$\Gamma(a_0(980)^\pm K^\mp,\ a_0^\pm \to \eta\pi^\pm)/\Gamma_{total}$ — Γ_{285}/Γ

VALUE (units 10^{-6})	CL%	DOCUMENT ID		TECN	COMMENT
<1.9	90	[1] AUBERT	07Y	BABR	$e^+e^- \to \Upsilon(4S)$
• • • We do not use the following data for averages, fits, limits, etc. • • •					
<2.1	90	[1] AUBERT,BE	04	BABR	Repl. by AUBERT 07Y

[1] Assumes equal production of B^+ and B^0 at the $\Upsilon(4S)$.

$\Gamma(b_1^- K^+,\ b_1^- \to \omega\pi^-)/\Gamma_{total}$ — Γ_{286}/Γ

VALUE (units 10^{-6})	DOCUMENT ID		TECN	COMMENT
7.4±1.0±1.0	[1] AUBERT	07BI	BABR	$e^+e^- \to \Upsilon(4S)$

[1] Assumes equal production of B^+ and B^0 at the $\Upsilon(4S)$.

$\Gamma(b_1^0 K^{*0},\ b_1^0 \to \omega\pi^0)/\Gamma_{total}$ — Γ_{287}/Γ

VALUE	CL%	DOCUMENT ID		TECN	COMMENT
$<8.0\times10^{-6}$	90	[1] AUBERT	09AF	BABR	$e^+e^- \to \Upsilon(4S)$

[1] Assumes equal production of B^+ and B^0 at the $\Upsilon(4S)$.

$\Gamma(b_1^- K^{*+},\ b_1^- \to \omega\pi^-)/\Gamma_{total}$ — Γ_{288}/Γ

VALUE	CL%	DOCUMENT ID		TECN	COMMENT
$<5.0\times10^{-6}$	90	[1] AUBERT	09AF	BABR	$e^+e^- \to \Upsilon(4S)$

[1] Assumes equal production of B^+ and B^0 at the $\Upsilon(4S)$.

$\Gamma(a_0(1450)^\pm K^\mp,\ a_0^\pm \to \eta\pi^\pm)/\Gamma_{total}$ — Γ_{289}/Γ

VALUE (units 10^{-6})	CL%	DOCUMENT ID		TECN	COMMENT
<3.1	90	[1] AUBERT	07Y	BABR	$e^+e^- \to \Upsilon(4S)$

[1] Assumes equal production of B^+ and B^0 at the $\Upsilon(4S)$.

$\Gamma(K_S^0 X^0(\text{Familon}))/\Gamma_{total}$ — Γ_{290}/Γ

VALUE (units 10^{-6})	CL%	DOCUMENT ID		TECN	COMMENT
<53	90	[1] AMMAR	01B	CLE2	$e^+e^- \to \Upsilon(4S)$

[1] AMMAR 01B searched for the two-body decay of the B meson to a massless neutral feebly-interacting particle X^0 such as the familon, the Nambu-Goldstone boson associated with a spontaneously broken global family symmetry.

$\Gamma(\omega K^*(892)^0)/\Gamma_{total}$ — Γ_{291}/Γ

VALUE (units 10^{-6})	CL%	DOCUMENT ID		TECN	COMMENT
2.0±0.5 OUR AVERAGE					
2.2±0.6±0.2		[1] AUBERT	09H	BABR	$e^+e^- \to \Upsilon(4S)$
1.8±0.7±0.3		[1] GOLDENZWE...	08	BELL	$e^+e^- \to \Upsilon(4S)$
• • • We do not use the following data for averages, fits, limits, etc. • • •					
< 4.2	90	[1] AUBERT,B	06T	BABR	Repl. by AUBERT 09H
< 6.0	90	[1] AUBERT	05O	BABR	Repl. by AUBERT,B 06T
<23	90	[1] BERGFELD	98	CLE2	

[1] Assumes equal production of B^+ and B^0 at the $\Upsilon(4S)$.

$\Gamma(\omega(K\pi)_0^{*0})/\Gamma_{total}$ — Γ_{292}/Γ

$(K\pi)_0^{*0}$ is the total S-wave composed of $K_0^*(1430)$ and nonresonant that are described using LASS shape.

VALUE (units 10^{-6})	DOCUMENT ID		TECN	COMMENT
18.4±1.8±1.7	[1] AUBERT	09H	BABR	$e^+e^- \to \Upsilon(4S)$

[1] Assumes equal production of B^+ and B^0 at the $\Upsilon(4S)$.

$\Gamma(\omega K_0^*(1430)^0)/\Gamma_{total}$ — Γ_{293}/Γ

VALUE (units 10^{-6})	DOCUMENT ID		TECN	COMMENT
16.0±1.6±3.0	[1] AUBERT	09H	BABR	$e^+e^- \to \Upsilon(4S)$

[1] Assumes equal production of B^+ and B^0 at the $\Upsilon(4S)$.

$\Gamma(\omega K_2^*(1430)^0)/\Gamma_{total}$ — Γ_{294}/Γ

VALUE (units 10^{-6})	DOCUMENT ID		TECN	COMMENT
10.1±2.0±1.1	[1] AUBERT	09H	BABR	$e^+e^- \to \Upsilon(4S)$

[1] Assumes equal production of B^+ and B^0 at the $\Upsilon(4S)$.

$\Gamma(\omega K^+\pi^- \text{nonresonant})/\Gamma_{total}$ — Γ_{295}/Γ

VALUE (units 10^{-6})	DOCUMENT ID		TECN	COMMENT
5.1±0.7±0.7	[1,2] GOLDENZWE...	08	BELL	$e^+e^- \to \Upsilon(4S)$

[1] Assumes equal production of B^+ and B^0 at the $\Upsilon(4S)$.
[2] For the $K\pi$ mass range 0.755–1.250 GeV/c^2, excluding $K^*(892)$.

$\Gamma(K^+\pi^-\pi^0)/\Gamma_{total}$ — Γ_{296}/Γ

VALUE (units 10^{-6})	CL%	DOCUMENT ID		TECN	COMMENT
37.8±3.2 OUR AVERAGE					
38.5±1.0±3.9		[1,2] LEES	11	BABR	$e^+e^- \to \Upsilon(4S)$
$36.6^{+4.2}_{-4.3}\pm3.0$		[1] CHANG	04	BELL	$e^+e^- \to \Upsilon(4S)$
• • • We do not use the following data for averages, fits, limits, etc. • • •					
$35.7^{+2.6}_{-1.5}\pm2.2$		[1] AUBERT	08AQ	BABR	Repl. by LEES 11
<40	90	[1] ECKHART	02	CLE2	$e^+e^- \to \Upsilon(4S)$

[1] Assumes equal production of B^+ and B^0 at the $\Upsilon(4S)$.
[2] Uses Dalitz plot analysis of $B^0 \to K^+\pi^-\pi^0$ decays.

$\Gamma(K^+\rho^-)/\Gamma_{total}$ — Γ_{297}/Γ

VALUE (units 10^{-6})	CL%	DOCUMENT ID		TECN	COMMENT
7.0±0.9 OUR AVERAGE					
6.6±0.5±0.8		[1,2] LEES	11	BABR	$e^+e^- \to \Upsilon(4S)$
$15.1^{+3.4}_{-3.3}{}^{+2.4}_{-2.6}$		[1] CHANG	04	BELL	$e^+e^- \to \Upsilon(4S)$
• • • We do not use the following data for averages, fits, limits, etc. • • •					
$8.0^{+0.8}_{-1.3}\pm0.6$		[1] AUBERT	08AQ	BABR	Repl. by LEES 11
$7.3^{+1.3}_{-1.2}\pm1.3$		[1] AUBERT	03T	BABR	Repl. by AUBERT 08AQ
<32	90	[1] JESSOP	00	CLE2	$e^+e^- \to \Upsilon(4S)$
<35	90	ASNER	96	CLE2	Repl. by JESSOP 00

[1] Assumes equal production of B^+ and B^0 at the $\Upsilon(4S)$.
[2] Uses Dalitz plot analysis of $B^0 \to K^+\pi^-\pi^0$ decays.

$\Gamma(K^+\rho(1450)^-)/\Gamma_{total}$ — Γ_{298}/Γ

VALUE (units 10^{-6})	CL%	DOCUMENT ID		TECN	COMMENT
2.4±1.0±0.6		[1,2] LEES	11	BABR	$e^+e^- \to \Upsilon(4S)$
• • • We do not use the following data for averages, fits, limits, etc. • • •					
<2.1	90	[1] AUBERT	08AQ	BABR	Repl. by LEES 11

[1] Assumes equal production of B^+ and B^0 at the $\Upsilon(4S)$.
[2] Uses Dalitz plot analysis of $B^0 \to K^+\pi^-\pi^0$ decays.

$\Gamma(K^+\rho(1700)^-)/\Gamma_{total}$ — Γ_{299}/Γ

VALUE (units 10^{-6})	CL%	DOCUMENT ID		TECN	COMMENT
0.6±0.6±0.4		[1,2] LEES	11	BABR	$e^+e^- \to \Upsilon(4S)$
• • • We do not use the following data for averages, fits, limits, etc. • • •					
<1.1	90	[1] AUBERT	08AQ	BABR	Repl. by LEES 11

[1] Assumes equal production of B^+ and B^0 at the $\Upsilon(4S)$.
[2] Uses Dalitz plot analysis of $B^0 \to K^+\pi^-\pi^0$ decays.

$\Gamma((K^+\pi^-\pi^0)\ \text{nonresonant})/\Gamma_{total}$ — Γ_{300}/Γ

VALUE (units 10^{-6})	CL%	DOCUMENT ID		TECN	COMMENT
2.8±0.5±0.4		[1,2] LEES	11	BABR	$e^+e^- \to \Upsilon(4S)$
• • • We do not use the following data for averages, fits, limits, etc. • • •					
4.4±0.9±0.5		[1] AUBERT	08AQ	BABR	Repl. by LEES 11
<9.4	90	[1] CHANG	04	BELL	$e^+e^- \to \Upsilon(4S)$

[1] Assumes equal production of B^+ and B^0 at the $\Upsilon(4S)$.
[2] Uses Dalitz plot analysis of $B^0 \to K^+\pi^-\pi^0$ decays. The quoted value is only for the flat part of the non-resonant component.

$\Gamma((K\pi)_0^{*+}\pi^-,\ (K\pi)_0^{*+} \to K^+\pi^0)/\Gamma_{total}$ — Γ_{301}/Γ

$(K\pi)_0^{*+}$ is the total S-wave composed of $K_0^*(1430)$ and nonresonant that are described using LASS shape.

VALUE (units 10^{-6})	CL%	DOCUMENT ID		TECN	COMMENT
34.2±2.4±4.1		[1,2] LEES	11	BABR	$e^+e^- \to \Upsilon(4S)$
• • • We do not use the following data for averages, fits, limits, etc. • • •					
$9.4^{+1.1}_{-1.3}{}^{+2.3}_{-2.1}$		[1] AUBERT	08AQ	BABR	Repl. by LEES 11

[1] Assumes equal production of B^+ and B^0 at the $\Upsilon(4S)$.
[2] Uses Dalitz plot analysis of $B^0 \to K^+\pi^-\pi^0$ decays.

$\Gamma((K\pi)_0^{*0}\pi^0,\ (K\pi)_0^{*0} \to K^+\pi^-)/\Gamma_{total}$ — Γ_{302}/Γ

$(K\pi)_0^{*0}$ is the total S-wave composed of $K_0^*(1430)$ and nonresonant that are described using LASS shape.

VALUE (units 10^{-6})	CL%	DOCUMENT ID		TECN	COMMENT
8.6±1.1±1.3		[1,2] LEES	11	BABR	$e^+e^- \to \Upsilon(4S)$
• • • We do not use the following data for averages, fits, limits, etc. • • •					
$8.7^{+1.1}_{-0.9}{}^{+2.8}_{-2.6}$		[1] AUBERT	08AQ	BABR	Repl. by LEES 11

[1] Assumes equal production of B^+ and B^0 at the $\Upsilon(4S)$.
[2] Uses Dalitz plot analysis of $B^0 \to K^+\pi^-\pi^0$ decays.

$\Gamma(K_2^*(1430)^0\pi^0)/\Gamma_{total}$ — Γ_{303}/Γ

VALUE (units 10^{-6})	CL%	DOCUMENT ID		TECN	COMMENT
<4.0	90	[1] AUBERT	08AQ	BABR	$e^+e^- \to \Upsilon(4S)$

[1] Assumes equal production of B^+ and B^0 at the $\Upsilon(4S)$.

Downloaded from https://academic.oup.com/ptep/article/2022/8/083C01/6651666 by KIT Library user on 27 September 2022

$\Gamma(K^*(1680)^0\pi^0)/\Gamma_{total}$ — Γ_{304}/Γ

VALUE (units 10^{-6})	CL%	DOCUMENT ID		TECN	COMMENT
<7.5	90	[1] AUBERT	08AQ	BABR	$e^+e^- \to \Upsilon(4S)$

[1] Assumes equal production of B^+ and B^0 at the $\Upsilon(4S)$.

$\Gamma(K_x^{*0}\pi^0)/\Gamma_{total}$ — Γ_{305}/Γ

K_x^{*0} stands for the possible candidates of $K^*(1410)$, $K_0^*(1430)$ and $K_2^*(1430)$.

VALUE (units 10^{-6})	DOCUMENT ID		TECN	COMMENT
$\mathbf{6.1^{+1.6+0.5}_{-1.5-0.6}}$	[1] CHANG	04	BELL	$e^+e^- \to \Upsilon(4S)$

[1] Assumes equal production of B^+ and B^0 at the $\Upsilon(4S)$.

$\Gamma(K^0\pi^+\pi^-)/\Gamma_{total}$ — Γ_{306}/Γ

VALUE (units 10^{-6})	CL%	DOCUMENT ID		TECN	COMMENT
49.7± 1.8 OUR FIT					
49.6± 2.0 OUR AVERAGE					
50.2± 1.5±1.8		[1] AUBERT	09AU	BABR	$e^+e^- \to \Upsilon(4S)$
47.5± 2.4±3.7		[2] GARMASH	07	BELL	$e^+e^- \to \Upsilon(4S)$
$50\ ^{+10}_{-9}\ \pm7$		[1] ECKHART	02	CLE2	$e^+e^- \to \Upsilon(4S)$
• • • We do not use the following data for averages, fits, limits, etc. • • •					
43.0± 2.3±2.3		[1] AUBERT	06I	BABR	Repl. by AUBERT 09AU
43.7± 3.8±3.4		[1] AUBERT,B	04O	BABR	Repl. by AUBERT 06I
45.4± 5.2±5.9		[1] GARMASH	04	BELL	Repl. by GARMASH 07
<440	90	ALBRECHT	91E	ARG	$e^+e^- \to \Upsilon(4S)$

[1] Assumes equal production of B^+ and B^0 at the $\Upsilon(4S)$.
[2] Uses Dalitz plot analysis of the $B^0 \to K^0\pi^+\pi^-$ final state decays.

$\Gamma(K^0\pi^+\pi^-\text{nonresonant})/\Gamma_{total}$ — Γ_{307}/Γ

VALUE (units 10^{-6})	DOCUMENT ID		TECN	COMMENT
$\mathbf{13.9^{+2.6}_{-1.8}}$ **OUR AVERAGE** Error includes scale factor of 1.6. See the ideogram below.				
12.1±0.6±2.9	[1] AAIJ	18F	LHCB	pp at 7, 8 TeV
$11.1^{+2.5}_{-1.0}\pm0.9$	[2] AUBERT	09AU	BABR	$e^+e^- \to \Upsilon(4S)$
$19.9\pm2.5^{+1.7}_{-2.0}$	[3] GARMASH	07	BELL	$e^+e^- \to \Upsilon(4S)$

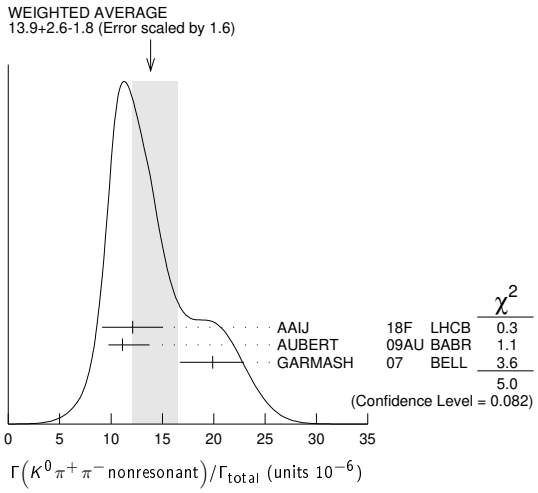

[1] Uses Dalitz plot analysis of the $B^0 \to K_S^0\pi^+\pi^-$ final state decays. For the branching fraction of the reference mode, the PDG 18 average $B(B^0 \to K_S^0\pi^+\pi^-) = (4.96 \pm 0.20) \times 10^{-5}$ is used.
[2] Assumes equal production of B^+ and B^0 at the $\Upsilon(4S)$.
[3] Uses Dalitz plot analysis of the $B^0 \to K^0\pi^+\pi^-$ final state decays.

$\Gamma(K^0\rho^0)/\Gamma_{total}$ — Γ_{308}/Γ

VALUE (units 10^{-6})	CL%	DOCUMENT ID		TECN	COMMENT
3.4 ±1.1 OUR AVERAGE Error includes scale factor of 2.3. See the ideogram below.					
$1.89^{+0.55}_{-0.79}\pm0.40$		[1] AAIJ	18F	LHCB	pp at 7, 8 TeV
$4.4\ ^{+0.7}_{-0.6}\ \pm0.3$		[2] AUBERT	09AU	BABR	$e^+e^- \to \Upsilon(4S)$
$6.1\ \pm1.0\ ^{+1.1}_{-1.2}$		[3] GARMASH	07	BELL	$e^+e^- \to \Upsilon(4S)$
• • • We do not use the following data for averages, fits, limits, etc. • • •					
4.9 ±0.8 ±0.9		[2] AUBERT	07F	BABR	Repl. by AUBERT 09AU
< 39	90	ASNER	96	CLEO	$e^+e^- \to \Upsilon(4S)$
<320	90	ALBRECHT	91B	ARG	$e^+e^- \to \Upsilon(4S)$
<500	90	[4] AVERY	89B	CLEO	$e^+e^- \to \Upsilon(4S)$

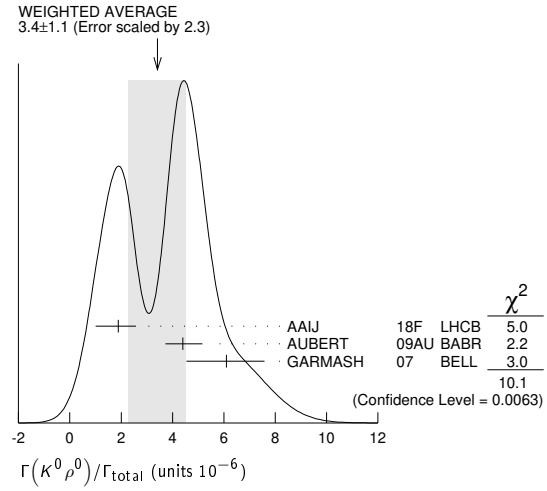

[1] Uses Dalitz plot analysis of the $B^0 \to K_S^0\pi^+\pi^-$ final state decays. For the branching fraction of the reference mode, the PDG 18 average $B(B^0 \to K_S^0\pi^+\pi^-) = (4.96 \pm 0.20) \times 10^{-5}$ is used.
[2] Assumes equal production of B^+ and B^0 at the $\Upsilon(4S)$.
[3] Uses Dalitz plot analysis of the $B^0 \to K^0\pi^+\pi^-$ final state decays.
[4] AVERY 89B reports $< 5.8 \times 10^{-4}$ assuming the $\Upsilon(4S)$ decays 43% to $B^0\overline{B}^0$. We rescale to 50%.

$\Gamma(K^*(892)^+\pi^-)/\Gamma_{total}$ — Γ_{309}/Γ

VALUE (units 10^{-6})	CL%	DOCUMENT ID		TECN	COMMENT
7.5 ±0.4 OUR AVERAGE					
7.02±0.30±0.45		[1] AAIJ	18F	LHCB	pp at 7, 8 TeV
8.0 ±1.1 ±0.8		[2,3] LEES	11	BABR	$e^+e^- \to \Upsilon(4S)$
$8.3\ ^{+0.9}_{-0.8}\ \pm0.8$		[3,4] AUBERT	09AU	BABR	$e^+e^- \to \Upsilon(4S)$
$8.4\ \pm1.1\ ^{+1.0}_{-0.9}$		[4] GARMASH	07	BELL	$e^+e^- \to \Upsilon(4S)$
$16\ ^{+6}_{-5}\ \pm2$		[3] ECKHART	02	CLE2	$e^+e^- \to \Upsilon(4S)$
• • • We do not use the following data for averages, fits, limits, etc. • • •					
$12.6\ ^{+2.7}_{-1.6}\ \pm0.9$		[2,3] AUBERT	08AQ	BABR	Repl. by LEES 11
11.0 ±1.5 ±0.71		[3] AUBERT	06I	BABR	Repl. by AUBERT 09AU
12.9 ±2.4 ±1.4		[3] AUBERT,B	04O	BABR	Repl. by AUBERT 06I
$14.8\ ^{+4.6}_{-4.4}\ ^{+2.8}_{-1.3}$		[3] CHANG	04	BELL	Repl. by GARMASH 07
< 72	90	ASNER	96	CLE2	$e^+e^- \to \Upsilon(4S)$
<620	90	ALBRECHT	91B	ARG	$e^+e^- \to \Upsilon(4S)$
<380	90	[5] AVERY	89B	CLEO	$e^+e^- \to \Upsilon(4S)$
<560	90	[6] AVERY	87	CLEO	$e^+e^- \to \Upsilon(4S)$

[1] Uses Dalitz plot analysis of the $B^0 \to K_S^0\pi^+\pi^-$ final state decays. For the branching fraction of the reference mode, the PDG 18 average $B(B^0 \to K_S^0\pi^+\pi^-) = (4.96 \pm 0.20) \times 10^{-5}$ is used.
[2] Uses Dalitz plot analysis of $B^0 \to K^+\pi^-\pi^0$ decays.
[3] Assumes equal production of B^+ and B^0 at the $\Upsilon(4S)$.
[4] Uses Dalitz plot analysis of the $B^0 \to K^0\pi^+\pi^-$ final state decays.
[5] AVERY 89B reports $< 4.4 \times 10^{-4}$ assuming the $\Upsilon(4S)$ decays 43% to $B^0\overline{B}^0$. We rescale to 50%.
[6] AVERY 87 reports $< 7 \times 10^{-4}$ assuming the $\Upsilon(4S)$ decays 40% to $B^0\overline{B}^0$. We rescale to 50%.

$\Gamma(K_0^*(1430)^+\pi^-)/\Gamma_{total}$ — Γ_{310}/Γ

VALUE (units 10^{-6})	DOCUMENT ID		TECN	COMMENT
33 ±7 OUR AVERAGE Error includes scale factor of 2.0.				
$29.9^{+2.3}_{-1.7}\pm3.6$	[1,2] AUBERT	09AU	BABR	$e^+e^- \to \Upsilon(4S)$
$49.7\pm3.8^{+6.8}_{-8.2}$	[2] GARMASH	07	BELL	$e^+e^- \to \Upsilon(4S)$

[1] Assumes equal production of B^+ and B^0 at the $\Upsilon(4S)$.
[2] Uses Dalitz plot analysis of the $B^0 \to K^0\pi^+\pi^-$ final state decays.

$\Gamma(K_x^{*+}\pi^-)/\Gamma_{total}$ — Γ_{311}/Γ

K_x^{*+} stands for the possible candidates of $K^*(1410)$, $K_0^*(1430)$ and $K_2^*(1430)$.

VALUE (units 10^{-6})	DOCUMENT ID		TECN	COMMENT
$\mathbf{5.1\pm1.5^{+0.6}_{-0.7}}$	[1] CHANG	04	BELL	$e^+e^- \to \Upsilon(4S)$

[1] Assumes equal production of B^+ and B^0 at the $\Upsilon(4S)$.

$\Gamma(K^*(1410)^+\pi^-,\ K^{*+} \to K^0\pi^+)/\Gamma_{total}$ — Γ_{312}/Γ

VALUE (units 10^{-6})	CL%	DOCUMENT ID		TECN	COMMENT
<3.8	90	[1] GARMASH	07	BELL	$e^+e^- \to \Upsilon(4S)$

[1] Uses Dalitz plot analysis of the $B^0 \to K^0\pi^+\pi^-$ final state decays.

Downloaded from https://academic.oup.com/ptep/article/2022/8/083C01/6651666 by KIT Library user on 27 September 2022

$\Gamma((K\pi)_0^{*+}\pi^-,\ (K\pi)_0^{*+}\to K^0\pi^+)/\Gamma_{total}$ — Γ_{313}/Γ

VALUE (units 10^{-6})		DOCUMENT ID		TECN	COMMENT
16.2±0.69±1.15		[1] AAIJ	18F	LHCB	pp at 7, 8 TeV

[1] Uses Dalitz plot analysis of the $B^0\to K^0_S\pi^+\pi^-$ final state decays. $(K\pi)_0^{*+}$ is the S-wave component of $K^0\pi^+$. For the branching fraction of the reference mode, the PDG 18 average $B(B^0\to K^0_S\pi^+\pi^-)=(4.96\pm0.20)\times10^{-5}$ is used.

$\Gamma(f_0(980)K^0,\ f_0\to\pi^+\pi^-)/\Gamma_{total}$ — Γ_{314}/Γ

VALUE (units 10^{-6})	CL%	DOCUMENT ID		TECN	COMMENT
8.1 ±0.8 OUR AVERAGE		Error includes scale factor of 1.3. See the ideogram below.			
9.23±0.40±0.79		[1] AAIJ	18F	LHCB	pp at 7, 8 TeV
6.9 ±0.8 ±0.6		[2] AUBERT	09AU	BABR	$e^+e^-\to\Upsilon(4S)$
7.6 ±1.7 $^{+0.9}_{-1.3}$		[3] GARMASH	07	BELL	$e^+e^-\to\Upsilon(4S)$
• • • We do not use the following data for averages, fits, limits, etc. • • •					
5.5 ±0.7 ±0.6		[2] AUBERT	06I	BABR	Repl. by AUBERT 09AU
<360	90	[4] AVERY	89B	CLEO	$e^+e^-\to\Upsilon(4S)$

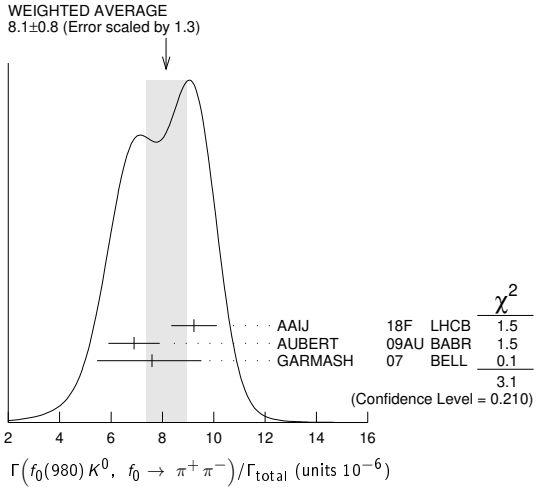

[1] Uses Dalitz plot analysis of the $B^0\to K^0_S\pi^+\pi^-$ final state decays. For the branching fraction of the reference mode, the PDG 18 average $B(B^0\to K^0_S\pi^+\pi^-)=(4.96\pm0.20)\times10^{-5}$ is used.
[2] Assumes equal production of B^+ and B^0 at the $\Upsilon(4S)$.
[3] Uses Dalitz plot analysis of the $B^0\to K^0\pi^+\pi^-$ final state decays.
[4] AVERY 89B reports $<4.2\times10^{-4}$ assuming the $\Upsilon(4S)$ decays 43% to $B^0\overline{B}^0$. We rescale to 50%.

$\Gamma(K^0f_0(500))/\Gamma_{total}$ — Γ_{315}/Γ

VALUE (units 10^{-6})	DOCUMENT ID		TECN	COMMENT
$0.16^{+0.20}_{-0.04}\pm0.15$	[1] AAIJ	18F	LHCB	pp at 7, 8 TeV

[1] Uses Dalitz plot analysis of the $B^0\to K^0_S\pi^+\pi^-$ final state decays. For the branching fraction of the reference mode, the PDG 18 average $B(B^0\to K^0_S\pi^+\pi^-)=(4.96\pm0.20)\times10^{-5}$ is used.

$\Gamma(K^0f_0(1500))/\Gamma_{total}$ — Γ_{316}/Γ

VALUE (units 10^{-6})	DOCUMENT ID		TECN	COMMENT
1.29±0.27±0.70	[1] AAIJ	18F	LHCB	pp at 7, 8 TeV

[1] Uses Dalitz plot analysis of the $B^0\to K^0_S\pi^+\pi^-$ final state decays. For the branching fraction of the reference mode, the PDG 18 average $B(B^0\to K^0_S\pi^+\pi^-)=(4.96\pm0.20)\times10^{-5}$ is used.

$\Gamma(f_2(1270)K^0)/\Gamma_{total}$ — Γ_{317}/Γ

VALUE (units 10^{-6})	CL%	DOCUMENT ID		TECN	COMMENT
$2.7^{+1.0}_{-0.8}\pm0.9$		[1] AUBERT	09AU	BABR	$e^+e^-\to\Upsilon(4S)$
• • • We do not use the following data for averages, fits, limits, etc. • • •					
<2.5	90	[2] GARMASH	07	BELL	$e^+e^-\to\Upsilon(4S)$

[1] Assumes equal production of B^+ and B^0 at the $\Upsilon(4S)$.
[2] GARMASH 07 reports $B(B^0\to f_2(1270)K^0)\times B(f_2(1270)\to\pi^+\pi^-)<1.4\times10^{-6}$ using Dalitz plot analysis. We compute $B(B^0\to f_2(1270)K^0)$ using the PDG value $B(f_2(1270)\to\pi\pi)=84.2\times10^{-2}$ and 2/3 for the $\pi^+\pi^-$ fraction.

$\Gamma(f_x(1300)K^0,f_x\to\pi^+\pi^-)/\Gamma_{total}$ — Γ_{318}/Γ

VALUE (units 10^{-6})	DOCUMENT ID		TECN	COMMENT
$1.81^{+0.55}_{-0.45}\pm0.48$	[1] AUBERT	09AU	BABR	$e^+e^-\to\Upsilon(4S)$

[1] Assumes equal production of B^+ and B^0 at the $\Upsilon(4S)$.

$\Gamma(K^*(892)^0\pi^0)/\Gamma_{total}$ — Γ_{319}/Γ

VALUE (units 10^{-6})	CL%	DOCUMENT ID		TECN	COMMENT
3.3±0.5±0.4		[1,2] LEES	11	BABR	$e^+e^-\to\Upsilon(4S)$
• • • We do not use the following data for averages, fits, limits, etc. • • •					
3.6±0.7±0.4		[1,2] AUBERT	08AQ	BABR	Repl. by LEES 11
<3.5	90	[2] CHANG	04	BELL	$e^+e^-\to\Upsilon(4S)$
<3.6	90	JESSOP	00	CLE2	$e^+e^-\to\Upsilon(4S)$
<28	90	ASNER	96	CLE2	Repl. by JESSOP 00

[1] Uses Dalitz plot analysis of $B^0\to K^+\pi^-\pi^0$ decays.
[2] Assumes equal production of B^+ and B^0 at the $\Upsilon(4S)$.

$\Gamma(K_2^*(1430)^+\pi^-)/\Gamma_{total}$ — Γ_{320}/Γ

VALUE (units 10^{-6})	CL%	DOCUMENT ID		TECN	COMMENT
$3.65^{+0.15}_{-0.12}\pm0.31$		[1] AAIJ	18F	LHCB	pp at 7, 8 TeV
• • • We do not use the following data for averages, fits, limits, etc. • • •					
< 16.2	90	[2,3] AUBERT	08AQ	BABR	$e^+e^-\to\Upsilon(4S)$
< 6	90	[4] GARMASH	07	BELL	$e^+e^-\to\Upsilon(4S)$
< 18	90	[3] GARMASH	04	BELL	Repl. by GARMASH 07
<2600	90	ALBRECHT	91B	ARG	$e^+e^-\to\Upsilon(4S)$

[1] Uses Dalitz plot analysis of the $B^0\to K^0_S\pi^+\pi^-$ final state decays. We compute $B(B^0\to K_2^*(1430)^+\pi^-)$ using the PDG 18 value $B(K_2^*(1430)\to K\pi)=49.9\times10^{-2}$ and 2/3 for the $K^0\pi^+$ fraction. For the branching fraction of the reference mode, the PDG 18 average $B(B^0\to K^0_S\pi^+\pi^-)=(4.96\pm0.20)\times10^{-5}$ is used.
[2] Uses Dalitz plot analysis of $B^0\to K^+\pi^-\pi^0$ decays.
[3] Assumes equal production of B^+ and B^0 at the $\Upsilon(4S)$.
[4] GARMASH 07 reports $B(B^0\to K_2^*(1430)^+\pi^-)\times B(K_2^{*+}\to K^0\pi^+)<2.1\times10^{-6}$ using Dalitz plot analysis. We compute $B(B^0\to K_2^*(1430)^+\pi^-)$ using the PDG value $B(K_2^*(1430)\to K\pi)=49.9\times10^{-2}$ and 2/3 for the $K^0\pi^+$ fraction.

$\Gamma(K^*(1680)^+\pi^-)/\Gamma_{total}$ — Γ_{321}/Γ

VALUE (units 10^{-6})	CL%	DOCUMENT ID		TECN	COMMENT
14.1±0.58±0.84		[1] AAIJ	18F	LHCB	pp at 7, 8 TeV
• • • We do not use the following data for averages, fits, limits, etc. • • •					
<25	90	[2,3] AUBERT	08AQ	BABR	$e^+e^-\to\Upsilon(4S)$
<10	90	[4] GARMASH	07	BELL	$e^+e^-\to\Upsilon(4S)$

[1] Uses Dalitz plot analysis of the $B^0\to K^0_S\pi^+\pi^-$ final state decays. We compute $B(B^0\to K_2^*(1430)^+\pi^-)$ using the PDG 18 value $B(K_2^*(1430)\to K\pi)=(49.9\pm1.2)\times10^{-2}$ and 2/3 for the $K^0\pi^+$ fraction. For the branching fraction of the reference mode, the PDG 18 average $B(B^0\to K^0_S\pi^+\pi^-)=(4.96\pm0.20)\times10^{-5}$ is used.
[2] Uses Dalitz plot analysis of $B^0\to K^+\pi^-\pi^0$ decays.
[3] Assumes equal production of B^+ and B^0 at the $\Upsilon(4S)$.
[4] GARMASH 07 reports $B(B^0\to K^*(1680)^+\pi^-)\times B(K^{*+}\to K^0\pi^+)<2.6\times10^{-6}$ using Dalitz plot analysis. We compute $B(B^0\to K^*(1680)^+\pi^-)$ using the PDG value $B(K^*(1680)\to K\pi)=38.7\times10^{-2}$ and 2/3 for the $K^0\pi^+$ fraction.

$\Gamma(K^+\pi^-\pi^+\pi^-)/\Gamma_{total}$ — Γ_{322}/Γ

VALUE	CL%	DOCUMENT ID		TECN	COMMENT
$<2.3\times10^{-4}$	90	[1] ADAM	96D	DLPH	$e^+e^-\to Z$
• • • We do not use the following data for averages, fits, limits, etc. • • •					
$<2.1\times10^{-4}$	90	[2] ABREU	95N	DLPH	Sup. by ADAM 96D

[1] ADAM 96D assumes $f_{B^0}=f_{B^-}=0.39$ and $f_{B_s}=0.12$. Contributions from B^0 and B_s decays cannot be separated. Limits are given for the weighted average of the decay rates for the two neutral B mesons.
[2] Assumes a B^0, B^- production fraction of 0.39 and a B_s production fraction of 0.12. Contributions from B^0 and B^0_s decays cannot be separated. Limits are given for the weighted average of the decay rates for the two neutral B mesons.

$\Gamma(\rho^0K^+\pi^-)/\Gamma_{total}$ — Γ_{323}/Γ

VALUE (units 10^{-6})	DOCUMENT ID		TECN	COMMENT
2.8±0.5±0.5	[1,2] KYEONG	09	BELL	$e^+e^-\to\Upsilon(4S)$

[1] Assumes equal production of B^+ and B^0 at the $\Upsilon(4S)$.
[2] Required $0.75<m_{K^+\pi^-}<1.20$ GeV/c^2.

$\Gamma(f_0(980)K^+\pi^-,\ f_0\to\pi\pi)/\Gamma_{total}$ — Γ_{324}/Γ

VALUE (units 10^{-6})	DOCUMENT ID		TECN	COMMENT
$1.4\pm0.4^{+0.3}_{-0.4}$	[1,2] KYEONG	09	BELL	$e^+e^-\to\Upsilon(4S)$

[1] Assumes equal production of B^+ and B^0 at the $\Upsilon(4S)$.
[2] Required $0.75<m_{K^+K^-}<1.2$ GeV/c^2.

$\Gamma(K^+\pi^-\pi^+\pi^-\text{ nonresonant})/\Gamma_{total}$ — Γ_{325}/Γ

VALUE	CL%	DOCUMENT ID		TECN	COMMENT
$<2.1\times10^{-6}$	90	[1,2] KYEONG	09	BELL	$e^+e^-\to\Upsilon(4S)$

[1] Assumes equal production of B^+ and B^0 at the $\Upsilon(4S)$.
[2] Required $0.55<m_{\pi^+\pi^-}<1.42$ and $0.75<m_{K^+\pi^-}<1.20$ GeV/c^2.

Downloaded from https://academic.oup.com/ptep/article/2022/8/083C01/6651666 by KIT Library user on 27 September 2022

$\Gamma(K^*(892)^0\pi^+\pi^-)/\Gamma_{total}$ — Γ_{326}/Γ

VALUE (units 10^{-6})	CL%	DOCUMENT ID		TECN	COMMENT
$54.5\pm2.9\pm4.3$		[1] AUBERT	07AS	BABR	$e^+e^-\to\Upsilon(4S)$
• • • We do not use the following data for averages, fits, limits, etc. • • •					
$4.5^{+1.1+0.9}_{-1.0-1.6}$		[1,2] KYEONG	09	BELL	$e^+e^-\to\Upsilon(4S)$
<1400	90	ALBRECHT	91E	ARG	$e^+e^-\to\Upsilon(4S)$

[1] Assumes equal production of B^+ and B^0 at the $\Upsilon(4S)$.
[2] Required $0.55 < m_{\pi^+\pi^-} < 1.42$ GeV/c^2.

$\Gamma(K^*(892)^0\rho^0)/\Gamma_{total}$ — Γ_{327}/Γ

VALUE (units 10^{-6})	CL%	DOCUMENT ID		TECN	COMMENT
3.9 ± 1.3 OUR AVERAGE		Error includes scale factor of 1.9.			
$5.1\pm0.6^{+0.6}_{-0.8}$		[1] LEES	12K	BABR	$e^+e^-\to\Upsilon(4S)$
$2.1^{+0.8+0.9}_{-0.7-0.5}$		[1] KYEONG	09	BELL	$e^+e^-\to\Upsilon(4S)$
• • • We do not use the following data for averages, fits, limits, etc. • • •					
$5.6\pm0.9\pm1.3$		[1] AUBERT,B	06G	BABR	Repl. by LEES 12K
< 34	90	[2] GODANG	02	CLE2	$e^+e^-\to\Upsilon(4S)$
<286	90	[3] ABE	00C	SLD	$e^+e^-\to Z$
<460	90	ALBRECHT	91B	ARG	$e^+e^-\to\Upsilon(4S)$
<580	90	[4] AVERY	89B	CLEO	$e^+e^-\to\Upsilon(4S)$
<960	90	[5] AVERY	87	CLEO	$e^+e^-\to\Upsilon(4S)$

[1] Assumes equal production of B^+ and B^0 at the $\Upsilon(4S)$.
[2] Assumes a helicity 00 configuration. For a helicity 11 configuration, the limit decreases to 2.4×10^{-5}.
[3] ABE 00C assumes $B(Z\to b\overline{b})=(21.7\pm0.1)\%$ and the B fractions $f_{B^0}=f_{B^+}=(39.7^{+1.8}_{-2.2})\%$ and $f_{B_s}=(10.5^{+1.8}_{-2.2})\%$.
[4] AVERY 89B reports $< 6.7\times10^{-4}$ assuming the $\Upsilon(4S)$ decays 43% to $B^0\overline{B}^0$. We rescale to 50%.
[5] AVERY 87 reports $< 1.2\times10^{-3}$ assuming the $\Upsilon(4S)$ decays 40% to $B^0\overline{B}^0$. We rescale to 50%.

$\Gamma(K^*(892)^0 f_0(980),\ f_0\to\pi\pi)/\Gamma_{total}$ — Γ_{328}/Γ

VALUE (units 10^{-6})	CL%	DOCUMENT ID		TECN	COMMENT
$3.9^{+2.1}_{-1.8}$ OUR AVERAGE		Error includes scale factor of 3.9.			
$5.7\pm0.6\pm0.4$		[1] LEES	12K	BABR	$e^+e^-\to\Upsilon(4S)$
$1.4^{+0.6+0.6}_{-0.5-0.4}$		[1,2] KYEONG	09	BELL	$e^+e^-\to\Upsilon(4S)$
• • • We do not use the following data for averages, fits, limits, etc. • • •					
< 4.3	90	[1] AUBERT,B	06G	BABR	$e^+e^-\to\Upsilon(4S)$
<170	90	[3] AVERY	89B	CLEO	$e^+e^-\to\Upsilon(4S)$

[1] Assumes equal production of B^+ and B^0 at the $\Upsilon(4S)$.
[2] The upper limit is 2.2×10^{-6} at 90% CL.
[3] AVERY 89B reports $< 2.0\times10^{-4}$ assuming the $\Upsilon(4S)$ decays 43% to $B^0\overline{B}^0$. We rescale to 50%.

$\Gamma(K_1(1270)^+\pi^-)/\Gamma_{total}$ — Γ_{329}/Γ

VALUE	CL%	DOCUMENT ID		TECN	COMMENT
$<3.0\times10^{-5}$	90	[1] AUBERT	10D	BABR	$e^+e^-\to\Upsilon(4S)$

[1] Assumes equal production of B^+ and B^0 at the $\Upsilon(4S)$.

$\Gamma(K_1(1400)^+\pi^-)/\Gamma_{total}$ — Γ_{330}/Γ

VALUE	CL%	DOCUMENT ID		TECN	COMMENT
$<2.7\times10^{-5}$	90	[1] AUBERT	10D	BABR	$e^+e^-\to\Upsilon(4S)$
• • • We do not use the following data for averages, fits, limits, etc. • • •					
$<1.1\times10^{-3}$	90	ALBRECHT	91B	ARG	$e^+e^-\to\Upsilon(4S)$

[1] Assumes equal production of B^+ and B^0 at the $\Upsilon(4S)$.

$\Gamma(a_1(1260)^-K^+)/\Gamma_{total}$ — Γ_{331}/Γ

VALUE (units 10^{-6})	CL%	DOCUMENT ID		TECN	COMMENT
$16.3\pm2.9\pm2.3$		[1,2] AUBERT	08F	BABR	$e^+e^-\to\Upsilon(4S)$
• • • We do not use the following data for averages, fits, limits, etc. • • •					
<230	90	[3] ADAM	96D	DLPH	$e^+e^-\to Z$
<390	90	[4] ABREU	95N	DLPH	Sup. by ADAM 96D

[1] Assumes equal production of B^+ and B^0 at the $\Upsilon(4S)$.
[2] Assumes $a_1^\pm$ decays only to 3π and $B(a_1^\pm\to\pi^\pm\pi^\mp\pi^\pm)=0.5$.
[3] ADAM 96D assumes $f_{B^0}=f_{B^-}=0.39$ and $f_{B_s}=0.12$. Contributions from B^0 and B_s decays cannot be separated. Limits are given for the weighted average of the decay rates for the two neutral B mesons.
[4] Assumes a B^0, B^- production fraction of 0.39 and a B_s production fraction of 0.12. Contributions from B^0 and B_s^0 decays cannot be separated. Limits are given for the weighted average of the decay rates for the two neutral B mesons.

$\Gamma(K^*(892)^+\rho^-)/\Gamma_{total}$ — Γ_{332}/Γ

VALUE (units 10^{-6})	CL%	DOCUMENT ID		TECN	COMMENT
$10.3\pm2.3\pm1.3$		[1] LEES	12K	BABR	$e^+e^-\to\Upsilon(4S)$
• • • We do not use the following data for averages, fits, limits, etc. • • •					
<12.0	90	[1] AUBERT,B	06G	BABR	Repl. by LEES 12K

[1] Assumes equal production of B^+ and B^0 at the $\Upsilon(4S)$.

$\Gamma(K_0^*(1430)^+\rho^-)/\Gamma_{total}$ — Γ_{333}/Γ

VALUE (units 10^{-6})	DOCUMENT ID		TECN	COMMENT
$28\pm10\pm6$	[1] LEES	12K	BABR	$e^+e^-\to\Upsilon(4S)$

[1] Assumes equal production of B^+ and B^0 at the $\Upsilon(4S)$.

$\Gamma(K_1(1400)^0\rho^0)/\Gamma_{total}$ — Γ_{334}/Γ

VALUE	CL%	DOCUMENT ID		TECN	COMMENT
$<3.0\times10^{-3}$	90	ALBRECHT	91B	ARG	$e^+e^-\to\Upsilon(4S)$

$\Gamma(K_0^*(1430)^0\rho^0)/\Gamma_{total}$ — Γ_{335}/Γ

VALUE (units 10^{-6})	DOCUMENT ID		TECN	COMMENT
$27\pm4\pm4$	[1] LEES	12K	BABR	$e^+e^-\to\Upsilon(4S)$

[1] Assumes equal production of B^+ and B^0 at the $\Upsilon(4S)$.

$\Gamma(K_0^*(1430)^0 f_0(980),\ f_0\to\pi\pi)/\Gamma_{total}$ — Γ_{336}/Γ

VALUE (units 10^{-6})	DOCUMENT ID		TECN	COMMENT
$2.7\pm0.7\pm0.6$	[1] LEES	12K	BABR	$e^+e^-\to\Upsilon(4S)$

[1] Assumes equal production of B^+ and B^0 at the $\Upsilon(4S)$.

$\Gamma(K_2^*(1430)^0 f_0(980),\ f_0\to\pi\pi)/\Gamma_{total}$ — Γ_{337}/Γ

VALUE (units 10^{-6})	DOCUMENT ID		TECN	COMMENT
$8.6\pm1.7\pm1.0$	[1] LEES	12K	BABR	$e^+e^-\to\Upsilon(4S)$

[1] Assumes equal production of B^+ and B^0 at the $\Upsilon(4S)$.

$\Gamma(K^+K^-)/\Gamma_{total}$ — Γ_{338}/Γ

VALUE (units 10^{-8})	CL%	DOCUMENT ID		TECN	COMMENT
$7.80\pm1.27\pm0.84$		[1] AAIJ	17G	LHCB	pp at 7 and 8 TeV
• • • We do not use the following data for averages, fits, limits, etc. • • •					
$10\pm8\pm4$		[2,3] DUH	13	BELL	$e^+e^-\to\Upsilon(4S)$
$12^{+8}_{-7}\pm1$		[4] AAIJ	12AR	LHCB	Repl. by AAIJ 17G
$23\pm10\pm10$		[5] AALTONEN	12L	CDF	$p\overline{p}$ at 1.96 TeV
< 70	90	[6] AALTONEN	09C	CDF	Repl. by AALTONEN 12L
< 50	90	[3] AUBERT	07B	BABR	$e^+e^-\to\Upsilon(4S)$
< 41	90	[3] LIN	07	BELL	Repl. by DUH 13
< 180	90	[7] ABULENCIA,A	06D	CDF	Repl. by AALTONEN 09C
< 37	90	ABE	05G	BELL	Repl. by LIN 07
< 70	90	CHAO	04	BELL	$e^+e^-\to\Upsilon(4S)$
< 80	90	[3] BORNHEIM	03	CLE2	$e^+e^-\to\Upsilon(4S)$
< 60	90	[3] AUBERT	02Q	BABR	$e^+e^-\to\Upsilon(4S)$
< 90	90	[3] CASEY	02	BELL	$e^+e^-\to\Upsilon(4S)$
< 270	90	[3] ABE	01H	BELL	$e^+e^-\to\Upsilon(4S)$
< 250	90	[3] AUBERT	01E	BABR	$e^+e^-\to\Upsilon(4S)$
< 6600	90	[8] ABE	00C	SLD	$e^+e^-\to Z$
< 190	90	[3] CRONIN-HEN..	00	CLE2	$e^+e^-\to\Upsilon(4S)$
< 430	90	GODANG	98	CLE2	Repl. by CRONIN-HENNESSY 00
< 4600		[9] ADAM	96D	DLPH	$e^+e^-\to Z$
< 400	90	ASNER	96	CLE2	Repl. by GODANG 98
< 1800	90	[10] BUSKULIC	96V	ALEP	$e^+e^-\to Z$
<12000	90	[11] ABREU	95N	DLPH	Sup. by ADAM 96D
< 700	90	[3] BATTLE	93	CLE2	$e^+e^-\to\Upsilon(4S)$

[1] Supercedes results of AAIJ 12AR.
[2] DUH 13 reports also for the same data $B(B^0\to K^+K^-)<0.20\times10^{-6}$ at 90% CL.
[3] Assumes equal production of B^+ and B^0 at the $\Upsilon(4S)$.
[4] AAIJ 12AR reports $[\Gamma(B^0\to K^+K^-)/\Gamma_{total}]\ /\ [B(B_s^0\to K^+K^-)]\ /\ [\Gamma(\overline{b}\to B_s^0)/\Gamma(\overline{b}\to B^0)]=0.018^{+0.008}_{-0.007}\pm0.009$ which we multiply by our best values $B(B_s^0\to K^+K^-)=(2.66\pm0.22)\times10^{-5}$, $\Gamma(\overline{b}\to B_s^0)/\Gamma(\overline{b}\to B^0)=0.246\pm0.023$. Our first error is their experiment's error and our second error is the systematic error from using our best values.
[5] Reported a central value of $(0.23\pm0.10\pm0.10)\times10^{-6}$ using $B(B^0\to K^+\pi^-)=(19.4\pm0.6)\times10^{-6}$.
[6] Obtains this result from $B(K^+K^-)/B(K^+\pi^-)=0.020\pm0.008\pm0.006$, assuming $B(B^0\to K^+\pi^-)=(19.4\pm0.6)\times10^{-6}$.
[7] ABULENCIA,A 06D obtains this from $\Gamma(K^+K^-)/\Gamma(K^+\pi^-)<0.10$ at 90% CL, assuming $B(B^0\to K^+\pi^-)=(18.9\pm0.7)\times10^{-6}$.
[8] ABE 00C assumes $B(Z\to b\overline{b})=(21.7\pm0.1)\%$ and the B fractions $f_{B^0}=f_{B^+}=(39.7^{+1.8}_{-2.2})\%$ and $f_{B_s}=(10.5^{+1.8}_{-2.2})\%$.
[9] ADAM 96D assumes $f_{B^0}=f_{B^-}=0.39$ and $f_{B_s}=0.12$. Contributions from B^0 and B_s decays cannot be separated. Limits are given for the weighted average of the decay rates for the two neutral B mesons.
[10] BUSKULIC 96V assumes PDG 96 production fractions for B^0, B^+, B_s, b baryons.
[11] Assumes a B^0, B^- production fraction of 0.39 and a B_s production fraction of 0.12. Contributions from B^0 and B_s^0 decays cannot be separated. Limits are given for the weighted average of the decay rates for the two neutral B mesons.

$\Gamma(K^0\overline{K}^0)/\Gamma_{total}$ — Γ_{339}/Γ

VALUE (units 10^{-6})	CL%	DOCUMENT ID		TECN	COMMENT
1.21 ± 0.16 OUR AVERAGE					
$1.26\pm0.19\pm0.05$		[1] DUH	13	BELL	$e^+e^-\to\Upsilon(4S)$
$1.08\pm0.28\pm0.11$		[1] AUBERT,BE	06C	BABR	$e^+e^-\to\Upsilon(4S)$

Downloaded from https://academic.oup.com/ptep/article/2022/8/083C01/6651666 by KIT Library user on 27 September 2022

• • • We do not use the following data for averages, fits, limits, etc. • • •

$0.87^{+0.25}_{-0.20}\pm0.09$		[1] LIN	07	BELL	Repl. by DUH 13
$0.8\ \pm0.3\ \pm0.9$		[1] ABE	05G	BELL	Repl. by LIN 07
$1.19^{+0.40}_{-0.35}\pm0.13$		[1] AUBERT,BE	05E	BABR	Repl. by AUBERT,BE 06C
<1.8	90	[1] AUBERT	04M	BABR	$e^+e^-\to\Upsilon(4S)$
<1.5	90	[1] CHAO	04	BELL	Repl. by ABE 05G
<3.3	90	[1] BORNHEIM	03	CLE2	$e^+e^-\to\Upsilon(4S)$
<4.1	90	[1] CASEY	02	BELL	$e^+e^-\to\Upsilon(4S)$
<17	90	GODANG	98	CLE2	$e^+e^-\to\Upsilon(4S)$

[1] Assumes equal production of B^+ and B^0 at the $\Upsilon(4S)$.

$\Gamma(K^0\overline{K}^0)/\Gamma(K^0\phi)$ — $\Gamma_{339}/\Gamma_{348}$

VALUE	DOCUMENT ID		TECN	COMMENT
$0.17\pm0.08\pm0.02$	[1] AAIJ	20F	LHCB	pp at 7, 8, 13 TeV

[1] Observed signal with a significance of 3.5 σ.

$\Gamma(K^0K^-\pi^+)/\Gamma_{total}$ — Γ_{340}/Γ

VALUE (units 10^{-6})	CL%	DOCUMENT ID		TECN	COMMENT
6.7 ± 0.5 OUR FIT					
7.0 ± 0.6 OUR AVERAGE					
$7.2\pm0.7\pm0.3$		[1] LAI	19	BELL	$e^+e^-\to\Upsilon(4S)$
$6.4\pm1.0\pm0.6$		[1] DEL-AMO-SA..	10E	BABR	$e^+e^-\to\Upsilon(4S)$
• • • We do not use the following data for averages, fits, limits, etc. • • •					
<18	90	[1] GARMASH	04	BELL	$e^+e^-\to\Upsilon(4S)$
<21	90	[1] ECKHART	02	CLE2	$e^+e^-\to\Upsilon(4S)$

[1] Assumes equal production of B^+ and B^0 at the $\Upsilon(4S)$.

$\Gamma(K^*(892)^\pm K^\mp)/\Gamma_{total}$ — Γ_{341}/Γ

VALUE	CL%	DOCUMENT ID		TECN	COMMENT
$<0.4\times10^{-6}$	90	AAIJ	14BM	LHCB	pp at 7 TeV

$\Gamma(K^0K^-\pi^+)/\Gamma(K^0\pi^+\pi^-)$ — $\Gamma_{340}/\Gamma_{306}$

VALUE	DOCUMENT ID		TECN	COMMENT
0.134 ± 0.011 OUR FIT				
$0.123\pm0.009\pm0.015$	AAIJ	17BP	LHCB	pp at 7, 8 TeV
• • • We do not use the following data for averages, fits, limits, etc. • • •				
$0.128\pm0.017\pm0.009$	AAIJ	13BP	LHCB	Repl. by AAIJ 17BP

$[\Gamma(\overline{K}^{*0}K^0)+\Gamma(K^{*0}\overline{K}^0)]/\Gamma_{total}$ — Γ_{342}/Γ

VALUE (units 10^{-6})	CL%	DOCUMENT ID		TECN	COMMENT
<0.96	90	[1] AAIJ	16	LHCB	pp at 7 TeV
• • • We do not use the following data for averages, fits, limits, etc. • • •					
<1.9	90	[2] AUBERT,BE	06N	BABR	$e^+e^-\to\Upsilon(4S)$

[1] Assumes $B(B^0\to K^0\pi^+\pi^-)=(4.96\pm0.20)\times10^{-5}$.
[2] Assumes equal production of B^+ and B^0 at the $\Upsilon(4S)$.

$\Gamma(K^+K^-\pi^0)/\Gamma_{total}$ — Γ_{343}/Γ

VALUE (units 10^{-6})	CL%	DOCUMENT ID		TECN	COMMENT
$2.17\pm0.60\pm0.24$		[1] GAUR	13	BELL	$e^+e^-\to\Upsilon(4S)$
• • • We do not use the following data for averages, fits, limits, etc. • • •					
<19	90	[1] ECKHART	02	CLE2	$e^+e^-\to\Upsilon(4S)$

[1] Assumes equal production of B^+ and B^0 at the $\Upsilon(4S)$.

$\Gamma(K^0_SK^0_S\pi^0)/\Gamma_{total}$ — Γ_{344}/Γ

VALUE	CL%	DOCUMENT ID		TECN	COMMENT
$<0.9\times10^{-6}$	90	[1] AUBERT	09AD	BABR	$e^+e^-\to\Upsilon(4S)$

[1] Assumes equal production of B^+ and B^0 at the $\Upsilon(4S)$.

$\Gamma(K^0_SK^0_S\eta)/\Gamma_{total}$ — Γ_{345}/Γ

VALUE	CL%	DOCUMENT ID		TECN	COMMENT
$<1.0\times10^{-6}$	90	[1] AUBERT	09AD	BABR	$e^+e^-\to\Upsilon(4S)$

[1] Assumes equal production of B^+ and B^0 at the $\Upsilon(4S)$.

$\Gamma(K^0_SK^0_S\eta')/\Gamma_{total}$ — Γ_{346}/Γ

VALUE	CL%	DOCUMENT ID		TECN	COMMENT
$<2.0\times10^{-6}$	90	[1] AUBERT	09AD	BABR	$e^+e^-\to\Upsilon(4S)$

[1] Assumes equal production of B^+ and B^0 at the $\Upsilon(4S)$.

$\Gamma(K^0K^+K^-)/\Gamma_{total}$ — Γ_{347}/Γ

VALUE (units 10^{-6})	CL%	DOCUMENT ID		TECN	COMMENT
26.8 ± 1.1 OUR FIT					
26.6 ± 1.2 OUR AVERAGE					
$26.5\pm0.9\pm0.8$		[1,2] LEES	12O	BABR	$e^+e^-\to\Upsilon(4S)$
$28.3\pm3.3\pm4.0$		[1] GARMASH	04	BELL	$e^+e^-\to\Upsilon(4S)$
• • • We do not use the following data for averages, fits, limits, etc. • • •					
$23.8\pm2.0\pm1.6$		[1] AUBERT,B	04V	BABR	Repl. by LEES 12O
<1300	90	ALBRECHT	91E	ARG	$e^+e^-\to\Upsilon(4S)$

[1] Assumes equal production of B^+ and B^0 at the $\Upsilon(4S)$.
[2] All intermediate charmonium and charm resonances are removed, except of χ_{c0}.

$\Gamma(K^0K^+K^-)/\Gamma(K^0\pi^+\pi^-)$ — $\Gamma_{347}/\Gamma_{306}$

VALUE	DOCUMENT ID		TECN	COMMENT
0.539 ± 0.025 OUR FIT				
$0.549\pm0.018\pm0.033$	AAIJ	17BP	LHCB	pp at 7, 8 TeV
• • • We do not use the following data for averages, fits, limits, etc. • • •				
$0.385\pm0.031\pm0.023$	AAIJ	13BP	LHCB	Repl. by AAIJ 17BP

$\Gamma(K^0\phi)/\Gamma_{total}$ — Γ_{348}/Γ

VALUE (units 10^{-6})	CL%	DOCUMENT ID		TECN	COMMENT
7.3 ± 0.7 OUR AVERAGE					
$7.1\pm0.6^{+0.4}_{-0.3}$		[1] LEES	12O	BABR	$e^+e^-\to\Upsilon(4S)$
$9.0^{+2.2}_{-1.8}\pm0.7$		[1] CHEN	03B	BELL	$e^+e^-\to\Upsilon(4S)$
• • • We do not use the following data for averages, fits, limits, etc. • • •					
$8.4^{+1.5}_{-1.3}\pm0.5$		[1] AUBERT	04A	BABR	Repl. by LEES 12O
$8.1^{+3.1}_{-2.5}\pm0.8$		[1] AUBERT	01D	BABR	$e^+e^-\to\Upsilon(4S)$
<12.3	90	[1] BRIERE	01	CLE2	$e^+e^-\to\Upsilon(4S)$
<31	90	[1] BERGFELD	98	CLE2	
<88	90	ASNER	96	CLE2	$e^+e^-\to\Upsilon(4S)$
<720	90	ALBRECHT	91B	ARG	$e^+e^-\to\Upsilon(4S)$
<420	90	[2] AVERY	89B	CLEO	$e^+e^-\to\Upsilon(4S)$
<1000	90	[3] AVERY	87	CLEO	$e^+e^-\to\Upsilon(4S)$

[1] Assumes equal production of B^+ and B^0 at the $\Upsilon(4S)$.
[2] AVERY 89B reports $<4.9\times10^{-4}$ assuming the $\Upsilon(4S)$ decays 43% to $B^0\overline{B}^0$. We rescale to 50%.
[3] AVERY 87 reports $<1.3\times10^{-3}$ assuming the $\Upsilon(4S)$ decays 40% to $B^0\overline{B}^0$. We rescale to 50%.

$\Gamma(f_0(980)K^0,\ f_0\to K^+K^-)/\Gamma_{total}$ — Γ_{349}/Γ

VALUE (units 10^{-6})	DOCUMENT ID		TECN	COMMENT
$7.0^{+2.6}_{-1.8}\pm2.4$	[1] LEES	12O	BABR	$e^+e^-\to\Upsilon(4S)$

[1] Assumes equal production of B^+ and B^0 at the $\Upsilon(4S)$.

$\Gamma(f_0(1500)K^0)/\Gamma_{total}$ — Γ_{350}/Γ

VALUE (units 10^{-6})	DOCUMENT ID		TECN	COMMENT
$13.3^{+5.8}_{-4.4}\pm3.2$	[1] LEES	12O	BABR	$e^+e^-\to\Upsilon(4S)$

[1] Assumes equal production of B^+ and B^0 at the $\Upsilon(4S)$.

$\Gamma(f'_2(1525)^0K^0)/\Gamma_{total}$ — Γ_{351}/Γ

VALUE (units 10^{-6})	DOCUMENT ID		TECN	COMMENT
$0.29^{+0.27}_{-0.18}\pm0.36$	[1] LEES	12O	BABR	$e^+e^-\to\Upsilon(4S)$

[1] Assumes equal production of B^+ and B^0 at the $\Upsilon(4S)$.

$\Gamma(f_0(1710)K^0,\ f_0\to K^+K^-)/\Gamma_{total}$ — Γ_{352}/Γ

VALUE (units 10^{-6})	DOCUMENT ID		TECN	COMMENT
$4.4\pm0.7\pm0.5$	[1] LEES	12O	BABR	$e^+e^-\to\Upsilon(4S)$

[1] Assumes equal production of B^+ and B^0 at the $\Upsilon(4S)$.

$\Gamma(K^0K^+K^-\text{nonresonant})/\Gamma_{total}$ — Γ_{353}/Γ

VALUE (units 10^{-6})	DOCUMENT ID		TECN	COMMENT
$33\pm5\pm9$	[1] LEES	12O	BABR	$e^+e^-\to\Upsilon(4S)$

[1] Assumes equal production of B^+ and B^0 at the $\Upsilon(4S)$.

$\Gamma(K^0_SK^0_SK^0_S)/\Gamma_{total}$ — Γ_{354}/Γ

VALUE (units 10^{-6})	DOCUMENT ID		TECN	COMMENT
$6.0\ \pm0.5$ OUR AVERAGE Error includes scale factor of 1.1.				
$6.19\pm0.48\pm0.19$	[1] LEES	12I	BABR	$e^+e^-\to\Upsilon(4S)$
$4.2\ ^{+1.6}_{-1.3}\ \pm0.8$	[1] GARMASH	04	BELL	$e^+e^-\to\Upsilon(4S)$
• • • We do not use the following data for averages, fits, limits, etc. • • •				
$6.9\ ^{+0.9}_{-0.8}\ \pm0.6$	[1] AUBERT,B	05	BABR	Repl. by LEES 12I

[1] Assumes equal production of B^+ and B^0 at the $\Upsilon(4S)$.

$\Gamma(f_0(980)K^0,\ f_0\to K^0_SK^0_S)/\Gamma_{total}$ — Γ_{355}/Γ

VALUE (units 10^{-6})	DOCUMENT ID		TECN	COMMENT
$2.7^{+1.3}_{-1.2}\pm1.3$	[1,2] LEES	12I	BABR	$e^+e^-\to\Upsilon(4S)$

[1] Assumes equal production of B^+ and B^0 at the $\Upsilon(4S)$.
[2] Uses Dalitz plot analysis of the $B^0\to K^0_SK^0_SK^0_S$ decay.

$\Gamma(f_0(1710)K^0,\ f_0\to K^0_SK^0_S)/\Gamma_{total}$ — Γ_{356}/Γ

VALUE (units 10^{-6})	DOCUMENT ID		TECN	COMMENT
$0.50^{+0.46}_{-0.24}\pm0.11$	[1,2] LEES	12I	BABR	$e^+e^-\to\Upsilon(4S)$

[1] Assumes equal production of B^+ and B^0 at the $\Upsilon(4S)$.
[2] Uses Dalitz plot analysis of the $B^0\to K^0_SK^0_SK^0_S$ decay.

Downloaded from https://academic.oup.com/ptep/article/2022/8/083C01/6651666 by KIT Library user on 27 September 2022

$\Gamma(f_2(2010)K^0,\ f_2 \to K^0_S K^0_S)/\Gamma_{total}$ — Γ_{357}/Γ

VALUE (units 10^{-6})	DOCUMENT ID		TECN	COMMENT
$0.54^{+0.21}_{-0.20} \pm 0.52$	[1,2] LEES	12I	BABR	$e^+e^- \to \Upsilon(4S)$

[1] Assumes equal production of B^+ and B^0 at the $\Upsilon(4S)$.
[2] Uses Dalitz plot analysis of the $B^0 \to K^0_S K^0_S K^0_S$ decay.

$\Gamma(K^0_S K^0_S K^0_S \text{ nonresonant})/\Gamma_{total}$ — Γ_{358}/Γ

VALUE (units 10^{-6})	DOCUMENT ID		TECN	COMMENT
$13.3^{+2.2}_{-2.3} \pm 2.2$	[1,2] LEES	12I	BABR	$e^+e^- \to \Upsilon(4S)$

[1] Assumes equal production of B^+ and B^0 at the $\Upsilon(4S)$.
[2] Uses Dalitz plot analysis of the $B^0 \to K^0_S K^0_S K^0_S$ decay.

$\Gamma(K^0_S K^0_S K^0_L)/\Gamma_{total}$ — Γ_{359}/Γ

VALUE (units 10^{-6})	CL%	DOCUMENT ID		TECN	COMMENT
<16	90	[1] AUBERT,B	06R	BABR	$e^+e^- \to \Upsilon(4S)$

[1] Assumes equal production of B^+ and B^0 at the $\Upsilon(4S)$.

$\Gamma(K^*(892)^0 K^+ K^-)/\Gamma_{total}$ — Γ_{360}/Γ

VALUE (units 10^{-6})	CL%	DOCUMENT ID		TECN	COMMENT
27.5±1.3±2.2		[1] AUBERT	07AS	BABR	$e^+e^- \to \Upsilon(4S)$
• • • We do not use the following data for averages, fits, limits, etc. • • •					
<610	90	ALBRECHT	91E	ARG	$e^+e^- \to \Upsilon(4S)$

[1] Assumes equal production of B^+ and B^0 at the $\Upsilon(4S)$.

$\Gamma(K^*(892)^0 \phi)/\Gamma_{total}$ — Γ_{361}/Γ

VALUE (units 10^{-6})	CL%	DOCUMENT ID		TECN	COMMENT
10.0±0.5 OUR FIT					
10.0±0.5 OUR AVERAGE					
10.4±0.5±0.6		[1] PRIM	13	BELL	$e^+e^- \to \Upsilon(4S)$
9.7±0.5±0.5		[1] AUBERT	08BG	BABR	$e^+e^- \to \Upsilon(4S)$
$11.5^{+4.5}_{-3.7}{}^{+1.8}_{-1.7}$		[1] BRIERE	01	CLE2	$e^+e^- \to \Upsilon(4S)$
• • • We do not use the following data for averages, fits, limits, etc. • • •					
9.2±0.7±0.6		[1] AUBERT	07D	BABR	Repl. by AUBERT 08BG
9.2±0.9±0.5		[1] AUBERT,B	04W	BABR	Repl. by AUBERT 07D
11.2±1.3±0.8		[1] AUBERT	03V	BABR	Repl. by AUBERT,B 04W
$10.0^{+1.6}_{-1.5}{}^{+0.7}_{-0.8}$		[1] CHEN	03B	BELL	Repl. by PRIM 13
$8.7^{+2.5}_{-2.1} \pm 1.1$		[1] AUBERT	01D	BABR	Repl. by AUBERT 03V
<384	90	[2] ABE	00C	SLD	$e^+e^- \to Z$
< 21	90	[1] BERGFELD	98	CLE2	
< 43	90	ASNER	96	CLE2	$e^+e^- \to \Upsilon(4S)$
<320	90	ALBRECHT	91B	ARG	$e^+e^- \to \Upsilon(4S)$
<380	90	[3] AVERY	89B	CLEO	$e^+e^- \to \Upsilon(4S)$
<380	90	[4] AVERY	87	CLEO	$e^+e^- \to \Upsilon(4S)$

[1] Assumes equal production of B^+ and B^0 at the $\Upsilon(4S)$.
[2] ABE 00C assumes $B(Z \to b\overline{b})=(21.7 \pm 0.1)\%$ and the B fractions $f_{B^0}=f_{B^+}=(39.7^{+1.8}_{-2.2})\%$ and $f_{B_s}=(10.5^{+1.8}_{-2.2})\%$.
[3] AVERY 89B reports $< 4.4 \times 10^{-4}$ assuming the $\Upsilon(4S)$ decays 43% to $B^0\overline{B}^0$. We rescale to 50%.
[4] AVERY 87 reports $< 4.7 \times 10^{-4}$ assuming the $\Upsilon(4S)$ decays 40% to $B^0\overline{B}^0$. We rescale to 50%.

$\Gamma(K^+ K^- \pi^+ \pi^- \text{ nonresonant})/\Gamma_{total}$ — Γ_{362}/Γ

VALUE (units 10^{-6})	CL%	DOCUMENT ID		TECN	COMMENT
<71.7	90	[1,2] CHIANG	10	BELL	$e^+e^- \to \Upsilon(4S)$

[1] Measured in the range $0.7 < m_{K\pi} < 1.7$ and corrected using PS assumption for the full $K\pi$ mass range.
[2] Assumes equal production of B^+ and B^0 at the $\Upsilon(4S)$.

$\Gamma(K^*(892)^0 K^- \pi^+)/\Gamma_{total}$ — Γ_{363}/Γ

VALUE (units 10^{-6})	DOCUMENT ID		TECN	COMMENT
4.5 ±1.3 OUR AVERAGE				
$2.11^{+5.63}_{-5.26}{}^{+4.85}_{-4.75}$	[1,2] CHIANG	10	BELL	$e^+e^- \to \Upsilon(4S)$
4.6 ±1.1 ±0.8	[2] AUBERT	07AS	BABR	$e^+e^- \to \Upsilon(4S)$

[1] Measured in the range $0.7 < m_{K\pi} < 1.7$ and corrected using PS assumption for the full $K\pi$ mass range. The quoted result is equivalent to the upper limit of $< 13.9 \times 10^{-6}$ at 90% CL.
[2] Assumes equal production of B^+ and B^0 at the $\Upsilon(4S)$.

$\Gamma(K^*(892)^0 \overline{K}^*(892)^0)/\Gamma_{total}$ — Γ_{364}/Γ

VALUE (units 10^{-6})	CL%	DOCUMENT ID		TECN	COMMENT
0.83±0.24 OUR AVERAGE Error includes scale factor of 1.5. See the ideogram below.					
0.85±0.07±0.20		[1] AAIJ	19L	LHCB	pp at 7 and 8 TeV
$0.26^{+0.33}_{-0.29}{}^{+0.10}_{-0.08}$		[2,3] CHIANG	10	BELL	$e^+e^- \to \Upsilon(4S)$
$1.28^{+0.35}_{-0.30} \pm 0.11$		[3] AUBERT	08I	BABR	$e^+e^- \to \Upsilon(4S)$
• • • We do not use the following data for averages, fits, limits, etc. • • •					
< 22	90	[4] GODANG	02	CLE2	$e^+e^- \to \Upsilon(4S)$
<469	90	[5] ABE	00C	SLD	$e^+e^- \to Z$

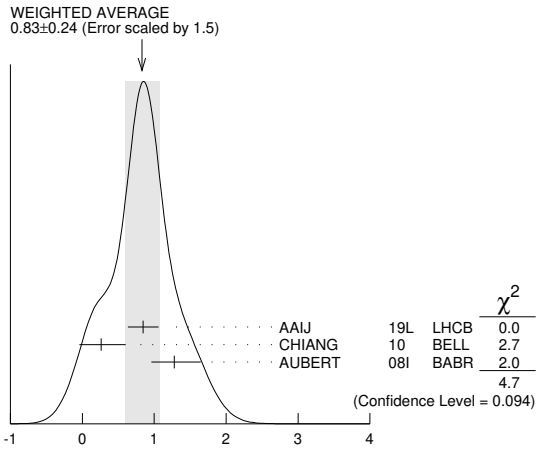

[1] AAIJ 19L reports $[\Gamma(B^0 \to K^*(892)^0\overline{K}^*(892)^0)/\Gamma_{total}] / [B(B^0_s \to \overline{K}^*(892)^0 K^*(892)^0)] = 0.0758 \pm 0.0057 \pm 0.0030$ which we multiply by our best value $B(B^0_s \to \overline{K}^*(892)^0 K^*(892)^0) = (1.11 \pm 0.27) \times 10^{-5}$. Our first error is their experiment's error and our second error is the systematic error from using our best value.
[2] Measured in the range $0.7 < m_{K\pi} < 1.7$ and corrected using PS assumption for the full $K\pi$ mass range. The quoted result is equivalent to the upper limit of $< 0.8 \times 10^{-6}$ at 90% CL.
[3] Assumes equal production of B^+ and B^0 at the $\Upsilon(4S)$.
[4] Assumes a helicity 00 configuration. For a helicity 11 configuration, the limit decreases to 1.9×10^{-5}.
[5] ABE 00C assumes $B(Z \to b\overline{b})=(21.7 \pm 0.1)\%$ and the B fractions $f_{B^0}=f_{B^+}=(39.7^{+1.8}_{-2.2})\%$ and $f_{B_s}=(10.5^{+1.8}_{-2.2})\%$.

$\Gamma(K^+ K^+ \pi^- \pi^- \text{ nonresonant})/\Gamma_{total}$ — Γ_{365}/Γ

VALUE (units 10^{-6})	CL%	DOCUMENT ID		TECN	COMMENT
<6.0	90	[1] CHIANG	10	BELL	$e^+e^- \to \Upsilon(4S)$

[1] Assumes equal production of B^+ and B^0 at the $\Upsilon(4S)$.

$\Gamma(K^*(892)^0 K^+ \pi^-)/\Gamma_{total}$ — Γ_{366}/Γ

VALUE (units 10^{-6})	CL%	DOCUMENT ID		TECN	COMMENT
<2.2	90	[1] AUBERT	07AS	BABR	$e^+e^- \to \Upsilon(4S)$
• • • We do not use the following data for averages, fits, limits, etc. • • •					
<7.6	90	[1] CHIANG	10	BELL	$e^+e^- \to \Upsilon(4S)$

[1] Assumes equal production of B^+ and B^0 at the $\Upsilon(4S)$.

$\Gamma(K^*(892)^0 K^*(892)^0)/\Gamma_{total}$ — Γ_{367}/Γ

VALUE (units 10^{-6})	CL%	DOCUMENT ID		TECN	COMMENT
< 0.2	90	[1] CHIANG	10	BELL	$e^+e^- \to \Upsilon(4S)$
• • • We do not use the following data for averages, fits, limits, etc. • • •					
< 0.41	90	[1] AUBERT	08I	BABR	$e^+e^- \to \Upsilon(4S)$
<37	90	[2] GODANG	02	CLE2	$e^+e^- \to \Upsilon(4S)$

[1] Assumes equal production of B^+ and B^0 at the $\Upsilon(4S)$.
[2] Assumes a helicity 00 configuration. For a helicity 11 configuration, the limit decreases to 2.9×10^{-5}.

$\Gamma(K^*(892)^+ K^*(892)^-)/\Gamma_{total}$ — Γ_{368}/Γ

VALUE (units 10^{-6})	CL%	DOCUMENT ID		TECN	COMMENT
< 2.0	90	[1] AUBERT	08AP	BABR	$e^+e^- \to \Upsilon(4S)$
• • • We do not use the following data for averages, fits, limits, etc. • • •					
<141	90	[2] GODANG	02	CLE2	$e^+e^- \to \Upsilon(4S)$

[1] Assumes equal production of B^+ and B^0 at the $\Upsilon(4S)$.
[2] Assumes a helicity 00 configuration. For a helicity 11 configuration, the limit decreases to 8.9×10^{-5}.

$\Gamma(K_1(1400)^0 \phi)/\Gamma_{total}$ — Γ_{369}/Γ

VALUE	CL%	DOCUMENT ID		TECN	COMMENT
$<5.0 \times 10^{-3}$	90	ALBRECHT	91B	ARG	$e^+e^- \to \Upsilon(4S)$

$\Gamma(\phi(K\pi)^*_0{}^0)/\Gamma_{total}$ — Γ_{370}/Γ

This decay refers to the coherent sum of resonant and nonresonant $J^P = 0^+$ $K\pi$ components with $1.13 < m_{K\pi} < 1.53$ GeV/c^2.

VALUE (units 10^{-6})	DOCUMENT ID		TECN	COMMENT
4.3±0.4 OUR AVERAGE				
4.3±0.4±0.4	[1] PRIM	13	BELL	$e^+e^- \to \Upsilon(4S)$
4.3±0.6±0.4	[1] AUBERT	08BG	BABR	$e^+e^- \to \Upsilon(4S)$

Downloaded from https://academic.oup.com/ptep/article/2022/8/083C01/6651666 by KIT Library user on 27 September 2022

• • • We do not use the following data for averages, fits, limits, etc. • • •

$5.0 \pm 0.8 \pm 0.3$	[1] AUBERT	07D	BABR	Repl. by AUBERT 08BG

[1] Assumes equal production of B^+ and B^0 at the $\Upsilon(4S)$.

$\Gamma(\phi(K\pi)_0^{*0}\ (1.60<m_{K\pi}<2.15))/\Gamma_{total}$ — Γ_{371}/Γ

This decay refers to the coherent sum of resonant and nonresonant $J^P = 0^+$ $K\pi$ components with $1.60 < m_{K\pi} < 2.15$ GeV/c^2.

VALUE (units 10^{-6})	CL%	DOCUMENT ID		TECN	COMMENT
<1.7	90	[1] AUBERT	07AO	BABR	$e^+e^- \to \Upsilon(4S)$

[1] Assumes equal production of B^+ and B^0 at the $\Upsilon(4S)$.

$\Gamma(K_0^*(1430)^0 K^-\pi^+)/\Gamma_{total}$ — Γ_{372}/Γ

VALUE (units 10^{-6})	CL%	DOCUMENT ID		TECN	COMMENT
<31.8	90	[1,2] CHIANG	10	BELL	$e^+e^- \to \Upsilon(4S)$

[1] Measured in the range $0.7 < m_{K\pi} < 1.7$ and corrected using PS assumption for the full $K\pi$ mass range.
[2] Assumes equal production of B^+ and B^0 at the $\Upsilon(4S)$.

$\Gamma(K_0^*(1430)^0 \overline{K}^*(892)^0)/\Gamma_{total}$ — Γ_{373}/Γ

VALUE (units 10^{-6})	CL%	DOCUMENT ID		TECN	COMMENT
<3.3	90	[1,2] CHIANG	10	BELL	$e^+e^- \to \Upsilon(4S)$

[1] Measured in the range $0.7 < m_{K\pi} < 1.7$ and corrected using PS assumption for the full $K\pi$ mass range.
[2] Assumes equal production of B^+ and B^0 at the $\Upsilon(4S)$.

$\Gamma(K_0^*(1430)^0 \overline{K}_0^*(1430)^0)/\Gamma_{total}$ — Γ_{374}/Γ

VALUE (units 10^{-6})	CL%	DOCUMENT ID		TECN	COMMENT
<8.4	90	[1,2] CHIANG	10	BELL	$e^+e^- \to \Upsilon(4S)$

[1] Measured in the range $0.7 < m_{K\pi} < 1.7$ and corrected using PS assumption for the full $K\pi$ mass range.
[2] Assumes equal production of B^+ and B^0 at the $\Upsilon(4S)$.

$\Gamma(K_0^*(1430)^0 \phi)/\Gamma_{total}$ — Γ_{375}/Γ

VALUE (units 10^{-6})	DOCUMENT ID		TECN	COMMENT
3.9±0.5±0.6	[1] AUBERT	08BG	BABR	$e^+e^- \to \Upsilon(4S)$

• • • We do not use the following data for averages, fits, limits, etc. • • •

$4.6 \pm 0.7 \pm 0.6$	[1] AUBERT	07D	BABR	Repl. by AUBERT 08BG
seen	[2] AUBERT,B	04W	BABR	Repl. by AUBERT 07D

[1] Assumes equal production of B^+ and B^0 at the $\Upsilon(4S)$.
[2] Observed 181 ± 17 events with statistical significance greater than 10 σ.

$\Gamma(K_0^*(1430)^0 K^*(892)^0)/\Gamma_{total}$ — Γ_{376}/Γ

VALUE (units 10^{-6})	CL%	DOCUMENT ID		TECN	COMMENT
<1.7	90	[1] CHIANG	10	BELL	$e^+e^- \to \Upsilon(4S)$

[1] Assumes equal production of B^+ and B^0 at the $\Upsilon(4S)$.

$\Gamma(K_0^*(1430)^0 K_0^*(1430)^0)/\Gamma_{total}$ — Γ_{377}/Γ

VALUE (units 10^{-6})	CL%	DOCUMENT ID		TECN	COMMENT
<4.7	90	[1] CHIANG	10	BELL	$e^+e^- \to \Upsilon(4S)$

[1] Assumes equal production of B^+ and B^0 at the $\Upsilon(4S)$.

$\Gamma(K^*(1680)^0 \phi)/\Gamma_{total}$ — Γ_{378}/Γ

VALUE (units 10^{-6})	CL%	DOCUMENT ID		TECN	COMMENT
<3.5	90	[1] AUBERT	07AO	BABR	$e^+e^- \to \Upsilon(4S)$

[1] Assumes equal production of B^+ and B^0 at the $\Upsilon(4S)$.

$\Gamma(K^*(1780)^0 \phi)/\Gamma_{total}$ — Γ_{379}/Γ

VALUE (units 10^{-6})	CL%	DOCUMENT ID		TECN	COMMENT
<2.7	90	[1] AUBERT	07AO	BABR	$e^+e^- \to \Upsilon(4S)$

[1] Assumes equal production of B^+ and B^0 at the $\Upsilon(4S)$.

$\Gamma(K^*(2045)^0 \phi)/\Gamma_{total}$ — Γ_{380}/Γ

VALUE (units 10^{-6})	CL%	DOCUMENT ID		TECN	COMMENT
<15.3	90	[1] AUBERT	07AO	BABR	$e^+e^- \to \Upsilon(4S)$

[1] Assumes equal production of B^+ and B^0 at the $\Upsilon(4S)$.

$\Gamma(K_2^*(1430)^0 \rho^0)/\Gamma_{total}$ — Γ_{381}/Γ

VALUE (units 10^{-6})	CL%	DOCUMENT ID		TECN	COMMENT
<1.1 × 10^3	90	ALBRECHT	91B	ARG	$e^+e^- \to \Upsilon(4S)$

$\Gamma(K_2^*(1430)^0 \phi)/\Gamma_{total}$ — Γ_{382}/Γ

VALUE (units 10^{-6})	CL%	DOCUMENT ID		TECN	COMMENT
6.8±0.9 OUR AVERAGE		Error includes scale factor of 1.2.			
$5.5^{+0.9}_{-0.7} \pm 1.0$		[1] PRIM	13	BELL	$e^+e^- \to \Upsilon(4S)$
$7.5 \pm 0.9 \pm 0.5$		[1] AUBERT	08BG	BABR	$e^+e^- \to \Upsilon(4S)$

• • • We do not use the following data for averages, fits, limits, etc. • • •

$7.8 \pm 1.1 \pm 0.6$		[1] AUBERT	07D	BABR	Repl. by AUBERT 08BG
seen		[2] AUBERT,B	04W	BABR	Repl. by AUBERT 07D
<1400	90	ALBRECHT	91B	ARG	$e^+e^- \to \Upsilon(4S)$

[1] Assumes equal production of B^+ and B^0 at the $\Upsilon(4S)$.
[2] The angular distribution of $B \to \phi K^*(1430)$ provides evidence with statistical significance of 3.2 σ.

$\Gamma(K^0\phi\phi)/\Gamma_{total}$ — Γ_{383}/Γ

VALUE (units 10^{-6})	DOCUMENT ID		TECN	COMMENT
3.7 ±0.7 OUR AVERAGE	Error includes scale factor of 1.3.			
$3.02^{+0.75}_{-0.66} \pm 0.20$	[1] MOHANTY	21	BELL	$e^+e^- \to \Upsilon(4S)$
$4.5 \pm 0.8 \pm 0.3$	[1] LEES	11A	BABR	$e^+e^- \to \Upsilon(4S)$

• • • We do not use the following data for averages, fits, limits, etc. • • •

$4.1\ ^{+1.7}_{-1.4} \pm 0.4$	[1] AUBERT,BE	06H	BABR	Repl. by LEES 11A

[1] Assumes equal production of B^0 and B^+ at the $\Upsilon(4S)$ and the $\phi\phi$ invariant mass below 2.85 GeV/c^2.

$\Gamma(\eta'\eta' K^0)/\Gamma_{total}$ — Γ_{384}/Γ

VALUE (units 10^{-6})	CL%	DOCUMENT ID		TECN	COMMENT
<31	90	[1] AUBERT,B	06P	BABR	$e^+e^- \to \Upsilon(4S)$

[1] Assumes equal production of B^+ and B^0 at the $\Upsilon(4S)$.

$\Gamma(\eta K^0\gamma)/\Gamma_{total}$ — Γ_{385}/Γ

VALUE (units 10^{-6})	DOCUMENT ID		TECN	COMMENT
7.6±1.8 OUR AVERAGE				
$7.1^{+2.1}_{-2.0} \pm 0.4$	[1,2] AUBERT	09	BABR	$e^+e^- \to \Upsilon(4S)$
$8.7^{+3.1}_{-2.7}{}^{+1.9}_{-1.6}$	[2,3] NISHIDA	05	BELL	$e^+e^- \to \Upsilon(4S)$

• • • We do not use the following data for averages, fits, limits, etc. • • •

$11.3^{+2.8}_{-1.6} \pm 0.6$	[1,2] AUBERT,B	06M	BABR	Repl. by AUBERT 09

[1] $m_{\eta K} < 3.25$ GeV/c^2.
[2] Assumes equal production of B^+ and B^0 at the $\Upsilon(4S)$.
[3] $m_{\eta K} < 2.4$ GeV/c^2

$\Gamma(\eta' K^0\gamma)/\Gamma_{total}$ — Γ_{386}/Γ

VALUE (units 10^{-6})	CL%	DOCUMENT ID		TECN	COMMENT
<6.4	90	[1,2] WEDD	10	BELL	$e^+e^- \to \Upsilon(4S)$

• • • We do not use the following data for averages, fits, limits, etc. • • •

<6.6	90	[1,3] AUBERT,B	06M	BABR	$e^+e^- \to \Upsilon(4S)$

[1] Assumes equal production of B^+ and B^0 at the $\Upsilon(4S)$.
[2] $m_{\eta' K} < 3.4$ GeV/c^2.
[3] $m_{\eta' K} < 3.25$ GeV/c^2.

$\Gamma(K^0\phi\gamma)/\Gamma_{total}$ — Γ_{387}/Γ

VALUE (units 10^{-6})	CL%	DOCUMENT ID		TECN	COMMENT
2.74±0.60±0.32		[1] SAHOO	11A	BELL	$e^+e^- \to \Upsilon(4S)$

• • • We do not use the following data for averages, fits, limits, etc. • • •

<2.7	90	[1] AUBERT	07Q	BABR	$e^+e^- \to \Upsilon(4S)$
<8.3	90	[1] DRUTSKOY	04	BELL	$e^+e^- \to \Upsilon(4S)$

[1] Assumes equal production of B^+ and B^0 at $\Upsilon(4S)$.

$\Gamma(K^+\pi^-\gamma)/\Gamma_{total}$ — Γ_{388}/Γ

VALUE	DOCUMENT ID		TECN	COMMENT
$(4.6^{+1.3}_{-1.2}{}^{+0.5}_{-0.7}) \times 10^{-6}$	[1,2] NISHIDA	02	BELL	$e^+e^- \to \Upsilon(4S)$

[1] Assumes equal production of B^+ and B^0 at the $\Upsilon(4S)$.
[2] 1.25 GeV/c^2 $< M_{K\pi} <$ 1.6 GeV/c^2

$\Gamma(K^*(892)^0\gamma)/\Gamma_{total}$ — Γ_{389}/Γ

VALUE (units 10^{-6})	CL%	DOCUMENT ID		TECN	COMMENT
41.8± 2.5 OUR AVERAGE		Error includes scale factor of 2.1.			
$39.6 \pm 0.7 \pm 1.4$		[1] HORIGUCHI	17	BELL	$e^+e^- \to \Upsilon(4S)$
$44.7 \pm 1.0 \pm 1.6$		[2] AUBERT	09AO	BABR	$e^+e^- \to \Upsilon(4S)$
$45.5^{+7.2}_{-6.8} \pm 3.4$		[3] COAN	00	CLE2	$e^+e^- \to \Upsilon(4S)$

• • • We do not use the following data for averages, fits, limits, etc. • • •

$39.2 \pm 2.0 \pm 2.4$		[4] AUBERT,BE	04A	BABR	Repl. by AUBERT 09AO
$40.1 \pm 2.1 \pm 1.7$		[5] NAKAO	04	BELL	Repl. by HORIGUCHI 17
< 110	90	ACOSTA	02G	CDF	$p\overline{p}$ at 1.8 TeV
$42.3 \pm 4.0 \pm 2.2$		[5] AUBERT	02C	BABR	Repl. by AUBERT,BE 04A
< 210	90	[6] ADAM	96D	DLPH	$e^+e^- \to Z$
$40 \pm 17 \pm 8$		[7] AMMAR	93	CLE2	Repl. by COAN 00
< 420	90	ALBRECHT	89G	ARG	$e^+e^- \to \Upsilon(4S)$
< 240	90	[8] AVERY	89B	CLEO	$e^+e^- \to \Upsilon(4S)$
<2100	90	AVERY	87	CLEO	$e^+e^- \to \Upsilon(4S)$

[1] Uses B($\Upsilon(4S) \to B^+B^-$) = (51.4 ± 0.6)% and B($\Upsilon(4S) \to B^0\overline{B}^0$) = (48.6 ± 0.6)%.
[2] Uses B($\Upsilon(4S) \to B^+B^-$) = (51.6 ± 0.6)% and B($\Upsilon(4S) \to B^0\overline{B}^0$) = (48.4 ± 0.6)%.
[3] Assumes equal production of B^+ and B^0 at the $\Upsilon(4S)$. No evidence for a nonresonant $K\pi\gamma$ contamination was seen; the central value assumes no contamination.
[4] Uses the production ratio of charged and neutral B from $\Upsilon(4S)$ decays $R^{+/0} = 1.006 \pm 0.048$.
[5] Assumes equal production of B^+ and B^0 at the $\Upsilon(4S)$.
[6] ADAM 96D assumes $f_{B^0} = f_{B^-} = 0.39$ and $f_{B_s} = 0.12$.
[7] AMMAR 93 observed 6.6 ± 2.8 events above background.
[8] AVERY 89B reports $< 2.8 \times 10^{-4}$ assuming the $\Upsilon(4S)$ decays 43% to $B^0\overline{B}^0$. We rescale to 50%.

Downloaded from https://academic.oup.com/ptep/article/2022/8/083C01/6651666 by KIT Library user on 27 September 2022

$\Gamma(K^*(1410)\gamma)/\Gamma_{total}$ — Γ_{390}/Γ

VALUE	CL%	DOCUMENT ID		TECN	COMMENT
$<1.3\times10^{-4}$	90	[1] NISHIDA	02	BELL	$e^+e^-\to\Upsilon(4S)$

[1] Assumes equal production of B^+ and B^0 at the $\Upsilon(4S)$.

$\Gamma(K^+\pi^-\gamma$ nonresonant$)/\Gamma_{total}$ — Γ_{391}/Γ

VALUE	CL%	DOCUMENT ID		TECN	COMMENT
$<2.6\times10^{-6}$	90	[1,2] NISHIDA	02	BELL	$e^+e^-\to\Upsilon(4S)$

[1] Assumes equal production of B^+ and B^0 at the $\Upsilon(4S)$.
[2] 1.25 GeV/c^2 $<M_{K\pi}<$ 1.6 GeV/c^2

$\Gamma(K^*(892)^0X(214),\ X\to\mu^+\mu^-)/\Gamma_{total}$ — Γ_{392}/Γ

$X(214)$ is a hypothetical particle of mass 214 MeV/c^2 reported by the HyperCP experiment (PARK 05)

VALUE (units 10^{-8})	CL%	DOCUMENT ID		TECN	COMMENT
<2.26	90	[1,2] HYUN	10	BELL	$e^+e^-\to\Upsilon(4S)$

[1] Assumes equal production of B^+ and B^0 at the $\Upsilon(4S)$.
[2] Based on scalar nature of X particle. With a vector X assumption, the upper limit is 2.27×10^{-8}.

$\Gamma(K^0\pi^+\pi^-)/\Gamma_{total}$ — Γ_{393}/Γ

VALUE (units 10^{-5})	DOCUMENT ID		TECN	COMMENT
1.99±0.18 OUR AVERAGE				
$2.05\pm0.20^{+0.26}_{-0.22}$	[1,2] DEL-AMO-SA...16		BABR	$e^+e^-\to\Upsilon(4S)$
$1.85\pm0.21\pm0.12$	[1,3] AUBERT	07R	BABR	$e^+e^-\to\Upsilon(4S)$
$2.40\pm0.4\ \pm0.3$	[3,4] YANG	05	BELL	$e^+e^-\to\Upsilon(4S)$

[1] $M_{K\pi\pi}<$ 1.8 GeV/c^2.
[2] Uses B($\Upsilon(4S)\to B^+B^-$) = 0.513 ± 0.006.
[3] Assumes equal production of B^+ and B^0 at the $\Upsilon(4S)$.
[4] $M_{K\pi\pi}<$ 2.0 GeV/c^2.

$\Gamma(K^+\pi^-\pi^0\gamma)/\Gamma_{total}$ — Γ_{394}/Γ

VALUE (units 10^{-5})	DOCUMENT ID		TECN	COMMENT
4.07±0.22±0.31	[1,2] AUBERT	07R	BABR	$e^+e^-\to\Upsilon(4S)$

[1] $M_{K\pi\pi}<$ 1.8 GeV/c^2.
[2] Assumes equal production of B^+ and B^0 at the $\Upsilon(4S)$.

$\Gamma(K_1(1270)^0\gamma)/\Gamma_{total}$ — Γ_{395}/Γ

VALUE (units 10^{-5})	CL%	DOCUMENT ID		TECN	COMMENT
< 5.8	90	[1] YANG	05	BELL	$e^+e^-\to\Upsilon(4S)$
• • • We do not use the following data for averages, fits, limits, etc. • • •					
<700	90	[2] ALBRECHT	89G	ARG	$e^+e^-\to\Upsilon(4S)$

[1] Assumes equal production of B^+ and B^0 at the $\Upsilon(4S)$.
[2] ALBRECHT 89G reports $<$ 0.0078 assuming the $\Upsilon(4S)$ decays 45% to $B^0\overline{B}^0$. We rescale to 50%.

$\Gamma(K_1(1400)^0\gamma)/\Gamma_{total}$ — Γ_{396}/Γ

VALUE (units 10^{-5})	CL%	DOCUMENT ID		TECN	COMMENT
< 1.2	90	[1] YANG	05	BELL	$e^+e^-\to\Upsilon(4S)$
• • • We do not use the following data for averages, fits, limits, etc. • • •					
<430	90	[2] ALBRECHT	89G	ARG	$e^+e^-\to\Upsilon(4S)$

[1] Assumes equal production of B^+ and B^0 at the $\Upsilon(4S)$.
[2] ALBRECHT 89G reports $<$ 0.0048 assuming the $\Upsilon(4S)$ decays 45% to $B^0\overline{B}^0$. We rescale to 50%.

$\Gamma(K_2^*(1430)^0\gamma)/\Gamma_{total}$ — Γ_{397}/Γ

VALUE (units 10^{-5})	CL%	DOCUMENT ID		TECN	COMMENT
1.24±0.24 OUR AVERAGE					
$1.22\pm0.25\pm0.10$		[1] AUBERT,B	04U	BABR	$e^+e^-\to\Upsilon(4S)$
$1.3\ \pm0.5\ \pm0.1$		[1] NISHIDA	02	BELL	$e^+e^-\to\Upsilon(4S)$
• • • We do not use the following data for averages, fits, limits, etc. • • •					
<40	90	[2] ALBRECHT	89G	ARG	$e^+e^-\to\Upsilon(4S)$

[1] Assumes equal production of B^+ and B^0 at the $\Upsilon(4S)$.
[2] ALBRECHT 89G reports $<4.4\times10^{-4}$ assuming the $\Upsilon(4S)$ decays 45% to $B^0\overline{B}^0$. We rescale to 50%.

$\Gamma(K^*(1680)^0\gamma)/\Gamma_{total}$ — Γ_{398}/Γ

VALUE	CL%	DOCUMENT ID		TECN	COMMENT
<0.0020	90	[1] ALBRECHT	89G	ARG	$e^+e^-\to\Upsilon(4S)$

[1] ALBRECHT 89G reports $<$ 0.0022 assuming the $\Upsilon(4S)$ decays 45% to $B^0\overline{B}^0$. We rescale to 50%.

$\Gamma(K_3^*(1780)^0\gamma)/\Gamma_{total}$ — Γ_{399}/Γ

VALUE (units 10^{-6})	CL%	DOCUMENT ID		TECN	COMMENT
< 83	90	[1,2] NISHIDA	05	BELL	$e^+e^-\to\Upsilon(4S)$
• • • We do not use the following data for averages, fits, limits, etc. • • •					
<10000	90	[3] ALBRECHT	89G	ARG	$e^+e^-\to\Upsilon(4S)$

[1] Assumes equal production of B^+ and B^0 at the $\Upsilon(4S)$.
[2] Uses B($K_3^*(1780)\to\eta K$) = $0.11^{+0.05}_{-0.04}$.
[3] ALBRECHT 89G reports $<$ 0.011 assuming the $\Upsilon(4S)$ decays 45% to $B^0\overline{B}^0$. We rescale to 50%.

$\Gamma(K_4^*(2045)^0\gamma)/\Gamma_{total}$ — Γ_{400}/Γ

VALUE	CL%	DOCUMENT ID		TECN	COMMENT
<0.0043	90	[1] ALBRECHT	89G	ARG	$e^+e^-\to\Upsilon(4S)$

[1] ALBRECHT 89G reports $<$ 0.0048 assuming the $\Upsilon(4S)$ decays 45% to $B^0\overline{B}^0$. We rescale to 50%.

$\Gamma(\rho^0\gamma)/\Gamma_{total}$ — Γ_{401}/Γ

VALUE (units 10^{-6})	CL%	DOCUMENT ID		TECN	COMMENT
0.86±0.15 OUR AVERAGE					
$0.97^{+0.24}_{-0.22}\pm0.06$		[1] AUBERT	08BH	BABR	$e^+e^-\to\Upsilon(4S)$
$0.78^{+0.17+0.09}_{-0.16-0.10}$		[1] TANIGUCHI	08	BELL	$e^+e^-\to\Upsilon(4S)$
• • • We do not use the following data for averages, fits, limits, etc. • • •					
$0.79^{+0.22}_{-0.20}\pm0.06$		[1] AUBERT	07L	BABR	Repl. by AUBERT 08BH
$1.25^{+0.37+0.07}_{-0.33-0.06}$		[1] MOHAPATRA	06	BELL	Repl. by TANIGUCHI 08
$0.0\ \pm0.2\ \pm0.1$	90	[1] AUBERT	05	BABR	Repl. by AUBERT 07L
< 0.8	90	[1] MOHAPATRA	05	BELL	$e^+e^-\to\Upsilon(4S)$
< 1.2	90	[1] AUBERT	04C	BABR	$e^+e^-\to\Upsilon(4S)$
<17	90	[1] COAN	00	CLE2	$e^+e^-\to\Upsilon(4S)$

[1] Assumes equal production of B^+ and B^0 at the $\Upsilon(4S)$.

$\Gamma(\rho^0X(214),\ X\to\mu^+\mu^-)/\Gamma_{total}$ — Γ_{402}/Γ

$X(214)$ is a hypothetical particle of mass 214 MeV/c^2 reported by the HyperCP experiment (PARK 05)

VALUE (units 10^{-8})	CL%	DOCUMENT ID		TECN	COMMENT
<1.73	90	[1,2] HYUN	10	BELL	$e^+e^-\to\Upsilon(4S)$

[1] Assumes equal production of B^+ and B^0 at the $\Upsilon(4S)$.
[2] The result is the same for a scalar or vector X particle.

$\Gamma(\rho^0\gamma)/\Gamma(K^*(892)^0\gamma)$ — $\Gamma_{401}/\Gamma_{389}$

VALUE (units 10^{-2})	DOCUMENT ID		TECN	COMMENT
$2.06^{+0.45+0.14}_{-0.43-0.16}$	TANIGUCHI	08	BELL	$e^+e^-\to\Upsilon(4S)$

$\Gamma(\omega\gamma)/\Gamma_{total}$ — Γ_{403}/Γ

VALUE (units 10^{-6})	CL%	DOCUMENT ID		TECN	COMMENT
$0.44^{+0.18}_{-0.16}$ OUR AVERAGE					
$0.50^{+0.27}_{-0.23}\pm0.09$		[1] AUBERT	08BH	BABR	$e^+e^-\to\Upsilon(4S)$
$0.40^{+0.19}_{-0.17}\pm0.13$		[1] TANIGUCHI	08	BELL	$e^+e^-\to\Upsilon(4S)$
• • • We do not use the following data for averages, fits, limits, etc. • • •					
$0.40^{+0.24}_{-0.20}\pm0.05$		[1] AUBERT	07L	BABR	Repl. by AUBERT 08BH
$0.56^{+0.34+0.05}_{-0.27-0.10}$		[1] MOHAPATRA	06	BELL	Repl. by TANIGUCHI 08
<1.0	90	[1] AUBERT	05	BABR	Repl. by AUBERT 07L
<0.8	90	[1] MOHAPATRA	05	BELL	Repl. by MOHAPATRA 06
<1.0	90	[1] AUBERT	04C	BABR	$e^+e^-\to\Upsilon(4S)$
<9.2	90	[1] COAN	00	CLE2	$e^+e^-\to\Upsilon(4S)$

[1] Assumes equal production of B^+ and B^0 at the $\Upsilon(4S)$.

$\Gamma(\phi\gamma)/\Gamma_{total}$ — Γ_{404}/Γ

VALUE	CL%	DOCUMENT ID		TECN	COMMENT
$<1.0\times10^{-7}$	90	[1] KING	16	BELL	$e^+e^-\to\Upsilon(4S)$
• • • We do not use the following data for averages, fits, limits, etc. • • •					
$<8.5\times10^{-7}$	90	[1] AUBERT,BE	05C	BABR	$e^+e^-\to\Upsilon(4S)$
$<3.3\times10^{-6}$	90	[1] COAN	00	CLE2	$e^+e^-\to\Upsilon(4S)$

[1] Assumes equal production of B^+ and B^0 at the $\Upsilon(4S)$.

$\Gamma(\pi^+\pi^-)/\Gamma_{total}$ — Γ_{405}/Γ

VALUE (units 10^{-6})	CL%	DOCUMENT ID		TECN	COMMENT
5.12±0.19 OUR FIT					
5.13±0.24 OUR AVERAGE					
$5.04\pm0.21\pm0.18$		[1] DUH	13	BELL	$e^+e^-\to\Upsilon(4S)$
$5.5\ \pm0.4\ \pm0.3$		[1] AUBERT	07B	BABR	$e^+e^-\to\Upsilon(4S)$
$4.5\ ^{+1.4}_{-1.2}\ ^{+0.5}_{-0.4}$		[1] BORNHEIM	03	CLE2	$e^+e^-\to\Upsilon(4S)$
• • • We do not use the following data for averages, fits, limits, etc. • • •					
$5.1\ \pm0.2\ \pm0.2$		[1] LIN	07A	BELL	Repl. by DUH 13
$4.4\ \pm0.6\ \pm0.3$		[1] CHAO	04	BELL	Repl. by LIN 07A
$4.7\ \pm0.6\ \pm0.2$		[1] AUBERT	02Q	BABR	Repl. by AUBERT 07B
$5.4\ \pm1.2\ \pm0.5$		[1] CASEY	02	BELL	Repl. by CHAO 04
$5.6\ ^{+2.3}_{-2.0}\ ^{+0.4}_{-0.5}$		[1] ABE	01H	BELL	Repl. by CASEY 02
$4.1\ \pm1.0\ \pm0.7$		[1] AUBERT	01E	BABR	Repl. by AUBERT 02Q
< 67	90	[2] ABE	00C	SLD	$e^+e^-\to Z$
$4.3\ ^{+1.6}_{-1.4}\ \pm0.5$		[1] CRONIN-HEN...00		CLE2	Repl. by BORNHEIM 03
< 15	90	GODANG	98	CLE2	Repl. by CRONIN-HENNESSY 00
< 45	90	[3] ADAM	96D	DLPH	$e^+e^-\to Z$

Downloaded from https://academic.oup.com/ptep/article/2022/8/083C01/6651666 by KIT Library user on 27 September 2022

< 20	90	ASNER	96	CLE2	Repl. by GODANG 98
< 41	90	[4] BUSKULIC	96V	ALEP	$e^+e^- \to Z$
< 55	90	[5] ABREU	95N	DLPH	Sup. by ADAM 96D
< 47	90	[6] AKERS	94L	OPAL	$e^+e^- \to Z$
< 29	90	[1] BATTLE	93	CLE2	$e^+e^- \to \Upsilon(4S)$
<130	90	[1] ALBRECHT	90B	ARG	$e^+e^- \to \Upsilon(4S)$
< 77	90	[7] BORTOLETTO	89	CLEO	$e^+e^- \to \Upsilon(4S)$
<260	90	[7] BEBEK	87	CLEO	$e^+e^- \to \Upsilon(4S)$
<500	90	GILES	84	CLEO	$e^+e^- \to \Upsilon(4S)$

[1] Assumes equal production of B^+ and B^0 at the $\Upsilon(4S)$.
[2] ABE 00C assumes $B(Z \to b\overline{b})=(21.7 \pm 0.1)\%$ and the B fractions $f_{B^0}=f_{B^+}=(39.7^{+1.8}_{-2.2})\%$ and $f_{B_s}=(10.5^{+1.8}_{-2.2})\%$.
[3] ADAM 96D assumes $f_{B^0} = f_{B^-} = 0.39$ and $f_{B_s} = 0.12$.
[4] BUSKULIC 96V assumes PDG 96 production fractions for B^0, B^+, B_s, b baryons.
[5] Assumes a B^0, B^- production fraction of 0.39 and a B_s production fraction of 0.12.
[6] Assumes $B(Z \to b\overline{b}) = 0.217$ and B^0_d (B^0_s) fraction 39.5% (12%).
[7] Paper assumes the $\Upsilon(4S)$ decays 43% to $B^0\overline{B}^0$. We rescale to 50%.

$\Gamma(\pi^+\pi^-)/\Gamma(K^+\pi^-)$ — $\Gamma_{405}/\Gamma_{272}$

VALUE	DOCUMENT ID		TECN	COMMENT
0.261±0.010 OUR FIT				
0.261±0.015 OUR AVERAGE				
0.262±0.009±0.017	AAIJ	12AR	LHCB	pp at 7 TeV
0.259±0.017±0.016	AALTONEN	11N	CDF	$p\overline{p}$ at 1.96 TeV
• • • We do not use the following data for averages, fits, limits, etc. • • •				
0.21 ±0.05 ±0.03	ABULENCIA,A	06D	CDF	Repl. by AALTONEN 11N

$\Gamma(\pi^0\pi^0)/\Gamma_{total}$ — Γ_{406}/Γ

VALUE (units 10^{-6})	CL%	DOCUMENT ID		TECN	COMMENT
1.59±0.26 OUR AVERAGE		Error includes scale factor of 1.4.			
1.31±0.19±0.19		[1] JULIUS	17	BELL	$e^+e^- \to \Upsilon(4S)$
1.83±0.21±0.13		[1] LEES	13D	BABR	$e^+e^- \to \Upsilon(4S)$
• • • We do not use the following data for averages, fits, limits, etc. • • •					
1.47±0.25±0.12		[1] AUBERT	07BC	BABR	Repl. by LEES 13D
1.17±0.32±0.10		[1] AUBERT	05L	BABR	Repl. by AUBERT 07BC
$2.3\ ^{+0.4}_{-0.5}\ ^{+0.2}_{-0.3}$		[1] CHAO	05	BELL	Repl. by JULIUS 17
< 3.6	90	[1] AUBERT	03L	BABR	$e^+e^- \to \Upsilon(4S)$
2.1 ±0.6 ±0.3		[1] AUBERT	03S	BABR	Repl. by AUBERT 05L
< 4.4	90	[1] BORNHEIM	03	CLE2	$e^+e^- \to \Upsilon(4S)$
1.7 ±0.6 ±0.2		[1] LEE	03	BELL	Repl. by CHAO 05
< 5.7	90	[1] ASNER	02	CLE2	$e^+e^- \to \Upsilon(4S)$
< 6.4	90	[1] CASEY	02	BELL	$e^+e^- \to \Upsilon(4S)$
< 9.3	90	GODANG	98	CLE2	Repl. by ASNER 02
< 9.1	90	ASNER	96	CLE2	Repl. by GODANG 98
<60	90	[2] ACCIARRI	95H	L3	$e^+e^- \to Z$

[1] Assumes equal production of B^+ and B^0 at the $\Upsilon(4S)$.
[2] ACCIARRI 95H assumes $f_{B^0} = 39.5 \pm 4.0$ and $f_{B_s} = 12.0 \pm 3.0\%$.

$\Gamma(\eta\pi^0)/\Gamma_{total}$ — Γ_{407}/Γ

VALUE (units 10^{-6})	CL%	DOCUMENT ID		TECN	COMMENT
$\mathbf{0.41^{+0.17}_{-0.15}{}^{+0.05}_{-0.07}}$		[1,2] PAL	15	BELL	$e^+e^- \to \Upsilon(4S)$
• • • We do not use the following data for averages, fits, limits, etc. • • •					
< 1.5	90	[2] AUBERT	08AH	BABR	$e^+e^- \to \Upsilon(4S)$
< 1.3	90	[2] AUBERT	06W	BABR	Repl. by AUBERT 08AH
< 2.5	90	[2] CHANG	05A	BELL	Repl. by PAL 15
< 2.5	90	[2] AUBERT,B	04D	BABR	Repl. by AUBERT 06W
< 2.9	90	[2] RICHICHI	00	CLE2	$e^+e^- \to \Upsilon(4S)$
< 8	90	BEHRENS	98	CLE2	Repl. by RICHICHI 00
< 250	90	[3] ACCIARRI	95H	L3	$e^+e^- \to Z$
<1800	90	[2] ALBRECHT	90B	ARG	$e^+e^- \to \Upsilon(4S)$

[1] PAL 15 signal significance is 3.0 standard deviations. The measurement corresponds to 90% CL upper limit of $< 6.5 \times 10^{-7}$.
[2] Assumes equal production of B^+ and B^0 at the $\Upsilon(4S)$.
[3] ACCIARRI 95H assumes $f_{B^0} = 39.5 \pm 4.0$ and $f_{B_s} = 12.0 \pm 3.0\%$.

$\Gamma(\eta\eta)/\Gamma_{total}$ — Γ_{408}/Γ

VALUE (units 10^{-6})	CL%	DOCUMENT ID		TECN	COMMENT
< 1.0	90	[1] AUBERT	09AV	BABR	$e^+e^- \to \Upsilon(4S)$
• • • We do not use the following data for averages, fits, limits, etc. • • •					
< 1.8	90	[1] AUBERT,B	06V	BABR	Repl. by AUBERT 09AV
< 2.0	90	[1] CHANG	05A	BELL	$e^+e^- \to \Upsilon(4S)$
< 2.8	90	[1] AUBERT,B	04X	BABR	$e^+e^- \to \Upsilon(4S)$
< 18	90	BEHRENS	98	CLE2	$e^+e^- \to \Upsilon(4S)$
<410	90	[2] ACCIARRI	95H	L3	$e^+e^- \to Z$

[1] Assumes equal production of B^+ and B^0 at the $\Upsilon(4S)$.
[2] ACCIARRI 95H assumes $f_{B^0} = 39.5 \pm 4.0$ and $f_{B_s} = 12.0 \pm 3.0\%$.

$\Gamma(\eta'\pi^0)/\Gamma_{total}$ — Γ_{409}/Γ

VALUE (units 10^{-6})	CL%	DOCUMENT ID		TECN	COMMENT
1.2±0.6 OUR AVERAGE		Error includes scale factor of 1.7.			
0.9±0.4±0.1		[1] AUBERT	08AH	BABR	$e^+e^- \to \Upsilon(4S)$
2.8±1.0±0.3		[1] SCHUEMANN	06	BELL	$e^+e^- \to \Upsilon(4S)$
• • • We do not use the following data for averages, fits, limits, etc. • • •					
$0.8^{+0.8}_{-0.6}\pm0.1$		[1] AUBERT	06W	BABR	Repl. by AUBERT 08AH
$1.0^{+1.4}_{-1.0}\pm0.8$	90	[1] AUBERT,B	04D	BABR	Repl. by AUBERT 06W
< 5.7	90	[1] RICHICHI	00	CLE2	$e^+e^- \to \Upsilon(4S)$
<11	90	BEHRENS	98	CLE2	Repl. by RICHICHI 00

[1] Assumes equal production of B^+ and B^0 at the $\Upsilon(4S)$.

$\Gamma(\eta'\eta')/\Gamma_{total}$ — Γ_{410}/Γ

VALUE (units 10^{-6})	CL%	DOCUMENT ID		TECN	COMMENT
< 1.7	90	[1] AUBERT	09AV	BABR	$e^+e^- \to \Upsilon(4S)$
• • • We do not use the following data for averages, fits, limits, etc. • • •					
< 6.5	90	[1] SCHUEMANN	07	BELL	$e^+e^- \to \Upsilon(4S)$
< 2.4	90	[1] AUBERT,B	06V	BABR	Repl. by AUBERT 09AV
<10	90	[1] AUBERT,B	04X	BABR	Repl. by AUBERT,B 06V
<47	90	BEHRENS	98	CLE2	$e^+e^- \to \Upsilon(4S)$

[1] Assumes equal production of B^+ and B^0 at the $\Upsilon(4S)$.

$\Gamma(\eta'\eta)/\Gamma_{total}$ — Γ_{411}/Γ

VALUE (units 10^{-6})	CL%	DOCUMENT ID		TECN	COMMENT
< 1.2	90	[1] AUBERT	08AH	BABR	$e^+e^- \to \Upsilon(4S)$
• • • We do not use the following data for averages, fits, limits, etc. • • •					
< 4.5	90	[1] SCHUEMANN	07	BELL	$e^+e^- \to \Upsilon(4S)$
< 1.7	90	[1] AUBERT	06W	BABR	Repl. by AUBERT 08AH
< 4.6	90	[1] AUBERT,B	04X	BABR	$e^+e^- \to \Upsilon(4S)$
<27	90	BEHRENS	98	CLE2	$e^+e^- \to \Upsilon(4S)$

[1] Assumes equal production of B^+ and B^0 at the $\Upsilon(4S)$.

$\Gamma(\eta'\rho^0)/\Gamma_{total}$ — Γ_{412}/Γ

VALUE (units 10^{-6})	CL%	DOCUMENT ID		TECN	COMMENT
< 1.3	90	[1] SCHUEMANN	07	BELL	$e^+e^- \to \Upsilon(4S)$
• • • We do not use the following data for averages, fits, limits, etc. • • •					
< 2.8	90	[1] DEL-AMO-SA...	10A	BABR	$e^+e^- \to \Upsilon(4S)$
< 3.7	90	AUBERT	07E	BABR	Repl. by DEL-AMO-SANCHEZ 10A
< 4.3	90	[1] AUBERT,B	04D	BABR	Repl. by AUBERT 07E
<12	90	[1] RICHICHI	00	CLE2	$e^+e^- \to \Upsilon(4S)$
<23	90	BEHRENS	98	CLE2	Repl. by RICHICHI 00

[1] Assumes equal production of B^+ and B^0 at the $\Upsilon(4S)$.

$\Gamma(\eta' f_0(980),\ f_0 \to \pi^+\pi^-)/\Gamma_{total}$ — Γ_{413}/Γ

VALUE (units 10^{-6})	CL%	DOCUMENT ID		TECN	COMMENT
<0.9	90	[1] DEL-AMO-SA...	10A	BABR	$e^+e^- \to \Upsilon(4S)$
• • • We do not use the following data for averages, fits, limits, etc. • • •					
<1.5	90	AUBERT	07E	BABR	Repl. by DEL-AMO-SANCHEZ 10A

[1] Assumes equal production of B^+ and B^0 at the $\Upsilon(4S)$.

$\Gamma(\eta\rho^0)/\Gamma_{total}$ — Γ_{414}/Γ

VALUE (units 10^{-6})	CL%	DOCUMENT ID		TECN	COMMENT
< 1.5	90	[1] AUBERT	07Y	BABR	$e^+e^- \to \Upsilon(4S)$
• • • We do not use the following data for averages, fits, limits, etc. • • •					
< 1.9	90	[1] WANG	07B	BELL	$e^+e^- \to \Upsilon(4S)$
< 1.5	90	[1] AUBERT,B	04D	BABR	Repl. by AUBERT 07Y
<10	90	[1] RICHICHI	00	CLE2	$e^+e^- \to \Upsilon(4S)$
<13	90	BEHRENS	98	CLE2	Repl. by RICHICHI 00

[1] Assumes equal production of B^+ and B^0 at the $\Upsilon(4S)$.

$\Gamma(\eta f_0(980),\ f_0 \to \pi^+\pi^-)/\Gamma_{total}$ — Γ_{415}/Γ

VALUE (units 10^{-6})	CL%	DOCUMENT ID		TECN	COMMENT
<0.4	90	[1] AUBERT	07Y	BABR	$e^+e^- \to \Upsilon(4S)$

[1] Assumes equal production of B^+ and B^0 at the $\Upsilon(4S)$.

$\Gamma(\omega\eta)/\Gamma_{total}$ — Γ_{416}/Γ

VALUE (units 10^{-6})	CL%	DOCUMENT ID		TECN	COMMENT
$\mathbf{0.94^{+0.35}_{-0.30}\pm0.09}$		[1] AUBERT	09AV	BABR	$e^+e^- \to \Upsilon(4S)$
• • • We do not use the following data for averages, fits, limits, etc. • • •					
< 1.9	90	[1] AUBERT,B	05K	BABR	Repl. by AUBERT 09AV
$4.0\ ^{+1.3}_{-1.2}\ \pm0.4$		[1] AUBERT,B	04X	BABR	Repl. by AUBERT,B 05K
<12	90	[1] BERGFELD	98	CLE2	

[1] Assumes equal production of B^+ and B^0 at the $\Upsilon(4S)$.

Downloaded from https://academic.oup.com/ptep/article/2022/8/083C01/6651666 by KIT Library user on 27 September 2022

$\Gamma(\omega\eta')/\Gamma_{total}$ — Γ_{417}/Γ

VALUE (units 10^{-6})	CL%	DOCUMENT ID		TECN	COMMENT
$1.01^{+0.46}_{-0.38}\pm0.09$		[1] AUBERT	09AV	BABR	$e^+e^-\to\Upsilon(4S)$
• • • We do not use the following data for averages, fits, limits, etc. • • •					
<2.2	90	[1] SCHUEMANN	07	BELL	$e^+e^-\to\Upsilon(4S)$
<2.8	90	[1] AUBERT,B	04X	BABR	$e^+e^-\to\Upsilon(4S)$
<60	90	[1] BERGFELD	98	CLE2	

[1] Assumes equal production of B^+ and B^0 at the $\Upsilon(4S)$.

$\Gamma(\omega\rho^0)/\Gamma_{total}$ — Γ_{418}/Γ

VALUE (units 10^{-6})	CL%	DOCUMENT ID		TECN	COMMENT
<1.6	90	[1] AUBERT	09H	BABR	$e^+e^-\to\Upsilon(4S)$
• • • We do not use the following data for averages, fits, limits, etc. • • •					
<1.5	90	[1] AUBERT,B	06T	BABR	Repl. by AUBERT 09H
<3.3	90	[1] AUBERT	05O	BABR	Repl. by AUBERT,B 06T
<11	90	[1] BERGFELD	98	CLE2	

[1] Assumes equal production of B^+ and B^0 at the $\Upsilon(4S)$.

$\Gamma(\omega f_0(980),\ f_0\to\pi^+\pi^-)/\Gamma_{total}$ — Γ_{419}/Γ

VALUE (units 10^{-6})	CL%	DOCUMENT ID		TECN	COMMENT
<1.5	90	[1] AUBERT	09H	BABR	$e^+e^-\to\Upsilon(4S)$
• • • We do not use the following data for averages, fits, limits, etc. • • •					
<1.5	90	[1] AUBERT,B	06T	BABR	Repl. by AUBERT 09H

[1] Assumes equal production of B^+ and B^0 at the $\Upsilon(4S)$.

$\Gamma(\omega\omega)/\Gamma_{total}$ — Γ_{420}/Γ

VALUE (units 10^{-6})	CL%	DOCUMENT ID		TECN	COMMENT
$1.2\pm0.3^{+0.3}_{-0.2}$		[1] LEES	14	BABR	$e^+e^-\to\Upsilon(4S)$
• • • We do not use the following data for averages, fits, limits, etc. • • •					
<4.0	90	[1] AUBERT,B	06T	BABR	Repl. by LEES 14
<19	90	[1] BERGFELD	98	CLE2	

[1] Assumes equal production of B^+ and B^0 at the $\Upsilon(4S)$.

$\Gamma(\phi\pi^0)/\Gamma_{total}$ — Γ_{421}/Γ

VALUE (units 10^{-6})	CL%	DOCUMENT ID		TECN	COMMENT
<0.15	90	[1] KIM	12A	BELL	$e^+e^-\to\Upsilon(4S)$
• • • We do not use the following data for averages, fits, limits, etc. • • •					
<0.28	90	[1] AUBERT,B	06C	BABR	$e^+e^-\to\Upsilon(4S)$
<1.0	90	[1] AUBERT,B	04D	BABR	Repl. by AUBERT,B 06C
<5	90	[1] BERGFELD	98	CLE2	

[1] Assumes equal production of B^+ and B^0 at the $\Upsilon(4S)$.

$\Gamma(\phi\eta)/\Gamma_{total}$ — Γ_{422}/Γ

VALUE (units 10^{-6})	CL%	DOCUMENT ID		TECN	COMMENT
<0.5	90	[1] AUBERT	09AV	BABR	$e^+e^-\to\Upsilon(4S)$
• • • We do not use the following data for averages, fits, limits, etc. • • •					
<0.6	90	[1] AUBERT,B	06V	BABR	Repl. by AUBERT 09AV
<1.0	90	[1] AUBERT,B	04X	BABR	Repl. by AUBERT,B 06V
<9	90	[1] BERGFELD	98	CLE2	

[1] Assumes equal production of B^+ and B^0 at the $\Upsilon(4S)$.

$\Gamma(\phi\eta')/\Gamma_{total}$ — Γ_{423}/Γ

VALUE (units 10^{-6})	CL%	DOCUMENT ID		TECN	COMMENT
<0.5	90	[1] SCHUEMANN	07	BELL	$e^+e^-\to\Upsilon(4S)$
• • • We do not use the following data for averages, fits, limits, etc. • • •					
<1.1	90	[1] AUBERT	09AV	BABR	$e^+e^-\to\Upsilon(4S)$
<1.0	90	[1] AUBERT,B	06V	BABR	Repl. by AUBERT 09AV
<4.5	90	[1] AUBERT,B	04X	BABR	Repl. by AUBERT,B 06V
<31	90	[1] BERGFELD	98	CLE2	

[1] Assumes equal production of B^+ and B^0 at the $\Upsilon(4S)$.

$\Gamma(\phi\pi^+\pi^-)/\Gamma_{total}$ — Γ_{424}/Γ

VALUE (units 10^{-7})	DOCUMENT ID		TECN	COMMENT
$1.82\pm0.25\pm0.43$	[1] AAIJ	17A	LHCB	pp at 7, 8 TeV

[1] Signal evidence is 4.5 standard deviations.

$\Gamma(\phi\rho^0)/\Gamma_{total}$ — Γ_{425}/Γ

VALUE (units 10^{-6})	CL%	DOCUMENT ID		TECN	COMMENT
<0.33	90	[1] AUBERT	08BK	BABR	$e^+e^-\to\Upsilon(4S)$
• • • We do not use the following data for averages, fits, limits, etc. • • •					
<156	90	[2] ABE	00C	SLD	$e^+e^-\to Z$
<13	90	[1] BERGFELD	98	CLE2	

[1] Assumes equal production of B^+ and B^0 at the $\Upsilon(4S)$.
[2] ABE 00C assumes $B(Z\to b\overline{b})=(21.7\pm0.1)\%$ and the B fractions $f_{B^0}=f_{B^+}=(39.7^{+1.8}_{-2.2})\%$ and $f_{B_s}=(10.5^{+1.8}_{-2.2})\%$.

$\Gamma(\phi f_0(980),\ f_0\to\pi^+\pi^-)/\Gamma_{total}$ — Γ_{426}/Γ

VALUE (units 10^{-6})	CL%	DOCUMENT ID		TECN	COMMENT
<0.38	90	[1] AUBERT	08BK	BABR	$e^+e^-\to\Upsilon(4S)$

[1] Assumes equal production of B^+ and B^0 at the $\Upsilon(4S)$.

$\Gamma(\phi\omega)/\Gamma_{total}$ — Γ_{427}/Γ

VALUE (units 10^{-6})	CL%	DOCUMENT ID		TECN	COMMENT
<0.7	90	[1] LEES	14	BABR	$e^+e^-\to\Upsilon(4S)$
• • • We do not use the following data for averages, fits, limits, etc. • • •					
<1.2	90	[1] AUBERT,B	06T	BABR	Repl. by LEES 14
<21	90	[1] BERGFELD	98	CLE2	

[1] Assumes equal production of B^+ and B^0 at the $\Upsilon(4S)$.

$\Gamma(\phi\phi)/\Gamma_{total}$ — Γ_{428}/Γ

VALUE	CL%	DOCUMENT ID		TECN	COMMENT
$<2.7\times10^{-8}$	90	AAIJ	19AP	LHCB	pp at 7, 8 and 13 TeV
• • • We do not use the following data for averages, fits, limits, etc. • • •					
$<2.8\times10^{-8}$	90	AAIJ	15AS	LHCB	Repl. by AAIJ 19AP
$<2\times10^{-7}$	90	[1] AUBERT	08BK	BABR	$e^+e^-\to\Upsilon(4S)$
$<1.5\times10^{-6}$	90	[1] AUBERT,B	04X	BABR	Repl. by AUBERT 08BK
$<3.21\times10^{-4}$	90	[2] ABE	00C	SLD	$e^+e^-\to Z$
$<1.2\times10^{-5}$	90	[1] BERGFELD	98	CLE2	
$<3.9\times10^{-5}$	90	ASNER	96	CLE2	$e^+e^-\to\Upsilon(4S)$

[1] Assumes equal production of B^+ and B^0 at the $\Upsilon(4S)$.
[2] ABE 00C assumes $B(Z\to b\overline{b})=(21.7\pm0.1)\%$ and the B fractions $f_{B^0}=f_{B^+}=(39.7^{+1.8}_{-2.2})\%$ and $f_{B_s}=(10.5^{+1.8}_{-2.2})\%$.

$\Gamma(a_0(980)^\pm\pi^\mp,\ a_0^\pm\to\eta\pi^\pm)/\Gamma_{total}$ — Γ_{429}/Γ

VALUE (units 10^{-6})	CL%	DOCUMENT ID		TECN	COMMENT
<3.1	90	[1] AUBERT	07Y	BABR	$e^+e^-\to\Upsilon(4S)$
• • • We do not use the following data for averages, fits, limits, etc. • • •					
<5.1	90	[1] AUBERT,BE	04	BABR	Repl. by AUBERT 07Y

[1] Assumes equal production of B^+ and B^0 at the $\Upsilon(4S)$.

$\Gamma(a_0(1450)^\pm\pi^\mp,\ a_0^\pm\to\eta\pi^\pm)/\Gamma_{total}$ — Γ_{430}/Γ

VALUE (units 10^{-6})	CL%	DOCUMENT ID		TECN	COMMENT
<2.3	90	[1] AUBERT	07Y	BABR	$e^+e^-\to\Upsilon(4S)$

[1] Assumes equal production of B^+ and B^0 at the $\Upsilon(4S)$.

$\Gamma(\pi^+\pi^-\pi^0)/\Gamma_{total}$ — Γ_{431}/Γ

VALUE	CL%	DOCUMENT ID		TECN	COMMENT
$<7.2\times10^{-4}$	90	[1] ALBRECHT	90B	ARG	$e^+e^-\to\Upsilon(4S)$

[1] ALBRECHT 90B limit assumes equal production of $B^0\overline{B}^0$ and B^+B^- at $\Upsilon(4S)$.

$\Gamma(\rho^0\pi^0)/\Gamma_{total}$ — Γ_{432}/Γ

VALUE (units 10^{-6})	CL%	DOCUMENT ID		TECN	COMMENT
2.0 ± 0.5 OUR AVERAGE					
$3.0\pm0.5\pm0.7$		[1,2] KUSAKA	08	BELL	$e^+e^-\to\Upsilon(4S)$
$1.4\pm0.6\pm0.3$		[1] AUBERT	04Z	BABR	$e^+e^-\to\Upsilon(4S)$
$1.6^{+2.0}_{-1.4}\pm0.8$		[1] JESSOP	00	CLEO	$e^+e^-\to\Upsilon(4S)$
• • • We do not use the following data for averages, fits, limits, etc. • • •					
$3.12^{+0.88+0.60}_{-0.82-0.76}$		[1] DRAGIC	06	BELL	Repl. by KUSAKA 08
$5.1\pm1.6\pm0.9$		DRAGIC	04	BELL	Repl. by DRAGIC 06
<5.3	90	[1] GORDON	02	BELL	Repl. by DRAGIC 04
<24	90	ASNER	96	CLEO	Repl. by JESSOP 00
<400	90	[1] ALBRECHT	90B	ARG	$e^+e^-\to\Upsilon(4S)$

[1] Assumes equal production of B^+ and B^0 at the $\Upsilon(4S)$.
[2] This is the first measurement that excludes contributions from $\rho(1450)$ and $\rho(1570)$ resonances.

$\Gamma(\rho^\mp\pi^\pm)/\Gamma_{total}$ — Γ_{433}/Γ

VALUE (units 10^{-6})	CL%	DOCUMENT ID		TECN	COMMENT
23.0 ± 2.3 OUR AVERAGE					
$22.6\pm1.1\pm4.4$		[1,2] KUSAKA	08	BELL	$e^+e^-\to\Upsilon(4S)$
$22.6\pm1.8\pm2.2$		[1] AUBERT	03T	BABR	$e^+e^-\to\Upsilon(4S)$
$27.6^{+8.4}_{-7.4}\pm4.2$		[1] JESSOP	00	CLE2	$e^+e^-\to\Upsilon(4S)$
• • • We do not use the following data for averages, fits, limits, etc. • • •					
$20.8^{+6.0+2.8}_{-6.3-3.1}$		[1] GORDON	02	BELL	Repl. by KUSAKA 08
<88	90	ASNER	96	CLE2	Repl. by JESSOP 00
<520	90	[1] ALBRECHT	90B	ARG	$e^+e^-\to\Upsilon(4S)$
<5200	90	[3] BEBEK	87	CLEO	$e^+e^-\to\Upsilon(4S)$

[1] Assumes equal production of B^+ and B^0 at the $\Upsilon(4S)$.
[2] This is the first measurement that excludes contributions from $\rho(1450)$ and $\rho(1570)$ resonances.
[3] BEBEK 87 reports $<6.1\times10^{-3}$ assuming the $\Upsilon(4S)$ decays 43% to $B^0\overline{B}^0$. We rescale to 50%.

Downloaded from https://academic.oup.com/ptep/article/2022/8/083C01/6651666 by KIT Library user on 27 September 2022

$\Gamma(\pi^+\pi^-\pi^+\pi^-)/\Gamma_{total}$ — Γ_{434}/Γ

VALUE	CL%	DOCUMENT ID		TECN	COMMENT
$<11.2\times10^{-6}$	90	[1] VANHOEFER	14	BELL	$e^+e^-\to\Upsilon(4S)$
• • • We do not use the following data for averages, fits, limits, etc. • • •					
$<23.1\times10^{-6}$	90	[1] AUBERT	08BB	BABR	$e^+e^-\to\Upsilon(4S)$
$<19.3\times10^{-6}$	90	[1] CHIANG	08	BELL	Repl. by VANHOEFER 14
$<2.3\times10^{-4}$	90	[2] ADAM	96D	DLPH	$e^+e^-\to Z$
$<2.8\times10^{-4}$	90	[3] ABREU	95N	DLPH	Sup. by ADAM 96D
$<6.7\times10^{-4}$	90	[1] ALBRECHT	90B	ARG	$e^+e^-\to\Upsilon(4S)$

[1] Assumes equal production of B^+ and B^0 at the $\Upsilon(4S)$.
[2] ADAM 96D assumes $f_{B^0}=f_{B^-}=0.39$ and $f_{B_s}=0.12$.
[3] Assumes a B^0, B^- production fraction of 0.39 and a B_s production fraction of 0.12.

$\Gamma(\rho^0\pi^+\pi^-)/\Gamma_{total}$ — Γ_{435}/Γ

VALUE (units 10^{-6})	CL%	DOCUMENT ID		TECN	COMMENT
< 8.8	90	[1] AUBERT	08BB	BABR	$e^+e^-\to\Upsilon(4S)$
• • • We do not use the following data for averages, fits, limits, etc. • • •					
<12.0	90	[1] VANHOEFER	14	BELL	$e^+e^-\to\Upsilon(4S)$
<12.0	90	[1] CHIANG	08	BELL	Repl. by VANHOEFER 14

[1] Assumes equal production of B^+ and B^0 at the $\Upsilon(4S)$.

$\Gamma(\rho^0\rho^0)/\Gamma_{total}$ — Γ_{436}/Γ

VALUE (units 10^{-6})	CL%	DOCUMENT ID		TECN	COMMENT
0.96±0.15 OUR FIT					
0.97±0.24 OUR AVERAGE					
1.02±0.30±0.15		[1,2] VANHOEFER	14	BELL	$e^+e^-\to\Upsilon(4S)$
0.92±0.32±0.14		[2] AUBERT	08BB	BABR	$e^+e^-\to\Upsilon(4S)$
• • • We do not use the following data for averages, fits, limits, etc. • • •					
$0.4\ \pm0.4\ ^{+0.2}_{-0.3}$		[2] CHIANG	08	BELL	Repl. by VANHOEFER 14
1.07±0.33±0.19		[2] AUBERT	07G	BABR	Repl. by AUBERT 08BB
< 1.1	90	[2] AUBERT	05I	BABR	Repl. by AUBERT 07G
< 2.1	90	[2] AUBERT	03V	BABR	Repl. by AUBERT 05I
< 18	90	[3] GODANG	02	CLE2	$e^+e^-\to\Upsilon(4S)$
<136	90	[4] ABE	00C	SLD	$e^+e^-\to Z$
<280	90	[2] ALBRECHT	90B	ARG	$e^+e^-\to\Upsilon(4S)$
<290	90	[5] BORTOLETTO	89	CLEO	$e^+e^-\to\Upsilon(4S)$
<430	90	[5] BEBEK	87	CLEO	$e^+e^-\to\Upsilon(4S)$

[1] Signal significance 3.4 standard deviations.
[2] Assumes equal production of B^+ and B^0 at the $\Upsilon(4S)$.
[3] Assumes a helicity 00 configuration. For a helicity 11 configuration, the limit decreases to 1.4×10^{-5}.
[4] ABE 00C assumes $B(Z\to b\overline{b})=(21.7\pm0.1)\%$ and the B fractions $f_{B^0}=f_{B^+}=(39.7\,^{+1.8}_{-2.2})\%$ and $f_{B_s}=(10.5\,^{+1.8}_{-2.2})\%$.
[5] Paper assumes the $\Upsilon(4S)$ decays 43% to $B^0\overline{B}^0$. We rescale to 50%.

$\Gamma(\rho^0\rho^0)/\Gamma(K^*(892)^0\phi)$ — $\Gamma_{436}/\Gamma_{361}$

VALUE (10^{-2})	DOCUMENT ID		TECN	COMMENT
9.5±1.5 OUR FIT				
9.4±1.7±0.9	AAIJ	15T	LHCB	pp at 7, 8 TeV

$\Gamma(f_0(980)\pi^+\pi^-,\ f_0\to\pi^+\pi^-)/\Gamma_{total}$ — Γ_{437}/Γ

VALUE	CL%	DOCUMENT ID		TECN	COMMENT
$<3.0\times10^{-6}$	90	[1] VANHOEFER	14	BELL	$e^+e^-\to\Upsilon(4S)$
• • • We do not use the following data for averages, fits, limits, etc. • • •					
$<3.8\times10^{-6}$	90	[1] CHIANG	08	BELL	$e^+e^-\to\Upsilon(4S)$

[1] Assumes equal production of B^+ and B^0 at the $\Upsilon(4S)$.

$\Gamma(\rho^0 f_0(980),\ f_0\to\pi^+\pi^-)/\Gamma_{total}$ — Γ_{438}/Γ

VALUE (units 10^{-7})	CL%	DOCUMENT ID		TECN	COMMENT
7.8±2.2±1.1		[1,2] VANHOEFER	14	BELL	$e^+e^-\to\Upsilon(4S)$
• • • We do not use the following data for averages, fits, limits, etc. • • •					
<8.1	90	AAIJ	15T	LHCB	pp at 7, 8 TeV
<4.0	90	[2] AUBERT	08BB	BABR	$e^+e^-\to\Upsilon(4S)$
<3	90	[2] CHIANG	08	BELL	Repl. by VANHOEFER 14
<5.3	90	[2] AUBERT	07G	BABR	Repl. by AUBERT 08BB

[1] Signal significance of 3.1 standard deviations.
[2] Assumes equal production of B^+ and B^0 at the $\Upsilon(4S)$.

$\Gamma(f_0(980)f_0(980),\ f_0\to\pi^+\pi^-,\ f_0\to\pi^+\pi^-)/\Gamma_{total}$ — Γ_{439}/Γ

VALUE (units 10^{-6})	CL%	DOCUMENT ID		TECN	COMMENT
<0.19	90	[1] AUBERT	08BB	BABR	$e^+e^-\to\Upsilon(4S)$
• • • We do not use the following data for averages, fits, limits, etc. • • •					
<0.2	90	[1] VANHOEFER	14	BELL	$e^+e^-\to\Upsilon(4S)$
<0.1	90	[1] CHIANG	08	BELL	Repl. by VANHOEFER 14
<0.16	90	[1] AUBERT	07G	BABR	Repl. by AUBERT 08BB

[1] Assumes equal production of B^+ and B^0 at the $\Upsilon(4S)$.

$\Gamma(f_0(980)f_0(980),\ f_0\to\pi^+\pi^-,\ f_0\to K^+K^-)/\Gamma_{total}$ — Γ_{440}/Γ

VALUE (units 10^{-6})	CL%	DOCUMENT ID		TECN	COMMENT
<0.23	90	[1] AUBERT	08BK	BABR	$e^+e^-\to\Upsilon(4S)$

[1] Assumes equal production of B^+ and B^0 at the $\Upsilon(4S)$.

$\Gamma(a_1(1260)^\mp\pi^\pm)/\Gamma_{total}$ — Γ_{441}/Γ

VALUE (units 10^{-6})	CL%	DOCUMENT ID		TECN	COMMENT
26 ±5 OUR AVERAGE		Error includes scale factor of 1.9.			
22.2±2.0±2.8		[1,2] DALSENO	12	BELL	$e^+e^-\to\Upsilon(4S)$
33.2±3.8±3.0		[2,3] AUBERT	06V	BABR	$e^+e^-\to\Upsilon(4S)$
• • • We do not use the following data for averages, fits, limits, etc. • • •					
< 630	90	[2] ALBRECHT	90B	ARG	$e^+e^-\to\Upsilon(4S)$
< 490	90	[4] BORTOLETTO	89	CLEO	$e^+e^-\to\Upsilon(4S)$
<1000	90	[4] BEBEK	87	CLEO	$e^+e^-\to\Upsilon(4S)$

[1] DALSENO 12 reports $B(B^0\to a_1^\pm\pi^\mp)\,B(a_1^\pm\to\pi^\pm\pi^+\pi^-)=(11.1\pm1.0\pm1.4)\times10^{-6}$ which we rescaled assuming $a_1(1260)$ decays only to 3π and $B(a_1^\pm\to\pi^\pm\pi^+\pi^-)=0.5$.
[2] Assumes equal production of B^+ and B^0 at the $\Upsilon(4S)$.
[3] Assumes $a_1(1260)$ decays only to 3π and $B(a_1^\pm\to\pi^\pm\pi^\mp\pi^\pm)=0.5$.
[4] Paper assumes the $\Upsilon(4S)$ decays 43% to $B^0\overline{B}^0$. We rescale to 50%.

$\Gamma(a_2(1320)^\mp\pi^\pm)/\Gamma_{total}$ — Γ_{442}/Γ

VALUE	CL%	DOCUMENT ID		TECN	COMMENT
$<6.3\times10^{-6}$	90	[1] DALSENO	12	BELL	$e^+e^-\to\Upsilon(4S)$
• • • We do not use the following data for averages, fits, limits, etc. • • •					
$<3.0\times10^{-4}$	90	[2] BORTOLETTO	89	CLEO	$e^+e^-\to\Upsilon(4S)$
$<1.4\times10^{-3}$	90	[2] BEBEK	87	CLEO	$e^+e^-\to\Upsilon(4S)$

[1] DALSENO 12 reports $B(B^0\to a_2^\pm\pi^\mp)\,B(a_2^\pm\to\pi^\pm\pi^+\pi^-)<2.2\times10^{-6}$ which we rescaled using $B(a_2^\pm\to\pi^\pm\pi^+\pi^-)=1/2\,B(a_2^\pm\to3\pi)=0.35\pm0.013$.
[2] Paper assumes the $\Upsilon(4S)$ decays 43% to $B^0\overline{B}^0$. We rescale to 50%.

$\Gamma(\pi^+\pi^-\pi^0\pi^0)/\Gamma_{total}$ — Γ_{443}/Γ

VALUE	CL%	DOCUMENT ID		TECN	COMMENT
$<3.1\times10^{-3}$	90	[1] ALBRECHT	90B	ARG	$e^+e^-\to\Upsilon(4S)$

[1] ALBRECHT 90B limit assumes equal production of $B^0\overline{B}^0$ and B^+B^- at $\Upsilon(4S)$.

$\Gamma(\rho^+\rho^-)/\Gamma_{total}$ — Γ_{444}/Γ

VALUE (units 10^{-6})	CL%	DOCUMENT ID		TECN	COMMENT
27.7±1.9 OUR AVERAGE					
28.3±1.5±1.5		[1] VANHOEFER	16	BELL	$e^+e^-\to\Upsilon(4S)$
$25.5\pm2.1\,^{+3.6}_{-3.9}$		[1] AUBERT	07BF	BABR	$e^+e^-\to\Upsilon(4S)$
• • • We do not use the following data for averages, fits, limits, etc. • • •					
$22.8\pm3.8\,^{+2.3}_{-2.6}$		[1] SOMOV	06	BELL	Repl. by VANHOEFER 16
$25\ ^{+7}_{-6}\ ^{+5}_{-6}$		[1] AUBERT	04G	BABR	Repl. by AUBERT,B 04R
$30\ \pm4\ \pm5$		[1,2] AUBERT,B	04R	BABR	Repl. by AUBERT 07BF
<2200	90	[1] ALBRECHT	90B	ARG	$e^+e^-\to\Upsilon(4S)$

[1] Assumes equal production of B^+ and B^0 at the $\Upsilon(4S)$.
[2] The quoted result is obtained after combining with AUBERT 04G result by AUBERT 04R alone gives $(33\pm4\pm5)\times10^{-6}$.

$\Gamma(a_1(1260)^0\pi^0)/\Gamma_{total}$ — Γ_{445}/Γ

VALUE	CL%	DOCUMENT ID		TECN	COMMENT
$<1.1\times10^{-3}$	90	[1] ALBRECHT	90B	ARG	$e^+e^-\to\Upsilon(4S)$

[1] ALBRECHT 90B limit assumes equal production of $B^0\overline{B}^0$ and B^+B^- at $\Upsilon(4S)$.

$\Gamma(\omega\pi^0)/\Gamma_{total}$ — Γ_{446}/Γ

VALUE (units 10^{-6})	CL%	DOCUMENT ID		TECN	COMMENT
< 0.5	90	[1] AUBERT	08AH	BABR	$e^+e^-\to\Upsilon(4S)$
• • • We do not use the following data for averages, fits, limits, etc. • • •					
< 2.0	90	[1] JEN	06	BELL	$e^+e^-\to\Upsilon(4S)$
< 1.2	90	[1] AUBERT,B	04D	BABR	Repl. by AUBERT 08AH
< 1.9	90	[1] WANG	04A	BELL	$e^+e^-\to\Upsilon(4S)$
< 3	90	[1] AUBERT	01G	BABR	$e^+e^-\to\Upsilon(4S)$
< 5.5	90	[1] JESSOP	00	CLE2	$e^+e^-\to\Upsilon(4S)$
< 14	90	[1] BERGFELD	98	CLE2	Repl. by JESSOP 00
<460	90	[2] ALBRECHT	90B	ARG	$e^+e^-\to\Upsilon(4S)$

[1] Assumes equal production of B^+ and B^0 at the $\Upsilon(4S)$.
[2] ALBRECHT 90B limit assumes equal production of $B^0\overline{B}^0$ and B^+B^- at $\Upsilon(4S)$.

$\Gamma(\pi^+\pi^+\pi^-\pi^-\pi^0)/\Gamma_{total}$ — Γ_{447}/Γ

VALUE	CL%	DOCUMENT ID		TECN	COMMENT
$<9.0\times10^{-3}$	90	[1] ALBRECHT	90B	ARG	$e^+e^-\to\Upsilon(4S)$

[1] ALBRECHT 90B limit assumes equal production of $B^0\overline{B}^0$ and B^+B^- at $\Upsilon(4S)$.

Downloaded from https://academic.oup.com/ptep/article/2022/8/083C01/6651666 by KIT Library user on 27 September 2022

$\Gamma(a_1(1260)^+\rho^-)/\Gamma_{total}$ — Γ_{448}/Γ

VALUE (units 10^{-6})	CL%	DOCUMENT ID		TECN	COMMENT
< 61	90	[1,2] AUBERT,B	06O	BABR	$e^+e^- \to \Upsilon(4S)$
• • • We do not use the following data for averages, fits, limits, etc. • • •					
<3400	90	[1] ALBRECHT	90B	ARG	$e^+e^- \to \Upsilon(4S)$

[1] Assumes equal production of B^+ and B^0 at the $\Upsilon(4S)$.
[2] Assumes $a_1(1260)$ decays only to 3π and $B(a_1^\pm \to \pi^\pm\pi^\mp\pi^\pm) = 0.5$.

$\Gamma(a_1(1260)^0\rho^0)/\Gamma_{total}$ — Γ_{449}/Γ

VALUE	CL%	DOCUMENT ID		TECN	COMMENT
$<2.4\times10^{-3}$	90	[1] ALBRECHT	90B	ARG	$e^+e^- \to \Upsilon(4S)$

[1] ALBRECHT 90B limit assumes equal production of $B^0\overline{B}^0$ and B^+B^- at $\Upsilon(4S)$.

$\Gamma(b_1^\mp\pi^\pm,\ b_1^\mp \to \omega\pi^\mp)/\Gamma_{total}$ — Γ_{450}/Γ

VALUE (units 10^{-6})	DOCUMENT ID		TECN	COMMENT
10.9±1.2±0.9	[1] AUBERT	07BI	BABR	$e^+e^- \to \Upsilon(4S)$

[1] Assumes equal production of B^+ and B^0 at the $\Upsilon(4S)$.

$\Gamma(b_1^0\pi^0,\ b_1^0 \to \omega\pi^0)/\Gamma_{total}$ — Γ_{451}/Γ

VALUE (units 10^{-6})	CL%	DOCUMENT ID		TECN	COMMENT
<1.9	90	[1] AUBERT	08AG	BABR	$e^+e^- \to \Upsilon(4S)$

[1] Assumes equal production of B^+ and B^0 at the $\Upsilon(4S)$.

$\Gamma(b_1^-\rho^+,\ b_1^- \to \omega\pi^-)/\Gamma_{total}$ — Γ_{452}/Γ

VALUE	CL%	DOCUMENT ID		TECN	COMMENT
$<1.4\times10^{-6}$	90	[1] AUBERT	09AF	BABR	$e^+e^- \to \Upsilon(4S)$

[1] Assumes equal production of B^+ and B^0 at the $\Upsilon(4S)$.

$\Gamma(b_1^0\rho^0,\ b_1^0 \to \omega\pi^0)/\Gamma_{total}$ — Γ_{453}/Γ

VALUE	CL%	DOCUMENT ID		TECN	COMMENT
$<3.4\times10^{-6}$	90	[1] AUBERT	09AF	BABR	$e^+e^- \to \Upsilon(4S)$

[1] Assumes equal production of B^+ and B^0 at the $\Upsilon(4S)$.

$\Gamma(\pi^+\pi^+\pi^+\pi^-\pi^-\pi^-)/\Gamma_{total}$ — Γ_{454}/Γ

VALUE	CL%	DOCUMENT ID		TECN	COMMENT
$<3.0\times10^{-3}$	90	[1] ALBRECHT	90B	ARG	$e^+e^- \to \Upsilon(4S)$

[1] ALBRECHT 90B limit assumes equal production of $B^0\overline{B}^0$ and B^+B^- at $\Upsilon(4S)$.

$\Gamma(a_1(1260)^+a_1(1260)^-,\ a_1^+ \to 2\pi^+\pi^-,\ a_1^- \to 2\pi^-\pi^+)/\Gamma_{total}$ — Γ_{455}/Γ

VALUE (units 10^{-6})	CL%	DOCUMENT ID		TECN	COMMENT
11.8±2.6±1.6		[1] AUBERT	09AL	BABR	$e^+e^- \to \Upsilon(4S)$
• • • We do not use the following data for averages, fits, limits, etc. • • •					
<6000	90	[1] ALBRECHT	90B	ARG	$e^+e^- \to \Upsilon(4S)$
<2800	90	[2] BORTOLETTO	89	CLEO	$e^+e^- \to \Upsilon(4S)$

[1] Assumes equal production of $B^0\overline{B}^0$ and B^+B^- at $\Upsilon(4S)$.
[2] BORTOLETTO 89 reports $< 3.2\times10^{-3}$ assuming the $\Upsilon(4S)$ decays 43% to $B^0\overline{B}^0$. We rescale to 50%.

$\Gamma(\pi^+\pi^+\pi^+\pi^-\pi^-\pi^-\pi^0)/\Gamma_{total}$ — Γ_{456}/Γ

VALUE	CL%	DOCUMENT ID		TECN	COMMENT
$<1.1\times10^{-2}$	90	[1] ALBRECHT	90B	ARG	$e^+e^- \to \Upsilon(4S)$

[1] ALBRECHT 90B limit assumes equal production of $B^0\overline{B}^0$ and B^+B^- at $\Upsilon(4S)$.

$\Gamma(p\overline{p})/\Gamma_{total}$ — Γ_{457}/Γ

VALUE (units 10^{-8})	CL%	DOCUMENT ID		TECN	COMMENT
1.25±0.27±0.18		[1] AAIJ	17BJ	LHCB	pp at 7 and 8 TeV
• • • We do not use the following data for averages, fits, limits, etc. • • •					
$1.47^{+0.62}_{-0.51}{}^{+0.35}_{-0.14}$		[2] AAIJ	13BQ	LHCB	Repl. by AAIJ 17BJ
< 11	90	[3] TSAI	07	BELL	$e^+e^- \to \Upsilon(4S)$
< 41	90	[3] CHANG	05	BELL	$e^+e^- \to \Upsilon(4S)$
< 27	90	[3] AUBERT	04U	BABR	$e^+e^- \to \Upsilon(4S)$
< 140	90	[3] BORNHEIM	03	CLE2	$e^+e^- \to \Upsilon(4S)$
< 120	90	[3] ABE	02O	BELL	$e^+e^- \to \Upsilon(4S)$
< 700	90	[3] COAN	99	CLE2	$e^+e^- \to \Upsilon(4S)$
< 1800	90	[4] BUSKULIC	96V	ALEP	$e^+e^- \to Z$
<35000	90	[5] ABREU	95N	DLPH	Sup. by ADAM 96D
< 3400	90	[6] BORTOLETTO	89	CLEO	$e^+e^- \to \Upsilon(4S)$
<12000	90	[7] ALBRECHT	88F	ARG	$e^+e^- \to \Upsilon(4S)$
<17000	90	[6] BEBEK	87	CLEO	$e^+e^- \to \Upsilon(4S)$

[1] Uses normalization mode $B(B^0 \to K^+\pi^-) = (19.6 \pm 0.5)\times10^{-6}$.
[2] Uses normalization mode $B(B^0 \to K^+\pi^-) = (19.55 \pm 0.54)\times10^{-6}$.
[3] Assumes equal production of B^+ and B^0 at the $\Upsilon(4S)$.
[4] BUSKULIC 96V assumes PDG 96 production fractions for B^0, B^+, B_s, b baryons.
[5] Assumes a B^0, B^- production fraction of 0.39 and a B_s production fraction of 0.12.
[6] Paper assumes the $\Upsilon(4S)$ decays 43% to $B^0\overline{B}^0$. We rescale to 50%.
[7] ALBRECHT 88F reports $< 1.3\times10^{-4}$ assuming the $\Upsilon(4S)$ decays 45% to $B^0\overline{B}^0$. We rescale to 50%.

$\Gamma(p\overline{p}\pi^+\pi^-)/\Gamma_{total}$ — Γ_{458}/Γ

VALUE (units 10^{-6})	CL%	DOCUMENT ID		TECN	COMMENT
2.87± 0.15± 0.11		[1,2] AAIJ	17BD	LHCB	pp at 7, 8 TeV
• • • We do not use the following data for averages, fits, limits, etc. • • •					
0.83± 0.17± 0.17		[3] CHU	20	BELL	$e^+e^- \to \Upsilon(4S)$
<950	90	[4] ABREU	95N	DLPH	Sup. by ADAM 96D
<250	90	[5] BEBEK	89	CLEO	$e^+e^- \to \Upsilon(4S)$
540 ±180 ±200		[6] ALBRECHT	88F	ARG	$e^+e^- \to \Upsilon(4S)$

[1] AAIJ 17BD reports $[\Gamma(B^0 \to p\overline{p}\pi^+\pi^-)/\Gamma_{total}]$ / $[B(B^0 \to J/\psi(1S)K^*(892)^0)]$ / $[B(J/\psi(1S) \to p\overline{p})]$ / $[B(K^*(892) \to (K\pi)^\pm)] = 1.07\pm0.04\pm0.04$ which we multiply by our best values $B(B^0 \to J/\psi(1S)K^*(892)^0) = (1.27\pm0.05)\times10^{-3}$, $B(J/\psi(1S) \to p\overline{p}) = (2.120\pm0.029)\times10^{-3}$, $B(K^*(892) \to (K\pi)^\pm) = (99.902\pm0.009)\times10^{-2}$. Our first error is their experiment's error and our second error is the systematic error from using our best values.
[2] The branching ratio is given for $m_{p\overline{p}} < 2.85$ GeV.
[3] Assumes equal production of B^0 and B^+ from $\Upsilon(4S)$ decays . This measurement is quoted for $M(\pi^+\pi^-) < 1.22$ GeV excluding the $0.46 < M(\pi^+\pi^-) < 0.53$ GeV region.
[4] Assumes a B^0, B^- production fraction of 0.39 and a B_s production fraction of 0.12.
[5] BEBEK 89 reports $< 2.9\times10^{-4}$ assuming the $\Upsilon(4S)$ decays 43% to $B^0\overline{B}^0$. We rescale to 50%.
[6] ALBRECHT 88F reports 6.0 ± 2.0 ± 2.2 assuming the $\Upsilon(4S)$ decays 45% to $B^0\overline{B}^0$. We rescale to 50%.

$\Gamma(p\overline{p}\pi^+\pi^-)/\Gamma(p\overline{p}K^+\pi^-)$ — $\Gamma_{458}/\Gamma_{459}$

VALUE	DOCUMENT ID		TECN	COMMENT
• • • We do not use the following data for averages, fits, limits, etc. • • •				
0.46±0.02±0.02	[1] AAIJ	17BD	LHCB	pp at 7, 8 TeV

[1] The ratio is given for $m_{p\overline{p}} < 2.85$ GeV.

$\Gamma(p\overline{p}K^0)/\Gamma_{total}$ — Γ_{460}/Γ

VALUE (units 10^{-6})	CL%	DOCUMENT ID		TECN	COMMENT
2.66±0.32 OUR AVERAGE					
$2.51^{+0.35}_{-0.29}\pm0.21$		[1,2] CHEN	08C	BELL	$e^+e^- \to \Upsilon(4S)$
3.0 ±0.5 ±0.3		[2] AUBERT	07AV	BABR	$e^+e^- \to \Upsilon(4S)$
• • • We do not use the following data for averages, fits, limits, etc. • • •					
$2.40^{+0.64}_{-0.44}\pm0.28$		[2,3,4] WANG	05A	BELL	Repl. by CHEN 08C
$1.88^{+0.77}_{-0.60}\pm0.23$		[2,3,5] WANG	04	BELL	Repl. by WANG 05A
<7.2	90	[2,3] ABE	02K	BELL	Repl. by WANG 04

[1] Explicitly vetoes resonant production of $p\overline{p}$ from charmonium states.
[2] Assumes equal production of B^+ and B^0 at the $\Upsilon(4S)$.
[3] Explicitly vetoes resonant production of $p\overline{p}$ from charmonium states and pK^0 production from Λ_c.
[4] Provides also results with $M_{p\overline{p}} < 2.85$ GeV/c^2 and angular asymmetry of $p\overline{p}$ system.
[5] The branching fraction for $M_{p\overline{p}} < 2.85$ is also reported.

$\Gamma(\Theta(1540)^+\overline{p},\ \Theta^+ \to pK^0_S)/\Gamma_{total}$ — Γ_{461}/Γ

VALUE (units 10^{-6})	CL%	DOCUMENT ID		TECN	COMMENT
<0.05	90	[1] AUBERT	07AV	BABR	$e^+e^- \to \Upsilon(4S)$
• • • We do not use the following data for averages, fits, limits, etc. • • •					
<0.23	90	[1] WANG	05A	BELL	$e^+e^- \to \Upsilon(4S)$

[1] Assumes equal production of B^+ and B^0 at the $\Upsilon(4S)$.

$\Gamma(f_J(2220)K^0,\ f_J \to p\overline{p})/\Gamma_{total}$ — Γ_{462}/Γ

VALUE (units 10^{-6})	CL%	DOCUMENT ID		TECN	COMMENT
<0.45	90	[1] AUBERT	07AV	BABR	$e^+e^- \to \Upsilon(4S)$

[1] Assumes equal production of B^+ and B^0 at the $\Upsilon(4S)$.

$\Gamma(p\overline{p}K^+\pi^-)/\Gamma_{total}$ — Γ_{459}/Γ

VALUE (units 10^{-6})	DOCUMENT ID		TECN	COMMENT
6.3±0.5±0.2	[1,2] AAIJ	17BD	LHCB	pp at 7, 8 TeV

[1] AAIJ 17BD reports $[\Gamma(B^0 \to p\overline{p}K^+\pi^-)/\Gamma_{total}]$ / $[B(B^0 \to J/\psi(1S)K^*(892)^0)]$ / $[B(J/\psi(1S) \to p\overline{p})]$ / $[B(K^*(892) \to (K\pi)^\pm)] = 2.34\pm0.12\pm0.12$ which we multiply by our best values $B(B^0 \to J/\psi(1S)K^*(892)^0) = (1.27\pm0.05)\times10^{-3}$, $B(J/\psi(1S) \to p\overline{p}) = (2.120\pm0.029)\times10^{-3}$, $B(K^*(892) \to (K\pi)^\pm) = (99.902\pm0.009)\times10^{-2}$. Our first error is their experiment's error and our second error is the systematic error from using our best values.
[2] The branching ratio is given for $m_{p\overline{p}} < 2.85$ GeV.

$\Gamma(p\overline{p}K^*(892)^0)/\Gamma_{total}$ — Γ_{463}/Γ

VALUE (units 10^{-6})	CL%	DOCUMENT ID		TECN	COMMENT
$1.24^{+0.28}_{-0.25}$ OUR AVERAGE					
$1.18^{+0.29}_{-0.25}\pm0.11$		[1,2] CHEN	08C	BELL	$e^+e^- \to \Upsilon(4S)$
1.47±0.45±0.40		[2] AUBERT	07AV	BABR	$e^+e^- \to \Upsilon(4S)$
• • • We do not use the following data for averages, fits, limits, etc. • • •					
<7.6	90	[2] WANG	04	BELL	$e^+e^- \to \Upsilon(4S)$

[1] Explicitly vetoes resonant production of $p\overline{p}$ from charmonium states.
[2] Assumes equal production of B^+ and B^0 at the $\Upsilon(4S)$.

Downloaded from https://academic.oup.com/ptep/article/2022/8/083C01/6651666 by KIT Library user on 27 September 2022

$\Gamma(p\overline{p}\pi^0)/\Gamma_{total}$ — Γ_{466}/Γ

VALUE (units 10^{-7})	DOCUMENT ID		TECN	COMMENT
5.0±1.8±0.6	PAL	19	BELL	$e^+e^- \to \Upsilon(4S)$

$\Gamma(f_J(2220)K^*_0,\ f_J \to p\overline{p})/\Gamma_{total}$ — Γ_{464}/Γ

VALUE (units 10^{-6})	CL%	DOCUMENT ID		TECN	COMMENT
<0.15	90	[1] AUBERT	07AV	BABR	$e^+e^- \to \Upsilon(4S)$

[1] Assumes equal production of B^+ and B^0 at the $\Upsilon(4S)$.

$\Gamma(p\overline{p}K^+K^-)/\Gamma_{total}$ — Γ_{465}/Γ

VALUE (units 10^{-8})	DOCUMENT ID		TECN	COMMENT
12.1±3.1±0.5	[1,2] AAIJ	17BD	LHCB	pp at 7, 8 TeV

[1] AAIJ 17BD reports $[\Gamma(B^0 \to p\overline{p}K^+K^-)/\Gamma_{total}]$ / $[B(B^0 \to J/\psi(1S)K^*(892)^0)]$ / $[B(J/\psi(1S) \to p\overline{p})]$ / $[B(K^*(892) \to (K\pi)^\pm)] = 0.045 \pm 0.011 \pm 0.004$ which we multiply by our best values $B(B^0 \to J/\psi(1S)K^*(892)^0) = (1.27 \pm 0.05) \times 10^{-3}$, $B(J/\psi(1S) \to p\overline{p}) = (2.120 \pm 0.029) \times 10^{-3}$, $B(K^*(892) \to (K\pi)^\pm) = (99.902 \pm 0.009) \times 10^{-2}$. Our first error is their experiment's error and our second error is the systematic error from using our best values.

[2] The branching ratio is given for $m_{p\overline{p}} < 2.85$ GeV.

$\Gamma(p\overline{p}K^+K^-)/\Gamma(p\overline{p}K^+\pi^-)$ — $\Gamma_{465}/\Gamma_{459}$

VALUE (%)	DOCUMENT ID		TECN	COMMENT
• • • We do not use the following data for averages, fits, limits, etc. • • •				
1.9±0.5±0.2	[1] AAIJ	17BD	LHCB	pp at 7, 8 TeV

[1] The ratio is given for $m_{p\overline{p}} < 2.85$ GeV.

$\Gamma(pp\overline{p}\overline{p})/\Gamma_{total}$ — Γ_{467}/Γ

VALUE	CL%	DOCUMENT ID		TECN	COMMENT
$<2.0 \times 10^{-7}$	90	[1] LEES	18C	BABR	$e^+e^- \to \Upsilon(4S)$

[1] Assumes equal production of B^+ and B^0 at the $\Upsilon(4S)$.

$\Gamma(p\overline{\Lambda}\pi^-)/\Gamma_{total}$ — Γ_{468}/Γ

VALUE (units 10^{-6})	CL%	DOCUMENT ID		TECN	COMMENT
3.14±0.29 OUR AVERAGE					
3.07±0.31±0.23		[1] AUBERT	09AC	BABR	$e^+e^- \to \Upsilon(4S)$
$3.23^{+0.33}_{-0.29}\pm0.29$		[1] WANG	07C	BELL	$e^+e^- \to \Upsilon(4S)$
• • • We do not use the following data for averages, fits, limits, etc. • • •					
$2.62^{+0.44}_{-0.40}\pm0.31$		[1,2] WANG	05A	BELL	Repl. by WANG 07C
$3.97^{+1.00}_{-0.80}\pm0.56$		[1] WANG	03	BELL	Repl. by WANG 05A
< 13	90	[1] COAN	99	CLE2	$e^+e^- \to \Upsilon(4S)$
<180	90	[3] ALBRECHT	88F	ARG	$e^+e^- \to \Upsilon(4S)$

[1] Assumes equal production of B^+ and B^0 at the $\Upsilon(4S)$.

[2] Provides also results with $M_{p\overline{p}} < 2.85$ GeV/c^2 and angular asymmetry of $p\overline{\Lambda}$ system.

[3] ALBRECHT 88F reports $< 2.0 \times 10^{-4}$ assuming the $\Upsilon(4S)$ decays 45% to $B^0\overline{B}^0$. We rescale to 50%.

$\Gamma(p\overline{\Lambda}\pi^-\gamma)/\Gamma_{total}$ — Γ_{469}/Γ

VALUE	CL%	DOCUMENT ID		TECN	COMMENT
$<6.5 \times 10^{-7}$	90	[1] LAI	14	BELL	$e^+e^- \to \Upsilon(4S)$

[1] Assumes equal production of B^+ and B^0 at the $\Upsilon(4S)$.

$\Gamma(p\overline{\Sigma}(1385)^-)/\Gamma_{total}$ — Γ_{470}/Γ

VALUE (units 10^{-6})	CL%	DOCUMENT ID		TECN	COMMENT
<0.26	90	[1] WANG	07C	BELL	$e^+e^- \to \Upsilon(4S)$

[1] Assumes equal production of B^+ and B^0 at the $\Upsilon(4S)$.

$[\Gamma(\Delta(1232)^+\overline{p}) + \Gamma(\Delta(1232)^-p)]/\Gamma_{total}$ — Γ_{471}/Γ

VALUE	DOCUMENT ID		TECN	COMMENT
$<1.6 \times 10^{-6}$	PAL	19	BELL	$e^+e^- \to \Upsilon(4S)$

$\Gamma(\Delta^0\overline{\Lambda})/\Gamma_{total}$ — Γ_{472}/Γ

VALUE (units 10^{-6})	CL%	DOCUMENT ID		TECN	COMMENT
<0.93	90	[1] WANG	07C	BELL	$e^+e^- \to \Upsilon(4S)$

[1] Assumes equal production of B^+ and B^0 at the $\Upsilon(4S)$.

$\Gamma(p\overline{\Lambda}K^-)/\Gamma_{total}$ — Γ_{473}/Γ

VALUE (units 10^{-6})	CL%	DOCUMENT ID		TECN	COMMENT
<0.82	90	[1] WANG	03	BELL	$e^+e^- \to \Upsilon(4S)$

[1] Assumes equal production of B^+ and B^0 at the $\Upsilon(4S)$.

$\Gamma(p\overline{\Lambda}D^-)/\Gamma_{total}$ — Γ_{474}/Γ

VALUE (units 10^{-6})	DOCUMENT ID		TECN	COMMENT
25.1±2.6±3.5	[1] CHANG	15	BELL	$e^+e^- \to \Upsilon(4S)$

[1] Assumes equal production of B^+ and B^0 at the $\Upsilon(4S)$.

$\Gamma(p\overline{\Lambda}D^{*-})/\Gamma_{total}$ — Γ_{475}/Γ

VALUE (units 10^{-6})	DOCUMENT ID		TECN	COMMENT
33.6±6.3±4.4	[1] CHANG	15	BELL	$e^+e^- \to \Upsilon(4S)$

[1] Assumes equal production of B^+ and B^0 at the $\Upsilon(4S)$.

$\Gamma(p\overline{\Sigma}^0\pi^-)/\Gamma_{total}$ — Γ_{476}/Γ

VALUE	CL%	DOCUMENT ID		TECN	COMMENT
$<3.8 \times 10^{-6}$	90	[1] WANG	03	BELL	$e^+e^- \to \Upsilon(4S)$

[1] Assumes equal production of B^+ and B^0 at the $\Upsilon(4S)$.

$\Gamma(\overline{\Lambda}\Lambda)/\Gamma_{total}$ — Γ_{477}/Γ

VALUE (units 10^{-6})	CL%	DOCUMENT ID		TECN	COMMENT
<0.32	90	[1] TSAI	07	BELL	$e^+e^- \to \Upsilon(4S)$
• • • We do not use the following data for averages, fits, limits, etc. • • •					
<0.69	90	[1] CHANG	05	BELL	Repl. by TSAI 07
<1.2	90	[1] BORNHEIM	03	CLE2	$e^+e^- \to \Upsilon(4S)$
<1.0	90	[1] ABE	02O	BELL	Repl. by CHANG 05
<3.9	90	[1] COAN	99	CLE2	$e^+e^- \to \Upsilon(4S)$

[1] Assumes equal production of B^+ and B^0 at the $\Upsilon(4S)$.

$\Gamma(\overline{\Lambda}\Lambda K^0)/\Gamma_{total}$ — Γ_{478}/Γ

VALUE (units 10^{-6})	DOCUMENT ID		TECN	COMMENT
$4.76^{+0.84}_{-0.68}\pm0.61$	[1,2] CHANG	09	BELL	$e^+e^- \to \Upsilon(4S)$

[1] Excluding charmonium events in $2.85 < m_{\Lambda\overline{\Lambda}} < 3.128$ GeV/c^2 and $3.315 < m_{\Lambda\overline{\Lambda}} < 3.735$ GeV/c^2. Measurements in various $m_{\Lambda\overline{\Lambda}}$ bins are also reported.

[2] Assumes equal production of B^+ and B^0 at the $\Upsilon(4S)$.

$\Gamma(\overline{\Lambda}\Lambda K^{*0})/\Gamma_{total}$ — Γ_{479}/Γ

VALUE (units 10^{-6})	DOCUMENT ID		TECN	COMMENT
$2.46^{+0.87}_{-0.72}\pm0.34$	[1,2] CHANG	09	BELL	$e^+e^- \to \Upsilon(4S)$

[1] Excluding charmonium events in $2.85 < m_{\Lambda\overline{\Lambda}} < 3.128$ GeV/c^2 and $3.315 < m_{\Lambda\overline{\Lambda}} < 3.735$ GeV/c^2. Measurements in various $m_{\Lambda\overline{\Lambda}}$ bins are also reported.

[2] Assumes equal production of B^+ and B^0 at the $\Upsilon(4S)$.

$\Gamma(\overline{\Lambda}\Lambda D^0)/\Gamma_{total}$ — Γ_{480}/Γ

VALUE (units 10^{-5})	DOCUMENT ID		TECN	COMMENT
$1.00^{+0.30}_{-0.26}$ OUR AVERAGE				
$0.98^{+0.29}_{-0.26}\pm0.19$	[1,2] LEES	14B	BABR	$e^+e^- \to \Upsilon(4S)$
$1.05^{+0.57}_{-0.44}\pm0.14$	[2] CHANG	09	BELL	$e^+e^- \to \Upsilon(4S)$

[1] Evidence for 3.4 st. dev. signal significance.

[2] Assumes equal production of B^+ and B^0 at the $\Upsilon(4S)$.

$\Gamma(D^0\Sigma^0\overline{\Lambda}+\text{c.c.})/\Gamma_{total}$ — Γ_{481}/Γ

VALUE	CL%	DOCUMENT ID		TECN	COMMENT
$<3.1 \times 10^{-5}$	90	[1,2] LEES	14B	BABR	$e^+e^- \to \Upsilon(4S)$

[1] Here $\Sigma^0 \to \Lambda\gamma$.

[2] Assumes equal production of B^+ and B^0 at the $\Upsilon(4S)$.

$\Gamma(\Delta^0\overline{\Delta}^0)/\Gamma_{total}$ — Γ_{482}/Γ

VALUE	CL%	DOCUMENT ID		TECN	COMMENT
<0.0015	90	[1] BORTOLETTO	89	CLEO	$e^+e^- \to \Upsilon(4S)$

[1] BORTOLETTO 89 reports < 0.0018 assuming $\Upsilon(4S)$ decays 43% to $B^0\overline{B}^0$. We rescale to 50%.

$\Gamma(\Delta^{++}\overline{\Delta}^{--})/\Gamma_{total}$ — Γ_{483}/Γ

VALUE	CL%	DOCUMENT ID		TECN	COMMENT
$<1.1 \times 10^{-4}$	90	[1] BORTOLETTO	89	CLEO	$e^+e^- \to \Upsilon(4S)$

[1] BORTOLETTO 89 reports $< 1.3 \times 10^{-4}$ assuming $\Upsilon(4S)$ decays 43% to $B^0\overline{B}^0$. We rescale to 50%.

$\Gamma(\overline{D}^0p\overline{p})/\Gamma_{total}$ — Γ_{484}/Γ

VALUE (units 10^{-4})	DOCUMENT ID		TECN	COMMENT
1.04±0.07 OUR AVERAGE				
1.02±0.04±0.06	[1,2] DEL-AMO-SA...12		BABR	$e^+e^- \to \Upsilon(4S)$
1.18±0.15±0.16	[2] ABE	02W	BELL	$e^+e^- \to \Upsilon(4S)$
• • • We do not use the following data for averages, fits, limits, etc. • • •				
1.13±0.06±0.08	[2] AUBERT,B	06S	BABR	Repl. by DEL-AMO-SANCHEZ 12

[1] Uses the values of D and D^* branching fractions from PDG 08.

[2] Assumes equal production of B^+ and B^0 at the $\Upsilon(4S)$.

$\Gamma(D_s^-\overline{\Lambda}p)/\Gamma_{total}$ — Γ_{485}/Γ

VALUE (units 10^{-5})	DOCUMENT ID		TECN	COMMENT
2.8±0.8±0.3	[1,2] MEDVEDEVA	07	BELL	$e^+e^- \to \Upsilon(4S)$

[1] Assumes equal production of B^+ and B^0 at the $\Upsilon(4S)$.

[2] MEDVEDEVA 07 reports $(2.9 \pm 0.7 \pm 0.5 \pm 0.4) \times 10^{-5}$ from a measurement of $[\Gamma(B^0 \to D_s^-\overline{\Lambda}p)/\Gamma_{total}] \times [B(D_s^+ \to \phi\pi^+)]$ assuming $B(D_s^+ \to \phi\pi^+) = (4.4 \pm 0.6) \times 10^{-2}$, which we rescale to our best value $B(D_s^+ \to \phi\pi^+) = (4.5 \pm 0.4) \times 10^{-2}$. Our first error is their experiment's error and our second error is the systematic error from using our best value.

Downloaded from https://academic.oup.com/ptep/article/2022/8/083C01/6651666 by KIT Library user on 27 September 2022

$\Gamma(\overline{D}^*(2007)^0 p\overline{p})/\Gamma_{total}$ — Γ_{486}/Γ

VALUE (units 10^{-4})	DOCUMENT ID		TECN	COMMENT
0.99±0.11 OUR AVERAGE				
0.97±0.07±0.09	[1,2] DEL-AMO-SA...12		BABR	$e^+e^- \to \Upsilon(4S)$
$1.20^{+0.33}_{-0.29}\pm0.21$	[2] ABE	02W	BELL	$e^+e^- \to \Upsilon(4S)$
• • • We do not use the following data for averages, fits, limits, etc. • • •				
1.01±0.10±0.09	[2] AUBERT,B	06S	BABR	Repl. by DEL-AMO-SANCHEZ 12

[1] Uses the values of D and D^* branching fractions from PDG 08.
[2] Assumes equal production of B^+ and B^0 at the $\Upsilon(4S)$.

$\Gamma(D^*(2010)^- p\overline{n})/\Gamma_{total}$ — Γ_{487}/Γ

VALUE (units 10^{-4})	DOCUMENT ID		TECN	COMMENT
$14.5^{+3.4}_{-3.0}\pm2.7$	[1] ANDERSON	01	CLE2	$e^+e^- \to \Upsilon(4S)$

[1] Assumes equal production of B^+ and B^0 at the $\Upsilon(4S)$.

$\Gamma(D^- p\overline{p}\pi^+)/\Gamma_{total}$ — Γ_{488}/Γ

VALUE (units 10^{-4})	DOCUMENT ID		TECN	COMMENT
3.32±0.10±0.29	[1,2] DEL-AMO-SA...12		BABR	$e^+e^- \to \Upsilon(4S)$
• • • We do not use the following data for averages, fits, limits, etc. • • •				
3.38±0.14±0.29	[2] AUBERT,B	06S	BABR	Repl. by DEL-AMO-SANCHEZ 12

[1] Uses the values of D and D^* branching fractions from PDG 08.
[2] Assumes equal production of B^+ and B^0 at the $\Upsilon(4S)$.

$\Gamma(D^*(2010)^- p\overline{p}\pi^+)/\Gamma_{total}$ — Γ_{489}/Γ

VALUE (units 10^{-4})	DOCUMENT ID		TECN	COMMENT
4.7 ±0.5 OUR AVERAGE Error includes scale factor of 1.2.				
4.55±0.16±0.39	[1,2] DEL-AMO-SA...12		BABR	$e^+e^- \to \Upsilon(4S)$
$6.5\ ^{+1.3}_{-1.2}\ \pm1.0$	[2] ANDERSON	01	CLE2	$e^+e^- \to \Upsilon(4S)$
• • • We do not use the following data for averages, fits, limits, etc. • • •				
4.81±0.22±0.44	[2] AUBERT,B	06S	BABR	Repl. by DEL-AMO-SANCHEZ 12

[1] Uses the values of D and D^* branching fractions from PDG 08.
[2] Assumes equal production of B^+ and B^0 at the $\Upsilon(4S)$.

$\Gamma(\overline{D}^0 p\overline{p}\pi^+\pi^-)/\Gamma_{total}$ — Γ_{490}/Γ

VALUE (units 10^{-4})	DOCUMENT ID		TECN	COMMENT
2.99±0.21±0.45	[1,2] DEL-AMO-SA...12		BABR	$e^+e^- \to \Upsilon(4S)$

[1] Uses the values of D and D^* branching fractions from PDG 08.
[2] Assumes equal production of B^+ and B^0 at the $\Upsilon(4S)$.

$\Gamma(\overline{D}^{*0} p\overline{p}\pi^+\pi^-)/\Gamma_{total}$ — Γ_{491}/Γ

VALUE (units 10^{-4})	DOCUMENT ID		TECN	COMMENT
1.91±0.36±0.29	[1,2] DEL-AMO-SA...12		BABR	$e^+e^- \to \Upsilon(4S)$

[1] Uses the values of D and D^* branching fractions from PDG 08.
[2] Assumes equal production of B^+ and B^0 at the $\Upsilon(4S)$.

$\Gamma(\Theta_c \overline{p}\pi^+,\ \Theta_c \to D^- p)/\Gamma_{total}$ — Γ_{492}/Γ

VALUE (units 10^{-6})	CL%	DOCUMENT ID		TECN	COMMENT
<9	90	[1] AUBERT,B	06S	BABR	$e^+e^- \to \Upsilon(4S)$

[1] Assumes equal production of B^+ and B^0 at the $\Upsilon(4S)$.

$\Gamma(\Theta_c \overline{p}\pi^+,\ \Theta_c \to D^{*-} p)/\Gamma_{total}$ — Γ_{493}/Γ

VALUE (units 10^{-6})	CL%	DOCUMENT ID		TECN	COMMENT
<14	90	[1] AUBERT,B	06S	BABR	$e^+e^- \to \Upsilon(4S)$

[1] Assumes equal production of B^+ and B^0 at the $\Upsilon(4S)$.

$\Gamma(\overline{\Sigma}_c^{--}\Delta^{++})/\Gamma_{total}$ — Γ_{494}/Γ

VALUE	CL%	DOCUMENT ID		TECN	COMMENT
$<8\times10^{-4}$	90	[1] PROCARIO	94	CLE2	$e^+e^- \to \Upsilon(4S)$

[1] PROCARIO 94 reports <0.0012 from a measurement of $[\Gamma(B^0 \to \overline{\Sigma}_c^{--}\Delta^{++})/\Gamma_{total}] \times [B(\Lambda_c^+ \to pK^-\pi^+)]$ assuming $B(\Lambda_c^+ \to pK^-\pi^+) = 0.043$, which we rescale to our best value $B(\Lambda_c^+ \to pK^-\pi^+) = 6.28\times10^{-2}$.

$\Gamma(\overline{\Lambda}_c^- p\pi^+\pi^-)/\Gamma_{total}$ — Γ_{495}/Γ

VALUE (units 10^{-3})	DOCUMENT ID		TECN	COMMENT
1.02±0.14 OUR AVERAGE Error includes scale factor of 1.3. See the ideogram below.				
1.23±0.05±0.33	[1,2] LEES	13H	BABR	$e^+e^- \to \Upsilon(4S)$
$0.89\pm0.11^{+0.05}_{-0.04}$	[1,3] PARK	07	BELL	$e^+e^- \to \Upsilon(4S)$
$1.33^{+0.22}_{-0.20}\pm0.07$	[4] DYTMAN	02	CLE2	$e^+e^- \to \Upsilon(4S)$
• • • We do not use the following data for averages, fits, limits, etc. • • •				
$0.88\pm0.16^{+0.05}_{-0.04}$	[5] GABYSHEV	02	BELL	Repl. by PARK 07
$1.33^{+0.46}_{-0.42}\pm0.37$	[6] FU	97	CLE2	Repl. by DYTMAN 02

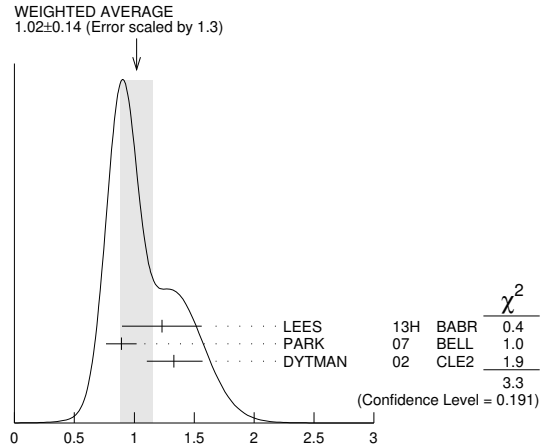

[1] Assumes equal production of B^+ and B^0 at the $\Upsilon(4S)$.
[2] Uses $\Lambda_c^+ \to pK^-\pi^+$ mode. The second error includes the uncertainty of the branching fraction of the Λ_c decay, $B(\Lambda_c^+ \to pK^-\pi^+) = (5.0\pm1.3)\%$.
[3] PARK 07 reports $(11.2\pm0.5\pm3.2)\times10^{-4}$ from a measurement of $[\Gamma(B^0 \to \overline{\Lambda}_c^- p\pi^+\pi^-)/\Gamma_{total}] \times [B(\Lambda_c^+ \to pK^-\pi^+)]$ assuming $B(\Lambda_c^+ \to pK^-\pi^+) = (5.0\pm1.3)\times10^{-2}$, which we rescale to our best value $B(\Lambda_c^+ \to pK^-\pi^+) = (6.28\pm0.32)\times10^{-2}$. Our first error is their experiment's error and our second error is the systematic error from using our best value.
[4] DYTMAN 02 reports $(1.67^{+0.27}_{-0.25})\times10^{-3}$ from a measurement of $[\Gamma(B^0 \to \overline{\Lambda}_c^- p\pi^+\pi^-)/\Gamma_{total}] \times [B(\Lambda_c^+ \to pK^-\pi^+)]$ assuming $B(\Lambda_c^+ \to pK^-\pi^+) = 0.05$, which we rescale to our best value $B(\Lambda_c^+ \to pK^-\pi^+) = (6.28\pm0.32)\times10^{-2}$. Our first error is their experiment's error and our second error is the systematic error from using our best value.
[5] GABYSHEV 02 reports $(1.1\pm0.2)\times10^{-3}$ from a measurement of $[\Gamma(B^0 \to \overline{\Lambda}_c^- p\pi^+\pi^-)/\Gamma_{total}] \times [B(\Lambda_c^+ \to pK^-\pi^+)]$ assuming $B(\Lambda_c^+ \to pK^-\pi^+) = 0.05$, which we rescale to our best value $B(\Lambda_c^+ \to pK^-\pi^+) = (6.28\pm0.32)\times10^{-2}$. Our first error is their experiment's error and our second error is the systematic error from using our best value.
[6] FU 97 uses PDG 96 values of Λ_c branching fraction.

$\Gamma(\overline{\Lambda}_c^- p)/\Gamma_{total}$ — Γ_{496}/Γ

VALUE (units 10^{-5})	CL%	DOCUMENT ID		TECN	COMMENT
1.54±0.18 OUR AVERAGE					
1.51±0.16±0.08		[1,2] AUBERT	08BN	BABR	$e^+e^- \to \Upsilon(4S)$
$2.19^{+0.56}_{-0.49}\pm0.65$		[1,3] GABYSHEV	03	BELL	$e^+e^- \to \Upsilon(4S)$
• • • We do not use the following data for averages, fits, limits, etc. • • •					
$2.10^{+0.67+0.77}_{-0.55-0.46}$		[1,4] AUBERT	07AV	BABR	Repl. by AUBERT 08BN
< 9	90	[1,5] DYTMAN	02	CLE2	$e^+e^- \to \Upsilon(4S)$
< 3.1	90	[1,4] GABYSHEV	02	BELL	$e^+e^- \to \Upsilon(4S)$
<21	90	[6] FU	97	CLE2	$e^+e^- \to \Upsilon(4S)$

[1] Assumes equal production of B^+ and B^0 at the $\Upsilon(4S)$.
[2] AUBERT 08BN reports $(1.89\pm0.21\pm0.49)\times10^{-5}$ from a measurement of $[\Gamma(B^0 \to \overline{\Lambda}_c^- p)/\Gamma_{total}] \times [B(\Lambda_c^+ \to pK^-\pi^+)]$ assuming $B(\Lambda_c^+ \to pK^-\pi^+) = (5.0\pm1.3)\times10^{-2}$, which we rescale to our best value $B(\Lambda_c^+ \to pK^-\pi^+) = (6.28\pm0.32)\times10^{-2}$. Our first error is their experiment's error and our second error is the systematic error from using our best value.
[3] The second error for GABYSHEV 03 includes the systematic and the error of $\Lambda_c \to \overline{p}K^+\pi^-$ decay branching fraction.
[4] Uses the value for $\Lambda_c \to pK^-\pi^+$ branching ratio $(5.0\pm1.3)\%$.
[5] DYTMAN 02 measurement uses $B(\Lambda_c^- \to \overline{p}K^+\pi^-) = 5.0\pm1.3\%$. The second error includes the systematic and the uncertainty of the branching ratio.
[6] FU 97 uses PDG 96 values of Λ_c branching ratio.

$\Gamma(\overline{\Lambda}_c^- p\pi^0)/\Gamma_{total}$ — Γ_{497}/Γ

VALUE (units 10^{-4})	CL%	DOCUMENT ID		TECN	COMMENT
1.55±0.17±0.08		[1,2] AUBERT	10H	BABR	$e^+e^- \to \Upsilon(4S)$
• • • We do not use the following data for averages, fits, limits, etc. • • •					
<5.9	90	[3] FU	97	CLE2	$e^+e^- \to \Upsilon(4S)$

[1] AUBERT 10H reports $(1.94\pm0.17\pm0.52)\times10^{-4}$ from a measurement of $[\Gamma(B^0 \to \overline{\Lambda}_c^- p\pi^0)/\Gamma_{total}] \times [B(\Lambda_c^+ \to pK^-\pi^+)]$ assuming $B(\Lambda_c^+ \to pK^-\pi^+) = (5.0\pm1.3)\times10^{-2}$, which we rescale to our best value $B(\Lambda_c^+ \to pK^-\pi^+) = (6.28\pm0.32)\times10^{-2}$. Our first error is their experiment's error and our second error is the systematic error from using our best value.
[2] Assumes equal production of B^+ and B^0 at the $\Upsilon(4S)$.
[3] FU 97 uses PDG 96 values of Λ_c branching ratio.

Downloaded from https://academic.oup.com/ptep/article/2022/8/083C01/6651666 by KIT Library user on 27 September 2022

$\Gamma(\Lambda_c^- p K^+ K^-)/\Gamma_{total}$ — Γ_{510}/Γ

VALUE (units 10^{-5})		DOCUMENT ID		TECN	COMMENT
2.0±0.4±0.1	[1,2]	LEES	15B	BABR	$e^+e^- \to \Upsilon(4S)$

[1] LEES 15B reports $[\Gamma(B^0 \to \Lambda_c^- p K^+ K^-)/\Gamma_{total}] \times [B(\Lambda_c^+ \to p K^- \pi^+)] = (12.5 \pm 2.0 \pm 1.0) \times 10^{-7}$ which we divide by our best value $B(\Lambda_c^+ \to p K^- \pi^+) = (6.28 \pm 0.32) \times 10^{-2}$. Our first error is their experiment's error and our second error is the systematic error from using our best value.
[2] Assumes equal production of B^+ and B^0 at the $\Upsilon(4S)$.

$\Gamma(\Lambda_c^- p \phi)/\Gamma_{total}$ — Γ_{511}/Γ

VALUE	CL%		DOCUMENT ID		TECN	COMMENT
<1.0 × 10⁻⁵	90	[1,2]	LEES	15B	BABR	$e^+e^- \to \Upsilon(4S)$

[1] LEES 15B reports $< 1.2 \times 10^{-5}$ from a measurement of $[\Gamma(B^0 \to \Lambda_c^- p \phi)/\Gamma_{total}] \times [B(\Lambda_c^+ \to p K^- \pi^+)]$ assuming $B(\Lambda_c^+ \to p K^- \pi^+) = (5.0 \pm 1.3) \times 10^{-2}$, which we rescale to our best value $B(\Lambda_c^+ \to p K^- \pi^+) = 6.28 \times 10^{-2}$.
[2] Assumes equal production of B^+ and B^0 at the $\Upsilon(4S)$.

$\Gamma(\Sigma_c(2455)^- p)/\Gamma_{total}$ — Γ_{498}/Γ

VALUE (units 10^{-6})		DOCUMENT ID		TECN	COMMENT
<24	[1,2]	AUBERT	10H	BABR	$e^+e^- \to \Upsilon(4S)$

[1] AUBERT 10H reports $[\Gamma(B^0 \to \Sigma_c(2455)^- p)/\Gamma_{total}] \times [B(\Lambda_c^+ \to p K^- \pi^+)] < 1.5 \times 10^{-6}$ which we divide by our best value $B(\Lambda_c^+ \to p K^- \pi^+) = 6.28 \times 10^{-2}$.
[2] Assumes equal production of B^+ and B^0 at the $\Upsilon(4S)$.

$\Gamma(\overline{\Lambda}_c^- p \pi^+ \pi^- \pi^0)/\Gamma_{total}$ — Γ_{499}/Γ

VALUE	CL%		DOCUMENT ID		TECN	COMMENT
<5.07 × 10⁻³	90	[1]	FU	97	CLE2	$e^+e^- \to \Upsilon(4S)$

[1] FU 97 uses PDG 96 values of Λ_c branching ratio.

$\Gamma(\overline{\Lambda}_c^- p \pi^+ \pi^- \pi^+ \pi^-)/\Gamma_{total}$ — Γ_{500}/Γ

VALUE	CL%		DOCUMENT ID		TECN	COMMENT
<2.74 × 10⁻³	90	[1]	FU	97	CLE2	$e^+e^- \to \Upsilon(4S)$

[1] FU 97 uses PDG 96 values of Λ_c branching ratio.

$\Gamma(\overline{\Lambda}_c^- p \pi^+ \pi^- (\text{nonresonant}))/\Gamma_{total}$ — Γ_{501}/Γ

VALUE (units 10^{-4})		DOCUMENT ID		TECN	COMMENT
5.5±1.0 OUR AVERAGE	Error includes scale factor of 1.3.				
7.9±0.4±2.0	[1,2]	LEES	13H	BABR	$e^+e^- \to \Upsilon(4S)$
5.1±0.8±0.3	[1,3]	PARK	07	BELL	$e^+e^- \to \Upsilon(4S)$

[1] Assumes equal production of B^+ and B^0 at the $\Upsilon(4S)$.
[2] Uses $\Lambda_c^+ \to p K^- \pi^+$ mode. The second error includes the uncertainty of the branching fraction of the Λ_c decay, $B(\Lambda_c^+ \to p K^- \pi^+) = (5.0 \pm 1.3)\%$.
[3] PARK 07 reports $(6.4 \pm 0.4 \pm 1.9) \times 10^{-4}$ from a measurement of $[\Gamma(B^0 \to \overline{\Lambda}_c^- p \pi^+ \pi^- (\text{nonresonant}))/\Gamma_{total}] \times [B(\Lambda_c^+ \to p K^- \pi^+)]$ assuming $B(\Lambda_c^+ \to p K^- \pi^+) = (5.0 \pm 1.3) \times 10^{-2}$, which we rescale to our best value $B(\Lambda_c^+ \to p K^- \pi^+) = (6.28 \pm 0.32) \times 10^{-2}$. Our first error is their experiment's error and our second error is the systematic error from using our best value.

$\Gamma(\overline{\Sigma}_c(2520)^{--} p \pi^+)/\Gamma_{total}$ — Γ_{502}/Γ

VALUE (units 10^{-4})		DOCUMENT ID		TECN	COMMENT
1.02±0.18 OUR AVERAGE					
1.15±0.10±0.30	[1,2]	LEES	13H	BABR	$e^+e^- \to \Upsilon(4S)$
0.96±0.21±0.05	[1,3]	PARK	07	BELL	$e^+e^- \to \Upsilon(4S)$
• • • We do not use the following data for averages, fits, limits, etc. • • •					
1.3 ±0.5 ±0.1	[4]	GABYSHEV	02	BELL	Repl. by PARK 07

[1] Assumes equal production of B^+ and B^0 at the $\Upsilon(4S)$.
[2] Uses $\Lambda_c^+ \to p K^- \pi^+$ mode. The second error includes the uncertainty of the branching fraction of the Λ_c decay, $B(\Lambda_c^+ \to p K^- \pi^+) = (5.0 \pm 1.3)\%$.
[3] PARK 07 reports $(1.2 \pm 0.1 \pm 0.4) \times 10^{-4}$ from a measurement of $[\Gamma(B^0 \to \overline{\Sigma}_c(2520)^{--} p \pi^+)/\Gamma_{total}] \times [B(\Lambda_c^+ \to p K^- \pi^+)]$ assuming $B(\Lambda_c^+ \to p K^- \pi^+) = (5.0 \pm 1.3) \times 10^{-2}$, which we rescale to our best value $B(\Lambda_c^+ \to p K^- \pi^+) = (6.28 \pm 0.32) \times 10^{-2}$. Our first error is their experiment's error and our second error is the systematic error from using our best value.
[4] GABYSHEV 02 reports $(1.63^{+0.64}_{-0.58}) \times 10^{-4}$ from a measurement of $[\Gamma(B^0 \to \overline{\Sigma}_c(2520)^{--} p \pi^+)/\Gamma_{total}] \times [B(\Lambda_c^+ \to p K^- \pi^+)]$ assuming $B(\Lambda_c^+ \to p K^- \pi^+) = 0.05$, which we rescale to our best value $B(\Lambda_c^+ \to p K^- \pi^+) = (6.28 \pm 0.32) \times 10^{-2}$. Our first error is their experiment's error and our second error is the systematic error from using our best value.

$\Gamma(\overline{\Sigma}_c(2520)^0 p \pi^-)/\Gamma_{total}$ — Γ_{503}/Γ

VALUE	CL%		DOCUMENT ID		TECN	COMMENT
<0.31 × 10⁻⁴	90	[1,2]	LEES	13H	BABR	$e^+e^- \to \Upsilon(4S)$
• • • We do not use the following data for averages, fits, limits, etc. • • •						
$<0.38 \times 10^{-4}$	90	[1]	PARK	07	BELL	$e^+e^- \to \Upsilon(4S)$
$<1.21 \times 10^{-4}$	90	[1,2]	GABYSHEV	02	BELL	Repl. by PARK 07

[1] Assumes equal production of B^+ and B^0 at the $\Upsilon(4S)$.
[2] Uses the value for $\Lambda_c \to p K^- \pi^+$ branching ratio $(5.0 \pm 1.3)\%$.

$\Gamma(\overline{\Sigma}_c(2455)^0 N^0,\ N^0 \to p \pi^-)/\Gamma_{total}$ — Γ_{505}/Γ

N^0 is the $N(1440)$ P_{11} or $N(1535)$ S_{11} or an admixture of the two baryonic states.

VALUE (units 10^{-4})		DOCUMENT ID		TECN	COMMENT
0.64±0.16±0.03	[1,2]	KIM	08	BELL	$e^+e^- \to \Upsilon(4S)$

[1] Assumes equal production of B^+ and B^0 at the $\Upsilon(4S)$.
[2] KIM 08 reports $(0.80 \pm 0.15 \pm 0.25) \times 10^{-4}$ from a measurement of $[\Gamma(B^0 \to \overline{\Sigma}_c(2455)^0 N^0,\ N^0 \to p \pi^-)/\Gamma_{total}] \times [B(\Lambda_c^+ \to p K^- \pi^+)]$ assuming $B(\Lambda_c^+ \to p K^- \pi^+) = (5.0 \pm 1.3) \times 10^{-2}$, which we rescale to our best value $B(\Lambda_c^+ \to p K^- \pi^+) = (6.28 \pm 0.32) \times 10^{-2}$. Our first error is their experiment's error and our second error is the systematic error from using our best value.

$\Gamma(\overline{\Sigma}_c(2455)^0 p \pi^-)/\Gamma_{total}$ — Γ_{504}/Γ

VALUE (units 10^{-4})	CL%		DOCUMENT ID		TECN	COMMENT
1.08±0.16 OUR AVERAGE						
0.91±0.07±0.24		[1,2]	LEES	13H	BABR	$e^+e^- \to \Upsilon(4S)$
1.12±0.21±0.06		[1,3]	PARK	07	BELL	$e^+e^- \to \Upsilon(4S)$
1.8 ±0.6 ±0.1		[4]	DYTMAN	02	CLE2	$e^+e^- \to \Upsilon(4S)$
• • • We do not use the following data for averages, fits, limits, etc. • • •						
$0.38^{+0.37}_{-0.33} \pm 0.02$	90	[5]	GABYSHEV	02	BELL	Repl. by PARK 07

[1] Assumes equal production of B^+ and B^0 at the $\Upsilon(4S)$.
[2] Uses $\Lambda_c^+ \to p K^- \pi^+$ mode. The second error includes the uncertainty of the branching fraction of the Λ_c decay, $B(\Lambda_c^+ \to p K^- \pi^+) = (5.0 \pm 1.3)\%$.
[3] PARK 07 reports $(1.4 \pm 0.2 \pm 0.4) \times 10^{-4}$ from a measurement of $[\Gamma(B^0 \to \overline{\Sigma}_c(2455)^0 p \pi^-)/\Gamma_{total}] \times [B(\Lambda_c^+ \to p K^- \pi^+)]$ assuming $B(\Lambda_c^+ \to p K^- \pi^+) = (5.0 \pm 1.3) \times 10^{-2}$, which we rescale to our best value $B(\Lambda_c^+ \to p K^- \pi^+) = (6.28 \pm 0.32) \times 10^{-2}$. Our first error is their experiment's error and our second error is the systematic error from using our best value.
[4] DYTMAN 02 reports $(2.2 \pm 0.7) \times 10^{-4}$ from a measurement of $[\Gamma(B^0 \to \overline{\Sigma}_c(2455)^0 p \pi^-)/\Gamma_{total}] \times [B(\Lambda_c^+ \to p K^- \pi^+)]$ assuming $B(\Lambda_c^+ \to p K^- \pi^+) = 0.05$, which we rescale to our best value $B(\Lambda_c^+ \to p K^- \pi^+) = (6.28 \pm 0.32) \times 10^{-2}$. Our first error is their experiment's error and our second error is the systematic error from using our best value.
[5] GABYSHEV 02 reports $(0.48^{+0.46}_{-0.41}) \times 10^{-4}$ from a measurement of $[\Gamma(B^0 \to \overline{\Sigma}_c(2455)^0 p \pi^-)/\Gamma_{total}] \times [B(\Lambda_c^+ \to p K^- \pi^+)]$ assuming $B(\Lambda_c^+ \to p K^- \pi^+) = 0.05$, which we rescale to our best value $B(\Lambda_c^+ \to p K^- \pi^+) = (6.28 \pm 0.32) \times 10^{-2}$. Our first error is their experiment's error and our second error is the systematic error from using our best value.

$\Gamma(\overline{\Sigma}_c(2455)^{--} p \pi^+)/\Gamma_{total}$ — Γ_{506}/Γ

VALUE (units 10^{-4})		DOCUMENT ID		TECN	COMMENT
1.83±0.24 OUR AVERAGE					
2.13±0.10±0.56	[1,2]	LEES	13H	BABR	$e^+e^- \to \Upsilon(4S)$
$1.67 \pm 0.25^{+0.09}_{-0.08}$	[1,3]	PARK	07	BELL	$e^+e^- \to \Upsilon(4S)$
$2.9 \pm 0.9^{+0.2}_{-0.1}$	[4]	DYTMAN	02	CLE2	$e^+e^- \to \Upsilon(4S)$
• • • We do not use the following data for averages, fits, limits, etc. • • •					
$1.9^{+0.6}_{-0.5} \pm 0.1$	[5]	GABYSHEV	02	BELL	Repl. by PARK 07

[1] Assumes equal production of B^+ and B^0 at the $\Upsilon(4S)$.
[2] Uses $\Lambda_c^+ \to p K^- \pi^+$ mode. The second error includes the uncertainty of the branching fraction of the Λ_c decay, $B(\Lambda_c^+ \to p K^- \pi^+) = (5.0 \pm 1.3)\%$.
[3] PARK 07 reports $(2.1 \pm 0.2 \pm 0.6) \times 10^{-4}$ from a measurement of $[\Gamma(B^0 \to \overline{\Sigma}_c(2455)^{--} p \pi^+)/\Gamma_{total}] \times [B(\Lambda_c^+ \to p K^- \pi^+)]$ assuming $B(\Lambda_c^+ \to p K^- \pi^+) = (5.0 \pm 1.3) \times 10^{-2}$, which we rescale to our best value $B(\Lambda_c^+ \to p K^- \pi^+) = (6.28 \pm 0.32) \times 10^{-2}$. Our first error is their experiment's error and our second error is the systematic error from using our best value.
[4] DYTMAN 02 reports $(3.7 \pm 1.1) \times 10^{-4}$ from a measurement of $[\Gamma(B^0 \to \overline{\Sigma}_c(2455)^{--} p \pi^+)/\Gamma_{total}] \times [B(\Lambda_c^+ \to p K^- \pi^+)]$ assuming $B(\Lambda_c^+ \to p K^- \pi^+) = 0.05$, which we rescale to our best value $B(\Lambda_c^+ \to p K^- \pi^+) = (6.28 \pm 0.32) \times 10^{-2}$. Our first error is their experiment's error and our second error is the systematic error from using our best value.
[5] GABYSHEV 02 reports $(2.38^{+0.75}_{-0.69}) \times 10^{-4}$ from a measurement of $[\Gamma(B^0 \to \overline{\Sigma}_c(2455)^{--} p \pi^+)/\Gamma_{total}] \times [B(\Lambda_c^+ \to p K^- \pi^+)]$ assuming $B(\Lambda_c^+ \to p K^- \pi^+) = 0.05$, which we rescale to our best value $B(\Lambda_c^+ \to p K^- \pi^+) = (6.28 \pm 0.32) \times 10^{-2}$. Our first error is their experiment's error and our second error is the systematic error from using our best value.

$\Gamma(\Lambda_c^- p K^+ \pi^-)/\Gamma_{total}$ — Γ_{507}/Γ

VALUE (units 10^{-5})		DOCUMENT ID		TECN	COMMENT
3.4±0.7±0.2	[1,2]	AUBERT	09AG	BABR	$e^+e^- \to \Upsilon(4S)$

[1] AUBERT 09AG reports $(4.33 \pm 0.82 \pm 0.33 \pm 1.13) \times 10^{-5}$ from a measurement of $[\Gamma(B^0 \to \Lambda_c^- p K^+ \pi^-)/\Gamma_{total}] \times [B(\Lambda_c^+ \to p K^- \pi^+)]$ assuming $B(\Lambda_c^+ \to p K^- \pi^+) = (5.0 \pm 1.3) \times 10^{-2}$, which we rescale to our best value $B(\Lambda_c^+ \to p K^- \pi^+) = (6.28 \pm 0.32) \times 10^{-2}$. Our first error is their experiment's error and our second error is the systematic error from using our best value.
[2] Assumes equal production of B^+ and B^0 at the $\Upsilon(4S)$.

Downloaded from https://academic.oup.com/ptep/article/2022/8/083C01/6651666 by KIT Library user on 27 September 2022

$\Gamma(\overline{\Sigma}_c(2455)^{--} p K^+, \overline{\Sigma}_c^{--} \to \overline{\Lambda}_c^- \pi^-)/\Gamma_{total}$ — Γ_{508}/Γ

VALUE (units 10^{-5})	DOCUMENT ID		TECN	COMMENT
$0.88 \pm 0.25^{+0.05}_{-0.04}$	[1,2] AUBERT	09AG	BABR	$e^+e^- \to \Upsilon(4S)$

[1] AUBERT 09AG reports $(1.11 \pm 0.30 \pm 0.09 \pm 0.29) \times 10^{-5}$ from a measurement of $[\Gamma(B^0 \to \overline{\Sigma}_c(2455)^{--} p K^+, \overline{\Sigma}_c^{--} \to \overline{\Lambda}_c^- \pi^-)/\Gamma_{total}] \times [B(\Lambda_c^+ \to p K^- \pi^+)]$ assuming $B(\Lambda_c^+ \to p K^- \pi^+) = (5.0 \pm 1.3) \times 10^{-2}$, which we rescale to our best value $B(\Lambda_c^+ \to p K^- \pi^+) = (6.28 \pm 0.32) \times 10^{-2}$. Our first error is their experiment's error and our second error is the systematic error from using our best value.
[2] Assumes equal production of B^+ and B^0 at the $\Upsilon(4S)$.

$\Gamma(\Lambda_c^- p K^*(892)^0)/\Gamma_{total}$ — Γ_{509}/Γ

VALUE (units 10^{-5})	CL%	DOCUMENT ID		TECN	COMMENT
<2.42	90	[1] AUBERT	09AG	BABR	$e^+e^- \to \Upsilon(4S)$

[1] Assumes equal production of B^+ and B^0 at the $\Upsilon(4S)$.

$\Gamma(\Lambda_c^- p \overline{p} p)/\Gamma_{total}$ — Γ_{512}/Γ

VALUE (units 10^{-6})	DOCUMENT ID		TECN	COMMENT
<2.8	[1] LEES	14C	BABR	$e^+e^- \to \Upsilon(4S)$

[1] Assumes equal production of B^+ and B^0 at the $\Upsilon(4S)$ and $B(\Lambda_c^+ \to p K^- \pi^+) = 0.050 \pm 0.013$.

$\Gamma(\overline{\Lambda}_c^- \Lambda K^+)/\Gamma_{total}$ — Γ_{513}/Γ

VALUE (units 10^{-5})	DOCUMENT ID		TECN	COMMENT
$4.8 \pm 1.1^{+0.2}_{-0.3}$	[1,2] LEES	11F	BABR	$e^+e^- \to \Upsilon(4S)$

[1] Assumes equal production of B^0 and B^+ from Upsilon(4S) decays.
[2] LEES 11F reports $(3.8 \pm 0.8 \pm 0.2 \pm 1.0) \times 10^{-5}$ from a measurement of $[\Gamma(B^0 \to \overline{\Lambda}_c^- \Lambda K^+)/\Gamma_{total}] / [B(\Lambda_c^+ \to p K^- \pi^+)] / [B(\Lambda \to p \pi^-)]$ assuming $B(\Lambda_c^+ \to p K^- \pi^+) = (5.0 \pm 1.3) \times 10^{-2}$, $B(\Lambda \to p \pi^-) = (63.9 \pm 0.5) \times 10^{-2}$, which we rescale to our best values $B(\Lambda_c^+ \to p K^- \pi^+) = (6.28 \pm 0.32) \times 10^{-2}$, $B(\Lambda \to p \pi^-) = (63.9 \pm 0.5) \times 10^{-2}$. Our first error is their experiment's error and our second error is the systematic error from using our best values. The reported uncertainties are statistical, systematic, and $\overline{\Lambda}_c^-$ branching fraction uncertainty.

$\Gamma(\overline{\Lambda}_c^- \Lambda_c^+)/\Gamma_{total}$ — Γ_{514}/Γ

VALUE (units 10^{-5})	CL%	DOCUMENT ID		TECN	COMMENT
<1.6	95	[1] AAIJ	14AA	LHCB	pp at 7 TeV
• • • We do not use the following data for averages, fits, limits, etc. • • •					
<6.2	90	[2] UCHIDA	08	BELL	$e^+e^- \to \Upsilon(4S)$

[1] Uses $B(\overline{B}^0 \to D^+ D_s^-) = (7.2 \pm 0.8) \times 10^{-3}$.
[2] Assumes equal production of B^+ and B^0 at the $\Upsilon(4S)$.

$\Gamma(\overline{\Lambda}_c(2593)^- / \overline{\Lambda}_c(2625)^- p)/\Gamma_{total}$ — Γ_{515}/Γ

VALUE	CL%	DOCUMENT ID		TECN	COMMENT
$<1.1 \times 10^{-4}$	90	[1,2] DYTMAN	02	CLE2	$e^+e^- \to \Upsilon(4S)$

[1] Assumes equal production of B^+ and B^0 at the $\Upsilon(4S)$.
[2] DYTMAN 02 measurement uses $B(\Lambda_c^- \to \overline{p} K^+ \pi^-) = 5.0 \pm 1.3\%$. The second error includes the systematic and the uncertainty of the branching ratio.

$\Gamma(\overline{\Xi}_c^- \Lambda_c^+)/\Gamma_{total}$ — Γ_{516}/Γ

VALUE (units 10^{-3})	DOCUMENT ID		TECN	COMMENT
$1.2 \pm 0.7 \pm 0.3$	[1,2] LI	19C	BELL	$e^+e^- \to \Upsilon(4S)$

[1] Uses fully reconstructed B^0 on tag side with recoil against Λ_c^+.
[2] LI 19C reports $(1.16 \pm 0.74 \pm 0.33) \times 10^{-3}$ from a measurement of $[\Gamma(B^0 \to \overline{\Xi}_c^- \Lambda_c^+)/\Gamma_{total}] \times [B(\Lambda_c^+ \to p K^- \pi^+)]$ assuming $B(\Lambda_c^+ \to p K^- \pi^+) = (6.28 \pm 0.32) \times 10^{-2}$.

$\Gamma(\overline{\Xi}_c^- \Lambda_c^+, \overline{\Xi}_c^- \to \overline{\Xi}^+ \pi^- \pi^-)/\Gamma_{total}$ — Γ_{517}/Γ

VALUE (units 10^{-5})	DOCUMENT ID		TECN	COMMENT
2.4 ± 1.1 OUR AVERAGE Error includes scale factor of 1.8.				
$3.3 \pm 0.7 \pm 0.3$	[1] LI	19C	BELL	$e^+e^- \to \Upsilon(4S)$
$1.2 \pm 0.9 \pm 0.1$	[2,3] AUBERT	08H	BABR	$e^+e^- \to \Upsilon(4S)$
• • • We do not use the following data for averages, fits, limits, etc. • • •				
$7.4^{+3.3}_{-2.7} \pm 0.4$	[3,4] CHISTOV	06A	BELL	Repl. by LI 19C

[1] LI 19C reports $(3.32 \pm 0.74 \pm 0.33) \times 10^{-5}$ from a measurement of $[\Gamma(B^0 \to \overline{\Xi}_c^- \Lambda_c^+, \overline{\Xi}_c^- \to \overline{\Xi}^+ \pi^- \pi^-)/\Gamma_{total}] \times [B(\Lambda_c^+ \to p K^- \pi^+)]$ assuming $B(\Lambda_c^+ \to p K^- \pi^+) = (6.28 \pm 0.32) \times 10^{-2}$.
[2] AUBERT 08H reports $(1.5 \pm 1.07 \pm 0.44) \times 10^{-5}$ from a measurement of $[\Gamma(B^0 \to \overline{\Xi}_c^- \Lambda_c^+, \overline{\Xi}_c^- \to \overline{\Xi}^+ \pi^- \pi^-)/\Gamma_{total}] \times [B(\Lambda_c^+ \to p K^- \pi^+)]$ assuming $B(\Lambda_c^+ \to p K^- \pi^+) = (5.0 \pm 1.3) \times 10^{-2}$, which we rescale to our best value $B(\Lambda_c^+ \to p K^- \pi^+) = (6.28 \pm 0.32) \times 10^{-2}$. Our first error is their experiment's error and our second error is the systematic error from using our best value.
[3] Assumes equal production of B^+ and B^0 at the $\Upsilon(4S)$.
[4] CHISTOV 06A reports $(9.3^{+3.7}_{-2.8} \pm 3.1) \times 10^{-5}$ from a measurement of $[\Gamma(B^0 \to \overline{\Xi}_c^- \Lambda_c^+, \overline{\Xi}_c^- \to \overline{\Xi}^+ \pi^- \pi^-)/\Gamma_{total}] \times [B(\Lambda_c^+ \to p K^- \pi^+)]$ assuming $B(\Lambda_c^+ \to p K^- \pi^+) = (5.0 \pm 1.3) \times 10^{-2}$, which we rescale to our best value $B(\Lambda_c^+ \to p K^- \pi^+) = (6.28 \pm 0.32) \times 10^{-2}$. Our first error is their experiment's error and our second error is the systematic error from using our best value.

$\Gamma(\overline{\Xi}_c^- \Lambda_c^+, \overline{\Xi}_c^- \to \overline{p} K^+ \pi^-)/\Gamma_{total}$ — Γ_{518}/Γ

VALUE (units 10^{-6})	DOCUMENT ID		TECN	COMMENT
$5.3 \pm 1.5 \pm 0.7$	[1] LI	19C	BELL	$e^+e^- \to \Upsilon(4S)$

[1] LI 19C reports $(5.27 \pm 1.51 \pm 0.69) \times 10^{-6}$ from a measurement of $[\Gamma(B^0 \to \overline{\Xi}_c^- \Lambda_c^+, \overline{\Xi}_c^- \to \overline{p} K^+ \pi^-)/\Gamma_{total}] \times [B(\Lambda_c^+ \to p K^- \pi^+)]$ assuming $B(\Lambda_c^+ \to p K^- \pi^+) = (6.28 \pm 0.32) \times 10^{-2}$.

$\Gamma(\Lambda_c^+ \Lambda_c^- K^0)/\Gamma_{total}$ — Γ_{519}/Γ

VALUE (units 10^{-4})	DOCUMENT ID		TECN	COMMENT
4.0 ± 0.9 OUR AVERAGE				
$3.99 \pm 0.76 \pm 0.51$	[1] LI	18D	BELL	$e^+e^- \to \Upsilon(4S)$
$3.8 \pm 3.1 \pm 2.1$	[2,3] AUBERT	08H	BABR	$e^+e^- \to \Upsilon(4S)$
• • • We do not use the following data for averages, fits, limits, etc. • • •				
$7.9^{+2.9}_{-2.3} \pm 4.3$	[2,3] GABYSHEV	06	BELL	Repl. by LI 18D

[1] Assumes $B(\Upsilon(4S) \to B^0 \overline{B}^0) = 48.6 \pm 0.6\%$ and $B(\Lambda_c^+ \to p K^- \pi^+) = 6.23 \pm 0.33\%$.
[2] Assumes $B(\Lambda_c^+ \to p K^- \pi^+) = 5.0 \pm 1.3\%$.
[3] Assumes equal production of B^+ and B^0 at the $\Upsilon(4S)$.

$\Gamma(\overline{\Xi}_c(2930)^- \Lambda_c^+, \overline{\Xi}_c^- \to \Lambda_c^- K^0)/\Gamma_{total}$ — Γ_{520}/Γ

VALUE (units 10^{-4})	DOCUMENT ID		TECN	COMMENT
$2.37 \pm 0.51 \pm 0.31$	[1] LI	18D	BELL	$e^+e^- \to \Upsilon(4S)$

[1] Assumes $B(\Upsilon(4S) \to B^0 \overline{B}^0) = 48.6 \pm 0.6\%$ and $B(\Lambda_c^+ \to p K^- \pi^+) = 6.23 \pm 0.33\%$.

$\Gamma(\gamma\gamma)/\Gamma_{total}$ — Γ_{521}/Γ

Test for $\Delta B=1$ weak neutral current. Allowed by higher-order electroweak interactions.

VALUE	CL%	DOCUMENT ID		TECN	COMMENT
$<3.2 \times 10^{-7}$	90	[1] DEL-AMO-SA...	11A	BABR	$e^+e^- \to \Upsilon(4S)$
• • • We do not use the following data for averages, fits, limits, etc. • • •					
$<6.2 \times 10^{-7}$	90	[1] VILLA	06	BELL	$e^+e^- \to \Upsilon(4S)$
$<1.7 \times 10^{-6}$	90	[1] AUBERT	01I	BABR	$e^+e^- \to \Upsilon(4S)$
$<3.9 \times 10^{-5}$	90	[2] ACCIARRI	95I	L3	$e^+e^- \to Z$

[1] Assumes equal production of B^+ and B^0 at the $\Upsilon(4S)$.
[2] ACCIARRI 95I assumes $f_{B^0} = 39.5 \pm 4.0$ and $f_{B_s} = 12.0 \pm 3.0\%$.

$\Gamma(e^+e^-)/\Gamma_{total}$ — Γ_{522}/Γ

Test for $\Delta B=1$ weak neutral current. Allowed by higher-order electroweak interactions.

VALUE	CL%	DOCUMENT ID		TECN	COMMENT
$< 2.5 \times 10^{-9}$	90	[1] AAIJ	20W	LHCB	pp at 7, 8, 13 TeV
• • • We do not use the following data for averages, fits, limits, etc. • • •					
$< 8.3 \times 10^{-8}$	90	AALTONEN	09P	CDF	$p\overline{p}$ at 1.96 TeV
$<11.3 \times 10^{-8}$	90	[2] AUBERT	08P	BABR	$e^+e^- \to \Upsilon(4S)$
$< 6.1 \times 10^{-8}$	90	[2] AUBERT	05W	BABR	Repl. by AUBERT 08P
$< 1.9 \times 10^{-7}$	90	[2] CHANG	03	BELL	$e^+e^- \to \Upsilon(4S)$
$< 8.3 \times 10^{-7}$	90	[2] BERGFELD	00B	CLE2	$e^+e^- \to \Upsilon(4S)$
$< 1.4 \times 10^{-5}$	90	[3] ACCIARRI	97B	L3	$e^+e^- \to Z$
$< 5.9 \times 10^{-6}$	90	AMMAR	94	CLE2	Repl. by BERGFELD 00B
$< 2.6 \times 10^{-5}$	90	[4] AVERY	89B	CLEO	$e^+e^- \to \Upsilon(4S)$
$< 7.6 \times 10^{-5}$	90	[5] ALBRECHT	87D	ARG	$e^+e^- \to \Upsilon(4S)$
$< 6.4 \times 10^{-5}$	90	[6] AVERY	87	CLEO	$e^+e^- \to \Upsilon(4S)$
$< 3 \times 10^{-4}$	90	GILES	84	CLEO	Repl. by AVERY 87

[1] Assumes no contribution from $B_s^0 \to e^+e^-$ decays.
[2] Assumes equal production of B^+ and B^0 at the $\Upsilon(4S)$.
[3] ACCIARRI 97B assume PDG 96 production fractions for B^+, B^0, B_s, and Λ_b.
[4] AVERY 89B reports $< 3 \times 10^{-5}$ assuming the $\Upsilon(4S)$ decays 43% to $B^0 \overline{B}^0$. We rescale to 50%.
[5] ALBRECHT 87D reports $< 8.5 \times 10^{-5}$ assuming the $\Upsilon(4S)$ decays 45% to $B^0 \overline{B}^0$. We rescale to 50%.
[6] AVERY 87 reports $< 8 \times 10^{-5}$ assuming the $\Upsilon(4S)$ decays 40% to $B^0 \overline{B}^0$. We rescale to 50%.

$\Gamma(e^+e^-\gamma)/\Gamma_{total}$ — Γ_{523}/Γ

Test for $\Delta B=1$ weak neutral current. Allowed by higher-order electroweak interactions.

VALUE	CL%	DOCUMENT ID		TECN	COMMENT
$<1.2 \times 10^{-7}$	90	AUBERT	08C	BABR	$e^+e^- \to \Upsilon(4S)$

$\Gamma(\mu^+\mu^-)/\Gamma_{total}$ — Γ_{524}/Γ

Test for $\Delta B=1$ weak neutral current. Allowed by higher-order electroweak interactions.

VALUE (units 10^{-9})	CL%	DOCUMENT ID		TECN	COMMENT
$0.07^{+0.13}_{-0.11}$ OUR AVERAGE Error includes scale factor of 1.8.					
$0.12^{+0.08}_{-0.07} \pm 0.01$		[1] AAIJ	22	LHCB	pp at 7, 8, 13 TeV
-0.19 ± 0.16		[2,3] AABOUD	19L	ATLS	pp at 7, 8, 13 TeV
• • • We do not use the following data for averages, fits, limits, etc. • • •					
< 0.36	95	[4] SIRUNYAN	20AG		pp at 7, 8, 13 TeV
$0.15^{+0.12+0.02}_{-0.10-0.01}$		[5] AAIJ	17AI	LHCB	Repl. by AAIJ 22
-0.25 ± 0.20		[6] AABOUD	16L	ATLS	Repl. by AABOUD 19L
$0.39^{+0.16}_{-0.14}$		[7] KHACHATRY...	15BE	LHC	pp at 7, 8 TeV
< 0.80	90	[8] AAIJ	13B	LHCB	Repl. by AAIJ 13BA
< 0.63	90	[9] AAIJ	13BA	LHCB	Repl. by KHACHATRYAN 15BE

Downloaded from https://academic.oup.com/ptep/article/2022/8/083C01/6651666 by KIT Library user on 27 September 2022

< 3.8	90	[10] AALTONEN	13F	CDF	$p\overline{p}$ at 1.96 TeV
$0.35^{+0.21}_{-0.18}$		[11] CHATRCHYAN	13AW	CMS	Repl. by SIRUNYAN 20AG
< 2.6	90	[8] AAIJ	12A	LHCB	Repl. by AAIJ 12W
< 0.81	90	[12] AAIJ	12W	LHCB	Repl. by AAIJ 13B
< 1.4	90	[12] CHATRCHYAN	12A	CMS	pp at 7 TeV
< 12	90	[13] AAIJ	11B	LHCB	Repl. by AAIJ 12A
< 5.0	90	[12] AALTONEN	11AG	CDF	$p\overline{p}$ at 1.96 TeV
< 3.7	90	[12] CHATRCHYAN	11T	CMS	Repl. by CHATRCHYAN 12A

[1] Corresponds to a 95% CL upper limit of $< 2.6 \times 10^{-10}$.
[2] Corresponds to a 95% CL upper limit of $< 2.1 \times 10^{-10}$.
[3] Uses normalization mode $B(B^+ \to J/\psi K^+) = (1.010 \pm 0.029) \times 10^{-3}$ and B production ratio $f(b \to B^0_s)/f(b \to B^0) = 0.256 \pm 0.013$.
[4] Uses normalization mode $B(B^+ \to J/\psi K^+) = (1.01 \pm 0.03) \times 10^{-3}$.
[5] Corresponds to a 95% CL upper limit of $< 3.4 \times 10^{-10}$.
[6] This value is obtained from a profile-likelihood fit, see Fig. 9. It corresponds to an uppper limit of $< 0.42 \times 10^{-9}$ at 95% C.L.
[7] Derived from the combined fit to CMS and LHCb data. Uncertainty includes both statistical and systematic component. Also reports $B(B^0 \to \mu^+\mu^-)/B(B_s \to \mu^+\mu^-) = 0.14^{+0.08}_{-0.06}$.
[8] Uses $B(B^+ \to J/\psi K^+ \to \mu^+\mu^- K^+) = (6.01 \pm 0.21) \times 10^{-5}$ and $B(B^0 \to K^+\pi^-) = (1.94 \pm 0.06) \times 10^{-5}$ for normalization.
[9] Reports also a limit of $< 7.4 \times 10^{-10}$ at 95% CL. Uses normalization modes $B^+ \to J/\psi K^+ \to \mu^+\mu^- K^+$ and $B^0 \to K^+\pi^-$.
[10] Uses normalization mode $B(B^+ \to J/\psi K^+) = (10.22 \pm 0.35) \times 10^{-4}$.
[11] Reports also a limit of $< 9.2 \times 10^{-10}$ at 90% CL. and uses $B(B^+ \to J/\psi K^+ \to \mu^+\mu^- K^+) = (6.0 \pm 0.2) \times 10^{-5}$ for normalization.
[12] Uses $B(B^+ \to J/\psi K^+ \to \mu^+\mu^- K^+) = (6.01 \pm 0.21) \times 10^{-5}$.
[13] Uses B production ratio $f(\overline{b} \to B^+)/f(\overline{b} \to B^0_s) = 3.71 \pm 0.47$ and three normalization modes.

$\Gamma(\mu^+\mu^-\gamma)/\Gamma_{total}$ — Γ_{525}/Γ

Test for ΔB=1 weak neutral current. Allowed by higher-order electroweak interactions.

VALUE	CL%	DOCUMENT ID		TECN	COMMENT
$< 2.0 \times 10^{-9}$	95	[1] AAIJ	22	LHCB	pp at 7, 8, 13 TeV
• • • We do not use the following data for averages, fits, limits, etc. • • •					
$< 1.6 \times 10^{-7}$	90	AUBERT	08C	BABR	$e^+e^- \to \Upsilon(4S)$

[1] The exclusion is limited to the range $m_{\mu\mu} > 4.9$ GeV/c^2.

$\Gamma(\tau^+\tau^-)/\Gamma_{total}$ — Γ_{528}/Γ

Test for ΔB=1 weak neutral current. Allowed by higher-order electroweak interactions.

VALUE	CL%	DOCUMENT ID		TECN	COMMENT
$< 2.1 \times 10^{-3}$	95	[1] AAIJ	17AJ	LHCB	pp at 7, 8 TeV
• • • We do not use the following data for averages, fits, limits, etc. • • •					
$< 4.1 \times 10^{-3}$	90	[2] AUBERT	06S	BABR	$e^+e^- \to \Upsilon(4S)$

[1] Assuming no contribution from $B^0_s \to \tau^+\tau^-$.
[2] Assumes equal production of B^+ and B^0 at the $\Upsilon(4S)$.

$\Gamma(\mu^+\mu^-\mu^+\mu^-)/\Gamma_{total}$ — Γ_{526}/Γ

VALUE	CL%	DOCUMENT ID		TECN	COMMENT
$< 6.9 \times 10^{-10}$	95	AAIJ	17N	LHCB	pp at 7, 8 TeV
• • • We do not use the following data for averages, fits, limits, etc. • • •					
$< 5.3 \times 10^{-9}$	90	[1] AAIJ	13AW	LHCB	Repl. by AAIJ 17N

[1] Also reports a limit of $< 6.6 \times 10^{-9}$ at 95% CL.

$\Gamma(SP, S \to \mu^+\mu^-, P \to \mu^+\mu^-)/\Gamma_{total}$ — Γ_{527}/Γ

Here S and P are the hypothetical scalar and pseudoscalar particles with masses of 2.5 GeV/c^2 and 214.3 MeV/c^2, respectively.

VALUE	CL%	DOCUMENT ID		TECN	COMMENT
$< 6.0 \times 10^{-10}$	95	AAIJ	17N	LHCB	pp at 7, 8 TeV
• • • We do not use the following data for averages, fits, limits, etc. • • •					
$< 5.1 \times 10^{-9}$	90	[1] AAIJ	13AW	LHCB	Repl. by AAIJ 17N

[1] Also reports a limit of $< 6.3 \times 10^{-9}$ at 95% CL.

$\Gamma(\pi^0\ell^+\ell^-)/\Gamma_{total}$ — Γ_{529}/Γ

VALUE	CL%	DOCUMENT ID		TECN	COMMENT
$< 5.3 \times 10^{-8}$	90	[1] LEES	13M	BABR	$e^+e^- \to \Upsilon(4S)$
• • • We do not use the following data for averages, fits, limits, etc. • • •					
$< 1.5 \times 10^{-7}$	90	[1] WEI	08A	BELL	$e^+e^- \to \Upsilon(4S)$
$< 1.2 \times 10^{-7}$	90	[1] AUBERT	07AG	BABR	Repl. by LEES 13M

[1] Assumes equal production of B^+ and B^0 at the $\Upsilon(4S)$.

$\Gamma(\pi^0\nu\overline{\nu})/\Gamma_{total}$ — Γ_{535}/Γ

Test for $\Delta B = 1$ weak neutral current. Allowed by higher-order electroweak interaction.

VALUE	CL%	DOCUMENT ID		TECN	COMMENT
$< 0.9 \times 10^{-5}$	90	[1] GRYGIER	17	BELL	$e^+e^- \to \Upsilon(4S)$
• • • We do not use the following data for averages, fits, limits, etc. • • •					
$< 6.9 \times 10^{-5}$	90	[1] LUTZ	13	BELL	$e^+e^- \to \Upsilon(4S)$
$< 2.2 \times 10^{-4}$	90	[1] CHEN	07D	BELL	Repl. by LUTZ 13

[1] Assumes equal production of B^+ and B^0 at the $\Upsilon(4S)$.

$\Gamma(\pi^0 e^+e^-)/\Gamma_{total}$ — Γ_{530}/Γ

VALUE	CL%	DOCUMENT ID		TECN	COMMENT
$< 8.4 \times 10^{-8}$	90	[1] LEES	13M	BABR	$e^+e^- \to \Upsilon(4S)$
• • • We do not use the following data for averages, fits, limits, etc. • • •					
$< 2.3 \times 10^{-7}$	90	[1] WEI	08A	BELL	$e^+e^- \to \Upsilon(4S)$
$< 1.4 \times 10^{-7}$	90	[1] AUBERT	07AG	BABR	Repl. by LEES 13M

[1] Assumes equal production of B^+ and B^0 at the $\Upsilon(4S)$.

$\Gamma(\pi^0\mu^+\mu^-)/\Gamma_{total}$ — Γ_{531}/Γ

VALUE	CL%	DOCUMENT ID		TECN	COMMENT
$< 6.9 \times 10^{-8}$	90	[1] LEES	13M	BABR	$e^+e^- \to \Upsilon(4S)$
• • • We do not use the following data for averages, fits, limits, etc. • • •					
$< 1.8 \times 10^{-7}$	90	[1] WEI	08A	BELL	$e^+e^- \to \Upsilon(4S)$
$< 5.1 \times 10^{-7}$	90	[1] AUBERT	07AG	BABR	$e^+e^- \to \Upsilon(4S)$

[1] Assumes equal production of B^+ and B^0 at the $\Upsilon(4S)$.

$\Gamma(\eta\ell^+\ell^-)/\Gamma_{total}$ — Γ_{532}/Γ

VALUE	CL%	DOCUMENT ID		TECN	COMMENT
$< 6.4 \times 10^{-8}$	90	[1] LEES	13M	BABR	$e^+e^- \to \Upsilon(4S)$

[1] Assumes equal production of B^+ and B^0 at the $\Upsilon(4S)$.

$\Gamma(\eta e^+e^-)/\Gamma_{total}$ — Γ_{533}/Γ

VALUE	CL%	DOCUMENT ID		TECN	COMMENT
$< 10.8 \times 10^{-8}$	90	[1] LEES	13M	BABR	$e^+e^- \to \Upsilon(4S)$

[1] Assumes equal production of B^+ and B^0 at the $\Upsilon(4S)$.

$\Gamma(\eta\mu^+\mu^-)/\Gamma_{total}$ — Γ_{534}/Γ

VALUE	CL%	DOCUMENT ID		TECN	COMMENT
$< 11.2 \times 10^{-8}$	90	[1] LEES	13M	BABR	$e^+e^- \to \Upsilon(4S)$

[1] Assumes equal production of B^+ and B^0 at the $\Upsilon(4S)$.

$\Gamma(K^0\ell^+\ell^-)/\Gamma_{total}$ — Γ_{536}/Γ

VALUE (units 10^{-7})	CL%	DOCUMENT ID		TECN	COMMENT
3.3 ±0.6 OUR AVERAGE					
$3.51^{+0.69}_{-0.60} \pm 0.10$		CHOUDHURY	21	BELL	$e^+e^- \to \Upsilon(4S)$
$2.1^{+1.5}_{-1.3} \pm 0.2$		[1] AUBERT	09T	BABR	$e^+e^- \to \Upsilon(4S)$
• • • We do not use the following data for averages, fits, limits, etc. • • •					
$3.4^{+0.9}_{-0.8} \pm 0.2$		[1,2] WEI	09A	BELL	$e^+e^- \to \Upsilon(4S)$
$2.9^{+1.6}_{-1.3} \pm 0.3$		[1] AUBERT,B	06J	BABR	Repl. by AUBERT 09T
< 6.8	90	[1] ISHIKAWA	03	BELL	$e^+e^- \to \Upsilon(4S)$

[1] Assumes equal production of B^0 and B^+ at $\Upsilon(4S)$.
[2] Superseded by CHOUDHURY 21.

$\Gamma(K^0 e^+e^-)/\Gamma_{total}$ — Γ_{537}/Γ

Test for ΔB=1 weak neutral current. Allowed by higher-order electroweak interactions.

VALUE (units 10^{-7})	CL%	DOCUMENT ID		TECN	COMMENT
$2.5^{+1.1}_{-0.9}$ OUR AVERAGE Error includes scale factor of 1.3.					
$3.1^{+1.0}_{-0.9} \pm 0.08$		CHOUDHURY	21	BELL	$e^+e^- \to \Upsilon(4S)$
$0.8^{+1.5}_{-1.2} \pm 0.1$		[1] AUBERT	09T	BABR	$e^+e^- \to \Upsilon(4S)$
• • • We do not use the following data for averages, fits, limits, etc. • • •					
$2.0^{+1.4}_{-1.0} \pm 0.1$		[1,2] WEI	09A	BELL	$e^+e^- \to \Upsilon(4S)$
$1.3^{+1.6}_{-1.1} \pm 0.2$		[1] AUBERT,B	06J	BABR	Repl. by AUBERT 09T
$2.1^{+2.3}_{-1.6} \pm 0.8$		[1] AUBERT	03U	BABR	$e^+e^- \to \Upsilon(4S)$
< 5.4	90	[3] ISHIKAWA	03	BELL	$e^+e^- \to \Upsilon(4S)$
< 27	90	[1] ABE	02	BELL	Repl. by ISHIKAWA 03
< 38	90	[1] AUBERT	02L	BABR	$e^+e^- \to \Upsilon(4S)$
< 84.5	90	[4] ANDERSON	01B	CLE2	$e^+e^- \to \Upsilon(4S)$
< 3000	90	ALBRECHT	91E	ARG	$e^+e^- \to \Upsilon(4S)$
< 5200	90	[5] AVERY	87	CLEO	$e^+e^- \to \Upsilon(4S)$

[1] Assumes equal production of B^+ and B^0 at the $\Upsilon(4S)$.
[2] Superseded by CHOUDHURY 21.
[3] Assumes equal production of B^0 and B^+ at $\Upsilon(4S)$.
[4] The result is for di-lepton masses above 0.5 GeV.
[5] AVERY 87 reports $< 6.5 \times 10^{-4}$ assuming the $\Upsilon(4S)$ decays 40% to $B^0\overline{B}^0$. We rescale to 50%.

$\Gamma(K^0\nu\overline{\nu})/\Gamma_{total}$ — Γ_{539}/Γ

Test for $\Delta B = 1$ weak neutral current. Allowed by higher-order electroweak interaction.

VALUE	CL%	DOCUMENT ID		TECN	COMMENT
$< 2.6 \times 10^{-5}$	90	[1] GRYGIER	17	BELL	$e^+e^- \to \Upsilon(4S)$
• • • We do not use the following data for averages, fits, limits, etc. • • •					
$< 4.9 \times 10^{-5}$	90	[1,2] LEES	13I	BABR	$e^+e^- \to \Upsilon(4S)$
$< 19.4 \times 10^{-5}$	90	[1] LUTZ	13	BELL	$e^+e^- \to \Upsilon(4S)$
$< 5.6 \times 10^{-5}$	90	[1] DEL-AMO-SA...10Q		BABR	Repl. by LEES 13I
$< 1.6 \times 10^{-4}$	90	[1] CHEN	07D	BELL	$e^+e^- \to \Upsilon(4S)$

[1] Assumes equal production of B^+ and B^0 at the $\Upsilon(4S)$.
[2] Also reported a limit $< 8.1 \times 10^{-5}$ at 90% CL obtained using a fully reconstructed hadronic B-tag evnets.

Downloaded from https://academic.oup.com/ptep/article/2022/8/083C01/6651666 by KIT Library user on 27 September 2022

$\Gamma(\rho^0 \nu\overline{\nu})/\Gamma_{total}$ — Γ_{540}/Γ

Test for $\Delta B = 1$ weak neutral current. Allowed by higher-order electroweak interaction.

VALUE	CL%	DOCUMENT ID		TECN	COMMENT
$<4.0 \times 10^{-5}$	90	[1] GRYGIER	17	BELL	$e^+e^- \to \Upsilon(4S)$
• • • We do not use the following data for averages, fits, limits, etc. • • •					
$<2.08 \times 10^{-4}$	90	[1] LUTZ	13	BELL	$e^+e^- \to \Upsilon(4S)$
$<4.4 \times 10^{-4}$	90	[1] CHEN	07D	BELL	Repl. by LUTZ 13

[1] Assumes equal production of B^+ and B^0 at the $\Upsilon(4S)$.

$\Gamma(K^0\mu^+\mu^-)/\Gamma_{total}$ — Γ_{538}/Γ

Test for ΔB=1 weak neutral current. Allowed by higher-order electroweak interactions.

VALUE (units 10^{-7})	CL%	DOCUMENT ID		TECN	COMMENT
3.39±0.35 OUR FIT Error includes scale factor of 1.1.					
3.39±0.35 OUR AVERAGE					
$3.9 \pm^{1.0}_{0.8} \pm 0.3$		CHOUDHURY	21	BELL	$e^+e^- \to \Upsilon(4S)$
$3.27 \pm 0.34 \pm 0.17$		[1] AAIJ	14M	LHCB	pp at 7, 8 TeV
$4.9 \pm^{2.9}_{2.5} \pm 0.3$		[2] AUBERT	09T	BABR	$e^+e^- \to \Upsilon(4S)$
• • • We do not use the following data for averages, fits, limits, etc. • • •					
$3.1 \pm^{0.7}_{0.6}$		AAIJ	12AH	LHCB	Repl. by AAIJ 14M
$4.4 \pm^{1.3}_{1.1} \pm 0.3$		[2,3] WEI	09A	BELL	$e^+e^- \to \Upsilon(4S)$
$5.9 \pm^{3.3}_{2.6} \pm 0.7$		[2] AUBERT,B	06J	BABR	Repl. by AUBERT 09T
$1.63 \pm^{0.82}_{0.63} \pm 0.14$		[2] AUBERT	03U	BABR	Repl. by AUBERT,B 06J
$5.6 \pm^{2.9}_{2.3} \pm 0.5$		[4] ISHIKAWA	03	BELL	Repl. by WEI 09A
<33	90	[2] ABE	02	BELL	Repl. by ISHIKAWA 03
<36	90	AUBERT	02L	BABR	$e^+e^- \to \Upsilon(4S)$
<66.4	90	[5] ANDERSON	01B	CLE2	$e^+e^- \to \Upsilon(4S)$
<5200	90	ALBRECHT	91E	ARG	$e^+e^- \to \Upsilon(4S)$
<3600	90	[6] AVERY	87	CLEO	$e^+e^- \to \Upsilon(4S)$

[1] Uses $B(B^0 \to J/\psi(1S)K^0) = (0.928 \pm 0.013 \pm 0.037) \times 10^{-3}$ for normalization.
[2] Assumes equal production of B^+ and B^0 at the $\Upsilon(4S)$.
[3] Superseded by CHOUDHURY 21.
[4] Assumes equal production of B^0 and B^+ at $\Upsilon(4S)$. The second error is a total of systematic uncertainties including model dependence.
[5] The result is for di-lepton masses above 0.5 GeV.
[6] AVERY 87 reports $< 4.5 \times 10^{-4}$ assuming the $\Upsilon(4S)$ decays 40% to $B^0\overline{B}^0$. We rescale to 50%.

$\Gamma(K^0\mu^+\mu^-)/\Gamma(J/\psi(1S)K^0)$ — $\Gamma_{538}/\Gamma_{200}$

VALUE (units 10^{-3})	DOCUMENT ID		TECN	COMMENT
0.38±0.04 OUR FIT Error includes scale factor of 1.1.				
0.37±0.12±0.02	AALTONEN	11AI	CDF	$p\overline{p}$ at 1.96 TeV

$\Gamma(K^*(892)^0\ell^+\ell^-)/\Gamma_{total}$ — Γ_{541}/Γ

Test for ΔB=1 weak neutral current. Allowed by higher-order electroweak interactions.

VALUE (units 10^{-7})	DOCUMENT ID		TECN	COMMENT
$9.9 \pm^{1.2}_{1.1}$ OUR AVERAGE				
$10.3 \pm^{2.2}_{2.1} \pm 0.7$	[1] AUBERT	09T	BABR	$e^+e^- \to \Upsilon(4S)$
$9.7 \pm^{1.3}_{1.1} \pm 0.7$	[1] WEI	09A	BELL	$e^+e^- \to \Upsilon(4S)$
• • • We do not use the following data for averages, fits, limits, etc. • • •				
$8.1 \pm^{2.1}_{1.9} \pm 0.9$	[1] AUBERT,B	06J	BABR	Repl. by AUBERT 09T
$11.7 \pm^{3.0}_{2.7} \pm 0.9$	[1] ISHIKAWA	03	BELL	Repl. by WEI 09A

[1] Assumes equal production of B^0 and B^+ at $\Upsilon(4S)$.

$\Gamma(K^*(892)^0 e^+e^-)/\Gamma_{total}$ — Γ_{542}/Γ

Test for ΔB=1 weak neutral current. Allowed by higher-order electroweak interactions.

VALUE (units 10^{-7})	CL%	DOCUMENT ID		TECN	COMMENT
$10.3 \pm^{1.9}_{1.7}$ OUR AVERAGE					
$8.6 \pm^{2.6}_{2.4} \pm 0.5$		[1] AUBERT	09T	BABR	$e^+e^- \to \Upsilon(4S)$
$11.8 \pm^{2.7}_{2.2} \pm 0.9$		[1] WEI	09A	BELL	$e^+e^- \to \Upsilon(4S)$
• • • We do not use the following data for averages, fits, limits, etc. • • •					
$10.4 \pm^{3.3}_{2.9} \pm 1.1$		[1] AUBERT,B	06J	BABR	Repl. by AUBERT 09T
$11.1 \pm^{5.6}_{4.7} \pm 1.1$		[1] AUBERT	03U	BABR	$e^+e^- \to \Upsilon(4S)$
< 24	90	[2] ISHIKAWA	03	BELL	$e^+e^- \to \Upsilon(4S)$
< 64	90	[1] ABE	02	BELL	Repl. by ISHIKAWA 03
< 67	90	[1] AUBERT	02L	BABR	$e^+e^- \to \Upsilon(4S)$
<2900	90	ALBRECHT	91E	ARG	$e^+e^- \to \Upsilon(4S)$

[1] Assumes equal production of B^+ and B^0 at the $\Upsilon(4S)$.
[2] Assumes equal production of B^0 and B^+ at $\Upsilon(4S)$.

$\Gamma(K^*(892)^0\mu^+\mu^-)/\Gamma_{total}$ — Γ_{543}/Γ

Test for ΔB=1 weak neutral current. Allowed by higher-order electroweak interactions.

VALUE (units 10^{-7})	CL%	DOCUMENT ID		TECN	COMMENT
9.4 ±0.5 OUR FIT					
9.4 ±0.6 OUR AVERAGE					
$9.04 \pm^{0.16}_{0.15} \pm 0.62$		[1] AAIJ	17Q	LHCB	pp at 7, 8 TeV
$13.5 \pm^{4.0}_{3.7} \pm 1.0$		[2] AUBERT	09T	BABR	$e^+e^- \to \Upsilon(4S)$
$10.6 \pm^{1.9}_{1.4} \pm 0.7$		[2] WEI	09A	BELL	$e^+e^- \to \Upsilon(4S)$
• • • We do not use the following data for averages, fits, limits, etc. • • •					
$10.36 \pm^{0.18}_{0.17} \pm 0.71$		[1] AAIJ	16AO	LHCB	Repl. by AAIJ 17Q
$8.7 \pm^{3.8}_{3.3} \pm 1.2$		[2] AUBERT,B	06J	BABR	Repl. by AUBERT 09T
$8.6 \pm^{7.9}_{5.8} \pm 1.1$		[2] AUBERT	03U	BABR	Repl. by AUBERT,B 06J
$13.3 \pm^{4.2}_{3.7} \pm 1.1$		[3] ISHIKAWA	03	BELL	Repl. by WEI 09A
<42	90	[2] ABE	02	BELL	$e^+e^- \to \Upsilon(4S)$
<33	90	AUBERT	02L	BABR	$e^+e^- \to \Upsilon(4S)$
<40	90	[4] AFFOLDER	99B	CDF	$p\overline{p}$ at 1.8 TeV

[1] Uses $B(B^0 \to J/\psi K^*(892)^0) = (1.19 \pm 0.01 \pm 0.08) \times 10^{-3}$. The second error is the total systematic uncertainty.
[2] Assumes equal production of B^+ and B^0 at the $\Upsilon(4S)$.
[3] Assumes equal production of B^0 and B^+ at $\Upsilon(4S)$. The second error is a total of systematic uncertainties including model dependence.
[4] AFFOLDER 99B measured relative to $B^0 \to J/\psi(1S)K^*(892)^0$.

$\Gamma(K^*(892)^0\mu^+\mu^-)/\Gamma(J/\psi(1S)K^*(892)^0)$ — $\Gamma_{543}/\Gamma_{202}$

VALUE (units 10^{-3})	DOCUMENT ID		TECN	COMMENT
0.75±0.05 OUR FIT				
0.77±0.08±0.03	AALTONEN	11AI	CDF	$p\overline{p}$ at 1.96 TeV
• • • We do not use the following data for averages, fits, limits, etc. • • •				
$0.80 \pm 0.10 \pm 0.06$	AALTONEN	11L	CDF	Repl. by AALTONEN 11AI
$0.61 \pm 0.23 \pm 0.07$	AALTONEN	09B	CDF	Repl. by AALTONEN 11L

$\Gamma(K^*(892)^0\chi,\ \chi \to \mu^+\mu^-)/\Gamma_{total}$ — Γ_{544}/Γ

VALUE	CL%	DOCUMENT ID		TECN	COMMENT
$< \sim 10^{-9}$	95	[1] AAIJ	15AZ	LHCB	pp at 7, 8 TeV

[1] The limt is obtained as a function of di-muon mass. A normalizing mode branching fraction value of $B(B^0 \to K^{*0}\mu^+\mu^-) = (1.6 \pm 0.3) \times 10^{-7}$ is used.

$\Gamma(\pi^+\pi^-\mu^+\mu^-)/\Gamma_{total}$ — Γ_{545}/Γ

VALUE (units 10^{-8})	DOCUMENT ID		TECN	COMMENT
2.1±0.5±0.1	[1] AAIJ	15S	LHCB	pp at 7, 8 TeV

[1] AAIJ 15S reports $(2.11 \pm 0.51 \pm 0.15 \pm 0.16) \times 10^{-8}$ from a measurement of $[\Gamma(B^0 \to \pi^+\pi^-\mu^+\mu^-)/\Gamma_{total}]$ / $[B(B^0 \to J/\psi(1S)K^*(892)^0)]$ assuming $B(B^0 \to J/\psi(1S)K^*(892)^0) = (1.3 \pm 0.1) \times 10^{-3}$, which we rescale to our best value $B(B^0 \to J/\psi(1S)K^*(892)^0) = (1.27 \pm 0.05) \times 10^{-3}$. Our first error is their experiment's error and our second error is the systematic error from using our best value.

$\Gamma(K^*(892)^0\nu\overline{\nu})/\Gamma_{total}$ — Γ_{546}/Γ

Test for ΔB=1 weak neutral current. Allowed by higher-order electroweak interactions.

VALUE	CL%	DOCUMENT ID		TECN	COMMENT
$<1.8 \times 10^{-5}$	90	[1] GRYGIER	17	BELL	$e^+e^- \to \Upsilon(4S)$
• • • We do not use the following data for averages, fits, limits, etc. • • •					
$<1.2 \times 10^{-4}$	90	[1,2] LEES	13I	BABR	$e^+e^- \to \Upsilon(4S)$
$<5.5 \times 10^{-5}$	90	[1] LUTZ	13	BELL	$e^+e^- \to \Upsilon(4S)$
$<1.2 \times 10^{-4}$	90	AUBERT	08BC	BABR	Repl. by LEES 13I
$<3.4 \times 10^{-4}$	90	[1] CHEN	07D	BELL	$e^+e^- \to \Upsilon(4S)$
$<1.0 \times 10^{-3}$	90	[3] ADAM	96D	DLPH	$e^+e^- \to Z$

[1] Assumes equal production of B^+ and B^0 at the $\Upsilon(4S)$.
[2] Also reported a limit $< 9.3 \times 10^{-5}$ at 90% CL obtained using a fully reconstructed hadronic B-tag evnets.
[3] ADAM 96D assumes $f_{B^0} = f_{B^-} = 0.39$ and $f_{B_s} = 0.12$.

$\Gamma(\text{invisible})/\Gamma_{total}$ — Γ_{547}/Γ

VALUE (units 10^{-5})	CL%	DOCUMENT ID		TECN	COMMENT
< 2.4	90	[1] LEES	12T	BABR	$e^+e^- \to \Upsilon(4S)$
• • • We do not use the following data for averages, fits, limits, etc. • • •					
< 7.8	90	[2] KU	20	BELL	$e^+e^- \to \Upsilon(4S)$
<13	90	[3] HSU	12	BELL	$e^+e^- \to \Upsilon(4S)$
<22	90	[1] AUBERT,B	04J	BABR	$e^+e^- \to \Upsilon(4S)$

[1] Uses the fully reconstructed $B^0 \to D^{(*)-}\ell^+\nu_\ell$ events as a tag.
[2] Identified by fully reconstructing a hadronic decay of the accompanying B meson .
[3] Identified by fully reconstructing a hadronic decay of the accompanying B meson and requiring no other particles in the event.

Downloaded from https://academic.oup.com/ptep/article/2022/8/083C01/6651666 by KIT Library user on 27 September 2022

$\Gamma(\nu\overline{\nu}\gamma)/\Gamma_{total}$ — Γ_{548}/Γ

VALUE (units 10^{-5})	CL%	DOCUMENT ID		TECN	COMMENT
<1.6	90	[1] KU	20	BELL	$e^+e^- \to \Upsilon(4S)$
• • • We do not use the following data for averages, fits, limits, etc. • • •					
<1.7	90	[2] LEES	12T	BABR	$e^+e^- \to \Upsilon(4S)$
<4.7	90	[2] AUBERT,B	04J	BABR	Repl. by LEES 12T

[1] Identified by fully reconstructing a hadronic decay of the accompanying B meson .
[2] Uses the fully reconstructed $B^0 \to D^{(*)-}\ell^+\nu_\ell$ events as a tag.

$\Gamma(\phi\nu\overline{\nu})/\Gamma_{total}$ — Γ_{549}/Γ

Test for $\Delta B = 1$ weak neutral current. Allowed by higher-order electroweak interaction.

VALUE	CL%	DOCUMENT ID		TECN	COMMENT
$<1.27 \times 10^{-4}$	90	[1] LUTZ	13	BELL	$e^+e^- \to \Upsilon(4S)$
• • • We do not use the following data for averages, fits, limits, etc. • • •					
$<5.8 \times 10^{-5}$	90	[1] CHEN	07D	BELL	Repl. by LUTZ 13

[1] Assumes equal production of B^+ and B^0 at the $\Upsilon(4S)$.

$\Gamma(e^\pm\mu^\mp)/\Gamma_{total}$ — Γ_{550}/Γ

Test of lepton family number conservation. Allowed by higher-order electroweak interactions.

VALUE	CL%	DOCUMENT ID		TECN	COMMENT
$< 1.0 \times 10^{-9}$	90	[1] AAIJ	18T	LHCB	pp at 7, 8 TeV
• • • We do not use the following data for averages, fits, limits, etc. • • •					
$< 2.8 \times 10^{-9}$	90	[2] AAIJ	13BM	LHCB	Repl. by AAIJ 18T
$< 6.4 \times 10^{-8}$	90	AALTONEN	09P	CDF	$p\overline{p}$ at 1.96 TeV
$< 9.2 \times 10^{-8}$	90	[3] AUBERT	08P	BABR	$e^+e^- \to \Upsilon(4S)$
$< 1.8 \times 10^{-7}$	90	[3] AUBERT	05W	BABR	$e^+e^- \to \Upsilon(4S)$
$< 1.7 \times 10^{-7}$	90	[3] CHANG	03	BELL	$e^+e^- \to \Upsilon(4S)$
$<15 \times 10^{-7}$	90	[3] BERGFELD	00B	CLE2	$e^+e^- \to \Upsilon(4S)$
$< 3.5 \times 10^{-6}$	90	ABE	98V	CDF	$p\overline{p}$ at 1.8 TeV
$< 1.6 \times 10^{-5}$	90	[4] ACCIARRI	97B	L3	$e^+e^- \to Z$
$< 5.9 \times 10^{-6}$	90	AMMAR	94	CLE2	$e^+e^- \to \Upsilon(4S)$
$< 3.4 \times 10^{-5}$	90	[5] AVERY	89B	CLEO	$e^+e^- \to \Upsilon(4S)$
$< 4.5 \times 10^{-5}$	90	[6] ALBRECHT	87D	ARG	$e^+e^- \to \Upsilon(4S)$
$< 7.7 \times 10^{-5}$	90	[7] AVERY	87	CLEO	$e^+e^- \to \Upsilon(4S)$
$< 3 \times 10^{-4}$	90	GILES	84	CLEO	Repl. by AVERY 87

[1] AAIJ 18T uses normalization modes $B(B^0 \to K^+\pi^-) = (19.6 \pm 0.5) \times 10^{-6}$ and $B(B^+ \to J/\psi K^+) = (1.026 \pm 0.031) \times 10^{-3}$.
[2] Uses normalization mode $B(B^0 \to K^+\pi^-) = (19.4 \pm 0.6) \times 10^{-6}$.
[3] Assumes equal production of B^+ and B^0 at the $\Upsilon(4S)$.
[4] ACCIARRI 97B assume PDG 96 production fractions for B^+, B^0, B_s, and Λ_b.
[5] Paper assumes the $\Upsilon(4S)$ decays 43% to $B^0\overline{B}^0$. We rescale to 50%.
[6] ALBRECHT 87D reports $< 5 \times 10^{-5}$ assuming the $\Upsilon(4S)$ decays 45% to $B^0\overline{B}^0$. We rescale to 50%.
[7] AVERY 87 reports $< 9 \times 10^{-5}$ assuming the $\Upsilon(4S)$ decays 40% to $B^0\overline{B}^0$. We rescale to 50%.

$\Gamma(\pi^0 e^\pm\mu^\mp)/\Gamma_{total}$ — Γ_{551}/Γ

VALUE	CL%	DOCUMENT ID		TECN	COMMENT
$<1.4 \times 10^{-7}$	90	[1] AUBERT	07AG	BABR	$e^+e^- \to \Upsilon(4S)$

[1] Assumes equal production of B^+ and B^0 at the $\Upsilon(4S)$.

$\Gamma(K^0 e^\pm\mu^\mp)/\Gamma_{total}$ — Γ_{552}/Γ

Test of lepton family number conservation.

VALUE	CL%	DOCUMENT ID		TECN	COMMENT
$< 3.8 \times 10^{-8}$	90	CHOUDHURY	21	BELL	$e^+e^- \to \Upsilon(4S)$
• • • We do not use the following data for averages, fits, limits, etc. • • •					
$< 2.7 \times 10^{-7}$	90	[1] AUBERT,B	06J	BABR	$e^+e^- \to \Upsilon(4S)$
$<40 \times 10^{-7}$	90	[1] AUBERT	02L	BABR	Repl. by AUBERT,B 06J

[1] Assumes equal production of B^+ and B^0 at the $\Upsilon(4S)$.

$\Gamma(K^*(892)^0 e^+\mu^-)/\Gamma_{total}$ — Γ_{553}/Γ

VALUE (units 10^{-7})	CL%	DOCUMENT ID		TECN	COMMENT
<1.6	90	[1] SANDILYA	18	BELL	$e^+e^- \to \Upsilon(4S)$
• • • We do not use the following data for averages, fits, limits, etc. • • •					
<5.3	90	[2] AUBERT,B	06J	BABR	$e^+e^- \to \Upsilon(4S)$

[1] Uses $B(\Upsilon(4S) \to B^0\overline{B}^0) = 0.486 \pm 0.006$.
[2] Assumes equal production of B^0 and B^+ at $\Upsilon(4S)$.

$\Gamma(K^*(892)^0 e^-\mu^+)/\Gamma_{total}$ — Γ_{554}/Γ

VALUE (units 10^{-7})	CL%	DOCUMENT ID		TECN	COMMENT
<1.2	90	[1] SANDILYA	18	BELL	$e^+e^- \to \Upsilon(4S)$
• • • We do not use the following data for averages, fits, limits, etc. • • •					
<3.4	90	[2] AUBERT,B	06J	BABR	$e^+e^- \to \Upsilon(4S)$

[1] Uses $B(\Upsilon(4S) \to B^0\overline{B}^0) = 0.486 \pm 0.006$.
[2] Assumes equal production of B^0 and B^+ at $\Upsilon(4S)$.

$\Gamma(K^*(892)^0 e^\pm\mu^\mp)/\Gamma_{total}$ — Γ_{555}/Γ

Test of lepton family number conservation.

VALUE (units 10^{-7})	CL%	DOCUMENT ID		TECN	COMMENT
< 1.8	90	[1] SANDILYA	18	BELL	$e^+e^- \to \Upsilon(4S)$
• • • We do not use the following data for averages, fits, limits, etc. • • •					
< 5.8	90	[2] AUBERT,B	06J	BABR	$e^+e^- \to \Upsilon(4S)$
<34	90	[2] AUBERT	02L	BABR	Repl. by AUBERT,B 06J

[1] Uses $B(\Upsilon(4S) \to B^0\overline{B}^0) = 0.486 \pm 0.006$.
[2] Assumes equal production of B^+ and B^0 at the $\Upsilon(4S)$.

$\Gamma(e^\pm\tau^\mp)/\Gamma_{total}$ — Γ_{556}/Γ

Test of lepton family number conservation. Allowed by higher-order electroweak interactions.

VALUE	CL%	DOCUMENT ID		TECN	COMMENT
$<1.6 \times 10^{-5}$	90	[1] ATMACAN	21	BELL	$e^+e^- \to \Upsilon(4S)$
• • • We do not use the following data for averages, fits, limits, etc. • • •					
$<2.8 \times 10^{-5}$	90	[2] AUBERT	08AD	BABR	$e^+e^- \to \Upsilon(4S)$
$<1.1 \times 10^{-4}$	90	BORNHEIM	04	CLE2	$e^+e^- \to \Upsilon(4S)$
$<5.3 \times 10^{-4}$	90	AMMAR	94	CLE2	Repl. by BORNHEIM 04

[1] Uses events in which one B meson is fully reconstructed in a hadronic decay mode.
[2] Assumes equal production of B^+ and B^0 at the $\Upsilon(4S)$.

$\Gamma(\mu^\pm\tau^\mp)/\Gamma_{total}$ — Γ_{557}/Γ

Test of lepton family number conservation. Allowed by higher-order electroweak interactions.

VALUE	CL%	DOCUMENT ID		TECN	COMMENT
$<1.4 \times 10^{-5}$	95	[1] AAIJ	19AK	LHCB	pp at 7, 8 TeV
• • • We do not use the following data for averages, fits, limits, etc. • • •					
$<1.5 \times 10^{-5}$	90	[2] ATMACAN	21	BELL	$e^+e^- \to \Upsilon(4S)$
$<2.2 \times 10^{-5}$	90	[3] AUBERT	08AD	BABR	$e^+e^- \to \Upsilon(4S)$
$<3.8 \times 10^{-5}$	90	BORNHEIM	04	CLE2	$e^+e^- \to \Upsilon(4S)$
$<8.3 \times 10^{-4}$	90	AMMAR	94	CLE2	Repl. by BORNHEIM 04

[1] Assuming no contribution from $B^0_s \to \mu^\pm\tau^\mp$.
[2] Uses events in which one B meson is fully reconstructed in a hadronic decay mode.
[3] Assumes equal production of B^+ and B^0 at the $\Upsilon(4S)$.

$\Gamma(\Lambda_c^+\mu^-)/\Gamma_{total}$ — Γ_{558}/Γ

VALUE	CL%	DOCUMENT ID		TECN	COMMENT
$<1.4 \times 10^{-6}$	90	[1,2] DEL-AMO-SA...	11K	BABR	$e^+e^- \to \Upsilon(4S)$

[1] DEL-AMO-SANCHEZ 11K reports $< 180 \times 10^{-8}$ from a measurement of $[\Gamma(B^0 \to \Lambda_c^+\mu^-)/\Gamma_{total}] \times [B(\Lambda_c^+ \to pK^-\pi^+)]$ assuming $B(\Lambda_c^+ \to pK^-\pi^+) = (5.0 \pm 1.3) \times 10^{-2}$, which we rescale to our best value $B(\Lambda_c^+ \to pK^-\pi^+) = 6.28 \times 10^{-2}$.
[2] Uses $B(\Upsilon(4S) \to B^0\overline{B}^0) = (51.6 \pm 0.6)\%$ and $B(\Upsilon(4S) \to B^+B^-) = (48.4 \pm 0.6)\%$.

$\Gamma(\Lambda_c^+ e^-)/\Gamma_{total}$ — Γ_{559}/Γ

VALUE	CL%	DOCUMENT ID		TECN	COMMENT
$<4 \times 10^{-6}$	90	[1,2] DEL-AMO-SA...	11K	BABR	$e^+e^- \to \Upsilon(4S)$

[1] DEL-AMO-SANCHEZ 11K reports $< 520 \times 10^{-8}$ from a measurement of $[\Gamma(B^0 \to \Lambda_c^+e^-)/\Gamma_{total}] \times [B(\Lambda_c^+ \to pK^-\pi^+)]$ assuming $B(\Lambda_c^+ \to pK^-\pi^+) = (5.0 \pm 1.3) \times 10^{-2}$, which we rescale to our best value $B(\Lambda_c^+ \to pK^-\pi^+) = 6.28 \times 10^{-2}$.
[2] Uses $B(\Upsilon(4S) \to B^0\overline{B}^0) = (51.6 \pm 0.6)\%$ and $B(\Upsilon(4S) \to B^+B^-) = (48.4 \pm 0.6)\%$.

B^0_s CROSS-PARTICLE BRANCHING RATIOS

$\Gamma([K^+K^-]_D K^*(892)^0)/\Gamma_{total} \times B(B^0_s \to [K^+K^-]_D K^*(892)^0)$ — $\Gamma_{143}/\Gamma \times B$

VALUE	DOCUMENT ID		TECN	COMMENT
0.10±0.02±0.01	AAIJ	14BN	LHCB	pp at 7, 8 TeV

$\Gamma([\pi^+\pi^-]_D K^*(892)^0)/\Gamma_{total} \times B(B^0_s \to [\pi^+\pi^-]_D K^*(892)^0)$ — $\Gamma_{144}/\Gamma \times B$

VALUE	DOCUMENT ID		TECN	COMMENT
0.15±0.04±0.01	AAIJ	14BN	LHCB	pp at 7, 8 TeV

See the related review(s):
Polarization in B Decays

POLARIZATION IN B^0 DECAY

In decays involving two vector mesons, one can distinguish among the states in which meson polarizations are both longitudinal (L) or both are transverse and parallel ($\|$) or perpendicular ($\perp$) to each other with the parameters Γ_L/Γ, $\Gamma_\perp/\Gamma$, and the relative phases $\phi_\|$ and $\phi_\perp$. See the definitions in the note on "Polarization in B Decays" review in the B^0 Particle Listings.

Γ_L/Γ in $B^0 \to J/\psi(1S)K^*(892)^0$

VALUE	EVTS	DOCUMENT ID		TECN	COMMENT
0.571±0.007 OUR AVERAGE					
0.572±0.006±0.014		[1] AAIJ	13AT	LHCB	pp at 7 TeV
0.587±0.011±0.013		[2] ABAZOV	09E	D0	$p\overline{p}$ at 1.96 TeV
0.556±0.009±0.010		[3] AUBERT	07AD	BABR	$e^+e^- \to \Upsilon(4S)$
0.562±0.026±0.018		ACOSTA	05	CDF	$p\overline{p}$ at 1.96 TeV
0.574±0.012±0.009		ITOH	05	BELL	$e^+e^- \to \Upsilon(4S)$
0.59 ±0.06 ±0.01		[4] AFFOLDER	00N	CDF	$p\overline{p}$ at 1.8 TeV
0.52 ±0.07 ±0.04		[5] JESSOP	97	CLE2	$e^+e^- \to \Upsilon(4S)$
0.65 ±0.10 ±0.04	65	ABE	95Z	CDF	$p\overline{p}$ at 1.8 TeV
0.97 ±0.16 ±0.15	13	[6] ALBRECHT	94G	ARG	$e^+e^- \to \Upsilon(4S)$

Downloaded from https://academic.oup.com/ptep/article/2022/8/083C01/6651666 by KIT Library user on 27 September 2022

• • • We do not use the following data for averages, fits, limits, etc. • • •

0.566±0.012±0.005	[3] AUBERT	05P	BABR	Repl. by AUBERT 07AD
0.62 ±0.02 ±0.03	[7] ABE	02N	BELL	Repl. by ITOH 05
0.597±0.028±0.024	[8] AUBERT	01H	BABR	Repl. by AUBERT 07AD
0.80 ±0.08 ±0.05 42	[6] ALAM	94	CLE2	Sup. by JESSOP 97

[1] AAIJ 13AT obtains $\Gamma_{\|}/\Gamma = 0.227 \pm 0.004 \pm 0.011$. The relation $1 = (\Gamma_L + \Gamma_\perp + \Gamma_{\|})/\Gamma$ is used to obtain Γ_L/Γ.

[2] Measured the angular and lifetime parameters for the time-dependent angular untagged decays $B^0_d \to J/\psi K^{*0}$ and $B^0_s \to J/\psi\phi$.

[3] Obtained by combining the B^0 and B^+ modes.

[4] AFFOLDER 00N measurements are based on 190 B^0 candidates obtained from a data sample of 89 pb^{-1}. The P-wave fraction is found to be $0.13^{+0.12}_{-0.09} \pm 0.06$.

[5] JESSOP 97 is the average over a mixture of B^0 and B^+ decays. The P-wave fraction is found to be $0.16 \pm 0.08 \pm 0.04$.

[6] Averaged over an admixture of B^0 and B^+ decays.

[7] Averaged over an admixture of B^0 and B^+ decays and the P wave fraction is $(19 \pm 2 \pm 3)\%$.

[8] Averaged over an admixture of B^0 and B^- decays and the P wave fraction is $(16.0 \pm 3.2 \pm 1.4) \times 10^{-2}$.

$\Gamma_\perp/\Gamma$ in $B^0 \to J/\psi K^{*0}$

VALUE	DOCUMENT ID		TECN	COMMENT
0.211±0.008 OUR AVERAGE	Error includes scale factor of 1.3.			See the ideogram below.
0.201±0.004±0.008	AAIJ	13AT	LHCB	pp at 7 TeV
0.230±0.013±0.025	[1] ABAZOV	09E	D0	$p\overline{p}$ at 1.96 TeV
0.233±0.010±0.005	[2] AUBERT	07AD	BABR	$e^+e^- \to \Upsilon(4S)$
0.215±0.032±0.006	ACOSTA	05	CDF	$p\overline{p}$ at 1.96 TeV
0.195±0.012±0.008	ITOH	05	BELL	$e^+e^- \to \Upsilon(4S)$

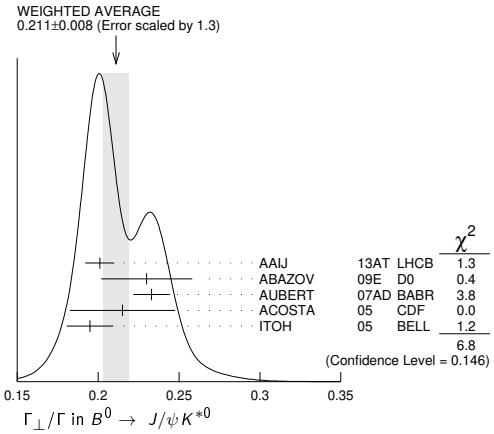

[1] Measured the angular and lifetime parameters for the time-dependent angular untagged decays $B^0_d \to J/\psi K^{*0}$ and $B^0_s \to J/\psi\phi$.

[2] Obtained by combining the B^0 and B^+ modes.

$\phi_{\|}$ in $B^0 \to J/\psi K^{*0}$

VALUE (rad)	DOCUMENT ID		TECN	COMMENT
−2.92±0.04 OUR AVERAGE	Error includes scale factor of 1.3.			See the ideogram below.
−2.94±0.02±0.03	AAIJ	13AT	LHCB	pp at 7 TeV
−2.69±0.08±0.11	[1] ABAZOV	09E	D0	$p\overline{p}$ at 1.96 TeV
−2.93±0.08±0.04	[2] AUBERT	07AD	BABR	$e^+e^- \to \Upsilon(4S)$

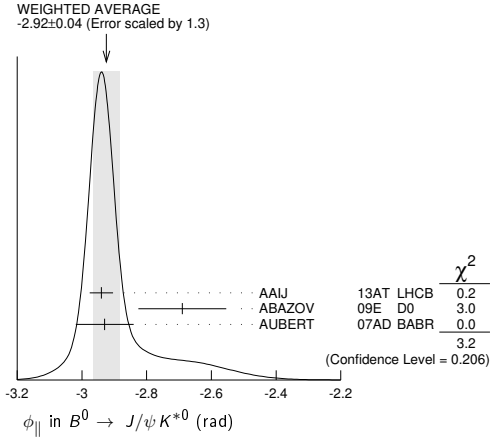

[1] Obtained $\phi_{\|}$ as $\delta_2 - \delta_1$, assuming they are uncorrelated.

[2] Obtained by combining the B^0 and B^+ modes.

$\phi_\perp$ in $B^0 \to J/\psi K^{*0}$

VALUE (rad)	DOCUMENT ID		TECN	COMMENT
2.96±0.05 OUR AVERAGE	Error includes scale factor of 2.2.			See the ideogram below.
2.94±0.02±0.02	AAIJ	13AT	LHCB	pp at 7 TeV
3.21±0.06±0.06	ABAZOV	09E	D0	$p\overline{p}$ at 1.96 TeV
2.91±0.05±0.03	[1] AUBERT	07AD	BABR	$e^+e^- \to \Upsilon(4S)$

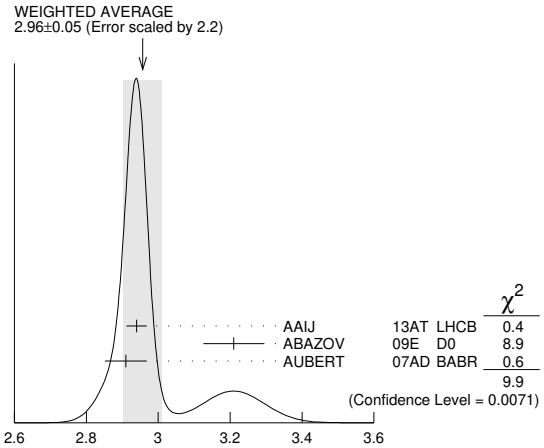

[1] Obtained by combining the B^0 and B^+ modes.

Γ_L/Γ in $B^0 \to \psi(2S) K^*(892)^0$

VALUE	DOCUMENT ID		TECN	COMMENT
$0.463^{+0.028}_{-0.040}$ OUR AVERAGE				
$0.455^{+0.031}_{-0.029}{}^{+0.014}_{-0.049}$	CHILIKIN	13	BELL	$e^+e^- \to \Upsilon(4S)$
0.48 ±0.05 ±0.02	[1] AUBERT	07AD	BABR	$e^+e^- \to \Upsilon(4S)$
0.45 ±0.11 ±0.04	[2] RICHICHI	01	CLE2	$e^+e^- \to \Upsilon(4S)$
• • • We do not use the following data for averages, fits, limits, etc. • • •				
$0.448^{+0.040}_{-0.027}{}^{+0.040}_{-0.053}$	MIZUK	09	BELL	$e^+e^- \to \Upsilon(4S)$

[1] Obtained by combining the B^0 and B^+ modes.

[2] Averages between charged and neutral B mesons.

$\Gamma_\perp/\Gamma$ in $B^0 \to \psi(2S) K^{*0}$

VALUE	DOCUMENT ID		TECN	COMMENT
0.30±0.06±0.02	[1] AUBERT	07AD	BABR	$e^+e^- \to \Upsilon(4S)$

[1] Obtained by combining the B^0 and B^+ modes.

$\phi_{\|}$ in $B^0 \to \psi(2S) K^{*0}$

VALUE (rad)	DOCUMENT ID		TECN	COMMENT
−2.8±0.4±0.1	[1] AUBERT	07AD	BABR	$e^+e^- \to \Upsilon(4S)$

[1] Obtained by combining the B^0 and B^+ modes.

$\phi_\perp$ in $B^0 \to \psi(2S) K^{*0}$

VALUE (rad)	DOCUMENT ID		TECN	COMMENT
2.8±0.3±0.1	[1] AUBERT	07AD	BABR	$e^+e^- \to \Upsilon(4S)$

[1] Obtained by combining the B^0 and B^+ modes.

Γ_L/Γ in $B^0 \to \chi_{c1} K^*(892)^0$

VALUE	DOCUMENT ID		TECN	COMMENT
$0.83\ ^{+0.06}_{-0.08}$ OUR AVERAGE	Error includes scale factor of 1.3.			
$0.947^{+0.038}_{-0.048}{}^{+0.046}_{-0.099}$	MIZUK	08	BELL	$e^+e^- \to \Upsilon(4S)$
0.77 ±0.07 ±0.04	[1] AUBERT	07AD	BABR	$e^+e^- \to \Upsilon(4S)$

[1] Obtained by combining the B^0 and B^+ modes.

$\Gamma_\perp/\Gamma$ in $B^0 \to \chi_{c1} K^*(892)^0$

VALUE	DOCUMENT ID		TECN	COMMENT
0.03±0.04±0.02	[1] AUBERT	07AD	BABR	$e^+e^- \to \Upsilon(4S)$

[1] Obtained by combining the B^0 and B^+ modes.

$\phi_{\|}$ in $B^0 \to \chi_{c1} K^*(892)^0$

VALUE (rad)	DOCUMENT ID		TECN	COMMENT
0.0±0.3±0.1	[1] AUBERT	07AD	BABR	$e^+e^- \to \Upsilon(4S)$

[1] Obtained by combining the B^0 and B^+ modes.

Downloaded from https://academic.oup.com/ptep/article/2022/8/083C01/6651666 by KIT Library user on 27 September 2022

Γ_L/Γ in $B^0 \to D_s^{*+} D^{*-}$

VALUE	DOCUMENT ID		TECN	COMMENT
0.574±0.014 OUR AVERAGE				
0.578±0.010±0.011	[1] AAIJ	21S	LHCB	pp at 13 TeV
0.519±0.050±0.028	[2] AUBERT	03I	BABR	$e^+e^- \to \Upsilon(4S)$
0.506±0.139±0.036	AHMED	00B	CLE2	$e^+e^- \to \Upsilon(4S)$

[1] AAIJ 21S uses $D_s^{*+} \to D_s^+ \gamma$ decays.
[2] Measurement performed using partial reconstruction of D^{*-} decay.

$|H_+|$ in $B^0 \to D_s^{*+} D^{*-}$

H_+, H_- define parity-even ($\|$) and parity-odd ($\perp$) polarization transversity amplitudes $A_{\|,\perp} = (H_+ \pm H_-)/\sqrt{2}$.

VALUE	DOCUMENT ID		TECN	COMMENT
0.195±0.022±0.032	[1] AAIJ	21S	BELL	pp at 13 TeV

[1] AAIJ 21S uses $D_s^{*+} \to D_s^+ \gamma$ decays.

$|H_-|$ in $B^0 \to D_s^{*+} D^{*-}$

H_+, H_- define parity-even ($\|$) and parity-odd ($\perp$) polarization transversity amplitudes $A_{\|,\perp} = (H_+ \pm H_-)/\sqrt{2}$.

VALUE	DOCUMENT ID		TECN	COMMENT
0.620±0.011±0.013	[1] AAIJ	21S	LHCB	pp at 13 TeV

[1] AAIJ 21S uses $D_s^{*+} \to D_s^+ \gamma$ decays.

ϕ_+ in $B^0 \to D_s^{*+} D^{*-}$

VALUE	DOCUMENT ID		TECN	COMMENT
−0.046±0.102±0.020	[1] AAIJ	21S	LHCB	pp at 13 TeV

[1] AAIJ 21S uses $D_s^{*+} \to D_s^+ \gamma$ decays.

ϕ_- in $B^0 \to D_s^{*+} D^{*-}$

VALUE	DOCUMENT ID		TECN	COMMENT
0.108±0.170±0.051	[1] AAIJ	21S	LHCB	pp at 13 TeV

[1] AAIJ 21S uses $D_s^{*+} \to D_s^+ \gamma$ decays.

Γ_L/Γ in $B^0 \to D^{*-} \rho^+$

VALUE	EVTS	DOCUMENT ID		TECN	COMMENT
0.885±0.016±0.012		CSORNA	03	CLE2	$e^+e^- \to \Upsilon(4S)$
• • • We do not use the following data for averages, fits, limits, etc. • • •					
0.93 ±0.05 ±0.05	76	ALAM	94	CLE2	$e^+e^- \to \Upsilon(4S)$

Γ_L/Γ in $B^0 \to D_s^{*+} \rho^-$

VALUE	DOCUMENT ID		TECN	COMMENT
$0.84^{+0.26}_{-0.28}$±0.13	[1] AUBERT	08AJ	BABR	$e^+e^- \to \Upsilon(4S)$

[1] Assumes equal production of B^+ and B^0 at the $\Upsilon(4S)$.

Γ_L/Γ in $B^0 \to D_s^{*+} K^{*-}$

VALUE	DOCUMENT ID		TECN	COMMENT
$0.92^{+0.37}_{-0.31}$±0.07	[1] AUBERT	08AJ	BABR	$e^+e^- \to \Upsilon(4S)$

[1] Assumes equal production of B^+ and B^0 at the $\Upsilon(4S)$.

Γ_L/Γ in $B^0 \to D^{*+} D^{*-}$

VALUE	DOCUMENT ID		TECN	COMMENT
0.624±0.029±0.011	KRONENBIT...	12	BELL	$e^+e^- \to \Upsilon(4S)$
• • • We do not use the following data for averages, fits, limits, etc. • • •				
0.57 ±0.08 ±0.02	MIYAKE	05	BELL	Repl. by KRONENBITTER 12

$\Gamma_\perp/\Gamma$ in $B^0 \to D^{*+} D^{*-}$

VALUE	DOCUMENT ID		TECN	COMMENT
0.147±0.019 OUR AVERAGE				
0.138±0.024±0.006	KRONENBIT...	12	BELL	$e^+e^- \to \Upsilon(4S)$
0.158±0.028±0.006	AUBERT	09C	BABR	$e^+e^- \to \Upsilon(4S)$
• • • We do not use the following data for averages, fits, limits, etc. • • •				
0.125±0.043±0.023	VERVINK	09	BELL	Repl. by KRONENBITTER 12
0.143±0.034±0.008	AUBERT	07BO	BABR	Repl. by AUBERT 09C
0.125±0.044±0.007	AUBERT,BE	05A	BABR	Repl. by AUBERT 07BO
0.19 ±0.08 ±0.01	MIYAKE	05	BELL	Repl. by VERVINK 09
0.063±0.055±0.009	AUBERT	03Q	BABR	Repl. by AUBERT,BE 05A

Γ_L/Γ in $B^0 \to \overline{D}^{*0} \omega$

VALUE	DOCUMENT ID		TECN	COMMENT
0.665±0.047±0.015	LEES	11M	BABR	$e^+e^- \to \Upsilon(4S)$

Γ_L/Γ in $B^0 \to \overline{D}_1(2430)^0 \omega$

VALUE (%)	DOCUMENT ID		TECN	COMMENT
$63.0 \pm 9.1^{+6.5}_{-6.0}$	[1,2] MATVIENKO	15	BELL	$e^+e^- \to \Upsilon(4S)$

[1] Obtained by amplitude analysis of $\overline{B}^0 \to D^{*-}\omega\pi^+$. The second uncertainty combines in qudrature experimental systematic and model uncertainties.
[2] Assumes equal production of B^0 and B^+ at $\Upsilon(4S)$.

Γ_L/Γ in $B^0 \to \overline{D}_1(2420)^0 \omega$

VALUE (%)	DOCUMENT ID		TECN	COMMENT
$67.1 \pm 11.7^{+2.3}_{-5.0}$	[1,2] MATVIENKO	15	BELL	$e^+e^- \to \Upsilon(4S)$

[1] Obtained by amplitude analysis of $\overline{B}^0 \to D^{*-}\omega\pi^+$. The second uncertainty combines in qudrature experimental systematic and model uncertainties.
[2] Assumes equal production of B^0 and B^+ at $\Upsilon(4S)$.

Γ_L/Γ in $B^0 \to \overline{D}_2^*(2460)^0 \omega$

VALUE (%)	DOCUMENT ID		TECN	COMMENT
$76.0^{+18.3}_{-8.5}{}^{+3.5}_{-2.8}$	[1,2] MATVIENKO	15	BELL	$e^+e^- \to \Upsilon(4S)$

[1] Obtained by amplitude analysis of $\overline{B}^0 \to D^{*-}\omega\pi^+$. The second uncertainty combines in qudrature experimental systematic and model uncertainties.
[2] Assumes equal production of B^0 and B^+ at $\Upsilon(4S)$.

Γ_L/Γ in $B^0 \to D^{*-} \omega \pi^+$

VALUE	DOCUMENT ID		TECN	COMMENT
0.654±0.042±0.016	[1] AUBERT	06L	BABR	$e^+e^- \to \Upsilon(4S)$

[1] Invariant mass of the $[\omega\pi]$ system is restricted in the region 1.1 and 1.9 GeV.

Γ_L/Γ in $B^0 \to \omega K^{*0}$

VALUE	DOCUMENT ID		TECN	COMMENT
0.69±0.11 OUR AVERAGE				
0.68±0.17±0.16	AAIJ	19J	LHCB	pp at 7, 8 TeV
0.72±0.14±0.02	AUBERT	09H	BABR	$e^+e^- \to \Upsilon(4S)$
$0.56 \pm 0.29^{+0.18}_{-0.08}$	GOLDENZWE..	08	BELL	$e^+e^- \to \Upsilon(4S)$

$\Gamma_\perp/\Gamma$ in $B^0 \to \omega K^*(892)^0$

VALUE	DOCUMENT ID		TECN	COMMENT
0.10±0.09±0.09	AAIJ	19J	LHCB	pp at 7, 8 TeV

A_{CP}^0 in $B^0 \to \omega K^*(892)^0$

VALUE	DOCUMENT ID		TECN	COMMENT
−0.13±0.27±0.13	AAIJ	19J	LHCB	pp at 7, 8 TeV

$A_{CP}^\perp$ in $B^0 \to \omega K^*(892)^0$

VALUE	DOCUMENT ID		TECN	COMMENT
0.3±0.8±0.4	AAIJ	19J	LHCB	pp at 7, 8 TeV

$A_{CP}^\|$ in $B^0 \to \omega K^*(892)^0$

VALUE	DOCUMENT ID		TECN	COMMENT
0.26±0.55±0.22	AAIJ	19J	LHCB	pp at 7, 8 TeV

ϕ_0 in $B^0 \to \omega K^*(892)^0$

VALUE	DOCUMENT ID		TECN	COMMENT
−0.86±0.29±0.71	AAIJ	19J	LHCB	pp at 7, 8 TeV

$\phi_\perp$ in $B^0 \to \omega K^*(892)^0$

VALUE	DOCUMENT ID		TECN	COMMENT
1.6±0.4±0.6	AAIJ	19J	LHCB	pp at 7, 8 TeV

$\phi_\|$ in $B^0 \to \omega K^*(892)^0$

VALUE	DOCUMENT ID		TECN	COMMENT
−1.83±0.29±0.32	AAIJ	19J	LHCB	pp at 7, 8 TeV

Γ_L/Γ in $B^0 \to \omega K_2^*(1430)^0$

VALUE	DOCUMENT ID		TECN	COMMENT
0.45±0.12±0.02	AUBERT	09H	BABR	$e^+e^- \to \Upsilon(4S)$

Γ_L/Γ in $B^0 \to K^{*0} \overline{K}^{*0}$

VALUE	DOCUMENT ID		TECN	COMMENT
0.74 ±0.05 OUR AVERAGE				
0.724±0.051±0.016	[1] AAIJ	19L	LHCB	pp at 7 and 8 TeV
$0.80 \pm^{+0.10}_{-0.12} \pm 0.06$	AUBERT	08I	BABR	$e^+e^- \to \Upsilon(4S)$

[1] Untagged and time-integrated analysis within 150 MeV of the K^{*0} mass.

Γ_L/Γ in $B^0 \to \phi K^*(892)^0$

VALUE	DOCUMENT ID		TECN	COMMENT
0.497±0.017 OUR AVERAGE				
0.497±0.019±0.015	AAIJ	14AM	LHCB	pp at 7 TeV
0.499±0.030±0.018	PRIM	13	BELL	$e^+e^- \to \Upsilon(4S)$
0.494±0.034±0.013	AUBERT	08BG	BABR	$e^+e^- \to \Upsilon(4S)$
• • • We do not use the following data for averages, fits, limits, etc. • • •				
0.506±0.040±0.015	AUBERT	07D	BABR	Repl. by AUBERT 08BG
0.45 ±0.05 ±0.02	CHEN	05A	BELL	Repl. by PRIM 13
0.52 ±0.05 ±0.02	[1] AUBERT,B	04W	BABR	Repl. by AUBERT 07D
0.65 ±0.07 ±0.02	AUBERT	03V	BABR	Repl. by AUBERT,B 04W
0.41 ±0.10 ±0.04	CHEN	03B	BELL	Repl. by CHEN 05A

[1] AUBERT,B 04W also measures the fraction of parity-odd transverse contribution $f_\perp = 0.22 \pm 0.05 \pm 0.02$ and the phases of the parity-even and parity-odd transverse amplitudes relative to the longitudinal amplitude.

Downloaded from https://academic.oup.com/ptep/article/2022/8/083C01/6651666 by KIT Library user on 27 September 2022

$\Gamma_\perp/\Gamma$ in $B^0 \to \phi K^*(892)^0$

VALUE	DOCUMENT ID		TECN	COMMENT
0.224±0.015 OUR AVERAGE				
0.221±0.016±0.013	AAIJ	14AM	LHCB	pp at 7 TeV
0.238±0.026±0.008	PRIM	13	BELL	$e^+e^- \to \Upsilon(4S)$
0.212±0.032±0.013	AUBERT	08BG	BABR	$e^+e^- \to \Upsilon(4S)$
• • • We do not use the following data for averages, fits, limits, etc. • • •				
0.227±0.038±0.013	AUBERT	07D	BABR	Repl. by AUBERT 08BG
0.31 $^{+0.06}_{-0.05}$ ±0.02	[1] CHEN	05A	BELL	Repl. by PRIM 13
0.22 ±0.05 ±0.02	AUBERT,B	04W	BABR	Repl. by AUBERT 07D

[1] This quantity was recalculated by the BELLE authors from numbers in the original paper.

$\phi_\parallel$ in $B^0 \to \phi K^*(892)^0$

VALUE (rad)	DOCUMENT ID		TECN	COMMENT
2.43 ±0.11 OUR AVERAGE	Error includes scale factor of 1.8. See the ideogram below.			
2.562±0.069±0.040	AAIJ	14AM	LHCB	pp at 7 TeV
2.23 ±0.10 ±0.02	PRIM	13	BELL	$e^+e^- \to \Upsilon(4S)$
2.40 ±0.13 ±0.08	AUBERT	08BG	BABR	$e^+e^- \to \Upsilon(4S)$
• • • We do not use the following data for averages, fits, limits, etc. • • •				
2.31 ±0.14 ±0.08	AUBERT	07D	BABR	Repl. by AUBERT 08BG
2.40 $^{+0.28}_{-0.24}$ ±0.07	[1] CHEN	05A	BELL	Repl. by PRIM 13
2.34 $^{+0.23}_{-0.20}$ ±0.05	AUBERT,B	04W	BABR	Repl. by AUBERT 07D

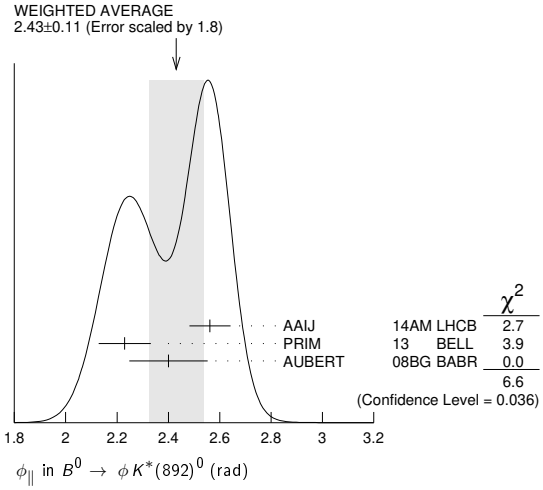

[1] This quantity was recalculated by the BELLE authors from numbers in the original paper.

$\phi_\perp$ in $B^0 \to \phi K^*(892)^0$

VALUE (rad)	DOCUMENT ID		TECN	COMMENT
2.53 ±0.09 OUR AVERAGE	Error includes scale factor of 1.7. See the ideogram below.			
2.633±0.062±0.037	AAIJ	14AM	LHCB	pp at 7 TeV
2.37 ±0.10 ±0.04	PRIM	13	BELL	$e^+e^- \to \Upsilon(4S)$
2.35 ±0.13 ±0.09	AUBERT	08BG	BABR	$e^+e^- \to \Upsilon(4S)$
• • • We do not use the following data for averages, fits, limits, etc. • • •				
2.24 ±0.15 ±0.09	AUBERT	07D	BABR	Repl. by AUBERT 08BG
2.51 ±0.25 ±0.06	[1] CHEN	05A	BELL	Repl. by PRIM 13
2.47 ±0.25 ±0.05	AUBERT,B	04W	BABR	Repl. by AUBERT 07D

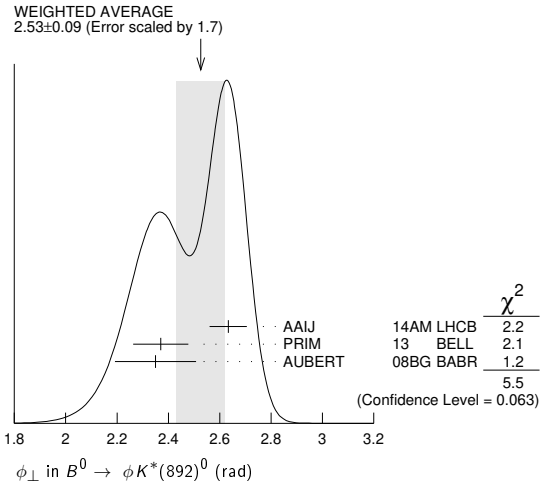

[1] This quantity was recalculated by the BELLE authors from numbers in the original paper.

$\delta_0(B^0 \to \phi K^*(892)^0)$

VALUE (rad)	DOCUMENT ID		TECN	COMMENT
2.88±0.10 OUR AVERAGE				
2.91±0.10±0.08	PRIM	13	BELL	$e^+e^- \to \Upsilon(4S)$
2.82±0.15±0.09	AUBERT	08BG	BABR	$e^+e^- \to \Upsilon(4S)$
• • • We do not use the following data for averages, fits, limits, etc. • • •				
2.78±0.17±0.09	AUBERT	07D	BABR	Repl. by AUBERT 08BG

A^0_{CP} in $B^0 \to \phi K^*(892)^0$

VALUE	DOCUMENT ID		TECN	COMMENT
−0.007±0.030 OUR AVERAGE				
−0.003±0.038±0.005	AAIJ	14AM	LHCB	pp at 7 TeV
−0.030±0.061±0.007	PRIM	13	BELL	$e^+e^- \to \Upsilon(4S)$
0.01 ±0.07 ±0.02	AUBERT	08BG	BABR	$e^+e^- \to \Upsilon(4S)$
• • • We do not use the following data for averages, fits, limits, etc. • • •				
−0.03 ±0.08 ±0.02	AUBERT	07D	BABR	Repl. by AUBERT 08BG
0.13 ±0.12 ±0.04	[1] CHEN	05A	BELL	Repl. by PRIM 13
−0.06 ±0.10 ±0.01	AUBERT,B	04W	BABR	Repl. by AUBERT 07D

[1] This quantity was recalculated by the BELLE authors from numbers in the original paper.

$A^\perp_{CP}$ in $B^0 \to \phi K^*(892)^0$

VALUE	DOCUMENT ID		TECN	COMMENT
−0.02 ±0.06 OUR AVERAGE				
0.047±0.074±0.009	AAIJ	14AM	LHCB	pp at 7 TeV
−0.14 ±0.11 ±0.01	PRIM	13	BELL	$e^+e^- \to \Upsilon(4S)$
−0.04 ±0.15 ±0.06	AUBERT	08BG	BABR	$e^+e^- \to \Upsilon(4S)$
• • • We do not use the following data for averages, fits, limits, etc. • • •				
−0.03 ±0.16 ±0.05	AUBERT	07D	BABR	Repl. by AUBERT 08BG
−0.20 ±0.18 ±0.04	[1] CHEN	05A	BELL	Repl. by PRIM 13
−0.10 ±0.24 ±0.05	AUBERT,B	04W	BABR	Repl. by AUBERT 07D

[1] This quantity was recalculated by the BELLE authors from numbers in the original paper.

$\Delta\phi_\parallel$ in $B^0 \to \phi K^*(892)^0$

VALUE (rad)	DOCUMENT ID		TECN	COMMENT
0.05 ±0.05 OUR AVERAGE				
0.045±0.069±0.015	AAIJ	14AM	LHCB	pp at 7 TeV
−0.02 ±0.10 ±0.01	PRIM	13	BELL	$e^+e^- \to \Upsilon(4S)$
0.22 ±0.12 ±0.08	AUBERT	08BG	BABR	$e^+e^- \to \Upsilon(4S)$
• • • We do not use the following data for averages, fits, limits, etc. • • •				
0.24 ±0.14 ±0.08	AUBERT	07D	BABR	Repl. by AUBERT 08BG
−0.32 ±0.27 ±0.07	[1] CHEN	05A	BELL	Repl. by PRIM 13
0.27 $^{+0.20}_{-0.23}$ ±0.05	AUBERT,B	04W	BABR	Repl. by AUBERT 07D

[1] This quantity was recalculated by the BELLE authors from numbers in the original paper.

$\Delta\phi_\perp$ in $B^0 \to \phi K^*(892)^0$

VALUE (rad)	DOCUMENT ID		TECN	COMMENT
0.08 ±0.05 OUR AVERAGE				
0.062±0.062±0.005	AAIJ	14AM	LHCB	pp at 7 TeV
0.05 ±0.10 ±0.02	PRIM	13	BELL	$e^+e^- \to \Upsilon(4S)$
0.21 ±0.13 ±0.08	AUBERT	08BG	BABR	$e^+e^- \to \Upsilon(4S)$
• • • We do not use the following data for averages, fits, limits, etc. • • •				
0.19 ±0.15 ±0.08	AUBERT	07D	BABR	Repl. by AUBERT 08BG
−0.30 ±0.25 ±0.06	[1] CHEN	05A	BELL	Repl. by PRIM 13
0.36 ±0.25 ±0.05	AUBERT,B	04W	BABR	Repl. by AUBERT 07D

[1] This quantity was recalculated by the BELLE authors from numbers in the original paper.

$\Delta\delta_0(B^0 \to \phi K^*(892)^0)$

VALUE (rad)	DOCUMENT ID		TECN	COMMENT
0.13±0.09 OUR AVERAGE				
0.08±0.10±0.01	PRIM	13	BELL	$e^+e^- \to \Upsilon(4S)$
0.27±0.14±0.08	AUBERT	08BG	BABR	$e^+e^- \to \Upsilon(4S)$
• • • We do not use the following data for averages, fits, limits, etc. • • •				
0.21±0.17±0.08	AUBERT	07D	BABR	Repl. by AUBERT 08BG

$\Delta\phi_{00}(B^0 \to \phi K^*_0(1430)^0)$

VALUE (rad)	DOCUMENT ID		TECN	COMMENT
0.28±0.42±0.04	AUBERT	08BG	BABR	$e^+e^- \to \Upsilon(4S)$

Γ_L/Γ in $B^0 \to \phi K^*_2(1430)^0$

VALUE	DOCUMENT ID		TECN	COMMENT
0.913 $^{+0.028}_{-0.050}$ OUR AVERAGE				
0.918 $^{+0.029}_{-0.060}$ ±0.012	PRIM	13	BELL	$e^+e^- \to \Upsilon(4S)$
0.901 $^{+0.046}_{-0.058}$ ±0.037	AUBERT	08BG	BABR	$e^+e^- \to \Upsilon(4S)$
• • • We do not use the following data for averages, fits, limits, etc. • • •				
0.853 $^{+0.061}_{-0.069}$ ±0.036	AUBERT	07D	BABR	Repl. by AUBERT 08BG

Downloaded from https://academic.oup.com/ptep/article/2022/8/083C01/6651666 by KIT Library user on 27 September 2022

$\Gamma_\perp/\Gamma$ in $B^0 \to \phi K_2^*(1430)^0$

VALUE	DOCUMENT ID		TECN	COMMENT
$0.027^{+0.031}_{-0.025}$ OUR AVERAGE	Error includes scale factor of 1.1.			
$0.056^{+0.050}_{-0.035}\pm0.009$	PRIM	13	BELL	$e^+e^- \to \Upsilon(4S)$
$0.002^{+0.018}_{-0.002}\pm0.031$	AUBERT	08BG	BABR	$e^+e^- \to \Upsilon(4S)$
• • • We do not use the following data for averages, fits, limits, etc. • • •				
$0.045^{+0.049}_{-0.040}\pm0.013$	AUBERT	07D	BABR	Repl. by AUBERT 08BG

$\phi_\parallel$ in $B^0 \to \phi K_2^*(1430)^0$

VALUE (rad)	DOCUMENT ID		TECN	COMMENT
4.0 ±0.4 OUR AVERAGE				
$3.76\pm2.88\pm1.32$	PRIM	13	BELL	$e^+e^- \to \Upsilon(4S)$
$3.96\pm0.38\pm0.06$	AUBERT	08BG	BABR	$e^+e^- \to \Upsilon(4S)$
• • • We do not use the following data for averages, fits, limits, etc. • • •				
$2.90\pm0.39\pm0.06$	AUBERT	07D	BABR	Repl. by AUBERT 08BG

$\phi_\perp$ in $B^0 \to \phi K_2^*(1430)^0$

VALUE (rad)	DOCUMENT ID		TECN	COMMENT
$4.45^{+0.43}_{-0.38}\pm0.13$	PRIM	13	BELL	$e^+e^- \to \Upsilon(4S)$
• • • We do not use the following data for averages, fits, limits, etc. • • •				
$5.72^{+0.55}_{-0.87}\pm0.11$	AUBERT	07D	BABR	Repl. by AUBERT 08BG

$\delta_0(B^0 \to \phi K_2^*(1430)^0)$

VALUE (rad)	DOCUMENT ID		TECN	COMMENT
3.46±0.14 OUR AVERAGE				
$3.53\pm0.11\pm0.19$	PRIM	13	BELL	$e^+e^- \to \Upsilon(4S)$
$3.41\pm0.13\pm0.13$	AUBERT	08BG	BABR	$e^+e^- \to \Upsilon(4S)$
• • • We do not use the following data for averages, fits, limits, etc. • • •				
$3.54^{+0.12}_{-0.14}\pm0.06$	AUBERT	07D	BABR	Repl. by AUBERT 08BG

A^0_{CP} in $B^0 \to \phi K_2^*(1430)^0$

VALUE	DOCUMENT ID		TECN	COMMENT
−0.03 ±0.04 OUR AVERAGE				
$-0.016^{+0.066}_{-0.051}\pm0.008$	PRIM	13	BELL	$e^+e^- \to \Upsilon(4S)$
−0.05 ±0.06 ±0.01	AUBERT	08BG	BABR	$e^+e^- \to \Upsilon(4S)$

$A^\perp_{CP}$ in $B^0 \to \phi K_2^*(1430)^0$

VALUE	DOCUMENT ID		TECN	COMMENT
$-0.01^{+0.85}_{-0.67}\pm0.09$	PRIM	13	BELL	$e^+e^- \to \Upsilon(4S)$

$\Delta\phi_\parallel(B^0 \to \phi K_2^*(1430)^0)$

VALUE (rad)	DOCUMENT ID		TECN	COMMENT
−0.9 ±0.4 OUR AVERAGE				
$-0.02\pm1.08\pm1.01$	PRIM	13	BELL	$e^+e^- \to \Upsilon(4S)$
$-1.00\pm0.38\pm0.09$	AUBERT	08BG	BABR	$e^+e^- \to \Upsilon(4S)$

$\Delta\phi_\perp(B^0 \to \phi K_2^*(1430)^0)$

VALUE	DOCUMENT ID		TECN	COMMENT
−0.19±0.42±0.11	PRIM	13	BELL	$e^+e^- \to \Upsilon(4S)$

$\Delta\delta_0$ in $B^0 \to \phi K_2^*(1430)^0$

VALUE (rad)	DOCUMENT ID		TECN	COMMENT
0.08±0.09 OUR AVERAGE				
$0.06\pm0.11\pm0.02$	PRIM	13	BELL	$e^+e^- \to \Upsilon(4S)$
$0.11\pm0.13\pm0.06$	AUBERT	08BG	BABR	$e^+e^- \to \Upsilon(4S)$

Γ_L/Γ in $B^0 \to K^*(892)^0\rho^0$

VALUE	DOCUMENT ID		TECN	COMMENT
0.173±0.026 OUR AVERAGE				
$0.164\pm0.015\pm0.022$	AAIJ	19J	LHCB	pp at 7, 8 TeV
0.40 ±0.08 ±0.11	LEES	12K	BABR	$e^+e^- \to \Upsilon(4S)$
• • • We do not use the following data for averages, fits, limits, etc. • • •				
0.57 ±0.09 ±0.08	AUBERT,B	06G	BABR	Repl. by LEES 12K

$\Gamma_\perp/\Gamma$ in $B^0 \to K^*(892)^0\rho^0$

VALUE	DOCUMENT ID		TECN	COMMENT
0.401±0.016±0.037	AAIJ	19J	LHCB	pp at 7, 8 TeV

A^0_{CP} in $B^0 \to K^*(892)^0\rho^0$

VALUE	DOCUMENT ID		TECN	COMMENT
−0.62±0.09±0.09	AAIJ	19J	LHCB	pp at 7, 8 TeV

$A^\perp_{CP}$ in $B^0 \to K^*(892)^0\rho^0$

VALUE	DOCUMENT ID		TECN	COMMENT
0.050±0.039±0.015	AAIJ	19J	LHCB	pp at 7, 8 TeV

$A^\parallel_{CP}$ in $B^0 \to K^*(892)^0\rho^0$

VALUE	DOCUMENT ID		TECN	COMMENT
0.188±0.037±0.022	AAIJ	19J	LHCB	pp at 7, 8 TeV

ϕ_0 in $B^0 \to K^*(892)^0\rho^0$

VALUE	DOCUMENT ID		TECN	COMMENT
1.57±0.08±0.18	AAIJ	19J	LHCB	pp at 7, 8 TeV

$\phi_\perp$ in $B^0 \to K^*(892)^0\rho^0$

VALUE	DOCUMENT ID		TECN	COMMENT
−2.365±0.032±0.054	AAIJ	19J	LHCB	pp at 7, 8 TeV

$\phi_\parallel$ in $B^0 \to K^*(892)^0\rho^0$

VALUE	DOCUMENT ID		TECN	COMMENT
0.795±0.030±0.068	AAIJ	19J	LHCB	pp at 7, 8 TeV

Γ_L/Γ in $B^0 \to K^{*+}\rho^-$

VALUE	DOCUMENT ID		TECN	COMMENT
0.38±0.13±0.03	LEES	12K	BABR	$e^+e^- \to \Upsilon(4S)$

Γ_L/Γ in $B^0 \to \rho^+\rho^-$

VALUE	DOCUMENT ID		TECN	COMMENT
$0.990^{+0.021}_{-0.019}$ OUR AVERAGE				
$0.988\pm0.012\pm0.023$	VANHOEFER	16	BELL	$e^+e^- \to \Upsilon(4S)$
$0.992\pm0.024^{+0.026}_{-0.013}$	AUBERT	07BF	BABR	$e^+e^- \to \Upsilon(4S)$
• • • We do not use the following data for averages, fits, limits, etc. • • •				
$0.941^{+0.034}_{-0.040}\pm0.030$	SOMOV	06	BELL	Repl. by VANHOEFER 16
$0.978\pm0.014^{+0.021}_{-0.029}$	AUBERT,B	05C	BABR	Repl. by AUBERT 07BF
$0.98\ ^{+0.02}_{-0.08}\ \pm0.03$	AUBERT	04G	BABR	Repl. by AUBERT,B 04R
$0.99\ \pm0.03\ ^{+0.04}_{-0.03}$	AUBERT,B	04R	BABR	Repl. by AUBERT,B 05C

Γ_L/Γ in $B^0 \to \rho^0\rho^0$

VALUE	DOCUMENT ID		TECN	COMMENT
$0.71\ ^{+0.08}_{-0.09}$ OUR AVERAGE	Error includes scale factor of 1.6. See the ideogram below.			
$0.745^{+0.048}_{-0.058}\pm0.034$	AAIJ	15T	LHCB	pp at 7, 8 TeV
$0.21\ ^{+0.18}_{-0.22}\ \pm0.15$	VANHOEFER	14	BELL	$e^+e^- \to \Upsilon(4S)$
$0.75\ ^{+0.11}_{-0.14}\ \pm0.05$	AUBERT	08BB	BABR	$e^+e^- \to \Upsilon(4S)$
• • • We do not use the following data for averages, fits, limits, etc. • • •				
0.87 ±0.13 ±0.04	AUBERT	07G	BABR	Repl. by AUBERT 08BB

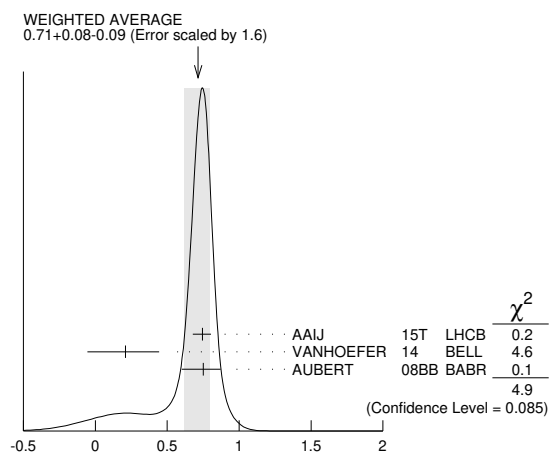

Γ_L/Γ in $B^0 \to \rho^0\rho^0$

Γ_L/Γ in $B^0 \to a_1(1260)^+ a_1(1260)^-$

VALUE	DOCUMENT ID		TECN	COMMENT
0.31±0.22±0.10	AUBERT	09AL	BABR	$e^+e^- \to \Upsilon(4S)$

Γ_L/Γ in $B^0 \to p\overline{p}K^*(892)^0$

VALUE	DOCUMENT ID		TECN	COMMENT
1.01±0.13±0.03	CHEN	08C	BELL	$e^+e^- \to \Upsilon(4S)$

Γ_L/Γ in $B^0 \to \Lambda\overline{\Lambda}K^*(892)^0$

VALUE	DOCUMENT ID		TECN	COMMENT
0.60±0.22±0.08	CHANG	09	BELL	$e^+e^- \to \Upsilon(4S)$

Downloaded from https://academic.oup.com/ptep/article/2022/8/083C01/6651666 by KIT Library user on 27 September 2022

Γ_L/Γ in $B^0 \to K^*(892)^0 \mu^+ \mu^-$ ($0.04 < q^2 < 6.0$ GeV^2/c^4)

VALUE	DOCUMENT ID		TECN	COMMENT
0.50±0.06±0.04	[1] AABOUD	18BY	ATLS	pp at 8 TeV

[1] A set of angular parameters obtained for this decay is also presented.

Γ_L/Γ in $B^0 \to K^*(892)^0 e^+ e^-$ (at low q^2)

VALUE	DOCUMENT ID		TECN	COMMENT
0.044±0.026±0.014	[1] AAIJ	20AO	LHCB	pp at 7, 8, 13 TeV
• • • We do not use the following data for averages, fits, limits, etc. • • •				
0.16 ±0.06 ±0.03	[2] AAIJ	15Z	LHCB	Repl. by AAIJ 20AO

[1] Determined in the effective dielectron invariant mass range $0.0008 < q^2 < 0.257$ GeV^2/c^4.
[2] Determined in the effective dielectron invariant mass range $0.002 < q^2 < 1.120$ GeV^2/c^4.

$A_T^{(2)}$ in $B^0 \to K^*(892)^0 e^+ e^-$ (at low q^2)

VALUE	DOCUMENT ID		TECN	COMMENT
0.11±0.10±0.02	[1] AAIJ	20AO	LHCB	pp at 7, 8, 13 TeV
• • • We do not use the following data for averages, fits, limits, etc. • • •				
−0.23±0.23±0.05	[2] AAIJ	15Z	LHCB	Repl. by AAIJ 20AO

[1] Determined in the effective dielectron invariant mass range $0.0008 < q^2 < 0.257$ GeV^2/c^4.
[2] Determined in the effective dielectron invariant mass range $0.002 < q^2 < 1.120$ GeV^2/c^4.

A_T^{Im} in $B^0 \to K^*(892)^0 e^+ e^-$ (at low q^2)

VALUE	DOCUMENT ID		TECN	COMMENT
0.02±0.10±0.01	[1] AAIJ	20AO	LHCB	pp at 7, 8, 13 TeV
• • • We do not use the following data for averages, fits, limits, etc. • • •				
0.14±0.22±0.05	[2] AAIJ	15Z	LHCB	Repl. by AAIJ 20AO

[1] Determined in the effective dielectron invariant mass range $0.0008 < q^2 < 0.257$ GeV^2/c^4.
[2] Determined in the effective dielectron invariant mass range $0.002 < q^2 < 1.120$ GeV^2/c^4.

A_T^{Re} in $B^0 \to K^*(892)^0 e^+ e^-$ (at low q^2)

Related to A_{FB}, F_L by $A_T^{Re} = (4/3)\ A_{FB}\ /\ (1 - F_L)$.

VALUE	DOCUMENT ID		TECN	COMMENT
−0.06±0.08±0.02	[1] AAIJ	20AO	LHCB	pp at 7, 8, 13 TeV
• • • We do not use the following data for averages, fits, limits, etc. • • •				
0.10±0.18±0.05	[2] AAIJ	15Z	LHCB	Repl. by AAIJ 20AO

[1] Determined in the effective dielectron invariant mass range $0.0008 < q^2 < 0.257$ GeV^2/c^4.
[2] Determined in the effective dielectron invariant mass range $0.002 < q^2 < 1.120$ GeV^2/c^4.

See the related review(s):

B^0 — $\overline{B}^0$ Mixing

B^0-$\overline{B}^0$ MIXING PARAMETERS

For a discussion of B^0-$\overline{B}^0$ mixing see the note on "B^0-$\overline{B}^0$ Mixing" in the B^0 Particle Listings above.

χ_d is a measure of the time-integrated B^0-$\overline{B}^0$ mixing probability that a produced $B^0(\overline{B}^0)$ decays as a $\overline{B}^0(B^0)$. Mixing violates $\Delta B \neq 2$ rule.

$$\chi_d = \frac{x_d^2}{2(1+x_d^2)}$$

$$x_d = \frac{\Delta m_{B^0}}{\Gamma_{B^0}} = (m_{B^0_H} - m_{B^0_L})\ \tau_{B^0}\ ,$$

where H, L stand for heavy and light states of two B^0 CP eigenstates and $\tau_{B^0} = \frac{1}{0.5(\Gamma_{B^0_H} + \Gamma_{B^0_L})}$.

χ_d

This B^0-$\overline{B}^0$ mixing parameter is the probability (integrated over time) that a produced B^0 (or $\overline{B}^0$) decays as a $\overline{B}^0$ (or B^0), e.g. for inclusive lepton decays

$$\chi_d = \Gamma(B^0 \to \ell^- X \text{ (via } \overline{B}^0))/\Gamma(B^0 \to \ell^\pm X)$$
$$= \Gamma(\overline{B}^0 \to \ell^+ X \text{ (via } B^0))/\Gamma(\overline{B}^0 \to \ell^\pm X)$$

Where experiments have measured the parameter $r = \chi/(1-\chi)$, we have converted to χ. Mixing violates the $\Delta B \neq 2$ rule.

Note that the measurement of χ at energies higher than the $\Upsilon(4S)$ have not separated χ_d from χ_s where the subscripts indicate $B^0(\overline{b}d)$ or $B^0_s(\overline{b}s)$. They are listed in the $B^\pm/B^0/B^0_s/b$-baryon ADMIXTURE section.

The experiments at $\Upsilon(4S)$ make an assumption about the $B^0\overline{B}^0$ fraction and about the ratio of the $B^\pm$ and B^0 semileptonic branching ratios (usually that it equals one).

"OUR EVALUATION" is an average using rescaled values of the data listed below. The average and rescaling were performed by the Heavy Flavor Averaging Group (HFLAV) and are described at https://hflav.web.cern.ch/. The averaging/rescaling procedure takes into account correlations between the measurements, includes χ_d calculated from Δm_{B^0} and τ_{B^0}.

VALUE	CL%	DOCUMENT ID		TECN	COMMENT
0.1858±0.0011 OUR EVALUATION					
0.182 ±0.015 OUR AVERAGE					
0.198 ±0.013 ±0.014		[1] BEHRENS	00B	CLE2	$e^+e^- \to \Upsilon(4S)$
0.16 ±0.04 ±0.04		[2] ALBRECHT	94	ARG	$e^+e^- \to \Upsilon(4S)$
0.149 ±0.023 ±0.022		[3] BARTELT	93	CLE2	$e^+e^- \to \Upsilon(4S)$
0.171 ±0.048		[4] ALBRECHT	92L	ARG	$e^+e^- \to \Upsilon(4S)$
• • • We do not use the following data for averages, fits, limits, etc. • • •					
0.20 ±0.13 ±0.12		[5] ALBRECHT	96D	ARG	$e^+e^- \to \Upsilon(4S)$
0.19 ±0.07 ±0.09		[6] ALBRECHT	96D	ARG	$e^+e^- \to \Upsilon(4S)$
0.24 ±0.12		[7] ELSEN	90	JADE	e^+e^- 35–44 GeV
0.158 $^{+0.052}_{-0.059}$		ARTUSO	89	CLEO	$e^+e^- \to \Upsilon(4S)$
0.17 ±0.05		[8] ALBRECHT	87I	ARG	$e^+e^- \to \Upsilon(4S)$
<0.19	90	[9] BEAN	87B	CLEO	$e^+e^- \to \Upsilon(4S)$
<0.27	90	[10] AVERY	84	CLEO	$e^+e^- \to \Upsilon(4S)$

[1] BEHRENS 00B uses high-momentum lepton tags and partially reconstructed $\overline{B}^0 \to D^{*+}\pi^-$, ρ^- decays to determine the flavor of the B meson.
[2] ALBRECHT 94 reports r=0.194 ± 0.062 ± 0.054. We convert to χ for comparison. Uses tagged events (lepton + pion from D^*).
[3] BARTELT 93 analysis performed using tagged events (lepton+pion from D^*). Using dilepton events they obtain 0.157 ± 0.016 $^{+0.033}_{-0.028}$.
[4] ALBRECHT 92L is a combined measurement employing several lepton-based techniques. It uses all previous ARGUS data in addition to new data and therefore supersedes ALBRECHT 87I. A value of r = 20.6 ± 7.0% is directly measured. The value can be used to measure $x = \Delta M/\Gamma = 0.72 \pm 0.15$ for the B_d meson. Assumes $f_{+-}/f_0 = 1.0 \pm 0.05$ and uses $\tau_{B^\pm}/\tau_{B^0} = (0.95 \pm 0.14)$ (f_{+-}/f_0).
[5] Uses $D^{*+}K^\pm$ correlations.
[6] Uses $(D^{*+}\ell^-)\ K^\pm$ correlations.
[7] These experiments see a combination of B_s and B_d mesons.
[8] ALBRECHT 87I is inclusive measurement with like-sign dileptons, with tagged B decays plus leptons, and one fully reconstructed event. Measures r=0.21 ± 0.08. We convert to χ for comparison. Superseded by ALBRECHT 92L.
[9] BEAN 87B measured $r <$ 0.24; we converted to χ.
[10] Same-sign dilepton events. Limit assumes semileptonic BR for B^+ and B^0 equal. If $B^0/B^\pm$ ratio <0.58, no limit exists. The limit was corrected in BEAN 87B from $r <$ 0.30 to $r <$ 0.37. We converted this limit to χ.

$\Delta m_{B^0} = m_{B^0_H} - m_{B^0_L}$

Δm_{B^0} is a measure of 2π times the B^0-$\overline{B}^0$ oscillation frequency in time-dependent mixing experiments.

"OUR EVALUATION" is an average using rescaled values of the data listed below. The average and rescaling were performed by the Heavy Flavor Averaging Group (HFLAV) and are described at https://hflav.web.cern.ch/. The averaging/rescaling procedure takes into account correlations between the measurements and includes Δm_d calculated from χ_d measured at $\Upsilon(4S)$.

VALUE ($10^{12}\ \hbar\ s^{-1}$)	DOCUMENT ID		TECN	COMMENT
0.5065±0.0019 OUR EVALUATION				
0.5050±0.0021±0.0010	[1] AAIJ	16AV	LHCB	pp at 7, 8 TeV
0.503 ±0.011 ±0.013	[2] AAIJ	13CF	LHCB	pp at 7 TeV
0.5156±0.0051±0.0033	[3] AAIJ	13F	LHCB	pp at 7 TeV
0.499 ±0.032 ±0.003	[4] AAIJ	12I	LHCB	pp at 7 TeV
0.506 ±0.020 ±0.016	[5] ABAZOV	06W	D0	$p\overline{p}$ at 1.96 TeV
0.511 ±0.007 $^{+0.007}_{-0.006}$	[6] AUBERT	06G	BABR	$e^+e^- \to \Upsilon(4S)$
0.511 ±0.005 ±0.006	[7] ABE	05B	BELL	$e^+e^- \to \Upsilon(4S)$
0.531 ±0.025 ±0.007	[8] ABDALLAH	03B	DLPH	$e^+e^- \to Z$
0.492 ±0.018 ±0.013	[9] AUBERT	03C	BABR	$e^+e^- \to \Upsilon(4S)$
0.503 ±0.008 ±0.010	[10] HASTINGS	03	BELL	$e^+e^- \to \Upsilon(4S)$
0.509 ±0.017 ±0.020	[11] ZHENG	03	BELL	$e^+e^- \to \Upsilon(4S)$
0.516 ±0.016 ±0.010	[12] AUBERT	02I	BABR	$e^+e^- \to \Upsilon(4S)$
0.493 ±0.012 ±0.009	[13] AUBERT	02J	BABR	$e^+e^- \to \Upsilon(4S)$
0.497 ±0.024 ±0.025	[14] ABBIENDI,G	00B	OPAL	$e^+e^- \to Z$
0.503 ±0.064 ±0.071	[15] ABE	99K	CDF	$p\overline{p}$ at 1.8 TeV
0.500 ±0.052 ±0.043	[16] ABE	99Q	CDF	$p\overline{p}$ at 1.8 TeV
0.516 ±0.099 $^{+0.029}_{-0.035}$	[17] AFFOLDER	99C	CDF	$p\overline{p}$ at 1.8 TeV
0.471 $^{+0.078}_{-0.068}$ $^{+0.033}_{-0.034}$	[18] ABE	98C	CDF	$p\overline{p}$ at 1.8 TeV
0.458 ±0.046 ±0.032	[19] ACCIARRI	98D	L3	$e^+e^- \to Z$
0.437 ±0.043 ±0.044	[20] ACCIARRI	98D	L3	$e^+e^- \to Z$
0.472 ±0.049 ±0.053	[21] ACCIARRI	98D	L3	$e^+e^- \to Z$
0.523 ±0.072 ±0.043	[22] ABREU	97N	DLPH	$e^+e^- \to Z$
0.493 ±0.042 ±0.027	[20] ABREU	97N	DLPH	$e^+e^- \to Z$
0.499 ±0.053 ±0.015	[23] ABREU	97N	DLPH	$e^+e^- \to Z$
0.480 ±0.040 ±0.051	[19] ABREU	97N	DLPH	$e^+e^- \to Z$
0.444 ±0.029 $^{+0.020}_{-0.017}$	[20] ACKERSTAFF	97U	OPAL	$e^+e^- \to Z$
0.430 ±0.043 $^{+0.028}_{-0.030}$	[19] ACKERSTAFF	97V	OPAL	$e^+e^- \to Z$
0.482 ±0.044 ±0.024	[24] BUSKULIC	97D	ALEP	$e^+e^- \to Z$
0.404 ±0.045 ±0.027	[20] BUSKULIC	97D	ALEP	$e^+e^- \to Z$
0.452 ±0.039 ±0.044	[19] BUSKULIC	97D	ALEP	$e^+e^- \to Z$
0.539 ±0.060 ±0.024	[25] ALEXANDER	96V	OPAL	$e^+e^- \to Z$
0.567 ±0.089 $^{+0.029}_{-0.023}$	[26] ALEXANDER	96V	OPAL	$e^+e^- \to Z$
• • • We do not use the following data for averages, fits, limits, etc. • • •				
0.516 ±0.016 ±0.010	[27] AUBERT	02N	BABR	$e^+e^- \to \Upsilon(4S)$
0.494 ±0.012 ±0.015	[28] HARA	02	BELL	Repl. by ABE 05B
0.528 ±0.017 ±0.011	[29] TOMURA	02	BELL	Repl. by ABE 05B
0.463 ±0.008 ±0.016	[13] ABE	01D	BELL	Repl. by HASTINGS 03
0.444 ±0.028 ±0.028	[30] ACCIARRI	98D	L3	$e^+e^- \to Z$
0.497 ±0.035	[31] ABREU	97N	DLPH	$e^+e^- \to Z$

Downloaded from https://academic.oup.com/ptep/article/2022/8/083C01/6651666 by KIT Library user on 27 September 2022

0.467	±0.022	$^{+0.017}_{-0.015}$	[32] ACKERSTAFF	97V	OPAL	$e^+e^- \to Z$
0.446	±0.032		[33] BUSKULIC	97D	ALEP	$e^+e^- \to Z$
0.531	$^{+0.050}_{-0.046}$	±0.078	[34] ABREU	96Q	DLPH	Sup. by ABREU 97N
0.496	$^{+0.055}_{-0.051}$	±0.043	[19] ACCIARRI	96E	L3	Repl. by ACCIARRI 98D
0.548	±0.050	$^{+0.023}_{-0.019}$	[35] ALEXANDER	96V	OPAL	$e^+e^- \to Z$
0.496	±0.046		[36] AKERS	95J	OPAL	Repl. by ACKERSTAFF 97V
0.462	$^{+0.040}_{-0.053}$	$^{+0.052}_{-0.035}$	[19] AKERS	95J	OPAL	Repl. by ACKERSTAFF 97V
0.50	±0.12	±0.06	[22] ABREU	94M	DLPH	Sup. by ABREU 97N
0.508	±0.075	±0.025	[25] AKERS	94C	OPAL	Repl. by ALEXANDER 96V
0.57	±0.11	±0.02	[26] AKERS	94H	OPAL	Repl. by ALEXANDER 96V
0.50	$^{+0.07}_{-0.06}$	$^{+0.11}_{-0.10}$	[19] BUSKULIC	94B	ALEP	Sup. by BUSKULIC 97D
0.52	$^{+0.10}_{-0.11}$	$^{+0.04}_{-0.03}$	[26] BUSKULIC	93K	ALEP	Sup. by BUSKULIC 97D

[1] Uses semileptonic decays of $B^0 \to D^-\mu^+\nu_\mu X$ and $B^0 \to D^{(*)-}\mu^+\nu_\mu X$, where the D mesons are reconstructed in $D^- \to K^+\pi^-\pi^-$ and $D^{(*)-} \to \overline{D}^0\pi^-$ with $\overline{D}^0 \to K^+\pi^-$.
[2] Uses semileptonic decays of $B^0 \to D^-\mu^+\nu_\mu X$ where the D^- mesons are reconstructed in $D^- \to K^+K^-\pi^-$.
[3] Measured using $B^0 \to D^-\pi^+$ and $B^0 \to J/\psi K^*(892)^0$ decays.
[4] Measured using $B^0 \to D^-\pi^+$.
[5] Uses opposite-side flavor-tagging with $B \to D^{(*)}\mu\nu_\mu X$ events.
[6] Measured using a simultaneous fit of the B^0 lifetime and $\overline{B}^0B^0$ oscillation frequency Δm_d in the partially reconstructed $B^0 \to D^{*-}\ell\nu$ decays.
[7] Measurement performed using a combined fit of CP-violation, mixing and lifetimes.
[8] Events with a high transverse momentum lepton were removed and an inclusively reconstructed vertex was required.
[9] AUBERT 03C uses a sample of approximately 14,000 exclusively reconstructed $B^0 \to D^*(2010)^-\ell\nu$ and simultaneously measures the lifetime and oscillation frequency.
[10] HASTINGS 03 measurement based on the time evolution of dilepton events. It also reports $f_+/f_0 = 1.01 \pm 0.03 \pm 0.09$ and CPT violation parameters in B^0-$\overline{B}^0$ mixing.
[11] ZHENG 03 data analyzed using partially reconstructed $\overline{B}^0 \to D^{*-}\pi^+$ decay and a flavor tag based on the charge of the lepton from the accompanying B decay.
[12] Uses a tagged sample of fully-reconstructed neutral B decays at $\Upsilon(4S)$.
[13] Measured based on the time evolution of dilepton events in $\Upsilon(4S)$ decays.
[14] Data analyzed using partially reconstructed $\overline{B}^0 \to D^{*+}\ell^-\overline{\nu}$ decay and a combination of flavor tags from the rest of the event.
[15] Uses di-muon events.
[16] Uses jet-charge and lepton-flavor tagging.
[17] Uses $\ell^-D^{*+}-\ell$ events.
[18] Uses π-B in the same side.
[19] Uses ℓ-ℓ.
[20] Uses ℓ-Q_{hem}.
[21] Uses ℓ-ℓ with impact parameters.
[22] Uses $D^{*\pm}$-Q_{hem}.
[23] Uses $\pi_s^\pm\ell$-Q_{hem}.
[24] Uses $D^{*\pm}$-ℓ/Q_{hem}.
[25] Uses $D^{*\pm}\ell$-Q_{hem}.
[26] Uses $D^{*\pm}$-ℓ.
[27] AUBERT 02N result based on the same analysis and data sample reported in AUBERT 02I.
[28] Uses a tagged sample of B^0 decays reconstructed in the mode $B^0 \to D^*\ell\nu$.
[29] Uses a tagged sample of fully-reconstructed hadronic B^0 decays at $\Upsilon(4S)$.
[30] ACCIARRI 98D combines results from ℓ-ℓ, ℓ-Q_{hem}, and ℓ-ℓ with impact parameters.
[31] ABREU 97N combines results from $D^{*\pm}$-Q_{hem}, ℓ-Q_{hem}, $\pi_s^\pm\ell$-Q_{hem}, and ℓ-ℓ.
[32] ACKERSTAFF 97V combines results from ℓ-ℓ, ℓ-Q_{hem}, D^*-ℓ, and $D^{*\pm}$-Q_{hem}.
[33] BUSKULIC 97D combines results from $D^{*\pm}$-ℓ/Q_{hem}, ℓ-Q_{hem}, and ℓ-ℓ.
[34] ABREU 96Q analysis performed using lepton, kaon, and jet-charge tags.
[35] ALEXANDER 96V combines results from $D^{*\pm}$-ℓ and $D^{*\pm}\ell$-Q_{hem}.
[36] AKERS 95J combines results from charge measurement, $D^{*\pm}\ell$-Q_{hem} and ℓ-ℓ.

$x_d = \Delta m_{B^0}/\Gamma_{B^0}$

"OUR EVALUATION" is an average using rescaled values of the data listed below. The average and rescaling were performed by the Heavy Flavor Averaging Group (HFLAV) and are described at https://hflav.web.cern.ch/. The averaging/rescaling procedure takes into account correlations between the measurements and includes Δm_d calculated from χ_d measured at $\Upsilon(4S)$.

VALUE	DOCUMENT ID
0.769±0.004 OUR EVALUATION	

Re(λ_{CP} / $|\lambda_{CP}|$) Re(z)

The λ_{CP} characterizes B^0 and $\overline{B}^0$ decays to states of charmonium plus K^0_L. Parameter z is used to describe CPT violation in mixing, see the review on "CP Violation" in the reviews section.

VALUE	DOCUMENT ID		TECN	COMMENT
0.047±0.022±0.003	[1] LEES	16E	BABR	$e^+e^- \to \Upsilon(4S)$
• • • We do not use the following data for averages, fits, limits, etc. • • •				
$0.014\pm0.035\pm0.034$	[2] AUBERT,B	04C	BABR	Repl. by LEES 16E

[1] The first uncertainty is the uncertainty from Re(z) and the second uncertainty is from Re($\lambda/|\lambda|$).
[2] Corresponds to 90% confidence range [−0.072, 0.101].

$\Delta\Gamma$ Re(z)

VALUE (ps^{-1})	DOCUMENT ID		TECN	COMMENT
−0.0071±0.0039±0.0020	AUBERT	06T	BABR	$e^+e^- \to \Upsilon(4S)$

Re(z)

VALUE (units 10^{-2})	DOCUMENT ID		TECN	COMMENT
−4 ± 4 OUR AVERAGE Error includes scale factor of 1.4.				
$-6.5\pm2.8\pm1.4$	[1] LEES	16E	BABR	$e^+e^- \to \Upsilon(4S)$
$1.9\pm3.7\pm3.3$	[2] HIGUCHI	12	BELL	$e^+e^- \to \Upsilon(4S)$
• • • We do not use the following data for averages, fits, limits, etc. • • •				
$0\pm12\pm1$	[3] HASTINGS	03	BELL	Repl. by HIGUCHI 12

[1] Measurement uses decays $B^0/\overline{B}^0 \to c\overline{c}K^0_S/K^0_L$.
[2] Measured using $B^0 \to J/\psi K^0_S$, $J/\psi K^0_L$, $D^-\pi^+$, $D^{*-}\pi^+$, $D^{*-}\rho^+$, and $D^{*-}\ell^+\nu$ decays.
[3] Measured using inclusive dilepton events from B^0 decay.

Im(z)

VALUE (units 10^{-2})	DOCUMENT ID		TECN	COMMENT
−0.8 ±0.4 OUR AVERAGE				
$1.0\pm3.0\pm1.3$	[1] LEES	16E	BABR	$e^+e^- \to \Upsilon(4S)$
$-0.57\pm0.33\pm0.33$	[2] HIGUCHI	12	BELL	$e^+e^- \to \Upsilon(4S)$
$-1.39\pm0.73\pm0.32$	[3] AUBERT	06T	BABR	$e^+e^- \to \Upsilon(4S)$
• • • We do not use the following data for averages, fits, limits, etc. • • •				
$3.8\pm2.9\pm2.5$	[4] AUBERT,B	04C	BABR	Repl. by AUBERT 06T
$-3\pm1\pm3$	[5] HASTINGS	03	BELL	Repl. by HIGUCHI 12

[1] Measurement uses decays $B^0/\overline{B}^0 \to c\overline{c}K^0_S/K^0_L$.
[2] Measured using $B^0 \to J/\psi K^0_S$, $J/\psi K^0_L$, $D^-\pi^+$, $D^{*-}\pi^+$, $D^{*-}\rho^+$, and $D^{*-}\ell^+\nu$ decays.
[3] Measurement uses $B^0/\overline{B}^0 \to \ell^+X/\ell^-X$ decays. Assuming $\Delta\Gamma = 0$, the result becomes Im(z) $= (-0.37 \pm 0.54) \times 10^{-2}$.
[4] Corresponds to 90% confidence range [−0.028, 0.104].
[5] Measured using inclusive dilepton events from B^0 decay.

CP VIOLATION PARAMETERS

Re(ϵ_{B^0})/(1+$|\epsilon_{B^0}|^2$)

CP impurity in B^0_d system. It is obtained from either $a_{\ell\ell}$, the charge asymmetry in like-sign dilepton events or a_{cp}, the time-dependent asymmetry of inclusive B^0 and $\overline{B}^0$ decays.

"OUR EVALUATION" is an average obtained by the Heavy Flavor Averaging Group (HFLAV) and described at https://hflav.web.cern.ch/. It is the result of a fit to B_d and B_s CP asymmetries, which includes the B_d measurements listed below and the B_s measurements listed in the B_s section, taking into account correlations between those measurements.

VALUE (units 10^{-3})	DOCUMENT ID		TECN	COMMENT
− 0.5 ± 0.4 OUR EVALUATION				
− 0.1 ± 0.4 OUR AVERAGE				
$-0.05\pm0.48\pm0.75$	[1] AAIJ	15F	LHCB	pp at 7, 8 TeV
$-0.975\pm0.875\pm0.475$	[2] LEES	15A	BABR	$e^+e^- \to \Upsilon(4S)$
1.55 ± 1.05	[3] ABAZOV	14	D0	$p\overline{p}$ at 1.96 TeV
$0.15\pm0.42\,^{+0.94}_{-0.81}$	[4] LEES	13N	BABR	$e^+e^- \to \Upsilon(4S)$
$-1.7\pm1.1\pm0.4$	[5] ABAZOV	12AC	D0	$p\overline{p}$ at 1.96 TeV
$0.4\pm1.3\pm0.9$	[6] AUBERT	06T	BABR	$e^+e^- \to \Upsilon(4S)$
$-0.3\pm2.0\pm2.1$	[7] NAKANO	06	BELL	$e^+e^- \to \Upsilon(4S)$
$3.5\pm10.3\pm1.5$	[8] JAFFE	01	CLE2	$e^+e^- \to \Upsilon(4S)$
• • • We do not use the following data for averages, fits, limits, etc. • • •				
-0.3 ± 1.3	[9] ABAZOV	11U	D0	Repl. by ABAZOV 14
$-2.3\pm1.1\pm0.8$	[10] ABAZOV	06S	D0	Repl. by ABAZOV 11U
$-14.7\pm6.7\pm5.7$	[11] AUBERT,B	04C	BABR	Repl. by AUBERT 06T
$1.2\pm2.9\pm3.6$	[2] AUBERT	02K	BABR	Repl. by LEES 15A
-3.2 ± 6.5	[12] BARATE	01D	ALEP	$e^+e^- \to Z$
$4\pm18\pm3$	[13] BEHRENS	00B	CLE2	Repl. by JAFFE 01
$1.2\pm13.8\pm3.2$	[14] ABBIENDI	99J	OPAL	$e^+e^- \to Z$
$2\pm7\pm3$	[15] ACKERSTAFF	97U	OPAL	$e^+e^- \to Z$
<45	[16] BARTELT	93	CLE2	$e^+e^- \to \Upsilon(4S)$

[1] AAIJ 15F uses semileptonic B^0 decays in the inclusive final states $D^-\mu^+$ and $D^{*-}\mu^+$, where the D^- meson decays into the $K^+\pi^-\pi^-$ final state, and the D^{*-} meson into the $\overline{D}^0(\to K^+\pi^-)\pi^-$ final state. Reports $A^d_{SL} = (-0.02 \pm 0.19 \pm 0.30)\%$, which equals to 4Re($\epsilon_{B^0}$)/(1+$|\epsilon_{B^0}|^2$).
[2] Uses the charge asymmetry in like-sign dilepton events. LEES 15A reports $A^d_{SL} = (-3.9 \pm 3.5 \pm 1.9) \times 10^{-3}$.
[3] ABAZOV 14 uses the dimuon charge asymmetry with different impact parameters from which it reports $A^d_{SL} = (-0.62 \pm 0.42) \times 10^{-2}$.
[4] Uses $B^0 \to D^{*-}X\ell^+\nu_\ell$ and a kaon-tagged sample which yields measurement of $A^d_{SL} = (0.06\pm0.17\,^{+0.38}_{-0.32})\%$, corresponding to $\Delta_{CP} = 1-|q/p| = (0.29\pm0.84\,^{+1.88}_{-1.61})\times10^{-3}$.
[5] ABAZOV 12AC uses $B^0 \to D^-\mu^+X$ and $B^0 \to D^*(2010)^-\mu^+X$ decays without initial state flavor tagging which yields measurement of $A^d_{SL} = (6.8 \pm 4.5 \pm 1.4) \times 10^{-3}$.
[6] AUBERT 06T reports $|q/p|-1=(-0.8\pm2.7\pm1.9)\times10^{-3}$. We convert to $(1-|q/p|^2)/4$.

Downloaded from https://academic.oup.com/ptep/article/2022/8/083C01/6651666 by KIT Library user on 27 September 2022

[7] Uses the charge asymmetry in like-sign dilepton events and reports $|q/p| = 1.0005 \pm 0.0040 \pm 0.0043$.
[8] JAFFE 01 finds $a_{\ell\ell} = 0.013 \pm 0.050 \pm 0.005$ and combines with the previous BEHRENS 00B independent measurement.
[9] ABAZOV 11U uses the dimuon charge asymmetry with different impact parameters from which it reports $A^d_{SL} = (-1.2 \pm 5.2) \times 10^{-3}$.
[10] Uses the dimuon charge asymmetry.
[11] AUBERT 04C reports $|q/p| = 1.029 \pm 0.013 \pm 0.011$ and we converted it to $(1-|q/p|^2)/4$.
[12] BARATE 01D measured by investigating time-dependent asymmetries in semileptonic and fully inclusive B^0_d decays.
[13] BEHRENS 00B uses high-momentum lepton tags and partially reconstructed $\overline{B}^0 \to D^{*+}\pi^-$, ρ^- decays to determine the flavor of the B meson.
[14] Data analyzed using the time-dependent asymmetry of inclusive B^0 decay. The production flavor of B^0 mesons is determined using both the jet charge and the charge of secondary vertex in the opposite hemisphere.
[15] ACKERSTAFF 97U assumes CPT and is based on measuring the charge asymmetry in a sample of B^0 decays defined by lepton and Q_{hem} tags. If CPT is not invoked, $\mathrm{Re}(\epsilon_B) = -0.006 \pm 0.010 \pm 0.006$ is found. The indirect CPT violation parameter is determined to $\mathrm{Im}(\delta B) = -0.020 \pm 0.016 \pm 0.006$.
[16] BARTELT 93 finds $a_{\ell\ell} = 0.031 \pm 0.096 \pm 0.032$ which corresponds to $|a_{\ell\ell}| < 0.18$, which yields the above $|\mathrm{Re}(\epsilon_{B^0})/(1+|\epsilon_{B^0}|^2)|$.

$A_{T/CP}$

$A_{T/CP}$ is defined as

$$\frac{P(\overline{B}^0 \to B^0) - P(B^0 \to \overline{B}^0)}{P(\overline{B}^0 \to B^0) + P(B^0 \to \overline{B}^0)},$$

the CPT invariant asymmetry between the oscillation probabilities $P(\overline{B}^0 \to B^0)$ and $P(B^0 \to \overline{B}^0)$.

VALUE	DOCUMENT ID		TECN	COMMENT
0.005±0.012±0.014	[1] AUBERT	02K	BABR	$e^+e^- \to \Upsilon(4S)$

[1] AUBERT 02K uses the charge asymmetry in like-sign dilepton events.

$A_{CP}(B^0 \to D^*(2010)^+ D^-)$

A_{CP} is defined as

$$\frac{B(\overline{B}^0 \to \overline{f}) - B(B^0 \to f)}{B(\overline{B}^0 \to \overline{f}) + B(B^0 \to f)},$$

the CP-violation charge asymmetry of exclusive B^0 and $\overline{B}^0$ decay.

VALUE	DOCUMENT ID		TECN	COMMENT
0.013±0.014 OUR AVERAGE				
0.008±0.014±0.006	AAIJ	20L	LHCB	pp at 7, 8, 13 TeV
0.06 ±0.05 ±0.02	ROHRKEN	12	BELL	$e^+e^- \to \Upsilon(4S)$
0.008±0.048±0.013	AUBERT	09C	BABR	$e^+e^- \to \Upsilon(4S)$
0.07 ±0.08 ±0.04	[1] AUSHEV	04	BELL	$e^+e^- \to \Upsilon(4S)$
• • • We do not use the following data for averages, fits, limits, etc. • • •				
−0.12 ±0.06 ±0.02	AUBERT	07AI	BABR	Repl. by AUBERT 09C
−0.03 ±0.10 ±0.02	AUBERT,B	06A	BABR	Repl. by AUBERT 07AI
−0.03 ±0.11 ±0.05	AUBERT	03J	BABR	Repl. by AUBERT,B 06B

[1] Combines results from fully and partially reconstructed $B^0 \to D^{*\pm}D^{\mp}$ decays.

$A_{CP}(B^0 \to [K^+K^-]_D K^*(892)^0)$

VALUE	DOCUMENT ID		TECN	COMMENT
−0.05±0.10±0.01	AAIJ	19N	LHCB	pp at 7, 8, 13 TeV
• • • We do not use the following data for averages, fits, limits, etc. • • •				
−0.20±0.15±0.02	AAIJ	14BN	LHCB	Repl. by AAIJ 16S
−0.45±0.23±0.02	AAIJ	13L	LHCB	Repl. by AAIJ 14BN

$A_{CP}(B^0 \to [K^+\pi^-]_D K^*(892)^0)$

VALUE	DOCUMENT ID		TECN	COMMENT
0.047±0.027±0.010	AAIJ	19N	LHCB	pp at 7, 8, 13 TeV
• • • We do not use the following data for averages, fits, limits, etc. • • •				
−0.03 ±0.04 ±0.02	AAIJ	14BN	LHCB	Repl. by AAIJ 19N
−0.08 ±0.08 ±0.01	AAIJ	13L	LHCB	Repl. by AAIJ 14BN

$A_{CP}(B^0 \to [K^+\pi^-\pi^+\pi^-]_D K^*(892)^0)$

VALUE	DOCUMENT ID		TECN	COMMENT
0.037±0.032±0.010	AAIJ	19N	LHCB	pp at 7, 8, 13 TeV

$A_{CP}(B^0 \to [K^-\pi^+]_D K^*(892)^0)$

VALUE	DOCUMENT ID		TECN	COMMENT
0.19±0.19±0.01	AAIJ	19N	LHCB	pp at 7, 8, 13 TeV

$A_{CP}(B^0 \to [K^-\pi^+\pi^+\pi^-]_D K^*(892)^0)$

VALUE	DOCUMENT ID		TECN	COMMENT
−0.01±0.24±0.01	AAIJ	19N	LHCB	pp at 7, 8, 13 TeV

$R^+_d = \Gamma(B^0 \to [\pi^+K^-]_D K^{*0}) / \Gamma(B^0 \to [\pi^-K^+]_D K^{*0})$

VALUE	DOCUMENT ID		TECN	COMMENT
0.064±0.021±0.002	AAIJ	19N	LHCB	pp at 7, 8, 13 TeV
• • • We do not use the following data for averages, fits, limits, etc. • • •				
0.06 ±0.03 ±0.01	AAIJ	14BN	LHCB	Repl. by AAIJ 19N

$R^-_d = \Gamma(\overline{B}^0 \to [\pi^-K^+]_D K^{*0}) / \Gamma(\overline{B}^0 \to [\pi^+K^-]_D K^{*0})$

VALUE	DOCUMENT ID		TECN	COMMENT
0.095±0.021±0.003	AAIJ	19N	LHCB	pp at 7, 8, 13 TeV
• • • We do not use the following data for averages, fits, limits, etc. • • •				
0.06 ±0.03 ±0.01	AAIJ	14BN	LHCB	Repl. by AAIJ 19N

$A_{CP}(B^0 \to [\pi^+\pi^-]_D K^*(892)^0)$

VALUE	DOCUMENT ID		TECN	COMMENT
−0.18±0.14±0.01	AAIJ	19N	LHCB	pp at 7, 8, 13 TeV
• • • We do not use the following data for averages, fits, limits, etc. • • •				
−0.09±0.22±0.02	AAIJ	14BN	LHCB	Repl. by AAIJ 16S

$A_{CP}(B^0 \to [\pi^+\pi^-\pi^+\pi^-]_D K^*(892)^0)$

VALUE	DOCUMENT ID		TECN	COMMENT
−0.03±0.15±0.01	AAIJ	19N	LHCB	pp at 7, 8, 13 TeV

$R^+_d = \Gamma(B^0 \to [\pi^+K^-\pi^+\pi^-]_D K^{*0}) / \Gamma(B^0 \to [\pi^-K^+\pi^+\pi^-]_D K^{*0})$

VALUE	DOCUMENT ID		TECN	COMMENT
0.074±0.026±0.002	AAIJ	19N	LHCB	pp at 7, 8, 13 TeV

$R^-_d = \Gamma(\overline{B}^0 \to [\pi^-K^+\pi^+\pi^-]_D K^{*0}) / \Gamma(\overline{B}^0 \to [\pi^+K^-\pi^+\pi^-]_D K^{*0})$

VALUE	DOCUMENT ID		TECN	COMMENT
0.072±0.025±0.003	AAIJ	19N	LHCB	pp at 7, 8, 13 TeV

$A_{CP}(B^0 \to K^+\pi^-)$

VALUE	DOCUMENT ID		TECN	COMMENT
−0.0834±0.0032 OUR AVERAGE				
−0.0824±0.0033±0.0033	AAIJ	21O	LHCB	pp at 13 TeV
−0.084 ±0.004 ±0.003	AAIJ	18O	LHCB	pp at 7, 8 TeV
−0.083 ±0.013 ±0.004	AALTONEN	14P	CDF	$p\overline{p}$ at 1.96 TeV
−0.069 ±0.014 ±0.007	DUH	13	BELL	$e^+e^- \to \Upsilon(4S)$
−0.107 ±0.016 $^{+0.006}_{-0.004}$	LEES	13D	BABR	$e^+e^- \to \Upsilon(4S)$
−0.04 ±0.16	[1] CHEN	00	CLE2	$e^+e^- \to \Upsilon(4S)$
• • • We do not use the following data for averages, fits, limits, etc. • • •				
−0.080 ±0.007 ±0.003	AAIJ	13AX	LHCB	Repl. by AAIJ 18O
−0.088 ±0.011 ±0.008	AAIJ	12V	LHCB	Repl. by AAIJ 13AX
−0.086 ±0.023 ±0.009	AALTONEN	11N	CDF	Repl. by AALTONEN 14P
−0.094 ±0.018 ±0.008	LIN	08	BELL	Repl. by DUH 13
−0.107 ±0.018 $^{+0.007}_{-0.004}$	AUBERT	07AF	BABR	Repl. by LEES 13D
−0.013 ±0.078 ±0.012	ABULENCIA,A	06D	CDF	Repl. by AALTONEN 11N
−0.088 ±0.035 ±0.013	[2] CHAO	05A	BELL	Repl. by CHAO 04B
−0.133 ±0.030 ±0.009	[3] AUBERT,B	04K	BABR	Repl. by AUBERT 07AF
−0.101 ±0.025 ±0.005	[4] CHAO	04B	BELL	Repl. by LIN 08
−0.07 ±0.08 ±0.02	[5] AUBERT	02D	BABR	Repl. by AUBERT 02Q
−0.102 ±0.050 ±0.016	[6] AUBERT	02Q	BABR	Repl. by AUBERT,B 04K
−0.06 ±0.09 $^{+0.01}_{-0.02}$	[7] CASEY	02	BELL	Repl. by CHAO 04B
0.044 $^{+0.186}_{-0.167}$ $^{+0.018}_{-0.021}$	[8] ABE	01K	BELL	Repl. by CASEY 02
−0.19 ±0.10 ±0.03	[9] AUBERT	01E	BABR	Repl. by AUBERT 02Q

[1] Corresponds to 90% confidence range $-0.30 < A_{CP} < 0.22$.
[2] Corresponds to a 90% CL interval of $-0.15 < A_{CP} < -0.03$.
[3] Based on a total signal yield of $N(K^-\pi^+) + N(K^+\pi^-) = 1606 \pm 51$ events.
[4] CHAO 04B reports significance of 3.9 standard deviation for deviation of A_{CP} from zero.
[5] Corresponds to 90% confidence range $-0.21 < A_{CP} < 0.07$.
[6] Corresponds to 90% confidence range $-0.188 < A_{CP} < -0.016$.
[7] Corresponds to 90% confidence range $-0.21 < A_{CP} < +0.09$.
[8] Corresponds to 90% confidence range $-0.25 < A_{CP} < 0.37$.
[9] Corresponds to 90% confidence range $-0.35 < A_{CP} < -0.03$.

$A_{CP}(B^0 \to \eta' K^*(892)^0)$

VALUE	DOCUMENT ID		TECN	COMMENT
−0.07±0.18 OUR AVERAGE				
−0.22±0.29±0.07	SATO	14	BELL	$e^+e^- \to \Upsilon(4S)$
0.02±0.23±0.02	DEL-AMO-SA...10A		BABR	$e^+e^- \to \Upsilon(4S)$
• • • We do not use the following data for averages, fits, limits, etc. • • •				
0.08±0.25±0.02	[1] AUBERT	07E	BABR	Repl. by DEL-AMO-SANCHEZ 10A

[1] Reports A_{CP} with the opposite sign convention.

$A_{CP}(B^0 \to \eta' K^*_0(1430)^0)$

VALUE	DOCUMENT ID		TECN	COMMENT
−0.19±0.17±0.02	DEL-AMO-SA...10A		BABR	$e^+e^- \to \Upsilon(4S)$

$A_{CP}(B^0 \to \eta' K^*_2(1430)^0)$

VALUE	DOCUMENT ID		TECN	COMMENT
0.14±0.18±0.02	DEL-AMO-SA...10A		BABR	$e^+e^- \to \Upsilon(4S)$

$A_{CP}(B^0 \to \eta K^*(892)^0)$

VALUE	DOCUMENT ID		TECN	COMMENT
0.19±0.05 OUR AVERAGE				
0.17±0.08±0.01	WANG	07B	BELL	$e^+e^- \to \Upsilon(4S)$
0.21±0.06±0.02	AUBERT,B	06H	BABR	$e^+e^- \to \Upsilon(4S)$
• • • We do not use the following data for averages, fits, limits, etc. • • •				
0.02±0.11±0.02	AUBERT,B	04D	BABR	Repl. by AUBERT,B 06H

Downloaded from https://academic.oup.com/ptep/article/2022/8/083C01/6651666 by KIT Library user on 27 September 2022

$A_{CP}(B^0 \to \eta K_0^*(1430)^0)$

VALUE	DOCUMENT ID		TECN	COMMENT
0.06±0.13±0.02	AUBERT,B	06H	BABR	$e^+e^- \to \Upsilon(4S)$

$A_{CP}(B^0 \to \eta K_2^*(1430)^0)$

VALUE	DOCUMENT ID		TECN	COMMENT
−0.07±0.19±0.02	AUBERT,B	06H	BABR	$e^+e^- \to \Upsilon(4S)$

$A_{CP}(B^0 \to b_1 K^+)$

VALUE	DOCUMENT ID		TECN	COMMENT
−0.07±0.12±0.02	AUBERT	07BI	BABR	$e^+e^- \to \Upsilon(4S)$

$A_{CP}(B^0 \to \omega K^{*0})$

VALUE	DOCUMENT ID		TECN	COMMENT
0.45±0.25±0.02	AUBERT	09H	BABR	$e^+e^- \to \Upsilon(4S)$

$A_{CP}(B^0 \to \omega (K\pi)_0^{*0})$

VALUE	DOCUMENT ID		TECN	COMMENT
−0.07±0.09±0.02	AUBERT	09H	BABR	$e^+e^- \to \Upsilon(4S)$

$A_{CP}(B^0 \to \omega K_2^*(1430)^0)$

VALUE	DOCUMENT ID		TECN	COMMENT
−0.37±0.17±0.02	AUBERT	09H	BABR	$e^+e^- \to \Upsilon(4S)$

$A_{CP}(B^0 \to K^+\pi^-\pi^0)$

VALUE (units 10^{-2})	DOCUMENT ID		TECN	COMMENT
0 ± 6 OUR AVERAGE				
$-3.0^{+4.5}_{-5.1}\pm5.5$	[1] AUBERT	08AQ	BABR	$e^+e^- \to \Upsilon(4S)$
7 ±11 ±1	[2] CHANG	04	BELL	$e^+e^- \to \Upsilon(4S)$

[1] Uses Dalitz plot analysis of $B^0 \to K^+\pi^-\pi^0$ decays.
[2] Corresponds to 90% confidence range $-0.12 < A^{CP} < 0.26$.

$A_{CP}(B^0 \to \rho^- K^+)$

VALUE	DOCUMENT ID		TECN	COMMENT
0.20±0.11 OUR AVERAGE				
0.20±0.09±0.08	[1] LEES	11	BABR	$e^+e^- \to \Upsilon(4S)$
$0.22^{+0.22+0.06}_{-0.23-0.02}$	[2] CHANG	04	BELL	$e^+e^- \to \Upsilon(4S)$
• • • We do not use the following data for averages, fits, limits, etc. • • •				
$0.11^{+0.14}_{-0.15}\pm0.07$	[1] AUBERT	08AQ	BABR	Repl. by LEES 11
−0.28±0.17±0.08	[3] AUBERT	03T	BABR	Repl. by AUBERT 08AQ

[1] Uses Dalitz plot analysis of $B^0 \to K^+\pi^-\pi^0$ decays.
[2] Corresponds to 90% confidence range $-0.18 < A_{CP} < 0.64$.
[3] The result reported corresponds to $-A_{CP}$.

$A_{CP}(B^0 \to \rho(1450)^- K^+)$

VALUE	DOCUMENT ID		TECN	COMMENT
−0.10±0.32±0.09	[1] LEES	11	BABR	$e^+e^- \to \Upsilon(4S)$

[1] Uses Dalitz plot analysis of $B^0 \to K^+\pi^-\pi^0$ decays.

$A_{CP}(B^0 \to \rho(1700)^- K^+)$

VALUE	DOCUMENT ID		TECN	COMMENT
−0.36±0.57±0.23	[1] LEES	11	BABR	$e^+e^- \to \Upsilon(4S)$

[1] Uses Dalitz plot analysis of $B^0 \to K^+\pi^-\pi^0$ decays.

$A_{CP}(B^0 \to K^+\pi^-\pi^0 \text{nonresonant})$

VALUE	DOCUMENT ID		TECN	COMMENT
0.10±0.16±0.08	[1] LEES	11	BABR	$e^+e^- \to \Upsilon(4S)$
• • • We do not use the following data for averages, fits, limits, etc. • • •				
$0.23^{+0.19+0.11}_{-0.27-0.10}$	[1] AUBERT	08AQ	BABR	Repl. by LEES 11

[1] Uses Dalitz plot analysis of $B^0 \to K^+\pi^-\pi^0$ decays. The quoted value is only for the flat part of the non-resonant component.

$A_{CP}(B^0 \to K^0\pi^+\pi^-)$

VALUE	DOCUMENT ID		TECN	COMMENT
−0.01±0.05±0.01	[1] AUBERT	09AU	BABR	$e^+e^- \to \Upsilon(4S)$

[1] Uses Dalitz plot analysis of $B^0 \to K^0\pi^+\pi^-$ decays and the first of two equivalent solutions is used.

$A_{CP}(B^0 \to K^*(892)^+\pi^-)$

VALUE	DOCUMENT ID		TECN	COMMENT
−0.27 ±0.04 OUR AVERAGE				
−0.308±0.060±0.016	[1] AAIJ	18F	LHCB	pp at 7, 8 TeV
−0.29 ±0.11 ±0.02	[2] LEES	11	BABR	$e^+e^- \to \Upsilon(4S)$
−0.21 ±0.10 ±0.02	[3,4] AUBERT	09AU	BABR	$e^+e^- \to \Upsilon(4S)$
−0.21 ±0.11 ±0.07	[5] DALSENO	09	BELL	$e^+e^- \to \Upsilon(4S)$
$0.26^{+0.33}_{-0.34}{}^{+0.10}_{-0.08}$	[6] EISENSTEIN	03	CLE2	$e^+e^- \to \Upsilon(4S)$
• • • We do not use the following data for averages, fits, limits, etc. • • •				
$-0.19^{+0.20}_{-0.15}\pm0.04$	[2] AUBERT	08AQ	BABR	Repl. by LEES 11
−0.11 ±0.14 ±0.05	[3] AUBERT	06I	BABR	Repl. by AUBERT 09AU
$0.23 \pm0.18^{+0.09}_{-0.06}$	AUBERT,B	04O	BABR	Repl. by AUBERT 06I

[1] Uses Dalitz plot analysis of the $B^0 \to K_S^0\pi^+\pi^-$ final state decays.
[2] Uses Dalitz plot analysis of $B^0 \to K^+\pi^-\pi^0$ decays.
[3] Uses Dalitz plot analysis of $B^0 \to K^0\pi^+\pi^-$ decays.
[4] The first of two equivalent solutions is used.
[5] Uses Dalitz plot analysis of $B^0 \to K^0\pi^+\pi^-$ decays and the first of two consistent solutions that may be preferred.
[6] Corresponds to 90% confidence range $-0.31 < A_{CP} < 0.78$.

$A_{CP}(B^0 \to (K\pi)_0^{*+}\pi^-)$

VALUE	DOCUMENT ID		TECN	COMMENT
0.02 ±0.04 OUR AVERAGE				
−0.032±0.047±0.031	[1] AAIJ	18F	LHCB	pp at 7, 8 TeV
0.07 ±0.14 ±0.01	[2] LEES	11	BABR	$e^+e^- \to \Upsilon(4S)$
0.09 ±0.07 ±0.03	[3] AUBERT	09AU	BABR	$e^+e^- \to \Upsilon(4S)$
• • • We do not use the following data for averages, fits, limits, etc. • • •				
$0.17^{+0.11}_{-0.16}\pm0.22$	[2] AUBERT	08AQ	BABR	Repl. by LEES 11

[1] Uses Dalitz plot analysis of the $B^0 \to K_S^0\pi^+\pi^-$ final states decays.
[2] Uses Dalitz plot analysis of $B^0 \to K^+\pi^-\pi^0$ decays.
[3] Uses Dalitz plot analysis of $B^0 \to K^0\pi^+\pi^-$ decays and the first of two equivalent solutions is used.

$A_{CP}(B^0 \to K_2^*(1430)^+\pi^-)$

VALUE	DOCUMENT ID		TECN	COMMENT
−0.29±0.22±0.09	[1] AAIJ	18F	LHCB	pp at 7, 8 TeV

[1] Uses Dalitz plot analysis of the $B^0 \to K_S^0\pi^+\pi^-$ final state decays.

$A_{CP}(B^0 \to K^*(1680)^+\pi^-)$

VALUE	DOCUMENT ID		TECN	COMMENT
−0.07±0.13±0.04	[1] AAIJ	18F	LHCB	pp at 7, 8 TeV

[1] Uses Dalitz plot analysis of the $B^0 \to K_S^0\pi^+\pi^-$ final state decays.

$A_{CP}(B^0 \to f_0(980) K_S^0)$

VALUE	DOCUMENT ID		TECN	COMMENT
0.28±0.27±0.15	[1] AAIJ	18F	LHCB	pp at 7, 8 TeV

[1] Uses Dalitz plot analysis of the $B^0 \to K_S^0\pi^+\pi^-$ final state decays.

$A_{CP}(B^0 \to (K\pi)_0^{*0}\pi^0)$

VALUE	DOCUMENT ID		TECN	COMMENT
−0.15±0.10±0.04	[1] LEES	11	BABR	$e^+e^- \to \Upsilon(4S)$
• • • We do not use the following data for averages, fits, limits, etc. • • •				
$-0.22\pm0.12^{+0.30}_{-0.29}$	[1] AUBERT	08AQ	BABR	Repl. by LEES 11

[1] Uses Dalitz plot analysis of $B^0 \to K^+\pi^-\pi^0$ decays.

$A_{CP}(B^0 \to K^{*0}\pi^0)$

VALUE	DOCUMENT ID		TECN	COMMENT
−0.15±0.12±0.04	[1] LEES	11	BABR	$e^+e^- \to \Upsilon(4S)$
• • • We do not use the following data for averages, fits, limits, etc. • • •				
$-0.09^{+0.21}_{-0.24}\pm0.09$	[1] AUBERT	08AQ	BABR	Repl. by LEES 11

[1] Uses Dalitz plot analysis of $B^0 \to K^+\pi^-\pi^0$ decays.

$A_{CP}(B^0 \to K^*(892)^0\pi^+\pi^-)$

VALUE	DOCUMENT ID		TECN	COMMENT
0.07±0.04±0.03	AUBERT	07AS	BABR	$e^+e^- \to \Upsilon(4S)$

$A_{CP}(B^0 \to K^*(892)^0\rho^0)$

VALUE	DOCUMENT ID		TECN	COMMENT
−0.06±0.09±0.02	LEES	12K	BABR	$e^+e^- \to \Upsilon(4S)$
• • • We do not use the following data for averages, fits, limits, etc. • • •				
0.09±0.19±0.02	AUBERT,B	06G	BABR	Repl. by LEES 12K

$A_{CP}(B^0 \to K^{*0} f_0(980))$

VALUE	DOCUMENT ID		TECN	COMMENT
0.07±0.10±0.02	LEES	12K	BABR	$e^+e^- \to \Upsilon(4S)$
• • • We do not use the following data for averages, fits, limits, etc. • • •				
−0.17±0.28±0.02	AUBERT,B	06G	BABR	Repl. by LEES 12K

$A_{CP}(B^0 \to K^{*+}\rho^-)$

VALUE	DOCUMENT ID		TECN	COMMENT
0.21±0.15±0.02	LEES	12K	BABR	$e^+e^- \to \Upsilon(4S)$

Downloaded from https://academic.oup.com/ptep/article/2022/8/083C01/6651666 by KIT Library user on 27 September 2022

$A_{CP}(B^0 \to K^*(892)^0 K^+ K^-)$

VALUE	DOCUMENT ID		TECN	COMMENT
0.01±0.05±0.02	AUBERT	07AS	BABR	$e^+e^- \to \Upsilon(4S)$

$A_{CP}(B^0 \to a_1^- K^+)$

VALUE	DOCUMENT ID		TECN	COMMENT
−0.16±0.12±0.01	AUBERT	08F	BABR	$e^+e^- \to \Upsilon(4S)$

$A_{CP}(B^0 \to K^0 K^0)$

VALUE	DOCUMENT ID		TECN	COMMENT
$-0.58^{+0.73}_{-0.66}\pm0.04$	LIN	07	BELL	$e^+e^- \to \Upsilon(4S)$

$A_{CP}(B^0 \to K^*(892)^0 \phi)$

VALUE	DOCUMENT ID		TECN	COMMENT
0.00 ±0.04 OUR AVERAGE				
−0.007±0.048±0.021	PRIM	13	BELL	$e^+e^- \to \Upsilon(4S)$
0.01 ±0.06 ±0.03	AUBERT	08BG	BABR	$e^+e^- \to \Upsilon(4S)$
• • • We do not use the following data for averages, fits, limits, etc. • • •				
−0.03 ±0.07 ±0.03	AUBERT	07D	BABR	Repl. by AUBERT 08BG
0.02 ±0.09 ±0.02	[1] CHEN	05A	BELL	Repl. by PRIM 13
−0.01 ±0.09 ±0.02	AUBERT,B	04W	BABR	Repl. by AUBERT 07D
0.04 ±0.12 ±0.02	AUBERT	03V	BABR	Repl. by AUBERT 04W
0.07 ±0.15 $^{+0.05}_{-0.03}$	[2] CHEN	03B	BELL	Repl. by CHEN 05A
0.00 ±0.27 ±0.03	[3] AUBERT	02E	BABR	Repl. by AUBERT 03V

[1] Corresponds to 90% confidence range $-0.14 < A_{CP} < 0.17$.
[2] Corresponds to 90% confidence range $-0.18 < A_{CP} < 0.33$.
[3] Corresponds to 90% confidence range $-0.44 < A_{CP} < 0.44$.

$A_{CP}(B^0 \to K^*(892)^0 K^- \pi^+)$

VALUE	DOCUMENT ID		TECN	COMMENT
0.22±0.33±0.20	AUBERT	07AS	BABR	$e^+e^- \to \Upsilon(4S)$

$A_{CP}(B^0 \to \phi(K\pi)_0^{*0})$

VALUE	DOCUMENT ID		TECN	COMMENT
0.12 ±0.08 OUR AVERAGE				
0.093±0.094±0.017	PRIM	13	BELL	$e^+e^- \to \Upsilon(4S)$
0.20 ±0.14 ±0.06	AUBERT	08BG	BABR	$e^+e^- \to \Upsilon(4S)$
• • • We do not use the following data for averages, fits, limits, etc. • • •				
0.17 ±0.15 ±0.03	AUBERT	07D	BABR	Repl. by AUBERT 08BG

$A_{CP}(B^0 \to \phi K_2^*(1430)^0)$

VALUE	DOCUMENT ID		TECN	COMMENT
−0.11 ±0.10 OUR AVERAGE				
$-0.155^{+0.152}_{-0.133}\pm0.033$	PRIM	13	BELL	$e^+e^- \to \Upsilon(4S)$
−0.08 ±0.12 ±0.05	AUBERT	08BG	BABR	$e^+e^- \to \Upsilon(4S)$
• • • We do not use the following data for averages, fits, limits, etc. • • •				
−0.12 ±0.14 ±0.04	AUBERT	07D	BABR	Repl. by AUBERT 08BG

$A_{CP}(B^0 \to K^*(892)^0 \gamma)$

VALUE	DOCUMENT ID		TECN	COMMENT
−0.006±0.011 OUR AVERAGE				
−0.013±0.017±0.004	[1] HORIGUCHI	17	BELL	$e^+e^- \to \Upsilon(4S)$
0.008±0.017±0.009	AAIJ	13	LHCB	pp at 7 TeV
−0.016±0.022±0.007	AUBERT	09AO	BABR	$e^+e^- \to \Upsilon(4S)$

[1] Uses B($\Upsilon(4S) \to B^+B^-$) = (51.4 ± 0.6)% and B($\Upsilon(4S) \to B^0\overline{B}^0$) = (48.6 ± 0.6)%.

$A_{CP}(B^0 \to K_2^*(1430)^0 \gamma)$

VALUE	DOCUMENT ID		TECN	COMMENT
−0.08±0.15±0.01	AUBERT,B	04U	BABR	$e^+e^- \to \Upsilon(4S)$

$A_{CP}(B^0 \to X_s \gamma)$

VALUE	DOCUMENT ID		TECN	COMMENT
−0.0094±0.0174±0.0047	[1] WATANUKI	19	BELL	$e^+e^- \to \Upsilon(4S)$

[1] Using a sum-of-exclusive technique with $m_{X_s} < 2.8$ GeV/c^2.

$A_{CP}(B^0 \to \rho^+ \pi^-)$

VALUE	DOCUMENT ID		TECN	COMMENT
0.13±0.06 OUR AVERAGE Error includes scale factor of 1.1.				
$0.09^{+0.05}_{-0.06}\pm0.04$	[1] LEES	13J	BABR	$e^+e^- \to \Upsilon(4S)$
0.21±0.08±0.04	[1] KUSAKA	07	BELL	$e^+e^- \to \Upsilon(4S)$
• • • We do not use the following data for averages, fits, limits, etc. • • •				
0.03±0.07±0.04	AUBERT	07AA	BABR	Repl. by LEES 13J
$-0.02\pm0.16^{+0.05}_{-0.02}$	WANG	05	BELL	Repl. by KUSAKA 07
−0.18±0.08±0.03	AUBERT	03T	BABR	Repl. by AUBERT 07AA

[1] Uses time-dependent Dalitz plot analysis of $B^0 \to \pi^+\pi^-\pi^0$ decays.

$A_{CP}(B^0 \to \rho^- \pi^+)$

VALUE	DOCUMENT ID		TECN	COMMENT
−0.08±0.08 OUR AVERAGE				
$-0.12\pm0.08^{+0.04}_{-0.05}$	[1] LEES	13J	BABR	$e^+e^- \to \Upsilon(4S)$
0.08±0.16±0.11	[1] KUSAKA	07	BELL	$e^+e^- \to \Upsilon(4S)$
• • • We do not use the following data for averages, fits, limits, etc. • • •				
$-0.37\pm0.16^{+0.09}_{-0.10}$	AUBERT	07AA	BABR	Repl. by LEES 13J
$-0.53\pm0.29^{+0.09}_{-0.04}$	WANG	05	BELL	Repl. by KUSAKA 07

[1] Uses time-dependent Dalitz plot analysis of $B^0 \to \pi^+\pi^-\pi^0$ decays.

$A_{CP}(B^0 \to a_1(1260)^\pm \pi^\mp)$

VALUE	DOCUMENT ID		TECN	COMMENT
−0.07±0.06 OUR AVERAGE				
−0.06±0.05±0.07	DALSENO	12	BELL	$e^+e^- \to \Upsilon(4S)$
−0.07±0.07±0.02	AUBERT	07O	BABR	$e^+e^- \to \Upsilon(4S)$

$A_{CP}(B^0 \to b_1^- \pi^+)$

VALUE	DOCUMENT ID		TECN	COMMENT
−0.05±0.10±0.02	AUBERT	07BI	BABR	$e^+e^- \to \Upsilon(4S)$

$A_{CP}(B^0 \to p\overline{p} K^*(892)^0)$

VALUE	DOCUMENT ID		TECN	COMMENT
0.05±0.12 OUR AVERAGE				
−0.08±0.20±0.02	CHEN	08C	BELL	$e^+e^- \to \Upsilon(4S)$
0.11±0.13±0.06	AUBERT	07AV	BABR	$e^+e^- \to \Upsilon(4S)$

$A_{CP}(B^0 \to p\overline{\Lambda}\pi^-)$

VALUE	DOCUMENT ID		TECN	COMMENT
0.04±0.07 OUR AVERAGE				
0.10±0.10±0.02	AUBERT	09AC	BABR	$e^+e^- \to \Upsilon(4S)$
−0.02±0.10±0.03	WANG	07C	BELL	$e^+e^- \to \Upsilon(4S)$

$A_{CP}(B^0 \to K^{*0} \ell^+ \ell^-)$

VALUE	DOCUMENT ID		TECN	COMMENT
−0.05±0.10 OUR AVERAGE				
0.02±0.20±0.02	AUBERT	09T	BABR	$e^+e^- \to \Upsilon(4S)$
−0.08±0.12±0.02	WEI	09A	BELL	$e^+e^- \to \Upsilon(4S)$

$A_{CP}(B^0 \to K^{*0} e^+ e^-)$

VALUE	DOCUMENT ID		TECN	COMMENT
−0.21±0.19±0.02	WEI	09A	BELL	$e^+e^- \to \Upsilon(4S)$

$A_{CP}(B^0 \to K^{*0} \mu^+ \mu^-)$

VALUE	DOCUMENT ID		TECN	COMMENT
−0.034±0.024 OUR AVERAGE				
−0.035±0.024±0.003	AAIJ	14AN	LHCB	pp at 7, 8 TeV
0.00 ±0.15 ±0.03	WEI	09A	BELL	$e^+e^- \to \Upsilon(4S)$
• • • We do not use the following data for averages, fits, limits, etc. • • •				
−0.072±0.040±0.005	AAIJ	13E	LHCB	Repl. by AAIJ 14AN

$C_{D^*(2010)^- D^+}$ $(B^0 \to D^*(2010)^- D^+)$

VALUE	DOCUMENT ID		TECN	COMMENT
−0.02 ±0.08 OUR AVERAGE				
−0.028±0.130±0.026	[1] AAIJ	20L	LHCB	pp at 7, 8, 13 TeV
−0.13 ±0.16 ±0.05	[2] ROHRKEN	12	BELL	$e^+e^- \to \Upsilon(4S)$
0.00 ±0.17 ±0.03	AUBERT	09C	BABR	$e^+e^- \to \Upsilon(4S)$
0.23 ±0.25 ±0.06	[3] AUSHEV	04	BELL	$e^+e^- \to \Upsilon(4S)$
• • • We do not use the following data for averages, fits, limits, etc. • • •				
0.23 ±0.15 ±0.04	AUBERT	07AI	BABR	Repl. by AUBERT 09C
0.17 ±0.24 ±0.04	AUBERT,B	05Z	BABR	Repl. by AUBERT 07AI
−0.22 ±0.37 ±0.10	AUBERT	03J	BABR	Repl. by AUBERT,B 05Z

[1] AAIJ 20L reports the measurements of C = −0.059 ± 0.092 ± 0.020 and ΔC = −0.031 ± 0.092 ± 0.016 such that $C_{D^*(2010)^- D^+}$ = C − ΔC .
[2] ROHRKEN 12 reports the measurements of C = −0.01 ± 0.11 ± 0.04 and ΔC = 0.12 ± 0.11 ± 0.03 such that $C_{D^*(2010)^- D^+}$ = C − ΔC .
[3] Combines results from fully and partially reconstructed $B^0 \to D^{*\pm} D^\mp$ decays.

$S_{D^*(2010)^- D^+}$ $(B^0 \to D^*(2010)^- D^+)$

VALUE	DOCUMENT ID		TECN	COMMENT
−0.83 ±0.09 OUR AVERAGE				
−0.880±0.107±0.022	[1] AAIJ	20L	LHCB	pp at 7, 8, 13 TeV
−0.65 ±0.22 ±0.07	[2] ROHRKEN	12	BELL	$e^+e^- \to \Upsilon(4S)$
−0.73 ±0.23 ±0.050	AUBERT	09C	BABR	$e^+e^- \to \Upsilon(4S)$
−0.96 ±0.43 ±0.12	[3] AUSHEV	04	BELL	$e^+e^- \to \Upsilon(4S)$
• • • We do not use the following data for averages, fits, limits, etc. • • •				
−0.44 ±0.22 ±0.06	AUBERT	07AI	BABR	Repl. by AUBERT 09C
−0.29 ±0.33 ±0.07	AUBERT,B	05Z	BABR	Repl. by AUBERT 07AI
−0.24 ±0.69 ±0.12	AUBERT	03J	BABR	Repl. by AUBERT,B 05Z

[1] AAIJ 20L reports the measurements of S = −0.861 ± 0.077 ± 0.019 and ΔS = 0.019 ± 0.075 ± 0.012 such that $S_{D^*(2010)^- D^+}$ = S − ΔS .
[2] ROHRKEN 12 reports the measurements of S = −0.78 ± 0.15 ± 0.05 and ΔS = −0.13 ± 0.15 ± 0.04 such that $S_{D^*(2010)^+ D^-}$ = S − ΔS.
[3] Combines results from fully and partially reconstructed $B^0 \to D^{*\pm} D^\mp$ decays.

Downloaded from https://academic.oup.com/ptep/article/2022/8/083C01/6651666 by KIT Library user on 27 September 2022

$C_{D^*(2010)^+D^-}$ ($B^0 \to D^*(2010)^+ D^-$)

VALUE	DOCUMENT ID		TECN	COMMENT
−0.03 ±0.09 OUR AVERAGE	Error includes scale factor of 1.1.			
−0.090±0.130±0.026	[1] AAIJ	20L	LHCB	pp at 7, 8, 13 TeV
0.11 ±0.14 ±0.06	[2] ROHRKEN	12	BELL	$e^+e^- \to \Upsilon(4S)$
0.08 ±0.17 ±0.04	AUBERT	09C	BABR	$e^+e^- \to \Upsilon(4S)$
−0.37 ±0.22 ±0.06	[3] AUSHEV	04	BELL	$e^+e^- \to \Upsilon(4S)$
• • • We do not use the following data for averages, fits, limits, etc. • • •				
0.18 ±0.15 ±0.04	AUBERT	07AI	BABR	Repl. by AUBERT 09C
0.09 ±0.25 ±0.06	AUBERT,B	05Z	BABR	Repl. by AUBERT 07AI
−0.47 ±0.40 ±0.12	AUBERT	03J	BABR	Repl. by AUBERT,B 05Z

[1] AAIJ 20L reports the measurements of $C = -0.059 \pm 0.092 \pm 0.020$ and $\Delta C = -0.031 \pm 0.092 \pm 0.016$ such that $C_{D^*(2010)^+D^-} = C + \Delta C$.

[2] ROHRKEN 12 reports the measurements of $C = -0.01 \pm 0.11 \pm 0.04$ and $\Delta C = 0.12 \pm 0.11 \pm 0.03$ such that $C_{D^*(2010)^+D^-} = C + \Delta C$.

[3] Combines results from fully and partially reconstructed $B^0 \to D^{*\pm} D^{\mp}$ decays.

$S_{D^*(2010)^+D^-}$ ($B^0 \to D^*(2010)^+ D^-$)

VALUE	DOCUMENT ID		TECN	COMMENT
−0.80 ±0.09 OUR AVERAGE				
−0.842±0.107±0.022	[1] AAIJ	20L	LHCB	pp at 7, 8, 13 TeV
−0.90 ±0.21 ±0.07	[2] ROHRKEN	12	BELL	$e^+e^- \to \Upsilon(4S)$
−0.62 ±0.21 ±0.03	AUBERT	09C	BABR	$e^+e^- \to \Upsilon(4S)$
−0.55 ±0.39 ±0.12	[3] AUSHEV	04	BELL	$e^+e^- \to \Upsilon(4S)$
• • • We do not use the following data for averages, fits, limits, etc. • • •				
−0.79 ±0.21 ±0.06	AUBERT	07AI	BABR	Repl. by AUBERT 09C
−0.54 ±0.35 ±0.07	AUBERT,B	05Z	BABR	Repl. by AUBERT 07AI
−0.82 ±0.75 ±0.14	AUBERT	03J	BABR	Repl. by AUBERT,B 05Z

[1] AAIJ 20L reports the measurements of $S = -0.861 \pm 0.077 \pm 0.019$ and $\Delta S = 0.019 \pm 0.075 \pm 0.012$ such that $S_{D^*(2010)^+D^-} = S + \Delta S$.

[2] ROHRKEN 12 reports the measurements of $S = -0.78 \pm 0.15 \pm 0.05$ and $\Delta S = -0.13 \pm 0.15 \pm 0.04$ such that $S_{D^*(2010)^+D^-} = S + \Delta S$.

[3] Combines results from fully and partially reconstructed $B^0 \to D^{*\pm} D^{\mp}$ decays.

$C_{D^{*+}D^{*-}}$ ($B^0 \to D^{*+} D^{*-}$)

VALUE	DOCUMENT ID		TECN	COMMENT
0.01±0.09 OUR AVERAGE	Error includes scale factor of 1.6. See the ideogram below.			
−0.15±0.08±0.04	[1,2] KRONENBIT...	12	BELL	$e^+e^- \to \Upsilon(4S)$
+0.15±0.09±0.04	[3] LEES	12AF	BABR	$e^+e^- \to \Upsilon(4S)$
0.05±0.09±0.02	AUBERT	09C	BABR	$e^+e^- \to \Upsilon(4S)$
• • • We do not use the following data for averages, fits, limits, etc. • • •				
−0.15±0.13±0.04	[2] VERVINK	09	BELL	Repl. by KRONENBITTER 12
−0.02±0.11±0.02	[1] AUBERT	07BO	BABR	Repl. by AUBERT 09C
0.26±0.26±0.06	[2] MIYAKE	05	BELL	Repl. by VERVINK 09
0.28±0.23±0.02	[4] AUBERT	03Q	BABR	Repl. by AUBERT 07BO

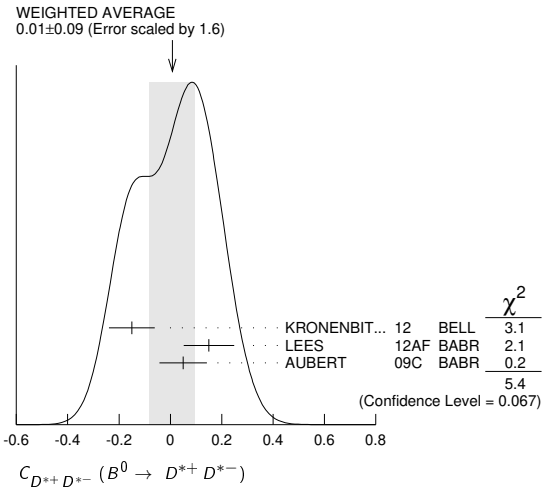

[1] Assumes both CP-even and CP-odd states having the CP asymmetry.

[2] Belle Collab. quotes $A_{D^{*+}D^{*-}}$ which is equal to $-C_{D^{*+}D^{*-}}$.

[3] Measured partially reconstructed candidates when one D^0 meson is not excplicitely reconstructed. Analysis does not separate CP-even and CP-odd component.

[4] AUBERT 03Q reports $|\lambda|$=0.75 ± 0.19 ± 0.02 and Im(λ)=0.05 ± 0.29 ± 0.10. We convert them to S and C parameters taking into account correlations.

$S_{D^{*+}D^{*-}}$ ($B^0 \to D^{*+} D^{*-}$)

VALUE	DOCUMENT ID		TECN	COMMENT
−0.59±0.14 OUR AVERAGE	Error includes scale factor of 1.8. See the ideogram below.			
−0.79±0.13±0.03	[1] KRONENBIT...	12	BELL	$e^+e^- \to \Upsilon(4S)$
−0.34±0.12±0.05	[2] LEES	12AF	BABR	$e^+e^- \to \Upsilon(4S)$
−0.70±0.16±0.03	[1] AUBERT	09C	BABR	$e^+e^- \to \Upsilon(4S)$
• • • We do not use the following data for averages, fits, limits, etc. • • •				
$-0.96 \pm 0.25^{+0.13}_{-0.16}$	VERVINK	09	BELL	Repl. by KRONENBITTER 12
−0.66±0.19±0.04	[1] AUBERT	07BO	BABR	Repl. by AUBERT 09C
−0.75±0.56±0.12	MIYAKE	05	BELL	Repl. by VERVINK 09
0.06±0.37±0.13	[3] AUBERT	03Q	BABR	Repl. by AUBERT 07BO

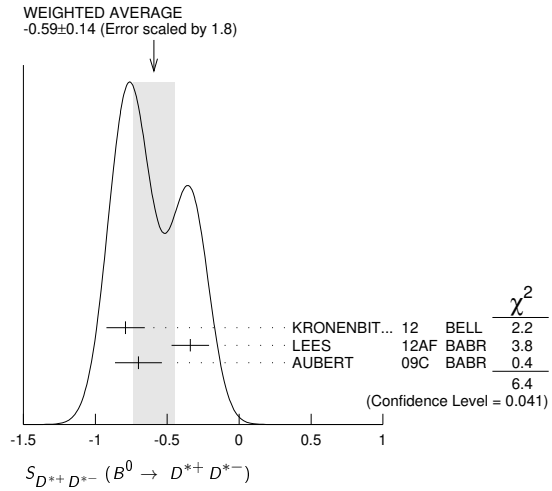

[1] Assumes both CP-even and CP-odd states having the CP asymmetry.

[2] Measured partially reconstructed candidates when one D^0 meson is not excplicitely reconstructed. Analysis does not separate CP-even and CP-odd component.

[3] AUBERT 03Q reports $|\lambda|$=0.75 ± 0.19 ± 0.02 and Im(λ)=0.05 ± 0.29 ± 0.10. We convert them to S and C parameters taking into account correlations.

C_+ ($B^0 \to D^{*+} D^{*-}$)

See the note in the $C_{\pi\pi}$ datablock, but for CP even final state.

VALUE	DOCUMENT ID		TECN	COMMENT
0.00±0.10 OUR AVERAGE	Error includes scale factor of 1.6. See the ideogram below.			
−0.18±0.10±0.05	[1] KRONENBIT...	12	BELL	$e^+e^- \to \Upsilon(4S)$
+0.15±0.09±0.04	[2] LEES	12AF	BABR	$e^+e^- \to \Upsilon(4S)$
0.00±0.12±0.02	AUBERT	09C	BABR	$e^+e^- \to \Upsilon(4S)$
• • • We do not use the following data for averages, fits, limits, etc. • • •				
−0.05±0.14±0.02	AUBERT	07BO	BABR	Repl. by AUBERT 09C
0.06±0.17±0.03	[3] AUBERT,BE	05A	BABR	Repl. by AUBERT 07BO

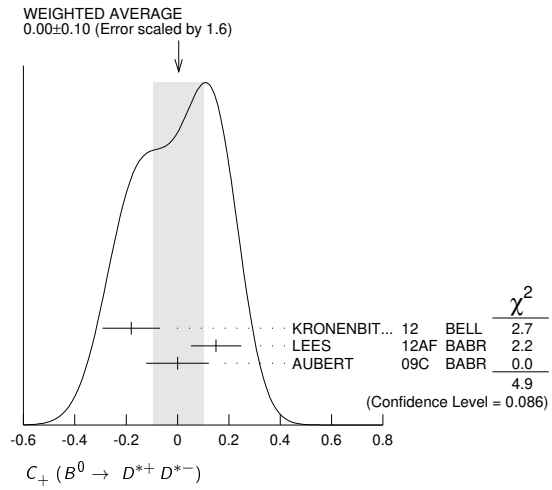

[1] Belle Collab. quotes $A_{D^{*+}D^{*-}}$ which is equal to $-C_{D^{*+}D^{*-}}$.

[2] Measured partially reconstructed candidates when one D^0 meson is not excplicitely reconstructed. Extracted under assumption of equal C_+ and C_-.

[3] AUBERT,BE 05A reports a CP-odd fraction $R_\perp = 0.125 \pm 0.044 \pm 0.007$.

S_+ ($B^0 \to D^{*+} D^{*-}$)

See the note in the $S_{\pi\pi}$ datablock, but for CP even final state.

VALUE	DOCUMENT ID		TECN	COMMENT
−0.73±0.09 OUR AVERAGE				
−0.81±0.13±0.03	KRONENBIT...	12	BELL	$e^+e^- \to \Upsilon(4S)$
−0.49±0.18±0.08	[1] LEES	12AF	BABR	$e^+e^- \to \Upsilon(4S)$
−0.76±0.16±0.04	AUBERT	09C	BABR	$e^+e^- \to \Upsilon(4S)$

Downloaded from https://academic.oup.com/ptep/article/2022/8/083C01/6651666 by KIT Library user on 27 September 2022

• • • We do not use the following data for averages, fits, limits, etc. • • •

$-0.72 \pm 0.19 \pm 0.05$	AUBERT	07BO	BABR	Repl. by AUBERT 09C
$-0.75 \pm 0.25 \pm 0.03$	[2] AUBERT,BE	05A	BABR	Repl. by AUBERT 07BO

[1] Measured partially reconstructed candidates when one D^0 meson is not excplicitely reconstructed. Analysis does not separate *CP*-even and *CP*-odd component. Value is obtained from $S = -0.34 \pm 0.12 \pm 0.05$ using $S = S_+ (1 - 2 R_\perp)$ with $R_\perp = 0.158 \pm 0.029$.

[2] AUBERT,BE 05A reports a *CP*-odd fraction $R_\perp = 0.125 \pm 0.044 \pm 0.007$.

C_- $(B^0 \to D^{*+} D^{*-})$

See the note in the $C_{\pi\pi}$ datablock, but for *CP* odd final state.

VALUE	DOCUMENT ID		TECN	COMMENT
0.19 ± 0.31 OUR AVERAGE				
$0.05 \pm 0.39 \pm 0.08$	[1] KRONENBIT...	12	BELL	$e^+ e^- \to \Upsilon(4S)$
$0.41 \pm 0.49 \pm 0.08$	AUBERT	09C	BABR	$e^+ e^- \to \Upsilon(4S)$
• • • We do not use the following data for averages, fits, limits, etc. • • •				
$0.23 \pm 0.67 \pm 0.10$	AUBERT	07BO	BABR	Repl. by AUBERT 09C
$-0.20 \pm 0.96 \pm 0.11$	[2] AUBERT,BE	05A	BABR	Repl. by AUBERT 07BO

[1] Belle Collab. quotes $A_{D^{*+}D^{*-}}$ which is equal to $-C_{D^{*+}D^{*-}}$.

[2] AUBERT,BE 05A reports a *CP*-odd fraction $R_\perp = 0.125 \pm 0.044 \pm 0.007$.

S_- $(B^0 \to D^{*+} D^{*-})$

See the note in the $S_{\pi\pi}$ datablock, but for *CP* odd final state.

VALUE	DOCUMENT ID		TECN	COMMENT
0.1 ± 1.6 OUR AVERAGE	Error includes scale factor of 3.5.			
$1.52 \pm 0.62 \pm 0.12$	KRONENBIT...	12	BELL	$e^+ e^- \to \Upsilon(4S)$
$-1.80 \pm 0.70 \pm 0.16$	AUBERT	09C	BABR	$e^+ e^- \to \Upsilon(4S)$
• • • We do not use the following data for averages, fits, limits, etc. • • •				
$-1.83 \pm 1.04 \pm 0.23$	AUBERT	07BO	BABR	Repl. by AUBERT 09C
$-1.75 \pm 1.78 \pm 0.22$	[1] AUBERT,BE	05A	BABR	Repl. by AUBERT 07BO

[1] AUBERT,BE 05A reports a *CP*-odd fraction $R_\perp = 0.125 \pm 0.044 \pm 0.007$.

C $(B^0 \to D^*(2010)^+ D^*(2010)^- K^0_S)$

VALUE	DOCUMENT ID		TECN	COMMENT
$0.01 \pm 0.28 \pm 0.09$	[1] DALSENO	07	BELL	$e^+ e^- \to \Upsilon(4S)$

[1] Reports value of A which is equal to $-C$.

S $(B^0 \to D^*(2010)^+ D^*(2010)^- K^0_S)$

VALUE	DOCUMENT ID		TECN	COMMENT
$0.06^{+0.45}_{-0.44} \pm 0.06$	[1] DALSENO	07	BELL	$e^+ e^- \to \Upsilon(4S)$

[1] This value includes an unknown *CP* dilution factor D due to possible contributions from intermediate resonances and different partial waves.

$C_{D^+D^-}$ $(B^0 \to D^+ D^-)$

VALUE	DOCUMENT ID		TECN	COMMENT
-0.22 ± 0.24 OUR AVERAGE	Error includes scale factor of 2.5. See the ideogram below.			
$0.26^{+0.18}_{-0.17} \pm 0.02$	AAIJ	16AN	LHCB	pp at 7, 8 TeV
$-0.43 \pm 0.16 \pm 0.05$	ROHRKEN	12	BELL	$e^+ e^- \to \Upsilon(4S)$
$-0.07 \pm 0.23 \pm 0.03$	AUBERT	09C	BABR	$e^+ e^- \to \Upsilon(4S)$
$-0.91 \pm 0.23 \pm 0.06$	[1] FRATINA	07	BELL	$e^+ e^- \to \Upsilon(4S)$
• • • We do not use the following data for averages, fits, limits, etc. • • •				
$0.11 \pm 0.22 \pm 0.07$	AUBERT	07AI	BABR	Repl. by AUBERT 09C
$0.11 \pm 0.35 \pm 0.06$	AUBERT,B	05Z	BABR	Repl. by AUBERT 07AI

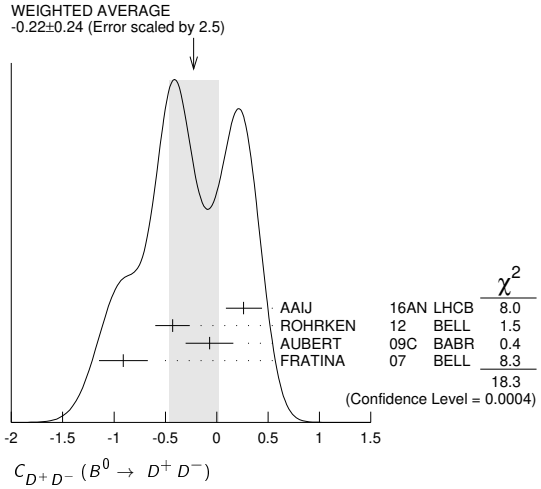

[1] The paper reports A, which is equal to $-C$.

$S_{D^+D^-}$ $(B^0 \to D^+ D^-)$

VALUE	DOCUMENT ID		TECN	COMMENT
$-0.76^{+0.15}_{-0.13}$ OUR AVERAGE	Error includes scale factor of 1.2.			
$-0.54^{+0.17}_{-0.16} \pm 0.05$	AAIJ	16AN	LHCB	pp at 7, 8 TeV
$-1.06^{+0.21}_{-0.14} \pm 0.08$	ROHRKEN	12	BELL	$e^+ e^- \to \Upsilon(4S)$
$-0.63 \pm 0.36 \pm 0.05$	AUBERT	09C	BABR	$e^+ e^- \to \Upsilon(4S)$
$-1.13 \pm 0.37 \pm 0.09$	FRATINA	07	BELL	$e^+ e^- \to \Upsilon(4S)$
• • • We do not use the following data for averages, fits, limits, etc. • • •				
$-0.54 \pm 0.34 \pm 0.06$	AUBERT	07AI	BABR	Repl. by AUBERT 09C
$-0.29 \pm 0.63 \pm 0.06$	AUBERT,B	05Z	BABR	Repl. by AUBERT 07AI

$C_{J/\psi(1S)\pi^0}$ $(B^0 \to J/\psi(1S)\pi^0)$

VALUE	DOCUMENT ID		TECN	COMMENT
0.03 ± 0.17 OUR AVERAGE	Error includes scale factor of 1.5.			
$0.15 \pm 0.14^{+0.04}_{-0.03}$	[1] PAL	18	BELL	$e^+ e^- \to \Upsilon(4S)$
$-0.20 \pm 0.19 \pm 0.03$	AUBERT	08AU	BABR	$e^+ e^- \to \Upsilon(4S)$
• • • We do not use the following data for averages, fits, limits, etc. • • •				
$-0.08 \pm 0.16 \pm 0.05$	[1] LEE	08A	BELL	Repl. by PAL 18
$-0.21 \pm 0.26 \pm 0.06$	AUBERT,B	06B	BABR	Repl. by AUBERT 08AU
$0.01 \pm 0.29 \pm 0.03$	[1] KATAOKA	04	BELL	Repl. by LEE 08A
$0.38 \pm 0.41 \pm 0.09$	AUBERT	03N	BABR	Repl. by AUBERT,B 06B

[1] BELLE Collab. quotes $A_{J/\psi\pi^0}$ which is equal to $-C_{J/\psi\pi^0}$.

$S_{J/\psi(1S)\pi^0}$ $(B^0 \to J/\psi(1S)\pi^0)$

VALUE	DOCUMENT ID		TECN	COMMENT
-0.88 ± 0.32 OUR AVERAGE	Error includes scale factor of 2.2.			
$-0.59 \pm 0.19 \pm 0.03$	PAL	18	BELL	$e^+ e^- \to \Upsilon(4S)$
$-1.23 \pm 0.21 \pm 0.04$	AUBERT	08AU	BABR	$e^+ e^- \to \Upsilon(4S)$
• • • We do not use the following data for averages, fits, limits, etc. • • •				
$-0.65 \pm 0.21 \pm 0.05$	LEE	08A	BELL	Repl. by PAL 18
$-0.68 \pm 0.30 \pm 0.04$	AUBERT,B	06B	BABR	Repl. by AUBERT 08AU
$-0.72 \pm 0.42 \pm 0.09$	KATAOKA	04	BELL	Repl. by LEE 08A
$0.05 \pm 0.49 \pm 0.16$	AUBERT	03N	BABR	Repl. by AUBERT,B 06B

$C(B^0 \to J/\psi(1S)\rho^0)$

VALUE	DOCUMENT ID		TECN	COMMENT
$-0.063 \pm 0.056^{+0.019}_{-0.014}$	[1] AAIJ	15J	LHCB	pp at 7, 8 TeV

[1] Time-dependent *CP* violation is measured in the $B^0 \to J/\psi\rho^0$ and was used to limit the size of penguin amplitude contributions to ϕ_S in $B^0_s \to J/\psi\phi$ decays to be between $[-1.05°, 1.18°]$ at 95% confidence level.

$S(B^0 \to J/\psi(1S)\rho^0)$

VALUE	DOCUMENT ID		TECN	COMMENT
$-0.66^{+0.13}_{-0.12} {}^{+0.09}_{-0.03}$	[1] AAIJ	15J	LHCB	pp at 7, 8 TeV

[1] Time-dependent *CP* violation is measured in the $B^0 \to J/\psi\rho^0$ and was used to limit the size of penguin amplitude contributions to ϕ_S in $B^0_s \to J/\psi\phi$ decays to be between $[-1.05°, 1.18°]$ at 95% confidence level.

$C_{D^{(*)}_{CP} h^0}$ $(B^0 \to D^{(*)}_{CP} h^0)$

VALUE	DOCUMENT ID		TECN	COMMENT
$-0.02 \pm 0.07 \pm 0.03$	[1] ABDESSALAM	15		$e^+ e^- \to \Upsilon(4S)$
• • • We do not use the following data for averages, fits, limits, etc. • • •				
$-0.23 \pm 0.16 \pm 0.04$	AUBERT	07AJ	BABR	Repl. by ABDESSALAM 15

[1] BABAR and BELLE combined analysis uses *CP*-eigenstate decay modes $D^0 \to K^+K^-$, $K^0_S\pi^0$, $K^0_S\omega$, and $h^0 = \pi^0, \eta, \omega$.

$S_{D^{(*)}_{CP} h^0}$ $(B^0 \to D^{(*)}_{CP} h^0)$

VALUE	DOCUMENT ID		TECN	COMMENT
$-0.66 \pm 0.10 \pm 0.06$	[1] ABDESSALAM	15		$e^+ e^- \to \Upsilon(4S)$
• • • We do not use the following data for averages, fits, limits, etc. • • •				
$-0.56 \pm 0.23 \pm 0.05$	AUBERT	07AJ	BABR	Repl. by ABDESSALAM 15

[1] BABAR and BELLE combined analysis uses *CP*-eigenstate decay modes $D^0 \to K^+K^-$, $K^0_S\pi^0$, $K^0_S\omega$, and $h^0 = \pi^0, \eta, \omega$.

$C_{K^0\pi^0}$ $(B^0 \to K^0\pi^0)$

VALUE	DOCUMENT ID		TECN	COMMENT
0.00 ± 0.13 OUR AVERAGE	Error includes scale factor of 1.4.			
$-0.14 \pm 0.13 \pm 0.06$	[1] FUJIKAWA	10A	BELL	$e^+ e^- \to \Upsilon(4S)$
$0.13 \pm 0.13 \pm 0.03$	AUBERT	09I	BABR	$e^+ e^- \to \Upsilon(4S)$
• • • We do not use the following data for averages, fits, limits, etc. • • •				
$0.24 \pm 0.15 \pm 0.03$	AUBERT	08E	BABR	Repl. by AUBERT 09I
$0.05 \pm 0.14 \pm 0.05$	[1] CHAO	07	BELL	Repl. by FUJIKAWA 10A
$0.06 \pm 0.18 \pm 0.03$	AUBERT	05Y	BABR	Repl. by AUBERT 08E

Downloaded from https://academic.oup.com/ptep/article/2022/8/083C01/6651666 by KIT Library user on 27 September 2022

$-0.16\pm0.29\pm0.05$	[1,2] CHAO	05A	BELL	Repl. by CHEN 05B
$0.11\pm0.20\pm0.09$	[1] CHEN	05B	BELL	Repl. by CHAO 07
$-0.03\pm0.36\pm0.11$	[1] AUBERT	04M	BABR	Repl. by AUBERT,B 04M
$0.40^{+0.27}_{-0.28}\pm0.09$	[3] AUBERT,B	04M	BABR	Repl. by AUBERT 05Y

[1] Reports A which is equal to $-C$.
[2] Corresponds to a 90% CL interval of $-0.33 < A_{CP} < 0.64$.
[3] Based on a total signal yield of 122 ± 16 events.

$S_{K^0\pi^0}$ ($B^0 \to K^0\pi^0$)

VALUE	DOCUMENT ID		TECN	COMMENT
0.58±0.17 OUR AVERAGE				
$0.67\pm0.31\pm0.08$	FUJIKAWA	10A	BELL	$e^+e^- \to \Upsilon(4S)$
$0.55\pm0.20\pm0.03$	AUBERT	09I	BABR	$e^+e^- \to \Upsilon(4S)$
• • • We do not use the following data for averages, fits, limits, etc. • • •				
$0.40\pm0.23\pm0.03$	AUBERT	08E	BABR	Repl. by AUBERT 09I
$0.33\pm0.35\pm0.08$	CHAO	07	BELL	Repl. by FUJIKAWA 10A
$0.35^{+0.30}_{-0.33}\pm0.04$	AUBERT	05Y	BABR	Repl. by AUBERT 08E
$0.32\pm0.61\pm0.13$	CHEN	05B	BELL	Repl. by CHAO 07
$0.48^{+0.38}_{-0.47}\pm0.06$	[1] AUBERT,B	04M	BABR	Repl. by AUBERT 05Y

[1] Based on a total signal yield of 122 ± 16 events.

$C_{\eta'(958)K^0_S}$ ($B^0 \to \eta'(958)K^0_S$)

See updated measurements in $C_{\eta' K^0}$

VALUE	DOCUMENT ID		TECN	COMMENT
−0.04±0.20 OUR AVERAGE Error includes scale factor of 2.5.				
$-0.21\pm0.10\pm0.02$	AUBERT	05M	BABR	$e^+e^- \to \Upsilon(4S)$
$0.19\pm0.11\pm0.05$	[1] CHEN	05B	BELL	$e^+e^- \to \Upsilon(4S)$
• • • We do not use the following data for averages, fits, limits, etc. • • •				
$-0.26\pm0.22\pm0.03$	[1] ABE	03C	BELL	Repl. by ABE 03H
$0.01\pm0.16\pm0.04$	[1] ABE	03H	BELL	Repl. by CHEN 05B
$0.10\pm0.22\pm0.04$	AUBERT	03W	BABR	Repl. by AUBERT 05M
$-0.13\pm0.32^{+0.06}_{-0.09}$	[1] CHEN	02B	BELL	Repl. by ABE 03C

[1] BELLE Collab. quotes $A_{\eta'(958)K^0_S}$ which is equal to $-C_{\eta'(958)K^0_S}$.

$S_{\eta'(958)K^0_S}$ ($B^0 \to \eta'(958)K^0_S$)

See updated measurements in $S_{\eta' K^0}$

VALUE	DOCUMENT ID		TECN	COMMENT
0.43±0.17 OUR AVERAGE Error includes scale factor of 1.5.				
$0.30\pm0.14\pm0.02$	AUBERT	05M	BABR	$e^+e^- \to \Upsilon(4S)$
$0.65\pm0.18\pm0.04$	CHEN	05B	BELL	$e^+e^- \to \Upsilon(4S)$
• • • We do not use the following data for averages, fits, limits, etc. • • •				
$0.71\pm0.37^{+0.05}_{-0.06}$	ABE	03C	BELL	Repl. by ABE 03H
$0.43\pm0.27\pm0.05$	ABE	03H	BELL	Repl. by CHEN 05B
$0.02\pm0.34\pm0.03$	AUBERT	03W	BABR	Repl. by AUBERT 05M
$0.28\pm0.55^{+0.07}_{-0.08}$	CHEN	02B	BELL	Repl. by ABE 03C

$C_{\eta' K^0}$ ($B^0 \to \eta' K^0$)

VALUE	DOCUMENT ID		TECN	COMMENT
−0.06±0.04 OUR AVERAGE				
$-0.03\pm0.05\pm0.04$	[1] SANTELJ	14	BELL	$e^+e^- \to \Upsilon(4S)$
$-0.08\pm0.06\pm0.02$	AUBERT	09I	BABR	$e^+e^- \to \Upsilon(4S)$
• • • We do not use the following data for averages, fits, limits, etc. • • •				
$-0.16\pm0.07\pm0.03$	[2] AUBERT	07A	BABR	Repl. by AUBERT 09I
$0.01\pm0.07\pm0.05$	[1,2] CHEN	07	BELL	Repl. by SANTELJ 14

[1] The paper reports A, which is equal to $-C$.
[2] The mixing-induced CP violation is reported with a significance of more than 5 standard deviations in this $b \to s$ penguin dominated mode.

$S_{\eta' K^0}$ ($B^0 \to \eta' K^0$)

VALUE	DOCUMENT ID		TECN	COMMENT
0.63±0.06 OUR AVERAGE				
$0.68\pm0.07\pm0.03$	SANTELJ	14	BELL	$e^+e^- \to \Upsilon(4S)$
$0.57\pm0.08\pm0.02$	AUBERT	09I	BABR	$e^+e^- \to \Upsilon(4S)$
• • • We do not use the following data for averages, fits, limits, etc. • • •				
$0.58\pm0.10\pm0.03$	[1] AUBERT	07A	BABR	Repl. by AUBERT 09I
$0.64\pm0.10\pm0.04$	[1] CHEN	07	BELL	Repl. by SANTELJ 14

[1] The mixing-induced CP violation is reported with a significance of more than 5 standard deviations in this $b \to s$ penguin dominated mode.

$C_{\omega K^0_S}$ ($B^0 \to \omega K^0_S$)

VALUE	DOCUMENT ID		TECN	COMMENT
0.0 ±0.4 OUR AVERAGE Error includes scale factor of 3.0.				
$0.36\pm0.19\pm0.05$	[1] CHOBANOVA	14	BELL	$e^+e^- \to \Upsilon(4S)$
$-0.52^{+0.22}_{-0.20}\pm0.03$	AUBERT	09I	BABR	$e^+e^- \to \Upsilon(4S)$
• • • We do not use the following data for averages, fits, limits, etc. • • •				
$0.09\pm0.29\pm0.06$	[1] CHAO	07	BELL	Repl. by CHOBANOVA 14
$-0.55^{+0.28}_{-0.26}\pm0.03$	AUBERT,B	06E	BABR	Repl. by AUBERT 09I
$-0.27\pm0.48\pm0.15$	[1] CHEN	05B	BELL	Repl. by CHAO 07

[1] Belle Collab. quotes $A_{\omega K^0_S}$ which is equal to $-C_{\omega K^0_S}$.

$S_{\omega K^0_S}$ ($B^0 \to \omega K^0_S$)

VALUE	DOCUMENT ID		TECN	COMMENT
0.70±0.21 OUR AVERAGE				
$0.91\pm0.32\pm0.05$	CHOBANOVA	14	BELL	$e^+e^- \to \Upsilon(4S)$
$0.55^{+0.26}_{-0.29}\pm0.02$	AUBERT	09I	BABR	$e^+e^- \to \Upsilon(4S)$
• • • We do not use the following data for averages, fits, limits, etc. • • •				
$0.11\pm0.46\pm0.07$	CHAO	07	BELL	Repl. by CHOBANOVA 14
$0.51^{+0.35}_{-0.39}\pm0.02$	AUBERT,B	06E	BABR	Repl. by AUBERT 09I
$0.76\pm0.65^{+0.13}_{-0.16}$	CHEN	05B	BELL	Repl. by CHAO 07

C ($B^0 \to K^0_S\pi^0\pi^0$)

VALUE	DOCUMENT ID		TECN	COMMENT
−0.21±0.20 OUR AVERAGE				
$-0.28\pm0.21\pm0.04$	[1] YUSA	19	BELL	$e^+e^- \to \Upsilon(4S)$
$0.23\pm0.52\pm0.13$	AUBERT	07AQ	BABR	$e^+e^- \to \Upsilon(4S)$

[1] Reports value of A which is equal to $-C$.

S ($B^0 \to K^0_S\pi^0\pi^0$)

VALUE	DOCUMENT ID		TECN	COMMENT
$0.89^{+0.27}_{-0.30}$ OUR AVERAGE				
$0.92^{+0.27}_{-0.31}\pm0.11$	YUSA	19	BELL	$e^+e^- \to \Upsilon(4S)$
$0.72\pm0.71\pm0.08$	AUBERT	07AQ	BABR	$e^+e^- \to \Upsilon(4S)$

$C_{\rho^0 K^0_S}$ ($B^0 \to \rho^0 K^0_S$)

VALUE	DOCUMENT ID		TECN	COMMENT
−0.04±0.20 OUR AVERAGE				
$-0.05\pm0.26\pm0.10$	[1] AUBERT	09AU	BABR	$e^+e^- \to \Upsilon(4S)$
$-0.03^{+0.24}_{-0.23}\pm0.15$	[2,3] DALSENO	09	BELL	$e^+e^- \to \Upsilon(4S)$
• • • We do not use the following data for averages, fits, limits, etc. • • •				
$0.64\pm0.41\pm0.20$	AUBERT	07F	BABR	Repl. by AUBERT 09AU

[1] Uses Dalitz plot analysis of $B^0 \to K^0\pi^+\pi^-$ decays and the first of two equivalent solutions is used.
[2] Quotes $A_{\rho^0(KS)^0}$ which is equal to $-C_{\rho^0 K^0_S}$.
[3] Uses Dalitz plot analysis of $B^0 \to K^0\pi^+\pi^-$ decays and the first of two consistent solutions that may be preferred.

$S_{\rho^0 K^0_S}$ ($B^0 \to \rho^0 K^0_S$)

VALUE	DOCUMENT ID		TECN	COMMENT
$0.50^{+0.17}_{-0.21}$ OUR AVERAGE				
$0.35^{+0.26}_{-0.31}\pm0.07$	[1] AUBERT	09AU	BABR	$e^+e^- \to \Upsilon(4S)$
$0.64^{+0.19}_{-0.25}\pm0.13$	[2] DALSENO	09	BELL	$e^+e^- \to \Upsilon(4S)$
• • • We do not use the following data for averages, fits, limits, etc. • • •				
$0.20\pm0.52\pm0.24$	AUBERT	07F	BABR	Repl. by AUBERT 09AU

[1] Uses Dalitz plot analysis of $B^0 \to K^0\pi^+\pi^-$ decays and the first of two equivalent solutions is used.
[2] Uses Dalitz plot analysis of $B^0 \to K^0\pi^+\pi^-$ decays and the first of two consistent solutions that may be preferred.

$C_{f_0(980)K^0_S}$ ($B^0 \to f_0(980)K^0_S$)

VALUE	DOCUMENT ID		TECN	COMMENT
0.29±0.20 OUR AVERAGE				
$0.28\pm0.24\pm0.09$	[1] LEES	12O	BABR	$e^+e^- \to \Upsilon(4S)$
$0.30\pm0.29\pm0.14$	[2,3] NAKAHAMA	10	BELL	$e^+e^- \to \Upsilon(4S)$
• • • We do not use the following data for averages, fits, limits, etc. • • •				
$0.08\pm0.19\pm0.05$	[4] AUBERT	09AU	BABR	Repl. by LEES 12O
$0.06\pm0.17\pm0.11$	[2,5] DALSENO	09	BELL	Repl. by NAKAHAMA 10
$-0.41\pm0.23\pm0.07$	[2] AUBERT	07AX	BABR	Repl. by AUBERT 09AU
$0.15\pm0.15\pm0.07$	[2] CHAO	07	BELL	Repl. by DALSENO 09
$0.39\pm0.27\pm0.09$	[2] CHEN	05B	BELL	Repl. by CHAO 07

[1] Uses Dalitz plot analysis of the $B^0 \to K^0_S K^+K^-$ decay.
[2] Quotes $A_{f_0(980)K^0_S}$ which is equal to $-C_{f_0(980)K^0_S}$.
[3] Uses Dalitz plot analysis of $B^0 \to K^0_S K^+K^-$ decays and the first of four consistent solutions that may be preferred.
[4] Uses Dalitz plot analysis of $B^0 \to K^0\pi^+\pi^-$ decays and the first of two equivalent solutions is used.
[5] Uses Dalitz plot analysis of $B^0 \to K^0\pi^+\pi^-$ decays and the first of two consistent solutions that may be preferred.

$S_{f_0(980)K^0_S}$ ($B^0 \to f_0(980)K^0_S$)

VALUE	DOCUMENT ID		TECN	COMMENT
−0.50±0.16 OUR AVERAGE				
$-0.55\pm0.18\pm0.12$	[1] LEES	12O	BABR	$e^+e^- \to \Upsilon(4S)$
$-0.43^{+0.22}_{-0.20}\pm0.14$	[2] DALSENO	09	BELL	$e^+e^- \to \Upsilon(4S)$

Downloaded from https://academic.oup.com/ptep/article/2022/8/083C01/6651666 by KIT Library user on 27 September 2022

• • • We do not use the following data for averages, fits, limits, etc. • • •

$-0.96^{+0.21}_{-0.04}\pm0.04$	[3] AUBERT	09AU	BABR	Repl. by LEES 12O
$-0.25\pm0.26\pm0.10$	[4] AUBERT	07AX	BABR	Repl. by AUBERT 09AU
$0.18\pm0.23\pm0.11$	CHAO	07	BELL	Repl. by DALSENO 09
$0.47\pm0.41\pm0.08$	CHEN	05B	BELL	Repl. by CHAO 07

[1] Uses Dalitz plot analysis of the $B^0 \to K^0_S K^+ K^-$ decay.
[2] Uses Dalitz plot analysis of $B^0 \to K^0\pi^+\pi^-$ decays and the first of two consistent solutions that may be preferred.
[3] Uses Dalitz plot analysis of $B^0 \to K^0\pi^+\pi^-$ decays and the first of two equivalent solutions is used.
[4] Reports β_{eff}. We quote S obtained from epaps: E-PRLTAO-99-076741.

$S_{f_2(1270)K^0_S}$ ($B^0 \to f_2(1270)K^0_S$)

VALUE	DOCUMENT ID		TECN	COMMENT
$-0.48\pm0.52\pm0.12$	[1] AUBERT	09AU	BABR	$e^+e^- \to \Upsilon(4S)$

[1] Uses Dalitz plot analysis of $B^0 \to K^0\pi^+\pi^-$ decays and the first of two equivalent solutions is used.

$C_{f_2(1270)K^0_S}$ ($B^0 \to f_2(1270)K^0_S$)

VALUE	DOCUMENT ID		TECN	COMMENT
$0.28^{+0.35}_{-0.40}\pm0.11$	[1] AUBERT	09AU	BABR	$e^+e^- \to \Upsilon(4S)$

[1] Uses Dalitz plot analysis of $B^0 \to K^0\pi^+\pi^-$ decays and the first of two equivalent solutions is used.

$S_{f_x(1300)K^0_S}$ ($B^0 \to f_x(1300)K^0_S$)

VALUE	DOCUMENT ID		TECN	COMMENT
$-0.20\pm0.52\pm0.10$	[1] AUBERT	09AU	BABR	$e^+e^- \to \Upsilon(4S)$

[1] Uses Dalitz plot analysis of $B^0 \to K^0\pi^+\pi^-$ decays and the first of two equivalent solutions is used.

$C_{f_x(1300)K^0_S}$ ($B^0 \to f_x(1300)K^0_S$)

VALUE	DOCUMENT ID		TECN	COMMENT
$0.13^{+0.33}_{-0.35}\pm0.10$	[1] AUBERT	09AU	BABR	$e^+e^- \to \Upsilon(4S)$

[1] Uses Dalitz plot analysis of $B^0 \to K^0\pi^+\pi^-$ decays and the first of two equivalent solutions is used.

$S_{K^0\pi^+\pi^-}$ ($B^0 \to K^0\pi^+\pi^-$ nonresonant)

VALUE	DOCUMENT ID		TECN	COMMENT
$-0.01\pm0.31\pm0.10$	[1] AUBERT	09AU	BABR	$e^+e^- \to \Upsilon(4S)$

[1] Uses Dalitz plot analysis of $B^0 \to K^0\pi^+\pi^-$ decays and the first of two equivalent solutions is used.

$C_{K^0\pi^+\pi^-}$ ($B^0 \to K^0\pi^+\pi^-$ nonresonant)

VALUE	DOCUMENT ID		TECN	COMMENT
$0.01\pm0.25\pm0.08$	[1] AUBERT	09AU	BABR	$e^+e^- \to \Upsilon(4S)$

[1] Uses Dalitz plot analysis of $B^0 \to K^0\pi^+\pi^-$ decays and the first of two equivalent solutions is used.

$C_{K^0_S K^0_S}$ ($B^0 \to K^0_S K^0_S$)

VALUE	DOCUMENT ID		TECN	COMMENT
0.0 ±0.4 OUR AVERAGE	Error includes scale factor of 1.4.			
$0.38\pm0.38\pm0.05$	[1] NAKAHAMA	08	BELL	$e^+e^- \to \Upsilon(4S)$
$-0.40\pm0.41\pm0.06$	AUBERT,BE	06C	BABR	$e^+e^- \to \Upsilon(4S)$

[1] Reports $A_{K^0_S K^0_S}$ which equals to $-C_{K^0_S K^0_S}$.

$S_{K^0_S K^0_S}$ ($B^0 \to K^0_S K^0_S$)

VALUE	DOCUMENT ID		TECN	COMMENT
−0.8 ±0.5 OUR AVERAGE				
$-0.38^{+0.69}_{-0.77}\pm0.09$	NAKAHAMA	08	BELL	$e^+e^- \to \Upsilon(4S)$
$-1.28^{+0.80}_{-0.73}+0.11_{-0.16}$	AUBERT,BE	06C	BABR	$e^+e^- \to \Upsilon(4S)$

$C_{K^+K^-K^0_S}$ ($B^0 \to K^+K^-K^0_S$ nonresonant)

VALUE	DOCUMENT ID		TECN	COMMENT
0.06 ±0.08 OUR AVERAGE				
0.02 ±0.09 ±0.03	[1,2] LEES	12O	BABR	$e^+e^- \to \Upsilon(4S)$
0.14 ±0.11 ±0.09	[3,4] NAKAHAMA	10	BELL	$e^+e^- \to \Upsilon(4S)$
• • • We do not use the following data for averages, fits, limits, etc. • • •				
$0.054\pm0.102\pm0.060$	[3,5] AUBERT	07AX	BABR	Repl. by LEES 12O
0.09 ±0.10 ±0.05	[3,5] CHAO	07	BELL	Repl. by NAKAHAMA 10
0.10 ±0.14 ±0.04	[5] AUBERT	05T	BABR	Repl. by AUBERT 07AX
0.09 ±0.12 ±0.07	[3] CHEN	05B	BELL	Repl. by CHAO 07
−0.10 ±0.19 ±0.10	[5] AUBERT,B	04V	BABR	Repl. by AUBERT 05T
$0.40 \pm0.33^{+0.28}_{-0.10}$	[3] ABE	03C	BELL	Repl. by ABE 03H
0.17 ±0.16 ±0.04	[3,5] ABE	03H	BELL	Repl. by CHEN 05B

[1] Uses Dalitz plot analysis of the $B^0 \to K^0_S K^+ K^-$ decay.
[2] This measurement is performed on all the isobar components, excluding ϕK^0_S and $f_0(980)\,K^0_S$.
[3] Quotes $A_{K^+K^-K^0_S}$ which is equal to $-C_{K^+K^-K^0_S}$.
[4] Uses Dalitz plot analysis of $B^0 \to K^0_S K^+ K^-$ decays and the first of four consistent solutions that may be preferred.
[5] Excludes the events from $B^0 \to \phi K^0_S$ decay. The results are derived from a combined sample of $K^+K^-K^0_S$ and $K^+K^-K^0_L$ decays.

$S_{K^+K^-K^0_S}$ ($B^0 \to K^+K^-K^0_S$ nonresonant)

VALUE	DOCUMENT ID		TECN	COMMENT
−0.66 ±0.11 OUR AVERAGE				
−0.65 ±0.12 ±0.03	[1,2] LEES	12O	BABR	$e^+e^- \to \Upsilon(4S)$
$-0.68 \pm0.15^{+0.21}_{-0.13}$	[3] CHAO	07	BELL	$e^+e^- \to \Upsilon(4S)$
• • • We do not use the following data for averages, fits, limits, etc. • • •				
$-0.764\pm0.111^{+0.071}_{-0.040}$	[3,4] AUBERT	07AX	BABR	Repl. by LEES 12O
−0.42 ±0.17 ±0.03	[3,5] AUBERT	05T	BABR	Repl. by AUBERT 07AX
−0.49 ±0.18 ±0.04	CHEN	05B	BELL	Repl. by CHAO 07
−0.56 ±0.25 ±0.04	[3,6] AUBERT,B	04V	BABR	Repl. by AUBERT 05T
−0.49 ±0.43 ±0.11	ABE	03C	BELL	Repl. by ABE 03H
−0.51 ±0.26 ±0.05	[3,7] ABE	03H	BELL	Repl. by CHEN 05B

[1] Uses Dalitz plot analysis of the $B^0 \to K^0_S K^+ K^-$ decay.
[2] This measurement is performed on all the isobar components, excluding ϕK^0_S and $f_0(980)\,K^0_S$. Note that the nonresonant component is not a CP eigenstate.
[3] Excludes events from $B^0 \to \phi K^0_S$ decay. The results are derived from a combined sample of $K^+K^-K^0_S$ and $K^+K^-K^0_L$ decays.
[4] Reports β_{eff}. We quote S obtained from epaps: E-PRLTAO-99-076741.
[5] The measured CP-even final states fraction is 0.89 ± 0.08 ± 0.06.
[6] The measured CP-even final states fraction is 0.98 ± 0.15 ± 0.04.
[7] The measured CP-even final states fraction is 1.03 ± 0.15 ± 0.05.

$C_{K^+K^-K^0_S}$ ($B^0 \to K^+K^-K^0_S$ inclusive)

VALUE	DOCUMENT ID		TECN	COMMENT
$0.015\pm0.077\pm0.053$	[1,2] AUBERT	07AX	BABR	$e^+e^- \to \Upsilon(4S)$

[1] Measured using full Dalitz plot fit including ϕ component.
[2] The results are derived from a combined sample of $K^+K^-K^0_S$ and $K^+K^-K^0_L$ decays.

$S_{K^+K^-K^0_S}$ ($B^0 \to K^+K^-K^0_S$ inclusive)

VALUE	DOCUMENT ID		TECN	COMMENT
$-0.647\pm0.116\pm0.040$	[1] AUBERT	07AX	BABR	$e^+e^- \to \Upsilon(4S)$

[1] Measured using full Dalitz plot fit including ϕ component.

$C_{\phi K^0_S}$ ($B^0 \to \phi K^0_S$)

VALUE	DOCUMENT ID		TECN	COMMENT
0.01±0.14 OUR AVERAGE				
$0.05\pm0.18\pm0.05$	[1] LEES	12O	BABR	$e^+e^- \to \Upsilon(4S)$
$-0.04\pm0.20\pm0.10$	[2,3] NAKAHAMA	10	BELL	$e^+e^- \to \Upsilon(4S)$
• • • We do not use the following data for averages, fits, limits, etc. • • •				
$0.08\pm0.18\pm0.04$	[2,4] AUBERT	07AX	BABR	Repl. by LEES 12O
$-0.07\pm0.15\pm0.05$	[2,4] CHEN	07	BELL	Repl. by NAKAHAMA 10
$0.00\pm0.23\pm0.05$	[4] AUBERT	05T	BABR	Repl. by AUBERT 07AX
$-0.08\pm0.22\pm0.09$	[2,4] CHEN	05B	BELL	Repl. by CHEN 07
$0.01\pm0.33\pm0.10$	[4] AUBERT,B	04G	BABR	Repl. by AUBERT 05T
$0.56\pm0.41\pm0.16$	[2] ABE	03C	BELL	Repl. by ABE 03H
$0.15\pm0.29\pm0.07$	[2] ABE	03H	BELL	Repl. by CHEN 05B

[1] Uses Dalitz plot analysis of the $B^0 \to K^0_S K^+ K^-$ decay.
[2] Quotes $A_{\phi K^0_S}$ which is equal to $-C_{\phi K^0_S}$.
[3] Uses Dalitz plot analysis of $B^0 \to K^0_S K^+ K^-$ decays and the first of four consistent solutions that may be preferred.
[4] Result combines B-meson final states ϕK^0_S and ϕK^0_L by assuming $S_{\phi K^0_S} = -S_{\phi K^0_L}$

$S_{\phi K^0_S}$ ($B^0 \to \phi K^0_S$)

VALUE	DOCUMENT ID		TECN	COMMENT
0.59±0.14 OUR AVERAGE				
$0.66\pm0.17\pm0.07$	[1] LEES	12O	BABR	$e^+e^- \to \Upsilon(4S)$
$0.50\pm0.21\pm0.06$	[2] CHEN	07	BELL	$e^+e^- \to \Upsilon(4S)$
• • • We do not use the following data for averages, fits, limits, etc. • • •				
$0.21\pm0.26\pm0.11$	[2,3] AUBERT	07AX	BABR	Repl. by LEES 12O
$0.50\pm0.25^{+0.07}_{-0.04}$	[2] AUBERT	05T	BABR	Repl. by AUBERT 07AX
$0.08\pm0.33\pm0.09$	[2] CHEN	05B	BELL	Repl. by CHEN 07
$0.47\pm0.34^{+0.08}_{-0.06}$	[2] AUBERT,B	04G	BABR	Repl. by AUBERT 05T
$-0.73\pm0.64\pm0.22$	ABE	03C	BELL	Repl. by ABE 03H
$-0.96\pm0.50^{+0.09}_{-0.11}$	ABE	03H	BELL	Repl. by CHEN 05B

[1] Uses Dalitz plot analysis of the $B^0 \to K^0_S K^+ K^-$ decay.
[2] Result combines B-meson final states ϕK^0_S and ϕK^0_L by assuming $S_{\phi K^0_S} = -S_{\phi K^0_L}$
[3] Reports β_{eff}. We quote S obtained from epaps: E-PRLTAO-99-076741.

Downloaded from https://academic.oup.com/ptep/article/2022/8/083C01/6651666 by KIT Library user on 27 September 2022

$C_{K_S K_S K_S}(B^0 \to K_S K_S K_S)$

VALUE	DOCUMENT ID		TECN	COMMENT
-0.14 ± 0.12 OUR AVERAGE				
$-0.12 \pm 0.16 \pm 0.05$	[1] KANG	21	BELL	$e^+e^- \to \Upsilon(4S)$
$-0.17 \pm 0.18 \pm 0.04$	LEES	12I	BABR	$e^+e^- \to \Upsilon(4S)$
• • • We do not use the following data for averages, fits, limits, etc. • • •				
$0.02 \pm 0.21 \pm 0.05$	AUBERT	07AT	BABR	Repl. by LEES 12I
$-0.31 \pm 0.20 \pm 0.07$	[1] CHEN	07	BELL	Repl. by KANG 21
$-0.34^{+0.28}_{-0.25} \pm 0.05$	AUBERT,B	05	BABR	Repl. by AUBERT 07AT
$-0.54 \pm 0.34 \pm 0.09$	[1] SUMISAWA	05	BELL	Repl. by CHEN 07

[1] KANG 21 quotes $A_{K^0_S K^0_S K^0_S}$ which is equal to $-C_{K^0_S K^0_S K^0_S}$.

$S_{K_S K_S K_S}(B^0 \to K_S K_S K_S)$

VALUE	DOCUMENT ID		TECN	COMMENT
-0.82 ± 0.17 OUR AVERAGE				
$-0.71 \pm 0.23 \pm 0.05$	KANG	21	BELL	$e^+e^- \to \Upsilon(4S)$
$-0.94^{+0.24}_{-0.21} \pm 0.06$	LEES	12I	BABR	$e^+e^- \to \Upsilon(4S)$
• • • We do not use the following data for averages, fits, limits, etc. • • •				
$-0.71 \pm 0.24 \pm 0.04$	AUBERT	07AT	BABR	Repl. by LEES 12I
$0.30 \pm 0.32 \pm 0.08$	CHEN	07	BELL	Repl. by KANG 21
$-0.71^{+0.38}_{-0.32} \pm 0.04$	AUBERT,B	05	BABR	Repl. by AUBERT 07AT
$1.26 \pm 0.68 \pm 0.20$	SUMISAWA	05	BELL	Repl. by CHEN 07.

$C_{K^0_S \pi^0 \gamma}(B^0 \to K^0_S \pi^0 \gamma)$

VALUE	DOCUMENT ID		TECN	COMMENT
$0.36 \pm 0.33 \pm 0.04$	[1] AUBERT	08BA	BABR	$e^+e^- \to \Upsilon(4S)$
• • • We do not use the following data for averages, fits, limits, etc. • • •				
$0.20 \pm 0.20 \pm 0.06$	[2,3] USHIRODA	06	BELL	$e^+e^- \to \Upsilon(4S)$
$-1.0 \pm 0.5 \pm 0.2$	[1] AUBERT,B	05P	BABR	Repl. by AUBERT 08BA
$-0.03 \pm 0.34 \pm 0.11$	[3] USHIRODA	05	BELL	Repl. by USHIRODA 06

[1] Requires $1.1 < M_{K^0_S \pi^0} < 1.8$ GeV/c^2.

[2] Requires $M_{K^0_S \pi^0} < 1.8$ GeV/c^2.

[3] Reports $A_{K^0_S \pi^0 \gamma}$, which is $-C_{K^0_S \pi^0 \gamma}$.

$S_{K^0_S \pi^0 \gamma}(B^0 \to K^0_S \pi^0 \gamma)$

VALUE	DOCUMENT ID		TECN	COMMENT
$-0.78 \pm 0.59 \pm 0.09$	[1] AUBERT	08BA	BABR	$e^+e^- \to \Upsilon(4S)$
• • • We do not use the following data for averages, fits, limits, etc. • • •				
$-0.10 \pm 0.31 \pm 0.07$	[2] USHIRODA	06	BELL	$e^+e^- \to \Upsilon(4S)$
$0.9 \pm 1.0 \pm 0.2$	[1] AUBERT,B	05P	BABR	Repl. by AUBERT 08BA
$-0.58^{+0.46}_{-0.38} \pm 0.11$	USHIRODA	05	BELL	Repl. by USHIRODA 06

[1] Requires $1.1 < M_{K^0_S \pi^0} < 1.8$ GeV/c^2.

[2] Requires $M_{K^0_S \pi^0} < 1.8$ GeV/c^2.

$C_{K^0_S \pi^+ \pi^- \gamma}(B^0 \to K^0_S \pi^+ \pi^- \gamma)$

VALUE	DOCUMENT ID		TECN	COMMENT
$-0.39 \pm 0.20^{+0.03}_{-0.02}$	[1] DEL-AMO-SA...16		BABR	$e^+e^- \to \Upsilon(4S)$

[1] Requires $M_{K\pi\pi} < 1.8$ GeV/c^2, 0.6 GeV/c^2 $< m_{\pi^+\pi^-} < 0.9$ GeV/c^2, $m_{K\pi} < 0.845$ GeV/c^2 or $m_{K\pi} > 0.945$ GeV/c^2.

$S_{K^0_S \pi^+ \pi^- \gamma}(B^0 \to K^0_S \pi^+ \pi^- \gamma)$

VALUE	DOCUMENT ID		TECN	COMMENT
$0.14 \pm 0.25 \pm 0.03$	[1] DEL-AMO-SA...16		BABR	$e^+e^- \to \Upsilon(4S)$

[1] Requires $M_{K\pi\pi} < 1.8$ GeV/c^2, 0.6 GeV/c^2 $< m_{\pi^+\pi^-} < 0.9$ GeV/c^2, $m_{K\pi} < 0.845$ GeV/c^2 or $m_{K\pi} > 0.945$ GeV/c^2.

$C_{K^*(892)^0 \gamma}(B^0 \to K^*(892)^0 \gamma)$

VALUE	DOCUMENT ID		TECN	COMMENT
-0.04 ± 0.16 OUR AVERAGE	Error includes scale factor of 1.2.			
$-0.14 \pm 0.16 \pm 0.03$	[1] AUBERT	08BA	BABR	$e^+e^- \to \Upsilon(4S)$
$0.20 \pm 0.24 \pm 0.05$	[1,2] USHIRODA	06	BELL	$e^+e^- \to \Upsilon(4S)$
• • • We do not use the following data for averages, fits, limits, etc. • • •				
$-0.40 \pm 0.23 \pm 0.03$	AUBERT,B	05P	BABR	Repl. by AUBERT 08BA
$-0.57 \pm 0.32 \pm 0.09$	[3] AUBERT,B	04Z	BABR	Repl. by AUBERT,B 05P

[1] Requires $0.8 < M_{K^0_S \pi^0} < 1.0$ GeV/c^2.

[2] Reports value of A which is equal to $-C$.

[3] Based on a total signal of 105 $\pm$ 14 events with $K^*(892)^0 \to K^0_S \pi^0$ only.

$S_{K^*(892)^0 \gamma}(B^0 \to K^*(892)^0 \gamma)$

VALUE	DOCUMENT ID		TECN	COMMENT
-0.15 ± 0.22 OUR AVERAGE				
$-0.03 \pm 0.29 \pm 0.03$	[1] AUBERT	08BA	BABR	$e^+e^- \to \Upsilon(4S)$
$-0.32^{+0.36}_{-0.33} \pm 0.05$	[1] USHIRODA	06	BELL	$e^+e^- \to \Upsilon(4S)$
• • • We do not use the following data for averages, fits, limits, etc. • • •				
$-0.21 \pm 0.40 \pm 0.05$	AUBERT,B	05P	BABR	Repl. by AUBERT 08BA
$-0.79^{+0.63}_{-0.50} \pm 0.10$	[2] USHIRODA	05	BELL	Repl. by USHIRODA 06
$0.25 \pm 0.63 \pm 0.14$	[3] AUBERT,B	04Z	BABR	Repl. by AUBERT,B 05P

[1] Requires $0.8 < M_{K^0_S \pi^0} < 1.0$ GeV/c^2.

[2] Assumes $C(B^0 \to K^*(892)^0 \gamma) = 0$.

[3] Based on a total signal of 105 $\pm$ 14 events with $K^*(892)^0 \to K^0_S \pi^0$ only.

$C_{\eta K^0 \gamma}(B^0 \to \eta K^0 \gamma)$

VALUE	DOCUMENT ID		TECN	COMMENT
0.1 $\pm$0.4 OUR AVERAGE	Error includes scale factor of 1.4.			
$0.48 \pm 0.41 \pm 0.07$	[1,2] NAKANO	18	BELL	$e^+e^- \to \Upsilon(4S)$
$-0.32^{+0.40}_{-0.39} \pm 0.07$	[3] AUBERT	09	BABR	$e^+e^- \to \Upsilon(4S)$

[1] Assuming $m_{\eta K^0_S} < 2.1$ GeV.

[2] Reversed the sign for C=-A.

[3] Assuming $m_{\eta K} < 3.25$ GeV.

$S_{\eta K^0 \gamma}(B^0 \to \eta K^0 \gamma)$

VALUE	DOCUMENT ID		TECN	COMMENT
-0.5 ± 0.5 OUR AVERAGE	Error includes scale factor of 1.2.			
$-1.32 \pm 0.77 \pm 0.36$	[1] NAKANO	18	BELL	$e^+e^- \to \Upsilon(4S)$
$-0.18^{+0.49}_{-0.46} \pm 0.12$	[2] AUBERT	09	BABR	$e^+e^- \to \Upsilon(4S)$

[1] Assuming $m_{\eta K^0_S} < 2.1$ GeV.

[2] Assuming $m_{\eta K} < 3.25$ GeV.

$C_{K^0 \phi \gamma}(B^0 \to K^0 \phi \gamma)$

VALUE	DOCUMENT ID		TECN	COMMENT
$-0.35 \pm 0.58^{+0.10}_{-0.23}$	[1] SAHOO	11A	BELL	$e^+e^- \to \Upsilon(4S)$

[1] Reports value of A, which is equal to $-C$.

$S_{K^0 \phi \gamma}(B^0 \to K^0 \phi \gamma)$

VALUE	DOCUMENT ID		TECN	COMMENT
$0.74^{+0.72}_{-1.05} {}^{+0.10}_{-0.24}$	SAHOO	11A	BELL	$e^+e^- \to \Upsilon(4S)$

$C(B^0 \to K^0_S \rho^0 \gamma)$

VALUE	DOCUMENT ID		TECN	COMMENT
$-0.05 \pm 0.18 \pm 0.06$	[1,2] LI	08F	BELL	$e^+e^- \to \Upsilon(4S)$

[1] Requires $M_{K^0_S \pi^+ \pi^-} < 1.8$ GeV/c^2 and $0.6 < M_{\pi^+\pi^-} < 0.9$ GeV/c^2.

[2] Reports value of $A_{\rm eff}$ which is equal to $-C$, and includes the non-resonant $\pi^+\pi^-$ contribution in the ρ^0 region.

$S(B^0 \to K^0_S \rho^0 \gamma)$

VALUE	DOCUMENT ID		TECN	COMMENT
-0.04 ± 0.23 OUR AVERAGE				
$-0.18 \pm 0.32^{+0.06}_{-0.05}$	[1] DEL-AMO-SA...16		BABR	$e^+e^- \to \Upsilon(4S)$
$0.11 \pm 0.33^{+0.05}_{-0.09}$	[2] LI	08F	BELL	$e^+e^- \to \Upsilon(4S)$

[1] Requires $M_{K\pi\pi} < 1.8$ GeV/c^2, 0.6 GeV/c^2 $< m_{\pi^+\pi^-} < 0.9$ GeV/c^2, $m_{K\pi} < 0.845$ GeV/c^2 or $m_{K\pi} > 0.945$ GeV/c^2.

[2] Requires $M_{K\pi\pi} < 1.8$ GeV/c^2.

$C(B^0 \to \rho^0 \gamma)$

VALUE	DOCUMENT ID		TECN	COMMENT
$0.44 \pm 0.49 \pm 0.14$	[1] USHIRODA	08	BELL	$e^+e^- \to \Upsilon(4S)$

[1] Reports value of A which is equal to $-C$.

$S(B^0 \to \rho^0 \gamma)$

VALUE	DOCUMENT ID		TECN	COMMENT
$-0.83 \pm 0.65 \pm 0.18$	USHIRODA	08	BELL	$e^+e^- \to \Upsilon(4S)$

$C_{\pi\pi}(B^0 \to \pi^+\pi^-)$

$C_{\pi\pi}$ is defined as $(1-|\lambda|^2)/(1+|\lambda|^2)$, where the quantity $\lambda = q/p\ \overline{A}_f/A_f$ is a phase convention independent observable quantity for the final state f. For details, see the review on "CP Violation" in the Reviews section.

VALUE	DOCUMENT ID		TECN	COMMENT
-0.314 ± 0.030 OUR AVERAGE				
$-0.311 \pm 0.045 \pm 0.015$	AAIJ	21O	LHCB	pp at 13 TeV
$-0.34 \pm 0.06 \pm 0.01$	AAIJ	18O	LHCB	pp at 7, 8 TeV
$-0.33 \pm 0.06 \pm 0.03$	[1] DALSENO	13	BELL	$e^+e^- \to \Upsilon(4S)$
$-0.25 \pm 0.08 \pm 0.02$	LEES	13D	BABR	$e^+e^- \to \Upsilon(4S)$
• • • We do not use the following data for averages, fits, limits, etc. • • •				
$-0.38 \pm 0.15 \pm 0.02$	AAIJ	13BO	LHCB	Repl. by AAIJ 18O
$-0.21 \pm 0.09 \pm 0.02$	AUBERT	07AF	BABR	Repl. by LEES 13D
$-0.55 \pm 0.08 \pm 0.05$	[1] ISHINO	07	BELL	Repl. by DALSENO 13
$-0.56 \pm 0.12 \pm 0.06$	[1] ABE	05D	BELL	Repl. by ISHINO 07
$-0.09 \pm 0.15 \pm 0.04$	AUBERT,BE	05	BABR	Repl. by AUBERT 07AF

Downloaded from https://academic.oup.com/ptep/article/2022/8/083C01/6651666 by KIT Library user on 27 September 2022

$-0.58 \pm 0.15 \pm 0.07$	[1] ABE	04E	BELL	Repl. by ABE 05D
$-0.77 \pm 0.27 \pm 0.08$	[1] ABE	03G	BELL	Repl. by ABE 04E.
$-0.94 \; ^{+0.31}_{-0.25} \pm 0.09$	[1] ABE	02M	BELL	Repl. by ABE 03G
$-0.25 \; ^{+0.45}_{-0.47} \pm 0.14$	[2] AUBERT	02D	BABR	Repl. by AUBERT 02Q
$-0.30 \pm 0.25 \pm 0.04$	[3] AUBERT	02Q	BABR	Repl. by AUBERT,BE 05

[1] Paper reports $A_{\pi\pi}$ which equals to $-C_{\pi\pi}$.
[2] Corresponds to 90% confidence range $-1.0 < C_{\pi\pi} < 0.47$.
[3] Corresponds to 90% confidence range $-0.72 < C_{\pi\pi} < 0.12$.

$S_{\pi\pi}$ ($B^0 \to \pi^+\pi^-$)

$S_{\pi\pi} = 2\mathrm{Im}\lambda/(1+|\lambda|^2)$, see the note in the $C_{\pi\pi}$ datablock above.

VALUE	DOCUMENT ID		TECN	COMMENT
-0.670 ± 0.030 OUR AVERAGE				
$-0.706 \pm 0.042 \pm 0.013$	AAIJ	21O	LHCB	pp at 13 TeV
$-0.63 \pm 0.05 \pm 0.01$	AAIJ	18O	LHCB	pp at 7, 8 TeV
$-0.64 \pm 0.08 \pm 0.03$	[1] DALSENO	13	BELL	$e^+e^- \to \Upsilon(4S)$
$-0.68 \pm 0.10 \pm 0.03$	LEES	13D	BABR	$e^+e^- \to \Upsilon(4S)$
• • • We do not use the following data for averages, fits, limits, etc. • • •				
$-0.71 \pm 0.13 \pm 0.02$	AAIJ	13BO	LHCB	Repl. by AAIJ 18O
$-0.60 \pm 0.11 \pm 0.03$	AUBERT	07AF	BABR	Repl. by LEES 13D
$-0.61 \pm 0.10 \pm 0.04$	ISHINO	07	BELL	Repl. by DALSENO 13
$-0.67 \pm 0.16 \pm 0.06$	[2] ABE	05D	BELL	Repl. by ISHINO 07
$-0.30 \pm 0.17 \pm 0.03$	AUBERT,BE	05	BABR	Repl. by AUBERT 07AF
$-1.00 \pm 0.21 \pm 0.07$	[3] ABE	04E	BELL	Repl. by ABE 05D
$-1.23 \pm 0.41 \; ^{+0.08}_{-0.07}$	ABE	03G	BELL	Repl. by ABE 04E.
$-1.21 \; ^{+0.38}_{-0.27} \; ^{+0.16}_{-0.13}$	ABE	02M	BELL	Repl. by ABE 03G
$0.03 \; ^{+0.52}_{-0.56} \pm 0.11$	[4] AUBERT	02D	BABR	Repl. by AUBERT 02Q
$0.02 \pm 0.34 \pm 0.05$	[5] AUBERT	02Q	BABR	Repl. by AUBERT,BE 05

[1] An isospin analysis using other BELLE measurements, disfavors the region of $23.8^\circ < \phi_2 < 66.8^\circ$ at 68% CL.
[2] Rule out the CP-conserving case, $C_{\pi\pi} = S_{\pi\pi} = 0$, at the 5.4 sigma level.
[3] Rule out the CP-conserving case, $C_{\pi\pi} = S_{\pi\pi} = 0$, at the 5.2 sigma level.
[4] Corresponds to 90% confidence range $-0.89 < S_{\pi\pi} < 0.85$.
[5] Corresponds to 90% confidence range $-0.54 < S_{\pi\pi} < 0.58$.

$C_{\pi^0\pi^0}$($B^0 \to \pi^0\pi^0$)

VALUE	DOCUMENT ID		TECN	COMMENT
-0.33 ± 0.22 OUR AVERAGE				
$-0.14 \pm 0.36 \pm 0.10$	[1] JULIUS	17	BELL	$e^+e^- \to \Upsilon(4S)$
$-0.43 \pm 0.26 \pm 0.05$	LEES	13D	BABR	$e^+e^- \to \Upsilon(4S)$
• • • We do not use the following data for averages, fits, limits, etc. • • •				
$-0.49 \pm 0.35 \pm 0.05$	AUBERT	07BC	BABR	Repl. by LEES 13D
$-0.12 \pm 0.56 \pm 0.06$	[2] AUBERT	05L	BABR	Repl. by AUBERT 07BC
$-0.44 \; ^{+0.52}_{-0.53} \pm 0.17$	[1] CHAO	05	BELL	Repl. by JULIUS 17

[1] BELLE Collab. quotes $A_{\pi^0\pi^0}$ which is equal to $-C_{\pi^0\pi^0}$.
[2] Corresponds to a 90% CL interval of $-0.88 < A_{CP} < 0.64$.

$C_{\rho\pi}$ ($B^0 \to \rho^+\pi^-$)

VALUE	DOCUMENT ID		TECN	COMMENT
-0.03 ± 0.07 OUR AVERAGE Error includes scale factor of 1.2.				
$0.016 \pm 0.059 \pm 0.036$	[1] LEES	13J	BABR	$e^+e^- \to \Upsilon(4S)$
$-0.13 \pm 0.09 \pm 0.05$	[1] KUSAKA	07	BELL	$e^+e^- \to \Upsilon(4S)$
• • • We do not use the following data for averages, fits, limits, etc. • • •				
$0.15 \pm 0.09 \pm 0.05$	AUBERT	07AA	BABR	Repl. by LEES 13J
$0.25 \pm 0.17 \; ^{+0.02}_{-0.06}$	WANG	05	BELL	Repl. by KUSAKA 07
$0.36 \pm 0.18 \pm 0.04$	AUBERT	03T	BABR	Repl. by AUBERT 07AA

[1] Uses time-dependent Dalitz plot analysis of $B^0 \to \pi^+\pi^-\pi^0$ decays.

$S_{\rho\pi}$ ($B^0 \to \rho^+\pi^-$)

VALUE	DOCUMENT ID		TECN	COMMENT
0.05 ± 0.07 OUR AVERAGE				
$0.053 \pm 0.081 \pm 0.034$	[1] LEES	13J	BABR	$e^+e^- \to \Upsilon(4S)$
$0.06 \pm 0.13 \pm 0.05$	[1] KUSAKA	07	BELL	$e^+e^- \to \Upsilon(4S)$
• • • We do not use the following data for averages, fits, limits, etc. • • •				
$-0.03 \pm 0.11 \pm 0.04$	AUBERT	07AA	BABR	Repl. by LEES 13J
$-0.28 \pm 0.23 \; ^{+0.10}_{-0.08}$	WANG	05	BELL	Repl. by KUSAKA 07
$0.19 \pm 0.24 \pm 0.03$	AUBERT	03T	BABR	Repl. by AUBERT 07AA

[1] Uses time-dependent Dalitz plot analysis of $B^0 \to \pi^+\pi^-\pi^0$ decays.

$\Delta C_{\rho\pi}$ ($B^0 \to \rho^+\pi^-$)

$\Delta C_{\rho\pi}$ describes the asymmetry between the rates $\Gamma(B^0 \to \rho^+\pi^-) + \Gamma(\overline{B}^0 \to \rho^-\pi^+)$ and $\Gamma(B^0 \to \rho^-\pi^+) + \Gamma(\overline{B}^0 \to \rho^+\pi^-)$.

VALUE	DOCUMENT ID		TECN	COMMENT
0.27 ± 0.06 OUR AVERAGE				
$0.234 \pm 0.061 \pm 0.048$	[1] LEES	13J	BABR	$e^+e^- \to \Upsilon(4S)$
$0.36 \pm 0.10 \pm 0.05$	[1] KUSAKA	07	BELL	$e^+e^- \to \Upsilon(4S)$
• • • We do not use the following data for averages, fits, limits, etc. • • •				
$0.39 \pm 0.09 \pm 0.09$	AUBERT	07AA	BABR	Repl. by LEES 13J
$0.38 \pm 0.18 \; ^{+0.02}_{-0.04}$	WANG	05	BELL	Repl. by KUSAKA 07
$0.28 \; ^{+0.18}_{-0.19} \pm 0.04$	AUBERT	03T	BABR	Repl. by AUBERT 07AA

[1] Uses time-dependent Dalitz plot analysis of $B^0 \to \pi^+\pi^-\pi^0$ decays.

$\Delta S_{\rho\pi}$ ($B^0 \to \rho^+\pi^-$)

$\Delta S_{\rho\pi}$ is related to the strong phase difference between the amplitudes contributing to $B^0 \to \rho^+\pi^-$.

VALUE	DOCUMENT ID		TECN	COMMENT
0.01 ± 0.08 OUR AVERAGE				
$0.054 \pm 0.082 \pm 0.039$	[1] LEES	13J	BABR	$e^+e^- \to \Upsilon(4S)$
$-0.08 \pm 0.13 \pm 0.05$	[1] KUSAKA	07	BELL	$e^+e^- \to \Upsilon(4S)$
• • • We do not use the following data for averages, fits, limits, etc. • • •				
$-0.01 \pm 0.14 \pm 0.06$	AUBERT	07AA	BABR	Repl. by LEES 13J
$-0.30 \pm 0.24 \pm 0.09$	WANG	05	BELL	Repl. by KUSAKA 07
$0.15 \pm 0.25 \pm 0.03$	AUBERT	03T	BABR	Repl. by AUBERT 07AA

[1] Uses time-dependent Dalitz plot analysis of $B^0 \to \pi^+\pi^-\pi^0$ decays.

$C_{\rho^0\pi^0}$ ($B^0 \to \rho^0\pi^0$)

VALUE	DOCUMENT ID		TECN	COMMENT
0.27 ± 0.24 OUR AVERAGE				
$0.19 \pm 0.23 \pm 0.15$	[1] LEES	13J	BABR	$e^+e^- \to \Upsilon(4S)$
$0.49 \pm 0.36 \pm 0.28$	[1,2] KUSAKA	07	BELL	$e^+e^- \to \Upsilon(4S)$
• • • We do not use the following data for averages, fits, limits, etc. • • •				
$-0.10 \pm 0.40 \pm 0.53$	AUBERT	07AA	BABR	Repl. by LEES 13J
$0.53 \; ^{+0.67}_{-0.84} \; ^{+0.10}_{-0.15}$	[2] DRAGIC	06	BELL	Repl. by KUSAKA 07

[1] Uses time-dependent Dalitz plot analysis of $B^0 \to \pi^+\pi^-\pi^0$ decays.
[2] Quotes $A_{\rho^0\pi^0}$ which is equal to $-C_{\rho^0\pi^0}$.

$S_{\rho^0\pi^0}$ ($B^0 \to \rho^0\pi^0$)

VALUE	DOCUMENT ID		TECN	COMMENT
-0.23 ± 0.34 OUR AVERAGE				
$-0.37 \pm 0.34 \pm 0.20$	[1] LEES	13J	BABR	$e^+e^- \to \Upsilon(4S)$
$0.17 \pm 0.57 \pm 0.35$	[1] KUSAKA	07	BELL	$e^+e^- \to \Upsilon(4S)$
• • • We do not use the following data for averages, fits, limits, etc. • • •				
$0.04 \pm 0.44 \pm 0.18$	AUBERT	07AA	BABR	Repl. by LEES 13J

[1] Uses time-dependent Dalitz plot analysis of $B^0 \to \pi^+\pi^-\pi^0$ decays.

$C_{a_1\pi}$ ($B^0 \to a_1(1260)^+\pi^-$)

VALUE	DOCUMENT ID		TECN	COMMENT
-0.05 ± 0.11 OUR AVERAGE				
$-0.01 \pm 0.11 \pm 0.09$	DALSENO	12	BELL	$e^+e^- \to \Upsilon(4S)$
$-0.10 \pm 0.15 \pm 0.09$	AUBERT	07O	BABR	$e^+e^- \to \Upsilon(4S)$

$S_{a_1\pi}$ ($B^0 \to a_1(1260)^+\pi^-$)

VALUE	DOCUMENT ID		TECN	COMMENT
-0.2 ± 0.4 OUR AVERAGE Error includes scale factor of 3.2.				
$-0.51 \pm 0.14 \pm 0.08$	DALSENO	12	BELL	$e^+e^- \to \Upsilon(4S)$
$0.37 \pm 0.21 \pm 0.07$	AUBERT	07O	BABR	$e^+e^- \to \Upsilon(4S)$

$\Delta C_{a_1\pi}$ ($B^0 \to a_1(1260)^+\pi^-$)

$\Delta C_{a_1\pi}$ describes the asymmetry between the rates $\Gamma(B^0 \to a_1^+\pi^-) + \Gamma(\overline{B}^0 \to a_1^-\pi^+)$ and $\Gamma(B^0 \to a_1^-\pi^+) + \Gamma(\overline{B}^0 \to a_1^+\pi^-)$.

VALUE	DOCUMENT ID		TECN	COMMENT
0.43 ± 0.14 OUR AVERAGE Error includes scale factor of 1.3.				
$0.54 \pm 0.11 \pm 0.07$	DALSENO	12	BELL	$e^+e^- \to \Upsilon(4S)$
$0.26 \pm 0.15 \pm 0.07$	AUBERT	07O	BABR	$e^+e^- \to \Upsilon(4S)$

$\Delta S_{a_1\pi}$ ($B^0 \to a_1(1260)^+\pi^-$)

$\Delta S_{a_1\pi}$ is related to the strong phase difference between the amplitudes contributing to $B^0 \to a_1\pi$ decays.

VALUE	DOCUMENT ID		TECN	COMMENT
-0.11 ± 0.12 OUR AVERAGE				
$-0.09 \pm 0.14 \pm 0.06$	DALSENO	12	BELL	$e^+e^- \to \Upsilon(4S)$
$-0.14 \pm 0.21 \pm 0.06$	AUBERT	07O	BABR	$e^+e^- \to \Upsilon(4S)$

C ($B^0 \to b_1^- K^+$)

VALUE	DOCUMENT ID		TECN	COMMENT
$-0.22 \pm 0.23 \pm 0.05$	AUBERT	07BI	BABR	$e^+e^- \to \Upsilon(4S)$

ΔC ($B^0 \to b_1^-\pi^+$)

VALUE	DOCUMENT ID		TECN	COMMENT
$-1.04 \pm 0.23 \pm 0.08$	AUBERT	07BI	BABR	$e^+e^- \to \Upsilon(4S)$

$C_{\rho^0\rho^0}$ ($B^0 \to \rho^0\rho^0$)

VALUE	DOCUMENT ID		TECN	COMMENT
$0.2 \pm 0.8 \pm 0.3$	AUBERT	08BB	BABR	$e^+e^- \to \Upsilon(4S)$

Downloaded from https://academic.oup.com/ptep/article/2022/8/083C01/6651666 by KIT Library user on 27 September 2022

$S_{\rho^0\rho^0}$ ($B^0 \to \rho^0\rho^0$)

VALUE	DOCUMENT ID		TECN	COMMENT
0.3±0.7±0.2	AUBERT	08BB	BABR	$e^+e^- \to \Upsilon(4S)$

$C_{\rho\rho}$ ($B^0 \to \rho^+\rho^-$)

VALUE	DOCUMENT ID		TECN	COMMENT
0.00±0.09 OUR AVERAGE				
0.00±0.10±0.06	[1] VANHOEFER	16	BELL	$e^+e^- \to \Upsilon(4S)$
0.01±0.15±0.06	AUBERT	07BF	BABR	$e^+e^- \to \Upsilon(4S)$
• • • We do not use the following data for averages, fits, limits, etc. • • •				
−0.16±0.21±0.08	[1] SOMOV	07	BELL	Repl. by VANHOEFER 16
−0.00±0.30±0.09	[1] SOMOV	06	BELL	Repl. by SOMOV 07
−0.03±0.18±0.09	AUBERT,B	05C	BABR	Repl. by AUBERT 07BF
−0.17±0.27±0.14	AUBERT,B	04R	BABR	Repl. by AUBERT,B 05C

[1] BELLE Collab. quotes A_{CP} which is equal to $-C$.

$S_{\rho\rho}$ ($B^0 \to \rho^+\rho^-$)

VALUE	DOCUMENT ID		TECN	COMMENT
−0.14±0.13 OUR AVERAGE				
−0.13±0.15±0.05	VANHOEFER	16	BELL	$e^+e^- \to \Upsilon(4S)$
$-0.17\pm0.20^{+0.05}_{-0.06}$	AUBERT	07BF	BABR	$e^+e^- \to \Upsilon(4S)$
• • • We do not use the following data for averages, fits, limits, etc. • • •				
0.19±0.30±0.08	SOMOV	07	BELL	Repl. by VANHOEFER 16
0.08±0.41±0.09	SOMOV	06	BELL	Repl. by SOMOV 07
$-0.33\pm0.24^{+0.08}_{-0.14}$	AUBERT,B	05C	BABR	Repl. by AUBERT 07BF
−0.42±0.42±0.14	AUBERT,B	04R	BABR	Repl. by AUBERT,B 05C

$|\lambda|$ ($B^0 \to J/\psi K^*(892)^0$)

VALUE	CL%	DOCUMENT ID		TECN	COMMENT
<0.25	95	[1] AUBERT,B	04H	BABR	$e^+e^- \to \Upsilon(4S)$

[1] Uses the measured cosine coefficients C and $\overline{C}$ and assumes $|q/p| = 1$.

cos 2β ($B^0 \to J/\psi K^*(892)^0$)

β (ϕ_1) is one of the angles of CMK unitarity triangle, see the review on "*CP*" Violation in the Reviews section.

VALUE	DOCUMENT ID		TECN	COMMENT
$1.7\ ^{+0.7}_{-0.9}$ OUR AVERAGE Error includes scale factor of 1.6.				
$2.72^{+0.50}_{-0.79}\pm0.27$	[1] AUBERT	05P	BABR	$e^+e^- \to \Upsilon(4S)$
0.87±0.74±0.12	[2] ITOH	05	BELL	$e^+e^- \to \Upsilon(4S)$

[1] The measurement is obtained when sin 2β is fixed to 0.726 and the sign of cos 2β is positive with 86% confidence level.
[2] The measurement is obtained with sin 2β fixed to 0.731.

cos 2β ($B^0 \to [K^0_S\pi^+\pi^-]_{D^{(*)}}\ h^0$)

VALUE	DOCUMENT ID		TECN	COMMENT
0.91±0.22±0.11	[1] ADACHI	18		$e^+e^- \to \Upsilon(4S)$
• • • We do not use the following data for averages, fits, limits, etc. • • •				
$1.06\pm0.33^{+0.21}_{-0.15}$	[2] VOROBYEV	16	BELL	$e^+e^- \to \Upsilon(4S)$
0.42±0.49±0.16	[3] AUBERT	07BH	BABR	$e^+e^- \to \Upsilon(4S)$
$1.87^{+0.40}_{-0.53}{}^{+0.22}_{-0.32}$	[4] KROKOVNY	06	BELL	Repl. by VOROBYEV 16

[1] Analyzes joint data sample of Belle and BaBar using Dalitz plot analysis of $D \to K^0_S\pi^+\pi^-$; the second error combines experimental systematic uncertainty and the Dalitz plot model uncertainty.
[2] A model-independent measurement uses the binned Dalitz plot technique.
[3] AUBERT 07BH evaluates the likelihoods for the positive and negative solutions assuming $\sin(2\beta_{eff}) = 0.678$. It quotes $L_+ / (L_+ + L_-) = 0.86$ corresponding to a likelihood ratio of $L_+/L_- = 6.14$ in favor of the positive solution.
[4] KROKOVNY 06 evaluates the likelihoods for the positive and negative solutions assuming $\sin(2\beta_{eff}) = 0.689$. It quotes $L_+ / (L_+ + L_-) = 0.983$ corresponding to a likelihood ratio of $L_+/L_- = 57.8$ in favor of the positive solution.

$(S_+ + S_-)/2$ ($B^0 \to D^{*-}\pi^+$)

$S_\pm = -\frac{2Im(\lambda_\pm)}{1+|\lambda_\pm|^2}$ where λ_+ and λ_- are defined in the $C_{\pi\pi}$ datablock above for $B^0 \to D^{*-}\pi^+$ and $\overline{B}^0 \to D^{*+}\pi^-$.

VALUE	DOCUMENT ID		TECN	COMMENT
−0.039±0.011 OUR AVERAGE				
−0.046±0.013±0.015	[1] BAHINIPATI	11	BELL	$e^+e^- \to \Upsilon(4S)$
−0.040±0.023±0.010	[2] AUBERT	06Y	BABR	$e^+e^- \to \Upsilon(4S)$
−0.034±0.014±0.009	[1] AUBERT	05Z	BABR	$e^+e^- \to \Upsilon(4S)$
• • • We do not use the following data for averages, fits, limits, etc. • • •				
−0.039±0.020±0.013	[3] RONGA	06	BELL	Repl. by BAHINIPATI 11
−0.030±0.028±0.018	[1] GERSHON	05	BELL	Repl. by RONGA 06
−0.068±0.038±0.020	[2] AUBERT	04V	BABR	Repl. by AUBERT 06Y
−0.063±0.024±0.014	[1] AUBERT	04W	BABR	Repl. by AUBERT 05Z
0.060±0.040±0.019	[2] SARANGI	04	BELL	Repl. by RONGA 06

[1] Uses partially reconstructed $B^0 \to D^{*\pm}\pi^\mp$ decays.
[2] Uses fully reconstructed $B^0 \to D^{*\pm}\pi^\mp$ decays.
[3] Combines the results from fully reconstructed and partially reconstructed $D^*\pi$ events by taking weighted averages. Assumes that systematic errors from physics parameters and fit biases in the two measurements are 100% correlated.

$(S_- - S_+)/2$ ($B^0 \to D^{*-}\pi^+$)

VALUE	DOCUMENT ID		TECN	COMMENT
−0.009±0.015 OUR AVERAGE				
−0.015±0.013±0.015	[1] BAHINIPATI	11	BELL	$e^+e^- \to \Upsilon(4S)$
0.049±0.042±0.015	[2] AUBERT	06Y	BABR	$e^+e^- \to \Upsilon(4S)$
−0.019±0.022±0.013	[1] AUBERT	05Z	BABR	$e^+e^- \to \Upsilon(4S)$
• • • We do not use the following data for averages, fits, limits, etc. • • •				
−0.011±0.020±0.013	[3] RONGA	06	BELL	Repl. by BAHINIPATI 11
−0.005±0.028±0.018	[1] GERSHON	05	BELL	Repl. by RONGA 06
0.031±0.070±0.033	[2] AUBERT	04V	BABR	Repl. by AUBERT 06Y
−0.004±0.037±0.014	[1] AUBERT	04W	BABR	Repl. by AUBERT 05Z
0.049±0.040±0.019	[2] SARANGI	04	BELL	Repl. by RONGA 06

[1] Uses partially reconstructed $B^0 \to D^{*\pm}\pi^\mp$ decays.
[2] Uses fully reconstructed $B^0 \to D^{*\pm}\pi^\mp$ decays.
[3] Combines the results from fully reconstructed and partially reconstructed $D^*\pi$ events by taking weighted averages. Assumes that systematic errors from physics parameters and fit biases in the two measurements are 100% correlated.

$(S_+ + S_-)/2$ ($B^0 \to D^-\pi^+$)

VALUE	DOCUMENT ID		TECN	COMMENT
−0.046±0.023 OUR AVERAGE				
−0.010±0.023±0.07	[1] AUBERT	06Y	BABR	$e^+e^- \to \Upsilon(4S)$
−0.050±0.021±0.012	[2] RONGA	06	BELL	$e^+e^- \to \Upsilon(4S)$
• • • We do not use the following data for averages, fits, limits, etc. • • •				
−0.022±0.038±0.020	[1] AUBERT	04V	BABR	Repl. by AUBERT 06Y
−0.062±0.037±0.018	[1] SARANGI	04	BELL	Repl. by RONGA 06

[1] Uses fully reconstructed $B^0 \to D^\pm\pi^\mp$ decays.
[2] Combines the results from fully reconstructed and partially reconstructed $D\pi$ events by taking weighted averages. Assumes that systematic errors from physics parameters and fit biases in the two measurements are 100% correlated.

$(S_- - S_+)/2$ ($B^0 \to D^-\pi^+$)

VALUE	DOCUMENT ID		TECN	COMMENT
−0.022±0.021 OUR AVERAGE				
−0.033±0.042±0.012	[1] AUBERT	06Y	BABR	$e^+e^- \to \Upsilon(4S)$
−0.019±0.021±0.012	[2] RONGA	06	BELL	$e^+e^- \to \Upsilon(4S)$
• • • We do not use the following data for averages, fits, limits, etc. • • •				
0.025±0.068±0.033	[1] AUBERT	04V	BABR	Repl. by AUBERT 06Y
−0.025±0.037±0.018	[1] SARANGI	04	BELL	Repl. by RONGA 06

[1] Uses fully reconstructed $B^0 \to D^\pm\pi^\mp$ decays.
[2] Combines the results from fully reconstructed and partially reconstructed $D\pi$ events by taking weighted averages. Assumes that systematic errors from physics parameters and fit biases in the two measurements are 100% correlated.

S_+ ($B^0 \to D^-\pi^+$)

VALUE	DOCUMENT ID		TECN	COMMENT
0.058±0.020±0.011	[1] AAIJ	18Z	LHCB	pp at 7, 8 TeV

[1] Measured in the simultaneous analysis of $B^0 \to D^\mp\pi^\pm$ decays. AAIJ 18Z reports a statistical (systematic) correlation of 0.6 (−0.41) with the measured value of $S_-(B^0 \to D^+\pi^-)$.

S_- ($B^0 \to D^+\pi^-$)

VALUE	DOCUMENT ID		TECN	COMMENT
0.038±0.020±0.007	[1] AAIJ	18Z	LHCB	pp at 7, 8 TeV

[1] Measured in the simultaneous analysis of $B^0 \to D^\mp\pi^\pm$ decays. AAIJ 18Z reports a statistical (systematic) correlation of 0.6 (−0.41) with the measured value of $S_+(B^0 \to D^-\pi^+)$.

$(S_+ + S_-)/2$ ($B^0 \to D^-\rho^+$)

VALUE	DOCUMENT ID		TECN	COMMENT
−0.024±0.031±0.009	[1] AUBERT	06Y	BABR	$e^+e^- \to \Upsilon(4S)$

[1] Uses fully reconstructed $B^0 \to D^-\rho^+$ decays.

$(S_- - S_+)/2$ ($B^0 \to D^-\rho^+$)

VALUE	DOCUMENT ID		TECN	COMMENT
−0.098±0.055±0.018	[1] AUBERT	06Y	BABR	$e^+e^- \to \Upsilon(4S)$

[1] Uses fully reconstructed $B^0 \to D^-\rho^+$ decays.

$C_{\eta_c K^0_S}$ ($B^0 \to \eta_c K^0_S$)

VALUE	DOCUMENT ID		TECN	COMMENT
0.080±0.124±0.029	AUBERT	09K	BABR	$e^+e^- \to \Upsilon(4S)$

$S_{\eta_c K^0_S}$ ($B^0 \to \eta_c K^0_S$)

VALUE	DOCUMENT ID		TECN	COMMENT
0.925±0.160±0.057	AUBERT	09K	BABR	$e^+e^- \to \Upsilon(4S)$

Downloaded from https://academic.oup.com/ptep/article/2022/8/083C01/6651666 by KIT Library user on 27 September 2022

$C_{c\overline{c}K^{(*)0}}$ ($B^0 \to c\overline{c}K^{(*)0}$)

"OUR EVALUATION" is an average using rescaled values of the data listed below. The average and rescaling were performed by the Heavy Flavor Averaging Group (HFLAV) and are described at https://hflav.web.cern.ch/. The averaging/rescaling procedure takes into account correlations between the measurements.

VALUE (units 10^{-2})	DOCUMENT ID		TECN	COMMENT
− 0.5± 1.5 OUR EVALUATION				
0.0± 1.4 OUR AVERAGE				
− 1.7± 2.9	[1,2] AAIJ	17BN	LHCB	pp at 7, 8 TeV
− 0.6± 1.6±1.2	[3] ADACHI	12A	BELL	$e^+e^- \to \Upsilon(4S)$
−29 $^{+53}_{-44}$ ±6	[4] AUBERT	09AU	BABR	$e^+e^- \to \Upsilon(4S)$
2.4± 2.0±1.6	[5] AUBERT	09K	BABR	$e^+e^- \to \Upsilon(4S)$
• • • We do not use the following data for averages, fits, limits, etc. • • •				
− 4 ± 7 ±5	[6] SAHOO	08	BELL	Repl. by ADACHI 12A
4.9± 2.3±1.8	[5] AUBERT	07AY	BABR	Repl. by AUBERT 09K
− 1.8± 2.1±1.4	[7] CHEN	07	BELL	Repl. by ADACHI 12A
− 0.7± 4.1±3.3	[8] ABE	05B	BELL	Repl. by CHEN 07
5.1± 3.2±1.4	[9] AUBERT	05F	BABR	Repl. by AUBERT 07AY
5.1± 5.1±2.6	[10] ABE	02Z	BELL	Repl. by ABE 05B
5.3± 5.4±3.2	[11] AUBERT	02P	BABR	Repl. by AUBERT 05F

[1] Measurement based on $B^0 \to J/\psi K^0_S$, $B^0 \to \psi(2S) K^0_S$ with $J/\psi \to \mu^+\mu^-$, $J/\psi \to e^+e^-$ and $\psi(2S) \to \mu^+\mu^-$.
[2] AAIJ 17BN provides the correlation coefficient ρ=0.42 between the uncertainties of $S_{B^0 \to c\overline{c}K^{(*)0}}(B^0 \to c\overline{c}K^{(*)0})$ and $C_{c\overline{c}K^{(*)0}}(B^0 \to c\overline{c}K^{(*)0})$ measurements.
[3] Measurement based on $B^0 \to J/\psi K^0_S$, $B^0 \to \psi(2S) K^0_S$, $B^0 \to J/\psi K^0_L$, and $B^0 \to \chi_{c1}(1P) K^0_S$ decays.
[4] Uses Dalitz plot analysis of $B^0 \to K^0\pi^+\pi^-$ decays and the first of two equivalent solutions is used.
[5] Measurement based on $B^0 \to c\overline{c}K^{(*)0}$ decays.
[6] Reports value of A of $B^0 \to \psi(2S) K^0$ which is equal to $-C$.
[7] Reports value of A of $B^0 \to J/\psi K^0$ which is equal to $-C$.
[8] Measurement based on 152×10^6 $B\overline{B}$ pairs.
[9] Measurement based on 227×10^6 $B\overline{B}$ pairs.
[10] Measured with both $\eta_f = \pm 1$ samples.
[11] Measured with the high purity of $\eta_f = -1$ samples.

sin(2β)

For a discussion of CP violation, see the review on "CP Violation" in the Reviews section. sin(2β) is a measure of the CP-violating amplitude in the $B^0_d \to J/\psi(1S) K^0_S$.

"OUR EVALUATION" is an average using rescaled values of the data listed below. The average and rescaling were performed by the Heavy Flavor Averaging Group (HFLAV) and are described at https://hflav.web.cern.ch/. The averaging/rescaling procedure takes into account correlations between the measurements.

VALUE	DOCUMENT ID		TECN	COMMENT
0.699±0.017 OUR EVALUATION				
0.698±0.027 OUR AVERAGE	Error includes scale factor of 1.6. See the ideogram below.			
0.760±0.034	[1,2] AAIJ	17BN	LHCB	pp at 7, 8 TeV
0.667±0.023±0.012	[3] ADACHI	12A	BELL	$e^+e^- \to \Upsilon(4S)$
0.57 ±0.58 ±0.06	[4] SATO	12	BELL	$e^+e^- \to \Upsilon(5S)$
0.69 ±0.52 ±0.08	[5] AUBERT	09AU	BABR	$e^+e^- \to \Upsilon(4S)$
0.687±0.028±0.012	[6] AUBERT	09K	BABR	$e^+e^- \to \Upsilon(4S)$
1.56 ±0.42 ±0.21	[7] AUBERT	04R	BABR	$e^+e^- \to \Upsilon(4S)$
0.79 $^{+0.41}_{-0.44}$	[8] AFFOLDER	00C	CDF	$p\overline{p}$ at 1.8 TeV
0.84 $^{+0.82}_{-1.04}$ ±0.16	[9] BARATE	00Q	ALEP	$e^+e^- \to Z$
3.2 $^{+1.8}_{-2.0}$ ±0.5	[10] ACKERSTAFF	98Z	OPAL	$e^+e^- \to Z$
• • • We do not use the following data for averages, fits, limits, etc. • • •				
0.72 ±0.09 ±0.03	[11] SAHOO	08	BELL	Repl. by ADACHI 12A
0.714±0.032±0.018	[6] AUBERT	07AY	BABR	Repl. by AUBERT 09K
0.642±0.031±0.017	CHEN	07	BELL	Repl. by ADACHI 12A
0.728±0.056±0.023	[12] ABE	05B	BELL	Repl. by CHEN 07
0.722±0.040±0.023	[13] AUBERT	05F	BABR	Repl. by AUBERT 07AY
0.99 ±0.14 ±0.06	[14] ABE	02U	BELL	$e^+e^- \to \Upsilon(4S)$
0.719±0.074±0.035	[15] ABE	02Z	BELL	Repl. by ABE 05B
0.59 ±0.14 ±0.05	[16] AUBERT	02N	BABR	$e^+e^- \to \Upsilon(4S)$
0.741±0.067±0.034	[17] AUBERT	02P	BABR	Repl. by AUBERT 05F
0.58 $^{+0.32}_{-0.34}$ $^{+0.09}_{-0.10}$	ABASHIAN	01	BELL	Repl. by ABE 01G
0.99 ±0.14 ±0.06	[18] ABE	01G	BELL	Repl. by ABE 02Z
0.34 ±0.20 ±0.05	AUBERT	01	BABR	Repl. by AUBERT 01B
0.59 ±0.14 ±0.05	[18] AUBERT	01B	BABR	Repl. by AUBERT 02P
1.8 ±1.1 ±0.3	[19] ABE	98U	CDF	Repl. by AFFOLDER 00C

[1] Measurement based on $B^0 \to J/\psi K^0_S$, $B^0 \to \psi(2S) K^0_S$ with $J/\psi \to \mu^+\mu^-$, $J/\psi \to e^+e^-$ and $\psi(2S) \to \mu^+\mu^-$.
[2] AAIJ 17BN provides the correlation coefficient $\rho = 0.42$ between the uncertainties of sin(2β) and cos(2β) measurements.
[3] Measurement based on $B^0 \to J/\psi K^0_S$, $B^0 \to \psi(2S) K^0_S$, $B^0 \to J/\psi K^0_L$, and $B^0 \to \chi_{c1}(1P) K^0_S$ decays.
[4] SATO 12 uses 121 fb^{-1} data collected on $\Upsilon(5S)$ resonance. Uses the "$B-\pi$ tagging" where $B\pi^+$ and $B\pi^-$ tagged $J/\psi K^0_S$ events are compared.
[5] Uses Dalitz plot analysis of $B^0 \to K^0\pi^+\pi^-$ decays and the first of two equivalent solutions.
[6] Measurement based on $B^0 \to c\overline{c}K^{(*)0}$ decays.
[7] Measurement in which the J/ψ decays to hadrons or to muons that do not satisfy the standard identification criteria.
[8] AFFOLDER 00C uses about 400 $B^0 \to J/\psi(1S) K^0_S$ events. The production flavor of B^0 was determined using three tagging algorithms: a same-side tag, a jet-charge tag, and a soft-lepton tag.
[9] BARATE 00Q uses 23 candidates for $B^0 \to J/\psi(1S) K^0_S$ decays. A combination of jet-charge, vertex-charge, and same-side tagging techniques were used to determine the B^0 production flavor.
[10] ACKERSTAFF 98Z uses 24 candidates for $B^0_d \to J/\psi(1S) K^0_S$ decay. A combination of jet-charge and vertex-charge techniques were used to tag the B^0_d production flavor.
[11] Based on $B^0 \to \psi(2S) K^0_S$ decays.
[12] Measurement based on 152×10^6 $B\overline{B}$ pairs.
[13] Measurement based on 227×10^6 $B\overline{B}$ pairs.
[14] ABE 02U result is based on the same analysis and data sample reported in ABE 01G.
[15] ABE 02Z result is based on 85×10^6 $B\overline{B}$ pairs.
[16] AUBERT 02N result based on the same analysis and data sample reported in AUBERT 01B.
[17] AUBERT 02P result is based on 88×10^6 $B\overline{B}$ pairs.
[18] First observation of CP violation in B^0 meson system.
[19] ABE 98U uses 198 ± 17 $B^0_d \to J/\psi(1S) K^0$ events. The production flavor of B^0 was determined using the same side tagging technique.

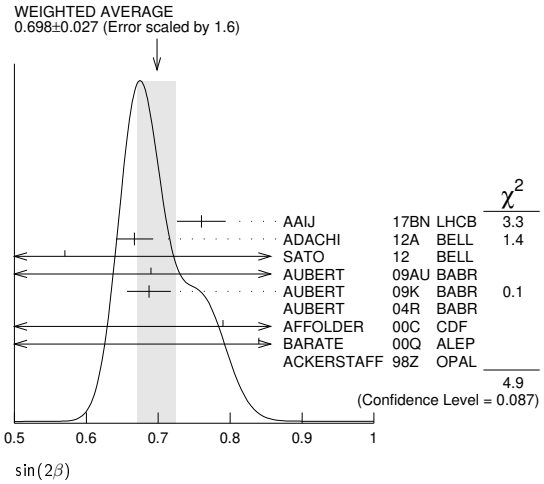

$C_{J/\psi(nS)K^0}$ ($B^0 \to J/\psi(nS)K^0$)

"OUR EVALUATION" is an average using rescaled values of the data listed below. The average and rescaling were performed by the Heavy Flavor Averaging Group (HFLAV) and are described at https://hflav.web.cern.ch/. The averaging/rescaling procedure takes into account correlations between the measurements.

VALUE (units 10^{-2})	DOCUMENT ID		TECN	COMMENT
− 0.8± 1.7 OUR EVALUATION				
− 0.5± 1.6 OUR AVERAGE				
− 1.7± 2.9	[1,2] AAIJ	17BN	LHCB	pp at 7, 8 TeV
1.5± 2.1$^{+2.3}_{-4.5}$	[3,4] ADACHI	12A	BELL	$e^+e^- \to \Upsilon(4S)$
−10.4± 5.5$^{+2.7}_{-4.7}$	[4,5] ADACHI	12A	BELL	$e^+e^- \to \Upsilon(4S)$
− 1.9± 2.6$^{+4.1}_{-1.7}$	[4,6] ADACHI	12A	BELL	$e^+e^- \to \Upsilon(4S)$
8.9± 7.6±2.0	[5] AUBERT	09K	BABR	$e^+e^- \to \Upsilon(4S)$
1.6± 2.3±1.8	AUBERT	09K	BABR	$e^+e^- \to \Upsilon(4S)$
• • • We do not use the following data for averages, fits, limits, etc. • • •				
− 1.4± 3.0	[7] AAIJ	17BN	LHCB	pp at 7, 8 TeV
− 5 ±10 ±1	[8] AAIJ	17BN	LHCB	pp at 7, 8 TeV
− 3.8± 3.2±0.5	[9] AAIJ	15N	LHCB	Repl. by AAIJ 17BN
3 ± 9 ±1	[10] AAIJ	13K	LHCB	Repl. by AAIJ 15N
− 4 ± 7 ±5	[4,5] SAHOO	08	BELL	Repl. by ADACHI 12A
− 1.8± 2.1±1.4	[4] CHEN	07	BELL	Repl. by ADACHI 12A

[1] Measurement based on $B^0 \to J/\psi K^0_S$, $B^0 \to \psi(2S) K^0_S$ with $J/\psi \to \mu^+\mu^-$, $J/\psi \to e^+e^-$ and $\psi(2S) \to \mu^+\mu^-$.
[2] AAIJ 17BN provides the correlation coefficient $\rho = 0.42$ between the uncertainties of $S_{J/\psi(nS)K^0}(B^0 \to J/\psi(nS)K^0)$ and $C_{J/\psi(nS)K^0}(B^0 \to J/\psi(nS)K^0)$ measurements.
[3] Uses $B^0 \to J/\psi K^0_S$ decays.
[4] The paper reports A, which is equal to $-C$.
[5] Uses $B^0 \to \psi(2S) K^0_S$ decays.
[6] Uses $B^0 \to J/\psi K^0_L$ decays.
[7] Measurement based on $B^0 \to J/\psi K^0_S$ with $J/\psi \to \mu^+\mu^-$ and $J/\psi \to e^+e^-$.
[8] Measurement based on $B^0 \to \psi(2S) K^0_S$ with $\psi(2S) \to \mu^+\mu^-$.
[9] AAIJ 15N uses 41,560 flavor-tagged $B_d \to J/\psi K^0_S$ events from 3 fb^{-1} of integrated luminosity. Provides the correlation coefficient $\rho = 0.483$ between the statistical uncertainties of and measurements.
[10] AAIJ 13K uses 8200 flavor-tagged $B_d \to J/\psi K^0_S$ events from 1 fb^{-1} of integrated luminosity. Provides the correlation coefficient $\rho = 0.42$ between the statistical uncertainties of $S_{J/\psi(nS)K^0}(B^0 \to J/\psi(nS)K^0)$ and $C_{J/\psi(nS)K^0}(B^0 \to J/\psi(nS)K^0)$ measurements.

Downloaded from https://academic.oup.com/ptep/article/2022/8/083C01/6651666 by KIT Library user on 27 September 2022

$S_{J/\psi(nS)K^0}$ ($B^0 \to J/\psi(nS)K^0$)

"OUR EVALUATION" is an average using rescaled values of the data listed below. The average and rescaling were performed by the Heavy Flavor Averaging Group (HFLAV) and are described at https://hflav.web.cern.ch/. The averaging/rescaling procedure takes into account correlations between the measurements.

VALUE	DOCUMENT ID		TECN	COMMENT
0.701±0.017 OUR EVALUATION				
0.698±0.024 OUR AVERAGE	Error includes scale factor of 1.4. See the ideogram below.			
0.760±0.034	[1,2] AAIJ	17BN	LHCB	pp at 7, 8 TeV
0.670±0.029±0.013	[3] ADACHI	12A	BELL	$e^+e^- \to \Upsilon(4S)$
0.738±0.079±0.036	[4] ADACHI	12A	BELL	$e^+e^- \to \Upsilon(4S)$
0.642±0.047±0.021	[5] ADACHI	12A	BELL	$e^+e^- \to \Upsilon(4S)$
0.57 ±0.58 ±0.06	[6] SATO	12	BELL	$e^+e^- \to \Upsilon(5S)$
0.897±0.100±0.036	[4] AUBERT	09K	BABR	$e^+e^- \to \Upsilon(4S)$
0.666±0.031±0.013	AUBERT	09K	BABR	$e^+e^- \to \Upsilon(4S)$
$0.79\ ^{+0.41}_{-0.44}$	[7] AFFOLDER	00C	CDF	$p\overline{p}$ at 1.8 TeV
$0.84\ ^{+0.82}_{-1.04}$ ±0.16	[8] BARATE	00Q	ALEP	$e^+e^- \to Z$
$3.2\ ^{+1.8}_{-2.0}$ ±0.5	[9] ACKERSTAFF	98Z	OPAL	$e^+e^- \to Z$
• • • We do not use the following data for averages, fits, limits, etc. • • •				
0.75 ±0.04	[10] AAIJ	17BN	LHCB	pp at 7, 8 TeV
0.84 ±0.10 ±0.01	[11] AAIJ	17BN	LHCB	pp at 7, 8 TeV
0.731±0.035±0.020	[12] AAIJ	15N	LHCB	Repl. by AAIJ 17BN
0.73 ±0.07 ±0.04	[13] AAIJ	13K	LHCB	Repl. by AAIJ 15N
0.650±0.029±0.018	[14] SAHOO	08	BELL	Repl. by ADACHI 12A
0.72 ±0.09 ±0.03	[4] SAHOO	08	BELL	Repl. by ADACHI 12A
0.642±0.031±0.017	CHEN	07	BELL	Repl. by ADACHI 12A

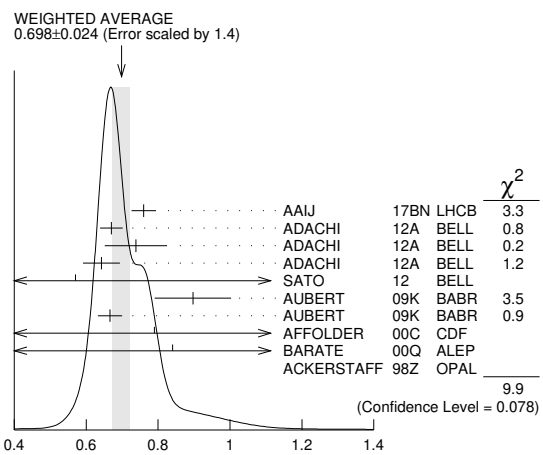

$S_{J/\psi(nS)K^0}$ ($B^0 \to J/\psi(nS)K^0$)

[1] Measurement based on $B^0 \to J/\psi K^0_S$, $B^0 \to \psi(2S)K^0_S$ with $J/\psi \to \mu^+\mu^-$, $J/\psi \to e^+e^-$ and $\psi(2S) \to \mu^+\mu^-$.

[2] AAIJ 17BN provides the correlation coefficient $\rho = 0.42$ between the uncertainties of $S_{J/\psi(nS)K^0}$ ($B^0 \to J/\psi(nS)K^0$) and $C_{J/\psi(nS)K^0}$ ($B^0 \to J/\psi(nS)K^0$) measurements.

[3] Uses $B^0 \to J/\psi K^0_S$ decays.

[4] Based on $B^0 \to \psi(2S)K^0_S$ decays.

[5] Uses $B^0 \to J/\psi K^0_L$ decays.

[6] SATO 12 uses 121 fb^{-1} data collected at $\Upsilon(5S)$ resonance. Uses the "$B-\pi$ tagging" where $B\pi^+$ and $B\pi^-$ tagged $J/\psi K^0_S$ events are compared.

[7] AFFOLDER 00C uses about 400 $B^0 \to J/\psi(1S)K^0_S$ events. The production flavor of B^0 was determined using three tagging algorithms: a same-side tag, a jet-charge tag, and a soft-lepton tag.

[8] BARATE 00Q uses 23 candidates for $B^0 \to J/\psi(1S)K^0_S$ decays. A combination of jet-charge, vertex-charge, and same-side tagging techniques were used to determine the B^0 production flavor.

[9] ACKERSTAFF 98Z uses 24 candidates for $B^0_d \to J/\psi(1S)K^0_S$ decay. A combination of jet-charge and vertex-charge techniques were used to tag the B^0_d production flavor.

[10] Measurement based on $B^0 \to J/\psi K^0_S$ with $J/\psi \to \mu^+\mu^-$ and $J/\psi \to e^+e^-$.

[11] Measurement based on $B^0 \to \psi(2S)K^0_S$ with $\psi(2S) \to \mu^+\mu^-$.

[12] AAIJ 15N uses 41,560 flavor-tagged $B_d \to J/\psi K^0_S$ events from 3 fb^{-1} of integrated luminosity. Provides the correlation coefficient $\rho = 0.483$ between the statistical uncertainties of and measurements.

[13] AAIJ 13K uses 8200 flavor-tagged $B_d \to J/\psi K^0_S$ events from 1 fb^{-1} of integrated luminosity. Provides the correlation coefficient $\rho = 0.42$ between the statistical uncertainties of $S_{J/\psi(nS)K^0}$ ($B^0 \to J/\psi(nS)K^0$) and $C_{J/\psi(nS)K^0}$ ($B^0 \to J/\psi(nS)K^0$) measurements.

[14] Combined result of CHEN 07 and SAHOO 08.

$C_{J/\psi K^{*0}}$ ($B^0 \to J/\psi K^{*0}$)

VALUE	DOCUMENT ID		TECN	COMMENT
0.025±0.083±0.054	[1] AUBERT	09K	BABR	$e^+e^- \to \Upsilon(4S)$

[1] Based on $B^0 \to J/\psi K^{*0}$, $K^{*0} \to K^0_S\pi^0$.

$S_{J/\psi K^{*0}}$ ($B^0 \to J/\psi K^{*0}$)

VALUE	DOCUMENT ID		TECN	COMMENT
0.601±0.239±0.087	[1,2] AUBERT	09K	BABR	$e^+e^- \to \Upsilon(4S)$

[1] Based on $B^0 \to J/\psi K^{*0}$, $K^{*0} \to K^0_S\pi^0$.

[2] This $S_{J/\psi K^{*0}}$ value has been corrected for the dilution of the sin(ΔM Δt) coefficient of the CP asymmetry by a factor of $1-R_\perp$, which arises from the mixture of CP-even and CP-odd B decay amplitudes.

$C_{\chi_{c0}K^0_S}$ ($B^0 \to \chi_{c0}K^0_S$)

VALUE	DOCUMENT ID		TECN	COMMENT
$\mathbf{-0.29^{+0.53}_{-0.44}\pm0.06}$	[1] AUBERT	09AU	BABR	$e^+e^- \to \Upsilon(4S)$

[1] Uses Dalitz plot analysis of $B^0 \to K^0\pi^+\pi^-$ decays and the first of two equivalent solutions is used.

$S_{\chi_{c0}K^0_S}$ ($B^0 \to \chi_{c0}K^0_S$)

VALUE	DOCUMENT ID		TECN	COMMENT
−0.69±0.52±0.08	[1] AUBERT	09AU	BABR	$e^+e^- \to \Upsilon(4S)$

[1] Uses Dalitz plot analysis of $B^0 \to K^0\pi^+\pi^-$ decays and the first of two equivalent solutions is used.

$C_{\chi_{c1}K^0_S}$ ($B^0 \to \chi_{c1}K^0_S$)

VALUE	DOCUMENT ID		TECN	COMMENT
0.06 ±0.07 OUR AVERAGE				
$0.017\pm0.083^{+0.026}_{-0.046}$	ADACHI	12A	BELL	$e^+e^- \to \Upsilon(4S)$
0.129±0.109±0.025	AUBERT	09K	BABR	$e^+e^- \to \Upsilon(4S)$

$S_{\chi_{c1}K^0_S}$ ($B^0 \to \chi_{c1}K^0_S$)

VALUE	DOCUMENT ID		TECN	COMMENT
0.63 ±0.10 OUR AVERAGE				
0.640±0.117±0.040	ADACHI	12A	BELL	$e^+e^- \to \Upsilon(4S)$
0.614±0.160±0.040	AUBERT	09K	BABR	$e^+e^- \to \Upsilon(4S)$

$\sin(2\beta_{\rm eff})(B^0 \to \phi K^0)$

VALUE	DOCUMENT ID		TECN	COMMENT
0.22±0.27±0.12	AUBERT	07AX	BABR	$e^+e^- \to \Upsilon(4S)$
• • • We do not use the following data for averages, fits, limits, etc. • • •				
$0.50\pm0.25\ ^{+0.07}_{-0.04}$	[1] AUBERT	05T	BABR	Repl. by AUBERT 07AX

[1] Obtained by constraining $C = 0$.

$\sin(2\beta_{\rm eff})(B^0 \to \phi K^*_0(1430)^0)$

VALUE	DOCUMENT ID		TECN	COMMENT
$\mathbf{0.97^{+0.03}_{-0.52}}$	[1] AUBERT	08BG	BABR	$e^+e^- \to \Upsilon(4S)$

[1] Measured using the CP-violation phase difference $\Delta\phi_{00}$ between the B and $\overline{B}$ decay amplitude.

$\sin(2\beta_{\rm eff})(B^0 \to K^+K^-K^0_S)$

VALUE	DOCUMENT ID		TECN	COMMENT
$\mathbf{0.77\pm0.11^{+0.07}_{-0.04}}$	AUBERT	07AX	BABR	$e^+e^- \to \Upsilon(4S)$
• • • We do not use the following data for averages, fits, limits, etc. • • •				
0.55±0.22±0.12	[1] AUBERT	05T	BABR	Repl. by AUBERT 07AX

[1] Obtained by constraining $C = 0$.

$\sin(2\beta_{\rm eff})(B^0 \to [K^0_S\pi^+\pi^-]_{D(*)}\, h^0)$

VALUE	DOCUMENT ID		TECN	COMMENT
0.80±0.14±0.07	[1] ADACHI	18		$e^+e^- \to \Upsilon(4S)$
• • • We do not use the following data for averages, fits, limits, etc. • • •				
0.43±0.27±0.08	[2] VOROBYEV	16	BELL	$e^+e^- \to \Upsilon(4S)$
0.29±0.34±0.06	AUBERT	07BH	BABR	$e^+e^- \to \Upsilon(4S)$
0.78±0.44±0.22	KROKOVNY	06	BELL	Repl. by VOROBYEV 16

[1] Analyzes joint data sample of Belle and BaBar using Dalitz plot analysis of $D \to K^0_S\pi^+\pi^-$; the second error combines experimental systematic uncertainty and the Dalitz plot model uncertainty.

[2] A model-independent measurement uses the binned Dalitz plot technique.

$\beta_{\rm eff}(B^0 \to [K^0_S\pi^+\pi^-]_{D(*)}\, h^0)$

VALUE (°)	DOCUMENT ID		TECN	COMMENT
22.5±4.4±1.3	[1] ADACHI	18		$e^+e^- \to \Upsilon(4S)$
• • • We do not use the following data for averages, fits, limits, etc. • • •				
11.7±7.8±2.1	[2] VOROBYEV	16	BELL	$e^+e^- \to \Upsilon(4S)$

[1] Analyzes joint data sample of Belle and BaBar using Dalitz plot analysis of $D \to K^0_S\pi^+\pi^-$; the second error combines experimental systematic uncertainty and the Dalitz plot model uncertainty.

[2] A model-independent measurement uses the binned Dalitz plot technique.

$2\beta_{\rm eff}(B^0 \to J/\psi\rho^0)$

VALUE (°)	DOCUMENT ID		TECN	COMMENT
$\mathbf{41.7\pm9.6^{+2.8}_{-6.3}}$	AAIJ	15J	LHCB	pp at 7, 8 TeV

Downloaded from https://academic.oup.com/ptep/article/2022/8/083C01/6651666 by KIT Library user on 27 September 2022

$|\lambda|$ ($B^0 \to [K^0_S \pi^+\pi^-]_{D^{(*)}} h^0$)

VALUE	DOCUMENT ID		TECN	COMMENT
1.01±0.08±0.02	AUBERT	07BH	BABR	$e^+e^- \to \Upsilon(4S)$

$|\sin(2\beta+\gamma)|$

β (ϕ_1) and γ (ϕ_3) are angles of CKM unitarity triangle, see the review on "*CP* Violation" in the Reviews section.

VALUE	CL%	DOCUMENT ID		TECN	COMMENT
>0.40	90	[1] AUBERT	06Y	BABR	$e^+e^- \to \Upsilon(4S)$
• • • We do not use the following data for averages, fits, limits, etc. • • •					
>0.77	68	[2] AAIJ	18Z	LHCB	pp at 7, 8 TeV
>0.13	95	[3] RONGA	06	BELL	$e^+e^- \to \Upsilon(4S)$
>0.07	95	[3] RONGA	06	BELL	$e^+e^- \to \Upsilon(4S)$
>0.35	90	[4] AUBERT	05Z	BABR	$e^+e^- \to \Upsilon(4S)$
>0.69	68	[5] AUBERT	04V	BABR	$e^+e^- \to \Upsilon(4S)$
>0.58	95	[6] AUBERT	04W	BABR	Repl. by AUBERT 05Z

[1] Uses fully reconstructed $B^0 \to D^{(*)\pm}\pi^\mp$ and $D^\pm\rho^\mp$ decays and some theoretical assumptions.
[2] Uses a time dependent CP violation measurement in $B^0 \to D^\mp\pi^\pm$ decays with external input and some theoretical assumptions.
[3] Combines the results from fully reconstructed and partially reconstructed $D^{(*)}\pi$ events by taking weighted averages. Assumes that systematic errors from physics parameters and fit biases in the two measurements are 100% correlated.
[4] Uses partially reconstructed $B^0 \to D^{*\pm}\pi^\mp$ decays and some theoretical assumptions.
[5] Uses fully reconstructed $B^0 \to D^{(*)\pm}\pi^\mp$ decays and some theoretical assumptions, such as the SU(3) symmetry relation.
[6] Combining this measurement with the results from AUBERT 04V for fully reconstructed $B^0 \to D^{(*)\pm}\pi^\mp$ and some theoretical assumptions, such as the SU(3) symmetry relation.

$2\beta+\gamma$

VALUE (°)	DOCUMENT ID		TECN	COMMENT
83±53±20	[1] AUBERT	08AC	BABR	$e^+e^- \to \Upsilon(4S)$

[1] Used a time-dependent Dalitz-plot analysis of $B^0 \to D^\mp K^0\pi^\pm$ assuming the ratio of the $b \to u$ and $b \to c$ decay amplitudes to be 0.3.

α

For angle $\alpha(\phi_2)$ of the CKM unitarity triangle, see the review on "*CP* violation" in the reviews section.

"OUR EVALUATION" is provided by the Heavy Flavor Averaging Group (HFLAV).

VALUE (°)	DOCUMENT ID		TECN	COMMENT
$85.2^{+4.8}_{-4.3}$ OUR EVALUATION				
• • • We do not use the following data for averages, fits, limits, etc. • • •				
93.7±10.6	[1] VANHOEFER	16	BELL	$e^+e^- \to \Upsilon(4S)$
84.9±13.5	[1] VANHOEFER	14	BELL	Repl. by VANHOEFER 16
79 ± 7 ±11	[2] AUBERT	10D	BABR	$e^+e^- \to \Upsilon(4S)$
$92.4^{+6.0}_{-6.5}$	[1] AUBERT	09G	BABR	$e^+e^- \to \Upsilon(4S)$
78.6± 7.3	[3] AUBERT	07O	BABR	$e^+e^- \to \Upsilon(4S)$
88 ±17	[4] SOMOV	06	BELL	Repl. by VANHOEFER 14
100 ±13	[5] AUBERT,B	05C	BABR	Repl. by AUBERT 09G
102^{+16}_{-12} ±14	[6] AUBERT,B	04R	BABR	Repl. by AUBERT,B 05C

[1] Based on an isospin analysis of the $B \to \rho\rho$ system.
[2] Obtained using the time dependent analysis of $B^0 \to a_1(1260)^\pm\pi^\mp$ and branching fraction measurements of $B \to a_1(1260)K$ and $B \to K_1\pi$. Uses SU(3) flavor relations.
[3] The angle $\alpha_{\rm eff}$ is obtained using the measured *CP* parameters of $B^0 \to a_1(1260)^\pm\pi^\mp$ and choosing one of the four solutions that is compatible with the result of SM-based fits.
[4] Obtained using isospin relation and selecting a solution closest to the CKM best fit average; the 90% CL allowed interval is $59^\circ < \phi_2\ (\equiv\alpha) < 115^\circ$.
[5] Obtained using isospin relation and selecting a solution closest to the CKM best fit average; 90% CL allowed interval is $79^\circ < \alpha < 123^\circ$.
[6] Obtained from the measured *CP* parameters of the longitudinal polarization by selecting the solution closest to the CKM best fit central value of $\alpha = 95^\circ - 98^\circ$.

CP VIOLATION PARAMETERS IN $B^0 \to D^0K^{*0}$ DECAY

The parameters r_{B^0} and δ_{B^0} are the magnitude ratio and strong phase difference between the amplitudes of A($B^0 \to D^0K^{*0}$) and A($B^0 \to \overline{D}^0K^{*0}$). The measured observables and are defined as $x_\pm = r_{B^0}\cos(\delta_{B^0} \pm \gamma)$ and $y_\pm = r_{B^0}\sin(\delta_{B^0} \pm \gamma)$ where γ is the CKM angle γ.

"OUR EVALUATION" is provided by the Heavy Flavor Averaging Group (HFLAV). The CKM angle γ is listed in the B^+ section for "*CP* VIOLATION PARAMETERS IN $B^+ \to DK^+$ AND SIMILAR DECAYS."

x_+ ($B^0 \to DK^{*0}$)

VALUE	DOCUMENT ID		TECN	COMMENT
0.04±0.17 OUR AVERAGE				
0.04±0.16±0.11	[1] AAIJ	16S	LHCB	pp at 7, 8 TeV
0.05±0.35±0.02	AAIJ	16Z	LHCB	pp at 7, 8 TeV
• • • We do not use the following data for averages, fits, limits, etc. • • •				
0.05±0.24±0.04	[2] AAIJ	16AA	LHCB	Repl. by AAIJ 16Z

[1] Uses Dalitz plof of $B^0 \to DK^+\pi^-$ with $D \to K^+K^-, \pi^+\pi^-$, or $K^+\pi^-$.
[2] Uses Dalitz plot analysis of $D \to K^0_S\pi^+\pi^-$ decays coming from $B^0 \to DK^*(892)^0$ modes.

x_- ($B^0 \to DK^{*0}$)

VALUE	DOCUMENT ID		TECN	COMMENT
−0.16±0.14 OUR AVERAGE				
−0.02±0.13±0.14	[1] AAIJ	16S	LHCB	pp at 7, 8 TeV
−0.31±0.20±0.04	AAIJ	16Z	LHCB	pp at 7, 8 TeV
• • • We do not use the following data for averages, fits, limits, etc. • • •				
−0.15±0.14±0.03	[2] AAIJ	16AA	LHCB	Repl. by AAIJ 16Z

[1] Uses Dalitz plot of $B^0 \to DK^+\pi^-$ with $D \to K^+K^-, \pi^+\pi^-$, or $K^+\pi^-$.
[2] Uses Dalitz plot analysis of $D \to K^0_S\pi^+\pi^-$ decays coming from $B^0 \to DK^*(892)^0$ modes.

y_+ ($B^0 \to DK^{*0}$)

VALUE	DOCUMENT ID		TECN	COMMENT
−0.68±0.22 OUR AVERAGE				
−0.47±0.28±0.22	[1] AAIJ	16S	LHCB	pp at 7, 8 TeV
−0.81±0.28±0.06	AAIJ	16Z	LHCB	pp at 7, 8 TeV
• • • We do not use the following data for averages, fits, limits, etc. • • •				
$-0.65^{+0.24}_{-0.23}$±0.08	[2] AAIJ	16AA	LHCB	Repl. by AAIJ 16Z

[1] Uses Dalitz plof of $B^0 \to DK^+\pi^-$ with $D \to K^+K^-, \pi^+\pi^-$, or $K^+\pi^-$.
[2] Uses Dalitz plot analysis of $D \to K^0_S\pi^+\pi^-$ decays coming from $B^0 \to DK^*(892)^0$ modes.

y_- ($B^0 \to DK^{*0}$)

VALUE	DOCUMENT ID		TECN	COMMENT
0.20±0.25 OUR AVERAGE Error includes scale factor of 1.2.				
−0.35±0.26±0.41	[1] AAIJ	16S	LHCB	pp at 7, 8 TeV
0.31±0.21±0.05	AAIJ	16Z	LHCB	pp at 7, 8 TeV
• • • We do not use the following data for averages, fits, limits, etc. • • •				
0.25±0.15±0.06	[2] AAIJ	16AA	LHCB	Repl. by AAIJ 16Z

[1] Uses Dalitz plof of $B^0 \to DK^+\pi^-$ with $D \to K^+K^-, \pi^+\pi^-$, or $K^+\pi^-$.
[2] Uses Dalitz plot analysis of $D \to K^0_S\pi^+\pi^-$ decays coming from $B^0 \to DK^*(892)^0$ modes.

r_{B^0} ($B^0 \to DK^{*0}$)

"OUR EVALUATION" is provided by the Heavy Flavor Averaging Group (HFLAV).

VALUE	DOCUMENT ID		TECN	COMMENT
$0.257^{+0.021}_{-0.023}$ OUR EVALUATION				
• • • We do not use the following data for averages, fits, limits, etc. • • •				
0.39 ±0.13	[1] AAIJ	16AA	LHCB	Repl. by AAIJ 16Z
0.56 ±0.17	[2] AAIJ	16Z	LHCB	pp at 7, 8 TeV

[1] Uses Dalitz plot analysis of $D \to K^0_S\pi^+\pi^-$ decays coming from $B^0 \to DK^*(892)^0$ modes.
[2] Measurement is performed with $K^+\pi^-$ masses within 50 MeV of the K^{*0} mass and an absolute value of the cosine of the K^{*0} helicity angle greater than 0.4. Angle γ is required to satisfy $0 < \gamma < 180$ degrees.

δ_{B^0} ($B^0 \to DK^{*0}$)

"OUR EVALUATION" is provided by the Heavy Flavor Averaging Group (HFLAV).

VALUE (°)	DOCUMENT ID		TECN	COMMENT
$194.1^{+9.6}_{-8.8}$ OUR EVALUATION				
• • • We do not use the following data for averages, fits, limits, etc. • • •				
197^{+24}_{-20}	[1] AAIJ	16AA	LHCB	Repl. by AAIJ 16Z
204^{+21}_{-20}	[2] AAIJ	16Z	LHCB	pp at 7, 8 TeV

[1] Uses Dalitz plot analysis of $D \to K^0_S\pi^+\pi^-$ decays coming from $B^0 \to DK^*(892)^0$ modes.
[2] Measurement is performed with $K^+\pi^-$ masses within 50 MeV of the K^{*0} mass and an absolute value of the cosine of the K^{*0} helicity angle greater than 0.4. Angle γ is required to satisfy $0 < \gamma < 180$ degrees.

T and *CPT* VIOLATION PARAMETERS

Measured values of the *T*-, *CP*-, and *CPT*-asymmetry parameters, defined as the differences in $S^\pm_{\alpha,\beta}$ and $C^\pm_{\alpha,\beta}$ between symmetry-transformed transitions. The indices $\alpha = \ell^+, \ell^-$ and $\beta = K^0_S, K^0_L$ stand for reconstructed the flavor final state and the *CP* final states from $\Upsilon(4S)$ decay. The sign $\pm$ indicates whether the decay to the flavor final state α occurs before or after the decay to the *CP* final state.

Alternatively, violations of *CPT* symmetry and Lorentz invariance are searched for by studying interference effects in B^0 mixing. Results are expressed in terms of the standard model extension parameter Δa, which describes the difference between the couplings of the valence quarks within B^0 meson with the Lorentz-violating fields.

ΔS^+_T ($S^-_{\ell^-,K^0_S} - S^+_{\ell^+,K^0_S}$)

VALUE	DOCUMENT ID		TECN	COMMENT
−1.37±0.14±0.06	LEES	12W	BABR	$e^+e^- \to \Upsilon(4S)$

ΔS^-_T ($S^+_{\ell^-,K^0_S} - S^-_{\ell^+,K^0_S}$)

VALUE	DOCUMENT ID		TECN	COMMENT
1.17±0.18±0.11	LEES	12W	BABR	$e^+e^- \to \Upsilon(4S)$

Downloaded from https://academic.oup.com/ptep/article/2022/8/083C01/6651666 by KIT Library user on 27 September 2022

$\Delta C_T^+ (C^-_{\ell^-,K^0_S} - C^+_{\ell^+,K^0_S})$

VALUE	DOCUMENT ID		TECN	COMMENT
0.10±0.14±0.08	LEES	12W	BABR	$e^+e^- \to \Upsilon(4S)$

$\Delta C_T^- (C^+_{\ell^-,K^0_S} - C^-_{\ell^+,K^0_S})$

VALUE	DOCUMENT ID		TECN	COMMENT
0.04±0.14±0.08	LEES	12W	BABR	$e^+e^- \to \Upsilon(4S)$

$\Delta S^+_{CP} (S^+_{\ell^-,K^0_S} - S^+_{\ell^+,K^0_S})$

VALUE	DOCUMENT ID		TECN	COMMENT
−1.30±0.11±0.07	LEES	12W	BABR	$e^+e^- \to \Upsilon(4S)$

$\Delta S^-_{CP} (S^-_{\ell^-,K^0_S} - S^-_{\ell^+,K^0_S})$

VALUE	DOCUMENT ID		TECN	COMMENT
1.33±0.12±0.06	LEES	12W	BABR	$e^+e^- \to \Upsilon(4S)$

$\Delta C^+_{CP} (C^+_{\ell^-,K^0_S} - C^+_{\ell^+,K^0_S})$

VALUE	DOCUMENT ID		TECN	COMMENT
0.07±0.09±0.03	LEES	12W	BABR	$e^+e^- \to \Upsilon(4S)$

$\Delta C^-_{CP} (C^-_{\ell^-,K^0_S} - C^-_{\ell^+,K^0_S})$

VALUE	DOCUMENT ID		TECN	COMMENT
0.08±0.10±0.04	LEES	12W	BABR	$e^+e^- \to \Upsilon(4S)$

$\Delta S^+_{CPT} (S^-_{\ell^+,K^0_S} - S^+_{\ell^+,K^0_S})$

VALUE	DOCUMENT ID		TECN	COMMENT
0.16±0.21±0.09	LEES	12W	BABR	$e^+e^- \to \Upsilon(4S)$

$\Delta S^-_{CPT} (S^+_{\ell^+,K^0_S} - S^-_{\ell^+,K^0_S})$

VALUE	DOCUMENT ID		TECN	COMMENT
−0.03±0.13±0.06	LEES	12W	BABR	$e^+e^- \to \Upsilon(4S)$

$\Delta C^+_{CPT} (C^-_{\ell^+,K^0_S} - C^+_{\ell^+,K^0_S})$

VALUE	DOCUMENT ID		TECN	COMMENT
0.14±0.15±0.07	LEES	12W	BABR	$e^+e^- \to \Upsilon(4S)$

$\Delta C^-_{CPT} (C^+_{\ell^+,K^0_S} - C^-_{\ell^+,K^0_S})$

VALUE	DOCUMENT ID		TECN	COMMENT
0.03±0.12±0.08	LEES	12W	BABR	$e^+e^- \to \Upsilon(4S)$

$\Delta a_\parallel$ CPT parameter in B^0 mixing

VALUE (10^{-15} GeV)	DOCUMENT ID		TECN	COMMENT
−0.10±0.82±0.54	[1] AAIJ	16E	LHCB	pp at 7, 8 TeV

[1] Uses $B^0 \to J/\psi K^0_S$ decays.

$\Delta a_\perp$ CPT parameter in B^0 mixing

VALUE (10^{-13} GeV)	DOCUMENT ID		TECN	COMMENT
−0.20±0.22±0.04	[1] AAIJ	16E	LHCB	pp at 7, 8 TeV

[1] Uses $B^0 \to J/\psi K^0_S$ decays.

Δa_X CPT parameter in B^0 mixing

VALUE (10^{-15} GeV)	DOCUMENT ID		TECN	COMMENT
+1.97±1.30±0.29	[1] AAIJ	16E	LHCB	pp at 7, 8 TeV

[1] Uses $B^0 \to J/\psi K^0_S$ decays.

Δa_Y CPT parameter in B^0 mixing

VALUE (10^{-15} GeV)	DOCUMENT ID		TECN	COMMENT
+0.44±1.26±0.29	[1] AAIJ	16E	LHCB	pp at 7, 8 TeV

[1] Uses $B^0 \to J/\psi K^0_S$ decays.

$B^0 \to D^{*-}\ell^+\nu_\ell$ FORM FACTORS

R_1 (form factor ratio $\sim V/A_1$)

VALUE	DOCUMENT ID		TECN	COMMENT
1.239±0.029 OUR AVERAGE				
1.229±0.028±0.009	[1] WAHEED	19	BELL	$e^+e^- \to \Upsilon(4S)$
1.56 ±0.07 ±0.15	AUBERT	09A	BABR	$e^+e^- \to \Upsilon(4S)$
1.18 ±0.30 ±0.12	DUBOSCQ	96	CLE2	$e^+e^- \to \Upsilon(4S)$
• • • We do not use the following data for averages, fits, limits, etc. • • •				
1.401±0.034±0.018	[1] DUNGEL	10	BELL	Repl. by WAHEED 19
1.429±0.061±0.044	AUBERT	08R	BABR	Repl. by AUBERT 09A
1.396±0.060±0.044	AUBERT,B	06Z	BABR	Repl. by AUBERT 08R

[1] Uses fully reconstructed $D^{*-}\ell^+\nu$ events ($\ell = e$ or μ).

R_2 (form factor ratio $\sim A_2/A_1$)

VALUE	DOCUMENT ID		TECN	COMMENT
0.84 ±0.04 OUR AVERAGE	Error includes scale factor of 1.8.			
0.852±0.021±0.006	[1] WAHEED	19	BELL	$e^+e^- \to \Upsilon(4S)$
0.66 ±0.05 ±0.09	AUBERT	09A	BABR	$e^+e^- \to \Upsilon(4S)$
0.71 ±0.22 ±0.07	DUBOSCQ	96	CLE2	$e^+e^- \to \Upsilon(4S)$
• • • We do not use the following data for averages, fits, limits, etc. • • •				
0.864±0.024±0.008	[1] DUNGEL	10	BELL	Repl. by WAHEED 19
0.827±0.038±0.022	AUBERT	08R	BABR	Repl. by AUBERT 09A
0.885±0.040±0.026	AUBERT,B	06Z	BABR	Repl. by AUBERT 08R

[1] Uses fully reconstructed $D^{*-}\ell^+\nu$ events ($\ell = e$ or μ).

$\rho^2_{A_1}$ (form factor slope)

VALUE	DOCUMENT ID		TECN	COMMENT
1.12 ±0.04 OUR AVERAGE	Error includes scale factor of 1.5.			
1.106±0.031±0.007	[1] WAHEED	19	BELL	$e^+e^- \to \Upsilon(4S)$
1.22 ±0.02 ±0.07	AUBERT	09A	BABR	$e^+e^- \to \Upsilon(4S)$
0.91 ±0.15 ±0.06	DUBOSCQ	96	CLE2	$e^+e^- \to \Upsilon(4S)$
• • • We do not use the following data for averages, fits, limits, etc. • • •				
1.214±0.034±0.009	[1] DUNGEL	10	BELL	Repl. by WAHEED 19
1.191±0.048±0.028	AUBERT	08R	BABR	Repl. by AUBERT 09A
1.145±0.059±0.046	AUBERT,B	06Z	BABR	Repl. by AUBERT 08R

[1] Uses fully reconstructed $D^{*-}\ell^+\nu$ events ($\ell = e$ or μ).

PARTIAL BRANCHING FRACTIONS IN $B^0 \to K^{(*)0}\ell^+\ell^-$

B($B^0 \to K^{*0}e^+e^-$) (0.0009 < q^2 < 1.0 GeV^2/c^4)

VALUE (units 10^{-7})	DOCUMENT ID		TECN	COMMENT
$3.1^{+0.9}_{-0.8}{}^{+0.2}_{-0.3}\pm0.2$	[1] AAIJ	13U	LHCB	pp at 7 TeV

[1] The last uncertainty is due to uncertainties of B($B^0 \to J/\psi K^{*0}$) and B($J/\psi \to e^+e^-$) branching fraction measurements.

B($B^0 \to K^{*0}\ell^+\ell^-$) (0.1 < q^2 < 2.0 GeV^2/c^4)

VALUE (units 10^{-7})	DOCUMENT ID		TECN	COMMENT
$1.24^{+0.23}_{-0.27}$ OUR AVERAGE	Error includes scale factor of 1.6.			
$1.14\pm0.11^{+0.11}_{-0.15}$	AAIJ	13Y	LHCB	pp at 7 TeV, $K^{*0}\mu^+\mu^-$
1.80±0.36±0.11	AALTONEN	11AI	CDF	$p\overline{p}$ at 1.96 TeV
• • • We do not use the following data for averages, fits, limits, etc. • • •				
$0.48^{+0.14}_{-0.12}\pm0.04$	[1] CHATRCHYAN	13BL	CMS	pp at 7 TeV
1.16±0.23±0.11	AAIJ	12U	LHCB	Repl. by AAIJ 13Y

[1] CHATRCHYAN 13BL uses, for this bin, 1.0 < q^2 < 2.0 GeV^2/c^4.

B($B^0 \to K^{*0}\ell^+\ell^-$) (2.0 < q^2 < 4.3 GeV^2/c^4)

VALUE (units 10^{-7})	DOCUMENT ID		TECN	COMMENT
0.76 ±0.07 OUR AVERAGE				
0.759±0.115±0.046	KHACHATRY...	16D	CMS	pp at 8 TeV
0.69 ±0.07 ±0.09	AAIJ	13Y	LHCB	pp at 7 TeV, $K^{*0}\mu^+\mu^-$
0.87 ±0.16 ±0.07	CHATRCHYAN	13BL	CMS	pp at 7 TeV
0.84 ±0.28 ±0.06	AALTONEN	11AI	CDF	$p\overline{p}$ at 1.96 TeV
• • • We do not use the following data for averages, fits, limits, etc. • • •				
0.78 ±0.21 ±0.05	AAIJ	12U	LHCB	Repl. by AAIJ 13Y

B($B^0 \to K^{*0}\ell^+\ell^-$) (4.3 < q^2 < 8.68 GeV^2/c^4)

VALUE (units 10^{-7})	DOCUMENT ID		TECN	COMMENT
1.87±0.21 OUR AVERAGE				
$2.15\pm0.18^{+0.22}_{-0.28}$	AAIJ	13Y	LHCB	pp at 7 TeV, $K^{*0}\mu^+\mu^-$
1.62±0.31±0.18	CHATRCHYAN	13BL	CMS	pp at 7 TeV
1.73±0.43±0.15	AALTONEN	11AI	CDF	$p\overline{p}$ at 1.96 TeV
• • • We do not use the following data for averages, fits, limits, etc. • • •				
3.02±0.35±0.22	AAIJ	12U	LHCB	Repl. by AAIJ 13Y

B($B^0 \to K^{*0}\ell^+\ell^-$) (10.09 < q^2 < 12.86 GeV^2/c^4)

VALUE (units 10^{-7})	DOCUMENT ID		TECN	COMMENT
1.49±0.15 OUR AVERAGE	Error includes scale factor of 1.3. See the ideogram below.			
1.72±0.11±0.14	KHACHATRY...	16D	CMS	pp at 8 TeV
$1.19\pm0.11^{+0.14}_{-0.17}$	AAIJ	13Y	LHCB	pp at 7 TeV, $K^{*0}\mu^+\mu^-$
1.50±0.25±0.25	CHATRCHYAN	13BL	CMS	pp at 7 TeV
1.77±0.36±0.12	AALTONEN	11AI	CDF	$p\overline{p}$ at 1.96 TeV
• • • We do not use the following data for averages, fits, limits, etc. • • •				
1.52±0.25±0.19	AAIJ	12U	LHCB	Repl. by AAIJ 13Y

Downloaded from https://academic.oup.com/ptep/article/2022/8/083C01/6651666 by KIT Library user on 27 September 2022

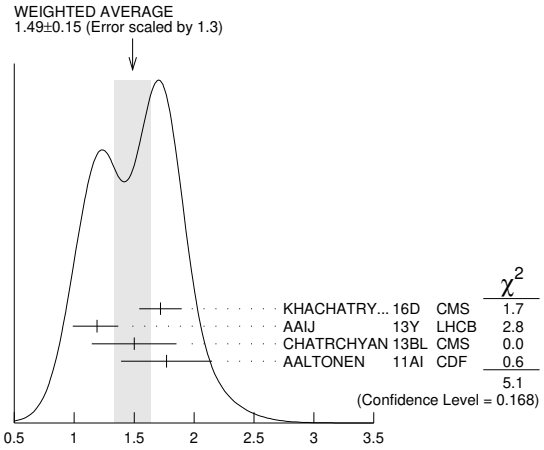

$B(B^0 \to K^{*0}\ell^+\ell^-)$ ($10.09 < q^2 < 12.86$ GeV$^2/c^4$) (units 10^{-7})

$B(B^0 \to K^{*0}\ell^+\ell^-)$ ($14.18 < q^2 < 16.0$ GeV$^2/c^4$)

VALUE (units 10^{-7})	DOCUMENT ID		TECN	COMMENT
1.09 ± 0.10 OUR AVERAGE	Error includes scale factor of 1.1.			
$1.22 \pm 0.11 \pm 0.09$	KHACHATRY...	16D	CMS	pp at 8 TeV
$1.02 \pm 0.11 {}^{+0.11}_{-0.15}$	AAIJ	13Y	LHCB	pp at 7 TeV, $K^{*0}\mu^+\mu^-$
$0.84 {}^{+0.16}_{-0.15} \pm 0.09$	CHATRCHYAN	13BL	CMS	pp at 7 TeV
$1.34 \pm 0.26 \pm 0.08$	AALTONEN	11AI	CDF	$p\overline{p}$ at 1.96 TeV
• • • We do not use the following data for averages, fits, limits, etc. • • •				
$1.15 \pm 0.20 \pm 0.09$	AAIJ	12U	LHCB	Repl. by AAIJ 13Y

$B(B^0 \to K^{*0}\ell^+\ell^-)$ ($16.0 < q^2 < 19.0$ GeV$^2/c^4$)

VALUE (units 10^{-7})	DOCUMENT ID		TECN	COMMENT
1.27 ± 0.09 OUR AVERAGE				
$1.26 \pm 0.09 \pm 0.09$	KHACHATRY...	16D	CMS	pp at 8 TeV
$1.23 \pm 0.12 {}^{+0.15}_{-0.18}$	AAIJ	13Y	LHCB	pp at 7 TeV, $K^{*0}\mu^+\mu^-$
$1.56 \pm 0.18 \pm 0.15$	CHATRCHYAN	13BL	CMS	pp at 7 TeV
$0.97 \pm 0.26 \pm 0.07$	AALTONEN	11AI	CDF	$p\overline{p}$ at 1.96 TeV
• • • We do not use the following data for averages, fits, limits, etc. • • •				
$1.50 \pm 0.24 \pm 0.15$	AAIJ	12U	LHCB	Repl. by AAIJ 13Y

$B(B^0 \to K^*(892)^0\ell^+\ell^-)$ ($15.0 < q^2 < 19.0$ GeV$^2/c^4$)

VALUE (units 10^{-7})	DOCUMENT ID		TECN	COMMENT
1.80 ± 0.13 OUR AVERAGE				
$2.2 {}^{+0.5}_{-0.4} \pm 0.2$	[1] WEHLE	21	BELL	$e^+e^- \to \Upsilon(4S)$
$2.0 {}^{+0.6}_{-0.5} \pm 0.2$	[2] WEHLE	21	BELL	$e^+e^- \to \Upsilon(4S)$
$1.744 {}^{+0.072}_{-0.076} \pm 0.123$	[1] AAIJ	17Q	LHCB	pp at 7, 8 TeV
• • • We do not use the following data for averages, fits, limits, etc. • • •				
$1.95 {}^{+0.08}_{-0.09} \pm 0.13$	[1] AAIJ	16AO	LHCB	Repl. by AAIJ 17Q

[1] Measured with $\mu^+\mu^-$ as lepton pair.
[2] Measured with e^+e^- as lepton pair.

$B(B^0 \to K^{*0}\ell^+\ell^-)$ ($1.0 < q^2 < 6.0$ GeV$^2/c^4$)

VALUE (units 10^{-7})	DOCUMENT ID		TECN	COMMENT
1.74 ± 0.11 OUR AVERAGE				
$1.9 {}^{+0.6}_{-0.5} \pm 0.3$	[1,2] WEHLE	21	BELL	$e^+e^- \to \Upsilon(4S)$
$1.8 {}^{+0.6}_{-0.6} \pm 0.2$	[1,3] WEHLE	21	BELL	$e^+e^- \to \Upsilon(4S)$
$1.68 \pm 0.083 \pm 0.12$	[1,2] AAIJ	17Q	LHCB	pp at 7, 8 TeV
1.90 ± 0.20	[2] KHACHATRY...	16D	CMS	pp at 7, 8 TeV
$1.42 \pm 0.41 \pm 0.12$	[2] AALTONEN	11AI	CDF	$p\overline{p}$ at 1.96 TeV
• • • We do not use the following data for averages, fits, limits, etc. • • •				
$1.92 {}^{+0.10}_{-0.09} \pm 0.14$	AAIJ	16AO	LHCB	Repl. by AAIJ 17Q
$1.70 \pm 0.15 {}^{+0.20}_{-0.25}$	AAIJ	13Y	LHCB	Repl. by AAIJ 16AO
$2.20 \pm 0.30 \pm 0.20$	CHATRCHYAN	13BL	CMS	Repl. by KHACHATRYAN 16D
$2.10 \pm 0.30 \pm 0.15$	AAIJ	12U	LHCB	Repl. by AAIJ 13Y

[1] Result is determined for the range $1.1 < q^2 < 6.0$ GeV$^4/c^2$.
[2] Measured with $\mu^+\mu^-$ as lepton pair.
[3] Measured with e^+e^- as lepton pair.

$B(B^0 \to K^{*0}\ell^+\ell^-)$ ($0.0 < q^2 < 4.3$ GeV$^2/c^4$)

VALUE (units 10^{-7})	DOCUMENT ID		TECN	COMMENT
$2.60 \pm 0.45 \pm 0.17$	AALTONEN	11AI	CDF	$p\overline{p}$ at 1.96 TeV

$B(B^0 \to K^{*0}\mu^+\mu^-)/B(B^0 \to K^{*0}e^+e^-)$ ($0.045 < q^2 < 1.1$ GeV$^2/c^4$)

VALUE	DOCUMENT ID		TECN	COMMENT
$0.65 {}^{+0.11}_{-0.07}$ OUR AVERAGE				
$0.46 {}^{+0.55}_{-0.27} \pm 0.13$	WEHLE	21	BELL	$e^+e^- \to \Upsilon(4S)$
$0.66 {}^{+0.11}_{-0.07} \pm 0.03$	AAIJ	17W	LHCB	pp at 7, 8 TeV

$B(B^0 \to K^{*0}\mu^+\mu^-)/B(B^0 \to K^{*0}e^+e^-)$ ($1.1 < q^2 < 6.0$ GeV$^2/c^4$)

VALUE	DOCUMENT ID		TECN	COMMENT
$0.71 {}^{+0.12}_{-0.08}$ OUR AVERAGE				
$1.06 {}^{+0.63}_{-0.38} \pm 0.13$	WEHLE	21	BELL	$e^+e^- \to \Upsilon(4S)$
$0.69 {}^{+0.11}_{-0.07} \pm 0.05$	AAIJ	17W	LHCB	pp at 7, 8 TeV

$B(B^0 \to K^{*0}\mu^+\mu^-)/B(B^0 \to K^{*0}e^+e^-)$ ($15.0 < q^2 < 19.0$ GeV$^2/c^4$)

VALUE	DOCUMENT ID		TECN	COMMENT
$1.12 {}^{+0.61}_{-0.36} \pm 0.10$	WEHLE	21	BELL	$e^+e^- \to \Upsilon(4S)$

$B(B^0 \to K^0\ell^+\ell^-)$ ($q^2 < 2.0$ GeV$^2/c^4$)

VALUE (units 10^{-7})	DOCUMENT ID		TECN	COMMENT
$0.24 {}^{+0.22}_{-0.20}$ OUR AVERAGE				
$0.21 {}^{+0.27}_{-0.23}$	AAIJ	12AH	LHCB	pp at 7 TeV
$0.31 \pm 0.37 \pm 0.02$	AALTONEN	11AI	CDF	$p\overline{p}$ at 1.96 TeV

$B(B^0 \to K^0\ell^+\ell^-)$ ($2.0 < q^2 < 4.3$ GeV$^2/c^4$)

VALUE (units 10^{-7})	DOCUMENT ID		TECN	COMMENT
$0.24 {}^{+0.35}_{-0.30}$ OUR AVERAGE	Error includes scale factor of 1.6.			
$0.07 {}^{+0.25}_{-0.21}$	AAIJ	12AH	LHCB	pp at 7 TeV
$0.93 \pm 0.49 \pm 0.07$	AALTONEN	11AI	CDF	$p\overline{p}$ at 1.96 TeV

$B(B^0 \to K^0\ell^+\ell^-)$ ($4.3 < q^2 < 8.68$ GeV$^2/c^4$)

VALUE (units 10^{-7})	DOCUMENT ID		TECN	COMMENT
1.08 ± 0.27 OUR AVERAGE				
1.23 ± 0.31	AAIJ	12AH	LHCB	pp at 7 TeV
$0.66 \pm 0.51 \pm 0.05$	AALTONEN	11AI	CDF	$p\overline{p}$ at 1.96 TeV

$B(B^0 \to K^0\ell^+\ell^-)$ ($10.09 < q^2 < 12.86$ GeV$^2/c^4$)

VALUE (units 10^{-7})	DOCUMENT ID		TECN	COMMENT
0.27 ± 0.27 OUR AVERAGE	Error includes scale factor of 1.8.			
$0.50 {}^{+0.22}_{-0.19}$	AAIJ	12AH	LHCB	pp at 7 TeV
$-0.03 \pm 0.22 \pm 0.01$	AALTONEN	11AI	CDF	$p\overline{p}$ at 1.96 TeV

$B(B^0 \to K^0\ell^+\ell^-)$ ($14.18 < q^2 < 16.0$ GeV$^2/c^4$)

VALUE (units 10^{-7})	DOCUMENT ID		TECN	COMMENT
$0.29 {}^{+0.21}_{-0.15}$ OUR AVERAGE	Error includes scale factor of 1.8.			
$0.20 {}^{+0.13}_{-0.09}$	AAIJ	12AH	LHCB	pp at 7 TeV
$0.73 \pm 0.26 \pm 0.06$	AALTONEN	11AI	CDF	$p\overline{p}$ at 1.96 TeV

$B(B^0 \to K^0\ell^+\ell^-)$ ($q^2 > 16.0$ GeV$^2/c^4$)

VALUE (units 10^{-7})	DOCUMENT ID		TECN	COMMENT
$0.31 {}^{+0.16}_{-0.12}$ OUR AVERAGE				
$0.35 {}^{+0.21}_{-0.14}$	AAIJ	12AH	LHCB	pp at 7 TeV
$0.21 \pm 0.18 \pm 0.16$	AALTONEN	11AI	CDF	$p\overline{p}$ at 1.96 TeV

$B(B^0 \to K^0\ell^+\ell^-)$ ($1.0 < q^2 < 6.0$ GeV$^2/c^4$)

VALUE (units 10^{-7})	DOCUMENT ID		TECN	COMMENT
$0.91 {}^{+0.15}_{-0.13}$ OUR AVERAGE				
$0.62 {}^{+0.44}_{-0.32} \pm 0.02$	[1] CHOUDHURY	21	BELL	$e^+e^- \to \Upsilon(4S)$
$1.12 {}^{+0.50}_{-0.40} \pm 0.04$	[2] CHOUDHURY	21	BELL	$e^+e^- \to \Upsilon(4S)$
$0.916 {}^{+0.172}_{-0.157} \pm 0.004$	[3] AAIJ	14M	LHCB	pp at 7, 8 TeV
$0.98 \pm 0.61 \pm 0.08$	AALTONEN	11AI	CDF	$p\overline{p}$ at 1.96 TeV
• • • We do not use the following data for averages, fits, limits, etc. • • •				
$0.65 {}^{+0.45}_{-0.35}$	AAIJ	12AH	LHCB	Repl. by AAIJ 14M

[1] Measured for $B^0 \to K^0_S\mu^+\mu^-$ decays. Measurements in other q^2 bins are also reported.
[2] Measured for $B^0 \to K^0_S e^+e^-$ decays. Measurements in other q^2 bins are also reported.
[3] Uses $B(B^0 \to J/\psi(1S)K^0) = (0.928 \pm 0.013 \pm 0.037) \times 10^{-3}$ for normalisation and $\mu^+\mu^-$ as a lepton pair. Measured in $1.1 < q^2 < 6.0$ GeV$^2/c^4$.

Downloaded from https://academic.oup.com/ptep/article/2022/8/083C01/6651666 by KIT Library user on 27 September 2022

$B(B^0 \to K^0\mu^+\mu^-)$ / $B(B^0 \to K^0 e^+ e^-)$ $(1.0 < q^2 < 6.0\ \mathrm{GeV}^2/c^4)$

VALUE	DOCUMENT ID		TECN	COMMENT
$0.55^{+0.46}_{-0.34} \pm 0.01$	[1] CHOUDHURY	21	BELL	$e^+e^- \to \Upsilon(4S)$

[1] Measured from the ratio of $K^0_S\mu^+\mu^-$ and $K^0_S e^+e^-$. Measurements in other q^2 bins are also reported.

$B(B^0 \to K^0\ell^+\ell^-)$ $(0.0 < q^2 < 4.3\ \mathrm{GeV}^2/c^4)$

VALUE (units 10^{-7})	DOCUMENT ID		TECN	COMMENT
$1.27 \pm 0.62 \pm 0.10$	AALTONEN	11AI	CDF	$p\overline{p}$ at 1.96 TeV

$B(B^0 \to K^0\ell^+\ell^-)$ $(15.0 < q^2 < 22.0\ \mathrm{GeV}^2/c^4)$

VALUE (units 10^{-7})	DOCUMENT ID		TECN	COMMENT
$0.67^{+0.11}_{-0.11} \pm 0.04$	[1] AAIJ	14M	LHCB	pp at 7, 8 TeV

[1] Uses $B(B^0 \to J/\psi(1S)K^0) = (0.928 \pm 0.013 \pm 0.037) \times 10^{-3}$ for normalisation and $\mu^+\mu^-$ as a lepton pair.

$B(B^0 \to K^*_{0,2}(1430)^0\mu^+\mu^-)$ $(1.10 < q^2 < 6.00\ \mathrm{GeV}^2/c^4)$

VALUE (units 10^{-8})	DOCUMENT ID		TECN	COMMENT
$4.02 \pm 0.44 \pm 0.31$	[1,2] AAIJ	16AP	LHCB	pp at 7, 8 TeV

[1] Measured the differential branching fraction and angular moments of the decay $B^0 \to K^+\pi^-\mu^+\mu^-$ in the $K^+\pi^-$ invariant mass range $1330 < m(K^+\pi^-) < 1530$ MeV/c^2.
[2] The reported value is converted from the measured $dB/dq^2 = (0.82 \pm 0.09 \pm 0.063) \times 10^{-8}\ (\mathrm{GeV}^2/c^4)^{-1}$ by multiplying by the $\Delta q^2 = 4.9\ \mathrm{GeV}^2/c^4$ range.

$F_H(B^0 \to K^0\mu^+\mu^-)$ $(1.1 < q^2 < 6.0\ \mathrm{GeV}^2/c^4)$

F_H is a fractional contribution of (pseudo) scalar and tensor amplitudes to the decay width in the massless muon approximation.

VALUE	DOCUMENT ID		TECN	COMMENT
$0.78 \pm 0.46 \pm 0.09$	[1] AAIJ	14O	LHCB	pp at 7, 8 TeV

[1] AAIJ 14O reports 68% C.L. interval, which we encode as midpoint with uncertainty as half of the width of interval.

$F_H(B^0 \to K^0\mu^+\mu^-)$ $(15.0 < q^2 < 22.0\ \mathrm{GeV}^2/c^4)$

VALUE	DOCUMENT ID		TECN	COMMENT
$0.34 \pm 0.25 \pm 0.03$	[1] AAIJ	14O	LHCB	pp at 7, 8 TeV

[1] AAIJ 14O reports 68% C.L. interval, which we encode as midpoint with uncertainty as half of the width of interval.

PRODUCTION ASYMMETRIES

$A_P(B^0)$

$A_P(B^0) = [\sigma(\overline{B}^0) - \sigma(B^0)] / [\sigma(\overline{B}^0) + \sigma(B^0)]$

VALUE (units 10^{-2})	DOCUMENT ID		TECN	COMMENT
-0.3 ± 0.6 OUR AVERAGE	Error includes scale factor of 1.7. See the ideogram below.			
$0.44 \pm 0.88 \pm 0.11$	[1] AAIJ	17BF	LHCB	pp at 7 TeV
$-1.40 \pm 0.55 \pm 0.10$	[1] AAIJ	17BF	LHCB	pp at 8 TeV
$0.25 \pm 0.48 \pm 0.05$	[2] AABOUD	16G	ATLS	pp at 7, 8 TeV
• • • We do not use the following data for averages, fits, limits, etc. • • •				
$-0.35 \pm 0.76 \pm 0.28$	[3] AAIJ	14BP	LHCB	Repl. by AAIJ 17BF, pp at 7 TeV

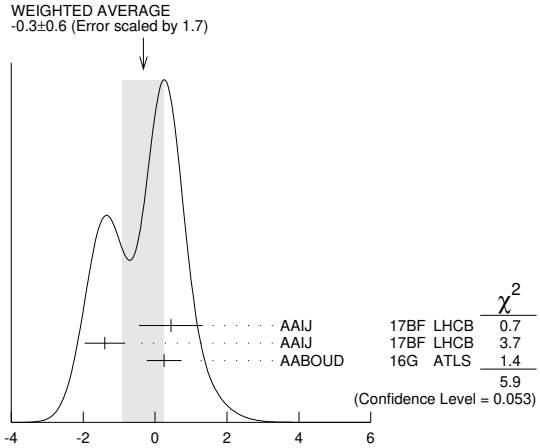

[1] AAIJ 17BF uses $B^0 \to J/\psi K^{*0}$ decays with B^0 transverse momenta p_T and rapidities y in the region of $0 < p_T < 30$ GeV/c and $2.1 < y < 4.5$.
[2] Based on time-dependent analysis of $B^0 \to J/\psi K^{*0}$ decay in kinematic range $p_T > 10$ GeV/c and $|\eta| < 2.5$.
[3] Based on time-dependent analysis of $B^0 \to J/\psi K^{*0}$ and $B^0 \to D^-\pi^+$ in kinematic range $4 < p_T < 30$ GeV/c and $2.5 < \eta < 4.5$.

$A(B^0+\overline{B}^0)$ in $K^0_S K^\mp\pi^\pm$

$A(B^0+\overline{B}^0) = [n(K^0_S K^-\pi^+) - n(K^0_S K^+\pi^-)] / [n(K^0_S K^-\pi^+) + n(K^0_S K^+\pi^-)]$

VALUE (units 10^{-2})	DOCUMENT ID		TECN	COMMENT
$-8.5 \pm 8.9 \pm 0.2$	LAI	19	BELL	$e^+e^- \to \Upsilon(4S)$

B^0 REFERENCES

AAIJ 22 PRL 128 041801 R. Aaij et al. (LHCb Collab.)
Also PR D105 012010 R. Aaij et al. (LHCb Collab.)
WAHEED 22 PR D105 012003 E. Waheed et al. (Belle Collab.)
AAIJ 21K CP C45 043001 R. Aaij et al. (LHCb Collab.)
AAIJ 21O JHEP 2103 075 R. Aaij et al. (LHCb Collab.)
AAIJ 21S JHEP 2106 177 R. Aaij et al. (LHCb Collab.)
AAIJ 21W EPJ C81 314 R. Aaij et al. (LHCb Collab.)
ATMACAN 21 PR D104 L091105 H. Atmacan et al. (BELLE Collab.)
CAO 21A PR D104 012008 L. Cao et al. (BELLE Collab.)
CHOUDHURY 21 JHEP 2103 105 S. Choudhury et al. (BELLE Collab.)
KANG 21 PR D103 032003 K.H. Kang et al. (BELLE Collab.)
MOHANTY 21 PR D103 052013 S. Mohanty et al. (Belle Collab.)
WAHEED 21 PR D103 079901 E. Waheed et al. (BELLE Collab.)
WEHLE 21 PRL 126 161801 S. Wehle et al. (BELLE Collab.)
AAIJ 20AG PR D102 051102 R. Aaij et al. (LHCb Collab.)
AAIJ 20AN JHEP 2012 139 R. Aaij et al. (LHCb Collab.)
AAIJ 20AO JHEP 2012 081 R. Aaij et al. (LHCb Collab.)
AAIJ 20F PR D102 012011 R. Aaij et al. (LHCb Collab.)
AAIJ 20L JHEP 2003 147 R. Aaij et al. (LHCb Collab.)
AAIJ 20W PRL 124 211802 R. Aaij et al. (LHCb Collab.)
CHILIKIN 20 JHEP 2005 034 K. Chilikin et al. (BELLE Collab.)
CHU 20 PR D101 052012 K. Chu et al. (BELLE Collab.)
KU 20 PR D102 012003 Y. Ku et al. (BELLE Collab.)
SIRUNYAN 20AG JHEP 2004 188 A.M. Sirunyan et al. (CMS Collab.)
AABOUD 19L JHEP 1904 098 M. Aaboud et al. (ATLAS Collab.)
AAIJ 19AK PRL 123 211801 R. Aaij et al. (LHCb Collab.)
AAIJ 19AP JHEP 1912 155 R. Aaij et al. (LHCb Collab.)
AAIJ 19J JHEP 1905 026 R. Aaij et al. (LHCb Collab.)
AAIJ 19L JHEP 1907 032 R. Aaij et al. (LHCb Collab.)
AAIJ 19N JHEP 1908 041 R. Aaij et al. (LHCb Collab.)
AAIJ 19U PRL 122 191804 R. Aaij et al. (LHCb Collab.)
CHILIKIN 19 PR D100 012001 K. Chilikin et al. (BELLE Collab.)
CHOU 19 PR D100 012002 P.-C. Chou et al. (BELLE Collab.)
GARG 19 PR D99 071102 R. Garg et al. (BELLE Collab.)
LAI 19 PR D100 011101 Y.-T. Lai et al. (BELLE Collab.)
LI 19C PR D100 031101 Y.B. Li et al. (BELLE Collab.)
PAL 19 PR D99 091104 B. Pal et al. (BELLE Collab.)
WAHEED 19 PR D100 052007 E. Waheed et al. (BELLE Collab.)
WATANUKI 19 PR D99 032012 S. Watanuki et al. (BELLE Collab.)
YUSA 19 PR D99 011102 Y. Yusa et al. (BELLE Collab.)
AABOUD 18BY JHEP 1810 047 M. Aaboud et al. (ATLAS Collab.)
AAIJ 18AN EPJ C78 1019 R. Aaij et al. (LHCb Collab.)
AAIJ 18AY PR D98 071103 R. Aaij et al. (LHCb Collab.)
AAIJ 18AZ PR D98 072006 R. Aaij et al. (LHCb Collab.)
AAIJ 18D PRL 120 171802 R. Aaij et al. (LHCb Collab.)
AAIJ 18F PRL 120 261801 R. Aaij et al. (LHCb Collab.)
AAIJ 18O PR D98 032004 R. Aaij et al. (LHCb Collab.)
AAIJ 18T JHEP 1803 078 R. Aaij et al. (LHCb Collab.)
AAIJ 18Z JHEP 1806 084 R. Aaij et al. (LHCb Collab.)
ABAZOV 18B PR D98 052010 V.M. Abazov et al. (D0 Collab.)
ADACHI 18 PR D98 112012 I. Adachi et al. (BELLE and BABAR Collabs.)
Also PRL 121 261801 I. Adachi et al. (BELLE and BABAR Collabs.)
LEES 18C PR D98 071102 J.P. Lees et al. (BABAR Collab.)
LI 18D EPJ C78 928 Y.B. Li et al. (BELLE Collab.)
NAKANO 18 PR D97 092003 H. Nakano et al. (BELLE Collab.)
PAL 18 PR D98 112008 B. Pal et al. (BELLE Collab.)
PDG 18 PR D98 030001 M. Tanabashi et al. (PDG Collab.)
SANDILYA 18 PR D98 071101 S. Sandilya et al. (BELLE Collab.)
SIRUNYAN 18BY EPJ C78 457 A.M. Sirunyan et al. (CMS Collab.)
SIRUNYAN 18DF EPJ C78 939 A.M. Sirunyan et al. (CMS Collab.)
VOSSEN 18 PR D98 012005 A. Vossen et al. (BELLE Collab.)
AAIJ 17A PR D95 012006 R. Aaij et al. (LHCb Collab.)
AAIJ 17AI PRL 118 191801 R. Aaij et al. (LHCb Collab.)
AAIJ 17AJ PRL 118 251802 R. Aaij et al. (LHCb Collab.)
AAIJ 17BD PR D96 051103 R. Aaij et al. (LHCb Collab.)
AAIJ 17BF PL B774 139 R. Aaij et al. (LHCb Collab.)
AAIJ 17BJ PRL 119 232001 R. Aaij et al. (LHCb Collab.)
AAIJ 17BN JHEP 1711 170 R. Aaij et al. (LHCb Collab.)
AAIJ 17BP JHEP 1711 027 R. Aaij et al. (LHCb Collab.)
AAIJ 17G PRL 118 081801 R. Aaij et al. (LHCb Collab.)
AAIJ 17N JHEP 1703 001 R. Aaij et al. (LHCb Collab.)
AAIJ 17Q JHEP 1704 142 R. Aaij et al. (LHCb Collab.)
AAIJ 17W JHEP 1708 055 R. Aaij et al. (LHCb Collab.)
GRYGIER 17 PR D96 091101 J. Grygier et al. (BELLE Collab.)
HORIGUCHI 17 PRL 119 191802 T. Horiguchi et al. (BELLE Collab.)
JULIUS 17 PR D96 032007 T. Julius et al. (BELLE Collab.)
AABOUD 16G JHEP 1606 081 M. Aaboud et al. (ATLAS Collab.)
AABOUD 16L EPJ C76 513 M. Aaboud et al. (ATLAS Collab.)
AAIJ 16 JHEP 1601 012 R. Aaij et al. (LHCb Collab.)
AAIJ 16AA JHEP 1608 137 R. Aaij et al. (LHCb Collab.)
AAIJ 16AN PRL 117 261801 R. Aaij et al. (LHCb Collab.)
AAIJ 16AO JHEP 1611 047 R. Aaij et al. (LHCb Collab.)
AAIJ 16AP JHEP 1612 065 R. Aaij et al. (LHCb Collab.)
AAIJ 16AV EPJ C76 412 R. Aaij et al. (LHCb Collab.)
AAIJ 16E PRL 116 241601 R. Aaij et al. (LHCb Collab.)
AAIJ 16S PR D93 112018 R. Aaij et al. (LHCb Collab.)
AAIJ 16Z JHEP 1606 131 R. Aaij et al. (LHCb Collab.)
BHARDWAJ 16 PR D93 052016 V. Bhardwaj et al. (BELLE Collab.)
CHOBANOVA 16 PR D93 031101 V. Chobanova et al. (BELLE Collab.)
DEL-AMO-SA... 16 PR D93 052013 P. del Amo Sanchez et al. (BABAR Collab.)
GLATTAUER 16 PR D93 032006 R. Glattauer et al. (BELLE Collab.)
HAMER 16 PR D93 032007 P. Hamer et al. (BELLE Collab.)
KHACHATRY... 16D PL B753 424 V. Khachatryan et al. (CMS Collab.)
KING 16 PR D93 111101 Z. King et al. (BELLE Collab.)
LEES 16 PRL 116 041801 J.P. Lees et al. (BABAR Collab.)
LEES 16E PR D94 011101 J.P. Lees et al. (BABAR Collab.)
LEES 16H PR D94 091101 J.P. Lees et al. (BABAR Collab.)
SATO 16B PR D94 072007 Y. Sato et al. (BELLE Collab.)
VANHOEFER 16 PR D93 032010 P. Vanhoefer et al. (BELLE Collab.)
Also PR D94 099903 (errat.) P. Vanhoefer et al. (BELLE Collab.)
VOROBYEV 16 PR D94 052004 V. Vorobyev et al. (BELLE Collab.)
AAIJ 15AC JHEP 1505 019 R. Aaij et al. (LHCb Collab.)
AAIJ 15AS JHEP 1510 053 R. Aaij et al. (LHCb Collab.)
AAIJ 15AZ PRL 115 161802 R. Aaij et al. (LHCb Collab.)
AAIJ 15BB PR D92 112002 R. Aaij et al. (LHCb Collab.)
AAIJ 15D JHEP 1501 024 R. Aaij et al. (LHCb Collab.)
AAIJ 15F PRL 114 041601 R. Aaij et al. (LHCb Collab.)
AAIJ 15J PL B742 38 R. Aaij et al. (LHCb Collab.)
AAIJ 15N PRL 115 031601 R. Aaij et al. (LHCb Collab.)
AAIJ 15Q PRL 115 111803 R. Aaij et al. (LHCb Collab.)
AAIJ 15S PL B743 46 R. Aaij et al. (LHCb Collab.)

Downloaded from https://academic.oup.com/ptep/article/2022/8/083C01/6651666 by KIT Library user on 27 September 2022

AAIJ	15T	PL B747 468	R. Aaij *et al.*	(LHCb Collab.)
AAIJ	15X	PR D92 012012	R. Aaij *et al.*	(LHCb Collab.)
AAIJ	15Y	PR D92 032002	R. Aaij *et al.*	(LHCb Collab.)
AAIJ	15Z	JHEP 1504 064	R. Aaij *et al.*	(LHCb Collab.)
ABAZOV	15A	PRL 114 062001	V.M. Abazov *et al.*	(D0 Collab.)
ABDESSALAM	15	PRL 115 121604	A. Abdessalam *et al.*	(BABAR and BELLE Collabs.)
BALA	15	PR D91 051101	A. Bala *et al.*	(BELLE Collab.)
CHANG	15	PRL 115 221803	Y.-Y. Chang *et al.*	(BELLE Collab.)
CHOI	15A	PR D91 092011	S.-K. Choi *et al.*	(BELLE Collab.)
KHACHATRY...	15BE	NAT 522 68	V. Khachatryan *et al.*	(CMS and LHCb Collab.)
LEES	15	PR D91 012003	J.P. Lees *et al.*	(BABAR Collab.)
LEES	15A	PRL 114 081801	J.P. Lees *et al.*	(BABAR Collab.)
LEES	15B	PR D91 031102	J.P. Lees *et al.*	(BABAR Collab.)
LEES	15C	PR D91 052002	J.P. Lees *et al.*	(BABAR Collab.)
MATVIENKO	15	PR D92 012013	D. Matvienko *et al.*	(BELLE Collab.)
PAL	15	PR D92 011101	B. Pal *et al.*	(BELLE Collab.)
WIECHCZYN...	15	PR D91 032008	J. Wiechczynski *et al.*	(BELLE Collab.)
AAIJ	14AA	PRL 112 202001	R. Aaij *et al.*	(LHCb Collab.)
AAIJ	14AM	JHEP 1405 069	R. Aaij *et al.*	(LHCb Collab.)
AAIJ	14AN	JHEP 1409 177	R. Aaij *et al.*	(LHCb Collab.)
AAIJ	14BM	NJP 16 123001	R. Aaij *et al.*	(LHCb Collab.)
AAIJ	14BN	PR D90 112002	R. Aaij *et al.*	(LHCb Collab.)
AAIJ	14BP	PL B739 218	R. Aaij *et al.*	(LHCb Collab.)
AAIJ	14E	JHEP 1404 114	R. Aaij *et al.*	(LHCb Collab.)
AAIJ	14L	JHEP 1407 140	R. Aaij *et al.*	(LHCb Collab.)
AAIJ	14M	JHEP 1406 133	R. Aaij *et al.*	(LHCb Collab.)
AAIJ	14O	JHEP 1405 082	R. Aaij *et al.*	(LHCb Collab.)
AAIJ	14R	PL B736 446	R. Aaij *et al.*	(LHCb Collab.)
AAIJ	14X	PR D90 012003	R. Aaij *et al.*	(LHCb Collab.)
AAIJ	14Y	PRL 112 091802	R. Aaij *et al.*	(LHCb Collab.)
AALTONEN	14P	PRL 113 242001	T. Aaltonen *et al.*	(CDF Collab.)
ABAZOV	14	PR D89 012002	V.M. Abazov *et al.*	(D0 Collab.)
CHILIKIN	14	PR D90 112009	K. Chilikin *et al.*	(BELLE Collab.)
CHOBANOVA	14	PR D90 012002	V. Chobanova *et al.*	(BELLE Collab.)
IWASHITA	14	PTEP 2014 043C01	T. Iwashita *et al.*	(BELLE Collab.)
LAI	14	PR D89 051103	Y.-T. Lai *et al.*	(BELLE Collab.)
LEES	14	PR D89 051101	J.P. Lees *et al.*	(BABAR Collab.)
LEES	14B	PR D89 112002	J.P. Lees *et al.*	(BABAR Collab.)
LEES	14C	PR D89 071102	J.P. Lees *et al.*	(BABAR Collab.)
PDG	14	CP C38 070001	K. Olive *et al.*	(PDG Collab.)
SANTELJ	14	JHEP 1410 165	L. Santelj *et al.*	(BELLE Collab.)
SATO	14	PR D90 072009	S. Sato *et al.*	(BELLE Collab.)
VANHOEFER	14	PR D89 072008	P. Vanhoefer *et al.*	(BELLE Collab.)
AAD	13U	PR D87 032002	G. Aad *et al.*	(ATLAS Collab.)
AAIJ	13	NP B867 1	R. Aaij *et al.*	(LHCb Collab.)
AAIJ	13A	NP B867 547	R. Aaij *et al.*	(LHCb Collab.)
AAIJ	13AA	NP B871 403	R. Aaij *et al.*	(LHCb Collab.)
AAIJ	13AC	NP B874 663	R. Aaij *et al.*	(LHCb Collab.)
AAIJ	13AO	PR D87 092001	R. Aaij *et al.*	(LHCb Collab.)
AAIJ	13AP	PR D87 092007	R. Aaij *et al.*	(LHCb Collab.)
AAIJ	13AQ	PR D87 112009	R. Aaij *et al.*	(LHCb Collab.)
AAIJ	13AT	PR D88 052002	R. Aaij *et al.*	(LHCb Collab.)
AAIJ	13AW	PRL 110 211801	R. Aaij *et al.*	(LHCb Collab.)
AAIJ	13AX	PRL 110 221601	R. Aaij *et al.*	(LHCb Collab.)
AAIJ	13B	PRL 110 021801	R. Aaij *et al.*	(LHCb Collab.)
AAIJ	13BA	PRL 111 101805	R. Aaij *et al.*	(LHCb Collab.)
AAIJ	13BM	PRL 111 141801	R. Aaij *et al.*	(LHCb Collab.)
AAIJ	13BO	JHEP 1310 183	R. Aaij *et al.*	(LHCb Collab.)
AAIJ	13BP	JHEP 1310 143	R. Aaij *et al.*	(LHCb Collab.)
AAIJ	13BQ	JHEP 1310 005	R. Aaij *et al.*	(LHCb Collab.)
AAIJ	13BT	PR D88 072005	R. Aaij *et al.*	(LHCb Collab.)
AAIJ	13CF	EPJ C73 2655	R. Aaij *et al.*	(LHCb Collab.)
AAIJ	13E	PRL 110 031801	R. Aaij *et al.*	(LHCb Collab.)
AAIJ	13F	PL B719 318	R. Aaij *et al.*	(LHCb Collab.)
AAIJ	13K	PL B721 24	R. Aaij *et al.*	(LHCb Collab.)
AAIJ	13L	JHEP 1303 067	R. Aaij *et al.*	(LHCb Collab.)
AAIJ	13M	PR D87 052001	R. Aaij *et al.*	(LHCb Collab.)
AAIJ	13P	JHEP 1304 001	R. Aaij *et al.*	(LHCb Collab.)
AAIJ	13U	JHEP 1305 159	R. Aaij *et al.*	(LHCb Collab.)
AAIJ	13Y	JHEP 1308 131	R. Aaij *et al.*	(LHCb Collab.)
AAIJ	13Z	JHEP 1309 006	R. Aaij *et al.*	(LHCb Collab.)
AALTONEN	13F	PR D87 072003	T. Aaltonen *et al.*	(CDF Collab.)
CHATRCHYAN	13AW	PRL 111 101804	S. Chatrchyan *et al.*	(CMS Collab.)
CHATRCHYAN	13BL	PL B727 77	S. Chatrchyan *et al.*	(CMS Collab.)
CHILIKIN	13	PR D88 074026	K. Chilikin *et al.*	(BELLE Collab.)
DALSENO	13	PR D88 092003	J. Dalseno *et al.*	(BELLE Collab.)
DUH	13	PR D87 031103	Y. T. Duh *et al.*	(BELLE Collab.)
GAUR	13	PR D87 091101	V. Gaur *et al.*	(BELLE Collab.)
LEES	13D	PR D87 052009	J.P. Lees *et al.*	(BABAR Collab.)
LEES	13H	PR D87 092004	J.P. Lees *et al.*	(BABAR Collab.)
LEES	13I	PR D87 112005	J.P. Lees *et al.*	(BABAR Collab.)
LEES	13J	PR D88 012003	J.P. Lees *et al.*	(BABAR Collab.)
LEES	13M	PR D88 032012	J.P. Lees *et al.*	(BABAR Collab.)
LEES	13N	PRL 111 101802	J.P. Lees *et al.*	(BABAR Collab.)
Also		PRL 111 159901(errat.)	J.P. Lees *et al.*	(BABAR Collab.)
Also		PR D93 032001	J.P. Lees *et al.*	(BABAR Collab.)
LUTZ	13	PR D87 111103	O. Lutz *et al.*	(BELLE Collab.)
PRIM	13	PR D88 072004	M. Prim *et al.*	(BELLE Collab.)
SIBIDANOV	13	PR D88 032005	A. Sibidanov *et al.*	(BELLE Collab.)
AAIJ	12A	PL B708 55	R. Aaij *et al.*	(LHCb Collab.)
AAIJ	12AH	JHEP 1207 133	R. Aaij *et al.*	(LHCb Collab.)
AAIJ	12AM	PRL 109 131801	R. Aaij *et al.*	(LHCb Collab.)
AAIJ	12AR	JHEP 1210 037	R. Aaij *et al.*	(LHCb Collab.)
AAIJ	12AX	PR D86 112005	R. Aaij *et al.*	(LHCb Collab.)
AAIJ	12E	PL B708 241	R. Aaij *et al.*	(LHCb Collab.)
AAIJ	12I	PL B709 177	R. Aaij *et al.*	(LHCb Collab.)
AAIJ	12L	EPJ C72 2118	R. Aaij *et al.*	(LHCb Collab.)
AAIJ	12T	PRL 108 161801	R. Aaij *et al.*	(LHCb Collab.)
AAIJ	12U	PRL 108 181806	R. Aaij *et al.*	(LHCb Collab.)
AAIJ	12V	PRL 108 201601	R. Aaij *et al.*	(LHCb Collab.)
AAIJ	12W	PRL 108 231801	R. Aaij *et al.*	(LHCb Collab.)
AALTONEN	12L	PRL 108 211803	T. Aaltonen *et al.*	(CDF Collab.)
ABAZOV	12AC	PR D86 072009	V.M. Abazov *et al.*	(D0 Collab.)
ABAZOV	12U	PR D85 112003	V.M. Abazov *et al.*	(D0 Collab.)
ADACHI	12A	PRL 108 171802	I. Adachi *et al.*	(BELLE Collab.)
CHANG	12	PR D85 091102	M.-C. Chang *et al.*	(BELLE Collab.)
CHATRCHYAN	12A	JHEP 1204 033	S. Chatrchyan *et al.*	(CMS Collab.)
DALSENO	12	PR D86 092012	J. Dalseno *et al.*	(BELLE Collab.)
DEL-AMO-SA...	12	PR D85 092017	P. del Amo Sanchez *et al.*	(BABAR Collab.)
HIGUCHI	12	PR D85 071105	T. Higuchi *et al.*	(BELLE Collab.)
HOI	12	PRL 108 031801	C.-T. Hoi *et al.*	(BELLE Collab.)
HSU	12	PR D86 032002	C.-L. Hsu *et al.*	(BELLE Collab.)
KIM	12A	PR D86 031101	J.H. Kim *et al.*	(BELLE Collab.)
KRONENBIT...	12	PR D86 071103	B. Kronenbitter *et al.*	(BELLE Collab.)
LEES	12AA	PR D86 092004	J.P. Lees *et al.*	(BABAR Collab.)
LEES	12AF	PR D86 112006	J.P. Lees *et al.*	(BABAR Collab.)
LEES	12B	PR D85 052003	J.P. Lees *et al.*	(BABAR Collab.)
LEES	12D	PRL 109 101802	J.P. Lees *et al.*	(BABAR Collab.)
Also		PR D88 072012	J.P. Lees *et al.*	(BABAR Collab.)
LEES	12I	PR D85 054023	J.P. Lees *et al.*	(BABAR Collab.)
LEES	12K	PR D85 072005	J.P. Lees *et al.*	(BABAR Collab.)
LEES	12O	PR D85 112010	J.P. Lees *et al.*	(BABAR Collab.)
LEES	12T	PR D86 051105	J.P. Lees *et al.*	(BABAR Collab.)
LEES	12W	PRL 109 211801	J.P. Lees *et al.*	(BABAR Collab.)
NEGISHI	12	PR D86 011101	K. Negishi *et al.*	(BELLE Collab.)
PDG	12	PR D86 010001	J. Beringer *et al.*	(PDG Collab.)
ROHRKEN	12	PR D85 091106	M. Rohrken *et al.*	(BELLE Collab.)
SATO	12	PRL 108 171801	Y. Sato *et al.*	(BELLE Collab.)
AAIJ	11B	PL B699 330	R. Aaij *et al.*	(LHCb Collab.)
AAIJ	11E	PR D84 092001	R. Aaij *et al.*	(LHCb Collab.)
Also		PR D85 039904 (errat.)	R. Aaij *et al.*	(LHCb Collab.)
AALTONEN	11	PRL 106 121804	T. Aaltonen *et al.*	(CDF Collab.)
AALTONEN	11AG	PRL 107 191801	T. Aaltonen *et al.*	(CDF Collab.)
Also		PRL 107 239903 (errat.)	T. Aaltonen *et al.*	(CDF Collab.)
AALTONEN	11AI	PRL 107 201802	T. Aaltonen *et al.*	(CDF Collab.)
AALTONEN	11L	PRL 106 161801	T. Aaltonen *et al.*	(CDF Collab.)
AALTONEN	11N	PRL 106 181802	T. Aaltonen *et al.*	(CDF Collab.)
ABAZOV	11U	PR D84 052007	V.M. Abazov *et al.*	(D0 Collab.)
AUSHEV	11	PR D83 051102	T. Aushev *et al.*	(BELLE Collab.)
BAHINIPATI	11	PR D84 021101	S. Bahinipati *et al.*	(BELLE Collab.)
BHARDWAJ	11	PRL 107 091803	V. Bhardwaj *et al.*	(BELLE Collab.)
CHATRCHYAN	11T	PRL 107 191802	S. Chatrchyan *et al.*	(CMS Collab.)
CHOI	11	PR D84 052004	S.-K. Choi *et al.*	(BELLE Collab.)
DEL-AMO-SA...	11A	PR D83 032006	P. del Amo Sanchez *et al.*	(BABAR Collab.)
DEL-AMO-SA...	11B	PR D83 032004	P. del Amo Sanchez *et al.*	(BABAR Collab.)
DEL-AMO-SA...	11C	PR D83 032007	P. del Amo Sanchez *et al.*	(BABAR Collab.)
DEL-AMO-SA...	11F	PR D83 052011	P. del Amo Sanchez *et al.*	(BABAR Collab.)
DEL-AMO-SA...	11K	PR D83 091101	P. del Amo Sanchez *et al.*	(BABAR Collab.)
HA	11	PR D83 071101	H. Ha *et al.*	(BELLE Collab.)
LEES	11	PR D83 112010	J.P. Lees *et al.*	(BABAR Collab.)
LEES	11A	PR D84 012001	J.P. Lees *et al.*	(BABAR Collab.)
LEES	11F	PR D84 071102	J.P. Lees *et al.*	(BABAR Collab.)
LEES	11M	PR D84 112007	J.P. Lees *et al.*	(BABAR Collab.)
Also		PR D87 039901 (errat.)	J.P. Lees *et al.*	(BABAR Collab.)
SAHOO	11A	PR D84 071101	H. Sahoo *et al.*	(BELLE Collab.)
AUBERT	10	PRL 104 011802	B. Aubert *et al.*	(BABAR Collab.)
AUBERT	10D	PR D81 052009	B. Aubert *et al.*	(BABAR Collab.)
AUBERT	10H	PR D82 031102	B. Aubert *et al.*	(BABAR Collab.)
AUSHEV	10	PR D81 031103	T. Aushev *et al.*	(BELLE Collab.)
CHIANG	10	PR D81 071101	C.-C. Chiang *et al.*	(BELLE Collab.)
DAS	10	PR D82 051103	A. Das *et al.*	(BELLE Collab.)
DEL-AMO-SA...	10A	PR D82 011502	P. del Amo Sanchez *et al.*	(BABAR Collab.)
DEL-AMO-SA...	10B	PR D82 011101	P. del Amo Sanchez *et al.*	(BABAR Collab.)
DEL-AMO-SA...	10E	PR D82 031101	P. del Amo Sanchez *et al.*	(BABAR Collab.)
DEL-AMO-SA...	10Q	PR D82 112002	P. del Amo Sanchez *et al.*	(BABAR Collab.)
DUNGEL	10	PR D82 112007	W. Dungel *et al.*	(BELLE Collab.)
FUJIKAWA	10A	PR D81 011101	M. Fujikawa *et al.*	(BELLE Collab.)
HYUN	10	PRL 105 091801	H.J. Hyun *et al.*	(BELLE Collab.)
JOSHI	10	PR D81 031101	N.J. Joshi *et al.*	(BELLE Collab.)
NAKAHAMA	10	PR D82 073011	Y. Nakahama *et al.*	(BELLE Collab.)
WEDD	10	PR D81 111104	R. Wedd *et al.*	(BELLE Collab.)
AALTONEN	09B	PR D79 011104	T. Aaltonen *et al.*	(CDF Collab.)
AALTONEN	09C	PRL 103 031801	T. Aaltonen *et al.*	(CDF Collab.)
AALTONEN	09E	PR D79 032001	T. Aaltonen *et al.*	(CDF Collab.)
AALTONEN	09P	PRL 102 201801	T. Aaltonen *et al.*	(CDF Collab.)
ABAZOV	09E	PRL 102 032001	V.M. Abazov *et al.*	(D0 Collab.)
AUBERT	09	PR D79 011102	B. Aubert *et al.*	(BABAR Collab.)
AUBERT	09A	PR D79 012002	B. Aubert *et al.*	(BABAR Collab.)
AUBERT	09AA	PR D79 112001	B. Aubert *et al.*	(BABAR Collab.)
AUBERT	09AC	PR D79 112009	B. Aubert *et al.*	(BABAR Collab.)
AUBERT	09AD	PR D80 011101	B. Aubert *et al.*	(BABAR Collab.)
AUBERT	09AE	PR D80 031102	B. Aubert *et al.*	(BABAR Collab.)
AUBERT	09AF	PR D80 051101	B. Aubert *et al.*	(BABAR Collab.)
AUBERT	09AG	PR D80 051105	B. Aubert *et al.*	(BABAR Collab.)
AUBERT	09AL	PR D80 092007	B. Aubert *et al.*	(BABAR Collab.)
AUBERT	09AO	PRL 103 211802	B. Aubert *et al.*	(BABAR Collab.)
AUBERT	09AU	PR D80 112001	B. Aubert *et al.*	(BABAR Collab.)
AUBERT	09AV	PR D80 112002	B. Aubert *et al.*	(BABAR Collab.)
AUBERT	09B	PRL 102 132001	B. Aubert *et al.*	(BABAR Collab.)
AUBERT	09C	PR D79 032002	B. Aubert *et al.*	(BABAR Collab.)
AUBERT	09G	PRL 102 141802	B. Aubert *et al.*	(BABAR Collab.)
AUBERT	09H	PR D79 052005	B. Aubert *et al.*	(BABAR Collab.)
AUBERT	09I	PR D79 052003	B. Aubert *et al.*	(BABAR Collab.)
AUBERT	09K	PR D79 072009	B. Aubert *et al.*	(BABAR Collab.)
AUBERT	09S	PR D79 092002	B. Aubert *et al.*	(BABAR Collab.)
AUBERT	09T	PRL 102 091803	B. Aubert *et al.*	(BABAR Collab.)
Also		EPAPS Document No. E-PRLTAO-102-060910		(BABAR Collab.)
AUBERT	09Y	PRL 103 051803	B. Aubert *et al.*	(BABAR Collab.)
CHANG	09	PR D79 052006	Y.-W. Chang *et al.*	(BELLE Collab.)
DALSENO	09	PR D79 072004	J. Dalseno *et al.*	(BELLE Collab.)
KYEONG	09	PR D80 051103	S.-H. Kyeong *et al.*	(BELLE Collab.)
MIZUK	09	PR D80 031104	R. Mizuk *et al.*	(BELLE Collab.)
VERVINK	09	PR D80 111104	K. Vervink *et al.*	(BELLE Collab.)
WEI	09A	PRL 103 171801	J.-T. Wei *et al.*	(BELLE Collab.)
Also		EPAPS Supplement EPAPS_appendix.pdf		(BELLE Collab.)
ADACHI	08	PR D77 091101	I. Adachi *et al.*	(BELLE Collab.)
AUBERT	08AB	PR D78 012006	B. Aubert *et al.*	(BABAR Collab.)
AUBERT	08AC	PR D77 071102	B. Aubert *et al.*	(BABAR Collab.)
AUBERT	08AD	PR D77 091104	B. Aubert *et al.*	(BABAR Collab.)
AUBERT	08AF	PR D78 011103	B. Aubert *et al.*	(BABAR Collab.)
AUBERT	08AG	PR D78 011104	B. Aubert *et al.*	(BABAR Collab.)
AUBERT	08AH	PR D78 011107	B. Aubert *et al.*	(BABAR Collab.)
AUBERT	08AJ	PR D78 032005	B. Aubert *et al.*	(BABAR Collab.)
AUBERT	08AP	PR D78 051103	B. Aubert *et al.*	(BABAR Collab.)
AUBERT	08AQ	PR D78 052005	B. Aubert *et al.*	(BABAR Collab.)
AUBERT	08AU	PRL 101 021801	B. Aubert *et al.*	(BABAR Collab.)
AUBERT	08AV	PRL 101 081801	B. Aubert *et al.*	(BABAR Collab.)
AUBERT	08B	PR D77 011102	B. Aubert *et al.*	(BABAR Collab.)
AUBERT	08BA	PR D78 071102	B. Aubert *et al.*	(BABAR Collab.)
AUBERT	08BB	PR D78 071104	B. Aubert *et al.*	(BABAR Collab.)
AUBERT	08BC	PR D78 072007	B. Aubert *et al.*	(BABAR Collab.)
AUBERT	08BD	PR D78 091101	B. Aubert *et al.*	(BABAR Collab.)
AUBERT	08BG	PR D78 092008	B. Aubert *et al.*	(BABAR Collab.)
AUBERT	08BH	PR D78 112001	B. Aubert *et al.*	(BABAR Collab.)
AUBERT	08BK	PRL 101 201801	B. Aubert *et al.*	(BABAR Collab.)
AUBERT	08BL	PRL 101 261802	B. Aubert *et al.*	(BABAR Collab.)
AUBERT	08BN	PR D78 112003	B. Aubert *et al.*	(BABAR Collab.)
AUBERT	08C	PR D77 011104	B. Aubert *et al.*	(BABAR Collab.)
AUBERT	08E	PR D77 012003	B. Aubert *et al.*	(BABAR Collab.)
AUBERT	08F	PRL 100 051803	B. Aubert *et al.*	(BABAR Collab.)
AUBERT	08G	PRL 100 171803	B. Aubert *et al.*	(BABAR Collab.)
AUBERT	08H	PR D77 031101	B. Aubert *et al.*	(BABAR Collab.)
AUBERT	08I	PRL 100 081801	B. Aubert *et al.*	(BABAR Collab.)
AUBERT	08N	PRL 100 021801	B. Aubert *et al.*	(BABAR Collab.)
Also		PR D79 092002	B. Aubert *et al.*	(BABAR Collab.)
AUBERT	08P	PR D77 032007	B. Aubert *et al.*	(BABAR Collab.)
AUBERT	08Q	PRL 100 151802	B. Aubert *et al.*	(BABAR Collab.)
AUBERT	08R	PR D77 032002	B. Aubert *et al.*	(BABAR Collab.)
AUBERT	08W	PRL 101 082001	B. Aubert *et al.*	(BABAR Collab.)
AUBERT	08Y	PR D77 111101	B. Aubert *et al.*	(BABAR Collab.)
CHEN	08C	PRL 100 251801	J.-H. Chen *et al.*	(BELLE Collab.)
CHIANG	08	PR D78 111102	C.C. Chiang *et al.*	(BELLE Collab.)
CHOI	08	PRL 100 142001	S.-K. Choi *et al.*	(BELLE Collab.)
GOLDENZWE...	08	PRL 101 231801	P. Goldenzweig *et al.*	(BELLE Collab.)

Downloaded from https://academic.oup.com/ptep/article/2022/8/083C01/6651666 by KIT Library user on 27 September 2022

KIM	08	PL B669 287	H.O. Kim *et al.*	(BELLE Collab.)
KUMAR	08	PR D78 091104	R. Kumar *et al.*	(BELLE Collab.)
KUSAKA	08	PR D77 072001	A. Kusaka *et al.*	(BELLE Collab.)
LEE	08A	PR D77 071101	S.E. Lee *et al.*	(BELLE Collab.)
LI	08F	PRL 101 251601	J. Li *et al.*	(BELLE Collab.)
LIN	08	NAT 452 332	S.-W. Lin *et al.*	(BELLE Collab.)
LIU	08I	PR D78 011106	Y. Liu *et al.*	(BELLE Collab.)
LIVENTSEV	08	PR D77 091503	D. Liventsev *et al.*	(BELLE Collab.)
MIZUK	08	PR D78 072004	R. Mizuk *et al.*	(BELLE Collab.)
NAKAHAMA	08	PRL 100 121601	Y. Nakahama *et al.*	(BELLE Collab.)
PDG	08	PL B667 1	C. Amsler *et al.*	(PDG Collab.)
SAHOO	08	PR D77 091103	H. Sahoo *et al.*	(BELLE Collab.)
TANIGUCHI	08	PRL 101 111801	N. Taniguchi *et al.*	(BELLE Collab.)
UCHIDA	08	PR D77 051101	Y. Uchida *et al.*	(BELLE Collab.)
USHIRODA	08	PRL 100 021602	Y. Ushiroda *et al.*	(BELLE Collab.)
WEI	08A	PR D78 011101	J.-T. Wei *et al.*	(BELLE Collab.)
ABAZOV	07S	PRL 99 142001	V.M. Abazov *et al.*	(D0 Collab.)
ABULENCIA	07A	PRL 98 122001	A. Abulencia *et al.*	(FNAL CDF Collab.)
ADAM	07	PRL 99 041802	N.E. Adam *et al.*	(CLEO Collab.)
Also		PR D76 012007	D.M. Asner *et al.*	(CLEO Collab.)
AUBERT	07A	PRL 98 031801	B. Aubert *et al.*	(BABAR Collab.)
AUBERT	07AA	PR D76 012004	B. Aubert *et al.*	(BABAR Collab.)
AUBERT	07AC	PR D76 031101	B. Aubert *et al.*	(BABAR Collab.)
AUBERT	07AD	PR D76 031102	B. Aubert *et al.*	(BABAR Collab.)
AUBERT	07AE	PR D76 031103	B. Aubert *et al.*	(BABAR Collab.)
AUBERT	07AF	PRL 99 021603	B. Aubert *et al.*	(BABAR Collab.)
AUBERT	07AG	PRL 99 051801	B. Aubert *et al.*	(BABAR Collab.)
AUBERT	07AI	PRL 99 071801	B. Aubert *et al.*	(BABAR Collab.)
AUBERT	07AJ	PRL 99 081801	B. Aubert *et al.*	(BABAR Collab.)
AUBERT	07AN	PR D76 051101	B. Aubert *et al.*	(BABAR Collab.)
AUBERT	07AO	PR D76 051103	B. Aubert *et al.*	(BABAR Collab.)
AUBERT	07AQ	PR D76 071101	B. Aubert *et al.*	(BABAR Collab.)
AUBERT	07AS	PR D76 071104	B. Aubert *et al.*	(BABAR Collab.)
AUBERT	07AT	PR D76 091101	B. Aubert *et al.*	(BABAR Collab.)
AUBERT	07AV	PR D76 092004	B. Aubert *et al.*	(BABAR Collab.)
AUBERT	07AX	PRL 99 161802	B. Aubert *et al.*	(BABAR Collab.)
AUBERT	07AY	PRL 99 171803	B. Aubert *et al.*	(BABAR Collab.)
AUBERT	07B	PR D75 012008	B. Aubert *et al.*	(BABAR Collab.)
AUBERT	07BC	PR D76 091102	B. Aubert *et al.*	(BABAR Collab.)
AUBERT	07BF	PR D76 052007	B. Aubert *et al.*	(BABAR Collab.)
AUBERT	07BH	PRL 99 231802	B. Aubert *et al.*	(BABAR Collab.)
AUBERT	07BI	PRL 99 241803	B. Aubert *et al.*	(BABAR Collab.)
AUBERT	07BO	PR D76 111102	B. Aubert *et al.*	(BABAR Collab.)
AUBERT	07D	PRL 98 051801	B. Aubert *et al.*	(BABAR Collab.)
AUBERT	07E	PRL 98 051802	B. Aubert *et al.*	(BABAR Collab.)
AUBERT	07F	PRL 98 051803	B. Aubert *et al.*	(BABAR Collab.)
AUBERT	07G	PRL 98 111801	B. Aubert *et al.*	(BABAR Collab.)
AUBERT	07H	PR D75 031101	B. Aubert *et al.*	(BABAR Collab.)
AUBERT	07J	PRL 98 091801	B. Aubert *et al.*	(BABAR Collab.)
AUBERT	07K	PRL 98 081801	B. Aubert *et al.*	(BABAR Collab.)
AUBERT	07L	PRL 98 151802	B. Aubert *et al.*	(BABAR Collab.)
AUBERT	07N	PR D75 072002	B. Aubert *et al.*	(BABAR Collab.)
AUBERT	07O	PRL 98 181803	B. Aubert *et al.*	(BABAR Collab.)
AUBERT	07Q	PR D75 051102	B. Aubert *et al.*	(BABAR Collab.)
AUBERT	07R	PRL 98 211804	B. Aubert *et al.*	(BABAR Collab.)
Also		PRL 100 189903E	B. Aubert *et al.*	(BABAR Collab.)
Also		PRL 100 199905E	B. Aubert *et al.*	(BABAR Collab.)
AUBERT	07Y	PR D75 111102	B. Aubert *et al.*	(BABAR Collab.)
CHANG	07A	PRL 98 131803	M.-C. Chang *et al.*	(BELLE Collab.)
CHANG	07B	PR D75 071104	P. Chang *et al.*	(BELLE Collab.)
CHAO	07	PR D76 091103	Y. Chao *et al.*	(BELLE Collab.)
CHEN	07	PRL 98 031802	K.-F. Chen *et al.*	(BELLE Collab.)
CHEN	07D	PRL 99 221802	K.-F. Chen *et al.*	(BELLE Collab.)
DALSENO	07	PR D76 072004	J. Dalseno *et al.*	(BELLE Collab.)
FRATINA	07	PRL 98 221802	S. Fratina *et al.*	(BELLE Collab.)
GARMASH	07	PR D75 012006	A. Garmash *et al.*	(BELLE Collab.)
HOKUUE	07	PL B648 139	T. Hokuue *et al.*	(BELLE Collab.)
ISHINO	07	PRL 98 211801	H. Ishino *et al.*	(BELLE Collab.)
KUSAKA	07	PRL 98 221602	A. Kusaka *et al.*	(BELLE Collab.)
Also		PR D77 072001	A. Kusaka *et al.*	(BELLE Collab.)
KUZMIN	07	PR D76 012006	A. Kuzmin *et al.*	(BELLE Collab.)
LIN	07	PRL 98 181804	S.-W. Lin *et al.*	(BELLE Collab.)
LIN	07A	PRL 99 121601	S.-W. Lin *et al.*	(BELLE Collab.)
MATYJA	07	PRL 99 191807	A. Matyja *et al.*	(BELLE Collab.)
MEDVEDEVA	07	PR D76 051102	T. Medvedeva *et al.*	(BELLE Collab.)
PARK	07	PR D75 011101	K.S. Park *et al.*	(BELLE Collab.)
SCHUEMANN	07	PR D75 092002	J. Schuemann *et al.*	(BELLE Collab.)
SOMOV	07	PR D76 011104	A. Somov *et al.*	(BELLE Collab.)
TSAI	07	PR D75 111101	Y.-T. Tsai *et al.*	(BELLE Collab.)
URQUIJO	07	PR D75 032001	P. Urquijo *et al.*	(BELLE Collab.)
WANG	07B	PR D75 092005	C.H. Wang *et al.*	(BELLE Collab.)
WANG	07C	PR D76 052004	M.-Z. Wang *et al.*	(BELLE Collab.)
XIE	07	PR D75 017101	Q.L. Xie *et al.*	(BELLE Collab.)
ZUPANC	07	PR D75 091102	A. Zupanc *et al.*	(BELLE Collab.)
ABAZOV	06S	PR D74 092001	V.M. Abazov *et al.*	(D0 Collab.)
ABAZOV	06W	PR D74 112002	V.M. Abazov *et al.*	(D0 Collab.)
ABULENCIA,A	06D	PRL 97 211802	A. Abulencia *et al.*	(CDF Collab.)
ACOSTA	06	PRL 96 202001	D. Acosta *et al.*	(CDF Collab.)
AUBERT	06	PR D73 011101	B. Aubert *et al.*	(BABAR Collab.)
AUBERT	06A	PRL 96 011803	B. Aubert *et al.*	(BABAR Collab.)
AUBERT	06E	PRL 96 052002	B. Aubert *et al.*	(BABAR Collab.)
AUBERT	06G	PR D73 012004	B. Aubert *et al.*	(BABAR Collab.)
AUBERT	06I	PR D73 031101	B. Aubert *et al.*	(BABAR Collab.)
AUBERT	06L	PR D74 012001	B. Aubert *et al.*	(BABAR Collab.)
AUBERT	06N	PR D74 031103	B. Aubert *et al.*	(BABAR Collab.)
AUBERT	06S	PRL 96 241802	B. Aubert *et al.*	(BABAR Collab.)
AUBERT	06T	PRL 96 251802	B. Aubert *et al.*	(BABAR Collab.)
AUBERT	06V	PRL 97 051802	B. Aubert *et al.*	(BABAR Collab.)
AUBERT	06W	PR D73 071102	B. Aubert *et al.*	(BABAR Collab.)
AUBERT	06X	PR D73 071103	B. Aubert *et al.*	(BABAR Collab.)
AUBERT	06Y	PR D73 111101	B. Aubert *et al.*	(BABAR Collab.)
AUBERT,B	06A	PR D73 112004	B. Aubert *et al.*	(BABAR Collab.)
AUBERT,B	06B	PR D74 011101	B. Aubert *et al.*	(BABAR Collab.)
AUBERT,B	06C	PR D74 011102	B. Aubert *et al.*	(BABAR Collab.)
AUBERT,B	06E	PR D74 011106	B. Aubert *et al.*	(BABAR Collab.)
AUBERT,B	06G	PRL 97 201801	B. Aubert *et al.*	(BABAR Collab.)
AUBERT,B	06H	PRL 97 201802	B. Aubert *et al.*	(BABAR Collab.)
AUBERT,B	06J	PR D73 092001	B. Aubert *et al.*	(BABAR Collab.)
AUBERT,B	06K	PRL 97 211801	B. Aubert *et al.*	(BABAR Collab.)
AUBERT,B	06L	PR D74 031101	B. Aubert *et al.*	(BABAR Collab.)
AUBERT,B	06M	PR D74 031102	B. Aubert *et al.*	(BABAR Collab.)
AUBERT,B	06O	PR D74 031104	B. Aubert *et al.*	(BABAR Collab.)
AUBERT,B	06P	PR D74 031105	B. Aubert *et al.*	(BABAR Collab.)
AUBERT,B	06Q	PR D74 091101	B. Aubert *et al.*	(BABAR Collab.)
AUBERT,B	06R	PR D74 032005	B. Aubert *et al.*	(BABAR Collab.)
AUBERT,B	06S	PR D74 051101	B. Aubert *et al.*	(BABAR Collab.)
AUBERT,B	06T	PR D74 051102	B. Aubert *et al.*	(BABAR Collab.)
AUBERT,B	06V	PR D74 051106	B. Aubert *et al.*	(BABAR Collab.)
AUBERT,B	06Y	PR D74 091105	B. Aubert *et al.*	(BABAR Collab.)
AUBERT,B	06Z	PR D74 092004	B. Aubert *et al.*	(BABAR Collab.)
AUBERT,BE	06C	PRL 97 171805	B. Aubert *et al.*	(BABAR Collab.)
AUBERT,BE	06H	PRL 97 261803	B. Aubert *et al.*	(BABAR Collab.)
AUBERT,BE	06J	PR D74 111102	B. Aubert *et al.*	(BABAR Collab.)
AUBERT,BE	06N	PR D74 072008	B. Aubert *et al.*	(BABAR Collab.)
BLYTH	06	PR D74 092002	S. Blyth *et al.*	(BELLE Collab.)
CHISTOV	06A	PR D74 111105	R. Chistov *et al.*	(BELLE Collab.)
DRAGIC	06	PR D73 111105	J. Dragic *et al.*	(BELLE Collab.)
GABYSHEV	06	PRL 97 202003	N. Gabyshev *et al.*	(BELLE Collab.)
GOKHROO	06	PRL 97 162002	G. Gokhroo *et al.*	(BELLE Collab.)
JEN	06	PR D74 111101	C.-M. Jen *et al.*	(BELLE Collab.)
KROKOVNY	06	PRL 97 081801	P. Krokovny *et al.*	(BELLE Collab.)
MOHAPATRA	06	PRL 96 221601	D. Mohapatra *et al.*	(BELLE Collab.)
NAKANO	06	PR D73 112002	E. Nakano *et al.*	(BELLE Collab.)
RONGA	06	PR D73 092003	F.J. Ronga *et al.*	(BELLE Collab.)
SCHUEMANN	06	PRL 97 061802	J. Schuemann *et al.*	(BELLE Collab.)
SOMOV	06	PRL 96 171801	A. Somov *et al.*	(BELLE Collab.)
SONI	06	PL B634 155	N. Soni *et al.*	(BELLE Collab.)
USHIRODA	06	PR D74 111104	Y. Ushiroda *et al.*	(BELLE Collab.)
VILLA	06	PR D73 051107	S. Villa *et al.*	(BELLE Collab.)
ABAZOV	05B	PRL 94 042001	V.M. Abazov *et al.*	(D0 Collab.)
ABAZOV	05C	PRL 94 102001	V.M. Abazov *et al.*	(D0 Collab.)
ABAZOV	05D	PRL 94 182001	V.M. Abazov *et al.*	(D0 Collab.)
ABAZOV	05W	PRL 95 171801	V.M. Abazov *et al.*	(D0 Collab.)
ABE	05A	PRL 94 221805	K. Abe *et al.*	(BELLE Collab.)
ABE	05B	PR D71 072003	K. Abe *et al.*	(BELLE Collab.)
Also		PR D71 079903 (errat.)	K. Abe *et al.*	(BELLE Collab.)
ABE	05D	PRL 95 101801	K. Abe *et al.*	(BELLE Collab.)
ABE	05G	PRL 95 231802	K. Abe *et al.*	(BELLE Collab.)
ACOSTA	05	PRL 94 101803	D. Acosta *et al.*	(CDF Collab.)
AUBERT	05	PRL 94 011801	B. Aubert *et al.*	(BABAR Collab.)
AUBERT	05B	PR D71 031501	B. Aubert *et al.*	(BABAR Collab.)
AUBERT	05E	PR D71 051502	B. Aubert *et al.*	(BABAR Collab.)
AUBERT	05F	PRL 94 161803	B. Aubert *et al.*	(BABAR Collab.)
AUBERT	05I	PRL 94 131801	B. Aubert *et al.*	(BABAR Collab.)
AUBERT	05J	PRL 94 141801	B. Aubert *et al.*	(BABAR Collab.)
AUBERT	05K	PRL 94 171801	B. Aubert *et al.*	(BABAR Collab.)
AUBERT	05L	PRL 94 181802	B. Aubert *et al.*	(BABAR Collab.)
AUBERT	05M	PRL 94 191802	B. Aubert *et al.*	(BABAR Collab.)
AUBERT	05O	PR D71 031103	B. Aubert *et al.*	(BABAR Collab.)
AUBERT	05P	PR D71 032005	B. Aubert *et al.*	(BABAR Collab.)
AUBERT	05T	PR D71 091102	B. Aubert *et al.*	(BABAR Collab.)
AUBERT	05U	PR D71 091103	B. Aubert *et al.*	(BABAR Collab.)
AUBERT	05V	PR D71 091104	B. Aubert *et al.*	(BABAR Collab.)
AUBERT	05W	PRL 94 221803	B. Aubert *et al.*	(BABAR Collab.)
AUBERT	05Y	PR D71 111102	B. Aubert *et al.*	(BABAR Collab.)
AUBERT	05Z	PR D71 112003	B. Aubert *et al.*	(BABAR Collab.)
AUBERT,B	05	PRL 95 011801	B. Aubert *et al.*	(BABAR Collab.)
AUBERT,B	05C	PRL 95 041805	B. Aubert *et al.*	(BABAR Collab.)
AUBERT,B	05K	PRL 95 131803	B. Aubert *et al.*	(BABAR Collab.)
AUBERT,B	05O	PR D72 051102	B. Aubert *et al.*	(BABAR Collab.)
AUBERT,B	05P	PR D72 051103	B. Aubert *et al.*	(BABAR Collab.)
AUBERT,B	05Q	PR D72 051106	B. Aubert *et al.*	(BABAR Collab.)
AUBERT,B	05Z	PRL 95 131802	B. Aubert *et al.*	(BABAR Collab.)
AUBERT,BE	05	PRL 95 151803	B. Aubert *et al.*	(BABAR Collab.)
AUBERT,BE	05A	PRL 95 151804	B. Aubert *et al.*	(BABAR Collab.)
AUBERT,BE	05B	PRL 95 171802	B. Aubert *et al.*	(BABAR Collab.)
AUBERT,BE	05C	PR D72 091103	B. Aubert *et al.*	(BABAR Collab.)
AUBERT,BE	05E	PRL 95 221801	B. Aubert *et al.*	(BABAR Collab.)
AUBERT,BE	05F	PR D72 111101	B. Aubert *et al.*	(BABAR Collab.)
CHANG	05	PR D71 072007	M.-C. Chang *et al.*	(BELLE Collab.)
CHANG	05A	PR D71 091106	P. Chang *et al.*	(BELLE Collab.)
CHAO	05	PRL 94 181803	Y. Chao *et al.*	(BELLE Collab.)
CHAO	05A	PR D71 031502	Y. Chao *et al.*	(BELLE Collab.)
CHEN	05A	PRL 94 221804	K.-F. Chen *et al.*	(BELLE Collab.)
CHEN	05B	PR D72 012004	K.-F. Chen *et al.*	(BELLE Collab.)
DRUTSKOY	05	PRL 94 061802	A. Drutskoy *et al.*	(BELLE Collab.)
GERSHON	05	PL B624 11	T. Gershon *et al.*	(BELLE Collab.)
ITOH	05	PRL 95 091601	R. Itoh *et al.*	(BELLE Collab.)
LIVENTSEV	05	PR D72 051109	D. Liventsev *et al.*	(BELLE Collab.)
MAJUMDER	05	PRL 95 041803	G. Majumder *et al.*	(BELLE Collab.)
MIYAKE	05	PL B618 34	H. Miyake *et al.*	(BELLE Collab.)
MOHAPATRA	05	PR D72 011101	D. Mohapatra *et al.*	(BELLE Collab.)
NISHIDA	05	PL B610 23	S. Nishida *et al.*	(BELLE Collab.)
OKABE	05	PL B614 27	T. Okabe *et al.*	(BELLE Collab.)
PARK	05	PRL 94 021801	H.K. Park *et al.*	(FNAL HyperCP Collab.)
SCHUMANN	05	PR D72 011103	J. Schumann *et al.*	(BELLE Collab.)
SUMISAWA	05	PRL 95 061801	K. Sumisawa *et al.*	(BELLE Collab.)
USHIRODA	05	PRL 94 231601	Y. Ushiroda *et al.*	(BELLE Collab.)
WANG	05	PRL 94 121801	C.C. Wang *et al.*	(BELLE Collab.)
WANG	05A	PL B617 141	M.-Z. Wang *et al.*	(BELLE Collab.)
XIE	05	PR D72 051105	Q.L. Xie *et al.*	(BELLE Collab.)
YANG	05	PRL 94 111802	H. Yang *et al.*	(BELLE Collab.)
ZHANG	05B	PR D71 091107	L.M. Zhang *et al.*	(BELLE Collab.)
ABDALLAH	04D	EPJ C33 213	J. Abdallah *et al.*	(DELPHI Collab.)
ABDALLAH	04E	EPJ C33 307	J. Abdallah *et al.*	(DELPHI Collab.)
ABE	04E	PRL 93 021601	K. Abe *et al.*	(BELLE Collab.)
AUBERT	04A	PR D69 011102	B. Aubert *et al.*	(BABAR Collab.)
AUBERT	04B	PR D69 032004	B. Aubert *et al.*	(BABAR Collab.)
AUBERT	04C	PRL 92 111801	B. Aubert *et al.*	(BABAR Collab.)
AUBERT	04G	PR D69 031102	B. Aubert *et al.*	(BABAR Collab.)
AUBERT	04H	PRL 92 061801	B. Aubert *et al.*	(BABAR Collab.)
AUBERT	04M	PRL 92 201802	B. Aubert *et al.*	(BABAR Collab.)
AUBERT	04R	PR D69 052001	B. Aubert *et al.*	(BABAR Collab.)
AUBERT	04U	PR D69 091503	B. Aubert *et al.*	(BABAR Collab.)
AUBERT	04V	PRL 92 251801	B. Aubert *et al.*	(BABAR Collab.)
AUBERT	04W	PRL 92 251802	B. Aubert *et al.*	(BABAR Collab.)
AUBERT	04Y	PRL 93 041801	B. Aubert *et al.*	(BABAR Collab.)
AUBERT	04Z	PRL 93 051802	B. Aubert *et al.*	(BABAR Collab.)
AUBERT,B	04B	PR D70 011101	B. Aubert *et al.*	(BABAR Collab.)
AUBERT,B	04C	PR D70 012007	B. Aubert *et al.*	(BABAR Collab.)
Also		PRL 92 181801	B. Aubert *et al.*	(BABAR Collab.)
AUBERT,B	04D	PR D70 032006	B. Aubert *et al.*	(BABAR Collab.)
AUBERT,B	04G	PRL 93 071801	B. Aubert *et al.*	(BABAR Collab.)
AUBERT,B	04H	PRL 93 081801	B. Aubert *et al.*	(BABAR Collab.)
AUBERT,B	04J	PRL 93 091802	B. Aubert *et al.*	(BABAR Collab.)
AUBERT,B	04K	PRL 93 131801	B. Aubert *et al.*	(BABAR Collab.)
AUBERT,B	04M	PRL 93 131805	B. Aubert	(BABAR Collab.)
AUBERT,B	04O	PR D70 091103	B. Aubert *et al.*	(BABAR Collab.)
AUBERT,B	04R	PRL 93 231801	B. Aubert *et al.*	(BABAR Collab.)
AUBERT,B	04S	PRL 93 181801	B. Aubert *et al.*	(BABAR Collab.)
AUBERT,B	04T	PR D70 091104	B. Aubert *et al.*	(BABAR Collab.)
AUBERT,B	04U	PR D70 091105	B. Aubert *et al.*	(BABAR Collab.)
AUBERT,B	04V	PRL 93 181805	B. Aubert *et al.*	(BABAR Collab.)
AUBERT,B	04W	PRL 93 231804	B. Aubert *et al.*	(BABAR Collab.)
AUBERT,B	04X	PRL 93 181806	B. Aubert *et al.*	(BABAR Collab.)
AUBERT,B	04Z	PRL 93 201801	B. Aubert *et al.*	(BABAR Collab.)
AUBERT,BE	04	PR D70 111102	B. Aubert *et al.*	(BABAR Collab.)
AUBERT,BE	04A	PR D70 112006	B. Aubert *et al.*	(BABAR Collab.)
AUBERT,BE	04B	PR D70 091106	B. Aubert *et al.*	(BABAR Collab.)
AUSHEV	04	PRL 93 201802	T. Aushev *et al.*	(BELLE Collab.)
BORNHEIM	04	PRL 93 241802	A. Bornheim *et al.*	(CLEO Collab.)
CHANG	04	PL B599 148	P. Chang *et al.*	(BELLE Collab.)
CHAO	04	PR D69 111102	Y. Chao *et al.*	(BELLE Collab.)
CHAO	04B	PRL 93 191802	Y. Chao *et al.*	(BELLE Collab.)

Downloaded from https://academic.oup.com/ptep/article/2022/8/083C01/6651666 by KIT Library user on 27 September 2022

DRAGIC	04	PRL 93 131802	J. Dragic	(BELLE Collab.)
DRUTSKOY	04	PRL 92 051801	A. Drutskoy *et al.*	(BELLE Collab.)
GARMASH	04	PR D69 012001	A. Garmash *et al.*	(BELLE Collab.)
KATAOKA	04	PRL 93 261801	S.U. Kataoka *et al.*	(BELLE Collab.)
MAJUMDER	04	PR D70 111103	G. Majumder *et al.*	(BELLE Collab.)
NAKAO	04	PR D69 112001	M. Nakao *et al.*	(BELLE Collab.)
SARANGI	04	PRL 93 031802	T.R. Sarangi *et al.*	(BELLE Collab.)
WANG	04	PRL 92 131801	M.Z. Wang *et al.*	(BELLE Collab.)
WANG	04A	PR D70 012001	C.H. Wang *et al.*	(BELLE Collab.)
ABDALLAH	03B	EPJ C28 155	J. Abdallah *et al.*	(DELPHI Collab.)
ABE	03B	PR D67 032003	K. Abe *et al.*	(BELLE Collab.)
ABE	03C	PR D67 031102	K. Abe *et al.*	(BELLE Collab.)
ABE	03G	PR D68 012001	K. Abe *et al.*	(BELLE Collab.)
ABE	03H	PRL 91 261602	K. Abe *et al.*	(BELLE Collab.)
ADAM	03	PR D67 032001	N.E. Adam *et al.*	(CLEO Collab.)
ATHAR	03	PR D68 072003	S.B. Athar *et al.*	(CLEO Collab.)
AUBERT	03B	PRL 90 091801	B. Aubert *et al.*	(BABAR Collab.)
AUBERT	03C	PR D67 072002	B. Aubert *et al.*	(BABAR Collab.)
AUBERT	03D	PRL 90 181803	B. Aubert *et al.*	(BABAR Collab.)
AUBERT	03E	PRL 90 181801	B. Aubert *et al.*	(BABAR Collab.)
AUBERT	03H	PR D67 091101	B. Aubert *et al.*	(BABAR Collab.)
AUBERT	03I	PR D67 092003	B. Aubert *et al.*	(BABAR Collab.)
AUBERT	03J	PRL 90 221801	B. Aubert *et al.*	(BABAR Collab.)
AUBERT	03K	PRL 90 231801	B. Aubert *et al.*	(BABAR Collab.)
AUBERT	03L	PRL 91 021801	B. Aubert *et al.*	(BABAR Collab.)
AUBERT	03N	PRL 91 061802	B. Aubert *et al.*	(BABAR Collab.)
AUBERT	03O	PRL 91 071801	B. Aubert *et al.*	(BABAR Collab.)
AUBERT	03Q	PRL 91 131801	B. Aubert *et al.*	(BABAR Collab.)
AUBERT	03S	PRL 91 241801	B. Aubert *et al.*	(BABAR Collab.)
AUBERT	03T	PRL 91 201802	B. Aubert *et al.*	(BABAR Collab.)
AUBERT	03U	PRL 91 221802	B. Aubert *et al.*	(BABAR Collab.)
AUBERT	03V	PRL 91 171802	B. Aubert *et al.*	(BABAR Collab.)
AUBERT	03W	PRL 91 161801	B. Aubert *et al.*	(BABAR Collab.)
AUBERT	03X	PR D68 092001	B. Aubert *et al.*	(BABAR Collab.)
BORNHEIM	03	PR D68 052002	A. Bornheim *et al.*	(CLEO Collab.)
CHANG	03	PR D68 111101	M.-C. Chang *et al.*	(BELLE Collab.)
CHEN	03B	PRL 91 201801	K.-F. Chen *et al.*	(BELLE Collab.)
CSORNA	03	PR D67 112002	S.E. Csorna *et al.*	(CLEO Collab.)
EISENSTEIN	03	PR D68 017101	B.I. Eisenstein *et al.*	(CLEO Collab.)
FANG	03	PRL 90 071801	F. Fang *et al.*	(BELLE Collab.)
GABYSHEV	03	PRL 90 121802	N. Gabyshev *et al.*	(BELLE Collab.)
HASTINGS	03	PR D67 052004	N.C. Hastings *et al.*	(BELLE Collab.)
ISHIKAWA	03	PRL 91 261601	A. Ishikawa *et al.*	(BELLE Collab.)
KROKOVNY	03	PRL 90 141802	P. Krokovny *et al.*	(BELLE Collab.)
KROKOVNY	03B	PRL 91 262002	P. Krokovny *et al.*	(BELLE Collab.)
LEE	03	PRL 91 261801	S.H. Lee *et al.*	(BELLE Collab.)
SATPATHY	03	PL B553 159	A. Satpathy *et al.*	(BELLE Collab.)
WANG	03	PRL 90 201802	M.-Z. Wang *et al.*	(BELLE Collab.)
ZHENG	03	PR D67 092004	Y. Zheng *et al.*	(BELLE Collab.)
ABE	02	PRL 88 021801	K. Abe *et al.*	(BELLE Collab.)
ABE	02E	PL B526 258	K. Abe *et al.*	(BELLE Collab.)
ABE	02F	PL B526 247	K. Abe *et al.*	(BELLE Collab.)
ABE	02H	PRL 88 171801	K. Abe *et al.*	(BELLE Collab.)
ABE	02J	PRL 88 052002	K. Abe *et al.*	(BELLE Collab.)
ABE	02K	PRL 88 181803	K. Abe *et al.*	(BELLE Collab.)
ABE	02M	PRL 89 071801	K. Abe *et al.*	(BELLE Collab.)
ABE	02N	PL B538 11	K. Abe *et al.*	(BELLE Collab.)
ABE	02O	PR D65 091103	K. Abe *et al.*	(BELLE Collab.)
ABE	02Q	PRL 89 122001	K. Abe *et al.*	(BELLE Collab.)
ABE	02U	PR D66 032007	K. Abe *et al.*	(BELLE Collab.)
ABE	02W	PRL 89 151802	K. Abe *et al.*	(BELLE Collab.)
ABE	02Z	PR D66 071102	K. Abe *et al.*	(BELLE Collab.)
ACOSTA	02C	PR D65 092009	D. Acosta *et al.*	(CDF Collab.)
ACOSTA	02G	PR D66 112002	D. Acosta *et al.*	(CDF Collab.)
AFFOLDER	02B	PRL 88 071801	T. Affolder *et al.*	(CDF Collab.)
AHMED	02B	PR D66 031101	S. Ahmed *et al.*	(CLEO Collab.)
ASNER	02	PR D65 031103	D.M. Asner *et al.*	(CLEO Collab.)
AUBERT	02	PR D65 032001	B. Aubert *et al.*	(BABAR Collab.)
AUBERT	02C	PRL 88 101805	B. Aubert *et al.*	(BABAR Collab.)
AUBERT	02D	PR D65 051502	B. Aubert *et al.*	(BABAR Collab.)
AUBERT	02E	PR D65 051101	B. Aubert *et al.*	(BABAR Collab.)
AUBERT	02H	PRL 89 011802	B. Aubert *et al.*	(BABAR Collab.)
Also		PRL 89 169903 (errat.)	B. Aubert *et al.*	(BABAR Collab.)
AUBERT	02I	PRL 88 221802	B. Aubert *et al.*	(BABAR Collab.)
AUBERT	02J	PRL 88 221803	B. Aubert *et al.*	(BABAR Collab.)
AUBERT	02K	PRL 88 231801	B. Aubert *et al.*	(BABAR Collab.)
AUBERT	02L	PRL 88 241801	B. Aubert *et al.*	(BABAR Collab.)
AUBERT	02M	PRL 89 061801	B. Aubert *et al.*	(BABAR Collab.)
AUBERT	02N	PR D66 032003	B. Aubert *et al.*	(BABAR Collab.)
AUBERT	02P	PRL 89 201802	B. Aubert *et al.*	(BABAR Collab.)
AUBERT	02Q	PRL 89 281802	B. Aubert *et al.*	(BABAR Collab.)
BRIERE	02	PRL 89 081803	R. Briere *et al.*	(CLEO Collab.)
CASEY	02	PR D66 092002	B.C.K. Casey *et al.*	(BELLE Collab.)
CHEN	02B	PL B546 196	K.-F. Chen *et al.*	(BELLE Collab.)
COAN	02	PRL 88 062001	T.E. Coan *et al.*	(CLEO Collab.)
Also		PRL 88 069902 (errat.)	T.E. Coan *et al.*	(CLEO Collab.)
DRUTSKOY	02	PL B542 171	A. Drutskoy *et al.*	(BELLE Collab.)
DYTMAN	02	PR D66 091101	S.A. Dytman *et al.*	(CLEO Collab.)
ECKHART	02	PRL 89 251801	E. Eckhart *et al.*	(CLEO Collab.)
EDWARDS	02	PR D65 012002	K.W. Edwards *et al.*	(CLEO Collab.)
GABYSHEV	02	PR D66 091102	N. Gabyshev *et al.*	(BELLE Collab.)
GODANG	02	PRL 88 021802	R. Godang *et al.*	(CLEO Collab.)
GORDON	02	PL B542 183	A. Gordon *et al.*	(BELLE Collab.)
HARA	02	PRL 89 251803	K. Hara *et al.*	(BELLE Collab.)
KROKOVNY	02	PRL 89 231804	P. Korkovny *et al.*	(BELLE Collab.)
MAHAPATRA	02	PRL 88 101803	R. Mahapatra *et al.*	(CLEO Collab.)
NISHIDA	02	PRL 89 231801	S. Nishida *et al.*	(BELLE Collab.)
TOMURA	02	PL B542 207	T. Tomura *et al.*	(BELLE Collab.)
ABASHIAN	01	PRL 86 2509	A. Abashian *et al.*	(BELLE Collab.)
ABE	01D	PRL 86 3228	K. Abe *et al.*	(BELLE Collab.)
ABE	01G	PRL 87 091802	K. Abe *et al.*	(BELLE Collab.)
ABE	01H	PRL 87 101801	K. Abe *et al.*	(BELLE Collab.)
ABE	01I	PRL 87 111801	K. Abe *et al.*	(BELLE Collab.)
ABE	01K	PR D64 071101	K. Abe *et al.*	(BELLE Collab.)
ABE	01L	PRL 87 161601	K. Abe *et al.*	(BELLE Collab.)
ABE	01M	PL B517 309	K. Abe *et al.*	(BELLE Collab.)
ABREU	01H	PL B510 55	P. Abreu *et al.*	(DELPHI Collab.)
ALEXANDER	01B	PR D64 092001	J.P. Alexander *et al.*	(CLEO Collab.)
AMMAR	01B	PRL 87 271801	R. Ammar *et al.*	(CLEO Collab.)
ANDERSON	01	PRL 86 2732	S. Anderson *et al.*	(CLEO Collab.)
ANDERSON	01B	PRL 87 181803	S. Anderson *et al.*	(CLEO Collab.)
AUBERT	01	PRL 86 2515	B. Aubert *et al.*	(BABAR Collab.)
AUBERT	01B	PRL 87 091801	B. Aubert *et al.*	(BABAR Collab.)
AUBERT	01D	PRL 87 151801	B. Aubert *et al.*	(BABAR Collab.)
AUBERT	01E	PRL 87 151802	B. Aubert *et al.*	(BABAR Collab.)
AUBERT	01F	PRL 87 201803	B. Aubert *et al.*	(BABAR Collab.)
AUBERT	01G	PRL 87 221802	B. Aubert *et al.*	(BABAR Collab.)
AUBERT	01H	PRL 87 241801	B. Aubert *et al.*	(BABAR Collab.)
AUBERT	01I	PRL 87 241803	B. Aubert *et al.*	(BABAR Collab.)
BARATE	01D	EPJ C20 431	R. Barate *et al.*	(ALEPH Collab.)
BRIERE	01	PRL 86 3718	R.A. Biere *et al.*	(CLEO Collab.)
EDWARDS	01	PRL 86 30	K.W. Edwards *et al.*	(CLEO Collab.)
JAFFE	01	PRL 86 5000	D. Jaffe *et al.*	(CLEO Collab.)
RICHICHI	01	PR D63 031103	S.J. Richichi *et al.*	(CLEO Collab.)
ABBIENDI	00Q	PL B482 15	G. Abbiendi *et al.*	(OPAL Collab.)
ABBIENDI,G	00B	PL B493 266	G. Abbiendi *et al.*	(OPAL Collab.)
ABE	00C	PR D62 071101	K. Abe *et al.*	(SLD Collab.)
AFFOLDER	00C	PR D61 072005	T. Affolder *et al.*	(CDF Collab.)
AFFOLDER	00N	PRL 85 4668	T. Affolder *et al.*	(CDF Collab.)
AHMED	00B	PR D62 112003	S. Ahmed *et al.*	(CLEO Collab.)
ANASTASSOV	00	PRL 84 1393	A. Anastassov *et al.*	(CLEO Collab.)
ARTUSO	00	PRL 84 4292	M. Artuso *et al.*	(CLEO Collab.)
AVERY	00	PR D62 051101	P. Avery *et al.*	(CLEO Collab.)
BARATE	00Q	PL B492 259	R. Barate *et al.*	(ALEPH Collab.)
BARATE	00R	PL B492 275	R. Barate *et al.*	(ALEPH Collab.)
BEHRENS	00	PR D61 052001	B.H. Behrens *et al.*	(CLEO Collab.)
BEHRENS	00B	PL B490 36	B.H. Behrens *et al.*	(CLEO Collab.)
BERGFELD	00B	PR D62 091102	T. Bergfeld *et al.*	(CLEO Collab.)
CHEN	00	PRL 85 525	S. Chen *et al.*	(CLEO Collab.)
COAN	00	PRL 84 5283	T.E. Coan *et al.*	(CLEO Collab.)
CRONIN-HEN...	00	PRL 85 515	D. Cronin-Hennessy *et al.*	(CLEO Collab.)
CSORNA	00	PR D61 111101	S.E. Csorna *et al.*	(CLEO Collab.)
JESSOP	00	PRL 85 2881	C.P. Jessop *et al.*	(CLEO Collab.)
LIPELES	00	PR D62 032005	E. Lipeles *et al.*	(CLEO Collab.)
RICHICHI	00	PRL 85 520	S.J. Richichi *et al.*	(CLEO Collab.)
ABBIENDI	99J	EPJ C12 609	G. Abbiendi *et al.*	(OPAL Collab.)
ABE	99K	PR D60 051101	F. Abe *et al.*	(CDF Collab.)
ABE	99Q	PR D60 072003	F. Abe *et al.*	(CDF Collab.)
AFFOLDER	99B	PRL 83 3378	T. Affolder *et al.*	(CDF Collab.)
AFFOLDER	99C	PR D60 112004	T. Affolder *et al.*	(CDF Collab.)
ARTUSO	99	PRL 82 3020	M. Artuso *et al.*	(CLEO Collab.)
BARTELT	99	PRL 82 3746	J. Bartelt *et al.*	(CLEO Collab.)
COAN	99	PR D59 111101	T.E. Coan *et al.*	(CLEO Collab.)
ABE	98B	PR D57 5382	F. Abe *et al.*	(CDF Collab.)
ABE	98C	PRL 80 2057	F. Abe *et al.*	(CDF Collab.)
Also		PR D59 032001	F. Abe *et al.*	(CDF Collab.)
ABE	98O	PR D58 072001	F. Abe *et al.*	(CDF Collab.)
ABE	98Q	PR D58 092002	F. Abe *et al.*	(CDF Collab.)
ABE	98U	PRL 81 5513	F. Abe *et al.*	(CDF Collab.)
ABE	98V	PRL 81 5742	F. Abe *et al.*	(CDF Collab.)
ACCIARRI	98D	EPJ C5 195	M. Acciarri *et al.*	(L3 Collab.)
ACCIARRI	98S	PL B438 417	M. Acciarri *et al.*	(L3 Collab.)
ACKERSTAFF	98Z	EPJ C5 379	K. Ackerstaff *et al.*	(OPAL Collab.)
BARATE	98Q	EPJ C4 387	R. Barate *et al.*	(ALEPH Collab.)
BEHRENS	98	PRL 80 3710	B.H. Behrens *et al.*	(CLEO Collab.)
BERGFELD	98	PRL 81 272	T. Bergfeld *et al.*	(CLEO Collab.)
BRANDENB...	98	PRL 80 2762	G. Brandenbrug *et al.*	(CLEO Collab.)
GODANG	98	PRL 80 3456	R. Godang *et al.*	(CLEO Collab.)
NEMATI	98	PR D57 5363	B. Nemati *et al.*	(CLEO Collab.)
ABE	97J	PRL 79 590	K. Abe *et al.*	(SLD Collab.)
ABREU	97F	ZPHY C74 19	P. Abreu *et al.*	(DELPHI Collab.)
Also		ZPHY C75 579 (erratum)	P. Abreu *et al.*	(DELPHI Collab.)
ABREU	97N	ZPHY C76 579	P. Abreu *et al.*	(DELPHI Collab.)
ACCIARRI	97B	PL B391 474	M. Acciarri *et al.*	(L3 Collab.)
ACCIARRI	97C	PL B391 481	M. Acciarri *et al.*	(L3 Collab.)
ACKERSTAFF	97G	PL B395 128	K. Ackerstaff *et al.*	(OPAL Collab.)
ACKERSTAFF	97U	ZPHY C76 401	K. Ackerstaff *et al.*	(OPAL Collab.)
ACKERSTAFF	97V	ZPHY C76 417	K. Ackerstaff *et al.*	(OPAL Collab.)
ARTUSO	97	PL B399 321	M. Artuso *et al.*	(CLEO Collab.)
ASNER	97	PRL 79 799	D. Asner *et al.*	(CLEO Collab.)
ATHANAS	97	PRL 79 2208	M. Athanas *et al.*	(CLEO Collab.)
BUSKULIC	97	PL B395 373	D. Buskulic *et al.*	(ALEPH Collab.)
BUSKULIC	97D	ZPHY C75 397	D. Buskulic *et al.*	(ALEPH Collab.)
FU	97	PRL 79 3125	X. Fu *et al.*	(CLEO Collab.)
JESSOP	97	PRL 79 4533	C.P. Jessop *et al.*	(CLEO Collab.)
ABE	96B	PR D53 3496	F. Abe *et al.*	(CDF Collab.)
ABE	96C	PRL 76 4462	F. Abe *et al.*	(CDF Collab.)
ABE	96H	PRL 76 2015	F. Abe *et al.*	(CDF Collab.)
ABE	96Q	PR D54 6596	F. Abe *et al.*	(CDF Collab.)
ABREU	96P	ZPHY C71 539	P. Abreu *et al.*	(DELPHI Collab.)
ABREU	96Q	ZPHY C72 17	P. Abreu *et al.*	(DELPHI Collab.)
ACCIARRI	96E	PL B383 487	M. Acciarri *et al.*	(L3 Collab.)
ADAM	96D	ZPHY C72 207	W. Adam *et al.*	(DELPHI Collab.)
ALBRECHT	96D	PL B374 256	H. Albrecht *et al.*	(ARGUS Collab.)
ALEXANDER	96T	PRL 77 5000	J.P. Alexander *et al.*	(CLEO Collab.)
ALEXANDER	96V	ZPHY C72 377	G. Alexander *et al.*	(OPAL Collab.)
ASNER	96	PR D53 1039	D.M. Asner *et al.*	(CLEO Collab.)
BARISH	96B	PRL 76 1570	B.C. Barish *et al.*	(CLEO Collab.)
BISHAI	96	PL B369 186	M. Bishai *et al.*	(CLEO Collab.)
BUSKULIC	96J	ZPHY C71 31	D. Buskulic *et al.*	(ALEPH Collab.)
BUSKULIC	96V	PL B384 471	D. Buskulic *et al.*	(ALEPH Collab.)
DUBOSCQ	96	PRL 76 3898	J.E. Duboscq *et al.*	(CLEO Collab.)
GIBAUT	96	PR D53 4734	D. Gibaut *et al.*	(CLEO Collab.)
PDG	96	PR D54 1	R. M. Barnett *et al.*	(PDG Collab.)
ABE	95Z	PRL 75 3068	F. Abe *et al.*	(CDF Collab.)
ABREU	95N	PL B357 255	P. Abreu *et al.*	(DELPHI Collab.)
ABREU	95Q	ZPHY C68 13	P. Abreu *et al.*	(DELPHI Collab.)
ACCIARRI	95H	PL B363 127	M. Acciarri *et al.*	(L3 Collab.)
ACCIARRI	95I	PL B363 137	M. Acciarri *et al.*	(L3 Collab.)
ADAM	95	ZPHY C68 363	W. Adam *et al.*	(DELPHI Collab.)
AKERS	95J	ZPHY C66 555	R. Akers *et al.*	(OPAL Collab.)
AKERS	95T	ZPHY C67 379	R. Akers *et al.*	(OPAL Collab.)
ALEXANDER	95	PL B341 435	J. Alexander *et al.*	(CLEO Collab.)
Also		PL B347 469 (erratum)	J. Alexander *et al.*	(CLEO Collab.)
BARISH	95	PR D51 1014	B.C. Barish *et al.*	(CLEO Collab.)
BUSKULIC	95N	PL B359 236	D. Buskulic *et al.*	(ALEPH Collab.)
ABE	94D	PRL 72 3456	F. Abe *et al.*	(CDF Collab.)
ABREU	94M	PL B338 409	P. Abreu *et al.*	(DELPHI Collab.)
AKERS	94C	PL B327 411	R. Akers *et al.*	(OPAL Collab.)
AKERS	94H	PL B336 585	R. Akers *et al.*	(OPAL Collab.)
AKERS	94J	PL B337 196	R. Akers *et al.*	(OPAL Collab.)
AKERS	94L	PL B337 393	R. Akers *et al.*	(OPAL Collab.)
ALAM	94	PR D50 43	M.S. Alam *et al.*	(CLEO Collab.)
ALBRECHT	94	PL B324 249	H. Albrecht *et al.*	(ARGUS Collab.)
ALBRECHT	94G	PL B340 217	H. Albrecht *et al.*	(ARGUS Collab.)
AMMAR	94	PR D49 5701	R. Ammar *et al.*	(CLEO Collab.)
ATHANAS	94	PRL 73 3503	M. Athanas *et al.*	(CLEO Collab.)
Also		PRL 74 3090 (erratum)	M. Athanas *et al.*	(CLEO Collab.)
BUSKULIC	94B	PL B322 441	D. Buskulic *et al.*	(ALEPH Collab.)
PDG	94	PR D50 1173	L. Montanet *et al.*	(CERN, LBL, BOST+)
PROCARIO	94	PRL 73 1472	M. Procario *et al.*	(CLEO Collab.)
STONE	94	HEPSY 93-11	S. Stone	
Published in B Decays, 2nd Edition, World Scientific, Singapore				
ABREU	93D	ZPHY C57 181	P. Abreu *et al.*	(DELPHI Collab.)
ABREU	93G	PL B312 253	P. Abreu *et al.*	(DELPHI Collab.)
ACTON	93C	PL B307 247	P.D. Acton *et al.*	(OPAL Collab.)
ALBRECHT	93	ZPHY C57 533	H. Albrecht *et al.*	(ARGUS Collab.)
ALBRECHT	93E	ZPHY C60 11	H. Albrecht *et al.*	(ARGUS Collab.)
ALEXANDER	93B	PL B319 365	J. Alexander *et al.*	(CLEO Collab.)
AMMAR	93	PRL 71 674	R. Ammar *et al.*	(CLEO Collab.)
BARTELT	93	PRL 71 1680	J.E. Bartelt *et al.*	(CLEO Collab.)
BATTLE	93	PRL 71 3922	M. Battle *et al.*	(CLEO Collab.)
BEAN	93B	PRL 70 2681	A. Bean *et al.*	(CLEO Collab.)

Downloaded from https://academic.oup.com/ptep/article/2022/8/083C01/6651666 by KIT Library user on 27 September 2022

BUSKULIC	93D	PL B307 194	D. Buskulic *et al.*	(ALEPH Collab.)
Also		PL B325 537 (erratum)	D. Buskulic *et al.*	(ALEPH Collab.)
BUSKULIC	93K	PL B313 498	D. Buskulic *et al.*	(ALEPH Collab.)
SANGHERA	93	PR D47 791	S. Sanghera *et al.*	(CLEO Collab.)
ALBRECHT	92C	PL B275 195	H. Albrecht *et al.*	(ARGUS Collab.)
ALBRECHT	92G	ZPHY C54 1	H. Albrecht *et al.*	(ARGUS Collab.)
ALBRECHT	92L	ZPHY C55 357	H. Albrecht *et al.*	(ARGUS Collab.)
BORTOLETTO	92	PR D45 21	D. Bortoletto *et al.*	(CLEO Collab.)
HENDERSON	92	PR D45 2212	S. Henderson *et al.*	(CLEO Collab.)
KRAMER	92	PL B279 181	G. Kramer, W.F. Palmer	(HAMB, OSU)
ALBAJAR	91E	PL B273 540	C. Albajar *et al.*	(UA1 Collab.)
ALBRECHT	91B	PL B254 288	H. Albrecht *et al.*	(ARGUS Collab.)
ALBRECHT	91C	PL B255 297	H. Albrecht *et al.*	(ARGUS Collab.)
ALBRECHT	91E	PL B262 148	H. Albrecht *et al.*	(ARGUS Collab.)
BERKELMAN	91	ARNPS 41 1	K. Berkelman, S. Stone	(CORN, SYRA)
"Decays of B Mesons"				
FULTON	91	PR D43 651	R. Fulton *et al.*	(CLEO Collab.)
ALBRECHT	90B	PL B241 278	H. Albrecht *et al.*	(ARGUS Collab.)
ALBRECHT	90J	ZPHY C48 543	H. Albrecht *et al.*	(ARGUS Collab.)
ANTREASYAN	90B	ZPHY C48 553	D. Antreasyan *et al.*	(Crystal Ball Collab.)
BORTOLETTO	90	PRL 64 2117	D. Bortoletto *et al.*	(CLEO Collab.)
ELSEN	90	ZPHY C46 349	E. Elsen *et al.*	(JADE Collab.)
ROSNER	90	PR D42 3732	J.L. Rosner	
WAGNER	90	PRL 64 1095	S.R. Wagner *et al.*	(Mark II Collab.)
ALBRECHT	89C	PL B219 121	H. Albrecht *et al.*	(ARGUS Collab.)
ALBRECHT	89G	PL B229 304	H. Albrecht *et al.*	(ARGUS Collab.)
ALBRECHT	89J	PL B229 175	H. Albrecht *et al.*	(ARGUS Collab.)
ALBRECHT	89L	PL B232 554	H. Albrecht *et al.*	(ARGUS Collab.)
ARTUSO	89	PRL 62 2233	M. Artuso *et al.*	(CLEO Collab.)
AVERILL	89	PR D39 123	D.A. Averill *et al.*	(HRS Collab.)
AVERY	89B	PL B223 470	P. Avery *et al.*	(CLEO Collab.)
BEBEK	89	PRL 62 8	C. Bebek *et al.*	(CLEO Collab.)
BORTOLETTO	89	PRL 62 2436	D. Bortoletto *et al.*	(CLEO Collab.)
BORTOLETTO	89B	PRL 63 1667	D. Bortoletto *et al.*	(CLEO Collab.)
ALBRECHT	88F	PL B209 119	H. Albrecht *et al.*	(ARGUS Collab.)
ALBRECHT	88K	PL B215 424	H. Albrecht *et al.*	(ARGUS Collab.)
ALBRECHT	87C	PL B185 218	H. Albrecht *et al.*	(ARGUS Collab.)
ALBRECHT	87D	PL B199 451	H. Albrecht *et al.*	(ARGUS Collab.)
ALBRECHT	87I	PL B192 245	H. Albrecht *et al.*	(ARGUS Collab.)
ALBRECHT	87J	PL B197 452	H. Albrecht *et al.*	(ARGUS Collab.)
AVERY	87	PL B183 429	P. Avery *et al.*	(CLEO Collab.)
BEAN	87B	PRL 58 183	A. Bean *et al.*	(CLEO Collab.)
BEBEK	87	PR D36 1289	C. Bebek *et al.*	(CLEO Collab.)
ALAM	86	PR D34 3279	M.S. Alam *et al.*	(CLEO Collab.)
ALBRECHT	86F	PL B182 95	H. Albrecht *et al.*	(ARGUS Collab.)
PDG	86	PL 170B 1	M. Aguilar-Benitez *et al.*	(CERN, CIT+)
CHEN	85	PR D31 2386	A. Chen *et al.*	(CLEO Collab.)
HAAS	85	PRL 55 1248	J. Haas *et al.*	(CLEO Collab.)
AVERY	84	PRL 53 1309	P. Avery *et al.*	(CLEO Collab.)
GILES	84	PR D30 2279	R. Giles *et al.*	(CLEO Collab.)
BEHRENDS	83	PRL 50 881	S. Behrends *et al.*	(CLEO Collab.)

$B^\pm/B^0$ ADMIXTURE

B DECAY MODES

The branching fraction measurements are for an admixture of B mesons at the $\Upsilon(4S)$. The values quoted assume that $B(\Upsilon(4S) \to B\overline{B}) = 100\%$.

For inclusive branching fractions, *e.g.*, $B \to D^\pm$ *anything*, the treatment of multiple D's in the final state must be defined. One possibility would be to count the number of events with one-or-more D's and divide by the total number of B's. Another possibility would be to count the total number of D's and divide by the total number of B's, which is the definition of average multiplicity. The two definitions are identical if only one D is allowed in the final state. Even though the "one-or-more" definition seems sensible, for practical reasons inclusive branching fractions are almost always measured using the multiplicity definition. For heavy final state particles, authors call their results inclusive branching fractions while for light particles some authors call their results multiplicities. In the B sections, we list all results as inclusive branching fractions, adopting a multiplicity definition. This means that inclusive branching fractions can exceed 100% and that inclusive partial widths can exceed total widths, just as inclusive cross sections can exceed total cross section.

$\overline{B}$ modes are charge conjugates of the modes below. Reactions indicate the weak decay vertex and do not include mixing.

	Mode		Fraction (Γ_i/Γ)	Scale factor/ Confidence level
	Semileptonic and leptonic modes			
Γ_1	$e^+\nu_e$ anything	[a]		
Γ_2	$\mu^+\nu_\mu$ anything	[a]		
Γ_3	$\ell^+\nu_\ell$ anything	[a,b]	(10.84 ± 0.16) %	
Γ_4	$D^-\ell^+\nu_\ell$ anything	[b]	(2.6 ± 0.5) %	
Γ_5	$\overline{D}^0\ell^+\nu_\ell$ anything	[b]	(7.3 ± 1.5) %	
Γ_6	$\overline{D}\ell^+\nu_\ell$		(2.42 ± 0.12) %	
Γ_7	$D^{*-}\ell^+\nu_\ell$ anything	[c]	$(6.7 \pm 1.3) \times 10^{-3}$	
Γ_8	$D^{*0}\ell^+\nu_\ell$ anything			
Γ_9	$\overline{D}^*\ell^+\nu_\ell$	[d]	(4.95 ± 0.11) %	
Γ_{10}	$\overline{D}^{**}\ell^+\nu_\ell$	[b,e]	(2.7 ± 0.7) %	
Γ_{11}	$\overline{D}_1(2420)\ell^+\nu_\ell$ anything		$(3.8 \pm 1.3) \times 10^{-3}$	S=2.4
Γ_{12}	$\overline{D}\pi\ell^+\nu_\ell$ anything + $\overline{D}^*\pi\ell^+\nu_\ell$ anything		(2.6 ± 0.5) %	S=1.5
Γ_{13}	$\overline{D}\pi\ell^+\nu_\ell$ anything		(1.5 ± 0.6) %	
Γ_{14}	$\overline{D}^*\pi\ell^+\nu_\ell$ anything		(1.9 ± 0.4) %	
Γ_{15}	$\overline{D}_2^*(2460)\ell^+\nu_\ell$ anything		$(4.4 \pm 1.6) \times 10^{-3}$	
Γ_{16}	$D^{*-}\pi^+\ell^+\nu_\ell$ anything		(1.00 ± 0.34) %	
Γ_{17}	$\overline{D}\pi^+\pi^-\ell^+\nu_\ell$		$(1.62 \pm 0.32) \times 10^{-3}$	
Γ_{18}	$\overline{D}^*\pi^+\pi^-\ell^+\nu_\ell$		$(9.4 \pm 3.2) \times 10^{-4}$	
Γ_{19}	$D_s^-\ell^+\nu_\ell$ anything	[b]	$< 7 \times 10^{-3}$	CL=90%
Γ_{20}	$D_s^-\ell^+\nu_\ell K^+$ anything	[b]	$< 5 \times 10^{-3}$	CL=90%
Γ_{21}	$D_s^-\ell^+\nu_\ell K^0$ anything	[b]	$< 7 \times 10^{-3}$	CL=90%
Γ_{22}	$X_c\ell^+\nu_\ell$		(10.65 ± 0.16) %	
Γ_{23}	$X_u\ell^+\nu_\ell$		$(1.91 \pm 0.27) \times 10^{-3}$	
Γ_{24}	$X_u e^+\nu_e$		$(1.57 \pm 0.19) \times 10^{-3}$	
Γ_{25}	$X_u\mu^+\nu_\mu$		$(1.62 \pm 0.21) \times 10^{-3}$	
Γ_{26}	$K^+\ell^+\nu_\ell$ anything	[b]	(6.3 ± 0.6) %	
Γ_{27}	$K^-\ell^+\nu_\ell$ anything	[b]	$(10 \pm 4) \times 10^{-3}$	
Γ_{28}	$K^0/\overline{K}^0\ell^+\nu_\ell$ anything	[b]	(4.6 ± 0.5) %	
Γ_{29}	$\overline{D}\tau^+\nu_\tau$		$(8.2 \pm 0.8) \times 10^{-3}$	
Γ_{30}	$\overline{D}^*\tau^+\nu_\tau$		(1.46 ± 0.08) %	
	D, D^*, or D_s modes			
Γ_{31}	$D^\pm$ anything		(23.1 ± 1.2) %	
Γ_{32}	$D^0/\overline{D}^0$ anything		(61.6 ± 2.9) %	S=1.3
Γ_{33}	$D^*(2010)^\pm$ anything		(22.5 ± 1.5) %	
Γ_{34}	$\overline{D}^*(2007)^0$ anything		(26.0 ± 2.7) %	
Γ_{35}	$D_s^\pm$ anything	[f]	(8.3 ± 0.8) %	
Γ_{36}	$D_s^{*\pm}$ anything		(6.3 ± 1.0) %	
Γ_{37}	$D_s^{*\pm}\overline{D}^{(*)}$		(3.4 ± 0.6) %	
Γ_{38}	$\overline{D}D_{s0}(2317)$		seen	
Γ_{39}	$\overline{D}D_{sJ}(2457)$		seen	
Γ_{40}	$D^{(*)}\overline{D}^{(*)}K^0 + D^{(*)}\overline{D}^{(*)}K^\pm$	[f,g]	$(7.1 {}^{+2.7}_{-1.7})$ %	
Γ_{41}	$b \to c\overline{c}s$		(22 ± 4) %	
Γ_{42}	$D_s^{(*)}\overline{D}^{(*)}$	[f,g]	(3.9 ± 0.4) %	
Γ_{43}	$D^*D^*(2010)^\pm$	[f]	$< 5.9 \times 10^{-3}$	CL=90%
Γ_{44}	$DD^*(2010)^\pm + D^*D^\pm$	[f]	$< 5.5 \times 10^{-3}$	CL=90%
Γ_{45}	$DD^\pm$	[f]	$< 3.1 \times 10^{-3}$	CL=90%
Γ_{46}	$D_s^{(*)\pm}\overline{D}^{(*)}X(n\pi^\pm)$	[f,g]	$(9 {}^{+5}_{-4})$ %	
Γ_{47}	$\overline{D}^*(2010)\gamma$		$< 1.1 \times 10^{-3}$	CL=90%
Γ_{48}	$D_s^+\pi^-$, $D_s^{*+}\pi^-$, $D_s^+\rho^-$, $D_s^{*+}\rho^-$, $D_s^+\pi^0$, $D_s^{*+}\pi^0$, $D_s^+\eta$, $D_s^{*+}\eta$, $D_s^+\rho^0$, $D_s^{*+}\rho^0$, $D_s^+\omega$, $D_s^{*+}\omega$	[f]	$< 4 \times 10^{-4}$	CL=90%
Γ_{49}	$D_{s1}(2536)^+$ anything		$< 9.5 \times 10^{-3}$	CL=90%
	Charmonium modes			
Γ_{50}	$J/\psi(1S)$ anything		(1.094 ± 0.032) %	S=1.1
Γ_{51}	$J/\psi(1S)$ (direct) anything		$(7.8 \pm 0.4) \times 10^{-3}$	S=1.1
Γ_{52}	$\psi(2S)$ anything		$(3.07 \pm 0.21) \times 10^{-3}$	
Γ_{53}	$\chi_{c1}(1P)$ anything		$(3.55 \pm 0.27) \times 10^{-3}$	S=1.3
Γ_{54}	$\chi_{c1}(1P)$ (direct) anything		$(3.08 \pm 0.19) \times 10^{-3}$	
Γ_{55}	$\chi_{c2}(1P)$ anything		$(10.0 \pm 1.7) \times 10^{-4}$	S=1.6
Γ_{56}	$\chi_{c2}(1P)$ (direct) anything		$(7.5 \pm 1.1) \times 10^{-4}$	
Γ_{57}	$\eta_c(1S)$ anything		$< 9 \times 10^{-3}$	CL=90%
Γ_{58}	$K\chi_{c1}(3872)$		$(2.3 \pm 0.7) \times 10^{-4}$	
Γ_{59}	$KX(3940)$, $X \to D^{*0}D^0$		$< 6.7 \times 10^{-5}$	CL=90%
Γ_{60}	$K\chi_{c0}(3915)$, $\chi_{c0} \to \omega J/\psi$	[h]	$(7.1 \pm 3.4) \times 10^{-5}$	
	K or K^* modes			
Γ_{61}	$K^\pm$ anything	[f]	(78.9 ± 2.5) %	
Γ_{62}	K^+ anything		(66 ± 5) %	
Γ_{63}	K^- anything		(13 ± 4) %	
Γ_{64}	$K^0/\overline{K}^0$ anything	[f]	(64 ± 4) %	
Γ_{65}	$K^*(892)^\pm$ anything		(18 ± 6) %	
Γ_{66}	$K^*(892)^0/\overline{K}^*(892)^0$ anything	[f]	(14.6 ± 2.6) %	
Γ_{67}	$K^*(892)\gamma$		$(4.2 \pm 0.6) \times 10^{-5}$	
Γ_{68}	$\eta K\gamma$		$(8.5 {}^{+1.8}_{-1.6}) \times 10^{-6}$	
Γ_{69}	$K_1(1400)\gamma$		$< 1.27 \times 10^{-4}$	CL=90%
Γ_{70}	$K_2^*(1430)\gamma$		$(1.7 {}^{+0.6}_{-0.5}) \times 10^{-5}$	
Γ_{71}	$K_2(1770)\gamma$		$< 1.2 \times 10^{-3}$	CL=90%
Γ_{72}	$K_3^*(1780)\gamma$		$< 3.7 \times 10^{-5}$	CL=90%
Γ_{73}	$K_4^*(2045)\gamma$		$< 1.0 \times 10^{-3}$	CL=90%
Γ_{74}	$K\eta'(958)$		$(8.3 \pm 1.1) \times 10^{-5}$	
Γ_{75}	$K^*(892)\eta'(958)$		$(4.1 \pm 1.1) \times 10^{-6}$	
Γ_{76}	$K\eta$		$< 5.2 \times 10^{-6}$	CL=90%
Γ_{77}	$K^*(892)\eta$		$(1.8 \pm 0.5) \times 10^{-5}$	

Downloaded from https://academic.oup.com/ptep/article/2022/8/083C01/6651666 by KIT Library user on 27 September 2022

Γ_{78}	$K\phi\phi$		$(2.3 \pm 0.9) \times 10^{-6}$	
Γ_{79}	$\overline{b} \to \overline{s}\gamma$		$(3.49 \pm 0.19) \times 10^{-4}$	
Γ_{80}	$\overline{b} \to \overline{d}\gamma$		$(9.2 \pm 3.0) \times 10^{-6}$	
Γ_{81}	$\overline{b} \to \overline{s}$gluon		< 6.8 %	CL=90%
Γ_{82}	η anything		$(2.6 {}^{+0.5}_{-0.8}) \times 10^{-4}$	
Γ_{83}	η' anything		$(4.2 \pm 0.9) \times 10^{-4}$	
Γ_{84}	K^+gluon (charmless)		$< 1.87 \times 10^{-4}$	CL=90%
Γ_{85}	K^0gluon (charmless)		$(1.9 \pm 0.7) \times 10^{-4}$	

Light unflavored meson modes

Γ_{86}	$\rho\gamma$		$(1.39 \pm 0.25) \times 10^{-6}$	S=1.2
Γ_{87}	$\rho/\omega\gamma$		$(1.30 \pm 0.23) \times 10^{-6}$	S=1.2
Γ_{88}	$\pi^{\pm}$ anything	[f,i]	(358 ± 7) %	
Γ_{89}	π^0 anything		(235 ± 11) %	
Γ_{90}	η anything		(17.6 ± 1.6) %	
Γ_{91}	ρ^0 anything		(21 ± 5) %	
Γ_{92}	ω anything		< 81 %	CL=90%
Γ_{93}	ϕ anything		(3.43 ± 0.12) %	
Γ_{94}	$\phi K^*(892)$		$< 2.2 \times 10^{-5}$	CL=90%
Γ_{95}	$\overline{b} \to \overline{d}$ gluon			
Γ_{96}	π^+ gluon (charmless)		$(3.7 \pm 0.8) \times 10^{-4}$	

Baryon modes

Γ_{97}	$\Lambda_c^+ / \overline{\Lambda}_c^-$ anything		(3.6 ± 0.4) %	
Γ_{98}	Λ_c^+ anything		< 1.3 %	CL=90%
Γ_{99}	$\overline{\Lambda}_c^-$ anything		< 7 %	CL=90%
Γ_{100}	$\overline{\Lambda}_c^- \ell^+$ anything		$< 9 \times 10^{-4}$	CL=90%
Γ_{101}	$\overline{\Lambda}_c^- e^+$ anything		$< 1.8 \times 10^{-3}$	CL=90%
Γ_{102}	$\overline{\Lambda}_c^- \mu^+$ anything		$< -1.4 \times 10^{-3}$	CL=90%
Γ_{103}	$\overline{\Lambda}_c^- p$ anything		(2.04 ± 0.33) %	
Γ_{104}	$\overline{\Lambda}_c^- p e^+ \nu_e$		$< 8 \times 10^{-4}$	CL=90%
Γ_{105}	$\overline{\Sigma}_c^{--}$anything		$(3.3 \pm 1.7) \times 10^{-3}$	
Γ_{106}	$\overline{\Sigma}_c^-$anything		$< 8 \times 10^{-3}$	CL=90%
Γ_{107}	$\overline{\Sigma}_c^0$anything		$(3.7 \pm 1.7) \times 10^{-3}$	
Γ_{108}	$\overline{\Sigma}_c^0 N$ ($N = p$ or n)		$< 1.2 \times 10^{-3}$	CL=90%
Γ_{109}	Ξ_c^0anything, $\Xi_c^0 \to \Xi^- \pi^+$		$(1.93 \pm 0.30) \times 10^{-4}$	S=1.1
Γ_{110}	Ξ_c^+, $\Xi_c^+ \to \Xi^- \pi^+ \pi^+$		$(4.5 {}^{+1.3}_{-1.2}) \times 10^{-4}$	
Γ_{111}	$p/\overline{p}$ anything	[f]	(8.0 ± 0.4) %	
Γ_{112}	$p/\overline{p}$ (direct) anything	[f]	(5.5 ± 0.5) %	
Γ_{113}	$\overline{p} e^+ \nu_e$ anything		$< 5.9 \times 10^{-4}$	CL=90%
Γ_{114}	$\Lambda/\overline{\Lambda}$ anything	[f]	(4.0 ± 0.5) %	
Γ_{115}	Λ anything		seen	
Γ_{116}	$\overline{\Lambda}$ anything		seen	
Γ_{117}	$\Xi^-/\overline{\Xi}^+$anything	[f]	$(2.7 \pm 0.6) \times 10^{-3}$	
Γ_{118}	baryons anything		(6.8 ± 0.6) %	
Γ_{119}	$p\overline{p}$ anything		(2.47 ± 0.23) %	
Γ_{120}	$\Lambda\overline{p}/\overline{\Lambda}p$ anything	[f]	(2.5 ± 0.4) %	
Γ_{121}	$\Lambda\overline{\Lambda}$ anything		$< 5 \times 10^{-3}$	CL=90%

Lepton Family number (*LF*) violating modes or $\Delta B = 1$ weak neutral current (*B1*) modes

Γ_{122}	$s e^+ e^-$	*B1*		$(6.7 \pm 1.7) \times 10^{-6}$	S=2.0
Γ_{123}	$s \mu^+ \mu^-$	*B1*		$(4.3 \pm 1.0) \times 10^{-6}$	
Γ_{124}	$s \ell^+ \ell^-$	*B1*	[b]	$(5.8 \pm 1.3) \times 10^{-6}$	S=1.8
Γ_{125}	$\pi \ell^+ \ell^-$	*B1*		$< 5.9 \times 10^{-8}$	CL=90%
Γ_{126}	$\pi e^+ e^-$	*B1*		$< 1.10 \times 10^{-7}$	CL=90%
Γ_{127}	$\pi \mu^+ \mu^-$	*B1*		$< 5.0 \times 10^{-8}$	CL=90%
Γ_{128}	$K e^+ e^-$	*B1*		$(4.4 \pm 0.6) \times 10^{-7}$	
Γ_{129}	$K^*(892) e^+ e^-$	*B1*		$(1.19 \pm 0.20) \times 10^{-6}$	S=1.2
Γ_{130}	$K \mu^+ \mu^-$	*B1*		$(4.4 \pm 0.4) \times 10^{-7}$	
Γ_{131}	$K^*(892) \mu^+ \mu^-$	*B1*		$(1.06 \pm 0.09) \times 10^{-6}$	
Γ_{132}	$K \ell^+ \ell^-$	*B1*		$(4.8 \pm 0.4) \times 10^{-7}$	
Γ_{133}	$K^*(892) \ell^+ \ell^-$	*B1*		$(1.05 \pm 0.10) \times 10^{-6}$	
Γ_{134}	$K \nu \overline{\nu}$	*B1*		$< 1.6 \times 10^{-5}$	CL=90%
Γ_{135}	$K^* \nu \overline{\nu}$	*B1*		$< 2.7 \times 10^{-5}$	CL=90%
Γ_{136}	$\pi \nu \overline{\nu}$	*B1*		$< 8 \times 10^{-6}$	CL=90%
Γ_{137}	$\rho \nu \overline{\nu}$	*B1*		$< 2.8 \times 10^{-5}$	CL=90%
Γ_{138}	$s e^{\pm} \mu^{\mp}$	*LF*	[f]	$< 2.2 \times 10^{-5}$	CL=90%
Γ_{139}	$\pi e^{\pm} \mu^{\mp}$	*LF*		$< 9.2 \times 10^{-8}$	CL=90%
Γ_{140}	$\rho e^{\pm} \mu^{\mp}$	*LF*		$< 3.2 \times 10^{-6}$	CL=90%
Γ_{141}	$K e^{\pm} \mu^{\mp}$	*LF*		$< 3.8 \times 10^{-8}$	CL=90%
Γ_{142}	$K^*(892) e^{\pm} \mu^{\mp}$	*LF*		$< 5.1 \times 10^{-7}$	CL=90%

[a] These values are model dependent.

[b] An ℓ indicates an e or a μ mode, not a sum over these modes.

[c] Here "anything" means at least one particle observed.

[d] This is a $B(B^0 \to D^{*-} \ell^+ \nu_\ell)$ value.

[e] D^{**} stands for the sum of the $D(1\,^1P_1)$, $D(1\,^3P_0)$, $D(1\,^3P_1)$, $D(1\,^3P_2)$, $D(2\,^1S_0)$, and $D(2\,^1S_1)$ resonances.

[f] The value is for the sum of the charge states or particle/antiparticle states indicated.

[g] $D^{(*)}\overline{D}^{(*)}$ stands for the sum of $D^*\overline{D}^*$, $D^*\overline{D}$, $D\overline{D}^*$, and $D\overline{D}$.

[h] $X(3915)$ denotes a near-threshold enhancement in the $\omega J/\psi$ mass spectrum.

[i] Inclusive branching fractions have a multiplicity definition and can be greater than 100%.

$B^{\pm}/B^0$ ADMIXTURE BRANCHING RATIOS

$\Gamma(\ell^+ \nu_\ell \text{anything})/\Gamma_{\text{total}}$ — Γ_3/Γ

These branching fraction values are model dependent.

"OUR EVALUATION" assumes lepton universality and is an average using rescaled values of the data listed below. The average and rescaling were performed by the Heavy Flavor Averaging Group (HFLAV) and are described at https://hflav.web.cern.ch/. The averaging/rescaling procedure takes into account correlations between the measurements.

VALUE (%)	DOCUMENT ID		TECN	COMMENT
10.84±0.16 OUR EVALUATION				
10.49±0.20 OUR AVERAGE	Error includes scale factor of 1.3. See the ideogram below.			
10.34±0.04±0.26	[1] LEES	17B	BABR	$e^+e^- \to \Upsilon(4S)$
10.28±0.18±0.24	[2] URQUIJO	07	BELL	$e^+e^- \to \Upsilon(4S)$
10.91±0.09±0.24	[3] MAHMOOD	04	CLEO	$e^+e^- \to \Upsilon(4S)$
9.7 ±0.5 ±0.4	[4] ALBRECHT	93H	ARG	$e^+e^- \to \Upsilon(4S)$
• • • We do not use the following data for averages, fits, limits, etc. • • •				
9.96±0.19±0.32	[5] AUBERT,B	06Y	BABR	Repl. by LEES 17B
10.85±0.21±0.36	[6] OKABE	05	BELL	Repl. by URQUIJO 07
10.83±0.16±0.06	[7] AUBERT	04X	BABR	Repl. by AUBERT,B 06Y
10.36±0.06±0.23	[8] AUBERT,B	04A	BABR	$e^+e^- \to \Upsilon(4S)$
10.87±0.18±0.30	[9] AUBERT	03	BABR	Repl. by AUBERT 04X
10.90±0.12±0.49	[10] ABE	02Y	BELL	Repl. by OKABE 05
10.49±0.17±0.43	[11] BARISH	96B	CLE2	Repl. by MAHMOOD 04
10.80±0.20±0.56	[12] HENDERSON	92	CLEO	$e^+e^- \to \Upsilon(4S)$
10.0 ±0.4 ±0.3	[13] YANAGISAWA	91	CSB2	$e^+e^- \to \Upsilon(4S)$
10.3 ±0.6 ±0.2	[14] ALBRECHT	90H	ARG	Direct e at $\Upsilon(4S)$
10.0 ±0.6 ±0.2	[15] ALBRECHT	90H	ARG	Direct μ at $\Upsilon(4S)$
11.7 ±0.4 ±1.0	[16] WACHS	89	CBAL	Direct e at $\Upsilon(4S)$
12.0 ±0.7 ±0.5	CHEN	84	CLEO	Direct e at $\Upsilon(4S)$
10.8 ±0.6 ±1.0	CHEN	84	CLEO	Direct μ at $\Upsilon(4S)$
11.2 ±0.9 ±1.0	LEVMAN	84	CUSB	Direct μ at $\Upsilon(4S)$
13.2 ±0.8 ±1.4	[17] KLOPFEN...	83B	CUSB	Direct e at $\Upsilon(4S)$

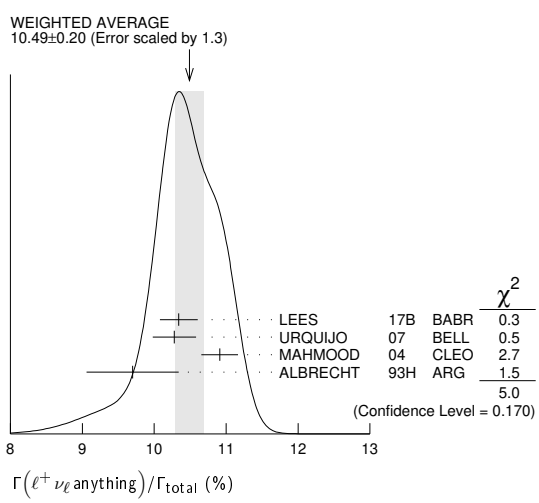

[1] LEES 17B measurement is obtained from semileptonic decays to electrons. The result is averaged over $B^{\pm}$ and B^0 mesons, assuming lepton universality.

[2] URQUIJO 07 report a measurement of $(10.07 \pm 0.18 \pm 0.21)$% for the partial branching fraction of $B \to e\nu_e X_c$ decay with electron energy above 0.6 GeV. We converted the result to $B \to e\nu_e X$ branching fraction.

[3] Uses charge and angular correlations in $\Upsilon(4S)$ events with a high-momentum lepton and an additional electron.

[4] ALBRECHT 93H analysis performed using tagged semileptonic decays of the B. This technique is almost model independent for the lepton branching ratio.

Downloaded from https://academic.oup.com/ptep/article/2022/8/083C01/6651666 by KIT Library user on 27 September 2022

[5] The measurements are obtained for charged and neutral B mesons partial rates of semileptonic decay to electrons with momentum above 0.6 GeV/c in the B rest frame. The best precision on the ratio is achieved for a momentum threshold of 1.0 GeV: $B(B^+ \to e^+\nu_e X)$ / $B(B^0 \to e^+\nu_e X) = 1.074 \pm 0.041 \pm 0.026$.

[6] The measurements are obtained for charged and neutral B mesons partial rates of semileptonic decay to electrons with momentum above 0.6 GeV/c in the B rest frame, and their ratio of $B(B^+ \to e^+\nu_e X)/B(B^0 \to e^+\nu_e X) = 1.08 \pm 0.05 \pm 0.02$.

[7] The semileptonic branching ratio, $|V_{cb}|$ and other heavy-quark parameters are determined from a simultaneous fit to moments of the hadronic-mass and lepton-energy distribution.

[8] Uses the high-momentum lepton tag method and requires the electron energy above 0.6 GeV.

[9] Uses the high-momentum lepton tag method. They also report $|V_{cb}| = 0.0423 \pm 0.0007(\text{exp}) \pm 0.0020(\text{theo.})$.

[10] Uses the high-momentum lepton tag method. ABE 02Y also reports $|V_{cb}| = 0.0408 \pm 0.0010(\text{exp}) \pm 0.0025(\text{theo.})$. The second error is due to uncertainties of theoretical inputs.

[11] BARISH 96B analysis performed using tagged semileptonic decays of the B. This technique is almost model independent for the lepton branching ratio.

[12] HENDERSON 92 measurement employs e and μ. The systematic error contains 0.004 in quadrature from model dependence. The authors average a variation of the Isgur, Scora, Grinstein, and Wise model with that of the Altarelli-Cabibbo-Corbò-Maiani-Martinelli model for semileptonic decays to correct the acceptance.

[13] YANAGISAWA 91 also measures an average semileptonic branching ratio at the $\Upsilon(5S)$ of 9.6–10.5% depending on assumptions about the relative production of different B meson species.

[14] ALBRECHT 90H uses the model of ALTARELLI 82 to correct over all lepton momenta. 0.099 ± 0.006 is obtained using ISGUR 89B.

[15] ALBRECHT 90H uses the model of ALTARELLI 82 to correct over all lepton momenta. 0.097 ± 0.006 is obtained using ISGUR 89B.

[16] Using data above $p(e) = 2.4$ GeV, WACHS 89 determine $\sigma(B \to e\nu\text{up})/\sigma(B \to e\nu\text{charm}) < 0.065$ at 90% CL.

[17] Ratio $\sigma(b \to e\nu\text{up})/\sigma(b \to e\nu\text{charm}) < 0.055$ at CL = 90%.

$\Gamma(D^-\ell^+\nu_\ell\text{anything})/\Gamma(\ell^+\nu_\ell\text{anything})$ — Γ_4/Γ_3

$\ell = e$ or μ.

VALUE	DOCUMENT ID		TECN	COMMENT
0.26±0.07±0.04	[1] FULTON	91	CLEO	$e^+e^- \to \Upsilon(4S)$

[1] FULTON 91 uses $B(D^+ \to K^-\pi^+\pi^+) = (9.1 \pm 1.3 \pm 0.4)\%$ as measured by MARK III.

$\Gamma(\overline{D}^0\ell^+\nu_\ell\text{anything})/\Gamma(\ell^+\nu_\ell\text{anything})$ — Γ_5/Γ_3

$\ell = e$ or μ.

VALUE	DOCUMENT ID		TECN	COMMENT
0.67±0.09±0.10	[1] FULTON	91	CLEO	$e^+e^- \to \Upsilon(4S)$

[1] FULTON 91 uses $B(D^0 \to K^-\pi^+) = (4.2 \pm 0.4 \pm 0.4)\%$ as measured by MARK III.

$\Gamma(\overline{D}\ell^+\nu_\ell)/\Gamma(\ell^+\nu_\ell\text{anything})$ — Γ_6/Γ_3

VALUE	DOCUMENT ID		TECN	COMMENT
0.223±0.006±0.009	[1] AUBERT	10	BABR	$e^+e^- \to \Upsilon(4S)$

[1] Uses a fully reconstructed B meson as a tag on the recoil side.

$\Gamma(D^{*-}\ell^+\nu_\ell\text{anything})/\Gamma_{\text{total}}$ — Γ_7/Γ

VALUE (units 10^{-2})	DOCUMENT ID		TECN	COMMENT
0.67±0.08±0.10	ABDALLAH	04D	DLPH	$e^+e^- \to Z^0$
• • • We do not use the following data for averages, fits, limits, etc. • • •				
0.6 ±0.3 ±0.1	[1] BARISH	95	CLE2	$e^+e^- \to \Upsilon(4S)$

[1] BARISH 95 use $B(D^0 \to K^-\pi^+) = (3.91 \pm 0.08 \pm 0.17)\%$ and $B(D^{*+} \to D^0\pi^+) = (68.1 \pm 1.0 \pm 1.3)\%$.

$\Gamma(D^{*0}\ell^+\nu_\ell\text{anything})/\Gamma_{\text{total}}$ — Γ_8/Γ

VALUE (units 10^{-2})	DOCUMENT ID		TECN	COMMENT
• • • We do not use the following data for averages, fits, limits, etc. • • •				
$0.6 \pm 0.6 \pm 0.1$	[1] BARISH	95	CLE2	$e^+e^- \to \Upsilon(4S)$

[1] BARISH 95 use $B(D^0 \to K^-\pi^+) = (3.91 \pm 0.08 \pm 0.17)\%$, $B(D^{*+} \to D^0\pi^+) = (68.1 \pm 1.0 \pm 1.3)\%$, $B(D^{*0} \to D^0\pi^0) = (63.6 \pm 2.3 \pm 3.3)\%$.

$\Gamma(\overline{D}^{**}\ell^+\nu_\ell)/\Gamma_{\text{total}}$ — Γ_{10}/Γ

D^{**} stands for the sum of the $D(1\,^1P_1)$, $D(1\,^3P_0)$, $D(1\,^3P_1)$, $D(1\,^3P_2)$, $D(2\,^1S_0)$, and $D(2\,^1S_1)$ resonances. $\ell = e$ or μ, not sum over e and μ modes.

VALUE	CL%	EVTS	DOCUMENT ID		TECN	COMMENT
0.027±0.005±0.005		63	[1] ALBRECHT	93	ARG	$e^+e^- \to \Upsilon(4S)$
• • • We do not use the following data for averages, fits, limits, etc. • • •						
<0.028	95		[2] BARISH	95	CLE2	$e^+e^- \to \Upsilon(4S)$

[1] ALBRECHT 93 assumes the GISW model to correct for unseen modes. Using the BHKT model, the result becomes $0.023 \pm 0.006 \pm 0.004$. Assumes $B(D^{*+} \to D^0\pi^+) = 68.1\%$, $B(D^0 \to K^-\pi^+) = 3.65\%$, $B(D^0 \to K^-\pi^+\pi^-\pi^+) = 7.5\%$. We have taken their average e and μ value.

[2] BARISH 95 use $B(D^0 \to K^-\pi^+) = (3.91 \pm 0.08 \pm 0.17)\%$, assume all nonresonant channels are zero, and use GISW model for relative abundances of D^{**} states.

$\Gamma(\overline{D}_1(2420)\ell^+\nu_\ell\text{anything})/\Gamma_{\text{total}}$ — Γ_{11}/Γ

VALUE	DOCUMENT ID		TECN	COMMENT
0.0038±0.0013 OUR AVERAGE	Error includes scale factor of 2.4.			
0.0033 ± 0.0006	[1] ABAZOV	05O	D0	$p\overline{p}$ at 1.96 TeV
0.0074 ± 0.0016	[2] BUSKULIC	97B	ALEP	$e^+e^- \to Z$
• • • We do not use the following data for averages, fits, limits, etc. • • •				
seen	[3] BUSKULIC	95B	ALEP	Repl. by BUSKULIC 97B

[1] Assumes $B(D_1 \to D^*\pi) = 1$, $B(D_1 \to D^*\pi^{\pm}) = 2/3$, and $B(b \to B) = 0.397$.

[2] BUSKULIC 97B assumes $B(D_1(2420) \to D^*\pi) = 1$, $B(D_1(2420) \to D^*\pi^{\pm}) = 2/3$, and $B(b \to B) = 0.378 \pm 0.022$.

[3] BUSKULIC 95B reports $f_B \times B(B \to \overline{D}_1(2420)^0\ell^+\nu_\ell\text{anything}) \times B(\overline{D}_1(2420)^0 \to \overline{D}^*(2010)^-\pi^+) = (2.04 \pm 0.58 \pm 0.34)10^{-3}$, where f_B is the production fraction for a single B charge state.

$[\Gamma(\overline{D}\pi\ell^+\nu_\ell\text{anything}) + \Gamma(\overline{D}^*\pi\ell^+\nu_\ell\text{anything})]/\Gamma_{\text{total}}$ — Γ_{12}/Γ

VALUE	DOCUMENT ID		TECN	COMMENT
0.026 ±0.005 OUR AVERAGE	Error includes scale factor of 1.5.			
$0.0340 \pm 0.0052 \pm 0.0032$	[1] ABREU	00R	DLPH	$e^+e^- \to Z$
$0.0226 \pm 0.0029 \pm 0.0033$	[2] BUSKULIC	97B	ALEP	$e^+e^- \to Z$

[1] Assumes no contribution from B_s and b baryons. Further assumes contributions from single pion ($D\pi$ and $D^*\pi$) states only, allowing isospin conservation to relate the relative π^0 and π^+ rates.

[2] BUSKULIC 97B assumes $B(b \to B) = 0.378 \pm 0.022$ and uses isospin invariance by assuming that all observed $D^0\pi^+$, $D^{*0}\pi^+$, $D^+\pi^-$, and $D^{*+}\pi^-$ are from D^{**} states. A correction has been applied to account for the production of B^0_s and Λ^0_b.

$\Gamma(\overline{D}\pi\ell^+\nu_\ell\text{anything})/\Gamma_{\text{total}}$ — Γ_{13}/Γ

VALUE	DOCUMENT ID		TECN	COMMENT
0.0154±0.0061	ABREU	00R	DLPH	$e^+e^- \to Z$

$\Gamma(\overline{D}^*\pi\ell^+\nu_\ell\text{anything})/\Gamma_{\text{total}}$ — Γ_{14}/Γ

VALUE	DOCUMENT ID		TECN	COMMENT
0.0186±0.0038	ABREU	00R	DLPH	$e^+e^- \to Z$

$\Gamma(\overline{D}^*_2(2460)\ell^+\nu_\ell\text{anything})/\Gamma_{\text{total}}$ — Γ_{15}/Γ

VALUE	CL%	DOCUMENT ID		TECN	COMMENT
0.0044±0.0016		[1] ABAZOV	05O	D0	$p\overline{p}$ at 1.96 TeV
• • • We do not use the following data for averages, fits, limits, etc. • • •					
<0.0065	95	[2] BUSKULIC	97B	ALEP	$e^+e^- \to Z$
not seen		[3] BUSKULIC	95B	ALEP	$e^+e^- \to Z$

[1] Assumes $B(D^*_2 \to D^*\pi^{\pm}) = 0.30 \pm 0.06$ and $B(b \to B) = 0.397$.

[2] A revised number based on BUSKULIC 97B which assumes $B(D^*_2(2460) \to D^*\pi^{\pm}) = 0.20$ and $B(b \to B) = 0.378 \pm 0.022$.

[3] BUSKULIC 95B reports $f_B \times B(B \to \overline{D}^*_2(2460)^0\ell^+\nu_\ell\text{anything}) \times B(\overline{D}^*_2(2460)^0 \to \overline{D}^*(2010)^-\pi^+) \leq 0.81 \times 10^{-3}$ at CL=95%, where f_B is the production fraction for a single B charge state.

$\Gamma(B \to \overline{D}^*_2(2460)\ell^+\nu_\ell\text{anything}) \times B(D^*_2(2460) \to D^{*-}\pi^+)$ / $\Gamma(B \to \overline{D}_1(2420)\ell^+\nu_\ell\text{anything}) \times B(\overline{D}_1(2420) \to D^{*-}\pi^+)$

VALUE	DOCUMENT ID		TECN	COMMENT
0.39±0.09±0.12	ABAZOV	05O	D0	$p\overline{p}$ at 1.96 TeV

$\Gamma(D^{*-}\pi^+\ell^+\nu_\ell\text{anything})/\Gamma_{\text{total}}$ — Γ_{16}/Γ

Includes resonant and nonresonant contributions.

VALUE (units 10^{-3})	DOCUMENT ID		TECN	COMMENT
10.0±2.7±2.1	[1] BUSKULIC	95B	ALEP	$e^+e^- \to Z$

[1] BUSKULIC 95B reports $f_B \times B(B \to \overline{D}^*(2010)^-\pi^+\ell^+\nu_\ell\text{anything}) = (3.7 \pm 1.0 \pm 0.7)10^{-3}$. Above value assumes $f_B = 0.37 \pm 0.03$.

$\Gamma(\overline{D}\pi^+\pi^-\ell^+\nu_\ell)/\Gamma(\overline{D}\ell^+\nu_\ell)$ — Γ_{17}/Γ_6

VALUE (units 10^{-2})	DOCUMENT ID		TECN	COMMENT
6.7±1.0±0.8	[1] LEES	16	BABR	$e^+e^- \to \Upsilon(4S)$

[1] Measurement used electrons and muons as leptons.

$\Gamma(\overline{D}^*\pi^+\pi^-\ell^+\nu_\ell)/\Gamma(\overline{D}^*\ell^+\nu_\ell)$ — Γ_{18}/Γ_9

VALUE (units 10^{-2})	DOCUMENT ID		TECN	COMMENT
1.9±0.5±0.4	[1] LEES	16	BABR	$e^+e^- \to \Upsilon(4S)$

[1] Measurement used electrons and muons as leptons.

$\Gamma(D^-_s\ell^+\nu_\ell\text{anything})/\Gamma_{\text{total}}$ — Γ_{19}/Γ

VALUE	CL%	DOCUMENT ID		TECN	COMMENT
$<7 \times 10^{-3}$	90	[1] ALBRECHT	93E	ARG	$e^+e^- \to \Upsilon(4S)$

[1] ALBRECHT 93E reports < 0.012 from a measurement of $[\Gamma(B \to D^-_s\ell^+\nu_\ell\text{anything})/\Gamma_{\text{total}}] \times [B(D^+_s \to \phi\pi^+)]$ assuming $B(D^+_s \to \phi\pi^+) = 0.027$, which we rescale to our best value $B(D^+_s \to \phi\pi^+) = 4.5 \times 10^{-2}$.

Downloaded from https://academic.oup.com/ptep/article/2022/8/083C01/6651666 by KIT Library user on 27 September 2022

$\Gamma(D_s^- \ell^+ \nu_\ell K^+ \text{anything})/\Gamma_{\text{total}}$ — Γ_{20}/Γ

VALUE	CL%	DOCUMENT ID		TECN	COMMENT
$<5 \times 10^{-3}$	90	[1] ALBRECHT	93E	ARG	$e^+e^- \to \Upsilon(4S)$

[1] ALBRECHT 93E reports < 0.008 from a measurement of $[\Gamma(B \to D_s^- \ell^+ \nu_\ell K^+ \text{anything})/\Gamma_{\text{total}}] \times [B(D_s^+ \to \phi\pi^+)]$ assuming $B(D_s^+ \to \phi\pi^+) = 0.027$, which we rescale to our best value $B(D_s^+ \to \phi\pi^+) = 4.5 \times 10^{-2}$.

$\Gamma(D_s^- \ell^+ \nu_\ell K^0 \text{anything})/\Gamma_{\text{total}}$ — Γ_{21}/Γ

VALUE	CL%	DOCUMENT ID		TECN	COMMENT
$<7 \times 10^{-3}$	90	[1] ALBRECHT	93E	ARG	$e^+e^- \to \Upsilon(4S)$

[1] ALBRECHT 93E reports < 0.012 from a measurement of $[\Gamma(B \to D_s^- \ell^+ \nu_\ell K^0 \text{anything})/\Gamma_{\text{total}}] \times [B(D_s^+ \to \phi\pi^+)]$ assuming $B(D_s^+ \to \phi\pi^+) = 0.027$, which we rescale to our best value $B(D_s^+ \to \phi\pi^+) = 4.5 \times 10^{-2}$.

$\Gamma(X_c \ell^+ \nu_\ell)/\Gamma_{\text{total}}$ — Γ_{22}/Γ

"OUR EVALUATION" is an average using rescaled values of the data listed below. The average and rescaling were performed by the Heavy Flavor Averaging Group (HFLAV) and are described at https://hflav.web.cern.ch/. The averaging/rescaling procedure takes into account correlations between the measurements.

VALUE (%)	DOCUMENT ID		TECN	COMMENT
10.65±0.16 OUR EVALUATION				
10.29±0.19 OUR AVERAGE				
10.18±0.03±0.24	[1] LEES	17B	BABR	$e^+e^- \to \Upsilon(4S)$
10.44±0.19±0.22	[2] URQUIJO	07	BELL	$e^+e^- \to \Upsilon(4S)$
• • • We do not use the following data for averages, fits, limits, etc. • • •				
10.64±0.17±0.06	[3] AUBERT	10A	BABR	Repl. by LEES 17B
10.61±0.16±0.06	[4] AUBERT	04X	BABR	Repl. by AUBERT 10A

[1] The measurement is obtained from semileptonic decays to electrons $B \to X e \nu$, and using a theoretical model (GAMBINO 07, GAMBINO 11) to predict the contribution from $B \to X_u e \nu$. The result is averaged over $B^{\pm}$ and B^0 mesons, assuming lepton universality.

[2] Measured the independent B^+ and B^0 partial branching fractions with electron energy above 0.4 GeV.

[3] Obtained from a combined fit to the moments of observed spectra in inclusive $B \to X_c \ell^+ \nu_\ell$ decay.

[4] The semileptonic branching ratio, $|V_{cb}|$ and other heavy-quark parameters are determined from a simultaneous fit to moments of the hadronic-mass and lepton-energy distribution.

$\Gamma(X_u \ell^+ \nu_\ell)/\Gamma_{\text{total}}$ — Γ_{23}/Γ

"OUR EVALUATION" is an average using rescaled values of the data listed below. The average and rescaling were performed by the Heavy Flavor Averaging Group (HFLAV) and are described at https://hflav.web.cern.ch/. The averaging/rescaling procedure takes into account correlations between the measurements.

VALUE (units 10^{-3})	DOCUMENT ID		TECN	COMMENT
1.91 ±0.27 OUR EVALUATION				
1.85 ±0.08 ±0.19	[1] CAO	21A	BELL	$e^+e^- \to \Upsilon(4S)$
$1.665 \pm 0.087^{+0.103}_{-0.094}$	[2] LEES	17B	BABR	$e^+e^- \to \Upsilon(4S)$
2.01 ±0.15 ±0.25	[3] LEES	12R	BABR	$e^+e^- \to \Upsilon(4S)$
2.53 ±0.24 ±0.24	[4] AUBERT,B	05X	BABR	$e^+e^- \to \Upsilon(4S)$
2.80 ±0.52 ±0.41	[5] LIMOSANI	05	BELL	$e^+e^- \to \Upsilon(4S)$
1.77 ±0.29 ±0.38	[6] BORNHEIM	02	CLE2	$e^+e^- \to \Upsilon(4S)$
• • • We do not use the following data for averages, fits, limits, etc. • • •				
1.963±0.173±0.159	[7] URQUIJO	10	BELL	Repl. by CAO 21A
1.18 ±0.09 ±0.07	[8] AUBERT	08AS	BABR	Repl. by LEES 12R
$2.27 \pm 0.26 \; ^{+0.37}_{-0.33}$	[9] AUBERT	06H	BABR	Repl. by LEES 17B
2.24 ±0.27 ±0.47	[10,11] AUBERT	04I	BABR	Repl. by AUBERT,B 05X

[1] Measures several partial branching fractions in different phase space regions. The most inclusive result of the full branching fraction is obtained in the region for lepton energy in B rest frame $E_\ell^* > 1$ GeV, where the measured partial branching fraction is $\Delta B = (1.59 \pm 0.07 \pm 0.16) \times 10^{-3}$. The acceptance in that region is reported to be 0.86.

[2] Obtained from the partial rate $\Delta B = (1.554 \pm 0.082^{+0.095}_{-0.086}) \times 10^{-3}$ for the electron momentum interval of 0.8–2.7 GeV/c based on GGOU1 method ($X_c \ell \nu$, m_c constraint fit of SF parameters).

[3] Measures several partial branching fractions in different phase space regions. The most precise result on the full branching fraction is obtained in the region for lepton momentum in B rest frame $p_\ell^* > 1$ GeV/c, where the measured partial branching fraction is $\Delta B = (1.80 \pm 0.13 \pm 0.15) \times 10^{-3}$. The acceptance in that region is reported in a private communication by the Authors to be 0.894. The corresponding $|V_{ub}|$ from the BLNP method is $(4.28 \pm 0.15 \pm 0.18 \pm 0.19) \times 10^{-3}$, where the last uncertainty comes from theoretical prediction.

[4] Determined from the partial rate $\Delta B = (4.41 \pm 0.42 \pm 0.42) \times 10^{-4}$ measured for electron energy > 2 GeV and hadronic mass squared < 3.5 GeV^2, and calculated acceptance 0.174 in that region. The V_{ub} is measured as $(4.41 \pm 0.30^{+0.65}_{-0.47} \pm 0.28) \times 10^{-3}$.

[5] Uses electrons in the momentum interval 1.9–2.6 GeV/c in the center-of-mass frame. The V_{ub} is found to be $(5.08 \pm 0.47^{+0.49}_{-0.48}) \times 10^{-3}$.

[6] BORNHEIM 02 uses the observed yield of leptons from semileptonic B decays in the end-point momentum interval 2.2–2.6 GeV/c with recent CLEO-2 data on $B \to X_s \gamma$. The V_{ub} is found to be $(4.08 \pm 0.34 \pm 0.53) \times 10^{-3}$.

[7] Uses a multivariate analysis method and requires lepton momentum in the B rest frame, $p_\ell^* > 1.0$ GeV/c.

[8] Measures several partial branching fractions in different phase space regions. The most precise result is obtained in the region for hadronic mass $M_X < 1.55$ GeV/c^2, and is $\Delta B = (1.18 \pm 0.09 \pm 0.07) \times 10^{-3}$. The corresponding $|V_{ub}|$ from the BLNP method is $(4.27 \pm 0.16 \pm 0.13 \pm 0.30) \times 10^{-3}$, where the last uncertainty comes from the theoretical prediction of the partial rate in the given phase-space region.

[9] Obtained from the partial rate $\Delta B = (0.572 \pm 0.041 \pm 0.065) \times 10^{-3}$ for the electron momentum interval of 2.0–2.6 GeV/c based on BLNP method.

[10] Used BaBar measurement of Semileptonic branching fraction $B(B \to X \ell \nu_\ell) = (10.87 \pm 0.18 \pm 0.30)\%$ to convert the ratio of rates to branching fraction.

[11] The third error includes the systematics and theoretical errors summed in quadrature.

$\Gamma(X_u \ell^+ \nu_\ell)/\Gamma(\ell^+ \nu_\ell \text{anything})$ — Γ_{23}/Γ_3

ℓ denotes e or μ, not the sum. These experiments measure this ratio in very limited momentum intervals.

VALUE (units 10^{-2})	CL%	EVTS	DOCUMENT ID		TECN	COMMENT
2.06±0.25±0.42			[1] AUBERT	04I	BABR	$e^+e^- \to \Upsilon(4S)$
• • • We do not use the following data for averages, fits, limits, etc. • • •						
			[2] ALBRECHT	94C	ARG	$e^+e^- \to \Upsilon(4S)$
		107	[3] BARTELT	93B	CLE2	$e^+e^- \to \Upsilon(4S)$
		77	[4] ALBRECHT	91C	ARG	$e^+e^- \to \Upsilon(4S)$
		41	[5] ALBRECHT	90	ARG	$e^+e^- \to \Upsilon(4S)$
		76	[6] FULTON	90	CLEO	$e^+e^- \to \Upsilon(4S)$
<4.0	90		[7] BEHRENDS	87	CLEO	$e^+e^- \to \Upsilon(4S)$
<4.0	90		CHEN	84	CLEO	Direct e at $\Upsilon(4S)$
<5.5	90		KLOPFEN...	83B	CUSB	Direct e at $\Upsilon(4S)$

[1] The third error includes the systematics and theoretical errors summed in quadrature.

[2] ALBRECHT 94C find $\Gamma(b \to c)/\Gamma(b \to \text{all}) = 0.99 \pm 0.02 \pm 0.04$.

[3] BARTELT 93B (CLEO II) measures an excess of $107 \pm 15 \pm 11$ leptons in the lepton momentum interval 2.3–2.6 GeV/c which is attributed to $b \to u \ell \nu_\ell$. This corresponds to a model-dependent partial branching ratio ΔB_{ub} between $(1.15 \pm 0.16 \pm 0.15) \times 10^{-4}$, as evaluated using the KS model (KOERNER 88), and $(1.54 \pm 0.22 \pm 0.20) \times 10^{-4}$ using the ACCMM model (ARTUSO 93). The corresponding values of $|V_{ub}|/|V_{cb}|$ are 0.056 ± 0.006 and 0.076 ± 0.008, respectively.

[4] ALBRECHT 91C result supersedes ALBRECHT 90. Two events are fully reconstructed providing evidence for the $b \to u$ transition. Using the model of ALTARELLI 82, they obtain $|V_{ub}/V_{cb}| = 0.11 \pm 0.012$ from 77 leptons in the 2.3–2.6 GeV momentum range.

[5] ALBRECHT 90 observes 41 ± 10 excess e and μ (lepton) events in the momentum interval $p = 2.3$–2.6 GeV signaling the presence of the $b \to u$ transition. The events correspond to a model-dependent measurement of $|V_{ub}/V_{cb}| = 0.10 \pm 0.01$.

[6] FULTON 90 observe 76 ± 20 excess e and μ (lepton) events in the momentum interval $p = 2.4$–2.6 GeV signaling the presence of the $b \to u$ transition. The average branching ratio, $(1.8 \pm 0.4 \pm 0.3) \times 10^{-4}$, corresponds to a model-dependent measurement of approximately $|V_{ub}/V_{cb}| = 0.1$ using $B(b \to c \ell \nu) = 10.2 \pm 0.2 \pm 0.7\%$.

[7] The quoted possible limits range from 0.018 to 0.04 for the ratio, depending on which model or momentum range is chosen. We select the most conservative limit they have calculated. This corresponds to a limit on $|V_{ub}|/|V_{cb}| < 0.20$. While the endpoint technique employed is more robust than their previous results in CHEN 84, these results do not provide a numerical improvement in the limit.

$\Gamma(X_u e^+ \nu_e)/\Gamma_{\text{total}}$ — Γ_{24}/Γ

Requires $E_e^* > 1$ GeV, where E_e^* is e^+ energy in B rest frame.

VALUE (units 10^{-3})	DOCUMENT ID		TECN	COMMENT
1.57±0.10±0.16	[1] CAO	21A	BELL	$e^+e^- \to \Upsilon(4S)$

[1] The correlation of 53% with $B(B \to X_u \mu^+ \nu_\mu)$(letpon energy in B rest frame $E_{\mu^+}^* > 1$ GeV) is reported.

$\Gamma(X_u \mu^+ \nu_\mu)/\Gamma_{\text{total}}$ — Γ_{25}/Γ

Requires $E_\mu^* > 1$ GeV, where E_μ^* is μ^+ energy in B rest frame.

VALUE (units 10^{-3})	DOCUMENT ID		TECN	COMMENT
1.62±0.10±0.18	[1] CAO	21A	BELL	$e^+e^- \to \Upsilon(4S)$

[1] The correlation of 53% with $B(B \to X_u e^+ \nu_e)$(letpon energy in B rest frame $E_{e^+}^* > 1$ GeV) is reported.

$\Gamma(K^+ \ell^+ \nu_\ell \text{anything})/\Gamma(\ell^+ \nu_\ell \text{anything})$ — Γ_{26}/Γ_3

ℓ denotes e or μ, not the sum.

VALUE	DOCUMENT ID		TECN	COMMENT
0.58 ±0.05 OUR AVERAGE				
0.594±0.021±0.056	ALBRECHT	94C	ARG	$e^+e^- \to \Upsilon(4S)$
0.54 ±0.07 ±0.06	[1] ALAM	87B	CLEO	$e^+e^- \to \Upsilon(4S)$

[1] ALAM 87B measurement relies on lepton-kaon correlations.

$\Gamma(K^- \ell^+ \nu_\ell \text{anything})/\Gamma(\ell^+ \nu_\ell \text{anything})$ — Γ_{27}/Γ_3

ℓ denotes e or μ, not the sum.

VALUE	DOCUMENT ID		TECN	COMMENT
0.092±0.035 OUR AVERAGE				
0.086±0.011±0.044	ALBRECHT	94C	ARG	$e^+e^- \to \Upsilon(4S)$
0.10 ±0.05 ±0.02	[1] ALAM	87B	CLEO	$e^+e^- \to \Upsilon(4S)$

[1] ALAM 87B measurement relies on lepton-kaon correlations.

Downloaded from https://academic.oup.com/ptep/article/2022/8/083C01/6651666 by KIT Library user on 27 September 2022

$\Gamma(K^0/\overline{K}^0\ell^+\nu_\ell \text{anything})/\Gamma(\ell^+\nu_\ell \text{anything})$ — Γ_{28}/Γ_3

ℓ denotes e or μ, not the sum. Sum over K^0 and $\overline{K}^0$ states.

VALUE	DOCUMENT ID		TECN	COMMENT
0.42 ±0.05 OUR AVERAGE				
0.452±0.038±0.056	[1] ALBRECHT	94C	ARG	$e^+e^- \to \Upsilon(4S)$
0.39 ±0.06 ±0.04	[2] ALAM	87B	CLEO	$e^+e^- \to \Upsilon(4S)$

[1] ALBRECHT 94C assume a $K^0/\overline{K}^0$ multiplicity twice that of K^0_S.
[2] ALAM 87B measurement relies on lepton-kaon correlations.

$\Gamma(\overline{D}\tau^+\nu_\tau)/\Gamma(\overline{D}\ell^+\nu_\ell)$ — Γ_{29}/Γ_6

"OUR EVALUATION" is an average using rescaled values of the data listed below. The average and rescaling were performed by the Heavy Flavor Averaging Group (HFLAV) and are described at https://hflav.web.cern.ch/. The averaging/rescaling procedure takes into account correlations between the measurements.

VALUE (units 10^{-2})	DOCUMENT ID		TECN	COMMENT
33.9 ± 3.0 OUR EVALUATION				
35 ± 4 OUR AVERAGE Error includes scale factor of 1.2.				
30.7 ± 3.7±1.6	[1] CARIA	20	BELL	$e^+e^- \to \Upsilon(4S)$
37.5 ± 6.4±2.6	[2,3] HUSCHLE	15	BELL	$e^+e^- \to \Upsilon(4S)$
44.0 ± 5.8±4.2	[2,3] LEES	12D	BABR	$e^+e^- \to \Upsilon(4S)$
• • • We do not use the following data for averages, fits, limits, etc. • • •				
4.16±11.7±5.2	[2] AUBERT	08N	BABR	Repl. by LEES 12D

[1] The tag-side B meson is reconstructed in a semileptonic decay mode and the signal-side τ is reconstructed in a purely leptonic decay. The Belle combination of HUSCHLE 15 and CARIA 20 yields $R(D) = (32.6 \pm 3.4) \times 10^{-2}$.
[2] Uses a fully reconstructed B meson as a tag on the recoil side.
[3] Uses $\tau^+ \to e^+\nu_e\overline{\nu}_\tau$ and $\tau^+ \to \mu^+\nu_\mu\overline{\nu}_\tau$ and e^+ or μ^+ as ℓ^+. Obtained from simultaneous fit to B+ and B0 assuming isospin symmetry.

$\Gamma(\overline{D}^*\tau^+\nu_\tau)/\Gamma(\overline{D}^*\ell^+\nu_\ell)$ — Γ_{30}/Γ_9

"OUR EVALUATION" is an average using rescaled values of the data listed below. The average and rescaling were performed by the Heavy Flavor Averaging Group (HFLAV) and are described at https://hflav.web.cern.ch/. The averaging/rescaling procedure takes into account correlations between the measurements.

VALUE (units 10^{-2})	DOCUMENT ID		TECN	COMMENT
29.5±1.4 OUR EVALUATION				
29.6±1.6 OUR AVERAGE				
28.3±1.8±1.4	[1] CARIA	20	BELL	$e^+e^- \to \Upsilon(4S)$
$27.0\pm3.5^{+2.8}_{-2.5}$	[2] HIROSE	17	BELL	$e^+e^- \to \Upsilon(4S)$
29.3±3.8±1.5	[3] HUSCHLE	15	BELL	$e^+e^- \to \Upsilon(4S)$
33.2±2.4±1.8	[3] LEES	12D	BABR	$e^+e^- \to \Upsilon(4S)$
• • • We do not use the following data for averages, fits, limits, etc. • • •				
29.7±5.6±1.8	[4] AUBERT	08N	BABR	Repl. by LEES 12D

[1] The tag-side B meson is reconstructed in a semileptonic decay mode and the signal-side τ is reconstructed in a purely leptonic decay. The Belle combination of HUSCHLE 15, HIROSE 17, and CARIA 20 yields $R(D^*) = 0.238 \pm 0.018$.
[2] Uses a fully reconstructed B meson as a tag on the recoil side.
[3] Uses $\tau^+ \to e^+\nu_e\overline{\nu}_\tau$ and $\tau^+ \to \mu^+\nu_\mu\overline{\nu}_\tau$ and e^+ or μ^+ as ℓ^+. Obtained from simultaneous fit to B+ and B0 assuming isospin symmetry. Uses a fully reconstructed B meson as a tag on the recoil side.
[4] Uses a fully reconstructed B meson as a tag on the recoil side. The results are normalized to the B^+ decay rate.

$\langle n_c \rangle$

VALUE	DOCUMENT ID		TECN	COMMENT
1.10±0.05	[1] GIBBONS	97B	CLE2	$e^+e^- \to \Upsilon(4S)$
• • • We do not use the following data for averages, fits, limits, etc. • • •				
0.98±0.16±0.12	[2] ALAM	87B	CLEO	$e^+e^- \to \Upsilon(4S)$

[1] GIBBONS 97B from charm counting using $B(D^+_s \to \phi\pi) = 0.036 \pm 0.009$ and $B(\Lambda^+_c \to pK^-\pi^+) = 0.044 \pm 0.006$.
[2] From the difference between K^- and K^+ widths. ALAM 87B measurement relies on lepton-kaon correlations. It does not consider the possibility of $B\overline{B}$ mixing. We have thus removed it from the average.

$\Gamma(D^{\pm}\text{anything})/\Gamma_{\text{total}}$ — Γ_{31}/Γ

VALUE	EVTS	DOCUMENT ID		TECN	COMMENT
0.231±0.012 OUR AVERAGE					
0.230±0.012±0.004		[1] GIBBONS	97B	CLE2	$e^+e^- \to \Upsilon(4S)$
0.241±0.037±0.004		[2] BORTOLETTO	92	CLEO	$e^+e^- \to \Upsilon(4S)$
0.223±0.051±0.004		[3] ALBRECHT	91H	ARG	$e^+e^- \to \Upsilon(4S)$
• • • We do not use the following data for averages, fits, limits, etc. • • •					
0.203±0.048±0.003	20k	[4] BORTOLETTO	87	CLEO	Sup. by BORTOLETTO 92

[1] GIBBONS 97B reports $[\Gamma(B \to D^{\pm}\text{anything})/\Gamma_{\text{total}}] \times [B(D^+ \to K^-2\pi^+)] = 0.0216 \pm 0.0008 \pm 0.00082$ which we divide by our best value $B(D^+ \to K^-2\pi^+) = (9.38 \pm 0.16) \times 10^{-2}$. Our first error is their experiment's error and our second error is the systematic error from using our best value.
[2] BORTOLETTO 92 reports $[\Gamma(B \to D^{\pm}\text{anything})/\Gamma_{\text{total}}] \times [B(D^+ \to K^-2\pi^+)] = 0.0226 \pm 0.0030 \pm 0.0018$ which we divide by our best value $B(D^+ \to K^-2\pi^+) = (9.38 \pm 0.16) \times 10^{-2}$. Our first error is their experiment's error and our second error is the systematic error from using our best value.
[3] ALBRECHT 91H reports $[\Gamma(B \to D^{\pm}\text{anything})/\Gamma_{\text{total}}] \times [B(D^+ \to K^-2\pi^+)] = 0.0209 \pm 0.0027 \pm 0.0040$ which we divide by our best value $B(D^+ \to K^-2\pi^+) = (9.38 \pm 0.16) \times 10^{-2}$. Our first error is their experiment's error and our second error is the systematic error from using our best value.
[4] BORTOLETTO 87 reports $[\Gamma(B \to D^{\pm}\text{anything})/\Gamma_{\text{total}}] \times [B(D^+ \to K^-2\pi^+)] = 0.019 \pm 0.004 \pm 0.002$ which we divide by our best value $B(D^+ \to K^-2\pi^+) = (9.38 \pm 0.16) \times 10^{-2}$. Our first error is their experiment's error and our second error is the systematic error from using our best value.

$\Gamma(D^0/\overline{D}^0\text{anything})/\Gamma_{\text{total}}$ — Γ_{32}/Γ

VALUE	EVTS	DOCUMENT ID		TECN	COMMENT
0.616±0.029 OUR AVERAGE Error includes scale factor of 1.3. See the ideogram below.					
0.636±0.024±0.005		[1] GIBBONS	97B	CLE2	$e^+e^- \to \Upsilon(4S)$
0.590±0.047±0.005		[2] BORTOLETTO	92	CLEO	$e^+e^- \to \Upsilon(4S)$
0.492±0.074±0.004		[3] ALBRECHT	91H	ARG	$e^+e^- \to \Upsilon(4S)$
• • • We do not use the following data for averages, fits, limits, etc. • • •					
0.532±0.065±0.004	21k	[4] BORTOLETTO	87	CLEO	$e^+e^- \to \Upsilon(4S)$
0.608±0.183±0.005		[5] GREEN	83	CLEO	Repl. by BORTOLETTO 87

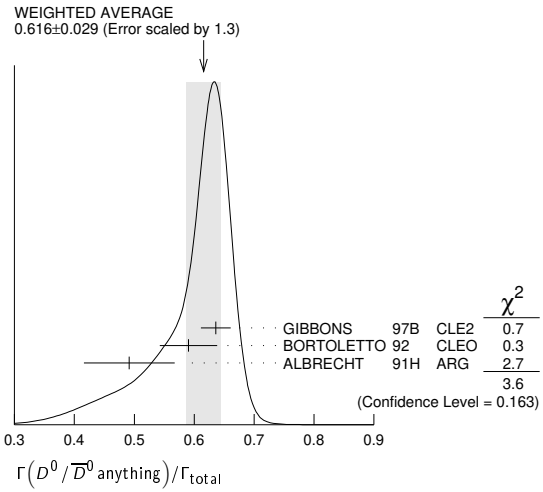

[1] GIBBONS 97B reports $[\Gamma(B \to D^0/\overline{D}^0\text{anything})/\Gamma_{\text{total}}] \times [B(D^0 \to K^-\pi^+)] = 0.0251 \pm 0.0006 \pm 0.00075$ which we divide by our best value $B(D^0 \to K^-\pi^+) = (3.947 \pm 0.030) \times 10^{-2}$. Our first error is their experiment's error and our second error is the systematic error from using our best value.
[2] BORTOLETTO 92 reports $[\Gamma(B \to D^0/\overline{D}^0\text{anything})/\Gamma_{\text{total}}] \times [B(D^0 \to K^-\pi^+)] = 0.0233 \pm 0.0012 \pm 0.0014$ which we divide by our best value $B(D^0 \to K^-\pi^+) = (3.947 \pm 0.030) \times 10^{-2}$. Our first error is their experiment's error and our second error is the systematic error from using our best value.
[3] ALBRECHT 91H reports $[\Gamma(B \to D^0/\overline{D}^0\text{anything})/\Gamma_{\text{total}}] \times [B(D^0 \to K^-\pi^+)] = 0.0194 \pm 0.0015 \pm 0.0025$ which we divide by our best value $B(D^0 \to K^-\pi^+) = (3.947 \pm 0.030) \times 10^{-2}$. Our first error is their experiment's error and our second error is the systematic error from using our best value.
[4] BORTOLETTO 87 reports $[\Gamma(B \to D^0/\overline{D}^0\text{anything})/\Gamma_{\text{total}}] \times [B(D^0 \to K^-\pi^+)] = 0.0210 \pm 0.0015 \pm 0.0021$ which we divide by our best value $B(D^0 \to K^-\pi^+) = (3.947 \pm 0.030) \times 10^{-2}$. Our first error is their experiment's error and our second error is the systematic error from using our best value.
[5] GREEN 83 reports $[\Gamma(B \to D^0/\overline{D}^0\text{anything})/\Gamma_{\text{total}}] \times [B(D^0 \to K^-\pi^+)] = 0.024 \pm 0.006 \pm 0.004$ which we divide by our best value $B(D^0 \to K^-\pi^+) = (3.947 \pm 0.030) \times 10^{-2}$. Our first error is their experiment's error and our second error is the systematic error from using our best value.

$\Gamma(D^-\ell^+\nu_\ell\text{anything})/\Gamma(\overline{D}^0\ell^+\nu_\ell\text{anything})$ — Γ_4/Γ_5

VALUE	DOCUMENT ID		TECN	COMMENT
0.359±0.006±0.009	[1] AAIJ	19AD	LHCB	pp at 13 TeV

[1] AAIJ 19AD uses $D^0 \to K^-\pi^+$ and $D^+ \to K^-\pi^+\pi^+$ modes.

$\Gamma(D^*(2010)^{\pm}\text{anything})/\Gamma_{\text{total}}$ — Γ_{33}/Γ

VALUE	EVTS	DOCUMENT ID		TECN	COMMENT
0.225±0.015 OUR AVERAGE					
0.247±0.019±0.01		[1] GIBBONS	97B	CLE2	$e^+e^- \to \Upsilon(4S)$
0.205±0.019±0.007		[2] ALBRECHT	96D	ARG	$e^+e^- \to \Upsilon(4S)$
0.230±0.028±0.009		[3] BORTOLETTO	92	CLEO	$e^+e^- \to \Upsilon(4S)$
• • • We do not use the following data for averages, fits, limits, etc. • • •					
0.283±0.053±0.002		[4] ALBRECHT	91H	ARG	Sup. by ALBRECHT 96D
$0.22 \pm0.04 ^{+0.07}_{-0.04}$	5200	[5] BORTOLETTO	87	CLEO	$e^+e^- \to \Upsilon(4S)$
$0.27 \pm0.06 ^{+0.08}_{-0.06}$	510	[6] CSORNA	85	CLEO	Repl. by BORTOLETTO 87

[1] GIBBONS 97B reports $B(B \to D^*(2010)^+\text{anything}) = 0.239 \pm 0.015 \pm 0.014 \pm 0.009$ using CLEO measured D and D^* branching fractions. We rescale to our PDG 96 values of D and D^* branching ratios. Our first error is their experiment's error and our second error is the systematic error from using our best value.
[2] ALBRECHT 96D reports $B(B \to D^*(2010)^+\text{anything})\ 0.196 \pm 0.019$ using CLEO measured $B(D^*(2010)^+ \to D^0\pi^+) = 0.681 \pm 0.01 \pm 0.013$, $B(D^0 \to K^-\pi^+) = 0.0401 \pm 0.0014$, $B(D^0 \to K^-\pi^+\pi^+\pi^-) = 0.081 \pm 0.005$., We rescale to our PDG 96

Downloaded from https://academic.oup.com/ptep/article/2022/8/083C01/6651666 by KIT Library user on 27 September 2022

values of D and D^* branching ratios. Our first error is their experiment's error and our second error is the systematic error from using our best value.

[3] BORTOLETTO 92 reports $B(B \to D^*(2010)^+ \text{anything}) = 0.25 \pm 0.03 \pm 0.04$ using MARK II $B(D^*(2010)^+ \to D^0\pi^+) = 0.57 \pm 0.06$ and $B(D^0 \to K^-\pi^+) = 0.042 \pm 0.008$. We rescale to our PDG 96 values of D and D^* branching ratios. Our first error is their experiment's error and our second error is the systematic error from using our best value.

[4] ALBRECHT 91H reports $0.348 \pm 0.060 \pm 0.035$ from a measurement of $[\Gamma(B \to D^*(2010)^{\pm}\text{anything})/\Gamma_{total}] \times [B(D^*(2010)^+ \to D^0\pi^+)]$ assuming $B(D^*(2010)^+ \to D^0\pi^+) = 0.55 \pm 0.04$, which we rescale to our best value $B(D^*(2010)^+ \to D^0\pi^+) = (67.7 \pm 0.5) \times 10^{-2}$. Our first error is their experiment's error and our second error is the systematic error from using our best value. Uses the PDG 90 $B(D^0 \to K^-\pi^+) = 0.0371 \pm 0.0025$.

[5] BORTOLETTO 87 uses old MARK III (BALTRUSAITIS 86E) branching ratios $B(D^0 \to K^-\pi^+) = 0.056 \pm 0.004 \pm 0.003$ and also assumes $B(D^*(2010)^+ \to D^0\pi^+) = 0.60^{+0.08}_{-0.15}$. The product branching ratio for $B(B \to D^*(2010)^+)\, B(D^*(2010)^+ \to D^0\pi^+)$ is $0.13 \pm 0.02 \pm 0.012$. Superseded by BORTOLETTO 92.

[6] $V-A$ momentum spectrum used to extrapolate below $p = 1$ GeV. We correct the value assuming $B(D^0 \to K^-\pi^+) = 0.042 \pm 0.006$ and $B(D^{*+} \to D^0\pi^+) = 0.6^{+0.08}_{-0.15}$. The product branching fraction is $B(B \to D^{*+}X)\cdot B(D^{*+} \to \pi^+ D^0)\cdot B(D^0 \to K^-\pi^+) = (68 \pm 15 \pm 9) \times 10^{-4}$.

$\Gamma(\overline{D}^*(2007)^0\text{anything})/\Gamma_{total}$ — Γ_{34}/Γ

VALUE	DOCUMENT ID		TECN	COMMENT
0.260±0.023±0.015	[1] GIBBONS	97B	CLE2	$e^+e^- \to \Upsilon(4S)$

[1] GIBBONS 97B reports $B(B \to D^*(2007)^0\text{anything})$ $0.247 \pm 0.012 \pm 0.018 \pm 0.018$ using CLEO measured D and D^* branching fractions. We rescale to our PDG 96 values of D and D^* branching ratios. Our first error is their experiment's error and our second error is the systematic error from using our best value.

$\Gamma(D_s^{\pm}\text{anything})/\Gamma_{total}$ — Γ_{35}/Γ

VALUE	EVTS	DOCUMENT ID		TECN	COMMENT
0.083±0.008 OUR AVERAGE					
0.089±0.010±0.008		[1] ARTUSO	05B	CLE2	$e^+e^- \to \Upsilon(5S)$
0.087±0.005±0.008		[2] AUBERT	02G	BABR	$e^+e^- \to \Upsilon(4S)$
0.065±0.011±0.006		[3] ALBRECHT	92G	ARG	$e^+e^- \to \Upsilon(4S)$
0.068±0.010±0.006	257	[4] BORTOLETTO	90	CLEO	$e^+e^- \to \Upsilon(4S)$
0.085±0.022±0.008		[5] HAAS	86	CLEO	$e^+e^- \to \Upsilon(4S)$
• • • We do not use the following data for averages, fits, limits, etc. • • •					
0.094±0.007±0.008		[6] GIBAUT	96	CLE2	Repl. by ARTUSO 05B
0.094±0.024±0.008		[7] ALBRECHT	87H	ARG	$e^+e^- \to \Upsilon(4S)$

[1] ARTUSO 05B reports $0.0905 \pm 0.0025 \pm 0.0140$ from a measurement of $[\Gamma(B \to D_s^{\pm}\text{anything})/\Gamma_{total}] \times [B(D_s^+ \to \phi\pi^+)]$ assuming $B(D_s^+ \to \phi\pi^+) = (4.4 \pm 0.5) \times 10^{-2}$, which we rescale to our best value $B(D_s^+ \to \phi\pi^+) = (4.5 \pm 0.4) \times 10^{-2}$. Our first error is their experiment's error and our second error is the systematic error from using our best value.

[2] AUBERT 02G reports $[\Gamma(B \to D_s^{\pm}\text{anything})/\Gamma_{total}] \times [B(D_s^+ \to \phi\pi^+)] = 0.00393 \pm 0.00007 \pm 0.00021$ which we divide by our best value $B(D_s^+ \to \phi\pi^+) = (4.5 \pm 0.4) \times 10^{-2}$. Our first error is their experiment's error and our second error is the systematic error from using our best value.

[3] ALBRECHT 92G reports $[\Gamma(B \to D_s^{\pm}\text{anything})/\Gamma_{total}] \times [B(D_s^+ \to \phi\pi^+)] = 0.00292 \pm 0.00039 \pm 0.00031$ which we divide by our best value $B(D_s^+ \to \phi\pi^+) = (4.5 \pm 0.4) \times 10^{-2}$. Our first error is their experiment's error and our second error is the systematic error from using our best value.

[4] BORTOLETTO 90 reports $[\Gamma(B \to D_s^{\pm}\text{anything})/\Gamma_{total}] \times [B(D_s^+ \to \phi\pi^+)] = 0.00306 \pm 0.00047$ which we divide by our best value $B(D_s^+ \to \phi\pi^+) = (4.5 \pm 0.4) \times 10^{-2}$. Our first error is their experiment's error and our second error is the systematic error from using our best value.

[5] HAAS 86 reports $[\Gamma(B \to D_s^{\pm}\text{anything})/\Gamma_{total}] \times [B(D_s^+ \to \phi\pi^+)] = 0.0038 \pm 0.0010$ which we divide by our best value $B(D_s^+ \to \phi\pi^+) = (4.5 \pm 0.4) \times 10^{-2}$. Our first error is their experiment's error and our second error is the systematic error from using our best value. $64 \pm 22\%$ decays are 2-body.

[6] GIBAUT 96 reports $0.1211 \pm 0.0039 \pm 0.0088$ from a measurement of $[\Gamma(B \to D_s^{\pm}\text{anything})/\Gamma_{total}] \times [B(D_s^+ \to \phi\pi^+)]$ assuming $B(D_s^+ \to \phi\pi^+) = 0.035$, which we rescale to our best value $B(D_s^+ \to \phi\pi^+) = (4.5 \pm 0.4) \times 10^{-2}$. Our first error is their experiment's error and our second error is the systematic error from using our best value.

[7] ALBRECHT 87H reports $[\Gamma(B \to D_s^{\pm}\text{anything})/\Gamma_{total}] \times [B(D_s^+ \to \phi\pi^+)] = 0.0042 \pm 0.0009 \pm 0.0006$ which we divide by our best value $B(D_s^+ \to \phi\pi^+) = (4.5 \pm 0.4) \times 10^{-2}$. Our first error is their experiment's error and our second error is the systematic error from using our best value. $46 \pm 16\%$ of $B \to D_s X$ decays are 2-body. Superseded by ALBRECHT 92G.

$\Gamma(D_s^{*\pm}\text{anything})/\Gamma_{total}$ — Γ_{36}/Γ

VALUE	DOCUMENT ID		TECN	COMMENT
0.063±0.009±0.006	[1] AUBERT	02G	BABR	$e^+e^- \to \Upsilon(4S)$

[1] AUBERT 02G reports $[\Gamma(B \to D_s^{*\pm}\text{anything})/\Gamma_{total}] \times [B(D_s^+ \to \phi\pi^+)] = 0.00284 \pm 0.00029 \pm 0.00025$ which we divide by our best value $B(D_s^+ \to \phi\pi^+) = (4.5 \pm 0.4) \times 10^{-2}$. Our first error is their experiment's error and our second error is the systematic error from using our best value.

$\Gamma(D_s^{*\pm}\overline{D}^{(*)})/\Gamma(D_s^{\pm}\text{anything})$ — Γ_{37}/Γ_{36}

Sum over modes

VALUE	DOCUMENT ID		TECN	COMMENT
0.533±0.037±0.037	AUBERT	02G	BABR	$e^+e^- \to \Upsilon(4S)$

$\Gamma(\overline{D}D_{s0}(2317))/\Gamma_{total}$ — Γ_{38}/Γ

VALUE	DOCUMENT ID		TECN	COMMENT
seen	[1] KROKOVNY	03B	BELL	$e^+e^- \to \Upsilon(4S)$

[1] The product branching ratio for $B(B \to \overline{D}D_{s0}(2317)^+)\times B(D_{s0}(2317)^+ \to D_s\pi^0)$ is measured to be $(8.5^{+2.1}_{-1.9} \pm 2.6) \times 10^{-4}$.

$\Gamma(\overline{D}D_{sJ}(2457))/\Gamma_{total}$ — Γ_{39}/Γ

VALUE	DOCUMENT ID		TECN	COMMENT
seen	[1] KROKOVNY	03B	BELL	$e^+e^- \to \Upsilon(4S)$

[1] The product branching ratio for $B(B \to \overline{D}D_{sJ}(2457)^+)\times B(D_{sJ}(2457)^+ \to D_s^{*+}\pi^0, D_s^+\gamma)$ are measured to be $(17.8^{+4.5}_{-3.9} \pm 5.3) \times 10^{-4}$ and $(6.7^{+1.3}_{-1.2} \pm 2.0) \times 10^{-4}$, respectively.

$[\Gamma(D^{(*)}\overline{D}^{(*)}K^0) + \Gamma(D^{(*)}\overline{D}^{(*)}K^{\pm})]/\Gamma_{total}$ — Γ_{40}/Γ

VALUE	DOCUMENT ID		TECN	COMMENT
$\mathbf{0.071^{+0.025}_{-0.015}{}^{+0.010}_{-0.009}}$	[1] BARATE	98Q	ALEP	$e^+e^- \to Z$

[1] The systematic error includes the uncertainties due to the charm branching ratios.

$\Gamma(b \to c\overline{c}s)/\Gamma_{total}$ — Γ_{41}/Γ

VALUE	DOCUMENT ID		TECN	COMMENT
0.219±0.037	[1] COAN	98	CLE2	$e^+e^- \to \Upsilon(4S)$

[1] COAN 98 uses D-ℓ correlation.

$\Gamma(D_s^{(*)}\overline{D}^{(*)})/\Gamma(D_s^{\pm}\text{anything})$ — Γ_{42}/Γ_{35}

Sum over modes.

VALUE	DOCUMENT ID		TECN	COMMENT
0.469±0.017 OUR AVERAGE				
0.464±0.013±0.015	AUBERT	02G	BABR	$e^+e^- \to \Upsilon(4S)$
$0.56\ ^{+0.21}_{-0.15}\ ^{+0.09}_{-0.08}$	[1] BARATE	98Q	ALEP	$e^+e^- \to Z$
0.457±0.019±0.037	GIBAUT	96	CLE2	$e^+e^- \to \Upsilon(4S)$
0.58 ±0.07 ±0.09	ALBRECHT	92G	ARG	$e^+e^- \to \Upsilon(4S)$
0.56 ±0.10	BORTOLETTO	90	CLEO	$e^+e^- \to \Upsilon(4S)$

[1] BARATE 98Q measures $B(B \to D_s^{(*)}\overline{D}^{(*)}) = 0.056^{+0.021}_{-0.015}{}^{+0.009}_{-0.008}{}^{+0.019}_{-0.011}$, where the third error results from the uncertainty on the different D branching ratios and is dominated by the uncertainty on $B(D_s^+ \to \phi\pi^+)$. We divide $B(B \to D_s^{(*)}\overline{D}^{(*)})$ by our best value of $B(B \to D_s\text{anything}) = 0.1 \pm 0.025$.

$\Gamma(D^*D^*(2010)^{\pm})/\Gamma_{total}$ — Γ_{43}/Γ

VALUE	CL%	DOCUMENT ID		TECN	COMMENT
$\mathbf{<5.9 \times 10^{-3}}$	90	BARATE	98Q	ALEP	$e^+e^- \to Z$

$[\Gamma(DD^*(2010)^{\pm}) + \Gamma(D^*D^{\pm})]/\Gamma_{total}$ — Γ_{44}/Γ

VALUE	CL%	DOCUMENT ID		TECN	COMMENT
$\mathbf{<5.5 \times 10^{-3}}$	90	BARATE	98Q	ALEP	$e^+e^- \to Z$

$\Gamma(DD^{\pm})/\Gamma_{total}$ — Γ_{45}/Γ

VALUE	CL%	DOCUMENT ID		TECN	COMMENT
$\mathbf{<3.1 \times 10^{-3}}$	90	BARATE	98Q	ALEP	$e^+e^- \to Z$

$\Gamma(D_s^{(*)\pm}\overline{D}^{(*)}X(n\pi^{\pm}))/\Gamma_{total}$ — Γ_{46}/Γ

VALUE	DOCUMENT ID		TECN	COMMENT
$\mathbf{0.094^{+0.040}_{-0.031}{}^{+0.034}_{-0.024}}$	[1] BARATE	98Q	ALEP	$e^+e^- \to Z$

[1] The systematic error includes the uncertainties due to the charm branching ratios.

$\Gamma(\overline{D}^*(2010)\gamma)/\Gamma_{total}$ — Γ_{47}/Γ

VALUE	CL%	DOCUMENT ID		TECN	COMMENT
$\mathbf{<1.1 \times 10^{-3}}$	90	[1] LESIAK	92	CBAL	$e^+e^- \to \Upsilon(4S)$

[1] LESIAK 92 set a limit on the inclusive process $B(b \to s\gamma) < 2.8 \times 10^{-3}$ at 90% CL for the range of masses of 892–2045 MeV, independent of assumptions about s-quark hadronization.

$\Gamma(D_s^+\pi^-, D_s^{*+}\pi^-, D_s^+\rho^-, D_s^{*+}\rho^-, D_s^+\pi^0, D_s^{*+}\pi^0, D_s^+\eta, D_s^{*+}\eta, D_s^+\rho^0, D_s^{*+}\rho^0, D_s^+\omega, D_s^{*+}\omega)/\Gamma_{total}$ — Γ_{48}/Γ

Sum over modes.

VALUE	CL%	DOCUMENT ID		TECN	COMMENT
$\mathbf{<4 \times 10^{-4}}$	90	[1] ALEXANDER	93B	CLE2	$e^+e^- \to \Upsilon(4S)$

[1] ALEXANDER 93B reports $< 4.8 \times 10^{-4}$ from a measurement of $[\Gamma(B \to D_s^+\pi^-, D_s^{*+}\pi^-, D_s^+\rho^-, D_s^{*+}\rho^-, D_s^+\pi^0, D_s^{*+}\pi^0, D_s^+\eta, D_s^{*+}\eta, D_s^+\rho^0, D_s^{*+}\rho^0, D_s^+\omega, D_s^{*+}\omega)/\Gamma_{total}] \times [B(D_s^+ \to \phi\pi^+)]$ assuming $B(D_s^+ \to \phi\pi^+) = 0.037$, which we rescale to our best value $B(D_s^+ \to \phi\pi^+) = 4.5 \times 10^{-2}$. This branching ratio limit provides a model-dependent upper limit $|V_{ub}|/|V_{cb}| < 0.16$ at CL=90%.

Downloaded from https://academic.oup.com/ptep/article/2022/8/083C01/6651666 by KIT Library user on 27 September 2022

$\Gamma(D_{s1}(2536)^{+}\text{ anything})/\Gamma_{\text{total}}$ — Γ_{49}/Γ

$D_{s1}(2536)^{+}$ is the narrow P-wave D_s^{+} meson with $J^P = 1^+$.

VALUE	CL%	DOCUMENT ID		TECN	COMMENT
<0.0095	90	[1] BISHAI	98	CLE2	$e^+e^- \to \Upsilon(4S)$

[1] Assuming factorization, the decay constant $f_{D_{s1}^+}$ is at least a factor of 2.5 times smaller than $f_{D_s^+}$.

$\Gamma(J/\psi(1S)\text{ anything})/\Gamma_{\text{total}}$ — Γ_{50}/Γ

VALUE (units 10^{-2})	EVTS	DOCUMENT ID		TECN	COMMENT
1.094±0.032 OUR AVERAGE		Error includes scale factor of 1.1.			
1.057±0.012±0.040		[1] AUBERT	03F	BABR	$e^+e^- \to \Upsilon(4S)$
1.121±0.013±0.042		ANDERSON	02	CLE2	$e^+e^- \to \Upsilon(4S)$
1.29 ±0.45 ±0.01	27	[2] MASCHMANN	90	CBAL	$e^+e^- \to \Upsilon(4S)$
1.24 ±0.27 ±0.01	120	[3] ALBRECHT	87D	ARG	$e^+e^- \to \Upsilon(4S)$
1.35 ±0.24 ±0.01	52	[4] ALAM	86	CLEO	$e^+e^- \to \Upsilon(4S)$
• • • We do not use the following data for averages, fits, limits, etc. • • •					
1.12 ±0.06 ±0.01	1489	[5] BALEST	95B	CLE2	$e^+e^- \to \Upsilon(4S)$
1.4 $^{+0.6}_{-0.5}$	7	[6] ALBRECHT	85H	ARG	$e^+e^- \to \Upsilon(4S)$
1.1 ±0.21 ±0.23	46	[7] HAAS	85	CLEO	Repl. by ALAM 86

[1] AUBERT 03F also reports the momentum distribution and helicity of $J/\psi \to \ell^+\ell^-$ in the $\Upsilon(4S)$ center-of-mass frame.

[2] MASCHMANN 90 reports $(1.12 \pm 0.33 \pm 0.25) \times 10^{-2}$ from a measurement of $[\Gamma(B \to J/\psi(1S)\text{ anything})/\Gamma_{\text{total}}] \times [B(J/\psi(1S) \to e^+e^-)]$ assuming $B(J/\psi(1S) \to e^+e^-) = 0.069 \pm 0.009$, which we rescale to our best value $B(J/\psi(1S) \to e^+e^-) = (5.971 \pm 0.032) \times 10^{-2}$. Our first error is their experiment's error and our second error is the systematic error from using our best value.

[3] ALBRECHT 87D reports $(1.07 \pm 0.16 \pm 0.22) \times 10^{-2}$ from a measurement of $[\Gamma(B \to J/\psi(1S)\text{ anything})/\Gamma_{\text{total}}] \times [B(J/\psi(1S) \to e^+e^-)]$ assuming $B(J/\psi(1S) \to e^+e^-) = 0.069 \pm 0.009$, which we rescale to our best value $B(J/\psi(1S) \to e^+e^-) = (5.971 \pm 0.032) \times 10^{-2}$. Our first error is their experiment's error and our second error is the systematic error from using our best value. ALBRECHT 87D find the branching ratio for J/ψ not from $\psi(2S)$ to be 0.0081 ± 0.0023.

[4] ALAM 86 reports $(1.09 \pm 0.16 \pm 0.21) \times 10^{-2}$ from a measurement of $[\Gamma(B \to J/\psi(1S)\text{ anything})/\Gamma_{\text{total}}] \times [B(J/\psi(1S) \to \mu^+\mu^-)]$ assuming $B(J/\psi(1S) \to \mu^+\mu^-) = 0.074 \pm 0.012$, which we rescale to our best value $B(J/\psi(1S) \to \mu^+\mu^-) = (5.961 \pm 0.033) \times 10^{-2}$. Our first error is their experiment's error and our second error is the systematic error from using our best value.

[5] BALEST 95B reports $(1.12 \pm 0.04 \pm 0.06) \times 10^{-2}$ from a measurement of $[\Gamma(B \to J/\psi(1S)\text{ anything})/\Gamma_{\text{total}}] \times [B(J/\psi(1S) \to e^+e^-)]$ assuming $B(J/\psi(1S) \to e^+e^-) = 0.0599 \pm 0.0025$, which we rescale to our best value $B(J/\psi(1S) \to e^+e^-) = (5.971 \pm 0.032) \times 10^{-2}$. Our first error is their experiment's error and our second error is the systematic error from using our best value. They measure $J/\psi(1S) \to e^+e^-$ and $\mu^+\mu^-$ and use PDG 1994 values for the branching fractions. The rescaling is the same for either mode so we use e^+e^-.

[6] Statistical and systematic errors were added in quadrature. ALBRECHT 85H also report a CL = 90% limit of 0.007 for $B \to J/\psi(1S) + X$ where m_X <1 GeV.

[7] Dimuon and dielectron events used.

$\Gamma(J/\psi(1S)\text{ (direct) anything})/\Gamma_{\text{total}}$ — Γ_{51}/Γ

VALUE	DOCUMENT ID		TECN	COMMENT
0.0078 ±0.0004 OUR AVERAGE	Error includes scale factor of 1.1.			
0.00740±0.00023±0.00043	[1] AUBERT	03F	BABR	$e^+e^- \to \Upsilon(4S)$
0.00813±0.00017±0.00037	[2] ANDERSON	02	CLE2	$e^+e^- \to \Upsilon(4S)$
• • • We do not use the following data for averages, fits, limits, etc. • • •				
0.0080 ±0.0008	[3] BALEST	95B	CLE2	$e^+e^- \to \Upsilon(4S)$

[1] AUBERT 03F also reports the helicity of $J/\psi \to \ell^+\ell^-$ produced directly in B decay.

[2] Also reports the measurement of $J/\psi \to \ell^+\ell^-$ polarization produced directly from B decay.

[3] BALEST 95B assume PDG 1994 values for sub mode branching ratios. $J/\psi(1S)$ mesons are reconstructed in $J/\psi(1S) \to e^+e^-$ and $J/\psi(1S) \to \mu^+\mu^-$. The $B \to J/\psi(1S)X$ branching ratio contains $J/\psi(1S)$ mesons directly from B decays and also from feeddown through $\psi(2S) \to J/\psi(1S)$, $\chi_{c1}(1P) \to J/\psi(1S)$, or $\chi_{c2}(1P) \to J/\psi(1S)$. Using the measured inclusive rates, BALEST 95B corrects for the feeddown and finds the $B \to J/\psi(1S)$ (direct) X branching ratio.

$\Gamma(\psi(2S)\text{ anything})/\Gamma_{\text{total}}$ — Γ_{52}/Γ

VALUE	EVTS	DOCUMENT ID		TECN	COMMENT
0.00307±0.00021 OUR AVERAGE					
0.00297±0.00020±0.00020		AUBERT	03F	BABR	$e^+e^- \to \Upsilon(4S)$
0.00316±0.00014±0.00028		[1] ANDERSON	02	CLE2	$e^+e^- \to \Upsilon(4S)$
0.0046 ±0.0017 ±0.0011	8	ALBRECHT	87D	ARG	$e^+e^- \to \Upsilon(4S)$
• • • We do not use the following data for averages, fits, limits, etc. • • •					
0.0034 ±0.0004 ±0.0003	240	[2] BALEST	95B	CLE2	$e^+e^- \to \Upsilon(4S)$

[1] Also reports the measurement of $\psi(2S) \to \ell^+\ell^-$ polarization produced directly from B decay.

[2] BALEST 95B assume PDG 1994 values for sub mode branching ratios. They find $B(B \to \psi(2S)X,\ \psi(2S) \to \ell^+\ell^-) = 0.30 \pm 0.05 \pm 0.04$ and $B(B \to \psi(2S)X,\ \psi(2S) \to J/\psi(1S)\pi^+\pi^-) = 0.37 \pm 0.05 \pm 0.05$. Weighted average is quoted for $B(B \to \psi(2S)X)$.

$\Gamma(\chi_{c1}(1P)\text{ anything})/\Gamma_{\text{total}}$ — Γ_{53}/Γ

VALUE (units 10^{-3})	EVTS	DOCUMENT ID		TECN	COMMENT
3.55±0.27 OUR AVERAGE		Error includes scale factor of 1.3. See the ideogram below.			
3.33±0.05±0.24		[1] BHARDWAJ	16	BELL	$e^+e^- \to \Upsilon(4S)$
3.67±0.35±0.44		AUBERT	03F	BABR	$e^+e^- \to \Upsilon(4S)$
4.35±0.29±0.40		ANDERSON	02	CLE2	$e^+e^- \to \Upsilon(4S)$
• • • We do not use the following data for averages, fits, limits, etc. • • •					
3.63±0.22±0.34		[2] ABE	02L	BELL	Repl. by BHARDWAJ 16
3.30±0.35±0.09		[3] CHEN	01	CLE2	$e^+e^- \to \Upsilon(4S)$
4.0 ±0.6 ±0.4	112	[4] BALEST	95B	CLE2	Repl. by CHEN 01
10.5 ±3.5 ±2.5		[5] ALBRECHT	92E	ARG	$e^+e^- \to \Upsilon(4S)$

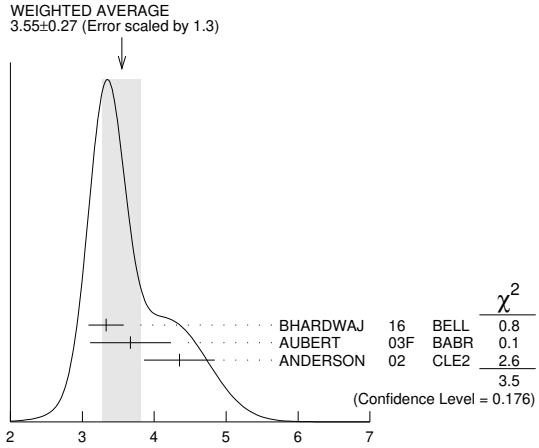

[1] Assumes equal production of B^+ and B^0 at the $\Upsilon(4S)$.

[2] ABE 02L uses PDG 01 values for $B(J/\psi(1S) \to \ell^+\ell^-)$ and $B(\chi_{c1,c2} \to J/\psi(1S)\gamma)$.

[3] CHEN 01 reports $0.00414 \pm 0.00031 \pm 0.00040$ from a measurement of $[\Gamma(B \to \chi_{c1}(1P)\text{ anything})/\Gamma_{\text{total}}] \times [B(\chi_{c1}(1P) \to \gamma J/\psi(1S))]$ assuming $B(\chi_{c1}(1P) \to \gamma J/\psi(1S)) = 0.273 \pm 0.016$, which we rescale to our best value $B(\chi_{c1}(1P) \to \gamma J/\psi(1S)) = (34.3 \pm 1.0) \times 10^{-2}$. Our first error is their experiment's error and our second error is the systematic error from using our best value. Assumes equal production of B^+ and B^0 at the $\Upsilon(4S)$.

[4] BALEST 95B assume $B(\chi_{c1}(1P) \to J/\psi(1S)\gamma) = (27.3 \pm 1.6) \times 10^{-2}$, the PDG 1994 value. Fit to ψ-photon invariant mass distribution allows for a $\chi_{c1}(1P)$ and a $\chi_{c2}(1P)$ component.

[5] ALBRECHT 92E assumes no $\chi_{c2}(1P)$ production.

$\Gamma(\chi_{c1}(1P)\text{ (direct) anything})/\Gamma_{\text{total}}$ — Γ_{54}/Γ

VALUE (units 10^{-3})	DOCUMENT ID		TECN	COMMENT
3.08±0.19 OUR AVERAGE				
3.03±0.05±0.24	[1] BHARDWAJ	16	BELL	$e^+e^- \to \Upsilon(4S)$
3.41±0.35±0.42	AUBERT	03F	BABR	$e^+e^- \to \Upsilon(4S)$
3.1 ±0.4 ±0.1	[2] CHEN	01	CLE2	$e^+e^- \to \Upsilon(4S)$
• • • We do not use the following data for averages, fits, limits, etc. • • •				
3.32±0.22±0.34	[3] ABE	02L	BELL	Repl. by BHARDWAJ 16
3.7 ±0.7	[4] BALEST	95B	CLE2	Repl. by CHEN 01

[1] Assumes equal production of B^+ and B^0 at the $\Upsilon(4S)$.

[2] CHEN 01 reports $0.00383 \pm 0.00031 \pm 0.00040$ from a measurement of $[\Gamma(B \to \chi_{c1}(1P)(\text{direct anything})/\Gamma_{\text{total}}] \times [B(\chi_{c1}(1P) \to \gamma J/\psi(1S))]$ assuming $B(\chi_{c1}(1P) \to \gamma J/\psi(1S)) = 0.273 \pm 0.016$, which we rescale to our best value $B(\chi_{c1}(1P) \to \gamma J/\psi(1S)) = (34.3 \pm 1.0) \times 10^{-2}$. Our first error is their experiment's error and our second error is the systematic error from using our best value. Assumes equal production of B^+ and B^0 at the $\Upsilon(4S)$.

[3] ABE 02L uses PDG 01 values for $B(J/\psi(1S) \to \ell^+\ell^-)$ and $B(\chi_{c1,c2} \to J/\psi(1S)\gamma)$.

[4] BALEST 95B assume PDG 1994 values. $J/\psi(1S)$ mesons are reconstructed in the e^+e^- and $\mu^+\mu^-$ modes. The $B \to \chi_{c1}(1P)X$ branching ratio contains $\chi_{c1}(1P)$ mesons directly from B decays and also from feeddown through $\psi(2S) \to \chi_{c1}(1P)\gamma$. Using the measured inclusive rates, BALEST 95B corrects for the feeddown and finds the $B \to \chi_{c1}(1P)$ (direct) X branching ratio.

$\Gamma(\chi_{c2}(1P)\text{ anything})/\Gamma_{\text{total}}$ — Γ_{55}/Γ

VALUE (units 10^{-4})	CL%	DOCUMENT ID		TECN	COMMENT
10.0±1.7 OUR AVERAGE		Error includes scale factor of 1.6. See the ideogram below.			
9.8±0.6±1.0		[1] BHARDWAJ	16	BELL	$e^+e^- \to \Upsilon(4S)$
21.0±4.5±3.1		AUBERT	03F	BABR	$e^+e^- \to \Upsilon(4S)$
7.0±3.5±0.2		[2] CHEN	01	CLE2	$e^+e^- \to \Upsilon(4S)$
• • • We do not use the following data for averages, fits, limits, etc. • • •					
18.0 $^{+2.3}_{-2.8}$ ±2.6		[3] ABE	02L	BELL	Repl. by BHARDWAJ 16
<38	90	[4] BALEST	95B	CLE2	Repl. by CHEN 01

[1] Assumes equal production of B^+ and B^0 at the $\Upsilon(4S)$.

Downloaded from https://academic.oup.com/ptep/article/2022/8/083C01/6651666 by KIT Library user on 27 September 2022

[2] CHEN 01 reports $(9.8 \pm 4.8 \pm 1.5) \times 10^{-4}$ from a measurement of $[\Gamma(B \to \chi_{c2}(1P)\text{anything})/\Gamma_{\text{total}}] \times [B(\chi_{c2}(1P) \to \gamma J/\psi(1S))]$ assuming $B(\chi_{c2}(1P) \to \gamma J/\psi(1S)) = 0.135 \pm 0.011$, which we rescale to our best value $B(\chi_{c2}(1P) \to \gamma J/\psi(1S)) = (19.0 \pm 0.5) \times 10^{-2}$. Our first error is their experiment's error and our second error is the systematic error from using our best value. Assumes equal production of B^+ and B^0 at the $\Upsilon(4S)$.

[3] ABE 02L uses PDG 01 values for $B(J/\psi(1S) \to \ell^+\ell^-)$ and $B(\chi_{c1,c2} \to J/\psi(1S)\gamma)$.

[4] BALEST 95B assume $B(\chi_{c2}(1P) \to J/\psi(1S)\gamma) = (13.5 \pm 1.1) \times 10^{-2}$, the PDG 1994 value. $J/\psi(1S)$ mesons are reconstructed in the e^+e^- and $\mu^+\mu^-$ modes, and PDG 1994 branching fractions are used. If interpreted as signal, the 35 ± 13 events correspond to $B(B \to \chi_{c2}(1P)X) = (0.25 \pm 0.10 \pm 0.03) \times 10^{-2}$.

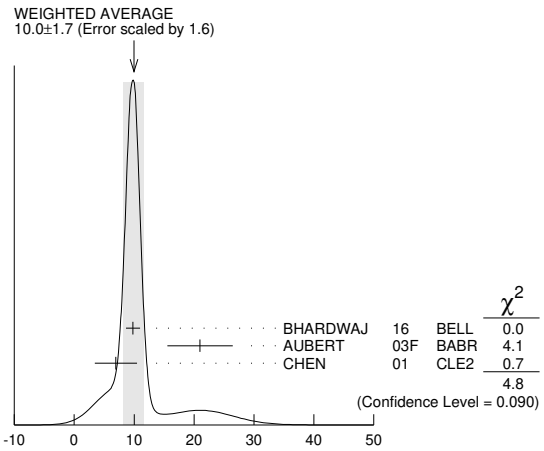

$\Gamma(\chi_{c2}(1P)\text{anything})/\Gamma_{\text{total}}$ Γ_{55}/Γ

$\Gamma(\chi_{c2}(1P)(\text{direct})\text{ anything})/\Gamma_{\text{total}}$ Γ_{56}/Γ

VALUE (units 10^{-3})	DOCUMENT ID		TECN	COMMENT
0.75±0.11 OUR AVERAGE				
0.70±0.06±0.10	[1] BHARDWAJ	16	BELL	$e^+e^- \to \Upsilon(4S)$
1.90±0.45±0.29	AUBERT	03F	BABR	$e^+e^- \to \Upsilon(4S)$
• • • We do not use the following data for averages, fits, limits, etc. • • •				
$1.53^{+0.23}_{-0.28} \pm 0.27$	[2] ABE	02L	BELL	Repl. by BHARDWAJ 16

[1] Assumes equal production of B^+ and B^0 at the $\Upsilon(4S)$.

[2] ABE 02L uses PDG 01 values for $B(J/\psi(1S) \to \ell^+\ell^-)$ and $B(\chi_{c1,c2} \to J/\psi(1S)\gamma)$.

$\Gamma(\eta_c(1S)\text{anything})/\Gamma_{\text{total}}$ Γ_{57}/Γ

VALUE	CL%	DOCUMENT ID		TECN	COMMENT
<0.009	90	[1] BALEST	95B	CLE2	$e^+e^- \to \Upsilon(4S)$

[1] BALEST 95B assume PDG 1994 values for sub mode branching ratios. $J/\psi(1S)$ mesons are reconstructed in $J/\psi(1S) \to e^+e^-$ and $J/\psi(1S) \to \mu^+\mu^-$. Search region $2960 < m_{\eta_c(1S)} < 3010$ MeV/c^2.

$\Gamma(K\chi_{c1}(3872))/\Gamma_{\text{total}}$ Γ_{58}/Γ

VALUE (units 10^{-4})	DOCUMENT ID		TECN	COMMENT
2.3±0.7 OUR AVERAGE				
2.2±0.6±0.5	[1] AUSHEV	10	BELL	$e^+e^- \to \Upsilon(4S)$
$2.5^{+0.8}_{-0.9}{}^{+1.0}_{-0.9}$	[2,3] GOKHROO	06	BELL	$e^+e^- \to \Upsilon(4S)$

[1] AUSHEV 10 reports $[\Gamma(B \to K\chi_{c1}(3872))/\Gamma_{\text{total}}] \times [B(\chi_{c1}(3872) \to \overline{D}^{*0}D^0)] = (0.80 \pm 0.20 \pm 0.10) \times 10^{-4}$ which we divide by our best value $B(\chi_{c1}(3872) \to \overline{D}^{*0}D^0) = (37 \pm 9) \times 10^{-2}$. Our first error is their experiment's error and our second error is the systematic error from using our best value.

[2] GOKHROO 06 reports $[\Gamma(B \to K\chi_{c1}(3872))/\Gamma_{\text{total}}] \times [B(\chi_{c1}(3872) \to D^0\overline{D}^0\pi^0)] = (1.22 \pm 0.31^{+0.23}_{-0.30}) \times 10^{-4}$ which we divide by our best value $B(\chi_{c1}(3872) \to D^0\overline{D}^0\pi^0) = (49^{+18}_{-20}) \times 10^{-2}$. Our first error is their experiment's error and our second error is the systematic error from using our best value.

[3] Measure the near-threshold enhancements in the $(D^0\overline{D}^0\pi^0)$ system at a mass $3875.2 \pm 0.7^{+0.3}_{-1.6} \pm 0.8$ MeV/c^2.

$\Gamma(KX(3940),\ X \to D^{*0}D^0)/\Gamma_{\text{total}}$ Γ_{59}/Γ

VALUE (units 10^{-4})	CL%	DOCUMENT ID		TECN	COMMENT
<0.67	90	AUSHEV	10	BELL	$e^+e^- \to \Upsilon(4S)$

$\Gamma(K\chi_{c0}(3915),\ \chi_{c0} \to \omega J/\psi)/\Gamma_{\text{total}}$ Γ_{60}/Γ

VALUE (units 10^{-5})	DOCUMENT ID		TECN	COMMENT
7.1±1.3±3.1	[1] CHOI	05	BELL	$e^+e^- \to \Upsilon(4S)$

[1] CHOI 05 reports the observation of a near-threshold enhancement in the $\omega J/\psi$ mass spectrum in exclusive $B \to K\omega J/\psi$. The new state, denoted as $\chi_{c0}(3915)$, is measured to have a mass of $3943 \pm 11 \pm 13$ GeV/c^2 and a width $\Gamma = 87 \pm 22 \pm 26$ MeV.

$\Gamma(K^{\pm}\text{anything})/\Gamma_{\text{total}}$ Γ_{61}/Γ

VALUE	DOCUMENT ID		TECN	COMMENT
0.789±0.025 OUR AVERAGE				
0.82 ±0.01 ±0.05	ALBRECHT	94C	ARG	$e^+e^- \to \Upsilon(4S)$
0.775±0.015±0.025	[1] ALBRECHT	93I	ARG	$e^+e^- \to \Upsilon(4S)$
0.85 ±0.07 ±0.09	ALAM	87B	CLEO	$e^+e^- \to \Upsilon(4S)$
• • • We do not use the following data for averages, fits, limits, etc. • • •				
seen	[2] BRODY	82	CLEO	$e^+e^- \to \Upsilon(4S)$
seen	[3] GIANNINI	82	CUSB	$e^+e^- \to \Upsilon(4S)$

[1] ALBRECHT 93I value is not independent of the sum of $B \to K^+$ anything and $B \to K^-$ anything ALBRECHT 94C values.

[2] Assuming $\Upsilon(4S) \to B\overline{B}$, a total of $3.38 \pm 0.34 \pm 0.68$ kaons per $\Upsilon(4S)$ decay is found (the second error is systematic). In the context of the standard B-decay model, this leads to a value for (b-quark $\to$ c-quark)/(b-quark $\to$ all) of $1.09 \pm 0.33 \pm 0.13$.

[3] GIANNINI 82 at CESR-CUSB observed 1.58 ± 0.35 K^0 per hadronic event much higher than 0.82 ± 0.10 below threshold. Consistent with predominant $b \to cX$ decay.

$\Gamma(K^+\text{anything})/\Gamma_{\text{total}}$ Γ_{62}/Γ

VALUE	DOCUMENT ID		TECN	COMMENT
0.66 ±0.05	[1] ALBRECHT	94C	ARG	$e^+e^- \to \Upsilon(4S)$
• • • We do not use the following data for averages, fits, limits, etc. • • •				
0.620±0.013±0.038	[2] ALBRECHT	94C	ARG	$e^+e^- \to \Upsilon(4S)$
0.66 ±0.05 ±0.07	[2] ALAM	87B	CLEO	$e^+e^- \to \Upsilon(4S)$

[1] Measurement relies on lepton-kaon correlations. It is for the weak decay vertex and does not include mixing of the neutral B meson. Mixing effects were corrected for by assuming a mixing parameter r of (18.1 ± 4.3)%.

[2] Measurement relies on lepton-kaon correlations. It includes production through mixing of the neutral B meson.

$\Gamma(K^-\text{anything})/\Gamma_{\text{total}}$ Γ_{63}/Γ

VALUE	DOCUMENT ID		TECN	COMMENT
0.13 ±0.04	[1] ALBRECHT	94C	ARG	$e^+e^- \to \Upsilon(4S)$
• • • We do not use the following data for averages, fits, limits, etc. • • •				
0.165±0.011±0.036	[2] ALBRECHT	94C	ARG	$e^+e^- \to \Upsilon(4S)$
0.19 ±0.05 ±0.02	[2] ALAM	87B	CLEO	$e^+e^- \to \Upsilon(4S)$

[1] Measurement relies on lepton-kaon correlations. It is for the weak decay vertex and does not include mixing of the neutral B meson. Mixing effects were corrected for by assuming a mixing parameter r of (18.1 ± 4.3)%.

[2] Measurement relies on lepton-kaon correlations. It includes production through mixing of the neutral B meson.

$\Gamma(K^0/\overline{K}^0\text{anything})/\Gamma_{\text{total}}$ Γ_{64}/Γ

VALUE	DOCUMENT ID		TECN	COMMENT
0.64 ±0.04 OUR AVERAGE				
0.642±0.010±0.042	[1] ALBRECHT	94C	ARG	$e^+e^- \to \Upsilon(4S)$
0.63 ±0.06 ±0.06	ALAM	87B	CLEO	$e^+e^- \to \Upsilon(4S)$

[1] ALBRECHT 94C assume a $K^0/\overline{K}^0$ multiplicity twice that of K^0_S.

$\Gamma(K^*(892)^{\pm}\text{anything})/\Gamma_{\text{total}}$ Γ_{65}/Γ

VALUE	DOCUMENT ID		TECN	COMMENT
0.182±0.054±0.024	ALBRECHT	94J	ARG	$e^+e^- \to \Upsilon(4S)$

$\Gamma(K^*(892)^0/\overline{K}^*(892)^0\text{anything})/\Gamma_{\text{total}}$ Γ_{66}/Γ

VALUE	DOCUMENT ID		TECN	COMMENT
0.146±0.016±0.020	ALBRECHT	94J	ARG	$e^+e^- \to \Upsilon(4S)$

$\Gamma(K^*(892)\gamma)/\Gamma_{\text{total}}$ Γ_{67}/Γ

VALUE (units 10^{-5})	CL%	DOCUMENT ID		TECN	COMMENT
4.24±0.54±0.32		[1] COAN	00	CLE2	$e^+e^- \to \Upsilon(4S)$
• • • We do not use the following data for averages, fits, limits, etc. • • •					
<150	90	[2] LESIAK	92	CBAL	$e^+e^- \to \Upsilon(4S)$
< 24	90	ALBRECHT	88H	ARG	$e^+e^- \to \Upsilon(4S)$

[1] An average of $B(B^+ \to K^*(892)^+\gamma)$ and $B(B^0 \to K^*(892)^0\gamma)$ measurements reported in COAN 00 by assuming full correlated systematic errors.

[2] LESIAK 92 set a limit on the inclusive process $B(b \to s\gamma) < 2.8 \times 10^{-3}$ at 90% CL for the range of masses of 892–2045 MeV, independent of assumptions about s-quark hadronization.

$\Gamma(\eta K\gamma)/\Gamma_{\text{total}}$ Γ_{68}/Γ

VALUE (units 10^{-6})	DOCUMENT ID		TECN	COMMENT
$\mathbf{8.5 \pm 1.3^{+1.2}_{-0.9}}$	[1] NISHIDA	05	BELL	$e^+e^- \to \Upsilon(4S)$

[1] $m_{\eta K} < 2.4$ GeV/c^2

$\Gamma(K_1(1400)\gamma)/\Gamma_{\text{total}}$ Γ_{69}/Γ

VALUE	CL%	DOCUMENT ID		TECN	COMMENT
$<12.7 \times 10^{-5}$	90	[1] COAN	00	CLE2	$e^+e^- \to \Upsilon(4S)$
• • • We do not use the following data for averages, fits, limits, etc. • • •					
$< 1.6 \times 10^{-3}$	90	[2] LESIAK	92	CBAL	$e^+e^- \to \Upsilon(4S)$
$< 4.1 \times 10^{-4}$	90	ALBRECHT	88H	ARG	$e^+e^- \to \Upsilon(4S)$

[1] Assumes equal production of B^+ and B^0 at the $\Upsilon(4S)$.

[2] LESIAK 92 set a limit on the inclusive process $B(b \to s\gamma) < 2.8 \times 10^{-3}$ at 90% CL for the range of masses of 892–2045 MeV, independent of assumptions about s-quark hadronization.

Downloaded from https://academic.oup.com/ptep/article/2022/8/083C01/6651666 by KIT Library user on 27 September 2022

$\Gamma(K_2^*(1430)\gamma)/\Gamma_{total}$ — Γ_{70}/Γ

VALUE (units 10^{-5})	CL%	DOCUMENT ID		TECN	COMMENT
$1.66^{+0.59}_{-0.53}\pm0.13$		[1] COAN	00	CLE2	$e^+e^-\to\Upsilon(4S)$
• • • We do not use the following data for averages, fits, limits, etc. • • •					
<83	90	ALBRECHT	88H	ARG	$e^+e^-\to\Upsilon(4S)$

[1] COAN 00 obtains a fitted signal yield of $15.9^{+5.7}_{-5.2}$ events. A search for contamination by $K^*(1410)$ yielded a rate consistent with 0; the central value assumes no contamination.

$\Gamma(K_2(1770)\gamma)/\Gamma_{total}$ — Γ_{71}/Γ

VALUE	CL%	DOCUMENT ID		TECN	COMMENT
$<1.2\times10^{-3}$	90	[1] LESIAK	92	CBAL	$e^+e^-\to\Upsilon(4S)$

[1] LESIAK 92 set a limit on the inclusive process $B(b\to s\gamma)<2.8\times10^{-3}$ at 90% CL for the range of masses of 892–2045 MeV, independent of assumptions about s-quark hadronization.

$\Gamma(K_3^*(1780)\gamma)/\Gamma_{total}$ — Γ_{72}/Γ

VALUE	CL%	DOCUMENT ID		TECN	COMMENT
$<3.7\times10^{-5}$	90	[1] NISHIDA	05	BELL	$e^+e^-\to\Upsilon(4S)$
• • • We do not use the following data for averages, fits, limits, etc. • • •					
$<3.0\times10^{-3}$	90	ALBRECHT	88H	ARG	$e^+e^-\to\Upsilon(4S)$

[1] Uses $B(K_3^*(1780)\to\eta K)=0.11^{+0.05}_{-0.04}$.

$\Gamma(K_4^*(2045)\gamma)/\Gamma_{total}$ — Γ_{73}/Γ

VALUE	CL%	DOCUMENT ID		TECN	COMMENT
$<1.0\times10^{-3}$	90	[1] LESIAK	92	CBAL	$e^+e^-\to\Upsilon(4S)$

[1] LESIAK 92 set a limit on the inclusive process $B(b\to s\gamma)<2.8\times10^{-3}$ at 90% CL for the range of masses of 892–2045 MeV, independent of assumptions about s-quark hadronization.

$\Gamma(K\eta'(958))/\Gamma_{total}$ — Γ_{74}/Γ

VALUE	DOCUMENT ID		TECN	COMMENT
$(8.3^{+0.9}_{-0.8}\pm0.7)\times10^{-5}$	[1] RICHICHI	00	CLE2	$e^+e^-\to\Upsilon(4S)$

[1] Assumes equal production of B^+ and B^0 at the $\Upsilon(4S)$.

$\Gamma(K^*(892)\eta'(958))/\Gamma_{total}$ — Γ_{75}/Γ

VALUE (units 10^{-6})	CL%	DOCUMENT ID		TECN	COMMENT
$4.1^{+1.0}_{-0.9}\pm0.5$		[1] AUBERT	07E	BABR	$e^+e^-\to\Upsilon(4S)$
• • • We do not use the following data for averages, fits, limits, etc. • • •					
<22	90	[1] RICHICHI	00	CLE2	$e^+e^-\to\Upsilon(4S)$

[1] Assumes equal production of B^+ and B^0 at the $\Upsilon(4S)$.

$\Gamma(K\eta)/\Gamma_{total}$ — Γ_{76}/Γ

VALUE	CL%	DOCUMENT ID		TECN	COMMENT
$<5.2\times10^{-6}$	90	[1] RICHICHI	00	CLE2	$e^+e^-\to\Upsilon(4S)$

[1] Assumes equal production of B^+ and B^0 at the $\Upsilon(4S)$.

$\Gamma(K^*(892)\eta)/\Gamma_{total}$ — Γ_{77}/Γ

VALUE	DOCUMENT ID		TECN	COMMENT
$(1.80^{+0.49}_{-0.43}\pm0.18)\times10^{-5}$	[1] RICHICHI	00	CLE2	$e^+e^-\to\Upsilon(4S)$

[1] Assumes equal production of B^+ and B^0 at the $\Upsilon(4S)$.

$\Gamma(K\phi\phi)/\Gamma_{total}$ — Γ_{78}/Γ

VALUE (units 10^{-6})	DOCUMENT ID		TECN	COMMENT
$2.3^{+0.9}_{-0.8}\pm0.3$	[1] HUANG	03	BELL	$e^+e^-\to\Upsilon(4S)$

[1] Assumes equal production of charged and neutral B meson pairs and isospin symmetry.

$\Gamma(\overline{b}\to\overline{s}\gamma)/\Gamma_{total}$ — Γ_{79}/Γ

VALUE (units 10^{-4})	DOCUMENT ID		TECN	COMMENT
3.49±0.19 OUR AVERAGE				
$3.75\pm0.18\pm0.35$	[1,2] SAITO	15	BELL	$e^+e^-\to\Upsilon(4S)$
$3.52\pm0.20\pm0.51$	[1,3] LEES	12U	BABR	$e^+e^-\to\Upsilon(4S)$
$3.32\pm0.16\pm0.31$	[1,4] LEES	12V	BABR	$e^+e^-\to\Upsilon(4S)$
$3.47\pm0.15\pm0.40$	[1,5] LIMOSANI	09	BELL	$e^+e^-\to\Upsilon(4S)$
$3.90\pm0.91\pm0.64$	[1,6] AUBERT	08O	BABR	$e^+e^-\to\Upsilon(4S)$
$3.29\pm0.44\pm0.29$	[1,7] CHEN	01C	CLE2	$e^+e^-\to\Upsilon(4S)$
• • • We do not use the following data for averages, fits, limits, etc. • • •				
$2.30\pm0.08\pm0.30$	[8] DEL-AMO-SA...10M		BABR	$e^+e^-\to\Upsilon(4S)$
$4.3\ \pm0.3\ \pm0.7$	[9] AUBERT	09U	BABR	Repl. by DEL-AMO-SANCHEZ 10M
$3.92\pm0.31\pm0.47$	[1,10] AUBERT,BE	06B	BABR	Repl. by LEES 12V
$3.49\pm0.20^{+0.59}_{-0.46}$	[1,11] AUBERT,B	05R	BABR	Repl. by LEES 12U
$3.50\pm0.32\pm0.31$	[1,12] KOPPENBURG	04	BELL	Repl. by LIMOSANI 09
$3.36\pm0.53^{+0.65}_{-0.68}$	[13] ABE	01F	BELL	Repl. by SAITO 15
$2.32\pm0.57\pm0.35$	ALAM	95	CLE2	Repl. by CHEN 01C

[1] We extrapolate the measured value to $E_\gamma>1.6$ GeV using the method of BUCHMUELLER 06 (average of three theoretical models).

[2] SAITO 15 measured $(3.51\pm0.17\pm0.33)\times10^{-4}$ using a sum-of-exclusive approach in which 38 of the hadronic final states with $m_{X_s}<2.8$ GeV/c^2 are reconstructed. The cut of minimum photon energy is $E_\gamma>1.9$ GeV.

[3] Reports $(3.29\pm0.19\pm0.48)\times10^{-4}$ for $E_\gamma>1.9$ GeV.

[4] Reports $(3.21\pm0.15\pm0.29\pm0.08)\times10^{-4}$ for $1.8<E_\gamma<2.8$ GeV, where the last systematic uncertainty is for model dependency. Results with other cutoffs are also reported.

[5] The measurement reported is $(3.45\pm0.15\pm0.40)\times10^{-4}$ for $E_\gamma>1.7$ GeV.

[6] Uses a fully reconstructed B meson as a tag on the recoil side. The measurement reported is $(3.66\pm0.85\pm0.60)\times10^{-4}$ for $E_\gamma>1.9$ GeV.

[7] The measurement reported is $(3.21\pm0.43^{+0.32}_{-0.29})\times10^{-4}$ for $E_\gamma>2.0$ GeV.

[8] Measured using sums of seven exclusive final states $B\to X_{d(s)}\gamma$ where $X_{d(s)}$ is a nonstrange (strange) charmless hadronic system in mass range 0.5–2.0 GeV/c^2.

[9] Measured using sums of seven exclusive final states $B\to X_{d(s)}\gamma$ where $X_{d(s)}$ is a nonstrange (strange) charmless hadronic system in mass range 0.6–1.8 GeV/c^2.

[10] The measurement reported is $(3.67\pm0.29\pm0.45)\times10^{-4}$ for $E_\gamma>1.9$ GeV.

[11] The measurement reported is $(3.27\pm0.18^{+0.55}_{-0.42})\times10^{-4}$ for $E_\gamma>1.9$ GeV.

[12] The measurement reported is $(3.55\pm0.32\pm0.32)\times10^{-4}$ for $E_\gamma>1.8$ GeV.

[13] ABE 01F reports their systematic errors $(\pm0.42^{+0.50}_{-0.54})\times10^{-4}$, where the second error is due to the theoretical uncertainty. We combine them in quadrature.

$\Gamma(\overline{b}\to\overline{d}\gamma)/\Gamma_{total}$ — Γ_{80}/Γ

VALUE (units 10^{-6})	DOCUMENT ID		TECN	COMMENT
$9.2\pm2.0\pm2.3$	[1] DEL-AMO-SA...10M		BABR	$e^+e^-\to\Upsilon(4S)$
• • • We do not use the following data for averages, fits, limits, etc. • • •				
$14\ \pm5\ \pm4$	[2] AUBERT	09U	BABR	Repl. by DEL-AMO-SANCHEZ 10M

[1] Measured using sums of seven exclusive final states $B\to X_{d(s)}\gamma$ where $X_{d(s)}$ is a nonstrange (strange) charmless hadronic system in mass range 0.5–2.0 GeV/c^2.

[2] Measured using sums of seven exclusive final states $B\to X_{d(s)}\gamma$ where $X_{d(s)}$ is a nonstrange (strange) charmless hadronic system in mass range 0.6–1.8 GeV/c^2.

$\Gamma(\overline{b}\to\overline{d}\gamma)/\Gamma(\overline{b}\to\overline{s}\gamma)$ — Γ_{80}/Γ_{79}

VALUE	DOCUMENT ID		TECN	COMMENT
0.040±0.009±0.010	[1] DEL-AMO-SA...10M		BABR	$e^+e^-\to\Upsilon(4S)$
• • • We do not use the following data for averages, fits, limits, etc. • • •				
$0.033\pm0.013\pm0.009$	[2] AUBERT	09U	BABR	Repl. by DEL-AMO-SANCHEZ 10M

[1] Measured using sums of seven exclusive final states $B\to X_{d(s)}\gamma$ where $X_{d(s)}$ is a nonstrange (strange) charmless hadronic system in mass range 0.5–2.0 GeV/c^2.

[2] Measured using sums of seven exclusive final states $B\to X_{d(s)}\gamma$ where $X_{d(s)}$ is a nonstrange (strange) charmless hadronic system in mass range 0.6–1.8 GeV/c^2.

$\Gamma(\overline{b}\to\overline{s}\text{gluon})/\Gamma_{total}$ — Γ_{81}/Γ

VALUE	CL%	EVTS	DOCUMENT ID		TECN	COMMENT
<0.068	90		[1] COAN	98	CLE2	$e^+e^-\to\Upsilon(4S)$
• • • We do not use the following data for averages, fits, limits, etc. • • •						
<0.08		2	[2] ALBRECHT	95D	ARG	$e^+e^-\to\Upsilon(4S)$

[1] COAN 98 uses D-ℓ correlation.

[2] ALBRECHT 95D use full reconstruction of one B decay as tag. Two candidate events for charmless B decay can be interpreted as either $b\to s$gluon or $b\to u$ transition. If interpreted as $b\to s$gluon they find a branching ratio of ~0.026 or the upper limit quoted above. Result is highly model dependent.

$\Gamma(\eta\text{ anything})/\Gamma_{total}$ — Γ_{82}/Γ

VALUE (units 10^{-4})	CL%	DOCUMENT ID		TECN	COMMENT
$2.61\pm0.30^{+0.44}_{-0.74}$		[1] NISHIMURA	10	BELL	$e^+e^-\to\Upsilon(4S)$
• • • We do not use the following data for averages, fits, limits, etc. • • •					
$1.69\pm0.29^{+0.36}_{-0.62}$		[2] NISHIMURA	10	BELL	$e^+e^-\to\Upsilon(4S)$
<4.4	90	[3] BROWDER	98	CLE2	$e^+e^-\to\Upsilon(4S)$

[1] Uses $B\to\eta X_s$ with $0.4<m_{X_s}<2.6$ GeV/c^2.

[2] Uses $B\to\eta X_s$ with $1.8<m_{X_s}<2.6$ GeV/c^2.

[3] BROWDER 98 search for high momentum $B\to\eta X_s$ between 2.1 and 2.7 GeV/c.

$\Gamma(\eta'\text{ anything})/\Gamma_{total}$ — Γ_{83}/Γ

VALUE (units 10^{-4})	DOCUMENT ID		TECN	COMMENT
4.2±0.9 OUR AVERAGE				
$3.9\pm0.8\pm0.9$	[1] AUBERT,B	04F	BABR	$e^+e^-\to\Upsilon(4S)$
$4.6\pm1.1\pm0.6$	[2] BONVICINI	03	CLE2	$e^+e^-\to\Upsilon(4S)$
• • • We do not use the following data for averages, fits, limits, etc. • • •				
$6.2\pm1.6^{+1.3}_{-2.0}$	[3] BROWDER	98	CLE2	$e^+e^-\to\Upsilon(4S)$

[1] AUBERT,B 04F reports branching ratio $B\to\eta' X_s$ for high momentum η' between 2.0 and 2.7 GeV/c in the $\Upsilon(4S)$ center-of-mass frame. X_s represents a recoil system consisting of a kaon and zero to four pions.

[2] BONVICINI 03 observed a signal of 61.2 ± 13.9 events in $B\to\eta' X_{nc}$ production for high momentum η' between 2.0 and 2.7 GeV/c in the $\Upsilon(4S)$ center-of-mass frame. The X_{nc} denotes "charmless" hadronic states recoiling against η'. The second error combines systematic and background subtraction uncertainties in quadrature.

[3] BROWDER 98 observed a signal of 39.0 ± 11.6 events in high momentum $B\to\eta' X_s$ production between 2.0 and 2.7 GeV/c. The branching fraction is based on the interpretation of $b\to sg$, where the last error includes additional uncertainties due to the color-suppressed $b\to$ backgrounds.

Downloaded from https://academic.oup.com/ptep/article/2022/8/083C01/6651666 by KIT Library user on 27 September 2022

$\Gamma(K^+ \text{gluon (charmless)})/\Gamma_{\text{total}}$ — Γ_{84}/Γ

VALUE (units 10^{-4})	CL%	DOCUMENT ID		TECN	COMMENT
<1.87	90	[1] DEL-AMO-SA...11		BABR	$e^+e^- \to \Upsilon(4S)$

[1] $B \to K^+X$ with $m_X < 1.69$ GeV/c^2.

$\Gamma(K^0 \text{gluon (charmless)})/\Gamma_{\text{total}}$ — Γ_{85}/Γ

VALUE (units 10^{-4})	DOCUMENT ID		TECN	COMMENT
$\mathbf{1.95^{+0.51}_{-0.45} \pm 0.50}$	[1] DEL-AMO-SA...11		BABR	$e^+e^- \to \Upsilon(4S)$

[1] $B \to K^0X$ with $m_X < 1.69$ GeV/c^2.

$\Gamma(\rho\gamma)/\Gamma_{\text{total}}$ — Γ_{86}/Γ

VALUE (units 10^{-6})	CL%	DOCUMENT ID		TECN	COMMENT
1.39±0.25 OUR AVERAGE		Error includes scale factor of 1.2.			
$1.73^{+0.34}_{-0.32} \pm 0.17$		[1,2] AUBERT	08BH	BABR	$e^+e^- \to \Upsilon(4S)$
$1.21^{+0.24}_{-0.22} \pm 0.12$		[1,2] TANIGUCHI	08	BELL	$e^+e^- \to \Upsilon(4S)$
• • • We do not use the following data for averages, fits, limits, etc. • • •					
$1.36^{+0.29}_{-0.27} \pm 0.10$		[1,3] AUBERT	07L	BABR	Repl. by AUBERT 08BH
< 1.9	90	[1,3] AUBERT	04C	BABR	Repl. by AUBERT 07L
<14	90	[1,4] COAN	00	CLE2	$e^+e^- \to \Upsilon(4S)$

[1] Assumes equal production of B^+ and B^0 at the $\Upsilon(4S)$.
[2] Assumes $\Gamma(B \to \rho\gamma) = \Gamma(B^+ \to \rho^+\gamma) = 2\,\Gamma(B^0 \to \rho^0\gamma)$ and uses lifetime ratio of $\tau_{B^+}/\tau_{B^0} = 1.071 \pm 0.009$.
[3] Assumes $\Gamma(B \to \rho\gamma) = \Gamma(B^+ \to \rho^+\gamma) = 2\,\Gamma(B^0 \to \rho^0\gamma)$ and uses lifetime ratio of $\tau_{B^+}/\tau_{B^0} = 1.083 \pm 0.017$.
[4] COAN 00 reports $B(B \to \rho\gamma)/B(B \to K^*(892)\gamma) < 0.32$ at 90%CL and scaled by the central value of $B(B \to K^*(892)\gamma)=(4.24 \pm 0.54 \pm 0.32) \times 10^{-5}$.

$\Gamma(\rho\gamma)/\Gamma(K^*(892)\gamma)$ — Γ_{86}/Γ_{67}

VALUE (units 10^{-2})	DOCUMENT ID		TECN	COMMENT
$\mathbf{3.02^{+0.60}_{-0.55}{}^{+0.26}_{-0.28}}$	TANIGUCHI	08	BELL	$e^+e^- \to \Upsilon(4S)$

$\Gamma(\rho/\omega\gamma)/\Gamma_{\text{total}}$ — Γ_{87}/Γ

VALUE (units 10^{-6})	CL%	DOCUMENT ID		TECN	COMMENT
1.30±0.23 OUR AVERAGE		Error includes scale factor of 1.2.			
$1.63^{+0.30}_{-0.28} \pm 0.16$		[1,2,3] AUBERT	08BH	BABR	$e^+e^- \to \Upsilon(4S)$
$1.14 \pm 0.20^{+0.10}_{-0.12}$		[1,3] TANIGUCHI	08	BELL	$e^+e^- \to \Upsilon(4S)$
• • • We do not use the following data for averages, fits, limits, etc. • • •					
$1.25^{+0.25}_{-0.24} \pm 0.09$		[4] AUBERT	07L	BABR	Repl. by AUBERT 08BH
$1.32^{+0.34}_{-0.31}{}^{+0.10}_{-0.09}$		[4] MOHAPATRA	06	BELL	Repl. by TANIGUCHI 08
0.6 ±0.3 ±0.1		[4] AUBERT	05	BABR	Repl. by AUBERT 07L
<1.4	90	[4] MOHAPATRA	05	BELL	$e^+e^- \to \Upsilon(4S)$

[1] Assumes $\Gamma(B \to \rho\gamma) = \Gamma(B^+ \to \rho^+\gamma) = 2\,\Gamma(B^0 \to \rho^0\gamma)$ and uses lifetime ratio of $\tau_{B^+}/\tau_{B^0} = 1.071 \pm 0.009$.
[2] Also reports $|V_{td}/V_{ts}| = 0.233^{+0.025}_{-0.024}{}^{+0.022}_{-0.021}$.
[3] Assumes equal production of B^+ and B^0 at the $\Upsilon(4S)$.
[4] Assumes $\Gamma(B \to \rho\gamma) = \Gamma(B^+ \to \rho^+\gamma) = 2\,\Gamma(B^0 \to \rho^0\gamma)$ and uses lifetime ratio of $\tau_{B^+}/\tau_{B^0} = 1.083 \pm 0.017$.

$\Gamma(\rho/\omega\gamma)/\Gamma(K^*(892)\gamma)$ — Γ_{87}/Γ_{67}

VALUE (units 10^{-2})	CL%	DOCUMENT ID		TECN	COMMENT
$\mathbf{2.84 \pm 0.50^{+0.27}_{-0.29}}$		[1] TANIGUCHI	08	BELL	$e^+e^- \to \Upsilon(4S)$
• • • We do not use the following data for averages, fits, limits, etc. • • •					
<3.5	90	MOHAPATRA	05	BELL	Repl. by TANIGUCHI 08

[1] Also reports $|V_{td}/V_{ts}| = 0.195^{+0.020}_{-0.019} \pm 0.015$.

$\Gamma(\pi^{\pm} \text{anything})/\Gamma_{\text{total}}$ — Γ_{88}/Γ

VALUE	DOCUMENT ID		TECN	COMMENT
3.585±0.025±0.070	[1] ALBRECHT	93I	ARG	$e^+e^- \to \Upsilon(4S)$

[1] ALBRECHT 93 excludes $\pi^{\pm}$ from K^0_S and Λ decays. If included, they find 4.105 ± 0.025 ± 0.080.

$\Gamma(\pi^0 \text{anything})/\Gamma_{\text{total}}$ — Γ_{89}/Γ

VALUE	DOCUMENT ID		TECN	COMMENT
2.35±0.02±0.11	[1] ABE	01J	BELL	$e^+e \to \Upsilon(4S)$

[1] From fully inclusive π^0 yield with no corrections from decays of K^0_S or other particles.

$\Gamma(\eta \text{anything})/\Gamma_{\text{total}}$ — Γ_{90}/Γ

VALUE	DOCUMENT ID		TECN	COMMENT
0.176±0.011±0.012	KUBOTA	96	CLE2	$e^+e^- \to \Upsilon(4S)$

$\Gamma(\rho^0 \text{anything})/\Gamma_{\text{total}}$ — Γ_{91}/Γ

VALUE	DOCUMENT ID		TECN	COMMENT
0.208±0.042±0.032	ALBRECHT	94J	ARG	$e^+e^- \to \Upsilon(4S)$

$\Gamma(\omega \text{anything})/\Gamma_{\text{total}}$ — Γ_{92}/Γ

VALUE	CL%	DOCUMENT ID		TECN	COMMENT
<0.81	90	ALBRECHT	94J	ARG	$e^+e^- \to \Upsilon(4S)$

$\Gamma(\phi \text{anything})/\Gamma_{\text{total}}$ — Γ_{93}/Γ

VALUE	DOCUMENT ID		TECN	COMMENT
0.0343±0.0012 OUR AVERAGE				
0.0353±0.0005±0.0030	HUANG	07	CLEO	$e^+e^- \to \Upsilon(4S)$
0.0341±0.0006±0.0012	AUBERT	04S	BABR	$e^+e^- \to \Upsilon(4S)$
0.0390±0.0030±0.0035	ALBRECHT	94J	ARG	$e^+e^- \to \Upsilon(4S)$
0.023 ±0.006 ±0.005	BORTOLETTO	86	CLEO	$e^+e^- \to \Upsilon(4S)$

$\Gamma(\phi K^*(892))/\Gamma_{\text{total}}$ — Γ_{94}/Γ

VALUE	CL%	DOCUMENT ID		TECN
$\mathbf{<2.2 \times 10^{-5}}$	90	[1] BERGFELD	98	CLE2

[1] Assumes equal production of B^+ and B^0 at the $\Upsilon(4S)$.

$\Gamma(\pi^+ \text{gluon (charmless)})/\Gamma_{\text{total}}$ — Γ_{96}/Γ

VALUE (units 10^{-4})	DOCUMENT ID		TECN	COMMENT
$\mathbf{3.72^{+0.50}_{-0.47} \pm 0.59}$	[1] DEL-AMO-SA...11		BABR	$e^+e^- \to \Upsilon(4S)$

[1] $B \to \pi^+X$ with $m_X < 1.71$ GeV/c^2.

$\Gamma(\Lambda_c^+ / \overline{\Lambda}_c^- \text{anything})/\Gamma_{\text{total}}$ — Γ_{97}/Γ

VALUE (%)	CL%	DOCUMENT ID		TECN	COMMENT
$\mathbf{3.59 \pm 0.32^{+0.19}_{-0.18}}$		[1] AUBERT	07C	BABR	$e^+e^- \to \Upsilon(4S)$
• • • We do not use the following data for averages, fits, limits, etc. • • •					
6.4 ±0.8 ±0.8		[2] CRAWFORD	92	CLEO	$e^+e^- \to \Upsilon(4S)$
14 ±9		[3] ALBRECHT	88E	ARG	$e^+e^- \to \Upsilon(4S)$
<11.2	90	[4] ALAM	87	CLEO	$e^+e^- \to \Upsilon(4S)$

[1] AUBERT 07C reports 0.045 ± 0.003 ± 0.012 from a measurement of $[\Gamma(B \to \Lambda_c^+ / \overline{\Lambda}_c^- \text{anything})/\Gamma_{\text{total}}] \times [B(\Lambda_c^+ \to pK^-\pi^+)]$ assuming $B(\Lambda_c^+ \to pK^-\pi^+) = (5.0 \pm 1.3) \times 10^{-2}$, which we rescale to our best value $B(\Lambda_c^+ \to pK^-\pi^+) = (6.28 \pm 0.32) \times 10^{-2}$. Our first error is their experiment's error and our second error is the systematic error from using our best value.
[2] CRAWFORD 92 result derived from lepton baryon correlations. Assumes all charmed baryons in B^0 and $B^{\pm}$ decay are Λ_c.
[3] ALBRECHT 88E measured $B(B \to \Lambda_c^+X)\cdot B(\Lambda_c^+ \to pK^-\pi^+) = (0.30 \pm 0.12 \pm 0.06)\%$ and used $B(\Lambda_c^+ \to pK^-\pi^+) = (2.2 \pm 1.0)\%$ from ABRAMS 80 to obtain above number.
[4] Assuming all baryons result from charmed baryons, ALAM 86 conclude the branching fraction is 7.4 ± 2.9%. The limit given above is model independent.

$\Gamma(\Lambda_c^+ \text{anything})/\Gamma(\overline{\Lambda}_c^- \text{anything})$ — Γ_{98}/Γ_{99}

VALUE	DOCUMENT ID		TECN	COMMENT
0.19±0.13±0.04	[1] AMMAR	97	CLE2	$e^+e^- \to \Upsilon(4S)$

[1] AMMAR 97 uses a high-momentum lepton tag ($P_\ell > 1.4$ GeV/c^2).

$\Gamma(\overline{\Lambda}_c^- \mu^+ \text{anything})/\Gamma(\overline{\Lambda}_c^- \text{anything})$ — Γ_{102}/Γ_{99}

VALUE (units 10^{-2})	DOCUMENT ID		TECN	COMMENT
−2.0±2.0±1.9	LEES	12	BABR	$e^+e^- \to \Upsilon(4S)$

$\Gamma(\overline{\Lambda}_c^- \ell^+ \text{anything})/\Gamma(\Lambda_c^+ / \overline{\Lambda}_c^- \text{anything})$ — Γ_{100}/Γ_{97}

VALUE	CL%	DOCUMENT ID		TECN	COMMENT
$\mathbf{<2.5 \times 10^{-2}}$	90	[1] LEES	12	BABR	$e^+e^- \to \Upsilon(4S)$

[1] LEES 12 quotes also the measurement $\Gamma(B \to \overline{\Lambda}_c^- \ell^+ \text{anything})/\Gamma(B \to \Lambda_c^+ / \overline{\Lambda}_c^- \text{anything}) = (1.2 \pm 0.7 \pm 0.4) \times 10^{-2}$.

$\Gamma(\overline{\Lambda}_c^- e^+ \text{anything})/\Gamma(\Lambda_c^+ / \overline{\Lambda}_c^- \text{anything})$ — Γ_{101}/Γ_{97}

VALUE	CL%	DOCUMENT ID		TECN	COMMENT
<0.05	90	[1] BONVICINI	98	CLE2	$e^+e^- \to \Upsilon(4S)$

[1] BONVICINI 98 uses the electron with momentum above 0.6 GeV/c.

$\Gamma(\overline{\Lambda}_c^- e^+ \text{anything})/\Gamma(\overline{\Lambda}_c^- \text{anything})$ — Γ_{101}/Γ_{99}

VALUE (units 10^{-2})	DOCUMENT ID		TECN	COMMENT
2.5±1.1±0.6	[1] LEES	12	BABR	$e^+e^- \to \Upsilon(4S)$

[1] Uses the full reconstruction of the recoiling B in a hadronic decay as a tag.

$\Gamma(\overline{\Lambda}_c^- \ell^+ \text{anything})/\Gamma(\overline{\Lambda}_c^- \text{anything})$ — Γ_{100}/Γ_{99}

VALUE	CL%	DOCUMENT ID		TECN	COMMENT
$\mathbf{<3.5 \times 10^{-2}}$	90	[1] LEES	12	BABR	$e^+e^- \to \Upsilon(4S)$

[1] LEES 12 quotes also the measurement $\Gamma(B \to \overline{\Lambda}_c^- \ell^+ \text{anything})/\Gamma(B \to \overline{\Lambda}_c^- \text{anything}) = (1.7 \pm 1.0 \pm 0.6) \times 10^{-2}$.

$\Gamma(\overline{\Lambda}_c^- p \text{anything})/\Gamma(\Lambda_c^+ / \overline{\Lambda}_c^- \text{anything})$ — Γ_{103}/Γ_{97}

VALUE	DOCUMENT ID		TECN	COMMENT
0.57±0.05±0.05	BONVICINI	98	CLE2	$e^+e^- \to \Upsilon(4S)$

Downloaded from https://academic.oup.com/ptep/article/2022/8/083C01/6651666 by KIT Library user on 27 September 2022

$\Gamma(\overline{\Lambda}_c^- p e^+ \nu_e)/\Gamma(\overline{\Lambda}_c^- p \text{ anything})$ — $\Gamma_{104}/\Gamma_{103}$

VALUE	CL%	DOCUMENT ID		TECN	COMMENT
<0.04	90	[1] BONVICINI	98	CLE2	$e^+e^- \to \Upsilon(4S)$

[1] BONVICINI 98 uses the electron with momentum above 0.6 GeV/c.

$\Gamma(\overline{\Sigma}_c^{--} \text{ anything})/\Gamma_{\text{total}}$ — Γ_{105}/Γ

VALUE	EVTS	DOCUMENT ID		TECN	COMMENT
0.0033±0.0017±0.0002	77	[1] PROCARIO	94	CLE2	$e^+e^- \to \Upsilon(4S)$

[1] PROCARIO 94 reports $[\Gamma(B \to \overline{\Sigma}_c^{--} \text{anything})/\Gamma_{\text{total}}] \times [B(\Lambda_c^+ \to pK^-\pi^+)] = 0.00021 \pm 0.00008 \pm 0.00007$ which we divide by our best value $B(\Lambda_c^+ \to pK^-\pi^+) = (6.28 \pm 0.32) \times 10^{-2}$. Our first error is their experiment's error and our second error is the systematic error from using our best value.

$\Gamma(\overline{\Sigma}_c^- \text{ anything})/\Gamma_{\text{total}}$ — Γ_{106}/Γ

VALUE	CL%	DOCUMENT ID		TECN	COMMENT
<8 × 10^{-3}	90	[1] PROCARIO	94	CLE2	$e^+e^- \to \Upsilon(4S)$

[1] PROCARIO 94 reports $[\Gamma(B \to \overline{\Sigma}_c^- \text{anything})/\Gamma_{\text{total}}] \times [B(\Lambda_c^+ \to pK^-\pi^+)] < 0.00048$ which we divide by our best value $B(\Lambda_c^+ \to pK^-\pi^+) = 6.28 \times 10^{-2}$.

$\Gamma(\Sigma_c^0 \text{ anything})/\Gamma_{\text{total}}$ — Γ_{107}/Γ

VALUE	EVTS	DOCUMENT ID		TECN	COMMENT
0.0037±0.0017±0.0002	76	[1] PROCARIO	94	CLE2	$e^+e^- \to \Upsilon(4S)$

[1] PROCARIO 94 reports $[\Gamma(B \to \overline{\Sigma}_c^0 \text{anything})/\Gamma_{\text{total}}] \times [B(\Lambda_c^+ \to pK^-\pi^+)] = 0.00023 \pm 0.00008 \pm 0.00007$ which we divide by our best value $B(\Lambda_c^+ \to pK^-\pi^+) = (6.28 \pm 0.32) \times 10^{-2}$. Our first error is their experiment's error and our second error is the systematic error from using our best value.

$\Gamma(\Sigma_c^0 N\,(N = p \text{ or } n))/\Gamma_{\text{total}}$ — Γ_{108}/Γ

VALUE	CL%	DOCUMENT ID		TECN	COMMENT
<1.2 × 10^{-3}	90	[1] PROCARIO	94	CLE2	$e^+e^- \to \Upsilon(4S)$

[1] PROCARIO 94 reports < 0.0017 from a measurement of $[\Gamma(B \to \overline{\Sigma}_c^0 N(N = p \text{ or } n))/\Gamma_{\text{total}}] \times [B(\Lambda_c^+ \to pK^-\pi^+)]$ assuming $B(\Lambda_c^+ \to pK^-\pi^+) = 0.043$, which we rescale to our best value $B(\Lambda_c^+ \to pK^-\pi^+) = 6.28 \times 10^{-2}$.

$\Gamma(\Xi_c^0 \text{ anything},\ \Xi_c^0 \to \Xi^-\pi^+)/\Gamma_{\text{total}}$ — Γ_{109}/Γ

VALUE (units 10^{-3})	DOCUMENT ID		TECN	COMMENT
0.193±0.030 OUR AVERAGE	Error includes scale factor of 1.1.			
0.211±0.019±0.025	[1] AUBERT,B	05M	BABR	$e^+e^- \to \Upsilon(4S)$
0.144±0.048±0.021	[2] BARISH	97	CLE2	$e^+e^- \to \Upsilon(4S)$

[1] The yield is obtained by requiring the momentum P < 2.15 GeV/c.
[2] BARISH 97 find 79 ± 27 Ξ_c^0 events.

$\Gamma(\Xi_c^+,\ \Xi_c^+ \to \Xi^-\pi^+\pi^+)/\Gamma_{\text{total}}$ — Γ_{110}/Γ

VALUE (units 10^{-3})	DOCUMENT ID		TECN	COMMENT
0.453±0.096$^{+0.085}_{-0.065}$	[1] BARISH	97	CLE2	$e^+e^- \to \Upsilon(4S)$

[1] BARISH 97 find 125 ± 28 Ξ_c^+ events.

$\Gamma(p/\overline{p} \text{ anything})/\Gamma_{\text{total}}$ — Γ_{111}/Γ

Includes p and $\overline{p}$ from Λ and $\overline{\Lambda}$ decay.

VALUE	EVTS	DOCUMENT ID		TECN	COMMENT
0.080±0.004 OUR AVERAGE					
0.080±0.005±0.005		ALBRECHT	93I	ARG	$e^+e^- \to \Upsilon(4S)$
0.080±0.005±0.003		CRAWFORD	92	CLEO	$e^+e^- \to \Upsilon(4S)$
0.082±0.005$^{+0.013}_{-0.010}$	2163	[1] ALBRECHT	89K	ARG	$e^+e^- \to \Upsilon(4S)$
• • • We do not use the following data for averages, fits, limits, etc. • • •					
>0.021		[2] ALAM	83B	CLEO	$e^+e^- \to \Upsilon(4S)$

[1] ALBRECHT 89K include direct and nondirect protons.
[2] ALAM 83B reported their result as > 0.036 ± 0.006 ± 0.009. Data are consistent with equal yields of p and $\overline{p}$. Using assumed yields below cut, $B(B \to p + X) = 0.03$ not including protons from Λ decays.

$\Gamma(p/\overline{p} \text{ (direct) anything})/\Gamma_{\text{total}}$ — Γ_{112}/Γ

VALUE	EVTS	DOCUMENT ID		TECN	COMMENT
0.055±0.005 OUR AVERAGE					
0.055±0.005±0.0035		ALBRECHT	93I	ARG	$e^+e^- \to \Upsilon(4S)$
0.056±0.006±0.005		CRAWFORD	92	CLEO	$e^+e^- \to \Upsilon(4S)$
0.055±0.016	1220	[1] ALBRECHT	89K	ARG	$e^+e^- \to \Upsilon(4S)$

[1] ALBRECHT 89K subtract contribution of Λ decay from the inclusive proton yield.

$\Gamma(\overline{p} e^+ \nu_e \text{ anything})/\Gamma_{\text{total}}$ — Γ_{113}/Γ

VALUE	CL%	DOCUMENT ID		TECN	COMMENT
< 5.9 × 10^{-4}	90	[1] ADAM	03B	CLE2	$e^+e^- \to \Upsilon(4S)$
• • • We do not use the following data for averages, fits, limits, etc. • • •					
<16 × 10^{-4}	90	ALBRECHT	90H	ARG	$e^+e^- \to \Upsilon(4S)$

[1] Based on $V-A$ model.

$\Gamma(\Lambda/\overline{\Lambda} \text{ anything})/\Gamma_{\text{total}}$ — Γ_{114}/Γ

VALUE	EVTS	DOCUMENT ID		TECN	COMMENT
0.040±0.005 OUR AVERAGE					
0.038±0.004±0.006	2998	CRAWFORD	92	CLEO	$e^+e^- \to \Upsilon(4S)$
0.042±0.005±0.006	943	ALBRECHT	89K	ARG	$e^+e^- \to \Upsilon(4S)$
• • • We do not use the following data for averages, fits, limits, etc. • • •					
0.022±0.003±0.0022		[1] ACKERSTAFF	97N	OPAL	$e^+e^- \to Z$
>0.011		[2] ALAM	83B	CLEO	$e^+e^- \to \Upsilon(4S)$

[1] ACKERSTAFF 97N assumes $B(b \to B) = 0.868 \pm 0.041$, *i.e.*, an admixture of B^0, $B^{\pm}$, and B_s.
[2] ALAM 83B reported their result as > 0.022 ± 0.007 ± 0.004. Values are for $(B(\Lambda X)+B(\overline{\Lambda} X))/2$. Data are consistent with equal yields of p and $\overline{p}$. Using assumed yields below cut, $B(B \to \Lambda X) = 0.03$.

$\Gamma(\Lambda \text{ anything})/\Gamma(\overline{\Lambda} \text{ anything})$ — $\Gamma_{115}/\Gamma_{116}$

VALUE	DOCUMENT ID		TECN	COMMENT
0.43±0.09±0.07	[1] AMMAR	97	CLE2	$e^+e^- \to \Upsilon(4S)$

[1] AMMAR 97 uses a high-momentum lepton tag ($P_\ell > 1.4$ GeV/c^2).

$\Gamma(\Xi^-/\overline{\Xi}^+ \text{ anything})/\Gamma_{\text{total}}$ — Γ_{117}/Γ

VALUE	EVTS	DOCUMENT ID		TECN	COMMENT
0.0027±0.0006 OUR AVERAGE					
0.0027±0.0005±0.0004	147	CRAWFORD	92	CLEO	$e^+e^- \to \Upsilon(4S)$
0.0028±0.0014	54	ALBRECHT	89K	ARG	$e^+e^- \to \Upsilon(4S)$

$\Gamma(\text{baryons anything})/\Gamma_{\text{total}}$ — Γ_{118}/Γ

VALUE	DOCUMENT ID		TECN	COMMENT
0.068±0.005±0.003	[1] ALBRECHT	92O	ARG	$e^+e^- \to \Upsilon(4S)$
• • • We do not use the following data for averages, fits, limits, etc. • • •				
0.076±0.014	[2] ALBRECHT	89K	ARG	$e^+e^- \to \Upsilon(4S)$

[1] ALBRECHT 92O result is from simultaneous analysis of p and Λ yields, $p\overline{p}$ and $\Lambda\overline{p}$ correlations, and various lepton-baryon and lepton-baryon-antibaryon correlations. Supersedes ALBRECHT 89K.
[2] ALBRECHT 89K obtain this result by adding their their measurements (5.5 ± 1.6)% for direct protons and (4.2 ± 0.5 ± 0.6)% for inclusive Λ production. They then assume (5.5 ± 1.6)% for neutron production and add it in also. Since each B decay has two baryons, they divide by 2 to obtain (7.6 ± 1.4)%.

$\Gamma(p\overline{p} \text{ anything})/\Gamma_{\text{total}}$ — Γ_{119}/Γ

Includes p and $\overline{p}$ from Λ and $\overline{\Lambda}$ decay.

VALUE	EVTS	DOCUMENT ID		TECN	COMMENT
0.0247±0.0023 OUR AVERAGE					
0.024 ±0.001 ±0.004		CRAWFORD	92	CLEO	$e^+e^- \to \Upsilon(4S)$
0.025 ±0.002 ±0.002	918	ALBRECHT	89K	ARG	$e^+e^- \to \Upsilon(4S)$

$\Gamma(p\overline{p} \text{ anything})/\Gamma(p/\overline{p} \text{ anything})$ — $\Gamma_{119}/\Gamma_{111}$

Includes p and $\overline{p}$ from Λ and $\overline{\Lambda}$ decay.

VALUE	DOCUMENT ID		TECN	COMMENT
• • • We do not use the following data for averages, fits, limits, etc. • • •				
0.30±0.02±0.05	[1] CRAWFORD	92	CLEO	$e^+e^- \to \Upsilon(4S)$

[1] CRAWFORD 92 value is not independent of their $\Gamma(p\overline{p}\text{anything})/\Gamma_{\text{total}}$ value.

$\Gamma(\Lambda\overline{p}/\overline{\Lambda}p \text{ anything})/\Gamma_{\text{total}}$ — Γ_{120}/Γ

Includes p and $\overline{p}$ from Λ and $\overline{\Lambda}$ decay.

VALUE	EVTS	DOCUMENT ID		TECN	COMMENT
0.025±0.004 OUR AVERAGE					
0.029±0.005±0.005		CRAWFORD	92	CLEO	$e^+e^- \to \Upsilon(4S)$
0.023±0.004±0.003	165	ALBRECHT	89K	ARG	$e^+e^- \to \Upsilon(4S)$

$\Gamma(\Lambda\overline{p}/\overline{\Lambda}p \text{ anything})/\Gamma(\Lambda/\overline{\Lambda} \text{ anything})$ — $\Gamma_{120}/\Gamma_{114}$

Includes p and $\overline{p}$ from Λ and $\overline{\Lambda}$ decay.

VALUE	DOCUMENT ID		TECN	COMMENT
• • • We do not use the following data for averages, fits, limits, etc. • • •				
0.76±0.11±0.08	[1] CRAWFORD	92	CLEO	$e^+e^- \to \Upsilon(4S)$

[1] CRAWFORD 92 value is not independent of their $[\Gamma(\Lambda\overline{p}\text{anything})+\Gamma(\overline{\Lambda}p\text{anything})]/\Gamma_{\text{total}}$ value.

$\Gamma(\Lambda\overline{\Lambda} \text{ anything})/\Gamma_{\text{total}}$ — Γ_{121}/Γ

VALUE	CL%	EVTS	DOCUMENT ID		TECN	COMMENT
<0.005	90		CRAWFORD	92	CLEO	$e^+e^- \to \Upsilon(4S)$
• • • We do not use the following data for averages, fits, limits, etc. • • •						
<0.0088	90	12	ALBRECHT	89K	ARG	$e^+e^- \to \Upsilon(4S)$

$\Gamma(\Lambda\overline{\Lambda} \text{ anything})/\Gamma(\Lambda/\overline{\Lambda} \text{ anything})$ — $\Gamma_{121}/\Gamma_{114}$

VALUE	CL%	DOCUMENT ID		TECN	COMMENT
• • • We do not use the following data for averages, fits, limits, etc. • • •					
<0.13	90	[1] CRAWFORD	92	CLEO	$e^+e^- \to \Upsilon(4S)$

[1] CRAWFORD 92 value is not independent of their $\Gamma(\Lambda\overline{\Lambda}\text{anything})/\Gamma_{\text{total}}$ value.

Downloaded from https://academic.oup.com/ptep/article/2022/8/083C01/6651666 by KIT Library user on 27 September 2022

$\Gamma(s e^+ e^-)/\Gamma_{total}$ — Γ_{122}/Γ

Test for $\Delta B = 1$ weak neutral current. Allowed by higher-order electroweak interactions.

VALUE (units 10^{-6})	CL%	DOCUMENT ID		TECN	COMMENT
6.7 ±1.7 OUR AVERAGE		Error includes scale factor of 2.0.			
$7.69^{+0.82+0.71}_{-0.77-0.60}$		[1] LEES	14D	BABR	$e^+e^- \to \Upsilon(4S)$
$4.04 \pm 1.30^{+0.87}_{-0.83}$		[2] IWASAKI	05	BELL	$e^+e^- \to \Upsilon(4S)$
• • • We do not use the following data for averages, fits, limits, etc. • • •					
6.0 ±1.7 ±1.3		[2] AUBERT,B	04I	BABR	Repl. by LEES 14D
$5.0 \pm 2.3^{+1.3}_{-1.1}$		[2] KANEKO	03	BELL	Repl. by IWASAKI 05
< 57	90	GLENN	98	CLEO	$e^+e^- \to \Upsilon(4S)$
<50000	90	BEBEK	81	CLEO	$e^+e^- \to \Upsilon(4S)$

[1] Measured from sum of exclusive modes through K^+, $K^+\pi^0$, $K^+\pi^-$, $K^+\pi^-\pi^0$, $K^+\pi^-\pi^+$, K^0_S, $K^0_S\pi^0$, $K^0_S\pi^+$, $K^0_S\pi^+\pi^0$, and $K^0_S\pi^+\pi^-$ corrected for unobserved modes.
[2] Requires $M_{\ell^+\ell^-} > 0.2$ GeV/c^2.

$\Gamma(s\mu^+\mu^-)/\Gamma_{total}$ — Γ_{123}/Γ

Test for $\Delta B = 1$ weak neutral current. Allowed by higher-order electroweak interactions.

VALUE (units 10^{-6})	CL%	DOCUMENT ID		TECN	COMMENT
4.3 ±1.0 OUR AVERAGE					
$4.41^{+1.31+0.63}_{-1.17-0.50}$		[1] LEES	14D	BABR	$e^+e^- \to \Upsilon(4S)$
$4.13 \pm 1.05^{+0.85}_{-0.81}$		[2] IWASAKI	05	BELL	$e^+e^- \to \Upsilon(4S)$
• • • We do not use the following data for averages, fits, limits, etc. • • •					
5.0 ±2.8 ±1.2		AUBERT,B	04I	BABR	Repl. by LEES 14D
$7.9 \pm 2.1^{+2.1}_{-1.5}$		KANEKO	03	BELL	Repl. by IWASAKI 05
< 58	90	GLENN	98	CLEO	$e^+e^- \to \Upsilon(4S)$
<17000	90	CHADWICK	81	CLEO	$e^+e^- \to \Upsilon(4S)$

[1] Measured from sum of exclusive modes through K^+, $K^+\pi^0$, $K^+\pi^-$, $K^+\pi^-\pi^0$, $K^+\pi^-\pi^+$, K^0_S, $K^0_S\pi^0$, $K^0_S\pi^+$, $K^0_S\pi^+\pi^0$, and $K^0_S\pi^+\pi^-$ corrected for unobserved modes.
[2] Requires $M_{\ell^+\ell^-} > 0.2$ GeV/c^2.

$[\Gamma(s e^+ e^-) + \Gamma(s\mu^+\mu^-)]/\Gamma_{total}$ — $(\Gamma_{122}+\Gamma_{123})/\Gamma$

Test for $\Delta B = 1$ weak neutral current. Allowed by higher-order electroweak interactions.

VALUE	CL%	DOCUMENT ID		TECN	COMMENT
<4.2 $\times 10^{-5}$	90	GLENN	98	CLEO	$e^+e^- \to \Upsilon(4S)$
• • • We do not use the following data for averages, fits, limits, etc. • • •					
<0.0024	90	[1] BEAN	87	CLEO	Repl. by GLENN 98
<0.0062	90	[2] AVERY	84	CLEO	Repl. by BEAN 87

[1] BEAN 87 reports $[(\mu^+\mu^-)+(e^+e^-)]/2$ and we converted it.
[2] Determine ratio of B^+ to B^0 semileptonic decays to be in the range 0.25–2.9.

$\Gamma(s\ell^+\ell^-)/\Gamma_{total}$ — Γ_{124}/Γ

Test for $\Delta B = 1$ weak neutral current.

VALUE (units 10^{-6})		DOCUMENT ID		TECN	COMMENT
5.8 ±1.3 OUR AVERAGE		Error includes scale factor of 1.8.			
$6.73^{+0.70+0.60}_{-0.64-0.56}$		[1] LEES	14D	BABR	$e^+e^- \to \Upsilon(4S)$
$4.11 \pm 0.83^{+0.85}_{-0.81}$		[2] IWASAKI	05	BELL	$e^+e^- \to \Upsilon(4S)$
• • • We do not use the following data for averages, fits, limits, etc. • • •					
5.6 ±1.5 ±1.3		[3] AUBERT,B	04I	BABR	Repl. by LEES 14D
$6.1 \pm 1.4^{+1.4}_{-1.1}$		[3] KANEKO	03	BELL	Repl. by IWASAKI 05

[1] Measured from sum of exclusive modes through K^+, $K^+\pi^0$, $K^+\pi^-$, $K^+\pi^-\pi^0$, $K^+\pi^-\pi^+$, K^0_S, $K^0_S\pi^0$, $K^0_S\pi^+$, $K^0_S\pi^+\pi^0$, and $K^0_S\pi^+\pi^-$ corrected for unobserved modes.
[2] Requires $M_{\ell^+\ell^-} > 0.2$ GeV/c^2.
[3] Requires $M_{e^+e^-} > 0.2$ GeV/c^2.

$\Gamma(\pi\ell^+\ell^-)/\Gamma_{total}$ — Γ_{125}/Γ

VALUE	CL%	DOCUMENT ID		TECN	COMMENT
<5.9 $\times 10^{-8}$	90	[1] LEES	13M	BABR	$e^+e^- \to \Upsilon(4S)$
• • • We do not use the following data for averages, fits, limits, etc. • • •					
<6.2 $\times 10^{-8}$	90	[1] WEI	08A	BELL	$e^+e^- \to \Upsilon(4S)$
<9.1 $\times 10^{-8}$	90	[1] AUBERT	07AG	BABR	$e^+e^- \to \Upsilon(4S)$

[1] Assumes equal production of B^+ and B^0 at the $\Upsilon(4S)$.

$\Gamma(\pi e^+ e^-)/\Gamma_{total}$ — Γ_{126}/Γ

VALUE	CL%	DOCUMENT ID		TECN	COMMENT
<11.0 $\times 10^{-8}$	90	[1] LEES	13M	BABR	$e^+e^- \to \Upsilon(4S)$

[1] Assumes equal production of B^+ and B^0 at the $\Upsilon(4S)$.

$\Gamma(\pi\mu^+\mu^-)/\Gamma_{total}$ — Γ_{127}/Γ

VALUE	CL%	DOCUMENT ID		TECN	COMMENT
<5.0 $\times 10^{-8}$	90	[1] LEES	13M	BABR	$e^+e^- \to \Upsilon(4S)$

[1] Assumes equal production of B^+ and B^0 at the $\Upsilon(4S)$.

$\Gamma(K e^+ e^-)/\Gamma_{total}$ — Γ_{128}/Γ

Test for $\Delta B = 1$ weak neutral current. Allowed by higher-order electroweak interactions.

VALUE (units 10^{-7})	CL%	DOCUMENT ID		TECN	COMMENT
4.4±0.6 OUR AVERAGE					
$3.9^{+0.9}_{-0.8} \pm 0.2$		[1] AUBERT	09T	BABR	$e^+e^- \to \Upsilon(4S)$
$4.8^{+0.8}_{-0.7} \pm 0.3$		[1] WEI	09A	BELL	$e^+e^- \to \Upsilon(4S)$
• • • We do not use the following data for averages, fits, limits, etc. • • •					
$3.3^{+0.9}_{-0.8} \pm 0.2$		[1] AUBERT,B	06J	BABR	Repl. by AUBERT 09T
$7.4^{+1.8}_{-1.6} \pm 0.5$		[1] AUBERT	03U	BABR	Repl. by AUBERT,B 06J
$4.8^{+1.5}_{-1.3} \pm 0.3$		[1,2] ISHIKAWA	03	BELL	Repl. by WEI 09A
<13	90	ABE	02	BELL	Repl. by ISHIKAWA 03

[1] Assumes equal production of B^+ and B^0 at the $\Upsilon(4S)$.
[2] The second error is a total of systematic uncertainties including model dependence.

$\Gamma(K^*(892) e^+ e^-)/\Gamma_{total}$ — Γ_{129}/Γ

Test for $\Delta B = 1$ weak neutral current. Allowed by higher-order electroweak interactions.

VALUE (units 10^{-7})	CL%	DOCUMENT ID		TECN	COMMENT
11.9±2.0 OUR AVERAGE		Error includes scale factor of 1.2.			
$9.9^{+2.3}_{-2.1} \pm 0.6$		[1] AUBERT	09T	BABR	$e^+e^- \to \Upsilon(4S)$
$13.9^{+2.3}_{-2.0} \pm 1.2$		[1] WEI	09A	BELL	$e^+e^- \to \Upsilon(4S)$
• • • We do not use the following data for averages, fits, limits, etc. • • •					
$9.7^{+3.0}_{-2.7} \pm 1.4$		[1] AUBERT,B	06J	BABR	Repl. by AUBERT 09T
$9.8^{+5.0}_{-4.2} \pm 1.1$		[1] AUBERT	03U	BABR	Repl. by AUBERT,B 06J
$14.9^{+5.2+1.2}_{-4.6-1.3}$		[2] ISHIKAWA	03	BELL	Repl. by WEI 09A
<56	90	ABE	02	BELL	Repl. by ISHIKAWA 03

[1] Assumes equal production of B^+ and B^0 at the $\Upsilon(4S)$.
[2] Assumes equal production of B^0 and B^+ at $\Upsilon(4S)$. The second error is a total of systematic uncertainties including model dependence.

$\Gamma(K\mu^+\mu^-)/\Gamma_{total}$ — Γ_{130}/Γ

Test for $\Delta B = 1$ weak neutral current. Allowed by higher-order electroweak interactions.

VALUE (units 10^{-7})	DOCUMENT ID		TECN	COMMENT
4.4±0.4 OUR AVERAGE				
4.2±0.4±0.2	AALTONEN	11AI	CDF	$p\overline{p}$ at 1.96 TeV
$4.1^{+1.3}_{-1.2} \pm 0.2$	[1] AUBERT	09T	BABR	$e^+e^- \to \Upsilon(4S)$
5.0±0.6±0.3	[1] WEI	09A	BELL	$e^+e^- \to \Upsilon(4S)$
• • • We do not use the following data for averages, fits, limits, etc. • • •				
$3.5^{+1.3}_{-1.1} \pm 0.3$	[1] AUBERT,B	06J	BABR	Repl. by AUBERT 09T
$4.5^{+2.3}_{-1.9} \pm 0.4$	[1] AUBERT	03U	BABR	Repl. by AUBERT,B 06J
$4.8^{+1.2}_{-1.1} \pm 0.4$	[1,2] ISHIKAWA	03	BELL	Repl. by WEI 09A
$9.9^{+4.0+1.3}_{-3.2-1.0}$	ABE	02	BELL	Repl. by ISHIKAWA 03

[1] Assumes equal production of B^+ and B^0 at the $\Upsilon(4S)$.
[2] The second error is a total of systematic uncertainties including model dependence.

$\Gamma(K\mu^+\mu^-)/\Gamma(K e^+ e^-)$ — $\Gamma_{130}/\Gamma_{128}$

VALUE	DOCUMENT ID		TECN	COMMENT
$1.01^{+0.19}_{-0.16}$ OUR AVERAGE				
$1.03^{+0.28}_{-0.24} \pm 0.01$	[1] CHOUDHURY	21	BELL	$e^+e^- \to \Upsilon(4S)$
$1.00^{+0.31}_{-0.25} \pm 0.07$	[2] LEES	12S	BABR	$e^+e^- \to \Upsilon(4S)$
$0.96^{+0.44}_{-0.34} \pm 0.05$	AUBERT	09T	BABR	$e^+e^- \to \Upsilon(4S)$
• • • We do not use the following data for averages, fits, limits, etc. • • •				
1.03±0.19±0.06	[3] WEI	09A	BELL	$e^+e^- \to \Upsilon(4S)$
1.06±0.48±0.08	AUBERT,B	06J	BABR	Repl. by AUBERT 09T

[1] For $1.0 < q^2 < 6.0$ GeV^2/c^4. Measurements in other q^2 bins are also reported.
[2] Measured in the union of $0.10 < q^2 < 8.12$ GeV^2/c^4 and $q^2 > 10.11$ GeV^2/c^4. LEES 12S reports also individual measurements $\Gamma(B \to K\mu^+\mu^-)/\Gamma(B \to Ke^+e^-) = 0.74^{+0.40}_{-0.31} \pm 0.06$ for $0.10 < q^2 < 8.12$ GeV^2/c^4 and $\Gamma(B \to K\mu^+\mu^-)/\Gamma(B \to Ke^+e^-) = 1.43^{+0.65}_{-0.44} \pm 0.12$ for $q^2 > 10.11$ GeV^2/c^4.
[3] Superseded by CHOUDHURY 21.

$\Gamma(K^*(892)\mu^+\mu^-)/\Gamma_{total}$ — Γ_{131}/Γ

Test for $\Delta B = 1$ weak neutral current. Allowed by higher-order electroweak interactions.

VALUE (units 10^{-7})	CL%	DOCUMENT ID		TECN	COMMENT
10.6±0.9 OUR AVERAGE					
10.1±1.0±0.5		AALTONEN	11AI	CDF	$p\overline{p}$ at 1.96 TeV
$13.5^{+3.5}_{-3.3} \pm 1.0$		[1] AUBERT	09T	BABR	$e^+e^- \to \Upsilon(4S)$
$11.0^{+1.6}_{-1.4} \pm 0.8$		[1] WEI	09A	BELL	$e^+e^- \to \Upsilon(4S)$

Downloaded from https://academic.oup.com/ptep/article/2022/8/083C01/6651666 by KIT Library user on 27 September 2022

• • • We do not use the following data for averages, fits, limits, etc. • • •

$8.8^{+3.5}_{-3.0}\pm1.2$		[1] AUBERT,B	06J	BABR	Repl. by AUBERT 09T
$12.7^{+7.6}_{-6.1}\pm1.6$		[1] AUBERT	03U	BABR	Repl. by AUBERT,B 06J
$11.7^{+3.6}_{-3.1}\pm1.0$		[2] ISHIKAWA	03	BELL	Repl. by WEI 09A
<31	90	ABE	02	BELL	Repl. by ISHIKAWA 03

[1] Assumes equal production of B^+ and B^0 at the $\Upsilon(4S)$.
[2] Assumes equal production of B^0 and B^+ at $\Upsilon(4S)$. The second error is a total of systematic uncertainties including model dependence.

$\Gamma(K^*(892)\mu^+\mu^-)/\Gamma(K^*(892)e^+e^-)$ — $\Gamma_{131}/\Gamma_{129}$

VALUE	DOCUMENT ID		TECN	COMMENT
0.98±0.15 OUR AVERAGE				
$1.13^{+0.34}_{-0.26}\pm0.10$	[1] LEES	12S	BABR	$e^+e^-\to\Upsilon(4S)$
$1.37^{+0.53}_{-0.40}\pm0.09$	AUBERT	09T	BABR	$e^+e^-\to\Upsilon(4S)$
$0.83\pm0.17\pm0.08$	WEI	09A	BELL	$e^+e^-\to\Upsilon(4S)$
• • • We do not use the following data for averages, fits, limits, etc. • • •				
$0.91\pm0.45\pm0.06$	AUBERT,B	06J	BABR	Repl. by AUBERT 09T

[1] Measured in the union of $0.10 < q^2 < 8.12$ GeV^2/c^4 and $q^2 > 10.11$ GeV^2/c^4. LEES 12S reports also individual measurements $\Gamma(B\to K^*(892)\mu^+\mu^-)/\Gamma(B\to K^*(892)e^+e^-) = 1.06^{+0.48}_{-0.33}\pm0.08$ for $0.10 < q^2 < 8.12$ GeV^2/c^4 and $\Gamma(B\to K^*(892)\mu^+\mu^-)/\Gamma(B\to K^*(892)e^+e^-) = 1.18^{+0.55}_{-0.37}\pm0.11$ for $q^2 > 10.11$ GeV^2/c^4.

$\Gamma(K\ell^+\ell^-)/\Gamma_{total}$ — Γ_{132}/Γ

Test for $\Delta B = 1$ weak neutral current. Allowed by higher-order electroweak interactions.

VALUE (units 10^{-7})	CL%	DOCUMENT ID		TECN	COMMENT
4.8±0.4 OUR AVERAGE					
$4.7\pm0.6\pm0.2$		LEES	12S	BABR	$e^+e^-\to\Upsilon(4S)$
$4.8^{+0.5}_{-0.4}\pm0.3$		WEI	09A	BELL	$e^+e^-\to\Upsilon(4S)$
• • • We do not use the following data for averages, fits, limits, etc. • • •					
$3.9\pm0.7\pm0.2$		[1] AUBERT	09T	BABR	Repl. by LEES 12S
$3.4\pm0.7\pm0.2$		[1] AUBERT,B	06J	BABR	Repl. by AUBERT 09T
$6.5^{+1.4}_{-1.3}\pm0.4$		[2] AUBERT	03U	BABR	Repl. by AUBERT,B 06J
$4.8^{+1.0}_{-0.9}\pm0.3$		[3] ISHIKAWA	03	BELL	Repl. by WEI 09A
$7.5^{+2.5}_{-2.1}\pm0.6$		[4] ABE	02	BELL	Repl. by ISHIKAWA 03
< 5.1	90	[1] AUBERT	02L	BABR	$e^+e^-\to\Upsilon(4S)$
<17	90	[5] ANDERSON	01B	CLE2	$e^+e^-\to\Upsilon(4S)$

[1] Assumes equal production of B^+ and B^0 at the $\Upsilon(4S)$.
[2] Assumes all four $B\to K\ell^+\ell^-$ modes having equal partial widths in the fit.
[3] Assumes equal production rate for charge and neutral B meson pairs, isospin invariance, lepton universality for $B\to K\ell^+\ell^-$, and $B(B\to K^*(892)\mu^+\mu^-) = 1.33$. The second error is total systematic uncertainties including model dependence.
[4] Assumes lepton universality.
[5] The result is for di-lepton masses above 0.5 GeV.

$\Gamma(K^*(892)\ell^+\ell^-)/\Gamma_{total}$ — Γ_{133}/Γ

Test for $\Delta B = 1$ weak neutral current. Allowed by higher-order electroweak interactions.

VALUE (units 10^{-7})	CL%	DOCUMENT ID		TECN	COMMENT
10.5±1.0 OUR AVERAGE					
$10.2^{+1.4}_{-1.3}\pm0.5$		LEES	12S	BABR	$e^+e^-\to\Upsilon(4S)$
$10.7^{+1.1}_{-1.0}\pm0.9$		WEI	09A	BELL	$e^+e^-\to\Upsilon(4S)$
• • • We do not use the following data for averages, fits, limits, etc. • • •					
$11.1^{+1.9}_{-1.8}\pm0.7$		[1] AUBERT	09T	BABR	Repl. by LEES 12S
$7.8^{+1.9}_{-1.7}\pm1.1$		[1] AUBERT,B	06J	BABR	Repl. by AUBERT 09T
$8.8^{+3.3}_{-2.9}\pm1.0$		[2] AUBERT	03U	BABR	Repl. by AUBERT,B 06J
$11.5^{+2.6}_{-2.4}\pm0.8$		[3] ISHIKAWA	03	BELL	Repl. by WEI 09A
<31	90	[1,4] AUBERT	02L	BABR	Repl. by AUBERT 03U
<33	90	[5] ANDERSON	01B	CLE2	$e^+e^-\to\Upsilon(4S)$

[1] Assumes equal production of B^+ and B^0 at the $\Upsilon(4S)$.
[2] Assumes the partial width ratio of electron and muon modes to be $\Gamma(B\to K^*(892)e^+e^-)/\Gamma(B\to K^*(892)\mu^+\mu^-) = 1.33$.
[3] Assumes equal production rate for charge and neutral B meson pairs, isospin invariance, lepton universality for $B\to K\ell^+\ell^-$, and $B(B\to K^*(892)\mu^+\mu^-) = 1.33$. The second error is total systematic uncertainties including model dependence.
[4] For averaging $K^*(892)\mu^+\mu^-$ and $K^*(892)e^+e^-$ modes, AUBERT 02L assumed $B(B\to K^*(892)e^+e^-)/B(B\to K^*(892)\mu^+\mu^-) = 1.2$.
[5] The result is for di-lepton masses above 0.5 GeV.

$\Gamma(K\nu\overline{\nu})/\Gamma_{total}$ — Γ_{134}/Γ

Test for $\Delta B = 1$ weak neutral current.

VALUE	CL%	DOCUMENT ID		TECN	COMMENT
<1.6 × 10^{-5}	90	[1] GRYGIER	17	BELL	$e^+e^-\to\Upsilon(4S)$
• • • We do not use the following data for averages, fits, limits, etc. • • •					
<1.7 × 10^{-5}	90	[1,2] LEES	13I	BABR	$e^+e^-\to\Upsilon(4S)$
<1.4 × 10^{-5}	90	[1] DEL-AMO-SA...10Q		BABR	Repl. by LEES 13I

[1] Assumes equal production of B^+ and B^0 at the $\Upsilon(4S)$.
[2] Also reported a limit $< 3.2\times10^{-5}$ at 90% CL obtained using a fully reconstructed hadronic B-tag evnets.

$\Gamma(K^*\nu\overline{\nu})/\Gamma_{total}$ — Γ_{135}/Γ

Test for $\Delta B = 1$ weak neutral current.

VALUE	CL%	DOCUMENT ID		TECN	COMMENT
<2.7 × 10^{-5}	90	[1] GRYGIER	17	BELL	$e^+e^-\to\Upsilon(4S)$
• • • We do not use the following data for averages, fits, limits, etc. • • •					
<7.6 × 10^{-5}	90	[1,2] LEES	13I	BABR	$e^+e^-\to\Upsilon(4S)$
<8 × 10^{-5}	90	AUBERT	08BC	BABR	Repl. by LEES 13I

[1] Assumes equal production of B^+ and B^0 at the $\Upsilon(4S)$.
[2] Also reported a limit $< 7.9\times10^{-5}$ at 90% CL obtained using a fully reconstructed hadronic B-tag evnets.

$\Gamma(\pi\nu\overline{\nu})/\Gamma_{total}$ — Γ_{136}/Γ

VALUE	CL%	DOCUMENT ID		TECN	COMMENT
<0.8 × 10^{-5}	90	[1] GRYGIER	17	BELL	$e^+e^-\to\Upsilon(4S)$

[1] Assumes equal production of B^+ and B^0 at the $\Upsilon(4S)$.

$\Gamma(\rho\nu\overline{\nu})/\Gamma_{total}$ — Γ_{137}/Γ

VALUE	CL%	DOCUMENT ID		TECN	COMMENT
<2.8 × 10^{-5}	90	[1] GRYGIER	17	BELL	$e^+e^-\to\Upsilon(4S)$

[1] Assumes equal production of B^+ and B^0 at the $\Upsilon(4S)$.

$\Gamma(se^{\pm}\mu^{\mp})/\Gamma_{total}$ — Γ_{138}/Γ

Test for lepton family number conservation. Allowed by higher-order electroweak interactions.

VALUE	CL%	DOCUMENT ID		TECN	COMMENT
<2.2 × 10^{-5}	90	GLENN	98	CLEO	$e^+e^-\to\Upsilon(4S)$

$\Gamma(\pi e^{\pm}\mu^{\mp})/\Gamma_{total}$ — Γ_{139}/Γ

Test of lepton family number conservation.

VALUE	CL%	DOCUMENT ID		TECN	COMMENT
<9.2 × 10^{-8}	90	[1] AUBERT	07AG	BABR	$e^+e^-\to\Upsilon(4S)$
• • • We do not use the following data for averages, fits, limits, etc. • • •					
<1.6 × 10^{-6}	90	[1] EDWARDS	02B	CLE2	$e^+e^-\to\Upsilon(4S)$

[1] Assumes equal production of B^+ and B^0 at the $\Upsilon(4S)$.

$\Gamma(\rho e^{\pm}\mu^{\mp})/\Gamma_{total}$ — Γ_{140}/Γ

Test of lepton family number conservation.

VALUE	CL%	DOCUMENT ID		TECN	COMMENT
<3.2 × 10^{-6}	90	[1] EDWARDS	02B	CLE2	$e^+e^-\to\Upsilon(4S)$

[1] Assumes equal production of B^+ and B^0 at the $\Upsilon(4S)$.

$\Gamma(Ke^{\pm}\mu^{\mp})/\Gamma_{total}$ — Γ_{141}/Γ

Test of lepton family number conservation.

VALUE (units 10^{-7})	CL%	DOCUMENT ID		TECN	COMMENT
< 0.38	90	[1] AUBERT,B	06J	BABR	$e^+e^-\to\Upsilon(4S)$
• • • We do not use the following data for averages, fits, limits, etc. • • •					
<16	90	[1] EDWARDS	02B	CLE2	$e^+e^-\to\Upsilon(4S)$

[1] Assumes equal production of B^+ and B^0 at the $\Upsilon(4S)$.

$\Gamma(K^*(892)e^{\pm}\mu^{\mp})/\Gamma_{total}$ — Γ_{142}/Γ

Test of lepton family number conservation.

VALUE (units 10^{-7})	CL%	DOCUMENT ID		TECN	COMMENT
< 5.1	90	[1] AUBERT,B	06J	BABR	$e^+e^-\to\Upsilon(4S)$
• • • We do not use the following data for averages, fits, limits, etc. • • •					
<62	90	[1] EDWARDS	02B	CLE2	$e^+e^-\to\Upsilon(4S)$

[1] Assumes equal production of B^+ and B^0 at the $\Upsilon(4S)$.

CP VIOLATION

A_{CP} is defined as

$$\frac{B(\overline{B}\to\overline{f})-B(B\to f)}{B(\overline{B}\to\overline{f})+B(B\to f)},$$

the *CP*-violation charge asymmetry of inclusive $B^{\pm}$ and B^0 decay.

$A_{CP}(B\to K^*(892)\gamma)$

VALUE	DOCUMENT ID		TECN	COMMENT
−0.003±0.011 OUR AVERAGE				
$-0.004\pm0.014\pm0.003$	[1] HORIGUCHI	17	BELL	$e^+e^-\to\Upsilon(4S)$
$-0.003\pm0.017\pm0.007$	[2] AUBERT	09AO	BABR	$e^+e^-\to\Upsilon(4S)$
$0.08\pm0.13\pm0.03$	[3] COAN	00	CLE2	$e^+e^-\to\Upsilon(4S)$

Downloaded from https://academic.oup.com/ptep/article/2022/8/083C01/6651666 by KIT Library user on 27 September 2022

• • • We do not use the following data for averages, fits, limits, etc. • • •

$-0.013 \pm 0.036 \pm 0.010$	[4] AUBERT,BE	04A	BABR	Repl. by AUBERT 09AO
$-0.015 \pm 0.044 \pm 0.012$	[3] NAKAO	04	BELL	Repl. by HORIGUCHI 17
$-0.044 \pm 0.076 \pm 0.012$	[5] AUBERT	02C	BABR	Repl. by AUBERT,BE 04A

[1] Uses B($\Upsilon(4S) \to B^+B^-$) = (51.4 ± 0.6)% and B($\Upsilon(4S) \to B^0\overline{B}^0$) = (48.6 ± 0.6)%.
[2] Corresponds to a 90% CL interval $-0.033 < A_{CP} < 0.028$.
[3] Assumes equal production of B^+ and B^0 at the $\Upsilon(4S)$.
[4] Corresponds to a 90% CL allowed region, $-0.074 < A_{CP} < 0.049$.
[5] A 90% CL range is $-0.170 < A_{CP} < 0.082$.

$A_{CP}(B \to s\gamma)$

VALUE	DOCUMENT ID		TECN	COMMENT
0.015 ±0.011 OUR AVERAGE				
$0.0144 \pm 0.0128 \pm 0.0011$	[1] WATANUKI	19	BELL	$e^+e^- \to \Upsilon(4S)$
$0.017 \pm 0.019 \pm 0.010$	[2] LEES	14K	BABR	$e^+e^- \to \Upsilon(4S)$
• • • We do not use the following data for averages, fits, limits, etc. • • •				
$-0.011 \pm 0.030 \pm 0.014$	[3] AUBERT	08BJ	BABR	Repl. by LEES 14K
$0.025 \pm 0.050 \pm 0.015$	[4] AUBERT,B	04E	BABR	Repl. by AUBERT 08BJ
$0.002 \pm 0.050 \pm 0.030$	[5] NISHIDA	04	BELL	Repl. by WATANUKI 19

[1] Using a sum-of-exclusive technique with $m_{X_s} < 2.8$ GeV/c^2.
[2] Measured with 16 exclusively reconstructed $B \to X_s\gamma$ decays with $0.6 < m_{X_s} < 2.0$ GeV/c^2 (ten charged and six neutral self-tagging B modes).
[3] Uses a sum of exclusively reconstructed $B \to X_s$ decay modes, with X_s mass between 0.6 and 2.8 GeV/c^2.
[4] Corresponds to $-0.06 < A_{CP} < 0.11$ at 90% CL.
[5] This measurement is performed inclusively for recoil mass X_s less than 2.1 GeV, which corresponds to $-0.093 < A_{CP} < 0.096$ at 90% CL.

$A_{CP}(B \to (s+d)\gamma)$

VALUE	DOCUMENT ID		TECN	COMMENT
0.010±0.031 OUR AVERAGE				
$0.022 \pm 0.039 \pm 0.009$	[1] PESANTEZ	15	BELL	$e^+e^- \to \Upsilon(4S)$
$0.057 \pm 0.060 \pm 0.018$	LEES	12V	BABR	$e^+e^- \to \Upsilon(4S)$
$-0.10 \pm 0.18 \pm 0.05$	[2] AUBERT	08O	BABR	$e^+e^- \to \Upsilon(4S)$
$-0.110 \pm 0.115 \pm 0.017$	AUBERT,BE	06B	BABR	$e^+e^- \to \Upsilon(4S)$
$-0.079 \pm 0.108 \pm 0.022$	[3] COAN	01	CLE2	$e^+e^- \to \Upsilon(4S)$

[1] Assumes equal production of B^+ and B^0 at the $\Upsilon(4S)$. Uses an opposite side lepton tag. Requires center-of-mass frame $E_\gamma > 2.1$ GeV.
[2] Uses a fully reconstructed B meson as a tag on the recoil side. Requires $E_\gamma > 2.2$ GeV.
[3] Corresponds to $-0.27 < A_{CP} < 0.10$ at 90% CL.

$A_{CP}(B \to X_s\ell^+\ell^-)$

VALUE	DOCUMENT ID		TECN	COMMENT
0.04±0.11±0.01	[1] LEES	14D	BABR	$e^+e^- \to \Upsilon(4S)$
• • • We do not use the following data for averages, fits, limits, etc. • • •				
$-0.22 \pm 0.26 \pm 0.02$	[2] AUBERT,B	04I	BABR	Repl. by LEES 14D

[1] Measured from sum of exclusive modes through K^+, $K^+\pi^0$, $K^+\pi^-$, $K^+\pi^-\pi^0$, $K^+\pi^-\pi^+$, $K^0_S\pi^+$, and $K^0_S\pi^+\pi^0$.
[2] The final state flavor is determined by the kaon and pion charges where modes with $X_s = K^0_S$, $K^0_S\pi^0$ or $K^0_S\pi^+\pi^-$ are not used.

$A_{CP}(B \to X_s\ell^+\ell^-)$ ($1.0 < q^2 < 6.0$ GeV^2/c^4)

VALUE	DOCUMENT ID		TECN	COMMENT
−0.06±0.22±0.01	[1] LEES	14D	BABR	$e^+e^- \to \Upsilon(4S)$

[1] Measured from sum of exclusive modes through K^+, $K^+\pi^0$, $K^+\pi^-$, $K^+\pi^-\pi^0$, $K^+\pi^-\pi^+$, $K^0_S\pi^+$, and $K^0_S\pi^+\pi^0$.

$A_{CP}(B \to X_s\ell^+\ell^-)$ ($1.0 < q^2 < 12.9$ or $q^2 > 14.2$ GeV^2/c^4)

VALUE	DOCUMENT ID		TECN	COMMENT
$\mathbf{0.19^{+0.18}_{-0.17} \pm 0.01}$	[1] LEES	14D	BABR	$e^+e^- \to \Upsilon(4S)$

[1] Measured from sum of exclusive modes through K^+, $K^+\pi^0$, $K^+\pi^-$, $K^+\pi^-\pi^0$, $K^+\pi^-\pi^+$, $K^0_S\pi^+$, and $K^0_S\pi + (pi-)^0$.

$A_{CP}(B \to K^* e^+e^-)$

VALUE	DOCUMENT ID		TECN	COMMENT
−0.18±0.15±0.01	WEI	09A	BELL	$e^+e^- \to \Upsilon(4S)$

$A_{CP}(B \to K^*\mu^+\mu^-)$

VALUE	DOCUMENT ID		TECN	COMMENT
−0.03±0.13±0.02	WEI	09A	BELL	$e^+e^- \to \Upsilon(4S)$

$A_{CP}(B \to K^*\ell^+\ell^-)$

VALUE	DOCUMENT ID		TECN	COMMENT
−0.04±0.07 OUR AVERAGE				
$0.03 \pm 0.13 \pm 0.01$	[1] LEES	12S	BABR	$e^+e^- \to \Upsilon(4S)$
$+0.01^{+0.16}_{-0.15} \pm 0.01$	AUBERT	09T	BABR	$e^+e^- \to \Upsilon(4S)$
$-0.10 \pm 0.10 \pm 0.01$	WEI	09A	BELL	$e^+e^- \to \Upsilon(4S)$

[1] Measured in the union of $0.10 < q^2 < 8.12$ GeV^2/c^4 and $q^2 > 10.11$ GeV^2/c^4. LEES 12S reports also individual measurements $A_{CP}(B \to K^*\ell^+\ell^-) = -0.13^{+0.18}_{-0.19} \pm 0.01$ for $0.10 < q^2 < 8.12$ GeV^2/c^4 and $A_{CP}(B \to K^*\ell^+\ell^-) = 0.16^{+0.18}_{-0.19} \pm 0.01$ for $q^2 > 10.11$ GeV^2/c^4.

$A_{CP}(B \to \eta$ anything$)$

VALUE	DOCUMENT ID		TECN	COMMENT
$\mathbf{-0.13 \pm 0.04^{+0.02}_{-0.03}}$	[1] NISHIMURA	10	BELL	$e^+e^- \to \Upsilon(4S)$

[1] Uses $B \to \eta X_s$ with $0.4 < m_{X_s} < 2.6$ GeV/c^2.

$\Delta A_{CP}(X_s\gamma) = A_{CP}(B^{\pm} \to X_s\gamma) - A_{CP}(B^0 \to X_s\gamma)$

This is the isospin difference of the CP asymmetries.

VALUE	DOCUMENT ID		TECN	COMMENT
0.041 ±0.023 OUR AVERAGE				
$0.0369 \pm 0.0265 \pm 0.0076$	[1] WATANUKI	19	BELL	$e^+e^- \to \Upsilon(4S)$
$0.050 \pm 0.039 \pm 0.015$	[2] LEES	14K	BABR	$e^+e^- \to \Upsilon(4S)$

[1] Using a sum-of-exclusive technique with $m_{X_s} < 2.8$ GeV/c^2.
[2] Measured with 16 exclusively reconstructed $B \to X_s\gamma$ decays with $0.6 < m_{X_s} < 2.0$ GeV/c^2 (ten charged and six neutral self-tagging B modes).

$\overline{A}_{CP}(B \to X_s\gamma) = (A_{CP}(B^+ \to X_s\gamma) + A_{CP}(B^0 \to X_s\gamma))/2$

VALUE	DOCUMENT ID		TECN	COMMENT
0.0091±0.0121±0.0013	[1] WATANUKI	19	BELL	$e^+e^- \to \Upsilon(4S)$

[1] Using a sum-of-exclusive technique with $m_{X_s} < 2.8$ GeV/c^2.

$\Delta A_{CP}(B \to K^*\gamma) = A_{CP}(B^+ \to K^{*+}\gamma) - A_{CP}(B^0 \to K^{*0}\gamma)$

This is the isospin difference of the CP asymmetries.

VALUE	DOCUMENT ID		TECN	COMMENT
0.024±0.028±0.005	[1] HORIGUCHI	17	BELL	$e^+e^- \to \Upsilon(4S)$

[1] Uses B($\Upsilon(4S) \to B^+B^-$) = (51.4 ± 0.6)% and B($\Upsilon(4S) \to B^0\overline{B}^0$) = (48.6 ± 0.6)%.

$\overline{A}_{CP}(B \to K^*\gamma) = (A_{CP}(B^+ \to K^{*+}\gamma) + A_{CP}(B^0 \to K^{*0}\gamma))/2$

This is the average CP asymmetry.

VALUE	DOCUMENT ID		TECN	COMMENT
−0.001±0.014±0.003	[1] HORIGUCHI	17	BELL	$e^+e^- \to \Upsilon(4S)$

[1] Uses B($\Upsilon(4S) \to B^+B^-$) = (51.4 ± 0.6)% and B($\Upsilon(4S) \to B^0\overline{B}^0$) = (48.6 ± 0.6)%.

POLARIZATION IN B DECAY

In decays involving two vector mesons, one can distinguish among the states in which meson polarizations are both longitudinal (L) or both are transverse and parallel ($\|$) or perpendicular ($\perp$) to each other with the parameters Γ_L/Γ, $\Gamma_\perp/\Gamma$, and the relative phases $\phi_\|$ and $\phi_\perp$. See the definitions in the note on "Polarization in B Decays" review in the B^0 Particle Listings.

$F_L(B \to K^*\ell^+\ell^-)$ ($q^2 > 0.1$ GeV^2/c^4)

VALUE	DOCUMENT ID		TECN	COMMENT
$\mathbf{0.63^{+0.18}_{-0.19} \pm 0.05}$	[1] AUBERT,B	06J	BABR	$e^+e^- \to \Upsilon(4S)$

[1] Results with different q^2 cuts are also reported.

$F_L(B \to K^*\ell^+\ell^-)$ ($m_{\ell\ell} < 2.5$ GeV/c^2)

VALUE	DOCUMENT ID		TECN	COMMENT
0.35±0.16±0.04	AUBERT	09N	BABR	$e^+e^- \to \Upsilon(4S)$

$F_L(B \to K^*\ell^+\ell^-)$ ($m_{\ell\ell} > 3.2$ GeV/c^2)

VALUE	DOCUMENT ID		TECN	COMMENT
$\mathbf{0.71^{+0.20}_{-0.22} \pm 0.04}$	AUBERT	09N	BABR	$e^+e^- \to \Upsilon(4S)$

$F_L(B \to K^*\ell^+\ell^-)$ ($0.10 < q^2 < 0.98$ GeV^2/c^4)

VALUE	DOCUMENT ID		TECN	COMMENT
$\mathbf{0.263^{+0.045}_{-0.044} \pm 0.017}$	AAIJ	16B	LHCB	pp at 7, 8 TeV

$F_L(B \to K^*\ell^+\ell^-)$ ($1.1 < q^2 < 2.5$ GeV^2/c^4)

VALUE	DOCUMENT ID		TECN	COMMENT
$\mathbf{0.660^{+0.083}_{-0.077} \pm 0.022}$	AAIJ	16B	LHCB	pp at 7, 8 TeV

$F_L(B \to K^*\ell^+\ell^-)$ ($0.1 < q^2 < 2.0$ GeV^2/c^4)

VALUE	DOCUMENT ID		TECN	COMMENT
$\mathbf{0.34^{+0.08}_{-0.07}}$ **OUR AVERAGE**				
$0.37^{+0.10}_{-0.09} \pm 0.04$ -0.03	AAIJ	13Y	LHCB	pp at 7 TeV, $K^{*0}\mu^+\mu^-$
$0.30 \pm 0.16 \pm 0.02$	AALTONEN	12I	CDF	$p\overline{p}$ at 1.96 TeV
$0.29^{+0.21}_{-0.18} \pm 0.02$	WEI	09A	BELL	$e^+e^- \to \Upsilon(4S)$
• • • We do not use the following data for averages, fits, limits, etc. • • •				
$0.60^{+0.00}_{-0.28} \pm 0.19$	[1] CHATRCHYAN	13BL	CMS	pp at 7 TeV
$0.00^{+0.13}_{-0.00} \pm 0.02$	AAIJ	12U	LHCB	Repl. by AAIJ 13Y
$0.53^{+0.32}_{-0.34} \pm 0.07$	AALTONEN	11L	CDF	Repl. by AALTONEN 12I

[1] CHATRCHYAN 13BL uses, for this bin, $1.0 < q^2 < 2.0$ GeV^2/c^4.

Downloaded from https://academic.oup.com/ptep/article/2022/8/083C01/6651666 by KIT Library user on 27 September 2022

$F_L(B \to K^* \ell^+ \ell^-)$ ($2.0 < q^2 < 4.3$ GeV^2/c^4)

VALUE	DOCUMENT ID		TECN	COMMENT
0.77 ±0.05 OUR AVERAGE				
$0.876^{+0.109}_{-0.097}\pm0.017$	[1] AAIJ	16B	LHCB	pp at 7, 8 TeV
0.80 ±0.08 ±0.06	KHACHATRY...	16D	CMS	pp at 8 TeV
$0.74\ ^{+0.10}_{-0.09}\ ^{+0.02}_{-0.03}$	AAIJ	13Y	LHCB	pp at 7 TeV, $K^{*0}\mu^+\mu^-$
0.65 ±0.17 ±0.03	CHATRCHYAN	13BL	CMS	pp at 7 TeV
$0.37\ ^{+0.25}_{-0.24}$ ±0.10	AALTONEN	12I	CDF	$p\overline{p}$ at 1.96 TeV
0.71 ±0.24 ±0.05	WEI	09A	BELL	$e^+e^- \to \Upsilon(4S)$
• • • We do not use the following data for averages, fits, limits, etc. • • •				
0.77 ±0.15 ±0.03	AAIJ	12U	LHCB	Repl. by AAIJ 13Y
$0.40\ ^{+0.32}_{-0.33}$ ±0.08	AALTONEN	11L	CDF	Repl. by AALTONEN 12I

[1] Measured in $2.5 < q^2 < 4.0$ GeV^2/c^4.

$F_L(B \to K^* \ell^+ \ell^-)$ ($4.0 < q^2 < 6.0$ GeV^2/c^4)

VALUE	DOCUMENT ID		TECN	COMMENT
$0.611^{+0.052}_{-0.053}\pm0.017$	AAIJ	16B	LHCB	pp at 7, 8 TeV

$F_L(B \to K^* \ell^+ \ell^-)$ ($6.0 < q^2 < 8.0$ GeV^2/c^4)

VALUE	DOCUMENT ID		TECN	COMMENT
0.579±0.046±0.015	AAIJ	16B	LHCB	pp at 7, 8 TeV

$F_L(B \to K^* \ell^+ \ell^-)$ ($4.3 < q^2 < 8.6$ GeV^2/c^4)

VALUE	DOCUMENT ID		TECN	COMMENT
0.64±0.06 OUR AVERAGE				
0.57±0.07±0.03	AAIJ	13Y	LHCB	pp at 7 TeV, $K^{*0}\mu^+\mu^-$
$0.81^{+0.13}_{-0.12}\pm0.05$	CHATRCHYAN	13BL	CMS	pp at 7 TeV
$0.68^{+0.15}_{-0.17}\pm0.09$	AALTONEN	12I	CDF	$p\overline{p}$ at 1.96 TeV
$0.64^{+0.23}_{-0.24}\pm0.07$	WEI	09A	BELL	$e^+e^- \to \Upsilon(4S)$
• • • We do not use the following data for averages, fits, limits, etc. • • •				
$0.60^{+0.06}_{-0.07}\pm0.01$	AAIJ	12U	LHCB	Repl. by AAIJ 13Y
$0.82^{+0.19}_{-0.23}\pm0.07$	AALTONEN	11L	CDF	Repl. by AALTONEN 12I

$F_L(B \to K^* \ell^+ \ell^-)$ ($10.09 < q^2 < 12.86$ GeV^2/c^4)

VALUE	DOCUMENT ID		TECN	COMMENT
0.448±0.033 OUR AVERAGE				
$0.493^{+0.049}_{-0.047}\pm0.013$	[1] AAIJ	16B	LHCB	pp at 7, 8 TeV
0.39 ±0.05 ±0.04	KHACHATRY...	16D	CMS	pp at 8 TeV
$0.48\ ^{+0.08}_{-0.09}$ ±0.03	AAIJ	13Y	LHCB	pp at 7 TeV, $K^{*0}\mu^+\mu^-$
$0.45\ ^{+0.10}_{-0.11}$ ±0.04	CHATRCHYAN	13BL	CMS	pp at 7 TeV
0.47 ±0.14 ±0.03	AALTONEN	12I	CDF	$p\overline{p}$ at 1.96 TeV
$0.17\ ^{+0.17}_{-0.15}$ ±0.03	WEI	09A	BELL	$e^+e^- \to \Upsilon(4S)$
• • • We do not use the following data for averages, fits, limits, etc. • • •				
0.41 ±0.11 ±0.03	AAIJ	12U	LHCB	Repl. by AAIJ 13Y
$0.31\ ^{+0.19}_{-0.18}$ ±0.02	AALTONEN	11L	CDF	Repl. by AALTONEN 12I

[1] Measured in $11.0 < q^2 < 12.5$ GeV^2/c^4.

$F_L(B \to K^* \ell^+ \ell^-)$ ($15.0 < q^2 < 17.0$ GeV^2/c^4)

VALUE	DOCUMENT ID		TECN	COMMENT
0.349±0.039±0.009	AAIJ	16B	LHCB	pp at 7, 8 TeV

$F_L(B \to K^* \ell^+ \ell^-)$ ($17.0 < q^2 < 19.0$ GeV^2/c^4)

VALUE	DOCUMENT ID		TECN	COMMENT
$0.354^{+0.049}_{-0.048}\pm0.025$	AAIJ	16B	LHCB	pp at 7, 8 TeV

$F_L(B \to K^* \ell^+ \ell^-)$ ($14.18 < q^2 < 16.0$ GeV^2/c^4)

VALUE	DOCUMENT ID		TECN	COMMENT
0.40±0.06 OUR AVERAGE Error includes scale factor of 1.4. See the ideogram below.				
$0.48^{+0.05}_{-0.06}\pm0.04$	KHACHATRY...	16D	CMS	pp at 8 TeV
$0.33^{+0.08}_{-0.07}\ ^{+0.02}_{-0.03}$	AAIJ	13Y	LHCB	pp at 7 TeV, $K^{*0}\mu^+\mu^-$
0.53±0.12±0.03	CHATRCHYAN	13BL	CMS	pp at 7 TeV
$0.29^{+0.14}_{-0.13}\pm0.05$	AALTONEN	12I	CDF	$p\overline{p}$ at 1.96 TeV
$-0.15^{+0.27}_{-0.23}\pm0.07$	WEI	09A	BELL	$e^+e^- \to \Upsilon(4S)$
• • • We do not use the following data for averages, fits, limits, etc. • • •				
0.37±0.09±0.05	AAIJ	12U	LHCB	Repl. by AAIJ 13Y
$0.55^{+0.17}_{-0.18}\pm0.02$	AALTONEN	11L	CDF	Repl. by AALTONEN 12I

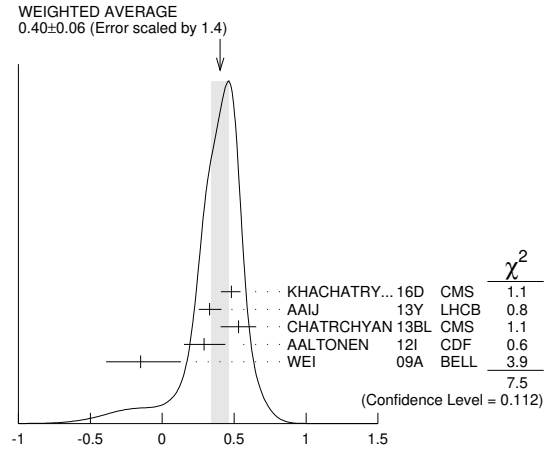

$F_L(B \to K^* \ell^+ \ell^-)$ ($14.18 < q^2 < 16.0$ GeV^2/c^4)

$F_L(B \to K^* \ell^+ \ell^-)$ ($16.0 < q^2 < 19.0$ GeV^2/c^4)

VALUE	DOCUMENT ID		TECN	COMMENT
0.350±0.019 OUR AVERAGE				
0.345±0.020±0.007	[1] AAIJ	20Y	LHCB	pp at 7, 8, 13 TeV
$0.38\ ^{+0.05}_{-0.06}$ ±0.04	KHACHATRY...	16D	CMS	pp at 8 TeV
$0.38\ ^{+0.09}_{-0.07}$ ±0.03	AAIJ	13Y	LHCB	pp at 7 TeV, $K^{*0}\mu^+\mu^-$
0.44 ±0.07 ±0.03	CHATRCHYAN	13BL	CMS	pp at 7 TeV
$0.20\ ^{+0.19}_{-0.17}$ ±0.05	AALTONEN	12I	CDF	$p\overline{p}$ at 1.96 TeV
$0.12\ ^{+0.15}_{-0.13}$ ±0.02	WEI	09A	BELL	$e^+e^- \to \Upsilon(4S)$
• • • We do not use the following data for averages, fits, limits, etc. • • •				
$0.344^{+0.028}_{-0.030}\pm0.008$	[1] AAIJ	16B	LHCB	Repl. by AAIJ 20Y
$0.26\ ^{+0.10}_{-0.08}$ ±0.03	AAIJ	12U	LHCB	Repl. by AAIJ 13Y
$0.09\ ^{+0.18}_{-0.14}$ ±0.03	AALTONEN	11L	CDF	Repl. by AALTONEN 12I

[1] Measured in $15.0 < q^2 < 19.0$ GeV^2/c^4.

$F_L(B \to K^* \ell^+ \ell^-)$ ($1.0 < q^2 < 6.0$ GeV^2/c^4)

VALUE	DOCUMENT ID		TECN	COMMENT
0.67 ±0.07 OUR AVERAGE Error includes scale factor of 2.8. See the ideogram below.				
0.700±0.025±0.013	[1] AAIJ	20Y	LHCB	pp at 7, 8, 13 TeV
0.72 ±0.06	KHACHATRY...	16D	CMS	pp at 7, 8 TeV
$0.24\ ^{+0.09}_{-0.08}$ ±0.02	[2] LEES	16C	BABR	$e^+e^- \to \Upsilon(4S)$
$0.65\ ^{+0.08}_{-0.07}$ ±0.03	AAIJ	13Y	LHCB	pp at 7 TeV, $K^{*0}\mu^+\mu^-$
$0.69\ ^{+0.19}_{-0.21}$ ±0.08	AALTONEN	12I	CDF	$p\overline{p}$ at 1.96 TeV
0.67 ±0.23 ±0.05	WEI	09A	BELL	$e^+e^- \to \Upsilon(4S)$
• • • We do not use the following data for averages, fits, limits, etc. • • •				
$0.690^{+0.035}_{-0.036}\pm0.017$	[1] AAIJ	16B	LHCB	Repl. by AAIJ 20Y
0.68 ±0.10 ±0.02	CHATRCHYAN	13BL	CMS	Repl. by KHACHATRYAN 16D
0.55 ±0.10 ±0.03	AAIJ	12U	LHCB	Repl. by AAIJ 13Y
$0.50\ ^{+0.27}_{-0.30}$ ±0.03	AALTONEN	11L	CDF	Repl. by AALTONEN 12I

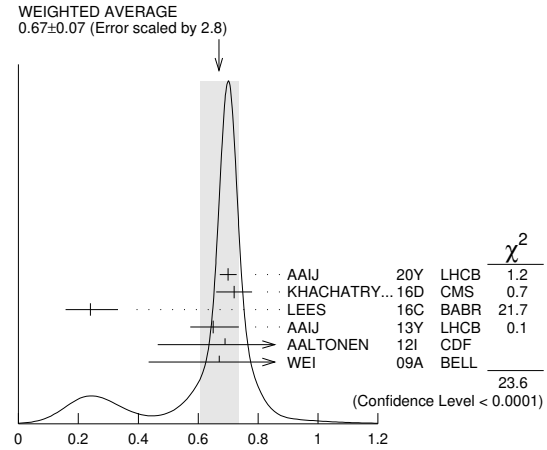

$F_L(B \to K^* \ell^+ \ell^-)$ ($1.0 < q^2 < 6.0$ GeV^2/c^4)

[1] Measured in $1.1 < q^2 < 6.0$ GeV^2/c^4.

Downloaded from https://academic.oup.com/ptep/article/2022/8/083C01/6651666 by KIT Library user on 27 September 2022

[2] Measured by combining B^0 and B^+ with e and μ as leptons. Results are also provided separately for B^0 and B^+.

$F_L(B \to K^* \ell^+ \ell^-)$ ($0.0 < q^2 < 4.3$ GeV^2/c^4)

VALUE	DOCUMENT ID		TECN	COMMENT
$0.33^{+0.14}_{-0.13} \pm 0.03$	AALTONEN	12I	CDF	$p\overline{p}$ at 1.96 TeV
• • • We do not use the following data for averages, fits, limits, etc. • • •				
$0.47^{+0.23}_{-0.24} \pm 0.03$	AALTONEN	11L	CDF	Repl. by AALTONEN 12I

$P_\tau(B \to D^* \tau^+ \nu_\tau)$

Measures difference in decay widths with positive and negative τ^+ helicities normalized to the sum of those decay widths.

VALUE	DOCUMENT ID		TECN	COMMENT
$-0.38 \pm 0.51^{+0.21}_{-0.16}$	[1] HIROSE	17	BELL	$e^+e^- \to \Upsilon(4S)$

[1] Uses a fully reconstructed B meson as a tag on the recoil side.

PARTIAL BRANCHING FRACTIONS IN $B \to K^{(*)} \ell^+ \ell^-$

B($B \to K^* \ell^+ \ell^-$) ($q^2 < 2.0$ GeV^2/c^4)

VALUE (units 10^{-7})	DOCUMENT ID		TECN	COMMENT
1.68±0.23 OUR AVERAGE				
$1.89^{+0.52}_{-0.46} \pm 0.06$	[1] LEES	12S	BABR	$e^+e^- \to \Upsilon(4S)$
$1.73 \pm 0.33 \pm 0.10$	AALTONEN	11AI	CDF	$p\overline{p}$ at 1.96 TeV
$1.46^{+0.40}_{-0.35} \pm 0.11$	WEI	09A	BELL	$e^+e^- \to \Upsilon(4S)$
• • • We do not use the following data for averages, fits, limits, etc. • • •				
$0.98 \pm 0.40 \pm 0.09$	AALTONEN	11L	CDF	Repl. by AALTONEN 11AI

[1] The value reported here from LEES 12S refers to $0.1 < q^2 < 2.0$ GeV^2/c^2.

B($B \to K^* \ell^+ \ell^-$) ($2.0 < q^2 < 4.3$ GeV^2/c^4)

VALUE (units 10^{-7})	DOCUMENT ID		TECN	COMMENT
0.87±0.17 OUR AVERAGE				
$0.95^{+0.35}_{-0.30} \pm 0.04$	LEES	12S	BABR	$e^+e^- \to \Upsilon(4S)$
$0.82 \pm 0.26 \pm 0.06$	AALTONEN	11AI	CDF	$p\overline{p}$ at 1.96 TeV
$0.86^{+0.31}_{-0.27} \pm 0.07$	WEI	09A	BELL	$e^+e^- \to \Upsilon(4S)$
• • • We do not use the following data for averages, fits, limits, etc. • • •				
$1.00 \pm 0.38 \pm 0.09$	AALTONEN	11L	CDF	Repl. by AALTONEN 11AI

B($B \to K^* \ell^+ \ell^-$) ($4.3 < q^2 < 8.68$ GeV^2/c^4)

VALUE (units 10^{-7})	DOCUMENT ID		TECN	COMMENT
1.67±0.29 OUR AVERAGE				
$1.82^{+0.56}_{-0.52} \pm 0.09$	[1] LEES	12S	BABR	$e^+e^- \to \Upsilon(4S)$
$1.72 \pm 0.41 \pm 0.14$	AALTONEN	11AI	CDF	$p\overline{p}$ at 1.96 TeV
$1.37^{+0.47}_{-0.42} \pm 0.39$	WEI	09A	BELL	$e^+e^- \to \Upsilon(4S)$
• • • We do not use the following data for averages, fits, limits, etc. • • •				
$1.69 \pm 0.57 \pm 0.15$	AALTONEN	11L	CDF	Repl. by AALTONEN 11AI

[1] The value reported here from LEES 12S refers to $4.3 < q^2 < 8.12$ GeV^2/c^2.

B($B \to K^* \ell^+ \ell^-$) ($10.09 < q^2 < 12.86$ GeV^2/c^4)

VALUE (units 10^{-7})	DOCUMENT ID		TECN	COMMENT
1.93±0.25 OUR AVERAGE				
$1.86^{+0.52}_{-0.48} \pm 0.10$	[1] LEES	12S	BABR	$e^+e^- \to \Upsilon(4S)$
$1.77 \pm 0.34 \pm 0.11$	AALTONEN	11AI	CDF	$p\overline{p}$ at 1.96 TeV
$2.24^{+0.44}_{-0.40} \pm 0.19$	WEI	09A	BELL	$e^+e^- \to \Upsilon(4S)$
• • • We do not use the following data for averages, fits, limits, etc. • • •				
$1.97 \pm 0.47 \pm 0.17$	AALTONEN	11L	CDF	Repl. by AALTONEN 11AI

[1] The value reported here from LEES 12S refers to $10.11 < q^2 < 12.89$ GeV^2/c^2.

B($B \to K^* \ell^+ \ell^-$) ($14.18 < q^2 < 16.0$ GeV^2/c^4)

VALUE (units 10^{-7})	DOCUMENT ID		TECN	COMMENT
1.21±0.17 OUR AVERAGE				
$1.46^{+0.41}_{-0.36} \pm 0.06$	[1] LEES	12S	BABR	$e^+e^- \to \Upsilon(4S)$
$1.21 \pm 0.24 \pm 0.07$	AALTONEN	11AI	CDF	$p\overline{p}$ at 1.96 TeV
$1.05^{+0.29}_{-0.26} \pm 0.08$	WEI	09A	BELL	$e^+e^- \to \Upsilon(4S)$
• • • We do not use the following data for averages, fits, limits, etc. • • •				
$1.51 \pm 0.36 \pm 0.13$	AALTONEN	11L	CDF	Repl. by AALTONEN 11AI

[1] The value reported here from LEES 12S refers to $14.21 < q^2 < 16.0$ GeV^2/c^2.

B($B \to K^* \ell^+ \ell^-$) ($16.0 < q^2$ GeV^2/c^4)

VALUE (units 10^{-7})	DOCUMENT ID		TECN	COMMENT
1.3 ±0.4 OUR AVERAGE	Error includes scale factor of 2.3. See the ideogram below.			
$1.02^{+0.47}_{-0.42} \pm 0.06$	LEES	12S	BABR	$e^+e^- \to \Upsilon(4S)$
$0.88 \pm 0.22 \pm 0.05$	AALTONEN	11AI	CDF	$p\overline{p}$ at 1.96 TeV
$2.04^{+0.27}_{-0.24} \pm 0.16$	WEI	09A	BELL	$e^+e^- \to \Upsilon(4S)$
• • • We do not use the following data for averages, fits, limits, etc. • • •				
$1.35 \pm 0.37 \pm 0.12$	AALTONEN	11L	CDF	Repl. by AALTONEN 11AI

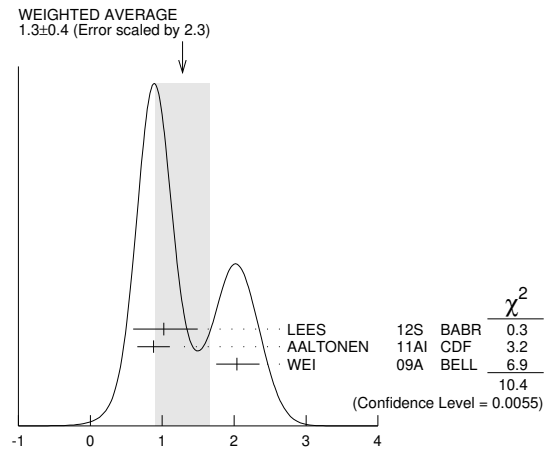

B($B \to K^* \ell^+ \ell^-$) ($16.0 < q^2$ GeV^2/c^4) (units 10^{-7})

B($B \to K^* \ell^+ \ell^-$) ($1.0 < q^2 < 6.0$ GeV^2/c^4)

VALUE (units 10^{-7})	DOCUMENT ID		TECN	COMMENT
1.64±0.26 OUR AVERAGE				
$2.05^{+0.53}_{-0.48} \pm 0.07$	LEES	12S	BABR	$e^+e^- \to \Upsilon(4S)$
$1.48 \pm 0.39 \pm 0.12$	AALTONEN	11AI	CDF	$p\overline{p}$ at 1.96 TeV
$1.49^{+0.45}_{-0.40} \pm 0.12$	WEI	09A	BELL	$e^+e^- \to \Upsilon(4S)$
• • • We do not use the following data for averages, fits, limits, etc. • • •				
$1.60 \pm 0.54 \pm 0.14$	AALTONEN	11L	CDF	Repl. by AALTONEN 11AI

B($B \to K^* \ell^+ \ell^-$) ($0.0 < q^2 < 4.3$ GeV^2/c^4)

VALUE (units 10^{-7})	DOCUMENT ID		TECN	COMMENT
2.53±0.43±0.15	AALTONEN	11AI	CDF	$p\overline{p}$ at 1.96 TeV
• • • We do not use the following data for averages, fits, limits, etc. • • •				
$1.98 \pm 0.55 \pm 0.18$	AALTONEN	11L	CDF	Repl. by AALTONEN 11AI

B($B^+ \to K^* \mu^+ \mu^-$) / B($B^+ \to K^* e^+ e^-$) ($0.045 < q^2 < 1.1$ GeV^2/c^4)

VALUE	DOCUMENT ID		TECN	COMMENT
$0.52^{+0.36}_{-0.26} \pm 0.05$	WEHLE	21	BELL	$e^+e^- \to \Upsilon(4S)$

B($B^+ \to K^* \mu^+ \mu^-$) / B($B^+ \to K^* e^+ e^-$) ($1.1 < q^2 < 6.0$ GeV^2/c^4)

VALUE	DOCUMENT ID		TECN	COMMENT
$0.96^{+0.45}_{-0.29} \pm 0.11$	WEHLE	21	BELL	$e^+e^- \to \Upsilon(4S)$

B($B^+ \to K^* \mu^+ \mu^-$) / B($B^+ \to K^* e^+ e^-$) ($15.0 < q^2 < 19.0$ GeV^2/c^4)

VALUE	DOCUMENT ID		TECN	COMMENT
$1.18^{+0.52}_{-0.32} \pm 0.10$	WEHLE	21	BELL	$e^+e^- \to \Upsilon(4S)$

B($B \to K \ell^+ \ell^-$) ($q^2 < 2.0$ GeV^2/c^4)

VALUE (units 10^{-7})	DOCUMENT ID		TECN	COMMENT
0.51±0.16 OUR AVERAGE	Error includes scale factor of 1.9. See the ideogram below.			
$0.71^{+0.20}_{-0.18} \pm 0.02$	[1] LEES	12S	BABR	$e^+e^- \to \Upsilon(4S)$
$0.33 \pm 0.10 \pm 0.02$	AALTONEN	11AI	CDF	$p\overline{p}$ at 1.96 TeV
$0.81^{+0.18}_{-0.16} \pm 0.05$	WEI	09A	BELL	$e^+e^- \to \Upsilon(4S)$
• • • We do not use the following data for averages, fits, limits, etc. • • •				
$0.38 \pm 0.16 \pm 0.03$	AALTONEN	11L	CDF	Repl. by AALTONEN 11AI

[1] The value reported here from LEES 12S refers to $0.1 < q^2 < 2.0$ GeV^2/c^2.

Downloaded from https://academic.oup.com/ptep/article/2022/8/083C01/6651666 by KIT Library user on 27 September 2022

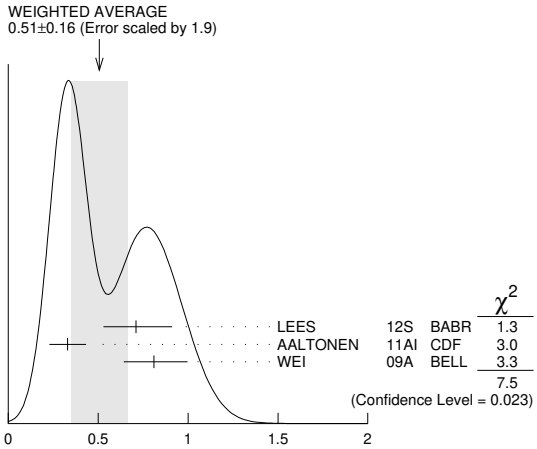

B($B \to K\ell^+\ell^-$) ($q^2 < 2.0$ GeV^2/c^4) (units 10^{-7})

B($B \to K\ell^+\ell^-$) ($2.0 < q^2 < 4.3$ GeV^2/c^4)

VALUE (units 10^{-7})	DOCUMENT ID		TECN	COMMENT
$0.57^{+0.10}_{-0.09}$ OUR AVERAGE	Error includes scale factor of 1.2.			
$0.49^{+0.15}_{-0.13} \pm 0.01$	LEES	12S	BABR	$e^+e^- \to \Upsilon(4S)$
$0.77 \pm 0.14 \pm 0.05$	AALTONEN	11AI	CDF	$p\overline{p}$ at 1.96 TeV
$0.46^{+0.14}_{-0.12} \pm 0.03$	WEI	09A	BELL	$e^+e^- \to \Upsilon(4S)$
• • • We do not use the following data for averages, fits, limits, etc. • • •				
$0.58 \pm 0.19 \pm 0.04$	AALTONEN	11L	CDF	Repl. by AALTONEN 11AI

B($B \to K\ell^+\ell^-$) ($4.3 < q^2 < 8.68$ GeV^2/c^4)

VALUE (units 10^{-7})	DOCUMENT ID		TECN	COMMENT
1.00±0.11 OUR AVERAGE				
$0.94^{+0.20}_{-0.19} \pm 0.02$	[1] LEES	12S	BABR	$e^+e^- \to \Upsilon(4S)$
$1.05 \pm 0.17 \pm 0.07$	AALTONEN	11AI	CDF	$p\overline{p}$ at 1.96 TeV
$1.00^{+0.19}_{-0.18} \pm 0.06$	WEI	09A	BELL	$e^+e^- \to \Upsilon(4S)$
• • • We do not use the following data for averages, fits, limits, etc. • • •				
$0.93 \pm 0.25 \pm 0.06$	AALTONEN	11L	CDF	Repl. by AALTONEN 11AI

[1] The value reported here from LEES 12S refers to $4.3 < q^2 < 8.12$ GeV^2/c^2.

B($B \to K\ell^+\ell^-$) ($10.09 < q^2 < 12.86$ GeV^2/c^4)

VALUE (units 10^{-7})	DOCUMENT ID		TECN	COMMENT
0.57±0.11 OUR AVERAGE	Error includes scale factor of 1.4. See the ideogram below.			
$0.90^{+0.20}_{-0.19} \pm 0.04$	[1] LEES	12S	BABR	$e^+e^- \to \Upsilon(4S)$
$0.48 \pm 0.10 \pm 0.03$	AALTONEN	11AI	CDF	$p\overline{p}$ at 1.96 TeV
$0.55^{+0.16}_{-0.14} \pm 0.03$	WEI	09A	BELL	$e^+e^- \to \Upsilon(4S)$
• • • We do not use the following data for averages, fits, limits, etc. • • •				
$0.72 \pm 0.17 \pm 0.05$	AALTONEN	11L	CDF	Repl. by AALTONEN 11AI

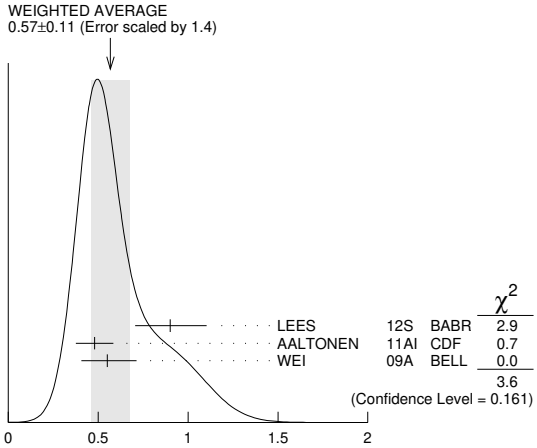

B($B \to K\ell^+\ell^-$) ($10.09 < q^2 < 12.86$ GeV^2/c^4) (units 10^{-7})

[1] The value reported here from LEES 12S refers to $10.11 < q^2 < 12.89$ GeV^2/c^2.

B($B \to K\ell^+\ell^-$) ($14.18 < q^2 < 16.0$ GeV^2/c^4)

VALUE (units 10^{-7})	DOCUMENT ID		TECN	COMMENT
0.49±0.07 OUR AVERAGE				
$0.49^{+0.15}_{-0.14} \pm 0.02$	[1] LEES	12S	BABR	$e^+e^- \to \Upsilon(4S)$
$0.52 \pm 0.09 \pm 0.03$	AALTONEN	11AI	CDF	$p\overline{p}$ at 1.96 TeV
$0.38^{+0.19}_{-0.12} \pm 0.02$	WEI	09A	BELL	$e^+e^- \to \Upsilon(4S)$
• • • We do not use the following data for averages, fits, limits, etc. • • •				
$0.38 \pm 0.12 \pm 0.03$	AALTONEN	11L	CDF	Repl. by AALTONEN 11AI

[1] The value reported here from LEES 12S refers to $14.21 < q^2 < 16.0$ GeV^2/c^2.

B($B \to K\ell^+\ell^-$) ($16.0 < q^2$ GeV^2/c^4)

VALUE (units 10^{-7})	DOCUMENT ID		TECN	COMMENT
0.52±0.16 OUR AVERAGE	Error includes scale factor of 2.1. See the ideogram below.			
$0.67^{+0.23}_{-0.21} \pm 0.05$	LEES	12S	BABR	$e^+e^- \to \Upsilon(4S)$
$0.38 \pm 0.09 \pm 0.02$	AALTONEN	11AI	CDF	$p\overline{p}$ at 1.96 TeV
$0.98^{+0.20}_{-0.18} \pm 0.06$	WEI	09A	BELL	$e^+e^- \to \Upsilon(4S)$
• • • We do not use the following data for averages, fits, limits, etc. • • •				
$0.35 \pm 0.13 \pm 0.02$	AALTONEN	11L	CDF	Repl. by AALTONEN 11AI

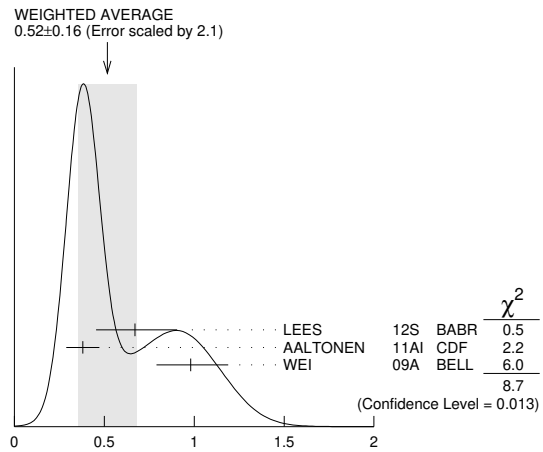

B($B \to K\ell^+\ell^-$) ($16.0 < q^2$ GeV^2/c^4) (units 10^{-7})

B($B \to K\ell^+\ell^-$) ($1.0 < q^2 < 6.0$ GeV^2/c^4)

VALUE (units 10^{-7})	DOCUMENT ID		TECN	COMMENT
1.33±0.13 OUR AVERAGE				
$1.36^{+0.27}_{-0.24} \pm 0.03$	LEES	12S	BABR	$e^+e^- \to \Upsilon(4S)$
$1.29 \pm 0.18 \pm 0.08$	AALTONEN	11AI	CDF	$p\overline{p}$ at 1.96 TeV
$1.36^{+0.23}_{-0.21} \pm 0.08$	WEI	09A	BELL	$e^+e^- \to \Upsilon(4S)$
• • • We do not use the following data for averages, fits, limits, etc. • • •				
$1.01 \pm 0.26 \pm 0.07$	AALTONEN	11L	CDF	Repl. by AALTONEN 11AI

B($B \to K\ell^+\ell^-$) ($0.0 < q^2 < 4.3$ GeV^2/c^4)

VALUE (units 10^{-7})	DOCUMENT ID		TECN	COMMENT
1.07±0.17±0.07	AALTONEN	11AI	CDF	$p\overline{p}$ at 1.96 TeV
• • • We do not use the following data for averages, fits, limits, etc. • • •				
$0.96 \pm 0.25 \pm 0.06$	AALTONEN	11L	CDF	Repl. by AALTONEN 11AI

B($B \to X_s\ell^+\ell^-$) ($1.0 < q^2 < 6.0$ GeV^2/c^4)

VALUE (units 10^{-6})	DOCUMENT ID		TECN	COMMENT
$1.60^{+0.41}_{-0.39}{}^{+0.25}_{-0.22}$	[1] LEES	14D	BABR	$e^+e^- \to \Upsilon(4S)$

[1] Measured from sum of exclusive modes through K^+, $K^+\pi^0$, $K^+\pi^-$, $K^+\pi^-\pi^0$, $K^+\pi^-\pi^+$, K^0_S, $K^0_S\pi^0$, $K^0_S\pi^+$, $K^0_S\pi^+\pi^0$, and $K^0_S\pi^+\pi^-$ corrected for unobserved modes.

B($B \to X_s e^+e^-$) ($1.0 < q^2 < 6.0$ GeV^2/c^4)

VALUE (units 10^{-6})	DOCUMENT ID		TECN	COMMENT
$1.93^{+0.47}_{-0.45}{}^{+0.28}_{-0.24}$	[1] LEES	14D	BABR	$e^+e^- \to \Upsilon(4S)$

[1] Measured from sum of exclusive modes through K^+, $K^+\pi^0$, $K^+\pi^-$, $K^+\pi^-\pi^0$, $K^+\pi^-\pi^+$, K^0_S, $K^0_S\pi^0$, $K^0_S\pi^+$, $K^0_S\pi^+\pi^0$, and $K^0_S\pi^+\pi^-$ corrected for unobserved modes.

B($B \to X_s\mu^+\mu^-$) ($1.0 < q^2 < 6.0$ GeV^2/c^4)

VALUE (units 10^{-6})	DOCUMENT ID		TECN	COMMENT
$0.66^{+0.82}_{-0.76}{}^{+0.31}_{-0.25}$	[1] LEES	14D	BABR	$e^+e^- \to \Upsilon(4S)$

[1] Measured from sum of exclusive modes through K^+, $K^+\pi^0$, $K^+\pi^-$, $K^+\pi^-\pi^0$, $K^+\pi^-\pi^+$, K^0_S, $K^0_S\pi^0$, $K^0_S\pi^+$, $K^0_S\pi^+\pi^0$, and $K^0_S\pi^+\pi^-$ corrected for unobserved modes.

Downloaded from https://academic.oup.com/ptep/article/2022/8/083C01/6651666 by KIT Library user on 27 September 2022

B($B \to X_s \ell^+ \ell^-$) (14.2 < q^2 GeV^2/c^4)

VALUE (units 10^{-6})	DOCUMENT ID		TECN	COMMENT
$0.57^{+0.16}_{-0.15}{}^{+0.03}_{-0.02}$	[1] LEES	14D	BABR	$e^+e^- \to \Upsilon(4S)$

[1] Measured from sum of exclusive modes through K^+, $K^+\pi^0$, $K^+\pi^-$, $K^+\pi^-\pi^0$, $K^+\pi^-\pi^+$, K^0_S, $K^0_S\pi^0$, $K^0_S\pi^+$, $K^0_S\pi^+\pi^0$, and $K^0_S\pi^+\pi^-$ corrected for unobserved modes.

B($B \to X_s e^+ e^-$) (14.2 < q^2 GeV^2/c^4)

VALUE (units 10^{-6})	DOCUMENT ID		TECN	COMMENT
$0.56^{+0.19}_{-0.18}{}^{+0.03}_{-0.03}$	[1] LEES	14D	BABR	$e^+e^- \to \Upsilon(4S)$

[1] Measured from sum of exclusive modes through K^+, $K^+\pi^0$, $K^+\pi^-$, $K^+\pi^-\pi^0$, $K^+\pi^-\pi^+$, K^0_S, $K^0_S\pi^0$, $K^0_S\pi^+$, $K^0_S\pi^+\pi^0$, and $K^0_S\pi^+\pi^-$ corrected for unobserved modes.

B($B \to X_s \mu^+ \mu^-$) (14.2 < q^2 GeV^2/c^4)

VALUE (units 10^{-6})	DOCUMENT ID		TECN	COMMENT
$0.60^{+0.31}_{-0.29}{}^{+0.05}_{-0.04}$	[1] LEES	14D	BABR	$e^+e^- \to \Upsilon(4S)$

[1] Measured from sum of exclusive modes through K^+, $K^+\pi^0$, $K^+\pi^-$, $K^+\pi^-\pi^0$, $K^+\pi^-\pi^+$, K^0_S, $K^0_S\pi^0$, $K^0_S\pi^+$, $K^0_S\pi^+\pi^0$, and $K^0_S\pi^+\pi^-$ corrected for unobserved modes.

LEPTON (HADRON) FORWARD-BACKWARD ASYMMETRY IN $B \to K^{(*)}\ell^+\ell^-$ ($B \to K/\pi h^+ h^-$) DECAY

The forward-backward angular asymmetry of the lepton pair in $B \to K^{(*)}\ell^+\ell^-$ ($B \to K/\pi h^+ h^-$) decay is defined as

$$A_{FB}(s) = \frac{N(cos\theta>0)-N(cos\theta<0)}{N(cos\theta>0)+N(cos\theta<0)},$$

where $s=q^2/m_B^2$, and θ is the angle of the ℓ^- (h^-) with respect to the flight direction of the B meson, measured in the dilepton (dihadron) rest frame. In addition, the fraction of longitudinal polarization F_L of the K^* and F_S, the relative contribution from scalar and pseudoscalar penguin amplitudes in $B \to K\ell^+\ell^-$, can be measured from the angular distribution of its decay products.

A_{FB}($B \to K^*\ell^+\ell^-$) (q^2 > 0.1 GeV^2/c^4)

VALUE	CL%	DOCUMENT ID		TECN	COMMENT
$0.50 \pm 0.15 \pm 0.02$		[1] ISHIKAWA	06	BELL	$e^+e^- \to \Upsilon(4S)$
• • • We do not use the following data for averages, fits, limits, etc. • • •					
>0.55	95	[2] AUBERT,B	06J	BABR	$e^+e^- \to \Upsilon(4S)$

[1] Using an unbinned max. likelihood fits to the M_{bc} distribution in five q^2 bins for cos θ >0 and cos θ <0.
[2] Results with different q^2 cuts are also reported.

A_{FB}($B \to K^*\ell^+\ell^-$) (0.1 < q^2 < 2.0 GeV^2/c^4)

VALUE	DOCUMENT ID		TECN	COMMENT
-0.01 ± 0.14 OUR AVERAGE	Error includes scale factor of 1.4. See the ideogram below.			
$-0.02 \pm 0.12 \pm 0.01$	AAIJ	13Y	LHCB	pp at 7 TeV, $K^{*0}\mu^+\mu^-$
$-0.35^{+0.26}_{-0.23} \pm 0.10$	AALTONEN	12I	CDF	$p\overline{p}$ at 1.96 TeV
$0.47^{+0.26}_{-0.32} \pm 0.03$	WEI	09A	BELL	$e^+e^- \to \Upsilon(4S)$
• • • We do not use the following data for averages, fits, limits, etc. • • •				
$-0.29^{+0.37}_{-0.00} \pm 0.18$	[1] CHATRCHYAN	13BL	CMS	pp at 7 TeV
$-0.15 \pm 0.20 \pm 0.06$	AAIJ	12U	LHCB	Repl. by AAIJ 13Y
$0.13^{+1.65}_{-0.75} \pm 0.25$	AALTONEN	11L	CDF	Repl. by AALTONEN 12I

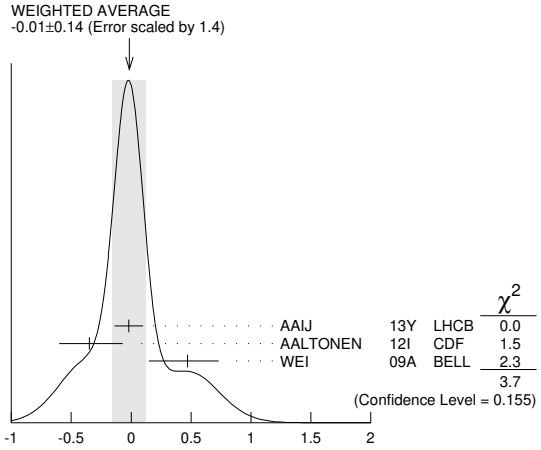

A_{FB}($B \to K^*\ell^+\ell^-$) (0.1 < q^2 < 2.0 GeV^2/c^4)

[1] CHATRCHYAN 13BL uses, for this bin, 1.0 < q^2 < 2.0 GeV^2/c^4.

A_{FB}($B \to K^*\ell^+\ell^-$) ($m_{\ell\ell}$ < 2.5 GeV/c^2)

VALUE	DOCUMENT ID		TECN	COMMENT
$0.24^{+0.18}_{-0.23} \pm 0.05$	AUBERT	09N	BABR	$e^+e^- \to \Upsilon(4S)$

A_{FB}($B \to K^*\ell^+\ell^-$) ($m_{\ell\ell}$ > 3.2 GeV/c^2)

VALUE	DOCUMENT ID		TECN	COMMENT
$0.76^{+0.52}_{-0.32} \pm 0.07$	AUBERT	09N	BABR	$e^+e^- \to \Upsilon(4S)$

A_{FB}($B \to K^*\ell^+\ell^-$) (0.10 < q^2 < 0.98 GeV^2/c^4)

VALUE	DOCUMENT ID		TECN	COMMENT
$-0.003^{+0.058}_{-0.057} \pm 0.009$	AAIJ	16B	LHCB	pp at 7, 8 TeV

A_{FB}($B \to K^*\ell^+\ell^-$) (1.1 < q^2 < 2.5 GeV^2/c^4)

VALUE	DOCUMENT ID		TECN	COMMENT
$-0.191^{+0.068}_{-0.080} \pm 0.012$	AAIJ	16B	LHCB	pp at 7, 8 TeV

A_{FB}($B \to K^*\ell^+\ell^-$) (2.0 < q^2 < 4.3 GeV^2/c^4)

VALUE	DOCUMENT ID		TECN	COMMENT
-0.14 ± 0.05 OUR AVERAGE				
$-0.118^{+0.082}_{-0.090} \pm 0.007$	[1] AAIJ	16B	LHCB	pp at 7, 8 TeV
$-0.12^{+0.15}_{-0.17} \pm 0.05$	KHACHATRY...	16D	CMS	pp at 8 TeV
$-0.20 \pm 0.08 \pm 0.01$	AAIJ	13Y	LHCB	pp at 7 TeV, $K^{*0}\mu^+\mu^-$
$-0.07 \pm 0.20 \pm 0.02$	CHATRCHYAN	13BL	CMS	pp at 7 TeV
$0.29^{+0.32}_{-0.35} \pm 0.15$	AALTONEN	12I	CDF	$p\overline{p}$ at 1.96 TeV
$0.11^{+0.31}_{-0.36} \pm 0.07$	WEI	09A	BELL	$e^+e^- \to \Upsilon(4S)$
• • • We do not use the following data for averages, fits, limits, etc. • • •				
$0.05^{+0.16}_{-0.20} \pm 0.04$	AAIJ	12U	LHCB	Repl. by AAIJ 13Y
$0.19^{+0.40}_{-0.41} \pm 0.14$	AALTONEN	11L	CDF	Repl. by AALTONEN 12I

[1] Measured in 2.5 < q^2 < 4.0 GeV^2/c^4.

A_{FB}($B \to K^*\ell^+\ell^-$) (0.0 < q^2 < 4.3 GeV^2/c^4)

VALUE	DOCUMENT ID		TECN	COMMENT
$-0.08^{+0.21}_{-0.20} \pm 0.05$	AALTONEN	12I	CDF	$p\overline{p}$ at 1.96 TeV
• • • We do not use the following data for averages, fits, limits, etc. • • •				
$0.21^{+0.31}_{-0.33} \pm 0.05$	AALTONEN	11L	CDF	Repl. by AALTONEN 12I

A_{FB}($B \to K^*\ell^+\ell^-$) (4.0 < q^2 < 6.0 GeV^2/c^4)

VALUE	DOCUMENT ID		TECN	COMMENT
$0.025^{+0.051}_{-0.052} \pm 0.004$	AAIJ	16B	LHCB	pp at 7, 8 TeV

A_{FB}($B \to K^*\ell^+\ell^-$) (6.0 < q^2 < 8.0 GeV^2/c^4)

VALUE	DOCUMENT ID		TECN	COMMENT
$0.152^{+0.041}_{-0.040} \pm 0.008$	AAIJ	16B	LHCB	pp at 7, 8 TeV

A_{FB}($B \to K^*\ell^+\ell^-$) (1.0 < q^2 < 6.0 GeV^2/c^4)

VALUE	DOCUMENT ID		TECN	COMMENT
-0.078 ± 0.022 OUR AVERAGE	Error includes scale factor of 1.1.			
$-0.073 \pm 0.021 \pm 0.002$	[1] AAIJ	20Y	LHCB	pp at 7, 8, 13 TeV
-0.12 ± 0.08	KHACHATRY...	16D	CMS	pp at 7, 8 TeV
$0.21^{+0.10}_{-0.15}{}^{+0.07}_{-0.09}$	[2] LEES	16C	BABR	$e^+e^- \to \Upsilon(4S)$
$-0.17 \pm 0.06 \pm 0.01$	AAIJ	13Y	LHCB	pp at 7 TeV, $K^{*0}\mu^+\mu^-$
$0.29^{+0.20}_{-0.23} \pm 0.07$	AALTONEN	12I	CDF	$p\overline{p}$ at 1.96 TeV
$0.26^{+0.27}_{-0.30} \pm 0.07$	WEI	09A	BELL	$e^+e^- \to \Upsilon(4S)$
• • • We do not use the following data for averages, fits, limits, etc. • • •				
$-0.075^{+0.032}_{-0.034} \pm 0.007$	[1] AAIJ	16B	LHCB	Repl. by AAIJ 20Y
0.55 ± 0.43	[3] SATO	16	BELL	$e^+e^- \to \Upsilon(4S)$
$-0.07 \pm 0.12 \pm 0.01$	CHATRCHYAN	13BL	CMS	Repl. by KHACHATRYAN 16D
$-0.06^{+0.13}_{-0.14} \pm 0.07$	AAIJ	12U	LHCB	Repl. by AAIJ 13Y
$0.43^{+0.36}_{-0.37} \pm 0.06$	AALTONEN	11L	CDF	Repl. by AALTONEN 12I

[1] Measured in 1.1 < q^2 < 6.0 GeV^2/c^4.
[2] Measured by combining B^0 and B^+ with e and μ as leptons. Results are also provided separately for B^0 and B^+.
[3] Uses $K^* \to K^-\pi^+$, $K^-\pi^0$, $K^0_S\pi^-$ in the range M($K\pi$) < 1.1 GeV/c^2. Uncertainty is statistical only.

Downloaded from https://academic.oup.com/ptep/article/2022/8/083C01/6651666 by KIT Library user on 27 September 2022

$A_{FB}(B \to K^* \ell^+ \ell^-)$ ($4.3 < q^2 < 8.6$ GeV^2/c^4)

VALUE	DOCUMENT ID		TECN	COMMENT
$0.13^{+0.06}_{-0.05}$ OUR AVERAGE	Error includes scale factor of 1.1.			
$0.16^{+0.06}_{-0.05} \pm 0.01$	AAIJ	13Y	LHCB	pp at 7 TeV, $K^{*0}\mu^+\mu^-$
$-0.01 \pm 0.11 \pm 0.03$	CHATRCHYAN	13BL	CMS	pp at 7 TeV
$0.01 \pm 0.20 \pm 0.09$	AALTONEN	12I	CDF	$p\overline{p}$ at 1.96 TeV
$0.45^{+0.15}_{-0.21} \pm 0.15$	WEI	09A	BELL	$e^+e^- \to \Upsilon(4S)$
• • • We do not use the following data for averages, fits, limits, etc. • • •				
$0.27^{+0.06}_{-0.08} \pm 0.02$	AAIJ	12U	LHCB	Repl. by AAIJ 13Y
$-0.06^{+0.30}_{-0.28} \pm 0.05$	AALTONEN	11L	CDF	Repl. by AALTONEN 12I

$A_{FB}(B \to K^* \ell^+ \ell^-)$ ($10.09 < q^2 < 12.86$ GeV^2/c^4)

VALUE	DOCUMENT ID		TECN	COMMENT
0.02 ± 0.13 OUR AVERAGE	Error includes scale factor of 4.5. See the ideogram below.			
$-0.318^{+0.044}_{-0.040} \pm 0.009$	[1] AAIJ	16B	LHCB	pp at 7, 8 TeV
$0.16 \pm 0.06 \pm 0.01$	KHACHATRY...	16D	CMS	pp at 8 TeV
$0.28^{+0.07}_{-0.06} \pm 0.02$	AAIJ	13Y	LHCB	pp at 7 TeV, $K^{*0}\mu^+\mu^-$
$0.40 \pm 0.08 \pm 0.05$	CHATRCHYAN	13BL	CMS	pp at 7 TeV
$0.38^{+0.16}_{-0.19} \pm 0.09$	AALTONEN	12I	CDF	$p\overline{p}$ at 1.96 TeV
$0.43^{+0.18}_{-0.20} \pm 0.03$	WEI	09A	BELL	$e^+e^- \to \Upsilon(4S)$
• • • We do not use the following data for averages, fits, limits, etc. • • •				
$0.27^{+0.11}_{-0.13} \pm 0.02$	AAIJ	12U	LHCB	Repl. by AAIJ 13Y
$0.66^{+0.23}_{-0.20} \pm 0.07$	AALTONEN	11L	CDF	Repl. by AALTONEN 12I

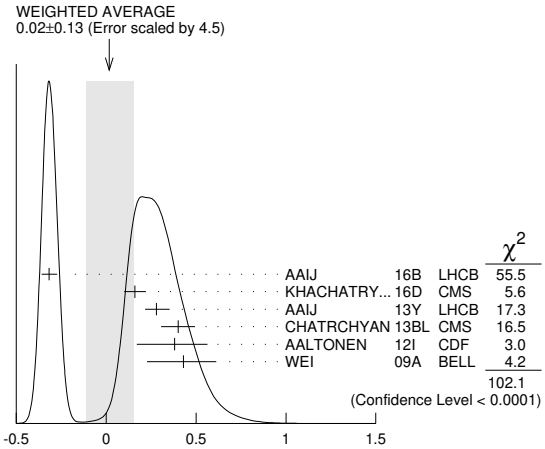

$A_{FB}(B \to K^* \ell^+ \ell^-)$ ($10.09 < q^2 < 12.86$ GeV^2/c^4)

[1] Measured in $11.0 < q^2 < 12.5$ GeV^2/c^4.

$A_{FB}(B \to K^* \ell^+ \ell^-)$ ($14.18 < q^2 < 16.0$ GeV^2/c^4)

VALUE	DOCUMENT ID		TECN	COMMENT
$0.43^{+0.05}_{-0.06}$ OUR AVERAGE	Error includes scale factor of 1.6. See the ideogram below.			
$0.39^{+0.04}_{-0.06} \pm 0.01$	KHACHATRY...	16D	CMS	pp at 8 TeV
$0.51^{+0.07}_{-0.05} \pm 0.02$	AAIJ	13Y	LHCB	pp at 7 TeV, $K^{*0}\mu^+\mu^-$
$0.29 \pm 0.09 \pm 0.05$	CHATRCHYAN	13BL	CMS	pp at 7 TeV
$0.44^{+0.18}_{-0.21} \pm 0.10$	AALTONEN	12I	CDF	$p\overline{p}$ at 1.96 TeV
$0.70^{+0.16}_{-0.22} \pm 0.10$	WEI	09A	BELL	$e^+e^- \to \Upsilon(4S)$
• • • We do not use the following data for averages, fits, limits, etc. • • •				
$0.47^{+0.06}_{-0.08} \pm 0.03$	AAIJ	12U	LHCB	Repl. by AAIJ 13Y
$0.42 \pm 0.16 \pm 0.09$	AALTONEN	11L	CDF	Repl. by AALTONEN 12I

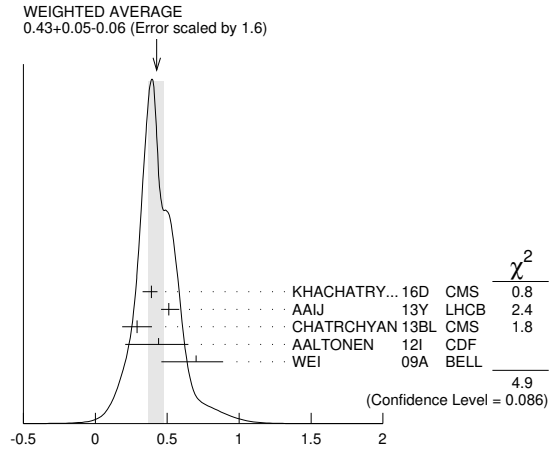

$A_{FB}(B \to K^* \ell^+ \ell^-)$ ($14.18 < q^2 < 16.0$ GeV^2/c^4)

$A_{FB}(B \to K^* \ell^+ \ell^-)$ ($15.0 < q^2 < 17.0$ GeV^2/c^4)

VALUE	DOCUMENT ID		TECN	COMMENT
$0.411^{+0.41}_{-0.037} \pm 0.008$	AAIJ	16B	LHCB	pp at 7, 8 TeV

$A_{FB}(B \to K^* \ell^+ \ell^-)$ ($17.0 < q^2 < 19.0$ GeV^2/c^4)

VALUE	DOCUMENT ID		TECN	COMMENT
$0.305^{+0.049}_{-0.048} \pm 0.013$	AAIJ	16B	LHCB	pp at 7, 8 TeV

$A_{FB}(B \to K^* \ell^+ \ell^-)$ ($16.0 < q^2 < 19.0$ GeV^2/c^4)

VALUE	DOCUMENT ID		TECN	COMMENT
0.362 ± 0.019 OUR AVERAGE				
$0.353 \pm 0.020 \pm 0.010$	[1] AAIJ	20Y	LHCB	pp at 7, 8, 13 TeV
$0.35 \pm 0.07 \pm 0.01$	KHACHATRY...	16D	CMS	pp at 8 TeV
$0.30 \pm 0.08^{+0.01}_{-0.02}$	AAIJ	13Y	LHCB	pp at 7 TeV, $K^{*0}\mu^+\mu^-$
$0.41 \pm 0.05 \pm 0.03$	CHATRCHYAN	13BL	CMS	pp at 7 TeV
$0.65^{+0.17}_{-0.18} \pm 0.16$	AALTONEN	12I	CDF	$p\overline{p}$ at 1.96 TeV
$0.66^{+0.11}_{-0.16} \pm 0.04$	WEI	09A	BELL	$e^+e^- \to \Upsilon(4S)$
• • • We do not use the following data for averages, fits, limits, etc. • • •				
$0.355 \pm 0.027 \pm 0.009$	[1] AAIJ	16B	LHCB	Repl. by AAIJ 20Y
$0.16^{+0.11}_{-0.13} \pm 0.06$	AAIJ	12U	LHCB	Repl. by AAIJ 13Y
$0.70^{+0.16}_{-0.25} \pm 0.10$	AALTONEN	11L	CDF	Repl. by AALTONEN 12I

[1] Measured in $15.0 < q^2 < 19.0$ GeV^2/c^4.

$A_{FB}(B \to K \ell^+ \ell^-)$ ($q^2 > 0.1$ GeV^2/c^4)

VALUE	DOCUMENT ID		TECN	COMMENT
0.11 ± 0.12 OUR AVERAGE				
$0.15^{+0.21}_{-0.23} \pm 0.08$	[1] AUBERT,B	06J	BABR	$e^+e^- \to \Upsilon(4S)$
$0.10 \pm 0.14 \pm 0.01$	[2] ISHIKAWA	06	BELL	$e^+e^- \to \Upsilon(4S)$

[1] Results with different q^2 cuts are also reported.
[2] Using an unbinned max. likelihood fits to the M_{bc} distribution in five q^2 bins for $\cos\theta > 0$ and $\cos\theta < 0$.

$A_{FB}(B \to K \ell^+ \ell^-)$ ($q^2 < 2.0$ GeV^2/c^4)

VALUE	DOCUMENT ID		TECN	COMMENT
$0.00^{+0.06}_{-0.05}$ OUR AVERAGE				
$0.00^{+0.06}_{-0.05}{}^{+0.03}_{-0.01}$	AAIJ	13H	LHCB	pp at 7 TeV
$0.13^{+0.42}_{-0.43} \pm 0.07$	AALTONEN	12I	CDF	$p\overline{p}$ at 1.96 TeV
$0.06^{+0.32}_{-0.35} \pm 0.02$	WEI	09A	BELL	$e^+e^- \to \Upsilon(4S)$
• • • We do not use the following data for averages, fits, limits, etc. • • •				
$-0.15^{+0.46}_{-0.39} \pm 0.08$	AALTONEN	11L	CDF	Repl. by AALTONEN 12I

$A_{FB}(B \to K \ell^+ \ell^-)$ ($2.0 < q^2 < 4.3$ GeV^2/c^4)

VALUE	DOCUMENT ID		TECN	COMMENT
$0.09^{+0.10}_{-0.07}$ OUR AVERAGE	Error includes scale factor of 1.4.			
$0.07^{+0.08}_{-0.05}{}^{+0.02}_{-0.01}$	AAIJ	13H	LHCB	pp at 7 TeV
$0.32^{+0.15}_{-0.16} \pm 0.05$	AALTONEN	12I	CDF	$p\overline{p}$ at 1.96 TeV
$-0.43^{+0.38}_{-0.40} \pm 0.09$	WEI	09A	BELL	$e^+e^- \to \Upsilon(4S)$

Downloaded from https://academic.oup.com/ptep/article/2022/8/083C01/6651666 by KIT Library user on 27 September 2022

• • • We do not use the following data for averages, fits, limits, etc. • • •

$0.72^{+0.40}_{-0.35}\pm0.07$	AALTONEN	11L	CDF	Repl. by AALTONEN 12I

$A_{FB}(B\to K\ell^+\ell^-)$ $(0.0<q^2<4.3\ \mathrm{GeV}^2/c^4)$

VALUE	DOCUMENT ID		TECN	COMMENT
$0.31\pm0.16\pm0.04$	AALTONEN	12I	CDF	$p\overline{p}$ at 1.96 TeV

• • • We do not use the following data for averages, fits, limits, etc. • • •

$0.36^{+0.24}_{-0.26}\pm0.06$	AALTONEN	11L	CDF	Repl. by AALTONEN 12I

$A_{FB}(B\to K\ell^+\ell^-)$ $(1.0<q^2<6.0\ \mathrm{GeV}^2/c^4)$

VALUE	DOCUMENT ID		TECN	COMMENT
$0.034^{+0.040}_{-0.029}$ OUR AVERAGE				
$0.02\ ^{+0.05}_{-0.03}\ ^{+0.02}_{-0.01}$	AAIJ	13H	LHCB	pp at 7 TeV
$0.13\ \pm0.09\ \pm0.02$	AALTONEN	12I	CDF	$p\overline{p}$ at 1.96 TeV
$-0.04\ ^{+0.13}_{-0.16}\ \pm0.05$	WEI	09A	BELL	$e^+e^-\to\Upsilon(4S)$

• • • We do not use the following data for averages, fits, limits, etc. • • •

$0.00\ \pm0.13$	[1] SATO	16	BELL	$e^+e^-\to\Upsilon(4S)$
$0.08\ ^{+0.27}_{-0.22}\ \pm0.07$	AALTONEN	11L	CDF	Repl. by AALTONEN 12I

[1] Statistical uncertainty only.

$A_{FB}(B\to K\ell^+\ell^-)$ $(4.3<q^2<8.6\ \mathrm{GeV}^2/c^4)$

VALUE	DOCUMENT ID		TECN	COMMENT
$-0.04^{+0.04}_{-0.05}$ OUR AVERAGE				
$-0.02^{+0.03}_{-0.05}\pm0.03$	AAIJ	13H	LHCB	pp at 7 TeV
$0.01^{+0.13}_{-0.10}\pm0.01$	AALTONEN	12I	CDF	$p\overline{p}$ at 1.96 TeV
$-0.20^{+0.12}_{-0.14}\pm0.03$	WEI	09A	BELL	$e^+e^-\to\Upsilon(4S)$

• • • We do not use the following data for averages, fits, limits, etc. • • •

$-0.20^{+0.17}_{-0.28}\pm0.03$	AALTONEN	11L	CDF	Repl. by AALTONEN 12I

$A_{FB}(B\to K\ell^+\ell^-)$ $(10.09<q^2<12.86\ \mathrm{GeV}^2/c^4)$

VALUE	DOCUMENT ID		TECN	COMMENT
-0.05 ± 0.06 OUR AVERAGE				
$-0.03\pm0.07\pm0.01$	AAIJ	13H	LHCB	pp at 7 TeV
$-0.03^{+0.11}_{-0.10}\pm0.04$	AALTONEN	12I	CDF	$p\overline{p}$ at 1.96 TeV
$-0.21^{+0.17}_{-0.15}\pm0.06$	WEI	09A	BELL	$e^+e^-\to\Upsilon(4S)$

• • • We do not use the following data for averages, fits, limits, etc. • • •

$-0.10^{+0.17}_{-0.15}\pm0.07$	AALTONEN	11L	CDF	Repl. by AALTONEN 12I

$A_{FB}(B\to K\ell^+\ell^-)$ $(14.18<q^2<16.0\ \mathrm{GeV}^2/c^4)$

VALUE	DOCUMENT ID		TECN	COMMENT
$-0.02^{+0.07}_{-0.05}$ OUR AVERAGE				
$-0.01^{+0.12}_{-0.06}\pm0.01$	AAIJ	13H	LHCB	pp at 7 TeV
$-0.05^{+0.09}_{-0.11}\pm0.03$	AALTONEN	12I	CDF	$p\overline{p}$ at 1.96 TeV
$0.04^{+0.32}_{-0.26}\pm0.05$	WEI	09A	BELL	$e^+e^-\to\Upsilon(4S)$

• • • We do not use the following data for averages, fits, limits, etc. • • •

$0.03^{+0.49}_{-0.16}\pm0.04$	AALTONEN	11L	CDF	Repl. by AALTONEN 12I

$A_{FB}(B\to K\ell^+\ell^-)$ $(16.0<q^2<18.0\ \mathrm{GeV}^2/c^4)$

VALUE	DOCUMENT ID		TECN	COMMENT
$-0.09^{+0.07+0.02}_{-0.09-0.01}$	AAIJ	13H	LHCB	pp at 7 TeV

$A_{FB}(B\to K\ell^+\ell^-)$ $(18.0<q^2<22.0\ \mathrm{GeV}^2/c^4)$

VALUE	DOCUMENT ID		TECN	COMMENT
$0.02\pm0.11\pm0.01$	AAIJ	13H	LHCB	pp at 7 TeV

$A_{FB}(B\to K\ell^+\ell^-)$ $(q^2>16.0\ \mathrm{GeV}^2/c^4)$

VALUE	DOCUMENT ID		TECN	COMMENT
$0.04^{+0.09}_{-0.07}$ OUR AVERAGE				
$0.09^{+0.17}_{-0.13}\pm0.03$	AALTONEN	12I	CDF	$p\overline{p}$ at 1.96 TeV
$0.02^{+0.11}_{-0.08}\pm0.02$	WEI	09A	BELL	$e^+e^-\to\Upsilon(4S)$

• • • We do not use the following data for averages, fits, limits, etc. • • •

$0.07^{+0.30}_{-0.23}\pm0.02$	AALTONEN	11L	CDF	Repl. by AALTONEN 12I

$A_{FB}(B\to X_s\ell^+\ell^-)$ $(1.0<q^2<6.0\ \mathrm{GeV}^2/c^4)$

VALUE	DOCUMENT ID		TECN	COMMENT
• • • We do not use the following data for averages, fits, limits, etc. • • •				
0.74 ± 0.54	[1] SATO	16	BELL	$e^+e^-\to\Upsilon(4S)$

[1] Uses the sum of 10 exclusive X_s modes in the range $M(X_s)>1.1\ \mathrm{GeV}/c^2$. Uncertainty is statistical only.

$F_S(B\to K\ell^+\ell^-)$ $(q^2>0.1\ \mathrm{GeV}^2/c^4)$

VALUE	DOCUMENT ID		TECN	COMMENT
$0.81^{+0.58}_{-0.61}\pm0.46$	[1] AUBERT,B	06J	BABR	$e^+e^-\to\Upsilon(4S)$

[1] Results with different q^2 cuts are also reported.

$A_{FB}(B\to Kp\overline{p})$ $(m_{p\overline{p}}<2.85\ \mathrm{GeV}/c^2)$

VALUE	DOCUMENT ID		TECN	COMMENT
$0.495\pm0.012\pm0.007$	[1] AAIJ	14AF	LHCB	pp at 7, 8 TeV

[1] Measured in $B^+\to K^+p\overline{p}$ decays.

$A_{FB}(B\to \pi p\overline{p})$ $(m_{p\overline{p}}<2.85\ \mathrm{GeV}/c^2)$

VALUE	DOCUMENT ID		TECN	COMMENT
$-0.409\pm0.033\pm0.006$	[1] AAIJ	14AF	LHCB	pp at 7, 8 TeV

[1] Measured in $B^+\to\pi^+p\overline{p}$ decays.

ISOSPIN ASYMMETRY

Δ_{0-} is defined as

$$\frac{\Gamma(\overline{B}^0\to f_d)-\Gamma(B^-\to f_u)}{\Gamma(\overline{B}^0\to f_d)+\Gamma(B^-\to f_u)},$$

the isospin asymmetry of inclusive neutral and charged B decay.

$\Delta_{0-}(B(B\to X_s\gamma))$

VALUE	DOCUMENT ID		TECN	COMMENT
$-0.005\ \pm0.020$ OUR AVERAGE				
$-0.0048\pm0.0149\pm0.0150$	[1] WATANUKI	19	BELL	$e^+e^-\to\Upsilon(4S)$
$-0.006\ \pm0.058\ \pm0.026$	AUBERT,B	05R	BABR	$e^+e^-\to\Upsilon(4S)$

[1] Using a sum-of-exclusive technique with $m_{X_s}<2.8\ \mathrm{GeV}/c^2$.

$\Delta_{0-}(B(B\to X_{s+d}\gamma))$

VALUE	DOCUMENT ID		TECN	COMMENT
$-0.06\pm0.15\pm0.07$	[1] AUBERT	08O	BABR	$e^+e^-\to\Upsilon(4S)$

[1] Uses a fully reconstructed B meson as a tag on the recoil side. The result is for $E_\gamma>2.2$ GeV.

$\Delta_{0+}(B\to K^*(892)\gamma)$

Δ_{0+} describes the isospin asymmetry between $\Gamma(B^0\to K^*(892)^0\gamma)$ and $\Gamma(B^+\to K^*(892)^+\gamma)$.

VALUE	DOCUMENT ID		TECN	COMMENT
0.063 ± 0.017 OUR AVERAGE				
$0.062\pm0.015\pm0.013$	[1] HORIGUCHI	17	BELL	$e^+e^-\to\Upsilon(4S)$
$0.066\pm0.021\pm0.022$	[2] AUBERT	09AO	BABR	$e^+e^-\to\Upsilon(4S)$

• • • We do not use the following data for averages, fits, limits, etc. • • •

$0.050\pm0.045\pm0.037$	[3] AUBERT,BE	04A	BABR	Repl. by AUBERT 09AO
$0.012\pm0.044\pm0.026$	NAKAO	04	BELL	Repl. by HORIGUCHI 17

[1] Uses $B(\Upsilon(4S)\to B^+B^-)=(51.4\pm0.6)\%$ and $B(\Upsilon(4S)\to B^0\overline{B}^0)=(48.6\pm0.6)\%$.

[2] Uses the production ratio of charged and neutral B from $\Upsilon(4S)$ decays and the lifetime ratio $\tau_{B^+}/\tau_{B^0}=1.071\pm0.009$. The 90% CL interval is $0.017<\Delta_{0+}<0.116$

[3] Uses the production ratio of charged and neutral B from $\Upsilon(4S)$ decays $R^{+/0}=1.006\pm0.048$ and the lifetime ratio of $\tau_{B^+}/\tau_{B^0}=1.083\pm0.017$. The 90% CL interval is $-0.046<\Delta_{0+}<0.146$.

$\Delta_{\rho\gamma}=\Gamma(B^+\to\rho^+\gamma)/(2\cdot\Gamma(B^0\to\rho^0\gamma))-1$

VALUE	DOCUMENT ID		TECN	COMMENT
-0.46 ± 0.17 OUR AVERAGE				
$-0.43^{+0.25}_{-0.22}\pm0.10$	AUBERT	08BH	BABR	$e^+e^-\to\Upsilon(4S)$
$-0.48^{+0.21+0.08}_{-0.19-0.09}$	TANIGUCHI	08	BELL	$e^+e^-\to\Upsilon(4S)$

$\Delta_{0-}(B(B\to K\ell^+\ell^-))$

VALUE	DOCUMENT ID		TECN	COMMENT
-0.15 ± 0.06 OUR AVERAGE Error includes scale factor of 1.2.				
$-0.31^{+0.13}_{-0.11}\pm0.01$	[1] CHOUDHURY	21	BELL	$e^+e^-\to\Upsilon(4S)$
$-0.10^{+0.08}_{-0.09}\pm0.02$	[2] AAIJ	14M	LHCB	pp at 7, 8 TeV
$-0.09^{+0.08}_{-0.08}\pm0.02$	[3] AAIJ	14M	LHCB	pp at 7, 8 TeV
$-0.58^{+0.29}_{-0.37}\pm0.02$	[4] LEES	12S	BABR	$e^+e^-\to\Upsilon(4S)$

• • • We do not use the following data for averages, fits, limits, etc. • • •

$-0.35^{+0.23}_{-0.27}$	[5] AAIJ	12AH	LHCB	Repl. by AAIJ 14M
$-1.43^{+0.56}_{-0.85}\pm0.05$	[6,7] AUBERT	09T	BABR	Repl. by LEES 12S
$-0.31^{+0.17}_{-0.14}\pm0.08$	[8,9] WEI	09A	BELL	$e^+e^-\to\Upsilon(4S)$

[1] For $1.0<q^2<6.0\ \mathrm{GeV}^2/c^4$ using both $\mu^+\mu^-$ and e^+e^- as a lepton pair. Measurements in other q^2 bins are also reported.

[2] For $1.1<q^2<6.0\ \mathrm{GeV}^2/c^4$ using $\mu^+\mu^-$ as a lepton pair and assuming isospin symmetry for the $B\to J/\psi(1S)K$. Measurements in other q^2 bins are also reported.

[3] For $15.0<q^2<19.0\ \mathrm{GeV}^2/c^4$ using $\mu^+\mu^-$ as a lepton pair and assuming isospin symmetry for the $B\to J/\psi(1S)K$. Measurements in other q^2 bins are also reported.

[4] For $0.10<q^2<8.12\ \mathrm{GeV}^2/c^4$. Measurements in other q^2 bins are also reported.

Downloaded from https://academic.oup.com/ptep/article/2022/8/083C01/6651666 by KIT Library user on 27 September 2022

[5] For $1 < q^2 < 6$ GeV^2/c^4.
[6] For $0.1 < m^2_{\ell^+\ell^-} < 7.02$ GeV^2/c^4.
[7] Assumes equal production of B^+ and B^0 at the $\Upsilon(4S)$.
[8] Superseded by CHOUDHURY 21.
[9] For $q^2 < 8.68$ GeV^2/c^4.

$\Delta_{0-}(B(B \to K^*\ell^+\ell^-))$

VALUE	DOCUMENT ID		TECN	COMMENT
$-0.03^{+0.08}_{-0.07}$ OUR AVERAGE	Error includes scale factor of 1.2.			
$0.00^{+0.12}_{-0.10}\pm0.02$	[1] AAIJ	14M	LHCB	pp at 7, 8 TeV
$0.06^{+0.10}_{-0.09}\pm0.02$	[2] AAIJ	14M	LHCB	pp at 7, 8 TeV
$-0.25^{+0.20}_{-0.17}\pm0.03$	[3] LEES	12S	BABR	$e^+e^- \to \Upsilon(4S)$
$-0.29\pm0.16\pm0.09$	[4] WEI	09A	BELL	$e^+e^- \to \Upsilon(4S)$
• • • We do not use the following data for averages, fits, limits, etc. • • •				
-0.15 ± 0.16	[5] AAIJ	12AH	LHCB	Repl. by AAIJ 14M
$-0.56^{+0.17}_{-0.15}\pm0.03$	[6,7] AUBERT	09T	BABR	Repl. by LEES 12S

[1] For $1.1 < q^2 < 6.0$ GeV^2/c^4 using $\mu^+\mu^-$ as a lepton pair and assuming isospin symmetry for the $B(B \to J/\psi(1S)K^*(892))$. Measurements in other q^2 bins are also reported.
[2] For $15.0 < q^2 < 22.0$ GeV^2/c^4 using $\mu^+\mu^-$ as a lepton pair and assuming isospin symmetry for the $B(B \to J/\psi(1S)K^*(892))$. Measurements in other q^2 bins are also reported.
[3] For $0.10 < q^2 < 8.12$ GeV^2/c^4. Measurements in other q^2 bins are also reported.
[4] For $q^2 < 8.68$ GeV^2/c^4.
[5] For $1 < q^2 < 6$ GeV^2/c^4.
[6] For $0.1 < m^2_{\ell^+\ell^-} < 7.02$ GeV^2/c^4.
[7] Assumes equal production of B^+ and B^0 at the $\Upsilon(4S)$.

$\Delta_{0-}(B(B \to K^{(*)}\ell^+\ell^-))$

VALUE	DOCUMENT ID		TECN	COMMENT
-0.45 ± 0.17 OUR AVERAGE	Error includes scale factor of 1.7.			
$-0.64^{+0.15}_{-0.14}\pm0.03$	[1,2] AUBERT	09T	BABR	$e^+e^- \to \Upsilon(4S)$
$-0.30^{+0.12}_{-0.11}\pm0.08$	[3] WEI	09A	BELL	$e^+e^- \to \Upsilon(4S)$

[1] For $0.1 < m^2_{\ell^+\ell^-} < 7.02$ GeV^2/c^4.
[2] Assumes equal production of B^+ and B^0 at the $\Upsilon(4S)$.
[3] For $q^2 < 8.68$ GeV^2/c^2.

$B \to X_c\ell\nu$ HADRONIC MASS MOMENTS

$\langle M_X^2 - \overline{M}_D^2\rangle$ (First Moments)

VALUE (GeV^2)	DOCUMENT ID		TECN	COMMENT
0.36 ±0.08 OUR AVERAGE	Error includes scale factor of 1.8.			
$0.467\pm0.038\pm0.068$	[1] ACOSTA	05F	CDF	$p\overline{p}$ at 1.96 TeV
$0.293\pm0.012\pm0.058$	[2] CSORNA	04	CLE2	$e^+e^- \to \Upsilon(4S)$
• • • We do not use the following data for averages, fits, limits, etc. • • •				
$0.251\pm0.023\pm0.062$	[3] CRONIN-HEN...	01B	CLE2	$e^+e^- \to \Upsilon(4S)$

[1] Moments are measured with a minimum lepton momentum of 0.7 GeV/c in the B rest frame;
[2] Uses minimum lepton energy of 1.5 GeV and also reports moments with $E_\ell > 1.0$ GeV.
[3] The leptons are required to have $P_\ell > 1.5$ GeV/c.

$\langle M_X^2\rangle$ (First Moments)

VALUE (GeV^2)	DOCUMENT ID		TECN	COMMENT
4.156±0.029 OUR AVERAGE				
$4.144\pm0.028\pm0.022$	[1] SCHWANDA	07	BELL	$e^+e^- \to \Upsilon(4S)$
$4.18\pm0.04\pm0.03$	[1] AUBERT,B	04	BABR	$e^+e^- \to \Upsilon(4S)$

[1] The leptons are required to have $E_\ell > 1.5$ GeV/c.

$\langle (M_X^2 - \overline{M}_X^2)^2\rangle$ (Second Moments)

VALUE (GeV^4)	DOCUMENT ID		TECN	COMMENT
0.55 ±0.08 OUR AVERAGE				
$0.515\pm0.061\pm0.064$	[1] SCHWANDA	07	BELL	$e^+e^- \to \Upsilon(4S)$
$0.629\pm0.031\pm0.143$	[2] CSORNA	04	CLE2	$e^+e^- \to \Upsilon(4S)$
• • • We do not use the following data for averages, fits, limits, etc. • • •				
$1.05\pm0.26\pm0.13$	[3] ACOSTA	05F	CDF	$p\overline{p}$ at 1.96 TeV
$0.576\pm0.048\pm0.168$	[1] CRONIN-HEN...	01B	CLE2	$e^+e^- \to \Upsilon(4S)$

[1] The leptons are required to have $E_\ell > 1.5$ GeV/c.
[2] Uses minimum lepton energy of 1.5 GeV and also reports moments with $E_\ell > 1.0$ GeV.
[3] Moments are measured with a minimum lepton momentum of 0.7 GeV/c in the B rest frame;

$\langle (M_X^2 - \overline{M}_D^2)^2\rangle$ (Second Moments)

VALUE (GeV^4)	DOCUMENT ID		TECN	COMMENT
0.639±0.056±0.178	[1] CRONIN-HEN...	01B	CLE2	$e^+e^- \to \Upsilon(4S)$

[1] The leptons are required to have $E_\ell > 1.5$ GeV/c.

$B \to X_c\ell\nu$ LEPTON MOMENTUM MOMENTS

R_0 ($\Gamma_{E_l>1.7GeV}$ / $\Gamma_{E_l>1.5GeV}$)

VALUE	DOCUMENT ID		TECN	COMMENT
0.6187±0.0014±0.0016	[1] MAHMOOD	03	CLE2	$e^+e^- \to \Upsilon(4S)$

[1] The leptons are required to have $E_l > 1.5$ GeV in the B rest frame.

R_1 ($\langle E_l\rangle_{E_l>1.5GeV}$)

VALUE	DOCUMENT ID		TECN	COMMENT
1.7797±0.0018 OUR AVERAGE	Error includes scale factor of 1.8. See the ideogram below.			
$1.7743\pm0.0019\pm0.0014$	[1] AUBERT,B	04A	BABR	$e^+e^- \to \Upsilon(4S)$
$1.7792\pm0.0021\pm0.0027$	[2] MAHMOOD	04	CLEO	$e^+e^- \to \Upsilon(4S)$
$1.7810\pm0.0007\pm0.0009$	[3] MAHMOOD	03	CLE2	$e^+e^- \to \Upsilon(4S)$

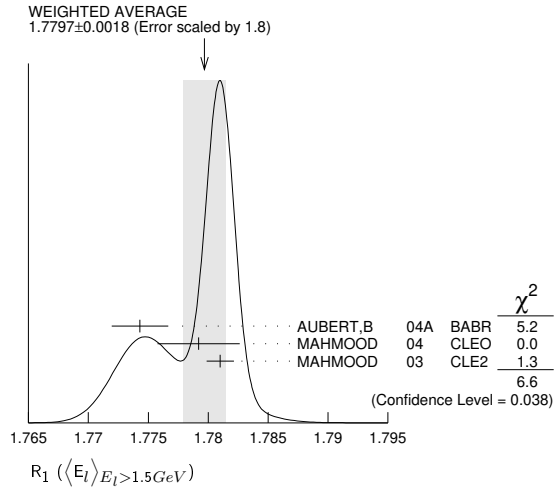

[1] The leptons are required to have $E_l > 1.5$ GeV in the B rest frame. The result with $E_l > 0.6$ GeV is also given.
[2] Uses $E_e > 1.5$ GeV and also reports moments with other minimum minimum E_e conditions, as low as $E_e > 0.6$ GeV.
[3] The leptons are required to have $E_l > 1.5$ GeV in the B rest frame.

R_2 ($\langle E_l^2 - \overline{E}_l^2\rangle_{E_l>1.5GeV}$)

VALUE (10^{-3} GeV^2)	DOCUMENT ID		TECN	COMMENT
30.8±0.8 OUR AVERAGE				
$30.3\pm0.9\pm0.5$	[1] AUBERT,B	04A	BABR	$e^+e^- \to \Upsilon(4S)$
$31.6\pm0.8\pm1.0$	[2] MAHMOOD	04	CLEO	$e^+e^- \to \Upsilon(4S)$

[1] The leptons are required to have $E_l > 1.5$ GeV in the B rest frame. The result with $E_l > 0.6$ GeV is also given.
[2] Uses $E_e > 1.5$ GeV and also reports moments with other minimum minimum E_e conditions, as low as $E_e > 0.6$ GeV.

R_3 ($\langle E_l^3 - \overline{E}_l^3\rangle_{E_l>1.5GeV}$)

VALUE (10^{-3} GeV^3)	DOCUMENT ID		TECN	COMMENT
2.12±0.47±0.20	[1] AUBERT,B	04A	BABR	$e^+e^- \to \Upsilon(4S)$

[1] The leptons are required to have $E_l > 1.5$ GeV in the B rest frame. The result with $E_l > 0.6$ GeV is also given.

$B \to X_s\gamma$ PHOTON ENERGY MOMENTS

$\langle E_\gamma\rangle$

VALUE (GeV)	DOCUMENT ID		TECN	COMMENT
2.314±0.011 OUR AVERAGE				
$2.346\pm0.018^{+0.027}_{-0.022}$	[1,2] LEES	12U	BABR	$e^+e^- \to \Upsilon(4S)$
$2.304\pm0.014\pm0.017$	[2,3] LEES	12V	BABR	$e^+e^- \to \Upsilon(4S)$
$2.311\pm0.009\pm0.015$	[3] LIMOSANI	09	BELL	$e^+e^- \to \Upsilon(4S)$
$2.289\pm0.058\pm0.027$	[3,4] AUBERT	08O	BABR	$e^+e^- \to \Upsilon(4S)$
$2.309\pm0.023\pm0.023$	[2,3] SCHWANDA	08	BELL	$e^+e^- \to \Upsilon(4S)$
• • • We do not use the following data for averages, fits, limits, etc. • • •				
$2.288\pm0.025\pm0.023$	[3] AUBERT,BE	06B	BABR	Repl. by LEES 12V

[1] LEES 12U uses $E_\gamma > 1.897$ GeV to calculate the moments; the moments are used to calculate the HQET parameters $m_b = 4.579^{+0.032}_{-0.029}$ GeV/c^2 and $\mu_\pi^2 = 0.257^{+0.034}_{-0.039}$ GeV^2 in the shape function model. The same HQET parameters are also determined in the kinetic model.
[2] Results for different E_γ threshold values are also measured.
[3] The result is for $E_\gamma > 1.9$ GeV.
[4] Uses a fully reconstructed B meson as a tag on the recoil side.

Downloaded from https://academic.oup.com/ptep/article/2022/8/083C01/6651666 by KIT Library user on 27 September 2022

$\langle E_\gamma^2 \rangle - \langle E_\gamma \rangle^2$

VALUE (10^{-2} GeV^2)	DOCUMENT ID		TECN	COMMENT
3.03±0.25 OUR AVERAGE				
$2.11 \pm 0.57^{+0.55}_{-0.69}$	[1,2] LEES	12U	BABR	$e^+e^- \to \Upsilon(4S)$
$3.62 \pm 0.33 \pm 0.33$	[2,3] LEES	12V	BABR	$e^+e^- \to \Upsilon(4S)$
$3.02 \pm 0.19 \pm 0.30$	[3] LIMOSANI	09	BELL	$e^+e^- \to \Upsilon(4S)$
$3.34 \pm 1.24 \pm 0.62$	[3,4] AUBERT	08O	BABR	$e^+e^- \to \Upsilon(4S)$
$2.17 \pm 0.60 \pm 0.55$	[2,3] SCHWANDA	08	BELL	$e^+e^- \to \Upsilon(4S)$
• • • We do not use the following data for averages, fits, limits, etc. • • •				
$3.28 \pm 0.40 \pm 0.43$	[3] AUBERT,BE	06B	BABR	Repl. by LEES 12V

[1] LEES 12U uses $E_\gamma > 1.897$ GeV to calculate the moments; the moments are used to calculate the HQET parameters $m_b = 4.579^{+0.032}_{-0.029}$ GeV/c^2 and $\mu_\pi^2 = 0.257^{+0.034}_{-0.039}$ GeV^2 in the shape function model. The same HQET parameters are also determined in the kinetic model.

[2] Results for different E_γ threshold values are also measured.

[3] The result is for $E_\gamma > 1.9$ GeV.

[4] Uses a fully reconstructed B meson as a tag on the recoil side.

$B^{\pm}/B^{0}$ ADMIXTURE REFERENCES

CAO	21A	PR D104 012008	L. Cao et al.	(BELLE Collab.)
CHOUDHURY	21	JHEP 2103 105	S. Choudhury et al.	(BELLE Collab.)
WEHLE	21	PRL 126 161801	S. Wehle et al.	(BELLE Collab.)
AAIJ	20Y	PRL 125 011802	R. Aaij et al.	(LHCb Collab.)
CARIA	20	PRL 124 161803	G. Caria et al.	(BELLE Collab.)
AAIJ	19AD	PR D100 031102	R. Aaij et al.	(LHCb Collab.)
WATANUKI	19	PR D99 032012	S. Watanuki et al.	(BELLE Collab.)
GRYGIER	17	PR D96 091101	J. Grygier et al.	(BELLE Collab.)
HIROSE	17	PRL 118 211801	S. Hirose et al.	(BELLE Collab.)
Also		PR D97 012004	S. Hirose et al.	(BELLE Collab.)
HORIGUCHI	17	PRL 119 191802	T. Horiguchi et al.	(BELLE Collab.)
LEES	17B	PR D95 072001	J.P. Lees et al.	(BABAR Collab.)
AAIJ	16B	JHEP 1602 104	R. Aaij et al.	(LHCb Collab.)
BHARDWAJ	16	PR D93 052016	V. Bhardwaj et al.	(BELLE Collab.)
KHACHATRY...	16D	PL B753 424	V. Khachatryan et al.	(CMS Collab.)
LEES	16	PRL 116 041801	J.P. Lees et al.	(BABAR Collab.)
LEES	16C	PR D93 052015	J.P. Lees et al.	(BABAR Collab.)
SATO	16	PR D93 032008	Y. Sato et al.	(BELLE Collab.)
Also		PR D93 059901 (errat.)	Y. Sato et al.	(BELLE Collab.)
HUSCHLE	15	PR D92 072014	M. Huschle et al.	(BELLE Collab.)
PESANTEZ	15	PRL 114 151601	L. Pesantez et al.	(BELLE Collab.)
SAITO	15	PR D91 052004	T. Saito et al.	(BELLE Collab.)
AAIJ	14AF	PRL 113 141801	R. Aaij et al.	(LHCb Collab.)
AAIJ	14M	JHEP 1406 133	R. Aaij et al.	(LHCb Collab.)
LEES	14D	PRL 112 211802	J.P. Lees et al.	(BABAR Collab.)
LEES	14K	PR D90 092001	J.P. Lees et al.	(BABAR Collab.)
AAIJ	13H	JHEP 1302 105	R. Aaij et al.	(LHCb Collab.)
AAIJ	13Y	JHEP 1308 131	R. Aaij et al.	(LHCb Collab.)
CHATRCHYAN	13BL	PL B727 77	S. Chatrchyan et al.	(CMS Collab.)
LEES	13I	PR D87 112005	J.P. Lees et al.	(BABAR Collab.)
LEES	13M	PR D88 032012	J.P. Lees et al.	(BABAR Collab.)
AAIJ	12AH	JHEP 1207 133	R. Aaij et al.	(LHCb Collab.)
AAIJ	12U	PRL 108 181806	R. Aaij et al.	(LHCb Collab.)
AALTONEN	12I	PRL 108 081807	T. Aaltonen et al.	(CDF Collab.)
LEES	12	PR D85 011102	J.P. Lees et al.	(BABAR Collab.)
LEES	12D	PRL 109 101802	J.P. Lees et al.	(BABAR Collab.)
Also		PR D88 072012	J.P. Lees et al.	(BABAR Collab.)
LEES	12R	PR D86 032004	J.P. Lees et al.	(BABAR Collab.)
LEES	12S	PR D86 032012	J.P. Lees et al.	(BABAR Collab.)
LEES	12U	PR D86 052012	J.P. Lees et al.	(BABAR Collab.)
LEES	12V	PRL 109 191801	J.P. Lees	(BABAR Collab.)
Also		PR D86 112008	J.P. Lees et al.	(BABAR Collab.)
AALTONEN	11AI	PRL 107 201802	T. Aaltonen et al.	(CDF Collab.)
AALTONEN	11L	PRL 106 161801	T. Aaltonen et al.	(CDF Collab.)
DEL-AMO-SA...	11	PR D83 031103	P. del Amo Sanchez et al.	(BABAR Collab.)
GAMBINO	11	JHEP 1109 055	P. Gambino	(LCGT)
AUBERT	10	PRL 104 011802	B. Aubert et al.	(BABAR Collab.)
AUBERT	10A	PR D81 032003	B. Aubert et al.	(BABAR Collab.)
AUSHEV	10	PR D81 031103	T. Aushev et al.	(BELLE Collab.)
DEL-AMO-SA...	10M	PR D82 051101	P. del Amo Sanchez et al.	(BABAR Collab.)
DEL-AMO-SA...	10Q	PR D82 112002	P. del Amo Sanchez et al.	(BABAR Collab.)
NISHIMURA	10	PRL 105 191803	K. Nishimura et al.	(BELLE Collab.)
URQUIJO	10	PRL 104 021801	P. Urquijo et al.	(BELLE Collab.)
AUBERT	09AO	PRL 103 211802	B. Aubert et al.	(BABAR Collab.)
AUBERT	09N	PR D79 031102	B. Aubert et al.	(BABAR Collab.)
AUBERT	09T	PRL 102 091803	B. Aubert et al.	(BABAR Collab.)
Also		EPAPS Document No. E-PRLTAO-102-060910		(BABAR Collab.)
AUBERT	09U	PRL 102 161803	B. Aubert et al.	(BABAR Collab.)
LIMOSANI	09	PRL 103 241801	A. Limosani et al.	(BELLE Collab.)
WEI	09A	PRL 103 171801	J.-T. Wei et al.	(BELLE Collab.)
Also		EPAPS Supplement EPAPS_appendix.pdf		(BELLE Collab.)
AUBERT	08AS	PRL 100 171802	B. Aubert et al.	(BABAR Collab.)
AUBERT	08BC	PR D78 072007	B. Aubert et al.	(BABAR Collab.)
AUBERT	08BH	PR D78 112001	B. Aubert et al.	(BABAR Collab.)
AUBERT	08BJ	PRL 101 171804	B. Aubert et al.	(BABAR Collab.)
AUBERT	08N	PRL 100 021801	B. Aubert et al.	(BABAR Collab.)
Also		PR D79 092002	B. Aubert et al.	(BABAR Collab.)
AUBERT	08O	PR D77 051103	B. Aubert et al.	(BABAR Collab.)
SCHWANDA	08	PR D78 032016	C. Schwanda et al.	(BELLE Collab.)
TANIGUCHI	08	PRL 101 111801	N. Taniguchi et al.	(BELLE Collab.)
WEI	08A	PR D78 011101	J.-T. Wei et al.	(BELLE Collab.)
AUBERT	07AG	PRL 99 051801	B. Aubert et al.	(BABAR Collab.)
AUBERT	07C	PR D75 012003	B. Aubert et al.	(BABAR Collab.)
AUBERT	07E	PRL 98 051802	B. Aubert et al.	(BABAR Collab.)
AUBERT	07L	PRL 98 151802	B. Aubert et al.	(BABAR Collab.)
GAMBINO	07	JHEP 0710 058	P. Gambino et al.	
HUANG	07	PR D75 012002	G.S. Huang et al.	(CLEO Collab.)
SCHWANDA	07	PR D75 032005	C. Schwanda et al.	(BELLE Collab.)
URQUIJO	07	PR D75 032001	P. Urquijo et al.	(BELLE Collab.)
AUBERT	06H	PR D73 012006	B. Aubert et al.	(BABAR Collab.)
AUBERT,B	06J	PR D73 092001	B. Aubert et al.	(BABAR Collab.)
AUBERT,B	06Y	PR D74 091105	B. Aubert et al.	(BABAR Collab.)
AUBERT,BE	06B	PRL 97 171803	B. Aubert et al.	(BABAR Collab.)
BUCHMUEL...	06	PR D73 073008	O.L. Buchmueller, H.U. Flacher	(RHBL)
GOKHROO	06	PRL 97 162002	G. Gokhroo et al.	(BELLE Collab.)
ISHIKAWA	06	PRL 96 251801	A. Ishikawa et al.	(BELLE Collab.)
MOHAPATRA	06	PRL 96 221601	D. Mohapatra et al.	(BELLE Collab.)
ABAZOV	05O	PRL 95 171803	V.M. Abazov et al.	(D0 Collab.)
ACOSTA	05F	PR D71 051103	D. Acosta et al.	(CDF Collab.)
ARTUSO	05B	PRL 95 261801	M. Artuso et al.	(CLEO Collab.)
AUBERT	05	PRL 94 011801	B. Aubert et al.	(BABAR Collab.)
AUBERT,B	05M	PRL 95 142003	B. Aubert et al.	(BABAR Collab.)
AUBERT,B	05R	PR D72 052004	B. Aubert et al.	(BABAR Collab.)
AUBERT,B	05X	PRL 95 111801	B. Aubert et al.	(BABAR Collab.)
Also		PRL 97 019903 (errat.)	B. Aubert et al.	(BABAR Collab.)
CHOI	05	PRL 94 182002	S.-K. Choi et al.	(BELLE Collab.)
IWASAKI	05	PR D72 092005	M. Iwasaki et al.	(BELLE Collab.)
LIMOSANI	05	PL B621 28	A. Limosani et al.	(BELLE Collab.)
MOHAPATRA	05	PR D72 011101	D. Mohapatra et al.	(BELLE Collab.)
NISHIDA	05	PL B610 23	S. Nishida et al.	(BELLE Collab.)
OKABE	05	PL B614 27	T. Okabe et al.	(BELLE Collab.)
ABDALLAH	04D	EPJ C33 213	J. Abdallah et al.	(DELPHI Collab.)
AUBERT	04C	PRL 92 111801	B. Aubert et al.	(BABAR Collab.)
AUBERT	04I	PRL 92 071802	B. Aubert et al.	(BABAR Collab.)
AUBERT	04S	PR D69 052005	B. Aubert et al.	(BABAR Collab.)
AUBERT	04X	PRL 93 011803	B. Aubert et al.	(BABAR Collab.)
AUBERT,B	04	PR D69 111103	B. Aubert et al.	(BABAR Collab.)
AUBERT,B	04A	PR D69 111104	B. Aubert et al.	(BABAR Collab.)
AUBERT,B	04E	PRL 93 021804	B. Aubert et al.	(BABAR Collab.)
AUBERT,B	04F	PRL 93 061801	B. Aubert et al.	(BABAR Collab.)
AUBERT,B	04I	PRL 93 081802	B. Aubert et al.	(BABAR Collab.)
AUBERT,BE	04A	PR D70 112006	B. Aubert et al.	(BABAR Collab.)
CSORNA	04	PR D70 032002	S.E. Csorna et al.	(CLEO Collab.)
KOPPENBURG	04	PRL 93 061803	P. Koppenburg et al.	(BELLE Collab.)
MAHMOOD	04	PR D70 032003	A.H. Mahmodd et al.	(CLEO Collab.)
NAKAO	04	PR D69 112001	M. Nakao et al.	(BELLE Collab.)
NISHIDA	04	PRL 93 031803	S. Nishida et al.	(BELLE Collab.)
ADAM	03B	PR D68 012004	N.E. Adam et al.	(CLEO Collab.)
AUBERT	03	PR D67 031101	B. Aubert et al.	(BABAR Collab.)
AUBERT	03F	PR D67 032002	B. Aubert et al.	(BABAR Collab.)
AUBERT	03U	PRL 91 221802	B. Aubert et al.	(BABAR Collab.)
BONVICINI	03	PR D68 011101	G. Bonvicini et al.	(CLEO Collab.)
HUANG	03	PRL 91 241802	H.-C. Huang et al.	(BELLE Collab.)
ISHIKAWA	03	PRL 91 261601	A. Ishikawa et al.	(BELLE Collab.)
KANEKO	03	PRL 90 021801	J. Kaneko et al.	(BELLE Collab.)
KROKOVNY	03B	PRL 91 262002	P. Krokovny et al.	(BELLE Collab.)
MAHMOOD	03	PR D67 072001	A.H. Mahmood et al.	(CLEO Collab.)
ABE	02	PRL 88 021801	K. Abe et al.	(BELLE Collab.)
ABE	02L	PRL 89 011803	K. Abe et al.	(BELLE Collab.)
ABE	02Y	PL B547 181	K. Abe et al.	(BELLE Collab.)
ANDERSON	02	PRL 89 282001	S. Anderson et al.	(CLEO Collab.)
AUBERT	02C	PRL 88 101805	B. Aubert et al.	(BABAR Collab.)
AUBERT	02G	PR D65 091104	B. Aubert et al.	(BABAR Collab.)
AUBERT	02L	PRL 88 241801	B. Aubert et al.	(BABAR Collab.)
BORNHEIM	02	PRL 88 231803	A. Bornheim et al.	(CLEO Collab.)
EDWARDS	02B	PR D65 111102	K.W. Edwards et al.	(CLEO Collab.)
ABE	01F	PL B511 151	K. Abe et al.	(BELLE Collab.)
ABE	01J	PR D64 072001	K. Abe et al.	(BELLE Collab.)
ANDERSON	01B	PRL 87 181803	S. Anderson et al.	(CLEO Collab.)
CHEN	01	PR D63 031102	S. Chen et al.	(CLEO Collab.)
CHEN	01C	PRL 87 251807	S. Chen et al.	(CLEO Collab.)
COAN	01	PRL 86 5661	T.E. Coan et al.	(CLEO Collab.)
CRONIN-HEN...	01B	PRL 87 251808	D. Cronin-Hennessy et al.	(CLEO Collab.)
PDG	01	Unofficial 2001 WWW edition		
ABREU	00R	PL B475 407	P. Abreu et al.	(DELPHI Collab.)
COAN	00	PRL 84 5283	T.E. Coan et al.	(CLEO Collab.)
RICHICHI	00	PRL 85 520	S.J. Richichi et al.	(CLEO Collab.)
BARATE	98Q	EPJ C4 387	R. Barate et al.	(ALEPH Collab.)
BERGFELD	98	PRL 81 272	T. Bergfeld et al.	(CLEO Collab.)
BISHAI	98	PR D57 3847	M. Bishai et al.	(CLEO Collab.)
BONVICINI	98	PR D57 6604	G. Bonvicini et al.	(CLEO Collab.)
BROWDER	98	PRL 81 1786	T.E. Browder et al.	(CLEO Collab.)
COAN	98	PRL 80 1150	T.E. Coan et al.	(CLEO Collab.)
GLENN	98	PRL 80 2289	S. Glenn et al.	(CLEO Collab.)
ACKERSTAFF	97N	ZPHY C74 423	K. Ackerstaff et al.	(OPAL Collab.)
AMMAR	97	PR D55 13	R. Ammar et al.	(CLEO Collab.)
BARISH	97	PRL 79 3599	B. Barish et al.	(CLEO Collab.)
BUSKULIC	97B	ZPHY C73 601	D. Buskulic et al.	(ALEPH Collab.)
GIBBONS	97B	PR D56 3783	L. Gibbons et al.	(CLEO Collab.)
ALBRECHT	96D	PL B374 256	H. Albrecht et al.	(ARGUS Collab.)
BARISH	96B	PRL 76 1570	B.C. Barish et al.	(CLEO Collab.)
GIBAUT	96	PR D53 4734	D. Gibaut et al.	(CLEO Collab.)
KUBOTA	96	PR D53 6033	Y. Kubota et al.	(CLEO Collab.)
PDG	96	PR D54 1	R. M. Barnett et al.	(PDG Collab.)
ALAM	95	PRL 74 2885	M.S. Alam et al.	(CLEO Collab.)
ALBRECHT	95D	PL B353 554	H. Albrecht et al.	(ARGUS Collab.)
BALEST	95B	PR D52 2661	R. Balest et al.	(CLEO Collab.)
BARISH	95	PR D51 1014	B.C. Barish et al.	(CLEO Collab.)
BUSKULIC	95B	PL B345 103	D. Buskulic et al.	(ALEPH Collab.)
ALBRECHT	94C	ZPHY C62 371	H. Albrecht et al.	(ARGUS Collab.)
ALBRECHT	94J	ZPHY C61 1	H. Albrecht et al.	(ARGUS Collab.)
PROCARIO	94	PRL 73 1472	M. Procario et al.	(CLEO Collab.)
ALBRECHT	93	ZPHY C57 533	H. Albrecht et al.	(ARGUS Collab.)
ALBRECHT	93E	ZPHY C60 11	H. Albrecht et al.	(ARGUS Collab.)
ALBRECHT	93H	PL B318 397	H. Albrecht et al.	(ARGUS Collab.)
ALBRECHT	93I	ZPHY C58 191	H. Albrecht et al.	(ARGUS Collab.)
ALEXANDER	93B	PL B319 365	J. Alexander et al.	(CLEO Collab.)
ARTUSO	93	PL B311 307	M. Artuso	(SYRA)
BARTELT	93B	PRL 71 4111	J.E. Bartelt et al.	(CLEO Collab.)
ALBRECHT	92E	PL B277 209	H. Albrecht et al.	(ARGUS Collab.)
ALBRECHT	92G	ZPHY C54 1	H. Albrecht et al.	(ARGUS Collab.)
ALBRECHT	92O	ZPHY C56 1	H. Albrecht et al.	(ARGUS Collab.)
BORTOLETTO	92	PR D45 21	D. Bortoletto et al.	(CLEO Collab.)
CRAWFORD	92	PR D45 752	G. Crawford et al.	(CLEO Collab.)
HENDERSON	92	PR D45 2212	S. Henderson et al.	(CLEO Collab.)
LESIAK	92	ZPHY C55 33	T. Lesiak et al.	(Crystal Ball Collab.)
ALBRECHT	91C	PL B255 297	H. Albrecht et al.	(ARGUS Collab.)
ALBRECHT	91H	ZPHY C52 353	H. Albrecht et al.	(ARGUS Collab.)
FULTON	91	PR D43 651	R. Fulton et al.	(CLEO Collab.)
YANAGISAWA	91	PRL 66 2436	C. Yanagisawa et al.	(CUSB II Collab.)
ALBRECHT	90	PL B234 409	H. Albrecht et al.	(ARGUS Collab.)
ALBRECHT	90H	PL B249 359	H. Albrecht et al.	(ARGUS Collab.)
BORTOLETTO	90	PRL 64 2117	D. Bortoletto et al.	(CLEO Collab.)
Also		PR D45 21	D. Bortoletto et al.	(CLEO Collab.)
FULTON	90	PRL 64 16	R. Fulton et al.	(CLEO Collab.)
MASCHMANN	90	ZPHY C46 555	W.S. Maschmann et al.	(Crystal Ball Collab.)
PDG	90	PL B239 1	J.J. Hernandez et al.	(IFIC, BOST, CIT+)
ALBRECHT	89K	ZPHY C42 519	H. Albrecht et al.	(ARGUS Collab.)
ISGUR	89B	PR D39 799	N. Isgur et al.	(TNTO, CIT)
WACHS	89	ZPHY C42 33	K. Wachs et al.	(Crystal Ball Collab.)
ALBRECHT	88E	PL B210 263	H. Albrecht et al.	(ARGUS Collab.)
ALBRECHT	88H	PL B210 258	H. Albrecht et al.	(ARGUS Collab.)
KOERNER	88	ZPHY C38 511	J.G. Korner, G.A. Schuler	(MAINZ, DESY)
ALAM	87	PRL 59 22	M.S. Alam et al.	(CLEO Collab.)
ALAM	87B	PRL 58 1814	M.S. Alam et al.	(CLEO Collab.)
ALBRECHT	87D	PL B199 451	H. Albrecht et al.	(ARGUS Collab.)
ALBRECHT	87H	PL B187 425	H. Albrecht et al.	(ARGUS Collab.)
BEAN	87	PR D35 3533	A. Bean et al.	(CLEO Collab.)
BEHRENDS	87	PRL 59 407	S. Behrends et al.	(CLEO Collab.)
BORTOLETTO	87	PR D35 19	D. Bortoletto et al.	(CLEO Collab.)
ALAM	86	PR D34 3279	M.S. Alam et al.	(CLEO Collab.)
BALTRUSAIT...	86E	PRL 56 2140	R.M. Baltrusaitis et al.	(Mark III Collab.)

Downloaded from https://academic.oup.com/ptep/article/2022/8/083C01/6651666 by KIT Library user on 27 September 2022

BORTOLETTO	86	PRL 56 800	D. Bortoletto *et al.*	(CLEO Collab.)
HAAS	86	PRL 56 2781	J. Haas *et al.*	(CLEO Collab.)
ALBRECHT	85H	PL 162B 395	H. Albrecht *et al.*	(ARGUS Collab.)
CSORNA	85	PRL 54 1894	S.E. Csorna *et al.*	(CLEO Collab.)
HAAS	85	PRL 55 1248	J. Haas *et al.*	(CLEO Collab.)
AVERY	84	PRL 53 1309	P. Avery *et al.*	(CLEO Collab.)
CHEN	84	PRL 52 1084	A. Chen *et al.*	(CLEO Collab.)
LEVMAN	84	PL 141B 271	G.M. Levman *et al.*	(CUSB Collab.)
ALAM	83B	PRL 51 1143	M.S. Alam *et al.*	(CLEO Collab.)
GREEN	83	PRL 51 347	J. Green *et al.*	(CLEO Collab.)
KLOPFEN...	83B	PL 130B 444	C. Klopfenstein *et al.*	(CUSB Collab.)
ALTARELLI	82	NP B208 365	G. Altarelli *et al.*	(ROMA, INFN, FRAS)
BRODY	82	PRL 48 1070	A.D. Brody *et al.*	(CLEO Collab.)
GIANNINI	82	NP B206 1	G. Giannini *et al.*	(CUSB Collab.)
BEBEK	81	PRL 46 84	C. Bebek *et al.*	(CLEO Collab.)
CHADWICK	81	PRL 46 88	K. Chadwick *et al.*	(CLEO Collab.)
ABRAMS	80	PRL 44 10	G.S. Abrams *et al.*	(SLAC, LBL)

$B^{\pm}/B^0/B^0_s/b$-baryon ADMIXTURE

$B^{\pm}/B^0/B^0_s/b$-baryon ADMIXTURE MEAN LIFE

Each measurement of the B mean life is an average over an admixture of various bottom mesons and baryons which decay weakly. Different techniques emphasize different admixtures of produced particles, which could result in a different B mean life.

"OUR EVALUATION" is an average using rescaled values of the data listed below. The average and rescaling were performed by the Heavy Flavor Averaging Group (HFLAV) and are described at https://hflav.web.cern.ch/. This is a weighted average of the lifetimes of the five main b-hadron species (B^+, B^0, B^0_{sH}, B^0_{sL}, and Λ_b) that assumes the production fractions in Z decays (given at the end of this section) and equal production fractions of B^0_{sH} and B^0_{sL} mesons.

VALUE (10^{-12} s)	EVTS	DOCUMENT ID		TECN	COMMENT
1.5672±0.0029 OUR EVALUATION					
• • • We do not use the following data for averages, fits, limits, etc. • • •					
1.570 ±0.005 ±0.008		[1] ABDALLAH	04E	DLPH	$e^+e^- \to Z$
1.533 $^{+0.035}_{-0.031}$		[2] ABE	98B	CDF	$p\overline{p}$ at 1.8 TeV
1.549 ±0.009 ±0.015		[3] ACCIARRI	98	L3	$e^+e^- \to Z$
1.611 ±0.010 ±0.027		[4] ACKERSTAFF	97F	OPAL	$e^+e^- \to Z$
1.582 ±0.011 ±0.027		[4] ABREU	96E	DLPH	$e^+e^- \to Z$
1.575 ±0.010 ±0.026		[5] ABREU	96E	DLPH	$e^+e^- \to Z$
1.533 ±0.013 ±0.022	29.8k	[6] BUSKULIC	96F	ALEP	$e^+e^- \to Z$
1.564 ±0.030 ±0.036		[7] ABE,K	95B	SLD	$e^+e^- \to Z$
1.542 ±0.021 ±0.045		[8] ABREU	94L	DLPH	$e^+e^- \to Z$
1.50 $^{+0.24}_{-0.21}$ ±0.03		[9] ABREU	94P	DLPH	$e^+e^- \to Z$
1.46 ±0.06 ±0.06	5344	[10] ABE	93J	CDF	Repl. by ABE 98B
1.23 $^{+0.14}_{-0.13}$ ±0.15	188	[11] ABREU	93D	DLPH	Sup. by ABREU 94L
1.49 ±0.11 ±0.12	253	[12] ABREU	93G	DLPH	Sup. by ABREU 94L
1.51 $^{+0.16}_{-0.14}$ ±0.11	130	[13] ACTON	93C	OPAL	$e^+e^- \to Z$
1.523 ±0.034 ±0.036	5372	[14] ACTON	93L	OPAL	$e^+e^- \to Z$
1.535 ±0.035 ±0.028	7357	[14] ADRIANI	93K	L3	Repl. by ACCIARRI 98
1.511 ±0.022 ±0.078		[15] BUSKULIC	93O	ALEP	$e^+e^- \to Z$
1.28 ±0.10		[16] ABREU	92	DLPH	Sup. by ABREU 94L
1.37 ±0.07 ±0.06	1354	[17] ACTON	92	OPAL	Sup. by ACTON 93L
1.49 ±0.03 ±0.06		[18] BUSKULIC	92F	ALEP	Sup. by BUSKULIC 96F
1.35 $^{+0.19}_{-0.17}$ ±0.05		[19] BUSKULIC	92G	ALEP	$e^+e^- \to Z$
1.32 ±0.08 ±0.09	1386	[20] ADEVA	91H	L3	Sup. by ADRIANI 93K
1.32 $^{+0.31}_{-0.25}$ ±0.15	37	[21] ALEXANDER	91G	OPAL	$e^+e^- \to Z$
1.29 ±0.06 ±0.10	2973	[22] DECAMP	91C	ALEP	Sup. by BUSKULIC 92F
1.36 $^{+0.25}_{-0.23}$		[23] HAGEMANN	90	JADE	E^{ee}_{cm}= 35 GeV
1.13 ±0.15		[24] LYONS	90	RVUE	
1.35 ±0.10 ±0.24		BRAUNSCH...	89B	TASS	E^{ee}_{cm}= 35 GeV
0.98 ±0.12 ±0.13		ONG	89	MRK2	E^{ee}_{cm}= 29 GeV
1.17 $^{+0.27}_{-0.22}$ $^{+0.17}_{-0.16}$		KLEM	88	DLCO	E^{ee}_{cm}= 29 GeV
1.29 ±0.20 ±0.21		[25] ASH	87	MAC	E^{ee}_{cm}= 29 GeV
1.02 $^{+0.42}_{-0.39}$	301	[26] BROM	87	HRS	E^{ee}_{cm}= 29 GeV

[1] Measurement performed using an inclusive reconstruction and B flavor identification technique.
[2] Measured using inclusive $J/\psi(1S) \to \mu^+\mu^-$ vertex.
[3] ACCIARRI 98 uses inclusively reconstructed secondary vertex and lepton impact parameter.
[4] ACKERSTAFF 97F uses inclusively reconstructed secondary vertices.
[5] Combines ABREU 96E secondary vertex result with ABREU 94L impact parameter result.
[6] BUSKULIC 96F analyzed using 3D impact parameter.
[7] ABE,K 95B uses an inclusive topological technique.
[8] ABREU 94L uses charged particle impact parameters. Their result from inclusively reconstructed secondary vertices is superseded by ABREU 96E.
[9] From proper time distribution of $b \to J/\psi(1S)$ anything.
[10] ABE 93J analyzed using $J/\psi(1S) \to \mu\mu$ vertices.
[11] ABREU 93D data analyzed using $D/D^*\ell$ anything event vertices.
[12] ABREU 93G data analyzed using charged and neutral vertices.
[13] ACTON 93C analysed using $D/D^*\ell$ anything event vertices.
[14] ACTON 93L and ADRIANI 93K analyzed using lepton (e and μ) impact parameter at Z.
[15] BUSKULIC 93O analyzed using dipole method.
[16] ABREU 92 is combined result of muon and hadron impact parameter analyses. Hadron tracks gave $(12.7 \pm 0.4 \pm 1.2) \times 10^{-13}$ s for an admixture of B species weighted by production fraction and mean charge multiplicity, while muon tracks gave $(13.0 \pm 1.0 \pm 0.8) \times 10^{-13}$ s for an admixture weighted by production fraction and semileptonic branching fraction.
[17] ACTON 92 is combined result of muon and electron impact parameter analyses.
[18] BUSKULIC 92F uses the lepton impact parameter distribution for data from the 1991 run.
[19] BUSKULIC 92G use $J/\psi(1S)$ tags to measure the average b lifetime. This is comparable to other methods only if the $J/\psi(1S)$ branching fractions of the different b-flavored hadrons are in the same ratio.
[20] Using $Z \to e^+X$ or μ^+X, ADEVA 91H determined the average lifetime for an admixture of B hadrons from the impact parameter distribution of the lepton.
[21] Using $Z \to J/\psi(1S)X$, $J/\psi(1S) \to \ell^+\ell^-$, ALEXANDER 91G determined the average lifetime for an admixture of B hadrons from the decay point of the $J/\psi(1S)$.
[22] Using $Z \to eX$ or μX, DECAMP 91C determines the average lifetime for an admixture of B hadrons from the signed impact parameter distribution of the lepton.
[23] HAGEMANN 90 uses electrons and muons in an impact parameter analysis.
[24] LYONS 90 combine the results of the B lifetime measurements of ONG 89, BRAUNSCHWEIG 89B, KLEM 88, and ASH 87, and JADE data by private communication. They use statistical techniques which include variation of the error with the mean life, and possible correlations between the systematic errors. This result is not independent of the measured results used in our average.
[25] We have combined an overall scale error of 15% in quadrature with the systematic error of ±0.7 to obtain ±2.1 systematic error.
[26] Statistical and systematic errors were combined by BROM 87.

CHARGED b-HADRON ADMIXTURE MEAN LIFE

VALUE (10^{-12} s)	DOCUMENT ID		TECN	COMMENT
1.72±0.08±0.06	[1] ADAM	95	DLPH	$e^+e^- \to Z$

[1] ADAM 95 data analyzed using vertex-charge technique to tag b-hadron charge.

NEUTRAL b-HADRON ADMIXTURE MEAN LIFE

VALUE (10^{-12} s)	DOCUMENT ID		TECN	COMMENT
1.58±0.11±0.09	[1] ADAM	95	DLPH	$e^+e^- \to Z$

[1] ADAM 95 data analyzed using vertex-charge technique to tag b-hadron charge.

MEAN LIFE RATIO $\tau_{\text{charged } b\text{-hadron}}/\tau_{\text{neutral } b\text{-hadron}}$

VALUE	DOCUMENT ID		TECN	COMMENT
$1.09^{+0.11}_{-0.10}$±0.08	[1] ADAM	95	DLPH	$e^+e^- \to Z$

[1] ADAM 95 data analyzed using vertex-charge technique to tag b-hadron charge.

$|\Delta\tau_b|/\tau_{b,\overline{b}}$

$\tau_{b,\overline{b}}$ and $|\Delta\tau_b|$ are the mean life average and difference between b and $\overline{b}$ hadrons.

VALUE	DOCUMENT ID		TECN	COMMENT
−0.001±0.012±0.008	[1] ABBIENDI	99J	OPAL	$e^+e^- \to Z$

[1] Data analyzed using both the jet charge and the charge of secondary vertex in the opposite hemisphere.

$\overline{b}$ PRODUCTION FRACTIONS AND DECAY MODES

The branching fraction measurements are for an admixture of B mesons and baryons at energies above the $\Upsilon(4S)$. Only the highest energy results (LHC, LEP, Tevatron, $Sp\overline{p}S$) are used in the branching fraction averages. In the following, we assume that the production fractions are the same at the LHC, LEP, and at the Tevatron.

For inclusive branching fractions, *e.g.*, $B \to D^{\pm}$ anything, the values usually are multiplicities, not branching fractions. They can be greater than one.

The modes below are listed for a $\overline{b}$ initial state. b modes are their charge conjugates. Reactions indicate the weak decay vertex and do not include mixing.

Mode	Fraction (Γ_i/Γ)	Scale factor/ Confidence level

Downloaded from https://academic.oup.com/ptep/article/2022/8/083C01/6651666 by KIT Library user on 27 September 2022

PRODUCTION FRACTIONS

The production fractions for weakly decaying b-hadrons at high energy have been calculated from the best values of mean lives, mixing parameters, and branching fractions in this edition by the Heavy Flavor Averaging Group (HFLAV) as described in the note "B^0-$\overline{B}^0$ Mixing" in the B^0 Particle Listings. We no longer provide world averages of the b-hadron production fractions, where results from LEP, Tevatron and LHC are averaged together; indeed the available data (from CDF and LHCb) shows that the fractions depend on the kinematics (in particular the p_T) of the produced b hadron. Hence we would like to list the fractions in Z decays instead, which are well-defined physics observables. The production fractions in $p\overline{p}$ collisions at the Tevatron are also listed at the end of the section. Values assume

$$B(\overline{b} \to B^+) = B(\overline{b} \to B^0)$$
$$B(\overline{b} \to B^+) + B(\overline{b} \to B^0) + B(\overline{b} \to B^0_s) + B(b \to b\text{-baryon}) = 100\%.$$

The correlation coefficients between production fractions are also reported:

$$cor(B^0_s, b\text{-baryon}) = 0.064$$
$$cor(B^0_s, B^{\pm}{=}B^0) = -0.633$$
$$cor(b\text{-baryon}, B^{\pm}{=}B^0) = -0.813.$$

The notation for production fractions varies in the literature (f_d, d_{B^0}, $f(b \to \overline{B}^0)$, $Br(b \to \overline{B}^0)$). We use our own branching fraction notation here, $B(\overline{b} \to B^0)$.

Note these production fractions are b-hadronization fractions, not the conventional branching fractions of b-quark to a B-hadron, which may have considerable dependence on the initial and final state kinematic and production environment.

Γ_1	B^+		(40.8 ± 0.7) %
Γ_2	B^0		(40.8 ± 0.7) %
Γ_3	B^0_s		(10.0 ± 0.8) %
Γ_4	B^+_c		
Γ_5	b-baryon		(8.4 ± 1.1) %

DECAY MODES

Semileptonic and leptonic modes

Γ_6	ν anything		(23.1 ± 1.5) %	
Γ_7	$\ell^+ \nu_\ell$ anything	[a]	(10.69 ± 0.22) %	
Γ_8	$e^+ \nu_e$ anything		(10.86 ± 0.35) %	
Γ_9	$\mu^+ \nu_\mu$ anything		($10.95^{+0.29}_{-0.25}$) %	
Γ_{10}	$D^- \ell^+ \nu_\ell$ anything	[a]	(2.2 ± 0.4) %	S=1.9
Γ_{11}	$D^- \pi^+ \ell^+ \nu_\ell$ anything		(4.9 ± 1.9) $\times 10^{-3}$	
Γ_{12}	$D^- \pi^- \ell^+ \nu_\ell$ anything		(2.6 ± 1.6) $\times 10^{-3}$	
Γ_{13}	$\overline{D}^0 \ell^+ \nu_\ell$ anything	[a]	(6.79 ± 0.34) %	
Γ_{14}	$\overline{D}^0 \pi^- \ell^+ \nu_\ell$ anything		(1.07 ± 0.27) %	
Γ_{15}	$\overline{D}^0 \pi^+ \ell^+ \nu_\ell$ anything		(2.3 ± 1.6) $\times 10^{-3}$	
Γ_{16}	$D^{*-} \ell^+ \nu_\ell$ anything	[a]	(2.75 ± 0.19) %	
Γ_{17}	$D^{*-} \pi^- \ell^+ \nu_\ell$ anything		(6 ± 7) $\times 10^{-4}$	
Γ_{18}	$D^{*-} \pi^+ \ell^+ \nu_\ell$ anything		(4.8 ± 1.0) $\times 10^{-3}$	
Γ_{19}	$\overline{D}^0_j \ell^+ \nu_\ell$ anything × $B(\overline{D}^0_j \to D^{*+} \pi^-)$	[a,b]	(2.6 ± 0.9) $\times 10^{-3}$	
Γ_{20}	$D^-_j \ell^+ \nu_\ell$ anything × $B(D^-_j \to D^0 \pi^-)$	[a,b]	(7.0 ± 2.3) $\times 10^{-3}$	
Γ_{21}	$\overline{D}^*_2(2460)^0 \ell^+ \nu_\ell$ anything × $B(\overline{D}^*_2(2460)^0 \to D^{*-} \pi^+)$		< 1.4 $\times 10^{-3}$	CL=90%
Γ_{22}	$D^*_2(2460)^- \ell^+ \nu_\ell$ anything × $B(D^*_2(2460)^- \to D^0 \pi^-)$		($4.2^{+1.5}_{-1.8}$) $\times 10^{-3}$	
Γ_{23}	$\overline{D}^*_2(2460)^0 \ell^+ \nu_\ell$ anything × $B(\overline{D}^*_2(2460)^0 \to D^- \pi^+)$		(1.6 ± 0.8) $\times 10^{-3}$	
Γ_{24}	charmless $\ell \overline{\nu}_\ell$	[a]	(1.7 ± 0.5) $\times 10^{-3}$	
Γ_{25}	$\tau^+ \nu_\tau$ anything		(2.41 ± 0.23) %	
Γ_{26}	$D^{*-} \tau \nu_\tau$ anything		(9 ± 4) $\times 10^{-3}$	
Γ_{27}	$\overline{c} \to \ell^- \overline{\nu}_\ell$ anything	[a]	(8.02 ± 0.19) %	
Γ_{28}	$c \to \ell^+ \nu$ anything		($1.6^{+0.4}_{-0.5}$) %	

Charmed meson and baryon modes

Γ_{29}	$\overline{D}^0$ anything		(58.7 ± 2.8) %	
Γ_{30}	$D^0 D^{\pm}_s$ anything	[c]	($9.1^{+4.0}_{-2.8}$) %	
Γ_{31}	$D^{\mp} D^{\pm}_s$ anything	[c]	($4.0^{+2.3}_{-1.8}$) %	
Γ_{32}	$\overline{D}^0 D^0$ anything	[c]	($5.1^{+2.0}_{-1.8}$) %	
Γ_{33}	$D^0 D^{\pm}$ anything	[c]	($2.7^{+1.8}_{-1.6}$) %	
Γ_{34}	$D^{\pm} D^{\mp}$ anything	[c]	< 9 $\times 10^{-3}$	CL=90%
Γ_{35}	D^0 anything			
Γ_{36}	D^+ anything			
Γ_{37}	D^- anything		(22.7 ± 1.6) %	
Γ_{38}	$D^*(2010)^+$ anything		(17.3 ± 2.0) %	
Γ_{39}	$D_1(2420)^0$ anything		(5.0 ± 1.5) %	
Γ_{40}	$D^*(2010)^{\mp} D^{\pm}_s$ anything	[c]	($3.3^{+1.6}_{-1.3}$) %	
Γ_{41}	$D^0 D^*(2010)^{\pm}$ anything	[c]	($3.0^{+1.1}_{-0.9}$) %	
Γ_{42}	$D^*(2010)^{\pm} D^{\mp}$ anything	[c]	($2.5^{+1.2}_{-1.0}$) %	
Γ_{43}	$D^*(2010)^{\pm} D^*(2010)^{\mp}$ anything	[c]	(1.2 ± 0.4) %	
Γ_{44}	$\overline{D} D$ anything		(10^{+11}_{-10}) %	
Γ_{45}	$D^*_2(2460)^0$ anything		(4.7 ± 2.7) %	
Γ_{46}	D^-_s anything		(14.7 ± 2.1) %	
Γ_{47}	D^+_s anything		(10.1 ± 3.1) %	
Γ_{48}	Λ^+_c anything		(7.7 ± 1.1) %	
Γ_{49}	$\overline{c}/c$ anything	[d]	(116.2 ± 3.2) %	

Charmonium modes

Γ_{50}	$J/\psi(1S)$ anything		(1.16 ± 0.10) %	
Γ_{51}	$\psi(2S)$ anything		(3.06 ± 0.30) $\times 10^{-3}$	
Γ_{52}	$\chi_{c0}(1P)$ anything		(1.5 ± 0.6) %	
Γ_{53}	$\chi_{c1}(1P)$ anything		(1.4 ± 0.4) %	
Γ_{54}	$\chi_{c2}(1P)$ anything		(6.2 ± 2.9) $\times 10^{-3}$	
Γ_{55}	$\chi_c(2P)$ anything, $\chi_c \to \phi\phi$		< 2.8 $\times 10^{-7}$	CL=95%
Γ_{56}	$\eta_c(1S)$ anything		(5.6 ± 0.9) $\times 10^{-3}$	
Γ_{57}	$\eta_c(2S)$ anything, $\eta_c \to \phi\phi$		(3.9 ± 1.4) $\times 10^{-7}$	
Γ_{58}	$\chi_{c1}(3872)$ anything, $\chi_{c1} \to \phi\phi$		< 4.5 $\times 10^{-7}$	CL=95%
Γ_{59}	$\chi_{c0}(3915)$ anything, $\chi_{c0} \to \phi\phi$		< 3.1 $\times 10^{-7}$	CL=95%

K or K^* modes

Γ_{60}	$\overline{s}\gamma$		(3.1 ± 1.1) $\times 10^{-4}$	
Γ_{61}	$\overline{s}\overline{\nu}\nu$	B1	< 6.4 $\times 10^{-4}$	CL=90%
Γ_{62}	$K^{\pm}$ anything		(74 ± 6) %	
Γ_{63}	K^0_S anything		(29.0 ± 2.9) %	

Pion modes

Γ_{64}	$\pi^{\pm}$ anything		(397 ± 21) %	
Γ_{65}	π^0 anything	[d]	(278 ± 60) %	
Γ_{66}	ϕ anything		(2.82 ± 0.23) %	

Baryon modes

Γ_{67}	$p/\overline{p}$ anything		(13.1 ± 1.1) %	
Γ_{68}	$\Lambda/\overline{\Lambda}$ anything		(5.9 ± 0.6) %	
Γ_{69}	b-baryon anything		(10.2 ± 2.8) %	
Γ_{70}	$\overline{\Lambda}^0_b$ anything			
Γ_{71}	Ξ^+_b anything			

Other modes

Γ_{72}	charged anything	[d]	(497 ± 7) %	
Γ_{73}	hadron$^+$ hadron$^-$		($1.7^{+1.0}_{-0.7}$) $\times 10^{-5}$	
Γ_{74}	charmless		(7 ± 21) $\times 10^{-3}$	

$\Delta B = 1$ weak neutral current ($B1$) modes

Γ_{75}	$e^+ e^-$ anything			
Γ_{76}	$\mu^+ \mu^-$ anything	B1	< 3.2 $\times 10^{-4}$	CL=90%
Γ_{77}	$\nu\overline{\nu}$ anything			

[a] An ℓ indicates an e or a μ mode, not a sum over these modes.

[b] D_j represents an unresolved mixture of pseudoscalar and tensor D^{**} (P-wave) states.

[c] The value is for the sum of the charge states or particle/antiparticle states indicated.

[d] Inclusive branching fractions have a multiplicity definition and can be greater than 100%.

Downloaded from https://academic.oup.com/ptep/article/2022/8/083C01/6651666 by KIT Library user on 27 September 2022

$B^{\pm}/B^0/B^0_s/b$-baryon ADMIXTURE BRANCHING RATIOS

$\Gamma(B^+)/\Gamma_{total}$ — Γ_1/Γ

"OUR EVALUATION" is an average from Z decay obtained by the Heavy Flavor Averaging Group (HFLAV) as described at https://hflav.web.cern.ch/.

VALUE	DOCUMENT ID		TECN	COMMENT
0.408 ±0.007 OUR EVALUATION				
0.4099±0.0082±0.0111	[1] ABDALLAH	03K	DLPH	$e^+e^- \to Z$

[1] The analysis is based on a neural network, to estimate the charge of the weakly-decaying b hadron by distinguishing its decay products from particles produced at the primary vertex.

$\Gamma(B^+)/\Gamma(B^0)$ — Γ_1/Γ_2

VALUE	DOCUMENT ID		TECN	COMMENT
$1.054\pm0.018^{+0.062}_{-0.074}$	AALTONEN	08N	CDF	$p\overline{p}$ at 1.96 TeV

$\Gamma(B^0_s)/\Gamma(B^+)$ — Γ_3/Γ_1

VALUE	DOCUMENT ID		TECN	COMMENT
• • • We do not use the following data for averages, fits, limits, etc. • • •				
$0.121\pm0.002\pm0.005$	[1,2] AAIJ	20V	LHCB	pp at 7 TeV
$0.124\pm0.002\pm0.005$	[1,3] AAIJ	20V	LHCB	pp at 8 TeV
$0.130\pm0.002\pm0.005$	[1,4,5] AAIJ	20V	LHCB	pp at 13 TeV

[1] AAIJ 20V measures the average value using the observed $B^0_s \to J/\psi\phi$ and $B^+ \to J/\psi K^+$ yields, over the ranges b-hadron p_T of 0.5 and 40 GeV and η of 2.0 and 6.5. The value is not used in averages as BR-related systematic uncertainties are not evaluated.

[2] AAIJ 20V reports $[\Gamma(\overline{b} \to B^0_s)/\Gamma(\overline{b} \to B^+)] \times [B(B^0_s \to J/\psi(1S)\phi)] / [B(B^+ \to J/\psi(1S)K^+)] = 0.1238 \pm 0.0010 \pm 0.0022$ which we multiply or divide by our best values $B(B^0_s \to J/\psi(1S)\phi) = (1.04 \pm 0.04) \times 10^{-3}$, $B(B^+ \to J/\psi(1S)K^+) = (1.020 \pm 0.019) \times 10^{-3}$. Our first error is their experiment's error and our second error is the systematic error from using our best values.

[3] AAIJ 20V reports $[\Gamma(\overline{b} \to B^0_s)/\Gamma(\overline{b} \to B^+)] \times [B(B^0_s \to J/\psi(1S)\phi)] / [B(B^+ \to J/\psi(1S)K^+)] = 0.1270 \pm 0.0007 \pm 0.0022$ which we multiply or divide by our best values $B(B^0_s \to J/\psi(1S)\phi) = (1.04 \pm 0.04) \times 10^{-3}$, $B(B^+ \to J/\psi(1S)K^+) = (1.020 \pm 0.019) \times 10^{-3}$. Our first error is their experiment's error and our second error is the systematic error from using our best values.

[4] AAIJ 20V reports the results in two different data sets, and we quote here the weighted average.

[5] AAIJ 20V reports $[\Gamma(\overline{b} \to B^0_s)/\Gamma(\overline{b} \to B^+)] \times [B(B^0_s \to J/\psi(1S)\phi)] / [B(B^+ \to J/\psi(1S)K^+)] = 0.1326 \pm 0.0007 \pm 0.0023$ which we multiply or divide by our best values $B(B^0_s \to J/\psi(1S)\phi) = (1.04 \pm 0.04) \times 10^{-3}$, $B(B^+ \to J/\psi(1S)K^+) = (1.020 \pm 0.019) \times 10^{-3}$. Our first error is their experiment's error and our second error is the systematic error from using our best values.

$\Gamma(B^0_s)/[\Gamma(B^+)+\Gamma(B^0)]$ — $\Gamma_3/(\Gamma_1+\Gamma_2)$

"OUR EVALUATION" is an average from Z decay obtained by the Heavy Flavor Averaging Group (HFLAV) as described at https://hflav.web.cern.ch/.

VALUE	DOCUMENT ID		TECN	COMMENT
0.1230±0.0115 OUR EVALUATION				
• • • We do not use the following data for averages, fits, limits, etc. • • •				
0.122 ± 0.006	[1] AAIJ	19AD	LHCB	pp at 13 TeV
$0.134 \pm0.004 ^{+0.011}_{-0.010}$	[2] AAIJ	12J	LHCB	pp at 7 TeV
$0.1265\pm0.0085\pm0.0131$	[3] AAIJ	11F	LHCB	pp at 7 TeV
$0.128 ^{+0.011}_{-0.010} \pm0.011$	[4] AALTONEN	08N	CDF	$p\overline{p}$ at 1.96 TeV
0.213 ± 0.068	[5] AFFOLDER	00E	CDF	$p\overline{p}$ at 1.8 TeV
$0.21 \pm0.036 ^{+0.038}_{-0.030}$	[6] ABE	99P	CDF	$\overline{p}p$ at 1.8 TeV

[1] AAIJ 19AD measured the average value using b-hadron semileptonic decays and assuming isospin symmetry for b-hadron p_T of 4 and 25 GeV and η of 2 and 5.

[2] AAIJ 12J measured this value using b-hadron semileptonic decays and assuming isospin symmetry.

[3] AAIJ 11F measured $f_s/f_d = 0.253 \pm 0.017 \pm 0.017 \pm 0.020$, where the errors are statistical, systematic, and theoretical. We divide their value by 2. Our second error combines systematic and theoretical uncertainties.

[4] AALTONEN 08N reports $[\Gamma(\overline{b} \to B^0_s)/\left[\Gamma(\overline{b} \to B^+) + \Gamma(\overline{b} \to B^0)\right]] \times [B(D^+_s \to \phi\pi^+)] = (5.76 \pm 0.18 ^{+0.45}_{-0.42}) \times 10^{-3}$ which we divide by our best value $B(D^+_s \to \phi\pi^+) = (4.5 \pm 0.4) \times 10^{-2}$. Our first error is their experiment's error and our second error is the systematic error from using our best value.

[5] AFFOLDER 00E uses several electron-charm final states in $b \to ce^-X$.

[6] ABE 99P uses the numbers of $K^*(892)^0$, $K^*(892)^+$, and $\phi(1020)$ events produced in association with the double semileptonic decays $b \to c\mu^-X$ with $c \to s\mu^+X$.

$\Gamma(B^0_s)/\Gamma(B^0)$ — Γ_3/Γ_2

"OUR EVALUATION" has been provided by the Heavy Flavor Averaging Group (HFLAV, https://hflav.web.cern.ch/).

VALUE	DOCUMENT ID		TECN	COMMENT
0.246 ±0.023 OUR EVALUATION				
0.239 ±0.016 OUR AVERAGE				
$0.240 \pm0.004 \pm0.020$	[1] AAD	15CM	ATLS	pp at 7 TeV
$0.238 \pm0.004 \pm0.026$	[2] AAIJ	13P	LHCB	pp at 7 TeV
• • • We do not use the following data for averages, fits, limits, etc. • • •				
0.2385 ± 0.0075	[3] AAIJ	21Y	LHCB	pp at 8 TeV
0.2539 ± 0.0079	[3] AAIJ	21Y	LHCB	pp at 13 TeV
0.2390 ± 0.0076	[3] AAIJ	21Y	LHCB	pp at 7 TeV

[1] AAD 15CM measurement is derived from the observed $B^0_s \to J/\psi\phi$ and $B^0_d \to J/\psi K^{*0}$ yields and a recent theory prediction of $B(B^0_s \to J/\psi\phi)/B(B^0_d \to J/\psi K^{*0})$. The second uncertainty combines in quadrature systematic and theoretical uncertainties.

[2] AAIJ 13P studies also separately the $p_T(B)$ and $\eta(B)$ dependency of $\Gamma(\overline{b} \to B^0_s)/\Gamma(\overline{b} \to B^0)$, finding $f_s/f_d(p_T) = (0.256 \pm 0.020) + (-2.0 \pm 0.6)\ 10^{-3}$ /GeV/c $(p_T - \langle p_T \rangle)$ and $f_s/f_d(\eta) = (0.256 \pm 0.020) + (0.005 \pm 0.006)\ (\eta - \langle \eta \rangle)$, where $\langle p_T \rangle = 10.4$ GeV/c and $\langle \eta \rangle = 3.28$. AAIJ 13P reports the measurement as $0.238 \pm 0.004 \pm 0.015 \pm 0.021$ where the last uncertainly is theoretical.

[3] AAIJ 21Y uses hadronic decays $B^0 \to D^-\pi^+$, $B^0 \to D^-K^+$, $B^0_s \to D^-_s\pi^+$ and $B^0_s \to J/\psi\phi$ as well as semileptonic B^0 and B^0_s decays. Measured within the p_T range [0.5,40] GeV/c, η range [2, 6.4].

$\Gamma(B^+_c)/[\Gamma(B^+)+\Gamma(B^0)]$ — $\Gamma_4/(\Gamma_1+\Gamma_2)$

VALUE (units 10^{-3})	DOCUMENT ID		TECN	COMMENT
3.7 ±0.6 OUR AVERAGE				
$3.63\pm0.08\pm0.87$	[1] AAIJ	19AI	LHCB	pp at 7 TeV
$3.78\pm0.04\pm0.90$	[1] AAIJ	19AI	LHCB	pp at 13 TeV

[1] Measured using B^+_c semileptonic decays.

$\Gamma(b\text{-baryon})/[\Gamma(B^+)+\Gamma(B^0)]$ — $\Gamma_5/(\Gamma_1+\Gamma_2)$

"OUR EVALUATION" is an average from Z decay obtained by the Heavy Flavor Averaging Group (HFLAV) as described at https://hflav.web.cern.ch/.

VALUE	DOCUMENT ID		TECN	COMMENT
0.103±0.015 OUR EVALUATION				
• • • We do not use the following data for averages, fits, limits, etc. • • •				
0.259 ± 0.018	[1] AAIJ	19AD	LHCB	pp at 13 TeV
$0.305\pm0.010\pm0.081$	[2] AAIJ	12J	LHCB	pp at 7 TeV
$0.31 \pm0.11 ^{+0.12}_{-0.08}$	[3] AALTONEN	09E	CDF	$p\overline{p}$ at 1.8 TeV
$0.22 ^{+0.08}_{-0.07} \pm0.01$	[4] AALTONEN	08N	CDF	$p\overline{p}$ at 1.96 TeV
0.118 ± 0.042	[3,5] AFFOLDER	00E	CDF	$p\overline{p}$ at 1.8 TeV

[1] AAIJ 19AD measured the average value for Λ^0_b using semileptonic decays and assuming isospin symmetry for b-hadron p_T of 4 and 25 GeV and η of 2 and 5.

[2] AAIJ 12J measured the ratio to be $(0.404 \pm 0.017 \pm 0.027 \pm 0.105) \times [1 - (0.031 \pm 0.004 \pm 0.003) \times P_T]$using b-hadron semileptonic decays where the P_T is the momentum of charmed hadron-muon pair in GeV/c.We quote their weighted average value where the second error combines systematic and the error on $B(\Lambda^+_c \to pK^-\pi^+)$.

[3] AALTONEN 09E errata to the measurement reported in AFFOLDER 00E using the p_T spectra from fully reconstructed B^0 and Λ_b decays.

[4] AALTONEN 08N reports $[\Gamma(\overline{b} \to b\text{-baryon})/\left[\Gamma(\overline{b} \to B^+) + \Gamma(\overline{b} \to B^0)\right]] \times [B(\Lambda^+_c \to pK^-\pi^+)] = (14.1 \pm 0.6 ^{+5.3}_{-4.4}) \times 10^{-3}$ which we divide by our best value $B(\Lambda^+_c \to pK^-\pi^+) = (6.28 \pm 0.32) \times 10^{-2}$. Our first error is their experiment's error and our second error is the systematic error from using our best value.

[5] AFFOLDER 00E uses several electron-charm final states in $b \to ce^-X$.

$\Gamma(\nu\text{anything})/\Gamma_{total}$ — Γ_6/Γ

VALUE	DOCUMENT ID		TECN	COMMENT
0.2308±0.0077±0.0124	[1,2] ACCIARRI	96C	L3	$e^+e^- \to Z$

[1] ACCIARRI 96C assumes relative b semileptonic decay rates e:μ:τ of 1:1:0.25. Based on missing-energy spectrum.

[2] Assumes Standard Model value for R_B.

$\Gamma(\ell^+\nu_\ell\text{anything})/\Gamma_{total}$ — Γ_7/Γ

"OUR EVALUATION" is an average of the data listed below, excluding all asymmetry measurements, performed by the LEP Electroweak Working Group as described in the "Note on the Z boson" in the Z Particle Listings.

VALUE	DOCUMENT ID		TECN	COMMENT
0.1069±0.0022 OUR EVALUATION				
0.1064±0.0016 OUR AVERAGE				
$0.1070\pm0.0010\pm0.0035$	[1] HEISTER	02G	ALEP	$e^+e^- \to Z$
$0.1070\pm0.0008^{+0.0037}_{-0.0049}$	[2] ABREU	01L	DLPH	$e^+e^- \to Z$
$0.1083\pm0.0010^{+0.0028}_{-0.0024}$	[3] ABBIENDI	00E	OPAL	$e^+e^- \to Z$
$0.1016\pm0.0013\pm0.0030$	[4] ACCIARRI	00	L3	$e^+e^- \to Z$
$0.1085\pm0.0012\pm0.0047$	[5,6] ACCIARRI	96C	L3	$e^+e^- \to Z$
• • • We do not use the following data for averages, fits, limits, etc. • • •				
$0.1106\pm0.0039\pm0.0022$	[7] ABREU	95D	DLPH	$e^+e^- \to Z$
$0.114 \pm0.003 \pm0.004$	[8] BUSKULIC	94G	ALEP	$e^+e^- \to Z$
$0.100 \pm0.007 \pm0.007$	[9] ABREU	93C	DLPH	$e^+e^- \to Z$
$0.105 \pm0.006 \pm0.005$	[10] AKERS	93B	OPAL	Repl. by ABBIENDI 00E

[1] Uses the combination of lepton transverse momentum spectrum and the correlation between the charge of the lepton and opposite jet charge. The first error is statistic and the second error is the total systematic error including the modeling.

[2] The experimental systematic and model uncertainties are combined in quadrature.

[3] ABBIENDI 00E result is determined by comparing the distribution of several kinematic variables of leptonic events in a lifetime tagged $Z \to b\overline{b}$ sample using artificial neural

Downloaded from https://academic.oup.com/ptep/article/2022/8/083C01/6651666 by KIT Library user on 27 September 2022

network techniques. The first error is statistic; the second error is the total systematic error.

[4] ACCIARRI 00 result obtained from a combined fit of $R_b = \Gamma(Z \to b\overline{b})/\Gamma(Z \to \text{hadrons})$ and $B(b \to \ell\nu X)$, using double-tagging method.

[5] ACCIARRI 96C result obtained by a fit to the single lepton spectrum.

[6] Assumes Standard Model value for R_B.

[7] ABREU 95D give systematic errors ± 0.0019 (model) and 0.0012 (R_c). We combine these in quadrature.

[8] BUSKULIC 94G uses e and μ events. This value is from a global fit to the lepton p and p_T (relative to jet) spectra which also determines the b and c production fractions, the fragmentation functions, and the forward-backward asymmetries. This branching ratio depends primarily on the ratio of dileptons to single leptons at high p_T, but the lower p_T portion of the lepton spectrum is included in the global fit to reduce the model dependence. The model dependence is ± 0.0026 and is included in the systematic error.

[9] ABREU 93C event count includes ee events. Combining ee, $\mu\mu$, and $e\mu$ events, they obtain $0.100 \pm 0.007 \pm 0.007$.

[10] AKERS 93B analysis performed using single and dilepton events.

$\Gamma(e^+\nu_e \text{anything})/\Gamma_{\text{total}}$ — Γ_8/Γ

VALUE	EVTS	DOCUMENT ID		TECN	COMMENT
0.1086 ± 0.0035 OUR AVERAGE					
$0.1078 \pm 0.0008 {}^{+0.0050}_{-0.0046}$		[1] ABBIENDI	00E	OPAL	$e^+e^- \to Z$
$0.1089 \pm 0.0020 \pm 0.0051$		[2,3] ACCIARRI	96C	L3	$e^+e^- \to Z$
$0.107 \pm 0.015 \pm 0.007$	260	[4] ABREU	93C	DLPH	$e^+e^- \to Z$
$0.138 \pm 0.032 \pm 0.008$		[5] ADEVA	91C	L3	$e^+e^- \to Z$
• • • We do not use the following data for averages, fits, limits, etc. • • •					
$0.086 \pm 0.027 \pm 0.008$		[6] ABE	93E	VNS	$E^{ee}_{cm} = 58$ GeV
$0.109 {}^{+0.014}_{-0.013} \pm 0.0055$	2719	[7] AKERS	93B	OPAL	Repl. by ABBIENDI 00E
$0.111 \pm 0.028 \pm 0.026$		BEHREND	90D	CELL	$E^{ee}_{cm} = 43$ GeV
$0.150 \pm 0.011 \pm 0.022$		BEHREND	90D	CELL	$E^{ee}_{cm} = 35$ GeV
$0.112 \pm 0.009 \pm 0.011$		ONG	88	MRK2	$E^{ee}_{cm} = 29$ GeV
$0.149 {}^{+0.022}_{-0.019}$		PAL	86	DLCO	$E^{ee}_{cm} = 29$ GeV
$0.110 \pm 0.018 \pm 0.010$		AIHARA	85	TPC	$E^{ee}_{cm} = 29$ GeV
$0.111 \pm 0.034 \pm 0.040$		ALTHOFF	84J	TASS	$E^{ee}_{cm} = 34.6$ GeV
0.146 ± 0.028		KOOP	84	DLCO	Repl. by PAL 86
$0.116 \pm 0.021 \pm 0.017$		NELSON	83	MRK2	$E^{ee}_{cm} = 29$ GeV

[1] ABBIENDI 00E result is determined by comparing the distribution of several kinematic variables of leptonic events in a lifetime tagged $Z \to b\overline{b}$ sample using artificial neural network techniques. The first error is statistic; the second error is the total systematic error.

[2] ACCIARRI 96C result obtained by a fit to the single lepton spectrum.

[3] Assumes Standard Model value for R_B.

[4] ABREU 93C event count includes ee events. Combining ee, $\mu\mu$, and $e\mu$ events, they obtain $0.100 \pm 0.007 \pm 0.007$.

[5] ADEVA 91C measure the average $B(b \to eX)$ branching ratio using single and double tagged b enhanced Z events. Combining e and μ results, they obtain $0.113 \pm 0.010 \pm 0.006$. Constraining the initial number of b quarks by the Standard Model prediction (378 ± 3 MeV) for the decay of the Z into $b\overline{b}$, the electron result gives $0.112 \pm 0.004 \pm 0.008$. They obtain $0.119 \pm 0.003 \pm 0.006$ when e and μ results are combined. Used to measure the $b\overline{b}$ width itself, this electron result gives $370 \pm 12 \pm 24$ MeV and combined with the muon result gives $385 \pm 7 \pm 22$ MeV.

[6] ABE 93E experiment also measures forward-backward asymmetries and fragmentation functions for b and c.

[7] AKERS 93B analysis performed using single and dilepton events.

$\Gamma(\mu^+\nu_\mu \text{anything})/\Gamma_{\text{total}}$ — Γ_9/Γ

VALUE	EVTS	DOCUMENT ID		TECN	COMMENT
$0.1095 {}^{+0.0029}_{-0.0025}$ OUR AVERAGE					
$0.1096 \pm 0.0008 {}^{+0.0034}_{-0.0027}$		[1] ABBIENDI	00E	OPAL	$e^+e^- \to Z$
$0.1082 \pm 0.0015 \pm 0.0059$		[2,3] ACCIARRI	96C	L3	$e^+e^- \to Z$
$0.110 \pm 0.012 \pm 0.007$	656	[4] ABREU	93C	DLPH	$e^+e^- \to Z$
$0.113 \pm 0.012 \pm 0.006$		[5] ADEVA	91C	L3	$e^+e^- \to Z$
• • • We do not use the following data for averages, fits, limits, etc. • • •					
$0.122 \pm 0.006 \pm 0.007$		[3] UENO	96	AMY	e^+e^- at 57.9 GeV
$0.101 {}^{+0.010}_{-0.009} \pm 0.0055$	4248	[6] AKERS	93B	OPAL	Repl. by ABBIENDI 00E
$0.104 \pm 0.023 \pm 0.016$		BEHREND	90D	CELL	$E^{ee}_{cm} = 43$ GeV
$0.148 \pm 0.010 \pm 0.016$		BEHREND	90D	CELL	$E^{ee}_{cm} = 35$ GeV
$0.118 \pm 0.012 \pm 0.010$		ONG	88	MRK2	$E^{ee}_{cm} = 29$ GeV
$0.117 \pm 0.016 \pm 0.015$		BARTEL	87	JADE	$E^{ee}_{cm} = 34.6$ GeV
$0.114 \pm 0.018 \pm 0.025$		BARTEL	85J	JADE	Repl. by BARTEL 87
$0.117 \pm 0.028 \pm 0.010$		ALTHOFF	84G	TASS	$E^{ee}_{cm} = 34.5$ GeV
$0.105 \pm 0.015 \pm 0.013$		ADEVA	83B	MRKJ	$E^{ee}_{cm} = 33$–38.5 GeV
$0.155 {}^{+0.054}_{-0.029}$		FERNANDEZ	83D	MAC	$E^{ee}_{cm} = 29$ GeV

[1] ABBIENDI 00E result is determined by comparing the distribution of several kinematic variables of leptonic events in a lifetime tagged $Z \to b\overline{b}$ sample using artificial neural network techniques. The first error is statistic; the second error is the total systematic error.

[2] ACCIARRI 96C result obtained by a fit to the single lepton spectrum.

[3] Assumes Standard Model value for R_B.

[4] ABREU 93C event count includes $\mu\mu$ events. Combining ee, $\mu\mu$, and $e\mu$ events, they obtain $0.100 \pm 0.007 \pm 0.007$.

[5] ADEVA 91C measure the average $B(b \to eX)$ branching ratio using single and double tagged b enhanced Z events. Combining e and μ results, they obtain $0.113 \pm 0.010 \pm 0.006$. Constraining the initial number of b quarks by the Standard Model prediction (378 ± 3 MeV) for the decay of the Z into $b\overline{b}$, the muon result gives $0.123 \pm 0.003 \pm 0.006$. They obtain $0.119 \pm 0.003 \pm 0.006$ when e and μ results are combined. Used to measure the $b\overline{b}$ width itself, this muon result gives $394 \pm 9 \pm 22$ MeV and combined with the electron result gives $385 \pm 7 \pm 22$ MeV.

[6] AKERS 93B analysis performed using single and dilepton events.

$\Gamma(D^-\ell^+\nu_\ell \text{anything})/\Gamma_{\text{total}}$ — Γ_{10}/Γ

VALUE	DOCUMENT ID		TECN	COMMENT
0.022 ± 0.004 OUR AVERAGE	Error includes scale factor of 1.9.			
$0.0272 \pm 0.0028 \pm 0.0018$	[1] ABREU	00R	DLPH	$e^+e^- \to Z$
$0.0194 \pm 0.0025 \pm 0.0003$	[2] AKERS	95Q	OPAL	$e^+e^- \to Z$

[1] ABREU 00R reports their experiment's uncertainties $\pm 0.0019 \pm 0.0016 \pm 0.0018$, where the first error is statistical, the second is systematic, and the third is the uncertainty due to the D branching fraction. We combine first two in quadrature.

[2] AKERS 95Q reports $[\Gamma(\overline{b} \to D^-\ell^+\nu_\ell \text{anything})/\Gamma_{\text{total}}] \times [B(D^+ \to K^-2\pi^+)] = (1.82 \pm 0.20 \pm 0.12) \times 10^{-3}$ which we divide by our best value $B(D^+ \to K^-2\pi^+) = (9.38 \pm 0.16) \times 10^{-2}$. Our first error is their experiment's error and our second error is the systematic error from using our best value.

$\Gamma(D^-\pi^+\ell^+\nu_\ell \text{anything})/\Gamma_{\text{total}}$ — Γ_{11}/Γ

VALUE	DOCUMENT ID		TECN	COMMENT
$0.0049 \pm 0.0018 \pm 0.0007$	ABREU	00R	DLPH	$e^+e^- \to Z$

$\Gamma(D^-\pi^-\ell^+\nu_\ell \text{anything})/\Gamma_{\text{total}}$ — Γ_{12}/Γ

VALUE	DOCUMENT ID		TECN	COMMENT
$0.0026 \pm 0.0015 \pm 0.0004$	ABREU	00R	DLPH	$e^+e^- \to Z$

$\Gamma(\overline{D}^0\ell^+\nu_\ell \text{anything})/\Gamma_{\text{total}}$ — Γ_{13}/Γ

VALUE	DOCUMENT ID		TECN	COMMENT
0.0679 ± 0.0034 OUR AVERAGE				
$0.0704 \pm 0.0040 \pm 0.0017$	[1] ABREU	00R	DLPH	$e^+e^- \to Z$
$0.0638 \pm 0.0056 \pm 0.0005$	[2] AKERS	95Q	OPAL	$e^+e^- \to Z$

[1] ABREU 00R reports their experiment's uncertainties $\pm 0.0034 \pm 0.0036 \pm 0.0017$, where the first error is statistical, the second is systematic, and the third is the uncertainty due to the D branching fraction. We combine first two in quadrature.

[2] AKERS 95Q reports $[\Gamma(\overline{b} \to \overline{D}^0\ell^+\nu_\ell \text{anything})/\Gamma_{\text{total}}] \times [B(D^0 \to K^-\pi^+)] = (2.52 \pm 0.14 \pm 0.17) \times 10^{-3}$ which we divide by our best value $B(D^0 \to K^-\pi^+) = (3.947 \pm 0.030) \times 10^{-2}$. Our first error is their experiment's error and our second error is the systematic error from using our best value.

$\Gamma(\overline{D}^0\pi^-\ell^+\nu_\ell \text{anything})/\Gamma_{\text{total}}$ — Γ_{14}/Γ

VALUE	DOCUMENT ID		TECN	COMMENT
$0.0107 \pm 0.0025 \pm 0.0011$	ABREU	00R	DLPH	$e^+e^- \to Z$

$\Gamma(\overline{D}^0\pi^+\ell^+\nu_\ell \text{anything})/\Gamma_{\text{total}}$ — Γ_{15}/Γ

VALUE	DOCUMENT ID		TECN	COMMENT
$0.0023 \pm 0.0015 \pm 0.0004$	ABREU	00R	DLPH	$e^+e^- \to Z$

$\Gamma(D^{*-}\ell^+\nu_\ell \text{anything})/\Gamma_{\text{total}}$ — Γ_{16}/Γ

VALUE	DOCUMENT ID		TECN	COMMENT
0.0275 ± 0.0019 OUR AVERAGE				
$0.0275 \pm 0.0021 \pm 0.0009$	[1] ABREU	00R	DLPH	$e^+e^- \to Z$
$0.0276 \pm 0.0027 \pm 0.0011$	[2] AKERS	95Q	OPAL	$e^+e^- \to Z$

[1] ABREU 00R reports their experiment's uncertainties $\pm 0.0017 \pm 0.0013 \pm 0.0009$, where the first error is statistical, the second is systematic, and the third is the uncertainty due to the D branching fraction. We combine first two in quadrature.

[2] AKERS 95Q reports $[B(\overline{b} \to D^*\ell^+\nu_\ell X) \times B(D^{*+} \to D^0\pi^+) \times B(D^0 \to K^-\pi^+)] = ((7.53 \pm 0.47 \pm 0.56) \times 10^{-4})$ and uses $B(D^{*+} \to D^0\pi^+) = 0.681 \pm 0.013$ and $B(D^0 \to K^-\pi^+) = 0.0401 \pm 0.0014$ to obtain the above result. The first error is the experiments error and the second error is the systematic error from the D^{*+} and D^0 branching ratios.

$\Gamma(D^{*-}\pi^-\ell^+\nu_\ell \text{anything})/\Gamma_{\text{total}}$ — Γ_{17}/Γ

VALUE	DOCUMENT ID		TECN	COMMENT
$0.0006 \pm 0.0007 \pm 0.0002$	ABREU	00R	DLPH	$e^+e^- \to Z$

$\Gamma(D^{*-}\pi^+\ell^+\nu_\ell \text{anything})/\Gamma_{\text{total}}$ — Γ_{18}/Γ

VALUE	DOCUMENT ID		TECN	COMMENT
$0.0048 \pm 0.0009 \pm 0.0005$	ABREU	00R	DLPH	$e^+e^- \to Z$

$\Gamma(\overline{D}^0_J\ell^+\nu_\ell \text{anything} \times B(\overline{D}^0_J \to D^{*+}\pi^-))/\Gamma_{\text{total}}$ — Γ_{19}/Γ

D_j represents an unresolved mixture of pseudoscalar and tensor D^{**} (P-wave) states.

VALUE (units 10^{-3})	DOCUMENT ID		TECN	COMMENT
$2.64 \pm 0.79 \pm 0.39$	ABBIENDI	03M	OPAL	$e^+e^- \to Z$
• • • We do not use the following data for averages, fits, limits, etc. • • •				
$6.1 \pm 1.3 \pm 1.3$	AKERS	95Q	OPAL	Repl. by ABBIENDI 03M

$\Gamma(D^-_J\ell^+\nu_\ell \text{anything} \times B(D^-_J \to D^0\pi^-))/\Gamma_{\text{total}}$ — Γ_{20}/Γ

D_j represents an unresolved mixture of pseudoscalar and tensor D^{**} (P-wave) states.

VALUE (units 10^{-3})	DOCUMENT ID		TECN	COMMENT
$7.0 \pm 1.9 {}^{+1.2}_{-1.3}$	AKERS	95Q	OPAL	$e^+e^- \to Z$

Downloaded from https://academic.oup.com/ptep/article/2022/8/083C01/6651666 by KIT Library user on 27 September 2022

$\Gamma(\overline{D}^*_2(2460)^0 \ell^+ \nu_\ell \text{anything} \times B(\overline{D}^*_2(2460)^0 \to D^{*-}\pi^+))/\Gamma_{total}$ — Γ_{21}/Γ

VALUE (units 10^{-3})	CL%	DOCUMENT ID		TECN	COMMENT
<1.4	90	ABBIENDI	03M	OPAL	$e^+e^- \to Z$

$\Gamma(D^*_2(2460)^- \ell^+ \nu_\ell \text{anything} \times B(D^*_2(2460)^- \to D^0\pi^-))/\Gamma_{total}$ — Γ_{22}/Γ

VALUE (units 10^{-3})	DOCUMENT ID		TECN	COMMENT
$4.2 \pm 1.3^{+0.7}_{-1.2}$	AKERS	95Q	OPAL	$e^+e^- \to Z$

$\Gamma(\overline{D}^*_2(2460)^0 \ell^+ \nu_\ell \text{anything} \times B(\overline{D}^*_2(2460)^0 \to D^-\pi^+))/\Gamma_{total}$ — Γ_{23}/Γ

VALUE (units 10^{-3})	DOCUMENT ID		TECN	COMMENT
$1.6 \pm 0.7 \pm 0.3$	AKERS	95Q	OPAL	$e^+e^- \to Z$

$\Gamma(\text{charmless } \ell\overline{\nu}_\ell)/\Gamma_{total}$ — Γ_{24}/Γ

"OUR EVALUATION" is an average of the data listed below performed by the LEP Heavy Flavour Steering Group. The averaging procedure takes into account correlations between the measurements.

VALUE	DOCUMENT ID		TECN	COMMENT
0.00171 ± 0.00052 OUR EVALUATION				
0.0017 ± 0.0004 OUR AVERAGE				
$0.00163 \pm 0.00053^{+0.00055}_{-0.00062}$	[1] ABBIENDI	01R	OPAL	$e^+e^- \to Z$
$0.00157 \pm 0.00035 \pm 0.00055$	[2] ABREU	00D	DLPH	$e^+e^- \to Z$
$0.00173 \pm 0.00055 \pm 0.00055$	[3] BARATE	99G	ALEP	$e^+e^- \to Z$
$0.0033 \pm 0.0010 \pm 0.0017$	[4] ACCIARRI	98K	L3	$e^+e^- \to Z$

[1] Obtained from the best fit of the MC simulated events to the data based on the $b \to X_u \ell\nu$ neutral network output distributions.
[2] ABREU 00D result obtained from a fit to the numbers of decays in $b \to u$ enriched and depleted samples and their lepton spectra, and assuming $|V_{cb}| = 0.0384 \pm 0.0033$ and $\tau_b = 1.564 \pm 0.014$ ps.
[3] Uses lifetime tagged $b\overline{b}$ sample.
[4] ACCIARRI 98K assumes $R_b = 0.2174 \pm 0.0009$ at Z decay.

$\Gamma(\tau^+ \nu_\tau \text{anything})/\Gamma_{total}$ — Γ_{25}/Γ

VALUE (units 10^{-2})	EVTS	DOCUMENT ID		TECN	COMMENT
2.41 ± 0.23 OUR AVERAGE					
$2.78 \pm 0.18 \pm 0.51$		[1] ABBIENDI	01Q	OPAL	$e^+e^- \to Z$
$2.43 \pm 0.20 \pm 0.25$		[2] BARATE	01E	ALEP	$e^+e^- \to Z$
$2.19 \pm 0.24 \pm 0.39$		[3] ABREU	00C	DLPH	$e^+e^- \to Z$
$1.7 \pm 0.5 \pm 1.1$		[4,5] ACCIARRI	96C	L3	$e^+e^- \to Z$
$2.4 \pm 0.7 \pm 0.8$	1032	[6] ACCIARRI	94C	L3	$e^+e^- \to Z$
• • • We do not use the following data for averages, fits, limits, etc. • • •					
$2.75 \pm 0.30 \pm 0.37$	405	[7] BUSKULIC	95	ALEP	Repl. by BARATE 01E
$4.08 \pm 0.76 \pm 0.62$		BUSKULIC	93B	ALEP	Repl. by BUSKULIC 95

[1] ABBIENDI 01Q uses a missing energy technique.
[2] The energy-flow and b-tagging algorithms were used.
[3] Uses the missing energy in $Z \to b\overline{b}$ decays without identifying leptons.
[4] ACCIARRI 96C result obtained from missing energy spectrum.
[5] Assumes Standard Model value for R_B.
[6] This is a direct result using tagged $b\overline{b}$ events at the Z, but species are not separated.
[7] BUSKULIC 95 uses missing-energy technique.

$\Gamma(D^{*-}\tau\nu_\tau \text{anything})/\Gamma_{total}$ — Γ_{26}/Γ

VALUE	DOCUMENT ID		TECN	COMMENT
$(0.88 \pm 0.31 \pm 0.28) \times 10^{-2}$	[1] BARATE	01E	ALEP	$e^+e^- \to Z$

[1] The energy-flow and b-tagging algorithms were used.

$\Gamma(\overline{b} \to \overline{c} \to \ell^-\overline{\nu}_\ell \text{anything})/\Gamma_{total}$ — Γ_{27}/Γ

"OUR EVALUATION" is an average of the data listed below, excluding all asymmetry measurements, performed by the LEP Electroweak Working Group as described in the "Note on the Z boson" in the Z Particle Listings.

VALUE	DOCUMENT ID		TECN	COMMENT
0.0802 ± 0.0019 OUR EVALUATION				
0.0817 ± 0.0020 OUR AVERAGE				
$0.0818 \pm 0.0015^{+0.0024}_{-0.0026}$	[1] HEISTER	02G	ALEP	$e^+e^- \to Z$
$0.0798 \pm 0.0022^{+0.0025}_{-0.0029}$	[2] ABREU	01L	DLPH	$e^+e^- \to Z$
$0.0840 \pm 0.0016^{+0.0039}_{-0.0036}$	[3] ABBIENDI	00E	OPAL	$e^+e^- \to Z$
• • • We do not use the following data for averages, fits, limits, etc. • • •				
$0.0770 \pm 0.0097 \pm 0.0046$	[4] ABREU	95D	DLPH	$e^+e^- \to Z$
$0.082 \pm 0.003 \pm 0.012$	[5] BUSKULIC	94G	ALEP	$e^+e^- \to Z$
$0.077 \pm 0.004 \pm 0.007$	[6] AKERS	93B	OPAL	Repl. by ABBIENDI 00E

[1] Uses the combination of lepton transverse momentum spectrum and the correlation between the charge of the lepton and opposite jet charge. The first error is statistic and the second error is the total systematic error including the modeling.
[2] The experimental systematic and model uncertainties are combined in quadrature.
[3] ABBIENDI 00E result is determined by comparing the distribution of several kinematic variables of leptonic events in a lifetime tagged $Z \to b\overline{b}$ sample using artificial neural network techniques. The first error is statistic; the second error is the total systematic error.
[4] ABREU 95D give systematic errors ± 0.0033 (model) and 0.0032 (R_c). We combine these in quadrature. This result is from the same global fit as their $\Gamma(\overline{b} \to \ell^+\nu_\ell X)$ data.
[5] BUSKULIC 94G uses e and μ events. This value is from the same global fit as their $\Gamma(\overline{b} \to \ell^+\nu_\ell \text{anything})/\Gamma_{total}$ data.
[6] AKERS 93B analysis performed using single and dilepton events.

$\Gamma(c \to \ell^+\nu \text{anything})/\Gamma_{total}$ — Γ_{28}/Γ

VALUE	DOCUMENT ID		TECN	COMMENT
$0.0161 \pm 0.0020^{+0.0034}_{-0.0047}$	[1] ABREU	01L	DLPH	$e^+e^- \to Z$

[1] The experimental systematic and model uncertainties are combined in quadrature.

$\Gamma(\overline{D}^0 \text{anything})/\Gamma_{total}$ — Γ_{29}/Γ

VALUE	DOCUMENT ID		TECN	COMMENT
$0.587 \pm 0.028 \pm 0.005$	[1] BUSKULIC	96Y	ALEP	$e^+e^- \to Z$

[1] BUSKULIC 96Y reports $0.605 \pm 0.024 \pm 0.016$ from a measurement of $[\Gamma(\overline{b} \to \overline{D}^0 \text{anything})/\Gamma_{total}] \times [B(D^0 \to K^-\pi^+)]$ assuming $B(D^0 \to K^-\pi^+) = 0.0383$, which we rescale to our best value $B(D^0 \to K^-\pi^+) = (3.947 \pm 0.030) \times 10^{-2}$. Our first error is their experiment's error and our second error is the systematic error from using our best value.

$\Gamma(D^0 D^{\pm}_s \text{anything})/\Gamma_{total}$ — Γ_{30}/Γ

VALUE	DOCUMENT ID		TECN	COMMENT
$0.091^{+0.020}_{-0.018}{}^{+0.034}_{-0.022}$	[1] BARATE	98Q	ALEP	$e^+e^- \to Z$

[1] The systematic error includes the uncertainties due to the charm branching ratios.

$\Gamma(D^{\mp} D^{\pm}_s \text{anything})/\Gamma_{total}$ — Γ_{31}/Γ

VALUE	DOCUMENT ID		TECN	COMMENT
$0.040^{+0.017}_{-0.014}{}^{+0.016}_{-0.011}$	[1] BARATE	98Q	ALEP	$e^+e^- \to Z$

[1] The systematic error includes the uncertainties due to the charm branching ratios.

$[\Gamma(D^0 D^{\pm}_s \text{anything}) + \Gamma(D^{\mp} D^{\pm}_s \text{anything})]/\Gamma_{total}$ — $(\Gamma_{30}+\Gamma_{31})/\Gamma$

VALUE	DOCUMENT ID		TECN	COMMENT
$0.131^{+0.026}_{-0.022}{}^{+0.048}_{-0.031}$	[1] BARATE	98Q	ALEP	$e^+e^- \to Z$

[1] The systematic error includes the uncertainties due to the charm branching ratios.

$\Gamma(\overline{D}^0 D^0 \text{anything})/\Gamma_{total}$ — Γ_{32}/Γ

VALUE	DOCUMENT ID		TECN	COMMENT
$0.051^{+0.016}_{-0.014}{}^{+0.012}_{-0.011}$	[1] BARATE	98Q	ALEP	$e^+e^- \to Z$

[1] The systematic error includes the uncertainties due to the charm branching ratios.

$\Gamma(D^0 D^{\pm} \text{anything})/\Gamma_{total}$ — Γ_{33}/Γ

VALUE	DOCUMENT ID		TECN	COMMENT
$0.027^{+0.015}_{-0.013}{}^{+0.010}_{-0.009}$	[1] BARATE	98Q	ALEP	$e^+e^- \to Z$

[1] The systematic error includes the uncertainties due to the charm branching ratios.

$[\Gamma(\overline{D}^0 D^0 \text{anything}) + \Gamma(D^0 D^{\pm} \text{anything})]/\Gamma_{total}$ — $(\Gamma_{32}+\Gamma_{33})/\Gamma$

VALUE	DOCUMENT ID		TECN	COMMENT
$0.078^{+0.020}_{-0.018}{}^{+0.018}_{-0.016}$	[1] BARATE	98Q	ALEP	$e^+e^- \to Z$

[1] The systematic error includes the uncertainties due to the charm branching ratios.

$\Gamma(D^{\pm} D^{\mp} \text{anything})/\Gamma_{total}$ — Γ_{34}/Γ

VALUE	CL%	DOCUMENT ID		TECN	COMMENT
<0.009	90	BARATE	98Q	ALEP	$e^+e^- \to Z$

$[\Gamma(D^0 \text{anything}) + \Gamma(D^+ \text{anything})]/\Gamma_{total}$ — $(\Gamma_{35}+\Gamma_{36})/\Gamma$

VALUE	DOCUMENT ID		TECN	COMMENT
$0.093 \pm 0.017 \pm 0.014$	[1] ABDALLAH	03E	DLPH	$e^+e^- \to Z$

[1] The second error is the total of systematic uncertainties including the branching fractions used in the measurement.

$\Gamma(D^- \text{anything})/\Gamma_{total}$ — Γ_{37}/Γ

VALUE	DOCUMENT ID		TECN	COMMENT
$0.227 \pm 0.016 \pm 0.004$	[1] BUSKULIC	96Y	ALEP	$e^+e^- \to Z$

[1] BUSKULIC 96Y reports $0.234 \pm 0.013 \pm 0.010$ from a measurement of $[\Gamma(\overline{b} \to D^- \text{anything})/\Gamma_{total}] \times [B(D^+ \to K^-2\pi^+)]$ assuming $B(D^+ \to K^-2\pi^+) = 0.091$, which we rescale to our best value $B(D^+ \to K^-2\pi^+) = (9.38 \pm 0.16) \times 10^{-2}$. Our first error is their experiment's error and our second error is the systematic error from using our best value.

$\Gamma(D^*(2010)^+ \text{anything})/\Gamma_{total}$ — Γ_{38}/Γ

VALUE	DOCUMENT ID		TECN	COMMENT
$0.173 \pm 0.016 \pm 0.012$	[1] ACKERSTAFF	98E	OPAL	$e^+e^- \to Z$

[1] Uses lepton tags to select $Z \to b\overline{b}$ events.

$\Gamma(D_1(2420)^0 \text{anything})/\Gamma_{total}$ — Γ_{39}/Γ

VALUE	DOCUMENT ID		TECN	COMMENT
$0.050 \pm 0.014 \pm 0.006$	[1] ACKERSTAFF	97W	OPAL	$e^+e^- \to Z$

[1] ACKERSTAFF 97W assumes $B(D^*_2(2460)^0 \to D^{*+}\pi^-) = 0.21 \pm 0.04$ and $\Gamma_{b\overline{b}}/\Gamma_{hadrons} = 0.216$ at Z decay.

Downloaded from https://academic.oup.com/ptep/article/2022/8/083C01/6651666 by KIT Library user on 27 September 2022

$\Gamma(D^*(2010)^{\mp} D_s^{\pm}\,\text{anything})/\Gamma_{\text{total}}$ — Γ_{40}/Γ

VALUE	DOCUMENT ID		TECN	COMMENT
$0.033^{+0.010}_{-0.009}{}^{+0.012}_{-0.009}$	[1] BARATE	98Q	ALEP	$e^+e^- \to Z$

[1] The systematic error includes the uncertainties due to the charm branching ratios.

$\Gamma(D^0 D^*(2010)^{\pm}\,\text{anything})/\Gamma_{\text{total}}$ — Γ_{41}/Γ

VALUE	DOCUMENT ID		TECN	COMMENT
$0.030^{+0.009}_{-0.008}{}^{+0.007}_{-0.005}$	[1] BARATE	98Q	ALEP	$e^+e^- \to Z$

[1] The systematic error includes the uncertainties due to the charm branching ratios.

$\Gamma(D^*(2010)^{\pm} D^{\mp}\,\text{anything})/\Gamma_{\text{total}}$ — Γ_{42}/Γ

VALUE	DOCUMENT ID		TECN	COMMENT
$0.025^{+0.010}_{-0.009}{}^{+0.006}_{-0.005}$	[1] BARATE	98Q	ALEP	$e^+e^- \to Z$

[1] The systematic error includes the uncertainties due to the charm branching ratios.

$\Gamma(D^*(2010)^{\pm} D^*(2010)^{\mp}\,\text{anything})/\Gamma_{\text{total}}$ — Γ_{43}/Γ

VALUE	DOCUMENT ID		TECN	COMMENT
$0.012^{+0.004}_{-0.003}\pm0.002$	[1] BARATE	98Q	ALEP	$e^+e^- \to Z$

[1] The systematic error includes the uncertainties due to the charm branching ratios.

$\Gamma(\overline{D}\,D\,\text{anything})/\Gamma_{\text{total}}$ — Γ_{44}/Γ

VALUE	DOCUMENT ID		TECN	COMMENT
$0.10\pm0.032^{+0.107}_{-0.095}$	[1] ABBIENDI	04I	OPAL	$e^+e^- \to Z$

[1] Measurement performed using an inclusive identification of B mesons and the D candidates.

$\Gamma(D_2^*(2460)^0\,\text{anything})/\Gamma_{\text{total}}$ — Γ_{45}/Γ

VALUE	DOCUMENT ID		TECN	COMMENT
$0.047\pm0.024\pm0.013$	[1] ACKERSTAFF	97W	OPAL	$e^+e^- \to Z$

[1] ACKERSTAFF 97W assumes $B(D_2^*(2460)^0 \to D^{*+}\pi^-) = 0.21 \pm 0.04$ and $\Gamma_{b\overline{b}}/\Gamma_{\text{hadrons}} = 0.216$ at Z decay.

$\Gamma(D_s^-\,\text{anything})/\Gamma_{\text{total}}$ — Γ_{46}/Γ

VALUE	DOCUMENT ID		TECN	COMMENT
$0.147\pm0.017\pm0.013$	[1] BUSKULIC	96Y	ALEP	$e^+e^- \to Z$

[1] BUSKULIC 96Y reports $0.183 \pm 0.019 \pm 0.009$ from a measurement of $[\Gamma(\overline{b} \to D_s^-\,\text{anything})/\Gamma_{\text{total}}] \times [B(D_s^+ \to \phi\pi^+)]$ assuming $B(D_s^+ \to \phi\pi^+) = 0.036$, which we rescale to our best value $B(D_s^+ \to \phi\pi^+) = (4.5 \pm 0.4) \times 10^{-2}$. Our first error is their experiment's error and our second error is the systematic error from using our best value.

$\Gamma(D_s^+\,\text{anything})/\Gamma_{\text{total}}$ — Γ_{47}/Γ

VALUE	DOCUMENT ID		TECN	COMMENT
$0.101\pm0.010\pm0.029$	[1] ABDALLAH	03E	DLPH	$e^+e^- \to Z$

[1] The second error is the total of systematic uncertainties including the branching fractions used in the measurement.

$\Gamma(b \to \Lambda_c^+\,\text{anything})/\Gamma_{\text{total}}$ — Γ_{48}/Γ

VALUE	DOCUMENT ID		TECN	COMMENT
$0.077\pm0.011\pm0.004$	[1] BUSKULIC	96Y	ALEP	$e^+e^- \to Z$

[1] BUSKULIC 96Y reports $0.110 \pm 0.014 \pm 0.006$ from a measurement of $[\Gamma(b \to \Lambda_c^+\,\text{anything})/\Gamma_{\text{total}}] \times [B(\Lambda_c^+ \to pK^-\pi^+)]$ assuming $B(\Lambda_c^+ \to pK^-\pi^+) = 0.044$, which we rescale to our best value $B(\Lambda_c^+ \to pK^-\pi^+) = (6.28 \pm 0.32) \times 10^{-2}$. Our first error is their experiment's error and our second error is the systematic error from using our best value.

$\Gamma(\overline{c}/c\,\text{anything})/\Gamma_{\text{total}}$ — Γ_{49}/Γ

VALUE	DOCUMENT ID		TECN	COMMENT
1.162 ± 0.032 OUR AVERAGE				
$1.12\ ^{+0.11}_{-0.10}$	[1] ABBIENDI	04I	OPAL	$e^+e^- \to Z$
$1.166\pm0.031\pm0.080$	[2] ABREU	00	DLPH	$e^+e^- \to Z$
1.147 ± 0.041	[3] ABREU	98D	DLPH	$e^+e^- \to Z$
$1.230\pm0.036\pm0.065$	[4] BUSKULIC	96Y	ALEP	$e^+e^- \to Z$

[1] Measurement performed using an inclusive identification of B mesons and the D candidates.
[2] Evaluated via summation of exclusive and inclusive channels.
[3] ABREU 98D results are extracted from a fit to the b-tagging probability distribution based on the impact parameter.
[4] BUSKULIC 96Y assumes PDG 96 production fractions for B^0, B^+, B_s, b baryons, and PDG 96 branching ratios for charm decays. This is sum of their inclusive $\overline{D}^0$, D^-, $\overline{D}_s$, and Λ_c branching ratios, corrected to include inclusive Ξ_c and charmonium.

$\Gamma(J/\psi(1S)\,\text{anything})/\Gamma_{\text{total}}$ — Γ_{50}/Γ

VALUE (units 10^{-2})	CL%	EVTS	DOCUMENT ID		TECN	COMMENT
1.16 ± 0.10 OUR AVERAGE						
$1.12\pm0.12\pm0.10$			[1] ABREU	94P	DLPH	$e^+e^- \to Z$
$1.16\pm0.16\pm0.14$		121	[2] ADRIANI	93J	L3	$e^+e^- \to Z$
$1.21\pm0.13\pm0.08$			BUSKULIC	92G	ALEP	$e^+e^- \to Z$
• • • We do not use the following data for averages, fits, limits, etc. • • •						
$1.3\ \pm0.2\ \pm0.2$			[3] ADRIANI	92	L3	$e^+e^- \to Z$
<4.9	90		MATTEUZZI	83	MRK2	$E^{ee}_{\text{cm}} = 29$ GeV

[1] ABREU 94P is an inclusive measurement from b decays at the Z. Uses $J/\psi(1S) \to e^+e^-$ and $\mu^+\mu^-$ channels. Assumes $\Gamma(Z \to b\overline{b})/\Gamma_{\text{hadron}} = 0.22$.
[2] ADRIANI 93J is an inclusive measurement from b decays at the Z. Uses $J/\psi(1S) \to \mu^+\mu^-$ and $J/\psi(1S) \to e^+e^-$ channels.
[3] ADRIANI 92 measurement is an inclusive result for $B(Z \to J/\psi(1S)X) = (4.1 \pm 0.7 \pm 0.3) \times 10^{-3}$ which is used to extract the b-hadron contribution to $J/\psi(1S)$ production.

$\Gamma(\psi(2S)\,\text{anything})/\Gamma_{\text{total}}$ — Γ_{51}/Γ

VALUE	DOCUMENT ID		TECN	COMMENT
• • • We do not use the following data for averages, fits, limits, etc. • • •				
$0.0048\pm0.0022\pm0.0010$	[1] ABREU	94P	DLPH	$e^+e^- \to Z$

[1] ABREU 94P is an inclusive measurement from b decays at the Z. Uses $\psi(2S) \to J/\psi(1S)\,\pi^+\pi^-$, $J/\psi(1S) \to \mu^+\mu^-$ channels. Assumes $\Gamma(Z \to b\overline{b})/\Gamma_{\text{hadron}} = 0.22$.

$\Gamma(\psi(2S)\,\text{anything})/\Gamma(J/\psi(1S)\,\text{anything})$ — Γ_{51}/Γ_{50}

VALUE	DOCUMENT ID		TECN	COMMENT
0.263 ± 0.013 OUR AVERAGE				
$0.265\pm0.002\pm0.016$	[1] AAIJ	20G	LHCB	pp at 13 TeV
$0.266\pm0.06\ \pm0.03$	[2,3] AAIJ	12BD	LHCB	pp at 7 TeV
$0.257\pm0.015\pm0.019$	[4,5] CHATRCHYAN	12AK	CMS	pp at 7 TeV

[1] The first error is statistic; the second error is the total systematic error.
[2] AAIJ 12BD reports $B(b \to \psi(2S)X) = (3.08 \pm 0.07 \pm 0.36 \pm 0.27) \times 10^{-3}$ and we divided our best value of $B(b \to \psi(1S)X) = (1.16 \pm 0.10) \times 10^{-2}$ as the ratio listed here.
[3] Assumes lepton universality imposing $B(\psi(2s) \to \mu^+\mu^-) = B(\psi(2s) \to e^+e^-)$.
[4] CHATRCHYAN 12AK really reports $\Gamma_{51}/\Gamma = (3.08\pm0.12\pm0.13\pm0.42)\times10^{-3}$ assuming PDG 10 value of $\Gamma_{50}/\Gamma = (1.16 \pm 0.10) \times 10^{-2}$ which we present as a ratio of $\Gamma_{51}/\Gamma_{50} = (26.5 \pm 1.0 \pm 1.1 \pm 2.8) \times 10^{-2}$.
[5] CHATRCHYAN 12AK reports $(26.5 \pm 1.0 \pm 1.1 \pm 2.8) \times 10^{-2}$ from a measurement of $[\Gamma(\overline{b} \to \psi(2S)\,\text{anything})/\Gamma(\overline{b} \to J/\psi(1S)\,\text{anything})] \times [B(\psi(2S) \to \mu^+\mu^-)] / [B(J/\psi(1S) \to \mu^+\mu^-)]$ assuming $B(\psi(2S) \to \mu^+\mu^-) = (7.7 \pm 0.8) \times 10^{-3}$, $B(J/\psi(1S) \to \mu^+\mu^-) = (5.93 \pm 0.06) \times 10^{-2}$, which we rescale to our best values $B(\psi(2S) \to \mu^+\mu^-) = (8.0 \pm 0.6) \times 10^{-3}$, $B(J/\psi(1S) \to \mu^+\mu^-) = (5.961 \pm 0.033) \times 10^{-2}$. Our first error is their experiment's error and our second error is the systematic error from using our best values.

$\Gamma(\chi_{c0}(1P)\,\text{anything})/\Gamma(\eta_c(1S)\,\text{anything})$ — Γ_{52}/Γ_{56}

VALUE	DOCUMENT ID		TECN	COMMENT
$0.32\pm0.06\pm0.05$	[1] AAIJ	17BB	LHCB	pp at 7, 8 TeV

[1] AAIJ 17BB reports $[\Gamma(\overline{b} \to \chi_{c0}(1P)\,\text{anything})/\Gamma(\overline{b} \to \eta_c(1S)\,\text{anything})] / [B(\eta_c(1S) \to \phi\phi)] \times [B(\chi_{c0}(1P) \to \phi\phi)] = 0.147 \pm 0.023 \pm 0.011$ which we multiply or divide by our best values $B(\eta_c(1S) \to \phi\phi) = (1.74 \pm 0.19) \times 10^{-3}$, $B(\chi_{c0}(1P) \to \phi\phi) = (8.0 \pm 0.7) \times 10^{-4}$. Our first error is their experiment's error and our second error is the systematic error from using our best values.

$\Gamma(\chi_{c1}(1P)\,\text{anything})/\Gamma_{\text{total}}$ — Γ_{53}/Γ

VALUE	EVTS	DOCUMENT ID		TECN	COMMENT
$0.014\ \pm0.004$ OUR AVERAGE					
$0.0112^{+0.0057}_{-0.0050}\pm0.0003$		[1] ABREU	94P	DLPH	$e^+e^- \to Z$
$0.019\ \pm0.007\ \pm0.001$	19	[2] ADRIANI	93J	L3	$e^+e^- \to Z$

[1] ABREU 94P reports $0.014 \pm 0.006^{+0.004}_{-0.002}$ from a measurement of $[\Gamma(\overline{b} \to \chi_{c1}(1P)\,\text{anything})/\Gamma_{\text{total}}] \times [B(\chi_{c1}(1P) \to \gamma J/\psi(1S))]$ assuming $B(\chi_{c1}(1P) \to \gamma J/\psi(1S)) = 0.273 \pm 0.016$, which we rescale to our best value $B(\chi_{c1}(1P) \to \gamma J/\psi(1S)) = (34.3 \pm 1.0) \times 10^{-2}$. Our first error is their experiment's error and our second error is the systematic error from using our best value. Assumes no $\chi_{c2}(1P)$ and $\Gamma(Z \to b\overline{b})/\Gamma_{\text{hadron}} = 0.22$.
[2] ADRIANI 93J reports $0.024 \pm 0.009 \pm 0.002$ from a measurement of $[\Gamma(\overline{b} \to \chi_{c1}(1P)\,\text{anything})/\Gamma_{\text{total}}] \times [B(\chi_{c1}(1P) \to \gamma J/\psi(1S))]$ assuming $B(\chi_{c1}(1P) \to \gamma J/\psi(1S)) = 0.273 \pm 0.016$, which we rescale to our best value $B(\chi_{c1}(1P) \to \gamma J/\psi(1S)) = (34.3 \pm 1.0) \times 10^{-2}$. Our first error is their experiment's error and our second error is the systematic error from using our best value.

$\Gamma(\chi_{c1}(1P)\,\text{anything})/\Gamma(J/\psi(1S)\,\text{anything})$ — Γ_{53}/Γ_{50}

VALUE	EVTS	DOCUMENT ID		TECN	COMMENT
• • • We do not use the following data for averages, fits, limits, etc. • • •					
1.92 ± 0.82	121	[1] ADRIANI	93J	L3	$e^+e^- \to Z$

[1] ADRIANI 93J is a ratio of inclusive measurements from b decays at the Z using only the $J/\psi(1S) \to \mu^+\mu^-$ channel since some systematics cancel.

Downloaded from https://academic.oup.com/ptep/article/2022/8/083C01/6651666 by KIT Library user on 27 September 2022

$\Gamma(\chi_{c1}(1P)\text{anything})/\Gamma(\chi_{c0}(1P)\text{anything})$ — Γ_{53}/Γ_{52}

VALUE	DOCUMENT ID		TECN	COMMENT
0.96±0.21±0.15	[1] AAIJ	17BB	LHCB	pp at 7, 8 TeV

[1] AAIJ 17BB reports $[\Gamma(\overline{b} \to \chi_{c1}(1P)\text{anything})/\Gamma(\overline{b} \to \chi_{c0}(1P)\text{anything})] / [B(\chi_{c0}(1P) \to \phi\phi)] \times [B(\chi_{c1}(1P) \to \phi\phi)] = 0.50 \pm 0.11 \pm 0.01$ which we multiply or divide by our best values $B(\chi_{c0}(1P) \to \phi\phi) = (8.0 \pm 0.7) \times 10^{-4}$, $B(\chi_{c1}(1P) \to \phi\phi) = (4.2 \pm 0.5) \times 10^{-4}$. Our first error is their experiment's error and our second error is the systematic error from using our best values.

$\Gamma(\chi_{c1}(1P)\text{anything})/\Gamma(\eta_c(1S)\text{anything})$ — Γ_{53}/Γ_{56}

VALUE	DOCUMENT ID		TECN	COMMENT
0.31±0.07±0.05	[1] AAIJ	17BB	LHCB	pp at 7, 8 TeV

[1] AAIJ 17BB reports $[\Gamma(\overline{b} \to \chi_{c1}(1P)\text{anything})/\Gamma(\overline{b} \to \eta_c(1S)\text{anything})] / [B(\eta_c(1S) \to \phi\phi)] \times [B(\chi_{c1}(1P) \to \phi\phi)] = 0.073 \pm 0.016 \pm 0.006$ which we multiply or divide by our best values $B(\eta_c(1S) \to \phi\phi) = (1.74 \pm 0.19) \times 10^{-3}$, $B(\chi_{c1}(1P) \to \phi\phi) = (4.2 \pm 0.5) \times 10^{-4}$. Our first error is their experiment's error and our second error is the systematic error from using our best values.

$\Gamma(\chi_{c2}(1P)\text{anything})/\Gamma(\chi_{c0}(1P)\text{anything})$ — Γ_{54}/Γ_{52}

VALUE	DOCUMENT ID		TECN	COMMENT
0.42±0.08±0.05	[1] AAIJ	17BB	LHCB	pp at 7, 8 TeV

[1] AAIJ 17BB reports $[\Gamma(\overline{b} \to \chi_{c2}(1P)\text{anything})/\Gamma(\overline{b} \to \chi_{c0}(1P)\text{anything})] / [B(\chi_{c0}(1P) \to \phi\phi)] \times [B(\chi_{c2}(1P) \to \phi\phi)] = 0.56 \pm 0.10 \pm 0.01$ which we multiply or divide by our best values $B(\chi_{c0}(1P) \to \phi\phi) = (8.0 \pm 0.7) \times 10^{-4}$, $B(\chi_{c2}(1P) \to \phi\phi) = (1.06 \pm 0.09) \times 10^{-3}$. Our first error is their experiment's error and our second error is the systematic error from using our best values.

$\Gamma(\chi_{c2}(1P)\text{anything})/\Gamma(\eta_c(1S)\text{anything})$ — Γ_{54}/Γ_{56}

VALUE	DOCUMENT ID		TECN	COMMENT
0.133±0.023±0.018	[1] AAIJ	17BB	LHCB	pp at 7, 8 TeV

[1] AAIJ 17BB reports $[\Gamma(\overline{b} \to \chi_{c2}(1P)\text{anything})/\Gamma(\overline{b} \to \eta_c(1S)\text{anything})] / [B(\eta_c(1S) \to \phi\phi)] \times [B(\chi_{c2}(1P) \to \phi\phi)] = 0.081 \pm 0.013 \pm 0.005$ which we multiply or divide by our best values $B(\eta_c(1S) \to \phi\phi) = (1.74 \pm 0.19) \times 10^{-3}$, $B(\chi_{c2}(1P) \to \phi\phi) = (1.06 \pm 0.09) \times 10^{-3}$. Our first error is their experiment's error and our second error is the systematic error from using our best values.

$\Gamma(\chi_c(2P)\text{anything},\ \chi_c \to \phi\phi)/\Gamma_{\text{total}}$ — Γ_{55}/Γ

VALUE	CL%	DOCUMENT ID		TECN	COMMENT
$<2.8 \times 10^{-7}$	95	AAIJ	17BB	LHCB	pp at 7, 8 TeV

$\Gamma(\eta_c(1S)\text{anything})/\Gamma(J/\psi(1S)\text{anything})$ — Γ_{56}/Γ_{50}

VALUE	DOCUMENT ID		TECN	COMMENT
0.48±0.03±0.06	AAIJ	20H	LHCB	pp at 13 TeV

$\Gamma(\eta_c(2S)\text{anything},\ \eta_c \to \phi\phi)/\Gamma(\eta_c(1S)\text{anything})$ — Γ_{57}/Γ_{56}

VALUE (units 10^{-5})	DOCUMENT ID		TECN	COMMENT
7.0±2.0±0.8	[1] AAIJ	17BB	LHCB	pp at 7, 8 TeV

[1] AAIJ 17BB reports $[\Gamma(\overline{b} \to \eta_c(2S)\text{anything},\ \eta_c \to \phi\phi)/\Gamma(\overline{b} \to \eta_c(1S)\text{anything})] / [B(\eta_c(1S) \to \phi\phi)] = 0.040 \pm 0.011 \pm 0.004$ which we multiply by our best value $B(\eta_c(1S) \to \phi\phi) = (1.74 \pm 0.19) \times 10^{-3}$. Our first error is their experiment's error and our second error is the systematic error from using our best value.

$\Gamma(\chi_{c1}(3872)\text{anything},\ \chi_{c1} \to \phi\phi)/\Gamma_{\text{total}}$ — Γ_{58}/Γ

VALUE	CL%	DOCUMENT ID		TECN	COMMENT
$<4.5 \times 10^{-7}$	95	AAIJ	17BB	LHCB	pp at 7, 8 TeV

$\Gamma(\chi_{c0}(3915)\text{anything},\ \chi_{c0} \to \phi\phi)/\Gamma_{\text{total}}$ — Γ_{59}/Γ

VALUE	CL%	DOCUMENT ID		TECN	COMMENT
$<3.1 \times 10^{-7}$	95	AAIJ	17BB	LHCB	pp at 7, 8 TeV

$\Gamma(\overline{s}\gamma)/\Gamma_{\text{total}}$ — Γ_{60}/Γ

VALUE (units 10^{-4})	CL%	DOCUMENT ID		TECN	COMMENT
3.11±0.80±0.72		[1] BARATE	98I	ALEP	$e^+e^- \to Z$
• • • We do not use the following data for averages, fits, limits, etc. • • •					
<5.4	90	[2] ADAM	96D	DLPH	$e^+e^- \to Z$
<12	90	[3] ADRIANI	93L	L3	$e^+e^- \to Z$

[1] BARATE 98I uses lifetime tagged $Z \to b\overline{b}$ sample.
[2] ADAM 96D assumes $f_{B^0} = f_{B^-} = 0.39$ and $f_{B_s} = 0.12$.
[3] ADRIANI 93L result is for $\overline{b} \to \overline{s}\gamma$ is performed inclusively.

$\Gamma(\overline{s}\nu\nu)/\Gamma_{\text{total}}$ — Γ_{61}/Γ

VALUE	CL%	DOCUMENT ID		TECN	COMMENT
$<6.4 \times 10^{-4}$	90	[1] BARATE	01E	ALEP	$e^+e^- \to Z$

[1] The energy-flow and b-tagging algorithms were used.

$\Gamma(K^{\pm}\text{anything})/\Gamma_{\text{total}}$ — Γ_{62}/Γ

VALUE	DOCUMENT ID		TECN	COMMENT
0.74±0.06 OUR AVERAGE				
0.72±0.02±0.06	BARATE	98V	ALEP	$e^+e^- \to Z$
0.88±0.05±0.18	ABREU	95C	DLPH	$e^+e^- \to Z$

$\Gamma(K^0_S\text{anything})/\Gamma_{\text{total}}$ — Γ_{63}/Γ

VALUE	DOCUMENT ID		TECN	COMMENT
0.290±0.011±0.027	ABREU	95C	DLPH	$e^+e^- \to Z$

$\Gamma(\pi^{\pm}\text{anything})/\Gamma_{\text{total}}$ — Γ_{64}/Γ

VALUE	DOCUMENT ID		TECN	COMMENT
3.97±0.02±0.21	BARATE	98V	ALEP	$e^+e^- \to Z$

$\Gamma(\pi^0\text{anything})/\Gamma_{\text{total}}$ — Γ_{65}/Γ

VALUE	DOCUMENT ID		TECN	COMMENT
2.78±0.15±0.60	[1] ADAM	96	DLPH	$e^+e^- \to Z$

[1] ADAM 96 measurement obtained from a fit to the rapidity distribution of $\pi^{0\prime s}$ in $Z \to b\,b$ events.

$\Gamma(\phi\text{anything})/\Gamma_{\text{total}}$ — Γ_{66}/Γ

VALUE	DOCUMENT ID		TECN	COMMENT
0.0282±0.0013±0.0019	ABBIENDI	00Z	OPAL	$e^+e^- \to Z$

$\Gamma(p/\overline{p}\text{anything})/\Gamma_{\text{total}}$ — Γ_{67}/Γ

VALUE	DOCUMENT ID		TECN	COMMENT
0.131±0.011 OUR AVERAGE				
0.131±0.004±0.011	BARATE	98V	ALEP	$e^+e^- \to Z$
0.141±0.018±0.056	ABREU	95C	DLPH	$e^+e^- \to Z$

$\Gamma(\Lambda/\overline{\Lambda}\text{anything})/\Gamma_{\text{total}}$ — Γ_{68}/Γ

VALUE	DOCUMENT ID		TECN	COMMENT
0.059 ±0.006 OUR AVERAGE				
0.0587±0.0046±0.0048	ACKERSTAFF	97N	OPAL	$e^+e^- \to Z$
0.059 ±0.007 ±0.009	ABREU	95C	DLPH	$e^+e^- \to Z$

$\Gamma(b\text{-baryon anything})/\Gamma_{\text{total}}$ — Γ_{69}/Γ

VALUE	DOCUMENT ID		TECN	COMMENT
0.102±0.007±0.027	[1] BARATE	98V	ALEP	$e^+e^- \to Z$

[1] BARATE 98V assumes $B(B_s \to pX) = 8 \pm 4\%$ and $B(b\text{-baryon} \to pX) = 58 \pm 6\%$.

$\Gamma(\Xi^+_b\text{anything})/\Gamma(\overline{\Lambda}^0_b\text{anything})$ — Γ_{71}/Γ_{70}

VALUE (units 10^{-2})	DOCUMENT ID		TECN	COMMENT
7.3±1.7 OUR AVERAGE				
6.7±0.5±2.1	[1] AAIJ	19AB	LHCB	pp at 7 and 8 TeV
8.2±0.7±2.6	[1] AAIJ	19AB	LHCB	pp at 13 TeV

[1] Measured from $R = [B(\overline{b} \to \Xi^+_b) \times B(\Xi_b \to J/\psi\Xi^+)]/[B(\overline{b} \to \overline{\Lambda}^0_b) \times B(\overline{\Lambda}^0_b \to J/\psi\overline{\Lambda}^0)]$ and assumes $\Gamma_{\Xi^+_b \to J/\psi\Xi^+}/\Gamma_{\overline{\Lambda}^0_b \to J/\psi\overline{\Lambda}^0} = 3/2$ related through SU(3) flavor symmetry.

$\Gamma(\text{charged anything})/\Gamma_{\text{total}}$ — Γ_{72}/Γ

VALUE	DOCUMENT ID		TECN	COMMENT
4.97±0.03±0.06	[1] ABREU	98H	DLPH	$e^+e^- \to Z$
• • • We do not use the following data for averages, fits, limits, etc. • • •				
5.84±0.04±0.38	ABREU	95C	DLPH	Repl. by ABREU 98H

[1] ABREU 98H measurement excludes the contribution from K^0 and Λ decay.

$\Gamma(\text{hadron}^+\text{hadron}^-)/\Gamma_{\text{total}}$ — Γ_{73}/Γ

VALUE (units 10^{-5})	DOCUMENT ID		TECN	COMMENT
$1.7^{+1.0}_{-0.7}\pm0.2$	[1,2] BUSKULIC	96V	ALEP	$e^+e^- \to Z$

[1] BUSKULIC 96V assumes PDG 96 production fractions for B^0, B^+, B_s, b baryons.
[2] Average branching fraction of weakly decaying B hadrons into two long-lived charged hadrons, weighted by their production cross section and lifetimes.

$\Gamma(\text{charmless})/\Gamma_{\text{total}}$ — Γ_{74}/Γ

VALUE	DOCUMENT ID		TECN	COMMENT
0.007±0.021	[1] ABREU	98D	DLPH	$e^+e^- \to Z$

[1] ABREU 98D results are extracted from a fit to the b-tagging probability distribution based on the impact parameter. The expected hidden charm contribution of 0.026 ± 0.004 has been subtracted.

$\Gamma(\mu^+\mu^-\text{anything})/\Gamma_{\text{total}}$ — Γ_{76}/Γ

Test for $\Delta B = 1$ weak neutral current.

VALUE	CL%	DOCUMENT ID		TECN	COMMENT
$<3.2 \times 10^{-4}$	90	ABBOTT	98B	D0	$p\overline{p}$ 1.8 TeV
• • • We do not use the following data for averages, fits, limits, etc. • • •					
$<5.0 \times 10^{-5}$	90	[1] ALBAJAR	91C	UA1	$E^{p\overline{p}}_{\text{cm}} = 630$ GeV
<0.02	95	ALTHOFF	84G	TASS	$E^{ee}_{\text{cm}} = 34.5$ GeV
<0.007	95	ADEVA	83	MRKJ	$E^{ee}_{\text{cm}} = 30$–38 GeV
<0.007	95	BARTEL	83B	JADE	$E^{ee}_{\text{cm}} = 33$–37 GeV

[1] Both ABBOTT 98B and GLENN 98 claim that the efficiency quoted in ALBAJAR 91C was overestimated by a large factor.

$[\Gamma(e^+e^-\text{anything}) + \Gamma(\mu^+\mu^-\text{anything})]/\Gamma_{\text{total}}$ — $(\Gamma_{75}+\Gamma_{76})/\Gamma$

Test for $\Delta B = 1$ weak neutral current.

VALUE	CL%	DOCUMENT ID		TECN	COMMENT
• • • We do not use the following data for averages, fits, limits, etc. • • •					
<0.008	90	MATTEUZZI	83	MRK2	$E^{ee}_{\text{cm}} = 29$ GeV

Downloaded from https://academic.oup.com/ptep/article/2022/8/083C01/6651666 by KIT Library user on 27 September 2022

$\Gamma(\nu\overline{\nu}\text{anything})/\Gamma_{\text{total}}$ — Γ_{77}/Γ

VALUE	DOCUMENT ID	TECN	COMMENT
• • • We do not use the following data for averages, fits, limits, etc. • • •			
$<3.9\times10^{-4}$	[1] GROSSMAN 96	RVUE	$e^+e^-\to Z$

[1] GROSSMAN 96 limit is derived from the ALEPH BUSKULIC 95 limit $B(B^+\to\tau^+\nu_\tau)<1.8\times10^{-3}$ at CL=90% using conservative simplifying assumptions.

χ_b AT HIGH ENERGY

For a discussion of B-$\overline{B}$ mixing, see the note on "B^0-$\overline{B}^0$ Mixing" in the B^0 Particle Listings.

χ_b is the average B-$\overline{B}$ mixing parameter at high-energy $\chi_b = f'_d\chi_d + f'_s\chi_s$ where f'_d and f'_s are the fractions of B^0 and B^0_s hadrons in an unbiased sample of semileptonic b-hadron decays.

"OUR EVALUATION" is an average using rescaled values of the data listed below. The average and rescaling were performed by the Heavy Flavor Averaging Group (HFLAV) and are described at https://hflav.web.cern.ch/. The averaging/rescaling procedure takes into account correlations between the measurements.

VALUE	EVTS	DOCUMENT ID		TECN	COMMENT
0.1284±0.0069 OUR EVALUATION					
0.129 ±0.004 OUR AVERAGE					
0.132 ±0.001 ±0.024		[1] ABAZOV	06S	D0	$p\overline{p}$ at 1.96 TeV
0.152 ±0.007 ±0.011		[2] ACOSTA	04A	CDF	$p\overline{p}$ at 1.8 TeV
0.1312±0.0049±0.0042		[3] ABBIENDI	03P	OPAL	$e^+e^-\to Z$
0.127 ±0.013 ±0.006		[4] ABREU	01L	DLPH	$e^+e^-\to Z$
0.1192±0.0068±0.0051		[5] ACCIARRI	99D	L3	$e^+e^-\to Z$
0.121 ±0.016 ±0.006		[6] ABREU	94J	DLPH	$e^+e^-\to Z$
0.114 ±0.014 ±0.008		[7] BUSKULIC	94G	ALEP	$e^+e^-\to Z$
0.129 ±0.022		[8] BUSKULIC	92B	ALEP	$e^+e^-\to Z$
0.176 ±0.031 ±0.032	1112	[9] ABE	91G	CDF	$p\overline{p}$ 1.8 TeV
0.148 ±0.029 ±0.017		[10] ALBAJAR	91D	UA1	$p\overline{p}$ 630 GeV
• • • We do not use the following data for averages, fits, limits, etc. • • •					
0.131 ±0.020 ±0.016		[11] ABE	97I	CDF	Repl. by ACOSTA 04A
0.1107±0.0062±0.0055		[12] ALEXANDER	96	OPAL	Rep. by ABBIENDI 03P
0.136 ±0.037 ±0.040		[13] UENO	96	AMY	e^+e^- at 57.9 GeV
0.144 ±0.014 $^{+0.017}_{-0.011}$		[14] ABREU	94F	DLPH	Sup. by ABREU 94J
0.131 ±0.014		[15] ABREU	94J	DLPH	$e^+e^-\to Z$
0.123 ±0.012 ±0.008		ACCIARRI	94D	L3	Repl. by ACCIARRI 99D
0.157 ±0.020 ±0.032		[16] ALBAJAR	94	UA1	$\sqrt{s}$ = 630 GeV
0.121 $^{+0.044}_{-0.040}$ ±0.017	1665	[17] ABREU	93C	DLPH	Sup. by ABREU 94J
0.143 $^{+0.022}_{-0.021}$ ±0.007		[18] AKERS	93B	OPAL	Sup. by ALEXANDER 96
0.145 $^{+0.041}_{-0.035}$ ±0.018		[19] ACTON	92C	OPAL	$e^+e^-\to Z$
0.121 ±0.017 ±0.006		[20] ADEVA	92C	L3	Sup. by ACCIARRI 94D
0.132 ±0.22 $^{+0.015}_{-0.012}$	823	[21] DECAMP	91	ALEP	$e^+e^-\to Z$
0.178 $^{+0.049}_{-0.040}$ ±0.020		[22] ADEVA	90P	L3	$e^+e^-\to Z$
0.17 $^{+0.15}_{-0.08}$		[23,24] WEIR	90	MRK2	e^+e^- 29 GeV
0.21 $^{+0.29}_{-0.15}$		[23] BAND	88	MAC	E^{ee}_{cm}= 29 GeV
>0.02 at 90% *CL*		[23] BAND	88	MAC	E^{ee}_{cm}= 29 GeV
0.121 ±0.047		[23,25] ALBAJAR	87C	UA1	Repl. by ALBAJAR 91D
<0.12 at 90% *CL*		[23,26] SCHAAD	85	MRK2	E^{ee}_{cm}= 29 GeV

[1] Uses the dimuon charge asymmetry. Averaged over the mix of b-flavored hadrons.
[2] Measurement performed using events containing a dimuon or an e/μ pair.
[3] The average B mixing parameter is determined simultaneously with b and c forward-backward asymmetries in the fit.
[4] The experimental systematic and model uncertainties are combined in quadrature.
[5] ACCIARRI 99D uses maximum-likelihood fits to extract χ_b as well as the A^b_{FB} in $Z\to b\overline{b}$ events containing prompt leptons.
[6] This ABREU 94J result is from 5182 $\ell\ell$ and 279 $\Lambda\ell$ events. The systematic error includes 0.004 for model dependence.
[7] BUSKULIC 94G data analyzed using ee, $e\mu$, and $\mu\mu$ events.
[8] BUSKULIC 92B uses a jet charge technique combined with electrons and muons.
[9] ABE 91G measurement of χ is done with $e\mu$ and ee events.
[10] ALBAJAR 91D measurement of χ is done with dimuons.
[11] Uses di-muon events.
[12] ALEXANDER 96 uses a maximum likelihood fit to simultaneously extract χ as well as the forward-backward asymmetries in $e^+e^-\to Z\to b\overline{b}$ and $c\overline{c}$.
[13] UENO 96 extracted χ from the energy dependence of the forward-backward asymmetry.
[14] ABREU 94F uses the average electric charge sum of the jets recoiling against a b-quark jet tagged by a high p_T muon. The result is for $\overline{\chi}=f_d\chi_d+0.9f_s\chi_s$.
[15] This ABREU 94J result combines $\ell\ell$, $\Lambda\ell$, and jet-charge ℓ (ABREU 94F) analyses. It is for $\overline{\chi}=f_d\chi_d+0.96f_s\chi_s$.
[16] ALBAJAR 94 uses dimuon events. Not independent of ALBAJAR 91D.
[17] ABREU 93C data analyzed using ee, $e\mu$, and $\mu\mu$ events.
[18] AKERS 93B analysis performed using dilepton events.
[19] ACTON 92C uses electrons and muons. Superseded by AKERS 93B.
[20] ADEVA 92C uses electrons and muons.
[21] DECAMP 91 done with opposite and like-sign dileptons. Superseded by BUSKULIC 92B.
[22] ADEVA 90P measurement uses ee, $\mu\mu$, and $e\mu$ events from 118k events at the Z. Superseded by ADEVA 92C.
[23] These experiments are not in the average because the combination of B_s and B_d mesons which they see could differ from those at higher energy.
[24] The WEIR 90 measurement supersedes the limit obtained in SCHAAD 85. The 90% CL are 0.06 and 0.38.
[25] ALBAJAR 87C measured $\chi=(\overline{B}^0\to B^0\to\mu^+X)$ divided by the average production weighted semileptonic branching fraction for B hadrons at 546 and 630 GeV.
[26] Limit is average probability for hadron containing B quark to produce a positive lepton.

CP VIOLATION PARAMETERS in semileptonic *b*-hadron decays.

$\text{Re}(\epsilon_b)/(1+|\epsilon_b|^2)$

CP impurity in semileptonic b-hadron decays.

VALUE (units 10^{-3})	DOCUMENT ID		TECN	COMMENT
• • • We do not use the following data for averages, fits, limits, etc. • • •				
−6.2 ±5.2 ±4.7	[1] AABOUD	17E	ATLS	pp at 8 TeV
−1.24±0.38±0.18	[2] ABAZOV	14	D0	$p\overline{p}$ at 1.96 TeV
−1.97±0.43±0.23	[3] ABAZOV	11U	D0	Repl. by ABAZOV 14
−2.39±0.63±0.37	[4] ABAZOV	10H	D0	Repl. by ABAZOV 11U

[1] AABOUD 17E reports a measurement of charge asymmetry of $A^b_{SL}=(-25\pm21\pm19)\times10^{-3}$ in lepton + jets $t\overline{t}$ events in which a b-hadron decays semileptonically to a soft muon.
[2] ABAZOV 14 reports a measurement of like-sign dimuon charge asymmetry of $A^b_{SL}=(-4.96\pm1.53\pm0.72)\times10^{-3}$ in semileptonic b-hadron decays.
[3] ABAZOV 11U reports a measurement of like-sign dimuon charge asymmetry of $A^b_{SL}=(-7.87\pm1.72\pm0.93)\times10^{-3}$ in semileptonic b-hadron decays.
[4] ABAZOV 10H reports a measurement of like-sign dimuon charge asymmetry of $A^b_{SL}=(-9.57\pm2.51\pm1.46)\times10^{-3}$ in semileptonic b-hadron decays. Using the measured production ratio of B^0_d and B^0_s, and the asymmetry of B^0_d $A^d_{SL}=(-4.7\pm4.6)\times10^{-3}$ measured from B-factories, they obtain the asymmetry for B^0_s as $A^s_{SL}=(-14.6\pm7.5)\times10^{-3}$.

B-HADRON PRODUCTION FRACTIONS IN $p\overline{p}$ COLLISIONS AT Tevatron

The production fractions for b-hadrons in $p\overline{p}$ collisions at the Tevatron have been calculated from the best values of mean lifetimes, mixing parameters, and branching fractions in this edition by the Heavy Flavor Averaging Group (HFLAV) (see https://hflav.web.cern.ch/).

The values reported below assume:

$f(\overline{b}\to B^+)=f(\overline{b}\to B^0)$

$f(\overline{b}\to B^+)+f(\overline{b}\to B^0)+f(\overline{b}\to B^0_s)+f(b\to b\text{-baryon})=1$

The values are:

$f(\overline{b}\to B^+)=f(\overline{b}\to B^0)=0.344\pm0.021$

$f(\overline{b}\to B^0_s)=0.115\pm0.013$

$f(b\to b\text{-baryon})=0.198\pm0.046$

$f(\overline{b}\to B^0_s)\ /\ f(\overline{b}\to B^0_d)=0.334\pm0.041$

and their correlation coefficients are:

$cor(B^0_s,\ b\text{-baryon})=-0.429$

$cor(B^0_s,\ B^+=B^0)=+0.159$

$cor(b\text{-baryon},\ B^+=B^0)=-0.960$

as obtained with the Tevatron average of time-integrated mixing parameter $\overline{\chi}=0.147\pm0.011$.

PRODUCTION ASYMMETRIES

$A^{b\overline{b}}_C$

$A^{b\overline{b}}_C=[N(\Delta y>0)-N(\Delta y<0)]\ /\ [N(\Delta y>0)+N(\Delta y<0)]$ with $\Delta y=|y_b|-|y_{\overline{b}}|$ where $y_{b/\overline{b}}$ is rapidity of b or $\overline{b}$ quarks.

VALUE (units 10^{-2})	DOCUMENT ID		TECN	COMMENT
Average is meaningless.				
0.4±0.4±0.3	[1] AAIJ	14AS	LHCB	pp at 7 TeV
2.0±0.9±0.6	[2] AAIJ	14AS	LHCB	pp at 7 TeV
1.6±1.7±0.6	[3] AAIJ	14AS	LHCB	pp at 7 TeV

[1] Measured for $40<M(b\overline{b})<75$ GeV/c^2.
[2] Measured for $75<M(b\overline{b})<105$ GeV/c^2.
[3] Measured for $M(b\overline{b})>105$ GeV/c^2.

$B^{\pm}/B^0/B^0_s/b$-baryon ADMIXTURE REFERENCES

AAIJ	21Y	PR D104 032005	R. Aaij *et al.*	(LHCb Collab.)
AAIJ	20G	EPJ C80 185	R. Aaij *et al.*	(LHCb Collab.)
AAIJ	20H	EPJ C80 191	R. Aaij *et al.*	(LHCb Collab.)
AAIJ	20V	PRL 124 122002	R. Aaij *et al.*	(LHCb Collab.)
AAIJ	19AB	PR D99 052006	R. Aaij *et al.*	(LHCb Collab.)
AAIJ	19AD	PR D100 031102	R. Aaij *et al.*	(LHCb Collab.)
AAIJ	19AI	PR D100 112006	R. Aaij *et al.*	(LHCb Collab.)
AABOUD	17E	JHEP 1702 071	M. Aaboud *et al.*	(ATLAS Collab.)
AAIJ	17BB	EPJ C77 609	R. Aaij *et al.*	(LHCb Collab.)
AAD	15CM	PRL 115 262001	G. Aad *et al.*	(ATLAS Collab.)
AAIJ	14AS	PRL 113 082003	R. Aaij *et al.*	(LHCb Collab.)

Downloaded from https://academic.oup.com/ptep/article/2022/8/083C01/6651666 by KIT Library user on 27 September 2022

ABAZOV	14	PR D89 012002	V.M. Abazov *et al.*	(D0 Collab.)
AAIJ	13P	JHEP 1304 001	R. Aaij *et al.*	(LHCb Collab.)
AAIJ	12BD	EPJ C72 2100	R. Aaij *et al.*	(LHCb Collab.)
Also		EPJ C80 49 (errat.)	R. Aaij *et al.*	(LHCb Collab.)
AAIJ	12J	PR D85 032008	R. Aaji *et al.*	(LHCb Collab.)
CHATRCHYAN	12AK	JHEP 1202 011	S. Chatrchyan *et al.*	(CMS Collab.)
AAIJ	11F	PRL 107 211801	R. Aaij *et al.*	(LHCb Collab.)
ABAZOV	11U	PR D84 052007	V.M. Abazov *et al.*	(D0 Collab.)
ABAZOV	10H	PRL 105 081801	V.M. Abazov *et al.*	(D0 Collab.)
Also		PR D82 032001	V.M. Abazov *et al.*	(D0 Collab.)
PDG	10	JP G37 075021	K. Nakamura *et al.*	(PDG Collab.)
AALTONEN	09E	PR D79 032001	T. Aaltonen *et al.*	(CDF Collab.)
AALTONEN	08N	PR D77 072003	T. Aaltonen *et al.*	(CDF Collab.)
ABAZOV	06S	PR D74 092001	V.M. Abazov *et al.*	(D0 Collab.)
ABBIENDI	04I	EPJ C35 149	G. Abbiendi *et al.*	(OPAL Collab.)
ABDALLAH	04E	EPJ C33 307	J. Abdallah *et al.*	(DELPHI Collab.)
ACOSTA	04A	PR D69 012002	D. Acosta *et al.*	(CDF Collab.)
ABBIENDI	03M	EPJ C30 467	G. Abbiendi *et al.*	(OPAL Collab.)
ABBIENDI	03P	PL B577 18	G. Abbiendi *et al.*	(OPAL Collab.)
ABDALLAH	03E	PL B561 26	J. Abdallah *et al.*	(DELPHI Collab.)
ABDALLAH	03K	PL B576 29	J. Abdallah *et al.*	(DELPHI Collab.)
HEISTER	02G	EPJ C22 613	A. Heister *et al.*	(ALEPH Collab.)
ABBIENDI	01Q	PL B520 1	G. Abbiendi *et al.*	(OPAL Collab.)
ABBIENDI	01R	EPJ C21 399	G. Abbiendi *et al.*	(OPAL Collab.)
ABREU	01L	EPJ C20 455	P. Abreu *et al.*	(DELPHI Collab.)
BARATE	01E	EPJ C19 213	R. Barate *et al.*	(ALEPH Collab.)
ABBIENDI	00E	EPJ C13 225	G. Abbiendi *et al.*	(OPAL Collab.)
ABBIENDI	00Z	PL B492 13	G. Abbiendi *et al.*	(OPAL Collab.)
ABREU	00	EPJ C12 225	P. Abreu *et al.*	(DELPHI Collab.)
ABREU	00C	PL B496 43	P. Abreu *et al.*	(DELPHI Collab.)
ABREU	00D	PL B478 14	P. Abreu *et al.*	(DELPHI Collab.)
ABREU	00R	PL B475 407	P. Abreu *et al.*	(DELPHI Collab.)
ACCIARRI	00	EPJ C13 47	M. Acciarri *et al.*	(L3 Collab.)
AFFOLDER	00E	PRL 84 1663	T. Affolder *et al.*	(CDF Collab.)
ABBIENDI	99J	EPJ C12 609	G. Abbiendi *et al.*	(OPAL Collab.)
ABE	99P	PR D60 092005	F. Abe *et al.*	(CDF Collab.)
ACCIARRI	99D	PL B448 152	M. Acciarri *et al.*	(L3 Collab.)
BARATE	99G	EPJ C6 555	R. Barate *et al.*	(ALEPH Collab.)
ABBOTT	98B	PL B423 419	B. Abbott *et al.*	(D0 Collab.)
ABE	98B	PR D57 5382	F. Abe *et al.*	(CDF Collab.)
ABREU	98D	PL B426 193	P. Abreu *et al.*	(DELPHI Collab.)
ABREU	98H	PL B425 399	P. Abreu *et al.*	(DELPHI Collab.)
ACCIARRI	98	PL B416 220	M. Acciarri *et al.*	(L3 Collab.)
ACCIARRI	98K	PL B436 174	M. Acciarri *et al.*	(L3 Collab.)
ACKERSTAFF	98E	EPJ C1 439	K. Ackerstaff *et al.*	(OPAL Collab.)
BARATE	98I	PL B429 169	R. Barate *et al.*	(ALEPH Collab.)
BARATE	98Q	EPJ C4 387	R. Barate *et al.*	(ALEPH Collab.)
BARATE	98V	EPJ C5 205	R. Barate *et al.*	(ALEPH Collab.)
GLENN	98	PRL 80 2289	S. Glenn *et al.*	(CLEO Collab.)
ABE	97I	PR D55 2546	F. Abe *et al.*	(CDF Collab.)
ACKERSTAFF	97F	ZPHY C73 397	K. Ackerstaff *et al.*	(OPAL Collab.)
ACKERSTAFF	97N	ZPHY C74 423	K. Ackerstaff *et al.*	(OPAL Collab.)
ACKERSTAFF	97W	ZPHY C76 425	K. Ackerstaff *et al.*	(OPAL Collab.)
ABREU	96E	PL B377 195	P. Abreu *et al.*	(DELPHI Collab.)
ACCIARRI	96C	ZPHY C71 379	M. Acciarri *et al.*	(L3 Collab.)
ADAM	96	ZPHY C69 561	W. Adam *et al.*	(DELPHI Collab.)
ADAM	96D	ZPHY C72 207	W. Adam *et al.*	(DELPHI Collab.)
ALEXANDER	96	ZPHY C70 357	G. Alexander *et al.*	(OPAL Collab.)
BUSKULIC	96F	PL B369 151	D. Buskulic *et al.*	(ALEPH Collab.)
BUSKULIC	96V	PL B384 471	D. Buskulic *et al.*	(ALEPH Collab.)
BUSKULIC	96Y	PL B388 648	D. Buskulic *et al.*	(ALEPH Collab.)
GROSSMAN	96	NP B465 369	Y. Grossman, Z. Ligeti, E. Nardi	(REHO, CIT)
Also		NP B480 753 (erratum)	Y. Grossman, Z. Ligeti, E. Nardi	
PDG	96	PR D54 1	R. M. Barnett *et al.*	(PDG Collab.)
UENO	96	PL B381 365	K. Ueno *et al.*	(AMY Collab.)
ABE,K	95B	PRL 75 3624	K. Abe *et al.*	(SLD Collab.)
ABREU	95C	PL B347 447	P. Abreu *et al.*	(DELPHI Collab.)
ABREU	95D	ZPHY C66 323	P. Abreu *et al.*	(DELPHI Collab.)
ADAM	95	ZPHY C68 363	W. Adam *et al.*	(DELPHI Collab.)
AKERS	95Q	ZPHY C67 57	R. Akers *et al.*	(OPAL Collab.)
BUSKULIC	95	PL B343 444	D. Buskulic *et al.*	(ALEPH Collab.)
ABREU	94F	PL B322 459	P. Abreu *et al.*	(DELPHI Collab.)
ABREU	94J	PL B332 488	P. Abreu *et al.*	(DELPHI Collab.)
ABREU	94L	ZPHY C63 3	P. Abreu *et al.*	(DELPHI Collab.)
ABREU	94P	PL B341 109	P. Abreu *et al.*	(DELPHI Collab.)
ACCIARRI	94C	PL B332 201	M. Acciarri *et al.*	(L3 Collab.)
ACCIARRI	94D	PL B335 542	M. Acciarri *et al.*	(L3 Collab.)
ALBAJAR	94	ZPHY C61 41	C. Albajar *et al.*	(UA1 Collab.)
BUSKULIC	94G	ZPHY C62 179	D. Buskulic *et al.*	(ALEPH Collab.)
ABE	93E	PL B313 288	K. Abe *et al.*	(VENUS Collab.)
ABE	93J	PRL 71 3421	F. Abe *et al.*	(CDF Collab.)
ABREU	93C	PL B301 145	P. Abreu *et al.*	(DELPHI Collab.)
ABREU	93D	ZPHY C57 181	P. Abreu *et al.*	(DELPHI Collab.)
ABREU	93G	PL B312 253	P. Abreu *et al.*	(DELPHI Collab.)
ACTON	93C	PL B307 247	P.D. Acton *et al.*	(OPAL Collab.)
ACTON	93L	ZPHY C60 217	P.D. Acton *et al.*	(OPAL Collab.)
ADRIANI	93J	PL B317 467	O. Adriani *et al.*	(L3 Collab.)
ADRIANI	93K	PL B317 474	O. Adriani *et al.*	(L3 Collab.)
ADRIANI	93L	PL B317 637	O. Adriani *et al.*	(L3 Collab.)
AKERS	93B	ZPHY C60 199	R. Akers *et al.*	(OPAL Collab.)
BUSKULIC	93B	PL B298 479	D. Buskulic *et al.*	(ALEPH Collab.)
BUSKULIC	93O	PL B314 459	D. Buskulic *et al.*	(ALEPH Collab.)
ABREU	92	ZPHY C53 567	P. Abreu *et al.*	(DELPHI Collab.)
ACTON	92	PL B274 513	D.P. Acton *et al.*	(OPAL Collab.)
ACTON	92C	PL B276 379	D.P. Acton *et al.*	(OPAL Collab.)
ADEVA	92C	PL B288 395	B. Adeva *et al.*	(L3 Collab.)
ADRIANI	92	PL B288 412	O. Adriani *et al.*	(L3 Collab.)
BUSKULIC	92B	PL B284 177	D. Buskulic *et al.*	(ALEPH Collab.)
BUSKULIC	92F	PL B295 174	D. Buskulic *et al.*	(ALEPH Collab.)
BUSKULIC	92G	PL B295 396	D. Buskulic *et al.*	(ALEPH Collab.)
ABE	91G	PRL 67 3351	F. Abe *et al.*	(CDF Collab.)
ADEVA	91C	PL B261 177	B. Adeva *et al.*	(L3 Collab.)
ADEVA	91H	PL B270 111	B. Adeva *et al.*	(L3 Collab.)
ALBAJAR	91C	PL B262 163	C. Albajar *et al.*	(UA1 Collab.)
ALBAJAR	91D	PL B262 171	C. Albajar *et al.*	(UA1 Collab.)
ALEXANDER	91G	PL B266 485	G. Alexander *et al.*	(OPAL Collab.)
DECAMP	91	PL B258 236	D. Decamp *et al.*	(ALEPH Collab.)
DECAMP	91C	PL B257 492	D. Decamp *et al.*	(ALEPH Collab.)
ADEVA	90P	PL B252 703	B. Adeva *et al.*	(L3 Collab.)
BEHREND	90D	ZPHY C47 333	H.J. Behrend *et al.*	(CELLO Collab.)
HAGEMANN	90	ZPHY C48 401	J. Hagemann *et al.*	(JADE Collab.)
LYONS	90	PR D41 982	L. Lyons, A.J. Martin, D.H. Saxon	(OXF, BRIS+)
WEIR	90	PL B240 289	A.J. Weir *et al.*	(Mark II Collab.)
BRAUNSCH...	89B	ZPHY C44 1	R. Braunschweig *et al.*	(TASSO Collab.)
ONG	89	PRL 62 1236	R.A. Ong *et al.*	(Mark II Collab.)
BAND	88	PL B200 221	H.R. Band *et al.*	(MAC Collab.)
KLEM	88	PR D37 41	D.E. Klem *et al.*	(DELCO Collab.)
ONG	88	PRL 60 2587	R.A. Ong *et al.*	(Mark II Collab.)
ALBAJAR	87C	PL B186 247	C. Albajar *et al.*	(UA1 Collab.)
ASH	87	PRL 58 640	W.W. Ash *et al.*	(MAC Collab.)
BARTEL	87	ZPHY C33 339	W. Bartel *et al.*	(JADE Collab.)
BROM	87	PL B195 301	J.M. Brom *et al.*	(HRS Collab.)
PAL	86	PR D33 2708	T. Pal *et al.*	(DELCO Collab.)
AIHARA	85	ZPHY C27 39	H. Aihara *et al.*	(TPC Collab.)
BARTEL	85J	PL 163B 277	W. Bartel *et al.*	(JADE Collab.)
SCHAAD	85	PL 160B 188	T. Schaad *et al.*	(Mark II Collab.)
ALTHOFF	84G	ZPHY C22 219	M. Althoff *et al.*	(TASSO Collab.)
ALTHOFF	84J	PL 146B 443	M. Althoff *et al.*	(TASSO Collab.)
KOOP	84	PRL 52 970	D.E. Koop *et al.*	(DELCO Collab.)
ADEVA	83	PRL 50 799	B. Adeva *et al.*	(Mark-J Collab.)
ADEVA	83B	PRL 51 443	B. Adeva *et al.*	(Mark-J Collab.)
BARTEL	83B	PL 132B 241	W. Bartel *et al.*	(JADE Collab.)
FERNANDEZ	83D	PRL 50 2054	E. Fernandez *et al.*	(MAC Collab.)
MATTEUZZI	83	PL 129B 141	C. Matteuzzi *et al.*	(Mark II Collab.)
NELSON	83	PRL 50 1542	M.E. Nelson *et al.*	(Mark II Collab.)

V_{cb} and V_{ub} CKM Matrix Elements

OMITTED FROM SUMMARY TABLE

See the related review(s):

Semileptonic B Hadron Decays, Determination of V_{cb} and V_{ub}

V_{cb} MEASUREMENTS

For the discussion of V_{cb} measurements, which is not repeated here, see the review on "Determination of $|V_{cb}|$ and $|V_{ub}|$."

The CKM matrix element $|V_{cb}|$ can be determined by studying the rate of the semileptonic decay $B \to D^{(*)}\ell\nu$ as a function of the recoil kinematics of $D^{(*)}$ mesons. Taking advantage of theoretical constraints on the normalization and a linear ω dependence of the form factors ($F(\omega)$, $G(\omega)$) provided by Heavy Quark Effective Theory (HQET), the $|V_{cb}|\times F(\omega)$ and ρ^2 can be simultaneously extracted from data, where ω is the scalar product of the two-meson four velocities, $F(1)$ is the form factor at zero recoil (ω=1) and ρ^2 is the slope. Using the theoretical input of $F(1)$, a value of $|V_{cb}|$ can be obtained.

"OUR EVALUATION" is an average using rescaled values of the data listed below. The average and rescaling were performed by the Heavy Flavor Averaging Group (HFLAV) and are described at https://hflav.web.cern.ch/. The averaging/rescaling procedure takes into account correlations between the measurements.

$|V_{cb}| \times F(1)$ (from $B^0 \to D^{*-}\ell^+\nu$)

VALUE (units 10^{-2})	DOCUMENT ID		TECN	COMMENT
3.500±0.036 OUR EVALUATION	with ρ^2=1.121 ± 0.024 and a correlation 0.317. The fitted χ^2 is 42.2 for 23 degrees of freedom.			
3.57 ±0.08 OUR AVERAGE	Error includes scale factor of 1.6. See the ideogram below.			
3.506±0.015±0.056	[1] WAHEED	21	BELL	$e^+e^- \to \Upsilon(4S)$
3.59 ±0.02 ±0.12	[2] AUBERT	09A	BABR	$e^+e^- \to \Upsilon(4S)$
3.92 ±0.18 ±0.23	[3] ABDALLAH	04D	DLPH	$e^+e^- \to Z^0$
4.31 ±0.13 ±0.18	[4] ADAM	03	CLE2	$e^+e^- \to \Upsilon(4S)$
3.55 ±0.14 $^{+0.23}_{-0.24}$	[5] ABREU	01H	DLPH	$e^+e^- \to Z$
3.71 ±0.10 ±0.20	[6] ABBIENDI	00Q	OPAL	$e^+e^- \to Z$
3.19 ±0.18 ±0.19	[7] BUSKULIC	97	ALEP	$e^+e^- \to Z$
• • • We do not use the following data for averages, fits, limits, etc. • • •				
3.483±0.015±0.056	[1] WAHEED	19	BELL	Repl. by WAHEED 21
3.46 ±0.02 ±0.10	[8] DUNGEL	10	BELL	Rep. by WAHEED 19
3.59 ±0.06 ±0.14	[9] AUBERT	08AT	BABR	Repl. by AUBERT 09A
3.44 ±0.03 ±0.11	[10] AUBERT	08R	BABR	Repl. by AUBERT 09A
3.55 ±0.03 ±0.16	[11] AUBERT	05E	BABR	Repl. by AUBERT 08R
3.77 ±0.11 ±0.19	[12] ABDALLAH	04D	DLPH	$e^+e^- \to Z^0$
3.54 ±0.19 ±0.18	[13] ABE	02F	BELL	Repl. by DUNGEL 10
4.31 ±0.13 ±0.18	[14] BRIERE	02	CLE2	$e^+e^- \to \Upsilon(4S)$
3.28 ±0.19 ±0.22	ACKERSTAFF	97G	OPAL	Repl. by ABBIENDI 00Q
3.50 ±0.19 ±0.23	[15] ABREU	96P	DLPH	Repl. by ABREU 01H
3.51 ±0.19 ±0.20	[16] BARISH	95	CLE2	Repl. by ADAM 03
3.14 ±0.23 ±0.25	BUSKULIC	95N	ALEP	Repl. by BUSKULIC 97

[1] WAHEED 21 uses fully reconstructed $D^{*-}\ell^+\nu$ events ($\ell = e$ or μ) and $\eta_{EW} = 1.0066$.

[2] Obtained from a global fit to $B \to D^{(*)}\ell\nu_\ell$ events, with reconstructed $D^0\ell$ and $D^+\ell$ final states and $\rho^2 = 1.22 \pm 0.02 \pm 0.07$.

[3] Measurement using fully reconstructed D^* sample with a $\rho^2 = 1.32 \pm 0.15 \pm 0.33$.

[4] Average of the $B^0 \to D^*(2010)^-\ell^+\nu$ and $B^+ \to \overline{D}^*(2007))\ell^+\nu$ modes with $\rho^2 = 1.61 \pm 0.09 \pm 0.21$ and $f_{+-} = 0.521 \pm 0.012$.

[5] ABREU 01H measured using about 5000 partial reconstructed D^* sample with a ρ^2=1.34 ± $0.14^{+0.24}_{-0.22}$.

[6] ABBIENDI 00Q: measured using both inclusively and exclusively reconstructed $D^{*\pm}$ samples with a ρ^2=1.21 ± 0.12 ± 0.20. The statistical and systematic correlations between $|V_{cb}|\times F(1)$ and ρ^2 are 0.90 and 0.54 respectively.

[7] BUSKULIC 97: measured using exclusively reconstructed $D^{*\pm}$ with a a^2=0.31 ± 0.17 ± 0.08. The statistical correlation is 0.92.

[8] Uses fully reconstructed $D^{*-}\ell^+\nu$ events ($\ell = e$ or μ).

[9] Measured using the dependence of $B^- \to D^{*0}e^-\overline{\nu}_e$ decay differential rate and the form factor description by CAPRINI 98 with $\rho^2 = 1.16 \pm 0.06 \pm 0.08$.

Downloaded from https://academic.oup.com/ptep/article/2022/8/083C01/6651666 by KIT Library user on 27 September 2022

[10] Measured using fully reconstructed D^* sample and a simultaneous fit to the Caprini-Lellouch-Neubert form factor parameters: $\rho^2 = 1.191 \pm 0.048 \pm 0.028$, $R_1(1) = 1.429 \pm 0.061 \pm 0.044$, and $R_2(1) = 0.827 \pm 0.038 \pm 0.022$.

[11] Measurement using fully reconstructed D^* sample with a $\rho^2 = 1.29 \pm 0.03 \pm 0.27$.

[12] Combines with previous partial reconstructed D^* measurement with a $\rho^2 = 1.39 \pm 0.10 \pm 0.33$.

[13] Measured using exclusive $B^0 \to D^*(892)^- e^+ \nu$ decays with $\rho^2 = 1.35 \pm 0.17 \pm 0.19$ and a correlation of 0.91.

[14] BRIERE 02 result is based on the same analysis and data sample reported in ADAM 03.

[15] ABREU 96P: measured using both inclusively and exclusively reconstructed $D^{*\pm}$ samples.

[16] BARISH 95: measured using both exclusive reconstructed $B^0 \to D^{*-} \ell^+ \nu$ and $B^+ \to D^{*0} \ell^+ \nu$ samples. They report their experiment's uncertainties $\pm 0.0019 \pm 0.0018 \pm 0.0008$, where the first error is statistical, the second is systematic, and the third is the uncertainty in the lifetimes. We combine the last two in quadrature.

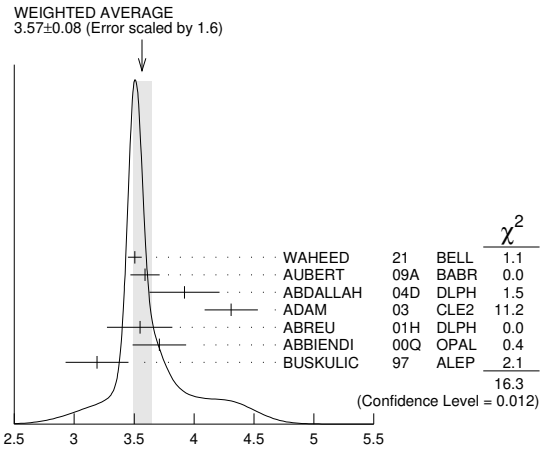

$|V_{cb}| \times F(1)$ (from $B^0 \to D^{*-} \ell^+ \nu$)

$|V_{cb}| \times G(1)$ (from $B \to D^- \ell^+ \nu$)

VALUE	DOCUMENT ID		TECN	COMMENT
0.04153±0.00098 OUR EVALUATION				with ρ^2=1.129 ± 0.033 and a correlation 0.758.
The fitted χ^2 is 4.6 for 8 degrees of freedom.				
0.0422 ±0.0010 OUR AVERAGE				
0.04229±0.00137	[1] GLATTAUER	16	BELL	$e^+e^- \to \Upsilon(4S)$
0.0423 ±0.0019 ±0.0014	[2] AUBERT	10	BABR	$e^+e^- \to \Upsilon(4S)$
0.0431 ±0.0008 ±0.0023	[3] AUBERT	09A	BABR	$e^+e^- \to \Upsilon(4S)$
0.0416 ±0.0047 ±0.0037	[4] BARTELT	99	CLE2	$e^+e^- \to \Upsilon(4S)$
0.0278 ±0.0068 ±0.0065	[5] BUSKULIC	97	ALEP	$e^+e^- \to Z$
• • • We do not use the following data for averages, fits, limits, etc. • • •				
0.0411 ±0.0044 ±0.0052	[6] ABE	02E	BELL	Repl. by GLATTAUER 16
0.0337 ±0.0044 $^{+0.0072}_{-0.0049}$	[7] ATHANAS	97	CLE2	Repl. by BARTELT 99

[1] Obtained from a fit to the combined partially reconstructed $B \to \overline{D} \ell \nu_\ell$ sample while tagged by the other fully reconstructed B meson in the event. Also reports fitted $\rho^2 = 1.09 \pm 0.05$.

[2] Obtained from a fit to the combined $B \to \overline{D} \ell^+ \nu_\ell$ sample in which a hadronic decay of the second B meson is fully reconstructed and $\rho^2 = 1.20 \pm 0.09 \pm 0.04$.

[3] Obtained from a global fit to $B \to D^{(*)} \ell \nu_\ell$ events, with reconstructed $D^0 \ell$ and $D^+ \ell$ final states and $\rho^2 = 1.20 \pm 0.04 \pm 0.07$.

[4] BARTELT 99: measured using both exclusive reconstructed $B^0 \to D^- \ell^+ \nu$ and $B^+ \to D^0 \ell^+ \nu$ samples.

[5] BUSKULIC 97: measured using exclusively reconstructed $D^\pm$ with a $a^2 = -0.05 \pm 0.53 \pm 0.38$. The statistical correlation is 0.99.

[6] Using the missing energy and momentum to extract kinematic information about the undetected neutrino in the $B^0 \to D^- \ell^+ \nu$ decay.

[7] ATHANAS 97: measured using both exclusive reconstructed $B^0 \to D^- \ell^+ \nu$ and $B^+ \to D^0 \ell^+ \nu$ samples with a $\rho^2 = 0.59 \pm 0.22 \pm 0.12 ^{+0.59}_{-0}$. They report their experiment's uncertainties $\pm 0.0044 \pm 0.0048 ^{+0.0053}_{-0.0012}$, where the first error is statistical, the second is systematic, and the third is the uncertainty due to the form factor model variations. We combine the last two in quadrature.

$|V_{cb}|$ (from $D_s^{*-} \mu^+ \nu_\mu$)

VALUE (units 10^{-3})	DOCUMENT ID		TECN	COMMENT
41.4±0.6±0.9±1.2	[1] AAIJ	20E	LHCB	pp at 7, 8 TeV

[1] Measured from an inclusive sample of $D_s^- \mu^+$ candidates using CNL parameterization of the form factor. AAIJ 20E provides also measurement of $|V_{cb}| = (42.3 \pm 0.8 \pm 0.9 \pm 1.2) \times 10^{-3}$ using BGL parameterization of the form factor. The third uncertainty is due to the external inputs used in the measurement.

V_{ub} MEASUREMENTS

For the discussion of V_{ub} measurements, which is not repeated here, see the review on "Determination of $|V_{cb}|$ and $|V_{ub}|$."

The CKM matrix element $|V_{ub}|$ can be determined by studying the rate of the charmless semileptonic decay $b \to u \ell \nu$. The relevant branching ratio measurements based on exclusive and inclusive decays can be found in the B Listings, and are not repeated here.

V_{cb} and V_{ub} CKM Matrix Elements REFERENCES

WAHEED	21	PR D103 079901	E. Waheed et al.	(BELLE Collab.)
AAIJ	20E	PR D101 072004	R. Aaij et al.	(LHCb Collab.)
WAHEED	19	PR D100 052007	E. Waheed et al.	(BELLE Collab.)
GLATTAUER	16	PR D93 032006	R. Glattauer et al.	(BELLE Collab.)
AUBERT	10	PRL 104 011802	B. Aubert et al.	(BABAR Collab.)
DUNGEL	10	PR D82 112007	W. Dungel et al.	(BELLE Collab.)
AUBERT	09A	PR D79 012002	B. Aubert et al.	(BABAR Collab.)
AUBERT	08AT	PRL 100 231803	B. Aubert et al.	(BABAR Collab.)
AUBERT	08R	PR D77 032002	B. Aubert et al.	(BABAR Collab.)
AUBERT	05E	PR D71 051502	B. Aubert et al.	(BABAR Collab.)
ABDALLAH	04D	EPJ C33 213	J. Abdallah et al.	(DELPHI Collab.)
ADAM	03	PR D67 032001	N.E. Adam et al.	(CLEO Collab.)
ABE	02E	PL B526 258	K. Abe et al.	(BELLE Collab.)
ABE	02F	PL B526 247	K. Abe et al.	(BELLE Collab.)
BRIERE	02	PRL 89 081803	R. Briere et al.	(CLEO Collab.)
ABREU	01H	PL B510 55	P. Abreu et al.	(DELPHI Collab.)
ABBIENDI	00Q	PL B482 15	G. Abbiendi et al.	(OPAL Collab.)
BARTELT	99	PRL 82 3746	J. Bartelt et al.	(CLEO Collab.)
CAPRINI	98	NP B530 153	I. Caprini, L. Lellouch, M. Neubert	(BCIP, CERN)
ACKERSTAFF	97G	PL B395 128	K. Ackerstaff et al.	(OPAL Collab.)
ATHANAS	97	PRL 79 2208	M. Athanas et al.	(CLEO Collab.)
BUSKULIC	97	PL B395 373	D. Buskulic et al.	(ALEPH Collab.)
ABREU	96P	ZPHY C71 539	P. Abreu et al.	(DELPHI Collab.)
BARISH	95	PR D51 1014	B.C. Barish et al.	(CLEO Collab.)
BUSKULIC	95N	PL B359 236	D. Buskulic et al.	(ALEPH Collab.)

B^*

$I(J^P) = \frac{1}{2}(1^-)$
I, J, P need confirmation.

Quantum numbers shown are quark-model predictions.

B^* MASS

From mass difference below and the average of our B masses $(m_{B^\pm} + m_{B^0})/2$.

VALUE (MeV)	DOCUMENT ID
5324.71±0.21 OUR FIT	

$m_{B^*} - m_B$

VALUE (MeV)	EVTS	DOCUMENT ID		TECN	COMMENT
45.21±0.21 OUR FIT					
45.42±0.26 OUR AVERAGE		Includes data from the datablock that follows this one.			
46.2 ±0.3 ±0.8		[1] ACKERSTAFF	97M	OPAL	$e^+e^- \to Z$
45.3 ±0.35±0.87	4227	[1] BUSKULIC	96D	ALEP	$E^{ee}_{\rm cm}$= 88–94 GeV
45.5 ±0.3 ±0.8		[1] ABREU	95R	DLPH	$E^{ee}_{\rm cm}$= 88–94 GeV
46.3 ±1.9	1378	[1] ACCIARRI	95B	L3	$E^{ee}_{\rm cm}$= 88–94 GeV
46.4 ±0.3 ±0.8		[2] AKERIB	91	CLE2	$e^+e^- \to \gamma X$
45.6 ±0.8		[2] WU	91	CSB2	$e^+e^- \to \gamma X, \gamma \ell X$
45.4 ±1.0		[3] LEE-FRANZINI	90	CSB2	$e^+e^- \to \Upsilon(5S)$
• • • We do not use the following data for averages, fits, limits, etc. • • •					
52 ±2 ±4	1400	[4] HAN	85	CUSB	$e^+e^- \to \gamma e X$

[1] u, d, s flavor averaged.

[2] These papers report E_γ in the B^* center of mass. The $m_{B^*} - m_B$ is 0.2 MeV higher. $E_{\rm cm}$ = 10.61–10.7 GeV. Admixture of B^0 and B^+ mesons, but not B_s.

[3] LEE-FRANZINI 90 value is for an admixture of B^0 and B^+. They measure 46.7 ± 0.4 ± 0.2 MeV for an admixture of B^0, B^+, and B_s, and use the shape of the photon line to separate the above value.

[4] HAN 85 is for $E_{\rm cm}$ = 10.6–11.2 GeV, giving an admixture of B^0, B^+, and B_s.

$m_{B^{*+}} - m_{B^+}$

VALUE (MeV)	DOCUMENT ID		TECN	COMMENT
The data in this block is included in the average printed for a previous datablock.				
45.37±0.21 OUR FIT				
45.01±0.30±0.23	[5] AAIJ	13O	LHCB	pp at 7 TeV

[5] Obtained the mass difference between $B^{*+} K^-$ and $B^+ K^-$ from $B^*_{s2}(5840)^0$ decay.

$|(m_{B^{*+}} - m_{B^+}) - (m_{B^{*0}} - m_{B^0})|$

VALUE (MeV)	CL%	DOCUMENT ID		TECN	COMMENT
<6	95	ABREU	95R	DLPH	$E^{ee}_{\rm cm}$= 88–94 GeV

$m_{B^{*0}} - m_{B^{*+}}$

VALUE (MeV)	DOCUMENT ID		TECN	COMMENT
0.91±0.24±0.09	[6] SIRUNYAN	18DF	CMS	pp at 8 TeV

[6] Uses exclusively reconstructed final states containing a $J/\psi \to \mu^+ \mu^-$ decay.

Downloaded from https://academic.oup.com/ptep/article/2022/8/083C01/6651666 by KIT Library user on 27 September 2022

B^* DECAY MODES

	Mode	Fraction (Γ_i/Γ)
Γ_1	$B\gamma$	seen

B^* REFERENCES

SIRUNYAN	18DF	EPJ C78 939	A.M. Sirunyan *et al.*	(CMS Collab.)
AAIJ	13O	PRL 110 151803	R. Aaij *et al.*	(LHCb Collab.)
ACKERSTAFF	97M	ZPHY C74 413	K. Ackerstaff *et al.*	(OPAL Collab.)
BUSKULIC	96D	ZPHY C69 393	D. Buskulic *et al.*	(ALEPH Collab.)
ABREU	95R	ZPHY C68 353	P. Abreu *et al.*	(DELPHI Collab.)
ACCIARRI	95B	PL B345 589	M. Acciarri *et al.*	(L3 Collab.)
AKERIB	91	PRL 67 1692	D.S. Akerib *et al.*	(CLEO Collab.)
WU	91	PL B273 177	Q.W. Wu *et al.*	(CUSB II Collab.)
LEE-FRANZINI	90	PRL 65 2947	J. Lee-Franzini *et al.*	(CUSB II Collab.)
HAN	85	PRL 55 36	K. Han *et al.*	(COLU, LSU, MPIM, STON)

$B_1(5721)$

$I(J^P) = \frac{1}{2}(1^+)$
I, J, P need confirmation.

Quantum numbers shown are quark-model predictions.

$B_1(5721)$ MASS

$B_1(5721)^+$ mass

OUR FIT uses $m_{B^{*0}}$ and $m_{B_1^+} - m_{B^{*0}}$ to determine $m_{B_1(5721)^+}$.

VALUE (MeV)	DOCUMENT ID
$5725.9^{+2.5}_{-2.7}$ OUR FIT	

$m_{B_1^+} - m_{B^{*0}}$

VALUE (MeV)	EVTS	DOCUMENT ID		TECN	COMMENT
$401.2^{+2.4}_{-2.7}$ OUR FIT					
$401.2^{+2.4}_{-2.7}$ OUR AVERAGE					
$400.5 \pm 1.8 \pm 3.1$	8k	[1] AAIJ	15AB	LHCB	pp at 7, 8 TeV
$402 \pm 3 \; ^{+1}_{-3}$		[2] AALTONEN	14I	CDF	$p\overline{p}$ at 1.96 TeV

[1] AAIJ 15AB reports $[m_{B_1^+} - m_{B^0}] - (m_{B^{*0}} - m_{B^0}) - m_{\pi^+} = 260.9 \pm 1.8 \pm 3.1$ MeV which we adjust by the π^+ mass and assume $(m_{B^{*0}} - m_{B^0}) = (m_{B^{*+}} - m_{B^+}) = 45.01 \pm 0.30 \pm 0.23$ MeV. The masses inside the square brackets were measured for each candidate event.

[2] AALTONEN 14I reports $m_{B_1(5721)^+} - m_{B^{*0}} - m_{\pi^+} = 262 \pm 3^{+1}_{-3}$ MeV which we adjusted by the π^+ mass.

$B_1(5721)^0$ mass

OUR FIT uses mass differences measurements listed below to determine the mass $m_{B_1(5721)^0}$.

VALUE (MeV)	DOCUMENT ID
5726.1 ± 1.3 OUR FIT Error includes scale factor of 1.2.	

$m_{B_1^0} - m_{B^+}$

VALUE (MeV)	DOCUMENT ID		TECN	COMMENT
446.7 ± 1.3 OUR FIT Error includes scale factor of 1.2.				
$441.5 \pm 2.4 \pm 1.3$	[1] ABAZOV	07T	D0	$p\overline{p}$ at 1.96 TeV
• • • We do not use the following data for averages, fits, limits, etc. • • •				
$446.2^{+1.9}_{-2.1}{}^{+1.0}_{-1.2}$	[1] AALTONEN	09D	CDF	Repl. by AALTONEN 14I

[1] Observed in $B_1^0 \to B^{*+}\pi^-$.

$m_{B_1^0} - m_{B^{*+}}$

VALUE (MeV)	EVTS	DOCUMENT ID		TECN	COMMENT
401.4 ± 1.2 OUR FIT Error includes scale factor of 1.2.					
402.8 ± 1.1 OUR AVERAGE					
$403.4 \pm 0.7 \pm 1.5$	35k	[1] AAIJ	15AB	LHCB	pp at 7, 8 TeV
$402.3 \pm 0.9^{+1.1}_{-1.2}$		[2] AALTONEN	14I	CDF	$p\overline{p}$ at 1.96 TeV

[1] AAIJ 15AB reports $[m_{B_1^0} - m_{B^+}] - (m_{B^{*+}} - m_{B^+}) - m_{\pi^-} = 263.9 \pm 0.7 \pm 1.4$ MeV which we adjust by the π^- mass and $(m_{B^{*+}} - m_{B^+}) = 45.01 \pm 0.30 \pm 0.23$ MeV. The masses inside the square brackets were measured for each candidate event.

[2] AALTONEN 14I reports $m_{B_1(5721)^0} - m_{B^{*+}} - m_{\pi^-} = 262.7 \pm 0.9^{+1.1}_{-1.2}$ MeV which we adjusted by the π^- mass.

$B_1(5721)$ WIDTH

$B_1(5721)^+$ width

VALUE (MeV)	EVTS	DOCUMENT ID		TECN	COMMENT
31 ± 6 OUR AVERAGE Error includes scale factor of 1.1.					
$29.1 \pm 3.6 \pm 4.3$	8k	AAIJ	15AB	LHCB	pp at 7, 8 TeV
$49 \; ^{+12}_{-10} \; ^{+2}_{-13}$		AALTONEN	14I	CDF	$p\overline{p}$ at 1.96 TeV

$B_1(5721)^0$ width

VALUE (MeV)	EVTS	DOCUMENT ID		TECN	COMMENT
27.5 ± 3.4 OUR AVERAGE Error includes scale factor of 1.1.					
$30.1 \pm 1.5 \pm 3.5$	35k	AAIJ	15AB	LHCB	pp at 7, 8 TeV
$23 \pm 3 \pm 4$		AALTONEN	14I	CDF	$p\overline{p}$ at 1.96 TeV

$B_1(5721)$ DECAY MODES

	Mode	Fraction (Γ_i/Γ)
Γ_1	$B^*\pi$	seen

$\Gamma(B^*\pi)/\Gamma_{total}$ — Γ_1/Γ

VALUE	DOCUMENT ID		TECN	CHG	COMMENT
seen	AAIJ	15AB	LHCB	± 0	pp at 7, 8 TeV
seen	AALTONEN	14I	CDF	$\pm$	$p\overline{p}$ at 1.96 TeV
seen	AALTONEN	09D	CDF	0	$p\overline{p}$ at 1.96 TeV
seen	[1] ABAZOV	07T	D0	0	$p\overline{p}$ at 1.96 TeV

[1] Observed in $B_1^0 \to B^{*+}\pi^-$ with $B^{*+} \to B^+\gamma$ and $B^+ \to J/\psi\pi^+$.

$B_1(5721)$ REFERENCES

AAIJ	15AB	JHEP 1504 024	R. Aaij *et al.*	(LHCb Collab.)
AALTONEN	14I	PR D90 012013	T. Aaltonen *et al.*	(CDF Collab.)
AALTONEN	09D	PRL 102 102003	T. Aaltonen *et al.*	(CDF Collab.)
ABAZOV	07T	PRL 99 172001	V.M. Abazov *et al.*	(D0 Collab.)

$B_J^*(5732)$

$I(J^P) = ?(?^?)$

OMITTED FROM SUMMARY TABLE
also known as B^{**}

Signal can be interpreted as stemming from several narrow and broad resonances.

$B_J^*(5732)$ MASS

VALUE (MeV)	EVTS	DOCUMENT ID		TECN	COMMENT
5698 ± 8 OUR AVERAGE Error includes scale factor of 1.2.					
5710 ± 20		[1] AFFOLDER	01F	CDF	$p\overline{p}$ at 1.8 TeV
5695^{+17}_{-19}		[2] BARATE	98L	ALEP	$e^+e^- \to Z$
$5704 \pm 4 \pm 10$	1944	[3] BUSKULIC	96D	ALEP	$E_{cm}^{ee} = 88$–94 GeV
$5732 \pm 5 \pm 20$	2157	ABREU	95B	DLPH	$E_{cm}^{ee} = 88$–94 GeV
5681 ± 11	1738	AKERS	95E	OPAL	$E_{cm}^{ee} = 88$–94 GeV
• • • We do not use the following data for averages, fits, limits, etc. • • •					
5713 ± 2		[4] ACCIARRI	99N	L3	$e^+e^- \to Z$

[1] AFFOLDER 01F uses the reconstructed B meson through semileptonic decay channels. The fraction of light B mesons that are produced at $L=1$ B^{**} states is measured to be $0.28 \pm 0.06 \pm 0.03$.

[2] BARATE 98L uses fully reconstructed B mesons to search for B^{**} production in the $B\pi^\pm$ system. In the framework of heavy quark symmetry (HQS), they also measured the mass of B_2^* to be $5739^{+8}_{-11}{}^{+6}_{-4}$ MeV/c^2 and the relative production rate of $B(b \to B_2^* \to B^{(*)}\pi)/B(b \to B_{u,d}) = (31 \pm 9^{+6}_{-5})\%$.

[3] Using $m_{B\pi} - m_B = 424 \pm 4 \pm 10$ MeV.

[4] ACCIARRI 99N uses inclusive reconstructed B mesons to search for B^{**} production in the $B^{(*)}\pi^\pm$ system. In the framework of HQET, they measured the mass of B_1^* and B_2^* to be $5670 \pm 10 \pm 13$ MeV and $5768 \pm 5 \pm 6$ with the $B(b \to B^{**}) = (32 \pm 3 \pm 6) \times 10^{-2}$. They also reported the evidence for the existence of an excited B-meson state or mixture of states in the region 5.9–6.0 GeV.

$B_J^*(5732)$ WIDTH

VALUE (MeV)	EVTS	DOCUMENT ID		TECN	COMMENT
128 ± 18 OUR AVERAGE					
145 ± 28	2157	ABREU	95B	DLPH	$E_{cm}^{ee} = 88$–94 GeV
116 ± 24	1738	AKERS	95E	OPAL	$E_{cm}^{ee} = 88$–94 GeV

$B_J^*(5732)$ DECAY MODES

	Mode	Fraction (Γ_i/Γ)
Γ_1	$B^*\pi + B\pi$	seen
Γ_2	$B^*\pi(X)$	[a] (85 ± 29) %

[a] X refers to decay modes with or without additional accompanying decay particles.

Downloaded from https://academic.oup.com/ptep/article/2022/8/083C01/6651666 by KIT Library user on 27 September 2022

$B_J^*(5732)$ BRANCHING RATIOS

X refers to decay modes with or without additional accompanying decay particles.

$\Gamma(B^*\pi(X))/\Gamma_{total}$ — Γ_2/Γ

VALUE	DOCUMENT ID		TECN	COMMENT
$0.85^{+0.26}_{-0.27}\pm0.12$	ABBIENDI	02E	OPAL	$e^+e^- \to Z$

$B_J^*(5732)$ REFERENCES

ABBIENDI	02E	EPJ C23 437	G. Abbiendi et al.	(OPAL Collab.)
AFFOLDER	01F	PR D64 072002	T. Affolder et al.	(CDF Collab.)
ACCIARRI	99N	PL B465 323	M. Acciarri et al.	(L3 Collab.)
BARATE	98L	PL B425 215	R. Barate et al.	(ALEPH Collab.)
BUSKULIC	96D	ZPHY C69 393	D. Buskulic et al.	(ALEPH Collab.)
ABREU	95B	PL B345 598	P. Abreu et al.	(DELPHI Collab.)
AKERS	95E	ZPHY C66 19	R. Akers et al.	(OPAL Collab.)

$B_2^*(5747)$

$I(J^P) = \frac{1}{2}(2^+)$
I, J, P need confirmation.

Quantum numbers shown are quark-model predictions.

$B_2^*(5747)$ MASS

$B_2^*(5747)^+$ mass

OUR FIT uses m_{B^0} and $m_{B_2^{*+}} - m_{B^0}$ to determine $m_{B_2^*(5747)^+}$.

VALUE (MeV)	DOCUMENT ID
5737.2±0.7 OUR FIT	

$m_{B_2^{*+}} - m_{B^0}$

VALUE (MeV)	EVTS	DOCUMENT ID		TECN	COMMENT
457.5 ±0.7 OUR FIT					
457.5 ±0.7 OUR AVERAGE					
457.62±0.72±0.40	4k	[1] AAIJ	15AB	LHCB	pp at 7, 8 TeV
457.3 $\pm1.3\ ^{+0.3}_{-0.9}$		[2] AALTONEN	14I	CDF	$p\overline{p}$ at 1.96 TeV

[1] AAIJ 15AB reports $[m_{B_2^{*+}} - m_{B^0}] - m_{\pi^+} = 318.1 \pm 0.7 \pm 0.4$ MeV which we adjust by the π^+ mass. The masses inside the square brackets were measured for each candidate event.

[2] AALTONEN 14I reports $m_{B_2^*(5747)^+} - m_{B^0} - m_{\pi^+} = 317.7 \pm 1.2^{+0.3}_{-0.9}$ MeV which we adjusted by the π^+ mass.

$B_2^*(5747)^0$ mass

OUR FIT uses m_{B^+}, $m_{B_1^0} - m_{B^+}$, and mass differences below to determine $m_{B_2^*(5747)^0}$. The −0.659 correlation between statistical uncertainties of $m_{B_1^0} - m_{B^+}$ and $m_{B_2^{*0}} - m_{B_1^0}$ measurements reported by ABAZOV 07T is taken into account.

VALUE (MeV)	DOCUMENT ID
5739.5±0.7 OUR FIT Error includes scale factor of 1.4.	

$m_{B_2^{*0}} - m_{B_1^0}$

VALUE (MeV)	DOCUMENT ID		TECN	COMMENT
13.4±1.4 OUR FIT Error includes scale factor of 1.3.				
26.2±3.1±0.9	[1] ABAZOV	07T	D0	$p\overline{p}$ at 1.96 TeV
• • • We do not use the following data for averages, fits, limits, etc. • • •				
$14.9^{+2.2}_{-2.5}\ ^{+1.2}_{-1.4}$	[1] AALTONEN	09D	CDF	Repl. by AALTONEN 14I

[1] Observed in $B_2^{*0} \to B^{*+}\pi^-$ and $B_2^{*0} \to B^+\pi^-$.

$m_{B_2^{*0}} - m_{B^+}$

VALUE (MeV)	EVTS	DOCUMENT ID		TECN	COMMENT
460.2 ±0.6 OUR FIT Error includes scale factor of 1.4.					
459.9 ±0.8 OUR AVERAGE Error includes scale factor of 1.8.					
460.18±0.37±0.33	17k	[1] AAIJ	15AB	LHCB	pp at 7, 8 TeV
457.5 $\pm1.2\ ^{+0.8}_{-0.9}$		[2] AALTONEN	14I	CDF	$p\overline{p}$ at 1.96 TeV

[1] AAIJ 15AB reports $[m_{B_2^{*0}} - m_{B^+}] - m_{\pi^-} = 320.6 \pm 0.4 \pm 0.3$ MeV which we adjust by the π^- mass. The masses inside the square brackets were measured for each candidate event.

[2] AALTONEN 14I reports $m_{B_2^*(5747)^0} - m_{B^+} - m_{\pi^-} = 317.9 \pm 1.2^{+0.8}_{-0.9}$ MeV which we adjusted by the π^- mass.

$B_2^*(5747)$ WIDTH

$B_2^*(5747)^+$ width

VALUE (MeV)	EVTS	DOCUMENT ID		TECN	COMMENT
20 ±5 OUR AVERAGE Error includes scale factor of 2.2.					
23.6±2.0±2.1	4k	AAIJ	15AB	LHCB	pp at 7, 8 TeV
11 $^{+4}_{-3}\ ^{+3}_{-4}$		AALTONEN	14I	CDF	$p\overline{p}$ at 1.96 TeV

$B_2^*(5747)^0$ width

VALUE (MeV)	EVTS	DOCUMENT ID		TECN	COMMENT
24.2±1.7 OUR AVERAGE					
24.5±1.0± 1.5	17k	AAIJ	15AB	LHCB	pp at 7, 8 TeV
22 $^{+3}_{-2}\ ^{+4}_{-5}$		AALTONEN	14I	CDF	$p\overline{p}$ at 1.96 TeV
• • • We do not use the following data for averages, fits, limits, etc. • • •					
$22.7^{+3.8}_{-3.2}\ ^{+3.2}_{-10.2}$		AALTONEN	09D	CDF	Repl. by AALTONEN 14I

$B_2^*(5747)$ DECAY MODES

	Mode	Fraction (Γ_i/Γ)
Γ_1	$B\pi$	seen
Γ_2	$B^*\pi$	seen

$\Gamma(B\pi)/\Gamma_{total}$ — Γ_1/Γ

VALUE	EVTS	DOCUMENT ID		TECN	CHG	COMMENT
seen	4k,17k	AAIJ	15AB	LHCB	±0	pp at 7, 8 TeV
seen		AALTONEN	14I	CDF	±	$p\overline{p}$ at 1.96 TeV
seen		AALTONEN	09D	CDF	0	$p\overline{p}$ at 1.96 TeV
seen		ABAZOV	07T	D0	0	$p\overline{p}$ at 1.96 TeV

$\Gamma(B^*\pi)/\Gamma_{total}$ — Γ_2/Γ

VALUE	EVTS	DOCUMENT ID		TECN	CHG	COMMENT
seen	4k,17k	AAIJ	15AB	LHCB	±0	pp at 7, 8 TeV
seen		AALTONEN	09D	CDF	0	$p\overline{p}$ at 1.96 TeV
seen		ABAZOV	07T	D0	0	$p\overline{p}$ at 1.96 TeV

$\Gamma(B^*\pi)/\Gamma(B\pi)$ — Γ_2/Γ_1

VALUE	EVTS	DOCUMENT ID		TECN	CHG	COMMENT
0.84±0.27 OUR AVERAGE						
0.71±0.14±0.30	17k	AAIJ	15AB	LHCB	0	pp at 7, 8 TeV
1.0 ±0.5 ±0.8	4k	AAIJ	15AB	LHCB	±	pp at 7, 8 TeV
1.10±0.42±0.31		[1] ABAZOV	07T	D0	0	$p\overline{p}$ at 1.96 TeV

[1] Converted from measured ratio of $R = B(B_2^{*0} \to B^{*+}\pi^-) / B(B_2^{*0} \to B^{(*)+}\pi^-) = 0.475 \pm 0.095 \pm 0.069$.

$B_2^*(5747)$ REFERENCES

AAIJ	15AB	JHEP 1504 024	R. Aaij et al.	(LHCb Collab.)
AALTONEN	14I	PR D90 012013	T. Aaltonen et al.	(CDF Collab.)
AALTONEN	09D	PRL 102 102003	T. Aaltonen et al.	(CDF Collab.)
ABAZOV	07T	PRL 99 172001	V.M. Abazov et al.	(D0 Collab.)

$B_J(5840)$

$I(J^P) = \frac{1}{2}(?^?)$
I, J, P need confirmation.

OMITTED FROM SUMMARY TABLE

Quantum numbers shown are quark-model predictions.

$B_J(5840)$ MASS

$B_J(5840)^+$ MASS

OUR FIT uses m_{B^0} and $m_{B_J(5840)^+} - m_{B^0}$ to determine $m_{B_J(5840)^+}$.

VALUE (MeV)	DOCUMENT ID
5851±19 OUR FIT	

$m_{B_J(5840)^+} - m_{B^0}$

VALUE (MeV)	EVTS	DOCUMENT ID		TECN	COMMENT
571±19 OUR FIT					
571±13±14	7k	[1] AAIJ	15AB	LHCB	pp at 7, 8 TeV
• • • We do not use the following data for averages, fits, limits, etc. • • •					
595±26±14	7k	[2] AAIJ	15AB	LHCB	pp at 7, 8 TeV

[1] AAIJ 15AB reports $[m_{B_J^+} - m_{B^0}] - m_{\pi^+} = 431 \pm 13 \pm 14$ MeV which we adjust by the π^+ mass. The masses inside the square brackets were measured for each candidate event. The result assumes $P = (-1)^J$ and uses two relativistic Breit-Wigner functions in the fit for mass difference.

[2] AAIJ 15AB reports $[m_{B_J^+} - m_{B^0}] - m_{\pi^+} = 455 \pm 26 \pm 14$ MeV which we adjust by the π^+ mass. The masses inside the square brackets were measured for each candidate event. The result assumes $P = (-1)^J$ and uses three relativistic Breit-Wigner functions in the fit for mass difference.

$m_{B_J(5840)^+} - m_{B^{*0}}$

VALUE (MeV)	EVTS	DOCUMENT ID		TECN	COMMENT
• • • We do not use the following data for averages, fits, limits, etc. • • •					
565±15±14	7k	[1] AAIJ	15AB	LHCB	pp at 7, 8 TeV

[1] AAIJ 15AB reports $[m_{B_J^+} - m_{B^0}] - (m_{B^{*+}} - m_{B^+}) - m_{\pi^+} = 425 \pm 15 \pm 14$ MeV which we adjust by the π^+ mass. The masses inside the square brackets were measured for each candidate event. The result assumes $P = -(-1)^J$, $(m_{B^{*0}} - m_{B^0}) = (m_{B^{*+}} - m_{B^+}) = 45.01 \pm 0.30 \pm 0.23$ MeV, and uses three relativistic Breit-Wigner functions in the fit for mass difference.

Downloaded from https://academic.oup.com/ptep/article/2022/8/083C01/6651666 by KIT Library user on 27 September 2022

$B_J(5840)^0$ MASS

OUR FIT uses m_{B^+} and $m_{B_J(5840)^0} - m_{B^+}$ to determine $m_{B_J(5840)^0}$.

VALUE (MeV)	DOCUMENT ID
5863±9 OUR FIT	

$m_{B_J(5840)^0} - m_{B^+}$

VALUE (MeV)	EVTS	DOCUMENT ID		TECN	COMMENT
584± 9 OUR FIT					
584± 5±7	12k	[1] AAIJ	15AB	LHCB	pp at 7, 8 TeV
• • • We do not use the following data for averages, fits, limits, etc. • • •					
610±22±7	12k	[2] AAIJ	15AB	LHCB	pp at 7, 8 TeV

[1] AAIJ 15AB reports $[m_{B_J^0} - m_{B^+}] - m_{\pi^-} = 444 \pm 5 \pm 7$ MeV which we adjust by the π^- mass. The masses inside the square brackets were measured for each candidate event. The result assumes $P = (-1)^J$ and uses two relativistic Breit-Wigner functions in the fit for mass difference.

[2] AAIJ 15AB reports $[m_{B_J^0} - m_{B^+}] - m_{\pi^-} = 471 \pm 22 \pm 7$ MeV which we adjust by the π^- mass. The masses inside the square brackets were measured for each candidate event. The result assumes $P = (-1)^J$ and uses three relativistic Breit-Wigner functions in the fit for mass difference.

$m_{B_J(5840)^0} - m_{B^{*+}}$

VALUE (MeV)	EVTS	DOCUMENT ID		TECN	COMMENT
• • • We do not use the following data for averages, fits, limits, etc. • • •					
584±5±7	12k	[1] AAIJ	15AB	LHCB	pp at 7, 8 TeV

[1] AAIJ 15AB reports $[m_{B_J^0} - m_{B^+}] - (m_{B^{*+}} - m_{B^+}) - m_{\pi^-} = 444 \pm 5 \pm 7$ MeV which we adjust by the π^- mass. The masses inside the square brackets were measured for each candidate event. The result assumes $P = -(-1)^J$, $(m_{B^{*+}} - m_{B^+}) = 45.01 \pm 0.30 \pm 0.23$ MeV, and uses three relativistic Breit-Wigner functions in the fit for mass difference.

$B_J(5840)$ WIDTH

$B_J(5840)^+$ WIDTH

VALUE (MeV)	EVTS	DOCUMENT ID		TECN	COMMENT
224±24±80	7k	[1] AAIJ	15AB	LHCB	pp at 7, 8 TeV
• • • We do not use the following data for averages, fits, limits, etc. • • •					
215±27±80	7k	[2] AAIJ	15AB	LHCB	pp at 7, 8 TeV
229±27±80	7k	[3] AAIJ	15AB	LHCB	pp at 7, 8 TeV

[1] Assuming $P = (-1)^J$ and using two relativistic Breit-Wigner functions in the fit for mass difference.

[2] Assuming $P = (-1)^J$ and using three relativistic Breit-Wigner functions in the fit for mass difference.

[3] Assuming $P = -(-1)^J$ and using three relativistic Breit-Wigner functions in the fit for mass difference.

$B_J(5840)^0$ WIDTH

VALUE (MeV)	EVTS	DOCUMENT ID		TECN	COMMENT
127±17±34	12k	[1] AAIJ	15AB	LHCB	pp at 7, 8 TeV
• • • We do not use the following data for averages, fits, limits, etc. • • •					
107±20±34	12k	[2] AAIJ	15AB	LHCB	pp at 7, 8 TeV
119±17±34	12k	[3] AAIJ	15AB	LHCB	pp at 7, 8 TeV

[1] Assuming $P = (-1)^J$ and using two relativistic Breit-Wigner functions in the fit for mass difference.

[2] Assuming $P = (-1)^J$ and using three relativistic Breit-Wigner functions in the fit for mass difference.

[3] Assuming $P = -(-1)^J$ and using three relativistic Breit-Wigner functions in the fit for mass difference.

$B_J(5840)$ DECAY MODES

	Mode	Fraction (Γ_i/Γ)
Γ_1	$B^*\pi$	seen
Γ_2	$B\pi$	possibly seen

$B_J(5840)$ BRANCHING RATIOS

$\Gamma(B^*\pi)/\Gamma_{total}$ — Γ_1/Γ

VALUE	EVTS	DOCUMENT ID		TECN	CHG	COMMENT
seen	7k	AAIJ	15AB	LHCB	±	pp at 7, 8 TeV
seen	12k	AAIJ	15AB	LHCB	0	pp at 7, 8 TeV

$\Gamma(B\pi)/\Gamma_{total}$ — Γ_2/Γ

VALUE	EVTS	DOCUMENT ID		TECN	CHG	COMMENT
possibly seen	7k	[1] AAIJ	15AB	LHCB	±	pp at 7, 8 TeV
possibly seen		[1] AAIJ	15AB	LHCB	0	pp at 7, 8 TeV

[1] A $B\pi$ decay is forbidden from a $P = -(-1)^J$ parent, whereas $B^*\pi$ is allowed.

$B_J(5840)$ REFERENCES

AAIJ 15AB JHEP 1504 024 R. Aaij *et al.* (LHCb Collab.)

$B_J(5970)$

$I(J^P) = \frac{1}{2}(?^?)$
I, J, P need confirmation.

Quantum numbers shown are quark-model predictions.

$B_J(5970)$ MASS

$B_J(5970)^+$ MASS

OUR FIT uses m_{B^0} and $m_{B_J(5970)^+} - m_{B^0}$ to determine $m_{B_J(5970)^+}$.

VALUE (MeV)	DOCUMENT ID
5964±5 OUR FIT	

$m_{B_J(5970)^+} - m_{B^0}$

VALUE (MeV)	EVTS	DOCUMENT ID		TECN	COMMENT
685 ±5 OUR FIT					
685 ±5 OUR AVERAGE					
685.3±4.1± 2.5	2k	[1] AAIJ	15AB	LHCB	pp at 7, 8 TeV
681 ±5 ±12	1.4k	[2] AALTONEN	14I	CDF	$p\overline{p}$ at 1.96 TeV
• • • We do not use the following data for averages, fits, limits, etc. • • •					
686.8±4.5± 2.5	2k	[3] AAIJ	15AB	LHCB	pp at 7, 8 TeV

[1] AAIJ 15AB reports $[m_{B_J^+} - m_{B^0}] - m_{\pi^+} = 545.8 \pm 4.1 \pm 2.5$ MeV which we adjust by the π^+ mass. The masses inside the square brackets were measured for each candidate event. The result assumes $P = (-1)^J$ and uses two relativistic Breit-Wigner functions in the fit for mass difference.

[2] AALTONEN 14I reports $m_{B_J(5970)^+} - m_{B^0} - m_{\pi^+} = 541 \pm 5 \pm 12$ MeV which we adjusted by the π^+ mass.

[3] AAIJ 15AB reports $[m_{B_J^+} - m_{B^0}] - m_{\pi^+} = 547 \pm 5 \pm 3$ MeV which we adjust by the π^+ mass. The masses inside the square brackets were measured for each candidate event. The result assumes $P = (-1)^J$ and uses three relativistic Breit-Wigner functions in the fit for mass difference.

$m_{B_J(5970)^+} - m_{B^{*0}}$

VALUE (MeV)	EVTS	DOCUMENT ID		TECN	COMMENT
• • • We do not use the following data for averages, fits, limits, etc. • • •					
686.0±4.0±2.5	2k	[1] AAIJ	15AB	LHCB	pp at 7, 8 TeV

[1] AAIJ 15AB reports $[m_{B_J^+} - m_{B^0}] - (m_{B^{*+}} - m_{B^+}) - m_{\pi^+} = 547 \pm 4 \pm 3$ MeV which we adjust by the π^+ mass. The masses inside the square brackets were measured for each candidate event. The result assumes $P = -(-1)^J$, $(m_{B^{*0}} - m_{B^0}) = (m_{B^{*+}} - m_{B^+}) = 45.01 \pm 0.30 \pm 0.23$ MeV, and uses three relativistic Breit-Wigner functions in the fit for mass difference.

$B_J(5970)^0$ MASS

OUR FIT uses m_{B^+} and $m_{B_J(5970)^0} - m_{B^+}$ to determine $m_{B_J(5970)^0}$.

VALUE (MeV)	DOCUMENT ID
5971±5 OUR FIT	

$m_{B_J(5970)^0} - m_{B^+}$

VALUE (MeV)	EVTS	DOCUMENT ID		TECN	COMMENT
691 ±5 OUR FIT					
691 ±5 OUR AVERAGE					
689.9±2.9± 5.1	10k	[1] AAIJ	15AB	LHCB	pp at 7, 8 TeV
698 ±5 ±12	2.6k	[2] AALTONEN	14I	CDF	$p\overline{p}$ at 1.96 TeV
• • • We do not use the following data for averages, fits, limits, etc. • • •					
714.3±6.4± 5.1	10k	[3] AAIJ	15AB	LHCB	pp at 7, 8 TeV

[1] AAIJ 15AB reports $[m_{B_J^0} - m_{B^+}] - m_{\pi^-} = 550.4 \pm 2.9 \pm 5.1$ MeV which we adjust by the π^- mass. The masses inside the square brackets were measured for each candidate event. The result assumes $P = (-1)^J$ and uses two relativistic Breit-Wigner functions in the fit for mass difference.

[2] AALTONEN 14I reports $m_{B_J(5970)^0} - m_{B^+} - m_{\pi^-} = 558 \pm 5 \pm 12$ MeV which we adjusted by the π^- mass.

[3] AAIJ 15AB reports $[m_{B_J^0} - m_{B^+}] - m_{\pi^-} = 575 \pm 6 \pm 5$ MeV which we adjust by the π^- mass. The masses inside the square brackets were measured for each candidate event. The result assumes $P = (-1)^J$ and uses three relativistic Breit-Wigner functions in the fit for mass difference.

$m_{B_J(5970)^0} - m_{B^{*+}}$

VALUE (MeV)	EVTS	DOCUMENT ID		TECN	COMMENT
• • • We do not use the following data for averages, fits, limits, etc. • • •					
691.6±3.7±5.1	10k	[1] AAIJ	15AB	LHCB	pp at 7, 8 TeV

[1] AAIJ 15AB reports $[m_{B_J^0} - m_{B^+}] - (m_{B^{*+}} - m_{B^+}) - m_{\pi^-} = 552 \pm 4 \pm 5$ MeV which we adjust by the π^- mass. The masses inside the square brackets were measured for each candidate event. The result assumes $P = -(-1)^J$, $(m_{B^{*+}} - m_{B^+}) = 45.01 \pm 0.30 \pm 0.23$ MeV, and uses three relativistic Breit-Wigner functions in the fit for mass difference.

Downloaded from https://academic.oup.com/ptep/article/2022/8/083C01/6651666 by KIT Library user on 27 September 2022

$B_J(5970)$ WIDTH

$B_J(5970)^+$ WIDTH

VALUE (MeV)	EVTS	DOCUMENT ID		TECN	COMMENT
62±20 OUR AVERAGE					
63±15±17	2k	[1] AAIJ	15AB	LHCB	pp at 7, 8 TeV
$60^{+30}_{-20}\pm40$	1.4k	AALTONEN	14I	CDF	$p\overline{p}$ at 1.96 TeV
• • • We do not use the following data for averages, fits, limits, etc. • • •					
61±14±17	2k	[2] AAIJ	15AB	LHCB	pp at 7, 8 TeV
61±15±17	2k	[3] AAIJ	15AB	LHCB	pp at 7, 8 TeV

[1] Assuming $P=(-1)^J$ and using two relativistic Breit-Wigner functions in the fit for mass difference.
[2] Assuming $P=(-1)^J$ and using three relativistic Breit-Wigner functions in the fit for mass difference.
[3] Assuming $P=-(-1)^J$ and using three relativistic Breit-Wigner functions in the fit for mass difference.

$B_J(5970)^0$ WIDTH

VALUE (MeV)	EVTS	DOCUMENT ID		TECN	COMMENT
81±12 OUR AVERAGE					
82± 8± 9	10k	[1] AAIJ	15AB	LHCB	pp at 7, 8 TeV
$70^{+30}_{-20}\pm30$	2.6k	AALTONEN	14I	CDF	$p\overline{p}$ at 1.96 TeV
• • • We do not use the following data for averages, fits, limits, etc. • • •					
56± 7± 9	10k	[2] AAIJ	15AB	LHCB	pp at 7, 8 TeV
82±10± 9	10k	[3] AAIJ	15AB	LHCB	pp at 7, 8 TeV

[1] Assuming $P=(-1)^J$ and using two relativistic Breit-Wigner functions in the fit for mass difference.
[2] Assuming $P=(-1)^J$ and using three relativistic Breit-Wigner functions in the fit for mass difference.
[3] Assuming $P=-(-1)^J$ and using three relativistic Breit-Wigner functions in the fit for mass difference.

$B_J(5970)$ DECAY MODES

	Mode	Fraction (Γ_i/Γ)
Γ_1	$B\pi$	possibly seen
Γ_2	$B^*\pi$	seen

$B_J(5970)$ BRANCHING RATIOS

$\Gamma(B\pi)/\Gamma_{total}$ — Γ_1/Γ

VALUE	EVTS	DOCUMENT ID		TECN	CHG	COMMENT
possibly seen	2k	[1] AAIJ	15AB	LHCB	±	pp at 7, 8 TeV
possibly seen	10k	[1] AAIJ	15AB	LHCB	0	pp at 7, 8 TeV
possibly seen	2.6k	AALTONEN	14I	CDF	0	$p\overline{p}$ at 1.96 TeV
possibly seen	1.4k	AALTONEN	14I	CDF	±	$p\overline{p}$ at 1.96 TeV

[1] A $B\pi$ decay is forbidden from a $P=-(-1)^J$ parent, whereas $B^*\pi$ is allowed.

$\Gamma(B^*\pi)/\Gamma_{total}$ — Γ_2/Γ

VALUE	EVTS	DOCUMENT ID		TECN	CHG	COMMENT
seen	10k	AAIJ	15AB	LHCB	0	pp at 7, 8 TeV
seen	2k	AAIJ	15AB	LHCB	±	pp at 7, 8 TeV
seen	2.6k	AALTONEN	14I	CDF	0	$p\overline{p}$ at 1.96 TeV
seen	1.4k	AALTONEN	14I	CDF	±	$p\overline{p}$ at 1.96 TeV

$B_J(5970)$ REFERENCES

AAIJ 15AB JHEP 1504 024 R. Aaij et al. (LHCb Collab.)
AALTONEN 14I PR D90 012013 T. Aaltonen et al. (CDF Collab.)

Downloaded from https://academic.oup.com/ptep/article/2022/8/083C01/6651666 by KIT Library user on 27 September 2022

BOTTOM, STRANGE MESONS ($B = \pm1$, $S = \mp1$)

$B_s^0 = s\overline{b}$, $\overline{B}_s^0 = \overline{s}b$, similarly for B_s^*'s

B_s^0

$I(J^P) = 0(0^-)$

I, J, P need confirmation. Quantum numbers shown are quark-model predictions.

B_s^0 MASS

VALUE (MeV)	EVTS	DOCUMENT ID		TECN	COMMENT
5366.92± 0.10 OUR FIT					
5366.91± 0.11 OUR AVERAGE					
5366.98± 0.07±0.13		[1] AAIJ	21C	LHCB	pp at 7, 8, 13 TeV
5366.85± 0.19±0.13		[2] AAIJ	19U	LHCB	pp at 7, 8, 13 TeV
5366.83± 0.25±0.27		[3] AAIJ	18AC	LHCB	pp at 7, 8, 13 TeV
5367.08± 0.38±0.15	128	[4] AAIJ	16U	LHCB	pp at 7, 8 TeV
5366.90± 0.28±0.23		[5] AAIJ	12E	LHCB	pp at 7 TeV
5364.4 ± 1.3 ±0.7		LOUVOT	09	BELL	$e^+e^- \to \Upsilon(5S)$
5366.01± 0.73±0.33		[6] ACOSTA	06	CDF	$p\overline{p}$ at 1.96 TeV
5369.9 ± 2.3 ±1.3	32	[7] ABE	96B	CDF	$p\overline{p}$ at 1.8 TeV
5374 ±16 ±2	3	ABREU	94D	DLPH	$e^+e^- \to Z$
5359 ±19 ±7	1	[7] AKERS	94J	OPAL	$e^+e^- \to Z$
5368.6 ± 5.6 ±1.5	2	BUSKULIC	93G	ALEP	$e^+e^- \to Z$
• • • We do not use the following data for averages, fits, limits, etc. • • •					
5370 ± 1 ±3		DRUTSKOY	07A	BELL	Repl. by LOUVOT 09
5370 ±40	6	[8] AKERS	94J	OPAL	$e^+e^- \to Z$
5383.3 ± 4.5 ±5.0	14	ABE	93F	CDF	Repl. by ABE 96B

[1] Uses $B_s^0 \to J/\psi\pi^+\pi^-K^+K^-$ decays.
[2] Uses $B_s^0 \to J/\psi p\overline{p}$ decays.
[3] Uses $B_s \to \chi_{c1}K^+K^-$ mode.
[4] Uses $J/\psi \to \mu^+\mu^-$, $\phi \to K^+K^-$ decays, and observes 128 ± 13 events of $B_s^0 \to J/\psi\phi\phi$.
[5] Uses $B_s^0 \to J/\psi\phi$ fully reconstructed decays.
[6] Uses exclusively reconstructed final states containing a $J/\psi \to \mu^+\mu^-$ decays.
[7] From the decay $B_s \to J/\psi(1S)\phi$.
[8] From the decay $B_s \to D_s^-\pi^+$.

$m_{B_s^0} - m_B$

m_B is the average of our B masses $(m_{B^\pm}+m_{B^0})/2$.

VALUE (MeV)	CL%	DOCUMENT ID		TECN	COMMENT
87.42±0.14 OUR FIT					
87.42±0.24 OUR AVERAGE					
87.60±0.44±0.09		[1] AAIJ	15U	LHCB	pp at 7, 8 TeV
87.42±0.30±0.09		[2] AAIJ	12E	LHCB	pp at 7 TeV
86.64±0.80±0.08		[3] ACOSTA	06	CDF	$p\overline{p}$ at 1.96 TeV
• • • We use the following data for averages but not for fits. • • •					
89.7 ±2.7 ±1.2		ABE	96B	CDF	$p\overline{p}$ at 1.8 TeV
• • • We do not use the following data for averages, fits, limits, etc. • • •					
80 to 130	68	LEE-FRANZINI	90	CSB2	$e^+e^- \to \Upsilon(5S)$

[1] The reported result is $m_{B_s^0} - m_{B^0} = 87.45 \pm 0.44 \pm 0.09$ MeV. We convert it to the mass difference with respect to the average of $(m_{B^\pm} + m_{B^0})/2$. Uses the mode $B_s^0 \to \psi(2S)K^-\pi^+$.
[2] The reported result is $m_{B_s^0} - m_{B^+} = 87.52 \pm 0.30 \pm 0.12$ MeV. We convert it to the mass difference with respect to the average of $(m_{B^\pm} + m_{B^0})/2$.
[3] The reported result is $m_{B_s^0} - m_{B^0} = 86.38 \pm 0.90 \pm 0.06$ MeV. We convert it to the mass difference with respect to the average of $(m_{B^\pm} + m_{B^0})/2$.

$m_{B_{sH}^0} - m_{B_{sL}^0}$

See the B_s^0-$\overline{B}_s^0$ MIXING section near the end of these B_s^0 Listings.

B_s^0 MEAN LIFE

"OUR EVALUATION" is provided by the Heavy Flavor Averaging Group (HFLAV, https://hflav.web.cern.ch/).

The mean B_s^0 lifetime is defined and computed as $1/\Gamma_{B_s^0}$, where $\Gamma_{B_s^0}$ is the average decay width of the B_s^0 mass eigenstates.

VALUE (10^{-12} s)	EVTS	DOCUMENT ID		TECN	COMMENT
1.520±0.005 OUR EVALUATION					
• • • We do not use the following data for averages, fits, limits, etc. • • •					
1.518±0.041±0.027		[1] AALTONEN	11AP	CDF	$p\overline{p}$ at 1.96 TeV
1.398±0.044$^{+0.028}_{-0.025}$		[2] ABAZOV	06V	D0	$p\overline{p}$ at 1.96 TeV
1.42 $^{+0.14}_{-0.13}$ ±0.03		[3] ABREU	00Y	DLPH	$e^+e^- \to Z$
1.53 $^{+0.16}_{-0.15}$ ±0.07		[4] ABREU,P	00G	DLPH	$e^+e^- \to Z$
1.36 ±0.09 $^{+0.06}_{-0.05}$		[5] ABE	99D	CDF	$p\overline{p}$ at 1.8 TeV
1.72 $^{+0.20}_{-0.19}$ $^{+0.18}_{-0.17}$		[6] ACKERSTAFF	98F	OPAL	$e^+e^- \to Z$
1.50 $^{+0.16}_{-0.15}$ ±0.04		[5] ACKERSTAFF	98G	OPAL	$e^+e^- \to Z$
1.47 ±0.14 ±0.08		[4] BARATE	98C	ALEP	$e^+e^- \to Z$
1.51 ±0.11		[7] BARATE	98C	ALEP	$e^+e^- \to Z$
1.56 $^{+0.29}_{-0.26}$ $^{+0.08}_{-0.07}$		[5] ABREU	96F	DLPH	Repl. by ABREU 00Y
1.65 $^{+0.34}_{-0.31}$ ±0.12		[4] ABREU	96F	DLPH	Repl. by ABREU 00Y
1.76 ±0.20 $^{+0.15}_{-0.10}$		[8] ABREU	96F	DLPH	Repl. by ABREU 00Y
1.60 ±0.26 $^{+0.13}_{-0.15}$		[9] ABREU	96F	DLPH	Repl. by ABREU,P 00G
1.67 ±0.14		[10] ABREU	96F	DLPH	$e^+e^- \to Z$
1.61 $^{+0.30}_{-0.29}$ $^{+0.18}_{-0.16}$	90	[4] BUSKULIC	96E	ALEP	Repl. by BARATE 98C
1.54 $^{+0.14}_{-0.13}$ ±0.04		[5] BUSKULIC	96M	ALEP	$e^+e^- \to Z$
1.42 $^{+0.27}_{-0.23}$ ±0.11	76	[5] ABE	95R	CDF	Repl. by ABE 99D
1.74 $^{+1.08}_{-0.69}$ ±0.07	8	[11] ABE	95R	CDF	Sup. by ABE 96N
1.54 $^{+0.25}_{-0.21}$ ±0.06	79	[5] AKERS	95G	OPAL	Repl. by ACKERSTAFF 98G
1.59 $^{+0.17}_{-0.15}$ ±0.03	134	[5] BUSKULIC	95O	ALEP	Sup. by BUSKULIC 96M
0.96 ±0.37	41	[12] ABREU	94E	DLPH	Sup. by ABREU 96F
1.92 $^{+0.45}_{-0.35}$ ±0.04	31	[5] BUSKULIC	94C	ALEP	Sup. by BUSKULIC 95O
1.13 $^{+0.35}_{-0.26}$ ±0.09	22	[5] ACTON	93H	OPAL	Sup. by AKERS 95G

[1] AALTONEN 11AP combines the fully reconstrcuted $B_s^0 \to D_s^-\pi^+$ decays and partially reconstructed $B_s^0 \to D_sX$ decays.
[2] Measured using $D_s\mu^+$ vertices.
[3] Uses $D_s^-\ell^+$, and $\phi\ell^+$ vertices.
[4] Measured using D_s hadron vertices.
[5] Measured using $D_s^-\ell^+$ vertices.
[6] ACKERSTAFF 98F use fully reconstructed $D_s^- \to \phi\pi^-$ and $D_s^- \to K^{*0}K^-$ in the inclusive B_s^0 decay.
[7] Combined results from $D_s^-\ell^+$ and D_s hadron.
[8] Measured using $\phi\ell$ vertices.
[9] Measured using inclusive D_s vertices.
[10] Combined result for the four ABREU 96F methods.
[11] Exclusive reconstruction of $B_s \to \psi\phi$.
[12] ABREU 94E uses the flight-distance distribution of D_s vertices, ϕ-lepton vertices, and $D_s\mu$ vertices.

$\Gamma_{B_s^0}$

"OUR EVALUATION" is an average performed by the Heavy Flavor Averaging Group (HFLAV, https://hflav.web.cern.ch/) as described in our "Review on B-$\overline{B}$ Mixing" in the B^0 section of these Listings. It includes the measurements of $\Gamma_{B_s^0}$ and $\Delta\Gamma_{B_s^0}$ listed in this section, as well as constraints from effective lifetimes with pure CP modes and flavor-specific modes.

VALUE (10^{12} s^{-1})	DOCUMENT ID		TECN	COMMENT
0.6578±0.0024 OUR EVALUATION Error includes scale factor of 2.6.				
0.662 ±0.004 OUR AVERAGE Error includes scale factor of 2.7. See the ideogram below.				
0.6703±0.0014±0.0018	[1] AAD	21AE	ATLS	pp at 7, 8, 13 TeV
0.608 ±0.018 ±0.012	[2] AAIJ	21AN	LHCB	pp at 7, 8 TeV
0.6590±0.0032±0.0023	[1] SIRUNYAN	21E	CMS	pp at 8, 13 TeV
0.6563±0.0021	[3] AAIJ	19Q	LHCB	pp at 7, 8, 13 TeV
0.668 ±0.011 ±0.006	[4] AAIJ	16AK	LHCB	pp at 7, 8 TeV
0.654 ±0.008 ±0.004	[1] AALTONEN	12AJ	CDF	$p\overline{p}$ at 1.96 TeV
0.693 $^{+0.018}_{-0.017}$	[1] ABAZOV	12D	D0	$p\overline{p}$ at 1.96 TeV
• • • We do not use the following data for averages, fits, limits, etc. • • •				
0.6531±0.0042±0.0026	[1] SIRUNYAN	21E	CMS	pp at 13 TeV
0.650 ±0.006 ±0.004	[3] AAIJ	17V	LHCB	Repl. by AAIJ 19Q
0.675 ±0.003 ±0.003	[1] AAD	16AP	ATLS	Repl. by AAD 21AE
0.6704±0.0043±0.0055	[1] KHACHATRY...	16S	CMS	pp at 8 TeV
0.6603±0.0027±0.0015	[5] AAIJ	15I	LHCB	Repl. by AAIJ 19Q
0.677 ±0.007 ±0.004	[1] AAD	14U	ATLS	Repl. by AAD 16AP
0.661 ±0.004 ±0.006	[6] AAIJ	13AR	LHCB	Repl. by AAIJ 15I
0.677 ±0.007 ±0.004	[1] AAD	12CV	ATLS	Repl. by AAD 14U

Downloaded from https://academic.oup.com/ptep/article/2022/8/083C01/6651666 by KIT Library user on 27 September 2022

0.657 ±0.009 ±0.008	[1] AAIJ	12D	LHCB	Repl. by AAIJ 13AR
0.654 ±0.011 ±0.005	[1,7] AALTONEN	12D	CDF	Repl. by AALTONEN 12AJ
0.672 ±0.027 ±0.013	[1] ABAZOV	09E	D0	Repl. by ABAZOV 08AM
0.658 ±0.017 ±0.009	[1,8] AALTONEN	08J	CDF	Repl. by AALTONEN 12D
0.658 ±0.022 ±0.004	[1] ABAZOV	08AM	D0	Repl. by ABAZOV 12D
0.658 ±0.035 $^{+0.0130}_{-0.004}$	[1,8] ABAZOV	07	D0	Repl. by ABAZOV 09E
0.714 $^{+0.007}_{-0.008}$ ±0.010	[1,8] ACOSTA	05	CDF	Repl. by AALTONEN 08J

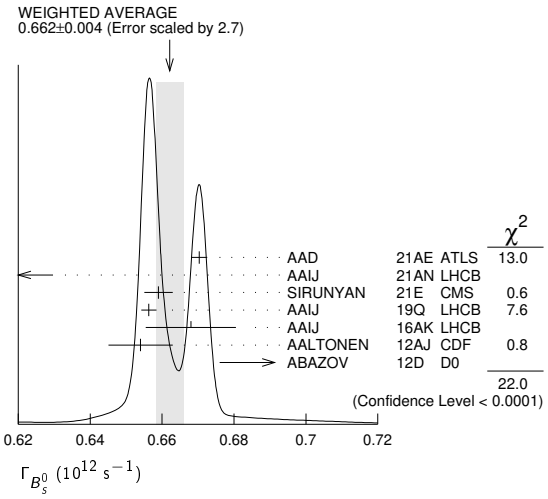

[1] Measured using a time-dependent angular analysis of $B^0_s \to J/\psi\phi$ decays.
[2] Measured using a time-dependent angular analysis of $B^0_s \to J/\psi\phi$ decays with $J/\psi \to e^+e^-$.
[3] Measured using time-dependent angular analysis of $B^0_s \to J/\psi K^+K^-$ in the region m(KK) > 1.05 GeV.
[4] Measured using a time-dependent angular analysis of $B^0_s \to \psi(2S)\phi$ decays.
[5] Measured using a time-dependent angular analysis of $B^0_s \to J/\psi K^+K^-$ decays.
[6] Measured using a combined time-dependent angular analysis of $B^0_s \to J/\psi K^+K^-$ and $B^0_s \to J/\psi\pi^+\pi^-$ decays.
[7] Assuming CPV phase $\phi_s = -0.04$.
[8] Assuming CPV phase $\phi_s = 0$.

$\Delta\Gamma_{B^0_s}$

"OUR EVALUATION" is an average performed by the Heavy Flavor Averaging Group (HFLAV, https://hflav.web.cern.ch/) as described in our "Review on B-$\overline{B}$ Mixing" in the B^0 section of these Listings. It includes the measurements of $\Gamma_{B^0_s}$ and $\Delta\Gamma_{B^0_s}$ listed in this section, as well as constraints from effective lifetimes with pure CP modes and flavor-specific modes.

VALUE (10^{12} s^{-1})	DOCUMENT ID		TECN	COMMENT
0.084 ±0.005 OUR EVALUATION Error includes scale factor of 1.7.				
0.075 ±0.007 OUR AVERAGE Error includes scale factor of 1.6. See the ideogram below.				
0.0657±0.0043±0.0037	[1] AAD	21AE	ATLS	pp at 7, 8, 13 TeV
0.115 ±0.045 ±0.011	[2] AAIJ	21AN	LHCB	pp at 7, 8 TeV
0.1032±0.0095±0.0048	[1] SIRUNYAN	21E	CMS	pp at 8, 13 TeV
0.077 ±0.008 ±0.003	[3] AAIJ	19Q	LHCB	pp at 13 TeV
0.066 ±0.018 ±0.010	[4] AAIJ	17V	LHCB	pp at 7, 8 TeV
0.066 $^{+0.041}_{-0.044}$ ±0.007	[5] AAIJ	16AK	LHCB	pp at 7, 8 TeV
0.068 ±0.026 ±0.009	[1] AALTONEN	12AJ	CDF	$p\overline{p}$ at 1.96 TeV
0.163 $^{+0.065}_{-0.064}$	[1,6] ABAZOV	12D	D0	$p\overline{p}$ at 1.96 TeV
• • • We do not use the following data for averages, fits, limits, etc. • • •				
0.114 ±0.014 ±0.007	[1] SIRUNYAN	21E	CMS	pp at 13 TeV
0.085 ±0.011 ±0.007	[1] AAD	16AP	ATLS	Repl. by AAD 21AE
0.095 ±0.013 ±0.007	[1] KHACHATRY...	16S	CMS	pp at 8 TeV
0.0805±0.0091±0.0032	[3] AAIJ	15I	LHCB	Repl. by AAIJ 19Q
0.053 ±0.021 ±0.010	[1] AAD	14U	ATLS	Repl. by AAD 16AP
0.106 ±0.011 ±0.007	[7] AAIJ	13AR	LHCB	Repl. by AAIJ 15I
0.053 ±0.021 ±0.010	[1] AAD	12CV	ATLS	Repl. by AAD 14U
0.123 ±0.029 ±0.011	[1] AAIJ	12D	LHCB	Repl. by AAIJ 13AR
0.075 ±0.035 ±0.006	[8] AALTONEN	12D	CDF	Repl. by AALTONEN 12AJ
0.085 $^{+0.072}_{-0.078}$ ±0.001	[9] ABAZOV	09E	D0	Repl. by ABAZOV 08AM
0.076 $^{+0.059}_{-0.063}$ ±0.006	[10] AALTONEN	08J	CDF	Repl. by AALTONEN 12D
0.19 ±0.07 $^{+0.02}_{-0.01}$	[1,11] ABAZOV	08AM	D0	Repl. by ABAZOV 12D
0.12 $^{+0.08}_{-0.10}$ ±0.02	[10,12] ABAZOV	07	D0	Repl. by ABAZOV 07N
0.13 ±0.09	[13] ABAZOV	07N	D0	Repl. by ABAZOV 09E
0.47 $^{+0.19}_{-0.24}$ ±0.01	[10] ACOSTA	05	CDF	Repl. by AALTONEN 08J

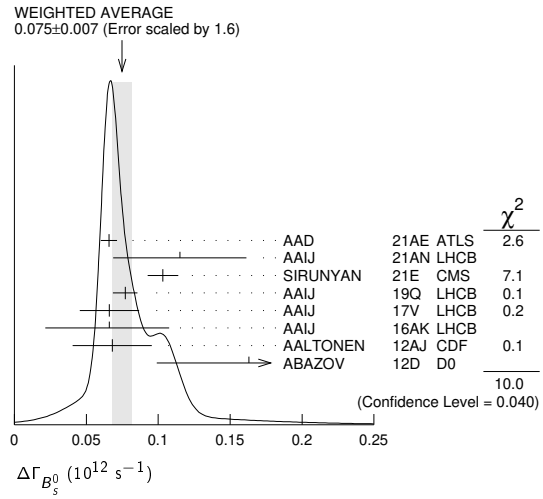

[1] Measured using the time-dependent angular analysis of $B^0_s \to J/\psi\phi$ decays.
[2] Measured using a time-dependent angular analysis of $B^0_s \to J/\psi\phi$ decays with $J/\psi \to e^+e^-$.
[3] Measured using time-dependent angular analysis of $B^0_s \to J/\psi K^+K^-$ decays.
[4] Measured using time-dependent angular analysis of $B^0_s \to J/\psi K^+K^-$ in the region m(KK) > 1.05 GeV.
[5] Measured using time-dependent angular analysis of $B^0_s \to \psi(2S)\phi$ decays.
[6] The error includes both statistical and systematic uncertainties.
[7] AAIJ 13AR result comes from a combined fit to $B^0_s \to J/\psi K^+K^-$ and $B^0_s \to J/\psi\pi^+\pi^-$ data sets. Also reports $\Delta\Gamma_s = 0.100 \pm 0.016 \pm 0.003$ ps^{-1} from a fit to $B^0_s \to J/\psi K^+K^-$ decays.
[8] Uses the time-dependent angular analysis of $B^0_s \to J/\psi\phi$ decays and assuming CP-violating angle $\beta_s(B^0 \to J/\psi\phi) = 0.02$.
[9] Measured the angular and lifetime parameters for the time-dependent angular untagged decays $B^0_d \to J/\psi K^{*0}$ and $B^0_s \to J/\psi\phi$.
[10] Measured using the time-dependent angular analysis of $B^0_s \to J/\psi\phi$ decays and assuming CP-violating phase $\phi_s = 0$.
[11] Obtaines 90% CL interval $-0.06 < \Delta\Gamma_s < 0.30$.
[12] ABAZOV 07 reports $0.17 \pm 0.09 \pm 0.02$ with CP-violating phase ϕ_s as a free parameter.
[13] Combines D^0 measurements of time-dependent angular distributions in $B^0_s \to J/\psi\phi$ and charge asymmetry in semileptonic decays. There is a 4-fold ambiguity in the solution.

$\Delta\Gamma_{B^0_s}/\Gamma_{B^0_s}$

$\Gamma_{B^0_s}$ and $\Delta\Gamma_{B^0_s}$ are the decay rate average and difference between two B^0_s CP eigenstates (light − heavy).

"OUR EVALUATION" is provided by the Heavy Flavor Averaging Group (HFLAV, https://hflav.web.cern.ch/). It is derived from the averages of $\Gamma_{B^0_s}$ and $\Delta\Gamma_{B^0_s}$ (and their correlation).

VALUE	CL%	DOCUMENT ID		TECN	COMMENT
0.128±0.007 OUR EVALUATION					
• • • We do not use the following data for averages, fits, limits, etc. • • •					
0.090±0.009±0.023		[1] ESEN	13	BELL	$e^+e^- \to \Upsilon(5S)$
		[2] AAIJ	12D	LHCB	pp at 7 TeV
		[3] AALTONEN	12D	CDF	$p\overline{p}$ at 1.96 TeV
		[4] ABAZOV	12D	D0	$p\overline{p}$ at 1.96 TeV
0.147 $^{+0.036}_{-0.030}$ $^{+0.042}_{-0.041}$		[1] ESEN	10	BELL	$e^+e^- \to \Upsilon(5S)$
0.072±0.021±0.022		[5] ABAZOV	09I	D0	$p\overline{p}$ at 1.96 TeV
>0.012	95	[5] AALTONEN	08F	CDF	$p\overline{p}$ at 1.96 TeV
0.116 $^{+0.09}_{-0.10}$ ±0.010		[6] AALTONEN	08J	CDF	Repl. by AALTONEN 12D
0.079 $^{+0.038}_{-0.035}$ $^{+0.031}_{-0.030}$		[5] ABAZOV	07Y	D0	Repl. by ABAZOV 09I
0.24 $^{+0.28}_{-0.38}$ $^{+0.03}_{-0.04}$		[6,7] ABAZOV	05W	D0	Repl. by ABAZOV 08AM
0.65 $^{+0.25}_{-0.33}$ ±0.01		[6] ACOSTA	05	CDF	Repl. by AALTONEN 08J
<0.46	95	[8] ABREU	00Y	DLPH	$e^+e^- \to Z$

Downloaded from https://academic.oup.com/ptep/article/2022/8/083C01/6651666 by KIT Library user on 27 September 2022

<0.69	95	[9] ABREU,P	00G	DLPH	$e^+e^- \to Z$
$0.25\ ^{+0.21}_{-0.14}$		[10] BARATE	00K	ALEP	$e^+e^- \to Z$
<0.83	95	[11] ABE	99D	CDF	$p\overline{p}$ at 1.8 TeV
<0.67	95	[12] ACCIARRI	98S	L3	$e^+e^- \to Z$

[1] Assumes CP violation is negligible.
[2] Measured using the time-dependent angular analysis of $B^0_s \to J/\psi\phi$ decays.
[3] Uses the time-dependent angular analysis of $B^0_s \to J/\psi\phi$ decays and assuming CP-violating angle $\beta_s(B^0 \to J/\psi\phi) = 0.02$.
[4] Measured using fully reconstructed $B_s \to J/\psi\phi$ decays.
[5] Assumes $2\,B(B^0_s \to D^{(*)}_s D^{(*)}_s) \simeq \Delta\Gamma^{CP}_s / \Gamma_s$.
[6] Measured using the time-dependent angular analysis of $B^0_s \to J/\psi\phi$ decays.
[7] Uses $|A_0|^2 - |A_\parallel|^2 = 0.355 \pm 0.066$ from ACOSTA 05.
[8] Uses $D^-_s \ell^+$, and $\phi\ell^+$ vertices.
[9] Measured using D_s hadron vertices.
[10] Uses $\phi\phi$ correlations from $B^0_s \to D^{(*)+}_s D^{(*)-}_s$.
[11] ABE 99D assumes $\tau_{B^0_s} = 1.55 \pm 0.05$ ps.
[12] ACCIARRI 98S assumes $\tau_{B^0_s} = 1.49 \pm 0.06$ ps and PDG 98 values of b production fraction.

B^0_{sH} MEAN LIFE

B^0_{sH} is the heavy mass state of two B^0_s CP eigenstates.

"OUR EVALUATION" is provided by the Heavy Flavor Averaging Group (HFLAV, https://hflav.web.cern.ch/). It is derived from the averages of $\Gamma_{B^0_s}$ and $\Delta\Gamma_{B^0_s}$ (and their correlation).

VALUE (10^{-12} s)	DOCUMENT ID		TECN	COMMENT
1.624±0.009 OUR EVALUATION				
• • • We do not use the following data for averages, fits, limits, etc. • • •				
$2.07 \pm 0.29 \pm 0.03$	[1] AAIJ	22	LHCB	pp at 7, 8, 13 TeV
$1.70\ ^{+0.60}_{-0.43} \pm 0.09$	[1] SIRUNYAN	20AG	CMS	pp at 7, 8, 13 TeV
$1.677 \pm 0.034 \pm 0.011$	[2] SIRUNYAN	18BY	CMS	pp at 8 TeV
$2.04 \pm 0.44 \pm 0.05$	[1] AAIJ	17AI	LHCB	pp at 7, 8, 13 TeV
$1.70 \pm 0.14 \pm 0.05$	[3] ABAZOV	16C	D0	$p\overline{p}$ at 1.96 TeV
$1.75 \pm 0.12 \pm 0.07$	[4] AAIJ	13AB	LHCB	pp at 7 TeV
$1.652 \pm 0.024 \pm 0.024$	[5] AAIJ	13AR	LHCB	pp at 7 TeV
$1.700 \pm 0.040 \pm 0.026$	[6] AAIJ	12AN	LHCB	pp at 7 TeV
	[7] AALTONEN	12D	CDF	$p\overline{p}$ at 1.96 TeV
$1.70\ ^{+0.12}_{-0.11} \pm 0.03$	[6] AALTONEN	11AB	CDF	$p\overline{p}$ at 1.96 TeV
$1.613\ ^{+0.123}_{-0.113}$	[8,9] AALTONEN	08J	CDF	Repl. by AALTONEN 12D
$1.58\ ^{+0.39}_{-0.42}\ ^{+0.01}_{-0.02}$	[9] ABAZOV	05W	D0	Repl. by ABAZOV 08AM
$2.07\ ^{+0.58}_{-0.46} \pm 0.03$	[9] ACOSTA	05	CDF	Repl. by AALTONEN 08J

[1] Measured using $B_s \to \mu^+\mu^-$ decays which, in the Standard Model, correspond to B^0_{sH} decays. Assumes $-2\,\mathrm{Re}(\lambda)/(1+|\lambda|^2) = 1$.
[2] Measured using $B^0_s \to J/\psi\pi^+\pi^-$ decays with $0.9240 < m(\pi\pi) < 1.0204$ GeV, which is dominated by the $f_0(980)$ resonance, making it a CP-odd state.
[3] Measured using $J/\psi\pi^+\pi^-$ mode with $0.880 < m(\pi\pi) < 1.080$ GeV/c^2, which is mostly $J/\psi f(0)(980)$ mode, a pure CP-odd final state.
[4] Measured using a pure CP-odd final state $J/\psi K^0_S$ with the assumption that contributions from penguin diagrams are small.
[5] Measured using $B_s \to J/\psi\pi^+\pi^-$ decays which, in the limit of $\phi_s = 0$ and $|\lambda| = 1$, correspond to B^0_{sH} decays.
[6] Measured using a pure CP-odd final state $J/\psi f_0(980)$.
[7] Uses the time-dependent angular analysis of $B^0_s \to J/\psi\phi$ decays assuming CP-violating angle $\beta_s(B^0 \to J/\psi\phi) = 0.02$.
[8] Obtained from $\Delta\Gamma_s$ and Γ_s fit with a correlation of 0.6.
[9] Measured using the time-dependent angular analysis of $B^0_s \to J/\psi\phi$ decays.

B^0_{sL} MEAN LIFE

B^0_{sL} is the light mass state of two B^0_s CP eigenstates.

"OUR EVALUATION" is provided by the Heavy Flavor Averaging Group (HFLAV, https://hflav.web.cern.ch/). It is derived from the averages of $\Gamma_{B^0_s}$ and $\Delta\Gamma_{B^0_s}$ (and their correlation).

VALUE (10^{-12} s)	DOCUMENT ID		TECN	COMMENT
1.429±0.007 OUR EVALUATION				
• • • We do not use the following data for averages, fits, limits, etc. • • •				
1.40 ± 0.02	[1] SIRUNYAN	18BY	CMS	pp at 8 TeV
$1.479 \pm 0.034 \pm 0.011$	[2] AAIJ	16AL	LHCB	pp at 7, 8 TeV
$1.379 \pm 0.026 \pm 0.017$	[3] AAIJ	14F	LHCB	pp at 7, 8 TeV
$1.407 \pm 0.016 \pm 0.007$	[4] AAIJ	14R	LHCB	pp at 7 TeV
$1.440 \pm 0.096 \pm 0.009$	[4] AAIJ	12	LHCB	Repl. by AAIJ 14R
$1.455 \pm 0.046 \pm 0.006$	[4] AAIJ	12R	LHCB	Repl. by AAIJ 14R
	[5] AALTONEN	12D	CDF	$p\overline{p}$ at 1.96 TeV
$1.437\ ^{+0.054}_{-0.047}$	[6,7] AALTONEN	08J	CDF	Repl. by AALTONEN 12D
$1.24\ ^{+0.14}_{-0.11}\ ^{+0.01}_{-0.02}$	[7] ABAZOV	05W	D0	Repl. by ABAZOV 08AM
$1.05\ ^{+0.16}_{-0.13} \pm 0.02$	[7] ACOSTA	05	CDF	Repl. by AALTONEN 08J
$1.27 \pm 0.33 \pm 0.08$	[8] BARATE	00K	ALEP	$e^+e^- \to Z$

[1] Measured using results in SIRUNYAN 18BY for the heavy B^0_s lifetime obtained from $B^0_s \to J/\psi\pi^+\pi^-$ decays and the average effective $B^0_s \to J/\psi\phi$ lifetime, and magnitude squared of the CP-odd amplitude $|A_\perp|^2 = 0.250 \pm 0.006$. The uncertainty includes all statistical and systematic contributions.
[2] Measured using $B^0_s \to J/\psi\eta$ decays.
[3] Measured using $B^0_s \to D^-_s D^+_s$. The effective lifetime is translated into a decay width of $\Gamma_L = 0.725 \pm 0.014 \pm 0.009$ ps^{-1}.
[4] Measured using $B^0_s \to K^+K^-$ decays. There may still be CPV in the decay.
[5] Uses the time-dependent angular analysis of $B^0_s \to J/\psi\phi$ decays and assuming CP-violating angle $\beta_s(B^0 \to J/\psi\phi) = 0.02$.
[6] Obtained from $\Delta\Gamma_s$ and Γ_s fit with a correlation of 0.6.
[7] Measured using the time-dependent angular analysis of $B^0_s \to J/\psi\phi$ decays.
[8] Uses $\phi\phi$ correlations from $B^0_s \to D^{(*)+}_s D^{(*)-}_s$.

B^0_s MEAN LIFE (Flavor specific)

VALUE (10^{-12} s)	DOCUMENT ID		TECN	COMMENT
1.527±0.011 OUR EVALUATION				
1.526±0.015 OUR AVERAGE	Error includes scale factor of 1.3. See the ideogram below.			
$1.547 \pm 0.013 \pm 0.011$	[1] AAIJ	17AN	LHCB	pp at 7, 8 TeV
$1.479 \pm 0.010 \pm 0.021$	[2] ABAZOV	15A	D0	$p\overline{p}$ at 1.96 TeV
$1.535 \pm 0.015 \pm 0.014$	[3] AAIJ	14AX	LHCB	pp at 7 TeV
$1.52 \pm 0.15 \pm 0.01$	[4] AAIJ	14F	LHCB	pp at 7, 8 TeV
$1.60 \pm 0.06 \pm 0.01$	[5] AAIJ	14R	LHCB	pp at 7 TeV
$1.518 \pm 0.041 \pm 0.027$	[6] AALTONEN	11AP	CDF	$p\overline{p}$ at 1.96 TeV
$1.42\ ^{+0.14}_{-0.13} \pm 0.03$	[7] ABREU	00Y	DLPH	$e^+e^- \to Z$
$1.36 \pm 0.09\ ^{+0.06}_{-0.05}$	[8] ABE	99D	CDF	$p\overline{p}$ at 1.8 TeV
$1.50\ ^{+0.16}_{-0.15} \pm 0.04$	[8] ACKERSTAFF	98G	OPAL	$e^+e^- \to Z$
$1.54\ ^{+0.14}_{-0.13} \pm 0.04$	[8] BUSKULIC	96M	ALEP	$e^+e^- \to Z$
• • • We do not use the following data for averages, fits, limits, etc. • • •				
$1.398 \pm 0.044\ ^{+0.028}_{-0.025}$	[9] ABAZOV	06V	D0	Repl. by ABAZOV 15A

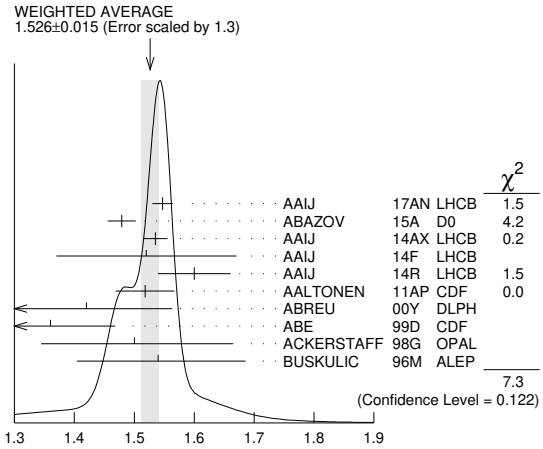

[1] AAIJ 17AN value was measured using $B^0_s \to D^{(*)-}_s \mu^+\nu_\mu$ decays relative to $B^0 \to D^{(*)-}\mu^+\nu_\mu$ decays.
[2] Measured using $B^0_s \to D^-_s \mu^+\nu_\mu X$ decays.
[3] Measured using the $B^0_s \to D^-_s \pi^+$ decays.
[4] Measured using $B^0_s \to D^+ D^-_s$.
[5] Measured using $B^0_s \to \pi^+ K^-$ decays.
[6] AALTONEN 11AP combines the fully reconstrcuted $B^0_s \to D^-_s \pi^+$ decays and partially reconstructed $B^0_s \to D_s X$ decays.
[7] Uses $D^-_s \ell^+$, and $\phi\ell^+$ vertices.
[8] Measured using $D^-_s \ell^+$ vertices.
[9] Measured using $D^-_s \mu^+$ vertices.

Downloaded from https://academic.oup.com/ptep/article/2022/8/083C01/6651666 by KIT Library user on 27 September 2022

B^0_s MEAN LIFE ($B_S \to J/\psi\phi$)

VALUE (10^{-12} s)	DOCUMENT ID		TECN	COMMENT
1.480±0.007 OUR EVALUATION				
1.480±0.007 OUR AVERAGE				
1.481±0.007±0.005	[1] SIRUNYAN	18BY	CMS	pp at 8 TeV
1.480±0.011±0.005	[1] AAIJ	14E	LHCB	pp at 7 TeV
$1.444^{+0.098}_{-0.090}\pm0.020$	[1] ABAZOV	05B	D0	$p\overline{p}$ at 1.96 TeV
$1.34\ ^{+0.23}_{-0.19}\ \pm0.05$	[2] ABE	98B	CDF	$p\overline{p}$ at 1.8 TeV
• • • We do not use the following data for averages, fits, limits, etc. • • •				
$1.39\ ^{+0.13}_{-0.16}\ ^{+0.01}_{-0.02}$	[2] ABAZOV	05W	D0	$p\overline{p}$ at 1.96 TeV
$1.34\ ^{+0.23}_{-0.19}\ \pm0.05$	[3] ABE	96N	CDF	Repl. by ABE 98B

[1] Measured using fully reconstructed $B_s \to J/\psi\phi$ decays.
[2] Measured using the time-dependent angular analysis of $B^0_s \to J/\psi\phi$ decays.
[3] ABE 96N uses 58 ± 12 exclusive $B_s \to J/\psi\phi$ events.

$\tau_{B^0_s}/\tau_{B^0}$ MEAN LIFE RATIO

$\tau_{B^0_s}/\tau_{B^0}$ (direct measurements)

VALUE	DOCUMENT ID		TECN	COMMENT
0.980±0.006±0.003	[1] SIRUNYAN	18BY	CMS	pp at 8 TeV

[1] Measured using $B^0_s \to J/\psi\phi(1020)$ and $B^0 \to J/\psi K^*(892)^0$ decays.

$\Gamma_{B^0_s} - \Gamma_{B^0}$

VALUE (10^{12} s^{-1})	DOCUMENT ID		TECN	COMMENT
−0.0041±0.0024±0.0015	[1] AAIJ	19Q	LHCB	pp at 13 TeV

[1] Measured using time-dependent angular analysis of $B^0_s \to J/\psi K^+K^-$ decays.

$\Gamma_{B^0_{sH}} - \Gamma_{B^0}$

VALUE (10^{12} s^{-1})	DOCUMENT ID		TECN	COMMENT
−0.05±0.004±0.004	[1] AAIJ	19AF	LHCB	pp at 7, 8, 13 TeV

[1] Measured in $B^0_s \to J/\psi\pi^+\pi^-$ decays.

B^0_s DECAY MODES

These branching fractions all scale with $B(\overline{b} \to B^0_s)$.

The branching fraction $B(B^0_s \to D^-_s \ell^+ \nu_\ell \text{anything})$ is not a pure measurement since the measured product branching fraction $B(\overline{b} \to B^0_s) \times B(B^0_s \to D^-_s \ell^+ \nu_\ell \text{anything})$ was used to determine $B(\overline{b} \to B^0_s)$, as described in the note on "B^0-$\overline{B}^0$ Mixing"

For inclusive branching fractions, *e.g.*, $B \to D^\pm$ anything, the values usually are multiplicities, not branching fractions. They can be greater than one.

	Mode		Fraction (Γ_i/Γ)	Scale factor/ Confidence level
Γ_1	D^-_s anything		(62 ± 6) %	
Γ_2	$\ell\nu_\ell X$		(9.6 ± 0.8) %	
Γ_3	$e^+\nu X^-$		(9.1 ± 0.8) %	
Γ_4	$\mu^+\nu X^-$		(10.2 ± 1.0) %	
Γ_5	$D^-_s \ell^+ \nu_\ell$ anything	[a]	(8.1 ± 1.3) %	
Γ_6	$D^{*-}_s \ell^+ \nu_\ell$ anything		(5.4 ± 1.1) %	
Γ_7	$D^-_s \mu^+ \nu_\mu$		(2.44± 0.23) %	
Γ_8	$D^{*-}_s \mu^+ \nu_\mu$		(5.3 ± 0.5) %	
Γ_9	$D_{s1}(2536)^- \mu^+ \nu_\mu$, $D^-_{s1} \to D^{*-} K^0_S$		(2.7 ± 0.7) $\times 10^{-3}$	
Γ_{10}	$D_{s1}(2536)^- X \mu^+ \nu$, $D^-_{s1} \to \overline{D}^0 K^+$		(4.4 ± 1.3) $\times 10^{-3}$	
Γ_{11}	$D_{s2}(2573)^- X \mu^+ \nu$, $D^-_{s2} \to \overline{D}^0 K^+$		(2.7 ± 1.0) $\times 10^{-3}$	
Γ_{12}	$K^- \mu^+ \nu_\mu$		(1.06± 0.09) $\times 10^{-4}$	
Γ_{13}	$D^-_s \pi^+$		(2.98± 0.14) $\times 10^{-3}$	
Γ_{14}	$D^-_s \rho^+$		(6.8 ± 1.4) $\times 10^{-3}$	
Γ_{15}	$D^-_s \pi^+\pi^+\pi^-$		(6.1 ± 1.0) $\times 10^{-3}$	
Γ_{16}	$D_{s1}(2536)^- \pi^+$, $D^-_{s1} \to D^-_s \pi^+\pi^-$		(2.4 ± 0.8) $\times 10^{-5}$	
Γ_{17}	$D^\mp_s K^\pm$		(2.25± 0.12) $\times 10^{-4}$	
Γ_{18}	$D^-_s K^+\pi^+\pi^-$		(3.2 ± 0.6) $\times 10^{-4}$	
Γ_{19}	$D^+_s D^-_s$		(4.4 ± 0.5) $\times 10^{-3}$	
Γ_{20}	$D^-_s D^+$		(2.8 ± 0.5) $\times 10^{-4}$	
Γ_{21}	$D^+ D^-$		(2.2 ± 0.6) $\times 10^{-4}$	
Γ_{22}	$D^{*+} D^-$			
Γ_{23}	$D^{*-} D^+$			
Γ_{24}	$D^0 \overline{D}^0$		(1.9 ± 0.5) $\times 10^{-4}$	
Γ_{25}	$D^{*-}_s \pi^+$		($1.9\ ^{+0.5}_{-0.4}$) $\times 10^{-3}$	
Γ_{26}	$D^{*\mp}_s K^\pm$		($1.32^{+0.40}_{-0.32}$) $\times 10^{-4}$	
Γ_{27}	$D^{*-}_s \rho^+$		(9.5 ± 2.0) $\times 10^{-3}$	
Γ_{28}	$D^{*+}_s D^-_s + D^{*-}_s D^+_s$		(1.39± 0.17) %	
Γ_{29}	$D^{*+}_s D^{*-}_s$		(1.44± 0.21) %	S=1.1
Γ_{30}	$D^{(*)+}_s D^{(*)-}_s$		(4.5 ± 1.4) %	
Γ_{31}	$D^{*-} D^+_s$		(3.9 ± 0.8) $\times 10^{-4}$	
Γ_{32}	$\overline{D}^{*0} \overline{K}^0$		(2.8 ± 1.1) $\times 10^{-4}$	
Γ_{33}	$\overline{D}^0 \overline{K}^0$		(4.3 ± 0.9) $\times 10^{-4}$	
Γ_{34}	$\overline{D}^0 K^- \pi^+$		(1.04± 0.13) $\times 10^{-3}$	
Γ_{35}	$\overline{D}^0 \overline{K}^*(892)^0$		(4.4 ± 0.6) $\times 10^{-4}$	
Γ_{36}	$\overline{D}^0 \overline{K}^*(1410)$		(3.9 ± 3.5) $\times 10^{-4}$	
Γ_{37}	$\overline{D}^0 \overline{K}^*_0(1430)$		(3.0 ± 0.7) $\times 10^{-4}$	
Γ_{38}	$\overline{D}^0 \overline{K}^*_2(1430)$		(1.1 ± 0.4) $\times 10^{-4}$	
Γ_{39}	$\overline{D}^0 \overline{K}^*(1680)$		< 7.8 $\times 10^{-5}$	CL=90%
Γ_{40}	$\overline{D}^0 \overline{K}^*_0(1950)$		< 1.1 $\times 10^{-4}$	CL=90%
Γ_{41}	$\overline{D}^0 \overline{K}^*_3(1780)$		< 2.6 $\times 10^{-5}$	CL=90%
Γ_{42}	$\overline{D}^0 \overline{K}^*_4(2045)$		< 3.1 $\times 10^{-5}$	CL=90%
Γ_{43}	$\overline{D}^0 K^- \pi^+$ (non-resonant)		(2.1 ± 0.8) $\times 10^{-4}$	
Γ_{44}	$D^*_{s2}(2573)^- \pi^+$, $D^*_{s2} \to \overline{D}^0 K^-$		(2.6 ± 0.4) $\times 10^{-4}$	
Γ_{45}	$D^*_{s1}(2700)^- \pi^+$, $D^*_{s1} \to \overline{D}^0 K^-$		(1.6 ± 0.8) $\times 10^{-5}$	
Γ_{46}	$D^*_{s1}(2860)^- \pi^+$, $D^*_{s1} \to \overline{D}^0 K^-$		(5 ± 4) $\times 10^{-5}$	
Γ_{47}	$D^*_{s3}(2860)^- \pi^+$, $D^*_{s3} \to \overline{D}^0 K^-$		(2.2 ± 0.6) $\times 10^{-5}$	
Γ_{48}	$\overline{D}^0 K^+ K^-$		(5.6 ± 0.9) $\times 10^{-5}$	
Γ_{49}	$\overline{D}^0 f_0(980)$		< 3.1 $\times 10^{-6}$	CL=90%
Γ_{50}	$\overline{D}^0 \phi$		(3.0 ± 0.5) $\times 10^{-5}$	
Γ_{51}	$\overline{D}^{*0} \phi$		(3.7 ± 0.6) $\times 10^{-5}$	
Γ_{52}	$D^{*\mp} \pi^\pm$		< 6.1 $\times 10^{-6}$	CL=90%
Γ_{53}	$\eta_c \phi$		(5.0 ± 0.9) $\times 10^{-4}$	
Γ_{54}	$\eta' X_{s\overline{s}}$			
Γ_{55}	$\eta_c \pi^+\pi^-$		(1.8 ± 0.7) $\times 10^{-4}$	
Γ_{56}	$J/\psi(1S)\phi$		(1.04± 0.04) $\times 10^{-3}$	
Γ_{57}	$J/\psi(1S)\phi\phi$		($1.20^{+0.14}_{-0.16}$) $\times 10^{-5}$	
Γ_{58}	$J/\psi(1S)\pi^0$		< 1.2 $\times 10^{-3}$	CL=90%
Γ_{59}	$J/\psi(1S)\eta$		(4.0 ± 0.7) $\times 10^{-4}$	S=1.4
Γ_{60}	$J/\psi(1S) K^0_S$		(1.92± 0.14) $\times 10^{-5}$	
Γ_{61}	$J/\psi(1S)\overline{K}^*(892)^0$		(4.1 ± 0.4) $\times 10^{-5}$	
Γ_{62}	$J/\psi(1S)\eta'$		(3.3 ± 0.4) $\times 10^{-4}$	
Γ_{63}	$J/\psi(1S)\pi^+\pi^-$		(2.02± 0.17) $\times 10^{-4}$	S=1.7
Γ_{64}	$J/\psi(1S) f_0(500)$, $f_0 \to \pi^+\pi^-$		< 4 $\times 10^{-6}$	CL=90%
Γ_{65}	$J/\psi(1S)\rho$, $\rho \to \pi^+\pi^-$		< 3.4 $\times 10^{-6}$	CL=90%
Γ_{66}	$J/\psi(1S) f_0(980)$, $f_0 \to \pi^+\pi^-$		(1.24± 0.15) $\times 10^{-4}$	S=2.1
Γ_{67}	$J/\psi(1S) f_2(1270)$, $f_2 \to \pi^+\pi^-$		(1.0 ± 0.4) $\times 10^{-6}$	
Γ_{68}	$J/\psi(1S) f_2(1270)_0$, $f_2 \to \pi^+\pi^-$		(7.3 ± 1.7) $\times 10^{-7}$	
Γ_{69}	$J/\psi(1S) f_2(1270)_\parallel$, $f_2 \to \pi^+\pi^-$		(1.05± 0.33) $\times 10^{-6}$	
Γ_{70}	$J/\psi(1S) f_2(1270)_\perp$, $f_2 \to \pi^+\pi^-$		(1.3 ± 0.7) $\times 10^{-6}$	
Γ_{71}	$J/\psi(1S) f_0(1370)$, $f_0 \to \pi^+\pi^-$		($4.4\ ^{+0.6}_{-4.0}$) $\times 10^{-5}$	
Γ_{72}	$J/\psi(1S) f_0(1500)$, $f_0 \to \pi^+\pi^-$		($2.04^{+0.32}_{-0.24}$) $\times 10^{-5}$	
Γ_{73}	$J/\psi(1S) f'_2(1525)_0$, $f'_2 \to \pi^+\pi^-$		(1.03± 0.22) $\times 10^{-6}$	
Γ_{74}	$J/\psi(1S) f'_2(1525)_\parallel$, $f'_2 \to \pi^+\pi^-$		($1.2\ ^{+2.6}_{-0.8}$) $\times 10^{-7}$	
Γ_{75}	$J/\psi(1S) f'_2(1525)_\perp$, $f'_2 \to \pi^+\pi^-$		(5 ± 4) $\times 10^{-7}$	
Γ_{76}	$J/\psi(1S) f_0(1790)$, $f_0 \to \pi^+\pi^-$		($4.9\ ^{+10.0}_{-1.0}$) $\times 10^{-6}$	
Γ_{77}	$J/\psi(1S)\pi^+\pi^-$ (nonresonant)		($1.74^{+1.10}_{-0.34}$) $\times 10^{-5}$	
Γ_{78}	$J/\psi(1S)\overline{K}^0\pi^+\pi^-$		< 4.4 $\times 10^{-5}$	CL=90%
Γ_{79}	$J/\psi(1S) K^+ K^-$		(7.9 ± 0.7) $\times 10^{-4}$	

Downloaded from https://academic.oup.com/ptep/article/2022/8/083C01/6651666 by KIT Library user on 27 September 2022

Γ_{80}	$J/\psi(1S) K^0 K^- \pi^+ +$ c.c.		$(9.5 \pm 1.3) \times 10^{-4}$	
Γ_{81}	$J/\psi(1S) \overline{K}^0 K^+ K^-$		$< 1.2 \times 10^{-5}$	CL=90%
Γ_{82}	$J/\psi K^*(892)^0 \overline{K}^*(892)^0$		$(1.10 \pm 0.09) \times 10^{-4}$	
Γ_{83}	$J/\psi(1S) f_2'(1525)$		$(2.6 \pm 0.6) \times 10^{-4}$	
Γ_{84}	$J/\psi(1S) p\overline{p}$		$(3.6 \pm 0.4) \times 10^{-6}$	
Γ_{85}	$J/\psi(1S)\gamma$		$< 7.3 \times 10^{-6}$	CL=90%
Γ_{86}	$J/\psi(1S)\pi^+\pi^-\pi^+\pi^-$		$(7.5 \pm 0.8) \times 10^{-5}$	
Γ_{87}	$J/\psi(1S) f_1(1285)$		$(7.2 \pm 1.4) \times 10^{-5}$	
Γ_{88}	$\psi(2S)\eta$		$(3.3 \pm 0.9) \times 10^{-4}$	
Γ_{89}	$\psi(2S)\eta'$		$(1.29 \pm 0.35) \times 10^{-4}$	
Γ_{90}	$\psi(2S)\pi^+\pi^-$		$(6.9 \pm 1.2) \times 10^{-5}$	
Γ_{91}	$\psi(2S)\phi$		$(5.2 \pm 0.4) \times 10^{-4}$	
Γ_{92}	$\psi(2S) K^- \pi^+$		$(3.1 \pm 0.4) \times 10^{-5}$	
Γ_{93}	$\psi(2S) \overline{K}^*(892)^0$		$(3.3 \pm 0.5) \times 10^{-5}$	
Γ_{94}	$\chi_{c1}\phi$		$(1.97 \pm 0.25) \times 10^{-4}$	
Γ_{95}	$\chi_{c1} K^+ K^-$			
Γ_{96}	$\chi_{c2} K^+ K^-$			
Γ_{97}	$\chi_{c1}(3872)\phi$		$(1.1 \pm 0.4) \times 10^{-4}$	
Γ_{98}	$\chi_{c1}(3872)(K^+K^-)_{non-\phi}$		$(8.6 \pm 3.5) \times 10^{-5}$	
Γ_{99}	$\pi^+\pi^-$		$(7.0 \pm 1.0) \times 10^{-7}$	
Γ_{100}	$\pi^0\pi^0$		$< 2.1 \times 10^{-4}$	CL=90%
Γ_{101}	$\eta\pi^0$		$< 1.0 \times 10^{-3}$	CL=90%
Γ_{102}	$\eta\eta$		$< 1.43 \times 10^{-4}$	CL=90%
Γ_{103}	$\rho^0\rho^0$		$< 3.20 \times 10^{-4}$	CL=90%
Γ_{104}	$\eta'\eta$		$< 6.5 \times 10^{-5}$	CL=90%
Γ_{105}	$\eta'\eta'$		$(3.3 \pm 0.7) \times 10^{-5}$	
Γ_{106}	$\eta'\phi$		$< 8.2 \times 10^{-7}$	CL=90%
Γ_{107}	$\phi f_0(980)$, $f_0(980) \to \pi^+\pi^-$		$(1.12 \pm 0.21) \times 10^{-6}$	
Γ_{108}	$\phi f_2(1270)$, $f_2(1270) \to \pi^+\pi^-$		$(6.1 {}^{+1.8}_{-1.5}) \times 10^{-7}$	
Γ_{109}	$\phi\rho^0$		$(2.7 \pm 0.8) \times 10^{-7}$	
Γ_{110}	$\phi\pi^+\pi^-$		$(3.5 \pm 0.5) \times 10^{-6}$	
Γ_{111}	$\phi\phi$		$(1.85 \pm 0.14) \times 10^{-5}$	
Γ_{112}	$\phi\phi\phi$		$(2.2 \pm 0.6) \times 10^{-6}$	
Γ_{113}	$\pi^+ K^-$		$(5.8 \pm 0.7) \times 10^{-6}$	
Γ_{114}	$K^+ K^-$		$(2.66 \pm 0.22) \times 10^{-5}$	
Γ_{115}	$K^0 \overline{K}^0$		$(1.76 \pm 0.31) \times 10^{-5}$	
Γ_{116}	$K^0\pi^+\pi^-$		$(9.5 \pm 2.1) \times 10^{-6}$	
Γ_{117}	$K^0 K^\pm \pi^\mp$		$(8.4 \pm 0.9) \times 10^{-5}$	
Γ_{118}	$K^*(892)^-\pi^+$		$(2.9 \pm 1.1) \times 10^{-6}$	
Γ_{119}	$K^*(892)^\pm K^\mp$		$(1.9 \pm 0.5) \times 10^{-5}$	
Γ_{120}	$K_0^*(1430)^\pm K^\mp$		$(3.1 \pm 2.5) \times 10^{-5}$	
Γ_{121}	$K_2^*(1430)^\pm K^\mp$		$(1.0 \pm 1.7) \times 10^{-5}$	
Γ_{122}	$K^*(892)^0 \overline{K}^0 +$ c.c.		$(2.0 \pm 0.6) \times 10^{-5}$	
Γ_{123}	$K_0^*(1430) \overline{K}^0 +$ c.c.		$(3.3 \pm 1.0) \times 10^{-5}$	
Γ_{124}	$K_2^*(1430)^0 \overline{K}^0 +$ c.c.		$(1.7 \pm 2.2) \times 10^{-5}$	
Γ_{125}	$K_S^0 \overline{K}^*(892)^0 +$ c.c.		$(1.6 \pm 0.4) \times 10^{-5}$	
Γ_{126}	$K^0 K^+ K^-$		$(1.3 \pm 0.6) \times 10^{-6}$	
Γ_{127}	$\overline{K}^*(892)^0\rho^0$		$< 7.67 \times 10^{-4}$	CL=90%
Γ_{128}	$\overline{K}^*(892)^0 K^*(892)^0$		$(1.11 \pm 0.27) \times 10^{-5}$	
Γ_{129}	$K^*(892)^0 \overline{K}_2^*(1430)^0$			
Γ_{130}	$K_2^*(1430)^0 \overline{K}^*(892)^0$			
Γ_{131}	$K_2^*(1430)^0 \overline{K}_2^*(1430)^0$			
Γ_{132}	$\phi K^*(892)^0$		$(1.14 \pm 0.30) \times 10^{-6}$	
Γ_{133}	$p\overline{p}$		$< 1.5 \times 10^{-8}$	CL=90%
Γ_{134}	$p\overline{p}K^+K^-$		$(4.5 \pm 0.5) \times 10^{-6}$	
Γ_{135}	$p\overline{p}K^+\pi^-$		$(1.39 \pm 0.26) \times 10^{-6}$	
Γ_{136}	$p\overline{p}\pi^+\pi^-$		$(4.3 \pm 2.0) \times 10^{-7}$	
Γ_{137}	$p\overline{\Lambda}K^- +$ c.c.		$(5.5 \pm 1.0) \times 10^{-6}$	
Γ_{138}	$\Lambda_c^-\Lambda\pi^+$		$(3.6 \pm 1.6) \times 10^{-4}$	
Γ_{139}	$\Lambda_c^-\Lambda_c^+$		$< 8.0 \times 10^{-5}$	CL=95%

Lepton Family number (*LF*) violating modes or $\Delta B = 1$ weak neutral current (*B1*) modes

Γ_{140}	$\gamma\gamma$	*B1*		$< 3.1 \times 10^{-6}$	CL=90%
Γ_{141}	$\phi\gamma$	*B1*		$(3.4 \pm 0.4) \times 10^{-5}$	
Γ_{142}	$\mu^+\mu^-$	*B1*		$(3.01 \pm 0.35) \times 10^{-9}$	
Γ_{143}	e^+e^-	*B1*		$< 9.4 \times 10^{-9}$	CL=90%
Γ_{144}	$\tau^+\tau^-$	*B1*		$< 6.8 \times 10^{-3}$	CL=95%
Γ_{145}	$\mu^+\mu^-\mu^+\mu^-$	*B1*		$< 2.5 \times 10^{-9}$	CL=95%
Γ_{146}	SP, $S \to \mu^+\mu^-$, $P \to \mu^+\mu^-$	*B1*	[b]	$< 2.2 \times 10^{-9}$	CL=95%
Γ_{147}	$\phi(1020)\mu^+\mu^-$	*B1*		$(8.4 \pm 0.4) \times 10^{-7}$	
Γ_{148}	$f_2'(1525)\mu^+\mu^-$			$(1.62 \pm 0.22) \times 10^{-7}$	
Γ_{149}	$\overline{K}^*(892)^0\mu^+\mu^-$	*B1*		$(2.9 \pm 1.1) \times 10^{-8}$	
Γ_{150}	$\pi^+\pi^-\mu^+\mu^-$	*B1*		$(8.4 \pm 1.7) \times 10^{-8}$	
Γ_{151}	$\phi\nu\overline{\nu}$	*B1*		$< 5.4 \times 10^{-3}$	CL=90%
Γ_{152}	$e^\pm\mu^\mp$	*LF*	[c]	$< 5.4 \times 10^{-9}$	CL=90%
Γ_{153}	$\mu^\pm\tau^\mp$	*LF*		$< 4.2 \times 10^{-5}$	CL=95%

[a] Not a pure measurement. See note at head of B_s^0 Decay Modes.

[b] Here S and P are the hypothetical scalar and pseudoscalar particles with masses of 2.5 GeV/c^2 and 214.3 MeV/c^2, respectively.

[c] The value is for the sum of the charge states or particle/antiparticle states indicated.

CONSTRAINED FIT INFORMATION

An overall fit to 12 branching ratios uses 20 measurements and one constraint to determine 8 parameters. The overall fit has a $\chi^2 = 26.9$ for 13 degrees of freedom.

The following *off-diagonal* array elements are the correlation coefficients $\langle \delta x_i \delta x_j \rangle / (\delta x_i \cdot \delta x_j)$, in percent, from the fit to the branching fractions, $x_i \equiv \Gamma_i/\Gamma_{total}$. The fit constrains the x_i whose labels appear in this array to sum to one.

	x_{13}	x_{15}	x_{17}	x_{56}	x_{63}	x_{66}
x_{15}	17					
x_{17}	82	14				
x_{56}	0	0	0			
x_{63}	0	0	0	43		
x_{66}	0	0	0	31	52	
x_{111}	0	0	0	15	6	5

B_s^0 BRANCHING RATIOS

$\Gamma(D_s^- \text{anything})/\Gamma_{total}$ — Γ_1/Γ

VALUE	EVTS	DOCUMENT ID		TECN	COMMENT
0.62 ±0.06 OUR AVERAGE					
0.602±0.058±0.023		[1] WANG	22	BELL	$e^+e^- \to \Upsilon(5S)$
0.91 ±0.18 ±0.41		[2] DRUTSKOY	07	BELL	$e^+e^- \to \Upsilon(4S)$
0.81 ±0.24 ±0.22	90	[3] BUSKULIC	96E	ALEP	$e^+e^- \to Z$
1.56 ±0.58 ±0.44	147	[4] ACTON	92N	OPAL	$e^+e^- \to Z$

[1] WANG 22 selects the B_s events by tagging the accompanying B_s via partial reconstruction of the semileptonic decays $B_s \to D_s X \ell^+ \nu$.

[2] The extraction of this result takes into account the correlation between the measurements of $B(\Upsilon(5S) \to D_s X)$ and $B(\Upsilon(5S) \to D^0 X)$.

[3] BUSKULIC 96E separate $c\overline{c}$ and $b\overline{b}$ sources of D_s^+ mesons using a lifetime tag, subtract generic $\overline{b} \to W^+ \to D_s^+$ events, and obtain $B(\overline{b} \to B_s^0) \times B(B_s^0 \to D_s^- \text{anything}) = 0.088 \pm 0.020 \pm 0.020$ assuming $B(D_s \to \phi\pi) = (3.5 \pm 0.4) \times 10^{-2}$ and PDG 1994 values for the relative partial widths to other D_s channels. We evaluate using our current values $B(\overline{b} \to B_s^0) = 0.107 \pm 0.014$ and $B(D_s \to \phi\pi) = 0.036 \pm 0.009$. Our first error is their experiment's and our second error is that due to $B(\overline{b} \to B_s^0)$ and $B(D_s \to \phi\pi)$.

[4] ACTON 92N assume that excess of 147 ± 48 D_s^0 events over that expected from B^0, B^+, and $c\overline{c}$ is all from B_s^0 decay. The product branching fraction is measured to be $B(\overline{b} \to B_s^0) B(B_s^0 \to D_s^- \text{anything}) \times B(D_s^- \to \phi\pi^-) = (5.9 \pm 1.9 \pm 1.1) \times 10^{-3}$. We evaluate using our current values $B(\overline{b} \to B_s^0) = 0.107 \pm 0.014$ and $B(D_s \to \phi\pi) = 0.036 \pm 0.009$. Our first error is their experiment's and our second error is that due to $B(\overline{b} \to B_s^0)$ and $B(D_s \to \phi\pi)$.

$\Gamma(\ell\nu_\ell X)/\Gamma_{total}$ — Γ_2/Γ

VALUE (units 10^{-2})	DOCUMENT ID		TECN	COMMENT
9.6±0.8 OUR AVERAGE				
9.6±0.4±0.7	[1] OSWALD	13	BELL	$e^+e^- \to \Upsilon(5S)$
$9.5 {}^{+2.5}_{-2.0} {}^{+1.1}_{-1.9}$	[2] LEES	12A	BABR	e^+e^-

[1] The measurement corresponds to the average of the electron and muon branching fractions.

[2] The measurement corresponds to a branching fraction where the lepton originates from bottom decay and is the average between the electron and muon branching fractions. LEES 12A uses the correlation of the production of ϕ mesons in association with a lepton in e^+e^- data taken at center-of-mass energies between 10.54 and 11.2 GeV.

$\Gamma(e^+\nu X^-)/\Gamma_{total}$ — Γ_3/Γ

VALUE (units 10^{-2})	DOCUMENT ID		TECN	COMMENT
9.1±0.5±0.6	OSWALD	13	BELL	$e^+e^- \to \Upsilon(5S)$

$\Gamma(\mu^+\nu X^-)/\Gamma_{total}$ — Γ_4/Γ

VALUE (units 10^{-2})	DOCUMENT ID		TECN	COMMENT
10.2±0.6±0.8	OSWALD	13	BELL	$e^+e^- \to \Upsilon(5S)$

Downloaded from https://academic.oup.com/ptep/article/2022/8/083C01/6651666 by KIT Library user on 27 September 2022

$\Gamma(D_s^- \ell^+ \nu_\ell \text{anything})/\Gamma_{\text{total}}$ — Γ_5/Γ

The values and averages in this section serve only to show what values result if one assumes our $B(\overline{b} \to B_s^0)$. They cannot be thought of as measurements since the underlying product branching fractions were also used to determine $B(\overline{b} \to B_s^0)$ as described in the note on "Production and Decay of b-Flavored Hadrons."

VALUE (units 10^{-2})	EVTS	DOCUMENT ID		TECN	COMMENT
8.1±1.3 OUR AVERAGE					
8.2±0.2±1.5		[1] OSWALD	15	BELL	$e^+e^- \to \Upsilon(5S)$
7.6±1.2±2.1	134	[2] BUSKULIC	95O	ALEP	$e^+e^- \to Z$
10.7±4.3±2.9		[3] ABREU	92M	DLPH	$e^+e^- \to Z$
10.3±3.6±2.8	18	[4] ACTON	92N	OPAL	$e^+e^- \to Z$
• • • We do not use the following data for averages, fits, limits, etc. • • •					
13 ±4 ±4	27	[5] BUSKULIC	92E	ALEP	$e^+e^- \to Z$

[1] Obtains $B_s \to D_s X e\nu$, and $D_s X \mu\nu$ separately, then combines them by assuming systematic uncertainties are fully correlated, except for the one on lepton identification. The third uncertainty adds in quadrature systematic uncertainties from external sources (number of B_s events, and $D_s^{(*)}$ branching fractions). OSWALD 15 also measures the cross-section $\sigma(e^+e^- \to B_s^{(*)}\overline{B}_s^{(*)}) = 53.8 \pm 1.4 \pm 5.3$ pb at $\sqrt{s} = 10.86$ GeV.

[2] BUSKULIC 95O use $D_s \ell$ correlations. The measured product branching ratio is $B(\overline{b} \to B_s) \times B(B_s \to D_s^- \ell^+ \nu_\ell \text{anything}) = (0.82 \pm 0.09^{+0.13}_{-0.14})\%$ assuming $B(D_s \to \phi\pi) = (3.5 \pm 0.4) \times 10^{-2}$ and PDG 1994 values for the relative partial widths to the six other D_s channels used in this analysis. Combined with results from $\Upsilon(4S)$ experiments this can be used to extract $B(\overline{b} \to B_s) = (11.0 \pm 1.2^{+2.5}_{-2.6})\%$. We evaluate using our current values $B(\overline{b} \to B_s^0) = 0.107 \pm 0.014$ and $B(D_s \to \phi\pi) = 0.036 \pm 0.009$. Our first error is their experiment's and our second error is that due to $B(\overline{b} \to B_s^0)$ and $B(D_s \to \phi\pi)$.

[3] ABREU 92M measured muons only and obtained product branching ratio $B(Z \to b \text{ or } \overline{b}) \times B(\overline{b} \to B_s) \times B(B_s \to D_s \mu^+ \nu_\mu \text{anything}) \times B(D_s \to \phi\pi) = (18 \pm 8) \times 10^{-5}$. We evaluate using our current values $B(\overline{b} \to B_s^0) = 0.107 \pm 0.014$ and $B(D_s \to \phi\pi) = 0.036 \pm 0.009$. Our first error is their experiment's and our second error is that due to $B(\overline{b} \to B_s^0)$ and $B(D_s \to \phi\pi)$. We use $B(Z \to b \text{ or } \overline{b}) = 2B(Z \to b\overline{b}) = 2\times(0.2212 \pm 0.0019)$.

[4] ACTON 92N is measured using $D_s \to \phi\pi^+$ and $K^*(892)^0 K^+$ events. The product branching fraction measured is measured to be $B(\overline{b} \to B_s^0)B(B_s^0 \to D_s^- \ell^+ \nu_\ell \text{anything}) \times B(D_s^- \to \phi\pi^-) = (3.9 \pm 1.1 \pm 0.8) \times 10^{-4}$. We evaluate using our current values $B(\overline{b} \to B_s^0) = 0.107 \pm 0.014$ and $B(D_s \to \phi\pi) = 0.036 \pm 0.009$. Our first error is their experiment's and our second error is that due to $B(\overline{b} \to B_s^0)$ and $B(D_s \to \phi\pi)$.

[5] BUSKULIC 92E is measured using $D_s \to \phi\pi^+$ and $K^*(892)^0 K^+$ events. They use $2.7 \pm 0.7\%$ for the $\phi\pi^+$ branching fraction. The average product branching fraction is measured to be $B(\overline{b} \to B_s^0)B(B_s^0 \to D_s^- \ell^+ \nu_\ell \text{anything}) = 0.020 \pm 0.0055^{+0.005}_{-0.006}$. We evaluate using our current values $B(\overline{b} \to B_s^0) = 0.107 \pm 0.014$ and $B(D_s \to \phi\pi) = 0.036 \pm 0.009$. Our first error is their experiment's and our second error is that due to $B(\overline{b} \to B_s^0)$ and $B(D_s \to \phi\pi)$. Superseded by BUSKULIC 95O.

$\Gamma(D_s^{*-} \ell^+ \nu_\ell \text{anything})/\Gamma_{\text{total}}$ — Γ_6/Γ

VALUE (units 10^{-2})	DOCUMENT ID		TECN	COMMENT
5.4±0.4±1.0	[1] OSWALD	15	BELL	$e^+e^- \to \Upsilon(5S)$

[1] Obtains $B_s \to D_s^* X e\nu$, and $D_s^* X \mu\nu$ separately, then combines them by assuming systematic uncertainties are fully correlated, except for the one on lepton identification. The third uncertainty adds in quadrature systematic uncertainties from external sources (number of B_s events, and $D_s^{(*)}$ branching fractions). OSWALD 15 also measures the cross-section $\sigma(e^+e^- \to B_s^{(*)}\overline{B}_s^{(*)}) = 53.8 \pm 1.4 \pm 5.3$ pb at $\sqrt{s} = 10.86$ GeV.

$\Gamma(D_s^- \mu^+ \nu_\mu)/\Gamma_{\text{total}}$ — Γ_7/Γ

VALUE (units 10^{-2})	DOCUMENT ID		TECN	COMMENT
2.44±0.21±0.10	[1] AAIJ	20E	LHCB	pp at 7, 8 TeV

[1] AAIJ 20E reports $[\Gamma(B_s^0 \to D_s^- \mu^+ \nu_\mu)/\Gamma_{\text{total}}] / [B(B^0 \to D^- \ell^+ \nu_\ell)] = 1.09 \pm 0.05 \pm 0.06 \pm 0.05$ which we multiply by our best value $B(B^0 \to D^- \ell^+ \nu_\ell) = (2.24 \pm 0.09) \times 10^{-2}$. Our first error is their experiment's error and our second error is the systematic error from using our best value.

$\Gamma(D_s^{*-} \mu^+ \nu_\mu)/\Gamma_{\text{total}}$ — Γ_8/Γ

VALUE (units 10^{-2})	DOCUMENT ID		TECN	COMMENT
5.3±0.5±0.1	[1] AAIJ	20E	LHCB	pp at 7, 8 TeV

[1] AAIJ 20E reports $[\Gamma(B_s^0 \to D_s^{*-} \mu^+ \nu_\mu)/\Gamma_{\text{total}}] / [B(B^0 \to D^*(2010)^- \ell^+ \nu_\ell)] = 1.06 \pm 0.05 \pm 0.07 \pm 0.05$ which we multiply by our best value $B(B^0 \to D^*(2010)^- \ell^+ \nu_\ell) = (4.97 \pm 0.12) \times 10^{-2}$. Our first error is their experiment's error and our second error is the systematic error from using our best value.

$\Gamma(D_s^- \mu^+ \nu_\mu)/\Gamma(D_s^{*-} \mu^+ \nu_\mu)$ — Γ_7/Γ_8

VALUE	DOCUMENT ID		TECN	COMMENT
• • • We do not use the following data for averages, fits, limits, etc. • • •				
0.464±0.013±0.043	[1] AAIJ	20E	LHCB	pp at 7, 8 TeV

[1] AAIJ 20E value is not independent of other reported measurements.

$\Gamma(D_{s1}(2536)^- \mu^+ \nu_\mu,\ D_{s1}^- \to D^{*-} K_S^0)/\Gamma_{\text{total}}$ — Γ_9/Γ

VALUE (units 10^{-3})	DOCUMENT ID		TECN	COMMENT
2.7±0.7±0.2	[1] ABAZOV	09G	D0	$p\overline{p}$ at 1.96 TeV

[1] ABAZOV 09G reports $[\Gamma(B_s^0 \to D_{s1}(2536)^- \mu^+ \nu_\mu,\ D_{s1}^- \to D^{*-} K_S^0)/\Gamma_{\text{total}}] \times [B(\overline{b} \to B_s^0)] = (2.66 \pm 0.52 \pm 0.45) \times 10^{-4}$ which we divide by our best value $B(\overline{b} \to B_s^0) = (10.0 \pm 0.8) \times 10^{-2}$. Our first error is their experiment's error and our second error is the systematic error from using our best value.

$\Gamma(D_{s1}(2536)^- X \mu^+ \nu,\ D_{s1}^- \to \overline{D}^0 K^+)/\Gamma(D_s^- \ell^+ \nu_\ell \text{anything})$ — Γ_{10}/Γ_5

VALUE (units 10^{-2})	DOCUMENT ID		TECN	COMMENT
5.4±1.2±0.5	AAIJ	11A	LHCB	pp at 7 TeV

$\Gamma(D_{s2}(2573)^- X \mu^+ \nu,\ D_{s2}^- \to \overline{D}^0 K^+)/\Gamma(D_s^- \ell^+ \nu_\ell \text{anything})$ — Γ_{11}/Γ_5

VALUE (units 10^{-2})	DOCUMENT ID		TECN	COMMENT
3.3±1.0±0.4	AAIJ	11A	LHCB	pp at 7 TeV

$\Gamma(D_{s1}(2536)^- X \mu^+ \nu,\ D_{s1}^- \to \overline{D}^0 K^+)/\Gamma(D_{s2}(2573)^- X \mu^+ \nu,\ D_{s2}^- \to \overline{D}^0 K^+)$ — Γ_{10}/Γ_{11}

VALUE	DOCUMENT ID		TECN	COMMENT
• • • We do not use the following data for averages, fits, limits, etc. • • •				
0.61±0.14±0.05	[1] AAIJ	11A	LHCB	pp at 7 TeV

[1] Not independent of other AAIJ 11A measurements.

$\Gamma(K^- \mu^+ \nu_\mu)/\Gamma(D_s^- \mu^+ \nu_\mu)$ — Γ_{12}/Γ_7

VALUE (units 10^{-3})	DOCUMENT ID		TECN	COMMENT
4.89±0.21±0.25	[1,2] AAIJ	21G	LHCB	pp at 8 TeV

[1] AAIJ 21G measures $B(B_s^0 \to K^- \mu^+ \nu_\mu)/B(B_s^0 \to D_s^- \mu^+ \nu_\mu) = (4.89 \pm 0.21^{+0.20}_{-0.21} \pm 0.14) \times 10^{-3}$ over the whole q^2 range, where the last uncertainty is due to the $D_s^- \to K^+ K^- \pi^-$ branching fraction.

[2] AAIJ 21G reports this branching ratio for $q^2 < 7$ GeV^2 as $(1.66 \pm 0.08 \pm 0.07 \pm 0.05) \times 10^{-3}$ and for $q^2 > 7$ GeV^2 as $(3.25 \pm 0.21^{+0.16}_{-0.17} \pm 0.09) \times 10^{-3}$.

$\Gamma(K^- \mu^+ \nu_\mu)/\Gamma_{\text{total}}$ — Γ_{12}/Γ

VALUE (units 10^{-4})	DOCUMENT ID		TECN	COMMENT
1.06±0.05±0.08	[1] AAIJ	21G	LHCB	pp at 8 TeV

[1] The total systematic error includes D_s^- branching fractions, B_s^0 lifetime, $|V_{cb}|$, and $B_s^0 \to D_s^-$ form factor integral uncertainties.

$\Gamma(D_s^- \pi^+)/\Gamma_{\text{total}}$ — Γ_{13}/Γ

VALUE (units 10^{-3})	EVTS	DOCUMENT ID		TECN	COMMENT
2.98±0.14 OUR FIT					
2.97±0.13 OUR AVERAGE					
2.96±0.10±0.09		[1] AAIJ	21Y	LHCB	pp at 7, 8, 13 TeV
3.6 ±0.5 ±0.5		[2] LOUVOT	09	BELL	$e^+e^- \to \Upsilon(5S)$
2.8 ±0.6 ±0.1		[3] ABULENCIA	07C	CDF	$p\overline{p}$ at 1.96 TeV
• • • We do not use the following data for averages, fits, limits, etc. • • •					
2.95±0.05$^{+0.25}_{-0.28}$		[4] AAIJ	12AG	LHCB	Repl. by AAIJ 21Y
6.8 ±2.2 ±1.6		DRUTSKOY	07A	BELL	Repl. by LOUVOT 09
3.3 ±1.1 ±0.1		[5] ABULENCIA	06J	CDF	Repl. by ABULENCIA 07C
<130	6	[6] AKERS	94J	OPAL	$e^+e^- \to Z$
seen	1	BUSKULIC	93G	ALEP	$e^+e^- \to Z$

[1] AAIJ 21Y reports $[\Gamma(B_s^0 \to D_s^- \pi^+)/\Gamma_{\text{total}}] / [B(B^0 \to D^- \pi^+)] = 1.18 \pm 0.04$ which we multiply by our best value $B(B^0 \to D^- \pi^+) = (2.51 \pm 0.08) \times 10^{-3}$. Our first error is their experiment's error and our second error is the systematic error from using our best value.

[2] LOUVOT 09 reports $(3.67^{+0.35+0.65}_{-0.33-0.645}) \times 10^{-3}$ from a measurement of $[\Gamma(B_s^0 \to D_s^- \pi^+)/\Gamma_{\text{total}}] \times [B(\Upsilon(10860) \to B_s^{(*)}\overline{B}_s^{(*)})]$ assuming $B(\Upsilon(10860) \to B_s^{(*)}\overline{B}_s^{(*)}) = (19.5 \pm 2.6) \times 10^{-2}$, which we rescale to our best value $B(\Upsilon(10860) \to B_s^{(*)}\overline{B}_s^{(*)}) = (20.1 \pm 3.1) \times 10^{-2}$. Our first error is their experiment's error and our second error is the systematic error from using our best value.

[3] ABULENCIA 07C reports $[\Gamma(B_s^0 \to D_s^- \pi^+)/\Gamma_{\text{total}}] / [B(B^0 \to D^- \pi^+)] = 1.13 \pm 0.08 \pm 0.23$ which we multiply by our best value $B(B^0 \to D^- \pi^+) = (2.51 \pm 0.08) \times 10^{-3}$. Our first error is their experiment's error and our second error is the systematic error from using our best value.

[4] AAIJ 12AG reports $(2.95 \pm 0.05 \pm 0.17^{+0.18}_{-0.22}) \times 10^{-3}$ where the last uncertainty comes from the semileptonic f_s/f_d measurement. We combined the systematics in quadrature.

[5] ABULENCIA 06J reports $[\Gamma(B_s^0 \to D_s^- \pi^+)/\Gamma_{\text{total}}] / [B(B^0 \to D^- \pi^+)] = 1.32 \pm 0.18 \pm 0.38$ which we multiply by our best value $B(B^0 \to D^- \pi^+) = (2.51 \pm 0.08) \times 10^{-3}$. Our first error is their experiment's error and our second error is the systematic error from using our best value.

[6] AKERS 94J sees ≤ 6 events and measures the limit on the product branching fraction $f(\overline{b} \to B_s^0) \cdot B(B_s^0 \to D_s^- \pi^+) < 1.3\%$ at CL = 90%. We divide by our current value $B(\overline{b} \to B_s^0) = 0.105$.

$\Gamma(D_s^- \rho^+)/\Gamma(D_s^- \pi^+)$ — Γ_{14}/Γ_{13}

VALUE	DOCUMENT ID		TECN	COMMENT
2.3±0.4±0.2	LOUVOT	10	BELL	$e^+e^- \to \Upsilon(5S)$

Downloaded from https://academic.oup.com/ptep/article/2022/8/083C01/6651666 by KIT Library user on 27 September 2022

$\Gamma(D_s^- \pi^+ \pi^+ \pi^-)/\Gamma_{total}$ — Γ_{15}/Γ

VALUE (units 10^{-3})	DOCUMENT ID		TECN	COMMENT
6.1±1.0 OUR FIT				
6.3±1.4±0.6	[1] ABULENCIA	07C	CDF	$p\overline{p}$ at 1.96 TeV

[1] ABULENCIA 07C reports $[\Gamma(B_s^0 \to D_s^- \pi^+ \pi^+ \pi^-)/\Gamma_{total}]$ / $[B(B^0 \to D^- \pi^+ \pi^+ \pi^-)] = 1.05 \pm 0.10 \pm 0.22$ which we multiply by our best value $B(B^0 \to D^- \pi^+ \pi^+ \pi^-) = (6.0 \pm 0.6) \times 10^{-3}$. Our first error is their experiment's error and our second error is the systematic error from using our best value.

$\Gamma(D_s^- \pi^+ \pi^+ \pi^-)/\Gamma(D_s^- \pi^+)$ — Γ_{15}/Γ_{13}

VALUE	DOCUMENT ID		TECN	COMMENT
2.05±0.33 OUR FIT				
2.01±0.37±0.20	AAIJ	11E	LHCB	pp at 7 TeV

$\Gamma(D_{s1}(2536)^- \pi^+,\ D_{s1}^- \to D_s^- \pi^+ \pi^-)/\Gamma(D_s^- \pi^+ \pi^+ \pi^-)$ — Γ_{16}/Γ_{15}

VALUE (units 10^{-3})	DOCUMENT ID		TECN	COMMENT
4.0±1.0±0.4	AAIJ	12AX	LHCB	pp at 7 TeV

$\Gamma(D_s^{\mp} K^{\pm})/\Gamma_{total}$ — Γ_{17}/Γ

VALUE (units 10^{-4})	DOCUMENT ID		TECN	COMMENT
2.25±0.12 OUR FIT				
$2.3\ ^{+1.2}_{-1.0}\ ^{+0.4}_{-0.3}$	[1] LOUVOT	09	BELL	$e^+e^- \to \Upsilon(5S)$

[1] LOUVOT 09 reports $(2.4\ ^{+1.2}_{-1.0} \pm 0.42) \times 10^{-4}$ from a measurement of $[\Gamma(B_s^0 \to D_s^{\mp} K^{\pm})/\Gamma_{total}] \times [B(\Upsilon(10860) \to B_s^{(*)} \overline{B}_s^{(*)})]$ assuming $B(\Upsilon(10860) \to B_s^{(*)} \overline{B}_s^{(*)}) = (19.5 \pm 2.6) \times 10^{-2}$, which we rescale to our best value $B(\Upsilon(10860) \to B_s^{(*)} \overline{B}_s^{(*)}) = (20.1 \pm 3.1) \times 10^{-2}$. Our first error is their experiment's error and our second error is the systematic error from using our best value.

$\Gamma(D_s^{\mp} K^{\pm})/\Gamma(D_s^- \pi^+)$ — Γ_{17}/Γ_{13}

VALUE (units 10^{-2})	DOCUMENT ID		TECN	COMMENT
7.55±0.24 OUR FIT				
7.55±0.24 OUR AVERAGE				
7.52±0.15±0.19	AAIJ	15AC	LHCB	pp at 7, 8 TeV
9.7 ±1.8 ±0.9	AALTONEN	09AQ	CDF	$p\overline{p}$ at 1.96 TeV
• • • We do not use the following data for averages, fits, limits, etc. • • •				
6.46±0.43±0.25	AAIJ	12AG	LHCB	Repl. by AAIJ 15AC

$\Gamma(D_s^- K^+ \pi^+ \pi^-)/\Gamma(D_s^- \pi^+ \pi^+ \pi^-)$ — Γ_{18}/Γ_{15}

VALUE (units 10^{-2})	DOCUMENT ID		TECN	COMMENT
5.2±0.5±0.3	AAIJ	12AX	LHCB	pp at 7 TeV

$\Gamma(D_s^+ D_s^-)/\Gamma_{total}$ — Γ_{19}/Γ

VALUE (units 10^{-3})	CL%	DOCUMENT ID		TECN	COMMENT
4.4±0.5 OUR AVERAGE					
4.0±0.2±0.5		[1] AAIJ	13AP	LHCB	pp at 7 TeV
$5.8\ ^{+1.1}_{-0.9}\pm1.3$		[2] ESEN	13	BELL	$e^+e^- \to \Upsilon(5S)$
5.4±0.8±0.8		[3] AALTONEN	12C	CDF	$p\overline{p}$ at 1.96 TeV
• • • We do not use the following data for averages, fits, limits, etc. • • •					
$10.3\ ^{+3.9}_{-3.2}\pm^{2.6}_{2.5}$		[4] ESEN	10	BELL	Repl. by ESEN 13
$10.4\ ^{+3.5}_{-3.2}\pm1.1$		[5] AALTONEN	08F	CDF	Repl. by AALTONEN 12C
<67	90	DRUTSKOY	07A	BELL	Repl. by ESEN 10

[1] Uses $B(B^0 \to D^- D_s^+) = (7.2 \pm 0.8) \times 10^{-3}$.

[2] Use $\Upsilon(5S) \to B_s^* \overline{B}_s^*$ decays assuming $B(\Upsilon(5S) \to B_s^* \overline{B}_s^*) = (17.1 \pm 3.0)\%$ and $\Gamma(\Upsilon(5S) \to B_s^* \overline{B}_s^*) / \Gamma(\Upsilon(5S) \to B_s^{(*)} \overline{B}_s^{(*)}) = (87.0 \pm 1.7)\%$.

[3] AALTONEN 12C reports $(f_s/f_d)\ (B(B_s^0 \to D_s^+ D_s^-) / B(B^0 \to D^- D_s^+)) = 0.183 \pm 0.021 \pm 0.017$. We multiply this result by our best value of $B(B^0 \to D^- D_s^+) = (7.2 \pm 0.8) \times 10^{-3}$ and divide by our best value of f_s/f_d, where $1/2\ f_s/f_d = 0.1230 \pm 0.0115$. Our first quoted uncertainty is the combined experiment's uncertainty and our second is the systematic uncertainty from using out best values.

[4] Uses $\Upsilon(10860) \to B_s^* \overline{B}_s^*$ assuming $B(\Upsilon(10860) \to B_s^{(*)} \overline{B}_s^{(*)}) = (19.3 \pm 2.9)\%$ and $\Gamma(\Upsilon(10860) \to B_s^* \overline{B}_s^*) / \Gamma(\Upsilon(10860) \to B_s^{(*)} \overline{B}_s^{(*)}) = (90.1\ ^{+3.8}_{-4.0})\%$.

[5] AALTONEN 08F reports $[\Gamma(B_s^0 \to D_s^+ D_s^-)/\Gamma_{total}]$ / $[B(B^0 \to D^- D_s^+)] = 1.44\ ^{+0.48}_{-0.44}$ which we multiply by our best value $B(B^0 \to D^- D_s^+) = (7.2 \pm 0.8) \times 10^{-3}$. Our first error is their experiment's error and our second error is the systematic error from using our best value.

$\Gamma(D_s^- D^+)/\Gamma_{total}$ — Γ_{20}/Γ

VALUE (units 10^{-4})	DOCUMENT ID		TECN	COMMENT
2.8±0.4±0.3	[1] AAIJ	14AA	LHCB	pp at 7 TeV
• • • We do not use the following data for averages, fits, limits, etc. • • •				
3.6±0.6±0.5	[2] AAIJ	13AP	LHCB	Repl. by AAIJ 14AA

[1] AAIJ 14AA reports $[\Gamma(B_s^0 \to D_s^- D^+)/\Gamma_{total}]$ / $[B(B^0 \to D^- D_s^+)] = 0.038 \pm 0.004 \pm 0.003$ which we multiply by our best value $B(B^0 \to D^- D_s^+) = (7.2 \pm 0.8) \times 10^{-3}$. Our first error is their experiment's error and our second error is the systematic error from using our best value..

[2] Uses $B(B^0 \to D^- D_s^+) = (7.2 \pm 0.8) \times 10^{-3}$.

$\Gamma(D^+ D^-)/\Gamma_{total}$ — Γ_{21}/Γ

VALUE (units 10^{-4})	DOCUMENT ID		TECN	COMMENT
2.2±0.4±0.4	[1] AAIJ	13AP	LHCB	pp at 7 TeV

[1] Uses $B(B^0 \to D^- D^+) = (2.11 \pm 0.31) \times 10^{-4}$ and $B(B^+ \to \overline{D}^0 D_s^+) = (10.1 \pm 1.7) \times 10^{-3}$.

$\Gamma(D^0 \overline{D}^0)/\Gamma_{total}$ — Γ_{24}/Γ

VALUE (units 10^{-4})	DOCUMENT ID		TECN	COMMENT
1.9±0.3±0.4	[1] AAIJ	13AP	LHCB	pp at 7 TeV

[1] Uses $B(B^0 \to D^- D^+) = (2.11 \pm 0.31) \times 10^{-4}$ and $B(B^+ \to \overline{D}^0 D_s^+) = (10.1 \pm 1.7) \times 10^{-3}$.

$\Gamma(D_s^{*-} \pi^+)/\Gamma(D_s^- \pi^+)$ — Γ_{25}/Γ_{13}

VALUE	DOCUMENT ID		TECN	COMMENT
$0.65\ ^{+0.15}_{-0.13}\pm0.07$	LOUVOT	10	BELL	$e^+e^- \to \Upsilon(5S)$

$\Gamma(D_s^{*\mp} K^{\pm})/\Gamma(D_s^{*-} \pi^+)$ — Γ_{26}/Γ_{25}

VALUE	DOCUMENT ID		TECN	COMMENT
$0.068\pm0.005\ ^{+0.003}_{-0.002}$	AAIJ	15AD	LHCB	pp at 7, 8 TeV

$\Gamma(D_s^{*-} \rho^+)/\Gamma(D_s^- \pi^+)$ — Γ_{27}/Γ_{13}

VALUE	DOCUMENT ID		TECN	COMMENT
3.2±0.6±0.3	LOUVOT	10	BELL	$e^+e^- \to \Upsilon(5S)$

$\Gamma(D_s^{*-} \rho^+)/\Gamma(D_s^- \rho^+)$ — Γ_{27}/Γ_{14}

VALUE	DOCUMENT ID		TECN	COMMENT
• • • We do not use the following data for averages, fits, limits, etc. • • •				
1.4±0.3±0.1	[1] LOUVOT	10	BELL	$e^+e^- \to \Upsilon(5S)$

[1] Not independent of other LOUVOT 10 measurements.

$[\Gamma(D_s^{*+} D_s^-) + \Gamma(D_s^{*-} D_s^+)]/\Gamma_{total}$ — Γ_{28}/Γ

VALUE (units 10^{-3})	CL%	DOCUMENT ID		TECN	COMMENT
13.9±1.7 OUR AVERAGE					
13.6±1.0±1.4		[1] AAIJ	16P	LHCB	pp at 7 TeV
$17.6\ ^{+2.3}_{-2.2}\pm4.0$		[2] ESEN	13	BELL	$e^+e^- \to \Upsilon(5S)$
12.5±1.7±1.8		[3] AALTONEN	12C	CDF	$p\overline{p}$ at 1.96 TeV
• • • We do not use the following data for averages, fits, limits, etc. • • •					
$27.5\ ^{+8.3}_{-7.1}\pm6.9$		[4] ESEN	10	BELL	Repl. by ESEN 13
<121	90	DRUTSKOY	07A	BELL	Repl. by ESEN 10

[1] AAIJ 16P reports $[\left[\Gamma(B_s^0 \to D_s^{*+} D_s^-) + \Gamma(D_s^{*-} D_s^+)\right]/\Gamma_{total}]$ / $[B(B^0 \to D^- D_s^+)] = 1.88 \pm 0.08 \pm 0.12$ which we multiply by our best value $B(B^0 \to D^- D_s^+) = (7.2 \pm 0.8) \times 10^{-3}$. Our first error is their experiment's error and our second error is the systematic error from using our best value.

[2] Use $\Upsilon(5S) \to B_s^* \overline{B}_s^*$ decays assuming $B(\Upsilon(5S) \to B_s^* \overline{B}_s^*) = (17.1 \pm 3.0)\%$ and $\Gamma(\Upsilon(5S) \to B_s^* \overline{B}_s^*) / \Gamma(\Upsilon(5S) \to B_s^{(*)} \overline{B}_s^{(*)}) = (87.0 \pm 1.7)\%$.

[3] AALTONEN 12C reports $(f_s/f_d)\ (B(B_s^0 \to D_s^{*+} D_s^- + D_s^{*-} D_s^+) / B(B^0 \to D^- D_s^+)) = 0.424 \pm 0.046 \pm 0.035$. We multiply this result by our best value of $B(B^0 \to D^- D_s^+) = (7.2 \pm 0.8) \times 10^{-3}$ and divide by our best value of f_s/f_d, where $1/2\ f_s/f_d = 0.1230 \pm 0.0115$. Our first quoted uncertainty is the combined experiment's uncertainty and our second is the systematic uncertainty from using out best values.

[4] Uses $\Upsilon(10860) \to B_s^* \overline{B}_s^*$ assuming $B(\Upsilon(10860) \to B_s^{(*)} \overline{B}_s^{(*)}) = (19.3 \pm 2.9)\%$ and $\Gamma(\Upsilon(10860) \to B_s^* \overline{B}_s^*) / \Gamma(\Upsilon(10860) \to B_s^{(*)} \overline{B}_s^{(*)}) = (90.1\ ^{+3.8}_{-4.0})\%$.

$\Gamma(D_s^{*+} D_s^{*-})/\Gamma_{total}$ — Γ_{29}/Γ

VALUE (units 10^{-3})	CL%	DOCUMENT ID		TECN	COMMENT
14.4± 2.1 OUR AVERAGE		Error includes scale factor of 1.1.			
12.7± 1.3±1.4		[1] AAIJ	16P	LHCB	pp at 7 TeV
$19.8\pm\ ^{3.3+5.2}_{3.1-5.0}$		[2] ESEN	13	BELL	$e^+e^- \to \Upsilon(5S)$
19.2± 2.9±2.7		[3] AALTONEN	12C	CDF	$p\overline{p}$ at 1.96 TeV
• • • We do not use the following data for averages, fits, limits, etc. • • •					
$30.8\ ^{+12.2+8.5}_{-10.4-8.6}$		[4] ESEN	10	BELL	Repl. by ESEN 13
<257	90	DRUTSKOY	07A	BELL	Repl. by ESEN 10

[1] AAIJ 16P reports $[\Gamma(B_s^0 \to D_s^{*+} D_s^{*-})/\Gamma_{total}]$ / $[B(B^0 \to D^- D_s^+)] = 1.76 \pm 0.11 \pm 0.14$ which we multiply by our best value $B(B^0 \to D^- D_s^+) = (7.2 \pm 0.8) \times 10^{-3}$. Our first error is their experiment's error and our second error is the systematic error from using our best value.

[2] Use $\Upsilon(5S) \to B_s^* \overline{B}_s^*$ decays assuming $B(\Upsilon(5S) \to B_s^* \overline{B}_s^*) = (17.1 \pm 3.0)\%$ and $\Gamma(\Upsilon(5S) \to B_s^* \overline{B}_s^*) / \Gamma(\Upsilon(5S) \to B_s^{(*)} \overline{B}_s^{(*)}) = (87.0 \pm 1.7)\%$.

[3] AALTONEN 12C reports $(f_s/f_d)\ (B(B_s^0 \to D_s^{*+} D_s^{*-}) / B(B^0 \to D^- D_s^+)) = 0.654 \pm 0.072 \pm 0.065$. We multiply this result by our best value of $B(B^0 \to D^- D_s^+) = (7.2 \pm 0.8) \times 10^{-3}$ and divide by our best value of f_s/f_d, where $1/2\ f_s/f_d = 0.1230 \pm 0.0115$. Our first quoted uncertainty is the combined experiment's uncertainty and our second is the systematic uncertainty from using out best values.

[4] Uses $\Upsilon(10860) \to B_s^* \overline{B}_s^*$ assuming $B(\Upsilon(10860) \to B_s^{(*)} \overline{B}_s^{(*)}) = (19.3 \pm 2.9)\%$ and $\Gamma(\Upsilon(10860) \to B_s^* \overline{B}_s^*) / \Gamma(\Upsilon(10860) \to B_s^{(*)} \overline{B}_s^{(*)}) = (90.1\ ^{+3.8}_{-4.0})\%$.

Downloaded from https://academic.oup.com/ptep/article/2022/8/083C01/6651666 by KIT Library user on 27 September 2022

$\Gamma(D_s^{(*)+} D_s^{(*)-})/\Gamma_{total}$ — Γ_{30}/Γ

"OUR EVALUATION" is an average using rescaled values of the data listed below. The average and rescaling were performed by the Heavy Flavor Averaging Group (HFLAV, https://hflav.web.cern.ch/) and are described at https://hflav.web.cern.ch/. The averaging/rescaling procedure takes into account correlations between the measurements.

VALUE (%)	CL%	DOCUMENT ID		TECN	COMMENT
4.5 ±1.4 OUR EVALUATION					
3.4 ±0.4 OUR AVERAGE					
3.07±0.22±0.33		[1] AAIJ	16P	LHCB	pp at 7 TeV
$4.32^{+0.42}_{-0.39}{}^{+1.04}_{-1.03}$		[2] ESEN	13	BELL	$e^+e^- \to \Upsilon(5S)$
3.7 ±0.4 ±0.5		[3] AALTONEN	12C	CDF	$p\overline{p}$ at 1.96 TeV
3.5 ±1.0 ±1.1		[4] ABAZOV	09I	D0	$p\overline{p}$ at 1.96 TeV
14 ±6 ±3		[5,6] BARATE	00K	ALEP	$e^+e^- \to Z$
• • • We do not use the following data for averages, fits, limits, etc. • • •					
$6.85^{+1.53}_{-1.30}{}^{+1.79}_{-1.80}$		[7,8] ESEN	10	BELL	Repl. by ESEN 13
$3.9^{+1.9}_{-1.7}{}^{+1.6}_{-1.5}$		[4] ABAZOV	07Y	D0	Repl. by ABAZOV 09I
<0.218	90	BARATE	98Q	ALEP	$e^+e^- \to Z$

[1] AAIJ 16P reports $[\Gamma(B_s^0 \to D_s^{(*)+} D_s^{(*)-})/\Gamma_{total}]$ / $[B(B^0 \to D^- D_s^+)] = 4.24 \pm 0.14 \pm 0.27$ which we multiply by our best value $B(B^0 \to D^- D_s^+) = (7.2 \pm 0.8) \times 10^{-3}$. Our first error is their experiment's error and our second error is the systematic error from using our best value.

[2] Use $\Upsilon(5S) \to B_s^* \overline{B}_s^*$ decays assuming $B(\Upsilon(5S) \to B_s^* \overline{B}_s^*) = (17.1 \pm 3.0)\%$ and $\Gamma(\Upsilon(5S) \to B_s^* \overline{B}_s^*)$ / $\Gamma(\Upsilon(5S) \to B_s^{(*)} \overline{B}_s^{(*)}) = (87.0 \pm 1.7)\%$.

[3] AALTONEN 12C reports (f_s/f_d) $(B(B_s^0 \to D_s^{(*)+} D_s^{(*)-})$ / $B(B^0 \to D^- D_s^+)) = 1.261 \pm 0.095 \pm 0.112$. We multiply this result by our best value of $B(B^0 \to D^- D_s^+) = (7.2 \pm 0.8) \times 10^{-3}$ and divide by our best value of f_s/f_d, where $1/2\ f_s/f_d = 0.1230 \pm 0.0115$. Our first quoted uncertainty is the combined experiment's uncertainty and our second is the systematic uncertainty from using out best values.

[4] Uses the final states where $D_s^+ \to \phi\pi^+$ and $D_s^- \to \phi\mu^-\overline{\nu}_\mu$.

[5] Reports $B(B_s^0(\text{short}) \to D_s^{(*)} D_s^{(*)}) = (0.23 \pm 0.10 \pm 0.05) \cdot [0.17/B(D_s \to \phi\chi)]^2$ assuming $B(B_s^0 \to B_s^0(\text{short})) = 50\%$. We use our best value $B(D_s \to \phi\chi) = 15.7 \pm 1.0\%$ to obtain the quoted result.

[6] Uses $\phi\phi$ correlations from $B_s^0(\text{short}) \to D_s^{(*)+} D_s^{(*)-}$.

[7] Sum of exclusive $B_s \to D_s^+ D_s^-$, $B_s \to D_s^{*\pm} D_s^{\mp}$ and $B_s \to D_s^{*+} D_s^{*-}$.

[8] Uses $\Upsilon(10860) \to B_s^* \overline{B}_s^*$ assuming $B(\Upsilon(10860) \to B_s^{(*)} \overline{B}_s^{(*)}) = (19.3 \pm 2.9)\%$ and $\Gamma(\Upsilon(10860) \to B_s^* \overline{B}_s^*)$ / $\Gamma(\Upsilon(10860) \to B_s^{(*)} \overline{B}_s^{(*)}) = (90.1^{+3.8}_{-4.0})\%$.

$\Gamma(D^{*-} D_s^+)/\Gamma_{total}$ — Γ_{31}/Γ

VALUE (units 10^{-4})	DOCUMENT ID		TECN	COMMENT
3.9±0.6±0.5	[1] AAIJ	21S	LHCB	pp at 13 TeV

[1] AAIJ 21S reports $[\Gamma(B_s^0 \to D^{*-} D_s^+)/\Gamma_{total}]$ / $[B(B^0 \to D^*(2010)^- D_s^+)] = 0.049 \pm 0.006 \pm 0.0036$ which we multiply by our best value $B(B^0 \to D^*(2010)^- D_s^+) = (8.0 \pm 1.1) \times 10^{-3}$. Our first error is their experiment's error and our second error is the systematic error from using our best value.

$[\Gamma(D^{*+} D^-) + \Gamma(D^{*-} D^+)]/\Gamma_{total}$ — $(\Gamma_{22}+\Gamma_{23})/\Gamma$

VALUE (units 10^{-5})	DOCUMENT ID		TECN	COMMENT
8.4±1.1±0.8	[1] AAIJ	21N	LHCB	pp at 7, 8, 13 TeV

[1] AAIJ 21N reports $[\left[\Gamma(B_s^0 \to D^{*+} D^-) + \Gamma(B_s^0 \to D^{*-} D^+)\right]/\Gamma_{total}]$ / $[B(B^0 \to D^\pm D^{*\mp}(CP\text{-averaged}))] = 0.137 \pm 0.017 \pm 0.006$ which we multiply by our best value $B(B^0 \to D^\pm D^{*\mp}(CP\text{-averaged})) = (6.1 \pm 0.6) \times 10^{-4}$. Our first error is their experiment's error and our second error is the systematic error from using our best value.

$\Gamma(\overline{D}^{*0} \overline{K}^0)/\Gamma_{total}$ — Γ_{32}/Γ

VALUE (units 10^{-4})	DOCUMENT ID		TECN	COMMENT
2.8±1.0±0.5	[1] AAIJ	16C	LHCB	pp at 7, 8 TeV

[1] Measured and normalized to the $B_s^0 \to \overline{D}^{*0} K_S^0$ decay with $f_s/f_d = 0.259 \pm 0.015$. Signal significance is 4.4 standard deviations.

$\Gamma(\overline{D}^0 \overline{K}^0)/\Gamma_{total}$ — Γ_{33}/Γ

VALUE (units 10^{-4})	DOCUMENT ID		TECN	COMMENT
4.3±0.5±0.7	[1] AAIJ	16C	LHCB	pp at 7, 8 TeV

[1] Measured and normalized to the $B^0 \to \overline{D}^0 K_S^0$ decay with $f_s/f_d = 0.259 \pm 0.015$.

$\Gamma(\overline{D}^0 K^- \pi^+)/\Gamma_{total}$ — Γ_{34}/Γ

VALUE (units 10^{-4})	DOCUMENT ID		TECN	COMMENT
10.4±1.1±0.5	[1] AAIJ	13AQ	LHCB	pp at 7 TeV

[1] AAIJ 13AQ reports $[\Gamma(B_s^0 \to \overline{D}^0 K^- \pi^+)/\Gamma_{total}]$ / $[B(B^0 \to \overline{D}^0 \pi^+ \pi^-)] = 1.18 \pm 0.05 \pm 0.12$ which we multiply by our best value $B(B^0 \to \overline{D}^0 \pi^+ \pi^-) = (8.8 \pm 0.5) \times 10^{-4}$. Our first error is their experiment's error and our second error is the systematic error from using our best value.

$\Gamma(\overline{D}^0 \overline{K}^*(892)^0)/\Gamma_{total}$ — Γ_{35}/Γ

VALUE (units 10^{-4})	DOCUMENT ID		TECN	COMMENT
4.4 ±0.6 OUR AVERAGE				
4.29±0.09±0.65	[1] AAIJ	14BH	LHCB	pp at 7, 8 TeV
4.7 ±1.2 ±0.3	[2] AAIJ	11D	LHCB	pp at 7 TeV
• • • We do not use the following data for averages, fits, limits, etc. • • •				
3.5 ±0.4 ±0.4	[3] AAIJ	13BX	LHCB	Repl. by AAIJ 14BH

[1] Uses Dalitz plot analysis of $B_s^0 \to \overline{D}^0 K^- \pi^+$ decays.

[2] AAIJ 11D reports $[\Gamma(B_s^0 \to \overline{D}^0 \overline{K}^*(892)^0)/\Gamma_{total}]$ / $[B(B^0 \to \overline{D}^0 \rho^0)] = 1.48 \pm 0.34 \pm 0.19$ which we multiply by our best value $B(B^0 \to \overline{D}^0 \rho^0) = (3.21 \pm 0.21) \times 10^{-4}$. Our first error is their experiment's error and our second error is the systematic error from using our best value.

[3] AAIJ 13BX reports $[\Gamma(B_s^0 \to \overline{D}^0 \overline{K}^*(892)^0)/\Gamma_{total}]$ / $[B(B^0 \to \overline{D}^0 K^*(892)^0)] = 7.8 \pm 0.7 \pm 0.3 \pm 0.6$ which we multiply by our best value $B(B^0 \to \overline{D}^0 K^*(892)^0) = (4.5 \pm 0.6) \times 10^{-5}$. Our first error is their experiment's error and our second error is the systematic error from using our best value.

$\Gamma(\overline{D}^0 \overline{K}^*(1410))/\Gamma_{total}$ — Γ_{36}/Γ

VALUE (units 10^{-5})	DOCUMENT ID		TECN	COMMENT
38.6±11.4±33.3	[1] AAIJ	14BH	LHCB	pp at 7, 8 TeV

[1] Uses Dalitz plot analysis of $B_s^0 \to \overline{D}^0 K^- \pi^+$ decays.

$\Gamma(\overline{D}^0 \overline{K}_0^*(1430))/\Gamma_{total}$ — Γ_{37}/Γ

VALUE (units 10^{-5})	DOCUMENT ID		TECN	COMMENT
30.0±2.4±6.8	[1] AAIJ	14BH	LHCB	pp at 7, 8 TeV

[1] Uses Dalitz plot analysis of $B_s^0 \to \overline{D}^0 K^- \pi^+$ decays. Corresponds to the resonant $K_0^*(1430)$ part of LASS parametrization.

$\Gamma(\overline{D}^0 \overline{K}_2^*(1430))/\Gamma_{total}$ — Γ_{38}/Γ

VALUE (units 10^{-5})	DOCUMENT ID		TECN	COMMENT
11.1±1.8±3.8	[1] AAIJ	14BH	LHCB	pp at 7, 8 TeV

[1] Uses Dalitz plot analysis of $B_s^0 \to \overline{D}^0 K^- \pi^+$ decays.

$\Gamma(\overline{D}^0 \overline{K}^*(1680))/\Gamma_{total}$ — Γ_{39}/Γ

VALUE (units 10^{-5})	CL%	DOCUMENT ID		TECN	COMMENT
<7.8	90	[1] AAIJ	14BH	LHCB	pp at 7, 8 TeV

[1] Uses Dalitz plot analysis of $B_s^0 \to \overline{D}^0 K^- \pi^+$ decays.

$\Gamma(\overline{D}^0 \overline{K}_0^*(1950))/\Gamma_{total}$ — Γ_{40}/Γ

VALUE (units 10^{-5})	CL%	DOCUMENT ID		TECN	COMMENT
<11	90	[1] AAIJ	14BH	LHCB	pp at 7, 8 TeV

[1] Uses Dalitz plot analysis of $B_s^0 \to \overline{D}^0 K^- \pi^+$ decays.

$\Gamma(\overline{D}^0 \overline{K}_3^*(1780))/\Gamma_{total}$ — Γ_{41}/Γ

VALUE (units 10^{-5})	CL%	DOCUMENT ID		TECN	COMMENT
<2.6	90	[1] AAIJ	14BH	LHCB	pp at 7, 8 TeV

[1] Uses Dalitz plot analysis of $B_s^0 \to \overline{D}^0 K^- \pi^+$ decays.

$\Gamma(\overline{D}^0 \overline{K}_4^*(2045))/\Gamma_{total}$ — Γ_{42}/Γ

VALUE (units 10^{-5})	CL%	DOCUMENT ID		TECN	COMMENT
<3.1	90	[1] AAIJ	14BH	LHCB	pp at 7, 8 TeV

[1] Uses Dalitz plot analysis of $B_s^0 \to \overline{D}^0 K^- \pi^+$ decays.

$\Gamma(\overline{D}^0 K^- \pi^+ (\text{non-resonant}))/\Gamma_{total}$ — Γ_{43}/Γ

VALUE (units 10^{-5})	DOCUMENT ID		TECN	COMMENT
20.6±3.8±7.3	[1] AAIJ	14BH	LHCB	pp at 7, 8 TeV

[1] Uses Dalitz plot analysis of $B_s^0 \to \overline{D}^0 K^- \pi^+$ decays. Corresponds to the non-resonant part of the LASS parametrization.

$\Gamma(D_{s2}^*(2573)^- \pi^+,\ D_{s2}^* \to \overline{D}^0 K^-)/\Gamma_{total}$ — Γ_{44}/Γ

VALUE (units 10^{-5})	DOCUMENT ID		TECN	COMMENT
25.7±0.7±4.0	[1] AAIJ	14BH	LHCB	pp at 7, 8 TeV

[1] Uses Dalitz plot analysis of $B_s^0 \to \overline{D}^0 K^- \pi^+$ decays.

$\Gamma(D_{s1}^*(2700)^- \pi^+,\ D_{s1}^* \to \overline{D}^0 K^-)/\Gamma_{total}$ — Γ_{45}/Γ

VALUE (units 10^{-5})	DOCUMENT ID		TECN	COMMENT
1.6±0.4±0.7	[1] AAIJ	14BH	LHCB	pp at 7, 8 TeV

[1] Uses Dalitz plot analysis of $B_s^0 \to \overline{D}^0 K^- \pi^+$ decays.

$\Gamma(D_{s1}^*(2860)^- \pi^+,\ D_{s1}^* \to \overline{D}^0 K^-)/\Gamma_{total}$ — Γ_{46}/Γ

VALUE (units 10^{-5})	DOCUMENT ID		TECN	COMMENT
5.0±1.2±3.4	[1] AAIJ	14BH	LHCB	pp at 7, 8 TeV

[1] Uses Dalitz plot analysis of $B_s^0 \to \overline{D}^0 K^- \pi^+$ decays.

Downloaded from https://academic.oup.com/ptep/article/2022/8/083C01/6651666 by KIT Library user on 27 September 2022

$\Gamma(D_{s3}^*(2860)^- \pi^+,\ D_{s3}^* \to \overline{D}^0 K^-)/\Gamma_{total}$ — Γ_{47}/Γ

VALUE (units 10^{-5})	DOCUMENT ID		TECN	COMMENT
2.2±0.1±0.6	[1] AAIJ	14BH	LHCB	pp at 7, 8 TeV

[1] Uses Dalitz plot analysis of $B_s^0 \to \overline{D}^0 K^- \pi^+$ decays.

$\Gamma(\overline{D}^0 K^+ K^-)/\Gamma_{total}$ — Γ_{48}/Γ

VALUE (units 10^{-5})	DOCUMENT ID		TECN	COMMENT
5.6±0.7±0.5	[1] AAIJ	18AZ	LHCB	pp at 7, 8 TeV
• • • We do not use the following data for averages, fits, limits, etc. • • •				
5.5±2.0±0.5	[2,3] AAIJ	12AM	LHCB	Repl. by AAIJ 18AZ

[1] AAIJ 18AZ reports $[\Gamma(B_s^0 \to \overline{D}^0 K^+ K^-)/\Gamma_{total}] / [B(B^0 \to \overline{D}^0 K^+ K^-)] = 0.930 \pm 0.089 \pm 0.069$ which we multiply by our best value $B(B^0 \to \overline{D}^0 K^+ K^-) = (6.1 \pm 0.5) \times 10^{-5}$. Our first error is their experiment's error and our second error is the systematic error from using our best value.

[2] AAIJ 12AM reports $[\Gamma(B_s^0 \to \overline{D}^0 K^+ K^-)/\Gamma_{total}] / [B(B^0 \to \overline{D}^0 K^+ K^-)] = 0.90 \pm 0.27 \pm 0.20$ which we multiply by our best value $B(B^0 \to \overline{D}^0 K^+ K^-) = (6.1 \pm 0.5) \times 10^{-5}$. Our first error is their experiment's error and our second error is the systematic error from using our best value.

[3] Uses $B(b \to B_s^0)/B(b \to B^0) = 0.267^{+0.023}_{-0.020}$ measured by the same authors.

$\Gamma(\overline{D}^0 f_0(980))/\Gamma_{total}$ — Γ_{49}/Γ

VALUE	CL%	DOCUMENT ID		TECN	COMMENT
$<3.1 \times 10^{-6}$	90	AAIJ	15AG	LHCB	pp at 7, 8 TeV

$\Gamma(\overline{D}^0 \phi)/\Gamma_{total}$ — Γ_{50}/Γ

VALUE (units 10^{-5})	DOCUMENT ID		TECN	COMMENT
3.0±0.4±0.2	[1] AAIJ	18AY	LHCB	pp at 7 and 8 TeV

[1] AAIJ 18AY reports $[\Gamma(B_s^0 \to \overline{D}^0 \phi)/\Gamma_{total}] / [B(B^0 \to \overline{D}^0 \pi^+ \pi^-)] = (3.4 \pm 0.4 \pm 0.3) \times 10^{-2}$ which we multiply by our best value $B(B^0 \to \overline{D}^0 \pi^+ \pi^-) = (8.8 \pm 0.5) \times 10^{-4}$. Our first error is their experiment's error and our second error is the systematic error from using our best value.

$\Gamma(\overline{D}^0 \phi)/\Gamma(\overline{D}^0 \overline{K}^*(892)^0)$ — Γ_{50}/Γ_{35}

VALUE	DOCUMENT ID		TECN	COMMENT
• • • We do not use the following data for averages, fits, limits, etc. • • •				
0.069±0.013±0.007	AAIJ	13BX	LHCB	Repl. by AAIJ 18AY

$\Gamma(\overline{D}^{*0} \phi)/\Gamma_{total}$ — Γ_{51}/Γ

VALUE (units 10^{-5})	DOCUMENT ID		TECN	COMMENT
3.7±0.6±0.2	[1] AAIJ	18AY	LHCB	pp at 7 and 8 TeV

[1] AAIJ 18AY reports $[\Gamma(B_s^0 \to \overline{D}^{*0} \phi)/\Gamma_{total}] / [B(B^0 \to \overline{D}^0 \pi^+ \pi^-)] = (4.2 \pm 0.5 \pm 0.4) \times 10^{-2}$ which we multiply by our best value $B(B^0 \to \overline{D}^0 \pi^+ \pi^-) = (8.8 \pm 0.5) \times 10^{-4}$. Our first error is their experiment's error and our second error is the systematic error from using our best value.

$\Gamma(D^{*\mp} \pi^\pm)/\Gamma_{total}$ — Γ_{52}/Γ

VALUE	CL%	DOCUMENT ID		TECN	COMMENT
$<6.1 \times 10^{-6}$	90	[1] AAIJ	13AL	LHCB	pp at 7 TeV

[1] Uses $f_s/f_d = 0.256 \pm 0.020$ and $B(B^0 \to D^{*-} \pi^+) = (2.76 \pm 0.13) \times 10^{-3}$.

$\Gamma(\eta_c \phi)/\Gamma_{total}$ — Γ_{53}/Γ

VALUE (units 10^{-4})	DOCUMENT ID		TECN	COMMENT
5.01±0.53±0.68	[1] AAIJ	17U	LHCB	pp at 7, 8 TeV

[1] The last uncertainty includes the limited knowledge of the external branching fractions where the η_c is reconstructed in the $p\overline{p}, K^+ K^- \pi^+ \pi^-$, $\pi^+ \pi^- \pi^+ \pi^-$, and $K^+ K^- K^+ K^-$ decays and $\phi(1020) \to K^+ K^-$.

$\Gamma(\eta_c \pi^+ \pi^-)/\Gamma_{total}$ — Γ_{55}/Γ

VALUE (units 10^{-4})	DOCUMENT ID		TECN	COMMENT
1.76±0.59±0.31	[1] AAIJ	17U	LHCB	pp at 7, 8 TeV

[1] The last uncertainty includes the limited knowledge of the external branching fractions where the η_c is reconstructed in the $p\overline{p}, K^+ K^- \pi^+ \pi^-$, $\pi^+ \pi^- \pi^+ \pi^-$, and $K^+ K^- K^+ K^-$ decays. The significance of the signal, including systematic uncertainties, is 4.6 standard deviations.

$\Gamma(J/\psi(1S)\phi)/\Gamma_{total}$ — Γ_{56}/Γ

VALUE (units 10^{-3})	EVTS	DOCUMENT ID		TECN	COMMENT
1.04 ±0.04 OUR FIT					
1.04 ±0.04 OUR AVERAGE					
1.037±0.032±0.022		[1] AAIJ	21Y	LHCB	pp at 7, 8, 13 TeV
1.25 ±0.07 ±0.23		[2] THORNE	13	BELL	$e^+ e^- \to \Upsilon(5S)$
1.5 ±0.5 ±0.1		[3] ABE	96Q	CDF	$p\overline{p}$
• • • We do not use the following data for averages, fits, limits, etc. • • •					
1.050±0.013±0.104		[4] AAIJ	13AN	LHCB	Repl. by AAIJ 21Y
<6	1	[5] AKERS	94J	OPAL	$e^+ e^- \to Z$
seen	14	[6] ABE	93F	CDF	$p\overline{p}$ at 1.8 TeV
seen	1	[7] ACTON	92N	OPAL	Sup. by AKERS 94J

[1] AAIJ 21Y reports $[\Gamma(B_s^0 \to J/\psi(1S)\phi)/\Gamma_{total}] \times [B(\phi(1020) \to K^+ K^-)] = (5.01 \pm 0.16 \pm 0.17) \times 10^{-4}$ from a measurement of $[\Gamma(B_s^0 \to J/\psi(1S)\phi)/\Gamma_{total}] \times [B(\phi(1020) \to K^+ K^-)] / [B(B^+ \to J/\psi(1S) K^+)]$ assuming $B(B^+ \to J/\psi(1S) K^+) = (1.003 \pm 0.035) \times 10^{-3}$, which we rescale to our best values $B(\phi(1020) \to K^+ K^-) = (49.1 \pm 0.5) \times 10^{-2}$, $B(B^+ \to J/\psi(1S) K^+) = (1.020 \pm 0.019) \times 10^{-3}$. Our first error is their experiment's error and our second error is the systematic error from using our best values.

[2] THORNE 13 uses $f_s = (17.2 \pm 3.0)\%$ as the fraction of $\Upsilon(5S)$ decaying to $B_s^{(*)} \overline{B}_s^{(*)}$.

[3] ABE 96Q reports $[\Gamma(B_s^0 \to J/\psi(1S)\phi)/\Gamma_{total}] \times [\Gamma(\overline{b} \to B_s^0)/\left[\Gamma(\overline{b} \to B^+) + \Gamma(\overline{b} \to B^0)\right]] = (0.185 \pm 0.055 \pm 0.020) \times 10^{-3}$ which we divide by our best value $\Gamma(\overline{b} \to B_s^0)/\left[\Gamma(\overline{b} \to B^+) + \Gamma(\overline{b} \to B^0)\right] = 0.1230 \pm 0.0115$. Our first error is their experiment's error and our second error is the systematic error from using our best value.

[4] AAIJ 13AN uses $f_s/f_d = 0.256 \pm 0.020$ and $B(B^+ \to J/\psi K^+) = (10.18 \pm 0.42) \times 10^{-4}$.

[5] AKERS 94J sees one event and measures the limit on the product branching fraction $f(\overline{b} \to B_s^0) \cdot B(B_s^0 \to J/\psi(1S)\phi) < 7 \times 10^{-4}$ at CL = 90%. We divide by $B(\overline{b} \to B_s^0) = 0.112$.

[6] ABE 93F measured using $J/\psi(1S) \to \mu^+ \mu^-$ and $\phi \to K^+ K^-$.

[7] In ACTON 92N a limit on the product branching fraction is measured to be $f(\overline{b} \to B_s^0) \cdot B(B_s^0 \to J/\psi(1S)\phi) \leq 0.22 \times 10^{-2}$.

$\Gamma(J/\psi(1S)\phi\phi)/\Gamma(J/\psi(1S)\phi)$ — Γ_{57}/Γ_{56}

VALUE (units 10^{-2})	EVTS	DOCUMENT ID		TECN	COMMENT
$1.15 \pm 0.12^{+0.05}_{-0.09}$	128	[1] AAIJ	16U	LHCB	pp at 7, 8 TeV

[1] Uses $J/\psi \to \mu^+ \mu^-$, $\phi \to K^+ K^-$ decays, and observes 128 ± 13 events of $B_s^0 \to J/\psi \phi \phi$.

$\Gamma(J/\psi(1S)\pi^0)/\Gamma_{total}$ — Γ_{58}/Γ

VALUE	CL%	DOCUMENT ID		TECN
$<1.2 \times 10^{-3}$	90	[1] ACCIARRI	97C	L3

[1] ACCIARRI 97C assumes B^0 production fraction (39.5 ± 4.0%) and B_s (12.0 ± 3.0%).

$\Gamma(J/\psi(1S)\eta)/\Gamma_{total}$ — Γ_{59}/Γ

VALUE (units 10^{-4})	CL%	DOCUMENT ID		TECN	COMMENT
4.0 ±0.7 OUR AVERAGE		Error includes scale factor of 1.4.			
$3.6\ ^{+0.5}_{-0.6}\ ^{+0.3}_{-0.2}$		[1] AAIJ	13A	LHCB	pp at 7 TeV
$5.10 \pm 0.50^{+1.17}_{-0.83}$		[2] LI	12	BELL	$e^+ e^- \to \Upsilon(4S)$
• • • We do not use the following data for averages, fits, limits, etc. • • •					
<38	90	[3] ACCIARRI	97C	L3	

[1] AAIJ 13A reports $[\Gamma(B_s^0 \to J/\psi(1S)\eta)/\Gamma_{total}] / [B(B^0 \to J/\psi(1S)\rho^0)] = 14.0 \pm 1.2^{+1.1}_{-1.5}{}^{+1.1}_{-1.0}$ which we multiply by our best value $B(B^0 \to J/\psi(1S)\rho^0) = (2.55^{+0.18}_{-0.16}) \times 10^{-5}$. Our first error is their experiment's error and our second error is the systematic error from using our best value.

[2] Observed for the first time with significances over 10 σ. The second error are total systematic uncertainties including the error on $N(B_s^{(*)} \overline{B}_s^{(*)})$.

[3] ACCIARRI 97C assumes B^0 production fraction (39.5 ± 4.0%) and B_s (12.0 ± 3.0%).

$\Gamma(J/\psi(1S) K_S^0)/\Gamma_{total}$ — Γ_{60}/Γ

VALUE (units 10^{-5})	DOCUMENT ID		TECN	COMMENT
1.92±0.14 OUR AVERAGE				
1.92±0.14±0.05	[1] AAIJ	15AL	LHCB	pp at 7, 8 TeV
2.0 ±0.4 ±0.2	[2] AALTONEN	11A	CDF	$p\overline{p}$ at 1.96 TeV
• • • We do not use the following data for averages, fits, limits, etc. • • •				
2.03±0.16±0.20	[3] AAIJ	13AB	LHCB	Repl. by AAIJ 15AL
2.03±0.26±0.20	[4] AAIJ	12O	LHCB	Repl. by AAIJ 13AB

[1] AAIJ 15AL reports $[\Gamma(B_s^0 \to J/\psi(1S) K_S^0)/\Gamma_{total}] / [B(B^0 \to J/\psi(1S) K_S^0)] = (4.31 \pm 0.17 \pm 0.12 \pm 0.25) \times 10^{-2}$ which we multiply by our best value $B(B^0 \to J/\psi(1S) K_S^0) = (4.45 \pm 0.11) \times 10^{-4}$. Our first error is their experiment's error and our second error is the systematic error from using our best value.

[2] AALTONEN 11A reports $[\Gamma(B_s^0 \to J/\psi(1S) K_S^0)/\Gamma_{total}] \times [B(\overline{b} \to B_s^0)] / [B(\overline{b} \to B^0)] / [B(B^0 \to J/\psi(1S) K_S^0)] = (1.09 \pm 0.19 \pm 0.11) \times 10^{-2}$ which we multiply or divide by our best values $B(\overline{b} \to B_s^0) = (10.0 \pm 0.8) \times 10^{-2}$, $B(\overline{b} \to B^0) = (40.8 \pm 0.7) \times 10^{-2}$, $B(B^0 \to J/\psi(1S) K_S^0) = 1/2 \times B(B^0 \to J/\psi(1S) K^0) = 1/2 \times (8.91 \pm 0.21) \times 10^{-4}$. Our firs t error is their experiment's error and our second error is the systematic error from using our best values.

Downloaded from https://academic.oup.com/ptep/article/2022/8/083C01/6651666 by KIT Library user on 27 September 2022

[3] AAIJ 13AB reports $(1.97 \pm 0.14 \pm 0.07 \pm 0.15 \pm 0.08) \times 10^{-5}$ from a measurement of $[\Gamma(B_s^0 \to J/\psi(1S) K_S^0)/\Gamma_{total}] / [B(B^0 \to J/\psi(1S) K^0)] \times [\Gamma(\overline{b} \to B_s^0)/\Gamma(\overline{b} \to B^0)]$ assuming $B(B^0 \to J/\psi(1S) K^0) = (8.98 \pm 0.35) \times 10^{-4}$, $\Gamma(\overline{b} \to B_s^0)/\Gamma(\overline{b} \to B^0) = 0.256 \pm 0.020$, which we rescale to our best values $B(B^0 \to J/\psi(1S) K^0) = (8.91 \pm 0.21) \times 10^{-4}$, $\Gamma(\overline{b} \to B_s^0)/\Gamma(\overline{b} \to B^0) = 0.246 \pm 0.023$. Our first error is their experiment's error and our second error is the systematic error from using our best values.

[4] AAIJ 12O reports $(1.83 \pm 0.21 \pm 0.10 \pm 0.14 \pm 0.07) \times 10^{-5}$ from a measurement of $[\Gamma(B_s^0 \to J/\psi(1S) K_S^0)/\Gamma_{total}] / [B(B^0 \to J/\psi(1S) K^0)] \times [\Gamma(\overline{b} \to B_s^0)/\Gamma(\overline{b} \to B^0)]$ assuming $B(B^0 \to J/\psi(1S) K^0) = (8.71 \pm 0.32) \times 10^{-4}$, $\Gamma(\overline{b} \to B_s^0)/\Gamma(\overline{b} \to B^0) = 0.267^{+0.021}_{-0.02}$, which we rescale to our best values $B(B^0 \to J/\psi(1S) K^0) = (8.91 \pm 0.21) \times 10^{-4}$, $\Gamma(\overline{b} \to B_s^0)/\Gamma(\overline{b} \to B^0) = 0.246 \pm 0.023$. Our first error is their experiment's error and our second error is the systematic error from using our best values.

$\Gamma(J/\psi(1S)\overline{K}^*(892)^0)/\Gamma_{total}$ — Γ_{61}/Γ

VALUE (units 10^{-5})	DOCUMENT ID		TECN	COMMENT
4.14±0.18±0.35	[1] AAIJ	15AV	LHCB	pp at 7, 8 TeV
• • • We do not use the following data for averages, fits, limits, etc. • • •				
$4.4\ ^{+0.5}_{-0.4} \pm 0.8$	[2] AAIJ	12AP	LHCB	Repl. by AAIJ 15AV
$9 \pm 4 \pm 1$	[3] AALTONEN	11A	CDF	$p\overline{p}$ at 1.96 TeV

[1] AAIJ 15AV result combines two measurements with different normalizing modes of $B^0 \to J/\psi K^*(892)^0$ and $B_s^0 \to J/\psi\phi$.

[2] AAIJ 12AP reports $B(B_s^0 \to J/\psi(1S)\overline{K}^*(892)^0)/B(B^0 \to J/\psi(1S) K^*(892)^0) = (3.43^{+0.34}_{-0.36} \pm 0.50) \times 10^{-2}$ and $B(B^0 \to J/\psi(1S) K^*(892)^0) = (1.29 \pm 0.05 \pm 0.13) \times 10^{-3}$ after correcting for the contribution from $K\pi$ S-wave beneath the K^* peak.

[3] AALTONEN 11A reports $[\Gamma(B_s^0 \to J/\psi(1S)\overline{K}^*(892)^0)/\Gamma_{total}] \times [B(\overline{b} \to B_s^0)] / [B(\overline{b} \to B^0)] / [B(B^0 \to J/\psi(1S) K^*(892)^0)] = 0.0168 \pm 0.0024 \pm 0.0068$ which we multiply or divide by our best values $B(\overline{b} \to B_s^0) = (10.0 \pm 0.8) \times 10^{-2}$, $B(\overline{b} \to B^0) = (40.8 \pm 0.7) \times 10^{-2}$, $B(B^0 \to J/\psi(1S) K^*(892)^0) = (1.27 \pm 0.05) \times 10^{-3}$. Our first error is their experiment's error and our second error is the systematic error from using our best values.

$\Gamma(J/\psi(1S)\eta')/\Gamma_{total}$ — Γ_{62}/Γ

VALUE (units 10^{-4})	DOCUMENT ID		TECN	COMMENT
3.3 ±0.4 OUR AVERAGE				
$3.2\ ^{+0.4}_{-0.5} \pm 0.2$	[1] AAIJ	13A	LHCB	pp at 7 TeV
$3.71 \pm 0.61\ ^{+0.85}_{-0.60}$	[2] LI	12	BELL	$e^+e^- \to \Upsilon(4S)$

[1] AAIJ 13A reports $[\Gamma(B_s^0 \to J/\psi(1S)\eta')/\Gamma_{total}] / [B(B^0 \to J/\psi(1S)\rho^0)] = 12.7 \pm 1.1\ ^{+0.5}_{-1.3}\ ^{+1.0}_{-0.9}$ which we multiply by our best value $B(B^0 \to J/\psi(1S)\rho^0) = (2.55^{+0.18}_{-0.16}) \times 10^{-5}$. Our first error is their experiment's error and our second error is the systematic error from using our best value.

[2] Observed for the first time with significances over 10 σ. The second error are total systematic uncertainties including the error on $N(B_s^{(*)}\overline{B}_s^{(*)})$.

$\Gamma(J/\psi(1S)\eta')/\Gamma(J/\psi(1S)\eta)$ — Γ_{62}/Γ_{59}

VALUE	DOCUMENT ID		TECN	COMMENT
0.87 ±0.06 OUR AVERAGE				
$0.902 \pm 0.072 \pm 0.045$	[1] AAIJ	15D	LHCB	pp at 7, 8 TeV
$0.90 \pm 0.09\ ^{+0.06}_{-0.02}$	[2] AAIJ	13A	LHCB	pp at 7 TeV
$0.73 \pm 0.14 \pm 0.02$	[2] LI	12	BELL	$e^+e^- \to \Upsilon(4S)$

[1] Uses $J/\psi \to \mu^+\mu^-$, $\eta' \to \rho^0\gamma$, and $\eta' \to \eta\pi^+\pi^-$ decays.

[2] Strongly correlated with measurements of $\Gamma(J/\psi(1S)\eta)/\Gamma$ and $\Gamma(J/\psi(1S)\eta')/\Gamma$ reported in the same reference.

$\Gamma(J/\psi(1S)\pi^+\pi^-)/\Gamma(J/\psi(1S)\phi)$ — Γ_{63}/Γ_{56}

VALUE (units 10^{-2})	DOCUMENT ID		TECN	COMMENT
19.4±1.5 OUR FIT Error includes scale factor of 2.2.				
19.9±0.7±0.2	[1] AAIJ	12AO	LHCB	pp at 7 TeV

[1] AAIJ 12AO reports $(19.79 \pm 0.47 \pm 0.52) \times 10^{-2}$ from a measurement of $[\Gamma(B_s^0 \to J/\psi(1S)\pi^+\pi^-)/\Gamma(B_s^0 \to J/\psi(1S)\phi)] / [B(\phi(1020) \to K^+K^-)]$ assuming $B(\phi(1020) \to K^+K^-) = (48.9 \pm 0.5) \times 10^{-2}$, which we rescale to our best value $B(\phi(1020) \to K^+K^-) = (49.1 \pm 0.5) \times 10^{-2}$. Our first error is their experiment's error and our second error is the systematic error from using our best value.

$\Gamma(J/\psi(1S) f_0(500),\ f_0 \to \pi^+\pi^-)/\Gamma(J/\psi(1S) f_0(980),\ f_0 \to \pi^+\pi^-)$ — Γ_{64}/Γ_{66}

VALUE	CL%	DOCUMENT ID		TECN	COMMENT
<0.034	90	[1] AAIJ	14BR	LHCB	pp at 7, 8 TeV

[1] Reported first of two solutions using the full Dalitz analysis.

$\Gamma(J/\psi(1S)\rho,\ \rho \to \pi^+\pi^-)/\Gamma(J/\psi(1S)\pi^+\pi^-)$ — Γ_{65}/Γ_{63}

VALUE	CL%	DOCUMENT ID		TECN	COMMENT
<0.017	90	[1] AAIJ	14BR	LHCB	pp at 7, 8 TeV

[1] Reported first of two solutions using the full Dalitz analysis.

$\Gamma(J/\psi(1S) f_0(980),\ f_0 \to \pi^+\pi^-)/\Gamma_{total}$ — Γ_{66}/Γ

VALUE (units 10^{-4})	DOCUMENT ID		TECN	COMMENT
1.24±0.15 OUR FIT Error includes scale factor of 2.1.				
$\mathbf{1.16^{+0.31}_{-0.19}\ ^{+0.30}_{-0.25}}$	[1] LI	11	BELL	$e^+e^- \to \Upsilon(5S)$

[1] The second error includes both the detector systematic and the uncertainty in the number of produced $Y(5S) \to B_s^{(*)}\overline{B}_s^{(*)}$ pairs.

$\Gamma(J/\psi(1S) f_0(980),\ f_0 \to \pi^+\pi^-)/\Gamma(J/\psi(1S)\phi)$ — Γ_{66}/Γ_{56}

VALUE	DOCUMENT ID		TECN	COMMENT
$\mathbf{0.119^{+0.013}_{-0.014}}$ **OUR FIT** Error includes scale factor of 2.4.				
$\mathbf{0.110^{+0.020}_{-0.018}}$ **OUR AVERAGE** Error includes scale factor of 2.5. See the ideogram below.				
$0.069 \pm 0.012 \pm 0.001$	[1] KHACHATRY...	16Q	CMS	pp at 7 TeV
$0.140^{+0.026}_{-0.013} \pm 0.002$	[2,3] AAIJ	12AO	LHCB	pp at 7 TeV
$0.135 \pm 0.036 \pm 0.001$	[4] ABAZOV	12C	D0	$p\overline{p}$ at 1.96 TeV
$0.126 \pm 0.012 \pm 0.001$	[5] AALTONEN	11AB	CDF	$p\overline{p}$ at 1.96 TeV
• • • We do not use the following data for averages, fits, limits, etc. • • •				
$0.124^{+0.026}_{-0.023} \pm 0.001$	[6] AAIJ	11	LHCB	Repl. by AAIJ 12AO

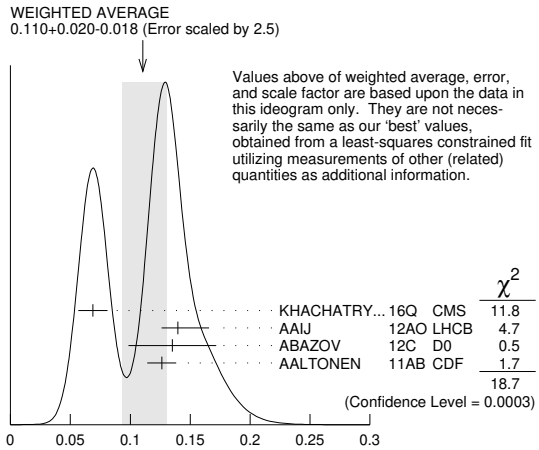

$\Gamma(J/\psi(1S) f_0(980),\ f_0 \to \pi^+\pi^-)/\Gamma(J/\psi(1S)\phi)$

[1] KHACHATRYAN 16Q reports $[\Gamma(B_s^0 \to J/\psi(1S) f_0(980),\ f_0 \to \pi^+\pi^-)/\Gamma(B_s^0 \to J/\psi(1S)\phi)] / [B(\phi(1020) \to K^+K^-)] = 0.140 \pm 0.008 \pm 0.023$ which we multiply by our best value $B(\phi(1020) \to K^+K^-) = (49.1 \pm 0.5) \times 10^{-2}$. Our first error is their experiment's error and our second error is the systematic error from using our best value.

[2] AAIJ 12AO reports $(13.9 \pm 0.6\ ^{+2.5}_{-1.2}) \times 10^{-2}$ from a measurement of $[\Gamma(B_s^0 \to J/\psi(1S) f_0(980),\ f_0 \to \pi^+\pi^-)/\Gamma(B_s^0 \to J/\psi(1S)\phi)] / [B(\phi(1020) \to K^+K^-)]$ assuming $B(\phi(1020) \to K^+K^-) = (48.9 \pm 0.5) \times 10^{-2}$, which we rescale to our best value $B(\phi(1020) \to K^+K^-) = (49.1 \pm 0.5) \times 10^{-2}$. Our first error is their experiment's error and our second error is the systematic error from using our best value.

[3] Measured in Dalitz plot like analysis of $B_s \to J/\psi\pi^+\pi^-$ decays.

[4] ABAZOV 12C reports $[\Gamma(B_s^0 \to J/\psi(1S) f_0(980),\ f_0 \to \pi^+\pi^-)/\Gamma(B_s^0 \to J/\psi(1S)\phi)] / [B(\phi(1020) \to K^+K^-)] = 0.275 \pm 0.041 \pm 0.061$ which we multiply by our best value $B(\phi(1020) \to K^+K^-) = (49.1 \pm 0.5) \times 10^{-2}$. Our first error is their experiment's error and our second error is the systematic error from using our best value.

[5] AALTONEN 11AB reports $[\Gamma(B_s^0 \to J/\psi(1S) f_0(980),\ f_0 \to \pi^+\pi^-)/\Gamma(B_s^0 \to J/\psi(1S)\phi)] / [B(\phi(1020) \to K^+K^-)] = 0.257 \pm 0.020 \pm 0.014$ which we multiply by our best value $B(\phi(1020) \to K^+K^-) = (49.1 \pm 0.5) \times 10^{-2}$. Our first error is their experiment's error and our second error is the systematic error from using our best value.

[6] AAIJ 11 reports $[\Gamma(B_s^0 \to J/\psi(1S) f_0(980),\ f_0 \to \pi^+\pi^-)/\Gamma(B_s^0 \to J/\psi(1S)\phi)] / [B(\phi(1020) \to K^+K^-)] = 0.252^{+0.046}_{-0.032}\ ^{+0.027}_{-0.033}$ which we multiply by our best value $B(\phi(1020) \to K^+K^-) = (49.1 \pm 0.5) \times 10^{-2}$. Our first error is their experiment's error and our second error is the systematic error from using our best value.

$\Gamma(J/\psi(1S) f_0(980),\ f_0 \to \pi^+\pi^-)/\Gamma(J/\psi(1S)\pi^+\pi^-)$ — Γ_{66}/Γ_{63}

VALUE	DOCUMENT ID		TECN	COMMENT
$\mathbf{0.61\ ^{+0.06}_{-0.07}}$ **OUR FIT** Error includes scale factor of 2.1.				
$\mathbf{0.703 \pm 0.015\ ^{+0.004}_{-0.051}}$	[1] AAIJ	14BR	LHCB	pp at 7, 8 TeV

[1] Reported first of two solutions using the full Dalitz analysis.

Downloaded from https://academic.oup.com/ptep/article/2022/8/083C01/6651666 by KIT Library user on 27 September 2022

$\Gamma(J/\psi(1S)f_2(1270),\ f_2\to\pi^+\pi^-)/\Gamma(J/\psi(1S)\phi)$ — Γ_{67}/Γ_{56}

VALUE (units 10^{-4})	DOCUMENT ID		TECN	COMMENT
$9.8^{+3.4}_{-3.6}\pm0.1$	[1,2] AAIJ	12AO	LHCB	pp at 7 TeV

[1] AAIJ 12AO reports $(0.098\pm0.033^{+0.006}_{-0.015})\times10^{-2}$ from a measurement of $[\Gamma(B_s^0\to J/\psi(1S)f_2(1270),\ f_2\to\pi^+\pi^-)/\Gamma(B_s^0\to J/\psi(1S)\phi)]$ / $[B(\phi(1020)\to K^+K^-)]$ assuming $B(\phi(1020)\to K^+K^-)=(48.9\pm0.5)\times10^{-2}$, which we rescale to our best value $B(\phi(1020)\to K^+K^-)=(49.1\pm0.5)\times10^{-2}$. Our first error is their experiment's error and our second error is the systematic error from using our best value.
[2] Measured in Dalitz plot like analysis of $B_s\to J/\psi\pi^+\pi^-$ decays for the f_2 helicity state $\lambda=0$.

$\Gamma(J/\psi(1S)f_2(1270)_0,\ f_2\to\pi^+\pi^-)/\Gamma(J/\psi(1S)\pi^+\pi^-)$ — Γ_{68}/Γ_{63}

VALUE (%)	DOCUMENT ID		TECN	COMMENT
$0.36\pm0.07\pm0.03$	[1] AAIJ	14BR	LHCB	pp at 7, 8 TeV

[1] Reported first of two solutions using the full Dalitz analysis.

$\Gamma(J/\psi(1S)f_2(1270)_\parallel,\ f_2\to\pi^+\pi^-)/\Gamma(J/\psi(1S)\pi^+\pi^-)$ — Γ_{69}/Γ_{63}

VALUE (%)	DOCUMENT ID		TECN	COMMENT
$0.52\pm0.15^{+0.05}_{-0.02}$	[1] AAIJ	14BR	LHCB	pp at 7, 8 TeV

[1] Reported first of two solutions using the full Dalitz analysis.

$\Gamma(J/\psi(1S)f_2(1270)_\perp,\ f_2\to\pi^+\pi^-)/\Gamma(J/\psi(1S)\pi^+\pi^-)$ — Γ_{70}/Γ_{63}

VALUE (%)	DOCUMENT ID		TECN	COMMENT
$0.63\pm0.34^{+0.16}_{-0.08}$	[1] AAIJ	14BR	LHCB	pp at 7, 8 TeV

[1] Reported first of two solutions using the full Dalitz analysis.

$\Gamma(J/\psi(1S)f_0(1370),\ f_0\to\pi^+\pi^-)/\Gamma_{total}$ — Γ_{71}/Γ

VALUE (units 10^{-4})	DOCUMENT ID		TECN	COMMENT
• • • We do not use the following data for averages, fits, limits, etc. • • •				
$0.34^{+0.11}_{-0.14}{}^{+0.085}_{-0.054}$	[1] LI	11	BELL	$e^+e^-\to\Upsilon(5S)$

[1] The second error includes both the detector systematic and the uncertainty in the number of produced $Y(5S)\to B_s^{(*)}\overline{B}_s^{(*)}$ pairs.

$\Gamma(J/\psi(1S)f_0(1370),\ f_0\to\pi^+\pi^-)/\Gamma(J/\psi(1S)\phi)$ — Γ_{71}/Γ_{56}

VALUE (units 10^{-2})	DOCUMENT ID		TECN	COMMENT
$4.21^{+0.54}_{-3.76}\pm0.05$	[1,2] AAIJ	12AO	LHCB	pp at 7 TeV

[1] AAIJ 12AO reports $(4.19\pm0.53^{+0.12}_{-3.7})\times10^{-2}$ from a measurement of $[\Gamma(B_s^0\to J/\psi(1S)f_0(1370),\ f_0\to\pi^+\pi^-)/\Gamma(B_s^0\to J/\psi(1S)\phi)]$ / $[B(\phi(1020)\to K^+K^-)]$ assuming $B(\phi(1020)\to K^+K^-)=(48.9\pm0.5)\times10^{-2}$, which we rescale to our best value $B(\phi(1020)\to K^+K^-)=(49.1\pm0.5)\times10^{-2}$. Our first error is their experiment's error and our second error is the systematic error from using our best value.
[2] Measured in Dalitz plot like analysis of $B_s\to J/\psi\pi^+\pi^-$ decays.

$\Gamma(J/\psi(1S)f_0(1500),\ f_0\to\pi^+\pi^-)/\Gamma(J/\psi(1S)\pi^+\pi^-)$ — Γ_{72}/Γ_{63}

VALUE	DOCUMENT ID		TECN	COMMENT
$0.101\pm0.008^{+0.011}_{-0.003}$	[1] AAIJ	14BR	LHCB	pp at 7, 8 TeV

[1] Reported first of two solutions using the full Dalitz analysis.

$\Gamma(J/\psi(1S)f_2'(1525)_0,\ f_2'\to\pi^+\pi^-)/\Gamma(J/\psi(1S)\pi^+\pi^-)$ — Γ_{73}/Γ_{63}

VALUE (%)	DOCUMENT ID		TECN	COMMENT
$0.51\pm0.09^{+0.05}_{-0.04}$	[1] AAIJ	14BR	LHCB	pp at 7, 8 TeV

[1] Reported first of two solutions using the full Dalitz analysis.

$\Gamma(J/\psi(1S)f_2'(1525)_\parallel,\ f_2'\to\pi^+\pi^-)/\Gamma(J/\psi(1S)\pi^+\pi^-)$ — Γ_{74}/Γ_{63}

VALUE (%)	DOCUMENT ID		TECN	COMMENT
$0.06^{+0.13}_{-0.04}\pm0.01$	[1] AAIJ	14BR	LHCB	pp at 7, 8 TeV

[1] Reported first of two solutions using the full Dalitz analysis.

$\Gamma(J/\psi(1S)f_2'(1525)_\perp,\ f_2'\to\pi^+\pi^-)/\Gamma(J/\psi(1S)\pi^+\pi^-)$ — Γ_{75}/Γ_{63}

VALUE (%)	DOCUMENT ID		TECN	COMMENT
$0.26\pm0.18^{+0.06}_{-0.04}$	[1] AAIJ	14BR	LHCB	pp at 7, 8 TeV

[1] Reported first of two solutions using the full Dalitz analysis.

$\Gamma(J/\psi(1S)f_0(1790),\ f_0\to\pi^+\pi^-)/\Gamma(J/\psi(1S)\pi^+\pi^-)$ — Γ_{76}/Γ_{63}

VALUE	DOCUMENT ID		TECN	COMMENT
$0.024\pm0.004^{+0.050}_{-0.002}$	[1] AAIJ	14BR	LHCB	pp at 7, 8 TeV

[1] Reported first of two solutions using the full Dalitz analysis.

$\Gamma(J/\psi(1S)\pi^+\pi^-(\text{nonresonant}))/\Gamma(J/\psi(1S)\phi)$ — Γ_{77}/Γ_{56}

VALUE (units 10^{-2})	DOCUMENT ID		TECN	COMMENT
$1.67^{+1.01}_{-0.32}\pm0.02$	[1,2] AAIJ	12AO	LHCB	pp at 7 TeV

[1] AAIJ 12AO reports $(1.66\pm0.31^{+0.96}_{-0.08})\times10^{-2}$ from a measurement of $[\Gamma(B_s^0\to J/\psi(1S)\pi^+\pi^-(\text{nonresonant}))/\Gamma(B_s^0\to J/\psi(1S)\phi)]$ / $[B(\phi(1020)\to K^+K^-)]$ assuming $B(\phi(1020)\to K^+K^-)=(48.9\pm0.5)\times10^{-2}$, which we rescale to our best value $B(\phi(1020)\to K^+K^-)=(49.1\pm0.5)\times10^{-2}$. Our first error is their experiment's error and our second error is the systematic error from using our best value.
[2] Measured in Dalitz plot like analysis of $B_s\to J/\psi\pi^+\pi^-$ decays.

$\Gamma(J/\psi(1S)\overline{K}^0\pi^+\pi^-)/\Gamma_{total}$ — Γ_{78}/Γ

VALUE	CL%	DOCUMENT ID		TECN	COMMENT
$<4.4\times10^{-5}$	90	[1] AAIJ	14L	LHCB	pp at 7 TeV

[1] Measured with $B(B_s^0\to J/\psi K_S^0\pi^+\pi^-)$ / $B(B^0\to J/\psi K_S^0\pi^+\pi^-)$ using PDG 12 values for the involved branching fractions.

$\Gamma(J/\psi(1S)K^+K^-)/\Gamma_{total}$ — Γ_{79}/Γ

VALUE (units 10^{-4})	DOCUMENT ID		TECN	COMMENT
7.9 ±0.7 OUR AVERAGE				
$7.70\pm0.08\pm0.72$	[1] AAIJ	13AN	LHCB	pp at 7 TeV
$10.1\ \pm0.9\ \pm2.1$	[2] THORNE	13	BELL	$e^+e^-\to\Upsilon(5S)$

[1] Uses $f_s/f_d=0.256\pm0.020$ and $B(B^+\to J/\psi K^+)=(10.18\pm0.42)\times10^{-4}$.
[2] Uses $f_s=(17.2\pm3.0)\%$ as the fraction of $\Upsilon(5S)$ decaying to $B_s^{(*)}\overline{B}_s^{(*)}$.

$\Gamma(J/\psi(1S)K^0K^-\pi^++\text{c.c.})/\Gamma_{total}$ — Γ_{80}/Γ

VALUE (units 10^{-4})	DOCUMENT ID		TECN	COMMENT
$9.5\pm1.0\pm0.8$	[1] AAIJ	14L	LHCB	pp at 7 TeV

[1] AAIJ 14L reports $[\Gamma(B_s^0\to J/\psi(1S)K^0K^-\pi^++\text{c.c.})/\Gamma_{total}]$ / $[B(B^0\to J/\psi(1S)K^0\pi^+\pi^-)]=2.12\pm0.15\pm0.18$ which we multiply by our best value $B(B^0\to J/\psi(1S)K^0\pi^+\pi^-)=(4.5\pm0.4)\times10^{-4}$. Our first error is their experiment's error and our second error is the systematic error from using our best value. This is an observation of $B_s^0\to J/\psi K_S^0K^\pm\pi^\mp$ with more than 10 standard deviations.

$\Gamma(J/\psi(1S)\overline{K}^0K^+K^-)/\Gamma_{total}$ — Γ_{81}/Γ

VALUE	CL%	DOCUMENT ID		TECN	COMMENT
$<12\times10^{-6}$	90	[1] AAIJ	14L	LHCB	pp at 7 TeV

[1] Measured with $B(B_s^0\to J/\psi K_S^0K^+K^-)/B(B^0\to J/\psi K_S^0\pi^+\pi^-)$ using PDG 12 values for the involved branching fractions.

$\Gamma(J/\psi(1S)f_2'(1525))/\Gamma_{total}$ — Γ_{83}/Γ

VALUE (units 10^{-4})	DOCUMENT ID		TECN	COMMENT
$2.61\pm0.20^{+0.56}_{-0.50}$	[1] AAIJ	13AN	LHCB	pp at 7 TeV

[1] Uses $f_s/f_d=0.256\pm0.020$ and $B(B^+\to J/\psi K^+)=(10.18\pm0.42)\times10^{-4}$.

$\Gamma(J/\psi(1S)f_2'(1525))/\Gamma(J/\psi(1S)\phi)$ — Γ_{83}/Γ_{56}

VALUE (units 10^{-2})	DOCUMENT ID		TECN	COMMENT
21 ±4 OUR AVERAGE				
$21.5\pm4.9\pm2.6$	[1] THORNE	13	BELL	$e^+e^-\to\Upsilon(5S)$
$21\ \pm7\ \pm1$	[2,3] ABAZOV	12AF	D0	$p\overline{p}$ at 1.96 TeV
• • • We do not use the following data for averages, fits, limits, etc. • • •				
$27\ \pm4\ \pm1$	[4] AAIJ	12S	LHCB	Repl. by AAIJ 13AN

[1] Uses $B(f_2'(1525)\to K^+K^-)=(44.4\pm1.1)\%$.
[2] ABAZOV 12AF reports $[\Gamma(B_s^0\to J/\psi(1S)f_2'(1525))/\Gamma(B_s^0\to J/\psi(1S)\phi)]\times B(f_2'(1525)\to K^+K^-)$ / $B(\phi(1020)\to K^+K^-)=0.19\pm0.05\pm0.04$ which we divide and multiply by our best values $B(f_2'(1525)\to K^+K^-)=\frac{1}{2}(87.6\pm2.2)\times10^{-2}$, $B(\phi(1020)\to K^+K^-)=(49.1\pm0.5)\times10^{-2}$. Our first error is their experiment's error and our second error is the systematic error from using our best values.
[3] ABAZOV 12AF fits the invariant masses of the K^+K^- pair in the range $1.35<M(K^+K^-)<2$ GeV.
[4] AAIJ 12S reports $[(26.4\pm2.7\pm2.4)\times10^{-2}$ from a measurement of $\Gamma(B_s^0\to J/\psi(1S)f_2'(1525))/\Gamma(B_s^0\to J/\psi(1S)\phi)]\times B(f_2'(1525)\to K^+K^-)$ / $B(\phi(1020)\to K^+K^-)$ assuming $B(f_2'(1525)\to K^+K^-)=(44.4\pm1.1)\times10^{-2}$, $B(\phi(1020)\to K^+K^-)=(48.9\pm0.5)\times10^{-2}$, which we rescale to our best values $B(f_2'(1525)\to K^+K^-)=\frac{1}{2}(87.6\pm2.2)\times10^{-2}$, $B(\phi(1020)\to K^+K^-)=(49.1\pm0.5)\times10^{-2}$. Our first error is their experiment's error and our second error is the systematic error from using our best values.

$\Gamma(J/\psi(1S)p\overline{p})/\Gamma_{total}$ — Γ_{84}/Γ

VALUE (units 10^{-6})	CL%	DOCUMENT ID		TECN	COMMENT
$3.58\pm0.19\pm0.39$		[1] AAIJ	19U	LHCB	pp at 7, 8, 13 TeV
• • • We do not use the following data for averages, fits, limits, etc. • • •					
<4.8	90	[2] AAIJ	13Z	LHCB	Repl. by AAIJ 19U

[1] Measured relative to $B_s^0\to J/\psi\phi$ assuming $B(B_s^0\to J/\psi\phi)=(10.5\pm0.13\pm0.64)\times10^{-4}$ and taking into account small K^+K^- S-wave contribution.
[2] Uses $B(B_s^0\to J/\psi(1S)\pi^+\pi^-)=(1.98\pm0.20)\times10^{-4}$.

Downloaded from https://academic.oup.com/ptep/article/2022/8/083C01/6651666 by KIT Library user on 27 September 2022

$\Gamma(J/\psi(1S)\gamma)/\Gamma_{total}$ — Γ_{85}/Γ

VALUE	CL%	DOCUMENT ID		TECN	COMMENT
$<7.3\times10^{-6}$	90	[1] AAIJ	15BB	LHCB	pp at 7, 8 TeV

[1] Branching fractions of normalization modes $B_s^0 \to J/\psi\gamma X$ taken from PDG 14. Uses $f_s/f_d = 0.259 \pm 0.015$.

$\Gamma(J/\psi(1S)\pi^+\pi^-\pi^+\pi^-)/\Gamma(J/\psi(1S)\pi^+\pi^-)$ — Γ_{86}/Γ_{63}

VALUE	DOCUMENT ID		TECN	COMMENT
0.371±0.015±0.022	[1] AAIJ	14Y	LHCB	pp at 7,8 TeV

[1] Excludes contributions from $\psi(2S)$ and $\chi_{c1}(3872)$ decaying to $J/\psi(1S)\pi^+\pi^-$.

$\Gamma(J/\psi(1S)f_1(1285))/\Gamma_{total}$ — Γ_{87}/Γ

VALUE (units 10^{-5})	DOCUMENT ID		TECN	COMMENT
7.2±1.3±0.4	[1] AAIJ	14Y	LHCB	pp at 7, 8 TeV

[1] AAIJ 14Y reports $(7.14 \pm 0.99^{+0.83}_{-0.91} \pm 0.41)\times10^{-5}$ from a measurement of $[\Gamma(B_s^0 \to J/\psi(1S)f_1(1285))/\Gamma_{total}] \times [B(f_1(1285) \to 2\pi^+2\pi^-)]$ assuming $B(f_1(1285) \to 2\pi^+2\pi^-) = 0.11^{+0.007}_{-0.006}$, which we rescale to our best value $B(f_1(1285) \to 2\pi^+2\pi^-) = (10.9 \pm 0.6)\times10^{-2}$. Our first error is their experiment's error and our second error is the systematic error from using our best value.

$\Gamma(\psi(2S)\eta)/\Gamma(J/\psi(1S)\eta)$ — Γ_{88}/Γ_{59}

VALUE	DOCUMENT ID		TECN	COMMENT
0.83±0.14±0.12	[1] AAIJ	13AA	LHCB	pp at 7 TeV

[1] Assuming lepton universality for dimuon decay modes of J/ψ and $\psi(2S)$ mesons, the ratio $B(J/\psi \to \mu^+\mu^-)/B(\psi(2S) \to \mu^+\mu^-) = B(J/\psi \to e^+e^-)/B(\psi(2S) \to e^+e^-) = 7.69 \pm 0.19$ was used.

$\Gamma(\psi(2S)\eta')/\Gamma(J/\psi(1S)\eta')$ — Γ_{89}/Γ_{62}

VALUE (units 10^{-2})	DOCUMENT ID		TECN	COMMENT
38.7±9.0±1.6	[1] AAIJ	15D	LHCB	pp at 7, 8 TeV

[1] Uses $J/\psi \to \mu^+\mu^-$, $\eta' \to \rho^0\gamma$, and $\eta' \to \eta\pi^+\pi^-$ decays.

$\Gamma(\psi(2S)\pi^+\pi^-)/\Gamma(J/\psi(1S)\pi^+\pi^-)$ — Γ_{90}/Γ_{63}

VALUE	DOCUMENT ID		TECN	COMMENT
0.34±0.04±0.03	[1] AAIJ	13AA	LHCB	pp at 7 TeV

[1] Assuming lepton universality for dimuon decay modes of J/ψ and $\psi(2S)$ mesons, the ratio $B(J/\psi \to \mu^+\mu^-)/B(\psi(2S) \to \mu^+\mu^-) = B(J/\psi \to e^+e^-)/B(\psi(2S) \to e^+e^-) = 7.69 \pm 0.19$ was used.

$\Gamma(\psi(2S)\phi)/\Gamma_{total}$ — Γ_{91}/Γ

VALUE (units 10^{-4})	EVTS	DOCUMENT ID		TECN	COMMENT
• • • We do not use the following data for averages, fits, limits, etc. • • •					
seen	1	BUSKULIC	93G	ALEP	$e^+e^- \to Z$

$\Gamma(\psi(2S)\phi)/\Gamma(J/\psi(1S)\phi)$ — Γ_{91}/Γ_{56}

VALUE	DOCUMENT ID		TECN	COMMENT
0.503±0.034 OUR AVERAGE				
0.500±0.034±0.011	[1,2] AAIJ	12L	LHCB	pp at 7 TeV
0.53 ±0.10 ±0.09	ABAZOV	09Y	D0	$p\overline{p}$ at 1.96 TeV
0.52 ±0.13 ±0.07	ABULENCIA	06N	CDF	$p\overline{p}$ at 1.96 TeV

[1] AAIJ 12L reports $0.489 \pm 0.026 \pm 0.021 \pm 0.012$ from a measurement of $[\Gamma(B_s^0 \to \psi(2S)\phi)/\Gamma(B_s^0 \to J/\psi(1S)\phi)] \times [B(J/\psi(1S) \to e^+e^-)] / [B(\psi(2S) \to e^+e^-)]$ assuming $B(J/\psi(1S) \to e^+e^-) = (5.94 \pm 0.06)\times10^{-2}$, $B(\psi(2S) \to e^+e^-) = (7.72 \pm 0.17)\times10^{-3}$, which we rescale to our best values $B(J/\psi(1S) \to e^+e^-) = (5.971 \pm 0.032)\times10^{-2}$, $B(\psi(2S) \to e^+e^-) = (7.93 \pm 0.17)\times10^{-3}$. Our first error is their experiment's error and our second error is the systematic error from using our best values.

[2] Assumes $B(J/\psi \to \mu^+\mu^-) / B(\psi(2S) \to \mu^+\mu^-) = B(J/\psi \to e^+e^-) / B(\psi(2S) \to e^+e^-) = 7.69 \pm 0.19$.

$\Gamma(\psi(2S)K^-\pi^+)/\Gamma_{total}$ — Γ_{92}/Γ

VALUE (units 10^{-5})	DOCUMENT ID		TECN	COMMENT
3.12±0.30±0.21	[1] AAIJ	15U	LHCB	pp at 7, 8 TeV

[1] AAIJ 15U reports $[\Gamma(B_s^0 \to \psi(2S)K^-\pi^+)/\Gamma_{total}] / [B(B^0 \to \psi(2S)K^+\pi^-)] = (5.38 \pm 0.36 \pm 0.22 \pm 0.31)\times10^{-2}$ which we multiply by our best value $B(B^0 \to \psi(2S)K^+\pi^-) = (5.8 \pm 0.4)\times10^{-4}$. Our first error is their experiment's error and our second error is the systematic error from using our best value.

$\Gamma(\psi(2S)\overline{K}^*(892)^0)/\Gamma_{total}$ — Γ_{93}/Γ

VALUE (units 10^{-5})	DOCUMENT ID		TECN	COMMENT
$3.3\pm0.5^{+0.2}_{-0.3}$	[1] AAIJ	15U	LHCB	pp at 7, 8 TeV

[1] AAIJ 15U reports $[\Gamma(B_s^0 \to \psi(2S)\overline{K}^*(892)^0)/\Gamma_{total}] / [B(B^0 \to \psi(2S)K^*(892)^0)] = (5.58 \pm 0.57 \pm 0.40 \pm 0.32)\times10^{-2}$ which we multiply by our best value $B(B^0 \to \psi(2S)K^*(892)^0) = (5.9 \pm 0.4)\times10^{-4}$. Our first error is their experiment's error and our second error is the systematic error from using our best value.

$\Gamma(\chi_{c1}\phi)/\Gamma(J/\psi(1S)\phi)$ — Γ_{94}/Γ_{56}

VALUE (units 10^{-2})	DOCUMENT ID		TECN	COMMENT
18.9±1.8±1.5	[1] AAIJ	13AC	LHCB	pp at 7 TeV

[1] Uses $B(\chi_{c1} \to J/\psi\gamma) = (34.4 \pm 1.5)\%$.

$\Gamma(\chi_{c2}K^+K^-)/\Gamma(\chi_{c1}K^+K^-)$ — Γ_{96}/Γ_{95}

VALUE (units 10^{-2})	DOCUMENT ID		TECN	COMMENT
17.1±3.1±1.0	[1] AAIJ	18AC	LHCB	pp at 7, 8, 13 TeV

[1] Measures the ratio for ±15 MeV window around ϕ mass.

$\Gamma(\chi_{c1}(3872)\phi)/\Gamma(\psi(2S)\phi)$ — Γ_{97}/Γ_{91}

VALUE	DOCUMENT ID		TECN	COMMENT
0.21±0.07 OUR AVERAGE				
0.22±0.02±0.07	[1] AAIJ	21C	LHCB	pp at 7, 8, 13 TeV
0.20±0.03±0.07	[2] SIRUNYAN	20BB	CMS	pp at 13 TeV

[1] AAIJ 21C reports $[\Gamma(B_s^0 \to \chi_{c1}(3872)\phi)/\Gamma(B_s^0 \to \psi(2S)\phi)] \times [B(\chi_{c1}(3872) \to \pi^+\pi^-J/\psi(1S))] / [B(\psi(2S) \to J/\psi(1S)\pi^+\pi^-)] = (2.42 \pm 0.23 \pm 0.07)\times10^{-2}$ which we multiply or divide by our best values $B(\chi_{c1}(3872) \to \pi^+\pi^-J/\psi(1S)) = (3.8 \pm 1.2)\times10^{-2}$, $B(\psi(2S) \to J/\psi(1S)\pi^+\pi^-) = (34.68 \pm 0.30)\times10^{-2}$. Our first error is their experiment's error and our second error is the systematic error from using our best values.

[2] SIRUNYAN 20BB reports $[\Gamma(B_s^0 \to \chi_{c1}(3872)\phi)/\Gamma(B_s^0 \to \psi(2S)\phi)] \times [B(\chi_{c1}(3872) \to \pi^+\pi^-J/\psi(1S))] / [B(\psi(2S) \to J/\psi(1S)\pi^+\pi^-)] = (2.21 \pm 0.29 \pm 0.17)\times10^{-2}$ which we multiply or divide by our best values $B(\chi_{c1}(3872) \to \pi^+\pi^-J/\psi(1S)) = (3.8 \pm 1.2)\times10^{-2}$, $B(\psi(2S) \to J/\psi(1S)\pi^+\pi^-) = (34.68 \pm 0.30)\times10^{-2}$. Our first error is their experiment's error and our second error is the systematic error from using our best values.

$\Gamma(J/\psi K^*(892)^0\overline{K}^*(892)^0)/\Gamma(\psi(2S)\phi)$ — Γ_{82}/Γ_{91}

VALUE	DOCUMENT ID		TECN	COMMENT
0.209±0.006±0.003	[1] AAIJ	21C	LHCB	pp at 7, 8, 13 TeV

[1] AAIJ 21C reports $\Gamma(B_s^0 \to J/\psi K^*(892)^0\overline{K}^*(892)^0)/\Gamma(B_s^0 \to \psi(2S)\phi)\ B^2(K^{*0} \to K^+\pi^-)/B(\psi(2S) \to J/\psi\pi^+\pi^-)/B(\phi \to K^+K^-) = 1.22 \pm 0.03 \pm 0.04$ which we adjust with PDG 20 values of $B(K^{*0} \to K^+\pi^-) = (99.902 \pm 0.009)\times10^{-2}$, $B(\psi(2S) \to J/\psi\pi^+\pi^-) = (34.68 \pm 0.30)\times10^{-2}$, and $B(\phi \to K^+K^-) = (49.2 \pm 0.5)\times10^{-2}$. The first uncertainty is the total experiment's one and the second is due to the adjustment branching fractions.

$\Gamma(\chi_{c1}(3872)(K^+K^-)_{non-\phi})/\Gamma(\chi_{c1}(3872)\phi)$ — Γ_{98}/Γ_{97}

VALUE	DOCUMENT ID		TECN	COMMENT
0.77±0.17±0.01	[1] AAIJ	21C	LHCB	pp at 7, 8, 13 TeV

[1] AAIJ 21C reports $[\Gamma(B_s^0 \to \chi_{c1}(3872)(K^+K^-)_{non-\phi})/\Gamma(B_s^0 \to \chi_{c1}(3872)\phi)] / [B(\phi(1020) \to K^+K^-)] = 1.57 \pm 0.32 \pm 0.12$ which we multiply by our best value $B(\phi(1020) \to K^+K^-) = (49.1 \pm 0.5)\times10^{-2}$. Our first error is their experiment's error and our second error is the systematic error from using our best value.

$\Gamma(\pi^+\pi^-)/\Gamma_{total}$ — Γ_{99}/Γ

VALUE (units 10^{-7})	CL%	DOCUMENT ID		TECN	COMMENT
7.0±1.0 OUR AVERAGE					
7.3±0.9±0.7		[1] AAIJ	17G	LHCB	pp at 7 and 8 TeV
6.4±1.8±0.6		[2] AALTONEN	12L	CDF	$p\overline{p}$ at 1.96 TeV
• • • We do not use the following data for averages, fits, limits, etc. • • •					
$10.4^{+2.4}_{-2.1}\pm1.0$		[3] AAIJ	12AR	LHCB	Repl. by AAIJ 17G
< 120	90	[4] PENG	10	BELL	$e^+e^- \to \Upsilon(5S)$
< 12	90	[5] AALTONEN	09C	CDF	Repl. by AALTONEN 12L
< 17	90	[6] ABULENCIA,A	06D	CDF	Repl. by AALTONEN 09C
<2320	90	[7] ABE	00C	SLD	$e^+e^- \to Z$
<1700	90	[8] BUSKULIC	96V	ALEP	$e^+e^- \to Z$

[1] AAIJ 17G reports $[\Gamma(B_s^0 \to \pi^+\pi^-)/\Gamma_{total}] / [B(B^0 \to K^+\pi^-)] \times [\Gamma(\overline{b} \to B_s^0)/\Gamma(\overline{b} \to B^0)] = (9.15 \pm 0.71 \pm 0.83)\times10^{-3}$ which we multiply or divide by our best values $B(B^0 \to K^+\pi^-) = (1.96 \pm 0.05)\times10^{-5}$, $\Gamma(\overline{b} \to B_s^0)/\Gamma(\overline{b} \to B^0) = 0.246 \pm 0.023$. Our first error is their experiment's error and our second error is the systematic error from using our best values.

[2] AALTONEN 12L reports $[\Gamma(B_s^0 \to \pi^+\pi^-)/\Gamma_{total}] / [B(B^0 \to K^+\pi^-)] \times [\Gamma(\overline{b} \to B_s^0)/\Gamma(\overline{b} \to B^0)] = 0.008 \pm 0.002 \pm 0.001$ which we multiply or divide by our best values $B(B^0 \to K^+\pi^-) = (1.96 \pm 0.05)\times10^{-5}$, $\Gamma(\overline{b} \to B_s^0)/\Gamma(\overline{b} \to B^0) = 0.246 \pm 0.023$. Our first error is their experiment's error and our second error is the systematic error from using our best values.

[3] AAIJ 12AR reports $[\Gamma(B_s^0 \to \pi^+\pi^-)/\Gamma_{total}] / [B(B^0 \to \pi^+\pi^-)] \times [\Gamma(\overline{b} \to B_s^0)/\Gamma(\overline{b} \to B^0)] = 0.050^{+0.011}_{-0.009} \pm 0.004$ which we multiply or divide by our best values $B(B^0 \to \pi^+\pi^-) = (5.12 \pm 0.19)\times10^{-6}$, $\Gamma(\overline{b} \to B_s^0)/\Gamma(\overline{b} \to B^0) = 0.246 \pm 0.023$. Our first error is their experiment's error and our second error is the systematic error from using our best values.

[4] Uses $\Upsilon(10860) \to B_s^*\overline{B}_s^*$ and assumes $B(\Upsilon(10860) \to B_s^{(*)}\overline{B}_s^{(*)}) = (19.3 \pm 2.9)\%$ and $\Gamma(\Upsilon(10860) \to B_s^*\overline{B}_s^*) / \Gamma(\Upsilon(10860) \to B_s^{(*)}\overline{B}_s^{(*)}) = (90.1^{+3.8}_{-4.0})\%$.

[5] Obtains this result from $(f_s/f_d) \cdot B(B_s \to \pi^+\pi^-)/B(B^0 \to K^+\pi^-) = 0.007 \pm 0.004 \pm 0.005$, assuming $f_s/f_d = 0.276 \pm 0.034$ and $B(B^0 \to K^+\pi^-) = (19.4 \pm 0.6)\times10^{-6}$.

[6] ABULENCIA,A 06D obtains this from $B(B_s \to \pi^+\pi^-) / B(B_s \to K^+K^-) < 0.05$ at 90% CL, assuming $B(B_s \to K^+K^-) = (33 \pm 6 \pm 7)\times10^{-6}$.

[7] ABE 00C assumes $B(Z \to b\overline{b}) = (21.7 \pm 0.1)\%$ and the B fractions $f_{B^0} = f_{B^+} = (39.7^{+1.8}_{-2.2})\%$ and $f_{B_s} = (10.5^{+1.8}_{-2.2})\%$.

[8] BUSKULIC 96V assumes PDG 96 production fractions for B^0, B^+, B_s, b baryons.

Downloaded from https://academic.oup.com/ptep/article/2022/8/083C01/6651666 by KIT Library user on 27 September 2022

$\Gamma(\pi^0\pi^0)/\Gamma_{total}$ — Γ_{100}/Γ

VALUE	CL%	DOCUMENT ID		TECN	COMMENT
$<2.1\times10^{-4}$	90	[1] ACCIARRI	95H	L3	$e^+e^-\to Z$

[1] ACCIARRI 95H assumes $f_{B^0}=39.5\pm4.0$ and $f_{B_s}=12.0\pm3.0\%$.

$\Gamma(\eta\pi^0)/\Gamma_{total}$ — Γ_{101}/Γ

VALUE	CL%	DOCUMENT ID		TECN	COMMENT
$<1.0\times10^{-3}$	90	[1] ACCIARRI	95H	L3	$e^+e^-\to Z$

[1] ACCIARRI 95H assumes $f_{B^0}=39.5\pm4.0$ and $f_{B_s}=12.0\pm3.0\%$.

$\Gamma(\eta\eta)/\Gamma_{total}$ — Γ_{102}/Γ

VALUE	CL%	DOCUMENT ID		TECN	COMMENT
$<1.43\times10^{-4}$	90	BHUYAN	22	BELL	$e^+e^-\to\Upsilon(5S)$
• • • We do not use the following data for averages, fits, limits, etc. • • •					
$<1.5\ \times10^{-3}$	90	[1] ACCIARRI	95H	L3	$e^+e^-\to Z$

[1] ACCIARRI 95H assumes $f_{B^0}=39.5\pm4.0$ and $f_{B_s}=12.0\pm3.0\%$.

$\Gamma(\rho^0\rho^0)/\Gamma_{total}$ — Γ_{103}/Γ

VALUE	CL%	DOCUMENT ID		TECN	COMMENT
$<3.20\times10^{-4}$	90	[1] ABE	00C	SLD	$e^+e^-\to Z$

[1] ABE 00C assumes $B(Z\to b\overline{b})=(21.7\pm0.1)\%$ and the B fractions $f_{B^0}=f_{B^+}=(39.7^{+1.8}_{-2.2})\%$ and $f_{B_s}=(10.5^{+1.8}_{-2.2})\%$.

$\Gamma(\eta'\eta)/\Gamma_{total}$ — Γ_{104}/Γ

VALUE	CL%	DOCUMENT ID		TECN	COMMENT
$<6.5\times10^{-5}$	90	[1] NISAR	21	BELL	$e^+e^-\to\Upsilon(5S)$

[1] Uses $\Upsilon(10860)\to B^*_s\overline{B}^*_s$ decays and assumes $B(\Upsilon(10860)\to B^{(*)}_s\overline{B}^{(*)}_s)=(20.1\pm3.1)\%$.

$\Gamma(\eta'\eta')/\Gamma_{total}$ — Γ_{105}/Γ

VALUE (units 10^{-5})	DOCUMENT ID		TECN	COMMENT
$3.3\pm0.7\pm0.1$	[1] AAIJ	15O	LHCB	pp at 7, 8 TeV

[1] AAIJ 15O reports $[\Gamma(B^0_s\to\eta'\eta')/\Gamma_{total}]\ /\ [B(B^+\to\eta'K^+)]=0.47\pm0.09\pm0.04$ which we multiply by our best value $B(B^+\to\eta'K^+)=(7.04\pm0.25)\times10^{-5}$. Our first error is their experiment's error and our second error is the systematic error from using our best value.

$\Gamma(\eta'\phi)/\Gamma_{total}$ — Γ_{106}/Γ

VALUE	CL%	DOCUMENT ID		TECN	COMMENT
$<0.82\times10^{-6}$	90	[1] AAIJ	17BA	LHCB	pp at 7, 8 TeV

[1] Corresponds to the 95% CL upper limit 1.01×10^{-6}. Uses the normalization mode $B^+\to\eta'K^+$ with branching fraction $(70.6\pm2.5)\times10^{-6}$ and the ratio of hadronisation fractions $f_s/f_d=0.259\pm0.015$, which is assumed equal to f_s/f_u.

$\Gamma(\eta'X_{s\overline{s}})/\Gamma_{total}$ — Γ_{54}/Γ

VALUE (units 10^{-3})	CL%	DOCUMENT ID		TECN	COMMENT
<1.4	90	[1] DUBEY	21	BELL	$e^+e^-\to\Upsilon(4S)$

[1] DUBEY 21 result is for $m(X_{s\overline{s}})<2.85$ GeV/c^2.

$\Gamma(\phi f_0(980),\ f_0(980)\to\pi^+\pi^-)/\Gamma_{total}$ — Γ_{107}/Γ

VALUE (units 10^{-6})	DOCUMENT ID		TECN	COMMENT
$1.12\pm0.16\pm0.14$	[1] AAIJ	17A	LHCB	pp at 7, 8 TeV

[1] Signal is observed with 8 standard deviations significance.

$\Gamma(\phi f_2(1270),\ f_2(1270)\to\pi^+\pi^-)/\Gamma_{total}$ — Γ_{108}/Γ

VALUE (units 10^{-6})	DOCUMENT ID		TECN	COMMENT
$0.61\pm0.13^{+0.13}_{-0.08}$	[1] AAIJ	17A	LHCB	pp at 7, 8 TeV

[1] Signal is observed with 5 standard deviations significance.

$\Gamma(\phi\rho^0)/\Gamma_{total}$ — Γ_{109}/Γ

VALUE (units 10^{-7})	CL%	DOCUMENT ID		TECN	COMMENT
$2.7\pm0.7\pm0.3$		[1] AAIJ	17A	LHCB	pp at 7, 8 TeV
• • • We do not use the following data for averages, fits, limits, etc. • • •					
<6170	90	[2] ABE	00C	SLD	$e^+e^-\to Z$

[1] Signal evidence is 4 standard deviations.
[2] ABE 00C assumes $B(Z\to b\overline{b})=(21.7\pm0.1)\%$ and the B fractions $f_{B^0}=f_{B^+}=(39.7^{+1.8}_{-2.2})\%$ and $f_{B_s}=(10.5^{+1.8}_{-2.2})\%$.

$\Gamma(\phi\pi^+\pi^-)/\Gamma_{total}$ — Γ_{110}/Γ

VALUE (units 10^{-6})	DOCUMENT ID		TECN	COMMENT
$3.48\pm0.23\pm0.39$	[1] AAIJ	17A	LHCB	pp at 7, 8 TeV

[1] Inclusive decays in mass range $400<m(\pi^+\pi^-)<1600$ MeV/c^2.

$\Gamma(\phi\phi)/\Gamma_{total}$ — Γ_{111}/Γ

VALUE (units 10^{-6})	CL%	DOCUMENT ID		TECN	COMMENT
18.5 ± 1.4 OUR FIT					
$18.5\pm1.4\pm1.0$		[1] AAIJ	15AS	LHCB	pp at 7, 8 TeV
• • • We do not use the following data for averages, fits, limits, etc. • • •					
$14\ ^{+6}_{-5}\ \pm6$		[2] ACOSTA	05J	CDF	Repl. by AALTONEN 11AN
<1183	90	[3] ABE	00C	SLD	$e^+e^-\to Z$

[1] AAIJ 15AS reports $[\Gamma(B^0_s\to\phi\phi)/\Gamma_{total}]\ /\ [B(B^0\to K^*(892)^0\phi)]=1.84\pm0.05\pm0.13$ which we multiply by our best value $B(B^0\to K^*(892)^0\phi)=(1.00\pm0.05)\times10^{-5}$. Our first error is their experiment's error and our second error is the systematic error from using our best value.
[2] Uses $B(B^0\to J/\psi\phi)=(1.38\pm0.49)\times10^{-3}$ and production cross-section ratio of $\sigma(B_s)/\sigma(B^0)=0.26\pm0.04$.
[3] ABE 00C assumes $B(Z\to b\overline{b})=(21.7\pm0.1)\%$ and the B fractions $f_{B^0}=f_{B^+}=(39.7^{+1.8}_{-2.2})\%$ and $f_{B_s}=(10.5^{+1.8}_{-2.2})\%$.

$\Gamma(\phi\phi)/\Gamma(J/\psi(1S)\phi)$ — Γ_{111}/Γ_{56}

VALUE (units 10^{-2})	DOCUMENT ID		TECN	COMMENT
1.77 ± 0.14 OUR FIT				
$1.78\pm0.14\pm0.20$	AALTONEN	11AN	CDF	$p\overline{p}$ at 1.96 TeV

$\Gamma(\phi\phi\phi)/\Gamma(\phi\phi)$ — $\Gamma_{112}/\Gamma_{111}$

VALUE	DOCUMENT ID		TECN	COMMENT
$0.117\pm0.030\pm0.015$	AAIJ	17BB	LHCB	pp at 7, 8 TeV

$\Gamma(\pi^+K^-)/\Gamma_{total}$ — Γ_{113}/Γ

VALUE (units 10^{-6})	CL%	DOCUMENT ID		TECN	COMMENT
5.8 ± 0.7 OUR AVERAGE					
$5.9\pm0.7\pm0.6$		[1] AAIJ	12AR	LHCB	pp at 7 TeV
$5.7\pm1.0\pm0.5$		[2] AALTONEN	09C	CDF	$p\overline{p}$ at 1.96 TeV
• • • We do not use the following data for averages, fits, limits, etc. • • •					
<26	90	[3] PENG	10	BELL	$e^+e^-\to\Upsilon(5S)$
<5.6	90	[4] ABULENCIA,A	06D	CDF	Repl. by AALTONEN 09C
<261	90	[5] ABE	00C	SLD	$e^+e^-\to Z$
<210	90	[6] BUSKULIC	96V	ALEP	$e^+e^-\to Z$
<260	90	[7] AKERS	94L	OPAL	$e^+e^-\to Z$

[1] AAIJ 12AR reports $[\Gamma(B^0_s\to\pi^+K^-)/\Gamma_{total}]\ /\ [B(B^0\to K^+\pi^-)]\times[\Gamma(\overline{b}\to B^0_s)/\Gamma(\overline{b}\to B^0)]=0.074\pm0.006\pm0.006$ which we multiply or divide by our best values $B(B^0\to K^+\pi^-)=(1.96\pm0.05)\times10^{-5}$, $\Gamma(\overline{b}\to B^0_s)/\Gamma(\overline{b}\to B^0)=0.246\pm0.023$. Our first error is their experiment's error and our second error is the systematic error from using our best values.
[2] AALTONEN 09C reports $[\Gamma(B^0_s\to\pi^+K^-)/\Gamma_{total}]\ /\ [B(B^0\to K^+\pi^-)]\times[B(\overline{b}\to B^0_s)]\ /\ [B(\overline{b}\to B^0)]=0.071\pm0.010\pm0.007$ which we multiply or divide by our best values $B(B^0\to K^+\pi^-)=(1.96\pm0.05)\times10^{-5}$, $B(\overline{b}\to B^0_s)=(10.0\pm0.8)\times10^{-2}$, $B(\overline{b}\to B^0)=(40.8\pm0.7)\times10^{-2}$. Our first error is their experiment's error and our second error is the systematic error from using our best values.
[3] Uses $\Upsilon(10860)\to B^*_s\overline{B}^*_s$ and assumes $B(\Upsilon(10860)\to B^{(*)}_s\overline{B}^{(*)}_s)=(19.3\pm2.9)\%$ and $\Gamma(\Upsilon(10860)\to B^*_s\overline{B}^*_s)\ /\ \Gamma(\Upsilon(10860)\to B^{(*)}_s\overline{B}^{(*)}_s)=(90.1^{+3.8}_{-4.0})\%$.
[4] ABULENCIA,A 06D obtains this from $(f_s/f_d)\ (B(B_s\to\pi^+K^-)\ /\ B(B^0\to K^+\pi^-))<0.08$ at 90% CL, assuming $f_s/f_d=0.260\pm0.039$ and $B(B^0\to K^+\pi^-)=(18.9\pm0.7)\times10^{-6}$.
[5] ABE 00C assumes $B(Z\to b\overline{b})=(21.7\pm0.1)\%$ and the B fractions $f_{B^0}=f_{B^+}=(39.7^{+1.8}_{-2.2})\%$ and $f_{B_s}=(10.5^{+1.8}_{-2.2})\%$.
[6] BUSKULIC 96V assumes PDG 96 production fractions for B^0, B^+, B_s, b baryons.
[7] Assumes $B(Z\to b\overline{b})=0.217$ and B^0_d (B^0_s) fraction 39.5% (12%).

$\Gamma(K^+K^-)/\Gamma_{total}$ — Γ_{114}/Γ

VALUE (units 10^{-6})	CL%	DOCUMENT ID		TECN	COMMENT
$26.6\pm\ 2.2$ OUR AVERAGE					
$25.2\pm\ 1.7\pm2.4$		[1] AAIJ	12AR	LHCB	pp at 7 TeV
$27.6\pm\ 2.3\pm2.7$		[2] AALTONEN	11N	CDF	$p\overline{p}$ at 1.96 TeV
$38\ ^{+10}_{-9}\ \pm7$		[3] PENG	10	BELL	$e^+e^-\to\Upsilon(5S)$
• • • We do not use the following data for averages, fits, limits, etc. • • •					
<310	90	DRUTSKOY	07A	BELL	$e^+e^-\to\Upsilon(5S)$
$33\ \pm\ 6\ \pm7$		[4] ABULENCIA,A	06D	CDF	Repl. by AALTONEN 11N
<283	90	[5] ABE	00C	SLD	$e^+e^-\to Z$
<59	90	[6] BUSKULIC	96V	ALEP	$e^+e^-\to Z$
<140	90	[7] AKERS	94L	OPAL	$e^+e^-\to Z$

[1] AAIJ 12AR reports $[\Gamma(B^0_s\to K^+K^-)/\Gamma_{total}]\ /\ [B(B^0\to K^+\pi^-)]\times[\Gamma(\overline{b}\to B^0_s)/\Gamma(\overline{b}\to B^0)]=0.316\pm0.009\pm0.019$ which we multiply or divide by our best values $B(B^0\to K^+\pi^-)=(1.96\pm0.05)\times10^{-5}$, $\Gamma(\overline{b}\to B^0_s)/\Gamma(\overline{b}\to B^0)=0.246\pm0.023$. Our first error is their experiment's error and our second error is the systematic error from using our best values.
[2] AALTONEN 11N reports $(f_s/f_d)\ (B(B^0_s\to K^+K^-)\ /\ B(B^0\to K^+\pi^-))=0.347\pm0.020\pm0.021$. We multiply this result by our best value of $B(B^0\to K^+\pi^-)=(1.96\pm0.05)\times10^{-5}$ and divide by our best value of f_s/f_d, where $1/2\ f_s/f_d=0.1230\pm0.0115$. Our first quoted uncertainty is the combined experiment's uncertainty and our second is the systematic uncertainty from using our best values.

Downloaded from https://academic.oup.com/ptep/article/2022/8/083C01/6651666 by KIT Library user on 27 September 2022

[3] Uses $\Upsilon(10860) \to B_s^* \overline{B}_s^*$ and assumes $B(\Upsilon(10860) \to B_s^{(*)} \overline{B}_s^{(*)}) = (19.3 \pm 2.9)\%$ and $\Gamma(\Upsilon(10860) \to B_s^* \overline{B}_s^*) / \Gamma(\Upsilon(10860) \to B_s^{(*)} \overline{B}_s^{(*)}) = (90.1^{+3.8}_{-4.0})\%$.

[4] ABULENCIA,A 06D obtains this from (f_s/f_d) $(B(B_s \to K^+K^-) / B(B^0 \to K^+\pi^-))$ $= 0.46 \pm 0.08 \pm 0.07$, assuming $f_s/f_d = 0.260 \pm 0.039$ and $B(B^0 \to K^+\pi^-) = (18.9 \pm 0.7) \times 10^{-6}$.

[5] ABE 00C assumes $B(Z \to b\overline{b})=(21.7 \pm 0.1)\%$ and the B fractions $f_{B^0}=f_{B^+}=(39.7^{+1.8}_{-2.2})\%$ and $f_{B_s}=(10.5^{+1.8}_{-2.2})\%$.

[6] BUSKULIC 96V assumes PDG 96 production fractions for B^0, B^+, B_s, b baryons.

[7] Assumes $B(Z \to b\overline{b}) = 0.217$ and B_d^0 (B_s^0) fraction 39.5% (12%).

$\Gamma(K^0\overline{K}^0)/\Gamma_{total}$ — Γ_{115}/Γ

VALUE (units 10^{-5})	CL%	DOCUMENT ID		TECN	COMMENT
1.76±0.31 OUR AVERAGE					
$1.68 \pm 0.34^{+0.16}_{-0.15}$		[1] AAIJ	20F	LHCB	pp at 7, 8, 13 TeV
$1.96^{+0.58}_{-0.51} \pm 0.10 \pm 0.20$		[2] PAL	16	BELL	$e^+e^- \to \Upsilon(5S)$
• • • We do not use the following data for averages, fits, limits, etc. • • •					
<6.6	90	[3] PENG	10	BELL	Repl. by PAL 16

[1] AAIJ 20F reports $[\Gamma(B_s^0 \to K^0\overline{K}^0)/\Gamma_{total}] / [B(B^0 \to K^0\phi)] = 2.3 \pm 0.4 \pm 0.2 \pm 0.1$ which we multiply by our best value $B(B^0 \to K^0\phi) = (7.3 \pm 0.7) \times 10^{-6}$. Our first error is their experiment's error and our second error is the systematic error from using our best value.

[2] Observed in $B_s^0 \to K_S^0 K_S^0$ with significance of 5.1 σ. The last uncertainty is due to the uncertainty of the total number of $B_s^0\overline{B}_s^0$ pairs.

[3] Uses $\Upsilon(10860) \to B_s^* \overline{B}_s^*$ and assumes $B(\Upsilon(10860) \to B_s^{(*)} \overline{B}_s^{(*)}) = (19.3 \pm 2.9)\%$ and $\Gamma(\Upsilon(10860) \to B_s^* \overline{B}_s^*) / \Gamma(\Upsilon(10860) \to B_s^{(*)} \overline{B}_s^{(*)}) = (90.1^{+3.8}_{-4.0})\%$.

$\Gamma(K^0\pi^+\pi^-)/\Gamma_{total}$ — Γ_{116}/Γ

VALUE (units 10^{-6})	DOCUMENT ID		TECN	COMMENT
9.5±2.1±0.3	[1,2] AAIJ	17BP	LHCB	pp at 7, 8 TeV
• • • We do not use the following data for averages, fits, limits, etc. • • •				
14 ±4 ±1	[3] AAIJ	13BP	LHCB	Repl. by AAIJ 17BP

[1] AAIJ 17BP reports $[\Gamma(B_s^0 \to K^0\pi^+\pi^-)/\Gamma_{total}] / [B(B^0 \to K^0\pi^+\pi^-)] = 0.191 \pm 0.027 \pm 0.033$ which we multiply by our best value $B(B^0 \to K^0\pi^+\pi^-) = (4.97 \pm 0.18) \times 10^{-5}$. Our first error is their experiment's error and our second error is the systematic error from using our best value.

[2] Used $f_s/f_d = 0.259 \pm 0.015$.

[3] AAIJ 13BP reports $[\Gamma(B_s^0 \to K^0\pi^+\pi^-)/\Gamma_{total}] / [B(B^0 \to K^0\pi^+\pi^-)] = 0.29 \pm 0.06 \pm 0.04$ which we multiply by our best value $B(B^0 \to K^0\pi^+\pi^-) = (4.97 \pm 0.18) \times 10^{-5}$. Our first error is their experiment's error and our second error is the systematic error from using our best value.

$\Gamma(K^0K^\pm\pi^\mp)/\Gamma_{total}$ — Γ_{117}/Γ

VALUE (units 10^{-5})	DOCUMENT ID		TECN	COMMENT
8.4±0.8±0.3	[1,2] AAIJ	17BP	LHCB	pp at 7, 8 TeV
• • • We do not use the following data for averages, fits, limits, etc. • • •				
7.4±0.9±0.3	[3] AAIJ	13BP	LHCB	Repl. by AAIJ 17BP

[1] AAIJ 17BP reports $[\Gamma(B_s^0 \to K^0K^\pm\pi^\mp)/\Gamma_{total}] / [B(B^0 \to K^0\pi^+\pi^-)] = 1.70 \pm 0.07 \pm 0.15$ which we multiply by our best value $B(B^0 \to K^0\pi^+\pi^-) = (4.97 \pm 0.18) \times 10^{-5}$. Our first error is their experiment's error and our second error is the systematic error from using our best value.

[2] Used $f_s/f_d = 0.259 \pm 0.015$.

[3] AAIJ 13BP reports $[\Gamma(B_s^0 \to K^0K^\pm\pi^\mp)/\Gamma_{total}] / [B(B^0 \to K^0\pi^+\pi^-)] = 1.48 \pm 0.12 \pm 0.14$ which we multiply by our best value $B(B^0 \to K^0\pi^+\pi^-) = (4.97 \pm 0.18) \times 10^{-5}$. Our first error is their experiment's error and our second error is the systematic error from using our best value.

$\Gamma(K^*(892)^-\pi^+)/\Gamma_{total}$ — Γ_{118}/Γ

VALUE (units 10^{-6})	DOCUMENT ID		TECN	COMMENT
2.9±1.0±0.2	[1,2] AAIJ	14BM	LHCB	pp at 7 TeV

[1] AAIJ 14BM reports $[\Gamma(B_s^0 \to K^*(892)^-\pi^+)/\Gamma_{total}] / [B(B^0 \to K^*(892)^+\pi^-)] = 0.39 \pm 0.13 \pm 0.05$ which we multiply by our best value $B(B^0 \to K^*(892)^+\pi^-) = (7.5 \pm 0.4) \times 10^{-6}$. Our first error is their experiment's error and our second error is the systematic error from using our best value.

[2] Uses $f_s/f_d = 0.259 \pm 0.015$.

$\Gamma(K^*(892)^\pm K^\mp)/\Gamma_{total}$ — Γ_{119}/Γ

VALUE (units 10^{-5})	DOCUMENT ID		TECN	COMMENT
1.86±0.12±0.45	[1,2] AAIJ	19K	LHCB	pp at 7, 8 TeV
• • • We do not use the following data for averages, fits, limits, etc. • • •				
$1.12 \pm 0.21^{+0.07}_{-0.06}$	[3,4] AAIJ	14BM	LHCB	Repl. by AAIJ 19K

[1] AAIJ 19K reports $(18.6 \pm 1.2 \pm 0.8 \pm 4.0 \pm 2.0) \times 10^{-6}$ as the measured value. We have combined in quadrature all systematic uncertainties into a single one.

[2] Measured in Dalitz plot analysis of $B_s^0 \to K_S^0 K^\pm\pi^\mp$ decays.

[3] AAIJ 14BM reports $[\Gamma(B_s^0 \to K^*(892)^\pm K^\mp)/\Gamma_{total}] / [B(B^0 \to K^*(892)^+\pi^-)] = 1.49 \pm 0.22 \pm 0.18$ which we multiply by our best value $B(B^0 \to K^*(892)^+\pi^-) = (7.5 \pm 0.4) \times 10^{-6}$. Our first error is their experiment's error and our second error is the systematic error from using our best value.

[4] Uses $f_s/f_d = 0.259 \pm 0.015$.

$\Gamma(K_0^*(1430)^\pm K^\mp)/\Gamma_{total}$ — Γ_{120}/Γ

VALUE (units 10^{-5})	DOCUMENT ID		TECN	COMMENT
3.13±0.23±2.53	[1,2] AAIJ	19K	LHCB	pp at 7, 8 TeV

[1] AAIJ 19K reports $(31.3 \pm 2.3 \pm 0.7 \pm 25.1 \pm 3.3) \times 10^{-6}$ as the measured value. We have combined in quadrature all systematic uncertainties into a single one.

[2] Measured in Dalitz plot analysis of $B_s^0 \to K_S^0 K^\pm\pi^\mp$ decays.

$\Gamma(K_2^*(1430)^\pm K^\mp)/\Gamma_{total}$ — Γ_{121}/Γ

VALUE (units 10^{-5})	DOCUMENT ID		TECN	COMMENT
1.03±0.25±1.64	[1,2] AAIJ	19K	LHCB	pp at 7, 8 TeV

[1] AAIJ 19K reports $(10.3 \pm 2.5 \pm 1.1 \pm 16.3 \pm 1.1) \times 10^{-6}$ as the measured value. We have combined in quadrature all systematic uncertainties into a single one.

[2] Measured in Dalitz plot analysis of $B_s^0 \to K_S^0 K^\pm\pi^\mp$ decays.

$\Gamma(K^*(892)^0\overline{K}^0 + c.c.)/\Gamma_{total}$ — Γ_{122}/Γ

VALUE (units 10^{-5})	DOCUMENT ID		TECN	COMMENT
1.98±0.28±0.50	[1,2] AAIJ	19K	LHCB	pp at 7, 8 TeV

[1] AAIJ 19K reports $(19.8 \pm 2.8 \pm 1.2 \pm 4.4 \pm 2.1) \times 10^{-6}$ as the measured value. We have combined in quadrature all systematic uncertainties into a single one.

[2] Measured in Dalitz plot analysis of $B_s^0 \to K_S^0 K^\pm\pi^\mp$ decays.

$\Gamma(K_0^*(1430)\overline{K}^0 + c.c.)/\Gamma_{total}$ — Γ_{123}/Γ

VALUE (units 10^{-5})	DOCUMENT ID		TECN	COMMENT
3.30±0.25±0.98	[1,2] AAIJ	19K	LHCB	pp at 7, 8 TeV

[1] AAIJ 19K reports $(33.0 \pm 2.5 \pm 0.9 \pm 9.1 \pm 3.5) \times 10^{-6}$ as the measured value. We have combined in quadrature all systematic uncertainties into a single one.

[2] Measured in Dalitz plot analysis of $B_s^0 \to K_S^0 K^\pm\pi^\mp$ decays.

$\Gamma(K_2^*(1430)^0\overline{K}^0 + c.c.)/\Gamma_{total}$ — Γ_{124}/Γ

VALUE (units 10^{-5})	DOCUMENT ID		TECN	COMMENT
1.68±0.45±2.13	[1,2] AAIJ	19K	LHCB	pp at 7, 8 TeV

[1] AAIJ 19K reports $(16.8 \pm 4.5 \pm 1.7 \pm 21.2 \pm 1.8) \times 10^{-6}$ as the measured value. We have combined in quadrature all systematic uncertainties into a single one.

[2] Measured in Dalitz plot analysis of $B_s^0 \to K_S^0 K^\pm\pi^\mp$ decays.

$\Gamma(K_S^0\overline{K}^*(892)^0 + c.c.)/\Gamma_{total}$ — Γ_{125}/Γ

VALUE (units 10^{-6})	DOCUMENT ID		TECN	COMMENT
16.4±3.4±2.3	[1] AAIJ	16	LHCB	pp at 7 TeV

[1] Measured relative to $B^0 \to K_S^0\pi^+\pi^-$ using the value of $B(B^0 \to K^0\pi^+\pi^-) = (4.96 \pm 0.2) \times 10^{-5}$.

$\Gamma(K^0K^+K^-)/\Gamma_{total}$ — Γ_{126}/Γ

VALUE (units 10^{-7})	CL%	DOCUMENT ID		TECN	COMMENT
12.9±6.5±0.5		[1,2,3] AAIJ	17BP	LHCB	pp at 7, 8 TeV
• • • We do not use the following data for averages, fits, limits, etc. • • •					
<34	90	[4] AAIJ	13BP	LHCB	Repl. by AAIJ 17BP

[1] AAIJ 17BP reports $[\Gamma(B_s^0 \to K^0K^+K^-)/\Gamma_{total}] / [B(B^0 \to K^0\pi^+\pi^-)] = 0.026 \pm 0.011 \pm 0.007$ which we multiply by our best value $B(B^0 \to K^0\pi^+\pi^-) = (4.97 \pm 0.18) \times 10^{-5}$. Our first error is their experiment's error and our second error is the systematic error from using our best value.

[2] AAIJ 17BP also set the limit range 4–25 $\times 10^{-7}$ at 90% CL using the world average value $B(B^0 \to K^0\pi^+\pi^-) = (4.96 \pm 0.20) \times 10^{-5}$.

[3] Used $f_s/f_d = 0.259 \pm 0.015$.

[4] AAIJ 13BP reports $[\Gamma(B_s^0 \to K^0K^+K^-)/\Gamma_{total}] / [B(B^0 \to K^0\pi^+\pi^-)] < 0.068$ which we multiply by our best value $B(B^0 \to K^0\pi^+\pi^-) = 4.97 \times 10^{-5}$.

$\Gamma(\overline{K}^*(892)^0\rho^0)/\Gamma_{total}$ — Γ_{127}/Γ

VALUE	CL%	DOCUMENT ID		TECN	COMMENT
<7.67 × 10^{-4}	90	[1] ABE	00C	SLD	$e^+e^- \to Z$

[1] ABE 00C assumes $B(Z \to b\overline{b})=(21.7 \pm 0.1)\%$ and the B fractions $f_{B^0}=f_{B^+}=(39.7^{+1.8}_{-2.2})\%$ and $f_{B_s}=(10.5^{+1.8}_{-2.2})\%$.

$\Gamma(\overline{K}^*(892)^0K^*(892)^0)/\Gamma_{total}$ — Γ_{128}/Γ

VALUE (units 10^{-5})	CL%	DOCUMENT ID		TECN	COMMENT
1.11±0.26±0.06		[1] AAIJ	15AF	LHCB	pp at 7 TeV
• • • We do not use the following data for averages, fits, limits, etc. • • •					
2.81±0.46±0.56		[2] AAIJ	12F	LHCB	Repl. by AAIJ 15AF
<168.1	90	[3] ABE	00C	SLD	$e^+e^- \to Z$

[1] AAIJ 15AF reports $[\Gamma(B_s^0 \to \overline{K}^*(892)^0K^*(892)^0)/\Gamma_{total}] / [B(B^0 \to K^*(892)^0\phi)] = 1.11 \pm 0.22 \pm 0.12 \pm 0.06$ which we multiply by our best value $B(B^0 \to K^*(892)^0\phi) = (1.00 \pm 0.05) \times 10^{-5}$. Our first error is their experiment's error and our second error is the systematic error from using our best value.

[2] Uses $B^0 \to J/\psi K^{*0}$ for normalization and assumes $B(B^0 \to J/\psi K^{*0})$ $B(J/\psi \to \mu^+\mu^-)$ $B(K^{*0} \to K^+\pi^-) = (1.33 \pm 0.06) \times 10^{-3}$ and $f_s/f_d = 0.253 \pm 0.031$. The second quoted error is total uncertainty including the error of 0.34 on f_s/f_d.

[3] ABE 00C assumes $B(Z \to b\overline{b})=(21.7 \pm 0.1)\%$ and the B fractions $f_{B^0}=f_{B^+}=(39.7^{+1.8}_{-2.2})\%$ and $f_{B_s}=(10.5^{+1.8}_{-2.2})\%$.

Downloaded from https://academic.oup.com/ptep/article/2022/8/083C01/6651666 by KIT Library user on 27 September 2022

$\Gamma(\phi K^*(892)^0)/\Gamma_{total}$ — Γ_{132}/Γ

VALUE (units 10^{-6})	CL%	DOCUMENT ID		TECN	COMMENT
1.14±0.29±0.06		[1] AAIJ	13BW	LHCB	pp at 7 TeV
• • • We do not use the following data for averages, fits, limits, etc. • • •					
<1013	90	[2] ABE	00C	SLD	$e^+e^- \to Z$

[1] AAIJ 13BW reports $[\Gamma(B^0_s \to \phi K^*(892)^0)/\Gamma_{total}]$ / $[B(B^0 \to K^*(892)^0\phi)] = 0.113 \pm 0.024 \pm 0.016$ which we multiply by our best value $B(B^0 \to K^*(892)^0\phi) = (1.00 \pm 0.05) \times 10^{-5}$. Our first error is their experiment's error and our second error is the systematic error from using our best value.

[2] ABE 00C assumes $B(Z \to b\overline{b})=(21.7 \pm 0.1)\%$ and the B fractions $f_{B^0}=f_{B^+}=(39.7^{+1.8}_{-2.2})\%$ and $f_{B_s}=(10.5^{+1.8}_{-2.2})\%$.

$\Gamma(p\overline{p})/\Gamma_{total}$ — Γ_{133}/Γ

Test for $\Delta B=1$ weak neutral current. Allowed by higher-order electroweak interactions.

VALUE (units 10^{-8})	CL%	DOCUMENT ID		TECN	COMMENT
< 1.5	90	[1] AAIJ	17BJ	LHCB	pp at 7 and 8 TeV
• • • We do not use the following data for averages, fits, limits, etc. • • •					
$2.84^{+2.03+0.85}_{-1.68-0.18}$		[2] AAIJ	13BQ	LHCB	Repl. by AAIJ 17BJ
<5900	90	[3] BUSKULIC	96V	ALEP	$e^+e^- \to Z$

[1] Uses normalization mode $B(B^0 \to K^+\pi^-) = (19.6 \pm 0.5) \times 10^{-6}$ and B production ratio $f(\overline{b} \to B^0_s)/f(\overline{b} \to B^0_d) = 0.259 \pm 0.015$.

[2] Uses normalization mode $B(B^0 \to K^+\pi^-) = (19.55 \pm 0.54) \times 10^{-6}$ and B production ratio $f(\overline{b} \to B^0_s)/f(\overline{b} \to B^0_d) = 0.256 \pm 0.020$.

[3] BUSKULIC 96V assumes PDG 96 production fractions for B^0, B^+, B_s, b baryons.

$\Gamma(p\overline{p}K^+K^-)/\Gamma_{total}$ — Γ_{134}/Γ

VALUE (units 10^{-6})		DOCUMENT ID		TECN	COMMENT
4.5±0.4±0.2		[1,2] AAIJ	17BD	LHCB	pp at 7, 8 TeV

[1] AAIJ 17BD reports $[\Gamma(B^0_s \to p\overline{p}K^+K^-)/\Gamma_{total}]$ / $[B(B^0 \to J/\psi(1S)K^*(892)^0)]$ / $[B(J/\psi(1S) \to p\overline{p})]$ / $[B(K^*(892) \to (K\pi)^\pm)] = 1.67 \pm 0.12 \pm 0.11$ which we multiply by our best values $B(B^0 \to J/\psi(1S)K^*(892)^0) = (1.27 \pm 0.05) \times 10^{-3}$, $B(J/\psi(1S) \to p\overline{p}) = (2.120 \pm 0.029) \times 10^{-3}$, $B(K^*(892) \to (K\pi)^\pm) = (99.902 \pm 0.009) \times 10^{-2}$. Our first error is their experiment's error and our second error is the systematic error from using our best values. Reported value assumes $f_s/f_d = 0.259 \pm 0.015$.

[2] The branching ratio is given for $m_{p\overline{p}}$ <2.85 GeV.

$\Gamma(p\overline{p}K^+\pi^-)/\Gamma_{total}$ — Γ_{135}/Γ

VALUE (units 10^{-7})		DOCUMENT ID		TECN	COMMENT
13.9±2.5±0.5		[1,2] AAIJ	17BD	LHCB	pp at 7, 8 TeV

[1] AAIJ 17BD reports $[\Gamma(B^0_s \to p\overline{p}K^+\pi^-)/\Gamma_{total}]$ / $[B(B^0 \to J/\psi(1S)K^*(892)^0)]$ / $[B(J/\psi(1S) \to p\overline{p})]$ / $[B(K^*(892) \to (K\pi)^\pm)] = 0.52 \pm 0.08 \pm 0.05$ which we multiply by our best values $B(B^0 \to J/\psi(1S)K^*(892)^0) = (1.27 \pm 0.05) \times 10^{-3}$, $B(J/\psi(1S) \to p\overline{p}) = (2.120 \pm 0.029) \times 10^{-3}$, $B(K^*(892) \to (K\pi)^\pm) = (99.902 \pm 0.009) \times 10^{-2}$. Our first error is their experiment's error and our second error is the systematic error from using our best values. Reported value assumes $f_s/f_d = 0.259 \pm 0.015$.

[2] The branching ratio is given for $m_{p\overline{p}}$ <2.85 GeV.

$\Gamma(p\overline{p}K^+\pi^-)/\Gamma(p\overline{p}K^+K^-)$ — $\Gamma_{135}/\Gamma_{134}$

VALUE		DOCUMENT ID		TECN	COMMENT
0.31±0.05±0.02		[1,2] AAIJ	17BD	LHCB	pp at 7, 8 TeV

[1] Reports $B(B^0_s \to p\overline{p}K^+\pi^-)$ / $B(B^0 \to p\overline{p}K^+\pi^-) = 0.22 \pm 0.04 \pm 0.02 \pm 0.01$, where the third error is due to f_s/f_d.

[2] The ratio is given for $m_{p\overline{p}}$ <2.85 GeV and assuming $f_s/f_d = 0.259 \pm 0.015$.

$\Gamma(p\overline{p}\pi^+\pi^-)/\Gamma_{total}$ — Γ_{136}/Γ

VALUE (units 10^{-7})		DOCUMENT ID		TECN	COMMENT
4.3±2.0±0.2		[1,2] AAIJ	17BD	LHCB	pp at 7, 8 TeV

[1] AAIJ 17BD reports $[\Gamma(B^0_s \to p\overline{p}\pi^+\pi^-)/\Gamma_{total}]$ / $[B(B^0 \to J/\psi(1S)K^*(892)^0)]$ / $[B(J/\psi(1S) \to p\overline{p})]$ / $[B(K^*(892) \to (K\pi)^\pm)] = 0.16 \pm 0.07 \pm 0.02$ which we multiply by our best values $B(B^0 \to J/\psi(1S)K^*(892)^0) = (1.27 \pm 0.05) \times 10^{-3}$, $B(J/\psi(1S) \to p\overline{p}) = (2.120 \pm 0.029) \times 10^{-3}$, $B(K^*(892) \to (K\pi)^\pm) = (99.902 \pm 0.009) \times 10^{-2}$. Our first error is their experiment's error and our second error is the systematic error from using our best values. Reported value assumes $f_s/f_d = 0.259 \pm 0.015$.

[2] The branching ratio is given for $m_{p\overline{p}}$ <2.85 GeV.

$\Gamma(p\overline{\Lambda}K^- + c.c.)/\Gamma_{total}$ — Γ_{137}/Γ

VALUE (units 10^{-6})		DOCUMENT ID		TECN	COMMENT
5.5±0.6±0.8		[1,2] AAIJ	17AL	LHCB	pp at 7, 8 TeV

[1] AAIJ 17AL reports $(5.46 \pm 0.61 \pm 0.82) \times 10^{-6}$ from a measurement of $[\Gamma(B^0_s \to p\overline{\Lambda}K^- + c.c.)/\Gamma_{total}]$ / $[B(B^0 \to p\overline{\Lambda}\pi^-)]$ assuming $B(B^0 \to p\overline{\Lambda}\pi^-) = (3.14 \pm 0.29) \times 10^{-6}$.

[2] AAIJ 17AL value represents the sum of $B^0_s \to p\overline{\Lambda}K^-$ and $B^0_s \to \overline{p}\Lambda K^+$ and assumes the fraction $f_s/f_d = 0.259 \pm 0.015$.

$\Gamma(\Lambda_c^-\Lambda\pi^+)/\Gamma_{total}$ — Γ_{138}/Γ

VALUE (units 10^{-4})	DOCUMENT ID		TECN	COMMENT
3.6±1.1±1.2	[1] SOLOVIEVA	13	BELL	$e^+e^- \to \Upsilon(4S)$

[1] The second error is the total systematic uncertainty including the Λ_c absolute branching fractions and the normalizion number of B_s events.

$\Gamma(\Lambda_c^-\Lambda_c^+)/\Gamma_{total}$ — Γ_{139}/Γ

VALUE	CL%	DOCUMENT ID		TECN	COMMENT
<8.0 × 10^{-5}	95	[1] AAIJ	14AA	LHCB	pp at 7 TeV

[1] Uses $B(\overline{B}^0 \to D^+D_s^-) = (7.2 \pm 0.8) \times 10^{-3}$.

$\Gamma(\gamma\gamma)/\Gamma_{total}$ — Γ_{140}/Γ

Test for $\Delta B=1$ weak neutral current.

VALUE (units 10^{-6})	CL%	DOCUMENT ID		TECN	COMMENT
< 3.1	90	[1] DUTTA	15	BELL	$e^+e^- \to \Upsilon(5S)$
• • • We do not use the following data for averages, fits, limits, etc. • • •					
< 8.7	90	[2] WICHT	08A	BELL	Repl. by DUTTA 15
< 53	90	DRUTSKOY	07A	BELL	Repl. by WICHT 08A
<148	90	[3] ACCIARRI	95I	L3	$e^+e^- \to Z$

[1] Assumes the fraction of $B_s^{(*)}\overline{B}_s^{(*)}$ in $b\overline{b}$ events is $f_s = (17.2 \pm 3.0)\%$.

[2] Assumes $\Upsilon(5S) \to B_s^*\overline{B}_s^* = (19.5^{+3.0}_{-2.3})\%$.

[3] ACCIARRI 95I assumes $f_{B^0} = 39.5 \pm 4.0$ and $f_{B_s} = (12.0 \pm 3.0)\%$.

$\Gamma(\phi\gamma)/\Gamma_{total}$ — Γ_{141}/Γ

VALUE (units 10^{-6})	CL%	DOCUMENT ID		TECN	COMMENT
34 ± 4 OUR AVERAGE					
36 ± 5 ± 7		[1] DUTTA	15	BELL	$e^+e^- \to \Upsilon(5S)$
33.8± 3.4± 2.0		[2] AAIJ	13	LHCB	pp at 7 TeV
• • • We do not use the following data for averages, fits, limits, etc. • • •					
39 ± 5		[3] AAIJ	12AE	LHCB	Repl. by AAIJ 13
$57^{+18}_{-15}{}^{+12}_{-11}$		[4] WICHT	08A	BELL	Repl. by DUTTA 15
<390	90	DRUTSKOY	07A	BELL	$e^+e^- \to \Upsilon(5S)$
<120	90	ACOSTA	02G	CDF	$p\overline{p}$ at 1.8 TeV
<700	90	[5] ADAM	96D	DLPH	$e^+e^- \to Z$

[1] Assumes the fraction of $B_s^{(*)}\overline{B}_s^{(*)}$ in $b\overline{b}$ events is $f_s = (17.2 \pm 3.0)\%$. The systematic uncertainty from f_s is 0.6×10^{-5}.

[2] AAIJ 13 reports $[\Gamma(B^0_s \to \phi\gamma)/\Gamma_{total}]$ / $[B(B^0 \to K^*(892)^0\gamma)] = 0.81 \pm 0.04 \pm 0.07$ which we multiply by our best value $B(B^0 \to K^*(892)^0\gamma) = (4.18 \pm 0.25) \times 10^{-5}$. Our first error is their experiment's error and our second error is the systematic error from using our best value.

[3] Measures $B(B^0 \to K^{*0}\gamma)/B(B_s \to \phi\gamma) = 1.12 \pm 0.08(\text{stat})^{+0.06}_{-0.04}(\text{sys})^{+0.09}_{-0.08}(f_s/f_d)$ and uses current world-average value of $B(B^0 \to K^{*0}\gamma) = (4.33 \pm 0.15) \times 10^{-5}$.

[4] Assumes $\Upsilon(5S) \to B_s^*\overline{B}_s^* = (19.5^{+3.0}_{-2.3})\%$.

[5] ADAM 96D assumes $f_{B^0} = f_{B^-} = 0.39$ and $f_{B_s} = 0.12$.

$\Gamma(\mu^+\mu^-)/\Gamma_{total}$ — Γ_{142}/Γ

Test for $\Delta B = 1$ weak neutral current.

VALUE (units 10^{-9})	CL%	DOCUMENT ID		TECN	COMMENT
3.01±0.35 OUR AVERAGE					
$3.09^{+0.46+0.15}_{-0.43-0.11}$		AAIJ	22	LHCB	pp at 7, 8, 13 TeV
2.9 ±0.6 ±0.4		[1] SIRUNYAN	20AG	CMS	pp at 7, 8, 13 TeV
$2.8^{+0.8}_{-0.7}$		[2] AABOUD	19L	ATLS	pp at 7, 8, 13 TeV
13^{+9}_{-7}		[3] AALTONEN	13F	CDF	$p\overline{p}$ at 1.96 TeV
• • • We do not use the following data for averages, fits, limits, etc. • • •					
$3.0 \pm 0.6^{+0.3}_{-0.2}$		AAIJ	17AI	LHCB	Repl. by AAIJ 22
$0.9^{+1.1}_{-0.8}$		[4] AABOUD	16L	ATLS	Repl. by AABOUD 19L
$2.8^{+0.7}_{-0.6}$		[5] KHACHATRY...	15BE	LHC	pp at 7, 8 TeV
$3.2^{+1.4}_{-1.2}{}^{+0.5}_{-0.3}$		[6] AAIJ	13B	LHCB	Repl. by AAIJ 13BA
$2.9^{+1.1}_{-1.0}{}^{+0.3}_{-0.1}$		[7] AAIJ	13BA	LHCB	Repl. by KHACHATRYAN 15BE
<12	90	[8] ABAZOV	13C	D0	$p\overline{p}$ at 1.96 TeV
$3.0^{+1.0}_{-0.9}$		[9] CHATRCHYAN	13AW	CMS	Repl. by SIRUNYAN 20AG
<19	90	[10] AAD	12AE	ATLS	pp at 7 TeV
<12	90	[11] AAIJ	12A	LHCB	Repl. by AAIJ 12W
< 3.8	90	[12] AAIJ	12W	LHCB	Repl. by AAIJ 13B
< 6.4	90	[13] CHATRCHYAN	12A	CMS	pp at 7 TeV
<43	90	[14] AAIJ	11B	LHCB	Repl. by AAIJ 12A
<35	90	[15] AALTONEN	11AG	CDF	$p\overline{p}$ at 1.96 TeV
<16	90	[16] CHATRCHYAN	11T	CMS	Repl. by CHATRCHYAN 12A
<42	90	[17] ABAZOV	10S	D0	$p\overline{p}$ at 1.96 TeV

[1] Uses normalization mode $B(B^+ \to J/\psi K^+) = (1.01 \pm 0.03) \times 10^{-3}$ and B production ratio $f(b \to B^0_s)/f(b \to B^+) = 0.252 \pm 0.012 \pm 0.015$.

[2] Uses normalization mode $B(B^+ \to J/\psi K^+) = (1.010 \pm 0.029) \times 10^{-3}$ and B production ratio $f(b \to B^0_s)/f(b \to B^0) = 0.256 \pm 0.013$.

[3] Uses normalization mode $B(B^+ \to J/\psi K^+) = (10.22 \pm 0.35) \times 10^{-4}$ and B production ratio $f(\overline{b} \to B^0_s)/f(\overline{b} \to B^0_d) = 0.28 \pm 0.04$.

[4] This value corresponds to an upper limit of $< 3.0 \times 10^{-9}$ at 95% C.L. It uses $f_s/f_d = 0.24 \pm 0.02$.

[5] Determined from the joint fit to CMS and LHCb data. Uncertainty includes both statistical and systematic component.

Downloaded from https://academic.oup.com/ptep/article/2022/8/083C01/6651666 by KIT Library user on 27 September 2022

[6] Uses B production ratio $f(\overline{b} \to B_s^0)/f(\overline{b} \to B_d^0) = 0.256 \pm 0.020$ and two normalization modes: $B(B^+ \to J/\psi K^+ \to \mu^+\mu^- K^+) = (6.01 \pm 0.21) \times 10^{-5}$ and $B(B^0 \to K^+\pi^-) = (1.94 \pm 0.06) \times 10^{-5}$.

[7] Uses B production ratio $f(\overline{b} \to B_s^0)/f(\overline{b} \to B_d^0) = 0.259 \pm 0.015$ and normalization modes $B^+ \to J/\psi K^+ \to \mu^+\mu^- K^+$ and $B^0 \to K^+\pi^-$.

[8] Uses normalization mode $B(B^+ \to J/\psi K^+ \to \mu^+\mu^- K^+) = (6.01 \pm 0.21) \times 10^{-5}$ and B production ratio $f(\overline{b} \to B_s^0)/f(\overline{b} \to B_d^0) = 0.263 \pm 0.017$.

[9] Uses B production ratio $f(\overline{b} \to B_s^0)/f(\overline{b} \to B_d^0) = 0.256 \pm 0.020$ and $B(B^+ \to J/\psi K^+ \to \mu^+\mu^- K^+) = (6.0 \pm 0.2) \times 10^{-5}$ for normalization.

[10] Uses B production ratio $f(\overline{b} \to B^+)/f(\overline{b} \to B_s^0) = 3.75 \pm 0.29$ and $B(B^+ \to J/\psi K^+ \to \mu^+\mu^- K^+) = (6.0 \pm 0.2) \times 10^{-5}$.

[11] Uses B production ratio $f(\overline{b} \to B_s^0)/f(\overline{b} \to B_d^0) = 0.267^{+0.021}_{-0.020}$ and three normalization modes $B(B^+ \to J/\psi K^+ \to \mu^+\mu^- K^+) = (6.01 \pm 0.21) \times 10^{-5}$, $B(B^0 \to K^+\pi^-) = (1.94 \pm 0.06) \times 10^{-5}$, and $B(B_s^0 \to J/\psi\phi \to \mu^+\mu^- K^+K^-) = (3.4 \pm 0.9) \times 10^{-5}$.

[12] Uses B production ratio $f(\overline{b} \to B_s^0)/f(\overline{b} \to B_d^0) = 0.267^{+0.021}_{-0.020}$ and three normalization modes of $B^+ \to J/\psi K^+$, $B^0 \to K^+\pi^-$, and $B_s^0 \to J/\psi\phi$.

[13] Uses $f_s/f_u = 0.267 \pm 0.021$ and $B(B^+ \to J/\psi K^+ \to \mu^+\mu^- K^+) = (6.0 \pm 0.2) \times 10^{-5}$.

[14] Uses B production ratio $f(\overline{b} \to B^+)/f(\overline{b} \to B_s^0) = 3.71 \pm 0.47$ and three normalization modes.

[15] Uses B production ratio $f(\overline{b} \to B^+)/f(\overline{b} \to B_s^0) = 3.55 \pm 0.47$ and $B(B^+ \to J/\psi K^+ \to \mu^+\mu^- K^+) = (6.01 \pm 0.21) \times 10^{-5}$.

[16] Uses B production ratio $f(\overline{b} \to B^+)/f(\overline{b} \to B_s^0) = 3.55 \pm 0.42$ and $B(B^+ \to J/\psi K^+ \to \mu^+\mu^- K^+) = (6.0 \pm 0.2) \times 10^{-5}$.

[17] Uses B production ratio $f(\overline{b} \to B^+)/f(\overline{b} \to B_s^0) = 3.86 \pm 0.59$, and the number of $B^+ \to J/\psi K^+$ decays.

$\Gamma(e^+e^-)/\Gamma_{total}$ — Γ_{143}/Γ

Test for $\Delta B = 1$ weak neutral current.

VALUE	CL%	DOCUMENT ID		TECN	COMMENT
$<9.4 \times 10^{-9}$	90	[1] AAIJ	20W	LHCB	pp at 7, 8, 13 TeV
• • • We do not use the following data for averages, fits, limits, etc. • • •					
$<2.8 \times 10^{-7}$	90	AALTONEN	09P	CDF	$p\overline{p}$ at 1.96 TeV
$<5.4 \times 10^{-5}$	90	[2] ACCIARRI	97B	L3	$e^+e^- \to Z$

[1] Assumes no contribution from $B^0 \to e^+e^-$ decays.

[2] ACCIARRI 97B assume PDG 96 production fractions for B^+, B^0, B_s, and Λ_b.

$\Gamma(\tau^+\tau^-)/\Gamma_{total}$ — Γ_{144}/Γ

VALUE	CL%	DOCUMENT ID		TECN	COMMENT
$<6.8 \times 10^{-3}$	95	[1] AAIJ	17AJ	LHCB	pp at 7, 8 TeV

[1] Assuming no contribution from $B^0 \to \tau^+\tau^-$.

$\Gamma(\mu^+\mu^-\mu^+\mu^-)/\Gamma_{total}$ — Γ_{145}/Γ

VALUE	CL%	DOCUMENT ID		TECN	COMMENT
$<2.5 \times 10^{-9}$	95	AAIJ	17N	LHCB	pp at 7, 8 TeV
• • • We do not use the following data for averages, fits, limits, etc. • • •					
$<1.2 \times 10^{-8}$	90	[1] AAIJ	13AW	LHCB	Repl. by AAIJ 17N

[1] Also reports a limit of $< 1.6 \times 10^{-8}$ at 95% CL.

$\Gamma(SP,\ S \to \mu^+\mu^-,\ P \to \mu^+\mu^-)/\Gamma_{total}$ — Γ_{146}/Γ

Here S and P are the hypothetical scalar and pseudoscalar particles with masses of 2.5 GeV/c^2 and 214.3 MeV/c^2, respectively.

VALUE	CL%	DOCUMENT ID		TECN	COMMENT
$<2.2 \times 10^{-9}$	95	AAIJ	17N	LHCB	pp at 7, 8 TeV
• • • We do not use the following data for averages, fits, limits, etc. • • •					
$<1.2 \times 10^{-8}$	90	[1] AAIJ	13AW	LHCB	Repl. by AAIJ 17N

[1] Also reports a limit of $< 1.6 \times 10^{-8}$ at 95% CL.

$\Gamma(\phi(1020)\mu^+\mu^-)/\Gamma_{total}$ — Γ_{147}/Γ

Test for $\Delta B = 1$ weak neutral current.

VALUE (units 10^{-7})	CL%	DOCUMENT ID		TECN	COMMENT
• • • We do not use the following data for averages, fits, limits, etc. • • •					
<32	90	[1] ABAZOV	06G	D0	$p\overline{p}$ at 1.96 TeV
$< 4.7 \times 10^2$	90	ACOSTA	02D	CDF	$p\overline{p}$ at 1.8 TeV

[1] Uses $B(B_s^0 \to J/\psi\phi) = 9.3 \times 10^{-4}$.

$\Gamma(\phi(1020)\mu^+\mu^-)/\Gamma(J/\psi(1S)\phi)$ — Γ_{147}/Γ_{56}

VALUE (units 10^{-3})	CL%	DOCUMENT ID		TECN	COMMENT
0.806±0.026 OUR AVERAGE					
$0.800 \pm 0.021 \pm 0.016$		AAIJ	21AG	LHCB	pp at 7, 8, 13 TeV
$1.13 \pm 0.19 \pm 0.07$		AALTONEN	11AI	CDF	$p\overline{p}$ at 1.96 TeV
• • • We do not use the following data for averages, fits, limits, etc. • • •					
$0.741^{+0.042}_{-0.040} \pm 0.029$		AAIJ	15AQ	LHCB	Repl. by AAIJ 21AG
$0.674^{+0.061}_{-0.056} \pm 0.016$		AAIJ	13X	LHCB	Repl. by AAIJ 15AQ
$1.11 \pm 0.25 \pm 0.09$		AALTONEN	11L	CDF	Repl. by AALTONEN 11AI
< 2.3	90	AALTONEN	09B	CDF	Repl. by AALTONEN 11L

$\Gamma(\overline{K}^*(892)^0\mu^+\mu^-)/\Gamma_{total}$ — Γ_{149}/Γ

VALUE (units 10^{-8})	DOCUMENT ID		TECN	COMMENT
2.9±1.0±0.4	[1] AAIJ	18AB	LHCB	pp at 7, 8, 13 TeV

[1] Normalizes to $B(B^0 \to J/\psi K^{*0}) = 1.19 \pm 0.01 \pm 0.08\%$ and $B(J/\psi \to \mu^+\mu^-) = 5.96 \pm 0.03\%$, and uses $f_s/f_d = 0.259 \pm 0.015$.

$\Gamma(f_2'(1525)\mu^+\mu^-)/\Gamma(J/\psi(1S)\phi)$ — Γ_{148}/Γ_{56}

VALUE (units 10^{-4})	DOCUMENT ID		TECN	COMMENT
1.55±0.19±0.08	[1] AAIJ	21AG	LHCB	pp at 7, 8, 13 TeV

[1] Measured by combining the q^2 regions [0.1, 0.98], [1.1, 8.0], and [11.0, 12.5] GeV^2/c^4.

$\Gamma(\pi^+\pi^-\mu^+\mu^-)/\Gamma_{total}$ — Γ_{150}/Γ

VALUE (units 10^{-8})	DOCUMENT ID		TECN	COMMENT
8.4±1.6±0.3	[1] AAIJ	15S	LHCB	pp at 7, 8 TeV

[1] AAIJ 15S reports $(8.6 \pm 1.5 \pm 0.7 \pm 0.7) \times 10^{-8}$ from a measurement of $[\Gamma(B_s^0 \to \pi^+\pi^-\mu^+\mu^-)/\Gamma_{total}]$ / $[B(B^0 \to J/\psi(1S)K^*(892)^0)]$ assuming $B(B^0 \to J/\psi(1S)K^*(892)^0) = (1.3 \pm 0.1) \times 10^{-3}$, which we rescale to our best value $B(B^0 \to J/\psi(1S)K^*(892)^0) = (1.27 \pm 0.05) \times 10^{-3}$. Our first error is their experiment's error and our second error is the systematic error from using our best value.

$\Gamma(\phi\nu\overline{\nu})/\Gamma_{total}$ — Γ_{151}/Γ

Test for $\Delta B = 1$ weak neutral current.

VALUE	CL%	DOCUMENT ID		TECN	COMMENT
$<5.4 \times 10^{-3}$	90	[1] ADAM	96D	DLPH	$e^+e^- \to Z$

[1] ADAM 96D assumes $f_{B^0} = f_{B^-} = 0.39$ and $f_{B_s} = 0.12$.

$\Gamma(e^\pm\mu^\mp)/\Gamma_{total}$ — Γ_{152}/Γ

Test of lepton family number conservation.

VALUE	CL%	DOCUMENT ID		TECN	COMMENT
$<5.4 \times 10^{-9}$	90	[1] AAIJ	18T	LHCB	pp at 7, 8 TeV
• • • We do not use the following data for averages, fits, limits, etc. • • •					
$<1.1 \times 10^{-8}$	90	[2] AAIJ	13BM	LHCB	Repl. by AAIJ 18T
$<2.0 \times 10^{-7}$	90	AALTONEN	09P	CDF	$p\overline{p}$ at 1.96 TeV
$<6.1 \times 10^{-6}$	90	ABE	98V	CDF	Repl. by AALTONEN 09P
$<4.1 \times 10^{-5}$	90	[3] ACCIARRI	97B	L3	$e^+e^- \to Z$

[1] AAIJ 18T uses normalization modes $B(B^0 \to K^+\pi^-) = (19.6 \pm 0.5) \times 10^{-6}$ and $B(B^+ \to J/\psi K^+) = (1.026 \pm 0.031) \times 10^{-3}$ with B production ratio $f(\overline{b} \to B_s^0)/f(\overline{b} \to B_d^0) = 0.259 \pm 0.015$. The upper limit increases to 6×10^{-9} with the assumption of B_L-dominated decay amplitude.

[2] Uses normalization mode $B(B^0 \to K^+\pi^-) = (19.4 \pm 0.6) \times 10^{-6}$ and B production ratio $f(\overline{b} \to B_s^0)/f(\overline{b} \to B_d^0) = 0.256 \pm 0.020$.

[3] ACCIARRI 97B assume PDG 96 production fractions for B^+, B^0, B_s, and Λ_b.

$\Gamma(\mu^\pm\tau^\mp)/\Gamma_{total}$ — Γ_{153}/Γ

VALUE	CL%	DOCUMENT ID		TECN	COMMENT
$<4.2 \times 10^{-5}$	95	[1] AAIJ	19AK	LHCB	pp at 7, 8 TeV

[1] Assuming no contribution from $B^0 \to \mu^\pm\tau^\mp$.

POLARIZATION IN B_s^0 DECAY

In decays involving two vector mesons, one can distinguish among the states in which meson polarizations are both longitudinal (L), or both are transverse and parallel ($\|$), or perpendicular ($\perp$) to each other with the parameters Γ_L/Γ, $\Gamma_\perp/\Gamma$, and the relative phases $\phi_\|$ and $\phi_\perp$. In decays involving two tensor mesons, the transverse polarization states are described by parameters $\Gamma_{\|1}$, $\Gamma_{\|2}$, $\Gamma_{\perp 1}$, $\Gamma_{\perp 2}$ and their relative phases $\phi_{\|1}$, $\phi_{\|2}$, $\phi_{\perp 1}$, $\phi_{\perp 2}$. See also the review on "Polarization in B Decays."

Γ_L/Γ in $B_s^0 \to D_s^*\rho^+$

VALUE	DOCUMENT ID		TECN	COMMENT
$1.05^{+0.08}_{-0.10}{}^{+0.03}_{-0.04}$	LOUVOT	10	BELL	$e^+e^- \to \Upsilon(5S)$

Γ_L/Γ in $B_s^0 \to J/\psi(1S)\phi$

VALUE	DOCUMENT ID		TECN	COMMENT
0.5196±0.0034 OUR AVERAGE Error includes scale factor of 1.5. See the ideogram below.				
$0.5152 \pm 0.0012 \pm 0.0034$	[1] AAD	21AE	ATLS	pp at 7, 8, 13 TeV
$0.5289 \pm 0.0038 \pm 0.0041$	[2] SIRUNYAN	21E	CMS	pp at 8, 13 TeV
$0.5186 \pm 0.0029 \pm 0.0023$	AAIJ	19Q	LHCB	pp at 13 TeV
$0.524 \pm 0.013 \pm 0.015$	[2] AALTONEN	12D	CDF	$p\overline{p}$ at 1.96 TeV
$0.558\ ^{+0.017}_{-0.019}$	[2,3] ABAZOV	12D	D0	$p\overline{p}$ at 1.96 TeV
$0.61 \pm 0.14 \pm 0.02$	[4] AFFOLDER	00N	CDF	$p\overline{p}$ at 1.8 TeV
$0.56 \pm 0.21\ ^{+0.02}_{-0.04}$	ABE	95Z	CDF	$p\overline{p}$ at 1.8 TeV

Downloaded from https://academic.oup.com/ptep/article/2022/8/083C01/6651666 by KIT Library user on 27 September 2022

• • • We do not use the following data for averages, fits, limits, etc. • • •

$0.5350 \pm 0.0047 \pm 0.0049$	[2] SIRUNYAN	21E	CMS	pp at 13 TeV
$0.522 \pm 0.003 \pm 0.007$	[1] AAD	16AP	ATLS	Repl. by AAD 21AE
$0.510 \pm 0.005 \pm 0.011$	[2] KHACHATRY...	16S	CMS	pp at 8 TeV
$0.5241 \pm 0.0034 \pm 0.0067$	AAIJ	15I	LHCB	Repl. by AAIJ 19Q
$0.529 \pm 0.006 \pm 0.012$	[1] AAD	14U	ATLS	Repl. by AAD 16AP
$0.539 \pm 0.014 \pm 0.016$	[2] AAD	12CV	ATLS	Repl. by AAD 14U
$0.555 \pm 0.027 \pm 0.006$	[5] ABAZOV	09E	D0	Repl. by ABAZOV 12D
$0.531 \pm 0.020 \pm 0.007$	[2] AALTONEN	08J	CDF	Repl. by AALTONEN 12D
$0.62 \pm 0.06 \pm 0.01$	ACOSTA	05	CDF	Repl. by AALTONEN 08J

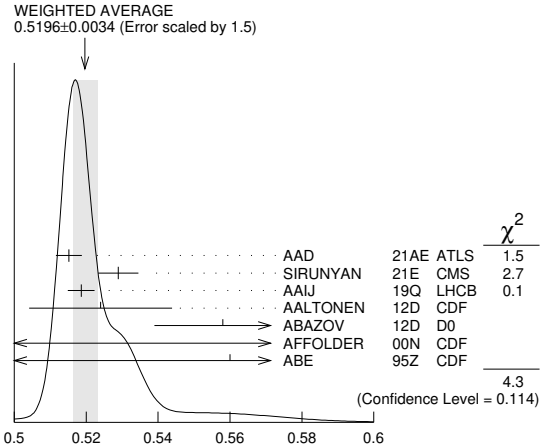

Γ_L/Γ in $B_s^0 \to J/\psi(1S)\phi$

[1] Measured using the flavor tagged, time-dependent angular analysis of $B_s^0 \to J/\psi\phi$ decays.

[2] Measured using the time-dependent angular analysis of $B_s^0 \to J/\psi\phi$ decays.

[3] The error includes both statistical and systematic uncertainties.

[4] AFFOLDER 00N measurements are based on 40 B_s^0 candidates obtained from a data sample of 89 pb^{-1}. The P-wave fraction is found to be $0.23 \pm 0.19 \pm 0.04$.

[5] Measured the angular and lifetime parameters for the time-dependent angular untagged decays $B_d^0 \to J/\psi K^{*0}$ and $B_s^0 \to J/\psi\phi$.

Γ_L/Γ in $B_s^0 \to D_s^{*+} D_s^{*-}$

VALUE	DOCUMENT ID		TECN	COMMENT
$0.06^{+0.18}_{-0.17} \pm 0.03$	ESEN	13	BELL	$e^+e^- \to \Upsilon(5S)$

$\Gamma_\parallel/\Gamma$ in $B_s^0 \to J/\psi(1S)\phi$

VALUE	DOCUMENT ID		TECN	COMMENT
0.2222±0.0027 OUR AVERAGE				
$0.2220 \pm 0.0017 \pm 0.0021$	[1] AAD	21AE	ATLS	pp at 7, 8, 13 TeV
$0.231 \pm 0.014 \pm 0.015$	[2] AALTONEN	12D	CDF	$p\overline{p}$ at 1.96 TeV
$0.231 {}^{+0.024}_{-0.030}$	[2,3] ABAZOV	12D	D0	$p\overline{p}$ at 1.96 TeV
• • • We do not use the following data for averages, fits, limits, etc. • • •				
$0.227 \pm 0.004 \pm 0.006$	[1] AAD	16AP	ATLS	Repl. by AAD 21AE
$0.220 \pm 0.008 \pm 0.009$	[1] AAD	14U	ATLS	Repl. by AAD 16AP
$0.224 \pm 0.010 \pm 0.009$	[2] AAD	12CV	ATLS	Repl. by AAD 14U
$0.244 \pm 0.032 \pm 0.014$	[4] ABAZOV	09E	D0	Repl. by ABAZOV 12D
$0.230 \pm 0.029 \pm 0.011$	[2] AALTONEN	08J	CDF	Repl. by AALTONEN 12D
$0.260 \pm 0.084 \pm 0.013$	ACOSTA	05	CDF	Repl. by AALTONEN 08J

[1] Measured using a tagged, time-dependent angular analysis of $B_s^0 \to J/\psi\phi$ decays.

[2] Measured using the time-dependent angular analysis of $B_s^0 \to J/\psi\phi$ decays.

[3] The error includes both statistical and systematic uncertainties.

[4] Measured the angular and lifetime parameters for the time-dependent angular untagged decays $B_d^0 \to J/\psi K^{*0}$ and $B_s^0 \to J/\psi\phi$.

$\Gamma_\perp/\Gamma$ in $B_s^0 \to J/\psi(1S)\phi$

VALUE	DOCUMENT ID		TECN	COMMENT
0.243 ±0.004 OUR AVERAGE				
$0.2393 \pm 0.0050 \pm 0.0037$	SIRUNYAN	21E	CMS	pp at 8, 13 TeV
$0.2456 \pm 0.0040 \pm 0.0019$	AAIJ	19Q	LHCB	pp at 13 TeV
• • • We do not use the following data for averages, fits, limits, etc. • • •				
$0.2337 \pm 0.0063 \pm 0.0045$	SIRUNYAN	21E	CMS	pp at 13 TeV
$0.243 \pm 0.008 \pm 0.012$	KHACHATRY...	16S	CMS	pp at 8 TeV
$0.2504 \pm 0.0049 \pm 0.0036$	AAIJ	15I	LHCB	Repl. by AAIJ 19Q

$\phi_\parallel$ in $B_s^0 \to J/\psi(1S)\phi$

VALUE (rad)	DOCUMENT ID		TECN	COMMENT
3.19±0.07 OUR AVERAGE Error includes scale factor of 1.3. See the ideogram below.				
$3.36 \pm 0.05 \pm 0.09$	[1] AAD	21AE	ATLS	pp at 7, 8, 13 TeV
$3.19 \pm 0.12 \pm 0.04$	SIRUNYAN	21E	CMS	pp at 8, 13 TeV
$3.06 {}^{+0.08}_{-0.07} \pm 0.04$	AAIJ	19Q	LHCB	pp at 13 TeV
3.15 ± 0.22	[2] ABAZOV	12D	D0	$p\overline{p}$ at 1.96 TeV
• • • We do not use the following data for averages, fits, limits, etc. • • •				
$3.18 \pm 0.12 \pm 0.003$	SIRUNYAN	21E	CMS	pp at 13 TeV
$3.15 \pm 0.10 \pm 0.05$	AAD	16AP	ATLS	Repl. by AAD 21AE
$3.48 {}^{+0.07}_{-0.09} \pm 0.68$	KHACHATRY...	16S	CMS	pp at 8 TeV
$3.26 {}^{+0.10}_{-0.17} {}^{+0.06}_{-0.07}$	AAIJ	15I	LHCB	Repl. by AAIJ 19Q
$2.72 {}^{+1.12}_{-0.27} \pm 0.26$	ABAZOV	09E	D0	Repl. by ABAZOV 12D

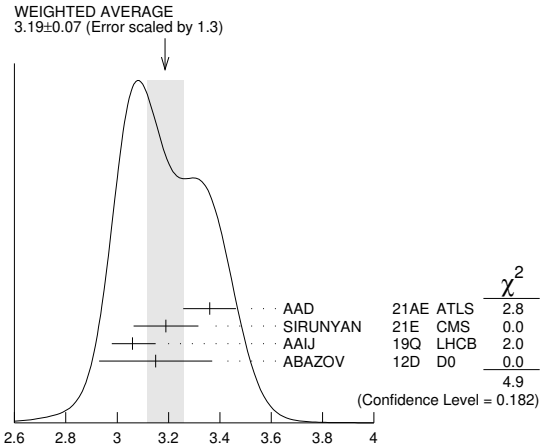

$\phi_\parallel$ in $B_s^0 \to J/\psi(1S)\phi$ (rad)

[1] The fit found another solution with $\phi_\parallel = 2.95 \pm 0.05 \pm 0.09$ rad.

[2] The error includes both statistical and systematic uncertainties.

$\phi_\perp$ in $B_s^0 \to J/\psi(1S)\phi$

VALUE (rad)	DOCUMENT ID		TECN	COMMENT
2.97±0.18 OUR AVERAGE Error includes scale factor of 2.3. See the ideogram below.				
$3.22 \pm 0.10 \pm 0.05$	[1] AAD	21AE	ATLS	pp at 7, 8, 13 TeV
$2.78 \pm 0.15 \pm 0.06$	[2] SIRUNYAN	21E	CMS	pp at 8, 13 TeV
$2.64 \pm 0.13 \pm 0.10$	AAIJ	19Q	LHCB	pp at 13 TeV
• • • We do not use the following data for averages, fits, limits, etc. • • •				
$2.77 \pm 0.16 \pm 0.05$	[2] SIRUNYAN	21E	CMS	pp at 13 TeV
$4.15 \pm 0.32 \pm 0.16$	[2] AAD	16AP	ATLS	Repl. by AAD 21AE
$2.98 \pm 0.36 \pm 0.66$	[2] KHACHATRY...	16S	CMS	pp at 8 TeV
$3.08 {}^{+0.14}_{-0.15} \pm 0.06$	AAIJ	15I	LHCB	Repl. by AAIJ 19Q
$3.89 \pm 0.47 \pm 0.11$	[2] AAD	14U	ATLS	Repl. by AAD 16AP

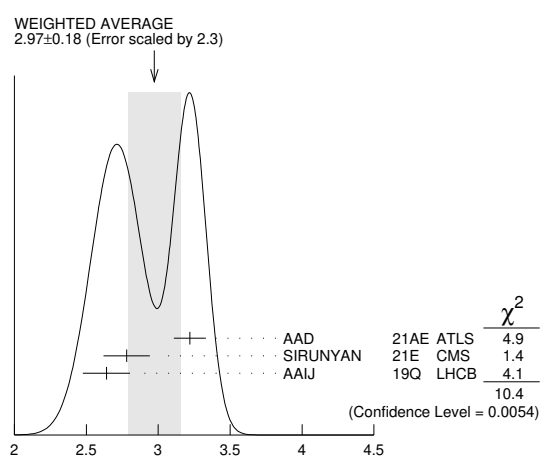

$\phi_\perp$ in $B_s^0 \to J/\psi(1S)\phi$ (rad)

[1] The fit found another solution with $\phi_\perp = 3.03 \pm 0.05 \pm 0.09$ rad.

[2] Measured using a tagged, time-dependent angular analysis of $B_s^0 \to J/\psi\phi$ decays.

Downloaded from https://academic.oup.com/ptep/article/2022/8/083C01/6651666 by KIT Library user on 27 September 2022

$\Gamma_\perp/\Gamma$ in $B_s^0 \to \psi(2S)\phi$

VALUE	DOCUMENT ID		TECN	COMMENT
$0.264^{+0.024}_{-0.023}\pm0.002$	[1] AAIJ	16AK	LHCB	pp at 7, 8 TeV

[1] Measured using time-dependent angular analysis of $B_s^0 \to \psi(2S)\phi$ decays.

$\phi_\parallel$ in $B_s^0 \to \psi(2S)\phi$

VALUE (rad)	DOCUMENT ID		TECN	COMMENT
$3.67^{+0.13}_{-0.18}\pm0.03$	[1] AAIJ	16AK	LHCB	pp at 7, 8 TeV

[1] Measured using time-dependent angular analysis of $B_s^0 \to \psi(2S)\phi$ decays.

$\phi_\perp$ in $B_s^0 \to \psi(2S)\phi$

VALUE (rad)	DOCUMENT ID		TECN	COMMENT
$3.29^{+0.43}_{-0.39}\pm0.04$	[1] AAIJ	16AK	LHCB	pp at 7, 8 TeV

[1] Measured using time-dependent angular analysis of $B_s^0 \to \psi(2S)\phi$ decays.

Γ_L/Γ for $B_s^0 \to J/\psi(1S)\overline{K}^*(892)^0$

Longitudinal polarization fraction, equals to f_L using notation of "Polarization in B decays" review.

VALUE	DOCUMENT ID		TECN	COMMENT
$0.497\pm0.025\pm0.025$	AAIJ	15AV	LHCB	pp at 7, 8 TeV
• • • We do not use the following data for averages, fits, limits, etc. • • •				
$0.50\ \pm0.08\ \pm0.02$	[1] AAIJ	12AP	LHCB	Repl. by AAIJ 15AV

[1] The non-resonant $K\pi$ background contributions are subtracted. Also reports an S-wave amplitude $|A_S|^2 = 0.07^{+0.15}_{-0.07}$.

$\Gamma_\parallel/\Gamma$ for $B_s^0 \to J/\psi(1S)\overline{K}^*(892)^0$

Parallel polarization fraction, equals to $1 - f_L - f_\perp$ using notation of "Polarization in B decays" review.

VALUE	DOCUMENT ID		TECN	COMMENT
$0.179\pm0.027\pm0.013$	AAIJ	15AV	LHCB	pp at 7, 8 TeV
• • • We do not use the following data for averages, fits, limits, etc. • • •				
$0.19\ ^{+0.10}_{-0.08}\ \pm0.02$	[1] AAIJ	12AP	LHCB	Repl. by AAIJ 15AV

[1] The non-resonant $K\pi$ background contributions are subtracted. Also reports an S-wave amplitude $|A_S|^2 = 0.07^{+0.15}_{-0.07}$.

$\Gamma_\parallel/\Gamma$ of $K^*(892)^0$ in $B_s^0 \to \psi(2S)\overline{K}^*(892)^0$

VALUE	DOCUMENT ID		TECN	COMMENT
$0.524\pm0.056\pm0.029$	AAIJ	15U	LHCB	pp at 7, 8 TeV

Γ_L/Γ in $B_s^0 \to \phi\phi$

VALUE	DOCUMENT ID		TECN	COMMENT
0.378 ± 0.013 OUR AVERAGE				
$0.381\pm0.007\pm0.012$	AAIJ	19AP	LHCB	pp at 7, 8 and 13 TeV
$0.348\pm0.041\pm0.021$	AALTONEN	11AN	CDF	$p\overline{p}$ at 1.96 TeV
• • • We do not use the following data for averages, fits, limits, etc. • • •				
$0.364\pm0.012\pm0.009$	AAIJ	14AE	LHCB	Repl. by AAIJ 19AP
$0.365\pm0.022\pm0.012$	AAIJ	12P	LHCB	Repl. by AAIJ 14AE

$\Gamma_\perp/\Gamma$ in $B_s^0 \to \phi\phi$

VALUE	DOCUMENT ID		TECN	COMMENT
0.292 ± 0.009 OUR AVERAGE				
$0.290\pm0.008\pm0.005$	[1] AAIJ	19AP	LHCB	pp at 7, 8 and 13 TeV
$0.365\pm0.044\pm0.027$	AALTONEN	11AN	CDF	$p\overline{p}$ at 1.96 TeV
• • • We do not use the following data for averages, fits, limits, etc. • • •				
$0.305\pm0.013\pm0.005$	AAIJ	14AE	LHCB	Repl. by AAIJ 19AP
$0.291\pm0.024\pm0.010$	AAIJ	12P	LHCB	Repl. by AAIJ 14AE

[1] Note: in the summary of AAIJ 19AP the systematic uncertainty is 0.007. We take the systematic uncertainty as given in Table 5 in the paper.

$\phi_\parallel$ in $B_s^0 \to \phi\phi$

VALUE (rad)	DOCUMENT ID		TECN	COMMENT
$2.56\ \pm0.06$ OUR AVERAGE				
$2.559\pm0.045\pm0.033$	AAIJ	19AP	LHCB	pp at 7, 8 and 13 TeV
$2.71\ ^{+0.31}_{-0.36}\ \pm0.22$	[1] AALTONEN	11AN	CDF	$p\overline{p}$ at 1.96 TeV
• • • We do not use the following data for averages, fits, limits, etc. • • •				
$2.54\ \pm0.07\ \pm0.09$	[2] AAIJ	14AE	LHCB	Repl. by AAIJ 19AP
$2.57\ \pm0.15\ \pm0.06$	[3] AAIJ	12P	LHCB	Repl. by AAIJ 14AE

[1] AALTONEN 11AN quotes $\cos\phi_\parallel = -0.91^{+0.15}_{-0.13} \pm 0.09$ which we convert to $\phi_\parallel$ taking the smaller solution.
[2] AAIJ 14AE reports measurement of $\phi_\perp$ and $\phi_\perp - \phi_\parallel$, which we convert into $\phi_\parallel$. Statistical uncertainty includes correlation between measured parameters, while systematic uncertainties are assumed uncorrelated.
[3] AAIJ 12P quotes $\cos\phi_\parallel = -0.844 \pm 0.068 \pm 0.029$ which we convert to $\phi_\parallel$, taking the smaller solution.

$\phi_\perp$ in $B_s^0 \to \phi\phi$

VALUE (rad)	DOCUMENT ID		TECN	COMMENT
$2.818\pm0.178\pm0.073$	AAIJ	19AP	LHCB	pp at 7, 8 and 13 TeV
• • • We do not use the following data for averages, fits, limits, etc. • • •				
$2.67\ \pm0.23\ \pm0.07$	AAIJ	14AE	LHCB	Repl. by AAIJ 19AP

Γ_L/Γ in $B_s^0 \to K^{*0}\overline{K}^{*0}$

VALUE	DOCUMENT ID		TECN	COMMENT
$0.240\pm0.031\pm0.025$	[1] AAIJ	19L	LHCB	pp at 7 and 8 TeV
• • • We do not use the following data for averages, fits, limits, etc. • • •				
$0.208\pm0.032\pm0.046$	[2] AAIJ	18S	LHCB	Repl. by AAIJ 19L
$0.201\pm0.057\pm0.040$	[3] AAIJ	15AF	LHCB	Repl. by AAIJ 18S
$0.31\ \pm0.12\ \pm0.04$	AAIJ	12F	LHCB	Repl. by AAIJ 15AF

[1] Untagged and time-integrated analysis within 150 MeV of the K^{*0} mass.
[2] Measured in angular analysis, which takes into account S-, P- and D-wave. contributions.
[3] Measured in angular analysis, which takes into account S-wave contributions.

$\Gamma_\perp/\Gamma$ in $B_s^0 \to K^{*0}\overline{K}^{*0}$

VALUE	DOCUMENT ID		TECN	COMMENT
$0.38\pm0.11\pm0.04$	AAIJ	12F	LHCB	pp at 7 TeV

$\Gamma_\parallel/\Gamma$ in $B_s^0 \to K^*(892)^0\overline{K}^*(892)^0$

VALUE	DOCUMENT ID		TECN	COMMENT
$0.297\pm0.029\pm0.042$	[1] AAIJ	18S	LHCB	pp at 7, 8 TeV
• • • We do not use the following data for averages, fits, limits, etc. • • •				
$0.215\pm0.046\pm0.015$	AAIJ	15AF	LHCB	Repl. by AAIJ 18S

[1] Measured in angular analysis, which takes into account S-, P- and D-wave. contributions.

$\Phi_\parallel$ in $B_s^0 \to K^*(892)^0\overline{K}^*(892)^0$

VALUE	DOCUMENT ID		TECN	COMMENT
$2.40\pm0.11\pm0.33$	[1] AAIJ	18S	LHCB	pp at 7, 8 TeV
• • • We do not use the following data for averages, fits, limits, etc. • • •				
$5.31\pm0.24\pm0.14$	AAIJ	15AF	LHCB	Repl. by AAIJ 18S

[1] Measured in angular analysis, which takes into account S-, P- and D-wave. contributions.

$\Phi_\perp$ in $B_s^0 \to K^*(892)^0\overline{K}^*(892)^0$

VALUE (rad)	DOCUMENT ID		TECN	COMMENT
$2.62\pm0.26\pm0.64$	[1] AAIJ	18S	LHCB	pp at 7, 8 TeV

[1] Measured in angular analysis, which takes into account S-, P- and D-wave. contributions.

Γ_L/Γ in $B_s^0 \to \phi\overline{K}^{*0}$

VALUE	DOCUMENT ID		TECN	COMMENT
$0.51\pm0.15\pm0.07$	AAIJ	13BW	LHCB	pp at 7 TeV

$\Gamma_\parallel/\Gamma$ in $B_s^0 \to \phi\overline{K}^{*0}$

VALUE	DOCUMENT ID		TECN	COMMENT
$0.21\pm0.11\pm0.02$	AAIJ	13BW	LHCB	pp at 7 TeV

$\phi_\parallel$ in $B_s^0 \to \phi\overline{K}^{*0}$

VALUE (rad)	DOCUMENT ID		TECN	COMMENT
$1.75\pm0.53\pm0.29$	[1] AAIJ	13BW	LHCB	pp at 7 TeV

[1] Measures $\cos(\phi_\parallel) = -0.18 \pm 0.52 \pm 0.29$, which we convert to $\phi_\parallel$ by taking the smaller solution.

Γ_L/Γ in $B_s^0 \to \overline{D}^{*0}\phi$

VALUE	DOCUMENT ID		TECN	COMMENT
$0.73\pm0.15\pm0.04$	AAIJ	18AY	LHCB	pp at 7 and 8 TeV

Γ_L/Γ in $B_s^0 \to K^*(892)^0\overline{K}_2^*(1430)^0$

VALUE	DOCUMENT ID		TECN	COMMENT
$0.911\pm0.020\pm0.165$	[1] AAIJ	18S	LHCB	pp at 7, 8 TeV

[1] Measured in angular analysis, which takes into account S-, P- and D-wave. contributions.

$\Gamma_\parallel/\Gamma$ in $B_s^0 \to K^*(892)^0\overline{K}_2^*(1430)^0$

VALUE	DOCUMENT ID		TECN	COMMENT
$0.012\pm0.008\pm0.053$	[1] AAIJ	18S	LHCB	pp at 7, 8 TeV

[1] Measured in angular analysis, which takes into account S-, P- and D-wave. contributions.

Γ_L/Γ in $B_s^0 \to K_2^*(1430)^0\overline{K}^*(892)^0$

VALUE	DOCUMENT ID		TECN	COMMENT
$0.62\pm0.16\pm0.25$	[1] AAIJ	18S	LHCB	pp at 7, 8 TeV

[1] Measured in angular analysis, which takes into account S-, P- and D-wave. contributions.

$\Gamma_\parallel/\Gamma$ in $B_s^0 \to K_2^*(1430)^0\overline{K}^*(892)^0$

VALUE	DOCUMENT ID		TECN	COMMENT
$0.24\pm0.10\pm0.14$	[1] AAIJ	18S	LHCB	pp at 7, 8 TeV

[1] Measured in angular analysis, which takes into account S-, P- and D-wave. contributions.

Γ_L/Γ in $B_s^0 \to K_2^*(1430)^0\overline{K}_2^*(1430)^0$

VALUE	DOCUMENT ID		TECN	COMMENT
$0.25\pm0.14\pm0.18$	[1] AAIJ	18S	LHCB	pp at 7, 8 TeV

[1] Measured in angular analysis, which takes into account S-, P- and D-wave. contributions.

$\Gamma_{\parallel 1}/\Gamma$ in $B_s^0 \to K_2^*(1430)^0\overline{K}_2^*(1430)^0$

VALUE	DOCUMENT ID		TECN	COMMENT
$0.17\pm0.11\pm0.14$	[1] AAIJ	18S	LHCB	pp at 7, 8 TeV

[1] Measured in angular analysis, which takes into account S-, P- and D-wave. contributions.

Downloaded from https://academic.oup.com/ptep/article/2022/8/083C01/6651666 by KIT Library user on 27 September 2022

$\Gamma_{\perp 1}/\Gamma$ in $B^0_s \to K^*_2(1430)^0 \overline{K}^*_2(1430)^0$

VALUE	DOCUMENT ID		TECN	COMMENT
0.30±0.18±0.21	[1] AAIJ	18S	LHCB	pp at 7, 8 TeV

[1] Measured in angular analysis, which takes into account S-, P- and D-wave. contributions.

$\Gamma_{\parallel 2}/\Gamma$ in $B^0_s \to K^*_2(1430)^0 \overline{K}^*_2(1430)^0$

VALUE	DOCUMENT ID		TECN	COMMENT
0.015±0.033±0.107	[1] AAIJ	18S	LHCB	pp at 7, 8 TeV

[1] Measured in angular analysis, which takes into account S-, P- and D-wave . contributions.

$F_L(B^0_s \to \phi\mu^+\mu^-)$ ($0.10 < q^2 < 2.00$ GeV$^2/c^4$)

VALUE	DOCUMENT ID		TECN	COMMENT
$0.20^{+0.08}_{-0.09}\pm0.02$	AAIJ	15AQ	LHCB	pp at 7, 8 TeV
• • • We do not use the following data for averages, fits, limits, etc. • • •				
$0.37^{+0.19}_{-0.17}\pm0.07$	AAIJ	13X	LHCB	Repl. by AAIJ 15AQ

$F_L(B^0_s \to \phi\mu^+\mu^-)$ ($2.00 < q^2 < 5.0$ GeV$^2/c^4$)

VALUE	DOCUMENT ID		TECN	COMMENT
$0.68^{+0.16}_{-0.13}\pm0.03$	AAIJ	15AQ	LHCB	pp at 7, 8 TeV
• • • We do not use the following data for averages, fits, limits, etc. • • •				
$0.53^{+0.25}_{-0.23}\pm0.10$	[1] AAIJ	13X	LHCB	Repl. by AAIJ 15AQ

[1] Measured in $2.0 < q^2 < 4.3$ GeV$^2/c^4$.

$F_L(B^0_s \to \phi\mu^+\mu^-)$ ($5.0 < q^2 < 8.0$ GeV$^2/c^4$)

VALUE	DOCUMENT ID		TECN	COMMENT
$0.54^{+0.10}_{-0.09}\pm0.02$	AAIJ	15AQ	LHCB	pp at 7, 8 TeV
• • • We do not use the following data for averages, fits, limits, etc. • • •				
$0.81^{+0.11}_{-0.13}\pm0.05$	[1] AAIJ	13X	LHCB	Repl. by AAIJ 15AQ

[1] Measured in $4.3 < q^2 < 8.68$ GeV$^2/c^4$.

$F_L(B^0_s \to \phi\mu^+\mu^-)$ ($11.0 < q^2 < 12.5$ GeV$^2/c^4$)

VALUE	DOCUMENT ID		TECN	COMMENT
0.29±0.11±0.04	AAIJ	15AQ	LHCB	pp at 7, 8 TeV
• • • We do not use the following data for averages, fits, limits, etc. • • •				
$0.33^{+0.14}_{-0.12}\pm0.06$	[1] AAIJ	13X	LHCB	Repl. by AAIJ 15AQ

[1] Measured in $10.09 < q^2 < 12.90$ GeV$^2/c^4$.

$F_L(B^0_s \to \phi\mu^+\mu^-)$ ($15.0 < q^2 < 17.0$ GeV$^2/c^4$)

VALUE	DOCUMENT ID		TECN	COMMENT
$0.23^{+0.09}_{-0.08}\pm0.02$	AAIJ	15AQ	LHCB	pp at 7, 8 TeV
• • • We do not use the following data for averages, fits, limits, etc. • • •				
$0.34^{+0.18}_{-0.17}\pm0.07$	[1] AAIJ	13X	LHCB	Repl. by AAIJ 15AQ

[1] Measured in $14.18 < q^2 < 16$ GeV$^2/c^4$.

$F_L(B^0_s \to \phi\mu^+\mu^-)$ ($17.0 < q^2 < 19.0$ GeV$^2/c^4$)

VALUE	DOCUMENT ID		TECN	COMMENT
$0.40^{+0.13}_{-0.15}\pm0.02$	AAIJ	15AQ	LHCB	pp at 7, 8 TeV
• • • We do not use the following data for averages, fits, limits, etc. • • •				
$0.16^{+0.17}_{-0.10}\pm0.07$	[1] AAIJ	13X	LHCB	Repl. by AAIJ 15AQ

[1] Measured in $16.0 < q^2 < 19.0$ GeV$^2/c^4$.

$F_L(B^0_s \to \phi\mu^+\mu^-)$ ($15.0 < q^2 < 18.9$ GeV$^2/c^4$)

VALUE	DOCUMENT ID		TECN	COMMENT
0.359±0.031±0.019	AAIJ	21AK	LHCB	pp at 7, 8, 13 TeV

$F_L(B^0_s \to \phi\mu^+\mu^-)$ ($1.00 < q^2 < 6.00$ GeV$^2/c^4$)

VALUE	DOCUMENT ID		TECN	COMMENT
0.715±0.036±0.013	AAIJ	21AK	LHCB	pp at 7, 8, 13 TeV
• • • We do not use the following data for averages, fits, limits, etc. • • •				
$0.63^{+0.09}_{-0.09}\pm0.03$	AAIJ	15AQ	LHCB	Repl. by AAIJ 21AK
$0.56^{+0.17}_{-0.16}\pm0.09$	AAIJ	13X	LHCB	Repl. by AAIJ 15AQ

B^0_s-$\overline{B}^0_s$ MIXING

For a discussion of B^0_s-$\overline{B}^0_s$ mixing see the note on "B^0-$\overline{B}^0$ Mixing" in the B^0 Particle Listings above.

χ_s is a measure of the time-integrated B^0_s-$\overline{B}^0_s$ mixing probability that produced $B^0_s(\overline{B}^0_s)$ decays as a $\overline{B}^0_s(B^0_s)$. Mixing violates $\Delta B \neq 2$ rule.

$$\chi_s = \frac{x_s^2}{2(1+x_s^2)}$$

$$x_s = \frac{\Delta m_{B^0_s}}{\Gamma_{B^0_s}} = (m_{B^0_{sH}} - m_{B^0_{sL}})\,\tau_{B^0_s}\,,$$

where H, L stand for heavy and light states of two B^0_s CP eigenstates and $\tau_{B^0_s} = \frac{1}{0.5(\Gamma_{B^0_{sH}}+\Gamma_{B^0_{sL}})}$.

$\Delta m_{B^0_s} = m_{B^0_{sH}} - m_{B^0_{sL}}$

$\Delta m_{B^0_s}$ is a measure of 2π times the B^0_s-$\overline{B}^0_s$ oscillation frequency in time-dependent mixing experiments.

"OUR EVALUATION" is provided by the Heavy Flavor Averaging Group (HFLAV, https://hflav.web.cern.ch/) by taking into account correlations between measurements.

VALUE ($10^{12}\,\hbar\,s^{-1}$)	CL%	DOCUMENT ID		TECN	COMMENT
17.765 ±0.006 OUR EVALUATION					
17.765 ±0.005 OUR AVERAGE					
17.7683±0.0051±0.0032		[1] AAIJ	22B	LHCB	pp at 13 TeV
17.757 ±0.007 ±0.008		[2] AAIJ	21M	LHCB	pp at 7, 8, 13 TeV
$17.51\ ^{+0.10}_{-0.09}\ \pm0.03$		[3] SIRUNYAN	21E	CMS	pp at 13 TeV
17.703 ±0.059 ±0.018		[4] AAIJ	19Q	LHCB	pp at 13 TeV
17.768 ±0.023 ±0.006		[1] AAIJ	13BI	LHCB	pp at 7 TeV
17.93 ±0.22 ±0.15		[5] AAIJ	13CF	LHCB	pp at 7 TeV
17.77 ±0.10 ±0.07		[6] ABULENCIA,A	06G	CDF	$p\overline{p}$ at 1.96 TeV
• • • We do not use the following data for averages, fits, limits, etc. • • •					
$17.711\ ^{+0.055}_{-0.057}\ \pm0.011$		[4] AAIJ	15I	LHCB	Repl. by AAIJ 19Q
17.63 ±0.11 ±0.02		[7] AAIJ	12I	LHCB	Repl. by AAIJ 21M
17–21	90	[8] ABAZOV	06B	D0	$p\overline{p}$ at 1.96 TeV
$17.31\ ^{+0.33}_{-0.18}\ \pm0.07$		[9] ABULENCIA	06Q	CDF	Repl. by ABULENCIA,A 06G
> 8.0	95	[10] ABDALLAH	04J	DLPH	$e^+e^- \to Z^0$
> 4.9	95	[11] ABDALLAH	04J	DLPH	$e^+e^- \to Z^0$
> 8.5	95	[12] ABDALLAH	04J	DLPH	$e^+e^- \to Z^0$
> 5.0	95	[13] ABDALLAH	03B	DLPH	$e^+e^- \to Z$
>10.3	95	[14] ABE	03	SLD	$e^+e^- \to Z$
>10.9	95	[15] HEISTER	03E	ALEP	$e^+e^- \to Z$
> 5.3	95	[16] ABE	02V	SLD	$e^+e^- \to Z$
> 1.0	95	[17] ABBIENDI	01D	OPAL	$e^+e^- \to Z$
> 7.4	95	[18] ABREU	00Y	DLPH	Repl. by ABDALLAH 04J
> 4.0	95	[19] ABREU,P	00G	DLPH	$e^+e^- \to Z$
> 5.2	95	[20] ABBIENDI	99S	OPAL	$e^+e^- \to Z$
<96	95	[21] ABE	99D	CDF	$p\overline{p}$ at 1.8 TeV
> 5.8	95	[22] ABE	99J	CDF	$p\overline{p}$ at 1.8 TeV
> 9.6	95	[23] BARATE	99J	ALEP	$e^+e^- \to Z$
> 7.9	95	[24] BARATE	98C	ALEP	Repl. by BARATE 99J
> 3.1	95	[25] ACKERSTAFF	97U	OPAL	Repl. by ABBIENDI 99S
> 2.2	95	[26] ACKERSTAFF	97V	OPAL	Repl. by ABBIENDI 99S
> 6.5	95	[27] ADAM	97	DLPH	Repl. by ABREU 00Y
> 6.6	95	[28] BUSKULIC	96M	ALEP	Repl. by BARATE 98C
> 2.2	95	[26] AKERS	95J	OPAL	Sup. by ACKERSTAFF 97V
> 5.7	95	[29] BUSKULIC	95J	ALEP	$e^+e^- \to Z$
> 1.8	95	[26] BUSKULIC	94B	ALEP	$e^+e^- \to Z$

[1] Measured using $B^0_s \to D^-_s\pi^+$ decays.
[2] Measured using $B^0_s \to D^-_s\pi^+\pi^-\pi^+$ decays.
[3] Measured using time-dependent angular analysis of $B^0_s \to J/\psi\phi$ decays.
[4] Measured using time-dependent angular analysis of $B^0_s \to J/\psi K^+K^-$ decays.
[5] Measured using $B^0_s \to D^-_s\mu^+\nu_\mu X$ decays.
[6] Significance of oscillation signal is 5.4 σ. Also reports $|V_{td}\ /\ V_{ts}| = 0.2060 \pm 0.0007\,^{+0.0081}_{-0.0060}$.
[7] Measured using $B^0_s \to D^-_s\pi^+$ and $D^-_s\pi^+\pi^-\pi^+$ decays.
[8] A likelihood scan over the oscillation frequency, Δm_s, gives a most probable value of 19 ps^{-1} and a range of $17 < \Delta m_s < 21$ (ps^{-1}) at 90% C.L. assuming Gaussian uncertainties. Also excludes $\Delta m_s < 14.8$ ps^{-1} at 95% C.L
[9] Significance of oscillation signal is 0.2%. Also reported the value $|V_{td}\ /\ V_{ts}| = 0.208\,^{+0.001}_{-0.002}\,^{+0.008}_{-0.006}$.
[10] Uses leptons emitted with large momentum transverse to a jet and improved techniques for vertexing and flavor-tagging.
[11] Updates of D_s-lepton analysis.
[12] Combined results from all Delphi analyses.

Downloaded from https://academic.oup.com/ptep/article/2022/8/083C01/6651666 by KIT Library user on 27 September 2022

[13] Events with a high transverse momentum lepton were removed and an inclusively reconstructed vertex was required.

[14] ABE 03 uses the novel "charge dipole" technique to reconstruct separate secondary and tertiary vertices originating from the $B \to D$ decay chain. The analysis excludes $\Delta m_s < 4.9\,\mathrm{ps}^{-1}$ and $7.9 < \Delta m_s < 10.3\,\mathrm{ps}^{-1}$.

[15] Three analyses based on complementary event selections: (1) fully-reconstructed hadronic decays; (2) semileptonic decays with D_s exclusively reconstructed; (3) inclusive semileptonic decays.

[16] ABE 02V uses exclusively reconstructed D_s^- mesons and excludes $\Delta m_s < 1.4\,\mathrm{ps}^{-1}$ and $2.4 < \Delta m_s < 5.3\,\mathrm{ps}^{-1}$ at 95%CL.

[17] Uses fully or partially reconstructed $D_s\ell$ vertices and a mixing tag as a flavor tagging.

[18] Replaced by ABDALLAH 04A. Uses $D_s^-\ell^+$, and $\phi\ell^+$ vertices, and a multi-variable discriminant as a flavor tagging.

[19] Uses inclusive D_s vertices and fully reconstructed B_s decays and a multi-variable discriminant as a flavor tagging.

[20] Uses ℓ-$Q_{\rm hem}$ and ℓ-ℓ.

[21] ABE 99D assumes $\tau_{B^0_s} = 1.55 \pm 0.05$ ps and $\Delta\Gamma/\Delta m = (5.6 \pm 2.6) \times 10^{-3}$.

[22] ABE 99J uses ϕ ℓ-ℓ correlation.

[23] BARATE 99J uses combination of an inclusive lepton and D_s^--based analyses.

[24] BARATE 98C combines results from $D_s h$-$\ell/Q_{\rm hem}$, $D_s h$-K in the same side, $D_s\ell$-$\ell/Q_{\rm hem}$ and $D_s\ell$-K in the same side.

[25] Uses ℓ-$Q_{\rm hem}$.

[26] Uses ℓ-ℓ.

[27] ADAM 97 combines results from $D_s\ell$-$Q_{\rm hem}$, ℓ-$Q_{\rm hem}$, and ℓ-ℓ.

[28] BUSKULIC 96M uses D_s lepton correlations and lepton, kaon, and jet charge tags.

[29] BUSKULIC 95J uses ℓ-$Q_{\rm hem}$. They find $\Delta m_s > 5.6$ [> 6.1] for f_s=10% [12%]. We interpolate to our central value f_s=10.5%.

$x_s = \Delta m_{B^0_s}/\Gamma_{B^0_s}$

This is derived by the Heavy Flavor Averaging Group (HFLAV, https://hflav.web.cern.ch/) from the results on $\Delta m_{B^0_s}$ and "OUR EVALUATION" of the B^0_s mean lifetime.

VALUE	DOCUMENT ID
27.01 ± 0.10 OUR EVALUATION	

χ_s

This is a B^0_s-$\overline{B}^0_s$ integrated mixing parameter derived from x_s above and OUR EVALUATION of $\Delta\Gamma_{B^0_s}/\Gamma_{B^0_s}$.

VALUE	DOCUMENT ID
0.499318 ± 0.000005 OUR EVALUATION	

CP VIOLATION PARAMETERS in B^0_s

$\mathrm{Re}(\epsilon_{B^0_s}) / (1 + |\epsilon_{B^0_s}|^2)$

CP impurity in B^0_s system.

"OUR EVALUATION" is an average obtained by the Heavy Flavor Averaging Group (HFLAV, https://hflav.web.cern.ch/) and described at https://hflav.web.cern.ch/. It is the result of a fit to B_d and B_s *CP* asymmetries, which includes the B_s measurements listed below and the B_d measurements listed in the B_d section, and takes into account correlations between those measurements.

VALUE (units 10^{-3})	DOCUMENT ID		TECN	COMMENT
−0.15 ± 0.70 OUR EVALUATION				
0.0 ± 1.1 OUR AVERAGE	Error includes scale factor of 1.6. See the ideogram below.			
0.98 ± 0.65 ± 0.5	[1] AAIJ	16G	LHCB	pp at 7, 8 TeV
−2.15 ± 1.85	[2] ABAZOV	14	D0	$p\overline{p}$ at 1.96 TeV
−2.8 ± 1.9 ± 0.4	[3] ABAZOV	13	D0	$p\overline{p}$ at 1.96 TeV
• • • We do not use the following data for averages, fits, limits, etc. • • •				
−0.15 ± 1.25 ± 0.90	[4] AAIJ	14D	LHCB	Repl. by AAIJ 16G
−4.5 ± 2.7	[5] ABAZOV	11U	D0	Repl. by ABAZOV 14
−0.4 ± 2.3 ± 0.4	[6] ABAZOV	10E	D0	Repl. by ABAZOV 13
−3.6 ± 1.9	[7] ABAZOV	10H	D0	Repl. by ABAZOV 11U
6.1 ± 4.8 ± 0.9	[8] ABAZOV	07A	D0	Repl. by ABAZOV 10E

[1] AAIJ 16G reports a measurement of time-integrated flavor-specific asymmetry in $B^0_s \to \mu^+ D_s^- X$ decays, $A^s_{SL} = (0.39 \pm 0.26 \pm 0.20)$%, which is approximately equal to $4 \times \mathrm{Re}(\epsilon_{B^0_s}) / (1 + |\epsilon_{B^0_s}|^2)$.

[2] ABAZOV 14 uses the dimuon charge asymmetry with different impact parameters from which it reports $A^s_{SL} = (-0.86 \pm 0.74) \times 10^{-2}$.

[3] ABAZOV 13 reports a measurement of time-integrated flavor-specific asymmetry in mixed semileptonic $B^0_s \to \mu^+ D_s^- X$ decays $A^s_{SL} = (-1.12 \pm 0.74 \pm 0.17)$% which is approximately equal to $4 \times \mathrm{Re}(\epsilon_{B^0_s}) / (1 + |\epsilon_{B^0_s}|^2)$.

[4] AAIJ 14D reports a measurement of time-integrated flavor-specific asymmetry in $B^0_s \to \mu^+ D_s^- X$ decays, $A^s_{SL} = (-0.06 \pm 0.50 \pm 0.36)$%, which is approximately equal to4 $\times \mathrm{Re}(\epsilon_{B^0_s}) / (1 + |\epsilon_{B^0_s}|^2)$.

[5] ABAZOV 11U uses the dimuon charge asymmetry with different impact parameters from which it reports $A^s_{SL} = (-18.1 \pm 10.6) \times 10^{-3}$.

[6] ABAZOV 10E reports a measurement of flavor-specific asymmetry in $B^0_{(s)} \to \mu^+ D^{*-}_{(s)} X$ decays with a decay-time analysis including initial-state flavor tagging, $A^s_{SL} = (-1.7 \pm 9.1^{+1.4}_{-1.5}) \times 10^{-3}$ which is approximately equal to $4 \times \mathrm{Re}(\epsilon_{B^0_s}) / (1 + |\epsilon_{B^0_s}|^2)$.

[7] ABAZOV 10H reports a measurement of like-sign dimuon charge asymmetry of $A^s_{SL} = (-9.57 \pm 2.51 \pm 1.46) \times 10^{-3}$ in semileptonic b-hadron decays. Using the measured production ratio of B^0_d and B^0_s, and the asymmetry of B^0_d $A^s_{SL} = (-4.7 \pm 4.6) \times 10^{-3}$ measured from B-factories, they obtain the asymmetry for B^0_s.

[8] The first direct measurement of the time integrated flavor untagged charge asymmetry in semileptonic B^0_s decays is reported as $2 \times A^s_{SL}(\text{untagged}) = A^s_{SL} = (2.45 \pm 1.93 \pm 0.35) \times 10^{-2}$.

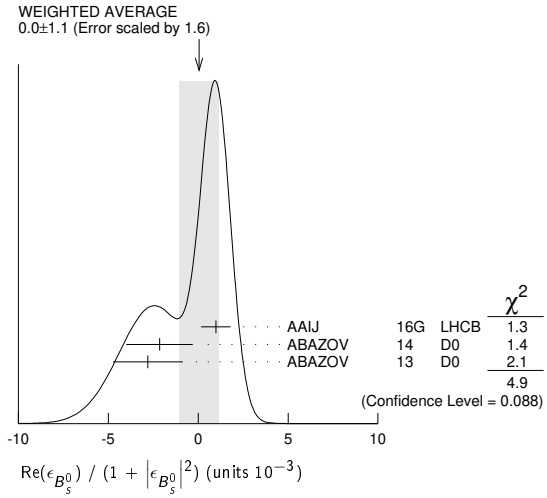

$C_{KK}(B^0_s \to K^+K^-)$

VALUE	DOCUMENT ID		TECN	COMMENT
0.162 ± 0.035 OUR AVERAGE				
0.164 ± 0.034 ± 0.014	AAIJ	21O	LHCB	pp at 13 TeV
0.14 ± 0.11 ± 0.03	AAIJ	13BO	LHCB	pp at 7 TeV

$S_{KK}(B^0_s \to K^+K^-)$

VALUE	DOCUMENT ID		TECN	COMMENT
0.14 ± 0.05 OUR AVERAGE	Error includes scale factor of 1.3.			
0.123 ± 0.034 ± 0.015	AAIJ	21O	LHCB	pp at 13 TeV
0.30 ± 0.12 ± 0.04	AAIJ	13BO	LHCB	pp at 7 TeV

$r_B(B^0_s \to D^{\mp}_s K^{\pm})$

r_B and δ_B are the amplitude ratio and relative strong phase between the amplitudes of $A(B^0_s \to D^+_s K^-)$ and $A(B^0_s \to D^-_s K^+)$,

VALUE	DOCUMENT ID		TECN	COMMENT
$\mathbf{0.37^{+0.10}_{-0.09}}$	[1] AAIJ	18U	LHCB	pp at 7, 8 TeV
• • • We do not use the following data for averages, fits, limits, etc. • • •				
$0.53^{+0.17}_{-0.16}$	[2] AAIJ	14BF	LHCB	Repl. by AAIJ 18U

[1] Measured in $B^0_s \to D^{\mp}_s K^{\pm}$ decays, constraining $-2\beta_s$ by the measurement of $\phi_s = -0.030 \pm 0.033$ from HFLAV.

[2] Measured in $B^0_s \to D^{\mp}_s K^{\pm}$ decays, constraining $-2\beta_s$ by the measurement of $\phi_s = 0.01 \pm 0.07 \pm 0.0$ from AAIJ 13AR. At 68% CL.

$r_B(B^0_s \to D^{\mp}_s K^{\pm}\pi^{\pm}\pi^{\mp})$

VALUE	DOCUMENT ID		TECN	COMMENT
$\mathbf{0.47 \pm 0.08^{+0.02}_{-0.03}}$	[1,2] AAIJ	21M	LHCB	pp at 7, 8, 13 TeV

[1] Measured in restricted phase space with $m(K^+\pi^+\pi^-) < 1950$ MeV, $m(K^+\pi^-) < 1200$ MeV and $m(\pi^+\pi^-) < 1200$ MeV.

[2] A model-independent coherence factor for the decay $B_s \to D_s K\pi\pi$ (in the restricted phase space region) is also reported.

$\delta_B(B^0_s \to D^{\pm}_s K^{\mp})$

VALUE (°)	DOCUMENT ID		TECN	COMMENT
$\mathbf{358^{+13}_{-14}}$	[1] AAIJ	18U	LHCB	pp at 7, 8 TeV
• • • We do not use the following data for averages, fits, limits, etc. • • •				
3^{+19}_{-20}	[2] AAIJ	14BF	LHCB	Repl. by AAIJ 18U

[1] Measured in $B^0_s \to D^{\mp}_s K^{\pm}$ decays, constraining $-2\beta_s$ by the measurement of $\phi_s = 0.030 \pm 0.033$ from HFLAV. The value is modulo 180°.

[2] Measured in $B^0_s \to D^{\mp}_s K^{\pm}$ decays, constraining $-2\beta_s$ by the measurement of $\phi_s = 0.01 \pm 0.07 \pm 0.0$ from AAIJ 13AR. The value is modulo 180° at 68% CL.

Downloaded from https://academic.oup.com/ptep/article/2022/8/083C01/6651666 by KIT Library user on 27 September 2022

$\delta_B(B^0_s \to D^\pm_s K^\mp \pi^\pm \pi^\mp)$

VALUE (°)	DOCUMENT ID		TECN	COMMENT
$-6^{+10}_{-12}{}^{+2}_{-4}$	[1,2] AAIJ	21M	LHCB	pp at 7, 8, 13 TeV

[1] Measured in restricted phase space with $m(K^+\pi^+\pi^-) < 1950$ MeV, $m(K^+\pi^-) < 1200$ MeV and $m(\pi^+\pi^-) < 1200$ MeV. The value is modulo 180°.
[2] A model-independent coherence factor for the decay $B_s \to D_s K\pi\pi$ (in the restricted phase space region) is also reported.

CP Violation phase β_s

$-2\beta_s$ is the weak phase difference between B^0_s mixing amplitude and the $B^0_s \to J/\psi\phi$ decay amplitude driven by the $b \to c\overline{c}s$ transition (such as $B_s \to J/\psi\phi$, $J/\psi K^+K^-$, $J/\psi\pi^+\pi^-$, and $D^+_s D^-_s$). The Standard Model value of β_s is $\arg(-\frac{V_{ts}V^*_{tb}}{V_{cs}V^*_{cb}})$ if penguin contributions are neglected.

"OUR EVALUATION" is an average using rescaled values of the data listed below. The average and rescaling were performed by the Heavy Flavor Averaging Group (HFLAV, https://hflav.web.cern.ch/) and are described at https://hflav.web.cern.ch/. The averaging/scaling procedure takes into account correlation between the measurements.

VALUE (10^{-2} rad)	DOCUMENT ID		TECN	COMMENT
2.5 ± 1.0 OUR EVALUATION				
2.3 ± 1.0 OUR AVERAGE				
4.35 ± 1.80 ± 1.05	[1] AAD	21AE	ATLS	pp at 7, 8, 13 TeV
0 ± 14 ± 4	[2] AAIJ	21AN	LHCB	pp at 7, 8 TeV
1.05 ± 2.20 ± 0.50	[3] SIRUNYAN	21E	CMS	pp at 8, 13 TeV
− 0.1 ± 2.2 ± 0.6	[4] AAIJ	19AF	LHCB	pp at 7, 8, 13 TeV
4.15 ± 2.05 ± 0.30	[5] AAIJ	19Q	LHCB	pp at 13 TeV
− 5.95 ± 5.35 ± 1.70	[6] AAIJ	17V	LHCB	pp at 7, 8 TeV
$-11.5\ ^{+14}_{-14.5} \pm 1$	[7] AAIJ	16AK	LHCB	pp at 7, 8 TeV
2.9 ± 2.5 ± 0.3	[8] AAIJ	15I	LHCB	pp at 7, 8 TeV
− 1 ± 9 ± 1	[9] AAIJ	14AY	LHCB	pp at 7, 8 TeV
	[10] AALTONEN	12AJ	CDF	$p\overline{p}$ at 1.96 TeV
$28\ ^{+18}_{-19}$	[11] ABAZOV	12D	D0	$p\overline{p}$ at 1.96 TeV
• • • We do not use the following data for averages, fits, limits, etc. • • •				
3.7 ± 5.8 ± 1.4	[12,13] AAIJ	19AP	LHCB	pp at 7, 8, 13 TeV
5.0 ± 6.5 ± 7.0	[14] AAIJ	18S	LHCB	pp at 7, 8 TeV
4.5 ± 3.9 ± 2.1	[15] AAD	16AP	ATLS	Repl. by AAD 21AE
3.75 ± 4.85 ± 1.55	[16] KHACHATRY...	16S	CMS	Repl. by SIRUNYAN 21E
$6\ ^{+8}_{-7}$	[17,18] AAIJ	15K	LHCB	pp at 7, 8 TeV
− 6 ± 13 ± 3	[19] AAD	14U	ATLS	Repl. by AAD 21AE
8.5 ± 7.5 ± 1.5	[20] AAIJ	14AE	LHCB	Repl. by AAIJ 19AP
− 3.5 ± 3.4 ± 0.4	[21] AAIJ	14S	LHCB	Repl. by AAIJ 19AF
− 0.5 ± 3.5 ± 0.5	[22] AAIJ	13AR	LHCB	Repl. by AAIJ 15I
	[23] AAIJ	13AY	LHCB	pp at 7 TeV
−11.0 ± 20.5 ± 5.0	[24] AAD	12CV	ATLS	Repl. by AAD 14U
22 ± 22 ± 1	[25] AAIJ	12B	LHCB	Repl. by AAIJ 12Q
− 8 ± 9 ± 3	[26] AAIJ	12D	LHCB	Repl. by AAIJ 13AR
$0.95\ ^{+8.70}_{-8.65} \pm ^{0.15}_{-0.20}$	[27] AAIJ	12Q	LHCB	Repl. by AAIJ 13AR
	[28] AALTONEN	12D	CDF	Repl. by AALTONEN 12AJ
	[29] AALTONEN	08G	CDF	Repl. by AALTONEN 12D
$28\ ^{+12}_{-15} \pm ^{4}_{-1}$	[11,30] ABAZOV	08AM	D0	Repl. by ABAZOV 12D
$39.5 \pm 28.0\ ^{+0.5}_{-7.0}$	[31,32] ABAZOV	07	D0	Repl. by ABAZOV 07N
$35\ ^{+20}_{-24}$	[32,33] ABAZOV	07N	D0	Repl. by ABAZOV 08AM

[1] AAD 21AE measured $\phi_s = -2\beta_s = -0.087 \pm 0.036 \pm 0.021$ rad. using a time-dependent angular analysis of $B^0_s \to J/\psi\phi$ decays.
[2] AAIJ 21AN measured $\phi_s = -2\beta_s = 0.00 \pm 0.28 \pm 0.07$ rad, using a time-dependent angular analysis of $B^0_s \to J/\psi\phi$ decays with $J/\psi \to e^+e^-$.
[3] SIRUNYAN 21E measured $\phi_s = -2\beta_s = -0.021 \pm 0.044 \pm 0.010$ rad. using a time-dependent angular analysis of $B^0_s \to J/\psi\phi$ decays.
[4] AAIJ 19AF reports $\phi_s = -2\beta_s = 0.002 \pm 0.044 \pm 0.012$ rad. and $|\lambda| = 0.949 \pm 0.036 \pm 0.019$, when direct *CP* violation is allowed. Measured using a time-dependent fit to $B^0_s \to J/\psi\pi^+\pi^-$ decays, which is sensitive to $\phi_s(s\overline{s}s)$, not $\phi_s(c\overline{c}s)$.
[5] AAIJ 19Q reports $\phi_s = -2\beta_s = -0.083 \pm 0.041 \pm 0.006$ rad. that was measured using a time-dependent angular analysis of $B^0_s \to J/\psi K^+K^-$ decays.
[6] Measured $\phi_s = -2\beta_s = 0.119 \pm 0.107 \pm 0.034$ rad using time-dependent angular analysis of $B^0_s \to J/\psi K^+K^-$ in the region $m(KK) > 1.05$ GeV.
[7] AAIJ 16AK reports $\phi_s = -2\beta_s = 0.23^{+0.29}_{-0.28} \pm 0.02$ rad. that was measured using a time-dependent angular analysis of $B^0_s \to \psi(2S)\phi$ decays.
[8] AAIJ 15I reports $\phi_s = -2\beta_s = -0.058 \pm 0.049 \pm 0.006$ rad. that was measured using a time-dependent angular analysis of $B^0_s \to J/\psi K^+K^-$ decays. It also combines this result with that of AAIJ 14S and quotes $\phi_s = -2\beta_s = -0.010 \pm 0.039$ rad.
[9] AAIJ 14AY reports $\phi_s = -2\beta_s = 0.02 \pm 0.17 \pm 0.02$ rad. in a time-dependent fit to $B^0_s \to D^+_s D^-_s$, while allowing *CP* violation in decay.
[10] AALTONEN 12AJ reports $-\pi/2 < \beta_s < -1.51$ or $-0.06 < \beta_s < 0.30$, or $1.26 < \beta_s < \pi/2$ rad. at 68% CL. Measured using the time-dependent angular analysis of $B^0_s \to J/\psi\phi$ decays.
[11] ABAZOV 12D reports $\phi_s = -2\beta_s = -0.55^{+0.38}_{-0.36}$ rad. that was measured using a time-dependent angular analysis of $B^0_s \to J/\psi\phi$ decays. A single error includes both statistical and systematic uncertainties.
[12] AAIJ 19AP reports $\phi_s^{s\overline{s}s} = -0.073 \pm 0.115 \pm 0.027$ rad and $|\lambda| = 0.99 \pm 0.05 \pm 0.01$. Measured using a time-dependent fit to $B^0_s \to \phi\phi$ decays, assuming independence of the helicity of the $\phi\phi$ decay.
[13] AAIJ 19AP reports also polarisation-dependent results assuming that the longitudinal weak phase is CP-conserving and that there is no direct CP violation, giving $\phi_{s,\parallel} = 0.014 \pm 0.055 \pm 0.011$ rad and $\phi_{s,\perp} = 0.044 \pm 0.059 \pm 0.019$ rad.
[14] AAIJ 18S reports $\phi_s = -2\beta_s = -0.10 \pm 0.13 \pm 0.14$ rad measured in $B^0_s \to (K^+\pi^-)(K^-\pi^+)$ in the region $0.75 < m(K^\pm\pi^\mp) < 1.6$ GeV. This is a $b \to d\overline{d}s$ transition with a decay amplitude phase different from that of $b \to c\overline{c}s$ transition.
[15] AAD 16AP reports $\phi_s = -2\beta_s = -0.090 \pm 0.078 \pm 0.041$ rad. that was measured using a time-dependent angular analysis of $B^0_s \to J/\psi\phi$ decays.
[16] KHACHATRYAN 16S reports $\phi_s = -2\beta_s = -0.075 \pm 0.097 \pm 0.031$ rad. that was measured using a time-dependent angular analysis of $B^0_s \to J/\psi\phi$ decays.
[17] AAIJ 15K reports $-2\beta_s = -0.12^{+0.14}_{-0.16}$ rad. The value was obtained by measuring time-dependent *CP* asymmetry in $B^0_s \to K^+K^-$ and using a U-spin relation between $B^0_s \to K^+K^-$ and $B^0 \to \pi^+\pi^-$.
[18] Results are also presented using additional inputs on $B^0 \to \pi^0\pi^0$ and $B^+ \to \pi^+\pi^0$ decays from other experiments and isospin symmetry assumptions. The dependence of the results on the maximum allowed amount of U-spin breaking up to 50% is also included.
[19] AAD 14U reports $\phi_s = -2\beta_s = 0.12 \pm 0.25 \pm 0.05$ rad. that was measured using a time-dependent angular analysis of $B^0_s \to J/\psi\phi$ decays.
[20] AAIJ 14AE value measured in $B^0_s \to \phi\phi$ decays.This is a $b \to s\overline{s}s$ transition with a decay amplitude phase different from that of $b \to c\overline{c}s$ transition. Also reports $\phi_s = -0.17 \pm 0.15 \pm 0.03$ rad.
[21] AAIJ 14S reports $\phi_s = -2\beta_s = 0.070 \pm 0.068 \pm 0.008$ rad. and $|\lambda| = 0.89 \pm 0.05 \pm 0.01$, when direct *CP* violation is allowed. Measured using a time-dependent fit to $B^0_s \to J/\psi\pi^+\pi^-$ decays.
[22] AAIJ 13AR reports $\phi_s = -2\beta_s = 0.01 \pm 0.07 \pm 0.01$ rad. obtained from combined fit to $B^0_s \to J/\psi K^+K^-$ and $B^0_s \to J/\psi\pi^+\pi^-$ data sets. Also reports separate results of $\phi_s = 0.07 \pm 0.09 \pm 0.01$ rad. from $B^0_s \to J/\psi K^+K^-$ decays and $\phi_s = -0.14^{+0.17}_{-0.16} \pm 0.01$ rad. from $B^0_s \to J/\psi\pi^+\pi^-$ decays.
[23] AAIJ 13AY uses $B^0_s \to \phi\phi$ mode, and reports the 68% CL interval of $\phi_s = -2\beta_s$ as $[-2.46, -0.76]$ rad.
[24] AAD 12CV reports $\phi_s = -2\beta_s = 0.22 \pm 0.41 \pm 0.10$ rad. that was measured using a time-dependent angular analysis of $B^0_s \to J/\psi\phi$ decays.
[25] Reports $\phi_s = -2\beta_s = -0.44 \pm 0.44 \pm 0.02$ rad. that was measured using a time-dependent fit to $B^0_s \to J/\psi f_0(980)$ decays.
[26] Reports $\phi_s = -2\beta_s = 0.15 \pm 0.18 \pm 0.06$ rad. that was measured using a time-dependent angular analysis of $B^0_s \to J/\psi\phi$ decays.
[27] Reports $\phi_s = -2\beta_s = -0.019^{+0.173}_{-0.174} {}^{+0.004}_{-0.003}$ rad. which was measured using a time-dependent fit to $B^0_s \to J/\psi\pi^+\pi^-$ decays, with the $\pi^+\pi^-$ mass within 775–1550 MeV. Searches for, but finds no evidence, for direct *CP* violation in $B^0_s \to J/\psi\pi\pi$ decays.
[28] Reports $0.02 < \phi_s < 0.52$ or $1.08 < \phi_s < 1.55$ rad. at 68% C.L. confidence regions in the two-dimensional space of ϕ_s and $\Delta\Gamma_{B^0_s}$ from $B^0_s \to J/\psi\phi$ decays.
[29] Reports $0.32 < 2\beta_s < 2.82$ rad. at 68% C.L. and confidence regions in the two-dimensional space of $2\beta_s$ and $\Delta\Gamma$ from the first measurement of $B^0_s \to J/\psi\phi$ decays using flavor tagging. The probability of a deviation from SM prediction as large as the level of observed data is 15%.
[30] Reports $\phi_s = -2\beta_s$ and obtains 90% CL interval $-0.03 < \beta_s < 0.60$ rad.
[31] The first direct measurement of the *CP*-violating mixing phase is reported from the time-dependent analysis of flavor untagged $B^0_s \to J/\psi\phi$ decays.
[32] Reports ϕ_s which equals to $-2\beta_s$.
[33] Combines D0 collaboration measurements of time-dependent angular distributions in $B^0_s \to J/\psi\phi$ and charge asymmetry in semileptonic decays. There is a 4-fold ambiguity in the solution.

$|\lambda|$ $(B^0_s \to J/\psi(1S)\phi)$

VALUE	DOCUMENT ID		TECN	COMMENT
1.001±0.018 OUR AVERAGE	Error includes scale factor of 1.2.			
0.972±0.026±0.008	[1] SIRUNYAN	21E	CMS	pp at 13 TeV
1.012±0.016±0.006	AAIJ	19Q	LHCB	pp at 13 TeV
• • • We do not use the following data for averages, fits, limits, etc. • • •				
0.964±0.019±0.007	AAIJ	15I	LHCB	Repl. by AAIJ 19Q

[1] Measured using time-dependent angular analysis of $B^0_s \to J/\psi\phi$ decays.

$|\lambda|$

VALUE	DOCUMENT ID		TECN	COMMENT
0.999±0.017 OUR AVERAGE				
0.99 ±0.05 ±0.01	[1] AAIJ	19AP	LHCB	pp at 7, 8, 13 TeV
1.035±0.034±0.089	[2] AAIJ	18S	LHCB	pp at 7, 8 TeV
0.994±0.018±0.006	[3] AAIJ	17V	LHCB	pp at 7, 8 TeV
$1.045^{+0.069}_{-0.050} \pm 0.007$	[4] AAIJ	16AK	LHCB	pp at 7, 8 TeV
$0.91\ ^{+0.18}_{-0.15} \pm 0.02$	[5] AAIJ	14AY	LHCB	pp at 7, 8 TeV

Downloaded from https://academic.oup.com/ptep/article/2022/8/083C01/6651666 by KIT Library user on 27 September 2022

• • • We do not use the following data for averages, fits, limits, etc. • • •

0.949±0.036±0.019	[6] AAIJ	19AF	LHCB	pp at 7, 8, 13 TeV
1.04 ±0.07 ±0.03	[7] AAIJ	14AE	LHCB	Repl. by AAIJ 19AP

[1] Measured in $B_s^0 \to \phi\phi$ decays.
[2] Measured in $B_s^0 \to (K^+\pi^-)(K^-\pi^+)$ in the region $0.75 < m(K^\pm\pi^\mp) < 1.6$ GeV.
[3] Measured using time-dependent angular analysis of $B_s^0 \to J/\psi K^+K^-$ in the region $m(KK) > 1.05$ GeV.
[4] Measured using time-dependent angular analysis of $B_s^0 \to \psi(2S)\phi$ decays.
[5] Measured in $B_s^0 \to D_s^+ D_s^-$ decays.
[6] Measured using time-dependent analysis of $B_s^0 \to J/\psi\pi^+\pi^-$ decays.
[7] Measured in $B_s^0 \to \phi\phi$ decays.

A, *CP* violation parameter

$A = -2\,\mathrm{Re}(\lambda) / (1 + |\lambda|^2)$

VALUE	DOCUMENT ID		TECN	COMMENT
−0.79±0.08 OUR AVERAGE				
−0.83±0.05±0.09	[1] AAIJ	21O	LHCB	pp at 13 TeV
−0.79±0.07±0.10	[1] AAIJ	18O	LHCB	pp at 7, 8 TeV
$0.49^{+0.77}_{-0.65}$±0.06	[2] AAIJ	15AL	LHCB	pp at 7, 8 TeV

[1] Measured in $B_s^0 \to K^+K^-$ decays.
[2] Measured in $B_s^0 \to J/\psi K_S^0$ decays.

C, *CP* violation parameter

$C = (1 - |\lambda|^2) / (1 + |\lambda|^2)$

VALUE	DOCUMENT ID		TECN	COMMENT
0.19±0.06 OUR AVERAGE				
0.20±0.06±0.02	[1] AAIJ	18O	LHCB	pp at 7, 8 TeV
−0.28±0.41±0.08	[2] AAIJ	15AL	LHCB	pp at 7, 8 TeV

[1] Measured in $B_s^0 \to K^+K^-$ decays.
[2] Measured in $B_s^0 \to J/\psi K_S^0$ decays.

S, *CP* violation parameter

$S = -2\,\mathrm{Im}(\lambda) / (1 + |\lambda|^2)$

VALUE	DOCUMENT ID		TECN	COMMENT
0.17±0.06 OUR AVERAGE				
0.18±0.06±0.02	[1] AAIJ	18O	LHCB	pp at 7, 8 TeV
−0.08±0.40±0.08	[2] AAIJ	15AL	LHCB	pp at 7, 8 TeV

[1] Measured in $B_s^0 \to K^+K^-$ decays.
[2] Measured in $B_s^0 \to J/\psi K_S^0$ decays.

$A_{CP}^L(B_s \to J/\psi \overline{K}^*(892)^0)$

VALUE	DOCUMENT ID		TECN	COMMENT
−0.048±0.057±0.020	AAIJ	15AV	LHCB	pp at 7, 8 TeV

$A_{CP}^\parallel(B_s \to J/\psi \overline{K}^*(892)^0)$

VALUE	DOCUMENT ID		TECN	COMMENT
0.171±0.152±0.028	AAIJ	15AV	LHCB	pp at 7, 8 TeV

$A_{CP}^\perp(B_s \to J/\psi \overline{K}^*(892)^0)$

VALUE	DOCUMENT ID		TECN	COMMENT
−0.049±0.096±0.025	AAIJ	15AV	LHCB	pp at 7, 8 TeV

$A_{CP}(B_s \to \pi^+K^-)$

A_{CP} is defined as

$$\frac{B(\overline{B}_s^0 \to f) - B(B_s^0 \to \overline{f})}{B(\overline{B}_s^0 \to f) + B(B_s^0 \to \overline{f})},$$

the *CP*-violation asymmetry of exclusive B_s^0 and $\overline{B}_s^0$ decay.

VALUE	DOCUMENT ID		TECN	COMMENT
0.224±0.012 OUR AVERAGE				
0.236±0.013±0.011	AAIJ	21O	LHCB	pp at 13 TeV
0.213±0.015±0.007	AAIJ	18O	LHCB	pp at 7, 8 TeV
0.22 ±0.07 ±0.02	AALTONEN	14P	CDF	$p\overline{p}$ at 1.96 TeV
• • • We do not use the following data for averages, fits, limits, etc. • • •				
0.27 ±0.04 ±0.01	AAIJ	13AX	LHCB	Repl. by AAIJ 18O
0.27 ±0.08 ±0.02	AAIJ	12V	LHCB	Repl. by AAIJ 13AX
0.39 ±0.15 ±0.08	AALTONEN	11N	CDF	Repl. by AALTONEN 14P

$A_{CP}(B_s^0 \to [K^+K^-]_D \overline{K}^*(892)^0)$

VALUE	DOCUMENT ID		TECN	COMMENT
−0.04±0.07±0.02	AAIJ	14BN	LHCB	pp at 7, 8 TeV
• • • We do not use the following data for averages, fits, limits, etc. • • •				
0.04±0.16±0.01	AAIJ	13L	LHCB	Repl. by AAIJ 14BN

$A_{CP}(B_s^0 \to [\pi^+K^-]_D K^*(892)^0)$

VALUE	DOCUMENT ID		TECN	COMMENT
−0.01±0.03±0.02	AAIJ	14BN	LHCB	pp at 7, 8 TeV

$A_{CP}(B_s^0 \to [\pi^+\pi^-]_D K^*(892)^0)$

VALUE	DOCUMENT ID		TECN	COMMENT
0.06±0.13±0.02	AAIJ	14BN	LHCB	pp at 7, 8 TeV

$S(B_s^0 \to \phi\gamma)$

VALUE	DOCUMENT ID		TECN	COMMENT
0.43±0.30±0.11	[1] AAIJ	19AE	LHCB	pp at 7, 8 TeV

[1] Measured in flavor tagged time dependent analysis.

$C(B_s^0 \to \phi\gamma)$

VALUE	DOCUMENT ID		TECN	COMMENT
0.11±0.29±0.11	[1] AAIJ	19AE	LHCB	pp at 7, 8 TeV

[1] Measured in flavor tagged time dependent analysis.

$A^\Delta(B_s^0 \to \phi\gamma)$

$A^\Delta(B_s \to \phi\gamma)$ is the multiplicative coefficient of the $\sinh(\Delta\Gamma t/2)$ term in the $B_s \to \phi\gamma$ decay rate time dependence.

VALUE	DOCUMENT ID		TECN	COMMENT
$-0.67^{+0.37}_{-0.41}$±0.17	[1] AAIJ	19AE	LHCB	pp at 7, 8 TeV
• • • We do not use the following data for averages, fits, limits, etc. • • •				
$-0.98^{+0.46}_{-0.52}{}^{+0.23}_{-0.20}$	[2] AAIJ	17B	LHCB	Repl. by AAIJ 19AE

[1] Measured in flavor tagged time dependent analysis, using tagged and un-tagged events. This result updates AAIJ 17B with better selection efficiency and other analysis improvements.
[2] Measured in time dependent analysis without initial flavor tagging.

CPT VIOLATION PARAMETERS

In the B_s^0 mixing, propagating mass eigenstates can be written as

$$|B_{sL}\rangle \propto p\sqrt{1-\xi}\,|B_s^0\rangle + q\sqrt{1+\xi}\,|\overline{B}_s^0\rangle$$
$$|B_{sH}\rangle \propto p\sqrt{1+\xi}\,|B_s^0\rangle - q\sqrt{1-\xi}\,|\overline{B}_s^0\rangle$$

where parameter ξ controls *CPT* violation. If ξ is zero, then *CPT* is conserved. The parameter ξ can be written as

$$\xi = \frac{2(M_{11}-M_{22}) - i(\Gamma_{11}-\Gamma_{22})}{-2\Delta m_s + i\Delta\Gamma_s} \approx \frac{-2\beta^\mu \Delta a_\mu}{2\Delta m_s - i\Delta\Gamma_s},$$

where M_{ii}, Γ_{ii}, Δm_s, and $\Delta\Gamma_s$ are parameters of Hamiltonian governing B_s oscillations, β^μ is the B_s^0 meson velocity and Δa_μ characterizes Lorentz-invariance violation.

$\Delta a_\perp$

VALUE (10^{-12} GeV)	CL%	DOCUMENT ID		TECN	COMMENT
−0.47±0.39±0.08		[1] AAIJ	16E	LHCB	pp at 7, 8 TeV
< 1.2	95	[2] ABAZOV	15L	D0	$p\overline{p}$ at 1.96 TeV

[1] Uses $B_s^0 \to J/\psi K^+K^-$ decays.
[2] Measured in semileptonic $B_s^0 \to D_s^- \mu^+ X$ decays. Also extracts limit on time and longitudinal components ($-0.8 < \Delta a_T - 0.396\,\Delta a_Z < 3.9$) 10^{-13} GeV.

$\Delta a_\parallel$

VALUE (10^{-14} GeV)	DOCUMENT ID		TECN	COMMENT
−0.89±1.41±0.36	[1] AAIJ	16E	LHCB	pp at 7, 8 TeV

[1] Uses $B_s^0 \to J/\psi K^+K^-$ decays.

Δa_X

VALUE (10^{-14} GeV)	DOCUMENT ID		TECN	COMMENT
+1.01±2.08±0.71	[1] AAIJ	16E	LHCB	pp at 7, 8 TeV

[1] Uses $B_s^0 \to J/\psi K^+K^-$ decays.

Δa_Y

VALUE (10^{-14} GeV)	DOCUMENT ID		TECN	COMMENT
−3.83±2.09±0.71	[1] AAIJ	16E	LHCB	pp at 7, 8 TeV

[1] Uses $B_s^0 \to J/\psi K^+K^-$ decays.

Re(ξ)

VALUE	DOCUMENT ID		TECN	COMMENT
−0.022±0.033±0.003	[1] AAIJ	16E	LHCB	pp at 7, 8 TeV

[1] Uses $B_s^0 \to J/\psi K^+K^-$ decays.

Im(ξ)

VALUE	DOCUMENT ID		TECN	COMMENT
0.004±0.011±0.002	[1] AAIJ	16E	LHCB	pp at 7, 8 TeV

[1] Uses $B_s^0 \to J/\psi K^+K^-$ decays.

PARTIAL BRANCHING FRACTIONS IN $B_s \to \phi\ell^+\ell^-$

$B(B_s \to \phi\ell^+\ell^-)$ ($0.1 < q^2 < 2.0$ GeV^2/c^4)

VALUE (units 10^{-7})	DOCUMENT ID		TECN	COMMENT
1.14 ±0.16 OUR AVERAGE				
1.11 $^{+0.14}_{-0.13}$ ±0.09	[1] AAIJ	15AQ	LHCB	pp at 7, 8 TeV
2.78 ±0.95 ±0.89	AALTONEN	11AI	CDF	$p\overline{p}$ at 1.96 TeV
• • • We do not use the following data for averages, fits, limits, etc. • • •				
$0.897^{+0.207}_{-0.186}$±0.097	[1] AAIJ	13X	LHCB	Repl. by AAIJ 15AQ

[1] Measured in $B_s^0 \to \phi\mu^+\mu^-$ decays.

Downloaded from https://academic.oup.com/ptep/article/2022/8/083C01/6651666 by KIT Library user on 27 September 2022

$B(B_s^0 \to \phi\ell^+\ell^-)$ $(0.1 < q^2 < 0.98\ GeV^2/c^4)$

VALUE (units 10^{-8})	DOCUMENT ID		TECN	COMMENT
6.81±0.47±0.34	[1] AAIJ	21AG	LHCB	pp at 7, 8, 13 TeV

[1] Measured in $B_s^0 \to \phi\mu^+\mu^-$ decays

$B(B_s^0 \to \phi\ell^+\ell^-)$ $(1.1 < q^2 < 2.5\ GeV^2/c^4)$

VALUE (units 10^{-8})	DOCUMENT ID		TECN	COMMENT
4.41±0.41±0.24	[1] AAIJ	21AG	LHCB	pp at 7, 8, 13 TeV

[1] Measured in $B_s^0 \to \phi\mu^+\mu^-$ decays

$B(B_s \to \phi\ell^+\ell^-)$ $(2.0 < q^2 < 5.0\ GeV^2/c^4)$

VALUE (units 10^{-7})	DOCUMENT ID		TECN	COMMENT
0.77 ±0.12 ±0.06	[1] AAIJ	15AQ	LHCB	pp at 7, 8 TeV
• • • We do not use the following data for averages, fits, limits, etc. • • •				
$0.529^{+0.182}_{-0.159}\pm0.057$	[1,2] AAIJ	13X	LHCB	Repl. by AAIJ 15AQ
0.58 ±0.55 ±0.19	[2] AALTONEN	11AI	CDF	$p\overline{p}$ at 1.96 TeV

[1] Measured in $B_s^0 \to \phi\mu^+\mu^-$ decays.
[2] Measured in $2<q^2<4.3\ GeV^2/c^4$.

$B(B_s^0 \to \phi\ell^+\ell^-)$ $(2.5 < q^2 < 4.0\ GeV^2/c^4)$

VALUE (units 10^{-8})	DOCUMENT ID		TECN	COMMENT
3.51±0.39±0.18	[1] AAIJ	21AG	LHCB	pp at 7, 8, 13 TeV

[1] Measured in $B_s^0 \to \phi\mu^+\mu^-$ decays

$B(B_s^0 \to \phi\ell^+\ell^-)$ $(4.0 < q^2 < 6.0\ GeV^2/c^4)$

VALUE (units 10^{-8})	DOCUMENT ID		TECN	COMMENT
6.22±0.48±0.32	[1] AAIJ	21AG	LHCB	pp at 7, 8, 13 TeV

[1] Measured in $B_s^0 \to \phi\mu^+\mu^-$ decays

$B(B_s \to \phi\ell^+\ell^-)$ $(5.0 < q^2 < 8.0\ GeV^2/c^4)$

VALUE (units 10^{-7})	DOCUMENT ID		TECN	COMMENT
0.96±0.13±0.08	[1] AAIJ	15AQ	LHCB	pp at 7, 8 TeV
• • • We do not use the following data for averages, fits, limits, etc. • • •				
$1.38^{+0.25}_{-0.23}\pm0.14$	[1,2] AAIJ	13X	LHCB	Repl. by AAIJ 15AQ
1.34±0.83±0.43	[2] AALTONEN	11AI	CDF	$p\overline{p}$ at 1.96 TeV

[1] Measured in $B_s^0 \to \phi\mu^+\mu^-$ decays.
[2] Measured in $4.3<q^2<8.68\ GeV^2/c^4$.

$B(B_s^0 \to \phi\ell^+\ell^-)$ $(6.0 < q^2 < 8.0\ GeV^2/c^4)$

VALUE (units 10^{-8})	DOCUMENT ID		TECN	COMMENT
6.30±0.48±0.32	[1] AAIJ	21AG	LHCB	pp at 7, 8, 13 TeV

[1] Measured in $B_s^0 \to \phi\mu^+\mu^-$ decays

$B(B_s \to \phi\ell^+\ell^-)$ $(11.0 < q^2 < 12.5\ GeV^2/c^4)$

VALUE (units 10^{-7})	DOCUMENT ID		TECN	COMMENT
0.717±0.045±0.036	[1] AAIJ	21AG	LHCB	pp at 7, 8, 13 TeV
• • • We do not use the following data for averages, fits, limits, etc. • • •				
0.71 ±0.10 ±0.06	[1] AAIJ	15AQ	LHCB	Repl. by AAIJ 21AG
$1.18\ ^{+0.22}_{-0.21}\ \pm0.14$	[1,2] AAIJ	13X	LHCB	Repl. by AAIJ 15AQ
2.98 ±0.95 ±0.95	[2] AALTONEN	11AI	CDF	$p\overline{p}$ at 1.96 TeV

[1] Measured in $B_s^0 \to \phi\mu^+\mu^-$ decays.
[2] Measured in $10.9<q^2<12.86\ GeV^2/c^4$.

$B(B_s^0 \to \phi\ell^+\ell^-)$ $(15.0 < q^2 < 19.0\ GeV^2/c^4)$

VALUE (units 10^{-8})	DOCUMENT ID		TECN	COMMENT
18.52±0.80±1.00	[1] AAIJ	21AG	LHCB	pp at 7, 8, 13 TeV

[1] Measured in $B_s^0 \to \phi\mu^+\mu^-$ decays

$B(B_s \to \phi\ell^+\ell^-)$ $(15.0 < q^2 < 17.0\ GeV^2/c^4)$

VALUE (units 10^{-7})	DOCUMENT ID		TECN	COMMENT
1.050±0.058±0.054	[1] AAIJ	21AG	LHCB	pp at 7, 8, 13 TeV
• • • We do not use the following data for averages, fits, limits, etc. • • •				
0.90 ±0.11 ±0.07	[1] AAIJ	15AQ	LHCB	Repl. by AAIJ 21AG
$0.760^{+0.189}_{-0.169}\pm0.087$	[1,2] AAIJ	13X	LHCB	Repl. by AAIJ 15AQ
1.86 ±0.66 ±0.59	[2] AALTONEN	11AI	CDF	$p\overline{p}$ at 1.96 TeV

[1] Measured in $B_s^0 \to \phi\mu^+\mu^-$ decays.
[2] Measured in $14.18<q^2<16\ GeV^2/c^4$.

$B(B_s \to \phi\ell^+\ell^-)$ $(17.0 < q^2 < 19.0\ GeV^2/c^4)$

VALUE (units 10^{-7})	DOCUMENT ID		TECN	COMMENT
0.838±0.058±0.046	[1] AAIJ	21AG	LHCB	pp at 7, 8, 13 TeV
• • • We do not use the following data for averages, fits, limits, etc. • • •				
0.79 ±0.11 ±0.07	[1] AAIJ	15AQ	LHCB	Repl. by AAIJ 21AG
$1.06\ ^{+0.23}_{-0.21}\ \pm0.12$	[1,2] AAIJ	13X	LHCB	Repl. by AAIJ 15AQ
2.32 ±0.76 ±0.74	[2] AALTONEN	11AI	CDF	$p\overline{p}$ at 1.96 TeV

[1] Measured in $B_s^0 \to \phi\mu^+\mu^-$ decays.
[2] Measured in $16<q^2<19\ GeV^2/c^4$.

$B(B_s \to \phi\ell^+\ell^-)$ $(1.0 < q^2 < 6.0\ GeV^2/c^4)$

VALUE (units 10^{-7})	DOCUMENT ID		TECN	COMMENT
1.44 ±0.11 OUR AVERAGE				
1.440±0.075±0.075	[1] AAIJ	21AG	LHCB	pp at 7, 8, 13 TeV
1.14 ±0.79 ±0.36	AALTONEN	11AI	CDF	$p\overline{p}$ at 1.96 TeV
• • • We do not use the following data for averages, fits, limits, etc. • • •				
1.29 ±0.16 ±0.10	[1] AAIJ	15AQ	LHCB	Repl. by AAIJ 21AG
$1.14\ ^{+0.25}_{-0.23}\ \pm0.13$	[1] AAIJ	13X	LHCB	Repl. by AAIJ 15AQ

[1] Measured in $B_s^0 \to \phi\mu^+\mu^-$ decays.

$B(B_s \to \phi\ell^+\ell^-)$ $(0.0 < q^2 < 4.3\ GeV^2/c^4)$

VALUE (units 10^{-7})	DOCUMENT ID		TECN	COMMENT
3.30±1.09±1.05	AALTONEN	11AI	CDF	$p\overline{p}$ at 1.96 TeV

PRODUCTION ASYMMETRIES

$A_P(B_s^0)$

$$A_P(B_s^0) = [\sigma(\overline{B}_s^0) - \sigma(B_s^0)]\ /\ [\sigma(\overline{B}_s^0) + \sigma(B_s^0)]$$

VALUE (units 10^{-2})	DOCUMENT ID		TECN	COMMENT
1.2 ±1.6 OUR AVERAGE				
−0.65±2.88±0.59	[1] AAIJ	17BF	LHCB	pp at 7 TeV
1.98±1.90±0.59	[1] AAIJ	17BF	LHCB	pp at 8 TeV
• • • We do not use the following data for averages, fits, limits, etc. • • •				
1.09±2.61±0.66	[2] AAIJ	14BP	LHCB	Repl. by AAIJ 17BF, pp at 7 TeV

[1] Based on time-dependent analysis of $B_s^0 \to D_s^- \pi^+$ in kinematic range $2 < p_T < 30$ GeV/c and $2.1 < \eta < 4.5$.
[2] Based on time-dependent analysis of $B_s^0 \to D_s^- \pi^+$ in kinematic range $4 < p_T < 30$ GeV/c and $2.5 < \eta < 4.5$.

$B_s^0 \to D_s^{*-} \ell^+ \nu_\ell$ FORM FACTORS

ρ^2 (form factor slope)

VALUE	DOCUMENT ID		TECN	COMMENT
1.17±0.08 OUR AVERAGE				
1.16±0.05±0.07	[1] AAIJ	20AW	LHCB	pp at 13 TeV
1.23±0.17±0.05	[2] AAIJ	20E	LHCB	pp at 7,8 TeV

[1] The $B_s^0 \to D_s^{*-} \mu^+ \nu_\mu$ decay is reconstructed through the decays of $D_s^{*-} \to D_s^- \gamma$, $D_s^- \to K^- K^+ \pi^-$.
[2] The $B_s^0 \to D_s^{*-} \mu^+ \nu_\mu$ decay is reconstructed inclusively without γ from the decays of $D_s^{*-} \to D_s^- \gamma$, $D_s^- \to K^- K^+ \pi^-$.

B_s^0 REFERENCES

AAIJ	22	PRL 128 041801	R. Aaij et al.	(LHCb Collab.)
Also		PR D105 012010	R. Aaij et al.	(LHCb Collab.)
AAIJ	22B	NATP 18 1	R. Aaij et al.	(LHCb Collab.)
BHUYAN	22	PR D105 012007	B. Bhuyan et al.	(Belle Collab.)
WANG	22	PR D105 012004	B. Wang et al.	(BELLE Collab.)
AAD	21AE	EPJ C81 342	G. Aad et al.	(ATLAS Collab.)
AAIJ	21AG	PRL 127 151801	R. Aaij et al.	(LHCb Collab.)
AAIJ	21AK	JHEP 2111 043	R. Aaij et al.	(LHCb Collab.)
AAIJ	21AN	EPJ C81 1026	R. Aaij et al.	(LHCb Collab.)
AAIJ	21C	JHEP 2102 024	R. Aaij et al.	(LHCb Collab.)
AAIJ	21G	PRL 126 081804	R. Aaij et al.	(LHCb Collab.)
AAIJ	21M	JHEP 2103 137	R. Aaij et al.	(LHCb Collab.)
AAIJ	21N	JHEP 2103 099	R. Aaij et al.	(LHCb Collab.)
AAIJ	21O	JHEP 2103 075	R. Aaij et al.	(LHCb Collab.)
AAIJ	21S	JHEP 2106 177	R. Aaij et al.	(LHCb Collab.)
AAIJ	21Y	PR D104 032005	R. Aaij et al.	(LHCb Collab.)
DUBEY	21	PR D104 012007	S. Dubey et al.	(Belle Collab.)
NISAR	21	PR D104 L031101	N. K. Nisar et al.	(BELLE Collab.)
SIRUNYAN	21E	PL B816 136188	A.M. Sirunyan et al.	(CMS Collab.)
AAIJ	20AW	JHEP 2012 144	R. Aaij et al.	(LHCb Collab.)
AAIJ	20E	PR D101 072004	R. Aaij et al.	(LHCb Collab.)
AAIJ	20F	PR D102 012011	R. Aaij et al.	(LHCb Collab.)
AAIJ	20W	PRL 124 211802	R. Aaij et al.	(LHCb Collab.)
PDG	20	PTEP 2020 083C01	P.A. Zyla et al.	(PDG Collab.)
SIRUNYAN	20AG	JHEP 2004 188	A.M. Sirunyan et al.	(CMS Collab.)
SIRUNYAN	20BB	PRL 125 152001	A.M. Sirunyan et al.	(CMS Collab.)
AABOUD	19L	JHEP 1904 098	M. Aaboud et al.	(ATLAS Collab.)
AAIJ	19AE	PRL 123 081802	R. Aaij et al.	(LHCb Collab.)
AAIJ	19AF	PL B797 134789	R. Aaij et al.	(LHCb Collab.)
AAIJ	19AK	PRL 123 211801	R. Aaij et al.	(LHCb Collab.)
AAIJ	19AP	JHEP 1912 155	R. Aaij et al.	(LHCb Collab.)
AAIJ	19K	JHEP 1906 114	R. Aaij et al.	(LHCb Collab.)
AAIJ	19L	JHEP 1907 032	R. Aaij et al.	(LHCb Collab.)
AAIJ	19Q	EPJ C79 706	R. Aaij et al.	(LHCb Collab.)
Also		EPJ C80 601 (errat.)	R. Aaij et al.	(LHCb Collab.)
AAIJ	19U	PRL 122 191804	R. Aaij et al.	(LHCb Collab.)

Downloaded from https://academic.oup.com/ptep/article/2022/8/083C01/6651666 by KIT Library user on 27 September 2022

AAIJ	18AB	JHEP 1807 020	R. Aaij *et al.*	(LHCb Collab.)
AAIJ	18AC	JHEP 1808 191	R. Aaij *et al.*	(LHCb Collab.)
AAIJ	18AY	PR D98 071103	R. Aaij *et al.*	(LHCb Collab.)
AAIJ	18AZ	PR D98 072006	R. Aaij *et al.*	(LHCb Collab.)
AAIJ	18O	PR D98 032004	R. Aaij *et al.*	(LHCb Collab.)
AAIJ	18S	JHEP 1803 140	R. Aaij *et al.*	(LHCb Collab.)
AAIJ	18T	JHEP 1803 078	R. Aaij *et al.*	(LHCb Collab.)
AAIJ	18U	JHEP 1803 059	R. Aaij *et al.*	(LHCb Collab.)
SIRUNYAN	18BY	EPJ C78 457	A.M. Sirunyan *et al.*	(CMS Collab.)
AAIJ	17A	PR D95 012006	R. Aaij *et al.*	(LHCb Collab.)
AAIJ	17AI	PRL 118 191801	R. Aaij *et al.*	(LHCb Collab.)
AAIJ	17AJ	PRL 118 251802	R. Aaij *et al.*	(LHCb Collab.)
AAIJ	17AL	PRL 119 041802	R. Aaij *et al.*	(LHCb Collab.)
AAIJ	17AN	PRL 119 101801	R. Aaij *et al.*	(LHCb Collab.)
AAIJ	17B	PRL 118 021801	R. Aaij *et al.*	(LHCb Collab.)
AAIJ	17BA	JHEP 1705 158	R. Aaij *et al.*	(LHCb Collab.)
AAIJ	17BB	EPJ C77 609	R. Aaij *et al.*	(LHCb Collab.)
AAIJ	17BD	PR D96 051103	R. Aaij *et al.*	(LHCb Collab.)
AAIJ	17BF	PL B774 139	R. Aaij *et al.*	(LHCb Collab.)
AAIJ	17BJ	PRL 119 232001	R. Aaij *et al.*	(LHCb Collab.)
AAIJ	17BP	JHEP 1711 027	R. Aaij *et al.*	(LHCb Collab.)
AAIJ	17G	PRL 118 081801	R. Aaij *et al.*	(LHCb Collab.)
AAIJ	17N	JHEP 1703 001	R. Aaij *et al.*	(LHCb Collab.)
AAIJ	17U	JHEP 1707 021	R. Aaij *et al.*	(LHCb Collab.)
AAIJ	17V	JHEP 1708 037	R. Aaij *et al.*	(LHCb Collab.)
AABOUD	16L	EPJ C76 513	M. Aaboud *et al.*	(ATLAS Collab.)
AAD	16AP	JHEP 1608 147	G. Aad *et al.*	(ATLAS Collab.)
AAIJ	16	JHEP 1601 012	R. Aaij *et al.*	(LHCb Collab.)
AAIJ	16AK	PL B762 253	R. Aaij *et al.*	(LHCb Collab.)
AAIJ	16AL	PL B762 484	R. Aaij *et al.*	(LHCb Collab.)
AAIJ	16C	PRL 116 161802	R. Aaij *et al.*	(LHCb Collab.)
AAIJ	16E	PRL 116 241601	R. Aaij *et al.*	(LHCb Collab.)
AAIJ	16G	PRL 117 061803	R. Aaij *et al.*	(LHCb Collab.)
AAIJ	16P	PR D93 092008	R. Aaij *et al.*	(LHCb Collab.)
AAIJ	16U	JHEP 1603 040	R. Aaij *et al.*	(LHCb Collab.)
ABAZOV	16C	PR D94 012001	V.M. Abazov *et al.*	(D0 Collab.)
KHACHATRY...	16Q	PL B756 84	V. Khachatryan *et al.*	(CMS Collab.)
KHACHATRY...	16S	PL B757 97	V. Khachatryan *et al.*	(CMS Collab.)
PAL	16	PRL 116 161801	B. Pal *et al.*	(BELLE Collab.)
AAIJ	15AC	JHEP 1505 019	R. Aaij *et al.*	(LHCb Collab.)
AAIJ	15AD	JHEP 1506 130	R. Aaij *et al.*	(LHCb Collab.)
AAIJ	15AF	JHEP 1507 166	R. Aaij *et al.*	(LHCb Collab.)
AAIJ	15AG	JHEP 1508 005	R. Aaij *et al.*	(LHCb Collab.)
AAIJ	15AL	JHEP 1506 131	R. Aaji *et al.*	(LHCb Collab.)
AAIJ	15AQ	JHEP 1509 179	R. Aaij *et al.*	(LHCb Collab.)
AAIJ	15AS	JHEP 1510 053	R. Aaij *et al.*	(LHCb Collab.)
AAIJ	15AV	JHEP 1511 082	R. Aaij *et al.*	(LHCb Collab.)
AAIJ	15BB	PR D92 112002	R. Aaij *et al.*	(LHCb Collab.)
AAIJ	15D	JHEP 1501 024	R. Aaij *et al.*	(LHCb Collab.)
AAIJ	15I	PRL 114 041801	R. Aaij *et al.*	(LHCb Collab.)
AAIJ	15K	PL B741 1	R. Aaij *et al.*	(LHCb Collab.)
AAIJ	15O	PRL 115 051801	R. Aaij *et al.*	(LHCb Collab.)
AAIJ	15S	PL B743 46	R. Aaij *et al.*	(LHCb Collab.)
AAIJ	15U	PL B747 484	R. Aaij *et al.*	(LHCb Collab.)
ABAZOV	15A	PRL 114 062001	V.M. Abazov *et al.*	(D0 Collab.)
ABAZOV	15L	PRL 115 161601	V.M. Abazov *et al.*	(D0 Collab.)
DUTTA	15	PR D91 011101	D. Dutta *et al.*	(BELLE Collab.)
KHACHATRY...	15BE	NAT 522 68	V. Khachatryan *et al.*	(CMS and LHCb Collab.)
OSWALD	15	PR D92 072013	C. Oswald *et al.*	(BELLE Collab.)
AAD	14U	PR D90 052007	G. Aad *et al.*	(ATLAS Collab.)
AAIJ	14AA	PRL 112 202001	R. Aaij *et al.*	(LHCb Collab.)
AAIJ	14AE	PR D90 052011	R. Aaij *et al.*	(LHCb Collab.)
AAIJ	14AX	PRL 113 172001	R. Aaij *et al.*	(LHCb Collab.)
AAIJ	14AY	PRL 113 211801	R. Aaij *et al.*	(LHCb Collab.)
AAIJ	14BF	JHEP 1411 060	R. Aaij *et al.*	(LHCb Collab.)
AAIJ	14BH	PR D90 072003	R. Aaij *et al.*	(LHCb Collab.)
AAIJ	14BM	NJP 16 123001	R. Aaij *et al.*	(LHCb Collab.)
AAIJ	14BN	PR D90 112002	R. Aaij *et al.*	(LHCb Collab.)
AAIJ	14BP	PL B739 218	R. Aaij *et al.*	(LHCb Collab.)
AAIJ	14BR	PR D89 092006	R. Aaij *et al.*	(LHCb Collab.)
AAIJ	14D	PL B728 607	R. Aaij *et al.*	(LHCb Collab.)
AAIJ	14E	JHEP 1404 114	R. Aaij *et al.*	(LHCb Collab.)
AAIJ	14F	PRL 112 111802	R. Aaij *et al.*	(LHCb Collab.)
AAIJ	14L	JHEP 1407 140	R. Aaij *et al.*	(LHCb Collab.)
AAIJ	14R	PL B736 446	R. Aaij *et al.*	(LHCb Collab.)
AAIJ	14S	PL B736 186	R. Aaij *et al.*	(LHCb Collab.)
AAIJ	14Y	PRL 112 091802	R. Aaij *et al.*	(LHCb Collab.)
AALTONEN	14P	PRL 113 242001	T. Aaltonen *et al.*	(CDF Collab.)
ABAZOV	14	PR D89 012002	V.M. Abazov *et al.*	(D0 Collab.)
PDG	14	CP C38 070001	K. Olive *et al.*	(PDG Collab.)
AAIJ	13	NP B867 1	R. Aaij *et al.*	(LHCb Collab.)
AAIJ	13A	NP B867 547	R. Aaij *et al.*	(LHCb Collab.)
AAIJ	13AA	NP B871 403	R. Aaij *et al.*	(LHCb Collab.)
AAIJ	13AB	NP B873 275	R. Aaij *et al.*	(LHCb Collab.)
AAIJ	13AC	NP B874 663	R. Aaij *et al.*	(LHCb Collab.)
AAIJ	13AL	PR D87 071101	R. Aaij *et al.*	(LHCb Collab.)
AAIJ	13AN	PR D87 072004	R. Aaij *et al.*	(LHCb Collab.)
AAIJ	13AP	PR D87 092007	R. Aaij *et al.*	(LHCb Collab.)
AAIJ	13AQ	PR D87 112009	R. Aaij *et al.*	(LHCb Collab.)
AAIJ	13AR	PR D87 112010	R. Aaij *et al.*	(LHCb Collab.)
AAIJ	13AW	PRL 110 211801	R. Aaij *et al.*	(LHCb Collab.)
AAIJ	13AX	PRL 110 221601	R. Aaij *et al.*	(LHCb Collab.)
AAIJ	13AY	PRL 110 241802	R. Aaij *et al.*	(LHCb Collab.)
AAIJ	13B	PRL 110 021801	R. Aaij *et al.*	(LHCb Collab.)
AAIJ	13BA	PRL 111 101805	R. Aaij *et al.*	(LHCb Collab.)
AAIJ	13BI	NJP 15 053021	R. Aaij *et al.*	(LHCb Collab.)
AAIJ	13BM	PRL 111 141801	R. Aaij *et al.*	(LHCb Collab.)
AAIJ	13BO	JHEP 1310 183	R. Aaij *et al.*	(LHCb Collab.)
AAIJ	13BP	JHEP 1310 143	R. Aaij *et al.*	(LHCb Collab.)
AAIJ	13BQ	JHEP 1310 005	R. Aaij *et al.*	(LHCb Collab.)
AAIJ	13BW	JHEP 1311 092	R. Aaij *et al.*	(LHCb Collab.)
AAIJ	13BX	PL B727 403	R. Aaij *et al.*	(LHCb Collab.)
AAIJ	13CF	EPJ C73 2655	R. Aaij *et al.*	(LHCb Collab.)
AAIJ	13L	JHEP 1303 067	R. Aaij *et al.*	(LHCb Collab.)
AAIJ	13X	JHEP 1307 084	R. Aaij *et al.*	(LHCb Collab.)
AAIJ	13Z	JHEP 1309 006	R. Aaij *et al.*	(LHCb Collab.)
AALTONEN	13F	PR D87 072003	T. Aaltonen *et al.*	(CDF Collab.)
ABAZOV	13	PRL 110 011801	V.M. Abazov *et al.*	(D0 Collab.)
ABAZOV	13C	PR D87 072006	V.M. Abazov *et al.*	(D0 Collab.)
CHATRCHYAN	13AW	PRL 111 101804	S. Chatrchyan *et al.*	(CMS Collab.)
ESEN	13	PR D87 031101	S. Esen *et al.*	(BELLE Collab.)
OSWALD	13	PR D87 072008	C. Oswald *et al.*	(BELLE Collab.)
Also		PR D90 119901 (errat.)	C. Oswald *et al.*	(BELLE Collab.)
SOLOVIEVA	13	PL B726 206	E. Solovieva *et al.*	(BELLE Collab.)
THORNE	13	PR D88 114006	F. Thorne *et al.*	(BELLE Collab.)
AAD	12AE	PL B713 387	G. Aad *et al.*	(ATLAS Collab.)
AAD	12CV	JHEP 1212 072	G. Aad *et al.*	(ATLAS Collab.)
AAIJ	12	PL B707 349	R. Aaij *et al.*	(LHCb Collab.)
AAIJ	12A	PL B708 55	R. Aaij *et al.*	(LHCb Collab.)
AAIJ	12AE	PR D85 112013	R. Aaij *et al.*	(LHCb Collab.)
AAIJ	12AG	JHEP 1206 115	R. Aaij *et al.*	(LHCb Collab.)
AAIJ	12AM	PRL 109 131801	R. Aaij *et al.*	(LHCb Collab.)
AAIJ	12AN	PRL 109 152002	R. Aaij *et al.*	(LHCb Collab.)
AAIJ	12AO	PR D86 052006	R. Aaij *et al.*	(LHCb Collab.)
AAIJ	12AP	PR D86 071102	R. Aaij *et al.*	(LHCb Collab.)
AAIJ	12AR	JHEP 1210 037	R. Aaij *et al.*	(LHCb Collab.)
AAIJ	12AX	PR D86 112005	R. Aaij *et al.*	(LHCb Collab.)
AAIJ	12B	PL B707 497	R. Aaij *et al.*	(LHCb Collab.)
AAIJ	12D	PRL 108 101803	R. Aaij *et al.*	(LHCb Collab.)
AAIJ	12E	PL B708 241	R. Aaij *et al.*	(LHCb Collab.)
AAIJ	12F	PL B709 50	R. Aaij *et al.*	(LHCb Collab.)
AAIJ	12I	PL B709 177	R. Aaij *et al.*	(LHCb Collab.)
AAIJ	12L	EPJ C72 2118	R. Aaij *et al.*	(LHCb Collab.)
AAIJ	12O	PL B713 172	R. Aaij *et al.*	(LHCb Collab.)
AAIJ	12P	PL B713 369	R. Aaij *et al.*	(LHCb Collab.)
AAIJ	12Q	PL B713 378	R. Aaij *et al.*	(LHCb Collab.)
AAIJ	12R	PL B716 393	R. Aaij *et al.*	(LHCb Collab.)
AAIJ	12S	PRL 108 151801	R. Aaij *et al.*	(LHCb Collab.)
AAIJ	12V	PRL 108 201601	R. Aaij *et al.*	(LHCb Collab.)
AAIJ	12W	PRL 108 231801	R. Aaij *et al.*	(LHCb Collab.)
AALTONEN	12AJ	PRL 109 171802	T. Aaltonen *et al.*	(CDF Collab.)
AALTONEN	12C	PRL 108 201801	T. Aaltonen *et al.*	(CDF Collab.)
AALTONEN	12D	PR D85 072002	T. Aaltonen *et al.*	(CDF Collab.)
AALTONEN	12L	PRL 108 211803	T. Aaltonen *et al.*	(CDF Collab.)
ABAZOV	12AF	PR D86 092011	V.M. Abazov *et al.*	(D0 Collab.)
ABAZOV	12C	PR D85 011103	V.M. Abazov *et al.*	(D0 Collab.)
ABAZOV	12D	PR D85 032006	V.M. Abazov *et al.*	(D0 Collab.)
CHATRCHYAN	12A	JHEP 1204 033	S. Chatrchyan *et al.*	(CMS Collab.)
LEES	12A	PR D85 011101	J.P. Lees *et al.*	(BABAR Collab.)
LI	12	PRL 108 181808	J. Li *et al.*	(BELLE Collab.)
PDG	12	PR D86 010001	J. Beringer *et al.*	(PDG Collab.)
AAIJ	11	PL B698 115	R. Aaij *et al.*	(LHCb Collab.)
AAIJ	11A	PL B698 14	R. Aaij *et al.*	(LHCb Collab.)
AAIJ	11B	PL B699 330	R. Aaij *et al.*	(LHCb Collab.)
AAIJ	11D	PL B706 32	R. Aaij	(LHCb Collab.)
AAIJ	11E	PR D84 092001	R. Aaij *et al.*	(LHCb Collab.)
Also		PR D85 039904 (errat.)	R. Aaij *et al.*	(LHCb Collab.)
AALTONEN	11A	PR D83 052012	T. Aaltonen *et al.*	(CDF Collab.)
AALTONEN	11AB	PR D84 052012	T. Aaltonen *et al.*	(CDF Collab.)
AALTONEN	11AG	PRL 107 191801	T. Aaltonen *et al.*	(CDF Collab.)
Also		PRL 107 239903 (errat.)	T. Aaltonen *et al.*	(CDF Collab.)
AALTONEN	11AI	PRL 107 201802	T. Aaltonen *et al.*	(CDF Collab.)
AALTONEN	11AN	PRL 107 261802	T. Aaltonen *et al.*	(CDF Collab.)
AALTONEN	11AP	PRL 107 272001	T. Aaltonen *et al.*	(CDF Collab.)
AALTONEN	11L	PRL 106 161801	T. Aaltonen *et al.*	(CDF Collab.)
AALTONEN	11N	PRL 106 181802	T. Aaltonen *et al.*	(CDF Collab.)
ABAZOV	11U	PR D84 052007	V.M. Abazov *et al.*	(D0 Collab.)
CHATRCHYAN	11T	PRL 107 191802	S. Chatrchyan *et al.*	(CMS Collab.)
LI	11	PRL 106 121802	J. Li *et al.*	(BELLE Collab.)
ABAZOV	10E	PR D82 012003	V.M. Abazov *et al.*	(D0 Collab.)
ABAZOV	10H	PRL 105 081801	V.M. Abazov *et al.*	(D0 Collab.)
Also		PR D82 032001	V.M. Abazov *et al.*	(D0 Collab.)
ABAZOV	10S	PL B693 539	V.M. Abazov *et al.*	(D0 Collab.)
ESEN	10	PRL 105 201802	S. Esen *et al.*	(BELLE Collab.)
LOUVOT	10	PRL 104 231801	R. LOUVOT *et al.*	(BELLE Collab.)
PENG	10	PR D82 072007	C.-C. Peng *et al.*	(BELLE Collab.)
AALTONEN	09AQ	PRL 103 191802	T. Aaltonen *et al.*	(CDF Collab.)
AALTONEN	09B	PR D79 011104	T. Aaltonen *et al.*	(CDF Collab.)
AALTONEN	09C	PRL 103 031801	T. Aaltonen *et al.*	(CDF Collab.)
AALTONEN	09P	PRL 102 201801	T. Aaltonen *et al.*	(CDF Collab.)
ABAZOV	09E	PRL 102 032001	V.M. Abazov *et al.*	(D0 Collab.)
ABAZOV	09G	PRL 102 051801	V.M. Abazov *et al.*	(D0 Collab.)
ABAZOV	09I	PRL 102 091801	V.M. Abazov *et al.*	(D0 Collab.)
ABAZOV	09Y	PR D79 111102	V.M. Abazov *et al.*	(D0 Collab.)
LOUVOT	09	PRL 102 021801	R. Louvot *et al.*	(BELLE Collab.)
AALTONEN	08F	PRL 100 021803	T. Aaltonen *et al.*	(CDF Collab.)
AALTONEN	08G	PRL 100 161802	T. Aaltonen *et al.*	(CDF Collab.)
AALTONEN	08J	PRL 100 121803	T. Aaltonen *et al.*	(CDF Collab.)
ABAZOV	08AM	PRL 101 241801	V.M. Abazov *et al.*	(D0 Collab.)
WICHT	08A	PRL 100 121801	J. Wicht *et al.*	(BELLE Collab.)
ABAZOV	07	PRL 98 121801	V.M. Abazov *et al.*	(D0 Collab.)
ABAZOV	07A	PRL 98 151801	V.M. Abazov *et al.*	(D0 Collab.)
ABAZOV	07N	PR D76 057101	V.M. Abazov *et al.*	(D0 Collab.)
ABAZOV	07Y	PRL 99 241801	V.M. Abazov *et al.*	(D0 Collab.)
ABULENCIA	07C	PRL 98 061802	A. Abulencia *et al.*	(CDF Collab.)
DRUTSKOY	07	PRL 98 052001	A. Drutskoy *et al.*	(BELLE Collab.)
DRUTSKOY	07A	PR D76 012002	A. Drutskoy *et al.*	(BELLE Collab.)
ABAZOV	06B	PRL 97 021802	V.M. Abazov *et al.*	(D0 Collab.)
ABAZOV	06G	PR D74 031107	V.M. Abazov *et al.*	(D0 Collab.)
ABAZOV	06V	PRL 97 241801	V.M. Abazov *et al.*	(D0 Collab.)
ABULENCIA	06J	PRL 96 191801	A. Abulencia *et al.*	(CDF Collab.)
ABULENCIA	06N	PRL 96 231801	A. Abulencia *et al.*	(CDF Collab.)
ABULENCIA	06Q	PRL 97 062003	A. Abulencia *et al.*	(CDF Collab.)
ABULENCIA,A	06D	PRL 97 211802	A. Abulencia *et al.*	(CDF Collab.)
ABULENCIA,A	06G	PRL 97 242003	A. Abulencia *et al.*	(CDF Collab.)
ACOSTA	06	PRL 96 202001	D. Acosta *et al.*	(CDF Collab.)
ABAZOV	05B	PRL 94 042001	V.M. Abazov *et al.*	(D0 Collab.)
ABAZOV	05W	PRL 95 171801	V.M. Abazov *et al.*	(D0 Collab.)
ACOSTA	05	PRL 94 101803	D. Acosta *et al.*	(CDF Collab.)
ACOSTA	05J	PRL 95 031801	D. Acosta *et al.*	(CDF Collab.)
ABDALLAH	04A	PL B585 63	J. Abdallah *et al.*	(DELPHI Collab.)
ABDALLAH	04J	EPJ C35 35	J. Abdallah *et al.*	(DELPHI Collab.)
ABDALLAH	03B	EPJ C28 155	J. Abdallah *et al.*	(DELPHI Collab.)
ABE	03	PR D67 012006	K. Abe *et al.*	(SLD Collab.)
HEISTER	03E	EPJ C29 143	A. Heister *et al.*	(ALEPH Collab.)
ABE	02V	PR D66 032009	K. Abe *et al.*	(SLD Collab.)
ACOSTA	02D	PR D65 111101	D. Acosta *et al.*	(CDF Collab.)
ACOSTA	02G	PR D66 112002	D. Acosta *et al.*	(CDF Collab.)
ABBIENDI	01D	EPJ C19 241	G. Abbiendi *et al.*	(OPAL Collab.)
ABE	00C	PR D62 071101	K. Abe *et al.*	(SLD Collab.)
ABREU	00Y	EPJ C16 555	P. Abreu *et al.*	(DELPHI Collab.)
ABREU,P	00G	EPJ C18 229	P. Abreu *et al.*	(DELPHI Collab.)
AFFOLDER	00N	PRL 85 4668	T. Affolder *et al.*	(CDF Collab.)
BARATE	00K	PL B486 286	R. Barate *et al.*	(ALEPH Collab.)
ABBIENDI	99S	EPJ C11 587	G. Abbiendi *et al.*	(OPAL Collab.)
ABE	99D	PR D59 032004	F. Abe *et al.*	(CDF Collab.)
ABE	99J	PRL 82 3576	F. Abe *et al.*	(CDF Collab.)
BARATE	99J	EPJ C7 553	R. Barate *et al.*	(ALEPH Collab.)
Also		EPJ C12 181 (errat.)	R. Barate *et al.*	(ALEPH Collab.)
ABE	98B	PR D57 5382	F. Abe *et al.*	(CDF Collab.)
ABE	98V	PRL 81 5742	F. Abe *et al.*	(CDF Collab.)
ACCIARRI	98S	PL B438 417	M. Acciarri *et al.*	(L3 Collab.)
ACKERSTAFF	98F	EPJ C2 407	K. Ackerstaff *et al.*	(OPAL Collab.)
ACKERSTAFF	98G	PL B426 161	K. Ackerstaff *et al.*	(OPAL Collab.)
BARATE	98C	EPJ C4 367	R. Barate *et al.*	(ALEPH Collab.)
BARATE	98Q	EPJ C4 387	R. Barate *et al.*	(ALEPH Collab.)
PDG	98	EPJ C3 1	C. Caso *et al.*	(PDG Collab.)
ACCIARRI	97B	PL B391 474	M. Acciarri *et al.*	(L3 Collab.)
ACCIARRI	97C	PL B391 481	M. Acciarri *et al.*	(L3 Collab.)
ACKERSTAFF	97U	ZPHY C76 401	K. Ackerstaff *et al.*	(OPAL Collab.)
ACKERSTAFF	97V	ZPHY C76 417	K. Ackerstaff *et al.*	(OPAL Collab.)
ADAM	97	PL B414 382	W. Adam *et al.*	(DELPHI Collab.)
ABE	96B	PR D53 3496	F. Abe *et al.*	(CDF Collab.)

Downloaded from https://academic.oup.com/ptep/article/2022/8/083C01/6651666 by KIT Library user on 27 September 2022

ABE	96N	PRL 77 1945	F. Abe et al.	(CDF Collab.)
ABE	96Q	PR D54 6596	F. Abe et al.	(CDF Collab.)
ABREU	96F	ZPHY C71 11	P. Abreu et al.	(DELPHI Collab.)
ADAM	96D	ZPHY C72 207	W. Adam et al.	(DELPHI Collab.)
BUSKULIC	96E	ZPHY C69 585	D. Buskulic et al.	(ALEPH Collab.)
BUSKULIC	96M	PL B377 205	D. Buskulic et al.	(ALEPH Collab.)
BUSKULIC	96V	PL B384 471	D. Buskulic et al.	(ALEPH Collab.)
PDG	96	PR D54 1	R. M. Barnett et al.	(PDG Collab.)
ABE	95R	PRL 74 4988	F. Abe et al.	(CDF Collab.)
ABE	95Z	PRL 75 3068	F. Abe et al.	(CDF Collab.)
ACCIARRI	95H	PL B363 127	M. Acciarri et al.	(L3 Collab.)
ACCIARRI	95I	PL B363 137	M. Acciarri et al.	(L3 Collab.)
AKERS	95G	PL B350 273	R. Akers et al.	(OPAL Collab.)
AKERS	95J	ZPHY C66 555	R. Akers et al.	(OPAL Collab.)
BUSKULIC	95J	PL B356 409	D. Buskulic et al.	(ALEPH Collab.)
BUSKULIC	95O	PL B361 221	D. Buskulic et al.	(ALEPH Collab.)
ABREU	94D	PL B324 500	P. Abreu et al.	(DELPHI Collab.)
ABREU	94E	ZPHY C61 407	P. Abreu et al.	(DELPHI Collab.)
Also		PL B289 199	P. Abreu et al.	(DELPHI Collab.)
AKERS	94J	PL B337 196	R. Akers et al.	(OPAL Collab.)
AKERS	94L	PL B337 393	R. Akers et al.	(OPAL Collab.)
BUSKULIC	94B	PL B322 441	D. Buskulic et al.	(ALEPH Collab.)
BUSKULIC	94C	PL B322 275	D. Buskulic et al.	(ALEPH Collab.)
ABE	93F	PRL 71 1685	F. Abe et al.	(CDF Collab.)
ACTON	93H	PL B312 501	P.D. Acton et al.	(OPAL Collab.)
BUSKULIC	93G	PL B311 425	D. Buskulic et al.	(ALEPH Collab.)
ABREU	92M	PL B289 199	P. Abreu et al.	(DELPHI Collab.)
ACTON	92N	PL B295 357	P.D. Acton et al.	(OPAL Collab.)
BUSKULIC	92E	PL B294 145	D. Buskulic et al.	(ALEPH Collab.)
LEE-FRANZINI	90	PRL 65 2947	J. Lee-Franzini et al.	(CUSB II Collab.)

B_s^*

$I(J^P) = 0(1^-)$

I, J, P need confirmation. Quantum numbers shown are quark-model predictions.

B_s^* MASS

From mass difference below and the B_s^0 mass.

VALUE (MeV)	DOCUMENT ID		TECN	COMMENT
$5415.4^{+1.8}_{-1.5}$ OUR FIT Error includes scale factor of 2.9.				
5415.8±1.5 OUR AVERAGE Error includes scale factor of 2.6.				
5416.4±0.4±0.5	LOUVOT	09	BELL	$e^+e^- \to \Upsilon(5S)$
5411.7±1.6±0.6	[1] AQUINES	06	CLEO	$e^+e^- \to \Upsilon(5S)$
• • • We do not use the following data for averages, fits, limits, etc. • • •				
5418 ±1 ±3	DRUTSKOY	07A	BELL	Repl. by LOUVOT 09
5414 ±1 ±3	[2] BONVICINI	06	CLEO	$e^+e^- \to \Upsilon(5S)$

[1] Utilized the beam constrained invariant mass peak positions for B^* and B_s^* to extract the measurement.
[2] Uses 14 candidates consistent with B_s decays into final states with a J/ψ and a $D_s^{(*)-}$.

$m_{B_s^*} - m_{B_s}$

VALUE (MeV)	DOCUMENT ID		TECN	COMMENT
$48.5^{+1.8}_{-1.5}$ OUR FIT Error includes scale factor of 2.9.				
46.1±1.5 OUR AVERAGE				
45.7±1.7±0.7	[3] AQUINES	06	CLEO	$e^+e^- \to \Upsilon(5S)$
47.0±2.6	[4] LEE-FRANZINI	90	CSB2	$e^+e^- \to \Upsilon(5S)$
• • • We do not use the following data for averages, fits, limits, etc. • • •				
48 ±1 ±3	[5] BONVICINI	06	CLEO	Repl. by AQUINES 06

[3] Utilized the beam constrained invariant mass peak positions for B^* and B_s^* to extract the measurement.
[4] LEE-FRANZINI 90 measure 46.7 ± 0.4 ± 0.2 MeV for an admixture of B^0, B^+, and B_s. They use the shape of the photon line to separate the above value for B_s.
[5] Uses 14 candidates consistent with B_s decays into final states with a J/ψ and a $D_s^{(*)-}$.

$|(m_{B_s^*} - m_{B_s}) - (m_{B^*} - m_B)|$

VALUE (MeV)	CL%	DOCUMENT ID		TECN	COMMENT
<6	95	ABREU	95R	DLPH	E^{ee}_{cm}= 88–94 GeV

B_s^* DECAY MODES

	Mode	Fraction (Γ_i/Γ)
Γ_1	$B_s\gamma$	seen

B_s^* REFERENCES

LOUVOT	09	PRL 102 021801	R. Louvot et al.	(BELLE Collab.)
DRUTSKOY	07A	PR D76 012002	A. Drutskoy et al.	(BELLE Collab.)
AQUINES	06	PRL 96 152001	O. Aquines et al.	(CLEO Collab.)
BONVICINI	06	PRL 96 022002	G. Bonvicini et al.	(CLEO Collab.)
ABREU	95R	ZPHY C68 353	P. Abreu et al.	(DELPHI Collab.)
LEE-FRANZINI	90	PRL 65 2947	J. Lee-Franzini et al.	(CUSB II Collab.)

$X(5568)^\pm$

$I(J^P) = ?(?^?)$

OMITTED FROM SUMMARY TABLE

Seen as a peak in the $B_s\pi^\pm$ mass spectrum with a significance of more than 3σ by ABAZOV 16E and ABAZOV 18A in inclusive $p\overline{p}$ collisions at 1.96 TeV. Not seen by AAIJ 16AI, AABOUD 18L, AALTONEN 18A, and SIRUNYAN 18J. Needs confirmation.

$X(5568)^\pm$ MASS

VALUE (MeV)	EVTS	DOCUMENT ID		TECN	COMMENT
$5566.9^{+3.2+0.6}_{-3.1-1.2}$	278	[1] ABAZOV	18A	D0	$p\overline{p} \to B_s^0\pi^\pm X$
• • • We do not use the following data for averages, fits, limits, etc. • • •					
$5567.8\pm2.9^{+0.9}_{-1.9}$	133	[2] ABAZOV	16E	D0	$p\overline{p} \to B_s^0\pi^\pm X$

[1] From the combined analysis of $B_s^0 \to J/\psi\phi$ and $B_s^0 \to D_s^\pm\mu^\mp X$ decays.
[2] Assumes $X(5568)^\pm \to B_s\pi^\pm$ decay. If $X(5568)^\pm \to B_s^*\pi^\pm$ decay is assumed, the mass shifts upward by 49 MeV.

$X(5568)^\pm$ WIDTH

VALUE (MeV)	EVTS	DOCUMENT ID		TECN	COMMENT
$18.6^{+7.9+3.5}_{-6.1-3.8}$	278	[1] ABAZOV	18A	D0	$p\overline{p} \to B_s\pi^\pm X$
• • • We do not use the following data for averages, fits, limits, etc. • • •					
$21.9\pm6.4^{+5.0}_{-2.5}$	133	ABAZOV	16E	D0	$p\overline{p} \to B_s\pi^\pm X$

[1] From the combined analysis of $B_s^0 \to J/\psi\phi$ and $B_s^0 \to D_s^\pm\mu^\mp X$ decays.

$X(5568)^\pm$ DECAY MODES

	Mode	Fraction (Γ_i/Γ)
Γ_1	$B_s\pi^\pm$	seen

$\Gamma(B_s\pi^\pm)/\Gamma_{total}$ — Γ_1/Γ

VALUE	EVTS	DOCUMENT ID		TECN	COMMENT
seen	145	[1] ABAZOV	18A	D0	$p\overline{p} \to B_s^0\pi^\pm X$
seen	133	[2] ABAZOV	16E	D0	$p\overline{p} \to B_s^0\pi^\pm X$
• • • We do not use the following data for averages, fits, limits, etc. • • •					
not seen		[3] AABOUD	18L	ATLS	$pp \to B_s^0\pi^\pm X$
not seen		[4] AALTONEN	18A	CDF	$p\overline{p} \to B_s^0\pi^\pm X$
not seen		[5] SIRUNYAN	18J	CMS	$pp \to B_s^0\pi^\pm X$
not seen		[6] AAIJ	16AI	LHCB	$pp \to B_s^0\pi^\pm X$

[1] With B_s mesons reconstructed in decays to $D_s^\pm\mu^\mp X$.
[2] Seen in $p\overline{p}$ collisions at 1.96 TeV at a rate of (8.6 ± 1.9 ± 1.4)% relative to inclusive B_s production in the kinematic region $10 < p_T(B_s) < 30$ GeV/c, with B_s mesons reconstructed in decays to $J/\psi\phi$.An alternative possibility, $X(5568)^\pm \to B_s^*\pi^\pm$ with a missing γ, could not be ruled out.
[3] Not seen in 24.4 fb^{-1} of pp collision data at $\sqrt{s}$ = 7 and 8 TeV with B_s mesons reconstructed in decays to $J/\psi\phi$. An upper limit on the production rate times branching fraction for $X(5568)^\pm \to B_s\pi^\pm$ relative to inclusive B_s production is less than 1.5% at $p_T(B_s) > 10$ GeV/c and less than 1.6% at $p_T(B_s) > 15$ GeV/c at 95% CL.
[4] Not seen in 9.6 fb^{-1} of $p\overline{p}$ collision data at $\sqrt{s}$ = 1.96 TeV with B_s mesons reconstructed in decays to $J/\psi\phi$. An upper limit on the production rate times branching fraction for $X(5568)^\pm \to B_s\pi^\pm$ relative to inclusive B_s production is less than 6.7% at 95% CL.
[5] Not seen in 19.7 fb^{-1} of pp collisions data at $\sqrt{s}$ = 8 TeV with B_s mesons reconstructed in decays to $J/\psi\phi$. An upper limit on the production rate times branching fraction for $X(5568)^\pm \to B_s\pi^\pm$ relative to inclusive B_s production is less than 1.1% at $p_T(B_s) > 10$ GeV/c and less than 1.0% at $p_T(B_s) > 15$ GeV/c at 95%CL.
[6] Not seen in 3 fb^{-1} of pp collision data at $\sqrt{s}$ = 7 and 8 TeV in a scan over the $X(5568)$ mass and width, with B_s mesons reconstructed in decays to $D_s^-\pi^+$ or $J/\psi\phi$. An upper limit on the production rate times branching fraction for $X(5568)^\pm \to B_s\pi^\pm$ relative to inclusive B_s production is less than 2.1% at $p_T(B_s) > 10$ GeV/c at 90% CL.

$X(5568)^\pm$ REFERENCES

AABOUD	18L	PRL 120 202007	M. Aaboud et al.	(ATLAS Collab.)
AALTONEN	18A	PRL 120 202006	T. Aaltonen et al.	(CDF Collab.)
ABAZOV	18A	PR D97 092004	V.M. Abazov et al.	(D0 Collab.)
SIRUNYAN	18J	PRL 120 202005	A.M. Sirunyan et al.	(CMS Collab.)
AAIJ	16AI	PRL 117 152003	R. Aaij et al.	(LHCb Collab.)
ABAZOV	16E	PRL 117 022003	V.M. Abazov et al.	(D0 Collab.)

Downloaded from https://academic.oup.com/ptep/article/2022/8/083C01/6651666 by KIT Library user on 27 September 2022

$B_{s1}(5830)^0$

$I(J^P) = 0(1^+)$
I, J, P need confirmation.

Quantum numbers shown are quark-model predictions.

$B_{s1}(5830)^0$ MASS

VALUE (MeV)	DOCUMENT ID		TECN	COMMENT
5828.70±0.20 OUR FIT				
5828.65±0.24 OUR AVERAGE				
5828.78±0.09±0.29	SIRUNYAN	18DF	CMS	pp at 8 TeV
5828.40±0.04±0.41	[1] AAIJ	13O	LHCB	pp at 7 TeV
• • • We do not use the following data for averages, fits, limits, etc. • • •				
5829.4 ±0.7	[2] AALTONEN	08K	CDF	Repl. by AALTONEN 14I

[1] Uses $B_{s1}(5830)^0 \to B^{*+} K^-$ decay.
[2] Uses two-body decays into K^- and B^+ mesons reconstructed as $B^+ \to J/\psi K^+$, $J/\psi \to \mu^+\mu^-$ or $B^+ \to \overline{D}^0\pi^+$, $\overline{D}^0 \to K^+\pi^-$.

$m_{B^0_{s1}} - m_{B^{*+}}$

VALUE (MeV)	DOCUMENT ID		TECN	COMMENT
503.99±0.17 OUR FIT				
504.03±0.12±0.15	[1] AALTONEN	14I	CDF	$p\overline{p}$ at 1.96 TeV
• • • We do not use the following data for averages, fits, limits, etc. • • •				
504.41±0.21±0.14	[2] AALTONEN	08K	CDF	Repl. by AALTONEN 14I

[1] AALTONEN 14I reports $m_{B_{s1}(5830)^0} - m_{B^{*+}} - m_{K^-} = 10.35 \pm 0.12 \pm 0.15$ MeV which we adjusted by the K^- mass.
[2] Uses two-body decays into K^- and B^+ mesons reconstructed as $B^+ \to J/\psi K^+$, $J/\psi \to \mu^+\mu^-$ or $B^+ \to \overline{D}^0\pi^+$, $\overline{D}^0 \to K^+\pi^-$.

$B_{s1}(5830)^0$ WIDTH

VALUE (MeV)	DOCUMENT ID		TECN	COMMENT
0.5±0.3±0.3	AALTONEN	14I	CDF	$p\overline{p}$ at 1.96 TeV

$B_{s1}(5830)^0$ DECAY MODES

	Mode	Fraction (Γ_i/Γ)
Γ_1	$B^{*+} K^-$	seen
Γ_2	$B^{*0} K^0_S$	

$B_{s1}(5830)^0$ BRANCHING RATIOS

$\Gamma(B^{*+} K^-)/\Gamma_{total}$ — Γ_1/Γ

VALUE	DOCUMENT ID		TECN	COMMENT
seen	AALTONEN	08K	CDF	$p\overline{p}$ at 1.96 TeV

$\Gamma(B^{*0} K^0_S)/\Gamma(B^{*+} K^-)$ — Γ_2/Γ_1

VALUE	DOCUMENT ID		TECN	COMMENT
0.49±0.12±0.07	[1] SIRUNYAN	18DF	CMS	pp at 8 TeV

[1] With the branching fractions $B(B^+ \to J/\psi K^+) = (1.026 \pm 0.031) \times 10^{-3}$ and $B(B^0 \to J/\psi K^{*0}) = (1.28 \pm 0.05) \times 10^{-3}$.

$B_{s1}(5830)^0$ REFERENCES

SIRUNYAN	18DF	EPJ C78 939	A.M. Sirunyan *et al.*	(CMS Collab.)
AALTONEN	14I	PR D90 012013	T. Aaltonen *et al.*	(CDF Collab.)
AAIJ	13O	PRL 110 151803	R. Aaij *et al.*	(LHCb Collab.)
AALTONEN	08K	PRL 100 082001	T. Aaltonen *et al.*	(CDF Collab.)

$B^*_{s2}(5840)^0$

$I(J^P) = 0(2^+)$
I, J, P need confirmation.

Quantum numbers shown are quark-model predictions.

$B^*_{s2}(5840)^0$ MASS

VALUE (MeV)	DOCUMENT ID		TECN	COMMENT
5839.86±0.12 OUR FIT				
5839.92±0.14 OUR AVERAGE				
5839.86±0.09±0.17	SIRUNYAN	18DF	CMS	pp at 8 TeV
5839.99±0.05±0.20	AAIJ	13O	LHCB	pp at 7 TeV
5839.6 ±1.1 ±0.7	[1] ABAZOV	08E	D0	$p\overline{p}$ at 1.96 TeV
• • • We do not use the following data for averages, fits, limits, etc. • • •				
5839.7 ±0.7	[2] AALTONEN	08K	CDF	Repl. by AALTONEN 14I

[1] Observed in $B^*_{s2}{}^0 \to B^+ K^-$. Measured production rate of $B^*_{s2}{}^0$ relative to B^+ to be $(1.15 \pm 0.23 \pm 0.13)$%.
[2] Uses two-body decays into K^- and B^+ mesons reconstructed as $B^+ \to J/\psi K^+$, $J/\psi \to \mu^+\mu^-$ or $B^+ \to \overline{D}^0\pi^+$, $\overline{D}^0 \to K^+\pi^-$.

$m_{B^*_{s2}{}^0} - m_{B^0_{s1}}$

VALUE (MeV)	DOCUMENT ID		TECN	COMMENT
• • • We do not use the following data for averages, fits, limits, etc. • • •				
10.5±0.6	[1] AALTONEN	08K	CDF	Repl. by AALTONEN 14I

[1] Uses two-body decays into K^- and B^+ mesons reconstructed as $B^+ \to J/\psi K^+$, $J/\psi \to \mu^+\mu^-$ or $B^+ \to \overline{D}^0\pi^+$, $\overline{D}^0 \to K^+\pi^-$.

$m_{B^*_{s2}{}^0} - m_{B^+}$

VALUE (MeV)	DOCUMENT ID		TECN	COMMENT
560.52±0.14 OUR FIT				
560.41±0.13±0.14	[1] AALTONEN	14I	CDF	$p\overline{p}$ at 1.96 TeV

[1] AALTONEN 14I reports $m_{B_{s2}(5840)^0} - m_{B^+} - m_{K^-} = 66.73 \pm 0.13 \pm 0.14$ MeV which we adjusted by the K^- mass.

$B^*_{s2}(5840)^0$ WIDTH

VALUE (MeV)	DOCUMENT ID		TECN	COMMENT
1.49±0.27 OUR AVERAGE				
1.52±0.34±0.30	SIRUNYAN	18DF	CMS	pp at 8 TeV
1.4 ±0.4 ±0.2	AALTONEN	14I	CDF	$p\overline{p}$ at 1.96 TeV
1.56±0.13±0.47	[1] AAIJ	13O	LHCB	pp at 7 TeV

[1] Uses $B^*_{s2}(5840)^0 \to B^{*+} K^-$ decays.

$B^*_{s2}(5840)^0$ DECAY MODES

Branching fractions are given relative to the one **DEFINED AS 1**.

	Mode	Fraction (Γ_i/Γ)
Γ_1	$B^+ K^-$	**DEFINED AS 1**
Γ_2	$B^{*+} K^-$	0.093±0.018
Γ_3	$B^0 K^0_S$	0.43 ±0.11
Γ_4	$B^{*0} K^0_S$	0.04 ±0.04

$B^*_{s2}(5840)^0$ BRANCHING RATIOS

$\Gamma(B^+ K^-)/\Gamma_{total}$ — Γ_1/Γ

VALUE	DOCUMENT ID		TECN	COMMENT
seen	AALTONEN	08K	CDF	$p\overline{p}$ at 1.96 TeV
seen	[1] ABAZOV	08E	D0	$p\overline{p}$ at 1.96 TeV

[1] Measured production rate of $B^*_{s2}{}^0$ relative to B^+ to be $(1.15 \pm 0.23 \pm 0.13)$%.

$\Gamma(B^{*+} K^-)/\Gamma(B^+ K^-)$ — Γ_2/Γ_1

VALUE	DOCUMENT ID		TECN	COMMENT
0.093±0.013±0.012	AAIJ	13O	LHCB	pp at 7 TeV

$\Gamma(B^{*0} K^0_S)/\Gamma(B^0 K^0_S)$ — Γ_4/Γ_3

VALUE	DOCUMENT ID		TECN	COMMENT
0.093±0.086±0.014	[1] SIRUNYAN	18DF	CMS	pp at 8 TeV

[1] With the branching fraction $B(B^0 \to J/\psi K^{*0}) = (1.28 \pm 0.05) \times 10^{-3}$.

$\Gamma(B^0 K^0_S)/\Gamma(B^+ K^-)$ — Γ_3/Γ_1

VALUE	DOCUMENT ID		TECN	COMMENT
0.432±0.077±0.078	[1] SIRUNYAN	18DF	CMS	pp at 8 TeV

[1] With the branching fractions $B(B^+ \to J/\psi K^+) = (1.026 \pm 0.031) \times 10^{-3}$ and $B(B^0 \to J/\psi K^{*0}) = (1.28 \pm 0.05) \times 10^{-3}$.

$\Gamma(B^{*+} K^-)/\Gamma(B^+ K^-)$ — Γ_2/Γ_1

VALUE	DOCUMENT ID		TECN	COMMENT
0.081±0.021±0.015	[1] SIRUNYAN	18DF	CMS	pp at 8 TeV

[1] With the branching fraction $B(B^+ \to J/\psi K^+) = (1.026 \pm 0.031) \times 10^{-3}$.

$B^*_{s2}(5840)^0$ REFERENCES

SIRUNYAN	18DF	EPJ C78 939	A.M. Sirunyan *et al.*	(CMS Collab.)
AALTONEN	14I	PR D90 012013	T. Aaltonen *et al.*	(CDF Collab.)
AAIJ	13O	PRL 110 151803	R. Aaij *et al.*	(LHCb Collab.)
AALTONEN	08K	PRL 100 082001	T. Aaltonen *et al.*	(CDF Collab.)
ABAZOV	08E	PRL 100 082002	V.M. Abazov *et al.*	(D0 Collab.)

$B^*_{sJ}(5850)$

$I(J^P) = ?(?^?)$

OMITTED FROM SUMMARY TABLE

Signal can be interpreted as coming from $\overline{b}s$ states. Needs confirmation.

$B^*_{sJ}(5850)$ MASS

VALUE (MeV)	EVTS	DOCUMENT ID		TECN	COMMENT
5853±15	141	AKERS	95E	OPAL	E^{ee}_{cm} = 88–94 GeV

Downloaded from https://academic.oup.com/ptep/article/2022/8/083C01/6651666 by KIT Library user on 27 September 2022

$B^*_{sJ}(5850)$ WIDTH

VALUE (MeV)	EVTS	DOCUMENT ID		TECN	COMMENT
47±22	141	AKERS	95E	OPAL	E^{ee}_{cm}= 88–94 GeV

$B^*_{sJ}(5850)$ REFERENCES

AKERS 95E ZPHY C66 19 R. Akers *et al.* (OPAL Collab.)

$B_{sJ}(6063)^0$ $I(J^P) = 0(?^?)$

OMITTED FROM SUMMARY TABLE

$B_{sJ}(6063)^0$ MASS

VALUE (MeV)	DOCUMENT ID		TECN	COMMENT
6063.5±1.2±0.8	[1] AAIJ	21D	LHCB	pp at 7, 8, 13 TeV

[1] Seen in the decay channel $B^\pm K^\mp$. Integrated luminosity = 9 fb^{-1}.

$B_{sJ}(6063)^0$ WIDTH

VALUE (MeV)	DOCUMENT ID		TECN	COMMENT
26±4±4	[1] AAIJ	21D	LHCB	pp at 7, 8, 13 TeV

[1] Seen in the decay channel $B^\pm K^\mp$. Integrated luminosity = 9 fb^{-1}.

$B_{sJ}(6063)^0$ DECAY MODES

	Mode	Fraction (Γ_i/Γ)
Γ_1	$B^+ K^-$	seen

$\Gamma(B^+K^-)/\Gamma_{total}$ — Γ_1/Γ

VALUE	DOCUMENT ID		TECN	COMMENT
seen	AAIJ	21D	LHCB	$B^\pm K^\mp$ mass spectrum

$B_{sJ}(6063)^0$ REFERENCES

AAIJ 21D EPJ C81 601 R. Aaij *et al.* (LHCb Collab.)

$B_{sJ}(6114)^0$ $I(J^P) = 0(?^?)$

OMITTED FROM SUMMARY TABLE

$B_{sJ}(6114)^0$ MASS

VALUE (MeV)	DOCUMENT ID		TECN	COMMENT
6114±3±5	[1] AAIJ	21D	LHCB	pp at 7, 8, 13 TeV

[1] Seen in the decay channel $B^\pm K^\mp$. Integrated luminosity = 9 fb^{-1}.

$B_{sJ}(6114)^0$ WIDTH

VALUE (MeV)	DOCUMENT ID		TECN	COMMENT
66±18±21	[1] AAIJ	21D	LHCB	pp at 7, 8, 13 TeV

[1] Seen in the decay channel $B^\pm K^\mp$. Integrated luminosity = 9 fb^{-1}.

$B_{sJ}(6114)^0$ DECAY MODES

	Mode	Fraction (Γ_i/Γ)
Γ_1	$B^+ K^-$	seen

$\Gamma(B^+K^-)/\Gamma_{total}$ — Γ_1/Γ

VALUE	DOCUMENT ID		TECN	COMMENT
seen	AAIJ	21D	LHCB	$B^\pm K^\mp$ mass spectrum

$B_{sJ}(6114)^0$ REFERENCES

AAIJ 21D EPJ C81 601 R. Aaij *et al.* (LHCb Collab.)

Downloaded from https://academic.oup.com/ptep/article/2022/8/083C01/6651666 by KIT Library user on 27 September 2022

BOTTOM, CHARMED MESONS
($B = C = \pm 1$)

$B_c^+ = c\overline{b}$, $B_c^- = \overline{c}b$, similarly for B_c^*'s

B_c^+

$I(J^P) = 0(0^-)$
I, J, P need confirmation.
Quantum numbers shown are quark-model predictions.

B_c^+ MASS

VALUE (MeV)	DOCUMENT ID		TECN	COMMENT
6274.47± 0.27± 0.17	[1] AAIJ	20R	LHCB	pp at 7, 8, 13 TeV
• • • We do not use the following data for averages, fits, limits, etc. • • •				
6274.28± 1.40± 0.32	[2] AAIJ	17L	LHCB	Repl. by AAIJ 20R
6274.0 ± 1.8 ± 0.4	[3] AAIJ	14AQ	LHCB	Repl. by AAIJ 20R
6276.28± 1.44± 0.36	[4] AAIJ	13AS	LHCB	Repl. by AAIJ 20R
6273.7 ± 1.3 ± 1.6	[5] AAIJ	12AV	LHCB	Repl. by AAIJ 20R
6275.6 ± 2.9 ± 2.5	[6] AALTONEN	08M	CDF	$p\overline{p}$ at 1.96 TeV
6300 ± 14 ± 5	[6] ABAZOV	08T	D0	$p\overline{p}$ at 1.96 TeV
6285.7 ± 5.3 ± 1.2	[6] ABULENCIA	06C	CDF	Repl. by AALTONEN 08M
6400 ±390 ±130	[7] ABE	98M	CDF	$p\overline{p}$ at 1.8 TeV
6320 ± 60	[8] ACKERSTAFF	98O	OPAL	$e^+e^- \to Z$

[1] AAIJ 20R uses the $B_c^+ \to J/\psi\pi^+$, $J/\psi\pi^+\pi^-\pi^+$, $J/\psi p\overline{p}\pi^+$, $J/\psi D_s^+$, $J/\psi D^0 K^+$ and $B_s^0\pi^+$ modes.
[2] Measured using $B_c^+ \to J/\psi D^0 K^+$ decays.
[3] Uses $B_c^+ \to J/\psi p\overline{p}\pi^+$ decays.
[4] AAIJ 13AS uses the $B_c^+ \to J/\psi D_s^+$.
[5] AAIJ 12AV uses the $B_c^+ \to J/\psi\pi^+$ mode and also measures the mass difference $M(B_c^+) - M(B^+) = 994.6 \pm 1.3 \pm 0.6$ MeV/c^2.
[6] Measured using a fully reconstructed decay mode of $B_c \to J/\psi\pi$.
[7] ABE 98M observed $20.4^{+6.2}_{-5.5}$ events in the $B_c^+ \to J/\psi(1s)\ell\nu_\ell$ with a significance of > 4.8 standard deviations. The mass value is estimated from $m(J/\psi(1S)\ell)$.
[8] ACKERSTAFF 98O observed 2 candidate events in the $B_c^+ \to J/\psi(1S)\pi^+$ channel with an estimated background of 0.63 ± 0.20 events.

$m_{B_c^+} - m_{B_s^0}$

VALUE (MeV)	DOCUMENT ID		TECN	COMMENT
907.75±0.37±0.27	[1] AAIJ	20R	LHCB	pp at 7, 8, 13 TeV

[1] AAIJ 20R uses the $B_c^+ \to J/\psi\pi^+$, $J/\psi\pi^+\pi^-\pi^+$, $J/\psi p\overline{p}\pi^+$, $J/\psi D_s^+$, $J/\psi D^0 K^+$ and $B_s^0\pi^+$ modes.

B_c^+ MEAN LIFE

"OUR EVALUATION" is an average using rescaled values of the data listed below. The average and rescaling were performed by the Heavy Flavor Averaging Group (HFLAV) and are described at https://hflav.web.cern.ch/. The averaging/rescaling procedure takes into account correlations between the measurements.

VALUE (10^{-12} s)	DOCUMENT ID		TECN	COMMENT
0.510 ±0.009 OUR EVALUATION				
0.510 ±0.009 OUR AVERAGE				
0.541 ±0.026 ±0.014	[1] SIRUNYAN	18BY	CMS	pp at 8 TeV
0.5134±0.0110±0.0057	[2,3] AAIJ	15G	LHCB	pp at 7, 8 TeV
0.509 ±0.008 ±0.012	[4] AAIJ	14G	LHCB	pp at 8 TeV
0.452 ±0.048 ±0.027	[3] AALTONEN	13	CDF	$p\overline{p}$ at 1.96 TeV
$0.448\ ^{+0.038}_{-0.036}$ ±0.032	[5] ABAZOV	09H	D0	$p\overline{p}$ at 1.96 TeV
$0.463\ ^{+0.073}_{-0.065}$ ±0.036	[5] ABULENCIA	06O	CDF	$p\overline{p}$ at 1.96 TeV
$0.46\ ^{+0.18}_{-0.16}$ ±0.03	[5] ABE	98M	CDF	$p\overline{p}$ 1.8 TeV

[1] The lifetime is measured using the decays $B_c^+ \to J/\psi\pi^+$ and $B^+ \to J/\psi K^+$.
[2] Also measures the width difference $\Delta\Gamma = \Gamma_{B_c^+} - \Gamma_{B^+} = 4.46 \pm 0.14 \pm 0.07$ mm^{-1} c.
[3] Uses fully reconstructed $B_c^+ \to J/\psi\pi^+$ decays.
[4] Measured using $B_c^+ \to J/\psi\mu^+\nu_\mu X$ decays.
[5] The lifetime is measured from the $J/\psi e$ decay vertices.

B_c^+ DECAY MODES × B($\overline{b} \to B_c$)

B_c^- modes are charge conjugates of the modes below.

	Mode	Fraction (Γ_i/Γ)	Confidence level
Γ_1	$J/\psi(1S)\ell^+\nu_\ell$anything	seen	
Γ_2	$J/\psi(1S)\mu^+\nu_\mu$	seen	
Γ_3	$J/\psi(1S)\tau^+\nu_\tau$	seen	
Γ_4	$J/\psi(1S)\pi^+$	seen	
Γ_5	$J/\psi(1S)K^+$	seen	
Γ_6	$J/\psi(1S)\pi^+\pi^+\pi^-$	seen	
Γ_7	$J/\psi(1S)a_1(1260)$	not seen	
Γ_8	$J/\psi(1S)K^+K^-\pi^+$	seen	
Γ_9	$J/\psi(1S)\pi^+\pi^+\pi^+\pi^-\pi^-$	seen	
Γ_{10}	$\psi(2S)\pi^+$	seen	
Γ_{11}	$J/\psi(1S)D^0K^+$	seen	
Γ_{12}	$J/\psi(1S)D^*(2007)^0K^+$	seen	
Γ_{13}	$J/\psi(1S)D^*(2010)^+K^{*0}$	seen	
Γ_{14}	$J/\psi(1S)D^+K^{*0}$	seen	
Γ_{15}	$J/\psi(1S)D_s^+$	seen	
Γ_{16}	$J/\psi(1S)D_s^{*+}$	seen	
Γ_{17}	$J/\psi(1S)p\overline{p}\pi^+$	seen	
Γ_{18}	$\chi_c^0\pi^+$	$(2.4^{+0.9}_{-0.8}) \times 10^{-5}$	
Γ_{19}	$p\overline{p}\pi^+$	not seen	
Γ_{20}	D^0K^+	seen	
Γ_{21}	$D^0\pi^+$	not seen	
Γ_{22}	$D^{*0}\pi^+$	not seen	
Γ_{23}	$D^{*0}K^+$	not seen	
Γ_{24}	$D_s^+\overline{D}^0$	$< 7.2 \times 10^{-4}$	90%
Γ_{25}	$D_s^+D^0$	$< 3.0 \times 10^{-4}$	90%
Γ_{26}	$D^+\overline{D}^0$	$< 1.9 \times 10^{-4}$	90%
Γ_{27}	D^+D^0	$< 1.4 \times 10^{-4}$	90%
Γ_{28}	$D_s^{*+}\overline{D}^0$	$< 5.3 \times 10^{-4}$	90%
Γ_{29}	$D_s^+\overline{D}^*(2007)^0$	$< 4.6 \times 10^{-4}$	90%
Γ_{30}	$D_s^{*+}D^0$	$< 9 \times 10^{-4}$	90%
Γ_{31}	$D_s^+D^*(2007)^0$	$< 6.6 \times 10^{-4}$	90%
Γ_{32}	$D^*(2010)^+\overline{D}^0$	$< 3.8 \times 10^{-4}$	90%
Γ_{33}	$D^*(2010)^+\overline{D}^0$, $D^{*+} \to D^+\pi^0/\gamma$	not seen	
Γ_{34}	$D^+\overline{D}^*(2007)^0$	$< 6.5 \times 10^{-4}$	90%
Γ_{35}	$D^*(2007)^+D^0$	$< 2.0 \times 10^{-4}$	90%
Γ_{36}	$D^*(2010)^+D^0$, $D^{*+} \to D^+\pi^0/\gamma$	not seen	
Γ_{37}	$D^+D^*(2007)^0$	$< 3.7 \times 10^{-4}$	90%
Γ_{38}	$D_s^{*+}\overline{D}^*(2007)^0$	$< 1.3 \times 10^{-3}$	90%
Γ_{39}	$D_s^{*+}D^*(2007)^0$	$< 1.3 \times 10^{-3}$	90%
Γ_{40}	$D^*(2010)^+\overline{D}^*(2007)^0$	$< 1.0 \times 10^{-3}$	90%
Γ_{41}	$D^*(2010)^+D^*(2007)^0$	$< 7.7 \times 10^{-4}$	90%
Γ_{42}	D^+K^{*0}	not seen	
Γ_{43}	$D^+\overline{K}^{*0}$	not seen	
Γ_{44}	$D_s^+K^{*0}$	not seen	
Γ_{45}	$D_s^+\overline{K}^{*0}$	not seen	
Γ_{46}	$D_s^+\phi$	not seen	
Γ_{47}	K^+K^0	not seen	
Γ_{48}	$B_s^0\pi^+$ / B($\overline{b} \to B_s$)	seen	

B_c^+ BRANCHING RATIOS

$\Gamma(J/\psi(1S)\ell^+\nu_\ell\text{anything})/\Gamma_{\text{total}} \times B(\overline{b} \to B_c)$ — $\Gamma_1/\Gamma \times B$

VALUE (units 10^{-5})	CL%	DOCUMENT ID		TECN	COMMENT
8.2±1.3 OUR AVERAGE		Error includes scale factor of 1.4.			
8.8±1.0±0.2		[1,2] AALTONEN	16A	CDF	$p\overline{p}$ at 1.96 TeV
$5.2^{+2.4}_{-2.1}$		[3] ABE	98M	CDF	$p\overline{p}$ 1.8 TeV
• • • We do not use the following data for averages, fits, limits, etc. • • •					
<16	90	[4] ACKERSTAFF	98O	OPAL	$e^+e^- \to Z$
<19	90	[5] ABREU	97E	DLPH	$e^+e^- \to Z$
<12	90	[6] BARATE	97H	ALEP	$e^+e^- \to Z$

[1] AALTONEN 16A reports $[\Gamma(B_c^+ \to J/\psi(1S)\ell^+\nu_\ell\text{anything})/\Gamma_{\text{total}} \times B(\overline{b} \to B_c)]$ / $[B(\overline{b} \to B^+)]$ / $[B(B^+ \to J/\psi(1S)K^+)] = 0.211 \pm 0.012^{+0.021}_{-0.020}$ which we multiply by our best values $B(\overline{b} \to B^+) = (40.8 \pm 0.7) \times 10^{-2}$, $B(B^+ \to J/\psi(1S)K^+) = (1.020 \pm 0.019) \times 10^{-3}$. Our first error is their experiment's error and our second error is the systematic error from using our best values.
[2] AALTONEN 16A also measures the cross-section $\sigma(B_c) \times B(B_c \to J/\psi\mu\nu_\mu) = 0.60 \pm 0.09$ nb and estimates the total cross-section $\sigma(B_c)$ to be in the range 25 ± 4 to 52 ± 8 nb for $p_T(B_c) > 6$ GeV/c and $|y(B_c)| < 1$.
[3] ABE 98M result is derived from the measurement of $[\sigma(B_c) \times B(B_c \to J/\psi(1S)\ell\nu_\ell)]$ / $[\sigma(B^+) \times B(B^+ \to J/\psi(1S)K^+)] = 0.132^{+0.041}_{-0.037}(\text{stat}) \pm 0.031(\text{sys})^{+0.032}_{-0.020}(\text{lifetime})$ by using PDG 98 values of $B(b \to B^+)$ and $B(B^+ \to J/\psi(1S)K^+)$.
[4] ACKERSTAFF 98O reports $B(Z \to B_c X)/B(Z \to qq) \times B(B_c \to J/\psi(1S)\ell\nu_\ell) < 6.95 \times 10^{-5}$ at 90%CL. We rescale to our PDG 98 values of $B(Z \to b\overline{b})$.
[5] ABREU 97E value listed is for an assumed $\tau_{B_c} = 0.4$ ps and improves to 1.6×10^{-4} for $\tau_{B_c} = 1.4$ ps.

Downloaded from https://academic.oup.com/ptep/article/2022/8/083C01/6651666 by KIT Library user on 27 September 2022

[6] BARATE 97H reports $B(Z \to B_c X)/B(Z \to q q) \cdot B(B_c \to J/\psi(1S)\ell\nu_\ell) < 5.2 \times 10^{-5}$ at 90%CL. We rescale to our PDG 96 values of $B(Z \to b\overline{b})$. A $B_c^+ \to J/\psi(1S)\mu^+\nu_\mu$ candidate event is found, compared to all the known background sources 2×10^{-3}, which gives $m_{B_c} = 5.96^{+0.25}_{-0.19}$ GeV and $\tau_{B_c} = 1.77 \pm 0.17$ ps.

$\Gamma(J/\psi(1S)\tau^+\nu_\tau)/\Gamma(J/\psi(1S)\mu^+\nu_\mu)$ — Γ_3/Γ_2

VALUE	DOCUMENT ID		TECN	COMMENT
0.71±0.17±0.18	[1] AAIJ	18C	LHCB	pp at 7, 8 TeV

[1] AAIJ 18C uses $\tau^+ \to \mu^+\nu_\mu\overline{\nu}_\tau$ mode to obtain the ratio value.

$\Gamma(J/\psi(1S)\pi^+)/\Gamma_{total} \times B(\overline{b} \to B_c)$ — $\Gamma_4/\Gamma \times B$

VALUE	CL%	DOCUMENT ID		TECN	COMMENT
seen		[1] AABOUD	21	ATLS	pp at 8 TeV
seen		[2] AAIJ	15M	LHCB	pp at 8 TeV
seen		[3] KHACHATRY...	15AA	CMS	pp at 7 TeV
seen		AALTONEN	13	CDF	$p\overline{p}$ at 1.96 TeV
seen		[4] AAIJ	12AV	LHCB	pp at 7 TeV
seen		AALTONEN	08M	CDF	$p\overline{p}$ at 1.96 TeV
seen		ABAZOV	08T	D0	$p\overline{p}$ at 1.96 TeV
• • • We do not use the following data for averages, fits, limits, etc. • • •					
$<2.4 \times 10^{-4}$	90	[5] ACKERSTAFF	98O	OPAL	$e^+e^- \to Z$
$<3.4 \times 10^{-4}$	90	[6] ABREU	97E	DLPH	$e^+e^- \to Z$
$<8.2 \times 10^{-5}$	90	[7] BARATE	97H	ALEP	$e^+e^- \to Z$
$<2.0 \times 10^{-5}$	95	[8] ABE	96R	CDF	$p\overline{p}$ 1.8 TeV

[1] AABOUD 21 reports a measurement of $B(B_c^+ \to J/\psi\pi^+)$ / $B(B^+ \to J/\psi K^+) \cdot f_c/f_u = (0.34 \pm 0.04^{+0.06}_{-0.02} \pm 0.01)$ %, at $p_T > 13$ GeV and $|y| < 2.3$.

[2] AAIJ 15M reports a measurement of $B(B_c^+ \to J/\psi\pi^+)$ / $B(B^+ \to J/\psi K^+) \cdot f_c/f_u = (0.683 \pm 0.018 \pm 0.009)$% at $p_T(B) < 20$ GeV and $2.0 < y(B) < 4.5$.

[3] KHACHATRYAN 15AA reports a measurement of $B(B_c^+ \to J/\psi\pi^+)$ / $B(B^+ \to J/\psi K^+) \cdot f_c/f_u = (0.48 \pm 0.05 \pm 0.03 \pm 0.05)$%, at $p_T > 15$ GeV and $|\eta(B)| < 1.6$.

[4] AAIJ 12AV reports a measurement of $B(B_c^+ \to J/\psi\pi^+)/B(B^+ \to J/\psi K^+)\ f_c/f_u = (0.68 \pm 0.10 \pm 0.03 \pm 0.05)$% at $p_T(B) > 4$ GeV and $2.5 < \eta(B) < 4.5$.

[5] ACKERSTAFF 98O reports $B(Z \to B_c X)/B(Z \to q q) \times B(B_c \to J/\psi(1S)\pi^+) < 1.06 \times 10^{-4}$ at 90%CL. We rescale to our PDG 98 values of $B(Z \to b\overline{b})$.

[6] ABREU 97E value listed is for an assumed $\tau_{B_c} = 0.4$ ps and improves to 2.7×10^{-4} for $\tau_{B_c} = 1.4$ ps.

[7] BARATE 97H reports $B(Z \to B_c X)/B(Z \to q q) \cdot B(B_c \to J/\psi(1S)\pi) < 3.6 \times 10^{-5}$ at 90%CL. We rescale to our PDG 96 values of $B(Z \to b\overline{b})$.

[8] ABE 96R reports $B(b \to B_c X)/B(b \to B^+ X) \cdot B(B_c^+ \to J/\psi(1S)\pi^+)/B(B^+ \to J/\psi(1S)K^+) < 0.053$ at 95%CL for $\tau_{B_c} = 0.8$ ps. It changes from 0.15 to 0.04 for 0.17 ps$< \tau_{B_c} < 1.6$ ps. We rescale to our PDG 96 values of $B(b \to B^+) = 0.378 \pm 0.022$ and $B(B^+ \to J/\psi(1S)K^+) = 0.00101 \pm 0.00014$.

$\Gamma(J/\psi(1S)\pi^+)/\Gamma(J/\psi(1S)\mu^+\nu_\mu)$ — Γ_4/Γ_2

VALUE (units 10^{-2})	DOCUMENT ID		TECN	COMMENT
4.69±0.28±0.46	[1] AAIJ	14W	LHCB	pp at 7 TeV

[1] AAIJ 14W reports also a measurement $B(B_c^+ \to J/\psi\pi^+)$ / $B(B_c^+ \to J/\psi\mu^+\nu_\mu) = 0.271 \pm 0.016 \pm 0.016$ in the region $m_{J/\psi\mu^+} > 5.3$ GeV.

$\Gamma(J/\psi(1S)K^+)/\Gamma(J/\psi(1S)\pi^+)$ — Γ_5/Γ_4

VALUE	EVTS	DOCUMENT ID		TECN	COMMENT
0.079±0.007±0.003		AAIJ	16AF	LHCB	pp at 7, 8 TeV
• • • We do not use the following data for averages, fits, limits, etc. • • •					
0.069±0.019±0.005	50	AAIJ	13BY	LHCB	Repl. by AAIJ 16AF

$\Gamma(J/\psi(1S)\pi^+\pi^+\pi^-)/\Gamma_{total} \times B(\overline{b} \to B_c)$ — $\Gamma_6/\Gamma \times B$

VALUE	CL%	DOCUMENT ID		TECN	COMMENT
seen		AAIJ	12Y	LHCB	pp at 7 TeV
• • • We do not use the following data for averages, fits, limits, etc. • • •					
$<5.7 \times 10^{-4}$	90	[1] ABREU	97E	DLPH	$e^+e^- \to Z$

[1] ABREU 97E value listed is independent of 0.4 ps$< \tau_{B_c} < 1.4$ ps.

$\Gamma(J/\psi(1S)\pi^+\pi^+\pi^-)/\Gamma(J/\psi(1S)\pi^+)$ — Γ_6/Γ_4

VALUE	DOCUMENT ID		TECN	COMMENT
2.4 ±0.4 OUR AVERAGE				
$2.55 \pm 0.80 \pm 0.33^{+0.04}_{-0.01}$	KHACHATRY...	15AA	CMS	pp at 7 TeV
2.41±0.30±0.33	AAIJ	12Y	LHCB	pp at 7 TeV

$\Gamma(J/\psi(1S)a_1(1260))/\Gamma_{total} \times B(\overline{b} \to B_c)$ — $\Gamma_7/\Gamma \times B$

VALUE	CL%	DOCUMENT ID		TECN	COMMENT
$<1.2 \times 10^{-3}$	90	[1] ACKERSTAFF	98O	OPAL	$e^+e^- \to Z$

[1] ACKERSTAFF 98O reports $B(Z \to B_c X)/B(Z \to q q) \times B(B_c \to J/\psi(1S)a_1(1260)) < 5.29 \times 10^{-4}$ at 90%CL. We rescale to our PDG 98 values of $B(Z \to b\overline{b})$.

$\Gamma(J/\psi(1S)K^+K^-\pi^+)/\Gamma_{total} \times B(\overline{b} \to B_c)$ — $\Gamma_8/\Gamma \times B$

VALUE	DOCUMENT ID		TECN	COMMENT
seen	[1] AAIJ	13CA	LHCB	pp at 7, 8 TeV

[1] A signal yield of 78 ± 14 decays is reported with a significance of 6.2 standard deviations using an integrated luminosity of 3 fb^{-1} data.

$\Gamma(J/\psi(1S)K^+K^-\pi^+)/\Gamma(J/\psi(1S)\pi^+)$ — Γ_8/Γ_4

VALUE	DOCUMENT ID		TECN	COMMENT
0.53±0.10±0.05	[1] AAIJ	13CA	LHCB	pp at 7, 8 TeV

[1] A signal yield of 78 ± 14 decays is reported with a significance of 6.2 standard deviations using an integrated luminosity of 3 fb^{-1} data.

$\Gamma(J/\psi(1S)\pi^+\pi^+\pi^+\pi^-\pi^-)/\Gamma(J/\psi(1S)\pi^+)$ — Γ_9/Γ_4

VALUE	DOCUMENT ID		TECN	COMMENT
1.74±0.44±0.24	[1] AAIJ	14P	LHCB	pp at 7, 8 TeV

[1] A signal yield of 32 ± 8 decays is reported with a significance of 4.5 standard deviations.

$\Gamma(\psi(2S)\pi^+)/\Gamma(J/\psi(1S)\pi^+)$ — Γ_{10}/Γ_4

VALUE	DOCUMENT ID		TECN	COMMENT
0.268±0.032±0.007±0.006	[1] AAIJ	15AY	LHCB	pp at 7, 8 TeV
• • • We do not use the following data for averages, fits, limits, etc. • • •				
0.250±0.068±0.014±0.006	[1] AAIJ	13AM	LHCB	Repl. by AAIJ 15AY

[1] The last uncertainty is due to the uncertainty of the $B(\psi(2S) \to \mu^+\mu^-)/B(J/\psi \to \mu^+\mu^-)$ ratio measurement.

$\Gamma(J/\psi(1S)D^0K^+)/\Gamma(J/\psi(1S)\pi^+)$ — Γ_{11}/Γ_4

VALUE	DOCUMENT ID		TECN	COMMENT
0.432±0.136±0.028	AAIJ	17L	LHCB	pp at 7, 8 TeV

$\Gamma(J/\psi(1S)D^*(2007)^0K^+)/\Gamma(J/\psi(1S)D^0K^+)$ — Γ_{12}/Γ_{11}

VALUE	DOCUMENT ID		TECN	COMMENT
5.1±1.8±0.4	AAIJ	17L	LHCB	pp at 7, 8 TeV

$\Gamma(J/\psi(1S)D^*(2010)^+K^{*0})/\Gamma(J/\psi(1S)D^0K^+)$ — Γ_{13}/Γ_{11}

VALUE	DOCUMENT ID		TECN	COMMENT
2.10±1.08±0.34	AAIJ	17L	LHCB	pp at 7, 8 TeV

$\Gamma(J/\psi(1S)D^+K^{*0})/\Gamma(J/\psi(1S)D^0K^+)$ — Γ_{14}/Γ_{11}

VALUE	DOCUMENT ID		TECN	COMMENT
0.63±0.39±0.08	AAIJ	17L	LHCB	pp at 7, 8 TeV

$\Gamma(J/\psi(1S)D_s^+)/\Gamma(J/\psi(1S)\pi^+)$ — Γ_{15}/Γ_4

VALUE	DOCUMENT ID		TECN	COMMENT
3.1 ±0.5 OUR AVERAGE				
3.8 ±1.1 ±0.4	AAD	16H	ATLS	pp at 7, 8 TeV
2.90±0.57±0.24	AAIJ	13AS	LHCB	pp at 7, 8 TeV

$\Gamma(J/\psi(1S)D_s^{*+})/\Gamma(J/\psi(1S)\pi^+)$ — Γ_{16}/Γ_4

VALUE	DOCUMENT ID		TECN	COMMENT
10.4±3.1±1.6	AAD	16H	ATLS	pp at 7, 8 TeV

$\Gamma(J/\psi(1S)D_s^{*+})/\Gamma(J/\psi(1S)D_s^+)$ — Γ_{16}/Γ_{15}

VALUE	DOCUMENT ID		TECN	COMMENT
2.5 ±0.5 OUR AVERAGE				
$2.8\ ^{+1.2}_{-0.8}\ \pm 0.3$	AAD	16H	ATLS	pp at 7, 8 TeV
2.37±0.56±0.10	AAIJ	13AS	LHCB	pp at 7, 8 TeV

$\Gamma(J/\psi(1S)p\overline{p}\pi^+)/\Gamma(J/\psi(1S)\pi^+)$ — Γ_{17}/Γ_4

VALUE	DOCUMENT ID		TECN	COMMENT
$0.143^{+0.041}_{-0.036}$	AAIJ	14AQ	LHCB	pp at 7, 8 TeV

$\Gamma(\chi_c^0\pi^+)/\Gamma_{total}$ — Γ_{18}/Γ

VALUE (units 10^{-6})	DOCUMENT ID		TECN	COMMENT
$24.0^{+8.6}_{-7.6} \pm 0.4$	[1,2] AAIJ	16AT	LHCB	pp at 7 and 8 TeV

[1] AAIJ 16AT reports $[\Gamma(B_c^+ \to \chi_c^0\pi^+)/\Gamma_{total}] \times [\Gamma(\overline{b} \to B^+)/\Gamma_{total}] = (9.8^{+3.4}_{-3.0} \pm 0.8) \times 10^{-6}$ which we divide by our best value $\Gamma(\overline{b} \to B^+)/\Gamma_{total} = 0.408 \pm 0.007$. Our first error is their experiment's error and our second error is the systematic error from using our best value.

[2] The significance of the observed signal is 4.0 standard deviations.

$\Gamma(p\overline{p}\pi^+)/\Gamma_{total}$ — Γ_{19}/Γ

VALUE	DOCUMENT ID		TECN	COMMENT
not seen	[1] AAIJ	16K	LHCB	pp at 7, 8 TeV

[1] Measures the ratio $(f_c/f_u) \times B(B_c^+ \to p\overline{p}\pi^+) < 3.6 \times 10^{-8}$ at 95% CL, in the region $m(p\overline{p}) < 2.85$ GeV/c^2, where f_c (f_u) represents the fragmentation fraction of the b-quark into the B_c^+ (B_u^+) meson.

Downloaded from https://academic.oup.com/ptep/article/2022/8/083C01/6651666 by KIT Library user on 27 September 2022

$\Gamma(D^0 K^+)/\Gamma_{total} \times B(\bar{b} \to B_c)$ — $\Gamma_{20}/\Gamma \times B$

VALUE (units 10^{-7})	DOCUMENT ID	TECN	COMMENT
$3.8^{+1.2}_{-1.0} \pm 0.1$	[1] AAIJ	17AG LHCB	pp at 7, 8 TeV

[1] AAIJ 17AG reports $[\Gamma(B_c^+ \to D^0 K^+)/\Gamma_{total} \times B(\bar{b} \to B_c)] / [B(\bar{b} \to B^+)] = (9.3^{+2.8}_{-2.5} \pm 0.6) \times 10^{-7}$ which we multiply by our best value $B(\bar{b} \to B^+) = (40.8 \pm 0.7) \times 10^{-2}$. Our first error is their experiment's error and our second error is the systematic error from using our best value.

$\Gamma(D^0 \pi^+)/\Gamma_{total} \times B(\bar{b} \to B_c)$ — $\Gamma_{21}/\Gamma \times B$

VALUE	CL%	DOCUMENT ID	TECN	COMMENT
$<1.6 \times 10^{-7}$	95	[1] AAIJ	17AG LHCB	pp at 7, 8 TeV

[1] AAIJ 17AG reports $[\Gamma(B_c^+ \to D^0 \pi^+)/\Gamma_{total} \times B(\bar{b} \to B_c)] / [B(\bar{b} \to B^+)] < 3.9 \times 10^{-7}$ which we multiply by our best value $B(\bar{b} \to B^+) = 40.8 \times 10^{-2}$.

$\Gamma(D^{*0} \pi^+)/\Gamma_{total} \times B(\bar{b} \to B_c)$ — $\Gamma_{22}/\Gamma \times B$

VALUE	CL%	DOCUMENT ID	TECN	COMMENT
$<4 \times 10^{-7}$	95	[1] AAIJ	17AG LHCB	pp at 7, 8 TeV

[1] AAIJ 17AG reports $[\Gamma(B_c^+ \to D^{*0} \pi^+)/\Gamma_{total} \times B(\bar{b} \to B_c)] / [B(\bar{b} \to B^+)] < 1.1 \times 10^{-6}$ which we multiply by our best value $B(\bar{b} \to B^+) = 40.8 \times 10^{-2}$.

$\Gamma(D^{*0} K^+)/\Gamma_{total} \times B(\bar{b} \to B_c)$ — $\Gamma_{23}/\Gamma \times B$

VALUE	CL%	DOCUMENT ID	TECN	COMMENT
$<4 \times 10^{-7}$	95	[1] AAIJ	17AG LHCB	pp at 7, 8 TeV

[1] AAIJ 17AG reports $[\Gamma(B_c^+ \to D^{*0} K^+)/\Gamma_{total} \times B(\bar{b} \to B_c)] / [B(\bar{b} \to B^+)] < 1.1 \times 10^{-6}$ which we multiply by our best value $B(\bar{b} \to B^+) = 40.8 \times 10^{-2}$.

$\Gamma(D_s^+ \overline{D}^0)/\Gamma_{total} \times B(\bar{b} \to B_c)$ — $\Gamma_{24}/\Gamma \times B$

VALUE	CL%	DOCUMENT ID	TECN	COMMENT
$<1.4 \times 10^{-7}$	90	[1] AAIJ	18P LHCB	pp at 7, 8 TeV

[1] AAIJ 18P reports $[\Gamma(B_c^+ \to D_s^+ \overline{D}^0)/\Gamma_{total} \times B(\bar{b} \to B_c)] / [B(\bar{b} \to B^+)] / [B(B^+ \to \overline{D}^0 D^+)] < 0.9 \times 10^{-3}$ which we multiply by our best values $B(\bar{b} \to B^+) = 40.8 \times 10^{-2}$, $B(B^+ \to \overline{D}^0 D^+) = 3.8 \times 10^{-4}$.

$\Gamma(D_s^+ D^0)/\Gamma_{total} \times B(\bar{b} \to B_c)$ — $\Gamma_{25}/\Gamma \times B$

VALUE	CL%	DOCUMENT ID	TECN	COMMENT
$<6 \times 10^{-8}$	90	[1] AAIJ	18P LHCB	pp at 7, 8 TeV

[1] AAIJ 18P reports $[\Gamma(B_c^+ \to D_s^+ D^0)/\Gamma_{total} \times B(\bar{b} \to B_c)] / [B(\bar{b} \to B^+)] / [B(B^+ \to \overline{D}^0 D^+)] < 3.7 \times 10^{-4}$ which we multiply by our best values $B(\bar{b} \to B^+) = 40.8 \times 10^{-2}$, $B(B^+ \to \overline{D}^0 D^+) = 3.8 \times 10^{-4}$.

$\Gamma(D^+ \overline{D}^0)/\Gamma_{total} \times B(\bar{b} \to B_c)$ — $\Gamma_{26}/\Gamma \times B$

VALUE	CL%	DOCUMENT ID	TECN	COMMENT
$<3.0 \times 10^{-6}$	90	[1] AAIJ	18P LHCB	pp at 7, 8 TeV

[1] AAIJ 18P reports $[\Gamma(B_c^+ \to D^+ \overline{D}^0)/\Gamma_{total} \times B(\bar{b} \to B_c)] / [B(\bar{b} \to B^+)] / [B(B^+ \to \overline{D}^0 D^+)] < 1.9 \times 10^{-2}$ which we multiply by our best values $B(\bar{b} \to B^+) = 40.8 \times 10^{-2}$, $B(B^+ \to \overline{D}^0 D^+) = 3.8 \times 10^{-4}$.

$\Gamma(D^+ D^0)/\Gamma_{total} \times B(\bar{b} \to B_c)$ — $\Gamma_{27}/\Gamma \times B$

VALUE	CL%	DOCUMENT ID	TECN	COMMENT
• • • We do not use the following data for averages, fits, limits, etc. • • •				
$<1.9 \times 10^{-6}$	90	[1] AAIJ	18P LHCB	Repl. by AAIJ 21AF

[1] AAIJ 18P reports $[\Gamma(B_c^+ \to D^+ D^0)/\Gamma_{total} \times B(\bar{b} \to B_c)] / [B(\bar{b} \to B^+)] / [B(B^+ \to \overline{D}^0 D^+)] < 1.2 \times 10^{-2}$ which we multiply by our best values $B(\bar{b} \to B^+) = 40.8 \times 10^{-2}$, $B(B^+ \to \overline{D}^0 D^+) = 3.8 \times 10^{-4}$.

$[\Gamma(D_s^{*+} \overline{D}^0) + \Gamma(D_s^+ \overline{D}^*(2007)^0)]/\Gamma_{total} \times B(\bar{b} \to B_c)$ — $(\Gamma_{28}+\Gamma_{29})/\Gamma \times B$

VALUE	CL%	DOCUMENT ID	TECN	COMMENT
• • • We do not use the following data for averages, fits, limits, etc. • • •				
$<4 \times 10^{-7}$	90	[1] AAIJ	18P LHCB	Repl. by AAIJ 21AF

[1] AAIJ 18P reports $[\left[\Gamma(B_c^+ \to D_s^{*+} \overline{D}^0) + \Gamma(B_c^+ \to D_s^+ \overline{D}^*(2007)^0)\right]/\Gamma_{total} \times B(\bar{b} \to B_c)] / [B(\bar{b} \to B^+)] / [B(B^+ \to \overline{D}^0 D^+)] < 2.8 \times 10^{-3}$ which we multiply by our best values $B(\bar{b} \to B^+) = 40.8 \times 10^{-2}$, $B(B^+ \to \overline{D}^0 D^+) = 3.8 \times 10^{-4}$.

$[\Gamma(D_s^{*+} D^0) + \Gamma(D_s^+ D^*(2007)^0)]/\Gamma_{total} \times B(\bar{b} \to B_c)$ — $(\Gamma_{30}+\Gamma_{31})/\Gamma \times B$

VALUE	CL%	DOCUMENT ID	TECN	COMMENT
• • • We do not use the following data for averages, fits, limits, etc. • • •				
$<5 \times 10^{-7}$	90	[1] AAIJ	18P LHCB	Repl. by AAIJ 21AF

[1] AAIJ 18P reports $[\left[\Gamma(B_c^+ \to D_s^{*+} D^0) + \Gamma(B_c^+ \to D_s^+ D^*(2007)^0)\right]/\Gamma_{total} \times B(\bar{b} \to B_c)] / [B(\bar{b} \to B^+)] / [B(B^+ \to \overline{D}^0 D^+)] < 3.0 \times 10^{-3}$ which we multiply by our best values $B(\bar{b} \to B^+) = 40.8 \times 10^{-2}$, $B(B^+ \to \overline{D}^0 D^+) = 3.8 \times 10^{-4}$.

$\Gamma(D^*(2010)^+ \overline{D}^0)/\Gamma_{total} \times B(\bar{b} \to B_c)$ — $\Gamma_{32}/\Gamma \times B$

VALUE	CL%	DOCUMENT ID	TECN	COMMENT
$<6.2 \times 10^{-3}$	90	[1] BARATE	98Q ALEP	$e^+ e^- \to Z$

[1] BARATE 98Q reports $B(Z \to B_c X) \times B(B_c \to D^*(2010)^+ \overline{D}^0) < 1.9 \times 10^{-3}$ at 90%CL. We rescale to our PDG 98 values of $B(Z \to b\bar{b})$.

$[\Gamma(D^*(2010)^+ \overline{D}^0,\ D^{*+} \to D^+ \pi^0/\gamma) + \Gamma(D^+ \overline{D}^*(2007)^0)]/\Gamma_{total} \times B(\bar{b} \to B_c)$ — $(\Gamma_{33}+\Gamma_{34})/\Gamma \times B$

VALUE	CL%	DOCUMENT ID	TECN	COMMENT
• • • We do not use the following data for averages, fits, limits, etc. • • •				
$<9 \times 10^{-6}$	90	[1] AAIJ	18P LHCB	Repl. by AAIJ 21AF

[1] AAIJ 18P reports $[\left[\Gamma(B_c^+ \to D^*(2010)^+ \overline{D}^0,\ D^{*+} \to D^+ \pi^0/\gamma) + \Gamma(B_c^+ \to D^+ \overline{D}^*(2007)^0)\right]/\Gamma_{total} \times B(\bar{b} \to B_c)] / [B(\bar{b} \to B^+)] / [B(B^+ \to \overline{D}^0 D^+)] < 5.5 \times 10^{-2}$ which we multiply by our best values $B(\bar{b} \to B^+) = 40.8 \times 10^{-2}$, $B(B^+ \to \overline{D}^0 D^+) = 3.8 \times 10^{-4}$.

$[\Gamma(D^*(2010)^+ D^0,\ D^{*+} \to D^+ \pi^0/\gamma) + \Gamma(D^+ D^*(2007)^0)]/\Gamma_{total} \times B(\bar{b} \to B_c)$ — $(\Gamma_{36}+\Gamma_{37})/\Gamma \times B$

VALUE	CL%	DOCUMENT ID	TECN	COMMENT
• • • We do not use the following data for averages, fits, limits, etc. • • •				
$<3.4 \times 10^{-6}$	90	[1] AAIJ	18P LHCB	Repl. by AAIJ 21AF

[1] AAIJ 18P reports $[\left[\Gamma(B_c^+ \to D^*(2010)^+ D^0,\ D^{*+} \to D^+ \pi^0/\gamma) + \Gamma(B_c^+ \to D^+ D^*(2007)^0)\right]/\Gamma_{total} \times B(\bar{b} \to B_c)] / [B(\bar{b} \to B^+)] / [B(B^+ \to \overline{D}^0 D^+)] < 2.2 \times 10^{-2}$ which we multiply by our best values $B(\bar{b} \to B^+) = 40.8 \times 10^{-2}$, $B(B^+ \to \overline{D}^0 D^+) = 3.8 \times 10^{-4}$.

$\Gamma(D_s^{*+} \overline{D}^*(2007)^0)/\Gamma_{total} \times B(\bar{b} \to B_c)$ — $\Gamma_{38}/\Gamma \times B$

VALUE	CL%	DOCUMENT ID	TECN	COMMENT
• • • We do not use the following data for averages, fits, limits, etc. • • •				
$<1.7 \times 10^{-6}$	90	[1] AAIJ	18P LHCB	Repl. by AAIJ 21AF

[1] AAIJ 18P reports $[\Gamma(B_c^+ \to D_s^{*+} \overline{D}^*(2007)^0)/\Gamma_{total} \times B(\bar{b} \to B_c)] / [B(\bar{b} \to B^+)] / [B(B^+ \to \overline{D}^0 D^+)] < 1.1 \times 10^{-2}$ which we multiply by our best values $B(\bar{b} \to B^+) = 40.8 \times 10^{-2}$, $B(B^+ \to \overline{D}^0 D^+) = 3.8 \times 10^{-4}$.

$\Gamma(D_s^{*+} D^*(2007)^0)/\Gamma_{total} \times B(\bar{b} \to B_c)$ — $\Gamma_{39}/\Gamma \times B$

VALUE	CL%	DOCUMENT ID	TECN	COMMENT
• • • We do not use the following data for averages, fits, limits, etc. • • •				
$<3.1 \times 10^{-6}$	90	[1] AAIJ	18P LHCB	Repl. by AAIJ 21AF

[1] AAIJ 18P reports $[\Gamma(B_c^+ \to D_s^{*+} D^*(2007)^0)/\Gamma_{total} \times B(\bar{b} \to B_c)] / [B(\bar{b} \to B^+)] / [B(B^+ \to \overline{D}^0 D^+)] < 2.0 \times 10^{-2}$ which we multiply by our best values $B(\bar{b} \to B^+) = 40.8 \times 10^{-2}$, $B(B^+ \to \overline{D}^0 D^+) = 3.8 \times 10^{-4}$.

$\Gamma(D^*(2010)^+ \overline{D}^*(2007)^0)/\Gamma_{total} \times B(\bar{b} \to B_c)$ — $\Gamma_{40}/\Gamma \times B$

VALUE	CL%	DOCUMENT ID	TECN	COMMENT
• • • We do not use the following data for averages, fits, limits, etc. • • •				
$<1.0 \times 10^{-4}$	90	[1] AAIJ	18P LHCB	Repl. by AAIJ 21AF

[1] AAIJ 18P reports $[\Gamma(B_c^+ \to D^*(2010)^+ \overline{D}^*(2007)^0)/\Gamma_{total} \times B(\bar{b} \to B_c)] / [B(\bar{b} \to B^+)] / [B(B^+ \to \overline{D}^0 D^+)] < 6.5 \times 10^{-1}$ which we multiply by our best values $B(\bar{b} \to B^+) = 40.8 \times 10^{-2}$, $B(B^+ \to \overline{D}^0 D^+) = 3.8 \times 10^{-4}$.

$\Gamma(D^*(2010)^+ D^*(2007)^0)/\Gamma_{total} \times B(\bar{b} \to B_c)$ — $\Gamma_{41}/\Gamma \times B$

VALUE	CL%	DOCUMENT ID	TECN	COMMENT
• • • We do not use the following data for averages, fits, limits, etc. • • •				
$<2.0 \times 10^{-5}$	90	[1] AAIJ	18P LHCB	Repl. by AAIJ 21AF

[1] AAIJ 18P reports $[\Gamma(B_c^+ \to D^*(2010)^+ D^*(2007)^0)/\Gamma_{total} \times B(\bar{b} \to B_c)] / [B(\bar{b} \to B^+)] / [B(B^+ \to \overline{D}^0 D^+)] < 1.3 \times 10^{-1}$ which we multiply by our best values $B(\bar{b} \to B^+) = 40.8 \times 10^{-2}$, $B(B^+ \to \overline{D}^0 D^+) = 3.8 \times 10^{-4}$.

$\Gamma(D^+ K^{*0})/\Gamma_{total} \times B(\bar{b} \to B_c)$ — $\Gamma_{42}/\Gamma \times B$

VALUE	CL%	DOCUMENT ID	TECN	COMMENT
$<2.0 \times 10^{-7}$	90	[1] AAIJ	13R LHCB	pp at 7 TeV

[1] AAIJ 13R reports $[\Gamma(B_c^+ \to D^+ K^{*0})/\Gamma_{total} \times B(\bar{b} \to B_c)] / [B(\bar{b} \to B^+)] < 0.5 \times 10^{-6}$ which we multiply by our best value $B(\bar{b} \to B^+) = 40.8 \times 10^{-2}$.

$\Gamma(D^+ \overline{K}^{*0})/\Gamma_{total} \times B(\bar{b} \to B_c)$ — $\Gamma_{43}/\Gamma \times B$

VALUE	CL%	DOCUMENT ID	TECN	COMMENT
$<1.6 \times 10^{-7}$	90	[1] AAIJ	13R LHCB	pp at 7 TeV

[1] AAIJ 13R reports $[\Gamma(B_c^+ \to D^+ \overline{K}^{*0})/\Gamma_{total} \times B(\bar{b} \to B_c)] / [B(\bar{b} \to B^+)] < 0.4 \times 10^{-6}$ which we multiply by our best value $B(\bar{b} \to B^+) = 40.8 \times 10^{-2}$.

$\Gamma(D_s^+ K^{*0})/\Gamma_{total} \times B(\bar{b} \to B_c)$ — $\Gamma_{44}/\Gamma \times B$

VALUE	CL%	DOCUMENT ID	TECN	COMMENT
$<2.9 \times 10^{-7}$	90	[1] AAIJ	13R LHCB	pp at 7 TeV

[1] AAIJ 13R reports $[\Gamma(B_c^+ \to D_s^+ K^{*0})/\Gamma_{total} \times B(\bar{b} \to B_c)] / [B(\bar{b} \to B^+)] < 0.7 \times 10^{-6}$ which we multiply by our best value $B(\bar{b} \to B^+) = 40.8 \times 10^{-2}$.

$\Gamma(D_s^+ \overline{K}^{*0})/\Gamma_{total} \times B(\bar{b} \to B_c)$ — $\Gamma_{45}/\Gamma \times B$

VALUE	CL%	DOCUMENT ID	TECN	COMMENT
$<4 \times 10^{-7}$	90	[1] AAIJ	13R LHCB	pp at 7 TeV

[1] AAIJ 13R reports $[\Gamma(B_c^+ \to D_s^+ \overline{K}^{*0})/\Gamma_{total} \times B(\bar{b} \to B_c)] / [B(\bar{b} \to B^+)] < 1.1 \times 10^{-6}$ which we multiply by our best value $B(\bar{b} \to B^+) = 40.8 \times 10^{-2}$.

Downloaded from https://academic.oup.com/ptep/article/2022/8/083C01/6651666 by KIT Library user on 27 September 2022

$\Gamma(D_s^+\phi)/\Gamma_{total} \times B(\overline{b}\to B_c)$ — $\Gamma_{46}/\Gamma \times B$

VALUE	CL%	DOCUMENT ID		TECN	COMMENT
$<3.3\times10^{-7}$	90	[1] AAIJ	13R	LHCB	pp at 7 TeV

[1] AAIJ 13R reports $[\Gamma(B_c^+\to D_s^+\phi)/\Gamma_{total}\times B(\overline{b}\to B_c)]$ / $[B(\overline{b}\to B^+)] < 0.8\times10^{-6}$ which we multiply by our best value $B(\overline{b}\to B^+) = 40.8\times10^{-2}$.

$\Gamma(K^+K^0)/\Gamma_{total} \times B(\overline{b}\to B_c)$ — $\Gamma_{47}/\Gamma \times B$

VALUE	CL%	DOCUMENT ID		TECN	COMMENT
$<4.6\times10^{-7}$	90	[1] AAIJ	13BS	LHCB	pp at 7 TeV

[1] Derived from $\Gamma(K^+K^0)/\Gamma\times B(\overline{b}\to B_c)$ / $(B(B^+\to K^0\pi^+)\,B(\overline{b}\to B^+)) < 5.8\%$ at 90% CL using normalization mode $B(B^+\to K^0\pi^+) = (23.97\pm0.53\pm0.71)\times10^{-6}$ and assuming a B production ratio $f(\overline{b}\to B_u^+) = 0.33$.

$\Gamma(B_s^0\pi^+ / B(\overline{b}\to B_s))/\Gamma_{total} \times B(\overline{b}\to B_c)$ — $\Gamma_{48}/\Gamma \times B$

VALUE (units 10^{-3})	DOCUMENT ID		TECN	COMMENT
$2.37\pm0.31\pm0.11^{+0.17}_{-0.13}$	[1] AAIJ	13BU	LHCB	pp at 7, 8 TeV

[1] The last uncertinty is due to the uncertainty of the B_c^+ lifetime measurument.

$\Gamma(D_s^+\overline{D}^0)/\Gamma_{total}$ — Γ_{24}/Γ

VALUE	CL%	DOCUMENT ID		TECN	COMMENT
$<7.2\times10^{-4}$	90	[1] AAIJ	21AF	LHCB	pp at 13 TeV

[1] Uses $B(\overline{b}\to B_c)/B(\overline{b}\to B^+) = 0.76\%$ determined by AAIJ 19AI.

$\Gamma(D_s^+D^0)/\Gamma_{total}$ — Γ_{25}/Γ

VALUE	CL%	DOCUMENT ID		TECN	COMMENT
$<3.0\times10^{-4}$	90	[1] AAIJ	21AF	LHCB	pp at 13 TeV

[1] Uses $B(\overline{b}\to B_c)/B(\overline{b}\to B^+) = 0.76\%$ determined by AAIJ 19AI.

$\Gamma(D^+\overline{D}^0)/\Gamma_{total}$ — Γ_{26}/Γ

VALUE	CL%	DOCUMENT ID		TECN	COMMENT
$<1.9\times10^{-4}$	90	[1] AAIJ	21AF	LHCB	pp at 13 TeV

[1] Uses $B(\overline{b}\to B_c)/B(\overline{b}\to B^+) = 0.76\%$ determined by AAIJ 19AI.

$\Gamma(D^+D^0)/\Gamma_{total}$ — Γ_{27}/Γ

VALUE	CL%	DOCUMENT ID		TECN	COMMENT
$<1.4\times10^{-4}$	90	[1] AAIJ	21AF	LHCB	pp at 13 TeV

[1] Uses $B(\overline{b}\to B_c)/B(\overline{b}\to B^+) = 0.76\%$ determined by AAIJ 19AI.

$\Gamma(D_s^{*+}\overline{D}^0)/\Gamma_{total}$ — Γ_{28}/Γ

VALUE	CL%	DOCUMENT ID		TECN	COMMENT
$<5.3\times10^{-4}$	90	[1] AAIJ	21AF	LHCB	pp at 13 TeV

[1] Uses $B(\overline{b}\to B_c)/B(\overline{b}\to B^+) = 0.76\%$ determined by AAIJ 19AI.

$\Gamma(D_s^+\overline{D}^*(2007)^0)/\Gamma_{total}$ — Γ_{29}/Γ

VALUE	CL%	DOCUMENT ID		TECN	COMMENT
$<4.6\times10^{-4}$	90	[1] AAIJ	21AF	LHCB	pp at 13 TeV

[1] Uses $B(\overline{b}\to B_c)/B(\overline{b}\to B^+) = 0.76\%$ determined by AAIJ 19AI.

$\Gamma(D_s^{*+}D^0)/\Gamma_{total}$ — Γ_{30}/Γ

VALUE	CL%	DOCUMENT ID		TECN	COMMENT
$<0.9\times10^{-3}$	90	[1] AAIJ	21AF	LHCB	pp at 13 TeV

[1] Uses $B(\overline{b}\to B_c)/B(\overline{b}\to B^+) = 0.76\%$ determined by AAIJ 19AI.

$\Gamma(D_s^+D^*(2007)^0)/\Gamma_{total}$ — Γ_{31}/Γ

VALUE	CL%	DOCUMENT ID		TECN	COMMENT
$<6.6\times10^{-4}$	90	[1] AAIJ	21AF	LHCB	pp at 13 TeV

[1] Uses $B(\overline{b}\to B_c)/B(\overline{b}\to B^+) = 0.76\%$ determined by AAIJ 19AI.

$\Gamma(D^*(2010)^+\overline{D}^0)/\Gamma_{total}$ — Γ_{32}/Γ

VALUE	CL%	DOCUMENT ID		TECN	COMMENT
$<3.8\times10^{-4}$	90	[1] AAIJ	21AF	LHCB	pp at 13 TeV

[1] Uses $B(\overline{b}\to B_c)/B(\overline{b}\to B^+) = 0.76\%$ determined by AAIJ 19AI.

$\Gamma(D^*(2007)^+D^0)/\Gamma_{total}$ — Γ_{35}/Γ

VALUE	CL%	DOCUMENT ID		TECN	COMMENT
$<2.0\times10^{-4}$	90	[1] AAIJ	21AF	LHCB	pp at 13 TeV

[1] Uses $B(\overline{b}\to B_c)/B(\overline{b}\to B^+) = 0.76\%$ determined by AAIJ 19AI.

$\Gamma(D^+\overline{D}^*(2007)^0)/\Gamma_{total}$ — Γ_{34}/Γ

VALUE	CL%	DOCUMENT ID		TECN	COMMENT
$<6.5\times10^{-4}$	90	[1] AAIJ	21AF	LHCB	pp at 13 TeV

[1] Uses $B(\overline{b}\to B_c)/B(\overline{b}\to B^+) = 0.76\%$ determined by AAIJ 19AI.

$\Gamma(D^+D^*(2007)^0)/\Gamma_{total}$ — Γ_{37}/Γ

VALUE	CL%	DOCUMENT ID		TECN	COMMENT
$<3.7\times10^{-4}$	90	[1] AAIJ	21AF	LHCB	pp at 13 TeV

[1] Uses $B(\overline{b}\to B_c)/B(\overline{b}\to B^+) = 0.76\%$ determined by AAIJ 19AI.

$\Gamma(D_s^{*+}\overline{D}^*(2007)^0)/\Gamma_{total}$ — Γ_{38}/Γ

VALUE	CL%	DOCUMENT ID		TECN	COMMENT
$<1.3\times10^{-3}$	90	[1] AAIJ	21AF	LHCB	pp at 13 TeV

[1] Uses $B(\overline{b}\to B_c)/B(\overline{b}\to B^+) = 0.76\%$ determined by AAIJ 19AI.

$\Gamma(D_s^{*+}D^*(2007)^0)/\Gamma_{total}$ — Γ_{39}/Γ

VALUE	CL%	DOCUMENT ID		TECN	COMMENT
$<1.3\times10^{-3}$	90	[1] AAIJ	21AF	LHCB	pp at 13 TeV

[1] Uses $B(\overline{b}\to B_c)/B(\overline{b}\to B^+) = 0.76\%$ determined by AAIJ 19AI.

$\Gamma(D^*(2010)^+\overline{D}^*(2007)^0)/\Gamma_{total}$ — Γ_{40}/Γ

VALUE	CL%	DOCUMENT ID		TECN	COMMENT
$<1.0\times10^{-3}$	90	[1] AAIJ	21AF	LHCB	pp at 13 TeV

[1] Uses $B(\overline{b}\to B_c)/B(\overline{b}\to B^+) = 0.76\%$ determined by AAIJ 19AI.

$\Gamma(D^*(2010)^+D^*(2007)^0)/\Gamma_{total}$ — Γ_{41}/Γ

VALUE	CL%	DOCUMENT ID		TECN	COMMENT
$<7.7\times10^{-4}$	90	[1] AAIJ	21AF	LHCB	pp at 13 TeV

[1] Uses $B(\overline{b}\to B_c)/B(\overline{b}\to B^+) = 0.76\%$ determined by AAIJ 19AI.

POLARIZATION IN B_c^+ DECAY

In decays involving two vector mesons, one can distinguish among the states in which meson polarizations are both longitudinal (L) or both are transverse and parallel ($\|$) or perpendicular ($\perp$) to each other with the parameters Γ_L/Γ, $\Gamma_\perp/\Gamma$, and the relative phases $\phi_\|$ and $\phi_\perp$. See the definitions in the note on "Polarization in B Decays" review in the B^0 Particle Listings.

Γ_L/Γ in $B_c^+\to J/\psi D_s^{*+}$

VALUE	DOCUMENT ID		TECN	COMMENT
0.54±0.15 OUR AVERAGE				
0.62±0.24	[1] AAD	16H	ATLS	pp at 7, 8 TeV
0.48±0.20	[2] AAIJ	13AS	LHCB	pp at 7, 8 TeV

[1] AAD 16H measures $1-\Gamma_L/\Gamma = 0.38\pm0.24$.
[2] AAIJ 13AS measures $1-\Gamma_L/\Gamma = 0.52\pm0.20$.

$A_P(B_c^+)$

$$A_P(B_c^+) = [\sigma(B_c^-)-\sigma(B_c^+)] \,/\, [\sigma(B_c^-)+\sigma(B_c^+)]$$

VALUE (units 10^{-2})	DOCUMENT ID		TECN	COMMENT
−1.0±1.0 OUR AVERAGE				
−2.5±2.1±0.5	[1] AAIJ	19AI	LHCB	pp at 7 TeV
−0.5±1.1±0.4	[1] AAIJ	19AI	LHCB	pp at 13 TeV

[1] Measured using B_c^+ semileptonic decays.

B_c^+ REFERENCES

AABOUD	21	PR D104 012010	M. Aaboud et al.	(ATLAS Collab.)
AAIJ	21AF	JHEP 2112 117	R. Aaij et al.	(LHCb Collab.)
AAIJ	20R	JHEP 2007 123	R. Aaij et al.	(LHCb Collab.)
AAIJ	19AI	PR D100 112006	R. Aaij et al.	(LHCb Collab.)
AAIJ	18C	PRL 120 121801	R. Aaij et al.	(LHCb Collab.)
AAIJ	18P	NP B930 563	R. Aaij et al.	(LHCb Collab.)
SIRUNYAN	18BY	EPJ C78 457	A.M. Sirunyan et al.	(CMS Collab.)
AAIJ	17AG	PRL 118 111803	R. Aaij et al.	(LHCb Collab.)
AAIJ	17L	PR D95 032005	R. Aaij et al.	(LHCb Collab.)
AAD	16H	EPJ C76 4	G. Aad et al.	(ATLAS Collab.)
AAIJ	16AF	JHEP 1609 153	R. Aaij et al.	(LHCb Collab.)
AAIJ	16AT	PR D94 091102	R. Aaij et al.	(LHCb Collab.)
AAIJ	16K	PL B759 313	R. Aaij et al.	(LHCb Collab.)
AALTONEN	16A	PR D93 052001	T. Aaltonen et al.	(CDF Collab.)
AAIJ	15AY	PR D92 072007	R. Aaij et al.	(LHCb Collab.)
AAIJ	15G	PL B742 29	R. Aaij et al.	(LHCb Collab.)
AAIJ	15M	PRL 114 132001	R. Aaij et al.	(LHCb Collab.)
KHACHATRY...	15AA	JHEP 1501 063	V. Khachatryan et al.	(CMS Collab.)
AAIJ	14AQ	PRL 113 152003	R. Aaij et al.	(LHCb Collab.)
AAIJ	14G	EPJ C74 2839	R. Aaij et al.	(LHCb Collab.)
AAIJ	14P	JHEP 1405 148	R. Aaij et al.	(LHCb Collab.)
AAIJ	14W	PR D90 032009	R. Aaij et al.	(LHCb Collab.)
AAIJ	13AM	PR D87 071103	R. Aaij et al.	(LHCb Collab.)
AAIJ	13AS	PR D87 112012	R. Aaij et al.	(LHCb Collab.)
Also		PR D89 019901 (errat.)	R. Aaij et al.	(LHCb Collab.)
AAIJ	13BS	PL B726 646	R. Aaij et al.	(LHCb Collab.)
AAIJ	13BU	PRL 111 181801	R. Aaij et al.	(LHCb Collab.)
AAIJ	13BY	JHEP 1309 075	R. Aaij et al.	(LHCb Collab.)
AAIJ	13CA	JHEP 1311 094	R. Aaij et al.	(LHCb Collab.)
AAIJ	13R	JHEP 1302 043	R. Aaij et al.	(LHCb Collab.)
AALTONEN	13	PR D87 011101	T. Aaltonen et al.	(CDF Collab.)
AAIJ	12AV	PRL 109 232001	R. Aaij et al.	(LHCb Collab.)
AAIJ	12Y	PRL 108 251802	R. Aaij et al.	(LHCb Collab.)
ABAZOV	09H	PRL 102 092001	V.M. Abazov et al.	(D0 Collab.)
AALTONEN	08M	PRL 100 182002	T. Aaltonen et al.	(CDF Collab.)
ABAZOV	08T	PRL 101 012001	V.M. Abazov et al.	(D0 Collab.)
ABULENCIA	06C	PRL 96 082002	A. Abulencia et al.	(CDF Collab.)
ABULENCIA	06O	PRL 97 012002	A. Abulencia et al.	(CDF Collab.)
ABE	98M	PRL 81 2432	F. Abe et al.	(CDF Collab.)
Also		PR D58 112004	F. Abe et al.	(CDF Collab.)
ACKERSTAFF	98O	PL B420 157	K. Ackerstaff et al.	(OPAL Collab.)
BARATE	98Q	EPJ C4 387	R. Barate et al.	(ALEPH Collab.)
PDG	98	EPJ C3 1	C. Caso et al.	(PDG Collab.)
ABREU	97E	PL B398 207	P. Abreu et al.	(DELPHI Collab.)
BARATE	97H	PL B402 213	R. Barate et al.	(ALEPH Collab.)
ABE	96R	PRL 77 5176	F. Abe et al.	(CDF Collab.)
PDG	96	PR D54 1	R. M. Barnett et al.	(PDG Collab.)

Downloaded from https://academic.oup.com/ptep/article/2022/8/083C01/6651666 by KIT Library user on 27 September 2022

$B_c(2S)^\pm$

$I(J^P) = 0(0^-)$

Quantum numbers neither measured nor confirmed.

$B_c(2S)^\pm$ MASS

VALUE (MeV)	EVTS	DOCUMENT ID		TECN	COMMENT
6871.2±1.0 OUR AVERAGE					
6871.7±1.3±0.3	24	[1,2] AAIJ	19Y	LHCB	pp at 7, 8, 13 TeV
6870.6±1.4±0.3	51	[3,4] SIRUNYAN	19M	CMS	pp at 13 TeV
• • • We do not use the following data for averages, fits, limits, etc. • • •					
not seen		[5] AAIJ	18AL	LHCB	pp at 8 TeV
6842 ±4 ±5	57	[6,7] AAD	14AQ	ATLS	pp at 7, 8 TeV

[1] AAIJ 19Y observed $B_c(2S)^+$ in the decay mode $B_c(2S)^+ \to B_c^+\pi^+\pi^-$ ($B_c^+ \to J/\psi\pi^+$) with 2.2 (3.2) global (local) standard deviations significance.

[2] AAIJ 19Y reports mass difference measurement of $M(B_c(2S)^+) - M(B_c^+) = 597.2 \pm 1.3 \pm 0.1$ MeV. We have adjusted this measurement with our best value of $M(B_c^+) = 6274.47 \pm 0.32$ MeV. The first uncertainty of the $M(B_c(2S)^+)$ value is a total of uncertainties reported by the experiment and the second one comes from our best value of $M(B_c^+)$.

[3] SIRUNYAN 19M observed $B_c(2S)^+$ in the decay mode $B_c(2S)^+ \to B_c^+\pi^+\pi^-$ ($B_c^+ \to J/\psi\pi^+$) with 6.5 standard deviations significance.

[4] SIRUNYAN 19M reports mass difference measurement of $M(B_c(2S)^+) - M(B_c^+) = 596.1 \pm 1.2 \pm 0.8$ MeV. We have adjusted this measurement with our best value of $M(B_c^+) = 6274.47 \pm 0.32$ MeV. The first uncertainty of the $M(B_c(2S)^+)$ value is a total of uncertainties reported by the experiment and the second one comes from our best value of $M(B_c^+)$.

[5] AAIJ 18AL reports an upper limit on the ratio of production cross sections for $[\sigma(B_c(2S)^+)/\sigma(B_c^+)]\cdot B(B_c(2S)^+ \to B_c^+\pi^+\pi^-) < 0.04$–$0.09$ at 95% CL for the mass value reported by AAD 14AQ.

[6] Observed in the decay mode $B_c(2S)^+ \to B_c^+\pi^+\pi^-$ ($B_c^+ \to J/\psi\pi^+$) with 5.2 standard deviations significance.

[7] Might be the $B_c^*(2S)$.

$B_c(2S)^\pm$ DECAY MODES

	Mode	Fraction (Γ_i/Γ)
Γ_1	$B_c^+\pi^+\pi^-$	seen

$B_c(2S)^\pm$ BRANCHING RATIOS

$\Gamma(B_c^+\pi^+\pi^-)/\Gamma_{total}$ — Γ_1/Γ

VALUE	EVTS	DOCUMENT ID		TECN	COMMENT
seen	57	[1] AAD	14AQ	ATLS	pp at 7, 8 TeV
• • • We do not use the following data for averages, fits, limits, etc. • • •					
not seen		[2] AAIJ	18AL	LHCB	pp at 8 TeV

[1] Observed with 5.2 standard deviations significance.

[2] AAIJ 18AL reports an upper limit on the ratio of production cross sections for $[\sigma(B_c(2S)^+)/\sigma(B_c^+)]\cdot B(B_c(2S)^+ \to B_c^+\pi^+\pi^-) < 0.04$–$0.09$ at 95% CL for the mass value reported by AAD 14AQ.

$B_c(2S)^\pm$ REFERENCES

AAIJ	19Y	PRL 122 232001	R. Aaij *et al.*	(LHCb Collab.)
SIRUNYAN	19M	PRL 122 132001	A.M. Sirunyan *et al.*	(CMS Collab.)
AAIJ	18AL	JHEP 1801 138	R. Aaij *et al.*	(LHCb Collab.)
AAD	14AQ	PRL 113 212004	G. Aad *et al.*	(ATLAS Collab.)

See the related review(s):

Spectroscopy of Mesons Containing Two Heavy Quarks

Downloaded from https://academic.oup.com/ptep/article/2022/8/083C01/6651666 by KIT Library user on 27 September 2022

$c\overline{c}$ MESONS (including possibly non-$q\overline{q}$ states)

Updated March 2022.

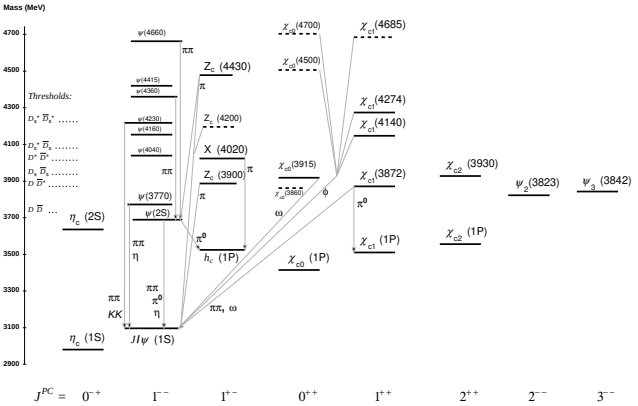

The level scheme of meson states containing a minimal quark content of $c\overline{c}$. The name of a state is determined by its quantum numbers $I^G J^{PC}$ (see the review "Naming Scheme for Hadrons"). States with unestablished quantum numbers are called X and are drawn according to our best estimate of their likely J^{PC}. States included in the Summary Tables are shown with solid lines; selected states not in the Summary Tables, but with assigned quantum numbers, are shown with dotted lines. The arrows indicate the most dominant hadronic transitions. Single photon transitions, including $\psi(nS) \to \gamma\eta_c(mS)$, $\psi(nS) \to \gamma\chi_{cJ}(1P)$, and $\chi_{cJ}(1P) \to \gamma J/\psi$, are omitted for clarity. For orientation, the location of the thresholds related to a pair of ground state open charm mesons is indicated in the figure.

$\eta_c(1S)$

$I^G(J^{PC}) = 0^+(0^{-+})$

$\eta_c(1S)$ MASS

VALUE (MeV)	EVTS	DOCUMENT ID		TECN	COMMENT
2983.9 ± 0.4 OUR AVERAGE		Error includes scale factor of 1.2.			
2983.9 ± 0.7 ± 0.1		[1] AAIJ	20H	LHCB	$pp \to bX \to p\overline{p}X$
2985.9 ± 0.7 ± 2.1	1705	ABLIKIM	19AV	BES3	$J/\psi \to \gamma\omega\omega$
2984.6 ± 0.7 ± 2.2	2673	XU	18	BELL	$e^+e^- \to e^+e^-\eta'\pi^+\pi^-$
2986.7 ± 0.5 ± 0.9	11k	[2] AAIJ	17AD	LHCB	$pp \to B^+X \to p\overline{p}K^+X$
2982.8 ± 1.0 ± 0.5	6.4k	[3] AAIJ	17BB	LHCB	$pp \to b\overline{b}X \to 2(K^+K^-)X$
2982.2 ± 1.5 ± 0.1	2.0k	[4] AAIJ	15BI	LHCB	$pp \to \eta_c(1S)X$
2983.5 ± 1.4 $^{+1.6}_{-3.6}$		[5] ANASHIN	14	KEDR	$J/\psi \to \gamma\eta_c$
2979.8 ± 0.8 ± 3.5	4.5k	[6,7] LEES	14E	BABR	$\gamma\gamma \to K^+K^-\pi^0$
2984.1 ± 1.1 ± 2.1	900	[6,7,8] LEES	14E	BABR	$\gamma\gamma \to K^+K^-\eta$
2984.3 ± 0.6 ± 0.6		[9,10] ABLIKIM	12F	BES3	$\psi(2S) \to \gamma\eta_c$
2984.49 ± 1.16 ± 0.52	832	[6] ABLIKIM	12N	BES3	$\psi(2S) \to \pi^0\gamma$ hadrons
2982.7 ± 1.8 ± 2.2	486	ZHANG	12A	BELL	$e^+e^- \to e^+e^-\eta'\pi^+\pi^-$
2984.5 ± 0.8 ± 3.1	11k	DEL-AMO-SA...	11M	BABR	$\gamma\gamma \to K^+K^-\pi^+\pi^-\pi^0$
2985.4 ± 1.5 $^{+0.5}_{-2.0}$	920	[10] VINOKUROVA	11	BELL	$B^\pm \to K^\pm(K^0_S K^\pm\pi^\mp)$
2982.2 ± 0.4 ± 1.6	14k	[11] LEES	10	BABR	10.6 $e^+e^- \to e^+e^-K^0_S K^\pm\pi^\mp$
2985.8 ± 1.5 ± 3.1	0.9k	AUBERT	08AB	BABR	$B \to \eta_c(1S)K^{(*)} \to K\overline{K}\pi K^{(*)}$
2986.1 ± 1.0 ± 2.5	7.5k	UEHARA	08	BELL	$\gamma\gamma \to \eta_c \to$ hadrons
2970 ± 5 ± 6	501	[12] ABE	07	BELL	$e^+e^- \to J/\psi(c\overline{c})$
2971 ± 3 $^{+2}_{-1}$	195	WU	06	BELL	$B^+ \to p\overline{p}K^+$
2974 ± 7 $^{+2}_{-1}$	20	WU	06	BELL	$B^+ \to \Lambda\overline{\Lambda}K^+$
2981.8 ± 1.3 ± 1.5	592	ASNER	04	CLEO	$\gamma\gamma \to \eta_c \to K^0_S K^\pm\pi^\mp$
2984.1 ± 2.1 ± 1.0	190	[13] AMBROGIANI	03	E835	$\overline{p}p \to \eta_c \to \gamma\gamma$
• • • We do not use the following data for averages, fits, limits, etc. • • •					
2982.5 ± 0.4 ± 1.4	12k	[14] DEL-AMO-SA...	11M	BABR	$\gamma\gamma \to K^0_S K^\pm\pi^\mp$
2982.2 ± 0.6		[15] MITCHELL	09	CLEO	$e^+e^- \to \gamma X$
2982 ± 5	270	[16] AUBERT	06E	BABR	$B^\pm \to K^\pm X_{c\overline{c}}$
2982.5 ± 1.1 ± 0.9	2.5k	[17] AUBERT	04D	BABR	$\gamma\gamma \to \eta_c(1S) \to K\overline{K}\pi$
2977.5 ± 1.0 ± 1.2		[15,18] BAI	03	BES	$J/\psi \to \gamma\eta_c$
2979.6 ± 2.3 ± 1.6	180	[19] FANG	03	BELL	$B \to \eta_c K$
2976.3 ± 2.3 ± 1.2		[15,20] BAI	00F	BES	$J/\psi,\ \psi(2S) \to \gamma\eta_c$
2976.6 ± 2.9 ± 1.3	140	[15,21] BAI	00F	BES	$J/\psi \to \gamma\eta_c$
2980.4 ± 2.3 ± 0.6		[22] BRANDENB...	00B	CLE2	$\gamma\gamma \to \eta_c \to K^\pm K^0_S\pi^\mp$
2975.8 ± 3.9 ± 1.2		[21] BAI	99B	BES	Sup. by BAI 00F
2999 ± 8	25	ABREU	98O	DLPH	$e^+e^- \to e^+e^-$ +hadrons
2988.3 $^{+3.3}_{-3.1}$		ARMSTRONG	95F	E760	$\overline{p}p \to \gamma\gamma$
2974.4 ± 1.9		[15,23] BISELLO	91	DM2	$J/\psi \to \eta_c\gamma$
2969 ± 4 ± 4	80	[15] BAI	90B	MRK3	$J/\psi \to \gamma K^+K^-K^+K^-$
2956 ±12 ±12		[15] BAI	90B	MRK3	$J/\psi \to \gamma K^+K^-K^0_S K^0_L$
2982.6 $^{+2.7}_{-2.3}$	12	BAGLIN	87B	SPEC	$\overline{p}p \to \gamma\gamma$
2980.2 ± 1.6		[15,23] BALTRUSAIT...	86	MRK3	$J/\psi \to \eta_c\gamma$
2984 ± 2.3 ± 4.0		[15] GAISER	86	CBAL	$J/\psi \to \gamma X$, $\psi(2S) \to \gamma X$
2976 ± 8		[15,24] BALTRUSAIT...	84	MRK3	$J/\psi \to 2\phi\gamma$
2982 ± 8	18	[25] HIMEL	80B	MRK2	e^+e^-
2980 ± 9		[25] PARTRIDGE	80B	CBAL	e^+e^-

[1] AAIJ 20H report $m_{J/\psi} - m_{\eta_c(1S)} = 113.0 \pm 0.7 \pm 0.1$ MeV. We use the current value $m_{J/\psi} = 3096.900 \pm 0.006$ MeV to obtain the quoted mass.
[2] AAIJ 17AD report $m_{J/\psi} - m_{\eta_c(1S)} = 110.2 \pm 0.5 \pm 0.9$ MeV. We use the current value $m_{J/\psi} = 3096.900 \pm 0.006$ MeV to obtain the quoted mass.
[3] From a fit of the $\phi\phi$ invariant mass with the mass and width of $\eta_c(1S)$ as free parameters.
[4] AAIJ 15BI reports $m_{J/\psi} - m_{\eta_c(1S)} = 114.7 \pm 1.5 \pm 0.1$ MeV from a sample of $\eta_c(1S)$ and J/ψ produced in b-hadron decays. We have used current value of $m_{J/\psi} = 3096.900 \pm 0.006$ MeV to arrive at the quoted $m_{\eta_c(1S)}$ result.
[5] Taking into account an asymmetric photon lineshape.
[6] With floating width.
[7] Ignoring possible interference with the non-resonant 0^- amplitude.
[8] Using both, $\eta \to \gamma\gamma$ and $\eta \to \pi^+\pi^-\pi^0$ decays.
[9] From a simultaneous fit to six decay modes of the η_c.
[10] Accounts for interference with non-resonant continuum.
[11] Taking into account interference with the non-resonant $J^P = 0^-$ amplitude.
[12] From a fit of the J/ψ recoil mass spectrum. Supersedes ABE,K 02 and ABE 04G.
[13] Using mass of $\psi(2S) = 3686.00$ MeV.
[14] Not independent from the measurements reported by LEES 10.
[15] MITCHELL 09 observes a significant asymmetry in the lineshapes of $\psi(2S) \to \gamma\eta_c$ and $J/\psi \to \gamma\eta_c$ transitions. If ignored, this asymmetry could lead to significant bias whenever the mass and width are measured in $\psi(2S)$ or J/ψ radiative decays.
[16] From the fit of the kaon momentum spectrum. Systematic errors not evaluated.
[17] Superseded by LEES 10.
[18] From a simultaneous fit of five decay modes of the η_c.
[19] Superseded by VINOKUROVA 11.
[20] Weighted average of the $\psi(2S)$ and $J/\psi(1S)$ samples. Using an η_c width of 13.2 MeV.
[21] Average of several decay modes. Using an η_c width of 13.2 MeV.
[22] Superseded by ASNER 04.
[23] Average of several decay modes.
[24] $\eta_c \to \phi\phi$.
[25] Mass adjusted by us to correspond to $J/\psi(1S)$ mass = 3097 MeV.

$\eta_c(1S)$ WIDTH

VALUE (MeV)	EVTS	DOCUMENT ID		TECN	COMMENT
32.0 ± 0.7 OUR FIT					
32.1 ± 0.8 OUR AVERAGE		Error includes scale factor of 1.1.			
33.8 ± 1.6 ± 4.1	1705	ABLIKIM	19AV	BES3	$J/\psi \to \gamma\omega\omega$
30.8 $^{+2.3}_{-2.2}$ ± 2.9	2673	XU	18	BELL	$e^+e^- \to e^+e^-\eta'\pi^+\pi^-$
34.0 ± 1.9 ± 1.3	11k	AAIJ	17AD	LHCB	$pp \to B^+X \to p\overline{p}K^+X$
31.4 ± 3.5 ± 2.0	6.4k	[1] AAIJ	17BB	LHCB	$pp \to b\overline{b}X \to 2(K^+K^-)X$
27.2 ± 3.1 $^{+5.4}_{-2.6}$		[2] ANASHIN	14	KEDR	$J/\psi \to \gamma\eta_c$

Downloaded from https://academic.oup.com/ptep/article/2022/8/083C01/6651666 by KIT Library user on 27 September 2022

$25.2\pm\ 2.6\pm2.4$	4.5k	[3,4] LEES	14E	BABR	$\gamma\gamma\to K^+K^-\pi^0$
$34.8\pm\ 3.1\pm4.0$	900	[3,4,5] LEES	14E	BABR	$\gamma\gamma\to K^+K^-\eta$
$32.0\pm\ 1.2\pm1.0$		[6,7] ABLIKIM	12F	BES3	$\psi(2S)\to\gamma\eta_c$
$36.4\pm\ 3.2\pm1.7$	832	[3] ABLIKIM	12N	BES3	$\psi(2S)\to\pi^0\gamma$ hadrons
$37.8^{+5.8}_{-5.3}\pm3.1$	486	ZHANG	12A	BELL	$e^+e^-\to e^+e^-\eta'\pi^+\pi^-$
$36.2\pm\ 2.8\pm3.0$	11k	DEL-AMO-SA...	11M	BABR	$\gamma\gamma\to K^+K^-\pi^+\pi^-\pi^0$
$35.1\pm\ 3.1^{+1.0}_{-1.6}$	920	[7] VINOKUROVA	11	BELL	$B^\pm\to K^\pm(K^0_SK^\pm\pi^\mp)$
$31.7\pm\ 1.2\pm0.8$	14k	[8] LEES	10	BABR	$10.6\ e^+e^-\to e^+e^-K^0_SK^\pm\pi^\mp$
$36.3^{+3.7}_{-3.6}\pm4.4$	0.9k	AUBERT	08AB	BABR	$B\to\eta_c(1S)K^{(*)}\to K\overline{K}\pi K^{(*)}$
$28.1\pm\ 3.2\pm2.2$	7.5k	UEHARA	08	BELL	$\gamma\gamma\to\eta_c\to$ hadrons
$48\ ^{+8}_{-7}\ \pm5$	195	WU	06	BELL	$B^+\to p\overline{p}K^+$
$40\ \pm19\ \pm5$	20	WU	06	BELL	$B^+\to\Lambda\overline{\Lambda}K^+$
$24.8\pm\ 3.4\pm3.5$	592	ASNER	04	CLEO	$\gamma\gamma\to\eta_c\to K^0_SK^\pm\pi^\mp$
$20.4^{+7.7}_{-6.7}\pm2.0$	190	AMBROGIANI	03	E835	$\overline{p}p\to\eta_c\to\gamma\gamma$
$23.9^{+12.6}_{-7.1}$		ARMSTRONG	95F	E760	$\overline{p}p\to\gamma\gamma$
• • • We do not use the following data for averages, fits, limits, etc. • • •					
$32.1\pm\ 1.1\pm1.3$	12k	[9] DEL-AMO-SA...	11M	BABR	$\gamma\gamma\to K^0_SK^\pm\pi^\mp$
$34.3\pm\ 2.3\pm0.9$	2.5k	[10] AUBERT	04D	BABR	$\gamma\gamma\to\eta_c(1S)\to K\overline{K}\pi$
$17.0\pm\ 3.7\pm7.4$		[11] BAI	03	BES	$J/\psi\to\gamma\eta_c$
$29\ \pm\ 8\ \pm6$	180	[12] FANG	03	BELL	$B\to\eta_cK$
$11.0\pm\ 8.1\pm4.1$		[13] BAI	00F	BES	$J/\psi\to\gamma\eta_c$ and $\psi(2S)\to\gamma\eta_c$
$27.0\pm\ 5.8\pm1.4$		[14] BRANDENB...	00B	CLE2	$\gamma\gamma\to\eta_c\to K^\pm K^0_S\pi^\mp$
$7.0^{+7.5}_{-7.0}$	12	BAGLIN	87B	SPEC	$\overline{p}p\to\gamma\gamma$
$10.1^{+33.0}_{-8.2}$	23	[15] BALTRUSAIT...	86	MRK3	$J/\psi\to\gamma p\overline{p}$
$11.5\pm\ 4.5$		GAISER	86	CBAL	$J/\psi\to\gamma X$, $\psi(2S)\to\gamma X$
<40 90% CL	18	HIMEL	80B	MRK2	e^+e^-
<20 90% CL		PARTRIDGE	80B	CBAL	e^+e^-

[1] From a fit of the $\phi\phi$ invariant mass with the mass and width of $\eta_c(1S)$ as free parameters.
[2] Taking into account an asymmetric photon lineshape.
[3] With floating mass.
[4] Ignoring possible interference with the non-resonant 0^- amplitude.
[5] Using both, $\eta\to\gamma\gamma$ and $\eta\to\pi^+\pi^-\pi^0$ decays.
[6] From a simultaneous fit to six decay modes of the η_c.
[7] Accounts for interference with non-resonant continuum.
[8] Taking into account interference with the non-resonant $J^P=0^-$ amplitude.
[9] Not independent from the measurements reported by LEES 10.
[10] Superseded by LEES 10.
[11] From a simultaneous fit of five decay modes of the η_c.
[12] Superseded by VINOKUROVA 11.
[13] From a fit to the 4-prong invariant mass in $\psi(2S)\to\gamma\eta_c$ and $J/\psi(1S)\to\gamma\eta_c$ decays.
[14] Superseded by ASNER 04.
[15] Positive and negative errors correspond to 90% confidence level.

$\eta_c(1S)$ DECAY MODES

	Mode	Fraction (Γ_i/Γ)	Confidence level
	Decays involving hadronic resonances		
Γ_1	$\eta'(958)\pi\pi$	$(4.1\ \pm1.7)$ %	
Γ_2	$\eta'(958)K\overline{K}$	$(3.5\ \pm1.5)$ %	
Γ_3	$\rho\rho$	$(1.8\ \pm0.5)$ %	
Γ_4	$K^*(892)^0K^-\pi^++$ c.c.	$(2.0\ \pm0.7)$ %	
Γ_5	$K^*(892)\overline{K}^*(892)$	$(6.9\ \pm1.3)\times10^{-3}$	
Γ_6	$K^*(892)^0\overline{K}^*(892)^0\pi^+\pi^-$	$(1.1\ \pm0.5)$ %	
Γ_7	ϕK^+K^-	$(2.9\ \pm1.4)\times10^{-3}$	
Γ_8	$\phi\phi$	$(1.74\pm0.19)\times10^{-3}$	
Γ_9	$\phi2(\pi^+\pi^-)$	$<4\ \times10^{-3}$	90%
Γ_{10}	$a_0(980)\pi$	seen	
Γ_{11}	$a_2(1320)\pi$	<2 %	90%
Γ_{12}	$K^*(892)\overline{K}+$ c.c.	<1.28 %	90%
Γ_{13}	$f_2(1270)\eta$	<1.1 %	90%
Γ_{14}	$f_2(1270)\eta'$	seen	
Γ_{15}	$\omega\omega$	$(2.9\ \pm0.8)\times10^{-3}$	
Γ_{16}	$\omega\phi$	$<2.5\ \times10^{-4}$	90%
Γ_{17}	$f_2(1270)f_2(1270)$	$(9.8\ \pm2.5)\times10^{-3}$	
Γ_{18}	$f_2(1270)f'_2(1525)$	$(9.5\ \pm3.2)\times10^{-3}$	
Γ_{19}	$f_0(500)\eta$	seen	
Γ_{20}	$f_0(500)\eta'$	seen	
Γ_{21}	$f_0(980)\eta$	seen	
Γ_{22}	$f_0(980)\eta'$	seen	
Γ_{23}	$f_0(1500)\eta$	seen	
Γ_{24}	$f_0(1710)\eta'$	seen	
Γ_{25}	$f_0(2100)\eta'$	seen	
Γ_{26}	$f_0(2200)\eta$	seen	
Γ_{27}	$a_0(1320)\pi$	seen	
Γ_{28}	$a_0(1450)\pi$	seen	
Γ_{29}	$a_0(1700)\pi$	seen	
Γ_{30}	$a_0(1950)\pi$	seen	
Γ_{31}	$K^*_0(1430)\overline{K}$	seen	
Γ_{32}	$K^*_2(1430)\overline{K}$	seen	
Γ_{33}	$K^*_0(1950)\overline{K}$	seen	
	Decays into stable hadrons		
Γ_{34}	$K\overline{K}\pi$	$(7.3\ \pm0.4)$ %	
Γ_{35}	$K\overline{K}\eta$	(1.36 ± 0.15) %	
Γ_{36}	$\eta\pi^+\pi^-$	$(1.7\ \pm0.6)$ %	
Γ_{37}	$\eta2(\pi^+\pi^-)$	$(4.4\ \pm1.6)$ %	
Γ_{38}	$K^+K^-\pi^+\pi^-$	$(6.6\ \pm1.1)\times10^{-3}$	
Γ_{39}	$K^+K^-\pi^+\pi^-\pi^0$	$(3.5\ \pm0.6)$ %	
Γ_{40}	$K^0K^-\pi^+\pi^-\pi^++$c.c.	$(5.6\ \pm1.9)$ %	
Γ_{41}	$K^+K^-2(\pi^+\pi^-)$	$(7.5\ \pm2.4)\times10^{-3}$	
Γ_{42}	$2(K^+K^-)$	$(1.43\pm0.30)\times10^{-3}$	
Γ_{43}	$\pi^+\pi^-\pi^0$	$<5\ \times10^{-4}$	90%
Γ_{44}	$\pi^+\pi^-\pi^0\pi^0$	$(4.7\ \pm1.4)$ %	
Γ_{45}	$2(\pi^+\pi^-)$	$(9.1\ \pm1.2)\times10^{-3}$	
Γ_{46}	$2(\pi^+\pi^-\pi^0)$	$(15.8\ \pm2.3)$ %	
Γ_{47}	$3(\pi^+\pi^-)$	$(1.7\ \pm0.4)$ %	
Γ_{48}	$p\overline{p}$	$(1.44\pm0.14)\times10^{-3}$	
Γ_{49}	$p\overline{p}\pi^0$	$(3.6\ \pm1.5)\times10^{-3}$	
Γ_{50}	$\Lambda\overline{\Lambda}$	$(1.06\pm0.23)\times10^{-3}$	
Γ_{51}	$K^+\overline{p}\Lambda+$ c.c.	$(2.5\ \pm0.4)\times10^{-3}$	
Γ_{52}	$\overline{\Lambda}(1520)\Lambda+$ c.c.	$(3.1\ \pm1.3)\times10^{-3}$	
Γ_{53}	$\Sigma^+\overline{\Sigma}^-$	$(2.1\ \pm0.6)\times10^{-3}$	
Γ_{54}	$\Xi^-\overline{\Xi}^+$	$(9.0\ \pm2.6)\times10^{-4}$	
Γ_{55}	$\pi^+\pi^-p\overline{p}$	$(5.3\ \pm2.1)\times10^{-3}$	
	Radiative decays		
Γ_{56}	$\gamma\gamma$	$(1.61\pm0.12)\times10^{-4}$	
	Charge conjugation (C), Parity (P), Lepton family number (LF) violating modes		
Γ_{57}	$\pi^+\pi^-$	P,CP $<1.1\ \times10^{-4}$	90%
Γ_{58}	$\pi^0\pi^0$	P,CP $<4\ \times10^{-5}$	90%
Γ_{59}	K^+K^-	P,CP $<6\ \times10^{-4}$	90%
Γ_{60}	$K^0_SK^0_S$	P,CP $<3.1\ \times10^{-4}$	90%

CONSTRAINED FIT INFORMATION

An overall fit to the total width, 8 combinations of partial widths obtained from integrated cross section, and 19 branching ratios uses 93 measurements and one constraint to determine 13 parameters. The overall fit has a $\chi^2=117.8$ for 81 degrees of freedom.

The following *off-diagonal* array elements are the correlation coefficients $\langle\delta p_i\delta p_j\rangle/(\delta p_i\cdot\delta p_j)$, in percent, from the fit to parameters p_i, including the branching fractions, $x_i\equiv\Gamma_i/\Gamma_{\rm total}$. The fit constrains the x_i whose labels appear in this array to sum to one.

x_8	16									
x_{17}	3	5								
x_{34}	18	35	6							
x_{35}	9	17	3	47						
x_{38}	10	18	3	21	10					
x_{42}	7	13	2	21	10	8				
x_{45}	12	22	4	25	12	14	10			
x_{48}	11	20	4	27	13	12	10	15		
x_{50}	3	5	1	6	3	3	2	4	23	
x_{56}	−27	−51	−9	−59	−28	−32	−23	−38	−38	−9
Γ	−1	−3	0	−3	−1	−2	−1	−2	6	1
	x_5	x_8	x_{17}	x_{34}	x_{35}	x_{38}	x_{42}	x_{45}	x_{48}	x_{50}

Γ	−27
	x_{56}

Downloaded from https://academic.oup.com/ptep/article/2022/8/083C01/6651666 by KIT Library user on 27 September 2022

	Mode	Rate (MeV)
Γ_5	$K^*(892)\overline{K}^*(892)$	0.22 ± 0.04
Γ_8	$\phi\phi$	0.056 ± 0.006
Γ_{17}	$f_2(1270)\, f_2(1270)$	0.31 ± 0.08
Γ_{34}	$K\overline{K}\pi$	2.32 ± 0.14
Γ_{35}	$K\overline{K}\eta$	0.43 ± 0.05
Γ_{38}	$K^+K^-\pi^+\pi^-$	0.210 ± 0.035
Γ_{42}	$2(K^+K^-)$	0.046 ± 0.010
Γ_{45}	$2(\pi^+\pi^-)$	0.29 ± 0.04
Γ_{48}	$p\overline{p}$	0.046 ± 0.005
Γ_{50}	$\Lambda\overline{\Lambda}$	0.034 ± 0.008
Γ_{56}	$\gamma\gamma$	0.00515 ± 0.00035

$\eta_c(1S)$ PARTIAL WIDTHS

$\Gamma(\gamma\gamma)$ — Γ_{56}

VALUE (keV)	EVTS	DOCUMENT ID		TECN	COMMENT
5.15± 0.35 OUR FIT					
• • • We do not use the following data for averages, fits, limits, etc. • • •					
5.8 ± 1.1	486	[1] ZHANG	12A	BELL	$e^+e^- \to e^+e^-\eta'\pi^+\pi^-$
5.2 ± 1.2	273 ± 43	[2,3] AUBERT	06E	BABR	$B^\pm \to K^\pm X_{c\overline{c}}$
5.5 ± 1.2 ± 1.8	157 ± 33	[4] KUO	05	BELL	$\gamma\gamma \to p\overline{p}$
7.4 ± 0.4 ± 2.3		[5] ASNER	04	CLEO	$\gamma\gamma \to \eta_c \to K^0_S K^\pm\pi^\mp$
13.9 ± 2.0 ± 3.0	41	[6] ABDALLAH	03J	DLPH	$\gamma\gamma \to \eta_c$
$3.8 {}^{+1.1}_{-1.0} {}^{+1.9}_{-1.0}$	190	[7] AMBROGIANI	03	E835	$\overline{p}p \to \eta_c \to \gamma\gamma$
7.6 ± 0.8 ± 2.3		[5,8] BRANDENB...	00B	CLE2	$\gamma\gamma \to \eta_c \to K^\pm K^0_S\pi^\mp$
6.9 ± 1.7 ± 2.1	76	[9] ACCIARRI	99T	L3	$e^+e^- \to e^+e^-\eta_c$
27 ±16 ±10	5	[5] SHIRAI	98	AMY	$58\ e^+e^-$
$6.7 {}^{+2.4}_{-1.7}$ ± 2.3		[4] ARMSTRONG	95F	E760	$\overline{p}p \to \gamma\gamma$
11.3 ± 4.2		[10] ALBRECHT	94H	ARG	$e^+e^- \to e^+e^-\eta_c$
8.0 ± 2.3 ± 2.4	17	[11] ADRIANI	93N	L3	$e^+e^- \to e^+e^-\eta_c$
$5.9 {}^{+2.1}_{-1.8}$ ± 1.9		[7] CHEN	90B	CLEO	$e^+e^- \to e^+e^-\eta_c$
$6.4 {}^{+5.0}_{-3.4}$		[12] AIHARA	88D	TPC	$e^+e^- \to e^+e^-X$
$4.3 {}^{+3.4}_{-3.7}$ ± 2.4		[4] BAGLIN	87B	SPEC	$\overline{p}p \to \gamma\gamma$
28 ±15		[5,13] BERGER	86	PLUT	$\gamma\gamma \to K\overline{K}\pi$

[1] Assuming there is no interference with the non-resonant background.
[2] Calculated by us using $\Gamma(\eta_c \to K\overline{K}\pi) \times \Gamma(\eta_c \to \gamma\gamma) / \Gamma = 0.44 \pm 0.05$ keV from PDG 06 and $B(\eta_c \to K\overline{K}\pi) = (8.5 \pm 1.8)\%$ from AUBERT 06E.
[3] Systematic errors not evaluated.
[4] Normalized to $B(\eta_c \to p\overline{p}) = (1.3 \pm 0.4) \times 10^{-3}$.
[5] Normalized to $B(\eta_c \to K^\pm K^0_S\pi^\mp)$.
[6] Average of $K^0_S K^\pm\pi^\mp$, $\pi^+\pi^-K^+K^-$, and $2(K^+K^-)$ decay modes.
[7] Normalized to the sum of $B(\eta_c \to K^\pm K^0_S\pi^\mp)$, $B(\eta_c \to K^+K^-\pi^+\pi^-)$, and $B(\eta_c \to 2\pi^+2\pi^-)$.
[8] Superseded by ASNER 04.
[9] Normalized to the sum of 9 branching ratios.
[10] Normalized to the sum of $B(\eta_c \to K^\pm K^0_S\pi^\mp)$, $B(\eta_c \to \phi\phi)$, $B(\eta_c \to K^+K^-\pi^+\pi^-)$, and $B(\eta_c \to 2\pi^+2\pi^-)$.
[11] Superseded by ACCIARRI 99T.
[12] Normalized to the sum of $B(\eta_c \to K^\pm K^0_S\pi^\mp)$, $B(\eta_c \to 2K^+2K^-)$, $B(\eta_c \to K^+K^-\pi^+\pi^-)$, and $B(\eta_c \to 2\pi^+2\pi^-)$.
[13] Re-evaluated by AIHARA 88D.

$\eta_c(1S)$ $\Gamma(i)\Gamma(\gamma\gamma)/\Gamma(\text{total})$

$\Gamma(\eta'(958)\pi\pi) \times \Gamma(\gamma\gamma)/\Gamma_{\text{total}}$ — $\Gamma_1\Gamma_{56}/\Gamma$

VALUE (eV)	EVTS	DOCUMENT ID		TECN	COMMENT
98.1±3.9±11.7	2673	XU	18	BELL	$e^+e^- \to e^+e^-\eta'\pi^+\pi^-$
• • • We do not use the following data for averages, fits, limits, etc. • • •					
$75.8 {}^{+6.3}_{-6.2}$ ± 8.4	486	[1] ZHANG	12A	BELL	$e^+e^- \to e^+e^-\eta'\pi^+\pi^-$

[1] Superseded by XU 18.

$\Gamma(\rho\rho) \times \Gamma(\gamma\gamma)/\Gamma_{\text{total}}$ — $\Gamma_3\Gamma_{56}/\Gamma$

VALUE (eV)	CL%	EVTS	DOCUMENT ID		TECN	COMMENT
• • • We do not use the following data for averages, fits, limits, etc. • • •						
<39	90	< 1556	UEHARA	08	BELL	$\gamma\gamma \to 2(\pi^+\pi^-)$

$\Gamma(K^*(892)\overline{K}^*(892)) \times \Gamma(\gamma\gamma)/\Gamma_{\text{total}}$ — $\Gamma_5\Gamma_{56}/\Gamma$

VALUE (eV)	EVTS	DOCUMENT ID		TECN	COMMENT
36 ±6 OUR FIT					
32.4±4.2±5.8	882 ± 115	UEHARA	08	BELL	$\gamma\gamma \to \pi^+\pi^-K^+K^-$

$\Gamma(\phi\phi) \times \Gamma(\gamma\gamma)/\Gamma_{\text{total}}$ — $\Gamma_8\Gamma_{56}/\Gamma$

VALUE (eV)	EVTS	DOCUMENT ID		TECN	COMMENT
9.0 ±0.8 OUR FIT					
7.75±0.66±0.62	386 ± 31	[1] LIU	12B	BELL	$\gamma\gamma \to 2(K^+K^-)$
• • • We do not use the following data for averages, fits, limits, etc. • • •					
6.8 ±1.2 ±1.3	132 ± 23	UEHARA	08	BELL	$\gamma\gamma \to 2(K^+K^-)$

[1] Supersedes UEHARA 08. Using $B(\phi \to K^+K^-) = (48.9 \pm 0.5)\%$.

$\Gamma(\omega\omega) \times \Gamma(\gamma\gamma)/\Gamma_{\text{total}}$ — $\Gamma_{15}\Gamma_{56}/\Gamma$

VALUE (eV)	EVTS	DOCUMENT ID		TECN	COMMENT
8.67±2.86±0.96	85 ± 29	[1] LIU	12B	BELL	$\gamma\gamma \to 2(\pi^+\pi^-\pi^0)$

[1] Using $B(\omega \to \pi^+\pi^-\pi^0) = (89.2 \pm 0.7)\%$.

$\Gamma(\omega\phi) \times \Gamma(\gamma\gamma)/\Gamma_{\text{total}}$ — $\Gamma_{16}\Gamma_{56}/\Gamma$

VALUE (eV)	CL%	DOCUMENT ID		TECN	COMMENT
• • • We do not use the following data for averages, fits, limits, etc. • • •					
<0.49	90	[1] LIU	12B	BELL	$\gamma\gamma \to K^+K^-\pi^+\pi^-\pi^0$

[1] Using $B(\phi \to K^+K^-) = (48.9 \pm 0.5)\%$ and $B(\omega \to \pi^+\pi^-\pi^0) = (89.2 \pm 0.7)\%$.

$\Gamma(f_2(1270)\, f_2(1270)) \times \Gamma(\gamma\gamma)/\Gamma_{\text{total}}$ — $\Gamma_{17}\Gamma_{56}/\Gamma$

VALUE (eV)	EVTS	DOCUMENT ID		TECN	COMMENT
50±13 OUR FIT					
69±17±12	3182±766	UEHARA	08	BELL	$\gamma\gamma \to 2(\pi^+\pi^-)$

$\Gamma(f_2(1270)\, f'_2(1525)) \times \Gamma(\gamma\gamma)/\Gamma_{\text{total}}$ — $\Gamma_{18}\Gamma_{56}/\Gamma$

VALUE (eV)	EVTS	DOCUMENT ID		TECN	COMMENT
49±9±13	1128±206	UEHARA	08	BELL	$\gamma\gamma \to \pi^+\pi^-K^+K^-$

$\Gamma(K\overline{K}\pi) \times \Gamma(\gamma\gamma)/\Gamma_{\text{total}}$ — $\Gamma_{34}\Gamma_{56}/\Gamma$

VALUE (keV)	CL%	EVTS	DOCUMENT ID		TECN	COMMENT
0.374±0.021 OUR FIT						
0.407±0.027 OUR AVERAGE Error includes scale factor of 1.2.						
0.374±0.009±0.031		14k	[1] LEES	10	BABR	$10.6\ e^+e^- \to e^+e^-K^0_S K^\pm\pi^\mp$
0.407±0.022±0.028			[2,3] ASNER	04	CLEO	$\gamma\gamma \to \eta_c \to K^0_S K^\pm\pi^\mp$
0.60 ±0.12 ±0.09		41	[3,4] ABDALLAH	03J	DLPH	$\gamma\gamma \to K^0_S K^\pm\pi^\mp$
1.47 ±0.87 ±0.27			[3] SHIRAI	98	AMY	$\gamma\gamma \to \eta_c \to K^\pm K^0_S\pi^\mp$
0.84 ±0.21			[3] ALBRECHT	94H	ARG	$\gamma\gamma \to K^\pm K^0_S\pi^\mp$
$0.60 {}^{+0.23}_{-0.20}$			[3] CHEN	90B	CLEO	$\gamma\gamma \to \eta_c K^\pm K^0_S\pi^\mp$
1.06 ±0.41 ±0.27		11	[3] BRAUNSCH...	89	TASS	$\gamma\gamma \to K\overline{K}\pi$
$1.5 {}^{+0.60}_{-0.45}$ ±0.3		7	[3] BERGER	86	PLUT	$\gamma\gamma \to K\overline{K}\pi$
• • • We do not use the following data for averages, fits, limits, etc. • • •						
0.386±0.008±0.021		12k	[5] DEL-AMO-SA...	11M	BABR	$\gamma\gamma \to K^0_S K^\pm\pi^\mp$
0.418±0.044±0.022			[3,6] BRANDENB...	00B	CLE2	$\gamma\gamma \to \eta_c \to K^\pm K^0_S\pi^\mp$
<0.63	95		[3] BEHREND	89	CELL	$\gamma\gamma \to K^0_S K^\pm\pi^\mp$
<4.4	95		ALTHOFF	85B	TASS	$\gamma\gamma \to K\overline{K}\pi$

[1] From the corrected and unfolded mass spectrum.
[2] Calculated by us from the value reported in ASNER 04 that assumes $B(\eta_c \to K\overline{K}\pi) = 5.5 \pm 1.7\%$
[3] We have multiplied $K^\pm K^0_S\pi^\mp$ measurement by 3 to obtain $K\overline{K}\pi$.
[4] Calculated by us from the value reported in ABDALLAH 03J, which uses $B(\eta_c \to K^0_S K^\pm\pi^\mp) = (1.5 \pm 0.4)\%$.
[5] Not independent from the measurements reported by LEES 10.
[6] Superseded by ASNER 04.

$\Gamma(K^+K^-\pi^+\pi^-) \times \Gamma(\gamma\gamma)/\Gamma_{\text{total}}$ — $\Gamma_{38}\Gamma_{56}/\Gamma$

VALUE (eV)	EVTS	DOCUMENT ID		TECN	COMMENT
34 ± 5 OUR FIT					
27 ± 6 OUR AVERAGE					
25.7± 3.2± 4.9	2019±248	UEHARA	08	BELL	$\gamma\gamma \to \pi^+\pi^-K^+K^-$
280 ±100 ±60	42	[1] ABDALLAH	03J	DLPH	$\gamma\gamma \to \pi^+\pi^-K^+K^-$
170 ± 80 ±20	13.9 ± 6.6	ALBRECHT	94H	ARG	$\gamma\gamma \to \pi^+\pi^-K^+K^-$

[1] Calculated by us from the value reported in ABDALLAH 03J, which uses $B(\eta_c \to \pi^+\pi^-K^+K^-) = (2.0 \pm 0.7)\%$.

$\Gamma(K^+K^-\pi^+\pi^-\pi^0) \times \Gamma(\gamma\gamma)/\Gamma_{\text{total}}$ — $\Gamma_{39}\Gamma_{56}/\Gamma$

VALUE (keV)	EVTS	DOCUMENT ID		TECN	COMMENT
• • • We do not use the following data for averages, fits, limits, etc. • • •					
0.190±0.006±0.028	11k	[1] DEL-AMO-SA...	11M	BABR	$\gamma\gamma \to K^+K^-\pi^+\pi^-\pi^0$

[1] Not independent from other measurements reported in DEL-AMO-SANCHEZ 11M.

Downloaded from https://academic.oup.com/ptep/article/2022/8/083C01/6651666 by KIT Library user on 27 September 2022

$\Gamma(2(K^+K^-)) \times \Gamma(\gamma\gamma)/\Gamma_{total}$ — $\Gamma_{42}\Gamma_{56}/\Gamma$

VALUE (eV)	EVTS	DOCUMENT ID		TECN	COMMENT
7.3± 1.5 OUR FIT					
5.8± 1.9 OUR AVERAGE					
5.6± 1.1± 1.6	216 ± 42	UEHARA	08	BELL	$\gamma\gamma \to 2(K^+K^-)$
350 ±90 ±60	46	[1] ABDALLAH	03J	DLPH	$\gamma\gamma \to 2(K^+K^-)$
231 ±90 ±23	9.1 ± 3.3	[2] ALBRECHT	94H	ARG	$\gamma\gamma \to 2(K^+K^-)$

[1] Calculated by us from the value reported in ABDALLAH 03J, which uses $B(\eta_c \to 2(K^+K^-)) = (2.1 \pm 1.2)\%$.
[2] Includes all topological modes except $\eta_c \to \phi\phi$.

$\Gamma(2(\pi^+\pi^-)) \times \Gamma(\gamma\gamma)/\Gamma_{total}$ — $\Gamma_{45}\Gamma_{56}/\Gamma$

VALUE (eV)	EVTS	DOCUMENT ID		TECN	COMMENT
47 ± 6 OUR FIT					
42 ± 6 OUR AVERAGE					
40.7± 3.7± 5.3	5381 ±492	UEHARA	08	BELL	$\gamma\gamma \to 2(\pi^+\pi^-)$
180 ±70 ±20	21.4 ± 8.6	ALBRECHT	94H	ARG	$\gamma\gamma \to 2(\pi^+\pi^-)$

$\Gamma(p\overline{p}) \times \Gamma(\gamma\gamma)/\Gamma_{total}$ — $\Gamma_{48}\Gamma_{56}/\Gamma$

VALUE (eV)	EVTS	DOCUMENT ID		TECN	COMMENT
7.4 ±0.7 OUR FIT					
$7.20 \pm 1.53^{+0.67}_{-0.75}$	157 ± 33	[1] KUO	05	BELL	$\gamma\gamma \to p\overline{p}$
• • • We do not use the following data for averages, fits, limits, etc. • • •					
$4.6\ ^{+1.3}_{-1.1} \pm 0.4$	190	[1] AMBROGIANI	03	E835	$\overline{p}p \to \gamma\gamma$
$8.1\ ^{+2.9}_{-2.0}$		[1] ARMSTRONG	95F	E760	$\overline{p}p \to \gamma\gamma$

[1] Not independent from the $\Gamma_{\gamma\gamma}$ reported by the same experiment.

$\Gamma(K^0_S K^0_S) \times \Gamma(\gamma\gamma)/\Gamma_{total}$ — $\Gamma_{60}\Gamma_{56}/\Gamma$

VALUE (eV)	CL%	DOCUMENT ID		TECN	COMMENT
<1.6	90	[1] UEHARA	13	BELL	$\gamma\gamma \to K^0_S K^0_S$
• • • We do not use the following data for averages, fits, limits, etc. • • •					
<0.29	90	[2] UEHARA	13	BELL	$\gamma\gamma \to K^0_S K^0_S$

[1] Taking into account interference with the non-resonant continuum.
[2] Neglecting interference with the non-resonant continuum.

$\eta_c(1S)$ BRANCHING RATIOS

HADRONIC DECAYS

$\Gamma(\eta'(958)\pi\pi)/\Gamma_{total}$ — Γ_1/Γ

VALUE	EVTS	DOCUMENT ID		TECN	COMMENT
0.041±0.017	14	[1] BALTRUSAIT...86		MRK3	$J/\psi \to \eta_c\gamma$

[1] The quoted branching ratios use $B(J/\psi(1S) \to \gamma\eta_c(1S)) = 0.0127 \pm 0.0036$.

$\Gamma(\rho\rho)/\Gamma_{total}$ — Γ_3/Γ

VALUE (units 10^{-3})	CL%	EVTS	DOCUMENT ID		TECN	COMMENT
18 ± 5 OUR AVERAGE						
12.6± 3.8±5.1		72	[1] ABLIKIM	05L	BES2	$J/\psi \to \pi^+\pi^-\pi^+\pi^-\gamma$
26.0± 2.4±8.8		113	[1] BISELLO	91	DM2	$J/\psi \to \gamma\rho^0\rho^0$
23.6±10.6±8.2		32	[1] BISELLO	91	DM2	$J/\psi \to \gamma\rho^+\rho^-$
• • • We do not use the following data for averages, fits, limits, etc. • • •						
<14	90		[1] BALTRUSAIT...86		MRK3	$J/\psi \to \eta_c\gamma$

[1] The quoted branching ratios use $B(J/\psi(1S) \to \gamma\eta_c(1S)) = 0.0127 \pm 0.0036$. Where relevant, the error in this branching ratio is treated as a common systematic in computing averages.

$\Gamma(K^*(892)^0 K^-\pi^+ + \text{c.c.})/\Gamma_{total}$ — Γ_4/Γ

VALUE	EVTS	DOCUMENT ID		TECN	COMMENT
0.02±0.007	63	[1,2] BALTRUSAIT...86		MRK3	$J/\psi \to \eta_c\gamma$

[1] BALTRUSAITIS 86 has an error according to Partridge.
[2] The quoted branching ratios use $B(J/\psi(1S) \to \gamma\eta_c(1S)) = 0.0127 \pm 0.0036$.

$\Gamma(K^*(892)\overline{K}^*(892))/\Gamma_{total}$ — Γ_5/Γ

VALUE (units 10^{-4})	EVTS	DOCUMENT ID		TECN	COMMENT
69±13 OUR FIT					
91±26 OUR AVERAGE					
108±25±44	60	[1] ABLIKIM	05L	BES2	$J/\psi \to K^+K^-\pi^+\pi^-\gamma$
82±28±27	14	[1] BISELLO	91	DM2	$e^+e^- \to \gamma K^+K^-\pi^+\pi^-$
90±50	9	[1] BALTRUSAIT...86		MRK3	$J/\psi \to \eta_c\gamma$

[1] The quoted branching ratios use $B(J/\psi(1S) \to \gamma\eta_c(1S)) = 0.0127 \pm 0.0036$. Where relevant, the error in this branching ratio is treated as a common systematic in computing averages.

$\Gamma(K^*(892)^0\overline{K}^*(892)^0\pi^+\pi^-)/\Gamma_{total}$ — Γ_6/Γ

VALUE (units 10^{-4})	EVTS	DOCUMENT ID		TECN	COMMENT
113±47±24	45	[1] ABLIKIM	06A	BES2	$J/\psi \to K^{*0}\overline{K}^{*0}\pi^+\pi^-\gamma$

[1] ABLIKIM 06A reports $[\Gamma(\eta_c(1S) \to K^*(892)^0\overline{K}^*(892)^0\pi^+\pi^-)/\Gamma_{total}] \times [B(J/\psi(1S) \to \gamma\eta_c(1S))] = (1.91 \pm 0.64 \pm 0.48) \times 10^{-4}$ which we divide by our best value $B(J/\psi(1S) \to \gamma\eta_c(1S)) = (1.7 \pm 0.4) \times 10^{-2}$. Our first error is their experiment's error and our second error is the systematic error from using our best value.

$\Gamma(\phi K^+K^-)/\Gamma_{total}$ — Γ_7/Γ

VALUE (units 10^{-3})	EVTS	DOCUMENT ID		TECN	COMMENT
$2.9^{+0.9}_{-0.8} \pm 1.1$	$14.1^{+4.4}_{-3.7}$	[1] HUANG	03	BELL	$B^+ \to (\phi K^+K^-) K^+$

[1] Using $B(B^+ \to \eta_c K^+) = (1.25 \pm 0.12^{+0.10}_{-0.12}) \times 10^{-3}$ from FANG 03 and $B(\eta_c \to K\overline{K}\pi) = (5.5 \pm 1.7) \times 10^{-2}$.

$\Gamma(\phi\phi)/\Gamma_{total}$ — Γ_8/Γ

VALUE (units 10^{-4})	EVTS	DOCUMENT ID		TECN	COMMENT
17.4± 1.9 OUR FIT					
28 ± 4 OUR AVERAGE					
$26\ ^{+4}_{-8} \pm 5$	1.2k	[1] ABLIKIM	17P	BES3	$J/\psi \to K^+K^-K^+K^-\gamma$
25.3± 5.1± 9.1	72	[2] ABLIKIM	05L	BES2	$J/\psi \to K^+K^-K^+K^-\gamma$
26 ± 9	357	[2] BAI	04	BES	$J/\psi \to \gamma K^+K^-K^+K^-$
31 ± 7 ±10	19	[2] BISELLO	91	DM2	$J/\psi \to \gamma K^+K^-K^+K^-$
$30\ ^{+18}_{-12} \pm 10$	5	[2] BISELLO	91	DM2	$J/\psi \to \gamma K^+K^-K^0_S K^0_L$
74 ±18 ±24	80	[2] BAI	90B	MRK3	$J/\psi \to \gamma K^+K^-K^+K^-$
67 ±21 ±24		[2] BAI	90B	MRK3	$J/\psi \to \gamma K^+K^-K^0_S K^0_L$
• • • We do not use the following data for averages, fits, limits, etc. • • •					
$18\ ^{+8}_{-6} \pm 7$	7	[3] HUANG	03	BELL	$B^+ \to (\phi\phi) K^+$

[1] ABLIKIM 17P reports $[\Gamma(\eta_c(1S) \to \phi\phi)/\Gamma_{total}] \times [B(J/\psi(1S) \to \gamma\eta_c(1S))] = (4.3 \pm 0.5^{+0.5}_{-1.2}) \times 10^{-5}$ which we divide by our best value $B(J/\psi(1S) \to \gamma\eta_c(1S)) = (1.7 \pm 0.4) \times 10^{-2}$. Our first error is their experiment's error and our second error is the systematic error from using our best value.
[2] The quoted branching ratios use $B(J/\psi(1S) \to \gamma\eta_c(1S)) = 0.0127 \pm 0.0036$. Where relevant, the error in this branching ratio is treated as a common systematic in computing averages.
[3] Using $B(B^+ \to \eta_c K^+) = (1.25 \pm 0.12^{+0.10}_{-0.12}) \times 10^{-3}$ from FANG 03 and $B(\eta_c \to K\overline{K}\pi) = (5.5 \pm 1.7) \times 10^{-2}$.

$\Gamma(\phi\phi)/\Gamma(K\overline{K}\pi)$ — Γ_8/Γ_{34}

VALUE	EVTS	DOCUMENT ID		TECN	COMMENT
0.0240±0.0025 OUR FIT					
$0.044\ ^{+0.012}_{-0.010}$ OUR AVERAGE					
0.055 ±0.014 ±0.005		AUBERT,B	04B	BABR	$B^\pm \to K^\pm\eta_c$
$0.032\ ^{+0.014}_{-0.010} \pm 0.009$	7	[1] HUANG	03	BELL	$B^\pm \to K^\pm\phi\phi$

[1] Using $B(B^+ \to \eta_c K^+) = (1.25 \pm 0.12^{+0.10}_{-0.12}) \times 10^{-3}$ from FANG 03 and $B(\eta_c \to K\overline{K}\pi) = (5.5 \pm 1.7) \times 10^{-2}$.

$\Gamma(\phi\phi)/\Gamma(p\overline{p})$ — Γ_8/Γ_{48}

VALUE	EVTS	DOCUMENT ID		TECN	COMMENT
1.79±0.14±0.32	6.4k	[1] AAIJ	17BB	LHCB	$pp \to b\overline{b}X \to 2(K^+K^-)X$

[1] Using inputs from AAIJ 15AS and AAIJ 15BI and $\Gamma(b \to J/\psi(1S)\text{ anything}))/\Gamma_{total} = (1.16 \pm 0.10)\%$ and $\Gamma(J/\psi(1S) \to p\overline{p})/\Gamma_{total} = (2.120 \pm 0.029) \times 10^{-3}$ from PDG 16.

$\Gamma(\phi 2(\pi^+\pi^-))/\Gamma_{total}$ — Γ_9/Γ

VALUE (units 10^{-4})	CL%	DOCUMENT ID		TECN	COMMENT
<40	90	[1] ABLIKIM	06A	BES2	$J/\psi \to \phi 2(\pi^+\pi^-)\gamma$

[1] ABLIKIM 06A reports $[\Gamma(\eta_c(1S) \to \phi 2(\pi^+\pi^-))/\Gamma_{total}] \times [B(J/\psi(1S) \to \gamma\eta_c(1S))] < 0.603 \times 10^{-4}$ which we divide by our best value $B(J/\psi(1S) \to \gamma\eta_c(1S)) = 1.7 \times 10^{-2}$.

$\Gamma(a_0(980)\pi)/\Gamma_{total}$ — Γ_{10}/Γ

VALUE	CL%	DOCUMENT ID		TECN	COMMENT
seen		LEES	21A	BABR	Dalitz anal. of $\eta_c \to \pi^+\pi^-\eta$
seen		LEES	14E	BABR	Dalitz anal. of $\eta_c \to K^+K^-\pi^0$
• • • We do not use the following data for averages, fits, limits, etc. • • •					
<0.02	90	[1,2] BALTRUSAIT...86		MRK3	$J/\psi \to \eta_c\gamma$

[1] The quoted branching ratios use $B(J/\psi(1S) \to \gamma\eta_c(1S)) = 0.0127 \pm 0.0036$.
[2] We are assuming $B(a_0(980) \to \eta\pi) > 0.5$.

$\Gamma(a_2(1320)\pi)/\Gamma_{total}$ — Γ_{11}/Γ

VALUE	CL%	DOCUMENT ID		TECN	COMMENT
seen		LEES	21A	BABR	Dalitz anal. of $\eta_c \to \pi^+\pi^-\eta$
<0.02	90	[1] BALTRUSAIT...86		MRK3	$J/\psi \to \eta_c\gamma$

[1] The quoted branching ratios use $B(J/\psi(1S) \to \gamma\eta_c(1S)) = 0.0127 \pm 0.0036$.

$\Gamma(K^*(892)\overline{K} + \text{c.c.})/\Gamma_{total}$ — Γ_{12}/Γ

VALUE	CL%	DOCUMENT ID		TECN	COMMENT
<0.0128	90	BISELLO	91	DM2	$J/\psi \to \gamma K^0_S K^\pm\pi^\mp$
<0.0132	90	[1] BISELLO	91	DM2	$J/\psi \to \gamma K^+K^-\pi^0$

[1] The quoted branching ratios use $B(J/\psi(1S) \to \gamma\eta_c(1S)) = 0.0127 \pm 0.0036$.

Downloaded from https://academic.oup.com/ptep/article/2022/8/083C01/6651666 by KIT Library user on 27 September 2022

$\Gamma(f_2(1270)\eta)/\Gamma_{total}$ — Γ_{13}/Γ

VALUE	CL%	DOCUMENT ID		TECN	COMMENT
seen		LEES	21A	BABR	Dalitz anal. of $\eta_c \to \pi^+\pi^-\eta$
<0.011	90	[1] BALTRUSAIT...86		MRK3	$J/\psi \to \eta_c\gamma$

[1] The quoted branching ratios use $B(J/\psi(1S) \to \gamma\eta_c(1S)) = 0.0127 \pm 0.0036$.

$\Gamma(f_2(1270)\eta')/\Gamma_{total}$ — Γ_{14}/Γ

VALUE	DOCUMENT ID		TECN	COMMENT
seen	LEES	21A	BABR	Dalitz anal. of $\eta_c \to \pi^+\pi^-\eta'$; $K^+K^-\eta'$

$\Gamma(\omega\omega)/\Gamma_{total}$ — Γ_{15}/Γ

VALUE (units 10^{-3})	CL%	EVTS	DOCUMENT ID		TECN	COMMENT
2.9±0.5±0.6		1705	[1] ABLIKIM	19AV	BES3	$J/\psi \to \gamma\omega\omega$
• • • We do not use the following data for averages, fits, limits, etc. • • •						
<6.3	90		[2] ABLIKIM	05L	BES2	$J/\psi \to 2(\pi^+\pi^-\pi^0)\gamma$
<6.3	90		[2] BISELLO	91	DM2	$J/\psi \to \gamma\omega\omega$
<3.1	90		[2] BALTRUSAIT...86		MRK3	$J/\psi \to \eta_c\gamma$

[1] ABLIKIM 19AV reports $[\Gamma(\eta_c(1S) \to \omega\omega)/\Gamma_{total}] \times [B(J/\psi(1S) \to \gamma\eta_c(1S))] = (4.90 \pm 0.17 \pm 0.77) \times 10^{-5}$ which we divide by our best value $B(J/\psi(1S) \to \gamma\eta_c(1S)) = (1.7 \pm 0.4) \times 10^{-2}$. Our first error is their experiment's error and our second error is the systematic error from using our best value.,

[2] The quoted branching ratios use $B(J/\psi(1S) \to \gamma\eta_c(1S)) = 0.0127 \pm 0.0036$. Where relevant, the error in this branching ratio is treated as a common systematic in computing averages.

$\Gamma(\omega\phi)/\Gamma_{total}$ — Γ_{16}/Γ

VALUE	CL%	DOCUMENT ID		TECN	COMMENT
< 2.5 × 10^{-4}	90	[1] ABLIKIM	17P	BES3	$J/\psi \to \pi^+\pi^-\pi^0 K^+K^-\gamma$
• • • We do not use the following data for averages, fits, limits, etc. • • •					
<17 × 10^{-4}	90	[2] ABLIKIM	05L	BES2	$J/\psi \to \pi^+\pi^-\pi^0 K^+K^-\gamma$

[1] Using $B(J/\psi \to \gamma\eta_c) = 0.017 \pm 0.004$.

[2] The quoted branching ratios use $B(J/\psi(1S) \to \gamma\eta_c(1S)) = 0.0127 \pm 0.0036$.

$\Gamma(f_2(1270)f_2(1270))/\Gamma_{total}$ — Γ_{17}/Γ

VALUE (units 10^{-2})	EVTS	DOCUMENT ID		TECN	COMMENT
0.98±0.25 OUR FIT					
$0.77^{+0.25}_{-0.30}$±0.17	91.2 ± 19.8	[1] ABLIKIM	04M	BES	$J/\psi \to \gamma 2\pi^+ 2\pi^-$

[1] ABLIKIM 04M reports $[\Gamma(\eta_c(1S) \to f_2(1270)f_2(1270))/\Gamma_{total}] \times [B(J/\psi(1S) \to \gamma\eta_c(1S))] = (1.3 \pm 0.3^{+0.3}_{-0.4}) \times 10^{-4}$ which we divide by our best value $B(J/\psi(1S) \to \gamma\eta_c(1S)) = (1.7 \pm 0.4) \times 10^{-2}$. Our first error is their experiment's error and our second error is the systematic error from using our best value.

$\Gamma(f_0(500)\eta)/\Gamma_{total}$ — Γ_{19}/Γ

VALUE	DOCUMENT ID		TECN	COMMENT
seen	LEES	21A	BABR	Dalitz anal. of $\eta_c \to \pi^+\pi^-\eta$

$\Gamma(f_0(500)\eta')/\Gamma_{total}$ — Γ_{20}/Γ

VALUE	DOCUMENT ID		TECN	COMMENT
seen	LEES	21A	BABR	Dalitz anal. of $\eta_c(1S) \to \pi^+\pi^-\eta'$

$\Gamma(f_0(980)\eta)/\Gamma_{total}$ — Γ_{21}/Γ

VALUE	DOCUMENT ID		TECN	COMMENT
seen	LEES	21A	BABR	Dalitz anal. of $\eta_c \to \pi^+\pi^-\eta$
seen	LEES	14E	BABR	Dalitz anal. of $\eta_c \to K^+K^-\eta$

$\Gamma(f_0(980)\eta')/\Gamma_{total}$ — Γ_{22}/Γ

VALUE	DOCUMENT ID		TECN	COMMENT
seen	LEES	21A	BABR	Dalitz anal. of $\eta_c \to \pi^+\pi^-\eta'$, $K^+K^-\eta'$

$\Gamma(f_0(1500)\eta)/\Gamma_{total}$ — Γ_{23}/Γ

VALUE	DOCUMENT ID		TECN	COMMENT
seen	LEES	21A	BABR	Dalitz anal. of $\eta_c \to \pi^+\pi^-\eta$
seen	LEES	14E	BABR	Dalitz anal. of $\eta_c \to K^+K^-\eta$

$\Gamma(f_0(1710)\eta')/\Gamma_{total}$ — Γ_{24}/Γ

VALUE	DOCUMENT ID		TECN	COMMENT
seen	LEES	21A	BABR	Dalitz anal. of $\eta_c \to K^+K^-\eta'$

$\Gamma(f_0(2100)\eta')/\Gamma_{total}$ — Γ_{25}/Γ

VALUE	DOCUMENT ID		TECN	COMMENT
seen	LEES	21A	BABR	Dalitz anal. of $\eta_c \to \pi^+\pi^-\eta$

$\Gamma(f_0(2200)\eta)/\Gamma_{total}$ — Γ_{26}/Γ

VALUE	DOCUMENT ID		TECN	COMMENT
seen	LEES	14E	BABR	Dalitz anal. of $\eta_c \to K^+K^-\eta$

$\Gamma(a_0(1320)\pi)/\Gamma_{total}$ — Γ_{27}/Γ

VALUE	DOCUMENT ID		TECN	COMMENT
seen	LEES	14E	BABR	Dalitz anal. of $\eta_c \to K^+K^-\pi^0$

$\Gamma(a_0(1450)\pi)/\Gamma_{total}$ — Γ_{28}/Γ

VALUE	DOCUMENT ID		TECN	COMMENT
seen	LEES	21A	BABR	Dalitz anal. of $\eta_c \to \pi^+\pi^-\eta$
seen	LEES	14E	BABR	Dalitz anal. of $\eta_c \to K^+K^-\pi^0$

$\Gamma(a_0(1700)\pi)/\Gamma_{total}$ — Γ_{29}/Γ

VALUE	DOCUMENT ID		TECN	COMMENT
seen	LEES	21A	BABR	Dalitz anal. of $\eta_c \to \pi^+\pi^-\eta'$

$\Gamma(a_0(1950)\pi)/\Gamma_{total}$ — Γ_{30}/Γ

VALUE	EVTS	DOCUMENT ID		TECN	COMMENT
seen		LEES	21A	BABR	Dalitz anal. of $\eta_c(1S) \to \pi^+\pi^-\eta'$
seen	12k	[1] LEES	16A	BABR	$\gamma\gamma \to \eta_c(1S) \to K\overline{K}\pi$

[1] From a model-independant partial wave analysis.

$\Gamma(K_0^*(1430)\overline{K})/\Gamma_{total}$ — Γ_{31}/Γ

VALUE	EVTS	DOCUMENT ID		TECN	COMMENT
seen	12k	[1] LEES	16A	BABR	$\gamma\gamma \to \eta_c(1S) \to K\overline{K}\pi$
seen		LEES	14E	BABR	Dalitz anal. of $\eta_c \to K^+K^-\eta/\pi^0$

[1] From a model-independant partial wave analysis.

$\Gamma(K_2^*(1430)\overline{K})/\Gamma_{total}$ — Γ_{32}/Γ

VALUE	DOCUMENT ID		TECN	COMMENT
seen	LEES	21A	BABR	Dalitz anal. of $\eta_c \to K^+K^-\eta'$
seen	LEES	14E	BABR	Dalitz anal. of $\eta_c \to K^+K^-\pi^0$

$\Gamma(K_0^*(1950)\overline{K})/\Gamma_{total}$ — Γ_{33}/Γ

VALUE	EVTS	DOCUMENT ID		TECN	COMMENT
seen		LEES	21A	BABR	Dalitz anal. of $\eta_c \to K^+K^-\eta'$
seen	12k	[1] LEES	16A	BABR	$\gamma\gamma \to \eta_c(1S) \to K\overline{K}\pi$
seen		LEES	14E	BABR	Dalitz anal. of $\eta_c \to K^+K^-\eta/\pi^0$

[1] From a Dalitz plot analysis using an isobar model.

$\Gamma(K\overline{K}\pi)/\Gamma_{total}$ — Γ_{34}/Γ

VALUE (units 10^{-2})	EVTS	DOCUMENT ID		TECN	COMMENT
7.3 ±0.4 OUR FIT					
6.9 ±0.5 OUR AVERAGE					
6.9 ±0.7 ±0.6	146	[1] ABLIKIM	19AP	BES3	$h_c \to \gamma\eta_c$
7.8 ±0.6 ±0.6	267	[2] ABLIKIM	19AP	BES3	$h_c \to \gamma\eta_c$
6.3 ±1.3 ±1.4	55	[3,4] ABLIKIM	12N	BES3	$\psi(2S) \to \pi^0\gamma K^+K^-\pi^0$
7.9 ±1.4 ±1.8	107	[5,6] ABLIKIM	12N	BES3	$\psi(2S) \to \pi^0\gamma K_S^0 K^\mp\pi^\pm$
8.5 ±1.8		[7] AUBERT	06E	BABR	$B^\pm \to K^\pm X_{c\overline{c}}$
5.1 ±2.1	0.6k	[8] BAI	04	BES	$J/\psi \to \gamma K^\pm\pi^\mp K_S^0$
6.90±1.42±1.32	33	[8] BISELLO	91	DM2	$J/\psi \to \gamma K^+K^-\pi^0$
5.43±0.94±0.94	68	[8] BISELLO	91	DM2	$J/\psi \to \gamma K^\pm\pi^\mp K_S^0$
4.8 ±1.7	95	[8,9] BALTRUSAIT...86		MRK3	$J/\psi \to \eta_c\gamma$
$16.1^{+9.2}_{-7.3}$		[10,11] HIMEL	80B	MRK2	$\psi(2S) \to \eta_c\gamma$
• • • We do not use the following data for averages, fits, limits, etc. • • •					
< 10.7 90% CL		[8,12] PARTRIDGE	80B	CBAL	$J/\psi \to \eta_c\gamma$

[1] ABLIKIM 19AP quotes $B(\eta_c \to K^+K^-\pi^0) = (1.15 \pm 0.12 \pm 0.10) \times 10^{-2}$ which we multiply by 6 to account for isospin symmetry.

[2] ABLIKIM 19AP quotes $B(\eta_c \to K_S^0 K^\pm\pi^\mp) = (2.60 \pm 0.21 \pm 0.20) \times 10^{-2}$ which we multiply by 3 to account for isospin symmetry.

[3] ABLIKIM 12N quotes $B(\psi(2S) \to \pi^0 h_c) \cdot B(h_c \to \gamma\eta_c) \cdot B(\eta_c \to K^+K^-\pi^0) = (4.54 \pm 0.76 \pm 0.48) \times 10^{-6}$ which we multiply by 6 to account for isospin symmetry.

[4] ABLIKIM 12N reports $[\Gamma(\eta_c(1S) \to K\overline{K}\pi)/\Gamma_{total}] \times [B(\psi(2S) \to h_c(1P)\pi^0)] \times [B(h_c(1P) \to \gamma\eta_c(1S))] = (27.24 \pm 4.56 \pm 2.88) \times 10^{-6}$ which we divide by our best values $B(\psi(2S) \to h_c(1P)\pi^0) = (8.6 \pm 1.3) \times 10^{-4}$, $B(h_c(1P) \to \gamma\eta_c(1S)) = (50 \pm 9) \times 10^{-2}$. Our first error is their experiment's error and our second error is the systematic error from using our best values.

[5] ABLIKIM 12N quotes $B(\psi(2S) \to \pi^0 h_c) \cdot B(h_c \to \gamma\eta_c) \cdot B(\eta_c \to K_S^0 K^\pm\pi^\mp) = (11.35 \pm 1.25 \pm 1.50) \times 10^{-6}$ which we multiply by 3 to account for isospin symmetry.

[6] ABLIKIM 12N reports $[\Gamma(\eta_c(1S) \to K\overline{K}\pi)/\Gamma_{total}] \times [B(\psi(2S) \to h_c(1P)\pi^0)] \times [B(h_c(1P) \to \gamma\eta_c(1S))] = (34.05 \pm 3.75 \pm 4.50) \times 10^{-6}$ which we divide by our best values $B(\psi(2S) \to h_c(1P)\pi^0) = (8.6 \pm 1.3) \times 10^{-4}$, $B(h_c(1P) \to \gamma\eta_c(1S)) = (50 \pm 9) \times 10^{-2}$. Our first error is their experiment's error and our second error is the systematic error from using our best values.

[7] Determined from the ratio of $B(B^\pm \to K^\pm\eta_c)\, B(\eta_c \to K\overline{K}\pi) = (7.4 \pm 0.5 \pm 0.7) \times 10^{-5}$ reported in AUBERT,B 04B and $B(B^\pm \to K^\pm\eta_c) = (8.7 \pm 1.5) \times 10^{-3}$ reported in AUBERT 06E.

[8] The quoted branching ratios use $B(J/\psi(1S) \to \gamma\eta_c(1S)) = 0.0127 \pm 0.0036$. Where relevant, the error in this branching ratio is treated as a common systematic in computing averages.

[9] Average from $K^+K^-\pi^0$ and $K^\pm K_S^0\pi^\mp$ decay channels.

[10] $K^\pm K_S^0\pi^\mp$ corrected to $K\overline{K}\pi$ by factor 3. KS, MR.

[11] Estimated using $B(\psi(2S) \to \gamma\eta_c(1S)) = 0.0028 \pm 0.0006$.

[12] $K^+K^-\pi^0$ corrected to $K\overline{K}\pi$ by factor 6. KS, MR

Downloaded from https://academic.oup.com/ptep/article/2022/8/083C01/6651666 by KIT Library user on 27 September 2022

$\Gamma(\phi K^+ K^-)/\Gamma(K\overline{K}\pi)$ — Γ_7/Γ_{34}

VALUE	EVTS	DOCUMENT ID		TECN	COMMENT
$0.052^{+0.016}_{-0.014}\pm0.014$	7	[1] HUANG	03	BELL	$B^\pm \to K^\pm\phi\phi$

[1] Using $B(B^+ \to \eta_c K^+) = (1.25 \pm 0.12^{+0.10}_{-0.12}) \times 10^{-3}$ from FANG 03 and $B(\eta_c \to K\overline{K}\pi) = (5.5 \pm 1.7) \times 10^{-2}$.

$\Gamma(K\overline{K}\eta)/\Gamma_{total}$ — Γ_{35}/Γ

VALUE (units 10^{-2})	CL%	EVTS	DOCUMENT ID		TECN	COMMENT
1.36±0.15 OUR FIT						
1.0 ±0.5 ±0.2		7	[1,2] ABLIKIM	12N	BES3	$\psi(2S) \to \pi^0\gamma\eta K^+K^-$
• • • We do not use the following data for averages, fits, limits, etc. • • •						
<3.1	90		[3] BALTRUSAIT...86		MRK3	$J/\psi \to \eta_c\gamma$

[1] ABLIKIM 12N quotes $B(\psi(2S) \to \pi^0 h_c) \cdot B(h_c \to \gamma\eta_c) \cdot B(\eta_c \to K^+K^-\eta) = (2.11 \pm 1.01 \pm 0.32) \times 10^{-6}$ which we multiply by 2 to account for isospin symmetry.

[2] ABLIKIM 12N reports $[\Gamma(\eta_c(1S) \to K\overline{K}\eta)/\Gamma_{total}] \times [B(\psi(2S) \to h_c(1P)\pi^0)] \times [B(h_c(1P) \to \gamma\eta_c(1S))] = (4.22 \pm 2.02 \pm 0.64) \times 10^{-6}$ which we divide by our best values $B(\psi(2S) \to h_c(1P)\pi^0) = (8.6 \pm 1.3) \times 10^{-4}$, $B(h_c(1P) \to \gamma\eta_c(1S)) = (50 \pm 9) \times 10^{-2}$. Our first error is their experiment's error and our second error is the systematic error from using our best values.

[3] The quoted branching ratios use $B(J/\psi(1S) \to \gamma\eta_c(1S)) = 0.0127 \pm 0.0036$.

$\Gamma(K\overline{K}\eta)/\Gamma(K\overline{K}\pi)$ — Γ_{35}/Γ_{34}

VALUE	EVTS	DOCUMENT ID		TECN	COMMENT
0.187±0.018 OUR FIT					
0.190±0.008±0.017	5.4k	[1] LEES	14E	BABR	$\gamma\gamma \to K^+K^-\eta/\pi^0$

[1] LEES 14E reports $B(\eta_c(1S) \to K^+K^-\eta)/B(\eta_c(1S) \to K^+K^-\pi^0) = 0.571 \pm 0.025 \pm 0.051$, which we divide by 3 to account for isospin symmetry. It uses both $\eta \to \gamma\gamma$ and $\eta \to \pi^+\pi^-\pi^0$ decays.

$\Gamma(\eta\pi^+\pi^-)/\Gamma_{total}$ — Γ_{36}/Γ

VALUE (units 10^{-2})	EVTS	DOCUMENT ID		TECN	COMMENT
1.7±0.4±0.4	33	[1] ABLIKIM	12N	BES3	$\psi(2S) \to \pi^0\gamma\eta\pi^+\pi^-$
• • • We do not use the following data for averages, fits, limits, etc. • • •					
5.4±2.0	75	[2] BALTRUSAIT...86		MRK3	$J/\psi \to \eta_c\gamma$
3.7±1.3±2.0	18	[2] PARTRIDGE	80B	CBAL	$J/\psi \to \eta\pi^+\pi^-\gamma$

[1] ABLIKIM 12N reports $[\Gamma(\eta_c(1S) \to \eta\pi^+\pi^-)/\Gamma_{total}] \times [B(\psi(2S) \to h_c(1P)\pi^0)] \times [B(h_c(1P) \to \gamma\eta_c(1S))] = (7.22 \pm 1.47 \pm 1.11) \times 10^{-6}$ which we divide by our best values $B(\psi(2S) \to h_c(1P)\pi^0) = (8.6 \pm 1.3) \times 10^{-4}$, $B(h_c(1P) \to \gamma\eta_c(1S)) = (50 \pm 9) \times 10^{-2}$. Our first error is their experiment's error and our second error is the systematic error from using our best values.

[2] The quoted branching ratios use $B(J/\psi(1S) \to \gamma\eta_c(1S)) = 0.0127 \pm 0.0036$. Where relevant, the error in this branching ratio is treated as a common systematic in computing averages.

$\Gamma(\eta 2(\pi^+\pi^-))/\Gamma_{total}$ — Γ_{37}/Γ

VALUE (units 10^{-2})	EVTS	DOCUMENT ID		TECN	COMMENT
4.4±1.2±1.0	39	[1] ABLIKIM	12N	BES3	$\psi(2S) \to \pi^0\gamma\eta 2(\pi^+\pi^-)$

[1] ABLIKIM 12N reports $[\Gamma(\eta_c(1S) \to \eta 2(\pi^+\pi^-))/\Gamma_{total}] \times [B(\psi(2S) \to h_c(1P)\pi^0)] \times [B(h_c(1P) \to \gamma\eta_c(1S))] = (19.17 \pm 3.77 \pm 3.72) \times 10^{-6}$ which we divide by our best values $B(\psi(2S) \to h_c(1P)\pi^0) = (8.6 \pm 1.3) \times 10^{-4}$, $B(h_c(1P) \to \gamma\eta_c(1S)) = (50 \pm 9) \times 10^{-2}$. Our first error is their experiment's error and our second error is the systematic error from using our best values.

$\Gamma(K^+K^-\pi^+\pi^-)/\Gamma_{total}$ — Γ_{38}/Γ

VALUE (units 10^{-3})	EVTS	DOCUMENT ID		TECN	COMMENT
6.6± 1.1 OUR FIT					
11.8± 2.3 OUR AVERAGE					
9.7± 2.2±2.2	38	[1] ABLIKIM	12N	BES3	$\psi(2S) \to \pi^0\gamma K^+K^-\pi^+\pi^-$
12 ± 4	0.4k	[2] BAI	04	BES	$J/\psi \to \gamma K^+K^-\pi^+\pi^-$
21 ± 7	110	[2] BALTRUSAIT...86		MRK3	$J/\psi \to \eta_c\gamma$
$14\ ^{+22}_{-9}$		[3] HIMEL	80B	MRK2	$\psi(2S) \to \eta_c\gamma$

[1] ABLIKIM 12N reports $[\Gamma(\eta_c(1S) \to K^+K^-\pi^+\pi^-)/\Gamma_{total}] \times [B(\psi(2S) \to h_c(1P)\pi^0)] \times [B(h_c(1P) \to \gamma\eta_c(1S))] = (4.16 \pm 0.76 \pm 0.59) \times 10^{-6}$ which we divide by our best values $B(\psi(2S) \to h_c(1P)\pi^0) = (8.6 \pm 1.3) \times 10^{-4}$, $B(h_c(1P) \to \gamma\eta_c(1S)) = (50 \pm 9) \times 10^{-2}$. Our first error is their experiment's error and our second error is the systematic error from using our best values.

[2] The quoted branching ratios use $B(J/\psi(1S) \to \gamma\eta_c(1S)) = 0.0127 \pm 0.0036$. Where relevant, the error in this branching ratio is treated as a common systematic in computing averages.

[3] Estimated using $B(\psi(2S) \to \gamma\eta_c(1S)) = 0.0028 \pm 0.0006$.

$\Gamma(K^+K^-\pi^+\pi^-\pi^0)/\Gamma(K\overline{K}\pi)$ — Γ_{39}/Γ_{34}

VALUE	EVTS	DOCUMENT ID		TECN	COMMENT
0.477±0.017±0.070	11k	[1] DEL-AMO-SA...11M		BABR	$\gamma\gamma \to K^+K^-\pi^+\pi^-\pi^0$

[1] We have multiplied the value of $\Gamma(K^+K^-\pi^+\pi^-\pi^0)/\Gamma(K^0_S K^\pm\pi^\mp)$ reported in DEL-AMO-SANCHEZ 11M by a factor 1/3 to obtain $\Gamma(K^+K^-\pi^+\pi^-\pi^0)/\Gamma(K\overline{K}\pi)$. Not independent from other measurements reported in DEL-AMO-SANCHEZ 11M.

$\Gamma(K^0K^-\pi^+\pi^-\pi^+ + c.c.)/\Gamma_{total}$ — Γ_{40}/Γ

VALUE (units 10^{-2})	EVTS	DOCUMENT ID		TECN	COMMENT
5.6±1.4±1.3	43	[1,2] ABLIKIM	12N	BES3	$\psi(2S) \to \pi^0\gamma K^0_S K^\mp\pi^\mp 2\pi^\pm$

[1] ABLIKIM 12N quotes $B(\psi(2S) \to \pi^0 h_c) \cdot B(h_c \to \gamma\eta_c) \cdot B(\eta_c \to K^0_S K^-\pi^-2\pi^+) = (12.01 \pm 2.22 \pm 2.04) \times 10^{-6}$ which we multiply by 2 to take c.c. into account.

[2] ABLIKIM 12N reports $[\Gamma(\eta_c(1S) \to K^0K^-\pi^+\pi^-\pi^+ + c.c.)/\Gamma_{total}] \times [B(\psi(2S) \to h_c(1P)\pi^0)] \times [B(h_c(1P) \to \gamma\eta_c(1S))] = (24.02 \pm 4.44 \pm 4.08) \times 10^{-6}$ which we divide by our best values $B(\psi(2S) \to h_c(1P)\pi^0) = (8.6 \pm 1.3) \times 10^{-4}$, $B(h_c(1P) \to \gamma\eta_c(1S)) = (50 \pm 9) \times 10^{-2}$. Our first error is their experiment's error and our second error is the systematic error from using our best values.

$\Gamma(K^+K^-2(\pi^+\pi^-))/\Gamma_{total}$ — Γ_{41}/Γ

VALUE (units 10^{-3})	EVTS	DOCUMENT ID		TECN	COMMENT
7.5±2.4 OUR AVERAGE					
8 ±4 ±2	10	[1] ABLIKIM	12N	BES3	$\psi(2S) \to \pi^0\gamma K^+K^-2(\pi^+\pi^-)$
7.2±2.4±1.5	100	[2] ABLIKIM	06A	BES2	$J/\psi \to K^+K^-2(\pi^+\pi^-)\gamma$

[1] ABLIKIM 12N reports $[\Gamma(\eta_c(1S) \to K^+K^-2(\pi^+\pi^-))/\Gamma_{total}] \times [B(\psi(2S) \to h_c(1P)\pi^0)] \times [B(h_c(1P) \to \gamma\eta_c(1S))] = (3.60 \pm 1.71 \pm 0.64) \times 10^{-6}$ which we divide by our best values $B(\psi(2S) \to h_c(1P)\pi^0) = (8.6 \pm 1.3) \times 10^{-4}$, $B(h_c(1P) \to \gamma\eta_c(1S)) = (50 \pm 9) \times 10^{-2}$. Our first error is their experiment's error and our second error is the systematic error from using our best values.

[2] ABLIKIM 06A reports $[\Gamma(\eta_c(1S) \to K^+K^-2(\pi^+\pi^-))/\Gamma_{total}] \times [B(J/\psi(1S) \to \gamma\eta_c(1S))] = (1.21 \pm 0.32 \pm 0.24) \times 10^{-4}$ which we divide by our best value $B(J/\psi(1S) \to \gamma\eta_c(1S)) = (1.7 \pm 0.4) \times 10^{-2}$. Our first error is their experiment's error and our second error is the systematic error from using our best value.

$\Gamma(2(K^+K^-))/\Gamma_{total}$ — Γ_{42}/Γ

VALUE (units 10^{-3})	EVTS	DOCUMENT ID		TECN	COMMENT
1.43± 0.30 OUR FIT					
2.2 ± 0.9 ±0.5	7	[1] ABLIKIM	12N	BES3	$\psi(2S) \to \pi^0\gamma 2(K^+K^-)$
• • • We do not use the following data for averages, fits, limits, etc. • • •					
$1.4\ ^{+0.5}_{-0.4}\ \pm0.6$	$14.5^{+4.6}_{-3.0}$	[2] HUANG	03	BELL	$B^+ \to 2(K^+K^-)\ K^+$
21 ±10 ±6		[3] ALBRECHT	94H	ARG	$\gamma\gamma \to K^+K^-K^+K^-$

[1] ABLIKIM 12N reports $[\Gamma(\eta_c(1S) \to 2(K^+K^-))/\Gamma_{total}] \times [B(\psi(2S) \to h_c(1P)\pi^0)] \times [B(h_c(1P) \to \gamma\eta_c(1S))] = (0.94 \pm 0.37 \pm 0.14) \times 10^{-6}$ which we divide by our best values $B(\psi(2S) \to h_c(1P)\pi^0) = (8.6 \pm 1.3) \times 10^{-4}$, $B(h_c(1P) \to \gamma\eta_c(1S)) = (50 \pm 9) \times 10^{-2}$. Our first error is their experiment's error and our second error is the systematic error from using our best values.

[2] Using $B(B^+ \to \eta_c K^+) = (1.25 \pm 0.12^{+0.10}_{-0.12}) \times 10^{-3}$ from FANG 03 and $B(\eta_c \to K\overline{K}\pi) = (5.5 \pm 1.7) \times 10^{-2}$.

[3] Normalized to the sum of $B(\eta_c \to K^\pm K^0_S\pi^\mp)$, $B(\eta_c \to \phi\phi)$, $B(\eta_c \to K^+K^-\pi^+\pi^-)$, and $B(\eta_c \to 2\pi^+2\pi^-)$.

$\Gamma(2(K^+K^-))/\Gamma(K\overline{K}\pi)$ — Γ_{42}/Γ_{34}

VALUE	EVTS	DOCUMENT ID		TECN	COMMENT
0.020±0.004 OUR FIT					
0.024±0.007 OUR AVERAGE					
0.023±0.007±0.006		AUBERT,B	04B	BABR	$B^\pm \to K^\pm\eta_c$
$0.026^{+0.009}_{-0.007}\pm0.007$	15	[1] HUANG	03	BELL	$B^\pm \to K^\pm(2K^+2K^-)$

[1] Using $B(B^+ \to \eta_c K^+) = (1.25 \pm 0.12^{+0.10}_{-0.12}) \times 10^{-3}$ from FANG 03 and $B(\eta_c \to K\overline{K}\pi) = (5.5 \pm 1.7) \times 10^{-2}$.

$\Gamma(\eta'(958)K\overline{K})/\Gamma(\eta'(958)\pi\pi)$ — Γ_2/Γ_1

VALUE	DOCUMENT ID		TECN	COMMENT
0.859±0.052±0.043	[1] LEES	21A	BABR	$\gamma\gamma \to \eta' K^+K^-$, $\eta'\pi^+\pi^-$

[1] Based on Dalitz-plot analysis of the $\eta_c \to \eta' K^+K^-$, $\eta'\pi^+\pi^-$ final states where the fit fractions and relative phases are determined for numerous two-body intermediate states.

$\Gamma(\pi^+\pi^-\pi^0)/\Gamma_{total}$ — Γ_{43}/Γ

VALUE	CL%	DOCUMENT ID		TECN	COMMENT
$<5 \times 10^{-4}$	90	[1] ABLIKIM	17AJ	BES3	$\psi(2S) \to \gamma\pi^+\pi^-\pi^0$

[1] ABLIKIM 17AJ reports $[\Gamma(\eta_c(1S) \to \pi^+\pi^-\pi^0)/\Gamma_{total}] \times [B(\psi(2S) \to \gamma\eta_c(1S))] < 1.6 \times 10^{-6}$ which we divide by our best value $B(\psi(2S) \to \gamma\eta_c(1S)) = 3.4 \times 10^{-3}$.

$\Gamma(\pi^+\pi^-\pi^0\pi^0)/\Gamma_{total}$ — Γ_{44}/Γ

VALUE (units 10^{-2})	EVTS	DOCUMENT ID		TECN	COMMENT
4.7±0.9±1.1	118	[1] ABLIKIM	12N	BES3	$\psi(2S) \to \pi^0\gamma\pi^+\pi^-2\pi^0$

[1] ABLIKIM 12N reports $[\Gamma(\eta_c(1S) \to \pi^+\pi^-\pi^0\pi^0)/\Gamma_{total}] \times [B(\psi(2S) \to h_c(1P)\pi^0)] \times [B(h_c(1P) \to \gamma\eta_c(1S))] = (20.31 \pm 2.20 \pm 3.33) \times 10^{-6}$ which we divide by our best values $B(\psi(2S) \to h_c(1P)\pi^0) = (8.6 \pm 1.3) \times 10^{-4}$, $B(h_c(1P) \to \gamma\eta_c(1S)) = (50 \pm 9) \times 10^{-2}$. Our first error is their experiment's error and our second error is the systematic error from using our best values.

Downloaded from https://academic.oup.com/ptep/article/2022/8/083C01/6651666 by KIT Library user on 27 September 2022

$\Gamma(2(\pi^+\pi^-))/\Gamma_{total}$ — Γ_{45}/Γ

VALUE (units 10^{-2})	EVTS	DOCUMENT ID		TECN	COMMENT
0.91±0.12 OUR FIT					
1.27±0.23 OUR AVERAGE					
1.7 ±0.3 ±0.4	100	[1] ABLIKIM	12N	BES3	$\psi(2S) \to \pi^0\gamma 2(\pi^+\pi^-)$
1.0 ±0.5	542 ± 75	[2] BAI	04	BES	$J/\psi \to \gamma\, 2(\pi^+\pi^-)$
1.05±0.17±0.34	137	[2] BISELLO	91	DM2	$J/\psi \to \gamma 2\pi^+ 2\pi^-$
1.3 ±0.6	25	[2] BALTRUSAIT...86		MRK3	$J/\psi \to \eta_c\gamma$
$2.0\ ^{+1.5}_{-1.0}$		[3] HIMEL	80B	MRK2	$\psi(2S) \to \eta_c\gamma$

[1] ABLIKIM 12N reports $[\Gamma(\eta_c(1S) \to 2(\pi^+\pi^-))/\Gamma_{total}] \times [B(\psi(2S) \to h_c(1P)\pi^0)] \times [B(h_c(1P) \to \gamma\eta_c(1S))] = (7.51 \pm 0.85 \pm 1.11) \times 10^{-6}$ which we divide by our best values $B(\psi(2S) \to h_c(1P)\pi^0) = (8.6 \pm 1.3) \times 10^{-4}$, $B(h_c(1P) \to \gamma\eta_c(1S)) = (50 \pm 9) \times 10^{-2}$. Our first error is their experiment's error and our second error is the systematic error from using our best values.

[2] The quoted branching ratios use $B(J/\psi(1S) \to \gamma\eta_c(1S)) = 0.0127 \pm 0.0036$. Where relevant, the error in this branching ratio is treated as a common systematic in computing averages.

[3] Estimated using $B(\psi(2S) \to \gamma\eta_c(1S)) = 0.0028 \pm 0.0006$.

$\Gamma(2(\pi^+\pi^-\pi^0))/\Gamma_{total}$ — Γ_{46}/Γ

VALUE (units 10^{-2})	EVTS	DOCUMENT ID		TECN	COMMENT
15.8±2.3 OUR AVERAGE					
15.3±1.8±1.8	333	ABLIKIM	19AP	BES3	$h_c \to \gamma\eta_c$
17 ±3 ±4	175	[1] ABLIKIM	12N	BES3	$\psi(2S) \to \pi^0\gamma 2(\pi^+\pi^-\pi^0)$

[1] ABLIKIM 12N reports $[\Gamma(\eta_c(1S) \to 2(\pi^+\pi^-\pi^0))/\Gamma_{total}] \times [B(\psi(2S) \to h_c(1P)\pi^0)] \times [B(h_c(1P) \to \gamma\eta_c(1S))] = (75.13 \pm 7.42 \pm 9.99) \times 10^{-6}$ which we divide by our best values $B(\psi(2S) \to h_c(1P)\pi^0) = (8.6 \pm 1.3) \times 10^{-4}$, $B(h_c(1P) \to \gamma\eta_c(1S)) = (50 \pm 9) \times 10^{-2}$. Our first error is their experiment's error and our second error is the systematic error from using our best values.

$\Gamma(3(\pi^+\pi^-))/\Gamma_{total}$ — Γ_{47}/Γ

VALUE (units 10^{-3})	EVTS	DOCUMENT ID		TECN	COMMENT
17 ±4 OUR AVERAGE					
20 ±5 ±5	51	[1] ABLIKIM	12N	BES3	$\psi(2S) \to \pi^0\gamma 3(\pi^+\pi^-)$
15.4±3.4±3.3	479	[2] ABLIKIM	06A	BES2	$J/\psi \to 3(\pi^+\pi^-)\gamma$

[1] ABLIKIM 12N reports $[\Gamma(\eta_c(1S) \to 3(\pi^+\pi^-))/\Gamma_{total}] \times [B(\psi(2S) \to h_c(1P)\pi^0)] \times [B(h_c(1P) \to \gamma\eta_c(1S))] = (8.82 \pm 1.57 \pm 1.59) \times 10^{-6}$ which we divide by our best values $B(\psi(2S) \to h_c(1P)\pi^0) = (8.6 \pm 1.3) \times 10^{-4}$, $B(h_c(1P) \to \gamma\eta_c(1S)) = (50 \pm 9) \times 10^{-2}$. Our first error is their experiment's error and our second error is the systematic error from using our best values.

[2] ABLIKIM 06A reports $[\Gamma(\eta_c(1S) \to 3(\pi^+\pi^-))/\Gamma_{total}] \times [B(J/\psi(1S) \to \gamma\eta_c(1S))] = (2.59 \pm 0.32 \pm 0.47) \times 10^{-4}$ which we divide by our best value $B(J/\psi(1S) \to \gamma\eta_c(1S)) = (1.7 \pm 0.4) \times 10^{-2}$. Our first error is their experiment's error and our second error is the systematic error from using our best value.

$\Gamma(p\overline{p})/\Gamma_{total}$ — Γ_{48}/Γ

VALUE (units 10^{-4})	EVTS	DOCUMENT ID		TECN	COMMENT
14.4± 1.4 OUR FIT					
12.6± 2.1 OUR AVERAGE					
12.0± 2.6±1.5	34	ABLIKIM	19AP	BES3	$h_c \to \gamma\eta_c$
15 ± 5 ±3	15	[1] ABLIKIM	12N	BES3	$\psi(2S) \to \pi^0\gamma p\overline{p}$
15 ± 6	213 ± 33	[2] BAI	04	BES	$J/\psi \to \gamma p\overline{p}$
10 ± 3 ±4	18	[2] BISELLO	91	DM2	$J/\psi \to \gamma p\overline{p}$
11 ± 6	23	[2] BALTRUSAIT...86		MRK3	$J/\psi \to \eta_c\gamma$
$29\ ^{+29}_{-15}$		[3] HIMEL	80B	MRK2	$\psi(2S) \to \eta_c\gamma$
• • • We do not use the following data for averages, fits, limits, etc. • • •					
$13.1\ ^{+1.8}_{-2.1} \pm 0.9$	195	[4] WU	06	BELL	$B^+ \to p\overline{p}K^+$

[1] ABLIKIM 12N reports $[\Gamma(\eta_c(1S) \to p\overline{p})/\Gamma_{total}] \times [B(\psi(2S) \to h_c(1P)\pi^0)] \times [B(h_c(1P) \to \gamma\eta_c(1S))] = (0.65 \pm 0.19 \pm 0.10) \times 10^{-6}$ which we divide by our best values $B(\psi(2S) \to h_c(1P)\pi^0) = (8.6 \pm 1.3) \times 10^{-4}$, $B(h_c(1P) \to \gamma\eta_c(1S)) = (50 \pm 9) \times 10^{-2}$. Our first error is their experiment's error and our second error is the systematic error from using our best values.

[2] The quoted branching ratios use $B(J/\psi(1S) \to \gamma\eta_c(1S)) = 0.0127 \pm 0.0036$. Where relevant, the error in this branching ratio is treated as a common systematic in computing averages.

[3] Estimated using $B(\psi(2S) \to \gamma\eta_c(1S)) = 0.0028 \pm 0.0006$.

[4] WU 06 reports $[\Gamma(\eta_c(1S) \to p\overline{p})/\Gamma_{total}] \times [B(B^+ \to \eta_c K^+)] = (1.42 \pm 0.11\ ^{+0.16}_{-0.20}) \times 10^{-6}$ which we divide by our best value $B(B^+ \to \eta_c K^+) = (1.09 \pm 0.08) \times 10^{-3}$. Our first error is their experiment's error and our second error is the systematic error from using our best value.

$\Gamma(p\overline{p})/\Gamma(K\overline{K}\pi)$ — Γ_{48}/Γ_{34}

VALUE	EVTS	DOCUMENT ID		TECN	COMMENT
0.0198±0.0019 OUR FIT					
$\mathbf{0.021 \pm 0.002\ ^{+0.004}_{-0.006}}$	195	[1] WU	06	BELL	$B^\pm \to K^\pm p\overline{p}$

[1] Using $B(B^+ \to \eta_c K^+) = (1.25 \pm 0.12\ ^{+0.10}_{-0.12}) \times 10^{-3}$ from FANG 03 and $B(\eta_c \to K\overline{K}\pi) = (5.5 \pm 1.7) \times 10^{-2}$.

$\Gamma(p\overline{p})/\Gamma_{total} \times \Gamma(\phi\phi)/\Gamma_{total}$ — $\Gamma_{48}/\Gamma \times \Gamma_8/\Gamma$

VALUE (units 10^{-5})	DOCUMENT ID		TECN	COMMENT
0.25±0.04 OUR FIT				
$\mathbf{4.0\ ^{+3.5}_{-3.2}}$	BAGLIN	89	SPEC	$\overline{p}p \to K^+K^-K^+K^-$

$\Gamma(p\overline{p}\pi^0)/\Gamma_{total}$ — Γ_{49}/Γ

VALUE (units 10^{-2})	EVTS	DOCUMENT ID		TECN	COMMENT
0.36±0.13±0.08	14	[1] ABLIKIM	12N	BES3	$\psi(2S) \to \pi^0\gamma p\overline{p}\pi^0$

[1] ABLIKIM 12N reports $[\Gamma(\eta_c(1S) \to p\overline{p}\pi^0)/\Gamma_{total}] \times [B(\psi(2S) \to h_c(1P)\pi^0)] \times [B(h_c(1P) \to \gamma\eta_c(1S))] = (1.53 \pm 0.49 \pm 0.23) \times 10^{-6}$ which we divide by our best values $B(\psi(2S) \to h_c(1P)\pi^0) = (8.6 \pm 1.3) \times 10^{-4}$, $B(h_c(1P) \to \gamma\eta_c(1S)) = (50 \pm 9) \times 10^{-2}$. Our first error is their experiment's error and our second error is the systematic error from using our best values.

$\Gamma(\Lambda\overline{\Lambda})/\Gamma_{total}$ — Γ_{50}/Γ

VALUE (units 10^{-4})	CL%	EVTS	DOCUMENT ID		TECN	COMMENT
10.6±2.3 OUR FIT						
11.8±2.3±2.5			[1] ABLIKIM	12B	BES3	
• • • We do not use the following data for averages, fits, limits, etc. • • •						
$8.7\ ^{+2.4}_{-2.3} \pm 0.6$		20	[2] WU	06	BELL	$B^+ \to \Lambda\overline{\Lambda}K^+$
<20		90	[3] BISELLO	91	DM2	$e^+e^- \to \gamma\Lambda\overline{\Lambda}$

[1] ABLIKIM 12B reports $[\Gamma(\eta_c(1S) \to \Lambda\overline{\Lambda})/\Gamma_{total}] \times [B(J/\psi(1S) \to \gamma\eta_c(1S))] = (0.198 \pm 0.021 \pm 0.032) \times 10^{-4}$ which we divide by our best value $B(J/\psi(1S) \to \gamma\eta_c(1S)) = (1.7 \pm 0.4) \times 10^{-2}$. Our first error is their experiment's error and our second error is the systematic error from using our best value.

[2] WU 06 reports $[\Gamma(\eta_c(1S) \to \Lambda\overline{\Lambda})/\Gamma_{total}] \times [B(B^+ \to \eta_c K^+)] = (0.95\ ^{+0.25+0.08}_{-0.22-0.11}) \times 10^{-6}$ which we divide by our best value $B(B^+ \to \eta_c K^+) = (1.09 \pm 0.08) \times 10^{-3}$. Our first error is their experiment's error and our second error is the systematic error from using our best value.

[3] The quoted branching ratios use $B(J/\psi(1S) \to \gamma\eta_c(1S)) = 0.0127 \pm 0.0036$.

$\Gamma(\Lambda\overline{\Lambda})/\Gamma(p\overline{p})$ — Γ_{50}/Γ_{48}

VALUE	DOCUMENT ID		TECN	COMMENT
0.74±0.16 OUR FIT				
$\mathbf{0.67\ ^{+0.19}_{-0.16} \pm 0.12}$	[1] WU	06	BELL	$B^+ \to p\overline{p}K^+, \Lambda\overline{\Lambda}K^+$

[1] Not independent from other $\eta_c \to \Lambda\overline{\Lambda}$, $p\overline{p}$ branching ratios reported by WU 06.

$\Gamma(K^+\overline{p}\Lambda + \text{c.c.})/\Gamma_{total}$ — Γ_{51}/Γ

VALUE (units 10^{-3})	EVTS	DOCUMENT ID		TECN	COMMENT
$\mathbf{2.50\ ^{+0.34+0.17}_{-0.32-0.18}}$	157	[1] LU	19	BELL	$B^+ \to \overline{p}\Lambda K^+K^+$

[1] LU 19 reports $(2.83\ ^{+0.36}_{-0.34} \pm 0.35) \times 10^{-3}$ from a measurement of $[\Gamma(\eta_c(1S) \to K^+\overline{p}\Lambda + \text{c.c.})/\Gamma_{total}] \times [B(B^+ \to \eta_c K^+)]$ assuming $B(B^+ \to \eta_c K^+) = (9.6 \pm 1.1) \times 10^{-4}$, which we rescale to our best value $B(B^+ \to \eta_c K^+) = (1.09 \pm 0.08) \times 10^{-3}$. Our first error is their experiment's error and our second error is the systematic error from using our best value.

$\Gamma(\overline{\Lambda}(1520)\Lambda + \text{c.c.})/\Gamma_{total}$ — Γ_{52}/Γ

VALUE (units 10^{-3})	EVTS	DOCUMENT ID		TECN	COMMENT
3.1±1.3±0.2	43	[1] LU	19	BELL	$B^+ \to \overline{p}\Lambda K^+K^+$

[1] LU 19 reports $(3.48 \pm 1.48 \pm 0.46) \times 10^{-3}$ from a measurement of $[\Gamma(\eta_c(1S) \to \overline{\Lambda}(1520)\Lambda + \text{c.c.})/\Gamma_{total}] \times [B(B^+ \to \eta_c K^+)]$ assuming $B(B^+ \to \eta_c K^+) = (9.6 \pm 1.1) \times 10^{-4}$, which we rescale to our best value $B(B^+ \to \eta_c K^+) = (1.09 \pm 0.08) \times 10^{-3}$. Our first error is their experiment's error and our second error is the systematic error from using our best value.

$\Gamma(\Sigma^+\overline{\Sigma}^-)/\Gamma_{total}$ — Γ_{53}/Γ

VALUE (units 10^{-3})	EVTS	DOCUMENT ID		TECN	COMMENT
2.1±0.3±0.5	112	[1] ABLIKIM	13C	BES3	$J/\psi \to \gamma p\overline{p}\pi^0\pi^0$

[1] ABLIKIM 13C reports $[\Gamma(\eta_c(1S) \to \Sigma^+\overline{\Sigma}^-)/\Gamma_{total}] \times [B(J/\psi(1S) \to \gamma\eta_c(1S))] = (3.60 \pm 0.48 \pm 0.31) \times 10^{-5}$ which we divide by our best value $B(J/\psi(1S) \to \gamma\eta_c(1S)) = (1.7 \pm 0.4) \times 10^{-2}$. Our first error is their experiment's error and our second error is the systematic error from using our best value.

$\Gamma(\Xi^-\overline{\Xi}^+)/\Gamma_{total}$ — Γ_{54}/Γ

VALUE (units 10^{-3})	EVTS	DOCUMENT ID		TECN	COMMENT
0.90±0.18±0.19	78	[1] ABLIKIM	13C	BES3	$J/\psi \to \gamma\Lambda\overline{\Lambda}\pi^+\pi^-$

[1] ABLIKIM 13C reports $[\Gamma(\eta_c(1S) \to \Xi^-\overline{\Xi}^+)/\Gamma_{total}] \times [B(J/\psi(1S) \to \gamma\eta_c(1S))] = (1.51 \pm 0.27 \pm 0.14) \times 10^{-5}$ which we divide by our best value $B(J/\psi(1S) \to \gamma\eta_c(1S)) = (1.7 \pm 0.4) \times 10^{-2}$. Our first error is their experiment's error and our second error is the systematic error from using our best value.

$\Gamma(\pi^+\pi^-p\overline{p})/\Gamma_{total}$ — Γ_{55}/Γ

VALUE (units 10^{-3})	CL%	EVTS	DOCUMENT ID		TECN	COMMENT
5.3±1.7±1.2		19	[1] ABLIKIM	12N	BES3	$\psi(2S) \to \pi^0\gamma p\overline{p}\pi^+\pi^-$
• • • We do not use the following data for averages, fits, limits, etc. • • •						
<12	90		HIMEL	80B	MRK2	$\psi(2S) \to \eta_c\gamma$

Downloaded from https://academic.oup.com/ptep/article/2022/8/083C01/6651666 by KIT Library user on 27 September 2022

[1] ABLIKIM 12N reports $[\Gamma(\eta_c(1S) \to \pi^+\pi^- p\overline{p})/\Gamma_{total}] \times [B(\psi(2S) \to h_c(1P)\pi^0)] \times [B(h_c(1P) \to \gamma\eta_c(1S))] = (2.30 \pm 0.65 \pm 0.36) \times 10^{-6}$ which we divide by our best values $B(\psi(2S) \to h_c(1P)\pi^0) = (8.6 \pm 1.3) \times 10^{-4}$, $B(h_c(1P) \to \gamma\eta_c(1S)) = (50 \pm 9) \times 10^{-2}$. Our first error is their experiment's error and our second error is the systematic error from using our best values.

RADIATIVE DECAYS

$\Gamma(\gamma\gamma)/\Gamma_{total}$ — Γ_{56}/Γ

VALUE (units 10^{-4})	CL%	EVTS	DOCUMENT ID		TECN	COMMENT
1.61±0.12 OUR FIT						
1.9 $^{+0.7}_{-0.6}$ OUR AVERAGE						
2.7 ±0.8 ±0.6			[1] ABLIKIM	13I	BES3	
1.4 $^{+0.7}_{-0.5}$ ±0.3		$1.2^{+2.8}_{-1.1}$	[2] ADAMS	08	CLEO	$\psi(2S) \to \pi^+\pi^- J/\psi$
• • • We do not use the following data for averages, fits, limits, etc. • • •						
2.0 $^{+0.9}_{-0.7}$ ±0.1		13	[3] WICHT	08	BELL	$B^\pm \to K^\pm\gamma\gamma$
2.80 $^{+0.67}_{-0.58}$ ±1.0			[4] ARMSTRONG	95F	E760	$\overline{p}p \to \gamma\gamma$
< 9	90		[5] BISELLO	91	DM2	$J/\psi \to \gamma\gamma\gamma$
6 $^{+4}_{-3}$ ±4			[4] BAGLIN	87B	SPEC	$\overline{p}p \to \gamma\gamma$
< 18	90		[6] BLOOM	83	CBAL	$J/\psi \to \eta_c\gamma$

[1] ABLIKIM 13I reports $[\Gamma(\eta_c(1S) \to \gamma\gamma)/\Gamma_{total}] \times [B(J/\psi(1S) \to \gamma\eta_c(1S))] = (4.5 \pm 1.2 \pm 0.6) \times 10^{-6}$ which we divide by our best value $B(J/\psi(1S) \to \gamma\eta_c(1S)) = (1.7 \pm 0.4) \times 10^{-2}$. Our first error is their experiment's error and our second error is the systematic error from using our best value.

[2] ADAMS 08 reports $[\Gamma(\eta_c(1S) \to \gamma\gamma)/\Gamma_{total}] \times [B(J/\psi(1S) \to \gamma\eta_c(1S))] = (2.4^{+1.1}_{-0.8} \pm 0.3) \times 10^{-6}$ which we divide by our best value $B(J/\psi(1S) \to \gamma\eta_c(1S)) = (1.7 \pm 0.4) \times 10^{-2}$. Our first error is their experiment's error and our second error is the systematic error from using our best value.

[3] WICHT 08 reports $[\Gamma(\eta_c(1S) \to \gamma\gamma)/\Gamma_{total}] \times [B(B^+ \to \eta_c K^+)] = (2.2^{+0.9}_{-0.7}{}^{+0.4}_{-0.2}) \times 10^{-7}$ which we divide by our best value $B(B^+ \to \eta_c K^+) = (1.09 \pm 0.08) \times 10^{-3}$. Our first error is their experiment's error and our second error is the systematic error from using our best value.

[4] Not independent from the values of the total and two-photon width quoted by the same experiment.

[5] The quoted branching ratios use $B(J/\psi(1S) \to \gamma\eta_c(1S)) = 0.0127 \pm 0.0036$.

[6] Using $B(J/\psi(1S) \to \gamma\eta_c(1S)) = 0.0127 \pm 0.0036$.

$\Gamma(\gamma\gamma)/\Gamma(K\overline{K}\pi)$ — Γ_{56}/Γ_{34}

VALUE (units 10^{-3})	EVTS	DOCUMENT ID		TECN	COMMENT
2.22±0.25 OUR FIT					
3.2 $^{+1.3}_{-1.0}$ $^{+0.8}_{-0.6}$	13	[1] WICHT	08	BELL	$B^\pm \to K^\pm\gamma\gamma$

[1] Using $B(B^+ \to \eta_c K^+) = (1.25 \pm 0.12^{+0.10}_{-0.12}) \times 10^{-3}$ from FANG 03 and $B(\eta_c \to K\overline{K}\pi) = (5.5 \pm 1.7) \times 10^{-2}$.

$\Gamma(p\overline{p})/\Gamma_{total} \times \Gamma(\gamma\gamma)/\Gamma_{total}$ — $\Gamma_{48}/\Gamma \times \Gamma_{56}/\Gamma$

VALUE (units 10^{-6})	EVTS	DOCUMENT ID		TECN	COMMENT
0.232±0.022 OUR FIT					
0.26 ±0.05 OUR AVERAGE	Error includes scale factor of 1.4.				
$0.224^{+0.038}_{-0.037} \pm 0.020$	190	AMBROGIANI	03	E835	$\overline{p}p \to \eta_c \to \gamma\gamma$
$0.336^{+0.080}_{-0.070}$		ARMSTRONG	95F	E760	$\overline{p}p \to \gamma\gamma$
$0.68^{+0.42}_{-0.31}$	12	BAGLIN	87B	SPEC	$\overline{p}p \to \gamma\gamma$

Charge conjugation (C), Parity (P), Lepton family number (LF) violating modes

$\Gamma(\pi^+\pi^-)/\Gamma_{total}$ — Γ_{57}/Γ

VALUE (units 10^{-5})	CL%	DOCUMENT ID		TECN	COMMENT
<11	90	[1] ABLIKIM	11G	BES3	$J/\psi \to \gamma\pi^+\pi^-$
• • • We do not use the following data for averages, fits, limits, etc. • • •					
<70	90	[2] ABLIKIM	06B	BES2	$J/\psi \to \pi^+\pi^-\gamma$

[1] ABLIKIM 11G reports $[\Gamma(\eta_c(1S) \to \pi^+\pi^-)/\Gamma_{total}] \times [B(J/\psi(1S) \to \gamma\eta_c(1S))] < 1.82\times10^{-6}$ which we divide by our best value $B(J/\psi(1S) \to \gamma\eta_c(1S)) = 1.7\times10^{-2}$.

[2] ABLIKIM 06B reports $[\Gamma(\eta_c(1S) \to \pi^+\pi^-)/\Gamma_{total}] \times [B(J/\psi(1S) \to \gamma\eta_c(1S))] < 1.1\times10^{-5}$ which we divide by our best value $B(J/\psi(1S) \to \gamma\eta_c(1S)) = 1.7\times10^{-2}$.

$\Gamma(\pi^0\pi^0)/\Gamma_{total}$ — Γ_{58}/Γ

VALUE (units 10^{-5})	CL%	DOCUMENT ID		TECN	COMMENT
< 4	90	[1] ABLIKIM	11G	BES3	$J/\psi \to \gamma\pi^0\pi^0$
• • • We do not use the following data for averages, fits, limits, etc. • • •					
<40	90	[2] ABLIKIM	06B	BES2	$J/\psi \to \pi^0\pi^0\gamma$

[1] ABLIKIM 11G reports $[\Gamma(\eta_c(1S) \to \pi^0\pi^0)/\Gamma_{total}] \times [B(J/\psi(1S) \to \gamma\eta_c(1S))] < 6.0\times10^{-7}$ which we divide by our best value $B(J/\psi(1S) \to \gamma\eta_c(1S)) = 1.7\times10^{-2}$.

[2] ABLIKIM 06B reports $[\Gamma(\eta_c(1S) \to \pi^0\pi^0)/\Gamma_{total}] \times [B(J/\psi(1S) \to \gamma\eta_c(1S))] < 0.71\times10^{-5}$ which we divide by our best value $B(J/\psi(1S) \to \gamma\eta_c(1S)) = 1.7\times10^{-2}$.

$\Gamma(K^+K^-)/\Gamma_{total}$ — Γ_{59}/Γ

VALUE (units 10^{-5})	CL%	DOCUMENT ID		TECN	COMMENT
<60	90	[1] ABLIKIM	06B	BES2	$J/\psi \to K^+K^-\gamma$

[1] ABLIKIM 06B reports $[\Gamma(\eta_c(1S) \to K^+K^-)/\Gamma_{total}] \times [B(J/\psi(1S) \to \gamma\eta_c(1S))] < 0.96\times10^{-5}$ which we divide by our best value $B(J/\psi(1S) \to \gamma\eta_c(1S)) = 1.7\times10^{-2}$.

$\Gamma(K^0_S K^0_S)/\Gamma_{total}$ — Γ_{60}/Γ

VALUE (units 10^{-5})	CL%	DOCUMENT ID		TECN	COMMENT
<31	90	[1] ABLIKIM	06B	BES2	$J/\psi \to K^0_S K^0_S\gamma$
• • • We do not use the following data for averages, fits, limits, etc. • • •					
<32	90	[2] UEHARA	13	BELL	$\gamma\gamma \to K^0_S K^0_S$
< 5.6	90	[3] UEHARA	13	BELL	$\gamma\gamma \to K^0_S K^0_S$

[1] ABLIKIM 06B reports $[\Gamma(\eta_c(1S) \to K^0_S K^0_S)/\Gamma_{total}] \times [B(J/\psi(1S) \to \gamma\eta_c(1S))] < 0.53\times10^{-5}$ which we divide by our best value $B(J/\psi(1S) \to \gamma\eta_c(1S)) = 1.7\times10^{-2}$.

[2] Taking into account interference with the non-resonant continuum.

[3] Neglecting interference with the non-resonant continuum.

$\eta_c(1S)$ REFERENCES

LEES	21A	PR D104 072002	J.P. Lees et al.	(BABAR Collab.)
AAIJ	20H	EPJ C80 191	R. Aaij et al.	(LHCb Collab.)
ABLIKIM	19AP	PR D100 012003	M. Ablikim et al.	(BESIII Collab.)
ABLIKIM	19AV	PR D100 052012	M. Ablikim et al.	(BESIII Collab.)
LU	19	PR D99 032003	P.-C. Lu et al.	(BELLE Collab.)
XU	18	PR D98 072001	Q.N. Xu et al.	(BELLE Collab.)
AAIJ	17AD	PL B769 305	R. Aaij et al.	(LHCb Collab.)
AAIJ	17BB	EPJ C77 609	R. Aaij et al.	(LHCb Collab.)
ABLIKIM	17AJ	PR D96 112008	M. Ablikim et al.	(BESIII Collab.)
ABLIKIM	17P	PR D95 092004	M. Ablikim et al.	(BESIII Collab.)
LEES	16A	PR D93 012005	J.P. Lees et al.	(BABAR Collab.)
PDG	16	CP C40 100001	C. Patrignani et al.	(PDG Collab.)
AAIJ	15AS	JHEP 1510 053	R. Aaij et al.	(LHCb Collab.)
AAIJ	15BI	EPJ C75 311	R. Aaij et al.	(LHCb Collab.)
ANASHIN	14	PL B738 391	V.V. Anashin et al.	(KEDR Collab.)
LEES	14E	PR D89 112004	J.P. Lees et al.	(BABAR Collab.)
ABLIKIM	13C	PR D87 012003	M. Ablikim et al.	(BESIII Collab.)
ABLIKIM	13I	PR D87 032003	M. Ablikim et al.	(BESIII Collab.)
UEHARA	13	PTEP 2013 123C01	S. Uehara et al.	(BELLE Collab.)
ABLIKIM	12B	PR D86 032008	M. Ablikim et al.	(BESIII Collab.)
ABLIKIM	12F	PRL 108 222002	M. Ablikim et al.	(BESIII Collab.)
ABLIKIM	12N	PR D86 092009	M. Ablikim et al.	(BESIII Collab.)
LIU	12B	PRL 108 232001	Z.Q. Liu et al.	(BELLE Collab.)
ZHANG	12A	PR D86 052002	C.C. Zhang et al.	(BELLE Collab.)
ABLIKIM	11G	PR D84 032006	M. Ablikim et al.	(BESIII Collab.)
DEL-AMO-SA...	11M	PR D84 012004	P. del Amo Sanchez et al.	(BABAR Collab.)
VINOKUROVA	11	PL B706 139	A. Vinokurova et al.	(BELLE Collab.)
LEES	10	PR D81 052010	J.P. Lees et al.	(BABAR Collab.)
MITCHELL	09	PRL 102 011801	R.E. Mitchell et al.	(CLEO Collab.)
ADAMS	08	PRL 101 101801	G.S. Adams et al.	(CLEO Collab.)
AUBERT	08AB	PR D78 012006	B. Aubert et al.	(BABAR Collab.)
UEHARA	08	EPJ C53 1	S. Uehara et al.	(BELLE Collab.)
WICHT	08	PL B662 323	J. Wicht et al.	(BELLE Collab.)
ABE	07	PRL 98 082001	K. Abe et al.	(BELLE Collab.)
ABLIKIM	06A	PL B633 19	M. Ablikim et al.	(BES Collab.)
ABLIKIM	06B	EPJ C45 337	M. Ablikim et al.	(BES Collab.)
AUBERT	06E	PRL 96 052002	B. Aubert et al.	(BABAR Collab.)
PDG	06	JP G33 1	W.-M. Yao et al.	(PDG Collab.)
WU	06	PRL 97 162003	C.-H. Wu et al.	(BELLE Collab.)
ABLIKIM	05L	PR D72 072005	M. Ablikim et al.	(BES Collab.)
KUO	05	PL B621 41	C.C. Kuo et al.	(BELLE Collab.)
ABE	04G	PR D70 071102	K. Abe et al.	(BELLE Collab.)
ABLIKIM	04M	PR D70 112008	M. Ablikim et al.	(BES Collab.)
ASNER	04	PRL 92 142001	D.M. Asner et al.	(CLEO Collab.)
AUBERT	04D	PRL 92 142002	B. Aubert et al.	(BABAR Collab.)
AUBERT,B	04B	PR D70 011101	B. Aubert et al.	(BABAR Collab.)
BAI	04	PL B578 16	J.Z. Bai et al.	(BES Collab.)
ABDALLAH	03J	EPJ C31 481	J. Abdallah et al.	(DELPHI Collab.)
AMBROGIANI	03	PL B566 45	M. Ambrogiani et al.	(FNAL E835 Collab.)
BAI	03	PL B555 174	J.Z. Bai et al.	(BES Collab.)
FANG	03	PRL 90 071801	F. Fang et al.	(BELLE Collab.)
HUANG	03	PRL 91 241802	H.-C. Huang et al.	(BELLE Collab.)
ABE,K	02	PRL 89 142001	K. Abe et al.	(BELLE Collab.)
BAI	00F	PR D62 072001	J.Z. Bai et al.	(BES Collab.)
BRANDENB...	00B	PRL 85 3095	G. Brandenburg et al.	(CLEO Collab.)
ACCIARRI	99T	PL B461 155	M. Acciarri et al.	(L3 Collab.)
BAI	99B	PR D60 072001	J.Z. Bai et al.	(BES Collab.)
ABREU	98O	PL B441 479	P. Abreu et al.	(DELPHI Collab.)
SHIRAI	98	PL B424 405	M. Shirai et al.	(AMY Collab.)
ARMSTRONG	95F	PR D52 4839	T.A. Armstrong et al.	(FNAL, FERR, GENO+)
ALBRECHT	94H	PL B338 390	H. Albrecht et al.	(ARGUS Collab.)
ADRIANI	93N	PL B318 575	O. Adriani et al.	(L3 Collab.)
BISELLO	91	NP B350 1	D. Bisello et al.	(DM2 Collab.)
BAI	90B	PRL 65 1309	Z. Bai et al.	(Mark III Collab.)
CHEN	90B	PL B243 169	W.Y. Chen et al.	(CLEO Collab.)
BAGLIN	89	PL B231 557	C. Baglin, S. Baird, G. Bassompierre	(R704 Collab.)
BEHREND	89	ZPHY C42 367	H.J. Behrend et al.	(CELLO Collab.)
BRAUNSCH...	89	ZPHY C41 533	W. Braunschweig et al.	(TASSO Collab.)
AIHARA	88D	PRL 60 2355	H. Aihara et al.	(TPC Collab.)
BAGLIN	87B	PL B187 191	C. Baglin et al.	(R704 Collab.)
BALTRUSAIT...	86	PR D33 629	R.M. Baltrusaitis et al.	(Mark III Collab.)
BERGER	86	PL 167B 120	C. Berger et al.	(PLUTO Collab.)
GAISER	86	PR D34 711	J. Gaiser et al.	(Crystal Ball Collab.)
ALTHOFF	85B	ZPHY C29 189	M. Althoff et al.	(TASSO Collab.)
BALTRUSAIT...	84	PRL 52 2126	R.M. Baltrusaitis et al.	(CIT, UCSC+) JP
BLOOM	83	ARNS 33 143	E.D. Bloom, C. Peck	(SLAC, CIT)
HIMEL	80B	PRL 45 1146	T.M. Himel et al.	(SLAC, LBL, UCB)
PARTRIDGE	80B	PRL 45 1150	R. Partridge et al.	(CIT, HARV, PRIN+)

Downloaded from https://academic.oup.com/ptep/article/2022/8/083C01/6651666 by KIT Library user on 27 September 2022

$J/\psi(1S)$

$I^G(J^{PC}) = 0^-(1^{--})$

$J/\psi(1S)$ MASS

VALUE (MeV)	EVTS	DOCUMENT ID		TECN	COMMENT
3096.900±0.006 OUR AVERAGE					
3096.900±0.002±0.006		[1] ANASHIN	15	KEDR	$e^+e^- \to$ hadrons
3096.89 ±0.09	502	[2] ARTAMONOV	00	OLYA	$e^+e^- \to$ hadrons
3096.91 ±0.03 ±0.01		[3] ARMSTRONG	93B	E760	$\overline{p}p \to e^+e^-$
3096.95 ±0.1 ±0.3	193	BAGLIN	87	SPEC	$\overline{p}p \to e^+e^-X$
• • • We do not use the following data for averages, fits, limits, etc. • • •					
3096.66 ±0.19 ±0.02	6.1k	[4] AAIJ	15BI	LHCB	$pp \to J/\psi X$
3096.917±0.010±0.007		AULCHENKO	03	KEDR	$e^+e^- \to$ hadrons
3097.5 ±0.3		GRIBUSHIN	96	FMPS	515 π^-Be $\to 2\mu X$
3098.4 ±2.0	38k	LEMOIGNE	82	GOLI	185 π^-Be $\to \gamma\mu^+\mu^-$A
3096.93 ±0.09	502	[5] ZHOLENTZ	80	REDE	e^+e^-
3097.0 ±1		[6] BRANDELIK	79C	DASP	e^+e^-

[1] Supersedes AULCHENKO 03.
[2] Reanalysis of ZHOLENTZ 80 using new electron mass (COHEN 87) and radiative corrections (KURAEV 85).
[3] Mass central value and systematic error recalculated by us according to Eq. (16) in ARMSTRONG 93B, using the value for the $\psi(2S)$ mass from AULCHENKO 03.
[4] From a sample of $\eta_c(1S)$ and J/ψ produced in b-hadron decays. Systematic uncertainties not estimated.
[5] Superseded by ARTAMONOV 00.
[6] From a simultaneous fit to e^+e^-, $\mu^+\mu^-$ and hadronic channels assuming $\Gamma(e^+e^-) = \Gamma(\mu^+\mu^-)$.

$J/\psi(1S)$ WIDTH

VALUE (keV)	EVTS	DOCUMENT ID		TECN	COMMENT
92.6 ± 1.7 OUR AVERAGE		Error includes scale factor of 1.1.			
92.45± 1.40±1.48		[1] ANASHIN	20	KEDR	e^+e^-
96.1 ± 3.2	13k	[2] ADAMS	06A	CLEO	$e^+e^- \to \mu^+\mu^-\gamma$
84.4 ± 8.9		BAI	95B	BES	e^+e^-
91 ±11 ±6		[3] ARMSTRONG	93B	E760	$\overline{p}p \to e^+e^-$
85.5 $^{+6.1}_{-5.8}$		[4] HSUEH	92	RVUE	See Υ mini-review
• • • We do not use the following data for averages, fits, limits, etc. • • •					
92.94± 1.83		[5,6] ANASHIN	18A	KEDR	e^+e^-
94.1 ± 2.7		[7] ANASHIN	10	KEDR	3.097 $e^+e^- \to e^+e^-, \mu^+\mu^-$
93.7 ± 3.5	7.8k	[2] AUBERT	04	BABR	$e^+e^- \to \mu^+\mu^-\gamma$

[1] Based on the same dataset as ANASHIN 18A and correlated to the values reported there.
[2] Calculated by us from the reported values of $\Gamma(e^+e^-)\times B(\mu^+\mu^-)$ using $B(e^+e^-) = (5.94 \pm 0.06)\%$ and $B(\mu^+\mu^-) = (5.93 \pm 0.06)\%$.
[3] The initial-state radiation correction reevaluated by ANDREOTTI 07 in its Ref. [4].
[4] Using data from COFFMAN 92, BALDINI-CELIO 75, BOYARSKI 75, ESPOSITO 75B, BRANDELIK 79C.
[5] Using $\Gamma(e^+e^-)$ from ANASHIN 18A and $B(J/\psi(1S) \to e^+e^-) = (5.971 \pm 0.032)\%$ from PDG 16.
[6] Superseded by ANASHIN 20 that is based on the same dataset .
[7] Assuming $\Gamma(e^+e^-) = \Gamma(\mu^+\mu^-)$ and using $\Gamma(e^+e^-)/\Gamma_{total} = (5.94 \pm 0.06)\%$.

$J/\psi(1S)$ DECAY MODES

	Mode		Fraction (Γ_i/Γ)	Scale factor/ Confidence level
Γ_1	hadrons		(87.7 ± 0.5) %	
Γ_2	virtual $\gamma \to$ hadrons		(13.50 ± 0.30) %	
Γ_3	ggg		(64.1 ± 1.0) %	
Γ_4	γgg		(8.8 ± 1.1) %	
Γ_5	e^+e^-		(5.971± 0.032) %	
Γ_6	$e^+e^-\gamma$	[a]	(8.8 ± 1.4) $\times 10^{-3}$	
Γ_7	$\mu^+\mu^-$		(5.961± 0.033) %	
	Decays involving hadronic resonances			
Γ_8	$\rho\pi$		(1.69 ± 0.15) %	S=2.4
Γ_9	$\rho^0\pi^0$		(5.6 ± 0.7) $\times 10^{-3}$	
Γ_{10}	$a_2(1320)\rho$		(1.09 ± 0.22) %	
Γ_{11}	$\eta\pi^+\pi^-$		(3.8 ± 0.7) $\times 10^{-4}$	
Γ_{12}	$\eta\pi^+\pi^-\pi^0$		(1.17 ± 0.20) %	
Γ_{13}	$\eta\pi^+\pi^-3\pi^0$		(4.9 ± 1.0) $\times 10^{-3}$	
Γ_{14}	$\eta\rho$		(1.93 ± 0.23) $\times 10^{-4}$	
Γ_{15}	$\eta\phi(2170) \to \eta\phi f_0(980) \to \eta\phi\pi^+\pi^-$		(1.2 ± 0.4) $\times 10^{-4}$	
Γ_{16}	$\eta\phi(2170) \to \eta K^*(892)^0\overline{K}^*(892)^0$		< 2.52 $\times 10^{-4}$	CL=90%
Γ_{17}	$\eta K^\pm K^0_S\pi^\mp$	[b]	(2.2 ± 0.4) $\times 10^{-3}$	
Γ_{18}	$\eta K^*(892)^0\overline{K}^*(892)^0$		(1.15 ± 0.26) $\times 10^{-3}$	
Γ_{19}	$\rho\eta'(958)$		(8.1 ± 0.8) $\times 10^{-5}$	S=1.6
Γ_{20}	$\rho^\pm\pi^\mp\pi^+\pi^-2\pi^0$		(2.8 ± 0.8) %	
Γ_{21}	$\rho^+\rho^-\pi^+\pi^-\pi^0$		(6 ± 4) $\times 10^{-3}$	
Γ_{22}	$\rho^\mp K^\pm K^0_S$		(1.9 ± 0.4) $\times 10^{-3}$	
Γ_{23}	$\rho(1450)\pi$			
Γ_{24}	$\rho(1450)\pi \to \pi^+\pi^-\pi^0$		(2.3 ± 0.7) $\times 10^{-3}$	
Γ_{25}	$\rho(1450)^\pm\pi^\mp \to K^0_S K^\pm\pi^\mp$		(3.5 ± 0.6) $\times 10^{-4}$	
Γ_{26}	$\rho(1450)^0\pi^0 \to K^+K^-\pi^0$		(2.7 ± 0.6) $\times 10^{-4}$	
Γ_{27}	$\rho(1450)\eta'(958) \to \pi^+\pi^-\eta'(958)$		(3.3 ± 0.7) $\times 10^{-6}$	
Γ_{28}	$\rho(1700)\pi$			
Γ_{29}	$\rho(1700)\pi \to \pi^+\pi^-\pi^0$		(1.7 ± 1.1) $\times 10^{-4}$	
Γ_{30}	$\rho(2150)\pi$			
Γ_{31}	$\rho(2150)\pi \to \pi^+\pi^-\pi^0$		(8 ±40) $\times 10^{-6}$	
Γ_{32}	$\rho_3(1690)\pi \to \pi^+\pi^-\pi^0$			
Γ_{33}	$\omega\pi^0$		(4.5 ± 0.5) $\times 10^{-4}$	S=1.4
Γ_{34}	$\omega\pi^0 \to \pi^+\pi^-\pi^0$		(1.7 ± 0.8) $\times 10^{-5}$	
Γ_{35}	$\omega\pi^+\pi^-$		(7.2 ± 1.0) $\times 10^{-3}$	
Γ_{36}	$\omega\pi^0\pi^0$		(3.4 ± 0.8) $\times 10^{-3}$	
Γ_{37}	$\omega 3\pi^0$		(1.9 ± 0.6) $\times 10^{-3}$	
Γ_{38}	$\omega f_2(1270)$		(4.3 ± 0.6) $\times 10^{-3}$	
Γ_{39}	$\omega\eta$		(1.74 ± 0.20) $\times 10^{-3}$	S=1.6
Γ_{40}	$\omega\pi^+\pi^-\pi^0$		(4.0 ± 0.7) $\times 10^{-3}$	
Γ_{41}	$\omega\pi^0\eta$		(3.4 ± 1.7) $\times 10^{-4}$	
Γ_{42}	$\omega\pi^+\pi^+\pi^-\pi^-$		(8.5 ± 3.4) $\times 10^{-3}$	
Γ_{43}	$\omega\pi^+\pi^-2\pi^0$		(3.3 ± 0.5) %	
Γ_{44}	$\omega\eta'\pi^+\pi^-$		(1.12 ± 0.13) $\times 10^{-3}$	
Γ_{45}	$\omega\eta'(958)$		(1.89 ± 0.18) $\times 10^{-4}$	
Γ_{46}	$\omega f_0(980)$		(1.4 ± 0.5) $\times 10^{-4}$	
Γ_{47}	$\omega f_0(1710) \to \omega K\overline{K}$		(4.8 ± 1.1) $\times 10^{-4}$	
Γ_{48}	$\omega f_1(1420)$		(6.8 ± 2.4) $\times 10^{-4}$	
Γ_{49}	$\omega f'_2(1525)$		< 2.2 $\times 10^{-4}$	CL=90%
Γ_{50}	$\omega X(1835) \to \omega p\overline{p}$		< 3.9 $\times 10^{-6}$	CL=95%
Γ_{51}	$\omega X(1835),\ X \to \eta'\pi^+\pi^-$		< 6.2 $\times 10^{-5}$	
Γ_{52}	$\omega K^\pm K^0_S\pi^\mp$	[b]	(3.4 ± 0.5) $\times 10^{-3}$	
Γ_{53}	$\omega K\overline{K}$		(1.9 ± 0.4) $\times 10^{-3}$	
Γ_{54}	$\omega K^*(892)\overline{K}$+ c.c.		(6.1 ± 0.9) $\times 10^{-3}$	
Γ_{55}	$\eta' K^{*\pm}K^\mp$		(1.48 ± 0.13) $\times 10^{-3}$	
Γ_{56}	$\eta' K^{*0}\overline{K}^0$ + c.c.		(1.66 ± 0.21) $\times 10^{-3}$	
Γ_{57}	$\eta' h_1(1415) \to \eta' K^*\overline{K}$+ c.c.		(2.16 ± 0.31) $\times 10^{-4}$	
Γ_{58}	$\eta' h_1(1415) \to \eta' K^{*\pm}K^\mp$		(1.51 ± 0.23) $\times 10^{-4}$	
Γ_{59}	$\overline{K}K^*(892)$+c.c.			
Γ_{60}	$\overline{K}K^*(892)$+c.c. $\to K^0_S K^\pm\pi^\mp$		(5.0 ± 0.5) $\times 10^{-3}$	
Γ_{61}	$K^+K^*(892)^-$+ c.c.		(6.0 $^{+0.8}_{-1.0}$) $\times 10^{-3}$	S=2.9
Γ_{62}	$K^+K^*(892)^-$+ c.c. $\to K^+K^-\pi^0$		(2.69 $^{+0.13}_{-0.20}$) $\times 10^{-3}$	
Γ_{63}	$K^+K^*(892)^-$+ c.c. $\to K^0K^\pm\pi^\mp$+ c.c.		(3.0 ± 0.4) $\times 10^{-3}$	
Γ_{64}	$K^0\overline{K}^*(892)^0$+ c.c.		(4.2 ± 0.4) $\times 10^{-3}$	
Γ_{65}	$K^0\overline{K}^*(892)^0$+ c.c. $\to K^0K^\pm\pi^\mp$+ c.c.		(3.2 ± 0.4) $\times 10^{-3}$	
Γ_{66}	$\overline{K}^*(892)^0K^+\pi^-$+ c.c.		(7.7 ± 1.6) $\times 10^{-3}$	
Γ_{67}	$K^*(892)^\pm K^\mp\pi^0$		(4.1 ± 1.3) $\times 10^{-3}$	
Γ_{68}	$K^*(892)^+K^0_S\pi^-$+ c.c.		(2.0 ± 0.5) $\times 10^{-3}$	
Γ_{69}	$K^*(892)^+K^0_S\pi^-$+ c.c. $\to K^0_S K^0_S\pi^+\pi^-$		(6.7 ± 2.2) $\times 10^{-4}$	
Γ_{70}	$K^*(892)^0K^0_S \to \gamma K^0_S K^0_S$		(6.3 $^{+0.6}_{-0.5}$) $\times 10^{-6}$	
Γ_{71}	$K^*(892)^0K^0_S\pi^0$		(7 ± 4) $\times 10^{-4}$	
Γ_{72}	$K^*(892)^\pm K^*(700)^\mp$		(1.1 $^{+1.0}_{-0.6}$) $\times 10^{-3}$	
Γ_{73}	$K^*(892)^0\overline{K}^*(892)^0$		(2.3 ± 0.6) $\times 10^{-4}$	
Γ_{74}	$K^*(892)^\pm K^*(892)^\mp$		(1.00 $^{+0.22}_{-0.40}$) $\times 10^{-3}$	
Γ_{75}	$K_1(1400)^\pm K^\mp$		(3.8 ± 1.4) $\times 10^{-3}$	
Γ_{76}	$K^*(1410)\overline{K}$+c.c.			
Γ_{77}	$K^*(1410)\overline{K}$+c.c $\to K^\pm K^\mp\pi^0$		(7 ± 4) $\times 10^{-5}$	
Γ_{78}	$K^*(1410)\overline{K}$+ c.c. $\to K^0_S K^\pm\pi^\mp$		(8 ± 6) $\times 10^{-5}$	
Γ_{79}	$K^*_2(1430)\overline{K}$+c.c.			
Γ_{80}	$K^*_2(1430)\overline{K}$+c.c. $\to K^\pm K^\mp\pi^0$		(1.0 ± 0.5) $\times 10^{-4}$	

Downloaded from https://academic.oup.com/ptep/article/2022/8/083C01/6651666 by KIT Library user on 27 September 2022

Γ_{81}	$K_2^*(1430)\overline{K}+$ c.c. $\to K_S^0 K^\pm \pi^\mp$		$(4.0 \pm 1.0) \times 10^{-4}$	
Γ_{82}	$\overline{K}_2^*(1430) K+$ c.c.		$< 4.0 \times 10^{-3}$	CL=90%
Γ_{83}	$K_2^*(1430)^+ K^- +$ c.c. $\to K^+ K^- \pi^0$		$(2.69 {}^{+0.25}_{-0.19}) \times 10^{-4}$	
Γ_{84}	$K_2^*(1430)^+ K_S^0 \pi^- +$ c.c.		$(3.6 \pm 1.8) \times 10^{-3}$	
Γ_{85}	$\overline{K}_2^*(1430)^0 K^*(892)^0 +$ c.c.		$(4.67 \pm 0.29) \times 10^{-3}$	
Γ_{86}	$K_2^*(1430)^- K^*(892)^+ +$ c.c.		$(3.4 \pm 2.9) \times 10^{-3}$	
Γ_{87}	$K_2^*(1430)^- K^*(892)^+ +$ c.c. $\to K^*(892)^+ K_S^0 \pi^- +$ c.c.		$(4 \pm 4) \times 10^{-4}$	
Γ_{88}	$K_2^*(1430)^0 \overline{K}_2^*(1430)^0$		$< 2.9 \times 10^{-3}$	CL=90%
Γ_{89}	$\overline{K}_2(1770)^0 K^*(892)^0 +$ c.c. $\to K^*(892)^0 K^- \pi^+ +$ c.c.		$(6.9 \pm 0.9) \times 10^{-4}$	
Γ_{90}	$K_2^*(1980)^+ K^- +$ c.c. $\to K^+ K^- \pi^0$		$(1.10 {}^{+0.60}_{-0.14}) \times 10^{-5}$	
Γ_{91}	$K_4^*(2045)^+ K^- +$ c.c. $\to K^+ K^- \pi^0$		$(6.2 {}^{+2.9}_{-1.6}) \times 10^{-6}$	
Γ_{92}	$K_1(1270)^\pm K^\mp$		$< 3.0 \times 10^{-3}$	CL=90%
Γ_{93}	$K_1(1270) K_S^0 \to \gamma K_S^0 K_S^0$		$(8.5 \pm 2.5) \times 10^{-7}$	
Γ_{94}	$a_2(1320)^\pm \pi^\mp$	[b]	$< 4.3 \times 10^{-3}$	CL=90%
Γ_{95}	$\phi\pi^0$		3×10^{-6} or 1×10^{-7}	
Γ_{96}	$\phi\pi^+\pi^-$		$(9.4 \pm 1.5) \times 10^{-4}$	S=1.7
Γ_{97}	$\phi\pi^0\pi^0$		$(5.0 \pm 1.0) \times 10^{-4}$	
Γ_{98}	$\phi 2(\pi^+\pi^-)$		$(1.60 \pm 0.32) \times 10^{-3}$	
Γ_{99}	$\phi\eta$		$(7.4 \pm 0.8) \times 10^{-4}$	S=1.5
Γ_{100}	$\phi\eta'(958)$		$(4.6 \pm 0.5) \times 10^{-4}$	S=2.2
Γ_{101}	$\phi\eta\eta'$		$(2.32 \pm 0.17) \times 10^{-4}$	
Γ_{102}	$\phi f_0(980)$		$(3.2 \pm 0.9) \times 10^{-4}$	S=1.9
Γ_{103}	$\phi f_0(980) \to \phi\pi^+\pi^-$		$(2.60 \pm 0.34) \times 10^{-4}$	
Γ_{104}	$\phi f_0(980) \to \phi\pi^0\pi^0$		$(1.8 \pm 0.5) \times 10^{-4}$	
Γ_{105}	$\phi\pi^0 f_0(980) \to \phi\pi^0\pi^+\pi^-$		$(4.5 \pm 1.0) \times 10^{-6}$	
Γ_{106}	$\phi\pi^0 f_0(980) \to \phi\pi^0 p^0\pi^0$		$(1.7 \pm 0.6) \times 10^{-6}$	
Γ_{107}	$\phi f_0(980)\eta \to \eta\phi\pi^+\pi^-$		$(3.2 \pm 1.0) \times 10^{-4}$	
Γ_{108}	$\phi a_0(980)^0 \to \phi\eta\pi^0$		$(4.4 \pm 1.4) \times 10^{-6}$	
Γ_{109}	$\phi f_2(1270)$		$(3.2 \pm 0.6) \times 10^{-4}$	
Γ_{110}	$\phi f_1(1285)$		$(2.6 \pm 0.5) \times 10^{-4}$	
Γ_{111}	$\phi f_1(1285) \to \phi\pi^0 f_0(980) \to \phi\pi^0\pi^+\pi^-$		$(9.4 \pm 2.8) \times 10^{-7}$	
Γ_{112}	$\phi f_1(1285) \to \phi\pi^0 f_0(980) \to \phi 3\pi^0$		$(2.1 \pm 2.2) \times 10^{-7}$	
Γ_{113}	$\phi\eta(1405) \to \phi\eta\pi^+\pi^-$		$(2.0 \pm 1.0) \times 10^{-5}$	
Γ_{114}	$\phi f_2'(1525)$		$(8 \pm 4) \times 10^{-4}$	S=2.7
Γ_{115}	$\phi X(1835) \to \phi p\overline{p}$		$< 2.1 \times 10^{-7}$	CL=90%
Γ_{116}	$\phi X(1835) \to \phi\eta\pi^+\pi^-$		$< 2.8 \times 10^{-4}$	CL=90%
Γ_{117}	$\phi X(1870) \to \phi\eta\pi^+\pi^-$		$< 6.13 \times 10^{-5}$	CL=90%
Γ_{118}	$\phi K\overline{K}$		$(1.77 \pm 0.16) \times 10^{-3}$	S=1.3
Γ_{119}	$\phi f_0(1710) \to \phi K\overline{K}$		$(3.6 \pm 0.6) \times 10^{-4}$	
Γ_{120}	ϕK^+K^-		$(8.3 \pm 1.1) \times 10^{-4}$	
Γ_{121}	$\phi K_S^0 K_S^0$		$(5.9 \pm 1.5) \times 10^{-4}$	
Γ_{122}	$\phi K^\pm K_S^0 \pi^\mp$	[b]	$(7.2 \pm 0.8) \times 10^{-4}$	
Γ_{123}	$\phi K^*(892)\overline{K}+$ c.c.		$(2.18 \pm 0.23) \times 10^{-3}$	
Γ_{124}	$b_1(1235)^\pm \pi^\mp$	[b]	$(3.0 \pm 0.5) \times 10^{-3}$	
Γ_{125}	$b_1(1235)^0 \pi^0$		$(2.3 \pm 0.6) \times 10^{-3}$	
Γ_{126}	$f_2'(1525) K^+K^-$		$(1.06 \pm 0.35) \times 10^{-3}$	
Γ_{127}	$\Delta(1232)^+\overline{p}$		$< 1 \times 10^{-4}$	CL=90%
Γ_{128}	$\Delta(1232)^{++}\overline{p}\pi^-$		$(1.6 \pm 0.5) \times 10^{-3}$	
Γ_{129}	$\Delta(1232)^{++}\overline{\Delta}(1232)^{--}$		$(1.10 \pm 0.29) \times 10^{-3}$	
Γ_{130}	$\overline{\Sigma}(1385)^0 p K^-$		$(5.1 \pm 3.2) \times 10^{-4}$	
Γ_{131}	$\Sigma(1385)^0\overline{\Lambda}+$ c.c.		$< 8.2 \times 10^{-6}$	CL=90%
Γ_{132}	$\Sigma(1385)^-\overline{\Sigma}^+$ (or c.c.)	[b]	$(3.1 \pm 0.5) \times 10^{-4}$	
Γ_{133}	$\Sigma(1385)^-\overline{\Sigma}(1385)^+$ (or c.c.)	[b]	$(1.16 \pm 0.05) \times 10^{-3}$	
Γ_{134}	$\Sigma(1385)^0\overline{\Sigma}(1385)^0$		$(1.07 \pm 0.08) \times 10^{-3}$	
Γ_{135}	$\Lambda(1520)\overline{\Lambda}+$ c.c. $\to \gamma\Lambda\overline{\Lambda}$		$< 4.1 \times 10^{-6}$	CL=90%
Γ_{136}	$\overline{\Lambda}(1520)\Lambda+$ c.c.		$< 1.80 \times 10^{-3}$	CL=90%
Γ_{137}	$\Xi^0\overline{\Xi}^0$		$(1.17 \pm 0.04) \times 10^{-3}$	
Γ_{138}	$\Xi(1530)^-\overline{\Xi}^+ +$ c.c.		$(3.18 \pm 0.08) \times 10^{-4}$	
Γ_{139}	$\Xi(1530)^0\overline{\Xi}^0$		$(3.2 \pm 1.4) \times 10^{-4}$	
Γ_{140}	$\Theta(1540)\overline{\Theta}(1540) \to K_S^0 p K^-\overline{n}+$ c.c.	[c]	$< 1.1 \times 10^{-5}$	CL=90%
Γ_{141}	$\Theta(1540) K^-\overline{n} \to K_S^0 p K^-\overline{n}$	[c]	$< 2.1 \times 10^{-5}$	CL=90%
Γ_{142}	$\Theta(1540) K_S^0\overline{p} \to K_S^0\overline{p}K^+ n$	[c]	$< 1.6 \times 10^{-5}$	CL=90%
Γ_{143}	$\overline{\Theta}(1540) K^+ n \to K_S^0\overline{p}K^+ n$	[c]	$< 5.6 \times 10^{-5}$	CL=90%
Γ_{144}	$\overline{\Theta}(1540) K_S^0 p \to K_S^0 p K^-\overline{n}$	[c]	$< 1.1 \times 10^{-5}$	CL=90%

Decays into stable hadrons

Γ_{145}	$2(\pi^+\pi^-)\pi^0$		(3.71 ± 0.28) %	S=1.3
Γ_{146}	$3(\pi^+\pi^-)\pi^0$		(2.9 ± 0.6) %	
Γ_{147}	$\pi^+\pi^- 3\pi^0$		(1.9 ± 0.9) %	
Γ_{148}	$\pi^+\pi^- 4\pi^0$		$(6.5 \pm 1.3) \times 10^{-3}$	
Γ_{149}	$\rho^\pm\pi^\mp\pi^0\pi^0$		(1.41 ± 0.22) %	
Γ_{150}	$\rho^+\rho^-\pi^0$		$(6.0 \pm 1.1) \times 10^{-3}$	
Γ_{151}	$\pi^+\pi^-\pi^0$		(2.10 ± 0.08) %	S=1.6
Γ_{152}	$2(\pi^+\pi^-\pi^0)$		(1.61 ± 0.20) %	
Γ_{153}	$\pi^+\pi^-\pi^0 K^+K^-$		(1.20 ± 0.30) %	
Γ_{154}	$\pi^+\pi^-$		$(1.47 \pm 0.14) \times 10^{-4}$	
Γ_{155}	$2(\pi^+\pi^-)$		$(3.57 \pm 0.30) \times 10^{-3}$	
Γ_{156}	$3(\pi^+\pi^-)$		$(4.3 \pm 0.4) \times 10^{-3}$	
Γ_{157}	$2(\pi^+\pi^-)3\pi^0$		(6.2 ± 0.9) %	
Γ_{158}	$4(\pi^+\pi^-)\pi^0$		$(9.0 \pm 3.0) \times 10^{-3}$	
Γ_{159}	$2(\pi^+\pi^-)\eta$		$(2.29 \pm 0.28) \times 10^{-3}$	
Γ_{160}	$3(\pi^+\pi^-)\eta$		$(7.2 \pm 1.5) \times 10^{-4}$	
Γ_{161}	$2(\pi^+\pi^-\pi^0)\eta$		$(1.6 \pm 0.5) \times 10^{-3}$	
Γ_{162}	$\pi^+\pi^-\pi^0\pi^0\eta$		$(2.4 \pm 0.5) \times 10^{-3}$	
Γ_{163}	$\rho^\pm\pi^\mp\pi^0\eta$		$(1.9 \pm 0.8) \times 10^{-3}$	
Γ_{164}	K^+K^-		$(2.86 \pm 0.21) \times 10^{-4}$	
Γ_{165}	$K_S^0 K_L^0$		$(1.95 \pm 0.11) \times 10^{-4}$	S=2.4
Γ_{166}	$K_S^0 K_S^0$		$< 1.4 \times 10^{-8}$	CL=95%
Γ_{167}	$K\overline{K}\pi$		$(6.1 \pm 1.0) \times 10^{-3}$	
Γ_{168}	$K^+K^-\pi^0$		$(2.88 \pm 0.12) \times 10^{-3}$	
Γ_{169}	$K_S^0 K^\pm\pi^\mp$		$(5.6 \pm 0.5) \times 10^{-3}$	
Γ_{170}	$K_S^0 K_L^0\pi^0$		$(2.06 \pm 0.26) \times 10^{-3}$	
Γ_{171}	$K^*(892)^0\overline{K}^0 +$ c.c. $\to K_S^0 K_L^0\pi^0$		$(1.21 \pm 0.18) \times 10^{-3}$	
Γ_{172}	$K_2^*(1430)^0\overline{K}^0 +$ c.c. $\to K_S^0 K_L^0\pi^0$		$(4.3 \pm 1.3) \times 10^{-4}$	
Γ_{173}	$K^+K^-\pi^+\pi^-$		$(6.86 \pm 0.28) \times 10^{-3}$	
Γ_{174}	$K^+K^-\pi^0\pi^0$		$(2.13 \pm 0.22) \times 10^{-3}$	
Γ_{175}	$K_S^0 K_L^0\pi^+\pi^-$		$(3.8 \pm 0.6) \times 10^{-3}$	
Γ_{176}	$K_S^0 K_L^0\pi^0\pi^0$		$(1.9 \pm 0.4) \times 10^{-3}$	
Γ_{177}	$K_S^0 K_L^0\eta$		$(1.45 \pm 0.33) \times 10^{-3}$	
Γ_{178}	$K_S^0 K_S^0\pi^+\pi^-$		$(1.68 \pm 0.19) \times 10^{-3}$	
Γ_{179}	$K^\mp K_S^0\pi^\pm\pi^0$		$(5.7 \pm 0.5) \times 10^{-3}$	
Γ_{180}	$K^+K^-2(\pi^+\pi^-)$		$(3.1 \pm 1.3) \times 10^{-3}$	
Γ_{181}	$K^+K^-\pi^+\pi^-\eta$		$(4.7 \pm 0.7) \times 10^{-3}$	
Γ_{182}	$2(K^+K^-)$		$(7.2 \pm 0.8) \times 10^{-4}$	
Γ_{183}	$K^+K^-K_S^0 K_S^0$		$(4.2 \pm 0.7) \times 10^{-4}$	
Γ_{184}	$p\overline{p}$		$(2.120 \pm 0.029) \times 10^{-3}$	
Γ_{185}	$p\overline{p}\pi^0$		$(1.19 \pm 0.08) \times 10^{-3}$	S=1.1
Γ_{186}	$p\overline{p}\pi^+\pi^-$		$(6.0 \pm 0.5) \times 10^{-3}$	S=1.3
Γ_{187}	$p\overline{p}\pi^+\pi^-\pi^0$	[d]	$(2.3 \pm 0.9) \times 10^{-3}$	S=1.9
Γ_{188}	$p\overline{p}\eta$		$(2.00 \pm 0.12) \times 10^{-3}$	
Γ_{189}	$p\overline{p}\rho$		$< 3.1 \times 10^{-4}$	CL=90%
Γ_{190}	$p\overline{p}\omega$		$(9.8 \pm 1.0) \times 10^{-4}$	S=1.3
Γ_{191}	$p\overline{p}\eta'(958)$		$(1.29 \pm 0.14) \times 10^{-4}$	S=2.0
Γ_{192}	$p\overline{p}a_0(980) \to p\overline{p}\pi^0\eta$		$(6.8 \pm 1.8) \times 10^{-5}$	
Γ_{193}	$p\overline{p}\phi$		$(5.19 \pm 0.33) \times 10^{-5}$	
Γ_{194}	$p\overline{n}\pi^-$		$(2.12 \pm 0.09) \times 10^{-3}$	
Γ_{195}	$n\overline{n}$		$(2.09 \pm 0.16) \times 10^{-3}$	
Γ_{196}	$n\overline{n}\pi^+\pi^-$		$(4 \pm 4) \times 10^{-3}$	
Γ_{197}	$nN(1440)$		seen	
Γ_{198}	$nN(1520)$		seen	
Γ_{199}	$nN(1535)$		seen	
Γ_{200}	$\Lambda\overline{\Lambda}$		$(1.89 \pm 0.09) \times 10^{-3}$	S=2.8
Γ_{201}	$\Lambda\overline{\Lambda}\pi^0$		$(3.8 \pm 0.4) \times 10^{-5}$	
Γ_{202}	$\Lambda\overline{\Lambda}\pi^+\pi^-$		$(4.3 \pm 1.0) \times 10^{-3}$	
Γ_{203}	$\Lambda\overline{\Lambda}\eta$		$(1.62 \pm 0.17) \times 10^{-4}$	
Γ_{204}	$\Lambda\overline{\Sigma}^-\pi^+$ (or c.c.)	[b]	$(8.3 \pm 0.7) \times 10^{-4}$	S=1.2
Γ_{205}	$pK^-\overline{\Lambda}+$c.c.		$(8.6 \pm 1.1) \times 10^{-4}$	
Γ_{206}	$pK^-\overline{\Sigma}^0$		$(2.9 \pm 0.8) \times 10^{-4}$	
Γ_{207}	$\overline{\Lambda}nK_S^0 +$ c.c.		$(6.5 \pm 1.1) \times 10^{-4}$	
Γ_{208}	$\Lambda\overline{\Sigma}+$ c.c.		$(2.83 \pm 0.23) \times 10^{-5}$	
Γ_{209}	$\Sigma^+\overline{\Sigma}^-$		$(1.07 \pm 0.04) \times 10^{-3}$	
Γ_{210}	$\Sigma^0\overline{\Sigma}^0$		$(1.172 \pm 0.032) \times 10^{-3}$	S=1.4
Γ_{211}	$\Xi^-\overline{\Xi}^+$		$(9.7 \pm 0.8) \times 10^{-4}$	S=1.4

Downloaded from https://academic.oup.com/ptep/article/2022/8/083C01/6651666 by KIT Library user on 27 September 2022

Radiative decays

Γ_{212}	$\gamma\eta_c(1S)$	(1.7 ± 0.4) %		S=1.5
Γ_{213}	$\gamma\eta_c(1S) \to 3\gamma$	$(3.8 {}^{+1.3}_{-1.0}) \times 10^{-6}$		S=1.1
Γ_{214}	$\gamma\eta_c(1S) \to \gamma\eta\eta\eta'$	$(4.9 \pm 0.8) \times 10^{-5}$		
Γ_{215}	3γ	$(1.16 \pm 0.22) \times 10^{-5}$		
Γ_{216}	4γ	$< 9 \times 10^{-6}$	CL=90%	
Γ_{217}	5γ	$< 1.5 \times 10^{-5}$	CL=90%	
Γ_{218}	$\gamma\pi^0$	$(3.56 \pm 0.17) \times 10^{-5}$		
Γ_{219}	$\gamma\pi^0\pi^0$	$(1.15 \pm 0.05) \times 10^{-3}$		
Γ_{220}	$\gamma 2\pi^+ 2\pi^-$	$(2.8 \pm 0.5) \times 10^{-3}$		S=1.9
Γ_{221}	$\gamma f_2(1270) f_2(1270)$	$(9.5 \pm 1.7) \times 10^{-4}$		
Γ_{222}	$\gamma f_2(1270) f_2(1270)$ (non resonant)	$(8.2 \pm 1.9) \times 10^{-4}$		
Γ_{223}	$\gamma\pi^+\pi^- 2\pi^0$	$(8.3 \pm 3.1) \times 10^{-3}$		
Γ_{224}	$\gamma K^0_S K^0_S$	$(8.1 \pm 0.4) \times 10^{-4}$		
Γ_{225}	$\gamma(K\overline{K}\pi)$ $[J^{PC} = 0^{-+}]$	$(7 \pm 4) \times 10^{-4}$		S=2.1
Γ_{226}	$\gamma K^+ K^- \pi^+\pi^-$	$(2.1 \pm 0.6) \times 10^{-3}$		
Γ_{227}	$\gamma K^*(892)\overline{K}^*(892)$	$(4.0 \pm 1.3) \times 10^{-3}$		
Γ_{228}	$\gamma\eta$	$(1.085 \pm 0.018) \times 10^{-3}$		
Γ_{229}	$\gamma\eta\pi^0$	$(2.14 \pm 0.31) \times 10^{-5}$		
Γ_{230}	$\gamma f_0(500) \to \gamma\pi\pi$			
Γ_{231}	$\gamma f_0(500) \to \gamma K\overline{K}$			
Γ_{232}	$\gamma f_0(500) \to \gamma\eta\eta$			
Γ_{233}	$\gamma a_0(980)^0 \to \gamma\eta\pi^0$	$< 2.5 \times 10^{-6}$	CL=95%	
Γ_{234}	$\gamma a_2(1320)^0 \to \gamma\eta\pi^0$	$< 6.6 \times 10^{-6}$	CL=95%	
Γ_{235}	$\gamma\eta\pi\pi$	$(6.1 \pm 1.0) \times 10^{-3}$		
Γ_{236}	$\gamma\eta_2(1870) \to \gamma\eta\pi^+\pi^-$	$(6.2 \pm 2.4) \times 10^{-4}$		
Γ_{237}	$\gamma\eta'(958)$	$(5.25 \pm 0.07) \times 10^{-3}$		S=1.3
Γ_{238}	$\gamma f_0(980) \to \gamma\pi\pi$			
Γ_{239}	$\gamma f_0(980) \to \gamma K\overline{K}$			
Γ_{240}	$\gamma\rho\rho$	$(4.5 \pm 0.8) \times 10^{-3}$		
Γ_{241}	$\gamma\rho\omega$	$< 5.4 \times 10^{-4}$	CL=90%	
Γ_{242}	$\gamma\rho\phi$	$< 8.8 \times 10^{-5}$	CL=90%	
Γ_{243}	$\gamma\omega\omega$	$(1.61 \pm 0.33) \times 10^{-3}$		
Γ_{244}	$\gamma\phi\phi$	$(4.0 \pm 1.2) \times 10^{-4}$		S=2.1
Γ_{245}	$\gamma\eta(1405/1475) \to \gamma K\overline{K}\pi$	$(2.8 \pm 0.6) \times 10^{-3}$		S=1.6
Γ_{246}	$\gamma\eta(1405/1475) \to \gamma\gamma\rho^0$	$(7.8 \pm 2.0) \times 10^{-5}$		S=1.8
Γ_{247}	$\gamma\eta(1405/1475) \to \gamma\eta\pi^+\pi^-$	$(3.0 \pm 0.5) \times 10^{-4}$		
Γ_{248}	$\gamma\eta(1405/1475) \to \gamma\rho^0\rho^0$	$(1.7 \pm 0.4) \times 10^{-3}$		S=1.3
Γ_{249}	$\gamma\eta(1405/1475) \to \gamma\gamma\phi$	$< 8.2 \times 10^{-5}$	CL=95%	
Γ_{250}	$\gamma\eta(1405) \to \gamma\gamma\gamma$	$< 2.63 \times 10^{-6}$	CL=90%	
Γ_{251}	$\gamma\eta(1475) \to \gamma\gamma\gamma$	$< 1.86 \times 10^{-6}$	CL=90%	
Γ_{252}	$\gamma\eta(1760) \to \gamma\rho^0\rho^0$	$(1.3 \pm 0.9) \times 10^{-4}$		
Γ_{253}	$\gamma\eta(1760) \to \gamma\omega\omega$	$(1.98 \pm 0.33) \times 10^{-3}$		
Γ_{254}	$\gamma\eta(1760) \to \gamma\gamma\gamma$	$< 4.80 \times 10^{-6}$	CL=90%	
Γ_{255}	$\gamma\eta(2225)$	$(3.14 {}^{+0.50}_{-0.19}) \times 10^{-4}$		
Γ_{256}	$\gamma f_2(1270)$	$(1.64 \pm 0.12) \times 10^{-3}$		S=1.3
Γ_{257}	$\gamma f_2(1270) \to \gamma K^0_S K^0_S$	$(2.58 {}^{+0.60}_{-0.22}) \times 10^{-5}$		
Γ_{258}	$\gamma f_1(1285)$	$(6.1 \pm 0.8) \times 10^{-4}$		
Γ_{259}	$\gamma f_0(1370) \to \gamma\pi\pi$			
Γ_{260}	$\gamma f_0(1370) \to \gamma K\overline{K}$	$(4.2 \pm 1.5) \times 10^{-4}$		
Γ_{261}	$\gamma f_0(1370) \to \gamma K^0_S K^0_S$	$(1.1 \pm 0.4) \times 10^{-5}$		
Γ_{262}	$\gamma f_0(1370) \to \gamma\eta\eta$			
Γ_{263}	$\gamma f_0(1370) \to \gamma\eta\eta'$			
Γ_{264}	$\gamma f_1(1420) \to \gamma K\overline{K}\pi$	$(7.9 \pm 1.3) \times 10^{-4}$		
Γ_{265}	$\gamma f_0(1500) \to \gamma\pi\pi$	$(1.09 \pm 0.24) \times 10^{-4}$		
Γ_{266}	$\gamma f_0(1500) \to \gamma\eta\eta$	$(1.7 {}^{+0.6}_{-1.4}) \times 10^{-5}$		
Γ_{267}	$\gamma f_0(1500) \to \gamma K^0_S K^0_S$	$(1.59 {}^{+0.24}_{-0.60}) \times 10^{-5}$		
Γ_{268}	$\gamma f_0(1500) \to \gamma\eta\eta'$			
Γ_{269}	$\gamma f_1(1510) \to \gamma\eta\pi^+\pi^-$	$(4.5 \pm 1.2) \times 10^{-4}$		
Γ_{270}	$\gamma f'_2(1525)$	$(5.7 {}^{+0.8}_{-0.5}) \times 10^{-4}$		S=1.5
Γ_{271}	$\gamma f'_2(1525) \to \gamma K^0_S K^0_S$	$(8.0 {}^{+0.7}_{-0.5}) \times 10^{-5}$		
Γ_{272}	$\gamma f'_2(1525) \to \gamma\eta\eta$	$(3.4 \pm 1.4) \times 10^{-5}$		
Γ_{273}	$\gamma f_2(1640) \to \gamma\omega\omega$	$(2.8 \pm 1.8) \times 10^{-4}$		
Γ_{274}	$\gamma f_0(1710) \to \gamma\pi\pi$	$(3.8 \pm 0.5) \times 10^{-4}$		
Γ_{275}	$\gamma f_0(1710) \to \gamma K\overline{K}$	$(9.5 {}^{+1.0}_{-0.5}) \times 10^{-4}$		S=1.5
Γ_{276}	$\gamma f_0(1710) \to \gamma\omega\omega$	$(3.1 \pm 1.0) \times 10^{-4}$		
Γ_{277}	$\gamma f_0(1710) \to \gamma\eta\eta$	$(2.4 {}^{+1.2}_{-0.7}) \times 10^{-4}$		
Γ_{278}	$\gamma f_0(1710) \to \gamma\eta\eta'$			
Γ_{279}	$\gamma f_0(1710) \to \gamma\omega\phi$	$(2.5 \pm 0.6) \times 10^{-4}$		
Γ_{280}	$\gamma f_0(1750) \to \gamma K^0_S K^0_S$	$(1.11 {}^{+0.20}_{-0.33}) \times 10^{-5}$		
Γ_{281}	$\gamma f_2(1810) \to \gamma\eta\eta$	$(5.4 {}^{+3.5}_{-2.4}) \times 10^{-5}$		
Γ_{282}	$\gamma f_2(1910) \to \gamma\omega\omega$	$(2.0 \pm 1.4) \times 10^{-4}$		
Γ_{283}	$\gamma f_2(1950) \to \gamma K^*(892)\overline{K}^*(892)$	$(7.0 \pm 2.2) \times 10^{-4}$		
Γ_{284}	$\gamma f_0(2020) \to \gamma\pi\pi$			
Γ_{285}	$\gamma f_0(2020) \to \gamma K\overline{K}$			
Γ_{286}	$\gamma f_0(2020) \to \gamma\eta\eta$			
Γ_{287}	$\gamma f_4(2050)$	$(2.7 \pm 0.7) \times 10^{-3}$		
Γ_{288}	$\gamma f_0(2100) \to \gamma\eta\eta$	$(1.13 {}^{+0.60}_{-0.30}) \times 10^{-4}$		
Γ_{289}	$\gamma f_0(2100) \to \gamma K\overline{K}$			
Γ_{290}	$\gamma f_0(2100) \to \gamma\pi\pi$	$(6.2 \pm 1.0) \times 10^{-4}$		
Γ_{291}	$\gamma f_0(2200)$			
Γ_{292}	$\gamma f_0(2200) \to \gamma K\overline{K}$	$(5.9 \pm 1.3) \times 10^{-4}$		
Γ_{293}	$\gamma f_0(2200) \to \gamma K^0_S K^0_S$	$(2.72 {}^{+0.19}_{-0.50}) \times 10^{-4}$		
Γ_{294}	$\gamma f_0(2200) \to \gamma\pi\pi$			
Γ_{295}	$\gamma f_0(2200) \to \gamma\eta\eta$			
Γ_{296}	$\gamma f_J(2220)$			
Γ_{297}	$\gamma f_J(2220) \to \gamma\pi\pi$	$< 3.9 \times 10^{-5}$	CL=90%	
Γ_{298}	$\gamma f_J(2220) \to \gamma K\overline{K}$	$< 4.1 \times 10^{-5}$	CL=90%	
Γ_{299}	$\gamma f_J(2220) \to \gamma p\overline{p}$	$(1.5 \pm 0.8) \times 10^{-5}$		
Γ_{300}	$\gamma f_0(2330) \to \gamma K^0_S K^0_S$	$(4.9 \pm 0.7) \times 10^{-5}$		
Γ_{301}	$\gamma f_0(2330) \to \gamma\pi\pi$			
Γ_{302}	$\gamma f_0(2330) \to \gamma\eta\eta$			
Γ_{303}	$\gamma f_2(2340) \to \gamma\eta\eta$	$(5.6 {}^{+2.4}_{-2.2}) \times 10^{-5}$		
Γ_{304}	$\gamma f_2(2340) \to \gamma K^0_S K^0_S$	$(5.5 {}^{+4.0}_{-1.5}) \times 10^{-5}$		
Γ_{305}	$\gamma X(1835) \to \gamma\pi^+\pi^-\eta'$	$(2.7 {}^{+0.6}_{-0.8}) \times 10^{-4}$		S=1.6
Γ_{306}	$\gamma X(1835) \to \gamma p\overline{p}$	$(7.7 {}^{+1.5}_{-0.9}) \times 10^{-5}$		
Γ_{307}	$\gamma X(1835) \to \gamma K^0_S K^0_S \eta$	$(3.3 {}^{+2.0}_{-1.3}) \times 10^{-5}$		
Γ_{308}	$\gamma X(1835) \to \gamma\gamma\phi(1020)$			
Γ_{309}	$\gamma X(1835) \to \gamma\gamma\gamma$	$< 3.56 \times 10^{-6}$	CL=90%	
Γ_{310}	$\gamma X(1835) \to \gamma 3(\pi^+\pi^-)$	$(2.4 {}^{+0.7}_{-0.8}) \times 10^{-5}$		
Γ_{311}	$\gamma X(2370) \to \gamma K^+ K^- \eta'$	$(1.8 \pm 0.7) \times 10^{-5}$		
Γ_{312}	$\gamma X(2370) \to \gamma K^0_S K^0_S \eta'$	$(1.2 \pm 0.5) \times 10^{-5}$		
Γ_{313}	$\gamma X(2370) \to \gamma\eta\eta\eta'$	$< 9.2 \times 10^{-6}$	CL=90%	
Γ_{314}	$\gamma p\overline{p}$	$(3.8 \pm 1.0) \times 10^{-4}$		
Γ_{315}	$\gamma p\overline{p}\pi^+\pi^-$	$< 7.9 \times 10^{-4}$	CL=90%	
Γ_{316}	$\gamma\Lambda\overline{\Lambda}$	$< 1.3 \times 10^{-4}$	CL=90%	
Γ_{317}	$\gamma A \to \gamma$ invisible	[e] $< 1.7 \times 10^{-6}$	CL=90%	
Γ_{318}	$\gamma A^0 \to \gamma\mu^+\mu^-$	[f] $< 5 \times 10^{-6}$	CL=90%	

Dalitz decays

Γ_{319}	$\pi^0 e^+ e^-$	$(7.6 \pm 1.4) \times 10^{-7}$		
Γ_{320}	$\eta e^+ e^-$	$(1.42 \pm 0.08) \times 10^{-5}$		
Γ_{321}	$\eta'(958) e^+ e^-$	$(6.59 \pm 0.18) \times 10^{-5}$		
Γ_{322}	$\eta U \to \eta e^+ e^-$	[g] $< 9.11 \times 10^{-7}$	CL=90%	
Γ_{323}	$\eta'(958) U \to \eta'(958) e^+ e^-$	[g] $< 2.0 \times 10^{-7}$	CL=90%	
Γ_{324}	$\phi e^+ e^-$	$< 1.2 \times 10^{-7}$	CL=90%	

Weak decays

Γ_{325}	$D^- e^+ \nu_e$ + c.c.	$< 7.1 \times 10^{-8}$	CL=90%	
Γ_{326}	$\overline{D}^0 e^+ e^-$ + c.c.	$< 8.5 \times 10^{-8}$	CL=90%	
Γ_{327}	$D^-_s e^+ \nu_e$ + c.c.	$< 1.3 \times 10^{-6}$	CL=90%	
Γ_{328}	$D^{*-}_s e^+ \nu_e$ + c.c.	$< 1.8 \times 10^{-6}$	CL=90%	
Γ_{329}	$D^- \pi^+$ + c.c.	$< 7.5 \times 10^{-5}$	CL=90%	
Γ_{330}	$\overline{D}^0 \overline{K}^0$ + c.c.	$< 1.7 \times 10^{-4}$	CL=90%	
Γ_{331}	$\overline{D}^0 \overline{K}^{*0}$ + c.c.	$< 2.5 \times 10^{-6}$	CL=90%	
Γ_{332}	$D^-_s \pi^+$ + c.c.	$< 1.3 \times 10^{-4}$	CL=90%	
Γ_{333}	$D^-_s \rho^+$ + c.c.	$< 1.3 \times 10^{-5}$	CL=90%	

Charge conjugation (C), Parity (P), Lepton Family number (LF) violating modes

Γ_{334}	$\gamma\gamma$	C	$< 2.7 \times 10^{-7}$	CL=90%	
Γ_{335}	$\gamma\phi$	C	$< 1.4 \times 10^{-6}$	CL=90%	
Γ_{336}	$e^\pm\mu^\mp$	LF	$< 1.6 \times 10^{-7}$	CL=90%	
Γ_{337}	$e^\pm\tau^\mp$	LF	$< 7.5 \times 10^{-8}$	CL=90%	
Γ_{338}	$\mu^\pm\tau^\mp$	LF	$< 2.0 \times 10^{-6}$	CL=90%	
Γ_{339}	$\Lambda^+_c e^-$ +c.c.		$< 6.9 \times 10^{-8}$	CL=90%	

Downloaded from https://academic.oup.com/ptep/article/2022/8/083C01/6651666 by KIT Library user on 27 September 2022

Other decays

Γ_{340} invisible	< 7	$\times 10^{-4}$	CL=90%

[a] For $E_\gamma > 100$ MeV.

[b] The value is for the sum of the charge states or particle/antiparticle states indicated.

[c] $\Theta(1540)$ is a hypothetical pentaquark state of 1.54 GeV/c^2 mass and a width of less than 25 MeV/c^2.

[d] Includes $p\overline{p}\pi^+\pi^-\gamma$ and excludes $p\overline{p}\eta$, $p\overline{p}\omega$, $p\overline{p}\eta'$.

[e] For a narrow state A with mass less than 960 MeV.

[f] For a narrow scalar or pseudoscalar A^0 with mass 0.21–3.0 GeV.

[g] For a dark photon U with mass between 100 and 2100 MeV.

$J/\psi(1S)$ PARTIAL WIDTHS

Γ(hadrons) — Γ_1

VALUE (keV)	DOCUMENT ID		TECN	COMMENT
81.37± 1.36±1.30	[1] ANASHIN	20	KEDR	e^+e^-
• • • We do not use the following data for averages, fits, limits, etc. • • •				
74.1 ± 8.1	BAI	95B	BES	e^+e^-
59 ±24	BALDINI-...	75	FRAG	e^+e^-
59 ±14	BOYARSKI	75	MRK1	e^+e^-
50 ±25	ESPOSITO	75B	FRAM	e^+e^-

[1] Based on the same dataset as ANASHIN 18A and correlated to the values reported there.

$\Gamma(e^+e^-)$ — Γ_5

VALUE (keV)	EVTS	DOCUMENT ID		TECN	COMMENT
5.53 ±0.10 OUR AVERAGE					
5.550±0.056±0.089		[1,2] ANASHIN	18A	KEDR	e^+e^-
$5.36^{+0.29}_{-0.28}$		[3] HSUEH	92	RVUE	See Υ mini-review
• • • We do not use the following data for averages, fits, limits, etc. • • •					
5.58 ±0.05 ±0.08		[4] ABLIKIM	16Q	BES3	3.773 $e^+e^-\to\mu^+\mu^-\gamma$
5.71 ±0.16	13k	[5] ADAMS	06A	CLEO	$e^+e^-\to\mu^+\mu^-\gamma$
5.57 ±0.19	7.8k	[5] AUBERT	04	BABR	$e^+e^-\to\mu^+\mu^-\gamma$
5.14 ±0.39		BAI	95B	BES	e^+e^-
4.72 ±0.35		ALEXANDER	89	RVUE	See Υ mini-review
4.4 ±0.6		[3] BRANDELIK	79C	DASP	e^+e^-
4.6 ±0.8		[6] BALDINI-...	75	FRAG	e^+e^-
4.8 ±0.6		BOYARSKI	75	MRK1	e^+e^-
4.6 ±1.0		ESPOSITO	75B	FRAM	e^+e^-

[1] From the cross sections of $e^+e^-\to e^+e^-$ and $e^+e^-\to$ hadrons near the $J/\psi(1S)$ peak.

[2] Based on the same dataset as ANASHIN 20 and correlated to the values reported there.

[3] From a simultaneous fit to e^+e^-, $\mu^+\mu^-$, and hadronic channels assuming $\Gamma(e^+e^-) = \Gamma(\mu^+\mu^-)$.

[4] Using $B(J/\psi\to\mu^+\mu^-) = (5.973 \pm 0.007 \pm 0.037)\%$ from ABLIKIM 13R.

[5] Calculated by us from the reported values of $\Gamma(e^+e^-)\times B(\mu^+\mu^-)$ using $B(\mu^+\mu^-) = (5.93 \pm 0.06)\%$.

[6] Assuming equal partial widths for e^+e^- and $\mu^+\mu^-$.

$\Gamma(\mu^+\mu^-)$ — Γ_7

VALUE (keV)	DOCUMENT ID		TECN	COMMENT
• • • We do not use the following data for averages, fits, limits, etc. • • •				
5.13±0.52	BAI	95B	BES	e^+e^-
4.8 ±0.6	BOYARSKI	75	MRK1	e^+e^-
5 ±1	ESPOSITO	75B	FRAM	e^+e^-

$\Gamma(\gamma\gamma)$ — Γ_{334}

VALUE (eV)	CL%	DOCUMENT ID		TECN	COMMENT
<5.4	90	BRANDELIK	79C	DASP	e^+e^-

$J/\psi(1S)\ \Gamma(i)\Gamma(e^+e^-)/\Gamma(\text{total})$

This combination of a partial width with the partial width into e^+e^- and with the total width is obtained from the integrated cross section into channel(I) in the e^+e^- annihilation.

$\Gamma(\text{hadrons}) \times \Gamma(e^+e^-)/\Gamma_{\text{total}}$ — $\Gamma_1\Gamma_5/\Gamma$

VALUE (keV)	DOCUMENT ID		TECN	COMMENT
• • • We do not use the following data for averages, fits, limits, etc. • • •				
4.884±0.048±0.078	[1,2] ANASHIN	18A	KEDR	e^+e^-
4 ±0.8	[3] BALDINI-...	75	FRAG	e^+e^-
3.9 ±0.8	[3] ESPOSITO	75B	FRAM	e^+e^-

[1] From the cross sections of $e^+e^-\to e^+e^-$ and $e^+e^-\to$ hadrons near the $J/\psi(1S)$ peak.

[2] Based on the same dataset as ANASHIN 20 and correlated to the values reported there.

[3] Data redundant with branching ratios or partial widths above.

$\Gamma(e^+e^-) \times \Gamma(e^+e^-)/\Gamma_{\text{total}}$ — $\Gamma_5\Gamma_5/\Gamma$

VALUE (eV)	DOCUMENT ID		TECN	COMMENT
• • • We do not use the following data for averages, fits, limits, etc. • • •				
333.1± 6.6±4.0	[1,2] ANASHIN	18A	KEDR	e^+e^-
332.3± 6.4±4.8	ANASHIN	10	KEDR	3.097 $e^+e^-\to e^+e^-$
350 ± 20	BRANDELIK	79C	DASP	e^+e^-
320 ± 70	[3] BALDINI-...	75	FRAG	e^+e^-
340 ± 90	[3] ESPOSITO	75B	FRAM	e^+e^-
360 ±100	[3] FORD	75	SPEC	e^+e^-

[1] From the cross sections of $e^+e^-\to e^+e^-$ and $e^+e^-\to$ hadrons near the $J/\psi(1S)$ peak.

[2] Based on the same dataset as ANASHIN 20 and correlated to the values reported there.

[3] Data redundant with branching ratios or partial widths above.

$\Gamma(\mu^+\mu^-) \times \Gamma(e^+e^-)/\Gamma_{\text{total}}$ — $\Gamma_7\Gamma_5/\Gamma$

VALUE (eV)	EVTS	DOCUMENT ID		TECN	COMMENT
333 ± 4 OUR AVERAGE					
333.4± 2.5±4.4		ABLIKIM	16Q	BES3	3.773 $e^+e^-\to\mu^+\mu^-\gamma$
331.8± 5.2±6.3		ANASHIN	10	KEDR	3.097 $e^+e^-\to\mu^+\mu^-$
338.4± 5.8±7.1	13k	ADAMS	06A	CLEO	$e^+e^-\to\mu^+\mu^-\gamma$
330.1± 7.7±7.3	7.8k	AUBERT	04	BABR	$e^+e^-\to\mu^+\mu^-\gamma$
• • • We do not use the following data for averages, fits, limits, etc. • • •					
510 ±90		DASP	75	DASP	e^+e^-
380 ±50		[1] ESPOSITO	75B	FRAM	e^+e^-

[1] Data redundant with branching ratios or partial widths above.

$\Gamma(\eta\pi^+\pi^-) \times \Gamma(e^+e^-)/\Gamma_{\text{total}}$ — $\Gamma_{11}\Gamma_5/\Gamma$

VALUE (eV)	EVTS	DOCUMENT ID		TECN	COMMENT
2.3 ±0.4 OUR AVERAGE					
2.34±0.43±0.16	49	LEES	18	BABR	$e^+e^-\to\eta\pi^+\pi^-\gamma$
2.22±0.96±0.02	9	[1] AUBERT	07AU	BABR	10.6 $e^+e^-\to\eta\pi^+\pi^-\gamma$

[1] AUBERT 07AU reports $[\Gamma(J/\psi(1S)\to\eta\pi^+\pi^-)\times\Gamma(J/\psi(1S)\to e^+e^-)/\Gamma_{\text{total}}]\times[B(\eta\to\pi^+\pi^-\pi^0)] = 0.51\pm0.22\pm0.03$ eV which we divide by our best value $B(\eta\to\pi^+\pi^-\pi^0) = (23.02\pm0.25)\times10^{-2}$. Our first error is their experiment's error and our second error is the systematic error from using our best value.

$\Gamma(\eta\pi^+\pi^-\pi^0) \times \Gamma(e^+e^-)/\Gamma_{\text{total}}$ — $\Gamma_{12}\Gamma_5/\Gamma$

VALUE (eV)	EVTS	DOCUMENT ID		TECN	COMMENT
64.8±11.1±0.4	200	[1] LEES	21C	BABR	$e^+e^-\to\gamma_{ISR}(\pi^+\pi^-4\pi^0)$

[1] LEES 21C reports $[\Gamma(J/\psi(1S)\to\eta\pi^+\pi^-\pi^0)\times\Gamma(J/\psi(1S)\to e^+e^-)/\Gamma_{\text{total}}]\times[B(\eta\to3\pi^0)] = 21.1\pm1.7\pm3.2$ eV which we divide by our best value $B(\eta\to3\pi^0) = (32.57\pm0.21)\times10^{-2}$. Our first error is their experiment's error and our second error is the systematic error from using our best value.

$\Gamma(\eta\pi^+\pi^-3\pi^0) \times \Gamma(e^+e^-)/\Gamma_{\text{total}}$ — $\Gamma_{13}\Gamma_5/\Gamma$

VALUE (eV)	EVTS	DOCUMENT ID		TECN	COMMENT
26.9±5.7±0.1	101	[1] LEES	21C	BABR	$e^+e^-\to\gamma_{ISR}(\pi^+\pi^-3\pi^0\gamma\gamma)$

[1] LEES 21C reports $[\Gamma(J/\psi(1S)\to\eta\pi^+\pi^-3\pi^0)\times\Gamma(J/\psi(1S)\to e^+e^-)/\Gamma_{\text{total}}]\times[B(\eta\to2\gamma)] = 10.6\pm1.6\pm1.6$ eV which we divide by our best value $B(\eta\to2\gamma) = (39.36\pm0.18)\times10^{-2}$. Our first error is their experiment's error and our second error is the systematic error from using our best value.

$\Gamma(\eta K^\pm K^0_S\pi^\mp) \times \Gamma(e^+e^-)/\Gamma_{\text{total}}$ — $\Gamma_{17}\Gamma_5/\Gamma$

VALUE (eV)	EVTS	DOCUMENT ID		TECN	COMMENT
7.3±1.4±0.4	44	LEES	17D	BABR	$e^+e^-\to K^0_S K^\pm\pi^\mp\pi^0\gamma$

$\Gamma(\rho^\pm\pi^\mp\pi^+\pi^-2\pi^0) \times \Gamma(e^+e^-)/\Gamma_{\text{total}}$ — $\Gamma_{20}\Gamma_5/\Gamma$

VALUE (eV)	EVTS	DOCUMENT ID		TECN	COMMENT
155±26±36	14k	LEES	21	BABR	10.6 $e^+e^-\to2(\pi^+\pi^-)3\pi^0\gamma$

$\Gamma(\rho^+\rho^-\pi^+\pi^-\pi^0) \times \Gamma(e^+e^-)/\Gamma_{\text{total}}$ — $\Gamma_{21}\Gamma_5/\Gamma$

VALUE (eV)	EVTS	DOCUMENT ID		TECN	COMMENT
32±13±15	14k	LEES	21	BABR	10.6 $e^+e^-\to2(\pi^+\pi^-)3\pi^0\gamma$

$\Gamma(\rho^\mp K^\pm K^0_S) \times \Gamma(e^+e^-)/\Gamma_{\text{total}}$ — $\Gamma_{22}\Gamma_5/\Gamma$

VALUE (eV)	EVTS	DOCUMENT ID		TECN	COMMENT
10.4±1.0±1.9	130	LEES	17D	BABR	$e^+e^-\to K^0_S K^\pm\pi^\mp\pi^0\gamma$

$\Gamma(\omega\pi^+\pi^-) \times \Gamma(e^+e^-)/\Gamma_{\text{total}}$ — $\Gamma_{35}\Gamma_5/\Gamma$

VALUE (eV)	EVTS	DOCUMENT ID		TECN	COMMENT
53.6±5.0±0.4	788	[1] AUBERT	07AU	BABR	10.6 $e^+e^-\to\omega\pi^+\pi^-\gamma$

[1] AUBERT 07AU reports $[\Gamma(J/\psi(1S)\to\omega\pi^+\pi^-)\times\Gamma(J/\psi(1S)\to e^+e^-)/\Gamma_{\text{total}}]\times[B(\omega(782)\to\pi^+\pi^-\pi^0)] = 47.8\pm3.1\pm3.2$ eV which we divide by our best value $B(\omega(782)\to\pi^+\pi^-\pi^0) = (89.2\pm0.7)\times10^{-2}$. Our first error is their experiment's error and our second error is the systematic error from using our best value.

$\Gamma(\omega\pi^0\pi^0) \times \Gamma(e^+e^-)/\Gamma_{\text{total}}$ — $\Gamma_{36}\Gamma_5/\Gamma$

VALUE (eV)	EVTS	DOCUMENT ID		TECN	COMMENT
27.8±3.5±0.2	398	[1] LEES	18E	BABR	10.6 $e^+e^-\to\pi^+\pi^-3\pi^0\gamma$

[1] LEES 18E reports $[\Gamma(J/\psi(1S)\to\omega\pi^0\pi^0)\times\Gamma(J/\psi(1S)\to e^+e^-)/\Gamma_{\text{total}}]\times[B(\omega(782)\to\pi^+\pi^-\pi^0)] = 24.8\pm1.8\pm2.5$ eV which we divide by our best value $B(\omega(782)\to\pi^+\pi^-\pi^0) = (89.2\pm0.7)\times10^{-2}$. Our first error is their experiment's error and our second error is the systematic error from using our best value.

Downloaded from https://academic.oup.com/ptep/article/2022/8/083C01/6651666 by KIT Library user on 27 September 2022

$\Gamma(\omega 3\pi^0) \times \Gamma(e^+e^-)/\Gamma_{total}$ — $\Gamma_{37}\Gamma_5/\Gamma$

VALUE (eV)	EVTS	DOCUMENT ID		TECN	COMMENT
10.5±3.1±0.1	89	[1] LEES	21C	BABR	$e^+e^- \to \gamma_{ISR}(\pi^+\pi^-4\pi^0)$

[1] LEES 21C reports $[\Gamma(J/\psi(1S) \to \omega 3\pi^0) \times \Gamma(J/\psi(1S) \to e^+e^-)/\Gamma_{total}] \times [B(\omega(782) \to \pi^+\pi^-\pi^0)] = 9.4 \pm 2.3 \pm 1.5$ eV which we divide by our best value $B(\omega(782) \to \pi^+\pi^-\pi^0) = (89.2 \pm 0.7) \times 10^{-2}$. Our first error is their experiment's error and our second error is the systematic error from using our best value.

$\Gamma(\omega\pi^+\pi^-\pi^0) \times \Gamma(e^+e^-)/\Gamma_{total}$ — $\Gamma_{40}\Gamma_5/\Gamma$

VALUE (10^{-2} keV)	EVTS	DOCUMENT ID		TECN	COMMENT
2.2±0.3±0.2	170	AUBERT	06D	BABR	$10.6\ e^+e^- \to \omega\pi^+\pi^-\pi^0\gamma$

$\Gamma(\omega\eta) \times \Gamma(e^+e^-)/\Gamma_{total}$ — $\Gamma_{39}\Gamma_5/\Gamma$

VALUE (eV)	DOCUMENT ID		TECN	COMMENT
16.9±7.6±0.2	[1] LEES	21C	BABR	$e^+e^- \to \gamma_{ISR}(\pi^+\pi^-4\pi^0)$

[1] Different final state as in AUBERT 06. LEES 21C reports $[\Gamma(J/\psi(1S) \to \omega\eta) \times \Gamma(J/\psi(1S) \to e^+e^-)/\Gamma_{total}] \times [B(\eta \to 3\pi^0)] \times [B(\omega(782) \to \pi^+\pi^-\pi^0)] = 4.9 \pm 2.1 \pm 0.7$ eV which we divide by our best values $B(\eta \to 3\pi^0) = (32.57 \pm 0.21) \times 10^{-2}$, $B(\omega(782) \to \pi^+\pi^-\pi^0) = (89.2 \pm 0.7) \times 10^{-2}$. Our first error is their experiment's error and our second error is the systematic error from using our best values.

$\Gamma(\omega\pi^0\eta) \times \Gamma(e^+e^-)/\Gamma_{total}$ — $\Gamma_{41}\Gamma_5/\Gamma$

VALUE (eV)	EVTS	DOCUMENT ID		TECN	COMMENT
1.90±0.96±0.01	27	[1] LEES	18E	BABR	$10.6\ e^+e^- \to \pi^+\pi^-\pi^0\pi^0\eta\gamma$

[1] LEES 18E reports $[\Gamma(J/\psi(1S) \to \omega\pi^0\eta) \times \Gamma(J/\psi(1S) \to e^+e^-)/\Gamma_{total}] \times [B(\omega(782) \to \pi^+\pi^-\pi^0)] = 1.7 \pm 0.8 \pm 0.3$ eV which we divide by our best value $B(\omega(782) \to \pi^+\pi^-\pi^0) = (89.2 \pm 0.7) \times 10^{-2}$. Our first error is their experiment's error and our second error is the systematic error from using our best value.

$\Gamma(\omega\pi^+\pi^-2\pi^0) \times \Gamma(e^+e^-)/\Gamma_{total}$ — $\Gamma_{43}\Gamma_5/\Gamma$

VALUE (eV)	EVTS	DOCUMENT ID		TECN	COMMENT
185±30±1	14k	[1] LEES	21	BABR	$10.6\ e^+e^- \to 2(\pi^+\pi^-)3\pi^0\gamma$

[1] LEES 21 reports $[\Gamma(J/\psi(1S) \to \omega\pi^+\pi^-2\pi^0) \times \Gamma(J/\psi(1S) \to e^+e^-)/\Gamma_{total}] \times [B(\omega(782) \to \pi^+\pi^-\pi^0)] = 165 \pm 9 \pm 25$ eV which we divide by our best value $B(\omega(782) \to \pi^+\pi^-\pi^0) = (89.2 \pm 0.7) \times 10^{-2}$. Our first error is their experiment's error and our second error is the systematic error from using our best value.

$\Gamma(\omega K\overline{K}) \times \Gamma(e^+e^-)/\Gamma_{total}$ — $\Gamma_{53}\Gamma_5/\Gamma$

VALUE (eV)	EVTS	DOCUMENT ID		TECN	COMMENT
3.70±1.98±0.03	24	[1] AUBERT	07AU	BABR	$10.6\ e^+e^- \to \omega K^+K^-\gamma$

[1] AUBERT 07AU reports $[\Gamma(J/\psi(1S) \to \omega K\overline{K}) \times \Gamma(J/\psi(1S) \to e^+e^-)/\Gamma_{total}] \times [B(\omega(782) \to \pi^+\pi^-\pi^0)] = 3.3 \pm 1.3 \pm 1.2$ eV which we divide by our best value $B(\omega(782) \to \pi^+\pi^-\pi^0) = (89.2 \pm 0.7) \times 10^{-2}$. Our first error is their experiment's error and our second error is the systematic error from using our best value.

$\Gamma(K^+K^*(892)^- + c.c.) \times \Gamma(e^+e^-)/\Gamma_{total}$ — $\Gamma_{61}\Gamma_5/\Gamma$

VALUE (eV)	DOCUMENT ID		TECN	COMMENT
29.0±1.7±1.3	AUBERT	08S	BABR	$10.6\ e^+e^- \to K^+K^*(892)^-\gamma$

$\Gamma(K^+K^*(892)^- + c.c. \to K^+K^-\pi^0) \times \Gamma(e^+e^-)/\Gamma_{total}$ — $\Gamma_{62}\Gamma_5/\Gamma$

VALUE (eV)	EVTS	DOCUMENT ID		TECN	COMMENT
10.96±0.85±0.70	155	AUBERT	08S	BABR	$10.6\ e^+e^- \to K^+K^-\pi^0\gamma$

$\Gamma(K^+K^*(892)^- + c.c. \to K^0K^\pm\pi^\mp + c.c.) \times \Gamma(e^+e^-)/\Gamma_{total}$ — $\Gamma_{63}\Gamma_5/\Gamma$

VALUE (eV)	EVTS	DOCUMENT ID		TECN	COMMENT
16.76±1.70±1.00	89	AUBERT	08S	BABR	$10.6\ e^+e^- \to K^0_S K^\pm\pi^\mp\gamma$

$\Gamma(K^0\overline{K}^*(892)^0 + c.c.) \times \Gamma(e^+e^-)/\Gamma_{total}$ — $\Gamma_{64}\Gamma_5/\Gamma$

VALUE (eV)	DOCUMENT ID		TECN	COMMENT
26.6±2.5±1.5	AUBERT	08S	BABR	$10.6\ e^+e^- \to K^0\overline{K}^*(892)^0\gamma$

$\Gamma(K^0\overline{K}^*(892)^0 + c.c. \to K^0K^\pm\pi^\mp + c.c.) \times \Gamma(e^+e^-)/\Gamma_{total}$ — $\Gamma_{65}\Gamma_5/\Gamma$

VALUE (eV)	EVTS	DOCUMENT ID		TECN	COMMENT
17.70±1.70±1.00	94	AUBERT	08S	BABR	$10.6\ e^+e^- \to K^0_S K^\pm\pi^\mp\gamma$

$\Gamma(\overline{K}^*(892)^0K^+\pi^- + c.c.) \times \Gamma(e^+e^-)/\Gamma_{total}$ — $\Gamma_{66}\Gamma_5/\Gamma$

VALUE (eV)	EVTS	DOCUMENT ID		TECN	COMMENT
42.6±4.8±7.2	99	[1] LEES	17D	BABR	$e^+e^- \to K^0_S K^\pm\pi^\mp\pi^0\gamma$

[1] Dividing by 1/6 to account for $B(K^*(892)^0 \to K^0_S\pi^0)$=1/6.

$\Gamma(K^*(892)^\pm K^\mp\pi^0) \times \Gamma(e^+e^-)/\Gamma_{total}$ — $\Gamma_{67}\Gamma_5/\Gamma$

VALUE (eV)	EVTS	DOCUMENT ID		TECN	COMMENT
22.8±2.8±6.8	80	[1] LEES	17D	BABR	$e^+e^- \to K^0_S K^\pm\pi^\mp\pi^0\gamma$

[1] Dividing by 1/4 to account for $B(K^*(892)^\pm \to K^0_S\pi^\pm) = 1/4$.

$\Gamma(K^*(892)^+K^0_S\pi^- + c.c.) \times \Gamma(e^+e^-)/\Gamma_{total}$ — $\Gamma_{68}\Gamma_5/\Gamma$

VALUE (eV)	EVTS	DOCUMENT ID		TECN	COMMENT
11.0±2.8 OUR AVERAGE					
9.2±1.2±3.2	64	[1] LEES	17D	BABR	$e^+e^- \to K^0_S K^\pm\pi^\mp\pi^0\gamma$
14.8±4.8±1.2	53	[2] LEES	14H	BABR	$e^+e^- \to \pi^+\pi^-K^0_S K^0_S\gamma$

[1] Dividing by 1/2 to take into account $B(K^*(892)^\pm \to K^\pm\pi^\mp) = 1/2$.
[2] Dividing by 1/4 to take into account $B(K^*(892) \to K^0_S\pi) = 1/4$.

$\Gamma(K^*(892)^+K^0_S\pi^- + c.c. \to K^0_S K^0_S\pi^+\pi^-) \times \Gamma(e^+e^-)/\Gamma_{total}$ — $\Gamma_{69}\Gamma_5/\Gamma$

VALUE (eV)	EVTS	DOCUMENT ID		TECN	COMMENT
3.7±1.2±0.3	53	LEES	14H	BABR	$e^+e^- \to \pi^+\pi^-K^0_S K^0_S\gamma$

$\Gamma(K^*(892)^0K^0_S\pi^0) \times \Gamma(e^+e^-)/\Gamma_{total}$ — $\Gamma_{71}\Gamma_5/\Gamma$

VALUE (eV)	EVTS	DOCUMENT ID		TECN	COMMENT
3.60±0.75±2.25	34	[1] LEES	17D	BABR	$e^+e^- \to K^0_S K^\pm\pi^\mp\pi^0\gamma$

[1] Dividing by 2/3 to account for $B(K^*(892)^0 \to K^+\pi^-) = 2/3$.

$\Gamma(K^*(892)^0\overline{K}^*(892)^0) \times \Gamma(e^+e^-)/\Gamma_{total}$ — $\Gamma_{73}\Gamma_5/\Gamma$

VALUE (eV)	EVTS	DOCUMENT ID		TECN	COMMENT
1.28±0.34±0.07	47±12	[1] LEES	12F	BABR	$10.6\ e^+e^- \to \pi^+\pi^-K^+K^-\gamma$
• • • We do not use the following data for averages, fits, limits, etc. • • •					
1.28±0.40±0.11	25 ± 8	[1,2] AUBERT	07AK	BABR	$10.6\ e^+e^- \to \pi^+\pi^-K^+K^-\gamma$

[1] Dividing by $(2/3)^2$ to take twice into account that $B(K^{*0} \to K^+\pi^-) = 2/3\ B(K^{*0} \to K\pi)$.
[2] Superseded by LEES 12F.

$\Gamma(K^*(892)^\pm K^*(892)^\mp) \times \Gamma(e^+e^-)/\Gamma_{total}$ — $\Gamma_{74}\Gamma_5/\Gamma$

VALUE (eV)	EVTS	DOCUMENT ID		TECN	COMMENT
0.80±0.48±0.32	1 ± 5	[1] LEES	14H	BABR	$e^+e^- \to \pi^+\pi^-K^0_S K^0_S\gamma$

[1] Dividing by $(1/4)^2$ to take twice into account $B(K^*(892) \to K^0_S\pi) = 1/4$.

$\Gamma(K^*_2(1430)^+K^0_S\pi^- + c.c.) \times \Gamma(e^+e^-)/\Gamma_{total}$ — $\Gamma_{84}\Gamma_5/\Gamma$

VALUE (eV)	EVTS	DOCUMENT ID		TECN	COMMENT
20.1±9.8±0.5	35	[1,2] LEES	14H	BABR	$e^+e^- \to \pi^+\pi^-K^0_S K^0_S\gamma$

[1] Dividing by 1/4 to take into account $B(K^*(1430) \to K^0_S\pi) = 1/4\ B(K^*(1430) \to K\pi)$.
[2] LEES 14H reports $[\Gamma(J/\psi(1S) \to K^*_2(1430)^+K^0_S\pi^- + c.c.) \times \Gamma(J/\psi(1S) \to e^+e^-)/\Gamma_{total}] \times [B(K^*_2(1430) \to K\pi)] = 10.0 \pm 4.8 \pm 0.8$ eV which we divide by our best value $B(K^*_2(1430) \to K\pi) = (49.9 \pm 1.2) \times 10^{-2}$. Our first error is their experiment's error and our second error is the systematic error from using our best value.

$\Gamma(\overline{K}^*_2(1430)^0K^*(892)^0 + c.c.) \times \Gamma(e^+e^-)/\Gamma_{total}$ — $\Gamma_{85}\Gamma_5/\Gamma$

VALUE (eV)	EVTS	DOCUMENT ID		TECN	COMMENT
25.8±1.4±0.6	710	[1,2,3] LEES	12F	BABR	$10.6\ e^+e^- \to \pi^+\pi^-K^+K^-\gamma$
• • • We do not use the following data for averages, fits, limits, etc. • • •					
33 ±4 ±1	317	[2,4] AUBERT	07AK	BABR	$10.6\ e^+e^- \to \pi^+\pi^-K^+K^-\gamma$

[1] LEES 12F reports $[\Gamma(J/\psi(1S) \to \overline{K}^*_2(1430)^0K^*(892)^0 + c.c.) \times \Gamma(J/\psi(1S) \to e^+e^-)/\Gamma_{total}] \times [B(K^*_2(1430) \to K\pi)] = 12.89 \pm 0.54 \pm 0.41$ eV which we divide by our best value $B(K^*_2(1430) \to K\pi) = (49.9 \pm 1.2) \times 10^{-2}$. Our first error is their experiment's error and our second error is the systematic error from using our best value.
[2] Dividing by 2/3 to take into account that $B(K^{*0} \to K^+\pi^-) = 2/3\ B(K^{*0} \to K\pi)$.
[3] The $K^*_2(1430)$ cannot be distinguished from the $K^*_0(1430)$.
[4] Superseded by LEES 12F. AUBERT 07AK reports $[\Gamma(J/\psi(1S) \to \overline{K}^*_2(1430)^0K^*(892)^0 + c.c.) \times \Gamma(J/\psi(1S) \to e^+e^-)/\Gamma_{total}] \times [B(K^*_2(1430) \to K\pi)] = 16.4 \pm 1.1 \pm 1.4$ eV which we divide by our best value $B(K^*_2(1430) \to K\pi) = (49.9 \pm 1.2) \times 10^{-2}$. Our first error is their experiment's error and our second error is the systematic error from using our best value.

$\Gamma(K^*_2(1430)^-K^*(892)^+ + c.c.) \times \Gamma(e^+e^-)/\Gamma_{total}$ — $\Gamma_{86}\Gamma_5/\Gamma$

VALUE (eV)	EVTS	DOCUMENT ID		TECN	COMMENT
18.6±16.1±0.4	8 ± 8	[1,2] LEES	14H	BABR	$e^+e^- \to \pi^+\pi^-K^0_S K^0_S\gamma$

[1] Dividing by $(1/4)^2$ to take into account $B(K^*(892) \to K^0_S\pi) = 1/4$ and $B(K^*(1430) \to K^0_S\pi) = 1/4\ B(K^*(1430) \to K\pi)$.
[2] LEES 14H reports $[\Gamma(J/\psi(1S) \to K^*_2(1430)^-K^*(892)^+ + c.c.) \times \Gamma(J/\psi(1S) \to e^+e^-)/\Gamma_{total}] \times [B(K^*_2(1430) \to K\pi)] = 9.28 \pm 8.0 \pm 0.32$ eV which we divide by our best value $B(K^*_2(1430) \to K\pi) = (49.9 \pm 1.2) \times 10^{-2}$. Our first error is their experiment's error and our second error is the systematic error from using our best value.

$\Gamma(K^*_2(1430)^-K^*(892)^+ + c.c. \to K^*(892)^+K^0_S\pi^- + c.c.) \times \Gamma(e^+e^-)/\Gamma_{total}$ — $\Gamma_{87}\Gamma_5/\Gamma$

VALUE (eV)	EVTS	DOCUMENT ID		TECN	COMMENT
2.32±2.00±0.08	8 ± 8	[1] LEES	14H	BABR	$e^+e^- \to \pi^+\pi^-K^0_S K^0_S\gamma$

[1] Dividing by 1/4 to take into account $B(K^*(892) \to K^0_S\pi) = 1/4$.

Downloaded from https://academic.oup.com/ptep/article/2022/8/083C01/6651666 by KIT Library user on 27 September 2022

$\Gamma(\overline{K}_2(1770)^0 K^*(892)^0 + \text{c.c.} \to K^*(892)^0 K^- \pi^+ + \text{c.c.}) \times \Gamma(e^+e^-)/\Gamma_{\text{total}}$ — $\Gamma_{89}\Gamma_5/\Gamma$

VALUE (eV)	EVTS	DOCUMENT ID		TECN	COMMENT
3.8±0.4±0.3	110 ± 14	[1] AUBERT	07AK	BABR	10.6 $e^+e^- \to \pi^+\pi^- K^+K^-\gamma$

[1] Dividing by 2/3 to take into account that $B(K^{*0} \to K^+\pi^-) = 2/3$.

$\Gamma(\phi\pi^+\pi^-) \times \Gamma(e^+e^-)/\Gamma_{\text{total}}$ — $\Gamma_{96}\Gamma_5/\Gamma$

VALUE (eV)	EVTS	DOCUMENT ID		TECN	COMMENT
4.48±0.35 OUR AVERAGE					
4.46±0.49±0.05	181	[1] LEES	12F	BABR	10.6 $e^+e^- \to K^+K^-\pi^+\pi^-\gamma$
4.51±0.48±0.05	254 ± 23	[2] SHEN	09	BELL	10.6 $e^+e^- \to K^+K^-\pi^+\pi^-\gamma$
• • • We do not use the following data for averages, fits, limits, etc. • • •					
5.3 ±0.7 ±0.1	103	[3] AUBERT,BE	06D	BABR	10.6 $e^+e^- \to K^+K^-\pi^+\pi^-\gamma$

[1] LEES 12F reports $[\Gamma(J/\psi(1S) \to \phi\pi^+\pi^-) \times \Gamma(J/\psi(1S) \to e^+e^-)/\Gamma_{\text{total}}] \times [B(\phi(1020) \to K^+K^-)] = 2.19 \pm 0.23 \pm 0.07$ eV which we divide by our best value $B(\phi(1020) \to K^+K^-) = (49.1 \pm 0.5) \times 10^{-2}$. Our first error is their experiment's error and our second error is the systematic error from using our best value.

[2] SHEN 09 reports $4.50 \pm 0.41 \pm 0.26$ eV from a measurement of $[\Gamma(J/\psi(1S) \to \phi\pi^+\pi^-) \times \Gamma(J/\psi(1S) \to e^+e^-)/\Gamma_{\text{total}}] \times [B(\phi(1020) \to K^+K^-)]$ assuming $B(\phi(1020) \to K^+K^-) = (49.2 \pm 0.6) \times 10^{-2}$, which we rescale to our best value $B(\phi(1020) \to K^+K^-) = (49.1 \pm 0.5) \times 10^{-2}$. Our first error is their experiment's error and our second error is the systematic error from using our best value.

[3] Superseded by LEES 12F. AUBERT,BE 06D reports $[\Gamma(J/\psi(1S) \to \phi\pi^+\pi^-) \times \Gamma(J/\psi(1S) \to e^+e^-)/\Gamma_{\text{total}}] \times [B(\phi(1020) \to K^+K^-)] = 2.61 \pm 0.30 \pm 0.18$ eV which we divide by our best value $B(\phi(1020) \to K^+K^-) = (49.1 \pm 0.5) \times 10^{-2}$. Our first error is their experiment's error and our second error is the systematic error from using our best value.

$\Gamma(\phi\pi^0\pi^0) \times \Gamma(e^+e^-)/\Gamma_{\text{total}}$ — $\Gamma_{97}\Gamma_5/\Gamma$

VALUE (eV)	EVTS	DOCUMENT ID		TECN	COMMENT
2.77±0.57±0.03	45	[1] LEES	12F	BABR	10.6 $e^+e^- \to K^+K^-\pi^0\pi^0\gamma$
• • • We do not use the following data for averages, fits, limits, etc. • • •					
3.13±0.88±0.03	23	[2] AUBERT,BE	06D	BABR	10.6 $e^+e^- \to K^+K^-\pi^0\pi^0\gamma$

[1] LEES 12F reports $[\Gamma(J/\psi(1S) \to \phi\pi^0\pi^0) \times \Gamma(J/\psi(1S) \to e^+e^-)/\Gamma_{\text{total}}] \times [B(\phi(1020) \to K^+K^-)] = 1.36 \pm 0.27 \pm 0.07$ eV which we divide by our best value $B(\phi(1020) \to K^+K^-) = (49.1 \pm 0.5) \times 10^{-2}$. Our first error is their experiment's error and our second error is the systematic error from using our best value.

[2] Superseded by LEES 12F. AUBERT,BE 06D reports $[\Gamma(J/\psi(1S) \to \phi\pi^0\pi^0) \times \Gamma(J/\psi(1S) \to e^+e^-)/\Gamma_{\text{total}}] \times [B(\phi(1020) \to K^+K^-)] = 1.54 \pm 0.40 \pm 0.16$ eV which we divide by our best value $B(\phi(1020) \to K^+K^-) = (49.1 \pm 0.5) \times 10^{-2}$. Our first error is their experiment's error and our second error is the systematic error from using our best value.

$\Gamma(\phi 2(\pi^+\pi^-)) \times \Gamma(e^+e^-)/\Gamma_{\text{total}}$ — $\Gamma_{98}\Gamma_5/\Gamma$

VALUE (10^{-2} keV)	EVTS	DOCUMENT ID		TECN	COMMENT
0.96±0.19±0.01	35	[1] AUBERT	06D	BABR	10.6 $e^+e^- \to \phi 2(\pi^+\pi^-)\gamma$

[1] AUBERT 06D reports $[\Gamma(J/\psi(1S) \to \phi 2(\pi^+\pi^-)) \times \Gamma(J/\psi(1S) \to e^+e^-)/\Gamma_{\text{total}}] \times [B(\phi(1020) \to K^+K^-)] = (0.47 \pm 0.09 \pm 0.03) \times 10^{-2}$ keV which we divide by our best value $B(\phi(1020) \to K^+K^-) = (49.1 \pm 0.5) \times 10^{-2}$. Our first error is their experiment's error and our second error is the systematic error from using our best value.

$\Gamma(\phi\eta) \times \Gamma(e^+e^-)/\Gamma_{\text{total}}$ — $\Gamma_{99}\Gamma_5/\Gamma$

VALUE (eV)	EVTS	DOCUMENT ID		TECN	COMMENT
6.1±2.7±0.4	6	[1] AUBERT	07AU	BABR	10.6 $e^+e^- \to \phi\eta\gamma$

[1] AUBERT 07AU quotes $\Gamma_{ee}^{J/\psi} \cdot B(J/\psi \to \phi\eta) \cdot B(\phi \to K^+K^-) \cdot B(\eta \to 3\pi) = 0.84 \pm 0.37 \pm 0.05$ eV.

$\Gamma(\phi f_0(980) \to \phi\pi^+\pi^-) \times \Gamma(e^+e^-)/\Gamma_{\text{total}}$ — $\Gamma_{103}\Gamma_5/\Gamma$

VALUE (eV)	EVTS	DOCUMENT ID		TECN	COMMENT
1.44±0.19 OUR AVERAGE					
1.40±0.25±0.02	57 ± 9	[1] LEES	12F	BABR	10.6 $e^+e^- \to \pi^+\pi^- K^+K^-\gamma$
1.48±0.27±0.09	60±11	[2] SHEN	09	BELL	10.6 $e^+e^- \to K^+K^-\pi^+\pi^-\gamma$
• • • We do not use the following data for averages, fits, limits, etc. • • •					
1.02±0.24±0.01	20 ± 5	[3] AUBERT	07AK	BABR	10.6 $e^+e^- \to \pi^+\pi^- K^+K^-\gamma$

[1] LEES 12F reports $[\Gamma(J/\psi(1S) \to \phi f_0(980) \to \phi\pi^+\pi^-) \times \Gamma(J/\psi(1S) \to e^+e^-)/\Gamma_{\text{total}}] \times [B(\phi(1020) \to K^+K^-)] = 0.69 \pm 0.11 \pm 0.05$ eV which we divide by our best value $B(\phi(1020) \to K^+K^-) = (49.1 \pm 0.5) \times 10^{-2}$. Our first error is their experiment's error and our second error is the systematic error from using our best value.

[2] Multiplied by 2/3 to take into account the $\phi\pi^+\pi^-$ mode only. Using $B(\phi \to K^+K^-) = (49.2 \pm 0.6)\%$.

[3] Superseded by LEES 12F. AUBERT 07AK reports $[\Gamma(J/\psi(1S) \to \phi f_0(980) \to \phi\pi^+\pi^-) \times \Gamma(J/\psi(1S) \to e^+e^-)/\Gamma_{\text{total}}] \times [B(\phi(1020) \to K^+K^-)] = 0.50 \pm 0.11 \pm 0.04$ eV which we divide by our best value $B(\phi(1020) \to K^+K^-) = (49.1 \pm 0.5) \times 10^{-2}$. Our first error is their experiment's error and our second error is the systematic error from using our best value.

$\Gamma(\phi f_0(980) \to \phi\pi^0\pi^0) \times \Gamma(e^+e^-)/\Gamma_{\text{total}}$ — $\Gamma_{104}\Gamma_5/\Gamma$

VALUE (eV)	EVTS	DOCUMENT ID		TECN	COMMENT
0.98±0.26±0.01	16 ± 4	[1] LEES	12F	BABR	10.6 $e^+e^- \to \pi^0\pi^0 K^+K^-\gamma$
• • • We do not use the following data for averages, fits, limits, etc. • • •					
0.96±0.40±0.01	7.0 ± 2.8	[2] AUBERT	07AK	BABR	10.6 $e^+e^- \to \pi^0\pi^0 K^+K^-\gamma$

[1] LEES 12F reports $[\Gamma(J/\psi(1S) \to \phi f_0(980) \to \phi\pi^0\pi^0) \times \Gamma(J/\psi(1S) \to e^+e^-)/\Gamma_{\text{total}}] \times [B(\phi(1020) \to K^+K^-)] = 0.48 \pm 0.12 \pm 0.05$ eV which we divide by our best value $B(\phi(1020) \to K^+K^-) = (49.1 \pm 0.5) \times 10^{-2}$. Our first error is their experiment's error and our second error is the systematic error from using our best value.

[2] Superseded by LEES 12F. AUBERT 07AK reports $[\Gamma(J/\psi(1S) \to \phi f_0(980) \to \phi\pi^0\pi^0) \times \Gamma(J/\psi(1S) \to e^+e^-)/\Gamma_{\text{total}}] \times [B(\phi(1020) \to K^+K^-)] = 0.47 \pm 0.19 \pm 0.05$ eV which we divide by our best value $B(\phi(1020) \to K^+K^-) = (49.1 \pm 0.5) \times 10^{-2}$. Our first error is their experiment's error and our second error is the systematic error from using our best value.

$\Gamma(\phi f_2(1270)) \times \Gamma(e^+e^-)/\Gamma_{\text{total}}$ — $\Gamma_{109}\Gamma_5/\Gamma$

VALUE (eV)	EVTS	DOCUMENT ID		TECN	COMMENT
$1.79 \pm 0.32^{+0.02}_{-0.06}$	61	[1,2,3] LEES	12F	BABR	10.6 $e^+e^- \to \pi^+\pi^- K^+K^-\gamma$
• • • We do not use the following data for averages, fits, limits, etc. • • •					
$4.08 \pm 0.73^{+0.04}_{-0.14}$	44	[2,4] AUBERT	07AK	BABR	10.6 $e^+e^- \to \pi^+\pi^- K^+K^-\gamma$

[1] LEES 12F reports $[\Gamma(J/\psi(1S) \to \phi f_2(1270)) \times \Gamma(J/\psi(1S) \to e^+e^-)/\Gamma_{\text{total}}] \times [B(f_2(1270) \to \pi\pi)] = 1.51 \pm 0.25 \pm 0.10$ eV which we divide by our best value $B(f_2(1270) \to \pi\pi) = (84.2^{+2.9}_{-0.9}) \times 10^{-2}$. Our first error is their experiment's error and our second error is the systematic error from using our best value.

[2] Using $B(\phi \to K^+K^-) = (48.9 \pm 0.5)\%$.

[3] Using $\pi^+\pi^-$ invariant mass between 1.1 and 1.5 GeV. May include other sources such as $f_0(1370)$.

[4] Superseded by LEES 12F. AUBERT 07AK reports $[\Gamma(J/\psi(1S) \to \phi f_2(1270)) \times \Gamma(J/\psi(1S) \to e^+e^-)/\Gamma_{\text{total}}] \times [B(f_2(1270) \to \pi\pi)] = 3.44 \pm 0.55 \pm 0.28$ eV which we divide by our best value $B(f_2(1270) \to \pi\pi) = (84.2^{+2.9}_{-0.9}) \times 10^{-2}$. Our first error is their experiment's error and our second error is the systematic error from using our best value.

$\Gamma(\phi f'_2(1525)) \times \Gamma(e^+e^-)/\Gamma_{\text{total}}$ — $\Gamma_{114}\Gamma_5/\Gamma$

VALUE (eV)	EVTS	DOCUMENT ID		TECN	COMMENT
8.2±3.2±0.2	11	[1,2] LEES	14H	BABR	$e^+e^- \to K^0_S K^0_S K^+K^-\gamma$

[1] Dividing by 1/4 to take into account $B(f'_2(1525) \to K^0_S K^0_S) = 1/4\ B(f'_2(1525) \to K\overline{K})$ and using $B(\phi \to K^+K^-) = (48.9 \pm 0.5)\%$.

[2] LEES 14H reports $[\Gamma(J/\psi(1S) \to \phi f'_2(1525)) \times \Gamma(J/\psi(1S) \to e^+e^-)/\Gamma_{\text{total}}] \times [B(f'_2(1525) \to K\overline{K})] = 7.2 \pm 2.8 \pm 0.3$ eV which we divide by our best value $B(f'_2(1525) \to K\overline{K}) = (87.6 \pm 2.2) \times 10^{-2}$. Our first error is their experiment's error and our second error is the systematic error from using our best value.

$\Gamma(\phi K^+K^-) \times \Gamma(e^+e^-)/\Gamma_{\text{total}}$ — $\Gamma_{120}\Gamma_5/\Gamma$

VALUE (eV)	EVTS	DOCUMENT ID		TECN	COMMENT
4.60±0.62±0.05	163	[1] LEES	12F	BABR	10.6 $e^+e^- \to K^+K^-K^+K^-\gamma$

[1] LEES 12F reports $[\Gamma(J/\psi(1S) \to \phi K^+K^-) \times \Gamma(J/\psi(1S) \to e^+e^-)/\Gamma_{\text{total}}] \times [B(\phi(1020) \to K^+K^-)] = 2.26 \pm 0.26 \pm 0.16$ eV which we divide by our best value $B(\phi(1020) \to K^+K^-) = (49.1 \pm 0.5) \times 10^{-2}$. Our first error is their experiment's error and our second error is the systematic error from using our best value.

$\Gamma(\phi K^0_S K^0_S) \times \Gamma(e^+e^-)/\Gamma_{\text{total}}$ — $\Gamma_{121}\Gamma_5/\Gamma$

VALUE (eV)	EVTS	DOCUMENT ID		TECN	COMMENT
3.26±0.84±0.04	29	[1] LEES	14H	BABR	$e^+e^- \to K^0_S K^0_S K^+K^-\gamma$

[1] LEES 14H reports $[\Gamma(J/\psi(1S) \to \phi K^0_S K^0_S) \times \Gamma(J/\psi(1S) \to e^+e^-)/\Gamma_{\text{total}}] \times [B(\phi(1020) \to K^+K^-)] = 1.6 \pm 0.4 \pm 0.1$ eV which we divide by our best value $B(\phi(1020) \to K^+K^-) = (49.1 \pm 0.5) \times 10^{-2}$. Our first error is their experiment's error and our second error is the systematic error from using our best value.

$\Gamma(f'_2(1525) K^+K^-) \times \Gamma(e^+e^-)/\Gamma_{\text{total}}$ — $\Gamma_{126}\Gamma_5/\Gamma$

VALUE (eV)	EVTS	DOCUMENT ID		TECN	COMMENT
5.8±1.9±0.1	16	[1,2] LEES	14H	BABR	$e^+e^- \to K^0_S K^0_S K^+K^-\gamma$

[1] Dividing by 1/4 to take into account $B(f'_2(1525) \to K^0_S K^0_S) = 1/4\ B(f'_2(1525) \to K\overline{K})$.

[2] LEES 14H reports $[\Gamma(J/\psi(1S) \to f'_2(1525) K^+K^-) \times \Gamma(J/\psi(1S) \to e^+e^-)/\Gamma_{\text{total}}] \times [B(f'_2(1525) \to K\overline{K})] = 5.12 \pm 1.68 \pm 0.20$ eV which we divide by our best value $B(f'_2(1525) \to K\overline{K}) = (87.6 \pm 2.2) \times 10^{-2}$. Our first error is their experiment's error and our second error is the systematic error from using our best value.

$\Gamma(2(\pi^+\pi^-)\pi^0) \times \Gamma(e^+e^-)/\Gamma_{\text{total}}$ — $\Gamma_{145}\Gamma_5/\Gamma$

VALUE (eV)	EVTS	DOCUMENT ID		TECN	COMMENT
303±5±18	4990	AUBERT	07AU	BABR	10.6 $e^+e^- \to 2(\pi^+\pi^-)\pi^0\gamma$

Downloaded from https://academic.oup.com/ptep/article/2022/8/083C01/6651666 by KIT Library user on 27 September 2022

$\Gamma(\pi^+\pi^-3\pi^0) \times \Gamma(e^+e^-)/\Gamma_{total}$ — $\Gamma_{147}\Gamma_5/\Gamma$

VALUE (eV)	EVTS	DOCUMENT ID		TECN	COMMENT
104 ±50 OUR AVERAGE		Error includes scale factor of 4.3.			
55.4±15.9± 0.5	14k	[1] LEES	21	BABR	$10.6\ e^+e^- \to 2(\pi^+\pi^-)3\pi^0\gamma$
150.0± 4.0±15.0	2.3k	LEES	18E	BABR	$10.6\ e^+e^- \to \pi^+\pi^-3\pi^0\gamma$

[1] LEES 21 reports $[\Gamma(J/\psi(1S) \to \pi^+\pi^-3\pi^0) \times \Gamma(J/\psi(1S) \to e^+e^-)/\Gamma_{total}] \times [\Gamma(\psi(2S) \to J/\psi(1S)\pi^+\pi^-)/\Gamma_{total}] = 19.2 \pm 4.5 \pm 3.2$ eV which we divide by our best value $\Gamma(\psi(2S) \to J/\psi(1S)\pi^+\pi^-)/\Gamma_{total} = 0.3468 \pm 0.0030$. Our first error is their experiment's error and our second error is the systematic error from using our best value.

$\Gamma(\pi^+\pi^-4\pi^0) \times \Gamma(e^+e^-)/\Gamma_{total}$ — $\Gamma_{148}\Gamma_5/\Gamma$

VALUE (eV)	EVTS	DOCUMENT ID		TECN	COMMENT
35.8±4.4±5.4	340	LEES	21C	BABR	$e^+e^- \to \gamma_{ISR}(\pi^+\pi^-4\pi^0)$

$\Gamma(\rho^\pm\pi^\mp\pi^0\pi^0) \times \Gamma(e^+e^-)/\Gamma_{total}$ — $\Gamma_{149}\Gamma_5/\Gamma$

VALUE (eV)	EVTS	DOCUMENT ID		TECN	COMMENT
78.0±9.0±8.0	1.2k	LEES	18E	BABR	$10.6\ e^+e^- \to \pi^+\pi^-3\pi^0\gamma$

$\Gamma(\rho^+\rho^-\pi^0) \times \Gamma(e^+e^-)/\Gamma_{total}$ — $\Gamma_{150}\Gamma_5/\Gamma$

VALUE (eV)	EVTS	DOCUMENT ID		TECN	COMMENT
33.0±5.0±3.3	529	LEES	18E	BABR	$10.6\ e^+e^- \to \pi^+\pi^-3\pi^0\gamma$

$\Gamma(\pi^+\pi^-\pi^0) \times \Gamma(e^+e^-)/\Gamma_{total}$ — $\Gamma_{151}\Gamma_5/\Gamma$

VALUE (keV)	DOCUMENT ID		TECN	COMMENT
0.1248±0.0019±0.0026	LEES	21B	BABR	$10.5\ e^+e^- \to \pi^+\pi^-\pi^0\gamma$
• • • We do not use the following data for averages, fits, limits, etc. • • •				
0.122 ±0.005 ±0.008	AUBERT,B	04N	BABR	$10.6\ e^+e^- \to \pi^+\pi^-\pi^0\gamma$

$\Gamma(2(\pi^+\pi^-\pi^0)) \times \Gamma(e^+e^-)/\Gamma_{total}$ — $\Gamma_{152}\Gamma_5/\Gamma$

VALUE (10^{-2} keV)	EVTS	DOCUMENT ID		TECN	COMMENT
8.9±0.5±1.0	761	AUBERT	06D	BABR	$10.6\ e^+e^- \to 2(\pi^+\pi^-\pi^0)\gamma$

$\Gamma(\pi^+\pi^-\pi^0K^+K^-) \times \Gamma(e^+e^-)/\Gamma_{total}$ — $\Gamma_{153}\Gamma_5/\Gamma$

VALUE (eV)	EVTS	DOCUMENT ID		TECN	COMMENT
107.0±4.3±6.4	768	AUBERT	07AU	BABR	$10.6\ e^+e^- \to K^+K^-\pi^+\pi^-\pi^0\gamma$

$\Gamma(2(\pi^+\pi^-)) \times \Gamma(e^+e^-)/\Gamma_{total}$ — $\Gamma_{155}\Gamma_5/\Gamma$

VALUE (eV)	EVTS	DOCUMENT ID		TECN	COMMENT
20.4±0.9±0.4		LEES	12E	BABR	$10.6\ e^+e^- \to 2\pi^+2\pi^-\gamma$
• • • We do not use the following data for averages, fits, limits, etc. • • •					
19.5±1.4±1.3	270	[1] AUBERT	05D	BABR	$10.6\ e^+e^- \to 2(\pi^+\pi^-)\gamma$

[1] Superseded by LEES 12E.

$\Gamma(3(\pi^+\pi^-)) \times \Gamma(e^+e^-)/\Gamma_{total}$ — $\Gamma_{156}\Gamma_5/\Gamma$

VALUE (10^{-2} keV)	EVTS	DOCUMENT ID		TECN	COMMENT
2.37±0.16±0.14	496	AUBERT	06D	BABR	$10.6\ e^+e^- \to 3(\pi^+\pi^-)\gamma$

$\Gamma(2(\pi^+\pi^-)3\pi^0) \times \Gamma(e^+e^-)/\Gamma_{total}$ — $\Gamma_{157}\Gamma_5/\Gamma$

VALUE (eV)	EVTS	DOCUMENT ID		TECN	COMMENT
345±10±50	14k	LEES	21	BABR	$10.6\ e^+e^- \to 2(\pi^+\pi^-)3\pi^0\gamma$

$\Gamma(2(\pi^+\pi^-)\eta) \times \Gamma(e^+e^-)/\Gamma_{total}$ — $\Gamma_{159}\Gamma_5/\Gamma$

VALUE (eV)	EVTS	DOCUMENT ID		TECN	COMMENT
13.1±2.4±0.1	85	[1] AUBERT	07AU	BABR	$10.6\ e^+e^- \to 2(\pi^+\pi^-)\eta\gamma$

[1] AUBERT 07AU reports $[\Gamma(J/\psi(1S) \to 2(\pi^+\pi^-)\eta) \times \Gamma(J/\psi(1S) \to e^+e^-)/\Gamma_{total}] \times [B(\eta \to 2\gamma)] = 5.16 \pm 0.85 \pm 0.39$ eV which we divide by our best value $B(\eta \to 2\gamma) = (39.36 \pm 0.18) \times 10^{-2}$. Our first error is their experiment's error and our second error is the systematic error from using our best value.

$\Gamma(2(\pi^+\pi^-\pi^0)\eta) \times \Gamma(e^+e^-)/\Gamma_{total}$ — $\Gamma_{161}\Gamma_5/\Gamma$

VALUE (eV)	EVTS	DOCUMENT ID		TECN	COMMENT
9.1±2.6±1.4	14k	LEES	21	BABR	$10.6\ e^+e^- \to 2(\pi^+\pi^-)3\pi^0\gamma$

$\Gamma(\pi^+\pi^-\pi^0\pi^0\eta) \times \Gamma(e^+e^-)/\Gamma_{total}$ — $\Gamma_{162}\Gamma_5/\Gamma$

VALUE (eV)	EVTS	DOCUMENT ID		TECN	COMMENT
13.1± 2.7 OUR AVERAGE					
26.1±17.9±0.3	14k	[1] LEES	21	BABR	$10.6\ e^+e^- \to 2(\pi^+\pi^-)3\pi^0\gamma$
12.8± 1.8±2.0	203	LEES	18E	BABR	$10.6\ e^+e^- \to \pi^+\pi^-\pi^0\pi^0\eta\gamma$

[1] LEES 21 reports $[\Gamma(J/\psi(1S) \to \pi^+\pi^-\pi^0\pi^0\eta) \times \Gamma(J/\psi(1S) \to e^+e^-)/\Gamma_{total}] \times [B(\eta \to \pi^+\pi^-\pi^0)] = 6 \pm 4 \pm 1$ eV which we divide by our best value $B(\eta \to \pi^+\pi^-\pi^0) = (23.02 \pm 0.25) \times 10^{-2}$. Our first error is their experiment's error and our second error is the systematic error from using our best value.

$\Gamma(\rho^\pm\pi^\mp\pi^0\eta) \times \Gamma(e^+e^-)/\Gamma_{total}$ — $\Gamma_{163}\Gamma_5/\Gamma$

VALUE (eV)	EVTS	DOCUMENT ID		TECN	COMMENT
10.5±4.1±1.6	168	LEES	18E	BABR	$10.6\ e^+e^- \to \pi^+\pi^-\pi^0\pi^0\eta\gamma$

$\Gamma(K^+K^-) \times \Gamma(e^+e^-)/\Gamma_{total}$ — $\Gamma_{164}\Gamma_5/\Gamma$

VALUE (eV)	EVTS	DOCUMENT ID		TECN	COMMENT
• • • We do not use the following data for averages, fits, limits, etc. • • •					
1.78±0.11±0.05	462	[1] LEES	15J	BABR	$e^+e^- \to K^+K^-\gamma$
1.94±0.11±0.05	462	[2] LEES	15J	BABR	$e^+e^- \to K^+K^-\gamma$
1.42±0.23±0.08	51	[3] LEES	13Q	BABR	$e^+e^- \to K^+K^-\gamma$

[1] $\sin\phi > 0$.
[2] $\sin\phi < 0$.
[3] Interference with non-resonant K^+K^- production not taken into account.

$\Gamma(K^0_SK^0_L\pi^0) \times \Gamma(e^+e^-)/\Gamma_{total}$ — $\Gamma_{170}\Gamma_5/\Gamma$

VALUE (eV)	EVTS	DOCUMENT ID		TECN	COMMENT
11.4±1.3±0.6	182	LEES	17A	BABR	$e^+e^- \to K^0_SK^0_L\pi^0\gamma$

$\Gamma(K^*(892)^0\overline{K}^0 + \text{c.c.} \to K^0_SK^0_L\pi^0) \times \Gamma(e^+e^-)/\Gamma_{total}$ — $\Gamma_{171}\Gamma_5/\Gamma$

VALUE (eV)	EVTS	DOCUMENT ID		TECN	COMMENT
6.7±0.9±0.4	106	LEES	17A	BABR	$e^+e^- \to K^0_SK^0_L\pi^0\gamma$

$\Gamma(K^*_2(1430)^0\overline{K}^0 + \text{c.c.} \to K^0_SK^0_L\pi^0) \times \Gamma(e^+e^-)/\Gamma_{total}$ — $\Gamma_{172}\Gamma_5/\Gamma$

VALUE (eV)	EVTS	DOCUMENT ID		TECN	COMMENT
2.4±0.7±0.1	37	LEES	17A	BABR	$e^+e^- \to K^0_SK^0_L\pi^0\gamma$

$\Gamma(K^+K^-\pi^+\pi^-) \times \Gamma(e^+e^-)/\Gamma_{total}$ — $\Gamma_{173}\Gamma_5/\Gamma$

VALUE (eV)	EVTS	DOCUMENT ID		TECN	COMMENT
37.94±0.81±1.10	3.1k	LEES	12F	BABR	$10.6\ e^+e^- \to \pi^+\pi^-K^+K^-\gamma$
• • • We do not use the following data for averages, fits, limits, etc. • • •					
36.3 ±1.3 ±2.1	1.5k	[1] AUBERT	07AK	BABR	$10.6\ e^+e^- \to \pi^+\pi^-K^+K^-\gamma$
33.6 ±2.7 ±2.7	233	[2] AUBERT	05D	BABR	$10.6\ e^+e^- \to K^+K^-\pi^+\pi^-\gamma$

[1] Superseded by LEES 12F.
[2] Superseded by AUBERT 07AK.

$\Gamma(K^+K^-\pi^0\pi^0) \times \Gamma(e^+e^-)/\Gamma_{total}$ — $\Gamma_{174}\Gamma_5/\Gamma$

VALUE (eV)	EVTS	DOCUMENT ID		TECN	COMMENT
11.75±0.81±0.90	388	LEES	12F	BABR	$10.6\ e^+e^- \to \pi^0\pi^0K^+K^-\gamma$
• • • We do not use the following data for averages, fits, limits, etc. • • •					
13.6 ±1.1 ±1.3	203	[1] AUBERT	07AK	BABR	$10.6\ e^+e^- \to \pi^0\pi^0K^+K^-\gamma$

[1] Superseded by LEES 12F.

$\Gamma(K^0_SK^0_L\pi^+\pi^-) \times \Gamma(e^+e^-)/\Gamma_{total}$ — $\Gamma_{175}\Gamma_5/\Gamma$

VALUE (eV)	EVTS	DOCUMENT ID		TECN	COMMENT
20.8±2.3±2.1	248	LEES	14H	BABR	$e^+e^- \to \pi^+\pi^-K^0_SK^0_L\gamma$

$\Gamma(K^0_SK^0_L\pi^0\pi^0) \times \Gamma(e^+e^-)/\Gamma_{total}$ — $\Gamma_{176}\Gamma_5/\Gamma$

VALUE (eV)	EVTS	DOCUMENT ID		TECN	COMMENT
10.3±2.3±0.5	47	LEES	17A	BABR	$e^+e^- \to K^0_SK^0_L\pi^0\pi^0\gamma$

$\Gamma(K^0_SK^0_L\eta) \times \Gamma(e^+e^-)/\Gamma_{total}$ — $\Gamma_{177}\Gamma_5/\Gamma$

VALUE (eV)	EVTS	DOCUMENT ID		TECN	COMMENT
8.0±1.8±0.4	45	LEES	17A	BABR	$e^+e^- \to K^0_SK^0_L\eta\gamma$

$\Gamma(K^0_SK^0_S\pi^+\pi^-) \times \Gamma(e^+e^-)/\Gamma_{total}$ — $\Gamma_{178}\Gamma_5/\Gamma$

VALUE (eV)	EVTS	DOCUMENT ID		TECN	COMMENT
9.3±0.9±0.5	133	LEES	14H	BABR	$e^+e^- \to \pi^+\pi^-K^0_SK^0_S\gamma$

$\Gamma(K^\mp K^0_S\pi^\pm\pi^0) \times \Gamma(e^+e^-)/\Gamma_{total}$ — $\Gamma_{179}\Gamma_5/\Gamma$

VALUE (eV)	EVTS	DOCUMENT ID		TECN	COMMENT
31.7±1.9±1.8	393	LEES	17D	BABR	$e^+e^- \to K^0_SK^\pm\pi^\mp\pi^0\gamma$

$\Gamma(K^+K^-2(\pi^+\pi^-)) \times \Gamma(e^+e^-)/\Gamma_{total}$ — $\Gamma_{180}\Gamma_5/\Gamma$

VALUE (10^{-2} keV)	EVTS	DOCUMENT ID		TECN	COMMENT
2.75±0.23±0.17	205	AUBERT	06D	BABR	$10.6\ e^+e^- \to K^+K^-2(\pi^+\pi^-)\gamma$

$\Gamma(K^+K^-\pi^+\pi^-\eta) \times \Gamma(e^+e^-)/\Gamma_{total}$ — $\Gamma_{181}\Gamma_5/\Gamma$

VALUE (eV)	EVTS	DOCUMENT ID		TECN	COMMENT
25.9±3.9±0.1	73	[1] AUBERT	07AU	BABR	$10.6\ e^+e^- \to K^+K^-\pi^+\pi^-\eta\gamma$

[1] AUBERT 07AU reports $[\Gamma(J/\psi(1S) \to K^+K^-\pi^+\pi^-\eta) \times \Gamma(J/\psi(1S) \to e^+e^-)/\Gamma_{total}] \times [B(\eta \to 2\gamma)] = 10.2 \pm 1.3 \pm 0.8$ eV which we divide by our best value $B(\eta \to 2\gamma) = (39.36 \pm 0.18) \times 10^{-2}$. Our first error is their experiment's error and our second error is the systematic error from using our best value.

$\Gamma(2(K^+K^-)) \times \Gamma(e^+e^-)/\Gamma_{total}$ — $\Gamma_{182}\Gamma_5/\Gamma$

VALUE (eV)	EVTS	DOCUMENT ID		TECN	COMMENT
4.00±0.33±0.29	287 ± 24	LEES	12F	BABR	$10.6\ e^+e^- \to 2(K^+K^-)\gamma$
• • • We do not use the following data for averages, fits, limits, etc. • • •					
4.11±0.39±0.30	156 ± 15	[1] AUBERT	07AK	BABR	$10.6\ e^+e^- \to 2(K^+K^-)\gamma$
4.0 ±0.7 ±0.6	38	[2] AUBERT	05D	BABR	$10.6\ e^+e^- \to 2(K^+K^-)\gamma$

[1] Superseded by LEES 12F.
[2] Superseded by AUBERT 07AK.

Downloaded from https://academic.oup.com/ptep/article/2022/8/083C01/6651666 by KIT Library user on 27 September 2022

$\Gamma(K^+K^-K^0_SK^0_S) \times \Gamma(e^+e^-)/\Gamma_{total}$ — $\Gamma_{183}\Gamma_5/\Gamma$

VALUE (eV)	EVTS	DOCUMENT ID		TECN	COMMENT
2.3±0.4±0.1	29	LEES	14H	BABR	$e^+e^- \to K^0_SK^0_SK^+K^-\gamma$

$\Gamma(p\overline{p}) \times \Gamma(e^+e^-)/\Gamma_{total}$ — $\Gamma_{184}\Gamma_5/\Gamma$

VALUE (eV)	EVTS	DOCUMENT ID		TECN	COMMENT
11.9±0.6 OUR AVERAGE	Error includes scale factor of 1.8. See the ideogram below.				
11.3±0.4±0.3	821	[1] LEES	13O	BABR	$e^+e^- \to p\overline{p}\gamma$
12.9±0.4±0.4	918	[2] LEES	13Y	BABR	$e^+e^- \to p\overline{p}\gamma$
9.7±1.7		[3] ARMSTRONG	93B	E760	$\overline{p}p \to e^+e^-$
• • • We do not use the following data for averages, fits, limits, etc. • • •					
12.0±0.6±0.5	438	[4] AUBERT	06B	BABR	$e^+e^- \to p\overline{p}\gamma$

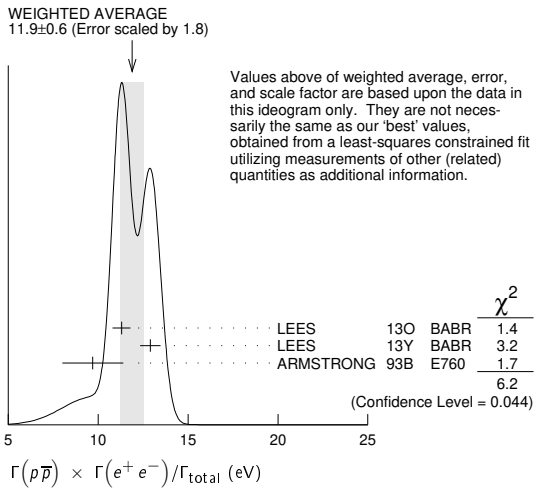

[1] ISR photon reconstructed in the detector
[2] ISR photon undetected
[3] Using $\Gamma_{total} = 85.5^{+6.1}_{-5.8}$ MeV.
[4] Superseded by LEES 13O

$\Gamma(\Lambda\overline{\Lambda}) \times \Gamma(e^+e^-)/\Gamma_{total}$ — $\Gamma_{200}\Gamma_5/\Gamma$

VALUE (eV)	DOCUMENT ID		TECN	COMMENT
10.7±0.9±0.7	AUBERT	07BD	BABR	$10.6\ e^+e^- \to \Lambda\overline{\Lambda}\gamma$

$\Gamma(\Sigma^0\overline{\Sigma}^0) \times \Gamma(e^+e^-)/\Gamma_{total}$ — $\Gamma_{210}\Gamma_5/\Gamma$

VALUE (eV)	DOCUMENT ID		TECN	COMMENT
6.4±1.2±0.6	AUBERT	07BD	BABR	$10.6\ e^+e^- \to \Sigma^0\overline{\Sigma}^0\gamma$

$J/\psi(1S)$ BRANCHING RATIOS

For the first four branching ratios, see also the partial widths, and (partial widths) $\times\ \Gamma(e^+e^-)/\Gamma_{total}$ above.

$\Gamma(\text{hadrons})/\Gamma_{total}$ — Γ_1/Γ

VALUE	DOCUMENT ID		TECN	COMMENT
0.877±0.005 OUR AVERAGE				
0.878±0.005	BAI	95B	BES	e^+e^-
0.86 ±0.02	BOYARSKI	75	MRK1	e^+e^-

$\Gamma(\text{virtual}\ \gamma \to \text{hadrons})/\Gamma_{total}$ — Γ_2/Γ

VALUE	DOCUMENT ID		TECN	COMMENT
0.135±0.003	[1,2] SETH	04	RVUE	e^+e^-
• • • We do not use the following data for averages, fits, limits, etc. • • •				
0.17 ±0.02	[1] BOYARSKI	75	MRK1	e^+e^-

[1] Included in $\Gamma(\text{hadrons})/\Gamma_{total}$.
[2] Using $B(J/\psi \to \ell^+\ell^-) = (5.90 \pm 0.09)\%$ from RPP-2002 and $R = 2.28 \pm 0.04$ determined by a fit to data from BAI 00 and BAI 02C.

$\Gamma(ggg)/\Gamma_{total}$ — Γ_3/Γ

VALUE (units 10^{-2})	EVTS	DOCUMENT ID		TECN	COMMENT
64.1±1.0	6 M	[1] BESSON	08	CLEO	$\psi(2S) \to \pi^+\pi^-+$ hadrons

[1] Calculated using the value $\Gamma(\gamma gg)/\Gamma(ggg) = 0.137 \pm 0.001 \pm 0.016 \pm 0.004$ from BESSON 08 and the PDG 08 values of $B(\ell^+\ell^-)$, B(virtual $\gamma \to$ hadrons), and $B(\gamma\eta_C)$. The statistical error is negligible and the systematic error is partially correlated with that of $\Gamma(\gamma gg)/\Gamma_{total}$ measurement of BESSON 08.

$\Gamma(\gamma gg)/\Gamma_{total}$ — Γ_4/Γ

VALUE (units 10^{-2})	EVTS	DOCUMENT ID		TECN	COMMENT
8.79±1.05	200 k	[1] BESSON	08	CLEO	$\psi(2S) \to \pi^+\pi^-\gamma+$ hadrons

[1] Calculated using the value $\Gamma(\gamma gg)/\Gamma(ggg) = 0.137 \pm 0.001 \pm 0.016 \pm 0.004$ from BESSON 08 and the value of $\Gamma(ggg)/\Gamma_{total}$. The statistical error is negligible and the systematic error is partially correlated with that of $\Gamma(ggg)/\Gamma_{total}$ measurement of BESSON 08.

$\Gamma(\gamma gg)/\Gamma(ggg)$ — Γ_4/Γ_3

VALUE (units 10^{-2})	EVTS	DOCUMENT ID		TECN	COMMENT
13.7±0.1±0.7	6 M	BESSON	08	CLEO	$\psi(2S) \to \pi^+\pi^-J/\psi$

$\Gamma(e^+e^-)/\Gamma_{total}$ — Γ_5/Γ

VALUE (units 10^{-2})	EVTS	DOCUMENT ID		TECN	COMMENT
5.971±0.032 OUR AVERAGE					
5.983±0.007±0.037	720k	ABLIKIM	13R	BES3	$\psi(2S) \to J/\psi\pi^+\pi^-$
5.945±0.067±0.042	15k	LI	05C	CLEO	$\psi(2S) \to J/\psi\pi^+\pi^-$
5.90 ±0.05 ±0.10		BAI	98D	BES	$\psi(2S) \to J/\psi\pi^+\pi^-$
6.09 ±0.33		BAI	95B	BES	e^+e^-
5.92 ±0.15 ±0.20		COFFMAN	92	MRK3	$\psi(2S) \to J/\psi\pi^+\pi^-$
6.9 ±0.9		BOYARSKI	75	MRK1	e^+e^-

$\Gamma(e^+e^-\gamma)/\Gamma_{total}$ — Γ_6/Γ

VALUE (units 10^{-3})	DOCUMENT ID		TECN	COMMENT
8.8±1.3±0.4	[1] ARMSTRONG	96	E760	$\overline{p}p \to e^+e^-\gamma$

[1] For $E_\gamma > 100$ MeV.

$\Gamma(\mu^+\mu^-)/\Gamma_{total}$ — Γ_7/Γ

VALUE (units 10^{-2})	EVTS	DOCUMENT ID		TECN	COMMENT
5.961±0.033 OUR AVERAGE					
5.973±0.007±0.038	770k	ABLIKIM	13R	BES3	$\psi(2S) \to J/\psi\pi^+\pi^-$
5.960±0.065±0.050	17k	LI	05C	CLEO	$\psi(2S) \to J/\psi\pi^+\pi^-$
5.84 ±0.06 ±0.10		BAI	98D	BES	$\psi(2S) \to J/\psi\pi^+\pi^-$
6.08 ±0.33		BAI	95B	BES	e^+e^-
5.90 ±0.15 ±0.19		COFFMAN	92	MRK3	$\psi(2S) \to J/\psi\pi^+\pi^-$
6.9 ±0.9		BOYARSKI	75	MRK1	e^+e^-

$\Gamma(e^+e^-)/\Gamma(\mu^+\mu^-)$ — Γ_5/Γ_7

VALUE	DOCUMENT ID		TECN	COMMENT
1.0016±0.0031 OUR AVERAGE				
1.0022±0.0044±0.0048	[1] AULCHENKO	14	KEDR	$3.097\ e^+e^- \to e^+e^-,\mu^+\mu^-$
1.0017±0.0017±0.0033	[2] ABLIKIM	13R	BES3	$\psi(2S) \to J/\psi\pi^+\pi^-$
1.002 ±0.021 ±0.013	[3] ANASHIN	10	KEDR	$3.097\ e^+e^- \to e^+e^-,\mu^+\mu^-$
0.997 ±0.012 ±0.006	LI	05C	CLEO	$\psi(2S) \to J/\psi\pi^+\pi^-$
• • • We do not use the following data for averages, fits, limits, etc. • • •				
1.011 ±0.013 ±0.016	BAI	98D	BES	$\psi(2S) \to J/\psi\pi^+\pi^-$
1.00 ±0.07	BAI	95B	BES	e^+e^-
1.00 ±0.05	BOYARSKI	75	MRK1	e^+e^-
0.91 ±0.15	ESPOSITO	75B	FRAM	e^+e^-
0.93 ±0.10	FORD	75	SPEC	e^+e^-

[1] From 235.3k $J/\psi \to e^+e^-$ and 156.6k $J/\psi \to \mu^+\mu^-$ observed events.
[2] Not independent of the corresponding measurements of $\Gamma(e+e-)/\Gamma_{total}$ and $\Gamma(mu+mu-)/\Gamma_{total}$.
[3] Not independent of the corresponding measurements of $\Gamma(e^+e^-) \times \Gamma(e^+e^-)/\Gamma_{total}$ and $\Gamma(\mu^+\mu^-) \times \Gamma(e^+e^-)/\Gamma_{total}$.

HADRONIC DECAYS

$\Gamma(\rho\pi)/\Gamma_{total}$ — Γ_8/Γ

VALUE (units 10^{-2})	EVTS	DOCUMENT ID		TECN	COMMENT
1.69 ±0.15 OUR AVERAGE	Error includes scale factor of 2.4. See the ideogram below.				
2.18 ±0.19		[1,2] AUBERT,B	04N	BABR	$10.6\ e^+e^- \to \pi^+\pi^-\pi^0\gamma$
2.184±0.005±0.201	220k	[2,3] BAI	04H	BES	$e^+e^- \to J/\psi \to \pi^+\pi^-\pi^0$
2.091±0.021±0.116		[2,4] BAI	04H	BES	$\psi(2S) \to \pi^+\pi^-J/\psi$
1.21 ±0.20		BAI	96D	BES	$e^+e^- \to \rho\pi$
1.42 ±0.01 ±0.19		COFFMAN	88	MRK3	e^+e^-
1.3 ±0.3	150	FRANKLIN	83	MRK2	e^+e^-
1.6 ±0.4	183	ALEXANDER	78	PLUT	e^+e^-
1.33 ±0.21		BRANDELIK	78B	DASP	e^+e^-
1.0 ±0.2	543	BARTEL	76	CNTR	e^+e^-
1.3 ±0.3	153	JEAN-MARIE	76	MRK1	e^+e^-

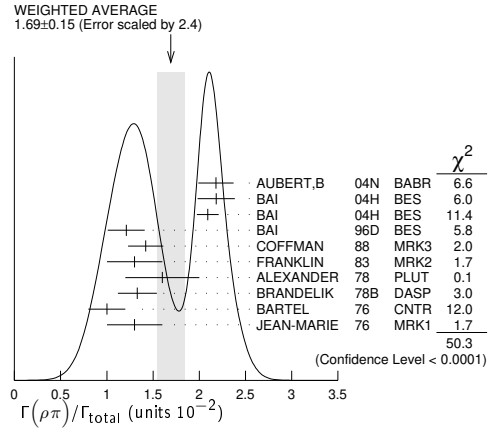

Downloaded from https://academic.oup.com/ptep/article/2022/8/083C01/6651666 by KIT Library user on 27 September 2022

[1] From the ratio of $\Gamma(e^+e^-)$ B$(\pi^+\pi^-\pi^0)$ and $\Gamma(e^+e^-)$ B$(\mu^+\mu^-)$ (AUBERT 04).
[2] Not independent of their B$(\pi^+\pi^-\pi^0)$.
[3] From $J/\psi \to \pi^+\pi^-\pi^0$ events directly.
[4] Obtained comparing the rates for $\pi^+\pi^-\pi^0$ and $\mu^+\mu^-$, using J/ψ events produced via $\psi(2S) \to \pi^+\pi^- J/\psi$ and with B$(J/\psi \to \mu^+\mu^-) = 5.88 \pm 0.10\%$.

$\Gamma(\rho\pi)/\Gamma(\pi^+\pi^-\pi^0)$ — Γ_8/Γ_{151}

VALUE	EVTS	DOCUMENT ID		TECN	COMMENT
1.142±0.011±0.026	20k	[1] LEES	17C	BABR	$J/\psi \to \pi^+\pi^-\pi^0$
• • • We do not use the following data for averages, fits, limits, etc. • • •					
1.331±0.033	20k	[2] LEES	17C	BABR	$J/\psi \to \pi^+\pi^-\pi^0$

[1] From a Dalitz plot analysis in an isobar model.
[2] From a Dalitz plot analysis in a Veneziano model.

$\Gamma(\rho^0\pi^0)/\Gamma(\rho\pi)$ — Γ_9/Γ_8

VALUE	DOCUMENT ID		TECN	COMMENT
0.328±0.005±0.027	COFFMAN	88	MRK3	e^+e^-
• • • We do not use the following data for averages, fits, limits, etc. • • •				
0.35 ±0.08	ALEXANDER	78	PLUT	e^+e^-
0.32 ±0.08	BRANDELIK	78B	DASP	e^+e^-
0.39 ±0.11	BARTEL	76	CNTR	e^+e^-
0.37 ±0.09	JEAN-MARIE	76	MRK1	e^+e^-

$\Gamma(a_2(1320)\rho)/\Gamma_{total}$ — Γ_{10}/Γ

VALUE (units 10^{-3})	EVTS	DOCUMENT ID		TECN	COMMENT
10.9±2.2 OUR AVERAGE					
11.7±0.7±2.5	7584	AUGUSTIN	89	DM2	$J/\psi \to \rho^0\rho^\pm\pi^\mp$
8.4±4.5	36	VANNUCCI	77	MRK1	$e^+e^- \to 2(\pi^+\pi^-)\pi^0$

$\Gamma(\eta\pi^+\pi^-)/\Gamma_{total}$ — Γ_{11}/Γ

VALUE (units 10^{-4})	EVTS	DOCUMENT ID		TECN	COMMENT
3.78±0.68	471	[1] ABLIKIM	19Q	BES3	$e^+e^- \to J/\psi \to \eta\pi^+\pi^-$

[1] From an energy scan of $e^+e^- \to J/\psi \to \eta\pi^+\pi^-$ assuming PDG 16 values for $\Gamma(e^+e^-)$, $\Gamma(\mu^+\mu^-)$, and Γ(total).

$\Gamma(\eta\rho)/\Gamma_{total}$ — Γ_{14}/Γ

VALUE (units 10^{-3})	EVTS	DOCUMENT ID		TECN	COMMENT
0.193±0.023 OUR AVERAGE					
0.194±0.017±0.029	299	JOUSSET	90	DM2	$J/\psi \to$ hadrons
0.193±0.013±0.029		COFFMAN	88	MRK3	$e^+e^- \to \pi^+\pi^-\eta$

$\Gamma(\eta\phi(2170) \to \eta\phi f_0(980) \to \eta\phi\pi^+\pi^-)/\Gamma_{total}$ — Γ_{15}/Γ

VALUE (units 10^{-4})	EVTS	DOCUMENT ID		TECN	COMMENT
1.20±0.14±0.37	471	ABLIKIM	15H	BES3	$e^+e^- \to J/\psi \to \phi\eta\pi^+\pi^-$

$\Gamma(\eta\phi(2170) \to \eta K^*(892)^0\overline{K}^*(892)^0)/\Gamma_{total}$ — Γ_{16}/Γ

VALUE	CL%	DOCUMENT ID		TECN	COMMENT
<2.52 × 10^{-4}	90	ABLIKIM	10C	BES2	$J/\psi \to \eta K^+\pi^-K^-\pi^+$

$\Gamma(\eta K^\pm K^0_S\pi^\mp)/\Gamma_{total}$ — Γ_{17}/Γ

VALUE (units 10^{-4})	EVTS	DOCUMENT ID		TECN	COMMENT
21.8±2.2±3.4	232 ± 23	ABLIKIM	08E	BES2	$e^+e^- \to J/\psi$

$\Gamma(\eta K^*(892)^0\overline{K}^*(892)^0)/\Gamma_{total}$ — Γ_{18}/Γ

VALUE (units 10^{-3})	EVTS	DOCUMENT ID		TECN	COMMENT
1.15±0.13±0.22	209	ABLIKIM	10C	BES2	$J/\psi \to \eta K^+\pi^-K^-\pi^+$

$\Gamma(\rho\eta'(958))/\Gamma_{total}$ — Γ_{19}/Γ

VALUE (units 10^{-5})	EVTS	DOCUMENT ID		TECN	COMMENT
8.1 ±0.8 OUR AVERAGE	Error includes scale factor of 1.6.				
7.90±0.19±0.49	3476	[1] ABLIKIM	17AK	BES3	$J/\psi \to \pi^+\pi^-\eta'$
8.3 ±3.0 ±1.2	19	JOUSSET	90	DM2	$J/\psi \to$ hadrons
11.4 ±1.4 ±1.6		COFFMAN	88	MRK3	$J/\psi \to \pi^+\pi^-\eta'$

[1] From a partial wave analysis of the decay $J/\psi \to \pi^+\pi^-\eta'$.

$\Gamma(\rho(1450)\pi \to \pi^+\pi^-\pi^0)/\Gamma(\pi^+\pi^-\pi^0)$ — Γ_{24}/Γ_{151}

VALUE (%)	EVTS	DOCUMENT ID		TECN	COMMENT
10.9 ±1.7 ±2.7	20k	[1] LEES	17C	BABR	$J/\psi \to \pi^+\pi^-\pi^0$
• • • We do not use the following data for averages, fits, limits, etc. • • •					
0.80±0.27	20k	[2] LEES	17C	BABR	$J/\psi \to \pi^+\pi^-\pi^0$

[1] From a Dalitz plot analysis in an isobar model.
[2] From a Dalitz plot analysis in a Veneziano model.

$\Gamma(\rho(1450)^\pm\pi^\mp \to K^0_S K^\pm\pi^\mp)/\Gamma(K^0_S K^\pm\pi^\mp)$ — Γ_{25}/Γ_{169}

VALUE (%)	EVTS	DOCUMENT ID		TECN	COMMENT
6.3±0.8±0.6	4k	[1] LEES	17C	BABR	$J/\psi \to K^0_S K^\pm\pi^\mp$

[1] From a Dalitz plot analysis in an isobar model.

$\Gamma(\rho(1450)^0\pi^0 \to K^+K^-\pi^0)/\Gamma(K^+K^-\pi^0)$ — Γ_{26}/Γ_{168}

VALUE (%)	EVTS	DOCUMENT ID		TECN	COMMENT
9.3±2.0±0.6	2k	[1] LEES	17C	BABR	$J/\psi \to K^+K^-\pi^0$

[1] From a Dalitz plot analysis in an isobar model.

$\Gamma(\rho(1450)\eta'(958) \to \pi^+\pi^-\eta'(958))/\Gamma_{total}$ — Γ_{27}/Γ

VALUE (units 10^{-6})	EVTS	DOCUMENT ID		TECN	COMMENT
3.28±0.55±0.44	119	[1] ABLIKIM	17AK	BES3	$J/\psi \to \pi^+\pi^-\eta'$

[1] From a partial wave analysis of the decay $J/\psi \to \pi^+\pi^-\eta'$.

$\Gamma(\rho(1700)\pi \to \pi^+\pi^-\pi^0)/\Gamma(\pi^+\pi^-\pi^0)$ — Γ_{29}/Γ_{151}

VALUE (units 10^{-3})	EVTS	DOCUMENT ID		TECN	COMMENT
8±2±5	20k	[1] LEES	17C	BABR	$J/\psi \to \pi^+\pi^-\pi^0$
• • • We do not use the following data for averages, fits, limits, etc. • • •					
22±6	20k	[2] LEES	17C	BABR	$J/\psi \to \pi^+\pi^-\pi^0$

[1] From a Dalitz plot analysis in an isobar model.
[2] From a Dalitz plot analysis in a Veneziano model.

$\Gamma(\rho(2150)\pi \to \pi^+\pi^-\pi^0)/\Gamma(\pi^+\pi^-\pi^0)$ — Γ_{31}/Γ_{151}

VALUE (units 10^{-4})	EVTS	DOCUMENT ID		TECN	COMMENT
4± 1±20	20k	[1] LEES	17C	BABR	$J/\psi \to \pi^+\pi^-\pi^0$
• • • We do not use the following data for averages, fits, limits, etc. • • •					
600±250	20k	[2] LEES	17C	BABR	$J/\psi \to \pi^+\pi^-\pi^0$

[1] From a Dalitz plot analysis in an isobar model.
[2] From a Dalitz plot analysis in a Veneziano model.

$\Gamma(\rho_3(1690)\pi \to \pi^+\pi^-\pi^0)/\Gamma(\pi^+\pi^-\pi^0)$ — Γ_{32}/Γ_{151}

VALUE (units 10^{-3})	EVTS	DOCUMENT ID		TECN	COMMENT
• • • We do not use the following data for averages, fits, limits, etc. • • •					
4.0±0.8	20k	[1] LEES	17C	BABR	$J/\psi \to \pi^+\pi^-\pi^0$

[1] From a Dalitz plot analysis in a Veneziano model.

$\Gamma(\omega\pi^0)/\Gamma_{total}$ — Γ_{33}/Γ

VALUE (units 10^{-3})	EVTS	DOCUMENT ID		TECN	COMMENT
0.45 ±0.05 OUR AVERAGE	Error includes scale factor of 1.4. See the ideogram below.				
0.538±0.012±0.065	2090	[1] ABLIKIM	06F	BES2	$J/\psi \to \omega\pi^0$
0.360±0.028±0.054	222	JOUSSET	90	DM2	$J/\psi \to$ hadrons
0.482±0.019±0.064		COFFMAN	88	MRK3	$e^+e^- \to \pi^0\pi^+\pi^-\pi^0$

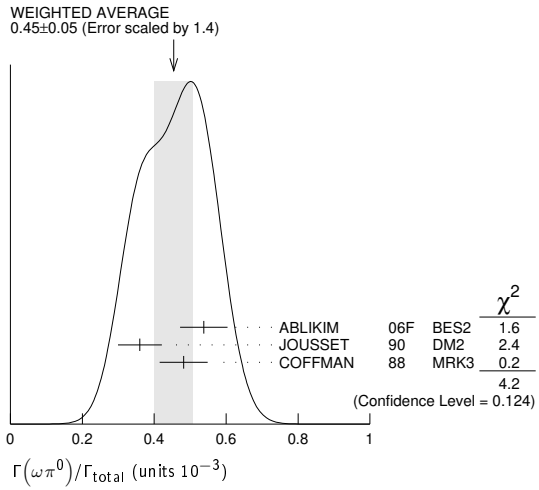

[1] Using B$(\omega \to \pi^+\pi^-\pi^0) = (89.1 \pm 0.7)\%$.

$\Gamma(\omega\pi^0 \to \pi^+\pi^-\pi^0)/\Gamma(\pi^+\pi^-\pi^0)$ — Γ_{34}/Γ_{151}

VALUE (units 10^{-4})	EVTS	DOCUMENT ID		TECN	COMMENT
8±3±2	20k	[1] LEES	17C	BABR	$J/\psi \to \pi^+\pi^-\pi^0$

[1] From a Dalitz plot analysis in an isobar model and significance 4.9 σ.

$\Gamma(\omega\pi^+\pi^-)/\Gamma_{total}$ — Γ_{35}/Γ

VALUE (units 10^{-3})	EVTS	DOCUMENT ID		TECN	COMMENT
7.2±1.0 OUR AVERAGE					
7.0±1.6	18058	AUGUSTIN	89	DM2	$J/\psi \to 2(\pi^+\pi^-)\pi^0$
7.8±1.6	215	BURMESTER	77D	PLUT	e^+e^-
6.8±1.9	348	VANNUCCI	77	MRK1	$e^+e^- \to 2(\pi^+\pi^-)\pi^0$

$\Gamma(\omega\pi^0\pi^0)/\Gamma_{total}$ — Γ_{36}/Γ

VALUE (units 10^{-3})	EVTS	DOCUMENT ID		TECN	COMMENT
3.4±0.3±0.7	509	AUGUSTIN	89	DM2	$J/\psi \to \pi^+\pi^-3\pi^0$

$\Gamma(\omega f_2(1270))/\Gamma_{total}$ — Γ_{38}/Γ

VALUE (units 10^{-3})	EVTS	DOCUMENT ID		TECN	COMMENT
4.3±0.6 OUR AVERAGE					
4.3±0.2±0.6	5860	AUGUSTIN	89	DM2	e^+e^-
4.0±1.6	70	BURMESTER	77D	PLUT	e^+e^-
• • • We do not use the following data for averages, fits, limits, etc. • • •					
1.9±0.8	81	VANNUCCI	77	MRK1	$e^+e^- \to 2(\pi^+\pi^-)\pi^0$

Downloaded from https://academic.oup.com/ptep/article/2022/8/083C01/6651666 by KIT Library user on 27 September 2022

$\Gamma(\omega\eta)/\Gamma_{total}$ — Γ_{39}/Γ

VALUE (units 10^{-3})	EVTS	DOCUMENT ID		TECN	COMMENT
1.74 ±0.20 OUR AVERAGE		Error includes scale factor of 1.6. See the ideogram below.			
2.352±0.273	5k	[1] ABLIKIM	06F	BES2	$J/\psi \to \omega\eta$
1.44 ±0.40 ±0.14	13	[2] AUBERT	06D	BABR	10.6 $e^+e^- \to \omega\eta\gamma$
1.43 ±0.10 ±0.21	378	JOUSSET	90	DM2	$J/\psi \to$ hadrons
1.71 ±0.08 ±0.20		COFFMAN	88	MRK3	$e^+e^- \to 3\pi\eta$

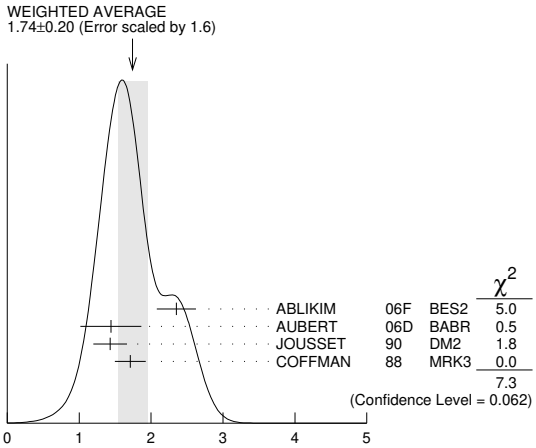

[1] Using $B(\eta \to 2\gamma) = (39.43 \pm 0.26)\%$, $B(\eta \to \pi^+\pi^-\pi^0) = 22.6 \pm 0.4\%$, $B(\eta \to \pi^+\pi^-\gamma) = 4.68 \pm 0.11\%$, and $B(\omega \to \pi^+\pi^-\pi^0) = (89.1 \pm 0.7)\%$.

[2] Using $\Gamma(J/\psi \to e^+e^-) = 5.52 \pm 0.14 \pm 0.04$ keV.

$\Gamma(\omega\pi^+\pi^+\pi^-\pi^-)/\Gamma_{total}$ — Γ_{42}/Γ

VALUE (units 10^{-4})	EVTS	DOCUMENT ID		TECN	COMMENT
85±34	140	VANNUCCI	77	MRK1	$e^+e^- \to 3(\pi^+\pi^-)\pi^0$

$\Gamma(\omega\eta'\pi^+\pi^-)/\Gamma_{total}$ — Γ_{44}/Γ

VALUE (units 10^{-3})	EVTS	DOCUMENT ID		TECN	COMMENT
1.12±0.02±0.13	14k	[1] ABLIKIM	19AC	BES3	$J/\psi \to \omega\eta'\pi^+\pi^-$

[1] Using the decays $\omega \to \pi^+\pi^-\pi^0$ and $\eta' \to \eta\pi^+\pi^-$.

$\Gamma(\omega\eta'(958))/\Gamma_{total}$ — Γ_{45}/Γ

VALUE (units 10^{-4})	EVTS	DOCUMENT ID		TECN	COMMENT
1.89±0.18 OUR AVERAGE					
2.08±0.30±0.14	137	[1] ABLIKIM	17AK	BES3	$J/\psi \to \pi^+\pi^-\eta'$
2.26±0.43	218	[2] ABLIKIM	06F	BES2	$J/\psi \to \omega\eta'$
$1.8\ ^{+1.0}_{-0.8}\ \pm0.3$	6	JOUSSET	90	DM2	$J/\psi \to$ hadrons
1.66±0.17±0.19		COFFMAN	88	MRK3	$e^+e^- \to 3\pi\eta'$

[1] From a partial wave analysis of the decay $J/\psi \to \pi^+\pi^-\eta'$.

[2] Using $B(\eta' \to \pi^+\pi^-\eta) = (44.3 \pm 1.5)\%$, $B(\eta' \to \pi^+\pi^-\gamma) = 29.5 \pm 1.0\%$, $B(\eta \to 2\gamma) = 39.43 \pm 0.26\%$, and $B(\omega \to \pi^+\pi^-\pi^0) = (89.1 \pm 0.7)\%$.

$\Gamma(\omega f_0(980))/\Gamma_{total}$ — Γ_{46}/Γ

VALUE (units 10^{-4})	DOCUMENT ID		TECN	COMMENT
1.41±0.27±0.47	[1] AUGUSTIN	89	DM2	$J/\psi \to 2(\pi^+\pi^-)\pi^0$

[1] Assuming $B(f_0(980) \to \pi\pi) = 0.78$.

$\Gamma(\omega f_0(1710) \to \omega K\overline{K})/\Gamma_{total}$ — Γ_{47}/Γ

VALUE (units 10^{-4})	DOCUMENT ID		TECN	COMMENT
4.8±1.1±0.3	[1,2] FALVARD	88	DM2	$J/\psi \to$ hadrons

[1] Includes unknown branching fraction $f_0(1710) \to K\overline{K}$.

[2] Addition of $f_0(1710) \to K^+K^-$ and $f_0(1710) \to K^0\overline{K}^0$ branching ratios.

$\Gamma(\omega f_1(1420))/\Gamma_{total}$ — Γ_{48}/Γ

VALUE (units 10^{-4})	EVTS	DOCUMENT ID		TECN	COMMENT
$\mathbf{6.8^{+1.9}_{-1.6}\pm1.7}$	111^{+31}_{-26}	BECKER	87	MRK3	$e^+e^- \to$ hadrons

$\Gamma(\omega f_2'(1525))/\Gamma_{total}$ — Γ_{49}/Γ

VALUE	CL%	DOCUMENT ID		TECN	COMMENT
$<2.2 \times 10^{-4}$	90	[1] VANNUCCI	77	MRK1	$e^+e^- \to \pi^+\pi^-\pi^0K^+K^-$
• • • We do not use the following data for averages, fits, limits, etc. • • •					
$<2.8 \times 10^{-4}$	90	[1] FALVARD	88	DM2	$J/\psi \to$ hadrons

[1] Re-evaluated assuming $B(f_2'(1525) \to K\overline{K}) = 0.713$.

$\Gamma(\omega X(1835) \to \omega p\overline{p})/\Gamma_{total}$ — Γ_{50}/Γ

VALUE	CL%	DOCUMENT ID		TECN	COMMENT
$<3.9 \times 10^{-6}$	95	ABLIKIM	13P	BES3	$J/\psi \to \gamma\pi^0p\overline{p}$

$\Gamma(\omega X(1835),\ X \to \eta'\pi^+\pi^-)/\Gamma_{total}$ — Γ_{51}/Γ

VALUE	DOCUMENT ID		TECN	COMMENT
$<6.2 \times 10^{-5}$	[1] ABLIKIM	19AC	BES3	$J/\psi \to \omega\eta'\pi^+\pi^-$

[1] Using the decays $\omega \to \pi^+\pi^-\pi^0$ and $\eta' \to \eta\pi^+\pi^-$.

$\Gamma(\omega K^\pm K^0_S\pi^\mp)/\Gamma_{total}$ — Γ_{52}/Γ

VALUE (units 10^{-4})	EVTS	DOCUMENT ID		TECN	COMMENT
34 ±5 OUR AVERAGE					
37.7±0.8±5.8	1972 ± 41	ABLIKIM	08E	BES2	$e^+e^- \to J/\psi$
29.5±1.4±7.0	879 ± 41	BECKER	87	MRK3	$e^+e^- \to$ hadrons

$\Gamma(\omega K\overline{K})/\Gamma_{total}$ — Γ_{53}/Γ

VALUE (units 10^{-4})	EVTS	DOCUMENT ID		TECN	COMMENT
19 ± 4 OUR AVERAGE					
19.8± 2.1±3.9		[1] FALVARD	88	DM2	$J/\psi \to$ hadrons
16 ±10	22	FELDMAN	77	MRK1	e^+e^-

[1] Addition of ωK^+K^- and $\omega K^0\overline{K}^0$ branching ratios.

$\Gamma(\omega K^*(892)\overline{K} + c.c.)/\Gamma_{total}$ — Γ_{54}/Γ

VALUE (units 10^{-4})	EVTS	DOCUMENT ID		TECN	COMMENT
61 ± 9 OUR AVERAGE					
62.0± 6.8±10.6	899 ± 98	ABLIKIM	08E	BES2	$J/\psi \to \omega K^0_S K^\pm\pi^\mp$
65.3±10.2±13.5	176 ± 28	ABLIKIM	08E	BES2	$J/\psi \to \omega K^+K^-\pi^0$
53 ±14 ±14	530 ± 140	BECKER	87	MRK3	$e^+e^- \to$ hadrons

$\Gamma(\eta' K^{*\pm}K^\mp)/\Gamma_{total}$ — Γ_{55}/Γ

VALUE (units 10^{-3})	DOCUMENT ID		TECN	COMMENT
1.48±0.13 OUR AVERAGE				
1.50±0.02±0.19	[1] ABLIKIM	18AB	BES3	$J/\psi \to \eta' K^*\overline{K}$
1.47±0.03±0.17	[2] ABLIKIM	18AB	BES3	$J/\psi \to \eta' K^*\overline{K}$

[1] From $\eta' K^+K^-\pi^0$.

[2] From $\eta' K^0_S K^\pm\pi^\mp$.

$\Gamma(\eta' K^{*0}\overline{K}^0 + c.c.)/\Gamma_{total}$ — Γ_{56}/Γ

VALUE (units 10^{-3})	DOCUMENT ID		TECN	COMMENT
1.66±0.03±0.21	[1] ABLIKIM	18AB	BES3	$J/\psi \to \eta' K^*\overline{K}$

[1] From $\eta' K^0_S K^\pm\pi^\mp$.

$\Gamma(\eta' h_1(1415) \to \eta' K^*\overline{K} + c.c.)/\Gamma_{total}$ — Γ_{57}/Γ

VALUE (units 10^{-4})	EVTS	DOCUMENT ID		TECN	COMMENT
2.16±0.12±0.29	1.1k	[1] ABLIKIM	18AB	BES3	$J/\psi \to \eta' h_1 \to \eta' K^*\overline{K}$

[1] From $\eta' K^0_S K^\pm\pi^\mp$.

$\Gamma(\eta' h_1(1415) \to \eta' K^{*\pm}K^\mp)/\Gamma_{total}$ — Γ_{58}/Γ

VALUE (units 10^{-4})	EVTS	DOCUMENT ID		TECN	COMMENT
1.51±0.09±0.21	1.0k	[1] ABLIKIM	18AB	BES3	$J/\psi \to \eta' h_1 \to \eta' K^*\overline{K}$

[1] From $\eta' K^+K^-\pi^0$.

$\Gamma(\overline{K}K^*(892) + c.c. \to K^0_S K^\pm\pi^\mp)/\Gamma(K^0_S K^\pm\pi^\mp)$ — Γ_{60}/Γ_{169}

VALUE (%)	EVTS	DOCUMENT ID		TECN	COMMENT
90.5±0.9±3.8	4k	[1] LEES	17C	BABR	$J/\psi \to K^0_S K^\pm\pi^\mp$

[1] From a Dalitz plot analysis in an isobar model.

$\Gamma(K^+K^*(892)^- + c.c.)/\Gamma_{total}$ — Γ_{61}/Γ

VALUE (units 10^{-3})	EVTS	DOCUMENT ID		TECN	COMMENT
$6.0\ ^{+0.8}_{-1.0}$ OUR AVERAGE		Error includes scale factor of 2.9. See the ideogram below.			
$8.07\pm0.04\ ^{+0.38}_{-0.61}$	183k	ABLIKIM	19AQ	BES	$J/\psi \to K^+K^-\pi^0$
4.57±0.17±0.70	2285	JOUSSET	90	DM2	$J/\psi \to$ hadrons
5.26±0.13±0.53		COFFMAN	88	MRK3	$J/\psi \to K^\pm K^0_S\pi^\mp$, $K^+K^-\pi^0$
• • • We do not use the following data for averages, fits, limits, etc. • • •					
2.6 ±0.6	24	FRANKLIN	83	MRK2	$J/\psi \to K^+K^-\pi^0$
3.2 ±0.6	48	VANNUCCI	77	MRK1	$J/\psi \to K^\pm K^0_S\pi^\mp$
4.1 ±1.2	39	BRAUNSCH...	76	DASP	$J/\psi \to K^\pm X$

Downloaded from https://academic.oup.com/ptep/article/2022/8/083C01/6651666 by KIT Library user on 27 September 2022

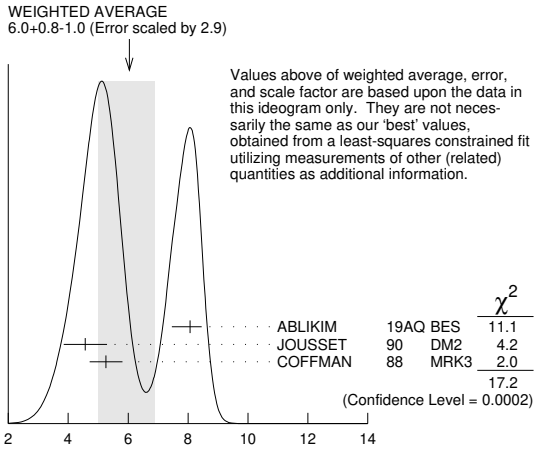

$\Gamma(K^+ K^*(892)^- + \text{c.c.} \to K^+ K^- \pi^0)/\Gamma_{\text{total}}$ — Γ_{62}/Γ

VALUE (units 10^{-3})	EVTS	DOCUMENT ID		TECN	COMMENT
$2.69 \pm 0.01^{+0.13}_{-0.20}$	183k	ABLIKIM	19AQ	BES	$J/\psi \to K^+ K^- \pi^0$

$\Gamma(K^+ K^*(892)^- + \text{c.c.} \to K^+ K^- \pi^0)/\Gamma(K^+ K^- \pi^0)$ — Γ_{62}/Γ_{168}

VALUE (%)	EVTS	DOCUMENT ID		TECN	COMMENT
$92.4 \pm 1.5 \pm 3.4$	2k	[1] LEES	17C	BABR	$J/\psi \to K^+ K^- \pi^0$

[1] From a Dalitz plot analysis in an isobar model.

$\Gamma(K^0 \overline{K}^*(892)^0 + \text{c.c.})/\Gamma_{\text{total}}$ — Γ_{64}/Γ

VALUE (units 10^{-3})	EVTS	DOCUMENT ID		TECN	COMMENT
4.2 ±0.4 OUR AVERAGE					
$3.96 \pm 0.15 \pm 0.60$	1192	JOUSSET	90	DM2	$J/\psi \to$ hadrons
$4.33 \pm 0.12 \pm 0.45$		COFFMAN	88	MRK3	$J/\psi \to K^\pm K^0_S \pi^\mp$
• • • We do not use the following data for averages, fits, limits, etc. • • •					
2.7 ± 0.6	45	VANNUCCI	77	MRK1	$J/\psi \to K^\pm K^0_S \pi^\mp$

$\Gamma(\overline{K}^*(892)^0 K^+ \pi^- + \text{c.c.})/\Gamma_{\text{total}}$ — Γ_{66}/Γ

VALUE	DOCUMENT ID		TECN	COMMENT
• • • We do not use the following data for averages, fits, limits, etc. • • •				
seen	[1] ABLIKIM	06C	BES2	$J/\psi \to \overline{K}^*(892)^0 K^+ \pi^-$

[1] A $K^*_0(700)$ is observed by ABLIKIM 06C in the $K^+\pi^-$ mass spectrum of the $\overline{K}^*(892)^0 K^+ \pi^-$ final state against the $\overline{K}^*(892)$. A corresponding branching fraction of the $J/\psi(1S)$ is not presented.

$\Gamma(K^*(892)^0 K^0_S \to \gamma K^0_S K^0_S)/\Gamma_{\text{total}}$ — Γ_{70}/Γ

VALUE (units 10^{-6})	DOCUMENT ID		TECN	COMMENT
$6.28^{+0.16+0.59}_{-0.17-0.52}$	ABLIKIM	18AA	BES3	$J/\psi \to \gamma K^0_S K^0_S$

$\Gamma(K^*(892)^\pm K^*(700)^\mp)/\Gamma_{\text{total}}$ — Γ_{72}/Γ

VALUE (units 10^{-3})	EVTS	DOCUMENT ID		TECN	COMMENT
$1.09 \pm 0.18^{+0.94}_{-0.54}$	655	ABLIKIM	10E	BES2	$J/\psi \to K^\pm K^0_S \pi^\mp \pi^0$

$\Gamma(K^*(892)^0 \overline{K}^*(892)^0)/\Gamma_{\text{total}}$ — Γ_{73}/Γ

VALUE (units 10^{-4})	CL%	DOCUMENT ID		TECN	COMMENT
• • • We do not use the following data for averages, fits, limits, etc. • • •					
<5	90	VANNUCCI	77	MRK1	$e^+e^- \to \pi^+\pi^- K^+ K^-$

$\Gamma(K^*(892)^\pm K^*(892)^\mp)/\Gamma_{\text{total}}$ — Γ_{74}/Γ

VALUE (units 10^{-3})	EVTS	DOCUMENT ID		TECN	COMMENT
$1.00 \pm 0.19^{+0.11}_{-0.32}$	323	ABLIKIM	10E	BES2	$J/\psi \to K^\pm K^0_S \pi^\mp \pi^0$

$\Gamma(K_1(1400)^\pm K^\mp)/\Gamma_{\text{total}}$ — Γ_{75}/Γ

VALUE (units 10^{-3})	DOCUMENT ID		TECN	COMMENT
$3.8 \pm 0.8 \pm 1.2$	[1] BAI	99C	BES	e^+e^-

[1] Assuming $B(K_1(1400) \to K^*\pi) = 0.94 \pm 0.06$

$\Gamma(K^*(1410)\overline{K} + \text{c.c.} \to K^\pm K^\mp \pi^0)/\Gamma(K^+ K^- \pi^0)$ — Γ_{77}/Γ_{168}

VALUE (%)	EVTS	DOCUMENT ID		TECN	COMMENT
$2.3 \pm 1.1 \pm 0.7$	2k	[1] LEES	17C	BABR	$J/\psi \to K^+ K^- \pi^0$

[1] From a Dalitz plot analysis in an isobar model.

$\Gamma(K^*(1410)\overline{K} + \text{c.c.} \to K^0_S K^\pm \pi^\mp)/\Gamma(K^0_S K^\pm \pi^\mp)$ — Γ_{78}/Γ_{169}

VALUE (%)	EVTS	DOCUMENT ID		TECN	COMMENT
$1.5 \pm 0.5 \pm 0.9$	4k	[1] LEES	17C	BABR	$J/\psi \to K^0_S K^\pm \pi^\mp$

[1] From a Dalitz plot analysis in an isobar model.

$\Gamma(K^*_2(1430)\overline{K} + \text{c.c.} \to K^\pm K^\mp \pi^0)/\Gamma(K^+ K^- \pi^0)$ — Γ_{80}/Γ_{168}

VALUE (%)	EVTS	DOCUMENT ID		TECN	COMMENT
$3.5 \pm 1.3 \pm 0.9$	2k	[1] LEES	17C	BABR	$J/\psi \to K^+ K^- \pi^0$

[1] From a Dalitz plot analysis in an isobar model.

$\Gamma(K^*_2(1430)\overline{K} + \text{c.c.} \to K^0_S K^\pm \pi^\mp)/\Gamma(K^0_S K^\pm \pi^\mp)$ — Γ_{81}/Γ_{169}

VALUE (%)	EVTS	DOCUMENT ID		TECN	COMMENT
$7.1 \pm 1.3 \pm 1.2$	4k	[1] LEES	17C	BABR	$J/\psi \to K^0_S K^\pm \pi^\mp$

[1] From a Dalitz plot analysis in an isobar model.

$\Gamma(\overline{K}^*_2(1430) K + \text{c.c.})/\Gamma_{\text{total}}$ — Γ_{82}/Γ

VALUE	CL%	DOCUMENT ID		TECN	COMMENT
$<40 \times 10^{-4}$	90	VANNUCCI	77	MRK1	$e^+e^- \to K^0 \overline{K}^{*0}_2$
• • • We do not use the following data for averages, fits, limits, etc. • • •					
$<66 \times 10^{-4}$	90	BRAUNSCH...	76	DASP	$e^+e^- \to K^\pm \overline{K}^{*\mp}_2$

$\Gamma(K^*_2(1430)^+ K^- + \text{c.c.} \to K^+ K^- \pi^0)/\Gamma_{\text{total}}$ — Γ_{83}/Γ

VALUE (units 10^{-4})	EVTS	DOCUMENT ID		TECN	COMMENT
$2.69 \pm 0.04^{+0.25}_{-0.19}$	183k	ABLIKIM	19AQ	BES	$J/\psi \to K^+ K^- \pi^0$

$\Gamma(\overline{K}^*_2(1430)^0 K^*(892)^0 + \text{c.c.})/\Gamma_{\text{total}}$ — Γ_{85}/Γ

VALUE (units 10^{-3})	EVTS	DOCUMENT ID		TECN	COMMENT
• • • We do not use the following data for averages, fits, limits, etc. • • •					
6.7 ± 2.6	40	VANNUCCI	77	MRK1	$e^+e^- \to \pi^+\pi^- K^+ K^-$

$\Gamma(K^*_2(1430)^0 \overline{K}^*_2(1430)^0)/\Gamma_{\text{total}}$ — Γ_{88}/Γ

VALUE	CL%	DOCUMENT ID		TECN	COMMENT
$<29 \times 10^{-4}$	90	VANNUCCI	77	MRK1	$e^+e^- \to \pi^+\pi^- K^+ K^-$

$\Gamma(K^*_2(1980)^+ K^- + \text{c.c.} \to K^+ K^- \pi^0)/\Gamma_{\text{total}}$ — Γ_{90}/Γ

VALUE (units 10^{-5})	EVTS	DOCUMENT ID		TECN	COMMENT
$1.1 \pm 0.1^{+0.6}_{-0.1}$	183k	ABLIKIM	19AQ	BES	$J/\psi \to K^+ K^- \pi^0$

$\Gamma(K^*_4(2045)^+ K^- + \text{c.c.} \to K^+ K^- \pi^0)/\Gamma_{\text{total}}$ — Γ_{91}/Γ

VALUE (units 10^{-6})	EVTS	DOCUMENT ID		TECN	COMMENT
$6.2 \pm 0.7^{+2.8}_{-1.4}$	183k	ABLIKIM	19AQ	BES	$J/\psi \to K^+ K^- \pi^0$

$\Gamma(K_1(1270)^\pm K^\mp)/\Gamma_{\text{total}}$ — Γ_{92}/Γ

VALUE	CL%	DOCUMENT ID		TECN	COMMENT
$<3.0 \times 10^{-3}$	90	[1] BAI	99C	BES	e^+e^-

[1] Assuming $B(K_1(1270) \to K\rho) = 0.42 \pm 0.06$

$\Gamma(K_1(1270) K^0_S \to \gamma K^0_S K^0_S)/\Gamma_{\text{total}}$ — Γ_{93}/Γ

VALUE (units 10^{-7})	DOCUMENT ID		TECN	COMMENT
$8.54^{+1.07+2.35}_{-1.20-2.13}$	ABLIKIM	18AA	BES3	$J/\psi \to \gamma K^0_S K^0_S$

$\Gamma(a_2(1320)^\pm \pi^\mp)/\Gamma_{\text{total}}$ — Γ_{94}/Γ

VALUE	CL%	DOCUMENT ID		TECN	COMMENT
$<43 \times 10^{-4}$	90	BRAUNSCH...	76	DASP	e^+e^-

$\Gamma(\phi\pi^0)/\Gamma_{\text{total}}$ — Γ_{95}/Γ

The two different fit values of ABLIKIM 15K below have the same statistical significance of 6.4 σ and cannot be distinguished at this moment.

VALUE (units 10^{-6})	CL%	EVTS	DOCUMENT ID		TECN	COMMENT
$2.94 \pm 0.16 \pm 0.16$		0.8k	[1] ABLIKIM	15K	BES3	$e^+e^- \to J/\psi \to K^+ K^- \gamma\gamma$
$0.124 \pm 0.033 \pm 0.030$		35 ± 9	[2] ABLIKIM	15K	BES3	$e^+e^- \to J/\psi \to K^+ K^- \gamma\gamma$
• • • We do not use the following data for averages, fits, limits, etc. • • •						
<6.4	90		[3] ABLIKIM	05B	BES2	$e^+e^- \to J/\psi \to \phi\gamma\gamma$
<6.8	90		COFFMAN	88	MRK3	$e^+e^- \to K^+ K^- \pi^0$

[1] Corresponding to one of the two fit solutions with $\delta = (-95.9 \pm 1.5)^\circ$ for the phase angle between the resonant $J/\psi \to \phi\pi^0$ and non-phi $J/\psi \to K^+ K^- \pi^0$ contributions.
[2] Corresponding to one of the two fit solutions with $\delta = (-152.1 \pm 7.7)^\circ$ for the phase angle between the resonant $J/\psi \to \phi\pi^0$ and non-phi $J/\psi \to K^+ K^- \pi^0$ contributions.
[3] Superseded by ABLIKIM 15K.

Downloaded from https://academic.oup.com/ptep/article/2022/8/083C01/6651666 by KIT Library user on 27 September 2022

$\Gamma(\phi\pi^+\pi^-)/\Gamma_{total}$ — Γ_{96}/Γ

VALUE (units 10^{-3})	EVTS	DOCUMENT ID		TECN	COMMENT
0.94±0.15 OUR AVERAGE		Error includes scale factor of 1.7.			
1.09±0.02±0.13		ABLIKIM	05	BES2	$J/\psi \to \phi\pi^+\pi^-$
0.78±0.03±0.12		FALVARD	88	DM2	$J/\psi \to$ hadrons
2.1 ±0.9	23	FELDMAN	77	MRK1	e^+e^-

$\Gamma(\phi 2(\pi^+\pi^-))/\Gamma_{total}$ — Γ_{98}/Γ

VALUE (units 10^{-4})	DOCUMENT ID		TECN	COMMENT
16.0±1.0±3.0	FALVARD	88	DM2	$J/\psi \to$ hadrons

$\Gamma(\phi\eta)/\Gamma_{total}$ — Γ_{99}/Γ

VALUE (units 10^{-3})	EVTS	DOCUMENT ID		TECN	COMMENT
0.74 ±0.08 OUR AVERAGE		Error includes scale factor of 1.5. See the ideogram below.			
0.898±0.024±0.089		ABLIKIM	05B	BES2	$e^+e^- \to J/\psi \to$ hadr
0.64 ±0.04 ±0.11	346	JOUSSET	90	DM2	$J/\psi \to$ hadrons
0.661±0.045±0.078		COFFMAN	88	MRK3	$e^+e^- \to K^+K^-\eta$

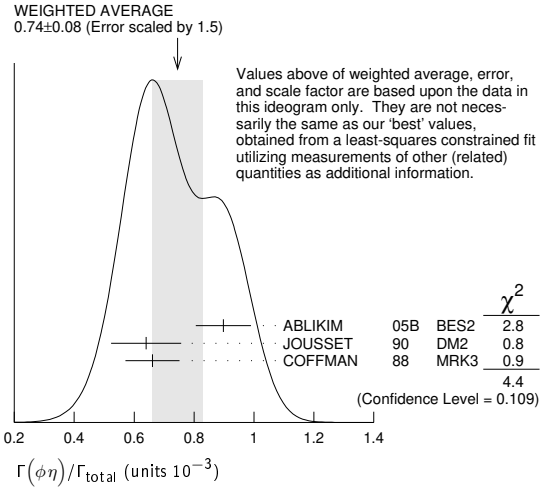

$\Gamma(\phi\eta'(958))/\Gamma_{total}$ — Γ_{100}/Γ

VALUE (units 10^{-4})	CL%	EVTS	DOCUMENT ID		TECN	COMMENT
4.6 ±0.5 OUR AVERAGE			Error includes scale factor of 2.2. See the ideogram below.			
5.10±0.03±0.32		31k	ABLIKIM	16M	BES3	$e^+e^- \to J/\psi \to$ hadrons
5.46±0.31±0.56			ABLIKIM	05B	BES2	$e^+e^- \to J/\psi \to$ hadrons
4.1 ±0.3 ±0.8		167	JOUSSET	90	DM2	$J/\psi \to$ hadrons
3.08±0.34±0.36			COFFMAN	88	MRK3	$e^+e^- \to K^+K^-\eta'$
• • • We do not use the following data for averages, fits, limits, etc. • • •						
< 13	90		VANNUCCI	77	MRK1	e^+e^-

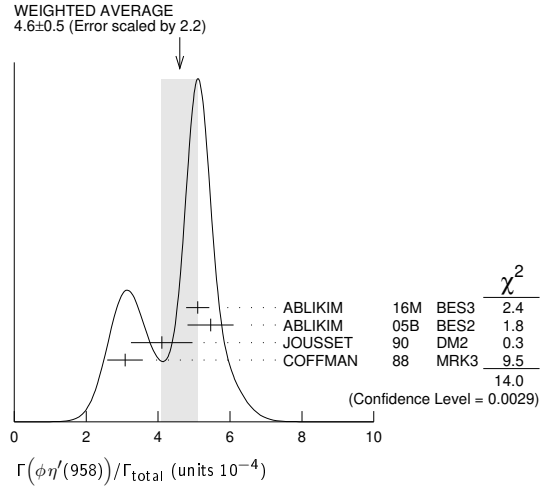

$\Gamma(\phi\eta\eta')/\Gamma_{total}$ — Γ_{101}/Γ

VALUE (units 10^{-4})	EVTS	DOCUMENT ID		TECN	COMMENT
2.32±0.06±0.16	2.2k	[1] ABLIKIM	19AN	BES3	$e^+e^- \to J/\psi \to$ hadrons

[1] Including contributions from intermediate resonances. Evidence for an intermediate resonance at M ≈ 2 GeV and Γ ≈ 150 MeV decaying to $\phi\eta'$ with $J^P = 1^+$ or $J^P = 1^-$, and $B(J/\psi \to \eta X) \times B(X \to \phi\eta') \approx 10^{-4}$.

$\Gamma(\phi f_0(980))/\Gamma_{total}$ — Γ_{102}/Γ

VALUE (units 10^{-4})	EVTS	DOCUMENT ID		TECN	COMMENT
3.2±0.9 OUR AVERAGE		Error includes scale factor of 1.9.			
4.6±0.4±0.8		[1] FALVARD	88	DM2	$J/\psi \to$ hadrons
2.6±0.6	50	[1] GIDAL	81	MRK2	$J/\psi \to K^+K^-K^+K^-$

[1] Assuming $B(f_0(980) \to \pi\pi) = 0.78$.

$\Gamma(\phi\pi^0 f_0(980) \to \phi\pi^0\pi^+\pi^-)/\Gamma_{total}$ — Γ_{105}/Γ

VALUE (units 10^{-6})	EVTS	DOCUMENT ID		TECN	COMMENT
4.50±0.80±0.61	355	ABLIKIM	15P	BES3	$J/\psi \to K^+K^-3\pi$

$\Gamma(\phi\pi^0 f_0(980) \to \phi\pi^0 p^0\pi^0)/\Gamma_{total}$ — Γ_{106}/Γ

VALUE (units 10^{-6})	EVTS	DOCUMENT ID		TECN	COMMENT
1.67±0.50±0.24	70	ABLIKIM	15P	BES3	$J/\psi \to K^+K^-3\pi$

$\Gamma(\phi f_0(980)\eta \to \eta\phi\pi^+\pi^-)/\Gamma_{total}$ — Γ_{107}/Γ

VALUE (units 10^{-4})	EVTS	DOCUMENT ID		TECN	COMMENT
3.23±0.75±0.73	52	ABLIKIM	08F	BES	$J/\psi \to \eta\phi f_0(980)$

$\Gamma(\phi a_0(980)^0 \to \phi\eta\pi^0)/\Gamma_{total}$ — Γ_{108}/Γ

VALUE (units 10^{-6})	DOCUMENT ID		TECN	COMMENT
4.37±1.35	[1] ABLIKIM	18D	BES3	$J/\psi \to \phi\eta\pi^0$
• • • We do not use the following data for averages, fits, limits, etc. • • •				
5.0 ±2.7 ±2.5	[2] ABLIKIM	11D	BES3	$J/\psi \to \phi\eta\pi^0$

[1] Assuming constructive interference between $a_0(980) - f_0(980)$ mixing and electromagnetic decay. Destructive interference gives a value of $(4.93 \pm 1.77) \times 10^{-6}$ for this branching fraction.

[2] Assuming $a_0(980) - f_0(980)$ mixing and isospin breaking via γ^* and K^*K loops.

$\Gamma(\phi f_2(1270))/\Gamma_{total}$ — Γ_{109}/Γ

VALUE (units 10^{-3})	CL%	DOCUMENT ID		TECN	COMMENT
• • • We do not use the following data for averages, fits, limits, etc. • • •					
< 0.45	90	FALVARD	88	DM2	$J/\psi \to$ hadrons
< 0.37	90	VANNUCCI	77	MRK1	$e^+e^- \to \pi^+\pi^-K^+K^-$

$\Gamma(\phi f_1(1285))/\Gamma_{total}$ — Γ_{110}/Γ

VALUE (units 10^{-4})	EVTS	DOCUMENT ID		TECN	COMMENT
2.6±0.5 OUR AVERAGE					
3.4±1.8±1.5	1.1k	[1] ABLIKIM	15H	BES3	$e^+e^- \to J/\psi \to \phi\eta\pi^+\pi^-$
3.2±0.6±0.4		JOUSSET	90	DM2	$J/\psi \to \phi 2(\pi^+\pi^-)$
2.1±0.5±0.4	25	[2] JOUSSET	90	DM2	$J/\psi \to \phi\eta\pi^+\pi^-$
• • • We do not use the following data for averages, fits, limits, etc. • • •					
0.6±0.2±0.1	16	BECKER	87	MRK3	$J/\psi \to \phi K\overline{K}\pi$

[1] ABLIKIM 15H reports $[\Gamma(J/\psi(1S) \to \phi f_1(1285))/\Gamma_{total}] \times [B(f_1(1285) \to \eta\pi^+\pi^-)] = (1.20 \pm 0.6 \pm 0.14) \times 10^{-4}$ which we divide by our best value $B(f_1(1285) \to \eta\pi^+\pi^-) = (35 \pm 15) \times 10^{-2}$. Our first error is their experiment's error and our second error is the systematic error from using our best value.

[2] We attribute to the $f_1(1285)$ the signal observed in the $\pi^+\pi^-\eta$ invariant mass distribution at 1297 MeV.

$\Gamma(\phi f_1(1285) \to \phi\pi^0 f_0(980) \to \phi\pi^0\pi^+\pi^-)/\Gamma_{total}$ — Γ_{111}/Γ

VALUE (units 10^{-7})	EVTS	DOCUMENT ID		TECN	COMMENT
9.36±2.31±1.54	78	ABLIKIM	15P	BES3	$J/\psi \to K^+K^-3\pi$

$\Gamma(\phi f_1(1285) \to \phi\pi^0 f_0(980) \to \phi 3\pi^0)/\Gamma_{total}$ — Γ_{112}/Γ

VALUE (units 10^{-7})	EVTS	DOCUMENT ID		TECN	COMMENT
2.08±1.63±1.47	9	ABLIKIM	15P	BES3	$J/\psi \to K^+K^-3\pi$

$\Gamma(\phi\eta(1405) \to \phi\eta\pi^+\pi^-)/\Gamma_{total}$ — Γ_{113}/Γ

VALUE (units 10^{-5})	CL%	EVTS	DOCUMENT ID		TECN	COMMENT
2.01±0.58±0.82		172	[1] ABLIKIM	15H	BES3	$e^+e^- \to J/\psi \to \phi\eta\pi^+\pi^-$
• • • We do not use the following data for averages, fits, limits, etc. • • •						
< 17	90		[2] FALVARD	88	DM2	$J/\psi \to$ hadrons

[1] With 3.6 σ significance.

[2] Includes unknown branching fraction $\eta(1405) \to \eta\pi\pi$.

$\Gamma(\phi f_2'(1525))/\Gamma_{total}$ — Γ_{114}/Γ

VALUE (units 10^{-4})	EVTS	DOCUMENT ID		TECN	COMMENT
8 ±4 OUR AVERAGE		Error includes scale factor of 2.7.			
12.3±0.6±2.0		[1,2] FALVARD	88	DM2	$J/\psi \to$ hadrons
4.8±1.8	46	[1] GIDAL	81	MRK2	$J/\psi \to K^+K^-K^+K^-$

[1] Re-evaluated using $B(f_2'(1525) \to K\overline{K}) = 0.713$.

[2] Including interference with $f_0(1710)$.

$\Gamma(\phi X(1835) \to \phi p\overline{p})/\Gamma_{total}$ — Γ_{115}/Γ

VALUE	CL%	DOCUMENT ID		TECN	COMMENT
<2.1 × 10^{-7}	90	[1] ABLIKIM	16K	BES3	$J/\psi \to p\overline{p}K^0_S K^0_L$, $p\overline{p}K^+K^-$

[1] Upper limit applies to any $p\overline{p}$ mass enhancement near threshold.

Downloaded from https://academic.oup.com/ptep/article/2022/8/083C01/6651666 by KIT Library user on 27 September 2022

$\Gamma(\phi X(1835) \to \phi\eta\pi^+\pi^-)/\Gamma_{total}$ — Γ_{116}/Γ

VALUE	CL%	DOCUMENT ID		TECN	COMMENT
$<2.8 \times 10^{-4}$	90	ABLIKIM	15H	BES3	$e^+e^- \to J/\psi \to \phi\eta\pi^+\pi^-$

$\Gamma(\phi X(1870) \to \phi\eta\pi^+\pi^-)/\Gamma_{total}$ — Γ_{117}/Γ

VALUE	CL%	DOCUMENT ID		TECN	COMMENT
$<6.13 \times 10^{-5}$	90	ABLIKIM	15H	BES3	$e^+e^- \to J/\psi \to \phi\eta\pi^+\pi^-$

$\Gamma(\phi K\overline{K})/\Gamma_{total}$ — Γ_{118}/Γ

VALUE (units 10^{-4})	EVTS	DOCUMENT ID		TECN	COMMENT
17.7± 1.6 OUR AVERAGE Error includes scale factor of 1.3. See the ideogram below.					
16.6± 1.9±1.2	163 ± 19	LEES	12F	BABR	10.6 $e^+e^- \to 2(K^+K^-)\gamma$
21.4± 0.4±2.2		ABLIKIM	05	BES2	$J/\psi \to \phi\pi^+\pi^-$
48 $^{+20}_{-16}$ ±6	$9.0^{+3.7}_{-3.0}$	[1,2] HUANG	03	BELL	$B^+ \to (\phi K^+K^-)\ K^+$
14.6± 0.8±2.1		[3] FALVARD	88	DM2	$J/\psi \to$ hadrons
18 ± 8	14	FELDMAN	77	MRK1	e^+e^-

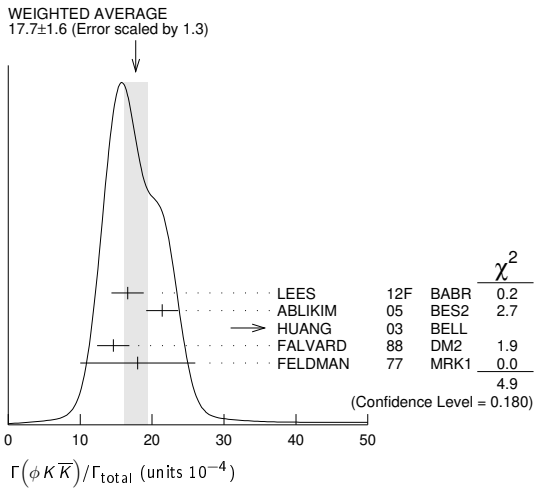

[1] We have multiplied K^+K^- measurement by 2 to obtain $K\overline{K}$.
[2] Using $B(B^+ \to J/\psi K^+) = (1.01 \pm 0.05) \times 10^{-3}$.
[3] Addition of ϕK^+K^- and $\phi K^0\overline{K}^0$ branching ratios.

$\Gamma(\phi f_0(1710) \to \phi K\overline{K})/\Gamma_{total}$ — Γ_{119}/Γ

VALUE (units 10^{-4})	DOCUMENT ID		TECN	COMMENT
3.6±0.2±0.6	[1,2] FALVARD	88	DM2	$J/\psi \to$ hadrons

[1] Including interference with $f_2'(1525)$.
[2] Includes unknown branching fraction $f_0(1710) \to K\overline{K}$.

$\Gamma(\phi K^\pm K^0_S \pi^\mp)/\Gamma_{total}$ — Γ_{122}/Γ

VALUE (units 10^{-4})	EVTS	DOCUMENT ID		TECN	COMMENT
7.2±0.8 OUR AVERAGE					
7.4±0.6±1.4	227 ± 19	ABLIKIM	08E	BES2	$e^+e^- \to J/\psi$
7.4±0.9±1.1		FALVARD	88	DM2	$J/\psi \to$ hadrons
7 ±0.6±1.0	163 ± 15	BECKER	87	MRK3	$e^+e^- \to$ hadrons

$\Gamma(\phi K^*(892)\overline{K} + c.c.)/\Gamma_{total}$ — Γ_{123}/Γ

VALUE (units 10^{-4})	EVTS	DOCUMENT ID		TECN	COMMENT
21.8±2.3 OUR AVERAGE					
20.8±2.7±3.9	195 ± 25	ABLIKIM	08E	BES2	$J/\psi \to \phi K^0_S K^\pm\pi^\mp$
29.6±3.7±4.7	238 ± 30	ABLIKIM	08E	BES2	$J/\psi \to \phi K^+K^-\pi^0$
20.7±2.4±3.0		FALVARD	88	DM2	$J/\psi \to$ hadrons
20 ±3 ±3	155 ± 20	BECKER	87	MRK3	$e^+e^- \to$ hadrons

$\Gamma(b_1(1235)^\pm\pi^\mp)/\Gamma_{total}$ — Γ_{124}/Γ

VALUE (units 10^{-4})	EVTS	DOCUMENT ID		TECN	COMMENT
30±5 OUR AVERAGE					
31±6	4600	AUGUSTIN	89	DM2	$J/\psi \to 2(\pi^+\pi^-)\pi^0$
29±7	87	BURMESTER	77D	PLUT	e^+e^-

$\Gamma(b_1(1235)^0\pi^0)/\Gamma_{total}$ — Γ_{125}/Γ

VALUE (units 10^{-4})	EVTS	DOCUMENT ID		TECN	COMMENT
23±3±5	229	AUGUSTIN	89	DM2	e^+e^-

$\Gamma(\Delta(1232)^+\overline{p})/\Gamma_{total}$ — Γ_{127}/Γ

VALUE	CL%	DOCUMENT ID		TECN	COMMENT
$<0.1 \times 10^{-3}$	90	HENRARD	87	DM2	e^+e^-

$\Gamma(\Delta(1232)^{++}\overline{p}\pi^-)/\Gamma_{total}$ — Γ_{128}/Γ

VALUE (units 10^{-3})	EVTS	DOCUMENT ID		TECN	COMMENT
1.58±0.23±0.40	332	EATON	84	MRK2	e^+e^-

$\Gamma(\Delta(1232)^{++}\overline{\Delta}(1232)^{--})/\Gamma_{total}$ — Γ_{129}/Γ

VALUE (units 10^{-3})	EVTS	DOCUMENT ID		TECN	COMMENT
1.10±0.09±0.28	233	EATON	84	MRK2	e^+e^-

$\Gamma(\overline{\Sigma}(1385)^0 pK^-)/\Gamma_{total}$ — Γ_{130}/Γ

VALUE (units 10^{-3})	EVTS	DOCUMENT ID		TECN	COMMENT
0.51±0.26±0.18	89	EATON	84	MRK2	e^+e^-

$\Gamma(\Sigma(1385)^0\overline{\Lambda} + c.c.)/\Gamma_{total}$ — Γ_{131}/Γ

VALUE	CL%	DOCUMENT ID		TECN	COMMENT
$<0.82 \times 10^{-5}$	90	ABLIKIM	13F	BES3	$J/\psi \to p\overline{p}\pi^+\pi^-\gamma\gamma$
• • • We do not use the following data for averages, fits, limits, etc. • • •					
$<0.2 \times 10^{-3}$	90	HENRARD	87	DM2	e^+e^-

$\Gamma(\Sigma(1385)^-\overline{\Sigma}^+$ (or c.c.))$/\Gamma_{total}$ — Γ_{132}/Γ

VALUE (units 10^{-3})	EVTS	DOCUMENT ID		TECN	COMMENT
0.31±0.05 OUR AVERAGE					
0.30±0.03±0.07	74 ± 8	HENRARD	87	DM2	$e^+e^- \to \Sigma^{*-}$
0.34±0.04±0.07	77 ± 9	HENRARD	87	DM2	$e^+e^- \to \Sigma^{*+}$
0.29±0.11±0.10	26	EATON	84	MRK2	$e^+e^- \to \Sigma^{*-}$
0.31±0.11±0.11	28	EATON	84	MRK2	$e^+e^- \to \Sigma^{*+}$

$\Gamma(\Sigma(1385)^-\overline{\Sigma}(1385)^+$ (or c.c.))$/\Gamma_{total}$ — Γ_{133}/Γ

VALUE (units 10^{-3})	EVTS	DOCUMENT ID		TECN	COMMENT
1.16 ±0.05 OUR AVERAGE					
1.096±0.012±0.071	43k	ABLIKIM	16L	BES3	$J/\psi \to \Sigma(1385)^-\overline{\Sigma}(1385)^+$
1.258±0.014±0.078	53k	ABLIKIM	16L	BES3	$J/\psi \to \Sigma(1385)^+\overline{\Sigma}(1385)^-$
1.23 ±0.07 ±0.30	0.8k	ABLIKIM	12P	BES2	$J/\psi \to \Sigma(1385)^-\overline{\Sigma}(1385)^+$
1.50 ±0.08 ±0.38	1k	ABLIKIM	12P	BES2	$J/\psi \to \Sigma(1385)^+\overline{\Sigma}(1385)^-$
1.00 ±0.04 ±0.21	0.6k	HENRARD	87	DM2	$e^+e^- \to \Sigma^{*-}$
1.19 ±0.04 ±0.25	0.7k	HENRARD	87	DM2	$e^+e^- \to \Sigma^{*+}$
0.86 ±0.18 ±0.22	56	EATON	84	MRK2	$e^+e^- \to \Sigma^{*-}$
1.03 ±0.24 ±0.25	68	EATON	84	MRK2	$e^+e^- \to \Sigma^{*+}$

$\Gamma(\Sigma(1385)^0\overline{\Sigma}(1385)^0)/\Gamma_{total}$ — Γ_{134}/Γ

VALUE (units 10^{-3})	EVTS	DOCUMENT ID		TECN	COMMENT
1.071±0.009±0.082	103k	ABLIKIM	17E	BES3	$e^+e^- \to J/\psi \to$ hadrons

$\Gamma(\Lambda(1520)\overline{\Lambda} + c.c. \to \gamma\Lambda\overline{\Lambda})/\Gamma_{total}$ — Γ_{135}/Γ

VALUE	CL%	DOCUMENT ID		TECN	COMMENT
$<4.1 \times 10^{-6}$	90	ABLIKIM	12B	BES3	$J/\psi \to \Lambda\overline{\Lambda}\gamma$

$\Gamma(\overline{\Lambda}(1520)\Lambda + c.c.)/\Gamma_{total}$ — Γ_{136}/Γ

VALUE	CL%	DOCUMENT ID		TECN	COMMENT
$<1.80 \times 10^{-3}$	90	LU	19	BELL	$B^+ \to \overline{p}\Lambda K^+K^+$

$\Gamma(\Xi^0\overline{\Xi}^0)/\Gamma_{total}$ — Γ_{137}/Γ

VALUE (units 10^{-3})	EVTS	DOCUMENT ID		TECN	COMMENT
1.17 ±0.04 OUR AVERAGE					
1.165±0.004±0.043	135k	ABLIKIM	17E	BES3	$e^+e^- \to J/\psi \to$ hadrons
1.20 ±0.12 ±0.21	206	ABLIKIM	08O	BES2	$e^+e^- \to J/\psi$

$\Gamma(\Xi(1530)^-\overline{\Xi}^+ + c.c.)/\Gamma_{total}$ — Γ_{138}/Γ

VALUE (units 10^{-3})	EVTS	DOCUMENT ID		TECN	COMMENT
0.318±0.008 OUR AVERAGE					
0.317±0.002±0.008	70k	ABLIKIM	20	BES3	$e^+e^- \to J/\psi$
0.59 ±0.09 ±0.12	75	HENRARD	87	DM2	e^+e^-

$\Gamma(\Xi(1530)^0\overline{\Xi}^0)/\Gamma_{total}$ — Γ_{139}/Γ

VALUE (units 10^{-3})	EVTS	DOCUMENT ID		TECN	COMMENT
0.32±0.12±0.07	24 ± 9	HENRARD	87	DM2	e^+e^-

$\Gamma(\Theta(1540)\overline{\Theta}(1540) \to K^0_S pK^-\overline{n} + c.c.)/\Gamma_{total}$ — Γ_{140}/Γ

VALUE	CL%	DOCUMENT ID		TECN	COMMENT
$<1.1 \times 10^{-5}$	90	BAI	04G	BES2	e^+e^-

$\Gamma(\Theta(1540)K^-\overline{n} \to K^0_S pK^-\overline{n})/\Gamma_{total}$ — Γ_{141}/Γ

VALUE	CL%	DOCUMENT ID		TECN	COMMENT
$<2.1 \times 10^{-5}$	90	BAI	04G	BES2	e^+e^-

$\Gamma(\Theta(1540)K^0_S\overline{p} \to K^0_S\overline{p}K^+n)/\Gamma_{total}$ — Γ_{142}/Γ

VALUE	CL%	DOCUMENT ID		TECN	COMMENT
$<1.6 \times 10^{-5}$	90	BAI	04G	BES2	e^+e^-

$\Gamma(\overline{\Theta}(1540)K^+n \to K^0_S\overline{p}K^+n)/\Gamma_{total}$ — Γ_{143}/Γ

VALUE	CL%	DOCUMENT ID		TECN	COMMENT
$<5.6 \times 10^{-5}$	90	BAI	04G	BES2	e^+e^-

$\Gamma(\overline{\Theta}(1540)K^0_S p \to K^0_S pK^-\overline{n})/\Gamma_{total}$ — Γ_{144}/Γ

VALUE	CL%	DOCUMENT ID		TECN	COMMENT
$<1.1 \times 10^{-5}$	90	BAI	04G	BES2	e^+e^-

Downloaded from https://academic.oup.com/ptep/article/2022/8/083C01/6651666 by KIT Library user on 27 September 2022

STABLE HADRONS

$\Gamma(2(\pi^+\pi^-)\pi^0)/\Gamma_{total}$ — Γ_{145}/Γ

VALUE (units 10^{-2})	EVTS	DOCUMENT ID		TECN	COMMENT
3.71±0.28 OUR AVERAGE		Error includes scale factor of 1.3. See the ideogram below.			
3.5 ±0.8 ±0.1	14k	[1] LEES	21	BABR	10.6 $e^+e^- \to 2(\pi^+\pi^-)3\pi^0\gamma$
4.73±0.44	228k	[2] ABLIKIM	19Q	BES3	$J/\psi \to 2(\pi^+\pi^-)\pi^0$
3.25±0.49	46055	AUGUSTIN	89	DM2	$J/\psi \to 2(\pi^+\pi^-)\pi^0$
3.17±0.42	147	FRANKLIN	83	MRK2	$e^+e^- \to$ hadrons
3.64±0.52	1500	BURMESTER	77D	PLUT	e^+e^-
4 ±1	675	JEAN-MARIE	76	MRK1	e^+e^-

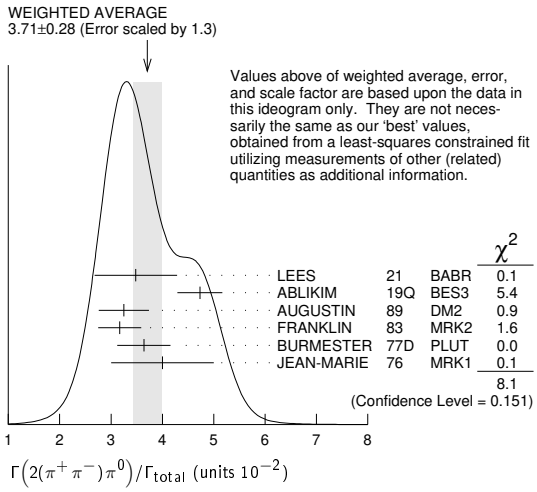

[1] LEES 21 reports $[\Gamma(J/\psi(1S) \to 2(\pi^+\pi^-)\pi^0)/\Gamma_{total}] \times [\Gamma(\psi(2S) \to e^+e^-)] \times [B(\psi(2S) \to J/\psi(1S)\pi^0\pi^0)] = (14.8 \pm 2.6 \pm 2.2) \times 10^{-3}$ keV which we divide by our best values $\Gamma(\psi(2S) \to e^+e^-) = 2.33 \pm 0.04$ keV, $B(\psi(2S) \to J/\psi(1S)\pi^0\pi^0) = (18.24 \pm 0.31) \times 10^{-2}$. Our first error is their experiment's error and our second error is the systematic error from using our best values.

[2] From an energy scan of $e^+e^- \to J/\psi \to 2(\pi^+\pi^-)\pi^0$, assuming PDG 16 values for $\Gamma(e^+e^-)$, $\Gamma(\mu^+\mu^-)$, and Γ(total), and for a phase difference between strong and electromagnetic amplitudes of $(84.9 \pm 3.6)^\circ$. An alternative solution is $(4.85 \pm 0.45)\%$ with a phase of $(-84.7 \pm 3.1)^\circ$.

$\Gamma(3(\pi^+\pi^-)\pi^0)/\Gamma_{total}$ — Γ_{146}/Γ

VALUE	EVTS	DOCUMENT ID		TECN	COMMENT
0.029±0.006 OUR AVERAGE					
0.028±0.009	11	FRANKLIN	83	MRK2	$e^+e^- \to$ hadrons
0.029±0.007	181	JEAN-MARIE	76	MRK1	e^+e^-

$\Gamma(\pi^+\pi^-\pi^0)/\Gamma_{total}$ — Γ_{151}/Γ

VALUE (units 10^{-3})	EVTS	DOCUMENT ID		TECN	COMMENT
21.0 ±0.8 OUR AVERAGE		Error includes scale factor of 1.6. See the ideogram below.			
$21.37 \pm 0.04^{+0.64}_{-0.62}$	1.8M	[1,2] ABLIKIM	12H	BES3	$e^+e^- \to J/\psi$
23.0 ±2.0 ±0.4	256	[3] AUBERT	07AU	BABR	10.6 $e^+e^- \to J/\psi\pi^+\pi^-\gamma$
21.84±0.05±2.01	220k	[1,4] BAI	04H	BES	e^+e^-
20.91±0.21±1.16		[4,5] BAI	04H	BES	e^+e^-
15 ±2	168	FRANKLIN	83	MRK2	e^+e^-

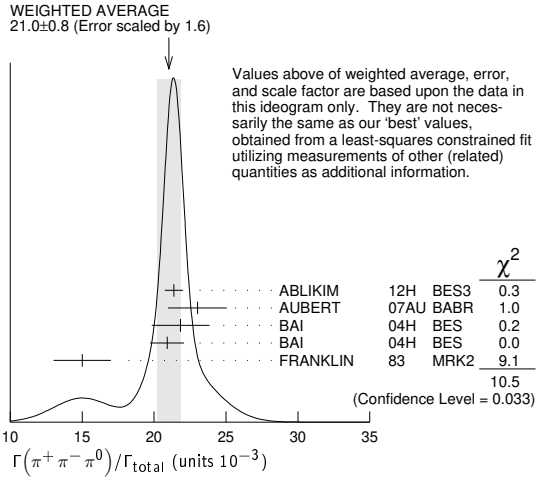

[1] From $J/\psi \to \pi^+\pi^-\pi^0$ events directly.

[2] The quoted systematic error includes a contribution of 1.23% (added in quadrature) from the uncertainty on the number of J/ψ events.

[3] AUBERT 07AU reports $[\Gamma(J/\psi(1S) \to \pi^+\pi^-\pi^0)/\Gamma_{total}] \times [\Gamma(\psi(2S) \to J/\psi(1S)\pi^+\pi^-) \times \Gamma(\psi(2S) \to e^+e^-)/\Gamma_{total}] = (18.6 \pm 1.2 \pm 1.1) \times 10^{-3}$ keV which we divide by our best value $\Gamma(\psi(2S) \to J/\psi(1S)\pi^+\pi^-) \times \Gamma(\psi(2S) \to e^+e^-)/\Gamma_{total} = 0.808 \pm 0.013$ keV. Our first error is their experiment's error and our second error is the systematic error from using our best value.

[4] Mostly $\rho\pi$, see also $\rho\pi$ subsection.

[5] Obtained comparing the rates for $\pi^+\pi^-\pi^0$ and $\mu^+\mu^-$, using J/ψ events produced via $\psi(2S) \to \pi^+\pi^- J/\psi$ and with $B(J/\psi \to \mu^+\mu^-) = 5.88 \pm 0.10\%$.

$\Gamma(\pi^+\pi^-\pi^0K^+K^-)/\Gamma_{total}$ — Γ_{153}/Γ

VALUE (units 10^{-2})	EVTS	DOCUMENT ID		TECN	COMMENT
1.2±0.3	309	VANNUCCI	77	MRK1	e^+e^-

$\Gamma(\pi^+\pi^-)/\Gamma_{total}$ — Γ_{154}/Γ

VALUE (units 10^{-4})	EVTS	DOCUMENT ID		TECN	COMMENT
1.47±0.14 OUR AVERAGE					
1.47±0.13±0.13	140	[1] METREVELI	12		$\psi(2S) \to 2(\pi^+\pi^-)$
1.58±0.20±0.15	84	BALTRUSAIT...85D		MRK3	e^+e^-
1.0 ±0.5	5	BRANDELIK	78B	DASP	e^+e^-
1.6 ±1.6	1	VANNUCCI	77	MRK1	e^+e^-

[1] Obtained by analyzing CLEO-c data but not authored by the CLEO Collaboration.

$\Gamma(2(\pi^+\pi^-))/\Gamma_{total}$ — Γ_{155}/Γ

VALUE (units 10^{-3})	EVTS	DOCUMENT ID		TECN	COMMENT
3.57±0.30 OUR AVERAGE					
3.53±0.12±0.29	1107	[1] ABLIKIM	05H	BES2	$e^+e^- \to \psi(2S) \to J/\psi\pi^+\pi^-$, $J/\psi \to 2(\pi^+\pi^-)$
4.0 ±1.0	76	JEAN-MARIE	76	MRK1	e^+e^-

[1] Computed using $B(J/\psi \to \mu^+\mu^-) = 0.0588 \pm 0.0010$.

$\Gamma(3(\pi^+\pi^-))/\Gamma_{total}$ — Γ_{156}/Γ

VALUE (units 10^{-4})	EVTS	DOCUMENT ID		TECN	COMMENT
• • • We do not use the following data for averages, fits, limits, etc. • • •					
40±20	32	JEAN-MARIE	76	MRK1	e^+e^-

$\Gamma(4(\pi^+\pi^-)\pi^0)/\Gamma_{total}$ — Γ_{158}/Γ

VALUE (units 10^{-4})	EVTS	DOCUMENT ID		TECN	COMMENT
90±30	13	JEAN-MARIE	76	MRK1	e^+e^-

$\Gamma(2(\pi^+\pi^-)\eta)/\Gamma_{total}$ — Γ_{159}/Γ

VALUE (units 10^{-3})	EVTS	DOCUMENT ID		TECN	COMMENT
2.29±0.28 OUR AVERAGE					
3.1 ±1.5 ±0.1	14k	[1] LEES	21	BABR	10.6 $e^+e^- \to 2(\pi^+\pi^-)3\pi^0\gamma$
2.26±0.08±0.27	4.8k	ABLIKIM	05C	BES2	$e^+e^- \to 2(\pi^+\pi^-)\eta$

[1] LEES 21 reports $[\Gamma(J/\psi(1S) \to 2(\pi^+\pi^-)\eta)/\Gamma_{total}] \times [\Gamma(J/\psi(1S) \to e^+e^-)] \times [B(\eta \to 3\pi^0)] = (5.6 \pm 2.6 \pm 0.8) \times 10^{-3}$ keV which we divide by our best values $\Gamma(J/\psi(1S) \to e^+e^-) = 5.53 \pm 0.10$ keV, $B(\eta \to 3\pi^0) = (32.57 \pm 0.21) \times 10^{-2}$. Our first error is their experiment's error and our second error is the systematic error from using our best values.

$\Gamma(3(\pi^+\pi^-)\eta)/\Gamma_{total}$ — Γ_{160}/Γ

VALUE (units 10^{-4})	EVTS	DOCUMENT ID		TECN	COMMENT
7.24±0.96±1.11	616	ABLIKIM	05C	BES2	$e^+e^- \to 3(\pi^+\pi^-)\eta$

$\Gamma(K^+K^-)/\Gamma_{total}$ — Γ_{164}/Γ

VALUE (units 10^{-4})	EVTS	DOCUMENT ID		TECN	COMMENT
2.86±0.09±0.19	1k	[1] METREVELI	12		$\psi(2S) \to \pi^+\pi^-K^+K^-$
• • • We do not use the following data for averages, fits, limits, etc. • • •					
2.39±0.24±0.22	107	[2] BALTRUSAIT...85D		MRK3	e^+e^-
2.2 ±0.9	6	[2] BRANDELIK	79C	DASP	e^+e^-

[1] Obtained by analyzing CLEO-c data but not authored by the CLEO Collaboration.

[2] Interference with non-resonant K^+K^- production not taken into account.

$\Gamma(K^0_SK^0_L)/\Gamma_{total}$ — Γ_{165}/Γ

VALUE (units 10^{-4})	EVTS	DOCUMENT ID		TECN	COMMENT
1.95±0.11 OUR AVERAGE		Error includes scale factor of 2.4. See the ideogram below.			
1.93±0.01±0.05	110k	ABLIKIM	17AH	BES3	$J/\psi \to K^0_SK^0_L \to \pi^+\pi^-X$
2.62±0.15±0.14	0.3k	[1] METREVELI	12		$\psi(2S) \to \pi^+\pi^-K^0_SK^0_L$
1.82±0.04±0.13	2.1k	[2] BAI	04A	BES2	$J/\psi \to K^0_SK^0_L \to \pi^+\pi^-X$
• • • We do not use the following data for averages, fits, limits, etc. • • •					
1.18±0.12±0.18		JOUSSET	90	DM2	$J/\psi \to$ hadrons
1.01±0.16±0.09	74	BALTRUSAIT...85D		MRK3	e^+e^-

[1] Obtained by analyzing CLEO-c data but not authored by the CLEO Collaboration.

[2] Using $B(K^0_S \to \pi^+\pi^-) = 0.6868 \pm 0.0027$.

Downloaded from https://academic.oup.com/ptep/article/2022/8/083C01/6651666 by KIT Library user on 27 September 2022

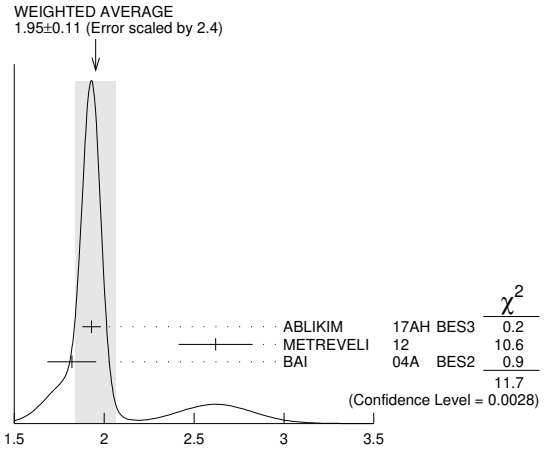

$\Gamma(K^0_S K^0_L)/\Gamma_{total}$ Γ_{165}/Γ

$\Gamma(K^0_S K^0_S)/\Gamma_{total}$ — Γ_{166}/Γ

VALUE	CL%	DOCUMENT ID		TECN	COMMENT
$<1.4\times10^{-8}$	95	[1] ABLIKIM	17AH	BES3	$J/\psi\to K^0_S K^0_S\to\pi^+\pi^-\pi^+\pi^-$
• • • We do not use the following data for averages, fits, limits, etc. • • •					
$<1\times10^{-6}$	95	[1] BAI	04D	BES	e^+e^-
$<5.2\times10^{-6}$	90	[1] BALTRUSAIT..	85C	MRK3	e^+e^-

[1] Forbidden by *CP*.

$\Gamma(K\overline{K}\pi)/\Gamma_{total}$ — Γ_{167}/Γ

VALUE (units 10^{-4})	EVTS	DOCUMENT ID		TECN	COMMENT
61 ±10 OUR AVERAGE					
55.2±12.0	25	FRANKLIN	83	MRK2	$e^+e^-\to K^+K^-\pi^0$
78.0±21.0	126	VANNUCCI	77	MRK1	$e^+e^-\to K^0_S K^\pm\pi^\mp$

$\Gamma(K^+K^-\pi^0)/\Gamma_{total}$ — Γ_{168}/Γ

VALUE (units 10^{-3})	EVTS	DOCUMENT ID		TECN	COMMENT
2.88±0.01±0.12	183k	ABLIKIM	19AQ	BES	$J/\psi\to K^+K^-\pi^0$

$\Gamma(K^+K^-\pi^0)/\Gamma(\pi^+\pi^-\pi^0)$ — $\Gamma_{168}/\Gamma_{151}$

VALUE (%)	EVTS	DOCUMENT ID		TECN	COMMENT
12.0±0.3±0.9	23k	LEES	17C	BABR	$J/\psi\to h^+h^-\pi^0$

$\Gamma(K^0_S K^\pm\pi^\mp)/\Gamma(\pi^+\pi^-\pi^0)$ — $\Gamma_{169}/\Gamma_{151}$

VALUE (%)	EVTS	DOCUMENT ID		TECN	COMMENT
26.5±0.5±2.1	24k	LEES	17C	BABR	$J/\psi\to h^0h^+h^-$

$\Gamma(K^+K^-\pi^+\pi^-)/\Gamma_{total}$ — Γ_{173}/Γ

VALUE (units 10^{-3})	EVTS	DOCUMENT ID		TECN	COMMENT
• • • We do not use the following data for averages, fits, limits, etc. • • •					
7.2±2.3	205	VANNUCCI	77	MRK1	e^+e^-

$\Gamma(K^+K^-2(\pi^+\pi^-))/\Gamma_{total}$ — Γ_{180}/Γ

VALUE (units 10^{-4})	EVTS	DOCUMENT ID		TECN	COMMENT
31±13	30	VANNUCCI	77	MRK1	e^+e^-

$\Gamma(2(K^+K^-))/\Gamma_{total}$ — Γ_{182}/Γ

VALUE (units 10^{-3})	EVTS	DOCUMENT ID		TECN	COMMENT
• • • We do not use the following data for averages, fits, limits, etc. • • •					
$1.4^{+0.5}_{-0.4}\pm0.2$	$11.0^{+4.3}_{-3.5}$	[1] HUANG	03	BELL	$B^+\to2(K^+K^-)K^+$
0.7±0.3		VANNUCCI	77	MRK1	e^+e^-

[1] Using $B(B^+\to J/\psi K^+)=(1.01\pm0.05)\times10^{-3}$.

$\Gamma(p\overline{p})/\Gamma_{total}$ — Γ_{184}/Γ

VALUE (units 10^{-3})	EVTS	DOCUMENT ID		TECN	COMMENT
2.120±0.029 OUR AVERAGE					
2.112±0.004±0.031	314k	ABLIKIM	12C	BES3	e^+e^-
2.17 ±0.16 ±0.04	317	[1] WU	06	BELL	$B^+\to p\overline{p}K^+$
2.26 ±0.01 ±0.14	63316	BAI	04E	BES2	$e^+e^-\to J/\psi$
1.97 ±0.22	99	BALDINI	98	FENI	e^+e^-
1.91 ±0.04 ±0.30		PALLIN	87	DM2	e^+e^-
2.16 ±0.07 ±0.15	1420	EATON	84	MRK2	e^+e^-
2.5 ±0.4	133	BRANDELIK	79C	DASP	e^+e^-
2.0 ±0.5		BESCH	78	BONA	e^+e^-
2.2 ±0.2	331	[2] PERUZZI	78	MRK1	e^+e^-
• • • We do not use the following data for averages, fits, limits, etc. • • •					
2.0 ±0.3	48	ANTONELLI	93	SPEC	e^+e^-

[1] WU 06 reports $[\Gamma(J/\psi(1S)\to p\overline{p})/\Gamma_{total}]\times[B(B^+\to J/\psi(1S)K^+)]=(2.21\pm0.13\pm0.10)\times10^{-6}$ which we divide by our best value $B(B^+\to J/\psi(1S)K^+)=(1.020\pm0.019)\times10^{-3}$. Our first error is their experiment's error and our second error is the systematic error from using our best value.

[2] Assuming angular distribution $(1+\cos^2\theta)$.

$\Gamma(p\overline{p}\pi^0)/\Gamma_{total}$ — Γ_{185}/Γ

VALUE (units 10^{-3})	EVTS	DOCUMENT ID		TECN	COMMENT
1.19±0.08 OUR AVERAGE Error includes scale factor of 1.1.					
1.33±0.02±0.11	11k	ABLIKIM	09B	BES2	e^+e^-
1.13±0.09±0.09	685	EATON	84	MRK2	e^+e^-
1.4 ±0.4		BRANDELIK	79C	DASP	e^+e^-
1.00±0.15	109	PERUZZI	78	MRK1	e^+e^-

$\Gamma(p\overline{p}\pi^+\pi^-)/\Gamma_{total}$ — Γ_{186}/Γ

VALUE (units 10^{-3})	EVTS	DOCUMENT ID		TECN	COMMENT
6.0 ±0.5 OUR AVERAGE Error includes scale factor of 1.3. See the ideogram below.					
6.46±0.17±0.43	1435	EATON	84	MRK2	e^+e^-
3.8 ±1.6	48	BESCH	81	BONA	e^+e^-
5.5 ±0.6	533	PERUZZI	78	MRK1	e^+e^-

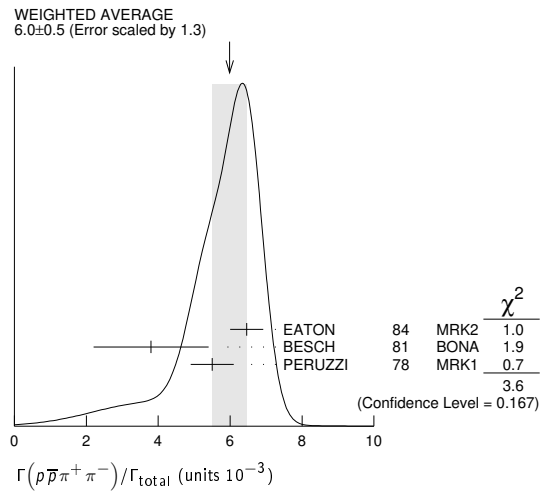

$\Gamma(p\overline{p}\pi^+\pi^-\pi^0)/\Gamma_{total}$ — Γ_{187}/Γ

Including $p\overline{p}\pi^+\pi^-\gamma$ and excluding ω, η, η'

VALUE (units 10^{-3})	EVTS	DOCUMENT ID		TECN	COMMENT
2.3 ±0.9 OUR AVERAGE Error includes scale factor of 1.9.					
3.36±0.65±0.28	364	EATON	84	MRK2	e^+e^-
1.6 ±0.6	39	PERUZZI	78	MRK1	e^+e^-

$\Gamma(p\overline{p}\eta)/\Gamma_{total}$ — Γ_{188}/Γ

VALUE (units 10^{-3})	EVTS	DOCUMENT ID		TECN	COMMENT
2.00±0.12 OUR AVERAGE					
1.91±0.02±0.17	13k	[1] ABLIKIM	09	BES2	e^+e^-
2.03±0.13±0.15	826	EATON	84	MRK2	e^+e^-
2.5 ±1.2		BRANDELIK	79C	DASP	e^+e^-
2.3 ±0.4	197	PERUZZI	78	MRK1	e^+e^-

[1] From the combination of $p\overline{p}\eta\to p\overline{p}\gamma\gamma$ and $p\overline{p}\eta\to p\overline{p}\pi^+\pi^-\pi^0$ channels.

$\Gamma(p\overline{p}\rho)/\Gamma_{total}$ — Γ_{189}/Γ

VALUE	CL%	DOCUMENT ID		TECN	COMMENT
$<0.31\times10^{-3}$	90	EATON	84	MRK2	$e^+e^-\to$ hadronsγ

$\Gamma(p\overline{p}\omega)/\Gamma_{total}$ — Γ_{190}/Γ

VALUE (units 10^{-3})	EVTS	DOCUMENT ID		TECN	COMMENT
0.98±0.10 OUR AVERAGE Error includes scale factor of 1.3. See the ideogram below.					
0.90±0.02±0.09	2670	ABLIKIM	13P	BES3	e^+e^-
0.98±0.03±0.14	2449	ABLIKIM	08	BES2	e^+e^-
1.10±0.17±0.18	486	EATON	84	MRK2	e^+e^-
1.6 ±0.3	77	PERUZZI	78	MRK1	e^+e^-

Downloaded from https://academic.oup.com/ptep/article/2022/8/083C01/6651666 by KIT Library user on 27 September 2022

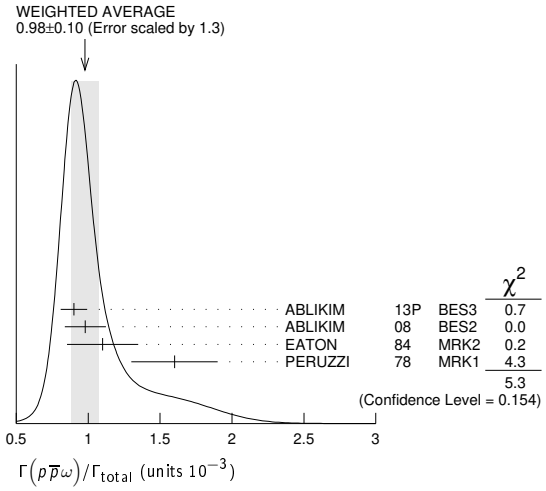

$\Gamma(p\overline{p}\eta'(958))/\Gamma_{total}$ — Γ_{191}/Γ

VALUE (units 10^{-3})	EVTS	DOCUMENT ID		TECN	COMMENT
0.129±0.014 OUR AVERAGE		Error includes scale factor of 2.0.			
0.126±0.002±0.007	16k	[1] ABLIKIM	19N	BES3	e^+e^-
0.200±0.023±0.028	265 ± 31	[2] ABLIKIM	09	BES2	e^+e^-
0.68 ±0.23 ±0.17	19	EATON	84	MRK2	e^+e^-
1.8 ±0.6	19	PERUZZI	78	MRK1	e^+e^-

[1] From the combination of $p\overline{p}\eta' \to p\overline{p}\pi^+\pi^-\eta$ and $p\overline{p}\eta' \to p\overline{p}\pi^+\pi^-\gamma$ channels.
[2] From the combination of $p\overline{p}\eta' \to p\overline{p}\pi^+\pi^-\eta$ and $p\overline{p}\eta' \to p\overline{p}\gamma\rho^0$ channels.

$\Gamma(p\overline{p}a_0(980) \to p\overline{p}\pi^0\eta)/\Gamma_{total}$ — Γ_{192}/Γ

VALUE (units 10^{-5})	DOCUMENT ID		TECN	COMMENT
6.8±1.2±1.3	ABLIKIM	14N	BES3	$e^+e^- \to J/\psi$

$\Gamma(p\overline{p}\phi)/\Gamma_{total}$ — Γ_{193}/Γ

VALUE (units 10^{-4})	EVTS	DOCUMENT ID		TECN	COMMENT
0.519±0.033 OUR AVERAGE					
0.523±0.006±0.033	14k	ABLIKIM	16K	BES3	$J/\psi \to p\overline{p}K^0_S K^0_L$, $p\overline{p}K^+K^-$
0.45 ±0.13 ±0.07		FALVARD	88	DM2	$J/\psi \to$ hadrons

$\Gamma(p\overline{n}\pi^-)/\Gamma_{total}$ — Γ_{194}/Γ

VALUE (units 10^{-3})	EVTS	DOCUMENT ID		TECN	COMMENT
2.12±0.09 OUR AVERAGE					
2.36±0.02±0.21	59k	ABLIKIM	06K	BES2	$J/\psi \to p\pi^-\overline{n}$
2.47±0.02±0.24	55k	ABLIKIM	06K	BES2	$J/\psi \to \overline{p}\pi^+n$
2.02±0.07±0.16	1288	EATON	84	MRK2	$e^+e^- \to p\pi^-$
1.93±0.07±0.16	1191	EATON	84	MRK2	$e^+e^- \to \overline{p}\pi^+$
1.7 ±0.7	32	BESCH	81	BONA	$e^+e^- \to p\pi^-$
1.6 ±1.2	5	BESCH	81	BONA	$e^+e^- \to \overline{p}\pi^+$
2.16±0.29	194	PERUZZI	78	MRK1	$e^+e^- \to p\pi^-$
2.04±0.27	204	PERUZZI	78	MRK1	$e^+e^- \to \overline{p}\pi^+$

$\Gamma(n\overline{n})/\Gamma_{total}$ — Γ_{195}/Γ

VALUE (units 10^{-3})	EVTS	DOCUMENT ID		TECN	COMMENT
2.09±0.16 OUR AVERAGE					
2.07±0.01±0.17	36k	ABLIKIM	12C	BES3	e^+e^-
2.31±0.49	79	BALDINI	98	FENI	e^+e^-
1.8 ±0.9		BESCH	78	BONA	e^+e^-
• • • We do not use the following data for averages, fits, limits, etc. • • •					
1.90±0.55	40	ANTONELLI	93	SPEC	e^+e^-

$\Gamma(n\overline{n}\pi^+\pi^-)/\Gamma_{total}$ — Γ_{196}/Γ

VALUE (units 10^{-3})	EVTS	DOCUMENT ID		TECN	COMMENT
3.8±3.6	5	BESCH	81	BONA	e^+e^-

$\Gamma(\Lambda\overline{\Lambda})/\Gamma_{total}$ — Γ_{200}/Γ

VALUE (units 10^{-3})	EVTS	DOCUMENT ID		TECN	COMMENT
1.89 ±0.09 OUR AVERAGE		Error includes scale factor of 2.8. See the ideogram below.			
1.943±0.003±0.033	441k	ABLIKIM	17L	BES3	e^+e^-
2.03 ±0.03 ±0.15	8887	ABLIKIM	06	BES2	$J/\psi \to \Lambda\overline{\Lambda}$
1.96 $^{+0.47}_{-0.44}$ ±0.04	46	[1] WU	06	BELL	$B^+ \to \Lambda\overline{\Lambda}K^+$
1.08 ±0.06 ±0.24	631	BAI	98G	BES	e^+e^-
1.38 ±0.05 ±0.20	1847	PALLIN	87	DM2	e^+e^-
1.58 ±0.08 ±0.19	365	EATON	84	MRK2	e^+e^-
2.6 ±1.6	5	BESCH	81	BONA	e^+e^-
1.1 ±0.2	196	PERUZZI	78	MRK1	e^+e^-

[1] WU 06 reports $[\Gamma(J/\psi(1S) \to \Lambda\overline{\Lambda})/\Gamma_{total}] \times [B(B^+ \to J/\psi(1S)K^+)] = (2.00^{+0.34}_{-0.29} \pm 0.34) \times 10^{-6}$ which we divide by our best value $B(B^+ \to J/\psi(1S)K^+) = (1.020 \pm 0.019) \times 10^{-3}$. Our first error is their experiment's error and our second error is the systematic error from using our best value.

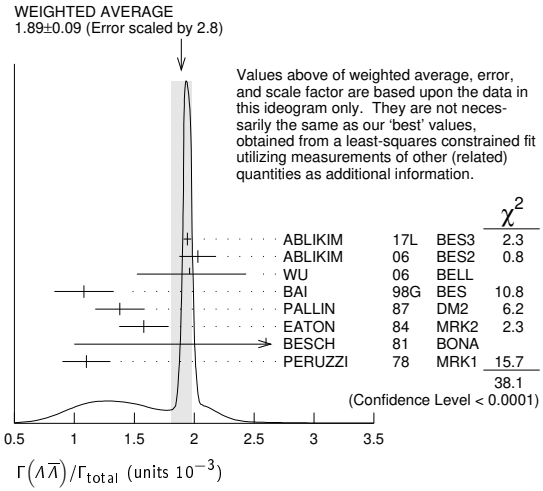

$\Gamma(\Lambda\overline{\Lambda}\pi^0)/\Gamma_{total}$ — Γ_{201}/Γ

VALUE (units 10^{-5})	CL%	EVTS	DOCUMENT ID		TECN	COMMENT
3.78±0.27±0.30		323	[1] ABLIKIM	13F	BES3	$J/\psi \to p\overline{p}\pi^+\pi^-\gamma\gamma$
• • • We do not use the following data for averages, fits, limits, etc. • • •						
< 6.4		90	[2] ABLIKIM	07H	BES2	$e^+e^- \to \psi(2S)$
23 ±7 ±8		11	BAI	98G	BES	e^+e^-
22 ±5 ±5		19	HENRARD	87	DM2	e^+e^-

[1] Using $B(\Lambda \to \pi^-p) = 63.9\%$ and $B(\pi^0 \to \gamma\gamma) = 98.8\%$.
[2] Using $B(\Lambda \to \pi^-p) = 63.9\%$.

$\Gamma(\Lambda\overline{\Lambda}\pi^+\pi^-)/\Gamma_{total}$ — Γ_{202}/Γ

VALUE (units 10^{-3})	EVTS	DOCUMENT ID		TECN	COMMENT
4.30±0.13±0.99	2.4k	ABLIKIM	12P	BES2	J/ψ

$\Gamma(\Lambda\overline{\Lambda}\eta)/\Gamma_{total}$ — Γ_{203}/Γ

VALUE (units 10^{-5})	EVTS	DOCUMENT ID		TECN	COMMENT
16.2±1.7 OUR AVERAGE					
15.7±0.80±1.54	454	[1] ABLIKIM	13F	BES3	$J/\psi \to p\overline{p}\pi^+\pi^-\gamma\gamma$
26.2±6.0 ±4.4	44	[2] ABLIKIM	07H	BES2	$e^+e^- \to \psi(2S)$

[1] Using $B(\Lambda \to \pi^-p) = 63.9\%$ and $B(\eta \to \gamma\gamma) = 39.31\%$.
[2] Using $B(\Lambda \to \pi^-p) = 63.9\%$ and $B(\eta \to \gamma\gamma) = 39.4\%$.

$\Gamma(\Lambda\overline{\Sigma}^-\pi^+ \text{(or c.c.)})/\Gamma_{total}$ — Γ_{204}/Γ

VALUE (units 10^{-3})	EVTS	DOCUMENT ID		TECN	COMMENT
0.83 ±0.07 OUR AVERAGE		Error includes scale factor of 1.2.			
0.770±0.051±0.083	335	[1] ABLIKIM	07H	BES2	$e^+e^- \to \overline{\Lambda}\Sigma^+\pi^-$
0.747±0.056±0.076	254	[1] ABLIKIM	07H	BES2	$e^+e^- \to \Lambda\overline{\Sigma}^-\pi^+$
0.90 ±0.06 ±0.16	225 ± 15	HENRARD	87	DM2	$e^+e^- \to \overline{\Lambda}\Sigma^+\pi^-$
1.11 ±0.06 ±0.20	342 ± 18	HENRARD	87	DM2	$e^+e^- \to \Lambda\overline{\Sigma}^-\pi^+$
1.53 ±0.17 ±0.38	135	EATON	84	MRK2	$e^+e^- \to \overline{\Lambda}\Sigma^+\pi^-$
1.38 ±0.21 ±0.35	118	EATON	84	MRK2	$e^+e^- \to \Lambda\overline{\Sigma}^-\pi^+$

[1] Using $B(\Lambda \to \pi^-p) = 63.9\%$ and $B(\Sigma^+ \to \pi^0p) = 51.6\%$.

$\Gamma(pK^-\overline{\Lambda}\text{+c.c.})/\Gamma_{total}$ — Γ_{205}/Γ

VALUE (units 10^{-3})	EVTS	DOCUMENT ID		TECN	COMMENT
0.86±0.11 OUR AVERAGE					
0.84 $^{+0.17}_{-0.15}$ ±0.02	45	[1] LU	19	BELL	$B^+ \to \overline{p}\Lambda K^+K^+$
0.89±0.07±0.14	307	EATON	84	MRK2	e^+e^-

[1] LU 19 reports $(8.32^{+1.63}_{-1.45} \pm 0.49) \times 10^{-4}$ from a measurement of $[\Gamma(J/\psi(1S) \to pK^-\overline{\Lambda}\text{+c.c.})/\Gamma_{total}] \times [B(B^+ \to J/\psi(1S)K^+)]$ assuming $B(B^+ \to J/\psi(1S)K^+) = (1.026 \pm 0.031) \times 10^{-3}$, which we rescale to our best value $B(B^+ \to J/\psi(1S)K^+) = (1.020 \pm 0.019) \times 10^{-3}$. Our first error is their experiment's error and our second error is the systematic error from using our best value.

$\Gamma(pK^-\overline{\Sigma}^0)/\Gamma_{total}$ — Γ_{206}/Γ

VALUE (units 10^{-3})	EVTS	DOCUMENT ID		TECN	COMMENT
0.29±0.06±0.05	90	EATON	84	MRK2	e^+e^-

$\Gamma(\overline{\Lambda}nK^0_S + \text{c.c.})/\Gamma_{total}$ — Γ_{207}/Γ

VALUE (units 10^{-4})	EVTS	DOCUMENT ID		TECN	COMMENT
6.46±0.20±1.07	1058	[1] ABLIKIM	08C	BES2	$e^+e^- \to J/\psi$

[1] Using $B(\overline{\Lambda} \to \overline{p}\pi^+) = 63.9\%$ and $B(K^0_S \to \pi^+\pi^-) = 69.2\%$.

Downloaded from https://academic.oup.com/ptep/article/2022/8/083C01/6651666 by KIT Library user on 27 September 2022

$\Gamma(\Lambda\overline{\Sigma}+\text{c.c.})/\Gamma_{\text{total}}$ — Γ_{208}/Γ

VALUE (units 10^{-5})	CL%	EVTS	DOCUMENT ID		TECN	COMMENT
2.83±0.23 OUR AVERAGE						
2.74±0.24±0.22		234 ± 21	[1] ABLIKIM	12B	BES3	$J/\psi \to \Lambda\overline{\Sigma}^0$
2.92±0.22±0.24		308 ± 24	[2] ABLIKIM	12B	BES3	$J/\psi \to \overline{\Lambda}\Sigma^0$
• • • We do not use the following data for averages, fits, limits, etc. • • •						
<18			[2] HENRARD	87	DM2	$J/\psi \to \overline{\Lambda}\Sigma^0$
<15	90		PERUZZI	78	MRK1	$e^+e^- \to \Lambda X$

[1] ABLIKIM 12B quotes $B(J/\psi \to \Lambda\overline{\Sigma}^0)$ which we multiply by 2.
[2] ABLIKIM 12B and HENRARD 87 quote results for $B(J/\psi \to \overline{\Lambda}\Sigma^0)$ which we multiply by 2.

$\Gamma(\Sigma^+\overline{\Sigma}^-)/\Gamma_{\text{total}}$ — Γ_{209}/Γ

VALUE (units 10^{-3})	EVTS	DOCUMENT ID		TECN	COMMENT
1.07 ±0.04 OUR AVERAGE					
1.061±0.004±0.036	87k	ABLIKIM	21AT	BES3	$J/\psi \to p\pi^0\overline{p}\pi^0$
1.50 ±0.10 ±0.22	399	ABLIKIM	08O	BES2	$e^+e^- \to J/\psi$

$\Gamma(\Sigma^0\overline{\Sigma}^0)/\Gamma_{\text{total}}$ — Γ_{210}/Γ

VALUE (units 10^{-3})	EVTS	DOCUMENT ID		TECN	COMMENT
1.172±0.032 OUR AVERAGE Error includes scale factor of 1.4.					
1.164±0.004±0.023	111k	ABLIKIM	17L	BES3	$J/\psi \to \Sigma^0\overline{\Sigma}^0$
1.33 ±0.04 ±0.11	1.7k	ABLIKIM	06	BES2	$J/\psi \to \Sigma^0\overline{\Sigma}^0$
1.06 ±0.04 ±0.23	884	PALLIN	87	DM2	$e^+e^- \to \Sigma^0\overline{\Sigma}^0$
1.58 ±0.16 ±0.25	90	EATON	84	MRK2	$e^+e^- \to \Sigma^0\overline{\Sigma}^0$
1.3 ±0.4	52	PERUZZI	78	MRK1	$e^+e^- \to \Sigma^0\overline{\Sigma}^0$
• • • We do not use the following data for averages, fits, limits, etc. • • •					
2.4 ±2.6	3	BESCH	81	BONA	$e^+e^- \to \Sigma^+\overline{\Sigma}^-$

$\Gamma(\Xi^-\overline{\Xi}^+)/\Gamma_{\text{total}}$ — Γ_{211}/Γ

VALUE (units 10^{-3})	EVTS	DOCUMENT ID		TECN	COMMENT
0.97 ±0.08 OUR AVERAGE Error includes scale factor of 1.4. See the ideogram below.					
1.040±0.006±0.074	43k	ABLIKIM	16L	BES3	$J/\psi \to \Xi^-\overline{\Xi}^+$
0.90 ±0.03 ±0.18	961	ABLIKIM	12P	BES2	$J/\psi \to \Xi^-\overline{\Xi}^+$
0.70 ±0.06 ±0.12	132	HENRARD	87	DM2	$e^+e^- \to \Xi^-\overline{\Xi}^+$
1.14 ±0.08 ±0.20	194	EATON	84	MRK2	$e^+e^- \to \Xi^-\overline{\Xi}^+$
1.4 ±0.5	51	PERUZZI	78	MRK1	$e^+e^- \to \Xi^-\overline{\Xi}^+$

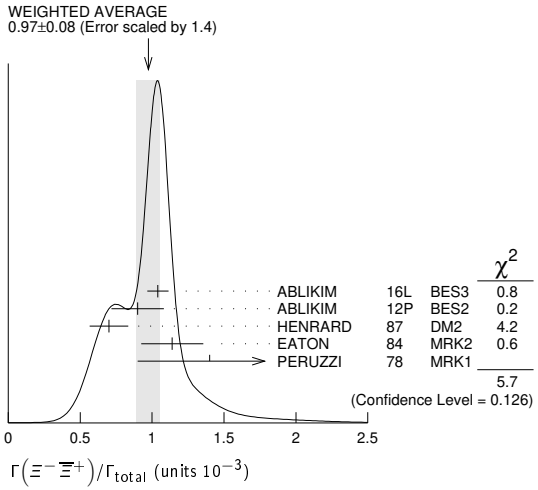

RADIATIVE DECAYS

$\Gamma(\gamma\eta_c(1S))/\Gamma_{\text{total}}$ — Γ_{212}/Γ

VALUE (units 10^{-2})	EVTS	DOCUMENT ID		TECN	COMMENT
1.7 ±0.4 OUR AVERAGE Error includes scale factor of 1.5.					
2.00±0.31±0.02		[1] MITCHELL	09	CLEO	$e^+e^- \to \gamma X$
1.27±0.36		GAISER	86	CBAL	$J/\psi \to \gamma X$
• • • We do not use the following data for averages, fits, limits, etc. • • •					
seen		ANASHIN	14	KEDR	$J/\psi \to \gamma\eta_c$
0.79±0.20	273 ± 43	[2] AUBERT	06E	BABR	$B^\pm \to K^\pm X_{c\overline{c}}$
seen	16	BALTRUSAIT...84		MRK3	$J/\psi \to 2\phi\gamma$

[1] MITCHELL 09 reports (1.98 ± 0.09 ± 0.30) × 10^{-2} from a measurement of $[\Gamma(J/\psi(1S) \to \gamma\eta_c(1S))/\Gamma_{\text{total}}] \times [B(\psi(2S) \to J/\psi(1S)\pi^+\pi^-)]$ assuming $B(\psi(2S) \to J/\psi(1S)\pi^+\pi^-) = (35.04 \pm 0.07 \pm 0.77) \times 10^{-2}$, which we rescale to our best value $B(\psi(2S) \to J/\psi(1S)\pi^+\pi^-) = (34.68 \pm 0.30) \times 10^{-2}$. Our first error is their experiment's error and our second error is the systematic error from using our best value.
[2] Calculated by the authors using an average of $B(J/\psi \to \gamma\eta_c) \times B(\eta_c \to K\overline{K}\pi)$ from BALTRUSAITIS 86, BISELLO 91, BAI 04 and $B(\eta_c \to K\overline{K}\pi) = (8.5 \pm 1.8)\%$ from AUBERT 06E.

$\Gamma(\gamma\eta_c(1S) \to 3\gamma)/\Gamma_{\text{total}}$ — Γ_{213}/Γ

VALUE (units 10^{-6})	EVTS	DOCUMENT ID		TECN	COMMENT
$3.8^{+1.3}_{-1.0}$ OUR AVERAGE Error includes scale factor of 1.1.					
4.5±1.2±0.6	33 ± 9	ABLIKIM	13I	BES3	$\psi(2S) \to \pi^+\pi^- J/\psi$
$1.2^{+2.7}_{-1.1}\pm0.3$	$1.2^{+2.8}_{-1.1}$	ADAMS	08	CLEO	$\psi(2S) \to \pi^+\pi^- J/\psi$

$\Gamma(\gamma\eta_c(1S) \to \gamma\eta\eta\eta')/\Gamma_{\text{total}}$ — Γ_{214}/Γ

VALUE (units 10^{-5})	EVTS	DOCUMENT ID		TECN	COMMENT
4.86±0.62±0.45	137	ABLIKIM	21C	BES3	$J/\psi(1S) \to \gamma\eta\eta\eta'$

$\Gamma(3\gamma)/\Gamma_{\text{total}}$ — Γ_{215}/Γ

VALUE (units 10^{-6})	CL%	EVTS	DOCUMENT ID		TECN	COMMENT
11.6±2.2 OUR AVERAGE						
11.3±1.8±2.0		113 ± 18	ABLIKIM	13I	BES3	$\psi(2S) \to \pi^+\pi^- J/\psi$
12 ±3 ±2		$24.2^{+7.2}_{-6.0}$	ADAMS	08	CLEO	$\psi(2S) \to \pi^+\pi^- J/\psi$
• • • We do not use the following data for averages, fits, limits, etc. • • •						
<55	90		PARTRIDGE	80	CBAL	e^+e^-

$\Gamma(4\gamma)/\Gamma_{\text{total}}$ — Γ_{216}/Γ

VALUE	CL%	DOCUMENT ID		TECN	COMMENT
<9 × 10^{-6}	90	ADAMS	08	CLEO	$\psi(2S) \to \pi^+\pi^- J/\psi$

$\Gamma(5\gamma)/\Gamma_{\text{total}}$ — Γ_{217}/Γ

VALUE	CL%	DOCUMENT ID		TECN	COMMENT
<15 × 10^{-6}	90	ADAMS	08	CLEO	$\psi(2S) \to \pi^+\pi^- J/\psi$

$\Gamma(\gamma\pi^0)/\Gamma_{\text{total}}$ — Γ_{218}/Γ

VALUE (units 10^{-5})	EVTS	DOCUMENT ID		TECN	COMMENT
3.56±0.17 OUR AVERAGE					
3.59±0.20±0.03	1.6k	[1] ABLIKIM	18O	BES3	$\psi(2S) \to \pi^+\pi^-\gamma\gamma\gamma$
3.63±0.36±0.13		PEDLAR	09	CLE3	$J/\psi \to \pi^0\gamma$
$3.13^{+0.65}_{-0.47}$	586	ABLIKIM	06E	BES2	$J/\psi \to \pi^0\gamma$
• • • We do not use the following data for averages, fits, limits, etc. • • •					
3.6 ±1.1 ±0.7		BLOOM	83	CBAL	e^+e^-
7.3 ±4.7	10	BRANDELIK	79C	DASP	e^+e^-

[1] ABLIKIM 18O reports $[\Gamma(J/\psi(1S) \to \gamma\pi^0)/\Gamma_{\text{total}}] \times [B(\pi^0 \to 2\gamma)] = (3.57 \pm 0.12 \pm 0.16) \times 10^{-5}$ from a measurement of $[\Gamma(J/\psi(1S) \to \gamma\pi^0)/\Gamma_{\text{total}}] \times [B(\pi^0 \to 2\gamma)] \times [B(\psi(2S) \to J/\psi(1S)\pi^+\pi^-)]$ assuming $B(\psi(2S) \to J/\psi(1S)\pi^+\pi^-) = (34.49 \pm 0.30) \times 10^{-2}$, which we rescale to our best values $B(\pi^0 \to 2\gamma) = (98.823 \pm 0.034) \times 10^{-2}$, $B(\psi(2S) \to J/\psi(1S)\pi^+\pi^-) = (34.68 \pm 0.30) \times 10^{-2}$. Our first error is their experiment's error and our second error is the systematic error from using our best values.

$\Gamma(\gamma\pi^0\pi^0)/\Gamma_{\text{total}}$ — Γ_{219}/Γ

VALUE (units 10^{-3})	DOCUMENT ID		TECN	COMMENT
1.15±0.05	[1] ABLIKIM	15AE	BES3	$J/\psi \to \gamma\pi^0\pi^0$

[1] The uncertainty is systematic as statistical is netligible.

$\Gamma(\gamma 2\pi^+ 2\pi^-)/\Gamma_{\text{total}}$ — Γ_{220}/Γ

VALUE (units 10^{-3})	DOCUMENT ID		TECN	COMMENT
2.8 ±0.5 OUR AVERAGE Error includes scale factor of 1.9. See the ideogram below.				
4.32±0.14±0.73	[1] BISELLO	89B	DM2	$J/\psi \to 4\pi\gamma$
2.08±0.13±0.35	[2] BISELLO	89B	DM2	$J/\psi \to 4\pi\gamma$
3.05±0.08±0.45	[2] BALTRUSAIT...	86B	MRK3	$J/\psi \to 4\pi\gamma$
4.85±0.45±1.20	[3] BURKE	82	MRK2	e^+e^-

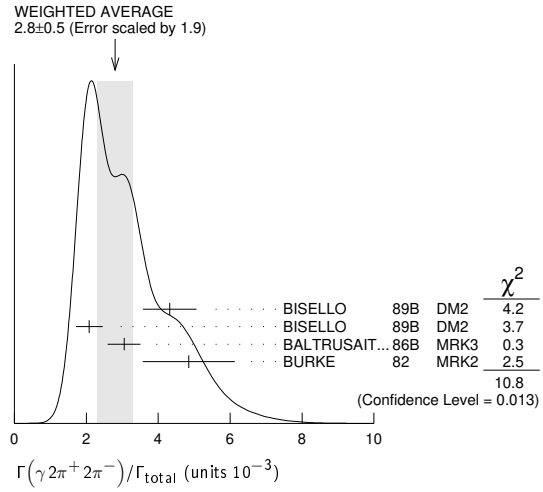

[1] 4π mass less than 3.0 GeV.

Downloaded from https://academic.oup.com/ptep/article/2022/8/083C01/6651666 by KIT Library user on 27 September 2022

[2] 4π mass less than 2.0 GeV.
[3] 4π mass less than 2.5 GeV.

$\Gamma(\gamma f_2(1270)\, f_2(1270))/\Gamma_{total}$ — Γ_{221}/Γ

VALUE (units 10^{-4})	EVTS	DOCUMENT ID		TECN	COMMENT
9.5±0.7±1.6	646 ± 45	ABLIKIM	04M	BES	$J/\psi \to \gamma 2\pi^+ 2\pi^-$

$\Gamma(\gamma f_2(1270)\, f_2(1270)\,(\text{non resonant}))/\Gamma_{total}$ — Γ_{222}/Γ

VALUE (units 10^{-4})	DOCUMENT ID		TECN	COMMENT
8.2±0.8±1.7	[1] ABLIKIM	04M	BES	$J/\psi \to \gamma 2\pi^+ 2\pi^-$

[1] Subtracting contribution from intermediate $\eta_c(1S)$ decays.

$\Gamma(\gamma\pi^+\pi^- 2\pi^0)/\Gamma_{total}$ — Γ_{223}/Γ

VALUE (units 10^{-3})	DOCUMENT ID		TECN	COMMENT
8.3±0.2±3.1	[1] BALTRUSAIT...86B		MRK3	$J/\psi \to 4\pi\gamma$

[1] 4π mass less than 2.0 GeV.

$\Gamma(\gamma K^0_S K^0_S)/\Gamma_{total}$ — Γ_{224}/Γ

VALUE (units 10^{-4})	DOCUMENT ID		TECN	COMMENT
8.1±0.4	ABLIKIM	18AA	BES3	$J/\psi \to \gamma K^0_S K^0_S$

$\Gamma(\gamma(K\overline{K}\pi)\,[J^{PC} = 0^{-+}])/\Gamma_{total}$ — Γ_{225}/Γ

VALUE (units 10^{-3})	DOCUMENT ID		TECN	COMMENT
0.7 ±0.4 OUR AVERAGE Error includes scale factor of 2.1.				
0.58±0.03±0.20	[1] BAI	00D	BES	$J/\psi \to \gamma K^\pm K^0_S \pi^\mp$
2.1 ±0.1 ±0.7	[2] BAI	00D	BES	$J/\psi \to \gamma K^\pm K^0_S \pi^\mp$

[1] For a broad structure around 1800 MeV.
[2] For a broad structure around 2040 MeV.

$\Gamma(\gamma K^+ K^- \pi^+\pi^-)/\Gamma_{total}$ — Γ_{226}/Γ

VALUE (units 10^{-3})	EVTS	DOCUMENT ID		TECN	COMMENT
2.1±0.1±0.6	1516	BAI	00B	BES	$J/\psi \to \gamma K^+ K^0 \pi^+\pi^-$

$\Gamma(\gamma K^*(892)\overline{K}^*(892))/\Gamma_{total}$ — Γ_{227}/Γ

VALUE (units 10^{-3})	EVTS	DOCUMENT ID		TECN	COMMENT
4.0±0.3±1.3	320	[1] BAI	00B	BES	$J/\psi \to \gamma K^+ K^0 \pi^+\pi^-$

[1] Summed over all charges.

$\Gamma(\gamma\eta)/\Gamma_{total}$ — Γ_{228}/Γ

VALUE (units 10^{-3})	EVTS	DOCUMENT ID		TECN	COMMENT
1.085±0.018 OUR AVERAGE					
1.067±0.005±0.023	87.9k	ABLIKIM	21AM	BES3	$e^+e^- \to J/\psi$
1.12 ±0.05 ±0.01	18.6k	[1] ABLIKIM	18O	BES3	$\psi(2S) \to \pi^+\pi^-\gamma\gamma\gamma$
1.101±0.029±0.022		PEDLAR	09	CLE3	$J/\psi \to \eta\gamma$
1.123±0.089	11k	ABLIKIM	06E	BES2	$J/\psi \to \eta\gamma$
• • • We do not use the following data for averages, fits, limits, etc. • • •					
0.88 ±0.08 ±0.11		BLOOM	83	CBAL	e^+e^-
0.82 ±0.10		BRANDELIK	79C	DASP	e^+e^-
1.3 ±0.4	21	BARTEL	77	CNTR	e^+e^-

[1] ABLIKIM 18O reports $[\Gamma(J/\psi(1S) \to \gamma\eta)/\Gamma_{total}] \times [B(\eta \to 2\gamma)] = (4.42 \pm 0.04 \pm 0.18) \times 10^{-4}$ from a measurement of $[\Gamma(J/\psi(1S) \to \gamma\eta)/\Gamma_{total}] \times [B(\eta \to 2\gamma)] \times [B(\psi(2S) \to J/\psi(1S)\pi^+\pi^-)]$ assuming $B(\psi(2S) \to J/\psi(1S)\pi^+\pi^-) = (34.49 \pm 0.30) \times 10^{-2}$, which we rescale to our best values $B(\eta \to 2\gamma) = (39.36 \pm 0.18) \times 10^{-2}$, $B(\psi(2S) \to J/\psi(1S)\pi^+\pi^-) = (34.68 \pm 0.30) \times 10^{-2}$. Our first error is their experiment's error and our second error is the systematic error from using our best values.

$\Gamma(\gamma\eta\pi^0)/\Gamma_{total}$ — Γ_{229}/Γ

VALUE (units 10^{-6})	EVTS	DOCUMENT ID		TECN	COMMENT
21.4±1.8±2.5	596	ABLIKIM	16P	BES3	$J/\psi \to 5\gamma$

$\Gamma(\gamma a_0(980)^0 \to \gamma\eta\pi^0)/\Gamma_{total}$ — Γ_{233}/Γ

VALUE	CL%	DOCUMENT ID		TECN	COMMENT
<2.5 × 10^{-6}	95	ABLIKIM	16P	BES3	$J/\psi \to 5\gamma$

$\Gamma(\gamma a_2(1320)^0 \to \gamma\eta\pi^0)/\Gamma_{total}$ — Γ_{234}/Γ

VALUE	CL%	DOCUMENT ID		TECN	COMMENT
<6.6 × 10^{-6}	95	ABLIKIM	16P	BES3	$J/\psi \to 5\gamma$

$\Gamma(\gamma\eta\pi\pi)/\Gamma_{total}$ — Γ_{235}/Γ

VALUE (units 10^{-3})	DOCUMENT ID		TECN	COMMENT
6.1 ±1.0 OUR AVERAGE				
5.85±0.3±1.05	[1] EDWARDS	83B	CBAL	$J/\psi \to \eta\pi^+\pi^-$
7.8 ±1.2±2.4	[1] EDWARDS	83B	CBAL	$J/\psi \to \eta 2\pi^0$

[1] Broad enhancement at 1700 MeV.

$\Gamma(\gamma\eta_2(1870) \to \gamma\eta\pi^+\pi^-)/\Gamma_{total}$ — Γ_{236}/Γ

VALUE (units 10^{-4})	DOCUMENT ID		TECN	COMMENT
6.2±2.2±0.9	BAI	99	BES	$J/\psi \to \gamma\eta\pi^+\pi^-$

$\Gamma(\gamma\eta'(958))/\Gamma_{total}$ — Γ_{237}/Γ

VALUE (units 10^{-3})	EVTS	DOCUMENT ID		TECN	COMMENT
5.25±0.07 OUR AVERAGE Error includes scale factor of 1.3. See the ideogram below.					
5.27±0.03±0.05	36k	ABLIKIM	19T	BES	$J/\psi \to \gamma\eta'$
5.43±0.23±0.09	5.0k	[1] ABLIKIM	18O	BES3	$\psi(2S) \to \pi^+\pi^-\gamma\gamma\gamma$
4.77±0.22±0.06		[2] ABLIKIM	11	BES3	$J/\psi \to \eta'\gamma$
5.24±0.12±0.11		PEDLAR	09	CLE3	$J/\psi \to \eta'\gamma$
5.55±0.44	35k	ABLIKIM	06E	BES2	$J/\psi \to \eta'\gamma$
• • • We do not use the following data for averages, fits, limits, etc. • • •					
4.50±0.14±0.53		BOLTON	92B	MRK3	$J/\psi \to \gamma\pi^+\pi^-\eta$, $\eta \to \gamma\gamma$
4.30±0.31±0.71		BOLTON	92B	MRK3	$J/\psi \to \gamma\pi^+\pi^-\eta$, $\eta \to \pi^+\pi^-\pi^0$
4.04±0.16±0.85	622	AUGUSTIN	90	DM2	$J/\psi \to \gamma\eta\pi^+\pi^-$
4.39±0.09±0.66	2420	AUGUSTIN	90	DM2	$J/\psi \to \gamma\gamma\pi^+\pi^-$
4.1 ±0.3 ±0.6		BLOOM	83	CBAL	$e^+e^- \to 3\gamma$ + hadrons
2.9 ±1.1	6	BRANDELIK	79C	DASP	$e^+e^- \to 3\gamma$
2.4 ±0.7	57	BARTEL	76	CNTR	$e^+e^- \to 2\gamma\rho$

[1] ABLIKIM 18O reports $[\Gamma(J/\psi(1S) \to \gamma\eta'(958))/\Gamma_{total}] \times [B(\eta'(958) \to \gamma\gamma)] = (1.26 \pm 0.02 \pm 0.05) \times 10^{-4}$ from a measurement of $[\Gamma(J/\psi(1S) \to \gamma\eta'(958))/\Gamma_{total}] \times [B(\eta'(958) \to \gamma\gamma)] \times [B(\psi(2S) \to J/\psi(1S)\pi^+\pi^-)]$ assuming $B(\psi(2S) \to J/\psi(1S)\pi^+\pi^-) = (34.49 \pm 0.30) \times 10^{-2}$, which we rescale to our best values $B(\eta'(958) \to \gamma\gamma) = (2.307 \pm 0.033) \times 10^{-2}$, $B(\psi(2S) \to J/\psi(1S)\pi^+\pi^-) = (34.68 \pm 0.30) \times 10^{-2}$. Our first error is their experiment's error and our second error is the systematic error from using our best values.

[2] ABLIKIM 11 reports $(4.84 \pm 0.03 \pm 0.24) \times 10^{-3}$ from a measurement of $[\Gamma(J/\psi(1S) \to \gamma\eta'(958))/\Gamma_{total}]$ / $[B(\eta'(958) \to \pi^+\pi^-\eta)]$ / $[B(\eta \to 2\gamma)]$ assuming $B(\eta'(958) \to \pi^+\pi^-\eta) = (43.2 \pm 0.7) \times 10^{-2}$, $B(\eta \to 2\gamma) = (39.31 \pm 0.20) \times 10^{-2}$, which we rescale to our best values $B(\eta'(958) \to \pi^+\pi^-\eta) = (42.5 \pm 0.5) \times 10^{-2}$, $B(\eta \to 2\gamma) = (39.36 \pm 0.18) \times 10^{-2}$. Our first error is their experiment's error and our second error is the systematic error from using our best values.

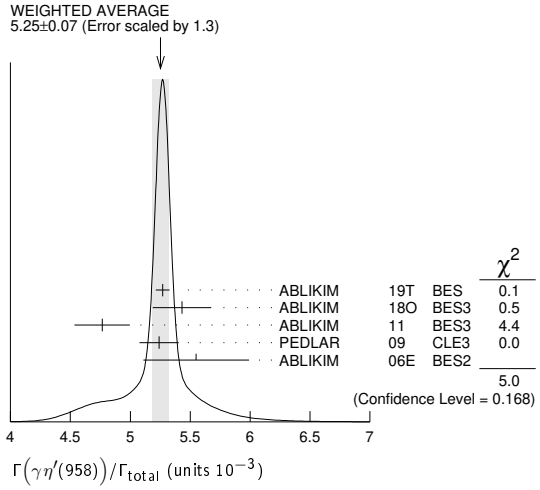

$\Gamma(\gamma f_0(500) \to \gamma\pi\pi)/\Gamma_{total}$ — Γ_{230}/Γ

VALUE (units 10^{-4})	DOCUMENT ID		TECN	COMMENT
• • • We do not use the following data for averages, fits, limits, etc. • • •				
10.5±2.0	SARANTSEV	21	RVUE	$J/\psi(1S) \to \gamma(\pi\pi,\ K\overline{K},\ \eta\eta,\ \omega\phi)$

$\Gamma(\gamma f_0(500) \to \gamma K\overline{K})/\Gamma_{total}$ — Γ_{231}/Γ

VALUE (units 10^{-5})	DOCUMENT ID		TECN	COMMENT
• • • We do not use the following data for averages, fits, limits, etc. • • •				
5±5	SARANTSEV	21	RVUE	$J/\psi(1S) \to \gamma(\pi\pi,\ K\overline{K},\ \eta\eta,\ \omega\phi)$

$\Gamma(\gamma f_0(500) \to \gamma\eta\eta)/\Gamma_{total}$ — Γ_{232}/Γ

VALUE (units 10^{-5})	DOCUMENT ID		TECN	COMMENT
• • • We do not use the following data for averages, fits, limits, etc. • • •				
4±3	SARANTSEV	21	RVUE	$J/\psi(1S) \to \gamma(\pi\pi,\ K\overline{K},\ \eta\eta,\ \omega\phi)$

$\Gamma(\gamma f_0(980) \to \gamma\pi\pi)/\Gamma_{total}$ — Γ_{238}/Γ

VALUE (units 10^{-5})	DOCUMENT ID		TECN	COMMENT
• • • We do not use the following data for averages, fits, limits, etc. • • •				
1.3±0.2	SARANTSEV	21	RVUE	$J/\psi(1S) \to \gamma(\pi\pi,\ K\overline{K},\ \eta\eta,\ \omega\phi)$

$\Gamma(\gamma f_0(980) \to \gamma K\overline{K})/\Gamma_{total}$ — Γ_{239}/Γ

VALUE (units 10^{-5})	DOCUMENT ID		TECN	COMMENT
• • • We do not use the following data for averages, fits, limits, etc. • • •				
0.8±0.3	SARANTSEV	21	RVUE	$J/\psi(1S) \to \gamma(\pi\pi,\ K\overline{K},\ \eta\eta,\ \omega\phi)$

Downloaded from https://academic.oup.com/ptep/article/2022/8/083C01/6651666 by KIT Library user on 27 September 2022

$\Gamma(\gamma\rho\rho)/\Gamma_{total}$ — Γ_{240}/Γ

VALUE (units 10^{-3})	CL%	DOCUMENT ID		TECN	COMMENT
4.5 ±0.8 OUR AVERAGE					
4.7 ±0.3 ±0.9		[1] BALTRUSAIT...	86B	MRK3	$J/\psi \to 4\pi\gamma$
3.75±1.05±1.20		[2] BURKE	82	MRK2	$J/\psi \to 4\pi\gamma$
• • • We do not use the following data for averages, fits, limits, etc. • • •					
<0.09	90	[3] BISELLO	89B		$J/\psi \to 4\pi\gamma$

[1] 4π mass less than 2.0 GeV.
[2] 4π mass less than 2.0 GeV. We have multiplied $2\rho^0$ measurement by 3 to obtain 2ρ.
[3] 4π mass in the range 2.0–25 GeV.

$\Gamma(\gamma\rho\omega)/\Gamma_{total}$ — Γ_{241}/Γ

VALUE	CL%	DOCUMENT ID		TECN	COMMENT
<5.4 × 10^{-4}	90	ABLIKIM	08A	BES2	$e^+e^- \to J/\psi$

$\Gamma(\gamma\rho\phi)/\Gamma_{total}$ — Γ_{242}/Γ

VALUE	CL%	DOCUMENT ID		TECN	COMMENT
<8.8 × 10^{-5}	90	ABLIKIM	08A	BES2	$e^+e^- \to J/\psi$

$\Gamma(\gamma\omega\omega)/\Gamma_{total}$ — Γ_{243}/Γ

VALUE (units 10^{-3})	EVTS	DOCUMENT ID		TECN	COMMENT
1.61±0.33 OUR AVERAGE					
6.0 ±4.8 ±1.8		ABLIKIM	08A	BES2	$J/\psi \to \gamma\omega\pi^+\pi^-$
1.41±0.2 ±0.42	120 ± 17	BISELLO	87	SPEC	e^+e^-, hadrons γ
1.76±0.09±0.45		BALTRUSAIT...	85C	MRK3	$e^+e^- \to$ hadrons γ

$\Gamma(\gamma\phi\phi)/\Gamma_{total}$ — Γ_{244}/Γ

VALUE (units 10^{-4})	EVTS	DOCUMENT ID		TECN	COMMENT
4.0±1.2 OUR AVERAGE Error includes scale factor of 2.1. See the ideogram below.					
7.5±0.6±1.2	168	BAI	90B	MRK3	$J/\psi \to \gamma 4K$
3.4±0.8±0.6	33 ± 7	[1] BISELLO	90	DM2	$J/\psi \to \gamma K^+K^-K^0_S K^0_L$
3.1±0.7±0.4		[1] BISELLO	86B	DM2	$J/\psi \to \gamma K^+K^-K^+K^-$

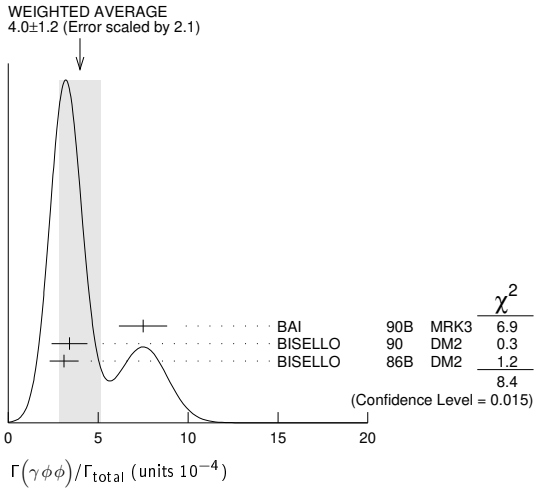

[1] $\phi\phi$ mass less than 2.9 GeV, η_c excluded.

$\Gamma(\gamma\eta(1405/1475) \to \gamma K\overline{K}\pi)/\Gamma_{total}$ — Γ_{245}/Γ

VALUE (units 10^{-3})	DOCUMENT ID		TECN	COMMENT
2.8 ±0.6 OUR AVERAGE Error includes scale factor of 1.6. See the ideogram below.				
1.66±0.1 ±0.58	[1,2] BAI	00D	BES	$J/\psi \to \gamma K^\pm K^0_S \pi^\mp$
3.8 ±0.3 ±0.6	[3] AUGUSTIN	90	DM2	$J/\psi \to \gamma K\overline{K}\pi$
4.0 ±0.7 ±1.0	[3] EDWARDS	82E	CBAL	$J/\psi \to K^+K^-\pi^0\gamma$
4.3 ±1.7	[3,4] SCHARRE	80	MRK2	e^+e^-
• • • We do not use the following data for averages, fits, limits, etc. • • •				
1.78±0.21±0.33	[3,5,6] AUGUSTIN	92	DM2	$J/\psi \to \gamma K\overline{K}\pi$
0.83±0.13±0.18	[3,7,8] AUGUSTIN	92	DM2	$J/\psi \to \gamma K\overline{K}\pi$
$0.66^{+0.17+0.24}_{-0.16-0.15}$	[3,6,9] BAI	90C	MRK3	$J/\psi \to \gamma K^0_S K^\pm\pi^\mp$
$1.03^{+0.21+0.26}_{-0.18-0.19}$	[3,8,10] BAI	90C	MRK3	$J/\psi \to \gamma K^0_S K^\pm\pi^\mp$

[1] Interference with the $J/\psi(1S)$ radiative transition to the broad $K\overline{K}\pi$ pseudoscalar state around 1800 is $(0.15 \pm 0.01 \pm 0.05) \times 10^{-3}$.
[2] Interference with $J/\psi \to \gamma f_1(1420)$ is $(-0.03 \pm 0.01 \pm 0.01) \times 10^{-3}$.
[3] Includes unknown branching fraction $\eta(1405) \to K\overline{K}\pi$.
[4] Corrected for spin-zero hypothesis for $\eta(1405)$.
[5] From fit to the $a_0(980)\pi$ 0^{-+} partial wave.
[6] $a_0(980)\pi$ mode.
[7] From fit to the $K^*(892)K$ 0^{-+} partial wave.
[8] K^*K mode.
[9] From $a_0(980)\pi$ final state.
[10] From $K^*(890)K$ final state.

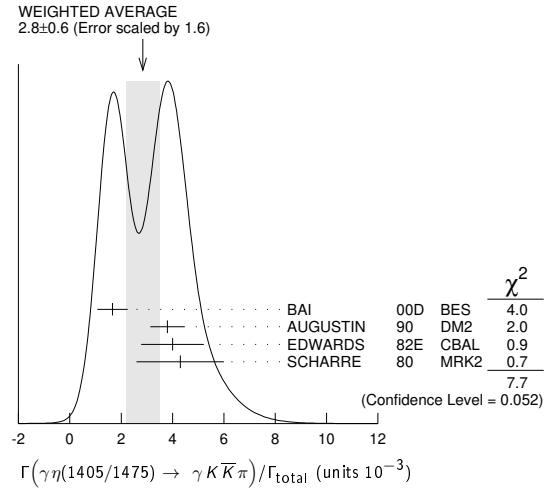

$\Gamma(\gamma\eta(1405/1475) \to \gamma\gamma\rho^0)/\Gamma_{total}$ — Γ_{246}/Γ

VALUE (units 10^{-4})	DOCUMENT ID		TECN	COMMENT
0.78±0.20 OUR AVERAGE Error includes scale factor of 1.8.				
1.07±0.17±0.11	[1] BAI	04J	BES2	$J/\psi \to \gamma\gamma\pi^+\pi^-$
0.64±0.12±0.07	[1] COFFMAN	90	MRK3	$J/\psi \to \gamma\gamma\pi^+\pi^-$

[1] Includes unknown branching fraction $\eta(1405) \to \gamma\rho^0$.

$\Gamma(\gamma\eta(1405/1475) \to \gamma\eta\pi^+\pi^-)/\Gamma_{total}$ — Γ_{247}/Γ

VALUE (units 10^{-4})	EVTS	DOCUMENT ID		TECN	COMMENT
3.0 ±0.5 OUR AVERAGE					
2.6 ±0.7 ±0.4		BAI	99	BES	$J/\psi \to \gamma\eta\pi^+\pi^-$
3.38±0.33±0.64		[1] BOLTON	92B	MRK3	$J/\psi \to \gamma\eta\pi^+\pi^-$
• • • We do not use the following data for averages, fits, limits, etc. • • •					
7.0 ±0.6 ±1.1	261	[2] AUGUSTIN	90	DM2	$J/\psi \to \gamma\eta\pi^+\pi^-$

[1] Via $a_0(980)\pi$.
[2] Includes unknown branching fraction to $\eta\pi^+\pi^-$.

$\Gamma(\gamma\eta(1405/1475) \to \gamma\rho^0\rho^0)/\Gamma_{total}$ — Γ_{248}/Γ

VALUE (units 10^{-3})	DOCUMENT ID		TECN	COMMENT
1.7 ±0.4 OUR AVERAGE Error includes scale factor of 1.3.				
2.1 ±0.4	BUGG	95	MRK3	$J/\psi \to \gamma\pi^+\pi^-\pi^+\pi^-$
1.36±0.38	[1,2] BISELLO	89B	DM2	$J/\psi \to 4\pi\gamma$

[1] Estimated by us from various fits.
[2] Includes unknown branching fraction to $\rho^0\rho^0$.

$\Gamma(\gamma\eta(1405/1475) \to \gamma\gamma\phi)/\Gamma_{total}$ — Γ_{249}/Γ

VALUE (units 10^{-6})	CL%	EVTS	DOCUMENT ID		TECN	COMMENT
<82	95		BAI	04J	BES2	$J/\psi \to \gamma\gamma K^+K^-$
• • • We do not use the following data for averages, fits, limits, etc. • • •						
7.03±0.92±0.91		1.3k	[1] ABLIKIM	18I	BES3	$J/\psi \to \gamma\gamma\phi(1020)$
10.36±1.51±1.54		1.9k	[2] ABLIKIM	18I	BES3	$J/\psi \to \gamma\gamma\phi(1020)$

[1] Constructive interference between the $X(1835)$ and $\eta(1405)/\eta(1475)$ is assumed in a fit to the $\gamma\phi$ invariant mass.
[2] Destructive interference between the $X(1835)$ and $\eta(1405)/\eta(1475)$ is assumed in a fit to the $\gamma\phi$ invariant mass.

$\Gamma(\gamma\eta(1405) \to \gamma\gamma\gamma)/\Gamma_{total}$ — Γ_{250}/Γ

VALUE	CL%	DOCUMENT ID		TECN	COMMENT
<2.63 × 10^{-6}	90	ABLIKIM	18O	BES3	$\psi(2S) \to \pi^+\pi^-\gamma\gamma\gamma$

$\Gamma(\gamma\eta(1475) \to \gamma\gamma\gamma)/\Gamma_{total}$ — Γ_{251}/Γ

VALUE	CL%	DOCUMENT ID		TECN	COMMENT
<1.86 × 10^{-6}	90	ABLIKIM	18O	BES3	$\psi(2S) \to \pi^+\pi^-\gamma\gamma\gamma$

$\Gamma(\gamma\eta(1760) \to \gamma\rho^0\rho^0)/\Gamma_{total}$ — Γ_{252}/Γ

VALUE (units 10^{-3})	DOCUMENT ID		TECN	COMMENT
0.13±0.09	[1,2] BISELLO	89B	DM2	$J/\psi \to 4\pi\gamma$

[1] Estimated by us from various fits.
[2] Includes unknown branching fraction to $\rho^0\rho^0$.

$\Gamma(\gamma\eta(1760) \to \gamma\omega\omega)/\Gamma_{total}$ — Γ_{253}/Γ

VALUE (units 10^{-3})	EVTS	DOCUMENT ID		TECN	COMMENT
1.98±0.08±0.32	1045	ABLIKIM	06H	BES	$J/\psi \to \gamma\omega\omega$

$\Gamma(\gamma\eta(1760) \to \gamma\gamma\gamma)/\Gamma_{total}$ — Γ_{254}/Γ

VALUE	CL%	DOCUMENT ID		TECN	COMMENT
<4.80 × 10^{-6}	90	ABLIKIM	18O	BES3	$\psi(2S) \to \pi^+\pi^-\gamma\gamma\gamma$

Downloaded from https://academic.oup.com/ptep/article/2022/8/083C01/6651666 by KIT Library user on 27 September 2022

$\Gamma(\gamma\eta(2225))/\Gamma_{total}$ — Γ_{255}/Γ

VALUE (units 10^{-4})	EVTS	DOCUMENT ID		TECN	COMMENT
$3.14^{+0.50}_{-0.19}$ OUR AVERAGE					
$2.40\pm0.10^{+2.47}_{-0.18}$		[1,2] ABLIKIM	16N	BES3	$J/\psi\to\gamma K^+K^-K^+K^-$
$4.4\pm0.4\pm0.8$	196	[2] ABLIKIM	08I	BES	$J/\psi\to\gamma K^+K^-K^0_SK^0_L$
$3.3\pm0.8\pm0.5$		[2] BAI	90B	MRK3	$J/\psi\to\gamma K^+K^-K^+K^-$
$2.7\pm0.6\pm0.6$		[2] BAI	90B	MRK3	$J/\psi\to\gamma K^+K^-K^0_SK^0_L$
$2.4\ ^{+1.5}_{-1.0}$		[3,4] BISELLO	89B	DM2	$J/\psi\to4\pi\gamma$

[1] From a partial wave analysis of $J/\psi\to\gamma\phi\phi$ that also finds significant signals for for $\eta(2100)$, 0^{-+} phase space, $f_0(2100)$, $f_2(2010)$, $f_2(2300)$, $f_2(2340)$, and a previously unseen 0^{-+} state $X(2500)$ ($M=2470^{+15+101}_{-19-23}$ MeV, $\Gamma=230^{+64+56}_{-35-33}$ MeV).
[2] Includes unknown branching fraction to $\phi\phi$.
[3] Estimated by us from various fits.
[4] Includes unknown branching fraction to $\rho^0\rho^0$.

$\Gamma(\gamma f_2(1270))/\Gamma_{total}$ — Γ_{256}/Γ

VALUE (units 10^{-3})	EVTS	DOCUMENT ID		TECN	COMMENT
1.64 ± 0.12 OUR AVERAGE		Error includes scale factor of 1.3. See the ideogram below.			
$2.07\pm0.16^{+0.02}_{-0.07}$	2.4k	[1,2] DOBBS	15		$J/\psi\to\gamma\pi\pi$
$1.63\pm0.26^{+0.02}_{-0.06}$		[3] ABLIKIM	06V	BES2	$e^+e^-\to J/\psi\to\gamma\pi^+\pi^-$
$1.42\pm0.21^{+0.01}_{-0.05}$		[4] ABLIKIM	06V	BES2	$e^+e^-\to J/\psi\to\gamma\pi^0\pi^0$
$1.33\pm0.05\pm0.20$		[5] AUGUSTIN	87	DM2	$J/\psi\to\gamma\pi^+\pi^-$
$1.36\pm0.09\pm0.23$		[5] BALTRUSAIT...	87	MRK3	$J/\psi\to\gamma\pi^+\pi^-$
$1.48\pm0.25\pm0.30$	178	EDWARDS	82B	CBAL	$e^+e^-\to2\pi^0\gamma$
2.0 ± 0.7	35	ALEXANDER	78	PLUT	e^+e^-
1.2 ± 0.6	30	[6] BRANDELIK	78B	DASP	$e^+e^-\to\pi^+\pi^-\gamma$

[1] Using CLEO-c data but not authored by the CLEO Collaboration.
[2] DOBBS 15 reports $[\Gamma(J/\psi(1S)\to\gamma f_2(1270))/\Gamma_{total}]\times[B(f_2(1270)\to\pi\pi)]=(1.744\pm0.052\pm0.122)\times10^{-3}$ which we divide by our best value $B(f_2(1270)\to\pi\pi)=(84.2^{+2.9}_{-0.9})\times10^{-2}$. Our first error is their experiment's error and our second error is the systematic error from using our best value.
[3] ABLIKIM 06V reports $[\Gamma(J/\psi(1S)\to\gamma f_2(1270))/\Gamma_{total}]\times[B(f_2(1270)\to\pi\pi)]=(1.371\pm0.010\pm0.222)\times10^{-3}$ which we divide by our best value $B(f_2(1270)\to\pi\pi)=(84.2^{+2.9}_{-0.9})\times10^{-2}$. Our first error is their experiment's error and our second error is the systematic error from using our best value.
[4] ABLIKIM 06V reports $[\Gamma(J/\psi(1S)\to\gamma f_2(1270))/\Gamma_{total}]\times[B(f_2(1270)\to\pi\pi)]=(1.200\pm0.027\pm0.174)\times10^{-3}$ which we divide by our best value $B(f_2(1270)\to\pi\pi)=(84.2^{+2.9}_{-0.9})\times10^{-2}$. Our first error is their experiment's error and our second error is the systematic error from using our best value.
[5] Estimated using $B(f_2(1270)\to\pi\pi)=0.843\pm0.012$. The errors do not contain the uncertainty in the $f_2(1270)$ decay.
[6] Restated by us to take account of spread of E1, M2, E3 transitions.

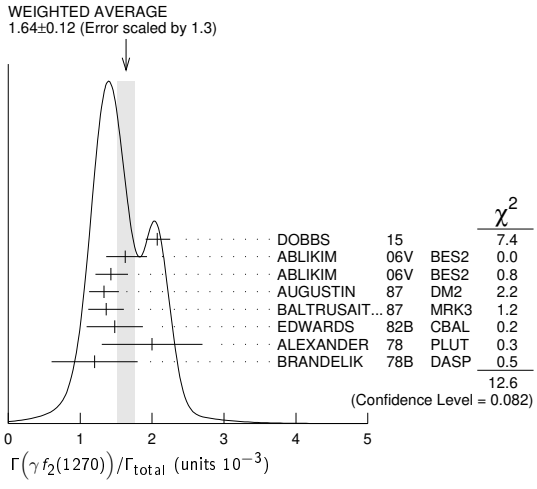

$\Gamma(\gamma f_2(1270)\to\gamma K^0_SK^0_S)/\Gamma_{total}$ — Γ_{257}/Γ

VALUE (units 10^{-5})	DOCUMENT ID		TECN	COMMENT
$2.58^{+0.08+0.59}_{-0.09-0.20}$	ABLIKIM	18AA	BES3	$J/\psi\to\gamma K^0_SK^0_S$

$\Gamma(\gamma f_1(1285))/\Gamma_{total}$ — Γ_{258}/Γ

VALUE (units 10^{-3})	DOCUMENT ID		TECN	COMMENT
0.61 ± 0.08 OUR AVERAGE				
$0.69\pm0.16\pm0.20$	[1] BAI	04J	BES2	$J/\psi\to\gamma\gamma\rho^0$
$0.61\pm0.04\pm0.21$	[2] BAI	00D	BES	$J/\psi\to\gamma K^\pm K^0_S\pi^\mp$
$0.45\pm0.09\pm0.17$	[3] BAI	99	BES	$J/\psi\to\gamma\eta\pi^+\pi^-$
$0.625\pm0.063\pm0.103$	[4] BOLTON	92	MRK3	$J/\psi\to\gamma f_1(1285)$
$0.70\pm0.08\pm0.16$	[5] BOLTON	92B	MRK3	$J/\psi\to\gamma\eta\pi^+\pi^-$

[1] Assuming $B(f_1(1285)\to\rho^0\gamma)=0.055\pm0.013$.
[2] Assuming $\Gamma(f_1(1285)\to K\overline{K}\pi)/\Gamma_{total}=0.090\pm0.004$.
[3] Assuming $\Gamma(f_1(1285)\to\eta\pi\pi)/\Gamma_{total}=0.5\pm0.18$.
[4] Obtained summing the sequential decay channels
$B(J/\psi\to\gamma f_1(1285), f_1(1285)\to\pi\pi\pi\pi)=(1.44\pm0.39\pm0.27)\times10^{-4}$;
$B(J/\psi\to\gamma f_1(1285), f_1(1285)\to a_0(980)\pi, a_0(980)\to\eta\pi)=(3.90\pm0.42\pm0.87)\times10^{-4}$;
$B(J/\psi\to\gamma f_1(1285), f_1(1285)\to a_0(980)\pi, a_0(980)\to K\overline{K})=(0.66\pm0.26\pm0.29)\times10^{-4}$;
$B(J/\psi\to\gamma f_1(1285), f_1(1285)\to\gamma\rho^0)=(0.25\pm0.07\pm0.03)\times10^{-4}$.
[5] Using $B(f_1(1285)\to a_0(980)\pi)=0.37$, and including unknown branching ratio for $a_0(980)\to\eta\pi$.

$\Gamma(\gamma f_0(1370)\to\gamma\pi\pi)/\Gamma_{total}$ — Γ_{259}/Γ

VALUE (units 10^{-5})	DOCUMENT ID		TECN	COMMENT
• • • We do not use the following data for averages, fits, limits, etc. • • •				
38 ± 10	SARANTSEV	21	RVUE	$J/\psi(1S)\to\gamma(\pi\pi,\ K\overline{K},\ \eta\eta,\ \omega\phi)$

$\Gamma(\gamma f_0(1370)\to\gamma K\overline{K})/\Gamma_{total}$ — Γ_{260}/Γ

VALUE (units 10^{-4})	EVTS	DOCUMENT ID		TECN	COMMENT
$4.19\pm0.73\pm1.34$	478	[1] DOBBS	15		$J/\psi\to\gamma K\overline{K}$
• • • We do not use the following data for averages, fits, limits, etc. • • •					
1.3 ± 0.4		SARANTSEV	21	RVUE	$J/\psi(1S)\to\gamma(\pi\pi,\ K\overline{K},\ \eta\eta,\ \omega\phi)$

[1] Using CLEO-c data but not authored by the CLEO Collaboration.

$\Gamma(\gamma f_0(1370)\to\gamma K^0_SK^0_S)/\Gamma_{total}$ — Γ_{261}/Γ

VALUE (units 10^{-5})	DOCUMENT ID		TECN	COMMENT
$1.07^{+0.08+0.36}_{-0.07-0.34}$	ABLIKIM	18AA	BES3	$J/\psi\to\gamma K^0_SK^0_S$

$\Gamma(\gamma f_0(1370)\to\gamma\eta\eta)/\Gamma_{total}$ — Γ_{262}/Γ

VALUE (units 10^{-5})	DOCUMENT ID		TECN	COMMENT
• • • We do not use the following data for averages, fits, limits, etc. • • •				
3.5 ± 1.0	SARANTSEV	21	RVUE	$J/\psi(1S)\to\gamma(\pi\pi,\ K\overline{K},\ \eta\eta,\ \omega\phi)$

$\Gamma(\gamma f_0(1370)\to\gamma\eta\eta')/\Gamma_{total}$ — Γ_{263}/Γ

VALUE (units 10^{-5})	DOCUMENT ID		TECN	COMMENT
• • • We do not use the following data for averages, fits, limits, etc. • • •				
0.9 ± 0.3	SARANTSEV	21	RVUE	$J/\psi(1S)\to\gamma(\pi\pi,\ K\overline{K},\ \eta\eta,\ \omega\phi)$

$\Gamma(\gamma f_1(1420)\to\gamma K\overline{K}\pi)/\Gamma_{total}$ — Γ_{264}/Γ

VALUE (units 10^{-3})	DOCUMENT ID		TECN	COMMENT
0.79 ± 0.13 OUR AVERAGE				
$0.68\pm0.04\pm0.24$	BAI	00D	BES	$J/\psi\to\gamma K^\pm K^0_S\pi^\mp$
$0.76\pm0.15\pm0.21$	[1,2] AUGUSTIN	92	DM2	$J/\psi\to\gamma K\overline{K}\pi$
$0.87\pm0.14^{+0.14}_{-0.11}$	[1] BAI	90C	MRK3	$J/\psi\to\gamma K^0_SK^\pm\pi^\mp$

[1] Included unknown branching fraction $f_1(1420)\to K\overline{K}\pi$.
[2] From fit to the $K^*(892)K$ 1^{++} partial wave.

$\Gamma(\gamma f_0(1500)\to\gamma\pi\pi)/\Gamma_{total}$ — Γ_{265}/Γ

VALUE (units 10^{-4})	EVTS	DOCUMENT ID		TECN	COMMENT
1.09 ± 0.24 OUR AVERAGE					
$1.21\pm0.29\pm0.24$	174	[1] DOBBS	15		$J/\psi\to\gamma\pi\pi$
$1.00\pm0.03\pm0.45$		[2] ABLIKIM	06V	BES2	$e^+e^-\to J/\psi\to\gamma\pi^+\pi^-$
$1.02\pm0.09\pm0.45$		[2] ABLIKIM	06V	BES2	$e^+e^-\to J/\psi\to\gamma\pi^0\pi^0$
• • • We do not use the following data for averages, fits, limits, etc. • • •					
0.90 ± 0.17		SARANTSEV	21	RVUE	$J/\psi(1S)\to\gamma(\pi\pi,\ K\overline{K},\ \eta\eta,\ \omega\phi)$
5.7 ± 0.8		[3,4] BUGG	95	MRK3	$J/\psi\to\gamma\pi^+\pi^-\pi^+\pi^-$

[1] Using CLEO-c data but not authored by the CLEO Collaboration.
[2] Including unknown branching fraction to $\pi\pi$.
[3] Including unknown branching ratio for $f_0(1500)\to\pi^+\pi^-\pi^+\pi^-$.
[4] Assuming that $f_0(1500)$ decays only to two S-wave dipions.

$\Gamma(\gamma f_0(1500)\to\gamma\eta\eta)/\Gamma_{total}$ — Γ_{266}/Γ

VALUE (units 10^{-5})	EVTS	DOCUMENT ID		TECN	COMMENT
$1.65^{+0.26+0.51}_{-0.31-1.40}$	5.5k	[1] ABLIKIM	13N	BES3	$J/\psi\to\gamma\eta\eta$
• • • We do not use the following data for averages, fits, limits, etc. • • •					
1.1 ± 0.4		SARANTSEV	21	RVUE	$J/\psi(1S)\to\gamma(\pi\pi,\ K\overline{K},\ \eta\eta,\ \omega\phi)$

[1] From partial wave analysis including all possible combinations of 0^{++}, 2^{++}, and 4^{++} resonances.

$\Gamma(\gamma f_0(1500)\to\gamma K^0_SK^0_S)/\Gamma_{total}$ — Γ_{267}/Γ

VALUE (units 10^{-5})	DOCUMENT ID		TECN	COMMENT
$1.59\pm0.16^{+0.18}_{-0.56}$	ABLIKIM	18AA	BES3	$J/\psi\to\gamma K^0_SK^0_S$
• • • We do not use the following data for averages, fits, limits, etc. • • •				
0.7 ± 0.3	SARANTSEV	21	RVUE	$J/\psi(1S)\to\gamma(\pi\pi,\ K\overline{K},\ \eta\eta,\ \omega\phi)$

Downloaded from https://academic.oup.com/ptep/article/2022/8/083C01/6651666 by KIT Library user on 27 September 2022

$\Gamma(\gamma f_0(1500) \to \gamma\eta\eta')/\Gamma_{total}$ — Γ_{268}/Γ

VALUE (units 10^{-5})	DOCUMENT ID	TECN	COMMENT
• • • We do not use the following data for averages, fits, limits, etc. • • •			
1.2±0.5	SARANTSEV 21	RVUE	$J/\psi(1S) \to \gamma(\pi\pi,\ K\overline{K},\ \eta\eta,\ \omega\phi)$

$\Gamma(\gamma f_1(1510) \to \gamma\eta\pi^+\pi^-)/\Gamma_{total}$ — Γ_{269}/Γ

VALUE (units 10^{-4})	DOCUMENT ID	TECN	COMMENT
4.5±1.0±0.7	BAI 99	BES	$J/\psi \to \gamma\eta\pi^+\pi^-$

$\Gamma(\gamma f_2'(1525))/\Gamma_{total}$ — Γ_{270}/Γ

VALUE (units 10^{-4})	CL%	EVTS	DOCUMENT ID	TECN	COMMENT
$5.7\ ^{+0.8}_{-0.5}$ OUR AVERAGE Error includes scale factor of 1.5. See the ideogram below.					
8.1 ±0.9 ±0.2		750	[1,2] DOBBS 15		$J/\psi \to \gamma K\overline{K}$
$3.85 \pm 0.17\ ^{+1.91}_{-0.73}$			[3] BAI 03G	BES	$J/\psi \to \gamma K\overline{K}$
$3.6 \pm 0.4\ ^{+1.4}_{-0.4}$			[3] BAI 96C	BES	$J/\psi \to \gamma K^+K^-$
5.6 ±1.4 ±0.9			[3] AUGUSTIN 88	DM2	$J/\psi \to \gamma K^+K^-$
4.5 ±0.4 ±0.9			[3] AUGUSTIN 88	DM2	$J/\psi \to \gamma K^0_S K^0_S$
6.8 ±1.6 ±1.4			[3] BALTRUSAIT...87	MRK3	$J/\psi \to \gamma K^+K^-$
• • • We do not use the following data for averages, fits, limits, etc. • • •					
<3.4	90	4	[4] BRANDELIK 79C	DASP	$e^+e^- \to \pi^+\pi^-\gamma$
<2.3	90	3	ALEXANDER 78	PLUT	$e^+e^- \to K^+K^-\gamma$

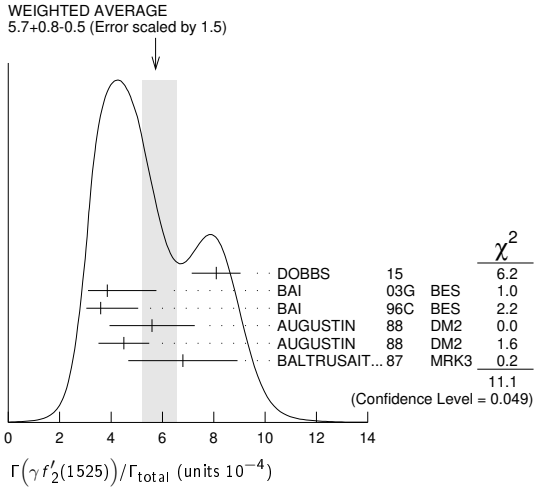

[1] Using CLEO-c data but not authored by the CLEO Collaboration.
[2] DOBBS 15 reports $[\Gamma(J/\psi(1S) \to \gamma f_2'(1525))/\Gamma_{total}] \times [B(f_2'(1525) \to K\overline{K})] = (7.09 \pm 0.46 \pm 0.67) \times 10^{-4}$ which we divide by our best value $B(f_2'(1525) \to K\overline{K}) = (87.6 \pm 2.2) \times 10^{-2}$. Our first error is their experiment's error and our second error is the systematic error from using our best value.
[3] Using $B(f_2'(1525) \to K\overline{K}) = 0.888$.
[4] Assuming isotropic production and decay of the $f_2'(1525)$ and isospin.

$\Gamma(\gamma f_2'(1525) \to \gamma K^0_S K^0_S)/\Gamma_{total}$ — Γ_{271}/Γ

VALUE (units 10^{-5})	DOCUMENT ID	TECN	COMMENT
$7.99\ ^{+0.03}_{-0.04}\ ^{+0.69}_{-0.50}$	ABLIKIM 18AA	BES3	$J/\psi \to \gamma K^0_S K^0_S$

$\Gamma(\gamma f_2'(1525) \to \gamma\eta\eta)/\Gamma_{total}$ — Γ_{272}/Γ

VALUE (units 10^{-5})	EVTS	DOCUMENT ID	TECN	COMMENT
$3.42\ ^{+0.43}_{-0.51}\ ^{+1.37}_{-1.30}$	5.5k	[1] ABLIKIM 13N	BES3	$J/\psi \to \gamma\eta\eta$

[1] From partial wave analysis including all possible combinations of 0^{++}, 2^{++}, and 4^{++} resonances.

$\Gamma(\gamma f_2(1640) \to \gamma\omega\omega)/\Gamma_{total}$ — Γ_{273}/Γ

VALUE (units 10^{-3})	EVTS	DOCUMENT ID	TECN	COMMENT
0.28±0.05±0.17	141	ABLIKIM 06H	BES	$J/\psi \to \gamma\omega\omega$

$\Gamma(\gamma f_0(1710) \to \gamma\pi\pi)/\Gamma_{total}$ — Γ_{274}/Γ

VALUE (units 10^{-4})	EVTS	DOCUMENT ID	TECN	COMMENT
3.8 ±0.5 OUR AVERAGE				
3.72±0.30±0.43	483	[1] DOBBS 15		$J/\psi \to \gamma\pi\pi$
3.96±0.06±1.12		[2] ABLIKIM 06V	BES2	$e^+e^- \to J/\psi \to \gamma\pi^+\pi^-$
3.99±0.15±2.64		[2] ABLIKIM 06V	BES2	$e^+e^- \to J/\psi \to \gamma\pi^0\pi^0$
• • • We do not use the following data for averages, fits, limits, etc. • • •				
0.6 ±0.2		[3] SARANTSEV 21	RVUE	$J/\psi(1S) \to \gamma(\pi\pi,\ K\overline{K},\ \eta\eta,\ \omega\phi)$
2.5 ±1.6 ±0.8		BAI 98H	BES	$J/\psi \to \gamma\pi^0\pi^0$

[1] Using CLEO-c data but not authored by the CLEO Collaboration.
[2] Including unknown branching fraction to $\pi\pi$.
[3] There is a further $(2.4 \pm 0.8) \times 10^{-4}$ scalar contribution at 1765 MeV.

$\Gamma(\gamma f_0(1710) \to \gamma K\overline{K})/\Gamma_{total}$ — Γ_{275}/Γ

VALUE (units 10^{-4})	CL%	EVTS	DOCUMENT ID	TECN	COMMENT
$9.5\ ^{+1.0}_{-0.5}$ OUR AVERAGE Error includes scale factor of 1.5. See the ideogram below.					
$8.00\ ^{+0.12}_{-0.08}\ ^{+1.24}_{-0.40}$			[1] ABLIKIM 18AA	BES3	$J/\psi \to \gamma K^0_S K^0_S$
11.76±0.54±0.94		1.2k	[2] DOBBS 15		$J/\psi \to \gamma K\overline{K}$
$9.62 \pm 029\ ^{+3.51}_{-1.86}$			[3] BAI 03G	BES	$J/\psi \to \gamma K\overline{K}$
$5.0 \pm 0.8\ ^{+1.8}_{-0.4}$			[1,4] BAI 96C	BES	$J/\psi \to \gamma K^+K^-$
9.2 ± 1.4 ±1.4			[1] AUGUSTIN 88	DM2	$J/\psi \to \gamma K^+K^-$
10.4 ± 1.2 ±1.6			[1] AUGUSTIN 88	DM2	$J/\psi \to \gamma K^0_S K^0_S$
9.6 ± 1.2 ±1.8			[1] BALTRUSAIT...87	MRK3	$J/\psi \to \gamma K^+K^-$
• • • We do not use the following data for averages, fits, limits, etc. • • •					
2.3 ± 0.8			[5] SARANTSEV 21	RVUE	$J/\psi(1S) \to \gamma(\pi\pi,\ K\overline{K},\ \eta\eta,\ \omega\phi)$
1.6 ± 0.2 ±0.3			[1,6] BAI 96C	BES	$J/\psi \to \gamma K^+K^-$
< 0.8	90		[7] BISELLO 89B		$J/\psi \to 4\pi\gamma$
1.6 ± 0.4 ±0.3			[8] BALTRUSAIT...87	MRK3	$J/\psi \to \gamma\pi^+\pi^-$
3.8 ± 1.6			[9] EDWARDS 82D	CBAL	$e^+e^- \to \eta\eta\gamma$

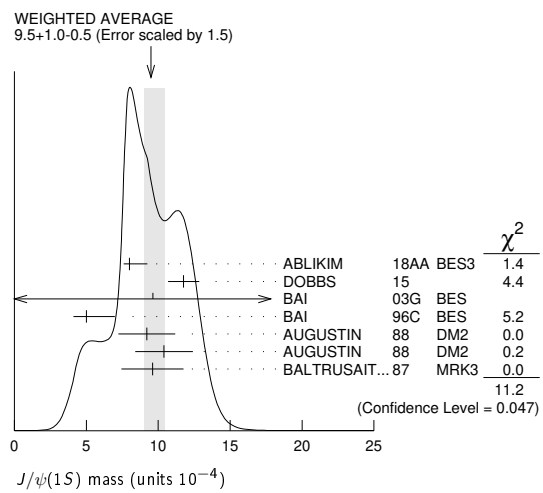

[1] Includes unknown branching fraction to K^+K^- or $K^0_S K^0_S$. We have multiplied K^+K^- measurement by 2, and $K^0_S K^0_S$ by 4 to obtain $K\overline{K}$ result.
[2] Using CLEO-c data but not authored by the CLEO Collaboration.
[3] Includes unknown branching ratio to K^+K^- or $K^0_S K^0_S$.
[4] Assuming $J^P = 2^+$ for $f_0(1710)$.
[5] There is a further $(6 \pm 2) \times 10^{-4}$ scalar contribution at 1765 MeV.
[6] Assuming $J^P = 0^+$ for $f_0(1710)$.
[7] Includes unknown branching fraction to $\rho^0\rho^0$.
[8] Includes unknown branching fraction to $\pi^+\pi^-$.
[9] Includes unknown branching fraction to $\eta\eta$.

$\Gamma(\gamma f_0(1710) \to \gamma\omega\omega)/\Gamma_{total}$ — Γ_{276}/Γ

VALUE (units 10^{-3})	EVTS	DOCUMENT ID	TECN	COMMENT
0.31±0.06±0.08	180	ABLIKIM 06H	BES	$J/\psi \to \gamma\omega\omega$

$\Gamma(\gamma f_0(1710) \to \gamma\eta\eta)/\Gamma_{total}$ — Γ_{277}/Γ

VALUE (units 10^{-4})	EVTS	DOCUMENT ID	TECN	COMMENT
$2.35\ ^{+0.13}_{-0.11}\ ^{+1.24}_{-0.74}$	5.5k	[1] ABLIKIM 13N	BES3	$J/\psi \to \gamma\eta\eta$
• • • We do not use the following data for averages, fits, limits, etc. • • •				
1.2 ±0.4		[2] SARANTSEV 21	RVUE	$J/\psi(1S) \to \gamma(\pi\pi,\ K\overline{K},\ \eta\eta,\ \omega\phi)$

[1] From partial wave analysis including all possible combinations of 0^{++}, 2^{++}, and 4^{++} resonances.
[2] There is a further $(0.7 \pm 0.1) \times 10^{-4}$ scalar contribution at 1765 MeV.

$\Gamma(\gamma f_0(1710) \to \gamma\eta\eta')/\Gamma_{total}$ — Γ_{278}/Γ

VALUE (units 10^{-5})	DOCUMENT ID	TECN	COMMENT
• • • We do not use the following data for averages, fits, limits, etc. • • •			
6.5±2.5	[1] SARANTSEV 21	RVUE	$J/\psi(1S) \to \gamma(\pi\pi,\ K\overline{K},\ \eta\eta,\ \omega\phi)$

[1] There is a further $(2.5 \pm 1.1) \times 10^{-5}$ scalar contribution at 1765 MeV.

Downloaded from https://academic.oup.com/ptep/article/2022/8/083C01/6651666 by KIT Library user on 27 September 2022

$\Gamma(\gamma f_0(1710) \to \gamma\omega\phi)/\Gamma_{total}$ — Γ_{279}/Γ

VALUE (units 10^{-4})	EVTS	DOCUMENT ID		TECN	COMMENT
2.5 ±0.6 OUR AVERAGE					
$2.00 \pm 0.08^{+1.38}_{-1.64}$	1.3k	ABLIKIM	13J	BES3	$J/\psi \to \gamma\omega\phi$
$2.61 \pm 0.27 \pm 0.65$	95	ABLIKIM	06J	BES2	$J/\psi \to \gamma\omega\phi$
• • • We do not use the following data for averages, fits, limits, etc. • • •					
0.1 ±0.1		[1] SARANTSEV	21	RVUE	$J/\psi(1S) \to \gamma(\pi\pi, K\overline{K}, \eta\eta, \omega\phi)$

[1] There is a further $(2.2 \pm 0.4) \times 10^{-4}$ scalar contribution at 1765 MeV.

$\Gamma(\gamma f_0(1750) \to \gamma K^0_S K^0_S)/\Gamma_{total}$ — Γ_{280}/Γ

VALUE (units 10^{-5})	DOCUMENT ID		TECN	COMMENT
$\mathbf{1.11 \pm 0.06^{+0.19}_{-0.32}}$	ABLIKIM	18AA	BES3	$J/\psi \to \gamma K^0_S K^0_S$

$\Gamma(\gamma f_2(1810) \to \gamma\eta\eta)/\Gamma_{total}$ — Γ_{281}/Γ

VALUE (units 10^{-5})	EVTS	DOCUMENT ID		COMMENT
$\mathbf{5.40^{+0.60+3.42}_{-0.67-2.35}}$	5.5k	[1] ABLIKIM	13N	$J/\psi \to \gamma\eta\eta$

[1] From partial wave analysis including all possible combinations of 0^{++}, 2^{++}, and 4^{++} resonances.

$\Gamma(\gamma f_2(1910) \to \gamma\omega\omega)/\Gamma_{total}$ — Γ_{282}/Γ

VALUE (units 10^{-3})	EVTS	DOCUMENT ID		TECN	COMMENT
0.20±0.04±0.13	151	ABLIKIM	06H	BES	$J/\psi \to \gamma\omega\omega$

$\Gamma(\gamma f_2(1950) \to \gamma K^*(892)\overline{K}^*(892))/\Gamma_{total}$ — Γ_{283}/Γ

VALUE (units 10^{-3})	DOCUMENT ID		TECN	COMMENT
0.7±0.1±0.2	BAI	00B	BES	$J/\psi \to \gamma K^+ K^0 \pi^+ \pi^-$

$\Gamma(\gamma f_0(2020) \to \gamma\pi\pi)/\Gamma_{total}$ — Γ_{284}/Γ

VALUE (units 10^{-5})	DOCUMENT ID		TECN	COMMENT
• • • We do not use the following data for averages, fits, limits, etc. • • •				
42±10	SARANTSEV	21	RVUE	$J/\psi(1S) \to \gamma(\pi\pi, K\overline{K}, \eta\eta, \omega\phi)$

$\Gamma(\gamma f_0(2020) \to \gamma K\overline{K})/\Gamma_{total}$ — Γ_{285}/Γ

VALUE (units 10^{-5})	DOCUMENT ID		TECN	COMMENT
• • • We do not use the following data for averages, fits, limits, etc. • • •				
55±25	SARANTSEV	21	RVUE	$J/\psi(1S) \to \gamma(\pi\pi, K\overline{K}, \eta\eta, \omega\phi)$

$\Gamma(\gamma f_0(2020) \to \gamma\eta\eta)/\Gamma_{total}$ — Γ_{286}/Γ

VALUE (units 10^{-5})	DOCUMENT ID		TECN	COMMENT
• • • We do not use the following data for averages, fits, limits, etc. • • •				
10±10	SARANTSEV	21	RVUE	$J/\psi(1S) \to \gamma(\pi\pi, K\overline{K}, \eta\eta, \omega\phi)$

$\Gamma(\gamma f_4(2050))/\Gamma_{total}$ — Γ_{287}/Γ

VALUE (units 10^{-3})	DOCUMENT ID		TECN	COMMENT
2.7±0.5±0.5	[1] BALTRUSAIT...87		MRK3	$J/\psi \to \gamma\pi^+\pi^-$

[1] Assuming branching fraction $f_4(2050) \to \pi\pi/$ total $= 0.167$.

$\Gamma(\gamma f_0(2100) \to \gamma\eta\eta)/\Gamma_{total}$ — Γ_{288}/Γ

VALUE (units 10^{-4})	EVTS	DOCUMENT ID		TECN	COMMENT
$\mathbf{1.13^{+0.09+0.64}_{-0.10-0.28}}$	5.5k	[1] ABLIKIM	13N	BES3	$J/\psi \to \gamma\eta\eta$
• • • We do not use the following data for averages, fits, limits, etc. • • •					
1.8 ±1.5		SARANTSEV	21	RVUE	$J/\psi(1S) \to \gamma(\pi\pi, K\overline{K}, \eta\eta, \omega\phi)$

[1] From partial wave analysis including all possible combinations of 0^{++}, 2^{++}, and 4^{++} resonances.

$\Gamma(\gamma f_0(2100) \to \gamma\pi\pi)/\Gamma_{total}$ — Γ_{290}/Γ

VALUE (units 10^{-4})	EVTS	DOCUMENT ID		TECN	COMMENT
6.24±0.48±0.87	744	[1] DOBBS	15		$J/\psi \to \gamma\pi\pi$
• • • We do not use the following data for averages, fits, limits, etc. • • •					
2.0 ±0.8		SARANTSEV	21	RVUE	$J/\psi(1S) \to \gamma(\pi\pi, K\overline{K}, \eta\eta, \omega\phi)$

[1] Using CLEO-c data but not authored by the CLEO Collaboration.

$\Gamma(\gamma f_0(2100) \to \gamma K\overline{K})/\Gamma_{total}$ — Γ_{289}/Γ

VALUE (units 10^{-5})	DOCUMENT ID		TECN	COMMENT
• • • We do not use the following data for averages, fits, limits, etc. • • •				
32±20	SARANTSEV	21	RVUE	$J/\psi(1S) \to \gamma(\pi\pi, K\overline{K}, \eta\eta, \omega\phi)$

$\Gamma(\gamma f_0(2200))/\Gamma_{total}$ — Γ_{291}/Γ

VALUE (units 10^{-4})	DOCUMENT ID		TECN	COMMENT
• • • We do not use the following data for averages, fits, limits, etc. • • •				
1.5	[1] AUGUSTIN	88	DM2	$J/\psi \to \gamma K^0_S K^0_S$

[1] Includes unknown branching fraction to $K^0_S K^0_S$.

$\Gamma(\gamma f_0(2200) \to \gamma\pi\pi)/\Gamma_{total}$ — Γ_{294}/Γ

VALUE (units 10^{-5})	DOCUMENT ID		TECN	COMMENT
• • • We do not use the following data for averages, fits, limits, etc. • • •				
5±2	SARANTSEV	21	RVUE	$J/\psi(1S) \to \gamma(\pi\pi, K\overline{K}, \eta\eta, \omega\phi)$

$\Gamma(\gamma f_0(2200) \to \gamma K\overline{K})/\Gamma_{total}$ — Γ_{292}/Γ

VALUE (units 10^{-4})	EVTS	DOCUMENT ID		TECN	COMMENT
5.86±0.49±1.20	490	[1] DOBBS	15		$J/\psi \to \gamma K\overline{K}$
• • • We do not use the following data for averages, fits, limits, etc. • • •					
0.5 ±0.5		SARANTSEV	21	RVUE	$J/\psi(1S) \to \gamma(\pi\pi, K\overline{K}, \eta\eta, \omega\phi)$

[1] Using CLEO-c data but not authored by the CLEO Collaboration.

$\Gamma(\gamma f_0(2200) \to \gamma K^0_S K^0_S)/\Gamma_{total}$ — Γ_{293}/Γ

VALUE (units 10^{-4})	DOCUMENT ID		TECN	COMMENT
$\mathbf{2.72^{+0.08+0.17}_{-0.06-0.47}}$	ABLIKIM	18AA	BES3	$J/\psi \to \gamma K^0_S K^0_S$

$\Gamma(\gamma f_0(2200) \to \gamma\eta\eta)/\Gamma_{total}$ — Γ_{295}/Γ

VALUE (units 10^{-5})	DOCUMENT ID		TECN	COMMENT
• • • We do not use the following data for averages, fits, limits, etc. • • •				
0.7±0.4	SARANTSEV	21	RVUE	$J/\psi(1S) \to \gamma(\pi\pi, K\overline{K}, \eta\eta, \omega\phi)$

$\Gamma(\gamma f_J(2220))/\Gamma_{total}$ — Γ_{296}/Γ

VALUE (units 10^{-5})	CL%	EVTS	DOCUMENT ID		TECN	COMMENT
• • • We do not use the following data for averages, fits, limits, etc. • • •						
>300			[1] BAI	96B	BES	$e^+e^- \to \gamma\overline{p}p, K\overline{K}$
>250	99.9		[2] HASAN	96	SPEC	$\overline{p}p \to \pi^+\pi^-$
< 2.3	95		[3] AUGUSTIN	88	DM2	$J/\psi \to \gamma K^+ K^-$
< 1.6	95		[3] AUGUSTIN	88	DM2	$J/\psi \to \gamma K^0_S K^0_S$
$12.4^{+6.4}_{-5.2} \pm 2.8$		23	[3] BALTRUSAIT...86D		MRK3	$J/\psi \to \gamma K^0_S K^0_S$
$8.4^{+3.4}_{-2.8} \pm 1.6$		93	[3] BALTRUSAIT...86D		MRK3	$J/\psi \to \gamma K^+ K^-$

[1] Using BARNES 93.
[2] Using BAI 96B.
[3] Includes unknown branching fraction to K^+K^- or $K^0_S K^0_S$.

$\Gamma(\gamma f_J(2220) \to \gamma\pi\pi)/\Gamma_{total}$ — Γ_{297}/Γ

VALUE (units 10^{-5})	CL%	DOCUMENT ID		TECN	COMMENT
< 3.9	90	[1,2] DOBBS	15		$J/\psi \to \gamma\pi\pi$
• • • We do not use the following data for averages, fits, limits, etc. • • •					
14 ±8 ±4		BAI	98H	BES	$J/\psi \to \gamma\pi^0\pi^0$
8.4±2.6±3.0		BAI	96B	BES	$e^+e^- \to J/\psi \to \gamma\pi^+\pi^-$

[1] Using CLEO-c data but not authored by the CLEO Collaboration.
[2] For $\Gamma = 20/50$ MeV, the 90% CL upper limits for $\pi^+\pi^-$ and $\pi^0\pi^0$ are $2.6/5.2 \times 10^{-5}$ and $1.3/1.9 \times 10^{-5}$, respectively.

$\Gamma(\gamma f_J(2220) \to \gamma K\overline{K})/\Gamma_{total}$ — Γ_{298}/Γ

VALUE (units 10^{-5})	CL%	DOCUMENT ID		TECN	COMMENT
< 4.1	90	[1,2] DOBBS	15		$J/\psi \to \gamma K\overline{K}$
• • • We do not use the following data for averages, fits, limits, etc. • • •					
< 3.6		[3] DEL-AMO-SA...10O		BABR	$e^+e^- \to J/\psi \to \gamma K^+K^-$
< 2.9		[3] DEL-AMO-SA...10O		BABR	$e^+e^- \to J/\psi \to \gamma K^0_S K^0_S$
6.6±2.9±2.4		BAI	96B	BES	$e^+e^- \to J/\psi \to \gamma K^+K^-$
10.8±4.0±3.2		BAI	96B	BES	$e^+e^- \to J/\psi \to \gamma K^0_S K^0_S$

[1] Using CLEO-c data but not authored by the CLEO Collaboration.
[2] For $\Gamma = 20/50$ MeV, the 90% CL upper limits for K^+K^- and $K^0_S K^0_S$ are $1.7/3.1 \times 10^{-5}$ and $1.2/2.0 \times 10^{-5}$, respectively.
[3] For spin 2 and helicity 0; other combinations lead to more stringent upper limits.

$\Gamma(\gamma f_J(2220) \to \gamma p\overline{p})/\Gamma_{total}$ — Γ_{299}/Γ

VALUE (units 10^{-5})	DOCUMENT ID		TECN	COMMENT
1.5±0.6±0.5	BAI	96B	BES	$e^+e^- \to J/\psi \to \gamma p\overline{p}$

$\Gamma(\gamma f_0(2330) \to \gamma K^0_S K^0_S)/\Gamma_{total}$ — Γ_{300}/Γ

VALUE (units 10^{-5})	DOCUMENT ID		TECN	COMMENT
$\mathbf{4.95 \pm 0.21^{+0.66}_{-0.72}}$	ABLIKIM	18AA	BES3	$J/\psi \to \gamma K^0_S K^0_S$
• • • We do not use the following data for averages, fits, limits, etc. • • •				
0.6 ±0.1	SARANTSEV	21	RVUE	$J/\psi(1S) \to \gamma(\pi\pi, K\overline{K}, \eta\eta, \omega\phi)$

$\Gamma(\gamma f_0(2330) \to \gamma\pi\pi)/\Gamma_{total}$ — Γ_{301}/Γ

VALUE (units 10^{-5})	DOCUMENT ID		TECN	COMMENT
• • • We do not use the following data for averages, fits, limits, etc. • • •				
4±2	SARANTSEV	21	RVUE	$J/\psi(1S) \to \gamma(\pi\pi, K\overline{K}, \eta\eta, \omega\phi)$

Downloaded from https://academic.oup.com/ptep/article/2022/8/083C01/6651666 by KIT Library user on 27 September 2022

$\Gamma(\gamma f_0(2330) \to \gamma\eta\eta)/\Gamma_{total}$ — Γ_{302}/Γ

VALUE (units 10^{-5})	DOCUMENT ID	TECN	COMMENT
• • • We do not use the following data for averages, fits, limits, etc. • • •			
1.5 ± 0.4	SARANTSEV 21 RVUE		$J/\psi(1S) \to \gamma(\pi\pi,\ K\overline{K},\ \eta\eta,\ \omega\phi)$

$\Gamma(\gamma f_2(2340) \to \gamma\eta\eta)/\Gamma_{total}$ — Γ_{303}/Γ

VALUE (units 10^{-5})	EVTS	DOCUMENT ID	TECN	COMMENT
$\mathbf{5.60^{+0.62+2.37}_{-0.65-2.07}}$	5.5k	[1] ABLIKIM 13N	BES3	$J/\psi \to \gamma\eta\eta$

[1] From partial wave analysis including all possible combinations of 0^{++}, 2^{++}, and 4^{++} resonances.

$\Gamma(\gamma f_2(2340) \to \gamma K^0_S K^0_S)/\Gamma_{total}$ — Γ_{304}/Γ

VALUE (units 10^{-5})	DOCUMENT ID	TECN	COMMENT
$\mathbf{5.54^{+0.34+3.82}_{-0.40-1.49}}$	ABLIKIM 18AA	BES3	$J/\psi \to \gamma K^0_S K^0_S$

$\Gamma(\gamma X(1835) \to \gamma\pi^+\pi^-\eta')/\Gamma_{total}$ — Γ_{305}/Γ

VALUE (units 10^{-4})	EVTS	DOCUMENT ID	TECN	COMMENT
$\mathbf{2.7\ ^{+0.6}_{-0.8}}$ **OUR AVERAGE** Error includes scale factor of 1.6.				
$3.93 \pm 0.38 ^{+0.31}_{-0.84}$		[1] ABLIKIM 16J	BES3	$J/\psi \to \gamma\pi^+\pi^-\eta'$
$2.2 \pm 0.4 \pm 0.4$	264	ABLIKIM 05R	BES2	$J/\psi \to \gamma\pi^+\pi^-\eta'$
• • • We do not use the following data for averages, fits, limits, etc. • • •				
$2.87 \pm 0.09 ^{+0.49}_{-0.52}$	4265	[2] ABLIKIM 11C	BES3	$J/\psi \to \gamma\pi^+\pi^-\eta'$

[1] From a fit of the measured $\pi^+\pi^-\eta'$ lineshape that accounts for the abrupt distortion observed at the $p\overline{p}$ threshold with a Flatte formula in addition to known backgrounds and contributors, as well as an *ad hoc* Breit-Wigner (M $\approx$ 1919 MeV; $\Gamma \approx$ 51 MeV) that is required for a good fit. Another explanation for the distortion provided by ABLIKIM 16J is that a second resonance near 1870 MeV interferes with the $X(1835)$; fits to this possibility yield product branching fraction values compatible with that shown within the respective systematic uncertainties.

[2] From a fit of the $\pi^+\pi^-\eta'$ mass distribution to a combination of $\gamma f_1(1510)$, $\gamma X(1835)$, and two states $\gamma X(2120)$ and $\gamma X(2370)$, for $M(\pi^+\pi^-\eta') < 2.8$ GeV,and accounting for backgrounds from non-η' events and $J/\psi \to \pi^0\pi^+\pi^-\eta'$.

$\Gamma(\gamma X(1835) \to \gamma p\overline{p})/\Gamma_{total}$ — Γ_{306}/Γ

VALUE (units 10^{-4})	EVTS	DOCUMENT ID	TECN	COMMENT
$\mathbf{0.77^{+0.15}_{-0.09}}$ **OUR AVERAGE**				
$0.90 ^{+0.04+0.27}_{-0.11-0.55}$		[1] ABLIKIM 12D	BES3	$J/\psi \to \gamma p\overline{p}$
$1.14 ^{+0.43+0.42}_{-0.30-0.26}$	231	[2] ALEXANDER 10	CLEO	$J/\psi \to \gamma p\overline{p}$
$0.70 \pm 0.04 ^{+0.19}_{-0.08}$		BAI 03F	BES2	$J/\psi \to \gamma p\overline{p}$

[1] From the fit including final state interaction effects in isospin 0 S-wave according to SIBIRTSEV 05A.

[2] From a fit of the $p\overline{p}$ mass distribution to a combination of $\gamma X(1835)$, γR with $M(R) = 2100$ MeV and $\Gamma(R) = 160$ MeV, and $\gamma p\overline{p}$ phase space, for $M(p\overline{p}) < 2.85$ GeV.

$\Gamma(\gamma X(1835) \to \gamma K^0_S K^0_S \eta)/\Gamma_{total}$ — Γ_{307}/Γ

VALUE (units 10^{-5})	DOCUMENT ID	TECN	COMMENT
$\mathbf{3.31^{+0.33+1.96}_{-0.30-1.29}}$	ABLIKIM 15T	BES3	$J/\psi \to \gamma K^0_S K^0_S \eta$

$\Gamma(\gamma X(1835) \to \gamma\gamma\phi(1020))/\Gamma_{total}$ — Γ_{308}/Γ

VALUE (units 10^{-6})	EVTS	DOCUMENT ID	TECN	COMMENT
• • • We do not use the following data for averages, fits, limits, etc. • • •				
$1.77 \pm 0.35 \pm 0.25$	305	[1] ABLIKIM 18I	BES3	$J/\psi \to \gamma\gamma\phi(1020)$
$8.09 \pm 1.99 \pm 1.36$	1.3k	[2] ABLIKIM 18I	BES3	$J/\psi \to \gamma\gamma\phi(1020)$

[1] Constructive interference between the $X(1835)$ and $\eta(1405)/\eta(1475)$ is assumed in a fit to the $\gamma\phi$ invariant mass.

[2] Destructive interference between the $X(1835)$ and $\eta(1405)/\eta(1475)$ is assumed in a fit to the $\gamma\phi$ invariant mass.

$\Gamma(\gamma X(1835) \to \gamma\gamma\gamma)/\Gamma_{total}$ — Γ_{309}/Γ

VALUE	CL%	DOCUMENT ID	TECN	COMMENT
$\mathbf{< 3.56 \times 10^{-6}}$	90	ABLIKIM 18O	BES3	$\psi(2S) \to \pi^+\pi^-\gamma\gamma\gamma$

$\Gamma(\gamma X(1835) \to \gamma 3(\pi^+\pi^-))/\Gamma_{total}$ — Γ_{310}/Γ

VALUE (units 10^{-5})	EVTS	DOCUMENT ID	TECN	COMMENT
$\mathbf{2.44 \pm 0.36 ^{+0.60}_{-0.74}}$	0.6k	ABLIKIM 13U	BES3	$J/\psi \to \gamma 3(\pi^+\pi^-)$

$\Gamma(\gamma X(2370) \to \gamma K^+K^-\eta')/\Gamma_{total}$ — Γ_{311}/Γ

VALUE (units 10^{-5})	DOCUMENT ID	TECN	COMMENT
$\mathbf{1.79 \pm 0.23 \pm 0.65}$	ABLIKIM 20Q	BES3	$J/\psi \to \gamma K^+K^-\eta'$

$\Gamma(\gamma X(2370) \to \gamma K^0_S K^0_S \eta')/\Gamma_{total}$ — Γ_{312}/Γ

VALUE (units 10^{-5})	DOCUMENT ID	TECN	COMMENT
$\mathbf{1.18 \pm 0.32 \pm 0.39}$	ABLIKIM 20Q	BES3	$J/\psi \to \gamma K^0_S K^0_S \eta'$

$\Gamma(\gamma X(2370) \to \gamma\eta\eta\eta')/\Gamma_{total}$ — Γ_{313}/Γ

VALUE (units 10^{-6})	CL%	DOCUMENT ID	TECN	COMMENT
$\mathbf{< 9.2}$	90	ABLIKIM 21C	BES3	$J/\psi(1S) \to \gamma\eta\eta\eta'$

$\Gamma(\gamma p\overline{p})/\Gamma_{total}$ — Γ_{314}/Γ

VALUE (units 10^{-3})	CL%	EVTS	DOCUMENT ID	TECN	COMMENT
$\mathbf{0.38 \pm 0.07 \pm 0.07}$		49	EATON 84	MRK2	e^+e^-
• • • We do not use the following data for averages, fits, limits, etc. • • •					
< 0.11	90		PERUZZI 78	MRK1	e^+e^-

$\Gamma(\gamma p\overline{p}\pi^+\pi^-)/\Gamma_{total}$ — Γ_{315}/Γ

VALUE	CL%	DOCUMENT ID	TECN	COMMENT
$\mathbf{< 0.79 \times 10^{-3}}$	90	EATON 84	MRK2	e^+e^-

$\Gamma(\gamma\Lambda\overline{\Lambda})/\Gamma_{total}$ — Γ_{316}/Γ

VALUE	CL%	DOCUMENT ID	TECN	COMMENT
$\mathbf{< 0.13 \times 10^{-3}}$	90	HENRARD 87	DM2	e^+e^-
• • • We do not use the following data for averages, fits, limits, etc. • • •				
$< 0.16 \times 10^{-3}$	90	BAI 98G	BES	e^+e^-

$\Gamma(\gamma A \to \gamma\text{invisible})/\Gamma_{total}$ — Γ_{317}/Γ

VALUE	CL%	EVTS	DOCUMENT ID	TECN	COMMENT
$\mathbf{< 1.7 \times 10^{-6}}$	90	88M	[1] ABLIKIM 20K	BES3	$\psi(2S) \to J/\psi\pi^+\pi^-$
• • • We do not use the following data for averages, fits, limits, etc. • • •					
$< 6.3 \times 10^{-6}$	90	3.7M	[2] INSLER 10	CLEO	$\psi(2S) \to J/\psi\pi^+\pi^-$

[1] For a narrow state A with mass $m_A < 1.2$ GeV. The limit varies with m_A, reaching its largest value of 1.7×10^{-6} at 1.2 GeV and being 7.0×10^{-7} for $m_A = 0$.

[2] The limit varies with mass m_A of a narrow state A and is 4.3×10^{-6} for $m_A = 0$,reaches its largest value of 6.3×10^{-6} at $m_A = 500$ MeV, and is 3.6×10^{-6} at $m_A = 960$ MeV.

$\Gamma(\gamma A^0 \to \gamma\mu^+\mu^-)/\Gamma_{total}$ (narrow state A^0 with 0.2 GeV $< m_{A^0} <$ 3 GeV) — Γ_{318}/Γ

VALUE	CL%	DOCUMENT ID	TECN	COMMENT
$\mathbf{< 0.5 \times 10^{-5}}$	90	[1] ABLIKIM 16E	BES3	$J/\psi \to \gamma\mu^+\mu^-$
• • • We do not use the following data for averages, fits, limits, etc. • • •				
$< 2.1 \times 10^{-5}$	90	[2] ABLIKIM 12	BES3	$J/\psi \to \gamma\mu^+\mu^-$

[1] For a narrow scalar or pseudoscalar, A^0, with a mass in the range 0.212–3 GeV. The measured 90% CL limit as a function of m_{A^0} is in the range $(2.8–495.3) \times 10^{-8}$.

[2] For a narrow scalar or pseudoscalar, A^0, with a mass in the range 0.21–3.00 GeV. The measured 90% CL limit as a function of m_{A^0} ranges from 4×10^{-7} to 2.1×10^{-5}.

DALITZ DECAYS

$\Gamma(\pi^0 e^+e^-)/\Gamma_{total}$ — Γ_{319}/Γ

VALUE (units 10^{-7})	EVTS	DOCUMENT ID	TECN	COMMENT
$\mathbf{7.56 \pm 1.32 \pm 0.50}$	39	ABLIKIM 14I	BES3	$J/\psi \to \pi^0 e^+e^-$

$\Gamma(\eta e^+e^-)/\Gamma_{total}$ — Γ_{320}/Γ

VALUE (units 10^{-5})	EVTS	DOCUMENT ID	TECN	COMMENT
$\mathbf{1.42 \pm 0.04 \pm 0.07}$	2.47k	[1,2] ABLIKIM 19A	BES3	$J/\psi \to \eta e^+e^-$
• • • We do not use the following data for averages, fits, limits, etc. • • •				
$1.16 \pm 0.07 \pm 0.06$	320	[1] ABLIKIM 14I	BES3	$J/\psi \to \eta e^+e^-$

[1] Using both $\eta \to \gamma\gamma$ and $\eta \to \pi^+\pi^-\pi^0$ decays.

[2] Approximation of the transition form factor squared as an incoherent sum of the ρ-meson and one-pole non-resonant amplitudes gives the pole mass $m(\Lambda) = 2.56 \pm 0.04 \pm 0.03$ GeV. Supersedes ABLIKIM 14I.

$\Gamma(\eta'(958) e^+e^-)/\Gamma_{total}$ — Γ_{321}/Γ

VALUE (units 10^{-5})	EVTS	DOCUMENT ID	TECN	COMMENT
$\mathbf{6.59 \pm 0.07 \pm 0.17}$	8.9k	[1] ABLIKIM 19H	BES3	$J/\psi \to \eta'(958) e^+e^-$
• • • We do not use the following data for averages, fits, limits, etc. • • •				
$5.81 \pm 0.16 \pm 0.31$	1.4k	[1,2] ABLIKIM 14I	BES3	$J/\psi \to \eta'(958) e^+e^-$

[1] Using both $\eta' \to \gamma\pi^+\pi^-$ and $\eta' \to \pi^+\pi^-\eta$ decays.

[2] Superseded by ABLIKIM 19H.

$\Gamma(\eta U \to \eta e^+e^-)/\Gamma_{total}$ — Γ_{322}/Γ

VALUE	CL%	DOCUMENT ID	TECN	COMMENT
$\mathbf{< 9.11 \times 10^{-7}}$	90	[1] ABLIKIM 19A	BES3	$J/\psi \to \eta e^+e^-$

[1] For a dark photon U with mass between 10 and 2400 MeV. Obtained 90% C.L. limits as a function of m_U range from 1.9×10^{-8} to 91.1×10^{-8}.

$\Gamma(\eta'(958) U \to \eta'(958) e^+e^-)/\Gamma_{total}$ — Γ_{323}/Γ

VALUE	CL%	DOCUMENT ID	TECN	COMMENT
$\mathbf{< 2.0 \times 10^{-7}}$	90	[1] ABLIKIM 19H	BES3	$J/\psi \to \eta'(958) e^+e^-$

[1] For a dark photon U with mass between 100 and 2100 MeV. Obtained 90% C.L. limits as a function of m_U range from 1.8×10^{-8} to 2.0×10^{-7}. The corresponding limits on the branching fraction $J/\psi \to \eta' U$ range from 5.7×10^{-8} to 7.4×10^{-7}.

Downloaded from https://academic.oup.com/ptep/article/2022/8/083C01/6651666 by KIT Library user on 27 September 2022

$\Gamma(\phi e^+ e^-)/\Gamma_{total}$ — Γ_{324}/Γ

VALUE (units 10^{-7})	CL%	DOCUMENT ID		TECN	COMMENT
<1.2	90	[1] ABLIKIM	19AB	BES3	$J/\psi \to \phi e^+ e^-$

[1] Using $B(\phi \to K^+ K^-) = (48.9 \pm 0.5)\%$ and $B(\psi(2S) \to \pi^+\pi^- J/\psi) = (34.49 \pm 0.30)\%$.

WEAK DECAYS

$\Gamma(D^- e^+ \nu_e + c.c.)/\Gamma_{total}$ — Γ_{325}/Γ

VALUE	CL%	DOCUMENT ID		TECN	COMMENT
$<7.1 \times 10^{-8}$	90	ABLIKIM	21Q	BES3	$e^+ e^- \to J/\psi$
• • • We do not use the following data for averages, fits, limits, etc. • • •					
$<1.2 \times 10^{-5}$	90	ABLIKIM	06M	BES2	$e^+ e^- \to J/\psi$

$\Gamma(\overline{D}^0 e^+ e^- + c.c.)/\Gamma_{total}$ — Γ_{326}/Γ

VALUE	CL%	DOCUMENT ID		TECN	COMMENT
$<8.5 \times 10^{-8}$	90	[1] ABLIKIM	17AF	BES3	$e^+ e^- \to J/\psi$
• • • We do not use the following data for averages, fits, limits, etc. • • •					
$<1.1 \times 10^{-5}$	90	ABLIKIM	06M	BES2	$e^+ e^- \to J/\psi$

[1] Using D^0 decays to $K^-\pi^+$, $K^-\pi^+\pi^0$, and $K^-\pi^+\pi^+\pi^-$.

$\Gamma(D_s^- e^+ \nu_e + c.c.)/\Gamma_{total}$ — Γ_{327}/Γ

VALUE	CL%	DOCUMENT ID		TECN	COMMENT
$<1.3 \times 10^{-6}$	90	ABLIKIM	14R	BES3	$e^+ e^- \to J/\psi$
• • • We do not use the following data for averages, fits, limits, etc. • • •					
$<3.6 \times 10^{-5}$	90	[1] ABLIKIM	06M	BES2	$e^+ e^- \to J/\psi$

[1] Using $B(D_s^- \to \phi\pi^-) = 4.4 \pm 0.5$ %.

$\Gamma(D_s^{*-} e^+ \nu_e + c.c.)/\Gamma_{total}$ — Γ_{328}/Γ

VALUE	CL%	DOCUMENT ID		TECN	COMMENT
$<1.8 \times 10^{-6}$	90	ABLIKIM	14R	BES3	$e^+ e^- \to J/\psi$

$\Gamma(D^- \pi^+ + c.c.)/\Gamma_{total}$ — Γ_{329}/Γ

VALUE	CL%	DOCUMENT ID		TECN	COMMENT
$<7.5 \times 10^{-5}$	90	ABLIKIM	08J	BES2	$e^+ e^- \to J/\psi$

$\Gamma(\overline{D}^0 \overline{K}^0 + c.c.)/\Gamma_{total}$ — Γ_{330}/Γ

VALUE	CL%	DOCUMENT ID		TECN	COMMENT
$<1.7 \times 10^{-4}$	90	ABLIKIM	08J	BES2	$e^+ e^- \to J/\psi$

$\Gamma(\overline{D}^0 \overline{K}^{*0} + c.c.)/\Gamma_{total}$ — Γ_{331}/Γ

VALUE	CL%	DOCUMENT ID		TECN	COMMENT
$<2.5 \times 10^{-6}$	90	ABLIKIM	14K	BES3	$e^+ e^- \to J/\psi$

$\Gamma(D_s^- \pi^+ + c.c.)/\Gamma_{total}$ — Γ_{332}/Γ

VALUE	CL%	DOCUMENT ID		TECN	COMMENT
$<1.3 \times 10^{-4}$	90	ABLIKIM	08J	BES2	$e^+ e^- \to J/\psi$

$\Gamma(D_s^- \rho^+ + c.c.)/\Gamma_{total}$ — Γ_{333}/Γ

VALUE	CL%	DOCUMENT ID		TECN	COMMENT
$<1.3 \times 10^{-5}$	90	ABLIKIM	14K	BES3	$e^+ e^- \to J/\psi$

CHARGE CONJUGATION (C), PARITY (P), LEPTON FAMILY NUMBER (LF) VIOLATING MODES

$\Gamma(\gamma\gamma)/\Gamma_{total}$ — Γ_{334}/Γ

VALUE	CL%	DOCUMENT ID		TECN	COMMENT
$< 2.7 \times 10^{-7}$	90	ABLIKIM	14Q	BES3	$\psi(2S) \to \pi^+\pi^- J/\psi$
• • • We do not use the following data for averages, fits, limits, etc. • • •					
$< 0.5 \times 10^{-5}$	90	ADAMS	08	CLEO	$\psi(2S) \to \pi^+\pi^- J/\psi$
$< 1.6 \times 10^{-4}$	90	[1] WICHT	08	BELL	$B^\pm \to K^\pm\gamma\gamma$
$< 2.2 \times 10^{-5}$	90	ABLIKIM	07J	BES2	$\psi(2S) \to J/\psi\pi^+\pi^-$
$<50 \times 10^{-5}$	90	BARTEL	77	CNTR	$e^+ e^-$

[1] WICHT 08 reports $[\Gamma(J/\psi(1S) \to \gamma\gamma)/\Gamma_{total}] \times [B(B^+ \to J/\psi(1S) K^+)] < 0.16 \times 10^{-6}$ which we divide by our best value $B(B^+ \to J/\psi(1S) K^+) = 1.020 \times 10^{-3}$.

$\Gamma(\gamma\phi)/\Gamma_{total}$ — Γ_{335}/Γ

VALUE	CL%	DOCUMENT ID		TECN	COMMENT
$<1.4 \times 10^{-6}$	90	ABLIKIM	14Q	BES3	$\psi(2S) \to \pi^+\pi^- J/\psi$

$\Gamma(e^\pm \mu^\mp)/\Gamma_{total}$ — Γ_{336}/Γ

VALUE	CL%	DOCUMENT ID		TECN	COMMENT
$<1.6 \times 10^{-7}$	90	ABLIKIM	13L	BES3	$e^+ e^- \to J/\psi$
• • • We do not use the following data for averages, fits, limits, etc. • • •					
$<1.1 \times 10^{-6}$	90	BAI	03D	BES	$e^+ e^- \to J/\psi$

$\Gamma(e^\pm \tau^\mp)/\Gamma_{total}$ — Γ_{337}/Γ

VALUE	CL%	DOCUMENT ID		TECN	COMMENT
$<7.5 \times 10^{-8}$	90	ABLIKIM	21M	BES3	$e^+ e^- \to J/\psi$
• • • We do not use the following data for averages, fits, limits, etc. • • •					
$<8.3 \times 10^{-6}$	90	[1] ABLIKIM	04	BES	$e^+ e^- \to J/\psi$

[1] Superseded by ABLIKIM 21M.

$\Gamma(\mu^\pm \tau^\mp)/\Gamma_{total}$ — Γ_{338}/Γ

VALUE	CL%	DOCUMENT ID		TECN	COMMENT
$<2.0 \times 10^{-6}$	90	ABLIKIM	04	BES	$e^+ e^- \to J/\psi$

$\Gamma(\Lambda_c^+ e^- + c.c.)/\Gamma_{total}$ — Γ_{339}/Γ

VALUE	CL%	DOCUMENT ID		TECN	COMMENT
$<6.9 \times 10^{-8}$	90	ABLIKIM	19AF	BES3	$e^+ e^- \to J/\psi \to p K^- \pi^+ e^-$ (+ c.c.)

OTHER DECAYS

$\Gamma(\text{invisible})/\Gamma(e^+ e^-)$ — Γ_{340}/Γ_5

VALUE	CL%	DOCUMENT ID		TECN	COMMENT
$<6.6 \times 10^{-2}$	90	LEES	13I	BABR	$B \to K^{(*)} J/\psi$

$\Gamma(\text{invisible})/\Gamma(\mu^+ \mu^-)$ — Γ_{340}/Γ_7

VALUE	CL%	DOCUMENT ID		TECN	COMMENT
$<1.2 \times 10^{-2}$	90	ABLIKIM	08G	BES2	$\psi(2S) \to \pi^+\pi^- J/\psi$

$J/\psi(1S)$ REFERENCES

ABLIKIM	21AM	PR D104 092004	M. Ablikim et al.	(BESIII Collab.)
ABLIKIM	21AT	JHEP 2111 226	M. Ablikim et al.	(BESIII Collab.)
ABLIKIM	21C	PR D103 012009	M. Ablikim et al.	(BESIII Collab.)
ABLIKIM	21M	PR D103 112007	M. Ablikim et al.	(BESIII Collab.)
ABLIKIM	21Q	JHEP 2106 157	M. Ablikim et al.	(BESIII Collab.)
LEES	21	PR D103 092001	J.P. Lees et al.	(BABAR Collab.)
LEES	21B	PR D104 112003	J.P. Lees et al.	(BABAR Collab.)
LEES	21C	PR D104 112004	J.P. Lees et al.	(BABAR Collab.)
SARANTSEV	21	PL B816 136227	A.V. Sarantsev et al.	(BONN, PNPI)
ABLIKIM	20	PR D101 012004	M. Ablikim et al.	(BESIII Collab.)
ABLIKIM	20K	PR D101 112005	M. Ablikim et al.	(BESIII Collab.)
ABLIKIM	20Q	EPJ C80 746	M. Ablikim et al.	(BESIII Collab.)
ANASHIN	20	JHEP 2007 112	V. V. Anashin et al.	(KEDR Collab.)
ABLIKIM	19A	PR D99 012006	M. Ablikim et al.	(BESIII Collab.)
Also		PR D104 099901 (errat.)	M. Ablikim et al.	(BESIII Collab.)
ABLIKIM	19AB	PR D99 052010	M. Ablikim et al.	(BESIII Collab.)
ABLIKIM	19AC	PR D99 071101	M. Ablikim et al.	(BESIII Collab.)
ABLIKIM	19AF	PR D99 072006	M. Ablikim et al.	(BESIII Collab.)
ABLIKIM	19AN	PR D99 112008	M. Ablikim et al.	(BESIII Collab.)
ABLIKIM	19AQ	PR D100 032004	M. Ablikim et al.	(BESIII Collab.)
ABLIKIM	19H	PR D99 012013	M. Ablikim et al.	(BESIII Collab.)
ABLIKIM	19N	PR D99 032006	M. Ablikim et al.	(BESIII Collab.)
ABLIKIM	19Q	PL B791 375	M. Ablikim et al.	(BESIII Collab.)
ABLIKIM	19T	PRL 122 142002	M. Ablikim et al.	(BESIII Collab.)
LU	19	PR D99 032003	P.-C. Lu et al.	(BELLE Collab.)
ABLIKIM	18AA	PR D98 072003	M. Ablikim et al.	(BESIII Collab.)
ABLIKIM	18AB	PR D98 072005	M. Ablikim et al.	(BESIII Collab.)
ABLIKIM	18D	PRL 121 022001	M. Ablikim et al.	(BESIII Collab.)
ABLIKIM	18I	PR D97 051101	M. Ablikim et al.	(BESIII Collab.)
ABLIKIM	18O	PR D97 072014	M. Ablikim et al.	(BESIII Collab.)
ANASHIN	18A	JHEP 1805 119	V.V. Anashin et al.	(KEDR Collab.)
LEES	18	PR D97 052007	J.P. Lees et al.	(BABAR Collab.)
LEES	18E	PR D98 112015	J.P. Lees et al.	(BABAR Collab.)
ABLIKIM	17AF	PR D96 111101	M. Ablikim et al.	(BESIII Collab.)
ABLIKIM	17AH	PR D96 112001	M. Ablikim et al.	(BESIII Collab.)
ABLIKIM	17AK	PR D96 112012	M. Ablikim et al.	(BESIII Collab.)
ABLIKIM	17E	PL B770 217	M. Ablikim et al.	(BESIII Collab.)
ABLIKIM	17L	PR D95 052003	M. Ablikim et al.	(BESIII Collab.)
LEES	17A	PR D95 052001	J.P. Lees et al.	(BABAR Collab.)
LEES	17C	PR D95 072007	J.P. Lees et al.	(BABAR Collab.)
LEES	17D	PR D95 092005	J.P. Lees et al.	(BABAR Collab.)
ABLIKIM	16E	PR D93 052005	M. Ablikim et al.	(BESIII Collab.)
ABLIKIM	16J	PRL 117 042002	M. Ablikim et al.	(BESIII Collab.)
ABLIKIM	16K	PR D93 052010	M. Ablikim et al.	(BESIII Collab.)
ABLIKIM	16L	PR D93 072003	M. Ablikim et al.	(BESIII Collab.)
ABLIKIM	16M	PR D93 072008	M. Ablikim et al.	(BESIII Collab.)
ABLIKIM	16N	PR D93 112011	M. Ablikim	(BESIII Collab.)
ABLIKIM	16P	PR D94 072005	M. Ablikim et al.	(BESIII Collab.)
ABLIKIM	16Q	PL B761 98	M. Ablikim et al.	(BESIII Collab.)
PDG	16	CP C40 100001	C. Patrignani et al.	(PDG Collab.)
AAIJ	15BI	EPJ C75 311	R. Aaij et al.	(LHCb Collab.)
ABLIKIM	15AE	PR D92 052003	M. Ablikim et al.	(BESIII Collab.)
ABLIKIM	15H	PR D91 052017	M. Ablikim et al.	(BESIII Collab.)
ABLIKIM	15K	PR D91 112001	M. Ablikim et al.	(BESIII Collab.)
ABLIKIM	15P	PR D92 012007	M. Ablikim et al.	(BESIII Collab.)
ABLIKIM	15T	PRL 115 091803	M. Ablikim et al.	(BESIII Collab.)
ANASHIN	15	PL B749 50	V.V. Anashin et al.	(KEDR Collab.)
DOBBS	15	PR D91 052006	S. Dobbs et al.	(NWES)
LEES	15J	PR D92 072008	J.P. Lees et al.	(BABAR Collab.)
ABLIKIM	14I	PR D89 092008	M. Ablikim et al.	(BESIII Collab.)
ABLIKIM	14K	PR D89 071101	M. Ablikim et al.	(BESIII Collab.)
ABLIKIM	14N	PR D90 052009	M. Ablikim et al.	(BESIII Collab.)
ABLIKIM	14Q	PR D90 092002	M. Ablikim et al.	(BESIII Collab.)
ABLIKIM	14R	PR D90 112014	M. Ablikim et al.	(BESIII Collab.)
ANASHIN	14	PL B738 391	V.V. Anashin et al.	(KEDR Collab.)
AULCHENKO	14	PL B731 227	V.M. Aulchenko et al.	(KEDR Collab.)
LEES	14H	PR D89 092002	J.P. Lees et al.	(BABAR Collab.)
ABLIKIM	13F	PR D87 052007	M. Ablikim et al.	(BESIII Collab.)
ABLIKIM	13I	PR D87 032003	M. Ablikim et al.	(BESIII Collab.)
ABLIKIM	13J	PR D87 032008	M. Ablikim et al.	(BESIII Collab.)
ABLIKIM	13L	PR D87 112007	M. Ablikim et al.	(BESIII Collab.)
ABLIKIM	13N	PR D87 092009	M. Ablikim et al.	(BESIII Collab.)
ABLIKIM	13P	PR D87 112004	M. Ablikim et al.	(BESIII Collab.)
ABLIKIM	13R	PR D88 032007	M. Ablikim et al.	(BESIII Collab.)
ABLIKIM	13U	PR D88 091502	M. Ablikim et al.	(BESIII Collab.)
LEES	13I	PR D87 112005	J.P. Lees et al.	(BABAR Collab.)
LEES	13O	PR D87 092005	J.P. Lees et al.	(BABAR Collab.)
LEES	13Q	PR D88 032013	J.P. Lees et al.	(BABAR Collab.)
LEES	13Y	PR D88 072009	J.P. Lees et al.	(BABAR Collab.)
ABLIKIM	12	PR D85 092012	M. Ablikim et al.	(BESIII Collab.)
ABLIKIM	12B	PR D86 032008	M. Ablikim et al.	(BESIII Collab.)
ABLIKIM	12C	PR D86 032014	M. Ablikim et al.	(BESIII Collab.)
ABLIKIM	12D	PRL 108 112003	M. Ablikim et al.	(BESIII Collab.)
ABLIKIM	12H	PL B710 594	M. Ablikim et al.	(BESIII Collab.)
ABLIKIM	12P	CP C36 1031	M. Ablikim et al.	(BES II Collab.)
LEES	12E	PR D85 112009	J.P. Lees et al.	(BABAR Collab.)
LEES	12F	PR D86 012008	J.P. Lees et al.	(BABAR Collab.)
METREVELI	12	PR D85 092007	Z. Metreveli et al.	(NWES, FLOR, WAYN+)
ABLIKIM	11	PR D83 012003	M. Ablikim et al.	(BESIII Collab.)
ABLIKIM	11C	PRL 106 072002	M. Ablikim et al.	(BESIII Collab.)
ABLIKIM	11D	PR D83 032003	M. Ablikim et al.	(BESIII Collab.)

Downloaded from https://academic.oup.com/ptep/article/2022/8/083C01/6651666 by KIT Library user on 27 September 2022

ABLIKIM	10C	PL B685 27	M. Ablikim *et al.*	(BES II Collab.)
ABLIKIM	10E	PL B693 88	M. Ablikim *et al.*	(BES II Collab.)
ALEXANDER	10	PR D82 092002	J.P. Alexander *et al.*	(CLEO Collab.)
ANASHIN	10	PL B685 134	V.V. Anashin *et al.*	(KEDR Collab.)
DEL-AMO-SA...	10O	PRL 105 172001	P. del Amo Sanchez *et al.*	(BABAR Collab.)
INSLER	10	PR D81 091101	J. Insler *et al.*	(CLEO Collab.)
ABLIKIM	09	PL B676 25	M. Ablikim *et al.*	(BES Collab.)
ABLIKIM	09B	PR D80 052004	M. Ablikim *et al.*	(BES II Collab.)
MITCHELL	09	PRL 102 011801	R.E. Mitchell *et al.*	(CLEO Collab.)
PEDLAR	09	PR D79 111101	T.K. Pedlar *et al.*	(CLEO Collab.)
SHEN	09	PR D80 031101	C.P. Shen *et al.*	(BELLE Collab.)
ABLIKIM	08	EPJ C53 15	M. Ablikim *et al.*	(BES Collab.)
ABLIKIM	08A	PR D77 012001	M. Ablikim *et al.*	(BES Collab.)
ABLIKIM	08C	PL B659 789	M. Ablikim *et al.*	(BES Collab.)
ABLIKIM	08E	PR D77 032005	M. Ablikim *et al.*	(BES Collab.)
ABLIKIM	08F	PRL 100 102003	M. Ablikim *et al.*	(BES Collab.)
ABLIKIM	08G	PRL 100 192001	M. Ablikim *et al.*	(BES Collab.)
ABLIKIM	08I	PL B662 330	M. Ablikim *et al.*	(BES Collab.)
ABLIKIM	08J	PL B663 297	M. Ablikim *et al.*	(BES Collab.)
ABLIKIM	08O	PR D78 092005	M. Ablikim *et al.*	(BES Collab.)
ADAMS	08	PRL 101 101801	G.S. Adams *et al.*	(CLEO Collab.)
AUBERT	08S	PR D77 092002	B. Aubert *et al.*	(BABAR Collab.)
BESSON	08	PR D78 032012	D. Besson *et al.*	(CLEO Collab.)
PDG	08	PL B667 1	C. Amsler *et al.*	(PDG Collab.)
WICHT	08	PL B662 323	J. Wicht *et al.*	(BELLE Collab.)
ABLIKIM	07H	PR D76 092003	M. Ablikim *et al.*	(BES Collab.)
ABLIKIM	07J	PR D76 117101	M. Ablikim *et al.*	(BES Collab.)
ANDREOTTI	07	PL B654 74	M. Andreotti *et al.*	(Femilab E835 Collab.)
AUBERT	07AK	PR D76 012008	B. Aubert *et al.*	(BABAR Collab.)
AUBERT	07AU	PR D76 092005	B. Aubert *et al.*	(BABAR Collab.)
Also		PR D77 119902E (errat.)	B. Aubert *et al.*	(BABAR Collab.)
AUBERT	07BD	PR D76 092006	B. Aubert *et al.*	(BABAR Collab.)
ABLIKIM	06	PL B632 181	M. Ablikim *et al.*	(BES Collab.)
ABLIKIM	06C	PL B633 681	M. Ablikim *et al.*	(BES Collab.)
ABLIKIM	06E	PR D73 052008	M. Ablikim *et al.*	(BES Collab.)
ABLIKIM	06F	PR D73 052007	M. Ablikim *et al.*	(BES Collab.)
ABLIKIM	06H	PR D73 112007	M. Ablikim *et al.*	(BES Collab.)
ABLIKIM	06J	PRL 96 162002	M. Ablikim *et al.*	(BES Collab.)
ABLIKIM	06K	PRL 97 062001	M. Ablikim *et al.*	(BES II Collab.)
ABLIKIM	06M	PL B639 418	M. Ablikim *et al.*	(BES Collab.)
ABLIKIM	06V	PL B642 441	M. Ablikim *et al.*	(BES Collab.)
ADAMS	06A	PR D73 051103	G.S. Adams *et al.*	(CLEO Collab.)
AUBERT	06	PR D73 011101	B. Aubert *et al.*	(BABAR Collab.)
AUBERT	06B	PR D73 012005	B. Aubert *et al.*	(BABAR Collab.)
AUBERT	06D	PR D73 052003	B. Aubert *et al.*	(BABAR Collab.)
AUBERT	06E	PRL 96 052002	B. Aubert *et al.*	(BABAR Collab.)
AUBERT,BE	06D	PR D74 091103	B. Aubert *et al.*	(BABAR Collab.)
WU	06	PRL 97 162003	C.-H. Wu *et al.*	(BELLE Collab.)
ABLIKIM	05	PL B607 243	M. Ablikim *et al.*	(BES Collab.)
ABLIKIM	05B	PR D71 032003	M. Ablikim *et al.*	(BES Collab.)
ABLIKIM	05C	PL B610 192	M. Ablikim *et al.*	(BES Collab.)
ABLIKIM	05H	PR D72 012002	M. Ablikim *et al.*	(BES Collab.)
ABLIKIM	05R	PRL 95 262001	M. Ablikim *et al.*	(BES Collab.)
AUBERT	05D	PR D71 052001	B. Aubert *et al.*	(BABAR Collab.)
LI	05C	PR D71 111103	Z. Li *et al.*	(CLEO Collab.)
SIBIRTSEV	05A	PR D71 054010	A. Sibirtsev, J. Haidenbauer	
ABLIKIM	04	PL B598 172	M. Ablikim *et al.*	(BES Collab.)
ABLIKIM	04M	PR D70 112008	M. Ablikim *et al.*	(BES Collab.)
AUBERT	04	PR D69 011103	B. Aubert *et al.*	(BABAR Collab.)
AUBERT,B	04N	PR D70 072004	B. Aubert *et al.*	(BABAR Collab.)
BAI	04	PL B578 16	J.Z. Bai *et al.*	(BES Collab.)
BAI	04A	PR D69 012003	J.Z. Bai *et al.*	(BES Collab.)
BAI	04D	PL B589 7	J.Z. Bai *et al.*	(BES Collab.)
BAI	04E	PL B591 42	J.Z. Bai *et al.*	(BES Collab.)
BAI	04G	PR D70 012004	J.Z. Bai *et al.*	(BES Collab.)
BAI	04H	PR D70 012005	J.Z. Bai *et al.*	(BES Collab.)
BAI	04J	PL B594 47	J.Z. Bai *et al.*	(BES Collab.)
SETH	04	PR D69 097503	K.K. Seth	
AULCHENKO	03	PL B573 63	V.M. Aulchenko *et al.*	(KEDR Collab.)
BAI	03D	PL B561 49	J.Z. Bai *et al.*	(BES Collab.)
BAI	03F	PRL 91 022001	J.Z. Bai *et al.*	(BES II Collab.)
BAI	03G	PR D68 052003	J.Z. Bai *et al.*	(BES Collab.)
HUANG	03	PRL 91 241802	H.-C. Huang *et al.*	(BELLE Collab.)
BAI	02C	PRL 88 101802	J.Z. Bai *et al.*	(BES Collab.)
ARTAMONOV	00	PL B474 427	A.S. Artamonov *et al.*	
BAI	00	PRL 84 594	J.Z. Bai *et al.*	(BES Collab.)
BAI	00B	PL B472 200	J.Z. Bai *et al.*	(BES Collab.)
BAI	00D	PL B476 25	J.Z. Bai *et al.*	(BES Collab.)
BAI	99	PL B446 356	J.Z. Bai *et al.*	(BES Collab.)
BAI	99C	PRL 83 1918	J.Z. Bai *et al.*	(BES Collab.)
BAI	98D	PR D58 092006	J.Z. Bai *et al.*	(BES Collab.)
BAI	98G	PL B424 213	J.Z. Bai *et al.*	(BES Collab.)
BAI	98H	PRL 81 1179	J.Z. Bai *et al.*	(BES Collab.)
BALDINI	98	PL B444 111	R. Baldini *et al.*	(FENICE Collab.)
ARMSTRONG	96	PR D54 7067	T.A. Armstrong *et al.*	(E760 Collab.)
BAI	96B	PRL 76 3502	J.Z. Bai *et al.*	(BES Collab.)
BAI	96C	PRL 77 3959	J.Z. Bai *et al.*	(BES Collab.)
BAI	96D	PR D54 1221	J.Z. Bai *et al.*	(BES Collab.)
GRIBUSHIN	96	PR D53 4723	A. Gribushin *et al.*	(E672 and E706 Collab.)
HASAN	96	PL B388 376	A. Hasan, D.V. Bugg	(BRUN, LOQM)
BAI	95B	PL B355 374	J.Z. Bai *et al.*	(BES Collab.)
BUGG	95	PL B353 378	D.V. Bugg *et al.*	(LOQM, PNPI, WASH)
ANTONELLI	93	PL B301 317	A. Antonelli *et al.*	(FENICE Collab.)
ARMSTRONG	93B	PR D47 772	T.A. Armstrong *et al.*	(FNAL E760 Collab.)
BARNES	93	PL B309 469	P.D. Barnes *et al.*	(PS185 Collab.)
AUGUSTIN	92	PR D46 1951	J.E. Augustin, G. Cosme	(DM2 Collab.)
BOLTON	92	PL B278 495	T. Bolton *et al.*	(Mark III Collab.)
BOLTON	92B	PRL 69 1328	T. Bolton *et al.*	(Mark III Collab.)
COFFMAN	92	PRL 68 282	D.M. Coffman *et al.*	(Mark III Collab.)
HSUEH	92	PR D45 2181	S. Hsueh, S. Palestini	(FNAL, TORI)
BISELLO	91	NP B350 1	D. Bisello *et al.*	(DM2 Collab.)
AUGUSTIN	90	PR D42 10	J.E. Augustin *et al.*	(DM2 Collab.)
BAI	90B	PRL 65 1309	Z. Bai *et al.*	(Mark III Collab.)
BAI	90C	PRL 65 2507	Z. Bai *et al.*	(Mark III Collab.)
BISELLO	90	PL B241 617	D. Bisello *et al.*	(DM2 Collab.)
COFFMAN	90	PR D41 1410	D.M. Coffman *et al.*	(Mark III Collab.)
JOUSSET	90	PR D41 1389	J. Jousset *et al.*	(DM2 Collab.)
ALEXANDER	89	NP B320 45	J.P. Alexander *et al.*	(LBL, MICH, SLAC)
AUGUSTIN	89	NP B320 1	J.E. Augustin, G. Cosme	(DM2 Collab.)
BISELLO	89B	PR D39 701	G. Busetto *et al.*	(DM2 Collab.)
AUGUSTIN	88	PRL 60 2238	J.E. Augustin *et al.*	(DM2 Collab.)
COFFMAN	88	PR D38 2695	D.M. Coffman *et al.*	(Mark III Collab.)
FALVARD	88	PR D38 2706	A. Falvard *et al.*	(CLER, FRAS, LALO+)
AUGUSTIN	87	ZPHY C36 369	J.E. Augustin *et al.*	(LALO, CLER, FRAS+)
BAGLIN	87	NP B286 592	C. Baglin *et al.*	(LAPP, CERN, GENO, LYON+)
BALTRUSAIT...	87	PR D35 2077	R.M. Baltrusaitis *et al.*	(Mark III Collab.)
BECKER	87	PRL 59 186	J.J. Becker *et al.*	(Mark III Collab.)
BISELLO	87	PL B192 239	D. Bisello *et al.*	(PADO, CLER, FRAS+)
COHEN	87	RMP 59 1121	E.R. Cohen, B.N. Taylor	(RISC, NBS)
HENRARD	87	NP B292 670	P. Henrard *et al.*	(CLER, FRAS, LALO+)
PALLIN	87	NP B292 653	D. Pallin *et al.*	(CLER, FRAS, LALO, PADO)
BALTRUSAIT...	86	PR D33 629	R.M. Baltrusaitis *et al.*	(Mark III Collab.)
BALTRUSAIT...	86B	PR D33 1222	R.M. Baltrusaitis *et al.*	(Mark III Collab.)
BALTRUSAIT...	86D	PRL 56 107	R.M. Baltrusaitis	(CIT, UCSC, ILL, SLAC+)
BISELLO	86B	PL B179 294	D. Bisello *et al.*	(DM2 Collab.)
GAISER	86	PR D34 711	J. Gaiser *et al.*	(Crystal Ball Collab.)
BALTRUSAIT...	85C	PRL 55 1723	R.M. Baltrusaitis *et al.*	(CIT, UCSC+)
BALTRUSAIT...	85D	PR D32 566	R.M. Baltrusaitis *et al.*	(CIT, UCSC+)
KURAEV	85	SJNP 41 466	E.A. Kuraev, V.S. Fadin	(NOVO)
		Translated from YAF 41 733.		
BALTRUSAIT...	84	PRL 52 2126	R.M. Baltrusaitis *et al.*	(CIT, UCSC+)
EATON	84	PR D29 804	M.W. Eaton *et al.*	(LBL, SLAC)
BLOOM	83	ARNS 33 143	E.D. Bloom, C. Peck	(SLAC, CIT)
EDWARDS	83B	PRL 51 859	C. Edwards *et al.*	(CIT, HARV, PRIN+)
FRANKLIN	83	PRL 51 963	M.E.B. Franklin *et al.*	(LBL, SLAC)
BURKE	82	PRL 49 632	D.L. Burke *et al.*	(LBL, SLAC)
EDWARDS	82B	PR D25 3065	C. Edwards *et al.*	(CIT, HARV, PRIN+)
EDWARDS	82D	PRL 48 458	C. Edwards *et al.*	(CIT, HARV, PRIN+)
Also		ARNS 33 143	E.D. Bloom, C. Peck	(SLAC, CIT)
EDWARDS	82E	PRL 49 259	C. Edwards *et al.*	(CIT, HARV, PRIN+)
LEMOIGNE	82	PL 113B 509	Y. Lemoigne *et al.*	(SACL, LOIC, SHMP+)
BESCH	81	ZPHY C8 1	H.J. Besch *et al.*	(BONN, DESY, MAINZ)
GIDAL	81	PL 107B 153	G. Gidal *et al.*	(SLAC, LBL)
PARTRIDGE	80	PRL 44 712	R. Partridge *et al.*	(CIT, HARV, PRIN+)
SCHARRE	80	PL 97B 329	D.L. Scharre *et al.*	(SLAC, LBL)
ZHOLENTZ	80	PL 96B 214	A.A. Zholents *et al.*	(NOVO)
Also		SJNP 34 814	A.A. Zholents *et al.*	(NOVO)
		Translated from YAF 34 1471.		
BRANDELIK	79C	ZPHY C1 233	R. Brandelik *et al.*	(DASP Collab.)
ALEXANDER	78	PL 72B 493	G. Alexander *et al.*	(DESY, HAMB, SIEG+)
BESCH	78	PL 78B 347	H.J. Besch *et al.*	(BONN, DESY, MAINZ)
BRANDELIK	78B	PL 74B 292	R. Brandelik *et al.*	(DASP Collab.)
PERUZZI	78	PR D17 2901	I. Peruzzi *et al.*	(SLAC, LBL)
BARTEL	77	PL 66B 489	W. Bartel *et al.*	(DESY, HEIDP)
BURMESTER	77D	PL 72B 135	J. Burmester *et al.*	(DESY, HAMB, SIEG+)
FELDMAN	77	PRPL 33C 285	G.J. Feldman, M.L. Perl	(LBL, SLAC)
VANNUCCI	77	PR D15 1814	F. Vannucci *et al.*	(SLAC, LBL)
BARTEL	76	PL 64B 483	W. Bartel *et al.*	(DESY, HEIDP)
BRAUNSCH...	76	PL 63B 487	W. Braunschweig *et al.*	(DASP Collab.)
JEAN-MARIE	76	PRL 36 291	B. Jean-Marie *et al.*	(SLAC, LBL) IG
BALDINI-...	75	PL 58B 471	R. Baldini-Celio *et al.*	(FRAS, ROMA)
BOYARSKI	75	PRL 34 1357	A.M. Boyarski *et al.*	(SLAC, LBL) JPC
DASP	75	PL 56B 491	W. Braunschweig *et al.*	(DASP Collab.)
ESPOSITO	75B	LNC 14 73	B. Esposito *et al.*	(FRAS, NAPL, PADO+)
FORD	75	PRL 34 604	R.L. Ford *et al.*	(SLAC, PENN)

BRANCHING RATIOS OF $\psi(2S)$ AND $\chi_{c0,1,2}$

Updated March 2022 by J.J. Hernández-Rey (IFIC, Valencia), S. Navas (U. of Granada), and C. Patrignani (Bologna Univ., INFN)

Since 2002, the treatment of the branching ratios of the $\psi(2S)$ and $\chi_{c0,1,2}$ has undergone an important restructuring.

When measuring a branching ratio experimentally, it is not always possible to normalize the number of events observed in the corresponding decay mode to the total number of particles produced. Therefore, the experimenters sometimes report the number of observed decays with respect to another decay mode of the same or another particle in the relevant decay chain. This is actually equivalent to measuring combinations of branching fractions of several decay modes.

To extract the branching ratio of a given decay mode, the collaborations use some previously reported measurements of the required branching ratios. However, the values are frequently taken from the *Review of Particle Physics* (RPP), which in turn uses the branching ratio reported by the experiment in the following edition, giving rise either to correlations or to plain vicious circles, as discussed in more detail in earlier editions of this review [1,2].

The way to avoid these dependencies and correlations is to extract the branching ratios through a fit that uses the truly measured combinations of branching fractions and partial widths. This fit, in fact, should involve decays from the four concerned particles, $\psi(2S)$, χ_{c0}, χ_{c1}, and χ_{c2}, and occasionally some combinations of branching ratios of more than one of them. This is what is done since the 2002 edition [3].

The PDG policy is to quote the results of the collaborations in a manner as close as possible to what appears in their original publications. However, in order to avoid the problems mentioned above, we had in some cases to work out the values originally measured, using the number of events and detection efficiencies

Downloaded from https://academic.oup.com/ptep/article/2022/8/083C01/6651666 by KIT Library user on 27 September 2022

given by the collaborations, or rescaling back the published results. The information was sometimes spread over several articles, and some articles referred to papers still unpublished, which in turn contained the relevant numbers in footnotes.

Even though the experimental collaborations are entitled to extract whatever branching ratios they consider appropriate by using other published results, we would like to encourage them to also quote explicitly in their articles the actual quantities measured, so that they can be used directly in averages and fits of different experimental determinations.

To inform the reader how we computed some of the values used in this edition of RPP, we use footnotes to indicate the branching ratios actually given by the experiments and the quantities they use to derive them from the true combination of branching ratios actually measured.

None of the branching ratios of the $\chi_{c0,1,2}$ are measured independently of the $\psi(2S)$ radiative decays. We tried to identify those branching ratios which can be correlated in a non-trivial way, and although we cannot preclude the existence of other cases, we are confident that the most relevant correlations have already been removed. Nevertheless, correlations in the errors of different quantities measured by the same experiment have not been taken into account.

Fit information

This is an overall fit to 4 total widths, 1 partial width, 26 combinations of partial widths, 24 branching ratios, and 108 combinations of branching ratios. Of the latter 62 involve decays of more than one particle.

The overall fit uses 248 measurements to determine 49 parameters and has a χ^2 of 379.8 for 199 degrees of freedom.

The relatively high χ^2 of the fit, 1.9 per d.o.f., can be traced back to a few specific discrepancies in the data. No scaling factors to fit uncertainties have been applied.

In the listing we provide the inter-particle correlation coefficients $< \delta x_i \delta x_j > / (\delta x_i \cdot \delta x_j)$, in percent, from the fit to the corresponding parameter x_i.

References

1. Y.F. Gu and X.H. Li, Phys. Lett. **B449**, 361 (1999).
2. C. Patrignani, Phys. Rev. **D64**, 034017 (2001).
3. K. Hagiwara *et al.* (Particle Data Group), Phys. Rev. **D68**, 010001 (2002).

$\chi_{c0}(1P)$

$I^G(J^{PC}) = 0^+(0^{++})$

$\chi_{c0}(1P)$ MASS

VALUE (MeV)	EVTS	DOCUMENT ID		TECN	COMMENT
3414.71 ± 0.30 OUR AVERAGE					
3413.0 ± 1.9 ±0.6	933	[1] AAIJ	17BB	LHCB	$pp \to b\overline{b}X \to 2(K^+K^-)X$
3414.2 ± 0.5 ±2.3	5.4k	UEHARA	08	BELL	$\gamma\gamma \to \chi_{c0} \to$ hadrons
3406 ± 7 ±6	230	[2] ABE	07	BELL	$e^+e^- \to J/\psi(c\overline{c})$
3414.21 ± 0.39 ±0.27		ABLIKIM	05G	BES2	$\psi(2S) \to \gamma\chi_{c0}$
3414.7 $^{+0.7}_{-0.6}$ ±0.2		[3] ANDREOTTI	03	E835	$\overline{p}p \to \chi_{c0} \to \pi^0\pi^0$
3415.5 ± 0.4 ±0.4	392	[4] BAGNASCO	02	E835	$\overline{p}p \to \chi_{c0} \to J/\psi\gamma$
3417.4 $^{+1.8}_{-1.9}$ ±0.2		[3] AMBROGIANI	99B	E835	$\overline{p}p \to e^+e^-\gamma$
3414.1 ± 0.6 ±0.8		BAI	99B	BES	$\psi(2S) \to \gamma X$
3417.8 ± 0.4 ±4		[3] GAISER	86	CBAL	$\psi(2S) \to \gamma X$
3416 ± 3 ±4		[5] TANENBAUM	78	MRK1	e^+e^-
• • • We do not use the following data for averages, fits, limits, etc. • • •					
3414.6 ± 1.1	266	UEHARA	13	BELL	$\gamma\gamma \to K^0_S K^0_S$
3416.5 ± 3.0		EISENSTEIN	01	CLE2	$e^+e^- \to e^+e^-\chi_{c0}$
3422 ±10		[5] BARTEL	78B	CNTR	$e^+e^- \to J/\psi 2\gamma$
3415 ± 9		[5] BIDDICK	77	CNTR	$e^+e^- \to \gamma X$

[1] From a fit of the $\phi\phi$ invariant mass with the width of $\chi_{c0}(1P)$ fixed to the PDG 16 value.
[2] From a fit of the J/ψ recoil mass spectrum. Supersedes ABE,K 02 and ABE 04G.
[3] Using mass of $\psi(2S)$ = 3686.0 MeV.
[4] Recalculated by ANDREOTTI 05A, using the value of $\psi(2S)$ mass from AULCHENKO 03.
[5] Mass value shifted by us by amount appropriate for $\psi(2S)$ mass = 3686 MeV and $J/\psi(1S)$ mass = 3097 MeV.

$\chi_{c0}(1P)$ WIDTH

VALUE (MeV)	EVTS	DOCUMENT ID		TECN	COMMENT
10.8±0.6 OUR FIT					
10.5±0.8 OUR AVERAGE Error includes scale factor of 1.1.					
10.6±1.9±2.6	5.4k	UEHARA	08	BELL	$\gamma\gamma \to \chi_{c0} \to$ hadrons
$12.6^{+1.5}_{-1.6}{}^{+0.9}_{-1.1}$		ABLIKIM	05G	BES2	$\psi(2S) \to \gamma\chi_{c0}$
$8.6^{+1.7}_{-1.3}$±0.1		ANDREOTTI	03	E835	$\overline{p}p \to \chi_{c0} \to \pi^0\pi^0$
9.7±1.0	392	[1] BAGNASCO	02	E835	$\overline{p}p \to \chi_{c0} \to J/\psi\gamma$
$16.6^{+5.2}_{-3.7}$±0.1		AMBROGIANI	99B	E835	$\overline{p}p \to e^+e^-\gamma$
14.3±2.0±3.0		BAI	98I	BES	$\psi(2S) \to \gamma\pi^+\pi^-$
13.5±3.3±4.2		GAISER	86	CBAL	$\psi(2S) \to \gamma X, \gamma\pi^0\pi^0$
• • • We do not use the following data for averages, fits, limits, etc. • • •					
13.2±2.1	266	UEHARA	13	BELL	$\gamma\gamma \to K^0_S K^0_S$

[1] Recalculated by ANDREOTTI 05A.

$\chi_{c0}(1P)$ DECAY MODES

	Mode	Fraction (Γ_i/Γ)	Scale factor/ Confidence level
	Hadronic decays		
Γ_1	$2(\pi^+\pi^-)$	(2.34±0.18) %	
Γ_2	$\rho^0\pi^+\pi^-$	(9.1 ±2.9) $\times 10^{-3}$	
Γ_3	$\rho^0\rho^0$		
Γ_4	$f_0(980)\,f_0(980)$	(6.6 ±2.1) $\times 10^{-4}$	
Γ_5	$\pi^+\pi^-\pi^0\pi^0$	(3.3 ±0.4) %	
Γ_6	$\rho^+\pi^-\pi^0$ + c.c.	(2.9 ±0.4) %	
Γ_7	$4\pi^0$	(3.3 ±0.4) $\times 10^{-3}$	
Γ_8	$\pi^+\pi^-K^+K^-$	(1.81±0.14) %	
Γ_9	$K^*_0(1430)^0\overline{K}^*_0(1430)^0 \to \pi^+\pi^-K^+K^-$	(9.8 $^{+4.0}_{-2.8}$) $\times 10^{-4}$	
Γ_{10}	$K^*_0(1430)^0\overline{K}^*_2(1430)^0$ + c.c. $\to \pi^+\pi^-K^+K^-$	(8.0 $^{+2.0}_{-2.4}$) $\times 10^{-4}$	
Γ_{11}	$K_1(1270)^+K^-$ + c.c. $\to \pi^+\pi^-K^+K^-$	(6.3 ±1.9) $\times 10^{-3}$	
Γ_{12}	$K_1(1400)^+K^-$ + c.c. $\to \pi^+\pi^-K^+K^-$	< 2.7 $\times 10^{-3}$	CL=90%
Γ_{13}	$f_0(980)\,f_0(980)$	(1.6 $^{+1.0}_{-0.9}$) $\times 10^{-4}$	
Γ_{14}	$f_0(980)\,f_0(2200)$	(7.9 $^{+2.0}_{-2.5}$) $\times 10^{-4}$	
Γ_{15}	$f_0(1370)\,f_0(1370)$	< 2.7 $\times 10^{-4}$	CL=90%
Γ_{16}	$f_0(1370)\,f_0(1500)$	< 1.7 $\times 10^{-4}$	CL=90%
Γ_{17}	$f_0(1370)\,f_0(1710)$	(6.7 $^{+3.5}_{-2.3}$) $\times 10^{-4}$	
Γ_{18}	$f_0(1500)\,f_0(1370)$	< 1.3 $\times 10^{-4}$	CL=90%
Γ_{19}	$f_0(1500)\,f_0(1500)$	< 5 $\times 10^{-5}$	CL=90%
Γ_{20}	$f_0(1500)\,f_0(1710)$	< 7 $\times 10^{-5}$	CL=90%
Γ_{21}	$K^+K^-\pi^+\pi^-\pi^0$	(8.6 ±0.9) $\times 10^{-3}$	
Γ_{22}	$K^0_S K^\pm\pi^\mp\pi^+\pi^-$	(4.2 ±0.4) $\times 10^{-3}$	
Γ_{23}	$K^+K^-\pi^0\pi^0$	(5.6 ±0.9) $\times 10^{-3}$	
Γ_{24}	$K^+\pi^-\overline{K}^0\pi^0$ + c.c.	(2.49±0.33) %	
Γ_{25}	$\rho^+K^-K^0$ + c.c.	(1.21±0.21) %	
Γ_{26}	$K^*(892)^-K^+\pi^0 \to K^+\pi^-\overline{K}^0\pi^0$ + c.c.	(4.6 ±1.2) $\times 10^{-3}$	
Γ_{27}	$K^0_S K^0_S\pi^+\pi^-$	(5.7 ±1.1) $\times 10^{-3}$	
Γ_{28}	$K^+K^-\eta\pi^0$	(3.0 ±0.7) $\times 10^{-3}$	
Γ_{29}	$3(\pi^+\pi^-)$	(1.20±0.18) %	
Γ_{30}	$K^+\overline{K}^*(892)^0\pi^-$ + c.c.	(7.5 ±1.6) $\times 10^{-3}$	
Γ_{31}	$K^*(892)^0\overline{K}^*(892)^0$	(1.7 ±0.6) $\times 10^{-3}$	

Downloaded from https://academic.oup.com/ptep/article/2022/8/083C01/6651666 by KIT Library user on 27 September 2022

Γ_{32}	$\pi\pi$	$(8.51\pm0.33)\times10^{-3}$		
Γ_{33}	$\pi^0\eta$	$<1.8\times10^{-4}$		
Γ_{34}	$\pi^0\eta'$	$<1.1\times10^{-3}$		
Γ_{35}	$\pi^0\eta_c$	$<1.6\times10^{-3}$		CL=90%
Γ_{36}	$\eta\eta$	$(3.01\pm0.19)\times10^{-3}$		
Γ_{37}	$\eta\eta'$	$(9.1\pm1.1)\times10^{-5}$		
Γ_{38}	$\eta'\eta'$	$(2.17\pm0.12)\times10^{-3}$		
Γ_{39}	$\omega\omega$	$(9.7\pm1.1)\times10^{-4}$		
Γ_{40}	$\omega\phi$	$(1.41\pm0.13)\times10^{-4}$		
Γ_{41}	ωK^+K^-	$(1.94\pm0.21)\times10^{-3}$		
Γ_{42}	K^+K^-	$(6.05\pm0.31)\times10^{-3}$		
Γ_{43}	$K^0_SK^0_S$	$(3.16\pm0.17)\times10^{-3}$		
Γ_{44}	$\pi^+\pi^-\eta$	$<2.0\times10^{-4}$		CL=90%
Γ_{45}	$\pi^+\pi^-\eta'$	$<4\times10^{-4}$		CL=90%
Γ_{46}	$\overline{K}^0K^+\pi^-+$ c.c.	$<9\times10^{-5}$		CL=90%
Γ_{47}	$K^+K^-\pi^0$	$<6\times10^{-5}$		CL=90%
Γ_{48}	$K^+K^-\eta$	$<2.3\times10^{-4}$		CL=90%
Γ_{49}	$K^+K^-K^0_SK^0_S$	$(1.4\pm0.5)\times10^{-3}$		
Γ_{50}	$K^0_SK^0_SK^0_SK^0_S$	$(5.8\pm0.5)\times10^{-4}$		
Γ_{51}	$K^+K^-K^+K^-$	$(2.82\pm0.29)\times10^{-3}$		
Γ_{52}	$K^+K^-\phi$	$(9.7\pm2.5)\times10^{-4}$		
Γ_{53}	$\overline{K}^0K^+\pi^-\phi+$ c.c.	$(3.7\pm0.6)\times10^{-3}$		
Γ_{54}	$K^+K^-\pi^0\phi$	$(1.90\pm0.35)\times10^{-3}$		
Γ_{55}	$\phi\pi^+\pi^-\pi^0$	$(1.18\pm0.15)\times10^{-3}$		
Γ_{56}	$\phi\phi$	$(8.0\pm0.7)\times10^{-4}$		
Γ_{57}	$\phi\phi\eta$	$(8.4\pm1.0)\times10^{-4}$		
Γ_{58}	$p\overline{p}$	$(2.21\pm0.08)\times10^{-4}$		
Γ_{59}	$p\overline{p}\pi^0$	$(7.0\pm0.7)\times10^{-4}$		S=1.3
Γ_{60}	$p\overline{p}\eta$	$(3.5\pm0.4)\times10^{-4}$		
Γ_{61}	$p\overline{p}\omega$	$(5.2\pm0.6)\times10^{-4}$		
Γ_{62}	$p\overline{p}\phi$	$(6.0\pm1.4)\times10^{-5}$		
Γ_{63}	$p\overline{p}\pi^+\pi^-$	$(2.1\pm0.7)\times10^{-3}$		S=1.4
Γ_{64}	$p\overline{p}\pi^0\pi^0$	$(1.04\pm0.28)\times10^{-3}$		
Γ_{65}	$p\overline{p}K^+K^-$ (non-resonant)	$(1.22\pm0.26)\times10^{-4}$		
Γ_{66}	$p\overline{p}K^0_SK^0_S$	$<8.8\times10^{-4}$		CL=90%
Γ_{67}	$p\overline{n}\pi^-$	$(1.27\pm0.11)\times10^{-3}$		
Γ_{68}	$\overline{p}n\pi^+$	$(1.37\pm0.12)\times10^{-3}$		
Γ_{69}	$p\overline{n}\pi^-\pi^0$	$(2.34\pm0.21)\times10^{-3}$		
Γ_{70}	$\overline{p}n\pi^+\pi^0$	$(2.21\pm0.18)\times10^{-3}$		
Γ_{71}	$\Lambda\overline{\Lambda}$	$(3.59\pm0.15)\times10^{-4}$		
Γ_{72}	$\Lambda\overline{\Lambda}\pi^+\pi^-$	$(1.18\pm0.13)\times10^{-3}$		
Γ_{73}	$\Lambda\overline{\Lambda}\pi^+\pi^-$ (non-resonant)	$<5\times10^{-4}$		CL=90%
Γ_{74}	$\Sigma(1385)^+\overline{\Lambda}\pi^-+$ c.c.	$<5\times10^{-4}$		CL=90%
Γ_{75}	$\Sigma(1385)^-\overline{\Lambda}\pi^++$ c.c.	$<5\times10^{-4}$		CL=90%
Γ_{76}	$K^+\overline{p}\Lambda+$ c.c.	$(1.25\pm0.12)\times10^{-3}$		S=1.3
Γ_{77}	$nK^0_S\overline{\Lambda}+$ c.c.	$(6.6\pm0.5)\times10^{-4}$		
Γ_{78}	$K^*(892)^+\overline{p}\Lambda+$ c.c.	$(4.8\pm0.9)\times10^{-4}$		
Γ_{79}	$K^+\overline{p}\Lambda(1520)+$ c.c.	$(2.9\pm0.7)\times10^{-4}$		
Γ_{80}	$\Lambda(1520)\overline{\Lambda}(1520)$	$(3.1\pm1.2)\times10^{-4}$		
Γ_{81}	$\Sigma^0\overline{\Sigma}^0$	$(4.68\pm0.32)\times10^{-4}$		
Γ_{82}	$\Sigma^+\overline{p}K^0_S+$ c.c.	$(3.52\pm0.27)\times10^{-4}$		
Γ_{83}	$\Sigma^0\overline{p}K^++$ c.c.	$(3.03\pm0.20)\times10^{-4}$		
Γ_{84}	$\Sigma^+\overline{\Sigma}^-$	$(4.6\pm0.8)\times10^{-4}$		S=2.6
Γ_{85}	$\Sigma^-\overline{\Sigma}^+$	$(5.1\pm0.5)\times10^{-4}$		
Γ_{86}	$\Sigma(1385)^+\overline{\Sigma}(1385)^-$	$(1.6\pm0.6)\times10^{-4}$		
Γ_{87}	$\Sigma(1385)^-\overline{\Sigma}(1385)^+$	$(2.3\pm0.7)\times10^{-4}$		
Γ_{88}	$K^-\Lambda\overline{\Xi}^++$ c.c.	$(1.94\pm0.35)\times10^{-4}$		
Γ_{89}	$\Xi^0\overline{\Xi}^0$	$(3.1\pm0.8)\times10^{-4}$		
Γ_{90}	$\Xi^-\overline{\Xi}^+$	$(4.8\pm0.7)\times10^{-4}$		
Γ_{91}	$\eta_c\pi^+\pi^-$	$<7\times10^{-4}$		CL=90%
	Radiative decays			
Γ_{92}	$\gamma J/\psi(1S)$	(1.40 ± 0.05) %		
Γ_{93}	$\gamma\rho^0$	$<9\times10^{-6}$		CL=90%
Γ_{94}	$\gamma\omega$	$<8\times10^{-6}$		CL=90%
Γ_{95}	$\gamma\phi$	$<6\times10^{-6}$		CL=90%
Γ_{96}	$\gamma\gamma$	$(2.04\pm0.09)\times10^{-4}$		
Γ_{97}	$e^+e^-J/\psi(1S)$	$(1.33\pm0.29)\times10^{-4}$		
Γ_{98}	$\mu^+\mu^-J/\psi(1S)$	$<1.9\times10^{-5}$		CL=90%

CONSTRAINED FIT INFORMATION

A multiparticle fit to $\chi_{c1}(1P)$, $\chi_{c0}(1P)$, $\chi_{c2}(1P)$, and $\psi(2S)$ with 4 total widths, a partial width, 25 combinations of partial widths obtained from integrated cross section, and 84 branching ratios uses 248 measurements to determine 49 parameters. The overall fit has a $\chi^2 = 379.8$ for 199 degrees of freedom.

The following *off-diagonal* array elements are the correlation coefficients $\langle\delta p_i\delta p_j\rangle/(\delta p_i\cdot\delta p_j)$, in percent, from the fit to parameters p_i, including the branching fractions, $x_i \equiv \Gamma_i/\Gamma_{\rm total}$.

	x_1	x_2	x_8	x_{30}	x_{32}	x_{36}	x_{42}	x_{43}	x_{51}	x_{56}
x_2	24									
x_8	9	2								
x_{30}	5	1	28							
x_{32}	8	2	10	3						
x_{36}	4	1	5	1	14					
x_{42}	8	2	8	3	18	11				
x_{43}	7	2	8	2	18	10	14			
x_{51}	5	1	5	2	9	5	7	7		
x_{56}	7	2	6	2	9	5	7	7	4	
x_{58}	3	1	4	1	3	−1	7	7	3	3
x_{71}	7	2	9	2	23	13	18	18	8	9
x_{92}	5	1	6	2	17	11	13	12	6	6
x_{96}	−8	−2	−2	−3	14	9	10	10	3	1
Γ	−26	−6	−19	−10	−15	−7	−14	−12	−10	−13

	x_{58}	x_{71}	x_{92}	x_{96}
x_{71}	9			
x_{92}	−19	16		
x_{96}	6	15	13	
Γ	−4	−13	−9	−38

$\chi_{c0}(1P)$ PARTIAL WIDTHS

$\chi_{c0}(1P)$ $\Gamma(i)\Gamma(\gamma J/\psi(1S))/\Gamma(\text{total})$

$\Gamma(p\overline{p}) \times \Gamma(\gamma J/\psi(1S))/\Gamma_{\rm total}$ — $\Gamma_{58}\Gamma_{92}/\Gamma$

VALUE (eV)	EVTS	DOCUMENT ID		TECN	COMMENT
33.6± 2.3 OUR FIT					
• • • We do not use the following data for averages, fits, limits, etc. • • •					
26.6± 2.6±1.4	392	[1,2] BAGNASCO	02	E835	$\overline{p}p \to \chi_{c0} \to J/\psi\gamma$
$48.7^{+11.3}_{-8.9}\pm2.4$		[1,2] AMBROGIANI	99B	E835	$\overline{p}p \to \gamma J/\psi$

[1] Calculated by us using $B(J/\psi(1S) \to e^+e^-) = 0.0593 \pm 0.0010$.
[2] Values in $(\Gamma(p\overline{p}) \times \Gamma(\gamma J/\psi(1S))/\Gamma_{\rm total})$ and $(\Gamma(p\overline{p})/\Gamma_{\rm total} \times \Gamma(\gamma J/\psi(1S))/\Gamma_{\rm total})$ are not independent. The latter is used in the fit since it is less correlated to the total width.

$\chi_{c0}(1P)$ $\Gamma(i)\Gamma(\gamma\gamma)/\Gamma(\text{total})$

$\Gamma(2(\pi^+\pi^-)) \times \Gamma(\gamma\gamma)/\Gamma_{\rm total}$ — $\Gamma_1\Gamma_{96}/\Gamma$

VALUE (eV)	EVTS	DOCUMENT ID		TECN	COMMENT
52 ± 4 OUR FIT					
49 ±10 OUR AVERAGE Error includes scale factor of 1.8.					
44.7± 3.6±4.9	3.6k	UEHARA	08	BELL	$\gamma\gamma \to \chi_{c0} \to 2(\pi^+\pi^-)$
75 ±13 ±8		EISENSTEIN	01	CLE2	$e^+e^- \to e^+e^-\chi_{c0}$

$\Gamma(\rho^0\rho^0) \times \Gamma(\gamma\gamma)/\Gamma_{\rm total}$ — $\Gamma_3\Gamma_{96}/\Gamma$

VALUE (eV)	CL%	EVTS	DOCUMENT ID		TECN	COMMENT
• • • We do not use the following data for averages, fits, limits, etc. • • •						
<12	90	<252	UEHARA	08	BELL	$\gamma\gamma \to \chi_{c0} \to 2(\pi^+\pi^-)$

$\Gamma(\pi^+\pi^-K^+K^-) \times \Gamma(\gamma\gamma)/\Gamma_{\rm total}$ — $\Gamma_8\Gamma_{96}/\Gamma$

VALUE (eV)	EVTS	DOCUMENT ID		TECN	COMMENT
40.0±3.5 OUR FIT					
38.8±3.7±4.7	1.7k	UEHARA	08	BELL	$\gamma\gamma \to \chi_{c0} \to K^+K^-\pi^+\pi^-$

$\Gamma(K^+K^-\pi^+\pi^-\pi^0) \times \Gamma(\gamma\gamma)/\Gamma_{\rm total}$ — $\Gamma_{21}\Gamma_{96}/\Gamma$

VALUE (eV)	EVTS	DOCUMENT ID		TECN	COMMENT
26±4±4	1094	DEL-AMO-SA...11M		BABR	$\gamma\gamma \to K^+K^-\pi^+\pi^-\pi^0$

$\Gamma(K^+\overline{K}^*(892)^0\pi^- + \text{c.c.}) \times \Gamma(\gamma\gamma)/\Gamma_{\rm total}$ — $\Gamma_{30}\Gamma_{96}/\Gamma$

VALUE (eV)	EVTS	DOCUMENT ID		TECN	COMMENT
16 ±4 OUR FIT					
16.7±6.1±3.0	495 ± 182	UEHARA	08	BELL	$\gamma\gamma \to \chi_{c0} \to K^+K^-\pi^+\pi^-$

Downloaded from https://academic.oup.com/ptep/article/2022/8/083C01/6651666 by KIT Library user on 27 September 2022

$\Gamma(K^*(892)^0\overline{K}^*(892)^0) \times \Gamma(\gamma\gamma)/\Gamma_{total}$ — $\Gamma_{31}\Gamma_{96}/\Gamma$

VALUE (eV)	CL%	EVTS	DOCUMENT ID		TECN	COMMENT
• • • We do not use the following data for averages, fits, limits, etc. • • •						
<6	90	<148	UEHARA	08	BELL	$\gamma\gamma \to \chi_{c0} \to K^+K^-\pi^+\pi^-$

$\Gamma(\pi\pi) \times \Gamma(\gamma\gamma)/\Gamma_{total}$ — $\Gamma_{32}\Gamma_{96}/\Gamma$

VALUE (eV)	EVTS	DOCUMENT ID		TECN	COMMENT
18.8± 1.3 OUR FIT					
23 ± 5 OUR AVERAGE					
$29.7^{+17.4}_{-12.0}\pm4.8$	103^{+60}_{-42}	[1] UEHARA	09	BELL	$10.6\ e^+e^- \to e^+e^-\pi^0\pi^0$
22.7± 3.2±3.5	129 ± 18	[2] NAKAZAWA	05	BELL	$10.6\ e^+e^- \to e^+e^-\pi^+\pi^-$

[1] We multiplied the measurement by 3 to convert from $\pi^0\pi^0$ to $\pi\pi$. Interference with the continuum included.
[2] We have multiplied $\pi^+\pi^-$ measurement by 3/2 to obtain $\pi\pi$.

$\Gamma(\eta\eta) \times \Gamma(\gamma\gamma)/\Gamma_{total}$ — $\Gamma_{36}\Gamma_{96}/\Gamma$

VALUE (eV)	EVTS	DOCUMENT ID		TECN	COMMENT
9.4±2.3±1.2	22	[1] UEHARA	10A	BELL	$10.6\ e^+e^- \to e^+e^-\eta\eta$

[1] Interference with the continuum not included.

$\Gamma(\omega\omega) \times \Gamma(\gamma\gamma)/\Gamma_{total}$ — $\Gamma_{39}\Gamma_{96}/\Gamma$

VALUE (eV)	CL%	DOCUMENT ID		TECN	COMMENT
• • • We do not use the following data for averages, fits, limits, etc. • • •					
<3.9	90	[1] LIU	12B	BELL	$\gamma\gamma \to 2(\pi^+\pi^-\pi^0)$

[1] Using $B(\omega \to \pi^+\pi^-\pi^0) = (89.2 \pm 0.7)\%$.

$\Gamma(\omega\phi) \times \Gamma(\gamma\gamma)/\Gamma_{total}$ — $\Gamma_{40}\Gamma_{96}/\Gamma$

VALUE (eV)	CL%	DOCUMENT ID		TECN	COMMENT
• • • We do not use the following data for averages, fits, limits, etc. • • •					
<0.34	90	[1] LIU	12B	BELL	$\gamma\gamma \to K^+K^-\pi^+\pi^-\pi^0$

[1] Using $B(\phi \to K^+K^-) = (48.9 \pm 0.5)\%$ and $B(\omega \to \pi^+\pi^-\pi^0) = (89.2 \pm 0.7)\%$.

$\Gamma(K^+K^-) \times \Gamma(\gamma\gamma)/\Gamma_{total}$ — $\Gamma_{42}\Gamma_{96}/\Gamma$

VALUE (eV)	EVTS	DOCUMENT ID		TECN	COMMENT
13.4±1.0 OUR FIT					
14.3±1.6±2.3	153 ± 17	NAKAZAWA	05	BELL	$10.6\ e^+e^- \to e^+e^-K^+K^-$

$\Gamma(K^0_SK^0_S) \times \Gamma(\gamma\gamma)/\Gamma_{total}$ — $\Gamma_{43}\Gamma_{96}/\Gamma$

VALUE (eV)	EVTS	DOCUMENT ID		TECN	COMMENT
7.0 ±0.5 OUR FIT					
8.7 ±1.7 ±0.9	266	[1] UEHARA	13	BELL	$\gamma\gamma \to K^0_SK^0_S$
• • • We do not use the following data for averages, fits, limits, etc. • • •					
7.00±0.65±0.71	134 ± 12	CHEN	07B	BELL	$e^+e^- \to e^+e^-\chi_{c0}$

[1] Supersedes CHEN 07B.

$\Gamma(K^+K^-K^+K^-) \times \Gamma(\gamma\gamma)/\Gamma_{total}$ — $\Gamma_{51}\Gamma_{96}/\Gamma$

VALUE (eV)	EVTS	DOCUMENT ID		TECN	COMMENT
6.2±0.7 OUR FIT					
7.9±1.3±1.1	215 ± 36	UEHARA	08	BELL	$\gamma\gamma \to \chi_{c0} \to 2(K^+K^-)$

$\Gamma(\phi\phi) \times \Gamma(\gamma\gamma)/\Gamma_{total}$ — $\Gamma_{56}\Gamma_{96}/\Gamma$

VALUE (eV)	EVTS	DOCUMENT ID		TECN	COMMENT
1.76±0.18 OUR FIT					
1.72±0.33±0.14	56 ± 11	[1] LIU	12B	BELL	$\gamma\gamma \to 2(K^+K^-)$
• • • We do not use the following data for averages, fits, limits, etc. • • •					
2.3 ±0.9 ±0.4	23.6 ± 9.6	UEHARA	08	BELL	$\gamma\gamma \to \chi_{c0} \to 2(K^+K^-)$

[1] Supersedes UEHARA 08. Using $B(\phi \to K^+K^-) = (48.9 \pm 0.5)\%$.

$\chi_{c0}(1P)$ BRANCHING RATIOS

HADRONIC DECAYS

$\Gamma(2(\pi^+\pi^-))/\Gamma_{total}$ — Γ_1/Γ

VALUE	DOCUMENT ID
0.0234±0.0018 OUR FIT	

$\Gamma(\rho^0\pi^+\pi^-)/\Gamma(2(\pi^+\pi^-))$ — Γ_2/Γ_1

VALUE	DOCUMENT ID		TECN	COMMENT
0.39±0.12 OUR FIT				
0.39±0.12	TANENBAUM	78	MRK1	$\psi(2S) \to \gamma\chi_{c0}$

$\Gamma(\rho^0\pi^+\pi^-)/\Gamma_{total}$ — Γ_2/Γ

VALUE	DOCUMENT ID
0.0091±0.0029 OUR FIT	

$\Gamma(f_0(980)f_0(980))/\Gamma_{total}$ — Γ_4/Γ

VALUE (units 10^{-4})	EVTS	DOCUMENT ID		TECN	COMMENT
6.6±2.1±0.1	36 ± 9	[1] ABLIKIM	04G	BES	$\psi(2S) \to \gamma 2\pi^+2\pi^-$

[1] ABLIKIM 04G reports $[\Gamma(\chi_{c0}(1P) \to f_0(980)f_0(980))/\Gamma_{total}] \times [B(\psi(2S) \to \gamma\chi_{c0}(1P))] = (6.5 \pm 1.6 \pm 1.3) \times 10^{-5}$ which we divide by our best value $B(\psi(2S) \to \gamma\chi_{c0}(1P)) = (9.79 \pm 0.20) \times 10^{-2}$. Our first error is their experiment's error and our second error is the systematic error from using our best value.

$\Gamma(\pi^+\pi^-\pi^0\pi^0)/\Gamma_{total}$ — Γ_5/Γ

VALUE (%)	EVTS	DOCUMENT ID		TECN	COMMENT
3.3±0.4±0.1	1751.4	[1] HE	08B	CLEO	$e^+e^- \to \gamma h^+h^-h^0h^0$

[1] HE 08B reports $3.54 \pm 0.10 \pm 0.43 \pm 0.18$ % from a measurement of $[\Gamma(\chi_{c0}(1P) \to \pi^+\pi^-\pi^0\pi^0)/\Gamma_{total}] \times [B(\psi(2S) \to \gamma\chi_{c0}(1P))]$ assuming $B(\psi(2S) \to \gamma\chi_{c0}(1P)) = (9.22 \pm 0.11 \pm 0.46) \times 10^{-2}$, which we rescale to our best value $B(\psi(2S) \to \gamma\chi_{c0}(1P)) = (9.79 \pm 0.20) \times 10^{-2}$. Our first error is their experiment's error and our second error is the systematic error from using our best value.

$\Gamma(\rho^+\pi^-\pi^0 + \text{c.c.})/\Gamma_{total}$ — Γ_6/Γ

VALUE (%)	EVTS	DOCUMENT ID		TECN	COMMENT
2.9±0.4±0.1	1358.5	[1,2] HE	08B	CLEO	$e^+e^- \to \gamma h^+h^-h^0h^0$

[1] HE 08B reports $3.04 \pm 0.18 \pm 0.42 \pm 0.16$ % from a measurement of $[\Gamma(\chi_{c0}(1P) \to \rho^+\pi^-\pi^0 + \text{c.c.})/\Gamma_{total}] \times [B(\psi(2S) \to \gamma\chi_{c0}(1P))]$ assuming $B(\psi(2S) \to \gamma\chi_{c0}(1P)) = (9.22 \pm 0.11 \pm 0.46) \times 10^{-2}$, which we rescale to our best value $B(\psi(2S) \to \gamma\chi_{c0}(1P)) = (9.79 \pm 0.20) \times 10^{-2}$. Our first error is their experiment's error and our second error is the systematic error from using our best value.
[2] Calculated by us. We have added the values from HE 08B for $\rho^+\pi^-\pi^0$ and $\rho^-\pi^+\pi^0$ decays assuming uncorrelated statistical and fully correlated systematic uncertainties.

$\Gamma(4\pi^0)/\Gamma_{total}$ — Γ_7/Γ

VALUE (units 10^{-3})	EVTS	DOCUMENT ID		TECN	COMMENT
3.3±0.4±0.1	3296	[1] ABLIKIM	11A	BES3	$e^+e^- \to \psi(2S) \to \gamma\chi_{c0}$

[1] ABLIKIM 11A reports $(3.34 \pm 0.06 \pm 0.44) \times 10^{-3}$ from a measurement of $[\Gamma(\chi_{c0}(1P) \to 4\pi^0)/\Gamma_{total}] \times [B(\psi(2S) \to \gamma\chi_{c0}(1P))]$ assuming $B(\psi(2S) \to \gamma\chi_{c0}(1P)) = (9.62 \pm 0.31) \times 10^{-2}$, which we rescale to our best value $B(\psi(2S) \to \gamma\chi_{c0}(1P)) = (9.79 \pm 0.20) \times 10^{-2}$. Our first error is their experiment's error and our second error is the systematic error from using our best value.

$\Gamma(\pi^+\pi^-K^+K^-)/\Gamma_{total}$ — Γ_8/Γ

VALUE (units 10^{-3})	DOCUMENT ID
18.1±1.4 OUR FIT	

$\Gamma(K^+\overline{K}^*(892)^0\pi^- + \text{c.c.})/\Gamma(\pi^+\pi^-K^+K^-)$ — Γ_{30}/Γ_8

VALUE	DOCUMENT ID		TECN	COMMENT
0.41±0.09 OUR FIT				
0.41±0.10	TANENBAUM	78	MRK1	$\psi(2S) \to \gamma\chi_{c0}$

$\Gamma(K^*_0(1430)^0\overline{K}^*_0(1430)^0 \to \pi^+\pi^-K^+K^-)/\Gamma_{total}$ — Γ_9/Γ

VALUE (units 10^{-4})	EVTS	DOCUMENT ID		TECN	COMMENT
$\mathbf{9.8^{+3.6}_{-2.8}\pm0.2}$	83	[1] ABLIKIM	05Q	BES2	$\psi(2S) \to \gamma\pi^+\pi^-K^+K^-$

[1] ABLIKIM 05Q reports $(10.44 \pm 2.37^{+3.05}_{-1.90}) \times 10^{-4}$ from a measurement of $[\Gamma(\chi_{c0}(1P) \to K^*_0(1430)^0\overline{K}^*_0(1430)^0 \to \pi^+\pi^-K^+K^-)/\Gamma_{total}] \times [B(\psi(2S) \to \gamma\chi_{c0}(1P))]$ assuming $B(\psi(2S) \to \gamma\chi_{c0}(1P)) = (9.22 \pm 0.11 \pm 0.46) \times 10^{-2}$, which we rescale to our best value $B(\psi(2S) \to \gamma\chi_{c0}(1P)) = (9.79 \pm 0.20) \times 10^{-2}$. Our first error is their experiment's error and our second error is the systematic error from using our best value.

$\Gamma(K^*_0(1430)^0\overline{K}^*_2(1430)^0 + \text{c.c.} \to \pi^+\pi^-K^+K^-)/\Gamma_{total}$ — Γ_{10}/Γ

VALUE (units 10^{-4})	EVTS	DOCUMENT ID		TECN	COMMENT
$\mathbf{8.0^{+2.0}_{-2.4}\pm0.2}$	62	[1] ABLIKIM	05Q	BES2	$\psi(2S) \to \gamma\pi^+\pi^-K^+K^-$

[1] ABLIKIM 05Q reports $(8.49 \pm 1.66^{+1.32}_{-1.99}) \times 10^{-4}$ from a measurement of $[\Gamma(\chi_{c0}(1P) \to K^*_0(1430)^0\overline{K}^*_2(1430)^0 + \text{c.c.} \to \pi^+\pi^-K^+K^-)/\Gamma_{total}] \times [B(\psi(2S) \to \gamma\chi_{c0}(1P))]$ assuming $B(\psi(2S) \to \gamma\chi_{c0}(1P)) = (9.22 \pm 0.11 \pm 0.46) \times 10^{-2}$, which we rescale to our best value $B(\psi(2S) \to \gamma\chi_{c0}(1P)) = (9.79 \pm 0.20) \times 10^{-2}$. Our first error is their experiment's error and our second error is the systematic error from using our best value.

$\Gamma(K_1(1270)^+K^- + \text{c.c.} \to \pi^+\pi^-K^+K^-)/\Gamma_{total}$ — Γ_{11}/Γ

VALUE (units 10^{-3})	EVTS	DOCUMENT ID		TECN	COMMENT
6.3±1.9±0.1	68	[1] ABLIKIM	05Q	BES2	$\psi(2S) \to \gamma\pi^+\pi^-K^+K^-$

[1] ABLIKIM 05Q reports $(6.66 \pm 1.31^{+1.60}_{-1.51}) \times 10^{-3}$ from a measurement of $[\Gamma(\chi_{c0}(1P) \to K_1(1270)^+K^-$ c.c. $\to \pi^+\pi^-K^+K^-)/\Gamma_{total}] \times [B(\psi(2S) \to \gamma\chi_{c0}(1P))]$ assuming $B(\psi(2S) \to \gamma\chi_{c0}(1P)) = (9.22 \pm 0.11 \pm 0.46) \times 10^{-2}$, which we rescale to our best value $B(\psi(2S) \to \gamma\chi_{c0}(1P)) = (9.79 \pm 0.20) \times 10^{-2}$. Our first error is their experiment's error and our second error is the systematic error from using our best value. The measurement assumes $B(K_1(1270) \to K\rho(770)) = 42 \pm 6\%$.

$\Gamma(K_1(1400)^+K^- + \text{c.c.} \to \pi^+\pi^-K^+K^-)/\Gamma_{total}$ — Γ_{12}/Γ

VALUE (units 10^{-3})	CL%	DOCUMENT ID		TECN	COMMENT
<2.7	90	[1] ABLIKIM	05Q	BES2	$\psi(2S) \to \gamma\pi^+\pi^-K^+K^-$

[1] ABLIKIM 05Q reports $< 2.85 \times 10^{-3}$ from a measurement of $[\Gamma(\chi_{c0}(1P) \to K_1(1400)^+K^-$ c.c. $\to \pi^+\pi^-K^+K^-)/\Gamma_{total}] \times [B(\psi(2S) \to \gamma\chi_{c0}(1P))]$ assuming $B(\psi(2S) \to \gamma\chi_{c0}(1P)) = (9.22 \pm 0.11 \pm 0.46) \times 10^{-2}$, which we rescale to our best value $B(\psi(2S) \to \gamma\chi_{c0}(1P)) = 9.79 \times 10^{-2}$. The measurement assumes $B(K_1(1400) \to K^*(892)\pi) = 94 \pm 6\%$.

Downloaded from https://academic.oup.com/ptep/article/2022/8/083C01/6651666 by KIT Library user on 27 September 2022

$\Gamma(f_0(980)\, f_0(980))/\Gamma_{total}$ — Γ_{13}/Γ

VALUE (units 10^{-5})	EVTS	DOCUMENT ID		TECN	COMMENT
$16.2^{+10.4}_{-9.0}\pm0.3$	28	[1] ABLIKIM	05Q	BES2	$\psi(2S)\to\gamma\pi^+\pi^-K^+K^-$

[1] ABLIKIM 05Q reports $[\Gamma(\chi_{c0}(1P)\to f_0(980)\,f_0(980))/\Gamma_{total}]\times[B(\psi(2S)\to\gamma\chi_{c0}(1P))]=(1.59\pm0.50^{+0.89}_{-0.72})\times10^{-5}$ which we divide by our best value $B(\psi(2S)\to\gamma\chi_{c0}(1P))=(9.79\pm0.20)\times10^{-2}$. Our first error is their experiment's error and our second error is the systematic error from using our best value. One of the $f_0(980)$ mesons is identified via decay to $\pi^+\pi^-$ while the other via K^+K^- decay.

$\Gamma(f_0(980)\, f_0(2200))/\Gamma_{total}$ — Γ_{14}/Γ

VALUE (units 10^{-4})	EVTS	DOCUMENT ID		TECN	COMMENT
$7.9^{+2.0}_{-2.5}\pm0.2$	77	[1] ABLIKIM	05Q	BES2	$\psi(2S)\to\gamma\pi^+\pi^-K^+K^-$

[1] ABLIKIM 05Q reports $(8.42\pm1.42^{+1.65}_{-2.29})\times10^{-4}$ from a measurement of $[\Gamma(\chi_{c0}(1P)\to f_0(980)\,f_0(2200))/\Gamma_{total}]\times[B(\psi(2S)\to\gamma\chi_{c0}(1P))]$ assuming $B(\psi(2S)\to\gamma\chi_{c0}(1P))=(9.22\pm0.11\pm0.46)\times10^{-2}$, which we rescale to our best value $B(\psi(2S)\to\gamma\chi_{c0}(1P))=(9.79\pm0.20)\times10^{-2}$. Our first error is their experiment's error and our second error is the systematic error from using our best value. The f_0 mesons are identified via $f_0(980)\to\pi^+\pi^-$ and $f_0(2200)\to K^+K^-$ decays.

$\Gamma(f_0(1370)\, f_0(1370))/\Gamma_{total}$ — Γ_{15}/Γ

VALUE (units 10^{-4})	CL%	DOCUMENT ID		TECN	COMMENT
<2.7	90	[1] ABLIKIM	05Q	BES2	$\psi(2S)\to\gamma\pi^+\pi^-K^+K^-$

[1] ABLIKIM 05Q reports $<2.9\times10^{-4}$ from a measurement of $[\Gamma(\chi_{c0}(1P)\to f_0(1370)\,f_0(1370))/\Gamma_{total}]\times[B(\psi(2S)\to\gamma\chi_{c0}(1P))]$ assuming $B(\psi(2S)\to\gamma\chi_{c0}(1P))=(9.22\pm0.11\pm0.46)\times10^{-2}$, which we rescale to our best value $B(\psi(2S)\to\gamma\chi_{c0}(1P))=9.79\times10^{-2}$. One of the $f_0(1370)$ mesons is identified via decay to $\pi^+\pi^-$ while the other via K^+K^- decay. Both branching fractions for these f_0 decays are implicitly included in the quoted result.

$\Gamma(f_0(1370)\, f_0(1500))/\Gamma_{total}$ — Γ_{16}/Γ

VALUE (units 10^{-4})	CL%	DOCUMENT ID		TECN	COMMENT
<1.7	90	[1] ABLIKIM	05Q	BES2	$\psi(2S)\to\gamma\pi^+\pi^-K^+K^-$

[1] ABLIKIM 05Q reports $<1.8\times10^{-4}$ from a measurement of $[\Gamma(\chi_{c0}(1P)\to f_0(1370)\,f_0(1500))/\Gamma_{total}]\times[B(\psi(2S)\to\gamma\chi_{c0}(1P))]$ assuming $B(\psi(2S)\to\gamma\chi_{c0}(1P))=(9.22\pm0.11\pm0.46)\times10^{-2}$, which we rescale to our best value $B(\psi(2S)\to\gamma\chi_{c0}(1P))=9.79\times10^{-2}$. The f_0 mesons are identified via $f_0(1370)\to\pi^+\pi^-$ and $f_0(1500)\to K^+K^-$ decays. Both branching fractions for these f_0 decays are implicitly included in the quoted result.

$\Gamma(f_0(1370)\, f_0(1710))/\Gamma_{total}$ — Γ_{17}/Γ

VALUE (units 10^{-4})	EVTS	DOCUMENT ID		TECN	COMMENT
$6.7^{+3.5}_{-2.3}\pm0.1$	61	[1] ABLIKIM	05Q	BES2	$\psi(2S)\to\gamma\pi^+\pi^-K^+K^-$

[1] ABLIKIM 05Q reports $(7.12\pm1.85^{+3.28}_{-1.68})\times10^{-4}$ from a measurement of $[\Gamma(\chi_{c0}(1P)\to f_0(1370)\,f_0(1710))/\Gamma_{total}]\times[B(\psi(2S)\to\gamma\chi_{c0}(1P))]$ assuming $B(\psi(2S)\to\gamma\chi_{c0}(1P))=(9.22\pm0.11\pm0.46)\times10^{-2}$, which we rescale to our best value $B(\psi(2S)\to\gamma\chi_{c0}(1P))=(9.79\pm0.20)\times10^{-2}$. Our first error is their experiment's error and our second error is the systematic error from using our best value. The f_0 mesons are identified via $f_0(1370)\to\pi^+\pi^-$ and $f_0(1710)\to K^+K^-$ decays. Both branching fractions for these f_0 decays are implicitly included in the quoted result.

$\Gamma(f_0(1500)\, f_0(1370))/\Gamma_{total}$ — Γ_{18}/Γ

VALUE (units 10^{-4})	CL%	DOCUMENT ID		TECN	COMMENT
<1.3	90	[1] ABLIKIM	05Q	BES2	$\psi(2S)\to\gamma\pi^+\pi^-K^+K^-$

[1] ABLIKIM 05Q reports $<1.4\times10^{-4}$ from a measurement of $[\Gamma(\chi_{c0}(1P)\to f_0(1500)\,f_0(1370))/\Gamma_{total}]\times[B(\psi(2S)\to\gamma\chi_{c0}(1P))]$ assuming $B(\psi(2S)\to\gamma\chi_{c0}(1P))=(9.22\pm0.11\pm0.46)\times10^{-2}$, which we rescale to our best value $B(\psi(2S)\to\gamma\chi_{c0}(1P))=9.79\times10^{-2}$. The f_0 mesons are identified via $f_0(1500)\to\pi^+\pi^-$ and $f_0(1370)\to K^+K^-$ decays. Both branching fractions for these f_0 decays are implicitly included in the quoted result.

$\Gamma(f_0(1500)\, f_0(1500))/\Gamma_{total}$ — Γ_{19}/Γ

VALUE (units 10^{-4})	CL%	DOCUMENT ID		TECN	COMMENT
<0.5	90	[1] ABLIKIM	05Q	BES2	$\psi(2S)\to\gamma\pi^+\pi^-K^+K^-$

[1] ABLIKIM 05Q reports $<0.55\times10^{-4}$ from a measurement of $[\Gamma(\chi_{c0}(1P)\to f_0(1500)\,f_0(1500))/\Gamma_{total}]\times[B(\psi(2S)\to\gamma\chi_{c0}(1P))]$ assuming $B(\psi(2S)\to\gamma\chi_{c0}(1P))=(9.22\pm0.11\pm0.46)\times10^{-2}$, which we rescale to our best value $B(\psi(2S)\to\gamma\chi_{c0}(1P))=9.79\times10^{-2}$. One of the $f_0(1500)$ is identified via decay to $\pi^+\pi^-$ while the other via K^+K^- decay. Both branching fractions for these f_0 decays are implicitly included in the quoted result.

$\Gamma(f_0(1500)\, f_0(1710))/\Gamma_{total}$ — Γ_{20}/Γ

VALUE (units 10^{-4})	CL%	DOCUMENT ID		TECN	COMMENT
<0.7	90	[1] ABLIKIM	05Q	BES2	$\psi(2S)\to\gamma\pi^+\pi^-K^+K^-$

[1] ABLIKIM 05Q reports $<0.73\times10^{-4}$ from a measurement of $[\Gamma(\chi_{c0}(1P)\to f_0(1500)\,f_0(1710))/\Gamma_{total}]\times[B(\psi(2S)\to\gamma\chi_{c0}(1P))]$ assuming $B(\psi(2S)\to\gamma\chi_{c0}(1P))=(9.22\pm0.11\pm0.46)\times10^{-2}$, which we rescale to our best value $B(\psi(2S)\to\gamma\chi_{c0}(1P))=9.79\times10^{-2}$. The f_0 mesons are identified via $f_0(1500)\to\pi^+\pi^-$ and $f_0(1710)\to K^+K^-$ decays. Both branching fractions for these f_0 decays are implicitly included in the quoted result.

$\Gamma(K^+K^-\pi^+\pi^-\pi^0)/\Gamma_{total}$ — Γ_{21}/Γ

VALUE (units 10^{-3})	EVTS	DOCUMENT ID		TECN	COMMENT
$8.61\pm0.13\pm0.94$	9.0k	[1] ABLIKIM	13B	BES3	$e^+e^-\to\psi(2S)\to\gamma\chi_{c0}$

[1] Using 1.06×10^8 $\psi(2S)$ mesons and $B(\psi(2S)\to\chi_{c0}\gamma)=(9.68\pm0.31)\%$.

$\Gamma(K^0_S K^\pm\pi^\mp\pi^+\pi^-)/\Gamma_{total}$ — Γ_{22}/Γ

VALUE (units 10^{-3})	EVTS	DOCUMENT ID		TECN	COMMENT
$4.22\pm0.10\pm0.43$	2.7k	[1] ABLIKIM	13B	BES3	$e^+e^-\to\psi(2S)\to\gamma\chi_{c0}$

[1] Using 1.06×10^8 $\psi(2S)$ mesons and $B(\psi(2S)\to\chi_{c0}\gamma)=(9.68\pm0.31)\%$.

$\Gamma(K^+K^-\pi^0\pi^0)/\Gamma_{total}$ — Γ_{23}/Γ

VALUE (%)	EVTS	DOCUMENT ID		TECN	COMMENT
$0.56\pm0.09\pm0.01$	213.5	[1] HE	08B	CLEO	$e^+e^-\to\gamma h^+h^-h^0h^0$

[1] HE 08B reports $0.59\pm0.05\pm0.08\pm0.03$ % from a measurement of $[\Gamma(\chi_{c0}(1P)\to K^+K^-\pi^0\pi^0)/\Gamma_{total}]\times[B(\psi(2S)\to\gamma\chi_{c0}(1P))]$ assuming $B(\psi(2S)\to\gamma\chi_{c0}(1P))=(9.22\pm0.11\pm0.46)\times10^{-2}$, which we rescale to our best value $B(\psi(2S)\to\gamma\chi_{c0}(1P))=(9.79\pm0.20)\times10^{-2}$. Our first error is their experiment's error and our second error is the systematic error from using our best value.

$\Gamma(K^+\pi^-\overline{K}^0\pi^0+\text{c.c.})/\Gamma_{total}$ — Γ_{24}/Γ

VALUE (%)	EVTS	DOCUMENT ID		TECN	COMMENT
$2.49\pm0.33\pm0.05$	401.7	[1] HE	08B	CLEO	$e^+e^-\to\gamma h^+h^-h^0h^0$

[1] HE 08B reports $2.64\pm0.15\pm0.31\pm0.14$ % from a measurement of $[\Gamma(\chi_{c0}(1P)\to K^+\pi^-\overline{K}^0\pi^0+\text{c.c.})/\Gamma_{total}]\times[B(\psi(2S)\to\gamma\chi_{c0}(1P))]$ assuming $B(\psi(2S)\to\gamma\chi_{c0}(1P))=(9.22\pm0.11\pm0.46)\times10^{-2}$, which we rescale to our best value $B(\psi(2S)\to\gamma\chi_{c0}(1P))=(9.79\pm0.20)\times10^{-2}$. Our first error is their experiment's error and our second error is the systematic error from using our best value.

$\Gamma(\rho^+K^-K^0+\text{c.c.})/\Gamma_{total}$ — Γ_{25}/Γ

VALUE (%)	EVTS	DOCUMENT ID		TECN	COMMENT
$1.21\pm0.21\pm0.02$	179.7	[1] HE	08B	CLEO	$e^+e^-\to\gamma h^+h^-h^0h^0$

[1] HE 08B reports $1.28\pm0.16\pm0.15\pm0.07$ % from a measurement of $[\Gamma(\chi_{c0}(1P)\to\rho^+K^-K^0+\text{c.c.})/\Gamma_{total}]\times[B(\psi(2S)\to\gamma\chi_{c0}(1P))]$ assuming $B(\psi(2S)\to\gamma\chi_{c0}(1P))=(9.22\pm0.11\pm0.46)\times10^{-2}$, which we rescale to our best value $B(\psi(2S)\to\gamma\chi_{c0}(1P))=(9.79\pm0.20)\times10^{-2}$. Our first error is their experiment's error and our second error is the systematic error from using our best value.

$\Gamma(K^*(892)^-K^+\pi^0\to K^+\pi^-\overline{K}^0\pi^0+\text{c.c.})/\Gamma_{total}$ — Γ_{26}/Γ

VALUE (%)	EVTS	DOCUMENT ID		TECN	COMMENT
$0.46\pm0.12\pm0.01$	64.1	[1] HE	08B	CLEO	$e^+e^-\to\gamma h^+h^-h^0h^0$

[1] HE 08B reports $0.49\pm0.10\pm0.07\pm0.03$ % from a measurement of $[\Gamma(\chi_{c0}(1P)\to K^*(892)^-K^+\pi^0\to K^+\pi^-\overline{K}^0\pi^0+\text{c.c.})/\Gamma_{total}]\times[B(\psi(2S)\to\gamma\chi_{c0}(1P))]$ assuming $B(\psi(2S)\to\gamma\chi_{c0}(1P))=(9.22\pm0.11\pm0.46)\times10^{-2}$, which we rescale to our best value $B(\psi(2S)\to\gamma\chi_{c0}(1P))=(9.79\pm0.20)\times10^{-2}$. Our first error is their experiment's error and our second error is the systematic error from using our best value.

$\Gamma(K^0_S K^0_S\pi^+\pi^-)/\Gamma_{total}$ — Γ_{27}/Γ

VALUE (units 10^{-3})	EVTS	DOCUMENT ID		TECN	COMMENT
$5.7\pm1.0\pm0.1$	152 ± 14	[1] ABLIKIM	05O	BES2	$\psi(2S)\to\gamma\chi_{c0}$

[1] ABLIKIM 05O reports $[\Gamma(\chi_{c0}(1P)\to K^0_S K^0_S\pi^+\pi^-)/\Gamma_{total}]\times[B(\psi(2S)\to\gamma\chi_{c0}(1P))]=(0.558\pm0.051\pm0.089)\times10^{-3}$ which we divide by our best value $B(\psi(2S)\to\gamma\chi_{c0}(1P))=(9.79\pm0.20)\times10^{-2}$. Our first error is their experiment's error and our second error is the systematic error from using our best value.

$\Gamma(K^+K^-\eta\pi^0)/\Gamma_{total}$ — Γ_{28}/Γ

VALUE (%)	EVTS	DOCUMENT ID		TECN	COMMENT
$0.30\pm0.07\pm0.01$	56.4	[1] HE	08B	CLEO	$e^+e^-\to\gamma h^+h^-h^0h^0$

[1] HE 08B reports $0.32\pm0.05\pm0.05\pm0.02$ % from a measurement of $[\Gamma(\chi_{c0}(1P)\to K^+K^-\eta\pi^0)/\Gamma_{total}]\times[B(\psi(2S)\to\gamma\chi_{c0}(1P))]$ assuming $B(\psi(2S)\to\gamma\chi_{c0}(1P))=(9.22\pm0.11\pm0.46)\times10^{-2}$, which we rescale to our best value $B(\psi(2S)\to\gamma\chi_{c0}(1P))=(9.79\pm0.20)\times10^{-2}$. Our first error is their experiment's error and our second error is the systematic error from using our best value.

$\Gamma(3(\pi^+\pi^-))/\Gamma_{total}$ — Γ_{29}/Γ

VALUE (units 10^{-3})	DOCUMENT ID		TECN	COMMENT
12.0±1.8 OUR EVALUATION	Treating systematic error as correlated.			
12.0±1.7 OUR AVERAGE				
$11.7\pm1.0\pm1.9$	[1] BAI	99B	BES	$\psi(2S)\to\gamma\chi_{c0}$
$12.5\pm2.9\pm0.5$	[1] TANENBAUM	78	MRK1	$\psi(2S)\to\gamma\chi_{c0}$

[1] Rescaled by us using $B(\psi(2S)\to\gamma\chi_{c0})=(9.4\pm0.4)\%$ and $B(\psi(2S)\to J/\psi(1S)\pi^+\pi^-)=(32.6\pm0.5)\%$.

$\Gamma(K^+\overline{K}^*(892)^0\pi^-+\text{c.c.})/\Gamma_{total}$ — Γ_{30}/Γ

VALUE	DOCUMENT ID
0.0075±0.0016 OUR FIT	

$\Gamma(K^*(892)^0\overline{K}^*(892)^0)/\Gamma_{total}$ — Γ_{31}/Γ

VALUE (units 10^{-3})	EVTS	DOCUMENT ID		TECN	COMMENT
$1.72^{+0.60}_{-0.54}\pm0.04$	64	[1] ABLIKIM	05Q	BES2	$\psi(2S)\to\gamma\pi^+\pi^-K^+K^-$

Downloaded from https://academic.oup.com/ptep/article/2022/8/083C01/6651666 by KIT Library user on 27 September 2022

• • • We do not use the following data for averages, fits, limits, etc. • • •

1.56±0.40±0.03	30 ± 6	[2,3] ABLIKIM	04H	BES	Repl. by ABLIKIM 05Q

[1] ABLIKIM 05Q reports $[\Gamma(\chi_{c0}(1P) \to K^*(892)^0\overline{K}^*(892)^0)/\Gamma_{total}] \times [B(\psi(2S) \to \gamma\chi_{c0}(1P))] = (0.168 \pm 0.035^{+0.047}_{-0.040}) \times 10^{-3}$ which we divide by our best value $B(\psi(2S) \to \gamma\chi_{c0}(1P)) = (9.79 \pm 0.20) \times 10^{-2}$. Our first error is their experiment's error and our second error is the systematic error from using our best value.

[2] Assumes $B(K^*(892)^0 \to K^-\pi^+) = 2/3$.

[3] ABLIKIM 04H reports $[\Gamma(\chi_{c0}(1P) \to K^*(892)^0\overline{K}^*(892)^0)/\Gamma_{total}] \times [B(\psi(2S) \to \gamma\chi_{c0}(1P))] = (1.53 \pm 0.29 \pm 0.26) \times 10^{-4}$ which we divide by our best value $B(\psi(2S) \to \gamma\chi_{c0}(1P)) = (9.79 \pm 0.20) \times 10^{-2}$. Our first error is their experiment's error and our second error is the systematic error from using our best value.

$\Gamma(\pi\pi)/\Gamma_{total}$ — Γ_{32}/Γ

VALUE (units 10^{-3})	DOCUMENT ID
8.51±0.33 OUR FIT	

$\Gamma(\pi^0\eta_c)/\Gamma_{total}$ — Γ_{35}/Γ

VALUE	CL%	DOCUMENT ID		TECN	COMMENT
$<1.6 \times 10^{-3}$	90	[1] ABLIKIM	15N	BES3	$\psi(2s)e^+e^- \to \gamma\pi^0\eta_c$

[1] Using $B(\eta_c \to K^0_S K^\pm\pi^\mp) \times B(K^0_S \to \pi^+\pi^-) \times B(\pi^0 \to \gamma\gamma) = (1.66 \pm 0.11) \times 10^{-2}$.

$\Gamma(\eta\eta)/\Gamma_{total}$ — Γ_{36}/Γ

VALUE (units 10^{-3})	DOCUMENT ID
3.01±0.19 OUR FIT	

$\Gamma(\eta\eta)/\Gamma(\pi\pi)$ — Γ_{36}/Γ_{32}

VALUE	DOCUMENT ID		TECN	COMMENT
0.353±0.025 OUR FIT				
• • • We do not use the following data for averages, fits, limits, etc. • • •				
$0.26 \pm 0.09 {}^{+0.03}_{-0.02}$	[1] ANDREOTTI	05C	E835	$\overline{p}p \to$ 2 mesons
0.24 ±0.10 ±0.08	[1] BAI	03C	BES	$\psi(2S) \to 5\gamma$

[1] We have multiplied $\pi^0\pi^0$ measurement by 3 to obtain $\pi\pi$.

$\Gamma(\eta\eta')/\Gamma_{total}$ — Γ_{37}/Γ

VALUE (units 10^{-5})	CL%	EVTS	DOCUMENT ID		TECN	COMMENT
9.1±1.1±0.2		85	[1] ABLIKIM	17AI	BES3	$\psi(2S) \to \gamma\eta'\eta$
• • • We do not use the following data for averages, fits, limits, etc. • • •						
<24	90	35 ± 13	[2] ASNER	09	CLEO	$\psi(2S) \to \gamma\eta'\eta$
<50	90		[3] ADAMS	07	CLEO	$\psi(2S) \to \gamma\chi_{c0}$

[1] ABLIKIM 17AI reports $(8.92 \pm 0.84 \pm 0.65) \times 10^{-5}$ from a measurement of $[\Gamma(\chi_{c0}(1P) \to \eta\eta')/\Gamma_{total}] \times [B(\psi(2S) \to \gamma\chi_{c0}(1P))]$ assuming $B(\psi(2S) \to \gamma\chi_{c0}(1P)) = (9.99 \pm 0.27) \times 10^{-2}$, which we rescale to our best value $B(\psi(2S) \to \gamma\chi_{c0}(1P)) = (9.79 \pm 0.20) \times 10^{-2}$. Our first error is their experiment's error and our second error is the systematic error from using our best value.

[2] ASNER 09 reports $< 0.25 \times 10^{-3}$ from a measurement of $[\Gamma(\chi_{c0}(1P) \to \eta\eta')/\Gamma_{total}] \times [B(\psi(2S) \to \gamma\chi_{c0}(1P))]$ assuming $B(\psi(2S) \to \gamma\chi_{c0}(1P)) = (9.22 \pm 0.11 \pm 0.46) \times 10^{-2}$, which we rescale to our best value $B(\psi(2S) \to \gamma\chi_{c0}(1P)) = 9.79 \times 10^{-2}$.

[3] Superseded by ASNER 09. ADAMS 07 reports $< 0.5 \times 10^{-3}$ from a measurement of $[\Gamma(\chi_{c0}(1P) \to \eta\eta')/\Gamma_{total}] \times [B(\psi(2S) \to \gamma\chi_{c0}(1P))]$ assuming $B(\psi(2S) \to \gamma\chi_{c0}(1P)) = (9.22 \pm 0.11 \pm 0.46) \times 10^{-2}$, which we rescale to our best value $B(\psi(2S) \to \gamma\chi_{c0}(1P)) = 9.79 \times 10^{-2}$.

$\Gamma(\eta'\eta')/\Gamma_{total}$ — Γ_{38}/Γ

VALUE (units 10^{-3})	EVTS	DOCUMENT ID		TECN	COMMENT
2.17±0.12 OUR AVERAGE					
2.23±0.13±0.05	2.5k	[1] ABLIKIM	17AI	BES3	$\psi(2S) \to \gamma\eta'\eta'$
2.00±0.21±0.04	0.4k	[2] ASNER	09	CLEO	$\psi(2S) \to \gamma\eta'\eta'$
• • • We do not use the following data for averages, fits, limits, etc. • • •					
1.60±0.41±0.03	23	[3] ADAMS	07	CLEO	$\psi(2S) \to \gamma\chi_{c0}$

[1] ABLIKIM 17AI reports $(2.19 \pm 0.03 \pm 0.14) \times 10^{-3}$ from a measurement of $[\Gamma(\chi_{c0}(1P) \to \eta'\eta')/\Gamma_{total}] \times [B(\psi(2S) \to \gamma\chi_{c0}(1P))]$ assuming $B(\psi(2S) \to \gamma\chi_{c0}(1P)) = (9.99 \pm 0.27) \times 10^{-2}$, which we rescale to our best value $B(\psi(2S) \to \gamma\chi_{c0}(1P)) = (9.79 \pm 0.20) \times 10^{-2}$. Our first error is their experiment's error and our second error is the systematic error from using our best value.

[2] ASNER 09 reports $(2.12 \pm 0.13 \pm 0.21) \times 10^{-3}$ from a measurement of $[\Gamma(\chi_{c0}(1P) \to \eta'\eta')/\Gamma_{total}] \times [B(\psi(2S) \to \gamma\chi_{c0}(1P))]$ assuming $B(\psi(2S) \to \gamma\chi_{c0}(1P)) = (9.22 \pm 0.11 \pm 0.46) \times 10^{-2}$, which we rescale to our best value $B(\psi(2S) \to \gamma\chi_{c0}(1P)) = (9.79 \pm 0.20) \times 10^{-2}$. Our first error is their experiment's error and our second error is the systematic error from using our best value.

[3] Superseded by ASNER 09. ADAMS 07 reports $(1.7 \pm 0.4 \pm 0.2) \times 10^{-3}$ from a measurement of $[\Gamma(\chi_{c0}(1P) \to \eta'\eta')/\Gamma_{total}] \times [B(\psi(2S) \to \gamma\chi_{c0}(1P))]$ assuming $B(\psi(2S) \to \gamma\chi_{c0}(1P)) = 0.0922 \pm 0.0011 \pm 0.0046$, which we rescale to our best value $B(\psi(2S) \to \gamma\chi_{c0}(1P)) = (9.79 \pm 0.20) \times 10^{-2}$. Our first error is their experiment's error and our second error is the systematic error from using our best value.

$\Gamma(\omega\omega)/\Gamma_{total}$ — Γ_{39}/Γ

VALUE (units 10^{-3})	EVTS	DOCUMENT ID		TECN	COMMENT
0.97±0.11 OUR AVERAGE					
0.93±0.11±0.02	991	[1] ABLIKIM	11K	BES3	$\psi(2S) \to \gamma$ hadrons
2.16±0.66±0.04	38.1 ± 9.6	[2] ABLIKIM	05N	BES2	$\psi(2S) \to \gamma\chi_{c0} \to \gamma 6\pi$

[1] ABLIKIM 11K reports $(0.95 \pm 0.03 \pm 0.11) \times 10^{-3}$ from a measurement of $[\Gamma(\chi_{c0}(1P) \to \omega\omega)/\Gamma_{total}] \times [B(\psi(2S) \to \gamma\chi_{c0}(1P))]$ assuming $B(\psi(2S) \to \gamma\chi_{c0}(1P)) = (9.62 \pm 0.31) \times 10^{-2}$, which we rescale to our best value $B(\psi(2S) \to \gamma\chi_{c0}(1P)) = (9.79 \pm 0.20) \times 10^{-2}$. Our first error is their experiment's error and our second error is the systematic error from using our best value.

[2] ABLIKIM 05N reports $[\Gamma(\chi_{c0}(1P) \to \omega\omega)/\Gamma_{total}] \times [B(\psi(2S) \to \gamma\chi_{c0}(1P))] = (0.212 \pm 0.053 \pm 0.037) \times 10^{-3}$ which we divide by our best value $B(\psi(2S) \to \gamma\chi_{c0}(1P)) = (9.79 \pm 0.20) \times 10^{-2}$. Our first error is their experiment's error and our second error is the systematic error from using our best value.

$\Gamma(\omega\phi)/\Gamma_{total}$ — Γ_{40}/Γ

VALUE (units 10^{-4})	EVTS	DOCUMENT ID		TECN	COMMENT
1.41±0.13±0.03	486	[1] ABLIKIM	19J	BES3	$\psi(2S) \to \gamma$ hadrons
• • • We do not use the following data for averages, fits, limits, etc. • • •					
1.18±0.22±0.02	76	[2,3] ABLIKIM	11K	BES3	$\psi(2S) \to \gamma$ hadrons

[1] ABLIKIM 19J reports $[\Gamma(\chi_{c0}(1P) \to \omega\phi)/\Gamma_{total}] \times [B(\psi(2S) \to \gamma\chi_{c0}(1P))] = (13.83 \pm 0.70 \pm 1.01) \times 10^{-6}$ which we divide by our best value $B(\psi(2S) \to \gamma\chi_{c0}(1P)) = (9.79 \pm 0.20) \times 10^{-2}$. Our first error is their experiment's error and our second error is the systematic error from using our best value.

[2] ABLIKIM 11K reports $(1.2 \pm 0.1 \pm 0.2) \times 10^{-4}$ from a measurement of $[\Gamma(\chi_{c0}(1P) \to \omega\phi)/\Gamma_{total}] \times [B(\psi(2S) \to \gamma\chi_{c0}(1P))]$ assuming $B(\psi(2S) \to \gamma\chi_{c0}(1P)) = (9.62 \pm 0.31) \times 10^{-2}$, which we rescale to our best value $B(\psi(2S) \to \gamma\chi_{c0}(1P)) = (9.79 \pm 0.20) \times 10^{-2}$. Our first error is their experiment's error and our second error is the systematic error from using our best value.

[3] Superseded by ABLIKIM 19J.

$\Gamma(\omega K^+K^-)/\Gamma_{total}$ — Γ_{41}/Γ

VALUE (units 10^{-3})	EVTS	DOCUMENT ID		TECN	COMMENT
1.94±0.06±0.20	1.4k	[1] ABLIKIM	13B	BES3	$e^+e^- \to \psi(2S) \to \gamma\chi_{c0}$

[1] Using 1.06×10^8 $\psi(2S)$ mesons and $B(\psi(2S) \to \chi_{c0}\gamma) = (9.68 \pm 0.31)\%$.

$\Gamma(K^+K^-)/\Gamma_{total}$ — Γ_{42}/Γ

VALUE (units 10^{-3})	DOCUMENT ID
6.05±0.31 OUR FIT	

$\Gamma(K^0_S K^0_S)/\Gamma_{total}$ — Γ_{43}/Γ

VALUE (units 10^{-3})	DOCUMENT ID
3.16±0.17 OUR FIT	

$\Gamma(K^0_S K^0_S)/\Gamma(\pi\pi)$ — Γ_{43}/Γ_{32}

VALUE	DOCUMENT ID		TECN	COMMENT
0.371±0.023 OUR FIT				
• • • We do not use the following data for averages, fits, limits, etc. • • •				
0.31 ±0.05 ±0.05	[1,2] CHEN	07B	BELL	$e^+e^- \to e^+e^-\chi_{c0}$

[1] Using $\Gamma(\pi\pi) \times \Gamma(\gamma\gamma)/\Gamma_{total}$ from the $\pi^+\pi^-$ measurement of NAKAZAWA 05 rescaled by 3/2 to convert to $\pi\pi$.

[2] Not independent from other measurements.

$\Gamma(K^0_S K^0_S)/\Gamma(K^+K^-)$ — Γ_{43}/Γ_{42}

VALUE	DOCUMENT ID		TECN	COMMENT
0.52±0.04 OUR FIT				
• • • We do not use the following data for averages, fits, limits, etc. • • •				
0.49±0.07±0.08	[1,2] CHEN	07B	BELL	$e^+e^- \to e^+e^-\chi_{c0}$

[1] Using $\Gamma(K^+K^-) \times \Gamma(\gamma\gamma)/\Gamma_{total}$ from NAKAZAWA 05.

[2] Not independent from other measurements.

$\Gamma(\pi^+\pi^-\eta)/\Gamma_{total}$ — Γ_{44}/Γ

VALUE (units 10^{-3})	CL%	DOCUMENT ID		TECN	COMMENT
<0.20	90	[1] ATHAR	07	CLEO	$\psi(2S) \to \gamma h^+h^-h^0$
• • • We do not use the following data for averages, fits, limits, etc. • • •					
<1.0	90	[2] ABLIKIM	06R	BES2	$\psi(2S) \to \gamma\chi_{c0}$

[1] ATHAR 07 reports $< 0.21 \times 10^{-3}$ from a measurement of $[\Gamma(\chi_{c0}(1P) \to \pi^+\pi^-\eta)/\Gamma_{total}] \times [B(\psi(2S) \to \gamma\chi_{c0}(1P))]$ assuming $B(\psi(2S) \to \gamma\chi_{c0}(1P)) = (9.22 \pm 0.11 \pm 0.46) \times 10^{-2}$, which we rescale to our best value $B(\psi(2S) \to \gamma\chi_{c0}(1P)) = 9.79 \times 10^{-2}$.

[2] ABLIKIM 06R reports $< 1.1 \times 10^{-3}$ from a measurement of $[\Gamma(\chi_{c0}(1P) \to \pi^+\pi^-\eta)/\Gamma_{total}] \times [B(\psi(2S) \to \gamma\chi_{c0}(1P))]$ assuming $B(\psi(2S) \to \gamma\chi_{c0}(1P)) = (9.2 \pm 0.4) \times 10^{-2}$, which we rescale to our best value $B(\psi(2S) \to \gamma\chi_{c0}(1P)) = 9.79 \times 10^{-2}$.

$\Gamma(\pi^+\pi^-\eta')/\Gamma_{total}$ — Γ_{45}/Γ

VALUE (units 10^{-3})	CL%	DOCUMENT ID		TECN	COMMENT
<0.4	90	[1] ATHAR	07	CLEO	$\psi(2S) \to \gamma h^+h^-h^0$

[1] ATHAR 07 reports $< 0.38 \times 10^{-3}$ from a measurement of $[\Gamma(\chi_{c0}(1P) \to \pi^+\pi^-\eta')/\Gamma_{total}] \times [B(\psi(2S) \to \gamma\chi_{c0}(1P))]$ assuming $B(\psi(2S) \to \gamma\chi_{c0}(1P)) = (9.22 \pm 0.11 \pm 0.46) \times 10^{-2}$, which we rescale to our best value $B(\psi(2S) \to \gamma\chi_{c0}(1P)) = 9.79 \times 10^{-2}$.

Downloaded from https://academic.oup.com/ptep/article/2022/8/083C01/6651666 by KIT Library user on 27 September 2022

$\Gamma(\overline{K}^0 K^+ \pi^- + \text{c.c.})/\Gamma_{\text{total}}$ — Γ_{46}/Γ

VALUE (units 10^{-3})	CL%	DOCUMENT ID		TECN	COMMENT
<0.09	90	[1] ATHAR	07	CLEO	$\psi(2S) \to \gamma h^+ h^- h^0$
• • • We do not use the following data for averages, fits, limits, etc. • • •					
<0.7	90	[2,3] ABLIKIM	06R	BES2	$\psi(2S) \to \gamma \chi_{c0}$
<0.7	90	[3,4] BAI	99B	BES	$\psi(2S) \to \gamma \chi_{c0}$

[1] ATHAR 07 reports $< 0.10 \times 10^{-3}$ from a measurement of $[\Gamma(\chi_{c0}(1P) \to \overline{K}^0 K^+ \pi^- + \text{c.c.})/\Gamma_{\text{total}}] \times [B(\psi(2S) \to \gamma\chi_{c0}(1P))]$ assuming $B(\psi(2S) \to \gamma\chi_{c0}(1P)) = (9.22 \pm 0.11 \pm 0.46) \times 10^{-2}$, which we rescale to our best value $B(\psi(2S) \to \gamma\chi_{c0}(1P)) = 9.79 \times 10^{-2}$.

[2] ABLIKIM 06R reports $< 0.70 \times 10^{-3}$ from a measurement of $[\Gamma(\chi_{c0}(1P) \to \overline{K}^0 K^+ \pi^- + \text{c.c.})/\Gamma_{\text{total}}] \times [B(\psi(2S) \to \gamma\chi_{c0}(1P))]$ assuming $B(\psi(2S) \to \gamma\chi_{c0}(1P)) = (9.2 \pm 0.4) \times 10^{-2}$, which we rescale to our best value $B(\psi(2S) \to \gamma\chi_{c0}(1P)) = 9.79 \times 10^{-2}$.

[3] We have multiplied the $K^0_S K^+ \pi^-$ measurement by a factor of 2 to convert to $K^0 K^+ \pi^-$.

[4] Rescaled by us using $B(\psi(2S) \to \gamma\chi_{c0}) = (9.4 \pm 0.4)\%$ and $B(\psi(2S) \to J/\psi(1S)\pi^+\pi^-) = (32.6 \pm 0.5)\%$.

$\Gamma(K^+ K^- \pi^0)/\Gamma_{\text{total}}$ — Γ_{47}/Γ

VALUE (units 10^{-3})	CL%	DOCUMENT ID		TECN	COMMENT
<0.06	90	[1] ATHAR	07	CLEO	$\psi(2S) \to \gamma h^+ h^- h^0$

[1] ATHAR 07 reports $< 0.06 \times 10^{-3}$ from a measurement of $[\Gamma(\chi_{c0}(1P) \to K^+ K^- \pi^0)/\Gamma_{\text{total}}] \times [B(\psi(2S) \to \gamma\chi_{c0}(1P))]$ assuming $B(\psi(2S) \to \gamma\chi_{c0}(1P)) = (9.22 \pm 0.11 \pm 0.46) \times 10^{-2}$, which we rescale to our best value $B(\psi(2S) \to \gamma\chi_{c0}(1P)) = 9.79 \times 10^{-2}$.

$\Gamma(K^+ K^- \eta)/\Gamma_{\text{total}}$ — Γ_{48}/Γ

VALUE (units 10^{-3})	CL%	DOCUMENT ID		TECN	COMMENT
<0.23	90	[1] ATHAR	07	CLEO	$\psi(2S) \to \gamma h^+ h^- h^0$

[1] ATHAR 07 reports $< 0.24 \times 10^{-3}$ from a measurement of $[\Gamma(\chi_{c0}(1P) \to K^+ K^- \eta)/\Gamma_{\text{total}}] \times [B(\psi(2S) \to \gamma\chi_{c0}(1P))]$ assuming $B(\psi(2S) \to \gamma\chi_{c0}(1P)) = (9.22 \pm 0.11 \pm 0.46) \times 10^{-2}$, which we rescale to our best value $B(\psi(2S) \to \gamma\chi_{c0}(1P)) = 9.79 \times 10^{-2}$.

$\Gamma(K^+ K^- K^0_S K^0_S)/\Gamma_{\text{total}}$ — Γ_{49}/Γ

VALUE (units 10^{-3})	EVTS	DOCUMENT ID		TECN	COMMENT
1.41±0.47±0.03	16.8±4.8	[1] ABLIKIM	05O	BES2	$\psi(2S) \to \gamma\chi_{c0}$

[1] ABLIKIM 05O reports $[\Gamma(\chi_{c0}(1P) \to K^+ K^- K^0_S K^0_S)/\Gamma_{\text{total}}] \times [B(\psi(2S) \to \gamma\chi_{c0}(1P))] = (0.138 \pm 0.039 \pm 0.025) \times 10^{-3}$ which we divide by our best value $B(\psi(2S) \to \gamma\chi_{c0}(1P)) = (9.79 \pm 0.20) \times 10^{-2}$. Our first error is their experiment's error and our second error is the systematic error from using our best value.

$\Gamma(K^0_S K^0_S K^0_S K^0_S)/\Gamma_{\text{total}}$ — Γ_{50}/Γ

VALUE (units 10^{-4})	EVTS	DOCUMENT ID		TECN	COMMENT
5.8±0.5±0.1	319	[1] ABLIKIM	19AA	BES3	$\psi(2S) \to \gamma 4K^0_S$

[1] Using $B(K^0_S \to \pi^+\pi^-) = (69.20 \pm 0.05)\%$. ABLIKIM 19AA reports $[\Gamma(\chi_{c0}(1P) \to K^0_S K^0_S K^0_S K^0_S)/\Gamma_{\text{total}}] \times [B(\psi(2S) \to \gamma\chi_{c0}(1P))] = (5.64 \pm 0.33 \pm 0.37) \times 10^{-5}$ which we divide by our best value $B(\psi(2S) \to \gamma\chi_{c0}(1P)) = (9.79 \pm 0.20) \times 10^{-2}$. Our first error is their experiment's error and our second error is the systematic error from using our best value..

$\Gamma(K^+ K^- K^+ K^-)/\Gamma_{\text{total}}$ — Γ_{51}/Γ

VALUE (units 10^{-3})	DOCUMENT ID
2.82±0.29 OUR FIT	

$\Gamma(K^+ K^- \phi)/\Gamma_{\text{total}}$ — Γ_{52}/Γ

VALUE (units 10^{-3})	EVTS	DOCUMENT ID		TECN	COMMENT
0.97±0.25±0.02	38	[1] ABLIKIM	06T	BES2	$\psi(2S) \to \gamma 2K^+ 2K^-$

[1] ABLIKIM 06T reports $(1.03 \pm 0.22 \pm 0.15) \times 10^{-3}$ from a measurement of $[\Gamma(\chi_{c0}(1P) \to K^+ K^- \phi)/\Gamma_{\text{total}}] \times [B(\psi(2S) \to \gamma\chi_{c0}(1P))]$ assuming $B(\psi(2S) \to \gamma\chi_{c0}(1P)) = (9.2 \pm 0.4) \times 10^{-2}$, which we rescale to our best value $B(\psi(2S) \to \gamma\chi_{c0}(1P)) = (9.79 \pm 0.20) \times 10^{-2}$. Our first error is their experiment's error and our second error is the systematic error from using our best value.

$\Gamma(\overline{K}^0 K^+ \pi^- \phi + \text{c.c.})/\Gamma_{\text{total}}$ — Γ_{53}/Γ

VALUE (units 10^{-3})	DOCUMENT ID		TECN	COMMENT
3.68±0.30±0.50	ABLIKIM	15M	BES3	$\psi(2S) \to \gamma\chi_{c0}$

$\Gamma(K^+ K^- \pi^0 \phi)/\Gamma_{\text{total}}$ — Γ_{54}/Γ

VALUE (units 10^{-3})	DOCUMENT ID		TECN	COMMENT
1.90±0.14±0.32	ABLIKIM	15M	BES3	$\psi(2S) \to \gamma\chi_{c0}$

$\Gamma(\phi\pi^+\pi^-\pi^0)/\Gamma_{\text{total}}$ — Γ_{55}/Γ

VALUE (units 10^{-3})	EVTS	DOCUMENT ID		TECN	COMMENT
1.18±0.07±0.13	538	[1] ABLIKIM	13B	BES3	$e^+e^- \to \psi(2S) \to \gamma\chi_{c0}$

[1] Using 1.06×10^8 $\psi(2S)$ mesons and $B(\psi(2S) \to \chi_{c0}\gamma) = (9.68 \pm 0.31)\%$.

$\Gamma(\phi\phi)/\Gamma_{\text{total}}$ — Γ_{56}/Γ

VALUE (units 10^{-3})	DOCUMENT ID
0.80±0.07 OUR FIT	

$\Gamma(\phi\phi\eta)/\Gamma_{\text{total}}$ — Γ_{57}/Γ

VALUE (units 10^{-4})	EVTS	DOCUMENT ID		TECN	COMMENT
8.4±0.7±0.6	186.6	[1] ABLIKIM	20B	BES3	$\psi(2S) \to \gamma\phi\phi\eta$

[1] ABLIKIM 20B reports $(8.41 \pm 0.74 \pm 0.62) \times 10^{-4}$ from a measurement of $[\Gamma(\chi_{c0}(1P) \to \phi\phi\eta)/\Gamma_{\text{total}}] \times [B(\psi(2S) \to \gamma\chi_{c0}(1P))]$ assuming $B(\psi(2S) \to \gamma\chi_{c0}(1P)) = (9.79 \pm 0.20) \times 10^{-2}$.

$\Gamma(p\overline{p})/\Gamma_{\text{total}}$ — Γ_{58}/Γ

VALUE (units 10^{-4})	DOCUMENT ID
2.21±0.08 OUR FIT	

$\Gamma(p\overline{p}\pi^0)/\Gamma_{\text{total}}$ — Γ_{59}/Γ

VALUE (units 10^{-3})	DOCUMENT ID		TECN	COMMENT
0.70±0.07 OUR AVERAGE Error includes scale factor of 1.3.				
0.73±0.06±0.01	[1] ONYISI	10	CLE3	$\psi(2S) \to \gamma p\overline{p}X$
0.56±0.12±0.01	[2] ATHAR	07	CLEO	$\psi(2S) \to \gamma h^+ h^- h^0$

[1] ONYISI 10 reports $(7.76 \pm 0.37 \pm 0.51 \pm 0.39) \times 10^{-4}$ from a measurement of $[\Gamma(\chi_{c0}(1P) \to p\overline{p}\pi^0)/\Gamma_{\text{total}}] \times [B(\psi(2S) \to \gamma\chi_{c0}(1P))]$ assuming $B(\psi(2S) \to \gamma\chi_{c0}(1P)) = (9.22 \pm 0.11 \pm 0.46) \times 10^{-2}$, which we rescale to our best value $B(\psi(2S) \to \gamma\chi_{c0}(1P)) = (9.79 \pm 0.20) \times 10^{-2}$. Our first error is their experiment's error and our second error is the systematic error from using our best value.

[2] ATHAR 07 reports $(0.59 \pm 0.10 \pm 0.08) \times 10^{-3}$ from a measurement of $[\Gamma(\chi_{c0}(1P) \to p\overline{p}\pi^0)/\Gamma_{\text{total}}] \times [B(\psi(2S) \to \gamma\chi_{c0}(1P))]$ assuming $B(\psi(2S) \to \gamma\chi_{c0}(1P)) = (9.22 \pm 0.11 \pm 0.46) \times 10^{-2}$, which we rescale to our best value $B(\psi(2S) \to \gamma\chi_{c0}(1P)) = (9.79 \pm 0.20) \times 10^{-2}$. Our first error is their experiment's error and our second error is the systematic error from using our best value.

$\Gamma(p\overline{p}\eta)/\Gamma_{\text{total}}$ — Γ_{60}/Γ

VALUE (units 10^{-3})	DOCUMENT ID		TECN	COMMENT
0.35±0.04 OUR AVERAGE				
0.35±0.04±0.01	[1] ONYISI	10	CLE3	$\psi(2S) \to \gamma p\overline{p}X$
0.37±0.11±0.01	[2] ATHAR	07	CLEO	$\psi(2S) \to \gamma h^+ h^- h^0$

[1] ONYISI 10 reports $(3.73 \pm 0.38 \pm 0.28 \pm 0.19) \times 10^{-4}$ from a measurement of $[\Gamma(\chi_{c0}(1P) \to p\overline{p}\eta)/\Gamma_{\text{total}}] \times [B(\psi(2S) \to \gamma\chi_{c0}(1P))]$ assuming $B(\psi(2S) \to \gamma\chi_{c0}(1P)) = (9.22 \pm 0.11 \pm 0.46) \times 10^{-2}$, which we rescale to our best value $B(\psi(2S) \to \gamma\chi_{c0}(1P)) = (9.79 \pm 0.20) \times 10^{-2}$. Our first error is their experiment's error and our second error is the systematic error from using our best value.

[2] ATHAR 07 reports $(0.39 \pm 0.11 \pm 0.04) \times 10^{-3}$ from a measurement of $[\Gamma(\chi_{c0}(1P) \to p\overline{p}\eta)/\Gamma_{\text{total}}] \times [B(\psi(2S) \to \gamma\chi_{c0}(1P))]$ assuming $B(\psi(2S) \to \gamma\chi_{c0}(1P)) = (9.22 \pm 0.11 \pm 0.46) \times 10^{-2}$, which we rescale to our best value $B(\psi(2S) \to \gamma\chi_{c0}(1P)) = (9.79 \pm 0.20) \times 10^{-2}$. Our first error is their experiment's error and our second error is the systematic error from using our best value.

$\Gamma(p\overline{p}\omega)/\Gamma_{\text{total}}$ — Γ_{61}/Γ

VALUE (units 10^{-3})	DOCUMENT ID		TECN	COMMENT
0.52±0.06±0.01	[1] ONYISI	10	CLE3	$\psi(2S) \to \gamma p\overline{p}X$

[1] ONYISI 10 reports $(5.57 \pm 0.48 \pm 0.42 \pm 0.14) \times 10^{-4}$ from a measurement of $[\Gamma(\chi_{c0}(1P) \to p\overline{p}\omega)/\Gamma_{\text{total}}] \times [B(\psi(2S) \to \gamma\chi_{c0}(1P))]$ assuming $B(\psi(2S) \to \gamma\chi_{c0}(1P)) = (9.22 \pm 0.11 \pm 0.46) \times 10^{-2}$, which we rescale to our best value $B(\psi(2S) \to \gamma\chi_{c0}(1P)) = (9.79 \pm 0.20) \times 10^{-2}$. Our first error is their experiment's error and our second error is the systematic error from using our best value.

$\Gamma(p\overline{p}\phi)/\Gamma_{\text{total}}$ — Γ_{62}/Γ

VALUE (units 10^{-5})	EVTS	DOCUMENT ID		TECN	COMMENT
6.0±1.4±0.1	42 ± 8	[1] ABLIKIM	11F	BES3	$\psi(2S) \to \gamma p\overline{p}K^+K^-$

[1] ABLIKIM 11F reports $(6.12 \pm 1.18 \pm 0.86) \times 10^{-5}$ from a measurement of $[\Gamma(\chi_{c0}(1P) \to p\overline{p}\phi)/\Gamma_{\text{total}}] \times [B(\psi(2S) \to \gamma\chi_{c0}(1P))]$ assuming $B(\psi(2S) \to \gamma\chi_{c0}(1P)) = (9.62 \pm 0.31) \times 10^{-2}$, which we rescale to our best value $B(\psi(2S) \to \gamma\chi_{c0}(1P)) = (9.79 \pm 0.20) \times 10^{-2}$. Our first error is their experiment's error and our second error is the systematic error from using our best value.

$\Gamma(p\overline{p}\pi^+\pi^-)/\Gamma_{\text{total}}$ — Γ_{63}/Γ

VALUE (units 10^{-3})	DOCUMENT ID		TECN	COMMENT
2.1 ±0.7 OUR EVALUATION Error includes scale factor of 1.4. Treating systematic error as correlated.				
2.1 ±1.0 OUR AVERAGE Error includes scale factor of 2.0.				
1.57±0.21±0.53	[1] BAI	99B	BES	$\psi(2S) \to \gamma\chi_{c0}$
4.20±1.15±0.18	[1] TANENBAUM	78	MRK1	$\psi(2S) \to \gamma\chi_{c0}$

[1] Rescaled by us using $B(\psi(2S) \to \gamma\chi_{c0}) = (9.4 \pm 0.4)\%$ and $B(\psi(2S) \to J/\psi(1S)\pi^+\pi^-) = (32.6 \pm 0.5)\%$.

$\Gamma(p\overline{p}\pi^0\pi^0)/\Gamma_{\text{total}}$ — Γ_{64}/Γ

VALUE (%)	EVTS	DOCUMENT ID		TECN	COMMENT
0.104±0.028±0.002	39.5	[1] HE	08B	CLEO	$e^+e^- \to \gamma h^+ h^- h^0 h^0$

[1] HE 08B reports $0.11 \pm 0.02 \pm 0.02 \pm 0.01$ % from a measurement of $[\Gamma(\chi_{c0}(1P) \to p\overline{p}\pi^0\pi^0)/\Gamma_{\text{total}}] \times [B(\psi(2S) \to \gamma\chi_{c0}(1P))]$ assuming $B(\psi(2S) \to \gamma\chi_{c0}(1P)) = (9.22 \pm 0.11 \pm 0.46) \times 10^{-2}$, which we rescale to our best value $B(\psi(2S) \to \gamma\chi_{c0}(1P)) = (9.79 \pm 0.20) \times 10^{-2}$. Our first error is their experiment's error and our second error is the systematic error from using our best value.

Downloaded from https://academic.oup.com/ptep/article/2022/8/083C01/6651666 by KIT Library user on 27 September 2022

$\Gamma(p\overline{p}K^+K^-(\text{non-resonant}))/\Gamma_{\text{total}}$ — Γ_{65}/Γ

VALUE (units 10^{-4})	EVTS	DOCUMENT ID		TECN	COMMENT
1.22±0.26±0.02	48 ± 8	[1] ABLIKIM	11F	BES3	$\psi(2S) \to \gamma p\overline{p}K^+K^-$

[1] ABLIKIM 11F reports $(1.24\pm0.20\pm0.18)\times10^{-4}$ from a measurement of $[\Gamma(\chi_{c0}(1P) \to p\overline{p}K^+K^-(\text{non-resonant}))/\Gamma_{\text{total}}] \times [B(\psi(2S) \to \gamma\chi_{c0}(1P))]$ assuming $B(\psi(2S) \to \gamma\chi_{c0}(1P)) = (9.62 \pm 0.31) \times 10^{-2}$, which we rescale to our best value $B(\psi(2S) \to \gamma\chi_{c0}(1P)) = (9.79 \pm 0.20) \times 10^{-2}$. Our first error is their experiment's error and our second error is the systematic error from using our best value.

$\Gamma(p\overline{p}K^0_SK^0_S)/\Gamma_{\text{total}}$ — Γ_{66}/Γ

VALUE (units 10^{-4})	CL%	DOCUMENT ID		TECN	COMMENT
<8.8	90	[1] ABLIKIM	06D	BES2	$\psi(2S) \to \chi_{c0}\gamma$

[1] Using $B(\psi(2S) \to \chi_{c0}\gamma) = (9.2 \pm 0.5)\%$

$\Gamma(p\overline{n}\pi^-)/\Gamma_{\text{total}}$ — Γ_{67}/Γ

VALUE (units 10^{-4})	EVTS	DOCUMENT ID		TECN	COMMENT
12.7±1.1 OUR AVERAGE					
12.9±1.1±0.3	5150	[1] ABLIKIM	12J	BES3	$\psi(2S) \to \gamma p\overline{n}\pi^-$
11.2±3.1±0.2		[2] ABLIKIM	06I	BES2	$\psi(2S) \to \gamma p\pi^-X$

[1] ABLIKIM 12J reports $[\Gamma(\chi_{c0}(1P) \to p\overline{n}\pi^-)/\Gamma_{\text{total}}] \times [B(\psi(2S) \to \gamma\chi_{c0}(1P))] = (1.26 \pm 0.02 \pm 0.11) \times 10^{-4}$ which we divide by our best value $B(\psi(2S) \to \gamma\chi_{c0}(1P)) = (9.79 \pm 0.20) \times 10^{-2}$. Our first error is their experiment's error and our second error is the systematic error from using our best value.

[2] ABLIKIM 06I reports $[\Gamma(\chi_{c0}(1P) \to p\overline{n}\pi^-)/\Gamma_{\text{total}}] \times [B(\psi(2S) \to \gamma\chi_{c0}(1P))] = (1.10 \pm 0.24 \pm 0.18) \times 10^{-4}$ which we divide by our best value $B(\psi(2S) \to \gamma\chi_{c0}(1P)) = (9.79 \pm 0.20) \times 10^{-2}$. Our first error is their experiment's error and our second error is the systematic error from using our best value.

$\Gamma(\overline{p}n\pi^+)/\Gamma_{\text{total}}$ — Γ_{68}/Γ

VALUE (units 10^{-4})	EVTS	DOCUMENT ID		TECN	COMMENT
13.7±1.2±0.3	5808	[1] ABLIKIM	12J	BES3	$\psi(2S) \to \gamma\overline{p}n\pi^+$

[1] ABLIKIM 12J reports $[\Gamma(\chi_{c0}(1P) \to \overline{p}n\pi^+)/\Gamma_{\text{total}}] \times [B(\psi(2S) \to \gamma\chi_{c0}(1P))] = (1.34 \pm 0.03 \pm 0.11) \times 10^{-4}$ which we divide by our best value $B(\psi(2S) \to \gamma\chi_{c0}(1P)) = (9.79 \pm 0.20) \times 10^{-2}$. Our first error is their experiment's error and our second error is the systematic error from using our best value.

$\Gamma(p\overline{n}\pi^-\pi^0)/\Gamma_{\text{total}}$ — Γ_{69}/Γ

VALUE (units 10^{-4})	EVTS	DOCUMENT ID		TECN	COMMENT
23.4±2.0±0.5	2480	[1] ABLIKIM	12J	BES3	$\psi(2S) \to \gamma p\overline{n}\pi^-\pi^0$

[1] ABLIKIM 12J reports $[\Gamma(\chi_{c0}(1P) \to p\overline{n}\pi^-\pi^0)/\Gamma_{\text{total}}] \times [B(\psi(2S) \to \gamma\chi_{c0}(1P))] = (2.29 \pm 0.08 \pm 0.18) \times 10^{-4}$ which we divide by our best value $B(\psi(2S) \to \gamma\chi_{c0}(1P)) = (9.79 \pm 0.20) \times 10^{-2}$. Our first error is their experiment's error and our second error is the systematic error from using our best value.

$\Gamma(\overline{p}n\pi^+\pi^0)/\Gamma_{\text{total}}$ — Γ_{70}/Γ

VALUE (units 10^{-4})	EVTS	DOCUMENT ID		TECN	COMMENT
22.1±1.8±0.5	2757	[1] ABLIKIM	12J	BES3	$\psi(2S) \to \gamma\overline{p}n\pi^+\pi^0$

[1] ABLIKIM 12J reports $[\Gamma(\chi_{c0}(1P) \to \overline{p}n\pi^+\pi^0)/\Gamma_{\text{total}}] \times [B(\psi(2S) \to \gamma\chi_{c0}(1P))] = (2.16 \pm 0.07 \pm 0.16) \times 10^{-4}$ which we divide by our best value $B(\psi(2S) \to \gamma\chi_{c0}(1P)) = (9.79 \pm 0.20) \times 10^{-2}$. Our first error is their experiment's error and our second error is the systematic error from using our best value.

$\Gamma(\Lambda\overline{\Lambda})/\Gamma_{\text{total}}$ — Γ_{71}/Γ

VALUE (units 10^{-4})	DOCUMENT ID
3.59±0.15 OUR FIT	

$\Gamma(\Lambda\overline{\Lambda}\pi^+\pi^-)/\Gamma_{\text{total}}$ — Γ_{72}/Γ

VALUE (units 10^{-5})	CL%	EVTS	DOCUMENT ID		TECN	COMMENT
118±12±2		426	[1] ABLIKIM	12I	BES3	$\psi(2S) \to \gamma\Lambda\overline{\Lambda}\pi^+\pi^-$
• • • We do not use the following data for averages, fits, limits, etc. • • •						
<400	90		[2] ABLIKIM	06D	BES2	$\psi(2S) \to \chi_{c0}\gamma$

[1] ABLIKIM 12I reports $(119.0\pm6.4\pm11.4)\times10^{-5}$ from a measurement of $[\Gamma(\chi_{c0}(1P) \to \Lambda\overline{\Lambda}\pi^+\pi^-)/\Gamma_{\text{total}}] \times [B(\psi(2S) \to \gamma\chi_{c0}(1P))]$ assuming $B(\psi(2S) \to \gamma\chi_{c0}(1P)) = (9.68 \pm 0.31) \times 10^{-2}$, which we rescale to our best value $B(\psi(2S) \to \gamma\chi_{c0}(1P)) = (9.79 \pm 0.20) \times 10^{-2}$. Our first error is their experiment's error and our second error is the systematic error from using our best value.

[2] Using $B(\psi(2S) \to \chi_{c0}\gamma) = (9.2 \pm 0.5)\%$

$\Gamma(\Lambda\overline{\Lambda}\pi^+\pi^-(\text{non-resonant}))/\Gamma_{\text{total}}$ — Γ_{73}/Γ

VALUE (units 10^{-5})	CL%	DOCUMENT ID		TECN	COMMENT
<50	90	[1] ABLIKIM	12I	BES3	$\psi(2S) \to \gamma\Lambda\overline{\Lambda}\pi^+\pi^-$

[1] ABLIKIM 12I reports $< 54 \times 10^{-5}$ from a measurement of $[\Gamma(\chi_{c0}(1P) \to \Lambda\overline{\Lambda}\pi^+\pi^-(\text{non-resonant}))/\Gamma_{\text{total}}] \times [B(\psi(2S) \to \gamma\chi_{c0}(1P))]$ assuming $B(\psi(2S) \to \gamma\chi_{c0}(1P)) = (9.68 \pm 0.31) \times 10^{-2}$, which we rescale to our best value $B(\psi(2S) \to \gamma\chi_{c0}(1P)) = 9.79 \times 10^{-2}$.

$\Gamma(\Sigma(1385)^+\overline{\Lambda}\pi^- + \text{c.c.})/\Gamma_{\text{total}}$ — Γ_{74}/Γ

VALUE (units 10^{-5})	CL%	DOCUMENT ID		TECN	COMMENT
<50	90	[1] ABLIKIM	12I	BES3	$\psi(2S) \to \gamma\Sigma(1385)^+\overline{\Lambda}\pi^-$

[1] ABLIKIM 12I reports $< 55 \times 10^{-5}$ from a measurement of $[\Gamma(\chi_{c0}(1P) \to \Sigma(1385)^+\overline{\Lambda}\pi^- + \text{c.c.})/\Gamma_{\text{total}}] \times [B(\psi(2S) \to \gamma\chi_{c0}(1P))]$ assuming $B(\psi(2S) \to \gamma\chi_{c0}(1P)) = (9.68 \pm 0.31) \times 10^{-2}$, which we rescale to our best value $B(\psi(2S) \to \gamma\chi_{c0}(1P)) = 9.79 \times 10^{-2}$.

$\Gamma(\Sigma(1385)^-\overline{\Lambda}\pi^+ + \text{c.c.})/\Gamma_{\text{total}}$ — Γ_{75}/Γ

VALUE (units 10^{-5})	CL%	DOCUMENT ID		TECN	COMMENT
<50	90	[1] ABLIKIM	12I	BES3	$\psi(2S) \to \gamma\Sigma(1385)^-\overline{\Lambda}\pi^+$

[1] ABLIKIM 12I reports $< 50 \times 10^{-5}$ from a measurement of $[\Gamma(\chi_{c0}(1P) \to \Sigma(1385)^-\overline{\Lambda}\pi^+ + \text{c.c.})/\Gamma_{\text{total}}] \times [B(\psi(2S) \to \gamma\chi_{c0}(1P))]$ assuming $B(\psi(2S) \to \gamma\chi_{c0}(1P)) = (9.68 \pm 0.31) \times 10^{-2}$, which we rescale to our best value $B(\psi(2S) \to \gamma\chi_{c0}(1P)) = 9.79 \times 10^{-2}$.

$\Gamma(K^+\overline{p}\Lambda + \text{c.c.})/\Gamma_{\text{total}}$ — Γ_{76}/Γ

VALUE (units 10^{-3})	EVTS	DOCUMENT ID		TECN	COMMENT
1.25±0.12 OUR AVERAGE Error includes scale factor of 1.3.					
1.30±0.09±0.03	9k	[1,2] ABLIKIM	13D	BES3	$\psi(2S) \to \gamma\Lambda\overline{p}K^+$
1.01±0.19±0.02		[3] ATHAR	07	CLEO	$\psi(2S) \to \gamma h^+h^-h^0$

[1] ABLIKIM 13D reports $(1.32\pm0.03\pm0.10)\times10^{-3}$ from a measurement of $[\Gamma(\chi_{c0}(1P) \to K^+\overline{p}\Lambda + \text{c.c.})/\Gamma_{\text{total}}] \times [B(\psi(2S) \to \gamma\chi_{c0}(1P))]$ assuming $B(\psi(2S) \to \gamma\chi_{c0}(1P)) = (9.68 \pm 0.31) \times 10^{-2}$, which we rescale to our best value $B(\psi(2S) \to \gamma\chi_{c0}(1P)) = (9.79 \pm 0.20) \times 10^{-2}$. Our first error is their experiment's error and our second error is the systematic error from using our best value.

[2] Using $B(\Lambda \to p\pi^-) = 63.9\%$.

[3] ATHAR 07 reports $(1.07 \pm 0.17 \pm 0.12) \times 10^{-3}$ from a measurement of $[\Gamma(\chi_{c0}(1P) \to K^+\overline{p}\Lambda + \text{c.c.})/\Gamma_{\text{total}}] \times [B(\psi(2S) \to \gamma\chi_{c0}(1P))]$ assuming $B(\psi(2S) \to \gamma\chi_{c0}(1P)) = (9.22 \pm 0.11 \pm 0.46) \times 10^{-2}$, which we rescale to our best value $B(\psi(2S) \to \gamma\chi_{c0}(1P)) = (9.79 \pm 0.20) \times 10^{-2}$. Our first error is their experiment's error and our second error is the systematic error from using our best value.

$\Gamma(K^*(892)^+\overline{p}\Lambda + \text{c.c.})/\Gamma_{\text{total}}$ — Γ_{78}/Γ

VALUE (units 10^{-4})	EVTS	DOCUMENT ID		TECN	COMMENT
4.8±0.9±0.1	254	[1] ABLIKIM	19AU	BES3	$\psi(2S) \to \gamma K^{*+}\overline{p}\Lambda$

[1] ABLIKIM 19AU reports $[\Gamma(\chi_{c0}(1P) \to K^*(892)^+\overline{p}\Lambda + \text{c.c.})/\Gamma_{\text{total}}] \times [B(\psi(2S) \to \gamma\chi_{c0}(1P))] = (4.7 \pm 0.7 \pm 0.5) \times 10^{-5}$ which we divide by our best value $B(\psi(2S) \to \gamma\chi_{c0}(1P)) = (9.79 \pm 0.20) \times 10^{-2}$. Our first error is their experiment's error and our second error is the systematic error from using our best value.

$\Gamma(K^+\overline{p}\Lambda(1520) + \text{c.c.})/\Gamma_{\text{total}}$ — Γ_{79}/Γ

VALUE (units 10^{-4})	EVTS	DOCUMENT ID		TECN	COMMENT
2.9±0.7±0.1	62 ± 12	[1] ABLIKIM	11F	BES3	$\psi(2S) \to \gamma p\overline{p}K^+K^-$

[1] ABLIKIM 11F reports $(3.00\pm0.58\pm0.50)\times10^{-4}$ from a measurement of $[\Gamma(\chi_{c0}(1P) \to K^+\overline{p}\Lambda(1520) + \text{c.c.})/\Gamma_{\text{total}}] \times [B(\psi(2S) \to \gamma\chi_{c0}(1P))]$ assuming $B(\psi(2S) \to \gamma\chi_{c0}(1P)) = (9.62 \pm 0.31) \times 10^{-2}$, which we rescale to our best value $B(\psi(2S) \to \gamma\chi_{c0}(1P)) = (9.79 \pm 0.20) \times 10^{-2}$. Our first error is their experiment's error and our second error is the systematic error from using our best value.

$\Gamma(nK^0_S\overline{\Lambda} + \text{c.c.})/\Gamma_{\text{total}}$ — Γ_{77}/Γ

VALUE (units 10^{-4})	EVTS	DOCUMENT ID		TECN	COMMENT
6.7±0.3±0.4	1284	[1] ABLIKIM	21AV	BES3	$\psi(2S) \to \gamma nK^0_S\overline{\Lambda}$ + c.c.

[1] ABLIKIM 21AV reports $(6.65 \pm 0.26 \pm 0.41) \times 10^{-4}$ from a measurement of $[\Gamma(\chi_{c0}(1P) \to nK^0_S\overline{\Lambda} + \text{c.c.})/\Gamma_{\text{total}}] \times [B(\psi(2S) \to \gamma\chi_{c0}(1P))]$ assuming $B(\psi(2S) \to \gamma\chi_{c0}(1P)) = 0.0979 \pm 0.0020$. Also uses $B(\overline{\Lambda} \to \overline{p}\pi^+) = (63.9 \pm 0.5)\%$ and $B(K^0_S \to \pi^+\pi^-) = (69.20 \pm 0.05)\%$.

$\Gamma(\Lambda(1520)\overline{\Lambda}(1520))/\Gamma_{\text{total}}$ — Γ_{80}/Γ

VALUE (units 10^{-4})	EVTS	DOCUMENT ID		TECN	COMMENT
3.1±1.2±0.1	28 ± 10	[1] ABLIKIM	11F	BES3	$\psi(2S) \to \gamma p\overline{p}K^+K^-$

[1] ABLIKIM 11F reports $(3.18 \pm 1.11 \pm 0.53) \times 10^{-4}$ from a measurement of $[\Gamma(\chi_{c0}(1P) \to \Lambda(1520)\overline{\Lambda}(1520))/\Gamma_{\text{total}}] \times [B(\psi(2S) \to \gamma\chi_{c0}(1P))]$ assuming $B(\psi(2S) \to \gamma\chi_{c0}(1P)) = (9.62 \pm 0.31) \times 10^{-2}$, which we rescale to our best value $B(\psi(2S) \to \gamma\chi_{c0}(1P)) = (9.79 \pm 0.20) \times 10^{-2}$. Our first error is their experiment's error and our second error is the systematic error from using our best value.

$\Gamma(\Sigma^0\overline{\Sigma}^0)/\Gamma_{\text{total}}$ — Γ_{81}/Γ

VALUE (units 10^{-4})	EVTS	DOCUMENT ID		TECN	COMMENT
4.68±0.32 OUR AVERAGE					
4.82±0.34±0.10	1046	[1] ABLIKIM	18V	BES3	$\psi(2S) \to \gamma\Sigma^0\overline{\Sigma}^0$
4.2 ±0.7 ±0.1	78 ± 10	[2] NAIK	08	CLEO	$\psi(2S) \to \gamma\Sigma^0\overline{\Sigma}^0$
• • • We do not use the following data for averages, fits, limits, etc. • • •					
4.7 ±0.5 ±0.1	243	[3,4] ABLIKIM	13H	BES3	$\psi(2S) \to \gamma\Sigma^0\overline{\Sigma}^0$

Downloaded from https://academic.oup.com/ptep/article/2022/8/083C01/6651666 by KIT Library user on 27 September 2022

[1] ABLIKIM 18V reports $[\Gamma(\chi_{c0}(1P) \to \Sigma^0\overline{\Sigma}^0)/\Gamma_{total}] \times [B(\psi(2S) \to \gamma\chi_{c0}(1P))] = (4.72 \pm 0.18 \pm 0.28) \times 10^{-5}$ which we divide by our best value $B(\psi(2S) \to \gamma\chi_{c0}(1P)) = (9.79 \pm 0.20) \times 10^{-2}$. Our first error is their experiment's error and our second error is the systematic error from using our best value.

[2] NAIK 08 reports $(4.41 \pm 0.56 \pm 0.47) \times 10^{-4}$ from a measurement of $[\Gamma(\chi_{c0}(1P) \to \Sigma^0\overline{\Sigma}^0)/\Gamma_{total}] \times [B(\psi(2S) \to \gamma\chi_{c0}(1P))]$ assuming $B(\psi(2S) \to \gamma\chi_{c0}(1P)) = (9.22 \pm 0.11 \pm 0.46) \times 10^{-2}$, which we rescale to our best value $B(\psi(2S) \to \gamma\chi_{c0}(1P)) = (9.79 \pm 0.20) \times 10^{-2}$. Our first error is their experiment's error and our second error is the systematic error from using our best value.

[3] ABLIKIM 13H reports $(4.78 \pm 0.34 \pm 0.39) \times 10^{-4}$ from a measurement of $[\Gamma(\chi_{c0}(1P) \to \Sigma^0\overline{\Sigma}^0)/\Gamma_{total}] \times [B(\psi(2S) \to \gamma\chi_{c0}(1P))]$ assuming $B(\psi(2S) \to \gamma\chi_{c0}(1P)) = (9.62 \pm 0.31) \times 10^{-2}$, which we rescale to our best value $B(\psi(2S) \to \gamma\chi_{c0}(1P)) = (9.79 \pm 0.20) \times 10^{-2}$. Our first error is their experiment's error and our second error is the systematic error from using our best value.

[4] Superseded by ABLIKIM 18V

$\Gamma(\Sigma^+\overline{\Sigma}^-)/\Gamma_{total}$ — Γ_{84}/Γ

VALUE (units 10^{-4})	EVTS	DOCUMENT ID		TECN	COMMENT
4.6 ±0.8 OUR AVERAGE Error includes scale factor of 2.6.					
5.10±0.35±0.10	747	[1] ABLIKIM	18V	BES3	$\psi(2S) \to \gamma\Sigma^+\overline{\Sigma}^-$
3.1 ±0.7 ±0.1	39 ± 7	[2] NAIK	08	CLEO	$\psi(2S) \to \gamma\Sigma^+\overline{\Sigma}^-$
• • • We do not use the following data for averages, fits, limits, etc. • • •					
4.5 ±0.5 ±0.1	148	[3,4] ABLIKIM	13H	BES3	$\psi(2S) \to \gamma\Sigma^+\overline{\Sigma}^-$

[1] ABLIKIM 18V reports $[\Gamma(\chi_{c0}(1P) \to \Sigma^+\overline{\Sigma}^-)/\Gamma_{total}] \times [B(\psi(2S) \to \gamma\chi_{c0}(1P))] = (4.99 \pm 0.24 \pm 0.24) \times 10^{-5}$ which we divide by our best value $B(\psi(2S) \to \gamma\chi_{c0}(1P)) = (9.79 \pm 0.20) \times 10^{-2}$. Our first error is their experiment's error and our second error is the systematic error from using our best value.

[2] NAIK 08 reports $(3.25 \pm 0.57 \pm 0.43) \times 10^{-4}$ from a measurement of $[\Gamma(\chi_{c0}(1P) \to \Sigma^+\overline{\Sigma}^-)/\Gamma_{total}] \times [B(\psi(2S) \to \gamma\chi_{c0}(1P))]$ assuming $B(\psi(2S) \to \gamma\chi_{c0}(1P)) = (9.22 \pm 0.11 \pm 0.46) \times 10^{-2}$, which we rescale to our best value $B(\psi(2S) \to \gamma\chi_{c0}(1P)) = (9.79 \pm 0.20) \times 10^{-2}$. Our first error is their experiment's error and our second error is the systematic error from using our best value.

[3] ABLIKIM 13H reports $(4.54 \pm 0.42 \pm 0.30) \times 10^{-4}$ from a measurement of $[\Gamma(\chi_{c0}(1P) \to \Sigma^+\overline{\Sigma}^-)/\Gamma_{total}] \times [B(\psi(2S) \to \gamma\chi_{c0}(1P))]$ assuming $B(\psi(2S) \to \gamma\chi_{c0}(1P)) = (9.62 \pm 0.31) \times 10^{-2}$, which we rescale to our best value $B(\psi(2S) \to \gamma\chi_{c0}(1P)) = (9.79 \pm 0.20) \times 10^{-2}$. Our first error is their experiment's error and our second error is the systematic error from using our best value.

[4] Superseded by ABLIKIM 18V

$\Gamma(\Sigma^-\overline{\Sigma}^+)/\Gamma_{total}$ — Γ_{85}/Γ

VALUE (units 10^{-4})	EVTS	DOCUMENT ID		TECN	COMMENT
5.1±0.2±0.4	2143	[1] ABLIKIM	20I	BES3	$\psi(2S) \to \gamma\Sigma^-\overline{\Sigma}^+$

[1] ABLIKIM 20I reports $(5.13 \pm 0.24 \pm 0.41) \times 10^{-4}$ from a measurement of $[\Gamma(\chi_{c0}(1P) \to \Sigma^-\overline{\Sigma}^+)/\Gamma_{total}] \times [B(\psi(2S) \to \gamma\chi_{c0}(1P))]$ assuming $B(\psi(2S) \to \gamma\chi_{c0}(1P)) = (9.79 \pm 0.20) \times 10^{-2}$.

$\Gamma(\Sigma(1385)^+\overline{\Sigma}(1385)^-)/\Gamma_{total}$ — Γ_{86}/Γ

VALUE (units 10^{-5})	EVTS	DOCUMENT ID		TECN	COMMENT
16.2±5.8±0.3	27	[1] ABLIKIM	12I	BES3	$\psi(2S) \to \gamma\Lambda\overline{\Lambda}\pi^+\pi^-$

[1] ABLIKIM 12I reports $(16.4 \pm 5.7 \pm 1.6) \times 10^{-5}$ from a measurement of $[\Gamma(\chi_{c0}(1P) \to \Sigma(1385)^+\overline{\Sigma}(1385)^-)/\Gamma_{total}] \times [B(\psi(2S) \to \gamma\chi_{c0}(1P))]$ assuming $B(\psi(2S) \to \gamma\chi_{c0}(1P)) = (9.68 \pm 0.31) \times 10^{-2}$, which we rescale to our best value $B(\psi(2S) \to \gamma\chi_{c0}(1P)) = (9.79 \pm 0.20) \times 10^{-2}$. Our first error is their experiment's error and our second error is the systematic error from using our best value.

$\Gamma(\Sigma(1385)^-\overline{\Sigma}(1385)^+)/\Gamma_{total}$ — Γ_{87}/Γ

VALUE (units 10^{-5})	EVTS	DOCUMENT ID		TECN	COMMENT
23.2±6.5±0.5	33	[1] ABLIKIM	12I	BES3	$\psi(2S) \to \gamma\Lambda\overline{\Lambda}\pi^+\pi^-$

[1] ABLIKIM 12I reports $(23.5 \pm 6.2 \pm 2.3) \times 10^{-5}$ from a measurement of $[\Gamma(\chi_{c0}(1P) \to \Sigma(1385)^-\overline{\Sigma}(1385)^+)/\Gamma_{total}] \times [B(\psi(2S) \to \gamma\chi_{c0}(1P))]$ assuming $B(\psi(2S) \to \gamma\chi_{c0}(1P)) = (9.68 \pm 0.31) \times 10^{-2}$, which we rescale to our best value $B(\psi(2S) \to \gamma\chi_{c0}(1P)) = (9.79 \pm 0.20) \times 10^{-2}$. Our first error is their experiment's error and our second error is the systematic error from using our best value.

$\Gamma(K^-\Lambda\overline{\Xi}^+ + \text{c.c.})/\Gamma_{total}$ — Γ_{88}/Γ

VALUE (units 10^{-4})	EVTS	DOCUMENT ID		TECN	COMMENT
1.94±0.35±0.04	57	[1] ABLIKIM	15I	BES3	$\psi(2S) \to \gamma K^-\Lambda\overline{\Xi}^+ + \text{c.c.}$

[1] ABLIKIM 15I reports $[\Gamma(\chi_{c0}(1P) \to K^-\Lambda\overline{\Xi}^+ + \text{c.c.})/\Gamma_{total}] \times [B(\psi(2S) \to \gamma\chi_{c0}(1P))] = (1.90 \pm 0.30 \pm 0.16) \times 10^{-5}$ which we divide by our best value $B(\psi(2S) \to \gamma\chi_{c0}(1P)) = (9.79 \pm 0.20) \times 10^{-2}$. Our first error is their experiment's error and our second error is the systematic error from using our best value.

$\Gamma(\Xi^0\overline{\Xi}^0)/\Gamma_{total}$ — Γ_{89}/Γ

VALUE (units 10^{-4})	EVTS	DOCUMENT ID		TECN	COMMENT
3.1±0.8±0.1	23.3±4.9	[1] NAIK	08	CLEO	$\psi(2S) \to \gamma\Xi^0\overline{\Xi}^0$

[1] NAIK 08 reports $(3.34 \pm 0.70 \pm 0.48) \times 10^{-4}$ from a measurement of $[\Gamma(\chi_{c0}(1P) \to \Xi^0\overline{\Xi}^0)/\Gamma_{total}] \times [B(\psi(2S) \to \gamma\chi_{c0}(1P))]$ assuming $B(\psi(2S) \to \gamma\chi_{c0}(1P)) = (9.22 \pm 0.11 \pm 0.46) \times 10^{-2}$, which we rescale to our best value $B(\psi(2S) \to \gamma\chi_{c0}(1P)) = (9.79 \pm 0.20) \times 10^{-2}$. Our first error is their experiment's error and our second error is the systematic error from using our best value.

$\Gamma(\Xi^-\overline{\Xi}^+)/\Gamma_{total}$ — Γ_{90}/Γ

VALUE (units 10^{-4})	CL%	EVTS	DOCUMENT ID		TECN	COMMENT
4.8±0.7±0.1		95 ± 11	[1] NAIK	08	CLEO	$\psi(2S) \to \gamma\Xi^+\overline{\Xi}^-$
• • • We do not use the following data for averages, fits, limits, etc. • • •						
<10.3	90		[2] ABLIKIM	06D	BES2	$\psi(2S) \to \chi_{c0}\gamma$

[1] NAIK 08 reports $(5.14 \pm 0.60 \pm 0.47) \times 10^{-4}$ from a measurement of $[\Gamma(\chi_{c0}(1P) \to \Xi^-\overline{\Xi}^+)/\Gamma_{total}] \times [B(\psi(2S) \to \gamma\chi_{c0}(1P))]$ assuming $B(\psi(2S) \to \gamma\chi_{c0}(1P)) = (9.22 \pm 0.11 \pm 0.46) \times 10^{-2}$, which we rescale to our best value $B(\psi(2S) \to \gamma\chi_{c0}(1P)) = (9.79 \pm 0.20) \times 10^{-2}$. Our first error is their experiment's error and our second error is the systematic error from using our best value.

[2] Using $B(\psi(2S) \to \chi_{c0}\gamma) = (9.2 \pm 0.5)\%$

$\Gamma(\eta_c\pi^+\pi^-)/\Gamma_{total}$ — Γ_{91}/Γ

VALUE	CL%	DOCUMENT ID		TECN	COMMENT
< 7 × 10⁻⁴	90	[1,2] ABLIKIM	13B	BES3	$e^+e^- \to \psi(2S) \to \gamma\chi_{c0}$
• • • We do not use the following data for averages, fits, limits, etc. • • •					
$<41 \times 10^{-4}$	90	[1,3] ABLIKIM	13B	BES3	$e^+e^- \to \psi(2S) \to \gamma\chi_{c0}$

[1] Using 1.06×10^8 $\psi(2S)$ mesons and $B(\psi(2S) \to \chi_{c0}\gamma) = (9.68 \pm 0.31)\%$.

[2] From the $\eta_c \to K^0_S K^\pm\pi^\mp$ decays.

[3] From the $\eta_c \to K^+K^-\pi^0$ decays.

$\Gamma(p\overline{p})/\Gamma_{total} \times \Gamma(\pi\pi)/\Gamma_{total}$ — $\Gamma_{58}/\Gamma \times \Gamma_{32}/\Gamma$

VALUE (units 10^{-7})	DOCUMENT ID		TECN	COMMENT
18.8±1.0 OUR FIT				
15.3±2.4±0.8	[1] ANDREOTTI	03	E835	$\overline{p}p \to \chi_{c0} \to \pi^0\pi^0$

[1] We have multiplied $B(p\overline{p})\cdot B(\pi^0\pi^0)$ measurement by 3 to obtain $B(p\overline{p})\cdot B(\pi\pi)$.

$\Gamma(p\overline{p})/\Gamma_{total} \times \Gamma(\pi^0\eta)/\Gamma_{total}$ — $\Gamma_{58}/\Gamma \times \Gamma_{33}/\Gamma$

VALUE (units 10^{-7})	DOCUMENT ID		TECN	COMMENT
<0.4	ANDREOTTI	05C	E835	$\overline{p}p \to \pi^0\eta$

$\Gamma(p\overline{p})/\Gamma_{total} \times \Gamma(\pi^0\eta')/\Gamma_{total}$ — $\Gamma_{58}/\Gamma \times \Gamma_{34}/\Gamma$

VALUE (units 10^{-7})	DOCUMENT ID		TECN	COMMENT
<2.5	ANDREOTTI	05C	E835	$\overline{p}p \to \pi^0\eta$

$\Gamma(p\overline{p})/\Gamma_{total} \times \Gamma(\eta\eta)/\Gamma_{total}$ — $\Gamma_{58}/\Gamma \times \Gamma_{36}/\Gamma$

VALUE (units 10^{-7})	DOCUMENT ID		TECN	COMMENT
6.7±0.5 OUR FIT				
$4.0 \pm 1.2^{+0.5}_{-0.3}$	ANDREOTTI	05C	E835	$\overline{p}p \to \eta\eta$

$\Gamma(p\overline{p})/\Gamma_{total} \times \Gamma(\eta\eta')/\Gamma_{total}$ — $\Gamma_{58}/\Gamma \times \Gamma_{37}/\Gamma$

VALUE (units 10^{-6})	DOCUMENT ID		TECN	COMMENT
• • • We do not use the following data for averages, fits, limits, etc. • • •				
$2.1^{+2.3}_{-1.5}$	ANDREOTTI	05C	E835	$\overline{p}p \to \pi^0\eta$

RADIATIVE DECAYS

$\Gamma(\gamma J/\psi(1S))/\Gamma_{total}$ — Γ_{92}/Γ

VALUE (units 10^{-2})	EVTS	DOCUMENT ID		TECN	COMMENT
1.40±0.05 OUR FIT					
• • • We do not use the following data for averages, fits, limits, etc. • • •					
0.25±0.16±2.15	12k	[1] ABLIKIM	17U	BES3	$e^+e^- \to \gamma X$
2.0 ±0.2 ±0.2		[2] ADAM	05A	CLEO	$e^+e^- \to \psi(2S) \to \gamma\chi_{c0}$

[1] Not independent from $B(\psi(2S) \to \gamma\chi_{c0}(1P))$ and the product $B(\psi(2S) \to \gamma\chi_{c0}(1P)) \times B(\chi_{c0}(1P) \to \gamma J/\psi(1S))$ also measured in ABLIKIM 17U.

[2] Uses $B(\psi(2S) \to \gamma\chi_{c0} \to \gamma\gamma J/\psi)$ from ADAM 05A and $B(\psi(2S) \to \gamma\chi_{c0})$ from ATHAR 04.

$\Gamma(\gamma\rho^0)/\Gamma_{total}$ — Γ_{93}/Γ

VALUE (units 10^{-6})	CL%	EVTS	DOCUMENT ID		TECN	COMMENT
< 9	90	1.2 ± 4.5	[1] BENNETT	08A	CLEO	$\psi(2S) \to \gamma\gamma\rho^0$
• • • We do not use the following data for averages, fits, limits, etc. • • •						
<10	90	6 ± 12	[2] ABLIKIM	11E	BES3	$\psi(2S) \to \gamma\gamma\rho^0$

[1] BENNETT 08A reports $< 9.6 \times 10^{-6}$ from a measurement of $[\Gamma(\chi_{c0}(1P) \to \gamma\rho^0)/\Gamma_{total}] \times [B(\psi(2S) \to \gamma\chi_{c0}(1P))]$ assuming $B(\psi(2S) \to \gamma\chi_{c0}(1P)) = (9.2 \pm 0.4) \times 10^{-2}$, which we rescale to our best value $B(\psi(2S) \to \gamma\chi_{c0}(1P)) = 9.79 \times 10^{-2}$.

[2] ABLIKIM 11E reports $< 10.5 \times 10^{-6}$ from a measurement of $[\Gamma(\chi_{c0}(1P) \to \gamma\rho^0)/\Gamma_{total}] \times [B(\psi(2S) \to \gamma\chi_{c0}(1P))]$ assuming $B(\psi(2S) \to \gamma\chi_{c0}(1P)) = (9.62 \pm 0.31) \times 10^{-2}$, which we rescale to our best value $B(\psi(2S) \to \gamma\chi_{c0}(1P)) = 9.79 \times 10^{-2}$.

$\Gamma(\gamma\omega)/\Gamma_{total}$ — Γ_{94}/Γ

VALUE (units 10^{-6})	CL%	EVTS	DOCUMENT ID		TECN	COMMENT
< 8	90	0.0 ± 2.8	[1] BENNETT	08A	CLEO	$\psi(2S) \to \gamma\gamma\omega$
• • • We do not use the following data for averages, fits, limits, etc. • • •						
<13	90	5 ± 11	[2] ABLIKIM	11E	BES3	$\psi(2S) \to \gamma\gamma\omega$

[1] BENNETT 08A reports $< 8.8 \times 10^{-6}$ from a measurement of $[\Gamma(\chi_{c0}(1P) \to \gamma\omega)/\Gamma_{total}] \times [B(\psi(2S) \to \gamma\chi_{c0}(1P))]$ assuming $B(\psi(2S) \to \gamma\chi_{c0}(1P)) = (9.2 \pm 0.4) \times 10^{-2}$, which we rescale to our best value $B(\psi(2S) \to \gamma\chi_{c0}(1P)) = 9.79 \times 10^{-2}$.

[2] ABLIKIM 11E reports $< 12.9 \times 10^{-6}$ from a measurement of $[\Gamma(\chi_{c0}(1P) \to \gamma\omega)/\Gamma_{total}] \times [B(\psi(2S) \to \gamma\chi_{c0}(1P))]$ assuming $B(\psi(2S) \to \gamma\chi_{c0}(1P)) = (9.62 \pm 0.31) \times 10^{-2}$, which we rescale to our best value $B(\psi(2S) \to \gamma\chi_{c0}(1P)) = 9.79 \times 10^{-2}$.

Downloaded from https://academic.oup.com/ptep/article/2022/8/083C01/6651666 by KIT Library user on 27 September 2022

$\Gamma(\gamma\phi)/\Gamma_{total}$ — Γ_{95}/Γ

VALUE (units 10^{-6})	CL%	EVTS	DOCUMENT ID		TECN	COMMENT
< 6	90	0.1 ± 1.6	[1] BENNETT	08A	CLEO	$\psi(2S) \to \gamma\gamma\phi$
• • • We do not use the following data for averages, fits, limits, etc. • • •						
<16	90	15 ± 7	[2] ABLIKIM	11E	BES3	$\psi(2S) \to \gamma\gamma\phi$

[1] BENNETT 08A reports $< 6.4 \times 10^{-6}$ from a measurement of $[\Gamma(\chi_{c0}(1P) \to \gamma\phi)/\Gamma_{total}] \times [B(\psi(2S) \to \gamma\chi_{c0}(1P))]$ assuming $B(\psi(2S) \to \gamma\chi_{c0}(1P)) = (9.2 \pm 0.4) \times 10^{-2}$, which we rescale to our best value $B(\psi(2S) \to \gamma\chi_{c0}(1P)) = 9.79 \times 10^{-2}$.

[2] ABLIKIM 11E reports $< 16.2 \times 10^{-6}$ from a measurement of $[\Gamma(\chi_{c0}(1P) \to \gamma\phi)/\Gamma_{total}] \times [B(\psi(2S) \to \gamma\chi_{c0}(1P))]$ assuming $B(\psi(2S) \to \gamma\chi_{c0}(1P)) = (9.62 \pm 0.31) \times 10^{-2}$, which we rescale to our best value $B(\psi(2S) \to \gamma\chi_{c0}(1P)) = 9.79 \times 10^{-2}$.

$\Gamma(\gamma\gamma)/\Gamma_{total}$ — Γ_{96}/Γ

VALUE (units 10^{-4})	CL%	DOCUMENT ID		TECN	COMMENT
2.04±0.09 OUR FIT					
• • • We do not use the following data for averages, fits, limits, etc. • • •					
<7	90	[1] WICHT	08	BELL	$B^{\pm} \to K^{\pm}\gamma\gamma$

[1] WICHT 08 reports $[\Gamma(\chi_{c0}(1P) \to \gamma\gamma)/\Gamma_{total}] \times [B(B^+ \to \chi_{c0} K^+)] < 0.11 \times 10^{-6}$ which we divide by our best value $B(B^+ \to \chi_{c0} K^+) = 1.51 \times 10^{-4}$.

$\Gamma(e^+e^- J/\psi(1S))/\Gamma_{total}$ — Γ_{97}/Γ

VALUE (units 10^{-4})	EVTS	DOCUMENT ID		TECN	COMMENT
• • • We do not use the following data for averages, fits, limits, etc. • • •					
1.54±0.33±0.03	56	[1,2] ABLIKIM	17I	BES3	$\psi(2S) \to \gamma e^+e^- J/\psi$

[1] ABLIKIM 17I reports $(1.51 \pm 0.30 \pm 0.13) \times 10^{-4}$ from a measurement of $[\Gamma(\chi_{c0}(1P) \to e^+e^- J/\psi(1S))/\Gamma_{total}] \times [B(\psi(2S) \to \gamma\chi_{c0}(1P))]$ assuming $B(\psi(2S) \to \gamma\chi_{c0}(1P)) = (9.99 \pm 0.27) \times 10^{-2}$, which we rescale to our best value $B(\psi(2S) \to \gamma\chi_{c0}(1P)) = (9.79 \pm 0.20) \times 10^{-2}$. Our first error is their experiment's error and our second error is the systematic error from using our best value.

[2] Not independent from other measurements reported by ABLIKIM 17I

$\Gamma(e^+e^- J/\psi(1S))/\Gamma(\gamma J/\psi(1S))$ — Γ_{97}/Γ_{92}

VALUE (units 10^{-3})	EVTS	DOCUMENT ID		TECN	COMMENT
9.5±1.9±0.7	56	[1] ABLIKIM	17I	BES3	$\psi(2S) \to e^+e^-\gamma J/\psi$

[1] Uses $B(\psi(2S) \to \gamma\chi_{c0}(1P)) \times B(\chi_{c0}(1P) \to \gamma J/\psi(1S)) = (15.8 \pm 0.3 \pm 0.6) \times 10^{-4}$ from ABLIKIM 17N and accounts for common systematic errors.

$\Gamma(\mu^+\mu^- J/\psi(1S))/\Gamma(e^+e^- J/\psi(1S))$ — Γ_{98}/Γ_{97}

VALUE	CL%	EVTS	DOCUMENT ID		TECN	COMMENT
<0.14	90	<9.5	ABLIKIM	19Z	BES3	$\psi(2S) \to \gamma\chi_c \to \gamma(\mu^+\mu^- J/\psi)$

$\Gamma(\gamma\gamma)/\Gamma(\gamma J/\psi(1S))$ — Γ_{96}/Γ_{92}

VALUE (units 10^{-2})	DOCUMENT ID		TECN	COMMENT
1.45±0.08 OUR FIT				
2.0 ±0.4 OUR AVERAGE				
$2.2 \pm 0.4^{+0.1}_{-0.2}$	[1] ANDREOTTI	04	E835	$\overline{p}p \to \chi_{c0} \to \gamma\gamma$
1.45±0.74	[2] AMBROGIANI	00B	E835	$\overline{p}p \to \chi_{c2} \to \gamma\gamma, \gamma J/\psi$

[1] The values of $B(p\overline{p})B(\gamma\gamma)$ and $B(\gamma\gamma)B(\gamma J/\psi)$ measured by ANDREOTTI 04 are not independent. The latter is used in the fit because of smaller systematics.

[2] Calculated by us using $B(J/\psi(1S) \to e^+e^-) = 0.0593 \pm 0.0010$.

$\Gamma(p\overline{p})/\Gamma_{total} \times \Gamma(\gamma J/\psi(1S))/\Gamma_{total}$ — $\Gamma_{58}/\Gamma \times \Gamma_{92}/\Gamma$

VALUE (units 10^{-7})	EVTS	DOCUMENT ID		TECN	COMMENT
31.1±1.5 OUR FIT					
28.2±2.1 OUR AVERAGE					
28.0±1.9±1.3	392	[1,2,3] BAGNASCO	02	E835	$\overline{p}p \to \chi_{c0} \to J/\psi\gamma$
$29.3^{+5.7}_{-4.7} \pm 1.5$	89	[1,2] AMBROGIANI	99B		$\overline{p}p \to \chi_{c0} \to J/\psi\gamma$

[1] Values in $(\Gamma(p\overline{p}) \times \Gamma(\gamma J/\psi(1S))/\Gamma_{total})$ and $(\Gamma(p\overline{p})/\Gamma_{total} \times \Gamma(\gamma J/\psi(1S))/\Gamma_{total})$ are not independent. The latter is used in the fit since it is less correlated to the total width.

[2] Calculated by us using $B(J/\psi(1S) \to e^+e^-) = 0.0593 \pm 0.0010$.

[3] Recalculated by ANDREOTTI 05A.

$\Gamma(p\overline{p})/\Gamma_{total} \times \Gamma(\gamma\gamma)/\Gamma_{total}$ — $\Gamma_{58}/\Gamma \times \Gamma_{96}/\Gamma$

VALUE (units 10^{-8})	DOCUMENT ID		TECN	COMMENT
4.52±0.27 OUR FIT				
• • • We do not use the following data for averages, fits, limits, etc. • • •				
$6.52 \pm 1.18^{+0.48}_{-0.72}$	[1] ANDREOTTI	04	E835	$p\overline{p} \to \chi_{c0} \to \gamma\gamma$

[1] The values of $B(p\overline{p})B(\gamma\gamma)$ and $B(\gamma\gamma)B(\gamma J/\psi)$ measured by ANDREOTTI 04 are not independent. The latter is used in the fit because of smaller systematics.

$\chi_{c0}(1P)$ CROSS-PARTICLE BRANCHING RATIOS

$\Gamma(\chi_{c0}(1P) \to p\overline{p})/\Gamma_{total} \times \Gamma(\psi(2S) \to \gamma\chi_{c0}(1P))/\Gamma_{total}$ — $\Gamma_{58}/\Gamma \times \Gamma_{162}^{\psi(2S)}/\Gamma^{\psi(2S)}$

VALUE (units 10^{-6})	EVTS	DOCUMENT ID		TECN	COMMENT
21.7±0.9 OUR FIT					
23.7±1.0 OUR AVERAGE					
23.7±0.8±0.9	1222	ABLIKIM	13V	BES3	$\psi(2S) \to \gamma p\overline{p}$
23.7±1.4±1.4	383 ± 22	[1] NAIK	08	CLEO	$\psi(2S) \to \gamma p\overline{p}$
$23.6^{+3.7}_{-3.4} \pm 3.4$	89.5^{+14}_{-13}	BAI	04F	BES	$\psi(2S) \to \gamma\chi_{c0}(1P) \to \gamma\overline{p}p$

[1] Calculated by us. NAIK 08 reports $B(\chi_{c0} \to p\overline{p}) = (25.7 \pm 1.5 \pm 1.5 \pm 1.3) \times 10^{-5}$ using $B(\psi(2S) \to \gamma\chi_{c0}) = (9.22 \pm 0.11 \pm 0.46)\%$.

$\Gamma(\chi_{c0}(1P) \to p\overline{p})/\Gamma_{total} \times \Gamma(\psi(2S) \to \gamma\chi_{c0}(1P))/\Gamma(\psi(2S) \to J/\psi(1S)\pi^+\pi^-)$ — $\Gamma_{58}/\Gamma \times \Gamma_{162}^{\psi(2S)}/\Gamma_{12}^{\psi(2S)}$

VALUE (units 10^{-5})	DOCUMENT ID		TECN	COMMENT
6.25±0.26 OUR FIT				
4.6 ±1.9	[1] BAI	98I	BES	$\psi(2S) \to \gamma\chi_{c0} \to \gamma\overline{p}p$

[1] Calculated by us. The value for $B(\chi_{c0} \to p\overline{p})$ reported in BAI 98I is derived using $B(\psi(2S) \to \gamma\chi_{c0}) = (9.3 \pm 0.8)\%$ and $B(\psi(2S) \to J/\psi(1S)\pi^+\pi^-) = (32.4 \pm 2.6)\%$ [BAI 98D].

$\Gamma(\chi_{c0}(1P) \to \Lambda\overline{\Lambda})/\Gamma_{total} \times \Gamma(\psi(2S) \to \gamma\chi_{c0}(1P))/\Gamma_{total}$ — $\Gamma_{71}/\Gamma \times \Gamma_{162}^{\psi(2S)}/\Gamma^{\psi(2S)}$

VALUE (units 10^{-6})	EVTS	DOCUMENT ID		TECN	COMMENT
35.2±1.3 OUR FIT					
35.1±1.4 OUR AVERAGE Error includes scale factor of 1.1.					
35.6±1.0±1.0	1486	ABLIKIM	21L	BES3	$\psi(2S) \to \gamma p\pi^-\overline{p}\pi^+$
31.2±3.3±2.0	131	[1] NAIK	08	CLEO	$\psi(2S) \to \gamma\Lambda\overline{\Lambda}$
• • • We do not use the following data for averages, fits, limits, etc. • • •					
32.0±1.9±2.2	369	[2,3] ABLIKIM	13H	BES3	$\psi(2S) \to \gamma\Lambda\overline{\Lambda}$

[1] Calculated by us. NAIK 08 reports $B(\chi_{c0} \to \Lambda\overline{\Lambda}) = (33.8 \pm 3.6 \pm 2.2 \pm 1.7) \times 10^{-5}$ using $B(\psi(2S) \to \gamma\chi_{c0}) = (9.22 \pm 0.11 \pm 0.46)\%$.

[2] Superseded by ABLIKIM 21L

[3] Calculated by us. ABLIKIM 13H reports $B(\chi_{c0} \to \Lambda\overline{\Lambda}) = (33.3 \pm 2.0 \pm 2.6) \times 10^{-5}$ from a measurement of $B(\chi_{c0} \to \Lambda\overline{\Lambda}) \times B(\psi(2S) \to \gamma\chi_{c0})$ assuming $B(\psi(2S) \to \gamma\chi_{c0}) = (9.62 \pm 0.31)\%$.

$\Gamma(\chi_{c0}(1P) \to \Lambda\overline{\Lambda})/\Gamma_{total} \times \Gamma(\psi(2S) \to \gamma\chi_{c0}(1P))/\Gamma(\psi(2S) \to J/\psi(1S)\pi^+\pi^-)$ — $\Gamma_{71}/\Gamma \times \Gamma_{162}^{\psi(2S)}/\Gamma_{12}^{\psi(2S)}$

VALUE (units 10^{-5})	EVTS	DOCUMENT ID		TECN	COMMENT
10.1±0.4 OUR FIT					
$\mathbf{13.0^{+3.6}_{-3.5} \pm 2.5}$	$15.2^{+4.2}_{-4.0}$	[1] BAI	03E	BES	$\psi(2S) \to \gamma\Lambda\overline{\Lambda}$

[1] BAI 03E reports $[B(\chi_{c0} \to \Lambda\overline{\Lambda}) B(\psi(2S) \to \gamma\chi_{c0}) / B(\psi(2S) \to J/\psi\pi^+\pi^-)] \times [B^2(\Lambda \to \pi^-p) / B(J/\psi \to p\overline{p})] = (2.45^{+0.68}_{-0.65} \pm 0.46)\%$. We calculate from this measurement the presented value using $B(\Lambda \to \pi^-p) = (63.9 \pm 0.5)\%$ and $B(J/\psi \to p\overline{p}) = (2.17 \pm 0.07) \times 10^{-3}$.

$\Gamma(\chi_{c0}(1P) \to \gamma J/\psi(1S))/\Gamma_{total} \times \Gamma(\psi(2S) \to \gamma\chi_{c0}(1P))/\Gamma_{total}$ — $\Gamma_{92}/\Gamma \times \Gamma_{162}^{\psi(2S)}/\Gamma^{\psi(2S)}$

VALUE (units 10^{-2})	EVTS	DOCUMENT ID		TECN	COMMENT
0.138±0.005 OUR FIT					
0.147±0.029 OUR AVERAGE Error includes scale factor of 4.6.					
0.158±0.003±0.006	4.8k	[1] ABLIKIM	17N	BES3	$\psi(2S) \to \gamma\gamma J/\psi$
0.024±0.015±0.205	12k	ABLIKIM	17U	BES3	$e^+e^- \to \gamma X$
0.069±0.018		[2] OREGLIA	82	CBAL	$\psi(2S) \to \gamma\chi_{c0}$
0.4 ±0.3		[3] BRANDELIK	79B	DASP	$\psi(2S) \to \gamma\chi_{c0}$
0.16 ±0.11		[3] BARTEL	78B	CNTR	$\psi(2S) \to \gamma\chi_{c0}$
3.3 ±1.7		[4] BIDDICK	77	CNTR	$e^+e^- \to \gamma X$
• • • We do not use the following data for averages, fits, limits, etc. • • •					
0.151±0.003±0.010	4.3k	[5] ABLIKIM	12O	BES3	$\psi(2S) \to \gamma\chi_{c0}$
0.125±0.007±0.013	560	[6] MENDEZ	08	CLEO	$\psi(2S) \to \gamma\chi_{c0}$
0.18 ±0.01 ±0.02	172	[7] ADAM	05A	CLEO	Repl. by MENDEZ 08

[1] Uses $B(J/\psi \to e^+e^-) = (5.971 \pm 0.032)\%$ and $B(J/\psi \to \mu^+\mu^-) = (5.961 \pm 0.033)\%$.

[2] Recalculated by us using $B(J/\psi(1S) \to \ell^+\ell^-) = 0.1181 \pm 0.0020$.

[3] Recalculated by us using $B(J/\psi(1S) \to \mu^+\mu^-) = 0.0588 \pm 0.0010$.

[4] Assumes isotropic gamma distribution.

[5] Superseded by ABLIKIM 17N.

[6] Not independent from other measurements of MENDEZ 08.

[7] Not independent from other values reported by ADAM 05A.

Downloaded from https://academic.oup.com/ptep/article/2022/8/083C01/6651666 by KIT Library user on 27 September 2022

$\Gamma(\chi_{c0}(1P)\to\gamma J/\psi(1S))/\Gamma_{total}\times\Gamma(\psi(2S)\to\gamma\chi_{c0}(1P))/\Gamma(\psi(2S)\to J/\psi(1S)\text{anything})$ — $\Gamma_{92}/\Gamma\times\Gamma_{162}^{\psi(2S)}/\Gamma_{10}^{\psi(2S)}$

$\Gamma_{92}/\Gamma\times\Gamma_{162}^{\psi(2S)}/\Gamma_{10}^{\psi(2S)}=\Gamma_{92}/\Gamma\times\Gamma_{162}^{\psi(2S)}/(\Gamma_{12}^{\psi(2S)}+\Gamma_{13}^{\psi(2S)}+\Gamma_{14}^{\psi(2S)}+0.343\Gamma_{163}^{\psi(2S)}+0.190\Gamma_{164}^{\psi(2S)})$

VALUE (units 10^{-2})	EVTS	DOCUMENT ID		TECN	COMMENT
0.224±0.009 OUR FIT					
• • • We do not use the following data for averages, fits, limits, etc. • • •					
0.201±0.011±0.021	560	[1] MENDEZ	08	CLEO	$\psi(2S)\to\gamma\chi_{c0}$
0.31 ±0.02 ±0.03	172	ADAM	05A	CLEO	Repl. by MENDEZ 08

[1] Not independent from other measurements of MENDEZ 08.

$\Gamma(\chi_{c0}(1P)\to\gamma J/\psi(1S))/\Gamma_{total}\times\Gamma(\psi(2S)\to\gamma\chi_{c0}(1P))/\Gamma(\psi(2S)\to J/\psi(1S)\pi^+\pi^-)$ — $\Gamma_{92}/\Gamma\times\Gamma_{162}^{\psi(2S)}/\Gamma_{12}^{\psi(2S)}$

VALUE (units 10^{-2})	EVTS	DOCUMENT ID		TECN	COMMENT
0.397±0.015 OUR FIT					
0.358±0.020±0.037	560	MENDEZ	08	CLEO	$\psi(2S)\to\gamma\chi_{c0}$
• • • We do not use the following data for averages, fits, limits, etc. • • •					
0.55 ±0.04 ±0.06	172	[1] ADAM	05A	CLEO	Repl. by MENDEZ 08

[1] Not independent from other values reported by ADAM 05A.

$\Gamma(\chi_{c0}(1P)\to\gamma\gamma)/\Gamma_{total}\times\Gamma(\psi(2S)\to\gamma\chi_{c0}(1P))/\Gamma_{total}$ — $\Gamma_{96}/\Gamma\times\Gamma_{162}^{\psi(2S)}/\Gamma^{\psi(2S)}$

VALUE (units 10^{-5})	EVTS	DOCUMENT ID		TECN	COMMENT
2.00±0.08 OUR FIT					
1.95±0.09 OUR AVERAGE					
1.93±0.08±0.05	3.5k	ABLIKIM	17AE	BES3	$\psi(2S)\to\gamma\chi_{c0}\to 3\gamma$
2.17±0.32±0.10	0.2k	ECKLUND	08A	CLEO	$\psi(2S)\to\gamma\chi_{c0}\to 3\gamma$
3.7 ±1.8 ±1.0		LEE	85	CBAL	$\psi(2S)\to\gamma\chi_{c0}$
• • • We do not use the following data for averages, fits, limits, etc. • • •					
2.17±0.17±0.12	0.8k	[1] ABLIKIM	12A	BES3	$\psi(2S)\to\gamma\chi_{c0}\to 3\gamma$

[1] Superseded by ABLIKIM 17AE.

$\Gamma(\chi_{c0}(1P)\to\pi\pi)/\Gamma_{total}\times\Gamma(\psi(2S)\to\gamma\chi_{c0}(1P))/\Gamma_{total}$ — $\Gamma_{32}/\Gamma\times\Gamma_{162}^{\psi(2S)}/\Gamma^{\psi(2S)}$

VALUE (units 10^{-4})	EVTS	DOCUMENT ID		TECN	COMMENT
8.34±0.29 OUR FIT					
8.80±0.34 OUR AVERAGE					
9.11±0.08±0.65	17k	[1] ABLIKIM	10A	BES3	$e^+e^-\to\psi(2S)\to\gamma\chi_{c0}$
8.81±0.11±0.43	8.9k	[2] ASNER	09	CLEO	$\psi(2S)\to\gamma\pi^+\pi^-$
8.13±0.19±0.89	2.8k	[3] ASNER	09	CLEO	$\psi(2S)\to\gamma\pi^0\pi^0$

[1] Calculated by us. ABLIKIM 10A reports $B(\chi_{c0}\to\pi^0\pi^0)=(3.23\pm0.03\pm0.23\pm0.14)\times10^{-3}$ using $B(\psi(2S)\to\gamma\chi_{c0})=(9.4\pm0.4)\%$. We have multiplied the $\pi^0\pi^0$ measurement by 3 to obtain $\pi\pi$.

[2] Calculated by us. ASNER 09 reports $B(\chi_{c0}\to\pi^+\pi^-)=(6.37\pm0.08\pm0.31\pm0.32)\times10^{-3}$ using $B(\psi(2S)\to\gamma\chi_{c0})=(9.22\pm0.11\pm0.46)\%$. We have multiplied the $\pi^+\pi^-$ measurement by 3/2 to obtain $\pi\pi$.

[3] Calculated by us. ASNER 09 reports $B(\chi_{c0}\to\pi^0\pi^0)=(2.94\pm0.07\pm0.32\pm0.15)\times10^{-3}$ using $B(\psi(2S)\to\gamma\chi_{c0})=(9.22\pm0.11\pm0.46)\%$. We have multiplied the $\pi^0\pi^0$ measurement by 3 to obtain $\pi\pi$.

$\Gamma(\chi_{c0}(1P)\to\pi\pi)/\Gamma_{total}\times\Gamma(\psi(2S)\to\gamma\chi_{c0}(1P))/\Gamma(\psi(2S)\to J/\psi(1S)\pi^+\pi^-)$ — $\Gamma_{32}/\Gamma\times\Gamma_{162}^{\psi(2S)}/\Gamma_{12}^{\psi(2S)}$

VALUE (units 10^{-4})	EVTS	DOCUMENT ID		TECN	COMMENT
24.0±0.8 OUR FIT					
20.7±1.7 OUR AVERAGE					
23.9±2.7±4.1	97 ± 11	[1] BAI	03C	BES	$\psi(2S)\to\gamma\chi_{c0}\to\gamma\pi^0\pi^0$
20.2±1.1±1.5	720 ± 32	[2] BAI	98I	BES	$\psi(2S)\to\gamma\chi_{c0}\to\gamma\pi^+\pi^-$

[1] We have multiplied $\pi^0\pi^0$ measurement by 3 to obtain $\pi\pi$.

[2] Calculated by us. The value for $B(\chi_{c0}\to\pi^+\pi^-)$ reported in BAI 98I is derived using $B(\psi'\to\gamma\chi_{c0})=(9.3\pm0.8)\%$ and $B(\psi'\to J/\psi\pi^+\pi^-)=(32.4\pm2.6)\%$ [BAI 98D]. We have multiplied $\pi^+\pi^-$ measurement by 3/2 to obtain $\pi\pi$.

$\Gamma(\chi_{c0}(1P)\to\eta\eta)/\Gamma_{total}\times\Gamma(\psi(2S)\to\gamma\chi_{c0}(1P))/\Gamma_{total}$ — $\Gamma_{36}/\Gamma\times\Gamma_{162}^{\psi(2S)}/\Gamma^{\psi(2S)}$

VALUE (units 10^{-4})	EVTS	DOCUMENT ID		TECN	COMMENT
2.95±0.18 OUR FIT					
3.12±0.19 OUR AVERAGE					
3.23±0.09±0.23	2132	[1] ABLIKIM	10A	BES3	$e^+e^-\to\psi(2S)\to\gamma\chi_{c0}$
2.93±0.12±0.29	0.9k	[2] ASNER	09	CLEO	$\psi(2S)\to\gamma\eta\eta$
• • • We do not use the following data for averages, fits, limits, etc. • • •					
2.86±0.46±0.37	48	[3] ADAMS	07	CLEO	$\psi(2S)\to\gamma\chi_{c0}$

[1] Calculated by us. ABLIKIM 10A reports $B(\chi_{c0}\to\eta\eta)=(3.44\pm0.10\pm0.24\pm0.13)\times10^{-3}$ using $B(\psi(2S)\to\gamma\chi_{c0})=(9.4\pm0.4)\%$.

[2] Calculated by us. ASNER 09 reports $B(\chi_{c0}\to\eta\eta)=(3.18\pm0.13\pm0.31\pm0.16)\times10^{-3}$ using $B(\psi(2S)\to\gamma\chi_{c0})=(9.22\pm0.11\pm0.46)\%$.

[3] Superseded by ASNER 09. Calculated by us. The value of $B(\chi_{c0}(1P)\to\eta\eta)$ reported by ADAMS 07 was derived using $B(\psi(2S)\to\gamma\chi_{c0}(1P))=(9.22\pm0.11\pm0.46)\%$ (ATHAR 04).

$\Gamma(\chi_{c0}(1P)\to\eta\eta)/\Gamma_{total}\times\Gamma(\psi(2S)\to\gamma\chi_{c0}(1P))/\Gamma(\psi(2S)\to J/\psi(1S)\pi^+\pi^-)$ — $\Gamma_{36}/\Gamma\times\Gamma_{162}^{\psi(2S)}/\Gamma_{12}^{\psi(2S)}$

VALUE (units 10^{-3})	DOCUMENT ID		TECN	COMMENT
0.85 ±0.05 OUR FIT				
0.578±0.241±0.158	BAI	03C	BES	$\psi(2S)\to\gamma\eta\eta$

$\Gamma(\chi_{c0}(1P)\to K^+K^-)/\Gamma_{total}\times\Gamma(\psi(2S)\to\gamma\chi_{c0}(1P))/\Gamma_{total}$ — $\Gamma_{42}/\Gamma\times\Gamma_{162}^{\psi(2S)}/\Gamma^{\psi(2S)}$

VALUE (units 10^{-4})	EVTS	DOCUMENT ID		TECN	COMMENT
5.92±0.28 OUR FIT					
5.97±0.07±0.32	8.1k	[1] ASNER	09	CLEO	$\psi(2S)\to\gamma K^+K^-$

[1] Calculated by us. ASNER 09 reports $B(\chi_{c0}\to K^+K^-)=(6.47\pm0.08\pm0.35\pm0.32)\times10^{-3}$ using $B(\psi(2S)\to\gamma\chi_{c0})=(9.22\pm0.11\pm0.46)\%$.

$\Gamma(\chi_{c0}(1P)\to K^+K^-)/\Gamma_{total}\times\Gamma(\psi(2S)\to\gamma\chi_{c0}(1P))/\Gamma(\psi(2S)\to J/\psi(1S)\pi^+\pi^-)$ — $\Gamma_{42}/\Gamma\times\Gamma_{162}^{\psi(2S)}/\Gamma_{12}^{\psi(2S)}$

VALUE (units 10^{-3})	EVTS	DOCUMENT ID		TECN	COMMENT
1.71±0.08 OUR FIT					
1.63±0.10±0.15	774 ± 38	[1] BAI	98I	BES	$\psi(2S)\to\gamma K^+K^-$

[1] Calculated by us. The value for $B(\chi_{c0}\to K^+K^-)$ reported by BAI 98I is derived using $B(\psi(2S)\to\gamma\chi_{c0})=(9.3\pm0.8)\%$ and $B(\psi(2S)\to J/\psi\pi^+\pi^-)=(32.4\pm2.6)\%$ [BAI 98D].

$\Gamma(\chi_{c0}(1P)\to K^0_SK^0_S)/\Gamma_{total}\times\Gamma(\psi(2S)\to\gamma\chi_{c0}(1P))/\Gamma_{total}$ — $\Gamma_{43}/\Gamma\times\Gamma_{162}^{\psi(2S)}/\Gamma^{\psi(2S)}$

VALUE (units 10^{-4})	EVTS	DOCUMENT ID		TECN	COMMENT
3.10±0.16 OUR FIT					
3.18±0.17 OUR AVERAGE					
3.22±0.07±0.17	2.1k	[1] ASNER	09	CLEO	$\psi(2S)\to\gamma K^0_SK^0_S$
3.02±0.19±0.33	322	ABLIKIM	05O	BES2	$\psi(2S)\to\gamma K^0_SK^0_S$

[1] Calculated by us. ASNER 09 reports $B(\chi_{c0}\to K^0_SK^0_S)=(3.49\pm0.08\pm0.18\pm0.17)\times10^{-3}$ using $B(\psi(2S)\to\gamma\chi_{c0})=(9.22\pm0.11\pm0.46)\%$.

$\Gamma(\chi_{c0}(1P)\to K^0_SK^0_S)/\Gamma_{total}\times\Gamma(\psi(2S)\to\gamma\chi_{c0}(1P))/\Gamma(\psi(2S)\to J/\psi(1S)\pi^+\pi^-)$ — $\Gamma_{43}/\Gamma\times\Gamma_{162}^{\psi(2S)}/\Gamma_{12}^{\psi(2S)}$

VALUE (units 10^{-4})	DOCUMENT ID		TECN	COMMENT
8.9±0.5 OUR FIT				
5.6±0.8±1.3	[1] BAI	99B	BES	$\psi(2S)\to\gamma K^0_SK^0_S$

[1] Calculated by us. The value of $B(\chi_{c0}\to K^0_SK^0_S)$ reported by BAI 99B was derived using $B(\psi(2S)\to\gamma\chi_{c0}(1P))=(9.3\pm0.8)\%$ and $B(\psi(2S)\to J/\psi\pi^+\pi^-)=(32.4\pm2.6)\%$ [BAI 98D].

$\Gamma(\chi_{c0}(1P)\to 2(\pi^+\pi^-))/\Gamma_{total}\times\Gamma(\psi(2S)\to\gamma\chi_{c0}(1P))/\Gamma(\psi(2S)\to J/\psi(1S)\pi^+\pi^-)$ — $\Gamma_1/\Gamma\times\Gamma_{162}^{\psi(2S)}/\Gamma_{12}^{\psi(2S)}$

VALUE (units 10^{-3})	DOCUMENT ID		TECN	COMMENT
6.6±0.5 OUR FIT				
6.9±2.4 OUR AVERAGE Error includes scale factor of 3.8.				
4.4±0.1±0.9	[1] BAI	99B	BES	$\psi(2S)\to\gamma\chi_{c0}$
9.3±0.9	[2] TANENBAUM	78	MRK1	$\psi(2S)\to\gamma\chi_{c0}$

[1] Calculated by us. The value for $B(\chi_{c0}\to 2\pi^+2\pi^-)$ reported in BAI 99B is derived using $B(\psi(2S)\to\gamma\chi_{c0})=(9.3\pm0.8)\%$ and $B(\psi(2S)\to J/\psi(1S)\pi^+\pi^-)=(32.4\pm2.6)\%$ [BAI 98D].

[2] The value $B(\psi(1S)\to\gamma\chi_{c0})\times B(\chi_{c0}\to 2\pi^+2\pi^-)$ reported in TANENBAUM 78 is derived using $B(\psi(2S)\to J/\psi(1S)\pi^+\pi^-)\times B(J/\psi(1S)\to\ell^+\ell^-)=(4.6\pm0.7)\%$. Calculated by us using $B(J/\psi(1S)\to\ell^+\ell^-)=0.1181\pm0.0020$.

$\Gamma(\chi_{c0}(1P)\to\pi^+\pi^-K^+K^-)/\Gamma_{total}\times\Gamma(\psi(2S)\to\gamma\chi_{c0}(1P))/\Gamma_{total}$ — $\Gamma_8/\Gamma\times\Gamma_{162}^{\psi(2S)}/\Gamma^{\psi(2S)}$

VALUE (units 10^{-3})	DOCUMENT ID		TECN	COMMENT
1.78±0.14 OUR FIT				
1.64±0.05±0.2	ABLIKIM	05Q	BES2	$\psi(2S)\to\gamma\chi_{c0}$

$\Gamma(\chi_{c0}(1P)\to\pi^+\pi^-K^+K^-)/\Gamma_{total}\times\Gamma(\psi(2S)\to\gamma\chi_{c0}(1P))/\Gamma(\psi(2S)\to J/\psi(1S)\pi^+\pi^-)$ — $\Gamma_8/\Gamma\times\Gamma_{162}^{\psi(2S)}/\Gamma_{12}^{\psi(2S)}$

VALUE (units 10^{-3})	DOCUMENT ID		TECN	COMMENT
5.1 ±0.4 OUR FIT				
5.8 ±1.6 OUR AVERAGE Error includes scale factor of 2.3.				
4.22±0.20±0.97	BAI	99B	BES	$\psi(2S)\to\gamma\chi_{c0}$
7.4 ±1.0	[1] TANENBAUM	78	MRK1	$\psi(2S)\to\gamma\chi_{c0}$

[1] The reported value is derived using $B(\psi(2S)\to\pi^+\pi^-J/\psi)\times B(J/\psi\to\ell^+\ell^-)=(4.6\pm0.7)\%$. Calculated by us using $B(J/\psi\to\ell^+\ell^-)=0.1181\pm0.0020$.

$\Gamma(\chi_{c0}(1P)\to K^+K^-K^+K^-)/\Gamma_{total}\times\Gamma(\psi(2S)\to\gamma\chi_{c0}(1P))/\Gamma_{total}$ — $\Gamma_{51}/\Gamma\times\Gamma_{162}^{\psi(2S)}/\Gamma^{\psi(2S)}$

VALUE (units 10^{-4})	EVTS	DOCUMENT ID		TECN	COMMENT
2.76±0.28 OUR FIT					
3.20±0.11±0.41	278	[1] ABLIKIM	06T	BES2	$\psi(2S)\to\gamma 2K^+2K^-$

[1] Calculated by us. The value of $B(\chi_{c0}\to 2K^+2K^-)$ reported by ABLIKIM 06T was derived using $B(\psi(2S)\to\gamma\chi_{c0}(1P))=(9.2\pm0.4)\%$.

Downloaded from https://academic.oup.com/ptep/article/2022/8/083C01/6651666 by KIT Library user on 27 September 2022

$\Gamma(\chi_{c0}(1P) \to K^+K^-K^+K^-)/\Gamma_{total} \times \Gamma(\psi(2S) \to \gamma\chi_{c0}(1P))/\Gamma(\psi(2S) \to J/\psi(1S)\pi^+\pi^-)$ $\quad \Gamma_{51}/\Gamma \times \Gamma_{162}^{\psi(2S)}/\Gamma_{12}^{\psi(2S)}$

VALUE (units 10^{-4})	DOCUMENT ID		TECN	COMMENT
8.0±0.8 OUR FIT				
6.1±0.8±0.9	[1] BAI	99B	BES	$\psi(2S) \to \gamma 2K^+2K^-$

[1] Calculated by us. The value of $B(\chi_{c0} \to 2K^+2K^-)$ reported by BAI 99B was derived using $B(\psi(2S) \to \gamma\chi_{c0}(1P)) = (9.3 \pm 0.8)\%$ and $B(\psi(2S) \to J/\psi\pi^+\pi^-) = (32.4 \pm 2.6)\%$ [BAI 98D].

$\Gamma(\chi_{c0}(1P) \to \phi\phi)/\Gamma_{total} \times \Gamma(\psi(2S) \to \gamma\chi_{c0}(1P))/\Gamma_{total}$ $\quad \Gamma_{56}/\Gamma \times \Gamma_{162}^{\psi(2S)}/\Gamma^{\psi(2S)}$

VALUE (units 10^{-4})	EVTS	DOCUMENT ID		TECN	COMMENT
0.78±0.07 OUR FIT					
0.78±0.08 OUR AVERAGE					
0.77±0.03±0.08	612	[1] ABLIKIM	11K	BES3	$\psi(2S) \to \gamma$ hadrons
0.86±0.19±0.12	26	[2] ABLIKIM	06T	BES2	$\psi(2S) \to \gamma 2K^+2K^-$

[1] Calculated by us. The value of $B(\chi_{c0} \to \phi\phi)$ reported by ABLIKIM 11K was derived using $B(\psi(2S) \to \gamma\chi_{c0}(1P)) = (9.62 \pm 0.31)\%$.

[2] Calculated by us. The value of $B(\chi_{c0} \to \phi\phi)$ reported by ABLIKIM 06T was derived using $B(\psi(2S) \to \gamma\chi_{c0}(1P)) = (9.2 \pm 0.4)\%$.

$\Gamma(\chi_{c0}(1P) \to \phi\phi)/\Gamma_{total} \times \Gamma(\psi(2S) \to \gamma\chi_{c0}(1P))/\Gamma(\psi(2S) \to J/\psi(1S)\pi^+\pi^-)$ $\quad \Gamma_{56}/\Gamma \times \Gamma_{162}^{\psi(2S)}/\Gamma_{12}^{\psi(2S)}$

VALUE (units 10^{-4})	DOCUMENT ID		TECN	COMMENT
2.25±0.21 OUR FIT				
2.6 ±1.0 ±1.1	[1] BAI	99B	BES	$\psi(2S) \to \gamma 2K^+2K^-$

[1] Calculated by us. The value of $B(\chi_{c0} \to \phi\phi)$ reported by BAI 99B was derived using $B(\psi(2S) \to \gamma\chi_{c0}(1P)) = (9.3 \pm 0.8)\%$ and $B(\psi(2S) \to J/\psi\pi^+\pi^-) = (32.4 \pm 2.6)\%$ [BAI 98D].

$\Gamma(\chi_{c0}(1P) \to \Sigma^+\overline{p}K^0_S + \text{c.c.})/\Gamma_{total} \times \Gamma(\psi(2S) \to \gamma\chi_{c0}(1P))/\Gamma_{total}$ $\quad \Gamma_{82}/\Gamma \times \Gamma_{162}^{\psi(2S)}/\Gamma^{\psi(2S)}$

VALUE (units 10^{-5})	EVTS	DOCUMENT ID		TECN	COMMENT
3.45±0.17±0.19	493	[1] ABLIKIM	19BB	BES3	$\psi(2S) \to \gamma\Sigma^+\overline{p}K^0_S$ + c.c.

[1] Calculated by us. ABLIKIM 19BB reports $B(\chi_c^0 \to \Sigma^+\overline{p}K^0_S + \text{c.c.}) = (3.52 \pm 0.19 \pm 0.21) \times 10^{-4}$ using $B(\psi(2S) \to \gamma\chi_c^0) = (9.79 \pm 0.20)\%$ and other branching fractions from PDG 18.

$\Gamma(\chi_{c0}(1P) \to \Sigma^0\overline{p}K^+ + \text{c.c.})/\Gamma_{total} \times \Gamma(\psi(2S) \to \gamma\chi_{c0}(1P))/\Gamma_{total}$ $\quad \Gamma_{83}/\Gamma \times \Gamma_{162}^{\psi(2S)}/\Gamma^{\psi(2S)}$

VALUE (units 10^{-5})	EVTS	DOCUMENT ID		TECN	COMMENT
2.97±0.12±0.14	871	[1] ABLIKIM	20AE	BES3	$\psi(2S) \to \gamma\Sigma^0\overline{p}K^+$ + c.c.

[1] Calculated by us. ABLIKIM 20AE reports $B(\chi_c^0 \to \Sigma^0\overline{p}K^+ + \text{c.c.}) = (3.03 \pm 0.12 \pm 0.15) \times 10^{-4}$ using $B(\psi(2S) \to \gamma\chi_c^0) = (9.79 \pm 0.20)\%$ and other branching fractions from PDG 20.

$\chi_{c0}(1P)$ REFERENCES

ABLIKIM	21AV	JHEP 2111 217	M. Ablikim et al.	(BESIII Collab.)
ABLIKIM	21L	PR D103 112004	M. Ablikim et al.	(BESIII Collab.)
ABLIKIM	20AE	PR D102 092006	M. Ablikim et al.	(BESIII Collab.)
ABLIKIM	20B	PR D101 012012	M. Ablikim et al.	(BESIII Collab.)
ABLIKIM	20I	PR D101 092002	M. Ablikim et al.	(BESIII Collab.)
PDG	20	PTEP 2020 083C01	P.A. Zyla et al.	(PDG Collab.)
ABLIKIM	19AA	PR D99 052008	M. Ablikim et al.	(BESIII Collab.)
ABLIKIM	19AU	PR D100 052010	M. Ablikim et al.	(BESIII Collab.)
ABLIKIM	19BB	PR D100 092006	M. Ablikim et al.	(BESIII Collab.)
ABLIKIM	19J	PR D99 012015	M. Ablikim et al.	(BESIII Collab.)
ABLIKIM	19Z	PR D99 051101	M. Ablikim et al.	(BESIII Collab.)
ABLIKIM	18V	PR D97 052011	M. Ablikim et al.	(BESIII Collab.)
PDG	18	PR D98 030001	M. Tanabashi et al.	(PDG Collab.)
AAIJ	17BB	EPJ C77 609	R. Aaij et al.	(LHCb Collab.)
ABLIKIM	17AE	PR D96 092007	M. Ablikim et al.	(BESIII Collab.)
ABLIKIM	17AI	PR D96 112006	M. Ablikim et al.	(BESIII Collab.)
ABLIKIM	17I	PRL 118 221802	M. Ablikim et al.	(BESIII Collab.)
ABLIKIM	17N	PR D95 072004	M. Ablikim et al.	(BESIII Collab.)
ABLIKIM	17U	PR D96 032001	M. Ablikim et al.	(BESIII Collab.)
PDG	16	CP C40 100001	C. Patrignani et al.	(PDG Collab.)
ABLIKIM	15I	PR D91 092006	M. Ablikim et al.	(BESIII Collab.)
ABLIKIM	15M	PR D91 112008	M. Ablikim et al.	(BESIII Collab.)
ABLIKIM	15N	PR D91 112018	M. Ablikim et al.	(BESIII Collab.)
ABLIKIM	13B	PR D87 012002	M. Ablikim et al.	(BESIII Collab.)
ABLIKIM	13D	PR D87 012007	M. Ablikim et al.	(BESIII Collab.)
ABLIKIM	13H	PR D87 032007	M. Ablikim et al.	(BESIII Collab.)
ABLIKIM	13V	PR D88 112001	M. Ablikim et al.	(BESIII Collab.)
UEHARA	13	PTEP 2013 123C01	S. Uehara et al.	(BELLE Collab.)
ABLIKIM	12A	PR D85 112008	M. Ablikim et al.	(BESIII Collab.)
ABLIKIM	12I	PR D86 052004	M. Ablikim et al.	(BESIII Collab.)
ABLIKIM	12J	PR D86 052011	M. Ablikim et al.	(BESIII Collab.)
ABLIKIM	12O	PRL 109 172002	M. Ablikim et al.	(BESIII Collab.)
LIU	12B	PRL 108 232001	Z.Q. Liu et al.	(BELLE Collab.)
ABLIKIM	11A	PR D83 012006	M. Ablikim et al.	(BESIII Collab.)
ABLIKIM	11E	PR D83 112005	M. Ablikim et al.	(BESIII Collab.)
ABLIKIM	11F	PR D83 112009	M. Ablikim et al.	(BESIII Collab.)
ABLIKIM	11K	PRL 107 092001	M. Ablikim et al.	(BESIII Collab.)
DEL-AMO-SA...	11M	PR D84 012004	P. del Amo Sanchez et al.	(BABAR Collab.)
ABLIKIM	10A	PR D81 052005	M. Ablikim et al.	(BESIII Collab.)
ONYISI	10	PR D82 011103	P.U.E. Onyisi et al.	(CLEO Collab.)
UEHARA	10A	PR D82 114031	S. Uehara et al.	(BELLE Collab.)
ASNER	09	PR D79 072007	D.M. Asner et al.	(CLEO Collab.)
UEHARA	09	PR D79 052009	S. Uehara et al.	(BELLE Collab.)
BENNETT	08A	PRL 101 151801	J.V. Bennett et al.	(CLEO Collab.)
ECKLUND	08A	PR D78 091501	K.M. Ecklund et al.	(CLEO Collab.)
HE	08B	PR D78 092004	Q. He et al.	(CLEO Collab.)
MENDEZ	08	PR D78 011102	H. Mendez et al.	(CLEO Collab.)
NAIK	08	PR D78 031101	P. Naik et al.	(CLEO Collab.)
UEHARA	08	EPJ C53 1	S. Uehara et al.	(BELLE Collab.)
WICHT	08	PL B662 323	J. Wicht et al.	(BELLE Collab.)
ABE	07	PRL 98 082001	K. Abe et al.	(BELLE Collab.)
ADAMS	07	PR D75 071101	G.S. Adams et al.	(CLEO Collab.)
ATHAR	07	PR D75 032002	S.B. Athar et al.	(CLEO Collab.)
CHEN	07B	PL B651 15	W.T. Chen et al.	(BELLE Collab.)
ABLIKIM	06D	PR D73 052006	M. Ablikim et al.	(BES Collab.)
ABLIKIM	06I	PR D74 012004	M. Ablikim et al.	(BES Collab.)
ABLIKIM	06R	PR D74 072001	M. Ablikim et al.	(BES Collab.)
ABLIKIM	06T	PL B642 197	M. Ablikim et al.	(BES Collab.)
ABLIKIM	05G	PR D71 092002	M. Ablikim et al.	(BES Collab.)
ABLIKIM	05N	PL B630 7	M. Ablikim et al.	(BES Collab.)
ABLIKIM	05O	PL B630 21	M. Ablikim et al.	(BES Collab.)
ABLIKIM	05Q	PR D72 092002	M. Ablikim et al.	(BES Collab.)
ADAM	05A	PRL 94 232002	N.E. Adam et al.	(CLEO Collab.)
ANDREOTTI	05A	NP B717 34	M. Andreotti et al.	(FNAL E835 Collab.)
ANDREOTTI	05C	PR D72 112002	M. Andreotti et al.	(FNAL E835 Collab.)
NAKAZAWA	05	PL B615 39	H. Nakazawa et al.	(BELLE Collab.)
ABE	04G	PR D70 071102	K. Abe et al.	(BELLE Collab.)
ABLIKIM	04G	PR D70 092002	M. Ablikim et al.	(BES Collab.)
ABLIKIM	04H	PR D70 092003	M. Ablikim et al.	(BES Collab.)
ANDREOTTI	04	PL B584 16	M. Andreotti et al.	(E835 Collab.)
ATHAR	04	PR D70 112002	S.B. Athar et al.	(CLEO Collab.)
BAI	04F	PR D69 092001	J.Z. Bai et al.	(BES Collab.)
ANDREOTTI	03	PRL 91 091801	M. Andreotti et al.	(FNAL E835 Collab.)
AULCHENKO	03	PL B573 63	V.M. Aulchenko et al.	(KEDR Collab.)
BAI	03C	PR D67 032004	J.Z. Bai et al.	(BES Collab.)
BAI	03E	PR D67 112001	J.Z. Bai et al.	(BES Collab.)
ABE,K	02	PRL 89 142001	K. Abe et al.	(BELLE Collab.)
BAGNASCO	02	PL B533 237	S. Bagnasco et al.	(FNAL E835 Collab.)
EISENSTEIN	01	PRL 87 061801	B.I. Eisenstein et al.	(CLEO Collab.)
AMBROGIANI	00B	PR D62 052002	M. Ambrogiani et al.	(FNAL E835 Collab.)
AMBROGIANI	99B	PRL 83 2902	M. Ambrogiani et al.	(FNAL E835 Collab.)
BAI	99B	PR D60 072001	J.Z. Bai et al.	(BES Collab.)
BAI	98D	PR D58 092006	J.Z. Bai et al.	(BES Collab.)
BAI	98I	PRL 81 3091	J.Z. Bai et al.	(BES Collab.)
GAISER	86	PR D34 711	J. Gaiser et al.	(Crystal Ball Collab.)
LEE	85	SLAC 282	R.A. Lee	(SLAC)
OREGLIA	82	PR D25 2259	M.J. Oreglia et al.	(SLAC, CIT, HARV+)
BRANDELIK	79B	NP B160 426	R. Brandelik et al.	(DASP Collab.)
BARTEL	78B	PL 79B 492	W. Bartel et al.	(DESY, HEIDP)
TANENBAUM	78	PR D17 1731	W.M. Tanenbaum et al.	(SLAC, LBL)
Also		Private Comm.	G. Trilling	(LBL, UCB)
BIDDICK	77	PRL 38 1324	C.J. Biddick et al.	(UCSD, UMD, PAVI+)

$\chi_{c1}(1P)$

$I^G(J^{PC}) = 0^+(1^{++})$

See the Review on "$\psi(2S)$ and χ_c branching ratios" before the $\chi_{c0}(1P)$ Listings.

$\chi_{c1}(1P)$ MASS

VALUE (MeV)	EVTS	DOCUMENT ID		TECN	COMMENT
3510.67 ± 0.05 OUR AVERAGE		Error includes scale factor of 1.2.			
3508.4 ± 1.9 ±0.7	460	[1] AAIJ	17BB	LHCB	$pp \to b\overline{b}X \to 2(K^+K^-)X$
3510.71 ± 0.04 ±0.09	4.8k	[2] AAIJ	17BI	LHCB	$\chi_{c1} \to J/\psi\mu^+\mu^-$
3510.30 ± 0.14 ±0.16		ABLIKIM	05G	BES2	$\psi(2S) \to \gamma\chi_{c1}$
3510.719± 0.051±0.019		ANDREOTTI	05A	E835	$p\overline{p} \to e^+e^-\gamma$
3509.4 ± 0.9		BAI	99B	BES	$\psi(2S) \to \gamma X$
3510.60 ± 0.087±0.019	513	[3] ARMSTRONG	92	E760	$\overline{p}p \to e^+e^-\gamma$
3511.3 ± 0.4 ±0.4	30	BAGLIN	86B	SPEC	$\overline{p}p \to e^+e^-X$
3512.3 ± 0.3 ±4.0		[4] GAISER	86	CBAL	$\psi(2S) \to \gamma X$
3507.4 ± 1.7	91	[5] LEMOIGNE	82	GOLI	185 π^-Be $\to \gamma\mu^+\mu^-$A
3510.4 ± 0.6		OREGLIA	82	CBAL	$e^+e^- \to J/\psi 2\gamma$
3510.1 ± 1.1	254	[6] HIMEL	80	MRK2	$e^+e^- \to J/\psi 2\gamma$
3509 ±11	21	BRANDELIK	79B	DASP	$e^+e^- \to J/\psi 2\gamma$
3507 ± 3		[6] BARTEL	78B	CNTR	$e^+e^- \to J/\psi 2\gamma$
3505.0 ± 4 ±4		[6,7] TANENBAUM	78	MRK1	e^+e^-
3513 ± 7	367	[6] BIDDICK	77	CNTR	$\psi(2S) \to \gamma X$
• • • We do not use the following data for averages, fits, limits, etc. • • •					
3500 ±10	40	TANENBAUM	75	MRK1	Hadrons γ

[1] From a fit of the $\phi\phi$ invariant mass with the width of $\chi_{c1}(1P)$ fixed to the PDG 16 value.

[2] AAIJ 17BI reports also $m(\chi_{c2}) - m(\chi_{c1}) = 45.39 \pm 0.07 \pm 0.03$ MeV.

[3] Recalculated by ANDREOTTI 05A, using the value of $\psi(2S)$ mass from AULCHENKO 03.

[4] Using mass of $\psi(2S) = 3686.0$ MeV.

[5] $J/\psi(1S)$ mass constrained to 3097 MeV.

[6] Mass value shifted by us by amount appropriate for $\psi(2S)$ mass = 3686 MeV and $J/\psi(1S)$ mass = 3097 MeV.

[7] From a simultaneous fit to radiative and hadronic decay channels.

$\chi_{c1}(1P)$ WIDTH

VALUE (MeV)	CL%	EVTS	DOCUMENT ID		TECN	COMMENT
0.84 ±0.04 OUR FIT						
0.88 ±0.05 OUR AVERAGE						
1.39 $^{+0.40}_{-0.38}$ $^{+0.26}_{-0.77}$			ABLIKIM	05G	BES2	$\psi(2S) \to \gamma\chi_{c1}$
0.876±0.045±0.026			ANDREOTTI	05A	E835	$p\overline{p} \to e^+e^-\gamma$
0.87 ±0.11 ±0.08		513	[1] ARMSTRONG	92	E760	$\overline{p}p \to e^+e^-\gamma$
• • • We do not use the following data for averages, fits, limits, etc. • • •						
<1.3	95		BAGLIN	86B	SPEC	$\overline{p}p \to e^+e^-X$
<3.8	90		GAISER	86	CBAL	$\psi(2S) \to \gamma X$

[1] Recalculated by ANDREOTTI 05A.

Downloaded from https://academic.oup.com/ptep/article/2022/8/083C01/6651666 by KIT Library user on 27 September 2022

$\chi_{c1}(1P)$ DECAY MODES

	Mode	Fraction (Γ_i/Γ)	Scale factor/ Confidence level
	Hadronic decays		
Γ_1	$3(\pi^+\pi^-)$	$(5.8 \pm 1.4) \times 10^{-3}$	S=1.2
Γ_2	$2(\pi^+\pi^-)$	$(7.6 \pm 2.6) \times 10^{-3}$	
Γ_3	$\pi^+\pi^-\pi^0\pi^0$	(1.19 ± 0.15) %	
Γ_4	$\rho^+\pi^-\pi^0$ + c.c.	(1.45 ± 0.24) %	
Γ_5	$\rho^0\pi^+\pi^-$	$(3.9 \pm 3.5) \times 10^{-3}$	
Γ_6	$4\pi^0$	$(5.4 \pm 0.8) \times 10^{-4}$	
Γ_7	$\pi^+\pi^-K^+K^-$	$(4.5 \pm 1.0) \times 10^{-3}$	
Γ_8	$K^+K^-\pi^0\pi^0$	$(1.12 \pm 0.27) \times 10^{-3}$	
Γ_9	$K^+K^-\pi^+\pi^-\pi^0$	(1.15 ± 0.13) %	
Γ_{10}	$K^0_S K^\pm\pi^\mp\pi^+\pi^-$	$(7.5 \pm 0.8) \times 10^{-3}$	
Γ_{11}	$K^+\pi^-\overline{K}^0\pi^0$ + c.c.	$(8.6 \pm 1.4) \times 10^{-3}$	
Γ_{12}	$\rho^- K^+\overline{K}^0$ + c.c.	$(5.0 \pm 1.2) \times 10^{-3}$	
Γ_{13}	$K^*(892)^0\overline{K}^0\pi^0 \to K^+\pi^-\overline{K}^0\pi^0$ + c.c.	$(2.3 \pm 0.6) \times 10^{-3}$	
Γ_{14}	$K^+K^-\eta\pi^0$	$(1.12 \pm 0.34) \times 10^{-3}$	
Γ_{15}	$\pi^+\pi^-K^0_S K^0_S$	$(6.9 \pm 2.9) \times 10^{-4}$	
Γ_{16}	$K^+K^-\eta$	$(3.2 \pm 1.0) \times 10^{-4}$	
Γ_{17}	$\overline{K}^0K^+\pi^-$ + c.c.	$(7.0 \pm 0.6) \times 10^{-3}$	
Γ_{18}	$K^*(892)^0\overline{K}^0$ + c.c.	$(10 \pm 4) \times 10^{-4}$	
Γ_{19}	$K^*(892)^+K^-$ + c.c.	$(1.4 \pm 0.6) \times 10^{-3}$	
Γ_{20}	$K^*_J(1430)^0\overline{K}^0$ + c.c. $\to K^0_S K^+\pi^-$ + c.c.	$< 8 \times 10^{-4}$	CL=90%
Γ_{21}	$K^*_J(1430)^+K^-$ + c.c. $\to K^0_S K^+\pi^-$ + c.c.	$< 2.1 \times 10^{-3}$	CL=90%
Γ_{22}	$K^+K^-\pi^0$	$(1.81 \pm 0.24) \times 10^{-3}$	
Γ_{23}	$\eta\pi^+\pi^-$	$(4.62 \pm 0.23) \times 10^{-3}$	
Γ_{24}	$a_0(980)^+\pi^-$ + c.c. $\to \eta\pi^+\pi^-$	$(3.2 \pm 0.4) \times 10^{-3}$	S=2.2
Γ_{25}	$a_2(1320)^+\pi^-$ + c.c. $\to \eta\pi^+\pi^-$	$(1.76 \pm 0.24) \times 10^{-4}$	
Γ_{26}	$a_2(1700)^+\pi^-$ + c.c. $\to \eta\pi^+\pi^-$	$(4.6 \pm 0.7) \times 10^{-5}$	
Γ_{27}	$f_2(1270)\eta \to \eta\pi^+\pi^-$	$(3.5 \pm 0.6) \times 10^{-4}$	
Γ_{28}	$f_4(2050)\eta \to \eta\pi^+\pi^-$	$(2.5 \pm 0.9) \times 10^{-5}$	
Γ_{29}	$\pi_1(1400)^+\pi^-$ + c.c. $\to \eta\pi^+\pi^-$	$< 5 \times 10^{-5}$	CL=90%
Γ_{30}	$\pi_1(1600)^+\pi^-$ + c.c. $\to \eta\pi^+\pi^-$	$< 1.5 \times 10^{-5}$	CL=90%
Γ_{31}	$\pi_1(2015)^+\pi^-$ + c.c. $\to \eta\pi^+\pi^-$	$< 8 \times 10^{-6}$	CL=90%
Γ_{32}	$f_2(1270)\eta$	$(6.7 \pm 1.1) \times 10^{-4}$	
Γ_{33}	$\pi^+\pi^-\eta'$	$(2.2 \pm 0.4) \times 10^{-3}$	
Γ_{34}	$K^+K^-\eta'(958)$	$(8.8 \pm 0.9) \times 10^{-4}$	
Γ_{35}	$K^*_0(1430)^+K^-$ + c.c.	$(6.4 {}^{+2.2}_{-2.8}) \times 10^{-4}$	
Γ_{36}	$f_0(980)\eta'(958)$	$(1.6 {}^{+1.4}_{-0.7}) \times 10^{-4}$	
Γ_{37}	$f_0(1710)\eta'(958)$	$(7 {}^{+7}_{-5}) \times 10^{-5}$	
Γ_{38}	$f'_2(1525)\eta'(958)$	$(9 \pm 6) \times 10^{-5}$	
Γ_{39}	$\pi^0 f_0(980) \to \pi^0\pi^+\pi^-$	$(3.5 \pm 0.9) \times 10^{-7}$	
Γ_{40}	$K^+\overline{K}^*(892)^0\pi^-$ + c.c.	$(3.2 \pm 2.1) \times 10^{-3}$	
Γ_{41}	$K^*(892)^0\overline{K}^*(892)^0$	$(1.4 \pm 0.4) \times 10^{-3}$	
Γ_{42}	$K^+K^-K^0_S K^0_S$	$< 4 \times 10^{-4}$	CL=90%
Γ_{43}	$K^0_S K^0_S K^0_S K^0_S$	$(3.5 \pm 1.0) \times 10^{-5}$	
Γ_{44}	$K^+K^-K^+K^-$	$(5.4 \pm 1.1) \times 10^{-4}$	
Γ_{45}	$K^+K^-\phi$	$(4.1 \pm 1.5) \times 10^{-4}$	
Γ_{46}	$\overline{K}^0K^+\pi^-\phi$ + c.c.	$(3.3 \pm 0.5) \times 10^{-3}$	
Γ_{47}	$K^+K^-\pi^0\phi$	$(1.62 \pm 0.30) \times 10^{-3}$	
Γ_{48}	$\phi\pi^+\pi^-\pi^0$	$(7.5 \pm 1.0) \times 10^{-4}$	
Γ_{49}	$\omega\omega$	$(5.7 \pm 0.7) \times 10^{-4}$	
Γ_{50}	ωK^+K^-	$(7.8 \pm 0.9) \times 10^{-4}$	
Γ_{51}	$\omega\phi$	$(2.7 \pm 0.4) \times 10^{-5}$	
Γ_{52}	$\phi\phi$	$(4.2 \pm 0.5) \times 10^{-4}$	
Γ_{53}	$\phi\phi\eta$	$(3.0 \pm 0.5) \times 10^{-4}$	
Γ_{54}	$p\overline{p}$	$(7.60 \pm 0.34) \times 10^{-5}$	
Γ_{55}	$p\overline{p}\pi^0$	$(1.55 \pm 0.18) \times 10^{-4}$	
Γ_{56}	$p\overline{p}\eta$	$(1.45 \pm 0.25) \times 10^{-4}$	
Γ_{57}	$p\overline{p}\omega$	$(2.12 \pm 0.31) \times 10^{-4}$	
Γ_{58}	$p\overline{p}\phi$	$< 1.7 \times 10^{-5}$	CL=90%
Γ_{59}	$p\overline{p}\pi^+\pi^-$	$(5.0 \pm 1.9) \times 10^{-4}$	
Γ_{60}	$p\overline{p}\pi^0\pi^0$	$< 5 \times 10^{-4}$	CL=90%
Γ_{61}	$p\overline{p}K^+K^-$ (non-resonant)	$(1.27 \pm 0.22) \times 10^{-4}$	
Γ_{62}	$p\overline{p}K^0_S K^0_S$	$< 4.5 \times 10^{-4}$	CL=90%
Γ_{63}	$p\overline{n}\pi^-$	$(3.8 \pm 0.5) \times 10^{-4}$	
Γ_{64}	$\overline{p}n\pi^+$	$(3.9 \pm 0.5) \times 10^{-4}$	
Γ_{65}	$p\overline{n}\pi^-\pi^0$	$(1.03 \pm 0.12) \times 10^{-3}$	
Γ_{66}	$\overline{p}n\pi^+\pi^0$	$(1.01 \pm 0.12) \times 10^{-3}$	
Γ_{67}	$\Lambda\overline{\Lambda}$	$(1.27 \pm 0.08) \times 10^{-4}$	
Γ_{68}	$\Lambda\overline{\Lambda}\pi^+\pi^-$	$(2.9 \pm 0.5) \times 10^{-4}$	
Γ_{69}	$\Lambda\overline{\Lambda}\pi^+\pi^-$ (non-resonant)	$(2.5 \pm 0.6) \times 10^{-4}$	
Γ_{70}	$\Sigma(1385)^+\overline{\Lambda}\pi^-$ + c.c.	$< 1.3 \times 10^{-4}$	CL=90%
Γ_{71}	$\Sigma(1385)^-\overline{\Lambda}\pi^+$ + c.c.	$< 1.3 \times 10^{-4}$	CL=90%
Γ_{72}	$K^+\overline{p}\Lambda$+c.c.	$(4.2 \pm 0.4) \times 10^{-4}$	S=1.2
Γ_{73}	$nK^0_S\overline{\Lambda}$ + c.c.	$(1.66 \pm 0.17) \times 10^{-4}$	
Γ_{74}	$K^*(892)^+\overline{p}\Lambda$+ c.c.	$(4.9 \pm 0.7) \times 10^{-4}$	
Γ_{75}	$K^+\overline{p}\Lambda(1520)$+ c.c.	$(1.7 \pm 0.4) \times 10^{-4}$	
Γ_{76}	$\Lambda(1520)\overline{\Lambda}(1520)$	$< 9 \times 10^{-5}$	CL=90%
Γ_{77}	$\Sigma^0\overline{\Sigma}^0$	$(4.2 \pm 0.6) \times 10^{-5}$	
Γ_{78}	$\Sigma^+\overline{p}K^0_S$ + c.c.	$(1.53 \pm 0.12) \times 10^{-4}$	
Γ_{79}	$\Sigma^0\overline{p}K^+$ + c.c.	$(1.46 \pm 0.10) \times 10^{-4}$	
Γ_{80}	$\Sigma^+\overline{\Sigma}^-$	$(3.6 \pm 0.7) \times 10^{-5}$	
Γ_{81}	$\Sigma^-\overline{\Sigma}^+$	$(5.7 \pm 1.5) \times 10^{-5}$	
Γ_{82}	$\Sigma(1385)^+\overline{\Sigma}(1385)^-$	$< 9 \times 10^{-5}$	CL=90%
Γ_{83}	$\Sigma(1385)^-\overline{\Sigma}(1385)^+$	$< 5 \times 10^{-5}$	CL=90%
Γ_{84}	$K^-\Lambda\overline{\Xi}^+$ + c.c.	$(1.35 \pm 0.24) \times 10^{-4}$	
Γ_{85}	$\Xi^0\overline{\Xi}^0$	$< 6 \times 10^{-5}$	CL=90%
Γ_{86}	$\Xi^-\overline{\Xi}^+$	$(8.0 \pm 2.1) \times 10^{-5}$	
Γ_{87}	$\pi^+\pi^-$ + K^+K^-	$< 2.1 \times 10^{-3}$	
Γ_{88}	$K^0_S K^0_S$	$< 6 \times 10^{-5}$	CL=90%
Γ_{89}	$\eta_C\pi^+\pi^-$	$< 3.2 \times 10^{-3}$	CL=90%
	Radiative decays		
Γ_{90}	$\gamma J/\psi(1S)$	(34.3 ± 1.0) %	
Γ_{91}	$\gamma\rho^0$	$(2.16 \pm 0.17) \times 10^{-4}$	
Γ_{92}	$\gamma\omega$	$(6.8 \pm 0.8) \times 10^{-5}$	
Γ_{93}	$\gamma\phi$	$(2.4 \pm 0.5) \times 10^{-5}$	
Γ_{94}	$\gamma\gamma$	$< 6.3 \times 10^{-6}$	CL=90%
Γ_{95}	$e^+e^-J/\psi(1S)$	$(3.46 \pm 0.22) \times 10^{-3}$	
Γ_{96}	$\mu^+\mu^-J/\psi(1S)$	$(2.33 \pm 0.29) \times 10^{-4}$	

CONSTRAINED FIT INFORMATION

A multiparticle fit to $\chi_{c1}(1P)$, $\chi_{c0}(1P)$, $\chi_{c2}(1P)$, and $\psi(2S)$ with 4 total widths, a partial width, 25 combinations of partial widths obtained from integrated cross section, and 84 branching ratios uses 248 measurements to determine 49 parameters. The overall fit has a $\chi^2 = 379.8$ for 199 degrees of freedom.

The following *off-diagonal* array elements are the correlation coefficients $\langle \delta p_i \delta p_j \rangle / (\delta p_i \cdot \delta p_j)$, in percent, from the fit to parameters p_i, including the branching fractions, $x_i \equiv \Gamma_i/\Gamma_{\rm total}$.

	x_{17}	x_{44}	x_{54}	x_{67}	x_{90}
x_{44}	3				
x_{54}	4	2			
x_{67}	11	4	5		
x_{90}	23	9	2	29	
Γ	−12	−5	−63	−15	−41

$\chi_{c1}(1P)$ PARTIAL WIDTHS

$\chi_{c1}(1P)\ \Gamma(i)\Gamma(\gamma J/\psi(1S))/\Gamma(\text{total})$

$\Gamma(p\overline{p}) \times \Gamma(\gamma J/\psi(1S))/\Gamma_{\rm total}$ — $\Gamma_{54}\Gamma_{90}/\Gamma$

VALUE (eV)	DOCUMENT ID		TECN	COMMENT
21.9±0.8 OUR FIT				
21.4±0.9 OUR AVERAGE				
21.5±0.5±0.8	[1] ANDREOTTI	05A	E835	$p\overline{p} \to e^+e^-\gamma$
21.4±1.5±2.2	[1,2] ARMSTRONG	92	E760	$\overline{p}p \to e^+e^-\gamma$
$19.9 {}^{+4.4}_{-4.0}$	[1] BAGLIN	86B	SPEC	$\overline{p}p \to e^+e^-X$

[1] Calculated by us using $B(J/\psi(1S) \to e^+e^-) = 0.0593 \pm 0.0010$.
[2] Recalculated by ANDREOTTI 05A.

$\chi_{c1}(1P)$ BRANCHING RATIOS

HADRONIC DECAYS

$\Gamma(3(\pi^+\pi^-))/\Gamma_{\rm total}$ — Γ_1/Γ

VALUE (units 10^{-3})	DOCUMENT ID		TECN	COMMENT
5.8±1.4 OUR EVALUATION Error includes scale factor of 1.2. Treating systematic error as correlated.				
5.8±1.1 OUR AVERAGE				
5.4±0.7±0.9	[1] BAI	99B	BES	$\psi(2S) \to \gamma\chi_{c1}$
16.0±5.9±0.8	[1] TANENBAUM	78	MRK1	$\psi(2S) \to \gamma\chi_{c1}$

[1] Rescaled by us using $B(\psi(2S) \to \gamma\chi_{c1}) = (8.8 \pm 0.4)$% and $B(\psi(2S) \to J/\psi(1S)\pi^+\pi^-) = (32.6 \pm 0.5)$%.

Downloaded from https://academic.oup.com/ptep/article/2022/8/083C01/6651666 by KIT Library user on 27 September 2022

$\Gamma(2(\pi^+\pi^-))/\Gamma_{total}$ — Γ_2/Γ

VALUE (units 10^{-3})	DOCUMENT ID		TECN	COMMENT
7.6±2.6 OUR EVALUATION	Treating systematic error as correlated.			
8 ±4 OUR AVERAGE	Error includes scale factor of 1.5.			
4.6±2.1±2.6	[1] BAI	99B	BES	$\psi(2S) \to \gamma\chi_{c1}$
12.5±4.2±0.6	[1] TANENBAUM	78	MRK1	$\psi(2S) \to \gamma\chi_{c1}$

[1] Rescaled by us using $B(\psi(2S) \to \gamma\chi_{c1}) = (8.8 \pm 0.4)\%$ and $B(\psi(2S) \to J/\psi(1S)\pi^+\pi^-) = (32.6 \pm 0.5)\%$.

$\Gamma(\pi^+\pi^-\pi^0\pi^0)/\Gamma_{total}$ — Γ_3/Γ

VALUE (%)	EVTS	DOCUMENT ID		TECN	COMMENT
1.19±0.15±0.03	604.7	[1] HE	08B	CLEO	$e^+e^- \to \gamma h^+h^-h^0h^0$

[1] HE 08B reports 1.28 ± 0.06 ± 0.15 ± 0.08 % from a measurement of $[\Gamma(\chi_{c1}(1P) \to \pi^+\pi^-\pi^0\pi^0)/\Gamma_{total}] \times [B(\psi(2S) \to \gamma\chi_{c1}(1P))]$ assuming $B(\psi(2S) \to \gamma\chi_{c1}(1P)) = (9.07 \pm 0.11 \pm 0.54) \times 10^{-2}$, which we rescale to our best value $B(\psi(2S) \to \gamma\chi_{c1}(1P)) = (9.75 \pm 0.24) \times 10^{-2}$. Our first error is their experiment's error and our second error is the systematic error from using our best value.

$\Gamma(\rho^+\pi^-\pi^0 + c.c.)/\Gamma_{total}$ — Γ_4/Γ

VALUE (%)	EVTS	DOCUMENT ID		TECN	COMMENT
1.45±0.24±0.04	712.3	[1,2] HE	08B	CLEO	$e^+e^- \to \gamma h^+h^-h^0h^0$

[1] HE 08B reports 1.56 ± 0.13 ± 0.22 ± 0.10 % from a measurement of $[\Gamma(\chi_{c1}(1P) \to \rho^+\pi^-\pi^0 + c.c.)/\Gamma_{total}] \times [B(\psi(2S) \to \gamma\chi_{c1}(1P))]$ assuming $B(\psi(2S) \to \gamma\chi_{c1}(1P)) = (9.07 \pm 0.11 \pm 0.54) \times 10^{-2}$, which we rescale to our best value $B(\psi(2S) \to \gamma\chi_{c1}(1P)) = (9.75 \pm 0.24) \times 10^{-2}$. Our first error is their experiment's error and our second error is the systematic error from using our best value.

[2] Calculated by us. We have added the values from HE 08B for $\rho^+\pi^-\pi^0$ and $\rho^-\pi^+\pi^0$ decays assuming uncorrelated statistical and fully correlated systematic uncertainties.

$\Gamma(\rho^0\pi^+\pi^-)/\Gamma_{total}$ — Γ_5/Γ

VALUE (units 10^{-3})	DOCUMENT ID		TECN	COMMENT
3.9±3.5	[1] TANENBAUM	78	MRK1	$\psi(2S) \to \gamma\chi_{c1}$

[1] Estimated using $B(\psi(2S) \to \gamma\chi_{c1}(1P)) = 0.087$. The errors do not contain the uncertainty in the $\psi(2S)$ decay.

$\Gamma(4\pi^0)/\Gamma_{total}$ — Γ_6/Γ

VALUE (units 10^{-4})	EVTS	DOCUMENT ID		TECN	COMMENT
5.4±0.8±0.1	608	[1] ABLIKIM	11A	BES3	$e^+e^- \to \psi(2S) \to \gamma\chi_{c1}$

[1] ABLIKIM 11A reports $(0.57 \pm 0.03 \pm 0.08) \times 10^{-3}$ from a measurement of $[\Gamma(\chi_{c1}(1P) \to 4\pi^0)/\Gamma_{total}] \times [B(\psi(2S) \to \gamma\chi_{c1}(1P))]$ assuming $B(\psi(2S) \to \gamma\chi_{c1}(1P)) = (9.2 \pm 0.4) \times 10^{-2}$, which we rescale to our best value $B(\psi(2S) \to \gamma\chi_{c1}(1P)) = (9.75 \pm 0.24) \times 10^{-2}$. Our first error is their experiment's error and our second error is the systematic error from using our best value.

$\Gamma(\pi^+\pi^-K^+K^-)/\Gamma_{total}$ — Γ_7/Γ

VALUE (units 10^{-3})	DOCUMENT ID		TECN	COMMENT
4.5±1.0 OUR EVALUATION	Treating systematic error as correlated.			
4.5±0.9 OUR AVERAGE				
4.2±0.4±0.9	[1] BAI	99B	BES	$\psi(2S) \to \gamma\chi_{c1}$
7.3±3.0±0.4	[1] TANENBAUM	78	MRK1	$\psi(2S) \to \gamma\chi_{c1}$

[1] Rescaled by us using $B(\psi(2S) \to \gamma\chi_{c1}) = (8.8 \pm 0.4)\%$ and $B(\psi(2S) \to J/\psi(1S)\pi^+\pi^-) = (32.6 \pm 0.5)\%$.

$\Gamma(K^+K^-\pi^0\pi^0)/\Gamma_{total}$ — Γ_8/Γ

VALUE (units 10^{-3})	EVTS	DOCUMENT ID		TECN	COMMENT
1.12±0.27±0.03	45.1	[1] HE	08B	CLEO	$e^+e^- \to \gamma h^+h^-h^0h^0$

[1] HE 08B reports $(0.12 \pm 0.02 \pm 0.02 \pm 0.01) \times 10^{-2}$ from a measurement of $[\Gamma(\chi_{c1}(1P) \to K^+K^-\pi^0\pi^0)/\Gamma_{total}] \times [B(\psi(2S) \to \gamma\chi_{c1}(1P))]$ assuming $B(\psi(2S) \to \gamma\chi_{c1}(1P)) = (9.07 \pm 0.11 \pm 0.54) \times 10^{-2}$, which we rescale to our best value $B(\psi(2S) \to \gamma\chi_{c1}(1P)) = (9.75 \pm 0.24) \times 10^{-2}$. Our first error is their experiment's error and our second error is the systematic error from using our best value.

$\Gamma(K^+K^-\pi^+\pi^-\pi^0)/\Gamma_{total}$ — Γ_9/Γ

VALUE (units 10^{-3})	EVTS	DOCUMENT ID		TECN	COMMENT
11.46±0.12±1.29	12k	[1] ABLIKIM	13B	BES3	$e^+e^- \to \psi(2S) \to \gamma\chi_{c1}$

[1] Using 1.06×10^8 $\psi(2S)$ mesons and $B(\psi(2S) \to \chi_{c1}\gamma) = (9.2 \pm 0.4)\%$.

$\Gamma(K^0_S K^\pm\pi^\mp\pi^+\pi^-)/\Gamma_{total}$ — Γ_{10}/Γ

VALUE (units 10^{-3})	EVTS	DOCUMENT ID		TECN	COMMENT
7.52±0.11±0.79	5.1k	[1] ABLIKIM	13B	BES3	$e^+e^- \to \psi(2S) \to \gamma\chi_{c1}$

[1] Using 1.06×10^8 $\psi(2S)$ mesons and $B(\psi(2S) \to \chi_{c1}\gamma) = (9.2 \pm 0.4)\%$.

$\Gamma(K^+\pi^-\overline{K}^0\pi^0 + c.c.)/\Gamma_{total}$ — Γ_{11}/Γ

VALUE (%)	EVTS	DOCUMENT ID		TECN	COMMENT
0.86±0.13±0.02	141.3	[1] HE	08B	CLEO	$e^+e^- \to \gamma h^+h^-h^0h^0$

[1] HE 08B reports 0.92 ± 0.09 ± 0.11 ± 0.06 % from a measurement of $[\Gamma(\chi_{c1}(1P) \to K^+\pi^-\overline{K}^0\pi^0 + c.c.)/\Gamma_{total}] \times [B(\psi(2S) \to \gamma\chi_{c1}(1P))]$ assuming $B(\psi(2S) \to \gamma\chi_{c1}(1P)) = (9.07 \pm 0.11 \pm 0.54) \times 10^{-2}$, which we rescale to our best value $B(\psi(2S) \to \gamma\chi_{c1}(1P)) = (9.75 \pm 0.24) \times 10^{-2}$. Our first error is their experiment's error and our second error is the systematic error from using our best value.

$\Gamma(\rho^-K^+\overline{K}^0 + c.c.)/\Gamma_{total}$ — Γ_{12}/Γ

VALUE (%)	EVTS	DOCUMENT ID		TECN	COMMENT
0.50±0.12±0.01	141.3	[1] HE	08B	CLEO	$e^+e^- \to \gamma h^+h^-h^0h^0$

[1] HE 08B reports 0.54 ± 0.11 ± 0.07 ± 0.03 % from a measurement of $[\Gamma(\chi_{c1}(1P) \to \rho^-K^+\overline{K}^0 + c.c.)/\Gamma_{total}] \times [B(\psi(2S) \to \gamma\chi_{c1}(1P))]$ assuming $B(\psi(2S) \to \gamma\chi_{c1}(1P)) = (9.07 \pm 0.11 \pm 0.54) \times 10^{-2}$, which we rescale to our best value $B(\psi(2S) \to \gamma\chi_{c1}(1P)) = (9.75 \pm 0.24) \times 10^{-2}$. Our first error is their experiment's error and our second error is the systematic error from using our best value.

$\Gamma(K^*(892)^0\overline{K}^0\pi^0 \to K^+\pi^-\overline{K}^0\pi^0 + c.c.)/\Gamma_{total}$ — Γ_{13}/Γ

VALUE (%)	EVTS	DOCUMENT ID		TECN	COMMENT
0.23±0.06±0.01	141.3	[1] HE	08B	CLEO	$e^+e^- \to \gamma h^+h^-h^0h^0$

[1] HE 08B reports 0.25 ± 0.06 ± 0.03 ± 0.02 % from a measurement of $[\Gamma(\chi_{c1}(1P) \to K^*(892)^0\overline{K}^0\pi^0 \to K^+\pi^-\overline{K}^0\pi^0 + c.c.)/\Gamma_{total}] \times [B(\psi(2S) \to \gamma\chi_{c1}(1P))]$ assuming $B(\psi(2S) \to \gamma\chi_{c1}(1P)) = (9.07 \pm 0.11 \pm 0.54) \times 10^{-2}$, which we rescale to our best value $B(\psi(2S) \to \gamma\chi_{c1}(1P)) = (9.75 \pm 0.24) \times 10^{-2}$. Our first error is their experiment's error and our second error is the systematic error from using our best value.

$\Gamma(K^+K^-\eta\pi^0)/\Gamma_{total}$ — Γ_{14}/Γ

VALUE (%)	EVTS	DOCUMENT ID		TECN	COMMENT
0.112±0.034±0.003	141.3	[1] HE	08B	CLEO	$e^+e^- \to \gamma h^+h^-h^0h^0$

[1] HE 08B reports 0.12 ± 0.03 ± 0.02 ± 0.01 % from a measurement of $[\Gamma(\chi_{c1}(1P) \to K^+K^-\eta\pi^0)/\Gamma_{total}] \times [B(\psi(2S) \to \gamma\chi_{c1}(1P))]$ assuming $B(\psi(2S) \to \gamma\chi_{c1}(1P)) = (9.07 \pm 0.11 \pm 0.54) \times 10^{-2}$, which we rescale to our best value $B(\psi(2S) \to \gamma\chi_{c1}(1P)) = (9.75 \pm 0.24) \times 10^{-2}$. Our first error is their experiment's error and our second error is the systematic error from using our best value.

$\Gamma(\pi^+\pi^-K^0_S K^0_S)/\Gamma_{total}$ — Γ_{15}/Γ

VALUE (units 10^{-4})	EVTS	DOCUMENT ID		TECN	COMMENT
6.9±2.9±0.2	19.8 ± 7.7	[1] ABLIKIM	05O	BES2	$\psi(2S) \to \chi_{c1}\gamma$

[1] ABLIKIM 05O reports $[\Gamma(\chi_{c1}(1P) \to \pi^+\pi^-K^0_S K^0_S)/\Gamma_{total}] \times [B(\psi(2S) \to \gamma\chi_{c1}(1P))] = (0.67 \pm 0.26 \pm 0.11) \times 10^{-4}$ which we divide by our best value $B(\psi(2S) \to \gamma\chi_{c1}(1P)) = (9.75 \pm 0.24) \times 10^{-2}$. Our first error is their experiment's error and our second error is the systematic error from using our best value.

$\Gamma(K^+K^-\eta)/\Gamma_{total}$ — Γ_{16}/Γ

VALUE (units 10^{-4})	DOCUMENT ID		TECN	COMMENT
3.2±1.0±0.1	[1] ATHAR	07	CLEO	$\psi(2S) \to \gamma h^+h^-h^0$

[1] ATHAR 07 reports $(0.34 \pm 0.10 \pm 0.04) \times 10^{-3}$ from a measurement of $[\Gamma(\chi_{c1}(1P) \to K^+K^-\eta)/\Gamma_{total}] \times [B(\psi(2S) \to \gamma\chi_{c1}(1P))]$ assuming $B(\psi(2S) \to \gamma\chi_{c1}(1P)) = 0.0907 \pm 0.0011 \pm 0.0054$, which we rescale to our best value $B(\psi(2S) \to \gamma\chi_{c1}(1P)) = (9.75 \pm 0.24) \times 10^{-2}$. Our first error is their experiment's error and our second error is the systematic error from using our best value.

$\Gamma(\overline{K}^0K^+\pi^- + c.c.)/\Gamma_{total}$ — Γ_{17}/Γ

VALUE (units 10^{-3})	DOCUMENT ID
7.0±0.6 OUR FIT	

$\Gamma(K^*(892)^0\overline{K}^0 + c.c.)/\Gamma_{total}$ — Γ_{18}/Γ

VALUE (units 10^{-3})	EVTS	DOCUMENT ID		TECN	COMMENT
0.98±0.37±0.02	22	[1] ABLIKIM	06R	BES2	$\psi(2S) \to \gamma\chi_{c1}$

[1] ABLIKIM 06R reports $(1.1 \pm 0.4 \pm 0.1) \times 10^{-3}$ from a measurement of $[\Gamma(\chi_{c1}(1P) \to K^*(892)^0\overline{K}^0 + c.c.)/\Gamma_{total}] \times [B(\psi(2S) \to \gamma\chi_{c1}(1P))]$ assuming $B(\psi(2S) \to \gamma\chi_{c1}(1P)) = (8.7 \pm 0.4) \times 10^{-2}$, which we rescale to our best value $B(\psi(2S) \to \gamma\chi_{c1}(1P)) = (9.75 \pm 0.24) \times 10^{-2}$. Our first error is their experiment's error and our second error is the systematic error from using our best value.

$\Gamma(K^*(892)^+K^- + c.c.)/\Gamma_{total}$ — Γ_{19}/Γ

VALUE (units 10^{-3})	EVTS	DOCUMENT ID		TECN	COMMENT
1.43±0.65±0.03	27	[1] ABLIKIM	06R	BES2	$\psi(2S) \to \gamma\chi_{c1}$

[1] ABLIKIM 06R reports $(1.6 \pm 0.7 \pm 0.2) \times 10^{-3}$ from a measurement of $[\Gamma(\chi_{c1}(1P) \to K^*(892)^+K^- + c.c.)/\Gamma_{total}] \times [B(\psi(2S) \to \gamma\chi_{c1}(1P))]$ assuming $B(\psi(2S) \to \gamma\chi_{c1}(1P)) = (8.7 \pm 0.4) \times 10^{-2}$, which we rescale to our best value $B(\psi(2S) \to \gamma\chi_{c1}(1P)) = (9.75 \pm 0.24) \times 10^{-2}$. Our first error is their experiment's error and our second error is the systematic error from using our best value.

$\Gamma(K^*_J(1430)^0\overline{K}^0 + c.c. \to K^0_S K^+\pi^- + c.c.)/\Gamma_{total}$ — Γ_{20}/Γ

VALUE	CL%	DOCUMENT ID		TECN	COMMENT
$<8 \times 10^{-4}$	90	[1] ABLIKIM	06R	BES2	$\psi(2S) \to \gamma\chi_{c1}$

[1] ABLIKIM 06R reports $< 0.9 \times 10^{-3}$ from a measurement of $[\Gamma(\chi_{c1}(1P) \to K^*_J(1430)^0\overline{K}^0 + c.c. \to K^0_S K^+\pi^- + c.c.)/\Gamma_{total}] \times [B(\psi(2S) \to \gamma\chi_{c1}(1P))]$ assuming $B(\psi(2S) \to \gamma\chi_{c1}(1P)) = (8.7 \pm 0.4) \times 10^{-2}$, which we rescale to our best value $B(\psi(2S) \to \gamma\chi_{c1}(1P)) = 9.75 \times 10^{-2}$.

$\Gamma(K^*_J(1430)^+K^- + c.c. \to K^0_S K^+\pi^- + c.c.)/\Gamma_{total}$ — Γ_{21}/Γ

VALUE	CL%	DOCUMENT ID		TECN	COMMENT
$<2.1 \times 10^{-3}$	90	[1] ABLIKIM	06R	BES2	$\psi(2S) \to \gamma\chi_{c1}$

[1] ABLIKIM 06R reports $< 2.4 \times 10^{-3}$ from a measurement of $[\Gamma(\chi_{c1}(1P) \to K^*_J(1430)^+K^- + c.c. \to K^0_S K^+\pi^- + c.c.)/\Gamma_{total}] \times [B(\psi(2S) \to \gamma\chi_{c1}(1P))]$ assuming $B(\psi(2S) \to \gamma\chi_{c1}(1P)) = (8.7 \pm 0.4) \times 10^{-2}$, which we rescale to our best value $B(\psi(2S) \to \gamma\chi_{c1}(1P)) = 9.75 \times 10^{-2}$.

Downloaded from https://academic.oup.com/ptep/article/2022/8/083C01/6651666 by KIT Library user on 27 September 2022

$\Gamma(K^+K^-\pi^0)/\Gamma_{total}$ — Γ_{22}/Γ

VALUE (units 10^{-3})	DOCUMENT ID		TECN	COMMENT
1.81±0.24±0.04	[1] ATHAR	07	CLEO	$\psi(2S) \to \gamma h^+ h^- h^0$

[1] ATHAR 07 reports $(1.95 \pm 0.16 \pm 0.23) \times 10^{-3}$ from a measurement of $[\Gamma(\chi_{c1}(1P) \to K^+K^-\pi^0)/\Gamma_{total}] \times [B(\psi(2S) \to \gamma\chi_{c1}(1P))]$ assuming $B(\psi(2S) \to \gamma\chi_{c1}(1P)) = 0.0907 \pm 0.0011 \pm 0.0054$, which we rescale to our best value $B(\psi(2S) \to \gamma\chi_{c1}(1P)) = (9.75 \pm 0.24) \times 10^{-2}$. Our first error is their experiment's error and our second error is the systematic error from using our best value.

$\Gamma(\eta\pi^+\pi^-)/\Gamma_{total}$ — Γ_{23}/Γ

VALUE (units 10^{-3})	EVTS	DOCUMENT ID		TECN	COMMENT
4.62±0.23 OUR AVERAGE					
4.58±0.23±0.11		[1,2] ABLIKIM	17K	BES3	$\psi(2S) \to \gamma\eta\pi^+\pi^-$
4.7 ±0.5 ±0.1		[3] ATHAR	07	CLEO	$\psi(2S) \to \gamma h^+ h^- h^0$
5.3 ±0.9 ±0.1	222	[4] ABLIKIM	06R	BES2	$\psi(2S) \to \gamma\chi_{c1}$

[1] From an amplitude analysis using an isobar model.
[2] ABLIKIM 17K reports $(4.67 \pm 0.03 \pm 0.23 \pm 0.16) \times 10^{-3}$ from a measurement of $[\Gamma(\chi_{c1}(1P) \to \eta\pi^+\pi^-)/\Gamma_{total}] \times [B(\psi(2S) \to \gamma\chi_{c1}(1P))]$ assuming $B(\psi(2S) \to \gamma\chi_{c1}(1P)) = (9.55 \pm 0.31) \times 10^{-2}$, which we rescale to our best value $B(\psi(2S) \to \gamma\chi_{c1}(1P)) = (9.75 \pm 0.24) \times 10^{-2}$. Our first error is their experiment's error and our second error is the systematic error from using our best value.
[3] ATHAR 07 reports $(5.0 \pm 0.3 \pm 0.5) \times 10^{-3}$ from a measurement of $[\Gamma(\chi_{c1}(1P) \to \eta\pi^+\pi^-)/\Gamma_{total}] \times [B(\psi(2S) \to \gamma\chi_{c1}(1P))]$ assuming $B(\psi(2S) \to \gamma\chi_{c1}(1P)) = 0.0907 \pm 0.0011 \pm 0.0054$, which we rescale to our best value $B(\psi(2S) \to \gamma\chi_{c1}(1P)) = (9.75 \pm 0.24) \times 10^{-2}$. Our first error is their experiment's error and our second error is the systematic error from using our best value.
[4] ABLIKIM 06R reports $(5.9 \pm 0.7 \pm 0.8) \times 10^{-3}$ from a measurement of $[\Gamma(\chi_{c1}(1P) \to \eta\pi^+\pi^-)/\Gamma_{total}] \times [B(\psi(2S) \to \gamma\chi_{c1}(1P))]$ assuming $B(\psi(2S) \to \gamma\chi_{c1}(1P)) = (8.7 \pm 0.4) \times 10^{-2}$, which we rescale to our best value $B(\psi(2S) \to \gamma\chi_{c1}(1P)) = (9.75 \pm 0.24) \times 10^{-2}$. Our first error is their experiment's error and our second error is the systematic error from using our best value.

$\Gamma(a_0(980)^+\pi^- + c.c. \to \eta\pi^+\pi^-)/\Gamma_{total}$ — Γ_{24}/Γ

VALUE (units 10^{-3})	EVTS	DOCUMENT ID		TECN	COMMENT
3.2 ±0.4 OUR AVERAGE		Error includes scale factor of 2.2.			
3.33±0.19±0.08		[1,2] ABLIKIM	17K	BES3	$\psi(2S) \to \gamma\eta\pi^+\pi^-$
1.79±0.63±0.04	58	[3] ABLIKIM	06R	BES2	$\psi(2S) \to \gamma\chi_{c1}$

[1] From an amplitude analysis using an isobar model.
[2] ABLIKIM 17K reports $(3.40 \pm 0.03 \pm 0.19 \pm 0.11) \times 10^{-3}$ from a measurement of $[\Gamma(\chi_{c1}(1P) \to a_0(980)^+\pi^- + c.c. \to \eta\pi^+\pi^-)/\Gamma_{total}] \times [B(\psi(2S) \to \gamma\chi_{c1}(1P))]$ assuming $B(\psi(2S) \to \gamma\chi_{c1}(1P)) = (9.55 \pm 0.31) \times 10^{-2}$, which we rescale to our best value $B(\psi(2S) \to \gamma\chi_{c1}(1P)) = (9.75 \pm 0.24) \times 10^{-2}$. Our first error is their experiment's error and our second error is the systematic error from using our best value.
[3] ABLIKIM 06R reports $(2.0 \pm 0.5 \pm 0.5) \times 10^{-3}$ from a measurement of $[\Gamma(\chi_{c1}(1P) \to a_0(980)^+\pi^- + c.c. \to \eta\pi^+\pi^-)/\Gamma_{total}] \times [B(\psi(2S) \to \gamma\chi_{c1}(1P))]$ assuming $B(\psi(2S) \to \gamma\chi_{c1}(1P)) = (8.7 \pm 0.4) \times 10^{-2}$, which we rescale to our best value $B(\psi(2S) \to \gamma\chi_{c1}(1P)) = (9.75 \pm 0.24) \times 10^{-2}$. Our first error is their experiment's error and our second error is the systematic error from using our best value.

$\Gamma(a_2(1320)^+\pi^- + c.c. \to \eta\pi^+\pi^-)/\Gamma_{total}$ — Γ_{25}/Γ

VALUE (units 10^{-3})	DOCUMENT ID		TECN	COMMENT
0.176±0.023±0.004	[1,2] ABLIKIM	17K	BES3	$\psi(2S) \to \gamma\eta\pi^+\pi^-$

[1] From an amplitude analysis using an isobar model.
[2] ABLIKIM 17K reports $(0.18 \pm 0.01 \pm 0.02 \pm 0.01) \times 10^{-3}$ from a measurement of $[\Gamma(\chi_{c1}(1P) \to a_2(1320)^+\pi^- + c.c. \to \eta\pi^+\pi^-)/\Gamma_{total}] \times [B(\psi(2S) \to \gamma\chi_{c1}(1P))]$ assuming $B(\psi(2S) \to \gamma\chi_{c1}(1P)) = (9.55 \pm 0.31) \times 10^{-2}$, which we rescale to our best value $B(\psi(2S) \to \gamma\chi_{c1}(1P)) = (9.75 \pm 0.24) \times 10^{-2}$. Our first error is their experiment's error and our second error is the systematic error from using our best value.

$\Gamma(a_2(1700)^+\pi^- + c.c. \to \eta\pi^+\pi^-)/\Gamma_{total}$ — Γ_{26}/Γ

VALUE (units 10^{-5})	DOCUMENT ID		TECN	COMMENT
4.6±0.7±0.1	[1,2] ABLIKIM	17K	BES3	$\psi(2S) \to \gamma\eta\pi^+\pi^-$

[1] From an amplitude analysis using an isobar model.
[2] ABLIKIM 17K reports $(4.7 \pm 0.4 \pm 0.6 \pm 0.2) \times 10^{-5}$ from a measurement of $[\Gamma(\chi_{c1}(1P) \to a_2(1700)^+\pi^- + c.c. \to \eta\pi^+\pi^-)/\Gamma_{total}] \times [B(\psi(2S) \to \gamma\chi_{c1}(1P))]$ assuming $B(\psi(2S) \to \gamma\chi_{c1}(1P)) = (9.55 \pm 0.31) \times 10^{-2}$, which we rescale to our best value $B(\psi(2S) \to \gamma\chi_{c1}(1P)) = (9.75 \pm 0.24) \times 10^{-2}$. Our first error is their experiment's error and our second error is the systematic error from using our best value.

$\Gamma(f_2(1270)\eta \to \eta\pi^+\pi^-)/\Gamma_{total}$ — Γ_{27}/Γ

VALUE (units 10^{-4})	DOCUMENT ID		TECN	COMMENT
3.5±0.6±0.1	[1,2] ABLIKIM	17K	BES3	$\psi(2S) \to \gamma\eta\pi^+\pi^-$

[1] From an amplitude analysis using an isobar model.
[2] ABLIKIM 17K reports $(0.36 \pm 0.01 \pm 0.06 \pm 0.01) \times 10^{-3}$ from a measurement of $[\Gamma(\chi_{c1}(1P) \to f_2(1270)\eta \to \eta\pi^+\pi^-)/\Gamma_{total}] \times [B(\psi(2S) \to \gamma\chi_{c1}(1P))]$ assuming $B(\psi(2S) \to \gamma\chi_{c1}(1P)) = (9.55 \pm 0.31) \times 10^{-2}$, which we rescale to our best value $B(\psi(2S) \to \gamma\chi_{c1}(1P)) = (9.75 \pm 0.24) \times 10^{-2}$. Our first error is their experiment's error and our second error is the systematic error from using our best value.

$\Gamma(f_4(2050)\eta \to \eta\pi^+\pi^-)/\Gamma_{total}$ — Γ_{28}/Γ

VALUE (units 10^{-5})	DOCUMENT ID		TECN	COMMENT
2.5±0.9±0.1	[1,2] ABLIKIM	17K	BES3	$\psi(2S) \to \gamma\eta\pi^+\pi^-$

[1] From an amplitude analysis using an isobar model.
[2] ABLIKIM 17K reports $(2.6 \pm 0.4 \pm 0.8 \pm 0.1) \times 10^{-5}$ from a measurement of $[\Gamma(\chi_{c1}(1P) \to f_4(2050)\eta \to \eta\pi^+\pi^-)/\Gamma_{total}] \times [B(\psi(2S) \to \gamma\chi_{c1}(1P))]$ assuming $B(\psi(2S) \to \gamma\chi_{c1}(1P)) = (9.55 \pm 0.31) \times 10^{-2}$, which we rescale to our best value $B(\psi(2S) \to \gamma\chi_{c1}(1P)) = (9.75 \pm 0.24) \times 10^{-2}$. Our first error is their experiment's error and our second error is the systematic error from using our best value.

$\Gamma(\pi_1(1400)^+\pi^- + c.c. \to \eta\pi^+\pi^-)/\Gamma_{total}$ — Γ_{29}/Γ

VALUE	CL%	DOCUMENT ID		TECN	COMMENT
$<5 \times 10^{-5}$	90	[1,2] ABLIKIM	17K	BES3	$\psi(2S) \to \gamma\eta\pi^+\pi^-$

[1] From an amplitude analysis using an isobar model.
[2] ABLIKIM 17K reports $< 4.6 \times 10^{-5}$ from a measurement of $[\Gamma(\chi_{c1}(1P) \to \pi_1(1400)^+\pi^- + c.c. \to \eta\pi^+\pi^-)/\Gamma_{total}] \times [B(\psi(2S) \to \gamma\chi_{c1}(1P))]$ assuming $B(\psi(2S) \to \gamma\chi_{c1}(1P)) = (9.55 \pm 0.31) \times 10^{-2}$, which we rescale to our best value $B(\psi(2S) \to \gamma\chi_{c1}(1P)) = 9.75 \times 10^{-2}$.

$\Gamma(\pi_1(1600)^+\pi^- + c.c. \to \eta\pi^+\pi^-)/\Gamma_{total}$ — Γ_{30}/Γ

VALUE	CL%	DOCUMENT ID		TECN	COMMENT
$<1.5 \times 10^{-5}$	90	[1,2] ABLIKIM	17K	BES3	$\psi(2S) \to \gamma\eta\pi^+\pi^-$

[1] From an amplitude analysis using an isobar model.
[2] ABLIKIM 17K reports $< 1.5 \times 10^{-5}$ from a measurement of $[\Gamma(\chi_{c1}(1P) \to \pi_1(1600)^+\pi^- + c.c. \to \eta\pi^+\pi^-)/\Gamma_{total}] \times [B(\psi(2S) \to \gamma\chi_{c1}(1P))]$ assuming $B(\psi(2S) \to \gamma\chi_{c1}(1P)) = (9.55 \pm 0.31) \times 10^{-2}$, which we rescale to our best value $B(\psi(2S) \to \gamma\chi_{c1}(1P)) = 9.75 \times 10^{-2}$.

$\Gamma(\pi_1(2015)^+\pi^- + c.c. \to \eta\pi^+\pi^-)/\Gamma_{total}$ — Γ_{31}/Γ

VALUE	CL%	DOCUMENT ID		TECN	COMMENT
$<8 \times 10^{-6}$	90	[1,2] ABLIKIM	17K	BES3	$\psi(2S) \to \gamma\eta\pi^+\pi^-$

[1] From an amplitude analysis using an isobar model.
[2] ABLIKIM 17K reports $< 8 \times 10^{-6}$ from a measurement of $[\Gamma(\chi_{c1}(1P) \to \pi_1(2015)^+\pi^- + c.c. \to \eta\pi^+\pi^-)/\Gamma_{total}] \times [B(\psi(2S) \to \gamma\chi_{c1}(1P))]$ assuming $B(\psi(2S) \to \gamma\chi_{c1}(1P)) = (9.55 \pm 0.31) \times 10^{-2}$, which we rescale to our best value $B(\psi(2S) \to \gamma\chi_{c1}(1P)) = 9.75 \times 10^{-2}$.

$\Gamma(f_2(1270)\eta)/\Gamma_{total}$ — Γ_{32}/Γ

VALUE (units 10^{-3})	EVTS	DOCUMENT ID		TECN	COMMENT
0.67±0.11 OUR AVERAGE					
0.63±0.11±0.02		[1,2] ABLIKIM	17K	BES3	$\psi(2S) \to \gamma\eta\pi^+\pi^-$
2.7 ±0.8 ±0.1	53	[3] ABLIKIM	06R	BES2	$\psi(2S) \to \gamma\chi_{c1}$

[1] ABLIKIM 17K reports $(6.4 \pm 1.1) \times 10^{-4}$ from a measurement of $[\Gamma(\chi_{c1}(1P) \to f_2(1270)\eta)/\Gamma_{total}] \times [B(\psi(2S) \to \gamma\chi_{c1}(1P))]$ assuming $B(\psi(2S) \to \gamma\chi_{c1}(1P)) = (9.55 \pm 0.31) \times 10^{-2}$, which we rescale to our best value $B(\psi(2S) \to \gamma\chi_{c1}(1P)) = (9.75 \pm 0.24) \times 10^{-2}$. Our first error is their experiment's error and our second error is the systematic error from using our best value.
[2] From an amplitude analysis using an isobar model.
[3] ABLIKIM 06R reports $(3.0 \pm 0.7 \pm 0.5) \times 10^{-3}$ from a measurement of $[\Gamma(\chi_{c1}(1P) \to f_2(1270)\eta)/\Gamma_{total}] \times [B(\psi(2S) \to \gamma\chi_{c1}(1P))]$ assuming $B(\psi(2S) \to \gamma\chi_{c1}(1P)) = (8.7 \pm 0.4) \times 10^{-2}$, which we rescale to our best value $B(\psi(2S) \to \gamma\chi_{c1}(1P)) = (9.75 \pm 0.24) \times 10^{-2}$. Our first error is their experiment's error and our second error is the systematic error from using our best value.

$\Gamma(\pi^+\pi^-\eta')/\Gamma_{total}$ — Γ_{33}/Γ

VALUE (units 10^{-3})	DOCUMENT ID		TECN	COMMENT
2.2±0.4±0.1	[1] ATHAR	07	CLEO	$\psi(2S) \to \gamma h^+ h^- h^0$

[1] ATHAR 07 reports $(2.4 \pm 0.4 \pm 0.3) \times 10^{-3}$ from a measurement of $[\Gamma(\chi_{c1}(1P) \to \pi^+\pi^-\eta')/\Gamma_{total}] \times [B(\psi(2S) \to \gamma\chi_{c1}(1P))]$ assuming $B(\psi(2S) \to \gamma\chi_{c1}(1P)) = 0.0907 \pm 0.0011 \pm 0.0054$, which we rescale to our best value $B(\psi(2S) \to \gamma\chi_{c1}(1P)) = (9.75 \pm 0.24) \times 10^{-2}$. Our first error is their experiment's error and our second error is the systematic error from using our best value.

$\Gamma(K^+K^-\eta'(958))/\Gamma_{total}$ — Γ_{34}/Γ

VALUE (units 10^{-4})	EVTS	DOCUMENT ID		TECN	COMMENT
8.75±0.87	310	[1] ABLIKIM	14J	BES3	$\psi(2S) \to \gamma K^+K^-\eta'(958)$

[1] Derived using $B(\psi(2S) \to \gamma\chi_{c1}) = (9.2 \pm 0.4)\%$. Uncertainty includes both statistical and systematic contributions combined in quadrature.

$\Gamma(K_0^*(1430)^+K^- + c.c.)/\Gamma_{total}$ — Γ_{35}/Γ

VALUE (units 10^{-4})	DOCUMENT ID		TECN	COMMENT
$6.41 \pm 0.57^{+2.09}_{-2.71}$	[1] ABLIKIM	14J	BES3	$\psi(2S) \to \gamma K^+K^-\eta'(958)$

[1] Normalized to $B(\chi_{c1} \to K^+K^-\eta'(958))$ branching fraction.

$\Gamma(f_0(980)\eta'(958))/\Gamma_{total}$ — Γ_{36}/Γ

VALUE (units 10^{-4})	DOCUMENT ID		TECN	COMMENT
$1.65 \pm 0.47^{+1.32}_{-0.56}$	[1] ABLIKIM	14J	BES3	$\psi(2S) \to \gamma K^+K^-\eta'(958)$

[1] Normalized to $B(\chi_{c1} \to K^+K^-\eta'(958))$ branching fraction.

Downloaded from https://academic.oup.com/ptep/article/2022/8/083C01/6651666 by KIT Library user on 27 September 2022

$\Gamma(f_0(1710)\eta'(958))/\Gamma_{total}$ — Γ_{37}/Γ

VALUE (units 10^{-4})	DOCUMENT ID		TECN	COMMENT
$0.71\pm0.22^{+0.68}_{-0.48}$	[1] ABLIKIM	14J	BES3	$\psi(2S)\to\gamma K^+K^-\eta'(958)$

[1] Normalized to $B(\chi_{c1}\to K^+K^-\eta'(958))$ branching fraction.

$\Gamma(f_2'(1525)\eta'(958))/\Gamma_{total}$ — Γ_{38}/Γ

VALUE (units 10^{-4})	DOCUMENT ID		TECN	COMMENT
$0.92\pm0.23^{+0.55}_{-0.51}$	[1] ABLIKIM	14J	BES3	$\psi(2S)\to\gamma K^+K^-\eta'(958)$

[1] Normalized to $B(\chi_{c1}\to K^+K^-\eta'(958))$ branching fraction.

$\Gamma(\pi^0 f_0(980)\to\pi^0\pi^+\pi^-)/\Gamma_{total}$ — Γ_{39}/Γ

VALUE (units 10^{-6})	CL%	DOCUMENT ID		TECN	COMMENT
0.35 ± 0.09		ABLIKIM	18D	BES3	$\psi(2S)\to\gamma\pi^0\pi^+\pi^-$
• • • We do not use the following data for averages, fits, limits, etc. • • •					
<6	90	[1] ABLIKIM	11D	BES3	$\psi(2S)\to\gamma\pi^0\pi^+\pi^-$

[1] ABLIKIM 11D reports $[\Gamma(\chi_{c1}(1P)\to\pi^0 f_0(980)\to\pi^0\pi^+\pi^-)/\Gamma_{total}]\times[B(\psi(2S)\to\gamma\chi_{c1}(1P))]<6.0\times10^{-7}$ which we divide by our best value $B(\psi(2S)\to\gamma\chi_{c1}(1P))=9.75\times10^{-2}$.

$\Gamma(K^+\overline{K}^*(892)^0\pi^-+\text{c.c.})/\Gamma_{total}$ — Γ_{40}/Γ

VALUE (units 10^{-4})	DOCUMENT ID		TECN	COMMENT
32 ± 21	[1] TANENBAUM	78	MRK1	$\psi(2S)\to\gamma\chi_{c1}$

[1] Estimated using $B(\psi(2S)\to\gamma\chi_{c1}(1P))=0.087$. The errors do not contain the uncertainty in the $\psi(2S)$ decay.

$\Gamma(K^*(892)^0\overline{K}^*(892)^0)/\Gamma_{total}$ — Γ_{41}/Γ

VALUE (units 10^{-3})	EVTS	DOCUMENT ID		TECN	COMMENT
$1.44\pm0.36\pm0.03$	28.4 ± 5.5	[1,2] ABLIKIM	04H	BES	$\psi(2S)\to\gamma K^+K^-\pi^+\pi^-$

[1] ABLIKIM 04H reports $[\Gamma(\chi_{c1}(1P)\to K^*(892)^0\overline{K}^*(892)^0)/\Gamma_{total}]\times[B(\psi(2S)\to\gamma\chi_{c1}(1P))]=(1.40\pm0.27\pm0.22)\times10^{-4}$ which we divide by our best value $B(\psi(2S)\to\gamma\chi_{c1}(1P))=(9.75\pm0.24)\times10^{-2}$. Our first error is their experiment's error and our second error is the systematic error from using our best value.

[2] Assumes $B(K^*(892)^0\to K^-\pi^+)=2/3$.

$\Gamma(K^+K^-K^0_SK^0_S)/\Gamma_{total}$ — Γ_{42}/Γ

VALUE	CL%	EVTS	DOCUMENT ID		TECN	COMMENT
$<4\times10^{-4}$	90	3.2 ± 2.4	[1] ABLIKIM	05O	BES2	$\psi(2S)\to\chi_{c1}\gamma$

[1] ABLIKIM 05O reports $[\Gamma(\chi_{c1}(1P)\to K^+K^-K^0_SK^0_S)/\Gamma_{total}]\times[B(\psi(2S)\to\gamma\chi_{c1}(1P))]<4.2\times10^{-5}$ which we divide by our best value $B(\psi(2S)\to\gamma\chi_{c1}(1P))=9.75\times10^{-2}$.

$\Gamma(K^0_SK^0_SK^0_SK^0_S)/\Gamma_{total}$ — Γ_{43}/Γ

VALUE (units 10^{-4})	EVTS	DOCUMENT ID		TECN	COMMENT
$0.35\pm0.10\pm0.01$	22	[1] ABLIKIM	19AA	BES3	$\psi(2S)\to\gamma4K^0_S$

[1] Using $B(K^0_S\to\pi^+\pi^-)=(69.20\pm0.05)\%$. ABLIKIM 19AA reports $[\Gamma(\chi_{c1}(1P)\to K^0_SK^0_SK^0_SK^0_S)/\Gamma_{total}]\times[B(\psi(2S)\to\gamma\chi_{c1}(1P))]=(3.4\pm0.9\pm0.3)\times10^{-6}$ which we divide by our best value $B(\psi(2S)\to\gamma\chi_{c1}(1P))=(9.75\pm0.24)\times10^{-2}$. Our first error is their experiment's error and our second error is the systematic error from using our best value..

$\Gamma(K^+K^-K^+K^-)/\Gamma_{total}$ — Γ_{44}/Γ

VALUE (units 10^{-3})	DOCUMENT ID
0.54 ± 0.11 OUR FIT	

$\Gamma(K^+K^-\phi)/\Gamma_{total}$ — Γ_{45}/Γ

VALUE (units 10^{-3})	EVTS	DOCUMENT ID		TECN	COMMENT
$0.41\pm0.15\pm0.01$	17	[1] ABLIKIM	06T	BES2	$\psi(2S)\to\gamma2K^+2K^-$

[1] ABLIKIM 06T reports $(0.46\pm0.16\pm0.06)\times10^{-3}$ from a measurement of $[\Gamma(\chi_{c1}(1P)\to K^+K^-\phi)/\Gamma_{total}]\times[B(\psi(2S)\to\gamma\chi_{c1}(1P))]$ assuming $B(\psi(2S)\to\gamma\chi_{c1}(1P))=(8.7\pm0.4)\times10^{-2}$, which we rescale to our best value $B(\psi(2S)\to\gamma\chi_{c1}(1P))=(9.75\pm0.24)\times10^{-2}$. Our first error is their experiment's error and our second error is the systematic error from using our best value.

$\Gamma(\overline{K}^0K^+\pi^-\phi+\text{c.c.})/\Gamma_{total}$ — Γ_{46}/Γ

VALUE (units 10^{-3})	DOCUMENT ID		TECN	COMMENT
$3.27\pm0.28\pm0.46$	ABLIKIM	15M	BES3	$\psi(2S)\to\gamma\chi_{c1}$

$\Gamma(K^+K^-\pi^0\phi)/\Gamma_{total}$ — Γ_{47}/Γ

VALUE (units 10^{-3})	DOCUMENT ID		TECN	COMMENT
$1.62\pm0.12\pm0.28$	ABLIKIM	15M	BES3	$\psi(2S)\to\gamma\chi_{c1}$

$\Gamma(\phi\pi^+\pi^-\pi^0)/\Gamma_{total}$ — Γ_{48}/Γ

VALUE (units 10^{-3})	EVTS	DOCUMENT ID		TECN	COMMENT
$0.75\pm0.06\pm0.08$	373	[1] ABLIKIM	13B	BES3	$e^+e^-\to\psi(2S)\to\gamma\chi_{c1}$

[1] Using 1.06×10^8 $\psi(2S)$ mesons and $B(\psi(2S)\to\chi_{c1}\gamma)=(9.2\pm0.4)\%$.

$\Gamma(\omega\omega)/\Gamma_{total}$ — Γ_{49}/Γ

VALUE (units 10^{-4})	EVTS	DOCUMENT ID		TECN	COMMENT
$5.7\pm0.7\pm0.1$	597	[1] ABLIKIM	11K	BES3	$\psi(2S)\to\gamma$ hadrons

[1] ABLIKIM 11K reports $(6.0\pm0.3\pm0.7)\times10^{-4}$ from a measurement of $[\Gamma(\chi_{c1}(1P)\to\omega\omega)/\Gamma_{total}]\times[B(\psi(2S)\to\gamma\chi_{c1}(1P))]$ assuming $B(\psi(2S)\to\gamma\chi_{c1}(1P))=(9.2\pm0.4)\times10^{-2}$, which we rescale to our best value $B(\psi(2S)\to\gamma\chi_{c1}(1P))=(9.75\pm0.24)\times10^{-2}$. Our first error is their experiment's error and our second error is the systematic error from using our best value.

$\Gamma(\omega K^+K^-)/\Gamma_{total}$ — Γ_{50}/Γ

VALUE (units 10^{-3})	EVTS	DOCUMENT ID		TECN	COMMENT
$0.78\pm0.04\pm0.08$	628	[1] ABLIKIM	13B	BES3	$e^+e^-\to\psi(2S)\to\gamma\chi_{c1}$

[1] Using 1.06×10^8 $\psi(2S)$ mesons and $B(\psi(2S)\to\chi_{c1}\gamma)=(9.2\pm0.4)\%$.

$\Gamma(\omega\phi)/\Gamma_{total}$ — Γ_{51}/Γ

VALUE (units 10^{-4})	EVTS	DOCUMENT ID		TECN	COMMENT
$0.27\pm0.04\pm0.01$	105	[1] ABLIKIM	19J	BES3	$\psi(2S)\to\gamma$ hadrons
• • • We do not use the following data for averages, fits, limits, etc. • • •					
$0.21\pm0.06\pm0.01$	15	[2,3] ABLIKIM	11K	BES3	$\psi(2S)\to\gamma$ hadrons

[1] ABLIKIM 19J reports $[\Gamma(\chi_{c1}(1P)\to\omega\phi)/\Gamma_{total}]\times[B(\psi(2S)\to\gamma\chi_{c1}(1P))]=(2.67\pm0.31\pm0.27)\times10^{-6}$ which we divide by our best value $B(\psi(2S)\to\gamma\chi_{c1}(1P))=(9.75\pm0.24)\times10^{-2}$. Our first error is their experiment's error and our second error is the systematic error from using our best value.

[2] ABLIKIM 11K reports $(0.22\pm0.06\pm0.02)\times10^{-4}$ from a measurement of $[\Gamma(\chi_{c1}(1P)\to\omega\phi)/\Gamma_{total}]\times[B(\psi(2S)\to\gamma\chi_{c1}(1P))]$ assuming $B(\psi(2S)\to\gamma\chi_{c1}(1P))=(9.2\pm0.4)\times10^{-2}$, which we rescale to our best value $B(\psi(2S)\to\gamma\chi_{c1}(1P))=(9.75\pm0.24)\times10^{-2}$. Our first error is their experiment's error and our second error is the systematic error from using our best value.

[3] Superseded by ABLIKIM 19J.

$\Gamma(\phi\phi)/\Gamma_{total}$ — Γ_{52}/Γ

VALUE (units 10^{-4})	EVTS	DOCUMENT ID		TECN	COMMENT
$4.2\pm0.5\pm0.1$	366	[1] ABLIKIM	11K	BES3	$\psi(2S)\to\gamma$ hadrons

[1] ABLIKIM 11K reports $(4.4\pm0.3\pm0.5)\times10^{-4}$ from a measurement of $[\Gamma(\chi_{c1}(1P)\to\phi\phi)/\Gamma_{total}]\times[B(\psi(2S)\to\gamma\chi_{c1}(1P))]$ assuming $B(\psi(2S)\to\gamma\chi_{c1}(1P))=(9.2\pm0.4)\times10^{-2}$, which we rescale to our best value $B(\psi(2S)\to\gamma\chi_{c1}(1P))=(9.75\pm0.24)\times10^{-2}$. Our first error is their experiment's error and our second error is the systematic error from using our best value.

$\Gamma(\phi\phi\eta)/\Gamma_{total}$ — Γ_{53}/Γ

VALUE (units 10^{-4})	EVTS	DOCUMENT ID		TECN	COMMENT
$3.0\pm0.4\pm0.2$	83.6	[1] ABLIKIM	20B	BES3	$\psi(2S)\to\gamma\phi\phi\eta$

[1] ABLIKIM 20B reports $(2.96\pm0.43\pm0.22)\times10^{-4}$ from a measurement of $[\Gamma(\chi_{c1}(1P)\to\phi\phi\eta)/\Gamma_{total}]\times[B(\psi(2S)\to\gamma\chi_{c1}(1P))]$ assuming $B(\psi(2S)\to\gamma\chi_{c1}(1P))=(9.75\pm0.24)\times10^{-2}$.

$\Gamma(p\overline{p})/\Gamma_{total}$ — Γ_{54}/Γ

VALUE (units 10^{-4})	DOCUMENT ID
0.760 ± 0.034 OUR FIT	

$\Gamma(p\overline{p}\pi^0)/\Gamma_{total}$ — Γ_{55}/Γ

VALUE (units 10^{-3})	DOCUMENT ID		TECN	COMMENT
0.155 ± 0.018 OUR AVERAGE				
$0.163\pm0.019\pm0.004$	[1] ONYISI	10	CLE3	$\psi(2S)\to\gamma p\overline{p}X$
$0.112\pm0.047\pm0.003$	[2] ATHAR	07	CLEO	$\psi(2S)\to\gamma h^+h^-h^0$

[1] ONYISI 10 reports $(1.75\pm0.16\pm0.13\pm0.11)\times10^{-4}$ from a measurement of $[\Gamma(\chi_{c1}(1P)\to p\overline{p}\pi^0)/\Gamma_{total}]\times[B(\psi(2S)\to\gamma\chi_{c1}(1P))]$ assuming $B(\psi(2S)\to\gamma\chi_{c1}(1P))=(9.07\pm0.11\pm0.54)\times10^{-2}$, which we rescale to our best value $B(\psi(2S)\to\gamma\chi_{c1}(1P))=(9.75\pm0.24)\times10^{-2}$. Our first error is their experiment's error and our second error is the systematic error from using our best value.

[2] ATHAR 07 reports $(1.2\pm0.5\pm0.1)\times10^{-4}$ from a measurement of $[\Gamma(\chi_{c1}(1P)\to p\overline{p}\pi^0)/\Gamma_{total}]\times[B(\psi(2S)\to\gamma\chi_{c1}(1P))]$ assuming $B(\psi(2S)\to\gamma\chi_{c1}(1P))=(9.07\pm0.11\pm0.54)\times10^{-2}$, which we rescale to our best value $B(\psi(2S)\to\gamma\chi_{c1}(1P))=(9.75\pm0.24)\times10^{-2}$. Our first error is their experiment's error and our second error is the systematic error from using our best value.

$\Gamma(p\overline{p}\eta)/\Gamma_{total}$ — Γ_{56}/Γ

VALUE (units 10^{-3})	CL%	DOCUMENT ID		TECN	COMMENT
$0.145\pm0.024\pm0.004$		[1] ONYISI	10	CLE3	$\psi(2S)\to\gamma p\overline{p}X$
• • • We do not use the following data for averages, fits, limits, etc. • • •					
<0.15	90	[2] ATHAR	07	CLEO	$\psi(2S)\to\gamma h^+h^-h^0$

[1] ONYISI 10 reports $(1.56\pm0.22\pm0.14\pm0.10)\times10^{-4}$ from a measurement of $[\Gamma(\chi_{c1}(1P)\to p\overline{p}\eta)/\Gamma_{total}]\times[B(\psi(2S)\to\gamma\chi_{c1}(1P))]$ assuming $B(\psi(2S)\to\gamma\chi_{c1}(1P))=(9.07\pm0.11\pm0.54)\times10^{-2}$, which we rescale to our best value $B(\psi(2S)\to\gamma\chi_{c1}(1P))=(9.75\pm0.24)\times10^{-2}$. Our first error is their experiment's error and our second error is the systematic error from using our best value.

[2] ATHAR 07 reports $<0.16\times10^{-3}$ from a measurement of $[\Gamma(\chi_{c1}(1P)\to p\overline{p}\eta)/\Gamma_{total}]\times[B(\psi(2S)\to\gamma\chi_{c1}(1P))]$ assuming $B(\psi(2S)\to\gamma\chi_{c1}(1P))=(9.07\pm0.11\pm0.54)\times10^{-2}$, which we rescale to our best value $B(\psi(2S)\to\gamma\chi_{c1}(1P))=9.75\times10^{-2}$.

Downloaded from https://academic.oup.com/ptep/article/2022/8/083C01/6651666 by KIT Library user on 27 September 2022

$\Gamma(p\overline{p}\omega)/\Gamma_{total}$ — Γ_{57}/Γ

VALUE (units 10^{-3})	DOCUMENT ID		TECN	COMMENT
0.212±0.030±0.005	[1] ONYISI	10	CLE3	$\psi(2S) \to \gamma p\overline{p}X$

[1] ONYISI 10 reports $(2.28 \pm 0.28 \pm 0.16 \pm 0.14) \times 10^{-4}$ from a measurement of $[\Gamma(\chi_{c1}(1P) \to p\overline{p}\omega)/\Gamma_{total}] \times [B(\psi(2S) \to \gamma\chi_{c1}(1P))]$ assuming $B(\psi(2S) \to \gamma\chi_{c1}(1P)) = (9.07 \pm 0.11 \pm 0.54) \times 10^{-2}$, which we rescale to our best value $B(\psi(2S) \to \gamma\chi_{c1}(1P)) = (9.75 \pm 0.24) \times 10^{-2}$. Our first error is their experiment's error and our second error is the systematic error from using our best value.

$\Gamma(p\overline{p}\phi)/\Gamma_{total}$ — Γ_{58}/Γ

VALUE	CL%	DOCUMENT ID		TECN	COMMENT
$<1.7 \times 10^{-5}$	90	[1] ABLIKIM	11F	BES3	$\psi(2S) \to \gamma p\overline{p}K^+K^-$

[1] ABLIKIM 11F reports $< 1.82 \times 10^{-5}$ from a measurement of $[\Gamma(\chi_{c1}(1P) \to p\overline{p}\phi)/\Gamma_{total}] \times [B(\psi(2S) \to \gamma\chi_{c1}(1P))]$ assuming $B(\psi(2S) \to \gamma\chi_{c1}(1P)) = (9.2 \pm 0.4) \times 10^{-2}$, which we rescale to our best value $B(\psi(2S) \to \gamma\chi_{c1}(1P)) = 9.75 \times 10^{-2}$.

$\Gamma(p\overline{p}\pi^+\pi^-)/\Gamma_{total}$ — Γ_{59}/Γ

VALUE (units 10^{-3})	DOCUMENT ID		TECN	COMMENT
0.50±0.19 OUR EVALUATION	Treating systematic error as correlated.			
0.50±0.19 OUR AVERAGE				
0.46±0.12±0.15	[1] BAI	99B	BES	$\psi(2S) \to \gamma\chi_{c1}$
1.08±0.77±0.05	[1] TANENBAUM	78	MRK1	$\psi(2S) \to \gamma\chi_{c1}$

[1] Rescaled by us using $B(\psi(2S) \to \gamma\chi_{c1}) = (8.8 \pm 0.4)\%$ and $B(\psi(2S) \to J/\psi(1S)\pi^+\pi^-) = (32.6 \pm 0.5)\%$.

$\Gamma(p\overline{p}\pi^0\pi^0)/\Gamma_{total}$ — Γ_{60}/Γ

VALUE	CL%	DOCUMENT ID		TECN	COMMENT
$<5 \times 10^{-4}$	90	[1] HE	08B	CLEO	$e^+e^- \to \gamma h^+h^-h^0h^0$

[1] HE 08B reports $< 0.05 \times 10^{-2}$ from a measurement of $[\Gamma(\chi_{c1}(1P) \to p\overline{p}\pi^0\pi^0)/\Gamma_{total}] \times [B(\psi(2S) \to \gamma\chi_{c1}(1P))]$ assuming $B(\psi(2S) \to \gamma\chi_{c1}(1P)) = (9.07 \pm 0.11 \pm 0.54) \times 10^{-2}$, which we rescale to our best value $B(\psi(2S) \to \gamma\chi_{c1}(1P)) = 9.75 \times 10^{-2}$.

$\Gamma(p\overline{p}K^+K^-(\text{non-resonant}))/\Gamma_{total}$ — Γ_{61}/Γ

VALUE (units 10^{-4})	EVTS	DOCUMENT ID		TECN	COMMENT
1.27±0.22±0.03	82 ± 9	[1] ABLIKIM	11F	BES3	$\psi(2S) \to \gamma p\overline{p}K^+K^-$

[1] ABLIKIM 11F reports $(1.35 \pm 0.15 \pm 0.19) \times 10^{-4}$ from a measurement of $[\Gamma(\chi_{c1}(1P) \to p\overline{p}K^+K^-(\text{non-resonant}))/\Gamma_{total}] \times [B(\psi(2S) \to \gamma\chi_{c1}(1P))]$ assuming $B(\psi(2S) \to \gamma\chi_{c1}(1P)) = (9.2 \pm 0.4) \times 10^{-2}$, which we rescale to our best value $B(\psi(2S) \to \gamma\chi_{c1}(1P)) = (9.75 \pm 0.24) \times 10^{-2}$. Our first error is their experiment's error and our second error is the systematic error from using our best value.

$\Gamma(p\overline{p}K^0_SK^0_S)/\Gamma_{total}$ — Γ_{62}/Γ

VALUE (units 10^{-4})	CL%	DOCUMENT ID		TECN	COMMENT
<4.5	90	[1] ABLIKIM	06D	BES2	$\psi(2S) \to \gamma\chi_{c1}$

[1] Using $B(\psi(2S) \to \chi_{c1}\gamma)$ (9.1 ± 0.6)%.

$\Gamma(p\overline{n}\pi^-)/\Gamma_{total}$ — Γ_{63}/Γ

VALUE (units 10^{-4})	EVTS	DOCUMENT ID		TECN	COMMENT
3.8±0.5±0.1	1412	[1] ABLIKIM	12J	BES3	$\psi(2S) \to \gamma p\overline{n}\pi^-$

[1] ABLIKIM 12J reports $[\Gamma(\chi_{c1}(1P) \to p\overline{n}\pi^-)/\Gamma_{total}] \times [B(\psi(2S) \to \gamma\chi_{c1}(1P))] = (0.37 \pm 0.02 \pm 0.04) \times 10^{-4}$ which we divide by our best value $B(\psi(2S) \to \gamma\chi_{c1}(1P)) = (9.75 \pm 0.24) \times 10^{-2}$. Our first error is their experiment's error and our second error is the systematic error from using our best value.

$\Gamma(\overline{p}n\pi^+)/\Gamma_{total}$ — Γ_{64}/Γ

VALUE (units 10^{-4})	EVTS	DOCUMENT ID		TECN	COMMENT
3.9±0.5±0.1	1625	[1] ABLIKIM	12J	BES3	$\psi(2S) \to \gamma\overline{p}n\pi^+$

[1] ABLIKIM 12J reports $[\Gamma(\chi_{c1}(1P) \to \overline{p}n\pi^+)/\Gamma_{total}] \times [B(\psi(2S) \to \gamma\chi_{c1}(1P))] = (0.38 \pm 0.02 \pm 0.04) \times 10^{-4}$ which we divide by our best value $B(\psi(2S) \to \gamma\chi_{c1}(1P)) = (9.75 \pm 0.24) \times 10^{-2}$. Our first error is their experiment's error and our second error is the systematic error from using our best value.

$\Gamma(p\overline{n}\pi^-\pi^0)/\Gamma_{total}$ — Γ_{65}/Γ

VALUE (units 10^{-4})	EVTS	DOCUMENT ID		TECN	COMMENT
10.3±1.1±0.2	1082	[1] ABLIKIM	12J	BES3	$\psi(2S) \to \gamma p\overline{n}\pi^-\pi^0$

[1] ABLIKIM 12J reports $[\Gamma(\chi_{c1}(1P) \to p\overline{n}\pi^-\pi^0)/\Gamma_{total}] \times [B(\psi(2S) \to \gamma\chi_{c1}(1P))] = (1.00 \pm 0.05 \pm 0.10) \times 10^{-4}$ which we divide by our best value $B(\psi(2S) \to \gamma\chi_{c1}(1P)) = (9.75 \pm 0.24) \times 10^{-2}$. Our first error is their experiment's error and our second error is the systematic error from using our best value.

$\Gamma(\overline{p}n\pi^+\pi^0)/\Gamma_{total}$ — Γ_{66}/Γ

VALUE (units 10^{-4})	EVTS	DOCUMENT ID		TECN	COMMENT
10.1±1.1±0.2	1261	[1] ABLIKIM	12J	BES3	$\psi(2S) \to \gamma\overline{p}n\pi^+\pi^0$

[1] ABLIKIM 12J reports $[\Gamma(\chi_{c1}(1P) \to \overline{p}n\pi^+\pi^0)/\Gamma_{total}] \times [B(\psi(2S) \to \gamma\chi_{c1}(1P))] = (0.98 \pm 0.05 \pm 0.10) \times 10^{-4}$ which we divide by our best value $B(\psi(2S) \to \gamma\chi_{c1}(1P)) = (9.75 \pm 0.24) \times 10^{-2}$. Our first error is their experiment's error and our second error is the systematic error from using our best value.

$\Gamma(\Lambda\overline{\Lambda})/\Gamma_{total}$ — Γ_{67}/Γ

VALUE (units 10^{-4})	DOCUMENT ID
1.27±0.08 OUR FIT	

$\Gamma(\Lambda\overline{\Lambda}\pi^+\pi^-)/\Gamma_{total}$ — Γ_{68}/Γ

VALUE (units 10^{-5})	CL%	EVTS	DOCUMENT ID		TECN	COMMENT
29±5±1		105	[1] ABLIKIM	12I	BES3	$\psi(2S) \to \gamma\Lambda\overline{\Lambda}\pi^+\pi^-$
• • • We do not use the following data for averages, fits, limits, etc. • • •						
<150		90	[2] ABLIKIM	06D	BES2	$\psi(2S) \to \gamma\chi_{c1}$

[1] ABLIKIM 12I reports $(31.1 \pm 3.4 \pm 3.9) \times 10^{-5}$ from a measurement of $[\Gamma(\chi_{c1}(1P) \to \Lambda\overline{\Lambda}\pi^+\pi^-)/\Gamma_{total}] \times [B(\psi(2S) \to \gamma\chi_{c1}(1P))]$ assuming $B(\psi(2S) \to \gamma\chi_{c1}(1P)) = (9.2 \pm 0.4) \times 10^{-2}$, which we rescale to our best value $B(\psi(2S) \to \gamma\chi_{c1}(1P)) = (9.75 \pm 0.24) \times 10^{-2}$. Our first error is their experiment's error and our second error is the systematic error from using our best value.

[2] Using $B(\psi(2S) \to \chi_{c1}\gamma)$ (9.1 ± 0.6)%.

$\Gamma(\Lambda\overline{\Lambda}\pi^+\pi^-(\text{non-resonant}))/\Gamma_{total}$ — Γ_{69}/Γ

VALUE (units 10^{-5})	EVTS	DOCUMENT ID		TECN	COMMENT
25±6±1	13	[1] ABLIKIM	12I	BES3	$\psi(2S) \to \gamma\Lambda\overline{\Lambda}\pi^+\pi^-$

[1] ABLIKIM 12I reports $(26.2 \pm 5.5 \pm 3.3) \times 10^{-5}$ from a measurement of $[\Gamma(\chi_{c1}(1P) \to \Lambda\overline{\Lambda}\pi^+\pi^-(\text{non-resonant}))/\Gamma_{total}] \times [B(\psi(2S) \to \gamma\chi_{c1}(1P))]$ assuming $B(\psi(2S) \to \gamma\chi_{c1}(1P)) = (9.2 \pm 0.4) \times 10^{-2}$, which we rescale to our best value $B(\psi(2S) \to \gamma\chi_{c1}(1P)) = (9.75 \pm 0.24) \times 10^{-2}$. Our first error is their experiment's error and our second error is the systematic error from using our best value.

$\Gamma(\Sigma(1385)^+\overline{\Lambda}\pi^- + \text{c.c.})/\Gamma_{total}$ — Γ_{70}/Γ

VALUE	CL%	DOCUMENT ID		TECN	COMMENT
$<1.3 \times 10^{-4}$	90	[1] ABLIKIM	12I	BES3	$\psi(2S) \to \gamma\Sigma(1385)^+\overline{\Lambda}\pi^-$

[1] ABLIKIM 12I reports $< 14 \times 10^{-5}$ from a measurement of $[\Gamma(\chi_{c1}(1P) \to \Sigma(1385)^+\overline{\Lambda}\pi^- + \text{c.c.})/\Gamma_{total}] \times [B(\psi(2S) \to \gamma\chi_{c1}(1P))]$ assuming $B(\psi(2S) \to \gamma\chi_{c1}(1P)) = (9.2 \pm 0.4) \times 10^{-2}$, which we rescale to our best value $B(\psi(2S) \to \gamma\chi_{c1}(1P)) = 9.75 \times 10^{-2}$.

$\Gamma(\Sigma(1385)^-\overline{\Lambda}\pi^+ + \text{c.c.})/\Gamma_{total}$ — Γ_{71}/Γ

VALUE (units 10^{-5})	CL%	DOCUMENT ID		TECN	COMMENT
<13	90	[1] ABLIKIM	12I	BES3	$\psi(2S) \to \gamma\Sigma(1385)^-\overline{\Lambda}\pi^+$

[1] ABLIKIM 12I reports $< 14 \times 10^{-5}$ from a measurement of $[\Gamma(\chi_{c1}(1P) \to \Sigma(1385)^-\overline{\Lambda}\pi^+ + \text{c.c.})/\Gamma_{total}] \times [B(\psi(2S) \to \gamma\chi_{c1}(1P))]$ assuming $B(\psi(2S) \to \gamma\chi_{c1}(1P)) = (9.2 \pm 0.4) \times 10^{-2}$, which we rescale to our best value $B(\psi(2S) \to \gamma\chi_{c1}(1P)) = 9.75 \times 10^{-2}$.

$\Gamma(K^+\overline{p}\Lambda + \text{c.c.})/\Gamma_{total}$ — Γ_{72}/Γ

VALUE (units 10^{-4})	EVTS	DOCUMENT ID		TECN	COMMENT
4.2±0.4 OUR AVERAGE	Error includes scale factor of 1.2.				
$9.2^{+2.8}_{-2.4} \pm 0.4$	24	[1] LU	19	BELL	$B^+ \to \overline{p}\Lambda K^+K^+$
4.2±0.4±0.1	3k	[2,3] ABLIKIM	13D	BES3	$\psi(2S) \to \gamma\Lambda\overline{p}K^+$
3.1±0.9±0.1		[4] ATHAR	07	CLEO	$\psi(2S) \to \gamma h^+h^-h^0$

[1] LU 19 reports $(9.15^{+2.63}_{-2.25} \pm 0.86) \times 10^{-4}$ from a measurement of $[\Gamma(\chi_{c1}(1P) \to K^+\overline{p}\Lambda + \text{c.c.})/\Gamma_{total}] \times [B(B^+ \to \chi_{c1}(1P)K^+)]$ assuming $B(B^+ \to \chi_{c1}(1P)K^+) = (4.79 \pm 0.23) \times 10^{-4}$, which we rescale to our best value $B(B^+ \to \chi_{c1}(1P)K^+) = (4.74 \pm 0.22) \times 10^{-4}$. Our first error is their experiment's error and our second error is the systematic error from using our best value.

[2] ABLIKIM 13D reports $(4.5 \pm 0.2 \pm 0.4) \times 10^{-4}$ from a measurement of $[\Gamma(\chi_{c1}(1P) \to K^+\overline{p}\Lambda + \text{c.c.})/\Gamma_{total}] \times [B(\psi(2S) \to \gamma\chi_{c1}(1P))]$ assuming $B(\psi(2S) \to \gamma\chi_{c1}(1P)) = (9.2 \pm 0.4) \times 10^{-2}$, which we rescale to our best value $B(\psi(2S) \to \gamma\chi_{c1}(1P)) = (9.75 \pm 0.24) \times 10^{-2}$. Our first error is their experiment's error and our second error is the systematic error from using our best value.

[3] Using $B(\Lambda \to p\pi^-) = 63.9\%$.

[4] ATHAR 07 reports $(3.3 \pm 0.9 \pm 0.4) \times 10^{-4}$ from a measurement of $[\Gamma(\chi_{c1}(1P) \to K^+\overline{p}\Lambda + \text{c.c.})/\Gamma_{total}] \times [B(\psi(2S) \to \gamma\chi_{c1}(1P))]$ assuming $B(\psi(2S) \to \gamma\chi_{c1}(1P)) = (9.07 \pm 0.11 \pm 0.54) \times 10^{-2}$, which we rescale to our best value $B(\psi(2S) \to \gamma\chi_{c1}(1P)) = (9.75 \pm 0.24) \times 10^{-2}$. Our first error is their experiment's error and our second error is the systematic error from using our best value.

$\Gamma(nK^0_S\overline{\Lambda} + \text{c.c.})/\Gamma_{total}$ — Γ_{73}/Γ

VALUE (units 10^{-4})	EVTS	DOCUMENT ID		TECN	COMMENT
1.66±0.12±0.12	399	[1] ABLIKIM	21AV	BES3	$\psi(2S) \to \gamma nK^0_S\overline{\Lambda}$ + c.c.

[1] ABLIKIM 21AV reports $(1.66 \pm 0.12 \pm 0.12) \times 10^{-4}$ from a measurement of $[\Gamma(\chi_{c1}(1P) \to nK^0_S\overline{\Lambda} + \text{c.c.})/\Gamma_{total}] \times [B(\psi(2S) \to \gamma\chi_{c1}(1P))]$ assuming $B(\psi(2S) \to \gamma\chi_{c1}(1P)) = 0.0975 \pm 0.0024$. Also uses $B(\overline{\Lambda} \to \overline{p}\pi^+) = (63.9 \pm 0.5)\%$ and $B(K^0_S \to \pi^+\pi^-) = (69.20 \pm 0.05)\%$.

$\Gamma(K^*(892)^+\overline{p}\Lambda + \text{c.c.})/\Gamma_{total}$ — Γ_{74}/Γ

VALUE (units 10^{-4})	EVTS	DOCUMENT ID		TECN	COMMENT
4.9±0.7±0.1	328	[1] ABLIKIM	19AU	BES3	$\psi(2S) \to \gamma K^{*+}\overline{p}\Lambda$

[1] ABLIKIM 19AU reports $[\Gamma(\chi_{c1}(1P) \to K^*(892)^+\overline{p}\Lambda + \text{c.c.})/\Gamma_{total}] \times [B(\psi(2S) \to \gamma\chi_{c1}(1P))] = (4.8 \pm 0.5 \pm 0.4) \times 10^{-5}$ which we divide by our best value $B(\psi(2S) \to \gamma\chi_{c1}(1P)) = (9.75 \pm 0.24) \times 10^{-2}$. Our first error is their experiment's error and our second error is the systematic error from using our best value.

Downloaded from https://academic.oup.com/ptep/article/2022/8/083C01/6651666 by KIT Library user on 27 September 2022

$\Gamma(K^+\overline{p}\Lambda(1520)+\text{c.c.})/\Gamma_{\text{total}}$ — Γ_{75}/Γ

VALUE (units 10^{-4})	EVTS	DOCUMENT ID		TECN	COMMENT
1.71±0.44±0.04	48 ± 10	[1] ABLIKIM	11F	BES3	$\psi(2S) \to \gamma p\overline{p}K^+K^-$

[1] ABLIKIM 11F reports $(1.81\pm0.38\pm0.28)\times10^{-4}$ from a measurement of $[\Gamma(\chi_{c1}(1P) \to K^+\overline{p}\Lambda(1520)+\text{c.c.})/\Gamma_{\text{total}}] \times [B(\psi(2S) \to \gamma\chi_{c1}(1P))]$ assuming $B(\psi(2S) \to \gamma\chi_{c1}(1P)) = (9.2 \pm 0.4)\times10^{-2}$, which we rescale to our best value $B(\psi(2S) \to \gamma\chi_{c1}(1P)) = (9.75 \pm 0.24)\times10^{-2}$. Our first error is their experiment's error and our second error is the systematic error from using our best value.

$\Gamma(\Lambda(1520)\overline{\Lambda}(1520))/\Gamma_{\text{total}}$ — Γ_{76}/Γ

VALUE	CL%	DOCUMENT ID		TECN	COMMENT
<9 × 10^{-5}	90	[1] ABLIKIM	11F	BES3	$\psi(2S) \to \gamma p\overline{p}K^+K^-$

[1] ABLIKIM 11F reports $< 1.00\times10^{-4}$ from a measurement of $[\Gamma(\chi_{c1}(1P) \to \Lambda(1520)\overline{\Lambda}(1520))/\Gamma_{\text{total}}] \times [B(\psi(2S) \to \gamma\chi_{c1}(1P))]$ assuming $B(\psi(2S) \to \gamma\chi_{c1}(1P)) = (9.2 \pm 0.4)\times10^{-2}$, which we rescale to our best value $B(\psi(2S) \to \gamma\chi_{c1}(1P)) = 9.75\times10^{-2}$.

$\Gamma(\Sigma^0\overline{\Sigma}^0)/\Gamma_{\text{total}}$ — Γ_{77}/Γ

VALUE (units 10^{-5})	CL%	EVTS	DOCUMENT ID		TECN	COMMENT
4.2±0.6±0.1		103	[1] ABLIKIM	18V	BES3	$\psi(2S) \to \gamma\Sigma^0\overline{\Sigma}^0$
• • • We do not use the following data for averages, fits, limits, etc. • • •						
<6	90		[2] ABLIKIM	13H	BES3	$\psi(2S) \to \gamma\Sigma^0\overline{\Sigma}^0$
<4	90	3.8 ± 2.5	[3] NAIK	08	CLEO	$\psi(2S) \to \gamma\Sigma^0\overline{\Sigma}^0$

[1] ABLIKIM 18V reports $[\Gamma(\chi_{c1}(1P) \to \Sigma^0\overline{\Sigma}^0)/\Gamma_{\text{total}}] \times [B(\psi(2S) \to \gamma\chi_{c1}(1P))] = (0.41 \pm 0.05 \pm 0.03)\times10^{-5}$ which we divide by our best value $B(\psi(2S) \to \gamma\chi_{c1}(1P)) = (9.75 \pm 0.24)\times10^{-2}$. Our first error is their experiment's error and our second error is the systematic error from using our best value.

[2] ABLIKIM 13H reports $< 0.62\times10^{-4}$ from a measurement of $[\Gamma(\chi_{c1}(1P) \to \Sigma^0\overline{\Sigma}^0)/\Gamma_{\text{total}}] \times [B(\psi(2S) \to \gamma\chi_{c1}(1P))]$ assuming $B(\psi(2S) \to \gamma\chi_{c1}(1P)) = (9.2 \pm 0.4)\times10^{-2}$, which we rescale to our best value $B(\psi(2S) \to \gamma\chi_{c1}(1P)) = 9.75\times10^{-2}$.

[3] NAIK 08 reports $< 0.44\times10^{-4}$ from a measurement of $[\Gamma(\chi_{c1}(1P) \to \Sigma^0\overline{\Sigma}^0)/\Gamma_{\text{total}}] \times [B(\psi(2S) \to \gamma\chi_{c1}(1P))]$ assuming $B(\psi(2S) \to \gamma\chi_{c1}(1P)) = (9.07 \pm 0.11 \pm 0.54)\times10^{-2}$, which we rescale to our best value $B(\psi(2S) \to \gamma\chi_{c1}(1P)) = 9.75\times10^{-2}$.

$\Gamma(\Sigma^+\overline{\Sigma}^-)/\Gamma_{\text{total}}$ — Γ_{80}/Γ

VALUE (units 10^{-5})	CL%	EVTS	DOCUMENT ID		TECN	COMMENT
3.6±0.6±0.1		59	[1] ABLIKIM	18V	BES3	$\psi(2S) \to \gamma\Sigma^+\overline{\Sigma}^-$
• • • We do not use the following data for averages, fits, limits, etc. • • •						
<8	90		[2] ABLIKIM	13H	BES3	$\psi(2S) \to \gamma\Sigma^+\overline{\Sigma}^-$
<6	90	4.3 ± 2.3	[3] NAIK	08	CLEO	$\psi(2S) \to \gamma\Sigma^+\overline{\Sigma}^-$

[1] ABLIKIM 18V reports $[\Gamma(\chi_{c1}(1P) \to \Sigma^+\overline{\Sigma}^-)/\Gamma_{\text{total}}] \times [B(\psi(2S) \to \gamma\chi_{c1}(1P))] = (0.35 \pm 0.06 \pm 0.02)\times10^{-5}$ which we divide by our best value $B(\psi(2S) \to \gamma\chi_{c1}(1P)) = (9.75 \pm 0.24)\times10^{-2}$. Our first error is their experiment's error and our second error is the systematic error from using our best value.

[2] ABLIKIM 13H reports $< 0.87\times10^{-4}$ from a measurement of $[\Gamma(\chi_{c1}(1P) \to \Sigma^+\overline{\Sigma}^-)/\Gamma_{\text{total}}] \times [B(\psi(2S) \to \gamma\chi_{c1}(1P))]$ assuming $B(\psi(2S) \to \gamma\chi_{c1}(1P)) = (9.2 \pm 0.4)\times10^{-2}$, which we rescale to our best value $B(\psi(2S) \to \gamma\chi_{c1}(1P)) = 9.75\times10^{-2}$.

[3] NAIK 08 reports $< 0.65\times10^{-4}$ from a measurement of $[\Gamma(\chi_{c1}(1P) \to \Sigma^+\overline{\Sigma}^-)/\Gamma_{\text{total}}] \times [B(\psi(2S) \to \gamma\chi_{c1}(1P))]$ assuming $B(\psi(2S) \to \gamma\chi_{c1}(1P)) = (9.07 \pm 0.11 \pm 0.54)\times10^{-2}$, which we rescale to our best value $B(\psi(2S) \to \gamma\chi_{c1}(1P)) = 9.75\times10^{-2}$.

$\Gamma(\Sigma^-\overline{\Sigma}^+)/\Gamma_{\text{total}}$ — Γ_{81}/Γ

VALUE (units 10^{-5})	EVTS	DOCUMENT ID		TECN	COMMENT
5.7±1.4±0.6	214	[1] ABLIKIM	20I	BES3	$\psi(2S) \to \gamma\Sigma^-\overline{\Sigma}^+$

[1] ABLIKIM 20I reports $(5.7 \pm 1.4 \pm 0.6)\times10^{-5}$ from a measurement of $[\Gamma(\chi_{c1}(1P) \to \Sigma^-\overline{\Sigma}^+)/\Gamma_{\text{total}}] \times [B(\psi(2S) \to \gamma\chi_{c1}(1P))]$ assuming $B(\psi(2S) \to \gamma\chi_{c1}(1P)) = (9.75 \pm 0.24)\times10^{-2}$.

$\Gamma(\Sigma(1385)^+\overline{\Sigma}(1385)^-)/\Gamma_{\text{total}}$ — Γ_{82}/Γ

VALUE	CL%	DOCUMENT ID		TECN	COMMENT
<9 × 10^{-5}	90	[1] ABLIKIM	12I	BES3	$\psi(2S) \to \gamma\Lambda\overline{\Lambda}\pi^+\pi^-$

[1] ABLIKIM 12I reports $< 10\times10^{-5}$ from a measurement of $[\Gamma(\chi_{c1}(1P) \to \Sigma(1385)^+\overline{\Sigma}(1385)^-)/\Gamma_{\text{total}}] \times [B(\psi(2S) \to \gamma\chi_{c1}(1P))]$ assuming $B(\psi(2S) \to \gamma\chi_{c1}(1P)) = (9.2 \pm 0.4)\times10^{-2}$, which we rescale to our best value $B(\psi(2S) \to \gamma\chi_{c1}(1P)) = 9.75\times10^{-2}$.

$\Gamma(\Sigma(1385)^-\overline{\Sigma}(1385)^+)/\Gamma_{\text{total}}$ — Γ_{83}/Γ

VALUE	CL%	DOCUMENT ID		TECN	COMMENT
<5 × 10^{-5}	90	[1] ABLIKIM	12I	BES3	$\psi(2S) \to \gamma\Lambda\overline{\Lambda}\pi^+\pi^-$

[1] ABLIKIM 12I reports $< 5.7\times10^{-5}$ from a measurement of $[\Gamma(\chi_{c1}(1P) \to \Sigma(1385)^-\overline{\Sigma}(1385)^+)/\Gamma_{\text{total}}] \times [B(\psi(2S) \to \gamma\chi_{c1}(1P))]$ assuming $B(\psi(2S) \to \gamma\chi_{c1}(1P)) = (9.2 \pm 0.4)\times10^{-2}$, which we rescale to our best value $B(\psi(2S) \to \gamma\chi_{c1}(1P)) = 9.75\times10^{-2}$.

$\Gamma(K^-\Lambda\overline{\Xi}^+ + \text{c.c.})/\Gamma_{\text{total}}$ — Γ_{84}/Γ

VALUE (units 10^{-4})	EVTS	DOCUMENT ID		TECN	COMMENT
1.35±0.24±0.03	49	[1] ABLIKIM	15I	BES3	$\psi(2S) \to \gamma K^-\Lambda\overline{\Xi}^+ + \text{c.c.}$

[1] ABLIKIM 15I reports $[\Gamma(\chi_{c1}(1P) \to K^-\Lambda\overline{\Xi}^+ + \text{c.c.})/\Gamma_{\text{total}}] \times [B(\psi(2S) \to \gamma\chi_{c1}(1P))] = (1.32 \pm 0.20 \pm 0.12)\times10^{-5}$ which we divide by our best value $B(\psi(2S) \to \gamma\chi_{c1}(1P)) = (9.75 \pm 0.24)\times10^{-2}$. Our first error is their experiment's error and our second error is the systematic error from using our best value.

$\Gamma(\Xi^0\overline{\Xi}^0)/\Gamma_{\text{total}}$ — Γ_{85}/Γ

VALUE	CL%	EVTS	DOCUMENT ID		TECN	COMMENT
<6 × 10^{-5}	90	1.7 ± 2.4	[1] NAIK	08	CLEO	$\psi(2S) \to \gamma\Xi^0\overline{\Xi}^0$

[1] NAIK 08 reports $< 0.60\times10^{-4}$ from a measurement of $[\Gamma(\chi_{c1}(1P) \to \Xi^0\overline{\Xi}^0)/\Gamma_{\text{total}}] \times [B(\psi(2S) \to \gamma\chi_{c1}(1P))]$ assuming $B(\psi(2S) \to \gamma\chi_{c1}(1P)) = (9.07 \pm 0.11 \pm 0.54)\times10^{-2}$, which we rescale to our best value $B(\psi(2S) \to \gamma\chi_{c1}(1P)) = 9.75\times10^{-2}$.

$\Gamma(\Xi^-\overline{\Xi}^+)/\Gamma_{\text{total}}$ — Γ_{86}/Γ

VALUE (units 10^{-4})	CL%	EVTS	DOCUMENT ID		TECN	COMMENT
0.80±0.21±0.02		16.4 ± 4.3	[1] NAIK	08	CLEO	$\psi(2S) \to \gamma\Xi^+\overline{\Xi}^-$
• • • We do not use the following data for averages, fits, limits, etc. • • •						
< 3.4	90		[2] ABLIKIM	06D	BES2	$\psi(2S) \to \gamma\chi_{c1}$

[1] NAIK 08 reports $(0.86 \pm 0.22 \pm 0.08)\times10^{-4}$ from a measurement of $[\Gamma(\chi_{c1}(1P) \to \Xi^-\overline{\Xi}^+)/\Gamma_{\text{total}}] \times [B(\psi(2S) \to \gamma\chi_{c1}(1P))]$ assuming $B(\psi(2S) \to \gamma\chi_{c1}(1P)) = (9.07 \pm 0.11 \pm 0.54)\times10^{-2}$, which we rescale to our best value $B(\psi(2S) \to \gamma\chi_{c1}(1P)) = (9.75 \pm 0.24)\times10^{-2}$. Our first error is their experiment's error and our second error is the systematic error from using our best value.

[2] Using $B(\psi(2S) \to \chi_{c1}\gamma)$ (9.1 ± 0.6)%.

$[\Gamma(\pi^+\pi^-)+\Gamma(K^+K^-)]/\Gamma_{\text{total}}$ — Γ_{87}/Γ

VALUE	CL%	DOCUMENT ID		TECN	COMMENT
<21 × 10^{-4}		[1] FELDMAN	77	MRK1	$\psi(2S) \to \gamma\chi_{c1}$
• • • We do not use the following data for averages, fits, limits, etc. • • •					
<38 × 10^{-4}	90	[1] BRANDELIK	79B	DASP	$\psi(2S) \to \gamma\chi_{c1}$

[1] Estimated using $B(\psi(2S) \to \gamma\chi_{c1}(1P)) = 0.087$. The errors do not contain the uncertainty in the $\psi(2S)$ decay.

$\Gamma(K^0_SK^0_S)/\Gamma_{\text{total}}$ — Γ_{88}/Γ

VALUE	CL%	DOCUMENT ID		TECN	COMMENT
<6 × 10^{-5}	90	[1] ABLIKIM	05O	BES2	$\psi(2S) \to \chi_{c1}\gamma$

[1] ABLIKIM 05O reports $[\Gamma(\chi_{c1}(1P) \to K^0_SK^0_S)/\Gamma_{\text{total}}] \times [B(\psi(2S) \to \gamma\chi_{c1}(1P))] < 0.6\times10^{-5}$ which we divide by our best value $B(\psi(2S) \to \gamma\chi_{c1}(1P)) = 9.75\times10^{-2}$.

$\Gamma(\eta_c\pi^+\pi^-)/\Gamma_{\text{total}}$ — Γ_{89}/Γ

VALUE	CL%	DOCUMENT ID		TECN	COMMENT
<3.2 × 10^{-3}	90	[1,2] ABLIKIM	13B	BES3	$e^+e^- \to \psi(2S) \to \gamma\chi_{c1}$
• • • We do not use the following data for averages, fits, limits, etc. • • •					
<4.4 × 10^{-3}	90	[1,3] ABLIKIM	13B	BES3	$e^+e^- \to \psi(2S) \to \gamma\chi_{c1}$

[1] Using 1.06×10^8 $\psi(2S)$ mesons and $B(\psi(2S) \to \chi_{c1}\gamma) = (9.2 \pm 0.4)\%$.

[2] Using the $\eta_c \to K^0_SK^\pm\pi^\mp$ decays.

[3] Using the $\eta_c \to K^+K^-\pi^0$ decays.

RADIATIVE DECAYS

$\Gamma(\gamma J/\psi(1S))/\Gamma_{\text{total}}$ — Γ_{90}/Γ

VALUE (units 10^{-2})	EVTS	DOCUMENT ID		TECN	COMMENT
34.3 ±1.0 OUR FIT					
• • • We do not use the following data for averages, fits, limits, etc. • • •					
34.75±0.11±1.70	1.9M	[1] ABLIKIM	17U	BES3	$e^+e^- \to \gamma X$
37.9 ±0.8 ±2.1		[2] ADAM	05A	CLEO	$e^+e^- \to \psi(2S) \to \gamma\chi_{c1}$

[1] Not independent from $B(\psi(2S) \to \gamma\chi_{c1}(1P))$ and the product $B(\psi(2S) \to \gamma\chi_{c1}(1P)) \times B(\chi_{c1}(1P) \to \gamma J/\psi(1S))$ also measured in ABLIKIM 17U.

[2] Uses $B(\psi(2S) \to \gamma\chi_{c1} \to \gamma\gamma J/\psi)$ from ADAM 05A and $B(\psi(2S) \to \gamma\chi_{c1})$ from ATHAR 04.

$\Gamma(\gamma\rho^0)/\Gamma_{\text{total}}$ — Γ_{91}/Γ

VALUE (units 10^{-6})	EVTS	DOCUMENT ID		TECN	COMMENT
216±17 OUR AVERAGE					
215±22±5	432 ± 25	[1] ABLIKIM	11E	BES3	$\psi(2S) \to \gamma\gamma\rho^0$
217±24±5	186 ± 15	[2] BENNETT	08A	CLEO	$\psi(2S) \to \gamma\gamma\rho^0$

[1] ABLIKIM 11E reports $(228 \pm 13 \pm 22)\times10^{-6}$ from a measurement of $[\Gamma(\chi_{c1}(1P) \to \gamma\rho^0)/\Gamma_{\text{total}}] \times [B(\psi(2S) \to \gamma\chi_{c1}(1P))]$ assuming $B(\psi(2S) \to \gamma\chi_{c1}(1P)) = (9.2 \pm 0.4)\times10^{-2}$, which we rescale to our best value $B(\psi(2S) \to \gamma\chi_{c1}(1P)) = (9.75 \pm 0.24)\times10^{-2}$. Our first error is their experiment's error and our second error is the systematic error from using our best value.

[2] BENNETT 08A reports $(243 \pm 19 \pm 22)\times10^{-6}$ from a measurement of $[\Gamma(\chi_{c1}(1P) \to \gamma\rho^0)/\Gamma_{\text{total}}] \times [B(\psi(2S) \to \gamma\chi_{c1}(1P))]$ assuming $B(\psi(2S) \to \gamma\chi_{c1}(1P)) = (8.7 \pm 0.4)\times10^{-2}$, which we rescale to our best value $B(\psi(2S) \to \gamma\chi_{c1}(1P)) = (9.75 \pm 0.24)\times10^{-2}$. Our first error is their experiment's error and our second error is the systematic error from using our best value.

Downloaded from https://academic.oup.com/ptep/article/2022/8/083C01/6651666 by KIT Library user on 27 September 2022

$\Gamma(\gamma\omega)/\Gamma_{total}$ — Γ_{92}/Γ

VALUE (units 10^{-6})	EVTS	DOCUMENT ID		TECN	COMMENT
68± 8 OUR AVERAGE					
66± 9±2	136 ± 14	[1] ABLIKIM	11E	BES3	$\psi(2S) \to \gamma\gamma\omega$
74±17±2	39 ± 7	[2] BENNETT	08A	CLEO	$\psi(2S) \to \gamma\gamma\omega$

[1] ABLIKIM 11E reports $(69.7 \pm 7.2 \pm 6.6) \times 10^{-6}$ from a measurement of $[\Gamma(\chi_{c1}(1P) \to \gamma\omega)/\Gamma_{total}] \times [B(\psi(2S) \to \gamma\chi_{c1}(1P))]$ assuming $B(\psi(2S) \to \gamma\chi_{c1}(1P)) = (9.2 \pm 0.4) \times 10^{-2}$, which we rescale to our best value $B(\psi(2S) \to \gamma\chi_{c1}(1P)) = (9.75 \pm 0.24) \times 10^{-2}$. Our first error is their experiment's error and our second error is the systematic error from using our best value.

[2] BENNETT 08A reports $(83 \pm 15 \pm 12) \times 10^{-6}$ from a measurement of $[\Gamma(\chi_{c1}(1P) \to \gamma\omega)/\Gamma_{total}] \times [B(\psi(2S) \to \gamma\chi_{c1}(1P))]$ assuming $B(\psi(2S) \to \gamma\chi_{c1}(1P)) = (8.7 \pm 0.4) \times 10^{-2}$, which we rescale to our best value $B(\psi(2S) \to \gamma\chi_{c1}(1P)) = (9.75 \pm 0.24) \times 10^{-2}$. Our first error is their experiment's error and our second error is the systematic error from using our best value.

$\Gamma(\gamma\phi)/\Gamma_{total}$ — Γ_{93}/Γ

VALUE (units 10^{-6})	CL%	EVTS	DOCUMENT ID		TECN	COMMENT
24±5±1		43 ± 9	[1] ABLIKIM	11E	BES3	$\psi(2S) \to \gamma\gamma\phi$
• • • We do not use the following data for averages, fits, limits, etc. • • •						
<23	90	5.2 ± 3.1	[2] BENNETT	08A	CLEO	$\psi(2S) \to \gamma\gamma\phi$

[1] ABLIKIM 11E reports $(25.8 \pm 5.2 \pm 2.3) \times 10^{-6}$ from a measurement of $[\Gamma(\chi_{c1}(1P) \to \gamma\phi)/\Gamma_{total}] \times [B(\psi(2S) \to \gamma\chi_{c1}(1P))]$ assuming $B(\psi(2S) \to \gamma\chi_{c1}(1P)) = (9.2 \pm 0.4) \times 10^{-2}$, which we rescale to our best value $B(\psi(2S) \to \gamma\chi_{c1}(1P)) = (9.75 \pm 0.24) \times 10^{-2}$. Our first error is their experiment's error and our second error is the systematic error from using our best value.

[2] BENNETT 08A reports $< 26 \times 10^{-6}$ from a measurement of $[\Gamma(\chi_{c1}(1P) \to \gamma\phi)/\Gamma_{total}] \times [B(\psi(2S) \to \gamma\chi_{c1}(1P))]$ assuming $B(\psi(2S) \to \gamma\chi_{c1}(1P)) = (8.7 \pm 0.4) \times 10^{-2}$, which we rescale to our best value $B(\psi(2S) \to \gamma\chi_{c1}(1P)) = 9.75 \times 10^{-2}$.

$\Gamma(\gamma\gamma)/\Gamma_{total}$ — Γ_{94}/Γ

VALUE	CL%	DOCUMENT ID		TECN	COMMENT
< 6.3×10^{-6}	90	ABLIKIM	17AE	BES3	$\psi(2S) \to \gamma\chi_{c1} \to 3\gamma$
• • • We do not use the following data for averages, fits, limits, etc. • • •					
< 3.5×10^{-5}	90	ECKLUND	08A	CLEO	$\psi(2S) \to \gamma\chi_{c1} \to 3\gamma$
<150 $\times 10^{-5}$	90	[1] YAMADA	77	DASP	$e^+e^- \to 3\gamma$

[1] Estimated using $B(\psi(2S) \to \gamma\chi_{c1}(1P)) = 0.087$. The errors do not contain the uncertainty in the $\psi(2S)$ decay.

$\Gamma(e^+e^- J/\psi(1S))/\Gamma_{total}$ — Γ_{95}/Γ

VALUE (units 10^{-3})	EVTS	DOCUMENT ID		TECN	COMMENT
• • • We do not use the following data for averages, fits, limits, etc. • • •					
3.65±0.23±0.09	1.9k	[1,2] ABLIKIM	17I	BES3	$\psi(2S) \to \gamma e^+e^- J/\psi$

[1] ABLIKIM 17I reports $(3.73 \pm 0.09 \pm 0.25) \times 10^{-3}$ from a measurement of $[\Gamma(\chi_{c1}(1P) \to e^+e^- J/\psi(1S))/\Gamma_{total}] \times [B(\psi(2S) \to \gamma\chi_{c1}(1P))]$ assuming $B(\psi(2S) \to \gamma\chi_{c1}(1P)) = (9.55 \pm 0.31) \times 10^{-2}$, which we rescale to our best value $B(\psi(2S) \to \gamma\chi_{c1}(1P)) = (9.75 \pm 0.24) \times 10^{-2}$. Our first error is their experiment's error and our second error is the systematic error from using our best value.

[2] Not independent from other measurements reported by ABLIKIM 17I

$\Gamma(e^+e^- J/\psi(1S))/\Gamma(\gamma J/\psi(1S))$ — Γ_{95}/Γ_{90}

VALUE (units 10^{-3})	EVTS	DOCUMENT ID		TECN	COMMENT
10.1±0.3±0.5	1.9k	[1] ABLIKIM	17I	BES3	$\psi(2S) \to e^+e^-\gamma J/\psi$

[1] Uses $B(\psi(2S) \to \gamma\chi_{c1}(1P)) \times B(\chi_{c1}(1P) \to \gamma J/\psi(1S)) = (351.8 \pm 1.0 \pm 12.0) \times 10^{-4}$ from ABLIKIM 17N and accounts for common systematic errors.

$\Gamma(\mu^+\mu^- J/\psi(1S))/\Gamma(e^+e^- J/\psi(1S))$ — Γ_{96}/Γ_{95}

VALUE (units 10^{-2})	EVTS	DOCUMENT ID		TECN	COMMENT
6.73±0.51±0.50	222	ABLIKIM	19Z	BES3	$\psi(2S) \to \gamma\chi_c \to \gamma(\mu^+\mu^- J/\psi)$

$\chi_{c1}(1P)$ CROSS-PARTICLE BRANCHING RATIOS

$\Gamma(\chi_{c1}(1P) \to p\overline{p})/\Gamma_{total} \times \Gamma(\psi(2S) \to \gamma\chi_{c1}(1P))/\Gamma(\psi(2S) \to J/\psi(1S)\pi^+\pi^-)$ — $\Gamma_{54}/\Gamma \times \Gamma_{163}^{\psi(2S)}/\Gamma_{12}^{\psi(2S)}$

VALUE (units 10^{-5})	DOCUMENT ID		TECN	COMMENT
2.14±0.10 OUR FIT				
1.1 ±1.0	[1] BAI	98I	BES	$\psi(2S) \to \gamma\chi_{c1} \to \gamma\overline{p}p$

[1] Calculated by us. The value for $B(\chi_{c1} \to p\overline{p})$ reported in BAI 98I is derived using $B(\psi(2S) \to \gamma\chi_{c1}) = (8.7 \pm 0.8)\%$ and $B(\psi(2S) \to J/\psi(1S)\pi^+\pi^-) = (32.4 \pm 2.6)\%$ [BAI 98D].

$\Gamma(\chi_{c1}(1P) \to \Lambda\overline{\Lambda})/\Gamma_{total} \times \Gamma(\psi(2S) \to \gamma\chi_{c1}(1P))/\Gamma_{total}$ — $\Gamma_{67}/\Gamma \times \Gamma_{163}^{\psi(2S)}/\Gamma^{\psi(2S)}$

VALUE (units 10^{-6})	EVTS	DOCUMENT ID		TECN	COMMENT
12.4±0.8 OUR FIT					
12.3±0.9 OUR AVERAGE Error includes scale factor of 1.2.					
12.8±0.6±0.6	528	ABLIKIM	21L	BES3	$\psi(2S) \to \gamma p\pi^-\overline{p}\pi^+$
10.5±1.6±0.6	46	[1] NAIK	08	CLEO	$\psi(2S) \to \gamma\Lambda\overline{\Lambda}$
• • • We do not use the following data for averages, fits, limits, etc. • • •					
11.2±1.0±0.9	136	[2,3] ABLIKIM	13H	BES3	$\psi(2S) \to \gamma\Lambda\overline{\Lambda}$

[1] Calculated by us. NAIK 08 reports $B(\chi_{c1} \to \Lambda\overline{\Lambda}) = (11.6 \pm 1.8 \pm 0.7 \pm 0.7) \times 10^{-5}$ using $B(\psi(2S) \to \gamma\chi_{c1}) = (9.07 \pm 0.11 \pm 0.54)\%$.

[2] Superseded by ABLIKIM 21L

[3] Calculated by us. ABLIKIM 13H reports $B(\chi_{c1} \to \Lambda\overline{\Lambda}) = (12.2 \pm 1.1 \pm 1.1) \times 10^{-5}$ from a measurement of $B(\chi_{c1} \to \Lambda\overline{\Lambda}) \times B(\psi(2S) \to \gamma\chi_{c1})$ assuming $B(\psi(2S) \to \gamma\chi_{c1}) = (9.2 \pm 0.4)\%$.

$\Gamma(\chi_{c1}(1P) \to \Lambda\overline{\Lambda})/\Gamma_{total} \times \Gamma(\psi(2S) \to \gamma\chi_{c1}(1P))/\Gamma(\psi(2S) \to J/\psi(1S)\pi^+\pi^-)$ — $\Gamma_{67}/\Gamma \times \Gamma_{163}^{\psi(2S)}/\Gamma_{12}^{\psi(2S)}$

VALUE (units 10^{-5})	EVTS	DOCUMENT ID		TECN	COMMENT
3.58±0.22 OUR FIT					
7.1 $^{+2.8}_{-2.4}$ ±1.3	$9.0^{+3.5}_{-3.1}$	[1] BAI	03E	BES	$\psi(2S) \to \gamma\Lambda\overline{\Lambda}$

[1] BAI 03E reports $[B(\chi_{c1} \to \Lambda\overline{\Lambda})\, B(\psi(2S) \to \gamma\chi_{c1}) / B(\psi(2S) \to J/\psi\pi^+\pi^-)] \times [B^2(\Lambda \to \pi^- p) / B(J/\psi \to p\overline{p})] = (1.33^{+0.52}_{-0.46} \pm 0.25)\%$. We calculate from this measurement the presented value using $B(\Lambda \to \pi^- p) = (63.9 \pm 0.5)\%$ and $B(J/\psi \to p\overline{p}) = (2.17 \pm 0.07) \times 10^{-3}$.

$\Gamma(\chi_{c1}(1P) \to \gamma J/\psi(1S))/\Gamma_{total} \times \Gamma(\psi(2S) \to \gamma\chi_{c1}(1P))/\Gamma_{total}$ — $\Gamma_{90}/\Gamma \times \Gamma_{163}^{\psi(2S)}/\Gamma^{\psi(2S)}$

VALUE (units 10^{-2})	EVTS	DOCUMENT ID		TECN	COMMENT
3.34 ±0.06 OUR FIT					
3.24 ±0.16 OUR AVERAGE Error includes scale factor of 2.1. See the ideogram below.					
3.518±0.010±0.120	143k	[1] ABLIKIM	17N	BES3	$\psi(2S) \to \gamma\gamma J/\psi$
3.442±0.010±0.132	1.9M	ABLIKIM	17U	BES3	$e^+e^- \to \gamma X$
2.81 ±0.05 ±0.23	13k	BAI	04I	BES2	$\psi(2S) \to J/\psi\gamma\gamma$
2.56 ±0.12 ±0.20		GAISER	86	CBAL	$\psi(2S) \to \gamma X$
2.78 ±0.30		[2] OREGLIA	82	CBAL	$\psi(2S) \to \gamma\chi_{c1}$
2.2 ±0.5		[3] BRANDELIK	79B	DASP	$\psi(2S) \to \gamma\chi_{c1}$
2.9 ±0.5		[3] BARTEL	78B	CNTR	$\psi(2S) \to \gamma\chi_{c1}$
5.0 ±1.5		[4] BIDDICK	77	CNTR	$e^+e^- \to \gamma X$
2.8 ±0.9		[2] WHITAKER	76	MRK1	e^+e^-
• • • We do not use the following data for averages, fits, limits, etc. • • •					
3.377±0.009±0.183	142k	[5] ABLIKIM	12O	BES3	$\psi(2S) \to \gamma\chi_{c1}$
3.56 ±0.03 ±0.12	24.9k	[6] MENDEZ	08	CLEO	$\psi(2S) \to \gamma\chi_{c1}$
3.44 ±0.06 ±0.13	3.7k	[7] ADAM	05A	CLEO	Repl. by MENDEZ 08

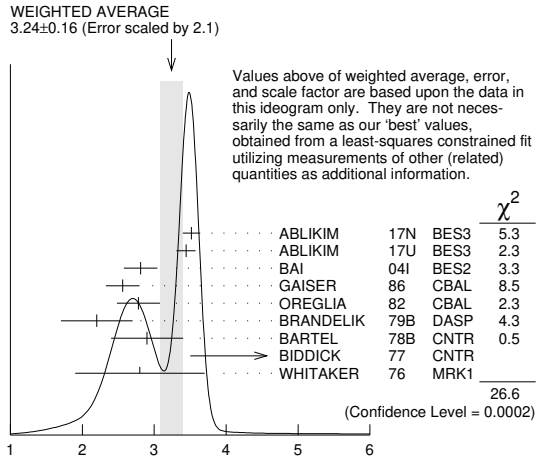

$\Gamma(\chi_{c1}(1P) \to \gamma J/\psi(1S))/\Gamma_{total} \times \Gamma(\psi(2S) \to \gamma\chi_{c1}(1P))/\Gamma_{total}$ (units 10^{-2})

[1] Uses $B(J/\psi \to e^+e^-) = (5.971 \pm 0.032)\%$ and $B(J/\psi \to \mu^+\mu^-) = (5.961 \pm 0.033)\%$.

[2] Recalculated by us using $B(J/\psi(1S) \to \ell^+\ell^-) = 0.1181 \pm 0.0020$.

[3] Recalculated by us using $B(J/\psi(1S) \to \mu^+\mu^-) = 0.0588 \pm 0.0010$.

[4] Assumes isotropic gamma distribution.

[5] Superseded by ABLIKIM 17N.

[6] Not independent from other measurements of MENDEZ 08.

[7] Not independent from other values reported by ADAM 05A.

$\Gamma(\chi_{c1}(1P) \to \gamma J/\psi(1S))/\Gamma_{total} \times \Gamma(\psi(2S) \to \gamma\chi_{c1}(1P))/\Gamma(\psi(2S) \to J/\psi(1S)\text{anything})$ — $\Gamma_{90}/\Gamma \times \Gamma_{163}^{\psi(2S)}/\Gamma_{10}^{\psi(2S)}$

$$\Gamma_{90}/\Gamma \times \Gamma_{163}^{\psi(2S)}/\Gamma_{10}^{\psi(2S)} = \Gamma_{90}/\Gamma \times \Gamma_{163}^{\psi(2S)}/(\Gamma_{12}^{\psi(2S)} + \Gamma_{13}^{\psi(2S)} + \Gamma_{14}^{\psi(2S)} + 0.343\Gamma_{163}^{\psi(2S)} + 0.190\Gamma_{164}^{\psi(2S)})$$

VALUE (units 10^{-2})	EVTS	DOCUMENT ID		TECN	COMMENT
5.43±0.10 OUR FIT					
• • • We do not use the following data for averages, fits, limits, etc. • • •					
5.70±0.04±0.15	24.9k	[1] MENDEZ	08	CLEO	$\psi(2S) \to \gamma\chi_{c1}$
5.77±0.10±0.12	3.7k	ADAM	05A	CLEO	Repl. by MENDEZ 08

[1] Not independent from other measurements of MENDEZ 08.

Downloaded from https://academic.oup.com/ptep/article/2022/8/083C01/6651666 by KIT Library user on 27 September 2022

$\Gamma(\chi_{c1}(1P) \to \gamma J/\psi(1S))/\Gamma_{total} \times \Gamma(\psi(2S) \to \gamma\chi_{c1}(1P))/\Gamma(\psi(2S) \to J/\psi(1S)\pi^+\pi^-)$ — $\Gamma_{90}/\Gamma \times \Gamma^{\psi(2S)}_{163}/\Gamma^{\psi(2S)}_{12}$

VALUE (units 10^{-2})	EVTS	DOCUMENT ID		TECN	COMMENT
9.63±0.17 OUR FIT					
10.15±0.28 OUR AVERAGE					
10.17±0.07±0.27	24.9k	MENDEZ	08	CLEO	$\psi(2S) \to \gamma\chi_{c1}$
12.6 ±0.3 ±3.8	3k	[1] ABLIKIM	04B	BES	$\psi(2S) \to J/\psi X$
8.5 ±2.1		[2] HIMEL	80	MRK2	$\psi(2S) \to \gamma\chi_{c1}$
• • • We do not use the following data for averages, fits, limits, etc. • • •					
10.24±0.17±0.23	3.7k	[3] ADAM	05A	CLEO	Repl. by MENDEZ 08

[1] From a fit to the J/ψ recoil mass spectra.
[2] The value for $B(\psi(2S) \to \gamma\chi_{c1}) \times B(\chi_{c1} \to \gamma J/\psi(1S))$ quoted in HIMEL 80 is derived using $B(\psi(2S) \to J/\psi(1S)\pi^+\pi^-) = (33 \pm 3)\%$ and $B(J/\psi(1S) \to \ell^+\ell^-) = 0.138 \pm 0.018$. Calculated by us using $B(J/\psi(1S) \to \ell^+\ell^-) = 0.1181 \pm 0.0020$.
[3] Not independent from other values reported by ADAM 05A.

$\Gamma(\chi_{c1}(1P) \to \overline{K}^0 K^+\pi^- + c.c.)/\Gamma_{total} \times \Gamma(\psi(2S) \to \gamma\chi_{c1}(1P))/\Gamma_{total}$ — $\Gamma_{17}/\Gamma \times \Gamma^{\psi(2S)}_{163}/\Gamma^{\psi(2S)}$

VALUE (units 10^{-4})	DOCUMENT ID		TECN	COMMENT
6.8±0.5 OUR FIT				
7.2±0.6 OUR AVERAGE				
7.3±0.5±0.5	[1] ATHAR	07	CLEO	$\psi(2S) \to \gamma K^0_S K^+\pi^-$
7.0±0.5±0.9	[2] ABLIKIM	06R	BES2	$\psi(2S) \to \gamma\chi_{c1}$

[1] Calculated by us. The value of $B(\chi_{c1} \to K^0 K^+\pi^- + c.c.)$ reported by ATHAR 07 was derived using $B(\psi(2S) \to \gamma\chi_{c1}(1P)) = (9.07 \pm 0.11 \pm 0.54)\%$.
[2] Calculated by us. ABLIKIM 06R reports $B(\chi_{c1} \to K^0_S K^+\pi^-) = (4.0 \pm 0.3 \pm 0.5) \times 10^{-3}$. We use $B(\psi(2S) \to \gamma\chi_{c1}) = (8.7 \pm 0.4) \times 10^{-2}$.

$\Gamma(\chi_{c1}(1P) \to \overline{K}^0 K^+\pi^- + c.c.)/\Gamma_{total} \times \Gamma(\psi(2S) \to \gamma\chi_{c1}(1P))/\Gamma(\psi(2S) \to J/\psi(1S)\pi^+\pi^-)$ — $\Gamma_{17}/\Gamma \times \Gamma^{\psi(2S)}_{163}/\Gamma^{\psi(2S)}_{12}$

VALUE (units 10^{-4})	DOCUMENT ID		TECN	COMMENT
19.6±1.6 OUR FIT				
13.2±2.4±3.2	[1] BAI	99B	BES	$\psi(2S) \to \gamma K^0_S K^+\pi^-$

[1] Calculated by us. The value of $B(\chi_{c1} \to K^0_S K^+\pi^-)$ reported by BAI 99B was derived using $B(\psi(2S) \to \gamma\chi_{c1}(1P)) = (8.7 \pm 0.8)\%$ and $B(\psi(2S) \to J/\psi\pi^+\pi^-) = (32.4 \pm 2.6)\%$ [BAI 98D].

$\Gamma(\chi_{c1}(1P) \to K^+K^-K^+K^-)/\Gamma_{total} \times \Gamma(\psi(2S) \to \gamma\chi_{c1}(1P))/\Gamma_{total}$ — $\Gamma_{44}/\Gamma \times \Gamma^{\psi(2S)}_{163}/\Gamma^{\psi(2S)}$

VALUE (units 10^{-4})	EVTS	DOCUMENT ID		TECN	COMMENT
0.53±0.11 OUR FIT					
0.61±0.11±0.08	54	[1] ABLIKIM	06T	BES2	$\psi(2S) \to \gamma K^+K^+K^-K^-$

[1] Calculated by us. The value of $B(\chi_{c1} \to 2K^+2K^-)$ reported by ABLIKIM 06T was derived using $B(\psi(2S) \to \gamma\chi_{c1}(1P)) = (8.7 \pm 0.8)\%$.

$\Gamma(\chi_{c1}(1P) \to K^+K^-K^+K^-)/\Gamma_{total} \times \Gamma(\psi(2S) \to \gamma\chi_{c1}(1P))/\Gamma(\psi(2S) \to J/\psi(1S)\pi^+\pi^-)$ — $\Gamma_{44}/\Gamma \times \Gamma^{\psi(2S)}_{163}/\Gamma^{\psi(2S)}_{12}$

VALUE (units 10^{-4})	DOCUMENT ID		TECN	COMMENT
1.52±0.31 OUR FIT				
1.13±0.40±0.29	[1] BAI	99B	BES	$\psi(2S) \to \gamma K^+K^+K^-K^-$

[1] Calculated by us. The value of $B(\chi_{c1} \to 2K^+2K^-)$ reported by BAI 99B was derived using $B(\psi(2S) \to \gamma\chi_{c1}(1P)) = (8.7 \pm 0.8)\%$ and $B(\psi(2S) \to J/\psi\pi^+\pi^-) = (32.4 \pm 2.6)\%$ [BAI 98D].

$\Gamma(\chi_{c1}(1P) \to p\overline{p})/\Gamma_{total} \times \Gamma(\psi(2S) \to \gamma\chi_{c1}(1P))/\Gamma_{total}$ — $\Gamma_{54}/\Gamma \times \Gamma^{\psi(2S)}_{163}/\Gamma^{\psi(2S)}$

VALUE (units 10^{-6})	EVTS	DOCUMENT ID		TECN	COMMENT
7.41±0.35 OUR FIT					
7.8 ±0.6 OUR AVERAGE	Error includes scale factor of 1.4. See the ideogram below.				
7.9 ±0.4 ±0.3	453	ABLIKIM	13V	BES3	$\psi(2S) \to \gamma p\overline{p}$
8.2 ±0.7 ±0.4	141 ± 13	[1] NAIK	08	CLEO	$\psi(2S) \to \gamma p\overline{p}$
4.8 $^{+1.4}_{-1.3}$ ±0.6	18.2$^{+5.5}_{-4.9}$	BAI	04F	BES	$\psi(2S) \to \gamma\chi_{c1}(1P) \to \gamma\overline{p}p$

[1] Calculated by us. NAIK 08 reports $B(\chi_{c1} \to p\overline{p}) = (9.0 \pm 0.8 \pm 0.4 \pm 0.5) \times 10^{-5}$ using $B(\psi(2S) \to \gamma\chi_{c1}) = (9.07 \pm 0.11 \pm 0.54)\%$.

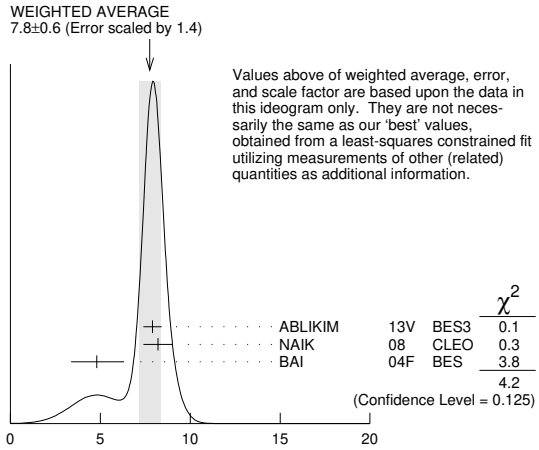

$\Gamma(\chi_{c1}(1P) \to p\overline{p})/\Gamma_{total} \times \Gamma(\psi(2S) \to \gamma\chi_{c1}(1P))/\Gamma_{total}$ (units 10^{-6})

$\Gamma(\chi_{c1}(1P) \to \Sigma^+\overline{p}K^0_S + c.c.)/\Gamma_{total} \times \Gamma(\psi(2S) \to \gamma\chi_{c1}(1P))/\Gamma_{total}$ — $\Gamma_{78}/\Gamma \times \Gamma^{\psi(2S)}_{163}/\Gamma^{\psi(2S)}$

VALUE (units 10^{-5})	EVTS	DOCUMENT ID		TECN	COMMENT
1.49±0.09±0.07	258	[1] ABLIKIM	19BB	BES3	$\psi(2S) \to \gamma\Sigma^+\overline{p}K^0_S$ + c.c.

[1] Calculated by us. ABLIKIM 19BB reports $B(\chi_{c1} \to \Sigma^+\overline{p}K^0_S + c.c.) = (1.53 \pm 0.10 \pm 0.08) \times 10^{-4}$ using $B(\psi(2S) \to \gamma\chi_{c1}) = (9.75 \pm 0.24)\%$ and other branching fractions from PDG 18.

$\Gamma(\chi_{c1}(1P) \to \Sigma^0\overline{p}K^+ + c.c.)/\Gamma_{total} \times \Gamma(\psi(2S) \to \gamma\chi_{c1}(1P))/\Gamma_{total}$ — $\Gamma_{79}/\Gamma \times \Gamma^{\psi(2S)}_{163}/\Gamma^{\psi(2S)}$

VALUE (units 10^{-5})	EVTS	DOCUMENT ID		TECN	COMMENT
1.42±0.07±0.06	493	[1] ABLIKIM	20AE	BES3	$\psi(2S) \to \gamma\Sigma^0\overline{p}K^+$ + c.c.

[1] Calculated by us. ABLIKIM 20AE reports $B(\chi_{c1} \to \Sigma^0\overline{p}K^+ + c.c.) = (1.46 \pm 0.07 \pm 0.07) \times 10^{-4}$ using $B(\psi(2S) \to \gamma\chi^0_c) = (9.75 \pm 0.24)\%$ and other branching fractions from PDG 20.

MULTIPOLE AMPLITUDES IN $\chi_{c1}(1P) \to \gamma J/\psi(1S)$

$a_2 = M2/\sqrt{E1^2 + M2^2}$ Magnetic quadrupole fractional transition amplitude

VALUE (units 10^{-2})	EVTS	DOCUMENT ID		TECN	COMMENT
−6.7 ±0.9 OUR AVERAGE	Error includes scale factor of 2.6. See the ideogram below.				
−7.40±0.33±0.34	164k	[1] ABLIKIM	17N	BES3	$\psi(2S) \to \gamma\gamma\ell^+\ell^-$
−6.26±0.63±0.24	39k	ARTUSO	09	CLEO	$\psi(2S) \to \gamma\gamma\ell^+\ell^-$
0.2 ±3.2 ±0.4	2090	AMBROGIANI	02	E835	$p\overline{p} \to \chi_{c1} \to J/\psi\gamma$
−0.2 $^{+0.8}_{-2.0}$	921	OREGLIA	82	CBAL	$\psi(2S) \to \chi_{c1}\gamma \to J/\psi\gamma\gamma$

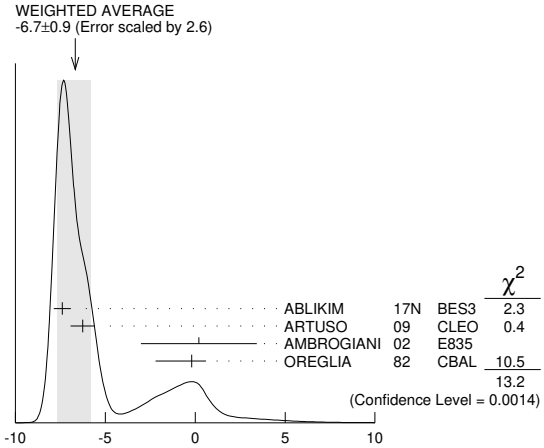

$a_2 = M2/\sqrt{E1^2 + M2^2}$ (units 10^{-2})

[1] Correlated with b_2 with correlation coefficient $\rho_{a_2 b_2} = 0.133$.

Downloaded from https://academic.oup.com/ptep/article/2022/8/083C01/6651666 by KIT Library user on 27 September 2022

MULTIPOLE AMPLITUDES IN $\psi(2S) \to \gamma\chi_{c1}(1S)$ RADIATIVE DECAY

$b_2 = M2/\sqrt{E1^2 + M2^2}$ Magnetic quadrupole fractional transition amplitude

VALUE (units 10^{-2})	EVTS	DOCUMENT ID		TECN	COMMENT
2.5 ±0.4 OUR AVERAGE					
2.29±0.39±0.27	164k	[1] ABLIKIM	17N	BES3	$\psi(2S) \to \gamma\gamma\ell^+\ell^-$
2.76±0.73±0.23	39k	ARTUSO	09	CLEO	$\psi(2S) \to \gamma\gamma\ell^+\ell^-$
$7.7\ ^{+5.0}_{-4.5}$	921	OREGLIA	82	CBAL	$\psi(2S) \to \gamma\gamma\ell^+\ell^-$

[1] Correlated with a_2 with correlation coefficient $\rho_{a_2 b_2} = 0.133$.

MULTIPOLE AMPLITUDE RATIOS IN RADIATIVE DECAYS $\psi(2S) \to \gamma\chi_{c1}(1S)$ and $\chi_{c1} \to \gamma J/\psi(1S)$

a_2/b_2 Magnetic quadrupole transition amplitude ratio

VALUE	EVTS	DOCUMENT ID		TECN	COMMENT
$\mathbf{-2.27^{+0.57}_{-0.99}}$	39k	[1] ARTUSO	09	CLEO	$\psi(2S) \to \gamma\gamma\ell^+\ell^-$

[1] Statistical and systematic errors combined. Not independent of $a_2(\chi_{c1})$ and $b_2(\chi_{c1})$ values from ARTUSO 09.

$\chi_{c1}(1P)$ REFERENCES

ABLIKIM	21AV	JHEP 2111 217	M. Ablikim et al.	(BESIII Collab.)
ABLIKIM	21L	PR D103 112004	M. Ablikim et al.	(BESIII Collab.)
ABLIKIM	20AE	PR D102 092006	M. Ablikim et al.	(BESIII Collab.)
ABLIKIM	20B	PR D101 012012	M. Ablikim et al.	(BESIII Collab.)
ABLIKIM	20I	PR D101 092002	M. Ablikim et al.	(BESIII Collab.)
PDG	20	PTEP 2020 083C01	P.A. Zyla et al.	(PDG Collab.)
ABLIKIM	19AA	PR D99 052008	M. Ablikim et al.	(BESIII Collab.)
ABLIKIM	19AU	PR D100 052010	M. Ablikim et al.	(BESIII Collab.)
ABLIKIM	19BB	PR D100 092006	M. Ablikim et al.	(BESIII Collab.)
ABLIKIM	19J	PR D99 012015	M. Ablikim et al.	(BESIII Collab.)
ABLIKIM	19Z	PR D99 051101	M. Ablikim et al.	(BESIII Collab.)
LU	19	PR D99 032003	P.-C. Lu et al.	(BELLE Collab.)
ABLIKIM	18D	PRL 121 022001	M. Ablikim et al.	(BESIII Collab.)
ABLIKIM	18V	PR D97 052011	M. Ablikim et al.	(BESIII Collab.)
PDG	18	PR D98 030001	M. Tanabashi et al.	(PDG Collab.)
AAIJ	17BB	EPJ C77 609	R. Aaij et al.	(LHCb Collab.)
AAIJ	17BI	PRL 119 221801	R. Aaij et al.	(LHCb Collab.)
ABLIKIM	17AE	PR D96 092007	M. Ablikim et al.	(BESIII Collab.)
ABLIKIM	17I	PRL 118 221802	M. Ablikim et al.	(BESIII Collab.)
ABLIKIM	17K	PR D95 032002	M. Ablikim et al.	(BESIII Collab.)
ABLIKIM	17N	PR D95 072004	M. Ablikim et al.	(BESIII Collab.)
ABLIKIM	17U	PR D96 032001	M. Ablikim et al.	(BESIII Collab.)
PDG	16	CP C40 100001	C. Patrignani et al.	(PDG Collab.)
ABLIKIM	15I	PR D91 092006	M. Ablikim et al.	(BESIII Collab.)
ABLIKIM	15M	PR D91 112008	M. Ablikim et al.	(BESIII Collab.)
ABLIKIM	14J	PR D89 074030	M. Ablikim et al.	(BESIII Collab.)
ABLIKIM	13B	PR D87 012002	M. Ablikim et al.	(BESIII Collab.)
ABLIKIM	13D	PR D87 012007	M. Ablikim et al.	(BESIII Collab.)
ABLIKIM	13H	PR D87 032007	M. Ablikim et al.	(BESIII Collab.)
ABLIKIM	13V	PR D88 112001	M. Ablikim et al.	(BESIII Collab.)
ABLIKIM	12I	PR D86 052004	M. Ablikim et al.	(BESIII Collab.)
ABLIKIM	12J	PR D86 052011	M. Ablikim et al.	(BESIII Collab.)
ABLIKIM	12O	PRL 109 172002	M. Ablikim et al.	(BESIII Collab.)
ABLIKIM	11A	PR D83 012006	M. Ablikim et al.	(BESIII Collab.)
ABLIKIM	11D	PR D83 032003	M. Ablikim et al.	(BESIII Collab.)
ABLIKIM	11E	PR D83 112005	M. Ablikim et al.	(BESIII Collab.)
ABLIKIM	11F	PR D83 112009	M. Ablikim et al.	(BESIII Collab.)
ABLIKIM	11K	PRL 107 092001	M. Ablikim et al.	(BESIII Collab.)
ONYISI	10	PR D82 011103	P.U.E. Onyisi et al.	(CLEO Collab.)
ARTUSO	09	PR D80 112003	M. Artuso et al.	(CLEO Collab.)
BENNETT	08A	PRL 101 151801	J.V. Bennett et al.	(CLEO Collab.)
ECKLUND	08A	PR D78 091501	K.M. Ecklund et al.	(CLEO Collab.)
HE	08B	PR D78 092004	Q. He et al.	(CLEO Collab.)
MENDEZ	08	PR D78 011102	H. Mendez et al.	(CLEO Collab.)
NAIK	08	PR D78 031101	P. Naik et al.	(CLEO Collab.)
ATHAR	07	PR D75 032002	S.B. Athar et al.	(CLEO Collab.)
ABLIKIM	06D	PR D73 052006	M. Ablikim et al.	(BES Collab.)
ABLIKIM	06R	PR D74 072001	M. Ablikim et al.	(BES Collab.)
ABLIKIM	06T	PL B642 197	M. Ablikim et al.	(BES Collab.)
ABLIKIM	05G	PR D71 092002	M. Ablikim et al.	(BES Collab.)
ABLIKIM	05O	PL B630 21	M. Ablikim et al.	(BES Collab.)
ADAM	05A	PRL 94 232002	N.E. Adam et al.	(CLEO Collab.)
ANDREOTTI	05A	NP B717 34	M. Andreotti et al.	(FNAL E835 Collab.)
ABLIKIM	04B	PR D70 012003	M. Ablikim et al.	(BES Collab.)
ABLIKIM	04H	PR D70 092003	M. Ablikim et al.	(BES Collab.)
ATHAR	04	PR D70 112002	S.B. Athar et al.	(CLEO Collab.)
BAI	04F	PR D69 092001	J.Z. Bai et al.	(BES Collab.)
BAI	04I	PR D70 012006	J.Z. Bai et al.	(BES Collab.)
AULCHENKO	03	PL B573 63	V.M. Aulchenko et al.	(KEDR Collab.)
BAI	03E	PR D67 112001	J.Z. Bai et al.	(BES Collab.)
AMBROGIANI	02	PR D65 052002	M. Ambrogiani et al.	(FNAL E835 Collab.)
BAI	99B	PR D60 072001	J.Z. Bai et al.	(BES Collab.)
BAI	98D	PR D58 092006	J.Z. Bai et al.	(BES Collab.)
BAI	98I	PRL 81 3091	J.Z. Bai et al.	(BES Collab.)
ARMSTRONG	92	NP B373 35	T.A. Armstrong et al.	(FNAL, FERR, GENO+)
Also		PRL 68 1468	T.A. Armstrong et al.	(FNAL, FERR, GENO+)
BAGLIN	86B	PL B172 455	C. Baglin	(LAPP, CERN, GENO, LYON, OSLO+)
GAISER	86	PR D34 711	J. Gaiser et al.	(Crystal Ball Collab.)
LEMOIGNE	82	PL 113B 509	Y. Lemoigne et al.	(SACL, LOIC, SHMP+)
OREGLIA	82	PR D25 2259	M.J. Oreglia et al.	(SLAC, CIT, HARV+)
Also		Private Comm.	M.J. Oreglia	(EFI)
HIMEL	80	PRL 44 920	T. Himel et al.	(LBL, SLAC)
Also		Private Comm.	G. Trilling	(LBL, UCB)
BRANDELIK	79B	NP B160 426	R. Brandelik et al.	(DASP Collab.)
BARTEL	78B	PL 79B 492	W. Bartel et al.	(DESY, HEIDP)
TANENBAUM	78	PR D17 1731	W.M. Tanenbaum et al.	(SLAC, LBL)
Also		Private Comm.	G. Trilling	(LBL, UCB)
BIDDICK	77	PRL 38 1324	C.J. Biddick et al.	(UCSD, UMD, PAVI+)
FELDMAN	77	PRPL 33C 285	G.J. Feldman, M.L. Perl	(LBL, SLAC)
YAMADA	77	Hamburg Conf. 69	S. Yamada	(DASP Collab.)
WHITAKER	76	PRL 37 1596	J.S. Whitaker et al.	(SLAC, LBL)
TANENBAUM	75	PRL 35 1323	W.M. Tanenbaum et al.	(LBL, SLAC)

$h_c(1P)$

$I^G(J^{PC}) = 0^-(1^{+-})$

Quantum numbers are quark model prediction, $C = -$ established by $\eta_c\gamma$ decay.

$h_c(1P)$ MASS

VALUE (MeV)	EVTS	DOCUMENT ID		TECN	COMMENT
3525.38±0.11 OUR AVERAGE					
3525.31±0.11±0.14	832	[1] ABLIKIM	12N	BES3	$\psi(2S) \to \pi^0\gamma$ hadrons
3525.40±0.13±0.18	3679	ABLIKIM	10B	BES3	$\psi(2S) \to \pi^0\gamma\eta_c$
3525.20±0.18±0.12	1282	[2] DOBBS	08A	CLEO	$\psi(2S) \to \pi^0\eta_c\gamma$
3525.8 ±0.2 ±0.2	13	ANDREOTTI	05B	E835	$\overline{p}p \to \eta_c\gamma$
• • • We do not use the following data for averages, fits, limits, etc. • • •					
3525.6 ±0.5	92^{+23}_{-22}	ADAMS	09	CLEO	$\psi(2S) \to 2(\pi^+\pi^-\pi^0)$
3524.4 ±0.6 ±0.4	168 ± 40	[3] ROSNER	05	CLEO	$\psi(2S) \to \pi^0\eta_c\gamma$
3527 ±8	42	ANTONIAZZI	94	E705	300 $\pi^\pm$, pLi $\to$ $J/\psi\pi^0$X
3526.28±0.18±0.19	59	[4] ARMSTRONG	92D	E760	$\overline{p}p \to J/\psi\pi^0$
3525.4 ±0.8 ±0.4	5	BAGLIN	86	SPEC	$\overline{p}p \to J/\psi$X

[1] With floating width.
[2] Combination of exclusive and inclusive analyses for the reaction $\psi(2S) \to \pi^0 h_c \to \pi^0\eta_c\gamma$. This result is the average of DOBBS 08A and ROSNER 05.
[3] Superseded by DOBBS 08A.
[4] Mass central value and systematic error recalculated by us according to Eq. (16) in ARMSTRONG 93B, using the value for the $\psi(2S)$ mass from AULCHENKO 03.

$h_c(1P)$ WIDTH

VALUE (MeV)	CL%	EVTS	DOCUMENT ID		TECN	COMMENT
0.70±0.28±0.22		832	[1] ABLIKIM	12N	BES3	$\psi(2S) \to \pi^0\gamma$ hadrons
• • • We do not use the following data for averages, fits, limits, etc. • • •						
< 1.44	90	3679	[2] ABLIKIM	10B	BES3	$\psi(2S) \to \pi^0\gamma\eta_c$
< 1		13	ANDREOTTI	05B	E835	$\overline{p}p \to \eta_c\gamma$
< 1.1	90	59	ARMSTRONG	92D	E760	$\overline{p}p \to J/\psi\pi^0$

[1] With floating mass.
[2] The central value is $\Gamma = 0.73 \pm 0.45 \pm 0.28$ MeV.

$h_c(1P)$ DECAY MODES

	Mode	Fraction (Γ_i/Γ)	Confidence level
Γ_1	$J/\psi(1S)\pi^0$		
Γ_2	$J/\psi(1S)\pi\pi$	not seen	
Γ_3	$J/\psi(1S)\pi^+\pi^-$	$< 2.3 \times 10^{-3}$	90%
Γ_4	$p\overline{p}$	$< 1.5 \times 10^{-4}$	90%
Γ_5	$p\overline{p}\pi^+\pi^-$	$(2.9\pm0.6) \times 10^{-3}$	
Γ_6	$p\overline{p}\pi^0\pi^0$	$< 5 \times 10^{-4}$	90%
Γ_7	$\pi^+\pi^-\pi^0$	$(1.6\pm0.5) \times 10^{-3}$	
Γ_8	$\pi^+\pi^-\pi^0\eta$	$(7.2\pm2.3) \times 10^{-3}$	
Γ_9	$2\pi^+2\pi^-\pi^0$	$(8.1\pm1.8) \times 10^{-3}$	
Γ_{10}	$3\pi^+3\pi^-\pi^0$	$< 9 \times 10^{-3}$	90%
Γ_{11}	$K^+K^-\pi^+\pi^-$	$< 6 \times 10^{-4}$	90%
Γ_{12}	$K^+K^-\pi^+\pi^-\pi^0$	$(3.2\pm0.8) \times 10^{-3}$	
Γ_{13}	$K^+K^-\pi^+\pi^-\eta$	$< 2.3 \times 10^{-3}$	90%
Γ_{14}	$K^+K^-\pi^0$	$< 6 \times 10^{-4}$	90%
Γ_{15}	$K^+K^-\pi^0\eta$	$< 2.1 \times 10^{-3}$	90%
Γ_{16}	$K^+K^-\eta$	$< 9 \times 10^{-4}$	90%
Γ_{17}	$2K^+2K^-\pi^0$	$< 2.4 \times 10^{-4}$	90%
Γ_{18}	$K^0_S K^\pm\pi^\mp$	$< 6 \times 10^{-4}$	90%
Γ_{19}	$K^0_S K^\pm\pi^\mp\pi^+\pi^-$	$(2.8\pm1.0) \times 10^{-3}$	
	Radiative decays		
Γ_{20}	$\gamma\eta$	$(4.7\pm2.1) \times 10^{-4}$	
Γ_{21}	$\gamma\eta'(958)$	$(1.5\pm0.4) \times 10^{-3}$	
Γ_{22}	$\gamma\eta_c(1S)$	(50 ±9) %	

$h_c(1P)$ PARTIAL WIDTHS

$h_c(1P)$ $\Gamma(i)\Gamma(\overline{p}p)/\Gamma(\text{total})$

$\Gamma(\gamma\eta_c(1S)) \times \Gamma(p\overline{p})/\Gamma_{\text{total}}$ — $\Gamma_{22}\Gamma_4/\Gamma$

VALUE (eV)	EVTS	DOCUMENT ID		TECN	COMMENT
• • • We do not use the following data for averages, fits, limits, etc. • • •					
12.0±4.5	13	[1] ANDREOTTI	05B	E835	$\overline{p}p \to \eta_c\gamma$

[1] Assuming $\Gamma = 1$ MeV.

Downloaded from https://academic.oup.com/ptep/article/2022/8/083C01/6651666 by KIT Library user on 27 September 2022

$h_c(1P)$ BRANCHING RATIOS

$\Gamma(J/\psi(1S)\pi\pi)/\Gamma(J/\psi(1S)\pi^0)$ — Γ_2/Γ_1

VALUE	CL%	DOCUMENT ID		TECN	COMMENT
<0.18	90	ARMSTRONG	92D	E760	$\overline{p}p \to J/\psi\pi^0$

$\Gamma(J/\psi(1S)\pi^+\pi^-)/\Gamma_{total}$ — Γ_3/Γ

VALUE	CL%	DOCUMENT ID		TECN	COMMENT
$<2.3\times10^{-3}$	90	[1] ABLIKIM	18M	BES3	$\psi(2S) \to \pi^0\pi^+\pi^- J/\psi$

[1] ABLIKIM 18M reports $[\Gamma(h_c(1P) \to J/\psi(1S)\pi^+\pi^-)/\Gamma_{total}] \times [B(\psi(2S) \to h_c(1P)\pi^0)] < 2.0\times10^{-6}$ which we divide by our best value $B(\psi(2S) \to h_c(1P)\pi^0) = 8.6\times10^{-4}$.

$\Gamma(p\overline{p})/\Gamma_{total}$ — Γ_4/Γ

VALUE	CL%	DOCUMENT ID		TECN	COMMENT
$<1.5\times10^{-4}$	90	[1] ABLIKIM	13V	BES3	$\psi(2S) \to \gamma p\overline{p}$

[1] ABLIKIM 13V reports $[\Gamma(h_c(1P) \to p\overline{p})/\Gamma_{total}] \times [B(\psi(2S) \to h_c(1P)\pi^0)] < 1.3\times10^{-7}$ which we divide by our best value $B(\psi(2S) \to h_c(1P)\pi^0) = 8.6\times10^{-4}$.

$\Gamma(\pi^+\pi^-\pi^0)/\Gamma_{total}$ — Γ_7/Γ

VALUE (units 10^{-3})	CL%	EVTS	DOCUMENT ID		TECN	COMMENT
1.6±0.5±0.2		101	[1] ABLIKIM	19AG	BES3	$\psi(2S) \to \pi^0 h_c(1P)$
• • • We do not use the following data for averages, fits, limits, etc. • • •						
<2.2	90		[2] ADAMS	09	CLEO	$\psi(2S) \to \pi^0\gamma\eta_c$

[1] ABLIKIM 19AG reports $[\Gamma(h_c(1P) \to \pi^+\pi^-\pi^0)/\Gamma_{total}] \times [B(\psi(2S) \to h_c(1P)\pi^0)] = (1.38\pm0.35\pm0.17)\times10^{-6}$ which we divide by our best value $B(\psi(2S) \to h_c(1P)\pi^0) = (8.6\pm1.3)\times10^{-4}$. Our first error is their experiment's error and our second error is the systematic error from using our best value.

[2] ADAMS 09 reports $[\Gamma(h_c(1P) \to \pi^+\pi^-\pi^0)/\Gamma_{total}] \times [B(\psi(2S) \to h_c(1P)\pi^0)] < 0.19\times10^{-5}$ which we divide by our best value $B(\psi(2S) \to h_c(1P)\pi^0) = 8.6\times10^{-4}$.

$\Gamma(\pi^+\pi^-\pi^0\eta)/\Gamma_{total}$ — Γ_8/Γ

VALUE (units 10^{-3})	EVTS	DOCUMENT ID		TECN	COMMENT
7.2±2.0±1.0	35	[1] ABLIKIM	20AH	BES3	$\psi(2S) \to \pi^0 h_c(1P)$

[1] ABLIKIM 20AH reports $[\Gamma(h_c(1P) \to \pi^+\pi^-\pi^0\eta)/\Gamma_{total}] \times [B(\psi(2S) \to h_c(1P)\pi^0)] = (6.2\pm1.6\pm0.7)\times10^{-6}$ which we divide by our best value $B(\psi(2S) \to h_c(1P)\pi^0) = (8.6\pm1.3)\times10^{-4}$. Our first error is their experiment's error and our second error is the systematic error from using our best value.

$\Gamma(2\pi^+2\pi^-\pi^0)/\Gamma_{total}$ — Γ_9/Γ

VALUE (units 10^{-2})	EVTS	DOCUMENT ID		TECN	COMMENT
0.81±0.18 OUR AVERAGE					
$0.74\pm0.14\pm0.11$	254	[1] ABLIKIM	19AG	BES3	$\psi(2S) \to \pi^0 h_c(1P)$
$2.2\ ^{+0.8}_{-0.6}\ \pm0.3$	92	[2] ADAMS	09	CLEO	$\psi(2S) \to \pi^0\gamma\eta_c$

[1] ABLIKIM 19AG reports $[\Gamma(h_c(1P) \to 2\pi^+2\pi^-\pi^0)/\Gamma_{total}] \times [B(\psi(2S) \to h_c(1P)\pi^0)] = (6.40\pm0.81\pm0.87)\times10^{-6}$ which we divide by our best value $B(\psi(2S) \to h_c(1P)\pi^0) = (8.6\pm1.3)\times10^{-4}$. Our first error is their experiment's error and our second error is the systematic error from using our best value.

[2] ADAMS 09 reports $[\Gamma(h_c(1P) \to 2\pi^+2\pi^-\pi^0)/\Gamma_{total}] \times [B(\psi(2S) \to h_c(1P)\pi^0)] = (1.88\ ^{+0.48}_{-0.45}\ ^{+0.47}_{-0.30})\times10^{-5}$ which we divide by our best value $B(\psi(2S) \to h_c(1P)\pi^0) = (8.6\pm1.3)\times10^{-4}$. Our first error is their experiment's error and our second error is the systematic error from using our best value.

$\Gamma(3\pi^+3\pi^-\pi^0)/\Gamma_{total}$ — Γ_{10}/Γ

VALUE	CL%	DOCUMENT ID		TECN	COMMENT
<9 $\times10^{-3}$	90	[1] ABLIKIM	19AG	BES3	$\psi(2S) \to \pi^0 h_c(1P)$
• • • We do not use the following data for averages, fits, limits, etc. • • •					
<0.029	90	[2] ADAMS	09	CLEO	$\psi(2S) \to \pi^0\gamma\eta_c$

[1] ABLIKIM 19AG reports $[\Gamma(h_c(1P) \to 3\pi^+3\pi^-\pi^0)/\Gamma_{total}] \times [B(\psi(2S) \to h_c(1P)\pi^0)] < 7.5\times10^{-6}$ which we divide by our best value $B(\psi(2S) \to h_c(1P)\pi^0) = 8.6\times10^{-4}$.

[2] ADAMS 09 reports $[\Gamma(h_c(1P) \to 3\pi^+3\pi^-\pi^0)/\Gamma_{total}] \times [B(\psi(2S) \to h_c(1P)\pi^0)] < 2.5\times10^{-5}$ which we divide by our best value $B(\psi(2S) \to h_c(1P)\pi^0) = 8.6\times10^{-4}$.

$\Gamma(p\overline{p}\pi^+\pi^-)/\Gamma_{total}$ — Γ_5/Γ

VALUE (units 10^{-3})	EVTS	DOCUMENT ID		TECN	COMMENT
2.9±0.5±0.4	230	[1] ABLIKIM	19AG	BES3	$\psi(2S) \to \pi^0 h_c(1P)$

[1] ABLIKIM 19AG reports $[\Gamma(h_c(1P) \to p\overline{p}\pi^+\pi^-)/\Gamma_{total}] \times [B(\psi(2S) \to h_c(1P)\pi^0)] = (2.49\pm0.27\pm0.28)\times10^{-6}$ which we divide by our best value $B(\psi(2S) \to h_c(1P)\pi^0) = (8.6\pm1.3)\times10^{-4}$. Our first error is their experiment's error and our second error is the systematic error from using our best value.

$\Gamma(p\overline{p}\pi^0\pi^0)/\Gamma_{total}$ — Γ_6/Γ

VALUE	CL%	EVTS	DOCUMENT ID		TECN	COMMENT
$<5\times10^{-4}$	90	12	[1] ABLIKIM	20AH	BES3	$\psi(2S) \to \pi^0 h_c(1P)$

[1] ABLIKIM 20AH reports $[\Gamma(h_c(1P) \to p\overline{p}\pi^0\pi^0)/\Gamma_{total}] \times [B(\psi(2S) \to h_c(1P)\pi^0)] < 4.4\times10^{-7}$ which we divide by our best value $B(\psi(2S) \to h_c(1P)\pi^0) = 8.6\times10^{-4}$.

$\Gamma(K^+K^-\pi^+\pi^-)/\Gamma_{total}$ — Γ_{11}/Γ

VALUE	CL%	DOCUMENT ID		TECN	COMMENT
$<6\times10^{-4}$	90	[1] ABLIKIM	19AG	BES3	$\psi(2S) \to \pi^0 h_c(1P)$

[1] ABLIKIM 19AG reports $[\Gamma(h_c(1P) \to K^+K^-\pi^+\pi^-)/\Gamma_{total}] \times [B(\psi(2S) \to h_c(1P)\pi^0)] < 0.5\times10^{-6}$ which we divide by our best value $B(\psi(2S) \to h_c(1P)\pi^0) = 8.6\times10^{-4}$.

$\Gamma(K^+K^-\pi^+\pi^-\pi^0)/\Gamma_{total}$ — Γ_{12}/Γ

VALUE (units 10^{-3})	EVTS	DOCUMENT ID		TECN	COMMENT
3.2±0.7±0.5	80	[1] ABLIKIM	20AH	BES3	$\psi(2S) \to \pi^0 h_c(1P)$

[1] ABLIKIM 20AH reports $[\Gamma(h_c(1P) \to K^+K^-\pi^+\pi^-\pi^0)/\Gamma_{total}] \times [B(\psi(2S) \to h_c(1P)\pi^0)] = (2.8\pm0.5\pm0.3)\times10^{-6}$ which we divide by our best value $B(\psi(2S) \to h_c(1P)\pi^0) = (8.6\pm1.3)\times10^{-4}$. Our first error is their experiment's error and our second error is the systematic error from using our best value.

$\Gamma(K^+K^-\pi^+\pi^-\eta)/\Gamma_{total}$ — Γ_{13}/Γ

VALUE	CL%	EVTS	DOCUMENT ID		TECN	COMMENT
$<2.3\times10^{-3}$	90	24	[1] ABLIKIM	20AH	BES3	$\psi(2S) \to \pi^0 h_c(1P)$

[1] ABLIKIM 20AH reports $[\Gamma(h_c(1P) \to K^+K^-\pi^+\pi^-\eta)/\Gamma_{total}] \times [B(\psi(2S) \to h_c(1P)\pi^0)] < 2.0\times10^{-6}$ which we divide by our best value $B(\psi(2S) \to h_c(1P)\pi^0) = 8.6\times10^{-4}$.

$\Gamma(K^+K^-\pi^0)/\Gamma_{total}$ — Γ_{14}/Γ

VALUE	CL%	EVTS	DOCUMENT ID		TECN	COMMENT
$<6\times10^{-4}$	90	20	[1] ABLIKIM	20AH	BES3	$\psi(2S) \to \pi^0 h_c(1P)$

[1] ABLIKIM 20AH reports $[\Gamma(h_c(1P) \to K^+K^-\pi^0)/\Gamma_{total}] \times [B(\psi(2S) \to h_c(1P)\pi^0)] < 4.8\times10^{-7}$ which we divide by our best value $B(\psi(2S) \to h_c(1P)\pi^0) = 8.6\times10^{-4}$.

$\Gamma(2K^+2K^-\pi^0)/\Gamma_{total}$ — Γ_{17}/Γ

VALUE	CL%	EVTS	DOCUMENT ID		TECN	COMMENT
$<2.4\times10^{-4}$	90	11	[1] ABLIKIM	20AH	BES3	$\psi(2S) \to \pi^0 h_c(1P)$

[1] ABLIKIM 20AH reports $[\Gamma(h_c(1P) \to 2K^+2K^-\pi^0)/\Gamma_{total}] \times [B(\psi(2S) \to h_c(1P)\pi^0)] < 2.1\times10^{-7}$ which we divide by our best value $B(\psi(2S) \to h_c(1P)\pi^0) = 8.6\times10^{-4}$.

$\Gamma(K^+K^-\pi^0\eta)/\Gamma_{total}$ — Γ_{15}/Γ

VALUE	CL%	EVTS	DOCUMENT ID		TECN	COMMENT
$<2.1\times10^{-3}$	90	20	[1] ABLIKIM	20AH	BES3	$\psi(2S) \to \pi^0 h_c(1P)$

[1] ABLIKIM 20AH reports $[\Gamma(h_c(1P) \to K^+K^-\pi^0\eta)/\Gamma_{total}] \times [B(\psi(2S) \to h_c(1P)\pi^0)] < 1.8\times10^{-6}$ which we divide by our best value $B(\psi(2S) \to h_c(1P)\pi^0) = 8.6\times10^{-4}$.

$\Gamma(K^+K^-\eta)/\Gamma_{total}$ — Γ_{16}/Γ

VALUE	CL%	EVTS	DOCUMENT ID		TECN	COMMENT
$<9\times10^{-4}$	90	18	[1] ABLIKIM	20AH	BES3	$\psi(2S) \to \pi^0 h_c(1P)$

[1] ABLIKIM 20AH reports $[\Gamma(h_c(1P) \to K^+K^-\eta)/\Gamma_{total}] \times [B(\psi(2S) \to h_c(1P)\pi^0)] < 7.5\times10^{-7}$ which we divide by our best value $B(\psi(2S) \to h_c(1P)\pi^0) = 8.6\times10^{-4}$.

$\Gamma(K^0_S K^\pm\pi^\mp)/\Gamma_{total}$ — Γ_{18}/Γ

VALUE	CL%	EVTS	DOCUMENT ID		TECN	COMMENT
$<6\times10^{-4}$	90	17	[1] ABLIKIM	20AH	BES3	$\psi(2S) \to \pi^0 h_c(1P)$

[1] ABLIKIM 20AH reports $[\Gamma(h_c(1P) \to K^0_S K^\pm\pi^\mp)/\Gamma_{total}] \times [B(\psi(2S) \to h_c(1P)\pi^0)] < 4.8\times10^{-7}$ which we divide by our best value $B(\psi(2S) \to h_c(1P)\pi^0) = 8.6\times10^{-4}$.

$\Gamma(K^0_S K^\pm\pi^\mp\pi^+\pi^-)/\Gamma_{total}$ — Γ_{19}/Γ

VALUE (units 10^{-3})	EVTS	DOCUMENT ID		TECN	COMMENT
2.8±0.9±0.4	41	[1] ABLIKIM	20AH	BES3	$\psi(2S) \to \pi^0 h_c(1P)$

[1] ABLIKIM 20AH reports $[\Gamma(h_c(1P) \to K^0_S K^\pm\pi^\mp\pi^+\pi^-)/\Gamma_{total}] \times [B(\psi(2S) \to h_c(1P)\pi^0)] = (2.4\pm0.7\pm0.3)\times10^{-6}$ which we divide by our best value $B(\psi(2S) \to h_c(1P)\pi^0) = (8.6\pm1.3)\times10^{-4}$. Our first error is their experiment's error and our second error is the systematic error from using our best value.

RADIATIVE DECAYS

$\Gamma(\gamma\eta)/\Gamma_{total}$ — Γ_{20}/Γ

VALUE (units 10^{-4})	EVTS	DOCUMENT ID		TECN	COMMENT
4.7±1.5±1.4	18	ABLIKIM	16I	BES3	$\psi(2S) \to \pi^0\gamma\eta$

$\Gamma(\gamma\eta'(958))/\Gamma_{total}$ — Γ_{21}/Γ

VALUE (units 10^{-3})	EVTS	DOCUMENT ID		TECN	COMMENT
1.52±0.27±0.29	44	ABLIKIM	16I	BES3	$\psi(2S) \to \pi^0\gamma\eta'(958)$

$\Gamma(\gamma\eta_c(1S))/\Gamma_{total}$ — Γ_{22}/Γ

VALUE (units 10^{-2})	EVTS	DOCUMENT ID		TECN	COMMENT
50± 9 OUR AVERAGE					
53± 7±8	3679	[1] ABLIKIM	10B	BES3	$\psi(2S) \to \pi^0\eta_c\gamma$
48± 6±7		[2] DOBBS	08A	CLEO	$\psi(2S) \to \pi^0\eta_c\gamma$

Downloaded from https://academic.oup.com/ptep/article/2022/8/083C01/6651666 by KIT Library user on 27 September 2022

• • • We do not use the following data for averages, fits, limits, etc. • • •

48± 6±7	1282	[3] DOBBS	08A	CLEO	$\psi(2S) \to \pi^0 \eta_c \gamma$
46±12±7	168	[4] ROSNER	05	CLEO	$\psi(2S) \to \pi^0 \eta_c \gamma$

[1] ABLIKIM 10B reports $[\Gamma(h_c(1P) \to \gamma\eta_c(1S))/\Gamma_{total}] \times [B(\psi(2S) \to h_c(1P)\pi^0)] = (4.58 \pm 0.40 \pm 0.50) \times 10^{-4}$ which we divide by our best value $B(\psi(2S) \to h_c(1P)\pi^0) = (8.6 \pm 1.3) \times 10^{-4}$. Our first error is their experiment's error and our second error is the systematic error from using our best value.

[2] Average of DOBBS 08A and ROSNER 05. DOBBS 08A reports $[\Gamma(h_c(1P) \to \gamma\eta_c(1S))/\Gamma_{total}] \times [B(\psi(2S) \to h_c(1P)\pi^0)] = (4.16 \pm 0.30 \pm 0.37) \times 10^{-4}$ which we divide by our best value $B(\psi(2S) \to h_c(1P)\pi^0) = (8.6 \pm 1.3) \times 10^{-4}$. Our first error is their experiment's error and our second error is the systematic error from using our best value.

[3] DOBBS 08A reports $[\Gamma(h_c(1P) \to \gamma\eta_c(1S))/\Gamma_{total}] \times [B(\psi(2S) \to h_c(1P)\pi^0)] = (4.19 \pm 0.32 \pm 0.45) \times 10^{-4}$ which we divide by our best value $B(\psi(2S) \to h_c(1P)\pi^0) = (8.6 \pm 1.3) \times 10^{-4}$. Our first error is their experiment's error and our second error is the systematic error from using our best value.

[4] ROSNER 05 reports $[\Gamma(h_c(1P) \to \gamma\eta_c(1S))/\Gamma_{total}] \times [B(\psi(2S) \to h_c(1P)\pi^0)] = (4.0 \pm 0.8 \pm 0.7) \times 10^{-4}$ which we divide by our best value $B(\psi(2S) \to h_c(1P)\pi^0) = (8.6 \pm 1.3) \times 10^{-4}$. Our first error is their experiment's error and our second error is the systematic error from using our best value.

$h_c(1P)$ REFERENCES

ABLIKIM	20AH	PR D102 112007	M. Ablikim *et al.*	(BESIII Collab.)
ABLIKIM	19AG	PR D99 072008	M. Ablikim *et al.*	(BESIII Collab.)
ABLIKIM	18M	PR D97 052008	M. Ablikim *et al.*	(BESIII Collab.)
ABLIKIM	16I	PRL 116 251802	M. Ablikim *et al.*	(BESIII Collab.)
ABLIKIM	13V	PR D88 112001	M. Ablikim *et al.*	(BESIII Collab.)
ABLIKIM	12N	PR D86 092009	M. Ablikim *et al.*	(BESIII Collab.)
ABLIKIM	10B	PRL 104 132002	M. Ablikim *et al.*	(BESIII Collab.)
ADAMS	09	PR D80 051106	G.S. Adams *et al.*	(CLEO Collab.)
DOBBS	08A	PRL 101 182003	S. Dobbs *et al.*	(CLEO Collab.)
ANDREOTTI	05B	PR D72 032001	M. Andreotti *et al.*	(FNAL E835 Collab.)
ROSNER	05	PRL 95 102003	J.L. Rosner *et al.*	(CLEO Collab.)
AULCHENKO	03	PL B573 63	V.M. Aulchenko *et al.*	(KEDR Collab.)
ANTONIAZZI	94	PR D50 4258	L. Antoniazzi *et al.*	(E705 Collab.)
ARMSTRONG	93B	PR D47 772	T.A. Armstrong *et al.*	(FNAL E760 Collab.)
ARMSTRONG	92D	PRL 69 2337	T.A. Armstrong *et al.*	(FNAL, FERR, GENO+)
BAGLIN	86	PL B171 135	C. Baglin *et al.*	(LAPP, CERN, TORI, STRB+)

$\chi_{c2}(1P)$

$I^G(J^{PC}) = 0^+(2^{++})$

See the Review on "$\psi(2S)$ and χ_c branching ratios" before the $\chi_{c0}(1P)$ Listings.

$\chi_{c2}(1P)$ MASS

VALUE (MeV)			EVTS	DOCUMENT ID		TECN	COMMENT
3556.17 ± 0.07 OUR AVERAGE							
3557.3	± 1.7	±0.7	611	[1] AAIJ	17BB	LHCB	$pp \to b\overline{b}X \to 2(K^+K^-)X$
3556.10	± 0.06	±0.11	4.0k	[2] AAIJ	17BI	LHCB	$\chi_{c2} \to J/\psi\mu^+\mu^-$
3555.3	± 0.6	±2.2	2.5k	UEHARA	08	BELL	$\gamma\gamma \to$ hadrons
3555.70	± 0.59	±0.39		ABLIKIM	05G	BES2	$\psi(2S) \to \gamma\chi_{c2}$
3556.173	± 0.123	±0.020		ANDREOTTI	05A	E835	$p\overline{p} \to e^+e^-\gamma$
3559.9	± 2.9			EISENSTEIN	01	CLE2	$e^+e^- \to e^+e^-\chi_{c2}$
3556.4	± 0.7			BAI	99B	BES	$\psi(2S) \to \gamma X$
3556.22	± 0.131	±0.020	585	[3] ARMSTRONG	92	E760	$\overline{p}p \to e^+e^-\gamma$
3556.9	± 0.4	±0.5	50	BAGLIN	86B	SPEC	$\overline{p}p \to e^+e^-X$
3557.8	± 0.2	±4		[4] GAISER	86	CBAL	$\psi(2S) \to \gamma X$
3553.4	± 2.2		66	[5] LEMOIGNE	82	GOLI	185 π^-Be $\to \gamma\mu^+\mu^-$A
3555.9	± 0.7			[6] OREGLIA	82	CBAL	$e^+e^- \to J/\psi 2\gamma$
3557	± 1.5		69	[7] HIMEL	80	MRK2	$e^+e^- \to J/\psi 2\gamma$
3551	±11		15	BRANDELIK	79B	DASP	$e^+e^- \to J/\psi 2\gamma$
3553	± 4			[7] BARTEL	78B	CNTR	$e^+e^- \to J/\psi 2\gamma$
3553	± 4	±4		[7,8] TANENBAUM	78	MRK1	e^+e^-
3563	± 7		360	[7] BIDDICK	77	CNTR	$e^+e^- \to \gamma X$

• • • We do not use the following data for averages, fits, limits, etc. • • •

3555.4	±1.3		53	UEHARA	13	BELL	$\gamma\gamma \to K^0_S K^0_S$
3543	±10		4	WHITAKER	76	MRK1	$e^+e^- \to J/\psi 2\gamma$

[1] From a fit of the $\phi\phi$ invariant mass with the width of $\chi_{c2}(1P)$ fixed to the PDG 16 value.

[2] AAIJ 17BI reports also $m(\chi_{c2}) - m(\chi_{c1}) = 45.39 \pm 0.07 \pm 0.03$ MeV.

[3] Recalculated by ANDREOTTI 05A, using the value of $\psi(2S)$ mass from AULCHENKO 03.

[4] Using mass of $\psi(2S) = 3686.0$ MeV.

[5] $J/\psi(1S)$ mass constrained to 3097 MeV.

[6] Assuming $\psi(2S)$ mass = 3686 MeV and $J/\psi(1S)$ mass = 3097 MeV.

[7] Mass value shifted by us by amount appropriate for $\psi(2S)$ mass = 3686 MeV and $J/\psi(1S)$ mass = 3097 MeV.

[8] From a simultaneous fit to radiative and hadronic decay channels.

$\chi_{c2}(1P)$ WIDTH

VALUE (MeV)	EVTS	DOCUMENT ID		TECN	COMMENT
1.97 ±0.09 OUR FIT					
2.00 ±0.11 OUR AVERAGE					
2.10 ±0.20 ±0.02	4.0k	AAIJ	17BI	LHCB	$\chi_{c2} \to J/\psi\mu^+\mu^-$
1.915±0.188±0.013		ANDREOTTI	05A	E835	$p\overline{p} \to e^+e^-\gamma$
1.96 ±0.17 ±0.07	585	[1] ARMSTRONG	92	E760	$\overline{p}p \to e^+e^-\gamma$
$2.6^{+1.4}_{-1.0}$	50	BAGLIN	86B	SPEC	$\overline{p}p \to e^+e^-X$
$2.8^{+2.1}_{-2.0}$		[2] GAISER	86	CBAL	$\psi(2S) \to \gamma X$

[1] Recalculated by ANDREOTTI 05A.

[2] Errors correspond to 90% confidence level; authors give only width range.

$\chi_{c2}(1P)$ DECAY MODES

	Mode	Fraction (Γ_i/Γ)	Confidence level
	Hadronic decays		
Γ_1	$2(\pi^+\pi^-)$	(1.02±0.09) %	
Γ_2	$\rho\rho$		
Γ_3	$\pi^+\pi^-\pi^0\pi^0$	(1.83±0.23) %	
Γ_4	$\rho^+\pi^-\pi^0$ + c.c.	(2.19±0.34) %	
Γ_5	$4\pi^0$	(1.11±0.15) $\times 10^{-3}$	
Γ_6	$K^+K^-\pi^0\pi^0$	(2.1 ±0.4) $\times 10^{-3}$	
Γ_7	$K^+\pi^-\overline{K}^0\pi^0$ + c.c.	(1.38±0.20) %	
Γ_8	$\rho^-K^+\overline{K}^0$ + c.c.	(4.1 ±1.2) $\times 10^{-3}$	
Γ_9	$K^*(892)^0K^-\pi^+ \to K^-\pi^+K^0\pi^0$ + c.c.	(2.9 ±0.8) $\times 10^{-3}$	
Γ_{10}	$K^*(892)^0\overline{K}^0\pi^0 \to K^+\pi^-\overline{K}^0\pi^0$ + c.c.	(3.8 ±0.9) $\times 10^{-3}$	
Γ_{11}	$K^*(892)^-K^+\pi^0 \to K^+\pi^-\overline{K}^0\pi^0$ + c.c.	(3.7 ±0.8) $\times 10^{-3}$	
Γ_{12}	$K^*(892)^+\overline{K}^0\pi^- \to K^+\pi^-\overline{K}^0\pi^0$ + c.c.	(2.9 ±0.8) $\times 10^{-3}$	
Γ_{13}	$K^+K^-\eta\pi^0$	(1.3 ±0.4) $\times 10^{-3}$	
Γ_{14}	$K^+K^-\pi^+\pi^-$	(8.4 ±0.9) $\times 10^{-3}$	
Γ_{15}	$K^+K^-\pi^+\pi^-\pi^0$	(1.17±0.13) %	
Γ_{16}	$K^0_SK^\pm\pi^\mp\pi^+\pi^-$	(7.3 ±0.8) $\times 10^{-3}$	
Γ_{17}	$K^+\overline{K}^*(892)^0\pi^-$ + c.c.	(2.1 ±1.1) $\times 10^{-3}$	
Γ_{18}	$K^*(892)^0\overline{K}^*(892)^0$	(2.3 ±0.4) $\times 10^{-3}$	
Γ_{19}	$3(\pi^+\pi^-)$	(8.6 ±1.8) $\times 10^{-3}$	
Γ_{20}	$\phi\phi$	(1.06±0.09) $\times 10^{-3}$	
Γ_{21}	$\phi\phi\eta$	(5.3 ±0.6) $\times 10^{-4}$	
Γ_{22}	$\omega\omega$	(8.4 ±1.0) $\times 10^{-4}$	
Γ_{23}	ωK^+K^-	(7.3 ±0.9) $\times 10^{-4}$	
Γ_{24}	$\omega\phi$	(9.6 ±2.7) $\times 10^{-6}$	
Γ_{25}	$\pi\pi$	(2.23±0.09) $\times 10^{-3}$	
Γ_{26}	$\rho^0\pi^+\pi^-$	(3.7 ±1.6) $\times 10^{-3}$	
Γ_{27}	$\pi^+\pi^-\pi^0$ (non-resonant)	(2.0 ±0.4) $\times 10^{-5}$	
Γ_{28}	$\rho(770)^\pm\pi^\mp$	(6 ±4) $\times 10^{-6}$	
Γ_{29}	$\pi^+\pi^-\eta$	(4.8 ±1.3) $\times 10^{-4}$	
Γ_{30}	$\pi^+\pi^-\eta'$	(5.0 ±1.8) $\times 10^{-4}$	
Γ_{31}	$\eta\eta$	(5.4 ±0.4) $\times 10^{-4}$	
Γ_{32}	K^+K^-	(1.01±0.06) $\times 10^{-3}$	
Γ_{33}	$K^0_SK^0_S$	(5.2 ±0.4) $\times 10^{-4}$	
Γ_{34}	$K^*(892)^\pm K^\mp$	(1.44±0.21) $\times 10^{-4}$	
Γ_{35}	$K^*(892)^0\overline{K}^0$ + c.c.	(1.24±0.27) $\times 10^{-4}$	
Γ_{36}	$K^*_2(1430)^\pm K^\mp$	(1.48±0.12) $\times 10^{-3}$	
Γ_{37}	$K^*_2(1430)^0\overline{K}^0$ + c.c.	(1.24±0.17) $\times 10^{-3}$	
Γ_{38}	$K^*_3(1780)^\pm K^\mp$	(5.2 ±0.8) $\times 10^{-4}$	
Γ_{39}	$K^*_3(1780)^0\overline{K}^0$ + c.c.	(5.6 ±2.1) $\times 10^{-4}$	
Γ_{40}	$a_2(1320)^0\pi^0$	(1.29±0.34) $\times 10^{-3}$	
Γ_{41}	$a_2(1320)^\pm\pi^\mp$	(1.8 ±0.6) $\times 10^{-3}$	
Γ_{42}	$\overline{K}^0K^+\pi^-$ + c.c.	(1.28±0.18) $\times 10^{-3}$	
Γ_{43}	$K^+K^-\pi^0$	(3.0 ±0.8) $\times 10^{-4}$	
Γ_{44}	$K^+K^-\eta$	< 3.2 $\times 10^{-4}$	90%
Γ_{45}	$K^+K^-\eta'(958)$	(1.94±0.34) $\times 10^{-4}$	
Γ_{46}	$\eta\eta'$	(2.2 ±0.5) $\times 10^{-5}$	
Γ_{47}	$\eta'\eta'$	(4.6 ±0.6) $\times 10^{-5}$	
Γ_{48}	$\pi^+\pi^-K^0_SK^0_S$	(2.2 ±0.5) $\times 10^{-3}$	
Γ_{49}	$K^+K^-K^0_SK^0_S$	< 4 $\times 10^{-4}$	90%
Γ_{50}	$K^0_SK^0_SK^0_SK^0_S$	(1.13±0.18) $\times 10^{-4}$	
Γ_{51}	$K^+K^-K^+K^-$	(1.65±0.20) $\times 10^{-3}$	
Γ_{52}	$K^+K^-\phi$	(1.42±0.29) $\times 10^{-3}$	
Γ_{53}	$\overline{K}^0K^+\pi^-\phi$ + c.c.	(4.8 ±0.7) $\times 10^{-3}$	
Γ_{54}	$K^+K^-\pi^0\phi$	(2.7 ±0.5) $\times 10^{-3}$	

Downloaded from https://academic.oup.com/ptep/article/2022/8/083C01/6651666 by KIT Library user on 27 September 2022

Γ_{55}	$\phi\pi^+\pi^-\pi^0$	$(9.3 \pm 1.2) \times 10^{-4}$	
Γ_{56}	$p\overline{p}$	$(7.33 \pm 0.33) \times 10^{-5}$	
Γ_{57}	$p\overline{p}\pi^0$	$(4.7 \pm 0.4) \times 10^{-4}$	
Γ_{58}	$p\overline{p}\eta$	$(1.74 \pm 0.25) \times 10^{-4}$	
Γ_{59}	$p\overline{p}\omega$	$(3.6 \pm 0.4) \times 10^{-4}$	
Γ_{60}	$p\overline{p}\phi$	$(2.8 \pm 0.9) \times 10^{-5}$	
Γ_{61}	$p\overline{p}\pi^+\pi^-$	$(1.32 \pm 0.34) \times 10^{-3}$	
Γ_{62}	$p\overline{p}\pi^0\pi^0$	$(7.8 \pm 2.3) \times 10^{-4}$	
Γ_{63}	$p\overline{p}K^+K^-$ (non-resonant)	$(1.91 \pm 0.32) \times 10^{-4}$	
Γ_{64}	$p\overline{p}K^0_SK^0_S$	$< 7.9 \times 10^{-4}$	90%
Γ_{65}	$p\overline{n}\pi^-$	$(8.5 \pm 0.9) \times 10^{-4}$	
Γ_{66}	$\overline{p}n\pi^+$	$(8.9 \pm 0.8) \times 10^{-4}$	
Γ_{67}	$p\overline{n}\pi^-\pi^0$	$(2.17 \pm 0.18) \times 10^{-3}$	
Γ_{68}	$\overline{p}n\pi^+\pi^0$	$(2.11 \pm 0.18) \times 10^{-3}$	
Γ_{69}	$\Lambda\overline{\Lambda}$	$(1.83 \pm 0.16) \times 10^{-4}$	
Γ_{70}	$\Lambda\overline{\Lambda}\pi^+\pi^-$	$(1.25 \pm 0.15) \times 10^{-3}$	
Γ_{71}	$\Lambda\overline{\Lambda}\pi^+\pi^-$ (non-resonant)	$(6.6 \pm 1.5) \times 10^{-4}$	
Γ_{72}	$\Sigma(1385)^+\overline{\Lambda}\pi^-$ + c.c.	$< 4 \times 10^{-4}$	90%
Γ_{73}	$\Sigma(1385)^-\overline{\Lambda}\pi^+$ + c.c.	$< 6 \times 10^{-4}$	90%
Γ_{74}	$K^+\overline{p}\Lambda$ + c.c.	$(7.8 \pm 0.5) \times 10^{-4}$	
Γ_{75}	$nK^0_S\overline{\Lambda}$ + c.c.	$(3.58 \pm 0.28) \times 10^{-4}$	
Γ_{76}	$K^*(892)^+\overline{p}\Lambda$ + c.c.	$(8.2 \pm 1.1) \times 10^{-4}$	
Γ_{77}	$K^+\overline{p}\Lambda(1520)$ + c.c.	$(2.8 \pm 0.7) \times 10^{-4}$	
Γ_{78}	$\Lambda(1520)\overline{\Lambda}(1520)$	$(4.6 \pm 1.5) \times 10^{-4}$	
Γ_{79}	$\Sigma^0\overline{\Sigma}^0$	$(3.7 \pm 0.6) \times 10^{-5}$	
Γ_{80}	$\Sigma^+\overline{p}K^0_S$ + c.c.	$(8.2 \pm 0.9) \times 10^{-5}$	
Γ_{81}	$\Sigma^0\overline{p}K^+$ + c.c.	$(9.1 \pm 0.8) \times 10^{-5}$	
Γ_{82}	$\Sigma^+\overline{\Sigma}^-$	$(3.4 \pm 0.7) \times 10^{-5}$	
Γ_{83}	$\Sigma^-\overline{\Sigma}^+$	$(4.4 \pm 1.8) \times 10^{-5}$	
Γ_{84}	$\Sigma(1385)^+\overline{\Sigma}(1385)^-$	$< 1.6 \times 10^{-4}$	90%
Γ_{85}	$\Sigma(1385)^-\overline{\Sigma}(1385)^+$	$< 8 \times 10^{-5}$	90%
Γ_{86}	$K^-\Lambda\overline{\Xi}^+$ + c.c.	$(1.76 \pm 0.32) \times 10^{-4}$	
Γ_{87}	$\Xi^0\overline{\Xi}^0$	$< 1.0 \times 10^{-4}$	90%
Γ_{88}	$\Xi^-\overline{\Xi}^+$	$(1.42 \pm 0.32) \times 10^{-4}$	
Γ_{89}	$J/\psi(1S)\pi^+\pi^-\pi^0$	< 1.5 %	90%
Γ_{90}	$\pi^0\eta_c$	$< 3.2 \times 10^{-3}$	90%
Γ_{91}	$\eta_c(1S)\pi^+\pi^-$	$< 5.4 \times 10^{-3}$	90%
	Radiative decays		
Γ_{92}	$\gamma J/\psi(1S)$	(19.0 ± 0.5) %	
Γ_{93}	$\gamma\rho^0$	$< 1.9 \times 10^{-5}$	90%
Γ_{94}	$\gamma\omega$	$< 6 \times 10^{-6}$	90%
Γ_{95}	$\gamma\phi$	$< 7 \times 10^{-6}$	90%
Γ_{96}	$\gamma\gamma$	$(2.85 \pm 0.10) \times 10^{-4}$	
Γ_{97}	$e^+e^-J/\psi(1S)$	$(2.15 \pm 0.14) \times 10^{-3}$	
Γ_{98}	$\mu^+\mu^-J/\psi(1S)$	$(2.02 \pm 0.33) \times 10^{-4}$	

CONSTRAINED FIT INFORMATION

A multiparticle fit to $\chi_{c1}(1P)$, $\chi_{c0}(1P)$, $\chi_{c2}(1P)$, and $\psi(2S)$ with 4 total widths, a partial width, 25 combinations of partial widths obtained from integrated cross section, and 84 branching ratios uses 248 measurements to determine 49 parameters. The overall fit has a $\chi^2 = 379.8$ for 199 degrees of freedom.

The following *off-diagonal* array elements are the correlation coefficients $\langle \delta p_i \delta p_j \rangle / (\delta p_i \cdot \delta p_j)$, in percent, from the fit to parameters p_i, including the branching fractions, $x_i \equiv \Gamma_i/\Gamma_{total}$.

	x_1	x_{14}	x_{17}	x_{18}	x_{20}	x_{25}	x_{26}	x_{31}	x_{32}	x_{33}
x_{14}		7								
x_{17}		2	21							
x_{18}		4	3	1						
x_{20}		7	5	1	3					
x_{25}		7	6	1	4	10				
x_{26}		18	2	0	1	1	1			
x_{31}		3	3	1	2	5	12	1		
x_{32}		5	4	1	3	7	15	1	8	
x_{33}		5	4	1	2	6	13	1	7	8
x_{42}		2	2	0	1	3	7	0	3	4	4
x_{51}		4	3	1	2	4	7	1	4	5	4
x_{56}		10	9	2	5	9	11	2	5	8	7
x_{69}		3	3	1	2	5	12	1	6	8	6
x_{92}		12	10	2	6	15	34	2	18	22	18
x_{96}		−6	−4	−1	−2	2	20	−2	12	12	10
Γ		−23	−19	−4	−11	−19	−25	−5	−12	−18	−15

	x_{42}	x_{51}	x_{56}	x_{69}	x_{92}	x_{96}
x_{51}	2					
x_{56}	4	5				
x_{69}	3	4	5			
x_{92}	10	11	4	17		
x_{96}	5	4	18	11	34	
Γ	−8	−11	−45	−12	−46	−43

$\chi_{c2}(1P)$ PARTIAL WIDTHS

$\chi_{c2}(1P)$ $\Gamma(i)\Gamma(\gamma J/\psi(1S))/\Gamma(total)$

$\Gamma(p\overline{p}) \times \Gamma(\gamma J/\psi(1S))/\Gamma_{total}$ — $\Gamma_{56}\Gamma_{92}/\Gamma$

VALUE (eV)	DOCUMENT ID		TECN	COMMENT
27.5±1.2 OUR FIT				
27.5±1.5 OUR AVERAGE				
27.0±1.5±1.1	[1] ANDREOTTI	05A	E835	$p\overline{p} \to e^+e^-\gamma$
27.7±1.5±2.0	[1,2] ARMSTRONG	92	E760	$\overline{p}p \to e^+e^-\gamma$
36 ±8	[1] BAGLIN	86B	SPEC	$\overline{p}p \to e^+e^-X$

[1] Calculated by us using $B(J/\psi(1S) \to e^+e^-) = 0.0593 \pm 0.0010$.
[2] Recalculated by ANDREOTTI 05A.

$\Gamma(\gamma\gamma) \times \Gamma(\gamma J/\psi(1S))/\Gamma_{total}$ — $\Gamma_{96}\Gamma_{92}/\Gamma$

VALUE (eV)	EVTS	DOCUMENT ID		TECN	COMMENT
107± 5 OUR FIT					
117± 10 OUR AVERAGE					
111± 12± 9	147 ± 15	[1] DOBBS	06	CLE3	10.4 $e^+e^- \to e^+e^-\chi_{c2}$
114± 11± 9	136 ± 13.3	[1,2] ABE	02T	BELL	$e^+e^- \to e^+e^-\chi_{c2}$
139± 55± 21		[1,3] ACCIARRI	99E	L3	$e^+e^- \to e^+e^-\chi_{c2}$
242± 65± 51		[1,4] ACKER..,K...	98	OPAL	$e^+e^- \to e^+e^-\chi_{c2}$
150± 42± 36		[1,5] DOMINICK	94	CLE2	$e^+e^- \to e^+e^-\chi_{c2}$
470±240±120		[1,6] BAUER	93	TPC	$e^+e^- \to e^+e^-\chi_{c2}$

[1] Calculated by us using $B(J/\psi \to \ell^+\ell^-) = 0.1187 \pm 0.0008$.
[2] All systematic errors added in quadrature.
[3] The value for $\Gamma(\chi_{c2} \to \gamma\gamma)$ reported in ACCIARRI 99E is derived using $B(\chi_{c2} \to \gamma J/\psi(1S)) \times B(J/\psi(1S) \to \ell^+\ell^-) = 0.0162 \pm 0.0014$.
[4] The value for $\Gamma(\chi_{c2} \to \gamma\gamma)$ reported in ACKERSTAFF,K 98 is derived using $B(\chi_{c2} \to \gamma J/\psi(1S)) = 0.135 \pm 0.011$ and $B(J/\psi(1S) \to \ell^+\ell^-) = 0.1203 \pm 0.0038$.
[5] The value for $\Gamma(\chi_{c2} \to \gamma\gamma)$ reported in DOMINICK 94 is derived using $B(\chi_{c2} \to \gamma J/\psi(1S)) = 0.135 \pm 0.011$, $B(J/\psi(1S) \to e^+e^-) = 0.0627 \pm 0.0020$, and $B(J/\psi(1S) \to \mu^+\mu^-) = 0.0597 \pm 0.0025$.
[6] The value for $\Gamma(\chi_{c2} \to \gamma\gamma)$ reported in BAUER 93 is derived using $B(\chi_{c2} \to \gamma J/\psi(1S)) = 0.135 \pm 0.011$, $B(J/\psi(1S) \to e^+e^-) = 0.0627 \pm 0.0020$, and $B(J/\psi(1S) \to \mu^+\mu^-) = 0.0597 \pm 0.0025$.

$\chi_{c2}(1P)$ $\Gamma(i)\Gamma(\gamma\gamma)/\Gamma(total)$

$\Gamma(2(\pi^+\pi^-)) \times \Gamma(\gamma\gamma)/\Gamma_{total}$ — $\Gamma_1\Gamma_{96}/\Gamma$

VALUE (eV)	EVTS	DOCUMENT ID		TECN	COMMENT
5.7 ±0.5 OUR FIT					
5.2 ±0.7 OUR AVERAGE					
5.01±0.44±0.55	1597±138	UEHARA	08	BELL	$\gamma\gamma \to \chi_{c2} \to 2(\pi^+\pi^-)$
6.4 ±1.8 ±0.8		EISENSTEIN	01	CLE2	$e^+e^- \to e^+e^-\chi_{c2}$

$\Gamma(\rho\rho) \times \Gamma(\gamma\gamma)/\Gamma_{total}$ — $\Gamma_2\Gamma_{96}/\Gamma$

VALUE (eV)	CL%	EVTS	DOCUMENT ID		TECN	COMMENT
• • • We do not use the following data for averages, fits, limits, etc. • • •						
<7.8	90	<598	UEHARA	08	BELL	$\gamma\gamma \to \chi_{c2} \to 2(\pi^+\pi^-)$

$\Gamma(K^+K^-\pi^+\pi^-) \times \Gamma(\gamma\gamma)/\Gamma_{total}$ — $\Gamma_{14}\Gamma_{96}/\Gamma$

VALUE (eV)	EVTS	DOCUMENT ID		TECN	COMMENT
4.7 ±0.5 OUR FIT					
4.42±0.42±0.53	780 ± 74	UEHARA	08	BELL	$\gamma\gamma \to \chi_{c2} \to K^+K^-\pi^+\pi^-$

$\Gamma(K^+K^-\pi^+\pi^-\pi^0) \times \Gamma(\gamma\gamma)/\Gamma_{total}$ — $\Gamma_{15}\Gamma_{96}/\Gamma$

VALUE (eV)	EVTS	DOCUMENT ID		TECN	COMMENT
6.5±0.9±1.5	1250	DEL-AMO-SA...11M		BABR	$\gamma\gamma \to K^+K^-\pi^+\pi^-\pi^0$

$\Gamma(K^*(892)^0\overline{K}^*(892)^0) \times \Gamma(\gamma\gamma)/\Gamma_{total}$ — $\Gamma_{18}\Gamma_{96}/\Gamma$

VALUE (eV)	EVTS	DOCUMENT ID		TECN	COMMENT
1.26±0.24 OUR FIT					
0.8 ±0.17±0.27	151 ± 30	UEHARA	08	BELL	$\gamma\gamma \to \chi_{c2} \to K^+K^-\pi^+\pi^-$

$\Gamma(\phi\phi) \times \Gamma(\gamma\gamma)/\Gamma_{total}$ — $\Gamma_{20}\Gamma_{96}/\Gamma$

VALUE (eV)	EVTS	DOCUMENT ID		TECN	COMMENT
0.60±0.05 OUR FIT					
0.62±0.07±0.05	89 ± 11	[1] LIU	12B	BELL	$\gamma\gamma \to 2(K^+K^-)$
• • • We do not use the following data for averages, fits, limits, etc. • • •					
0.58±0.18±0.16	26.5 ± 8.1	UEHARA	08	BELL	$\gamma\gamma \to \chi_{c2} \to 2(K^+K^-)$

[1] Supersedes UEHARA 08. Using $B(\phi \to K^+K^-) = (48.9 \pm 0.5)\%$.

Downloaded from https://academic.oup.com/ptep/article/2022/8/083C01/6651666 by KIT Library user on 27 September 2022

$\Gamma(\omega\omega) \times \Gamma(\gamma\gamma)/\Gamma_{total}$ — $\Gamma_{22}\Gamma_{96}/\Gamma$

VALUE (eV)	CL%	DOCUMENT ID		TECN	COMMENT
• • • We do not use the following data for averages, fits, limits, etc. • • •					
<0.64	90	[1] LIU	12B	BELL	$\gamma\gamma \to 2(\pi^+\pi^-\pi^0)$

[1] Using $B(\omega \to \pi^+\pi^-\pi^0) = (89.2 \pm 0.7)\%$.

$\Gamma(\omega\phi) \times \Gamma(\gamma\gamma)/\Gamma_{total}$ — $\Gamma_{24}\Gamma_{96}/\Gamma$

VALUE (eV)	CL%	DOCUMENT ID		TECN	COMMENT
• • • We do not use the following data for averages, fits, limits, etc. • • •					
<0.04	90	[1] LIU	12B	BELL	$\gamma\gamma \to K^+K^-\pi^+\pi^-\pi^0$

[1] Using $B(\phi \to K^+K^-) = (48.9 \pm 0.5)\%$ and $B(\omega \to \pi^+\pi^-\pi^0) = (89.2 \pm 0.7)\%$.

$\Gamma(\pi\pi) \times \Gamma(\gamma\gamma)/\Gamma_{total}$ — $\Gamma_{25}\Gamma_{96}/\Gamma$

VALUE (eV)	EVTS	DOCUMENT ID		TECN	COMMENT
1.25±0.07 OUR FIT					
1.18±0.25 OUR AVERAGE					
$1.44 \pm 0.54 \pm 0.47$	34 ± 13	[1] UEHARA	09	BELL	$10.6\ e^+e^- \to e^+e^-\pi^0\pi^0$
$1.14 \pm 0.21 \pm 0.17$	54 ± 10	[2] NAKAZAWA	05	BELL	$10.6\ e^+e^- \to e^+e^-\pi^+\pi^-$

[1] We multiplied the measurement by 3 to convert from $\pi^0\pi^0$ to $\pi\pi$. Interference with the continuum included.
[2] We have multiplied $\pi^+\pi^-$ measurement by 3/2 to obtain $\pi\pi$.

$\Gamma(\rho^0\pi^+\pi^-) \times \Gamma(\gamma\gamma)/\Gamma_{total}$ — $\Gamma_{26}\Gamma_{96}/\Gamma$

VALUE (eV)	EVTS	DOCUMENT ID		TECN	COMMENT
2.1±0.9 OUR FIT					
3.2±1.9±0.5	986 ± 578	UEHARA	08	BELL	$\gamma\gamma \to \chi_{c2} \to 2(\pi^+\pi^-)$

$\Gamma(\eta\eta) \times \Gamma(\gamma\gamma)/\Gamma_{total}$ — $\Gamma_{31}\Gamma_{96}/\Gamma$

VALUE (eV)	EVTS	DOCUMENT ID		TECN	COMMENT
0.53±0.22±0.09	8	[1] UEHARA	10A	BELL	$10.6\ e^+e^- \to e^+e^-\eta\eta$

[1] Interference with the continuum not included.

$\Gamma(K^+K^-) \times \Gamma(\gamma\gamma)/\Gamma_{total}$ — $\Gamma_{32}\Gamma_{96}/\Gamma$

VALUE (eV)	EVTS	DOCUMENT ID		TECN	COMMENT
0.56±0.04 OUR FIT					
0.44±0.11±0.07	33 ± 8	NAKAZAWA	05	BELL	$10.6\ e^+e^- \to e^+e^-K^+K^-$

$\Gamma(K^0_S K^0_S) \times \Gamma(\gamma\gamma)/\Gamma_{total}$ — $\Gamma_{33}\Gamma_{96}/\Gamma$

VALUE (eV)	EVTS	DOCUMENT ID		TECN	COMMENT
0.294±0.025 OUR FIT					
$0.27\ ^{+0.07}_{-0.06} \pm 0.03$	53	[1] UEHARA	13	BELL	$\gamma\gamma \to K^0_S K^0_S$
• • • We do not use the following data for averages, fits, limits, etc. • • •					
$0.31 \pm 0.05 \pm 0.03$	38 ± 7	CHEN	07B	BELL	$e^+e^- \to e^+e^-\chi_{c2}$

[1] Supersedes CHEN 07B.

$\Gamma(\overline{K}^0K^+\pi^- + \text{c.c.}) \times \Gamma(\gamma\gamma)/\Gamma_{total}$ — $\Gamma_{42}\Gamma_{96}/\Gamma$

VALUE (eV)	EVTS	DOCUMENT ID		TECN	COMMENT
0.72±0.11 OUR FIT					
1.20±0.33±0.13	126	[1] DEL-AMO-SA...	11M	BABR	$\gamma\gamma \to K^0_S K^\pm\pi^\mp$

[1] We have multiplied $\overline{K}K\pi$ by 2/3 to obtain $\overline{K}^0K^+\pi^- + \text{c.c.}$

$\Gamma(K^+K^-K^+K^-) \times \Gamma(\gamma\gamma)/\Gamma_{total}$ — $\Gamma_{51}\Gamma_{96}/\Gamma$

VALUE (eV)	EVTS	DOCUMENT ID		TECN	COMMENT
0.93±0.11 OUR FIT					
1.10±0.21±0.15	126 ± 24	UEHARA	08	BELL	$\gamma\gamma \to \chi_{c2} \to 2(K^+K^-)$

$\Gamma(\eta_c(1S)\pi^+\pi^-) \times \Gamma(\gamma\gamma)/\Gamma_{total}$ — $\Gamma_{91}\Gamma_{96}/\Gamma$

VALUE (eV)	CL%	DOCUMENT ID		TECN	COMMENT
<15.7	90	LEES	12AE	BABR	$e^+e^- \to e^+e^-\pi^+\pi^-\eta_c$

$\chi_{c2}(1P)$ BRANCHING RATIOS

HADRONIC DECAYS

$\Gamma(2(\pi^+\pi^-))/\Gamma_{total}$ — Γ_1/Γ

VALUE	DOCUMENT ID
0.0102±0.0009 OUR FIT	

$\Gamma(\rho^0\pi^+\pi^-)/\Gamma(2(\pi^+\pi^-))$ — Γ_{26}/Γ_1

VALUE	DOCUMENT ID		TECN	COMMENT
0.36±0.15 OUR FIT				
0.31±0.17	TANENBAUM	78	MRK1	$\psi(2S) \to \gamma\chi_{c2}$

$\Gamma(\pi^+\pi^-\pi^0\pi^0)/\Gamma_{total}$ — Γ_3/Γ

VALUE (%)	EVTS	DOCUMENT ID		TECN	COMMENT
1.83±0.23±0.04	903.5	[1] HE	08B	CLEO	$e^+e^- \to \gamma h^+h^-h^0h^0$

[1] HE 08B reports $1.87 \pm 0.07 \pm 0.22 \pm 0.13$ % from a measurement of $[\Gamma(\chi_{c2}(1P) \to \pi^+\pi^-\pi^0\pi^0)/\Gamma_{total}] \times [B(\psi(2S) \to \gamma\chi_{c2}(1P))]$ assuming $B(\psi(2S) \to \gamma\chi_{c2}(1P)) = (9.33 \pm 0.14 \pm 0.61) \times 10^{-2}$, which we rescale to our best value $B(\psi(2S) \to \gamma\chi_{c2}(1P)) = (9.52 \pm 0.20) \times 10^{-2}$. Our first error is their experiment's error and our second error is the systematic error from using our best value.

$\Gamma(\rho^+\pi^-\pi^0 + \text{c.c.})/\Gamma_{total}$ — Γ_4/Γ

VALUE (%)	EVTS	DOCUMENT ID		TECN	COMMENT
2.19±0.34±0.05	1031.9	[1,2] HE	08B	CLEO	$e^+e^- \to \gamma h^+h^-h^0h^0$

[1] HE 08B reports $2.23 \pm 0.11 \pm 0.32 \pm 0.16$ % from a measurement of $[\Gamma(\chi_{c2}(1P) \to \rho^+\pi^-\pi^0 + \text{c.c.})/\Gamma_{total}] \times [B(\psi(2S) \to \gamma\chi_{c2}(1P))]$ assuming $B(\psi(2S) \to \gamma\chi_{c2}(1P)) = (9.33 \pm 0.14 \pm 0.61) \times 10^{-2}$, which we rescale to our best value $B(\psi(2S) \to \gamma\chi_{c2}(1P)) = (9.52 \pm 0.20) \times 10^{-2}$. Our first error is their experiment's error and our second error is the systematic error from using our best value.
[2] Calculated by us. We have added the values from HE 08B for $\rho^+\pi^-\pi^0$ and $\rho^-\pi^+\pi^0$ decays assuming uncorrelated statistical and fully correlated systematic uncertainties.

$\Gamma(4\pi^0)/\Gamma_{total}$ — Γ_5/Γ

VALUE (units 10^{-3})	EVTS	DOCUMENT ID		TECN	COMMENT
1.11±0.15±0.02	1164	[1] ABLIKIM	11A	BES3	$e^+e^- \to \psi(2S) \to \gamma\chi_{c2}$

[1] ABLIKIM 11A reports $(1.21 \pm 0.05 \pm 0.16) \times 10^{-3}$ from a measurement of $[\Gamma(\chi_{c2}(1P) \to 4\pi^0)/\Gamma_{total}] \times [B(\psi(2S) \to \gamma\chi_{c2}(1P))]$ assuming $B(\psi(2S) \to \gamma\chi_{c2}(1P)) = (8.74 \pm 0.35) \times 10^{-2}$, which we rescale to our best value $B(\psi(2S) \to \gamma\chi_{c2}(1P)) = (9.52 \pm 0.20) \times 10^{-2}$. Our first error is their experiment's error and our second error is the systematic error from using our best value.

$\Gamma(K^+K^-\pi^0\pi^0)/\Gamma_{total}$ — Γ_6/Γ

VALUE (%)	EVTS	DOCUMENT ID		TECN	COMMENT
0.206±0.040±0.004	76.9	[1] HE	08B	CLEO	$e^+e^- \to \gamma h^+h^-h^0h^0$

[1] HE 08B reports $0.21 \pm 0.03 \pm 0.03 \pm 0.01$ % from a measurement of $[\Gamma(\chi_{c2}(1P) \to K^+K^-\pi^0\pi^0)/\Gamma_{total}] \times [B(\psi(2S) \to \gamma\chi_{c2}(1P))]$ assuming $B(\psi(2S) \to \gamma\chi_{c2}(1P)) = (9.33 \pm 0.14 \pm 0.61) \times 10^{-2}$, which we rescale to our best value $B(\psi(2S) \to \gamma\chi_{c2}(1P)) = (9.52 \pm 0.20) \times 10^{-2}$. Our first error is their experiment's error and our second error is the systematic error from using our best value.

$\Gamma(K^+\pi^-\overline{K}^0\pi^0 + \text{c.c.})/\Gamma_{total}$ — Γ_7/Γ

VALUE (%)	EVTS	DOCUMENT ID		TECN	COMMENT
1.38±0.19±0.03	211.6	[1] HE	08B	CLEO	$e^+e^- \to \gamma h^+h^-h^0h^0$

[1] HE 08B reports $1.41 \pm 0.11 \pm 0.16 \pm 0.10$ % from a measurement of $[\Gamma(\chi_{c2}(1P) \to K^+\pi^-\overline{K}^0\pi^0 + \text{c.c.})/\Gamma_{total}] \times [B(\psi(2S) \to \gamma\chi_{c2}(1P))]$ assuming $B(\psi(2S) \to \gamma\chi_{c2}(1P)) = (9.33 \pm 0.14 \pm 0.61) \times 10^{-2}$, which we rescale to our best value $B(\psi(2S) \to \gamma\chi_{c2}(1P)) = (9.52 \pm 0.20) \times 10^{-2}$. Our first error is their experiment's error and our second error is the systematic error from using our best value.

$\Gamma(\rho^-K^+\overline{K}^0 + \text{c.c.})/\Gamma_{total}$ — Γ_8/Γ

VALUE (%)	EVTS	DOCUMENT ID		TECN	COMMENT
0.41±0.12±0.01	62.9	[1] HE	08B	CLEO	$e^+e^- \to \gamma h^+h^-h^0h^0$

[1] HE 08B reports $0.42 \pm 0.11 \pm 0.06 \pm 0.03$ % from a measurement of $[\Gamma(\chi_{c2}(1P) \to \rho^-K^+\overline{K}^0 + \text{c.c.})/\Gamma_{total}] \times [B(\psi(2S) \to \gamma\chi_{c2}(1P))]$ assuming $B(\psi(2S) \to \gamma\chi_{c2}(1P)) = (9.33 \pm 0.14 \pm 0.61) \times 10^{-2}$, which we rescale to our best value $B(\psi(2S) \to \gamma\chi_{c2}(1P)) = (9.52 \pm 0.20) \times 10^{-2}$. Our first error is their experiment's error and our second error is the systematic error from using our best value.

$\Gamma(K^*(892)^0K^-\pi^+ \to K^-\pi^+K^0\pi^0 + \text{c.c.})/\Gamma_{total}$ — Γ_9/Γ

VALUE (%)	EVTS	DOCUMENT ID		TECN	COMMENT
0.29±0.08±0.01	38.7	[1] HE	08B	CLEO	$e^+e^- \to \gamma h^+h^-h^0h^0$

[1] HE 08B reports $0.30 \pm 0.07 \pm 0.04 \pm 0.02$ % from a measurement of $[\Gamma(\chi_{c2}(1P) \to K^*(892)^0K^-\pi^+ \to K^-\pi^+K^0\pi^0 + \text{c.c.})/\Gamma_{total}] \times [B(\psi(2S) \to \gamma\chi_{c2}(1P))]$ assuming $B(\psi(2S) \to \gamma\chi_{c2}(1P)) = (9.33 \pm 0.14 \pm 0.61) \times 10^{-2}$, which we rescale to our best value $B(\psi(2S) \to \gamma\chi_{c2}(1P)) = (9.52 \pm 0.20) \times 10^{-2}$. Our first error is their experiment's error and our second error is the systematic error from using our best value.

$\Gamma(K^*(892)^0\overline{K}^0\pi^0 \to K^+\pi^-\overline{K}^0\pi^0 + \text{c.c.})/\Gamma_{total}$ — Γ_{10}/Γ

VALUE (%)	EVTS	DOCUMENT ID		TECN	COMMENT
0.38±0.09±0.01	63.0	[1] HE	08B	CLEO	$e^+e^- \to \gamma h^+h^-h^0h^0$

[1] HE 08B reports $0.39 \pm 0.07 \pm 0.05 \pm 0.03$ % from a measurement of $[\Gamma(\chi_{c2}(1P) \to K^*(892)^0\overline{K}^0\pi^0 \to K^+\pi^-\overline{K}^0\pi^0 + \text{c.c.})/\Gamma_{total}] \times [B(\psi(2S) \to \gamma\chi_{c2}(1P))]$ assuming $B(\psi(2S) \to \gamma\chi_{c2}(1P)) = (9.33 \pm 0.14 \pm 0.61) \times 10^{-2}$, which we rescale to our best value $B(\psi(2S) \to \gamma\chi_{c2}(1P)) = (9.52 \pm 0.20) \times 10^{-2}$. Our first error is their experiment's error and our second error is the systematic error from using our best value.

$\Gamma(K^*(892)^-K^+\pi^0 \to K^+\pi^-\overline{K}^0\pi^0 + \text{c.c.})/\Gamma_{total}$ — Γ_{11}/Γ

VALUE (%)	EVTS	DOCUMENT ID		TECN	COMMENT
0.37±0.08±0.01	51.1	[1] HE	08B	CLEO	$e^+e^- \to \gamma h^+h^-h^0h^0$

[1] HE 08B reports $0.38 \pm 0.07 \pm 0.04 \pm 0.03$ % from a measurement of $[\Gamma(\chi_{c2}(1P) \to K^*(892)^-K^+\pi^0 \to K^+\pi^-\overline{K}^0\pi^0 + \text{c.c.})/\Gamma_{total}] \times [B(\psi(2S) \to \gamma\chi_{c2}(1P))]$ assuming $B(\psi(2S) \to \gamma\chi_{c2}(1P)) = (9.33 \pm 0.14 \pm 0.61) \times 10^{-2}$, which we rescale to our best value $B(\psi(2S) \to \gamma\chi_{c2}(1P)) = (9.52 \pm 0.20) \times 10^{-2}$. Our first error is their experiment's error and our second error is the systematic error from using our best value.

$\Gamma(K^*(892)^+\overline{K}^0\pi^- \to K^+\pi^-\overline{K}^0\pi^0 + \text{c.c.})/\Gamma_{total}$ — Γ_{12}/Γ

VALUE (%)	EVTS	DOCUMENT ID		TECN	COMMENT
0.29±0.08±0.01	39.3	[1] HE	08B	CLEO	$e^+e^- \to \gamma h^+h^-h^0h^0$

[1] HE 08B reports $0.30 \pm 0.07 \pm 0.04 \pm 0.02$ % from a measurement of $[\Gamma(\chi_{c2}(1P) \to K^*(892)^+\overline{K}^0\pi^- \to K^+\pi^-\overline{K}^0\pi^0 + \text{c.c.})/\Gamma_{total}] \times [B(\psi(2S) \to \gamma\chi_{c2}(1P))]$ assuming $B(\psi(2S) \to \gamma\chi_{c2}(1P)) = (9.33 \pm 0.14 \pm 0.61) \times 10^{-2}$, which we rescale to our best value $B(\psi(2S) \to \gamma\chi_{c2}(1P)) = (9.52 \pm 0.20) \times 10^{-2}$. Our first error is their experiment's error and our second error is the systematic error from using our best value.

Downloaded from https://academic.oup.com/ptep/article/2022/8/083C01/6651666 by KIT Library user on 27 September 2022

$\Gamma(K^+K^-\eta\pi^0)/\Gamma_{total}$ — Γ_{13}/Γ

VALUE (%)	EVTS	DOCUMENT ID		TECN	COMMENT
0.127±0.044±0.003	22.9	[1] HE	08B	CLEO	$e^+e^- \to \gamma h^+ h^- h^0 h^0$

[1] HE 08B reports 0.13 ± 0.04 ± 0.02 ± 0.01 % from a measurement of $[\Gamma(\chi_{c2}(1P) \to K^+K^-\eta\pi^0)/\Gamma_{total}] \times [B(\psi(2S) \to \gamma\chi_{c2}(1P))]$ assuming $B(\psi(2S) \to \gamma\chi_{c2}(1P)) = (9.33 \pm 0.14 \pm 0.61) \times 10^{-2}$, which we rescale to our best value $B(\psi(2S) \to \gamma\chi_{c2}(1P)) = (9.52 \pm 0.20) \times 10^{-2}$. Our first error is their experiment's error and our second error is the systematic error from using our best value.

$\Gamma(K^+K^-\pi^+\pi^-)/\Gamma_{total}$ — Γ_{14}/Γ

VALUE (units 10^{-3})	DOCUMENT ID
8.4±0.9 OUR FIT	

$\Gamma(K^+K^-\pi^+\pi^-\pi^0)/\Gamma_{total}$ — Γ_{15}/Γ

VALUE (units 10^{-3})	EVTS	DOCUMENT ID		TECN	COMMENT
11.69±0.13±1.31	11k	[1] ABLIKIM	13B	BES3	$e^+e^- \to \psi(2S) \to \gamma\chi_{c2}$

[1] Using 1.06×10^8 $\psi(2S)$ mesons and $B(\psi(2S) \to \chi_{c2}\gamma) = (8.72 \pm 0.34)\%$.

$\Gamma(K^0_S K^\pm\pi^\mp\pi^+\pi^-)/\Gamma_{total}$ — Γ_{16}/Γ

VALUE (units 10^{-3})	EVTS	DOCUMENT ID		TECN	COMMENT
7.30±0.11±0.75	4.5k	[1] ABLIKIM	13B	BES3	$e^+e^- \to \psi(2S) \to \gamma\chi_{c2}$

[1] Using 1.06×10^8 $\psi(2S)$ mesons and $B(\psi(2S) \to \chi_{c2}\gamma) = (8.72 \pm 0.34)\%$.

$\Gamma(K^+\overline{K}^*(892)^0\pi^- + c.c.)/\Gamma(K^+K^-\pi^+\pi^-)$ — Γ_{17}/Γ_{14}

VALUE	DOCUMENT ID		TECN	COMMENT
0.25±0.13 OUR FIT				
0.25±0.13	TANENBAUM	78	MRK1	$\psi(2S) \to \gamma\chi_{c2}$

$\Gamma(K^+\overline{K}^*(892)^0\pi^- + c.c.)/\Gamma_{total}$ — Γ_{17}/Γ

VALUE (units 10^{-4})	DOCUMENT ID
21±11 OUR FIT	

$\Gamma(K^*(892)^0\overline{K}^*(892)^0)/\Gamma_{total}$ — Γ_{18}/Γ

VALUE (units 10^{-3})	DOCUMENT ID
2.3±0.4 OUR FIT	

$\Gamma(3(\pi^+\pi^-))/\Gamma_{total}$ — Γ_{19}/Γ

VALUE (units 10^{-3})	DOCUMENT ID		TECN	COMMENT
8.6±1.8 OUR EVALUATION	Treating systematic error as correlated.			
8.6±1.8 OUR AVERAGE				
8.6±0.9±1.6	[1] BAI	99B	BES	$\psi(2S) \to \gamma\chi_{c2}$
8.7±5.9±0.4	[1] TANENBAUM	78	MRK1	$\psi(2S) \to \gamma\chi_{c2}$

[1] Rescaled by us using $B(\psi(2S) \to \gamma\chi_{c2}) = (8.3 \pm 0.4)\%$ and $B(\psi(2S) \to J/\psi(1S)\pi^+\pi^-) = (32.6 \pm 0.5)\%$. Multiplied by a factor of 2 to convert from $K^0_S K^+\pi^-$ to $K^0 K^+\pi^-$ decay.

$\Gamma(\phi\phi)/\Gamma_{total}$ — Γ_{20}/Γ

VALUE (units 10^{-3})	DOCUMENT ID
1.06±0.09 OUR FIT	

$\Gamma(\phi\phi\eta)/\Gamma_{total}$ — Γ_{21}/Γ

VALUE (units 10^{-4})	EVTS	DOCUMENT ID		TECN	COMMENT
5.3±0.5±0.4	143.6	[1] ABLIKIM	20B	BES3	$\psi(2S) \to \gamma\phi\phi\eta$

[1] ABLIKIM 20B reports $(5.33 \pm 0.52 \pm 0.39) \times 10^{-4}$ from a measurement of $[\Gamma(\chi_{c2}(1P) \to \phi\phi\eta)/\Gamma_{total}] \times [B(\psi(2S) \to \gamma\chi_{c2}(1P))]$ assuming $B(\psi(2S) \to \gamma\chi_{c2}(1P)) = (9.52 \pm 0.20) \times 10^{-2}$.

$\Gamma(\omega\omega)/\Gamma_{total}$ — Γ_{22}/Γ

VALUE (units 10^{-3})	EVTS	DOCUMENT ID		TECN	COMMENT
0.84±0.10 OUR AVERAGE					
0.82±0.10±0.02	762	[1] ABLIKIM	11K	BES3	$\psi(2S) \to \gamma$ hadrons
1.73±0.57±0.04	27.7±7.4	[2] ABLIKIM	05N	BES2	$\psi(2S) \to \gamma\chi_{c2} \to \gamma 6\pi$

[1] ABLIKIM 11K reports $(8.9 \pm 0.3 \pm 1.1) \times 10^{-4}$ from a measurement of $[\Gamma(\chi_{c2}(1P) \to \omega\omega)/\Gamma_{total}] \times [B(\psi(2S) \to \gamma\chi_{c2}(1P))]$ assuming $B(\psi(2S) \to \gamma\chi_{c2}(1P)) = (8.74 \pm 0.35) \times 10^{-2}$, which we rescale to our best value $B(\psi(2S) \to \gamma\chi_{c2}(1P)) = (9.52 \pm 0.20) \times 10^{-2}$. Our first error is their experiment's error and our second error is the systematic error from using our best value.

[2] ABLIKIM 05N reports $[\Gamma(\chi_{c2}(1P) \to \omega\omega)/\Gamma_{total}] \times [B(\psi(2S) \to \gamma\chi_{c2}(1P))] = (0.165 \pm 0.044 \pm 0.032) \times 10^{-3}$ which we divide by our best value $B(\psi(2S) \to \gamma\chi_{c2}(1P)) = (9.52 \pm 0.20) \times 10^{-2}$. Our first error is their experiment's error and our second error is the systematic error from using our best value.

$\Gamma(\omega K^+K^-)/\Gamma_{total}$ — Γ_{23}/Γ

VALUE (units 10^{-3})	EVTS	DOCUMENT ID		TECN	COMMENT
0.73±0.04±0.08	512	[1] ABLIKIM	13B	BES3	$e^+e^- \to \psi(2S) \to \gamma\chi_{c2}$

[1] Using 1.06×10^8 $\psi(2S)$ mesons and $B(\psi(2S) \to \chi_{c2}\gamma) = (8.72 \pm 0.34)\%$.

$\Gamma(\omega\phi)/\Gamma_{total}$ — Γ_{24}/Γ

VALUE (units 10^{-6})	CL%	EVTS	DOCUMENT ID		TECN	COMMENT
9.6±2.7±0.2		33	[1] ABLIKIM	19J	BES3	$\psi(2S) \to \gamma$ hadrons
• • • We do not use the following data for averages, fits, limits, etc. • • •						
<18	90		[2,3] ABLIKIM	11K	BES3	$\psi(2S) \to \gamma$ hadrons

[1] ABLIKIM 19J reports $[\Gamma(\chi_{c2}(1P) \to \omega\phi)/\Gamma_{total}] \times [B(\psi(2S) \to \gamma\chi_{c2}(1P))] = (0.91 \pm 0.23 \pm 0.12) \times 10^{-6}$ which we divide by our best value $B(\psi(2S) \to \gamma\chi_{c2}(1P)) = (9.52 \pm 0.20) \times 10^{-2}$. Our first error is their experiment's error and our second error is the systematic error from using our best value.

[2] ABLIKIM 11K reports $< 2 \times 10^{-5}$ from a measurement of $[\Gamma(\chi_{c2}(1P) \to \omega\phi)/\Gamma_{total}] \times [B(\psi(2S) \to \gamma\chi_{c2}(1P))]$ assuming $B(\psi(2S) \to \gamma\chi_{c2}(1P)) = (8.74 \pm 0.35) \times 10^{-2}$, which we rescale to our best value $B(\psi(2S) \to \gamma\chi_{c2}(1P)) = 9.52 \times 10^{-2}$.

[3] Superseded by ABLIKIM 19J.

$\Gamma(\pi\pi)/\Gamma_{total}$ — Γ_{25}/Γ

VALUE (units 10^{-3})	DOCUMENT ID
2.23±0.09 OUR FIT	

$\Gamma(\rho^0\pi^+\pi^-)/\Gamma_{total}$ — Γ_{26}/Γ

VALUE (units 10^{-4})	DOCUMENT ID
37±16 OUR FIT	

$\Gamma(\pi^+\pi^-\pi^0(\text{non-resonant}))/\Gamma_{total}$ — Γ_{27}/Γ

VALUE (units 10^{-5})	EVTS	DOCUMENT ID		TECN	COMMENT
2.01±0.42±0.04	64	[1] ABLIKIM	17AG	BES3	$\psi(2S) \to \gamma\pi^+\pi^-\pi^0$

[1] ABLIKIM 17AG reports $(2.1 \pm 0.4 \pm 0.2) \times 10^{-5}$ from a measurement of $[\Gamma(\chi_{c2}(1P) \to \pi^+\pi^-\pi^0(\text{non-resonant}))/\Gamma_{total}] \times [B(\psi(2S) \to \gamma\chi_{c2}(1P))]$ assuming $B(\psi(2S) \to \gamma\chi_{c2}(1P)) = (9.11 \pm 0.31) \times 10^{-2}$, which we rescale to our best value $B(\psi(2S) \to \gamma\chi_{c2}(1P)) = (9.52 \pm 0.20) \times 10^{-2}$. Our first error is their experiment's error and our second error is the systematic error from using our best value.

$\Gamma(\rho(770)^\pm\pi^\mp)/\Gamma_{total}$ — Γ_{28}/Γ

VALUE (units 10^{-5})	EVTS	DOCUMENT ID		TECN	COMMENT
0.61±0.38±0.01	15	[1] ABLIKIM	17AG	BES3	$\psi(2S) \to \gamma\pi^+\pi^-\pi^0$

[1] ABLIKIM 17AG reports $(0.64 \pm 0.39 \pm 0.07) \times 10^{-5}$ from a measurement of $[\Gamma(\chi_{c2}(1P) \to \rho(770)^\pm\pi^\mp)/\Gamma_{total}] \times [B(\psi(2S) \to \gamma\chi_{c2}(1P))]$ assuming $B(\psi(2S) \to \gamma\chi_{c2}(1P)) = (9.11 \pm 0.31) \times 10^{-2}$, which we rescale to our best value $B(\psi(2S) \to \gamma\chi_{c2}(1P)) = (9.52 \pm 0.20) \times 10^{-2}$. Our first error is their experiment's error and our second error is the systematic error from using our best value.

$\Gamma(\pi^+\pi^-\eta)/\Gamma_{total}$ — Γ_{29}/Γ

VALUE (units 10^{-3})	CL%	DOCUMENT ID		TECN	COMMENT
0.48±0.13±0.01		[1] ATHAR	07	CLEO	$\psi(2S) \to \gamma h^+h^-h^0$
• • • We do not use the following data for averages, fits, limits, etc. • • •					
<1.4	90	[2] ABLIKIM	06R	BES2	$\psi(2S) \to \gamma\chi_{c2}$

[1] ATHAR 07 reports $(0.49 \pm 0.12 \pm 0.06) \times 10^{-3}$ from a measurement of $[\Gamma(\chi_{c2}(1P) \to \pi^+\pi^-\eta)/\Gamma_{total}] \times [B(\psi(2S) \to \gamma\chi_{c2}(1P))]$ assuming $B(\psi(2S) \to \gamma\chi_{c2}(1P)) = (9.33 \pm 0.14 \pm 0.61) \times 10^{-2}$, which we rescale to our best value $B(\psi(2S) \to \gamma\chi_{c2}(1P)) = (9.52 \pm 0.20) \times 10^{-2}$. Our first error is their experiment's error and our second error is the systematic error from using our best value.

[2] ABLIKIM 06R reports $< 1.7 \times 10^{-3}$ from a measurement of $[\Gamma(\chi_{c2}(1P) \to \pi^+\pi^-\eta)/\Gamma_{total}] \times [B(\psi(2S) \to \gamma\chi_{c2}(1P))]$ assuming $B(\psi(2S) \to \gamma\chi_{c2}(1P)) = (8.1 \pm 0.4) \times 10^{-2}$, which we rescale to our best value $B(\psi(2S) \to \gamma\chi_{c2}(1P)) = 9.52 \times 10^{-2}$.

$\Gamma(\pi^+\pi^-\eta')/\Gamma_{total}$ — Γ_{30}/Γ

VALUE (units 10^{-3})	DOCUMENT ID		TECN	COMMENT
0.50±0.18±0.01	[1] ATHAR	07	CLEO	$\psi(2S) \to \gamma h^+h^-h^0$

[1] ATHAR 07 reports $(0.51 \pm 0.18 \pm 0.06) \times 10^{-3}$ from a measurement of $[\Gamma(\chi_{c2}(1P) \to \pi^+\pi^-\eta')/\Gamma_{total}] \times [B(\psi(2S) \to \gamma\chi_{c2}(1P))]$ assuming $B(\psi(2S) \to \gamma\chi_{c2}(1P)) = (9.33 \pm 0.14 \pm 0.61) \times 10^{-2}$, which we rescale to our best value $B(\psi(2S) \to \gamma\chi_{c2}(1P)) = (9.52 \pm 0.20) \times 10^{-2}$. Our first error is their experiment's error and our second error is the systematic error from using our best value.

$\Gamma(\eta\eta)/\Gamma_{total}$ — Γ_{31}/Γ

VALUE (units 10^{-4})	DOCUMENT ID
5.4±0.4 OUR FIT	

$\Gamma(K^+K^-)/\Gamma_{total}$ — Γ_{32}/Γ

VALUE (units 10^{-3})	DOCUMENT ID
1.01±0.06 OUR FIT	

$\Gamma(K^0_S K^0_S)/\Gamma_{total}$ — Γ_{33}/Γ

VALUE (units 10^{-3})	DOCUMENT ID
0.52±0.04 OUR FIT	

Downloaded from https://academic.oup.com/ptep/article/2022/8/083C01/6651666 by KIT Library user on 27 September 2022

$\Gamma(K^0_S K^0_S)/\Gamma(\pi\pi)$ — Γ_{33}/Γ_{25}

VALUE	DOCUMENT ID		TECN	COMMENT
0.235±0.019 OUR FIT				
• • • We do not use the following data for averages, fits, limits, etc. • • •				
0.27 ±0.07 ±0.04	[1,2] CHEN	07B	BELL	$e^+e^- \to e^+e^-\chi_{c2}$

[1] Using $\Gamma(\pi\pi)\times\Gamma(\gamma\gamma)/\Gamma_{total}$ from the $\pi^+\pi^-$ measurement of NAKAZAWA 05 rescaled by 3/2 to convert to $\pi\pi$.
[2] Not independent from other measurements.

$\Gamma(K^0_S K^0_S)/\Gamma(K^+K^-)$ — Γ_{33}/Γ_{32}

VALUE	DOCUMENT ID		TECN	COMMENT
0.52±0.05 OUR FIT				
• • • We do not use the following data for averages, fits, limits, etc. • • •				
0.70±0.21±0.12	[1,2] CHEN	07B	BELL	$e^+e^- \to e^+e^-\chi_{c2}$

[1] Using $\Gamma(K^+K^-)\times\Gamma(\gamma\gamma)/\Gamma_{total}$ from NAKAZAWA 05.
[2] Not independent from other measurements.

$\Gamma(K^*(892)^\pm K^\mp)/\Gamma_{total}$ — Γ_{34}/Γ

VALUE (units 10^{-4})	DOCUMENT ID		TECN	COMMENT
1.44±0.21±0.03	[1] ABLIKIM	17AG	BES3	$\psi(2S)\to\gamma K\overline{K}\pi$
• • • We do not use the following data for averages, fits, limits, etc. • • •				
1.72±0.26±0.04	[2] ABLIKIM	17AG	BES3	$\psi(2S)\to\gamma K^+K^-\pi^0$
1.34±0.27±0.03	[3] ABLIKIM	17AG	BES3	$\psi(2S)\to\gamma K^0_S K^\pm\pi^\mp$

[1] ABLIKIM 17AG reports $(1.5\pm0.1\pm0.2)\times10^{-4}$ from a measurement of $[\Gamma(\chi_{c2}(1P)\to K^*(892)^\pm K^\mp)/\Gamma_{total}]\times[B(\psi(2S)\to\gamma\chi_{c2}(1P))]$ assuming $B(\psi(2S)\to\gamma\chi_{c2}(1P)) = (9.11\pm0.31)\times10^{-2}$, which we rescale to our best value $B(\psi(2S)\to\gamma\chi_{c2}(1P)) = (9.52\pm0.20)\times10^{-2}$. Our first error is their experiment's error and our second error is the systematic error from using our best value.
[2] ABLIKIM 17AG reports $(1.8\pm0.2\pm0.2)\times10^{-4}$ from a measurement of $[\Gamma(\chi_{c2}(1P)\to K^*(892)^\pm K^\mp)/\Gamma_{total}]\times[B(\psi(2S)\to\gamma\chi_{c2}(1P))]$ assuming $B(\psi(2S)\to\gamma\chi_{c2}(1P)) = (9.11\pm0.31)\times10^{-2}$, which we rescale to our best value $B(\psi(2S)\to\gamma\chi_{c2}(1P)) = (9.52\pm0.20)\times10^{-2}$. Our first error is their experiment's error and our second error is the systematic error from using our best value.
[3] ABLIKIM 17AG reports $(1.4\pm0.2\pm0.2)\times10^{-4}$ from a measurement of $[\Gamma(\chi_{c2}(1P)\to K^*(892)^\pm K^\mp)/\Gamma_{total}]\times[B(\psi(2S)\to\gamma\chi_{c2}(1P))]$ assuming $B(\psi(2S)\to\gamma\chi_{c2}(1P)) = (9.11\pm0.31)\times10^{-2}$, which we rescale to our best value $B(\psi(2S)\to\gamma\chi_{c2}(1P)) = (9.52\pm0.20)\times10^{-2}$. Our first error is their experiment's error and our second error is the systematic error from using our best value.

$\Gamma(K^*(892)^0\overline{K}^0+\text{c.c.})/\Gamma_{total}$ — Γ_{35}/Γ

VALUE (units 10^{-4})	DOCUMENT ID		TECN	COMMENT
1.24±0.27±0.03	[1] ABLIKIM	17AG	BES3	$\psi(2S)\to\gamma K^0_S K^\pm\pi^\mp$

[1] ABLIKIM 17AG reports $(1.3\pm0.2\pm0.2)\times10^{-4}$ from a measurement of $[\Gamma(\chi_{c2}(1P)\to K^*(892)^0\overline{K}^0+\text{c.c.})/\Gamma_{total}]\times[B(\psi(2S)\to\gamma\chi_{c2}(1P))]$ assuming $B(\psi(2S)\to\gamma\chi_{c2}(1P)) = (9.11\pm0.31)\times10^{-2}$, which we rescale to our best value $B(\psi(2S)\to\gamma\chi_{c2}(1P)) = (9.52\pm0.20)\times10^{-2}$. Our first error is their experiment's error and our second error is the systematic error from using our best value.

$\Gamma(K^*_2(1430)^\pm K^\mp)/\Gamma_{total}$ — Γ_{36}/Γ

VALUE (units 10^{-4})	DOCUMENT ID		TECN	COMMENT
14.8±1.2±0.3	[1] ABLIKIM	17AG	BES3	$\psi(2S)\to\gamma K\overline{K}\pi$
• • • We do not use the following data for averages, fits, limits, etc. • • •				
17.4±1.6±0.4	[2] ABLIKIM	17AG	BES3	$\psi(2S)\to\gamma K^+K^-\pi^0$
13.0±1.5±0.3	[3] ABLIKIM	17AG	BES3	$\psi(2S)\to\gamma K^0_S K^\pm\pi^\mp$

[1] ABLIKIM 17AG reports $(15.5\pm0.6\pm1.2)\times10^{-4}$ from a measurement of $[\Gamma(\chi_{c2}(1P)\to K^*_2(1430)^\pm K^\mp)/\Gamma_{total}]\times[B(\psi(2S)\to\gamma\chi_{c2}(1P))]$ assuming $B(\psi(2S)\to\gamma\chi_{c2}(1P)) = (9.11\pm0.31)\times10^{-2}$, which we rescale to our best value $B(\psi(2S)\to\gamma\chi_{c2}(1P)) = (9.52\pm0.20)\times10^{-2}$. Our first error is their experiment's error and our second error is the systematic error from using our best value.
[2] ABLIKIM 17AG reports $(18.2\pm0.8\pm1.6)\times10^{-4}$ from a measurement of $[\Gamma(\chi_{c2}(1P)\to K^*_2(1430)^\pm K^\mp)/\Gamma_{total}]\times[B(\psi(2S)\to\gamma\chi_{c2}(1P))]$ assuming $B(\psi(2S)\to\gamma\chi_{c2}(1P)) = (9.11\pm0.31)\times10^{-2}$, which we rescale to our best value $B(\psi(2S)\to\gamma\chi_{c2}(1P)) = (9.52\pm0.20)\times10^{-2}$. Our first error is their experiment's error and our second error is the systematic error from using our best value.
[3] ABLIKIM 17AG reports $(13.6\pm0.8\pm1.4)\times10^{-4}$ from a measurement of $[\Gamma(\chi_{c2}(1P)\to K^*_2(1430)^\pm K^\mp)/\Gamma_{total}]\times[B(\psi(2S)\to\gamma\chi_{c2}(1P))]$ assuming $B(\psi(2S)\to\gamma\chi_{c2}(1P)) = (9.11\pm0.31)\times10^{-2}$, which we rescale to our best value $B(\psi(2S)\to\gamma\chi_{c2}(1P)) = (9.52\pm0.20)\times10^{-2}$. Our first error is their experiment's error and our second error is the systematic error from using our best value.

$\Gamma(K^*_2(1430)^0\overline{K}^0+\text{c.c.})/\Gamma_{total}$ — Γ_{37}/Γ

VALUE (units 10^{-4})	DOCUMENT ID		TECN	COMMENT
12.4±1.7±0.3	[1] ABLIKIM	17AG	BES3	$\psi(2S)\to\gamma K^0_S K^\pm\pi^\mp$

[1] ABLIKIM 17AG reports $(13.0\pm1.0\pm1.5)\times10^{-4}$ from a measurement of $[\Gamma(\chi_{c2}(1P)\to K^*_2(1430)^0\overline{K}^0+\text{c.c.})/\Gamma_{total}]\times[B(\psi(2S)\to\gamma\chi_{c2}(1P))]$ assuming $B(\psi(2S)\to\gamma\chi_{c2}(1P)) = (9.11\pm0.31)\times10^{-2}$, which we rescale to our best value $B(\psi(2S)\to\gamma\chi_{c2}(1P)) = (9.52\pm0.20)\times10^{-2}$. Our first error is their experiment's error and our second error is the systematic error from using our best value.

$\Gamma(K^*_3(1780)^\pm K^\mp)/\Gamma_{total}$ — Γ_{38}/Γ

VALUE (units 10^{-4})	DOCUMENT ID		TECN	COMMENT
5.2±0.8±0.1	[1] ABLIKIM	17AG	BES3	$\psi(2S)\to\gamma K\overline{K}\pi$
• • • We do not use the following data for averages, fits, limits, etc. • • •				
5.1±1.0±0.1	[2] ABLIKIM	17AG	BES3	$\psi(2S)\to\gamma K^+K^-\pi^0$
5.6±1.8±0.1	[3] ABLIKIM	17AG	BES3	$\psi(2S)\to\gamma K^0_S K^\pm\pi^\mp$

[1] ABLIKIM 17AG reports $(5.4\pm0.5\pm0.7)\times10^{-4}$ from a measurement of $[\Gamma(\chi_{c2}(1P)\to K^*_3(1780)^\pm K^\mp)/\Gamma_{total}]\times[B(\psi(2S)\to\gamma\chi_{c2}(1P))]$ assuming $B(\psi(2S)\to\gamma\chi_{c2}(1P)) = (9.11\pm0.31)\times10^{-2}$, which we rescale to our best value $B(\psi(2S)\to\gamma\chi_{c2}(1P)) = (9.52\pm0.20)\times10^{-2}$. Our first error is their experiment's error and our second error is the systematic error from using our best value.
[2] ABLIKIM 17AG reports $(5.3\pm0.5\pm0.9)\times10^{-4}$ from a measurement of $[\Gamma(\chi_{c2}(1P)\to K^*_3(1780)^\pm K^\mp)/\Gamma_{total}]\times[B(\psi(2S)\to\gamma\chi_{c2}(1P))]$ assuming $B(\psi(2S)\to\gamma\chi_{c2}(1P)) = (9.11\pm0.31)\times10^{-2}$, which we rescale to our best value $B(\psi(2S)\to\gamma\chi_{c2}(1P)) = (9.52\pm0.20)\times10^{-2}$. Our first error is their experiment's error and our second error is the systematic error from using our best value.
[3] ABLIKIM 17AG reports $(5.9\pm1.1\pm1.5)\times10^{-4}$ from a measurement of $[\Gamma(\chi_{c2}(1P)\to K^*_3(1780)^\pm K^\mp)/\Gamma_{total}]\times[B(\psi(2S)\to\gamma\chi_{c2}(1P))]$ assuming $B(\psi(2S)\to\gamma\chi_{c2}(1P)) = (9.11\pm0.31)\times10^{-2}$, which we rescale to our best value $B(\psi(2S)\to\gamma\chi_{c2}(1P)) = (9.52\pm0.20)\times10^{-2}$. Our first error is their experiment's error and our second error is the systematic error from using our best value.

$\Gamma(K^*_3(1780)^0\overline{K}^0+\text{c.c.})/\Gamma_{total}$ — Γ_{39}/Γ

VALUE (units 10^{-4})	DOCUMENT ID		TECN	COMMENT
5.6±2.1±0.1	[1] ABLIKIM	17AG	BES3	$\psi(2S)\to\gamma K^0_S K^\pm\pi^\mp$

[1] ABLIKIM 17AG reports $(5.9\pm1.6\pm1.5)\times10^{-4}$ from a measurement of $[\Gamma(\chi_{c2}(1P)\to K^*_3(1780)^0\overline{K}^0+\text{c.c.})/\Gamma_{total}]\times[B(\psi(2S)\to\gamma\chi_{c2}(1P))]$ assuming $B(\psi(2S)\to\gamma\chi_{c2}(1P)) = (9.11\pm0.31)\times10^{-2}$, which we rescale to our best value $B(\psi(2S)\to\gamma\chi_{c2}(1P)) = (9.52\pm0.20)\times10^{-2}$. Our first error is their experiment's error and our second error is the systematic error from using our best value.

$\Gamma(a_2(1320)^0\pi^0)/\Gamma_{total}$ — Γ_{40}/Γ

VALUE (units 10^{-4})	DOCUMENT ID		TECN	COMMENT
12.9±3.4±0.3	[1] ABLIKIM	17AG	BES3	$\psi(2S)\to\gamma K^+K^-\pi^0$

[1] ABLIKIM 17AG reports $(13.5\pm1.6\pm3.2)\times10^{-4}$ from a measurement of $[\Gamma(\chi_{c2}(1P)\to a_2(1320)^0\pi^0)/\Gamma_{total}]\times[B(\psi(2S)\to\gamma\chi_{c2}(1P))]$ assuming $B(\psi(2S)\to\gamma\chi_{c2}(1P)) = (9.11\pm0.31)\times10^{-2}$, which we rescale to our best value $B(\psi(2S)\to\gamma\chi_{c2}(1P)) = (9.52\pm0.20)\times10^{-2}$. Our first error is their experiment's error and our second error is the systematic error from using our best value.

$\Gamma(a_2(1320)^\pm\pi^\mp)/\Gamma_{total}$ — Γ_{41}/Γ

VALUE (units 10^{-4})	DOCUMENT ID		TECN	COMMENT
17.6±6.1±0.4	[1] ABLIKIM	17AG	BES3	$\psi(2S)\to\gamma K^0_S K^\pm\pi^\mp$

[1] ABLIKIM 17AG reports $(18.4\pm3.3\pm5.5)\times10^{-4}$ from a measurement of $[\Gamma(\chi_{c2}(1P)\to a_2(1320)^\pm\pi^\mp)/\Gamma_{total}]\times[B(\psi(2S)\to\gamma\chi_{c2}(1P))]$ assuming $B(\psi(2S)\to\gamma\chi_{c2}(1P)) = (9.11\pm0.31)\times10^{-2}$, which we rescale to our best value $B(\psi(2S)\to\gamma\chi_{c2}(1P)) = (9.52\pm0.20)\times10^{-2}$. Our first error is their experiment's error and our second error is the systematic error from using our best value.

$\Gamma(K^+K^-\pi^0)/\Gamma_{total}$ — Γ_{43}/Γ

VALUE (units 10^{-3})	DOCUMENT ID		TECN	COMMENT
0.30±0.08±0.01	[1] ATHAR	07	CLEO	$\psi(2S)\to\gamma h^+h^-h^0$

[1] ATHAR 07 reports $(0.31\pm0.07\pm0.04)\times10^{-3}$ from a measurement of $[\Gamma(\chi_{c2}(1P)\to K^+K^-\pi^0)/\Gamma_{total}]\times[B(\psi(2S)\to\gamma\chi_{c2}(1P))]$ assuming $B(\psi(2S)\to\gamma\chi_{c2}(1P)) = (9.33\pm0.14\pm0.61)\times10^{-2}$, which we rescale to our best value $B(\psi(2S)\to\gamma\chi_{c2}(1P)) = (9.52\pm0.20)\times10^{-2}$. Our first error is their experiment's error and our second error is the systematic error from using our best value.

$\Gamma(K^+K^-\eta)/\Gamma_{total}$ — Γ_{44}/Γ

VALUE (units 10^{-3})	CL%	DOCUMENT ID		TECN	COMMENT
<0.32	90	[1] ATHAR	07	CLEO	$\psi(2S)\to\gamma h^+h^-h^0$

[1] ATHAR 07 reports $<0.33\times10^{-3}$ from a measurement of $[\Gamma(\chi_{c2}(1P)\to K^+K^-\eta)/\Gamma_{total}]\times[B(\psi(2S)\to\gamma\chi_{c2}(1P))]$ assuming $B(\psi(2S)\to\gamma\chi_{c2}(1P)) = (9.33\pm0.14\pm0.61)\times10^{-2}$, which we rescale to our best value $B(\psi(2S)\to\gamma\chi_{c2}(1P)) = 9.52\times10^{-2}$.

$\Gamma(K^+K^-\eta'(958))/\Gamma_{total}$ — Γ_{45}/Γ

VALUE (units 10^{-4})	EVTS	DOCUMENT ID		TECN	COMMENT
1.94±0.34	107	[1] ABLIKIM	14J	BES3	$\psi(2S)\to\gamma K^+K^-\eta'(958)$

[1] Derived using $B(\psi(2S)\to\gamma\chi_{c2}) = (8.72\pm0.34)\%$. Uncertainty includes both statistical and systematic contributions combined in quadrature.

$\Gamma(\eta\eta')/\Gamma_{total}$ — Γ_{46}/Γ

VALUE (units 10^{-5})	CL%	EVTS	DOCUMENT ID		TECN	COMMENT
2.17±0.47±0.05		20	[1] ABLIKIM	17AI	BES3	$\psi(2S)\to\gamma\eta'\eta$

Downloaded from https://academic.oup.com/ptep/article/2022/8/083C01/6651666 by KIT Library user on 27 September 2022

• • • We do not use the following data for averages, fits, limits, etc. • • •

< 6	90	3.3 ± 8.0	[2] ASNER	09	CLEO	$\psi(2S) \to \gamma\eta\eta'$
<23	90		[3] ADAMS	07	CLEO	$\psi(2S) \to \gamma\chi_{c2}$

[1] ABLIKIM 17AI reports $(2.27\pm0.43\pm0.25)\times10^{-5}$ from a measurement of $[\Gamma(\chi_{c2}(1P) \to \eta\eta')/\Gamma_{total}] \times [B(\psi(2S) \to \gamma\chi_{c2}(1P))]$ assuming $B(\psi(2S) \to \gamma\chi_{c2}(1P)) = (9.11 \pm 0.31) \times 10^{-2}$, which we rescale to our best value $B(\psi(2S) \to \gamma\chi_{c2}(1P)) = (9.52 \pm 0.20) \times 10^{-2}$. Our first error is their experiment's error and our second error is the systematic error from using our best value.

[2] ASNER 09 reports $< 0.6\times10^{-4}$ from a measurement of $[\Gamma(\chi_{c2}(1P) \to \eta\eta')/\Gamma_{total}] \times [B(\psi(2S) \to \gamma\chi_{c2}(1P))]$ assuming $B(\psi(2S) \to \gamma\chi_{c2}(1P)) = (9.33 \pm 0.14 \pm 0.61) \times 10^{-2}$, which we rescale to our best value $B(\psi(2S) \to \gamma\chi_{c2}(1P)) = 9.52 \times 10^{-2}$.

[3] Superseded by ASNER 09. ADAMS 07 reports $< 2.3 \times 10^{-4}$ from a measurement of $[\Gamma(\chi_{c2}(1P) \to \eta\eta')/\Gamma_{total}] \times [B(\psi(2S) \to \gamma\chi_{c2}(1P))]$ assuming $B(\psi(2S) \to \gamma\chi_{c2}(1P)) = 0.0933 \pm 0.0014 \pm 0.0061$, which we rescale to our best value $B(\psi(2S) \to \gamma\chi_{c2}(1P)) = 9.52 \times 10^{-2}$.

$\Gamma(\eta'\eta')/\Gamma_{total}$ — Γ_{47}/Γ

VALUE (units 10^{-5})	CL%	EVTS	DOCUMENT ID		TECN	COMMENT
$4.6\pm0.6\pm0.1$		60	[1] ABLIKIM	17AI	BES3	$\psi(2S) \to \gamma\eta'\eta'$

• • • We do not use the following data for averages, fits, limits, etc. • • •

<10	90	12 ± 7	[2] ASNER	09	CLEO	$\psi(2S) \to \gamma\eta'\eta'$
<30	90		[3] ADAMS	07	CLEO	$\psi(2S) \to \gamma\chi_{c2}$

[1] ABLIKIM 17AI reports $(4.76\pm0.56\pm0.38)\times10^{-5}$ from a measurement of $[\Gamma(\chi_{c2}(1P) \to \eta'\eta')/\Gamma_{total}] \times [B(\psi(2S) \to \gamma\chi_{c2}(1P))]$ assuming $B(\psi(2S) \to \gamma\chi_{c2}(1P)) = (9.11 \pm 0.31) \times 10^{-2}$, which we rescale to our best value $B(\psi(2S) \to \gamma\chi_{c2}(1P)) = (9.52 \pm 0.20) \times 10^{-2}$. Our first error is their experiment's error and our second error is the systematic error from using our best value.

[2] ASNER 09 reports $< 1.0 \times 10^{-4}$ from a measurement of $[\Gamma(\chi_{c2}(1P) \to \eta'\eta')/\Gamma_{total}] \times [B(\psi(2S) \to \gamma\chi_{c2}(1P))]$ assuming $B(\psi(2S) \to \gamma\chi_{c2}(1P)) = (9.33 \pm 0.14 \pm 0.61) \times 10^{-2}$, which we rescale to our best value $B(\psi(2S) \to \gamma\chi_{c2}(1P)) = 9.52 \times 10^{-2}$.

[3] Superseded by ASNER 09. ADAMS 07 reports $< 3.1 \times 10^{-4}$ from a measurement of $[\Gamma(\chi_{c2}(1P) \to \eta'\eta')/\Gamma_{total}] \times [B(\psi(2S) \to \gamma\chi_{c2}(1P))]$ assuming $B(\psi(2S) \to \gamma\chi_{c2}(1P)) = 0.0933 \pm 0.0014 \pm 0.0061$, which we rescale to our best value $B(\psi(2S) \to \gamma\chi_{c2}(1P)) = 9.52 \times 10^{-2}$.

$\Gamma(\pi^+\pi^- K^0_S K^0_S)/\Gamma_{total}$ — Γ_{48}/Γ

VALUE (units 10^{-3})	EVTS	DOCUMENT ID		TECN	COMMENT
$2.17\pm0.54\pm0.05$	57 ± 11	[1] ABLIKIM	05O	BES2	$\psi(2S) \to \gamma\chi_{c2}$

[1] ABLIKIM 05O reports $[\Gamma(\chi_{c2}(1P) \to \pi^+\pi^- K^0_S K^0_S)/\Gamma_{total}] \times [B(\psi(2S) \to \gamma\chi_{c2}(1P))] = (0.207 \pm 0.039 \pm 0.033) \times 10^{-3}$ which we divide by our best value $B(\psi(2S) \to \gamma\chi_{c2}(1P)) = (9.52 \pm 0.20) \times 10^{-2}$. Our first error is their experiment's error and our second error is the systematic error from using our best value.

$\Gamma(K^+K^- K^0_S K^0_S)/\Gamma_{total}$ — Γ_{49}/Γ

VALUE (units 10^{-4})	CL%	EVTS	DOCUMENT ID		TECN	COMMENT
<4	90	2.3 ± 2.2	[1] ABLIKIM	05O	BES2	$e^+e^- \to \chi_{c2}\gamma$

[1] ABLIKIM 05O reports $[\Gamma(\chi_{c2}(1P) \to K^+K^- K^0_S K^0_S)/\Gamma_{total}] \times [B(\psi(2S) \to \gamma\chi_{c2}(1P))] < 3.5 \times 10^{-5}$ which we divide by our best value $B(\psi(2S) \to \gamma\chi_{c2}(1P)) = 9.52 \times 10^{-2}$.

$\Gamma(K^0_S K^0_S K^0_S K^0_S)/\Gamma_{total}$ — Γ_{50}/Γ

VALUE (units 10^{-4})	EVTS	DOCUMENT ID		TECN	COMMENT
$1.13\pm0.18\pm0.02$	68	[1] ABLIKIM	19AA	BES3	$\psi(2S) \to \gamma 4K^0_S$

[1] Using $B(K^0_S \to \pi^+\pi^-) = (69.20 \pm 0.05)\%$. ABLIKIM 19AA reports $[\Gamma(\chi_{c2}(1P) \to K^0_S K^0_S K^0_S K^0_S)/\Gamma_{total}] \times [B(\psi(2S) \to \gamma\chi_{c2}(1P))] = (10.8 \pm 1.5 \pm 0.8) \times 10^{-6}$ which we divide by our best value $B(\psi(2S) \to \gamma\chi_{c2}(1P)) = (9.52 \pm 0.20) \times 10^{-2}$. Our first error is their experiment's error and our second error is the systematic error from using our best value..

$\Gamma(K^+K^-K^+K^-)/\Gamma_{total}$ — Γ_{51}/Γ

VALUE (units 10^{-3})	DOCUMENT ID
1.65 ± 0.20 OUR FIT	

$\Gamma(K^+K^-\phi)/\Gamma_{total}$ — Γ_{52}/Γ

VALUE (units 10^{-3})	EVTS	DOCUMENT ID		TECN	COMMENT
$1.42\pm0.29\pm0.03$	52	[1] ABLIKIM	06T	BES2	$\psi(2S) \to \gamma 2K^+2K^-$

[1] ABLIKIM 06T reports $(1.67\pm0.26\pm0.24)\times10^{-3}$ from a measurement of $[\Gamma(\chi_{c2}(1P) \to K^+K^-\phi)/\Gamma_{total}] \times [B(\psi(2S) \to \gamma\chi_{c2}(1P))]$ assuming $B(\psi(2S) \to \gamma\chi_{c2}(1P)) = (8.1 \pm 0.4) \times 10^{-2}$, which we rescale to our best value $B(\psi(2S) \to \gamma\chi_{c2}(1P)) = (9.52 \pm 0.20) \times 10^{-2}$. Our first error is their experiment's error and our second error is the systematic error from using our best value.

$\Gamma(\overline{K}^0 K^+\pi^-\phi + \text{c.c.})/\Gamma_{total}$ — Γ_{53}/Γ

VALUE (units 10^{-3})	DOCUMENT ID		TECN	COMMENT
$4.83\pm0.32\pm0.66$	ABLIKIM	15M	BES3	$\psi(2S) \to \gamma\chi_{c2}$

$\Gamma(K^+K^-\pi^0\phi)/\Gamma_{total}$ — Γ_{54}/Γ

VALUE (units 10^{-3})	DOCUMENT ID		TECN	COMMENT
$2.74\pm0.16\pm0.44$	ABLIKIM	15M	BES3	$\psi(2S) \to \gamma\chi_{c2}$

$\Gamma(\phi\pi^+\pi^-\pi^0)/\Gamma_{total}$ — Γ_{55}/Γ

VALUE (units 10^{-3})	EVTS	DOCUMENT ID		TECN	COMMENT
$0.93\pm0.06\pm0.10$	408	[1] ABLIKIM	13B	BES3	$e^+e^- \to \psi(2S) \to \gamma\chi_{c2}$

[1] Using 1.06×10^8 $\psi(2S)$ mesons and $B(\psi(2S) \to \chi_{c2}\gamma) = (8.72 \pm 0.34)\%$.

$\Gamma(p\overline{p})/\Gamma_{total}$ — Γ_{56}/Γ

VALUE (units 10^{-4})	DOCUMENT ID
0.733 ± 0.033 OUR FIT	

$\Gamma(p\overline{p}\pi^0)/\Gamma_{total}$ — Γ_{57}/Γ

VALUE (units 10^{-3})	DOCUMENT ID		TECN	COMMENT
0.47 ± 0.04 OUR AVERAGE				
$0.47\pm0.04\pm0.01$	[1] ONYISI	10	CLE3	$\psi(2S) \to \gamma p\overline{p}X$
$0.43\pm0.09\pm0.01$	[2] ATHAR	07	CLEO	$\psi(2S) \to \gamma h^+h^-h^0$

[1] ONYISI 10 reports $(4.83 \pm 0.25 \pm 0.35 \pm 0.31) \times 10^{-4}$ from a measurement of $[\Gamma(\chi_{c2}(1P) \to p\overline{p}\pi^0)/\Gamma_{total}] \times [B(\psi(2S) \to \gamma\chi_{c2}(1P))]$ assuming $B(\psi(2S) \to \gamma\chi_{c2}(1P)) = (9.33\pm0.14\pm0.61)\times10^{-2}$, which we rescale to our best value $B(\psi(2S) \to \gamma\chi_{c2}(1P)) = (9.52 \pm 0.20) \times 10^{-2}$. Our first error is their experiment's error and our second error is the systematic error from using our best value.

[2] ATHAR 07 reports $(0.44 \pm 0.08 \pm 0.05) \times 10^{-3}$ from a measurement of $[\Gamma(\chi_{c2}(1P) \to p\overline{p}\pi^0)/\Gamma_{total}] \times [B(\psi(2S) \to \gamma\chi_{c2}(1P))]$ assuming $B(\psi(2S) \to \gamma\chi_{c2}(1P)) = (9.33 \pm 0.14 \pm 0.61) \times 10^{-2}$, which we rescale to our best value $B(\psi(2S) \to \gamma\chi_{c2}(1P)) = (9.52 \pm 0.20) \times 10^{-2}$. Our first error is their experiment's error and our second error is the systematic error from using our best value.

$\Gamma(p\overline{p}\eta)/\Gamma_{total}$ — Γ_{58}/Γ

VALUE (units 10^{-3})	DOCUMENT ID		TECN	COMMENT
0.174 ± 0.025 OUR AVERAGE				
$0.172\pm0.026\pm0.004$	[1] ONYISI	10	CLE3	$\psi(2S) \to \gamma p\overline{p}X$
$0.186\pm0.070\pm0.004$	[2] ATHAR	07	CLEO	$\psi(2S) \to \gamma h^+h^-h^0$

[1] ONYISI 10 reports $(1.76 \pm 0.23 \pm 0.14 \pm 0.11) \times 10^{-4}$ from a measurement of $[\Gamma(\chi_{c2}(1P) \to p\overline{p}\eta)/\Gamma_{total}] \times [B(\psi(2S) \to \gamma\chi_{c2}(1P))]$ assuming $B(\psi(2S) \to \gamma\chi_{c2}(1P)) = (9.33\pm0.14\pm0.61)\times10^{-2}$, which we rescale to our best value $B(\psi(2S) \to \gamma\chi_{c2}(1P)) = (9.52 \pm 0.20) \times 10^{-2}$. Our first error is their experiment's error and our second error is the systematic error from using our best value.

[2] ATHAR 07 reports $(0.19 \pm 0.07 \pm 0.02) \times 10^{-3}$ from a measurement of $[\Gamma(\chi_{c2}(1P) \to p\overline{p}\eta)/\Gamma_{total}] \times [B(\psi(2S) \to \gamma\chi_{c2}(1P))]$ assuming $B(\psi(2S) \to \gamma\chi_{c2}(1P)) = (9.33 \pm 0.14 \pm 0.61) \times 10^{-2}$, which we rescale to our best value $B(\psi(2S) \to \gamma\chi_{c2}(1P)) = (9.52 \pm 0.20) \times 10^{-2}$. Our first error is their experiment's error and our second error is the systematic error from using our best value.

$\Gamma(p\overline{p}\omega)/\Gamma_{total}$ — Γ_{59}/Γ

VALUE (units 10^{-3})	DOCUMENT ID		TECN	COMMENT
$0.36\pm0.04\pm0.01$	[1] ONYISI	10	CLE3	$\psi(2S) \to \gamma p\overline{p}X$

[1] ONYISI 10 reports $(3.68 \pm 0.35 \pm 0.26 \pm 0.24) \times 10^{-4}$ from a measurement of $[\Gamma(\chi_{c2}(1P) \to p\overline{p}\omega)/\Gamma_{total}] \times [B(\psi(2S) \to \gamma\chi_{c2}(1P))]$ assuming $B(\psi(2S) \to \gamma\chi_{c2}(1P)) = (9.33\pm0.14\pm0.61)\times10^{-2}$, which we rescale to our best value $B(\psi(2S) \to \gamma\chi_{c2}(1P)) = (9.52 \pm 0.20) \times 10^{-2}$. Our first error is their experiment's error and our second error is the systematic error from using our best value.

$\Gamma(p\overline{p}\phi)/\Gamma_{total}$ — Γ_{60}/Γ

VALUE (units 10^{-5})	EVTS	DOCUMENT ID		TECN	COMMENT
$2.8\pm0.9\pm0.1$	24 ± 7	[1] ABLIKIM	11F	BES3	$\psi(2S) \to \gamma p\overline{p}K^+K^-$

[1] ABLIKIM 11F reports $(3.04\pm0.85\pm0.43)\times10^{-5}$ from a measurement of $[\Gamma(\chi_{c2}(1P) \to p\overline{p}\phi)/\Gamma_{total}] \times [B(\psi(2S) \to \gamma\chi_{c2}(1P))]$ assuming $B(\psi(2S) \to \gamma\chi_{c2}(1P)) = (8.74 \pm 0.35) \times 10^{-2}$, which we rescale to our best value $B(\psi(2S) \to \gamma\chi_{c2}(1P)) = (9.52 \pm 0.20) \times 10^{-2}$. Our first error is their experiment's error and our second error is the systematic error from using our best value.

$\Gamma(p\overline{p}\pi^+\pi^-)/\Gamma_{total}$ — Γ_{61}/Γ

VALUE (units 10^{-3})	DOCUMENT ID		TECN	COMMENT
1.32 ± 0.34 OUR EVALUATION Treating systematic error as correlated.				
1.3 ± 0.4 OUR AVERAGE Error includes scale factor of 1.3.				
$1.17\pm0.19\pm0.30$	[1] BAI	99B	BES	$\psi(2S) \to \gamma\chi_{c2}$
$2.64\pm1.03\pm0.14$	[1] TANENBAUM	78	MRK1	$\psi(2S) \to \gamma\chi_{c2}$

[1] Rescaled by us using $B(\psi(2S) \to \gamma\chi_{c2}) = (8.3 \pm 0.4)\%$ and $B(\psi(2S) \to J/\psi(1S)\pi^+\pi^-) = (32.6 \pm 0.5)\%$. Multiplied by a factor of 2 to convert from $K^0_S K^+\pi^-$ to $K^0 K^+\pi^-$ decay.

$\Gamma(p\overline{p}\pi^0\pi^0)/\Gamma_{total}$ — Γ_{62}/Γ

VALUE (%)	EVTS	DOCUMENT ID		TECN	COMMENT
$0.078\pm0.023\pm0.002$	29.2	[1] HE	08B	CLEO	$e^+e^- \to \gamma h^+h^-h^0h^0$

[1] HE 08B reports $0.08 \pm 0.02 \pm 0.01 \pm 0.01$ % from a measurement of $[\Gamma(\chi_{c2}(1P) \to p\overline{p}\pi^0\pi^0)/\Gamma_{total}] \times [B(\psi(2S) \to \gamma\chi_{c2}(1P))]$ assuming $B(\psi(2S) \to \gamma\chi_{c2}(1P)) = (9.33 \pm 0.14 \pm 0.61) \times 10^{-2}$, which we rescale to our best value $B(\psi(2S) \to \gamma\chi_{c2}(1P)) = (9.52 \pm 0.20) \times 10^{-2}$. Our first error is their experiment's error and our second error is the systematic error from using our best value.

Downloaded from https://academic.oup.com/ptep/article/2022/8/083C01/6651666 by KIT Library user on 27 September 2022

$\Gamma(p\overline{p}K^+K^-(\text{non-resonant}))/\Gamma_{\text{total}}$ — Γ_{63}/Γ

VALUE (units 10^{-4})	EVTS	DOCUMENT ID		TECN	COMMENT
1.91±0.32±0.04	131 ± 12	[1] ABLIKIM	11F	BES3	$\psi(2S) \to \gamma p\overline{p}K^+K^-$

[1] ABLIKIM 11F reports $(2.08\pm0.19\pm0.30)\times10^{-4}$ from a measurement of $[\Gamma(\chi_{c2}(1P) \to p\overline{p}K^+K^-(\text{non-resonant}))/\Gamma_{\text{total}}] \times [B(\psi(2S) \to \gamma\chi_{c2}(1P))]$ assuming $B(\psi(2S) \to \gamma\chi_{c2}(1P)) = (8.74 \pm 0.35) \times 10^{-2}$, which we rescale to our best value $B(\psi(2S) \to \gamma\chi_{c2}(1P)) = (9.52 \pm 0.20) \times 10^{-2}$. Our first error is their experiment's error and our second error is the systematic error from using our best value.

$\Gamma(p\overline{p}K^0_SK^0_S)/\Gamma_{\text{total}}$ — Γ_{64}/Γ

VALUE (units 10^{-4})	CL%	DOCUMENT ID		TECN	COMMENT
<7.9	90	[1] ABLIKIM	06D	BES2	$\psi(2S) \to \chi_{c2}\gamma$

[1] Using $B(\psi(2S) \to \chi_{c2}\gamma) = (9.3 \pm 0.6)\%$.

$\Gamma(p\overline{n}\pi^-)/\Gamma_{\text{total}}$ — Γ_{65}/Γ

VALUE (units 10^{-4})	EVTS	DOCUMENT ID		TECN	COMMENT
8.5±0.9 OUR AVERAGE					
8.4±1.0±0.2	3309	[1] ABLIKIM	12J	BES3	$\psi(2S) \to \gamma p\overline{n}\pi^-$
10.2±3.4±0.2		[2] ABLIKIM	06I	BES2	$\psi(2S) \to \gamma p\pi^- X$

[1] ABLIKIM 12J reports $[\Gamma(\chi_{c2}(1P) \to p\overline{n}\pi^-)/\Gamma_{\text{total}}] \times [B(\psi(2S) \to \gamma\chi_{c2}(1P))] = (0.80 \pm 0.02 \pm 0.09) \times 10^{-4}$ which we divide by our best value $B(\psi(2S) \to \gamma\chi_{c2}(1P)) = (9.52 \pm 0.20) \times 10^{-2}$. Our first error is their experiment's error and our second error is the systematic error from using our best value.

[2] ABLIKIM 06I reports $[\Gamma(\chi_{c2}(1P) \to p\overline{n}\pi^-)/\Gamma_{\text{total}}] \times [B(\psi(2S) \to \gamma\chi_{c2}(1P))] = (0.97 \pm 0.20 \pm 0.26) \times 10^{-4}$ which we divide by our best value $B(\psi(2S) \to \gamma\chi_{c2}(1P)) = (9.52 \pm 0.20) \times 10^{-2}$. Our first error is their experiment's error and our second error is the systematic error from using our best value.

$\Gamma(\overline{p}n\pi^+)/\Gamma_{\text{total}}$ — Γ_{66}/Γ

VALUE (units 10^{-4})	EVTS	DOCUMENT ID		TECN	COMMENT
8.9±0.8±0.2	3732	[1] ABLIKIM	12J	BES3	$\psi(2S) \to \gamma\overline{p}n\pi^+$

[1] ABLIKIM 12J reports $[\Gamma(\chi_{c2}(1P) \to \overline{p}n\pi^+)/\Gamma_{\text{total}}] \times [B(\psi(2S) \to \gamma\chi_{c2}(1P))] = (0.85 \pm 0.02 \pm 0.07) \times 10^{-4}$ which we divide by our best value $B(\psi(2S) \to \gamma\chi_{c2}(1P)) = (9.52 \pm 0.20) \times 10^{-2}$. Our first error is their experiment's error and our second error is the systematic error from using our best value.

$\Gamma(p\overline{n}\pi^-\pi^0)/\Gamma_{\text{total}}$ — Γ_{67}/Γ

VALUE (units 10^{-4})	EVTS	DOCUMENT ID		TECN	COMMENT
21.7±1.7±0.5	2128	[1] ABLIKIM	12J	BES3	$\psi(2S) \to \gamma p\overline{n}\pi^-\pi^0$

[1] ABLIKIM 12J reports $[\Gamma(\chi_{c2}(1P) \to p\overline{n}\pi^-\pi^0)/\Gamma_{\text{total}}] \times [B(\psi(2S) \to \gamma\chi_{c2}(1P))] = (2.07 \pm 0.06 \pm 0.15) \times 10^{-4}$ which we divide by our best value $B(\psi(2S) \to \gamma\chi_{c2}(1P)) = (9.52 \pm 0.20) \times 10^{-2}$. Our first error is their experiment's error and our second error is the systematic error from using our best value.

$\Gamma(\overline{p}n\pi^+\pi^0)/\Gamma_{\text{total}}$ — Γ_{68}/Γ

VALUE (units 10^{-4})	EVTS	DOCUMENT ID		TECN	COMMENT
21.1±1.8±0.4	2352	[1] ABLIKIM	12J	BES3	$\psi(2S) \to \gamma\overline{p}n\pi^+\pi^0$

[1] ABLIKIM 12J reports $[\Gamma(\chi_{c2}(1P) \to \overline{p}n\pi^+\pi^0)/\Gamma_{\text{total}}] \times [B(\psi(2S) \to \gamma\chi_{c2}(1P))] = (2.01 \pm 0.06 \pm 0.16) \times 10^{-4}$ which we divide by our best value $B(\psi(2S) \to \gamma\chi_{c2}(1P)) = (9.52 \pm 0.20) \times 10^{-2}$. Our first error is their experiment's error and our second error is the systematic error from using our best value.

$\Gamma(\Lambda\overline{\Lambda})/\Gamma_{\text{total}}$ — Γ_{69}/Γ

VALUE (units 10^{-4})	DOCUMENT ID
1.83±0.16 OUR FIT	

$\Gamma(\Lambda\overline{\Lambda}\pi^+\pi^-)/\Gamma_{\text{total}}$ — Γ_{70}/Γ

VALUE (units 10^{-5})	CL%	EVTS	DOCUMENT ID		TECN	COMMENT
125±15±3		371	[1] ABLIKIM	12I	BES3	$\psi(2S) \to \gamma\Lambda\overline{\Lambda}\pi^+\pi^-$
• • • We do not use the following data for averages, fits, limits, etc. • • •						
<350	90		[2] ABLIKIM	06D	BES2	$\psi(2S) \to \chi_{c2}\gamma$

[1] ABLIKIM 12I reports $(137.0\pm7.6\pm15.7)\times10^{-5}$ from a measurement of $[\Gamma(\chi_{c2}(1P) \to \Lambda\overline{\Lambda}\pi^+\pi^-)/\Gamma_{\text{total}}] \times [B(\psi(2S) \to \gamma\chi_{c2}(1P))]$ assuming $B(\psi(2S) \to \gamma\chi_{c2}(1P)) = (8.72 \pm 0.34) \times 10^{-2}$, which we rescale to our best value $B(\psi(2S) \to \gamma\chi_{c2}(1P)) = (9.52 \pm 0.20) \times 10^{-2}$. Our first error is their experiment's error and our second error is the systematic error from using our best value.

[2] Using $B(\psi(2S) \to \chi_{c2}\gamma) = (9.3 \pm 0.6)\%$.

$\Gamma(\Lambda\overline{\Lambda}\pi^+\pi^-(\text{non-resonant}))/\Gamma_{\text{total}}$ — Γ_{71}/Γ

VALUE (units 10^{-5})	EVTS	DOCUMENT ID		TECN	COMMENT
66±15±1	36	[1] ABLIKIM	12I	BES3	$\psi(2S) \to \gamma\Lambda\overline{\Lambda}\pi^+\pi^-$

[1] ABLIKIM 12I reports $(71.8\pm14.5\pm8.2)\times10^{-5}$ from a measurement of $[\Gamma(\chi_{c2}(1P) \to \Lambda\overline{\Lambda}\pi^+\pi^-(\text{non-resonant}))/\Gamma_{\text{total}}] \times [B(\psi(2S) \to \gamma\chi_{c2}(1P))]$ assuming $B(\psi(2S) \to \gamma\chi_{c2}(1P)) = (8.72 \pm 0.34) \times 10^{-2}$, which we rescale to our best value $B(\psi(2S) \to \gamma\chi_{c2}(1P)) = (9.52 \pm 0.20) \times 10^{-2}$. Our first error is their experiment's error and our second error is the systematic error from using our best value.

$\Gamma(\Sigma(1385)^+\overline{\Lambda}\pi^- + \text{c.c.})/\Gamma_{\text{total}}$ — Γ_{72}/Γ

VALUE (units 10^{-5})	CL%	DOCUMENT ID		TECN	COMMENT
<40	90	[1] ABLIKIM	12I	BES3	$\psi(2S) \to \gamma\Sigma(1385)^+\overline{\Lambda}\pi^-$

[1] ABLIKIM 12I reports $< 42 \times 10^{-5}$ from a measurement of $[\Gamma(\chi_{c2}(1P) \to \Sigma(1385)^+\overline{\Lambda}\pi^- + \text{c.c.})/\Gamma_{\text{total}}] \times [B(\psi(2S) \to \gamma\chi_{c2}(1P))]$ assuming $B(\psi(2S) \to \gamma\chi_{c2}(1P)) = (8.72 \pm 0.34) \times 10^{-2}$, which we rescale to our best value $B(\psi(2S) \to \gamma\chi_{c2}(1P)) = 9.52 \times 10^{-2}$.

$\Gamma(\Sigma(1385)^-\overline{\Lambda}\pi^+ + \text{c.c.})/\Gamma_{\text{total}}$ — Γ_{73}/Γ

VALUE (units 10^{-5})	CL%	DOCUMENT ID		TECN	COMMENT
<60	90	[1] ABLIKIM	12I	BES3	$\psi(2S) \to \gamma\Sigma(1385)^-\overline{\Lambda}\pi^+$

[1] ABLIKIM 12I reports $< 61 \times 10^{-5}$ from a measurement of $[\Gamma(\chi_{c2}(1P) \to \Sigma(1385)^-\overline{\Lambda}\pi^+ + \text{c.c.})/\Gamma_{\text{total}}] \times [B(\psi(2S) \to \gamma\chi_{c2}(1P))]$ assuming $B(\psi(2S) \to \gamma\chi_{c2}(1P)) = (8.72 \pm 0.34) \times 10^{-2}$, which we rescale to our best value $B(\psi(2S) \to \gamma\chi_{c2}(1P)) = 9.52 \times 10^{-2}$.

$\Gamma(K^+\overline{p}\Lambda + \text{c.c.})/\Gamma_{\text{total}}$ — Γ_{74}/Γ

VALUE (units 10^{-4})	EVTS	DOCUMENT ID		TECN	COMMENT
7.8±0.5 OUR AVERAGE					
7.7±0.5±0.2	5k	[1,2] ABLIKIM	13D	BES3	$\psi(2S) \to \gamma\Lambda\overline{p}K^+$
8.3±1.6±0.2		[3] ATHAR	07	CLEO	$\psi(2S) \to \gamma h^+h^-h^0$

[1] ABLIKIM 13D reports $(8.4 \pm 0.3 \pm 0.6) \times 10^{-4}$ from a measurement of $[\Gamma(\chi_{c2}(1P) \to K^+\overline{p}\Lambda + \text{c.c.})/\Gamma_{\text{total}}] \times [B(\psi(2S) \to \gamma\chi_{c2}(1P))]$ assuming $B(\psi(2S) \to \gamma\chi_{c2}(1P)) = (8.72 \pm 0.34) \times 10^{-2}$, which we rescale to our best value $B(\psi(2S) \to \gamma\chi_{c2}(1P)) = (9.52 \pm 0.20) \times 10^{-2}$. Our first error is their experiment's error and our second error is the systematic error from using our best value.

[2] Using $B(\Lambda \to p\pi^-) = 63.9\%$.

[3] ATHAR 07 reports $(8.5 \pm 1.4 \pm 1.0) \times 10^{-4}$ from a measurement of $[\Gamma(\chi_{c2}(1P) \to K^+\overline{p}\Lambda + \text{c.c.})/\Gamma_{\text{total}}] \times [B(\psi(2S) \to \gamma\chi_{c2}(1P))]$ assuming $B(\psi(2S) \to \gamma\chi_{c2}(1P)) = (9.33 \pm 0.14 \pm 0.61) \times 10^{-2}$, which we rescale to our best value $B(\psi(2S) \to \gamma\chi_{c2}(1P)) = (9.52 \pm 0.20) \times 10^{-2}$. Our first error is their experiment's error and our second error is the systematic error from using our best value.

$\Gamma(nK^0_S\overline{\Lambda} + \text{c.c.})/\Gamma_{\text{total}}$ — Γ_{75}/Γ

VALUE (units 10^{-4})	EVTS	DOCUMENT ID		TECN	COMMENT
3.58±0.16±0.23	879	[1] ABLIKIM	21AV	BES3	$\psi(2S) \to \gamma nK^0_S\overline{\Lambda} + \text{c.c.}$

[1] ABLIKIM 21AV reports $(3.58 \pm 0.16 \pm 0.23) \times 10^{-4}$ from a measurement of $[\Gamma(\chi_{c2}(1P) \to nK^0_S\overline{\Lambda} + \text{c.c.})/\Gamma_{\text{total}}] \times [B(\psi(2S) \to \gamma\chi_{c2}(1P))]$ assuming $B(\psi(2S) \to \gamma\chi_{c2}(1P)) = 0.0952 \pm 0.0020$. Also uses $B(\overline{\Lambda} \to \overline{p}\pi^+) = (63.9 \pm 0.5)\%$ and $B(K^0_S \to \pi^+\pi^-) = (69.20 \pm 0.05)\%$.

$\Gamma(K^*(892)^+\overline{p}\Lambda + \text{c.c.})/\Gamma_{\text{total}}$ — Γ_{76}/Γ

VALUE (units 10^{-4})	EVTS	DOCUMENT ID		TECN	COMMENT
8.2±1.1±0.2	476	[1] ABLIKIM	19AU	BES3	$\psi(2S) \to \gamma K^{*+}\overline{p}\Lambda$

[1] ABLIKIM 19AU reports $[\Gamma(\chi_{c2}(1P) \to K^*(892)^+\overline{p}\Lambda + \text{c.c.})/\Gamma_{\text{total}}] \times [B(\psi(2S) \to \gamma\chi_{c2}(1P))] = (7.8 \pm 0.9 \pm 0.6) \times 10^{-5}$ which we divide by our best value $B(\psi(2S) \to \gamma\chi_{c2}(1P)) = (9.52 \pm 0.20) \times 10^{-2}$. Our first error is their experiment's error and our second error is the systematic error from using our best value.

$\Gamma(K^+\overline{p}\Lambda(1520) + \text{c.c.})/\Gamma_{\text{total}}$ — Γ_{77}/Γ

VALUE (units 10^{-4})	EVTS	DOCUMENT ID		TECN	COMMENT
2.8±0.7±0.1	79 ± 13	[1] ABLIKIM	11F	BES3	$\psi(2S) \to \gamma p\overline{p}K^+K^-$

[1] ABLIKIM 11F reports $(3.06\pm0.50\pm0.54)\times10^{-4}$ from a measurement of $[\Gamma(\chi_{c2}(1P) \to K^+\overline{p}\Lambda(1520) + \text{c.c.})/\Gamma_{\text{total}}] \times [B(\psi(2S) \to \gamma\chi_{c2}(1P))]$ assuming $B(\psi(2S) \to \gamma\chi_{c2}(1P)) = (8.74 \pm 0.35) \times 10^{-2}$, which we rescale to our best value $B(\psi(2S) \to \gamma\chi_{c2}(1P)) = (9.52 \pm 0.20) \times 10^{-2}$. Our first error is their experiment's error and our second error is the systematic error from using our best value.

$\Gamma(\Lambda(1520)\overline{\Lambda}(1520))/\Gamma_{\text{total}}$ — Γ_{78}/Γ

VALUE (units 10^{-4})	EVTS	DOCUMENT ID		TECN	COMMENT
4.6±1.4±0.1	29 ± 7	[1] ABLIKIM	11F	BES3	$\psi(2S) \to \gamma p\overline{p}K^+K^-$

[1] ABLIKIM 11F reports $(5.05 \pm 1.29 \pm 0.93) \times 10^{-4}$ from a measurement of $[\Gamma(\chi_{c2}(1P) \to \Lambda(1520)\overline{\Lambda}(1520))/\Gamma_{\text{total}}] \times [B(\psi(2S) \to \gamma\chi_{c2}(1P))]$ assuming $B(\psi(2S) \to \gamma\chi_{c2}(1P)) = (8.74 \pm 0.35) \times 10^{-2}$, which we rescale to our best value $B(\psi(2S) \to \gamma\chi_{c2}(1P)) = (9.52 \pm 0.20) \times 10^{-2}$. Our first error is their experiment's error and our second error is the systematic error from using our best value.

$\Gamma(\Sigma^0\overline{\Sigma}^0)/\Gamma_{\text{total}}$ — Γ_{79}/Γ

VALUE (units 10^{-5})	CL%	EVTS	DOCUMENT ID		TECN	COMMENT
3.7±0.6±0.1		91	[1] ABLIKIM	18V	BES3	$\psi(2S) \to \gamma\Sigma^0\overline{\Sigma}^0$
• • • We do not use the following data for averages, fits, limits, etc. • • •						
<6	90		[2] ABLIKIM	13H	BES3	$\psi(2S) \to \gamma\Sigma^0\overline{\Sigma}^0$
<7	90	7.5 ± 3.4	[3] NAIK	08	CLEO	$\psi(2S) \to \gamma\Sigma^0\overline{\Sigma}^0$

Downloaded from https://academic.oup.com/ptep/article/2022/8/083C01/6651666 by KIT Library user on 27 September 2022

[1] ABLIKIM 18V reports $[\Gamma(\chi_{c2}(1P) \to \Sigma^0\overline{\Sigma}^0)/\Gamma_{total}] \times [B(\psi(2S) \to \gamma\chi_{c2}(1P))] = (0.35 \pm 0.05 \pm 0.02) \times 10^{-5}$ which we divide by our best value $B(\psi(2S) \to \gamma\chi_{c2}(1P)) = (9.52 \pm 0.20) \times 10^{-2}$. Our first error is their experiment's error and our second error is the systematic error from using our best value.

[2] ABLIKIM 13H reports $< 0.65 \times 10^{-4}$ from a measurement of $[\Gamma(\chi_{c2}(1P) \to \Sigma^0\overline{\Sigma}^0)/\Gamma_{total}] \times [B(\psi(2S) \to \gamma\chi_{c2}(1P))]$ assuming $B(\psi(2S) \to \gamma\chi_{c2}(1P)) = (8.74 \pm 0.35) \times 10^{-2}$, which we rescale to our best value $B(\psi(2S) \to \gamma\chi_{c2}(1P)) = 9.52 \times 10^{-2}$.

[3] NAIK 08 reports $< 0.75 \times 10^{-4}$ from a measurement of $[\Gamma(\chi_{c2}(1P) \to \Sigma^0\overline{\Sigma}^0)/\Gamma_{total}] \times [B(\psi(2S) \to \gamma\chi_{c2}(1P))]$ assuming $B(\psi(2S) \to \gamma\chi_{c2}(1P)) = (9.33 \pm 0.14 \pm 0.61) \times 10^{-2}$, which we rescale to our best value $B(\psi(2S) \to \gamma\chi_{c2}(1P)) = 9.52 \times 10^{-2}$.

$\Gamma(\Sigma^+\overline{\Sigma}^-)/\Gamma_{total}$ — Γ_{82}/Γ

VALUE (units 10^{-5})	CL%	EVTS	DOCUMENT ID		TECN	COMMENT
3.4±0.7±0.1		55	[1] ABLIKIM	18V	BES3	$\psi(2S) \to \gamma\Sigma^+\overline{\Sigma}^-$
• • • We do not use the following data for averages, fits, limits, etc. • • •						
<8	90		[2] ABLIKIM	13H	BES3	$\psi(2S) \to \gamma\Sigma^+\overline{\Sigma}^-$
<7	90	4.0 ± 3.5	[3] NAIK	08	CLEO	$\psi(2S) \to \gamma\Sigma^+\overline{\Sigma}^-$

[1] ABLIKIM 18V reports $[\Gamma(\chi_{c2}(1P) \to \Sigma^+\overline{\Sigma}^-)/\Gamma_{total}] \times [B(\psi(2S) \to \gamma\chi_{c2}(1P))] = (0.32 \pm 0.06 \pm 0.03) \times 10^{-5}$ which we divide by our best value $B(\psi(2S) \to \gamma\chi_{c2}(1P)) = (9.52 \pm 0.20) \times 10^{-2}$. Our first error is their experiment's error and our second error is the systematic error from using our best value.

[2] ABLIKIM 13H reports $< 0.88 \times 10^{-4}$ from a measurement of $[\Gamma(\chi_{c2}(1P) \to \Sigma^+\overline{\Sigma}^-)/\Gamma_{total}] \times [B(\psi(2S) \to \gamma\chi_{c2}(1P))]$ assuming $B(\psi(2S) \to \gamma\chi_{c2}(1P)) = (8.74 \pm 0.35) \times 10^{-2}$, which we rescale to our best value $B(\psi(2S) \to \gamma\chi_{c2}(1P)) = 9.52 \times 10^{-2}$.

[3] NAIK 08 reports $< 0.67 \times 10^{-4}$ from a measurement of $[\Gamma(\chi_{c2}(1P) \to \Sigma^+\overline{\Sigma}^-)/\Gamma_{total}] \times [B(\psi(2S) \to \gamma\chi_{c2}(1P))]$ assuming $B(\psi(2S) \to \gamma\chi_{c2}(1P)) = (9.33 \pm 0.14 \pm 0.61) \times 10^{-2}$, which we rescale to our best value $B(\psi(2S) \to \gamma\chi_{c2}(1P)) = 9.52 \times 10^{-2}$.

$\Gamma(\Sigma^-\overline{\Sigma}^+)/\Gamma_{total}$ — Γ_{83}/Γ

VALUE (units 10^{-5})	EVTS	DOCUMENT ID		TECN	COMMENT
4.4±1.7±0.5	131	[1] ABLIKIM	20I	BES3	$\psi(2S) \to \gamma\Sigma^-\overline{\Sigma}^+$

[1] ABLIKIM 20I reports $(4.4 \pm 1.7 \pm 0.5) \times 10^{-5}$ from a measurement of $[\Gamma(\chi_{c2}(1P) \to \Sigma^-\overline{\Sigma}^+)/\Gamma_{total}] \times [B(\psi(2S) \to \gamma\chi_{c2}(1P))]$ assuming $B(\psi(2S) \to \gamma\chi_{c2}(1P)) = (9.52 \pm 0.20) \times 10^{-2}$.

$\Gamma(\Sigma(1385)^+\overline{\Sigma}(1385)^-)/\Gamma_{total}$ — Γ_{84}/Γ

VALUE (units 10^{-5})	CL%	DOCUMENT ID		TECN	COMMENT
<16	90	[1] ABLIKIM	12I	BES3	$\psi(2S) \to \gamma\Sigma(1385)^+\overline{\Sigma}(1385)^-$

[1] ABLIKIM 12I reports $< 17 \times 10^{-5}$ from a measurement of $[\Gamma(\chi_{c2}(1P) \to \Sigma(1385)^+\overline{\Sigma}(1385)^-)/\Gamma_{total}] \times [B(\psi(2S) \to \gamma\chi_{c2}(1P))]$ assuming $B(\psi(2S) \to \gamma\chi_{c2}(1P)) = (8.72 \pm 0.34) \times 10^{-2}$, which we rescale to our best value $B(\psi(2S) \to \gamma\chi_{c2}(1P)) = 9.52 \times 10^{-2}$.

$\Gamma(\Sigma(1385)^-\overline{\Sigma}(1385)^+)/\Gamma_{total}$ — Γ_{85}/Γ

VALUE (units 10^{-5})	CL%	DOCUMENT ID		TECN	COMMENT
<8	90	[1] ABLIKIM	12I	BES3	$\psi(2S) \to \gamma\Sigma(1385)^-\overline{\Sigma}(1385)^+$

[1] ABLIKIM 12I reports $< 8.5 \times 10^{-5}$ from a measurement of $[\Gamma(\chi_{c2}(1P) \to \Sigma(1385)^-\overline{\Sigma}(1385)^+)/\Gamma_{total}] \times [B(\psi(2S) \to \gamma\chi_{c2}(1P))]$ assuming $B(\psi(2S) \to \gamma\chi_{c2}(1P)) = (8.72 \pm 0.34) \times 10^{-2}$, which we rescale to our best value $B(\psi(2S) \to \gamma\chi_{c2}(1P)) = 9.52 \times 10^{-2}$.

$\Gamma(K^-\Lambda\overline{\Xi}^+ + \text{c.c.})/\Gamma_{total}$ — Γ_{86}/Γ

VALUE (units 10^{-4})	EVTS	DOCUMENT ID		TECN	COMMENT
1.76±0.32±0.04	51	[1] ABLIKIM	15I	BES3	$\psi(2S) \to \gamma K^-\Lambda\overline{\Xi}^+ + \text{c.c.}$

[1] ABLIKIM 15I reports $[\Gamma(\chi_{c2}(1P) \to K^-\Lambda\overline{\Xi}^+ + \text{c.c.})/\Gamma_{total}] \times [B(\psi(2S) \to \gamma\chi_{c2}(1P))] = (1.68 \pm 0.26 \pm 0.15) \times 10^{-5}$ which we divide by our best value $B(\psi(2S) \to \gamma\chi_{c2}(1P)) = (9.52 \pm 0.20) \times 10^{-2}$. Our first error is their experiment's error and our second error is the systematic error from using our best value.

$\Gamma(\Xi^0\overline{\Xi}^0)/\Gamma_{total}$ — Γ_{87}/Γ

VALUE (units 10^{-4})	CL%	EVTS	DOCUMENT ID		TECN	COMMENT
<1.0	90	2.9 ± 1.7	[1] NAIK	08	CLEO	$\psi(2S) \to \gamma\Xi^0\overline{\Xi}^0$

[1] NAIK 08 reports $< 1.06 \times 10^{-4}$ from a measurement of $[\Gamma(\chi_{c2}(1P) \to \Xi^0\overline{\Xi}^0)/\Gamma_{total}] \times [B(\psi(2S) \to \gamma\chi_{c2}(1P))]$ assuming $B(\psi(2S) \to \gamma\chi_{c2}(1P)) = (9.33 \pm 0.14 \pm 0.61) \times 10^{-2}$, which we rescale to our best value $B(\psi(2S) \to \gamma\chi_{c2}(1P)) = 9.52 \times 10^{-2}$.

$\Gamma(\Xi^-\overline{\Xi}^+)/\Gamma_{total}$ — Γ_{88}/Γ

VALUE (units 10^{-4})	CL%	EVTS	DOCUMENT ID		TECN	COMMENT
1.42±0.31±0.03		29 ± 5	[1] NAIK	08	CLEO	$\psi(2S) \to \gamma\Xi^+\overline{\Xi}^-$
• • • We do not use the following data for averages, fits, limits, etc. • • •						
< 3.7	90		[2] ABLIKIM	06D	BES2	$\psi(2S) \to \chi_{c2}\gamma$

[1] NAIK 08 reports $(1.45 \pm 0.30 \pm 0.15) \times 10^{-4}$ from a measurement of $[\Gamma(\chi_{c2}(1P) \to \Xi^-\overline{\Xi}^+)/\Gamma_{total}] \times [B(\psi(2S) \to \gamma\chi_{c2}(1P))]$ assuming $B(\psi(2S) \to \gamma\chi_{c2}(1P)) = (9.33 \pm 0.14 \pm 0.61) \times 10^{-2}$, which we rescale to our best value $B(\psi(2S) \to \gamma\chi_{c2}(1P)) = (9.52 \pm 0.20) \times 10^{-2}$. Our first error is their experiment's error and our second error is the systematic error from using our best value.

[2] Using $B(\psi(2S) \to \chi_{c2}\gamma) = (9.3 \pm 0.6)\%$.

$\Gamma(J/\psi(1S)\pi^+\pi^-\pi^0)/\Gamma_{total}$ — Γ_{89}/Γ

VALUE	CL%	DOCUMENT ID		TECN	COMMENT
<0.015	90	BARATE	81	SPEC	190 GeV π^-Be $\to 2\pi 2\mu$

$\Gamma(\pi^0\eta_c)/\Gamma_{total}$ — Γ_{90}/Γ

VALUE	CL%	DOCUMENT ID		TECN	COMMENT
<3.2 × 10^{-3}	90	[1] ABLIKIM	15N	BES3	$\psi(2S)e^+e^- \to \gamma\pi^0\eta_c$

[1] Using $B(\eta_c \to K^0_S K^\pm\pi^\mp) \times B(K^0_S \to \pi^+\pi^-) \times B(\pi^0 \to \gamma\gamma) = (1.66 \pm 0.11) \times 10^{-2}$.

$\Gamma(\eta_c(1S)\pi^+\pi^-)/\Gamma_{total}$ — Γ_{91}/Γ

VALUE	CL%	DOCUMENT ID		TECN	COMMENT
<0.54 × 10^{-2}	90	[1,2] ABLIKIM	13B	BES3	$e^+e^- \to \psi(2S) \to \gamma\chi_{c2}$
• • • We do not use the following data for averages, fits, limits, etc. • • •					
<1.2 × 10^{-2}	90	[1,3] ABLIKIM	13B	BES3	$e^+e^- \to \psi(2S) \to \gamma\chi_{c2}$

[1] Using 1.06×10^8 $\psi(2S)$ mesons and $B(\psi(2S) \to \chi_{c2}\gamma) = (8.72 \pm 0.34)\%$.

[2] From the $\eta_c \to K^0_S K^\pm\pi^\mp$ decays.

[3] From the $\eta_c \to K^+K^-\pi^0$ decays.

$\Gamma(\eta_c(1S)\pi^+\pi^-)/\Gamma(\overline{K}^0K^+\pi^- + \text{c.c.})$ — Γ_{91}/Γ_{42}

VALUE	CL%	DOCUMENT ID		TECN	COMMENT
<16.4	90	[1] LEES	12AE	BABR	$e^+e^- \to e^+e^-\pi^+\pi^-\eta_c$

[1] We divided the reported limit by 2 to take into account the $K^0_L K^+\pi^-$ mode.

RADIATIVE DECAYS

$\Gamma(\gamma J/\psi(1S))/\Gamma_{total}$ — Γ_{92}/Γ

VALUE (units 10^{-2})	EVTS	DOCUMENT ID		TECN	COMMENT
19.0 ±0.5 OUR FIT					
• • • We do not use the following data for averages, fits, limits, etc. • • •					
18.64±0.08±1.69	1.0M	[1] ABLIKIM	17U	BES3	$e^+e^- \to \gamma X$
19.9 ±0.5 ±1.2		[2] ADAM	05A	CLEO	$e^+e^- \to \psi(2S) \to \gamma\chi_{c2}$

[1] Not independent from $B(\psi(2S) \to \gamma\chi_{c2}(1P))$ and the product $B(\psi(2S) \to \gamma\chi_{c2}(1P)) \times B(\chi_{c2}(1P) \to \gamma J/\psi(1S))$ also measured in ABLIKIM 17U.

[2] Uses $B(\psi(2S) \to \gamma\chi_{c2} \to \gamma\gamma J/\psi)$ from ADAM 05A and $B(\psi(2S) \to \gamma\chi_{c2})$ from ATHAR 04.

$\Gamma(\gamma\rho^0)/\Gamma_{total}$ — Γ_{93}/Γ

VALUE (units 10^{-6})	CL%	EVTS	DOCUMENT ID		TECN	COMMENT
<19	90	13 ± 11	[1] ABLIKIM	11E	BES3	$\psi(2S) \to \gamma\gamma\rho^0$
• • • We do not use the following data for averages, fits, limits, etc. • • •						
<40	90	17.2 ± 6.8	[2] BENNETT	08A	CLEO	$\psi(2S) \to \gamma\gamma\rho^0$

[1] ABLIKIM 11E reports $< 20.8 \times 10^{-6}$ from a measurement of $[\Gamma(\chi_{c2}(1P) \to \gamma\rho^0)/\Gamma_{total}] \times [B(\psi(2S) \to \gamma\chi_{c2}(1P))]$ assuming $B(\psi(2S) \to \gamma\chi_{c2}(1P)) = (8.74 \pm 0.35) \times 10^{-2}$, which we rescale to our best value $B(\psi(2S) \to \gamma\chi_{c2}(1P)) = 9.52 \times 10^{-2}$.

[2] BENNETT 08A reports $< 50 \times 10^{-6}$ from a measurement of $[\Gamma(\chi_{c2}(1P) \to \gamma\rho^0)/\Gamma_{total}] \times [B(\psi(2S) \to \gamma\chi_{c2}(1P))]$ assuming $B(\psi(2S) \to \gamma\chi_{c2}(1P)) = (8.1 \pm 0.4) \times 10^{-2}$, which we rescale to our best value $B(\psi(2S) \to \gamma\chi_{c2}(1P)) = 9.52 \times 10^{-2}$.

$\Gamma(\gamma\omega)/\Gamma_{total}$ — Γ_{94}/Γ

VALUE (units 10^{-6})	CL%	EVTS	DOCUMENT ID		TECN	COMMENT
<6	90	1 ± 6	[1] ABLIKIM	11E	BES3	$\psi(2S) \to \gamma\gamma\omega$
• • • We do not use the following data for averages, fits, limits, etc. • • •						
<6	90	0.0 ± 1.8	[2] BENNETT	08A	CLEO	$\psi(2S) \to \gamma\gamma\omega$

[1] ABLIKIM 11E reports $< 6.1 \times 10^{-6}$ from a measurement of $[\Gamma(\chi_{c2}(1P) \to \gamma\omega)/\Gamma_{total}] \times [B(\psi(2S) \to \gamma\chi_{c2}(1P))]$ assuming $B(\psi(2S) \to \gamma\chi_{c2}(1P)) = (8.74 \pm 0.35) \times 10^{-2}$, which we rescale to our best value $B(\psi(2S) \to \gamma\chi_{c2}(1P)) = 9.52 \times 10^{-2}$.

[2] BENNETT 08A reports $< 7.0 \times 10^{-6}$ from a measurement of $[\Gamma(\chi_{c2}(1P) \to \gamma\omega)/\Gamma_{total}] \times [B(\psi(2S) \to \gamma\chi_{c2}(1P))]$ assuming $B(\psi(2S) \to \gamma\chi_{c2}(1P)) = (8.1 \pm 0.4) \times 10^{-2}$, which we rescale to our best value $B(\psi(2S) \to \gamma\chi_{c2}(1P)) = 9.52 \times 10^{-2}$.

$\Gamma(\gamma\phi)/\Gamma_{total}$ — Γ_{95}/Γ

VALUE (units 10^{-6})	CL%	EVTS	DOCUMENT ID		TECN	COMMENT
< 7	90	5 ± 5	[1] ABLIKIM	11E	BES3	$\psi(2S) \to \gamma\gamma\phi$
• • • We do not use the following data for averages, fits, limits, etc. • • •						
<11	90	1.3 ± 2.5	[2] BENNETT	08A	CLEO	$\psi(2S) \to \gamma\gamma\phi$

[1] ABLIKIM 11E reports $< 8.1 \times 10^{-6}$ from a measurement of $[\Gamma(\chi_{c2}(1P) \to \gamma\phi)/\Gamma_{total}] \times [B(\psi(2S) \to \gamma\chi_{c2}(1P))]$ assuming $B(\psi(2S) \to \gamma\chi_{c2}(1P)) = (8.74 \pm 0.35) \times 10^{-2}$, which we rescale to our best value $B(\psi(2S) \to \gamma\chi_{c2}(1P)) = 9.52 \times 10^{-2}$.

[2] BENNETT 08A reports $< 13 \times 10^{-6}$ from a measurement of $[\Gamma(\chi_{c2}(1P) \to \gamma\phi)/\Gamma_{total}] \times [B(\psi(2S) \to \gamma\chi_{c2}(1P))]$ assuming $B(\psi(2S) \to \gamma\chi_{c2}(1P)) = (8.1 \pm 0.4) \times 10^{-2}$, which we rescale to our best value $B(\psi(2S) \to \gamma\chi_{c2}(1P)) = 9.52 \times 10^{-2}$.

$\Gamma(\gamma\gamma)/\Gamma_{total}$ — Γ_{96}/Γ

VALUE (units 10^{-4})	DOCUMENT ID
2.85±0.10 OUR FIT	

Downloaded from https://academic.oup.com/ptep/article/2022/8/083C01/6651666 by KIT Library user on 27 September 2022

$\Gamma(e^+e^-J/\psi(1S))/\Gamma_{total}$ — Γ_{97}/Γ

VALUE (units 10^{-3})	EVTS	DOCUMENT ID		TECN	COMMENT
• • • We do not use the following data for averages, fits, limits, etc. • • •					
$2.37\pm0.15\pm0.05$	1.3k	[1,2] ABLIKIM	17I	BES3	$\psi(2S)\to\gamma e^+e^-J/\psi$

[1] ABLIKIM 17I reports $(2.48\pm0.08\pm0.16)\times10^{-3}$ from a measurement of $[\Gamma(\chi_{c2}(1P)\to e^+e^-J/\psi(1S))/\Gamma_{total}]\times[B(\psi(2S)\to\gamma\chi_{c2}(1P))]$ assuming $B(\psi(2S)\to\gamma\chi_{c2}(1P)) = (9.11\pm0.31)\times10^{-2}$, which we rescale to our best value $B(\psi(2S)\to\gamma\chi_{c2}(1P)) = (9.52\pm0.20)\times10^{-2}$. Our first error is their experiment's error and our second error is the systematic error from using our best value.
[2] Not independent from other measurements reported by ABLIKIM 17I

$\Gamma(e^+e^-J/\psi(1S))/\Gamma(\gamma J/\psi(1S))$ — Γ_{97}/Γ_{92}

VALUE (units 10^{-3})	EVTS	DOCUMENT ID		TECN	COMMENT
11.3±0.4±0.5	1.3k	[1] ABLIKIM	17I	BES3	$\psi(2S)\to e^+e^-\gamma J/\psi$

[1] Uses $B(\psi(2S)\to\gamma\chi_{c2}(1P))\times B(\chi_{c2}(1P)\to\gamma J/\psi(1S)) = (199.6\pm0.8\pm7.0)\times10^{-4}$ from ABLIKIM 17N and accounts for common systematic errors.

$\Gamma(\mu^+\mu^-J/\psi(1S))/\Gamma(e^+e^-J/\psi(1S))$ — Γ_{98}/Γ_{97}

VALUE (units 10^{-2})	EVTS	DOCUMENT ID		TECN	COMMENT
9.40±0.79±1.15	219	ABLIKIM	19Z	BES3	$\psi(2S)\to\gamma\chi_c\to\gamma(\mu^+\mu^-J/\psi)$

$\Gamma(\gamma\gamma)/\Gamma(\gamma J/\psi(1S))$ — Γ_{96}/Γ_{92}

VALUE (units 10^{-3})	DOCUMENT ID		TECN	COMMENT
1.50±0.05 OUR FIT				
0.99±0.18	[1] AMBROGIANI	00B	E835	$\overline{p}p\to\chi_{c2}\to\gamma\gamma,\gamma J/\psi$

[1] Calculated by us using $B(J/\psi(1S)\to e^+e^-) = 0.0593\pm0.0010$.

$\Gamma(\gamma\gamma)/\Gamma_{total}\times\Gamma(p\overline{p})/\Gamma_{total}$ — $\Gamma_{96}/\Gamma\times\Gamma_{56}/\Gamma$

VALUE (units 10^{-8})	DOCUMENT ID		TECN	COMMENT
2.09±0.13 OUR FIT				
1.7 ±0.4 OUR AVERAGE				
1.60 ± 0.42	ARMSTRONG	93	E760	$\overline{p}p\to\gamma\gamma X$
9.9 ± 4.5	BAGLIN	87B	SPEC	$\overline{p}p\to\gamma\gamma X$

$\chi_{c2}(1P)$ CROSS-PARTICLE BRANCHING RATIOS

$\Gamma(\chi_{c2}(1P)\to K^+K^-\pi^+\pi^-)/\Gamma_{total}\times\Gamma(\psi(2S)\to\gamma\chi_{c2}(1P))/\Gamma(\psi(2S)\to J/\psi(1S)\pi^+\pi^-)$ — $\Gamma_{14}/\Gamma\times\Gamma_{164}^{\psi(2S)}/\Gamma_{12}^{\psi(2S)}$

VALUE (units 10^{-3})	DOCUMENT ID		TECN	COMMENT
2.31±0.26 OUR FIT				
2.5 ±0.9 OUR AVERAGE Error includes scale factor of 2.3.				
$1.90\pm0.14\pm0.44$	BAI	99B	BES	$\psi(2S)\to\gamma\chi_{c2}$
3.8 ± 0.67	[1] TANENBAUM	78	MRK1	$\psi(2S)\to\gamma\chi_{c2}$

[1] The reported value is derived using $B(\psi(2S)\to\pi^+\pi^-J/\psi)\times B(J/\psi\to\ell^+\ell^-) = (4.6\pm0.7)\%$. Calculated by us using $B(J/\psi\to\ell^+\ell^-) = 0.1181\pm0.0020$.

$\Gamma(\chi_{c2}(1P)\to K^*(892)^0\overline{K}^*(892)^0)/\Gamma_{total}\times\Gamma(\psi(2S)\to\gamma\chi_{c2}(1P))/\Gamma_{total}$ — $\Gamma_{18}/\Gamma\times\Gamma_{164}^{\psi(2S)}/\Gamma^{\psi(2S)}$

VALUE (units 10^{-4})	DOCUMENT ID		TECN	COMMENT
2.1 ±0.4 OUR FIT				
3.11±0.36±0.48	ABLIKIM	04H	BES2	$\psi(2S)\to\gamma\chi_{c2}$

$\Gamma(\chi_{c2}(1P)\to p\overline{p})/\Gamma_{total}\times\Gamma(\psi(2S)\to\gamma\chi_{c2}(1P))/\Gamma(\psi(2S)\to J/\psi(1S)\pi^+\pi^-)$ — $\Gamma_{56}/\Gamma\times\Gamma_{164}^{\psi(2S)}/\Gamma_{12}^{\psi(2S)}$

VALUE (units 10^{-5})	DOCUMENT ID		TECN	COMMENT
2.01±0.09 OUR FIT				
1.4 ±1.1	[1] BAI	98I	BES	$\psi(2S)\to\gamma\chi_{c2}\to\gamma\overline{p}p$

[1] Calculated by us. The value for $B(\chi_{c2}\to p\overline{p})$ reported in BAI 98I is derived using $B(\psi(2S)\to\gamma\chi_{c2}) = (7.8\pm0.8)\%$ and $B(\psi(2S)\to J/\psi(1S)\pi^+\pi^-) = (32.4\pm2.6)\%$ [BAI 98D].

$\Gamma(\chi_{c2}(1P)\to p\overline{p})/\Gamma_{total}\times\Gamma(\psi(2S)\to\gamma\chi_{c2}(1P))/\Gamma_{total}$ — $\Gamma_{56}/\Gamma\times\Gamma_{164}^{\psi(2S)}/\Gamma^{\psi(2S)}$

VALUE (units 10^{-6})	EVTS	DOCUMENT ID		TECN	COMMENT
6.98±0.32 OUR FIT					
7.1 ±0.5 OUR AVERAGE Error includes scale factor of 1.2.					
$7.3\pm0.4\pm0.3$	405	ABLIKIM	13V	BES3	$\psi(2S)\to\gamma p\overline{p}$
$7.2\pm0.7\pm0.4$	121 ± 12	[1] NAIK	08	CLEO	$\psi(2S)\to\gamma p\overline{p}$
$4.4\ ^{+1.6}_{-1.4}\pm0.6$	$14.3^{+5.2}_{-4.7}$	BAI	04F	BES	$\psi(2S)\to\gamma\chi_{c2}(1P)\to\gamma\overline{p}p$

[1] Calculated by us. NAIK 08 reports $B(\chi_{c2}\to p\overline{p}) = (7.7\pm0.8\pm0.4\pm0.5)\times10^{-5}$ using $B(\psi(2S)\to\gamma\chi_{c2}) = (9.33\pm0.14\pm0.61)\%$.

$\Gamma(\chi_{c2}(1P)\to\Lambda\overline{\Lambda})/\Gamma_{total}\times\Gamma(\psi(2S)\to\gamma\chi_{c2}(1P))/\Gamma_{total}$ — $\Gamma_{69}/\Gamma\times\Gamma_{164}^{\psi(2S)}/\Gamma^{\psi(2S)}$

VALUE (units 10^{-6})	EVTS	DOCUMENT ID		TECN	COMMENT
17.4±1.4 OUR FIT					
17.3±1.5 OUR AVERAGE					
$18.2\pm0.8\pm1.7$	670	ABLIKIM	21L	BES3	$\psi(2S)\to\gamma p\pi^-\overline{p}\pi^+$
$15.9\pm2.1\pm1.0$	71	[1] NAIK	08	CLEO	$\psi(2S)\to\gamma\Lambda\overline{\Lambda}$
• • • We do not use the following data for averages, fits, limits, etc. • • •					
$18.2\pm1.4\pm0.9$	207	[2,3] ABLIKIM	13H	BES3	$\psi(2S)\to\gamma\Lambda\overline{\Lambda}$

[1] Calculated by us. NAIK 08 reports $B(\chi_{c2}\to\Lambda\overline{\Lambda}) = (17.0\pm2.2\pm1.1\pm1.1)\times10^{-5}$ using $B(\psi(2S)\to\gamma\chi_{c2}) = (9.33\pm0.14\pm0.61)\%$.
[2] Superseded by ABLIKIM 21L
[3] Calculated by us. ABLIKIM 13H reports $B(\chi_{c2}\to\Lambda\overline{\Lambda}) = (20.8\pm1.6\pm2.3)\times10^{-5}$ from a measurement of $B(\chi_{c2}\to\Lambda\overline{\Lambda})\times B(\psi(2S)\to\gamma\chi_{c2})$ assuming $B(\psi(2S)\to\gamma\chi_{c2}) = (8.74\pm0.35)\%$.

$\Gamma(\chi_{c2}(1P)\to\Lambda\overline{\Lambda})/\Gamma_{total}\times\Gamma(\psi(2S)\to\gamma\chi_{c2}(1P))/\Gamma(\psi(2S)\to J/\psi(1S)\pi^+\pi^-)$ — $\Gamma_{69}/\Gamma\times\Gamma_{164}^{\psi(2S)}/\Gamma_{12}^{\psi(2S)}$

VALUE (units 10^{-5})	EVTS	DOCUMENT ID		TECN	COMMENT
5.0±0.4 OUR FIT					
$\mathbf{7.1\ ^{+3.1}_{-2.9}\pm1.3}$	$8.3^{+3.7}_{-3.4}$	[1] BAI	03E	BES	$\psi(2S)\to\gamma\Lambda\overline{\Lambda}$

[1] BAI 03E reports $[B(\chi_{c2}\to\Lambda\overline{\Lambda})\,B(\psi(2S)\to\gamma\chi_{c2})\,/\,B(\psi(2S)\to J/\psi\pi^+\pi^-)]\times[B^2(\Lambda\to\pi^-p)\,/\,B(J/\psi\to p\overline{p})] = (1.33^{+0.59}_{-0.55}\pm0.25)\%$. We calculate from this measurement the presented value using $B(\Lambda\to\pi^-p) = (63.9\pm0.5)\%$ and $B(J/\psi\to p\overline{p}) = (2.17\pm0.07)\times10^{-3}$.

$\Gamma(\chi_{c2}(1P)\to\pi\pi)/\Gamma_{total}\times\Gamma(\psi(2S)\to\gamma\chi_{c2}(1P))/\Gamma_{total}$ — $\Gamma_{25}/\Gamma\times\Gamma_{164}^{\psi(2S)}/\Gamma^{\psi(2S)}$

VALUE (units 10^{-4})	EVTS	DOCUMENT ID		TECN	COMMENT
2.12±0.08 OUR FIT					
2.17±0.09 OUR AVERAGE					
$2.19\pm0.05\pm0.15$	4.5k	[1] ABLIKIM	10A	BES3	$e^+e^-\to\psi(2S)\to\gamma\chi_{c2}$
$2.23\pm0.06\pm0.10$	2.5k	[2] ASNER	09	CLEO	$\psi(2S)\to\gamma\pi^+\pi^-$
$1.90\pm0.08\pm0.20$	0.8k	[3] ASNER	09	CLEO	$\psi(2S)\to\gamma\pi^0\pi^0$

[1] Calculated by us. ABLIKIM 10A reports $B(\chi_{c2}\to\pi^0\pi^0) = (0.88\pm0.02\pm0.06\pm0.04)\times10^{-3}$ using $B(\psi(2S)\to\gamma\chi_{c2}) = (8.3\pm0.4)\%$. We have multiplied the $\pi^0\pi^0$ measurement by 3 to obtain $\pi\pi$.
[2] Calculated by us. ASNER 09 reports $B(\chi_{c2}\to\pi^+\pi^-) = (1.59\pm0.04\pm0.07\pm0.10)\times10^{-3}$ using $B(\psi(2S)\to\gamma\chi_{c2}) = (9.33\pm0.14\pm0.61)\%$. We have multiplied the $\pi^+\pi^-$ measurement by 3/2 to obtain $\pi\pi$.
[3] Calculated by us. ASNER 09 reports $B(\chi_{c2}\to\pi^0\pi^0) = (0.68\pm0.03\pm0.07\pm0.04)\times10^{-3}$ using $B(\psi(2S)\to\gamma\chi_{c2}) = (9.33\pm0.14\pm0.61)\%$. We have multiplied the $\pi^0\pi^0$ measurement by 3 to obtain $\pi\pi$.

$\Gamma(\chi_{c2}(1P)\to\pi\pi)/\Gamma_{total}\times\Gamma(\psi(2S)\to\gamma\chi_{c2}(1P))/\Gamma(\psi(2S)\to J/\psi(1S)\pi^+\pi^-)$ — $\Gamma_{25}/\Gamma\times\Gamma_{164}^{\psi(2S)}/\Gamma_{12}^{\psi(2S)}$

VALUE (units 10^{-3})	EVTS	DOCUMENT ID		TECN	COMMENT
0.612±0.023 OUR FIT					
0.54 ±0.06 OUR AVERAGE					
$0.66\pm0.18\pm0.37$	21 ± 6	[1] BAI	03C	BES	$\psi(2S)\to\gamma\pi^0\pi^0$
$0.54\pm0.05\pm0.04$	185 ± 16	[2] BAI	98I	BES	$\psi(2S)\to\gamma\pi^+\pi^-$

[1] We have multiplied $\pi^0\pi^0$ measurement by 3 to obtain $\pi\pi$.
[2] Calculated by us. The value for $B(\chi_{c2}\to\pi^+\pi^-)$ reported by BAI 98I is derived using $B(\psi(2S)\to\gamma\chi_{c2}) = (7.8\pm0.8)\%$ and $B(\psi(2S)\to J/\psi\pi^+\pi^-) = (32.4\pm2.6)\%$ [BAI 98D]. We have multiplied $\pi^+\pi^-$ measurement by 3/2 to obtain $\pi\pi$.

$\Gamma(\chi_{c2}(1P)\to\eta\eta)/\Gamma_{total}\times\Gamma(\psi(2S)\to\gamma\chi_{c2}(1P))/\Gamma_{total}$ — $\Gamma_{31}/\Gamma\times\Gamma_{164}^{\psi(2S)}/\Gamma^{\psi(2S)}$

VALUE (units 10^{-4})	CL%	EVTS	DOCUMENT ID		TECN	COMMENT
0.52±0.04 OUR FIT						
0.52±0.04 OUR AVERAGE						
$0.54\pm0.03\pm0.04$		386	[1] ABLIKIM	10A	BES3	$e^+e^-\to\psi(2S)\to\gamma\chi_{c2}$
$0.47\pm0.05\pm0.05$		156	ASNER	09	CLEO	$\psi(2S)\to\gamma\eta\eta$
• • • We do not use the following data for averages, fits, limits, etc. • • •						
<0.44	90		[2] ADAMS	07	CLEO	$\psi(2S)\to\gamma\chi_{c2}$
<3	90		BAI	03C	BES	$\psi(2S)\to\gamma\eta\eta\to5\gamma$
$0.62\pm0.31\pm0.19$			LEE	85	CBAL	$\psi(2S)\to$ photons

[1] Calculated by us. ABLIKIM 10A reports $B(\chi_{c2}\to\eta\eta) = (0.65\pm0.04\pm0.05\pm0.03)\times10^{-3}$ using $B(\psi(2S)\to\gamma\chi_{c2}) = (8.3\pm0.4)\%$.
[2] Superseded by ASNER 09.

$\Gamma(\chi_{c2}(1P)\to K^+K^-)/\Gamma_{total}\times\Gamma(\psi(2S)\to\gamma\chi_{c2}(1P))/\Gamma_{total}$ — $\Gamma_{32}/\Gamma\times\Gamma_{164}^{\psi(2S)}/\Gamma^{\psi(2S)}$

VALUE (units 10^{-5})	EVTS	DOCUMENT ID		TECN	COMMENT
9.6±0.6 OUR FIT					
10.5±0.3±0.6	1.6k	[1] ASNER	09	CLEO	$\psi(2S)\to\gamma K^+K^-$

[1] Calculated by us. ASNER 09 reports $B(\chi_{c2}\to K^+K^-) = (1.13\pm0.03\pm0.06\pm0.07)\times10^{-3}$ using $B(\psi(2S)\to\gamma\chi_{c2}) = (9.33\pm0.14\pm0.61)\%$.

$\Gamma(\chi_{c2}(1P)\to K^+K^-)/\Gamma_{total}\times\Gamma(\psi(2S)\to\gamma\chi_{c2}(1P))/\Gamma(\psi(2S)\to J/\psi(1S)\pi^+\pi^-)$ — $\Gamma_{32}/\Gamma\times\Gamma_{164}^{\psi(2S)}/\Gamma_{12}^{\psi(2S)}$

VALUE (units 10^{-3})	EVTS	DOCUMENT ID		TECN	COMMENT
0.276±0.017 OUR FIT					
0.190±0.034±0.019	115 ± 13	[1] BAI	98I	BES	$\psi(2S)\to\gamma K^+K^-$

[1] Calculated by us. The value for $B(\chi_{c2}\to K^+K^-)$ reported by BAI 98I is derived using $B(\psi(2S)\to\gamma\chi_{c2}) = (7.8\pm0.8)\%$ and $B(\psi(2S)\to J/\psi\pi^+\pi^-) = (32.4\pm2.6)\%$ [BAI 98D].

Downloaded from https://academic.oup.com/ptep/article/2022/8/083C01/6651666 by KIT Library user on 27 September 2022

$\Gamma(\chi_{c2}(1P) \to K^0_S K^0_S)/\Gamma_{total} \times \Gamma(\psi(2S) \to \gamma\chi_{c2}(1P))/\Gamma_{total}$ — $\Gamma_{33}/\Gamma \times \Gamma^{\psi(2S)}_{164}/\Gamma^{\psi(2S)}$

VALUE (units 10^{-5})	EVTS	DOCUMENT ID		TECN	COMMENT
5.0 ±0.4 OUR FIT					
5.0 ±0.4 OUR AVERAGE					
4.9 ±0.3 ±0.3	373 ± 20	[1] ASNER	09	CLEO	$\psi(2S) \to \gamma K^0_S K^0_S$
5.72±0.76±0.63	65	ABLIKIM	05O	BES2	$\psi(2S) \to \gamma K^0_S K^0_S$

[1] Calculated by us. ASNER 09 reports $B(\chi_{c2} \to K^0_S K^0_S) = (0.53 \pm 0.03 \pm 0.03 \pm 0.03) \times 10^{-3}$ using $B(\psi(2S) \to \gamma\chi_{c2}) = (9.33 \pm 0.14 \pm 0.61)\%$.

$\Gamma(\chi_{c2}(1P) \to K^0_S K^0_S)/\Gamma_{total} \times \Gamma(\psi(2S) \to \gamma\chi_{c2}(1P))/\Gamma(\psi(2S) \to J/\psi(1S)\pi^+\pi^-)$ — $\Gamma_{33}/\Gamma \times \Gamma^{\psi(2S)}_{164}/\Gamma^{\psi(2S)}_{12}$

VALUE (units 10^{-5})	DOCUMENT ID		TECN	COMMENT
14.4±1.1 OUR FIT				
14.7±4.1±3.3	[1] BAI	99B	BES	$\psi(2S) \to \gamma K^0_S K^0_S$

[1] Calculated by us. The value of $B(\chi_{c2} \to K^0_S K^0_S)$ reported by BAI 99B was derived using $B(\psi(2S) \to \gamma\chi_{c2}(1P)) = (7.8 \pm 0.8)\%$ and $B(\psi(2S) \to J/\psi\pi^+\pi^-) = (32.4 \pm 2.6)\%$ [BAI 98D].

$\Gamma(\chi_{c2}(1P) \to \overline{K}^0 K^+\pi^- + \text{c.c.})/\Gamma_{total} \times \Gamma(\psi(2S) \to \gamma\chi_{c2}(1P))/\Gamma_{total}$ — $\Gamma_{42}/\Gamma \times \Gamma^{\psi(2S)}_{164}/\Gamma^{\psi(2S)}$

VALUE (units 10^{-4})	EVTS	DOCUMENT ID		TECN	COMMENT
1.22±0.17 OUR FIT					
1.15±0.18 OUR AVERAGE					
1.21±0.19±0.09	37	[1] ATHAR	07	CLEO	$\psi(2S) \to \gamma K^0_S K^\pm\pi^\mp$
0.97±0.32±0.13	28	[2] ABLIKIM	06R	BES2	$\psi(2S) \to \gamma K^0_S K^\pm\pi^\mp$

[1] Calculated by us. ATHAR 07 reports $B(\chi_{c2} \to \overline{K}^0 K^+\pi^- + \text{c.c.}) = (1.3 \pm 0.2 \pm 0.1 \pm 0.1) \times 10^{-3}$ using $B(\psi(2S) \to \gamma\chi_{c2}) = (9.33 \pm 0.14 \pm 0.61)\%$.

[2] Calculated by us. ABLIKIM 06R reports $B(\chi_{c2} \to K^0_S K^\pm\pi^\mp) = (0.6 \pm 0.2 \pm 0.1) \times 10^{-3}$ using $B(\psi(2S) \to \gamma\chi_{c2}) = (8.1 \pm 0.6)\%$. We have multiplied by 2 to obtain $\overline{K}^0 K^+\pi^- + \text{c.c.}$ from $K^0_S K^\pm\pi^\mp$.

$\Gamma(\chi_{c2}(1P) \to 2(\pi^+\pi^-))/\Gamma_{total} \times \Gamma(\psi(2S) \to \gamma\chi_{c2}(1P))/\Gamma(\psi(2S) \to J/\psi(1S)\pi^+\pi^-)$ — $\Gamma_1/\Gamma \times \Gamma^{\psi(2S)}_{164}/\Gamma^{\psi(2S)}_{12}$

VALUE (units 10^{-3})	DOCUMENT ID		TECN	COMMENT
2.79±0.26 OUR FIT				
3.1 ±1.0 OUR AVERAGE Error includes scale factor of 2.5.				
2.3 ±0.1 ±0.5	[1] BAI	99B	BES	$\psi(2S) \to \gamma\chi_{c2}$
4.3 ±0.6	[2] TANENBAUM	78	MRK1	$\psi(2S) \to \gamma\chi_{c2}$

[1] Calculated by us. The value for $B(\chi_{c2} \to 2\pi^+2\pi^-)$ reported in BAI 99B is derived using $B(\psi(2S) \to \gamma\chi_{c2}) = (7.8 \pm 0.8)\%$ and $B(\psi(2S) \to J/\psi(1S)\pi^+\pi^-) = (32.4 \pm 2.6)\%$ [BAI 98D].

[2] The value for $B(\psi(2S) \to \gamma\chi_{c2}) \times B(\chi_{c2} \to 2\pi^+\pi^-)$ reported in TANENBAUM 78 is derived using $B(\psi(2S) \to J/\psi(1S)\pi^+\pi^-) \times B(J/\psi(1S)\ell^+\ell^-) = (4.6 \pm 0.7)\%$. Calculated by us using $B(J/\psi(1S) \to \ell^+\ell^-) = 0.1181 \pm 0.0020$.

$\Gamma(\chi_{c2}(1P) \to K^+K^-K^+K^-)/\Gamma_{total} \times \Gamma(\psi(2S) \to \gamma\chi_{c2}(1P))/\Gamma_{total}$ — $\Gamma_{51}/\Gamma \times \Gamma^{\psi(2S)}_{164}/\Gamma^{\psi(2S)}$

VALUE (units 10^{-4})	EVTS	DOCUMENT ID		TECN	COMMENT
1.57±0.19 OUR FIT					
1.76±0.16±0.24	160	[1] ABLIKIM	06T	BES2	$\psi(2S) \to \gamma 2K^+2K^-$

[1] Calculated by us. The value of $B(\chi_{c2} \to 2K^+2K^-)$ reported by ABLIKIM 06T was derived using $B(\psi(2S) \to \gamma\chi_{c2}(1P)) = (8.1 \pm 0.4)\%$.

$\Gamma(\chi_{c2}(1P) \to K^+K^-K^+K^-)/\Gamma_{total} \times \Gamma(\psi(2S) \to \gamma\chi_{c2}(1P))/\Gamma(\psi(2S) \to J/\psi(1S)\pi^+\pi^-)$ — $\Gamma_{51}/\Gamma \times \Gamma^{\psi(2S)}_{164}/\Gamma^{\psi(2S)}_{12}$

VALUE (units 10^{-4})	DOCUMENT ID		TECN	COMMENT
4.5±0.5 OUR FIT				
3.6±0.6±0.6	[1] BAI	99B	BES	$\psi(2S) \to \gamma 2K^+2K^-$

[1] Calculated by us. The value of $B(\chi_{c2} \to 2K^+2K^-)$ reported by BAI 99B was derived using $B(\psi(2S) \to \gamma\chi_{c2}(1P)) = (7.8 \pm 0.8)\%$ and $B(\psi(2S) \to J/\psi\pi^+\pi^-) = (32.4 \pm 2.6)\%$ [BAI 98D].

$\Gamma(\chi_{c2}(1P) \to \phi\phi)/\Gamma_{total} \times \Gamma(\psi(2S) \to \gamma\chi_{c2}(1P))/\Gamma_{total}$ — $\Gamma_{20}/\Gamma \times \Gamma^{\psi(2S)}_{164}/\Gamma^{\psi(2S)}$

VALUE (units 10^{-4})	EVTS	DOCUMENT ID		TECN	COMMENT
1.01±0.08 OUR FIT					
0.98±0.13 OUR AVERAGE Error includes scale factor of 1.3.					
0.94±0.03±0.10	849	[1] ABLIKIM	11K	BES3	$\psi(2S) \to \gamma$ hadrons
1.38±0.24±0.23	41	[2] ABLIKIM	06T	BES2	$\psi(2S) \to \gamma 2K^+2K^-$

[1] Calculated by us. The value of $B(\chi_{c2} \to \phi\phi)$ reported by ABLIKIM 11K was derived using $B(\psi(2S) \to \gamma\chi_{c2}(1P)) = (8.74 \pm 0.35)\%$.

[2] Calculated by us. The value of $B(\chi_{c2} \to \phi\phi)$ reported by ABLIKIM 06T was derived using $B(\psi(2S) \to \gamma\chi_{c2}(1P)) = (8.1 \pm 0.4)\%$.

$\Gamma(\chi_{c2}(1P) \to \phi\phi)/\Gamma_{total} \times \Gamma(\psi(2S) \to \gamma\chi_{c2}(1P))/\Gamma(\psi(2S) \to J/\psi(1S)\pi^+\pi^-)$ — $\Gamma_{20}/\Gamma \times \Gamma^{\psi(2S)}_{164}/\Gamma^{\psi(2S)}_{12}$

VALUE (units 10^{-4})	DOCUMENT ID		TECN	COMMENT
2.92±0.24 OUR FIT				
4.8 ±1.3 ±1.3	[1] BAI	99B	BES	$\psi(2S) \to \gamma 2K^+2K^-$

[1] Calculated by us. The value of $B(\chi_{c2} \to \phi\phi)$ reported by BAI 99B was derived using $B(\psi(2S) \to \gamma\chi_{c2}(1P)) = (7.8 \pm 0.8)\%$ and $B(\psi(2S) \to J/\psi\pi^+\pi^-) = (32.4 \pm 2.6)\%$ [BAI 98D].

$\Gamma(\chi_{c2}(1P) \to \Sigma^+\overline{p}K^0_S + \text{c.c.})/\Gamma_{total} \times \Gamma(\psi(2S) \to \gamma\chi_{c2}(1P))/\Gamma_{total}$ — $\Gamma_{80}/\Gamma \times \Gamma^{\psi(2S)}_{164}/\Gamma^{\psi(2S)}$

VALUE (units 10^{-6})	EVTS	DOCUMENT ID		TECN	COMMENT
7.85±0.77±0.44	129	[1] ABLIKIM	19BB	BES3	$\psi(2S) \to \gamma\Sigma^+\overline{p}K^0_S + \text{c.c.}$

[1] Calculated by us. ABLIKIM 19BB reports $B(\chi_{c2} \to \Sigma^+\overline{p}K^0_S + \text{c.c.}) = (8.25 \pm 0.83 \pm 0.49) \times 10^{-5}$ using $B(\psi(2S) \to \gamma\chi_{c2}) = (9.52 \pm 0.20)\%$ and other branching fractions from PDG 18.

$\Gamma(\chi_{c2}(1P) \to \Sigma^0\overline{p}K^+ + \text{c.c.})/\Gamma_{total} \times \Gamma(\psi(2S) \to \gamma\chi_{c2}(1P))/\Gamma_{total}$ — $\Gamma_{81}/\Gamma \times \Gamma^{\psi(2S)}_{164}/\Gamma^{\psi(2S)}$

VALUE (units 10^{-5})	EVTS	DOCUMENT ID		TECN	COMMENT
0.87±0.06±0.04	271	[1] ABLIKIM	20AE	BES3	$\psi(2S) \to \gamma\Sigma^0\overline{p}K^+ + \text{c.c.}$

[1] Calculated by us. ABLIKIM 20AE reports $B(\chi_{c2} \to \Sigma^0\overline{p}K^+ + \text{c.c.}) = (0.91 \pm 0.06 \pm 0.05) \times 10^{-4}$ using $B(\psi(2S) \to \gamma\chi_{c2}) = (9.52 \pm 0.20)\%$ and other branching fractions from PDG 20.

$\Gamma(\chi_{c2}(1P) \to \gamma J/\psi(1S))/\Gamma_{total} \times \Gamma(\psi(2S) \to \gamma\chi_{c2}(1P))/\Gamma_{total}$ — $\Gamma_{92}/\Gamma \times \Gamma^{\psi(2S)}_{164}/\Gamma^{\psi(2S)}$

VALUE (units 10^{-2})	EVTS	DOCUMENT ID		TECN	COMMENT
1.81 ±0.04 OUR FIT					
1.69 ±0.16 OUR AVERAGE Error includes scale factor of 3.4. See the ideogram below.					
1.996±0.008±0.070	81k	[1] ABLIKIM	17N	BES3	$\psi(2S) \to \gamma\gamma J/\psi$
1.793±0.008±0.163	1.0M	ABLIKIM	17U	BES3	$e^+e^- \to \gamma X$
1.62 ±0.04 ±0.12	5.8k	BAI	04I	BES2	$\psi(2S) \to J/\psi\gamma\gamma$
0.99 ±0.10 ±0.08		GAISER	86	CBAL	$\psi(2S) \to \gamma X$
1.47 ±0.17		[2] OREGLIA	82	CBAL	$\psi(2S) \to \gamma\chi_{c2}$
1.8 ±0.5		[3] BRANDELIK	79B	DASP	$\psi(2S) \to \gamma\chi_{c2}$
1.2 ±0.2		[3] BARTEL	78B	CNTR	$\psi(2S) \to \gamma\chi_{c2}$
2.2 ±1.2		[4] BIDDICK	77	CNTR	$e^+e^- \to \gamma X$
1.2 ±0.7		[2] WHITAKER	76	MRK1	e^+e^-
• • • We do not use the following data for averages, fits, limits, etc. • • •					
1.874±0.007±0.102	76k	[5] ABLIKIM	12O	BES3	$\psi(2S) \to \gamma\chi_{c2}$
1.95 ±0.02 ±0.07	12.4k	[6] MENDEZ	08	CLEO	$\psi(2S) \to \gamma\chi_{c2}$
1.85 ±0.04 ±0.07	1.9k	[7] ADAM	05A	CLEO	Repl. by MENDEZ 08

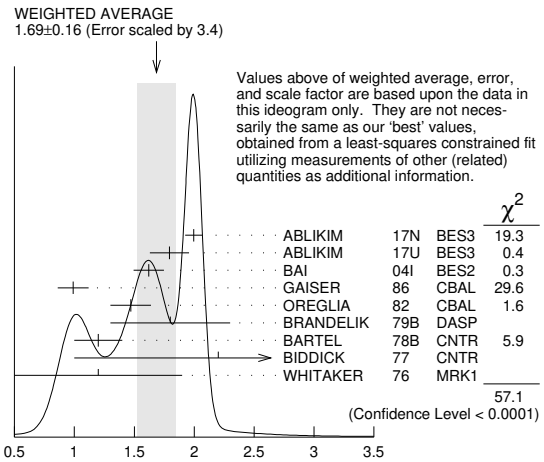

$\Gamma(\chi_{c2}(1P) \to \gamma J/\psi(1S))/\Gamma_{total} \times \Gamma(\psi(2S) \to \gamma\chi_{c2}(1P))/\Gamma_{total}$ (units 10^{-2})

[1] Uses $B(J/\psi \to e^+e^-) = (5.971 \pm 0.032)\%$ and $B(J/\psi \to \mu^+\mu^-) = (5.961 \pm 0.033)\%$.

[2] Recalculated by us using $B(J/\psi(1S) \to \ell^+\ell^-) = 0.1181 \pm 0.0020$.

[3] Recalculated by us using $B(J/\psi(1S) \to \mu^+\mu^-) = 0.0588 \pm 0.0010$.

[4] Assumes isotropic gamma distribution.

[5] Superseded by ABLIKIM 17N.

[6] Not independent from other measurements of MENDEZ 08.

[7] Not independent from other values reported by ADAM 05A.

Downloaded from https://academic.oup.com/ptep/article/2022/8/083C01/6651666 by KIT Library user on 27 September 2022

$\Gamma(\chi_{c2}(1P)\to\gamma J/\psi(1S))/\Gamma_{total}\times\Gamma(\psi(2S)\to\gamma\chi_{c2}(1P))/\Gamma(\psi(2S)\to J/\psi(1S)\text{anything})$ $\Gamma_{92}/\Gamma\times\Gamma_{164}^{\psi(2S)}/\Gamma_{10}^{\psi(2S)}$

$\Gamma_{92}/\Gamma\times\Gamma_{164}^{\psi(2S)}/\Gamma_{10}^{\psi(2S)}=\Gamma_{92}/\Gamma\times\Gamma_{164}^{\psi(2S)}/(\Gamma_{12}^{\psi(2S)}+\Gamma_{13}^{\psi(2S)}+\Gamma_{14}^{\psi(2S)}+0.343\Gamma_{163}^{\psi(2S)}+0.190\Gamma_{164}^{\psi(2S)})$

VALUE (units 10^{-2})	EVTS	DOCUMENT ID		TECN	COMMENT
2.95±0.06 OUR FIT					
• • • We do not use the following data for averages, fits, limits, etc. • • •					
3.12±0.03±0.09	12.4k	[1] MENDEZ	08	CLEO	$\psi(2S)\to\gamma\chi_{c2}$
3.11±0.07±0.07	1.9k	ADAM	05A	CLEO	Repl. by MENDEZ 08

[1] Not independent from other measurements of MENDEZ 08.

$\Gamma(\chi_{c2}(1P)\to\gamma J/\psi(1S))/\Gamma_{total}\times\Gamma(\psi(2S)\to\gamma\chi_{c2}(1P))/\Gamma(\psi(2S)\to J/\psi(1S)\pi^+\pi^-)$ $\Gamma_{92}/\Gamma\times\Gamma_{164}^{\psi(2S)}/\Gamma_{12}^{\psi(2S)}$

VALUE (units 10^{-2})	EVTS	DOCUMENT ID		TECN	COMMENT
5.22±0.11 OUR FIT					
5.53±0.17 OUR AVERAGE					
5.56±0.05±0.16	12.4k	MENDEZ	08	CLEO	$\psi(2S)\to\gamma\chi_{c2}$
6.0 ±2.8	1.3k	[1] ABLIKIM	04B	BES	$\psi(2S)\to J/\psi X$
3.9 ±1.2		[2] HIMEL	80	MRK2	$\psi(2S)\to\gamma\chi_{c2}$
• • • We do not use the following data for averages, fits, limits, etc. • • •					
5.52±0.13±0.13	1.9k	[3] ADAM	05A	CLEO	Repl. by MENDEZ 08

[1] From a fit to the J/ψ recoil mass spectra.
[2] The value for $B(\psi(2S)\to\gamma\chi_{c2})\times B(\chi_{c2}\to\gamma J/\psi(1S))$ reported in HIMEL 80 is derived using $B(\psi(2S)\to J/\psi(1S)\pi^+\pi^-)=(33\pm3)\%$ and $B(J/\psi(1S)\to\ell^+\ell^-)=0.138\pm0.018$. Calculated by us using $B(J/\psi(1S)\to\ell^+\ell^-)=(0.1181\pm0.0020)$.
[3] Not independent from other values reported by ADAM 05A.

$\Gamma(\chi_{c2}(1P)\to\gamma\gamma)/\Gamma_{total}\times\Gamma(\psi(2S)\to\gamma\chi_{c2}(1P))/\Gamma_{total}$ $\Gamma_{96}/\Gamma\times\Gamma_{164}^{\psi(2S)}/\Gamma^{\psi(2S)}$

VALUE (units 10^{-5})	EVTS	DOCUMENT ID		TECN	COMMENT
2.71±0.08 OUR FIT					
2.82±0.10 OUR AVERAGE					
2.83±0.08±0.06	5k	[1] ABLIKIM	17AE	BES3	$\psi(2S)\to\gamma\chi_{c2}\to3\gamma$
2.68±0.28±0.15	0.3k	ECKLUND	08A	CLEO	$\psi(2S)\to\gamma\chi_{c2}\to3\gamma$
7.0 ±2.1 ±2.0		LEE	85	CBAL	$\psi(2S)\to\gamma\chi_{c2}$
• • • We do not use the following data for averages, fits, limits, etc. • • •					
2.81±0.17±0.15	1.1k	[2] ABLIKIM	12A	BES3	$\psi(2S)\to\gamma\chi_{c2}\to3\gamma$

[1] ABLIKIM 17AE measures the ratio of two-photon partial widths for the helicity $\lambda=0$ and helicity $\lambda=2$ components to be $f_{0/2}=\Gamma_{\gamma\gamma}^{\lambda=0}/\Gamma_{\gamma\gamma}^{\lambda=2}=0.000\pm0.006\pm0.012$.
[2] ABLIKIM 12A measures the ratio of two-photon partial widths for the helicity $\lambda=0$ and helicity $\lambda=2$ components to be $f_{0/2}=\Gamma_{\gamma\gamma}^{\lambda=0}/\Gamma_{\gamma\gamma}^{\lambda=2}=0.00\pm0.02\pm0.02$. Superseded by ABLIKIM 17AE.

$\Gamma(\chi_{c2}(1P)\to\gamma\gamma)/\Gamma(\chi_{c0}(1P)\to\gamma\gamma)$ $\Gamma_{96}/\Gamma_{96}^{\chi_{c0}(1P)}$

VALUE	EVTS	DOCUMENT ID		TECN	COMMENT
0.292±0.028 OUR AVERAGE					
0.295±0.014±0.028	8k	[1] ABLIKIM	17AE	BES3	$\psi(2S)\to\gamma\chi_{cJ}\to3\gamma$
0.278±0.050±0.036	0.5k	[1] ECKLUND	08A	CLEO	$\psi(2S)\to\gamma\chi_{cJ}\to3\gamma$
• • • We do not use the following data for averages, fits, limits, etc. • • •					
0.271±0.029±0.030	1.9k	[1,2] ABLIKIM	12A	BES3	$\psi(2S)\to\gamma\chi_{cJ}\to3\gamma$

[1] Not independent from the values of $\Gamma(\chi_{c0},\chi_{c2})$ and $B(\psi(2S)\to\chi_{c0},\chi_{c2})$.
[2] Superseded by ABLIKIM 17AE.

MULTIPOLE AMPLITUDES IN $\chi_{c2}(1P)\to\gamma J/\psi(1S)$ RADIATIVE DECAY

$a_2=M2/\sqrt{E1^2+M2^2+E3^2}$ Magnetic quadrupole fractional transition amplitude

VALUE (units 10^{-2})	EVTS	DOCUMENT ID		TECN	COMMENT
−11.0± 1.0 OUR AVERAGE					
−12.0± 1.3±0.4	89k	[1] ABLIKIM	17N	BES3	$\psi(2S)\to\gamma\gamma\ell^+\ell^-$
− 9.3± 1.6±0.3	19.8k	[2] ARTUSO	09	CLEO	$\psi(2S)\to\gamma\gamma\ell^+\ell^-$
$-9.3^{+3.9}_{-4.1}\pm0.6$	5.9k	[3] AMBROGIANI	02	E835	$p\overline{p}\to\chi_{c2}\to J/\psi\gamma$
−14 ± 6	1.9k	[3] ARMSTRONG	93E	E760	$p\overline{p}\to\chi_{c2}\to J/\psi\gamma$
$-33.3^{+11.6}_{-29.2}$	441	[3] OREGLIA	82	CBAL	$\psi(2S)\to\chi_{c1}\gamma\to J/\psi\gamma\gamma$
• • • We do not use the following data for averages, fits, limits, etc. • • •					
− 7.9± 1.9±0.3	19.8k	[4] ARTUSO	09	CLEO	$\psi(2S)\to\gamma\gamma\ell^+\ell^-$

[1] Correlated with a_3, b_2, and b_3 with correlation coefficients $\rho_{a_2a_3}=0.733$, $\rho_{a_2b_2}=-0.605$, and $\rho_{a_2b_3}=-0.095$.
[2] From a fit with floating $M2$ amplitudes a_2 and b_2, and fixed $E3$ amplitudes $a_3=b_3=0$.
[3] Assuming $a_3=0$.
[4] From a fit with floating $M2$ and $E3$ amplitudes a_2, b_2, and a_3, and b_3.

$a_3=E3/\sqrt{E1^2+M2^2+E3^2}$ Electric octupole fractional transition amplitude

VALUE (units 10^{-2})	EVTS	DOCUMENT ID		TECN	COMMENT
−0.3±1.0 OUR AVERAGE Error includes scale factor of 1.3. See the ideogram below.					
−1.3±0.9±0.4	89k	[1] ABLIKIM	17N	BES3	$\psi(2S)\to\gamma\gamma\ell^+\ell^-$
1.7±1.4±0.3	19.8k	[2] ARTUSO	09	CLEO	$\psi(2S)\to\gamma\gamma\ell^+\ell^-$
$2.0^{+5.5}_{-4.4}\pm0.9$	5908	AMBROGIANI	02	E835	$p\overline{p}\to\chi_{c2}\to J/\psi\gamma$
0^{+6}_{-5}	1904	ARMSTRONG	93E	E760	$p\overline{p}\to\chi_{c2}\to J/\psi\gamma$

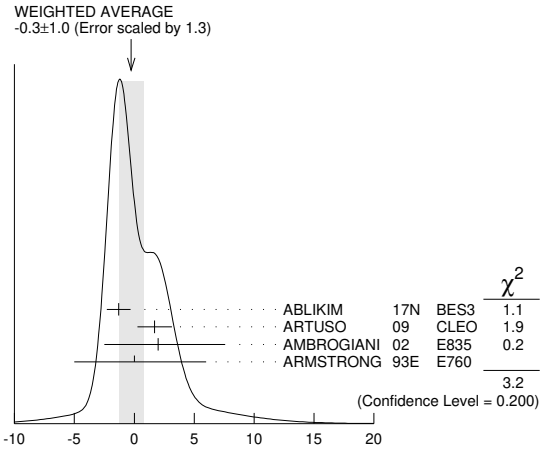

$a_3=E3/\sqrt{E1^2+M2^2+E3^2}$ Electric octupole fractional transition amplitude (units 10^{-2})

[1] Correlated with a_2, b_2, and b_3 with correlation coefficients $\rho_{a_2a_3}=0.733$, $\rho_{a_3b_2}=-0.422$, and $\rho_{a_3b_3}=-0.024$.
[2] From a fit with floating $M2$ and $E3$ amplitudes a_2, b_2, and a_3, and b_3.

MULTIPOLE AMPLITUDES IN $\psi(2S)\to\gamma\chi_{c2}(1P)$ RADIATIVE DECAY

$b_2=M2/\sqrt{E1^2+M2^2+E3^2}$ Magnetic quadrupole fractional transition amplitude

VALUE (units 10^{-2})	EVTS	DOCUMENT ID		TECN	COMMENT
1.9±0.9 OUR AVERAGE Error includes scale factor of 1.4. See the ideogram below.					
1.7±0.8±0.2	89k	[1] ABLIKIM	17N	BES3	$\psi(2S)\to\gamma\gamma\ell^+\ell^-$
4.6±1.0±1.3	13.8k	[2] ABLIKIM	11I	BES3	$\psi(2S)\to\gamma\pi^+\pi^-,\gamma K^+K^-$
0.2±1.5±0.4	19.8k	[3] ARTUSO	09	CLEO	$\psi(2S)\to\gamma\gamma\ell^+\ell^-$
$-5.1^{+5.4}_{-3.6}$	721	[2] ABLIKIM	04I	BES2	$\psi(2S)\to\gamma\pi^+\pi^-,\gamma K^+K^-$
$13.2^{+9.8}_{-7.5}$	441	[4] OREGLIA	82	CBAL	$\psi(2S)\to\gamma\gamma\ell^+\ell^-$
• • • We do not use the following data for averages, fits, limits, etc. • • •					
1.0±1.3±0.3	19.8k	[4] ARTUSO	09	CLEO	$\psi(2S)\to\gamma\gamma\ell^+\ell^-$

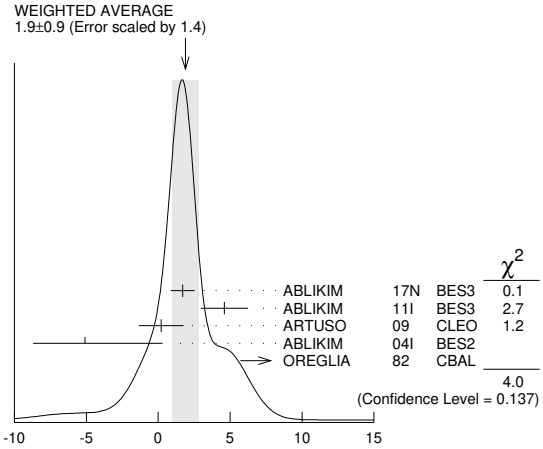

$b_2=M2/\sqrt{E1^2+M2^2+E3^2}$ Magnetic quadrupole fractional transition amplitude (units 10^{-2})

[1] Correlated with a_2, a_3, and b_3 with correlation coefficients $\rho_{a_2b_2}=-0.605$, $\rho_{a_3b_2}=-0.422$, and $\rho_{b_2b_3}=0.384$.
[2] From a fit with floating $M2$ and $E3$ amplitudes b_2 and b_3.
[3] From a fit with floating $M2$ and $E3$ amplitudes a_2, b_2, and a_3, and b_3.

Downloaded from https://academic.oup.com/ptep/article/2022/8/083C01/6651666 by KIT Library user on 27 September 2022

[4] From a fit with floating $M2$ amplitudes a_2 and b_2, and fixed $E3$ amplitudes $a_3 = b_3 = 0$.

$b_3 = E3/\sqrt{E1^2 + M2^2 + E3^2}$ Electric octupole fractional transition amplitude

VALUE (units 10^{-2})	EVTS	DOCUMENT ID		TECN	COMMENT
-1.0 ± 0.6 OUR AVERAGE					
$-1.4 \pm 0.7 \pm 0.4$	89k	[1] ABLIKIM	17N	BES3	$\psi(2S) \to \gamma\gamma\ell^+\ell^-$
$1.5 \pm 0.8 \pm 1.8$	13.8k	[2] ABLIKIM	11I	BES3	$\psi(2S) \to \gamma\pi^+\pi^-, \gamma K^+K^-$
$-0.8 \pm 1.2 \pm 0.2$	19.8k	ARTUSO	09	CLEO	$\psi(2S) \to \gamma\gamma\ell^+\ell^-$
$-2.7^{+4.3}_{-2.9}$	721	[2] ABLIKIM	04I	BES2	$\psi(2S) \to \gamma\pi^+\pi^-, \gamma K^+K^-$

[1] Correlated with a_2, a_3, and b_2 with correlation coefficients $\rho_{a_2 b_3} = -0.095$, $\rho_{a_3 b_3} = -0.024$, and $\rho_{b_2 b_3} = 0.384$.

[2] From a fit with floating $M2$ and $E3$ amplitudes b_2 and b_3.

MULTIPOLE AMPLITUDE RATIOS IN RADIATIVE DECAYS $\psi(2S) \to \gamma\chi_{c2}(1P)$ and $\chi_{c2} \to \gamma J/\psi(1S)$

b_2/a_2 Magnetic quadrupole transition amplitude ratio

VALUE (units 10^{-2})	EVTS	DOCUMENT ID		TECN	COMMENT
$\mathbf{-11^{+14}_{-15}}$	19.8k	[1] ARTUSO	09	CLEO	$\psi(2S) \to \gamma\gamma\ell^+\ell^-$

[1] Statistical and systematic errors combined. From a fit with floating $M2$ amplitudes a_2 and b_2, and fixed $E3$ amplitudes $a_3 = b_3 = 0$. Not independent of values for $a_2(\chi_{c2}(1P))$ and $b_2(\chi_{c2}(1P))$ from ARTUSO 09.

$\chi_{c2}(1P)$ REFERENCES

ABLIKIM	21AV	JHEP 2111 217	M. Ablikim et al.	(BESIII Collab.)
ABLIKIM	21L	PR D103 112004	M. Ablikim et al.	(BESIII Collab.)
ABLIKIM	20AE	PR D102 092006	M. Ablikim et al.	(BESIII Collab.)
ABLIKIM	20B	PR D101 012012	M. Ablikim et al.	(BESIII Collab.)
ABLIKIM	20I	PR D101 092002	M. Ablikim et al.	(BESIII Collab.)
PDG	20	PTEP 2020 083C01	P.A. Zyla et al.	(PDG Collab.)
ABLIKIM	19AA	PR D99 052008	M. Ablikim et al.	(BESIII Collab.)
ABLIKIM	19AU	PR D100 052010	M. Ablikim et al.	(BESIII Collab.)
ABLIKIM	19BB	PR D100 092006	M. Ablikim et al.	(BESIII Collab.)
ABLIKIM	19J	PR D99 012015	M. Ablikim et al.	(BESIII Collab.)
ABLIKIM	19Z	PR D99 051101	M. Ablikim et al.	(BESIII Collab.)
ABLIKIM	18V	PR D97 052011	M. Ablikim et al.	(BESIII Collab.)
PDG	18	PR D98 030001	M. Tanabashi et al.	(PDG Collab.)
AAIJ	17BB	EPJ C77 609	R. Aaij et al.	(LHCb Collab.)
AAIJ	17BI	PRL 119 221801	R. Aaij et al.	(LHCb Collab.)
ABLIKIM	17AE	PR D96 092007	M. Ablikim et al.	(BESIII Collab.)
ABLIKIM	17AG	PR D96 111102	M. Ablikim et al.	(BESIII Collab.)
ABLIKIM	17AI	PR D96 112006	M. Ablikim et al.	(BESIII Collab.)
ABLIKIM	17I	PRL 118 221802	M. Ablikim et al.	(BESIII Collab.)
ABLIKIM	17N	PR D95 072004	M. Ablikim et al.	(BESIII Collab.)
ABLIKIM	17U	PR D96 032001	M. Ablikim et al.	(BESIII Collab.)
PDG	16	CP C40 100001	C. Patrignani et al.	(PDG Collab.)
ABLIKIM	15I	PR D91 092006	M. Ablikim et al.	(BESIII Collab.)
ABLIKIM	15M	PR D91 112008	M. Ablikim et al.	(BESIII Collab.)
ABLIKIM	15N	PR D91 112018	M. Ablikim et al.	(BESIII Collab.)
ABLIKIM	14J	PR D89 074030	M. Ablikim et al.	(BESIII Collab.)
ABLIKIM	13B	PR D87 012002	M. Ablikim et al.	(BESIII Collab.)
ABLIKIM	13D	PR D87 012007	M. Ablikim et al.	(BESIII Collab.)
ABLIKIM	13H	PR D87 032007	M. Ablikim et al.	(BESIII Collab.)
ABLIKIM	13V	PR D88 112001	M. Ablikim et al.	(BESIII Collab.)
UEHARA	13	PTEP 2013 123C01	S. Uehara et al.	(BELLE Collab.)
ABLIKIM	12A	PR D85 112008	M. Ablikim et al.	(BESIII Collab.)
ABLIKIM	12I	PR D86 052004	M. Ablikim et al.	(BESIII Collab.)
ABLIKIM	12J	PR D86 052011	M. Ablikim et al.	(BESIII Collab.)
ABLIKIM	12O	PRL 109 172002	M. Ablikim et al.	(BESIII Collab.)
LEES	12AE	PR D86 092005	J.P. Lees et al.	(BABAR Collab.)
LIU	12B	PRL 108 232001	Z.Q. Liu et al.	(BELLE Collab.)
ABLIKIM	11A	PR D83 012006	M. Ablikim et al.	(BESIII Collab.)
ABLIKIM	11E	PR D83 112005	M. Ablikim et al.	(BESIII Collab.)
ABLIKIM	11F	PR D83 112009	M. Ablikim et al.	(BESIII Collab.)
ABLIKIM	11I	PR D84 092006	M. Ablikim et al.	(BESIII Collab.)
ABLIKIM	11K	PRL 107 092001	M. Ablikim et al.	(BESIII Collab.)
DEL-AMO-SA...	11M	PR D84 012004	P. del Amo Sanchez et al.	(BABAR Collab.)
ABLIKIM	10A	PR D81 052005	M. Ablikim et al.	(BESIII Collab.)
ONYISI	10	PR D82 011103	P.U.E. Onyisi et al.	(CLEO Collab.)
UEHARA	10A	PR D82 114031	S. Uehara et al.	(BELLE Collab.)
ARTUSO	09	PR D80 112003	M. Artuso et al.	(CLEO Collab.)
ASNER	09	PR D79 072007	D.M. Asner et al.	(CLEO Collab.)
UEHARA	09	PR D79 052009	S. Uehara et al.	(BELLE Collab.)
BENNETT	08A	PRL 101 151801	J.V. Bennett et al.	(CLEO Collab.)
ECKLUND	08A	PR D78 091501	K.M. Ecklund et al.	(CLEO Collab.)
HE	08B	PR D78 092004	Q. He et al.	(CLEO Collab.)
MENDEZ	08	PR D78 011102	H. Mendez et al.	(CLEO Collab.)
NAIK	08	PR D78 031101	P. Naik et al.	(CLEO Collab.)
UEHARA	08	EPJ C53 1	S. Uehara et al.	(BELLE Collab.)
ADAMS	07	PR D75 071101	G.S. Adams et al.	(CLEO Collab.)
ATHAR	07	PR D75 032002	S.B. Athar et al.	(CLEO Collab.)
CHEN	07B	PL B651 15	W.T. Chen et al.	(BELLE Collab.)
ABLIKIM	06D	PR D73 052006	M. Ablikim et al.	(BES Collab.)
ABLIKIM	06I	PR D74 012004	M. Ablikim et al.	(BES Collab.)
ABLIKIM	06R	PR D74 072001	M. Ablikim et al.	(BES Collab.)
ABLIKIM	06T	PL B642 197	M. Ablikim et al.	(BES Collab.)
DOBBS	06	PR D73 071101	S. Dobbs et al.	(CLEO Collab.)
ABLIKIM	05G	PR D71 092002	M. Ablikim et al.	(BES Collab.)
ABLIKIM	05N	PL B630 7	M. Ablikim et al.	(BES Collab.)
ABLIKIM	05O	PL B630 21	M. Ablikim et al.	(BES Collab.)
ADAM	05A	PRL 94 232002	N.E. Adam et al.	(CLEO Collab.)
ANDREOTTI	05A	NP B717 34	M. Andreotti et al.	(FNAL E835 Collab.)
NAKAZAWA	05	PL B615 39	H. Nakazawa et al.	(BELLE Collab.)
ABLIKIM	04B	PR D70 012003	M. Ablikim et al.	(BES Collab.)
ABLIKIM	04H	PR D70 092003	M. Ablikim et al.	(BES Collab.)
ABLIKIM	04I	PR D70 092004	M. Ablikim et al.	(BES Collab.)
ATHAR	04	PR D70 112002	S.B. Athar et al.	(CLEO Collab.)
BAI	04F	PR D69 092001	J.Z. Bai et al.	(BES Collab.)
BAI	04I	PR D70 012006	J.Z. Bai et al.	(BES Collab.)
AULCHENKO	03	PL B573 63	V.M. Aulchenko et al.	(KEDR Collab.)
BAI	03C	PR D67 032004	J.Z. Bai et al.	(BES Collab.)
BAI	03E	PR D67 112001	J.Z. Bai et al.	(BES Collab.)
ABE	02T	PL B540 33	K. Abe et al.	(BELLE Collab.)
AMBROGIANI	02	PR D65 052002	M. Ambrogiani et al.	(FNAL E835 Collab.)
EISENSTEIN	01	PRL 87 061801	B.I. Eisenstein et al.	(CLEO Collab.)
AMBROGIANI	00B	PR D62 052002	M. Ambrogiani et al.	(FNAL E835 Collab.)
ACCIARRI	99E	PL B453 73	M. Acciarri et al.	(L3 Collab.)
BAI	99B	PR D60 072001	J.Z. Bai et al.	(BES Collab.)
ACKER..,K...	98	PL B439 197	K. Ackerstaff et al.	(OPAL Collab.)
BAI	98D	PR D58 092006	J.Z. Bai et al.	(BES Collab.)
BAI	98I	PRL 81 3091	J.Z. Bai et al.	(BES Collab.)
DOMINICK	94	PR D50 4265	J. Dominick et al.	(CLEO Collab.)
ARMSTRONG	93	PRL 70 2988	T.A. Armstrong et al.	(FNAL E760 Collab.)
ARMSTRONG	93E	PR D48 3037	T.A. Armstrong et al.	(FNAL-E760 Collab.)
BAUER	93	PL B302 345	D.A. Bauer et al.	(TPC Collab.)
ARMSTRONG	92	NP B373 35	T.A. Armstrong et al.	(FNAL, FERR, GENO+)
Also		PRL 68 1468	T.A. Armstrong et al.	(FNAL, FERR, GENO+)
BAGLIN	87B	PL B187 191	C. Baglin et al.	(R704 Collab.)
BAGLIN	86B	PL B172 455	C. Baglin	(LAPP, CERN, GENO, LYON, OSLO+)
GAISER	86	PR D34 711	J. Gaiser et al.	(Crystal Ball Collab.)
LEE	85	SLAC 282	R.A. Lee	(SLAC)
LEMOIGNE	82	PL 113B 509	Y. Lemoigne et al.	(SACL, LOIC, SHMP+)
OREGLIA	82	PR D25 2259	M.J. Oreglia et al.	(SLAC, CIT, HARV+)
Also		Private Comm.	M.J. Oreglia	(EFI)
BARATE	81	PR D24 2994	R. Barate et al.	(SACL, LOIC, SHMP, CERN+)
HIMEL	80	PRL 44 920	T. Himel et al.	(LBL, SLAC)
Also		Private Comm.	G. Trilling	(LBL, UCB)
BRANDELIK	79B	NP B160 426	R. Brandelik et al.	(DASP Collab.)
BARTEL	78B	PL 79B 492	W. Bartel et al.	(DESY, HEIDP)
TANENBAUM	78	PR D17 1731	W.M. Tanenbaum et al.	(SLAC, LBL)
Also		Private Comm.	G. Trilling	(LBL, UCB)
BIDDICK	77	PRL 38 1324	C.J. Biddick et al.	(UCSD, UMD, PAVI+)
WHITAKER	76	PRL 37 1596	J.S. Whitaker et al.	(SLAC, LBL)

$\eta_c(2S)$

$I^G(J^{PC}) = 0^+(0^{-+})$

Quantum numbers are quark model predictions.

$\eta_c(2S)$ MASS

VALUE (MeV)	EVTS	DOCUMENT ID		TECN	COMMENT
3637.5 ± 1.1 OUR AVERAGE Error includes scale factor of 1.2.					
$3635.1 \pm 3.7 \pm 2.9$	106	XU	18	BELL	$e^+e^- \to e^+e^-\eta'\pi^+\pi^-$
$3633.6 \pm 1.7 \pm 0.6$	106	[1] AAIJ	17AD	LHCB	$pp \to B^+X \to p\overline{p}K^+X$
$3636.4 \pm 4.1 \pm 0.7$	365	[2] AAIJ	17BB	LHCB	$pp \to b\overline{b}X \to 2(K^+K^-)X$
$3637.0 \pm 5.7 \pm 3.4$	178	[3,4] LEES	14E	BABR	$\gamma\gamma \to K^+K^-\pi^0$
$3635.1 \pm 5.8 \pm 2.1$	47	[3,5] LEES	14E	BABR	$\gamma\gamma \to K^+K^-\eta$
$3646.9 \pm 1.6 \pm 3.6$	57 ± 17	ABLIKIM	13K	BES3	$\psi(2S) \to \gamma K^0_S K^\pm\pi^\mp\pi^+\pi^-$
$3637.6 \pm 2.9 \pm 1.6$	127 ± 18	[6] ABLIKIM	12G	BES3	$\psi(2S) \to \gamma K^0 K\pi, KK\pi^0$
$3638.5 \pm 1.5 \pm 0.8$	624	[3] DEL-AMO-SA...	11M	BABR	$\gamma\gamma \to K^0_S K^\pm\pi^\mp$
$3640.5 \pm 3.2 \pm 2.5$	1201	[3] DEL-AMO-SA...	11M	BABR	$\gamma\gamma \to K^+K^-\pi^+\pi^-\pi^0$
$3636.1^{+3.9+0.7}_{-4.2-2.0}$	128	[7] VINOKUROVA	11	BELL	$B^\pm \to K^\pm(K^0_S K^\pm\pi^\mp)$
$3626 \pm 5 \pm 6$	311	[8] ABE	07	BELL	$e^+e^- \to J/\psi(c\overline{c})$
$3645.0 \pm 5.5^{+4.9}_{-7.8}$	121 ± 27	AUBERT	05C	BABR	$e^+e^- \to J/\psi c\overline{c}$
$3642.9 \pm 3.1 \pm 1.5$	61	ASNER	04	CLEO	$\gamma\gamma \to \eta_c \to K^0_S K^\pm\pi^\mp$
• • • We do not use the following data for averages, fits, limits, etc. • • •					
3639 ± 7	98 ± 52	[9] AUBERT	06E	BABR	$B^\pm \to K^\pm X_{c\overline{c}}$
$3630.8 \pm 3.4 \pm 1.0$	112 ± 24	[10] AUBERT	04D	BABR	$\gamma\gamma \to \eta_c(2S) \to K\overline{K}\pi$
$3654 \pm 6 \pm 8$	39 ± 11	[11] CHOI	02	BELL	$B \to KK_SK^-\pi^+$
3594 ± 5		[12] EDWARDS	82C	CBAL	$e^+e^- \to \gamma X$

[1] AAIJ 17AD report $m_{\psi(2S)} - m_{\eta_c(2S)} = 52.5 \pm 1.7 \pm 0.6$ MeV. We use the current value $m_{\psi(2S)} = 3686.097 \pm 0.025$ MeV to obtain the quoted mass.

[2] From a fit of the $\phi\phi$ invariant mass with the width of $\eta_c(2S)$ fixed to the PDG 16 value.

[3] Ignoring possible interference with continuum.

[4] With a width fixed to 11.3 MeV.

[5] With a width fixed to 11.3 MeV. Using both $\eta \to \gamma\gamma$ and $\eta \to \pi^+\pi^-\pi^0$ decays.

[6] From a simultaneous fit to $K^0_S K^\pm\pi^\mp$ and $K^+K^-\pi^0$ decay modes.

[7] Accounts for interference with non-resonant continuum.

[8] From a fit of the J/ψ recoil mass spectrum. Supersedes ABE,K 02 and ABE 04G.

[9] From the fit of the kaon momentum spectrum. Systematic errors not evaluated.

[10] Superseded by DEL-AMO-SANCHEZ 11M.

[11] Superseded by VINOKUROVA 11.

[12] Assuming mass of $\psi(2S) = 3686$ MeV.

$\eta_c(2S)$ WIDTH

VALUE (MeV)	CL%	EVTS	DOCUMENT ID		TECN	COMMENT
$11.3^{+3.2}_{-2.9}$ OUR AVERAGE						
$9.9 \pm 4.8 \pm 2.9$		57 ± 17	ABLIKIM	13K	BES3	$\psi(2S) \to \gamma K^0_S K^\pm\pi^\mp\pi^+\pi^-$
$16.9 \pm 6.4 \pm 4.8$		127 ± 18	[13] ABLIKIM	12G	BES3	$\psi(2S) \to \gamma K^0 K\pi, KK\pi^0$
$13.4 \pm 4.6 \pm 3.2$		624	[14] DEL-AMO-SA...	11M	BABR	$\gamma\gamma \to K^0_S K^\pm\pi^\mp$
$6.6^{+8.4+2.6}_{-5.1-0.9}$		128	[15] VINOKUROVA	11	BELL	$B^\pm \to K^\pm(K^0_S K^\pm\pi^\mp)$
$6.3 \pm 12.4 \pm 4.0$		61	ASNER	04	CLEO	$\gamma\gamma \to \eta_c \to K^0_S K^\pm\pi^\mp$

Downloaded from https://academic.oup.com/ptep/article/2022/8/083C01/6651666 by KIT Library user on 27 September 2022

• • • We do not use the following data for averages, fits, limits, etc. • • •

< 23	90	98 ± 52	[16] AUBERT	06E	BABR	$B^\pm \to K^\pm X_{c\overline{c}}$
22 ±14		121 ± 27	AUBERT	05C	BABR	$e^+e^- \to J/\psi c\overline{c}$
17.0± 8.3±2.5		112 ± 24	[17] AUBERT	04D	BABR	$\gamma\gamma \to \eta_c(2S) \to K\overline{K}\pi$
<55	90	39 ± 11	[18] CHOI	02	BELL	$B \to K K_S K^-\pi^+$
<8.0	95		[19] EDWARDS	82C	CBAL	$e^+e^- \to \gamma X$

[13] From a simultaneous fit to $K^0_S K^\pm\pi^\mp$ and $K^+K^-\pi^0$ decay modes.
[14] Ignoring possible interference with continuum.
[15] Accounts for interference with non-resonant continuum.
[16] From the fit of the kaon momentum spectrum. Systematic errors not evaluated.
[17] Superseded by DEL-AMO-SANCHEZ 11M.
[18] For a mass value of 3654 ± 6 MeV. Superseded by VINOKUROVA 11.
[19] For a mass value of 3594 ± 5 MeV

$\eta_c(2S)$ DECAY MODES

	Mode	Fraction (Γ_i/Γ)	Confidence level
Γ_1	hadrons	not seen	
Γ_2	$K\overline{K}\pi$	(1.9±1.2) %	
Γ_3	$K\overline{K}\eta$	(5 ±4) $\times 10^{-3}$	
Γ_4	$2\pi^+2\pi^-$	not seen	
Γ_5	$\rho^0\rho^0$	not seen	
Γ_6	$3\pi^+3\pi^-$	not seen	
Γ_7	$K^+K^-\pi^+\pi^-$	not seen	
Γ_8	$K^{*0}\overline{K}^{*0}$	not seen	
Γ_9	$K^+K^-\pi^+\pi^-\pi^0$	(1.4±1.0) %	
Γ_{10}	$K^+K^-2\pi^+2\pi^-$	not seen	
Γ_{11}	$K^0_S K^-2\pi^+\pi^-$ + c.c.	seen	
Γ_{12}	$2K^+2K^-$	not seen	
Γ_{13}	$\phi\phi$	not seen	
Γ_{14}	$p\overline{p}$	seen	
Γ_{15}	$p\overline{p}\pi^+\pi^-$	seen	
Γ_{16}	$\gamma\gamma$	(1.9±1.3) $\times 10^{-4}$	
Γ_{17}	$\gamma J/\psi(1S)$	< 1.4 %	90%
Γ_{18}	$\pi^+\pi^-\eta$	not seen	
Γ_{19}	$\pi^+\pi^-\eta'$	not seen	
Γ_{20}	$\pi^+\pi^-\eta_c(1S)$	< 25 %	90%

$\eta_c(2S)$ PARTIAL WIDTHS

$\Gamma(\gamma\gamma)$ — Γ_{16}

VALUE (keV)	EVTS	DOCUMENT ID		TECN	COMMENT
• • • We do not use the following data for averages, fits, limits, etc. • • •					
0.44±0.14	106	[20] XU	18	BELL	$e^+e^- \to e^+e^-\eta'\pi^+\pi^-$
1.3 ±0.6		[21] ASNER	04	CLEO	$\gamma\gamma \to \eta_c \to K^0_S K^\pm\pi^\mp$

[20] Assuming that the branching fraction into $\eta'\pi^+\pi^-$ is the same as for $\eta_c(1S)$.
[21] They measure $\Gamma(\eta_c(2S)\gamma\gamma)\,B(\eta_c(2S) \to K\overline{K}\pi) = (0.18 \pm 0.05 \pm 0.02)\,\Gamma(\eta_c(1S)\gamma\gamma)\,B(\eta_c(1S) \to K\overline{K}\pi)$. The value for $\Gamma(\eta_c(2S) \to \gamma\gamma)$ is derived assuming that the branching fractions for $\eta_c(2S)$ and $\eta_c(1S)$ decays to $K_S K\pi$ are equal and using $\Gamma(\eta_c(1S) \to \gamma\gamma) = 7.4 \pm 0.4 \pm 2.3$ keV.

$\Gamma(\gamma\gamma) \times \Gamma(\pi^+\pi^-\eta')/\Gamma_{total}$ — $\Gamma_{16}\Gamma_{19}/\Gamma$

VALUE (eV)	EVTS	DOCUMENT ID		TECN	COMMENT
$5.6^{+1.2}_{-1.1}\pm1.1$	106	XU	18	BELL	$e^+e^- \to e^+e^-\eta'\pi^+\pi^-$

$\eta_c(2S)$ $\Gamma(i)\Gamma(\gamma\gamma)/\Gamma(total)$

$\Gamma(2\pi^+2\pi^-) \times \Gamma(\gamma\gamma)/\Gamma_{total}$ — $\Gamma_4\Gamma_{16}/\Gamma$

VALUE (eV)	CL%	DOCUMENT ID		TECN	COMMENT
<6.5	90	UEHARA	08	BELL	$\gamma\gamma \to \eta_c(2S) \to 2(\pi^+\pi^-)$

$\Gamma(K\overline{K}\pi) \times \Gamma(\gamma\gamma)/\Gamma_{total}$ — $\Gamma_2\Gamma_{16}/\Gamma$

VALUE (eV)	EVTS	DOCUMENT ID		TECN	COMMENT
41±4±6	624	[22] DEL-AMO-SA...11M		BABR	$\gamma\gamma \to K^0_S K^\pm\pi^\mp$

[22] Not independent from other measurements reported in DEL-AMO-SANCHEZ 11M.

$\Gamma(K^+K^-\pi^+\pi^-) \times \Gamma(\gamma\gamma)/\Gamma_{total}$ — $\Gamma_7\Gamma_{16}/\Gamma$

VALUE (eV)	CL%	DOCUMENT ID		TECN	COMMENT
<5.0	90	UEHARA	08	BELL	$\gamma\gamma \to \eta_c(2S) \to K^+K^-\pi^+\pi^-$

$\Gamma(K^+K^-\pi^+\pi^-\pi^0) \times \Gamma(\gamma\gamma)/\Gamma_{total}$ — $\Gamma_9\Gamma_{16}/\Gamma$

VALUE (eV)	EVTS	DOCUMENT ID		TECN	COMMENT
30±6±5	1201	[23] DEL-AMO-SA...11M		BABR	$\gamma\gamma \to K^+K^-\pi^+\pi^-\pi^0$

[23] Not independent from other measurements reported in DEL-AMO-SANCHEZ 11M.

$\Gamma(2K^+2K^-) \times \Gamma(\gamma\gamma)/\Gamma_{total}$ — $\Gamma_{12}\Gamma_{16}/\Gamma$

VALUE (eV)	CL%	DOCUMENT ID		TECN	COMMENT
<2.9	90	UEHARA	08	BELL	$\gamma\gamma \to \eta_c(2S) \to 2(K^+K^-)$

$\Gamma(\pi^+\pi^-\eta_c(1S)) \times \Gamma(\gamma\gamma)/\Gamma_{total}$ — $\Gamma_{20}\Gamma_{16}/\Gamma$

VALUE (eV)	CL%	DOCUMENT ID		TECN	COMMENT
<133	90	LEES	12AE	BABR	$e^+e^- \to e^+e^-\pi^+\pi^-\eta_c$

$\eta_c(2S)$ $\Gamma(i)\Gamma(\gamma\gamma)/\Gamma^2(total)$

$\Gamma(p\overline{p})/\Gamma_{total} \times \Gamma(\gamma\gamma)/\Gamma_{total}$ — $\Gamma_{14}/\Gamma \times \Gamma_{16}/\Gamma$

VALUE (units 10^{-8})	CL%	DOCUMENT ID		TECN	COMMENT
< 5.6	90[24,25,26]	AMBROGIANI	01	E835	$\overline{p}p \to \gamma\gamma$
• • • We do not use the following data for averages, fits, limits, etc. • • •					
< 8.0	90[24,25,27]	AMBROGIANI	01	E835	$\overline{p}p \to \gamma\gamma$
<12.0	90 [25,27]	AMBROGIANI	01	E835	$\overline{p}p \to \gamma\gamma$

[24] Including the measurements of of ARMSTRONG 95F in the AMBROGIANI 01 analysis.
[25] For a total width Γ=5 MeV.
[26] For the resonance mass region 3589–3599 MeV/c^2.
[27] For the resonance mass region 3575–3660 MeV/c^2.

$\eta_c(2S)$ BRANCHING RATIOS

$\Gamma(hadrons)/\Gamma_{total}$ — Γ_1/Γ

VALUE	DOCUMENT ID		TECN	COMMENT
not seen	ABREU	98O	DLPH	$e^+e^- \to e^+e^-$ + hadrons
• • • We do not use the following data for averages, fits, limits, etc. • • •				
seen	[28] EDWARDS	82C	CBAL	$e^+e^- \to \gamma X$

[28] For a mass value of 3594 ± 5 MeV

$\Gamma(K\overline{K}\pi)/\Gamma_{total}$ — Γ_2/Γ

VALUE (units 10^{-2})	EVTS	DOCUMENT ID		TECN	COMMENT
1.9±0.4±1.1	59 ± 12	[29] AUBERT	08AB	BABR	$B \to \eta_c(2S)K \to K\overline{K}\pi K$
• • • We do not use the following data for averages, fits, limits, etc. • • •					
seen	127 ± 18	ABLIKIM	13K	BES3	$\psi(2S) \to \gamma K\overline{K}\pi$
seen	39 ± 11	[30] CHOI	02	BELL	$B \to K K_S K^-\pi^+$

[29] Derived from a measurement of $[B(B^+ \to \eta_c(2S)K^+) \times B(\eta_c(2S) \to K\overline{K}\pi)]$ / $[B(B^+ \to \eta_c K^+) \times B(\eta_c \to K\overline{K}\pi)] = (9.6^{+2.0}_{-1.9} \pm 2.5)\%$ and using $B(B^+ \to \eta_c(2S)K^+) = (3.4 \pm 1.8) \times 10^{-4}$, and $[B(B^+ \to \eta_c K^+) \times B(\eta_c \to K\overline{K}\pi)] = (6.88 \pm 0.77^{+0.55}_{-0.66}) \times 10^{-5}$.
[30] For a mass value of 3654 ± 6 MeV

$\Gamma(K\overline{K}\eta)/\Gamma(K\overline{K}\pi)$ — Γ_3/Γ_2

VALUE (units 10^{-2})	EVTS	DOCUMENT ID		TECN	COMMENT
27.3±7.0±9.0	225	[31] LEES	14E	BABR	$\gamma\gamma \to K^+K^-\gamma\gamma$

[31] LEES 14E reports $B(\eta_c(2S) \to K^+K^-\eta)/B(\eta_c(2S) \to K^+K^-\pi^0) = 0.82 \pm 0.21 \pm 0.27$, which we divide by 3 to account for isospin symmetry.

$\Gamma(2\pi^+2\pi^-)/\Gamma_{total}$ — Γ_4/Γ

VALUE	DOCUMENT ID		TECN	COMMENT
not seen	UEHARA	08	BELL	$\gamma\gamma \to \eta_c(2S)$

$\Gamma(\rho^0\rho^0)/\Gamma_{total}$ — Γ_5/Γ

VALUE	DOCUMENT ID		TECN	COMMENT
not seen	ABLIKIM	11H	BES3	$\psi(2S) \to \gamma 2\pi^+2\pi^-$

$\Gamma(K^+K^-\pi^+\pi^-)/\Gamma_{total}$ — Γ_7/Γ

VALUE	DOCUMENT ID		TECN	COMMENT
not seen	UEHARA	08	BELL	$\gamma\gamma \to \eta_c(2S)$

$\Gamma(K^+K^-\pi^+\pi^-\pi^0)/\Gamma(K\overline{K}\pi)$ — Γ_9/Γ_2

VALUE	EVTS	DOCUMENT ID		TECN	COMMENT
0.73±0.17±0.17	1201	[32] DEL-AMO-SA...11M		BABR	$\gamma\gamma \to K^+K^-\pi^+\pi^-\pi^0$

[32] We have multiplied the value of $\Gamma(K^+K^-\pi^+\pi^-\pi^0)/\Gamma(K^0_S K^\pm\pi^\mp)$ reported in DEL-AMO-SANCHEZ 11M by a factor 1/3 to obtain $\Gamma(K^+K^-\pi^+\pi^-\pi^0)/\Gamma(K\overline{K}\pi)$. Not independent from other measurements reported in DEL-AMO-SANCHEZ 11M.

$\Gamma(K^{*0}\overline{K}^{*0})/\Gamma_{total}$ — Γ_8/Γ

VALUE	DOCUMENT ID		TECN	COMMENT
not seen	ABLIKIM	11H	BES3	$\psi(2S) \to \gamma K^+K^-\pi^+\pi^-$

$\Gamma(K^0_S K^-2\pi^+\pi^-$ + c.c.$)/\Gamma_{total}$ — Γ_{11}/Γ

VALUE	EVTS	DOCUMENT ID		TECN	COMMENT
seen	57±17	ABLIKIM	13K	BES3	$\psi(2S) \to \gamma K^0_S K^\pm\pi^\mp\pi^+\pi^-$

$\Gamma(2K^+2K^-)/\Gamma_{total}$ — Γ_{12}/Γ

VALUE	DOCUMENT ID		TECN	COMMENT
not seen	UEHARA	08	BELL	$\gamma\gamma \to \eta_c(2S)$

Downloaded from https://academic.oup.com/ptep/article/2022/8/083C01/6651666 by KIT Library user on 27 September 2022

$\Gamma(\phi\phi)/\Gamma_{total}$ — Γ_{13}/Γ

VALUE	DOCUMENT ID		TECN	COMMENT
not seen	ABLIKIM	11H	BES3	$\psi(2S) \to \gamma K^+ K^- K^+ K^-$

$\Gamma(p\overline{p})/\Gamma_{total}$ — Γ_{14}/Γ

VALUE	EVTS	DOCUMENT ID		TECN	COMMENT
seen	106	[33] AAIJ	17AD	LHCB	$pp \to B^+ X \to p\overline{p} K^+ X$

[33] AAIJ 17AD report a 6.4 standard deviation signal, with $B(B^+ \to \eta_c(2S) K^+ \to p\overline{p} K^+)/B(B^+ \to J/\psi K^+ \to p\overline{p} K^+) = (1.58 \pm 0.33 \pm 0.09) \times 10^{-2}$.

$\Gamma(p\overline{p}\pi^+\pi^-)/\Gamma_{total}$ — Γ_{15}/Γ

VALUE	EVTS	DOCUMENT ID		TECN	COMMENT
seen	110	[34] CHILIKIN	19	BELL	$e^+e^- \to \Upsilon(4S)$

[34] CHILIKIN 19 reports signals in $B^+ \to \eta_c(2S) K^+$ and $B^0 \to \eta_c(2S) K^0_S$ with 12.3 and 5.9 standard deviations, respectively.

$\Gamma(\gamma\gamma)/\Gamma_{total}$ — Γ_{16}/Γ

VALUE	CL%	DOCUMENT ID		TECN	COMMENT
• • • We do not use the following data for averages, fits, limits, etc. • • •					
$<4 \times 10^{-4}$	90	[35] WICHT	08	BELL	$B^\pm \to K^\pm\gamma\gamma$
not seen		AMBROGIANI	01	E835	$\overline{p}p \to \gamma\gamma$
<0.01	90	LEE	85	CBAL	$\psi' \to$ photons

[35] WICHT 08 reports $[\Gamma(\eta_c(2S) \to \gamma\gamma)/\Gamma_{total}] \times [B(B^+ \to \eta_c(2S) K^+)] < 0.18 \times 10^{-6}$ which we divide by our best value $B(B^+ \to \eta_c(2S) K^+) = 4.4 \times 10^{-4}$.

$\Gamma(\pi^+\pi^-\eta_c(1S))/\Gamma(K\overline{K}\pi)$ — Γ_{20}/Γ_2

VALUE	CL%	DOCUMENT ID		TECN	COMMENT
<3.33	90	[36] LEES	12AE	BABR	$e^+e^- \to e^+e^-\pi^+\pi^-\eta_c$

[36] We divided the reported limit by 3 to take into account isospin relations.

$\eta_c(2S)$ CROSS-PARTICLE BRANCHING RATIOS

$\Gamma(\eta_c(2S) \to K\overline{K}\eta)/\Gamma_{total} \times \Gamma(\psi(2S) \to \gamma\eta_c(2S))/\Gamma_{total}$ — $\Gamma_3/\Gamma \times \Gamma^{\psi(2S)}_{166}/\Gamma^{\psi(2S)}$

VALUE	CL%	DOCUMENT ID		TECN	COMMENT
• • • We do not use the following data for averages, fits, limits, etc. • • •					
$<11.8 \times 10^{-6}$	90	[37] CRONIN-HEN..	10	CLEO	$\psi(2S) \to \gamma K^+ K^- \eta$

[37] CRONIN-HENNESSY 10 reports a limit of $< 5.9 \times 10^{-6}$ for the decay $\eta_c(2S) \to K^+ K^- \eta$ which we multiply by 2 account for isospin symmetry. It assumes $\Gamma(\eta_c(2S)) = 14$ MeV. It also gives the analytic dependence of limits on width.

$\Gamma(\eta_c(2S) \to 2\pi^+ 2\pi^-)/\Gamma_{total} \times \Gamma(\psi(2S) \to \gamma\eta_c(2S))/\Gamma_{total}$ — $\Gamma_4/\Gamma \times \Gamma^{\psi(2S)}_{166}/\Gamma^{\psi(2S)}$

VALUE	CL%	DOCUMENT ID		TECN	COMMENT
$<14.6 \times 10^{-6}$	90	[38] CRONIN-HEN..	10	CLEO	$\psi(2S) \to \gamma 2\pi^+ 2\pi^-$

[38] Assuming $\Gamma(\eta_c(2S)) = 14$ MeV. CRONIN-HENNESSY 10 gives the analytic dependence of limits on width.

$\Gamma(\eta_c(2S) \to \rho^0\rho^0)/\Gamma_{total} \times \Gamma(\psi(2S) \to \gamma\eta_c(2S))/\Gamma_{total}$ — $\Gamma_5/\Gamma \times \Gamma^{\psi(2S)}_{166}/\Gamma^{\psi(2S)}$

VALUE	CL%	DOCUMENT ID		TECN	COMMENT
$<12.7 \times 10^{-7}$	90	ABLIKIM	11H	BES3	$\psi(2S) \to \gamma 2\pi^+ 2\pi^-$

$\Gamma(\eta_c(2S) \to 3\pi^+ 3\pi^-)/\Gamma_{total} \times \Gamma(\psi(2S) \to \gamma\eta_c(2S))/\Gamma_{total}$ — $\Gamma_6/\Gamma \times \Gamma^{\psi(2S)}_{166}/\Gamma^{\psi(2S)}$

VALUE	CL%	DOCUMENT ID		TECN	COMMENT
$<13.2 \times 10^{-6}$	90	[39] CRONIN-HEN..	10	CLEO	$\psi(2S) \to \gamma 3\pi^+ 3\pi^-$

[39] Assuming $\Gamma(\eta_c(2S)) = 14$ MeV. CRONIN-HENNESSY 10 gives the analytic dependence of limits on width.

$\Gamma(\eta_c(2S) \to K^+ K^- \pi^+\pi^-)/\Gamma_{total} \times \Gamma(\psi(2S) \to \gamma\eta_c(2S))/\Gamma_{total}$ — $\Gamma_7/\Gamma \times \Gamma^{\psi(2S)}_{166}/\Gamma^{\psi(2S)}$

VALUE	CL%	DOCUMENT ID		TECN	COMMENT
$<9.6 \times 10^{-6}$	90	[40] CRONIN-HEN..	10	CLEO	$\psi(2S) \to \gamma K^+ K^- \pi^+\pi^-$

[40] Assuming $\Gamma(\eta_c(2S)) = 14$ MeV. CRONIN-HENNESSY 10 gives the analytic dependence of limits on width.

$\Gamma(\eta_c(2S) \to K^{*0}\overline{K}^{*0})/\Gamma_{total} \times \Gamma(\psi(2S) \to \gamma\eta_c(2S))/\Gamma_{total}$ — $\Gamma_8/\Gamma \times \Gamma^{\psi(2S)}_{166}/\Gamma^{\psi(2S)}$

VALUE	CL%	DOCUMENT ID		TECN	COMMENT
$<19.6 \times 10^{-7}$	90	ABLIKIM	11H	BES3	$\psi(2S) \to \gamma K^+ K^- \pi^+\pi^-$

$\Gamma(\eta_c(2S) \to K^+ K^- \pi^+\pi^-\pi^0)/\Gamma_{total} \times \Gamma(\psi(2S) \to \gamma\eta_c(2S))/\Gamma_{total}$ — $\Gamma_9/\Gamma \times \Gamma^{\psi(2S)}_{166}/\Gamma^{\psi(2S)}$

VALUE	CL%	DOCUMENT ID		TECN	COMMENT
$<43.0 \times 10^{-6}$	90	[41] CRONIN-HEN..	10	CLEO	$\psi(2S) \to \gamma K^+ K^- \pi^+\pi^-\pi^0$

[41] Assuming $\Gamma(\eta_c(2S)) = 14$ MeV. CRONIN-HENNESSY 10 gives the analytic dependence of limits on width.

$\Gamma(\eta_c(2S) \to K^+ K^- 2\pi^+ 2\pi^-)/\Gamma_{total} \times \Gamma(\psi(2S) \to \gamma\eta_c(2S))/\Gamma_{total}$ — $\Gamma_{10}/\Gamma \times \Gamma^{\psi(2S)}_{166}/\Gamma^{\psi(2S)}$

VALUE	CL%	DOCUMENT ID		TECN	COMMENT
$<9.7 \times 10^{-6}$	90	[42] CRONIN-HEN..	10	CLEO	$\psi(2S) \to \gamma K^+ K^- 2\pi^+ 2\pi^-$

[42] Assuming $\Gamma(\eta_c(2S)) = 14$ MeV. CRONIN-HENNESSY 10 gives the analytic dependence of limits on width.

$\Gamma(\eta_c(2S) \to K^0_S K^- 2\pi^+\pi^- + \text{c.c.})/\Gamma_{total} \times \Gamma(\psi(2S) \to \gamma\eta_c(2S))/\Gamma_{total}$ — $\Gamma_{11}/\Gamma \times \Gamma^{\psi(2S)}_{166}/\Gamma^{\psi(2S)}$

VALUE (units 10^{-6})	CL%	EVTS	DOCUMENT ID		TECN	COMMENT
$7.03 \pm 2.10 \pm 0.7$		60	ABLIKIM	13K	BES3	$\psi(2S) \to \gamma K^0_S K^- 2\pi^+\pi^- +$c.c.
• • • We do not use the following data for averages, fits, limits, etc. • • •						
< 15.2	90		[43] CRONIN-HEN..	10	CLEO	$\psi(2S) \to \gamma K^0_S K^- 2\pi^+\pi^- +$c.c.

[43] Assuming $\Gamma(\eta_c(2S)) = 14$ MeV. CRONIN-HENNESSY 10 gives the analytic dependence of limits on width.

$\Gamma(\eta_c(2S) \to \phi\phi)/\Gamma_{total} \times \Gamma(\psi(2S) \to \gamma\eta_c(2S))/\Gamma_{total}$ — $\Gamma_{13}/\Gamma \times \Gamma^{\psi(2S)}_{166}/\Gamma^{\psi(2S)}$

VALUE	CL%	DOCUMENT ID		TECN	COMMENT
$<7.8 \times 10^{-7}$	90	ABLIKIM	11H	BES3	$\psi(2S) \to \gamma K^+ K^- K^+ K^-$

$\Gamma(\eta_c(2S) \to p\overline{p})/\Gamma_{total} \times \Gamma(\psi(2S) \to \gamma\eta_c(2S))/\Gamma_{total}$ — $\Gamma_{14}/\Gamma \times \Gamma^{\psi(2S)}_{166}/\Gamma^{\psi(2S)}$

VALUE	CL%	DOCUMENT ID		TECN	COMMENT
$<1.4 \times 10^{-6}$	90	ABLIKIM	13V	BES3	$\psi(2S) \to \gamma p\overline{p}$

$\Gamma(\eta_c(2S) \to \gamma J/\psi(1S))/\Gamma_{total} \times \Gamma(\psi(2S) \to \gamma\eta_c(2S))/\Gamma_{total}$ — $\Gamma_{17}/\Gamma \times \Gamma^{\psi(2S)}_{166}/\Gamma^{\psi(2S)}$

VALUE	CL%	EVTS	DOCUMENT ID		TECN	COMMENT
$<9.7 \times 10^{-6}$	90	33	[44] ABLIKIM	17N	BES3	$\psi(2S) \to \gamma\gamma J/\psi$

[44] Uses $B(J/\psi \to e^+e^-) = (5.971 \pm 0.032)\%$ and $B(J/\psi \to \mu^+\mu^-) = (5.961 \pm 0.033)\%$.

$\Gamma(\eta_c(2S) \to \pi^+\pi^-\eta)/\Gamma_{total} \times \Gamma(\psi(2S) \to \gamma\eta_c(2S))/\Gamma_{total}$ — $\Gamma_{18}/\Gamma \times \Gamma^{\psi(2S)}_{166}/\Gamma^{\psi(2S)}$

VALUE	CL%	DOCUMENT ID		TECN	COMMENT
$<4.3 \times 10^{-6}$	90	[45] CRONIN-HEN..	10	CLEO	$\psi(2S) \to \gamma\pi^+\pi^-\eta$

[45] Assuming $\Gamma(\eta_c(2S)) = 14$ MeV. CRONIN-HENNESSY 10 gives the analytic dependence of limits on width.

$\Gamma(\eta_c(2S) \to \pi^+\pi^-\eta')/\Gamma_{total} \times \Gamma(\psi(2S) \to \gamma\eta_c(2S))/\Gamma_{total}$ — $\Gamma_{19}/\Gamma \times \Gamma^{\psi(2S)}_{166}/\Gamma^{\psi(2S)}$

VALUE	CL%	DOCUMENT ID		TECN	COMMENT
$<14.2 \times 10^{-6}$	90	[46] CRONIN-HEN..	10	CLEO	$\psi(2S) \to \gamma\pi^+\pi^-\eta'$

[46] Assuming $\Gamma(\eta_c(2S)) = 14$ MeV. CRONIN-HENNESSY 10 gives the analytic dependence of limits on width.

$\Gamma(\eta_c(2S) \to \pi^+\pi^-\eta_c(1S))/\Gamma_{total} \times \Gamma(\psi(2S) \to \gamma\eta_c(2S))/\Gamma_{total}$ — $\Gamma_{20}/\Gamma \times \Gamma^{\psi(2S)}_{166}/\Gamma^{\psi(2S)}$

VALUE	CL%	DOCUMENT ID		TECN	COMMENT
$<1.7 \times 10^{-4}$	90	[47] CRONIN-HEN..	10	CLEO	$\psi(2S) \to \gamma\pi^+\pi^-\eta_c(1S)$

[47] Assuming $\Gamma(\eta_c(2S)) = 14$ MeV. CRONIN-HENNESSY 10 gives the analytic dependence of limits on width.

$\eta_c(2S)$ REFERENCES

CHILIKIN	19	PR D100 012001	K. Chilikin *et al.*	(BELLE Collab.)
XU	18	PR D98 072001	Q.N. Xu *et al.*	(BELLE Collab.)
AAIJ	17AD	PL B769 305	R. Aaij *et al.*	(LHCb Collab.)
AAIJ	17BB	EPJ C77 609	R. Aaij *et al.*	(LHCb Collab.)
ABLIKIM	17N	PR D95 072004	M. Ablikim *et al.*	(BESIII Collab.)
PDG	16	CP C40 100001	C. Patrignani *et al.*	(PDG Collab.)
LEES	14E	PR D89 112004	J.P. Lees *et al.*	(BABAR Collab.)
ABLIKIM	13K	PR D87 052005	M. Ablikim *et al.*	(BESIII Collab.)
ABLIKIM	13V	PR D88 112001	M. Ablikim *et al.*	(BESIII Collab.)
ABLIKIM	12G	PRL 109 042003	M. Ablikim *et al.*	(BESIII Collab.)
LEES	12AE	PR D86 092005	J.P. Lees *et al.*	(BABAR Collab.)
ABLIKIM	11H	PR D84 091102	M. Ablikim *et al.*	(BESIII Collab.)
DEL-AMO-SA...	11M	PR D84 012004	P. del Amo Sanchez *et al.*	(BABAR Collab.)
VINOKUROVA	11	PL B706 139	A. Vinokurova *et al.*	(BELLE Collab.)
CRONIN-HEN...	10	PR D81 052002	D. Cronin-Hennessey *et al.*	(CLEO Collab.)
AUBERT	08AB	PR D78 012006	B. Aubert *et al.*	(BABAR Collab.)
UEHARA	08	EPJ C53 1	S. Uehara *et al.*	(BELLE Collab.)
WICHT	08	PL B662 323	J. Wicht *et al.*	(BELLE Collab.)
ABE	07	PRL 98 082001	K. Abe *et al.*	(BELLE Collab.)
AUBERT	06E	PRL 96 052002	B. Aubert *et al.*	(BABAR Collab.)
AUBERT	05C	PR D72 031101	B. Aubert *et al.*	(BABAR Collab.)
ABE	04G	PR D70 071102	K. Abe *et al.*	(BELLE Collab.)
ASNER	04	PRL 92 142001	D.M. Asner *et al.*	(CLEO Collab.)
AUBERT	04D	PRL 92 142002	B. Aubert *et al.*	(BABAR Collab.)
ABE,K	02	PRL 89 142001	K. Abe *et al.*	(BELLE Collab.)
CHOI	02	PRL 89 102001	S.-K. Choi *et al.*	(BELLE Collab.)
AMBROGIANI	01	PR D64 052003	M. Ambrogiani *et al.*	(FNAL E835 Collab.)
ABREU	98O	PL B441 479	P. Abreu *et al.*	(DELPHI Collab.)
ARMSTRONG	95F	PR D52 4839	T.A. Armstrong *et al.*	(FNAL, FERR, GENO+)
LEE	85	SLAC 282	R.A. Lee	(SLAC)
EDWARDS	82C	PRL 48 70	C. Edwards *et al.*	(CIT, HARV, PRIN+)

Downloaded from https://academic.oup.com/ptep/article/2022/8/083C01/6651666 by KIT Library user on 27 September 2022

$\psi(2S)$

$I^G(J^{PC}) = 0^-(1^{--})$

See the Review on "$\psi(2S)$ and χ_c branching ratios" before the $\chi_{c0}(1P)$ Listings.

$\psi(2S)$ MASS

OUR FIT includes measurements of $m_{\psi(2S)}$, $m_{\psi(3770)}$, and $m_{\psi(3770)} - m_{\psi(2S)}$.

VALUE (MeV)	EVTS	DOCUMENT ID		TECN	COMMENT
3686.10 ±0.06 OUR FIT Error includes scale factor of 5.9.					
3686.097±0.010 OUR AVERAGE					
3686.099±0.004±0.009		[1] ANASHIN	15	KEDR	$e^+e^- \to$ hadrons
3686.12 ±0.06 ±0.10	4k	AAIJ	12H	LHCB	$pp \to J/\psi\pi^+\pi^- X$
3685.95 ±0.10	413	[2] ARTAMONOV	00	OLYA	$e^+e^- \to$ hadrons
3685.98 ±0.09 ±0.04		[3] ARMSTRONG	93B	E760	$\overline{p}p \to e^+e^-$
• • • We do not use the following data for averages, fits, limits, etc. • • •					
3686.114±0.007$^{+0.011}_{-0.016}$		[4] ANASHIN	12	KEDR	$e^+e^- \to$ hadrons
3686.111±0.025±0.009		AULCHENKO	03	KEDR	$e^+e^- \to$ hadrons
3686.00 ±0.10	413	[5] ZHOLENTZ	80	OLYA	e^+e^-

[1] Supersedes AULCHENKO 03 and ANASHIN 12.
[2] Reanalysis of ZHOLENTZ 80 using new electron mass (COHEN 87) and radiative corrections (KURAEV 85).
[3] Mass central value and systematic error recalculated by us according to Eq. (16) in ARMSTRONG 93B, using the value for the $J/\psi(1S)$ mass from AULCHENKO 03.
[4] From the scans in 2004 and 2006. ANASHIN 12 reports the value 3686.114 ± 0.007 ± 0.011$^{+0.002}_{-0.012}$ MeV, where the third uncertainty is due to assumptions on the interference between the resonance and hadronic continuum. We combined the two systematic uncertainties.
[5] Superseded by ARTAMONOV 00.

$m_{\psi(2S)} - m_{J/\psi(1S)}$

VALUE (MeV)	DOCUMENT ID		TECN	COMMENT
589.188±0.028 OUR AVERAGE				
589.194±0.027±0.011	[1] AULCHENKO	03	KEDR	$e^+e^- \to$ hadrons
589.7 ±1.2	LEMOIGNE	82	GOLI	185 π^-Be $\to \gamma\mu^+\mu^-$A
589.07 ±0.13	[1] ZHOLENTZ	80	OLYA	e^+e^-
588.7 ±0.8	LUTH	75	MRK1	
• • • We do not use the following data for averages, fits, limits, etc. • • •				
588 ±1	[2] BAI	98E	BES	e^+e^-

[1] Redundant with data in mass above.
[2] Systematic errors not evaluated.

$\psi(2S)$ WIDTH

VALUE (keV)	EVTS	DOCUMENT ID		TECN	COMMENT
294± 8 OUR FIT					
286±16 OUR AVERAGE					
358±88± 4		ABLIKIM	08B	BES2	$e^+e^- \to$ hadrons
290±25± 4	2.7k	ANDREOTTI	07	E835	$p\overline{p} \to e^+e^-$, $J/\psi X$
331±58± 2		ABLIKIM	06L	BES2	$e^+e^- \to$ hadrons
264±27		[1] BAI	02B	BES2	e^+e^-
287±37±16		[2] ARMSTRONG	93B	E760	$\overline{p}p \to e^+e^-$

[1] From a simultaneous fit to the hadronic and $\mu^+\mu^-$ cross section, assuming $\Gamma = \Gamma_h + \Gamma_e + \Gamma_\mu + \Gamma_\tau$ and lepton universality. Does not include vacuum polarization correction.
[2] The initial-state radiation correction reevaluated by ANDREOTTI 07 in its Ref. [4].

$\psi(2S)$ DECAY MODES

	Mode	Fraction (Γ_i/Γ)	Scale factor/ Confidence level
Γ_1	hadrons	(97.85 ±0.13) %	
Γ_2	virtual $\gamma \to$ hadrons	(1.73 ±0.14) %	S=1.5
Γ_3	ggg	(10.6 ±1.6) %	
Γ_4	γgg	(1.03 ±0.29) %	
Γ_5	light hadrons	(15.4 ±1.5) %	
Γ_6	K^0_S anything	(16.0 ±1.1) %	
Γ_7	e^+e^-	(7.93 ±0.17) $\times 10^{-3}$	
Γ_8	$\mu^+\mu^-$	(8.0 ±0.6) $\times 10^{-3}$	
Γ_9	$\tau^+\tau^-$	(3.1 ±0.4) $\times 10^{-3}$	
	Decays into $J/\psi(1S)$ and anything		
Γ_{10}	$J/\psi(1S)$ anything	(61.4 ±0.6) %	
Γ_{11}	$J/\psi(1S)$ neutrals	(25.38 ±0.32) %	
Γ_{12}	$J/\psi(1S)\pi^+\pi^-$	(34.68 ±0.30) %	
Γ_{13}	$J/\psi(1S)\pi^0\pi^0$	(18.24 ±0.31) %	
Γ_{14}	$J/\psi(1S)\eta$	(3.37 ±0.05) %	
Γ_{15}	$J/\psi(1S)\pi^0$	(1.268±0.032) $\times 10^{-3}$	
	Hadronic decays		
Γ_{16}	$\pi^+\pi^-$	(7.8 ±2.6) $\times 10^{-6}$	
Γ_{17}	$\pi^+\pi^-\pi^0$	(2.01 ±0.17) $\times 10^{-4}$	S=1.7
Γ_{18}	$\rho(770)\pi \to \pi^+\pi^-\pi^0$	(3.2 ±1.2) $\times 10^{-5}$	S=1.8
Γ_{19}	$\rho(2150)\pi \to \pi^+\pi^-\pi^0$	(1.9 $^{+1.2}_{-0.4}$) $\times 10^{-4}$	
Γ_{20}	$2(\pi^+\pi^-)$	(2.4 ±0.6) $\times 10^{-4}$	S=2.2
Γ_{21}	$\rho^0\pi^+\pi^-$	(2.2 ±0.6) $\times 10^{-4}$	S=1.4
Γ_{22}	$2(\pi^+\pi^-)\pi^0$	(2.9 ±1.0) $\times 10^{-3}$	S=4.7
Γ_{23}	$\rho a_2(1320)$	(2.6 ±0.9) $\times 10^{-4}$	
Γ_{24}	$\pi^+\pi^-\pi^0\pi^0\pi^0$	(5.3 ±0.9) $\times 10^{-3}$	
Γ_{25}	$\pi^+\pi^-4\pi^0$	(1.4 ±1.0) $\times 10^{-3}$	
Γ_{26}	$\rho^\pm\pi^\mp\pi^0\pi^0$	< 2.7 $\times 10^{-3}$	CL=90%
Γ_{27}	$3(\pi^+\pi^-)$	(3.5 ±2.0) $\times 10^{-4}$	S=2.8
Γ_{28}	$2(\pi^+\pi^-\pi^0)$	(4.8 ±1.5) $\times 10^{-3}$	
Γ_{29}	$3(\pi^+\pi^-)\pi^0$	(3.5 ±1.6) $\times 10^{-3}$	
Γ_{30}	$2(\pi^+\pi^-)3\pi^0$	(1.42 ±0.31) %	
Γ_{31}	$\eta\pi^+\pi^-$	< 1.6 $\times 10^{-4}$	CL=90%
Γ_{32}	$\eta\pi^+\pi^-\pi^0$	(9.5 ±1.7) $\times 10^{-4}$	
Γ_{33}	$\eta 2(\pi^+\pi^-)$	(1.2 ±0.6) $\times 10^{-3}$	
Γ_{34}	$\eta\pi^+\pi^-\pi^0\pi^0$	< 4 $\times 10^{-4}$	CL=90%
Γ_{35}	$\eta\pi^+\pi^-3\pi^0$	< 2.1 $\times 10^{-3}$	CL=90%
Γ_{36}	$\eta 2(\pi^+\pi^-\pi^0)$	< 2.1 $\times 10^{-3}$	CL=90%
Γ_{37}	$\rho\eta$	(2.2 ±0.6) $\times 10^{-5}$	S=1.1
Γ_{38}	$\eta'\pi^+\pi^-\pi^0$	(4.5 ±2.1) $\times 10^{-4}$	
Γ_{39}	$\eta'\rho$	(1.9 $^{+1.7}_{-1.2}$) $\times 10^{-5}$	
Γ_{40}	$\omega\pi^0$	(2.1 ±0.6) $\times 10^{-5}$	
Γ_{41}	$\omega\pi^+\pi^-$	(7.3 ±1.2) $\times 10^{-4}$	S=2.1
Γ_{42}	$\omega\pi^+\pi^-2\pi^0$	(8.7 ±2.4) $\times 10^{-3}$	
Γ_{43}	$b_1^\pm\pi^\mp$	(4.0 ±0.6) $\times 10^{-4}$	S=1.1
Γ_{44}	$\omega f_2(1270)$	(2.2 ±0.4) $\times 10^{-4}$	
Γ_{45}	$\omega\pi^0\pi^0$	(1.11 ±0.35) $\times 10^{-3}$	
Γ_{46}	$\omega 3\pi^0$	< 8 $\times 10^{-4}$	CL=90%
Γ_{47}	$b_1^0\pi^0$	(2.4 ±0.6) $\times 10^{-4}$	
Γ_{48}	$\omega\eta$	< 1.1 $\times 10^{-5}$	CL=90%
Γ_{49}	$\omega\eta'$	(3.2 $^{+2.5}_{-2.1}$) $\times 10^{-5}$	
Γ_{50}	$\phi\pi^0$	< 4 $\times 10^{-7}$	CL=90%
Γ_{51}	$\phi\pi^+\pi^-$	(1.18 ±0.26) $\times 10^{-4}$	S=1.5
Γ_{52}	$\phi f_0(980) \to \pi^+\pi^-$	(7.5 ±3.3) $\times 10^{-5}$	S=1.6
Γ_{53}	$\phi\eta$	(3.10 ±0.31) $\times 10^{-5}$	
Γ_{54}	$\eta\phi(2170)$, $\phi(2170) \to \phi f_0(980)$, $f_0 \to \pi^+\pi^-$	< 2.2 $\times 10^{-6}$	CL=90%
Γ_{55}	$\phi\eta'$	(1.54 ±0.20) $\times 10^{-5}$	
Γ_{56}	$\phi f_1(1285)$	(3.0 ±1.3) $\times 10^{-5}$	
Γ_{57}	$\phi\eta(1405) \to \phi\pi^+\pi^-\eta$	(8.5 ±1.7) $\times 10^{-6}$	
Γ_{58}	$\phi f_2'(1525)$	(4.4 ±1.6) $\times 10^{-5}$	
Γ_{59}	K^+K^-	(7.5 ±0.5) $\times 10^{-5}$	
Γ_{60}	$K^+K^-\pi^+$	(7.3 ±0.5) $\times 10^{-4}$	
Γ_{61}	$K^+K^-\pi^0$	(4.07 ±0.31) $\times 10^{-5}$	
Γ_{62}	$K^0_S K^0_S$	< 4.6 $\times 10^{-6}$	
Γ_{63}	$K^0_S K^0_L$	(5.34 ±0.33) $\times 10^{-5}$	
Γ_{64}	$K^0_S K^0_L \pi^0$	< 3.0 $\times 10^{-4}$	CL=90%
Γ_{65}	$K^+K^-\pi^0\pi^0$	(2.6 ±1.3) $\times 10^{-4}$	
Γ_{66}	$K^+K^-\pi^+\pi^-\pi^0$	(1.26 ±0.09) $\times 10^{-3}$	
Γ_{67}	$\omega f_0(1710) \to \omega K^+K^-$	(5.9 ±2.2) $\times 10^{-5}$	
Γ_{68}	$K^*(892)^0 K^-\pi^+\pi^0$ + c.c.	(8.6 ±2.2) $\times 10^{-4}$	
Γ_{69}	$K^*(892)^+ K^-\pi^+\pi^-$ + c.c.	(9.6 ±2.8) $\times 10^{-4}$	
Γ_{70}	$K^*(892)^+ K^-\rho^0$ + c.c.	(7.3 ±2.6) $\times 10^{-4}$	
Γ_{71}	$K^*(892)^0 K^-\rho^+$ + c.c.	(6.1 ±1.8) $\times 10^{-4}$	
Γ_{72}	$K^0_S K^0_S \pi^+\pi^-$	(2.2 ±0.4) $\times 10^{-4}$	
Γ_{73}	$K^0_S K^0_L \pi^0\pi^0$	(1.3 ±0.6) $\times 10^{-3}$	
Γ_{74}	$K^0_S K^0_L \eta$	(1.3 ±0.5) $\times 10^{-3}$	
Γ_{75}	$K^+K^-\rho^0$	(2.2 ±0.4) $\times 10^{-4}$	
Γ_{76}	$K^*(892)^0 \overline{K}^*_2(1430)^0$	(1.9 ±0.5) $\times 10^{-4}$	
Γ_{77}	$K^+K^-\pi^+\pi^-\eta$	(1.3 ±0.7) $\times 10^{-3}$	
Γ_{78}	$K^+K^-2(\pi^+\pi^-)$	(1.9 ±0.9) $\times 10^{-3}$	
Γ_{79}	$K^+K^-2(\pi^+\pi^-)\pi^0$	(1.00 ±0.31) $\times 10^{-3}$	
Γ_{80}	$K^+K^*(892)^-$ + c.c.	(2.9 ±0.4) $\times 10^{-5}$	S=1.2
Γ_{81}	$2(K^+K^-)$	(6.3 ±1.3) $\times 10^{-5}$	
Γ_{82}	$2(K^+K^-)\pi^0$	(1.10 ±0.28) $\times 10^{-4}$	
Γ_{83}	$K^+K^-\phi$	(7.0 ±1.6) $\times 10^{-5}$	
Γ_{84}	$K_1(1270)^\pm K^\mp$	(1.00 ±0.28) $\times 10^{-3}$	
Γ_{85}	$K^+\overline{K}^*(892)^0\pi^-$ + c.c.	(6.7 ±2.5) $\times 10^{-4}$	
Γ_{86}	ηK^+K^-, no $\eta\phi$	(3.49 ±0.17) $\times 10^{-5}$	

Downloaded from https://academic.oup.com/ptep/article/2022/8/083C01/6651666 by KIT Library user on 27 September 2022

Γ_{87}	$X(1750)\eta \to K^+K^-\eta$	$(4.8 \pm 2.8) \times 10^{-6}$	
Γ_{88}	$K_1(1400)^\pm K^\mp$	$< 3.1 \times 10^{-4}$	CL=90%
Γ_{89}	$K_2^*(1430)^\pm K^\mp$	$(7.1 {}^{+1.3}_{-0.9}) \times 10^{-5}$	
Γ_{90}	$K^*(892)^0\overline{K}^0 +$ c.c.	$(1.09 \pm 0.20) \times 10^{-4}$	
Γ_{91}	ωK^+K^-	$(1.62 \pm 0.11) \times 10^{-4}$	S=1.1
Γ_{92}	$\omega K^0_S K^0_S$	$(7.0 \pm 0.5) \times 10^{-5}$	
Γ_{93}	$\omega K^*(892)^+K^-+$ c.c.	$(2.07 \pm 0.26) \times 10^{-4}$	
Γ_{94}	$\omega K_2^*(1430)^+K^-+$ c.c.	$(6.1 \pm 1.2) \times 10^{-5}$	
Γ_{95}	$\omega\overline{K}^*(892)^0K^0$	$(1.68 \pm 0.30) \times 10^{-4}$	
Γ_{96}	$\omega\overline{K}_2^*(1430)^0K^0$	$(5.8 \pm 2.2) \times 10^{-5}$	
Γ_{97}	$\omega X(1440) \to \omega K^0_S K^-\pi^+ +$ c.c.	$(1.6 \pm 0.4) \times 10^{-5}$	
Γ_{98}	$\omega X(1440) \to \omega K^+K^-\pi^0$	$(1.09 \pm 0.26) \times 10^{-5}$	
Γ_{99}	$\omega f_1(1285) \to \omega K^0_S K^-\pi^+ +$ c.c.	$(3.0 \pm 1.0) \times 10^{-6}$	
Γ_{100}	$\omega f_1(1285) \to \omega K^+K^-\pi^0$	$(1.2 \pm 0.7) \times 10^{-6}$	
Γ_{101}	$p\overline{p}$	$(2.94 \pm 0.08) \times 10^{-4}$	
Γ_{102}	$n\overline{n}$	$(3.06 \pm 0.15) \times 10^{-4}$	
Γ_{103}	$p\overline{p}\pi^0$	$(1.53 \pm 0.07) \times 10^{-4}$	
Γ_{104}	$N(940)\overline{p}+$ c.c. $\to p\overline{p}\pi^0$	$(6.4 {}^{+1.8}_{-1.3}) \times 10^{-5}$	
Γ_{105}	$N(1440)\overline{p}+$ c.c. $\to p\overline{p}\pi^0$	$(7.3 {}^{+1.7}_{-1.5}) \times 10^{-5}$	S=2.5
Γ_{106}	$N(1520)\overline{p}+$ c.c. $\to p\overline{p}\pi^0$	$(6.4 {}^{+2.3}_{-1.8}) \times 10^{-6}$	
Γ_{107}	$N(1535)\overline{p}+$ c.c. $\to p\overline{p}\pi^0$	$(2.5 \pm 1.0) \times 10^{-5}$	
Γ_{108}	$N(1650)\overline{p}+$ c.c. $\to p\overline{p}\pi^0$	$(3.8 {}^{+1.4}_{-1.7}) \times 10^{-5}$	
Γ_{109}	$N(1720)\overline{p}+$ c.c. $\to p\overline{p}\pi^0$	$(1.79 {}^{+0.26}_{-0.70}) \times 10^{-5}$	
Γ_{110}	$N(2300)\overline{p}+$ c.c. $\to p\overline{p}\pi^0$	$(2.6 {}^{+1.2}_{-0.7}) \times 10^{-5}$	
Γ_{111}	$N(2570)\overline{p}+$ c.c. $\to p\overline{p}\pi^0$	$(2.13 {}^{+0.40}_{-0.31}) \times 10^{-5}$	
Γ_{112}	$p\overline{p}\pi^+\pi^-$	$(6.0 \pm 0.4) \times 10^{-4}$	
Γ_{113}	$p\overline{p}K^+K^-$	$(2.7 \pm 0.7) \times 10^{-5}$	
Γ_{114}	$p\overline{p}\eta$	$(6.0 \pm 0.4) \times 10^{-5}$	
Γ_{115}	$N(1535)\overline{p}+$ c.c. $\to p\overline{p}\eta$	$(4.5 {}^{+0.7}_{-0.6}) \times 10^{-5}$	
Γ_{116}	$p\overline{p}\pi^+\pi^-\pi^0$	$(7.3 \pm 0.7) \times 10^{-4}$	
Γ_{117}	$p\overline{p}\rho^0$	$(5.0 \pm 2.2) \times 10^{-5}$	
Γ_{118}	$p\overline{p}\omega$	$(6.9 \pm 2.1) \times 10^{-5}$	
Γ_{119}	$p\overline{p}\eta'$	$(1.10 \pm 0.13) \times 10^{-5}$	
Γ_{120}	$p\overline{p}\phi$	$(6.1 \pm 0.6) \times 10^{-6}$	
Γ_{121}	$\phi X(1835) \to p\overline{p}\phi$	$< 1.82 \times 10^{-7}$	CL=90%
Γ_{122}	$p\overline{n}\pi^-$ or c.c.	$(2.48 \pm 0.17) \times 10^{-4}$	
Γ_{123}	$p\overline{n}\pi^-\pi^0$	$(3.2 \pm 0.7) \times 10^{-4}$	
Γ_{124}	$\Lambda\overline{\Lambda}$	$(3.81 \pm 0.13) \times 10^{-4}$	S=1.4
Γ_{125}	$\Lambda\overline{\Lambda}\pi^0$	$< 2.9 \times 10^{-6}$	CL=90%
Γ_{126}	$\Lambda\overline{\Lambda}\eta$	$(2.5 \pm 0.4) \times 10^{-5}$	
Γ_{127}	$\Lambda\overline{\Lambda}\pi^+\pi^-$	$(2.8 \pm 0.6) \times 10^{-4}$	
Γ_{128}	$\Lambda\overline{p}K^+$	$(1.00 \pm 0.14) \times 10^{-4}$	
Γ_{129}	$\Lambda\overline{p}K^*(892)^+ +$ c.c.	$(6.3 \pm 0.7) \times 10^{-5}$	
Γ_{130}	$\Lambda\overline{p}K^+\pi^+\pi^-$	$(1.8 \pm 0.4) \times 10^{-4}$	
Γ_{131}	$\overline{\Lambda}nK^0_S +$ c.c.	$(8.1 \pm 1.8) \times 10^{-5}$	
Γ_{132}	$\Delta^{++}\overline{\Delta}^{--}$	$(1.28 \pm 0.35) \times 10^{-4}$	
Γ_{133}	$\Lambda\overline{\Sigma}^+\pi^- +$ c.c.	$(1.40 \pm 0.13) \times 10^{-4}$	
Γ_{134}	$\Lambda\overline{\Sigma}^-\pi^+ +$ c.c.	$(1.54 \pm 0.14) \times 10^{-4}$	
Γ_{135}	$\Lambda\overline{\Sigma}^0 +$ c.c.	$(1.6 \pm 0.7) \times 10^{-6}$	
Γ_{136}	$\Lambda\overline{\Sigma}^0$		
Γ_{137}	$\Sigma^0\overline{p}K^+ +$ c.c.	$(1.67 \pm 0.18) \times 10^{-5}$	
Γ_{138}	$\Sigma^+\overline{\Sigma}^-$	$(2.43 \pm 0.10) \times 10^{-4}$	S=1.4
Γ_{139}	$\Sigma^0\overline{\Sigma}^0$	$(2.35 \pm 0.09) \times 10^{-4}$	S=1.1
Γ_{140}	$\Sigma(1385)^+\overline{\Sigma}(1385)^-$	$(8.5 \pm 0.7) \times 10^{-5}$	
Γ_{141}	$\Sigma(1385)^-\overline{\Sigma}(1385)^+$	$(8.5 \pm 0.8) \times 10^{-5}$	
Γ_{142}	$\Sigma(1385)^0\overline{\Sigma}(1385)^0$	$(6.9 \pm 0.7) \times 10^{-5}$	
Γ_{143}	$\Xi^-\overline{\Xi}^+$	$(2.87 \pm 0.11) \times 10^{-4}$	S=1.1
Γ_{144}	$\Xi^0\overline{\Xi}^0$	$(2.3 \pm 0.4) \times 10^{-4}$	S=4.2
Γ_{145}	$\Xi(1530)^0\overline{\Xi}(1530)^0$	$(6.8 \pm 0.4) \times 10^{-5}$	
Γ_{146}	$\Lambda\overline{\Xi}^+K^- +$ c.c.	$(3.9 \pm 0.4) \times 10^{-5}$	
Γ_{147}	$\Xi(1530)^-\overline{\Xi}(1530)^+$	$(1.15 \pm 0.07) \times 10^{-4}$	
Γ_{148}	$\Xi(1530)^-\overline{\Xi}^+$	$(7.0 \pm 1.2) \times 10^{-6}$	
Γ_{149}	$\Xi(1530)^0\overline{\Xi}^0$	$(5.3 \pm 0.5) \times 10^{-6}$	
Γ_{150}	$\Xi(1690)^-\overline{\Xi}^+ \to K^-\Lambda\overline{\Xi}^+ +$ c.c.	$(5.2 \pm 1.6) \times 10^{-6}$	
Γ_{151}	$\Xi(1820)^-\overline{\Xi}^+ \to K^-\Lambda\overline{\Xi}^+ +$ c.c.	$(1.20 \pm 0.32) \times 10^{-5}$	
Γ_{152}	$\Sigma^0\overline{\Xi}^+K^- +$ c.c.	$(3.7 \pm 0.4) \times 10^{-5}$	
Γ_{153}	$\Omega^-\overline{\Omega}^+$	$(5.66 \pm 0.30) \times 10^{-5}$	S=1.3
Γ_{154}	$\eta_c\pi^+\pi^-\pi^0$	$< 1.0 \times 10^{-3}$	CL=90%
Γ_{155}	$h_c(1P)\pi^0$	$(8.6 \pm 1.3) \times 10^{-4}$	
Γ_{156}	$\Lambda_c^+\overline{p}e^+e^-+$ c.c.	$< 1.7 \times 10^{-6}$	CL=90%
Γ_{157}	$\Theta(1540)\overline{\Theta}(1540) \to K^0_S pK^-\overline{n}+$ c.c.	[a] $< 8.8 \times 10^{-6}$	CL=90%
Γ_{158}	$\Theta(1540)K^-\overline{n} \to K^0_S pK^-\overline{n}$	[a] $< 1.0 \times 10^{-5}$	CL=90%
Γ_{159}	$\Theta(1540)K^0_S\overline{p} \to K^0_S\overline{p}K^+n$	[a] $< 7.0 \times 10^{-6}$	CL=90%
Γ_{160}	$\overline{\Theta}(1540)K^+n \to K^0_S\overline{p}K^+n$	[a] $< 2.6 \times 10^{-5}$	CL=90%
Γ_{161}	$\overline{\Theta}(1540)K^0_S p \to K^0_S pK^-\overline{n}$	[a] $< 6.0 \times 10^{-6}$	CL=90%
	Radiative decays		
Γ_{162}	$\gamma\chi_{c0}(1P)$	(9.79 ± 0.20) %	
Γ_{163}	$\gamma\chi_{c1}(1P)$	(9.75 ± 0.24) %	
Γ_{164}	$\gamma\chi_{c2}(1P)$	(9.52 ± 0.20) %	
Γ_{165}	$\gamma\eta_c(1S)$	$(3.4 \pm 0.5) \times 10^{-3}$	S=1.3
Γ_{166}	$\gamma\eta_c(2S)$	$(7 \pm 5) \times 10^{-4}$	
Γ_{167}	$\gamma\pi^0$	$(1.04 \pm 0.22) \times 10^{-6}$	S=1.4
Γ_{168}	$\gamma 2(\pi^+\pi^-)$	$(4.0 \pm 0.6) \times 10^{-4}$	
Γ_{169}	$\gamma 3(\pi^+\pi^-)$	$< 1.7 \times 10^{-4}$	CL=90%
Γ_{170}	$\gamma\eta'(958)$	$(1.24 \pm 0.04) \times 10^{-4}$	
Γ_{171}	$\gamma f_2(1270)$	$(2.73 {}^{+0.29}_{-0.25}) \times 10^{-4}$	S=1.8
Γ_{172}	$\gamma f_0(1370) \to \gamma K\overline{K}$	$(3.1 \pm 1.7) \times 10^{-5}$	
Γ_{173}	$\gamma f_0(1500)$	$(9.3 \pm 1.9) \times 10^{-5}$	
Γ_{174}	$\gamma f'_2(1525)$	$(3.3 \pm 0.8) \times 10^{-5}$	
Γ_{175}	$\gamma f_0(1710)$		
Γ_{176}	$\gamma f_0(1710) \to \gamma\pi\pi$	$(3.5 \pm 0.6) \times 10^{-5}$	
Γ_{177}	$\gamma f_0(1710) \to \gamma K\overline{K}$	$(6.6 \pm 0.7) \times 10^{-5}$	
Γ_{178}	$\gamma f_0(2100) \to \gamma\pi\pi$	$(4.8 \pm 1.0) \times 10^{-6}$	
Γ_{179}	$\gamma f_0(2200) \to \gamma K\overline{K}$	$(3.2 \pm 1.0) \times 10^{-6}$	
Γ_{180}	$\gamma f_J(2220) \to \gamma\pi\pi$	$< 5.8 \times 10^{-6}$	CL=90%
Γ_{181}	$\gamma f_J(2220) \to \gamma K\overline{K}$	$< 9.5 \times 10^{-6}$	CL=90%
Γ_{182}	$\gamma\eta$	$(9.2 \pm 1.8) \times 10^{-7}$	
Γ_{183}	$\gamma\eta\pi^+\pi^-$	$(8.7 \pm 2.1) \times 10^{-4}$	
Γ_{184}	$\gamma\eta(1405)$		
Γ_{185}	$\gamma\eta(1405) \to \gamma K\overline{K}\pi$	$< 9 \times 10^{-5}$	CL=90%
Γ_{186}	$\gamma\eta(1405) \to \gamma\eta\pi^+\pi^-$	$(3.6 \pm 2.5) \times 10^{-5}$	
Γ_{187}	$\gamma\eta(1405) \to \gamma f_0(980)\pi^0 \to \gamma\pi^+\pi^-\pi^0$	$< 5.0 \times 10^{-7}$	CL=90%
Γ_{188}	$\gamma\eta(1475)$		
Γ_{189}	$\gamma\eta(1475) \to \gamma K\overline{K}\pi$	$< 1.4 \times 10^{-4}$	CL=90%
Γ_{190}	$\gamma\eta(1475) \to \gamma\eta\pi^+\pi^-$	$< 8.8 \times 10^{-5}$	CL=90%
Γ_{191}	$\gamma K^{*0}K^+\pi^- +$ c.c.	$(3.7 \pm 0.9) \times 10^{-4}$	
Γ_{192}	$\gamma K^{*0}\overline{K}^{*0}$	$(2.4 \pm 0.7) \times 10^{-4}$	
Γ_{193}	$\gamma K^0_S K^+\pi^- +$ c.c.	$(2.6 \pm 0.5) \times 10^{-4}$	
Γ_{194}	$\gamma K^+K^-\pi^+\pi^-$	$(1.9 \pm 0.5) \times 10^{-4}$	
Γ_{195}	$\gamma K^+K^-2(\pi^+\pi^-)$	$< 2.2 \times 10^{-4}$	CL=90%
Γ_{196}	$\gamma 2(K^+K^-)$	$< 4 \times 10^{-5}$	CL=90%
Γ_{197}	$\gamma p\overline{p}$	$(3.9 \pm 0.5) \times 10^{-5}$	S=2.0
Γ_{198}	$\gamma f_2(1950) \to \gamma p\overline{p}$	$(1.20 \pm 0.22) \times 10^{-5}$	
Γ_{199}	$\gamma f_2(2150) \to \gamma p\overline{p}$	$(7.2 \pm 1.8) \times 10^{-6}$	
Γ_{200}	$\gamma X(1835) \to \gamma p\overline{p}$	$(4.6 {}^{+1.8}_{-4.0}) \times 10^{-6}$	
Γ_{201}	$\gamma X \to \gamma p\overline{p}$	[b] $< 2 \times 10^{-6}$	CL=90%
Γ_{202}	$\gamma p\overline{p}\pi^+\pi^-$	$(2.8 \pm 1.4) \times 10^{-5}$	
Γ_{203}	$\gamma\gamma$	$< 1.5 \times 10^{-4}$	CL=90%
Γ_{204}	$\gamma\gamma J/\psi$	$(3.1 {}^{+1.0}_{-1.2}) \times 10^{-4}$	
Γ_{205}	$e^+e^-\eta'$	$(1.90 \pm 0.26) \times 10^{-6}$	
Γ_{206}	$e^+e^-\chi_{c0}(1P)$	$(1.06 \pm 0.24) \times 10^{-3}$	
Γ_{207}	$e^+e^-\chi_{c1}(1P)$	$(8.5 \pm 0.6) \times 10^{-4}$	
Γ_{208}	$e^+e^-\chi_{c2}(1P)$	$(7.0 \pm 0.8) \times 10^{-4}$	
	Weak decays		
Γ_{209}	$D^0e^+e^-+$ c.c.	$< 1.4 \times 10^{-7}$	CL=90%
	Other decays		
Γ_{210}	invisible	< 1.6 %	CL=90%

[a] $\Theta(1540)$ is a hypothetical pentaquark state of 1.54 GeV/c^2 mass and a width of less than 25 MeV/c^2.

[b] For a narrow resonance in the range $2.2 < M(X) < 2.8$ GeV.

Downloaded from https://academic.oup.com/ptep/article/2022/8/083C01/6651666 by KIT Library user on 27 September 2022

CONSTRAINED FIT INFORMATION

A multiparticle fit to $\chi_{c1}(1P)$, $\chi_{c0}(1P)$, $\chi_{c2}(1P)$, and $\psi(2S)$ with 4 total widths, a partial width, 25 combinations of partial widths obtained from integrated cross section, and 84 branching ratios uses 248 measurements to determine 49 parameters. The overall fit has a $\chi^2 = 379.8$ for 199 degrees of freedom.

The following *off-diagonal* array elements are the correlation coefficients $\langle \delta p_i \delta p_j \rangle / (\delta p_i \cdot \delta p_j)$, in percent, from the fit to parameters p_i, including the branching fractions, $x_i \equiv \Gamma_i/\Gamma_{total}$.

	x_7	x_8	x_9	x_{12}	x_{13}	x_{14}	x_{101}	x_{162}	x_{163}	x_{164}
x_8	3									
x_9	1	0								
x_{12}	29	11	2							
x_{13}	28	6	1	48						
x_{14}	13	4	1	36	15					
x_{101}	0	0	0	4	3	2				
x_{162}	1	0	0	2	1	1	0			
x_{163}	1	0	0	2	1	1	0	0		
x_{164}	1	0	0	3	1	1	0	0	0	
Γ	−81	−4	−1	−38	−34	−16	−7	−1	−1	−1

$\psi(2S)$ PARTIAL WIDTHS

Γ(hadrons) — Γ_1

VALUE (keV)	DOCUMENT ID		TECN	COMMENT
• • • We do not use the following data for averages, fits, limits, etc. • • •				
258±26	BAI	02B	BES2	e^+e^-
224±56	LUTH	75	MRK1	e^+e^-

$\Gamma(e^+e^-)$ — Γ_7

VALUE (keV)	DOCUMENT ID		TECN	COMMENT
2.33 ±0.04 OUR FIT				
2.29 ±0.06 OUR AVERAGE				
2.23 ±0.10 ±0.02	[1] ABLIKIM	15V	BES3	4.0–4.4 $e^+e^- \to \pi^+\pi^- J/\psi$
2.338±0.037±0.096	ABLIKIM	08B	BES2	$e^+e^- \to$ hadrons
2.330±0.036±0.110	ABLIKIM	06L	BES2	$e^+e^- \to$ hadrons
2.44 ±0.21	[2] BAI	02B	BES2	e^+e^-
2.14 ±0.21	ALEXANDER	89	RVUE	See Υ mini-review
• • • We do not use the following data for averages, fits, limits, etc. • • •				
2.279±0.015±0.042	[3] ANASHIN	18	KEDR	e^+e^-
2.282±0.015±0.042	[4] ANASHIN	18	KEDR	e^+e^-
2.0 ±0.3	BRANDELIK	79C	DASP	e^+e^-
2.1 ±0.3	[5] LUTH	75	MRK1	e^+e^-

[1] ABLIKIM 15V reports 2.213 ± 0.018 ± 0.099 keV from a measurement of $[\Gamma(\psi(2S) \to e^+e^-)] \times [B(\psi(2S) \to J/\psi(1S)\pi^+\pi^-)]$ assuming $B(\psi(2S) \to J/\psi(1S)\pi^+\pi^-) = (34.95 \pm 0.45)\times 10^{-2}$, which we rescale to our best value $B(\psi(2S) \to J/\psi(1S)\pi^+\pi^-) = (34.68 \pm 0.30)\times 10^{-2}$. Our first error is their experiment's error and our second error is the systematic error from using our best value.

[2] From a simultaneous fit to e^+e^-, $\mu^+\mu^-$, and hadronic channel, assuming $\Gamma_e = \Gamma_\mu = \Gamma_\tau/0.38847$.

[3] Combining $\Gamma_{e^+e^-} \cdot B(\mu^+\mu^-)$ from ANASHIN 18 with $\Gamma_{e^+e^-} \cdot B$(hadrons) from ANASHIN 12 and assuming lepton universality.

[4] From the sum of $\Gamma_{e^+e^-} \cdot B$(hadrons) from ANASHIN 12, $\Gamma_{e^+e^-} \cdot B(e^+e^-)$ and $\Gamma_{e^+e^-} \cdot B(\mu^+\mu^-)$ from ANASHIN 18, and $\Gamma_{e^+e^-} \cdot B(\tau^+\tau^-)$ from ANASHIN 07.

[5] From a simultaneous fit to e^+e^-, $\mu^+\mu^-$, and hadronic channels assuming $\Gamma(e^+e^-) = \Gamma(\mu^+\mu^-)$.

$\Gamma(\gamma\gamma)$ — Γ_{203}

VALUE (eV)	CL%	DOCUMENT ID		TECN	COMMENT
<43	90	BRANDELIK	79C	DASP	e^+e^-

$\psi(2S)$ $\Gamma(i)\Gamma(e^+e^-)/\Gamma$(total)

This combination of a partial width with the partial width into e^+e^- and with the total width is obtained from the integrated cross section into channel(i) in the e^+e^- annihilation. We list only data that have not been used to determine the partial width $\Gamma(i)$ or the branching ratio $\Gamma(i)/$total.

Γ(hadrons) × $\Gamma(e^+e^-)/\Gamma_{total}$ — $\Gamma_1\Gamma_7/\Gamma$

VALUE (keV)	DOCUMENT ID		TECN	COMMENT
2.233±0.015±0.042	[1] ANASHIN	12	KEDR	$e^+e^- \to$ hadrons
• • • We do not use the following data for averages, fits, limits, etc. • • •				
2.2 ±0.4	ABRAMS	75	MRK1	e^+e^-

[1] ANASHIN 12 reports the value 2.233 ± 0.015 ± 0.037 ± 0.020 keV, where the third uncertainty is due to assumptions on the interference between the resonance and hadronic continuum. We combined the two systematic uncertainties.

$\Gamma(K^0_S$anything$)$ × $\Gamma(e^+e^-)/\Gamma_{total}$ — $\Gamma_6\Gamma_7/\Gamma$

VALUE (keV)	DOCUMENT ID		TECN	COMMENT
0.3738±0.0067±0.0200	ABLIKIM	21S	BES3	$e^+e^- \to K^0_S$ anything

$\Gamma(e^+e^-)$ × $\Gamma(e^+e^-)/\Gamma_{total}$ — $\Gamma_7\Gamma_7/\Gamma$

VALUE (eV)	DOCUMENT ID		TECN	COMMENT
21.2±0.7±1.2	[1] ANASHIN	18	KEDR	e^+e^-

[1] From the average of nine scans of the $\psi(2S)$.

$\Gamma(\mu^+\mu^-)$ × $\Gamma(e^+e^-)/\Gamma_{total}$ — $\Gamma_8\Gamma_7/\Gamma$

VALUE (eV)	DOCUMENT ID		TECN	COMMENT
19.3±0.3±0.5	[1] ANASHIN	18	KEDR	$\psi(2S) \to \mu^+\mu^-$

[1] From the average of nine scans of the $\psi(2S)$.

$\Gamma(\tau^+\tau^-)$ × $\Gamma(e^+e^-)/\Gamma_{total}$ — $\Gamma_9\Gamma_7/\Gamma$

VALUE (eV)	EVTS	DOCUMENT ID		TECN	COMMENT
• • • We do not use the following data for averages, fits, limits, etc. • • •					
9.0±2.6	79	[1] ANASHIN	07	KEDR	$e^+e^- \to \psi(2S) \to \tau^+\tau^-$

[1] Using $\psi(2S)$ total width of 337 ± 13 keV. Systematic errors not evaluated.

$\Gamma(J/\psi(1S)\pi^+\pi^-)$ × $\Gamma(e^+e^-)/\Gamma_{total}$ — $\Gamma_{12}\Gamma_7/\Gamma$

VALUE (keV)	EVTS	DOCUMENT ID		TECN	COMMENT
0.808±0.013 OUR FIT					
0.837±0.025 OUR AVERAGE		Error includes scale factor of 1.3. See the ideogram below.			
0.837±0.028±0.005		[1] LEES	12E	BABR	10.6 $e^+e^- \to 2\pi^+2\pi^-\gamma$
0.852±0.010±0.026	19.5k	ADAM	06	CLEO	3.773 $e^+e^- \to \gamma\psi(2S)$
0.68 ±0.09		[2] BAI	98E	BES	e^+e^-
• • • We do not use the following data for averages, fits, limits, etc. • • •					
0.88 ±0.08 ±0.03	256	[3] AUBERT	07AU	BABR	10.6 $e^+e^- \to J/\psi\pi^+\pi^-\gamma$
0.755±0.048±0.004	544	[4] AUBERT	05D	BABR	10.6 $e^+e^- \to \pi^+\pi^-\mu^+\mu^-\gamma$

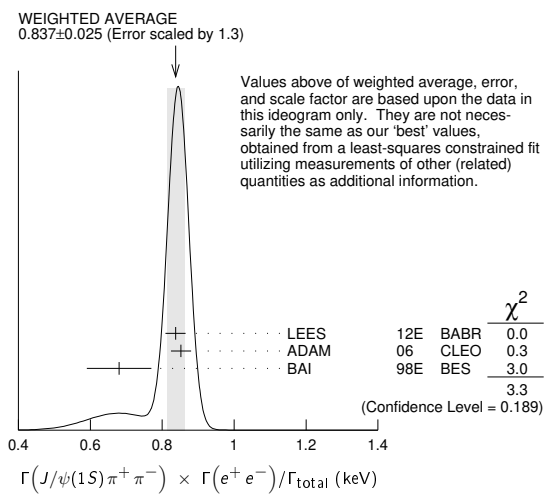

[1] LEES 12E reports $[\Gamma(\psi(2S) \to J/\psi(1S)\pi^+\pi^-) \times \Gamma(\psi(2S) \to e^+e^-)/\Gamma_{total}] \times [B(J/\psi(1S) \to \mu^+\mu^-)] = (49.9 \pm 1.3 \pm 1.0)\times 10^{-3}$ keV which we divide by our best value $B(J/\psi(1S) \to \mu^+\mu^-) = (5.961 \pm 0.033)\times 10^{-2}$. Our first error is their experiment's error and our second error is the systematic error from using our best value.

[2] The value of $\Gamma(e^+e^-)$ quoted in BAI 98E is derived using $B(\psi(2S) \to J/\psi(1S)\pi^+\pi^-) = (32.4 \pm 2.6)\times 10^{-2}$ and $B(J/\psi(1S) \to \ell^+\ell^-) = 0.1203 \pm 0.0038$. Recalculated by us using $B(J/\psi(1S) \to \ell^+\ell^-) = 0.1181 \pm 0.0020$.

[3] AUBERT 07AU reports $[\Gamma(\psi(2S) \to J/\psi(1S)\pi^+\pi^-) \times \Gamma(\psi(2S) \to e^+e^-)/\Gamma_{total}] \times [B(J/\psi(1S) \to \pi^+\pi^-\pi^0)] = 0.0186 \pm 0.0012 \pm 0.0011$ keV which we divide by our best value $B(J/\psi(1S) \to \pi^+\pi^-\pi^0) = (2.10 \pm 0.08)\times 10^{-2}$. Our first error is their experiment's error and our second error is the systematic error from using our best value.

[4] AUBERT 05D reports $[\Gamma(\psi(2S) \to J/\psi(1S)\pi^+\pi^-) \times \Gamma(\psi(2S) \to e^+e^-)/\Gamma_{total}] \times [B(J/\psi(1S) \to \mu^+\mu^-)] = 0.0450 \pm 0.0018 \pm 0.0022$ keV which we divide by our best value $B(J/\psi(1S) \to \mu^+\mu^-) = (5.961 \pm 0.033)\times 10^{-2}$. Our first error is their experiment's error and our second error is the systematic error from using our best value. Superseded by LEES 12E.

$\Gamma(J/\psi(1S)\pi^0\pi^0)$ × $\Gamma(e^+e^-)/\Gamma_{total}$ — $\Gamma_{13}\Gamma_7/\Gamma$

VALUE (keV)	EVTS	DOCUMENT ID		TECN	COMMENT
0.425±0.009 OUR FIT					
0.411±0.008±0.018	3.6k	ADAM	06	CLEO	3.773 $e^+e^- \to \gamma\psi(2S)$
• • • We do not use the following data for averages, fits, limits, etc. • • •					
0.48 ±0.09 ±0.02	142	[1] LEES	18E	BABR	10.6 $e^+e^- \to J/\psi\pi^0\pi^0\gamma$

[1] LEES 18E reports $[\Gamma(\psi(2S) \to J/\psi(1S)\pi^0\pi^0) \times \Gamma(\psi(2S) \to e^+e^-)/\Gamma_{total}] \times [B(J/\psi(1S) \to \pi^+\pi^-\pi^0)] = 0.0101 \pm 0.0015 \pm 0.0011$ keV which we divide by our best value $B(J/\psi(1S) \to \pi^+\pi^-\pi^0) = (2.10 \pm 0.08)\times 10^{-2}$. Our first error is their experiment's error and our second error is the systematic error from using our best value.

Downloaded from https://academic.oup.com/ptep/article/2022/8/083C01/6651666 by KIT Library user on 27 September 2022

$\Gamma(J/\psi(1S)\eta) \times \Gamma(e^+e^-)/\Gamma_{total}$ — $\Gamma_{14}\Gamma_7/\Gamma$

VALUE (eV)	EVTS	DOCUMENT ID		TECN	COMMENT
78.6± 1.6 OUR FIT					
87 ± 9 OUR AVERAGE					
83 ±25 ±5	14	[1] AUBERT	07AU	BABR	10.6 $e^+e^- \to J/\psi\pi^+\pi^-\pi^0\gamma$
88 ± 6 ±7	291 ± 24	ADAM	06	CLEO	3.773 $e^+e^- \to \gamma\psi(2S)$

[1] AUBERT 07AU quotes $\Gamma_{ee}^{\psi(2S)} \cdot B(\psi(2S) \to J/\psi\eta) \cdot B(J/\psi \to \mu^+\mu^-) \cdot B(\eta \to \pi^+\pi^-\pi^0) = 1.11 \pm 0.33 \pm 0.07$ eV.

$\Gamma(J/\psi(1S)\pi^0) \times \Gamma(e^+e^-)/\Gamma_{total}$ — $\Gamma_{15}\Gamma_7/\Gamma$

VALUE (eV)	CL%	EVTS	DOCUMENT ID		TECN	COMMENT
<8	90	<37	ADAM	06	CLEO	3.773 $e^+e^- \to \gamma\psi(2S)$

$\Gamma(2(\pi^+\pi^-)\pi^0) \times \Gamma(e^+e^-)/\Gamma_{total}$ — $\Gamma_{22}\Gamma_7/\Gamma$

VALUE (eV)	EVTS	DOCUMENT ID		TECN	COMMENT
29.7±2.2±1.8	410	AUBERT	07AU	BABR	10.6 $e^+e^- \to 2(\pi^+\pi^-)\pi^0\gamma$

$\Gamma(\pi^+\pi^-\pi^0\pi^0\pi^0) \times \Gamma(e^+e^-)/\Gamma_{total}$ — $\Gamma_{24}\Gamma_7/\Gamma$

VALUE (eV)	EVTS	DOCUMENT ID		TECN	COMMENT
12.4±1.8±1.2	177	LEES	18E	BABR	10.6 $e^+e^- \to \pi^+\pi^-3\pi^0\gamma$

$\Gamma(\pi^+\pi^-4\pi^0) \times \Gamma(e^+e^-)/\Gamma_{total}$ — $\Gamma_{25}\Gamma_7/\Gamma$

VALUE (eV)	EVTS	DOCUMENT ID		TECN	COMMENT
3.3±2.3±0.5	18	LEES	21C	BABR	$e^+e^- \to \gamma_{ISR}(\pi^+\pi^-4\pi^0)$

$\Gamma(\rho^\pm\pi^\mp\pi^0\pi^0) \times \Gamma(e^+e^-)/\Gamma_{total}$ — $\Gamma_{26}\Gamma_7/\Gamma$

VALUE (eV)	CL%	DOCUMENT ID		TECN	COMMENT
<6.2	90	LEES	18E	BABR	10.6 $e^+e^- \to \pi^+\pi^-3\pi^0\gamma$

$\Gamma(2(\pi^+\pi^-\pi^0)) \times \Gamma(e^+e^-)/\Gamma_{total}$ — $\Gamma_{28}\Gamma_7/\Gamma$

VALUE (eV)	EVTS	DOCUMENT ID		TECN	COMMENT
11.2±3.3±1.3	43	AUBERT	06D	BABR	10.6 $e^+e^- \to 2(\pi^+\pi^-\pi^0)\gamma$

$\Gamma(2(\pi^+\pi^-)3\pi^0) \times \Gamma(e^+e^-)/\Gamma_{total}$ — $\Gamma_{30}\Gamma_7/\Gamma$

VALUE (eV)	EVTS	DOCUMENT ID		TECN	COMMENT
33±5±5	14k	LEES	21	BABR	10.6 $e^+e^- \to 2(\pi^+\pi^-)3\pi^0\gamma$

$\Gamma(\eta 2(\pi^+\pi^-)) \times \Gamma(e^+e^-)/\Gamma_{total}$ — $\Gamma_{33}\Gamma_7/\Gamma$

VALUE (eV)	CL%	EVTS	DOCUMENT ID		TECN	COMMENT
2.87±1.41±0.01		16	[1] AUBERT	07AU	BABR	10.6 $e^+e^- \to 2(\pi^+\pi^-)\eta\gamma$
• • • We do not use the following data for averages, fits, limits, etc. • • •						
<7	90	14k	[2] LEES	21	BABR	10.6 $e^+e^- \to 2(\pi^+\pi^-)3\pi^0\gamma$

[1] AUBERT 07AU reports $[\Gamma(\psi(2S) \to \eta 2(\pi^+\pi^-)) \times \Gamma(\psi(2S) \to e^+e^-)/\Gamma_{total}] \times [B(\eta \to 2\gamma)] = 1.13 \pm 0.55 \pm 0.08$ eV which we divide by our best value $B(\eta \to 2\gamma) = (39.36 \pm 0.18) \times 10^{-2}$. Our first error is their experiment's error and our second error is the systematic error from using our best value.

[2] LEES 21 reports $[\Gamma(\psi(2S) \to \eta 2(\pi^+\pi^-)) \times \Gamma(\psi(2S) \to e^+e^-)/\Gamma_{total}] \times [B(\eta \to 3\pi^0)] < 2.3$ eV which we divide by our best value $B(\eta \to 3\pi^0) = 32.57 \times 10^{-2}$.

$\Gamma(\eta\pi^+\pi^-\pi^0\pi^0) \times \Gamma(e^+e^-)/\Gamma_{total}$ — $\Gamma_{34}\Gamma_7/\Gamma$

VALUE (eV)	CL%	DOCUMENT ID		TECN	COMMENT
<0.85	90	LEES	18E	BABR	10.6 $e^+e^- \to \pi^+\pi^-\pi^0\pi^0\eta\gamma$

$\Gamma(\eta\pi^+\pi^-3\pi^0) \times \Gamma(e^+e^-)/\Gamma_{total}$ — $\Gamma_{35}\Gamma_7/\Gamma$

VALUE (eV)	CL%	DOCUMENT ID		TECN	COMMENT
<5	90	[1] LEES	21C	BABR	$e^+e^- \to \gamma_{ISR}(\pi^+\pi^-3\pi^0\gamma\gamma)$

[1] LEES 21C reports $[\Gamma(\psi(2S) \to \eta\pi^+\pi^-3\pi^0) \times \Gamma(\psi(2S) \to e^+e^-)/\Gamma_{total}] \times [B(\eta \to 2\gamma)] < 1.9$ eV which we divide by our best value $B(\eta \to 2\gamma) = 39.36 \times 10^{-2}$.

$\Gamma(\eta 2(\pi^+\pi^-\pi^0)) \times \Gamma(e^+e^-)/\Gamma_{total}$ — $\Gamma_{36}\Gamma_7/\Gamma$

VALUE (eV)	CL%	EVTS	DOCUMENT ID		TECN	COMMENT
<5	90	14k	[1] LEES	21	BABR	10.6 $e^+e^- \to 2(\pi^+\pi^-)3\pi^0\gamma$

[1] LEES 21 reports $[\Gamma(\psi(2S) \to \eta 2(\pi^+\pi^-\pi^0)) \times \Gamma(\psi(2S) \to e^+e^-)/\Gamma_{total}] \times [B(\eta \to 2\gamma)] < 1.9$ eV which we divide by our best value $B(\eta \to 2\gamma) = 39.36 \times 10^{-2}$.

$\Gamma(\omega\pi^+\pi^-) \times \Gamma(e^+e^-)/\Gamma_{total}$ — $\Gamma_{41}\Gamma_7/\Gamma$

VALUE (eV)	EVTS	DOCUMENT ID		TECN	COMMENT
3.01±0.84±0.02	37	[1] AUBERT	07AU	BABR	10.6 $e^+e^- \to \omega\pi^+\pi^-\gamma$

[1] AUBERT 07AU reports $[\Gamma(\psi(2S) \to \omega\pi^+\pi^-) \times \Gamma(\psi(2S) \to e^+e^-)/\Gamma_{total}] \times [B(\omega(782) \to \pi^+\pi^-\pi^0)] = 2.69 \pm 0.73 \pm 0.16$ eV which we divide by our best value $B(\omega(782) \to \pi^+\pi^-\pi^0) = (89.2 \pm 0.7) \times 10^{-2}$. Our first error is their experiment's error and our second error is the systematic error from using our best value.

$\Gamma(\omega\pi^+\pi^-2\pi^0) \times \Gamma(e^+e^-)/\Gamma_{total}$ — $\Gamma_{42}\Gamma_7/\Gamma$

VALUE (eV)	EVTS	DOCUMENT ID		TECN	COMMENT
20.2±5.6±0.1	14k	[1] LEES	21	BABR	10.6 $e^+e^- \to 2(\pi^+\pi^-)3\pi^0\gamma$

[1] LEES 21 reports $[\Gamma(\psi(2S) \to \omega\pi^+\pi^-2\pi^0) \times \Gamma(\psi(2S) \to e^+e^-)/\Gamma_{total}] \times [B(\omega(782) \to \pi^+\pi^-\pi^0)] = 18 \pm 4 \pm 3$ eV which we divide by our best value $B(\omega(782) \to \pi^+\pi^-\pi^0) = (89.2 \pm 0.7) \times 10^{-2}$. Our first error is their experiment's error and our second error is the systematic error from using our best value.

$\Gamma(\omega\pi^0\pi^0) \times \Gamma(e^+e^-)/\Gamma_{total}$ — $\Gamma_{45}\Gamma_7/\Gamma$

VALUE (eV)	EVTS	DOCUMENT ID		TECN	COMMENT
2.58±0.82±0.02	33	[1] LEES	18E	BABR	10.6 $e^+e^- \to \pi^+\pi^-3\pi^0\gamma$

[1] LEES 18E reports $[\Gamma(\psi(2S) \to \omega\pi^0\pi^0) \times \Gamma(\psi(2S) \to e^+e^-)/\Gamma_{total}] \times [B(\omega(782) \to \pi^+\pi^-\pi^0)] = 2.3 \pm 0.7 \pm 0.2$ eV which we divide by our best value $B(\omega(782) \to \pi^+\pi^-\pi^0) = (89.2 \pm 0.7) \times 10^{-2}$. Our first error is their experiment's error and our second error is the systematic error from using our best value.

$\Gamma(\omega 3\pi^0) \times \Gamma(e^+e^-)/\Gamma_{total}$ — $\Gamma_{46}\Gamma_7/\Gamma$

VALUE (eV)	CL%	DOCUMENT ID		TECN	COMMENT
<1.8	90	[1] LEES	21C	BABR	$e^+e^- \to \gamma_{ISR}(\pi^+\pi^-4\pi^0)$

[1] LEES 21C reports $[\Gamma(\psi(2S) \to \omega 3\pi^0) \times \Gamma(\psi(2S) \to e^+e^-)/\Gamma_{total}] \times [B(\omega(782) \to \pi^+\pi^-\pi^0)] < 1.6$ eV which we divide by our best value $B(\omega(782) \to \pi^+\pi^-\pi^0) = 89.2 \times 10^{-2}$.

$\Gamma(\phi\pi^+\pi^-) \times \Gamma(e^+e^-)/\Gamma_{total}$ — $\Gamma_{51}\Gamma_7/\Gamma$

VALUE (eV)	EVTS	DOCUMENT ID		TECN	COMMENT
0.55±0.19±0.01	19	[1] LEES	12F	BABR	10.6 $e^+e^- \to K^+K^-\pi^+\pi^-\gamma$
• • • We do not use the following data for averages, fits, limits, etc. • • •					
0.57±0.23±0.01	10	[2] AUBERT,BE	06D	BABR	10.6 $e^+e^- \to K^+K^-\pi^+\pi^-\gamma$

[1] LEES 12F reports $[\Gamma(\psi(2S) \to \phi\pi^+\pi^-) \times \Gamma(\psi(2S) \to e^+e^-)/\Gamma_{total}] \times [B(\phi(1020) \to K^+K^-)] = 0.27 \pm 0.09 \pm 0.02$ eV which we divide by our best value $B(\phi(1020) \to K^+K^-) = (49.1 \pm 0.5) \times 10^{-2}$. Our first error is their experiment's error and our second error is the systematic error from using our best value.

[2] Superseded by LEES 12F. AUBERT,BE 06D reports $[\Gamma(\psi(2S) \to \phi\pi^+\pi^-) \times \Gamma(\psi(2S) \to e^+e^-)/\Gamma_{total}] \times [B(\phi(1020) \to K^+K^-)] = 0.28 \pm 0.11 \pm 0.02$ eV which we divide by our best value $B(\phi(1020) \to K^+K^-) = (49.1 \pm 0.5) \times 10^{-2}$. Our first error is their experiment's error and our second error is the systematic error from using our best value.

$\Gamma(\phi f_0(980) \to \pi^+\pi^-) \times \Gamma(e^+e^-)/\Gamma_{total}$ — $\Gamma_{52}\Gamma_7/\Gamma$

VALUE (eV)	EVTS	DOCUMENT ID		TECN	COMMENT
0.346±0.129±0.004	12	[1] LEES	12F	BABR	10.6 $e^+e^- \to \pi^+\pi^-K^+K^-\gamma$
• • • We do not use the following data for averages, fits, limits, etc. • • •					
0.346±0.168±0.004	6 ± 3	[2] AUBERT	07AK	BABR	10.6 $e^+e^- \to \pi^+\pi^-K^+K^-\gamma$

[1] LEES 12F reports $[\Gamma(\psi(2S) \to \phi f_0(980) \to \pi^+\pi^-) \times \Gamma(\psi(2S) \to e^+e^-)/\Gamma_{total}] \times [B(\phi(1020) \to K^+K^-)] = 0.17 \pm 0.06 \pm 0.02$ eV which we divide by our best value $B(\phi(1020) \to K^+K^-) = (49.1 \pm 0.5) \times 10^{-2}$. Our first error is their experiment's error and our second error is the systematic error from using our best value.

[2] Superseded by LEES 12F. AUBERT 07AK reports $[\Gamma(\psi(2S) \to \phi f_0(980) \to \pi^+\pi^-) \times \Gamma(\psi(2S) \to e^+e^-)/\Gamma_{total}] \times [B(\phi(1020) \to K^+K^-)] = 0.17 \pm 0.08 \pm 0.02$ eV which we divide by our best value $B(\phi(1020) \to K^+K^-) = (49.1 \pm 0.5) \times 10^{-2}$. Our first error is their experiment's error and our second error is the systematic error from using our best value.

$\Gamma(K^+K^-) \times \Gamma(e^+e^-)/\Gamma_{total}$ — $\Gamma_{59}\Gamma_7/\Gamma$

VALUE (eV)	EVTS	DOCUMENT ID		TECN	COMMENT
• • • We do not use the following data for averages, fits, limits, etc. • • •					
0.147±0.035±0.005	66	[1] LEES	15J	BABR	$e^+e^- \to K^+K^-\gamma$
0.197±0.035±0.005	66	[2] LEES	15J	BABR	$e^+e^- \to K^+K^-\gamma$
0.35 ±0.14 ±0.03	11	[3] LEES	13Q	BABR	$e^+e^- \to K^+K^-\gamma$

[1] $\sin\phi > 0$.
[2] $\sin\phi < 0$.
[3] Interference with non-resonant K^+K^- production not taken into account.

$\Gamma(K^+K^-\pi^+) \times \Gamma(e^+e^-)/\Gamma_{total}$ — $\Gamma_{60}\Gamma_7/\Gamma$

VALUE (eV)	EVTS	DOCUMENT ID		TECN	COMMENT
1.92±0.30±0.06	133	LEES	12F	BABR	10.6 $e^+e^- \to \pi^+\pi^-K^+K^-\gamma$
• • • We do not use the following data for averages, fits, limits, etc. • • •					
2.56±0.42±0.16	85	[1] AUBERT	07AK	BABR	10.6 $e^+e^- \to \pi^+\pi^-K^+K^-\gamma$

[1] Superseded by LEES 12F.

$\Gamma(K^0_S K^0_L \pi^0) \times \Gamma(e^+e^-)/\Gamma_{total}$ — $\Gamma_{64}\Gamma_7/\Gamma$

VALUE (eV)	CL%	EVTS	DOCUMENT ID		TECN	COMMENT
<0.7	90	8	LEES	17A	BABR	$e^+e^- \to K^0_S K^0_L \pi^0\gamma$

$\Gamma(K^+K^-\pi^0\pi^0) \times \Gamma(e^+e^-)/\Gamma_{total}$ — $\Gamma_{65}\Gamma_7/\Gamma$

VALUE (eV)	EVTS	DOCUMENT ID		TECN	COMMENT
0.60±0.31±0.03	17	LEES	12F	BABR	10.6 $e^+e^- \to \pi^0\pi^0K^+K^-\gamma$

Downloaded from https://academic.oup.com/ptep/article/2022/8/083C01/6651666 by KIT Library user on 27 September 2022

$\Gamma(K^+K^-\pi^+\pi^-\pi^0) \times \Gamma(e^+e^-)/\Gamma_{total}$ — $\Gamma_{66}\Gamma_7/\Gamma$

VALUE (eV)	EVTS	DOCUMENT ID		TECN	COMMENT
4.4±1.3±0.3	32	AUBERT	07AU	BABR	10.6 $e^+e^- \to K^+K^-\pi^+\pi^-\pi^0\gamma$

$\Gamma(K^0_S K^0_L \pi^0\pi^0) \times \Gamma(e^+e^-)/\Gamma_{total}$ — $\Gamma_{73}\Gamma_7/\Gamma$

VALUE (eV)	EVTS	DOCUMENT ID		TECN	COMMENT
2.92±1.27±0.15	14	LEES	17A	BABR	$e^+e^- \to K^0_S K^0_L \pi^0\pi^0\gamma$

$\Gamma(K^0_S K^0_L \eta) \times \Gamma(e^+e^-)/\Gamma_{total}$ — $\Gamma_{74}\Gamma_7/\Gamma$

VALUE (eV)	EVTS	DOCUMENT ID		TECN	COMMENT
3.14±1.08±0.16	16	LEES	17A	BABR	$e^+e^- \to K^0_S K^0_L \eta\gamma$

$\Gamma(K^+K^-\pi^+\pi^-\eta) \times \Gamma(e^+e^-)/\Gamma_{total}$ — $\Gamma_{77}\Gamma_7/\Gamma$

VALUE (eV)	EVTS	DOCUMENT ID		TECN	COMMENT
3.05±1.80±0.01	7	[1] AUBERT	07AU	BABR	10.6 $e^+e^- \to K^+K^-\pi^+\pi^-\eta\gamma$

[1] AUBERT 07AU reports $[\Gamma(\psi(2S) \to K^+K^-\pi^+\pi^-\eta) \times \Gamma(\psi(2S) \to e^+e^-)/\Gamma_{total}] \times [B(\eta \to 2\gamma)] = 1.2 \pm 0.7 \pm 0.1$ eV which we divide by our best value $B(\eta \to 2\gamma) = (39.36 \pm 0.18) \times 10^{-2}$. Our first error is their experiment's error and our second error is the systematic error from using our best value.

$\Gamma(K^+K^-2(\pi^+\pi^-)) \times \Gamma(e^+e^-)/\Gamma_{total}$ — $\Gamma_{78}\Gamma_7/\Gamma$

VALUE (eV)	EVTS	DOCUMENT ID		TECN	COMMENT
4.4±2.1±0.3	26	AUBERT	06D	BABR	10.6 $e^+e^- \to K^+K^-2(\pi^+\pi^-)\gamma$

$\Gamma(2(K^+K^-)) \times \Gamma(e^+e^-)/\Gamma_{total}$ — $\Gamma_{81}\Gamma_7/\Gamma$

VALUE (eV)	EVTS	DOCUMENT ID		TECN	COMMENT
0.22±0.10±0.02	13	LEES	12F	BABR	10.6 $e^+e^- \to K^+K^-K^+K^-\gamma$

$\Gamma(p\overline{p}) \times \Gamma(e^+e^-)/\Gamma_{total}$ — $\Gamma_{101}\Gamma_7/\Gamma$

VALUE (eV)	EVTS	DOCUMENT ID		TECN	COMMENT
0.686±0.019 OUR FIT					
0.63 ±0.05 OUR AVERAGE		Error includes scale factor of 1.2.			
0.67 ±0.12 ±0.02	43	[1] LEES	13O	BABR	$e^+e^- \to p\overline{p}\gamma$
0.74 ±0.07 ±0.04	142	[2] LEES	13Y	BABR	$e^+e^- \to p\overline{p}\gamma$
0.579±0.038±0.036	2.7k	ANDREOTTI	07	E835	$p\overline{p} \to e^+e^-$, $J/\psi X$
• • • We do not use the following data for averages, fits, limits, etc. • • •					
0.70 ±0.17 ±0.03	22	[3] AUBERT	06B	BABR	$e^+e^- \to p\overline{p}\gamma$

[1] ISR photon reconstructed in the detector
[2] ISR photon undetected
[3] Superseded by LEES 13O

$\Gamma(\Lambda\overline{\Lambda}) \times \Gamma(e^+e^-)/\Gamma_{total}$ — $\Gamma_{124}\Gamma_7/\Gamma$

VALUE (eV)	DOCUMENT ID		TECN	COMMENT
1.5±0.4±0.1	AUBERT	07BD	BABR	10.6 $e^+e^- \to \Lambda\overline{\Lambda}\gamma$

$\psi(2S)$ BRANCHING RATIOS

$\Gamma(\text{hadrons})/\Gamma_{total}$ — Γ_1/Γ

VALUE	DOCUMENT ID		TECN	COMMENT
0.9785±0.0013 OUR AVERAGE				
0.9779±0.0015	[1] BAI	02B	BES2	e^+e^-
0.981 ±0.003	[1] LUTH	75	MRK1	e^+e^-

[1] Includes cascade decay into $J/\psi(1S)$.

$\Gamma(\text{virtual}\,\gamma \to \text{hadrons})/\Gamma_{total}$ — Γ_2/Γ

VALUE	DOCUMENT ID		TECN	COMMENT
0.0173±0.0014 OUR AVERAGE	Error includes scale factor of 1.5.			
0.0166±0.0010	[1,2] SETH	04	RVUE	e^+e^-
0.0199±0.0019	[1] BAI	02B	BES2	e^+e^-
• • • We do not use the following data for averages, fits, limits, etc. • • •				
0.029 ±0.004	[1] LUTH	75	MRK1	e^+e^-

[1] Included in $\Gamma(\text{hadrons})/\Gamma_{total}$.
[2] Using $B(\psi(2S) \to \ell^+\ell^-) = (0.73 \pm 0.04)\%$ from RPP-2002 and $R = 2.28 \pm 0.04$ determined by a fit to data from BAI 00 and BAI 02C.

$\Gamma(ggg)/\Gamma_{total}$ — Γ_3/Γ

VALUE (units 10^{-2})	EVTS	DOCUMENT ID		TECN	COMMENT
10.58±1.62	2.9 M	[1] LIBBY	09	CLEO	$\psi(2S) \to$ hadrons

[1] Calculated using $\Gamma(\gamma gg)/\Gamma(ggg) = 0.097 \pm 0.026 \pm 0.016$ from LIBBY 09, $B(\psi(2S) \to X J/\psi)$ relative and absolute branching fractions from MENDEZ 08, $B(\psi(2S) \to \gamma\eta_C)$ from MITCHELL 09, and $B(\psi(2S) \to$ virtual $\gamma \to$ hadrons), $B(\psi(2S) \to \gamma\chi_{cJ})$, and $B(\psi(2S) \to \ell^+\ell^-)$ from PDG 08. The statistical error is negligible and the systematic error is largely uncorrelated with that of $\Gamma(\gamma gg)/\Gamma_{total}$ LIBBY 09 measurement.

$\Gamma(\gamma gg)/\Gamma_{total}$ — Γ_4/Γ

VALUE (units 10^{-2})	EVTS	DOCUMENT ID		TECN	COMMENT
1.025±0.288	200 k	[1] LIBBY	09	CLEO	$\psi(2S) \to \gamma +$ hadrons

[1] Calculated using $\Gamma(\gamma gg)/\Gamma(ggg) = 0.097 \pm 0.026 \pm 0.016$ from LIBBY 09. The statistical error is negligible and the systematic error is largely uncorrelated with that of $\Gamma(ggg)/\Gamma_{total}$ LIBBY 09 measurement.

$\Gamma(\gamma gg)/\Gamma(ggg)$ — Γ_4/Γ_3

VALUE (units 10^{-2})	EVTS	DOCUMENT ID		TECN	COMMENT
9.7±2.6±1.6	2.9 M	LIBBY	09	CLEO	$\psi(2S) \to (\gamma +)$ hadrons

$\Gamma(\text{light hadrons})/\Gamma_{total}$ — Γ_5/Γ

VALUE	DOCUMENT ID		TECN	COMMENT
0.154±0.015	[1] MENDEZ	08	CLEO	$e^+e^- \to \psi(2S)$
• • • We do not use the following data for averages, fits, limits, etc. • • •				
0.169±0.026	[2] ADAM	05A	CLEO	$e^+e^- \to \psi(2S)$

[1] Uses $B(\psi(2S) \to J/\psi X)$ from MENDEZ 08 and other branching fractions from PDG 07.
[2] Uses $B(J/\psi X)$ from ADAM 05A, $B(\chi_{cJ}\gamma)$, $B(\eta_C\gamma)$ from ATHAR 04 and $B(\ell^+\ell^-)$ from PDG 04. Superseded by MENDEZ 08.

$\Gamma(e^+e^-)/\Gamma_{total}$ — Γ_7/Γ

VALUE (units 10^{-4})	DOCUMENT ID		TECN	COMMENT
79.3± 1.7 OUR FIT				
• • • We do not use the following data for averages, fits, limits, etc. • • •				
88 ±13	[1] FELDMAN	77	RVUE	e^+e^-

[1] From an overall fit assuming equal partial widths for e^+e^- and $\mu^+\mu^-$. For a measurement of the ratio see the entry $\Gamma(\mu^+\mu^-)/\Gamma(e^+e^-)$ below. Includes LUTH 75, HILGER 75, BURMESTER 77.

$\Gamma(\mu^+\mu^-)/\Gamma_{total}$ — Γ_8/Γ

VALUE (units 10^{-4})	DOCUMENT ID
80±6 OUR FIT	

$\Gamma(\mu^+\mu^-)/\Gamma(e^+e^-)$ — Γ_8/Γ_7

VALUE	DOCUMENT ID		TECN	COMMENT
1.00±0.08 OUR FIT				
• • • We do not use the following data for averages, fits, limits, etc. • • •				
0.89±0.16	BOYARSKI	75C	MRK1	e^+e^-

$\Gamma(\tau^+\tau^-)/\Gamma_{total}$ — Γ_9/Γ

VALUE (units 10^{-4})	DOCUMENT ID		TECN	COMMENT
31 ±4 OUR FIT				
30.8±2.1±3.8	[1] ABLIKIM	06W	BES	$e^+e^- \to \psi(2S)$

[1] Computed using PDG 02 value of $B(\psi(2S) \to$ hadrons$) = 0.9810 \pm 0.0030$ to estimate the total number of $\psi(2S)$ events.

DECAYS INTO $J/\psi(1S)$ AND ANYTHING

$\Gamma(J/\psi(1S)\,\text{anything})/\Gamma_{total}$

$$\Gamma_{10}/\Gamma = (\Gamma_{12}+\Gamma_{13}+\Gamma_{14}+0.343\Gamma_{163}+0.190\Gamma_{164})/\Gamma$$

VALUE	EVTS	DOCUMENT ID		TECN	COMMENT
0.614 ±0.006 OUR FIT					
0.55 ±0.07 OUR AVERAGE					
0.51 ±0.12		BRANDELIK	79C	DASP	$e^+e^- \to \mu^+\mu^-X$
0.57 ±0.08		ABRAMS	75B	MRK1	$e^+e^- \to \mu^+\mu^-X$
• • • We do not use the following data for averages, fits, limits, etc. • • •					
0.644 ±0.006 ±0.016		[1] ABLIKIM	21Z	BES3	$e^+e^- \to \ell^+\ell^-X$
0.6254±0.0016±0.0155	1.1M	[2] MENDEZ	08	CLEO	$\psi(2S) \to \ell^+\ell^-X$
0.5950±0.0015±0.0190	151k	ADAM	05A	CLEO	Repl. by MENDEZ 08

[1] From a fit to the $e^+e^- \to J/\psi X$ cross section between 3.645 and 3.891 GeV, with $\Gamma(ee)$ and Γ fixed to the PDG 20 values of the cross particle fit which are correlated to "OUR FIT" value for $B(\psi(2S) \to J/\psi X)$.
[2] Not independent from other measurements of MENDEZ 08.

$\Gamma(e^+e^-)/\Gamma(J/\psi(1S)\,\text{anything})$ — Γ_7/Γ_{10}

VALUE (units 10^{-2})	EVTS	DOCUMENT ID		TECN	COMMENT
1.291±0.026 OUR FIT					
1.28 ±0.04 OUR AVERAGE		Error includes scale factor of 1.6. See the ideogram below.			
1.22 ±0.02 ±0.05	5097 ± 73	[1] ANDREOTTI	05	E835	$p\overline{p} \to \psi(2S) \to e^+e^-$
1.28 ±0.03 ±0.02		[1] AMBROGIANI	00A	E835	$p\overline{p} \to \psi(2S)$
1.44 ±0.08 ±0.02		[1] ARMSTRONG	97	E760	$\overline{p}p \to \psi(2S)$

Downloaded from https://academic.oup.com/ptep/article/2022/8/083C01/6651666 by KIT Library user on 27 September 2022

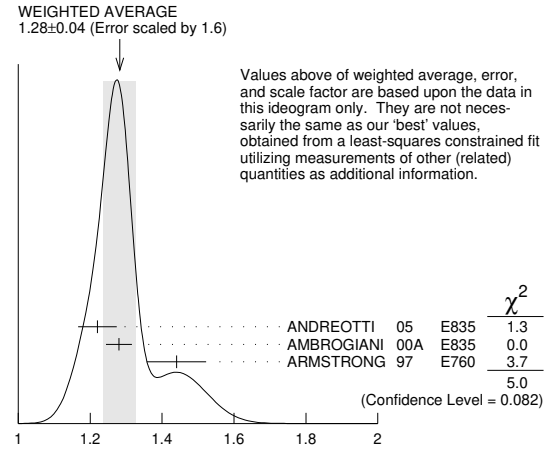

$\Gamma(e^+e^-)/\Gamma(J/\psi(1S)\,\text{anything})$ (units 10^{-2}) — Γ_7/Γ_{10}

[1] Using $B(J/\psi(1S) \to e^+e^-) = 0.0593 \pm 0.0010$.

$\Gamma(\mu^+\mu^-)/\Gamma(J/\psi(1S)\,\text{anything})$ — Γ_8/Γ_{10}

VALUE	DOCUMENT ID		TECN	COMMENT
0.0130±0.0010 OUR FIT				
0.014 ±0.003	HILGER	75	SPEC	e^+e^-

$\Gamma(J/\psi(1S)\,\text{neutrals})/\Gamma_{\text{total}}$ — Γ_{11}/Γ

VALUE	DOCUMENT ID
0.2538±0.0032 OUR FIT	

$\Gamma(J/\psi(1S)\pi^+\pi^-)/\Gamma_{\text{total}}$ — Γ_{12}/Γ

VALUE	EVTS	DOCUMENT ID		TECN	COMMENT
0.3468±0.0030 OUR FIT					
0.348 ±0.005 OUR AVERAGE Error includes scale factor of 1.3. See the ideogram below.					
0.3498±0.0002±0.0045	20M	ABLIKIM	13R	BES3	$\psi(2S) \to J/\psi\pi^+\pi^-$
0.3504±0.0007±0.0077	565k	MENDEZ	08	CLEO	$\psi(2S) \to \ell^+\ell^-\pi^+\pi^-$
0.323 ±0.014		BAI	02B	BES2	e^+e^-
0.32 ±0.04		ABRAMS	75B	MRK1	$e^+e^- \to J/\psi\pi^+\pi^-$
• • • We do not use the following data for averages, fits, limits, etc. • • •					
0.3354±0.0014±0.0110	60k	[1] ADAM	05A	CLEO	Repl. by MENDEZ 08

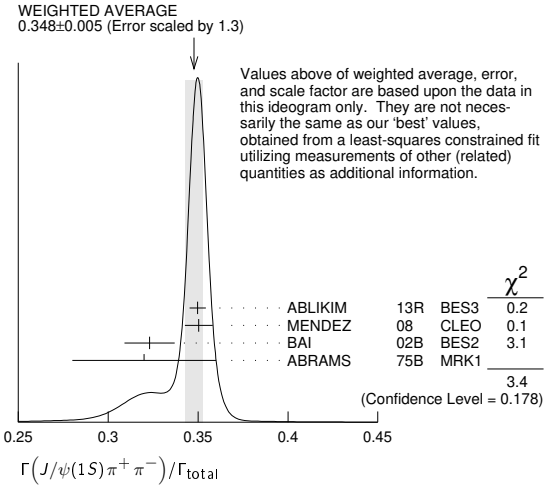

$\Gamma(J/\psi(1S)\pi^+\pi^-)/\Gamma_{\text{total}}$

[1] Not independent from other values reported by ADAM 05A.

$\Gamma(e^+e^-)/\Gamma(J/\psi(1S)\pi^+\pi^-)$ — Γ_7/Γ_{12}

VALUE	DOCUMENT ID		TECN	COMMENT
0.0229±0.0005 OUR FIT				
0.0252±0.0028±0.0011	[1] AUBERT	02B	BABR	e^+e^-

[1] Using $B(J/\psi(1S) \to e^+e^-) = 0.0593 \pm 0.0010$.

$\Gamma(\mu^+\mu^-)/\Gamma(J/\psi(1S)\pi^+\pi^-)$ — Γ_8/Γ_{12}

VALUE	DOCUMENT ID		TECN	COMMENT
0.0230±0.0017 OUR FIT				
0.0228±0.0018 OUR AVERAGE				
0.0230±0.0020±0.0012	[1] AAIJ	16Y	LHCB	$\Lambda_b^0 \to \psi(2S)X$
0.0216±0.0026±0.0014	[2] AUBERT	02B	BABR	e^+e^-
0.0327±0.0077±0.0072	[2] GRIBUSHIN	96	FMPS	$515\ \pi^-\text{Be} \to 2\mu X$

[1] Using $B(J/\psi(1S) \to \mu^+\mu^-) = (5.961 \pm 0.033) \times 10^{-2}$.
[2] Using $B(J/\psi(1S) \to \mu^+\mu^-) = (5.88 \pm 0.10) \times 10^{-2}$.

$\Gamma(\tau^+\tau^-)/\Gamma(J/\psi(1S)\pi^+\pi^-)$ — Γ_9/Γ_{12}

VALUE (units 10^{-3})	DOCUMENT ID		TECN	COMMENT
8.8 ±1.1 OUR FIT				
8.73±1.39±1.57	BAI	02	BES	e^+e^-

$\Gamma(J/\psi(1S)\pi^+\pi^-)/\Gamma(J/\psi(1S)\,\text{anything})$ — Γ_{12}/Γ_{10}

VALUE	EVTS	DOCUMENT ID		TECN	COMMENT
0.5645±0.0026 OUR FIT					
0.554 ±0.008 OUR AVERAGE Error includes scale factor of 1.3. See the ideogram below.					
0.5604±0.0009±0.0062	565k	MENDEZ	08	CLEO	$\psi(2S) \to \ell^+\ell^-\pi^+\pi^-$
0.525 ±0.009 ±0.022	4k	ANDREOTTI	05	E835	$\psi(2S) \to J/\psi X$
0.536 ±0.007 ±0.016	20k	[1,2] ABLIKIM	04B	BES	$\psi(2S) \to J/\psi X$
0.496 ±0.037		ARMSTRONG	97	E760	$\overline{p}p \to \psi(2S)$
• • • We do not use the following data for averages, fits, limits, etc. • • •					
0.5637±0.0027±0.0046	60k	ADAM	05A	CLEO	Repl. by MENDEZ 08

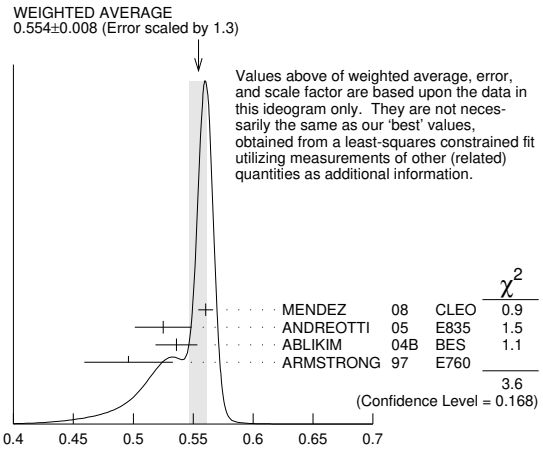

$\Gamma(J/\psi(1S)\pi^+\pi^-)/\Gamma(J/\psi(1S)\,\text{anything})$

[1] From a fit to the J/ψ recoil mass spectra.
[2] ABLIKIM 04B quotes $B(\psi(2S) \to J/\psi X)\ /\ B(\psi(2S) \to J/\psi\pi^+\pi^-)$.

$\Gamma(J/\psi(1S)\,\text{neutrals})/\Gamma(J/\psi(1S)\pi^+\pi^-)$
$\Gamma_{11}/\Gamma_{12} = (0.9761\Gamma_{13}+0.719\Gamma_{14}+0.343\Gamma_{163}+0.190\Gamma_{164})/\Gamma_{12}$

VALUE	DOCUMENT ID		TECN	COMMENT
0.732±0.008 OUR FIT				
0.73 ±0.09	TANENBAUM	76	MRK1	e^+e^-

$\Gamma(J/\psi(1S)\pi^0\pi^0)/\Gamma_{\text{total}}$ — Γ_{13}/Γ

VALUE	EVTS	DOCUMENT ID		TECN	COMMENT
0.1824±0.0031 OUR FIT					
• • • We do not use the following data for averages, fits, limits, etc. • • •					
0.1769±0.0008±0.0053	61k	[1] MENDEZ	08	CLEO	$\psi(2S) \to \ell^+\ell^-2\pi^0$
0.1652±0.0014±0.0058	13.4k	[2] ADAM	05A	CLEO	Repl. by MENDEZ 08

[1] Not independent from other measurements of MENDEZ 08.
[2] Not independent from other values reported by ADAM 05A.

$\Gamma(J/\psi(1S)\pi^0\pi^0)/\Gamma(J/\psi(1S)\,\text{anything})$ — Γ_{13}/Γ_{10}

VALUE	EVTS	DOCUMENT ID		TECN	COMMENT
0.2968±0.0031 OUR FIT					
0.320 ±0.012 OUR AVERAGE					
0.300 ±0.008 ±0.022	1655 ± 44	ANDREOTTI	05	E835	$\psi(2S) \to J/\psi X$
0.328 ±0.013 ±0.008		AMBROGIANI	00A	E835	$p\overline{p} \to \psi(2S)$
0.323 ±0.033		ARMSTRONG	97	E760	$\overline{p}p \to \psi(2S)$
• • • We do not use the following data for averages, fits, limits, etc. • • •					
0.2829±0.0012±0.0056	61k	MENDEZ	08	CLEO	$\psi(2S) \to \ell^+\ell^-2\pi^0$
0.2776±0.0025±0.0043	13.4k	ADAM	05A	CLEO	Repl. by MENDEZ 08

$\Gamma(J/\psi(1S)\pi^0\pi^0)/\Gamma(J/\psi(1S)\pi^+\pi^-)$ — Γ_{13}/Γ_{12}

VALUE	EVTS	DOCUMENT ID		TECN	COMMENT
0.526 ±0.008 OUR FIT					
0.513 ±0.022 OUR AVERAGE Error includes scale factor of 2.2.					
0.5047±0.0022±0.0102	61k	MENDEZ	08	CLEO	$\psi(2S) \to \ell^+\ell^-2\pi^0$
0.570 ±0.009 ±0.026	14k	[1] ABLIKIM	04B	BES	$\psi(2S) \to J/\psi X$
• • • We do not use the following data for averages, fits, limits, etc. • • •					
0.4924±0.0047±0.0086	73k	[2,3] ADAM	05A	CLEO	Repl. by MENDEZ 08
0.571 ±0.018 ±0.044		[4] ANDREOTTI	05	E835	$\psi(2S) \to J/\psi X$
0.53 ±0.06		TANENBAUM	76	MRK1	e^+e^-
0.64 ±0.15		[5] HILGER	75	SPEC	e^+e^-

[1] From a fit to the J/ψ recoil mass spectra.
[2] Not independent from other values reported by ADAM 05A.
[3] Using 13,217 $J/\psi\pi^0\pi^0$ and 60,010 $J/\psi\pi^+\pi^-$ events.
[4] Not independent from other values reported by ANDREOTTI 05.
[5] Ignoring the $J/\psi(1S)\eta$ and $J/\psi(1S)\gamma\gamma$ decays.

Downloaded from https://academic.oup.com/ptep/article/2022/8/083C01/6651666 by KIT Library user on 27 September 2022

$\Gamma(J/\psi(1S)\eta)/\Gamma_{total}$ — Γ_{14}/Γ

VALUE (units 10^{-3})	EVTS	DOCUMENT ID		TECN	COMMENT
33.7 ± 0.5 OUR FIT					
32.9 ± 1.7 OUR AVERAGE Error includes scale factor of 2.1. See the ideogram below.					
33.75 ± 0.17 ± 0.86	68.2k	ABLIKIM	12M	BES3	$e^+e^- \to \ell^+\ell^-2\gamma$
29.8 ± 0.9 ± 2.3	5.7k	BAI	04I	BES2	$\psi(2S) \to J/\psi\gamma\gamma$
25.5 ± 2.9	386	[1] OREGLIA	80	CBAL	$e^+e^- \to J/\psi 2\gamma$
45 ± 12	17	[2] BRANDELIK	79B	DASP	$e^+e^- \to J/\psi 2\gamma$
42 ± 6	164	[2] BARTEL	78B	CNTR	e^+e^-
• • • We do not use the following data for averages, fits, limits, etc. • • •					
34.3 ± 0.4 ± 0.9	18.4k	[3] MENDEZ	08	CLEO	$\psi(2S) \to \ell^+\ell^-\eta$
32.5 ± 0.6 ± 1.1	2.8k	[4] ADAM	05A	CLEO	Repl. by MENDEZ 08
43 ± 8	44	TANENBAUM	76	MRK1	e^+e^-

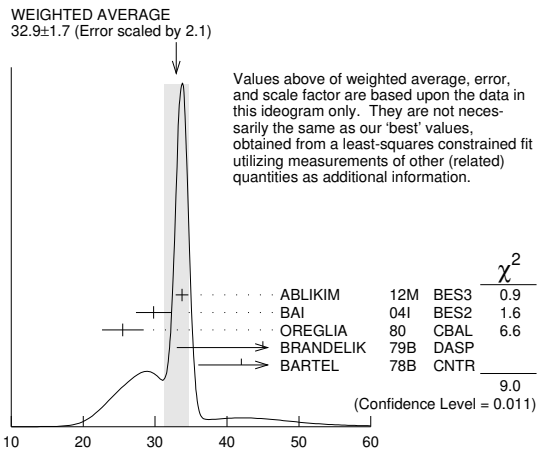

[1] Recalculated by us using $B(J/\psi(1S) \to \ell^+\ell^-) = 0.1181 \pm 0.0020$.
[2] Recalculated by us using $B(J/\psi(1S) \to \mu^+\mu^-) = 0.0588 \pm 0.0010$.
[3] Not independent from other measurements of MENDEZ 08.
[4] Not independent from other values reported by ADAM 05A.

$\Gamma(J/\psi(1S)\eta)/\Gamma(J/\psi(1S)\text{anything})$ — Γ_{14}/Γ_{10}

VALUE	EVTS	DOCUMENT ID		TECN	COMMENT
0.0549±0.0008 OUR FIT					
0.058 ±0.007 OUR AVERAGE Error includes scale factor of 1.4. See the ideogram below.					
0.050 ±0.006 ±0.003	298 ± 20	ANDREOTTI	05	E835	$\psi(2S) \to J/\psi X$
0.072 ±0.009		AMBROGIANI	00A	E835	$p\overline{p} \to \psi(2S)$
0.061 ±0.015		ARMSTRONG	97	E760	$\overline{p}p \to \psi(2S)$
• • • We do not use the following data for averages, fits, limits, etc. • • •					
0.0549±0.0006±0.0009	18.4k	[1] MENDEZ	08	CLEO	$\psi(2S) \to \ell^+\ell^-\eta$
0.0546±0.0010±0.0007	2.8k	ADAM	05A	CLEO	Repl. by MENDEZ 08

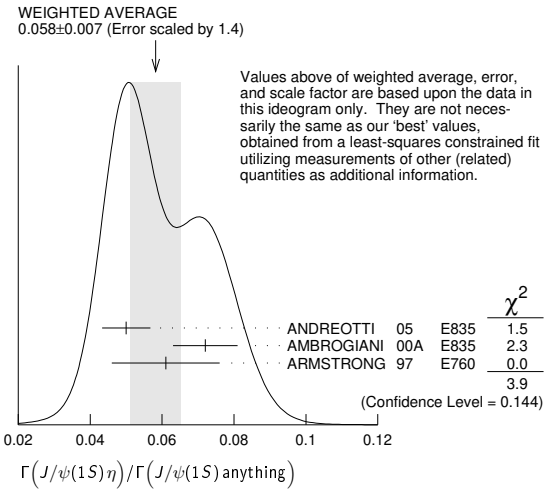

[1] Not independent from other measurements of MENDEZ 08.

$\Gamma(J/\psi(1S)\eta)/\Gamma(J/\psi(1S)\pi^+\pi^-)$ — Γ_{14}/Γ_{12}

VALUE	EVTS	DOCUMENT ID		TECN	COMMENT
0.0972±0.0014 OUR FIT					
0.0979±0.0018 OUR AVERAGE					
0.0979±0.0010±0.0015	18.4k	MENDEZ	08	CLEO	$\psi(2S) \to \ell^+\ell^-\eta$
0.098 ±0.005 ±0.010	2k	[1] ABLIKIM	04B	BES	$\psi(2S) \to J/\psi X$
0.091 ±0.021		[2] HIMEL	80	MRK2	$e^+e^- \to \psi(2S)X$
• • • We do not use the following data for averages, fits, limits, etc. • • •					
0.0968±0.0019±0.0013	2.8k	[3] ADAM	05A	CLEO	Repl. by MENDEZ 08
0.095 ±0.007 ±0.007		[4] ANDREOTTI	05	E835	$\psi(2S) \to J/\psi X$

[1] From a fit to the J/ψ recoil mass spectra.
[2] The value for $B(\psi(2S) \to J/\psi(1s)\eta)$ reported in HIMEL 80 is derived using $B(\psi(2S)) \to J/\psi(1S)\pi^+\pi^-) = (33 \pm 3))\%$ and $B(J/\psi(1S) \to \ell^+\ell^-) = 0.138 \pm 0.018$. Calculated by us using $B(J/\psi(1S) \to \ell^+\ell^-) = (0.1181 \pm 0.0020)$.
[3] Not independent from other values reported by ADAM 05A.
[4] Not independent from other values reported by ANDREOTTI 05.

$\Gamma(J/\psi(1S)\pi^0)/\Gamma_{total}$ — Γ_{15}/Γ

VALUE (units 10^{-4})	EVTS	DOCUMENT ID		TECN	COMMENT
12.68±0.32 OUR AVERAGE					
12.6 ±0.2 ±0.3	4.1k	ABLIKIM	12M	BES3	$e^+e^- \to \ell^+\ell^-2\gamma$
13.3 ±0.8 ±0.3	530	MENDEZ	08	CLEO	$\psi(2S) \to \ell^+\ell^-2\gamma$
14.3 ±1.4 ±1.2	280	BAI	04I	BES2	$\psi(2S) \to J/\psi\gamma\gamma$
14 ±6	7	HIMEL	80	MRK2	e^+e^-
9 ±2 ±1	23	[1] OREGLIA	80	CBAL	$\psi(2S) \to J/\psi 2\gamma$
• • • We do not use the following data for averages, fits, limits, etc. • • •					
13 ±1 ±1	88	ADAM	05A	CLEO	Repl. by MENDEZ 08

[1] Recalculated by us using $B(J/\psi(1S) \to \ell^+\ell^-) = 0.1181 \pm 0.0020$.

$\Gamma(J/\psi(1S)\pi^0)/\Gamma(J/\psi(1S)\text{anything})$
$\Gamma_{15}/\Gamma_{10} = \Gamma_{15}/(\Gamma_{12}+\Gamma_{13}+\Gamma_{14}+0.343\Gamma_{163}+0.190\Gamma_{164})$

VALUE (units 10^{-2})	EVTS	DOCUMENT ID		TECN	COMMENT
• • • We do not use the following data for averages, fits, limits, etc. • • •					
0.213±0.012±0.003	527	[1] MENDEZ	08	CLEO	$e^+e^- \to J/\psi\gamma\gamma$
0.22 ±0.02 ±0.01		[2] ADAM	05A	CLEO	$e^+e^- \to \psi(2S) \to J/\psi\gamma\gamma$

[1] Not independent from other values reported by MENDEZ 08. Supersedes ADAM 05A.
[2] Not independent from other values reported by ADAM 05A.

$\Gamma(J/\psi(1S)\pi^0)/\Gamma(J/\psi(1S)\pi^+\pi^-)$ — Γ_{15}/Γ_{12}

VALUE (units 10^{-2})	EVTS	DOCUMENT ID		TECN	COMMENT
• • • We do not use the following data for averages, fits, limits, etc. • • •					
0.380±0.022±0.005	527	[1] MENDEZ	08	CLEO	$e^+e^- \to J/\psi\gamma\gamma$
0.39 ±0.04 ±0.01		[2] ADAM	05A	CLEO	$e^+e^- \to \psi(2S) \to J/\psi\gamma\gamma$

[1] Not independent from other values reported by MENDEZ 08. Supersedes ADAM 05A.
[2] Not independent from other values reported by ADAM 05A.

HADRONIC DECAYS

$\Gamma(\pi^+\pi^-)/\Gamma_{total}$ — Γ_{16}/Γ

VALUE (units 10^{-5})	CL%	EVTS	DOCUMENT ID		TECN	COMMENT
0.78±0.26 OUR AVERAGE						
0.76±0.25±0.06		30	[1] METREVELI	12		$\psi(2S) \to \pi^+\pi^-$
8 ±5			BRANDELIK	79C	DASP	e^+e^-
• • • We do not use the following data for averages, fits, limits, etc. • • •						
<2.1	90		DOBBS	06A	CLEO	$e^+e^- \to \psi(2S)$
<5	90		FELDMAN	77	MRK1	e^+e^-

[1] Obtained by analyzing CLEO-c data but not authored by the CLEO Collaboration. Using $\psi(3770) \to \pi^+\pi^-$ for continuum subtraction.

$\Gamma(\pi^+\pi^-\pi^0)/\Gamma_{total}$ — Γ_{17}/Γ

VALUE (units 10^{-4})	EVTS	DOCUMENT ID		TECN	COMMENT
2.01±0.17 OUR AVERAGE Error includes scale factor of 1.7. See the ideogram below.					
$2.14 \pm 0.03^{+0.12}_{-0.11}$	7k	[1] ABLIKIM	12H	BES3	$e^+e^- \to \psi(2S)$
1.81±0.18±0.19	260 ± 19	[2] ABLIKIM	05J	BES2	$e^+e^- \to \psi(2S)$
$1.88^{+0.16}_{-0.15} \pm 0.28$	194	ADAM	05	CLEO	$e^+e^- \to \psi(2S)$
0.85±0.46	4	FRANKLIN	83	MRK2	$e^+e^- \to$ hadrons

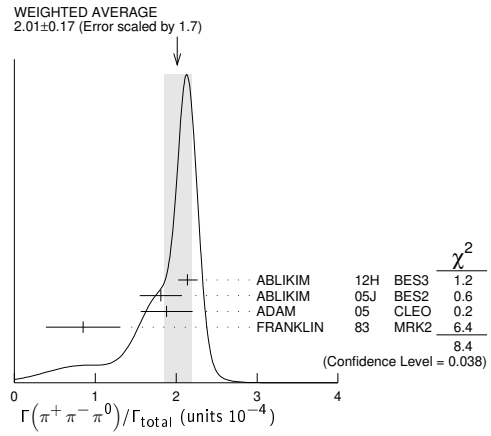

Downloaded from https://academic.oup.com/ptep/article/2022/8/083C01/6651666 by KIT Library user on 27 September 2022

[1] From $\psi(2S) \to \pi^+\pi^-\pi^0$ events directly. The quoted systematic error includes a contribution of 4% (added in quadrature) from the uncertainty on the number of $\psi(2S)$ events.

[2] From a PW analysis of $\psi(2S) \to \pi^+\pi^-\pi^0$.

$\Gamma(\rho(770)\pi \to \pi^+\pi^-\pi^0)/\Gamma_{total}$ — Γ_{18}/Γ

VALUE (units 10^{-4})	CL%	EVTS	DOCUMENT ID		TECN	COMMENT
0.32±0.12 OUR AVERAGE	Error includes scale factor of 1.8.					
$0.51 \pm 0.07 \pm 0.11$			[1] ABLIKIM	05J	BES2	$\psi(2S) \to \rho(770)\pi \to \pi^+\pi^-\pi^0$
$0.24^{+0.08}_{-0.07} \pm 0.02$		22	ADAM	05	CLEO	$e^+e^- \to \psi(2S)$
• • • We do not use the following data for averages, fits, limits, etc. • • •						
<0.83	90	1	FRANKLIN	83	MRK2	e^+e^-
<10	90		BARTEL	76	CNTR	e^+e^-
<10	90		[2] ABRAMS	75	MRK1	e^+e^-

[1] From a PW analysis of $\psi(2S) \to \pi^+\pi^-\pi^0$.

[2] Final state $\rho^0\pi^0$.

$\Gamma(\rho(2150)\pi \to \pi^+\pi^-\pi^0)/\Gamma_{total}$ — Γ_{19}/Γ

VALUE (units 10^{-4})	DOCUMENT ID		TECN	COMMENT
$\mathbf{1.94 \pm 0.25^{+1.15}_{-0.34}}$	[1] ABLIKIM	05J	BES2	$\psi(2S) \to \rho(2150)\pi \to \pi^+\pi^-\pi^0$

[1] From a PW analysis of $\psi(2S) \to \pi^+\pi^-\pi^0$.

$\Gamma(2(\pi^+\pi^-))/\Gamma_{total}$ — Γ_{20}/Γ

VALUE (units 10^{-4})	EVTS	DOCUMENT ID		TECN	COMMENT
2.4±0.6 OUR AVERAGE	Error includes scale factor of 2.2.				
$2.2 \pm 0.2 \pm 0.2$	308	BRIERE	05	CLEO	$e^+e^- \to \psi(2S) \to 2(\pi^+\pi^-)$
4.5 ± 1.0		TANENBAUM	78	MRK1	e^+e^-

$\Gamma(\rho^0\pi^+\pi^-)/\Gamma_{total}$ — Γ_{21}/Γ

VALUE (units 10^{-4})	EVTS	DOCUMENT ID		TECN	COMMENT
2.2±0.6 OUR AVERAGE	Error includes scale factor of 1.4.				
$2.0 \pm 0.2 \pm 0.4$	285.5	BRIERE	05	CLEO	$e^+e^- \to \psi(2S) \to 2(\pi^+\pi^-)$
4.2 ± 1.5		TANENBAUM	78	MRK1	e^+e^-

$\Gamma(2(\pi^+\pi^-)\pi^0)/\Gamma_{total}$ — Γ_{22}/Γ

VALUE (units 10^{-4})	EVTS	DOCUMENT ID		TECN	COMMENT
29 ±10 OUR AVERAGE	Error includes scale factor of 4.7. See the ideogram below.				
$24.9 \pm 0.7 \pm 3.6$	2173	ABLIKIM	07D	BES2	$e^+e^- \to \psi(2S)$
$127 \pm 12 \pm 2$	410	[1] AUBERT	07AU	BABR	$10.6\ e^+e^- \to 2(\pi^+\pi^-)\pi^0\gamma$
$26.1 \pm 0.7 \pm 3.0$	1703	BRIERE	05	CLEO	$e^+e^- \to \psi(2S) \to 2(\pi^+\pi^-)\pi^0$
30 ± 8	42	FRANKLIN	83	MRK2	e^+e^-

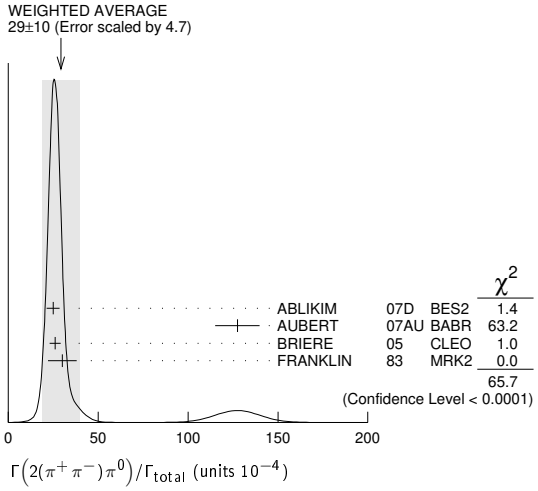

[1] AUBERT 07AU reports $[\Gamma(\psi(2S) \to 2(\pi^+\pi^-)\pi^0)/\Gamma_{total}] \times [\Gamma(\psi(2S) \to e^+e^-)] = (297 \pm 22 \pm 18) \times 10^{-4}$ keV which we divide by our best value $\Gamma(\psi(2S) \to e^+e^-) = 2.33 \pm 0.04$ keV. Our first error is their experiment's error and our second error is the systematic error from using our best value.

$\Gamma(\rho a_2(1320))/\Gamma_{total}$ — Γ_{23}/Γ

VALUE (units 10^{-4})	CL%	EVTS	DOCUMENT ID		TECN	COMMENT
2.55±0.73±0.47		112 ± 31	BAI	04C	BES2	$\psi(2S) \to 2(\pi^+\pi^-)\pi^0$
• • • We do not use the following data for averages, fits, limits, etc. • • •						
<2.3	90		BAI	98J	BES	e^+e^-

$\Gamma(3(\pi^+\pi^-))/\Gamma_{total}$ — Γ_{27}/Γ

VALUE (units 10^{-4})	EVTS	DOCUMENT ID		TECN	COMMENT
3.5 ±2.0 OUR AVERAGE	Error includes scale factor of 2.8.				
$5.45 \pm 0.42 \pm 0.87$	671	ABLIKIM	05H	BES2	$e^+e^- \to \psi(2S) \to 3(\pi^+\pi^-)$
1.5 ± 1.0		[1] TANENBAUM	78	MRK1	e^+e^-

[1] Assuming entirely strong decay.

$\Gamma(3(\pi^+\pi^-)\pi^0)/\Gamma_{total}$ — Γ_{29}/Γ

VALUE (units 10^{-4})	EVTS	DOCUMENT ID		TECN	COMMENT
35±16	6	FRANKLIN	83	MRK2	$e^+e^- \to$ hadrons

$\Gamma(\eta\pi^+\pi^-)/\Gamma_{total}$ — Γ_{31}/Γ

VALUE (units 10^{-4})	CL%	DOCUMENT ID		TECN	COMMENT
<1.6	90	BRIERE	05	CLEO	$e^+e^- \to \psi(2S) \to 2(\pi^+\pi^-)\pi^0$

$\Gamma(\eta\pi^+\pi^-\pi^0)/\Gamma_{total}$ — Γ_{32}/Γ

VALUE (units 10^{-4})	EVTS	DOCUMENT ID		TECN	COMMENT
9.5±0.7±1.5		[1] BRIERE	05	CLEO	$e^+e^- \to \psi(2S) \to$ hadr
• • • We do not use the following data for averages, fits, limits, etc. • • •					
$10.3 \pm 0.8 \pm 1.4$	201.7	[2] BRIERE	05	CLEO	$e^+e^- \to \psi(2S) \to \eta 3\pi(\eta \to \gamma\gamma)$
$8.1 \pm 1.4 \pm 1.6$	50.0	[2] BRIERE	05	CLEO	$e^+e^- \to \psi(2S) \to \eta 3\pi(\eta \to 3\pi)$

[1] Average of $\eta \to \gamma\gamma$ and $\eta \to 3\pi$.

[2] Not independent from other values reported by BRIERE 05.

$\Gamma(\rho\eta)/\Gamma_{total}$ — Γ_{37}/Γ

VALUE (units 10^{-5})	EVTS	DOCUMENT ID		TECN	COMMENT
2.2 ±0.6 OUR AVERAGE	Error includes scale factor of 1.1.				
$3.0\ ^{+1.1}_{-0.9} \pm 0.2$	18	ADAM	05	CLEO	$e^+e^- \to \psi(2S)$
$1.78^{+0.67}_{-0.62} \pm 0.17$	13	ABLIKIM	04L	BES	$e^+e^- \to \psi(2S)$

$\Gamma(\eta'\pi^+\pi^-\pi^0)/\Gamma_{total}$ — Γ_{38}/Γ

VALUE (units 10^{-4})	EVTS	DOCUMENT ID		TECN	COMMENT
4.5±1.6±1.3	12.8	BRIERE	05	CLEO	$e^+e^- \to \psi(2S) \to$ hadr

$\Gamma(\eta'\rho)/\Gamma_{total}$ — Γ_{39}/Γ

VALUE (units 10^{-5})	EVTS	DOCUMENT ID		TECN	COMMENT
$\mathbf{1.87\ ^{+1.64}_{-1.11} \pm 0.33}$	2	ABLIKIM	04L	BES	$e^+e^- \to \psi(2S)$
• • • We do not use the following data for averages, fits, limits, etc. • • •					
$1.02 \pm 0.11 \pm 0.24$	143	[1] ABLIKIM	17AK	BES3	$e^+e^- \to \psi(2S)$
$0.569 \pm 0.128 \pm 0.236$	80	[2] ABLIKIM	17AK	BES3	$e^+e^- \to \psi(2S)$

[1] Destructive-interference solution of a partial wave analysis of the decay $\psi(2S) \to \pi^+\pi^-\eta'$.

[2] Constructive-interference solution of a partial wave analysis of the decay $\psi(2S) \to \pi^+\pi^-\eta'$.

$\Gamma(\omega\pi^0)/\Gamma_{total}$ — Γ_{40}/Γ

VALUE (units 10^{-5})	EVTS	DOCUMENT ID		TECN	COMMENT
2.1 ±0.6 OUR AVERAGE					
$2.5\ ^{+1.2}_{-1.0} \pm 0.2$	14	ADAM	05	CLEO	$e^+e^- \to \psi(2S)$
$1.87^{+0.68}_{-0.62} \pm 0.28$	14	ABLIKIM	04L	BES	$e^+e^- \to \psi(2S)$

$\Gamma(\omega\pi^+\pi^-)/\Gamma_{total}$ — Γ_{41}/Γ

VALUE (units 10^{-4})	EVTS	DOCUMENT ID		TECN	COMMENT
7.3±1.2 OUR AVERAGE	Error includes scale factor of 2.1. See the ideogram below.				
$8.4 \pm 0.5 \pm 1.2$	386	ABLIKIM	07D	BES2	$e^+e^- \to \psi(2S)$
$12.2 \pm 2.2 \pm 0.7$	37	[1] AUBERT	07AU	BABR	$10.6\ e^+e^- \to \omega\pi^+\pi^-\gamma$
$8.2 \pm 0.5 \pm 0.7$	391	BRIERE	05	CLEO	$e^+e^- \to \psi(2S) \to 2(\pi^+\pi^-)\pi^0$
$4.8 \pm 0.6 \pm 0.7$	100 ± 22	[2] BAI	03B	BES	$\psi(2S) \to 2(\pi^+\pi^-)\pi^0$

[1] AUBERT 07AU quotes $\Gamma_{ee}^{\psi(2S)} \cdot B(\psi(2S) \to \omega\pi^+\pi^-) \cdot B(\omega \to 3\pi) = 2.69 \pm 0.73 \pm 0.16$ eV.

[2] Normalized to $B(\psi(2S) \to J/\psi\pi^+\pi^-) = 0.305 \pm 0.016$.

Downloaded from https://academic.oup.com/ptep/article/2022/8/083C01/6651666 by KIT Library user on 27 September 2022

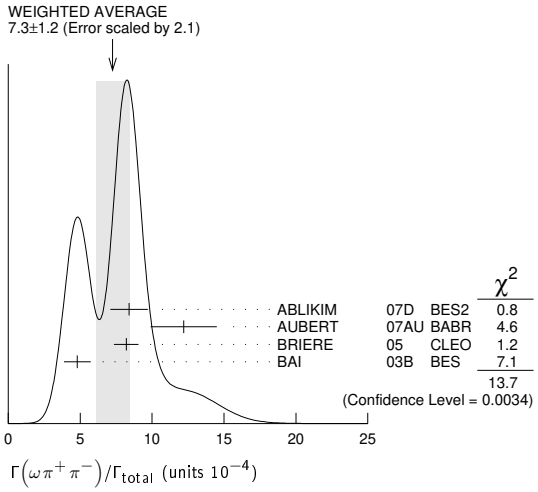

$\Gamma(b_1^{\pm}\pi^{\mp})/\Gamma_{total}$ — Γ_{43}/Γ

VALUE (units 10^{-4})	EVTS	DOCUMENT ID		TECN	COMMENT
4.0 ±0.6 OUR AVERAGE	Error includes scale factor of 1.1.				
5.1 ±0.6 ±0.8	202	ABLIKIM	07D	BES2	$e^+e^- \to \psi(2S)$
$4.18^{+0.43}_{-0.42} \pm 0.92$	170	ADAM	05	CLEO	$e^+e^- \to \psi(2S)$
3.2 ±0.6 ±0.5	61 ± 11	[1,2] BAI	03B	BES	$\psi(2S) \to 2(\pi^+\pi^-)\pi^0$
• • • We do not use the following data for averages, fits, limits, etc. • • •					
5.2 ±0.8 ±1.0		[1] BAI	99C	BES	Repl. by BAI 03B

[1] Assuming $B(b_1 \to \omega\pi)=1$.
[2] Normalized to $B(\psi(2S) \to J/\psi\pi^+\pi^-) = 0.305 \pm 0.016$.

$\Gamma(\omega f_2(1270))/\Gamma_{total}$ — Γ_{44}/Γ

VALUE (units 10^{-4})	CL%	EVTS	DOCUMENT ID		TECN	COMMENT
2.2 ±0.4 OUR AVERAGE						
2.3 ±0.5 ±0.4		57	ABLIKIM	07D	BES2	$e^+e^- \to \psi(2S)$
2.05±0.41±0.38		62±12	BAI	04C	BES2	$\psi(2S) \to 2(\pi^+\pi^-)\pi^0$
• • • We do not use the following data for averages, fits, limits, etc. • • •						
<1.5	90		[1] BAI	03B	BES	$\psi(2S) \to 2(\pi^+\pi^-)\pi^0$
<1.7	90		BAI	98J	BES	Repl. by BAI 03B

[1] Normalized to $B(\psi(2S) \to J/\psi\pi^+\pi^-) = 0.305 \pm 0.016$.

$\Gamma(b_1^0\pi^0)/\Gamma_{total}$ — Γ_{47}/Γ

VALUE (units 10^{-4})	EVTS	DOCUMENT ID		TECN	COMMENT
$\mathbf{2.35^{+0.47}_{-0.42} \pm 0.40}$	45	ADAM	05	CLEO	$e^+e^- \to \psi(2S)$

$\Gamma(\omega\eta)/\Gamma_{total}$ — Γ_{48}/Γ

VALUE (units 10^{-5})	CL%	DOCUMENT ID		TECN	COMMENT
<1.1	90	ADAM	05	CLEO	$e^+e^- \to \psi(2S)$
• • • We do not use the following data for averages, fits, limits, etc. • • •					
<3.1	90	ABLIKIM	04K	BES	$e^+e^- \to \psi(2S)$

$\Gamma(\omega\eta')/\Gamma_{total}$ — Γ_{49}/Γ

VALUE (units 10^{-5})	EVTS	DOCUMENT ID		TECN	COMMENT
$\mathbf{3.2^{+2.4}_{-2.0} \pm 0.7}$	4	[1] ABLIKIM	04K	BES	$e^+e^- \to \psi(2S)$

[1] Calculated combining $\eta' \to \gamma\rho$ and $\eta\pi^+\pi^-$ channels.

$\Gamma(\phi\pi^0)/\Gamma_{total}$ — Γ_{50}/Γ

VALUE (units 10^{-5})	CL%	DOCUMENT ID		TECN	COMMENT
<0.04	90	ABLIKIM	12L	BES3	$e^+e^- \to \psi(2S)$
• • • We do not use the following data for averages, fits, limits, etc. • • •					
<0.7	90	ADAM	05	CLEO	$e^+e^- \to \psi(2S)$
<0.4	90	ABLIKIM	04K	BES	$e^+e^- \to \psi(2S)$

$\Gamma(\phi\pi^+\pi^-)/\Gamma_{total}$ — Γ_{51}/Γ

VALUE (units 10^{-4})	EVTS	DOCUMENT ID		TECN	COMMENT
1.18±0.26 OUR AVERAGE	Error includes scale factor of 1.5. See the ideogram below.				
2.3 ±0.8 ±0.1	19 ± 6	LEES	12F	BABR	10.6 $e^+e^- \to \pi^+\pi^-K^+K^-\gamma$
0.9 ±0.2 ±0.1	47.6	BRIERE	05	CLEO	$e^+e^- \to \psi(2S) \to K^+K^-\pi^+\pi^-$
1.5 ±0.2 ±0.2	51.5 ± 8.3	[1] BAI	03B	BES	$\psi(2S) \to K^+K^-\pi^+\pi^-$
• • • We do not use the following data for averages, fits, limits, etc. • • •					
2.45±0.96±0.04	10 ± 4	[2,3] AUBERT	07AK	BABR	10.6 $e^+e^- \to \pi^+\pi^-K^+K^-\gamma$

[1] Normalized to $B(\psi(2S) \to J/\psi\pi^+\pi^-) = 0.305 \pm 0.016$.
[2] Superseded by LEES 12F. AUBERT 07AK reports $[\Gamma(\psi(2S) \to \phi\pi^+\pi^-)/\Gamma_{total}] \times [\Gamma(\psi(2S) \to e^+e^-)] = (0.57 \pm 0.22 \pm 0.04) \times 10^{-3}$ keV which we divide by our best value $\Gamma(\psi(2S) \to e^+e^-) = 2.33 \pm 0.04$ keV. Our first error is their experiment's error and our second error is the systematic error from using our best value.
[3] Using $B(\phi \to K^+K^-) = (49.3 \pm 0.6)\%$.

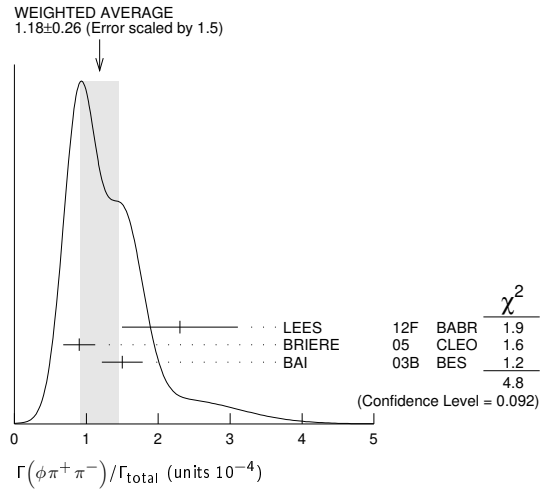

$\Gamma(\phi f_0(980) \to \pi^+\pi^-)/\Gamma_{total}$ — Γ_{52}/Γ

VALUE (units 10^{-4})	EVTS	DOCUMENT ID		TECN	COMMENT
0.75±0.33 OUR AVERAGE	Error includes scale factor of 1.6.				
1.5 ±0.5 ±0.1	12 ± 4	LEES	12F	BABR	10.6 $e^+e^- \to \pi^+\pi^-K^+K^-\gamma$
0.6 ±0.2 ±0.1	18.4±6.4	[1] BAI	03B	BES	$\psi(2S) \to K^+K^-\pi^+\pi^-$
• • • We do not use the following data for averages, fits, limits, etc. • • •					
1.46±0.71±0.02	6 ± 3	[2,3] AUBERT	07AK	BABR	10.6 $e^+e^- \to \pi^+\pi^-K^+K^-\gamma$

[1] Normalized to $B(\psi(2S) \to J/\psi\pi^+\pi^-) = 0.305 \pm 0.016$.
[2] Superseded by LEES 12F. AUBERT 07AK reports $[\Gamma(\psi(2S) \to \phi f_0(980) \to \pi^+\pi^-)/\Gamma_{total}] \times [\Gamma(\psi(2S) \to e^+e^-)] = (0.34 \pm 0.16 \pm 0.04) \times 10^{-3}$ keV which we divide by our best value $\Gamma(\psi(2S) \to e^+e^-) = 2.33 \pm 0.04$ keV. Our first error is their experiment's error and our second error is the systematic error from using our best value.
[3] Using $B(\phi \to K^+K^-) = (49.3 \pm 0.6)\%$.

$\Gamma(\phi\eta)/\Gamma_{total}$ — Γ_{53}/Γ

VALUE (units 10^{-5})	EVTS	DOCUMENT ID		TECN	COMMENT
3.10±0.31 OUR AVERAGE					
3.14±0.23±0.23	0.2k	ABLIKIM	12L	BES3	$e^+e^- \to \psi(2S)$
$2.0\ ^{+1.5}_{-1.1} \pm 0.4$	6	ADAM	05	CLEO	$e^+e^- \to \psi(2S)$
3.3 ±1.1 ±0.5	17	ABLIKIM	04K	BES	$e^+e^- \to \psi(2S)$

$\Gamma(\eta\phi(2170), \phi(2170) \to \phi f_0(980), f_0 \to \pi^+\pi^-)/\Gamma_{total}$ — Γ_{54}/Γ

VALUE	CL%	DOCUMENT ID		TECN	COMMENT
$\mathbf{<2.2 \times 10^{-6}}$	90	ABLIKIM	19I	BES3	$e^+e^- \to \eta\phi f_0(980)$

$\Gamma(\phi\eta')/\Gamma_{total}$ — Γ_{55}/Γ

VALUE (units 10^{-5})	EVTS	DOCUMENT ID		TECN	COMMENT
1.54±0.20 OUR AVERAGE					
1.51±0.16±0.12	201	ABLIKIM	19BA	BES3	$e^+e^- \to \psi(2S)$
3.1 ±1.4 ±0.7	8	[1] ABLIKIM	04K	BES	$e^+e^- \to \psi(2S)$

[1] Calculated combining $\eta' \to \gamma\rho$ and $\eta\pi^+\pi^-$ channels.

$\Gamma(\phi f_1(1285))/\Gamma_{total}$ — Γ_{56}/Γ

VALUE (units 10^{-5})	EVTS	DOCUMENT ID		TECN	COMMENT
3.0±0.4±1.3	234	[1] ABLIKIM	19BA	BES3	$e^+e^- \to \psi(2S)$

[1] ABLIKIM 19BA reports $[\Gamma(\psi(2S) \to \phi f_1(1285))/\Gamma_{total}] \times [B(f_1(1285) \to \eta\pi^+\pi^-)] = (1.03 \pm 0.10 \pm 0.09) \times 10^{-5}$ which we divide by our best value $B(f_1(1285) \to \eta\pi^+\pi^-) = (35 \pm 15) \times 10^{-2}$. Our first error is their experiment's error and our second error is the systematic error from using our best value.

$\Gamma(\phi\eta(1405) \to \phi\pi^+\pi^-\eta)/\Gamma_{total}$ — Γ_{57}/Γ

VALUE (units 10^{-6})	EVTS	DOCUMENT ID		TECN	COMMENT
8.46±1.37±0.92	195	ABLIKIM	19BA	BES3	$e^+e^- \to \psi(2S)$

$\Gamma(\phi f_2'(1525))/\Gamma_{total}$ — Γ_{58}/Γ

VALUE (units 10^{-4})	CL%	EVTS	DOCUMENT ID		TECN	COMMENT
0.44±0.12±0.11		20 ± 6	BAI	04C		$\psi(2S) \to 2(K^+K^-)$
• • • We do not use the following data for averages, fits, limits, etc. • • •						
<0.45	90		BAI	98J	BES	$e^+e^- \to 2(K^+K^-)$

Downloaded from https://academic.oup.com/ptep/article/2022/8/083C01/6651666 by KIT Library user on 27 September 2022

$\Gamma(K^+K^-)/\Gamma_{total}$ — Γ_{59}/Γ

VALUE (units 10^{-5})	CL%	EVTS	DOCUMENT ID		TECN	COMMENT
7.48±0.23±0.39		1.3k	[1] METREVELI	12		$\psi(2S) \to K^+K^-$
• • • We do not use the following data for averages, fits, limits, etc. • • •						
6.2 ±1.5 ±0.2		66	[2,3] LEES	15J	BABR	$e^+e^- \to K^+K^-\gamma$
8.3 ±1.5 ±0.2		66	[3,4] LEES	15J	BABR	$e^+e^- \to K^+K^-\gamma$
6.3 ±0.6 ±0.3			[5] DOBBS	06A	CLEO	e^+e^-
10 ±7			[5] BRANDELIK	79C	DASP	e^+e^-
< 5	90		FELDMAN	77	MRK1	e^+e^-

[1] Obtained by analyzing CLEO-c data but not authored by the CLEO Collaboration.
[2] $\sin\phi > 0$.
[3] Using $\Gamma(\psi(2S) \to e^+e^-) = (2.37 \pm 0.04)$ keV.
[4] $\sin\phi < 0$.
[5] Interference with non-resonant K^+K^- production not taken into account.

$\Gamma(K^+K^-\pi^+)/\Gamma_{total}$ — Γ_{60}/Γ

VALUE (units 10^{-4})	EVTS	DOCUMENT ID		TECN	COMMENT
7.3±0.5 OUR AVERAGE					
8.1±1.3±0.3	133	LEES	12F	BABR	10.6 $e^+e^- \to \pi^+\pi^-K^+K^-\gamma$
7.1±0.3±0.4	817.2	BRIERE	05	CLEO	$e^+e^- \to \psi(2S) \to K^+K^-\pi^+\pi^-$
16 ±4		[1] TANENBAUM	78	MRK1	e^+e^-
• • • We do not use the following data for averages, fits, limits, etc. • • •					
11.0±1.9±0.2	85	[2] AUBERT	07AK	BABR	10.6 $e^+e^- \to \pi^+\pi^-K^+K^-\gamma$

[1] Assuming entirely strong decay.
[2] Superseded by LEES 12F. AUBERT 07AK reports $[\Gamma(\psi(2S) \to K^+K^-\pi^+)/\Gamma_{total}] \times [\Gamma(\psi(2S) \to e^+e^-)] = (2.56 \pm 0.42 \pm 0.16) \times 10^{-3}$ keV which we divide by our best value $\Gamma(\psi(2S) \to e^+e^-) = 2.33 \pm 0.04$ keV. Our first error is their experiment's error and our second error is the systematic error from using our best value.

$\Gamma(K^+K^-\pi^0)/\Gamma_{total}$ — Γ_{61}/Γ

VALUE (units 10^{-5})	CL%	EVTS	DOCUMENT ID		TECN	COMMENT
4.07±0.16±0.26		0.9k	ABLIKIM	12L	BES3	$e^+e^- \to \psi(2S)$
• • • We do not use the following data for averages, fits, limits, etc. • • •						
<8.9	90	1	FRANKLIN	83	MRK2	$e^+e^- \to$ hadrons

$\Gamma(K^0_SK^0_S)/\Gamma_{total}$ — Γ_{62}/Γ

VALUE (units 10^{-4})	DOCUMENT ID		TECN	COMMENT
<0.046	[1] BAI	04D	BES	e^+e^-

[1] Forbidden by *CP*.

$\Gamma(K^0_SK^0_L)/\Gamma_{total}$ — Γ_{63}/Γ

VALUE (units 10^{-5})	EVTS	DOCUMENT ID		TECN	COMMENT
5.34±0.33 OUR AVERAGE					
5.28±0.25±0.34	478 ± 23	[1] METREVELI	12		$\psi(2S) \to K^0_SK^0_L$
5.8 ±0.8 ±0.4		DOBBS	06A	CLEO	e^+e^-
5.24±0.47±0.48	156 ± 14	[2] BAI	04B	BES2	$\psi(2S) \to K^0_SK^0_L \to \pi^+\pi^-X$

[1] Obtained by analyzing CLEO-c data but not authored by the CLEO Collaboration.
[2] Using $B(K^0_S \to \pi^+\pi^-) = 0.6860 \pm 0.0027$.

$\Gamma(K^+K^-\pi^+\pi^-\pi^0)/\Gamma_{total}$ — Γ_{66}/Γ

VALUE (units 10^{-4})	EVTS	DOCUMENT ID		TECN	COMMENT
12.6±0.9 OUR AVERAGE					
18.9±5.7±0.3	32	[1] AUBERT	07AU	BABR	10.6 $e^+e^- \to K^+K^-\pi^+\pi^-\pi^0\gamma$
11.7±1.0±1.5	597	ABLIKIM	06G	BES2	$\psi(2S) \to K^+K^-\pi^+\pi^-\pi^0$
12.7±0.5±1.0	711.6	BRIERE	05	CLEO	$e^+e^- \to \psi(2S) \to K^+K^-\pi^+\pi^-\pi^0$

[1] AUBERT 07AU reports $[\Gamma(\psi(2S) \to K^+K^-\pi^+\pi^-\pi^0)/\Gamma_{total}] \times [\Gamma(\psi(2S) \to e^+e^-)] = (44 \pm 13 \pm 3) \times 10^{-4}$ keV which we divide by our best value $\Gamma(\psi(2S) \to e^+e^-) = 2.33 \pm 0.04$ keV. Our first error is their experiment's error and our second error is the systematic error from using our best value.

$\Gamma(\omega f_0(1710) \to \omega K^+K^-)/\Gamma_{total}$ — Γ_{67}/Γ

VALUE (units 10^{-5})	EVTS	DOCUMENT ID		TECN	COMMENT
5.9±2.0±0.9	19	ABLIKIM	06G	BES2	$\psi(2S) \to K^+K^-\pi^+\pi^-\pi^0$

$\Gamma(K^*(892)^0K^-\pi^+\pi^0 + \text{c.c.})/\Gamma_{total}$ — Γ_{68}/Γ

VALUE (units 10^{-4})	EVTS	DOCUMENT ID		TECN	COMMENT
8.6±1.3±1.8	238	ABLIKIM	06G	BES2	$\psi(2S) \to K^+K^-\pi^+\pi^-\pi^0$

$\Gamma(K^*(892)^+K^-\pi^+\pi^- + \text{c.c.})/\Gamma_{total}$ — Γ_{69}/Γ

VALUE (units 10^{-4})	EVTS	DOCUMENT ID		TECN	COMMENT
9.6±2.2±1.7	133	ABLIKIM	06G	BES2	$\psi(2S) \to K^+K^-\pi^+\pi^-\pi^0$

$\Gamma(K^*(892)^+K^-\rho^0 + \text{c.c.})/\Gamma_{total}$ — Γ_{70}/Γ

VALUE (units 10^{-4})	EVTS	DOCUMENT ID		TECN	COMMENT
7.3±2.2±1.4	78	ABLIKIM	06G	BES2	$\psi(2S) \to K^+K^-\pi^+\pi^-\pi^0$

$\Gamma(K^*(892)^0K^-\rho^+ + \text{c.c.})/\Gamma_{total}$ — Γ_{71}/Γ

VALUE (units 10^{-4})	EVTS	DOCUMENT ID		TECN	COMMENT
6.1±1.3±1.2	125	ABLIKIM	06G	BES2	$\psi(2S) \to K^+K^-\pi^+\pi^-\pi^0$

$\Gamma(K^0_SK^0_S\pi^+\pi^-)/\Gamma_{total}$ — Γ_{72}/Γ

VALUE (units 10^{-4})	EVTS	DOCUMENT ID		TECN	COMMENT
2.20±0.25±0.37	83 ± 9	ABLIKIM	05O	BES2	$e^+e^- \to \psi(2S)$

$\Gamma(K^+K^-\rho^0)/\Gamma_{total}$ — Γ_{75}/Γ

VALUE (units 10^{-4})	EVTS	DOCUMENT ID		TECN	COMMENT
2.2±0.2±0.4	223.8	BRIERE	05	CLEO	$e^+e^- \to \psi(2S) \to K^+K^-\pi^+\pi^-$

$\Gamma(K^*(892)^0\overline{K}^*_2(1430)^0)/\Gamma_{total}$ — Γ_{76}/Γ

VALUE (units 10^{-4})	CL%	EVTS	DOCUMENT ID		TECN	COMMENT
1.86±0.32±0.43		93 ± 16	BAI	04C		$\psi(2S) \to K^+K^-\pi^+\pi^-$
• • • We do not use the following data for averages, fits, limits, etc. • • •						
<1.2	90		BAI	98J	BES	e^+e^-

$\Gamma(K^+K^-\pi^+\pi^-\eta)/\Gamma_{total}$ — Γ_{77}/Γ

VALUE (units 10^{-3})	EVTS	DOCUMENT ID		TECN	COMMENT
1.3±0.7±0.1	7	[1] AUBERT	07AU	BABR	10.6 $e^+e^- \to K^+K^-\pi^+\pi^-\eta\gamma$

[1] AUBERT 07AU quotes $\Gamma^{\psi(2S)}_{ee} \cdot B(\psi(2S) \to 2(\pi^+\pi)\eta) \cdot B(\eta \to \gamma\gamma) = 1.2 \pm 0.7 \pm 0.1$ eV.

$\Gamma(K^+K^-2(\pi^+\pi^-)\pi^0)/\Gamma_{total}$ — Γ_{79}/Γ

VALUE (units 10^{-4})	EVTS	DOCUMENT ID		TECN	COMMENT
10.0±2.5±1.8	65	ABLIKIM	07D	BES2	$e^+e^- \to \psi(2S)$

$\Gamma(K^+K^*(892)^- + \text{c.c.})/\Gamma_{total}$ — Γ_{80}/Γ

VALUE (units 10^{-5})	CL%	EVTS	DOCUMENT ID		TECN	COMMENT
2.9 ±0.4 OUR AVERAGE Error includes scale factor of 1.2.						
$3.18 \pm 0.30^{+0.26}_{-0.31}$		0.2k	ABLIKIM	12L	BES3	$e^+e^- \to \psi(2S)$
$2.9\ ^{+1.3}_{-1.7}$ ±0.4		9.6 ± 4.2	ABLIKIM	05I	BES2	$e^+e^- \to \psi(2S)$
$1.3\ ^{+1.0}_{-0.7}$ ±0.3		7	ADAM	05	CLEO	$e^+e^- \to \psi(2S)$
• • • We do not use the following data for averages, fits, limits, etc. • • •						
<5.4	90		FRANKLIN	83	MRK2	$e^+e^- \to$ hadrons

$\Gamma(2(K^+K^-))/\Gamma_{total}$ — Γ_{81}/Γ

VALUE (units 10^{-4})	EVTS	DOCUMENT ID		TECN	COMMENT
0.63±0.13 OUR AVERAGE					
0.9 ±0.4 ±0.1	13	LEES	12F	BABR	10.6 $e^+e^- \to 2(K^+K^-)\gamma$
0.6 ±0.1 ±0.1	59.2	BRIERE	05	CLEO	$e^+e^- \to \psi(2S) \to 2(K^+K^-)$

$\Gamma(2(K^+K^-)\pi^0)/\Gamma_{total}$ — Γ_{82}/Γ

VALUE (units 10^{-4})	EVTS	DOCUMENT ID		TECN	COMMENT
1.1±0.2±0.2	44.7	BRIERE	05	CLEO	$e^+e^- \to \psi(2S) \to 2(K^+K^-)\pi^0$

$\Gamma(K^+K^-\phi)/\Gamma_{total}$ — Γ_{83}/Γ

VALUE (units 10^{-4})	EVTS	DOCUMENT ID		TECN	COMMENT
0.70±0.16 OUR AVERAGE					
0.8 ±0.2 ±0.1	36.8	BRIERE	05	CLEO	$e^+e^- \to \psi(2S) \to 2(K^+K^-)$
0.6 ±0.2 ±0.1	16.1 ± 5.0	[1] BAI	03B	BES	$\psi(2S) \to 2(K^+K^-)$

[1] Normalized to $B(\psi(2S) \to J/\psi\pi^+\pi^-) = 0.305 \pm 0.016$.

$\Gamma(K_1(1270)^\pm K^\mp)/\Gamma_{total}$ — Γ_{84}/Γ

VALUE (units 10^{-4})	DOCUMENT ID		TECN	COMMENT
10.0±1.8±2.1	[1] BAI	99C	BES	e^+e^-

[1] Assuming $B(K_1(1270) \to K\rho) = 0.42 \pm 0.06$

$\Gamma(K^+\overline{K}^*(892)^0\pi^- + \text{c.c.})/\Gamma_{total}$ — Γ_{85}/Γ

VALUE (units 10^{-4})	DOCUMENT ID		TECN	COMMENT
6.7±2.5	TANENBAUM	78	MRK1	e^+e^-

Downloaded from https://academic.oup.com/ptep/article/2022/8/083C01/6651666 by KIT Library user on 27 September 2022

$\Gamma(\eta K^+ K^-, \text{no } \eta\phi)/\Gamma_{\text{total}}$ — Γ_{86}/Γ

VALUE (units 10^{-5})	CL%	EVTS	DOCUMENT ID		TECN	COMMENT
3.49±0.09±0.15		1.8k	[1] ABLIKIM	20F	BES3	$\psi(2S) \to K^+ K^- \gamma\gamma$
• • • We do not use the following data for averages, fits, limits, etc. • • •						
3.08±0.29±0.25		0.3k	[1,2] ABLIKIM	12L	BES3	$\psi(2S) \to K^+ K^- \gamma\gamma$
<13	90		BRIERE	05	CLEO	$e^+ e^- \to \psi(2S) \to K^+ K^- \pi^+ \pi^- \pi^0$

[1] Excluding $\eta\phi$.
[2] Superseded by ABLIKIM 20F.

$\Gamma(X(1750)\eta \to K^+ K^- \eta)/\Gamma_{\text{total}}$ — Γ_{87}/Γ

VALUE (units 10^{-6})	DOCUMENT ID		TECN	COMMENT
4.8±1.0±2.6	ABLIKIM	20F	BES3	$\psi(2S) \to K^+ K^- \eta$

$\Gamma(K_1(1400)^\pm K^\mp)/\Gamma_{\text{total}}$ — Γ_{88}/Γ

VALUE (units 10^{-4})	CL%	DOCUMENT ID		TECN	COMMENT
<3.1	90	[1] BAI	99C	BES	$e^+ e^-$

[1] Assuming $B(K_1(1400) \to K^* \pi) = 0.94 \pm 0.06$

$\Gamma(K_2^*(1430)^\pm K^\mp)/\Gamma_{\text{total}}$ — Γ_{89}/Γ

VALUE (units 10^{-5})	EVTS	DOCUMENT ID		TECN	COMMENT
$7.12\pm0.62^{+1.13}_{-0.61}$	251 ± 22	ABLIKIM	12L	BES3	$e^+ e^- \to \psi(2S)$

$\Gamma(K^*(892)^0 \overline{K}^0 + \text{c.c.})/\Gamma_{\text{total}}$ — Γ_{90}/Γ

VALUE (units 10^{-5})	EVTS	DOCUMENT ID		TECN	COMMENT
10.9±2.0 OUR AVERAGE					
$13.3^{+2.4}_{-2.8}\pm1.7$	65.6 ± 9.0	ABLIKIM	05I	BES2	$e^+ e^- \to \psi(2S)$
$9.2^{+2.7}_{-2.2}\pm0.9$	25	ADAM	05	CLEO	$e^+ e^- \to \psi(2S)$

$\Gamma(K^+ K^*(892)^- + \text{c.c.})/\Gamma(K^*(892)^0 \overline{K}^0 + \text{c.c.})$ — Γ_{80}/Γ_{90}

VALUE	DOCUMENT ID		TECN	COMMENT
0.16±0.06 OUR AVERAGE				
$0.22^{+0.10}_{-0.14}$	ABLIKIM	05I	BES2	$e^+ e^- \to \psi(2S)$
$0.14^{+0.08}_{-0.06}$	ADAM	05	CLEO	$e^+ e^- \to \psi(2S)$

$\Gamma(\omega K^+ K^-)/\Gamma_{\text{total}}$ — Γ_{91}/Γ

VALUE (units 10^{-4})	EVTS	DOCUMENT ID		TECN	COMMENT
1.62±0.11 OUR AVERAGE		Error includes scale factor of 1.1.			
1.56±0.04±0.11	2.8k	ABLIKIM	14G	BES3	$\psi(2S) \to K^+ K^- \pi^+ \pi^- \pi^0$
2.38±0.37±0.29	78	ABLIKIM	06G	BES2	$\psi(2S) \to K^+ K^- \pi^+ \pi^- \pi^0$
1.9 ±0.3 ±0.3	76.8	BRIERE	05	CLEO	$e^+ e^- \to \psi(2S) \to K^+ K^- \pi^+ \pi^- \pi^0$
1.5 ±0.3 ±0.2	23	[1] BAI	03B	BES	$\psi(2S) \to K^+ K^- \pi^+ \pi^- \pi^0$

[1] Normalized to $B(\psi(2S) \to J/\psi\pi^+\pi^-) = 0.305 \pm 0.016$.

$\Gamma(\omega K_S^0 K_S^0)/\Gamma_{\text{total}}$ — Γ_{92}/Γ

VALUE (units 10^{-5})	EVTS	DOCUMENT ID		TECN	COMMENT
7.04±0.39±0.36	1.5k	ABLIKIM	21AL	BES3	$\psi(2S) \to \pi^+ \pi^- \pi^0 K_S^0 K_S^0$

$\Gamma(\omega K^*(892)^+ K^- + \text{c.c.})/\Gamma_{\text{total}}$ — Γ_{93}/Γ

VALUE (units 10^{-5})	EVTS	DOCUMENT ID		TECN	COMMENT
20.7±2.6 OUR AVERAGE					
18.9±2.9±2.2	396	ABLIKIM	13M	BES3	$\psi(2S) \to \omega K_S^0 K^- \pi^+$
22.6±3.0±2.4	535	ABLIKIM	13M	BES3	$\psi(2S) \to \omega K^+ K^- \pi^0$

$\Gamma(\omega K_2^*(1430)^+ K^- + \text{c.c.})/\Gamma_{\text{total}}$ — Γ_{94}/Γ

VALUE (units 10^{-5})	EVTS	DOCUMENT ID		TECN	COMMENT
6.1 ±1.2 OUR AVERAGE					
6.39±1.50±0.78	128	ABLIKIM	13M	BES3	$\psi(2S) \to \omega K_S^0 K^- \pi^+$
5.86±1.61±0.83	143	ABLIKIM	13M	BES3	$\psi(2S) \to \omega K^+ K^- \pi^0$

$\Gamma(\omega \overline{K}^*(892)^0 K^0)/\Gamma_{\text{total}}$ — Γ_{95}/Γ

VALUE (units 10^{-5})	EVTS	DOCUMENT ID		TECN	COMMENT
16.8±2.5±1.6	356	ABLIKIM	13M	BES3	$\psi(2S) \to \omega K_S^0 K^- \pi^+$

$\Gamma(\omega \overline{K}_2^*(1430)^0 K^0)/\Gamma_{\text{total}}$ — Γ_{96}/Γ

VALUE (units 10^{-5})	EVTS	DOCUMENT ID		TECN	COMMENT
5.82±2.08±0.72	116	ABLIKIM	13M	BES3	$\psi(2S) \to \omega K_S^0 K^- \pi^+$

$\Gamma(\omega X(1440) \to \omega K_S^0 K^- \pi^+ + \text{c.c.})/\Gamma_{\text{total}}$ — Γ_{97}/Γ

VALUE (units 10^{-5})	EVTS	DOCUMENT ID		TECN	COMMENT
1.60±0.27±0.24	109	[1] ABLIKIM	13M	BES3	$\psi(2S) \to \omega K_S^0 K^- \pi^+$

[1] $X(1440)$ compatible with $\eta(1405)$ and $\eta(1475)$. A $f_1(1420)$ is also possible.

$\Gamma(\omega X(1440) \to \omega K^+ K^- \pi^0)/\Gamma_{\text{total}}$ — Γ_{98}/Γ

VALUE (units 10^{-5})	EVTS	DOCUMENT ID		TECN	COMMENT
1.09±0.20±0.16	82	[1] ABLIKIM	13M	BES3	$\psi(2S) \to \omega K^+ K^- \pi^0$

[1] $X(1440)$ compatible with $\eta(1405)$ and $\eta(1475)$. A $f_1(1420)$ is also possible.

$\Gamma(\omega f_1(1285) \to \omega K_S^0 K^- \pi^+ + \text{c.c.})/\Gamma_{\text{total}}$ — Γ_{99}/Γ

VALUE (units 10^{-5})	EVTS	DOCUMENT ID		TECN	COMMENT
0.302±0.098±0.027	22	[1] ABLIKIM	13M	BES3	$\psi(2S) \to \omega K_S^0 K^- \pi^+$

[1] Statistical signficance 4.5 σ. This measurement is equivalent to a limit of $< 0.478\times10^{-5}$ at 90% C.L.

$\Gamma(\omega f_1(1285) \to \omega K^+ K^- \pi^0)/\Gamma_{\text{total}}$ — Γ_{100}/Γ

VALUE (units 10^{-5})	EVTS	DOCUMENT ID		TECN	COMMENT
0.125±0.070±0.013	10	[1] ABLIKIM	13M	BES3	$\psi(2S) \to \omega K^+ K^- \pi^0$

[1] Statistical signficance 3.2 σ. This measurement is equivalent to a limit of $< 0.221\times10^{-5}$ at 90% C.L.

$\Gamma(p\overline{p})/\Gamma_{\text{total}}$ — Γ_{101}/Γ

VALUE (units 10^{-4})	EVTS	DOCUMENT ID		TECN	COMMENT
2.94±0.08 OUR FIT					
3.02±0.08 OUR AVERAGE					
3.05±0.02±0.12	19k	ABLIKIM	18T	BES3	$e^+ e^- \to \psi(2S) \to p\overline{p}$
3.08±0.05±0.18	4.5k	[1] DOBBS	14		$e^+ e^- \to \psi(2S) \to p\overline{p}$
3.36±0.09±0.25	1.6k	ABLIKIM	07C	BES	$e^+ e^- \to \psi(2S) \to p\overline{p}$
2.87±0.12±0.15	557	PEDLAR	05	CLEO	$e^+ e^- \to \psi(2S) \to p\overline{p}$
1.4 ±0.8	4	BRANDELIK	79C	DASP	$e^+ e^- \to \psi(2S) \to p\overline{p}$
2.3 ±0.7		FELDMAN	77	MRK1	$e^+ e^- \to \psi(2S) \to p\overline{p}$

[1] Using CLEO-c data but not authored by the CLEO Collaboration.

$\Gamma(p\overline{p})/\Gamma(J/\psi(1S)\pi^+\pi^-)$ — Γ_{101}/Γ_{12}

VALUE (units 10^{-4})	DOCUMENT ID		TECN	COMMENT
8.49±0.23 OUR FIT				
6.98±0.49±0.97	BAI	01	BES	$e^+ e^- \to \psi(2S) \to p\overline{p}$

$\Gamma(n\overline{n})/\Gamma_{\text{total}}$ — Γ_{102}/Γ

VALUE (units 10^{-4})	EVTS	DOCUMENT ID		TECN	COMMENT
3.06±0.06±0.14	6k	ABLIKIM	18T	BES3	$e^+ e^- \to \psi(2S) \to n\overline{n}$

$\Gamma(p\overline{p}\pi^0)/\Gamma_{\text{total}}$ — Γ_{103}/Γ

VALUE (units 10^{-4})	EVTS	DOCUMENT ID		TECN	COMMENT
1.53±0.07 OUR AVERAGE					
1.65±0.03±0.15	4.5k	ABLIKIM	13A	BES3	$\psi(2S) \to p\overline{p}\pi^0$
1.54±0.06±0.06	948	ALEXANDER	10	CLEO	$\psi(2S) \to \pi^0 p\overline{p}$
1.32±0.10±0.15	256	[1] ABLIKIM	05E	BES2	$e^+ e^- \to \psi(2S) \to p\overline{p}\gamma\gamma$
1.4 ±0.5	9	FRANKLIN	83	MRK2	$e^+ e^-$

[1] Computed using $B(\pi^0 \to \gamma\gamma) = (98.80 \pm 0.03)\%$.

$\Gamma(N(940)\overline{p} + \text{c.c.} \to p\overline{p}\pi^0)/\Gamma_{\text{total}}$ — Γ_{104}/Γ

VALUE (units 10^{-5})	EVTS	DOCUMENT ID		TECN	COMMENT
$6.42\pm0.20^{+1.78}_{-1.28}$	1.9k	[1] ABLIKIM	13A	BES3	$\psi(2S) \to p\overline{p}\pi^0$

[1] From a fit of $\pi^0 p\overline{p}$ data to eight distinct intermediate $N\overline{p}$ resonant states.

$\Gamma(N(1440)\overline{p} + \text{c.c.} \to p\overline{p}\pi^0)/\Gamma_{\text{total}}$ — Γ_{105}/Γ

VALUE (units 10^{-5})	EVTS	DOCUMENT ID		TECN	COMMENT
$7.3\ ^{+1.7}_{-1.5}$ OUR AVERAGE	Error includes scale factor of 2.5.				
$3.58\pm0.25^{+1.59}_{-0.84}$	1.1k	[1] ABLIKIM	13A	BES3	$\psi(2S) \to p\overline{p}\pi^0$
8.1 ±0.7 ±0.3	474	[2] ALEXANDER	10	CLEO	$\psi(2S) \to \pi^0 p\overline{p}$

[1] From a fit of $\pi^0 p\overline{p}$ data to eight distinct intermediate $N\overline{p}$ resonant states.
[2] From a fit of the $p\overline{p}$ and $p\pi^0$ mass distributions to a combination of $N(1440)\overline{p}$, a broad $p\overline{p}$ enhancement around 2100 MeV, and two other broad, unestablished resonances.

$\Gamma(N(1520)\overline{p} + \text{c.c.} \to p\overline{p}\pi^0)/\Gamma_{\text{total}}$ — Γ_{106}/Γ

VALUE (units 10^{-5})	EVTS	DOCUMENT ID		TECN	COMMENT
$0.64\pm0.05^{+0.22}_{-0.17}$	0.2k	[1] ABLIKIM	13A	BES3	$\psi(2S) \to p\overline{p}\pi^0$

[1] From a fit of $\pi^0 p\overline{p}$ data to eight distinct intermediate $N\overline{p}$ resonant states.

$\Gamma(N(1535)\overline{p} + \text{c.c.} \to p\overline{p}\pi^0)/\Gamma_{\text{total}}$ — Γ_{107}/Γ

VALUE (units 10^{-5})	EVTS	DOCUMENT ID		TECN	COMMENT
$2.47\pm0.28^{+0.99}_{-0.97}$	0.7k	[1] ABLIKIM	13A	BES3	$\psi(2S) \to p\overline{p}\pi^0$

[1] From a fit of $\pi^0 p\overline{p}$ data to eight distinct intermediate $N\overline{p}$ resonant states.

$\Gamma(N(1650)\overline{p} + \text{c.c.} \to p\overline{p}\pi^0)/\Gamma_{\text{total}}$ — Γ_{108}/Γ

VALUE (units 10^{-5})	EVTS	DOCUMENT ID		TECN	COMMENT
$3.76\pm0.28^{+1.37}_{-1.66}$	1.1k	[1] ABLIKIM	13A	BES3	$\psi(2S) \to p\overline{p}\pi^0$

[1] From a fit of $\pi^0 p\overline{p}$ data to eight distinct intermediate $N\overline{p}$ resonant states.

Downloaded from https://academic.oup.com/ptep/article/2022/8/083C01/6651666 by KIT Library user on 27 September 2022

$\Gamma(N(1720)\overline{p}+\text{c.c.}\to p\overline{p}\pi^0)/\Gamma_{\text{total}}$ — Γ_{109}/Γ

VALUE (units 10^{-5})	EVTS	DOCUMENT ID		TECN	COMMENT
$\mathbf{1.79\pm0.10^{+0.24}_{-0.71}}$	0.5k	[1] ABLIKIM	13A	BES3	$\psi(2S)\to p\overline{p}\pi^0$

[1] From a fit of $\pi^0 p\overline{p}$ data to eight distinct intermediate $N\overline{p}$ resonant states.

$\Gamma(N(2300)\overline{p}+\text{c.c.}\to p\overline{p}\pi^0)/\Gamma_{\text{total}}$ — Γ_{110}/Γ

VALUE (units 10^{-5})	EVTS	DOCUMENT ID		TECN	COMMENT
$\mathbf{2.62\pm0.28^{+1.12}_{-0.64}}$	0.9k	[1] ABLIKIM	13A	BES3	$\psi(2S)\to p\overline{p}\pi^0$

[1] From a fit of $\pi^0 p\overline{p}$ data to eight distinct intermediate $N\overline{p}$ resonant states.

$\Gamma(N(2570)\overline{p}+\text{c.c.}\to p\overline{p}\pi^0)/\Gamma_{\text{total}}$ — Γ_{111}/Γ

VALUE (units 10^{-5})	EVTS	DOCUMENT ID		TECN	COMMENT
$\mathbf{2.13\pm0.08^{+0.40}_{-0.30}}$	0.8k	[1] ABLIKIM	13A	BES3	$\psi(2S)\to p\overline{p}\pi^0$

[1] From a fit of $\pi^0 p\overline{p}$ data to eight distinct intermediate $N\overline{p}$ resonant states.

$\Gamma(p\overline{p}\pi^+\pi^-)/\Gamma_{\text{total}}$ — Γ_{112}/Γ

VALUE (units 10^{-4})	EVTS	DOCUMENT ID		TECN	COMMENT
6.0±0.4 OUR AVERAGE					
$5.9\pm0.2\pm0.4$	904.5	BRIERE	05	CLEO	$e^+e^-\to\psi(2S)\to p\overline{p}\pi^+\pi^-$
$8\ \pm2$		[1] TANENBAUM	78	MRK1	e^+e^-

[1] Assuming entirely strong decay.

$\Gamma(p\overline{p}K^+K^-)/\Gamma_{\text{total}}$ — Γ_{113}/Γ

VALUE (units 10^{-5})	EVTS	DOCUMENT ID		TECN	COMMENT
2.7±0.6±0.4	30.1	BRIERE	05	CLEO	$e^+e^-\to\psi(2S)\to p\overline{p}K^+K^-$

$\Gamma(p\overline{p}\eta)/\Gamma_{\text{total}}$ — Γ_{114}/Γ

VALUE (units 10^{-5})	EVTS	DOCUMENT ID		TECN	COMMENT
6.0±0.4 OUR AVERAGE					
$6.4\pm0.2\pm0.6$	679	[1] ABLIKIM	13S	BES3	$\psi(2S)\to\eta p\overline{p}$
$5.6\pm0.6\pm0.3$	154	[1] ALEXANDER	10	CLEO	$\psi(2S)\to\eta p\overline{p}$
$5.8\pm1.1\pm0.7$	44.8 ± 8.5	[2] ABLIKIM	05E	BES2	$e^+e^-\to\psi(2S)\to p\overline{p}\gamma\gamma$
$8\ \pm3\ \pm3$	9.8	BRIERE	05	CLEO	$e^+e^-\to\psi(2S)\to p\overline{p}\pi^+\pi^-\pi^0$

[1] With $N(1535)$ decaying to $p\eta$.
[2] Computed using $B(\eta\to\gamma\gamma)=(39.43\pm0.26)\%$.

$\Gamma(N(1535)\overline{p}+\text{c.c.}\to p\overline{p}\eta)/\Gamma_{\text{total}}$ — Γ_{115}/Γ

VALUE (units 10^{-5})	EVTS	DOCUMENT ID		TECN	COMMENT
$\mathbf{4.5^{+0.7}_{-0.6}}$ **OUR AVERAGE**					
$5.2\pm0.3^{+3.2}_{-1.2}$	527	[1] ABLIKIM	13S	BES3	$\psi(2S)\to\eta p\overline{p}$
$4.4\pm0.6\pm0.3$	123	[2] ALEXANDER	10	CLEO	$\psi(2S)\to\eta p\overline{p}$

[1] With $N(1535)$ decaying to $p\eta$.
[2] From a fit of the $p\overline{p}$ and $p\eta$ distributions to a combination of $N^*(1535)\overline{p}$ and a broad $p\overline{p}$ enhancement around 2100 MeV.

$\Gamma(p\overline{p}\pi^+\pi^-\pi^0)/\Gamma_{\text{total}}$ — Γ_{116}/Γ

VALUE (units 10^{-4})	EVTS	DOCUMENT ID		TECN	COMMENT
7.3±0.4±0.6	434.9	BRIERE	05	CLEO	$e^+e^-\to\psi(2S)\to p\overline{p}\pi^+\pi^-\pi^0$

$\Gamma(p\overline{p}\rho^0)/\Gamma_{\text{total}}$ — Γ_{117}/Γ

VALUE (units 10^{-4})	EVTS	DOCUMENT ID		TECN	COMMENT
0.5±0.1±0.2	61.1	BRIERE	05	CLEO	$e^+e^-\to\psi(2S)\to p\overline{p}\pi^+\pi^-$

$\Gamma(p\overline{p}\omega)/\Gamma_{\text{total}}$ — Γ_{118}/Γ

VALUE (units 10^{-4})	EVTS	DOCUMENT ID		TECN	COMMENT
0.69±0.21 OUR AVERAGE					
$0.6\ \pm0.2\ \pm0.2$	21.2	BRIERE	05	CLEO	$e^+e^-\to\psi(2S)\to p\overline{p}\pi^+\pi^-\pi^0$
$0.8\ \pm0.3\ \pm0.1$	14.9 ± 0.1	[1] BAI	03B	BES	$\psi(2S)\to p\overline{p}\pi^+\pi^-\pi^0$

[1] Normalized to $B(\psi(2S)\to J/\psi\pi^+\pi^-)=0.305\pm0.016$.

$\Gamma(p\overline{p}\eta')/\Gamma_{\text{total}}$ — Γ_{119}/Γ

VALUE (units 10^{-5})	EVTS	DOCUMENT ID		TECN	COMMENT
1.10±0.10±0.08	491	[1] ABLIKIM	19N	BES3	$\psi(2S)\to\eta' p\overline{p}$

[1] From the combination of $p\overline{p}\eta'\to p\overline{p}\pi^+\pi^-\eta$ and $p\overline{p}\eta'\to p\overline{p}\pi^+\pi^-\gamma$ channels.

$\Gamma(p\overline{p}\phi)/\Gamma_{\text{total}}$ — Γ_{120}/Γ

VALUE (units 10^{-6})	CL%	EVTS	DOCUMENT ID		TECN	COMMENT
6.06±0.38±0.48		753	ABLIKIM	19AO	BES3	$e^+e^-\to\psi(2S)\to p\overline{p}K^+K^-$
• • • We do not use the following data for averages, fits, limits, etc. • • •						
<24	90		BRIERE	05	CLEO	$e^+e^-\to\psi(2S)\to p\overline{p}K^+K^-$
<26	90		[1] BAI	03B	BES	$\psi(2S)\to K^+K^-p\overline{p}$

[1] Normalized to $B(\psi(2S)\to J/\psi\pi^+\pi^-)=0.305\pm0.016$.

$\Gamma(\phi X(1835)\to p\overline{p}\phi)/\Gamma_{\text{total}}$ — Γ_{121}/Γ

VALUE	CL%	DOCUMENT ID		TECN	COMMENT
$\mathbf{<1.82\times10^{-7}}$	90	ABLIKIM	19AO	BES3	$e^+e^-\to\psi(2S)\to p\overline{p}K^+K^-$

$\Gamma(p\overline{n}\pi^-\text{ or c.c.})/\Gamma_{\text{total}}$ — Γ_{122}/Γ

VALUE (units 10^{-4})	EVTS	DOCUMENT ID		TECN	COMMENT
2.48±0.17 OUR AVERAGE					
$2.45\pm0.11\pm0.21$	851	ABLIKIM	06I	BES2	$e^+e^-\to p\pi^-X$
$2.52\pm0.12\pm0.22$	849	ABLIKIM	06I	BES2	$e^+e^-\to\overline{p}\pi^+X$

$\Gamma(p\overline{n}\pi^-\pi^0)/\Gamma_{\text{total}}$ — Γ_{123}/Γ

VALUE (units 10^{-4})	EVTS	DOCUMENT ID		TECN	COMMENT
3.18±0.50±0.50	135 ± 21	ABLIKIM	06I	BES2	$e^+e^-\to p\pi^-\pi^0X$

$\Gamma(\Lambda\overline{\Lambda})/\Gamma_{\text{total}}$ — Γ_{124}/Γ

VALUE (units 10^{-4})	CL%	EVTS	DOCUMENT ID		TECN	COMMENT
3.81±0.13 OUR AVERAGE Error includes scale factor of 1.4. See the ideogram below.						
$3.97\pm0.02\pm0.12$		31k	ABLIKIM	17L	BES3	$e^+e^-\to\Lambda\overline{\Lambda}$
$3.71\pm0.05\pm0.15$		6.5k	[1] DOBBS	17		$e^+e^-\to\Lambda\overline{\Lambda}$
$3.39\pm0.20\pm0.32$		337	ABLIKIM	07C	BES	$e^+e^-\to\psi(2S)\to$ hadrons
$6.4\ \pm1.8\ \pm0.1$			[2] AUBERT	07BD	BABR	$10.6\ e^+e^-\to\Lambda\overline{\Lambda}\gamma$
$3.28\pm0.23\pm0.25$		208	PEDLAR	05	CLEO	$e^+e^-\to\psi(2S)\to$ hadrons
• • • We do not use the following data for averages, fits, limits, etc. • • •						
$3.75\pm0.09\pm0.23$		1.9k	[1,3] DOBBS	14		$e^+e^-\to\Lambda\overline{\Lambda}$
$1.81\pm0.20\pm0.27$		80	[4] BAI	01	BES	$e^+e^-\to\psi(2S)\to$ hadrons
<4	90		FELDMAN	77	MRK1	$e^+e^-\to\psi(2S)\to$ hadrons

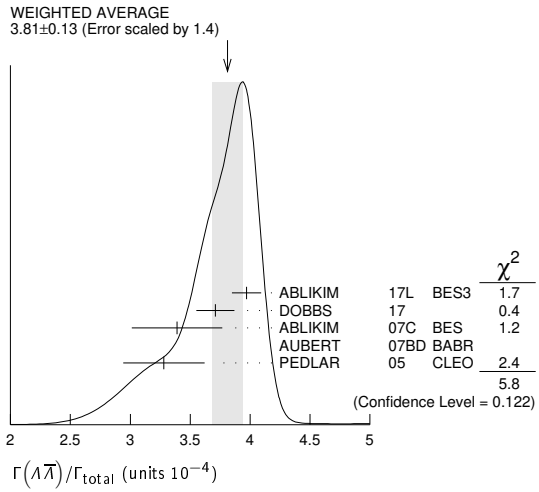

[1] Using CLEO-c data but not authored by the CLEO Collaboration.
[2] AUBERT 07BD reports $[\Gamma(\psi(2S)\to\Lambda\overline{\Lambda})/\Gamma_{\text{total}}]\times[\Gamma(\psi(2S)\to e^+e^-)]=(15\pm4\pm1)\times10^{-4}$ keV which we divide by our best value $\Gamma(\psi(2S)\to e^+e^-)=2.33\pm0.04$ keV. Our first error is their experiment's error and our second error is the systematic error from using our best value.
[3] Superseded by DOBBS 17.
[4] Estimated using $B(\psi(2S)\to J/\psi\pi^+\pi^-)=0.310\pm0.028$.

$\Gamma(\Lambda\overline{\Lambda}\pi^0)/\Gamma_{\text{total}}$ — Γ_{125}/Γ

VALUE (units 10^{-5})	CL%	DOCUMENT ID		TECN	COMMENT
< 0.29	90	[1] ABLIKIM	13F	BES3	$\psi(2S)\to p\overline{p}\pi^+\pi^-\gamma\gamma$
• • • We do not use the following data for averages, fits, limits, etc. • • •					
<12	90	[2] ABLIKIM	07H	BES2	$e^+e^-\to\psi(2S)$

[1] Using $B(\Lambda\to\pi^-p)=63.9\%$ and $B(\pi^0\to\gamma\gamma)=98.8\%$.
[2] Using $B(\Lambda\to\pi^-p)=63.9\%$ and $B(\eta\to\gamma\gamma)=39.4\%$.

Downloaded from https://academic.oup.com/ptep/article/2022/8/083C01/6651666 by KIT Library user on 27 September 2022

$\Gamma(\Lambda\overline{\Lambda}\eta)/\Gamma_{total}$ — Γ_{126}/Γ

VALUE (units 10^{-5})	CL%	EVTS	DOCUMENT ID		TECN	COMMENT
2.48±0.34±0.19		60	[1] ABLIKIM	13F	BES3	$\psi(2S) \to p\overline{p}\pi^+\pi^-\gamma\gamma$
• • • We do not use the following data for averages, fits, limits, etc. • • •						
<4.9	90		[2] ABLIKIM	07H	BES2	$e^+e^- \to \psi(2S)$

[1] Using $B(\Lambda \to \pi^- p) = 63.9\%$ and $B(\eta \to \gamma\gamma) = 39.31\%$.
[2] Using $B(\Lambda \to \pi^- p) = 63.9\%$.

$\Gamma(\Lambda\overline{\Lambda}\pi^+\pi^-)/\Gamma_{total}$ — Γ_{127}/Γ

VALUE (units 10^{-4})	EVTS	DOCUMENT ID		TECN	COMMENT
2.8±0.4±0.5	73.4	BRIERE	05	CLEO	$e^+e^- \to \psi(2S) \to p\overline{p}2(\pi^+\pi^-)$

$\Gamma(\Lambda\overline{p}K^+)/\Gamma_{total}$ — Γ_{128}/Γ

VALUE (units 10^{-4})	EVTS	DOCUMENT ID		TECN	COMMENT
1.0±0.1±0.1	74.0	BRIERE	05	CLEO	$e^+e^- \to \psi(2S) \to p\overline{p}K^+\pi^-$

$\Gamma(\Lambda\overline{p}K^*(892)^+ + c.c.)/\Gamma_{total}$ — Γ_{129}/Γ

VALUE (units 10^{-5})	EVTS	DOCUMENT ID		TECN	COMMENT
6.3±0.5±0.5	1011	ABLIKIM	19AU	BES3	$e^+e^- \to \psi(2S)$

$\Gamma(\Lambda\overline{p}K^+\pi^+\pi^-)/\Gamma_{total}$ — Γ_{130}/Γ

VALUE (units 10^{-4})	EVTS	DOCUMENT ID		TECN	COMMENT
1.8±0.3±0.3	45.8	BRIERE	05	CLEO	$e^+e^- \to \psi(2S) \to p\overline{p}K^+\pi^+\pi^-\pi^-$

$\Gamma(\overline{\Lambda}nK^0_S + c.c.)/\Gamma_{total}$ — Γ_{131}/Γ

VALUE (units 10^{-4})	EVTS	DOCUMENT ID		TECN	COMMENT
0.81±0.11±0.14	50	[1] ABLIKIM	08C	BES2	$e^+e^- \to J/\psi$

[1] Using $B(\overline{\Lambda} \to \overline{p}\pi^+) = 63.9\%$ and $B(K^0_S \to \pi^+\pi^-) = 69.2\%$.

$\Gamma(\Delta^{++}\overline{\Delta}^{--})/\Gamma_{total}$ — Γ_{132}/Γ

VALUE (units 10^{-5})	EVTS	DOCUMENT ID		TECN	COMMENT
12.8±1.0±3.4	157	[1] BAI	01	BES	$e^+e^- \to \psi(2S) \to$ hadrons

[1] Estimated using $B(\psi(2S) \to J/\psi\pi^+\pi^-) = 0.310 \pm 0.028$.

$\Gamma(\Lambda\overline{\Sigma}^+\pi^- + c.c.)/\Gamma_{total}$ — Γ_{133}/Γ

VALUE (units 10^{-4})	EVTS	DOCUMENT ID		TECN	COMMENT
1.40±0.03±0.13	2.8k	ABLIKIM	13W	BES3	$\psi(2S) \to$ hadrons

$\Gamma(\Lambda\overline{\Sigma}^-\pi^+ + c.c.)/\Gamma_{total}$ — Γ_{134}/Γ

VALUE (units 10^{-4})	EVTS	DOCUMENT ID		TECN	COMMENT
1.54±0.04±0.13	2.8k	ABLIKIM	13W	BES3	$\psi(2S) \to$ hadrons

$\Gamma(\Lambda\overline{\Sigma}^0 + c.c.)/\Gamma_{total}$ — Γ_{135}/Γ

VALUE (units 10^{-6})	EVTS	DOCUMENT ID		TECN	COMMENT
1.60±0.31±0.59	60	ABLIKIM	21L	BES3	$e^+e^- \to \psi(2S) \to$ hadrons

$\Gamma(\Lambda\overline{\Sigma}^0)/\Gamma_{total}$ — Γ_{136}/Γ

VALUE (units 10^{-5})	EVTS	DOCUMENT ID		COMMENT
• • • We do not use the following data for averages, fits, limits, etc. • • •				
1.23±0.23±0.08	30	[1] DOBBS	17	$e^+e^- \to \psi(2S) \to$ hadrons

[1] Using CLEO-c data but not authored by the CLEO Collaboration.

$\Gamma(\Sigma^0\overline{p}K^+ + c.c.)/\Gamma_{total}$ — Γ_{137}/Γ

VALUE (units 10^{-5})	EVTS	DOCUMENT ID		TECN	COMMENT
1.67±0.13±0.12	276	[1] ABLIKIM	13D	BES3	$\psi(2S) \to \gamma\Lambda\overline{p}K^+$

[1] Using $B(\Lambda \to p\pi^-) = 63.9\%$, and $B(\Sigma^0 \to \Lambda\gamma) = 100\%$.

$\Gamma(\Sigma^+\overline{\Sigma}^-)/\Gamma_{total}$ — Γ_{138}/Γ

VALUE (units 10^{-4})	EVTS	DOCUMENT ID		TECN	COMMENT
2.43±0.10 OUR AVERAGE		Error includes scale factor of 1.4.			
2.52±0.04±0.09	5.4k	ABLIKIM	21AT	BES3	$\psi(2S) \to p\pi^0\overline{p}\pi^0$
2.31±0.06±0.10	1.9k	[1] DOBBS	17		$e^+e^- \to \psi(2S) \to$ hadrons
2.57±0.44±0.68	35	PEDLAR	05	CLEO	$e^+e^- \to \psi(2S) \to$ hadrons
• • • We do not use the following data for averages, fits, limits, etc. • • •					
2.51±0.15±0.16	281	[1,2] DOBBS	14		$e^+e^- \to \psi(2S) \to$ hadrons

[1] Using CLEO-c data but not authored by the CLEO Collaboration.
[2] Superseded by DOBBS 17.

$\Gamma(\Sigma^0\overline{\Sigma}^0)/\Gamma_{total}$ — Γ_{139}/Γ

VALUE (units 10^{-4})	EVTS	DOCUMENT ID		TECN	COMMENT
2.35±0.09 OUR AVERAGE		Error includes scale factor of 1.1.			
2.44±0.03±0.11	7k	ABLIKIM	17L	BES3	$e^+e^- \to \psi(2S) \to$ hadrons
2.22±0.05±0.11	2.6k	[1] DOBBS	17		$e^+e^- \to \psi(2S) \to$ hadrons
2.35±0.36±0.32	59	ABLIKIM	07C	BES	$e^+e^- \to \psi(2S) \to$ hadrons
2.63±0.35±0.21	58	PEDLAR	05	CLEO	$e^+e^- \to \psi(2S) \to$ hadrons
• • • We do not use the following data for averages, fits, limits, etc. • • •					
2.25±0.11±0.16	439	[1,2] DOBBS	14		$e^+e^- \to \psi(2S) \to$ hadrons
1.2 ±0.4 ±0.4	8	[3] BAI	01	BES	$e^+e^- \to \psi(2S) \to$ hadrons

[1] Using CLEO-c data but not authored by the CLEO Collaboration.
[2] Superseded by DOBBS 17.
[3] Estimated using $B(\psi(2S) \to J/\psi\pi^+\pi^-) = 0.310 \pm 0.028$.

$\Gamma(\Sigma(1385)^+\overline{\Sigma}(1385)^-)/\Gamma_{total}$ — Γ_{140}/Γ

VALUE (units 10^{-5})	EVTS	DOCUMENT ID		TECN	COMMENT
8.5±0.7 OUR AVERAGE					
8.4±0.5±0.5	1.5k	ABLIKIM	16L	BES3	$\psi(2S) \to \Sigma(1385)^+\overline{\Sigma}(1385)^-$
11 ±3 ±3	14	[1] BAI	01	BES	$e^+e^- \to \psi(2S) \to$ hadrons

[1] Estimated using $B(\psi(2S) \to J/\psi\pi^+\pi^-) = 0.310 \pm 0.028$.

$\Gamma(\Sigma(1385)^-\overline{\Sigma}(1385)^+)/\Gamma_{total}$ — Γ_{141}/Γ

VALUE (units 10^{-5})	EVTS	DOCUMENT ID		TECN	COMMENT
8.5±0.6±0.6	1.4k	ABLIKIM	16L	BES3	$\psi(2S) \to \Sigma(1385)^-\overline{\Sigma}(1385)^+$

$\Gamma(\Sigma(1385)^0\overline{\Sigma}(1385)^0)/\Gamma_{total}$ — Γ_{142}/Γ

VALUE (units 10^{-4})	EVTS	DOCUMENT ID		TECN	COMMENT
0.69±0.05±0.05	2.2k	ABLIKIM	17E	BES3	$e^+e^- \to \psi(2S) \to$ hadrons

$\Gamma(\Xi^-\overline{\Xi}^+)/\Gamma_{total}$ — Γ_{143}/Γ

VALUE (units 10^{-4})	CL%	EVTS	DOCUMENT ID		TECN	COMMENT
2.87±0.11 OUR AVERAGE			Error includes scale factor of 1.1.			
3.03±0.05±0.14		3.6k	[1] DOBBS	17		$e^+e^- \to \psi(2S) \to$ hadrons
2.78±0.05±0.14		5k	ABLIKIM	16L	BES3	$\psi(2S) \to \Xi^-\overline{\Xi}^+$
3.03±0.40±0.32		67	ABLIKIM	07C	BES	$e^+e^- \to \psi(2S) \to$ hadrons
2.38±0.30±0.21		63	PEDLAR	05	CLEO	$e^+e^- \to \psi(2S) \to$ hadrons
• • • We do not use the following data for averages, fits, limits, etc. • • •						
2.66±0.12±0.20		548	[1,2] DOBBS	14		$e^+e^- \to \psi(2S) \to$ hadrons
0.94±0.27±0.15		12	[3] BAI	01	BES	$e^+e^- \to \psi(2S) \to$ hadrons
<2	90		FELDMAN	77	MRK1	$e^+e^- \to \psi(2S) \to$ hadrons

[1] Using CLEO-c data but not authored by the CLEO Collaboration.
[2] Superseded by DOBBS 17.
[3] Estimated using $B(\psi(2S) \to J/\psi\pi^+\pi^-) = 0.310 \pm 0.028$.

$\Gamma(\Xi^0\overline{\Xi}^0)/\Gamma_{total}$ — Γ_{144}/Γ

VALUE (units 10^{-4})	EVTS	DOCUMENT ID		TECN	COMMENT
2.3 ±0.4 OUR AVERAGE		Error includes scale factor of 4.2.			
2.73±0.03±0.13	11k	ABLIKIM	17E	BES3	$e^+e^- \to \psi(2S) \to$ hadrons
1.97±0.06±0.11	1.2k	[1] DOBBS	17		$e^+e^- \to \psi(2S) \to$ hadrons
2.75±0.64±0.61	19	PEDLAR	05	CLEO	$e^+e^- \to \psi(2S) \to$ hadrons
• • • We do not use the following data for averages, fits, limits, etc. • • •					
2.02±0.19±0.15	112	[1,2] DOBBS	14		$e^+e^- \to \psi(2S) \to$ hadrons

[1] Using CLEO-c data but not authored by the CLEO Collaboration.
[2] Superseded by DOBBS 17.

$\Gamma(\Xi(1530)^0\overline{\Xi}(1530)^0)/\Gamma_{total}$ — Γ_{145}/Γ

VALUE (units 10^{-5})	CL%	EVTS	DOCUMENT ID		TECN	COMMENT
6.77±0.14±0.39		2951	ABLIKIM	21AO	BES3	$e^+e^- \to \psi(2S) \to$ hadrons
• • • We do not use the following data for averages, fits, limits, etc. • • •						
<32	90		PEDLAR	05	CLEO	$e^+e^- \to \psi(2S) \to$ hadrons
< 8.1	90		[1] BAI	01	BES	$e^+e^- \to \psi(2S) \to$ hadrons

[1] Estimated using $B(\psi(2S) \to J/\psi\pi^+\pi^-) = 0.310 \pm 0.028$.

$\Gamma(\Lambda\overline{\Xi}^+K^- + c.c.)/\Gamma_{total}$ — Γ_{146}/Γ

VALUE (units 10^{-5})	EVTS	DOCUMENT ID		TECN	COMMENT
3.86±0.27±0.32	236	ABLIKIM	15I	BES3	$e^+e^- \to \psi(2S) \to K^-\Lambda\overline{\Xi}^+ +$ c.c.

$\Gamma(\Xi(1530)^-\overline{\Xi}(1530)^+)/\Gamma_{total}$ — Γ_{147}/Γ

VALUE (units 10^{-5})	EVTS	DOCUMENT ID		TECN	COMMENT
11.45±0.40±0.59	5k	ABLIKIM	19AT	BES3	$e^+e^- \to \psi(2S) \to$ hadrons

$\Gamma(\Xi(1530)^-\overline{\Xi}^+)/\Gamma_{total}$ — Γ_{148}/Γ

VALUE (units 10^{-6})	EVTS	DOCUMENT ID		TECN	COMMENT
7.0±1.1±0.4	399	ABLIKIM	19AT	BES3	$e^+e^- \to \psi(2S) \to$ hadrons

$\Gamma(\Xi(1530)^0\overline{\Xi}^0)/\Gamma_{total}$ — Γ_{149}/Γ

VALUE (units 10^{-5})	EVTS	DOCUMENT ID		TECN	COMMENT
0.53±0.04±0.03	278	ABLIKIM	21AO	BES3	$e^+e^- \to \psi(2S) \to$ hadrons

$\Gamma(\Xi(1690)^-\overline{\Xi}^+ \to K^-\Lambda\overline{\Xi}^+ + c.c.)/\Gamma_{total}$ — Γ_{150}/Γ

VALUE (units 10^{-6})	EVTS	DOCUMENT ID		TECN	COMMENT
5.21±1.48±0.57	74	ABLIKIM	15I	BES3	$e^+e^- \to \psi(2S) \to K^-\Lambda\overline{\Xi}^+ +$ c.c.

Downloaded from https://academic.oup.com/ptep/article/2022/8/083C01/6651666 by KIT Library user on 27 September 2022

$\Gamma(\Xi(1820)^-\overline{\Xi}^+ \to K^-\Lambda\overline{\Xi}^+ + \text{c.c.})/\Gamma_{\text{total}}$ — Γ_{151}/Γ

VALUE (units 10^{-6})	EVTS	DOCUMENT ID		TECN	COMMENT
12.03±2.94±1.22	136	ABLIKIM	15I	BES3	$e^+e^- \to \psi(2S) \to K^-\Lambda\overline{\Xi}^+ +$ c.c.

$\Gamma(\Sigma^0\overline{\Xi}^+K^- + \text{c.c.})/\Gamma_{\text{total}}$ — Γ_{152}/Γ

VALUE (units 10^{-5})	EVTS	DOCUMENT ID		TECN	COMMENT
3.67±0.33±0.28	142	ABLIKIM	15I	BES3	$e^+e^- \to \psi(2S) \to K^-\Sigma^0\overline{\Xi}^+ +$ c.c.

$\Gamma(\Omega^-\overline{\Omega}^+)/\Gamma_{\text{total}}$ — Γ_{153}/Γ

VALUE (units 10^{-5})	CL%	EVTS	DOCUMENT ID		TECN	COMMENT
5.66±0.30 OUR AVERAGE			Error includes scale factor of 1.3.			
5.85±0.12±0.25		4k	[1] ABLIKIM	21E	BES3	$\psi(2S) \to \Omega^-\overline{\Omega}^+ \to \Lambda K^-\overline{\Lambda}K^+$
5.2 ±0.3 ±0.3		326	[1,2] DOBBS	17		$e^+e^- \to \psi(2S) \to$ hadrons
• • • We do not use the following data for averages, fits, limits, etc. • • •						
4.7 ±0.9 ±0.5		27	[1,2,3] DOBBS	14		$e^+e^- \to \psi(2S) \to$ hadrons
<15	90		ABLIKIM	12Q	BES2	$e^+e^- \to \psi(2S) \to$ hadrons
<16	90		PEDLAR	05	CLEO	$e^+e^- \to \psi(2S) \to$ hadrons
< 7.3	90		[4] BAI	01	BES	$e^+e^- \to \psi(2S) \to$ hadrons

[1] Using B($\Omega^- \to \Lambda K^-$) = (67.8 ± 0.7)% and B($\Lambda \to p\pi^-$) = (63.9 ± 0.5)%.
[2] Using CLEO-c data but not authored by the CLEO Collaboration.
[3] Superseded by DOBBS 17.
[4] Estimated using B($\psi(2S) \to J/\psi\pi^+\pi^-$) = 0.310 ± 0.028.

$\Gamma(\eta_c\pi^+\pi^-\pi^0)/\Gamma_{\text{total}}$ — Γ_{154}/Γ

VALUE (units 10^{-3})	CL%	DOCUMENT ID		TECN	COMMENT
<1.0	90	PEDLAR	07	CLEO	$e^+e^- \to \psi(2S)$

$\Gamma(h_c(1P)\pi^0)/\Gamma_{\text{total}}$ — Γ_{155}/Γ

VALUE (units 10^{-4})	EVTS	DOCUMENT ID		TECN	COMMENT
8.6±1.3 OUR AVERAGE					
9.0±1.5±1.3	3k	[1] GE	11	CLEO	$\psi(2S) \to \pi^0$ anything
8.4±1.3±1.0	11k	ABLIKIM	10B	BES3	$\psi(2S) \to \pi^0 h_c$
• • • We do not use the following data for averages, fits, limits, etc. • • •					
seen	92^{+23}_{-22}	ADAMS	09	CLEO	$\psi(2S) \to 2\pi^+2\pi^-2\pi^0$
seen	1282	DOBBS	08A	CLEO	$\psi(2S) \to \pi^0\eta_c\gamma$
seen	168 ± 40	ROSNER	05	CLEO	$\psi(2S) \to \pi^0\eta_c\gamma$

[1] Assuming a width $\Gamma(h_c(1P))$ = 0.86 MeV $\equiv \Gamma_0$, a measured dependence of the central value of $B = (7.6 + 1.4 \times \Gamma(h_c(1P)/\Gamma_0) \times 10^{-4}$, and with a systematic error that accounts for the width variation range 0.43–1.29 MeV.

$\Gamma(\Lambda_c^+\overline{p}e^+e^- + \text{c.c.})/\Gamma_{\text{total}}$ — Γ_{156}/Γ

VALUE	CL%	EVTS	DOCUMENT ID		TECN	COMMENT
<1.7 × 10^{-6}	90	450M	ABLIKIM	18Q	BES3	$e^+e^- \to \psi(2S)$

$\Gamma(\Theta(1540)\overline{\Theta}(1540) \to K^0_S pK^-\overline{n} + \text{c.c.})/\Gamma_{\text{total}}$ — Γ_{157}/Γ

VALUE (units 10^{-5})	CL%	DOCUMENT ID		TECN	COMMENT
<0.88	90	BAI	04G	BES2	e^+e^-

$\Gamma(\Theta(1540)K^-\overline{n} \to K^0_S pK^-\overline{n})/\Gamma_{\text{total}}$ — Γ_{158}/Γ

VALUE (units 10^{-5})	CL%	DOCUMENT ID		TECN	COMMENT
<1.0	90	BAI	04G	BES2	e^+e^-

$\Gamma(\Theta(1540)K^0_S\overline{p} \to K^0_S\overline{p}K^+n)/\Gamma_{\text{total}}$ — Γ_{159}/Γ

VALUE (units 10^{-5})	CL%	DOCUMENT ID		TECN	COMMENT
<0.70	90	BAI	04G	BES2	e^+e^-

$\Gamma(\overline{\Theta}(1540)K^+n \to K^0_S\overline{p}K^+n)/\Gamma_{\text{total}}$ — Γ_{160}/Γ

VALUE (units 10^{-5})	CL%	DOCUMENT ID		TECN	COMMENT
<2.6	90	BAI	04G	BES2	e^+e^-

$\Gamma(\overline{\Theta}(1540)K^0_S p \to K^0_S pK^-\overline{n})/\Gamma_{\text{total}}$ — Γ_{161}/Γ

VALUE (units 10^{-5})	CL%	DOCUMENT ID		TECN	COMMENT
<0.60	90	BAI	04G	BES2	e^+e^-

RADIATIVE DECAYS

$\Gamma(\gamma\chi_{c0}(1P))/\Gamma_{\text{total}}$ — Γ_{162}/Γ

VALUE (units 10^{-2})	EVTS	DOCUMENT ID		TECN	COMMENT
9.79 ±0.20 OUR FIT					
9.33 ±0.26 OUR AVERAGE					
9.389±0.014±0.332	4.7M	ABLIKIM	17U	BES3	$e^+e^- \to \gamma X$
9.22 ±0.11 ±0.46	72k	ATHAR	04	CLEO	$e^+e^- \to \gamma X$
9.9 ±0.5 ±0.8		[1] GAISER	86	CBAL	$e^+e^- \to \gamma X$
7.2 ±2.3		[1] BIDDICK	77	CNTR	$e^+e^- \to \gamma X$
7.5 ±2.6		[1] WHITAKER	76	MRK1	e^+e^-

[1] Angular distribution (1+$\cos^2\theta$) assumed.

$\Gamma(\gamma\chi_{c1}(1P))/\Gamma_{\text{total}}$ — Γ_{163}/Γ

VALUE (units 10^{-2})	EVTS	DOCUMENT ID		TECN	COMMENT
9.75 ±0.24 OUR FIT					
9.54 ±0.29 OUR AVERAGE					
9.905±0.011±0.353	5.0M	ABLIKIM	17U	BES3	$e^+e^- \to \gamma X$
9.07 ±0.11 ±0.54	76k	ATHAR	04	CLEO	$e^+e^- \to \gamma X$
9.0 ±0.5 ±0.7		[1] GAISER	86	CBAL	$e^+e^- \to \gamma X$
7.1 ±1.9		[2] BIDDICK	77	CNTR	$e^+e^- \to \gamma X$

[1] Angular distribution (1−0.189 $\cos^2\theta$) assumed.
[2] Valid for isotropic distribution of the photon.

$\Gamma(\gamma\chi_{c0}(1P))/\Gamma(\gamma\chi_{c1}(1P))$ — $\Gamma_{162}/\Gamma_{163}$

VALUE	DOCUMENT ID		TECN	COMMENT
• • • We do not use the following data for averages, fits, limits, etc. • • •				
1.02±0.01±0.07	[1] ATHAR	04	CLEO	$e^+e^- \to \gamma X$

[1] Not independent from ATHAR 04 measurements of B($\gamma\chi_{cJ}$).

$\Gamma(\gamma\chi_{c2}(1P))/\Gamma_{\text{total}}$ — Γ_{164}/Γ

VALUE (units 10^{-2})	EVTS	DOCUMENT ID		TECN	COMMENT
9.52 ±0.20 OUR FIT					
9.42 ±0.31 OUR AVERAGE		Error includes scale factor of 1.3. See the ideogram below.			
9.621±0.013±0.272	4.2M	ABLIKIM	17U	BES3	$e^+e^- \to \gamma X$
9.33 ±0.14 ±0.61	79k	ATHAR	04	CLEO	$e^+e^- \to \gamma X$
8.0 ±0.5 ±0.7		[1] GAISER	86	CBAL	$e^+e^- \to \gamma X$
7.0 ±2.0		[2] BIDDICK	77	CNTR	$e^+e^- \to \gamma X$

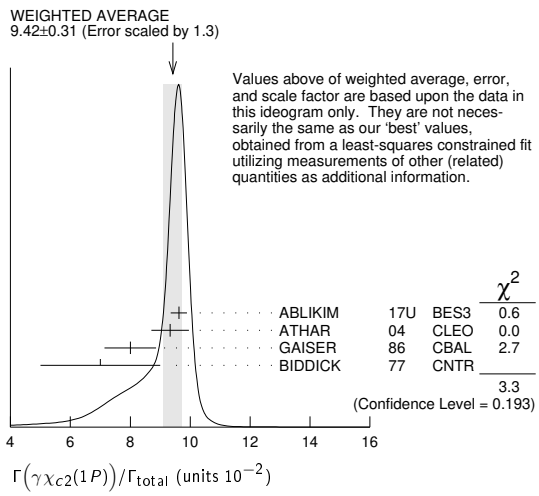

[1] Angular distribution (1−0.052 $\cos^2\theta$) assumed.
[2] Valid for isotropic distribution of the photon.

$[\Gamma(\gamma\chi_{c0}(1P)) + \Gamma(\gamma\chi_{c1}(1P)) + \Gamma(\gamma\chi_{c2}(1P))]/\Gamma_{\text{total}}$ — $(\Gamma_{162}+\Gamma_{163}+\Gamma_{164})/\Gamma$

VALUE	DOCUMENT ID		TECN	COMMENT
• • • We do not use the following data for averages, fits, limits, etc. • • •				
27.6±0.3±2.0	[1] ATHAR	04	CLEO	$e^+e^- \to \gamma X$

[1] Not independent from ATHAR 04 measurements of B($\gamma\chi_{cJ}$).

$\Gamma(\gamma\chi_{c0}(1P))/\Gamma(\gamma\chi_{c2}(1P))$ — $\Gamma_{162}/\Gamma_{164}$

VALUE	DOCUMENT ID		TECN	COMMENT
• • • We do not use the following data for averages, fits, limits, etc. • • •				
0.99±0.02±0.08	[1] ATHAR	04	CLEO	$e^+e^- \to \gamma X$

[1] Not independent from ATHAR 04 measurements of B($\gamma\chi_{cJ}$).

$\Gamma(\gamma\chi_{c2}(1P))/\Gamma(\gamma\chi_{c1}(1P))$ — $\Gamma_{164}/\Gamma_{163}$

VALUE	DOCUMENT ID		TECN	COMMENT
• • • We do not use the following data for averages, fits, limits, etc. • • •				
1.03±0.02±0.03	[1] ATHAR	04	CLEO	$e^+e^- \to \gamma X$

[1] Not independent from ATHAR 04 measurements of B($\gamma\chi_{cJ}$).

$\Gamma(\gamma\eta_c(1S))/\Gamma_{\text{total}}$ — Γ_{165}/Γ

VALUE (units 10^{-2})	EVTS	DOCUMENT ID		TECN	COMMENT
0.34 ±0.05 OUR AVERAGE		Error includes scale factor of 1.3. See the ideogram below.			
0.432±0.016±0.060		MITCHELL	09	CLEO	$e^+e^- \to \gamma X$
0.32 ±0.04 ±0.06	2.5k	[1] ATHAR	04	CLEO	$e^+e^- \to \gamma X$
0.28 ±0.06		[2] GAISER	86	CBAL	$e^+e^- \to \gamma X$

Downloaded from https://academic.oup.com/ptep/article/2022/8/083C01/6651666 by KIT Library user on 27 September 2022

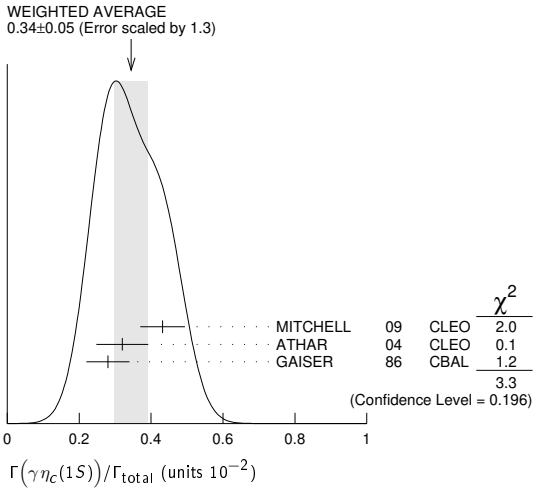

[1] ATHAR 04 used $\Gamma_{\eta_c(1S)} = 24.8 \pm 4.9$ MeV to obtain this result.
[2] GAISER 86 used $\Gamma_{\eta_c(1S)} = 11.5 \pm 4.5$ MeV to obtain this result.

$\Gamma(\gamma\eta_c(2S))/\Gamma_{total}$ — Γ_{166}/Γ

VALUE (units 10^{-4})	CL%	DOCUMENT ID		TECN	COMMENT
7±2±4		[1] ABLIKIM	12G	BES3	$\psi(2S) \to \gamma K^0 K\pi$, $K K \pi^0$
• • • We do not use the following data for averages, fits, limits, etc. • • •					
< 8	90	[2] CRONIN-HEN..	10	CLEO	$\psi(2S) \to \gamma K\overline{K}\pi$
<20	90	ATHAR	04	CLEO	$e^+e^- \to \gamma X$
20–130	95	EDWARDS	82C	CBAL	$e^+e^- \to \gamma X$

[1] ABLIKIM 12G reports $[\Gamma(\psi(2S) \to \gamma\eta_c(2S))/\Gamma_{total}] \times [B(\eta_c(2S) \to K\overline{K}\pi)] = (1.30 \pm 0.20 \pm 0.30) \times 10^{-5}$ which we divide by our best value $B(\eta_c(2S) \to K\overline{K}\pi) = (1.9 \pm 1.2) \times 10^{-2}$. Our first error is their experiment's error and our second error is the systematic error from using our best value.
[2] CRONIN-HENNESSY 10 reports $[\Gamma(\psi(2S) \to \gamma\eta_c(2S))/\Gamma_{total}] \times [B(\eta_c(2S) \to K\overline{K}\pi)] < 14.5 \times 10^{-6}$ which we divide by our best value $B(\eta_c(2S) \to K\overline{K}\pi) = 1.9 \times 10^{-2}$. This measurement assumes $\Gamma(\eta_c(2S)) = 14$ MeV. CRONIN-HENNESSY 10 gives the analytic dependence of limits on width.

$\Gamma(\gamma\pi^0)/\Gamma_{total}$ — Γ_{167}/Γ

VALUE (units 10^{-6})	CL%	EVTS	DOCUMENT ID		TECN	COMMENT
1.04±0.22 OUR AVERAGE Error includes scale factor of 1.4.						
0.95±0.16±0.05		423	ABLIKIM	17X	BES3	$\psi(2S) \to \gamma\pi^0$
1.58±0.40±0.13		37	ABLIKIM	10F	BES3	$\psi(2S) \to \gamma\pi^0$
• • • We do not use the following data for averages, fits, limits, etc. • • •						
< 5	90		PEDLAR	09	CLE3	$\psi(2S) \to \gamma X$
<5400	95		[1] LIBERMAN	75	SPEC	e^+e^-
$< 1 \times 10^4$	90		WIIK	75	DASP	e^+e^-

[1] Restated by us using $B(\psi(2S) \to \mu^+\mu^-) = 0.0077$.

$\Gamma(\gamma 2(\pi^+\pi^-))/\Gamma_{total}$ — Γ_{168}/Γ

VALUE (units 10^{-5})	EVTS	DOCUMENT ID		TECN	COMMENT
39.6±2.8±5.0	583	ABLIKIM	07D	BES2	$e^+e^- \to \psi(2S)$

$\Gamma(\gamma 3(\pi^+\pi^-))/\Gamma_{total}$ — Γ_{169}/Γ

VALUE (units 10^{-5})	CL%	DOCUMENT ID		TECN	COMMENT
<17	90	ABLIKIM	07D	BES2	$e^+e^- \to \psi(2S)$

$\Gamma(\gamma\eta'(958))/\Gamma_{total}$ — Γ_{170}/Γ

VALUE (units 10^{-4})	CL%	EVTS	DOCUMENT ID		TECN	COMMENT
1.24 ±0.04 OUR AVERAGE						
1.251±0.022±0.062		56k	ABLIKIM	17X	BES3	$\psi(2S) \to \gamma\pi^+\pi^-\eta$, $\gamma\pi^0\pi^0\eta$
1.26 ±0.03 ±0.08		2226	[1] ABLIKIM	10F	BES3	$\psi(2S) \to 3\gamma\pi^+\pi^-$, $2\gamma\pi^+\pi^-$
1.19 ±0.08 ±0.03			PEDLAR	09	CLE3	$\psi(2S) \to \gamma X$
1.24 ±0.27 ±0.15		23	ABLIKIM	06R	BES2	$e^+e^- \to \psi(2S)$
1.54 ±0.31 ±0.20		~ 43	BAI	98F	BES	$\psi(2S) \to \pi^+\pi^- 2\gamma$, $\pi^+\pi^- 3\gamma$
• • • We do not use the following data for averages, fits, limits, etc. • • •						
< 60	90		[2] BRAUNSCH...	77	DASP	e^+e^-
< 11	90		[3] BARTEL	76	CNTR	e^+e^-

[1] Combining the results from $\eta' \to \pi^+\pi^-\eta$ and $\eta' \to \pi^+\pi^-\gamma$ decay modes.
[2] Restated by us using total decay width 228 keV.
[3] The value is normalized to the branching ratio for $\Gamma(J/\psi(1S)\eta)/\Gamma_{total}$.

$\Gamma(\gamma f_2(1270))/\Gamma_{total}$ — Γ_{171}/Γ

VALUE (units 10^{-4})	EVTS	DOCUMENT ID		TECN	COMMENT
$2.73^{+0.29}_{-0.25}$ OUR AVERAGE Error includes scale factor of 1.8.					
$2.84 \pm 0.15^{+0.03}_{-0.10}$	1.9k	[1,2] DOBBS	15		$\psi(2S) \to \gamma\pi\pi$
2.12±0.19±0.32		[3,4] BAI	03C	BES	$\psi(2S) \to \gamma\pi\pi$
• • • We do not use the following data for averages, fits, limits, etc. • • •					
2.08±0.19±0.33	200.6 ± 18.8	[3] BAI	03C	BES	$\psi(2S) \to \gamma\pi^+\pi^-$
2.90±1.08±1.07	29.9 ± 11.1	[3] BAI	03C	BES	$\psi(2S) \to \gamma\pi^0\pi^0$

[1] Using CLEO-c data but not authored by the CLEO Collaboration.
[2] DOBBS 15 reports $[\Gamma(\psi(2S) \to \gamma f_2(1270))/\Gamma_{total}] \times [B(f_2(1270) \to \pi\pi)] = (2.39 \pm 0.09 \pm 0.09) \times 10^{-4}$ which we divide by our best value $B(f_2(1270) \to \pi\pi) = (84.2^{+2.9}_{-0.9}) \times 10^{-2}$. Our first error is their experiment's error and our second error is the systematic error from using our best value.
[3] Normalized to $B(\psi(2S) \to J/\psi\pi^+\pi^-) = 0.305 \pm 0.016$.
[4] Combining the results from $\pi^+\pi^-$ and $\pi^0\pi^0$ decay modes.

$\Gamma(\gamma f_0(1370) \to \gamma K\overline{K})/\Gamma_{total}$ — Γ_{172}/Γ

VALUE (units 10^{-5})	EVTS	DOCUMENT ID		COMMENT
3.1±1.0±1.4	175	[1] DOBBS	15	$\psi(2S) \to \gamma K\overline{K}$

[1] Using CLEO-c data but not authored by the CLEO Collaboration.

$\Gamma(\gamma f_0(1500))/\Gamma_{total}$ — Γ_{173}/Γ

VALUE (units 10^{-5})	EVTS	DOCUMENT ID		COMMENT
9.3±1.8±0.6	274	[1,2] DOBBS	15	$\psi(2S) \to \gamma\pi\pi$

[1] DOBBS 15 reports $[\Gamma(\psi(2S) \to \gamma f_0(1500))/\Gamma_{total}] \times [B(f_0(1500) \to \pi\pi)] = (3.2 \pm 0.6 \pm 0.2) \times 10^{-5}$ which we divide by our best value $B(f_0(1500) \to \pi\pi) = (34.5 \pm 2.2) \times 10^{-2}$. Our first error is their experiment's error and our second error is the systematic error from using our best value.
[2] Using CLEO-c data but not authored by the CLEO Collaboration.

$\Gamma(\gamma f_2'(1525))/\Gamma_{total}$ — Γ_{174}/Γ

VALUE (units 10^{-5})	EVTS	DOCUMENT ID		COMMENT
3.3±0.8±0.1	136	[1,2] DOBBS	15	$\psi(2S) \to \gamma K\overline{K}$

[1] DOBBS 15 reports $[\Gamma(\psi(2S) \to \gamma f_2'(1525))/\Gamma_{total}] \times [B(f_2'(1525) \to K\overline{K})] = (2.9 \pm 0.6 \pm 0.3) \times 10^{-5}$ which we divide by our best value $B(f_2'(1525) \to K\overline{K}) = (87.6 \pm 2.2) \times 10^{-2}$. Our first error is their experiment's error and our second error is the systematic error from using our best value.
[2] Using CLEO-c data but not authored by the CLEO Collaboration.

$\Gamma(\gamma f_0(1710) \to \gamma\pi\pi)/\Gamma_{total}$ — Γ_{176}/Γ

VALUE (units 10^{-5})	EVTS	DOCUMENT ID		TECN	COMMENT
3.5 ±0.6 OUR AVERAGE					
3.6 ±0.4 ±0.5	290	[1] DOBBS	15		$\psi(2S) \to \gamma\pi\pi$
3.01±0.41±1.24	35.6 ± 4.8	[2] BAI	03C	BES	$\psi(2S) \to \gamma\pi^+\pi^-$

[1] Using CLEO-c data but not authored by the CLEO Collaboration.
[2] Normalized to $B(\psi(2S) \to J/\psi\pi^+\pi^-) = 0.305 \pm 0.016$.

$\Gamma(\gamma f_0(1710) \to \gamma K\overline{K})/\Gamma_{total}$ — Γ_{177}/Γ

VALUE (units 10^{-5})	CL%	EVTS	DOCUMENT ID		TECN	COMMENT
6.6 ±0.7 OUR AVERAGE						
6.7 ±0.6 ±0.6		375	[1] DOBBS	15		$\psi(2S) \to \gamma K\overline{K}$
6.04±0.90±1.32		39.6±5.9	[2,3] BAI	03C	BES	$\psi(2S) \to \gamma K^+K^-$
• • • We do not use the following data for averages, fits, limits, etc. • • •						
< 15.6	90	6.8 ± 3.1	[2,3] BAI	03C	BES	$\psi(2S) \to \gamma K^0_S K^0_S$

[1] Using CLEO-c data but not authored by the CLEO Collaboration.
[2] Includes unknown branching fractions to K^+K^- or $K^0_S K^0_S$. We have multiplied the K^+K^- result by a factor of 2 and the $K^0_S K^0_S$ result by a factor of 4 to obtain the $K\overline{K}$ result.
[3] Normalized to $B(\psi(2S) \to J/\psi\pi^+\pi^-) = 0.305 \pm 0.016$.

$\Gamma(\gamma f_0(2100) \to \gamma\pi\pi)/\Gamma_{total}$ — Γ_{178}/Γ

VALUE (units 10^{-6})	EVTS	DOCUMENT ID		COMMENT
4.8±0.5±0.9	373	[1] DOBBS	15	$\psi(2S) \to \gamma\pi\pi$

[1] Using CLEO-c data but not authored by the CLEO Collaboration.

$\Gamma(\gamma f_0(2200) \to \gamma K\overline{K})/\Gamma_{total}$ — Γ_{179}/Γ

VALUE (units 10^{-6})	EVTS	DOCUMENT ID		COMMENT
3.2±0.6±0.8	207	[1] DOBBS	15	$\psi(2S) \to \gamma K\overline{K}$

[1] Using CLEO-c data but not authored by the CLEO Collaboration.

$\Gamma(\gamma f_J(2220) \to \gamma\pi\pi)/\Gamma_{total}$ — Γ_{180}/Γ

VALUE	CL%	DOCUMENT ID		COMMENT
$<5.8 \times 10^{-6}$	90	[1,2] DOBBS	15	$\psi(2S) \to \gamma\pi\pi$

[1] Using CLEO-c data but not authored by the CLEO Collaboration.
[2] For $\Gamma = 20/50$ MeV, the 90% CL upper limits for $\pi^+\pi^-$ and $\pi^0\pi^0$ are $3.2/4.3 \times 10^{-6}$ and $2.6/4.0 \times 10^{-6}$, respectively.

Downloaded from https://academic.oup.com/ptep/article/2022/8/083C01/6651666 by KIT Library user on 27 September 2022

$\Gamma(\gamma f_J(2220) \to \gamma K\overline{K})/\Gamma_{total}$ — Γ_{181}/Γ

VALUE	CL%	DOCUMENT ID		COMMENT
$<9.5 \times 10^{-6}$	90	[1,2] DOBBS	15	$\psi(2S) \to \gamma K\overline{K}$

[1] Using CLEO-c data but not authored by the CLEO Collaboration.
[2] For $\Gamma = 20/50$ MeV, the 90% CL upper limits for K^+K^- and $K^0_S K^0_S$ are $2.1/4.3\times10^{-6}$ and $3.7/5.5 \times 10^{-6}$, respectively.

$\Gamma(\gamma\eta)/\Gamma_{total}$ — Γ_{182}/Γ

VALUE (units 10^{-6})	CL%	EVTS	DOCUMENT ID		TECN	COMMENT
0.92±0.18 OUR AVERAGE						
0.85±0.18±0.04		382	[1] ABLIKIM	17X	BES3	$\psi(2S) \to \gamma\pi^+\pi^-\pi^0$, $\gamma 3\pi^0$
1.38±0.48±0.09		13	[1] ABLIKIM	10F	BES3	$\psi(2S) \to \gamma\pi^+\pi^-\pi^0$, $\gamma 3\pi^0$
• • • We do not use the following data for averages, fits, limits, etc. • • •						
< 2	90		PEDLAR	09	CLE3	$\psi(2S) \to \gamma X$
< 90	90		BAI	98F	BES	$\psi(2S) \to \pi^+\pi^- 3\gamma$
<200	90		YAMADA	77	DASP	$e^+e^- \to 3\gamma$

[1] Combining the results from $\eta \to \pi^+\pi^-\pi^0$ and $\eta \to 3\pi^0$ decay modes.

$\Gamma(\gamma\eta\pi^+\pi^-)/\Gamma_{total}$ — Γ_{183}/Γ

VALUE (units 10^{-4})	EVTS	DOCUMENT ID		TECN	COMMENT
8.71±1.25±1.64	418	ABLIKIM	06R	BES2	$\psi(2S) \to \gamma\eta\pi^+\pi^-$

$\Gamma(\gamma\eta(1405) \to \gamma K\overline{K}\pi)/\Gamma_{total}$ — Γ_{185}/Γ

VALUE (units 10^{-4})	CL%	DOCUMENT ID		TECN	COMMENT
<0.9	90	ABLIKIM	06R	BES2	$\psi(2S) \to \gamma K^0_S K^+\pi^- +$ c.c.
• • • We do not use the following data for averages, fits, limits, etc. • • •					
<1.3	90	ABLIKIM	06R	BES2	$\psi(2S) \to \gamma K^+K^-\pi^0$
<1.2	90	[1] SCHARRE	80	MRK1	e^+e^-

[1] Includes unknown branching fraction $\eta(1405) \to K\overline{K}\pi$.

$\Gamma(\gamma\eta(1405) \to \gamma\eta\pi^+\pi^-)/\Gamma_{total}$ — Γ_{186}/Γ

VALUE (units 10^{-4})	EVTS	DOCUMENT ID		TECN	COMMENT
0.36±0.25±0.05	10	ABLIKIM	06R	BES2	$\psi(2S) \to \gamma\eta\pi^+\pi^-$

$\Gamma(\gamma\eta(1405) \to \gamma f_0(980)\pi^0 \to \gamma\pi^+\pi^-\pi^0)/\Gamma_{total}$ — Γ_{187}/Γ

VALUE	CL%	DOCUMENT ID		TECN	COMMENT
$<5.0 \times 10^{-7}$	90	ABLIKIM	17AJ	BES3	$\psi(2S) \to \gamma\pi^+\pi^-\pi^0$

$\Gamma(\gamma\eta(1475) \to \gamma K\overline{K}\pi)/\Gamma_{total}$ — Γ_{189}/Γ

VALUE (units 10^{-4})	CL%	DOCUMENT ID		TECN	COMMENT
<1.4	90	ABLIKIM	06R	BES2	$\psi(2S) \to \gamma K^+K^-\pi^0$
• • • We do not use the following data for averages, fits, limits, etc. • • •					
<1.5	90	ABLIKIM	06R	BES2	$\psi(2S) \to \gamma K^0_S K^+\pi^- +$ c.c.

$\Gamma(\gamma\eta(1475) \to \gamma\eta\pi^+\pi^-)/\Gamma_{total}$ — Γ_{190}/Γ

VALUE (units 10^{-4})	CL%	DOCUMENT ID		TECN	COMMENT
<0.88	90	ABLIKIM	06R	BES2	$\psi(2S) \to \gamma\eta\pi^+\pi^-$

$\Gamma(\gamma K^{*0} K^+\pi^- + \text{c.c.})/\Gamma_{total}$ — Γ_{191}/Γ

VALUE (units 10^{-5})	EVTS	DOCUMENT ID		TECN	COMMENT
37.0±6.1±7.2	237	ABLIKIM	07D	BES2	$e^+e^- \to \psi(2S)$

$\Gamma(\gamma K^{*0}\overline{K}^{*0})/\Gamma_{total}$ — Γ_{192}/Γ

VALUE (units 10^{-5})	EVTS	DOCUMENT ID		TECN	COMMENT
24.0±4.5±5.0	41	ABLIKIM	07D	BES2	$e^+e^- \to \psi(2S)$

$\Gamma(\gamma K^0_S K^+\pi^- + \text{c.c.})/\Gamma_{total}$ — Γ_{193}/Γ

VALUE (units 10^{-5})	EVTS	DOCUMENT ID		TECN	COMMENT
25.6±3.6±3.6	115	ABLIKIM	07D	BES2	$e^+e^- \to \psi(2S)$

$\Gamma(\gamma K^+K^-\pi^+\pi^-)/\Gamma_{total}$ — Γ_{194}/Γ

VALUE (units 10^{-5})	EVTS	DOCUMENT ID		TECN	COMMENT
19.1±2.7±4.3	132	ABLIKIM	07D	BES2	$e^+e^- \to \psi(2S)$

$\Gamma(\gamma K^+K^- 2(\pi^+\pi^-))/\Gamma_{total}$ — Γ_{195}/Γ

VALUE (units 10^{-5})	CL%	DOCUMENT ID		TECN	COMMENT
<22	90	ABLIKIM	07D	BES2	$e^+e^- \to \psi(2S)$

$\Gamma(\gamma 2(K^+K^-))/\Gamma_{total}$ — Γ_{196}/Γ

VALUE (units 10^{-5})	CL%	DOCUMENT ID		TECN	COMMENT
<4	90	ABLIKIM	07D	BES2	$e^+e^- \to \psi(2S)$

$\Gamma(\gamma p\overline{p})/\Gamma_{total}$ — Γ_{197}/Γ

VALUE (units 10^{-5})	EVTS	DOCUMENT ID		TECN	COMMENT
3.9 ±0.5 OUR AVERAGE Error includes scale factor of 2.0.					
4.18±0.26±0.18	348	[1] ALEXANDER	10	CLEO	$\psi(2S) \to \gamma p\overline{p}$
2.9 ±0.4 ±0.4	142	ABLIKIM	07D	BES2	$e^+e^- \to \psi(2S)$

[1] From a fit of the $p\overline{p}$ mass distribution to a combination of $\gamma f_2(1950)$, $\gamma f_2(2150)$, and $\gamma p\overline{p}$ phase space, for $M(p\overline{p} < 2.85$ GeV, and accounting for backgrounds from $\psi(2S) \to \pi^0 p\overline{p}$ and continuum.

$\Gamma(\gamma f_2(1950) \to \gamma p\overline{p})/\Gamma_{total}$ — Γ_{198}/Γ

VALUE (units 10^{-5})	EVTS	DOCUMENT ID		TECN	COMMENT
1.2±0.2±0.1	111	[1] ALEXANDER	10	CLEO	$\psi(2S) \to \gamma p\overline{p}$

[1] From a fit of the $p\overline{p}$ mass distribution to a combination of $\gamma f_2(1950)$, $\gamma f_2(2150)$, and $\gamma p\overline{p}$ phase space, for $M(p\overline{p} < 2.85$ GeV, and accounting for backgrounds from $\psi(2S) \to \pi^0 p\overline{p}$ and continuum.

$\Gamma(\gamma f_2(2150) \to \gamma p\overline{p})/\Gamma_{total}$ — Γ_{199}/Γ

VALUE (units 10^{-5})	EVTS	DOCUMENT ID		TECN	COMMENT
0.72±0.18±0.03	73	[1] ALEXANDER	10	CLEO	$\psi(2S) \to \gamma p\overline{p}$

[1] From a fit of the $p\overline{p}$ mass distribution to a combination of $\gamma f_2(1950)$, $\gamma f_2(2150)$, and $\gamma p\overline{p}$ phase space, for $M(p\overline{p} < 2.85$ GeV, and accounting for backgrounds from $\psi(2S) \to \pi^0 p\overline{p}$ and continuum.

$\Gamma(\gamma X(1835) \to \gamma p\overline{p})/\Gamma_{total}$ — Γ_{200}/Γ

VALUE (units 10^{-6})	CL%	DOCUMENT ID		TECN	COMMENT
$4.57 \pm 0.36^{+1.77}_{-4.26}$		ABLIKIM	12D	BES3	$J/\psi \to \gamma p\overline{p}$
• • • We do not use the following data for averages, fits, limits, etc. • • •					
<1.6	90	ALEXANDER	10	CLEO	$\psi(2S) \to \gamma p\overline{p}$
<5.4	90	ABLIKIM	07D	BES	$\psi(2S) \to \gamma p\overline{p}$

$\Gamma(\gamma X \to \gamma p\overline{p})/\Gamma_{total}$ — Γ_{201}/Γ

For a narrow resonance in the range $2.2 < M(X) < 2.8$ GeV.

VALUE (units 10^{-6})	CL%	DOCUMENT ID		TECN	COMMENT
<2	90	ALEXANDER	10	CLEO	$\psi(2S) \to \gamma p\overline{p}$

$\Gamma(\gamma p\overline{p}\pi^+\pi^-)/\Gamma_{total}$ — Γ_{202}/Γ

VALUE (units 10^{-5})	EVTS	DOCUMENT ID		TECN	COMMENT
2.8±1.2±0.7	17	ABLIKIM	07D	BES2	$e^+e^- \to \psi(2S)$

$\Gamma(\gamma\gamma J/\psi)/\Gamma_{total}$ — Γ_{204}/Γ

VALUE (units 10^{-4})	EVTS	DOCUMENT ID		TECN	COMMENT
$3.1 \pm 0.6^{+0.8}_{-1.0}$	1.1k	ABLIKIM	12O	BES3	$e^+e^- \to \psi(2S)$
• • • We do not use the following data for averages, fits, limits, etc. • • •					
3.2±0.6	1.1k	[1] ABLIKIM	17N	BES3	$\psi(2S) \to \gamma\gamma J/\psi$

[1] Uses B($J/\psi \to e^+e^-$) = (5.971 ± 0.032)% and B($J/\psi \to \mu^+\mu^-$) = (5.961 ± 0.033)%. No systematic error estimation.

$\Gamma(e^+e^-\eta')/\Gamma_{total}$ — Γ_{205}/Γ

VALUE (units 10^{-6})	EVTS	DOCUMENT ID		TECN	COMMENT
1.90±0.26 OUR AVERAGE					
1.99±0.33±0.12	57	ABLIKIM	18Z	BES3	$\psi(2S) \to \eta' e^+e^-$, $\eta' \to \gamma\pi^+\pi^-$
1.79±0.38±0.11	20	ABLIKIM	18Z	BES3	$\psi(2S) \to \eta' e^+e^-$, $\eta' \to \eta\pi^+\pi^-$

$\Gamma(e^+e^-\chi_{c0}(1P))/\Gamma_{total}$ — Γ_{206}/Γ

VALUE (units 10^{-4})	EVTS	DOCUMENT ID		TECN	COMMENT
10.6±2.4±0.4	48	[1] ABLIKIM	17I	BES3	$\psi(2S) \to e^+e^-\gamma J/\psi$

[1] ABLIKIM 17I reports $(11.7 \pm 2.5 \pm 1.0) \times 10^{-4}$ from a measurement of $[\Gamma(\psi(2S) \to e^+e^-\chi_{c0}(1P))/\Gamma_{total}] \times [B(\chi_{c0}(1P) \to \gamma J/\psi(1S))]$ assuming $B(\chi_{c0}(1P) \to \gamma J/\psi(1S)) = (1.27 \pm 0.06) \times 10^{-2}$, which we rescale to our best value $B(\chi_{c0}(1P) \to \gamma J/\psi(1S)) = (1.40 \pm 0.05) \times 10^{-2}$. Our first error is their experiment's error and our second error is the systematic error from using our best value.

$\Gamma(e^+e^-\chi_{c0}(1P))/\Gamma(\gamma\chi_{c0}(1P))$ — $\Gamma_{206}/\Gamma_{162}$

VALUE (units 10^{-3})	EVTS	DOCUMENT ID		TECN	COMMENT
9.4±1.9±0.6	48	[1] ABLIKIM	17I	BES3	$\psi(2S) \to e^+e^-\gamma J/\psi$

[1] Uses $B(\psi(2S) \to \gamma\chi_{c0}(1P)) \times B(\chi_{c0}(1P) \to \gamma J/\psi(1S)) = (15.8 \pm 0.3 \pm 0.6) \times 10^{-4}$ from ABLIKIM 17N and accounts for common systematic errors.

$\Gamma(e^+e^-\chi_{c1}(1P))/\Gamma_{total}$ — Γ_{207}/Γ

VALUE (units 10^{-4})	EVTS	DOCUMENT ID		TECN	COMMENT
8.5±0.6±0.2	873	[1] ABLIKIM	17I	BES3	$\psi(2S) \to e^+e^-\gamma J/\psi$

[1] ABLIKIM 17I reports $(8.6 \pm 0.3 \pm 0.6) \times 10^{-4}$ from a measurement of $[\Gamma(\psi(2S) \to e^+e^-\chi_{c1}(1P))/\Gamma_{total}] \times [B(\chi_{c1}(1P) \to \gamma J/\psi(1S))]$ assuming $B(\chi_{c1}(1P) \to \gamma J/\psi(1S)) = (33.9 \pm 1.2) \times 10^{-2}$, which we rescale to our best value $B(\chi_{c1}(1P) \to \gamma J/\psi(1S)) = (34.3 \pm 1.0) \times 10^{-2}$. Our first error is their experiment's error and our second error is the systematic error from using our best value.

Downloaded from https://academic.oup.com/ptep/article/2022/8/083C01/6651666 by KIT Library user on 27 September 2022

$\Gamma(e^+e^-\chi_{c1}(1P))/\Gamma(\gamma\chi_{c1}(1P))$ — $\Gamma_{207}/\Gamma_{163}$

VALUE (units 10^{-3})	EVTS	DOCUMENT ID		TECN	COMMENT
8.3±0.3±0.4	873	[1] ABLIKIM	17I	BES3	$\psi(2S) \to e^+e^-\gamma J/\psi$

[1] Uses B($\psi(2S) \to \gamma\chi_{c1}(1P)$) × B($\chi_{c1}(1P) \to \gamma J/\psi(1S)$) = (351.8 ± 1.0 ± 12.0) × 10^{-4} from ABLIKIM 17N and accounts for common systematic errors.

$\Gamma(e^+e^-\chi_{c2}(1P))/\Gamma_{total}$ — Γ_{208}/Γ

VALUE (units 10^{-4})	EVTS	DOCUMENT ID		TECN	COMMENT
7.0±0.7±0.2	227	[1] ABLIKIM	17I	BES3	$\psi(2S) \to e^+e^-\gamma J/\psi$

[1] ABLIKIM 17I reports (6.9 ± 0.5 ± 0.6) × 10^{-4} from a measurement of [$\Gamma(\psi(2S) \to e^+e^-\chi_{c2}(1P))/\Gamma_{total}$] × [B($\chi_{c2}(1P) \to \gamma J/\psi(1S)$)] assuming B($\chi_{c2}(1P) \to \gamma J/\psi(1S)$) = (19.2 ± 0.7) × 10^{-2}, which we rescale to our best value B($\chi_{c2}(1P) \to \gamma J/\psi(1S)$) = (19.0 ± 0.5) × 10^{-2}. Our first error is their experiment's error and our second error is the systematic error from using our best value.

$\Gamma(e^+e^-\chi_{c2}(1P))/\Gamma(\gamma\chi_{c2}(1P))$ — $\Gamma_{208}/\Gamma_{164}$

VALUE (units 10^{-3})	EVTS	DOCUMENT ID		TECN	COMMENT
6.6±0.5±0.4	227	[1] ABLIKIM	17I	BES3	$\psi(2S) \to e^+e^-\gamma J/\psi$

[1] Uses B($\psi(2S) \to \gamma\chi_{c2}(1P)$) × B($\chi_{c2}(1P) \to \gamma J/\psi(1S)$) = (199.6 ± 0.8 ± 7.0) × 10^{-4} from ABLIKIM 17N and accounts for common systematic errors.

WEAK DECAYS

$\Gamma(D^0e^+e^- + c.c.)/\Gamma_{total}$ — Γ_{209}/Γ

VALUE	CL%	DOCUMENT ID		TECN	COMMENT
<1.4 × 10^{-7}	90	[1] ABLIKIM	17AF	BES3	$e^+e^- \to \psi(2S)$

[1] Using D^0 decays to $K^-\pi^+$, $K^-\pi^+\pi^0$, and $K^-\pi^+\pi^+\pi^-$.

OTHER DECAYS

Γ(invisible)/$\Gamma(e^+e^-)$ — Γ_{210}/Γ_7

VALUE	CL%	DOCUMENT ID		TECN	COMMENT
<2.0	90	LEES	13I	BABR	$B \to K^{(*)}\psi(2S)$

$\psi(2S)$ CROSS-PARTICLE BRANCHING RATIOS

For measurements involving B($\psi(2S) \to \gamma\chi_{cJ}(1P)$)×B($\chi_{cJ}(1P) \to X$) see the corresponding entries in the $\chi_{cJ}(1P)$ sections.

MULTIPOLE AMPLITUDE RATIOS IN RADIATIVE DECAYS $\psi(2S) \to \gamma\chi_{cJ}(1P)$ and $\chi_{cJ} \to \gamma J/\psi(1S)$

$a_2(\chi_{c1})/a_2(\chi_{c2})$ Magnetic quadrupole transition amplitude ratio

VALUE (units 10^{-2})	EVTS	DOCUMENT ID		TECN	COMMENT
63 ± 7 OUR AVERAGE					
61.7± 8.3	253k	[1] ABLIKIM	17N	BES3	$\psi(2S) \to \gamma\gamma\ell^+\ell^-$
67^{+19}_{-13}	59k	[2] ARTUSO	09	CLEO	$\psi(2S) \to \gamma\gamma\ell^+\ell^-$

[1] Statistical and systematic errors combined.
[2] Statistical and systematic errors combined. Using values from fits with floating *M2* amplitudes $a_2(\chi_{c1})$, $a_2(\chi_{c2})$, $b_2(\chi_{c1})$, $b_2(\chi_{c2})$ and fixed *E3* amplitudes of $a_3(\chi_{c2}) = b_3(\chi_{c2}) = 0$. Not independent of values for $a_2(\chi_{c1}(1P))$ and $a_2(\chi_{c2}(1P))$ from ARTUSO 09.

$b_2(\chi_{c2})/b_2(\chi_{c1})$ Magnetic quadrupole transition amplitude ratio

VALUE (units 10^{-2})	EVTS	DOCUMENT ID		TECN	COMMENT
60±31 OUR AVERAGE					
74±40	253k	[1] ABLIKIM	17N	BES3	$\psi(2S) \to \gamma\gamma\ell^+\ell^-$
37^{+53}_{-47}	59k	[2] ARTUSO	09	CLEO	$\psi(2S) \to \gamma\gamma\ell^+\ell^-$

[1] Statistical and systematic errors combined. Derived from the reported measurement of $b_2(\chi_{c1})/b_2(\chi_{c2}) = 1.35 \pm 0.72$.
[2] Statistical and systematic errors combined. Using values from fits with floating *M2* amplitudes $a_2(\chi_{c1})$, $a_2(\chi_{c2})$, $b_2(\chi_{c1})$, $b_2(\chi_{c2})$ and fixed *E3* amplitudes of $a_3(\chi_{c2}) = b_3(\chi_{c2}) = 0$. Not independent of values for $b_2(\chi_{c1}(1P))$ and $b_2(\chi_{c2}(1P))$ from ARTUSO 09.

$\psi(2S)$ REFERENCES

ABLIKIM	21AL	PR D104 092003	M. Ablikim et al.	(BESIII Collab.)
ABLIKIM	21AO	PR D104 092012	M. Ablikim et al.	(BESIII Collab.)
ABLIKIM	21AT	JHEP 2111 226	M. Ablikim et al.	(BESIII Collab.)
ABLIKIM	21E	PRL 126 092002	M. Ablikim et al.	(BESIII Collab.)
ABLIKIM	21L	PR D103 112004	M. Ablikim et al.	(BESIII Collab.)
ABLIKIM	21S	PL B820 136576	M. Ablikim et al.	(BESIII Collab.)
ABLIKIM	21Z	PRL 127 082002	M. Ablikim et al.	(BESIII Collab.)
LEES	21	PR D103 092001	J.P. Lees et al.	(BABAR Collab.)
LEES	21C	PR D104 112004	J.P. Lees et al.	(BABAR Collab.)
ABLIKIM	20F	PR D101 032008	M. Ablikim et al.	(BESIII Collab.)
PDG	20	PTEP 2020 083C01	P.A. Zyla et al.	(PDG Collab.)
ABLIKIM	19AO	PR D99 112010	M. Ablikim et al.	(BESIII Collab.)
ABLIKIM	19AT	PR D100 051101	M. Ablikim et al.	(BESIII Collab.)
ABLIKIM	19AU	PR D100 052010	M. Ablikim et al.	(BESIII Collab.)
ABLIKIM	19BA	PR D100 092003	M. Ablikim et al.	(BESIII Collab.)
ABLIKIM	19I	PR D99 012014	M. Ablikim et al.	(BESIII Collab.)
ABLIKIM	19N	PR D99 032006	M. Ablikim et al.	(BESIII Collab.)
ABLIKIM	18Q	PR D97 091102	M. Ablikim et al.	(BESIII Collab.)
ABLIKIM	18T	PR D98 032006	M. Ablikim et al.	(BESIII Collab.)
ABLIKIM	18Z	PL B783 452	M. Ablikim et al.	(BESIII Collab.)
ANASHIN	18	PL B781 174	V.V. Anashin et al.	(KEDR Collab.)
LEES	18E	PR D98 112015	J.P. Lees et al.	(BABAR Collab.)
ABLIKIM	17AF	PR D96 111101	M. Ablikim et al.	(BESIII Collab.)
ABLIKIM	17AJ	PR D96 112008	M. Ablikim et al.	(BESIII Collab.)
ABLIKIM	17AK	PR D96 112012	M. Ablikim et al.	(BESIII Collab.)
ABLIKIM	17E	PL B770 217	M. Ablikim et al.	(BESIII Collab.)
ABLIKIM	17I	PRL 118 221802	M. Ablikim et al.	(BESIII Collab.)
ABLIKIM	17L	PR D95 052003	M. Ablikim et al.	(BESIII Collab.)
ABLIKIM	17N	PR D95 072004	M. Ablikim et al.	(BESIII Collab.)
ABLIKIM	17U	PR D96 032001	M. Ablikim et al.	(BESIII Collab.)
ABLIKIM	17X	PR D96 052003	M. Ablikim et al.	(BESIII Collab.)
DOBBS	17	PR D96 092004	S. Dobbs et al.	(NWES, WAYN)
LEES	17A	PR D95 052001	J.P. Lees et al.	(BABAR Collab.)
AAIJ	16Y	JHEP 1605 132	R. Aaij et al.	(LHCb Collab.)
ABLIKIM	16L	PR D93 072003	M. Ablikim et al.	(BESIII Collab.)
ABLIKIM	15I	PR D91 092006	M. Ablikim et al.	(BESIII Collab.)
ABLIKIM	15V	PL B749 414	M. Ablikim et al.	(BESIII Collab.)
ANASHIN	15	PL B749 50	V.V. Anashin et al.	(KEDR Collab.)
DOBBS	15	PR D91 052006	S. Dobbs et al.	(NWES)
LEES	15J	PR D92 072008	J.P. Lees et al.	(BABAR Collab.)
ABLIKIM	14G	PR D89 112006	M. Ablikim et al.	(BESIII Collab.)
DOBBS	14	PL B739 90	S. Dobbs et al.	(NWES, WAYN)
ABLIKIM	13A	PRL 110 022001	M. Ablikim et al.	(BESIII Collab.)
ABLIKIM	13D	PR D87 012007	M. Ablikim et al.	(BESIII Collab.)
ABLIKIM	13F	PR D87 052007	M. Ablikim et al.	(BESIII Collab.)
ABLIKIM	13M	PR D87 092006	M. Ablikim et al.	(BESIII Collab.)
ABLIKIM	13R	PR D88 032007	M. Ablikim et al.	(BESIII Collab.)
ABLIKIM	13S	PR D88 032010	M. Ablikim et al.	(BESIII Collab.)
ABLIKIM	13W	PR D88 112007	M. Ablikim et al.	(BESIII Collab.)
LEES	13I	PR D87 112005	J.P. Lees et al.	(BABAR Collab.)
LEES	13O	PR D87 092005	J.P. Lees et al.	(BABAR Collab.)
LEES	13Q	PR D88 032013	J.P. Lees et al.	(BABAR Collab.)
LEES	13Y	PR D88 072009	J.P. Lees et al.	(BABAR Collab.)
AAIJ	12H	EPJ C72 1972	R. Aaij et al.	(LHCb Collab.)
ABLIKIM	12D	PRL 108 112003	M. Ablikim et al.	(BESIII Collab.)
ABLIKIM	12G	PRL 109 042003	M. Ablikim et al.	(BESIII Collab.)
ABLIKIM	12H	PL B710 594	M. Ablikim et al.	(BESIII Collab.)
ABLIKIM	12L	PR D86 072011	M. Ablikim et al.	(BESIII Collab.)
ABLIKIM	12M	PR D86 092008	M. Ablikim et al.	(BESIII Collab.)
ABLIKIM	12O	PRL 109 172002	M. Ablikim et al.	(BESIII Collab.)
ABLIKIM	12Q	CP C36 1040	M. Ablikim et al.	(BES II Collab.)
ANASHIN	12	PL B711 280	V.V. Anashin et al.	(KEDR Collab.)
LEES	12E	PR D85 112009	J.P. Lees et al.	(BABAR Collab.)
LEES	12F	PR D86 012008	J.P. Lees et al.	(BABAR Collab.)
METREVELI	12	PR D85 092007	Z. Metreveli et al.	(NWES, FLOR, WAYN+)
GE	11	PR D84 032008	J.Y. Ge et al.	(CLEO Collab.)
ABLIKIM	10B	PRL 104 132002	M. Ablikim et al.	(BESIII Collab.)
ABLIKIM	10F	PRL 105 261801	M. Ablikim et al.	(BESIII Collab.)
ALEXANDER	10	PR D82 092002	J.P. Alexander et al.	(CLEO Collab.)
CRONIN-HEN...	10	PR D81 052002	D. Cronin-Hennessey et al.	(CLEO Collab.)
ADAMS	09	PR D80 051106	G.S. Adams et al.	(CLEO Collab.)
ARTUSO	09	PR D80 112003	M. Artuso et al.	(CLEO Collab.)
LIBBY	09	PR D80 072002	J. Libby et al.	(CLEO Collab.)
MITCHELL	09	PRL 102 011801	R.E. Mitchell et al.	(CLEO Collab.)
PEDLAR	09	PR D79 111101	T.K. Pedlar et al.	(CLEO Collab.)
ABLIKIM	08B	PL B659 74	M. Ablikim et al.	(BES Collab.)
ABLIKIM	08C	PL B659 789	M. Ablikim et al.	(BES Collab.)
DOBBS	08A	PRL 101 182003	S. Dobbs et al.	(CLEO Collab.)
MENDEZ	08	PR D78 011102	H. Mendez et al.	(CLEO Collab.)
PDG	08	PL B667 1	C. Amsler et al.	(PDG Collab.)
ABLIKIM	07C	PL B648 149	M. Ablikim et al.	(BES Collab.)
ABLIKIM	07D	PRL 99 011802	M. Ablikim et al.	(BES II Collab.)
ABLIKIM	07H	PR D76 092003	M. Ablikim et al.	(BES Collab.)
ANASHIN	07	JETPL 85 347	V.V. Anashin et al.	(KEDR Collab.)
		Translated from ZETFP 85 429.		
ANDREOTTI	07	PL B654 74	M. Andreotti et al.	(Fermilab E835 Collab.)
AUBERT	07AK	PR D76 012008	B. Aubert et al.	(BABAR Collab.)
AUBERT	07AU	PR D76 092005	B. Aubert et al.	(BABAR Collab.)
Also		PR D77 119902E (errat.)	B. Aubert et al.	(BABAR Collab.)
AUBERT	07BD	PR D76 092006	B. Aubert et al.	(BABAR Collab.)
PDG	07	Unofficial 2007 WWW edition		(PDG Collab.)
PEDLAR	07	PR D75 011102	T.K. Pedlar et al.	(CLEO Collab.)
ABLIKIM	06G	PR D73 052004	M. Ablikim et al.	(BES Collab.)
ABLIKIM	06I	PR D74 012004	M. Ablikim et al.	(BES Collab.)
ABLIKIM	06L	PRL 97 121801	M. Ablikim et al.	(BES Collab.)
ABLIKIM	06R	PR D74 072001	M. Ablikim et al.	(BES Collab.)
ABLIKIM	06W	PR D74 112003	M. Ablikim et al.	(BES Collab.)
ADAM	06	PRL 96 082004	N.E. Adam et al.	(CLEO Collab.)
AUBERT	06B	PR D73 012005	B. Aubert et al.	(BABAR Collab.)
AUBERT	06D	PR D73 052003	B. Aubert et al.	(BABAR Collab.)
AUBERT,BE	06D	PR D74 091103	B. Aubert et al.	(BABAR Collab.)
DOBBS	06A	PR D74 111105	S. Dobbs et al.	(CLEO Collab.)
ABLIKIM	05E	PR D71 072006	M. Ablikim et al.	(BES Collab.)
ABLIKIM	05H	PR D72 012002	M. Ablikim et al.	(BES Collab.)
ABLIKIM	05I	PL B614 37	M. Ablikim et al.	(BES Collab.)
ABLIKIM	05J	PL B619 247	M. Ablikim et al.	(BES Collab.)
ABLIKIM	05O	PL B630 21	M. Ablikim et al.	(BES Collab.)
ADAM	05	PRL 94 012005	N.E. Adam et al.	(CLEO Collab.)
ADAM	05A	PRL 94 232002	N.E. Adam et al.	(CLEO Collab.)
ANDREOTTI	05	PR D71 032006	M. Andreotti et al.	(FNAL E835 Collab.)
AUBERT	05D	PR D71 052001	B. Aubert et al.	(BABAR Collab.)
BRIERE	05	PRL 95 062001	R.A. Briere et al.	(CLEO Collab.)
PEDLAR	05	PR D72 051108	T.K. Pedlar et al.	(CLEO Collab.)
ROSNER	05	PRL 95 102003	J.L. Rosner et al.	(CLEO Collab.)
ABLIKIM	04B	PR D70 012003	M. Ablikim et al.	(BES Collab.)
ABLIKIM	04K	PR D70 112003	M. Ablikim et al.	(BES Collab.)
ABLIKIM	04L	PR D70 112007	M. Ablikim et al.	(BES Collab.)
ATHAR	04	PR D70 112002	S.B. Athar et al.	(CLEO Collab.)
BAI	04B	PRL 92 052001	J.Z. Bai et al.	(BES Collab.)
BAI	04C	PR D69 072001	J.Z. Bai et al.	(BES Collab.)
BAI	04D	PL B589 7	J.Z. Bai et al.	(BES Collab.)
BAI	04G	PR D70 012004	J.Z. Bai et al.	(BES Collab.)
BAI	04I	PR D70 012006	J.Z. Bai et al.	(BES Collab.)
PDG	04	PL B592 1	S. Eidelman et al.	(PDG Collab.)
SETH	04	PR D69 097503	K.K. Seth	
AULCHENKO	03	PL B573 63	V.M. Aulchenko et al.	(KEDR Collab.)
BAI	03B	PR D67 052002	J.Z. Bai et al.	(BES Collab.)
BAI	03C	PR D67 032004	J.Z. Bai et al.	(BES Collab.)
AUBERT	02B	PR D65 031101	B. Aubert et al.	(BABAR Collab.)
BAI	02	PR D65 052004	J.Z. Bai et al.	(BES Collab.)
BAI	02B	PL B550 24	J.Z. Bai et al.	(BES Collab.)
BAI	02C	PRL 88 101802	J.Z. Bai et al.	(BES Collab.)
PDG	02	PR D66 010001	K. Hagiwara et al.	(PDG Collab.)
BAI	01	PR D63 032002	J.Z. Bai et al.	(BES Collab.)
AMBROGIANI	00A	PR D62 032004	M. Ambrogiani et al.	(FNAL E835 Collab.)
ARTAMONOV	00	PL B474 427	A.S. Artamonov et al.	
BAI	00	PRL 84 594	J.Z. Bai et al.	(BES Collab.)
BAI	99C	PRL 83 1918	J.Z. Bai et al.	(BES Collab.)
BAI	98E	PR D57 3854	J.Z. Bai et al.	(BES Collab.)
BAI	98F	PR D58 097101	J.Z. Bai et al.	(BES Collab.)
BAI	98J	PRL 81 5080	J.Z. Bai et al.	(BES Collab.)
ARMSTRONG	97	PR D55 1153	T.A. Armstrong et al.	(E760 Collab.)
GRIBUSHIN	96	PR D53 4723	A. Gribushin et al.	(E672 and E706 Collab.)
ARMSTRONG	93B	PR D47 772	T.A. Armstrong et al.	(FNAL E760 Collab.)

Downloaded from https://academic.oup.com/ptep/article/2022/8/083C01/6651666 by KIT Library user on 27 September 2022

ALEXANDER	89	NP B320 45	J.P. Alexander *et al.*	(LBL, MICH, SLAC)
COHEN	87	RMP 59 1121	E.R. Cohen, B.N. Taylor	(RISC, NBS)
GAISER	86	PR D34 711	J. Gaiser *et al.*	(Crystal Ball Collab.)
KURAEV	85	SJNP 41 466	E.A. Kuraev, V.S. Fadin	(NOVO)
		Translated from YAF 41 733.		
FRANKLIN	83	PRL 51 963	M.E.B. Franklin *et al.*	(LBL, SLAC)
EDWARDS	82C	PRL 48 70	C. Edwards *et al.*	(CIT, HARV, PRIN+)
LEMOIGNE	82	PL 113B 509	Y. Lemoigne *et al.*	(SACL, LOIC, SHMP+)
HIMEL	80	PRL 44 920	T. Himel *et al.*	(LBL, SLAC)
OREGLIA	80	PRL 45 959	M.J. Oreglia *et al.*	(SLAC, CIT, HARV+)
SCHARRE	80	PL 97B 329	D.L. Scharre *et al.*	(SLAC, LBL)
ZHOLENTZ	80	PL 96B 214	A.A. Zholents *et al.*	(NOVO)
Also		SJNP 34 814	A.A. Zholents *et al.*	(NOVO)
		Translated from YAF 34 1471.		
BRANDELIK	79B	NP B160 426	R. Brandelik *et al.*	(DASP Collab.)
BRANDELIK	79C	ZPHY C1 233	R. Brandelik *et al.*	(DASP Collab.)
BARTEL	78B	PL 79B 492	W. Bartel *et al.*	(DESY, HEIDP)
TANENBAUM	78	PR D17 1731	W.M. Tanenbaum *et al.*	(SLAC, LBL)
BIDDICK	77	PRL 38 1324	C.J. Biddick *et al.*	(UCSD, UMD, PAVI+)
BRAUNSCH...	77	PL 67B 249	W. Braunschweig *et al.*	(DASP Collab.)
BURMESTER	77	PL 66B 395	J. Burmester *et al.*	(DESY, HAMB, SIEG+)
FELDMAN	77	PRPL 33C 285	G.J. Feldman, M.L. Perl	(LBL, SLAC)
YAMADA	77	Hamburg Conf. 69	S. Yamada	(DASP Collab.)
BARTEL	76	PL 64B 483	W. Bartel *et al.*	(DESY, HEIDP)
TANENBAUM	76	PRL 36 402	W.M. Tanenbaum *et al.*	(SLAC, LBL) IG
WHITAKER	76	PRL 37 1596	J.S. Whitaker *et al.*	(SLAC, LBL)
ABRAMS	75	Stanford Symp. 25	G.S. Abrams	(LBL)
ABRAMS	75B	PRL 34 1181	G.S. Abrams *et al.*	(LBL, SLAC)
BOYARSKI	75C	Palermo Conf. 54	A.M. Boyarski *et al.*	(SLAC, LBL)
HILGER	75	PRL 35 625	E. Hilger *et al.*	(STAN, PENN)
LIBERMAN	75	Stanford Symp. 55	A.D. Liberman	(STAN)
LUTH	75	PRL 35 1124	V. Luth *et al.*	(SLAC, LBL) JPC
WIIK	75	Stanford Symp. 69	B.H. Wiik	(DESY)

$\psi(3770)$

$I^G(J^{PC}) = 0^-(1^{--})$

$\psi(3770)$ MASS (MeV)

OUR FIT includes measurements of $m_{\psi(2S)}$, $m_{\psi(3770)}$, and $m_{\psi(3770)} - m_{\psi(2S)}$.

VALUE (MeV)	EVTS	DOCUMENT ID		TECN	COMMENT
3773.7±0.4 OUR FIT Error includes scale factor of 1.4.					
3778.1±0.7 OUR AVERAGE					
3778.1±0.7±0.6		[1] AAIJ	19M	LHCB	$pp \to D\overline{D}$ + anything
$3779.2^{+1.8+0.6}_{-1.7-0.8}$		[2] ANASHIN	12A	KEDR	$e^+e^- \to D\overline{D}$
3775.5±2.4±0.5	57	AUBERT	08B	BABR	$B \to D\overline{D}K$
3776 ±5 ±4	68	BRODZICKA	08	BELL	$B^+ \to D^0\overline{D}^0K^+$
3778.8±1.9±0.9		AUBERT	07BE	BABR	$e^+e^- \to D\overline{D}\gamma$
• • • We do not use the following data for averages, fits, limits, etc. • • •					
3779.8±0.6		[3] SHAMOV	17	RVUE	$e^+e^- \to D\overline{D}$, hadrons
3772.0±1.9		[4,5] ABLIKIM	08D	BES2	$e^+e^- \to$ hadrons
3778.4±3.0±1.3	34	CHISTOV	04	BELL	Sup. by BRODZICKA 08

[1] Measured in prompt hadroproduction.
[2] Taking into account interference between the resonant and non-resonant $D\overline{D}$ production.
[3] From the joint analysis of the data on the $D\overline{D}$ and inclusive hadronic cross sections in the $\psi(3770)$ region from BaBar, Belle, BES-II, CLEO and KEDR.
[4] Reanalysis of data presented in BAI 02C. From a global fit over the center-of-mass energy region 3.7–5.0 GeV covering the $\psi(3770)$, $\psi(4040)$, $\psi(4160)$, and $\psi(4415)$ resonances. Phase angle fixed in the fit to $\delta = 0°$.
[5] Interference between the resonant and non-resonant $D\overline{D}$ production not taken into account.

$m_{\psi(3770)} - m_{\psi(2S)}$

OUR FIT includes measurements of $m_{\psi(2S)}$, $m_{\psi(3770)}$, and $m_{\psi(3770)} - m_{\psi(2S)}$.

VALUE (MeV)	DOCUMENT ID		TECN	COMMENT
87.6±0.4 OUR FIT Error includes scale factor of 1.4.				
86.6±0.7 OUR AVERAGE Error includes scale factor of 2.0. See the ideogram below.				
86.9±0.4	[1] ABLIKIM	07E	BES2	$e^+e^- \to$ hadrons
86.7±0.7	ABLIKIM	06L	BES2	$e^+e^- \to$ hadrons
80 ±2	SCHINDLER	80	MRK2	e^+e^-
86 ±2	[2] BACINO	78	DLCO	e^+e^-
88 ±3	RAPIDIS	77	LGW	e^+e^-

[1] BES-II $\psi(2S)$ mass subtracted (see ABLIKIM 06L).
[2] SPEAR $\psi(2S)$ mass subtracted (see SCHINDLER 80).

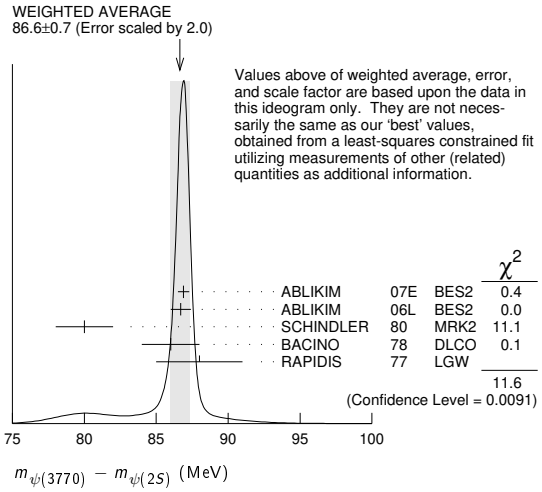

$\psi(3770)$ WIDTH

VALUE (MeV)	EVTS	DOCUMENT ID		TECN	COMMENT
27.2± 1.0 OUR FIT					
27.5± 0.9 OUR AVERAGE					
$24.9^{+4.6+0.5}_{-4.0-1.1}$		[1] ANASHIN	12A	KEDR	$e^+e^- \to D\overline{D}$
30.4± 8.5		[2,3] ABLIKIM	08D	BES2	$e^+e^- \to$ hadrons
27 ±10 ±5	68	BRODZICKA	08	BELL	$B^+ \to D^0\overline{D}^0K^+$
28.5± 1.2±0.2		[3] ABLIKIM	07E	BES2	$e^+e^- \to$ hadrons
23.5± 3.7±0.9		AUBERT	07BE	BABR	$e^+e^- \to D\overline{D}\gamma$
26.9± 2.4±0.3		[3] ABLIKIM	06L	BES2	$e^+e^- \to$ hadrons
24 ± 5		[3] SCHINDLER	80	MRK2	e^+e^-
24 ± 5		[3] BACINO	78	DLCO	e^+e^-
28 ± 5		[3] RAPIDIS	77	LGW	e^+e^-
• • • We do not use the following data for averages, fits, limits, etc. • • •					
25.8± 1.3		[4] SHAMOV	17	RVUE	$e^+e^- \to D\overline{D}$, hadrons

[1] Taking into account interference between the resonant and non-resonant $D\overline{D}$ production.
[2] Reanalysis of data presented in BAI 02C. From a global fit over the center-of-mass energy region 3.7–5.0 GeV covering the $\psi(3770)$, $\psi(4040)$, $\psi(4160)$, and $\psi(4415)$ resonances. Phase angle fixed in the fit to $\delta = 0°$.
[3] Interference between the resonant and non-resonant $D\overline{D}$ production not taken into account.
[4] From the joint analysis of the data on the $D\overline{D}$ and inclusive hadronic cross sections in the $\psi(3770)$ region from BaBar, Belle, BES-II, CLEO and KEDR.

$\psi(3770)$ DECAY MODES

	Mode	Fraction (Γ_i/Γ)	Scale factor/ Confidence level
Γ_1	$D\overline{D}$	$(93\ ^{+8}_{-9})$ %	S=2.0
Γ_2	$D^0\overline{D}^0$	$(52\ ^{+4}_{-5})$ %	S=2.0
Γ_3	D^+D^-	(41 ±4) %	S=2.0
Γ_4	$J/\psi X$	$(5.0 \pm 2.2) \times 10^{-3}$	
Γ_5	$J/\psi\pi^+\pi^-$	$(1.93 \pm 0.28) \times 10^{-3}$	
Γ_6	$J/\psi\pi^0\pi^0$	$(8.0 \pm 3.0) \times 10^{-4}$	
Γ_7	$J/\psi\eta$	$(9 \pm 4) \times 10^{-4}$	
Γ_8	$J/\psi\pi^0$	$< 2.8 \times 10^{-4}$	CL=90%
Γ_9	e^+e^-	$(9.6 \pm 0.7) \times 10^{-6}$	S=1.3
	Decays to light hadrons		
Γ_{10}	$b_1(1235)\pi$	$< 1.4 \times 10^{-5}$	CL=90%
Γ_{11}	$\phi\eta'$	$< 7 \times 10^{-4}$	CL=90%
Γ_{12}	$\omega\eta'$	$< 4 \times 10^{-4}$	CL=90%
Γ_{13}	$\rho^0\eta'$	$< 6 \times 10^{-4}$	CL=90%
Γ_{14}	$\phi\eta$	$(3.1 \pm 0.7) \times 10^{-4}$	
Γ_{15}	$\omega\eta$	$< 1.4 \times 10^{-5}$	CL=90%
Γ_{16}	$\rho^0\eta$	$< 5 \times 10^{-4}$	CL=90%
Γ_{17}	$\phi\pi^0$	$< 3 \times 10^{-5}$	CL=90%
Γ_{18}	$\omega\pi^0$	$< 6 \times 10^{-4}$	CL=90%
Γ_{19}	$\pi^+\pi^-\pi^0$	$< 5 \times 10^{-6}$	CL=90%
Γ_{20}	$\rho\pi$	$< 5 \times 10^{-6}$	CL=90%
Γ_{21}	K^+K^-		
Γ_{22}	$K^*(892)^+K^-$ + c.c.	$< 1.4 \times 10^{-5}$	CL=90%
Γ_{23}	$K^*(892)^0\overline{K}^0$ + c.c.	$< 1.2 \times 10^{-3}$	CL=90%
Γ_{24}	$K^0_S K^0_L$	$< 1.2 \times 10^{-5}$	CL=90%
Γ_{25}	$2(\pi^+\pi^-)$	$< 1.12 \times 10^{-3}$	CL=90%

Downloaded from https://academic.oup.com/ptep/article/2022/8/083C01/6651666 by KIT Library user on 27 September 2022

Γ_{26}	$2(\pi^+\pi^-)\pi^0$	< 1.06	$\times 10^{-3}$	CL=90%
Γ_{27}	$2(\pi^+\pi^-\pi^0)$	< 5.85	%	CL=90%
Γ_{28}	$\omega\pi^+\pi^-$	< 6.0	$\times 10^{-4}$	CL=90%
Γ_{29}	$3(\pi^+\pi^-)$	< 9.1	$\times 10^{-3}$	CL=90%
Γ_{30}	$3(\pi^+\pi^-)\pi^0$	< 1.37	%	CL=90%
Γ_{31}	$3(\pi^+\pi^-)2\pi^0$	< 11.74	%	CL=90%
Γ_{32}	$\eta\pi^+\pi^-$	< 1.24	$\times 10^{-3}$	CL=90%
Γ_{33}	$\pi^+\pi^-2\pi^0$	< 8.9	$\times 10^{-3}$	CL=90%
Γ_{34}	$\rho^0\pi^+\pi^-$	< 6.9	$\times 10^{-3}$	CL=90%
Γ_{35}	$\eta 3\pi$	< 1.34	$\times 10^{-3}$	CL=90%
Γ_{36}	$\eta 2(\pi^+\pi^-)$	< 2.43	%	CL=90%
Γ_{37}	$\eta\rho^0\pi^+\pi^-$	< 1.45	%	CL=90%
Γ_{38}	$\eta' 3\pi$	< 2.44	$\times 10^{-3}$	CL=90%
Γ_{39}	$K^+K^-\pi^+\pi^-$	< 9.0	$\times 10^{-4}$	CL=90%
Γ_{40}	$\phi\pi^+\pi^-$	< 4.1	$\times 10^{-4}$	CL=90%
Γ_{41}	$K^+K^-2\pi^0$	< 4.2	$\times 10^{-3}$	CL=90%
Γ_{42}	$4(\pi^+\pi^-)$	< 1.67	%	CL=90%
Γ_{43}	$4(\pi^+\pi^-)\pi^0$	< 3.06	%	CL=90%
Γ_{44}	$\phi f_0(980)$	< 4.5	$\times 10^{-4}$	CL=90%
Γ_{45}	$K^+K^-\pi^+\pi^-\pi^0$	< 2.36	$\times 10^{-3}$	CL=90%
Γ_{46}	$K^+K^-\rho^0\pi^0$	< 8	$\times 10^{-4}$	CL=90%
Γ_{47}	$K^+K^-\rho^+\pi^-$	< 1.46	%	CL=90%
Γ_{48}	ωK^+K^-	< 3.4	$\times 10^{-4}$	CL=90%
Γ_{49}	$\phi\pi^+\pi^-\pi^0$	< 3.8	$\times 10^{-3}$	CL=90%
Γ_{50}	$K^{*0}K^-\pi^+\pi^0$ + c.c.	< 1.62	%	CL=90%
Γ_{51}	$K^{*+}K^-\pi^+\pi^-$ + c.c.	< 3.23	%	CL=90%
Γ_{52}	$K^+K^-\pi^+\pi^-2\pi^0$	< 2.67	%	CL=90%
Γ_{53}	$K^+K^-2(\pi^+\pi^-)$	< 1.03	%	CL=90%
Γ_{54}	$K^+K^-2(\pi^+\pi^-)\pi^0$	< 3.60	%	CL=90%
Γ_{55}	ηK^+K^-	< 4.1	$\times 10^{-4}$	CL=90%
Γ_{56}	$\eta K^+K^-\pi^+\pi^-$	< 1.24	%	CL=90%
Γ_{57}	$\rho^0K^+K^-$	< 5.0	$\times 10^{-3}$	CL=90%
Γ_{58}	$2(K^+K^-)$	< 6.0	$\times 10^{-4}$	CL=90%
Γ_{59}	ϕK^+K^-	< 7.5	$\times 10^{-4}$	CL=90%
Γ_{60}	$2(K^+K^-)\pi^0$	< 2.9	$\times 10^{-4}$	CL=90%
Γ_{61}	$2(K^+K^-)\pi^+\pi^-$	< 3.2	$\times 10^{-3}$	CL=90%
Γ_{62}	$K^0_S K^-\pi^+$	< 3.2	$\times 10^{-3}$	CL=90%
Γ_{63}	$K^0_S K^-\pi^+\pi^0$	< 1.33	%	CL=90%
Γ_{64}	$K^0_S K^-\rho^+$	< 6.6	$\times 10^{-3}$	CL=90%
Γ_{65}	$K^0_S K^-2\pi^+\pi^-$	< 8.7	$\times 10^{-3}$	CL=90%
Γ_{66}	$K^0_S K^-\pi^+\rho^0$	< 1.6	%	CL=90%
Γ_{67}	$K^0_S K^-\pi^+\eta$	< 1.3	%	CL=90%
Γ_{68}	$K^0_S K^-2\pi^+\pi^-\pi^0$	< 4.18	%	CL=90%
Γ_{69}	$K^0_S K^-2\pi^+\pi^-\eta$	< 4.8	%	CL=90%
Γ_{70}	$K^0_S K^-\pi^+2(\pi^+\pi^-)$	< 1.22	%	CL=90%
Γ_{71}	$K^0_S K^-\pi^+2\pi^0$	< 2.65	%	CL=90%
Γ_{72}	$K^0_S K^-K^+K^-\pi^+$	< 4.9	$\times 10^{-3}$	CL=90%
Γ_{73}	$K^0_S K^-K^+K^-\pi^+\pi^0$	< 3.0	%	CL=90%
Γ_{74}	$K^0_S K^-K^+K^-\pi^+\eta$	< 2.2	%	CL=90%
Γ_{75}	$K^{*0}K^-\pi^+$ + c.c.	< 9.7	$\times 10^{-3}$	CL=90%
Γ_{76}	$p\overline{p}$			
Γ_{77}	$p\overline{p}\pi^0$	< 4	$\times 10^{-5}$	CL=90%
Γ_{78}	$p\overline{p}\pi^+\pi^-$	< 5.8	$\times 10^{-4}$	CL=90%
Γ_{79}	$\Lambda\overline{\Lambda}$	< 1.2	$\times 10^{-4}$	CL=90%
Γ_{80}	$p\overline{p}\pi^+\pi^-\pi^0$	< 1.85	$\times 10^{-3}$	CL=90%
Γ_{81}	$\omega p\overline{p}$	< 2.9	$\times 10^{-4}$	CL=90%
Γ_{82}	$\Lambda\overline{\Lambda}\pi^0$	< 7	$\times 10^{-5}$	CL=90%
Γ_{83}	$p\overline{p}2(\pi^+\pi^-)$	< 2.6	$\times 10^{-3}$	CL=90%
Γ_{84}	$\eta p\overline{p}$	< 5.4	$\times 10^{-4}$	CL=90%
Γ_{85}	$\eta p\overline{p}\pi^+\pi^-$	< 3.3	$\times 10^{-3}$	CL=90%
Γ_{86}	$\rho^0 p\overline{p}$	< 1.7	$\times 10^{-3}$	CL=90%
Γ_{87}	$p\overline{p}K^+K^-$	< 3.2	$\times 10^{-4}$	CL=90%
Γ_{88}	$\eta p\overline{p}K^+K^-$	< 6.9	$\times 10^{-3}$	CL=90%
Γ_{89}	$\pi^0 p\overline{p}K^+K^-$	< 1.2	$\times 10^{-3}$	CL=90%
Γ_{90}	$\phi p\overline{p}$	< 1.3	$\times 10^{-4}$	CL=90%
Γ_{91}	$\Lambda\overline{\Lambda}\pi^+\pi^-$	< 2.5	$\times 10^{-4}$	CL=90%
Γ_{92}	$\Lambda\overline{p}K^+$	< 2.8	$\times 10^{-4}$	CL=90%
Γ_{93}	$\Lambda\overline{p}K^+\pi^+\pi^-$	< 6.3	$\times 10^{-4}$	CL=90%
Γ_{94}	$\Lambda\overline{\Lambda}\eta$	< 1.9	$\times 10^{-4}$	CL=90%
Γ_{95}	$\Sigma^+\overline{\Sigma}^-$	< 1.0	$\times 10^{-4}$	CL=90%
Γ_{96}	$\Sigma^0\overline{\Sigma}^0$	< 4	$\times 10^{-5}$	CL=90%
Γ_{97}	$\Xi^+\overline{\Xi}^-$	< 1.5	$\times 10^{-4}$	CL=90%
Γ_{98}	$\Xi^0\overline{\Xi}^0$	< 1.4	$\times 10^{-4}$	CL=90%

Radiative decays

Γ_{99}	$\gamma\chi_{c2}$	< 6.4	$\times 10^{-4}$	CL=90%
Γ_{100}	$\gamma\chi_{c1}$	(2.49±0.23)	$\times 10^{-3}$	
Γ_{101}	$\gamma\chi_{c0}$	(6.9 ±0.6)	$\times 10^{-3}$	
Γ_{102}	$\gamma\eta_c$	< 7	$\times 10^{-4}$	CL=90%
Γ_{103}	$\gamma\eta_c(2S)$	< 9	$\times 10^{-4}$	CL=90%
Γ_{104}	$\gamma\eta'$	< 1.8	$\times 10^{-4}$	CL=90%
Γ_{105}	$\gamma\eta$	< 1.5	$\times 10^{-4}$	CL=90%
Γ_{106}	$\gamma\pi^0$	< 2	$\times 10^{-4}$	CL=90%

CONSTRAINED FIT INFORMATION

An overall fit to the total width, a partial width, and 3 branching ratios uses 23 measurements and one constraint to determine 5 parameters. The overall fit has a χ^2 = 20.1 for 19 degrees of freedom.

The following *off-diagonal* array elements are the correlation coefficients $\langle \delta p_i \delta p_j \rangle / (\delta p_i \cdot \delta p_j)$, in percent, from the fit to parameters p_i, including the branching fractions, $x_i \equiv \Gamma_i/\Gamma_{\rm total}$. The fit constrains the x_i whose labels appear in this array to sum to one.

	x_2	x_3	x_9
x_3	99		
x_9	0	0	
Γ	0	0	−44

	Mode	Rate (MeV)	Scale factor
Γ_2	$D^0\overline{D}^0$	14.0 ±1.4	1.8
Γ_3	D^+D^-	11.2 ±1.1	1.7
Γ_9	e^+e^-	(2.62±0.18) $\times 10^{-4}$	1.4

$\psi(3770)$ PARTIAL WIDTHS

$\Gamma(e^+e^-)$ — Γ_9

VALUE (keV)	EVTS	DOCUMENT ID		TECN	COMMENT
0.262±0.018 OUR FIT Error includes scale factor of 1.4.					
0.256±0.016 OUR AVERAGE Error includes scale factor of 1.2.					
$0.154^{+0.079}_{-0.058}{}^{+0.021}_{-0.027}$		[1,2] ANASHIN	12A	KEDR	$e^+e^- \to D\overline{D}$
0.22 ±0.05		[3,4] ABLIKIM	08D	BES2	$e^+e^- \to$ hadrons
0.277±0.011±0.013		[4] ABLIKIM	07E	BES2	$e^+e^- \to$ hadrons
$0.203\pm0.003^{+0.041}_{-0.027}$	1.4M	[4,5] BESSON	06	CLEO	$e^+e^- \to$ hadrons
0.276±0.050		[4] SCHINDLER	80	MRK2	e^+e^-
0.18 ±0.06		[4] BACINO	78	DLCO	e^+e^-
• • • We do not use the following data for averages, fits, limits, etc. • • •					
0.196±0.018		[6] SHAMOV	17	RVUE	$e^+e^- \to D\overline{D}$, hadrons
$0.414^{+0.072}_{-0.080}{}^{+0.093}_{-0.028}$		[2,7] ANASHIN	12A	KEDR	$e^+e^- \to D\overline{D}$
0.37 ±0.09		[8] RAPIDIS	77	LGW	e^+e^-

[1] Solution I of the two solutions.
[2] Taking into account interference between the resonant and non-resonant $D\overline{D}$ production.
[3] Reanalysis of data presented in BAI 02C. From a global fit over the center-of-mass energy region 3.7–5.0 GeV covering the $\psi(3770)$, $\psi(4040)$, $\psi(4160)$, and $\psi(4415)$ resonances. Phase angle fixed in the fit to $\delta = 0°$.
[4] Interference between the resonant and non-resonant $D\overline{D}$ production not taken into account.
[5] BESSON 06 (as corrected in BESSON 10) measure $\sigma(e^+e^- \to \psi(3770) \to$ hadrons) $= 6.36 \pm 0.08^{+0.41}_{-0.30}$ nb at $\sqrt{s} = 3773 \pm 1$ MeV, and obtain Γ_{ee} from the Born-level cross section calculated using $\psi(3770)$ mass and width from our 2004 edition, PDG 04.
[6] From the joint analysis of the data on the $D\overline{D}$ and inclusive hadronic cross sections in the $\psi(3770)$ region from BaBar, Belle, BES-II, CLEO and KEDR.
[7] Solution II of the two solutions.
[8] See also $\Gamma(e^+e^-)/\Gamma_{\rm total}$ below.

$\psi(3770)$ BRANCHING RATIOS

$\Gamma(D\overline{D})/\Gamma_{\rm total}$ — $\Gamma_1/\Gamma = (\Gamma_2+\Gamma_3)/\Gamma$

VALUE	EVTS	DOCUMENT ID		TECN	COMMENT
$0.93\ ^{+0.08}_{-0.09}$ OUR FIT Error includes scale factor of 2.0.					
$0.93\ ^{+0.08}_{-0.09}$ OUR AVERAGE Error includes scale factor of 2.1.					
0.849±0.056±0.018		[1] ABLIKIM	08B	BES2	$e^+e^- \to$ non-$D\overline{D}$
$1.033\pm0.014^{+0.048}_{-0.066}$	1.427M	[2] BESSON	06	CLEO	$e^+e^- \to$ hadrons
• • • We do not use the following data for averages, fits, limits, etc. • • •					
0.836±0.049		[3] SHAMOV	17	RVUE	$e^+e^- \to D\overline{D}$, hadrons
0.866±0.050±0.036		[4,5] ABLIKIM	07K	BES2	$e^+e^- \to$ non-$D\overline{D}$
0.836±0.073±0.042		[5] ABLIKIM	06L	BES2	$e^+e^- \to D\overline{D}$
0.855±0.017±0.058		[5,6] ABLIKIM	06N	BES2	$e^+e^- \to D\overline{D}$

[1] Neglecting interference.

Downloaded from https://academic.oup.com/ptep/article/2022/8/083C01/6651666 by KIT Library user on 27 September 2022

[2] Obtained by comparing a measurement of the total cross section (corrected in BESSON 10) with that of $D\overline{D}$ reported by CLEO in DOBBS 07.
[3] From the joint analysis of the data on the $D\overline{D}$ and inclusive hadronic cross sections in the $\psi(3770)$ region from BaBar, Belle, BES-II, CLEO and KEDR.
[4] Using $\sigma^{obs} = 7.07 \pm 0.58$ nb and neglecting interference.
[5] Not independent of ABLIKIM 08B.
[6] From a measurement of $\sigma(e^+e^- \to D\overline{D})$ at $\sqrt{s} = 3773$ MeV, using the $\psi(3770)$ resonance parameters measured by ABLIKIM 06L.

$\Gamma(D^0\overline{D}^0)/\Gamma_{total}$ — Γ_2/Γ

VALUE	DOCUMENT ID		TECN	COMMENT
$0.52\ ^{+0.04}_{-0.05}$ OUR FIT Error includes scale factor of 2.0.				
• • • We do not use the following data for averages, fits, limits, etc. • • •				
$0.467 \pm 0.047 \pm 0.023$	ABLIKIM	06L	BES2	$e^+e^- \to D^0\overline{D}^0$
$0.499 \pm 0.013 \pm 0.038$	[1] ABLIKIM	06N	BES2	$e^+e^- \to D^0\overline{D}^0$

[1] From a measurement of $\sigma(e^+e^- \to D\overline{D})$ at $\sqrt{s} = 3773$ MeV, using the $\psi(3770)$ resonance parameters measured by ABLIKIM 06L.

$\Gamma(D^+D^-)/\Gamma_{total}$ — Γ_3/Γ

VALUE	DOCUMENT ID		TECN	COMMENT
0.41 ± 0.04 OUR FIT Error includes scale factor of 2.0.				
• • • We do not use the following data for averages, fits, limits, etc. • • •				
$0.369 \pm 0.037 \pm 0.028$	ABLIKIM	06L	BES2	$e^+e^- \to D^+D^-$
$0.357 \pm 0.011 \pm 0.034$	[1] ABLIKIM	06N	BES2	$e^+e^- \to D^+D^-$

[1] From a measurement of $\sigma(e^+e^- \to D\overline{D})$ at $\sqrt{s} = 3773$ MeV, using the $\psi(3770)$ resonance parameters measured by ABLIKIM 06L.

$\Gamma(D^0\overline{D}^0)/\Gamma(D^+D^-)$ — Γ_2/Γ_3

VALUE	EVTS	DOCUMENT ID		TECN	COMMENT
1.253 ± 0.016 OUR FIT					
1.253 ± 0.016 OUR AVERAGE					
$1.252 \pm 0.009 \pm 0.013$	5.3M	BONVICINI	14	CLEO	$e^+e^- \to D\overline{D}$
$1.39 \pm 0.31 \pm 0.12$		PAKHLOVA	08	BELL	10.6 $e^+e^- \to D\overline{D}\gamma$
$1.78 \pm 0.33 \pm 0.24$		AUBERT	07BE	BABR	$e^+e^- \to D\overline{D}\gamma$
$1.27 \pm 0.12 \pm 0.08$		ABLIKIM	06L	BES2	$e^+e^- \to D\overline{D}$
$2.43 \pm 1.50 \pm 0.43$	34	[1] CHISTOV	04	BELL	$B^+ \to \psi(3770) K^+$
• • • We do not use the following data for averages, fits, limits, etc. • • •					
$1.258 \pm 0.016 \pm 0.014$		[2] DOBBS	07	CLEO	$e^+e^- \to D\overline{D}$

[1] See ADLER 88C for older measurements of this quantity.
[2] Superseded by BONVICINI 14.

$\Gamma(J/\psi X)/\Gamma_{total}$ — Γ_4/Γ

VALUE (%)	DOCUMENT ID		TECN	COMMENT
$0.5 \pm 0.2 \pm 0.1$	[1] ABLIKIM	21Z	BES3	$e^+e^- \to \ell^+\ell^- X$

[1] From a fit to the $e^+e^- \to J/\psi X$ cross section between 3.645 and 3.891 GeV, with $\psi(2S)$ and $\psi(3770)$ masses, total widths and leptonic widths fixed to the values from the PDG 20. An alternative fit with an improved χ^2, corresponding to a significance of 5.3 σ, uses an additional resonance with a mass of $3766.2 \pm 3.8 \pm 0.4$ MeV/c^2, a total width of $22.2 \pm 5.9 \pm 1.4$ MeV, and $\Gamma(e\,e)\cdot B(J/\psi X) = 79.4 \pm 85.5 \pm 11.7$ eV, possibly compatible with the results of ABLIKIM 08H.

$\Gamma(J/\psi\pi^+\pi^-)/\Gamma_{total}$ — Γ_5/Γ

VALUE (units 10^{-3})	EVTS	DOCUMENT ID		TECN	COMMENT
1.93 ± 0.28 OUR AVERAGE					
$1.89 \pm 0.20 \pm 0.20$	231 ± 33	ADAM	06	CLEO	$e^+e^- \to \psi(3770)$
$3.4 \pm 1.4 \pm 0.9$	17.8 ± 4.8	BAI	05	BES2	$e^+e^- \to \psi(3770)$

$\Gamma(J/\psi\pi^0\pi^0)/\Gamma_{total}$ — Γ_6/Γ

VALUE (units 10^{-2})	EVTS	DOCUMENT ID		TECN	COMMENT
$0.080 \pm 0.025 \pm 0.016$	39 ± 14	ADAM	06	CLEO	$e^+e^- \to \psi(3770)$

$\Gamma(J/\psi\eta)/\Gamma_{total}$ — Γ_7/Γ

VALUE (units 10^{-5})	EVTS	DOCUMENT ID		TECN	COMMENT
$87 \pm 33 \pm 22$	22 ± 10	ADAM	06	CLEO	$e^+e^- \to \psi(3770)$

$\Gamma(J/\psi\pi^0)/\Gamma_{total}$ — Γ_8/Γ

VALUE (units 10^{-5})	CL%	EVTS	DOCUMENT ID		TECN	COMMENT
<28	90	<10	ADAM	06	CLEO	$e^+e^- \to \psi(3770)$

$\Gamma(e^+e^-)/\Gamma_{total}$ — Γ_9/Γ

VALUE (units 10^{-5})	DOCUMENT ID		TECN	COMMENT
0.96 ± 0.07 OUR FIT Error includes scale factor of 1.3.				
1.3 ± 0.2	RAPIDIS	77	LGW	e^+e^-

DECAYS TO LIGHT HADRONS

$\Gamma(b_1(1235)\pi)/\Gamma_{total}$ — Γ_{10}/Γ

VALUE (units 10^{-5})	CL%	DOCUMENT ID		TECN	COMMENT
<1.4	90	[1] ADAMS	06	CLEO	$e^+e^- \to \psi(3770)$

[1] Comparing cross sections at $\sqrt{s} = 3.773$ GeV and $\sqrt{s} = 3.671$ GeV, neglecting interference, and using $\sigma(\psi(3770) \to D\overline{D}) = 6.39 \pm 0.20$ nb.

$\Gamma(\phi\eta')/\Gamma_{total}$ — Γ_{11}/Γ

VALUE (units 10^{-4})	CL%	DOCUMENT ID		TECN	COMMENT
<7	90	[1] ADAMS	06	CLEO	$e^+e^- \to \psi(3770)$

[1] Comparing cross sections at $\sqrt{s} = 3.773$ GeV and $\sqrt{s} = 3.671$ GeV, neglecting interference, and using $\sigma(\psi(3770) \to D\overline{D}) = 6.39 \pm 0.20$ nb.

$\Gamma(\omega\eta')/\Gamma_{total}$ — Γ_{12}/Γ

VALUE (units 10^{-4})	CL%	DOCUMENT ID		TECN	COMMENT
<4	90	[1] ADAMS	06	CLEO	$e^+e^- \to \psi(3770)$

[1] Comparing cross sections at $\sqrt{s} = 3.773$ GeV and $\sqrt{s} = 3.671$ GeV, neglecting interference, and using $\sigma(\psi(3770) \to D\overline{D}) = 6.39 \pm 0.20$ nb.

$\Gamma(\rho^0\eta')/\Gamma_{total}$ — Γ_{13}/Γ

VALUE (units 10^{-4})	CL%	DOCUMENT ID		TECN	COMMENT
<6	90	[1] ADAMS	06	CLEO	$e^+e^- \to \psi(3770)$

[1] Comparing cross sections at $\sqrt{s} = 3.773$ GeV and $\sqrt{s} = 3.671$ GeV, neglecting interference, and using $\sigma(\psi(3770) \to D\overline{D}) = 6.39 \pm 0.20$ nb.

$\Gamma(\phi\eta)/\Gamma_{total}$ — Γ_{14}/Γ

VALUE (units 10^{-4})	CL%	DOCUMENT ID		TECN	COMMENT
$3.1 \pm 0.6 \pm 0.3$		[1] ADAMS	06	CLEO	3.773 $e^+e^- \to \phi\eta$
• • • We do not use the following data for averages, fits, limits, etc. • • •					
<19	90	[2] ABLIKIM	07B	BES2	$e^+e^- \to \psi(3770)$

[1] Comparing cross sections at $\sqrt{s} = 3.773$ GeV and $\sqrt{s} = 3.671$ GeV, neglecting interference, and using $\sigma(\psi(3770) \to D\overline{D}) = 6.39 \pm 0.20$ nb.
[2] Assuming that interference effects between resonance and continuum can be neglected and using $\sigma^{obs}(e^+e^- \to \psi(3770)) = 7.15 \pm 0.38$ nb.

$\Gamma(\omega\eta)/\Gamma_{total}$ — Γ_{15}/Γ

VALUE (units 10^{-5})	CL%	DOCUMENT ID		TECN	COMMENT
<1.4	90	[1] ADAMS	06	CLEO	$e^+e^- \to \psi(3770)$

[1] Comparing cross sections at $\sqrt{s} = 3.773$ GeV and $\sqrt{s} = 3.671$ GeV, neglecting interference, and using $\sigma(\psi(3770) \to D\overline{D}) = 6.39 \pm 0.20$ nb.

$\Gamma(\rho^0\eta)/\Gamma_{total}$ — Γ_{16}/Γ

VALUE (units 10^{-4})	CL%	DOCUMENT ID		TECN	COMMENT
<5	90	[1] ADAMS	06	CLEO	$e^+e^- \to \psi(3770)$

[1] Comparing cross sections at $\sqrt{s} = 3.773$ GeV and $\sqrt{s} = 3.671$ GeV, neglecting interference, and using $\sigma(\psi(3770) \to D\overline{D}) = 6.39 \pm 0.20$ nb.

$\Gamma(\phi\pi^0)/\Gamma_{total}$ — Γ_{17}/Γ

VALUE (units 10^{-5})	CL%	DOCUMENT ID		TECN	COMMENT
< 3	90	[1] ADAMS	06	CLEO	$e^+e^- \to \psi(3770)$
• • • We do not use the following data for averages, fits, limits, etc. • • •					
<50	90	[2] ABLIKIM	07B	BES2	$e^+e^- \to \psi(3770)$

[1] Comparing cross sections at $\sqrt{s} = 3.773$ GeV and $\sqrt{s} = 3.671$ GeV, neglecting interference, and using $\sigma(\psi(3770) \to D\overline{D}) = 6.39 \pm 0.20$ nb.
[2] Assuming that interference effects between resonance and continuum can be neglected and using $\sigma^{obs}(e^+e^- \to \psi(3770)) = 7.15 \pm 0.38$ nb.

$\Gamma(\omega\pi^0)/\Gamma_{total}$ — Γ_{18}/Γ

VALUE (units 10^{-4})	CL%	DOCUMENT ID		TECN	COMMENT
<6	90	[1] ADAMS	06	CLEO	$e^+e^- \to \psi(3770)$

[1] Comparing cross sections at $\sqrt{s} = 3.773$ GeV and $\sqrt{s} = 3.671$ GeV, neglecting interference, and using $\sigma(\psi(3770) \to D\overline{D}) = 6.39 \pm 0.20$ nb.

$\Gamma(\pi^+\pi^-\pi^0)/\Gamma_{total}$ — Γ_{19}/Γ

VALUE (units 10^{-6})	CL%	DOCUMENT ID		TECN	COMMENT
<5	90	[1,2] ADAMS	06	CLEO	$e^+e^- \to \psi(3770)$

[1] Data suggest possible destructive interference with continuum.
[2] Comparing cross sections at $\sqrt{s} = 3.773$ GeV and $\sqrt{s} = 3.671$ GeV, neglecting interference, and using $\sigma(\psi(3770) \to D\overline{D}) = 6.39 \pm 0.20$ nb.

$\Gamma(\rho\pi)/\Gamma_{total}$ — Γ_{20}/Γ

VALUE (units 10^{-6})	CL%	DOCUMENT ID		TECN	COMMENT
<5	90	[1,2] ADAMS	06	CLEO	$e^+e^- \to \psi(3770)$

[1] Comparing cross sections at $\sqrt{s} = 3.773$ GeV and $\sqrt{s} = 3.671$ GeV, neglecting interference, and using $\sigma(\psi(3770) \to D\overline{D}) = 6.39 \pm 0.20$ nb.
[2] Data suggest possible destructive interference with continuum.

$\Gamma(K^+K^-)/\Gamma_{total}$ — Γ_{21}/Γ

VALUE	DOCUMENT ID		TECN	COMMENT
• • • We do not use the following data for averages, fits, limits, etc. • • •				
$\sim 10^{-5}$	[1] DRUZHININ	15	RVUE	$e^+e^- \to \psi(3770)$

[1] DRUZHININ 15 uses BABAR and CLEO data takitaking into account interference of the processes $e^+e^- \to K^+K^-$ and $e^+e^- \to K^0_S K^0_L$.

Downloaded from https://academic.oup.com/ptep/article/2022/8/083C01/6651666 by KIT Library user on 27 September 2022

$\Gamma(K^*(892)^+ K^- + \text{c.c.})/\Gamma_{\text{total}}$ — Γ_{22}/Γ

VALUE (units 10^{-5})	CL%	DOCUMENT ID		TECN	COMMENT
<1.4	90	[1] ADAMS	06	CLEO	$e^+e^- \to \psi(3770)$

[1] Comparing cross sections at $\sqrt{s} = 3.773$ GeV and $\sqrt{s} = 3.671$ GeV, neglecting interference, and using $\sigma(\psi(3770) \to D\overline{D}) = 6.39 \pm 0.20$ nb.

$\Gamma(K^*(892)^0 \overline{K}^0 + \text{c.c.})/\Gamma_{\text{total}}$ — Γ_{23}/Γ

VALUE (units 10^{-3})	CL%	DOCUMENT ID		TECN	COMMENT
<1.2	90	[1] ADAMS	06	CLEO	$e^+e^- \to \psi(3770)$

[1] Comparing cross sections at $\sqrt{s} = 3.773$ GeV and $\sqrt{s} = 3.671$ GeV, neglecting interference, and using $\sigma(\psi(3770) \to D\overline{D}) = 6.39 \pm 0.20$ nb.

$\Gamma(K^0_S K^0_L)/\Gamma_{\text{total}}$ — Γ_{24}/Γ

VALUE (units 10^{-5})	CL%	DOCUMENT ID		TECN	COMMENT
< 1.2	90	[1] CRONIN-HEN...	06	CLEO	$e^+e^- \to \psi(3770)$
• • • We do not use the following data for averages, fits, limits, etc. • • •					
<21	90	[2] ABLIKIM	04F	BES	$e^+e^- \to \psi(3770)$

[1] Using $\sigma(e^+e^- \to \psi(3770) \to \text{hadrons}) = (6.38 \pm 0.08^{+0.41}_{-0.30})$ nb from BESSON 06 and $B(K^0_S \to \pi^+\pi^-) = 0.6895 \pm 0.0014$.
[2] Using $B(K^0_S \to \pi^+\pi^-) = 0.6860 \pm 0.0027$.

$\Gamma(2(\pi^+\pi^-))/\Gamma_{\text{total}}$ — Γ_{25}/Γ

VALUE (units 10^{-4})	CL%	DOCUMENT ID		TECN	COMMENT
<11.2	90	[1] HUANG	06A	CLEO	$e^+e^- \to \psi(3770)$
• • • We do not use the following data for averages, fits, limits, etc. • • •					
<48	90	[2] ABLIKIM	07B	BES2	$e^+e^- \to \psi(3770)$

[1] Using $\sigma_{tot}(e^+e^- \to \psi(3770)) = 7.9 \pm 0.6$ nb at the resonance.
[2] Assuming that interference effects between resonance and continuum can be neglected and using $\sigma^{obs}(e^+e^- \to \psi(3770)) = 7.15 \pm 0.38$ nb.

$\Gamma(2(\pi^+\pi^-)\pi^0)/\Gamma_{\text{total}}$ — Γ_{26}/Γ

VALUE (units 10^{-4})	CL%	DOCUMENT ID		TECN	COMMENT
<10.6	90	[1] HUANG	06A	CLEO	$e^+e^- \to \psi(3770)$
• • • We do not use the following data for averages, fits, limits, etc. • • •					
<62	90	[2] ABLIKIM	07B	BES2	$e^+e^- \to \psi(3770)$

[1] Using $\sigma_{tot}(e^+e^- \to \psi(3770)) = 7.9 \pm 0.6$ nb at the resonance.
[2] Assuming that interference effects between resonance and continuum can be neglected and using $\sigma^{obs}(e^+e^- \to \psi(3770)) = 7.15 \pm 0.38$ nb.

$\Gamma(2(\pi^+\pi^-\pi^0))/\Gamma_{\text{total}}$ — Γ_{27}/Γ

VALUE (units 10^{-3})	CL%	EVTS	DOCUMENT ID		TECN	COMMENT
<58.5	90	305	ABLIKIM	08N	BES2	$e^+e^- \to \psi(3770)$

$\Gamma(\omega\pi^+\pi^-)/\Gamma_{\text{total}}$ — Γ_{28}/Γ

VALUE (units 10^{-4})	CL%	DOCUMENT ID		TECN	COMMENT
< 6.0	90	[1] HUANG	06A	CLEO	$e^+e^- \to \psi(3770)$
• • • We do not use the following data for averages, fits, limits, etc. • • •					
<55	90	[2] ABLIKIM	07I	BES2	3.77 e^+e^-

[1] Using $\sigma_{tot}(e^+e^- \to \psi(3770)) = 7.9 \pm 0.6$ nb at the resonance.
[2] Assuming that interference effects between resonance and continuum can be neglected and using $\sigma^{obs}(e^+e^- \to \psi(3770)) = 7.15 \pm 0.38$ nb.

$\Gamma(3(\pi^+\pi^-))/\Gamma_{\text{total}}$ — Γ_{29}/Γ

VALUE (units 10^{-4})	CL%	DOCUMENT ID		TECN	COMMENT
<91	90	[1] ABLIKIM	07B	BES2	$e^+e^- \to \psi(3770)$

[1] Assuming that interference effects between resonance and continuum can be neglected and using $\sigma^{obs}(e^+e^- \to \psi(3770)) = 7.15 \pm 0.38$ nb.

$\Gamma(3(\pi^+\pi^-)\pi^0)/\Gamma_{\text{total}}$ — Γ_{30}/Γ

VALUE (units 10^{-4})	CL%	DOCUMENT ID		TECN	COMMENT
<137	90	[1] ABLIKIM	07B	BES2	$e^+e^- \to \psi(3770)$

[1] Assuming that interference effects between resonance and continuum can be neglected and using $\sigma^{obs}(e^+e^- \to \psi(3770)) = 7.15 \pm 0.38$ nb.

$\Gamma(3(\pi^+\pi^-)2\pi^0)/\Gamma_{\text{total}}$ — Γ_{31}/Γ

VALUE (units 10^{-3})	CL%	EVTS	DOCUMENT ID		TECN	COMMENT
<117.4	90	59	ABLIKIM	08N	BES2	$e^+e^- \to \psi(3770)$

$\Gamma(\eta\pi^+\pi^-)/\Gamma_{\text{total}}$ — Γ_{32}/Γ

VALUE (units 10^{-3})	CL%	DOCUMENT ID		TECN	COMMENT
<1.24	90	[1] HUANG	06A	CLEO	$e^+e^- \to \psi(3770)$
• • • We do not use the following data for averages, fits, limits, etc. • • •					
<2.3	90	[2] ABLIKIM	10D	BES2	$e^+e^- \to \psi(3770)$

[1] Using $\sigma_{tot}(e^+e^- \to \psi(3770)) = 7.9 \pm 0.6$ nb at the resonance.
[2] Assuming that interference effects between resonance and continuum can be neglected and using $\sigma^{obs}(e^+e^- \to \psi(3770)) = 7.15 \pm 0.38$ nb.

$\Gamma(\pi^+\pi^-2\pi^0)/\Gamma_{\text{total}}$ — Γ_{33}/Γ

VALUE (units 10^{-3})	CL%	EVTS	DOCUMENT ID		TECN	COMMENT
<8.9	90	218	ABLIKIM	08N	BES2	$e^+e^- \to \psi(3770)$

$\Gamma(\rho^0\pi^+\pi^-)/\Gamma_{\text{total}}$ — Γ_{34}/Γ

VALUE (units 10^{-3})	CL%	DOCUMENT ID		TECN	COMMENT
<6.9	90	[1] ABLIKIM	07F	BES2	$e^+e^- \to \psi(3770)$

[1] Assuming that interference effects between resonance and continuum can be neglected and using $\sigma^{obs}(e^+e^- \to \psi(3770)) = 7.15 \pm 0.38$ nb.

$\Gamma(\eta 3\pi)/\Gamma_{\text{total}}$ — Γ_{35}/Γ

VALUE (units 10^{-4})	CL%	DOCUMENT ID		TECN	COMMENT
<13.4	90	[1] HUANG	06A	CLEO	$e^+e^- \to \psi(3770)$

[1] Using $\sigma_{tot}(e^+e^- \to \psi(3770)) = 7.9 \pm 0.6$ nb at the resonance.

$\Gamma(\eta 2(\pi^+\pi^-))/\Gamma_{\text{total}}$ — Γ_{36}/Γ

VALUE (units 10^{-4})	CL%	DOCUMENT ID		TECN	COMMENT
<243	90	[1] ABLIKIM	07B	BES2	$e^+e^- \to \psi(3770)$

[1] Assuming that interference effects between resonance and continuum can be neglected and using $\sigma^{obs}(e^+e^- \to \psi(3770)) = 7.15 \pm 0.38$ nb.

$\Gamma(\eta\rho^0\pi^+\pi^-)/\Gamma_{\text{total}}$ — Γ_{37}/Γ

VALUE (units 10^{-2})	CL%	DOCUMENT ID		TECN	COMMENT
<1.45	90	[1] ABLIKIM	10D	BES2	$e^+e^- \to \psi(3770)$

[1] Assuming that interference effects between resonance and continuum can be neglected and using $\sigma^{obs}(e^+e^- \to \psi(3770)) = 7.15 \pm 0.38$ nb.

$\Gamma(\eta' 3\pi)/\Gamma_{\text{total}}$ — Γ_{38}/Γ

VALUE (units 10^{-4})	CL%	DOCUMENT ID		TECN	COMMENT
<24.4	90	[1] HUANG	06A	CLEO	$e^+e^- \to \psi(3770)$

[1] Using $\sigma_{tot}(e^+e^- \to \psi(3770)) = 7.9 \pm 0.6$ nb at the resonance.

$\Gamma(K^+K^-\pi^+\pi^-)/\Gamma_{\text{total}}$ — Γ_{39}/Γ

VALUE (units 10^{-4})	CL%	DOCUMENT ID		TECN	COMMENT
< 9.0	90	[1] HUANG	06A	CLEO	$e^+e^- \to \psi(3770)$
• • • We do not use the following data for averages, fits, limits, etc. • • •					
<48	90	[2] ABLIKIM	07B	BES2	$e^+e^- \to \psi(3770)$

[1] Using $\sigma_{tot}(e^+e^- \to \psi(3770)) = 7.9 \pm 0.6$ nb at the resonance.
[2] Assuming that interference effects between resonance and continuum can be neglected and using $\sigma^{obs}(e^+e^- \to \psi(3770)) = 7.15 \pm 0.38$ nb.

$\Gamma(\phi\pi^+\pi^-)/\Gamma_{\text{total}}$ — Γ_{40}/Γ

VALUE (units 10^{-4})	CL%	DOCUMENT ID		TECN	COMMENT
< 4.1	90	[1] HUANG	06A	CLEO	$e^+e^- \to \psi(3770)$
• • • We do not use the following data for averages, fits, limits, etc. • • •					
<16	90	[2] ABLIKIM	07B	BES2	$e^+e^- \to \psi(3770)$

[1] Using $\sigma_{tot}(e^+e^- \to \psi(3770)) = 7.9 \pm 0.6$ nb at the resonance.
[2] Assuming that interference effects between resonance and continuum can be neglected and using $\sigma^{obs}(e^+e^- \to \psi(3770)) = 7.15 \pm 0.38$ nb.

$\Gamma(K^+K^-2\pi^0)/\Gamma_{\text{total}}$ — Γ_{41}/Γ

VALUE (units 10^{-3})	CL%	EVTS	DOCUMENT ID		TECN	COMMENT
<4.2	90	14	ABLIKIM	08N	BES2	$e^+e^- \to \psi(3770)$

$\Gamma(4(\pi^+\pi^-))/\Gamma_{\text{total}}$ — Γ_{42}/Γ

VALUE (units 10^{-3})	CL%	DOCUMENT ID		TECN	COMMENT
<16.7	90	[1] ABLIKIM	07F	BES2	$e^+e^- \to \psi(3770)$

[1] Assuming that interference effects between resonance and continuum can be neglected and using $\sigma^{obs}(e^+e^- \to \psi(3770)) = 7.15 \pm 0.38$ nb.

$\Gamma(4(\pi^+\pi^-)\pi^0)/\Gamma_{\text{total}}$ — Γ_{43}/Γ

VALUE (units 10^{-3})	CL%	DOCUMENT ID		TECN	COMMENT
<30.6	90	[1] ABLIKIM	07F	BES2	$e^+e^- \to \psi(3770)$

[1] Assuming that interference effects between resonance and continuum can be neglected and using $\sigma^{obs}(e^+e^- \to \psi(3770)) = 7.15 \pm 0.38$ nb.

$\Gamma(\phi f_0(980))/\Gamma_{\text{total}}$ — Γ_{44}/Γ

VALUE (units 10^{-4})	CL%	DOCUMENT ID		TECN	COMMENT
<4.5	90	[1] HUANG	06A	CLEO	$e^+e^- \to \psi(3770)$

[1] Using $\sigma_{tot}(e^+e^- \to \psi(3770)) = 7.9 \pm 0.6$ nb at the resonance.

$\Gamma(K^+K^-\pi^+\pi^-\pi^0)/\Gamma_{\text{total}}$ — Γ_{45}/Γ

VALUE (units 10^{-4})	CL%	DOCUMENT ID		TECN	COMMENT
< 23.6	90	[1] HUANG	06A	CLEO	$e^+e^- \to \psi(3770)$
• • • We do not use the following data for averages, fits, limits, etc. • • •					
<111	90	[2] ABLIKIM	07B	BES2	$e^+e^- \to \psi(3770)$

[1] Using $\sigma_{tot}(e^+e^- \to \psi(3770)) = 7.9 \pm 0.6$ nb at the resonance.
[2] Assuming that interference effects between resonance and continuum can be neglected and using $\sigma^{obs}(e^+e^- \to \psi(3770)) = 7.15 \pm 0.38$ nb.

Downloaded from https://academic.oup.com/ptep/article/2022/8/083C01/6651666 by KIT Library user on 27 September 2022

$\Gamma(K^+K^-\rho^0\pi^0)/\Gamma_{total}$ — Γ_{46}/Γ

VALUE (units 10^{-4})	CL%	DOCUMENT ID		TECN	COMMENT
<8	90	[1] ABLIKIM	07I	BES2	3.77 e^+e^-

[1] Assuming that interference effects between resonance and continuum can be neglected and using $\sigma^{obs}(e^+e^- \to \psi(3770)) = 7.15 \pm 0.38$ nb.

$\Gamma(K^+K^-\rho^+\pi^-)/\Gamma_{total}$ — Γ_{47}/Γ

VALUE (units 10^{-4})	CL%	DOCUMENT ID		TECN	COMMENT
<146	90	[1] ABLIKIM	07I	BES2	3.77 e^+e^-

[1] Assuming that interference effects between resonance and continuum can be neglected and using $\sigma^{obs}(e^+e^- \to \psi(3770)) = 7.15 \pm 0.38$ nb.

$\Gamma(\omega K^+K^-)/\Gamma_{total}$ — Γ_{48}/Γ

VALUE (units 10^{-4})	CL%	DOCUMENT ID		TECN	COMMENT
< 3.4	90	[1] HUANG	06A	CLEO	$e^+e^- \to \psi(3770)$
• • • We do not use the following data for averages, fits, limits, etc. • • •					
<66	90	[2] ABLIKIM	07I	BES2	3.77 e^+e^-

[1] Using $\sigma_{tot}(e^+e^- \to \psi(3770)) = 7.9 \pm 0.6$ nb at the resonance.
[2] Assuming that interference effects between resonance and continuum can be neglected and using $\sigma^{obs}(e^+e^- \to \psi(3770)) = 7.15 \pm 0.38$ nb.

$\Gamma(\phi\pi^+\pi^-\pi^0)/\Gamma_{total}$ — Γ_{49}/Γ

VALUE (units 10^{-4})	CL%	DOCUMENT ID		TECN	COMMENT
<38	90	[1] ABLIKIM	07I	BES2	3.77 e^+e^-

[1] Assuming that interference effects between resonance and continuum can be neglected and using $\sigma^{obs}(e^+e^- \to \psi(3770)) = 7.15 \pm 0.38$ nb.

$\Gamma(K^{*0}K^-\pi^+\pi^0 + c.c.)/\Gamma_{total}$ — Γ_{50}/Γ

VALUE (units 10^{-4})	CL%	DOCUMENT ID		TECN	COMMENT
<162	90	[1] ABLIKIM	07I	BES2	3.77 e^+e^-

[1] Assuming that interference effects between resonance and continuum can be neglected and using $\sigma^{obs}(e^+e^- \to \psi(3770)) = 7.15 \pm 0.38$ nb.

$\Gamma(K^{*+}K^-\pi^+\pi^- + c.c.)/\Gamma_{total}$ — Γ_{51}/Γ

VALUE (units 10^{-4})	CL%	DOCUMENT ID		TECN	COMMENT
<323	90	[1] ABLIKIM	07I	BES2	3.77 e^+e^-

[1] Assuming that interference effects between resonance and continuum can be neglected and using $\sigma^{obs}(e^+e^- \to \psi(3770)) = 7.15 \pm 0.38$ nb.

$\Gamma(K^+K^-\pi^+\pi^-2\pi^0)/\Gamma_{total}$ — Γ_{52}/Γ

VALUE (units 10^{-3})	CL%	EVTS	DOCUMENT ID		TECN	COMMENT
<26.7	90	24	ABLIKIM	08N	BES2	$e^+e^- \to \psi(3770)$

$\Gamma(K^+K^-2(\pi^+\pi^-))/\Gamma_{total}$ — Γ_{53}/Γ

VALUE (units 10^{-3})	CL%	DOCUMENT ID		TECN	COMMENT
<10.3	90	[1] ABLIKIM	07F	BES2	$e^+e^- \to \psi(3770)$

[1] Assuming that interference effects between resonance and continuum can be neglected and using $\sigma^{obs}(e^+e^- \to \psi(3770)) = 7.15 \pm 0.38$ nb.

$\Gamma(K^+K^-2(\pi^+\pi^-)\pi^0)/\Gamma_{total}$ — Γ_{54}/Γ

VALUE (units 10^{-3})	CL%	DOCUMENT ID		TECN	COMMENT
<36.0	90	[1] ABLIKIM	07F	BES2	$e^+e^- \to \psi(3770)$

[1] Assuming that interference effects between resonance and continuum can be neglected and using $\sigma^{obs}(e^+e^- \to \psi(3770)) = 7.15 \pm 0.38$ nb.

$\Gamma(\eta K^+K^-)/\Gamma_{total}$ — Γ_{55}/Γ

VALUE (units 10^{-4})	CL%	DOCUMENT ID		TECN	COMMENT
< 4.1	90	[1] HUANG	06A	CLEO	$e^+e^- \to \psi(3770)$
• • • We do not use the following data for averages, fits, limits, etc. • • •					
<31	90	[2] ABLIKIM	10D	BES2	$e^+e^- \to \psi(3770)$

[1] Using $\sigma_{tot}(e^+e^- \to \psi(3770)) = 7.9 \pm 0.6$ nb at the resonance.
[2] Assuming that interference effects between resonance and continuum can be neglected and using $\sigma^{obs}(e^+e^- \to \psi(3770)) = 7.15 \pm 0.38$ nb.

$\Gamma(\eta K^+K^-\pi^+\pi^-)/\Gamma_{total}$ — Γ_{56}/Γ

VALUE (units 10^{-2})	CL%	DOCUMENT ID		TECN	COMMENT
<1.24	90	[1] ABLIKIM	10D	BES2	$e^+e^- \to \psi(3770)$

[1] Assuming that interference effects between resonance and continuum can be neglected and using $\sigma^{obs}(e^+e^- \to \psi(3770)) = 7.15 \pm 0.38$ nb.

$\Gamma(\rho^0K^+K^-)/\Gamma_{total}$ — Γ_{57}/Γ

VALUE (units 10^{-3})	CL%	DOCUMENT ID		TECN	COMMENT
<5.0	90	[1] ABLIKIM	07F	BES2	$e^+e^- \to \psi(3770)$

[1] Assuming that interference effects between resonance and continuum can be neglected and using $\sigma^{obs}(e^+e^- \to \psi(3770)) = 7.15 \pm 0.38$ nb.

$\Gamma(2(K^+K^-))/\Gamma_{total}$ — Γ_{58}/Γ

VALUE (units 10^{-4})	CL%	DOCUMENT ID		TECN	COMMENT
< 6.0	90	[1] HUANG	06A	CLEO	$e^+e^- \to \psi(3770)$
• • • We do not use the following data for averages, fits, limits, etc. • • •					
<17	90	[2] ABLIKIM	07B	BES2	$e^+e^- \to \psi(3770)$

[1] Using $\sigma_{tot}(e^+e^- \to \psi(3770)) = 7.9 \pm 0.6$ nb at the resonance.
[2] Assuming that interference effects between resonance and continuum can be neglected and using $\sigma^{obs}(e^+e^- \to \psi(3770)) = 7.15 \pm 0.38$ nb.

$\Gamma(\phi K^+K^-)/\Gamma_{total}$ — Γ_{59}/Γ

VALUE (units 10^{-4})	CL%	DOCUMENT ID		TECN	COMMENT
< 7.5	90	[1] HUANG	06A	CLEO	$e^+e^- \to \psi(3770)$
• • • We do not use the following data for averages, fits, limits, etc. • • •					
<24	90	[2] ABLIKIM	07B	BES2	$e^+e^- \to \psi(3770)$

[1] Using $\sigma_{tot}(e^+e^- \to \psi(3770)) = 7.9 \pm 0.6$ nb at the resonance.
[2] Assuming that interference effects between resonance and continuum can be neglected and using $\sigma^{obs}(e^+e^- \to \psi(3770)) = 7.15 \pm 0.38$ nb.

$\Gamma(2(K^+K^-)\pi^0)/\Gamma_{total}$ — Γ_{60}/Γ

VALUE (units 10^{-4})	CL%	DOCUMENT ID		TECN	COMMENT
< 2.9	90	[1] HUANG	06A	CLEO	$e^+e^- \to \psi(3770)$
• • • We do not use the following data for averages, fits, limits, etc. • • •					
<46	90	[2] ABLIKIM	07B	BES2	$e^+e^- \to \psi(3770)$

[1] Using $\sigma_{tot}(e^+e^- \to \psi(3770)) = 7.9 \pm 0.6$ nb at the resonance.
[2] Assuming that interference effects between resonance and continuum can be neglected and using $\sigma^{obs}(e^+e^- \to \psi(3770)) = 7.15 \pm 0.38$ nb.

$\Gamma(2(K^+K^-)\pi^+\pi^-)/\Gamma_{total}$ — Γ_{61}/Γ

VALUE (units 10^{-3})	CL%	DOCUMENT ID		TECN	COMMENT
<3.2	90	[1] ABLIKIM	07F	BES2	$e^+e^- \to \psi(3770)$

[1] Assuming that interference effects between resonance and continuum can be neglected and using $\sigma^{obs}(e^+e^- \to \psi(3770)) = 7.15 \pm 0.38$ nb.

$\Gamma(K^0_SK^-\pi^+)/\Gamma_{total}$ — Γ_{62}/Γ

VALUE (units 10^{-3})	CL%	EVTS	DOCUMENT ID		TECN	COMMENT
<3.2	90	18	ABLIKIM	08M	BES2	$e^+e^- \to \psi(3770)$

$\Gamma(K^0_SK^-\pi^+\pi^0)/\Gamma_{total}$ — Γ_{63}/Γ

VALUE (units 10^{-3})	CL%	EVTS	DOCUMENT ID		TECN	COMMENT
<13.3	90	40	ABLIKIM	08M	BES2	$e^+e^- \to \psi(3770)$

$\Gamma(K^0_SK^-\rho^+)/\Gamma_{total}$ — Γ_{64}/Γ

VALUE (units 10^{-3})	CL%	DOCUMENT ID		TECN	COMMENT
<6.6	90	ABLIKIM	09C	BES2	$e^+e^- \to \psi(3770)$

$\Gamma(K^0_SK^-2\pi^+\pi^-)/\Gamma_{total}$ — Γ_{65}/Γ

VALUE (units 10^{-3})	CL%	EVTS	DOCUMENT ID		TECN	COMMENT
<8.7	90	39	ABLIKIM	08M	BES2	$e^+e^- \to \psi(3770)$

$\Gamma(K^0_SK^-\pi^+\rho^0)/\Gamma_{total}$ — Γ_{66}/Γ

VALUE (units 10^{-2})	CL%	DOCUMENT ID		TECN	COMMENT
<1.6	90	ABLIKIM	09C	BES2	$e^+e^- \to \psi(3770)$

$\Gamma(K^0_SK^-\pi^+\eta)/\Gamma_{total}$ — Γ_{67}/Γ

VALUE (units 10^{-2})	CL%	DOCUMENT ID		TECN	COMMENT
<1.3	90	ABLIKIM	09C	BES2	$e^+e^- \to \psi(3770)$

$\Gamma(K^0_SK^-2\pi^+\pi^-\pi^0)/\Gamma_{total}$ — Γ_{68}/Γ

VALUE (units 10^{-3})	CL%	EVTS	DOCUMENT ID		TECN	COMMENT
<41.8	90	23	ABLIKIM	08M	BES2	$e^+e^- \to \psi(3770)$

$\Gamma(K^0_SK^-2\pi^+\pi^-\eta)/\Gamma_{total}$ — Γ_{69}/Γ

VALUE (units 10^{-2})	CL%	DOCUMENT ID		TECN	COMMENT
<4.8	90	ABLIKIM	09C	BES2	$e^+e^- \to \psi(3770)$

$\Gamma(K^0_SK^-\pi^+2(\pi^+\pi^-))/\Gamma_{total}$ — Γ_{70}/Γ

VALUE (units 10^{-3})	CL%	EVTS	DOCUMENT ID		TECN	COMMENT
<12.2	90	4	ABLIKIM	08M	BES2	$e^+e^- \to \psi(3770)$

$\Gamma(K^0_SK^-\pi^+2\pi^0)/\Gamma_{total}$ — Γ_{71}/Γ

VALUE (units 10^{-3})	CL%	EVTS	DOCUMENT ID		TECN	COMMENT
<26.5	90	17	ABLIKIM	08M	BES2	$e^+e^- \to \psi(3770)$

$\Gamma(K^0_SK^-K^+K^-\pi^+)/\Gamma_{total}$ — Γ_{72}/Γ

VALUE (units 10^{-3})	CL%	DOCUMENT ID		TECN	COMMENT
<4.9	90	ABLIKIM	09C	BES2	$e^+e^- \to \psi(3770)$

Downloaded from https://academic.oup.com/ptep/article/2022/8/083C01/6651666 by KIT Library user on 27 September 2022

$\Gamma(K^0_S K^- K^+ K^- \pi^+ \pi^0)/\Gamma_{total}$ — Γ_{73}/Γ

VALUE (units 10^{-2})	CL%	DOCUMENT ID		TECN	COMMENT
<3.0	90	ABLIKIM	09C	BES2	$e^+e^- \to \psi(3770)$

$\Gamma(K^0_S K^- K^+ K^- \pi^+ \eta)/\Gamma_{total}$ — Γ_{74}/Γ

VALUE (units 10^{-2})	CL%	DOCUMENT ID		TECN	COMMENT
<2.2	90	ABLIKIM	09C	BES2	$e^+e^- \to \psi(3770)$

$\Gamma(K^{*0} K^- \pi^+ + \text{c.c.})/\Gamma_{total}$ — Γ_{75}/Γ

VALUE (units 10^{-3})	CL%	DOCUMENT ID		TECN	COMMENT
<9.7	90	[1] ABLIKIM	07F	BES2	$e^+e^- \to \psi(3770)$

[1] Assuming that interference effects between resonance and continuum can be neglected and using $\sigma^{obs}(e^+e^- \to \psi(3770)) = 7.15 \pm 0.38$ nb.

$\Gamma(p\overline{p})/\Gamma_{total}$ — Γ_{76}/Γ

VALUE (units 10^{-6})	EVTS	DOCUMENT ID		TECN	COMMENT
• • • We do not use the following data for averages, fits, limits, etc. • • •					
not seen		[1] AAIJ	17AD	LHCB	$pp \to B^+X \to p\overline{p}K^+X$
$7.1^{+8.6}_{-2.9}$	684	[2] ABLIKIM	14L	BES3	$e^+e^- \to \psi(3770)$
310 ± 30	684	[3] ABLIKIM	14L	BES3	$e^+e^- \to \psi(3770)$

[1] AAIJ 17AD reports $B(B^+ \to \psi(3770)K^+ \to p\overline{p}K^+)/B(B^+ \to J/\psi K^+ \to p\overline{p}K^+) < 0.09$ (0.10) at 90% (95%) CL.
[2] Solution I of two equivalent solutions in a fit with a resonance interfering with continuum.
[3] Solution II of two equivalent solutions in a fit with a resonance interfering with continuum.

$\Gamma(p\overline{p}\pi^0)/\Gamma_{total}$ — Γ_{77}/Γ

VALUE (units 10^{-4})	CL%	DOCUMENT ID		TECN	COMMENT
< 0.4	90	[1,2] ABLIKIM	14O	BES3	$e^+e^- \to \psi(3770)$
• • • We do not use the following data for averages, fits, limits, etc. • • •					
$59^{+3}_{-2} \pm 5$		[1,3] ABLIKIM	14O	BES3	$e^+e^- \to \psi(3770)$
<12	90	[4] ABLIKIM	07B	BES2	$e^+e^- \to \psi(3770)$

[1] Calculated by the authors using $\sigma(e^+e^- \to \psi(3770) \to \text{hadrons}) = 6.36 \pm 0.08^{+0.41}_{-0.30}$ nb from BESSON 10.
[2] Solution I of two equivalent solutions in a fit with a resonance interfering with continuum.
[3] Solution II of two equivalent solutions in a fit with a resonance interfering with continuum.
[4] Assuming that interference effects between resonance and continuum can be neglected and using $\sigma^{obs}(e^+e^- \to \psi(3770)) = 7.15 \pm 0.38$ nb.

$\Gamma(p\overline{p}\pi^+\pi^-)/\Gamma_{total}$ — Γ_{78}/Γ

VALUE (units 10^{-4})	CL%	DOCUMENT ID		TECN	COMMENT
< 5.8	90	[1] HUANG	06A	CLEO	$e^+e^- \to \psi(3770)$
• • • We do not use the following data for averages, fits, limits, etc. • • •					
<16	90	[2] ABLIKIM	07B	BES2	$e^+e^- \to \psi(3770)$

[1] Using $\sigma_{tot}(e^+e^- \to \psi(3770)) = 7.9 \pm 0.6$ nb at the resonance.
[2] Assuming that interference effects between resonance and continuum can be neglected and using $\sigma^{obs}(e^+e^- \to \psi(3770)) = 7.15 \pm 0.38$ nb.

$\Gamma(\Lambda\overline{\Lambda})/\Gamma_{total}$ — Γ_{79}/Γ

VALUE	CL%	DOCUMENT ID		TECN	COMMENT
$<1.2 \times 10^{-4}$	90	[1] HUANG	06A	CLEO	$e^+e^- \to \psi(3770)$
• • • We do not use the following data for averages, fits, limits, etc. • • •					
$<1.8 \times 10^{-4}$	90	[2] ABLIKIM	21AS	BES3	$e^+e^- \to \psi(3770)$
$<4 \times 10^{-4}$	90	[3] ABLIKIM	07F	BES2	$e^+e^- \to \psi(3770)$

[1] Using $\sigma_{tot}(e^+e^- \to \psi(3770)) = 7.9 \pm 0.6$ nb at the resonance.
[2] From a measurement of the $e^+e^- \to \Lambda\overline{\Lambda}$ cross section between 3.5 and 4.6 GeV. At a 90% CL the lower bound is $> 2.4 \times 10^{-6}$.
[3] Assuming that interference effects between resonance and continuum can be neglected and using $\sigma^{obs}(e^+e^- \to \psi(3770)) = 7.15 \pm 0.38$ nb.

$\Gamma(p\overline{p}\pi^+\pi^-\pi^0)/\Gamma_{total}$ — Γ_{80}/Γ

VALUE (units 10^{-4})	CL%	DOCUMENT ID		TECN	COMMENT
<18.5	90	[1] HUANG	06A	CLEO	$e^+e^- \to \psi(3770)$
• • • We do not use the following data for averages, fits, limits, etc. • • •					
<73	90	[2] ABLIKIM	07B	BES2	$e^+e^- \to \psi(3770)$

[1] Using $\sigma_{tot}(e^+e^- \to \psi(3770)) = 7.9 \pm 0.6$ nb at the resonance.
[2] Assuming that interference effects between resonance and continuum can be neglected and using $\sigma^{obs}(e^+e^- \to \psi(3770)) = 7.15 \pm 0.38$ nb.

$\Gamma(\omega p\overline{p})/\Gamma_{total}$ — Γ_{81}/Γ

VALUE (units 10^{-4})	CL%	DOCUMENT ID		TECN	COMMENT
< 2.9	90	[1] HUANG	06A	CLEO	$e^+e^- \to \psi(3770)$
• • • We do not use the following data for averages, fits, limits, etc. • • •					
<30	90	[2] ABLIKIM	07I	BES2	3.77 e^+e^-

[1] Using $\sigma_{tot}(e^+e^- \to \psi(3770)) = 7.9 \pm 0.6$ nb at the resonance.
[2] Using $\sigma^{obs} = 7.15 \pm 0.27 \pm 0.27$ nb and neglecting interference.

$\Gamma(\Lambda\overline{\Lambda}\pi^0)/\Gamma_{total}$ — Γ_{82}/Γ

VALUE (units 10^{-4})	CL%	DOCUMENT ID		TECN	COMMENT
< 0.7	90	[1] ABLIKIM	13Q	BES3	$e^+e^- \to \psi(3770)$
• • • We do not use the following data for averages, fits, limits, etc. • • •					
<12	90	[2] ABLIKIM	07I	BES2	3.77 e^+e^-

[1] Assuming that interference effects between resonance and continuum can be neglected.
[2] Assuming that interference effects between resonance and continuum can be neglected and using $\sigma^{obs}(e^+e^- \to \psi(3770)) = 7.15 \pm 0.38$ nb.

$\Gamma(p\overline{p}2(\pi^+\pi^-))/\Gamma_{total}$ — Γ_{83}/Γ

VALUE (units 10^{-3})	CL%	DOCUMENT ID		TECN	COMMENT
<2.6	90	[1] ABLIKIM	07F	BES2	$e^+e^- \to \psi(3770)$

[1] Assuming that interference effects between resonance and continuum can be neglected and using $\sigma^{obs}(e^+e^- \to \psi(3770)) = 7.15 \pm 0.38$ nb.

$\Gamma(\eta p\overline{p})/\Gamma_{total}$ — Γ_{84}/Γ

VALUE (units 10^{-4})	CL%	DOCUMENT ID		TECN	COMMENT
< 5.4	90	[1] HUANG	06A	CLEO	$e^+e^- \to \psi(3770)$
• • • We do not use the following data for averages, fits, limits, etc. • • •					
<11	90	[2] ABLIKIM	10D	BES2	$e^+e^- \to \psi(3770)$

[1] Using $\sigma_{tot}(e^+e^- \to \psi(3770)) = 7.9 \pm 0.6$ nb at the resonance.
[2] Assuming that interference effects between resonance and continuum can be neglected and using $\sigma^{obs}(e^+e^- \to \psi(3770)) = 7.15 \pm 0.38$ nb.

$\Gamma(\eta p\overline{p}\pi^+\pi^-)/\Gamma_{total}$ — Γ_{85}/Γ

VALUE (units 10^{-3})	CL%	DOCUMENT ID		TECN	COMMENT
<3.3	90	[1] ABLIKIM	10D	BES2	$e^+e^- \to \psi(3770)$

[1] Assuming that interference effects between resonance and continuum can be neglected and using $\sigma^{obs}(e^+e^- \to \psi(3770)) = 7.15 \pm 0.38$ nb.

$\Gamma(\rho^0 p\overline{p})/\Gamma_{total}$ — Γ_{86}/Γ

VALUE (units 10^{-3})	CL%	DOCUMENT ID		TECN	COMMENT
<1.7	90	[1] ABLIKIM	07F	BES2	$e^+e^- \to \psi(3770)$

[1] Assuming that interference effects between resonance and continuum can be neglected and using $\sigma^{obs}(e^+e^- \to \psi(3770)) = 7.15 \pm 0.38$ nb.

$\Gamma(p\overline{p}K^+K^-)/\Gamma_{total}$ — Γ_{87}/Γ

VALUE (units 10^{-4})	CL%	DOCUMENT ID		TECN	COMMENT
< 3.2	90	[1] HUANG	06A	CLEO	$e^+e^- \to \psi(3770)$
• • • We do not use the following data for averages, fits, limits, etc. • • •					
<11	90	[2] ABLIKIM	07B	BES2	$e^+e^- \to \psi(3770)$

[1] Using $\sigma_{tot}(e^+e^- \to \psi(3770)) = 7.9 \pm 0.6$ nb at the resonance.
[2] Assuming that interference effects between resonance and continuum can be neglected and using $\sigma^{obs}(e^+e^- \to \psi(3770)) = 7.15 \pm 0.38$ nb.

$\Gamma(\eta p\overline{p}K^+K^-)/\Gamma_{total}$ — Γ_{88}/Γ

VALUE (units 10^{-3})	CL%	DOCUMENT ID		TECN	COMMENT
<6.9	90	[1] ABLIKIM	10D	BES2	$e^+e^- \to \psi(3770)$

[1] Assuming that interference effects between resonance and continuum can be neglected and using $\sigma^{obs}(e^+e^- \to \psi(3770)) = 7.15 \pm 0.38$ nb.

$\Gamma(\pi^0 p\overline{p}K^+K^-)/\Gamma_{total}$ — Γ_{89}/Γ

VALUE (units 10^{-3})	CL%	DOCUMENT ID		TECN	COMMENT
<1.2	90	[1] ABLIKIM	10D	BES2	$e^+e^- \to \psi(3770)$

[1] Assuming that interference effects between resonance and continuum can be neglected and using $\sigma^{obs}(e^+e^- \to \psi(3770)) = 7.15 \pm 0.38$ nb.

$\Gamma(\phi p\overline{p})/\Gamma_{total}$ — Γ_{90}/Γ

VALUE (units 10^{-4})	CL%	DOCUMENT ID		TECN	COMMENT
<1.3	90	[1] HUANG	06A	CLEO	$e^+e^- \to \psi(3770)$
• • • We do not use the following data for averages, fits, limits, etc. • • •					
<9	90	[2] ABLIKIM	07B	BES2	$e^+e^- \to \psi(3770)$

[1] Using $\sigma_{tot}(e^+e^- \to \psi(3770)) = 7.9 \pm 0.6$ nb at the resonance.
[2] Assuming that interference effects between resonance and continuum can be neglected and using $\sigma^{obs}(e^+e^- \to \psi(3770)) = 7.15 \pm 0.38$ nb.

$\Gamma(\Lambda\overline{\Lambda}\pi^+\pi^-)/\Gamma_{total}$ — Γ_{91}/Γ

VALUE (units 10^{-4})	CL%	DOCUMENT ID		TECN	COMMENT
< 2.5	90	[1] HUANG	06A	CLEO	$e^+e^- \to \psi(3770)$
• • • We do not use the following data for averages, fits, limits, etc. • • •					
< 4.7	90	[2] ABLIKIM	13Q	BES3	$e^+e^- \to \psi(3770)$
<39	90	[3] ABLIKIM	07F	BES2	$e^+e^- \to \psi(3770)$

[1] Using $\sigma_{tot}(e^+e^- \to \psi(3770)) = 7.9 \pm 0.6$ nb at the resonance.
[2] Assuming that interference effects between resonance and continuum can be neglected.
[3] Assuming that interference effects between resonance and continuum can be neglected and using $\sigma^{obs}(e^+e^- \to \psi(3770)) = 7.15 \pm 0.38$ nb.

Downloaded from https://academic.oup.com/ptep/article/2022/8/083C01/6651666 by KIT Library user on 27 September 2022

$\Gamma(\Lambda\overline{p}K^+)/\Gamma_{total}$ — Γ_{92}/Γ

VALUE (units 10^{-4})	CL%	DOCUMENT ID		TECN	COMMENT
<2.8	90	[1] HUANG	06A	CLEO	$e^+e^- \to \psi(3770)$

[1] Using $\sigma_{tot}(e^+e^- \to \psi(3770)) = 7.9 \pm 0.6$ nb at the resonance.

$\Gamma(\Lambda\overline{p}K^+\pi^+\pi^-)/\Gamma_{total}$ — Γ_{93}/Γ

VALUE (units 10^{-4})	CL%	DOCUMENT ID		TECN	COMMENT
<6.3	90	[1] HUANG	06A	CLEO	$e^+e^- \to \psi(3770)$

[1] Using $\sigma_{tot}(e^+e^- \to \psi(3770)) = 7.9 \pm 0.6$ nb at the resonance.

$\Gamma(\Lambda\overline{\Lambda}\eta)/\Gamma_{total}$ — Γ_{94}/Γ

VALUE (units 10^{-4})	CL%	DOCUMENT ID		TECN	COMMENT
<1.9	90	[1] ABLIKIM	13Q	BES3	$e^+e^- \to \psi(3770)$

[1] Assuming that interference effects between resonance and continuum can be neglected.

$\Gamma(\Sigma^+\overline{\Sigma}^-)/\Gamma_{total}$ — Γ_{95}/Γ

VALUE (units 10^{-4})	CL%	DOCUMENT ID		TECN	COMMENT
<1.0	90	[1] ABLIKIM	13Q	BES3	$e^+e^- \to \psi(3770)$

[1] Assuming that interference effects between resonance and continuum can be neglected.

$\Gamma(\Sigma^0\overline{\Sigma}^0)/\Gamma_{total}$ — Γ_{96}/Γ

VALUE (units 10^{-4})	CL%	DOCUMENT ID		TECN	COMMENT
<0.4	90	[1] ABLIKIM	13Q	BES3	$e^+e^- \to \psi(3770)$

[1] Assuming that interference effects between resonance and continuum can be neglected.

$\Gamma(\Xi^+\overline{\Xi}^-)/\Gamma_{total}$ — Γ_{97}/Γ

VALUE (units 10^{-4})	CL%	DOCUMENT ID		TECN	COMMENT
<1.5	90	[1] ABLIKIM	13Q	BES3	$e^+e^- \to \psi(3770)$

[1] Assuming that interference effects between resonance and continuum can be neglected.

$\Gamma(\Xi^0\overline{\Xi}^0)/\Gamma_{total}$ — Γ_{98}/Γ

VALUE (units 10^{-4})	CL%	DOCUMENT ID		TECN	COMMENT
<1.4	90	[1] ABLIKIM	13Q	BES3	$e^+e^- \to \psi(3770)$

[1] Assuming that interference effects between resonance and continuum can be neglected.

RADIATIVE DECAYS

$\Gamma(\gamma\chi_{c2})/\Gamma_{total}$ — Γ_{99}/Γ

VALUE (units 10^{-3})	CL%	DOCUMENT ID		TECN	COMMENT
<0.64	90	[1] ABLIKIM	15J	BES3	$e^+e^- \to \psi(3770) \to \gamma\gamma J/\psi$
• • • We do not use the following data for averages, fits, limits, etc. • • •					
<2.0	90	[2] BRIERE	06	CLEO	$e^+e^- \to \psi(3770) \to \gamma +$ hadrons
<0.9	90	[3] COAN	06A	CLEO	$e^+e^- \to \psi(3770) \to \gamma\gamma J/\psi$

[1] This limit is equivalent to $(0.25 \pm 0.21 \pm 0.18) \times 10^{-3}$ branching fraction value.
[2] Uses $B(\psi(2S) \to \gamma\chi_{c2}) = 9.22 \pm 0.11 \pm 0.46$ % from ATHAR 04, $\psi(2S)$ mass and width from PDG 04, and $\Gamma_{ee}(\psi(2S)) = 2.54 \pm 0.03 \pm 0.11$ keV from ADAM 06.
[3] Using $\Gamma_{ee}(\psi(2S)) = (2.54 \pm 0.03 \pm 0.11)$ keV from ADAM 06 and taking $\sigma(e^+e^- \to D\overline{D})$ from HE 05 for $\sigma(e^+e^- \to \psi(3770))$.

$\Gamma(\gamma\chi_{c1})/\Gamma_{total}$ — Γ_{100}/Γ

VALUE (units 10^{-3})	EVTS	DOCUMENT ID		TECN	COMMENT
2.49±0.23 OUR AVERAGE					
1.98±0.78±0.05	202	[1] ABLIKIM	16B	BES3	$e^+e^- \to \psi(3770) \to \gamma +$ hadrons
2.48±0.15±0.23	0.6k	ABLIKIM	15J	BES3	$e^+e^- \to \psi(3770) \to \gamma\gamma J/\psi$
2.4 ±0.8 ±0.2		[2] ABLIKIM	14H	BES3	$e^+e^- \to \psi(3770) \to K^0_S K^\pm\pi^\mp$
2.9 ±0.5 ±0.4		[3] BRIERE	06	CLEO	$e^+e^- \to \psi(3770) \to \gamma +$ hadrons, $\gamma\gamma J/\psi$
• • • We do not use the following data for averages, fits, limits, etc. • • •					
3.9 ±1.4 ±0.6	54	[4] BRIERE	06	CLEO	$e^+e^- \to \psi(3770) \to \gamma +$ hadrons
2.8 ±0.5 ±0.4	53	[5] COAN	06A	CLEO	$e^+e^- \to \psi(3770) \to \gamma\gamma J/\psi$

[1] ABLIKIM 16B reports $(1.94 \pm 0.42 \pm 0.64) \times 10^{-3}$ from a measurement of $[\Gamma(\psi(3770) \to \gamma\chi_{c1})/\Gamma_{total}]$ / $[B(\psi(2S) \to \gamma\chi_{c1}(1P))]$ assuming $B(\psi(2S) \to \gamma\chi_{c1}(1P)) = (9.55 \pm 0.31) \times 10^{-2}$, which we rescale to our best value $B(\psi(2S) \to \gamma\chi_{c1}(1P)) = (9.75 \pm 0.24) \times 10^{-2}$. Our first error is their experiment's error and our second error is the systematic error from using our best value.
[2] ABLIKIM 14H reports $[\Gamma(\psi(3770) \to \gamma\chi_{c1})/\Gamma_{total}] \times [B(\chi_{c1}(1P) \to K^0_S K^\pm\pi^\mp)] = (8.51 \pm 2.39 \pm 1.42) \times 10^{-6}$ which we divide by our best value $B(\chi_{c1}(1P) \to K^0_S K^\pm\pi^\mp) = 0.00349 \pm 0.00029$. Our first error is their experiment's error and our second error is the systematic error from using our best value. We have calculated the best value of $B(\chi_{c1}(1P) \to K^0_S K^\pm\pi^\mp)$ as 1/2 of $B(\chi_{c1}(1P) \to \overline{K}^0 K^+\pi^- + \text{c.c.}) = (7.0 \pm 0.6) \times 10^{-3}$.
[3] Averages the two measurements from COAN 06A and BRIERE 06.
[4] Uses $B(\psi(2S) \to \gamma\chi_{c1}) = 9.07 \pm 0.11 \pm 0.54$ % from ATHAR 04, $\psi(2S)$ mass and width from PDG 04, and $\Gamma_{ee}(\psi(2S)) = 2.54 \pm 0.03 \pm 0.11$ keV from ADAM 06.
[5] Using $\Gamma_{ee}(\psi(2S)) = (2.54 \pm 0.03 \pm 0.11)$ keV from ADAM 06 and taking $\sigma(e^+e^- \to D\overline{D})$ from HE 05 for $\sigma(e^+e^- \to \psi(3770))$.

$\Gamma(\gamma\chi_{c1})/\Gamma(J/\psi\pi^+\pi^-)$ — Γ_{100}/Γ_5

VALUE	EVTS	DOCUMENT ID		TECN	COMMENT
1.49±0.31±0.26	53 ± 10	[1] COAN	06A	CLEO	$e^+e^- \to \psi(3770) \to \gamma\gamma J/\psi$

[1] Using $B(\psi(3770) \to J/\psi\pi^+\pi^-) = (1.89 \pm 0.20 \pm 0.20) \times 10^{-3}$ from ADAM 06.

$\Gamma(\gamma\chi_{c0})/\Gamma_{total}$ — Γ_{101}/Γ

VALUE (units 10^{-3})	CL%	EVTS	DOCUMENT ID		TECN	COMMENT
6.9±0.6 OUR AVERAGE						
6.7±0.7±0.1		2.2k	[1] ABLIKIM	16B	BES3	$e^+e^- \to \psi(3770) \to \gamma +$ hadrons
7.3±0.7±0.6		274	BRIERE	06	CLEO	$e^+e^- \to \psi(3770) \to \gamma +$ hadrons
• • • We do not use the following data for averages, fits, limits, etc. • • •						
< 44	90		[2] COAN	06A	CLEO	$e^+e^- \to \psi(3770) \to \gamma\gamma J/\psi$

[1] ABLIKIM 16B reports $(6.88 \pm 0.28 \pm 0.67) \times 10^{-3}$ from a measurement of $[\Gamma(\psi(3770) \to \gamma\chi_{c0})/\Gamma_{total}]$ / $[B(\psi(2S) \to \gamma\chi_{c0}(1P))]$ assuming $B(\psi(2S) \to \gamma\chi_{c0}(1P)) = (9.99 \pm 0.27) \times 10^{-2}$, which we rescale to our best value $B(\psi(2S) \to \gamma\chi_{c0}(1P)) = (9.79 \pm 0.20) \times 10^{-2}$. Our first error is their experiment's error and our second error is the systematic error from using our best value.
[2] Using $\Gamma_{ee}(\psi(2S)) = (2.54 \pm 0.03 \pm 0.11)$ keV from ADAM 06 and taking $\sigma(e^+e^- \to D\overline{D})$ from HE 05 for $\sigma(e^+e^- \to \psi(3770))$.

$\Gamma(\gamma\chi_{c0})/\Gamma(\gamma\chi_{c2})$ — Γ_{101}/Γ_{99}

VALUE	CL%	DOCUMENT ID		TECN	COMMENT
• • • We do not use the following data for averages, fits, limits, etc. • • •					
>8	90	[1] BRIERE	06	CLEO	$e^+e^- \to \psi(3770)$

[1] Not independent of other results in BRIERE 06.

$\Gamma(\gamma\chi_{c0})/\Gamma(\gamma\chi_{c1})$ — $\Gamma_{101}/\Gamma_{100}$

VALUE	DOCUMENT ID		TECN	COMMENT
• • • We do not use the following data for averages, fits, limits, etc. • • •				
2.5±0.6	[1] BRIERE	06	CLEO	$e^+e^- \to \psi(3770)$

[1] Not independent of other results in BRIERE 06.

$\Gamma(\gamma\eta_c)/\Gamma_{total}$ — Γ_{102}/Γ

VALUE	CL%	DOCUMENT ID		TECN
<7 × 10^{-4}	90	[1] ABLIKIM	14H	BES3

[1] ABLIKIM 14H reports $[\Gamma(\psi(3770) \to \gamma\eta_c)/\Gamma_{total}] \times [B(\eta_c(1S) \to K^0_S K^\pm\pi^\mp)] < 16 \times 10^{-6}$ which we divide by our best value $B(\eta_c(1S) \to K^0_S K^\pm\pi^\mp) = 2.42 \times 10^{-2}$. We have calculated the best value of $B(\eta_c(1S) \to K^0_S K^\pm\pi^\mp)$ as 1/3 of $B(\eta_c(1S) \to K\overline{K}\pi) = 7.3 \times 10^{-2}$.

$\Gamma(\gamma\eta_c(2S))/\Gamma_{total}$ — Γ_{103}/Γ

VALUE	CL%	DOCUMENT ID		TECN
<9 × 10^{-4}	90	[1] ABLIKIM	14H	BES3

[1] ABLIKIM 14H reports $[\Gamma(\psi(3770) \to \gamma\eta_c(2S))/\Gamma_{total}] \times [B(\eta_c(2S) \to K^0_S K^\pm\pi^\mp)] < 5.6 \times 10^{-6}$ which we divide by our best value $B(\eta_c(2S) \to K^0_S K^\pm\pi^\mp) = 6 \times 10^{-3}$. We have calculated the best value of $B(\eta_c(2S) \to K^0_S K^\pm\pi^\mp)$ as 1/3 of $B(\eta_c(2S) \to K\overline{K}\pi) = 1.9 \times 10^{-2}$.

$\Gamma(\gamma\eta')/\Gamma_{total}$ — Γ_{104}/Γ

VALUE (units 10^{-4})	CL%	DOCUMENT ID		TECN	COMMENT
<1.8	90	[1] PEDLAR	09	CLE3	$\psi(2S) \to \gamma X$

[1] Assuming maximal destructive interference between $\psi(3770)$ and continuum sources.

$\Gamma(\gamma\eta)/\Gamma_{total}$ — Γ_{105}/Γ

VALUE (units 10^{-4})	CL%	DOCUMENT ID		TECN	COMMENT
<1.5	90	[1] PEDLAR	09	CLE3	$\psi(2S) \to \gamma X$

[1] Assuming maximal destructive interference between $\psi(3770)$ and continuum sources.

$\Gamma(\gamma\pi^0)/\Gamma_{total}$ — Γ_{106}/Γ

VALUE (units 10^{-4})	CL%	DOCUMENT ID		TECN	COMMENT
<2	90	PEDLAR	09	CLE3	$\psi(2S) \to \gamma X$

$\psi(3770)$ REFERENCES

ABLIKIM	21AS	PR D104 L091104	M. Ablikim et al.	(BESIII Collab.)
ABLIKIM	21Z	PRL 127 082002	M. Ablikim et al.	(BESIII Collab.)
PDG	20	PTEP 2020 083C01	P.A. Zyla et al.	(PDG Collab.)
AAIJ	19M	JHEP 1907 035	R. Aaij et al.	(LHCb Collab.)
AAIJ	17AD	PL B769 305	R. Aaij et al.	(LHCb Collab.)
SHAMOV	17	PL B769 187	A.G. Shamov, K.Yu. Todyshev	
ABLIKIM	16B	PL B753 103	M. Ablikim et al.	(BESIII Collab.)
ABLIKIM	15J	PR D91 092009	M. Ablikim et al.	(BESIII Collab.)
DRUZHININ	15	PR D92 054024	V.P. Druzhinin	(NOVO)
ABLIKIM	14H	PR D89 112005	M. Ablikim et al.	(BESIII Collab.)
ABLIKIM	14L	PL B735 101	M. Ablikim et al.	(BESIII Collab.)
ABLIKIM	14O	PR D90 032007	M. Ablikim et al.	(BESIII Collab.)
BONVICINI	14	PR D89 072002	G. Bonvicini et al.	(CLEO Collab.)
ABLIKIM	13Q	PR D87 112011	M. Ablikim et al.	(BESIII Collab.)
ANASHIN	12A	PL B711 292	V.V. Anashin et al.	(KEDR Collab.)
ABLIKIM	10D	EPJ C66 11	M. Ablikim et al.	(BES II Collab.)
BESSON	10	PRL 104 159901 (errat.)	D. Besson et al.	(CLEO Collab.)
ABLIKIM	09C	EPJ C64 243	M. Ablikim et al.	(BES Collab.)
PEDLAR	09	PR D79 111101	T.K. Pedlar et al.	(CLEO Collab.)

Downloaded from https://academic.oup.com/ptep/article/2022/8/083C01/6651666 by KIT Library user on 27 September 2022

ABLIKIM	08B	PL B659 74	M. Ablikim *et al.*	(BES Collab.)
ABLIKIM	08D	PL B660 315	M. Ablikim *et al.*	(BES Collab.)
ABLIKIM	08H	PRL 101 102004	M. Ablikim *et al.*	(BES Collab.)
ABLIKIM	08M	PL B670 179	M. Ablikim *et al.*	(BES Collab.)
ABLIKIM	08N	PL B670 184	M. Ablikim *et al.*	(BES Collab.)
AUBERT	08B	PR D77 011102	B. Aubert *et al.*	(BABAR Collab.)
BRODZICKA	08	PRL 100 092001	J. Brodzicka *et al.*	(BELLE Collab.)
PAKHLOVA	08	PR D77 011103	G. Pakhlova *et al.*	(BELLE Collab.)
ABLIKIM	07B	PL B650 111	M. Ablikim *et al.*	(BES Collab.)
ABLIKIM	07E	PL B652 238	M. Ablikim *et al.*	(BES Collab.)
ABLIKIM	07F	PL B656 30	M. Ablikim *et al.*	(BES Collab.)
ABLIKIM	07I	EPJ C52 805	M. Ablikim *et al.*	(BES Collab.)
ABLIKIM	07K	PR D76 122002	M. Ablikim *et al.*	(BES Collab.)
AUBERT	07BE	PR D76 111105	B. Aubert *et al.*	(BABAR Collab.)
DOBBS	07	PR D76 112001	S. Dobbs *et al.*	(CLEO Collab.)
ABLIKIM	06L	PRL 97 121801	M. Ablikim *et al.*	(BES Collab.)
ABLIKIM	06N	PL B641 145	M. Ablikim *et al.*	(BES Collab.)
ADAM	06	PRL 96 082004	N.E. Adam *et al.*	(CLEO Collab.)
ADAMS	06	PR D73 012002	G.S. Adams *et al.*	(CLEO Collab.)
BESSON	06	PRL 96 092002	D. Besson *et al.*	(CLEO Collab.)
Also		PRL 104 159901 (errat.)	D. Besson *et al.*	(CLEO Collab.)
BRIERE	06	PR D74 031106	R.A. Briere *et al.*	(CLEO Collab.)
COAN	06A	PRL 96 182002	T.E. Coan *et al.*	(CLEO Collab.)
CRONIN-HEN...	06	PR D74 012005	D. Cronin-Hennessy *et al.*	(CLEO Collab.)
HUANG	06A	PRL 96 032003	G.S. Huang *et al.*	(CLEO Collab.)
BAI	05	PL B605 63	J.Z. Bai *et al.*	(BES Collab.)
HE	05	PRL 95 121801	Q. He *et al.*	(CLEO Collab.)
Also		PRL 96 199903 (errat.)	Q. He *et al.*	(CLEO Collab.)
ABLIKIM	04F	PR D70 077101	M. Ablikim *et al.*	(BES Collab.)
ATHAR	04	PR D70 112002	S.B. Athar *et al.*	(CLEO Collab.)
CHISTOV	04	PRL 93 051803	R. Chistov *et al.*	(BELLE Collab.)
PDG	04	PL B592 1	S. Eidelman *et al.*	(PDG Collab.)
BAI	02C	PRL 88 101802	J.Z. Bai *et al.*	(BES Collab.)
ADLER	88C	PRL 60 89	J. Adler *et al.*	(Mark III Collab.)
SCHINDLER	80	PR D21 2716	R.H. Schindler *et al.*	(Mark II Collab.)
BACINO	78	PRL 40 671	W.J. Bacino *et al.*	(SLAC, UCLA, UCI)
RAPIDIS	77	PRL 39 526	P.A. Rapidis *et al.*	(LGW Collab.)

$\psi_2(3823)$

$I^G(J^{PC}) = 0^-(2^{--})$
I, J, P need confirmation.

was $\psi(3823)$, $X(3823)$

Seen by BHARDWAJ 13 in $B \to \chi_{c1}\gamma K$ and ABLIKIM 15S in $e^+e^- \to \pi^+\pi^-\gamma\chi_{c1}$ decays as a narrow peak in the invariant mass distribution of the $\chi_{c1}\gamma$ system. Properties consistent with the $\psi_2(1^3D_2)$ $c\bar{c}$ state.

$\psi_2(3823)$ MASS

VALUE (MeV)	EVTS	DOCUMENT ID		TECN	COMMENT
3823.7 ±0.5 OUR AVERAGE		Error includes scale factor of 1.1.			
3824.08±0.53±0.14	137	[1] AAIJ	20s	LHCB	$B^+ \to J/\psi\pi^+\pi^-K^+$
3821.7 ±1.3 ±0.7	19 ± 5	[2] ABLIKIM	15s	BES3	$e^+e^- \to \pi^+\pi^-\chi_{c1}\gamma$
3823.1 ±1.8 ±0.7	33±10	[3] BHARDWAJ	13	BELL	$B^\pm \to \chi_{c1}\gamma K^\pm$

[1] Using the measured $m_{\psi_2(3823)} - m_{\psi(2S)} = 137.98 \pm 0.53 \pm 0.14$ MeV.

[2] From a simultaneous unbinned maximum likelihood fit of $e^+e^- \to \pi^+\pi^-\chi_{c1}\gamma$ data (the $\pi^+\pi^-$ recoil mass) taken at $\sqrt{s}$ values of 4.23, 4.26, 4.36, 4.42, and 4.60 GeV to simulated events including both $\psi(2S) \to \chi_{c1}\gamma$ and $\psi_2(3823) \to \chi_{c1}\gamma$ together, with floating mass scale offset for $\psi(2S)$, floating $\psi_2(3823)$ mass, and zero $\psi_2(3823)$ width, resulting in a significance of 5.9σ when including systematic uncertainties.

[3] From a simultaneous fit to $B^\pm \to (\chi_{c1}\gamma)K^\pm$ and $B^0 \to (\chi_{c1}\gamma)K^0_S$ with significance 4.0σ including systematics. Corrected for the measured $\psi(2S)$ mass using $B \to \psi(2S)K \to (\gamma\chi_{c1})K$ decays.

$m_{\psi_2(3823)} - m_{\psi(2S)}$

VALUE (MeV)	EVTS	DOCUMENT ID		TECN	COMMENT
• • • We do not use the following data for averages, fits, limits, etc. • • •					
137.98±0.53±0.14	137	[1] AAIJ	20s	LHCB	$B^+ \to J/\psi\pi^+\pi^-K^+$

[1] AAIJ 20s also reports $m_{\chi_{c1}(3872)} - m_{\psi_2(3823)} = 47.50 \pm 0.53 \pm 0.13$ MeV.

$\psi_2(3823)$ WIDTH

VALUE (MeV)	CL%	DOCUMENT ID		TECN	COMMENT
< 5.2	90	[1] AAIJ	20s	LHCB	$B^+ \to J/\psi\pi^+\pi^-K^+$
• • • We do not use the following data for averages, fits, limits, etc. • • •					
<16	90	[2] ABLIKIM	15s	BES3	$e^+e^- \to \pi^+\pi^-\chi_{c1}\gamma$
<24	90	[3] BHARDWAJ	13	BELL	$B^\pm \to \chi_{c1}\gamma K^\pm$

[1] AAIJ 20s also provides a limit of < 6.6 MeV with 95% CL.

[2] From a fit of $e^+e^- \to \pi^+\pi^-\chi_{c1}\gamma$ data (the $\pi^+\pi^-$ recoil mass) taken at $\sqrt{s}$ values of 4.23, 4.26, 4.36, 4.42, and 4.60 GeV to a Breit-Wigner function with the mass fixed from the likelihood fit above, Gaussian resolution smearing, and floating width.

[3] From a simultaneous fit to $B^\pm \to (\chi_{c1}\gamma)K^\pm$ and $B^0 \to (\chi_{c1}\gamma)K^0_S$ with significance 4.0σ including systematics.

$\psi_2(3823)$ DECAY MODES

Branching fractions are given relative to the one **DEFINED AS 1**.

	Mode	Fraction (Γ_i/Γ)	Confidence level
Γ_1	$J/\psi(1S)\pi^+\pi^-$	<0.06	90%
Γ_2	$J/\psi(1S)\pi^0\pi^0$	<0.11	90%
Γ_3	$J/\psi(1S)\pi^0$	<0.030	90%
Γ_4	$J/\psi(1S)\eta$	<0.14	90%
Γ_5	$\chi_{c0}\gamma$	<0.24	90%
Γ_6	$\chi_{c1}\gamma$	**DEFINED AS 1**	
Γ_7	$\chi_{c2}\gamma$	$0.28\ ^{+0.14}_{-0.11}$	

$\psi_2(3823)$ BRANCHING RATIOS

$\Gamma(J/\psi(1S)\pi^+\pi^-)/\Gamma_{total}$ — Γ_1/Γ

VALUE	EVTS	DOCUMENT ID		TECN	COMMENT
• • • We do not use the following data for averages, fits, limits, etc. • • •					
not seen		[1] ABLIKIM	21O	BES3	$e^+e^- \to \pi^+\pi^-X$
seen	137 ± 26	AAIJ	20s	LHCB	$B^+ \to J/\psi\pi^+\pi^-K^+$

[1] From a simultaneous unbinned maximum likelihood fit of the $\pi^+\pi^-$ recoil mass distributions of seven decay channels in the process $e^+e^- \to \pi^+\pi^-X$.

$\Gamma(J/\psi(1S)\pi^+\pi^-)/\Gamma(\chi_{c1}\gamma)$ — Γ_1/Γ_6

VALUE	CL%	DOCUMENT ID		TECN	COMMENT
<0.06	90	[1] ABLIKIM	21O	BES3	$e^+e^- \to \pi^+\pi^-X$

[1] From a simultaneous unbinned maximum likelihood fit of the $\pi^+\pi^-$ recoil mass distributions of seven decay channels in the process $e^+e^- \to \pi^+\pi^-X$.

$\Gamma(J/\psi(1S)\pi^0\pi^0)/\Gamma(\chi_{c1}\gamma)$ — Γ_2/Γ_6

VALUE	CL%	DOCUMENT ID		TECN	COMMENT
<0.11	90	[1] ABLIKIM	21O	BES3	$e^+e^- \to \pi^+\pi^-X$

[1] From a simultaneous unbinned maximum likelihood fit of the $\pi^+\pi^-$ recoil mass distributions of seven decay channels in the process $e^+e^- \to \pi^+\pi^-X$.

$\Gamma(J/\psi(1S)\pi^0)/\Gamma(\chi_{c1}\gamma)$ — Γ_3/Γ_6

VALUE	CL%	DOCUMENT ID		TECN	COMMENT
<0.03	90	[1] ABLIKIM	21O	BES3	$e^+e^- \to \pi^+\pi^-X$

[1] From a simultaneous unbinned maximum likelihood fit of the $\pi^+\pi^-$ recoil mass distributions of seven decay channels in the process $e^+e^- \to \pi^+\pi^-X$.

$\Gamma(J/\psi(1S)\eta)/\Gamma(\chi_{c1}\gamma)$ — Γ_4/Γ_6

VALUE	CL%	DOCUMENT ID		TECN	COMMENT
<0.14	90	[1] ABLIKIM	21O	BES3	$e^+e^- \to \pi^+\pi^-X$

[1] From a simultaneous unbinned maximum likelihood fit of the $\pi^+\pi^-$ recoil mass distributions of seven decay channels in the process $e^+e^- \to \pi^+\pi^-X$.

$\Gamma(\chi_{c0}\gamma)/\Gamma_{total}$ — Γ_5/Γ

VALUE	DOCUMENT ID		TECN	COMMENT
• • • We do not use the following data for averages, fits, limits, etc. • • •				
not seen	[1] ABLIKIM	21O	BES3	$e^+e^- \to \pi^+\pi^-X$

[1] From a simultaneous unbinned maximum likelihood fit of the $\pi^+\pi^-$ recoil mass distributions of seven decay channels in the process $e^+e^- \to \pi^+\pi^-X$.

$\Gamma(\chi_{c1}\gamma)/\Gamma_{total}$ — Γ_6/Γ

VALUE	EVTS	DOCUMENT ID		TECN	COMMENT
seen	33 ± 10	[1] BHARDWAJ	13	BELL	$B^\pm \to \chi_{c1}\gamma K^\pm$
• • • We do not use the following data for averages, fits, limits, etc. • • •					
seen	63 ± 9	[2] ABLIKIM	21O	BES3	$e^+e^- \to \pi^+\pi^-X$
seen	16 ± 5	[3] ABLIKIM	21O	BES3	$e^+e^- \to \pi^0\pi^0X$

[1] BHARDWAJ 13 reports $B(B^\pm \to \psi_2(3823)K^\pm) \times B(\psi_2(3823) \to \gamma\chi_{c1}) = (9.7 \pm 2.8 \pm 1.1) \times 10^{-6}$ with statistical significance 3.8 σ.

[2] From a simultaneous unbinned maximum likelihood fit of the $\pi^+\pi^-$ recoil mass distributions of seven decay channels in the process $e^+e^- \to \pi^+\pi^-X$. Signal has a 11.8 σ significance.

[3] From a fit of the invariant $\pi^0\pi^0$ recoil-mass distribution. Signal has a 4.3 σ significance.

$\Gamma(\chi_{c0}\gamma)/\Gamma(\chi_{c1}\gamma)$ — Γ_5/Γ_6

VALUE	CL%	DOCUMENT ID		TECN	COMMENT
<0.24	90	[1] ABLIKIM	21O	BES3	$e^+e^- \to \pi^+\pi^-X$

[1] From a simultaneous unbinned maximum likelihood fit of the $\pi^+\pi^-$ recoil mass distributions of seven decay channels in the process $e^+e^- \to \pi^+\pi^-X$.

$\Gamma(\chi_{c2}\gamma)/\Gamma_{total}$ — Γ_7/Γ

VALUE	DOCUMENT ID		TECN	COMMENT
• • • We do not use the following data for averages, fits, limits, etc. • • •				
seen	[1] ABLIKIM	21O	BES3	$e^+e^- \to \pi^+\pi^-X$
not seen	[2] ABLIKIM	15s	BES3	$e^+e^- \to \pi^+\pi^-\chi_{c2}\gamma$
not seen	[3] BHARDWAJ	13	BELL	$B^\pm \to \chi_{c2}\gamma K^\pm$

[1] From a simultaneous unbinned maximum likelihood fit of the $\pi^+\pi^-$ recoil mass distributions of seven decay channels in the process $e^+e^- \to \pi^+\pi^-X$. Signal has a 3.2 σ significance.

[2] From a simultaneous unbinned maximum likelihood fit of $e^+e^- \to \pi^+\pi^-\chi_{c2}\gamma$ data (the $\pi^+\pi^-$ recoil mass) taken at $\sqrt{s}$ values of 4.23, 4.26, 4.36, 4.42, and 4.60 GeV to simulated events including both $\psi(2S) \to \chi_{c2}\gamma$ and $\psi_2(3823) \to \chi_{c2}\gamma$ together, with floating mass scale offset for $\psi(2S)$, $\psi_2(3823)$ mass floating (fixed to that above), and zero $\psi_2(3823)$ width.

[3] BHARDWAJ 13 reports $B(B^\pm \to \psi_2(3823)K^\pm) \times B(\psi_2(3823) \to \gamma\chi_{c2}) < 3.6 \times 10^{-6}$ at 90% CL.

Downloaded from https://academic.oup.com/ptep/article/2022/8/083C01/6651666 by KIT Library user on 27 September 2022

$\Gamma(\chi_{c2}\gamma)/\Gamma(\chi_{c1}\gamma)$ — Γ_7/Γ_6

VALUE	CL%	EVTS	DOCUMENT ID		TECN	COMMENT
$0.28^{+0.14}_{-0.11}\pm0.02$		9 ± 4	[1] ABLIKIM	21O	BES3	$e^+e^-\to\pi^+\pi^-\chi_{c2}\gamma$
• • • We do not use the following data for averages, fits, limits, etc. • • •						
<0.42	90		[2] ABLIKIM	15S	BES3	$e^+e^-\to\pi^+\pi^-\chi_{c2}\gamma$
<0.41	90		BHARDWAJ	13	BELL	$B^\pm\to\chi_{c1/c2}\gamma K^\pm$

[1] From a simultaneous unbinned maximum likelihood fit of the $\pi^+\pi^-$ recoil mass distributions of seven decay channels in the process $e^+e^-\to\pi^+\pi^-X$.

[2] From a simultaneous unbinned maximum likelihood fit of $e^+e^-\to\pi^+\pi^-\chi_{c1(2)}\gamma$ data (the $\pi^+\pi^-$ recoil mass) taken at $\sqrt{s}$ values of 4.23, 4.26, 4.36, 4.42, and 4.60 GeV to simulated events including both $\psi(2S)\to\chi_{c1(2)}\gamma$ and $\psi_2(3823)\to\chi_{c1(2)}\gamma$ together, with floating mass scale offset for $\psi(2S)$, $\psi_2(3823)$ mass floating (fixed to that above), and zero $\psi_2(3823)$ width.

$\psi_2(3823)$ REFERENCES

ABLIKIM	21O	PR D103 L091102	M. Ablikim et al.	(BESIII Collab.)
AAIJ	20S	JHEP 2008 123	R. Aaij et al.	(LHCb Collab.)
ABLIKIM	15S	PRL 115 011803	M. Ablikim et al.	(BESIII Collab.)
BHARDWAJ	13	PRL 111 032001	V. Bhardwaj et al.	(BELLE Collab.)

$\psi_3(3842)$

$I^G(J^{PC}) = 0^-(3^{--})$

J, P need confirmation.

J^P has not been measured, 3^- is the quark model prediction.

$\psi_3(3842)$ MASS

VALUE (MeV)	DOCUMENT ID		TECN	COMMENT
$3842.71\pm0.16\pm0.12$	AAIJ	19M	LHCB	$pp\to D\overline{D}+$ anything

$\psi_3(3842)$ WIDTH

VALUE (MeV)	DOCUMENT ID		TECN	COMMENT
$2.79\pm0.51\pm0.35$	AAIJ	19M	LHCB	$pp\to D\overline{D}+$ anything

$\psi_3(3842)$ DECAY MODES

	Mode	Fraction (Γ_i/Γ)
Γ_1	D^+D^-	seen
Γ_2	$D^0\overline{D}^0$	seen

$\psi_3(3842)$ BRANCHING RATIOS

$\Gamma(D^+D^-)/\Gamma_{total}$ — Γ_1/Γ

VALUE	DOCUMENT ID		TECN	COMMENT
seen	AAIJ	19M	LHCB	$pp\to D\overline{D}+$ anything

$\Gamma(D^0\overline{D}^0)/\Gamma_{total}$ — Γ_2/Γ

VALUE	DOCUMENT ID		TECN	COMMENT
seen	AAIJ	19M	LHCB	$pp\to D\overline{D}+$ anything

$\psi_3(3842)$ REFERENCES

AAIJ	19M	JHEP 1907 035	R. Aaij et al.	(LHCb Collab.)

$\chi_{c0}(3860)$

$I^G(J^{PC}) = 0^+(0^{++})$

OMITTED FROM SUMMARY TABLE

The assignment $J^P=0^+$ is preferred over 2^+ by 2.5 sigma.

Observed by CHILIKIN 17 using full amplitude analysis of the process $e^+e^-\to J/\psi D\overline{D}$, where $D=D^0$, D^+. Not seen by AAIJ 20AI in the decay $B^+\to D^+D^-K^+$.

$\chi_{c0}(3860)$ MASS

VALUE (MeV)	DOCUMENT ID		TECN	COMMENT
3862^{+26+40}_{-32-13}	CHILIKIN	17	BELL	$e^+e^-\to J/\psi D\overline{D}$

$\chi_{c0}(3860)$ WIDTH

VALUE (MeV)	DOCUMENT ID		TECN	COMMENT
$201^{+154+88}_{-67-82}$	CHILIKIN	17	BELL	$e^+e^-\to J/\psi D\overline{D}$

$\chi_{c0}(3860)$ DECAY MODES

	Mode	Fraction (Γ_i/Γ)
Γ_1	$D^0\overline{D}^0$	seen
Γ_2	D^+D^-	seen

$\chi_{c0}(3860)$ BRANCHING RATIOS

$\Gamma(D^0\overline{D}^0)/\Gamma_{total}$ — Γ_1/Γ

VALUE	DOCUMENT ID		TECN	COMMENT
seen	CHILIKIN	17	BELL	$e^+e^-\to J/\psi D^0\overline{D}^0$

$\Gamma(D^+D^-)/\Gamma_{total}$ — Γ_2/Γ

VALUE	DOCUMENT ID		TECN	COMMENT
seen	CHILIKIN	17	BELL	$e^+e^-\to J/\psi D^+D^-$

$\chi_{c0}(3860)$ REFERENCES

AAIJ	20AI	PR D102 112003	R. Aaij et al.	(LHCb Collab.)
CHILIKIN	17	PR D95 112003	K. Chilikin et al.	(BELLE Collab.) JPC

$\chi_{c1}(3872)$

$I^G(J^{PC}) = 0^+(1^{++})$

also known as $X(3872)$

This state shows properties different from a conventional $q\overline{q}$ state. A candidate for an exotic structure. See the review on non-$q\overline{q}$ states.

First observed by CHOI 03 in $B\to K\pi^+\pi^-J/\psi(1S)$ decays as a narrow peak in the invariant mass distribution of the $\pi^+\pi^-J/\psi(1S)$ final state. Isovector hypothesis excluded by AUBERT 05B and CHOI 11.

AAIJ 13Q perform a full five-dimensional amplitude analysis of the angular correlations between the decay products in $B^+\to\chi_{c1}(3872)K^+$ decays, where $\chi_{c1}(3872)\to J/\psi\pi^+\pi^-$ and $J/\psi\to\mu^+\mu^-$, which unambiguously gives the $J^{PC}=1^{++}$ assignment under the assumption that the $\pi^+\pi^-$ and J/ψ are in an S-wave. AAIJ 15AO extend this analysis with more data to limit D-wave contributions to $<4\%$ at 95% CL.

See the review on "Spectroscopy of Mesons Containing Two Heavy Quarks."

$\chi_{c1}(3872)$ MASS FROM $J/\psi X$ MODE

VALUE (MeV)	EVTS	DOCUMENT ID		TECN	COMMENT
3871.65 ± 0.06 OUR AVERAGE					
$3871.64\pm0.06\pm0.01$	19.8k	[1] AAIJ	20S	LHCB	$B^+\to J/\psi\pi^+\pi^-K^+$
$3871.9\pm0.7\pm0.2$	20	ABLIKIM	14	BES3	$e^+e^-\to J/\psi\pi^+\pi^-\gamma$
$3871.95\pm0.48\pm0.12$	0.6k	AAIJ	12H	LHCB	$pp\to J/\psi\pi^+\pi^-X$
$3871.85\pm0.27\pm0.19$	170	[2] CHOI	11	BELL	$B\to K\pi^+\pi^-J/\psi$
$3873^{+1.8}_{-1.6}\pm1.3$	27	[3] DEL-AMO-SA...	10B	BABR	$B\to\omega J/\psi K$
$3871.61\pm0.16\pm0.19$	6k	[3,4] AALTONEN	09AU	CDF2	$p\overline{p}\to J/\psi\pi^+\pi^-X$
$3871.4\pm0.6\pm0.1$	93.4	AUBERT	08Y	BABR	$B^+\to K^+J/\psi\pi^+\pi^-$
$3868.7\pm1.5\pm0.4$	9.4	AUBERT	08Y	BABR	$B^0\to K^0_SJ/\psi\pi^+\pi^-$
$3871.8\pm3.1\pm3.0$	522	[3,5] ABAZOV	04F	D0	$p\overline{p}\to J/\psi\pi^+\pi^-X$
• • • We do not use the following data for averages, fits, limits, etc. • • •					
$3871.695\pm0.067\pm0.068$	15.6k	[6] AAIJ	20AD	LHCB	$pp\to J/\psi\pi^+\pi^-X$
$3871.59\pm0.06\pm0.03$	4.2k	[7] AAIJ	20S	LHCB	$B^+\to J/\psi\pi^+\pi^-K^+$
$3873.3\pm1.1\pm1.0$	45	[8] ABLIKIM	19V	BES	$e^+e^-\to\gamma\omega J/\psi$
3860.0 ± 10.4	13.6	[3,9] AGHASYAN	18A	COMP	$\gamma^*N\to X\pi^\pm N'$
$3868.6\pm1.2\pm0.2$	8	[10] AUBERT	06	BABR	$B^0\to K^0_SJ/\psi\pi^+\pi^-$
$3871.3\pm0.6\pm0.1$	61	[10] AUBERT	06	BABR	$B^-\to K^-J/\psi\pi^+\pi^-$
3873.4 ± 1.4	25	[11] AUBERT	05R	BABR	$B^+\to K^+J/\psi\pi^+\pi^-$
$3871.3\pm0.7\pm0.4$	730	[3,12] ACOSTA	04	CDF2	$p\overline{p}\to J/\psi\pi^+\pi^-X$
$3872.0\pm0.6\pm0.5$	36	[13] CHOI	03	BELL	$B\to K\pi^+\pi^-J/\psi$
3836 ± 13	58	[3,14] ANTONIAZZI	94	E705	$300\ \pi^\pm\mathrm{Li}\to J/\psi\pi^+\pi^-X$

[1] Calculated from $m_{\chi_{c1}(3872)}-m_{\psi(2S)}=185.54\pm0.06$ MeV obtained by combining the data with $\chi_{c1}(3872)$ produced in B^+ decays from AAIJ 20s and inclusive b-hadron decays from AAIJ 20AD and using $m_{\psi(2S)}=3686.097$ MeV. Breit-Wigner parametrization.

[2] The mass difference for the $\chi_{c1}(3872)$ produced in B^+ and B^0 decays is $(-0.71\pm0.96\pm0.19)$ MeV.

Downloaded from https://academic.oup.com/ptep/article/2022/8/083C01/6651666 by KIT Library user on 27 September 2022

[3] Width consistent with detector resolution.
[4] A possible equal mixture of two states with a mass difference greater than 3.6 MeV/c^2 is excluded at 95% CL.
[5] Calculated from the corresponding $m_{\chi_{c1}(3872)} - m_{J/\psi}$ using $m_{J/\psi}$=3096.916 MeV.
[6] Using $\chi_{c1}(3872)$ produced in inclusive b-hadron decays and $m_{\psi(2S)} = 3686.097 \pm 0.010$ MeV. Breit-Wigner parametrization. Superseded by the combined value in AAIJ 20S.
[7] Using Breit-Wigner parametrization. Superseded by the combined value in AAIJ 20S.
[8] Fit with fixed width and including two resonances, $\chi_{c0}(3915)$ and $X(3960)$.
[9] Could be a different state.
[10] Calculated from the corresponding $m_{\chi_{c1}(3872)} - m_{\psi(2S)}$ using $m_{\psi(2S)} = 3686.093$ MeV. Superseded by AUBERT 08Y.
[11] Calculated from the corresponding $m_{\chi_{c1}(3872)} - m_{\psi(2S)}$ using $m_{\psi(2S)} = 3685.96$MeV. Superseded by AUBERT 06.
[12] Superseded by AALTONEN 09AU.
[13] Superseded by CHOI 11.
[14] A lower mass value can be due to an incorrect momentum scale for soft pions.

$\chi_{c1}(3872)$ MASS FROM $\overline{D}^{*0} D^0$ MODE

VALUE (MeV)	EVTS	DOCUMENT ID		TECN	COMMENT
• • • We do not use the following data for averages, fits, limits, etc. • • •					
$3872.9^{+0.6}_{-0.4}{}^{+0.4}_{-0.5}$	50	[1,2] AUSHEV	10	BELL	$B \to \overline{D}^{*0} D^0 K$
$3875.1^{+0.7}_{-0.5} \pm 0.5$	33 ± 6	[2] AUBERT	08B	BABR	$B \to \overline{D}^{*0} D^0 K$
$3875.2 \pm 0.7^{+0.9}_{-1.8}$	24 ± 6	[2,3] GOKHROO	06	BELL	$B \to D^0 \overline{D}^0 \pi^0 K$

[1] Calculated from the measured $m_{\chi_{c1}(3872)} - m_{D^{*0}} - m_{\overline{D}^0} = 1.1^{+0.6}_{-0.4}{}^{+0.1}_{-0.3}$ MeV.
[2] Experiments report $D^{*0}\overline{D}^0$ invariant mass above $D^{*0}\overline{D}^0$ threshold because D^{*0} decay products are kinematically constrained to the D^{*0} mass, even though the D^{*0} may decay off-shell.
[3] Superseded by AUSHEV 10.

$m_{\chi_{c1}(3872)} - m_{J/\psi}$

VALUE (MeV)	EVTS	DOCUMENT ID		TECN	COMMENT
774.9±3.1±3.0	522	ABAZOV	04F	D0	$p\overline{p} \to J/\psi \pi^+ \pi^- X$

$m_{\chi_{c1}(3872)} - m_{\psi(2S)}$

VALUE (MeV)	EVTS	DOCUMENT ID		TECN	COMMENT
• • • We do not use the following data for averages, fits, limits, etc. • • •					
185.598±0.067±0.068	15.6k	[1] AAIJ	20AD	LHCB	$pp \to J/\psi \pi^+ \pi^- X$
185.54 ±0.06	19.8k	[2] AAIJ	20S	LHCB	$pp \to J/\psi \pi^+ \pi^- X$
187.4 ±1.4	25	[3] AUBERT	05R	BABR	$B^+ \to K^+ J/\psi \pi^+ \pi^-$

[1] Using $\chi_{c1}(3872)$ produced in inclusive b-hadron decays. Breit-Wigner parametrization. Superseded by the combined value in AAIJ 20S.
[2] Combining $m_{\chi_{c1}(3872)} - m_{\psi(2S)} = 185.49 \pm 0.06 \pm 0.03$ MeV from AAIJ 20S and the measured mass difference from AAIJ 20AD. Breit-Wigner parametrization.
[3] Superseded by AUBERT 06.

$\chi_{c1}(3872)$ WIDTH

VALUE (MeV)	CL%	EVTS	DOCUMENT ID		TECN	COMMENT
1.19±0.21 OUR AVERAGE Error includes scale factor of 1.1.						
1.39±0.24±0.10		15.6k	[1] AAIJ	20AD	LHCB	$pp \to J/\psi \pi^+ \pi^- X$
$0.96^{+0.19}_{-0.18} \pm 0.21$		4.2k	[2] AAIJ	20S	LHCB	$B^+ \to J/\psi \pi^+ \pi^- K^+$
• • • We do not use the following data for averages, fits, limits, etc. • • •						
<2.4	90		ABLIKIM	14	BES3	$e^+ e^- \to J/\psi \pi^+ \pi^- \gamma$
<1.2	90		CHOI	11	BELL	$B \to K \pi^+ \pi^- J/\psi$
<3.3	90		AUBERT	08Y	BABR	$B^+ \to K^+ J/\psi \pi^+ \pi^-$
<4.1	90	69	AUBERT	06	BABR	$B \to K \pi^+ \pi^- J/\psi$
<2.3	90	36	[3] CHOI	03	BELL	$B \to K \pi^+ \pi^- J/\psi$

[1] Using $\chi_{c1}(3872)$ produced in inclusive b-hadron decays. Breit-Wigner parametrization.
[2] Using Breit-Wigner parametrization. Partially overlapping dataset with that of AAIJ 20AD.
[3] Superseded by CHOI 11.

$\chi_{c1}(3872)$ WIDTH FROM $\overline{D}^{*0} D^0$ MODE

VALUE (MeV)	EVTS	DOCUMENT ID		TECN	COMMENT
• • • We do not use the following data for averages, fits, limits, etc. • • •					
$3.9^{+2.8}_{-1.4}{}^{+0.2}_{-1.1}$	50	[1] AUSHEV	10	BELL	$B \to \overline{D}^{*0} D^0 K$
$3.0^{+1.9}_{-1.4} \pm 0.9$	33 ± 6	AUBERT	08B	BABR	$B \to \overline{D}^{*0} D^0 K$

[1] With a measured value of $B(B \to \chi_{c1}(3872) K) \times B(\chi_{c1}(3872) \to D^{*0}\overline{D}^0) = (0.80 \pm 0.20 \pm 0.10) \times 10^{-4}$, assumed to be equal for both charged and neutral modes.

$\chi_{c1}(3872)$ DECAY MODES

	Mode	Fraction (Γ_i/Γ)	Confidence level
Γ_1	$e^+ e^-$	$< 2.8 \times 10^{-6}$	90%
Γ_2	$\pi^+ \pi^- J/\psi(1S)$	(3.8± 1.2) %	
Γ_3	$\pi^+ \pi^- \pi^0 J/\psi(1S)$	not seen	
Γ_4	$\omega \eta_c(1S)$	< 33 %	90%
Γ_5	$\omega J/\psi(1S)$	(4.3± 2.1) %	
Γ_6	$\phi\phi$	not seen	
Γ_7	$D^0 \overline{D}^0 \pi^0$	$(49\ ^{+18}_{-20})$ %	
Γ_8	$\overline{D}^{*0} D^0$	(37 ± 9) %	
Γ_9	$\gamma\gamma$	< 11 %	90%
Γ_{10}	$D^0 \overline{D}^0$	< 29 %	90%
Γ_{11}	$D^+ D^-$	< 19 %	90%
Γ_{12}	$\pi^0 \chi_{c2}$	< 4 %	90%
Γ_{13}	$\pi^0 \chi_{c1}$	(3.4± 1.6) %	
Γ_{14}	$\pi^0 \chi_{c0}$	< 70 %	90%
Γ_{15}	$\pi^+ \pi^- \eta_c(1S)$	< 14 %	90%
Γ_{16}	$\pi^+ \pi^- \chi_{c1}$	$< 7 \times 10^{-3}$	90%
Γ_{17}	$p\overline{p}$	$< 2.4 \times 10^{-5}$	95%
	Radiative decays		
Γ_{18}	$\gamma D^+ D^-$	< 4 %	90%
Γ_{19}	$\gamma \overline{D}^0 D^0$	< 6 %	90%
Γ_{20}	$\gamma J/\psi$	$(8 \pm 4) \times 10^{-3}$	
Γ_{21}	$\gamma \chi_{c1}$	$< 9 \times 10^{-3}$	90%
Γ_{22}	$\gamma \chi_{c2}$	< 3.2 %	90%
Γ_{23}	$\gamma \psi(2S)$	(4.5± 2.0) %	
	***C*-violating decays**		
Γ_{24}	$\eta J/\psi$	< 1.8 %	90%

$\chi_{c1}(3872)$ PARTIAL WIDTHS

$\Gamma(e^+ e^-)$ — Γ_1

VALUE (eV)	CL%	DOCUMENT ID		TECN	COMMENT
• • • We do not use the following data for averages, fits, limits, etc. • • •					
< 4.3	90	[1] ABLIKIM	15V	BES3	4.0–4.4 $e^+ e^- \to \pi^+ \pi^- J/\psi$
<280	90	[2] YUAN	04	RVUE	$e^+ e^- \to \pi^+ \pi^- J/\psi$

[1] ABLIKIM 15V reports this limit from the measurement of $\Gamma(\chi_{c1}(3872) \to \pi^+ \pi^- J/\psi(1S)) \times \Gamma(\chi_{c1}(3872) \to e^+ e^-)/\Gamma < 0.13$ eV using $\Gamma(\chi_{c1}(3872) \to \pi^+ \pi^- J/\psi(1S))/\Gamma = 3\%$.
[2] Using BAI 98E data on $e^+ e^- \to \pi^+ \pi^- \ell^+ \ell^-$. Assuming that $\Gamma(\pi^+ \pi^- J/\psi)$ of $\chi_{c1}(3872)$ is the same as that of $\psi(2S)$ (85.4 keV).

$\Gamma(\gamma\gamma) \times \Gamma(\pi^+ \pi^- J/\psi(1S))/\Gamma_{total}$ — $\Gamma_9\Gamma_2/\Gamma$

$\chi_{c1}(3872)$ $\Gamma(i)\Gamma(e^+ e^-)/\Gamma(total)$

$\Gamma(\pi^+ \pi^- J/\psi(1S)) \times \Gamma(e^+ e^-)/\Gamma_{total}$ — $\Gamma_2\Gamma_1/\Gamma$

VALUE (eV)	CL%	DOCUMENT ID		TECN	COMMENT
< 0.13	90	ABLIKIM	15V	BES3	4.0–4.4 $e^+ e^- \to \pi^+ \pi^- J/\psi$
• • • We do not use the following data for averages, fits, limits, etc. • • •					
< 6.2	90	[1,2] AUBERT	05D	BABR	10.6 $e^+ e^- \to K^+ K^- \pi^+ \pi^- \gamma$
< 8.3	90	[2] DOBBS	05	CLE3	$e^+ e^- \to \pi^+ \pi^- J/\psi$
<10	90	[3] YUAN	04	RVUE	$e^+ e^- \to \pi^+ \pi^- J/\psi$

[1] Using $B(\chi_{c1}(3872) \to J/\psi \pi^+ \pi^-) \cdot B(J/\psi \to \mu^+ \mu^-) \cdot \Gamma(\chi_{c1}(3872) \to e^+ e^-) < 0.37$ eV from AUBERT 05D and $B(J/\psi \to \mu^+ \mu^-) = 0.0588 \pm 0.0010$ from the PDG 04.
[2] Assuming $\chi_{c1}(3872)$ has $J^{PC} = 1^{--}$.
[3] Using BAI 98E data on $e^+ e^- \to \pi^+ \pi^- \ell^+ \ell^-$. From theoretical calculation of the production cross section and using $B(J/\psi \to \mu^+ \mu^-) = (5.88 \pm 0.10)\%$.

$\chi_{c1}(3872)$ $\Gamma(i)\Gamma(\gamma\gamma)/\Gamma(total)$

$\Gamma(\pi^+ \pi^- J/\psi(1S)) \times \Gamma(\gamma\gamma)/\Gamma_{total}$ — $\Gamma_2\Gamma_9/\Gamma$

VALUE (eV)	CL%	EVTS	DOCUMENT ID		TECN	COMMENT
• • • We do not use the following data for averages, fits, limits, etc. • • •						
$5.5^{+4.1}_{-3.8} \pm 0.7$		3	[1] TERAMOTO	21	BELL	$e^+ e^- \to \gamma^* \gamma$ at Υ(nS)
<12.9	90		[2] DOBBS	05	CLE3	$e^+ e^- \to \pi^+ \pi^- J/\psi \gamma$

[1] Measured in single-tag two-photon production assuming Q^2 dependence of a $c\overline{c}$ meson model. Here, $\Gamma(\chi_{c1}(3872) \to \gamma\gamma)$ is the reduced two-photon decay width, $\tilde{\Gamma}_{\gamma\gamma}$.
[2] Assuming $\chi_{c1}(3872)$ has positive C parity and spin 0.

Downloaded from https://academic.oup.com/ptep/article/2022/8/083C01/6651666 by KIT Library user on 27 September 2022

$\Gamma(\omega J/\psi(1S)) \times \Gamma(\gamma\gamma)/\Gamma_{total}$ — $\Gamma_5\Gamma_9/\Gamma$

VALUE (eV)	CL%	DOCUMENT ID		TECN	COMMENT
• • • We do not use the following data for averages, fits, limits, etc. • • •					
<1.7	90	[1] LEES	12AD	BABR	$e^+e^- \to e^+e^-\omega J/\psi$

[1] Assuming $\chi_{c1}(3872)$ has spin 2.

$\Gamma(\pi^+\pi^-\eta_c(1S)) \times \Gamma(\gamma\gamma)/\Gamma_{total}$ — $\Gamma_{15}\Gamma_9/\Gamma$

VALUE (eV)	CL%	DOCUMENT ID		TECN	COMMENT
<11.1	90	LEES	12AE	BABR	$e^+e^- \to e^+e^-\pi^+\pi^-\eta_c$

$\chi_{c1}(3872)$ BRANCHING RATIOS

$\Gamma(\pi^+\pi^- J/\psi(1S))/\Gamma_{total}$ — Γ_2/Γ

VALUE	EVTS	DOCUMENT ID		TECN	COMMENT
0.038±0.012 OUR AVERAGE					
0.038±0.002±0.012		[1] AAIJ	20S	LHCB	$B^+ \to J/\psi\pi^+\pi^-K^+$
0.041±0.005±0.013		[2] CHOI	11	BELL	$B^+ \to \pi^+\pi^- J/\psi K^+$
0.040±0.008±0.013	93	[3,4] AUBERT	08Y	BABR	$B \to \chi_{c1}(3872)K$
• • • We do not use the following data for averages, fits, limits, etc. • • •					
seen	151	[5] BALA	15	BELL	$B \to \chi_{c1}(3872)K\pi$
0.061±0.020±0.020	30	[6] AUBERT	05R	BABR	$B^+ \to K^+\pi^+\pi^- J/\psi$
0.065±0.014±0.021	36	[7] CHOI	03	BELL	$B^+ \to K^+\pi^+\pi^- J/\psi$

[1] AAIJ 20S reports $[\Gamma(\chi_{c1}(3872) \to \pi^+\pi^- J/\psi(1S))/\Gamma_{total}] \times [B(B^+ \to \chi_{c1}(3872)K^+)] = (7.95 \pm 0.15 \pm 0.33) \times 10^{-6}$ which we divide by our best value $B(B^+ \to \chi_{c1}(3872)K^+) = (2.1 \pm 0.7) \times 10^{-4}$. Our first error is their experiment's error and our second error is the systematic error from using our best value.

[2] CHOI 11 reports $[\Gamma(\chi_{c1}(3872) \to \pi^+\pi^- J/\psi(1S))/\Gamma_{total}] \times [B(B^+ \to \chi_{c1}(3872)K^+)] = (8.63 \pm 0.82 \pm 0.52) \times 10^{-6}$ which we divide by our best value $B(B^+ \to \chi_{c1}(3872)K^+) = (2.1 \pm 0.7) \times 10^{-4}$. Our first error is their experiment's error and our second error is the systematic error from using our best value.

[3] AUBERT 08Y reports $[\Gamma(\chi_{c1}(3872) \to \pi^+\pi^- J/\psi(1S))/\Gamma_{total}] \times [B(B^+ \to \chi_{c1}(3872)K^+)] = (8.4 \pm 1.5 \pm 0.7) \times 10^{-6}$ which we divide by our best value $B(B^+ \to \chi_{c1}(3872)K^+) = (2.1 \pm 0.7) \times 10^{-4}$. Our first error is their experiment's error and our second error is the systematic error from using our best value.

[4] superseded by LEES 20C

[5] BALA 15 reports $B(\chi_{c1}(3872) \to \pi^+\pi^- J/\psi) \times B(B^0 \to \chi_{c1}(3872)K^+\pi^-) = (7.9 \pm 1.3 \pm 0.4) \times 10^{-6}$ and $B(\chi_{c1}(3872) \to \pi^+\pi^- J/\psi) \times B(B^+ \to \chi_{c1}(3872)K^0\pi^+) = (10.6 \pm 3.0 \pm 0.9) \times 10^{-6}$.

[6] Superseded by AUBERT 08Y. AUBERT 05R reports $[\Gamma(\chi_{c1}(3872) \to \pi^+\pi^- J/\psi(1S))/\Gamma_{total}] \times [B(B^+ \to \chi_{c1}(3872)K^+)] = (1.28 \pm 0.41) \times 10^{-5}$ which we divide by our best value $B(B^+ \to \chi_{c1}(3872)K^+) = (2.1 \pm 0.7) \times 10^{-4}$. Our first error is their experiment's error and our second error is the systematic error from using our best value.

[7] CHOI 03 reports $[\Gamma(\chi_{c1}(3872) \to \pi^+\pi^- J/\psi(1S))/\Gamma_{total}] \times [B(B^+ \to \chi_{c1}(3872)K^+)] / [B(B^+ \to \psi(2S)K^+)] / [B(\psi(2S) \to J/\psi(1S)\pi^+\pi^-)] = 0.063 \pm 0.012 \pm 0.007$ which we multiply or divide by our best values $B(B^+ \to \chi_{c1}(3872)K^+) = (2.1 \pm 0.7) \times 10^{-4}$, $B(B^+ \to \psi(2S)K^+) = (6.24 \pm 0.20) \times 10^{-4}$, $B(\psi(2S) \to J/\psi(1S)\pi^+\pi^-) = (34.68 \pm 0.30) \times 10^{-2}$. Our first error is their experiment's error and our second error is the systematic error from using our best values.

$\Gamma(\pi^+\pi^-\pi^0 J/\psi(1S))/\Gamma_{total}$ — Γ_3/Γ

VALUE	DOCUMENT ID		TECN	COMMENT
not seen	[1] WANG	11B	BELL	$\Upsilon(2S) \to \gamma X$
not seen	[2] SHEN	10A	BELL	$\Upsilon(1S) \to \gamma X$

[1] WANG 11B reports $B(\Upsilon(2S) \to \gamma\chi_{c1}(3872)) \times B(\chi_{c1} \to \pi^+\pi^-\pi^0 J/\psi) < 2.4 \times 10^{-6}$ at 95% CL.

[2] SHEN 10A reports $B(\Upsilon(1S) \to \gamma\chi_{c1}(3872)) \times B(\chi_{c1} \to \pi^+\pi^-\pi^0 J/\psi) < 2.8 \times 10^{-6}$ at 95% CL.

$\Gamma(\omega\eta_c(1S))/\Gamma_{total}$ — Γ_4/Γ

VALUE	CL%	DOCUMENT ID		TECN	COMMENT
<0.33	90	[1] VINOKUROVA	15	BELL	$B^+ \to \omega\eta_c K^+$

[1] VINOKUROVA 15 reports $[\Gamma(\chi_{c1}(3872) \to \omega\eta_c(1S))/\Gamma_{total}] \times [B(B^+ \to \chi_{c1}(3872)K^+)] < 6.9 \times 10^{-5}$ which we divide by our best value $B(B^+ \to \chi_{c1}(3872)K^+) = 2.1 \times 10^{-4}$.

$\Gamma(\omega J/\psi(1S))/\Gamma_{total}$ — Γ_5/Γ

VALUE	EVTS	DOCUMENT ID		TECN	COMMENT
• • • We do not use the following data for averages, fits, limits, etc. • • •					
0.029±0.011±0.009	21 ± 7	[1] DEL-AMO-SA...	10B	BABR	$B^+ \to \omega J/\psi K^+$

[1] DEL-AMO-SANCHEZ 10B reports $[\Gamma(\chi_{c1}(3872) \to \omega J/\psi(1S))/\Gamma_{total}] \times [B(B^+ \to \chi_{c1}(3872)K^+)] = (6 \pm 2 \pm 1) \times 10^{-6}$ which we divide by our best value $B(B^+ \to \chi_{c1}(3872)K^+) = (2.1 \pm 0.7) \times 10^{-4}$. Our first error is their experiment's error and our second error is the systematic error from using our best value. DEL-AMO-SANCHEZ 10B also reports $B(B^0 \to \chi_{c1}(3872)K^0) \times B(\chi_{c1}(3872) \to J/\psi\omega) = (6 \pm 3 \pm 1) \times 10^{-6}$.

$\Gamma(\omega J/\psi(1S))/\Gamma(\pi^+\pi^- J/\psi(1S))$ — Γ_5/Γ_2

VALUE	DOCUMENT ID		TECN	COMMENT
1.1±0.4 OUR AVERAGE Error includes scale factor of 1.7.				
$1.6^{+0.4}_{-0.3}\pm0.2$	[1] ABLIKIM	19V	BES	$e^+e^- \to \gamma\omega J/\psi$
0.8±0.3	[2] DEL-AMO-SA...	10B	BABR	$B \to \omega J/\psi K$

[1] Fit with fixed width and including two resonances, $\chi_{c0}(3915)$ and $X(3960)$.

[2] Statistical and systematic errors added in quadrature. Uses the values of $B(B \to \chi_{c1}(3872)K) \times B(\chi_{c1}(3872) \to J/\psi\pi^+\pi^-)$ reported in AUBERT 08Y, taking into account the common systematics.

$\Gamma(\phi\phi)/\Gamma_{total}$ — Γ_6/Γ

VALUE	DOCUMENT ID		TECN	COMMENT
not seen	[1] AAIJ	17BB	LHCB	pp at 7, 8 TeV

[1] AAIJ 17BB reports $B(b \to \chi_{c1}(3872)\text{ anything}) \times B(\chi_{c1}(3872) \to \phi\phi) < 4.5 \times 10^{-7}$ at 95% CL.

$\Gamma(D^0\overline{D}^0\pi^0)/\Gamma_{total}$ — Γ_7/Γ

VALUE	CL%	EVTS	DOCUMENT ID		TECN	COMMENT
$\mathbf{0.49^{+0.18}_{-0.20}\pm0.16}$		17	[1] GOKHROO	06	BELL	$B^+ \to D^0\overline{D}^0\pi^0K^+$
• • • We do not use the following data for averages, fits, limits, etc. • • •						
<0.29	90		[2] CHISTOV	04	BELL	Sup. by GOKHROO 06

[1] GOKHROO 06 reports $[\Gamma(\chi_{c1}(3872) \to D^0\overline{D}^0\pi^0)/\Gamma_{total}] \times [B(B^+ \to \chi_{c1}(3872)K^+)] = (1.02 \pm 0.31^{+0.21}_{-0.29}) \times 10^{-4}$ which we divide by our best value $B(B^+ \to \chi_{c1}(3872)K^+) = (2.1 \pm 0.7) \times 10^{-4}$. Our first error is their experiment's error and our second error is the systematic error from using our best value.

[2] CHISTOV 04 reports $[\Gamma(\chi_{c1}(3872) \to D^0\overline{D}^0\pi^0)/\Gamma_{total}] \times [B(B^+ \to \chi_{c1}(3872)K^+)] < 0.6 \times 10^{-4}$ which we divide by our best value $B(B^+ \to \chi_{c1}(3872)K^+) = 2.1 \times 10^{-4}$.

$\Gamma(D^0\overline{D}^0\pi^0)/\Gamma(\pi^+\pi^- J/\psi(1S))$ — Γ_7/Γ_2

VALUE	CL%	DOCUMENT ID		TECN	COMMENT
• • • We do not use the following data for averages, fits, limits, etc. • • •					
<1.16	90	ABLIKIM	20W	BES3	$e^+e^- \to \gamma\chi_{c1}(3872)$

$\Gamma(\overline{D}^{*0}D^0)/\Gamma_{total}$ — Γ_8/Γ

VALUE	EVTS	DOCUMENT ID		TECN	COMMENT
0.37±0.09±0.12	41^{+9}_{-8}	[1] AUSHEV	10	BELL	$B^+ \to D^{*0}\overline{D}^0K^+$
• • • We do not use the following data for averages, fits, limits, etc. • • •					
0.80±0.28±0.26	27 ± 6	[2] AUBERT	08B	BABR	$B^+ \to \overline{D}^{*0}D^0K^+$

[1] AUSHEV 10 reports $[\Gamma(\chi_{c1}(3872) \to \overline{D}^{*0}D^0)/\Gamma_{total}] \times [B(B^+ \to \chi_{c1}(3872)K^+)] = (0.77 \pm 0.16 \pm 0.10) \times 10^{-4}$ which we divide by our best value $B(B^+ \to \chi_{c1}(3872)K^+) = (2.1 \pm 0.7) \times 10^{-4}$. Our first error is their experiment's error and our second error is the systematic error from using our best value.

[2] AUBERT 08B reports $[\Gamma(\chi_{c1}(3872) \to \overline{D}^{*0}D^0)/\Gamma_{total}] \times [B(B^+ \to \chi_{c1}(3872)K^+)] = (1.67 \pm 0.36 \pm 0.47) \times 10^{-4}$ which we divide by our best value $B(B^+ \to \chi_{c1}(3872)K^+) = (2.1 \pm 0.7) \times 10^{-4}$. Our first error is their experiment's error and our second error is the systematic error from using our best value.

$\Gamma(\overline{D}^{*0}D^0)/\Gamma(\pi^+\pi^- J/\psi(1S))$ — Γ_8/Γ_2

VALUE	EVTS	DOCUMENT ID		TECN	COMMENT
11.77±3.09	50	ABLIKIM	20W	BES3	$e^+e^- \to \gamma\chi_{c1}(3872)$

$\Gamma(\gamma\gamma)/\Gamma_{total}$ — Γ_9/Γ

VALUE	CL%	DOCUMENT ID		TECN	COMMENT
<0.11	90	[1] WICHT	08	BELL	$e^+e^- \to \Upsilon(4S)$

[1] WICHT 08 reports $[\Gamma(\chi_{c1}(3872) \to \gamma\gamma)/\Gamma_{total}] \times [B(B^+ \to \chi_{c1}(3872)K^+)] < 2.4 \times 10^{-5}$ which we divide by our best value $B(B^+ \to \chi_{c1}(3872)K^+) = 2.1 \times 10^{-4}$.

$\Gamma(D^0\overline{D}^0)/\Gamma_{total}$ — Γ_{10}/Γ

VALUE	CL%	DOCUMENT ID		TECN	COMMENT
<0.29	90	[1] CHISTOV	04	BELL	$B \to KD^0\overline{D}^0$

[1] CHISTOV 04 reports $[\Gamma(\chi_{c1}(3872) \to D^0\overline{D}^0)/\Gamma_{total}] \times [B(B^+ \to \chi_{c1}(3872)K^+)] < 6 \times 10^{-5}$ which we divide by our best value $B(B^+ \to \chi_{c1}(3872)K^+) = 2.1 \times 10^{-4}$.

$\Gamma(D^+D^-)/\Gamma_{total}$ — Γ_{11}/Γ

VALUE	CL%	DOCUMENT ID		TECN	COMMENT
<0.19	90	[1] CHISTOV	04	BELL	$B \to KD^+D^-$

[1] CHISTOV 04 reports $[\Gamma(\chi_{c1}(3872) \to D^+D^-)/\Gamma_{total}] \times [B(B^+ \to \chi_{c1}(3872)K^+)] < 4 \times 10^{-5}$ which we divide by our best value $B(B^+ \to \chi_{c1}(3872)K^+) = 2.1 \times 10^{-4}$.

$\Gamma(\pi^0\chi_{c2})/\Gamma(\pi^+\pi^- J/\psi(1S))$ — Γ_{12}/Γ_2

VALUE	CL%	DOCUMENT ID		TECN	COMMENT
<1.1	90	ABLIKIM	19U	BES3	$e^+e^- \to \gamma\chi_{c1}(3872)$

Downloaded from https://academic.oup.com/ptep/article/2022/8/083C01/6651666 by KIT Library user on 27 September 2022

$\Gamma(\pi^0\chi_{c1})/\Gamma_{total}$ — Γ_{13}/Γ

VALUE	CL%	DOCUMENT ID		TECN	COMMENT
• • • We do not use the following data for averages, fits, limits, etc. • • •					
<0.04	90	[1] BHARDWAJ	19	BELL	$B^\pm \to \pi^0\chi_{c1}K^\pm$

[1] BHARDWAJ 19 reports $[\Gamma(\chi_{c1}(3872) \to \pi^0\chi_{c1})/\Gamma_{total}] \times [B(B^+ \to \chi_{c1}(3872)K^+)] < 8.1 \times 10^{-6}$ which we divide by our best value $B(B^+ \to \chi_{c1}(3872)K^+) = 2.1 \times 10^{-4}$.

$\Gamma(\pi^0\chi_{c1})/\Gamma(\pi^+\pi^-J/\psi(1S))$ — Γ_{13}/Γ_2

VALUE (units 10^{-2})	EVTS	DOCUMENT ID		TECN	COMMENT
$88^{+33}_{-27}\pm10$	10.8	ABLIKIM	19U	BES3	$e^+e^- \to \gamma\chi_{c1}(3872)$

$\Gamma(\pi^0\chi_{c0})/\Gamma(\pi^+\pi^-J/\psi(1S))$ — Γ_{14}/Γ_2

VALUE	CL%	DOCUMENT ID		TECN	COMMENT
<19	90	ABLIKIM	19U	BES3	$e^+e^- \to \gamma\chi_{c1}(3872)$

$\Gamma(\pi^+\pi^-\eta_c(1S))/\Gamma_{total}$ — Γ_{15}/Γ

VALUE	CL%	DOCUMENT ID		TECN	COMMENT
<0.14	90	[1] VINOKUROVA	15	BELL	$B^+ \to \pi^+\pi^-\eta_c K^+$

[1] VINOKUROVA 15 reports $[\Gamma(\chi_{c1}(3872) \to \pi^+\pi^-\eta_c(1S))/\Gamma_{total}] \times [B(B^+ \to \chi_{c1}(3872)K^+)] < 3.0 \times 10^{-5}$ which we divide by our best value $B(B^+ \to \chi_{c1}(3872)K^+) = 2.1 \times 10^{-4}$.

$\Gamma(\pi^+\pi^-\chi_{c1})/\Gamma_{total}$ — Γ_{16}/Γ

VALUE	CL%	DOCUMENT ID		TECN	COMMENT
$<7\times10^{-3}$	90	[1] BHARDWAJ	16	BELL	$B^+ \to \pi^+\pi^-\chi_{c1}K^+$

[1] BHARDWAJ 16 reports $[\Gamma(\chi_{c1}(3872) \to \pi^+\pi^-\chi_{c1})/\Gamma_{total}] \times [B(B^+ \to \chi_{c1}(3872)K^+)] < 1.5 \times 10^{-6}$ which we divide by our best value $B(B^+ \to \chi_{c1}(3872)K^+) = 2.1 \times 10^{-4}$.

$\Gamma(p\overline{p})/\Gamma_{total}$ — Γ_{17}/Γ

VALUE	CL%	DOCUMENT ID		TECN	COMMENT
$<2.4\times10^{-5}$	95	[1] AAIJ	17AD	LHCB	$B^+ \to p\overline{p}K^+$
• • • We do not use the following data for averages, fits, limits, etc. • • •					
$<8 \times10^{-5}$	95	[2] AAIJ	13S	LHCB	$B^+ \to p\overline{p}K^+$

[1] AAIJ 17AD reports $[\Gamma(\chi_{c1}(3872) \to p\overline{p})/\Gamma_{total}] \times [B(B^+ \to \chi_{c1}(3872)K^+)] < 0.5 \times 10^{-8}$ which we divide by our best value $B(B^+ \to \chi_{c1}(3872)K^+) = 2.1 \times 10^{-4}$.

[2] AAIJ 13S reports $[\Gamma(\chi_{c1}(3872) \to p\overline{p})/\Gamma_{total}] \times [B(B^+ \to \chi_{c1}(3872)K^+)] < 1.7 \times 10^{-8}$ which we divide by our best value $B(B^+ \to \chi_{c1}(3872)K^+) = 2.1 \times 10^{-4}$.

Radiative decays

$\Gamma(\gamma D^+D^-)/\Gamma(\pi^+\pi^-J/\psi(1S))$ — Γ_{18}/Γ_2

VALUE	CL%	DOCUMENT ID		TECN	COMMENT
<0.99	90	ABLIKIM	20W	BES3	$e^+e^- \to \gamma\chi_{c1}(3872)$

$\Gamma(\gamma\overline{D}^0D^0)/\Gamma(\pi^+\pi^-J/\psi(1S))$ — Γ_{19}/Γ_2

VALUE	CL%	DOCUMENT ID		TECN	COMMENT
<1.58	90	ABLIKIM	20W	BES3	$e^+e^- \to \gamma\chi_{c1}(3872)$

$\Gamma(\gamma J/\psi)/\Gamma_{total}$ — Γ_{20}/Γ

VALUE	EVTS	DOCUMENT ID		TECN	COMMENT
$0.0085^{+0.0024}_{-0.0022}\pm0.0027$		[1] BHARDWAJ	11	BELL	$B^\pm \to \gamma J/\psi K^\pm$
• • • We do not use the following data for averages, fits, limits, etc. • • •					
$0.013 \pm0.004 \pm0.004$	20	[2] AUBERT	09B	BABR	$B^+ \to \gamma J/\psi K^+$
$0.016 \pm0.005 \pm0.005$	19	[3] AUBERT,BE	06M	BABR	$B^+ \to \gamma J/\psi K^+$

[1] BHARDWAJ 11 reports $[\Gamma(\chi_{c1}(3872) \to \gamma J/\psi)/\Gamma_{total}] \times [B(B^+ \to \chi_{c1}(3872)K^+)] = (1.78^{+0.48}_{-0.44} \pm 0.12) \times 10^{-6}$ which we divide by our best value $B(B^+ \to \chi_{c1}(3872)K^+) = (2.1 \pm 0.7) \times 10^{-4}$. Our first error is their experiment's error and our second error is the systematic error from using our best value.

[2] AUBERT 09B reports $[\Gamma(\chi_{c1}(3872) \to \gamma J/\psi)/\Gamma_{total}] \times [B(B^+ \to \chi_{c1}(3872)K^+)] = (2.8 \pm 0.8 \pm 0.1) \times 10^{-6}$ which we divide by our best value $B(B^+ \to \chi_{c1}(3872)K^+) = (2.1 \pm 0.7) \times 10^{-4}$. Our first error is their experiment's error and our second error is the systematic error from using our best value.

[3] Superseded by AUBERT 09B. AUBERT,BE 06M reports $[\Gamma(\chi_{c1}(3872) \to \gamma J/\psi)/\Gamma_{total}] \times [B(B^+ \to \chi_{c1}(3872)K^+)] = (3.3 \pm 1.0 \pm 0.3) \times 10^{-6}$ which we divide by our best value $B(B^+ \to \chi_{c1}(3872)K^+) = (2.1 \pm 0.7) \times 10^{-4}$. Our first error is their experiment's error and our second error is the systematic error from using our best value.

$\Gamma(\gamma J/\psi)/\Gamma(\pi^+\pi^-J/\psi(1S))$ — Γ_{20}/Γ_2

VALUE	DOCUMENT ID		TECN	COMMENT
0.79±0.28	ABLIKIM	20W	BES3	$e^+e^- \to \gamma\chi_{c1}(3872)$

$\Gamma(\gamma\chi_{c1})/\Gamma_{total}$ — Γ_{21}/Γ

VALUE	CL%	DOCUMENT ID		TECN	COMMENT
$<9\times10^{-3}$	90	[1] BHARDWAJ	13	BELL	$B^\pm \to \chi_{c1}\gamma K^\pm$

[1] BHARDWAJ 13 reports $[\Gamma(\chi_{c1}(3872) \to \gamma\chi_{c1})/\Gamma_{total}] \times [B(B^+ \to \chi_{c1}(3872)K^+)] < 1.9\times10^{-6}$ which we divide by our best value $B(B^+ \to \chi_{c1}(3872)K^+) = 2.1\times10^{-4}$.

$\Gamma(\gamma\chi_{c1})/\Gamma(\pi^+\pi^-J/\psi(1S))$ — Γ_{21}/Γ_2

VALUE	CL%	DOCUMENT ID		TECN	COMMENT
<0.89	90	CHOI	03	BELL	$B \to K\pi^+\pi^-J/\psi$

$\Gamma(\gamma\chi_{c2})/\Gamma_{total}$ — Γ_{22}/Γ

VALUE	CL%	DOCUMENT ID		TECN	COMMENT
<0.032	90	[1] BHARDWAJ	13	BELL	$B^\pm \to \chi_{c2}\gamma K^\pm$

[1] BHARDWAJ 13 reports $[\Gamma(\chi_{c1}(3872) \to \gamma\chi_{c2})/\Gamma_{total}] \times [B(B^+ \to \chi_{c1}(3872)K^+)] < 6.7\times10^{-6}$ which we divide by our best value $B(B^+ \to \chi_{c1}(3872)K^+) = 2.1\times10^{-4}$.

$\Gamma(\gamma\psi(2S))/\Gamma_{total}$ — Γ_{23}/Γ

VALUE	EVTS	DOCUMENT ID		TECN	COMMENT
$0.045\pm0.013\pm0.015$	25 ± 7	[1] AUBERT	09B	BABR	$B^+ \to \gamma\psi(2S)K^+$
• • • We do not use the following data for averages, fits, limits, etc. • • •					
seen	36 ± 9	[2] AAIJ	14AH	LHCB	$B^+ \to \gamma\psi(2S)K^+$
not seen		[3] BHARDWAJ	11	BELL	$B^+ \to \gamma\psi(2S)K^+$

[1] AUBERT 09B reports $[\Gamma(\chi_{c1}(3872) \to \gamma\psi(2S))/\Gamma_{total}] \times [B(B^+ \to \chi_{c1}(3872)K^+)] = (9.5 \pm 2.7 \pm 0.6) \times 10^{-6}$ which we divide by our best value $B(B^+ \to \chi_{c1}(3872)K^+) = (2.1 \pm 0.7) \times 10^{-4}$. Our first error is their experiment's error and our second error is the systematic error from using our best value.

[2] From 36.4 ± 9.0 events of $\chi_{c1}(3872) \to J/\psi\gamma$ decays with a statistical significance of 4.4σ.

[3] BHARDWAJ 11 reports $B(B^+ \to K^+\chi_{c1}(3872)) \times B(\chi_{c1} \to \gamma\psi(2S)) < 3.45\times10^{-6}$ at 90% CL.

$\Gamma(\gamma\psi(2S))/\Gamma(\pi^+\pi^-J/\psi(1S))$ — Γ_{23}/Γ_2

VALUE	CL%	DOCUMENT ID		TECN	COMMENT
<0.42	90	ABLIKIM	20W	BES3	$e^+e^- \to \gamma\chi_{c1}(3872)$

$\Gamma(\gamma\psi(2S))/\Gamma(\gamma J/\psi)$ — Γ_{23}/Γ_{20}

VALUE	CL%	EVTS	DOCUMENT ID		TECN	COMMENT
2.6 ±0.6 OUR AVERAGE						
$2.46\pm0.64\pm0.29$		36 ± 9	[1] AAIJ	14AH	LHCB	$B^+ \to \gamma\psi(2S)K^+$
3.4 ± 1.4			AUBERT	09B	BABR	$B^+ \to \gamma c\overline{c}K'$
• • • We do not use the following data for averages, fits, limits, etc. • • •						
<2.1	90		BHARDWAJ	11	BELL	$B^+ \to \gamma\psi(2S)K^+$

[1] From 36.4 ± 9.0 events of $\chi_{c1}(3872) \to J/\psi\gamma$ decays with a statistical significance of 4.4σ.

C-violating decays

$\Gamma(\eta J/\psi)/\Gamma_{total}$ — Γ_{24}/Γ

VALUE	CL%	DOCUMENT ID		TECN	COMMENT
<0.018	90	[1,2] IWASHITA	14	BELL	$B \to K\eta J/\psi$
• • • We do not use the following data for averages, fits, limits, etc. • • •					
<0.04	90	[3] AUBERT	04Y	BABR	$B \to K\eta J/\psi$

[1] IWASHITA 14 reports $[\Gamma(\chi_{c1}(3872) \to \eta J/\psi)/\Gamma_{total}] \times [B(B^+ \to \chi_{c1}(3872)K^+)] < 3.8\times10^{-6}$ which we divide by our best value $B(B^+ \to \chi_{c1}(3872)K^+) = 2.1\times10^{-4}$.

[2] IWASHITA 14 also scans the $\eta J/\psi$ mass range 3.8–4.75 GeV and sets upper limits for $B(B^\pm \to \chi_{c1}(3872)K^\pm)\times B(\chi_{c1}(3872) \to \eta J/\psi)$ in 5 MeV intervals.

[3] AUBERT 04Y reports $[\Gamma(\chi_{c1}(3872) \to \eta J/\psi)/\Gamma_{total}] \times [B(B^+ \to \chi_{c1}(3872)K^+)] < 7.7\times10^{-6}$ which we divide by our best value $B(B^+ \to \chi_{c1}(3872)K^+) = 2.1\times10^{-4}$.

$\chi_{c1}(3872)$ REFERENCES

TERAMOTO	21	PRL 126 122001	Y. Teramoto et al.	(BELLE Collab.)
AAIJ	20AD	PR D102 092005	R. Aaij et al.	(LHCb Collab.)
AAIJ	20S	JHEP 2008 123	R. Aaij et al.	(LHCb Collab.)
ABLIKIM	20W	PRL 124 242001	M. Ablikim et al.	(BESIII Collab.)
LEES	20C	PRL 124 152001	J.P. Lees et al.	(BABAR Collab.)
ABLIKIM	19U	PRL 122 202001	M. Ablikim et al.	(BESIII Collab.)
ABLIKIM	19V	PRL 122 232002	M. Ablikim et al.	(BESIII Collab.)
BHARDWAJ	19	PR D99 111101	V. Bhardwaj et al.	(BELLE Collab.)
AGHASYAN	18A	PL B783 334	M. Aghasyan et al.	(COMPASS Collab.)
AAIJ	17AD	PL B769 305	R. Aaij et al.	(LHCb Collab.)
AAIJ	17BB	EPJ C77 609	R. Aaij et al.	(LHCb Collab.)
BHARDWAJ	16	PR D93 052016	V. Bhardwaj et al.	(BELLE Collab.)
AAIJ	15AO	PR D92 011102	R. Aaij et al.	(LHCb Collab.)
ABLIKIM	15V	PL B749 414	M. Ablikim et al.	(BESIII Collab.)
BALA	15	PR D91 051101	A. Bala et al.	(BELLE Collab.)
VINOKUROVA	15	JHEP 1506 132	A. Vinokurova et al.	(BELLE Collab.)
Also		JHEP 1702 088 (errat.)	A. Vinokurava et al.	(BELLE Collab.)
AAIJ	14AH	NP B886 665	R. Aaij et al.	(LHCb Collab.)
ABLIKIM	14	PRL 112 092001	M. Ablikim et al.	(BESIII Collab.)
IWASHITA	14	PTEP 2014 043C01	T. Iwashita et al.	(BELLE Collab.)
AAIJ	13Q	PRL 110 222001	R. Aaij et al.	(LHCb Collab.) JP
AAIJ	13S	EPJ C73 2462	R. Aaij et al.	(LHCb Collab.)
BHARDWAJ	13	PRL 111 032001	V. Bhardwaj et al.	(BELLE Collab.)
AAIJ	12H	EPJ C72 1972	R. Aaij et al.	(LHCb Collab.)
LEES	12AD	PR D86 072002	J.P. Lees et al.	(BABAR Collab.)
LEES	12AE	PR D86 092005	J.P. Lees et al.	(BABAR Collab.)
BHARDWAJ	11	PRL 107 091803	V. Bhardwaj et al.	(BELLE Collab.)
CHOI	11	PR D84 052004	S.-K. Choi et al.	(BELLE Collab.)
WANG	11B	PR D84 071107	X.L. Wang et al.	(BELLE Collab.)
AUSHEV	10	PR D81 031103	T. Aushev et al.	(BELLE Collab.)
DEL-AMO-SA...	10B	PR D82 011101	P. del Amo Sanchez et al.	(BABAR Collab.)
SHEN	10A	PR D82 051504	C.P. Shen et al.	(BELLE Collab.)
AALTONEN	09AU	PRL 103 152001	T. Aaltonen et al.	(CDF Collab.)
AUBERT	09B	PRL 102 132001	B. Aubert et al.	(BABAR Collab.)
AUBERT	08B	PR D77 011102	B. Aubert et al.	(BABAR Collab.)
AUBERT	08Y	PR D77 111101	B. Aubert et al.	(BABAR Collab.)
WICHT	08	PL B662 323	J. Wicht et al.	(BELLE Collab.)
AUBERT	06	PR D73 011101	B. Aubert et al.	(BABAR Collab.)
AUBERT,BE	06M	PR D74 071101	B. Aubert et al.	(BABAR Collab.)
GOKHROO	06	PRL 97 162002	G. Gokhroo et al.	(BELLE Collab.)

Downloaded from https://academic.oup.com/ptep/article/2022/8/083C01/6651666 by KIT Library user on 27 September 2022

AUBERT	05B	PR D71 031501	B. Aubert *et al.*	(BABAR Collab.)
AUBERT	05D	PR D71 052001	B. Aubert *et al.*	(BABAR Collab.)
AUBERT	05R	PR D71 071103	B. Aubert *et al.*	(BABAR Collab.)
DOBBS	05	PRL 94 032004	S. Dobbs *et al.*	(CLEO Collab.)
ABAZOV	04F	PRL 93 162002	V.M. Abazov *et al.*	(D0 Collab.)
ACOSTA	04	PRL 93 072001	D. Acosta *et al.*	(CDF Collab.)
AUBERT	04Y	PRL 93 041801	B. Aubert *et al.*	(BABAR Collab.)
CHISTOV	04	PRL 93 051803	R. Chistov *et al.*	(BELLE Collab.)
PDG	04	PL B592 1	S. Eidelman *et al.*	(PDG Collab.)
YUAN	04	PL B579 74	C.Z. Yuan *et al.*	
CHOI	03	PRL 91 262001	S.-K. Choi *et al.*	(BELLE Collab.)
BAI	98E	PR D57 3854	J.Z. Bai *et al.*	(BES Collab.)
ANTONIAZZI	94	PR D50 4258	L. Antoniazzi *et al.*	(E705 Collab.)

$Z_c(3900)$

$I^G(J^{PC}) = 1^+(1^{+-})$

was $X(3900)$

Properties incompatible with a $q\overline{q}$ structure (exotic state). See the review on non-$q\overline{q}$ states.

Charged $Z_c(3900)$ seen as a peak in the invariant mass distribution of the $J/\psi\pi^\pm$ system by BES III (ABLIKIM 13T) in $e^+e^- \to \pi^+\pi^- J/\psi$ at c.m. energy of 4.26 GeV and by radiative return from e^+e^- collisions at $\sqrt{s}$ from 9.46 to 10.86 GeV at Belle (LIU 13B). Partial wave analysis of ABLIKIM 17J determines $J^P = 1^+$ with more than 7σ significance. Neutral $Z_c(3900)$ seen in the $J/\psi\pi^0$ invariant mass distribution in $e^+e^- \to \pi^0\pi^0 J/\psi$ at c.m. energies of 4.23, 4.26, and 4.36 GeV by BES III (ABLIKIM 15U) and at 4.17 GeV by XIAO 13A. Peaks in $(D\overline{D}^*)^{0,\pm}$ reported by BES III (ABLIKIM 14A, ABLIKIM 15AB) are assumed to be related.

$Z_c(3900)$ MASS

VALUE (MeV)	EVTS	DOCUMENT ID		TECN	CHG	COMMENT
3887.1±2.6 OUR AVERAGE		Error includes scale factor of 1.7. See the ideogram below.				
$3893.1\pm2.2\pm3.0$		[1] ABLIKIM	20N	BES3	0	$e^+e^- \to \pi^0\pi^0 J/\psi$
$3902.6^{+5.2}_{-5.0}{}^{+3.3}_{-1.4}$		[2,3] ABAZOV	19	D0	±	1.96 TeV $p\overline{p} \to J/\psi\pi^+\pi^- X$
$3881.2\pm4.2\pm52.7$	6k	[4] ABLIKIM	17J	BES3	±	$e^+e^- \to \pi^+\pi^- J/\psi$
$3885.7^{+4.3}_{-5.7}\pm8.4$		[2,4] ABLIKIM	15AB	BES3	0	$e^+e^- \to \pi^0(D\overline{D}^*)^0$
$3881.7\pm1.6\pm1.6$	1.2k	[2,4] ABLIKIM	15AC	BES3	±	$e^+e^- \to \pi^\pm(D\overline{D}^*)^\mp$
$3883.9\pm1.5\pm4.2$	1.2k	[2,4] ABLIKIM	14A	BES3	±	$e^+e^- \to \pi^\pm(D\overline{D}^*)^\mp$
$3894.5\pm6.6\pm4.5$	159	[2] LIU	13B	BELL	±	$e^+e^- \to \gamma\pi^+\pi^- J/\psi$
$3886\pm4\pm2$	81	[2,5] XIAO	13A		±	4.17 $e^+e^- \to \pi^+\pi^- J/\psi$
$3904\pm9\pm5$	25	[2,5] XIAO	13A		0	4.17 $e^+e^- \to \pi^0\pi^0 J/\psi$
• • • We do not use the following data for averages, fits, limits, etc. • • •						
$3895.0\pm5.2^{+4.0}_{-2.7}$	502	[2,6] ABAZOV	18B	D0	±	1.96 TeV $p\overline{p} \to J/\psi\pi^+\pi^- X$
$3894.8\pm2.3\pm3.2$	356	[2,7] ABLIKIM	15U	BES3	0	$e^+e^- \to \pi^0\pi^0 J/\psi$
$3899.0\pm3.6\pm4.9$	307	[2,8] ABLIKIM	13T	BES3	±	$e^+e^- \to \pi^+\pi^- J/\psi$

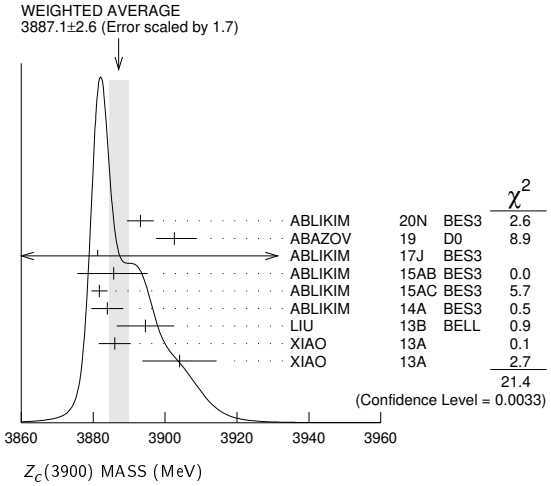

[1] Pole mass obtained from a fit to a relativistic Breit-Wigner.
[2] Neglecting interference between the $Z_c(3900)$ and other processes.
[3] Measured in weak decays of b-flavored hadrons (nonprompt).
[4] Pole mass obtained from a fit to a Flatte-like formula.
[5] For $M^2(\pi^+\pi^-) < 0.65$ GeV^2. Obtained by analyzing CLEO-c data but not authored by the CLEO Collaboration.
[6] The signal of the $Z_c(3900)$ is correlated with a parent $J/\psi\pi^+\pi^-$ system in the invariant mass range 4.2–4.7 GeV. Superseded by ABAZOV 19.
[7] Superseded by ABLIKIM 20N.
[8] Superseded by ABLIKIM 17J.

$Z_c(3900)$ WIDTH

VALUE (MeV)	EVTS	DOCUMENT ID		TECN	CHG	COMMENT
28.4± 2.6 OUR AVERAGE						
$44.4\pm5.2\pm14.0$		[1] ABLIKIM	20N	BES3	0	$e^+e^- \to \pi^0\pi^0 J/\psi$
$32^{+28}_{-21}{}^{+26}_{-7}$		[2,3] ABAZOV	19	D0	±	1.96 TeV $p\overline{p} \to \pi^+\pi^- J/\psi X$ (nonprompt)
$51.8\pm4.6\pm36.0$	6 k	[4] ABLIKIM	17J	BES3	±	$e^+e^- \to \pi^+\pi^- J/\psi$
$35^{+11}_{-12}\pm15$		[2,4] ABLIKIM	15AB	BES3	0	$e^+e^- \to \pi^0(D\overline{D}^*)^0$
$26.6\pm2.0\pm2.1$	1248	[2,4] ABLIKIM	15AC	BES3	±	$e^+e^- \to \pi^\pm(D\overline{D}^*)^\mp$
$24.8\pm3.3\pm11.0$	1212	[2,4] ABLIKIM	14A	BES3	±	$e^+e^- \to \pi^\pm(D\overline{D}^*)^\mp$
$63\pm24\pm26$	159	[2] LIU	13B	BELL	±	$e^+e^- \to \gamma\pi^+\pi^- J/\psi$
$37\pm4\pm8$	81	[2,5] XIAO	13A		±	4.17 $e^+e^- \to \pi^+\pi^- J/\psi$
• • • We do not use the following data for averages, fits, limits, etc. • • •						
$29.6\pm8.2\pm8.2$	356	[2,6] ABLIKIM	15U	BES3	0	$e^+e^- \to \pi^0\pi^0 J/\psi$
$46\pm10\pm20$	307	[2,7] ABLIKIM	13T	BES3	±	$e^+e^- \to \pi^+\pi^- J/\psi$

[1] Pole width obtained from a fit to a relativistic Breit-Wigner.
[2] Neglecting interference between the $Z_c(3900)$ and other processes.
[3] Measured in weak decays of b-flavored hadrons (nonprompt).
[4] Pole width obtained from a fit to a Flatte-like formula.
[5] For $M^2(\pi^+\pi^-) < 0.65$ GeV^2. Obtained by analyzing CLEO-c data but not authored by the CLEO Collaboration.
[6] Superseded by ABLIKIM 20N.
[7] Superseded by ABLIKIM 17J.

$Z_c(3900)$ DECAY MODES

	Mode	Fraction (Γ_i/Γ)
Γ_1	$J/\psi\pi$	seen
Γ_2	$h_c\pi^\pm$	not seen
Γ_3	$\eta_c\pi^+\pi^-$	not seen
Γ_4	$\eta_c(1S)\rho(770)^\pm$	
Γ_5	$(D\overline{D}^*)^\pm$	seen
Γ_6	D^0D^{*-} + c.c.	seen
Γ_7	D^-D^{*0} + c.c.	seen
Γ_8	$\omega\pi^\pm$	not seen
Γ_9	$J/\psi\eta$	not seen
Γ_{10}	D^+D^{*-} + c.c	seen
Γ_{11}	$D^0\overline{D}^{*0}$ + c.c	seen

$Z_c(3900)$ BRANCHING RATIOS

$\Gamma(J/\psi\pi)/\Gamma_{total}$ — Γ_1/Γ

VALUE	EVTS	DOCUMENT ID		TECN	CHG	COMMENT
seen		ABLIKIM	20N	BES3	0	$e^+e^- \to \pi^0\pi^0 J/\psi$
seen		[1] ABAZOV	19	D0	±	1.96 TeV $p\overline{p} \to \pi^+\pi^- J/\psi X$ (prompt)
seen		ABLIKIM	17J	BES3	±	$e^+e^- \to \pi^+\pi^- J/\psi$
seen	356	ABLIKIM	15U	BES3	0	$e^+e^- \to \pi^0\pi^0 J/\psi$
not seen		[2] ADOLPH	15D	COMP	±	$\gamma N \to J/\psi\pi^\pm N$
seen	307	ABLIKIM	13T	BES3	±	$e^+e^- \to \pi^+\pi^- J/\psi$
seen	25	[3] XIAO	13A		0	4.17 $e^+e^- \to \pi^0\pi^0 J/\psi$

[1] But not seen in the "prompt" sample (no b-hadron enhancement).
[2] ADOLPH 15D measure $B(Z_c(3900)^\pm \to J/\psi\pi^\pm)\,\sigma(\gamma N \to Z_c(3900)^\pm N)/\sigma(\gamma N \to J/\psi N) < 3.7\times10^{-3}$ at 90% CL.
[3] Obtained by analyzing CLEO-c data but not authored by the CLEO Collaboration.

$\Gamma(h_c\pi^\pm)/\Gamma_{total}$ — Γ_2/Γ

VALUE	DOCUMENT ID		TECN	CHG	COMMENT
not seen	ABLIKIM	13X	BES3	±	$e^+e^- \to h_c\pi^+\pi^-$

$\Gamma(\eta_c\pi^+\pi^-)/\Gamma_{total}$ — Γ_3/Γ

VALUE	DOCUMENT ID		TECN	CHG	COMMENT
not seen	[1] VINOKUROVA	15	BELL	0	$B^+ \to K^+\eta_c\pi^+\pi^-$

[1] VINOKUROVA 15 reports $B(B^+ \to K^+Z_c(3900)^0)\times B(X \to \eta_c\pi^+\pi^-) < 4.7\times10^{-5}$ at 90% CL.

$\Gamma((D\overline{D}^*)^\pm)/\Gamma(J/\psi\pi)$ — Γ_5/Γ_1

VALUE	DOCUMENT ID		TECN	CHG	COMMENT
6.2±1.1±2.7	[1] ABLIKIM	14A	BES3	±	$e^+e^- \to \pi^\pm(D\overline{D}^*)^\mp$

[1] Assuming the same origin of the $(D\overline{D}^*)^\pm$ and $\pi^\pm J/\psi$ decay modes.

$\Gamma(D^0D^{*-}+\text{c.c.})/\Gamma_{total}$ — Γ_6/Γ

VALUE	DOCUMENT ID		TECN	CHG	COMMENT
seen	ABLIKIM	15AC	BES3	±	$e^+e^- \to \pi^+D^0D^{*-}$ + c.c.
seen	ABLIKIM	14A	BES3	±	$e^+e^- \to \pi^+D^0D^{*-}$ + c.c.

Downloaded from https://academic.oup.com/ptep/article/2022/8/083C01/6651666 by KIT Library user on 27 September 2022

$\Gamma(D^- D^{*0} + \text{c.c.})/\Gamma_{\text{total}}$ — Γ_7/Γ

VALUE	DOCUMENT ID		TECN	CHG	COMMENT
seen	ABLIKIM	15AC	BES3	±	$e^+e^- \to \pi^+ D^- D^{*0}$ + c.c.
seen	ABLIKIM	14A	BES3	±	$e^+e^- \to \pi^+ D^- D^{*0}$ + c.c.

$\Gamma(\omega\pi^\pm)/\Gamma_{\text{total}}$ — Γ_8/Γ

VALUE	DOCUMENT ID		TECN	CHG	COMMENT
not seen	ABLIKIM	15R	BES3	±	$e^+e^- \to \omega\pi^+\pi^-$

$\Gamma(J/\psi\eta)/\Gamma_{\text{total}}$ — Γ_9/Γ

VALUE	DOCUMENT ID		TECN	CHG	COMMENT
not seen	ABLIKIM	15Q	BES3	0	4.0–4.6 $e^+e^- \to J/\psi\eta\pi^0$

$\Gamma(J/\psi\eta)/\Gamma(J/\psi\pi)$ — Γ_9/Γ_1

VALUE	CL%	DOCUMENT ID		TECN	CHG	COMMENT
<0.15	90	ABLIKIM	15Q	BES3	0	4.226 $e^+e^- \to J/\psi\eta\pi^0$
• • • We do not use the following data for averages, fits, limits, etc. • • •						
<0.65	90	ABLIKIM	15Q	BES3	0	4.257 $e^+e^- \to J/\psi\eta\pi^0$

$\Gamma(\eta_c(1S)\rho(770)^\pm)/\Gamma(J/\psi\pi)$ — Γ_4/Γ_1

VALUE	EVTS	DOCUMENT ID		TECN	COMMENT
2.3±0.8	332	[1] ABLIKIM	19BC	BES3	$e^+e^- \to \pi^+\pi^-\pi^0\eta_c(1S)$

[1] Using $e^+e^- \to \pi^\mp(Z_c(3900)^\pm \to J/\psi\pi^\pm)$ cross section at 4.23 and 4.26 GeV from ABLIKIM 17J.

$\Gamma(D^+ D^{*-} + \text{c.c})/\Gamma_{\text{total}}$ — Γ_{10}/Γ

VALUE	DOCUMENT ID		TECN	CHG	COMMENT
seen	ABLIKIM	15AB	BES3	0	$e^+e^- \to \pi^0(D\overline{D}^*)^0$

$\Gamma(D^0\overline{D}^{*0} + \text{c.c})/\Gamma_{\text{total}}$ — Γ_{11}/Γ

VALUE	DOCUMENT ID		TECN	CHG	COMMENT
seen	ABLIKIM	15AB	BES3	0	$e^+e^- \to \pi^0(D\overline{D}^*)^0$

$\Gamma(D^+ D^{*-} + \text{c.c})/\Gamma(D^0\overline{D}^{*0} + \text{c.c})$ — Γ_{10}/Γ_{11}

VALUE	DOCUMENT ID		TECN	CHG	COMMENT
0.96±0.18±0.12	ABLIKIM	15AB	BES3	0	$e^+e^- \to \pi^0(D\overline{D}^*)^0$

$Z_c(3900)$ REFERENCES

ABLIKIM	20N	PR D102 012009	M. Ablikim *et al.*	(BESIII Collab.) JP
ABAZOV	19	PR D100 012005	V.M. Abazov *et al.*	(D0 Collab.)
ABLIKIM	19BC	PR D100 111102	M. Ablikim *et al.*	(BESIII Collab.)
ABAZOV	18B	PR D98 052010	V.M. Abazov *et al.*	(D0 Collab.)
ABLIKIM	17J	PRL 119 072001	M. Ablikim *et al.*	(BESIII Collab.) JP
ABLIKIM	15AB	PRL 115 222002	M. Ablikim *et al.*	(BESIII Collab.)
ABLIKIM	15AC	PR D92 092006	M. Ablikim *et al.*	(BESIII Collab.) JP
ABLIKIM	15Q	PR D92 012008	M. Ablikim *et al.*	(BESIII Collab.)
ABLIKIM	15R	PR D92 032009	M. Ablikim *et al.*	(BESIII Collab.)
ABLIKIM	15U	PRL 115 112003	M. Ablikim *et al.*	(BESIII Collab.)
ADOLPH	15D	PL B742 330	C. Adolph *et al.*	(COMPASS Collab.)
VINOKUROVA	15	JHEP 1506 132	A. Vinokurova *et al.*	(BELLE Collab.)
Also		JHEP 1702 088 (errat.)	A. Vinokurova *et al.*	(BELLE Collab.)
ABLIKIM	14A	PRL 112 022001	M. Ablikim *et al.*	(BESIII Collab.) JP
ABLIKIM	13T	PRL 110 252001	M. Ablikim *et al.*	(BESIII Collab.)
ABLIKIM	13X	PRL 111 242001	M. Ablikim *et al.*	(BESIII Collab.)
LIU	13B	PRL 110 252002	Z.Q. Liu *et al.*	(BELLE Collab.)
XIAO	13A	PL B727 366	T. Xiao *et al.*	(NWES)

$\chi_{c0}(3915)$

$I^G(J^{PC}) = 0^+(0^{++})$

was $X(3915)$

The $\chi_{c0}(3915)$ was originally seen by BELLE in its $\omega J/\psi$ decay mode and was produced in both B decays in CHOI 05 and $\gamma\gamma$ collisions in UEHARA 10. The J^{PC} was determined to be 0^{++} by BABAR in LEES 12AD but this assignment was questioned by ZHOU 15C. In AAIJ 20AI LHCb found the D^+D^- decay mode of the $\chi_{c0}(3915)$ using B decays and determined its J^{PC} to be 0^{++}. Based on their compatible mass, width, and J^{PC}, we assume the state decaying to $\omega J/\psi$ and the state decaying to D^+D^- are both the $\chi_{c0}(3915)$. See also the $\chi_{c2}(3930)$.

$\chi_{c0}(3915)$ MASS

VALUE (MeV)	EVTS	DOCUMENT ID		TECN	COMMENT
3921.7± 1.8 OUR AVERAGE		Error includes scale factor of 1.5. See the ideogram below.			
3923.8± 1.5± 0.4	1.2k	[1] AAIJ	20AI	LHCB	$B^+ \to D^+D^-K^+$
3919.4± 2.2± 1.6	59 ± 10	LEES	12AD	BABR	$e^+e^- \to e^+e^-\omega J/\psi$
$3919.1^{+3.8}_{-3.4}$ ± 2.0		DEL-AMO-SA...	10B	BABR	$B \to \omega J/\psi K$
3915 ± 3 ± 2	49 ± 15	UEHARA	10	BELL	10.6 $e^+e^- \to e^+e^-\omega J/\psi$
3943 ±11 ±13	58 ± 11	[2] CHOI	05	BELL	$B \to \omega J/\psi K$
• • • We do not use the following data for averages, fits, limits, etc. • • •					
3926.4± 2.2± 1.2		[3] ABLIKIM	19V	BES	$e^+e^- \to \gamma\omega J/\psi$
$3914.6^{+3.8}_{-3.4}$ ± 2.0		[2] AUBERT	08W	BABR	Superseded by DEL-AMO-SANCHEZ 10B

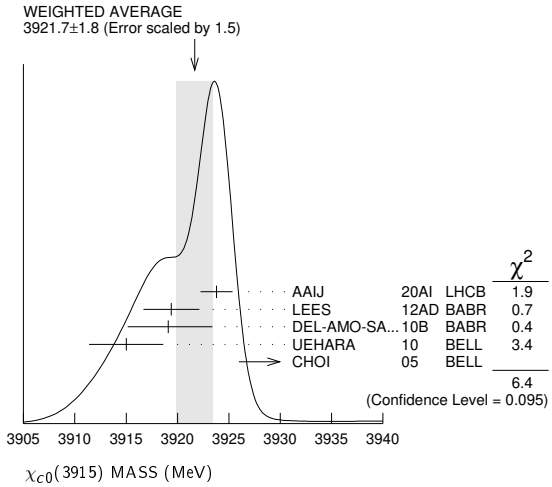

[1] Obtained from the full amplitude analysis. Parameterized with the relativistic Breit-Wigner line shape.
[2] $\omega J/\psi$ threshold enhancement fitted as an S-wave Breit-Wigner resonance.
[3] Could also be $X(3940)$. Significance 3.1σ. Fit with additional resonance at 3963.7 ± 5.7 MeV, significance 3.4σ.

$\chi_{c0}(3915)$ WIDTH

VALUE (MeV)	EVTS	DOCUMENT ID		TECN	COMMENT
18.8± 3.5 OUR AVERAGE					
17.4± 5.1± 0.8	1.2k	[1] AAIJ	20AI	LHCB	$B^+ \to D^+D^-K^+$
13 ± 6 ± 3	59	LEES	12AD	BABR	$e^+e^- \to e^+e^-\omega J/\psi$
$31\ ^{+10}_{-8}$ ± 5		DEL-AMO-SA...	10B	BABR	$B \to \omega J/\psi K$
17 ±10 ± 3	49	UEHARA	10	BELL	10.6 $e^+e^- \to e^+e^-\omega J/\psi$
87 ±22 ±26	58	[2] CHOI	05	BELL	$B \to \omega J/\psi K$
• • • We do not use the following data for averages, fits, limits, etc. • • •					
3.8± 7.5± 2.6		[3] ABLIKIM	19V	BES	$e^+e^- \to \gamma\omega J/\psi$
$34\ ^{+12}_{-8}$ ± 5		[2] AUBERT	08W	BABR	Superseded by DEL-AMO-SANCHEZ 10B

[1] Obtained from the full amplitude analysis. Parameterized with the relativistic Breit-Wigner line shape.
[2] $\omega J/\psi$ threshold enhancement fitted as an S-wave Breit-Wigner resonance.
[3] Could also be $X(3940)$. Significance 3.1σ. Fit with additional resonance at 3963.7 ± 5.7 MeV, significance 3.4σ.

$\chi_{c0}(3915)$ DECAY MODES

	Mode	Fraction (Γ_i/Γ)
Γ_1	$\omega J/\psi$	seen
Γ_2	$\overline{D}^{*0}D^0$	not seen
Γ_3	D^+D^-	seen
Γ_4	$\pi^+\pi^-\eta_c(1S)$	not seen
Γ_5	$\eta_c\eta$	not seen
Γ_6	$\eta_c\pi^0$	not seen
Γ_7	$K\overline{K}$	not seen
Γ_8	$\gamma\gamma$	seen
Γ_9	$\pi^0\chi_{c1}$	not seen

$\chi_{c0}(3915)$ $\Gamma(i)\Gamma(\gamma\gamma)/\Gamma(\text{total})$

$\Gamma(\omega J/\psi) \times \Gamma(\gamma\gamma)/\Gamma_{\text{total}}$ — $\Gamma_1\Gamma_8/\Gamma$

VALUE (eV)	EVTS	DOCUMENT ID		TECN	COMMENT
54± 9 OUR AVERAGE					
52±10±3	59 ± 10	[1] LEES	12AD	BABR	$e^+e^- \to e^+e^-\omega J/\psi$
61±17±8	49 ± 15	[1] UEHARA	10	BELL	10.6 $e^+e^- \to e^+e^-\omega J/\psi$
• • • We do not use the following data for averages, fits, limits, etc. • • •					
18± 5±2	49 ± 15	[2] UEHARA	10	BELL	10.6 $e^+e^- \to e^+e^-\omega J/\psi$

[1] For $J^P = 0^+$.
[2] For $J^P = 2^+$, helicity-2.

$\Gamma(\pi^+\pi^-\eta_c(1S)) \times \Gamma(\gamma\gamma)/\Gamma_{\text{total}}$ — $\Gamma_4\Gamma_8/\Gamma$

VALUE (eV)	CL%	DOCUMENT ID		TECN	COMMENT
<16	90	LEES	12AE	BABR	$e^+e^- \to e^+e^-\pi^+\pi^-\eta_c$

$\Gamma(K\overline{K}) \times \Gamma(\gamma\gamma)/\Gamma_{\text{total}}$ — $\Gamma_7\Gamma_8/\Gamma$

VALUE (eV)	CL%	DOCUMENT ID		TECN	COMMENT
<1.96	90	UEHARA	13	BELL	$\gamma\gamma \to K^0_S K^0_S$

Downloaded from https://academic.oup.com/ptep/article/2022/8/083C01/6651666 by KIT Library user on 27 September 2022

$\chi_{c0}(3915)$ BRANCHING RATIOS

$\Gamma(\omega J/\psi)/\Gamma_{total}$ — Γ_1/Γ

VALUE	DOCUMENT ID		TECN	COMMENT
seen	[1] DEL-AMO-SA...	10B	BABR	$B \to \omega J/\psi K$
seen	[2] CHOI	05	BELL	$B \to \omega J/\psi K$

[1] DEL-AMO-SANCHEZ 10B reports $B(B^{\pm} \to \chi_{c0}(3915) K^{\pm}) \times B(\chi_{c0}(3915) \to J/\psi\omega) = (3.0^{+0.7}_{-0.6}{}^{+0.5}_{-0.3}) \times 10^{-5}$ and $B(B^0 \to \chi_{c0}(3915) K^0) \times B(\chi_{c0}(3915) \to J/\psi\omega) = (2.1 \pm 0.9 \pm 0.3) \times 10^{-5}$.

[2] CHOI 05 reports $B(B \to \chi_{c0}(3915) K) \times B(\chi_{c0}(3915) \to J/\psi\omega) = (7.1 \pm 1.3 \pm 3.1) \times 10^{-5}$.

$\Gamma(\omega J/\psi)/\Gamma(\overline{D}^{*0} D^0)$ — Γ_1/Γ_2

VALUE	CL%	DOCUMENT ID		TECN	COMMENT
>0.71	90	[1] AUSHEV	10	BELL	$B \to \overline{D}^{*0} D^0 K$

[1] By combining the upper limit $B(B \to \chi_{c0}(3915) K) \times B(\chi_{c0}(3915) \to D^{*0}\overline{D}^0) < 0.67 \times 10^{-4}$ from AUSHEV 10 with the average of CHOI 05 and AUBERT 08W measurements $B(B \to \chi_{c0}(3915) K) \times B(\chi_{c0}(3915) \to \omega J/\psi) = (0.51 \pm 0.11) \times 10^{-4}$.

$\Gamma(D^+ D^-)/\Gamma_{total}$ — Γ_3/Γ

VALUE	DOCUMENT ID		TECN	COMMENT
seen	AAIJ	20AI	LHCB	$B^+ \to D^+ D^- K^+$

$\Gamma(\eta_c \eta)/\Gamma_{total}$ — Γ_5/Γ

VALUE	CL%	DOCUMENT ID		TECN	COMMENT
not seen	90	[1] VINOKUROVA	15	BELL	$B^+ \to K^+ \eta_c \eta$

[1] VINOKUROVA 15 reports $B(B^+ \to K^+ \chi_{c0}(3915)) \times B(\chi_{c0}(3915) \to \eta_c \eta) < 4.7 \times 10^{-5}$ at 90% CL.

$\Gamma(\eta_c \pi^0)/\Gamma_{total}$ — Γ_6/Γ

VALUE	CL%	DOCUMENT ID		TECN	COMMENT
not seen	90	[1] VINOKUROVA	15	BELL	$B^+ \to K^+ \eta_c \pi^0$

[1] VINOKUROVA 15 reports $B(B^+ \to K^+ \chi_{c0}(3915)^0) \times B(\chi_{c0}(3915) \to \eta_c \pi^0) < 1.7 \times 10^{-5}$ at 90% CL.

$\Gamma(\gamma\gamma)/\Gamma_{total}$ — Γ_8/Γ

VALUE	EVTS	DOCUMENT ID		TECN	COMMENT
seen	59 ± 10	LEES	12AD	BABR	$e^+ e^- \to e^+ e^- \omega J/\psi$
seen		UEHARA	10	BELL	10.6 $e^+ e^- \to e^+ e^- \omega J/\psi$

$\Gamma(\pi^0 \chi_{c1})/\Gamma_{total}$ — Γ_9/Γ

VALUE	EVTS	DOCUMENT ID		TECN	COMMENT
not seen	42 ± 14	[1] BHARDWAJ	19	BELL	$B^{\pm} \to \chi_{c1} \pi^0 K^{\pm}$

[1] BHARDWAJ 19 reports $B(B^+ \to K^+ \chi_{c0}(3915)) \times B(\chi_{c0}(3915) \to \chi_{c1} \pi^0) < 3.8 \times 10^{-5}$ at 90% CL. A signal significance 2.3 standard deviations.

$\chi_{c0}(3915)$ REFERENCES

AAIJ	20AI	PR D102 112003	R. Aaij *et al.*	(LHCb Collab.) JPC
ABLIKIM	19V	PRL 122 232002	M. Ablikim *et al.*	(BESIII Collab.)
BHARDWAJ	19	PR D99 111101	V. Bhardwaj *et al.*	(BELLE Collab.)
VINOKUROVA	15	JHEP 1506 132	A. Vinokurova *et al.*	(BELLE Collab.)
Also		JHEP 1702 088 (errat.)	A. Vinokurova *et al.*	(BELLE Collab.)
ZHOU	15C	PRL 115 022001	Z.-Y. Zhou, Z. Xiao, H.-Q. Zhou	(BEIJT, NANJ)
UEHARA	13	PTEP 2013 123C01	S. Uehara *et al.*	(BELLE Collab.)
LEES	12AD	PR D86 072002	J.P. Lees *et al.*	(BABAR Collab.)
LEES	12AE	PR D86 092005	J.P. Lees *et al.*	(BABAR Collab.)
AUSHEV	10	PR D81 031103	T. Aushev *et al.*	(BELLE Collab.)
DEL-AMO-SA...	10B	PR D82 011101	P. del Amo Sanchez *et al.*	(BABAR Collab.)
UEHARA	10	PRL 104 092001	S. Uehara *et al.*	(BELLE Collab.)
AUBERT	08W	PRL 101 082001	B. Aubert *et al.*	(BABAR Collab.)
CHOI	05	PRL 94 182002	S.-K. Choi *et al.*	(BELLE Collab.)

$\chi_{c2}(3930)$

$I^G(J^{PC}) = 0^+(2^{++})$

$\chi_{c2}(3930)$ MASS

VALUE (MeV)	EVTS	DOCUMENT ID		TECN	COMMENT
3922.5±1.0 OUR AVERAGE		Error includes scale factor of 1.7. See the ideogram below.			
$3926.8 \pm 2.4 \pm 0.8$	1.2k	[1] AAIJ	20AI	LHCB	$B^+ \to D^+ D^- K^+$
$3921.9 \pm 0.6 \pm 0.2$		[2] AAIJ	19M	LHCB	$pp \to D\overline{D} +$ anything
$3926.7 \pm 2.7 \pm 1.1$	76 ± 17	AUBERT	10G	BABR	10.6 $e^+ e^- \to e^+ e^- D\overline{D}$
$3929 \pm 5 \pm 2$	64	UEHARA	06	BELL	10.6 $e^+ e^- \to e^+ e^- D\overline{D}$

[1] Obtained from the full amplitude analysis. Parameterized with the relativistic Breit-Wigner line shape. Previous measurements assumed a single state in this region. This analysis revealed the presence of $\chi_{c0}(3930)$ with the same mass.

[2] Measured in prompt hadroproduction.

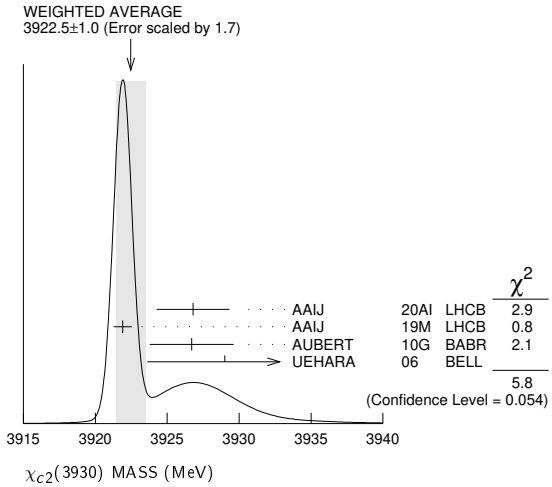

$\chi_{c2}(3930)$ WIDTH

VALUE (MeV)	EVTS	DOCUMENT ID		TECN	COMMENT
35.2± 2.2 OUR AVERAGE		Error includes scale factor of 1.2.			
$34.2 \pm 6.6 \pm 1.1$	1.2k	[1] AAIJ	20AI	LHCB	$B^+ \to D^+ D^- K^+$
$36.6 \pm 1.9 \pm 0.9$		[2] AAIJ	19M	LHCB	$pp \to D\overline{D} +$ anything
$21.3 \pm 6.8 \pm 3.6$	76 ± 17	AUBERT	10G	BABR	10.6 $e^+ e^- \to e^+ e^- D\overline{D}$
$29 \pm 10 \pm 2$	64	UEHARA	06	BELL	10.6 $e^+ e^- \to e^+ e^- D\overline{D}$

[1] Obtained from the full amplitude analysis. Parameterized with the relativistic Breit-Wigner line shape. Previous measurements assumed a single state in this region. This analysis revealed the presence of $\chi_{c0}(3930)$ with the same mass.

[2] Measured in prompt hadroproduction.

$\chi_{c2}(3930)$ DECAY MODES

	Mode	Fraction (Γ_i/Γ)
Γ_1	$\gamma\gamma$	seen
Γ_2	$K\overline{K}\pi$	
Γ_3	$K^+ K^- \pi^+ \pi^- \pi^0$	
Γ_4	$D\overline{D}$	seen
Γ_5	$D^+ D^-$	seen
Γ_6	$D^0 \overline{D}^0$	seen
Γ_7	$\pi^+ \pi^- \eta_c(1S)$	not seen
Γ_8	$K\overline{K}$	not seen

$\chi_{c2}(3930)$ PARTIAL WIDTHS

$\chi_{c2}(3930)$ $\Gamma(i)\Gamma(\gamma\gamma)/\Gamma(total)$

$\Gamma(K\overline{K}\pi) \times \Gamma(\gamma\gamma)/\Gamma_{total}$ — $\Gamma_2\Gamma_1/\Gamma$

VALUE (eV)	CL%	DOCUMENT ID		TECN	COMMENT
<2.1	90	DEL-AMO-SA...	11M	BABR	$\gamma\gamma \to K^0_S K^{\pm} \pi^{\mp}$

$\Gamma(K^+ K^- \pi^+ \pi^- \pi^0) \times \Gamma(\gamma\gamma)/\Gamma_{total}$ — $\Gamma_3\Gamma_1/\Gamma$

VALUE (eV)	CL%	DOCUMENT ID		TECN	COMMENT
<3.4	90	DEL-AMO-SA...	11M	BABR	$\gamma\gamma \to K^+ K^- \pi^+ \pi^- \pi^0$

$\Gamma(D\overline{D}) \times \Gamma(\gamma\gamma)/\Gamma_{total}$ — $\Gamma_4\Gamma_1/\Gamma$

VALUE (keV)	EVTS	DOCUMENT ID		TECN	COMMENT
0.21±0.04 OUR AVERAGE					
$0.24 \pm 0.05 \pm 0.04$	76 ± 17	AUBERT	10G	BABR	10.6 $e^+ e^- \to e^+ e^- D\overline{D}$
$0.18 \pm 0.05 \pm 0.03$	64	[1] UEHARA	06	BELL	10.6 $e^+ e^- \to e^+ e^- D\overline{D}$

[1] Assuming $B(D^+ D^-) = 0.89\, B(D^0 \overline{D}^0)$.

$\Gamma(\pi^+ \pi^- \eta_c(1S)) \times \Gamma(\gamma\gamma)/\Gamma_{total}$ — $\Gamma_7\Gamma_1/\Gamma$

VALUE (eV)	CL%	DOCUMENT ID		TECN	COMMENT
<18	90	LEES	12AE	BABR	$e^+ e^- \to e^+ e^- \pi^+ \pi^- \eta_c$

$\Gamma(K\overline{K}) \times \Gamma(\gamma\gamma)/\Gamma_{total}$ — $\Gamma_8\Gamma_1/\Gamma$

VALUE (eV)	CL%	DOCUMENT ID		TECN	COMMENT
<0.256	90	UEHARA	13	BELL	$\gamma\gamma \to K^0_S K^0_S$

Downloaded from https://academic.oup.com/ptep/article/2022/8/083C01/6651666 by KIT Library user on 27 September 2022

$\chi_{c2}(3930)$ BRANCHING RATIOS

$\Gamma(D^+D^-)/\Gamma(D^0\overline{D}^0)$ — Γ_5/Γ_6

VALUE	EVTS	DOCUMENT ID		TECN	COMMENT
0.74±0.43±0.16	64	UEHARA	06	BELL	10.6 $e^+e^- \to e^+e^- D\overline{D}$

$\chi_{c2}(3930)$ REFERENCES

AAIJ	20AI	PR D102 112003	R. Aaij *et al.*	(LHCb Collab.)
AAIJ	19M	JHEP 1907 035	R. Aaij *et al.*	(LHCb Collab.)
UEHARA	13	PTEP 2013 123C01	S. Uehara *et al.*	(BELLE Collab.)
LEES	12AE	PR D86 092005	J.P. Lees *et al.*	(BABAR Collab.)
DEL-AMO-SA...	11M	PR D84 012004	P. del Amo Sanchez *et al.*	(BABAR Collab.)
AUBERT	10G	PR D81 092003	B. Aubert *et al.*	(BABAR Collab.)
UEHARA	06	PRL 96 082003	S. Uehara *et al.*	(BELLE Collab.)

$X(3940)$

$I^G(J^{PC}) = ?^?(?^{??})$

OMITTED FROM SUMMARY TABLE

Reported by ABE 07, observed in $e^+e^- \to J/\psi X$.

$X(3940)$ MASS

VALUE (MeV)	EVTS	DOCUMENT ID		TECN	COMMENT
$3942^{+7}_{-6}\pm6$	52	PAKHLOV	08	BELL	$e^+e^- \to J/\psi X$
• • • We do not use the following data for averages, fits, limits, etc. • • •					
3943± 6±6	25	[1] ABE	07	BELL	$e^+e^- \to J/\psi X$
3936±14	266	[2] ABE	07	BELL	$e^+e^- \to J/\psi(c\overline{c})$

[1] From a fit to $D^{*+}D^-$ and $D^{*0}\overline{D}^0$ events.
[2] From the inclusive fit. Not independent of the exclusive measurement by ABE 07.

$X(3940)$ WIDTH

VALUE (MeV)	CL%	EVTS	DOCUMENT ID		TECN	COMMENT
$37^{+26}_{-15}\pm8$		52	PAKHLOV	08	BELL	$e^+e^- \to J/\psi X$
• • • We do not use the following data for averages, fits, limits, etc. • • •						
<52	90	25	ABE	07	BELL	$e^+e^- \to J/\psi X$

$X(3940)$ DECAY MODES

	Mode	Fraction (Γ_i/Γ)
Γ_1	$D\overline{D}^*$ + c.c.	seen
Γ_2	$D\overline{D}$	not seen
Γ_3	$J/\psi\omega$	not seen

$X(3940)$ BRANCHING RATIOS

$\Gamma(D\overline{D}^*+\text{c.c.})/\Gamma_{total}$ — Γ_1/Γ

VALUE	CL%	EVTS	DOCUMENT ID		TECN	COMMENT
• • • We do not use the following data for averages, fits, limits, etc. • • •						
>0.45	90	25	[1,2] ABE	07	BELL	$e^+e^- \to J/\psi X$

[1] For $X(3940)$ decaying to final states with more than two tracks.
[2] PAKHLOV 08 finds that the inclusive peak near 3940 MeV/c^2 may consist of several states.

$\Gamma(D\overline{D})/\Gamma_{total}$ — Γ_2/Γ

VALUE	CL%	DOCUMENT ID		TECN	COMMENT
• • • We do not use the following data for averages, fits, limits, etc. • • •					
<0.41	90	[1,2] ABE	07	BELL	$e^+e^- \to J/\psi X$

[1] For $X(3940)$ decaying to final states with more than two tracks.
[2] PAKHLOV 08 finds that the inclusive peak near 3940 MeV/c^2 may consist of several states.

$\Gamma(J/\psi\omega)/\Gamma_{total}$ — Γ_3/Γ

VALUE	CL%	DOCUMENT ID		TECN	COMMENT
• • • We do not use the following data for averages, fits, limits, etc. • • •					
<0.26	90	[1,2] ABE	07	BELL	$e^+e^- \to J/\psi X$

[1] For $X(3940)$ decaying to final states with more than two tracks.
[2] PAKHLOV 08 finds that the inclusive peak near 3940 MeV/c^2 may consist of several states.

$X(3940)$ REFERENCES

PAKHLOV	08	PRL 100 202001	P. Pakhlov *et al.*	(BELLE Collab.)
ABE	07	PRL 98 082001	K. Abe *et al.*	(BELLE Collab.)

$X(4020)^{\pm}$

$I^G(J^{PC}) = 1^+(?^{?-})$

Properties incompatible with a $q\overline{q}$ structure (exotic state). See the review on non-$q\overline{q}$ states.

Charged $X(4020)$ seen by ABLIKIM 13X from $e^+e^- \to \pi^+\pi^- h_c(1P)$ at c.m. energy from 3.90 to 4.42 GeV as a peak in the invariant mass distribution of the $\pi^{\pm}h_c(1P)$ system, and by ABLIKIM 14B from $e^+e^- \to (D^*\overline{D}^*)^{\pm}\pi^{\mp}$ events in $(D^*\overline{D}^*)^{\pm}$ mass. A neutral $X(4020)$ seen by ABLIKIM 14P at three c.m. energies in the same range in $e^+e^- \to \pi^0\pi^0 h_c(1P)$ as a peak in the larger of the two masses recoiling against a π^0. ABLIKIM 15AA observes a 5.9 σ signal in $(D^*\overline{D}^*)^0$ in $e^+e^- \to (D^*\overline{D}^*)^0\pi^0$ events using collisions at two c.m. energies. Production rates and mass values support grouping neutral and charged $X(4020)$ together as manifestations of a single $I = 1$ particle.

$X(4020)^{\pm}$ MASS

VALUE (MeV)	EVTS	DOCUMENT ID		TECN	CHG	COMMENT
4024.1±1.9 OUR AVERAGE						
$4025.5^{+2.0}_{-4.7}\pm3.1$	116	[1] ABLIKIM	15AA	BES3	0	$e^+e^- \to (D^*\overline{D}^*)^0\pi^0$
4026.3±2.6±3.7	401	[1] ABLIKIM	14B	BES3	±	$e^+e^- \to (D^*\overline{D}^*)^{\pm}\pi^{\mp}$
4023.9±2.2±3.8	61	[1,2] ABLIKIM	14P	BES3	0	$e^+e^- \to \pi^0\pi^0 h_c$
4022.9±0.8±2.7	253	[1] ABLIKIM	13X	BES3	±	$e^+e^- \to \pi^+\pi^- h_c$

[1] Neglecting interference between the $X(4020)$ and non-resonant continuum.
[2] Assuming $J^P = 1^+$ and width of 7.9 ± 2.6 MeV.

$X(4020)^{\pm}$ WIDTH

VALUE (MeV)	EVTS	DOCUMENT ID		TECN	CHG	COMMENT
13 ±5 OUR AVERAGE		Error includes scale factor of 1.7. See the ideogram below.				
23.0±6.0±1.0	116	[1] ABLIKIM	15AA	BES3	0	$e^+e^- \to (D^*\overline{D}^*)^0\pi^0$
24.8±5.6±7.7	401	[1] ABLIKIM	14B	BES3	±	$e^+e^- \to (D^*\overline{D}^*)^{\pm}\pi^{\mp}$
7.9±2.7±2.6	253	[1] ABLIKIM	13X	BES3	±	$e^+e^- \to \pi^+\pi^- h_c$

[1] Neglecting interference between the $X(4020)$ and non-resonant continuum.

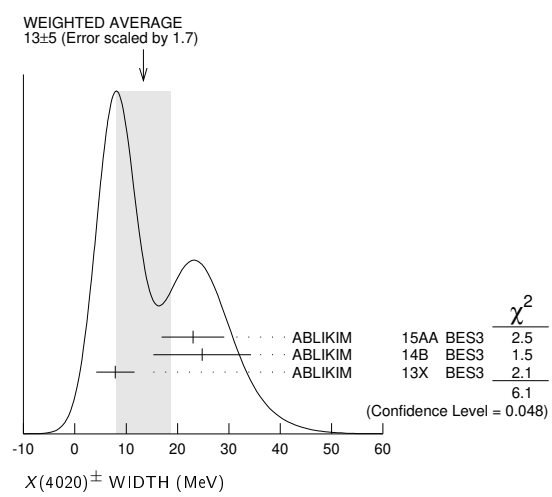

$X(4020)^{\pm}$ DECAY MODES

	Mode	Fraction (Γ_i/Γ)
Γ_1	$h_c(1P)\pi$	seen
Γ_2	$D^*\overline{D}^*$	seen
Γ_3	$D\overline{D}^*$ + c.c.	not seen
Γ_4	$\eta_c\pi^+\pi^-$	not seen
Γ_5	$\eta_c(1S)\rho(770)^{\pm}$	
Γ_6	$J/\psi(1S)\pi^{\pm}$	not seen

$X(4020)^{\pm}$ BRANCHING RATIOS

$\Gamma(h_c(1P)\pi)/\Gamma_{total}$ — Γ_1/Γ

VALUE	EVTS	DOCUMENT ID		TECN	CHG	COMMENT
seen	61	ABLIKIM	14P	BES3	0	$e^+e^- \to \pi^0\pi^0 h_c$
seen	253	ABLIKIM	13X	BES3	±	$e^+e^- \to \pi^+\pi^- h_c$

Downloaded from https://academic.oup.com/ptep/article/2022/8/083C01/6651666 by KIT Library user on 27 September 2022

$\Gamma(D^*\overline{D}^*)/\Gamma_{total}$ — Γ_2/Γ

VALUE	EVTS	DOCUMENT ID		TECN	CHG	COMMENT
seen	116	[1] ABLIKIM	15AA	BES3	0	$e^+e^- \to (D^*\overline{D}^*)^0\pi^0$
seen	401	[1] ABLIKIM	14B	BES3	$\pm$	$e^+e^- \to (D^*\overline{D}^*)^{\pm}\pi^{\mp}$

[1] Neglecting interference between the $X(4020)$ and non-resonant continuum.

$\Gamma(D\overline{D}^* + \text{c.c.})/\Gamma_{total}$ — Γ_3/Γ

VALUE	DOCUMENT ID		TECN	CHG	COMMENT
not seen	ABLIKIM	15AC	BES3	$\pm$	$e^+e^- \to \pi^{\pm}(D\overline{D}^*)^{\mp}$

$\Gamma(\eta_c\pi^+\pi^-)/\Gamma_{total}$ — Γ_4/Γ

VALUE	DOCUMENT ID		TECN	COMMENT
not seen	[1] VINOKUROVA	15	BELL	$B^+ \to K^+\eta_c\pi^+\pi^-$

[1] VINOKUROVA 15 reports $B(B^+ \to K^+X(4020)^0) \times B(X \to \eta_c\pi^+\pi^-) < 1.6 \times 10^{-5}$ at 90% CL.

$\Gamma(\eta_c(1S)\rho(770)^{\pm})/\Gamma(h_c(1P)\pi)$ — Γ_5/Γ_1

VALUE	CL%	DOCUMENT ID		TECN	COMMENT
<1.2	90	[1] ABLIKIM	19BC	BES3	$e^+e^- \to \pi^+\pi^-\pi^0\eta_c(1S)$

[1] Using $e^+e^- \to \pi^{\mp}(Z_c(4020)^{\pm} \to h_c(1P)\pi^{\pm})$ cross section at 4.23, 4.26 and 4.36 GeV from ABLIKIM 13X.

$\Gamma(J/\psi(1S)\pi^{\pm})/\Gamma_{total}$ — Γ_6/Γ

VALUE	DOCUMENT ID		TECN	COMMENT
not seen	[1] ABLIKIM	17J	BES3	$e^+e^- \to \pi^+\pi^- J/\psi$

[1] From Partial Wave Analysis assuming $J^P = 1^+$.

$X(4020)^{\pm}$ REFERENCES

ABLIKIM	19BC	PR D100 111102	M. Ablikim *et al.*	(BESIII Collab.)
ABLIKIM	17J	PRL 119 072001	M. Ablikim *et al.*	(BESIII Collab.)
ABLIKIM	15AA	PRL 115 182002	M. Ablikim *et al.*	(BESIII Collab.)
ABLIKIM	15AC	PR D92 092006	M. Ablikim *et al.*	(BESIII Collab.)
VINOKUROVA	15	JHEP 1506 132	A. Vinokurova *et al.*	(BELLE Collab.)
Also		JHEP 1702 088 (errat.)	A. Vinokurava *et al.*	(BELLE Collab.)
ABLIKIM	14B	PRL 112 132001	M. Ablikim *et al.*	(BESIII Collab.)
ABLIKIM	14P	PRL 113 212002	M. Ablikim *et al.*	(BESIII Collab.)
ABLIKIM	13X	PRL 111 242001	M. Ablikim *et al.*	(BESIII Collab.)

$\psi(4040)$

$I^G(J^{PC}) = 0^-(1^{--})$

$\psi(4040)$ MASS

VALUE (MeV)	DOCUMENT ID		TECN	COMMENT
4039 ± 1 OUR ESTIMATE				
4039.6± 4.3	[1] ABLIKIM	08D	BES2	$e^+e^- \to$ hadrons
• • • We do not use the following data for averages, fits, limits, etc. • • •				
4034 ± 6	[2] MO	10	RVUE	$e^+e^- \to$ hadrons
4037 ± 2	[3] SETH	05A	RVUE	$e^+e^- \to$ hadrons
4040 ± 1	[4] SETH	05A	RVUE	$e^+e^- \to$ hadrons
4040 ±10	BRANDELIK	78C	DASP	e^+e^-

[1] Reanalysis of data presented in BAI 02C. From a global fit over the center-of-mass energy region 3.7–5.0 GeV covering the $\psi(3770)$, $\psi(4040)$, $\psi(4160)$, and $\psi(4415)$ resonances. Phase angle fixed in the fit to $\delta = (130 \pm 46)^{\circ}$.

[2] Reanalysis of data presented in BAI 00 and BAI 02C. From a global fit over the center-of-mass energy 3.8-4.8 GeV covering the $\psi(4040)$, $\psi(4160)$ and $\psi(4415)$ resonances and including interference effects.

[3] From a fit to Crystal Ball (OSTERHELD 86) data.

[4] From a fit to BES (BAI 02C) data.

$\psi(4040)$ WIDTH

VALUE (MeV)	DOCUMENT ID		TECN	COMMENT
80 ±10 OUR ESTIMATE				
84.5±12.3	[5] ABLIKIM	08D	BES2	$e^+e^- \to$ hadrons
• • • We do not use the following data for averages, fits, limits, etc. • • •				
87 ±11	[6] MO	10	RVUE	$e^+e^- \to$ hadrons
85 ±10	[7] SETH	05A	RVUE	$e^+e^- \to$ hadrons
89 ± 6	[8] SETH	05A	RVUE	$e^+e^- \to$ hadrons
52 ±10	BRANDELIK	78C	DASP	e^+e^-

[5] Reanalysis of data presented in BAI 02C. From a global fit over the center-of-mass energy region 3.7–5.0 GeV covering the $\psi(3770)$, $\psi(4040)$, $\psi(4160)$, and $\psi(4415)$ resonances. Phase angle fixed in the fit to $\delta = (130 \pm 46)^{\circ}$.

[6] Reanalysis of data presented in BAI 00 and BAI 02C. From a global fit over the center-of-mass energy 3.8-4.8 GeV covering the $\psi(4040)$, $\psi(4160)$ and $\psi(4415)$ resonances and including interference effects.

[7] From a fit to Crystal Ball (OSTERHELD 86) data.

[8] From a fit to BES (BAI 02C) data.

$\psi(4040)$ DECAY MODES

Due to the complexity of the $c\overline{c}$ threshold region, in this listing, "seen" ("not seen") means that a cross section for the mode in question has been measured at effective $\sqrt{s}$ near this particle's central mass value, more (less) than 2σ above zero, without regard to any peaking behavior in $\sqrt{s}$ or absence thereof. See mode listing(s) for details and references.

	Mode	Fraction (Γ_i/Γ)	Confidence level
Γ_1	e^+e^-	$(1.07\pm0.16)\times10^{-5}$	
Γ_2	$D\overline{D}$	seen	
Γ_3	$D^0\overline{D}^0$	seen	
Γ_4	D^+D^-	seen	
Γ_5	$D^*\overline{D}+$ c.c.	seen	
Γ_6	$D^*(2007)^0\overline{D}^0+$ c.c.	seen	
Γ_7	$D^*(2010)^+D^-+$ c.c.	seen	
Γ_8	$D^*\overline{D}^*$	seen	
Γ_9	$D^*(2007)^0\overline{D}^*(2007)^0$	seen	
Γ_{10}	$D^*(2010)^+D^*(2010)^-$	seen	
Γ_{11}	$D\overline{D}\pi$ (excl. $D^*\overline{D}$)		
Γ_{12}	$D^0D^-\pi^+$+c.c. (excl. $D^*(2007)^0\overline{D}^0$ +c.c., $D^*(2010)^+D^-$ +c.c.)	not seen	
Γ_{13}	$D\overline{D}^*\pi$ (excl. $D^*\overline{D}^*$)	not seen	
Γ_{14}	$D^0\overline{D}^{*-}\pi^+$+c.c. (excl. $D^*(2010)^+D^*(2010)^-$)	seen	
Γ_{15}	$D_s^+D_s^-$	seen	
Γ_{16}	$\pi^+\pi^+\pi^-\pi^-\pi^0$		
Γ_{17}	$J/\psi(1S)$ hadrons		
Γ_{18}	$J/\psi\pi^+\pi^-$	$<4\times10^{-3}$	90%
Γ_{19}	$J/\psi\pi^0\pi^0$	$<2\times10^{-3}$	90%
Γ_{20}	$J/\psi\eta$	$(5.2\pm0.7)\times10^{-3}$	
Γ_{21}	$J/\psi\pi^0$	$<2.8\times10^{-4}$	90%
Γ_{22}	$J/\psi\pi^+\pi^-\pi^0$	$<2\times10^{-3}$	90%
Γ_{23}	$\chi_{c1}\gamma$	$<3.4\times10^{-3}$	90%
Γ_{24}	$\chi_{c2}\gamma$	$<5\times10^{-3}$	90%
Γ_{25}	$\chi_{c1}\pi^+\pi^-\pi^0$	<1.1 %	90%
Γ_{26}	$\chi_{c2}\pi^+\pi^-\pi^0$	<3.2 %	90%
Γ_{27}	$h_c(1P)\pi^+\pi^-$	$<3\times10^{-3}$	90%
Γ_{28}	$\phi\pi^+\pi^-$	$<3\times10^{-3}$	90%
Γ_{29}	$\Lambda\overline{\Lambda}\pi^+\pi^-$	$<2.9\times10^{-4}$	90%
Γ_{30}	$\Lambda\overline{\Lambda}\pi^0$	$<9\times10^{-5}$	90%
Γ_{31}	$\Lambda\overline{\Lambda}\eta$	$<3.0\times10^{-4}$	90%
Γ_{32}	$\Lambda\overline{\Lambda}$	$<6\times10^{-6}$	90%
Γ_{33}	$\Sigma^+\overline{\Sigma}^-$	$<1.3\times10^{-4}$	90%
Γ_{34}	$\Sigma^0\overline{\Sigma}^0$	$<7\times10^{-5}$	90%
Γ_{35}	$\Xi^+\overline{\Xi}^-$	$<1.6\times10^{-4}$	90%
Γ_{36}	$\Xi^0\overline{\Xi}^0$	$<1.8\times10^{-4}$	90%
Γ_{37}	$\mu^+\mu^-$	$(9\pm6)\times10^{-6}$	

$\psi(4040)$ PARTIAL WIDTHS

$\Gamma(e^+e^-)$ — Γ_1

VALUE (keV)	DOCUMENT ID		TECN	COMMENT
0.86±0.07 OUR ESTIMATE				
0.83±0.20	[9] ABLIKIM	08D	BES2	$e^+e^- \to$ hadrons
• • • We do not use the following data for averages, fits, limits, etc. • • •				
0.6 to 1.4	[10] MO	10	RVUE	$e^+e^- \to$ hadrons
0.88±0.11	[11] SETH	05A	RVUE	$e^+e^- \to$ hadrons
0.91±0.13	[12] SETH	05A	RVUE	$e^+e^- \to$ hadrons
0.75±0.15	BRANDELIK	78C	DASP	e^+e^-

[9] Reanalysis of data presented in BAI 02C. From a global fit over the center-of-mass energy region 3.7–5.0 GeV covering the $\psi(3770)$, $\psi(4040)$, $\psi(4160)$, and $\psi(4415)$ resonances. Phase angle fixed in the fit to $\delta = (130 \pm 46)^{\circ}$.

[10] Reanalysis of data presented in BAI 00 and BAI 02C. From a global fit over the center-of-mass energy 3.8-4.8 GeV covering the $\psi(4040)$, $\psi(4160)$ and $\psi(4415)$ resonances and including interference effects. Four sets of solutions are obtained with the same fit quality, mass and total width, but with different e^+e^- partial widths. We quote only the range of values.

[11] From a fit to Crystal Ball (OSTERHELD 86) data.

[12] From a fit to BES (BAI 02C) data.

$\Gamma(\mu^+\mu^-)$ — Γ_{37}

VALUE (keV)	DOCUMENT ID		TECN	COMMENT
0.73±0.48±0.12	[13,14] ABLIKIM	20AG	BES3	$e^+e^- \to \mu^+\mu^-$

[13] From a fit to the $e^+e^- \to \mu^+\mu^-$ cross section between 3.8 and 4.6 GeV to the coherent sum of four resonant amplitudes assuming $\Gamma(\mu^+\mu^-) = \Gamma(e^+e^-)$.

[14] From solution 1 of 8 with equal fit quality. Other solutions range from $0.58 \pm 0.52 \pm 0.10$ to $0.80 \pm 0.48 \pm 0.13$ keV.

Downloaded from https://academic.oup.com/ptep/article/2022/8/083C01/6651666 by KIT Library user on 27 September 2022

$\psi(4040)$ $\Gamma(i) \times \Gamma(e^+e^-)/\Gamma(\text{total})$

$\Gamma(\chi_{c1}\gamma) \times \Gamma(e^+e^-)/\Gamma_{\text{total}}$ — $\Gamma_{23}\Gamma_1/\Gamma$

VALUE (eV)	CL%	DOCUMENT ID		TECN	COMMENT
<2.9	90	[15] HAN	15	BELL	10.58 $e^+e^- \to \chi_{c1}\gamma$

[15] Using $B(\eta \to \gamma\gamma) = (39.41 \pm 0.21)\%$.

$\Gamma(\chi_{c2}\gamma) \times \Gamma(e^+e^-)/\Gamma_{\text{total}}$ — $\Gamma_{24}\Gamma_1/\Gamma$

VALUE (eV)	CL%	DOCUMENT ID		TECN	COMMENT
<4.6	90	[16] HAN	15	BELL	10.58 $e^+e^- \to \chi_{c2}\gamma$

[16] Using $B(\eta \to \gamma\gamma) = (39.41 \pm 0.21)\%$.

$\Gamma(J/\psi\eta) \times \Gamma(e^+e^-)/\Gamma_{\text{total}}$ — $\Gamma_{20}\Gamma_1/\Gamma$

VALUE (eV)	DOCUMENT ID		TECN	COMMENT
• • • We do not use the following data for averages, fits, limits, etc. • • •				
1.5 ± 0.3	[17] ABLIKIM	20O	BES3	$e^+e^- \to \eta J/\psi$
1.4 ± 0.3	[18] ABLIKIM	20O	BES3	$e^+e^- \to \eta J/\psi$
7.0 ± 0.6	[19] ABLIKIM	20O	BES3	$e^+e^- \to \eta J/\psi$

[17] Solution 1 of three equivalent fit solutions using three resonant structures.
[18] Solution 2 of three equivalent fit solutions using three resonant structures.
[19] Solution 3 of three equivalent fit solutions using three resonant structures.

$\psi(4040)$ $\Gamma(i) \times \Gamma(e^+e^-)/\Gamma^2(\text{total})$

$\Gamma(J/\psi\eta)/\Gamma_{\text{total}} \times \Gamma(e^+e^-)/\Gamma_{\text{total}}$ — $\Gamma_{20}/\Gamma \times \Gamma_1/\Gamma$

VALUE (units 10^{-8})	DOCUMENT ID		TECN	COMMENT
• • • We do not use the following data for averages, fits, limits, etc. • • •				
$5.1 \pm 1.4 \pm 1.5$	[20] WANG	13B	BELL	$e^+e^- \to J/\psi\eta\gamma$
$12.8 \pm 2.1 \pm 1.9$	[21] WANG	13B	BELL	$e^+e^- \to J/\psi\eta\gamma$

[20] Solution I of two equivalent solutions in a fit using two interfering resonances. Mass and width fixed at 4039 MeV and 80 MeV, respectively.
[21] Solution II of two equivalent solutions in a fit using two interfering resonances. Mass and width fixed at 4039 MeV and 80 MeV, respectively.

$\Gamma(\Lambda\overline{\Lambda}) \times \Gamma(e^+e^-)/\Gamma_{\text{total}}$ — $\Gamma_{32}\Gamma_1/\Gamma$

VALUE (eV)	CL%	DOCUMENT ID		TECN	COMMENT
$<5.5 \times 10^{-3}$	90	[22] ABLIKIM	21AS	BES3	$e^+e^- \to \psi(4040)$

[22] From a measurement of the $e^+e^- \to \Lambda\overline{\Lambda}$ cross section between 3.5 and 4.6 GeV.

$\psi(4040)$ BRANCHING RATIOS

$\Gamma(e^+e^-)/\Gamma_{\text{total}}$ — Γ_1/Γ

VALUE (units 10^{-5})	DOCUMENT ID		TECN	COMMENT
• • • We do not use the following data for averages, fits, limits, etc. • • •				
~ 1.0	FELDMAN	77	MRK1	e^+e^-

$\Gamma(D^0\overline{D}^0)/\Gamma_{\text{total}}$ — Γ_3/Γ

VALUE	DOCUMENT ID		TECN	COMMENT
seen	AUBERT	09M	BABR	$e^+e^- \to D^0\overline{D}^0\gamma$
seen	CRONIN-HEN...	09	CLEO	$e^+e^- \to D^0\overline{D}^0$
seen	PAKHLOVA	08	BELL	$e^+e^- \to D^0\overline{D}^0\gamma$

$\Gamma(D^+D^-)/\Gamma_{\text{total}}$ — Γ_4/Γ

VALUE	DOCUMENT ID		TECN	COMMENT
seen	AUBERT	09M	BABR	$e^+e^- \to D^+D^-\gamma$
seen	CRONIN-HEN...	09	CLEO	$e^+e^- \to D^+D^-$
seen	PAKHLOVA	08	BELL	$e^+e^- \to D^+D^-\gamma$

$\Gamma(D\overline{D})/\Gamma(D^*\overline{D} + \text{c.c.})$ — Γ_2/Γ_5

VALUE	DOCUMENT ID		TECN	COMMENT
$0.24 \pm 0.05 \pm 0.12$	AUBERT	09M	BABR	$e^+e^- \to \gamma D^{(*)}\overline{D}$

$\Gamma(D^0\overline{D}^0)/\Gamma(D^*(2007)^0\overline{D}^0 + \text{c.c.})$ — Γ_3/Γ_6

VALUE	DOCUMENT ID		TECN	COMMENT
0.05 ± 0.03	[23] GOLDHABER	77	MRK1	e^+e^-

[23] Phase-space factor (p^3) explicitly removed.

$\Gamma(D^*(2007)^0\overline{D}^0 + \text{c.c.})/\Gamma_{\text{total}}$ — Γ_6/Γ

VALUE	DOCUMENT ID		TECN	COMMENT
seen	AUBERT	09M	BABR	$e^+e^- \to D^{*0}\overline{D}^0\gamma$
seen	CRONIN-HEN...	09	CLEO	$e^+e^- \to D^{*0}\overline{D}^0$

$\Gamma(D^*(2010)^+D^- + \text{c.c.})/\Gamma_{\text{total}}$ — Γ_7/Γ

VALUE	DOCUMENT ID		TECN	COMMENT
seen	[24] ZHUKOVA	18	BELL	$e^+e^- \to D^{*+}D^-\gamma$
seen	AUBERT	09M	BABR	$e^+e^- \to D^{*+}D^-\gamma$
seen	CRONIN-HEN...	09	CLEO	$e^+e^- \to D^{*+}D^-$
• • • We do not use the following data for averages, fits, limits, etc. • • •				
seen	PAKHLOVA	07	BELL	$e^+e^- \to D^{*+}D^-\gamma$

[24] Supersedes PAKHLOVA 07.

$\Gamma(D^*(2010)^+D^- + \text{c.c.})/\Gamma(D^*(2007)^0\overline{D}^0 + \text{c.c.})$ — Γ_7/Γ_6

VALUE	DOCUMENT ID		TECN	COMMENT
$0.95 \pm 0.09 \pm 0.10$	AUBERT	09M	BABR	$e^+e^- \to \gamma D^*\overline{D}$

$\Gamma(D^*\overline{D}^*)/\Gamma(D^*\overline{D} + \text{c.c.})$ — Γ_8/Γ_5

VALUE	DOCUMENT ID		TECN	COMMENT
$0.18 \pm 0.14 \pm 0.03$	AUBERT	09M	BABR	$e^+e^- \to \gamma D^{(*)}\overline{D}^{(*)}$

$\Gamma(D^*(2007)^0\overline{D}^*(2007)^0)/\Gamma_{\text{total}}$ — Γ_9/Γ

VALUE	DOCUMENT ID		TECN	COMMENT
seen	AUBERT	09M	BABR	$e^+e^- \to D^{*0}\overline{D}^{*0}\gamma$
seen	CRONIN-HEN...	09	CLEO	$e^+e^- \to D^{*0}\overline{D}^{*0}$

$\Gamma(D^*(2007)^0\overline{D}^*(2007)^0)/\Gamma(D^*(2007)^0\overline{D}^0 + \text{c.c.})$ — Γ_9/Γ_6

VALUE	DOCUMENT ID		TECN	COMMENT
32.0 ± 12.0	[25] GOLDHABER	77	MRK1	e^+e^-

[25] Phase-space factor (p^3) explicitly removed.

$\Gamma(D^*(2010)^+D^*(2010)^-)/\Gamma_{\text{total}}$ — Γ_{10}/Γ

VALUE	DOCUMENT ID		TECN	COMMENT
seen	[26] ZHUKOVA	18	BELL	$e^+e^- \to D^{*+}D^{*-}\gamma$
seen	AUBERT	09M	BABR	$e^+e^- \to D^{*+}D^{*-}\gamma$
seen	CRONIN-HEN...	09	CLEO	$e^+e^- \to D^{*+}D^{*-}$
• • • We do not use the following data for averages, fits, limits, etc. • • •				
seen	PAKHLOVA	07	BELL	$e^+e^- \to D^{*+}D^{*-}\gamma$

[26] Supersedes PAKHLOVA 07.

$\Gamma(D^0D^-\pi^+ + \text{c.c. (excl. } D^*(2007)^0\overline{D}^0 + \text{c.c.}, D^*(2010)^+D^- + \text{c.c.}))/\Gamma_{\text{total}}$ — Γ_{12}/Γ

VALUE	DOCUMENT ID		TECN	COMMENT
not seen	PAKHLOVA	08A	BELL	$e^+e^- \to D^0D^-\pi^+\gamma$

$\Gamma(D\overline{D}^*\pi \text{ (excl. } D^*\overline{D}^*))/\Gamma_{\text{total}}$ — Γ_{13}/Γ

VALUE	DOCUMENT ID		TECN	COMMENT
not seen	CRONIN-HEN...	09	CLEO	$e^+e^- \to D\overline{D}^*\pi$

$\Gamma(D^0\overline{D}^{*-}\pi^+ + \text{c.c. (excl. } D^*(2010)^+D^*(2010)^-))/\Gamma_{\text{total}}$ — Γ_{14}/Γ

VALUE	DOCUMENT ID		TECN	COMMENT
seen	PAKHLOVA	09	BELL	$e^+e^- \to D^0D^{*-}\pi^+\gamma$

$\Gamma(D_s^+D_s^-)/\Gamma_{\text{total}}$ — Γ_{15}/Γ

VALUE	DOCUMENT ID		TECN	COMMENT
seen	PAKHLOVA	11	BELL	$e^+e^- \to D_s^+D_s^-\gamma$
seen	DEL-AMO-SA...	10N	BABR	$e^+e^- \to D_s^+D_s^-\gamma$
seen	CRONIN-HEN...	09	CLEO	$e^+e^- \to D_s^+D_s^-$

$\Gamma(\pi^+\pi^+\pi^-\pi^-\pi^0)/\Gamma_{\text{total}}$ — Γ_{16}/Γ

VALUE	DOCUMENT ID		TECN	COMMENT
• • • We do not use the following data for averages, fits, limits, etc. • • •				
$(3.51 \pm 1.89 \pm 1.24) \times 10^{-5}$	[27] ABLIKIM	21AW	BES3	$e^+e^- \to 2\pi^+2\pi^-\pi^0$
$(2.41 \pm 0.05 \pm 0.79) \times 10^{-2}$	[28] ABLIKIM	21AW	BES3	$e^+e^- \to 2\pi^+2\pi^-\pi^0$

[27] Solution 1 of two solutions with equal fit quality. The significance of the $\psi(4040)$ signal is 3.6 σ.
[28] Solution 2 of two solutions with equal fit quality. The significance of the $\psi(4040)$ signal is 3.6 σ.

$\Gamma(J/\psi\pi^+\pi^-)/\Gamma_{\text{total}}$ — Γ_{18}/Γ

VALUE (units 10^{-3})	CL%	DOCUMENT ID		TECN	COMMENT
<4	90	COAN	06	CLEO	3.97–4.06 $e^+e^- \to$ hadrons

$\Gamma(J/\psi\pi^0\pi^0)/\Gamma_{\text{total}}$ — Γ_{19}/Γ

VALUE (units 10^{-3})	CL%	DOCUMENT ID		TECN	COMMENT
<2	90	COAN	06	CLEO	3.97–4.06 $e^+e^- \to$ hadrons

$\Gamma(J/\psi\eta)/\Gamma_{\text{total}}$ — Γ_{20}/Γ

VALUE (units 10^{-3})	CL%	DOCUMENT ID		TECN	COMMENT
$5.2 \pm 0.5 \pm 0.5$		[29] ABLIKIM	12K	BES3	$e^+e^- \to \ell^+\ell^- 2\gamma$
• • • We do not use the following data for averages, fits, limits, etc. • • •					
<7	90	COAN	06	CLEO	3.97–4.06 $e^+e^- \to$ hadrons

[29] ABLIKIM 12K measure $\sigma(e^+e^- \to J/\psi\eta) = 32.1 \pm 2.8 \pm 1.3$ pb. They assume the $\eta J/\psi$ fully originates from $\psi(4040)$ decays.

$\Gamma(J/\psi\pi^0)/\Gamma_{\text{total}}$ — Γ_{21}/Γ

VALUE (units 10^{-3})	CL%	DOCUMENT ID		TECN	COMMENT
<0.28	90	[30] ABLIKIM	12K	BES3	$e^+e^- \to \ell^+\ell^- 2\gamma$
• • • We do not use the following data for averages, fits, limits, etc. • • •					
<2	90	COAN	06	CLEO	3.97–4.06 $e^+e^- \to$ hadrons

[30] ABLIKIM 12K measure $\sigma(e^+e^- \to J/\psi\pi^0) < 1.6$ pb. They assume the $\eta J/\psi$ fully originates from $\psi(4040)$ decays.

Downloaded from https://academic.oup.com/ptep/article/2022/8/083C01/6651666 by KIT Library user on 27 September 2022

$\Gamma(J/\psi\pi^+\pi^-\pi^0)/\Gamma_{total}$ — Γ_{22}/Γ

VALUE (units 10^{-3})	CL%	DOCUMENT ID		TECN	COMMENT
<2	90	COAN	06	CLEO	3.97–4.06 $e^+e^- \to$ hadrons

$\Gamma(\chi_{c1}\gamma)/\Gamma_{total}$ — Γ_{23}/Γ

VALUE (units 10^{-3})	CL%	DOCUMENT ID		TECN	COMMENT
• • • We do not use the following data for averages, fits, limits, etc. • • •					
<11	90	COAN	06	CLEO	3.97–4.06 $e^+e^- \to$ hadrons

$\Gamma(\chi_{c2}\gamma)/\Gamma_{total}$ — Γ_{24}/Γ

VALUE (units 10^{-3})	CL%	DOCUMENT ID		TECN	COMMENT
• • • We do not use the following data for averages, fits, limits, etc. • • •					
<17	90	COAN	06	CLEO	3.97–4.06 $e^+e^- \to$ hadrons

$\Gamma(\chi_{c1}\pi^+\pi^-\pi^0)/\Gamma_{total}$ — Γ_{25}/Γ

VALUE (units 10^{-3})	CL%	DOCUMENT ID		TECN	COMMENT
<11	90	COAN	06	CLEO	3.97–4.06 $e^+e^- \to$ hadrons

$\Gamma(\chi_{c2}\pi^+\pi^-\pi^0)/\Gamma_{total}$ — Γ_{26}/Γ

VALUE (units 10^{-3})	CL%	DOCUMENT ID		TECN	COMMENT
<32	90	COAN	06	CLEO	3.97–4.06 $e^+e^- \to$ hadrons

$\Gamma(h_c(1P)\pi^+\pi^-)/\Gamma_{total}$ — Γ_{27}/Γ

VALUE (units 10^{-3})	CL%	DOCUMENT ID		TECN	COMMENT
<3	90	[31] PEDLAR	11	CLEO	$e^+e^- \to h_c(1P)\pi^+\pi^-$

[31] From several values of $\sqrt{s}$ near the peak of the $\psi(4040)$, PEDLAR 11 measures $\sigma(e^+e^- \to h_c(1P)\pi^+\pi^-) = 1.0 \pm 8.0 \pm 5.4 \pm 0.2$ pb, where the errors are statistical, systematic, and due to uncertainty in $B(\psi(2S) \to \pi^0 h_c(1P))$, respectively.

$\Gamma(\phi\pi^+\pi^-)/\Gamma_{total}$ — Γ_{28}/Γ

VALUE (units 10^{-3})	CL%	DOCUMENT ID		TECN	COMMENT
<3	90	COAN	06	CLEO	3.97–4.06 $e^+e^- \to$ hadrons

$\Gamma(\Lambda\overline{\Lambda}\pi^+\pi^-)/\Gamma_{total}$ — Γ_{29}/Γ

VALUE (units 10^{-4})	CL%	DOCUMENT ID		TECN	COMMENT
<2.9	90	[32] ABLIKIM	13Q	BES3	$e^+e^- \to \psi(4040)$

[32] Assuming that interference effects between resonance and continuum can be neglected.

$\Gamma(\Lambda\overline{\Lambda}\pi^0)/\Gamma_{total}$ — Γ_{30}/Γ

VALUE (units 10^{-4})	CL%	DOCUMENT ID		TECN	COMMENT
<0.9	90	[33] ABLIKIM	13Q	BES3	$e^+e^- \to \psi(4040)$

[33] Assuming that interference effects between resonance and continuum can be neglected.

$\Gamma(\Lambda\overline{\Lambda}\eta)/\Gamma_{total}$ — Γ_{31}/Γ

VALUE (units 10^{-4})	CL%	DOCUMENT ID		TECN	COMMENT
<3.0	90	[34] ABLIKIM	13Q	BES3	$e^+e^- \to \psi(4040)$

[34] Assuming that interference effects between resonance and continuum can be neglected.

$\Gamma(\Sigma^+\overline{\Sigma}^-)/\Gamma_{total}$ — Γ_{33}/Γ

VALUE (units 10^{-4})	CL%	DOCUMENT ID		TECN	COMMENT
<1.3	90	[35] ABLIKIM	13Q	BES3	$e^+e^- \to \psi(4040)$

[35] Assuming that interference effects between resonance and continuum can be neglected.

$\Gamma(\Sigma^0\overline{\Sigma}^0)/\Gamma_{total}$ — Γ_{34}/Γ

VALUE (units 10^{-4})	CL%	DOCUMENT ID		TECN	COMMENT
<0.7	90	[36] ABLIKIM	13Q	BES3	$e^+e^- \to \psi(4040)$

[36] Assuming that interference effects between resonance and continuum can be neglected.

$\Gamma(\Xi^+\overline{\Xi}^-)/\Gamma_{total}$ — Γ_{35}/Γ

VALUE (units 10^{-4})	CL%	DOCUMENT ID		TECN	COMMENT
<1.6	90	[37] ABLIKIM	13Q	BES3	$e^+e^- \to \psi(4040)$

[37] Assuming that interference effects between resonance and continuum can be neglected.

$\Gamma(\Xi^0\overline{\Xi}^0)/\Gamma_{total}$ — Γ_{36}/Γ

VALUE (units 10^{-4})	CL%	DOCUMENT ID		TECN	COMMENT
<1.8	90	[38] ABLIKIM	13Q	BES3	$e^+e^- \to \psi(4040)$

[38] Assuming that interference effects between resonance and continuum can be neglected.

$\psi(4040)$ REFERENCES

ABLIKIM	21AS	PR D104 L091104	M. Ablikim et al.	(BESIII Collab.)
ABLIKIM	21AW	PR D104 112009	M. Ablikim et al.	(BESIII Collab.)
ABLIKIM	20AG	PR D102 112009	M. Ablikim et al.	(BESIII Collab.)
ABLIKIM	20O	PR D102 031101	M. Ablikim et al.	(BESIII Collab.)
ZHUKOVA	18	PR D97 012002	V. Zhukova et al.	(BELLE Collab.)
HAN	15	PR D92 012011	Y.L. Han et al.	(BELLE Collab.)
ABLIKIM	13Q	PR D87 112011	M. Ablikim et al.	(BESIII Collab.)
WANG	13B	PR D87 051101	X.L. Wang et al.	(BELLE Collab.)
ABLIKIM	12K	PR D86 071101	M. Ablikim et al.	(BESIII Collab.)
PAKHLOVA	11	PR D83 011101	G. Pakhlova et al.	(BELLE Collab.)
PEDLAR	11	PRL 107 041803	T. Pedlar et al.	(CLEO Collab.)
DEL-AMO-SA...	10N	PR D82 052004	P. del Amo Sanchez et al.	(BABAR Collab.)
MO	10	PR D82 077501	X.H. Mo, C.Z. Yuan, P. Wang	(BHEP)
AUBERT	09M	PR D79 092001	B. Aubert et al.	(BABAR Collab.)
CRONIN-HEN...	09	PR D80 072001	D. Cronin-Hennessy et al.	(CLEO Collab.)
PAKHLOVA	09	PR D80 091101	G. Pakhlova et al.	(BELLE Collab.)
ABLIKIM	08D	PL B660 315	M. Ablikim et al.	(BES Collab.)
PAKHLOVA	08	PR D77 011103	G. Pakhlova et al.	(BELLE Collab.)
PAKHLOVA	08A	PRL 100 062001	G. Pakhlova et al.	(BELLE Collab.)
PAKHLOVA	07	PRL 98 092001	G. Pakhlova et al.	(BELLE Collab.)
COAN	06	PRL 96 162003	T.E. Coan et al.	(CLEO Collab.)
SETH	05A	PR D72 017501	K.K. Seth	
BAI	02C	PRL 88 101802	J.Z. Bai et al.	(BES Collab.)
BAI	00	PRL 84 594	J.Z. Bai et al.	(BES Collab.)
OSTERHELD	86	SLAC-PUB-4160	A. Osterheld et al.	(SLAC Crystal Ball Collab.)
BRANDELIK	78C	PL 76B 361	R. Brandelik et al.	(DASP Collab.)
Also		ZPHY C1 233	R. Brandelik et al.	(DASP Collab.)
FELDMAN	77	PRPL 33C 285	G.J. Feldman, M.L. Perl	(LBL, SLAC)
GOLDHABER	77	PL 69B 503	G. Goldhaber et al.	(Mark I Collab.)

$X(4050)^{\pm}$

$I^G(J^{PC}) = 1^-(?^{?+})$

I, G, C need confirmation.

OMITTED FROM SUMMARY TABLE

Properties incompatible with a $q\overline{q}$ structure (exotic state). See the review on non-$q\overline{q}$ states.

Observed by MIZUK 08 in the $\pi^+\chi_{c1}(1P)$ invariant mass distribution in $\overline{B}^0 \to K^-\pi^+\chi_{c1}(1P)$ decays. Not seen by LEES 12B in this same mode after accounting for $K\pi$ resonant mass and angular structure.

$X(4050)^{\pm}$ MASS

VALUE (MeV)	DOCUMENT ID		TECN	COMMENT
$4051 \pm 14^{+20}_{-41}$	[1] MIZUK	08	BELL	$\overline{B}^0 \to K^-\pi^+\chi_{c1}(1P)$

[1] From a Dalitz plot analysis with two Breit-Wigner amplitudes.

$X(4050)^{\pm}$ WIDTH

VALUE (MeV)	DOCUMENT ID		TECN	COMMENT
$82^{+21}_{-17}{}^{+47}_{-22}$	[1] MIZUK	08	BELL	$\overline{B}^0 \to K^-\pi^+\chi_{c1}(1P)$

[1] From a Dalitz plot analysis with two Breit-Wigner amplitudes.

$X(4050)^{\pm}$ DECAY MODES

	Mode	Fraction (Γ_i/Γ)
Γ_1	$\pi^+\chi_{c1}(1P)$	seen
Γ_2	$\pi^{\pm}\psi(3770)$	not seen
Γ_3	$\pi^{\pm}\chi_{c0}(1P)$	not seen
Γ_4	$\pi^{\pm}\chi_{c2}(1P)$	not seen

$X(4050)^{\pm}$ BRANCHING RATIOS

$\Gamma(\pi^+\chi_{c1}(1P))/\Gamma_{total}$ — Γ_1/Γ

VALUE	EVTS	DOCUMENT ID		TECN	COMMENT
seen		[1] MIZUK	08	BELL	$\overline{B}^0 \to K^-\pi^+\chi_{c1}(1P)$
• • • We do not use the following data for averages, fits, limits, etc. • • •					
not seen	16	[2] ABLIKIM	21W	BES3	$e^+e^- \to \chi_{c,J}\pi^+\pi^+$
not seen		[3] LEES	12B	BABR	$B \to K\pi\chi_{c1}(1P)$

[1] With a product branching fraction measurement of $B(\overline{B}^0 \to K^-X(4050)^+) \times B(X(4050)^+ \to \pi^+\chi_{c1}(1P)) = (3.0^{+1.5}_{-0.8}{}^{+3.7}_{-1.6}) \times 10^{-5}$.

[2] ABLIKIM 21W measurement is limited by statistics.

[3] With a product branching fraction limit of $B(\overline{B}^0 \to X(4050)^+K^-) \times B(X(4050)^+ \to \chi_{c1}\pi^+) < 1.8 \times 10^{-5}$ at 90% CL.

$\Gamma(\pi^{\pm}\chi_{c0}(1P))/\Gamma_{total}$ — Γ_3/Γ

VALUE	EVTS	DOCUMENT ID		TECN	COMMENT
not seen	18	[1] ABLIKIM	21W	BES3	$e^+e^- \to \chi_{c,J}\pi^+\pi^+$

[1] ABLIKIM 21W measurement is limited by statistics.

$\Gamma(\pi^{\pm}\chi_{c2}(1P))/\Gamma_{total}$ — Γ_4/Γ

VALUE	EVTS	DOCUMENT ID		TECN	COMMENT
not seen	14	[1] ABLIKIM	21W	BES3	$e^+e^- \to \chi_{c,J}\pi^+\pi^+$

[1] ABLIKIM 21W measurement is limited by statistics.

$\Gamma(\pi^{\pm}\psi(3770))/\Gamma_{total}$ — Γ_2/Γ

VALUE	DOCUMENT ID		TECN	COMMENT
not seen	[1] ABLIKIM	19AR	BES3	$e^+e^- \to \pi^+\pi^-D\overline{D}$

[1] From a measurement of $\sigma(e^+e^- \to \pi^+\pi^-D\overline{D})$ between $\sqrt{s} = 4.08$ and 4.6 GeV.

$X(4050)^{\pm}$ REFERENCES

ABLIKIM	21W	PR D103 052010	M. Ablikim et al.	(BESIII Collab.)
ABLIKIM	19AR	PR D100 032005	M. Ablikim et al.	(BESIII Collab.)
LEES	12B	PR D85 052003	J.P. Lees et al.	(BABAR Collab.)
MIZUK	08	PR D78 072004	R. Mizuk et al.	(BELLE Collab.)

Downloaded from https://academic.oup.com/ptep/article/2022/8/083C01/6651666 by KIT Library user on 27 September 2022

$X(4055)^{\pm}$

$I^G(J^{PC}) = 1^+(?^{?-})$
I, G, C need confirmation.

OMITTED FROM SUMMARY TABLE

Properties incompatible with a $q\overline{q}$ structure (exotic state). See the review on non-$q\overline{q}$ states.

Needs confirmation. Seen by WANG 15A in the $\psi(2S)\pi^+$ invariant mass distribution in $\psi(4360) \to \psi(2S)\pi^+\pi^-$ decay.

$X(4055)^{\pm}$ MASS

VALUE (MeV)	DOCUMENT ID		TECN	COMMENT
4054 ±3 ±1	[1] WANG	15A	BELL	10.58 $e^+e^- \to \gamma\pi^+\pi^-\psi(2S)$
• • • We do not use the following data for averages, fits, limits, etc. • • •				
4039.3±6.0	[2] ABLIKIM	18K	BES3	$e^+e^- \to \pi^0\pi^0\psi(2S)$
4032.1±2.4	[3] ABLIKIM	17V	BES3	$e^+e^- \to \pi^+\pi^-\psi(2S)$

[1] Statistical significance of 3.5 σ.
[2] Statistical error only, with significance of 5.9 σ (from a fit with a 19% CL). Identified as the same structure observed in ABLIKIM 17V in $e^+e^- \to \pi^+\pi^-\psi(2S)$ decays.
[3] Statistical error only, with significance of 9.2 σ. From an unbinned maximum likelihood fit of the $\pi^+\pi^-\psi(2S)$ Dalitz plot from data collected at $\sqrt{s} = 4.416$ GeV for a $J^C = 1^+$ state. The fit does not match the detailed structure of the data, having a C.L. of only 8%.

$X(4055)^{\pm}$ WIDTH

VALUE (MeV)	DOCUMENT ID		TECN	COMMENT
45 ±11 ±6	[1] WANG	15A	BELL	10.58 $e^+e^- \to \gamma\pi^+\pi^-\psi(2S)$
• • • We do not use the following data for averages, fits, limits, etc. • • •				
31.9±14.8	[2] ABLIKIM	18K	BES3	$e^+e^- \to \pi^0\pi^0\psi(2S)$
26.1± 5.3	[3] ABLIKIM	17V	BES3	$e^+e^- \to \pi^+\pi^-\psi(2S)$

[1] Statistical significance of 3.5 σ.
[2] Statistical error only, with significance of 5.9 σ (from a fit with a 19% CL). Identified as the same structure observed in ABLIKIM 17V in $e^+e^- \to \pi^+\pi^-\psi(2S)$ decays.
[3] Statistical error only, with significance of 9.2 σ. From an unbinned maximum likelihood fit of the $\pi^+\pi^-\psi(2S)$ Dalitz plot from data collected at $\sqrt{s} = 4.416$ GeV for a $J^C = 1^+$ state. The fit does not match the detailed structure of the data, having a C.L. of only 8%.

$X(4055)^{\pm}$ DECAY MODES

	Mode	Fraction (Γ_i/Γ)
Γ_1	$\pi^+\psi(2S)$	seen
Γ_2	$\pi^{\pm}\psi(3770)$	not seen

$X(4055)^{\pm}$ BRANCHING RATIOS

$\Gamma(\pi^+\psi(2S))/\Gamma_{total}$ — Γ_1/Γ

VALUE	DOCUMENT ID		TECN	COMMENT
seen	[1] WANG	15A	BELL	10.58 $e^+e^- \to \gamma\pi^+\pi^-\psi(2S)$

[1] Statistical significance of 3.5 σ.

$\Gamma(\pi^{\pm}\psi(3770))/\Gamma_{total}$ — Γ_2/Γ

VALUE	DOCUMENT ID		TECN	COMMENT
not seen	[1] ABLIKIM	19AR	BES3	$e^+e^- \to \pi^+\pi^- D\overline{D}$

[1] From a measurement of $\sigma(e^+e^- \to \pi^+\pi^- D\overline{D})$ between $\sqrt{s} = 4.08$ and 4.6 GeV.

$X(4055)^{\pm}$ REFERENCES

ABLIKIM 19AR PR D100 032005 M. Ablikim et al. (BESIII Collab.)
ABLIKIM 18K PR D97 052001 M. Ablikim et al. (BESIII Collab.)
ABLIKIM 17V PR D96 032004 M. Ablikim et al. (BESIII Collab.)
Also PR D99 019903 (errat.) M. Ablikim et al. (BESIII Collab.)
WANG 15A PR D91 112007 X.L. Wang et al. (BELLE Collab.)

$X(4100)^{\pm}$

$I^G(J^{PC}) = 1^-(?^{??})$

OMITTED FROM SUMMARY TABLE

Properties incompatible with a $q\overline{q}$ structure (exotic state). See the review on non-$q\overline{q}$ states.

Reported by AAIJ 18AN in the $\eta_c(1S)\pi^-$ invariant mass distribution in $B^0 \to \eta_c(1S)K^+\pi^-$ decays with a significance of 3.4σ. $J^P = 0^+$ or 1^- assignment consistent with data.

$X(4100)^{\pm}$ MASS

VALUE (MeV)	DOCUMENT ID		TECN	COMMENT
$4096 \pm 20^{+18}_{-22}$	AAIJ	18AN	LHCB	$B^0 \to \eta_c(1S)K^+\pi^-$

$X(4100)^{\pm}$ WIDTH

VALUE (MeV)	DOCUMENT ID		TECN	COMMENT
$152 \pm 58^{+60}_{-35}$	AAIJ	18AN	LHCB	$B^0 \to \eta_c(1S)K^+\pi^-$

$X(4100)^{\pm}$ DECAY MODES

	Mode	Fraction (Γ_i/Γ)
Γ_1	$\eta_c(1S)\pi^-$	seen
Γ_2	$\pi^{\pm}\psi(3770)$	not seen

$X(4100)^{\pm}$ BRANCHING RATIOS

$\Gamma(\eta_c(1S)\pi^-)/\Gamma_{total}$ — Γ_1/Γ

VALUE	DOCUMENT ID		TECN	COMMENT
seen	[1] AAIJ	18AN	LHCB	$B^0 \to \eta_c(1S)K^+\pi^-$

[1] AAIJ 18AN quotes a fit fraction for $B^0 \to X(4100)^-K^+ \to \eta_c(1S)\pi^-K^+$ of $(3.3 \pm 1.1^{+1.2}_{-1.1})$% from an amplitude analysis.

$\Gamma(\pi^{\pm}\psi(3770))/\Gamma_{total}$ — Γ_2/Γ

VALUE	DOCUMENT ID		TECN	COMMENT
not seen	[1] ABLIKIM	19AR	BES3	$e^+e^- \to \pi^+\pi^- D\overline{D}$

[1] From a measurement of $\sigma(e^+e^- \to \pi^+\pi^- D\overline{D})$ between $\sqrt{s} = 4.08$ and 4.6 GeV.

$X(4100)^{\pm}$ REFERENCES

ABLIKIM 19AR PR D100 032005 M. Ablikim et al. (BESIII Collab.)
AAIJ 18AN EPJ C78 1019 R. Aaij et al. (LHCb Collab.)

$\chi_{c1}(4140)$

$I^G(J^{PC}) = 0^+(1^{++})$

was $X(4140)$

This state shows properties different from a conventional $q\overline{q}$ state. A candidate for an exotic structure. See the review on non-$q\overline{q}$ states.

Seen by AALTONEN 09AH, ABAZOV 14A, CHATRCHYAN 14M, AAIJ 17C in $B^+ \to \chi_{c1}K^+$, $\chi_{c1} \to J/\psi\phi$, and by ABAZOV 15M separately in both prompt (4.7 σ) and non-prompt (5.6 σ) production in $p\overline{p} \to J/\psi\phi +$ anything. Not seen by SHEN 10 in $\gamma\gamma \to J/\psi\phi$ and ABLIKIM 15 in $e^+e^- \to \gamma J/\psi\phi$ at $\sqrt{s} = 4.23$, 4.26, 4.36 GeV.

$\chi_{c1}(4140)$ MASS

VALUE (MeV)	EVTS	DOCUMENT ID		TECN	COMMENT
4146.5± 3.0 OUR AVERAGE	Error includes scale factor of 1.3. See the ideogram below.				
4118 ±11 $^{+19}_{-36}$	24k	[1] AAIJ	21E	LHCB	$B^+ \to J/\psi\phi K^+$
4143.4$^{+2.9}_{-3.0}$± 0.6	19	[2] AALTONEN	17	CDF	$B^+ \to J/\psi\phi K^+$
4152.5± 1.7$^{+6.2}_{-5.4}$	616	[3] ABAZOV	15M	D0	$p\overline{p} \to J/\psi\phi +$ anything
4159.0± 4.3± 6.6	52	[4] ABAZOV	14A	D0	$B^+ \to J/\psi\phi K^+$
4148.0± 2.4± 6.3	0.3k	[5] CHATRCHYAN	14M	CMS	$B^+ \to J/\psi\phi K^+$
• • • We do not use the following data for averages, fits, limits, etc. • • •					
4146.5± 4.5$^{+4.6}_{-2.8}$	4289	[6,7] AAIJ	17C	LHCB	$B^+ \to J/\psi\phi K^+$
4143.0± 2.9± 1.2	14	[8,9] AALTONEN	09AH	CDF	$B^+ \to J/\psi\phi K^+$

[1] From an amplitude analysis of the decay $B^+ \to J/\psi\phi K^+$ with a significance of 13 σ.
[2] Statistical significance of more than 5 σ.
[3] Statistical significance of more than 6 σ.
[4] Statistical significance of 3.1 σ.
[5] From a fit assuming an S-wave relativistic Breit-Wigner shape above a three-body phase-space non-resonant component with statistical significance of more than 5 σ.
[6] From an amplitude analysis of the decay $B^+ \to J/\psi\phi K^+$ with a significance of 8.4 σ.
[7] Superseded by AAIJ 21E.
[8] Statistical significance of 3.8 σ.
[9] Superseded by AALTONEN 17.

Downloaded from https://academic.oup.com/ptep/article/2022/8/083C01/6651666 by KIT Library user on 27 September 2022

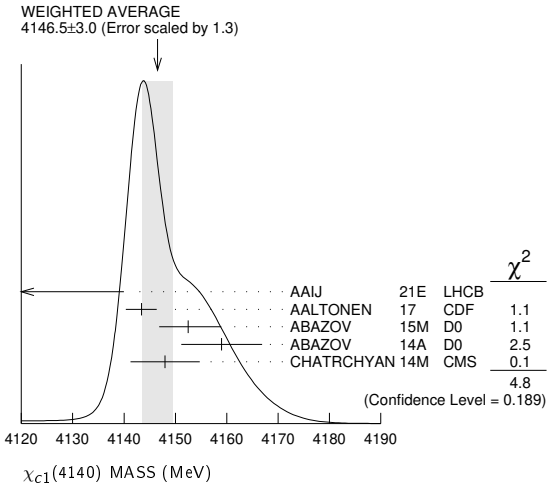

$\chi_{c1}(4140)$ WIDTH

VALUE (MeV)	EVTS	DOCUMENT ID		TECN	COMMENT
19^{+7}_{-5} OUR AVERAGE					
$162 \pm 21^{+24}_{-49}$	24k	[1] AAIJ	21E	LHCB	$B^+ \to J/\psi\phi K^+$
$15.3^{+10.4}_{-6.1} \pm 2.5$	19	[2] AALTONEN	17	CDF	$B^+ \to J/\psi\phi K^+$
$16.3 \pm 5.6 \pm 11.4$	616	[3] ABAZOV	15M	D0	$p\overline{p} \to J/\psi\phi +$ anything
$20 \pm 13^{+3}_{-8}$	52	[4] ABAZOV	14A	D0	$B^+ \to J/\psi\phi K^+$
$28^{+15}_{-11} \pm 19$	0.3k	[5] CHATRCHYAN	14M	CMS	$B^+ \to J/\psi\phi K^+$
• • • We do not use the following data for averages, fits, limits, etc. • • •					
$83 \pm 21^{+21}_{-14}$	4289	[6,7] AAIJ	17C	LHCB	$B^+ \to J/\psi\phi K^+$
$11.7^{+8.3}_{-5.0} \pm 3.7$	14	[8,9] AALTONEN	09AH	CDF	$B^+ \to J/\psi\phi K^+$

[1] From an amplitude analysis of the decay $B^+ \to J/\psi\phi K^+$ with a significance of 13 σ.
[2] Statistical significance of more than 5 σ.
[3] Statistical significance of more than 6 σ.
[4] Statistical significance of 3.1 σ.
[5] From a fit assuming an S-wave relativistic Breit-Wigner shape above a three-body phase-space non-resonant component with statistical significance of more than 5 σ.
[6] From an amplitude analysis of the decay $B^+ \to J/\psi\phi K^+$ with a significance of 8.4 σ.
[7] Superseded by AAIJ 21E.
[8] Statistical significance of 3.8 σ.
[9] Superseded by AALTONEN 17.

$\chi_{c1}(4140)$ DECAY MODES

	Mode	Fraction (Γ_i/Γ)
Γ_1	$J/\psi\phi$	seen
Γ_2	$\gamma\gamma$	not seen

$\chi_{c1}(4140)$ $\Gamma(i)\Gamma(\gamma\gamma)/\Gamma(\text{total})$

$\Gamma(\gamma\gamma) \times \Gamma(J/\psi\phi)/\Gamma_{\text{total}}$ — $\Gamma_2\Gamma_1/\Gamma$

VALUE (eV)	CL%	DOCUMENT ID		TECN	COMMENT
<41	90	[1] SHEN	10	BELL	10.6 $e^+e^- \to e^+e^- J/\psi\phi$
• • • We do not use the following data for averages, fits, limits, etc. • • •					
< 6	90	[2] SHEN	10	BELL	10.6 $e^+e^- \to e^+e^- J/\psi\phi$

[1] For $J^P = 0^+$.
[2] For $J^P = 2^+$.

$\chi_{c1}(4140)$ BRANCHING RATIOS

$\Gamma(J/\psi\phi)/\Gamma_{\text{total}}$ — Γ_1/Γ

VALUE	EVTS	DOCUMENT ID		TECN	COMMENT
seen	24k	[1] AAIJ	21E	LHCB	$B^+ \to J/\psi\phi K^+$
seen	616	[2] ABAZOV	15M	D0	$p\overline{p} \to J/\psi\phi +$ anything
seen	52	[3] ABAZOV	14A	D0	$B^+ \to J/\psi\phi K^+$
seen	0.3k	[4] CHATRCHYAN	14M	CMS	$B^+ \to J/\psi\phi K^+$
seen	14	[5] AALTONEN	09AH	CDF	$B^+ \to J/\psi\phi K^+$
• • • We do not use the following data for averages, fits, limits, etc. • • •					
seen	4289	[6,7] AAIJ	17C	LHCB	$B^+ \to J/\psi\phi K^+$
not seen		[8] ABLIKIM	15	BES3	$e^+e^- \to \gamma\phi J/\psi$
not seen		[9] AAIJ	12AA	LHCB	$pp \to B^+X$ at 7 TeV

[1] From an amplitude analysis of the decay $B^+ \to J/\psi\phi K^+$ with a significance of 13 σ.
[2] Statistical significance of more than 6 σ.
[3] ABAZOV 14A reports $B(B^+ \to \chi_{c1}(4140)K^+ \to J/\psi\phi K^+)/B(B^+ \to J/\psi\phi K^+) = (19 \pm 7 \pm 4)\%$ with 3.1 σ signficance.
[4] From a fit assuming an S-wave relativistic Breit-Wigner shape above a three-body phase-space non-resonant component with statistical significance of more than 5 σ.
[5] Statistical significance of 3.8 σ.
[6] From an amplitude analysis of the decay $B^+ \to J/\psi\phi K^+$ with a significance of 8.4 σ.
[7] Superseded by AAIJ 21E.
[8] Reported $\sigma(e^+e^- \to \gamma\chi_{c1}(4140))\cdot B(\chi_{c1}(4140) \to J/\psi\phi) < 0.35$, 0.28, and 0.33 pb at 4.23, 4.26, and 4.36 GeV, respectively, at 90% CL.
[9] Reported $B(B^+ \to \chi_{c1}(4140)K^+)\cdot B(\chi_{c1}(4140) \to J/\psi\phi)/B(B^+ \to J/\psi\phi K^+) < 0.07$ at 90% CL.

$\Gamma(\gamma\gamma)/\Gamma_{\text{total}}$ — Γ_2/Γ

VALUE	DOCUMENT ID		TECN	COMMENT
not seen	SHEN	10	BELL	10.6 $e^+e^- \to e^+e^- J/\psi\phi$

$\chi_{c1}(4140)$ REFERENCES

AAIJ	21E	PRL 127 082001	R. Aaij et al.	(LHCb Collab.)
AAIJ	17C	PRL 118 022003	R. Aaij et al.	(LHCb Collab.) JP
Also		PR D95 012002	R. Aaij et al.	(LHCb Collab.)
AALTONEN	17	MPL A32 1750139	T. Aaltonen et al.	(CDF Collab.)
ABAZOV	15M	PRL 115 232001	V.M. Abazov et al.	(D0 Collab.)
ABLIKIM	15	PR D91 032002	M. Ablikim et al.	(BESIII Collab.)
ABAZOV	14A	PR D89 012004	V.M. Abazov et al.	(D0 Collab.)
CHATRCHYAN	14M	PL B734 261	S. Chatrchyan et al.	(CMS Collab.)
AAIJ	12AA	PR D85 091103	R. Aaij et al.	(LHCb Collab.)
SHEN	10	PRL 104 112004	C.P. Shen et al.	(BELLE Collab.)
AALTONEN	09AH	PRL 102 242002	T. Aaltonen et al.	(CDF Collab.)

$\psi(4160)$

$I^G(J^{PC}) = 0^-(1^{--})$

$\psi(4160)$ MASS

VALUE (MeV)	DOCUMENT ID		TECN	COMMENT
4191 ± 5 OUR AVERAGE				
4191^{+9}_{-8}	AAIJ	13BC	LHCB	$B^+ \to K^+\mu^+\mu^-$
4191.7 ± 6.5	[1] ABLIKIM	08D	BES2	$e^+e^- \to$ hadrons
• • • We do not use the following data for averages, fits, limits, etc. • • •				
4193 ± 7	[2] MO	10	RVUE	$e^+e^- \to$ hadrons
4151 ± 4	[3] SETH	05A	RVUE	$e^+e^- \to$ hadrons
4155 ± 5	[4] SETH	05A	RVUE	$e^+e^- \to$ hadrons
4159 ± 20	BRANDELIK	78C	DASP	e^+e^-

[1] Reanalysis of data presented in BAI 02C. From a global fit over the center-of-mass energy region 3.7–5.0 GeV covering the $\psi(3770)$, $\psi(4040)$, $\psi(4160)$, and $\psi(4415)$ resonances. Phase angle fixed in the fit to $\delta = (293 \pm 57)^\circ$.
[2] Reanalysis of data presented in BAI 00 and BAI 02C. From a global fit over the center-of-mass energy 3.8-4.8 GeV covering the $\psi(4040)$, $\psi(4160)$ and $\psi(4415)$ resonances and including interference effects.
[3] From a fit to Crystal Ball (OSTERHELD 86) data.
[4] From a fit to BES (BAI 02C) data.

$\psi(4160)$ WIDTH

VALUE (MeV)	DOCUMENT ID		TECN	COMMENT
70 ± 10 OUR AVERAGE				
65^{+22}_{-16}	AAIJ	13BC	LHCB	$B^+ \to K^+\mu^+\mu^-$
71.8 ± 12.3	[1] ABLIKIM	08D	BES2	$e^+e^- \to$ hadrons
• • • We do not use the following data for averages, fits, limits, etc. • • •				
79 ± 14	[2] MO	10	RVUE	$e^+e^- \to$ hadrons
107 ± 10	[3] SETH	05A	RVUE	$e^+e^- \to$ hadrons
107 ± 16	[4] SETH	05A	RVUE	$e^+e^- \to$ hadrons
78 ± 20	BRANDELIK	78C	DASP	e^+e^-

[1] Reanalysis of data presented in BAI 02C. From a global fit over the center-of-mass energy region 3.7–5.0 GeV covering the $\psi(3770)$, $\psi(4040)$, $\psi(4160)$, and $\psi(4415)$ resonances. Phase angle fixed in the fit to $\delta = (293 \pm 57)^\circ$.
[2] Reanalysis of data presented in BAI 00 and BAI 02C. From a global fit over the center-of-mass energy 3.8-4.8 GeV covering the $\psi(4040)$, $\psi(4160)$ and $\psi(4415)$ resonances and including interference effects.
[3] From a fit to Crystal Ball (OSTERHELD 86) data.
[4] From a fit to BES (BAI 02C) data.

Downloaded from https://academic.oup.com/ptep/article/2022/8/083C01/6651666 by KIT Library user on 27 September 2022

$\psi(4160)$ DECAY MODES

Due to the complexity of the $c\overline{c}$ threshold region, in this listing, "seen" ("not seen") means that a cross section for the mode in question has been measured at effective $\sqrt{s}$ near this particle's central mass value, more (less) than 2σ above zero, without regard to any peaking behavior in $\sqrt{s}$ or absence thereof. See mode listing(s) for details and references.

	Mode	Fraction (Γ_i/Γ)	Confidence level
Γ_1	e^+e^-	$(6.9 \pm 3.3) \times 10^{-6}$	
Γ_2	$\mu^+\mu^-$	seen	
Γ_3	$D\overline{D}$	seen	
Γ_4	$D^0\overline{D}^0$	seen	
Γ_5	D^+D^-	seen	
Γ_6	$D^*\overline{D}+$ c.c.	seen	
Γ_7	$D^*(2007)^0\overline{D}^0+$ c.c.	seen	
Γ_8	$D^*(2010)^+D^-+$ c.c.	seen	
Γ_9	$D^*\overline{D}^*$	seen	
Γ_{10}	$D^*(2007)^0\overline{D}^*(2007)^0$	seen	
Γ_{11}	$D^*(2010)^+D^*(2010)^-$	seen	
Γ_{12}	$D^0D^-\pi^+$+c.c. (excl. $D^*(2007)^0\overline{D}^0$ +c.c., $D^*(2010)^+D^-$ +c.c.)	not seen	
Γ_{13}	$D\overline{D}^*\pi$+c.c. (excl. $D^*\overline{D}^*$)	seen	
Γ_{14}	$D^0D^{*-}\pi^+$+c.c. (excl. $D^*(2010)^+D^*(2010)^-$)	not seen	
Γ_{15}	$D_s^+D_s^-$	not seen	
Γ_{16}	$D_s^{*+}D_s^-$+c.c.	seen	
Γ_{17}	$J/\psi\pi^+\pi^-$	$< 3 \times 10^{-3}$	90%
Γ_{18}	$J/\psi\pi^0\pi^0$	$< 3 \times 10^{-3}$	90%
Γ_{19}	$J/\psi K^+K^-$	$< 2 \times 10^{-3}$	90%
Γ_{20}	$J/\psi\eta$	$< 8 \times 10^{-3}$	90%
Γ_{21}	$J/\psi\pi^0$	$< 1 \times 10^{-3}$	90%
Γ_{22}	$J/\psi\eta'$	$< 5 \times 10^{-3}$	90%
Γ_{23}	$J/\psi\pi^+\pi^-\pi^0$	$< 1 \times 10^{-3}$	90%
Γ_{24}	$\psi(2S)\pi^+\pi^-$	$< 4 \times 10^{-3}$	90%
Γ_{25}	$\chi_{c1}\gamma$	$< 5 \times 10^{-3}$	90%
Γ_{26}	$\chi_{c2}\gamma$	< 1.3 %	90%
Γ_{27}	$\chi_{c1}\pi^+\pi^-\pi^0$	$< 2 \times 10^{-3}$	90%
Γ_{28}	$\chi_{c2}\pi^+\pi^-\pi^0$	$< 8 \times 10^{-3}$	90%
Γ_{29}	$h_c(1P)\pi^+\pi^-$	$< 5 \times 10^{-3}$	90%
Γ_{30}	$h_c(1P)\pi^0\pi^0$	$< 2 \times 10^{-3}$	90%
Γ_{31}	$h_c(1P)\eta$	$< 2 \times 10^{-3}$	90%
Γ_{32}	$h_c(1P)\pi^0$	$< 4 \times 10^{-4}$	90%
Γ_{33}	$\phi\pi^+\pi^-$	$< 2 \times 10^{-3}$	90%
Γ_{34}	$\gamma\chi_{c1}(3872)$	$< 1.8 \times 10^{-3}$	90%
Γ_{35}	$\gamma\chi_{c0}(3915) \to \gamma J/\psi\pi^+\pi^-$	$< 1.36 \times 10^{-4}$	90%
Γ_{36}	$\gamma X(3930) \to \gamma J/\psi\pi^+\pi^-$	$< 1.18 \times 10^{-4}$	90%
Γ_{37}	$\gamma X(3940) \to \gamma J/\psi\pi^+\pi^-$	$< 1.47 \times 10^{-4}$	90%
Γ_{38}	$\gamma\chi_{c0}(3915) \to \gamma\gamma J/\psi$	$< 1.26 \times 10^{-4}$	90%
Γ_{39}	$\gamma X(3930) \to \gamma\gamma J/\psi$	$< 8.8 \times 10^{-5}$	90%
Γ_{40}	$\gamma X(3940) \to \gamma\gamma J/\psi$	$< 1.79 \times 10^{-4}$	90%
Γ_{41}	K^+K^-		
Γ_{42}	$K_S^0K^\pm\pi^\mp$		
Γ_{43}	$p\overline{p}p\overline{p}$	not seen	
Γ_{44}	$\Lambda\overline{\Lambda}$	$< 1.5 \times 10^{-6}$	90%

$\psi(4160)$ PARTIAL WIDTHS

$\Gamma(e^+e^-)$ — Γ_1

VALUE (keV)	DOCUMENT ID		TECN	COMMENT
0.48±0.22	[1] ABLIKIM	08D	BES2	$e^+e^- \to$ hadrons
• • • We do not use the following data for averages, fits, limits, etc. • • •				
0.4 to 1.1	[2] MO	10	RVUE	$e^+e^- \to$ hadrons
0.83±0.08	[3] SETH	05A	RVUE	$e^+e^- \to$ hadrons
0.84±0.13	[4] SETH	05A	RVUE	$e^+e^- \to$ hadrons
0.77±0.23	BRANDELIK	78C	DASP	e^+e^-

[1] Reanalysis of data presented in BAI 02C. From a global fit over the center-of-mass energy region 3.7–5.0 GeV covering the $\psi(3770)$, $\psi(4040)$, $\psi(4160)$, and $\psi(4415)$ resonances. Phase angle fixed in the fit to $\delta = (293 \pm 57)^\circ$.

[2] Reanalysis of data presented in BAI 00 and BAI 02C. From a global fit over the center-of-mass energy 3.8-4.8 GeV covering the $\psi(4040)$, $\psi(4160)$ and $\psi(4415)$ resonances and including interference effects. Four sets of solutions are obtained with the same fit quality, mass and total width, but with different e^+e^- partial widths. We quote only the range of values.

[3] From a fit to Crystal Ball (OSTERHELD 86) data.

[4] From a fit to BES (BAI 02C) data.

$\Gamma(\mu^+\mu^-)$ — Γ_2

VALUE (keV)	DOCUMENT ID		TECN	COMMENT
2.45±1.24±0.94	[1,2] ABLIKIM	20AG	BES3	$e^+e^- \to \mu^+\mu^-$

[1] From a fit to the $e^+e^- \to \mu^+\mu^-$ cross section between 3.8 and 4.6 GeV to the coherent sum of four resonant amplitudes assuming $\Gamma(\mu^+\mu^-) = \Gamma(e^+e^-)$.

[2] From solution 1 of 8 with equal fit quality. Other solutions range from 2.08 ± 0.99 ± 0.80 to 2.45 ± 1.24 ± 0.94 keV.

$\psi(4160)$ $\Gamma(i) \times \Gamma(e^+e^-)/\Gamma(\text{total})$

$\Gamma(J/\psi\eta') \times \Gamma(e^+e^-)/\Gamma_{\text{total}}$ — $\Gamma_{22}\Gamma_1/\Gamma$

VALUE (eV)	EVTS	DOCUMENT ID		TECN	COMMENT
• • • We do not use the following data for averages, fits, limits, etc. • • •					
0.17±0.04	86	[1,2] ABLIKIM	20A	BES3	$e^+e^- \to \eta' J/\psi$
1.07±0.09	86	[1,3] ABLIKIM	20A	BES3	$e^+e^- \to \eta' J/\psi$

[1] Based on a fit to $\sigma(e^+e^- \to \eta' J/\psi)$ from $\sqrt{s} = 4.18$ to 4.60 GeV assuming interfering $\psi(4160)$ and $\psi(4260)$ contributions. At $\sqrt{s} = 4.18$ GeV, $\sigma(e^+e^- \to \eta' J/\psi) = 2.4 \pm 0.3 \pm 0.2$ pb.

[2] Solution I of the fit, corresponding to a phase of -0.03 ± 0.44 rad.

[3] Solution II of the fit, corresponding to a phase of 2.54 ± 0.04 rad.

$\Gamma(\chi_{c1}\gamma) \times \Gamma(e^+e^-)/\Gamma_{\text{total}}$ — $\Gamma_{25}\Gamma_1/\Gamma$

VALUE (eV)	CL%	DOCUMENT ID		TECN	COMMENT
<2.2	90	[1] HAN	15	BELL	10.58 $e^+e^- \to \chi_{c1}\gamma$

[1] Using $B(\eta \to \gamma\gamma) = (39.41 \pm 0.21)$%.

$\Gamma(\chi_{c2}\gamma) \times \Gamma(e^+e^-)/\Gamma_{\text{total}}$ — $\Gamma_{26}\Gamma_1/\Gamma$

VALUE (eV)	CL%	DOCUMENT ID		TECN	COMMENT
• • • We do not use the following data for averages, fits, limits, etc. • • •					
<6.1	90	[1] HAN	15	BELL	10.58 $e^+e^- \to \chi_{c2}\gamma$

[1] Using $B(\eta \to \gamma\gamma) = (39.41 \pm 0.21)$%.

$\Gamma(K_S^0K^\pm\pi^\mp) \times \Gamma(e^+e^-)/\Gamma_{\text{total}}$ — $\Gamma_{42}\Gamma_1/\Gamma$

VALUE (eV)	DOCUMENT ID		TECN	COMMENT
• • • We do not use the following data for averages, fits, limits, etc. • • •				
2.71 ±0.13 ±0.12	[1] ABLIKIM	19AE	BES3	$e^+e^- \to K_S^0K^\pm\pi^\mp$
0.0095±0.0088±0.0004	[2] ABLIKIM	19AE	BES3	$e^+e^- \to K_S^0K^\pm\pi^\mp$

[1] Solution I of the fit including the $\psi(4160)$ with mass 4191 ± 5 MeV and width 70 ± 10 MeV from PDG 16 and the $\psi(4230)$ with mass 4219.6 ± 3.3 ± 5.1 MeV and width 56.0 ± 3.6 ± 6.9 MeV from GAO 17.

[2] Solution II of the fit including the $\psi(4160)$ with mass 4191 ± 5 MeV and width 70 ± 10 MeV from PDG 16 and the $\psi(4230)$ with mass 4219.6 ± 3.3 ± 5.1 MeV and width 56.0 ± 3.6 ± 6.9 MeV from GAO 17.

$\psi(4160)$ $\Gamma(i) \times \Gamma(e^+e^-)/\Gamma^2(\text{total})$

$\Gamma(J/\psi\eta)/\Gamma_{\text{total}} \times \Gamma(e^+e^-)/\Gamma_{\text{total}}$ — $\Gamma_{20}/\Gamma \times \Gamma_1/\Gamma$

VALUE (units 10^{-8})	DOCUMENT ID		TECN	COMMENT
• • • We do not use the following data for averages, fits, limits, etc. • • •				
2.8±0.9±0.9	[1] WANG	13B	BELL	$e^+e^- \to J/\psi\eta\gamma$
12.8±1.7±2.0	[2] WANG	13B	BELL	$e^+e^- \to J/\psi\eta\gamma$

[1] Solution I of two equivalent solutions in a fit using two interfering resonances. Mass and width fixed at 4153 MeV and 103 MeV, respectively.

[2] Solution II of two equivalent solutions in a fit using two interfering resonances. Mass and width fixed at 4153 MeV and 103 MeV, respectively.

$\psi(4160)$ BRANCHING RATIOS

$\Gamma(\mu^+\mu^-)/\Gamma_{\text{total}}$ — Γ_2/Γ

VALUE	DOCUMENT ID		TECN	COMMENT
seen	[1] AAIJ	13BC	LHCB	$B^+ \to K^+\mu^+\mu^-$

[1] AAIJ 13BC report $B(B^+ \to K^+\psi(4160))\,B(\psi(4160) \to \mu^+\mu^-) = (3.5^{+0.9}_{-0.8}) \times 10^{-9}$.

$\Gamma(D\overline{D})/\Gamma(D^*\overline{D}^*)$ — Γ_3/Γ_9

VALUE	DOCUMENT ID		TECN	COMMENT
0.02±0.03±0.02	AUBERT	09M	BABR	$e^+e^- \to \gamma D^{(*)}\overline{D}^{(*)}$

$\Gamma(D^0\overline{D}^0)/\Gamma_{\text{total}}$ — Γ_4/Γ

VALUE	DOCUMENT ID		TECN	COMMENT
seen	CRONIN-HEN...09		CLEO	$e^+e^- \to D^0\overline{D}^0$
seen	PAKHLOVA	08	BELL	$e^+e^- \to D^0\overline{D}^0\gamma$
• • • We do not use the following data for averages, fits, limits, etc. • • •				
not seen	AUBERT	09M	BABR	$e^+e^- \to D^0\overline{D}^0\gamma$

$\Gamma(D^+D^-)/\Gamma_{\text{total}}$ — Γ_5/Γ

VALUE	DOCUMENT ID		TECN	COMMENT
seen	CRONIN-HEN...09		CLEO	$e^+e^- \to D^+D^-$
seen	PAKHLOVA	08	BELL	$e^+e^- \to D^+D^-\gamma$
• • • We do not use the following data for averages, fits, limits, etc. • • •				
not seen	AUBERT	09M	BABR	$e^+e^- \to D^+D^-\gamma$

Downloaded from https://academic.oup.com/ptep/article/2022/8/083C01/6651666 by KIT Library user on 27 September 2022

$\Gamma(D^*(2007)^0\overline{D}^0 + \text{c.c.})/\Gamma_{\text{total}}$ — Γ_7/Γ

VALUE	DOCUMENT ID		TECN	COMMENT
seen	AUBERT	09M	BABR	$e^+e^- \to D^{*0}\overline{D}^0\gamma$
seen	CRONIN-HEN...	09	CLEO	$e^+e^- \to D^{*0}\overline{D}^0$

$\Gamma(D^*(2010)^+ D^- + \text{c.c.})/\Gamma_{\text{total}}$ — Γ_8/Γ

VALUE	DOCUMENT ID		TECN	COMMENT
seen	[1] ZHUKOVA	18	BELL	$e^+e^- \to D^{*+}D^-\gamma$
seen	AUBERT	09M	BABR	$e^+e^- \to D^{*+}D^-\gamma$
seen	CRONIN-HEN...	09	CLEO	$e^+e^- \to D^{*+}D^-$
• • • We do not use the following data for averages, fits, limits, etc. • • •				
seen	PAKHLOVA	07	BELL	$e^+e^- \to D^{*+}D^-\gamma$

[1] Supersedes PAKHLOVA 07.

$\Gamma(D^*\overline{D} + \text{c.c.})/\Gamma(D^*\overline{D}^*)$ — Γ_6/Γ_9

VALUE	DOCUMENT ID		TECN	COMMENT
$0.34 \pm 0.14 \pm 0.05$	AUBERT	09M	BABR	$e^+e^- \to \gamma D^{(*)}\overline{D}^{(*)}$

$\Gamma(D^*(2007)^0\overline{D}^*(2007)^0)/\Gamma_{\text{total}}$ — Γ_{10}/Γ

VALUE	DOCUMENT ID		TECN	COMMENT
seen	AUBERT	09M	BABR	$e^+e^- \to D^{*0}\overline{D}^{*0}\gamma$
seen	CRONIN-HEN...	09	CLEO	$e^+e^- \to D^{*0}\overline{D}^{*0}$

$\Gamma(D^*(2010)^+ D^*(2010)^-)/\Gamma_{\text{total}}$ — Γ_{11}/Γ

VALUE	DOCUMENT ID		TECN	COMMENT
seen	[1] ZHUKOVA	18	BELL	$e^+e^- \to D^{*+}D^{*-}\gamma$
seen	AUBERT	09M	BABR	$e^+e^- \to D^{*+}D^{*-}\gamma$
seen	CRONIN-HEN...	09	CLEO	$e^+e^- \to D^{*+}D^{*-}$
• • • We do not use the following data for averages, fits, limits, etc. • • •				
seen	PAKHLOVA	07	BELL	$e^+e^- \to D^{*+}D^{*-}\gamma$

[1] Supersedes PAKHLOVA 07.

$\Gamma(D^0 D^-\pi^+ + \text{c.c. (excl. } D^*(2007)^0\overline{D}^0 + \text{c.c., } D^*(2010)^+ D^- + \text{c.c.}))/\Gamma_{\text{total}}$ — Γ_{12}/Γ

VALUE	DOCUMENT ID		TECN	COMMENT
not seen	PAKHLOVA	08A	BELL	$e^+e^- \to D^0 D^-\pi^+\gamma$

$\Gamma(D\overline{D}^*\pi + \text{c.c. (excl. } D^*\overline{D}^*))/\Gamma_{\text{total}}$ — Γ_{13}/Γ

VALUE	DOCUMENT ID		TECN	COMMENT
seen	CRONIN-HEN...	09	CLEO	$e^+e^- \to D\overline{D}^*\pi$

$\Gamma(D^0 D^{*-}\pi^+ + \text{c.c. (excl. } D^*(2010)^+ D^*(2010)^-))/\Gamma_{\text{total}}$ — Γ_{14}/Γ

VALUE	DOCUMENT ID		TECN	COMMENT
not seen	PAKHLOVA	09	BELL	$e^+e^- \to D^0 D^{*-}\pi^+\gamma$

$\Gamma(D_s^+ D_s^-)/\Gamma_{\text{total}}$ — Γ_{15}/Γ

VALUE	DOCUMENT ID		TECN	COMMENT
not seen	PAKHLOVA	11	BELL	$e^+e^- \to D_s^+ D_s^-\gamma$
not seen	DEL-AMO-SA...	10N	BABR	$e^+e^- \to D_s^+ D_s^-\gamma$
not seen	CRONIN-HEN...	09	CLEO	$e^+e^- \to D_s^+ D_s^-$

$\Gamma(D_s^{*+} D_s^- + \text{c.c.})/\Gamma_{\text{total}}$ — Γ_{16}/Γ

VALUE	DOCUMENT ID		TECN	COMMENT
seen	PAKHLOVA	11	BELL	$e^+e^- \to D_s^{*+} D_s^-\gamma$
seen	DEL-AMO-SA...	10N	BABR	$e^+e^- \to D_s^{*+} D_s^-\gamma$
seen	CRONIN-HEN...	09	CLEO	$e^+e^- \to D_s^{*+} D_s^-$

$\Gamma(J/\psi\pi^+\pi^-)/\Gamma_{\text{total}}$ — Γ_{17}/Γ

VALUE (units 10^{-3})	CL%	DOCUMENT ID		TECN	COMMENT
<3	90	COAN	06	CLEO	4.12–4.2 $e^+e^- \to$ hadrons

$\Gamma(J/\psi\pi^0\pi^0)/\Gamma_{\text{total}}$ — Γ_{18}/Γ

VALUE (units 10^{-3})	CL%	DOCUMENT ID		TECN	COMMENT
<3	90	COAN	06	CLEO	4.12–4.2 $e^+e^- \to$ hadrons

$\Gamma(J/\psi K^+K^-)/\Gamma_{\text{total}}$ — Γ_{19}/Γ

VALUE (units 10^{-3})	CL%	DOCUMENT ID		TECN	COMMENT
<2	90	COAN	06	CLEO	4.12–4.2 $e^+e^- \to$ hadrons

$\Gamma(J/\psi\eta)/\Gamma_{\text{total}}$ — Γ_{20}/Γ

VALUE (units 10^{-3})	CL%	DOCUMENT ID		TECN	COMMENT
<8	90	COAN	06	CLEO	4.12–4.2 $e^+e^- \to$ hadrons
• • • We do not use the following data for averages, fits, limits, etc. • • •					
possibly seen	[1] ABLIKIM	15L	BES3		$e^+e^- \to J/\psi\eta$
seen	WANG	13B	BELL		$e^+e^- \to J/\psi\eta\gamma$

[1] An enhancement around 4.2 GeV is observed.

$\Gamma(J/\psi\pi^0)/\Gamma_{\text{total}}$ — Γ_{21}/Γ

VALUE (units 10^{-3})	CL%	DOCUMENT ID		TECN	COMMENT
<1	90	COAN	06	CLEO	4.12–4.2 $e^+e^- \to$ hadrons

$\Gamma(J/\psi\eta')/\Gamma_{\text{total}}$ — Γ_{22}/Γ

VALUE (units 10^{-3})	CL%	DOCUMENT ID		TECN	COMMENT
<5	90	COAN	06	CLEO	4.12–4.2 $e^+e^- \to$ hadrons

$\Gamma(J/\psi\pi^+\pi^-\pi^0)/\Gamma_{\text{total}}$ — Γ_{23}/Γ

VALUE (units 10^{-3})	CL%	DOCUMENT ID		TECN	COMMENT
<1	90	COAN	06	CLEO	4.12–4.2 $e^+e^- \to$ hadrons

$\Gamma(\psi(2S)\pi^+\pi^-)/\Gamma_{\text{total}}$ — Γ_{24}/Γ

VALUE (units 10^{-3})	CL%	DOCUMENT ID		TECN	COMMENT
<4	90	COAN	06	CLEO	4.12–4.2 $e^+e^- \to$ hadrons

$\Gamma(\chi_{c1}\gamma)/\Gamma_{\text{total}}$ — Γ_{25}/Γ

VALUE (units 10^{-3})	CL%	DOCUMENT ID		TECN	COMMENT
• • • We do not use the following data for averages, fits, limits, etc. • • •					
<7	90	COAN	06	CLEO	4.12–4.2 $e^+e^- \to$ hadrons

$\Gamma(\chi_{c2}\gamma)/\Gamma_{\text{total}}$ — Γ_{26}/Γ

VALUE (units 10^{-3})	CL%	DOCUMENT ID		TECN	COMMENT
<13	90	COAN	06	CLEO	4.12–4.2 $e^+e^- \to$ hadrons

$\Gamma(\chi_{c1}\pi^+\pi^-\pi^0)/\Gamma_{\text{total}}$ — Γ_{27}/Γ

VALUE (units 10^{-3})	CL%	DOCUMENT ID		TECN	COMMENT
<2	90	COAN	06	CLEO	4.12–4.2 $e^+e^- \to$ hadrons

$\Gamma(\chi_{c2}\pi^+\pi^-\pi^0)/\Gamma_{\text{total}}$ — Γ_{28}/Γ

VALUE (units 10^{-3})	CL%	DOCUMENT ID		TECN	COMMENT
<8	90	COAN	06	CLEO	4.12–4.2 $e^+e^- \to$ hadrons

$\Gamma(h_c(1P)\pi^+\pi^-)/\Gamma_{\text{total}}$ — Γ_{29}/Γ

VALUE (units 10^{-3})	CL%	DOCUMENT ID		TECN	COMMENT
<5	90	[1] PEDLAR	11	CLEO	$e^+e^- \to h_c(1P)\pi^+\pi^-$

[1] At $\sqrt{s} = 4170$ MeV, PEDLAR 11 measures $\sigma(e^+e^- \to h_c(1P)\pi^+\pi^-) = 15.6 \pm 2.3 \pm 1.9 \pm 3.0$ pb, where the errors are statistical, systematic, and due to uncertainty in $B(\psi(2S) \to \pi^0 h_c(1P))$, respectively.

$\Gamma(h_c(1P)\pi^0\pi^0)/\Gamma_{\text{total}}$ — Γ_{30}/Γ

VALUE (units 10^{-3})	CL%	DOCUMENT ID		TECN	COMMENT
<2	90	[1] PEDLAR	11	CLEO	$e^+e^- \to h_c(1P)\pi^0\pi^0$

[1] At $\sqrt{s} = 4170$ MeV, PEDLAR 11 measures $\sigma(e^+e^- \to h_c(1P)\pi^0\pi^0) = 3.0 \pm 3.3 \pm 1.1 \pm 0.6$ pb, where the errors are statistical, systematic, and due to uncertainty in $B(\psi(2S) \to \pi^0 h_c(1P))$, respectively.

$\Gamma(h_c(1P)\eta)/\Gamma_{\text{total}}$ — Γ_{31}/Γ

VALUE (units 10^{-3})	CL%	EVTS	DOCUMENT ID		TECN	COMMENT
<2	90		[1] PEDLAR	11	CLEO	$e^+e^- \to h_c(1P)\eta$
• • • We do not use the following data for averages, fits, limits, etc. • • •						
possibly seen		41	[2] ABLIKIM	17R	BES3	$e^+e^- \to h_c(1P)\eta$

[1] At $\sqrt{s} = 4170$ MeV, PEDLAR 11 measures $\sigma(e^+e^- \to h_c(1P)\eta) = 4.7 \pm 1.7 \pm 1.0 \pm 0.9$ pb, where the errors are statistical, systematic, and due to uncertainty in $B(\psi(2S) \to \pi^0 h_c(1P))$, respectively.

[2] An enhancement around 4.2 GeV is observed.

$\Gamma(h_c(1P)\pi^0)/\Gamma_{\text{total}}$ — Γ_{32}/Γ

VALUE (units 10^{-3})	CL%	DOCUMENT ID		TECN	COMMENT
<0.4	90	[1] PEDLAR	11	CLEO	$e^+e^- \to h_c(1P)\pi^0$

[1] At $\sqrt{s} = 4170$ MeV, PEDLAR 11 measures $\sigma(e^+e^- \to h_c(1P)\pi^0) = -0.7 \pm 1.8 \pm 0.7 \pm 0.1$ pb, where the errors are statistical, systematic, and due to uncertainty in $B(\psi(2S) \to \pi^0 h_c(1P))$, respectively.

$\Gamma(\phi\pi^+\pi^-)/\Gamma_{\text{total}}$ — Γ_{33}/Γ

VALUE (units 10^{-3})	CL%	DOCUMENT ID		TECN	COMMENT
<2	90	COAN	06	CLEO	4.12–4.2 $e^+e^- \to$ hadrons

$\Gamma(\gamma\chi_{c1}(3872))/\Gamma_{\text{total}}$ — Γ_{34}/Γ

VALUE	CL%	DOCUMENT ID		COMMENT
$<1.8 \times 10^{-3}$	90	[1,2] XIAO	13	$\psi(4160) \to \gamma J/\psi\pi^+\pi^-$
• • • We do not use the following data for averages, fits, limits, etc. • • •				
<0.012	90	[1,3] XIAO	13	$\psi(4160) \to \gamma J/\psi\pi^+\pi^-$

[1] Obtained by analyzing CLEO data but not authored by the CLEO Collaboration.

[2] XIAO 13 reports $[\Gamma(\psi(4160) \to \gamma\chi_{c1}(3872))/\Gamma_{\text{total}}] \times [B(\chi_{c1}(3872) \to \pi^+\pi^- J/\psi(1S))] < 0.68 \times 10^{-4}$ which we divide by our best value $B(\chi_{c1}(3872) \to \pi^+\pi^- J/\psi(1S)) = 3.8 \times 10^{-2}$.

[3] XIAO 13 reports $[\Gamma(\psi(4160) \to \gamma\chi_{c1}(3872))/\Gamma_{\text{total}}] \times [B(\chi_{c1}(3872) \to \gamma J/\psi)] < 1.05 \times 10^{-4}$ which we divide by our best value $B(\chi_{c1}(3872) \to \gamma J/\psi) = 8 \times 10^{-3}$.

$\Gamma(\gamma\chi_{c0}(3915) \to \gamma J/\psi\pi^+\pi^-)/\Gamma_{\text{total}}$ — Γ_{35}/Γ

VALUE	CL%	DOCUMENT ID		COMMENT
$<1.36 \times 10^{-4}$	90	[1] XIAO	13	$\psi(4160) \to \gamma J/\psi\pi^+\pi^-$

[1] Obtained by analyzing CLEO data but not authored by the CLEO Collaboration.

Downloaded from https://academic.oup.com/ptep/article/2022/8/083C01/6651666 by KIT Library user on 27 September 2022

$\Gamma(\gamma X(3930) \to \gamma J/\psi\pi^+\pi^-)/\Gamma_{total}$ — Γ_{36}/Γ

VALUE	CL%	DOCUMENT ID		COMMENT
$<1.18 \times 10^{-4}$	90	[1] XIAO	13	$\psi(4160) \to \gamma J/\psi\pi^+\pi^-$

[1] Obtained by analyzing CLEO data but not authored by the CLEO Collaboration.

$\Gamma(\gamma X(3940) \to \gamma J/\psi\pi^+\pi^-)/\Gamma_{total}$ — Γ_{37}/Γ

VALUE	CL%	DOCUMENT ID		COMMENT
$<1.47 \times 10^{-4}$	90	[1] XIAO	13	$\psi(4160) \to \gamma J/\psi\pi^+\pi^-$

[1] Obtained by analyzing CLEO data but not authored by the CLEO Collaboration.

$\Gamma(\gamma \chi_{c0}(3915) \to \gamma\gamma J/\psi)/\Gamma_{total}$ — Γ_{38}/Γ

VALUE	CL%	DOCUMENT ID		COMMENT
$<1.26 \times 10^{-4}$	90	[1] XIAO	13	$\psi(4160) \to \gamma\gamma J/\psi$

[1] Obtained by analyzing CLEO data but not authored by the CLEO Collaboration.

$\Gamma(\gamma X(3930) \to \gamma\gamma J/\psi)/\Gamma_{total}$ — Γ_{39}/Γ

VALUE	CL%	DOCUMENT ID		COMMENT
$<0.88 \times 10^{-4}$	90	[1] XIAO	13	$\psi(4160) \to \gamma\gamma J/\psi$

[1] Obtained by analyzing CLEO data but not authored by the CLEO Collaboration.

$\Gamma(\gamma X(3940) \to \gamma\gamma J/\psi)/\Gamma_{total}$ — Γ_{40}/Γ

VALUE	CL%	DOCUMENT ID		COMMENT
$<1.79 \times 10^{-4}$	90	[1] XIAO	13	$\psi(4160) \to \gamma\gamma J/\psi$

[1] Obtained by analyzing CLEO data but not authored by the CLEO Collaboration.

$\Gamma(K^+K^-)/\Gamma_{total}$ — Γ_{41}/Γ

VALUE	CL%	DOCUMENT ID		TECN	COMMENT
• • • We do not use the following data for averages, fits, limits, etc. • • •					
$<2 \times 10^{-5}$	90	[1] DRUZHININ	15	RVUE	$e^+e^- \to \psi(3770)$

[1] DRUZHININ 15 uses BABAR and CLEO data taking into account interference of the processes $e^+e^- \to K^+K^-$ and $e^+e^- \to K^0_S K^0_L$.

$\Gamma(p\overline{p}p\overline{p})/\Gamma_{total}$ — Γ_{43}/Γ

VALUE	DOCUMENT ID		TECN	COMMENT
not seen	ABLIKIM	21D	BES3	4.0–4.6 $e^+e^- \to p\overline{p}p\overline{p}$

$\Gamma(\Lambda\overline{\Lambda}) \times \Gamma(e^+e^-)/\Gamma_{total}$ — $\Gamma_{44}\Gamma_1/\Gamma$

VALUE (eV)	CL%	DOCUMENT ID		TECN	COMMENT
$<0.7 \times 10^{-3}$	90	[1] ABLIKIM	21AS	BES3	$e^+e^- \to \psi(4160)$

[1] From a measurement of the $e^+e^- \to \Lambda\overline{\Lambda}$ cross section between 3.5 and 4.6 GeV.

$\psi(4160)$ REFERENCES

ABLIKIM	21AS	PR D104 L091104	M. Ablikim et al.	(BESIII Collab.)
ABLIKIM	21D	PR D103 052003	M. Ablikim et al.	(BESIII Collab.)
ABLIKIM	20A	PR D101 012008	M. Ablikim et al.	(BESIII Collab.)
ABLIKIM	20AG	PR D102 112009	M. Ablikim et al.	(BESIII Collab.)
ABLIKIM	19AE	PR D99 072005	M. Ablikim et al.	(BESIII Collab.)
ZHUKOVA	18	PR D97 012002	V. Zhukova et al.	(BELLE Collab.)
ABLIKIM	17R	PR D96 012001	M. Ablikim et al.	(BESIII Collab.)
GAO	17	PR D95 092007	X.Y. Gao, C.P. Shen, C.Z. Yuan	
PDG	16	CP C40 100001	C. Patrignani et al.	(PDG Collab.)
ABLIKIM	15L	PR D91 112005	M. Ablikim et al.	(BESIII Collab.)
DRUZHININ	15	PR D92 054024	V.P. Druzhinin	(NOVO)
HAN	15	PR D92 012011	Y.L. Han et al.	(BELLE Collab.)
AAIJ	13BC	PRL 111 112003	R. Aaij et al.	(LHCb Collab.)
WANG	13B	PR D87 051101	X.L. Wang et al.	(BELLE Collab.)
XIAO	13	PR D87 057501	T. Xiao et al.	(NWES, WAYN)
PAKHLOVA	11	PR D83 011101	G. Pakhlova et al.	(BELLE Collab.)
PEDLAR	11	PRL 107 041803	T. Pedlar et al.	(CLEO Collab.)
DEL-AMO-SA...	10N	PR D82 052004	P. del Amo Sanchez et al.	(BABAR Collab.)
MO	10	PR D82 077501	X.H. Mo, C.Z. Yuan, P. Wang	(BHEP)
AUBERT	09M	PR D79 092001	B. Aubert et al.	(BABAR Collab.)
CRONIN-HEN...	09	PR D80 072001	D. Cronin-Hennessy et al.	(CLEO Collab.)
PAKHLOVA	09	PR D80 091101	G. Pakhlova et al.	(BELLE Collab.)
ABLIKIM	08D	PL B660 315	M. Ablikim et al.	(BES Collab.)
PAKHLOVA	08	PR D77 011103	G. Pakhlova et al.	(BELLE Collab.)
PAKHLOVA	08A	PRL 100 062001	G. Pakhlova et al.	(BELLE Collab.)
PAKHLOVA	07	PRL 98 092001	G. Pakhlova et al.	(BELLE Collab.)
COAN	06	PRL 96 162003	T.E. Coan et al.	(CLEO Collab.)
SETH	05A	PR D72 017501	K.K. Seth	
BAI	02C	PRL 88 101802	J.Z. Bai et al.	(BES Collab.)
BAI	00	PRL 84 594	J.Z. Bai et al.	(BES Collab.)
OSTERHELD	86	SLAC-PUB-4160	A. Osterheld et al.	(SLAC Crystal Ball Collab.)
BRANDELIK	78C	PL 76B 361	R. Brandelik et al.	(DASP Collab.)

$X(4160)$

$I^G(J^{PC}) = ?^?(?^{??})$

OMITTED FROM SUMMARY TABLE

Seen by PAKHLOV 08 in $e^+e^- \to J/\psi X$, $X \to D^*\overline{D}^*$

A state with consistent mass and width is seen by AAIJ 21E in $B^+ \to X(4160)K^+$ with $X(4160) \to J/\psi\phi$ using an amplitude analysis of $B^+ \to J/\psi\phi K^+$ with a significance (accounting for systematic uncertainties) of 4.8 σ. The $J^{PC} = 2^{-+}$ assignment is favored over other assignments with a significance of more than 4 σ.

$X(4160)$ MASS

VALUE (MeV)	EVTS	DOCUMENT ID		TECN	COMMENT
4153^{+23}_{-21} **OUR AVERAGE**					
$4146 \pm 18 \pm 33$	24k	[1] AAIJ	21E	LHCB	$B^+ \to J/\psi\phi K^+$
$4156^{+25}_{-20} \pm 15$	24	PAKHLOV	08	BELL	$e^+e^- \to J/\psi X$

[1] From an amplitude analysis of the decay $B^+ \to J/\psi\phi K^+$ with a significance of 4.8 σ.

$X(4160)$ WIDTH

VALUE (MeV)	EVTS	DOCUMENT ID		TECN	COMMENT
136^{+60}_{-35} **OUR AVERAGE**					
$135 \pm 28^{+59}_{-30}$	24k	[1] AAIJ	21E	LHCB	$B^+ \to J/\psi\phi K^+$
$139^{+111}_{-61} \pm 21$	24	PAKHLOV	08	BELL	$e^+e^- \to J/\psi X$

[1] From an amplitude analysis of the decay $B^+ \to J/\psi\phi K^+$ with a significance of 4.8 σ.

$X(4160)$ DECAY MODES

	Mode	Fraction (Γ_i/Γ)
Γ_1	$D\overline{D}$	not seen
Γ_2	$D^*\overline{D}$ + c.c.	not seen
Γ_3	$D^*\overline{D}^*$	seen
Γ_4	$J/\psi\phi$	seen

$X(4160)$ BRANCHING RATIOS

$\Gamma(D\overline{D})/\Gamma(D^*\overline{D}^*)$ — Γ_1/Γ_3

VALUE	CL%	DOCUMENT ID		TECN	COMMENT
<0.09	90	PAKHLOV	08	BELL	$e^+e^- \to J/\psi X$

$\Gamma(D^*\overline{D}$ + c.c.$)/\Gamma(D^*\overline{D}^*)$ — Γ_2/Γ_3

VALUE	CL%	DOCUMENT ID		TECN	COMMENT
<0.22	90	PAKHLOV	08	BELL	$e^+e^- \to J/\psi X$

$\Gamma(J/\psi\phi)/\Gamma_{total}$ — Γ_4/Γ

VALUE	EVTS	DOCUMENT ID		TECN	COMMENT
seen	24k	[1] AAIJ	21E	LHCB	$B^+ \to J/\psi\phi K^+$

[1] From an amplitude analysis of the decay $B^+ \to J/\psi\phi K^+$ with a significance of 4.8 σ.

$X(4160)$ REFERENCES

AAIJ	21E	PRL 127 082001	R. Aaij et al.	(LHCb Collab.)
PAKHLOV	08	PRL 100 202001	P. Pakhlov et al.	(BELLE Collab.)

$Z_c(4200)$

$I^G(J^{PC}) = 1^+(1^{+-})$

I, G, C need confirmation.

OMITTED FROM SUMMARY TABLE

was $X(4200)^\pm$

This state shows properties different from a conventional $q\overline{q}$ state. A candidate for an exotic structure. See the review on non-$q\overline{q}$ states.

Reported by CHILIKIN 14 in $J/\psi\pi^+$ at a significance of 6.2σ. Assignments of 0^-, 1^-, 2^-, and 2^+ excluded at 6.1σ, 7.4σ, 4.4σ, and 7.0σ level, respectively. Needs confirmation.

$Z_c(4200)$ MASS

VALUE (MeV)	DOCUMENT ID		TECN	COMMENT
4196^{+31+17}_{-29-13}	CHILIKIN	14	BELL	$\overline{B}^0 \to J/\psi K^-\pi^+$

$Z_c(4200)$ WIDTH

VALUE (MeV)	DOCUMENT ID		TECN	COMMENT
$370 \pm 70^{+70}_{-132}$	CHILIKIN	14	BELL	$\overline{B}^0 \to J/\psi K^-\pi^+$

$Z_c(4200)$ DECAY MODES

	Mode	Fraction (Γ_i/Γ)
Γ_1	$J/\psi\pi^+$	seen

Downloaded from https://academic.oup.com/ptep/article/2022/8/083C01/6651666 by KIT Library user on 27 September 2022

$Z_c(4200)$ BRANCHING RATIOS

$\Gamma(J/\psi\pi^+)/\Gamma_{total}$ — Γ_1/Γ

VALUE	DOCUMENT ID		TECN	COMMENT
seen	CHILIKIN	14	BELL	$\overline{B}^0 \to J/\psi K^- \pi^+$
• • • We do not use the following data for averages, fits, limits, etc. • • •				
possibly seen	[1] AAIJ	19R	LHCB	$B^0 \to K^+\pi^- J/\psi$ + c.c.

[1] From a model-independent analysis.

$Z_c(4200)$ REFERENCES

AAIJ	19R	PRL 122 152002	R. Aaij *et al.*	(LHCb Collab.)
CHILIKIN	14	PR D90 112009	K. Chilikin *et al.*	(BELLE Collab.)

$\psi(4230)$

$I^G(J^{PC}) = 0^-(1^{--})$

also known as $Y(4230)$; was $\psi(4260)$

The original $\psi(4260)$ (also known as $Y(4260)$) was observed by AUBERT,B 05I as a peak in the energy dependence of the $e^+e^- \to \pi^+\pi^- J/\psi$ cross section and was confirmed by HE 06B, YUAN 07, LEES 12AC, and LIU 13B in the same process. A higher-statistics analysis by ABLIKIM 17B revealed an asymmetry in the cross section and resulted in a shift of the peak position to a lower mass. The $\psi(4260)$ was therefore renamed $\psi(4230)$. The energy-dependent cross sections for e^+e^- to other channels also exhibit peaks in the same mass region. The parameters corresponding to those peaks are also listed here, but the number of states in this region remains to be determined.

For details see the review on "Spectroscopy of mesons containing two heavy quarks."

$\psi(4230)$ MASS

VALUE (MeV)	EVTS	DOCUMENT ID		TECN	COMMENT
4222.7± 2.6 OUR AVERAGE Error includes scale factor of 1.7. See the ideogram below.					
4234.4± 3.2± 0.2		[1] ABLIKIM	21AJ	BES3	$e^+e^- \to \pi^+\pi^-\psi(2S)$
4216.7± 8.9± 4.1		[2] ABLIKIM	20AG	BES3	$e^+e^- \to \mu^+\mu^-$
4220.4± 2.4± 2.3		[3] ABLIKIM	20N	BES3	$e^+e^- \to \pi^0\pi^0 J/\psi$
4218.6± 3.8± 2.5		[3] ABLIKIM	20O	BES3	$e^+e^- \to \eta J/\psi$
4218.5± 1.6± 4.0		[4] ABLIKIM	19AI	BES3	$e^+e^- \to \omega\chi_{c0}$
4228.6± 4.1± 6.3		ABLIKIM	19R	BES3	$e^+e^- \to \pi^+D^0D^{*-}$ + c.c.
$4200.6^{+7.9}_{-13.3}$± 3.0		[5] ABLIKIM	19V	BES3	$e^+e^- \to \gamma\chi_{c1}(3872)$
4222.0± 3.1± 1.4		[6] ABLIKIM	17B	BES3	$e^+e^- \to \pi^+\pi^- J/\psi$
$4218^{+5.5}_{-4.5}$± 0.9		ABLIKIM	17G	BES3	$e^+e^- \to \pi^+\pi^- h_c$
• • • We do not use the following data for averages, fits, limits, etc. • • •					
4231.9± 5.3± 4.9		ABLIKIM	20N	BES3	$e^+e^- \to \pi^0 Z_c(3900)^0$, $Z_c^0 \to \pi^0 J/\psi$
4209.5± 7.4± 1.4		[7] ABLIKIM	17V	BES3	$e^+e^- \to \pi^+\pi^-\psi(2S)$
4209.1± 6.8± 7.0		[6] ZHANG	17B	RVUE	$e^+e^- \to \pi^+\pi^-\psi(2S)$
4223.3± 1.6± 2.5		[8] ZHANG	17C	RVUE	$e^+e^- \to \pi^+\pi^- J/\psi$ or $\psi(2S)$
4230 ± 8 ± 6	180	[9] ABLIKIM	15C	BES3	$e^+e^- \to \omega\chi_{c0}$
4258.6± 8.3±12.1		[10] LIU	13B	BELL	$e^+e^- \to \gamma\pi^+\pi^- J/\psi$
4245 ± 5 ± 4		[11] LEES	12AC	BABR	10.58 $e^+e^- \to \gamma\pi^+\pi^- J/\psi$
4247 ±12 $^{+17}_{-32}$		[10,12] YUAN	07	BELL	10.58 $e^+e^- \to \gamma\pi^+\pi^- J/\psi$
4284 $^{+17}_{-16}$ ± 41	3.6	HE	06B	CLEO	9.4–10.6 $e^+e^- \to \gamma\pi^+\pi^- J/\psi$
4259 ± 8 $^{+2}_{-6}$	125	[13] AUBERT,B	05I	BABR	10.58 $e^+e^- \to \gamma\pi^+\pi^- J/\psi$

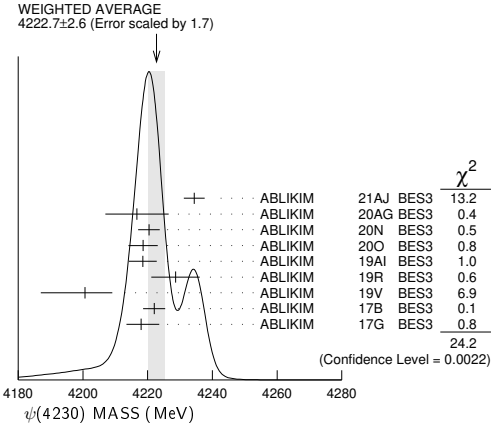

[1] From a three-resonance fit to the Born cross section in the range $\sqrt{s}$ = 4.008–4.698 GeV.

[2] Solution 1 of 8 with equal fit quality to the $e^+e^- \to \mu^+\mu^-$ cross section between 3.8 and 4.6 GeV to the coherent sum of four resonant amplitudes. Other solutions range from 4212.8 ± 7.2 ± 4.0 to 4219.4 ± 11.2 ± 4.1 MeV.

[3] From a fit of the measured cross section in the range $\sqrt{s}$ = 3.808–4.600 GeV.

[4] From a fit of the measured cross section from $\sqrt{s}$ = 4.178–4.278 GeV. Supersedes ABLIKIM 15C.

[5] Simultaneous fit to $\chi_{c1} \to \omega J/\psi$ and $\chi_{c1} \to \pi^+\pi^- J/\psi$.

[6] From a three-resonance fit.

[7] From a fit to the cross section for $e^+e^- \to \pi^+\pi^-\psi(2S) \to 2(\pi^+\pi^-)\ell^+\ell^-$ obtained from 16 center-of-mass energies between 4.008 and 4.600 GeV and comprising 5.1 fb^{-1}. Superseded by ABLIKIM 21AJ.

[8] From a combined fit of BELLE, BABAR and BES3 $e^+e^- \to \pi^+\pi^- J/\psi$ and $e^+e^- \to \pi^+\pi^-\psi(2S)$ data.

[9] From a 3-parameter fit of measured cross sections from $\sqrt{s}$ = 4.21–4.42 GeV to a phase-space modified Breit-Wigner function, using the decays $\chi_{c0} \to \pi^+\pi^-$, $\chi_{c0} \to K^+K^-$, and $\omega \to \pi^+\pi^-\pi^0$.

[10] From a two-resonance fit.

[11] From a single-resonance fit. Supersedes AUBERT,B 05I.

[12] Superseded by LIU 13B.

[13] From a single-resonance fit. Two interfering resonances are not excluded. Superseded by LEES 12AC.

$\psi(4230)$ WIDTH

VALUE (MeV)	EVTS	DOCUMENT ID		TECN	COMMENT
49 ± 8 OUR AVERAGE Error includes scale factor of 3.5. See the ideogram below.					
17.6±18.1± 0.9		[1] ABLIKIM	21AJ	BES3	$e^+e^- \to \pi^+\pi^-\psi(2S)$
47.2±22.8±10.5		[2] ABLIKIM	20AG	BES3	$e^+e^- \to \mu^+\mu^-$
46.2± 4.7± 2.1		[3] ABLIKIM	20N	BES3	$e^+e^- \to \pi^0\pi^0 J/\psi$
82.0± 5.7± 0.4		[3] ABLIKIM	20O	BES3	$e^+e^- \to \eta J/\psi$
28.2± 3.9± 1.6		[4] ABLIKIM	19AI	BES3	$e^+e^- \to \omega\chi_{c0}$
77.0± 6.8± 6.3		ABLIKIM	19R	BES3	$e^+e^- \to \pi^+D^0D^{*-}$ + c.c.
115 $^{+38}_{-26}$ ±12		[5] ABLIKIM	19V	BES3	$e^+e^- \to \gamma\chi_{c1}(3872)$
44.1± 4.3± 2.0		[6] ABLIKIM	17B	BES3	$e^+e^- \to \pi^+\pi^- J/\psi$
$66.0^{+12.3}_{-8.3}$± 0.4		ABLIKIM	17G	BES3	$e^+e^- \to \pi^+\pi^- h_c$
• • • We do not use the following data for averages, fits, limits, etc. • • •					
41.2±16.0±16.4		ABLIKIM	20N	BES3	$e^+e^- \to \pi^0 Z_c(3900)^0$, $Z_c^0 \to \pi^0 J/\psi$
80.1±24.6± 2.9		[7] ABLIKIM	17V	BES3	$e^+e^- \to \pi^+\pi^-\psi(2S)$
76.6±14.2± 2.4		[6] ZHANG	17B	RVUE	$e^+e^- \to \pi^+\pi^-\psi(2S)$
54.2± 2.6± 1.0		[8] ZHANG	17C	RVUE	$e^+e^- \to \pi^+\pi^- J/\psi$ or $\psi(2S)$
38 ±12 ± 2	180	[9] ABLIKIM	15C	BES3	$e^+e^- \to \omega\chi_{c0}$
134.1±16.4± 5.5		[10] LIU	13B	BELL	$e^+e^- \to \gamma\pi^+\pi^- J/\psi$
114 $^{+16}_{-15}$ ± 7		[11] LEES	12AC	BABR	10.58 $e^+e^- \to \gamma\pi^+\pi^- J/\psi$
108 ±19 ±10		[10,12] YUAN	07	BELL	10.58 $e^+e^- \to \gamma\pi^+\pi^- J/\psi$
73 $^{+39}_{-25}$ ± 5	13.6	HE	06B	CLEO	9.4–10.6 $e^+e^- \to \gamma\pi^+\pi^- J/\psi$
88 ±23 $^{+6}_{-4}$	125	[13] AUBERT,B	05I	BABR	10.58 $e^+e^- \to \gamma\pi^+\pi^- J/\psi$

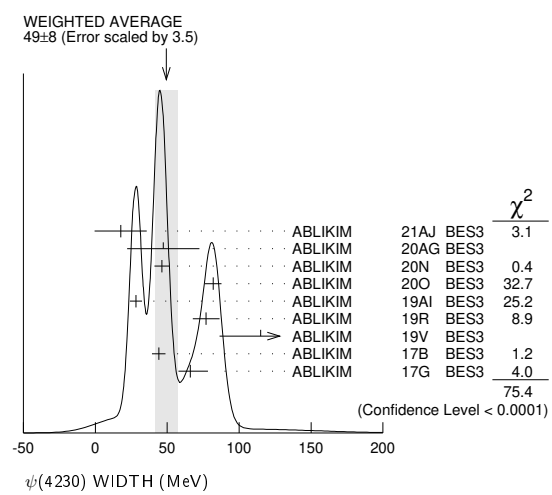

[1] From a three-resonance fit to the Born cross section in the range $\sqrt{s}$ = 4.008–4.698 GeV.

[2] Solution 1 of 8 with equal fit quality to the $e^+e^- \to \mu^+\mu^-$ cross section between 3.8 and 4.6 GeV to the coherent sum of four resonant amplitudes. Other solutions range from 36.4 ± 16.8 ± 8.1 to 49.6 ± 22.6 ± 11.0 MeV.

[3] From a fit of the measured cross section in the range $\sqrt{s}$ = 3.808–4.600 GeV.

[4] From a fit of the measured cross section from $\sqrt{s}$ = 4.178–4.278 GeV. Supersedes ABLIKIM 15C.

[5] Simultaneous fit to $\chi_{c1} \to \omega J/\psi$ and $\chi_{c1} \to \pi^+\pi^- J/\psi$.

[6] From a three-resonance fit.

[7] From a fit to the cross section for $e^+e^- \to \pi^+\pi^-\psi(2S) \to 2(\pi^+\pi^-)\ell^+\ell^-$ obtained from 16 center-of-mass energies between 4.008 and 4.600 GeV and comprising 5.1 fb^{-1}. Superseded by ABLIKIM 21AJ.

Downloaded from https://academic.oup.com/ptep/article/2022/8/083C01/6651666 by KIT Library user on 27 September 2022

[8] From a combined fit of BELLE, BABAR and BES3 $e^+e^- \to \pi^+\pi^- J/\psi$ and $e^+e^- \to \pi^+\pi^-\psi(2S)$ data.
[9] From a 3-parameter fit of measured cross sections from $\sqrt{s}$ = 4.21–4.42 GeV to a phase-space modified Breit-Wigner function, using the decays $\chi_{c0} \to \pi^+\pi^-$, $\chi_{c0} \to K^+K^-$, and $\omega \to \pi^+\pi^-\pi^0$.
[10] From a two-resonance fit.
[11] From a single-resonance fit. Supersedes AUBERT,B 05I.
[12] Superseded by LIU 13B.
[13] From a single-resonance fit. Two interfering resonances are not excluded. Superseded by LEES 12AC.

$\psi(4230)$ DECAY MODES

	Mode	Fraction (Γ_i/Γ)
Γ_1	e^+e^-	
Γ_2	$\mu^+\mu^-$	$(3.1\pm2.8)\times10^{-5}$
Γ_3	$\eta_c(1S)\pi^+\pi^-$	not seen
Γ_4	$\eta_c(1S)\pi^+\pi^-\pi^0$	seen
Γ_5	$J/\psi\pi^+\pi^-$	seen
Γ_6	$J/\psi f_0(980)$, $f_0(980) \to \pi^+\pi^-$	seen
Γ_7	$Z_c(3900)^\pm\pi^\mp$, $Z_c^\pm \to J/\psi\pi^\pm$	seen
Γ_8	$J/\psi\pi^0\pi^0$	seen
Γ_9	$J/\psi K^+K^-$	seen
Γ_{10}	$J/\psi K^0_S K^0_S$	not seen
Γ_{11}	$J/\psi\eta$	seen
Γ_{12}	$J/\psi\pi^0$	not seen
Γ_{13}	$J/\psi\eta'$	seen
Γ_{14}	$J/\psi\pi^+\pi^-\pi^0$	not seen
Γ_{15}	$J/\psi\eta\pi^0$	not seen
Γ_{16}	$J/\psi\eta\eta$	not seen
Γ_{17}	$\psi(2S)\pi^+\pi^-$	seen
Γ_{18}	$\psi(2S)\eta$	not seen
Γ_{19}	$\chi_{c0}\omega$	seen
Γ_{20}	$\chi_{c1}\pi^+\pi^-\pi^0$	not seen
Γ_{21}	$\chi_{c2}\pi^+\pi^-\pi^0$	not seen
Γ_{22}	$h_c(1P)\pi^+\pi^-$	seen
Γ_{23}	$\phi\pi^+\pi^-$	not seen
Γ_{24}	$\phi f_0(980) \to \phi\pi^+\pi^-$	not seen
Γ_{25}	$D\overline{D}$	not seen
Γ_{26}	$D^0\overline{D}^0$	not seen
Γ_{27}	D^+D^-	not seen
Γ_{28}	$D^*\overline{D}$+c.c.	not seen
Γ_{29}	$D^*(2007)^0\overline{D}^0$+c.c.	not seen
Γ_{30}	$D^*(2010)^+D^-$+c.c.	not seen
Γ_{31}	$D^*\overline{D}^*$	
Γ_{32}	$D^*(2007)^0\overline{D}^*(2007)^0$	not seen
Γ_{33}	$D^*(2010)^+D^*(2010)^-$	not seen
Γ_{34}	$D\overline{D}\pi$+c.c.	
Γ_{35}	$D^0D^-\pi^+$+c.c. (excl. $D^*(2007)^0\overline{D}^{*0}$ +c.c., $D^*(2010)^+D^-$ +c.c.)	not seen
Γ_{36}	$D\overline{D}^*\pi$+c.c. (excl. $D^*\overline{D}^*$)	not seen
Γ_{37}	$D^0D^{*-}\pi^+$+c.c. (excl. $D^*(2010)^+D^*(2010)^-$)	not seen
Γ_{38}	$D^0D^*(2010)^-\pi^+$+c.c.	seen
Γ_{39}	$D_1(2420)\overline{D}$+ c.c.	not seen
Γ_{40}	$D^*\overline{D}^*\pi$	not seen
Γ_{41}	$D_s^+D_s^-$	not seen
Γ_{42}	$D_s^{*+}D_s^-$+c.c.	not seen
Γ_{43}	$D_s^{*+}D_s^{*-}$	not seen
Γ_{44}	$p\overline{p}$	not seen
Γ_{45}	$p\overline{p}\pi^0$	not seen
Γ_{46}	$p\overline{p}\eta$	not seen
Γ_{47}	$p\overline{p}\omega$	not seen
Γ_{48}	$\Xi^-\overline{\Xi}^+$	not seen
Γ_{49}	$\pi^+\pi^+\pi^-\pi^-$	not seen
Γ_{50}	$\pi^+\pi^+\pi^-\pi^-\pi^0$	not seen
Γ_{51}	$K^0_S K^\pm\pi^\mp$	not seen
Γ_{52}	$K^0_S K^\pm\pi^\mp\pi^0$	not seen
Γ_{53}	$K^0_S K^\pm\pi^\mp\eta$	not seen
Γ_{54}	$K^+K^-\pi^0$	not seen
Γ_{55}	$K^+K^-\pi^+\pi^-$	not seen
Γ_{56}	$K^+K^-\pi^+\pi^-\pi^0$	not seen
Γ_{57}	$K^+K^+K^-K^-$	not seen
Γ_{58}	$K^+K^+K^-K^-\pi^0$	not seen
Γ_{59}	$p\overline{p}\pi^+\pi^-$	not seen
Γ_{60}	$p\overline{p}\pi^+\pi^-\pi^0$	not seen
Γ_{61}	$p\overline{p}p\overline{p}$	not seen
Γ_{62}	$\Lambda\overline{\Lambda}$	not seen
	Radiative decays	
Γ_{63}	$\eta_c(1S)\gamma$	possibly seen
Γ_{64}	$\eta_c(1S)\pi^0\gamma$	not seen
Γ_{65}	$\chi_{c1}\gamma$	not seen
Γ_{66}	$\chi_{c2}\gamma$	not seen
Γ_{67}	$\chi_{c1}(3872)\gamma$	seen

$\psi(4230)$ PARTIAL WIDTHS

$\Gamma(\mu^+\mu^-)$ — Γ_2

VALUE (keV)		DOCUMENT ID		TECN	COMMENT
1.53±1.26±0.54	[1,2]	ABLIKIM	20AG	BES3	$e^+e^- \to \mu^+\mu^-$

[1] From a fit to the $e^+e^- \to \mu^+\mu^-$ cross section between 3.8 and 4.6 GeV to the coherent sum of four resonant amplitudes assuming $\Gamma(\mu^+\mu^-) = \Gamma(e^+e^-)$.
[2] From solution 1 of 8 with equal fit quality. Other solutions range from 1.09 ± 0.84 ± 0.39 to 1.53 ± 1.26 ± 0.54 keV.

$\psi(4230)$ $\Gamma(i)\times\Gamma(e^+e^-)/\Gamma(\text{total})$

$\Gamma(J/\psi\pi^+\pi^-)\times\Gamma(e^+e^-)/\Gamma_{total}$ — $\Gamma_5\Gamma_1/\Gamma$

VALUE (eV)	EVTS	DOCUMENT ID		TECN	COMMENT
9.2±1.0 OUR AVERAGE					
9.2±0.8±0.7		[1] LEES	12AC	BABR	10.58 $e^+e^- \to \gamma\pi^+\pi^- J/\psi$
$8.9^{+3.9}_{-3.1}\pm1.8$	8.1	HE	06B	CLEO	9.4–10.6 $e^+e^- \to \gamma\pi^+\pi^- J/\psi$
• • • We do not use the following data for averages, fits, limits, etc. • • •					
6.4±0.8±0.6		[2] LIU	13B	BELL	$e^+e^- \to \gamma\pi^+\pi^- J/\psi$
20.5±1.4±2.0		[3] LIU	13B	BELL	$e^+e^- \to \gamma\pi^+\pi^- J/\psi$
$6.0\pm1.2^{+4.7}_{-0.5}$		[2,4] YUAN	07	BELL	10.58 $e^+e^- \to \gamma\pi^+\pi^- J/\psi$
$20.6\pm2.3^{+9.1}_{-1.7}$		[3,4] YUAN	07	BELL	10.58 $e^+e^- \to \gamma\pi^+\pi^- J/\psi$
$5.5\pm1.0^{+0.8}_{-0.7}$	125	[5] AUBERT,B	05I	BABR	10.58 $e^+e^- \to \gamma\pi^+\pi^- J/\psi$

[1] From a single-resonance fit. Supersedes AUBERT,B 05I.
[2] Solution I of two equivalent solutions in a fit using two interfering resonances.
[3] Solution II of two equivalent solutions in a fit using two interfering resonances.
[4] Superseded by LIU 13B.
[5] From a single-resonance fit. Two interfering resonances are not excluded. Superseded by LEES 12AC.

$\Gamma(J/\psi K^+K^-)\times\Gamma(e^+e^-)/\Gamma_{total}$ — $\Gamma_9\Gamma_1/\Gamma$

VALUE (eV)	CL%	DOCUMENT ID		TECN	COMMENT
<1.7	90	[1] SHEN	14	BELL	9.4–10.9 $e^+e^- \to \gamma K^+K^- J/\psi$
• • • We do not use the following data for averages, fits, limits, etc. • • •					
<1.2	90	[2] YUAN	08	BELL	$e^+e^- \to \gamma K^+K^- J/\psi$

[1] From a fit of the broad $K^+K^- J/\psi$ enhancement including a coherent $\psi(4260)$ amplitude with mass and width from LIU 13B. Supersedes YUAN 08. The shape of the cross section observed by ABLIKIM 18N between 2.2 and 2.3 GeV is incompatible with that of $e^+e^- \to \pi^+\pi^- J/\psi$ in ABLIKIM 13T and ABLIKIM 17B. They also observe a broad enhancement around 2.5 GeV.
[2] From a fit of the broad $K^+K^- J/\psi$ enhancement including a coherent $\psi(4260)$ amplitude with mass and width from YUAN 07.

$\Gamma(J/\psi K^0_S K^0_S)\times\Gamma(e^+e^-)/\Gamma_{total}$ — $\Gamma_{10}\Gamma_1/\Gamma$

VALUE (eV)	CL%	DOCUMENT ID		TECN	COMMENT
<0.85	90	[1] SHEN	14	BELL	9.4–10.9 $e^+e^- \to \gamma K^0_S K^0_S J/\psi$

[1] From a fit of the $K^0_S K^0_S J/\psi$ mass range from 4.4 to 5.5 GeV including a coherent $\psi(4260)$ amplitude with mass and width from LIU 13B.

$\Gamma(J/\psi\eta)\times\Gamma(e^+e^-)/\Gamma_{total}$ — $\Gamma_{11}\Gamma_1/\Gamma$

VALUE (eV)	CL%	DOCUMENT ID		TECN	COMMENT
• • • We do not use the following data for averages, fits, limits, etc. • • •					
8.0±1.7		[1] ABLIKIM	20O	BES3	$e^+e^- \to \eta J/\psi$
4.8±1.0		[2] ABLIKIM	20O	BES3	$e^+e^- \to \eta J/\psi$
7.0±1.5		[3] ABLIKIM	20O	BES3	$e^+e^- \to \eta J/\psi$
<14.2	90	WANG	13B	BELL	$e^+e^- \to J/\psi\eta\gamma$

[1] Solution 1 of three equivalent fit solutions using three resonant structures.
[2] Solution 2 of three equivalent fit solutions using three resonant structures.
[3] Solution 3 of three equivalent fit solutions using three resonant structures.

$\Gamma(J/\psi\eta')\times\Gamma(e^+e^-)/\Gamma_{total}$ — $\Gamma_{13}\Gamma_1/\Gamma$

VALUE (eV)	EVTS	DOCUMENT ID		TECN	COMMENT
• • • We do not use the following data for averages, fits, limits, etc. • • •					
0.06±0.03	46	[1,2] ABLIKIM	20A	BES3	$e^+e^- \to \eta' J/\psi$
1.38±0.11	46	[1,3] ABLIKIM	20A	BES3	$e^+e^- \to \eta' J/\psi$

[1] Based on a fit to $\sigma(e^+e^- \to \eta' J/\psi)$ from $\sqrt{s}$ = 4.18 to 4.60 GeV assuming interfering $\psi(4160)$ and $\psi(4260)$ contributions. At $\sqrt{s}$ = 4.23 GeV, $\sigma(e^+e^- \to \eta' J/\psi)$ = 3.6 ± 0.6 ± 0.3 pb.
[2] Solution I of the fit, corresponding to a phase of −0.03 ± 0.44 rad.
[3] Solution II of the fit, corresponding to a phase of 2.54 ± 0.04 rad.

Downloaded from https://academic.oup.com/ptep/article/2022/8/083C01/6651666 by KIT Library user on 27 September 2022

$\Gamma(\psi(2S)\pi^+\pi^-) \times \Gamma(e^+e^-)/\Gamma_{total}$ — $\Gamma_{17}\Gamma_1/\Gamma$

VALUE (eV)	CL%	DOCUMENT ID		TECN	COMMENT
• • • We do not use the following data for averages, fits, limits, etc. • • •					
1.59 ± 0.75		[1] ABLIKIM	21AJ	BES3	$e^+e^- \to \pi^+\pi^-\psi(2S)$
1.63 ± 0.78		[2] ABLIKIM	21AJ	BES3	$e^+e^- \to \pi^+\pi^-\psi(2S)$
0.02 ± 0.01		[3] ABLIKIM	21AJ	BES3	$e^+e^- \to \pi^+\pi^-\psi(2S)$
1.6 ± 1.3		[4] ABLIKIM	19K	BES3	$e^+e^- \to \pi^+\pi^-\psi(2S)$
1.8 ± 1.4		[5] ABLIKIM	19K	BES3	$e^+e^- \to \pi^+\pi^-\psi(2S)$
<4.3	90	[6] LIU	08H	RVUE	$10.58\ e^+e^- \to \psi(2S)\pi^+\pi^-\gamma$
$7.4\ ^{+2.1}_{-1.7}$		[7] LIU	08H	RVUE	$10.58\ e^+e^- \to \psi(2S)\pi^+\pi^-\gamma$

[1] Solution I of four equivalent solutions in a fit using three interfering resonances.
[2] Solution II of four equivalent solutions in a fit using three interfering resonances
[3] Solutions III and IV of four equivalent solutions in a fit using three interfering resonances.
[4] Solution I of two equivalent solutions in a fit using two interfering resonances.
[5] Solution II of two equivalent solutions in a fit using two interfering resonances.
[6] For constructive interference with the $\psi(4360)$ in a combined fit of AUBERT 07S and WANG 07D data with three resonances.
[7] For destructive interference with the $\psi(4360)$ in a combined fit of AUBERT 07S and WANG 07D data with three resonances.

$\Gamma(\chi_{c0}\omega) \times \Gamma(e^+e^-)/\Gamma_{total}$ — $\Gamma_{19}\Gamma_1/\Gamma$

VALUE (eV)	EVTS	DOCUMENT ID		TECN	COMMENT
$2.5 \pm 0.2 \pm 0.3$		[1] ABLIKIM	19AI	BES3	$e^+e^- \to \omega\chi_{c0}$
• • • We do not use the following data for averages, fits, limits, etc. • • •					
$2.7 \pm 0.5 \pm 0.4$	180	[2] ABLIKIM	15C	BES3	$e^+e^- \to \omega\chi_{c0}$

[1] From a fit of the measured cross section from $\sqrt{s} = 4.178$–4.278 GeV. Supersedes ABLIKIM 15C.
[2] From a 3-parameter fit of measured cross sections from $\sqrt{s} = 4.21$–4.42 GeV to a phase-space modified Breit-Wigner function, using the decays $\chi_{c0} \to \pi^+\pi^-$, $\chi_{c0} \to K^+K^-$, and $\omega \to \pi^+\pi^-\pi^0$.

$\Gamma(h_c(1P)\pi^+\pi^-) \times \Gamma(e^+e^-)/\Gamma_{total}$ — $\Gamma_{22}\Gamma_1/\Gamma$

VALUE (eV)	DOCUMENT ID		TECN	COMMENT
$4.6\ ^{+2.9}_{-1.4} \pm 0.8$	ABLIKIM	17G	BES3	$e^+e^- \to \pi^+\pi^- h_c$

$\Gamma(\phi\pi^+\pi^-) \times \Gamma(e^+e^-)/\Gamma_{total}$ — $\Gamma_{23}\Gamma_1/\Gamma$

VALUE (eV)	CL%	DOCUMENT ID		TECN	COMMENT
<0.4	90	AUBERT,BE	06D	BABR	$10.6\ e^+e^- \to K^+K^-\pi^+\pi^-\gamma$

$\Gamma(\phi f_0(980) \to \phi\pi^+\pi^-) \times \Gamma(e^+e^-)/\Gamma_{total}$ — $\Gamma_{24}\Gamma_1/\Gamma$

VALUE (eV)	CL%	DOCUMENT ID		TECN	COMMENT
<0.28	90	[1] AUBERT	07AK	BABR	$10.6\ e^+e^- \to \pi^+\pi^-K^+K^-\gamma$

[1] AUBERT 07AK reports $[\Gamma(\psi(4230) \to \phi f_0(980) \to \phi\pi^+\pi^-) \times \Gamma(\psi(4230) \to e^+e^-)/\Gamma_{total}] \times [B(\phi(1020) \to K^+K^-)] < 0.14$ eV which we divide by our best value $B(\phi(1020) \to K^+K^-) = 49.1 \times 10^{-2}$.

$\Gamma(\Xi^-\overline{\Xi}^+) \times \Gamma(e^+e^-)/\Gamma_{total}$ — $\Gamma_{48}\Gamma_1/\Gamma$

VALUE (eV)	CL%	DOCUMENT ID		TECN	COMMENT
$<2.7 \times 10^{-4}$	90	ABLIKIM	20C	BES3	$e^+e^- \to \Xi^-\overline{\Xi}^+$

$\Gamma(\pi^+\pi^+\pi^-\pi^-) \times \Gamma(e^+e^-)/\Gamma_{total}$ — $\Gamma_{49}\Gamma_1/\Gamma$

VALUE (eV)	CL%	DOCUMENT ID		TECN	COMMENT
<32	90	ABLIKIM	21AW	BES3	$e^+e^- \to 2\pi^+2\pi^-$

$\Gamma(\pi^+\pi^+\pi^-\pi^-\pi^0) \times \Gamma(e^+e^-)/\Gamma_{total}$ — $\Gamma_{50}\Gamma_1/\Gamma$

VALUE (eV)	CL%	DOCUMENT ID		TECN	COMMENT
<16	90	ABLIKIM	21AW	BES3	$e^+e^- \to 2\pi^+2\pi^-\pi^0$

$\Gamma(K^0_S K^\pm\pi^\mp) \times \Gamma(e^+e^-)/\Gamma_{total}$ — $\Gamma_{51}\Gamma_1/\Gamma$

VALUE (eV)	DOCUMENT ID		TECN	COMMENT
• • • We do not use the following data for averages, fits, limits, etc. • • •				
$2.04 \pm 0.19 \pm 0.09$	[1] ABLIKIM	19AE	BES3	$e^+e^- \to K^0_S K^\pm\pi^\mp$
$0.0027 \pm 0.0023 \pm 0.0001$	[2] ABLIKIM	19AE	BES3	$e^+e^- \to K^0_S K^\pm\pi^\mp$
<0.5 at 90% CL	AUBERT	08S	BABR	$10.6\ e^+e^- \to K^0_S K^\pm\pi^\mp\gamma$

[1] Solution I of the fit including the $\psi(4160)$ with mass 4191 ± 5 MeV and width 70 ± 10 MeV from PDG 16 and the $\psi(4230)$ with mass $4219.6 \pm 3.3 \pm 5.1$ MeV and width $56.0 \pm 3.6 \pm 6.9$ MeV from GAO 17.
[2] Solution II of the fit including the $\psi(4160)$ with mass 4191 ± 5 MeV and width 70 ± 10 MeV from PDG 16 and the $\psi(4230)$ with mass $4219.6 \pm 3.3 \pm 5.1$ MeV and width $56.0 \pm 3.6 \pm 6.9$ MeV from GAO 17.

$\Gamma(K^0_S K^\pm\pi^\mp\pi^0) \times \Gamma(e^+e^-)/\Gamma_{total}$ — $\Gamma_{52}\Gamma_1/\Gamma$

VALUE (eV)	CL%	DOCUMENT ID		TECN	COMMENT
<0.05	90	ABLIKIM	19	BES3	$e^+e^- \to K^0_S K^\pm\pi^\mp\pi^0$

$\Gamma(K^0_S K^\pm\pi^\mp\eta) \times \Gamma(e^+e^-)/\Gamma_{total}$ — $\Gamma_{53}\Gamma_1/\Gamma$

VALUE (eV)	CL%	DOCUMENT ID		TECN	COMMENT
<0.19	90	ABLIKIM	19	BES3	$e^+e^- \to K^0_S K^\pm\pi^\mp\eta$

$\Gamma(K^+K^-\pi^0) \times \Gamma(e^+e^-)/\Gamma_{total}$ — $\Gamma_{54}\Gamma_1/\Gamma$

VALUE (eV)	CL%	DOCUMENT ID		TECN	COMMENT
• • • We do not use the following data for averages, fits, limits, etc. • • •					
<0.6	90	AUBERT	08S	BABR	$10.6\ e^+e^- \to K^+K^-\pi^0\gamma$

$\Gamma(K^+K^-\pi^+\pi^-) \times \Gamma(e^+e^-)/\Gamma_{total}$ — $\Gamma_{55}\Gamma_1/\Gamma$

VALUE (eV)	CL%	DOCUMENT ID		TECN	COMMENT
<20	90	ABLIKIM	21AW	BES3	$e^+e^- \to K^+K^-\pi^+\pi^-$

$\Gamma(K^+K^-\pi^+\pi^-\pi^0) \times \Gamma(e^+e^-)/\Gamma_{total}$ — $\Gamma_{56}\Gamma_1/\Gamma$

VALUE (eV)	CL%	DOCUMENT ID		TECN	COMMENT
<43	90	ABLIKIM	21AW	BES3	$e^+e^- \to K^+K^-\pi^+\pi^-\pi^0$

$\Gamma(K^+K^+K^-K^-) \times \Gamma(e^+e^-)/\Gamma_{total}$ — $\Gamma_{57}\Gamma_1/\Gamma$

VALUE (eV)	CL%	DOCUMENT ID		TECN	COMMENT
<3.8	90	ABLIKIM	21AW	BES3	$e^+e^- \to 2K^+2K^-$

$\Gamma(K^+K^+K^-K^-\pi^0) \times \Gamma(e^+e^-)/\Gamma_{total}$ — $\Gamma_{58}\Gamma_1/\Gamma$

VALUE (eV)	CL%	DOCUMENT ID		TECN	COMMENT
<2.1	90	ABLIKIM	21AW	BES3	$e^+e^- \to 2K^+2K^-\pi^0$

$\Gamma(p\overline{p}\pi^+\pi^-) \times \Gamma(e^+e^-)/\Gamma_{total}$ — $\Gamma_{59}\Gamma_1/\Gamma$

VALUE (eV)	CL%	DOCUMENT ID		TECN	COMMENT
<7.2	90	ABLIKIM	21AW	BES3	$e^+e^- \to p\overline{p}\pi^+\pi^-$

$\Gamma(p\overline{p}\pi^+\pi^-\pi^0) \times \Gamma(e^+e^-)/\Gamma_{total}$ — $\Gamma_{60}\Gamma_1/\Gamma$

VALUE (eV)	CL%	DOCUMENT ID		TECN	COMMENT
<15	90	ABLIKIM	21AW	BES3	$e^+e^- \to p\overline{p}\pi^+\pi^-\pi^0$

$\Gamma(\Lambda\overline{\Lambda}) \times \Gamma(e^+e^-)/\Gamma_{total}$ — $\Gamma_{62}\Gamma_1/\Gamma$

VALUE (eV)	CL%	DOCUMENT ID		TECN	COMMENT
$<0.8 \times 10^{-3}$	90	[1] ABLIKIM	21AS	BES3	$e^+e^- \to \psi(4260)$

[1] From a measurement of the $e^+e^- \to \Lambda\overline{\Lambda}$ cross section between 3.5 and 4.6 GeV.

$\Gamma(\chi_{c1}\gamma) \times \Gamma(e^+e^-)/\Gamma_{total}$ — $\Gamma_{65}\Gamma_1/\Gamma$

VALUE (eV)	CL%	DOCUMENT ID		TECN	COMMENT
<1.4	90	[1] HAN	15	BELL	$10.58\ e^+e^- \to \chi_{c1}\gamma$

[1] Using $B(\eta \to \gamma\gamma) = (39.41 \pm 0.21)\%$.

$\Gamma(\chi_{c2}\gamma) \times \Gamma(e^+e^-)/\Gamma_{total}$ — $\Gamma_{66}\Gamma_1/\Gamma$

VALUE (eV)	CL%	DOCUMENT ID		TECN	COMMENT
<4.0	90	[1] HAN	15	BELL	$10.58\ e^+e^- \to \chi_{c2}\gamma$

[1] Using $B(\eta \to \gamma\gamma) = (39.41 \pm 0.21)\%$.

$\psi(4230)$ BRANCHING RATIOS

$\Gamma(\eta_c(1S)\pi^+\pi^-)/\Gamma_{total}$ — Γ_3/Γ

VALUE	DOCUMENT ID		TECN	COMMENT
not seen	[1] ABLIKIM	21B	BES3	$e^+e^- \to \pi^+\pi^-\eta_c$

[1] Not seen in $e^+e^- \to \pi^+\pi^-\eta_c$ at $\sqrt{s} = 4.226$ GeV with a 90% C.L. upper limit on the cross section of 16.8 pb.

$\Gamma(\eta_c(1S)\pi^+\pi^-\pi^0)/\Gamma_{total}$ — Γ_4/Γ

VALUE	DOCUMENT ID		TECN	COMMENT
seen	[1] ABLIKIM	21B	BES3	$e^+e^- \to \pi^+\pi^-\pi^0\eta_c$

[1] Seen as a peak in the $e^+e^- \to \pi^+\pi^-\pi^0\eta_c$ cross section with a peak value of $46.1\ ^{+9.5}_{-9.4} \pm 6.6$ pb at $\sqrt{s} = 4.226$ GeV.

$\Gamma(J/\psi\pi^+\pi^-)/\Gamma_{total}$ — Γ_5/Γ

VALUE	DOCUMENT ID		TECN	COMMENT
seen	ABLIKIM	17B	BES3	$e^+e^- \to \pi^+\pi^- J/\psi$

$\Gamma(J/\psi f_0(980),\ f_0(980) \to \pi^+\pi^-)/\Gamma(J/\psi\pi^+\pi^-)$ — Γ_6/Γ_5

VALUE	DOCUMENT ID		TECN	COMMENT
• • • We do not use the following data for averages, fits, limits, etc. • • •				
0.17 ± 0.13	[1] LEES	12AC	BABR	$10.58\ e^+e^- \to \gamma\pi^+\pi^- J/\psi$

[1] Systematic uncertainties not estimated.

$\Gamma(Z_c(3900)^\pm\pi^\mp,\ Z_c^\pm \to J/\psi\pi^\pm)/\Gamma(J/\psi\pi^+\pi^-)$ — Γ_7/Γ_5

VALUE	DOCUMENT ID		TECN	COMMENT
$0.215 \pm 0.033 \pm 0.075$	[1] ABLIKIM	13T	BES3	$e^+e^- \to \pi^+\pi^- J/\psi$
• • • We do not use the following data for averages, fits, limits, etc. • • •				
0.29 ± 0.08	[2] LIU	13B	BELL	$e^+e^- \to \gamma\pi^+\pi^- J/\psi$

[1] Assuming that the cross section of $e^+e^- \to \pi^+\pi^- J/\psi$ is fully due to the $\psi(4260)$.
[2] Systematic error not evaluated.

$\Gamma(J/\psi\pi^0\pi^0)/\Gamma_{total}$ — Γ_8/Γ

VALUE	DOCUMENT ID		TECN	COMMENT
seen	[1] ABLIKIM	20N	BES3	$e^+e^- \to \pi^0\pi^0 J/\psi$

[1] From a fit to the cross section $e^+e^- \to \pi^0\pi^0 J/\psi$ at center-of-mass energies between 3.808 and 4.600 GeV.

Downloaded from https://academic.oup.com/ptep/article/2022/8/083C01/6651666 by KIT Library user on 27 September 2022

$\Gamma(J/\psi K^0_S K^0_S)/\Gamma_{total}$ — Γ_{10}/Γ

VALUE	DOCUMENT ID		TECN	COMMENT
not seen	SHEN	14	BELL	9.4–10.9 $e^+e^- \to \gamma K^0_S K^0_S J/\psi$

$\Gamma(J/\psi\eta)/\Gamma_{total}$ — Γ_{11}/Γ

VALUE	DOCUMENT ID		TECN	COMMENT
seen	ABLIKIM	20O	BES3	$e^+e^- \to \eta J/\psi$

$\Gamma(J/\psi\eta\pi^0)/\Gamma_{total}$ — Γ_{15}/Γ

VALUE	DOCUMENT ID		TECN	COMMENT
not seen	ABLIKIM	15Q	BES3	4.0–4.6 $e^+e^- \to J/\psi\eta\pi^0$

$\Gamma(\psi(2S)\pi^+\pi^-)/\Gamma_{total}$ — Γ_{17}/Γ

VALUE	DOCUMENT ID		TECN	COMMENT
seen	[1] ABLIKIM	17V	BES3	$e^+e^- \to \pi^+\pi^-\psi(2S)$

[1] From a fit to the cross section for $e^+e^- \to \pi^+\pi^-\psi(2S) \to 2(\pi^+\pi^-)\ell^+\ell^-$ obtained from 16 center-of-mass energies between 4.008 and 4.600 GeV and comprising 5.1 fb^{-1}.

$\Gamma(\psi(2S)\pi^+\pi^-)/\Gamma(J/\psi\pi^+\pi^-)$ — Γ_{17}/Γ_5

VALUE	DOCUMENT ID		TECN	COMMENT
• • • We do not use the following data for averages, fits, limits, etc. • • •				
$(0.11 \pm 0.03 \pm 0.03)$ to $(0.55 \pm 0.18 \pm 0.19)$	[1] ZHANG	17C	RVUE	$e^+e^- \to \pi^+\pi^- J/\psi$ or $\psi(2S)$

[1] From a combined fit of BELLE, BABAR and BES3 $e^+e^- \to \pi^+\pi^- J/\psi$ and $e^+e^- \to \pi^+\pi^-\psi(2S)$ data.

$\Gamma(\chi_{c0}\omega)/\Gamma_{total}$ — Γ_{19}/Γ

VALUE	EVTS	DOCUMENT ID		TECN	COMMENT
seen	180	[1] ABLIKIM	15C	BES3	$e^+e^- \to \omega\chi_{c0}$

[1] From a 3-parameter fit of measured cross sections from $\sqrt{s} = 4.21$–4.42 GeV to a phase-space modified Breit-Wigner function, using the decays $\chi_{c0} \to \pi^+\pi^-$, $\chi_{c0} \to K^+K^-$, and $\omega \to \pi^+\pi^-\pi^0$.

$\Gamma(h_c(1P)\pi^+\pi^-)/\Gamma_{total}$ — Γ_{22}/Γ

VALUE	DOCUMENT ID		TECN	COMMENT
seen	ABLIKIM	17G	BES3	$e^+e^- \to \pi^+\pi^- h_c$

$\Gamma(h_c(1P)\pi^+\pi^-)/\Gamma(J/\psi\pi^+\pi^-)$ — Γ_{22}/Γ_5

VALUE	CL%	DOCUMENT ID		TECN	COMMENT
<1.0	90	[1] PEDLAR	11	CLEO	$e^+e^- \to h_c(1P)\pi^+\pi^-$

[1] At $\sqrt{s} = 4260$ MeV, PEDLAR 11 measures $\sigma(e^+e^- \to h_c(1P)\pi^+\pi^-) = 32 \pm 17 \pm 6 \pm 6$ pb, where the errors are statistical, systematic, and due to uncertainty in $B(\psi(2S) \to \pi^0 h_c(1P))$, respectively.

$\Gamma(D\overline{D})/\Gamma(J/\psi\pi^+\pi^-)$ — Γ_{25}/Γ_5

VALUE	CL%	DOCUMENT ID		TECN	COMMENT
<1.0	90	[1] AUBERT	07BE	BABR	$e^+e^- \to D\overline{D}\gamma$
• • • We do not use the following data for averages, fits, limits, etc. • • •					
<4.0	90	CRONIN-HEN...	09	CLEO	e^+e^-

[1] Using 4259 ± 10 MeV for the mass and 88 ± 24 MeV for the width of $\psi(4260)$.

$\Gamma(D^0\overline{D}^0)/\Gamma_{total}$ — Γ_{26}/Γ

VALUE	DOCUMENT ID		TECN	COMMENT
not seen	CRONIN-HEN...	09	CLEO	$e^+e^- \to D^0\overline{D}^0$
• • • We do not use the following data for averages, fits, limits, etc. • • •				
not seen	AUBERT	09M	BABR	$e^+e^- \to D^0\overline{D}^0\gamma$
not seen	PAKHLOVA	08	BELL	$e^+e^- \to D^0\overline{D}^0\gamma$

$\Gamma(D^+D^-)/\Gamma_{total}$ — Γ_{27}/Γ

VALUE	DOCUMENT ID		TECN	COMMENT
not seen	CRONIN-HEN...	09	CLEO	$e^+e^- \to D^+D^-$
• • • We do not use the following data for averages, fits, limits, etc. • • •				
not seen	AUBERT	09M	BABR	$e^+e^- \to D^+D^-\gamma$
not seen	PAKHLOVA	08	BELL	$e^+e^- \to D^+D^-\gamma$

$\Gamma(D^*\overline{D}+\text{c.c.})/\Gamma(J/\psi\pi^+\pi^-)$ — Γ_{28}/Γ_5

VALUE	CL%	DOCUMENT ID		TECN	COMMENT
<34	90	AUBERT	09M	BABR	$e^+e^- \to \gamma D^*\overline{D}$
• • • We do not use the following data for averages, fits, limits, etc. • • •					
<45	90	CRONIN-HEN...	09	CLEO	e^+e^-

$\Gamma(D^*(2007)^0\overline{D}^0+\text{c.c.})/\Gamma_{total}$ — Γ_{29}/Γ

VALUE	DOCUMENT ID		TECN	COMMENT
not seen	CRONIN-HEN...	09	CLEO	$e^+e^- \to D^{*0}\overline{D}^0$
• • • We do not use the following data for averages, fits, limits, etc. • • •				
not seen	AUBERT	09M	BABR	$e^+e^- \to D^{*0}\overline{D}^0\gamma$

$\Gamma(D^*(2010)^+D^-+\text{c.c.})/\Gamma_{total}$ — Γ_{30}/Γ

VALUE	DOCUMENT ID		TECN	COMMENT
not seen	CRONIN-HEN...	09	CLEO	$e^+e^- \to D^{*+}D^-$
not seen	PAKHLOVA	07	BELL	$e^+e^- \to D^{*+}D^-\gamma$
• • • We do not use the following data for averages, fits, limits, etc. • • •				
not seen	AUBERT	09M	BABR	$e^+e^- \to D^{*+}D^-\gamma$

$\Gamma(D^*\overline{D}^*)/\Gamma(J/\psi\pi^+\pi^-)$ — Γ_{31}/Γ_5

VALUE	CL%	DOCUMENT ID		TECN	COMMENT
<11	90	CRONIN-HEN...	09	CLEO	e^+e^-
• • • We do not use the following data for averages, fits, limits, etc. • • •					
<40	90	AUBERT	09M	BABR	$e^+e^- \to \gamma D^*\overline{D}^*$

$\Gamma(D^*(2007)^0\overline{D}^*(2007)^0)/\Gamma_{total}$ — Γ_{32}/Γ

VALUE	DOCUMENT ID		TECN	COMMENT
not seen	CRONIN-HEN...	09	CLEO	$e^+e^- \to D^{*0}\overline{D}^{*0}$
• • • We do not use the following data for averages, fits, limits, etc. • • •				
not seen	AUBERT	09M	BABR	$e^+e^- \to D^{*0}\overline{D}^{*0}\gamma$

$\Gamma(D^*(2010)^+D^*(2010)^-)/\Gamma_{total}$ — Γ_{33}/Γ

VALUE	DOCUMENT ID		TECN	COMMENT
not seen	CRONIN-HEN...	09	CLEO	$e^+e^- \to D^{*+}D^{*-}$
not seen	PAKHLOVA	07	BELL	$e^+e^- \to D^{*+}D^{*-}\gamma$
• • • We do not use the following data for averages, fits, limits, etc. • • •				
not seen	AUBERT	09M	BABR	$e^+e^- \to D^{*+}D^{*-}\gamma$

$\Gamma(D^0D^-\pi^++\text{c.c.}\ (\text{excl. } D^*(2007)^0\overline{D}^{*0}+\text{c.c.}, D^*(2010)^+D^-+\text{c.c.}))/\Gamma_{total}$ — Γ_{35}/Γ

VALUE	DOCUMENT ID		TECN	COMMENT
not seen	PAKHLOVA	08A	BELL	10.6 $e^+e^- \to D^0D^-\pi^+\gamma$

$\Gamma(D\overline{D}^*\pi+\text{c.c.}\ (\text{excl. } D^*\overline{D}^*))/\Gamma_{total}$ — Γ_{36}/Γ

VALUE	DOCUMENT ID		TECN	COMMENT
not seen	CRONIN-HEN...	09	CLEO	$e^+e^- \to D^*\overline{D}\pi$

$\Gamma(D\overline{D}^*\pi+\text{c.c.}\ (\text{excl. } D^*\overline{D}^*))/\Gamma(J/\psi\pi^+\pi^-)$ — Γ_{36}/Γ_5

VALUE	CL%	DOCUMENT ID		TECN	COMMENT
<15	90	CRONIN-HEN...	09	CLEO	e^+e^-

$\Gamma(D^0D^{*-}\pi^++\text{c.c.}\ (\text{excl. } D^*(2010)^+D^*(2010)^-))/\Gamma_{total}$ — Γ_{37}/Γ

VALUE	DOCUMENT ID		TECN	COMMENT
not seen	PAKHLOVA	09	BELL	$e^+e^- \to D^0D^{*-}\pi^+\gamma$

$\Gamma(D^0D^*(2010)^-\pi^++\text{c.c.})/\Gamma_{total}$ — Γ_{38}/Γ

VALUE	DOCUMENT ID		TECN	COMMENT
seen	ABLIKIM	19R	BES3	$e^+e^- \to \pi^+D^0D^{*-}$ + c.c.

$\Gamma(D^0D^*(2010)^-\pi^++\text{c.c.})/\Gamma(J/\psi\pi^+\pi^-)$ — Γ_{38}/Γ_5

VALUE	CL%	DOCUMENT ID		TECN	COMMENT
<9	90	PAKHLOVA	09	BELL	$e^+e^- \to D^0D^{*-}\pi^+$

$\Gamma(D^0D^*(2010)^-\pi^++\text{c.c.})/\Gamma_{total} \times \Gamma(e^+e^-)/\Gamma_{total}$ — $\Gamma_{38}/\Gamma \times \Gamma_1/\Gamma$

VALUE	CL%	DOCUMENT ID		TECN	COMMENT
$<0.42 \times 10^{-6}$	90	[1] PAKHLOVA	09	BELL	$e^+e^- \to D^0D^{*-}\pi^+$

[1] Using 4263^{+8}_{-9} MeV for the mass of $\psi(4260)$.

$\Gamma(D_1(2420)\overline{D}+\text{c.c.})/\Gamma_{total}$ — Γ_{39}/Γ

VALUE	DOCUMENT ID		TECN	COMMENT
not seen	[1] ABLIKIM	19AR	BES3	$e^+e^- \to \pi^+\pi^-D\overline{D}$

[1] Results from a measurement of $\sigma(e^+e^- \to D_1(2420)\overline{D}+\text{c.c.})$ between $\sqrt{s} = 4.3$ and 4.6 GeV.

$\Gamma(D^*\overline{D}^*\pi)/\Gamma_{total}$ — Γ_{40}/Γ

VALUE	DOCUMENT ID		TECN	COMMENT
not seen	CRONIN-HEN...	09	CLEO	$e^+e^- \to D^*\overline{D}^*\pi$

$\Gamma(D^*\overline{D}^*\pi)/\Gamma(J/\psi\pi^+\pi^-)$ — Γ_{40}/Γ_5

VALUE	CL%	DOCUMENT ID		TECN	COMMENT
<8.2	90	CRONIN-HEN...	09	CLEO	e^+e^-

$\Gamma(D_s^+D_s^-)/\Gamma_{total}$ — Γ_{41}/Γ

VALUE	DOCUMENT ID		TECN	COMMENT
not seen	DEL-AMO-SA...	10N	BABR	$e^+e^- \to D_s^+D_s^-\gamma$
not seen	CRONIN-HEN...	09	CLEO	$e^+e^- \to D_s^+D_s^-$
• • • We do not use the following data for averages, fits, limits, etc. • • •				
not seen	PAKHLOVA	11	BELL	$e^+e^- \to D_s^+D_s^-\gamma$

Downloaded from https://academic.oup.com/ptep/article/2022/8/083C01/6651666 by KIT Library user on 27 September 2022

$\Gamma(D_s^+ D_s^-)/\Gamma(J/\psi\pi^+\pi^-)$ — Γ_{41}/Γ_5

VALUE	CL%	DOCUMENT ID		TECN	COMMENT
<0.7	95	DEL-AMO-SA...	10N	BABR	10.6 e^+e^-
• • • We do not use the following data for averages, fits, limits, etc. • • •					
<1.3	90	CRONIN-HEN..	09	CLEO	e^+e^-

$\Gamma(D_s^{*+} D_s^- + \text{c.c.})/\Gamma_{\text{total}}$ — Γ_{42}/Γ

VALUE	DOCUMENT ID		TECN	COMMENT
not seen	DEL-AMO-SA...	10N	BABR	$e^+e^- \to D_s^{*+} D_s^- \gamma$
not seen	CRONIN-HEN..	09	CLEO	$e^+e^- \to D_s^{*+} D_s^-$
• • • We do not use the following data for averages, fits, limits, etc. • • •				
not seen	PAKHLOVA	11	BELL	$e^+e^- \to D_s^{*+} D_s^- \gamma$

$\Gamma(D_s^{*+} D_s^- + \text{c.c.})/\Gamma(J/\psi\pi^+\pi^-)$ — Γ_{42}/Γ_5

VALUE	CL%	DOCUMENT ID		TECN	COMMENT
< 0.8	90	CRONIN-HEN..	09	CLEO	e^+e^-
• • • We do not use the following data for averages, fits, limits, etc. • • •					
<44	95	DEL-AMO-SA...	10N	BABR	10.6 e^+e^-

$\Gamma(D_s^{*+} D_s^{*-})/\Gamma_{\text{total}}$ — Γ_{43}/Γ

VALUE	DOCUMENT ID		TECN	COMMENT
not seen	CRONIN-HEN..	09	CLEO	$e^+e^- \to D_s^{*+} D_s^{*-}$
• • • We do not use the following data for averages, fits, limits, etc. • • •				
not seen	PAKHLOVA	11	BELL	$e^+e^- \to D_s^{*+} D_s^{*-} \gamma$
not seen	DEL-AMO-SA...	10N	BABR	$e^+e^- \to D_s^{*+} D_s^{*-} \gamma$

$\Gamma(D_s^{*+} D_s^{*-})/\Gamma(J/\psi\pi^+\pi^-)$ — Γ_{43}/Γ_5

VALUE	CL%	DOCUMENT ID		TECN	COMMENT
< 9.5	90	CRONIN-HEN..	09	CLEO	e^+e^-
• • • We do not use the following data for averages, fits, limits, etc. • • •					
<30	95	DEL-AMO-SA...	10N	BABR	10.6 e^+e^-

$\Gamma(p\overline{p})/\Gamma(J/\psi\pi^+\pi^-)$ — Γ_{44}/Γ_5

VALUE	CL%	DOCUMENT ID		TECN	COMMENT
<0.13	90	[1] AUBERT	06B	BABR	$e^+e^- \to p\overline{p}\gamma$

[1] Using 4259 ± 10 MeV for the mass and 88 ± 24 MeV for the width of $\psi(4260)$.

$\Gamma(p\overline{p}\pi^0)/\Gamma(J/\psi\pi^+\pi^-)$ — Γ_{45}/Γ_5

VALUE	CL%	DOCUMENT ID		TECN	COMMENT
$<2\times10^{-4}$	90	ABLIKIM	17F	BES3	$e^+e^- \to \psi(4260) \to$ hadrons

$\Gamma(p\overline{p}\eta)/\Gamma_{\text{total}}$ — Γ_{46}/Γ

VALUE	DOCUMENT ID		TECN	COMMENT
not seen	ABLIKIM	21AN	BES3	$e^+e^- \to p\overline{p}\eta$

$\Gamma(p\overline{p}\omega)/\Gamma_{\text{total}}$ — Γ_{47}/Γ

VALUE	DOCUMENT ID		TECN	COMMENT
not seen	ABLIKIM	21AN	BES3	$e^+e^- \to p\overline{p}\omega$

$\Gamma(p\overline{p}p\overline{p})/\Gamma_{\text{total}}$ — Γ_{61}/Γ

VALUE	DOCUMENT ID		TECN	COMMENT
not seen	ABLIKIM	21D	BES3	4.0–4.6 $e^+e^- \to p\overline{p}p\overline{p}$

Radiative decays

$\Gamma(\eta_c(1S)\gamma)/\Gamma_{\text{total}}$ — Γ_{63}/Γ

VALUE	DOCUMENT ID		COMMENT
possibly seen	[1] ABLIKIM	17W	$e^+e^- \to \gamma\eta_c(1S)$

[1] Significance ranges from 4.2 σ to as low as 1.5 σ for a flat component plus $\psi(4260)$ spectrum. Needs confirmation.

$\Gamma(\eta_c(1S)\pi^0\gamma)/\Gamma_{\text{total}}$ — Γ_{64}/Γ

VALUE	DOCUMENT ID		TECN	COMMENT
not seen	[1] ABLIKIM	21B	BES3	$e^+e^- \to \gamma\pi^0\eta_c$

[1] Not seen in $e^+e^- \to \gamma\pi^0\eta_c$ at $\sqrt{s} = 4.226$ GeV with a 90% C.L. upper limit on the cross section of 11.2 pb.

$\Gamma(\chi_{c1}(3872)\gamma)/\Gamma_{\text{total}}$ — Γ_{67}/Γ

VALUE	EVTS	DOCUMENT ID		TECN	COMMENT
seen		ABLIKIM	19V	BES3	$e^+e^- \to \gamma\chi_{c1}(3872)$
seen	20 ± 5	ABLIKIM	14	BES3	$e^+e^- \to J/\psi\pi^+\pi^-\gamma$

$\psi(4230)$ REFERENCES

ABLIKIM	21AJ	PR D104 052012	M. Ablikim et al.	(BESIII Collab.)
ABLIKIM	21AN	PR D104 092008	M. Ablikim et al.	(BESIII Collab.)
ABLIKIM	21AS	PR D104 L091104	M. Ablikim et al.	(BESIII Collab.)
ABLIKIM	21AW	PR D104 112009	M. Ablikim et al.	(BESIII Collab.)
ABLIKIM	21B	PR D103 032006	M. Ablikim et al.	(BESIII Collab.)
ABLIKIM	21D	PR D103 052003	M. Ablikim et al.	(BESIII Collab.)
ABLIKIM	20A	PR D101 012008	M. Ablikim et al.	(BESIII Collab.)
ABLIKIM	20AG	PR D102 112009	M. Ablikim et al.	(BESIII Collab.)
ABLIKIM	20C	PRL 124 032002	M. Ablikim et al.	(BESIII Collab.)
ABLIKIM	20N	PR D102 012009	M. Ablikim et al.	(BESIII Collab.)
ABLIKIM	20O	PR D102 031101	M. Ablikim et al.	(BESIII Collab.)
ABLIKIM	19	PR D99 012003	M. Ablikim et al.	(BESIII Collab.)
ABLIKIM	19AE	PR D99 072005	M. Ablikim et al.	(BESIII Collab.)
ABLIKIM	19AI	PR D99 091103	M. Ablikim et al.	(BESIII Collab.)
ABLIKIM	19AR	PR D100 032005	M. Ablikim et al.	(BESIII Collab.)
ABLIKIM	19K	PR D99 019903 (errat.)	M. Ablikim et al.	(BESIII Collab.)
ABLIKIM	19R	PRL 122 102002	M. Ablikim et al.	(BESIII Collab.)
ABLIKIM	19V	PRL 122 232002	M. Ablikim et al.	(BESIII Collab.)
ABLIKIM	18N	PR D97 071101	M. Ablikim et al.	(BESIII Collab.)
ABLIKIM	17B	PRL 118 092001	M. Ablikim et al.	(BESIII Collab.)
ABLIKIM	17F	PL B771 45	M. Ablikim et al.	(BESIII Collab.)
ABLIKIM	17G	PRL 118 092002	M. Ablikim et al.	(BESIII Collab.)
ABLIKIM	17V	PR D96 032004	M. Ablikim et al.	(BESIII Collab.)
Also		PR D99 019903 (errat.)	M. Ablikim et al.	(BESIII Collab.)
ABLIKIM	17W	PR D96 051101	M. Ablikim et al.	(BESIII Collab.)
GAO	17	PR D95 092007	X.Y. Gao, C.P. Shen, C.Z. Yuan	
ZHANG	17B	PR D96 054008	J. Zhang, J. Zhang	
ZHANG	17C	EPJ C77 727	J. Zhang, L. Yuan	
PDG	16	CP C40 100001	C. Patrignani et al.	(PDG Collab.)
ABLIKIM	15C	PRL 114 092003	M. Ablikim et al.	(BESIII Collab.)
ABLIKIM	15Q	PR D92 012008	M. Ablikim et al.	(BESIII Collab.)
HAN	15	PR D92 012011	Y.L. Han et al.	(BELLE Collab.)
ABLIKIM	14	PRL 112 092001	M. Ablikim et al.	(BESIII Collab.)
SHEN	14	PR D89 072015	C.P. Shen et al.	(BELLE Collab.)
ABLIKIM	13T	PRL 110 252001	M. Ablikim et al.	(BESIII Collab.)
LIU	13B	PRL 110 252002	Z.Q. Liu et al.	(BELLE Collab.)
WANG	13B	PR D87 051101	X.L. Wang et al.	(BELLE Collab.)
LEES	12AC	PR D86 051102	J.P. Lees et al.	(BABAR Collab.)
PAKHLOVA	11	PR D83 011101	G. Pakhlova et al.	(BELLE Collab.)
PEDLAR	11	PRL 107 041803	T. Pedlar et al.	(CLEO Collab.)
DEL-AMO-SA...	10N	PR D82 052004	P. del Amo Sanchez et al.	(BABAR Collab.)
AUBERT	09M	PR D79 092001	B. Aubert et al.	(BABAR Collab.)
CRONIN-HEN...	09	PR D80 072001	D. Cronin-Hennessy et al.	(CLEO Collab.)
PAKHLOVA	09	PR D80 091101	G. Pakhlova et al.	(BELLE Collab.)
AUBERT	08S	PR D77 092002	B. Aubert et al.	(BABAR Collab.)
LIU	08H	PR D78 014032	Z.Q. Liu, X.S. Qin, C.Z. Yuan	
PAKHLOVA	08	PR D77 011103	G. Pakhlova et al.	(BELLE Collab.)
PAKHLOVA	08A	PRL 100 062001	G. Pakhlova et al.	(BELLE Collab.)
YUAN	08	PR D77 011105	C.Z. Yuan et al.	(BELLE Collab.)
AUBERT	07AK	PR D76 012008	B. Aubert et al.	(BABAR Collab.)
AUBERT	07BE	PR D76 111105	B. Aubert et al.	(BABAR Collab.)
AUBERT	07S	PRL 98 212001	B. Aubert et al.	(BABAR Collab.)
PAKHLOVA	07	PRL 98 092001	G. Pakhlova et al.	(BELLE Collab.)
WANG	07D	PRL 99 142002	X.L. Wang et al.	(BELLE Collab.)
YUAN	07	PRL 99 182004	C.Z. Yuan et al.	(BELLE Collab.)
AUBERT	06B	PR D73 012005	B. Aubert et al.	(BABAR Collab.)
AUBERT,BE	06D	PR D74 091103	B. Aubert et al.	(BABAR Collab.)
HE	06B	PR D74 091104	Q. He et al.	(CLEO Collab.)
AUBERT,B	05I	PRL 95 142001	B. Aubert et al.	(BABAR Collab.)

$R_{c0}(4240)$

$I^G(J^{PC}) = 1^+(0^{--})$

I, G, C need confirmation.

OMITTED FROM SUMMARY TABLE

was $X(4240)^{\pm}$

Properties incompatible with a $q\overline{q}$ structure (exotic state). See the review on non-$q\overline{q}$ states.

Spin and parity assigment $J^P = 0^-$ is favored over 1^-, 2^-, and 2^+ by 8 σ and over 1^+ by 1 σ, according to the four-dimensional amplitude analysis of AAIJ 14AG.

$R_{c0}(4240)$ MASS

VALUE (MeV)	DOCUMENT ID		TECN	COMMENT
$4239\pm18^{+45}_{-10}$	[1] AAIJ	14AG	LHCB	$B^0 \to K^+\pi^-\psi(2S)$

[1] From a 4-dimensional analysis when a second, lower mass resonance is allowed in the $Z_c(4430)$ fit, with significance 6 σ including systematic variations.

$R_{c0}(4240)$ WIDTH

VALUE (MeV)	DOCUMENT ID		TECN	COMMENT
$220\pm47^{+108}_{-74}$	[1] AAIJ	14AG	LHCB	$B^0 \to K^+\pi^-\psi(2S)$

[1] From a 4-dimensional analysis when a second, lower mass resonance is allowed in the $Z_c(4430)$ fit, with significance 6 σ including systematic variations.

$R_{c0}(4240)$ DECAY MODES

	Mode	Fraction (Γ_i/Γ)
Γ_1	$\pi^-\psi(2S)$	seen

$R_{c0}(4240)$ BRANCHING RATIOS

$\Gamma(\pi^-\psi(2S))/\Gamma_{\text{total}}$ — Γ_1/Γ

VALUE	DOCUMENT ID		TECN	COMMENT
seen	[1] AAIJ	14AG	LHCB	$B^0 \to K^+\pi^-\psi(2S)$

[1] From a 4-dimensional analysis when a second, lower mass resonance is allowed in the $Z_c(4430)$ fit. No partial branching fraction quoted.

$R_{c0}(4240)$ REFERENCES

AAIJ	14AG	PRL 112 222002	R. Aaij et al.	(LHCb Collab.)

Downloaded from https://academic.oup.com/ptep/article/2022/8/083C01/6651666 by KIT Library user on 27 September 2022

$X(4250)^{\pm}$

$I^G(J^{PC}) = 1^-(?^{?+})$
I, G, C need confirmation.

OMITTED FROM SUMMARY TABLE

Properties incompatible with a $q\overline{q}$ structure (exotic state). See the review on non-$q\overline{q}$ states.

Observed by MIZUK 08 in the $\pi^+\chi_{c1}(1P)$ invariant mass distribution in $\overline{B}^0 \to K^-\pi^+\chi_{c1}(1P)$ decays. Not seen by LEES 12B in this same mode after accounting for $K\pi$ resonant mass and angular structure.

$X(4250)^{\pm}$ MASS

VALUE (MeV)	DOCUMENT ID		TECN	COMMENT
$\mathbf{4248^{+44}_{-29}{}^{+180}_{-35}}$	[1] MIZUK	08	BELL	$\overline{B}^0 \to K^-\pi^+\chi_{c1}(1P)$

[1] From a Dalitz plot analysis with two Breit-Wigner amplitudes.

$X(4250)^{\pm}$ WIDTH

VALUE (MeV)	DOCUMENT ID		TECN	COMMENT
$\mathbf{177^{+54}_{-39}{}^{+316}_{-61}}$	[1] MIZUK	08	BELL	$\overline{B}^0 \to K^-\pi^+\chi_{c1}(1P)$

[1] From a Dalitz plot analysis with two Breit-Wigner amplitudes.

$X(4250)^{\pm}$ DECAY MODES

	Mode	Fraction (Γ_i/Γ)
Γ_1	$\pi^+\chi_{c1}(1P)$	seen

$X(4250)^{\pm}$ BRANCHING RATIOS

$\Gamma(\pi^+\chi_{c1}(1P))/\Gamma_{total}$ — Γ_1/Γ

VALUE	DOCUMENT ID		TECN	COMMENT
seen	[1] MIZUK	08	BELL	$\overline{B}^0 \to K^-\pi^+\chi_{c1}(1P)$
• • • We do not use the following data for averages, fits, limits, etc. • • •				
not seen	[2] LEES	12B	BABR	$B \to K\pi\chi_{c1}(1P)$

[1] With a product branching fraction measurement of $B(\overline{B}^0 \to K^-X(4250)^+) \times B(X(4250)^+ \to \pi^+\chi_{c1}(1P)) = (4.0^{+2.3}_{-0.9}{}^{+19.7}_{-0.5}) \times 10^{-5}$.
[2] With a product branching fraction limit of $B(\overline{B}^0 \to X(4250)^+K^-) \times B(X(4250)^+ \to \chi_{c1}\pi^+) < 4.0 \times 10^{-5}$ at 90% CL.

$X(4250)^{\pm}$ REFERENCES

LEES	12B	PR D85 052003	J.P. Lees *et al.*	(BABAR Collab.)
MIZUK	08	PR D78 072004	R. Mizuk *et al.*	(BELLE Collab.)

$\chi_{c1}(4274)$

$I^G(J^{PC}) = 0^+(1^{++})$

was $X(4274)$

This state shows properties different from a conventional $q\overline{q}$ state. A candidate for an exotic structure. See the review on non-$q\overline{q}$ states.

Seen by AAIJ 17C in $B^+ \to \chi_{c1}K^+$, $\chi_{c1} \to J/\psi\phi$ using an amplitude analysis of $B^+ \to J/\psi\phi K^+$ with a significance (accounting for systematic uncertainties) of 6.0 σ.

$\chi_{c1}(4274)$ MASS

VALUE (MeV)	EVTS	DOCUMENT ID		TECN	COMMENT
4286^{+8}_{-9} OUR AVERAGE Error includes scale factor of 1.7.					
$4294 \pm 4^{+3}_{-6}$	24k	[1] AAIJ	21E	LHCB	$B^+ \to J/\psi\phi K^+$
$4274.4^{+8.4}_{-6.7} \pm 1.9$	22	[2] AALTONEN	17	CDF	$B^+ \to J/\psi\phi K^+$
• • • We do not use the following data for averages, fits, limits, etc. • • •					
$4273.3 \pm 8.3^{+17.2}_{-3.6}$	4289	[3,4] AAIJ	17C	LHCB	$B^+ \to J/\psi\phi K^+$

[1] From an amplitude analysis of the decay $B^+ \to J/\psi\phi K^+$ with a significance of 18 σ.
[2] From a fit to the invariant mass spectrum with a significance of 3.1 σ.
[3] From an amplitude analysis of the decay $B^+ \to J/\psi\phi K^+$ with a significance of 6.0 σ.
[4] Superseded by AAIJ 21E.

$\chi_{c1}(4274)$ WIDTH

VALUE (MeV)	EVTS	DOCUMENT ID		TECN	COMMENT
51 ± 7 OUR AVERAGE					
$53 \pm 5 \pm 5$	24k	[1] AAIJ	21E	LHCB	$B^+ \to J/\psi\phi K^+$
$32.3^{+21.9}_{-15.3} \pm 7.6$	22	[2] AALTONEN	17	CDF	$B^+ \to J/\psi\phi K^+$
• • • We do not use the following data for averages, fits, limits, etc. • • •					
$56 \pm 11^{+8}_{-11}$	4289	[3,4] AAIJ	17C	LHCB	$B^+ \to J/\psi\phi K^+$

[1] From an amplitude analysis of the decay $B^+ \to J/\psi\phi K^+$ with a significance of 18 σ.
[2] From a fit to the invariant mass spectrum with a significance of 3.1 σ.
[3] From an amplitude analysis of the decay $B^+ \to J/\psi\phi K^+$ with a significance of 6.0 σ.
[4] Superseded by AAIJ 21E.

$\chi_{c1}(4274)$ DECAY MODES

	Mode	Fraction (Γ_i/Γ)
Γ_1	$J/\psi\phi$	seen

$\chi_{c1}(4274)$ BRANCHING RATIOS

$\Gamma(J/\psi\phi)/\Gamma_{total}$ — Γ_1/Γ

VALUE	EVTS	DOCUMENT ID		TECN	COMMENT
seen	24k	[1] AAIJ	21E	LHCB	$B^+ \to J/\psi\phi K^+$
• • • We do not use the following data for averages, fits, limits, etc. • • •					
seen	4289	[2,3] AAIJ	17C	LHCB	$B^+ \to J/\psi\phi K^+$

[1] From an amplitude analysis of the decay $B^+ \to J/\psi\phi K^+$ with a significance of 18 σ.
[2] From an amplitude analysis of the decay $B^+ \to J/\psi\phi K^+$ with a significance of 6.0 σ.
[3] Superseded by AAIJ 21E.

$\chi_{c1}(4274)$ REFERENCES

AAIJ	21E	PRL 127 082001	R. Aaij *et al.*	(LHCb Collab.)
AAIJ	17C	PRL 118 022003	R. Aaij *et al.*	(LHCb Collab.) JP
Also		PR D95 012002	R. Aaij *et al.*	(LHCb Collab.)
AALTONEN	17	MPL A32 1750139	T. Altonen *et al.*	(CDF Collab.)

$X(4350)$

$I^G(J^{PC}) = 0^+(?^{?+})$

OMITTED FROM SUMMARY TABLE

Seen by SHEN 10 in the $\gamma\gamma \to J/\psi\phi$. Needs confirmation.

$X(4350)$ MASS

VALUE (MeV)	EVTS	DOCUMENT ID		TECN	COMMENT
$\mathbf{4350.6^{+4.6}_{-5.1} \pm 0.7}$	$8.8^{+4.2}_{-3.2}$	[1] SHEN	10	BELL	10.6 $e^+e^- \to e^+e^-J/\psi\phi$

[1] Statistical significance of 3.2 σ.

$X(4350)$ WIDTH

VALUE (MeV)	EVTS	DOCUMENT ID		TECN	COMMENT
$\mathbf{13^{+18}_{-9} \pm 4}$	$8.8^{+4.2}_{-3.2}$	[1] SHEN	10	BELL	10.6 $e^+e^- \to e^+e^-J/\psi\phi$

[1] Statistical significance of 3.2 σ.

$X(4350)$ DECAY MODES

	Mode	Fraction (Γ_i/Γ)
Γ_1	$J/\psi\phi$	seen
Γ_2	$\gamma\gamma$	seen

$X(4350)$ $\Gamma(i)\Gamma(\gamma\gamma)/\Gamma(total)$

$\Gamma(\gamma\gamma) \times \Gamma(J/\psi\phi)/\Gamma_{total}$ — $\Gamma_2\Gamma_1/\Gamma$

VALUE (eV)	EVTS	DOCUMENT ID		TECN	COMMENT
$\mathbf{6.7^{+3.2}_{-2.4} \pm 1.1}$	$8.8^{+4.2}_{-3.2}$	[1] SHEN	10	BELL	10.6 $e^+e^- \to e^+e^-J/\psi\phi$
• • • We do not use the following data for averages, fits, limits, etc. • • •					
$1.5^{+0.7}_{-0.6} \pm 0.3$	$8.8^{+4.2}_{-3.2}$	[2] SHEN	10	BELL	10.6 $e^+e^- \to e^+e^-J/\psi\phi$

[1] For $J^P = 0^+$. Statistical significance of 3.2 σ.
[2] For $J^P = 2^+$. Statistical significance of 3.2 σ.

$X(4350)$ BRANCHING RATIOS

$\Gamma(J/\psi\phi)/\Gamma_{total}$ — Γ_1/Γ

VALUE	DOCUMENT ID		TECN	COMMENT
seen	[1] SHEN	10	BELL	10.6 $e^+e^- \to e^+e^-J/\psi\phi$

[1] Statistical significance of 3.2 σ.

$\Gamma(\gamma\gamma)/\Gamma_{total}$ — Γ_2/Γ

VALUE	DOCUMENT ID		TECN	COMMENT
seen	[1] SHEN	10	BELL	10.6 $e^+e^- \to e^+e^-J/\psi\phi$

[1] Statistical significance of 3.2 σ.

$X(4350)$ REFERENCES

SHEN	10	PRL 104 112004	C.P. Shen *et al.*	(BELLE Collab.)

Downloaded from https://academic.oup.com/ptep/article/2022/8/083C01/6651666 by KIT Library user on 27 September 2022

$\psi(4360)$

$I^G(J^{PC}) = 0^-(1^{--})$

also known as $Y(4360)$; was $X(4360)$

This state shows properties different from a conventional $q\overline{q}$ state. A candidate for an exotic structure. See the review on non-$q\overline{q}$ states.

Seen in radiative return from e^+e^- collisions at $\sqrt{s}$ = 9.54–10.58 GeV by AUBERT 07S, WANG 07D, and LEES 14F. See also the review on "Spectroscopy of mesons containing two heavy quarks."

$\psi(4360)$ MASS

VALUE (MeV)	EVTS	DOCUMENT ID		TECN	COMMENT
4372 ± 9 OUR AVERAGE		Error includes scale factor of 2.9. See the ideogram below.			
4390.3 ± 6.0 ± 0.7		[1] ABLIKIM	21AJ	BES3	$e^+e^- \to \pi^+\pi^-\psi(2S)$
4371.7 ± 7.5 ± 1.8		[2] ABLIKIM	21AK	BES3	$e^+e^- \to \gamma\chi_{c2} \to \gamma\gamma J/\psi$
4382.0 ± 13.3 ± 1.7		[3] ABLIKIM	20O	BES3	$e^+e^- \to \eta J/\psi$
4320.0 ± 10.4 ± 7.0		[4] ABLIKIM	17B	BES3	$e^+e^- \to \pi^+\pi^- J/\psi$
$4391.5^{+6.3}_{-6.8} \pm 1.0$		ABLIKIM	17G	BES3	$e^+e^- \to \pi^+\pi^- h_c$
4347 ± 6 ± 3	279	[5] WANG	15A	BELL	10.58 $e^+e^- \to \gamma\pi^+\pi^-\psi(2S)$
4340 ± 16 ± 9	37	[6] LEES	14F	BABR	10.58 $e^+e^- \to \gamma\pi^+\pi^-\psi(2S)$
• • • We do not use the following data for averages, fits, limits, etc. • • •					
4383.8 ± 4.2 ± 0.8		[7] ABLIKIM	17V	BES3	$e^+e^- \to \pi^+\pi^-\psi(2S)$
4383.7 ± 2.9 ± 6.2		[8] ZHANG	17B	RVUE	$e^+e^- \to \pi^+\pi^-\psi(2S)$
4386.4 ± 2.1 ± 6.4		[9] ZHANG	17C	RVUE	$e^+e^- \to \pi^+\pi^- J/\psi$ or $\psi(2S)$
$4355^{+9}_{-10} \pm 9$	74	[10] LIU	08H	RVUE	10.58 $e^+e^- \to \gamma\pi^+\pi^-\psi(2S)$
4324 ± 24		[11] AUBERT	07S	BABR	10.58 $e^+e^- \to \gamma\pi^+\pi^-\psi(2S)$
4361 ± 9 ± 9	47	[6] WANG	07D	BELL	10.58 $e^+e^- \to \gamma\pi^+\pi^-\psi(2S)$

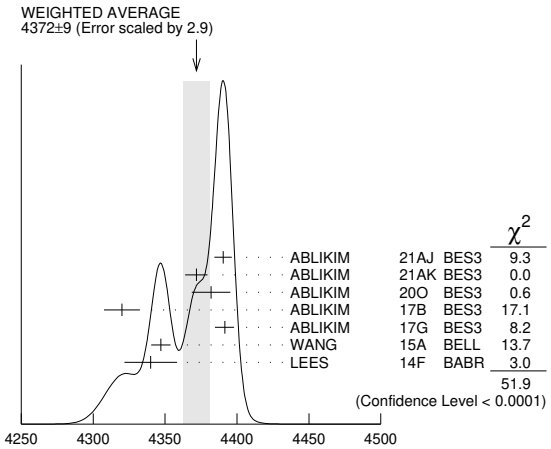

[1] From a three-resonance fit to the Born cross section in the range $\sqrt{s}$ = 4.008–4.698 GeV.
[2] From a five-resonance fit to the cross section for $e^+e^- \to \gamma\gamma J/\psi \to \gamma\gamma\ell^+\ell^-$.
[3] From a fit of the measured cross section in the range $\sqrt{s}$ = 3.808–4.600 GeV.
[4] From a three-resonance fit.
[5] From a two-resonance fit. Supersedes WANG 07D.
[6] From a two-resonance fit.
[7] From a fit to the cross section for $e^+e^- \to \pi^+\pi^-\psi(2S) \to 2(\pi^+\pi^-)\ell^+\ell^-$ obtained from 16 center-of-mass energies between 4.008 and 4.600 GeV and comprising 5.1 fb^{-1}. Superseded by ABLIKIM 21AJ.
[8] From a three-resonance fit.
[9] From a combined fit of BELLE, BABAR and BES3 $e^+e^- \to \pi^+\pi^- J/\psi$ and $e^+e^- \to \pi^+\pi^-\psi(2S)$ data.
[10] From a combined fit of AUBERT 07S and WANG 07D data with two resonances.
[11] From a single-resonance fit. Systematic errors not estimated.

$\psi(4360)$ WIDTH

VALUE (MeV)	EVTS	DOCUMENT ID		TECN	COMMENT
115 ±13 OUR AVERAGE		Error includes scale factor of 2.2. See the ideogram below.			
143.3 ± 10.0 ± 0.5		[1] ABLIKIM	21AJ	BES3	$e^+e^- \to \pi^+\pi^-\psi(2S)$
51.1 ± 17.6 ± 1.9		[2] ABLIKIM	21AK	BES3	$e^+e^- \to \gamma\chi_{c2} \to \gamma\gamma J/\psi$
135.8 ± 60.8 ± 22.5		[3] ABLIKIM	20O	BES3	$e^+e^- \to \eta J/\psi$
$101.4^{+25.3}_{-19.7} \pm 10.2$		[4] ABLIKIM	17B	BES3	$e^+e^- \to \pi^+\pi^- J/\psi$
$139.5^{+16.2}_{-20.6} \pm 0.6$		ABLIKIM	17G	BES3	$e^+e^- \to \pi^+\pi^- h_c$
103 ± 9 ± 5	279	[5] WANG	15A	BELL	10.58 $e^+e^- \to \gamma\pi^+\pi^-\psi(2S)$
94 ± 32 ± 13	37	[6] LEES	14F	BABR	10.58 $e^+e^- \to \gamma\pi^+\pi^-\psi(2S)$
• • • We do not use the following data for averages, fits, limits, etc. • • •					
84.2 ± 12.5 ± 2.1		[7] ABLIKIM	17V	BES3	$e^+e^- \to \pi^+\pi^-\psi(2S)$
94.2 ± 7.3 ± 2.0		[8] ZHANG	17B	RVUE	$e^+e^- \to \pi^+\pi^-\psi(2S)$
96.0 ± 6.7 ± 2.7		[9] ZHANG	17C	RVUE	$e^+e^- \to \pi^+\pi^- J/\psi$ or $\psi(2S)$
$103^{+17}_{-15} \pm 11$	74	[10] LIU	08H	RVUE	10.58 $e^+e^- \to \gamma\pi^+\pi^-\psi(2S)$
172 ± 33		[11] AUBERT	07S	BABR	10.58 $e^+e^- \to \gamma\pi^+\pi^-\psi(2S)$
74 ± 15 ± 10	47	[6] WANG	07D	BELL	10.58 $e^+e^- \to \gamma\pi^+\pi^-\psi(2S)$

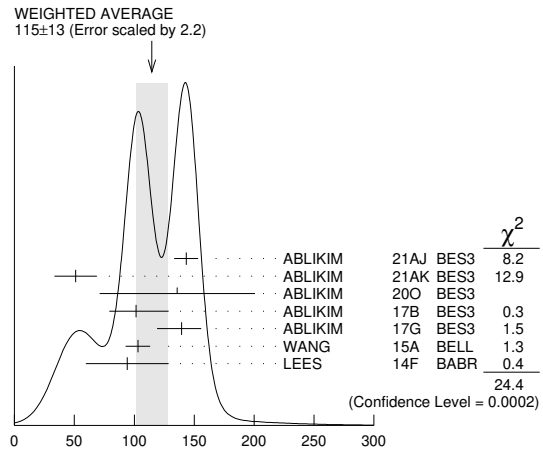

[1] From a three-resonance fit to the Born cross section in the range $\sqrt{s}$ = 4.008–4.698 GeV.
[2] From a five-resonance fit to the cross section for $e^+e^- \to \gamma\gamma J/\psi \to \gamma\gamma\ell^+\ell^-$.
[3] From a fit of the measured cross section in the range $\sqrt{s}$ = 3.808–4.600 GeV.
[4] From a three-resonance fit.
[5] From a two-resonance fit. Supersedes WANG 07D.
[6] From a two-resonance fit.
[7] From a fit to the cross section for $e^+e^- \to \pi^+\pi^-\psi(2S) \to 2(\pi^+\pi^-)\ell^+\ell^-$ obtained from 16 center-of-mass energies between 4.008 and 4.600 GeV and comprising 5.1 fb^{-1}. Superseded by ABLIKIM 21AJ.
[8] From a three-resonance fit.
[9] From a combined fit of BELLE, BABAR and BES3 $e^+e^- \to \pi^+\pi^- J/\psi$ and $e^+e^- \to \pi^+\pi^-\psi(2S)$ data.
[10] From a combined fit of AUBERT 07S and WANG 07D data with two resonances.
[11] From a single-resonance fit. Systematic errors not estimated.

$\psi(4360)$ DECAY MODES

	Mode	Fraction (Γ_i/Γ)
Γ_1	e^+e^-	
Γ_2	$h_c\pi^+\pi^-$	seen
Γ_3	$J/\psi\pi^+\pi^-$	
Γ_4	$\psi(2S)\pi^+\pi^-$	seen
Γ_5	$\psi(3770)\pi^+\pi^-$	possibly seen
Γ_6	$\psi_2(3823)\pi^+\pi^-$	possibly seen
Γ_7	$J/\psi\eta$	seen
Γ_8	$D^0D^{*-}\pi^+$	
Γ_9	$D_1(2420)\overline{D}+$ c.c.	possibly seen
Γ_{10}	$p\overline{p}\eta$	not seen
Γ_{11}	$p\overline{p}\omega$	not seen
Γ_{12}	$\chi_{c1}\gamma$	
Γ_{13}	$\chi_{c2}\gamma$	

$\psi(4360)$ $\Gamma(i) \times \Gamma(e^+e^-)/\Gamma(\text{total})$

$\Gamma(h_c\pi^+\pi^-) \times \Gamma(e^+e^-)/\Gamma_{\text{total}}$ — $\Gamma_2\Gamma_1/\Gamma$

VALUE (eV)	DOCUMENT ID		TECN	COMMENT
$\mathbf{11.6^{+5.0}_{-4.4} \pm 1.9}$	ABLIKIM	17G	BES3	$e^+e^- \to \pi^+\pi^- h_c$

$\Gamma(\psi(2S)\pi^+\pi^-) \times \Gamma(e^+e^-)/\Gamma_{\text{total}}$ — $\Gamma_4\Gamma_1/\Gamma$

VALUE (eV)	EVTS	DOCUMENT ID		TECN	COMMENT
• • • We do not use the following data for averages, fits, limits, etc. • • •					
10.7 ± 4.1		[1] ABLIKIM	21AJ	BES3	$e^+e^- \to \pi^+\pi^-\psi(2S)$
20.7 ± 2.5		[2] ABLIKIM	21AJ	BES3	$e^+e^- \to \pi^+\pi^-\psi(2S)$
9.9 ± 4.1		[3] ABLIKIM	21AJ	BES3	$e^+e^- \to \pi^+\pi^-\psi(2S)$
19.4 ± 2.0		[4] ABLIKIM	21AJ	BES3	$e^+e^- \to \pi^+\pi^-\psi(2S)$
7.3 ± 2.8		[5] ABLIKIM	19K	BES3	$e^+e^- \to \pi^+\pi^-\psi(2S)$

Downloaded from https://academic.oup.com/ptep/article/2022/8/083C01/6651666 by KIT Library user on 27 September 2022

11.0±3.8		[6] ABLIKIM	19K	BES3	$e^+e^- \to \pi^+\pi^-\psi(2S)$
9.2±0.6±0.6	279	[7] WANG	15A	BELL	10.58 $e^+e^- \to \gamma\pi^+\pi^-\psi(2S)$
10.9±0.6±0.7	279	[8] WANG	15A	BELL	10.58 $e^+e^- \to \gamma\pi^+\pi^-\psi(2S)$
6.0±1.0±0.5	37	[5] LEES	14F	BABR	10.58 $e^+e^- \to \gamma\pi^+\pi^-\psi(2S)$
7.2±1.0±0.6	37	[6] LEES	14F	BABR	10.58 $e^+e^- \to \gamma\pi^+\pi^-\psi(2S)$
$11.1^{+1.3}_{-1.2}$	74	[9] LIU	08H	RVUE	10.58 $e^+e^- \to \gamma\pi^+\pi^-\psi(2S)$
12.3±1.2	74	[10] LIU	08H	RVUE	10.58 $e^+e^- \to \gamma\pi^+\pi^-\psi(2S)$
10.4±1.7±1.5	47	[5] WANG	07D	BELL	10.58 $e^+e^- \to \gamma\pi^+\pi^-\psi(2S)$
11.8±1.8±1.4	47	[6] WANG	07D	BELL	10.58 $e^+e^- \to \gamma\pi^+\pi^-\psi(2S)$

[1] Solution I of four equivalent solutions in a fit using three interfering resonances. Supersedes ABLIKIM 19K.
[2] Solution II of four equivalent solutions in a fit using three interfering resonances. Supersedes ABLIKIM 19K.
[3] Solution III of four equivalent solutions in a fit using three interfering resonances. Supersedes ABLIKIM 19K.
[4] Solution IV of four equivalent solutions in a fit using three interfering resonances. Supersedes ABLIKIM 19K.
[5] Solution I of two equivalent solutions in a fit using two interfering resonances.
[6] Solution II of two equivalent solutions in a fit using two interfering resonances.
[7] Solution I of two equivalent solutions from a fit using two interfering resonances. Supersedes WANG 07D.
[8] Solution II of two equivalent solutions from a fit using two interfering resonances. Supersedes WANG 07D.
[9] Solution I in a combined fit of AUBERT 07S and WANG 07D data with two resonances.
[10] Solution II in a combined fit of AUBERT 07S and WANG 07D data with two resonances.

$\Gamma(J/\psi\eta) \times \Gamma(e^+e^-)/\Gamma_{total}$ — $\Gamma_7\Gamma_1/\Gamma$

VALUE (eV)	CL%	DOCUMENT ID		TECN	COMMENT
• • • We do not use the following data for averages, fits, limits, etc. • • •					
3.4±2.2		[1] ABLIKIM	20O	BES3	$e^+e^- \to \eta J/\psi$
1.5±1.0		[2] ABLIKIM	20O	BES3	$e^+e^- \to \eta J/\psi$
1.7±1.1		[3] ABLIKIM	20O	BES3	$e^+e^- \to \eta J/\psi$
<6.8	90	WANG	13B	BELL	$e^+e^- \to J/\psi\eta\gamma$

[1] Solution 1 of three equivalent fit solutions using three resonant structures.
[2] Solution 2 of three equivalent fit solutions using three resonant structures.
[3] Solution 3 of three equivalent fit solutions using three resonant structures.

$\Gamma(\chi_{c1}\gamma) \times \Gamma(e^+e^-)/\Gamma_{total}$ — $\Gamma_{12}\Gamma_1/\Gamma$

VALUE (eV)	CL%	DOCUMENT ID		TECN	COMMENT
<0.57	90	[1] HAN	15	BELL	10.58 $e^+e^- \to \chi_{c1}\gamma$

[1] Using B($\eta \to \gamma\gamma$) = (39.41 ± 0.21)%.

$\Gamma(\chi_{c2}\gamma) \times \Gamma(e^+e^-)/\Gamma_{total}$ — $\Gamma_{13}\Gamma_1/\Gamma$

VALUE (eV)	CL%	DOCUMENT ID		TECN	COMMENT
<1.9	90	[1] HAN	15	BELL	10.58 $e^+e^- \to \chi_{c2}\gamma$

[1] Using B($\eta \to \gamma\gamma$) = (39.41 ± 0.21)%.

$\psi(4360)$ BRANCHING RATIOS

$\Gamma(h_c\pi^+\pi^-)/\Gamma_{total}$ — Γ_2/Γ

VALUE	DOCUMENT ID		TECN	COMMENT
seen	ABLIKIM	17G	BES3	$e^+e^- \to \pi^+\pi^- h_c$

$\Gamma(\psi(2S)\pi^+\pi^-)/\Gamma_{total}$ — Γ_4/Γ

VALUE	DOCUMENT ID		TECN	COMMENT
seen	[1] ABLIKIM	17V	BES3	$e^+e^- \to \pi^+\pi^-\psi(2S)$

[1] From a fit to the cross section for $e^+e^- \to \pi^+\pi^-\psi(2S) \to 2(\pi^+\pi^-)\ell^+\ell^-$ obtained from 16 center-of-mass energies between 4.008 and 4.600 GeV and comprising 5.1 fb^{-1}.

$\Gamma(\psi(2S)\pi^+\pi^-)/\Gamma(J/\psi\pi^+\pi^-)$ — Γ_4/Γ_3

VALUE	DOCUMENT ID		TECN	COMMENT
• • • We do not use the following data for averages, fits, limits, etc. • • •				
(0.81 ± 0.12 ± 0.13) to (42 ± 15 ± 15)	[1] ZHANG	17C	RVUE	$e^+e^- \to \pi^+\pi^- J/\psi$ or $\psi(2S)$

[1] From a combined fit of BELLE, BABAR and BES3 $e^+e^- \to \pi^+\pi^- J/\psi$ and $e^+e^- \to \pi^+\pi^-\psi(2S)$ data.

$\Gamma(\psi(3770)\pi^+\pi^-)/\Gamma_{total}$ — Γ_5/Γ

VALUE	DOCUMENT ID		TECN	COMMENT
possibly seen	[1] ABLIKIM	19AR	BES3	$e^+e^- \to \pi^+\pi^- D\overline{D}$

[1] Observe $e^+e^- \to \pi^+\pi^-\psi(3770)$ at $\sqrt{s}$ = 4.26, 4.36, and 4.42 GeV but cannot establish if continuum or resonant.

$\Gamma(\psi_2(3823)\pi^+\pi^-)/\Gamma_{total}$ — Γ_6/Γ

VALUE	EVTS	DOCUMENT ID		TECN	COMMENT
possibly seen	19	[1] ABLIKIM	15S	BES3	$e^+e^- \to \pi^+\pi^-\chi_{c1}\gamma$

[1] From a fit of $e^+e^- \to \pi^+\pi^-\psi_2(3823)$, $\psi_2(3823) \to \chi_{c1}\gamma$ cross sections taken at $\sqrt{s}$ values of 4.23, 4.26, 4.36, 4.42, and 4.60 GeV to the $\psi(4360)$ line shape.

$\Gamma(J/\psi\eta)/\Gamma_{total}$ — Γ_7/Γ

VALUE	DOCUMENT ID		TECN	COMMENT
seen	[1] ABLIKIM	20O	BES3	$e^+e^- \to \eta J/\psi$

[1] With a significance of 6.0 σ.

$\Gamma(D^0D^{*-}\pi^+)/\Gamma_{total} \times \Gamma(e^+e^-)/\Gamma_{total}$ — $\Gamma_8/\Gamma \times \Gamma_1/\Gamma$

VALUE	CL%	DOCUMENT ID		TECN	COMMENT
$<0.72 \times 10^{-6}$	90	[1] PAKHLOVA	09	BELL	$e^+e^- \to \psi(4360) \to D^0D^{*-}\pi^+$

[1] Using 4355^{+9}_{-10} ± 9 MeV for the mass of $\psi(4360)$.

$\Gamma(D^0D^{*-}\pi^+)/\Gamma(\psi(2S)\pi^+\pi^-)$ — Γ_8/Γ_4

VALUE	CL%	DOCUMENT ID		TECN	COMMENT
<8	90	PAKHLOVA	09	BELL	$e^+e^- \to \psi(4360) \to D^0D^{*-}\pi^+$

$\Gamma(D_1(2420)\overline{D}+\text{c.c.})/\Gamma_{total}$ — Γ_9/Γ

VALUE	DOCUMENT ID		TECN	COMMENT
possibly seen	[1] ABLIKIM	19AR	BES3	$e^+e^- \to \pi^+\pi^- D\overline{D}$

[1] Evidence for $e^+e^- \to D_1(2420)\overline{D}+$ c.c. between $\sqrt{s}$ = 4.3 and 4.6 GeV, not necessarily resonant.

$\Gamma(p\overline{p}\eta)/\Gamma_{total}$ — Γ_{10}/Γ

VALUE	DOCUMENT ID		TECN	COMMENT
not seen	ABLIKIM	21AN	BES3	$e^+e^- \to p\overline{p}\eta$

$\Gamma(p\overline{p}\omega)/\Gamma_{total}$ — Γ_{11}/Γ

VALUE	DOCUMENT ID		TECN	COMMENT
not seen	ABLIKIM	21AN	BES3	$e^+e^- \to p\overline{p}\omega$

$\psi(4360)$ REFERENCES

ABLIKIM	21AJ	PR D104 052012	M. Ablikim et al.	(BESIII Collab.)
ABLIKIM	21AK	PR D104 092001	M. Ablikim et al.	(BESIII Collab.)
ABLIKIM	21AN	PR D104 092008	M. Ablikim et al.	(BESIII Collab.)
ABLIKIM	20O	PR D102 031101	M. Ablikim et al.	(BESIII Collab.)
ABLIKIM	19AR	PR D100 032005	M. Ablikim et al.	(BESIII Collab.)
ABLIKIM	19K	PR D99 019903 (errat.)	M. Ablikim et al.	(BESIII Collab.)
ABLIKIM	17B	PRL 118 092001	M. Ablikim et al.	(BESIII Collab.)
ABLIKIM	17G	PRL 118 092002	M. Ablikim et al.	(BESIII Collab.)
ABLIKIM	17V	PR D96 032004	M. Ablikim et al.	(BESIII Collab.)
Also		PR D99 019903 (errat.)	M. Ablikim et al.	(BESIII Collab.)
ZHANG	17B	PR D96 054008	J. Zhang, J. Zhang	
ZHANG	17C	EPJ C77 727	J. Zhang, L. Yuan	
ABLIKIM	15S	PRL 115 011803	M. Ablikim et al.	(BESIII Collab.)
HAN	15	PR D92 012011	Y.L. Han et al.	(BELLE Collab.)
WANG	15A	PR D91 112007	X.L. Wang et al.	(BELLE Collab.)
LEES	14F	PR D89 111103	J.P. Lees et al.	(BABAR Collab.)
WANG	13B	PR D87 051101	X.L. Wang et al.	(BELLE Collab.)
PAKHLOVA	09	PR D80 091101	G. Pakhlova et al.	(BELLE Collab.)
LIU	08H	PR D78 014032	Z.Q. Liu, X.S. Qin, C.Z. Yuan	
AUBERT	07S	PRL 98 212001	B. Aubert et al.	(BABAR Collab.)
WANG	07D	PRL 99 142002	X.L. Wang et al.	(BELLE Collab.)

$\psi(4415)$

$I^G(J^{PC}) = 0^-(1^{--})$

$\psi(4415)$ MASS

VALUE (MeV)	DOCUMENT ID		TECN	COMMENT
4421 ± 4 OUR ESTIMATE				
4415.1 ± 7.9	[1] ABLIKIM	08D	BES2	$e^+e^- \to$ hadrons
• • • We do not use the following data for averages, fits, limits, etc. • • •				
4412 ±15	[2] MO	10	RVUE	$e^+e^- \to$ hadrons
4411 ± 7	[3] PAKHLOVA	08A	BELL	10.6 $e^+e^- \to D^0D^-\pi^+\gamma$
4425 ± 6	[4] SETH	05A	RVUE	$e^+e^- \to$ hadrons
4429 ± 9	[5] SETH	05A	RVUE	$e^+e^- \to$ hadrons
4417 ±10	BRANDELIK	78C	DASP	e^+e^-
4414 ± 7	SIEGRIST	76	MRK1	e^+e^-

[1] Reanalysis of data presented in BAI 02C. From a global fit over the center-of-mass energy region 3.7–5.0 GeV covering the $\psi(3770)$, $\psi(4040)$, $\psi(4160)$, and $\psi(4415)$ resonances. Phase angle fixed in the fit to $\delta = (234 \pm 88)^\circ$.
[2] Reanalysis of data presented in BAI 00 and BAI 02C. From a global fit over the center-of-mass energy 3.8-4.8 GeV covering the $\psi(4040)$, $\psi(4160)$ and $\psi(4415)$ resonances and including interference effects.
[3] Systematic uncertainties not estimated.
[4] From a fit to Crystal Ball (OSTERHELD 86) data.
[5] From a fit to BES (BAI 02C) data.

$\psi(4415)$ WIDTH

VALUE (MeV)	DOCUMENT ID		TECN	COMMENT
62 ±20 OUR ESTIMATE				
71.5±19.0	[6] ABLIKIM	08D	BES2	$e^+e^- \to$ hadrons
• • • We do not use the following data for averages, fits, limits, etc. • • •				
118 ±32	[7] MO	10	RVUE	$e^+e^- \to$ hadrons
77 ±20	[8] PAKHLOVA	08A	BELL	10.6 $e^+e^- \to D^0D^-\pi^+\gamma$
119 ±16	[9] SETH	05A	RVUE	$e^+e^- \to$ hadrons
118 ±35	[10] SETH	05A	RVUE	$e^+e^- \to$ hadrons

Downloaded from https://academic.oup.com/ptep/article/2022/8/083C01/6651666 by KIT Library user on 27 September 2022

66 ±15	BRANDELIK	78C	DASP	e^+e^-
33 ±10	SIEGRIST	76	MRK1	e^+e^-

[6] Reanalysis of data presented in BAI 02C. From a global fit over the center-of-mass energy region 3.7–5.0 GeV covering the $\psi(3770)$, $\psi(4040)$, $\psi(4160)$, and $\psi(4415)$ resonances. Phase angle fixed in the fit to $\delta = (234 \pm 88)^\circ$.

[7] Reanalysis of data presented in BAI 00 and BAI 02C. From a global fit over the center-of-mass energy 3.8-4.8 GeV covering the $\psi(4040)$, $\psi(4160)$ and $\psi(4415)$ resonances and including interference effects.

[8] Systematic uncertainties not estimated.

[9] From a fit to Crystal Ball (OSTERHELD 86) data.

[10] From a fit to BES (BAI 02C) data.

$\psi(4415)$ DECAY MODES

Due to the complexity of the $c\overline{c}$ threshold region, in this listing, "seen" ("not seen") means that a cross section for the mode in question has been measured at effective $\sqrt{s}$ near this particle's central mass value, more (less) than 2σ above zero, without regard to any peaking behavior in $\sqrt{s}$ or absence thereof. See mode listing(s) for details and references.

	Mode	Fraction (Γ_i/Γ)	Confidence level
Γ_1	$D\overline{D}$	seen	
Γ_2	$D^0\overline{D}^0$	seen	
Γ_3	D^+D^-	seen	
Γ_4	$D^*\overline{D}$ + c.c.	seen	
Γ_5	$D^*(2007)^0\overline{D}^0$ + c.c.	seen	
Γ_6	$D^*(2010)^+D^-$ + c.c.	seen	
Γ_7	$D^*\overline{D}^*$	seen	
Γ_8	$D^*(2007)^0\overline{D}^*(2007)^0$ + c.c.	seen	
Γ_9	$D^*(2010)^+D^*(2010)^-$ + c.c.	seen	
Γ_{10}	$D^0D^-\pi^+$ (excl. $D^*(2007)^0\overline{D}^0$ + c.c., $D^*(2010)^+D^-$ + c.c.	< 2.3 %	90%
Γ_{11}	$D\overline{D}_2^*(2460) \rightarrow D^0D^-\pi^+$ + c.c.	(10 ± 4) %	
Γ_{12}	$D^0D^{*-}\pi^+$ + c.c.	< 11 %	90%
Γ_{13}	$D_1(2420)\overline{D}$ + c.c.	possibly seen	
Γ_{14}	$D_s^+D_s^-$	not seen	
Γ_{15}	$\omega\chi_{c2}$	possibly seen	
Γ_{16}	$D_s^{*+}D_s^-$ + c.c.	seen	
Γ_{17}	$D_s^{*+}D_s^{*-}$	not seen	
Γ_{18}	$\psi_2(3823)\pi^+\pi^-$	possibly seen	
Γ_{19}	$\psi(3770)\pi^+\pi^-$	possibly seen	
Γ_{20}	$J/\psi\eta$	$< 6 \times 10^{-3}$	90%
Γ_{21}	$\chi_{c1}\gamma$	$< 8 \times 10^{-4}$	90%
Γ_{22}	$\chi_{c2}\gamma$	$< 4 \times 10^{-3}$	90%
Γ_{23}	$\Lambda\overline{\Lambda}$	$< 3.1 \times 10^{-6}$	90%
Γ_{24}	e^+e^-	$(9.4 \pm 3.2) \times 10^{-6}$	
Γ_{25}	$\mu^+\mu^-$	$(2.0 \pm 1.0) \times 10^{-5}$	

$\psi(4415)$ PARTIAL WIDTHS

$\Gamma(e^+e^-)$ — Γ_{24}

VALUE (keV)	DOCUMENT ID		TECN	COMMENT
0.58±0.07 OUR ESTIMATE				
0.35±0.12	[11] ABLIKIM	08D	BES2	$e^+e^- \rightarrow$ hadrons
• • • We do not use the following data for averages, fits, limits, etc. • • •				
0.4 to 0.8	[12] MO	10	RVUE	$e^+e^- \rightarrow$ hadrons
0.72±0.11	[13] SETH	05A	RVUE	$e^+e^- \rightarrow$ hadrons
0.64±0.23	[14] SETH	05A	RVUE	$e^+e^- \rightarrow$ hadrons
0.49±0.13	BRANDELIK	78C	DASP	e^+e^-
0.44±0.14	SIEGRIST	76	MRK1	e^+e^-

[11] Reanalysis of data presented in BAI 02C. From a global fit over the center-of-mass energy region 3.7–5.0 GeV covering the $\psi(3770)$, $\psi(4040)$, $\psi(4160)$, and $\psi(4415)$ resonances. Phase angle fixed in the fit to $\delta = (234 \pm 88)^\circ$.

[12] Reanalysis of data presented in BAI 00 and BAI 02C. From a global fit over the center-of-mass energy 3.8-4.8 GeV covering the $\psi(4040)$, $\psi(4160)$ and $\psi(4415)$ resonances and including interference effects. Four sets of solutions are obtained with the same fit quality, mass and total width, but with different e^+e^- partial widths. We quote only the range of values.

[13] From a fit to Crystal Ball (OSTERHELD 86) data.

[14] From a fit to BES (BAI 02C) data.

$\Gamma(\mu^+\mu^-)$ — Γ_{25}

VALUE (keV)	DOCUMENT ID		TECN	COMMENT
1.25±0.28±0.35	[15,16] ABLIKIM	20AG	BES3	$e^+e^- \rightarrow \mu^+\mu^-$

[15] From a fit to the $e^+e^- \rightarrow \mu^+\mu^-$ cross section between 3.8 and 4.6 GeV to the coherent sum of four resonant amplitudes assuming $\Gamma(\mu^+\mu^-) = \Gamma(e^+e^-)$.

[16] From solution 1 of 8 with equal fit quality. Other solutions range from $1.24 \pm 0.28 \pm 0.35$ to $1.27 \pm 0.41 \pm 0.36$ keV.

$\psi(4415)$ $\Gamma(i) \times \Gamma(e^+e^-)/\Gamma(\text{total})$

$\Gamma(J/\psi\eta) \times \Gamma(e^+e^-)/\Gamma_{\text{total}}$ — $\Gamma_{20}\Gamma_{24}/\Gamma$

VALUE (eV)	CL%	DOCUMENT ID		TECN	COMMENT
<3.6	90	WANG	13B	BELL	$e^+e^- \rightarrow J/\psi\eta\gamma$

$\Gamma(\chi_{c1}\gamma) \times \Gamma(e^+e^-)/\Gamma_{\text{total}}$ — $\Gamma_{21}\Gamma_{24}/\Gamma$

VALUE (eV)	CL%	DOCUMENT ID		TECN	COMMENT
<0.47	90	[17] HAN	15	BELL	10.58 $e^+e^- \rightarrow \chi_{c1}\gamma$

[17] Using $B(\eta \rightarrow \gamma\gamma) = (39.41 \pm 0.21)$%.

$\Gamma(\chi_{c2}\gamma) \times \Gamma(e^+e^-)/\Gamma_{\text{total}}$ — $\Gamma_{22}\Gamma_{24}/\Gamma$

VALUE (eV)	CL%	DOCUMENT ID		TECN	COMMENT
<2.3	90	[18] HAN	15	BELL	10.58 $e^+e^- \rightarrow \chi_{c2}\gamma$

[18] Using $B(\eta \rightarrow \gamma\gamma) = (39.41 \pm 0.21)$%.

$\Gamma(\Lambda\overline{\Lambda}) \times \Gamma(e^+e^-)/\Gamma_{\text{total}}$ — $\Gamma_{23}\Gamma_{24}/\Gamma$

VALUE (eV)	CL%	DOCUMENT ID		TECN	COMMENT
$<1.8 \times 10^{-3}$	90	[19] ABLIKIM	21AS	BES3	$e^+e^- \rightarrow \psi(4415)$

[19] From a measurement of the $e^+e^- \rightarrow \Lambda\overline{\Lambda}$ cross section between 3.5 and 4.6 GeV.

$\psi(4415)$ BRANCHING RATIOS

$\Gamma(D^0\overline{D}^0)/\Gamma_{\text{total}}$ — Γ_2/Γ

VALUE	DOCUMENT ID		TECN	COMMENT
seen	PAKHLOVA	08	BELL	$e^+e^- \rightarrow D^0\overline{D}^0\gamma$
• • • We do not use the following data for averages, fits, limits, etc. • • •				
not seen	AUBERT	09M	BABR	$e^+e^- \rightarrow D^0\overline{D}^0\gamma$

$\Gamma(D^+D^-)/\Gamma_{\text{total}}$ — Γ_3/Γ

VALUE	DOCUMENT ID		TECN	COMMENT
seen	PAKHLOVA	08	BELL	$e^+e^- \rightarrow D^+D^-\gamma$
• • • We do not use the following data for averages, fits, limits, etc. • • •				
not seen	AUBERT	09M	BABR	$e^+e^- \rightarrow D^+D^-\gamma$

$\Gamma(D\overline{D})/\Gamma(D^*\overline{D}^*)$ — Γ_1/Γ_7

VALUE	DOCUMENT ID		TECN	COMMENT
0.14±0.12±0.03	AUBERT	09M	BABR	$e^+e^- \rightarrow \gamma D^{(*)}\overline{D}^{(*)}$

$\Gamma(D^*(2007)^0\overline{D}^0 + \text{c.c.})/\Gamma_{\text{total}}$ — Γ_5/Γ

VALUE	DOCUMENT ID		TECN	COMMENT
seen	AUBERT	09M	BABR	$e^+e^- \rightarrow D^{*0}\overline{D}^0\gamma$

$\Gamma(D^*(2010)^+D^- + \text{c.c.})/\Gamma_{\text{total}}$ — Γ_6/Γ

VALUE	DOCUMENT ID		TECN	COMMENT
seen	[20] ZHUKOVA	18	BELL	$e^+e^- \rightarrow D^{*+}D^-\gamma$
seen	AUBERT	09M	BABR	$e^+e^- \rightarrow D^{*+}D^-\gamma$
• • • We do not use the following data for averages, fits, limits, etc. • • •				
seen	PAKHLOVA	07	BELL	$e^+e^- \rightarrow D^{*+}D^-\gamma$

[20] Supersedes PAKHLOVA 07.

$\Gamma(D^*\overline{D} + \text{c.c.})/\Gamma(D^*\overline{D}^*)$ — Γ_4/Γ_7

VALUE	DOCUMENT ID		TECN	COMMENT
0.17±0.25±0.03	AUBERT	09M	BABR	$e^+e^- \rightarrow \gamma D^{(*)}\overline{D}^{(*)}$

$\Gamma(D^*(2007)^0\overline{D}^*(2007)^0 + \text{c.c.})/\Gamma_{\text{total}}$ — Γ_8/Γ

VALUE	DOCUMENT ID		TECN	COMMENT
seen	AUBERT	09M	BABR	$e^+e^- \rightarrow D^{*0}\overline{D}^{*0}\gamma$

$\Gamma(D^*(2010)^+D^*(2010)^- + \text{c.c.})/\Gamma_{\text{total}}$ — Γ_9/Γ

VALUE	DOCUMENT ID		TECN	COMMENT
seen	[21] ZHUKOVA	18	BELL	$e^+e^- \rightarrow D^{*+}D^{*-}\gamma$
seen	AUBERT	09M	BABR	$e^+e^- \rightarrow D^{*+}D^{*-}\gamma$
• • • We do not use the following data for averages, fits, limits, etc. • • •				
seen	PAKHLOVA	07	BELL	$e^+e^- \rightarrow D^{*+}D^{*-}\gamma$

[21] Supersedes PAKHLOVA 07.

$\Gamma(D\overline{D}_2^*(2460) \rightarrow D^0D^-\pi^+ + \text{c.c.})/\Gamma_{\text{total}}$ — Γ_{11}/Γ

VALUE (units 10^{-2})	DOCUMENT ID		TECN	COMMENT
10.5±2.4±3.8	[22] PAKHLOVA	08A	BELL	10.6 $e^+e^- \rightarrow D^0D^-\pi^+\gamma$

[22] Using 4421 ± 4 MeV for the mass and 62 ± 20 MeV for the width of $\psi(4415)$.

$\Gamma(D^0D^-\pi^+$ (excl. $D^*(2007)^0\overline{D}^0$ + c.c., $D^*(2010)^+D^-$ + c.c.)/ $\Gamma(D\overline{D}_2^*(2460) \rightarrow D^0D^-\pi^+ + \text{c.c.})$ — Γ_{10}/Γ_{11}

VALUE	CL%	DOCUMENT ID		TECN	COMMENT
<0.22	90	[23] PAKHLOVA	08A	BELL	10.6 $e^+e^- \rightarrow D^0D^-\pi^+\gamma$

[23] Using 4421 ± 4 MeV for the mass and 62 ± 20 MeV for the width of $\psi(4415)$.

Downloaded from https://academic.oup.com/ptep/article/2022/8/083C01/6651666 by KIT Library user on 27 September 2022

$\Gamma(D^0 D^{*-}\pi^+ + \text{c.c.})/\Gamma_{total} \times \Gamma(e^+e^-)/\Gamma_{total}$ — $\Gamma_{12}/\Gamma \times \Gamma_{24}/\Gamma$

VALUE	CL%	DOCUMENT ID		TECN	COMMENT
$<0.99 \times 10^{-6}$	90	[24] PAKHLOVA	09	BELL	$e^+e^- \to D^0 D^{*-}\pi^+$

[24] Using 4421 ± 4 MeV for the mass of $\psi(4415)$.

$\Gamma(D_1(2420)\overline{D} + \text{c.c.})/\Gamma_{total}$ — Γ_{13}/Γ

VALUE	DOCUMENT ID		TECN	COMMENT
possibly seen	[25] ABLIKIM	19AR	BES3	$e^+e^- \to \pi^+\pi^- D\overline{D}$

[25] Evidence for $e^+e^- \to D_1(2420)\overline{D} +$ c.c. between $\sqrt{s} = 4.3$ and 4.6 GeV, not necessarily resonant.

$\Gamma(D_s^+ D_s^-)/\Gamma_{total}$ — Γ_{14}/Γ

VALUE	DOCUMENT ID		TECN	COMMENT
not seen	PAKHLOVA	11	BELL	$e^+e^- \to D_s^+ D_s^- \gamma$
not seen	DEL-AMO-SA...	10N	BABR	$e^+e^- \to D_s^+ D_s^- \gamma$

$\Gamma(\omega\chi_{c2})/\Gamma_{total}$ — Γ_{15}/Γ

VALUE	DOCUMENT ID		TECN	COMMENT
possibly seen	ABLIKIM	16A	BES3	$e^+e^- \to \gamma\pi^+\pi^-\pi^0\ell^+\ell^-$

$\Gamma(D_s^{*+} D_s^- + \text{c.c.})/\Gamma_{total}$ — Γ_{16}/Γ

VALUE	DOCUMENT ID		TECN	COMMENT
seen	PAKHLOVA	11	BELL	$e^+e^- \to D_s^{*+} D_s^- \gamma$
seen	DEL-AMO-SA...	10N	BABR	$e^+e^- \to D_s^{*+} D_s^- \gamma$

$\Gamma(D_s^{*+} D_s^{*-})/\Gamma_{total}$ — Γ_{17}/Γ

VALUE	DOCUMENT ID		TECN	COMMENT
not seen	PAKHLOVA	11	BELL	$e^+e^- \to D_s^{*+} D_s^{*-} \gamma$
not seen	DEL-AMO-SA...	10N	BABR	$e^+e^- \to D_s^{*+} D_s^{*-} \gamma$

$\Gamma(\psi(3770)\pi^+\pi^-)/\Gamma_{total}$ — Γ_{19}/Γ

VALUE	DOCUMENT ID		TECN	COMMENT
possibly seen	[26] ABLIKIM	19AR	BES3	$e^+e^- \to \pi^+\pi^- D\overline{D}$

[26] Observe $e^+e^- \to \pi^+\pi^-\psi(3770)$ at $\sqrt{s} = 4.26$, 4.36, and 4.42 GeV but cannot establish if continuum or resonant.

$\Gamma(\psi_2(3823)\pi^+\pi^-)/\Gamma_{total}$ — Γ_{18}/Γ

VALUE	EVTS	DOCUMENT ID		TECN	COMMENT
possibly seen	19	[27] ABLIKIM	15S	BES3	$e^+e^- \to \pi^+\pi^-\chi_{c1}\gamma$

[27] From a fit of $e^+e^- \to \pi^+\pi^-\psi_2(3823)$, $\psi_2(3823) \to \chi_{c1}\gamma$ cross sections taken at $\sqrt{s}$ values of 4.23, 4.26, 4.36, 4.42, and 4.60 GeV to the $\psi(4415)$ line shape.

$\psi(4415)$ REFERENCES

ABLIKIM	21AS	PR D104 L091104	M. Ablikim *et al.*	(BESIII Collab.)
ABLIKIM	20AG	PR D102 112009	M. Ablikim *et al.*	(BESIII Collab.)
ABLIKIM	19AR	PR D100 032005	M. Ablikim *et al.*	(BESIII Collab.)
ZHUKOVA	18	PR D97 012002	V. Zhukova *et al.*	(BELLE Collab.)
ABLIKIM	16A	PR D93 011102	M. Ablikim *et al.*	(BESIII Collab.)
ABLIKIM	15S	PRL 115 011803	M. Ablikim *et al.*	(BESIII Collab.)
HAN	15	PR D92 012011	Y.L. Han *et al.*	(BELLE Collab.)
WANG	13B	PR D87 051101	X.L. Wang *et al.*	(BELLE Collab.)
PAKHLOVA	11	PR D83 011101	G. Pakhlova *et al.*	(BELLE Collab.)
DEL-AMO-SA...	10N	PR D82 052004	P. del Amo Sanchez *et al.*	(BABAR Collab.)
MO	10	PR D82 077501	X.H. Mo, C.Z. Yuan, P. Wang	(BHEP)
AUBERT	09M	PR D79 092001	B. Aubert *et al.*	(BABAR Collab.)
PAKHLOVA	09	PR D80 091101	G. Pakhlova *et al.*	(BELLE Collab.)
ABLIKIM	08D	PL B660 315	M. Ablikim *et al.*	(BES Collab.)
PAKHLOVA	08	PR D77 011103	G. Pakhlova *et al.*	(BELLE Collab.)
PAKHLOVA	08A	PRL 100 062001	G. Pakhlova *et al.*	(BELLE Collab.)
PAKHLOVA	07	PRL 98 092001	G. Pakhlova *et al.*	(BELLE Collab.)
SETH	05A	PR D72 017501	K.K. Seth	
BAI	02C	PRL 88 101802	J.Z. Bai *et al.*	(BES Collab.)
BAI	00	PRL 84 594	J.Z. Bai *et al.*	(BES Collab.)
OSTERHELD	86	SLAC-PUB-4160	A. Osterheld *et al.*	(SLAC Crystal Ball Collab.)
BRANDELIK	78C	PL 76B 361	R. Brandelik *et al.*	(DASP Collab.)
SIEGRIST	76	PRL 36 700	J.L. Siegrist *et al.*	(LBL, SLAC)

$Z_c(4430)$

$I^G(J^{PC}) = 1^+(1^{+-})$
G, C need confirmation.

was $X(4430)^\pm$

Properties incompatible with a $q\overline{q}$ structure (exotic state). See the review on non-$q\overline{q}$ states.

First seen by CHOI 08 in $B \to K\pi^+\psi(2S)$ decays, confirmed by AAIJ 14AG, and confirmed in a model-independent way by AAIJ 15BH. Also seen by CHILIKIN 14 in $B \to K^+\pi J/\psi$ decays. J^P was determined by CHILIKIN 13 and AAIJ 14AG.

$Z_c(4430)$ MASS

VALUE (MeV)	DOCUMENT ID		TECN	COMMENT
4478^{+15}_{-18} OUR AVERAGE				
$4475 \pm 7^{+15}_{-25}$	[1] AAIJ	14AG	LHCB	$B^0 \to K^+\pi^-\psi(2S)$
$4485 \pm 22^{+28}_{-11}$	[1] CHILIKIN	13	BELL	$B^0 \to K^+\pi^-\psi(2S)$
• • • We do not use the following data for averages, fits, limits, etc. • • •				
4443^{+15+19}_{-12-13}	[2] MIZUK	09	BELL	$B \to K\pi^+\psi(2S)$
$4433 \pm 4 \pm 2$	[3] CHOI	08	BELL	$B \to K\pi^+\psi(2S)$

[1] From a four-dimensional amplitude analysis.
[2] From a Dalitz plot analysis. Superseded by CHILIKIN 13.
[3] Superseded by MIZUK 09 and CHILIKIN 13.

$Z_c(4430)$ WIDTH

VALUE (MeV)	DOCUMENT ID		TECN	COMMENT
181±31 OUR AVERAGE				
$172 \pm 13^{+37}_{-34}$	[1] AAIJ	14AG	LHCB	$B^0 \to K^+\pi^-\psi(2S)$
200^{+41+26}_{-46-35}	[1] CHILIKIN	13	BELL	$B^0 \to K^+\pi^-\psi(2S)$
• • • We do not use the following data for averages, fits, limits, etc. • • •				
107^{+86+74}_{-43-56}	[2] MIZUK	09	BELL	$B \to K\pi^+\psi(2S)$
45^{+18+30}_{-13-13}	[3] CHOI	08	BELL	$B \to K\pi^+\psi(2S)$

[1] From a four-dimensional amplitude analysis.
[2] From a Dalitz plot analysis. Superseded by CHILIKIN 13.
[3] Superseded by MIZUK 09 and CHILIKIN 13.

$Z_c(4430)$ DECAY MODES

	Mode	Fraction (Γ_i/Γ)
Γ_1	$\pi^+\psi(2S)$	seen
Γ_2	$\pi^+ J/\psi$	seen

$Z_c(4430)$ BRANCHING RATIOS

$\Gamma(\pi^+\psi(2S))/\Gamma_{total}$ — Γ_1/Γ

VALUE	DOCUMENT ID		TECN	COMMENT
seen	[1] AAIJ	14AG	LHCB	$B^0 \to K^+\pi^-\psi(2S)$
seen	[2] CHILIKIN	13	BELL	$B^0 \to K^+\pi^-\psi(2S)$
• • • We do not use the following data for averages, fits, limits, etc. • • •				
not seen	[3] AUBERT	09AA	BABR	$B \to K\pi^+\psi(2S)$
seen	[4] MIZUK	09	BELL	$B \to K\pi^+\psi(2S)$

[1] From a four-dimensional amplitude analysis. No product of branching fractions quoted.
[2] From a four-dimensional amplitude analysis. Measured a product of branching fractions $B(B^0 \to Z_c(4430)^- K^+) \times B(Z_c(4430)^- \to \psi(2S)\pi^-) = (6.0^{+1.7+2.5}_{-2.0-1.4}) \times 10^{-5}$.
[3] AUBERT 09AA quotes $B(B^+ \to \overline{K}^0 Z_c(4430)^+) \times B(Z_c(4430)^+ \to \pi^+\psi(2S)) < 4.7 \times 10^{-5}$ and $B(\overline{B}^0 \to K^- Z_c(4430)^+) \times B(Z_c(4430)^+ \to \pi^+\psi(2S)) < 3.1 \times 10^{-5}$ at 95% CL.
[4] Measured a product of branching fractions $B(\overline{B}^0 \to K^- Z_c(4430)^+) \times B(Z_c(4430)^+ \to \pi^+\psi(2S)) = (3.2^{+1.8+5.3}_{-0.9-1.6}) \times 10^{-5}$. Superseded by CHILIKIN 13.

$\Gamma(\pi^+ J/\psi)/\Gamma_{total}$ — Γ_2/Γ

VALUE	DOCUMENT ID		TECN	COMMENT
seen	[1,2] CHILIKIN	14	BELL	$\overline{B}^0 \to K^-\pi^+ J/\psi$
• • • We do not use the following data for averages, fits, limits, etc. • • •				
not seen	[3] AUBERT	09AA	BABR	$B \to K\pi^+ J/\psi$

[1] CHILIKIN 14 reports $B(\overline{B}^0 \to Z_c(4430)^+ K^-) \times B(Z_c(4430)^+ \to J/\psi\pi^+) = (5.4^{+4.0+1.1}_{-1.0-0.9}) \times 10^{-6}$.
[2] A broad enhancement seen by AAIJ 19R in the decays $B^0 \to J/\psi\pi^+ K^-$ at 4600 MeV can be due to an interplay of $Z_c(4430)$, $Z_c(4200)$ and the fitting polynomials.
[3] AUBERT 09AA quotes $B(B^+ \to \overline{K}^0 Z_c(4430)^+) \times B(Z_c(4430)^+ \to \pi^+ J/\psi) < 1.5 \times 10^{-5}$ and $B(\overline{B}^0 \to K^- Z_c(4430)^+) \times B(Z_c(4430)^+ \to \pi^+ J/\psi) < 0.4 \times 10^{-5}$ at 95% CL.

$Z_c(4430)$ REFERENCES

AAIJ	19R	PRL 122 152002	R. Aaij *et al.*	(LHCb Collab.)
AAIJ	15BH	PR D92 112009	R. Aaij *et al.*	(LHCb Collab.)
AAIJ	14AG	PRL 112 222002	R. Aaij *et al.*	(LHCb Collab.) JP
CHILIKIN	14	PR D90 112009	K. Chilikin *et al.*	(BELLE Collab.)
CHILIKIN	13	PR D88 074026	K. Chilikin *et al.*	(BELLE Collab.) JP
AUBERT	09AA	PR D79 112001	B. Aubert *et al.*	(BABAR Collab.)
MIZUK	09	PR D80 031104	R. Mizuk *et al.*	(BELLE Collab.)
CHOI	08	PRL 100 142001	S.-K. Choi *et al.*	(BELLE Collab.)

$\chi_{c0}(4500)$

$I^G(J^{PC}) = 0^+(0^{++})$

OMITTED FROM SUMMARY TABLE

was $X(4500)$

This state shows properties different from a conventional $q\overline{q}$ state. A candidate for an exotic structure. See the review on non-$q\overline{q}$ states.

Seen by AAIJ 17C in $B^+ \to \chi_{c0} K^+$, $\chi_{c0} \to J/\psi\phi$ using an amplitude analysis of $B^+ \to J/\psi\phi K^+$ with a significance (accounting for systematic uncertainties) of 6.1 σ.

Downloaded from https://academic.oup.com/ptep/article/2022/8/083C01/6651666 by KIT Library user on 27 September 2022

$\chi_{c0}(4500)$ MASS

VALUE (MeV)	EVTS	DOCUMENT ID		TECN	COMMENT
4474± 3± 3	24k	[1] AAIJ	21E	LHCB	$B^+ \to J/\psi\phi K^+$
• • • We do not use the following data for averages, fits, limits, etc. • • •					
$4506 \pm 11 ^{+12}_{-15}$	4289	[2,3] AAIJ	17C	LHCB	$B^+ \to J/\psi\phi K^+$

[1] From an amplitude analysis of the decay $B^+ \to J/\psi\phi K^+$ with a significance of 20 σ.
[2] From an amplitude analysis of the decay $B^+ \to J/\psi\phi K^+$ with a significance of 6.1 σ.
[3] Superseded by AAIJ 21E.

$\chi_{c0}(4500)$ WIDTH

VALUE (MeV)	EVTS	DOCUMENT ID		TECN	COMMENT
77± 6$^{+10}_{-8}$	24k	[1] AAIJ	21E	LHCB	$B^+ \to J/\psi\phi K^+$
• • • We do not use the following data for averages, fits, limits, etc. • • •					
$92 \pm 21 ^{+21}_{-20}$	4289	[2,3] AAIJ	17C	LHCB	$B^+ \to J/\psi\phi K^+$

[1] From an amplitude analysis of the decay $B^+ \to J/\psi\phi K^+$ with a significance of 20 σ.
[2] From an amplitude analysis of the decay $B^+ \to J/\psi\phi K^+$ with a significance of 6.1 σ.
[3] Superseded by AAIJ 21E.

$\chi_{c0}(4500)$ DECAY MODES

	Mode	Fraction (Γ_i/Γ)
Γ_1	$J/\psi\phi$	seen

$\chi_{c0}(4500)$ BRANCHING RATIOS

$\Gamma(J/\psi\phi)/\Gamma_{total}$ — **Γ_1/Γ**

VALUE	EVTS	DOCUMENT ID		TECN	COMMENT
seen	24k	[1] AAIJ	21E	LHCB	$B^+ \to J/\psi\phi K^+$
• • • We do not use the following data for averages, fits, limits, etc. • • •					
seen	4289	[2,3] AAIJ	17C	LHCB	$B^+ \to J/\psi\phi K^+$

[1] From an amplitude analysis of the decay $B^+ \to J/\psi\phi K^+$ with a significance of 20 σ.
[2] From an amplitude analysis of the decay $B^+ \to J/\psi\phi K^+$ with a significance of 6.1 σ.
[3] Superseded by AAIJ 21E.

$\chi_{c0}(4500)$ REFERENCES

AAIJ	21E	PRL 127 082001	R. Aaij *et al.*	(LHCb Collab.)
AAIJ	17C	PRL 118 022003	R. Aaij *et al.*	(LHCb Collab.) JP
Also		PR D95 012002	R. Aaij *et al.*	(LHCb Collab.)

$X(4630)$

$I^G(J^{PC}) = 0^+(?^{?+})$

OMITTED FROM SUMMARY TABLE

This state shows properties different from a conventional $q\overline{q}$ state. A candidate for an exotic structure. See the review on "Heavy Non-$q\overline{q}$ Mesons."

Seen by AAIJ 21E in $B^+ \to X(4630)K^+$ with $X(4630) \to J/\psi\phi$ using an amplitude analysis of $B^+ \to J/\psi\phi K^+$ with a significance (accounting for systematic uncertainties) of 5.5 σ. The $J^P = 1^-$ assignment is favored over 2^- with a significance of 3 σ and other assignments are disfavored by more than 5 σ.

$X(4630)$ MASS

VALUE (MeV)	EVTS	DOCUMENT ID		TECN	COMMENT
$4626 \pm 16 ^{+18}_{-110}$	24k	[1] AAIJ	21E	LHCB	$B^+ \to J/\psi\phi K^+$

[1] From an amplitude analysis of the decay $B^+ \to J/\psi\phi K^+$ with a significance of 5.5 σ.

$X(4630)$ WIDTH

VALUE (MeV)	EVTS	DOCUMENT ID		TECN	COMMENT
$174 \pm 27 ^{+134}_{-73}$	24k	[1] AAIJ	21E	LHCB	$B^+ \to J/\psi\phi K^+$

[1] From an amplitude analysis of the decay $B^+ \to J/\psi\phi K^+$ with a significance of 5.5 σ.

$X(4630)$ DECAY MODES

	Mode	Fraction (Γ_i/Γ)
Γ_1	$J/\psi\phi$	seen

$\Gamma(J/\psi\phi)/\Gamma_{total}$ — **Γ_1/Γ**

VALUE	EVTS	DOCUMENT ID		TECN	COMMENT
seen	24k	[1] AAIJ	21E	LHCB	$B^+ \to J/\psi\phi K^+$

[1] From an amplitude analysis of the decay $B^+ \to J/\psi\phi K^+$ with a significance of 5.5 σ.

$X(4630)$ REFERENCES

AAIJ	21E	PRL 127 082001	R. Aaij *et al.*	(LHCb Collab.)

$\psi(4660)$

$I^G(J^{PC}) = 0^-(1^{--})$

also known as $Y(4660)$; was $X(4660)$

This state shows properties different from a conventional $q\overline{q}$ state. A candidate for an exotic structure. See the review on non-$q\overline{q}$ states.

Seen in radiative return from e^+e^- collisions at $\sqrt{s} = 9.54$–10.58 GeV by WANG 07D. Also obtained in a combined fit of WANG 07D, AUBERT 07S, and LEES 14F. See also the review on "Spectroscopy of mesons containing two heavy quarks."

$\psi(4660)$ MASS

VALUE (MeV)	EVTS	DOCUMENT ID		TECN	COMMENT
4630 ± 6 OUR AVERAGE		Error includes scale factor of 1.4. See the ideogram below.			
$4651.0 \pm 37.8 \pm 2.1$		[1] ABLIKIM	21AJ	BES3	$e^+e^- \to \pi^+\pi^-\psi(2S)$
$4619.8 ^{+8.9}_{-8.0} \pm 2.3$	66	[2] JIA	20	BELL	$e^+e^- \to \gamma D_s^+ D_{s2}^*(2573)^-$
$4625.9 ^{+6.2}_{-6.0} \pm 0.4$	89	[3] JIA	19A	BELL	$e^+e^- \to \gamma D_s^+ D_{s1}(2536)^-$
$4652 \pm 10 \pm 11$	279	[4] WANG	15A	BELL	10.58 $e^+e^- \to \gamma\pi^+\pi^-\psi(2S)$
$4669 \pm 21 \pm 3$	37	[5] LEES	14F	BABR	10.58 $e^+e^- \to \gamma\pi^+\pi^-\psi(2S)$
$4634 ^{+8}_{-7} ^{+5}_{-8}$	142	[6] PAKHLOVA	08B	BELL	$e^+e^- \to \Lambda_c^+\Lambda_c^-$
• • • We do not use the following data for averages, fits, limits, etc. • • •					
$4652.5 \pm 3.4 \pm 1.1$		[7] DAI	17	RVUE	$e^+e^- \to \Lambda_c^+\Lambda_c^-$
$4645.2 \pm 9.5 \pm 6.0$		[8] ZHANG	17B	RVUE	$e^+e^- \to \pi^+\pi^-\psi(2S)$
$4646.4 \pm 9.7 \pm 4.8$		[9] ZHANG	17C	RVUE	$e^+e^- \to \pi^+\pi^- J/\psi$ or $\psi(2S)$
$4661 ^{+9}_{-8} \pm 6$	44	[10] LIU	08H	RVUE	10.58 $e^+e^- \to \gamma\pi^+\pi^-\psi(2S)$
$4664 \pm 11 \pm 5$	44	WANG	07D	BELL	10.58 $e^+e^- \to \gamma\pi^+\pi^-\psi(2S)$

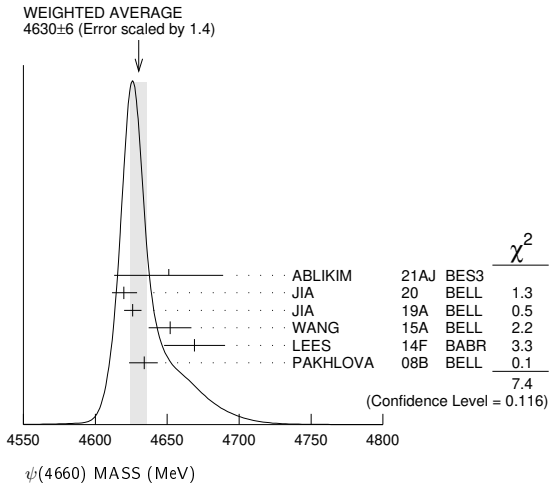

[1] From a three-resonance fit to the Born cross section in the range $\sqrt{s} = 4.008$–4.698 GeV.
[2] Using $D_{s2}^*(2573)^- \to \overline{D}^0 K^-$ decays.
[3] From a fit of a Breit-Wigner convolved with a Gaussian.
[4] From a two-resonance fit. Supersedes WANG 07D.
[5] From a two-resonance fit.
[6] The $\pi^+\pi^-\psi(2S)$ and $\Lambda_c^+\Lambda_c^-$ states are not necessarily the same.
[7] The pole parameters are extracted from the speed plot.
[8] From a three-resonance fit.
[9] From a combined fit of BELLE, BABAR and BES3 $e^+e^- \to \pi^+\pi^- J/\psi$ and $e^+e^- \to \pi^+\pi^-\psi(2S)$ data.
[10] From a combined fit of AUBERT 07S and WANG 07D data with two resonances.

$\psi(4660)$ WIDTH

VALUE (MeV)	EVTS	DOCUMENT ID		TECN	COMMENT
72 $^{+14}_{-12}$ OUR AVERAGE		Error includes scale factor of 1.7. See the ideogram below.			
$155.4 \pm 24.8 \pm 0.8$		[1] ABLIKIM	21AJ	BES3	$e^+e^- \to \pi^+\pi^-\psi(2S)$
$47.0 ^{+31.3}_{-14.8} \pm 4.6$	66	[2] JIA	20	BELL	$e^+e^- \to \gamma D_s^+ D_{s2}^*(2573)^-$
$49.8 ^{+13.9}_{-11.5} \pm 4.0$	89	[3] JIA	19A	BELL	$e^+e^- \to \gamma D_s^+ D_{s1}(2536)^-$

Downloaded from https://academic.oup.com/ptep/article/2022/8/083C01/6651666 by KIT Library user on 27 September 2022

68 ±11 ± 5	279	[4] WANG	15A	BELL	10.58 $e^+e^- \to \gamma\pi^+\pi^-\psi(2S)$
104 ±48 ±10	37	[5] LEES	14F	BABR	10.58 $e^+e^- \to \gamma\pi^+\pi^-\psi(2S)$
92 $^{+40}_{-24}$ $^{+10}_{-21}$	142	[6] PAKHLOVA	08B	BELL	$e^+e^- \to \Lambda_c^+\Lambda_c^-$

• • • We do not use the following data for averages, fits, limits, etc. • • •

62.6± 5.6± 4.3		[7] DAI	17	RVUE	$e^+e^- \to \Lambda_c^+\Lambda_c^-$
113.8±18.1± 3.4		[8] ZHANG	17B	RVUE	$e^+e^- \to \pi^+\pi^-\psi(2S)$
103.5±15.6± 4.0		[9] ZHANG	17C	RVUE	$e^+e^- \to \pi^+\pi^- J/\psi$ or $\psi(2S)$
42 $^{+17}_{-12}$ ± 6	44	[10] LIU	08H	RVUE	10.58 $e^+e^- \to \gamma\pi^+\pi^-\psi(2S)$
48 ±15 ± 3	44	WANG	07D	BELL	10.58 $e^+e^- \to \gamma\pi^+\pi^-\psi(2S)$

[1] From a three-resonance fit to the Born cross section in the range $\sqrt{s}$ = 4.008–4.698 GeV.
[2] Using $D_{s2}^*(2573)^- \to \overline{D}^0 K^-$ decays.
[3] From a fit of a Breit-Wigner convolved with a Gaussian.
[4] From a two-resonance fit. Supersedes WANG 07D.
[5] From a two-resonance fit.
[6] The $\pi^+\pi^-\psi(2S)$ and $\Lambda_c^+\Lambda_c^-$ states are not necessarily the same.
[7] The pole parameters are extracted from the speed plot.
[8] From a three-resonance fit.
[9] From a combined fit of BELLE, BABAR and BES3 $e^+e^- \to \pi^+\pi^- J/\psi$ and $e^+e^- \to \pi^+\pi^-\psi(2S)$ data.
[10] From a combined fit of AUBERT 07S and WANG 07D data with two resonances.

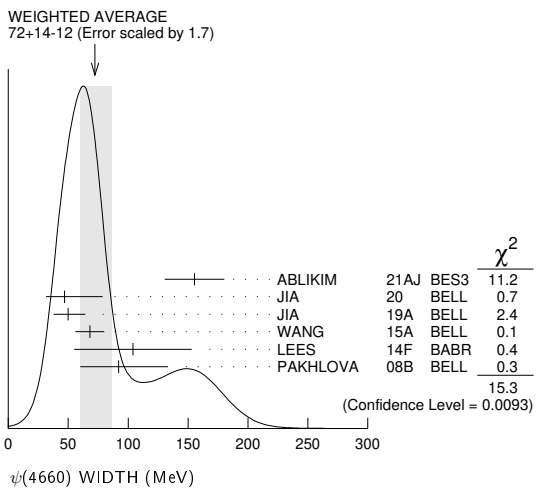

$\psi(4660)$ DECAY MODES

	Mode	Fraction (Γ_i/Γ)
Γ_1	e^+e^-	not seen
Γ_2	$\psi(2S)\pi^+\pi^-$	seen
Γ_3	$J/\psi\eta$	not seen
Γ_4	$D^0D^{*-}\pi^+$	not seen
Γ_5	$\chi_{c1}\gamma$	not seen
Γ_6	$\chi_{c2}\gamma$	not seen
Γ_7	$\Lambda_c^+\Lambda_c^-$	seen
Γ_8	$D_s^+D_{s1}(2536)^-$	seen
Γ_9	$D_s^+D_{s2}^*(2573)^-$	

$\psi(4660)$ $\Gamma(i) \times \Gamma(e^+e^-)/\Gamma(\text{total})$

$\Gamma(\psi(2S)\pi^+\pi^-) \times \Gamma(e^+e^-)/\Gamma_{\text{total}}$ — $\Gamma_2\Gamma_1/\Gamma$

VALUE (eV)	EVTS	DOCUMENT ID		TECN	COMMENT
• • • We do not use the following data for averages, fits, limits, etc. • • •					
4.7±3.8		[1] ABLIKIM	21AJ	BES3	$e^+e^- \to \pi^+\pi^-\psi(2S)$
11.2±3.2		[2] ABLIKIM	21AJ	BES3	$e^+e^- \to \pi^+\pi^-\psi(2S)$
4.7±4.2		[3] ABLIKIM	21AJ	BES3	$e^+e^- \to \pi^+\pi^-\psi(2S)$
11.3±3.3		[4] ABLIKIM	21AJ	BES3	$e^+e^- \to \pi^+\pi^-\psi(2S)$
2.0±0.3±0.2	279	[5] WANG	15A	BELL	10.58 $e^+e^- \to \gamma\pi^+\pi^-\psi(2S)$
8.1±1.1±1.0	279	[6] WANG	15A	BELL	10.58 $e^+e^- \to \gamma\pi^+\pi^-\psi(2S)$
2.7±1.3±0.5	37	[7] LEES	14F	BABR	10.58 $e^+e^- \to \gamma\pi^+\pi^-\psi(2S)$
7.5±1.7±0.7	37	[8] LEES	14F	BABR	10.58 $e^+e^- \to \gamma\pi^+\pi^-\psi(2S)$
2.2$^{+0.7}_{-0.6}$	44	[9] LIU	08H	RVUE	10.58 $e^+e^- \to \gamma\pi^+\pi^-\psi(2S)$
5.9±1.6	44	[10] LIU	08H	RVUE	10.58 $e^+e^- \to \gamma\pi^+\pi^-\psi(2S)$
3.0±0.9±0.3	44	[7] WANG	07D	BELL	10.58 $e^+e^- \to \gamma\pi^+\pi^-\psi(2S)$
7.6±1.8±0.8	44	[8] WANG	07D	BELL	10.58 $e^+e^- \to \gamma\pi^+\pi^-\psi(2S)$

[1] Solution I of four equivalent solutions in a fit using three interfering resonances.
[2] Solution II of four equivalent solutions in a fit using three interfering resonances.
[3] Solution III of four equivalent solutions in a fit using three interfering resonances.
[4] Solution IV of four equivalent solutions in a fit using three interfering resonances.
[5] Solution I of two equivalent solutions from a fit using two interfering resonances. Supersedes WANG 07D.
[6] Solution II of two equivalent solutions from a fit using two interfering resonances. Supersedes WANG 07D.
[7] Solution I of two equivalent solutions in a fit using two interfering resonances.
[8] Solution II of two equivalent solutions in a fit using two interfering resonances.
[9] Solution I in a combined fit of AUBERT 07S and WANG 07D data with two resonances.
[10] Solution II in a combined fit of AUBERT 07S and WANG 07D data with two resonances.

$\Gamma(J/\psi\eta) \times \Gamma(e^+e^-)/\Gamma_{\text{total}}$ — $\Gamma_3\Gamma_1/\Gamma$

VALUE (eV)	CL%	DOCUMENT ID		TECN	COMMENT
• • • We do not use the following data for averages, fits, limits, etc. • • •					
<0.94	90	WANG	13B	BELL	$e^+e^- \to J/\psi\eta\gamma$

$\Gamma(\chi_{c1}\gamma) \times \Gamma(e^+e^-)/\Gamma_{\text{total}}$ — $\Gamma_5\Gamma_1/\Gamma$

VALUE (eV)	CL%	DOCUMENT ID		TECN	COMMENT
<0.45	90	[1] HAN	15	BELL	10.58 $e^+e^- \to \chi_{c1}\gamma$

[1] Using B($\eta \to \gamma\gamma$) = (39.41 ± 0.21)%.

$\Gamma(\chi_{c2}\gamma) \times \Gamma(e^+e^-)/\Gamma_{\text{total}}$ — $\Gamma_6\Gamma_1/\Gamma$

VALUE (eV)	CL%	DOCUMENT ID		TECN	COMMENT
<2.1	90	[1] HAN	15	BELL	10.58 $e^+e^- \to \chi_{c2}\gamma$

[1] Using B($\eta \to \gamma\gamma$) = (39.41 ± 0.21)%.

$\Gamma(D_s^+D_{s1}(2536)^-) \times \Gamma(e^+e^-)/\Gamma_{\text{total}}$ — $\Gamma_8\Gamma_1/\Gamma$

VALUE (eV)	EVTS	DOCUMENT ID		TECN	COMMENT
14.3$^{+2.8}_{-2.6}$±1.5	89	[1] JIA	19A	BELL	$e^+e^- \to \gamma D_s^+D_{s1}(2536)^-$

[1] Assuming B($D_{s1}(2536)^- \to \overline{D}^{*0}K^-$) = 1.

$\Gamma(D_s^+D_{s2}^*(2573)^-) \times \Gamma(e^+e^-)/\Gamma_{\text{total}}$ — $\Gamma_9\Gamma_1/\Gamma$

VALUE (eV)	EVTS	DOCUMENT ID		TECN	COMMENT
14.7$^{+5.9}_{-4.5}$±3.6	66	[1] JIA	20	BELL	$e^+e^- \to \gamma D_s^+D_{s2}^*(2573)^-$

[1] Assuming B($D_{s2}^*(2573)^- \to \overline{D}^0K^-$) = 1.

$\psi(4660)$ BRANCHING RATIOS

$\Gamma(D^0D^{*-}\pi^+)/\Gamma(\psi(2S)\pi^+\pi^-)$ — Γ_4/Γ_2

VALUE	CL%	DOCUMENT ID		TECN	COMMENT
<10	90	PAKHLOVA	09	BELL	$e^+e^- \to D^0D^{*-}\pi^+$

$\Gamma(D^0D^{*-}\pi^+)/\Gamma_{\text{total}} \times \Gamma(e^+e^-)/\Gamma_{\text{total}}$ — $\Gamma_4/\Gamma \times \Gamma_1/\Gamma$

VALUE	CL%	DOCUMENT ID		TECN	COMMENT
<0.37 × 10^{-6}	90	[1] PAKHLOVA	09	BELL	$e^+e^- \to D^0D^{*-}\pi^+$

[1] Using 4664 ± 11 ± 5 MeV for the mass of $\psi(4660)$.

$\Gamma(\Lambda_c^+\Lambda_c^-)/\Gamma_{\text{total}} \times \Gamma(e^+e^-)/\Gamma_{\text{total}}$ — $\Gamma_7/\Gamma \times \Gamma_1/\Gamma$

VALUE (units 10^{-6})	EVTS	DOCUMENT ID		TECN	COMMENT
0.68$^{+0.16}_{-0.15}$$^{+0.29}_{-0.30}$	142	[1] PAKHLOVA	08B	BELL	$e^+e^- \to \Lambda_c^+\Lambda_c^-$

[1] The $\pi^+\pi^-\psi(2S)$ and $\Lambda_c^+\Lambda_c^-$ states are not necessarily the same.

$\psi(4660)$ REFERENCES

ABLIKIM	21AJ	PR D104 052012	M. Ablikim *et al.*	(BESIII Collab.)
JIA	20	PR D101 091101	S. Jia *et al.*	(BELLE Collab.)
JIA	19A	PR D100 111103	S. Jia *et al.*	(BELLE Collab.)
DAI	17	PR D96 116001	L.-Y. Dai, J. Haidenbauer, U.-G. Meissner	(JULI+)
ZHANG	17B	PR D96 054008	J. Zhang, J. Zhang	
ZHANG	17C	EPJ C77 727	J. Zhang, L. Yuan	
HAN	15	PR D92 012011	Y.L. Han *et al.*	(BELLE Collab.)
WANG	15A	PR D91 112007	X.L. Wang *et al.*	(BELLE Collab.)
LEES	14F	PR D89 111103	J.P. Lees *et al.*	(BABAR Collab.)
WANG	13B	PR D87 051101	X.L. Wang *et al.*	(BELLE Collab.)
PAKHLOVA	09	PR D80 091101	G. Pakhlova *et al.*	(BELLE Collab.)
LIU	08H	PR D78 014032	Z.Q. Liu, X.S. Qin, C.Z. Yuan	
PAKHLOVA	08B	PRL 101 172001	C. Pakhlova *et al.*	(BELLE Collab.)
AUBERT	07S	PRL 98 212001	B. Aubert *et al.*	(BABAR Collab.)
WANG	07D	PRL 99 142002	X.L. Wang *et al.*	(BELLE Collab.)

Downloaded from https://academic.oup.com/ptep/article/2022/8/083C01/6651666 by KIT Library user on 27 September 2022

$\chi_{c1}(4685)$

$I^G(J^{PC}) = 0^+(1^{++})$

OMITTED FROM SUMMARY TABLE

This state shows properties different from a conventional $q\overline{q}$ state. A candidate for an exotic structure. See the review on "Heavy Non-$q\overline{q}$ Mesons."

Seen by AAIJ 21E in $B^+ \to \chi_{c1}(4685) K^+$ with $\chi_{c1}(4685) \to J/\psi\phi$ using an amplitude analysis of $B^+ \to J/\psi\phi K^+$ with a significance (accounting for systematic uncertainties) of 15 σ. The $J^P = 1^+$ assignment is favored with high significance.

$\chi_{c1}(4685)$ MASS

VALUE (MeV)	EVTS	DOCUMENT ID		TECN	COMMENT
$4684 \pm 7^{+13}_{-16}$	24k	[1] AAIJ	21E	LHCB	$B^+ \to J/\psi\phi K^+$

[1] From an amplitude analysis of the decay $B^+ \to J/\psi\phi K^+$ with a significance of 15 σ.

$\chi_{c1}(4685)$ WIDTH

VALUE (MeV)	EVTS	DOCUMENT ID		TECN	COMMENT
$126 \pm 15^{+37}_{-41}$	24k	[1] AAIJ	21E	LHCB	$B^+ \to J/\psi\phi K^+$

[1] From an amplitude analysis of the decay $B^+ \to J/\psi\phi K^+$ with a significance of 15 σ.

$\chi_{c1}(4685)$ DECAY MODES

	Mode	Fraction (Γ_i/Γ)
Γ_1	$J/\psi\phi$	seen

$\Gamma(J/\psi\phi)/\Gamma_{total}$ — Γ_1/Γ

VALUE	EVTS	DOCUMENT ID		TECN	COMMENT
seen	24k	[1] AAIJ	21E	LHCB	$B^+ \to J/\psi\phi K^+$

[1] From an amplitude analysis of the decay $B^+ \to J/\psi\phi K^+$ with a significance of 15 σ.

$\chi_{c1}(4685)$ REFERENCES

AAIJ 21E PRL 127 082001 R. Aaij et al. (LHCb Collab.) JP

$\chi_{c0}(4700)$

$I^G(J^{PC}) = 0^+(0^{++})$

OMITTED FROM SUMMARY TABLE

was $X(4700)$

This state shows properties different from a conventional $q\overline{q}$ state. A candidate for an exotic structure. See the review on non-$q\overline{q}$ states.

Seen by AAIJ 17C in $B^+ \to \chi_{c0} K^+$, $\chi_{c0} \to J/\psi\phi$ using an amplitude analysis of $B^+ \to J/\psi\phi K^+$ with a significance (accounting for systematic uncertainties) of 5.6 σ.

$\chi_{c0}(4700)$ MASS

VALUE (MeV)	EVTS	DOCUMENT ID		TECN	COMMENT
$4694 \pm 4^{+16}_{-3}$	24k	[1] AAIJ	21E	LHCB	$B^+ \to J/\psi\phi K^+$
• • • We do not use the following data for averages, fits, limits, etc. • • •					
$4741 \pm 6 \pm 6$	175	[2] AAIJ	21C	LHCB	$B_s^0 \to J/\psi\phi\pi^+\pi^-$
$4704 \pm 10^{+14}_{-24}$	4289	[3,4] AAIJ	17C	LHCB	$B^+ \to J/\psi\phi K^+$

[1] From an amplitude analysis of the decay $B^+ \to J/\psi\phi K^+$ with a significance of 17 σ.
[2] From a 1D fit to the $J/\psi\phi$ mass distribution with a significance of 5.3 σ. The identification of this structure as the $\chi_{c0}(4700)$ needs confirmation.
[3] From an amplitude analysis of the decay $B^+ \to J/\psi\phi K^+$ with a significance of 5.6 σ.
[4] Superseded by AAIJ 21E.

$\chi_{c0}(4700)$ WIDTH

VALUE (MeV)	EVTS	DOCUMENT ID		TECN	COMMENT
$87 \pm 8^{+16}_{-6}$	24k	[1] AAIJ	21E	LHCB	$B^+ \to J/\psi\phi K^+$
• • • We do not use the following data for averages, fits, limits, etc. • • •					
$53 \pm 15 \pm 11$	175	[2] AAIJ	21C	LHCB	$B_s^0 \to J/\psi\phi\pi^+\pi^-$
$120 \pm 31^{+42}_{-33}$	4289	[3,4] AAIJ	17C	LHCB	$B^+ \to J/\psi\phi K^+$

[1] From an amplitude analysis of the decay $B^+ \to J/\psi\phi K^+$ with a significance of 17 σ.
[2] From a 1D fit to the $J/\psi\phi$ mass distribution with a significance of 5.3 σ. The identification of this structure as the $\chi_{c0}(4700)$ needs confirmation.
[3] From an amplitude analysis of the decay $B^+ \to J/\psi\phi K^+$ with a significance of 5.6 σ.
[4] Superseded by AAIJ 21E.

$\chi_{c0}(4700)$ DECAY MODES

	Mode	Fraction (Γ_i/Γ)
Γ_1	$J/\psi\phi$	seen

$\chi_{c0}(4700)$ BRANCHING RATIOS

$\Gamma(J/\psi\phi)/\Gamma_{total}$ — Γ_1/Γ

VALUE	EVTS	DOCUMENT ID		TECN	COMMENT
seen	24k	[1] AAIJ	21E	LHCB	$B^+ \to J/\psi\phi K^+$
• • • We do not use the following data for averages, fits, limits, etc. • • •					
seen	175	[2] AAIJ	21C	LHCB	$B_s^0 \to J/\psi\phi\pi^+\pi^-$
seen	4289	[3,4] AAIJ	17C	LHCB	$B^+ \to J/\psi\phi K^+$

[1] From an amplitude analysis of the decay $B^+ \to J/\psi\phi K^+$ with a significance of 17 σ.
[2] From a 1D fit to the $J/\psi\phi$ mass distribution with a significance of 5.3 σ. The identification of this structure as the $\chi_{c0}(4700)$ needs confirmation.
[3] From an amplitude analysis of the decay $B^+ \to J/\psi\phi K^+$ with a significance of 5.6 σ.
[4] Superseded by AAIJ 21E.

$\chi_{c0}(4700)$ REFERENCES

AAIJ 21C JHEP 2102 024 R. Aaij et al. (LHCb Collab.)
AAIJ 21E PRL 127 082001 R. Aaij et al. (LHCb Collab.)
AAIJ 17C PRL 118 022003 R. Aaij et al. (LHCb Collab.) JP
Also PR D95 012002 R. Aaij et al. (LHCb Collab.)

Downloaded from https://academic.oup.com/ptep/article/2022/8/083C01/6651666 by KIT Library user on 27 September 2022

$b\bar{b}$ MESONS (including possibly non-$q\bar{q}$ states)

Updated July 2021.

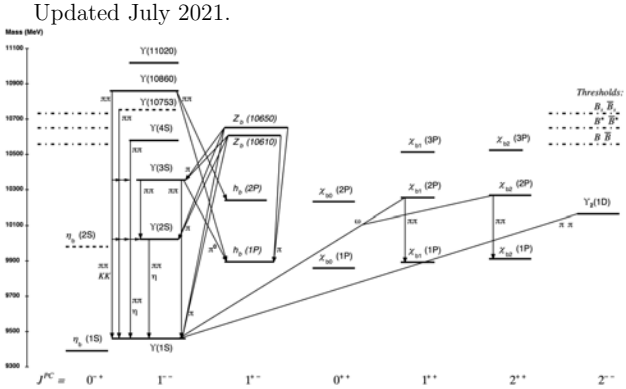

The level scheme of meson states containing a minimal quark content of $b\bar{b}$. The name of a state is determined by its quantum numbers $I^G J^{PC}$ (see the review "Naming Scheme for Hadrons"). States included in the Summary Tables are shown with solid lines; those requiring confirmation are shown with dotted lines. The arrows indicate the most dominant hadronic transitions. Single photon transitions, including $\Upsilon(nS) \to \gamma\eta_b(mS)$, $\Upsilon(nS) \to \gamma\chi_{bJ}(mP)$, and $\chi_{bJ}(nP) \to \gamma\Upsilon(mS)$, are omitted for clarity. For orientation, the location of the thresholds related to a pair of ground state open bottom mesons is indicated in the figure.

WIDTH DETERMINATIONS OF THE Υ STATES

As is the case for the $J/\psi(1S)$ and $\psi(2S)$, the full widths of the $b\bar{b}$ states $\Upsilon(1S)$, $\Upsilon(2S)$, and $\Upsilon(3S)$ are not directly measurable, since they are much narrower than the energy resolution of the e^+e^- storage rings where these states are produced. The common indirect method to determine Γ starts from

$$\Gamma = \Gamma_{\ell\ell}/B_{\ell\ell} \ , \tag{1}$$

where $\Gamma_{\ell\ell}$ is one leptonic partial width and $B_{\ell\ell}$ is the corresponding branching fraction ($\ell = e$, μ, or τ). One then assumes e-μ-τ universality and uses

$$\Gamma_{\ell\ell} = \Gamma_{ee}$$

$$B_{\ell\ell} = \text{average of } B_{ee},\ B_{\mu\mu},\ \text{and } B_{\tau\tau} \ . \tag{2}$$

The electronic partial width Γ_{ee} is also not directly measurable at e^+e^- storage rings, only in the combination $\Gamma_{ee}\Gamma_{\rm had}/\Gamma$, where $\Gamma_{\rm had}$ is the hadronic partial width and

$$\Gamma_{\rm had} + 3\Gamma_{ee} = \Gamma \ . \tag{3}$$

This combination is obtained experimentally from the energy-integrated hadronic cross section

$$\int_{\text{resonance}} \sigma(e^+e^- \to \Upsilon \to \text{hadrons})dE$$

$$= \frac{6\pi^2}{M^2}\frac{\Gamma_{ee}\Gamma_{\rm had}}{\Gamma}C_r = \frac{6\pi^2}{M^2}\frac{\Gamma_{ee}^{(0)}\Gamma_{\rm had}}{\Gamma}C_r^{(0)} \ , \tag{4}$$

where M is the Υ mass, and C_r and $C_r^{(0)}$ are radiative correction factors. C_r is used for obtaining Γ_{ee} as defined in Eq. (1), and contains corrections from all orders of QED for describing $(b\bar{b}) \to e^+e^-$. The lowest order QED value $\Gamma_{ee}^{(0)}$, relevant for comparison with potential-model calculations, is defined by the lowest order QED graph (Born term) alone, and is about 7% lower than Γ_{ee}.

The Listings give experimental results on B_{ee}, $B_{\mu\mu}$, $B_{\tau\tau}$, and $\Gamma_{ee}\Gamma_{\rm had}/\Gamma$. The entries of the last quantity have been re-evaluated consistently using the correction procedure of KURAEV 85 [1]. The partial width Γ_{ee} is obtained from the average values for $\Gamma_{ee}\Gamma_{\rm had}/\Gamma$ and $B_{\ell\ell}$ using

$$\Gamma_{ee} = \frac{\Gamma_{ee}\Gamma_{\rm had}}{\Gamma(1-3B_{\ell\ell})} \ . \tag{5}$$

The total width Γ is then obtained from Eq. (1). We do not list Γ_{ee} and Γ values of individual experiments. The Γ_{ee} values in the Meson Summary Table are also those defined in Eq. (1).

References

1. E.A. Kuraev, V.S. Fadin, Sov. J. Nucl. Phys. **41**, 466 (1985).

$\eta_b(1S)$

$I^G(J^{PC}) = 0^+(0^{-+})$

Quantum numbers shown are quark-model predictions. Observed in radiative decay of the $\Upsilon(3S)$, therefore $C = +$.

$\eta_b(1S)$ MASS

VALUE (MeV)	EVTS	DOCUMENT ID		TECN	COMMENT
9398.7 ± 2.0 OUR AVERAGE		Error includes scale factor of 1.5. See the ideogram below.			
$9394.8^{+2.7}_{-3.1}{}^{+4.5}_{-2.7}$	29k	FULSOM	18	BELL	$\Upsilon(2S) \to \gamma X$
9400.7 ± 1.7 ± 1.6	33.1k	TAMPONI	15	BELL	$e^+e^- \to \gamma\eta +$ hadrons
9402.4 ± 1.5 ± 1.8	34k	[1] MIZUK	12	BELL	$e^+e^- \to \gamma\pi^+\pi^- +$ hadrons
9391.8 ± 6.6 ± 2.0	2.3k	[2] BONVICINI	10	CLEO	$\Upsilon(3S) \to \gamma X$
$9394.2^{+4.8}_{-4.9} \pm 2.0$	13k	[2] AUBERT	09AQ	BABR	$\Upsilon(2S) \to \gamma X$
$9388.9^{+3.1}_{-2.3} \pm 2.7$	19k	[2] AUBERT	08V	BABR	$\Upsilon(3S) \to \gamma X$
• • • We do not use the following data for averages, fits, limits, etc. • • •					
9393.2 ± 3.4 ± 2.3	10	[2,3] DOBBS	12		$\Upsilon(2S) \to \gamma$ hadrons
9300 ± 20 ± 20		HEISTER	02D	ALEP	181–209 e^+e^-

[1] With floating width. Not independent of the corresponding mass difference measurement.
[2] Assuming $\Gamma_{\eta_b(1S)} = 10$ MeV. Not independent of the corresponding γ energy or mass difference measurements.
[3] Obtained by analyzing CLEO III data but not authored by the CLEO Collaboration.

Downloaded from https://academic.oup.com/ptep/article/2022/8/083C01/6651666 by KIT Library user on 27 September 2022

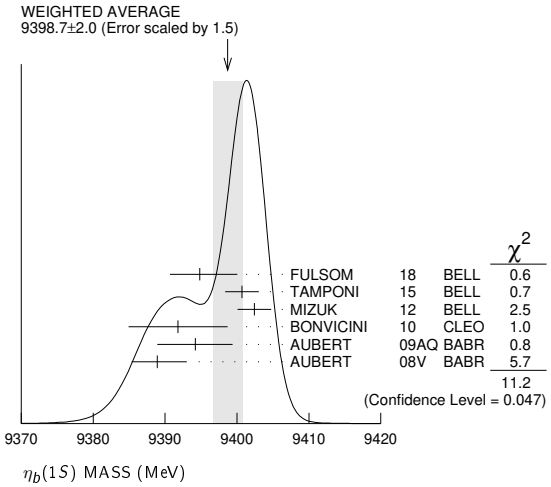

$m_{\Upsilon(1S)} - m_{\eta_b}$

VALUE (MeV)	EVTS	DOCUMENT ID		TECN	COMMENT
62.3±3.2 OUR AVERAGE	Error includes scale factor of 1.8. See the ideogram below.				
57.9±1.5±1.8	34k	[1] MIZUK	12	BELL	$e^+e^- \to \gamma\pi^+\pi^-$ + hadrons
68.5±6.6±2.0	2.3 ± 0.5k	[2] BONVICINI	10	CLEO	$\Upsilon(3S) \to \gamma X$
$66.1^{+4.8}_{-4.9}$±2.0	13 ± 5k	[2] AUBERT	09AQ	BABR	$\Upsilon(2S) \to \gamma X$
$71.4^{+2.3}_{-3.1}$±2.7	19 ± 3k	[2] AUBERT	08V	BABR	$\Upsilon(3S) \to \gamma X$
• • • We do not use the following data for averages, fits, limits, etc. • • •					
67.1±3.4±2.3	10^{+5}_{-4}	[2,3] DOBBS	12		$\Upsilon(2S) \to \gamma$ hadrons

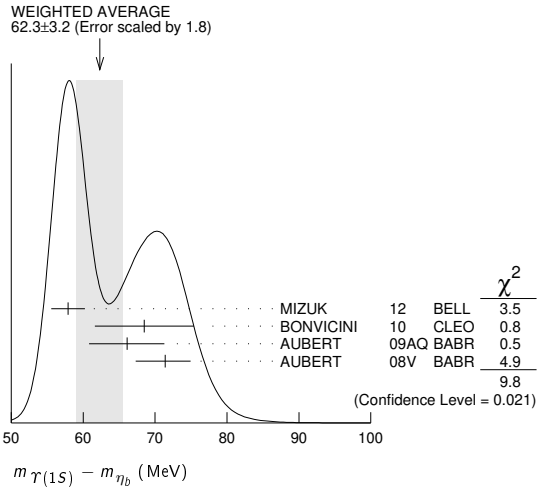

[1] With floating width. Not independent of the corresponding mass measurement.
[2] Assuming $\Gamma_{\eta_b(1S)}$ = 10 MeV. Not independent of the corresponding γ energy or mass measurements.
[3] Obtained by analyzing CLEO III data but not authored by the CLEO Collaboration.

γ ENERGY IN $\Upsilon(3S)$ DECAY

VALUE (MeV)	EVTS	DOCUMENT ID		TECN	COMMENT
$920.6^{+2.8}_{-3.2}$ OUR AVERAGE					
918.6±6.0±1.9	2.3 ± 0.5k	[1] BONVICINI	10	CLEO	$\Upsilon(3S) \to \gamma X$
$921.2^{+2.1}_{-2.8}$±2.4	19 ± 3k	[1] AUBERT	08V	BABR	$\Upsilon(3S) \to \gamma X$

[1] Assuming $\Gamma_{\eta_b(1S)}$ = 10 MeV. Not independent of the corresponding mass or mass difference measurements.

γ ENERGY IN $\Upsilon(2S)$ DECAY

VALUE (MeV)	EVTS	DOCUMENT ID		TECN	COMMENT
$609.3^{+4.6}_{-4.5}$±1.9	13 ± 5k	[1] AUBERT	09AQ	BABR	$\Upsilon(2S) \to \gamma X$

[1] Assuming $\Gamma_{\eta_b(1S)}$ = 10 MeV. Not independent of the corresponding mass or mass difference measurements.

$\eta_b(1S)$ WIDTH

VALUE (MeV)	EVTS	DOCUMENT ID		TECN	COMMENT
10^{+5}_{-4} OUR AVERAGE					
8^{+6}_{-5} ±5	33.1k	[1] TAMPONI	15	BELL	$e^+e^- \to \gamma\eta +$ hadrons
$10.8^{+4.0}_{-3.7}{}^{+4.5}_{-2.0}$	34k	[1] MIZUK	12	BELL	$e^+e^- \to \gamma\pi^+\pi^- +$ hadrons

[1] With floating mass.

$\eta_b(1S)$ DECAY MODES

	Mode	Fraction (Γ_i/Γ)	Confidence level
Γ_1	hadrons	seen	
Γ_2	$3h^+3h^-$	not seen	
Γ_3	$2h^+2h^-$	not seen	
Γ_4	$4h^+4h^-$	not seen	
Γ_5	$\gamma\gamma$	not seen	
Γ_6	$\mu^+\mu^-$	$<9\times10^{-3}$	90%
Γ_7	$\tau^+\tau^-$	<8 %	90%

$\eta_b(1S)$ $\Gamma(i)\Gamma(\gamma\gamma)/\Gamma(\text{total})$

$\Gamma(3h^+3h^-) \times \Gamma(\gamma\gamma)/\Gamma_{\text{total}}$ — $\Gamma_2\Gamma_5/\Gamma$

VALUE (eV)	CL%	DOCUMENT ID		TECN	COMMENT
• • • We do not use the following data for averages, fits, limits, etc. • • •					
<470	95	ABDALLAH	06	DLPH	161–209 e^+e^-
<132	95	HEISTER	02D	ALEP	181–209 e^+e^-

$\Gamma(2h^+2h^-) \times \Gamma(\gamma\gamma)/\Gamma_{\text{total}}$ — $\Gamma_3\Gamma_5/\Gamma$

VALUE (eV)	CL%	DOCUMENT ID		TECN	COMMENT
• • • We do not use the following data for averages, fits, limits, etc. • • •					
<190	95	ABDALLAH	06	DLPH	161–209 e^+e^-
< 48	95	HEISTER	02D	ALEP	181–209 e^+e^-

$\Gamma(4h^+4h^-) \times \Gamma(\gamma\gamma)/\Gamma_{\text{total}}$ — $\Gamma_4\Gamma_5/\Gamma$

VALUE (eV)	CL%	DOCUMENT ID		TECN	COMMENT
• • • We do not use the following data for averages, fits, limits, etc. • • •					
<660	95	ABDALLAH	06	DLPH	161–209 e^+e^-

$\eta_b(1S)$ BRANCHING RATIOS

$\Gamma(\text{hadrons})/\Gamma_{\text{total}}$ — Γ_1/Γ

VALUE	EVTS	DOCUMENT ID		TECN	COMMENT
seen	34k	MIZUK	12	BELL	$e^+e^- \to \gamma\pi^+\pi^- +$ hadrons

$\Gamma(\mu^+\mu^-)/\Gamma_{\text{total}}$ — Γ_6/Γ

VALUE	CL%	DOCUMENT ID		TECN	COMMENT
$<9\times10^{-3}$	90	[1] AUBERT	09Z	BABR	$e^+e^- \to \Upsilon(2S,3S) \to \gamma\eta_b$

[1] Obtained using $B(\Upsilon(2S) \to \gamma\eta_b) = (4.2^{+1.1}_{-1.0} \pm 0.9)\times10^{-4}$ and $B(\Upsilon(3S) \to \gamma\eta_b) = (4.8 \pm 0.5 \pm 0.6)\times10^{-4}$. This limit is equivalent to $B(\eta_b \to \mu^+\mu^-) = (-0.25 \pm 0.51 \pm 0.33)$% measurement.

$\Gamma(\tau^+\tau^-)/\Gamma_{\text{total}}$ — Γ_7/Γ

VALUE	CL%	DOCUMENT ID		TECN	COMMENT
$<8\times10^{-2}$	90	AUBERT	09P	BABR	$e^+e^- \to \gamma\tau^+\tau^-$

$\eta_b(1S)$ REFERENCES

FULSOM	18	PRL 121 232001	B.G. Fulsom *et al.*	(BELLE Collab.)
TAMPONI	15	PRL 115 142001	U. Tamponi *et al.*	(BELLE Collab.)
DOBBS	12	PRL 109 082001	S. Dobbs *et al.*	
MIZUK	12	PRL 109 232002	R. Mizuk *et al.*	(BELLE Collab.)
BONVICINI	10	PR D81 031104	G. Bonvicini *et al.*	(CLEO Collab.)
AUBERT	09AQ	PRL 103 161801	B. Aubert *et al.*	(BABAR Collab.)
AUBERT	09P	PRL 103 181801	B. Aubert *et al.*	(BABAR Collab.)
AUBERT	09Z	PRL 103 081803	B. Aubert *et al.*	(BABAR Collab.)
AUBERT	08V	PRL 101 071801	B. Aubert *et al.*	(BABAR Collab.)
ABDALLAH	06	PL B634 340	J.M. Abdallah *et al.*	(DELPHI Collab.)
HEISTER	02D	PL B530 56	A. Heister *et al.*	(ALEPH Collab.)

Downloaded from https://academic.oup.com/ptep/article/2022/8/083C01/6651666 by KIT Library user on 27 September 2022

$\Upsilon(1S)$

$I^G(J^{PC}) = 0^-(1^{--})$

$\Upsilon(1S)$ MASS

VALUE (MeV)	DOCUMENT ID		TECN	COMMENT
9460.30±0.26 OUR AVERAGE	Error includes scale factor of 3.3.			
9460.51±0.09±0.05	[1] ARTAMONOV	00	MD1	$e^+e^- \to$ hadrons
9459.97±0.11±0.07	MACKAY	84	REDE	$e^+e^- \to$ hadrons
• • • We do not use the following data for averages, fits, limits, etc. • • •				
9460.60±0.09±0.05	[2,3] BARU	92B	REDE	$e^+e^- \to$ hadrons
9460.59±0.12	BARU	86	REDE	$e^+e^- \to$ hadrons
9460.6 ±0.4	[3,4] ARTAMONOV	84	REDE	$e^+e^- \to$ hadrons

[1] Reanalysis of BARU 92B and ARTAMONOV 84 using new electron mass (COHEN 87).
[2] Superseding BARU 86.
[3] Superseded by ARTAMONOV 00.
[4] Value includes data of ARTAMONOV 82.

$\Upsilon(1S)$ WIDTH

VALUE (keV)	DOCUMENT ID
54.02±1.25 OUR EVALUATION	See the Note on "Width Determinations of the Υ States"

$\Upsilon(1S)$ DECAY MODES

	Mode	Fraction (Γ_i/Γ)	Scale factor/ Confidence level
Γ_1	$\tau^+\tau^-$	(2.60 ±0.10) %	
Γ_2	e^+e^-	(2.38 ±0.11) %	
Γ_3	$\mu^+\mu^-$	(2.48 ±0.05) %	
	Hadronic decays		
Γ_4	ggg	(81.7 ±0.7) %	
Γ_5	γgg	(2.2 ±0.6) %	
Γ_6	$\eta'(958)$ anything	(2.94 ±0.24) %	
Γ_7	$J/\psi(1S)$ anything	(5.4 ±0.4) $\times 10^{-4}$	S=1.4
Γ_8	$J/\psi(1S)\eta_c$	< 2.2 $\times 10^{-6}$	CL=90%
Γ_9	$J/\psi(1S)\chi_{c0}$	< 3.4 $\times 10^{-6}$	CL=90%
Γ_{10}	$J/\psi(1S)\chi_{c1}$	(3.9 ±1.2) $\times 10^{-6}$	
Γ_{11}	$J/\psi(1S)\chi_{c2}$	< 1.4 $\times 10^{-6}$	CL=90%
Γ_{12}	$J/\psi(1S)\eta_c(2S)$	< 2.2 $\times 10^{-6}$	CL=90%
Γ_{13}	$J/\psi(1S)X(3940)$	< 5.4 $\times 10^{-6}$	CL=90%
Γ_{14}	$J/\psi(1S)X(4160)$	< 5.4 $\times 10^{-6}$	CL=90%
Γ_{15}	$X(4350)$ anything, $X \to J/\psi(1S)\phi$	< 8.1 $\times 10^{-6}$	CL=90%
Γ_{16}	$Z_c(3900)^\pm$ anything, $Z_c \to J/\psi(1S)\pi^\pm$	< 1.3 $\times 10^{-5}$	CL=90%
Γ_{17}	$Z_c(4200)^\pm$ anything, $Z_c \to J/\psi(1S)\pi^\pm$	< 6.0 $\times 10^{-5}$	CL=90%
Γ_{18}	$Z_c(4430)^\pm$ anything, $Z_c \to J/\psi(1S)\pi^\pm$	< 4.9 $\times 10^{-5}$	CL=90%
Γ_{19}	$X_{cs}^\pm$ anything, $X \to J/\psi K^\pm$	< 5.7 $\times 10^{-6}$	CL=90%
Γ_{20}	$\psi(4230)$ anything, $\psi \to J/\psi(1S)\pi^+\pi^-$	< 3.8 $\times 10^{-5}$	CL=90%
Γ_{21}	$\psi(4230)$ anything, $\psi \to J/\psi(1S)K^+K^-$	< 7.5 $\times 10^{-6}$	CL=90%
Γ_{22}	$\chi_{c1}(4140)$ anything, $\chi_{c1} \to J/\psi(1S)\phi$	< 5.2 $\times 10^{-6}$	CL=90%
Γ_{23}	χ_{c0} anything	< 4 $\times 10^{-3}$	CL=90%
Γ_{24}	χ_{c1} anything	(1.90 ±0.35) $\times 10^{-4}$	
Γ_{25}	$\chi_{c1}(1P)X_{tetra}$	< 3.78 $\times 10^{-5}$	CL=90%
Γ_{26}	χ_{c2} anything	(2.8 ±0.8) $\times 10^{-4}$	
Γ_{27}	$\psi(2S)$ anything	(1.23 ±0.20) $\times 10^{-4}$	
Γ_{28}	$\psi(2S)\eta_c$	< 3.6 $\times 10^{-6}$	CL=90%
Γ_{29}	$\psi(2S)\chi_{c0}$	< 6.5 $\times 10^{-6}$	CL=90%
Γ_{30}	$\psi(2S)\chi_{c1}$	< 4.5 $\times 10^{-6}$	CL=90%
Γ_{31}	$\psi(2S)\chi_{c2}$	< 2.1 $\times 10^{-6}$	CL=90%
Γ_{32}	$\psi(2S)\eta_c(2S)$	< 3.2 $\times 10^{-6}$	CL=90%
Γ_{33}	$\psi(2S)X(3940)$	< 2.9 $\times 10^{-6}$	CL=90%
Γ_{34}	$\psi(2S)X(4160)$	< 2.9 $\times 10^{-6}$	CL=90%
Γ_{35}	$\psi(4230)$ anything, $\psi \to \psi(2S)\pi^+\pi^-$	< 7.9 $\times 10^{-5}$	CL=90%
Γ_{36}	$\psi(4360)$ anything, $\psi \to \psi(2S)\pi^+\pi^-$	< 5.2 $\times 10^{-5}$	CL=90%
Γ_{37}	$\psi(4660)$ anything, $\psi \to \psi(2S)\pi^+\pi^-$	< 2.2 $\times 10^{-5}$	CL=90%
Γ_{38}	$X(4050)^\pm$ anything, $X \to \psi(2S)\pi^\pm$	< 8.8 $\times 10^{-5}$	CL=90%
Γ_{39}	$Z_c(4430)^\pm$ anything, $Z_c \to \psi(2S)\pi^\pm$	< 6.7 $\times 10^{-5}$	CL=90%
Γ_{40}	$\chi_{c1}(3872)$ anything	< 2.5 $\times 10^{-4}$	CL=90%
Γ_{41}	$Z_c(4200)^+Z_c(4200)^-$	< 2.23 $\times 10^{-5}$	CL=90%
Γ_{42}	$Z_c(3900)^\pm Z_c(4200)^\mp$	< 8.1 $\times 10^{-6}$	CL=90%
Γ_{43}	$Z_c(3900)^+Z_c(3900)^-$	< 1.8 $\times 10^{-6}$	CL=90%
Γ_{44}	$X(4050)^+X(4050)^-$	< 1.58 $\times 10^{-5}$	CL=90%
Γ_{45}	$X(4250)^+X(4250)^-$	< 2.66 $\times 10^{-5}$	CL=90%
Γ_{46}	$X(4050)^\pm X(4250)^\mp$	< 4.42 $\times 10^{-5}$	CL=90%
Γ_{47}	$Z_c(4430)^+Z_c(4430)^-$	< 2.03 $\times 10^{-5}$	CL=90%
Γ_{48}	$X(4055)^\pm X(4055)^\mp$	< 2.33 $\times 10^{-5}$	CL=90%
Γ_{49}	$X(4055)^\pm Z_c(4430)^\mp$	< 4.55 $\times 10^{-5}$	CL=90%
Γ_{50}	$\rho\pi$	< 3.68 $\times 10^{-6}$	CL=90%
Γ_{51}	$\omega\pi^0$	< 3.90 $\times 10^{-6}$	CL=90%
Γ_{52}	$\pi^+\pi^-$	< 5 $\times 10^{-4}$	CL=90%
Γ_{53}	K^+K^-	< 5 $\times 10^{-4}$	CL=90%
Γ_{54}	$p\overline{p}$	< 5 $\times 10^{-4}$	CL=90%
Γ_{55}	$\pi^+\pi^-\pi^0$	(2.1 ±0.8) $\times 10^{-6}$	
Γ_{56}	ϕK^+K^-	(2.4 ±0.5) $\times 10^{-6}$	
Γ_{57}	$\omega\pi^+\pi^-$	(4.5 ±1.0) $\times 10^{-6}$	
Γ_{58}	$K^*(892)^0K^-\pi^+$ + c.c.	(4.4 ±0.8) $\times 10^{-6}$	
Γ_{59}	$\phi f_2'(1525)$	< 1.63 $\times 10^{-6}$	CL=90%
Γ_{60}	$\omega f_2(1270)$	< 1.79 $\times 10^{-6}$	CL=90%
Γ_{61}	$\rho(770)a_2(1320)$	< 2.24 $\times 10^{-6}$	CL=90%
Γ_{62}	$K^*(892)^0\overline{K}_2^*(1430)^0$ + c.c.	(3.0 ±0.8) $\times 10^{-6}$	
Γ_{63}	$K_1(1270)^\pm K^\mp$	< 2.41 $\times 10^{-6}$	CL=90%
Γ_{64}	$K_1(1400)^\pm K^\mp$	(1.0 ±0.4) $\times 10^{-6}$	
Γ_{65}	$b_1(1235)^\pm\pi^\mp$	< 1.25 $\times 10^{-6}$	CL=90%
Γ_{66}	$\pi^+\pi^-\pi^0\pi^0$	(1.28 ±0.30) $\times 10^{-5}$	
Γ_{67}	$K_S^0K^+\pi^-$ + c.c.	(1.6 ±0.4) $\times 10^{-6}$	
Γ_{68}	$K^*(892)^0\overline{K}^0$ + c.c.	(2.9 ±0.9) $\times 10^{-6}$	
Γ_{69}	$K^*(892)^-K^+$ + c.c.	< 1.11 $\times 10^{-6}$	CL=90%
Γ_{70}	$f_1(1285)$ anything	(4.6 ±3.1) $\times 10^{-3}$	
Γ_{71}	$D^*(2010)^\pm$ anything	(2.52 ±0.20) %	
Γ_{72}	$f_1(1285)X_{tetra}$	< 6.24 $\times 10^{-5}$	CL=90%
Γ_{73}	^2H anything	(2.85 ±0.25) $\times 10^{-5}$	
Γ_{74}	Sum of 100 exclusive modes	(1.200±0.017) %	
	Radiative decays		
Γ_{75}	$\gamma\pi^+\pi^-$	(6.3 ±1.8) $\times 10^{-5}$	
Γ_{76}	$\gamma\pi^0\pi^0$	(1.7 ±0.7) $\times 10^{-5}$	
Γ_{77}	$\gamma\pi\pi$ (S-wave)	(4.6 ±0.7) $\times 10^{-5}$	
Γ_{78}	$\gamma\pi^0\eta$	< 2.4 $\times 10^{-6}$	CL=90%
Γ_{79}	γK^+K^-	[a] (1.14 ±0.13) $\times 10^{-5}$	
Γ_{80}	$\gamma p\overline{p}$	[b] < 6 $\times 10^{-6}$	CL=90%
Γ_{81}	$\gamma 2h^+2h^-$	(7.0 ±1.5) $\times 10^{-4}$	
Γ_{82}	$\gamma 3h^+3h^-$	(5.4 ±2.0) $\times 10^{-4}$	
Γ_{83}	$\gamma 4h^+4h^-$	(7.4 ±3.5) $\times 10^{-4}$	
Γ_{84}	$\gamma\pi^+\pi^-K^+K^-$	(2.9 ±0.9) $\times 10^{-4}$	
Γ_{85}	$\gamma 2\pi^+2\pi^-$	(2.5 ±0.9) $\times 10^{-4}$	
Γ_{86}	$\gamma 3\pi^+3\pi^-$	(2.5 ±1.2) $\times 10^{-4}$	
Γ_{87}	$\gamma 2\pi^+2\pi^-K^+K^-$	(2.4 ±1.2) $\times 10^{-4}$	
Γ_{88}	$\gamma\pi^+\pi^-p\overline{p}$	(1.5 ±0.6) $\times 10^{-4}$	
Γ_{89}	$\gamma 2\pi^+2\pi^-p\overline{p}$	(4 ±6) $\times 10^{-5}$	
Γ_{90}	$\gamma 2K^+2K^-$	(2.0 ±2.0) $\times 10^{-5}$	
Γ_{91}	$\gamma\eta'(958)$	< 1.9 $\times 10^{-6}$	CL=90%
Γ_{92}	$\gamma\eta$	< 1.0 $\times 10^{-6}$	CL=90%
Γ_{93}	$\gamma f_0(980)$	< 3 $\times 10^{-5}$	CL=90%
Γ_{94}	$\gamma f_2'(1525)$	(2.9 ±0.6) $\times 10^{-5}$	
Γ_{95}	$\gamma f_2(1270)$	(1.01 ±0.06) $\times 10^{-4}$	
Γ_{96}	$\gamma\eta(1405)$	< 8.2 $\times 10^{-5}$	CL=90%
Γ_{97}	$\gamma f_0(1500)$	< 1.5 $\times 10^{-5}$	CL=90%
Γ_{98}	$\gamma f_0(1500) \to \gamma K^+K^-$	(1.0 ±0.4) $\times 10^{-5}$	
Γ_{99}	$\gamma f_0(1710)$	< 2.6 $\times 10^{-4}$	CL=90%
Γ_{100}	$\gamma f_0(1710) \to \gamma K^+K^-$	(1.01 ±0.32) $\times 10^{-5}$	
Γ_{101}	$\gamma f_0(1710) \to \gamma\pi^+\pi^-$	(5.3 ±2.0) $\times 10^{-6}$	
Γ_{102}	$\gamma f_0(1710) \to \gamma\pi^0\pi^0$	< 1.4 $\times 10^{-6}$	CL=90%
Γ_{103}	$\gamma f_0(1710) \to \gamma\eta\eta$	< 1.8 $\times 10^{-6}$	CL=90%
Γ_{104}	$\gamma f_4(2050)$	< 5.3 $\times 10^{-5}$	CL=90%
Γ_{105}	$\gamma f_0(2200) \to \gamma K^+K^-$	< 2 $\times 10^{-4}$	CL=90%
Γ_{106}	$\gamma f_J(2220) \to \gamma K^+K^-$	< 8 $\times 10^{-7}$	CL=90%
Γ_{107}	$\gamma f_J(2220) \to \gamma\pi^+\pi^-$	< 6 $\times 10^{-7}$	CL=90%
Γ_{108}	$\gamma f_J(2220) \to \gamma p\overline{p}$	< 1.1 $\times 10^{-6}$	CL=90%

Downloaded from https://academic.oup.com/ptep/article/2022/8/083C01/6651666 by KIT Library user on 27 September 2022

Γ_{109}	$\gamma\eta(2225) \to \gamma\phi\phi$	< 3	$\times 10^{-3}$	CL=90%
Γ_{110}	$\gamma\eta_c(1S)$	< 2.9	$\times 10^{-5}$	CL=90%
Γ_{111}	$\gamma\eta_c(2S)$	< 4	$\times 10^{-4}$	CL=90%
Γ_{112}	$\gamma\chi_{c0}$	< 6.6	$\times 10^{-5}$	CL=90%
Γ_{113}	$\gamma\chi_{c1}$	$(4.7\ ^{+2.4}_{-1.9})$	$\times 10^{-5}$	
Γ_{114}	$\gamma\chi_{c2}$	< 7.6	$\times 10^{-6}$	CL=90%
Γ_{115}	$\gamma\chi_{c1}(3872)$	< 4	$\times 10^{-5}$	CL=90%
Γ_{116}	$\gamma\chi_{c1}(3872)$, $\chi_{c1} \to \pi^+\pi^-\pi^0 J/\psi$	< 2.8	$\times 10^{-6}$	CL=90%
Γ_{117}	$\gamma\chi_{c0}(3915) \to \omega J/\psi$	< 3.0	$\times 10^{-6}$	CL=90%
Γ_{118}	$\gamma\chi_{c1}(4140) \to \phi J/\psi$	< 2.2	$\times 10^{-6}$	CL=90%
Γ_{119}	γX	[c] < 4.5	$\times 10^{-6}$	CL=90%
Γ_{120}	$\gamma X \overline{X}(m_X < 3.1$ GeV)	[d] < 1	$\times 10^{-3}$	CL=90%
Γ_{121}	$\gamma X \overline{X}(m_X < 4.5$ GeV)	[e] < 2.4	$\times 10^{-4}$	CL=90%
Γ_{122}	$\gamma X \to \gamma + \geq 4$ prongs	[f] < 1.78	$\times 10^{-4}$	CL=95%
Γ_{123}	$\gamma a_1^0 \to \gamma\mu^+\mu^-$	[g] < 9	$\times 10^{-6}$	CL=90%
Γ_{124}	$\gamma a_1^0 \to \gamma\tau^+\tau^-$	[a] < 1.30	$\times 10^{-4}$	CL=90%
Γ_{125}	$\gamma a_1^0 \to \gamma gg$	[h] < 1	%	CL=90%
Γ_{126}	$\gamma a_1^0 \to \gamma s\overline{s}$	[h] < 1	$\times 10^{-3}$	CL=90%
	Lepton Family number (*LF*) violating modes			
Γ_{127}	$\mu^\pm\tau^\mp$ *LF*	< 6.0	$\times 10^{-6}$	CL=95%
	Other decays			
Γ_{128}	invisible	< 3.0	$\times 10^{-4}$	CL=90%
Γ_{129}	hadrons	(97 ± 5) %		

[a] $2m_\tau < M(\tau^+\tau^-) < 9.2$ GeV

[b] 2 GeV $< m_{K^+K^-} <$ 3 GeV

[c] X = scalar with $m < 8.0$ GeV

[d] $X\overline{X}$ = vectors with $m < 3.1$ GeV

[e] X and $\overline{X}$ = zero spin with $m < 4.5$ GeV

[f] 1.5 GeV $< m_X <$ 5.0 GeV

[g] 201 MeV $< M(\mu^+\mu^-) <$ 3565 MeV

[h] 0.5 GeV $< m_X <$ 9.0 GeV, where m_X is the invariant mass of the hadronic final state.

$\Upsilon(1S)$ $\Gamma(i)\Gamma(e^+e^-)/\Gamma(\text{total})$

$\Gamma(\mu^+\mu^-) \times \Gamma(e^+e^-)/\Gamma_{\text{total}}$ — $\Gamma_3\Gamma_2/\Gamma$

VALUE (eV)	DOCUMENT ID		TECN	COMMENT
31.2±1.6±1.7	KOBEL	92	CBAL	$e^+e^- \to \mu^+\mu^-$

$\Gamma(\text{hadrons}) \times \Gamma(e^+e^-)/\Gamma_{\text{total}}$ — $\Gamma_{129}\Gamma_2/\Gamma$

VALUE (keV)	DOCUMENT ID		TECN	COMMENT
1.240±0.016 OUR AVERAGE				
1.252±0.004±0.019	[1] ROSNER	06	CLEO	9.5 $e^+e^- \to$ hadrons
1.187±0.023±0.031	[1] BARU	92B	MD1	$e^+e^- \to$ hadrons
1.23 ±0.02 ±0.05	[1] JAKUBOWSKI	88	CBAL	$e^+e^- \to$ hadrons
1.37 ±0.06 ±0.09	[2] GILES	84B	CLEO	$e^+e^- \to$ hadrons
1.23 ±0.08 ±0.04	[2] ALBRECHT	82	DASP	$e^+e^- \to$ hadrons
1.13 ±0.07 ±0.11	[2] NICZYPORUK	82	LENA	$e^+e^- \to$ hadrons
1.09 ±0.25	[2] BOCK	80	CNTR	$e^+e^- \to$ hadrons
1.35 ±0.14	[3] BERGER	79	PLUT	$e^+e^- \to$ hadrons

[1] Radiative corrections evaluated following KURAEV 85.
[2] Radiative corrections reevaluated by BUCHMUELLER 88 following KURAEV 85.
[3] Radiative corrections reevaluated by ALEXANDER 89 using $B(\mu\mu) = 0.026$.

$\Upsilon(1S)$ PARTIAL WIDTHS

$\Gamma(e^+e^-)$ — Γ_2

VALUE (keV)	DOCUMENT ID
1.340±0.018 OUR EVALUATION	

$\Upsilon(1S)$ BRANCHING RATIOS

$\Gamma(\tau^+\tau^-)/\Gamma_{\text{total}}$ — Γ_1/Γ

VALUE (units 10^{-2})	EVTS	DOCUMENT ID		TECN	COMMENT
2.60±0.10 OUR AVERAGE					
2.53±0.13±0.05	60k	[1] BESSON	07	CLEO	$e^+e^- \to \Upsilon(1S) \to \tau^+\tau^-$
$2.61 \pm 0.12 ^{+0.09}_{-0.13}$	25k	CINABRO	94B	CLE2	$e^+e^- \to \tau^+\tau^-$
2.7 ±0.4 ±0.2		[2] ALBRECHT	85C	ARG	$\Upsilon(2S) \to \pi^+\pi^-\tau^+\tau^-$
3.4 ±0.4 ±0.4		GILES	83	CLEO	$e^+e^- \to \tau^+\tau^-$

[1] BESSON 07 reports $[\Gamma(\Upsilon(1S) \to \tau^+\tau^-)/\Gamma_{\text{total}}] / [B(\Upsilon(1S) \to \mu^+\mu^-)] = 1.02 \pm 0.02 \pm 0.05$ which we multiply by our best value $B(\Upsilon(1S) \to \mu^+\mu^-) = (2.48 \pm 0.05) \times 10^{-2}$. Our first error is their experiment's error and our second error is the systematic error from using our best value.
[2] Using $B(\Upsilon(1S) \to ee) = B(\Upsilon(1S) \to \mu\mu) = 0.0256$; not used for width evaluations.

$\Gamma(e^+e^-)/\Gamma_{\text{total}}$ — Γ_2/Γ

VALUE (units 10^{-2})	EVTS	DOCUMENT ID		TECN	COMMENT
2.38±0.11 OUR AVERAGE					
2.29±0.08±0.11		ALEXANDER	98	CLE2	$\Upsilon(2S) \to \pi^+\pi^-e^+e^-$
2.42±0.14±0.14	307	ALBRECHT	87	ARG	$\Upsilon(2S) \to \pi^+\pi^-e^+e^-$
2.8 ±0.3 ±0.2	826	BESSON	84	CLEO	$\Upsilon(2S) \to \pi^+\pi^-e^+e^-$
5.1 ±3.0		BERGER	80C	PLUT	$e^+e^- \to e^+e^-$

$\Gamma(\mu^+\mu^-)/\Gamma_{\text{total}}$ — Γ_3/Γ

VALUE	EVTS	DOCUMENT ID		TECN	COMMENT
0.0248±0.0005 OUR AVERAGE					
0.0249±0.0002±0.0007	345k	ADAMS	05	CLEO	$e^+e^- \to \mu^+\mu^-$
0.0249±0.0008±0.0013		ALEXANDER	98	CLE2	$\Upsilon(2S) \to \pi^+\pi^-\mu^+\mu^-$
0.0212±0.0020±0.0010		[1] BARU	92	MD1	$e^+e^- \to \mu^+\mu^-$
0.0231±0.0012±0.0010		[1] KOBEL	92	CBAL	$e^+e^- \to \mu^+\mu^-$
0.0252±0.0007±0.0007		CHEN	89B	CLEO	$e^+e^- \to \mu^+\mu^-$
0.0261±0.0009±0.0011		KAARSBERG	89	CSB2	$e^+e^- \to \mu^+\mu^-$
0.0230±0.0025±0.0013	86	ALBRECHT	87	ARG	$\Upsilon(2S) \to \pi^+\pi^-\mu^+\mu^-$
0.029 ±0.003 ±0.002	864	BESSON	84	CLEO	$\Upsilon(2S) \to \pi^+\pi^-\mu^+\mu^-$
0.027 ±0.003 ±0.003		ANDREWS	83	CLEO	$e^+e^- \to \mu^+\mu^-$
0.032 ±0.013 ±0.003		ALBRECHT	82	DASP	$e^+e^- \to \mu^+\mu^-$
0.038 ±0.015 ±0.002		NICZYPORUK	82	LENA	$e^+e^- \to \mu^+\mu^-$
$0.014\ ^{+0.034}_{-0.014}$		BOCK	80	CNTR	$e^+e^- \to \mu^+\mu^-$
0.022 ±0.020		BERGER	79	PLUT	$e^+e^- \to \mu^+\mu^-$

[1] Taking into account interference between the resonance and continuum.

$\Gamma(\tau^+\tau^-)/\Gamma(\mu^+\mu^-)$ — Γ_1/Γ_3

VALUE	EVTS	DOCUMENT ID		TECN	COMMENT
1.008±0.023 OUR AVERAGE					
1.005±0.013±0.022	0.7M	[1] DEL-AMO-SA...10C		BABR	$\Upsilon(3S) \to \pi^+\pi^-\Upsilon(1S)$
1.02 ±0.02 ±0.05	60k	BESSON	07	CLEO	$e^+e^- \to \Upsilon(1S)$

[1] Allows any number of extra photons with total energy < 500 MeV.

$\Gamma(ggg)/\Gamma_{\text{total}}$ — Γ_4/Γ

VALUE (units 10^{-2})	EVTS	DOCUMENT ID		TECN	COMMENT
81.7±0.7	20M	[1] BESSON	06A	CLEO	$\Upsilon(1S) \to$ hadrons

[1] Calculated using the value $\Gamma(\gamma gg)/\Gamma(ggg) = (2.70 \pm 0.01 \pm 0.13 \pm 0.24)\%$ from BESSON 06A and PDG 08 values of $B(\mu^+\mu^-) = (2.48 \pm 0.05)\%$ and $R_{\text{hadrons}} = 3.51$. The statistical error is negligible and the systematic error is partially correlated with that of $\Gamma(\gamma gg)/\Gamma_{\text{total}}$ measurement of BESSON 06A.

$\Gamma(\gamma gg)/\Gamma_{\text{total}}$ — Γ_5/Γ

VALUE (units 10^{-2})	EVTS	DOCUMENT ID		TECN	COMMENT
2.20±0.60	400k	[1] BESSON	06A	CLEO	$\Upsilon(1S) \to \gamma +$ hadrons

[1] Calculated using BESSON 06A values of $\Gamma(\gamma gg)/\Gamma(ggg) = (2.70 \pm 0.01 \pm 0.13 \pm 0.24)\%$ and $\Gamma(ggg)/\Gamma_{\text{total}}$. The statistical error is negligible and the systematic error is partially correlated with that of $\Gamma(ggg)/\Gamma_{\text{total}}$ measurement of BESSON 06A.

$\Gamma(\gamma gg)/\Gamma(ggg)$ — Γ_5/Γ_4

VALUE (units 10^{-2})	EVTS	DOCUMENT ID		TECN	COMMENT
2.70±0.01±0.27	20M	BESSON	06A	CLEO	$\Upsilon(1S) \to (\gamma +)$ hadrons

$\Gamma(\eta'(958)\text{ anything})/\Gamma_{\text{total}}$ — Γ_6/Γ

VALUE	DOCUMENT ID		TECN	COMMENT
0.0294±0.0024 OUR AVERAGE				
0.030 ±0.002 ±0.002	AQUINES	06A	CLE3	$\Upsilon(1S) \to \eta'$ anything
0.028 ±0.004 ±0.002	ARTUSO	03	CLE2	$\Upsilon(1S) \to \eta'$ anything

$\Gamma(J/\psi(1S)\text{ anything})/\Gamma_{\text{total}}$ — Γ_7/Γ

VALUE (units 10^{-4})	CL%	EVTS	DOCUMENT ID		TECN	COMMENT
5.4 ±0.4 OUR FIT Error includes scale factor of 1.4.						
5.4 ±0.4 OUR AVERAGE Error includes scale factor of 1.5.						
5.25±0.13±0.25		3k	SHEN	16	BELL	$e^+e^- \to J/\psi X$
6.4 ±0.4 ±0.6		730	BRIERE	04	CLEO	$e^+e^- \to J/\psi X$
11 ±4 ±2			[1] FULTON	89	CLEO	$e^+e^- \to \mu^+\mu^- X$
• • • We do not use the following data for averages, fits, limits, etc. • • •						
<6.8	90		ALBRECHT	92J	ARG	$e^+e^- \to e^+e^- X$, $\mu^+\mu^- X$
<17	90		MASCHMANN	90	CBAL	$e^+e^- \to$ hadrons
<200	90		NICZYPORUK	83	LENA	

[1] Using $B((J/\psi) \to \mu^+\mu^-) = (6.9 \pm 0.9)\%$.

$\Gamma(J/\psi(1S)\eta_c)/\Gamma_{\text{total}}$ — Γ_8/Γ

VALUE	CL%	DOCUMENT ID		TECN	COMMENT
$<2.2 \times 10^{-6}$	90	YANG	14	BELL	$e^+e^- \to J/\psi X$

$\Gamma(J/\psi(1S)\chi_{c0})/\Gamma_{\text{total}}$ — Γ_9/Γ

VALUE	CL%	DOCUMENT ID		TECN	COMMENT
$<3.4 \times 10^{-6}$	90	YANG	14	BELL	$e^+e^- \to J/\psi X$

Downloaded from https://academic.oup.com/ptep/article/2022/8/083C01/6651666 by KIT Library user on 27 September 2022

$\Gamma(J/\psi(1S)\chi_{c1})/\Gamma_{total}$ — Γ_{10}/Γ

VALUE (units 10^{-6})	EVTS	DOCUMENT ID		TECN	COMMENT
3.90±1.21±0.23	20	YANG	14	BELL	$e^+e^- \to J/\psi X$

$\Gamma(J/\psi(1S)\chi_{c2})/\Gamma_{total}$ — Γ_{11}/Γ

VALUE	CL%	DOCUMENT ID		TECN	COMMENT
$<1.4\times10^{-6}$	90	YANG	14	BELL	$e^+e^- \to J/\psi X$

$\Gamma(J/\psi(1S)\eta_c(2S))/\Gamma_{total}$ — Γ_{12}/Γ

VALUE	CL%	DOCUMENT ID		TECN	COMMENT
$<2.2\times10^{-6}$	90	YANG	14	BELL	$e^+e^- \to J/\psi X$

$\Gamma(J/\psi(1S)X(3940))/\Gamma_{total}$ — Γ_{13}/Γ

VALUE	CL%	DOCUMENT ID		TECN	COMMENT
$<5.4\times10^{-6}$	90	YANG	14	BELL	$e^+e^- \to J/\psi X$

$\Gamma(J/\psi(1S)X(4160))/\Gamma_{total}$ — Γ_{14}/Γ

VALUE	CL%	DOCUMENT ID		TECN	COMMENT
$<5.4\times10^{-6}$	90	YANG	14	BELL	$e^+e^- \to J/\psi X$

$\Gamma(X(4350)$ anything, $X \to J/\psi(1S)\phi)/\Gamma_{total}$ — Γ_{15}/Γ

VALUE	CL%	DOCUMENT ID		TECN	COMMENT
$<8.1\times10^{-6}$	90	SHEN	16	BELL	$\Upsilon(1S) \to J/\psi K^+K^-X$

$\Gamma(Z_c(3900)^\pm$ anything, $Z_c \to J/\psi(1S)\pi^\pm)/\Gamma_{total}$ — Γ_{16}/Γ

VALUE	CL%	DOCUMENT ID		TECN	COMMENT
$<1.3\times10^{-5}$	90	SHEN	16	BELL	$\Upsilon(1S) \to J/\psi\pi^\pm X$

$\Gamma(Z_c(4200)^\pm$ anything, $Z_c \to J/\psi(1S)\pi^\pm)/\Gamma_{total}$ — Γ_{17}/Γ

VALUE	CL%	DOCUMENT ID		TECN	COMMENT
$<6.0\times10^{-5}$	90	SHEN	16	BELL	$\Upsilon(1S) \to J/\psi\pi^\pm X$

$\Gamma(Z_c(4430)^\pm$ anything, $Z_c \to J/\psi(1S)\pi^\pm)/\Gamma_{total}$ — Γ_{18}/Γ

VALUE	CL%	DOCUMENT ID		TECN	COMMENT
$<4.9\times10^{-5}$	90	SHEN	16	BELL	$\Upsilon(1S) \to J/\psi\pi^\pm X$

$\Gamma(X_{cs}^\pm$ anything, $X \to J/\psi K^\pm)/\Gamma_{total}$ — Γ_{19}/Γ

VALUE	CL%	DOCUMENT ID		TECN	COMMENT
$<5.7\times10^{-6}$	90	SHEN	16	BELL	$\Upsilon(1S) \to J/\psi K^-X$

$\Gamma(\psi(4230)$ anything, $\psi \to J/\psi(1S)\pi^+\pi^-)/\Gamma_{total}$ — Γ_{20}/Γ

VALUE	CL%	DOCUMENT ID		TECN	COMMENT
$<3.8\times10^{-5}$	90	SHEN	16	BELL	$\Upsilon(1S) \to J/\psi\pi^+\pi^-X$

$\Gamma(\psi(4230)$ anything, $\psi \to J/\psi(1S)K^+K^-)/\Gamma_{total}$ — Γ_{21}/Γ

VALUE	CL%	DOCUMENT ID		TECN	COMMENT
$<7.5\times10^{-6}$	90	SHEN	16	BELL	$\Upsilon(1S) \to J/\psi K^+K^-X$

$\Gamma(\chi_{c1}(4140)$ anything, $\chi_{c1} \to J/\psi(1S)\phi)/\Gamma_{total}$ — Γ_{22}/Γ

VALUE	CL%	DOCUMENT ID		TECN	COMMENT
$<5.2\times10^{-6}$	90	SHEN	16	BELL	$\Upsilon(1S) \to J/\psi K^+K^-X$

$\Gamma(\chi_{c0}$ anything$)/\Gamma(J/\psi(1S)$ anything$)$ — Γ_{23}/Γ_7

VALUE	CL%	DOCUMENT ID		TECN	COMMENT
<7.4	90	BRIERE	04	CLEO	$e^+e^- \to J/\psi X$

$\Gamma(\chi_{c1}$ anything$)/\Gamma_{total}$ — Γ_{24}/Γ

VALUE (units 10^{-4})	EVTS	DOCUMENT ID		TECN	COMMENT
1.90±0.35 OUR FIT					
1.90±0.43±0.14	215	JIA	17	BELL	$\Upsilon(1S) \to \gamma J/\psi(1S)$

$\Gamma(\chi_{c1}$ anything$)/\Gamma(J/\psi(1S)$ anything$)$ — Γ_{24}/Γ_7

VALUE	EVTS	DOCUMENT ID		TECN	COMMENT
0.35±0.07 OUR FIT					
0.35±0.08±0.06	52 ± 12	BRIERE	04	CLEO	$e^+e^- \to J/\psi X$

$\Gamma(\chi_{c1}(1P)X_{tetra})/\Gamma_{total}$ — Γ_{25}/Γ

VALUE	CL%	DOCUMENT ID		TECN	COMMENT
$<37.8\times10^{-6}$	90	[1] JIA	17A	BELL	$e^+e^- \to$ hadrons

[1] For a tetraquark state X_{tetra}, with mass in the range 1.16–2.46 GeV and width in the range 0–0.3 GeV. Measured 90% CL limits as a function of X_{tetra} mass and width range from 4.4×10^{-6} to 37.8×10^{-6}.

$\Gamma(\chi_{c2}$ anything$)/\Gamma(J/\psi(1S)$ anything$)$ — Γ_{26}/Γ_7

VALUE	EVTS	DOCUMENT ID		TECN	COMMENT
0.52±0.12±0.09	47 ± 11	BRIERE	04	CLEO	$e^+e^- \to J/\psi X$

$\Gamma(\psi(2S)$ anything$)/\Gamma_{total}$ — Γ_{27}/Γ

VALUE (units 10^{-4})	EVTS	DOCUMENT ID		TECN	COMMENT
1.23±0.17±0.11	215	SHEN	16	BELL	$e^+e^- \to \psi(2S)X$

$\Gamma(\psi(2S)$ anything$)/\Gamma(J/\psi(1S)$ anything$)$ — Γ_{27}/Γ_7

VALUE	EVTS	DOCUMENT ID		TECN	COMMENT
0.41±0.11±0.08	42 ± 11	BRIERE	04	CLEO	$e^+e^- \to J/\psi\pi^+\pi^-X$

$\Gamma(\psi(2S)\eta_c)/\Gamma_{total}$ — Γ_{28}/Γ

VALUE	CL%	DOCUMENT ID		TECN	COMMENT
$<3.6\times10^{-6}$	90	YANG	14	BELL	$e^+e^- \to \psi(2S)X$

$\Gamma(\psi(2S)\chi_{c0})/\Gamma_{total}$ — Γ_{29}/Γ

VALUE	CL%	DOCUMENT ID		TECN	COMMENT
$<6.5\times10^{-6}$	90	YANG	14	BELL	$e^+e^- \to \psi(2S)X$

$\Gamma(\psi(2S)\chi_{c1})/\Gamma_{total}$ — Γ_{30}/Γ

VALUE	CL%	DOCUMENT ID		TECN	COMMENT
$<4.5\times10^{-6}$	90	YANG	14	BELL	$e^+e^- \to \psi(2S)X$

$\Gamma(\psi(2S)\chi_{c2})/\Gamma_{total}$ — Γ_{31}/Γ

VALUE	CL%	DOCUMENT ID		TECN	COMMENT
$<2.1\times10^{-6}$	90	YANG	14	BELL	$e^+e^- \to \psi(2S)X$

$\Gamma(\psi(2S)\eta_c(2S))/\Gamma_{total}$ — Γ_{32}/Γ

VALUE	CL%	DOCUMENT ID		TECN	COMMENT
$<3.2\times10^{-6}$	90	YANG	14	BELL	$e^+e^- \to \psi(2S)X$

$\Gamma(\psi(2S)X(3940))/\Gamma_{total}$ — Γ_{33}/Γ

VALUE	CL%	DOCUMENT ID		TECN	COMMENT
$<2.9\times10^{-6}$	90	YANG	14	BELL	$e^+e^- \to \psi(2S)X$

$\Gamma(\psi(2S)X(4160))/\Gamma_{total}$ — Γ_{34}/Γ

VALUE	CL%	DOCUMENT ID		TECN	COMMENT
$<2.9\times10^{-6}$	90	YANG	14	BELL	$e^+e^- \to \psi(2S)X$

$\Gamma(\psi(4230)$ anything, $\psi \to \psi(2S)\pi^+\pi^-)/\Gamma_{total}$ — Γ_{35}/Γ

VALUE	CL%	DOCUMENT ID		TECN	COMMENT
$<7.9\times10^{-5}$	90	SHEN	16	BELL	$\Upsilon(1S) \to \psi(2S)\pi^+\pi^-X$

$\Gamma(\psi(4360)$ anything, $\psi \to \psi(2S)\pi^+\pi^-)/\Gamma_{total}$ — Γ_{36}/Γ

VALUE	CL%	DOCUMENT ID		TECN	COMMENT
$<5.2\times10^{-5}$	90	SHEN	16	BELL	$\Upsilon(1S) \to \psi(2S)\pi^+\pi^-X$

$\Gamma(\psi(4660)$ anything, $\psi \to \psi(2S)\pi^+\pi^-)/\Gamma_{total}$ — Γ_{37}/Γ

VALUE	CL%	DOCUMENT ID		TECN	COMMENT
$<2.2\times10^{-5}$	90	SHEN	16	BELL	$\Upsilon(1S) \to \psi(2S)\pi^+\pi^-X$

$\Gamma(X(4050)^\pm$ anything, $X \to \psi(2S)\pi^\pm)/\Gamma_{total}$ — Γ_{38}/Γ

VALUE	CL%	DOCUMENT ID		TECN	COMMENT
$<8.8\times10^{-5}$	90	SHEN	16	BELL	$\Upsilon(1S) \to \psi(2S)\pi^\pm X$

$\Gamma(Z_c(4430)^\pm$ anything, $Z_c \to \psi(2S)\pi^\pm)/\Gamma_{total}$ — Γ_{39}/Γ

VALUE	CL%	DOCUMENT ID		TECN	COMMENT
$<6.7\times10^{-5}$	90	SHEN	16	BELL	$\Upsilon(1S) \to \psi(2S)\pi^\pm X$

$\Gamma(\chi_{c1}(3872)$ anything$)/\Gamma_{total}$ — Γ_{40}/Γ

VALUE	CL%	DOCUMENT ID		TECN	COMMENT
$<2.5\times10^{-4}$	90	[1] SHEN	16	BELL	$\Upsilon(1S) \to J/\psi\pi^+\pi^-X$

[1] SHEN 16 reports $[\Gamma(\Upsilon(1S) \to \chi_{c1}(3872)\text{anything})/\Gamma_{total}] \times [B(\chi_{c1}(3872) \to \pi^+\pi^-J/\psi(1S))] < 9.5\times10^{-6}$ which we divide by our best value $B(\chi_{c1}(3872) \to \pi^+\pi^-J/\psi(1S)) = 3.8\times10^{-2}$.

$\Gamma(Z_c(4200)^+Z_c(4200)^-)/\Gamma_{total}$ — Γ_{41}/Γ

VALUE	CL%	DOCUMENT ID		TECN	COMMENT
$<22.3\times10^{-6}$	90	[1] JIA	18	BELL	$\Upsilon(1S) \to J/\psi\pi^\pm X$

[1] Assuming $B(Z_c(4200)^\pm \to J/\psi\pi^\pm) = 1$.

$\Gamma(Z_c(3900)^\pm Z_c(4200)^\mp)/\Gamma_{total}$ — Γ_{42}/Γ

VALUE	CL%	DOCUMENT ID		TECN	COMMENT
$<8.1\times10^{-6}$	90	[1] JIA	18	BELL	$\Upsilon(1S) \to J/\psi\pi^\pm X$

[1] Assuming $B(Z_c(4200)^\pm \to J/\psi\pi^\pm) = 1 = B(Z_c(3900)^\pm \to J/\psi\pi^\pm)$.

$\Gamma(Z_c(3900)^+Z_c(3900)^-)/\Gamma_{total}$ — Γ_{43}/Γ

VALUE	CL%	DOCUMENT ID		TECN	COMMENT
$<1.8\times10^{-6}$	90	[1] JIA	18	BELL	$\Upsilon(1S) \to J/\psi\pi^\pm X$

[1] Assuming $B(Z_c(3900)^\pm \to J/\psi\pi^\pm) = 1$

$\Gamma(X(4050)^+X(4050)^-)/\Gamma_{total}$ — Γ_{44}/Γ

VALUE	CL%	DOCUMENT ID		TECN	COMMENT
$<15.8\times10^{-6}$	90	[1] JIA	18	BELL	$\Upsilon(1S) \to \chi_{c1}(1P)\pi^\pm X$

[1] Assuming $B(X(4050)^\pm \to \chi_{c1}(1P)\pi^\pm) = 1$

Downloaded from https://academic.oup.com/ptep/article/2022/8/083C01/6651666 by KIT Library user on 27 September 2022

$\Gamma(X(4250)^+ X(4250)^-)/\Gamma_{total}$ — Γ_{45}/Γ

VALUE	CL%	DOCUMENT ID		TECN	COMMENT
$<26.6 \times 10^{-6}$	90	[1] JIA	18	BELL	$\Upsilon(1S) \to \chi_{c1}(1P)\pi^\pm X$

[1] Assuming $B(X(4250)^\pm \to \chi_{c1}(1P)\pi^\pm) = 1$

$\Gamma(X(4050)^\pm X(4250)^\mp)/\Gamma_{total}$ — Γ_{46}/Γ

VALUE	CL%	DOCUMENT ID		TECN	COMMENT
$<44.2 \times 10^{-6}$	90	[1] JIA	18	BELL	$\Upsilon(1S) \to \chi_{c1}(1P)\pi^\pm X$

[1] Assuming $B(X(4050)^\pm \to \chi_{c1}(1P)\pi^\pm) = 1 = B(X(4250)^\pm \to \chi_{c1}(1P)\pi^\pm)$

$\Gamma(Z_c(4430)^+ Z_c(4430)^-)/\Gamma_{total}$ — Γ_{47}/Γ

VALUE	CL%	DOCUMENT ID		TECN	COMMENT
$<20.3 \times 10^{-6}$	90	[1] JIA	18	BELL	$\Upsilon(2S) \to \psi(2S)\pi^\pm X$

[1] Assuming $B(Z_c(4430)^\pm \to \psi(2S)\pi^\pm) = 1$

$\Gamma(X(4055)^\pm X(4055)^\mp)/\Gamma_{total}$ — Γ_{48}/Γ

VALUE	CL%	DOCUMENT ID		TECN	COMMENT
$<23.3 \times 10^{-6}$	90	[1] JIA	18	BELL	$\Upsilon(1S) \to \psi(2S)\pi^\pm X$

[1] Assuming $B(X(4055)^\pm \to \psi(2S)\pi^\pm) = 1$

$\Gamma(X(4055)^\pm Z_c(4430)^\mp)/\Gamma_{total}$ — Γ_{49}/Γ

VALUE	CL%	DOCUMENT ID		TECN	COMMENT
$<45.5 \times 10^{-6}$	90	[1] JIA	18	BELL	$\Upsilon(1S) \to \psi(2S)\pi^\pm X$

[1] Assuming $B(X(4055)^\pm \to \psi(2S)\pi^\pm) = 1 = B(Z_c(4430)^\pm \to \psi(2S)\pi^\pm)$

$\Gamma(\rho\pi)/\Gamma_{total}$ — Γ_{50}/Γ

VALUE (units 10^{-6})	CL%	DOCUMENT ID		TECN	COMMENT
<3.68	90	SHEN	13	BELL	$\Upsilon(1S) \to \pi^+\pi^-\pi^0$
• • • We do not use the following data for averages, fits, limits, etc. • • •					
$<1 \times 10^3$	90	BLINOV	90	MD1	$\Upsilon(1S) \to \rho^0\pi^0$
$<2 \times 10^2$	90	FULTON	90B		$\Upsilon(1S) \to \rho^0\pi^0$
$<2.1 \times 10^3$	90	NICZYPORUK	83	LENA	$\Upsilon(1S) \to \rho^0\pi^0$

$\Gamma(\omega\pi^0)/\Gamma_{total}$ — Γ_{51}/Γ

VALUE (units 10^{-6})	CL%	DOCUMENT ID		TECN	COMMENT
<3.90	90	SHEN	13	BELL	$\Upsilon(1S) \to \pi^+\pi^-\pi^0\pi^0$

$\Gamma(\pi^+\pi^-)/\Gamma_{total}$ — Γ_{52}/Γ

VALUE (units 10^{-4})	CL%	DOCUMENT ID		TECN	COMMENT
<5	90	BARU	92	MD1	$\Upsilon(1S) \to \pi^+\pi^-$

$\Gamma(K^+K^-)/\Gamma_{total}$ — Γ_{53}/Γ

VALUE (units 10^{-4})	CL%	DOCUMENT ID		TECN	COMMENT
<5	90	BARU	92	MD1	$\Upsilon(1S) \to K^+K^-$

$\Gamma(p\overline{p})/\Gamma_{total}$ — Γ_{54}/Γ

VALUE (units 10^{-4})	CL%	DOCUMENT ID		TECN	COMMENT
<5	90	[1] BARU	96	MD1	$\Upsilon(1S) \to p\overline{p}$

[1] Supersedes BARU 92 in this node.

$\Gamma(\pi^+\pi^-\pi^0)/\Gamma_{total}$ — Γ_{55}/Γ

VALUE (units 10^{-6})	CL%	EVTS	DOCUMENT ID		TECN	COMMENT
2.14±0.72±0.34		26 ± 9	SHEN	13	BELL	$\Upsilon(1S) \to \pi^+\pi^-\pi^0$
• • • We do not use the following data for averages, fits, limits, etc. • • •						
<18.4	90		ANASTASSOV	99	CLE2	$e^+e^- \to$ hadrons

$\Gamma(\phi K^+K^-)/\Gamma_{total}$ — Γ_{56}/Γ

VALUE (units 10^{-6})	EVTS	DOCUMENT ID		TECN	COMMENT
2.36±0.37±0.29	56	SHEN	12A	BELL	$\Upsilon(1S) \to 2(K^+K^-)$

$\Gamma(\omega\pi^+\pi^-)/\Gamma_{total}$ — Γ_{57}/Γ

VALUE (units 10^{-6})	EVTS	DOCUMENT ID		TECN	COMMENT
4.46±0.67±0.72	64	SHEN	12A	BELL	$\Upsilon(1S) \to 2(\pi^+\pi^-)\pi^0$

$\Gamma(K^*(892)^0 K^-\pi^+ + \text{c.c.})/\Gamma_{total}$ — Γ_{58}/Γ

VALUE (units 10^{-6})	EVTS	DOCUMENT ID		TECN	COMMENT
4.42±0.50±0.58	173	SHEN	12A	BELL	$\Upsilon(1S) \to K^+K^-\pi^+\pi^-$

$\Gamma(\phi f_2'(1525))/\Gamma_{total}$ — Γ_{59}/Γ

VALUE (units 10^{-6})	CL%	DOCUMENT ID		TECN	COMMENT
<1.63	90	SHEN	12A	BELL	$\Upsilon(1S) \to 2(K^+K^-)$

$\Gamma(\omega f_2(1270))/\Gamma_{total}$ — Γ_{60}/Γ

VALUE (units 10^{-6})	CL%	DOCUMENT ID		TECN	COMMENT
<1.79	90	SHEN	12A	BELL	$\Upsilon(1S) \to 2(\pi^+\pi^-)\pi^0$

$\Gamma(\rho(770)a_2(1320))/\Gamma_{total}$ — Γ_{61}/Γ

VALUE (units 10^{-6})	CL%	DOCUMENT ID		TECN	COMMENT
<2.24	90	SHEN	12A	BELL	$\Upsilon(1S) \to 2(\pi^+\pi^-)\pi^0$

$\Gamma(K^*(892)^0\overline{K}_2^*(1430)^0 + \text{c.c.})/\Gamma_{total}$ — Γ_{62}/Γ

VALUE (units 10^{-6})	EVTS	DOCUMENT ID		TECN	COMMENT
3.02±0.68±0.34	42	SHEN	12A	BELL	$\Upsilon(1S) \to K^+K^-\pi^+\pi^-$

$\Gamma(K_1(1270)^\pm K^\mp)/\Gamma_{total}$ — Γ_{63}/Γ

VALUE (units 10^{-6})	CL%	DOCUMENT ID		TECN	COMMENT
<2.41	90	SHEN	12A	BELL	$\Upsilon(1S) \to K^+K^-\pi^+\pi^-$

$\Gamma(K_1(1400)^\pm K^\mp)/\Gamma_{total}$ — Γ_{64}/Γ

VALUE (units 10^{-6})	EVTS	DOCUMENT ID		TECN	COMMENT
1.02±0.35±0.22	24	SHEN	12A	BELL	$\Upsilon(1S) \to K^+K^-\pi^+\pi^-$

$\Gamma(b_1(1235)^\pm\pi^\mp)/\Gamma_{total}$ — Γ_{65}/Γ

VALUE (units 10^{-6})	CL%	DOCUMENT ID		TECN	COMMENT
<1.25	90	SHEN	12A	BELL	$\Upsilon(1S) \to 2(\pi^+\pi^-)\pi^0$

$\Gamma(\pi^+\pi^-\pi^0\pi^0)/\Gamma_{total}$ — Γ_{66}/Γ

VALUE (units 10^{-6})	EVTS	DOCUMENT ID		TECN	COMMENT
12.8±2.0±2.3	143 ± 22	SHEN	13	BELL	$\Upsilon(1S) \to \pi^+\pi^-\pi^0\pi^0$

$\Gamma(K_S^0 K^+\pi^- + \text{c.c.})/\Gamma_{total}$ — Γ_{67}/Γ

VALUE (units 10^{-6})	CL%	EVTS	DOCUMENT ID		TECN	COMMENT
1.59±0.33±0.18		37 ± 8	SHEN	13	BELL	$\Upsilon(1S) \to K_S^0 K^-\pi^+$
• • • We do not use the following data for averages, fits, limits, etc. • • •						
<3.4	90		[1] DOBBS	12A		$\Upsilon(1S) \to K_S^0 K^-\pi^+$

[1] Obtained by analyzing CLEO III data but not authored by the CLEO Collaboration.

$\Gamma(K^*(892)^0\overline{K}^0 + \text{c.c.})/\Gamma_{total}$ — Γ_{68}/Γ

VALUE (units 10^{-6})	EVTS	DOCUMENT ID		TECN	COMMENT
2.92±0.85±0.37	16 ± 5	SHEN	13	BELL	$\Upsilon(1S) \to K_S^0 K^-\pi^+$

$\Gamma(K^*(892)^- K^+ + \text{c.c.})/\Gamma_{total}$ — Γ_{69}/Γ

VALUE (units 10^{-6})	CL%	DOCUMENT ID		TECN	COMMENT
<1.11	90	SHEN	13	BELL	$\Upsilon(1S) \to K_S^0 K^-\pi^+$

$\Gamma(f_1(1285)\text{ anything})/\Gamma_{total}$ — Γ_{70}/Γ

VALUE (units 10^{-3})	EVTS	DOCUMENT ID		TECN	COMMENT
4.6±2.8±1.3	3.1k	JIA	17A	BELL	$e^+e^- \to$ hadrons

$\Gamma(D^*(2010)^\pm\text{ anything})/\Gamma_{total}$ — Γ_{71}/Γ

VALUE (units 10^{-3})	CL%	EVTS	DOCUMENT ID		TECN	COMMENT
25.2±1.3±1.5		≈ 2k	[1] AUBERT	10C	BABR	$\Upsilon(2S) \to \pi^+\pi^-\Upsilon(1S)$
• • • We do not use the following data for averages, fits, limits, etc. • • •						
<19	90		[2] ALBRECHT	92J	ARG	$e^+e^- \to D^0\pi^\pm X$

[1] For $x_p > 0.1$.
[2] For $x_p > 0.2$.

$\Gamma(f_1(1285)X_{tetra})/\Gamma_{total}$ — Γ_{72}/Γ

VALUE	CL%	DOCUMENT ID		TECN	COMMENT
$<62.4 \times 10^{-6}$	90	[1] JIA	17A	BELL	$e^+e^- \to$ hadrons

[1] For a tetraquark state X_{tetra}, with mass in the range 1.16–2.46 GeV and width in the range 0–0.3 GeV. Measured 90% CL limits as a function of X_{tetra} mass and width range from 4.6×10^{-6} to 62.4×10^{-6}.

$\Gamma(\overline{^2H}\text{ anything})/\Gamma_{total}$ — Γ_{73}/Γ

VALUE (units 10^{-5})	EVTS	DOCUMENT ID		TECN	COMMENT
2.85±0.25 OUR AVERAGE					
$2.81 \pm 0.49^{+0.20}_{-0.24}$		LEES	14G	BABR	$e^+e^- \to \overline{^2H} X$
2.86±0.19±0.21	455	ASNER	07	CLEO	$e^+e^- \to \overline{^2H} X$

$\Gamma(\text{Sum of 100 exclusive modes})/\Gamma_{total}$ — Γ_{74}/Γ

VALUE (units 10^{-2})	DOCUMENT ID		COMMENT
1.200±0.017	[1,2] DOBBS	12A	$\Upsilon(1S) \to$ hadrons

[1] DOBBS 12A presents individual exclusive branching fractions or upper limits for 100 modes of four to ten pions, kaons, or protons.
[2] Obtained by analyzing CLEO III data but not authored by the CLEO Collaboration.

$\Gamma(ggg, \gamma gg \to \overline{d}\text{ anything})/\Gamma(ggg, \gamma gg \to \text{anything})$

VALUE (units 10^{-5})	EVTS	DOCUMENT ID		TECN	COMMENT
3.36±0.23±0.25	455	ASNER	07	CLEO	$e^+e^- \to \overline{d}X$

$\Gamma(\gamma\pi^+\pi^-)/\Gamma_{total}$ — Γ_{75}/Γ

VALUE (units 10^{-5})	DOCUMENT ID		TECN	COMMENT
6.3±1.2±1.3	[1] ANASTASSOV	99	CLE2	$e^+e^- \to$ hadrons

[1] For $m_{\pi\pi} > 1$ GeV.

Downloaded from https://academic.oup.com/ptep/article/2022/8/083C01/6651666 by KIT Library user on 27 September 2022

$\Gamma(\gamma\pi^0\pi^0)/\Gamma_{total}$ — Γ_{76}/Γ

VALUE (units 10^{-5})	DOCUMENT ID	TECN	COMMENT
1.7±0.6±0.3	[1] ANASTASSOV 99	CLE2	$e^+e^- \to$ hadrons

[1] For $m_{\pi\pi}$ >1 GeV.

$\Gamma(\gamma\pi\pi(\text{S-wave}))/\Gamma_{total}$ — Γ_{77}/Γ

VALUE (units 10^{-5})	DOCUMENT ID	TECN	COMMENT
4.63±0.56±0.48	LEES 18A	BABR	$\Upsilon(1S) \to \gamma\pi^+\pi^-$

$\Gamma(\gamma\pi^0\eta)/\Gamma_{total}$ — Γ_{78}/Γ

VALUE (units 10^{-6})	CL%	DOCUMENT ID	TECN	COMMENT
<2.4	90	[1] BESSON 07A	CLEO	$e^+e^- \to \Upsilon(1S)$

[1] BESSON 07A obtained this limit for $0.7 < m_{\pi^0\eta} < 3$ GeV.

$\Gamma(\gamma K^+K^-)/\Gamma_{total}$ — Γ_{79}/Γ
($2 < m_{K^+K^-} < 3$ GeV)

VALUE (units 10^{-5})	CL%	DOCUMENT ID	TECN	COMMENT
1.14±0.08±0.10	90	ATHAR 06	CLE3	$\Upsilon(1S) \to \gamma K^+K^-$

$\Gamma(\gamma p\overline{p})/\Gamma_{total}$ — Γ_{80}/Γ
($2 < m_{p\overline{p}} < 3$ GeV)

VALUE (units 10^{-5})	CL%	DOCUMENT ID	TECN	COMMENT
<0.6	90	ATHAR 06	CLE3	$\Upsilon(1S) \to \gamma p\overline{p}$

$\Gamma(\gamma 2h^+2h^-)/\Gamma_{total}$ — Γ_{81}/Γ

VALUE (units 10^{-4})	EVTS	DOCUMENT ID	TECN	COMMENT
7.0±1.1±1.0	80 ± 12	FULTON 90B	CLEO	$e^+e^- \to$ hadrons

$\Gamma(\gamma 3h^+3h^-)/\Gamma_{total}$ — Γ_{82}/Γ

VALUE (units 10^{-4})	EVTS	DOCUMENT ID	TECN	COMMENT
5.4±1.5±1.3	39 ± 11	FULTON 90B	CLEO	$e^+e^- \to$ hadrons

$\Gamma(\gamma 4h^+4h^-)/\Gamma_{total}$ — Γ_{83}/Γ

VALUE (units 10^{-4})	EVTS	DOCUMENT ID	TECN	COMMENT
7.4±2.5±2.5	36 ± 12	FULTON 90B	CLEO	$e^+e^- \to$ hadrons

$\Gamma(\gamma\pi^+\pi^-K^+K^-)/\Gamma_{total}$ — Γ_{84}/Γ

VALUE (units 10^{-4})	EVTS	DOCUMENT ID	TECN	COMMENT
2.9±0.7±0.6	29 ± 8	FULTON 90B	CLEO	$e^+e^- \to$ hadrons

$\Gamma(\gamma 2\pi^+2\pi^-)/\Gamma_{total}$ — Γ_{85}/Γ

VALUE (units 10^{-4})	EVTS	DOCUMENT ID	TECN	COMMENT
2.5±0.7±0.5	26 ± 7	FULTON 90B	CLEO	$e^+e^- \to$ hadrons

$\Gamma(\gamma 3\pi^+3\pi^-)/\Gamma_{total}$ — Γ_{86}/Γ

VALUE (units 10^{-4})	EVTS	DOCUMENT ID	TECN	COMMENT
2.5±0.9±0.8	17 ± 5	FULTON 90B	CLEO	$e^+e^- \to$ hadrons

$\Gamma(\gamma 2\pi^+2\pi^-K^+K^-)/\Gamma_{total}$ — Γ_{87}/Γ

VALUE (units 10^{-4})	EVTS	DOCUMENT ID	TECN	COMMENT
2.4±0.9±0.8	18 ± 7	FULTON 90B	CLEO	$e^+e^- \to$ hadrons

$\Gamma(\gamma\pi^+\pi^-p\overline{p})/\Gamma_{total}$ — Γ_{88}/Γ

VALUE (units 10^{-4})	EVTS	DOCUMENT ID	TECN	COMMENT
1.5±0.5±0.3	22 ± 6	FULTON 90B	CLEO	$e^+e^- \to$ hadrons

$\Gamma(\gamma 2\pi^+2\pi^-p\overline{p})/\Gamma_{total}$ — Γ_{89}/Γ

VALUE (units 10^{-4})	EVTS	DOCUMENT ID	TECN	COMMENT
0.4±0.4±0.4	7 ± 6	FULTON 90B	CLEO	$e^+e^- \to$ hadrons

$\Gamma(\gamma 2K^+2K^-)/\Gamma_{total}$ — Γ_{90}/Γ

VALUE (units 10^{-4})	EVTS	DOCUMENT ID	TECN	COMMENT
0.2±0.2	2 ± 2	FULTON 90B	CLEO	$e^+e^- \to$ hadrons

$\Gamma(\gamma\eta'(958))/\Gamma_{total}$ — Γ_{91}/Γ

VALUE (units 10^{-6})	CL%	DOCUMENT ID	TECN	COMMENT
< 1.9	90	ATHAR 07A	CLEO	$\Upsilon(1S) \to \gamma\eta' \to \gamma\pi^+\pi^-\eta, \gamma\rho$
• • • We do not use the following data for averages, fits, limits, etc. • • •				
<16	90	RICHICHI 01B	CLE2	$\Upsilon(1S) \to \gamma\eta' \to \gamma\eta\pi^+\pi^-$

$\Gamma(\gamma\eta)/\Gamma_{total}$ — Γ_{92}/Γ

VALUE (units 10^{-6})	CL%	DOCUMENT ID	TECN	COMMENT
< 1.0	90	ATHAR 07A	CLEO	$\Upsilon(1S) \to \gamma\eta \to \gamma\gamma\gamma$, $\gamma\pi^+\pi^-\pi^0$, $\gamma 3\pi^0$
• • • We do not use the following data for averages, fits, limits, etc. • • •				
<21	90	MASEK 02	CLEO	$\Upsilon(1S) \to \gamma\eta$

$\Gamma(\gamma f_0(980))/\Gamma_{total}$ — Γ_{93}/Γ

VALUE (units 10^{-5})	CL%	DOCUMENT ID	TECN	COMMENT
<3	90	[1] ATHAR 06	CLE3	$\Upsilon(1S) \to \gamma\pi^+\pi^-$

[1] Assuming $B(f_0(980) \to \pi\pi) = 1$.

$\Gamma(\gamma f_2'(1525))/\Gamma_{total}$ — Γ_{94}/Γ

VALUE (units 10^{-5})	CL%	EVTS	DOCUMENT ID	TECN	COMMENT
2.9 ±0.6 OUR AVERAGE					
$2.13\pm0.28\pm0.72$			[1] LEES 18A	BABR	$\Upsilon(1S) \to \gamma K^+K^-$
$4.1 \pm1.4 \pm0.1$		17	[2] BESSON 11	CLEO	$\Upsilon(1S) \to K^0_S K^0_S$
$3.7 \ ^{+0.9}_{-0.7} \pm0.8$			ATHAR 06	CLE3	$\Upsilon(1S) \to \gamma K^+K^-$
• • • We do not use the following data for averages, fits, limits, etc. • • •					
<14	90		[3] FULTON 90B	CLEO	$\Upsilon(1S) \to \gamma K^+K^-$
<19.4	90		[3] ALBRECHT 89	ARG	$\Upsilon(1S) \to \gamma K^+K^-$

[1] Using $B(f_2'(1525) \to K\overline{K}) = 0.887 \pm 0.022$ and $B(K^0\overline{K}^0) = 1/2\ B(K\overline{K})$.

[2] BESSON 11 reports $(4.0 \pm 1.3 \pm 0.6) \times 10^{-5}$ from a measurement of $[\Gamma(\Upsilon(1S) \to \gamma f_2'(1525))/\Gamma_{total}] \times [B(f_2'(1525) \to K\overline{K})]$ assuming $B(f_2'(1525) \to K\overline{K}) = (88.8 \pm 3.1) \times 10^{-2}$, which we rescale to our best value $B(f_2'(1525) \to K\overline{K}) = (87.6 \pm 2.2) \times 10^{-2}$. Our first error is their experiment's error and our second error is the systematic error from using our best value. The result also assumes $B(K^0_S \to \pi^+\pi^-) = (69.20 \pm 0.05)\%$ and $B(f_2'(1525) \to K\overline{K}) = 4\ B(f_2'(1525) \to K^0_S K^0_S)$.

[3] Assuming $B(f_2'(1525) \to K\overline{K}) = 0.71$.

$\Gamma(\gamma f_2(1270))/\Gamma_{total}$ — Γ_{95}/Γ

VALUE (units 10^{-5})	CL%	DOCUMENT ID	TECN	COMMENT
10.1 ±0.6 OUR AVERAGE				
$10.15\pm0.59\ ^{+0.54}_{-0.43}$		[1] LEES 18A	BABR	$\Upsilon(1S) \to \gamma\pi^+\pi^-$
$10.5 \pm1.6\ ^{+1.9}_{-1.8}$		[2] BESSON 07A	CLE3	$\Upsilon(1S) \to \gamma\pi^0\pi^0$
$10.2 \pm0.8 \pm0.7$		ATHAR 06	CLE3	$\Upsilon(1S) \to \gamma\pi^+\pi^-$
$8.1 \pm2.3\ ^{+2.9}_{-2.7}$		[3] ANASTASSOV 99	CLE2	$e^+e^- \to$ hadrons
• • • We do not use the following data for averages, fits, limits, etc. • • •				
<21	90	[3] FULTON 90B	CLEO	$\Upsilon(1S) \to \gamma\pi^+\pi^-$
<13	90	[3] ALBRECHT 89	ARG	$\Upsilon(1S) \to \gamma\pi^+\pi^-$
<81	90	SCHMITT 88	CBAL	$\Upsilon(1S) \to \gamma X$

[1] Using $B(f_2(1270) \to \pi^0\pi^0) = 1/3\ B(f_2(1270) \to \pi\pi)$ and $B(f_2(1270) \to \pi\pi) = (84.2\ ^{+2.9}_{-0.9})\%$.

[2] Using $B(f_2(1270) \to \pi^0\pi^0) = B(f_2(1270) \to \pi\pi)/3$ and $B(f_2(1270) \to \pi\pi) = (84.7\ ^{+2.5}_{-1.2})\%$.

[3] Using $B(f_2(1270) \to \pi\pi) = 0.84$.

$\Gamma(\gamma\eta(1405))/\Gamma_{total}$ — Γ_{96}/Γ

VALUE (units 10^{-5})	CL%	DOCUMENT ID	TECN	COMMENT
<8.2	90	[1] FULTON 90B	CLEO	$\Upsilon(1S) \to \gamma K^\pm\pi^\mp K^0_S$

[1] Includes unknown branching ratio of $\eta(1405) \to K^\pm\pi^\mp K^0_S$.

$\Gamma(\gamma f_0(1500))/\Gamma_{total}$ — Γ_{97}/Γ

VALUE (units 10^{-5})	CL%	DOCUMENT ID	TECN	COMMENT
<1.5	90	[1] BESSON 07A	CLEO	$e^+e^- \to \Upsilon(1S) \to \gamma\pi^0\pi^0$
• • • We do not use the following data for averages, fits, limits, etc. • • •				
<6.1	90	[2] BESSON 07A	CLEO	$e^+e^- \to \Upsilon(1S) \to \gamma\eta\eta$

[1] Using $B(f_0(1500) \to \pi^0\pi^0) = B(f_0(1500) \to \pi\pi)/3$ and $B(f_0(1500) \to \pi\pi) = (0.349 \pm 0.023)\%$.

[2] Calculated by us using $B(f_0(1500) \to \eta\eta) = (5.1 \pm 0.9)\%$.

$\Gamma(\gamma f_0(1500) \to \gamma K^+K^-)/\Gamma_{total}$ — Γ_{98}/Γ

VALUE (units 10^{-5})	DOCUMENT ID	TECN	COMMENT
1.04±0.14±0.33	[1] LEES 18A	BABR	$e^+e^- \to \Upsilon(1S) \to \gamma K^+K^-$

[1] LEES 18A quotes $B(\Upsilon(1S) \to \gamma f_0(1500) \to \gamma K\overline{K}) = (2.08 \pm 0.27 \pm 0.65) \times 10^{-5}$ assuming $B(K^0\overline{K}^0) = 1/2\ B(K\overline{K})$.

$\Gamma(\gamma f_0(1710))/\Gamma_{total}$ — Γ_{99}/Γ

VALUE (units 10^{-4})	CL%	DOCUMENT ID	TECN	COMMENT
< 2.6	90	[1] ALBRECHT 89	ARG	$\Upsilon(1S) \to \gamma K^+K^-$
• • • We do not use the following data for averages, fits, limits, etc. • • •				
< 6.3	90	[1] FULTON 90B	CLEO	$\Upsilon(1S) \to \gamma K^+K^-$
<19	90	[1] FULTON 90B	CLEO	$\Upsilon(1S) \to \gamma K^0_S K^0_S$
< 8	90	[2] ALBRECHT 89	ARG	$\Upsilon(1S) \to \gamma\pi^+\pi^-$
<24	90	[3] SCHMITT 88	CBAL	$\Upsilon(1S) \to \gamma X$

[1] Assuming $B(f_0(1710) \to K\overline{K}) = 0.38$.

[2] Assuming $B(f_0(1710) \to \pi\pi) = 0.04$.

[3] Assuming $B(f_0(1710) \to \eta\eta) = 0.18$.

Downloaded from https://academic.oup.com/ptep/article/2022/8/083C01/6651666 by KIT Library user on 27 September 2022

$\Gamma(\gamma f_0(1710) \to \gamma K^+ K^-)/\Gamma_{total}$ — Γ_{100}/Γ

VALUE (units 10^{-5})	CL%	DOCUMENT ID		TECN	COMMENT
$1.01 \pm 0.26 \pm 0.18$		[1] LEES	18A	BABR	$e^+e^- \to \Upsilon(1S) \to \gamma K^+ K^-$
• • • We do not use the following data for averages, fits, limits, etc. • • •					
<0.7	90	ATHAR	06	CLEO	$e^+e^- \to \Upsilon(1S) \to \gamma K^+ K^-$

[1] LEES 18A quotes $B(\Upsilon(1S) \to \gamma f_0(1710) \to \gamma K\overline{K}) = (2.02 \pm 0.51 \pm 0.35) \times 10^{-5}$ assuming $B(K^0\overline{K}^0) = 1/2\ B(K\overline{K})$.

$\Gamma(\gamma f_0(1710) \to \gamma \pi^+ \pi^-)/\Gamma_{total}$ — Γ_{101}/Γ

VALUE (units 10^{-5})	DOCUMENT ID		TECN	COMMENT
$0.53 \pm 0.17 \pm 0.11$	[1] LEES	18A	BABR	$\Upsilon(1S) \to \gamma \pi^+ \pi^-$

[1] LEES 18A quotes $B(\Upsilon(1S) \to \gamma f_0(1710) \to \gamma \pi\pi) = (0.79 \pm 0.26 \pm 0.17) \times 10^{-5}$ assuming $B(\pi^0\pi^0) = 1/3\ B(\pi\pi)$.

$\Gamma(\gamma f_0(1710) \to \gamma \pi^0 \pi^0)/\Gamma_{total}$ — Γ_{102}/Γ

VALUE (units 10^{-6})	CL%	DOCUMENT ID		TECN	COMMENT
<1.4	90	BESSON	07A	CLEO	$e^+e^- \to \Upsilon(1S) \to \gamma \pi^0 \pi^0$

$\Gamma(\gamma f_0(1710) \to \gamma \eta\eta)/\Gamma_{total}$ — Γ_{103}/Γ

VALUE (units 10^{-6})	CL%	DOCUMENT ID		TECN	COMMENT
<1.8	90	BESSON	07A	CLEO	$e^+e^- \to \Upsilon(1S) \to \gamma\eta\eta$

$\Gamma(\gamma f_4(2050))/\Gamma_{total}$ — Γ_{104}/Γ

VALUE (units 10^{-5})	CL%	DOCUMENT ID		TECN	COMMENT
<5.3	90	[1] ATHAR	06	CLE3	$\Upsilon(1S) \to \gamma \pi^+ \pi^-$

[1] Assuming $B(f_4(2050) \to \pi\pi) = 0.17$.

$\Gamma(\gamma f_0(2200) \to \gamma K^+ K^-)/\Gamma_{total}$ — Γ_{105}/Γ

VALUE	CL%	DOCUMENT ID		TECN	COMMENT
<0.0002	90	BARU	89	MD1	$\Upsilon(1S) \to \gamma K^+ K^-$

$\Gamma(\gamma f_J(2220) \to \gamma K^+ K^-)/\Gamma_{total}$ — Γ_{106}/Γ

VALUE (units 10^{-7})	CL%	DOCUMENT ID		TECN	COMMENT
$<$ 8	90	ATHAR	06	CLE3	$\Upsilon(1S) \to \gamma K^+ K^-$
• • • We do not use the following data for averages, fits, limits, etc. • • •					
<160	90	MASEK	02	CLEO	$\Upsilon(1S) \to \gamma K^+ K^-$
<150	90	FULTON	90B	CLEO	$\Upsilon(1S) \to \gamma K^+ K^-$
<290	90	ALBRECHT	89	ARG	$\Upsilon(1S) \to \gamma K^+ K^-$
<2000	90	BARU	89	MD1	$\Upsilon(1S) \to \gamma K^+ K^-$

$\Gamma(\gamma f_J(2220) \to \gamma \pi^+ \pi^-)/\Gamma_{total}$ — Γ_{107}/Γ

VALUE (units 10^{-7})	CL%	DOCUMENT ID		TECN	COMMENT
$<$ 6	90	ATHAR	06	CLE3	$\Upsilon(1S) \to \gamma \pi^+ \pi^-$
• • • We do not use the following data for averages, fits, limits, etc. • • •					
<120	90	MASEK	02	CLEO	$\Upsilon(1S) \to \gamma \pi^+ \pi^-$

$\Gamma(\gamma f_J(2220) \to \gamma p\overline{p})/\Gamma_{total}$ — Γ_{108}/Γ

VALUE (units 10^{-7})	CL%	DOCUMENT ID		TECN	COMMENT
$<$ 11	90	ATHAR	06	CLE3	$\Upsilon(1S) \to \gamma p\overline{p}$
• • • We do not use the following data for averages, fits, limits, etc. • • •					
<160	90	MASEK	02	CLEO	$\Upsilon(1S) \to \gamma p\overline{p}$

$\Gamma(\gamma\eta(2225) \to \gamma\phi\phi)/\Gamma_{total}$ — Γ_{109}/Γ

VALUE	CL%	DOCUMENT ID		TECN	COMMENT
<0.003	90	BARU	89	MD1	$\Upsilon(1S) \to \gamma K^+ K^- K^+ K^-$

$\Gamma(\gamma\eta_c(1S))/\Gamma_{total}$ — Γ_{110}/Γ

VALUE	CL%	DOCUMENT ID		TECN	COMMENT
$<2.9 \times 10^{-5}$	90	[1] KATRENKO	20	BELL	$e^+e^- \to \gamma +$ hadrons
• • • We do not use the following data for averages, fits, limits, etc. • • •					
$<5.7 \times 10^{-5}$	90	SHEN	10A	BELL	$\Upsilon(1S) \to \gamma X$

[1] Using $\Upsilon(2S) \to \Upsilon(1S)\pi^+\pi^-$ decays.

$\Gamma(\gamma\eta_c(2S))/\Gamma_{total}$ — Γ_{111}/Γ

VALUE	CL%	DOCUMENT ID		TECN	COMMENT
$<4 \times 10^{-4}$	90	[1] KATRENKO	20	BELL	$e^+e^- \to \gamma +$ hadrons

[1] Using $\Upsilon(2S) \to \Upsilon(1S)\pi^+\pi^-$ decays.

$\Gamma(\gamma\chi_{c0})/\Gamma_{total}$ — Γ_{112}/Γ

VALUE	CL%	DOCUMENT ID		TECN	COMMENT
$<6.6 \times 10^{-5}$	90	[1] KATRENKO	20	BELL	$\Upsilon(1S) \to \gamma +$ hadrons
• • • We do not use the following data for averages, fits, limits, etc. • • •					
$<6.5 \times 10^{-4}$	90	SHEN	10A	BELL	$\Upsilon(1S) \to \gamma X$

[1] Using $\Upsilon(2S) \to \Upsilon(1S)\pi^+\pi^-$ decays.

$\Gamma(\gamma\chi_{c1})/\Gamma_{total}$ — Γ_{113}/Γ

VALUE (units 10^{-5})	CL%	EVTS	DOCUMENT ID		TECN	COMMENT
$4.7^{+2.4}_{-1.8}{}^{+0.4}_{-0.5}$		5	[1] KATRENKO	20	BELL	$\Upsilon(1S) \to \gamma +$ hadrons
• • • We do not use the following data for averages, fits, limits, etc. • • •						
<2.3	90		SHEN	10A	BELL	$\Upsilon(1S) \to \gamma X$

[1] Using $\Upsilon(2S) \to \Upsilon(1S)\pi^+\pi^-$ decays.

$\Gamma(\gamma\chi_{c2})/\Gamma_{total}$ — Γ_{114}/Γ

VALUE	CL%	DOCUMENT ID		TECN	COMMENT
$<7.6 \times 10^{-6}$	90	SHEN	10A	BELL	$\Upsilon(1S) \to \gamma X$
• • • We do not use the following data for averages, fits, limits, etc. • • •					
$<3.3 \times 10^{-5}$	90	[1] KATRENKO	20	BELL	$\Upsilon(1S) \to \gamma +$ hadrons

[1] Using $\Upsilon(2S) \to \Upsilon(1S)\pi^+\pi^-$ decays.

$\Gamma(\gamma\chi_{c1}(3872))/\Gamma_{total}$ — Γ_{115}/Γ

VALUE	CL%	DOCUMENT ID		TECN	COMMENT
$<4 \times 10^{-5}$	90	[1] SHEN	10A	BELL	$\Upsilon(1S) \to \gamma X$

[1] SHEN 10A reports $[\Gamma(\Upsilon(1S) \to \gamma\chi_{c1}(3872))/\Gamma_{total}] \times [B(\chi_{c1}(3872) \to \pi^+\pi^- J/\psi(1S))] < 1.6 \times 10^{-6}$ which we divide by our best value $B(\chi_{c1}(3872) \to \pi^+\pi^- J/\psi(1S)) = 3.8 \times 10^{-2}$.

$\Gamma(\gamma\chi_{c1}(3872), \chi_{c1} \to \pi^+\pi^-\pi^0 J/\psi)/\Gamma_{total}$ — Γ_{116}/Γ

VALUE	CL%	DOCUMENT ID		TECN	COMMENT
$<2.8 \times 10^{-6}$	90	SHEN	10A	BELL	$\Upsilon(1S) \to \gamma X$

$\Gamma(\gamma\chi_{c0}(3915) \to \omega J/\psi)/\Gamma_{total}$ — Γ_{117}/Γ

VALUE (units 10^{-6})	CL%	DOCUMENT ID		TECN	COMMENT
<3.0	90	SHEN	10A	BELL	$\Upsilon(1S) \to \gamma X$

$\Gamma(\gamma\chi_{c1}(4140) \to \phi J/\psi)/\Gamma_{total}$ — Γ_{118}/Γ

VALUE (units 10^{-6})	CL%	DOCUMENT ID		TECN	COMMENT
<2.2	90	SHEN	10A	BELL	$\Upsilon(1S) \to \gamma X$

$\Gamma(\gamma X)/\Gamma_{total}$ — Γ_{119}/Γ

(X = scalar with $m < 8.0$ GeV)

VALUE (units 10^{-6})	CL%	DOCUMENT ID		TECN	COMMENT
$<$ 4.5	90	[1] DEL-AMO-SA...11J		BABR	$e^+e^- \to \gamma + X$
• • • We do not use the following data for averages, fits, limits, etc. • • •					
<30	90	[2] BALEST	95	CLEO	$e^+e^- \to \gamma + X$

[1] For a noninteracting scalar X with mass $m < 8.0$ GeV.
[2] For a noninteracting pseudoscalar X with mass < 7.2 GeV.

$\Gamma(\gamma X\overline{X}(m_X < 3.1\ \text{GeV}))/\Gamma_{total}$ — Γ_{120}/Γ

($X\overline{X}$ = vectors with $m < 3.1$ GeV)

VALUE (units 10^{-3})	CL%	DOCUMENT ID		TECN	COMMENT
<1	90	[1] BALEST	95	CLEO	$e^+e^- \to \gamma + X\overline{X}$

[1] For a noninteracting vector X with mass < 3.1 GeV.

$\Gamma(\gamma X\overline{X}(m_X < 4.5\ \text{GeV}))/\Gamma_{total}$ — Γ_{121}/Γ

X and $\overline{X}$ = zero spin with $m < 4.5$ GeV

VALUE (units 10^{-5})	CL%	DOCUMENT ID		TECN	COMMENT
<24	90	[1] DEL-AMO-SA...11J		BABR	$e^+e^- \to \gamma + X\overline{X}$

[1] For a noninteracting scalar X with mass $m < 4.5$ GeV.

$\Gamma(\gamma X \to \gamma + \geq 4\ \text{prongs})/\Gamma_{total}$ — Γ_{122}/Γ

($1.5\ \text{GeV} < m_X < 5.0$ GeV)

VALUE (units 10^{-4})	CL%	DOCUMENT ID		TECN	COMMENT
<1.78	95	ROSNER	07A	CLEO	$e^+e^- \to \gamma X$

$\Gamma(\gamma a_1^0 \to \gamma\mu^+\mu^-)/\Gamma_{total}$ — Γ_{123}/Γ

($201 < M(\mu^+\mu^-) < 3565$ MeV)

VALUE (units 10^{-6})	CL%	DOCUMENT ID		TECN	COMMENT
<9	90	[1] LOVE	08	CLEO	$e^+e^- \to \gamma a_1^0 \to \gamma\mu^+\mu^-$
• • • We do not use the following data for averages, fits, limits, etc. • • •					
<9.7	90	[2] LEES	13C	BABR	$e^+e^- \to \gamma a_1^0 \to \gamma\mu^+\mu^-$

[1] For a narrow scalar or pseudoscalar a_1^0 with $201 < M(\mu^+\mu^-) < 3565$ MeV, excluding J/ψ. Measured 90% CL limits as a function of $M(\mu^+\mu^-)$ range from 1–9 $\times 10^{-6}$.
[2] For a narrow scalar or pseudoscalar a_1^0 with mass in the range 212–9200 MeV, excluding J/ψ and $\psi(2S)$. Measured 90% CL limits as a function of $m_{a_1^0}$ range from 0.28–9.7 $\times 10^{-6}$.

Downloaded from https://academic.oup.com/ptep/article/2022/8/083C01/6651666 by KIT Library user on 27 September 2022

$\Gamma(\gamma a_1^0 \to \gamma\tau^+\tau^-)/\Gamma_{total}$ — Γ_{124}/Γ

$(2m_\tau < M(\tau^+\tau^-) < 9.2$ GeV)

VALUE (units 10^{-6})	CL%	DOCUMENT ID		TECN	COMMENT
<130	90	[1] LEES	13R	BABR	$\Upsilon(2S) \to \gamma\tau^+\tau^-\pi^+\pi^-$
• • • We do not use the following data for averages, fits, limits, etc. • • •					
< 50	90	[2] LOVE	08	CLEO	$e^+e^- \to \gamma a_1^0 \to \gamma\tau^+\tau^-$

[1] For a narrow scalar a_1^0 with $2m_\tau < M(a_1^0) < 9.2$ GeV, which result in a 90% CL upper limits of 0.9×10^{-5} at $M(a_1^0) = 2m_\tau$, $\approx 1.5\times10^{-5}$ at $M(a_1^0) = 7.5$ GeV, and 13×10^{-5} at $M(a_1^0) = 9.2$ GeV.

[2] For a narrow scalar or pseudoscalar a_1^0 with $2m_\tau < M(a_1^0) < 7.5$ GeV, which result in a 90% CL limits ranging from 1×10^{-5} at $M(a_1^0)=2m_\tau$ to 5×10^{-5} at $M(a_1^0)=7.5$ GeV.

$\Gamma(\gamma a_1^0 \to \gamma gg)/\Gamma_{total}$ — Γ_{125}/Γ

(0.5 GeV $< m <$ 9.0 GeV)

VALUE	CL%	DOCUMENT ID		TECN	COMMENT
$<1\times10^{-2}$	90	[1] LEES	13L	BABR	$\Upsilon(1S) \to \gamma X$

[1] For a narrow, *CP*-odd pseudoscalar a_1^0 searched for in 26 hadronic decay modes with invariant mass 0.5 GeV $< m_X <$ 9.0 GeV. Measured 90% CL limit as a function of m_X range from 10^{-6} to 10^{-2}.

$\Gamma(\gamma a_1^0 \to \gamma s\bar{s})/\Gamma_{total}$ — Γ_{126}/Γ

(0.5 GeV $< m <$ 9.0 GeV)

VALUE	CL%	DOCUMENT ID		TECN	COMMENT
$<1\times10^{-3}$	90	[1] LEES	13L	BABR	$\Upsilon(1S) \to \gamma X$

[1] For a narrow, *CP*-odd pseudoscalar a_1^0 searched for in 14 hadronic decay modes with invariant mass 1.5 GeV $< m_X <$ 9.0 GeV. Measured 90% CL limit as a function of m_X range from 10^{-5} to 10^{-3}.

LEPTON FAMILY NUMBER (*LF*) VIOLATING MODES

$\Gamma(\mu^\pm\tau^\mp)/\Gamma_{total}$ — Γ_{127}/Γ

VALUE (units 10^{-6})	CL%	DOCUMENT ID		TECN	COMMENT
<6.0	95	LOVE	08A	CLEO	$e^+e^- \to \mu^\pm\tau^\mp$

OTHER DECAYS

$\Gamma(\text{invisible})/\Gamma_{total}$ — Γ_{128}/Γ

VALUE (units 10^{-4})	CL%	DOCUMENT ID		TECN	COMMENT
< 3.0	90	AUBERT	09AX	BABR	$\Upsilon(3S) \to \pi^+\pi^-\Upsilon(1S)$
• • • We do not use the following data for averages, fits, limits, etc. • • •					
<39	90	RUBIN	07	CLEO	$\Upsilon(2S) \to \pi^+\pi^-\Upsilon(1S)$
<25	90	TAJIMA	07	BELL	$\Upsilon(3S) \to \pi^+\pi^-\Upsilon(1S)$

$\Upsilon(1S)$ REFERENCES

KATRENKO	20	PRL 124 122001	P. Katrenko *et al.*	(BELLE Collab.)
JIA	18	PR D97 112004	S. Jia *et al.*	(BELLE Collab.)
LEES	18A	PR D97 112006	J.P. Lees *et al.*	(BABAR Collab.)
JIA	17	PR D95 012001	S. Jia *et al.*	(BELLE Collab.)
JIA	17A	PR D96 112002	S. Jia *et al.*	(BELLE Collab.)
SHEN	16	PR D93 112013	C.P. Shen *et al.*	(BELLE Collab.)
LEES	14G	PR D89 111102	J.P. Lees *et al.*	(BABAR Collab.)
YANG	14	PR D90 112008	S.D. Yang *et al.*	(BELLE Collab.)
LEES	13C	PR D87 031102	J.P. Lees *et al.*	(BABAR Collab.)
LEES	13L	PR D88 031701	J.P. Lees *et al.*	(BABAR Collab.)
LEES	13R	PR D88 071102	J.P. Lees *et al.*	(BABAR Collab.)
SHEN	13	PR D88 011102	C.P. Shen *et al.*	(BELLE Collab.)
DOBBS	12A	PR D86 052003	S. Dobbs *et al.*	
SHEN	12A	PR D86 031102	C.P. Shen *et al.*	(BELLE Collab.)
BESSON	11	PR D83 037101	D. Besson *et al.*	(CLEO Collab.)
DEL-AMO-SA...	11J	PRL 107 021804	P. del Amo Sanchez *et al.*	(BABAR Collab.)
AUBERT	10C	PR D81 011102	B. Aubert *et al.*	(BABAR Collab.)
DEL-AMO-SA...	10C	PRL 104 191801	P. del Amo Sanchez *et al.*	(BABAR Collab.)
SHEN	10A	PR D82 051504	C.P. Shen *et al.*	(BELLE Collab.)
AUBERT	09AX	PRL 103 251801	B. Aubert *et al.*	(BABAR Collab.)
LOVE	08	PRL 101 151802	W. Love *et al.*	(CLEO Collab.)
LOVE	08A	PRL 101 201601	W. Love *et al.*	(CLEO Collab.)
PDG	08	PL B667 1	C. Amsler *et al.*	(PDG Collab.)
ASNER	07	PR D75 012009	D.M. Asner *et al.*	(CLEO Collab.)
ATHAR	07A	PR D76 072003	S.B. Athar *et al.*	(CLEO Collab.)
BESSON	07	PRL 98 052002	D. Besson *et al.*	(CLEO Collab.)
BESSON	07A	PR D75 072001	D. Besson *et al.*	(CLEO Collab.)
ROSNER	07A	PR D76 117102	J.L. Rosner *et al.*	(CLEO Collab.)
RUBIN	07	PR D75 031104	P. Rubin *et al.*	(CLEO Collab.)
TAJIMA	07	PRL 98 132001	O. Tajima *et al.*	(BELLE Collab.)
AQUINES	06A	PR D74 092006	O. Aquines *et al.*	(CLEO Collab.)
ATHAR	06	PR D73 032001	S.B. Athar *et al.*	(CLEO Collab.)
BESSON	06A	PR D74 012003	D. Besson *et al.*	(CLEO Collab.)
ROSNER	06	PRL 96 092003	J.L. Rosner *et al.*	(CLEO Collab.)
ADAMS	05	PRL 94 012001	G.S. Adams *et al.*	(CLEO Collab.)
BRIERE	04	PR D70 072001	R.A. Briere *et al.*	(CLEO Collab.)
ARTUSO	03	PR D67 052003	M. Artuso *et al.*	(CLEO Collab.)
MASEK	02	PR D65 072002	G. Masek *et al.*	(CLEO Collab.)
RICHICHI	01B	PRL 87 141801	S.J. Richichi *et al.*	(CLEO Collab.)
ARTAMONOV	00	PL B474 427	A.S. Artamonov *et al.*	
ANASTASSOV	99	PRL 82 286	A. Anastassov *et al.*	(CLEO Collab.)
ALEXANDER	98	PR D58 052004	J.P. Alexander *et al.*	(CLEO Collab.)
BARU	96	PRPL 267 71	S.E. Baru *et al.*	(NOVO)
BALEST	95	PR D51 2053	R. Balest *et al.*	(CLEO Collab.)
CINABRO	94B	PL B340 129	D. Cinabro *et al.*	(CLEO Collab.)
ALBRECHT	92J	ZPHY C55 25	H. Albrecht *et al.*	(ARGUS Collab.)
BARU	92	ZPHY C54 229	S.E. Baru *et al.*	(NOVO)
BARU	92B	ZPHY C56 547	S.E. Baru *et al.*	(NOVO)
KOBEL	92	ZPHY C53 193	M. Kobel *et al.*	(Crystal Ball Collab.)
BLINOV	90	PL B245 311	A.E. Blinov *et al.*	(NOVO)
FULTON	90B	PR D41 1401	R. Fulton *et al.*	(CLEO Collab.)
MASCHMANN	90	ZPHY C46 555	W.S. Maschmann *et al.*	(Crystal Ball Collab.)
ALBRECHT	89	ZPHY C42 349	H. Albrecht *et al.*	(ARGUS Collab.)
ALEXANDER	89	NP B320 45	J.P. Alexander *et al.*	(LBL, MICH, SLAC)
BARU	89	ZPHY C42 505	S.E. Baru *et al.*	(NOVO)
CHEN	89B	PR D39 3528	W.Y. Chen *et al.*	(CLEO Collab.)
FULTON	89	PL B224 445	R. Fulton *et al.*	(CLEO Collab.)
KAARSBERG	89	PRL 62 2077	T.M. Kaarsberg *et al.*	(CUSB Collab.)
BUCHMUEL...	88	HE e^+e^- Physics 412 Editors: A. Ali and P. Soeding, World Scientific, Singapore	W. Buchmueller, S. Cooper	(HANN, DESY, MIT)
JAKUBOWSKI	88	ZPHY C40 49	Z. Jakubowski *et al.*	(Crystal Ball Collab.) IGJPC
SCHMITT	88	ZPHY C40 199	P. Schmitt *et al.*	(Crystal Ball Collab.)
ALBRECHT	87	ZPHY C35 283	H. Albrecht *et al.*	(ARGUS Collab.)
COHEN	87	RMP 59 1121	E.R. Cohen, B.N. Taylor	(RISC, NBS)
BARU	86	ZPHY C30 551	S.E. Baru *et al.*	(NOVO)
ALBRECHT	85C	PL 154B 452	H. Albrecht *et al.*	(ARGUS Collab.)
KURAEV	85	SJNP 41 466 Translated from YAF 41 733.	E.A. Kuraev, V.S. Fadin	(NOVO)
ARTAMONOV	84	PL 137B 272	A.S. Artamonov *et al.*	(NOVO)
BESSON	84	PR D30 1433	D. Besson *et al.*	(CLEO Collab.)
GILES	84B	PR D29 1285	R. Giles *et al.*	(CLEO Collab.)
MACKAY	84	PR D29 2483	W.W. MacKay *et al.*	(CUSB Collab.)
ANDREWS	83	PRL 50 807	D.E. Andrews *et al.*	(CLEO Collab.)
GILES	83	PRL 50 877	R. Giles *et al.*	(HARV, OSU, ROCH, RUTG+)
NICZYPORUK	83	ZPHY C17 197	B. Niczyporuk *et al.*	(LENA Collab.)
ALBRECHT	82	PL 116B 383	H. Albrecht *et al.*	(DESY, DORT, HEIDH+)
ARTAMONOV	82	PL 118B 225	A.S. Artamonov *et al.*	(NOVO)
NICZYPORUK	82	ZPHY C15 299	B. Niczyporuk *et al.*	(LENA Collab.)
BERGER	80C	PL 93B 497	C. Berger *et al.*	(PLUTO Collab.)
BOCK	80	ZPHY C6 125	P. Bock *et al.*	(HEIDP, MPIM, DESY, HAMB)
BERGER	79	ZPHY C1 343	C. Berger *et al.*	(PLUTO Collab.)

$\chi_{b0}(1P)$

$I^G(J^{PC}) = 0^+(0^{++})$
J needs confirmation.

Observed in radiative decay of the $\Upsilon(2S)$, therefore $C = +$. Branching ratio requires E1 transition, M1 is strongly disfavored, therefore $P = +$.

$\chi_{b0}(1P)$ MASS

VALUE (MeV)	DOCUMENT ID
9859.44±0.42±0.31 OUR EVALUATION From average γ energy below, using $\Upsilon(2S)$ mass = 10023.26 ± 0.31 MeV	

$m_{\chi_{b1}(1P)} - m_{\chi_{b0}(1P)}$

VALUE (MeV)	DOCUMENT ID		TECN	COMMENT
32.49±0.93	LEES	14M	BABR	$\Upsilon(2S) \to \gamma\gamma\mu^+\mu^-$

γ ENERGY IN $\Upsilon(2S)$ DECAY

VALUE (MeV)	DOCUMENT ID		TECN	COMMENT
162.5 ±0.4 OUR AVERAGE				
162.56±0.19±0.42	ARTUSO	05	CLEO	$\Upsilon(2S) \to \gamma X$
162.0 ±0.8 ±1.2	EDWARDS	99	CLE2	$\Upsilon(2S) \to \gamma\chi(1P)$
162.1 ±0.5 ±1.4	ALBRECHT	85E	ARG	$\Upsilon(2S) \to$ conv.γX
163.8 ±1.6 ±2.7	NERNST	85	CBAL	$\Upsilon(2S) \to \gamma$X
158.0 ±7 ±1	HAAS	84	CLEO	$\Upsilon(2S) \to$ conv.γX
• • • We do not use the following data for averages, fits, limits, etc. • • •				
149.4 ±0.7 ±5.0	KLOPFEN...	83	CUSB	$\Upsilon(2S) \to \gamma$X

$\chi_{b0}(1P)$ DECAY MODES

	Mode	Fraction (Γ_i/Γ)	Confidence level
Γ_1	$\gamma\Upsilon(1S)$	(1.94±0.27) %	
Γ_2	D^0X	< 10.4 %	90%
Γ_3	$\pi^+\pi^-K^+K^-\pi^0$	< 1.6 $\times10^{-4}$	90%
Γ_4	$2\pi^+\pi^-K^-K^0_S$	< 5 $\times10^{-5}$	90%
Γ_5	$2\pi^+\pi^-K^-K^0_S2\pi^0$	< 5 $\times10^{-4}$	90%
Γ_6	$2\pi^+2\pi^-2\pi^0$	< 2.1 $\times10^{-4}$	90%
Γ_7	$2\pi^+2\pi^-K^+K^-$	(1.1 ±0.6) $\times10^{-4}$	
Γ_8	$2\pi^+2\pi^-K^+K^-\pi^0$	< 2.7 $\times10^{-4}$	90%
Γ_9	$2\pi^+2\pi^-K^+K^-2\pi^0$	< 5 $\times10^{-4}$	90%
Γ_{10}	$3\pi^+2\pi^-K^-K^0_S\pi^0$	< 1.6 $\times10^{-4}$	90%
Γ_{11}	$3\pi^+3\pi^-$	< 8 $\times10^{-5}$	90%
Γ_{12}	$3\pi^+3\pi^-2\pi^0$	< 6 $\times10^{-4}$	90%
Γ_{13}	$3\pi^+3\pi^-K^+K^-$	(2.4 ±1.2) $\times10^{-4}$	
Γ_{14}	$3\pi^+3\pi^-K^+K^-\pi^0$	< 1.0 $\times10^{-3}$	90%
Γ_{15}	$4\pi^+4\pi^-$	< 8 $\times10^{-5}$	90%
Γ_{16}	$4\pi^+4\pi^-2\pi^0$	< 2.1 $\times10^{-3}$	90%
Γ_{17}	$J/\psi J/\psi$	< 7 $\times10^{-5}$	90%
Γ_{18}	$J/\psi\psi(2S)$	< 1.2 $\times10^{-4}$	90%
Γ_{19}	$\psi(2S)\psi(2S)$	< 3.1 $\times10^{-5}$	90%
Γ_{20}	$J/\psi(1S)$anything	< 2.3 $\times10^{-3}$	90%

Downloaded from https://academic.oup.com/ptep/article/2022/8/083C01/6651666 by KIT Library user on 27 September 2022

$\chi_{b0}(1P)$ BRANCHING RATIOS

$\Gamma(\gamma\Upsilon(1S))/\Gamma_{total}$ — Γ_1/Γ

VALUE (%)	CL%	EVTS	DOCUMENT ID		TECN	COMMENT
1.94±0.27 OUR AVERAGE						
2.07±0.24±0.21			[1,2] LEES	14M	BABR	$\Upsilon(2S) \to \gamma\gamma\mu^+\mu^-$
1.76±0.30±0.18		87	[3,4] KORNICER	11	CLEO	$e^+e^- \to \gamma\gamma\ell^+\ell^-$
• • • We do not use the following data for averages, fits, limits, etc. • • •						
< 4.6	90		[5] LEES	11J	BABR	$\Upsilon(2S) \to X\gamma$
< 6	90		WALK	86	CBAL	$\Upsilon(2S) \to \gamma\gamma\ell^+\ell^-$
<11	90		PAUSS	83	CUSB	$\Upsilon(2S) \to \gamma\gamma\ell^+\ell^-$

[1] LEES 14M quotes $\Gamma(\chi_{b0}(1P) \to \gamma\Upsilon(1S))/\Gamma_{total} \times \Gamma(\Upsilon(2S) \to \gamma\chi_{b0}(1P))/\Gamma_{total} = (7.75 \pm 0.91) \times 10^{-4}$ combining the results from samples of $\Upsilon(2S) \to \gamma\gamma\mu^+\mu^-$ with and without converted photons. Assumes $B(\Upsilon(1S) \to \mu^+\mu^-) = (2.48 \pm 0.05)\%$.

[2] LEES 14M reports $[\Gamma(\chi_{b0}(1P) \to \gamma\Upsilon(1S))/\Gamma_{total}] \times [B(\Upsilon(2S) \to \gamma\chi_{b0}(1P))] = (7.75 \pm 0.91) \times 10^{-4}$ which we divide by our best value $B(\Upsilon(2S) \to \gamma\chi_{b0}(1P)) = (3.8 \pm 0.4) \times 10^{-2}$. Our first error is their experiment's error and our second error is the systematic error from using our best value.

[3] Assuming $B(\Upsilon(1S) \to \ell^+\ell^-) = (2.48 \pm 0.05)\%$.

[4] KORNICER 11 reports $[\Gamma(\chi_{b0}(1P) \to \gamma\Upsilon(1S))/\Gamma_{total}] \times [B(\Upsilon(2S) \to \gamma\chi_{b0}(1P))] = (6.59 \pm 0.96 \pm 0.60) \times 10^{-4}$ which we divide by our best value $B(\Upsilon(2S) \to \gamma\chi_{b0}(1P)) = (3.8 \pm 0.4) \times 10^{-2}$. Our first error is their experiment's error and our second error is the systematic error from using our best value.

[5] LEES 11J quotes a central value of $\Gamma(\chi_{b0}(1P) \to \gamma\Upsilon(1S))/\Gamma_{total} \times \Gamma(\Upsilon(2S) \to \gamma\chi_{b0}(1P))/\Gamma_{total} = (8.3 \pm 5.6^{+3.7}_{-2.6}) \times 10^{-4}$.

$\Gamma(D^0X)/\Gamma_{total}$ — Γ_2/Γ

VALUE	CL%	DOCUMENT ID		TECN	COMMENT
<10.4 × 10⁻²	90	[6,7] BRIERE	08	CLEO	$\Upsilon(2S) \to \gamma D^0X$

[6] For $p_{D^0} > 2.5$ GeV/c.

[7] The authors also present their result as $(5.6 \pm 3.6 \pm 0.5) \times 10^{-2}$.

$\Gamma(\pi^+\pi^-K^+K^-\pi^0)/\Gamma_{total}$ — Γ_3/Γ

VALUE (units 10^{-4})	CL%	DOCUMENT ID		TECN	COMMENT
<1.6	90	[8] ASNER	08A	CLEO	$\Upsilon(2S) \to \gamma\pi^+\pi^-K^+K^-\pi^0$

[8] ASNER 08A reports $[\Gamma(\chi_{b0}(1P) \to \pi^+\pi^-K^+K^-\pi^0)/\Gamma_{total}] \times [B(\Upsilon(2S) \to \gamma\chi_{b0}(1P))] < 6 \times 10^{-6}$ which we divide by our best value $B(\Upsilon(2S) \to \gamma\chi_{b0}(1P)) = 3.8 \times 10^{-2}$.

$\Gamma(2\pi^+\pi^-K^-K^0_S)/\Gamma_{total}$ — Γ_4/Γ

VALUE (units 10^{-4})	CL%	DOCUMENT ID		TECN	COMMENT
<0.5	90	[9] ASNER	08A	CLEO	$\Upsilon(2S) \to \gamma 2\pi^+\pi^-K^-K^0_S$

[9] ASNER 08A reports $[\Gamma(\chi_{b0}(1P) \to 2\pi^+\pi^-K^-K^0_S)/\Gamma_{total}] \times [B(\Upsilon(2S) \to \gamma\chi_{b0}(1P))] < 2 \times 10^{-6}$ which we divide by our best value $B(\Upsilon(2S) \to \gamma\chi_{b0}(1P)) = 3.8 \times 10^{-2}$.

$\Gamma(2\pi^+\pi^-K^-K^0_S2\pi^0)/\Gamma_{total}$ — Γ_5/Γ

VALUE (units 10^{-4})	CL%	DOCUMENT ID		TECN	COMMENT
<5	90	[10] ASNER	08A	CLEO	$\Upsilon(2S) \to \gamma 2\pi^+\pi^-K^-2\pi^0$

[10] ASNER 08A reports $[\Gamma(\chi_{b0}(1P) \to 2\pi^+\pi^-K^-K^0_S2\pi^0)/\Gamma_{total}] \times [B(\Upsilon(2S) \to \gamma\chi_{b0}(1P))] < 18 \times 10^{-6}$ which we divide by our best value $B(\Upsilon(2S) \to \gamma\chi_{b0}(1P)) = 3.8 \times 10^{-2}$.

$\Gamma(2\pi^+2\pi^-2\pi^0)/\Gamma_{total}$ — Γ_6/Γ

VALUE (units 10^{-4})	CL%	DOCUMENT ID		TECN	COMMENT
<2.1	90	[11] ASNER	08A	CLEO	$\Upsilon(2S) \to \gamma 2\pi^+2\pi^-2\pi^0$

[11] ASNER 08A reports $[\Gamma(\chi_{b0}(1P) \to 2\pi^+2\pi^-2\pi^0)/\Gamma_{total}] \times [B(\Upsilon(2S) \to \gamma\chi_{b0}(1P))] < 8 \times 10^{-6}$ which we divide by our best value $B(\Upsilon(2S) \to \gamma\chi_{b0}(1P)) = 3.8 \times 10^{-2}$.

$\Gamma(2\pi^+2\pi^-K^+K^-)/\Gamma_{total}$ — Γ_7/Γ

VALUE (units 10^{-4})	EVTS	DOCUMENT ID		TECN	COMMENT
1.1±0.6±0.1	7	[12] ASNER	08A	CLEO	$\Upsilon(2S) \to \gamma 2\pi^+2\pi^-K^+K^-$

[12] ASNER 08A reports $[\Gamma(\chi_{b0}(1P) \to 2\pi^+2\pi^-K^+K^-)/\Gamma_{total}] \times [B(\Upsilon(2S) \to \gamma\chi_{b0}(1P))] = (4 \pm 2 \pm 1) \times 10^{-6}$ which we divide by our best value $B(\Upsilon(2S) \to \gamma\chi_{b0}(1P)) = (3.8 \pm 0.4) \times 10^{-2}$. Our first error is their experiment's error and our second error is the systematic error from using our best value.

$\Gamma(2\pi^+2\pi^-K^+K^-\pi^0)/\Gamma_{total}$ — Γ_8/Γ

VALUE (units 10^{-4})	CL%	DOCUMENT ID		TECN	COMMENT
<2.7	90	[13] ASNER	08A	CLEO	$\Upsilon(2S) \to \gamma 2\pi^+2\pi^-K^+K^-\pi^0$

[13] ASNER 08A reports $[\Gamma(\chi_{b0}(1P) \to 2\pi^+2\pi^-K^+K^-\pi^0)/\Gamma_{total}] \times [B(\Upsilon(2S) \to \gamma\chi_{b0}(1P))] < 10 \times 10^{-6}$ which we divide by our best value $B(\Upsilon(2S) \to \gamma\chi_{b0}(1P)) = 3.8 \times 10^{-2}$.

$\Gamma(2\pi^+2\pi^-K^+K^-2\pi^0)/\Gamma_{total}$ — Γ_9/Γ

VALUE (units 10^{-4})	CL%	DOCUMENT ID		TECN	COMMENT
<5	90	[14] ASNER	08A	CLEO	$\Upsilon(2S) \to \gamma 2\pi^+2\pi^-K^+K^-2\pi^0$

[14] ASNER 08A reports $[\Gamma(\chi_{b0}(1P) \to 2\pi^+2\pi^-K^+K^-2\pi^0)/\Gamma_{total}] \times [B(\Upsilon(2S) \to \gamma\chi_{b0}(1P))] < 20 \times 10^{-6}$ which we divide by our best value $B(\Upsilon(2S) \to \gamma\chi_{b0}(1P)) = 3.8 \times 10^{-2}$.

$\Gamma(3\pi^+2\pi^-K^-K^0_S\pi^0)/\Gamma_{total}$ — Γ_{10}/Γ

VALUE (units 10^{-4})	CL%	DOCUMENT ID		TECN	COMMENT
<1.6	90	[15] ASNER	08A	CLEO	$\Upsilon(2S) \to \gamma 3\pi^+2\pi^-K^-K^0_S\pi^0$

[15] ASNER 08A reports $[\Gamma(\chi_{b0}(1P) \to 3\pi^+2\pi^-K^-K^0_S\pi^0)/\Gamma_{total}] \times [B(\Upsilon(2S) \to \gamma\chi_{b0}(1P))] < 6 \times 10^{-6}$ which we divide by our best value $B(\Upsilon(2S) \to \gamma\chi_{b0}(1P)) = 3.8 \times 10^{-2}$.

$\Gamma(3\pi^+3\pi^-)/\Gamma_{total}$ — Γ_{11}/Γ

VALUE (units 10^{-4})	CL%	DOCUMENT ID		TECN	COMMENT
<0.8	90	[16] ASNER	08A	CLEO	$\Upsilon(2S) \to \gamma 3\pi^+3\pi^-$

[16] ASNER 08A reports $[\Gamma(\chi_{b0}(1P) \to 3\pi^+3\pi^-)/\Gamma_{total}] \times [B(\Upsilon(2S) \to \gamma\chi_{b0}(1P))] < 3 \times 10^{-6}$ which we divide by our best value $B(\Upsilon(2S) \to \gamma\chi_{b0}(1P)) = 3.8 \times 10^{-2}$.

$\Gamma(3\pi^+3\pi^-2\pi^0)/\Gamma_{total}$ — Γ_{12}/Γ

VALUE (units 10^{-4})	CL%	DOCUMENT ID		TECN	COMMENT
<6	90	[17] ASNER	08A	CLEO	$\Upsilon(2S) \to \gamma 3\pi^+3\pi^-2\pi^0$

[17] ASNER 08A reports $[\Gamma(\chi_{b0}(1P) \to 3\pi^+3\pi^-2\pi^0)/\Gamma_{total}] \times [B(\Upsilon(2S) \to \gamma\chi_{b0}(1P))] < 22 \times 10^{-6}$ which we divide by our best value $B(\Upsilon(2S) \to \gamma\chi_{b0}(1P)) = 3.8 \times 10^{-2}$.

$\Gamma(3\pi^+3\pi^-K^+K^-)/\Gamma_{total}$ — Γ_{13}/Γ

VALUE (units 10^{-4})	EVTS	DOCUMENT ID		TECN	COMMENT
2.4±1.2±0.2	9	[18] ASNER	08A	CLEO	$\Upsilon(2S) \to \gamma 3\pi^+3\pi^-K^+K^-$

[18] ASNER 08A reports $[\Gamma(\chi_{b0}(1P) \to 3\pi^+3\pi^-K^+K^-)/\Gamma_{total}] \times [B(\Upsilon(2S) \to \gamma\chi_{b0}(1P))] = (9 \pm 4 \pm 2) \times 10^{-6}$ which we divide by our best value $B(\Upsilon(2S) \to \gamma\chi_{b0}(1P)) = (3.8 \pm 0.4) \times 10^{-2}$. Our first error is their experiment's error and our second error is the systematic error from using our best value.

$\Gamma(3\pi^+3\pi^-K^+K^-\pi^0)/\Gamma_{total}$ — Γ_{14}/Γ

VALUE (units 10^{-4})	CL%	DOCUMENT ID		TECN	COMMENT
<10	90	[19] ASNER	08A	CLEO	$\Upsilon(2S) \to \gamma 3\pi^+3\pi^-K^+K^-\pi^0$

[19] ASNER 08A reports $[\Gamma(\chi_{b0}(1P) \to 3\pi^+3\pi^-K^+K^-\pi^0)/\Gamma_{total}] \times [B(\Upsilon(2S) \to \gamma\chi_{b0}(1P))] < 37 \times 10^{-6}$ which we divide by our best value $B(\Upsilon(2S) \to \gamma\chi_{b0}(1P)) = 3.8 \times 10^{-2}$.

$\Gamma(4\pi^+4\pi^-)/\Gamma_{total}$ — Γ_{15}/Γ

VALUE (units 10^{-4})	CL%	DOCUMENT ID		TECN	COMMENT
<0.8	90	[20] ASNER	08A	CLEO	$\Upsilon(2S) \to \gamma 4\pi^+4\pi^-$

[20] ASNER 08A reports $[\Gamma(\chi_{b0}(1P) \to 4\pi^+4\pi^-)/\Gamma_{total}] \times [B(\Upsilon(2S) \to \gamma\chi_{b0}(1P))] < 3 \times 10^{-6}$ which we divide by our best value $B(\Upsilon(2S) \to \gamma\chi_{b0}(1P)) = 3.8 \times 10^{-2}$.

$\Gamma(4\pi^+4\pi^-2\pi^0)/\Gamma_{total}$ — Γ_{16}/Γ

VALUE (units 10^{-4})	CL%	DOCUMENT ID		TECN	COMMENT
<21	90	[21] ASNER	08A	CLEO	$\Upsilon(2S) \to \gamma 4\pi^+4\pi^-2\pi^0$

[21] ASNER 08A reports $[\Gamma(\chi_{b0}(1P) \to 4\pi^+4\pi^-2\pi^0)/\Gamma_{total}] \times [B(\Upsilon(2S) \to \gamma\chi_{b0}(1P))] < 77 \times 10^{-6}$ which we divide by our best value $B(\Upsilon(2S) \to \gamma\chi_{b0}(1P)) = 3.8 \times 10^{-2}$.

$\Gamma(J/\psi J/\psi)/\Gamma_{total}$ — Γ_{17}/Γ

VALUE (units 10^{-5})	CL%	DOCUMENT ID		TECN	COMMENT
<7	90	[22] SHEN	12	BELL	$\Upsilon(2S) \to \gamma\psi X$

[22] SHEN 12 reports $< 7.1 \times 10^{-5}$ from a measurement of $[\Gamma(\chi_{b0}(1P) \to J/\psi J/\psi)/\Gamma_{total}] \times [B(\Upsilon(2S) \to \gamma\chi_{b0}(1P))]$ assuming $B(\Upsilon(2S) \to \gamma\chi_{b0}(1P)) = (3.8 \pm 0.4) \times 10^{-2}$.

$\Gamma(J/\psi\psi(2S))/\Gamma_{total}$ — Γ_{18}/Γ

VALUE (units 10^{-5})	CL%	DOCUMENT ID		TECN	COMMENT
<12	90	[23] SHEN	12	BELL	$\Upsilon(2S) \to \gamma\psi X$

[23] SHEN 12 reports $< 12 \times 10^{-5}$ from a measurement of $[\Gamma(\chi_{b0}(1P) \to J/\psi\psi(2S))/\Gamma_{total}] \times [B(\Upsilon(2S) \to \gamma\chi_{b0}(1P))]$ assuming $B(\Upsilon(2S) \to \gamma\chi_{b0}(1P)) = (3.8 \pm 0.4) \times 10^{-2}$.

$\Gamma(\psi(2S)\psi(2S))/\Gamma_{total}$ — Γ_{19}/Γ

VALUE (units 10^{-5})	CL%	DOCUMENT ID		TECN	COMMENT
<3.1	90	[24] SHEN	12	BELL	$\Upsilon(2S) \to \gamma\psi X$

[24] SHEN 12 reports $< 3.1 \times 10^{-5}$ from a measurement of $[\Gamma(\chi_{b0}(1P) \to \psi(2S)\psi(2S))/\Gamma_{total}] \times [B(\Upsilon(2S) \to \gamma\chi_{b0}(1P))]$ assuming $B(\Upsilon(2S) \to \gamma\chi_{b0}(1P)) = (3.8 \pm 0.4) \times 10^{-2}$.

$\Gamma(J/\psi(1S)\text{anything})/\Gamma_{total}$ — Γ_{20}/Γ

VALUE	CL%	DOCUMENT ID		TECN	COMMENT
<2.3 × 10⁻³	90	JIA	17A	BELL	$e^+e^- \to$ hadrons

$\chi_{b0}(1P)$ CROSS-PARTICLE BRANCHING RATIOS

$\Gamma(\chi_{b0}(1P) \to \gamma\Upsilon(1S))/\Gamma_{total} \times \Gamma(\Upsilon(2S) \to \gamma\chi_{b0}(1P))/\Gamma_{total}$ — $\Gamma_1/\Gamma \times \Gamma_{61}^{\Upsilon(2S)}/\Gamma^{\Upsilon(2S)}$

VALUE	CL%	DOCUMENT ID		TECN	COMMENT
<1.7 × 10⁻³	90	[25] LEES	11J	BABR	$\Upsilon(2S) \to X\gamma$

[25] LEES 11J quotes a central value of $\Gamma(\chi_{b0}(1P) \to \gamma\Upsilon(1S))/\Gamma_{total} \times \Gamma(\Upsilon(2S) \to \gamma\chi_{b0}(1P))/\Gamma_{total} = (8.3 \pm 5.6^{+3.7}_{-2.6}) \times 10^{-4}$ and derives a 90% CL upper limit of $\Gamma(\gamma\Upsilon(1S))/\Gamma_{total} < 4.6\%$ using $B(\Upsilon(2S) \to \gamma\chi_{b0}(1P)) = (3.8 \pm 0.4)\%$.

Downloaded from https://academic.oup.com/ptep/article/2022/8/083C01/6651666 by KIT Library user on 27 September 2022

$B(\chi_{b0}(1P) \to \gamma\Upsilon(1S)) \times B(\Upsilon(2S) \to \gamma\chi_{b0}(1P)) \times B(\Upsilon(1S) \to \ell^+\ell^-)$

VALUE (units 10^{-5})	EVTS	DOCUMENT ID		TECN	COMMENT
1.67±0.28 OUR AVERAGE					
$2.9\ ^{+1.7}_{-1.4}\ ^{+0.1}_{-0.8}$		[26] LEES	14M	BABR	$\Upsilon(2S) \to \gamma\gamma\mu^+\mu^-$
1.63±0.24±0.15	87	KORNICER	11	CLEO	$e^+e^- \to \gamma\gamma\ell^+\ell^-$

[26] From a sample of $\Upsilon(2S) \to \gamma\gamma\mu^+\mu^-$ with one converted photon.

$[B(\chi_{b0}(1P) \to \gamma\Upsilon(1S)) \times B(\Upsilon(2S) \to \gamma\chi_{b0}(1P))] / [B(\chi_{b1}(1P) \to \gamma\Upsilon(1S)) \times B(\Upsilon(2S) \to \gamma\chi_{b1}(1P))]$

VALUE (%)	DOCUMENT ID		TECN	COMMENT
3.28±0.37	[27] LEES	14M	BABR	$\Upsilon(2S) \to \gamma\gamma\mu^+\mu^-$

[27] From a sample of $\Upsilon(2S) \to \gamma\gamma\mu^+\mu^-$ without converted photons.

$\chi_{b0}(1P)$ REFERENCES

JIA	17A	PR D96 112002	S. Jia et al.	(BELLE Collab.)
LEES	14M	PR D90 112010	J.P. Lees et al.	(BABAR Collab.)
SHEN	12	PR D85 071102	C.P. Shen et al.	(BELLE Collab.)
KORNICER	11	PR D83 054003	M. Kornicer et al.	(CLEO Collab.)
LEES	11J	PR D84 072002	J.P. Lees et al.	(BABAR Collab.)
ASNER	08A	PR D78 091103	D.M. Asner et al.	(CLEO Collab.)
BRIERE	08	PR D78 092007	R.A. Briere et al.	(CLEO Collab.)
ARTUSO	05	PRL 94 032001	M. Artuso et al.	(CLEO Collab.)
EDWARDS	99	PR D59 032003	K.W. Edwards et al.	(CLEO Collab.)
WALK	86	PR D34 2611	W.S. Walk et al.	(Crystal Ball Collab.)
ALBRECHT	85E	PL 160B 331	H. Albrecht et al.	(ARGUS Collab.)
NERNST	85	PRL 54 2195	R. Nernst et al.	(Crystal Ball Collab.)
HAAS	84	PRL 52 799	J. Haas et al.	(CLEO Collab.)
KLOPFEN...	83	PRL 51 160	C. Klopfenstein et al.	(CUSB Collab.)
PAUSS	83	PL 130B 439	F. Pauss et al.	(MPIM, COLU, CORN, LSU+)

$\chi_{b1}(1P)$

$I^G(J^{PC}) = 0^+(1^{++})$
J needs confirmation.

Observed in radiative decay of the $\Upsilon(2S)$, therefore $C = +$. Branching ratio requires E1 transition, M1 is strongly disfavored, therefore $P = +$. $J = 1$ from SKWARNICKI 87.

$\chi_{b1}(1P)$ MASS

VALUE (MeV)	DOCUMENT ID
9892.78±0.26±0.31 OUR EVALUATION	From average γ energy below, using $\Upsilon(2S)$ mass = 10023.26 ± 0.31 MeV

γ ENERGY IN $\Upsilon(2S)$ DECAY

VALUE (MeV)	DOCUMENT ID		TECN	COMMENT
129.63±0.33 OUR AVERAGE	Error includes scale factor of 1.3.			See the ideogram below.
129.58±0.09±0.29	ARTUSO	05	CLEO	$\Upsilon(2S) \to \gamma X$
128.8 ±0.4 ±0.6	EDWARDS	99	CLE2	$\Upsilon(2S) \to \gamma\chi(1P)$
131.7 ±0.9 ±1.3	WALK	86	CBAL	$\Upsilon(2S) \to \gamma\gamma\ell^+\ell^-$
131.7 ±0.3 ±1.1	ALBRECHT	85E	ARG	$\Upsilon(2S) \to$ conv.γX
130.6 ±0.8 ±2.4	NERNST	85	CBAL	$\Upsilon(2S) \to \gamma X$
129 ±0.8 ±1	HAAS	84	CLEO	$\Upsilon(2S) \to$ conv.γX
128.1 ±0.4 ±3.0	KLOPFEN...	83	CUSB	$\Upsilon(2S) \to \gamma X$
130.6 ±3.0	PAUSS	83	CUSB	$\Upsilon(2S) \to \gamma\gamma\ell^+\ell^-$

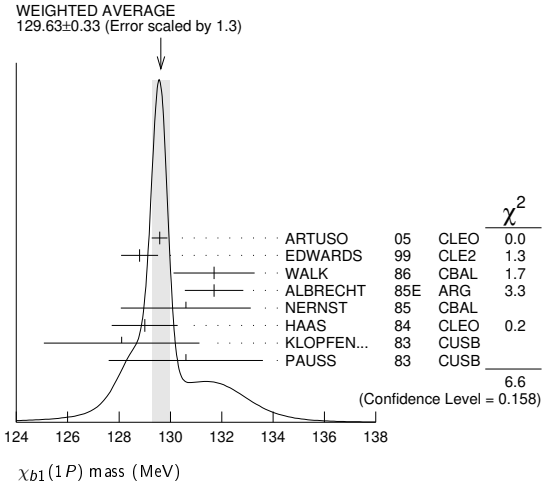

$\chi_{b1}(1P)$ DECAY MODES

	Mode	Fraction (Γ_i/Γ)	Confidence level
Γ_1	$\gamma\Upsilon(1S)$	(35.2 ±2.0) %	
Γ_2	D^0X	(12.6 ±2.2) %	
Γ_3	$\pi^+\pi^-K^+K^-\pi^0$	(2.0 ±0.6) $\times 10^{-4}$	
Γ_4	$2\pi^+\pi^-K^-K^0_S$	(1.3 ±0.5) $\times 10^{-4}$	
Γ_5	$2\pi^+\pi^-K^-K^0_S 2\pi^0$	< 6 $\times 10^{-4}$	90%
Γ_6	$2\pi^+2\pi^-2\pi^0$	(8.0 ±2.5) $\times 10^{-4}$	
Γ_7	$2\pi^+2\pi^-K^+K^-$	(1.5 ±0.5) $\times 10^{-4}$	
Γ_8	$2\pi^+2\pi^-K^+K^-\pi^0$	(3.5 ±1.2) $\times 10^{-4}$	
Γ_9	$2\pi^+2\pi^-K^+K^-2\pi^0$	(8.6 ±3.2) $\times 10^{-4}$	
Γ_{10}	$3\pi^+2\pi^-K^-K^0_S\pi^0$	(9.3 ±3.3) $\times 10^{-4}$	
Γ_{11}	$3\pi^+3\pi^-$	(1.9 ±0.6) $\times 10^{-4}$	
Γ_{12}	$3\pi^+3\pi^-2\pi^0$	(1.7 ±0.5) $\times 10^{-3}$	
Γ_{13}	$3\pi^+3\pi^-K^+K^-$	(2.6 ±0.8) $\times 10^{-4}$	
Γ_{14}	$3\pi^+3\pi^-K^+K^-\pi^0$	(7.5 ±2.6) $\times 10^{-4}$	
Γ_{15}	$4\pi^+4\pi^-$	(2.6 ±0.9) $\times 10^{-4}$	
Γ_{16}	$4\pi^+4\pi^-2\pi^0$	(1.4 ±0.6) $\times 10^{-3}$	
Γ_{17}	ω anything	(4.9 ±1.4) %	
Γ_{18}	ωX_{tetra}	< 4.44 $\times 10^{-4}$	90%
Γ_{19}	$J/\psi J/\psi$	< 2.7 $\times 10^{-5}$	90%
Γ_{20}	$J/\psi\psi(2S)$	< 1.7 $\times 10^{-5}$	90%
Γ_{21}	$\psi(2S)\psi(2S)$	< 6 $\times 10^{-5}$	90%
Γ_{22}	$J/\psi(1S)$ anything	< 1.1 $\times 10^{-3}$	90%
Γ_{23}	$J/\psi(1S)X_{tetra}$	< 2.27 $\times 10^{-4}$	90%

$\chi_{b1}(1P)$ BRANCHING RATIOS

$\Gamma(\gamma\Upsilon(1S))/\Gamma_{total}$ — Γ_1/Γ

VALUE	EVTS	DOCUMENT ID		TECN	COMMENT
0.352±0.020 OUR AVERAGE					
$0.356^{+0.016}_{-0.022}$±0.019	964k	[1] FULSOM	18	BELL	$\Upsilon(2S) \to \gamma X$
0.364±0.017±0.019		[2,3,4] LEES	14M	BABR	$\Upsilon(2S) \to \gamma\gamma\mu^+\mu^-$
0.331±0.018±0.017	3222	[4,5] KORNICER	11	CLEO	$e^+e^- \to \gamma\gamma\ell^+\ell^-$
0.350±0.023±0.018	13k	[6] LEES	11J	BABR	$\Upsilon(2S) \to X\gamma$
0.34 ±0.07 ±0.02	53	[4,7,8] WALK	86	CBAL	$\Upsilon(2S) \to \gamma\gamma\ell^+\ell^-$
0.47 ±0.18		KLOPFEN...	83	CUSB	$\Upsilon(2S) \to \gamma\gamma\ell^+\ell^-$

[1] FULSOM 18 reports $[\Gamma(\chi_{b1}(1P) \to \gamma\Upsilon(1S))/\Gamma_{total}] \times [B(\Upsilon(2S) \to \gamma\chi_{b1}(1P))] = (2.45 \pm 0.02^{+0.11}_{-0.15}) \times 10^{-2}$ which we divide by our best value $B(\Upsilon(2S) \to \gamma\chi_{b1}(1P)) = (6.9 \pm 0.4) \times 10^{-2}$. Our first error is their experiment's error and our second error is the systematic error from using our best value.

[2] LEES 14M quotes $\Gamma(\chi_{b1}(1P) \to \gamma\Upsilon(1S))/\Gamma_{total} \times \Gamma(\Upsilon(2S) \to \gamma\chi_{b1}(1P))/\Gamma_{total} = (2.51 \pm 0.12)$ % combining the results from samples of $\Upsilon(2S) \to \gamma\gamma\mu^+\mu^-$ with and without converted photons.

[3] LEES 14M reports $[\Gamma(\chi_{b1}(1P) \to \gamma\Upsilon(1S))/\Gamma_{total}] \times [B(\Upsilon(2S) \to \gamma\chi_{b1}(1P))] = (2.51 \pm 0.12) \times 10^{-2}$ which we divide by our best value $B(\Upsilon(2S) \to \gamma\chi_{b1}(1P)) = (6.9 \pm 0.4) \times 10^{-2}$. Our first error is their experiment's error and our second error is the systematic error from using our best value.

[4] Assuming $B(\Upsilon(1S) \to \mu^+\mu^-) = (2.48 \pm 0.05)$%.

[5] KORNICER 11 reports $[\Gamma(\chi_{b1}(1P) \to \gamma\Upsilon(1S))/\Gamma_{total}] \times [B(\Upsilon(2S) \to \gamma\chi_{b1}(1P))] = (22.8 \pm 0.4 \pm 1.2) \times 10^{-3}$ which we divide by our best value $B(\Upsilon(2S) \to \gamma\chi_{b1}(1P)) = (6.9 \pm 0.4) \times 10^{-2}$. Our first error is their experiment's error and our second error is the systematic error from using our best value.

[6] LEES 11J reports $[\Gamma(\chi_{b1}(1P) \to \gamma\Upsilon(1S))/\Gamma_{total}] \times [B(\Upsilon(2S) \to \gamma\chi_{b1}(1P))] = (24.1 \pm 0.6 \pm 1.5) \times 10^{-3}$ which we divide by our best value $B(\Upsilon(2S) \to \gamma\chi_{b1}(1P)) = (6.9 \pm 0.4) \times 10^{-2}$. Our first error is their experiment's error and our second error is the systematic error from using our best value.

[7] WALK 86 quotes $B(\Upsilon(2S) \to \gamma\chi_{b1}(1P)) \times B(\chi_{b1}(1P) \to \gamma\Upsilon(1S)) \times B(\Upsilon(1S) \to \ell^+\ell^-) = (5.8 \pm 0.9 \pm 0.7)$ %.

[8] WALK 86 reports $[\Gamma(\chi_{b1}(1P) \to \gamma\Upsilon(1S))/\Gamma_{total}] \times [B(\Upsilon(2S) \to \gamma\chi_{b1}(1P))] = (23.4 \pm 3.63 \pm 2.82) \times 10^{-3}$ which we divide by our best value $B(\Upsilon(2S) \to \gamma\chi_{b1}(1P)) = (6.9 \pm 0.4) \times 10^{-2}$. Our first error is their experiment's error and our second error is the systematic error from using our best value.

$\Gamma(D^0X)/\Gamma_{total}$ — Γ_2/Γ

VALUE (units 10^{-2})	EVTS	DOCUMENT ID		TECN	COMMENT
12.6±1.9±1.1	2310	[1] BRIERE	08	CLEO	$\Upsilon(2S) \to \gamma D^0X$

[1] For $p_{D^0} > 2.5$ GeV/c.

$\Gamma(\pi^+\pi^-K^+K^-\pi^0)/\Gamma_{total}$ — Γ_3/Γ

VALUE (units 10^{-4})	EVTS	DOCUMENT ID		TECN	COMMENT
2.0±0.6±0.1	18	[1] ASNER	08A	CLEO	$\Upsilon(2S) \to \gamma\pi^+\pi^-K^+K^-\pi^0$

[1] ASNER 08A reports $[\Gamma(\chi_{b1}(1P) \to \pi^+\pi^-K^+K^-\pi^0)/\Gamma_{total}] \times [B(\Upsilon(2S) \to \gamma\chi_{b1}(1P))] = (14 \pm 3 \pm 3) \times 10^{-6}$ which we divide by our best value $B(\Upsilon(2S) \to \gamma\chi_{b1}(1P)) = (6.9 \pm 0.4) \times 10^{-2}$. Our first error is their experiment's error and our second error is the systematic error from using our best value.

Downloaded from https://academic.oup.com/ptep/article/2022/8/083C01/6651666 by KIT Library user on 27 September 2022

$\Gamma(2\pi^+\pi^-K^-K^0_S)/\Gamma_{total}$ — Γ_4/Γ

VALUE (units 10^{-4})	EVTS	DOCUMENT ID		TECN	COMMENT
1.3±0.5±0.1	11	[1] ASNER	08A	CLEO	$\Upsilon(2S) \to \gamma 2\pi^+\pi^-K^-K^0_S$

[1] ASNER 08A reports $[\Gamma(\chi_{b1}(1P) \to 2\pi^+\pi^-K^-K^0_S)/\Gamma_{total}] \times [B(\Upsilon(2S) \to \gamma\chi_{b1}(1P))] = (9 \pm 3 \pm 2) \times 10^{-6}$ which we divide by our best value $B(\Upsilon(2S) \to \gamma\chi_{b1}(1P)) = (6.9 \pm 0.4) \times 10^{-2}$. Our first error is their experiment's error and our second error is the systematic error from using our best value.

$\Gamma(2\pi^+\pi^-K^-K^0_S 2\pi^0)/\Gamma_{total}$ — Γ_5/Γ

VALUE (units 10^{-4})	CL%	DOCUMENT ID		TECN	COMMENT
<6	90	[1] ASNER	08A	CLEO	$\Upsilon(2S) \to \gamma 2\pi^+\pi^-K^-2\pi^0$

[1] ASNER 08A reports $[\Gamma(\chi_{b1}(1P) \to 2\pi^+\pi^-K^-K^0_S 2\pi^0)/\Gamma_{total}] \times [B(\Upsilon(2S) \to \gamma\chi_{b1}(1P))] < 42 \times 10^{-6}$ which we divide by our best value $B(\Upsilon(2S) \to \gamma\chi_{b1}(1P)) = 6.9 \times 10^{-2}$.

$\Gamma(2\pi^+2\pi^-2\pi^0)/\Gamma_{total}$ — Γ_6/Γ

VALUE (units 10^{-4})	EVTS	DOCUMENT ID		TECN	COMMENT
8.0±2.4±0.4	46	[1] ASNER	08A	CLEO	$\Upsilon(2S) \to \gamma 2\pi^+2\pi^-2\pi^0$

[1] ASNER 08A reports $[\Gamma(\chi_{b1}(1P) \to 2\pi^+2\pi^-2\pi^0)/\Gamma_{total}] \times [B(\Upsilon(2S) \to \gamma\chi_{b1}(1P))] = (55 \pm 9 \pm 14) \times 10^{-6}$ which we divide by our best value $B(\Upsilon(2S) \to \gamma\chi_{b1}(1P)) = (6.9 \pm 0.4) \times 10^{-2}$. Our first error is their experiment's error and our second error is the systematic error from using our best value.

$\Gamma(2\pi^+2\pi^-K^+K^-)/\Gamma_{total}$ — Γ_7/Γ

VALUE (units 10^{-4})	EVTS	DOCUMENT ID		TECN	COMMENT
1.5±0.5±0.1	18	[1] ASNER	08A	CLEO	$\Upsilon(2S) \to \gamma 2\pi^+2\pi^-K^+K^-$

[1] ASNER 08A reports $[\Gamma(\chi_{b1}(1P) \to 2\pi^+2\pi^-K^+K^-)/\Gamma_{total}] \times [B(\Upsilon(2S) \to \gamma\chi_{b1}(1P))] = (10 \pm 3 \pm 2) \times 10^{-6}$ which we divide by our best value $B(\Upsilon(2S) \to \gamma\chi_{b1}(1P)) = (6.9 \pm 0.4) \times 10^{-2}$. Our first error is their experiment's error and our second error is the systematic error from using our best value.

$\Gamma(2\pi^+2\pi^-K^+K^-\pi^0)/\Gamma_{total}$ — Γ_8/Γ

VALUE (units 10^{-4})	EVTS	DOCUMENT ID		TECN	COMMENT
3.5±1.2±0.2	22	[1] ASNER	08A	CLEO	$\Upsilon(2S) \to \gamma 2\pi^+2\pi^-K^+K^-\pi^0$

[1] ASNER 08A reports $[\Gamma(\chi_{b1}(1P) \to 2\pi^+2\pi^-K^+K^-\pi^0)/\Gamma_{total}] \times [B(\Upsilon(2S) \to \gamma\chi_{b1}(1P))] = (24 \pm 6 \pm 6) \times 10^{-6}$ which we divide by our best value $B(\Upsilon(2S) \to \gamma\chi_{b1}(1P)) = (6.9 \pm 0.4) \times 10^{-2}$. Our first error is their experiment's error and our second error is the systematic error from using our best value.

$\Gamma(2\pi^+2\pi^-K^+K^-2\pi^0)/\Gamma_{total}$ — Γ_9/Γ

VALUE (units 10^{-4})	EVTS	DOCUMENT ID		TECN	COMMENT
8.6±3.2±0.4	26	[1] ASNER	08A	CLEO	$\Upsilon(2S) \to \gamma 2\pi^+2\pi^-K^+K^-2\pi^0$

[1] ASNER 08A reports $[\Gamma(\chi_{b1}(1P) \to 2\pi^+2\pi^-K^+K^-2\pi^0)/\Gamma_{total}] \times [B(\Upsilon(2S) \to \gamma\chi_{b1}(1P))] = (59 \pm 14 \pm 17) \times 10^{-6}$ which we divide by our best value $B(\Upsilon(2S) \to \gamma\chi_{b1}(1P)) = (6.9 \pm 0.4) \times 10^{-2}$. Our first error is their experiment's error and our second error is the systematic error from using our best value.

$\Gamma(3\pi^+2\pi^-K^-K^0_S\pi^0)/\Gamma_{total}$ — Γ_{10}/Γ

VALUE (units 10^{-4})	EVTS	DOCUMENT ID		TECN	COMMENT
9.3±3.3±0.5	21	[1] ASNER	08A	CLEO	$\Upsilon(2S) \to \gamma 3\pi^+2\pi^-K^-K^0_S\pi^0$

[1] ASNER 08A reports $[\Gamma(\chi_{b1}(1P) \to 3\pi^+2\pi^-K^-K^0_S\pi^0)/\Gamma_{total}] \times [B(\Upsilon(2S) \to \gamma\chi_{b1}(1P))] = (64 \pm 16 \pm 16) \times 10^{-6}$ which we divide by our best value $B(\Upsilon(2S) \to \gamma\chi_{b1}(1P)) = (6.9 \pm 0.4) \times 10^{-2}$. Our first error is their experiment's error and our second error is the systematic error from using our best value.

$\Gamma(3\pi^+3\pi^-)/\Gamma_{total}$ — Γ_{11}/Γ

VALUE (units 10^{-4})	EVTS	DOCUMENT ID		TECN	COMMENT
1.9±0.6±0.1	25	[1] ASNER	08A	CLEO	$\Upsilon(2S) \to \gamma 3\pi^+3\pi^-$

[1] ASNER 08A reports $[\Gamma(\chi_{b1}(1P) \to 3\pi^+3\pi^-)/\Gamma_{total}] \times [B(\Upsilon(2S) \to \gamma\chi_{b1}(1P))] = (13 \pm 3 \pm 3) \times 10^{-6}$ which we divide by our best value $B(\Upsilon(2S) \to \gamma\chi_{b1}(1P)) = (6.9 \pm 0.4) \times 10^{-2}$. Our first error is their experiment's error and our second error is the systematic error from using our best value.

$\Gamma(3\pi^+3\pi^-2\pi^0)/\Gamma_{total}$ — Γ_{12}/Γ

VALUE (units 10^{-4})	EVTS	DOCUMENT ID		TECN	COMMENT
17±5±1	56	[1] ASNER	08A	CLEO	$\Upsilon(2S) \to \gamma 3\pi^+3\pi^-2\pi^0$

[1] ASNER 08A reports $[\Gamma(\chi_{b1}(1P) \to 3\pi^+3\pi^-2\pi^0)/\Gamma_{total}] \times [B(\Upsilon(2S) \to \gamma\chi_{b1}(1P))] = (119 \pm 18 \pm 32) \times 10^{-6}$ which we divide by our best value $B(\Upsilon(2S) \to \gamma\chi_{b1}(1P)) = (6.9 \pm 0.4) \times 10^{-2}$. Our first error is their experiment's error and our second error is the systematic error from using our best value.

$\Gamma(3\pi^+3\pi^-K^+K^-)/\Gamma_{total}$ — Γ_{13}/Γ

VALUE (units 10^{-4})	EVTS	DOCUMENT ID		TECN	COMMENT
2.6±0.8±0.1	21	[1] ASNER	08A	CLEO	$\Upsilon(2S) \to \gamma 3\pi^+3\pi^-K^+K^-$

[1] ASNER 08A reports $[\Gamma(\chi_{b1}(1P) \to 3\pi^+3\pi^-K^+K^-)/\Gamma_{total}] \times [B(\Upsilon(2S) \to \gamma\chi_{b1}(1P))] = (18 \pm 4 \pm 4) \times 10^{-6}$ which we divide by our best value $B(\Upsilon(2S) \to \gamma\chi_{b1}(1P)) = (6.9 \pm 0.4) \times 10^{-2}$. Our first error is their experiment's error and our second error is the systematic error from using our best value.

$\Gamma(3\pi^+3\pi^-K^+K^-\pi^0)/\Gamma_{total}$ — Γ_{14}/Γ

VALUE (units 10^{-4})	EVTS	DOCUMENT ID		TECN	COMMENT
7.5±2.6±0.4	28	[1] ASNER	08A	CLEO	$\Upsilon(2S) \to \gamma 3\pi^+3\pi^-K^+K^-\pi^0$

[1] ASNER 08A reports $[\Gamma(\chi_{b1}(1P) \to 3\pi^+3\pi^-K^+K^-\pi^0)/\Gamma_{total}] \times [B(\Upsilon(2S) \to \gamma\chi_{b1}(1P))] = (52 \pm 11 \pm 14) \times 10^{-6}$ which we divide by our best value $B(\Upsilon(2S) \to \gamma\chi_{b1}(1P)) = (6.9 \pm 0.4) \times 10^{-2}$. Our first error is their experiment's error and our second error is the systematic error from using our best value.

$\Gamma(4\pi^+4\pi^-)/\Gamma_{total}$ — Γ_{15}/Γ

VALUE (units 10^{-4})	EVTS	DOCUMENT ID		TECN	COMMENT
2.6±0.9±0.1	24	[1] ASNER	08A	CLEO	$\Upsilon(2S) \to \gamma 4\pi^+4\pi^-$

[1] ASNER 08A reports $[\Gamma(\chi_{b1}(1P) \to 4\pi^+4\pi^-)/\Gamma_{total}] \times [B(\Upsilon(2S) \to \gamma\chi_{b1}(1P))] = (18 \pm 4 \pm 5) \times 10^{-6}$ which we divide by our best value $B(\Upsilon(2S) \to \gamma\chi_{b1}(1P)) = (6.9 \pm 0.4) \times 10^{-2}$. Our first error is their experiment's error and our second error is the systematic error from using our best value.

$\Gamma(4\pi^+4\pi^-2\pi^0)/\Gamma_{total}$ — Γ_{16}/Γ

VALUE (units 10^{-4})	EVTS	DOCUMENT ID		TECN	COMMENT
14±5±1	26	[1] ASNER	08A	CLEO	$\Upsilon(2S) \to \gamma 4\pi^+4\pi^-2\pi^0$

[1] ASNER 08A reports $[\Gamma(\chi_{b1}(1P) \to 4\pi^+4\pi^-2\pi^0)/\Gamma_{total}] \times [B(\Upsilon(2S) \to \gamma\chi_{b1}(1P))] = (96 \pm 24 \pm 29) \times 10^{-6}$ which we divide by our best value $B(\Upsilon(2S) \to \gamma\chi_{b1}(1P)) = (6.9 \pm 0.4) \times 10^{-2}$. Our first error is their experiment's error and our second error is the systematic error from using our best value.

$\Gamma(\omega\,\text{anything})/\Gamma_{total}$ — Γ_{17}/Γ

VALUE (units 10^{-2})	EVTS	DOCUMENT ID		TECN	COMMENT
4.9±1.3±0.6	51k	JIA	17A	BELL	$e^+e^- \to$ hadrons

$\Gamma(\omega X_{tetra})/\Gamma_{total}$ — Γ_{18}/Γ

VALUE	CL%	DOCUMENT ID		TECN	COMMENT
<44.4 × 10^{-5}	90	[1] JIA	17A	BELL	$e^+e^- \to$ hadrons

[1] For a tetraquark state X_{tetra}, with mass in the range 1.16–2.46 GeV and width in the range 0–0.3 GeV. Measured 90% CL limits as a function of X_{tetra} mass and width range from 3.3×10^{-5} to 44.4×10^{-5}.

$\Gamma(J/\psi J/\psi)/\Gamma_{total}$ — Γ_{19}/Γ

VALUE (units 10^{-5})	CL%	DOCUMENT ID		TECN	COMMENT
<2.7	90	[1] SHEN	12	BELL	$\Upsilon(2S) \to \gamma\psi X$

[1] SHEN 12 reports $< 2.7 \times 10^{-5}$ from a measurement of $[\Gamma(\chi_{b1}(1P) \to J/\psi J/\psi)/\Gamma_{total}] \times [B(\Upsilon(2S) \to \gamma\chi_{b1}(1P))]$ assuming $B(\Upsilon(2S) \to \gamma\chi_{b1}(1P)) = (6.9 \pm 0.4) \times 10^{-2}$.

$\Gamma(J/\psi\psi(2S))/\Gamma_{total}$ — Γ_{20}/Γ

VALUE (units 10^{-5})	CL%	DOCUMENT ID		TECN	COMMENT
<1.7	90	[1] SHEN	12	BELL	$\Upsilon(2S) \to \gamma\psi X$

[1] SHEN 12 reports $< 1.7 \times 10^{-5}$ from a measurement of $[\Gamma(\chi_{b1}(1P) \to J/\psi\psi(2S))/\Gamma_{total}] \times [B(\Upsilon(2S) \to \gamma\chi_{b1}(1P))]$ assuming $B(\Upsilon(2S) \to \gamma\chi_{b1}(1P)) = (6.9 \pm 0.4) \times 10^{-2}$.

$\Gamma(\psi(2S)\psi(2S))/\Gamma_{total}$ — Γ_{21}/Γ

VALUE (units 10^{-5})	CL%	DOCUMENT ID		TECN	COMMENT
<6	90	[1] SHEN	12	BELL	$\Upsilon(2S) \to \gamma\psi X$

[1] SHEN 12 reports $< 6.2 \times 10^{-5}$ from a measurement of $[\Gamma(\chi_{b1}(1P) \to \psi(2S)\psi(2S))/\Gamma_{total}] \times [B(\Upsilon(2S) \to \gamma\chi_{b1}(1P))]$ assuming $B(\Upsilon(2S) \to \gamma\chi_{b1}(1P)) = (6.9 \pm 0.4) \times 10^{-2}$.

$\Gamma(J/\psi(1S)\,\text{anything})/\Gamma_{total}$ — Γ_{22}/Γ

VALUE	CL%	DOCUMENT ID		TECN	COMMENT
<1.1 × 10^{-3}	90	JIA	17A	BELL	$e^+e^- \to$ hadrons

$\Gamma(J/\psi(1S)X_{tetra})/\Gamma_{total}$ — Γ_{23}/Γ

VALUE	CL%	DOCUMENT ID		TECN	COMMENT
<22.7 × 10^{-5}	90	[1] JIA	17A	BELL	$e^+e^- \to$ hadrons

[1] For a tetraquark state X_{tetra}, with mass in the range 1.16–2.46 GeV and width in the range 0–0.3 GeV. Measured 90% CL limits as a function of X_{tetra} mass and width range from 1.8×10^{-5} to 22.7×10^{-5}.

$\chi_{b1}(1P)$ Cross-Particle Branching Ratios

$\Gamma(\chi_{b1}(1P) \to \gamma\Upsilon(1S))/\Gamma_{total} \times \Gamma(\Upsilon(2S) \to \gamma\chi_{b1}(1P))/\Gamma_{total}$ / $\Gamma_1/\Gamma \times \Gamma^{\Upsilon(2S)}_{59}/\Gamma^{\Upsilon(2S)}$

VALUE (units 10^{-3})	EVTS	DOCUMENT ID		TECN	COMMENT
24.1±0.6±1.5	13k	LEES	11J	BABR	$\Upsilon(2S) \to X\gamma$

$B(\chi_{b1}(1P) \to \gamma\Upsilon(1S)) \times B(\Upsilon(2S) \to \gamma\chi_{b1}(1P)) \times B(\Upsilon(1S) \to \ell^+\ell^-)$

VALUE (units 10^{-4})	EVTS	DOCUMENT ID		TECN	COMMENT
5.90±0.34 OUR AVERAGE	Error includes scale factor of 1.3. See the ideogram below.				
$6.86^{+0.47}_{-0.45}{}^{+0.44}_{-0.35}$		[1] LEES	14M	BABR	$\Upsilon(2S) \to \gamma\gamma\mu^+\mu^-$

Downloaded from https://academic.oup.com/ptep/article/2022/8/083C01/6651666 by KIT Library user on 27 September 2022

$5.65 \pm 0.11 \pm 0.27$	3222	KORNICER	11	CLEO	$e^+e^- \to \gamma\gamma\ell^+\ell^-$
$5.8 \pm 0.9 \pm 0.7$	53	WALK	86	CBAL	$\Upsilon(2S) \to \gamma\gamma\ell^+\ell^-$

[1] From a sample of $\Upsilon(2S) \to \gamma\gamma\mu^+\mu^-$ with one converted photon.

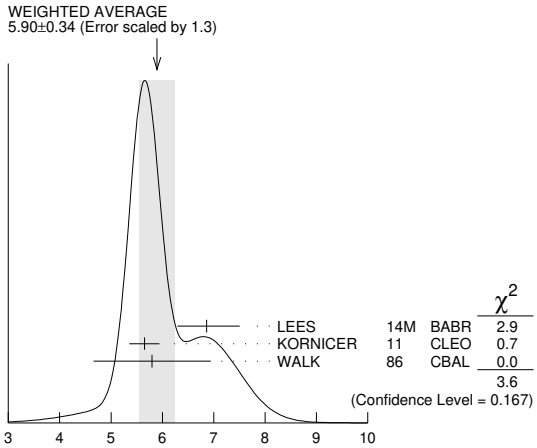

$B(\chi_{b1}(1P) \to \gamma\Upsilon(1S)) \times B(\Upsilon(2S) \to \gamma\chi_{b1}(1P)) \times B(\Upsilon(1S) \to \ell^+\ell^-)$ (units 10^{-4})

$B(\chi_{b1}(1P) \to \gamma\Upsilon(1S)) \times B(\Upsilon(3S) \to \gamma\chi_{b1}(1P)) \times B(\Upsilon(1S) \to \ell^+\ell^-)$

VALUE (units 10^{-5})	EVTS	DOCUMENT ID		TECN	COMMENT
1.30±0.34 OUR AVERAGE					
$1.16^{+0.78}_{-0.67} \pm 0.14$		[1] LEES	14M	BABR	$\Upsilon(3S) \to \gamma\gamma\mu^+\mu^-$
$1.33 \pm 0.30 \pm 0.23$	50	KORNICER	11	CLEO	$e^+e^- \to \gamma\gamma\ell^+\ell^-$

[1] From a sample of $\Upsilon(3S) \to \gamma\gamma\mu^+\mu^-$ with converted photons.

$B(\chi_{b2}(1P) \to pX + \bar{p}X)/B(\chi_{b1}(1P) \to pX + \bar{p}X)$

VALUE	DOCUMENT ID		TECN	COMMENT
1.068±0.010±0.040	BRIERE	07	CLEO	$\Upsilon(2S) \to \gamma\chi_{bJ}(1P)$

$B(\chi_{b0}(1P) \to pX + \bar{p}X)/B(\chi_{b1}(1P) \to pX + \bar{p}X)$

VALUE	DOCUMENT ID		TECN	COMMENT
1.11±0.15±0.20	BRIERE	07	CLEO	$\Upsilon(2S) \to \gamma\chi_{bJ}(1P)$

$\chi_{b1}(1P)$ REFERENCES

FULSOM	18	PRL 121 232001	B.G. Fulsom *et al.*	(BELLE Collab.)
JIA	17A	PR D96 112002	S. Jia *et al.*	(BELLE Collab.)
LEES	14M	PR D90 112010	J.P. Lees *et al.*	(BABAR Collab.)
SHEN	12	PR D85 071102	C.P. Shen *et al.*	(BELLE Collab.)
KORNICER	11	PR D83 054003	M. Kornicer *et al.*	(CLEO Collab.)
LEES	11J	PR D84 072002	J.P. Lees *et al.*	(BABAR Collab.)
ASNER	08A	PR D78 091103	D.M. Asner *et al.*	(CLEO Collab.)
BRIERE	08	PR D78 092007	R.A. Briere *et al.*	(CLEO Collab.)
BRIERE	07	PR D76 012005	R.A. Briere *et al.*	(CLEO Collab.)
ARTUSO	05	PRL 94 032001	M. Artuso *et al.*	(CLEO Collab.)
EDWARDS	99	PR D59 032003	K.W. Edwards *et al.*	(CLEO Collab.)
SKWARNICKI	87	PRL 58 972	T. Skwarnicki *et al.*	(Crystal Ball Collab.) J
WALK	86	PR D34 2611	W.S. Walk *et al.*	(Crystal Ball Collab.)
ALBRECHT	85E	PL 160B 331	H. Albrecht *et al.*	(ARGUS Collab.)
NERNST	85	PRL 54 2195	R. Nernst *et al.*	(Crystal Ball Collab.)
HAAS	84	PRL 52 799	J. Haas *et al.*	(CLEO Collab.)
KLOPFEN...	83	PRL 51 160	C. Klopfenstein *et al.*	(CUSB Collab.)
PAUSS	83	PL 130B 439	F. Pauss *et al.*	(MPIM, COLU, CORN, LSU+)

$h_b(1P)$

$I^G(J^{PC}) = 0^-(1^{+-})$

Quantum numbers are quark model predictions, $C = -$ established by $\eta_b\gamma$ decay.

$h_b(1P)$ MASS

VALUE (MeV)	EVTS	DOCUMENT ID		TECN	COMMENT
9899.3±0.8 OUR AVERAGE					
$9899.3 \pm 0.4 \pm 1.0$	112k	TAMPONI	15	BELL	$e^+e^- \to \gamma\eta +$ hadrons
$9899.1 \pm 0.4 \pm 1.0$	70k	MIZUK	12	BELL	$e^+e^- \to \pi^+\pi^-$ hadrons
$9902 \pm 4 \pm 2$	10.8k	LEES	11K	BABR	$\Upsilon(3S) \to \eta_b\gamma\pi^0$
• • • We do not use the following data for averages, fits, limits, etc. • • •					
$9898.2^{+1.1}_{-1.0} \pm 1.0$	50.0k	[1] ADACHI	12	BELL	10.86 $e^+e^- \to \pi^+\pi^-$ MM

[1] Superseded by MIZUK 12.

$h_b(1P)$ DECAY MODES

	Mode	Fraction (Γ_i/Γ)
Γ_1	$\eta_b(1S)\gamma$	(52^{+6}_{-5}) %

$h_b(1P)$ BRANCHING RATIOS

$\Gamma(\eta_b(1S)\gamma)/\Gamma_{total}$ — **Γ_1/Γ**

VALUE (units 10^{-2})	EVTS	DOCUMENT ID		TECN	COMMENT
52^{+6}_{-5} OUR AVERAGE					
$56 \pm 8 \pm 4$	33.1k	[1] TAMPONI	15	BELL	$e^+e^- \to \gamma\eta +$ hadrons
$49.2 \pm 5.7^{+5.6}_{-3.3}$	24k	MIZUK	12	BELL	$e^+e^- \to (\gamma)\pi^+\pi^-$ hadrons
• • • We do not use the following data for averages, fits, limits, etc. • • •					
seen	10.8k	LEES	11K	BABR	$\Upsilon(3S) \to \eta_b\gamma\pi^0$

[1] Using $B(\eta \to 2\gamma) = (39.41 \pm 0.20)$%.

$h_b(1P)$ REFERENCES

TAMPONI	15	PRL 115 142001	U. Tamponi *et al.*	(BELLE Collab.)
ADACHI	12	PRL 108 032001	I. Adachi *et al.*	(BELLE Collab.)
MIZUK	12	PRL 109 232002	R. Mizuk *et al.*	(BELLE Collab.)
LEES	11K	PR D84 091101	J.P. Lees *et al.*	(BABAR Collab.)

$\chi_{b2}(1P)$

$I^G(J^{PC}) = 0^+(2^{++})$
J needs confirmation.

Observed in radiative decay of the $\Upsilon(2S)$, therefore $C = +$. Branching ratio requires E1 transition, M1 is strongly disfavored, therefore $P = +$. $J = 2$ from SKWARNICKI 87.

$\chi_{b2}(1P)$ MASS

VALUE (MeV)	DOCUMENT ID
9912.21±0.26±0.31 OUR EVALUATION	From average γ energy below, using $\Upsilon(2S)$ mass = 10023.26 ± 0.31 MeV

$m_{\chi_{b2}(1P)} - m_{\chi_{b1}(1P)}$

VALUE (MeV)	DOCUMENT ID		TECN	COMMENT
19.10±0.25 OUR AVERAGE	Error includes scale factor of 1.1.			
$19.81 \pm 0.65 \pm 0.20$	[1] AAIJ	14BG	LHCB	$pp \to \gamma\mu^+\mu^- X$
19.01 ± 0.24	LEES	14M	BABR	$\Upsilon(2S) \to \gamma\gamma\mu^+\mu^-$

[1] From the $\chi_{bj}(1P) \to \Upsilon(1S)\gamma$ transition.

γ ENERGY IN $\Upsilon(2S)$ DECAY

VALUE (MeV)	DOCUMENT ID		TECN	COMMENT
110.44±0.29 OUR AVERAGE	Error includes scale factor of 1.1.			
$110.58 \pm 0.08 \pm 0.30$	ARTUSO	05	CLEO	$\Upsilon(2S) \to \gamma X$
$110.8 \pm 0.3 \pm 0.6$	EDWARDS	99	CLE2	$\Upsilon(2S) \to \gamma\chi(1P)$
$107.0 \pm 1.1 \pm 1.3$	WALK	86	CBAL	$\Upsilon(2S) \to \gamma\gamma\ell^+\ell^-$
$110.6 \pm 0.3 \pm 0.9$	ALBRECHT	85E	ARG	$\Upsilon(2S) \to$ conv. γX
$110.4 \pm 0.8 \pm 2.2$	NERNST	85	CBAL	$\Upsilon(2S) \to \gamma X$
$109.5 \pm 0.7 \pm 1.0$	HAAS	84	CLEO	$\Upsilon(2S) \to$ conv. γX
$108.2 \pm 0.3 \pm 2.0$	KLOPFEN...	83	CUSB	$\Upsilon(2S) \to \gamma X$
108.8 ± 4.0	PAUSS	83	CUSB	$\Upsilon(2S) \to \gamma\gamma\ell^+\ell^-$

$\chi_{b2}(1P)$ DECAY MODES

	Mode	Fraction (Γ_i/Γ)	Confidence level
Γ_1	$\gamma\Upsilon(1S)$	(18.0 ± 1.0) %	
Γ_2	D^0X	< 7.9 %	90%
Γ_3	$\pi^+\pi^-K^+K^-\pi^0$	$(8 \pm 5) \times 10^{-5}$	
Γ_4	$2\pi^+\pi^-K^-K^0_S$	$< 1.0 \times 10^{-4}$	90%
Γ_5	$2\pi^+\pi^-K^-K^0_S2\pi^0$	$(5.3 \pm 2.4) \times 10^{-4}$	
Γ_6	$2\pi^+2\pi^-2\pi^0$	$(3.5 \pm 1.4) \times 10^{-4}$	
Γ_7	$2\pi^+2\pi^-K^+K^-$	$(1.1 \pm 0.4) \times 10^{-4}$	
Γ_8	$2\pi^+2\pi^-K^+K^-\pi^0$	$(2.1 \pm 0.9) \times 10^{-4}$	
Γ_9	$2\pi^+2\pi^-K^+K^-2\pi^0$	$(3.9 \pm 1.8) \times 10^{-4}$	
Γ_{10}	$3\pi^+2\pi^-K^-K^0_S\pi^0$	$< 5 \times 10^{-4}$	90%
Γ_{11}	$3\pi^+3\pi^-$	$(7.0 \pm 3.1) \times 10^{-5}$	
Γ_{12}	$3\pi^+3\pi^-2\pi^0$	$(1.0 \pm 0.4) \times 10^{-3}$	
Γ_{13}	$3\pi^+3\pi^-K^+K^-$	$< 8 \times 10^{-5}$	90%
Γ_{14}	$3\pi^+3\pi^-K^+K^-\pi^0$	$(3.6 \pm 1.5) \times 10^{-4}$	
Γ_{15}	$4\pi^+4\pi^-$	$(8 \pm 4) \times 10^{-5}$	
Γ_{16}	$4\pi^+4\pi^-2\pi^0$	$(1.8 \pm 0.7) \times 10^{-3}$	
Γ_{17}	$J/\psi J/\psi$	$< 4 \times 10^{-5}$	90%
Γ_{18}	$J/\psi\psi(2S)$	$< 5 \times 10^{-5}$	90%
Γ_{19}	$\psi(2S)\psi(2S)$	$< 1.6 \times 10^{-5}$	90%
Γ_{20}	$J/\psi(1S)$anything	$(1.5 \pm 0.4) \times 10^{-3}$	

Downloaded from https://academic.oup.com/ptep/article/2022/8/083C01/6651666 by KIT Library user on 27 September 2022

$\chi_{b2}(1P)$ BRANCHING RATIOS

$\Gamma(\gamma\Upsilon(1S))/\Gamma_{total}$ — Γ_1/Γ

VALUE	EVTS	DOCUMENT ID		TECN	COMMENT
0.180±0.010 OUR AVERAGE					
$0.164^{+0.009}_{-0.010}\pm0.008$	503k	[1] FULSOM	18	BELL	$\Upsilon(2S)\to\gamma X$
$0.185\pm0.008\pm0.009$		[2,3,4] LEES	14M	BABR	$\Upsilon(2S)\to\gamma\gamma\mu^+\mu^-$
$0.186\pm0.011\pm0.009$	1770	[4,5] KORNICER	11	CLEO	$e^+e^-\to\gamma\gamma\ell^+\ell^-$
$0.194^{+0.014}_{-0.017}\pm0.009$	8k	[6] LEES	11J	BABR	$\Upsilon(2S)\to X\gamma$
$0.25\pm0.06\pm0.01$	35	[4,7,8] WALK	86	CBAL	$\Upsilon(2S)\to\gamma\gamma\ell^+\ell^-$
0.20 ± 0.05		KLOPFEN...	83	CUSB	$\Upsilon(2S)\to\gamma\gamma\ell^+\ell^-$

[1] FULSOM 18 reports $[\Gamma(\chi_{b2}(1P)\to\gamma\Upsilon(1S))/\Gamma_{total}]\times[B(\Upsilon(2S)\to\gamma\chi_{b2}(1P))] = (1.17\pm0.01^{+0.06}_{-0.07})\times10^{-2}$ which we divide by our best value $B(\Upsilon(2S)\to\gamma\chi_{b2}(1P)) = (7.15\pm0.35)\times10^{-2}$. Our first error is their experiment's error and our second error is the systematic error from using our best value.

[2] LEES 14M quotes $\Gamma(\chi_{b2}(1P)\to\gamma\Upsilon(1S))/\Gamma_{total}\times\Gamma(\Upsilon(2S)\to\gamma\chi_{b2}(1P))/\Gamma_{total} = (1.32\pm0.06)\%$ combining the results from samples of $\Upsilon(2S)\to\gamma\gamma\mu^+\mu^-$ with and without converted photons.

[3] LEES 14M reports $[\Gamma(\chi_{b2}(1P)\to\gamma\Upsilon(1S))/\Gamma_{total}]\times[B(\Upsilon(2S)\to\gamma\chi_{b2}(1P))] = (1.32\pm0.06)\times10^{-2}$ which we divide by our best value $B(\Upsilon(2S)\to\gamma\chi_{b2}(1P)) = (7.15\pm0.35)\times10^{-2}$. Our first error is their experiment's error and our second error is the systematic error from using our best value.

[4] Assuming $B(\Upsilon(1S)\to\mu^+\mu^-) = (2.48\pm0.05)\%$.

[5] KORNICER 11 reports $[\Gamma(\chi_{b2}(1P)\to\gamma\Upsilon(1S))/\Gamma_{total}]\times[B(\Upsilon(2S)\to\gamma\chi_{b2}(1P))] = (1.33\pm0.04\pm0.07)\times10^{-2}$ which we divide by our best value $B(\Upsilon(2S)\to\gamma\chi_{b2}(1P)) = (7.15\pm0.35)\times10^{-2}$. Our first error is their experiment's error and our second error is the systematic error from using our best value.

[6] LEES 11J reports $[\Gamma(\chi_{b2}(1P)\to\gamma\Upsilon(1S))/\Gamma_{total}]\times[B(\Upsilon(2S)\to\gamma\chi_{b2}(1P))] = (13.9\pm0.5^{+0.9}_{-1.1})\times10^{-3}$ which we divide by our best value $B(\Upsilon(2S)\to\gamma\chi_{b2}(1P)) = (7.15\pm0.35)\times10^{-2}$. Our first error is their experiment's error and our second error is the systematic error from using our best value.

[7] WALK 86 quotes $B(\Upsilon(2S)\to\gamma\chi_{b2}(1P))\times B(\chi_{b2}(1P)\to\gamma\Upsilon(1S))\times B(\Upsilon(1S)\to\ell^+\ell^-) = (4.4\pm0.9\pm0.5)\%$.

[8] WALK 86 reports $[\Gamma(\chi_{b2}(1P)\to\gamma\Upsilon(1S))/\Gamma_{total}]\times[B(\Upsilon(2S)\to\gamma\chi_{b2}(1P))] = (17.7\pm3.6\pm2.0)\times10^{-3}$ which we divide by our best value $B(\Upsilon(2S)\to\gamma\chi_{b2}(1P)) = (7.15\pm0.35)\times10^{-2}$. Our first error is their experiment's error and our second error is the systematic error from using our best value.

$\Gamma(D^0X)/\Gamma_{total}$ — Γ_2/Γ

VALUE	CL%	DOCUMENT ID		TECN	COMMENT
$<7.9\times10^{-2}$	90	[1,2] BRIERE	08	CLEO	$\Upsilon(2S)\to\gamma D^0X$

[1] For $p_{D^0}>2.5$ GeV/c.

[2] The authors also present their result as $(5.4\pm1.9\pm0.5)\times10^{-2}$.

$\Gamma(\pi^+\pi^-K^+K^-\pi^0)/\Gamma_{total}$ — Γ_3/Γ

VALUE (units 10^{-4})	EVTS	DOCUMENT ID		TECN	COMMENT
0.84±0.50±0.04	8	[1] ASNER	08A	CLEO	$\Upsilon(2S)\to\gamma\pi^+\pi^-K^+K^-\pi^0$

[1] ASNER 08A reports $[\Gamma(\chi_{b2}(1P)\to\pi^+\pi^-K^+K^-\pi^0)/\Gamma_{total}]\times[B(\Upsilon(2S)\to\gamma\chi_{b2}(1P))] = (6\pm3\pm2)\times10^{-6}$ which we divide by our best value $B(\Upsilon(2S)\to\gamma\chi_{b2}(1P)) = (7.15\pm0.35)\times10^{-2}$. Our first error is their experiment's error and our second error is the systematic error from using our best value.

$\Gamma(2\pi^+\pi^-K^-K^0_S)/\Gamma_{total}$ — Γ_4/Γ

VALUE (units 10^{-4})	CL%	DOCUMENT ID		TECN	COMMENT
<1.0	90	[1] ASNER	08A	CLEO	$\Upsilon(2S)\to\gamma2\pi^+\pi^-K^-K^0_S$

[1] ASNER 08A reports $[\Gamma(\chi_{b2}(1P)\to2\pi^+\pi^-K^-K^0_S)/\Gamma_{total}]\times[B(\Upsilon(2S)\to\gamma\chi_{b2}(1P))] < 7\times10^{-6}$ which we divide by our best value $B(\Upsilon(2S)\to\gamma\chi_{b2}(1P)) = 7.15\times10^{-2}$.

$\Gamma(2\pi^+\pi^-K^-K^0_S2\pi^0)/\Gamma_{total}$ — Γ_5/Γ

VALUE (units 10^{-4})	EVTS	DOCUMENT ID		TECN	COMMENT
5.3±2.4±0.3	11	[1] ASNER	08A	CLEO	$\Upsilon(2S)\to\gamma2\pi^+\pi^-K^-2\pi^0$

[1] ASNER 08A reports $[\Gamma(\chi_{b2}(1P)\to2\pi^+\pi^-K^-K^0_S2\pi^0)/\Gamma_{total}]\times[B(\Upsilon(2S)\to\gamma\chi_{b2}(1P))] = (38\pm14\pm10)\times10^{-6}$ which we divide by our best value $B(\Upsilon(2S)\to\gamma\chi_{b2}(1P)) = (7.15\pm0.35)\times10^{-2}$. Our first error is their experiment's error and our second error is the systematic error from using our best value.

$\Gamma(2\pi^+2\pi^-2\pi^0)/\Gamma_{total}$ — Γ_6/Γ

VALUE (units 10^{-4})	EVTS	DOCUMENT ID		TECN	COMMENT
3.5±1.4±0.2	19	[1] ASNER	08A	CLEO	$\Upsilon(2S)\to\gamma2\pi^+2\pi^-2\pi^0$

[1] ASNER 08A reports $[\Gamma(\chi_{b2}(1P)\to2\pi^+2\pi^-2\pi^0)/\Gamma_{total}]\times[B(\Upsilon(2S)\to\gamma\chi_{b2}(1P))] = (25\pm8\pm6)\times10^{-6}$ which we divide by our best value $B(\Upsilon(2S)\to\gamma\chi_{b2}(1P)) = (7.15\pm0.35)\times10^{-2}$. Our first error is their experiment's error and our second error is the systematic error from using our best value.

$\Gamma(2\pi^+2\pi^-K^+K^-)/\Gamma_{total}$ — Γ_7/Γ

VALUE (units 10^{-4})	EVTS	DOCUMENT ID		TECN	COMMENT
1.1±0.4±0.1	14	[1] ASNER	08A	CLEO	$\Upsilon(2S)\to\gamma2\pi^+2\pi^-K^+K^-$

[1] ASNER 08A reports $[\Gamma(\chi_{b2}(1P)\to2\pi^+2\pi^-K^+K^-)/\Gamma_{total}]\times[B(\Upsilon(2S)\to\gamma\chi_{b2}(1P))] = (8\pm2\pm2)\times10^{-6}$ which we divide by our best value $B(\Upsilon(2S)\to\gamma\chi_{b2}(1P)) = (7.15\pm0.35)\times10^{-2}$. Our first error is their experiment's error and our second error is the systematic error from using our best value.

$\Gamma(2\pi^+2\pi^-K^+K^-\pi^0)/\Gamma_{total}$ — Γ_8/Γ

VALUE (units 10^{-4})	EVTS	DOCUMENT ID		TECN	COMMENT
2.1±0.9±0.1	13	[1] ASNER	08A	CLEO	$\Upsilon(2S)\to\gamma2\pi^+2\pi^-K^+K^-\pi^0$

[1] ASNER 08A reports $[\Gamma(\chi_{b2}(1P)\to2\pi^+2\pi^-K^+K^-\pi^0)/\Gamma_{total}]\times[B(\Upsilon(2S)\to\gamma\chi_{b2}(1P))] = (15\pm5\pm4)\times10^{-6}$ which we divide by our best value $B(\Upsilon(2S)\to\gamma\chi_{b2}(1P)) = (7.15\pm0.35)\times10^{-2}$. Our first error is their experiment's error and our second error is the systematic error from using our best value.

$\Gamma(2\pi^+2\pi^-K^+K^-2\pi^0)/\Gamma_{total}$ — Γ_9/Γ

VALUE (units 10^{-4})	EVTS	DOCUMENT ID		TECN	COMMENT
3.9±1.8±0.2	11	[1] ASNER	08A	CLEO	$\Upsilon(2S)\to\gamma2\pi^+2\pi^-K^+K^-2\pi^0$

[1] ASNER 08A reports $[\Gamma(\chi_{b2}(1P)\to2\pi^+2\pi^-K^+K^-2\pi^0)/\Gamma_{total}]\times[B(\Upsilon(2S)\to\gamma\chi_{b2}(1P))] = (28\pm11\pm7)\times10^{-6}$ which we divide by our best value $B(\Upsilon(2S)\to\gamma\chi_{b2}(1P)) = (7.15\pm0.35)\times10^{-2}$. Our first error is their experiment's error and our second error is the systematic error from using our best value.

$\Gamma(3\pi^+2\pi^-K^-K^0_S\pi^0)/\Gamma_{total}$ — Γ_{10}/Γ

VALUE (units 10^{-4})	CL%	DOCUMENT ID		TECN	COMMENT
<5	90	[1] ASNER	08A	CLEO	$\Upsilon(2S)\to\gamma3\pi^+2\pi^-K^-K^0_S\pi^0$

[1] ASNER 08A reports $[\Gamma(\chi_{b2}(1P)\to3\pi^+2\pi^-K^-K^0_S\pi^0)/\Gamma_{total}]\times[B(\Upsilon(2S)\to\gamma\chi_{b2}(1P))] < 36\times10^{-6}$ which we divide by our best value $B(\Upsilon(2S)\to\gamma\chi_{b2}(1P)) = 7.15\times10^{-2}$.

$\Gamma(3\pi^+3\pi^-)/\Gamma_{total}$ — Γ_{11}/Γ

VALUE (units 10^{-4})	EVTS	DOCUMENT ID		TECN	COMMENT
0.70±0.31±0.03	9	[1] ASNER	08A	CLEO	$\Upsilon(2S)\to\gamma3\pi^+3\pi^-$

[1] ASNER 08A reports $[\Gamma(\chi_{b2}(1P)\to3\pi^+3\pi^-)/\Gamma_{total}]\times[B(\Upsilon(2S)\to\gamma\chi_{b2}(1P))] = (5\pm2\pm1)\times10^{-6}$ which we divide by our best value $B(\Upsilon(2S)\to\gamma\chi_{b2}(1P)) = (7.15\pm0.35)\times10^{-2}$. Our first error is their experiment's error and our second error is the systematic error from using our best value.

$\Gamma(3\pi^+3\pi^-2\pi^0)/\Gamma_{total}$ — Γ_{12}/Γ

VALUE (units 10^{-4})	EVTS	DOCUMENT ID		TECN	COMMENT
10.2±3.6±0.5	34	[1] ASNER	08A	CLEO	$\Upsilon(2S)\to\gamma3\pi^+3\pi^-2\pi^0$

[1] ASNER 08A reports $[\Gamma(\chi_{b2}(1P)\to3\pi^+3\pi^-2\pi^0)/\Gamma_{total}]\times[B(\Upsilon(2S)\to\gamma\chi_{b2}(1P))] = (73\pm16\pm20)\times10^{-6}$ which we divide by our best value $B(\Upsilon(2S)\to\gamma\chi_{b2}(1P)) = (7.15\pm0.35)\times10^{-2}$. Our first error is their experiment's error and our second error is the systematic error from using our best value.

$\Gamma(3\pi^+3\pi^-K^+K^-)/\Gamma_{total}$ — Γ_{13}/Γ

VALUE (units 10^{-4})	CL%	DOCUMENT ID		TECN	COMMENT
<0.8	90	[1] ASNER	08A	CLEO	$\Upsilon(2S)\to\gamma3\pi^+3\pi^-K^+K^-$

[1] ASNER 08A reports $[\Gamma(\chi_{b2}(1P)\to3\pi^+3\pi^-K^+K^-)/\Gamma_{total}]\times[B(\Upsilon(2S)\to\gamma\chi_{b2}(1P))] < 6\times10^{-6}$ which we divide by our best value $B(\Upsilon(2S)\to\gamma\chi_{b2}(1P)) = 7.15\times10^{-2}$.

$\Gamma(3\pi^+3\pi^-K^+K^-\pi^0)/\Gamma_{total}$ — Γ_{14}/Γ

VALUE (units 10^{-4})	EVTS	DOCUMENT ID		TECN	COMMENT
3.6±1.5±0.2	14	[1] ASNER	08A	CLEO	$\Upsilon(2S)\to\gamma3\pi^+3\pi^-K^+K^-\pi^0$

[1] ASNER 08A reports $[\Gamma(\chi_{b2}(1P)\to3\pi^+3\pi^-K^+K^-\pi^0)/\Gamma_{total}]\times[B(\Upsilon(2S)\to\gamma\chi_{b2}(1P))] = (26\pm8\pm7)\times10^{-6}$ which we divide by our best value $B(\Upsilon(2S)\to\gamma\chi_{b2}(1P)) = (7.15\pm0.35)\times10^{-2}$. Our first error is their experiment's error and our second error is the systematic error from using our best value.

$\Gamma(4\pi^+4\pi^-)/\Gamma_{total}$ — Γ_{15}/Γ

VALUE (units 10^{-4})	EVTS	DOCUMENT ID		TECN	COMMENT
0.84±0.40±0.04	7	[1] ASNER	08A	CLEO	$\Upsilon(2S)\to\gamma4\pi^+4\pi^-$

[1] ASNER 08A reports $[\Gamma(\chi_{b2}(1P)\to4\pi^+4\pi^-)/\Gamma_{total}]\times[B(\Upsilon(2S)\to\gamma\chi_{b2}(1P))] = (6\pm2\pm2)\times10^{-6}$ which we divide by our best value $B(\Upsilon(2S)\to\gamma\chi_{b2}(1P)) = (7.15\pm0.35)\times10^{-2}$. Our first error is their experiment's error and our second error is the systematic error from using our best value.

$\Gamma(4\pi^+4\pi^-2\pi^0)/\Gamma_{total}$ — Γ_{16}/Γ

VALUE (units 10^{-4})	EVTS	DOCUMENT ID		TECN	COMMENT
18±7±1	29	[1] ASNER	08A	CLEO	$\Upsilon(2S)\to\gamma4\pi^+4\pi^-2\pi^0$

[1] ASNER 08A reports $[\Gamma(\chi_{b2}(1P)\to4\pi^+4\pi^-2\pi^0)/\Gamma_{total}]\times[B(\Upsilon(2S)\to\gamma\chi_{b2}(1P))] = (132\pm31\pm40)\times10^{-6}$ which we divide by our best value $B(\Upsilon(2S)\to\gamma\chi_{b2}(1P)) = (7.15\pm0.35)\times10^{-2}$. Our first error is their experiment's error and our second error is the systematic error from using our best value.

Downloaded from https://academic.oup.com/ptep/article/2022/8/083C01/6651666 by KIT Library user on 27 September 2022

$\Gamma(J/\psi J/\psi)/\Gamma_{total}$ — Γ_{17}/Γ

VALUE (units 10^{-5})	CL%	DOCUMENT ID		TECN	COMMENT
<5	90	[1] SHEN	12	BELL	$\Upsilon(2S) \to \gamma\psi X$

[1] SHEN 12 reports $< 4.5\times10^{-5}$ from a measurement of $[\Gamma(\chi_{b2}(1P) \to J/\psi J/\psi)/\Gamma_{total}] \times [B(\Upsilon(2S) \to \gamma\chi_{b2}(1P))]$ assuming $B(\Upsilon(2S) \to \gamma\chi_{b2}(1P)) = (7.15\pm0.35)\times10^{-2}$.

$\Gamma(J/\psi\psi(2S))/\Gamma_{total}$ — Γ_{18}/Γ

VALUE (units 10^{-5})	CL%	DOCUMENT ID		TECN	COMMENT
<5	90	[1] SHEN	12	BELL	$\Upsilon(2S) \to \gamma\psi X$

[1] SHEN 12 reports $< 4.9\times10^{-5}$ from a measurement of $[\Gamma(\chi_{b2}(1P) \to J/\psi\psi(2S))/\Gamma_{total}] \times [B(\Upsilon(2S) \to \gamma\chi_{b2}(1P))]$ assuming $B(\Upsilon(2S) \to \gamma\chi_{b2}(1P)) = (7.15 \pm 0.35)\times10^{-2}$.

$\Gamma(\psi(2S)\psi(2S))/\Gamma_{total}$ — Γ_{19}/Γ

VALUE (units 10^{-5})	CL%	DOCUMENT ID		TECN	COMMENT
<1.6	90	[1] SHEN	12	BELL	$\Upsilon(2S) \to \gamma\psi X$

[1] SHEN 12 reports $< 1.6\times10^{-5}$ from a measurement of $[\Gamma(\chi_{b2}(1P) \to \psi(2S)\psi(2S))/\Gamma_{total}] \times [B(\Upsilon(2S) \to \gamma\chi_{b2}(1P))]$ assuming $B(\Upsilon(2S) \to \gamma\chi_{b2}(1P)) = (7.15 \pm 0.35)\times10^{-2}$.

$\Gamma(J/\psi(1S)\,\text{anything})/\Gamma_{total}$ — Γ_{20}/Γ

VALUE (units 10^{-3})	EVTS	DOCUMENT ID		TECN	COMMENT
1.50±0.34±0.22	462	JIA	17A	BELL	$e^+e^- \to$ hadrons

$\chi_{b2}(1P)$ Cross-Particle Branching Ratios

$\Gamma(\chi_{b2}(1P) \to \gamma\Upsilon(1S))/\Gamma_{total} \times \Gamma(\Upsilon(2S) \to \gamma\chi_{b2}(1P))/\Gamma_{total}$ — $\Gamma_1/\Gamma \times \Gamma_{60}^{\Upsilon(2S)}/\Gamma^{\Upsilon(2S)}$

VALUE (units 10^{-3})	EVTS	DOCUMENT ID		TECN	COMMENT
$13.9\pm0.5^{+0.9}_{-1.1}$	8k	LEES	11J	BABR	$\Upsilon(2S) \to X\gamma$

$B(\chi_{b2}(1P) \to \gamma\Upsilon(1S)) \times B(\Upsilon(2S) \to \gamma\chi_{b2}(1P)) \times B(\Upsilon(1S) \to \ell^+\ell^-)$

VALUE (units 10^{-4})	EVTS	DOCUMENT ID		TECN	COMMENT
3.38±0.16 OUR AVERAGE					
$3.63^{+0.36}_{-0.34}{}^{+0.18}_{-0.19}$		[1] LEES	14M	BABR	$\Upsilon(2S) \to \gamma\gamma\mu^+\mu^-$
3.29±0.09±0.16	1770	KORNICER	11	CLEO	$e^+e^- \to \gamma\gamma\ell^+\ell^-$
4.4 ±0.9 ±0.5	35	WALK	86	CBAL	$\Upsilon(2S) \to \gamma\gamma\ell^+\ell^-$

[1] From a sample of $\Upsilon(2S) \to \gamma\gamma\mu^+\mu^-$ with converted photons.

$[B(\chi_{b2}(1P) \to \gamma\Upsilon(1S)) \times B(\Upsilon(2S) \to \gamma\chi_{b2}(1P))]$ / $[B(\chi_{b1}(1P) \to \gamma\Upsilon(1S)) \times B(\Upsilon(2S) \to \gamma\chi_{b1}(1P))]$

VALUE (%)	DOCUMENT ID		TECN	COMMENT
55.6±1.6	[1] LEES	14M	BABR	$\Upsilon(2S) \to \gamma\gamma\mu^+\mu^-$

[1] From a sample of $\Upsilon(2S) \to \gamma\gamma\mu^+\mu^-$ events without converted photons.

$B(\chi_{b2}(1P) \to \gamma\Upsilon(1S)) \times B(\Upsilon(3S) \to \gamma\chi_{b2}(1P)) \times B(\Upsilon(1S) \to \ell^+\ell^-)$

VALUE (units 10^{-5})	EVTS	DOCUMENT ID		TECN	COMMENT
3.8 ±0.5 OUR AVERAGE					
$4.68^{+0.99}_{-0.92}\pm0.37$		[1] LEES	14M	BABR	$\Upsilon(3S) \to \gamma\gamma\mu^+\mu^-$
3.56±0.40±0.41	126	KORNICER	11	CLEO	$e^+e^- \to \gamma\gamma\ell^+\ell^-$

[1] From a sample of $\Upsilon(3S) \to \gamma\gamma\mu^+\mu^-$ with converted photons.

$\chi_{b2}(1P)$ REFERENCES

FULSOM	18	PRL 121 232001	B.G. Fulsom *et al.*	(BELLE Collab.)
JIA	17A	PR D96 112002	S. Jia *et al.*	(BELLE Collab.)
AAIJ	14BG	JHEP 1410 088	R. Aaij *et al.*	(LHCb Collab.)
LEES	14M	PR D90 112010	J.P. Lees *et al.*	(BABAR Collab.)
SHEN	12	PR D85 071102	C.P. Shen *et al.*	(BELLE Collab.)
KORNICER	11	PR D83 054003	M. Kornicer *et al.*	(CLEO Collab.)
LEES	11J	PR D84 072002	J.P. Lees *et al.*	(BABAR Collab.)
ASNER	08A	PR D78 091103	D.M. Asner *et al.*	(CLEO Collab.)
BRIERE	08	PR D78 092007	R.A. Briere *et al.*	(CLEO Collab.)
ARTUSO	05	PRL 94 032001	M. Artuso *et al.*	(CLEO Collab.)
EDWARDS	99	PR D59 032003	K.W. Edwards *et al.*	(CLEO Collab.)
SKWARNICKI	87	PRL 58 972	T. Skwarnicki *et al.*	(Crystal Ball Collab.) J
WALK	86	PR D34 2611	W.S. Walk *et al.*	(Crystal Ball Collab.)
ALBRECHT	85E	PL 160B 331	H. Albrecht *et al.*	(ARGUS Collab.)
NERNST	85	PRL 54 2195	R. Nernst *et al.*	(Crystal Ball Collab.)
HAAS	84	PRL 52 799	J. Haas *et al.*	(CLEO Collab.)
KLOPFEN...	83	PRL 51 160	C. Klopfenstein *et al.*	(CUSB Collab.)
PAUSS	83	PL 130B 439	F. Pauss *et al.*	(MPIM, COLU, CORN, LSU+)

$\eta_b(2S)$

$I^G(J^{PC}) = 0^+(0^{-+})$

OMITTED FROM SUMMARY TABLE

Quantum numbers shown are quark-model predictions.

$\eta_b(2S)$ MASS

VALUE (MeV)	EVTS	DOCUMENT ID		TECN	COMMENT
$9999.0\pm3.5^{+2.8}_{-1.9}$	26k	[1] MIZUK	12	BELL	$e^+e^- \to \gamma\pi^+\pi^-$ + hadrons
• • • We do not use the following data for averages, fits, limits, etc. • • •					
9974.6±2.3±2.1	11 ± 4	[2,3,4] DOBBS	12		$\Upsilon(2S) \to \gamma$ hadrons

[1] Assuming $\Gamma_{\eta_b(2S)} = 4.9$ MeV. Not independent of the corresponding mass difference measurement.
[2] SANDILYA 13 (Belle Collab.) search for such a state reconstructed in the same 26 exclusive hadronic final states as DOBBS 12 using a sample of $(157.8\pm3.6)\times10^6$ $\Upsilon(2S)$ decays or about 17 times larger and find no evidence for a signal. Their 90% C.L. upper limit on the branching fraction $B(\Upsilon(2S) \to \eta_b(2S)\gamma) \times \sum_i B(\eta_b(2S) \to X_i) < 4.9\times10^{-6}$, summed over the exclusive hadronic final states X_i, is an order of magnitude smaller than that reported by DOBBS 12.
[3] Obtained by analyzing CLEO III data but not authored by the CLEO Collaboration.
[4] Assuming $\Gamma_{\eta_b(2S)} = 5$ MeV. Not independent of the corresponding mass difference measurement.

$m_{\Upsilon(2S)} - m_{\eta_b(2S)}$

VALUE (MeV)	EVTS	DOCUMENT ID		TECN	COMMENT
$24.3\pm3.5^{+2.8}_{-1.9}$	26k	[5] MIZUK	12	BELL	$e^+e^- \to \gamma\pi^+\pi^-$ + hadrons
• • • We do not use the following data for averages, fits, limits, etc. • • •					
48.7±2.3±2.1	11 ± 4	[6,7,8] DOBBS	12		$\Upsilon(2S) \to \gamma$ hadrons

[5] Assuming $\Gamma_{\eta_b(2S)} = 4.9$ MeV. Not independent of the corresponding mass measurement.
[6] SANDILYA 13 (Belle Collab.) search for such a state reconstructed in the same 26 exclusive hadronic final states as DOBBS 12 using a sample of $(157.8\pm3.6)\times10^6$ $\Upsilon(2S)$ decays or about 17 times larger and find no evidence for a signal. Their 90% C.L. upper limit on the branching fraction $B(\Upsilon(2S) \to \eta_b(2S)\gamma) \times \sum_i B(\eta_b(2S) \to X_i) < 4.9\times10^{-6}$, summed over the exclusive hadronic final states X_i, is an order of magnitude smaller than that reported by DOBBS 12.
[7] Obtained by analyzing CLEO III data but not authored by the CLEO Collaboration.
[8] Assuming $\Gamma_{\eta_b(2S)} = 5$ MeV. Not independent of the corresponding mass measurement.

$\eta_b(2S)$ WIDTH

VALUE (MeV)	CL%	DOCUMENT ID		TECN	COMMENT
<24	90	MIZUK	12	BELL	$e^+e^- \to \gamma\pi^+\pi^-$ hadrons

$\eta_b(2S)$ DECAY MODES

	Mode	Fraction (Γ_i/Γ)
Γ_1	hadrons	seen

$\eta_b(2S)$ BRANCHING RATIOS

$\Gamma(\text{hadrons})/\Gamma_{total}$ — Γ_1/Γ

VALUE	EVTS	DOCUMENT ID		TECN	COMMENT
seen	26k	MIZUK	12	BELL	$e^+e^- \to \gamma\pi^+\pi^-$ hadrons
• • • We do not use the following data for averages, fits, limits, etc. • • •					
seen		[9,10] DOBBS	12		$\Upsilon(2S) \to \gamma$ hadrons

[9] SANDILYA 13 (Belle Collab.) search for such a state reconstructed in the same 26 exclusive hadronic final states as DOBBS 12 using a sample of $(157.8\pm3.6)\times10^6$ $\Upsilon(2S)$ decays or about 17 times larger and find no evidence for a signal. Their 90% C.L. upper limit on the branching fraction $B(\Upsilon(2S) \to \eta_b(2S)\gamma) \times \sum_i B(\eta_b(2S) \to X_i) < 4.9\times10^{-6}$, summed over the exclusive hadronic final states X_i, is an order of magnitude smaller than that reported by DOBBS 12.
[10] Obtained by analyzing CLEO III data but not authored by the CLEO Collaboration.

$\eta_b(2S)$ REFERENCES

SANDILYA	13	PRL 111 112001	S. Sandilya *et al.*	(BELLE Collab.)
DOBBS	12	PRL 109 082001	S. Dobbs *et al.*	
MIZUK	12	PRL 109 232002	R. Mizuk *et al.*	(BELLE Collab.)

$\Upsilon(2S)$

$I^G(J^{PC}) = 0^-(1^{--})$

$\Upsilon(2S)$ MASS

VALUE (MeV)	DOCUMENT ID		TECN	COMMENT
10023.26±0.31 OUR AVERAGE				
10023.5 ±0.5	[1] ARTAMONOV	00	MD1	$e^+e^- \to$ hadrons
10023.1 ±0.4	BARBER	84	REDE	$e^+e^- \to$ hadrons
• • • We do not use the following data for averages, fits, limits, etc. • • •				
10023.6 ±0.5	[2,3] BARU	86B	REDE	$e^+e^- \to$ hadrons

[1] Reanalysis of BARU 86B using new electron mass (COHEN 87).
[2] Reanalysis of ARTAMONOV 84.
[3] Superseded by ARTAMONOV 00.

$m_{\Upsilon(3S)} - m_{\Upsilon(2S)}$

VALUE (MeV)	DOCUMENT ID		TECN	COMMENT
331.50±0.02±0.13	LEES	11C	BABR	$e^+e^- \to \pi^+\pi^- X$

$\Upsilon(2S)$ WIDTH

VALUE (keV)	DOCUMENT ID
31.98±2.63 OUR EVALUATION	See the Note on "Width Determinations of the Υ States"

Downloaded from https://academic.oup.com/ptep/article/2022/8/083C01/6651666 by KIT Library user on 27 September 2022

$\Upsilon(2S)$ DECAY MODES

	Mode	Fraction (Γ_i/Γ)	Scale factor/ Confidence level
Γ_1	$\Upsilon(1S)\pi^+\pi^-$	(17.85 ± 0.26) %	
Γ_2	$\Upsilon(1S)\pi^0\pi^0$	(8.6 ± 0.4) %	
Γ_3	$\tau^+\tau^-$	(2.00 ± 0.21) %	
Γ_4	$\mu^+\mu^-$	(1.93 ± 0.17) %	S=2.2
Γ_5	e^+e^-	(1.91 ± 0.16) %	
Γ_6	$\Upsilon(1S)\pi^0$	$< 4 \times 10^{-5}$	CL=90%
Γ_7	$\Upsilon(1S)\eta$	$(2.9 \pm 0.4) \times 10^{-4}$	S=2.0
Γ_8	$J/\psi(1S)$ anything	$< 6 \times 10^{-3}$	CL=90%
Γ_9	$J/\psi(1S)\eta_c$	$< 5.4 \times 10^{-6}$	CL=90%
Γ_{10}	$J/\psi(1S)\chi_{c0}$	$< 3.4 \times 10^{-6}$	CL=90%
Γ_{11}	$J/\psi(1S)\chi_{c1}$	$< 1.2 \times 10^{-6}$	CL=90%
Γ_{12}	$J/\psi(1S)\chi_{c2}$	$< 2.0 \times 10^{-6}$	CL=90%
Γ_{13}	$J/\psi(1S)\eta_c(2S)$	$< 2.5 \times 10^{-6}$	CL=90%
Γ_{14}	$J/\psi(1S)X(3940)$	$< 2.0 \times 10^{-6}$	CL=90%
Γ_{15}	$J/\psi(1S)X(4160)$	$< 2.0 \times 10^{-6}$	CL=90%
Γ_{16}	χ_{c1} anything	$(2.2 \pm 0.5) \times 10^{-4}$	
Γ_{17}	$\chi_{c1}(1P)^0 X_{tetra}$	$< 3.67 \times 10^{-5}$	CL=90%
Γ_{18}	χ_{c2} anything	$(2.3 \pm 0.8) \times 10^{-4}$	
Γ_{19}	$\psi(2S)\eta_c$	$< 5.1 \times 10^{-6}$	CL=90%
Γ_{20}	$\psi(2S)\chi_{c0}$	$< 4.7 \times 10^{-6}$	CL=90%
Γ_{21}	$\psi(2S)\chi_{c1}$	$< 2.5 \times 10^{-6}$	CL=90%
Γ_{22}	$\psi(2S)\chi_{c2}$	$< 1.9 \times 10^{-6}$	CL=90%
Γ_{23}	$\psi(2S)\eta_c(2S)$	$< 3.3 \times 10^{-6}$	CL=90%
Γ_{24}	$\psi(2S)X(3940)$	$< 3.9 \times 10^{-6}$	CL=90%
Γ_{25}	$\psi(2S)X(4160)$	$< 3.9 \times 10^{-6}$	CL=90%
Γ_{26}	$Z_c(3900)^+ Z_c(3900)^-$	$< 1.0 \times 10^{-6}$	CL=90%
Γ_{27}	$Z_c(4200)^+ Z_c(4200)^-$	$< 1.67 \times 10^{-5}$	CL=90%
Γ_{28}	$Z_c(3900)^\pm Z_c(4200)^\mp$	$< 7.3 \times 10^{-6}$	CL=90%
Γ_{29}	$X(4050)^+ X(4050)^-$	$< 1.35 \times 10^{-5}$	CL=90%
Γ_{30}	$X(4250)^+ X(4250)^-$	$< 2.67 \times 10^{-5}$	CL=90%
Γ_{31}	$X(4050)^\pm X(4250)^\mp$	$< 2.72 \times 10^{-5}$	CL=90%
Γ_{32}	$Z_c(4430)^+ Z_c(4430)^-$	$< 2.03 \times 10^{-5}$	CL=90%
Γ_{33}	$X(4055)^\pm X(4055)^\mp$	$< 1.11 \times 10^{-5}$	CL=90%
Γ_{34}	$X(4055)^\pm Z_c(4430)^\mp$	$< 2.11 \times 10^{-5}$	CL=90%
Γ_{35}	$\overline{{}^2H}$ anything	$(2.78^{+0.30}_{-0.26}) \times 10^{-5}$	S=1.2
Γ_{36}	hadrons	(94 ± 11) %	
Γ_{37}	ggg	(58.8 ± 1.2) %	
Γ_{38}	γgg	(1.87 ± 0.28) %	
Γ_{39}	$\phi K^+ K^-$	$(1.6 \pm 0.4) \times 10^{-6}$	
Γ_{40}	$\omega\pi^+\pi^-$	$< 2.58 \times 10^{-6}$	CL=90%
Γ_{41}	$K^*(892)^0 K^-\pi^+ +$ c.c.	$(2.3 \pm 0.7) \times 10^{-6}$	
Γ_{42}	$\phi f_2'(1525)$	$< 1.33 \times 10^{-6}$	CL=90%
Γ_{43}	$\omega f_2(1270)$	$< 5.7 \times 10^{-7}$	CL=90%
Γ_{44}	$\rho(770) a_2(1320)$	$< 8.8 \times 10^{-7}$	CL=90%
Γ_{45}	$K^*(892)^0 \overline{K}_2^*(1430)^0 +$ c.c.	$(1.5 \pm 0.6) \times 10^{-6}$	
Γ_{46}	$K_1(1270)^\pm K^\mp$	$< 3.22 \times 10^{-6}$	CL=90%
Γ_{47}	$K_1(1400)^\pm K^\mp$	$< 8.3 \times 10^{-7}$	CL=90%
Γ_{48}	$b_1(1235)^\pm \pi^\mp$	$< 4.0 \times 10^{-7}$	CL=90%
Γ_{49}	$\rho\pi$	$< 1.16 \times 10^{-6}$	CL=90%
Γ_{50}	$\pi^+\pi^-\pi^0$	$< 8.0 \times 10^{-7}$	CL=90%
Γ_{51}	$\omega\pi^0$	$< 1.63 \times 10^{-6}$	CL=90%
Γ_{52}	$\pi^+\pi^-\pi^0\pi^0$	$(1.30 \pm 0.28) \times 10^{-5}$	
Γ_{53}	$K_S^0 K^+\pi^-+$ c.c.	$(1.14 \pm 0.33) \times 10^{-6}$	
Γ_{54}	$K^*(892)^0 \overline{K}^0 +$ c.c.	$< 4.22 \times 10^{-6}$	CL=90%
Γ_{55}	$K^*(892)^- K^+ +$ c.c.	$< 1.45 \times 10^{-6}$	CL=90%
Γ_{56}	$f_1(1285)$ anything	$(2.2 \pm 1.6) \times 10^{-3}$	
Γ_{57}	$f_1(1285) X_{tetra}$	$< 6.47 \times 10^{-5}$	CL=90%
Γ_{58}	Sum of 100 exclusive modes	$(2.90 \pm 0.30) \times 10^{-3}$	
	Radiative decays		
Γ_{59}	$\gamma\chi_{b1}(1P)$	(6.9 ± 0.4) %	
Γ_{60}	$\gamma\chi_{b2}(1P)$	(7.15 ± 0.35) %	
Γ_{61}	$\gamma\chi_{b0}(1P)$	(3.8 ± 0.4) %	
Γ_{62}	$\gamma f_0(1710)$	$< 5.9 \times 10^{-4}$	CL=90%
Γ_{63}	$\gamma f_2'(1525)$	$< 5.3 \times 10^{-4}$	CL=90%
Γ_{64}	$\gamma f_2(1270)$	$< 2.41 \times 10^{-4}$	CL=90%
Γ_{65}	$\gamma f_J(2220)$		
Γ_{66}	$\gamma\eta_c(1S)$	$< 2.7 \times 10^{-5}$	CL=90%
Γ_{67}	$\gamma\chi_{c0}$	$< 1.0 \times 10^{-4}$	CL=90%
Γ_{68}	$\gamma\chi_{c1}$	$< 3.6 \times 10^{-6}$	CL=90%
Γ_{69}	$\gamma\chi_{c2}$	$< 1.5 \times 10^{-5}$	CL=90%
Γ_{70}	$\gamma\chi_{c1}(3872)$	$< 2.1 \times 10^{-5}$	CL=90%
Γ_{71}	$\gamma\chi_{c1}(3872)$, $\chi_{c1} \to \pi^+\pi^-\pi^0 J/\psi$	$< 2.4 \times 10^{-6}$	CL=90%
Γ_{72}	$\gamma\chi_{c0}(3915) \to \omega J/\psi$	$< 2.8 \times 10^{-6}$	CL=90%
Γ_{73}	$\gamma\chi_{c1}(4140) \to \phi J/\psi$	$< 1.2 \times 10^{-6}$	CL=90%
Γ_{74}	$\gamma X(4350) \to \phi J/\psi$	$< 1.3 \times 10^{-6}$	CL=90%
Γ_{75}	$\gamma\eta_b(1S)$	$(5.5 \pm^{1.1}_{0.9}) \times 10^{-4}$	S=1.2
Γ_{76}	$\gamma\eta_b(1S) \to \gamma$ Sum of 26 exclusive modes	$< 3.7 \times 10^{-6}$	CL=90%
Γ_{77}	$\gamma X_{b\overline{b}} \to \gamma$ Sum of 26 exclusive modes	$< 4.9 \times 10^{-6}$	CL=90%
Γ_{78}	$\gamma X \to \gamma + \geq 4$ prongs	[a] $< 1.95 \times 10^{-4}$	CL=95%
Γ_{79}	$\gamma A^0 \to \gamma$ hadrons	$< 8 \times 10^{-5}$	CL=90%
Γ_{80}	$\gamma a_1^0 \to \gamma\mu^+\mu^-$	$< 8.3 \times 10^{-6}$	CL=90%
	Lepton Family number (*LF*) violating modes		
Γ_{81}	$e^\pm\tau^\mp$ *LF*	$< 3.2 \times 10^{-6}$	CL=90%
Γ_{82}	$\mu^\pm\tau^\mp$ *LF*	$< 3.3 \times 10^{-6}$	CL=90%

[a] 1.5 GeV $< m_X <$ 5.0 GeV

CONSTRAINED FIT INFORMATION

An overall fit to 3 branching ratios uses 13 measurements and one constraint to determine 3 parameters. The overall fit has a $\chi^2 =$ 11.8 for 11 degrees of freedom.

The following *off-diagonal* array elements are the correlation coefficients $\langle \delta x_i \delta x_j \rangle / (\delta x_i \cdot \delta x_j)$, in percent, from the fit to the branching fractions, $x_i \equiv \Gamma_i/\Gamma_{total}$. The fit constrains the x_i whose labels appear in this array to sum to one.

x_7 2

x_1

$\Upsilon(2S)$ $\Gamma(i)\Gamma(e^+e^-)/\Gamma(total)$

$\Gamma(\mu^+\mu^-) \times \Gamma(e^+e^-)/\Gamma_{total}$ — $\Gamma_4\Gamma_5/\Gamma$

VALUE (eV)	DOCUMENT ID		TECN	COMMENT
6.5±1.5±1.0	KOBEL	92	CBAL	$e^+e^- \to \mu^+\mu^-$

$\Gamma(\Upsilon(1S)\pi^+\pi^-) \times \Gamma(e^+e^-)/\Gamma_{total}$ — $\Gamma_1\Gamma_5/\Gamma$

VALUE (eV)	EVTS	DOCUMENT ID		TECN	COMMENT
105.4±1.0±4.2	11.8k	[1] AUBERT	08BP	BABR	10.58 $e^+e^- \to \gamma\pi^+\pi^-\ell^+\ell^-$

[1] Using B($\Upsilon(1S) \to e^+e^-$) = (2.38 ± 0.11)% and B($\Upsilon(1S) \to \mu^+\mu^-$) = (2.48 ± 0.05)%.

$\Gamma(\text{hadrons}) \times \Gamma(e^+e^-)/\Gamma_{total}$ — $\Gamma_{36}\Gamma_5/\Gamma$

VALUE (keV)	DOCUMENT ID		TECN	COMMENT
0.577±0.009 OUR AVERAGE				
0.581±0.004±0.009	[1] ROSNER	06	CLEO	10.0 $e^+e^- \to$ hadrons
0.552±0.031±0.017	[1] BARU	96	MD1	$e^+e^- \to$ hadrons
0.54 ±0.04 ±0.02	[1] JAKUBOWSKI	88	CBAL	$e^+e^- \to$ hadrons
0.58 ±0.03 ±0.04	[2] GILES	84B	CLEO	$e^+e^- \to$ hadrons
0.60 ±0.12 ±0.07	[2] ALBRECHT	82	DASP	$e^+e^- \to$ hadrons
0.54 ±0.07 $^{+0.09}_{-0.05}$	[2] NICZYPORUK	81C	LENA	$e^+e^- \to$ hadrons
0.41 ±0.18	[2] BOCK	80	CNTR	$e^+e^- \to$ hadrons

[1] Radiative corrections evaluated following KURAEV 85.
[2] Radiative corrections reevaluated by BUCHMUELLER 88 following KURAEV 85.

$\Upsilon(2S)$ PARTIAL WIDTHS

$\Gamma(e^+e^-)$ — Γ_5

VALUE (keV)	DOCUMENT ID
0.612±0.011 OUR EVALUATION	

$\Upsilon(2S)$ BRANCHING RATIOS

$\Gamma(\Upsilon(1S)\pi^+\pi^-)/\Gamma_{total}$ — Γ_1/Γ

Abbreviation MM in the *COMMENT* field below stands for missing mass.

VALUE (units 10^{-2})	EVTS	DOCUMENT ID		TECN	COMMENT
17.85±0.26 OUR FIT					
17.92±0.26 OUR AVERAGE					
16.8 ±1.1 ±1.3	906k	[1] LEES	11C	BABR	$e^+e^- \to \pi^+\pi^- X$
17.80±0.05±0.37	170k	[2] LEES	11L	BABR	$\Upsilon(2S) \to \pi^+\pi^-\mu^+\mu^-$
18.02±0.02±0.61	851k	[3] BHARI	09	CLEO	$e^+e^- \to \pi^+\pi^-$ MM
17.22±0.17±0.75	11.8k	[4] AUBERT	08BP	BABR	$e^+e^- \to \gamma\pi^+\pi^-\ell^+\ell^-$
19.2 ±0.2 ±1.0	52.6k	[5] ALEXANDER	98	CLE2	$\pi^+\pi^-\ell^+\ell^-$, $\pi^+\pi^-$ MM

Downloaded from https://academic.oup.com/ptep/article/2022/8/083C01/6651666 by KIT Library user on 27 September 2022

18.1 ±0.5 ±1.0	11.6k	ALBRECHT	87	ARG	$e^+e^- \to \pi^+\pi^-$ MM
16.9 ±4.0		GELPHMAN	85	CBAL	$e^+e^- \to e^+e^-\pi^+\pi^-$
19.1 ±1.2 ±0.6		BESSON	84	CLEO	$\pi^+\pi^-$ MM
18.9 ±2.6		FONSECA	84	CUSB	$e^+e^- \to \ell^+\ell^-\pi^+\pi^-$
21 ±7	7	NICZYPORUK	81B	LENA	$e^+e^- \to \ell^+\ell^-\pi^+\pi^-$

[1] LEES 11C reports $[\Gamma(\Upsilon(2S) \to \Upsilon(1S)\pi^+\pi^-)/\Gamma_{total}] \times [B(\Upsilon(3S) \to \Upsilon(2S)\text{anything})] = (1.78 \pm 0.02 \pm 0.11) \times 10^{-2}$ which we divide by our best value $B(\Upsilon(3S) \to \Upsilon(2S)\text{anything}) = (10.6 \pm 0.8) \times 10^{-2}$. Our first error is their experiment's error and our second error is the systematic error from using our best value.
[2] Using $B(\Upsilon(1S) \to \mu^+\mu^-) = (2.48 \pm 0.05)\%$.
[3] A weighted average of the inclusive and exclusive results.
[4] Using $B(\Upsilon(2S) \to e^+e^-) = (1.91 \pm 0.16)\%$, $B(\Upsilon(2S) \to \mu^+\mu^-) = (1.93 \pm 0.17)\%$ and, $\Gamma_{ee}(\Upsilon(2S)) = 0.612 \pm 0.011$ keV.
[5] Using $B(\Upsilon(1S) \to e^+e^-) = (2.52 \pm 0.17)\%$ and $B(\Upsilon(1S) \to \mu^+\mu^-) = (2.48 \pm 0.07)\%$.

$\Gamma(\Upsilon(1S)\pi^0\pi^0)/\Gamma_{total}$ — Γ_2/Γ

VALUE (units 10^{-2})	EVTS	DOCUMENT ID		TECN	COMMENT
8.6 ±0.4 OUR AVERAGE					
8.43±0.16±0.42	38k	[1] BHARI	09	CLEO	$e^+e^- \to \pi^0\pi^0\ell^+\ell^-$
9.2 ±0.6 ±0.8	275	[2] ALEXANDER	98	CLE2	$e^+e^- \to \pi^0\pi^0\ell^+\ell^-$
9.5 ±1.9 ±1.9	25	ALBRECHT	87	ARG	$e^+e^- \to \pi^0\pi^0\ell^+\ell^-$
8.0 ±1.5		GELPHMAN	85	CBAL	$e^+e^- \to \pi^0\pi^0\ell^+\ell^-$
10.3 ±2.3		FONSECA	84	CUSB	$e^+e^- \to \pi^0\pi^0\ell^+\ell^-$

[1] Authors assume $B(\Upsilon(1S) \to e^+e^-) + B(\Upsilon(1S) \to \mu^+\mu^-) = 4.96\%$.
[2] Using $B(\Upsilon(1S) \to e^+e^-) = (2.52 \pm 0.17)\%$ and $B(\Upsilon(1S) \to \mu^+\mu^-) = (2.48 \pm 0.07)\%$.

$\Gamma(\Upsilon(1S)\pi^0\pi^0)/\Gamma(\Upsilon(1S)\pi^+\pi^-)$ — Γ_2/Γ_1

VALUE	DOCUMENT ID		TECN	COMMENT
• • • We do not use the following data for averages, fits, limits, etc. • • •				
0.462±0.037	[1] BHARI	09	CLEO	$e^+e^- \to \Upsilon(2S)$

[1] Not independent of other values reported by BHARI 09.

$\Gamma(\tau^+\tau^-)/\Gamma_{total}$ — Γ_3/Γ

VALUE (units 10^{-2})	EVTS	DOCUMENT ID		TECN	COMMENT
2.00±0.21 OUR AVERAGE					
2.00±0.12±0.18	22k	[1] BESSON	07	CLEO	$e^+e^- \to \Upsilon(2S) \to \tau^+\tau^-$
1.7 ±1.5 ±0.6		HAAS	84B	CLEO	$e^+e^- \to \tau^+\tau^-$

[1] BESSON 07 reports $[\Gamma(\Upsilon(2S) \to \tau^+\tau^-)/\Gamma_{total}] / [B(\Upsilon(2S) \to \mu^+\mu^-)] = 1.04 \pm 0.04 \pm 0.05$ which we multiply by our best value $B(\Upsilon(2S) \to \mu^+\mu^-) = (1.93 \pm 0.17) \times 10^{-2}$. Our first error is their experiment's error and our second error is the systematic error from using our best value.

$\Gamma(\mu^+\mu^-)/\Gamma_{total}$ — Γ_4/Γ

VALUE	CL%	EVTS	DOCUMENT ID		TECN	COMMENT
0.0193±0.0017 OUR AVERAGE Error includes scale factor of 2.2. See the ideogram below.						
0.0203±0.0003±0.0008		120k	ADAMS	05	CLEO	$e^+e^- \to \mu^+\mu^-$
0.0122±0.0028±0.0019			[1] KOBEL	92	CBAL	$e^+e^- \to \mu^+\mu^-$
0.0138±0.0025±0.0015			KAARSBERG	89	CSB2	$e^+e^- \to \mu^+\mu^-$
0.009 ±0.006 ±0.006			[2] ALBRECHT	85	ARG	$e^+e^- \to \mu^+\mu^-$
0.018 ±0.008 ±0.005			HAAS	84B	CLEO	$e^+e^- \to \mu^+\mu^-$
• • • We do not use the following data for averages, fits, limits, etc. • • •						
<0.038	90		NICZYPORUK	81C	LENA	$e^+e^- \to \mu^+\mu^-$

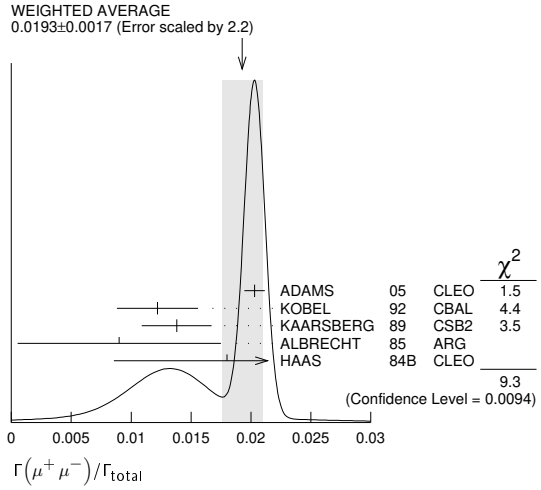

[1] Taking into account interference between the resonance and continuum.
[2] Re-evaluated using $B(\Upsilon(1S) \to \mu^+\mu^-) = 0.026$.

$\Gamma(\tau^+\tau^-)/\Gamma(\mu^+\mu^-)$ — Γ_3/Γ_4

VALUE	EVTS	DOCUMENT ID		TECN	COMMENT
1.04±0.04±0.05	22k	BESSON	07	CLEO	$e^+e^- \to \Upsilon(2S)$

$\Gamma(\Upsilon(1S)\pi^0)/\Gamma_{total}$ — Γ_6/Γ

VALUE (units 10^{-5})	CL%	DOCUMENT ID		TECN	COMMENT
• • • We do not use the following data for averages, fits, limits, etc. • • •					
< 4	90	[1] TAMPONI	13	BELL	$e^+e^- \to \Upsilon(1S)\pi^0$
< 18	90	[2] HE	08A	CLEO	$e^+e^- \to \ell^+\ell^-\gamma\gamma$
<110	90	ALEXANDER	98	CLE2	$e^+e^- \to \ell^+\ell^-\gamma\gamma$
<800	90	LURZ	87	CBAL	$e^+e^- \to \ell^+\ell^-\gamma\gamma$

[1] TAMPONI 13 reports $[\Gamma(\Upsilon(2S) \to \Upsilon(1S)\pi^0)/\Gamma_{total}] / [B(\Upsilon(2S) \to \Upsilon(1S)\pi^+\pi^-)] < 2.3 \times 10^{-4}$ which we multiply by our best value $B(\Upsilon(2S) \to \Upsilon(1S)\pi^+\pi^-) = 17.85 \times 10^{-2}$.
[2] Authors assume $B(\Upsilon(1S) \to e^+e^-) + B(\Upsilon(1S) \to \mu^+\mu^-) = 4.96\%$.

$\Gamma(\Upsilon(1S)\pi^0)/\Gamma(\Upsilon(1S)\pi^+\pi^-)$ — Γ_6/Γ_1

VALUE (units 10^{-4})	CL%	DOCUMENT ID		TECN	COMMENT
<2.3	90	TAMPONI	13	BELL	$e^+e^- \to \Upsilon(1S)\pi^0$

$\Gamma(\Upsilon(1S)\eta)/\Gamma_{total}$ — Γ_7/Γ

VALUE (units 10^{-4})	CL%	EVTS	DOCUMENT ID		TECN	COMMENT
2.9 ±0.4 OUR FIT Error includes scale factor of 2.0.						
2.9 ±0.4 OUR AVERAGE Error includes scale factor of 1.9. See the ideogram below.						
2.39±0.31±0.14		112	[1] LEES	11L	BABR	$\Upsilon(2S) \to \ell^+\ell^-\eta$
$2.1^{+0.7}_{-0.6}$ ±0.3		14	[2] HE	08A	CLEO	$e^+e^- \to \ell^+\ell^-\eta$
• • • We use the following data for averages but not for fits. • • •						
3.55±0.32±0.05		241	[3] TAMPONI	13	BELL	$e^+e^- \to \Upsilon(1S)\eta$
• • • We do not use the following data for averages, fits, limits, etc. • • •						
< 9	90		[1,4] AUBERT	08BP	BABR	$e^+e^- \to \gamma\pi^+\pi^-\pi^0\ell^+\ell^-$
< 28	90		ALEXANDER	98	CLE2	$e^+e^- \to \ell^+\ell^-\eta$
< 50	90		ALBRECHT	87	ARG	$e^+e^- \to \pi^+\pi^-\ell^+\ell^-$ MM
< 70	90		LURZ	87	CBAL	$e^+e^- \to \ell^+\ell^-(\gamma\gamma, 3\pi^0)$
< 100	90		BESSON	84	CLEO	$e^+e^- \to \pi^+\pi^-\ell^+\ell^-$ MM
< 20	90		FONSECA	84	CUSB	$e^+e^- \to \ell^+\ell^-(\gamma\gamma, \pi^+\pi^-\pi^0)$

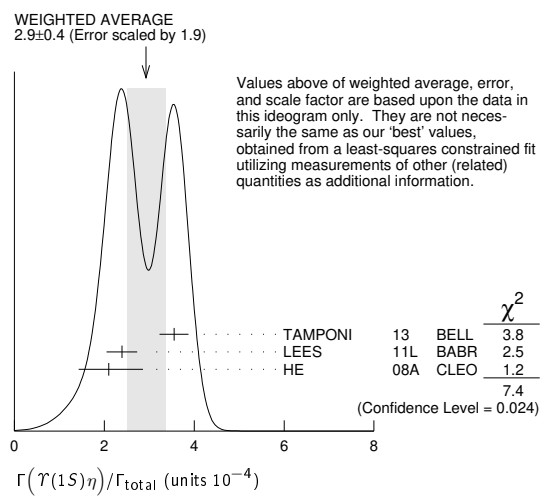

[1] Using $B(\Upsilon(1S) \to e^+e^-) = (2.38 \pm 0.11)\%$ and $B(\Upsilon(1S) \to \mu^+\mu^-) = (2.48 \pm 0.05)\%$.
[2] Authors assume $B(\Upsilon(1S) \to e^+e^-) + B(\Upsilon(1S) \to \mu^+\mu^-) = 4.96\%$.
[3] TAMPONI 13 reports $[\Gamma(\Upsilon(2S) \to \Upsilon(1S)\eta)/\Gamma_{total}] / [B(\Upsilon(2S) \to \Upsilon(1S)\pi^+\pi^-)] = (1.99 \pm 0.14 \pm 0.11) \times 10^{-3}$ which we multiply by our best value $B(\Upsilon(2S) \to \Upsilon(1S)\pi^+\pi^-) = (17.85 \pm 0.26) \times 10^{-2}$. Our first error is their experiment's error and our second error is the systematic error from using our best value.
[4] Using $\Gamma_{ee}(\Upsilon(2S)) = 0.612 \pm 0.011$ keV.

$\Gamma(\Upsilon(1S)\eta)/\Gamma(\Upsilon(1S)\pi^+\pi^-)$ — Γ_7/Γ_1

VALUE (units 10^{-3})	CL%	EVTS	DOCUMENT ID		TECN	COMMENT
1.64±0.25 OUR FIT Error includes scale factor of 2.0.						
1.99±0.14±0.11		241	TAMPONI	13	BELL	$e^+e^- \to \Upsilon(1S)\eta$
• • • We do not use the following data for averages, fits, limits, etc. • • •						
1.35±0.17±0.08			[1] LEES	11L	BABR	$\Upsilon(2S) \to (\pi^+\pi^-)(\gamma\gamma)\mu^+\mu^-$
< 5.2	90		[2] AUBERT	08BP	BABR	$e^+e^- \to \gamma\pi^+\pi^-(\pi^0)\ell^+\ell^-$

[1] Not independent of other values reported by LEES 11L.
[2] Not independent of other values reported by AUBERT 08BP.

$\Gamma(\Upsilon(1S)\pi^0)/\Gamma(\Upsilon(1S)\eta)$ — Γ_6/Γ_7

VALUE	CL%	DOCUMENT ID		TECN	COMMENT
• • • We do not use the following data for averages, fits, limits, etc. • • •					
<0.13	90	TAMPONI	13	BELL	$e^+e^- \to \Upsilon(1S)\pi^0$

Downloaded from https://academic.oup.com/ptep/article/2022/8/083C01/6651666 by KIT Library user on 27 September 2022

$\Gamma(J/\psi(1S)\text{ anything})/\Gamma_{total}$ — Γ_8/Γ

VALUE	CL%	DOCUMENT ID		TECN	COMMENT
<0.006	90	MASCHMANN	90	CBAL	$e^+e^- \to$ hadrons

$\Gamma(J/\psi(1S)\eta_c)/\Gamma_{total}$ — Γ_9/Γ

VALUE	CL%	DOCUMENT ID		TECN	COMMENT
$<5.4\times10^{-6}$	90	YANG	14	BELL	$e^+e^- \to J/\psi X$

$\Gamma(J/\psi(1S)\chi_{c0})/\Gamma_{total}$ — Γ_{10}/Γ

VALUE	CL%	DOCUMENT ID		TECN	COMMENT
$<3.4\times10^{-6}$	90	YANG	14	BELL	$e^+e^- \to J/\psi X$

$\Gamma(J/\psi(1S)\chi_{c1})/\Gamma_{total}$ — Γ_{11}/Γ

VALUE	CL%	DOCUMENT ID		TECN	COMMENT
$<1.2\times10^{-6}$	90	YANG	14	BELL	$e^+e^- \to J/\psi X$

$\Gamma(J/\psi(1S)\chi_{c2})/\Gamma_{total}$ — Γ_{12}/Γ

VALUE	CL%	DOCUMENT ID		TECN	COMMENT
$<2.0\times10^{-6}$	90	YANG	14	BELL	$e^+e^- \to J/\psi X$

$\Gamma(J/\psi(1S)\eta_c(2S))/\Gamma_{total}$ — Γ_{13}/Γ

VALUE	CL%	DOCUMENT ID		TECN	COMMENT
$<2.5\times10^{-6}$	90	YANG	14	BELL	$e^+e^- \to J/\psi X$

$\Gamma(J/\psi(1S)X(3940))/\Gamma_{total}$ — Γ_{14}/Γ

VALUE	CL%	DOCUMENT ID		TECN	COMMENT
$<2.0\times10^{-6}$	90	YANG	14	BELL	$e^+e^- \to J/\psi X$

$\Gamma(J/\psi(1S)X(4160))/\Gamma_{total}$ — Γ_{15}/Γ

VALUE	CL%	DOCUMENT ID		TECN	COMMENT
$<2.0\times10^{-6}$	90	YANG	14	BELL	$e^+e^- \to J/\psi X$

$\Gamma(\chi_{c1}\text{ anything})/\Gamma_{total}$ — Γ_{16}/Γ

VALUE (units 10^{-4})	EVTS	DOCUMENT ID		TECN	COMMENT
$2.24\pm0.44\pm0.20$	376	JIA	17	BELL	$\Upsilon(2S) \to \gamma J/\psi(1S)$

$\Gamma(\chi_{c1}(1P)^0 X_{tetra})/\Gamma_{total}$ — Γ_{17}/Γ

VALUE	CL%	DOCUMENT ID		TECN	COMMENT
$<36.7\times10^{-6}$	90	[1] JIA	17A	BELL	$e^+e^- \to$ hadrons

[1] For a tetraquark state X_{tetra}, with mass in the range 1.16–2.46 GeV and width in the range 0–0.3 GeV. Measured 90% CL limits as a function of X_{tetra} mass and width range from 4.4×10^{-6} to 36.7×10^{-6}.

$\Gamma(\chi_{c2}\text{ anything})/\Gamma_{total}$ — Γ_{18}/Γ

VALUE (units 10^{-4})	DOCUMENT ID		TECN	COMMENT
$2.28\pm0.73\pm0.34$	JIA	17	BELL	$\Upsilon(2S) \to \gamma J/\psi(1S)$

$\Gamma(\psi(2S)\eta_c)/\Gamma_{total}$ — Γ_{19}/Γ

VALUE	CL%	DOCUMENT ID		TECN	COMMENT
$<5.1\times10^{-6}$	90	YANG	14	BELL	$e^+e^- \to \psi(2S)X$

$\Gamma(\psi(2S)\chi_{c0})/\Gamma_{total}$ — Γ_{20}/Γ

VALUE	CL%	DOCUMENT ID		TECN	COMMENT
$<4.7\times10^{-6}$	90	YANG	14	BELL	$e^+e^- \to \psi(2S)X$

$\Gamma(\psi(2S)\chi_{c1})/\Gamma_{total}$ — Γ_{21}/Γ

VALUE	CL%	DOCUMENT ID		TECN	COMMENT
$<2.5\times10^{-6}$	90	YANG	14	BELL	$e^+e^- \to \psi(2S)X$

$\Gamma(\psi(2S)\chi_{c2})/\Gamma_{total}$ — Γ_{22}/Γ

VALUE	CL%	DOCUMENT ID		TECN	COMMENT
$<1.9\times10^{-6}$	90	YANG	14	BELL	$e^+e^- \to \psi(2S)X$

$\Gamma(\psi(2S)\eta_c(2S))/\Gamma_{total}$ — Γ_{23}/Γ

VALUE	CL%	DOCUMENT ID		TECN	COMMENT
$<3.3\times10^{-6}$	90	YANG	14	BELL	$e^+e^- \to \psi(2S)X$

$\Gamma(\psi(2S)X(3940))/\Gamma_{total}$ — Γ_{24}/Γ

VALUE	CL%	DOCUMENT ID		TECN	COMMENT
$<3.9\times10^{-6}$	90	YANG	14	BELL	$e^+e^- \to \psi(2S)X$

$\Gamma(\psi(2S)X(4160))/\Gamma_{total}$ — Γ_{25}/Γ

VALUE	CL%	DOCUMENT ID		TECN	COMMENT
$<3.9\times10^{-6}$	90	YANG	14	BELL	$e^+e^- \to \psi(2S)X$

$\Gamma(Z_c(3900)^+ Z_c(3900)^-)/\Gamma_{total}$ — Γ_{26}/Γ

VALUE	CL%	DOCUMENT ID		TECN	COMMENT
$<1.0\times10^{-6}$	90	[1] JIA	18	BELL	$\Upsilon(2S) \to J/\psi\pi^\pm X$

[1] Assuming $B(Z_c(3900)^\pm \to J/\psi\pi^\pm) = 1$.

$\Gamma(Z_c(4200)^+ Z_c(4200)^-)/\Gamma_{total}$ — Γ_{27}/Γ

VALUE	CL%	DOCUMENT ID		TECN	COMMENT
$<16.7\times10^{-6}$	90	[1] JIA	18	BELL	$\Upsilon(1S) \to J/\psi\pi^\pm X$

[1] Assuming $B(Z_c(4200)^\pm \to J/\psi\pi^\pm) = 1$

$\Gamma(Z_c(3900)^\pm Z_c(4200)^\mp)/\Gamma_{total}$ — Γ_{28}/Γ

VALUE	CL%	DOCUMENT ID		TECN	COMMENT
$<7.3\times10^{-6}$	90	[1] JIA	18	BELL	$\Upsilon(2S) \to J/\psi\pi^\pm X$

[1] Assuming $B(Z_c(4200)^\pm \to J/\psi\pi^\pm) = 1 = B(Z_c(3900)^\pm \to J/\psi\pi^\pm)$.

$\Gamma(X(4050)^+ X(4050)^-)/\Gamma_{total}$ — Γ_{29}/Γ

VALUE	CL%	DOCUMENT ID		TECN	COMMENT
$<13.5\times10^{-6}$	90	[1] JIA	18	BELL	$\Upsilon(2S) \to \chi_{c1}(1P)\pi^\pm X$

[1] Assuming $B(X(4050)^\pm \to \chi_{c1}(1P)\pi^\pm)$

$\Gamma(X(4250)^+ X(4250)^-)/\Gamma_{total}$ — Γ_{30}/Γ

VALUE	CL%	DOCUMENT ID		TECN	COMMENT
$<26.7\times10^{-6}$	90	[1] JIA	18	BELL	$\Upsilon(2S) \to \chi_{c1}(1P)\pi^\pm X$

[1] Assuming $B(X(4250)^\pm \to \chi_{c1}(1P)\pi^\pm) = 1$

$\Gamma(X(4050)^\pm X(4250)^\mp)/\Gamma_{total}$ — Γ_{31}/Γ

VALUE	CL%	DOCUMENT ID		TECN	COMMENT
$<27.2\times10^{-6}$	90	[1] JIA	18	BELL	$\Upsilon(2S) \to \chi_{c1}(1P)\pi^\pm X$

[1] Assuming $B(X(4050)^\pm \to \chi_{c1}(1P)\pi^\pm) = 1 = B(X(4250)^\pm \to \chi_{c1}(1P)\pi^\pm)$

$\Gamma(Z_c(4430)^+ Z_c(4430)^-)/\Gamma_{total}$ — Γ_{32}/Γ

VALUE	CL%	DOCUMENT ID		TECN	COMMENT
$<20.3\times10^{-6}$	90	[1] JIA	18	BELL	$\Upsilon(2S) \to \psi(2S)\pi^\pm X$

[1] Assuming $B(Z_c(4430)^\pm \to \psi(2P)\pi^\pm) = 1$

$\Gamma(X(4055)^\pm X(4055)^\mp)/\Gamma_{total}$ — Γ_{33}/Γ

VALUE	CL%	DOCUMENT ID		TECN	COMMENT
$<11.1\times10^{-6}$	90	[1] JIA	18	BELL	$\Upsilon(2S) \to \psi(2S)\pi^\pm X$

[1] Assuming $B(X(4055)^\pm \to \psi(2S)\pi^\pm) = 1$

$\Gamma(X(4055)^\pm Z_c(4430)^\mp)/\Gamma_{total}$ — Γ_{34}/Γ

VALUE	CL%	DOCUMENT ID		TECN	COMMENT
$<21.1\times10^{-6}$	90	[1] JIA	18	BELL	$\Upsilon(2S) \to \psi(2S)\pi^\pm X$

[1] Assuming $B(X(4055)^\pm \to \psi(2S)\pi^\pm) = 1 = B(Z_c(4430)^\pm \to \psi(2S)\pi^\pm)$

$\Gamma(\overline{^2H}\text{ anything})/\Gamma_{total}$ — Γ_{35}/Γ

VALUE (units 10^{-5})	EVTS	DOCUMENT ID		TECN	COMMENT
$2.78^{+0.30}_{-0.26}$ OUR AVERAGE	Error includes scale factor of 1.2.				
$2.64\pm0.11^{+0.26}_{-0.21}$		LEES	14G	BABR	$e^+e^- \to \overline{^2H}X$
$3.37\pm0.50\pm0.25$	58	ASNER	07	CLEO	$e^+e^- \to \overline{^2H}X$

$\Gamma(ggg)/\Gamma_{total}$ — Γ_{37}/Γ

VALUE (units 10^{-2})	EVTS	DOCUMENT ID		TECN	COMMENT
58.8±1.2	6M	[1] BESSON	06A	CLEO	$\Upsilon(2S) \to$ hadrons

[1] Calculated using the value $\Gamma(\gamma gg)/\Gamma(ggg) = (3.18 \pm 0.04 \pm 0.22 \pm 0.41)\%$ from BESSON 06A and PDG 08 values of $B(\pi^+\pi^-\Upsilon(1S)) = (18.1\pm0.4)\%$, $B(\pi^0\pi^0\Upsilon(1S)) = (8.6\pm0.4)\%$, $B(\mu^+\mu^-) = (1.93\pm0.17)\%$, and $R_{hadrons} = 3.51$. The statistical error is negligible and the systematic error is partially correlated with that of $\Gamma(\gamma gg)/\Gamma_{total}$ measurement of BESSON 06A.

$\Gamma(\gamma gg)/\Gamma(ggg)$ — Γ_{38}/Γ_{37}

VALUE (units 10^{-2})	EVTS	DOCUMENT ID		TECN	COMMENT
3.18±0.04±0.47	6M	BESSON	06A	CLEO	$\Upsilon(2S) \to (\gamma +)$ hadrons

$\Gamma(\phi K^+K^-)/\Gamma_{total}$ — Γ_{39}/Γ

VALUE (units 10^{-6})	EVTS	DOCUMENT ID		TECN	COMMENT
1.58±0.33±0.18	58	SHEN	12A	BELL	$\Upsilon(1S) \to 2(K^+K^-)$

$\Gamma(\omega\pi^+\pi^-)/\Gamma_{total}$ — Γ_{40}/Γ

VALUE (units 10^{-6})	CL%	DOCUMENT ID		TECN	COMMENT
<2.58	90	SHEN	12A	BELL	$\Upsilon(1S) \to 2(\pi^+\pi^-)\pi^0$

$\Gamma(K^*(892)^0 K^-\pi^+ + \text{c.c.})/\Gamma_{total}$ — Γ_{41}/Γ

VALUE (units 10^{-6})	EVTS	DOCUMENT ID		TECN	COMMENT
2.32±0.40±0.54	135	SHEN	12A	BELL	$\Upsilon(1S) \to K^+K^-\pi^+\pi^-$

$\Gamma(\phi f_2'(1525))/\Gamma_{total}$ — Γ_{42}/Γ

VALUE (units 10^{-6})	CL%	DOCUMENT ID		TECN	COMMENT
<1.33	90	SHEN	12A	BELL	$\Upsilon(1S) \to 2(K^+K^-)$

$\Gamma(\omega f_2(1270))/\Gamma_{total}$ — Γ_{43}/Γ

VALUE (units 10^{-6})	CL%	DOCUMENT ID		TECN	COMMENT
<0.57	90	SHEN	12A	BELL	$\Upsilon(1S) \to 2(\pi^+\pi^-)\pi^0$

$\Gamma(\rho(770)a_2(1320))/\Gamma_{total}$ — Γ_{44}/Γ

VALUE (units 10^{-6})	CL%	DOCUMENT ID		TECN	COMMENT
<0.88	90	SHEN	12A	BELL	$\Upsilon(1S) \to 2(\pi^+\pi^-)\pi^0$

Downloaded from https://academic.oup.com/ptep/article/2022/8/083C01/6651666 by KIT Library user on 27 September 2022

$\Gamma(K^*(892)^0\overline{K}_2^*(1430)^0 + \text{c.c.})/\Gamma_{total}$ — Γ_{45}/Γ

VALUE (units 10^{-6})	EVTS	DOCUMENT ID		TECN	COMMENT
1.53±0.52±0.19	32	SHEN	12A	BELL	$\Upsilon(1S) \to K^+K^-\pi^+\pi^-$

$\Gamma(K_1(1270)^\pm K^\mp)/\Gamma_{total}$ — Γ_{46}/Γ

VALUE (units 10^{-6})	CL%	DOCUMENT ID		TECN	COMMENT
<3.22	90	SHEN	12A	BELL	$\Upsilon(1S) \to K^+K^-\pi^+\pi^-$

$\Gamma(K_1(1400)^\pm K^\mp)/\Gamma_{total}$ — Γ_{47}/Γ

VALUE (units 10^{-6})	CL%	DOCUMENT ID		TECN	COMMENT
<0.83	90	SHEN	12A	BELL	$\Upsilon(1S) \to K^+K^-\pi^+\pi^-$

$\Gamma(b_1(1235)^\pm\pi^\mp)/\Gamma_{total}$ — Γ_{48}/Γ

VALUE (units 10^{-6})	CL%	DOCUMENT ID		TECN	COMMENT
<0.40	90	SHEN	12A	BELL	$\Upsilon(1S) \to 2(\pi^+\pi^-)\pi^0$

$\Gamma(\rho\pi)/\Gamma_{total}$ — Γ_{49}/Γ

VALUE (units 10^{-6})	CL%	DOCUMENT ID		TECN	COMMENT
<1.16	90	SHEN	13	BELL	$\Upsilon(2S) \to \pi^+\pi^-\pi^0$

$\Gamma(\pi^+\pi^-\pi^0)/\Gamma_{total}$ — Γ_{50}/Γ

VALUE (units 10^{-6})	CL%	DOCUMENT ID		TECN	COMMENT
<0.80	90	SHEN	13	BELL	$\Upsilon(2S) \to \pi^+\pi^-\pi^0$

$\Gamma(\omega\pi^0)/\Gamma_{total}$ — Γ_{51}/Γ

VALUE (units 10^{-6})	CL%	DOCUMENT ID		TECN	COMMENT
<1.63	90	SHEN	13	BELL	$\Upsilon(2S) \to \pi^+\pi^-\pi^0\pi^0$

$\Gamma(\pi^+\pi^-\pi^0\pi^0)/\Gamma_{total}$ — Γ_{52}/Γ

VALUE (units 10^{-6})	EVTS	DOCUMENT ID		TECN	COMMENT
13.0±1.9±2.1	261 ± 37	SHEN	13	BELL	$\Upsilon(2S) \to \pi^+\pi^-\pi^0\pi^0$

$\Gamma(K^0_S K^+\pi^- + \text{c.c.})/\Gamma_{total}$ — Γ_{53}/Γ

VALUE (units 10^{-6})	CL%	EVTS	DOCUMENT ID		TECN	COMMENT
1.14±0.30±0.13		40 ± 10	SHEN	13	BELL	$\Upsilon(2S) \to K^0_S K^-\pi^+$
• • • We do not use the following data for averages, fits, limits, etc. • • •						
<3.2	90		[1] DOBBS	12A		$\Upsilon(2S) \to K^0_S K^-\pi^+$

[1] Obtained by analyzing CLEO III data but not authored by the CLEO Collaboration.

$\Gamma(K^*(892)^0\overline{K}^0 + \text{c.c.})/\Gamma_{total}$ — Γ_{54}/Γ

VALUE (units 10^{-6})	CL%	DOCUMENT ID		TECN	COMMENT
<4.22	90	SHEN	13	BELL	$\Upsilon(2S) \to K^0_S K^-\pi^+$

$\Gamma(K^*(892)^- K^+ + \text{c.c.})/\Gamma_{total}$ — Γ_{55}/Γ

VALUE (units 10^{-6})	CL%	DOCUMENT ID		TECN	COMMENT
<1.45	90	SHEN	13	BELL	$\Upsilon(2S) \to K^0_S K^-\pi^+$

$\Gamma(f_1(1285)\,\text{anything})/\Gamma_{total}$ — Γ_{56}/Γ

VALUE (units 10^{-3})	EVTS	DOCUMENT ID		TECN	COMMENT
2.20±1.50±0.63	2.9k	JIA	17A	BELL	$e^+e^- \to$ hadrons

$\Gamma(f_1(1285)X_{tetra})/\Gamma_{total}$ — Γ_{57}/Γ

VALUE	CL%	DOCUMENT ID		TECN	COMMENT
<64.7 × 10^{-6}	90	[1] JIA	17A	BELL	$e^+e^- \to$ hadrons

[1] For a tetraquark state X_{tetra}, with mass in the range 1.16–2.46 GeV and width in the range 0–0.3 GeV. Measured 90% CL limits as a function of X_{tetra} mass and width range from 7.8×10^{-6} to 64.7×10^{-6}.

$\Gamma(\text{Sum of 100 exclusive modes})/\Gamma_{total}$ — Γ_{58}/Γ

VALUE (units 10^{-2})	DOCUMENT ID		COMMENT
0.29±0.03	[1,2] DOBBS	12A	$\Upsilon(2S) \to$ hadrons

[1] DOBBS 12A presents individual exclusive branching fractions or upper limits for 100 modes of four to ten pions, kaons, or protons.
[2] Obtained by analyzing CLEO III data but not authored by the CLEO Collaboration.

$\Gamma(\gamma\chi_{b1}(1P))/\Gamma_{total}$ — Γ_{59}/Γ

VALUE	EVTS	DOCUMENT ID		TECN	COMMENT
0.069 ±0.004 OUR AVERAGE					
0.0693±0.0012±0.0041	407k	ARTUSO	05	CLEO	$e^+e^- \to \gamma X$
0.069 ±0.005 ±0.009		EDWARDS	99	CLE2	$\Upsilon(2S) \to \gamma\chi(1P)$
0.091 ±0.018 ±0.022		ALBRECHT	85E	ARG	$e^+e^- \to \gamma$conv. X
0.065 ±0.007 ±0.012		NERNST	85	CBAL	$e^+e^- \to \gamma X$
0.080 ±0.017 ±0.016		HAAS	84	CLEO	$e^+e^- \to \gamma$conv. X
0.059 ±0.014		KLOPFEN...	83	CUSB	$e^+e^- \to \gamma X$

$\Gamma(\gamma\chi_{b2}(1P))/\Gamma_{total}$ — Γ_{60}/Γ

VALUE	EVTS	DOCUMENT ID		TECN	COMMENT
0.0715±0.0035 OUR AVERAGE					
0.0724±0.0011±0.0040	410k	ARTUSO	05	CLEO	$e^+e^- \to \gamma X$
0.074 ±0.005 ±0.008		EDWARDS	99	CLE2	$\Upsilon(2S) \to \gamma\chi(1P)$
0.098 ±0.021 ±0.024		ALBRECHT	85E	ARG	$e^+e^- \to \gamma$conv. X
0.058 ±0.007 ±0.010		NERNST	85	CBAL	$e^+e^- \to \gamma X$
0.102 ±0.018 ±0.021		HAAS	84	CLEO	$e^+e^- \to \gamma$conv. X
0.061 ±0.014		KLOPFEN...	83	CUSB	$e^+e^- \to \gamma X$

$\Gamma(\gamma\chi_{b0}(1P))/\Gamma_{total}$ — Γ_{61}/Γ

VALUE	EVTS	DOCUMENT ID		TECN	COMMENT
0.038 ±0.004 OUR AVERAGE					
0.0375±0.0012±0.0047	198k	ARTUSO	05	CLEO	$e^+e^- \to \gamma X$
0.034 ±0.005 ±0.006		EDWARDS	99	CLE2	$\Upsilon(2S) \to \gamma\chi(1P)$
0.064 ±0.014 ±0.016		ALBRECHT	85E	ARG	$e^+e^- \to \gamma$conv. X
0.036 ±0.008 ±0.009		NERNST	85	CBAL	$e^+e^- \to \gamma X$
0.044 ±0.023 ±0.009		HAAS	84	CLEO	$e^+e^- \to \gamma$conv. X
• • • We do not use the following data for averages, fits, limits, etc. • • •					
0.035 ±0.014		KLOPFEN...	83	CUSB	$e^+e^- \to \gamma X$

$\Gamma(\gamma f_0(1710))/\Gamma_{total}$ — Γ_{62}/Γ

VALUE (units 10^{-5})	CL%	DOCUMENT ID		TECN	COMMENT
<59	90	[1] ALBRECHT	89	ARG	$\Upsilon(2S) \to \gamma K^+K^-$
• • • We do not use the following data for averages, fits, limits, etc. • • •					
< 5.9	90	[2] ALBRECHT	89	ARG	$\Upsilon(2S) \to \gamma\pi^+\pi^-$

[1] Re-evaluated assuming $B(f_0(1710) \to K^+K^-) = 0.19$.
[2] Includes unknown branching ratio of $f_0(1710) \to \pi^+\pi^-$.

$\Gamma(\gamma f'_2(1525))/\Gamma_{total}$ — Γ_{63}/Γ

VALUE (units 10^{-5})	CL%	DOCUMENT ID		TECN	COMMENT
<53	90	[1] ALBRECHT	89	ARG	$\Upsilon(2S) \to \gamma K^+K^-$

[1] Re-evaluated assuming $B(f'_2(1525) \to K\overline{K}) = 0.71$.

$\Gamma(\gamma f_2(1270))/\Gamma_{total}$ — Γ_{64}/Γ

VALUE (units 10^{-5})	CL%	DOCUMENT ID		TECN	COMMENT
<24.1	90	[1] ALBRECHT	89	ARG	$\Upsilon(2S) \to \gamma\pi^+\pi^-$

[1] Using $B(f_2(1270) \to \pi\pi) = 0.84$.

$\Gamma(\gamma f_J(2220))/\Gamma_{total}$ — Γ_{65}/Γ

VALUE (units 10^{-5})	CL%	DOCUMENT ID		TECN	COMMENT
• • • We do not use the following data for averages, fits, limits, etc. • • •					
<6.8	90	[1] ALBRECHT	89	ARG	$\Upsilon(2S) \to \gamma K^+K^-$

[1] Includes unknown branching ratio of $f_J(2220) \to K^+K^-$.

$\Gamma(\gamma\eta_c(1S))/\Gamma_{total}$ — Γ_{66}/Γ

VALUE	CL%	DOCUMENT ID		TECN	COMMENT
<2.7 × 10^{-5}	90	WANG	11B	BELL	$\Upsilon(2S) \to \gamma X$

$\Gamma(\gamma\chi_{c0})/\Gamma_{total}$ — Γ_{67}/Γ

VALUE	CL%	DOCUMENT ID		TECN	COMMENT
<1.0 × 10^{-4}	90	WANG	11B	BELL	$\Upsilon(2S) \to \gamma X$

$\Gamma(\gamma\chi_{c1})/\Gamma_{total}$ — Γ_{68}/Γ

VALUE	CL%	DOCUMENT ID		TECN	COMMENT
<3.6 × 10^{-6}	90	WANG	11B	BELL	$\Upsilon(2S) \to \gamma X$

$\Gamma(\gamma\chi_{c2})/\Gamma_{total}$ — Γ_{69}/Γ

VALUE	CL%	DOCUMENT ID		TECN	COMMENT
<1.5 × 10^{-5}	90	WANG	11B	BELL	$\Upsilon(2S) \to \gamma X$

$\Gamma(\gamma\chi_{c1}(3872))/\Gamma_{total}$ — Γ_{70}/Γ

VALUE	CL%	DOCUMENT ID		TECN	COMMENT
<2.1 × 10^{-5}	90	[1] WANG	11B	BELL	$\Upsilon(2S) \to \gamma X$

[1] WANG 11B reports $[\Gamma(\Upsilon(2S) \to \gamma\chi_{c1}(3872))/\Gamma_{total}] \times [B(\chi_{c1}(3872) \to \pi^+\pi^- J/\psi(1S))] < 0.8 \times 10^{-6}$ which we divide by our best value $B(\chi_{c1}(3872) \to \pi^+\pi^- J/\psi(1S)) = 3.8 \times 10^{-2}$.

$\Gamma(\gamma\chi_{c1}(3872),\ \chi_{c1} \to \pi^+\pi^-\pi^0 J/\psi)/\Gamma_{total}$ — Γ_{71}/Γ

VALUE	CL%	DOCUMENT ID		TECN	COMMENT
<2.4 × 10^{-6}	90	WANG	11B	BELL	$\Upsilon(2S) \to \gamma X$

$\Gamma(\gamma\chi_{c0}(3915) \to \omega J/\psi)/\Gamma_{total}$ — Γ_{72}/Γ

VALUE	CL%	DOCUMENT ID		TECN	COMMENT
<2.8 × 10^{-6}	90	WANG	11B	BELL	$\Upsilon(2S) \to \gamma X$

$\Gamma(\gamma\chi_{c1}(4140) \to \phi J/\psi)/\Gamma_{total}$ — Γ_{73}/Γ

VALUE	CL%	DOCUMENT ID		TECN	COMMENT
<1.2 × 10^{-6}	90	WANG	11B	BELL	$\Upsilon(2S) \to \gamma X$

$\Gamma(\gamma X(4350) \to \phi J/\psi)/\Gamma_{total}$ — Γ_{74}/Γ

VALUE	CL%	DOCUMENT ID		TECN	COMMENT
<1.3 × 10^{-6}	90	WANG	11B	BELL	$\Upsilon(2S) \to \gamma X$

Downloaded from https://academic.oup.com/ptep/article/2022/8/083C01/6651666 by KIT Library user on 27 September 2022

$\Gamma(\gamma\eta_b(1S))/\Gamma_{total}$ — Γ_{75}/Γ

VALUE (units 10^{-4})	CL%	EVTS	DOCUMENT ID		TECN	COMMENT
$5.5^{+1.1}_{-0.9}$ OUR AVERAGE	Error includes scale factor of 1.2.					
$6.1^{+0.6+0.9}_{-0.7-0.6}$		29k	FULSOM	18	BELL	$\Upsilon(2S) \to \gamma X$
$3.9 \pm 1.1^{+1.1}_{-0.9}$		13 ± 5k	[1] AUBERT	09AQ	BABR	$\Upsilon(2S) \to \gamma X$
• • • We do not use the following data for averages, fits, limits, etc. • • •						
<21	90		LEES	11J	BABR	$\Upsilon(2S) \to X\gamma$
< 8.4	90		[1] BONVICINI	10	CLEO	$\Upsilon(2S) \to \gamma X$
< 5.1	90		[2] ARTUSO	05	CLEO	$e^+e^- \to \gamma X$

[1] Assuming $\Gamma_{\eta_b(1S)} = 10$ MeV.

[2] Superseded by BONVICINI 10.

$\Gamma(\gamma\eta_b(1S) \to \gamma \text{Sum of 26 exclusive modes})/\Gamma_{total}$ — Γ_{76}/Γ

VALUE	CL%	DOCUMENT ID		TECN	COMMENT
$<3.7 \times 10^{-6}$	90	SANDILYA	13	BELL	$\Upsilon(2S) \to \gamma$ hadrons

$\Gamma(\gamma X_{b\overline{b}} \to \gamma \text{Sum of 26 exclusive modes})/\Gamma_{total}$ — Γ_{77}/Γ

VALUE (units 10^{-6})	CL%	EVTS	DOCUMENT ID		TECN	COMMENT
< 4.9	90		SANDILYA	13	BELL	$\Upsilon(2S) \to \gamma$ hadrons
• • • We do not use the following data for averages, fits, limits, etc. • • •						
$46.2^{+29.7}_{-14.2} \pm 10.6$		10	[1] DOBBS	12		$\Upsilon(2S) \to \gamma$ hadrons

[1] Obtained by analyzing CLEO III data but not authored by the CLEO Collaboration.

$\Gamma(\gamma X \to \gamma + \geq 4 \text{ prongs})/\Gamma_{total}$ — Γ_{78}/Γ

(1.5 GeV $< m_X <$ 5.0 GeV)

VALUE (units 10^{-4})	CL%	DOCUMENT ID		TECN	COMMENT
<1.95	95	ROSNER	07A	CLEO	$e^+e^- \to \gamma X$

$\Gamma(\gamma A^0 \to \gamma \text{hadrons})/\Gamma_{total}$ — Γ_{79}/Γ

(0.3 GeV $< m_{A^0} <$ 7 GeV)

VALUE	CL%	DOCUMENT ID		TECN	COMMENT
$<8 \times 10^{-5}$	90	[1] LEES	11H	BABR	$\Upsilon(2S) \to \gamma$ hadrons

[1] For a narrow scalar or pseudoscalar A^0, excluding known resonances, with mass in the range 0.3–7 GeV. Measured 90% CL limits as a function of m_{A^0} range from 1×10^{-6} to 8×10^{-5}.

$\Gamma(\gamma a_1^0 \to \gamma\mu^+\mu^-)/\Gamma_{total}$ — Γ_{80}/Γ

VALUE (units 10^{-6})	CL%	DOCUMENT ID		TECN	COMMENT
<8.3	90	[1] AUBERT	09Z	BABR	$e^+e^- \to \gamma a_1^0 \to \gamma\mu^+\mu^-$

[1] For a narrow scalar or pseudoscalar a_1^0 with mass in the range 212–9300 MeV, excluding J/ψ and $\psi(2S)$. Measured 90% CL limits as a function of $m_{a_1^0}$ range from 0.26–8.3 $\times 10^{-6}$.

LEPTON FAMILY NUMBER (*LF*) VIOLATING MODES

$\Gamma(e^\pm\tau^\mp)/\Gamma_{total}$ — Γ_{81}/Γ

VALUE (units 10^{-6})	CL%	DOCUMENT ID		TECN	COMMENT
<3.2	90	LEES	10B	BABR	$e^+e^- \to e^\pm\tau^\mp$

$\Gamma(\mu^\pm\tau^\mp)/\Gamma_{total}$ — Γ_{82}/Γ

VALUE (units 10^{-6})	CL%	DOCUMENT ID		TECN	COMMENT
< 3.3	90	LEES	10B	BABR	$e^+e^- \to \mu^\pm\tau^\mp$
• • • We do not use the following data for averages, fits, limits, etc. • • •					
<14.4	95	LOVE	08A	CLEO	$e^+e^- \to \mu^\pm\tau^\mp$

$\Upsilon(2S)$ Cross-Particle Branching Ratios

$B(\Upsilon(2S) \to \pi^+\pi^-) \times B(\Upsilon(3S) \to \Upsilon(2S)X)$

VALUE (units 10^{-2})	EVTS	DOCUMENT ID		TECN	COMMENT
$1.78 \pm 0.02 \pm 0.11$	906k	LEES	11C	BABR	$e^+e^- \to \pi^+\pi^- X$

$\Upsilon(2S)$ REFERENCES

FULSOM	18	PRL 121 232001	B.G. Fulsom *et al.*	(BELLE Collab.)
JIA	18	PR D97 112004	S. Jia *et al.*	(BELLE Collab.)
JIA	17	PR D95 012001	S. Jia *et al.*	(BELLE Collab.)
JIA	17A	PR D96 112002	S. Jia *et al.*	(BELLE Collab.)
LEES	14G	PR D89 111102	J.P. Lees *et al.*	(BABAR Collab.)
YANG	14	PR D90 112008	S.D. Yang *et al.*	(BELLE Collab.)
SANDILYA	13	PRL 111 112001	S. Sandilya *et al.*	(BELLE Collab.)
SHEN	13	PR D88 011102	C.P. Shen *et al.*	(BELLE Collab.)
TAMPONI	13	PR D87 011104	U. Tamponi *et al.*	(BELLE Collab.)
DOBBS	12	PRL 109 082001	S. Dobbs *et al.*	
DOBBS	12A	PR D86 052003	S. Dobbs *et al.*	
SHEN	12A	PR D86 031102	C.P. Shen *et al.*	(BELLE Collab.)
LEES	11C	PR D84 011104	J.P. Lees *et al.*	(BABAR Collab.)
LEES	11H	PRL 107 221803	J.P. Lees *et al.*	(BABAR Collab.)
LEES	11J	PR D84 072002	J.P. Lees *et al.*	(BABAR Collab.)
LEES	11L	PR D84 092003	J.P. Lees *et al.*	(BABAR Collab.)
WANG	11B	PR D84 071107	X.L. Wang *et al.*	(BELLE Collab.)
BONVICINI	10	PR D81 031104	G. Bonvicini *et al.*	(CLEO Collab.)
LEES	10B	PRL 104 151802	J.P. Lees *et al.*	(BABAR Collab.)
AUBERT	09AQ	PRL 103 161801	B. Aubert *et al.*	(BABAR Collab.)
AUBERT	09Z	PRL 103 081803	B. Aubert *et al.*	(BABAR Collab.)
BHARI	09	PR D79 011103	S.R. Bhari *et al.*	(CLEO Collab.)
AUBERT	08BP	PR D78 112002	B. Aubert *et al.*	(BABAR Collab.)
HE	08A	PRL 101 192001	Q. He *et al.*	(CLEO Collab.)
LOVE	08A	PRL 101 201601	W. Love *et al.*	(CLEO Collab.)
PDG	08	PL B667 1	C. Amsler *et al.*	(PDG Collab.)
ASNER	07	PR D75 012009	D.M. Asner *et al.*	(CLEO Collab.)
BESSON	07	PRL 98 052002	D. Besson *et al.*	(CLEO Collab.)
ROSNER	07A	PR D76 117102	J.L. Rosner *et al.*	(CLEO Collab.)
BESSON	06A	PR D74 012003	D. Besson *et al.*	(CLEO Collab.)
ROSNER	06	PRL 96 092003	J.L. Rosner *et al.*	(CLEO Collab.)
ADAMS	05	PRL 94 012001	G.S. Adams *et al.*	(CLEO Collab.)
ARTUSO	05	PRL 94 032001	M. Artuso *et al.*	(CLEO Collab.)
ARTAMONOV	00	PL B474 427	A.S. Artamonov *et al.*	
EDWARDS	99	PR D59 032003	K.W. Edwards *et al.*	(CLEO Collab.)
ALEXANDER	98	PR D58 052004	J.P. Alexander *et al.*	(CLEO Collab.)
BARU	96	PRPL 267 71	S.E. Baru *et al.*	(NOVO)
KOBEL	92	ZPHY C53 193	M. Kobel *et al.*	(Crystal Ball Collab.)
MASCHMANN	90	ZPHY C46 555	W.S. Maschmann *et al.*	(Crystal Ball Collab.)
ALBRECHT	89	ZPHY C42 349	H. Albrecht *et al.*	(ARGUS Collab.)
KAARSBERG	89	PRL 62 2077	T.M. Kaarsberg *et al.*	(CUSB Collab.)
BUCHMUEL...	88	HE e^+e^- Physics 412 Editors: A. Ali and P. Soeding, World Scientific, Singapore	W. Buchmueller, S. Cooper	(HANN, DESY, MIT)
JAKUBOWSKI	88	ZPHY C40 49	Z. Jakubowski *et al.*	(Crystal Ball Collab.) IGJPC
ALBRECHT	87	ZPHY C35 283	H. Albrecht *et al.*	(ARGUS Collab.)
COHEN	87	RMP 59 1121	E.R. Cohen, B.N. Taylor	(RISC, NBS)
LURZ	87	ZPHY C36 383	B. Lurz *et al.*	(Crystal Ball Collab.)
BARU	86B	ZPHY C32 622 (erratum)	S.E. Baru *et al.*	(NOVO)
ALBRECHT	85	ZPHY C28 45	H. Albrecht *et al.*	(ARGUS Collab.)
ALBRECHT	85E	PL 160B 331	H. Albrecht *et al.*	(ARGUS Collab.)
GELPHMAN	85	PR D32 2893	D. Gelphman *et al.*	(Crystal Ball Collab.)
KURAEV	85	SJNP 41 466 Translated from YAF 41 733.	E.A. Kuraev, V.S. Fadin	(NOVO)
NERNST	85	PRL 54 2195	R. Nernst *et al.*	(Crystal Ball Collab.)
ARTAMONOV	84	PL 137B 272	A.S. Artamonov *et al.*	(NOVO)
BARBER	84	PL 135B 498	D.P. Barber *et al.*	
BESSON	84	PR D30 1433	D. Besson *et al.*	(CLEO Collab.)
FONSECA	84	NP B242 31	V. Fonseca *et al.*	(CUSB Collab.)
GILES	84B	PR D29 1285	R. Giles *et al.*	(CLEO Collab.)
HAAS	84	PRL 52 799	J. Haas *et al.*	(CLEO Collab.)
HAAS	84B	PR D30 1996	J. Haas *et al.*	(CLEO Collab.)
KLOPFEN...	83	PRL 51 160	C. Klopfenstein *et al.*	(CUSB Collab.)
ALBRECHT	82	PL 116B 383	H. Albrecht *et al.*	(DESY, DORT, HEIDH+)
NICZYPORUK	81B	PL 100B 95	B. Niczyporuk *et al.*	(LENA Collab.)
NICZYPORUK	81C	PL 99B 169	B. Niczyporuk *et al.*	(LENA Collab.)
BOCK	80	ZPHY C6 125	P. Bock *et al.*	(HEIDP, MPIM, DESY, HAMB)

$\Upsilon_2(1D)$

$I^G(J^{PC}) = 0^-(2^{--})$

was $\Upsilon(1D)$

First observed by BONVICINI 04 in the decay to $\gamma\gamma\,\Upsilon(1S)$ and confirmed by DEL-AMO-SANCHEZ 10R in the decay to $\pi^+\pi^-\,\Upsilon(1S)$. Data consistent with $J^P = 2^-$. The states with $J = 1$ and 3 also possibly seen, but need confirmation.

$\Upsilon_2(1D)$ MASS

VALUE (MeV)	EVTS	DOCUMENT ID		TECN	COMMENT
10163.7 ± 1.4 OUR AVERAGE	Error includes scale factor of 1.7.				
$10164.5 \pm 0.8 \pm 0.5$		DEL-AMO-SA...	10R	BABR	$\Upsilon(3S) \to \gamma\gamma\pi^+\pi^-\ell^+\ell^-$
$10161.1 \pm 0.6 \pm 1.6$	38	BONVICINI	04	CLE3	$\Upsilon(3S) \to 4\gamma\ell^+\ell^-$

$\Upsilon_2(1D)$ DECAY MODES

	Mode	Fraction (Γ_i/Γ)
Γ_1	$\gamma\gamma\,\Upsilon(1S)$	seen
Γ_2	$\gamma\chi_{bJ}(1P)$	seen
Γ_3	$\eta\,\Upsilon(1S)$	not seen
Γ_4	$\pi^+\pi^-\,\Upsilon(1S)$	$(6.6 \pm 1.6) \times 10^{-3}$

$\Upsilon_2(1D)$ BRANCHING RATIOS

$\Gamma(\eta\,\Upsilon(1S))/\Gamma(\gamma\gamma\,\Upsilon(1S))$ — Γ_3/Γ_1

VALUE	CL%	DOCUMENT ID		TECN	COMMENT
<0.25	90	BONVICINI	04	CLE3	$\Upsilon(3S) \to 4\gamma\ell^+\ell^-$

$\Gamma(\pi^+\pi^-\,\Upsilon(1S))/\Gamma_{total}$ — Γ_4/Γ

VALUE (units 10^{-2})	DOCUMENT ID		TECN	COMMENT
$0.66^{+0.15}_{-0.14} \pm 0.06$	[1] DEL-AMO-SA...	10R	BABR	$\Upsilon(3S) \to \gamma\gamma\pi^+\pi^-\ell^+\ell^-$

[1] Using theoretical predictions for $B(\chi_{bJ}(2P) \to \gamma\,\Upsilon_2(1D))$.

$\Gamma(\pi^+\pi^-\,\Upsilon(1S))/\Gamma(\gamma\gamma\,\Upsilon(1S))$ — Γ_4/Γ_1

VALUE	CL%	DOCUMENT ID		TECN	COMMENT
<1.2	90	[2] BONVICINI	04	CLE3	$\Upsilon(3S) \to 4\gamma\ell^+\ell^-$

[2] Assuming $J = 2$.

$\Upsilon_2(1D)$ REFERENCES

DEL-AMO-SA...	10R	PR D82 111102	P. del Amo Sanchez *et al.*	(BABAR Collab.)
BONVICINI	04	PR D70 032001	G. Bonvicini *et al.*	(CLEO Collab.)

Downloaded from https://academic.oup.com/ptep/article/2022/8/083C01/6651666 by KIT Library user on 27 September 2022

$\chi_{b0}(2P)$

$I^G(J^{PC}) = 0^+(0^{++})$
J needs confirmation.

Observed in radiative decay of the $\Upsilon(3S)$, therefore $C = +$. Branching ratio requires E1 transition, M1 is strongly disfavored, therefore $P = +$.

$\chi_{b0}(2P)$ MASS

VALUE (MeV)	DOCUMENT ID
10232.5±0.4±0.5 OUR EVALUATION	From γ energy below, using $\Upsilon(3S)$ mass = 10355.2 ± 0.5 MeV

$m_{\chi_{b1}(2P)} - m_{\chi_{b0}(2P)}$

VALUE (MeV)	DOCUMENT ID		TECN	COMMENT
23.8±1.7	LEES	14M	BABR	$\Upsilon(3S) \to \gamma\gamma\mu^+\mu^-$

γ ENERGY IN $\Upsilon(3S)$ DECAY

VALUE (MeV)	EVTS	DOCUMENT ID		TECN	COMMENT
121.9 ±0.4 OUR EVALUATION		Treating systematic errors as correlated			
122.2 ±0.5 OUR AVERAGE		Error includes scale factor of 1.4. See the ideogram below.			
121.55±0.16±0.46		ARTUSO	05	CLEO	$\Upsilon(3S) \to \gamma X$
123.0 ±0.8	4959	[1] HEINTZ	92	CSB2	$e^+e^- \to \gamma X$
124.6 ±1.4	17	[2] HEINTZ	92	CSB2	$e^+e^- \to \ell^+\ell^-\gamma\gamma$
122.3 ±0.3 ±0.6	9903	MORRISON	91	CLE2	$e^+e^- \to \gamma X$

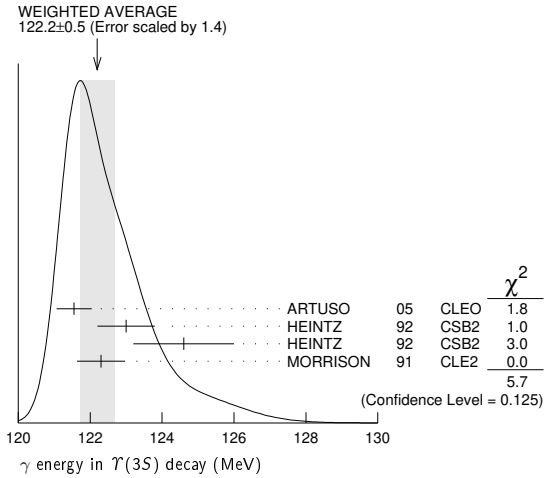

[1] A systematic uncertainty on the energy scale of 0.9% not included. Supersedes NARAIN 91.

[2] A systematic uncertainty on the energy scale of 0.9% not included. Supersedes HEINTZ 91.

$\chi_{b0}(2P)$ DECAY MODES

	Mode	Fraction (Γ_i/Γ)		Confidence level
Γ_1	$\gamma\Upsilon(2S)$	(1.38±0.30)	%	
Γ_2	$\gamma\Upsilon(1S)$	(3.8 ±1.7)	$\times 10^{-3}$	
Γ_3	D^0X	< 8.2	%	90%
Γ_4	$\pi^+\pi^-K^+K^-\pi^0$	< 3.4	$\times 10^{-5}$	90%
Γ_5	$2\pi^+\pi^-K^-K^0_S$	< 5	$\times 10^{-5}$	90%
Γ_6	$2\pi^+\pi^-K^-K^0_S2\pi^0$	< 2.2	$\times 10^{-4}$	90%
Γ_7	$2\pi^+2\pi^-2\pi^0$	< 2.4	$\times 10^{-4}$	90%
Γ_8	$2\pi^+2\pi^-K^+K^-$	< 1.5	$\times 10^{-4}$	90%
Γ_9	$2\pi^+2\pi^-K^+K^-\pi^0$	< 2.2	$\times 10^{-4}$	90%
Γ_{10}	$2\pi^+2\pi^-K^+K^-2\pi^0$	< 1.1	$\times 10^{-3}$	90%
Γ_{11}	$3\pi^+2\pi^-K^-K^0_S\pi^0$	< 7	$\times 10^{-4}$	90%
Γ_{12}	$3\pi^+3\pi^-$	< 7	$\times 10^{-5}$	90%
Γ_{13}	$3\pi^+3\pi^-2\pi^0$	< 1.2	$\times 10^{-3}$	90%
Γ_{14}	$3\pi^+3\pi^-K^+K^-$	< 1.5	$\times 10^{-4}$	90%
Γ_{15}	$3\pi^+3\pi^-K^+K^-\pi^0$	< 7	$\times 10^{-4}$	90%
Γ_{16}	$4\pi^+4\pi^-$	< 1.7	$\times 10^{-4}$	90%
Γ_{17}	$4\pi^+4\pi^-2\pi^0$	< 6	$\times 10^{-4}$	90%

$\chi_{b0}(2P)$ BRANCHING RATIOS

$\Gamma(\gamma\Upsilon(2S))/\Gamma_{total}$ — Γ_1/Γ

VALUE (%)	CL%	DOCUMENT ID		TECN	COMMENT
1.38±0.30 OUR AVERAGE					
$1.31 \pm 0.27^{+0.13}_{-0.12}$		[3,4] LEES	14M	BABR	$\Upsilon(3S) \to \gamma\gamma\mu^+\mu^-$
3.6 ±1.6 ±0.3		[3,5] HEINTZ	92	CSB2	$e^+e^- \to \ell^+\ell^-\gamma\gamma$
• • • We do not use the following data for averages, fits, limits, etc. • • •					
<2.8	90	[6] LEES	11J	BABR	$\Upsilon(3S) \to X\gamma$
<8.9	90	[7] CRAWFORD	92B	CLE2	$e^+e^- \to \ell^+\ell^-\gamma\gamma$

[3] Assuming $B(\Upsilon(2S) \to \mu^+\mu^-) = (1.93 \pm 0.17)\%$.

[4] LEES 14M reports $[\Gamma(\chi_{b0}(2P) \to \gamma\Upsilon(2S))/\Gamma_{total}] \times [B(\Upsilon(3S) \to \gamma\chi_{b0}(2P))] = (7.7 \pm 1.6) \times 10^{-4}$ which we divide by our best value $B(\Upsilon(3S) \to \gamma\chi_{b0}(2P)) = (5.9 \pm 0.6) \times 10^{-2}$. Our first error is their experiment's error and our second error is the systematic error from using our best value.

[5] Recalculated by us. HEINTZ 92 quotes $B(\Upsilon(3S) \to \gamma\chi_{b0}(2P)) \times B(\chi_{b0}(2P) \to \gamma\Upsilon(2S)) = (0.28 \pm 0.12 \pm 0.03)\%$ using $B(\Upsilon(2S) \to \mu^+\mu^-) = (1.44 \pm 0.10)\%$. Supersedes HEINTZ 91.

[6] LEES 11J quotes a central value of $\Gamma(\chi_{b0}(2P) \to \gamma\Upsilon(2S))/\Gamma_{total} \times \Gamma(\Upsilon(3S) \to \gamma\chi_{b0}(2P))/\Gamma_{total} = (-0.3 \pm 0.2^{+0.5}_{-0.4})\%$.

[7] Using $B(\Upsilon(2S) \to \mu^+\mu^-) = (1.37 \pm 0.26)\%$, $B(\Upsilon(3S) \to \gamma\gamma\Upsilon(2S)) \times 2\, B(\Upsilon(2S) \to \mu^+\mu^-) < 1.19 \times 10^{-4}$, and $B(\Upsilon(3S) \to \chi_{b0}(2P)\gamma) = 0.049$.

$\Gamma(\gamma\Upsilon(1S))/\Gamma_{total}$ — Γ_2/Γ

VALUE (%)	CL%	DOCUMENT ID		TECN	COMMENT
0.38±0.17 OUR AVERAGE					
0.36±0.17±0.03		[8,9,10] LEES	14M	BABR	$\Upsilon(3S) \to \gamma\gamma\mu^+\mu^-$
0.9 ±0.7 ±0.1		[9,11] HEINTZ	92	CSB2	$e^+e^- \to \ell^+\ell^-\gamma\gamma$
• • • We do not use the following data for averages, fits, limits, etc. • • •					
<1.2	90	[12] LEES	11J	BABR	$\Upsilon(3S) \to X\gamma$
<2.5	90	[13] CRAWFORD	92B	CLE2	$e^+e^- \to \ell^+\ell^-\gamma\gamma$

[8] LEES 14M quotes $\Gamma(\chi_{b0}(2P) \to \gamma\Upsilon(1S))/\Gamma_{total} \times \Gamma(\Upsilon(3S) \to \gamma\chi_{b0}(2P))/\Gamma_{total} = (2.1 \pm 1.0) \times 10^{-4}$ combining the results from $\Upsilon(3S) \to \gamma\gamma\mu^+\mu^-$ samples with and without photon conversions.

[9] Assuming $B(\Upsilon(1S) \to \mu^+\mu^-) = (2.48 \pm 0.05)\%$.

[10] LEES 14M reports $[\Gamma(\chi_{b0}(2P) \to \gamma\Upsilon(1S))/\Gamma_{total}] \times [B(\Upsilon(3S) \to \gamma\chi_{b0}(2P))] = (2.1 \pm 1.0) \times 10^{-4}$ which we divide by our best value $B(\Upsilon(3S) \to \gamma\chi_{b0}(2P)) = (5.9 \pm 0.6) \times 10^{-2}$. Our first error is their experiment's error and our second error is the systematic error from using our best value.

[11] Recalculated by us. HEINTZ 92 quotes $B(\Upsilon(3S) \to \gamma\chi_{b0}(2P)) \times B(\chi_{b0}(2P) \to \gamma\Upsilon(1S)) = (0.05 \pm 0.04 \pm 0.01)\%$ using $B(\Upsilon(1S) \to \mu^+\mu^-) = (2.57 \pm 0.05)\%$. Supersedes HEINTZ 91.

[12] LEES 11J quotes a central value of $\Gamma(\chi_{b0}(2P) \to \gamma\Upsilon(1S))/\Gamma_{total} \times \Gamma(\Upsilon(3S) \to \gamma\chi_{b0}(2P))/\Gamma_{total} = (3.9 \pm 2.2^{+1.2}_{-0.6}) \times 10^{-4}$.

[13] Using $B(\Upsilon(1S) \to \mu^+\mu^-) = (2.57 \pm 0.07)\%$, $B(\Upsilon(3S) \to \gamma\gamma\Upsilon(1S)) \times 2\, B(\Upsilon(1S) \to \mu^+\mu^-) < 0.63 \times 10^{-4}$, and $B(\Upsilon(3S) \to \chi_{b0}(2P)\gamma) = 0.049$.

$\Gamma(D^0X)/\Gamma_{total}$ — Γ_3/Γ

VALUE	CL%	DOCUMENT ID		TECN	COMMENT
<8.2 × 10⁻²	90	[14,15] BRIERE	08	CLEO	$\Upsilon(3S) \to \gamma D^0X$

[14] For $p_{D^0} > 2.5$ GeV/c.

[15] The authors also present their result as $(4.1 \pm 3.0 \pm 0.4) \times 10^{-2}$.

$\Gamma(\pi^+\pi^-K^+K^-\pi^0)/\Gamma_{total}$ — Γ_4/Γ

VALUE (units 10^{-4})	CL%	DOCUMENT ID		TECN	COMMENT
<0.34	90	[16] ASNER	08A	CLEO	$\Upsilon(3S) \to \gamma\pi^+\pi^-K^+K^-\pi^0$

[16] ASNER 08A reports $[\Gamma(\chi_{b0}(2P) \to \pi^+\pi^-K^+K^-\pi^0)/\Gamma_{total}] \times [B(\Upsilon(3S) \to \gamma\chi_{b0}(2P))] < 2 \times 10^{-6}$ which we divide by our best value $B(\Upsilon(3S) \to \gamma\chi_{b0}(2P)) = 5.9 \times 10^{-2}$.

$\Gamma(2\pi^+\pi^-K^-K^0_S)/\Gamma_{total}$ — Γ_5/Γ

VALUE (units 10^{-4})	CL%	DOCUMENT ID		TECN	COMMENT
<0.5	90	[17] ASNER	08A	CLEO	$\Upsilon(3S) \to \gamma 2\pi^+\pi^-K^-K^0_S$

[17] ASNER 08A reports $[\Gamma(\chi_{b0}(2P) \to 2\pi^+\pi^-K^-K^0_S)/\Gamma_{total}] \times [B(\Upsilon(3S) \to \gamma\chi_{b0}(2P))] < 3 \times 10^{-6}$ which we divide by our best value $B(\Upsilon(3S) \to \gamma\chi_{b0}(2P)) = 5.9 \times 10^{-2}$.

$\Gamma(2\pi^+\pi^-K^-K^0_S2\pi^0)/\Gamma_{total}$ — Γ_6/Γ

VALUE (units 10^{-4})	CL%	DOCUMENT ID		TECN	COMMENT
<2.2	90	[18] ASNER	08A	CLEO	$\Upsilon(3S) \to \gamma 2\pi^+\pi^-K^-2\pi^0$

[18] ASNER 08A reports $[\Gamma(\chi_{b0}(2P) \to 2\pi^+\pi^-K^-K^0_S2\pi^0)/\Gamma_{total}] \times [B(\Upsilon(3S) \to \gamma\chi_{b0}(2P))] < 13 \times 10^{-6}$ which we divide by our best value $B(\Upsilon(3S) \to \gamma\chi_{b0}(2P)) = 5.9 \times 10^{-2}$.

$\Gamma(2\pi^+2\pi^-2\pi^0)/\Gamma_{total}$ — Γ_7/Γ

VALUE (units 10^{-4})	CL%	DOCUMENT ID		TECN	COMMENT
<2.4	90	[19] ASNER	08A	CLEO	$\Upsilon(3S) \to \gamma 2\pi^+2\pi^-2\pi^0$

[19] ASNER 08A reports $[\Gamma(\chi_{b0}(2P) \to 2\pi^+2\pi^-2\pi^0)/\Gamma_{total}] \times [B(\Upsilon(3S) \to \gamma\chi_{b0}(2P))] < 14 \times 10^{-6}$ which we divide by our best value $B(\Upsilon(3S) \to \gamma\chi_{b0}(2P)) = 5.9 \times 10^{-2}$.

$\Gamma(2\pi^+2\pi^-K^+K^-)/\Gamma_{total}$ — Γ_8/Γ

VALUE (units 10^{-4})	CL%	DOCUMENT ID		TECN	COMMENT
<1.5	90	[20] ASNER	08A	CLEO	$\Upsilon(3S) \to \gamma 2\pi^+2\pi^-K^+K^-$

[20] ASNER 08A reports $[\Gamma(\chi_{b0}(2P) \to 2\pi^+2\pi^-K^+K^-)/\Gamma_{total}] \times [B(\Upsilon(3S) \to \gamma\chi_{b0}(2P))] < 9 \times 10^{-6}$ which we divide by our best value $B(\Upsilon(3S) \to \gamma\chi_{b0}(2P)) = 5.9 \times 10^{-2}$.

Downloaded from https://academic.oup.com/ptep/article/2022/8/083C01/6651666 by KIT Library user on 27 September 2022

$\Gamma(2\pi^+2\pi^-K^+K^-\pi^0)/\Gamma_{total}$ — Γ_9/Γ

VALUE (units 10^{-4})	CL%	DOCUMENT ID		TECN	COMMENT
<2.2	90	[21] ASNER	08A	CLEO	$\Upsilon(3S) \to \gamma 2\pi^+2\pi^-K^+K^-\pi^0$

[21] ASNER 08A reports $[\Gamma(\chi_{b0}(2P) \to 2\pi^+2\pi^-K^+K^-\pi^0)/\Gamma_{total}] \times [B(\Upsilon(3S) \to \gamma\chi_{b0}(2P))] < 13\times10^{-6}$ which we divide by our best value $B(\Upsilon(3S) \to \gamma\chi_{b0}(2P)) = 5.9\times10^{-2}$.

$\Gamma(2\pi^+2\pi^-K^+K^-2\pi^0)/\Gamma_{total}$ — Γ_{10}/Γ

VALUE (units 10^{-4})	CL%	DOCUMENT ID		TECN	COMMENT
<11	90	[22] ASNER	08A	CLEO	$\Upsilon(3S) \to \gamma 2\pi^+2\pi^-K^+K^-2\pi^0$

[22] ASNER 08A reports $[\Gamma(\chi_{b0}(2P) \to 2\pi^+2\pi^-K^+K^-2\pi^0)/\Gamma_{total}] \times [B(\Upsilon(3S) \to \gamma\chi_{b0}(2P))] < 63\times10^{-6}$ which we divide by our best value $B(\Upsilon(3S) \to \gamma\chi_{b0}(2P)) = 5.9\times10^{-2}$.

$\Gamma(3\pi^+2\pi^-K^-K^0_S\pi^0)/\Gamma_{total}$ — Γ_{11}/Γ

VALUE (units 10^{-4})	CL%	DOCUMENT ID		TECN	COMMENT
<7	90	[23] ASNER	08A	CLEO	$\Upsilon(3S) \to \gamma 3\pi^+2\pi^-K^-K^0_S\pi^0$

[23] ASNER 08A reports $[\Gamma(\chi_{b0}(2P) \to 3\pi^+2\pi^-K^-K^0_S\pi^0)/\Gamma_{total}] \times [B(\Upsilon(3S) \to \gamma\chi_{b0}(2P))] < 39\times10^{-6}$ which we divide by our best value $B(\Upsilon(3S) \to \gamma\chi_{b0}(2P)) = 5.9\times10^{-2}$.

$\Gamma(3\pi^+3\pi^-)/\Gamma_{total}$ — Γ_{12}/Γ

VALUE (units 10^{-4})	CL%	DOCUMENT ID		TECN	COMMENT
<0.7	90	[24] ASNER	08A	CLEO	$\Upsilon(3S) \to \gamma 3\pi^+3\pi^-$

[24] ASNER 08A reports $[\Gamma(\chi_{b0}(2P) \to 3\pi^+3\pi^-)/\Gamma_{total}] \times [B(\Upsilon(3S) \to \gamma\chi_{b0}(2P))] < 4\times10^{-6}$ which we divide by our best value $B(\Upsilon(3S) \to \gamma\chi_{b0}(2P)) = 5.9\times10^{-2}$.

$\Gamma(3\pi^+3\pi^-2\pi^0)/\Gamma_{total}$ — Γ_{13}/Γ

VALUE (units 10^{-4})	CL%	DOCUMENT ID		TECN	COMMENT
<12	90	[25] ASNER	08A	CLEO	$\Upsilon(3S) \to \gamma 3\pi^+3\pi^-2\pi^0$

[25] ASNER 08A reports $[\Gamma(\chi_{b0}(2P) \to 3\pi^+3\pi^-2\pi^0)/\Gamma_{total}] \times [B(\Upsilon(3S) \to \gamma\chi_{b0}(2P))] < 72\times10^{-6}$ which we divide by our best value $B(\Upsilon(3S) \to \gamma\chi_{b0}(2P)) = 5.9\times10^{-2}$.

$\Gamma(3\pi^+3\pi^-K^+K^-)/\Gamma_{total}$ — Γ_{14}/Γ

VALUE (units 10^{-4})	CL%	DOCUMENT ID		TECN	COMMENT
<1.5	90	[26] ASNER	08A	CLEO	$\Upsilon(3S) \to \gamma 3\pi^+3\pi^-K^+K^-$

[26] ASNER 08A reports $[\Gamma(\chi_{b0}(2P) \to 3\pi^+3\pi^-K^+K^-)/\Gamma_{total}] \times [B(\Upsilon(3S) \to \gamma\chi_{b0}(2P))] < 9\times10^{-6}$ which we divide by our best value $B(\Upsilon(3S) \to \gamma\chi_{b0}(2P)) = 5.9\times10^{-2}$.

$\Gamma(3\pi^+3\pi^-K^+K^-\pi^0)/\Gamma_{total}$ — Γ_{15}/Γ

VALUE (units 10^{-4})	CL%	DOCUMENT ID		TECN	COMMENT
<7	90	[27] ASNER	08A	CLEO	$\Upsilon(3S) \to \gamma 3\pi^+3\pi^-K^+K^-\pi^0$

[27] ASNER 08A reports $[\Gamma(\chi_{b0}(2P) \to 3\pi^+3\pi^-K^+K^-\pi^0)/\Gamma_{total}] \times [B(\Upsilon(3S) \to \gamma\chi_{b0}(2P))] < 43\times10^{-6}$ which we divide by our best value $B(\Upsilon(3S) \to \gamma\chi_{b0}(2P)) = 5.9\times10^{-2}$.

$\Gamma(4\pi^+4\pi^-)/\Gamma_{total}$ — Γ_{16}/Γ

VALUE (units 10^{-4})	CL%	DOCUMENT ID		TECN	COMMENT
<1.7	90	[28] ASNER	08A	CLEO	$\Upsilon(3S) \to \gamma 4\pi^+4\pi^-$

[28] ASNER 08A reports $[\Gamma(\chi_{b0}(2P) \to 4\pi^+4\pi^-)/\Gamma_{total}] \times [B(\Upsilon(3S) \to \gamma\chi_{b0}(2P))] < 10\times10^{-6}$ which we divide by our best value $B(\Upsilon(3S) \to \gamma\chi_{b0}(2P)) = 5.9\times10^{-2}$.

$\Gamma(4\pi^+4\pi^-2\pi^0)/\Gamma_{total}$ — Γ_{17}/Γ

VALUE (units 10^{-4})	CL%	DOCUMENT ID		TECN	COMMENT
<6	90	[29] ASNER	08A	CLEO	$\Upsilon(3S) \to \gamma 4\pi^+4\pi^-2\pi^0$

[29] ASNER 08A reports $[\Gamma(\chi_{b0}(2P) \to 4\pi^+4\pi^-2\pi^0)/\Gamma_{total}] \times [B(\Upsilon(3S) \to \gamma\chi_{b0}(2P))] < 38\times10^{-6}$ which we divide by our best value $B(\Upsilon(3S) \to \gamma\chi_{b0}(2P)) = 5.9\times10^{-2}$.

$\Gamma(\chi_{b0}(2P) \to \gamma\Upsilon(1S))/\Gamma_{total} \times \Gamma(\Upsilon(3S) \to \gamma\chi_{b0}(2P))/\Gamma_{total}$ — $\Gamma_2/\Gamma \times \Gamma_{22}^{\Upsilon(3S)}/\Gamma^{\Upsilon(3S)}$

VALUE (units 10^{-4})	CL%	DOCUMENT ID		TECN	COMMENT
<8.2	90	[30] LEES	11J	BABR	$\Upsilon(3S) \to X\gamma$

[30] LEES 11J quotes a central value of $\Gamma(\chi_{b0}(2P) \to \gamma\Upsilon(1S))/\Gamma_{total} \times \Gamma(\Upsilon(3S) \to \gamma\chi_{b0}(2P))/\Gamma_{total} = (3.9 \pm 2.2^{+1.2}_{-0.6}) \times 10^{-4}$ and derives a 90% CL upper limit of $B(\chi_{b0}(2P) \to \gamma\Upsilon(1S)) < 1.2\%$ using $B(\Upsilon(3S) \to \gamma\chi_{b0}(2P)) = (5.9 \pm 0.6)\%$.

$B(\chi_{b0}(2P) \to \gamma\Upsilon(1S)) \times B(\Upsilon(3S) \to \gamma\chi_{b0}(2P)) \times B(\Upsilon(1S) \to \ell^+\ell^-)$

VALUE (units 10^{-5})	DOCUMENT ID		TECN	COMMENT
1.4±0.9 OUR AVERAGE				
$1.7^{+1.5+0.1}_{-1.4-1.2}$	[31] LEES	14M	BABR	$\Upsilon(3S) \to \gamma\gamma\mu^+\mu^-$
1.3±1.0±0.3	[32] HEINTZ	92	CSB2	$\Upsilon(3S) \to \gamma\gamma\ell^+\ell^-$

[31] From a sample of $\Upsilon(3S) \to \gamma\gamma\mu^+\mu^-$ with one converted photon.

[32] Calculated by us. HEINTZ 92 quotes $B(\Upsilon(3S) \to \gamma\chi_{b0}(2P)) \times B(\chi_{b0}(2P) \to \gamma\Upsilon(1S)) = (0.05 \pm 0.04 \pm 0.01)\%$ using $B(\Upsilon(1S) \to \mu^+\mu^-) = (2.57 \pm 0.05)\%$.

$[B(\chi_{b0}(2P) \to \gamma\Upsilon(1S)) \times B(\Upsilon(3S) \to \gamma\chi_{b0}(2P))] / [B(\chi_{b1}(2P) \to \gamma\Upsilon(1S)) \times B(\Upsilon(3S) \to \gamma\chi_{b1}(2P))]$

VALUE (%)	DOCUMENT ID		TECN	COMMENT
1.71±0.80	[33] LEES	14M	BABR	$\Upsilon(3S) \to \gamma\gamma\mu^+\mu^-$

[33] From a sample of $\Upsilon(3S) \to \gamma\gamma\mu^+\mu^-$ without converted photons.

$\Gamma(\chi_{b0}(2P) \to \gamma\Upsilon(2S))/\Gamma_{total} \times \Gamma(\Upsilon(3S) \to \gamma\chi_{b0}(2P))/\Gamma_{total}$ — $\Gamma_1/\Gamma \times \Gamma_{22}^{\Upsilon(3S)}/\Gamma^{\Upsilon(3S)}$

VALUE (units 10^{-3})	CL%	DOCUMENT ID		TECN	COMMENT
<1.6	90	[34] LEES	11J	BABR	$\Upsilon(3S) \to X\gamma$

[34] LEES 11J quotes a central value of $\Gamma(\chi_{b0}(2P) \to \gamma\Upsilon(2S))/\Gamma_{total} \times \Gamma(\Upsilon(3S) \to \gamma\chi_{b0}(2P))/\Gamma_{total} = (-0.3 \pm 0.2^{+0.5}_{-0.4})\%$ and derives a 90% CL upper limit of $B(\chi_{b0}(2P) \to \gamma\Upsilon(2S)) < 2.8\%$ using $B(\Upsilon(3S) \to \gamma\chi_{b0}(2P)) = (5.9 \pm 0.6)\%$.

$B(\chi_{b0}(2P) \to \gamma\Upsilon(2S)) \times B(\Upsilon(3S) \to \gamma\chi_{b0}(2P)) \times B(\Upsilon(2S) \to \ell^+\ell^-)$

VALUE (units 10^{-5})	DOCUMENT ID		TECN	COMMENT
4.4±1.6 OUR AVERAGE				
$6.6^{+4.9+2.0}_{-4.0-0.3}$	[35] LEES	14M	BABR	$\Upsilon(3S) \to \gamma\gamma\mu^+\mu^-$
4.0±1.7±0.3	[36] HEINTZ	92	CSB2	$\Upsilon(3S) \to \gamma\gamma\ell^+\ell^-$

[35] From a sample of $\Upsilon(3S) \to \gamma\gamma\mu^+\mu^-$ with one converted photon.

[36] Calculated by us. HEINTZ 92 quotes $B(\Upsilon(3S) \to \gamma\chi_{b0}(2P)) \times B(\chi_{b0}(2P) \to \gamma\Upsilon(2S)) = (0.28 \pm 0.12 \pm 0.03)\%$ using $B(\Upsilon(2S) \to \mu^+\mu^-) = (1.44 \pm 0.10)\%$.

$[B(\chi_{b0}(2P) \to \gamma\Upsilon(2S)) \times B(\Upsilon(3S) \to \gamma\chi_{b0}(2P))] / [B(\chi_{b1}(2P) \to \gamma\Upsilon(2S)) \times B(\Upsilon(3S) \to \gamma\chi_{b1}(2P))]$

VALUE (%)	DOCUMENT ID		TECN	COMMENT
3.31±0.56	[37] LEES	14M	BABR	$\Upsilon(3S) \to \gamma\gamma\mu^+\mu^-$

[37] From a sample of $\Upsilon(3S) \to \gamma\gamma\mu^+\mu^-$ without converted photons.

$\chi_{b0}(2P)$ REFERENCES

LEES	14M	PR D90 112010	J.P. Lees *et al.*	(BABAR Collab.)
LEES	11J	PR D84 072002	J.P. Lees *et al.*	(BABAR Collab.)
ASNER	08A	PR D78 091103	D.M. Asner *et al.*	(CLEO Collab.)
BRIERE	08	PR D78 092007	R.A. Briere *et al.*	(CLEO Collab.)
ARTUSO	05	PRL 94 032001	M. Artuso *et al.*	(CLEO Collab.)
CRAWFORD	92B	PL B294 139	G. Crawford *et al.*	(CLEO Collab.)
HEINTZ	92	PR D46 1928	U. Heintz *et al.*	(CUSB II Collab.)
HEINTZ	91	PRL 66 1563	U. Heintz *et al.*	(CUSB Collab.)
MORRISON	91	PRL 67 1696	R.J. Morrison *et al.*	(CLEO Collab.)
NARAIN	91	PRL 66 3113	M. Narain *et al.*	(CUSB Collab.)

$\chi_{b1}(2P)$

$I^G(J^{PC}) = 0^+(1^{++})$
J needs confirmation.

Observed in radiative decay of the $\Upsilon(3S)$, therefore $C = +$. Branching ratio requires E1 transition, M1 is strongly disfavored, therefore $P = +$.

$\chi_{b1}(2P)$ MASS

VALUE (MeV)	DOCUMENT ID
10255.46±0.22±0.50 OUR EVALUATION	From γ energy below, using $\Upsilon(3S)$ mass = 10355.2 ± 0.5 MeV

$m_{\chi_{b1}(2P)} - m_{\chi_{b0}(2P)}$

VALUE (MeV)	DOCUMENT ID		TECN	COMMENT
23.5±0.7±0.7	[1] HEINTZ	92	CSB2	$e^+e^- \to \gamma X, \ell^+\ell^-\gamma\gamma$

[1] From the average photon energy for inclusive and exclusive events. Supersedes NARAIN 91.

γ ENERGY IN $\Upsilon(3S)$ DECAY

VALUE (MeV)	EVTS	DOCUMENT ID		TECN	COMMENT
99.26±0.22 OUR EVALUATION		Treating systematic errors as correlated			
99.53±0.23 OUR AVERAGE		Error includes scale factor of 1.3. See the ideogram below.			
99.15±0.07±0.25		ARTUSO	05	CLEO	$\Upsilon(3S) \to \gamma X$
99 ±1	169	CRAWFORD	92B	CLE2	$e^+e^- \to \ell^+\ell^-\gamma\gamma$
100.1 ±0.4	11147	[2] HEINTZ	92	CSB2	$e^+e^- \to \gamma X$
100.2 ±0.5	223	[3] HEINTZ	92	CSB2	$e^+e^- \to \ell^+\ell^-\gamma\gamma$
99.5 ±0.1 ±0.5	25759	MORRISON	91	CLE2	$e^+e^- \to \gamma X$

[2] A systematic uncertainty on the energy scale of 0.9% not included. Supersedes NARAIN 91.

[3] A systematic uncertainty on the energy scale of 0.9% not included. Supersedes HEINTZ 91.

Downloaded from https://academic.oup.com/ptep/article/2022/8/083C01/6651666 by KIT Library user on 27 September 2022

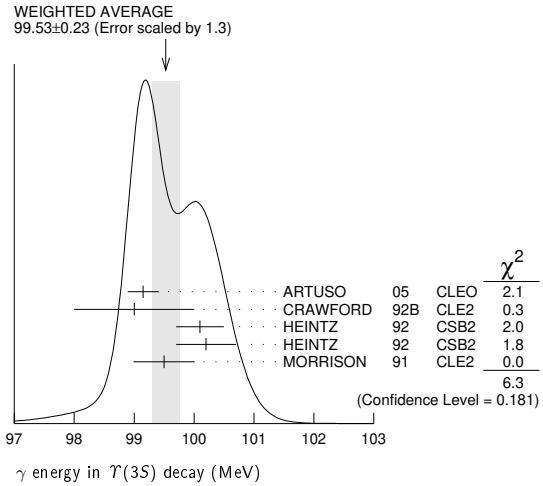

$\chi_{b1}(2P)$ DECAY MODES

	Mode	Fraction (Γ_i/Γ)
Γ_1	$\omega\,\Upsilon(1S)$	$(1.63^{+0.40}_{-0.34})$ %
Γ_2	$\gamma\,\Upsilon(2S)$	(18.1 ± 1.9) %
Γ_3	$\gamma\,\Upsilon(1S)$	(9.9 ± 1.0) %
Γ_4	$\pi\pi\chi_{b1}(1P)$	$(9.1 \pm 1.3) \times 10^{-3}$
Γ_5	$D^0 X$	(8.8 ± 1.7) %
Γ_6	$\pi^+\pi^-K^+K^-\pi^0$	$(3.1 \pm 1.0) \times 10^{-4}$
Γ_7	$2\pi^+\pi^-K^-K^0_S$	$(1.1 \pm 0.5) \times 10^{-4}$
Γ_8	$2\pi^+\pi^-K^-K^0_S 2\pi^0$	$(7.7 \pm 3.2) \times 10^{-4}$
Γ_9	$2\pi^+2\pi^-2\pi^0$	$(5.9 \pm 2.0) \times 10^{-4}$
Γ_{10}	$2\pi^+2\pi^-K^+K^-$	$(10 \pm 4) \times 10^{-5}$
Γ_{11}	$2\pi^+2\pi^-K^+K^-\pi^0$	$(5.5 \pm 1.8) \times 10^{-4}$
Γ_{12}	$2\pi^+2\pi^-K^+K^-2\pi^0$	$(10 \pm 4) \times 10^{-4}$
Γ_{13}	$3\pi^+2\pi^-K^-K^0_S\pi^0$	$(6.7 \pm 2.6) \times 10^{-4}$
Γ_{14}	$3\pi^+3\pi^-$	$(1.2 \pm 0.4) \times 10^{-4}$
Γ_{15}	$3\pi^+3\pi^-2\pi^0$	$(1.2 \pm 0.4) \times 10^{-3}$
Γ_{16}	$3\pi^+3\pi^-K^+K^-$	$(2.0 \pm 0.8) \times 10^{-4}$
Γ_{17}	$3\pi^+3\pi^-K^+K^-\pi^0$	$(6.1 \pm 2.2) \times 10^{-4}$
Γ_{18}	$4\pi^+4\pi^-$	$(1.7 \pm 0.6) \times 10^{-4}$
Γ_{19}	$4\pi^+4\pi^-2\pi^0$	$(1.9 \pm 0.7) \times 10^{-3}$

$\chi_{b1}(2P)$ BRANCHING RATIOS

$\Gamma(\omega\,\Upsilon(1S))/\Gamma_{total}$ — Γ_1/Γ

VALUE (units 10^{-2})	EVTS	DOCUMENT ID	TECN	COMMENT
$\mathbf{1.63^{+0.35}_{-0.31}{}^{+0.16}_{-0.15}}$	$32.6^{+6.9}_{-6.1}$	[4] CRONIN-HEN..04	CLE3	$\Upsilon(3S) \to \gamma\omega\,\Upsilon(1S)$

[4] Using $B(\Upsilon(3S) \to \gamma\chi_{b1}(2P)) = (11.3 \pm 0.6)\%$ and $B(\Upsilon(1S) \to \ell^+\ell^-) = 2\,B(\Upsilon(1S) \to \mu^+\mu^-) = 2\,(2.48 \pm 0.06)\%$.

$\Gamma(\gamma\,\Upsilon(2S))/\Gamma_{total}$ — Γ_2/Γ

VALUE	EVTS	DOCUMENT ID		TECN	COMMENT
0.181±0.019 OUR AVERAGE					
0.211±0.017±0.019		[5,6,7] LEES	14M	BABR	$\Upsilon(3S) \to \gamma\gamma\mu^+\mu^-$
0.190±0.018±0.017	4.3k	[8] LEES	11J	BABR	$\Upsilon(3S) \to X\gamma$
0.206±0.035±0.019		[5,9] CRAWFORD	92B	CLE2	$e^+e^- \to \ell^+\ell^-\gamma\gamma$
0.132±0.018±0.012		[5,10] HEINTZ	92	CSB2	$e^+e^- \to \ell^+\ell^-\gamma\gamma$

[5] Assuming $B(\Upsilon(2S) \to \mu^+\mu^-) = (1.93 \pm 0.17)\%$.

[6] LEES 14M quotes $\Gamma(\chi_{b1}(2P) \to \gamma\,\Upsilon(2S))/\Gamma_{total} \times \Gamma(\Upsilon(3S) \to \gamma\chi_{b1}(2P))/\Gamma_{total} = (2.66 \pm 0.22)\%$ combining the results from $\Upsilon(3S) \to \gamma\gamma\mu^+\mu^-$ samples with and without photon conversions.

[7] LEES 14M reports $[\Gamma(\chi_{b1}(2P) \to \gamma\,\Upsilon(2S))/\Gamma_{total}] \times [B(\Upsilon(3S) \to \gamma\chi_{b1}(2P))] = (2.66 \pm 0.22) \times 10^{-2}$ which we divide by our best value $B(\Upsilon(3S) \to \gamma\chi_{b1}(2P)) = (12.6 \pm 1.2) \times 10^{-2}$. Our first error is their experiment's error and our second error is the systematic error from using our best value.

[8] LEES 11J reports $[\Gamma(\chi_{b1}(2P) \to \gamma\,\Upsilon(2S))/\Gamma_{total}] \times [B(\Upsilon(3S) \to \gamma\chi_{b1}(2P))] = (2.4 \pm 0.1 \pm 0.2) \times 10^{-2}$ which we divide by our best value $B(\Upsilon(3S) \to \gamma\chi_{b1}(2P)) = (12.6 \pm 1.2) \times 10^{-2}$. Our first error is their experiment's error and our second error is the systematic error from using our best value.

[9] CRAWFORD 92B quotes $B(\Upsilon(3S) \to \gamma\chi_{b1}(2P)) \times B(\chi_{b1}(2P) \to \gamma\,\Upsilon(2S)) \times 2\,B(\Upsilon(2S) \to \ell^+\ell^-) = (10.23 \pm 1.20 \pm 1.26)\ 10^{-4}$.

[10] Recalculated by us. HEINTZ 92 quotes $B(\Upsilon(3S) \to \gamma\chi_{b1}(2P)) \times B(\chi_{b1}(2P) \to \gamma\,\Upsilon(2S)) = (2.29 \pm 0.23 \pm 0.21)$ % using $B(\Upsilon(2S) \to \mu^+\mu^-) = (1.44 \pm 0.10)\%$. Supersedes HEINTZ 91.

$\Gamma(\gamma\,\Upsilon(1S))/\Gamma_{total}$ — Γ_3/Γ

VALUE	EVTS	DOCUMENT ID		TECN	COMMENT
0.099±0.010 OUR AVERAGE					
0.107±0.006±0.010		[11,12,13] LEES	14M	BABR	$\Upsilon(3S) \to \gamma\gamma\mu^+\mu^-$
0.098±0.005±0.009	15k	[14] LEES	11J	BABR	$\Upsilon(3S) \to X\gamma$
0.103±0.023±0.009		[11,15] CRAWFORD	92B	CLE2	$e^+e^- \to \ell^+\ell^-\gamma\gamma$
0.075±0.010±0.007		[11,16] HEINTZ	92	CSB2	$e^+e^- \to \ell^+\ell^-\gamma\gamma$

[11] Assuming $B(\Upsilon(1S) \to \mu^+\mu^-) = (2.48 \pm 0.05)\%$.

[12] LEES 14M quotes $\Gamma(\chi_{b1}(2P) \to \gamma\,\Upsilon(1S))/\Gamma_{total} \times \Gamma(\Upsilon(3S) \to \gamma\chi_{b1}(2P))/\Gamma_{total} = (13.48 \pm 0.72) \times 10^{-3}$ combining the results from samples of $\Upsilon(3S) \to \gamma\gamma\mu^+\mu^-$ with and without converted photons.

[13] LEES 14M reports $[\Gamma(\chi_{b1}(2P) \to \gamma\,\Upsilon(1S))/\Gamma_{total}] \times [B(\Upsilon(3S) \to \gamma\chi_{b1}(2P))] = (13.48 \pm 0.72) \times 10^{-3}$ which we divide by our best value $B(\Upsilon(3S) \to \gamma\chi_{b1}(2P)) = (12.6 \pm 1.2) \times 10^{-2}$. Our first error is their experiment's error and our second error is the systematic error from using our best value.

[14] LEES 11J reports $[\Gamma(\chi_{b1}(2P) \to \gamma\,\Upsilon(1S))/\Gamma_{total}] \times [B(\Upsilon(3S) \to \gamma\chi_{b1}(2P))] = (12.4 \pm 0.3 \pm 0.6) \times 10^{-3}$ which we divide by our best value $B(\Upsilon(3S) \to \gamma\chi_{b1}(2P)) = (12.6 \pm 1.2) \times 10^{-2}$. Our first error is their experiment's error and our second error is the systematic error from using our best value.

[15] CRAWFORD 92B quotes $B(\Upsilon(3S) \to \gamma\chi_{b1}(2P)) \times B(\chi_{b1}(2P) \to \gamma\,\Upsilon(1S)) \times 2\,B(\Upsilon(1S) \to \ell^+\ell^-) = (6.47 \pm 1.12 \pm 0.82)\ 10^{-4}$.

[16] Recalculated by us. HEINTZ 92 quotes $B(\Upsilon(3S) \to \gamma\chi_{b1}(2P)) \times B(\chi_{b1}(2P) \to \gamma\,\Upsilon(1S)) = (0.91 \pm 0.11 \pm 0.06)\%$ using $B(\Upsilon(1S) \to \mu^+\mu^-) = (2.57 \pm 0.05)\%$. Supersedes HEINTZ 91.

$\Gamma(\pi\pi\chi_{b1}(1P))/\Gamma_{total}$ — Γ_4/Γ

VALUE (units 10^{-3})	EVTS	DOCUMENT ID		TECN	COMMENT
9.1±1.3 OUR AVERAGE					
9.2±1.1±0.8	31k	[17] LEES	11C	BABR	$e^+e^- \to \pi^+\pi^-X$
8.6±2.3±2.1		[18] CAWLFIELD	06	CLE3	$\Upsilon(3S) \to 2(\gamma\pi\ell)$

[17] LEES 11C measures $B(\Upsilon(3S) \to \chi_{b1}(2P)X) \times B(\chi_{b1}(2P) \to \chi_{b1}(1P)\pi^+\pi^-) = (1.16 \pm 0.07 \pm 0.12) \times 10^{-3}$. We derive the value assuming $B(\Upsilon(3S) \to \chi_{b1}(2P)X) = B(\Upsilon(3S) \to \chi_{b1}(2P)\gamma) = (12.6 \pm 1.2) \times 10^{-2}$.

[18] CAWLFIELD 06 quote $\Gamma(\chi_b(2P) \to \pi\pi\chi_b(1P)) = 0.83 \pm 0.22 \pm 0.08 \pm 0.19$ keV assuming l-spin conservation, no D-wave contribution, $\Gamma(\chi_{b1}(2P)) = 96 \pm 16$keV, and $\Gamma(\chi_{b2}(2P)) = 138 \pm 19$ keV.

$\Gamma(D^0X)/\Gamma_{total}$ — Γ_5/Γ

VALUE (units 10^{-2})	EVTS	DOCUMENT ID		TECN	COMMENT
8.8±1.5±0.8	2243	[19] BRIERE	08	CLEO	$\Upsilon(3S) \to \gamma D^0X$

[19] For $p_{D^0} > 2.5$ GeV/c.

$\Gamma(\pi^+\pi^-K^+K^-\pi^0)/\Gamma_{total}$ — Γ_6/Γ

VALUE (units 10^{-4})	EVTS	DOCUMENT ID		TECN	COMMENT
3.1±1.0±0.3	30	[20] ASNER	08A	CLEO	$\Upsilon(3S) \to \gamma\pi^+\pi^-K^+K^-\pi^0$

[20] ASNER 08A reports $[\Gamma(\chi_{b1}(2P) \to \pi^+\pi^-K^+K^-\pi^0)/\Gamma_{total}] \times [B(\Upsilon(3S) \to \gamma\chi_{b1}(2P))] = (39 \pm 8 \pm 9) \times 10^{-6}$ which we divide by our best value $B(\Upsilon(3S) \to \gamma\chi_{b1}(2P)) = (12.6 \pm 1.2) \times 10^{-2}$. Our first error is their experiment's error and our second error is the systematic error from using our best value.

$\Gamma(2\pi^+\pi^-K^-K^0_S)/\Gamma_{total}$ — Γ_7/Γ

VALUE (units 10^{-4})	EVTS	DOCUMENT ID		TECN	COMMENT
1.1±0.5±0.1	10	[21] ASNER	08A	CLEO	$\Upsilon(3S) \to \gamma 2\pi^+\pi^-K^-K^0_S$

[21] ASNER 08A reports $[\Gamma(\chi_{b1}(2P) \to 2\pi^+\pi^-K^-K^0_S)/\Gamma_{total}] \times [B(\Upsilon(3S) \to \gamma\chi_{b1}(2P))] = (14 \pm 5 \pm 3) \times 10^{-6}$ which we divide by our best value $B(\Upsilon(3S) \to \gamma\chi_{b1}(2P)) = (12.6 \pm 1.2) \times 10^{-2}$. Our first error is their experiment's error and our second error is the systematic error from using our best value.

$\Gamma(2\pi^+\pi^-K^-K^0_S 2\pi^0)/\Gamma_{total}$ — Γ_8/Γ

VALUE (units 10^{-4})	EVTS	DOCUMENT ID		TECN	COMMENT
7.7±3.1±0.7	15	[22] ASNER	08A	CLEO	$\Upsilon(3S) \to \gamma 2\pi^+\pi^-K^-2\pi^0$

[22] ASNER 08A reports $[\Gamma(\chi_{b1}(2P) \to 2\pi^+\pi^-K^-K^0_S 2\pi^0)/\Gamma_{total}] \times [B(\Upsilon(3S) \to \gamma\chi_{b1}(2P))] = (97 \pm 30 \pm 26) \times 10^{-6}$ which we divide by our best value $B(\Upsilon(3S) \to \gamma\chi_{b1}(2P)) = (12.6 \pm 1.2) \times 10^{-2}$. Our first error is their experiment's error and our second error is the systematic error from using our best value.

$\Gamma(2\pi^+2\pi^-2\pi^0)/\Gamma_{total}$ — Γ_9/Γ

VALUE (units 10^{-4})	EVTS	DOCUMENT ID		TECN	COMMENT
5.9±2.0±0.5	36	[23] ASNER	08A	CLEO	$\Upsilon(3S) \to \gamma 2\pi^+2\pi^-2\pi^0$

[23] ASNER 08A reports $[\Gamma(\chi_{b1}(2P) \to 2\pi^+2\pi^-2\pi^0)/\Gamma_{total}] \times [B(\Upsilon(3S) \to \gamma\chi_{b1}(2P))] = (74 \pm 16 \pm 19) \times 10^{-6}$ which we divide by our best value $B(\Upsilon(3S) \to \gamma\chi_{b1}(2P)) = (12.6 \pm 1.2) \times 10^{-2}$. Our first error is their experiment's error and our second error is the systematic error from using our best value.

$\Gamma(2\pi^+2\pi^-K^+K^-)/\Gamma_{total}$ — Γ_{10}/Γ

VALUE (units 10^{-4})	EVTS	DOCUMENT ID		TECN	COMMENT
1.0±0.4±0.1	12	[24] ASNER	08A	CLEO	$\Upsilon(3S) \to \gamma 2\pi^+2\pi^-K^+K^-$

[24] ASNER 08A reports $[\Gamma(\chi_{b1}(2P) \to 2\pi^+2\pi^-K^+K^-)/\Gamma_{total}] \times [B(\Upsilon(3S) \to \gamma\chi_{b1}(2P))] = (12 \pm 4 \pm 3) \times 10^{-6}$ which we divide by our best value $B(\Upsilon(3S) \to \gamma\chi_{b1}(2P)) = (12.6 \pm 1.2) \times 10^{-2}$. Our first error is their experiment's error and our second error is the systematic error from using our best value.

Downloaded from https://academic.oup.com/ptep/article/2022/8/083C01/6651666 by KIT Library user on 27 September 2022

$\Gamma(2\pi^+2\pi^-K^+K^-\pi^0)/\Gamma_{total}$ — Γ_{11}/Γ

VALUE (units 10^{-4})	EVTS	DOCUMENT ID		TECN	COMMENT
5.5±1.7±0.5	38	[25] ASNER	08A	CLEO	$\Upsilon(3S) \to \gamma 2\pi^+2\pi^-K^+K^-\pi^0$

[25] ASNER 08A reports $[\Gamma(\chi_{b1}(2P) \to 2\pi^+2\pi^-K^+K^-\pi^0)/\Gamma_{total}] \times [B(\Upsilon(3S) \to \gamma\chi_{b1}(2P))] = (69 \pm 13 \pm 17) \times 10^{-6}$ which we divide by our best value $B(\Upsilon(3S) \to \gamma\chi_{b1}(2P)) = (12.6 \pm 1.2) \times 10^{-2}$. Our first error is their experiment's error and our second error is the systematic error from using our best value.

$\Gamma(2\pi^+2\pi^-K^+K^-2\pi^0)/\Gamma_{total}$ — Γ_{12}/Γ

VALUE (units 10^{-4})	EVTS	DOCUMENT ID		TECN	COMMENT
9.6±3.5±0.9	27	[26] ASNER	08A	CLEO	$\Upsilon(3S) \to \gamma 2\pi^+2\pi^-K^+K^-2\pi^0$

[26] ASNER 08A reports $[\Gamma(\chi_{b1}(2P) \to 2\pi^+2\pi^-K^+K^-2\pi^0)/\Gamma_{total}] \times [B(\Upsilon(3S) \to \gamma\chi_{b1}(2P))] = (121 \pm 29 \pm 33) \times 10^{-6}$ which we divide by our best value $B(\Upsilon(3S) \to \gamma\chi_{b1}(2P)) = (12.6 \pm 1.2) \times 10^{-2}$. Our first error is their experiment's error and our second error is the systematic error from using our best value.

$\Gamma(3\pi^+2\pi^-K^-K^0_S\pi^0)/\Gamma_{total}$ — Γ_{13}/Γ

VALUE (units 10^{-4})	EVTS	DOCUMENT ID		TECN	COMMENT
6.7±2.5±0.6	17	[27] ASNER	08A	CLEO	$\Upsilon(3S) \to \gamma 3\pi^+2\pi^-K^-K^0_S\pi^0$

[27] ASNER 08A reports $[\Gamma(\chi_{b1}(2P) \to 3\pi^+2\pi^-K^-K^0_S\pi^0)/\Gamma_{total}] \times [B(\Upsilon(3S) \to \gamma\chi_{b1}(2P))] = (85 \pm 23 \pm 22) \times 10^{-6}$ which we divide by our best value $B(\Upsilon(3S) \to \gamma\chi_{b1}(2P)) = (12.6 \pm 1.2) \times 10^{-2}$. Our first error is their experiment's error and our second error is the systematic error from using our best value.

$\Gamma(3\pi^+3\pi^-)/\Gamma_{total}$ — Γ_{14}/Γ

VALUE (units 10^{-4})	EVTS	DOCUMENT ID		TECN	COMMENT
1.2±0.4±0.1	18	[28] ASNER	08A	CLEO	$\Upsilon(3S) \to \gamma 3\pi^+3\pi^-$

[28] ASNER 08A reports $[\Gamma(\chi_{b1}(2P) \to 3\pi^+3\pi^-)/\Gamma_{total}] \times [B(\Upsilon(3S) \to \gamma\chi_{b1}(2P))] = (15 \pm 4 \pm 3) \times 10^{-6}$ which we divide by our best value $B(\Upsilon(3S) \to \gamma\chi_{b1}(2P)) = (12.6 \pm 1.2) \times 10^{-2}$. Our first error is their experiment's error and our second error is the systematic error from using our best value.

$\Gamma(3\pi^+3\pi^-2\pi^0)/\Gamma_{total}$ — Γ_{15}/Γ

VALUE (units 10^{-4})	EVTS	DOCUMENT ID		TECN	COMMENT
12±4±1	44	[29] ASNER	08A	CLEO	$\Upsilon(3S) \to \gamma 3\pi^+3\pi^-2\pi^0$

[29] ASNER 08A reports $[\Gamma(\chi_{b1}(2P) \to 3\pi^+3\pi^-2\pi^0)/\Gamma_{total}] \times [B(\Upsilon(3S) \to \gamma\chi_{b1}(2P))] = (150 \pm 30 \pm 40) \times 10^{-6}$ which we divide by our best value $B(\Upsilon(3S) \to \gamma\chi_{b1}(2P)) = (12.6 \pm 1.2) \times 10^{-2}$. Our first error is their experiment's error and our second error is the systematic error from using our best value.

$\Gamma(3\pi^+3\pi^-K^+K^-)/\Gamma_{total}$ — Γ_{16}/Γ

VALUE (units 10^{-4})	EVTS	DOCUMENT ID		TECN	COMMENT
2.0±0.7±0.2	16	[30] ASNER	08A	CLEO	$\Upsilon(3S) \to \gamma 3\pi^+3\pi^-K^+K^-$

[30] ASNER 08A reports $[\Gamma(\chi_{b1}(2P) \to 3\pi^+3\pi^-K^+K^-)/\Gamma_{total}] \times [B(\Upsilon(3S) \to \gamma\chi_{b1}(2P))] = (25 \pm 7 \pm 6) \times 10^{-6}$ which we divide by our best value $B(\Upsilon(3S) \to \gamma\chi_{b1}(2P)) = (12.6 \pm 1.2) \times 10^{-2}$. Our first error is their experiment's error and our second error is the systematic error from using our best value.

$\Gamma(3\pi^+3\pi^-K^+K^-\pi^0)/\Gamma_{total}$ — Γ_{17}/Γ

VALUE (units 10^{-4})	EVTS	DOCUMENT ID		TECN	COMMENT
6.1±2.1±0.6	25	[31] ASNER	08A	CLEO	$\Upsilon(3S) \to \gamma 3\pi^+3\pi^-K^+K^-\pi^0$

[31] ASNER 08A reports $[\Gamma(\chi_{b1}(2P) \to 3\pi^+3\pi^-K^+K^-\pi^0)/\Gamma_{total}] \times [B(\Upsilon(3S) \to \gamma\chi_{b1}(2P))] = (77 \pm 17 \pm 21) \times 10^{-6}$ which we divide by our best value $B(\Upsilon(3S) \to \gamma\chi_{b1}(2P)) = (12.6 \pm 1.2) \times 10^{-2}$. Our first error is their experiment's error and our second error is the systematic error from using our best value.

$\Gamma(4\pi^+4\pi^-)/\Gamma_{total}$ — Γ_{18}/Γ

VALUE (units 10^{-4})	EVTS	DOCUMENT ID		TECN	COMMENT
1.7±0.6±0.2	16	[32] ASNER	08A	CLEO	$\Upsilon(3S) \to \gamma 4\pi^+4\pi^-$

[32] ASNER 08A reports $[\Gamma(\chi_{b1}(2P) \to 4\pi^+4\pi^-)/\Gamma_{total}] \times [B(\Upsilon(3S) \to \gamma\chi_{b1}(2P))] = (22 \pm 6 \pm 5) \times 10^{-6}$ which we divide by our best value $B(\Upsilon(3S) \to \gamma\chi_{b1}(2P)) = (12.6 \pm 1.2) \times 10^{-2}$. Our first error is their experiment's error and our second error is the systematic error from using our best value.

$\Gamma(4\pi^+4\pi^-2\pi^0)/\Gamma_{total}$ — Γ_{19}/Γ

VALUE (units 10^{-4})	EVTS	DOCUMENT ID		TECN	COMMENT
19±7±2	41	[33] ASNER	08A	CLEO	$\Upsilon(3S) \to \gamma 4\pi^+4\pi^-2\pi^0$

[33] ASNER 08A reports $[\Gamma(\chi_{b1}(2P) \to 4\pi^+4\pi^-2\pi^0)/\Gamma_{total}] \times [B(\Upsilon(3S) \to \gamma\chi_{b1}(2P))] = (241 \pm 47 \pm 72) \times 10^{-6}$ which we divide by our best value $B(\Upsilon(3S) \to \gamma\chi_{b1}(2P)) = (12.6 \pm 1.2) \times 10^{-2}$. Our first error is their experiment's error and our second error is the systematic error from using our best value.

$\chi_{b1}(2P)$ Cross-Particle Branching Ratios

$\Gamma(\chi_{b1}(2P) \to \gamma\Upsilon(1S))/\Gamma_{total} \times \Gamma(\Upsilon(3S) \to \gamma\chi_{b1}(2P))/\Gamma_{total}$ — $\Gamma_3/\Gamma \times \Gamma_{21}^{\Upsilon(3S)}/\Gamma^{\Upsilon(3S)}$

VALUE (units 10^{-3})	EVTS	DOCUMENT ID		TECN	COMMENT
12.4±0.3±0.6	15k	LEES	11J	BABR	$\Upsilon(3S) \to X\gamma$

$B(\chi_{b1}(2P) \to \gamma\Upsilon(1S)) \times B(\Upsilon(3S) \to \gamma\chi_{b1}(2P)) \times B(\Upsilon(1S) \to \ell^+\ell^-)$

VALUE (units 10^{-4})	EVTS	DOCUMENT ID		TECN	COMMENT
2.9 ±0.4 OUR AVERAGE	Error includes scale factor of 1.9. See the ideogram below.				
$3.52^{+0.28+0.17}_{-0.27-0.18}$		[34] LEES	14M	BABR	$\Upsilon(3S) \to \gamma\gamma\mu^+\mu^-$
$3.24 \pm 0.56 \pm 0.41$	58	[35] CRAWFORD	92B	CLE2	$\Upsilon(3S) \to \gamma\gamma\ell^+\ell^-$
$2.34 \pm 0.28 \pm 0.15$		[36] HEINTZ	92	CSB2	$\Upsilon(3S) \to \gamma\gamma\ell^+\ell^-$

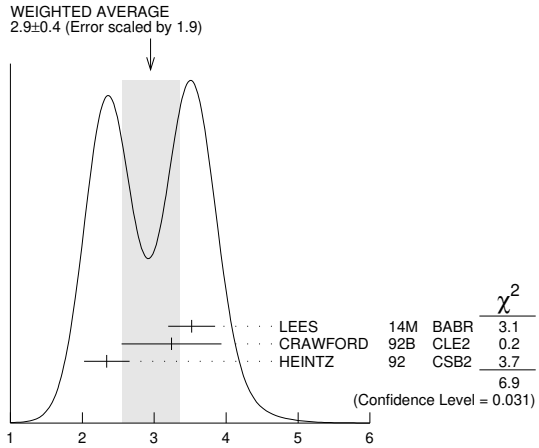

$B(\chi_{b1}(2P) \to \gamma\Upsilon(1S)) \times B(\Upsilon(3S) \to \gamma\chi_{b1}(2P)) \times B(\Upsilon(1S) \to \ell^+\ell^-)$ (units 10^{-4})

[34] From a sample of $\Upsilon(3S) \to \gamma\gamma\mu^+\mu^-$ with one converted photon.

[35] CRAWFORD 92B quotes $2\times B(\Upsilon(3S) \to \gamma\chi_{bJ}(2P))\ B(\chi_{bJ}(2P) \to \gamma\Upsilon(nS))\ B(\Upsilon(nS) \to \ell^+\ell^-)$.

[36] Calculated by us. HEINTZ 92 quotes $B(\Upsilon(3S) \to \gamma\chi_{b1}(2P)) \times B(\chi_{b1}(2P) \to \gamma\Upsilon(1S)) = (0.91 \pm 0.11 \pm 0.06)\%$ using $B(\Upsilon(1S) \to \mu^+\mu^-) = (2.57 \pm 0.05)\%$.

$\Gamma(\chi_{b1}(2P) \to \gamma\Upsilon(2S))/\Gamma_{total} \times \Gamma(\Upsilon(3S) \to \gamma\chi_{b1}(2P))/\Gamma_{total}$ — $\Gamma_2/\Gamma \times \Gamma_{21}^{\Upsilon(3S)}/\Gamma^{\Upsilon(3S)}$

VALUE (units 10^{-2})	EVTS	DOCUMENT ID		TECN	COMMENT
2.4±0.1±0.2	4.3k	LEES	11J	BABR	$\Upsilon(3S) \to X\gamma$

$B(\chi_{b1}(2P) \to \gamma\Upsilon(2S)) \times B(\Upsilon(3S) \to \gamma\chi_{b1}(2P)) \times B(\Upsilon(2S) \to \ell^+\ell^-)$

VALUE (units 10^{-4})	EVTS	DOCUMENT ID		TECN	COMMENT
3.8 ±0.6 OUR AVERAGE	Error includes scale factor of 1.8. See the ideogram below.				
$4.95^{+0.75+1.01}_{-0.70-0.24}$		[37] LEES	14M	BABR	$\Upsilon(3S) \to \gamma\gamma\mu^+\mu^-$
$5.12 \pm 0.60 \pm 0.63$	111	[38] CRAWFORD	92B	CLE2	$\Upsilon(3S) \to \gamma\gamma\ell^+\ell^-$
$3.30 \pm 0.33 \pm 0.20$		[39] HEINTZ	92	CSB2	$\Upsilon(3S) \to \gamma\gamma\ell^+\ell^-$

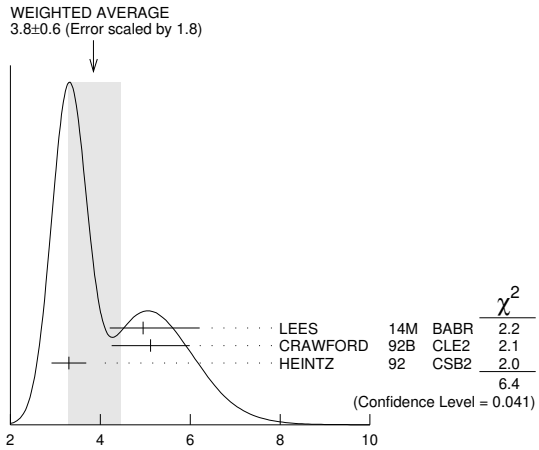

$B(\chi_{b1}(2P) \to \gamma\Upsilon(2S)) \times B(\Upsilon(3S) \to \gamma\chi_{b1}(2P)) \times B(\Upsilon(2S) \to \ell^+\ell^-)$ (units 10^{-4})

[37] From a sample of $\Upsilon(3S) \to \gamma\gamma\mu^+\mu^-$ with one converted photon.

[38] CRAWFORD 92B quotes $2\times B(\Upsilon(3S) \to \gamma\chi_{bJ}(2P))\ B(\chi_{bJ}(2P) \to \gamma\Upsilon(nS))\ B(\Upsilon(nS) \to \ell^+\ell^-)$.

[39] Calculated by us. HEINTZ 92 quotes $B(\Upsilon(3S) \to \gamma\chi_{b1}(2P)) \times B(\chi_{b1}(2P) \to \gamma\Upsilon(2S)) = (2.29 \pm 0.23 \pm 0.21)$ % using $B(\Upsilon(2S) \to \mu^+\mu^-) = (1.44 \pm 0.10)\%$.

$B(\chi_{b1}(2P) \to \chi_{b1}(1P)\pi^+\pi^-) \times B(\Upsilon(3S) \to \chi_{b1}(2P)X)$

VALUE (units 10^{-3})	EVTS	DOCUMENT ID		TECN	COMMENT
1.16±0.07±0.12	31k	LEES	11C	BABR	$e^+e^- \to \pi^+\pi^-X$

Downloaded from https://academic.oup.com/ptep/article/2022/8/083C01/6651666 by KIT Library user on 27 September 2022

$B(\chi_{b2}(2P) \to pX + \bar{p}X)/B(\chi_{b1}(2P) \to pX + \bar{p}X)$

VALUE	DOCUMENT ID		TECN	COMMENT
1.109±0.007±0.040	BRIERE	07	CLEO	$\Upsilon(3S) \to \gamma\chi_{bJ}(2P)$

$B(\chi_{b0}(2P) \to pX + \bar{p}X)/B(\chi_{b1}(2P) \to pX + \bar{p}X)$

VALUE	DOCUMENT ID		TECN	COMMENT
1.082±0.025±0.060	BRIERE	07	CLEO	$\Upsilon(3S) \to \gamma\chi_{bJ}(2P)$

$\chi_{b1}(2P)$ REFERENCES

LEES	14M	PR D90 112010	J.P. Lees et al.	(BABAR Collab.)
LEES	11C	PR D84 011104	J.P. Lees et al.	(BABAR Collab.)
LEES	11J	PR D84 072002	J.P. Lees et al.	(BABAR Collab.)
ASNER	08A	PR D78 091103	D.M. Asner et al.	(CLEO Collab.)
BRIERE	08	PR D78 092007	R.A. Briere et al.	(CLEO Collab.)
BRIERE	07	PR D76 012005	R.A. Briere et al.	(CLEO Collab.)
CAWLFIELD	06	PR D73 012003	C. Cawlfield et al.	(CLEO Collab.)
ARTUSO	05	PRL 94 032001	M. Artuso et al.	(CLEO Collab.)
CRONIN-HEN...	04	PRL 92 222002	D. Cronin-Hennessy et al.	(CLEO Collab.)
CRAWFORD	92B	PL B294 139	G. Crawford et al.	(CLEO Collab.)
HEINTZ	92	PR D46 1928	U. Heintz et al.	(CUSB II Collab.)
HEINTZ	91	PRL 66 1563	U. Heintz et al.	(CUSB Collab.)
MORRISON	91	PRL 67 1696	R.J. Morrison et al.	(CLEO Collab.)
NARAIN	91	PRL 66 3113	M. Narain et al.	(CUSB Collab.)

$h_b(2P)$

$I^G(J^{PC}) = 0^-(1^{+-})$

Quantum numbers are quark model predictions. $C = -$ established by $\eta_b\gamma$ decay.

$h_b(2P)$ MASS

VALUE (MeV)	EVTS	DOCUMENT ID		TECN	COMMENT
10259.8±0.5±1.1	90k	[1] MIZUK	12	BELL	$e^+e^- \to \pi^+\pi^-$ hadrons
• • • We do not use the following data for averages, fits, limits, etc. • • •					
$10259.8 \pm 0.6^{+1.4}_{-1.0}$	83.9k	[2] ADACHI	12	BELL	10.86 $e^+e^- \to \pi^+\pi^-$ MM

[1] Observed with 9 standard deviations significance.
[2] Superseded by MIZUK 12.

$h_b(2P)$ DECAY MODES

	Mode	Fraction (Γ_i/Γ)
Γ_1	hadrons	not seen
Γ_2	$\eta_b(1S)\gamma$	(22± 5) %
Γ_3	$\eta_b(2S)\gamma$	(48±13) %

$h_b(2P)$ BRANCHING RATIOS

$\Gamma(\text{hadrons})/\Gamma_{total}$ — Γ_1/Γ

VALUE	EVTS	DOCUMENT ID		TECN	COMMENT
not seen	83.9k	ADACHI	12	BELL	10.86 $e^+e^- \to \pi^+\pi^-$ MM

$\Gamma(\eta_b(1S)\gamma)/\Gamma_{total}$ — Γ_2/Γ

VALUE (units 10^{-2})	EVTS	DOCUMENT ID		TECN	COMMENT
$22.3 \pm 3.8^{+3.1}_{-3.3}$	10k	MIZUK	12	BELL	$e^+e^- \to (\gamma)\pi^+\pi^-$ hadrons

$\Gamma(\eta_b(2S)\gamma)/\Gamma_{total}$ — Γ_3/Γ

VALUE (units 10^{-2})	EVTS	DOCUMENT ID		TECN	COMMENT
$47.5 \pm 10.5^{+6.8}_{-7.7}$	26k	MIZUK	12	BELL	$e^+e^- \to (\gamma)\pi^+\pi^-$ hadrons

$h_b(2P)$ REFERENCES

ADACHI	12	PRL 108 032001	I. Adachi et al.	(BELLE Collab.)
MIZUK	12	PRL 109 232002	R. Mizuk et al.	(BELLE Collab.)

$\chi_{b2}(2P)$

$I^G(J^{PC}) = 0^+(2^{++})$
J needs confirmation.

Observed in radiative decay of the $\Upsilon(3S)$, therefore $C = +$. Branching ratio requires E1 transition, M1 is strongly disfavored, therefore $P = +$.

$\chi_{b2}(2P)$ MASS

VALUE (MeV)	DOCUMENT ID
10268.65±0.22±0.50 OUR EVALUATION	From γ energy below, using $\Upsilon(3S)$ mass = 10355.2 ± 0.5 MeV

$m_{\chi_{b2}(2P)} - m_{\chi_{b1}(2P)}$

VALUE (MeV)	DOCUMENT ID		TECN	COMMENT
13.10±0.24 OUR AVERAGE				
12.3 ±2.6 ±0.6	[1] AAIJ	14BG	LHCB	$pp \to \gamma\mu^+\mu^- X$
13.04±0.26	LEES	14M	BABR	$\Upsilon(3S) \to \gamma\gamma\mu^+\mu^-$
13.5 ±0.4 ±0.5	[2] HEINTZ	92	CSB2	$e^+e^- \to \gamma X, \ell^+\ell^-\gamma\gamma$

[1] From the $\chi_{bj}(2P) \to \Upsilon(1S)\gamma$ transition.
[2] From the average photon energy for inclusive and exclusive events. Supersedes NARAIN 91.

γ ENERGY IN $\Upsilon(3S)$ DECAY

VALUE (MeV)	EVTS	DOCUMENT ID		TECN	COMMENT
86.19±0.22 OUR EVALUATION	Treating systematic errors as correlated				
86.40±0.18 OUR AVERAGE					
86.04±0.06±0.27		ARTUSO	05	CLEO	$\Upsilon(3S) \to \gamma X$
86 ±1	101	CRAWFORD	92B	CLE2	$e^+e^- \to \ell^+\ell^-\gamma\gamma$
86.7 ±0.4	10319	[3] HEINTZ	92	CSB2	$e^+e^- \to \gamma X$
86.9 ±0.4	157	[4] HEINTZ	92	CSB2	$e^+e^- \to \ell^+\ell^-\gamma\gamma$
86.4 ±0.1 ±0.4	30741	MORRISON	91	CLE2	$e^+e^- \to \gamma X$

[3] A systematic uncertainty on the energy scale of 0.9% not included. Supersedes NARAIN 91.
[4] A systematic uncertainty on the energy scale of 0.9% not included. Supersedes HEINTZ 91.

$\chi_{b2}(2P)$ DECAY MODES

	Mode	Fraction (Γ_i/Γ)	Confidence level
Γ_1	$\omega\Upsilon(1S)$	$(1.10^{+0.34}_{-0.30})$ %	
Γ_2	$\gamma\Upsilon(2S)$	(8.9 ±1.2) %	
Γ_3	$\gamma\Upsilon(1S)$	(6.6 ±0.8) %	
Γ_4	$\pi\pi\chi_{b2}(1P)$	(5.1 ±0.9) $\times 10^{-3}$	
Γ_5	$D^0 X$	< 2.4 %	90%
Γ_6	$\pi^+\pi^- K^+K^-\pi^0$	< 1.1 $\times 10^{-4}$	90%
Γ_7	$2\pi^+\pi^- K^- K^0_S$	< 9 $\times 10^{-5}$	90%
Γ_8	$2\pi^+\pi^- K^- K^0_S 2\pi^0$	< 7 $\times 10^{-4}$	90%
Γ_9	$2\pi^+2\pi^-2\pi^0$	(3.9 ±1.6) $\times 10^{-4}$	
Γ_{10}	$2\pi^+2\pi^- K^+K^-$	(9 ±4) $\times 10^{-5}$	
Γ_{11}	$2\pi^+2\pi^- K^+K^-\pi^0$	(2.4 ±1.1) $\times 10^{-4}$	
Γ_{12}	$2\pi^+2\pi^- K^+K^-2\pi^0$	(4.7 ±2.3) $\times 10^{-4}$	
Γ_{13}	$3\pi^+2\pi^- K^- K^0_S\pi^0$	< 4 $\times 10^{-4}$	90%
Γ_{14}	$3\pi^+3\pi^-$	(9 ±4) $\times 10^{-5}$	
Γ_{15}	$3\pi^+3\pi^-2\pi^0$	(1.2 ±0.4) $\times 10^{-3}$	
Γ_{16}	$3\pi^+3\pi^- K^+K^-$	(1.4 ±0.7) $\times 10^{-4}$	
Γ_{17}	$3\pi^+3\pi^- K^+K^-\pi^0$	(4.2 ±1.7) $\times 10^{-4}$	
Γ_{18}	$4\pi^+4\pi^-$	(9 ±5) $\times 10^{-5}$	
Γ_{19}	$4\pi^+4\pi^-2\pi^0$	(1.3 ±0.5) $\times 10^{-3}$	

$\chi_{b2}(2P)$ BRANCHING RATIOS

$\Gamma(\omega\Upsilon(1S))/\Gamma_{total}$ — Γ_1/Γ

VALUE (units 10^{-2})	EVTS	DOCUMENT ID		TECN	COMMENT
$1.10^{+0.32}_{-0.28}{}^{+0.11}_{-0.10}$	$20.1^{+5.8}_{-5.1}$	[5] CRONIN-HEN...04		CLE3	$\Upsilon(3S) \to \gamma\omega\Upsilon(1S)$

[5] Using $B(\Upsilon(3S) \to \gamma\chi_{b2}(2P)) = (11.4 \pm 0.8)\%$ and $B(\Upsilon(1S) \to \ell^+\ell^-) = 2\,B(\Upsilon(1S) \to \mu^+\mu^-) = 2\,(2.48 \pm 0.06)\%$.

$\Gamma(\gamma\Upsilon(2S))/\Gamma_{total}$ — Γ_2/Γ

VALUE	EVTS	DOCUMENT ID		TECN	COMMENT
0.089±0.012 OUR AVERAGE					
0.085±0.010±0.010		[6,7,8] LEES	14M	BABR	$\Upsilon(3S) \to \gamma\gamma\mu^+\mu^-$
0.084±0.011±0.010	2.5k	[9] LEES	11J	BABR	$\Upsilon(3S) \to X\gamma$
0.096±0.022±0.012		[7,10] CRAWFORD	92B	CLE2	$e^+e^- \to \ell^+\ell^-\gamma\gamma$
0.106±0.016±0.013		[7,11] HEINTZ	92	CSB2	$e^+e^- \to \ell^+\ell^-\gamma\gamma$

[6] LEES 14M quotes $\Gamma(\chi_{b2}(2P) \to \gamma\Upsilon(2S))/\Gamma_{total} \times \Gamma(\Upsilon(3S) \to \gamma\chi_{b2}(2P))/\Gamma_{total} = (1.12 \pm 0.13)\%$ combining the results from samples of $\Upsilon(3S) \to \gamma\gamma\mu^+\mu^-$ with and without converted photons.
[7] Assuming $B(\Upsilon(2S) \to \mu^+\mu^-) = (1.93 \pm 0.17)\%$.
[8] LEES 14M reports $[\Gamma(\chi_{b2}(2P) \to \gamma\Upsilon(2S))/\Gamma_{total}] \times [B(\Upsilon(3S) \to \gamma\chi_{b2}(2P))] = (1.12 \pm 0.13) \times 10^{-2}$ which we divide by our best value $B(\Upsilon(3S) \to \gamma\chi_{b2}(2P)) = (13.1 \pm 1.6) \times 10^{-2}$. Our first error is their experiment's error and our second error is the systematic error from using our best value.
[9] LEES 11J reports $[\Gamma(\chi_{b2}(2P) \to \gamma\Upsilon(2S))/\Gamma_{total}] \times [B(\Upsilon(3S) \to \gamma\chi_{b2}(2P))] = (1.1 \pm 0.1 \pm 0.1) \times 10^{-2}$ which we divide by our best value $B(\Upsilon(3S) \to \gamma\chi_{b2}(2P)) = (13.1 \pm 1.6) \times 10^{-2}$. Our first error is their experiment's error and our second error is the systematic error from using our best value.
[10] CRAWFORD 92B quotes $B(\Upsilon(3S) \to \gamma\chi_{b1}(2P)) \times B(\chi_{b2}(2P) \to \gamma\Upsilon(2S)) \times 2\,B(\Upsilon(2S) \to \ell^+\ell^-) = (4.98 \pm 0.94 \pm 0.62)\,10^{-4}$.
[11] Recalculated by us. HEINTZ 92 quotes $B(\Upsilon(3S) \to \gamma\chi_{b2}(2P)) \times B(\chi_{b2}(2P) \to \gamma\Upsilon(2S)) = (1.90 \pm 0.23 \pm 0.18)$ % using $B(\Upsilon(2S) \to \mu^+\mu^-) = (1.44 \pm 0.10)\%$. Supersedes HEINTZ 91.

$\Gamma(\gamma\Upsilon(1S))/\Gamma_{total}$ — Γ_3/Γ

VALUE	EVTS	DOCUMENT ID		TECN	COMMENT
0.066±0.008 OUR AVERAGE					
0.061±0.004±0.007		[12,13,14] LEES	14M	BABR	$\Upsilon(3S) \to \gamma\gamma\mu^+\mu^-$
0.070±0.004±0.008	11k	[15] LEES	11J	BABR	$\Upsilon(3S) \to X\gamma$

Downloaded from https://academic.oup.com/ptep/article/2022/8/083C01/6651666 by KIT Library user on 27 September 2022

$0.077 \pm 0.018 \pm 0.009$	[13,16] CRAWFORD	92B	CLE2	$e^+e^- \to \ell^+\ell^-\gamma\gamma$
$0.061 \pm 0.009 \pm 0.007$	[13,17] HEINTZ	92	CSB2	$e^+e^- \to \ell^+\ell^-\gamma\gamma$

[12] LEES 14M quotes $\Gamma(\chi_{b2}(2P) \to \gamma\Upsilon(1S))/\Gamma_{total} \times \Gamma(\Upsilon(3S) \to \gamma\chi_{b2}(2P))/\Gamma_{total} = (8.03 \pm 0.50) \times 10^{-3}$ combining the results from samples of $\Upsilon(3S) \to \gamma\gamma\mu^+\mu^-$ with and without converted photons.

[13] Assuming $B(\Upsilon(1S) \to \mu^+\mu^-) = (2.48 \pm 0.05)\%$.

[14] LEES 14M reports $[\Gamma(\chi_{b2}(2P) \to \gamma\Upsilon(1S))/\Gamma_{total}] \times [B(\Upsilon(3S) \to \gamma\chi_{b2}(2P))] = (8.03 \pm 0.50) \times 10^{-3}$ which we divide by our best value $B(\Upsilon(3S) \to \gamma\chi_{b2}(2P)) = (13.1 \pm 1.6) \times 10^{-2}$. Our first error is their experiment's error and our second error is the systematic error from using our best value.

[15] LEES 11J reports $[\Gamma(\chi_{b2}(2P) \to \gamma\Upsilon(1S))/\Gamma_{total}] \times [B(\Upsilon(3S) \to \gamma\chi_{b2}(2P))] = (9.2 \pm 0.3 \pm 0.4) \times 10^{-3}$ which we divide by our best value $B(\Upsilon(3S) \to \gamma\chi_{b2}(2P)) = (13.1 \pm 1.6) \times 10^{-2}$. Our first error is their experiment's error and our second error is the systematic error from using our best value.

[16] CRAWFORD 92B quotes $B(\Upsilon(3S) \to \gamma\chi_{b2}(2P)) \times B(\chi_{b2}(2P) \to \gamma\Upsilon(1S)) \times 2\, B(\Upsilon(1S) \to \ell^+\ell^-) = (5.03 \pm 0.94 \pm 0.63)\ 10^{-4}$.

[17] Recalculated by us. HEINTZ 92 quotes $B(\Upsilon(3S) \to \gamma\chi_{b2}(2P)) \times B(\chi_{b2}(2P) \to \gamma\Upsilon(1S)) = (0.77 \pm 0.11 \pm 0.05)\%$ using $B(\Upsilon(1S) \to \mu^+\mu^-) = (2.57 \pm 0.05)\%$. Supersedes HEINTZ 91.

$\Gamma(\pi\pi\chi_{b2}(1P))/\Gamma_{total}$ — Γ_4/Γ

VALUE (units 10^{-3})	EVTS	DOCUMENT ID		TECN	COMMENT
5.1±0.9 OUR AVERAGE					
$4.9 \pm 0.7 \pm 0.6$	17k	[18] LEES	11C	BABR	$e^+e^- \to \pi^+\pi^- X$
$6.0 \pm 1.6 \pm 1.4$		[19] CAWLFIELD	06	CLE3	$\Upsilon(3S) \to 2(\gamma\pi\ell)$

[18] $(0.64 \pm 0.05 \pm 0.08) \times 10^{-3}$. We derive the value assuming $B(\Upsilon(3S) \to \chi_{b2}(2P)X) = B(\Upsilon(3S) \to \chi_{b2}(2P)\gamma) = (13.1 \pm 1.6) \times 10^{-2}$.

[19] CAWLFIELD 06 quote $\Gamma(\chi_b(2P) \to \pi\pi\chi_b(1P)) = 0.83 \pm 0.22 \pm 0.08 \pm 0.19$ keV assuming l-spin conservation, no D-wave contribution, $\Gamma(\chi_{b1}(2P)) = 96 \pm 16$keV, and $\Gamma(\chi_{b2}(2P)) = 138 \pm 19$ keV.

$\Gamma(D^0X)/\Gamma_{total}$ — Γ_5/Γ

VALUE	CL%	DOCUMENT ID		TECN	COMMENT
$<2.4 \times 10^{-2}$	90	[20,21] BRIERE	08	CLEO	$\Upsilon(3S) \to \gamma D^0 X$

[20] For $p_{D^0} > 2.5$ GeV/c.

[21] The authors also present their result as $(0.2 \pm 1.4 \pm 0.1) \times 10^{-2}$.

$\Gamma(\pi^+\pi^-K^+K^-\pi^0)/\Gamma_{total}$ — Γ_6/Γ

VALUE (units 10^{-4})	CL%	DOCUMENT ID		TECN	COMMENT
<1.1	90	[22] ASNER	08A	CLEO	$\Upsilon(3S) \to \gamma\pi^+\pi^-K^+K^-\pi^0$

[22] ASNER 08A reports $[\Gamma(\chi_{b2}(2P) \to \pi^+\pi^-K^+K^-\pi^0)/\Gamma_{total}] \times [B(\Upsilon(3S) \to \gamma\chi_{b2}(2P))] < 14 \times 10^{-6}$ which we divide by our best value $B(\Upsilon(3S) \to \gamma\chi_{b2}(2P)) = 13.1 \times 10^{-2}$.

$\Gamma(2\pi^+\pi^-K^-K^0_S)/\Gamma_{total}$ — Γ_7/Γ

VALUE (units 10^{-4})	CL%	DOCUMENT ID		TECN	COMMENT
<0.9	90	[23] ASNER	08A	CLEO	$\Upsilon(3S) \to \gamma 2\pi^+\pi^-K^-K^0_S$

[23] ASNER 08A reports $[\Gamma(\chi_{b2}(2P) \to 2\pi^+\pi^-K^-K^0_S)/\Gamma_{total}] \times [B(\Upsilon(3S) \to \gamma\chi_{b2}(2P))] < 12 \times 10^{-6}$ which we divide by our best value $B(\Upsilon(3S) \to \gamma\chi_{b2}(2P)) = 13.1 \times 10^{-2}$.

$\Gamma(2\pi^+\pi^-K^-K^0_S2\pi^0)/\Gamma_{total}$ — Γ_8/Γ

VALUE (units 10^{-4})	CL%	DOCUMENT ID		TECN	COMMENT
<7	90	[24] ASNER	08A	CLEO	$\Upsilon(3S) \to \gamma 2\pi^+\pi^-K^-2\pi^0$

[24] ASNER 08A reports $[\Gamma(\chi_{b2}(2P) \to 2\pi^+\pi^-K^-K^0_S2\pi^0)/\Gamma_{total}] \times [B(\Upsilon(3S) \to \gamma\chi_{b2}(2P))] < 87 \times 10^{-6}$ which we divide by our best value $B(\Upsilon(3S) \to \gamma\chi_{b2}(2P)) = 13.1 \times 10^{-2}$.

$\Gamma(2\pi^+2\pi^-2\pi^0)/\Gamma_{total}$ — Γ_9/Γ

VALUE (units 10^{-4})	EVTS	DOCUMENT ID		TECN	COMMENT
3.9±1.6±0.5	23	[25] ASNER	08A	CLEO	$\Upsilon(3S) \to \gamma 2\pi^+2\pi^-2\pi^0$

[25] ASNER 08A reports $[\Gamma(\chi_{b2}(2P) \to 2\pi^+2\pi^-2\pi^0)/\Gamma_{total}] \times [B(\Upsilon(3S) \to \gamma\chi_{b2}(2P))] = (51 \pm 16 \pm 13) \times 10^{-6}$ which we divide by our best value $B(\Upsilon(3S) \to \gamma\chi_{b2}(2P)) = (13.1 \pm 1.6) \times 10^{-2}$. Our first error is their experiment's error and our second error is the systematic error from using our best value.

$\Gamma(2\pi^+2\pi^-K^+K^-)/\Gamma_{total}$ — Γ_{10}/Γ

VALUE (units 10^{-4})	EVTS	DOCUMENT ID		TECN	COMMENT
0.9±0.4±0.1	11	[26] ASNER	08A	CLEO	$\Upsilon(3S) \to \gamma 2\pi^+2\pi^-K^+K^-$

[26] ASNER 08A reports $[\Gamma(\chi_{b2}(2P) \to 2\pi^+2\pi^-K^+K^-)/\Gamma_{total}] \times [B(\Upsilon(3S) \to \gamma\chi_{b2}(2P))] = (12 \pm 4 \pm 3) \times 10^{-6}$ which we divide by our best value $B(\Upsilon(3S) \to \gamma\chi_{b2}(2P)) = (13.1 \pm 1.6) \times 10^{-2}$. Our first error is their experiment's error and our second error is the systematic error from using our best value.

$\Gamma(2\pi^+2\pi^-K^+K^-\pi^0)/\Gamma_{total}$ — Γ_{11}/Γ

VALUE (units 10^{-4})	EVTS	DOCUMENT ID		TECN	COMMENT
2.4±1.0±0.3	16	[27] ASNER	08A	CLEO	$\Upsilon(3S) \to \gamma 2\pi^+2\pi^-K^+K^-\pi^0$

[27] ASNER 08A reports $[\Gamma(\chi_{b2}(2P) \to 2\pi^+2\pi^-K^+K^-\pi^0)/\Gamma_{total}] \times [B(\Upsilon(3S) \to \gamma\chi_{b2}(2P))] = (32 \pm 11 \pm 8) \times 10^{-6}$ which we divide by our best value $B(\Upsilon(3S) \to \gamma\chi_{b2}(2P)) = (13.1 \pm 1.6) \times 10^{-2}$. Our first error is their experiment's error and our second error is the systematic error from using our best value.

$\Gamma(2\pi^+2\pi^-K^+K^-2\pi^0)/\Gamma_{total}$ — Γ_{12}/Γ

VALUE (units 10^{-4})	EVTS	DOCUMENT ID		TECN	COMMENT
4.7±2.2±0.6	14	[28] ASNER	08A	CLEO	$\Upsilon(3S) \to \gamma 2\pi^+2\pi^-K^+K^-2\pi^0$

[28] ASNER 08A reports $[\Gamma(\chi_{b2}(2P) \to 2\pi^+2\pi^-K^+K^-2\pi^0)/\Gamma_{total}] \times [B(\Upsilon(3S) \to \gamma\chi_{b2}(2P))] = (62 \pm 23 \pm 17) \times 10^{-6}$ which we divide by our best value $B(\Upsilon(3S) \to \gamma\chi_{b2}(2P)) = (13.1 \pm 1.6) \times 10^{-2}$. Our first error is their experiment's error and our second error is the systematic error from using our best value.

$\Gamma(3\pi^+2\pi^-K^-K^0_S\pi^0)/\Gamma_{total}$ — Γ_{13}/Γ

VALUE (units 10^{-4})	CL%	DOCUMENT ID		TECN	COMMENT
<4	90	[29] ASNER	08A	CLEO	$\Upsilon(3S) \to \gamma 3\pi^+2\pi^-K^-K^0_S\pi^0$

[29] ASNER 08A reports $[\Gamma(\chi_{b2}(2P) \to 3\pi^+2\pi^-K^-K^0_S\pi^0)/\Gamma_{total}] \times [B(\Upsilon(3S) \to \gamma\chi_{b2}(2P))] < 58 \times 10^{-6}$ which we divide by our best value $B(\Upsilon(3S) \to \gamma\chi_{b2}(2P)) = 13.1 \times 10^{-2}$.

$\Gamma(3\pi^+3\pi^-)/\Gamma_{total}$ — Γ_{14}/Γ

VALUE (units 10^{-4})	EVTS	DOCUMENT ID		TECN	COMMENT
0.9±0.4±0.1	14	[30] ASNER	08A	CLEO	$\Upsilon(3S) \to \gamma 3\pi^+3\pi^-$

[30] ASNER 08A reports $[\Gamma(\chi_{b2}(2P) \to 3\pi^+3\pi^-)/\Gamma_{total}] \times [B(\Upsilon(3S) \to \gamma\chi_{b2}(2P))] = (12 \pm 4 \pm 3) \times 10^{-6}$ which we divide by our best value $B(\Upsilon(3S) \to \gamma\chi_{b2}(2P)) = (13.1 \pm 1.6) \times 10^{-2}$. Our first error is their experiment's error and our second error is the systematic error from using our best value.

$\Gamma(3\pi^+3\pi^-2\pi^0)/\Gamma_{total}$ — Γ_{15}/Γ

VALUE (units 10^{-4})	EVTS	DOCUMENT ID		TECN	COMMENT
12±4±1	45	[31] ASNER	08A	CLEO	$\Upsilon(3S) \to \gamma 3\pi^+3\pi^-2\pi^0$

[31] ASNER 08A reports $[\Gamma(\chi_{b2}(2P) \to 3\pi^+3\pi^-2\pi^0)/\Gamma_{total}] \times [B(\Upsilon(3S) \to \gamma\chi_{b2}(2P))] = (159 \pm 33 \pm 43) \times 10^{-6}$ which we divide by our best value $B(\Upsilon(3S) \to \gamma\chi_{b2}(2P)) = (13.1 \pm 1.6) \times 10^{-2}$. Our first error is their experiment's error and our second error is the systematic error from using our best value.

$\Gamma(3\pi^+3\pi^-K^+K^-)/\Gamma_{total}$ — Γ_{16}/Γ

VALUE (units 10^{-4})	EVTS	DOCUMENT ID		TECN	COMMENT
1.4±0.7±0.2	12	[32] ASNER	08A	CLEO	$\Upsilon(3S) \to \gamma 3\pi^+3\pi^-K^+K^-$

[32] ASNER 08A reports $[\Gamma(\chi_{b2}(2P) \to 3\pi^+3\pi^-K^+K^-)/\Gamma_{total}] \times [B(\Upsilon(3S) \to \gamma\chi_{b2}(2P))] = (19 \pm 7 \pm 5) \times 10^{-6}$ which we divide by our best value $B(\Upsilon(3S) \to \gamma\chi_{b2}(2P)) = (13.1 \pm 1.6) \times 10^{-2}$. Our first error is their experiment's error and our second error is the systematic error from using our best value.

$\Gamma(3\pi^+3\pi^-K^+K^-\pi^0)/\Gamma_{total}$ — Γ_{17}/Γ

VALUE (units 10^{-4})	EVTS	DOCUMENT ID		TECN	COMMENT
4.2±1.7±0.5	16	[33] ASNER	08A	CLEO	$\Upsilon(3S) \to \gamma 3\pi^+3\pi^-K^+K^-\pi^0$

[33] ASNER 08A reports $[\Gamma(\chi_{b2}(2P) \to 3\pi^+3\pi^-K^+K^-\pi^0)/\Gamma_{total}] \times [B(\Upsilon(3S) \to \gamma\chi_{b2}(2P))] = (55 \pm 16 \pm 15) \times 10^{-6}$ which we divide by our best value $B(\Upsilon(3S) \to \gamma\chi_{b2}(2P)) = (13.1 \pm 1.6) \times 10^{-2}$. Our first error is their experiment's error and our second error is the systematic error from using our best value.

$\Gamma(4\pi^+4\pi^-)/\Gamma_{total}$ — Γ_{18}/Γ

VALUE (units 10^{-4})	EVTS	DOCUMENT ID		TECN	COMMENT
0.9±0.4±0.1	9	[34] ASNER	08A	CLEO	$\Upsilon(3S) \to \gamma 4\pi^+4\pi^-$

[34] ASNER 08A reports $[\Gamma(\chi_{b2}(2P) \to 4\pi^+4\pi^-)/\Gamma_{total}] \times [B(\Upsilon(3S) \to \gamma\chi_{b2}(2P))] = (12 \pm 5 \pm 3) \times 10^{-6}$ which we divide by our best value $B(\Upsilon(3S) \to \gamma\chi_{b2}(2P)) = (13.1 \pm 1.6) \times 10^{-2}$. Our first error is their experiment's error and our second error is the systematic error from using our best value.

$\Gamma(4\pi^+4\pi^-2\pi^0)/\Gamma_{total}$ — Γ_{19}/Γ

VALUE (units 10^{-4})	EVTS	DOCUMENT ID		TECN	COMMENT
13±5±2	27	[35] ASNER	08A	CLEO	$\Upsilon(3S) \to \gamma 4\pi^+4\pi^-2\pi^0$

[35] ASNER 08A reports $[\Gamma(\chi_{b2}(2P) \to 4\pi^+4\pi^-2\pi^0)/\Gamma_{total}] \times [B(\Upsilon(3S) \to \gamma\chi_{b2}(2P))] = (165 \pm 46 \pm 50) \times 10^{-6}$ which we divide by our best value $B(\Upsilon(3S) \to \gamma\chi_{b2}(2P)) = (13.1 \pm 1.6) \times 10^{-2}$. Our first error is their experiment's error and our second error is the systematic error from using our best value.

$\chi_{b2}(2P)$ Cross-Particle Branching Ratios

$\Gamma(\chi_{b2}(2P) \to \gamma\Upsilon(1S))/\Gamma_{total} \times \Gamma(\Upsilon(3S) \to \gamma\chi_{b2}(2P))/\Gamma_{total}$ — $\Gamma_3/\Gamma \times \Gamma^{\Upsilon(3S)}_{20}/\Gamma^{\Upsilon(3S)}$

VALUE (units 10^{-3})	EVTS	DOCUMENT ID		TECN	COMMENT
9.2±0.3±0.4	11k	LEES	11J	BABR	$\Upsilon(3S) \to X\gamma$

$\Gamma(\chi_{b2}(2P) \to \gamma\Upsilon(2S))/\Gamma_{total} \times \Gamma(\Upsilon(3S) \to \gamma\chi_{b2}(2P))/\Gamma_{total}$ — $\Gamma_2/\Gamma \times \Gamma^{\Upsilon(3S)}_{20}/\Gamma^{\Upsilon(3S)}$

VALUE (units 10^{-2})	EVTS	DOCUMENT ID		TECN	COMMENT
1.1±0.1±0.1	2.5k	LEES	11J	BABR	$\Upsilon(3S) \to X\gamma$

$B(\chi_{b2}(2P) \to \chi_{b2}(1P)\pi^+\pi^-) \times B(\Upsilon(3S) \to \chi_{b2}(2P)X)$

VALUE (units 10^{-3})	EVTS	DOCUMENT ID		TECN	COMMENT
0.64±0.05±0.08	17k	LEES	11C	BABR	$e^+e^- \to \pi^+\pi^- X$

Downloaded from https://academic.oup.com/ptep/article/2022/8/083C01/6651666 by KIT Library user on 27 September 2022

$B(\chi_{b2}(2P) \to \gamma\Upsilon(1S)) \times B(\Upsilon(3S) \to \gamma\chi_{b2}(2P)) \times B(\Upsilon(1S) \to \ell^+\ell^-)$

VALUE (units 10^{-4})	EVTS	DOCUMENT ID		TECN	COMMENT
2.02±0.18 OUR AVERAGE					
$1.95^{+0.22}_{-0.21}{}^{+0.10}_{-0.16}$		[36] LEES	14M	BABR	$\Upsilon(3S) \to \gamma\gamma\mu^+\mu^-$
2.52±0.47±0.32	48	[37] CRAWFORD	92B	CLE2	$\Upsilon(3S) \to \gamma\gamma\ell^+\ell^-$
1.98±0.28±0.12		[38] HEINTZ	92	CSB2	$\Upsilon(3S) \to \gamma\gamma\ell^+\ell^-$

[36] From a sample of $\Upsilon(3S) \to \gamma\gamma\mu^+\mu^-$ with converted photons.
[37] CRAWFORD 92B quotes $2\times B(\Upsilon(3S) \to \gamma\chi_{bJ}(2P))\ B(\chi_{bJ}(2P) \to \gamma\Upsilon(nS))\ B(\Upsilon(nS) \to \ell^+\ell^-)$.
[38] Calculated by us. HEINTZ 92 quotes $B(\Upsilon(3S) \to \gamma\chi_{b2}(2P))\times B(\chi_{b2}(2P) \to \gamma\Upsilon(1S)) = (0.77 \pm 0.11 \pm 0.05)\%$ using $B(\Upsilon(1S) \to \mu^+\mu^-) = (2.57 \pm 0.05)\%$.

$[B(\chi_{b2}(2P) \to \gamma\Upsilon(1S)) \times B(\Upsilon(3S) \to \gamma\chi_{b2}(2P))]$ / $[B(\chi_{b1}(2P) \to \gamma\Upsilon(1S)) \times B(\Upsilon(3S) \to \gamma\chi_{b1}(2P))]$

VALUE (%)	DOCUMENT ID		TECN	COMMENT
66.6±3.0	[39] LEES	14M	BABR	$\Upsilon(3S) \to \gamma\gamma\mu^+\mu^-$

[39] From a sample of $\Upsilon(3S) \to \gamma\gamma\mu^+\mu^-$ events without converted photons.

$B(\chi_{b2}(2P) \to \gamma\Upsilon(2S)) \times B(\Upsilon(3S) \to \gamma\chi_{b2}(2P)) \times B(\Upsilon(2S) \to \ell^+\ell^-)$

VALUE (units 10^{-4})	EVTS	DOCUMENT ID		TECN	COMMENT
2.74±0.29 OUR AVERAGE					
$3.22^{+0.58}_{-0.53}{}^{+0.16}_{-0.71}$		[40] LEES	14M	BABR	$\Upsilon(3S) \to \gamma\gamma\mu^+\mu^-$
2.49±0.47±0.31	53	[41] CRAWFORD	92B	CLE2	$\Upsilon(3S) \to \gamma\gamma\ell^+\ell^-$
2.74±0.33±0.18		[42] HEINTZ	92	CSB2	$\Upsilon(3S) \to \gamma\gamma\ell^+\ell^-$

[40] From a sample of $\Upsilon(3S) \to \gamma\gamma\mu^+\mu^-$ with converted photons.
[41] CRAWFORD 92B quotes $2\times B(\Upsilon(3S) \to \gamma\chi_{bJ}(2P))\ B(\chi_{bJ}(2P) \to \gamma\Upsilon(nS))\ B(\Upsilon(nS) \to \ell^+\ell^-)$.
[42] Calculated by us. HEINTZ 92 quotes $B(\Upsilon(3S) \to \gamma\chi_{b2}(2P)) \times B(\chi_{b2}(2P) \to \gamma\Upsilon(2S)) = (1.90 \pm 0.23 \pm 0.18)$ % using $B(\Upsilon(2S) \to \mu^+\mu^-) = (1.44 \pm 0.10)\%$.

$[B(\chi_{b2}(2P) \to \gamma\Upsilon(2S)) \times B(\Upsilon(3S) \to \gamma\chi_{b2}(2P))]$ / $[B(\chi_{b1}(2P) \to \gamma\Upsilon(2S)) \times B(\Upsilon(3S) \to \gamma\chi_{b1}(2P))]$

VALUE (%)	DOCUMENT ID		TECN	COMMENT
46.9±2.0	[43] LEES	14M	BABR	$\Upsilon(3S) \to \gamma\gamma\mu^+\mu^-$

[43] From a sample of $\Upsilon(3S) \to \gamma\gamma\mu^+\mu^-$ without converted photons.

$\chi_{b2}(2P)$ REFERENCES

AAIJ	14BG	JHEP 1410 088	R. Aaij et al.	(LHCb Collab.)
LEES	14M	PR D90 112010	J.P. Lees et al.	(BABAR Collab.)
LEES	11C	PR D84 011104	J.P. Lees et al.	(BABAR Collab.)
LEES	11J	PR D84 072002	J.P. Lees et al.	(BABAR Collab.)
ASNER	08A	PR D78 091103	D.M. Asner et al.	(CLEO Collab.)
BRIERE	08	PR D78 092007	R.A. Briere et al.	(CLEO Collab.)
CAWLFIELD	06	PR D73 012003	C. Cawlfield et al.	(CLEO Collab.)
ARTUSO	05	PRL 94 032001	M. Artuso et al.	(CLEO Collab.)
CRONIN-HEN...	04	PRL 92 222002	D. Cronin-Hennessy et al.	(CLEO Collab.)
CRAWFORD	92B	PL B294 139	G. Crawford et al.	(CLEO Collab.)
HEINTZ	92	PR D46 1928	U. Heintz et al.	(CUSB II Collab.)
HEINTZ	91	PRL 66 1563	U. Heintz et al.	(CUSB Collab.)
MORRISON	91	PRL 67 1696	R.J. Morrison et al.	(CLEO Collab.)
NARAIN	91	PRL 66 3113	M. Narain et al.	(CUSB Collab.)

$\Upsilon(3S)$

$I^G(J^{PC}) = 0^-(1^{--})$

$\Upsilon(3S)$ MASS

VALUE (MeV)	DOCUMENT ID		TECN	COMMENT
10355.2±0.5	[1] ARTAMONOV	00	MD1	$e^+e^- \to$ hadrons
• • • We do not use the following data for averages, fits, limits, etc. • • •				
10355.3±0.5	[2,3] BARU	86B	REDE	$e^+e^- \to$ hadrons

[1] Reanalysis of BARU 86B using new electron mass (COHEN 87).
[2] Reanalysis of ARTAMONOV 84.
[3] Superseded by ARTAMONOV 00.

$m_{\Upsilon(3S)} - m_{\Upsilon(2S)}$

VALUE (MeV)	DOCUMENT ID		TECN	COMMENT
331.50±0.02±0.13	LEES	11C	BABR	$e^+e^- \to \pi^+\pi^- X$

$\Upsilon(3S)$ WIDTH

VALUE (keV)	DOCUMENT ID
20.32±1.85 OUR EVALUATION	See the Note on "Width Determinations of the Υ States"

$\Upsilon(3S)$ DECAY MODES

	Mode	Fraction (Γ_i/Γ)	Scale factor/ Confidence level
Γ_1	$\Upsilon(2S)$ anything	(10.6 ± 0.8) %	
Γ_2	$\Upsilon(2S)\pi^+\pi^-$	(2.82± 0.18) %	S=1.6
Γ_3	$\Upsilon(2S)\pi^0\pi^0$	(1.85± 0.14) %	
Γ_4	$\Upsilon(2S)\gamma\gamma$	(5.0 ± 0.7) %	
Γ_5	$\Upsilon(2S)\pi^0$	< 5.1 $\times 10^{-4}$	CL=90%
Γ_6	$\Upsilon(1S)\pi^+\pi^-$	(4.37± 0.08) %	
Γ_7	$\Upsilon(1S)\pi^0\pi^0$	(2.20± 0.13) %	
Γ_8	$\Upsilon(1S)\eta$	< 1 $\times 10^{-4}$	CL=90%
Γ_9	$\Upsilon(1S)\pi^0$	< 7 $\times 10^{-5}$	CL=90%
Γ_{10}	$h_b(1P)\pi^0$	< 1.2 $\times 10^{-3}$	CL=90%
Γ_{11}	$h_b(1P)\pi^0 \to \gamma\eta_b(1S)\pi^0$	(4.3 ± 1.4) $\times 10^{-4}$	
Γ_{12}	$h_b(1P)\pi^+\pi^-$	< 1.2 $\times 10^{-4}$	CL=90%
Γ_{13}	$\tau^+\tau^-$	(2.29± 0.30) %	
Γ_{14}	$\mu^+\mu^-$	(2.18± 0.21) %	S=2.1
Γ_{15}	e^+e^-	(2.18± 0.20) %	
Γ_{16}	hadrons	(93 ±12) %	
Γ_{17}	ggg	(35.7 ± 2.6) %	
Γ_{18}	γgg	(9.7 ± 1.8) $\times 10^{-3}$	
Γ_{19}	^2H anything	(2.33± 0.33) $\times 10^{-5}$	
	Radiative decays		
Γ_{20}	$\gamma\chi_{b2}(2P)$	(13.1 ± 1.6) %	S=3.4
Γ_{21}	$\gamma\chi_{b1}(2P)$	(12.6 ± 1.2) %	S=2.4
Γ_{22}	$\gamma\chi_{b0}(2P)$	(5.9 ± 0.6) %	S=1.4
Γ_{23}	$\gamma\chi_{b2}(1P)$	(10.0 ± 1.0) $\times 10^{-3}$	S=1.7
Γ_{24}	$\gamma\chi_{b1}(1P)$	(9 ± 5) $\times 10^{-4}$	S=1.8
Γ_{25}	$\gamma\chi_{b0}(1P)$	(2.7 ± 0.4) $\times 10^{-3}$	
Γ_{26}	$\gamma\eta_b(2S)$	< 6.2 $\times 10^{-4}$	CL=90%
Γ_{27}	$\gamma\eta_b(1S)$	(5.1 ± 0.7) $\times 10^{-4}$	
Γ_{28}	$\gamma A^0 \to \gamma$ hadrons	< 8 $\times 10^{-5}$	CL=90%
Γ_{29}	$\gamma X \to \gamma + \geq 4$ prongs	[a] < 2.2 $\times 10^{-4}$	CL=95%
Γ_{30}	$\gamma a_1^0 \to \gamma\mu^+\mu^-$	< 5.5 $\times 10^{-6}$	CL=90%
Γ_{31}	$\gamma a_1^0 \to \gamma\tau^+\tau^-$	[b] < 1.6 $\times 10^{-4}$	CL=90%
	Lepton Family number (*LF*) violating modes		
Γ_{32}	$e^\pm\tau^\mp$	*LF* < 4.2 $\times 10^{-6}$	CL=90%
Γ_{33}	$\mu^\pm\tau^\mp$	*LF* < 3.1 $\times 10^{-6}$	CL=90%

[a] 1.5 GeV $< m_X <$ 5.0 GeV
[b] For $m_{\tau^+\tau^-}$ in the ranges 4.03–9.52 and 9.61–10.10 GeV.

$\Upsilon(3S)\ \Gamma(i)\Gamma(e^+e^-)/\Gamma(\text{total})$

$\Gamma(\text{hadrons}) \times \Gamma(e^+e^-)/\Gamma_{\text{total}}$ — $\Gamma_{16}\Gamma_{15}/\Gamma$

VALUE (keV)	DOCUMENT ID		TECN	COMMENT
0.414±0.007 OUR AVERAGE				
0.413±0.004±0.006	ROSNER	06	CLEO	10.4 $e^+e^- \to$ hadrons
0.45 ±0.03 ±0.03	[4] GILES	84B	CLEO	$e^+e^- \to$ hadrons

[4] Radiative corrections reevaluated by BUCHMUELLER 88 following KURAEV 85.

$\Gamma(\Upsilon(1S)\pi^+\pi^-) \times \Gamma(e^+e^-)/\Gamma_{\text{total}}$ — $\Gamma_6\Gamma_{15}/\Gamma$

VALUE (eV)	EVTS	DOCUMENT ID		TECN	COMMENT
18.46±0.27±0.77	6.4k	[5] AUBERT	08BP	BABR	$e^+e^- \to \gamma\pi^+\pi^-\ell^+\ell^-$

[5] Using $B(\Upsilon(1S) \to e^+e^-) = (2.38 \pm 0.11)\%$ and $B(\Upsilon(1S) \to \mu^+\mu^-) = (2.48 \pm 0.05)\%$.

$\Upsilon(3S)$ PARTIAL WIDTHS

$\Gamma(e^+e^-)$ — Γ_{15}

VALUE (keV)	DOCUMENT ID
0.443±0.008 OUR EVALUATION	

$\Upsilon(3S)$ BRANCHING RATIOS

$\Gamma(\Upsilon(2S)\text{anything})/\Gamma_{\text{total}}$ — Γ_1/Γ

VALUE	EVTS	DOCUMENT ID		TECN	COMMENT
0.106 ±0.008 OUR AVERAGE					
0.1023±0.0105	4625	[6,7,8] BUTLER	94B	CLE2	$e^+e^- \to \ell^+\ell^- X$
0.111 ±0.012	4891	[7,8,9] BROCK	91	CLEO	$e^+e^- \to \pi^+\pi^- X$, $\pi^+\pi^-\ell^+\ell^-$

[6] Using $B(\Upsilon(2S) \to \Upsilon(1S)\gamma\gamma) = (0.038 \pm 0.007)\%$, and $B(\Upsilon(2S) \to \Upsilon(1S)\pi^0\pi^0) = (1/2)B(\Upsilon(2S) \to \Upsilon(1S)\pi^+\pi^-)$.
[7] Using $B(\Upsilon(1S) \to \mu^+\mu^-) = (2.48 \pm 0.06)\%$. With the assumption of $e\mu$ universality.
[8] Using $B(\Upsilon(2S) \to \Upsilon(1S)\pi^+\pi^-) = (18.5 \pm 0.8)\%$.
[9] Using $B(\Upsilon(2S) \to \mu^+\mu^-) = (1.31 \pm 0.21)\%$, $B(\Upsilon(2S) \to \Upsilon(1S)\gamma\gamma)\times 2B(\Upsilon(1S) \to \mu^+\mu^-) = (0.188 \pm 0.035)\%$, and $B(\Upsilon(2S) \to \Upsilon(1S)\pi^0\pi^0)\times 2B(\Upsilon(1S) \to \mu^+\mu^-) = (0.436 \pm 0.056)\%$. With the assumption of $e\mu$ universality.

$\Gamma(\Upsilon(2S)\pi^+\pi^-)/\Gamma_{\text{total}}$ — Γ_2/Γ

VALUE (units 10^{-2})	EVTS	DOCUMENT ID		TECN	COMMENT
2.82±0.18 OUR AVERAGE Error includes scale factor of 1.6. See the ideogram below.					
3.00±0.02±0.14	543k	LEES	11C	BABR	$e^+e^- \to \pi^+\pi^- X$
2.40±0.10±0.26	800	[10] AUBERT	08BP	BABR	$e^+e^- \to \gamma\pi^+\pi^- e^+e^-$

Downloaded from https://academic.oup.com/ptep/article/2022/8/083C01/6651666 by KIT Library user on 27 September 2022

3.12±0.49	980	[11,12] BUTLER	94B	CLE2	$e^+e^- \to \pi^+\pi^-\ell^+\ell^-$
2.13±0.38	974	[13] BROCK	91	CLEO	$e^+e^- \to \pi^+\pi^-$X, $\pi^+\pi^-\ell^+\ell^-$
• • • We do not use the following data for averages, fits, limits, etc. • • •					
4.82±0.65±0.53	138	[13] WU	93	CUSB	$\Upsilon(3S) \to \pi^+\pi^-\ell^+\ell^-$
3.1 ±2.0	5	MAGERAS	82	CUSB	$\Upsilon(3S) \to \pi^+\pi^-\ell^+\ell^-$

[10] Using B($\Upsilon(1S) \to e^+e^-$) = (2.38 ± 0.11)%, B($\Upsilon(1S) \to \mu^+\mu^-$) = (2.48 ± 0.05)%, and $\Gamma_{ee}(\Upsilon(3S))$ = 0.443 ± 0.008 keV.

[11] From the exclusive mode.

[12] Using B($\Upsilon(2S) \to \Upsilon(1S)\gamma\gamma$) = (0.038 ± 0.007)%, and B($\Upsilon(2S) \to \Upsilon(1S)\pi^0\pi^0$) = (1/2)B($\Upsilon(2S) \to \Upsilon(1S)\pi^+\pi^-$).

[13] Using B($\Upsilon(2S) \to \mu^+\mu^-$) = (1.31 ± 0.21)%, B($\Upsilon(2S) \to \Upsilon(1S)\gamma\gamma$)×2B($\Upsilon(1S) \to \mu^+\mu^-$) = (0.188 ± 0.035)%, and B($\Upsilon(2S) \to \Upsilon(1S)\pi^0\pi^0$)×2B($\Upsilon(1S) \to \mu^+\mu^-$) = (0.436 ± 0.056)%. With the assumption of $e\mu$ universality.

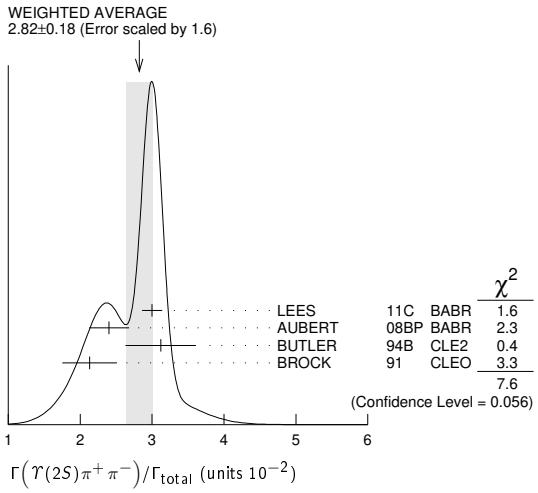

$\Gamma(\Upsilon(2S)\pi^0\pi^0)/\Gamma_{total}$ — Γ_3/Γ

VALUE (units 10^{-2})	EVTS	DOCUMENT ID		TECN	COMMENT
1.85±0.14 OUR AVERAGE					
1.82±0.09±0.12	4391	[14] BHARI	09	CLEO	$e^+e^- \to \pi^0\pi^0\ell^+\ell^-$
2.16±0.39		[15,16] BUTLER	94B	CLE2	$e^+e^- \to \pi^0\pi^0\ell^+\ell^-$
1.7 ±0.5 ±0.2	10	[17] HEINTZ	92	CSB2	$e^+e^- \to \pi^0\pi^0\ell^+\ell^-$

[14] Authors assume B($\Upsilon(1S) \to e^+e^-$) + B($\Upsilon(1S) \to \mu^+\mu^-$) = 4.06%.

[15] B($\Upsilon(2S) \to \mu^+\mu^-$) = (1.31 ± 0.21)% and assuming $e\mu$ universality.

[16] From the exclusive mode.

[17] B($\Upsilon(2S) \to \mu^+\mu^-$) = (1.44 ± 0.10)% and assuming $e\mu$ universality. Supersedes HEINTZ 91.

$\Gamma(\Upsilon(2S)\gamma\gamma)/\Gamma_{total}$ — Γ_4/Γ

VALUE	DOCUMENT ID		TECN	COMMENT
0.0502±0.0069	[18] BUTLER	94B	CLE2	$e^+e^- \to \ell^+\ell^-2\gamma$

[18] From the exclusive mode.

$\Gamma(\Upsilon(2S)\pi^0)/\Gamma_{total}$ — Γ_5/Γ

VALUE (units 10^{-3})	CL%	DOCUMENT ID		TECN	COMMENT
<0.51	90	[19] HE	08A	CLEO	$e^+e^- \to \ell^+\ell^-\gamma\gamma$

[19] Authors assume B($\Upsilon(2S) \to e^+e^-$) + B($\Upsilon(1S) \to \mu^+\mu^-$) = 4.06%.

$\Gamma(\Upsilon(1S)\pi^+\pi^-)/\Gamma_{total}$ — Γ_6/Γ

Abbreviation MM in the *COMMENT* field below stands for missing mass.

VALUE (units 10^{-2})	EVTS	DOCUMENT ID		TECN	COMMENT
4.37±0.08 OUR AVERAGE					
4.32±0.07±0.13	90k	[20] LEES	11L	BABR	$\Upsilon(3S) \to \pi^+\pi^-\ell^+\ell^-$
4.46±0.01±0.13	190k	[21] BHARI	09	CLEO	$e^+e^- \to \pi^+\pi^-$ MM
4.17±0.06±0.19	6.4k	[22] AUBERT	08BP	BABR	10.58 $e^+e^- \to \gamma\pi^+\pi^-\ell^+\ell^-$
4.52±0.35	11830	[23] BUTLER	94B	CLE2	$e^+e^- \to \pi^+\pi^-$X, $\pi^+\pi^-\ell^+\ell^-$
4.46±0.34±0.50	451	[23] WU	93	CUSB	$\Upsilon(3S) \to \pi^+\pi^-\ell^+\ell^-$
4.46±0.30	11221	[23] BROCK	91	CLEO	$e^+e^- \to \pi^+\pi^-$X, $\pi^+\pi^-\ell^+\ell^-$
• • • We do not use the following data for averages, fits, limits, etc. • • •					
4.9 ±1.0	22	GREEN	82	CLEO	$\Upsilon(3S) \to \pi^+\pi^-\ell^+\ell^-$
3.9 ±1.3	26	MAGERAS	82	CUSB	$\Upsilon(3S) \to \pi^+\pi^-\ell^+\ell^-$

[20] Using B($\Upsilon(1S) \to e^+e^-$) = (2.38 ± 0.11)% and B($\Upsilon(1S) \to \mu^+\mu^-$) = (2.48 ± 0.05)%.

[21] A weighted average of the inclusive and exclusive results.

[22] Using B($\Upsilon(2S) \to e^+e^-$) = (1.91 ± 0.16)%, B($\Upsilon(2S) \to \mu^+\mu^-$) = (1.93 ± 0.17)%, and $\Gamma_{ee}(\Upsilon(3S))$ = 0.443 ± 0.008 keV.

[23] Using B($\Upsilon(1S) \to \mu^+\mu^-$) = (2.48 ± 0.06)%. With the assumption of $e\mu$ universality.

$\Gamma(\Upsilon(2S)\pi^+\pi^-)/\Gamma(\Upsilon(1S)\pi^+\pi^-)$ — Γ_2/Γ_6

VALUE	EVTS	DOCUMENT ID		TECN	COMMENT
• • • We do not use the following data for averages, fits, limits, etc. • • •					
0.577±0.026±0.060	800	[24] AUBERT	08BP	BABR	$e^+e^- \to \gamma\pi^+\pi^-\ell^+\ell^-$

[24] Using B($\Upsilon(1S) \to e^+e^-$) = (2.38 ± 0.11)%, B($\Upsilon(1S) \to \mu^+\mu^-$) = (2.48 ± 0.05)%, B($\Upsilon(2S) \to e^+e^-$) = (1.91 ± 0.16)%, and B($\Upsilon(2S) \to \mu^+\mu^-$) = (1.93 ± 0.17)%. Not independent of other values reported by AUBERT 08BP.

$\Gamma(\Upsilon(1S)\pi^0\pi^0)/\Gamma_{total}$ — Γ_7/Γ

VALUE (units 10^{-2})	EVTS	DOCUMENT ID		TECN	COMMENT
2.20±0.13 OUR AVERAGE					
2.24±0.09±0.11	6584	[25] BHARI	09	CLEO	$e^+e^- \to \pi^0\pi^0\ell^+\ell^-$
1.99±0.34	56	[26] BUTLER	94B	CLE2	$e^+e^- \to \pi^0\pi^0\ell^+\ell^-$
2.2 ±0.4 ±0.3	33	[27] HEINTZ	92	CSB2	$e^+e^- \to \pi^0\pi^0\ell^+\ell^-$

[25] Authors assume B($\Upsilon(1S) \to e^+e^-$) + B($\Upsilon(1S) \to \mu^+\mu^-$) = 4.96%.

[26] Using B($\Upsilon(1S) \to \mu^+\mu^-$) = (2.48 ± 0.06)% and assuming $e\mu$ universality.

[27] Using B($\Upsilon(1S) \to \mu^+\mu^-$) = (2.57 ± 0.07)% and assuming $e\mu$ universality. Supersedes HEINTZ 91.

$\Gamma(\Upsilon(1S)\pi^0\pi^0)/\Gamma(\Upsilon(1S)\pi^+\pi^-)$ — Γ_7/Γ_6

VALUE	DOCUMENT ID		TECN	COMMENT
• • • We do not use the following data for averages, fits, limits, etc. • • •				
0.501±0.043	[28] BHARI	09	CLEO	$e^+e^- \to \Upsilon(3S)$

[28] Not independent of other values reported by BHARI 09.

$\Gamma(\Upsilon(1S)\eta)/\Gamma_{total}$ — Γ_8/Γ

VALUE (units 10^{-3})	CL%	DOCUMENT ID		TECN	COMMENT
<0.1	90	[29] LEES	11L	BABR	$\Upsilon(3S) \to (\pi^+\pi^-)(\gamma\gamma)\ell^+\ell^-$
• • • We do not use the following data for averages, fits, limits, etc. • • •					
<0.8	90	[29,30] AUBERT	08BP	BABR	$e^+e^- \to \gamma\pi^+\pi^-\pi^0\ell^+\ell^-$
<0.18	90	[31] HE	08A	CLEO	$e^+e^- \to \ell^+\ell^-\eta$
<2.2	90	BROCK	91	CLEO	$e^+e^- \to \ell^+\ell^-\eta$

[29] Using B($\Upsilon(1S) \to e^+e^-$) = (2.38 ± 0.11)%, B($\Upsilon(1S) \to \mu^+\mu^-$) = (2.48 ± 0.05)%.

[30] Using $\Gamma_{ee}(\Upsilon(3S))$ = 0.443 ± 0.008 keV.

[31] Authors assume B($\Upsilon(1S) \to e^+e^-$) + B($\Upsilon(1S) \to \mu^+\mu^-$) = 4.96%.

$\Gamma(\Upsilon(1S)\eta)/\Gamma(\Upsilon(1S)\pi^+\pi^-)$ — Γ_8/Γ_6

VALUE (units 10^{-2})	CL%	DOCUMENT ID		TECN	COMMENT
<0.23	90	[32] LEES	11L	BABR	$\Upsilon(3S) \to (\pi^+\pi^-)(\gamma\gamma)\ell^+\ell^-$
• • • We do not use the following data for averages, fits, limits, etc. • • •					
<1.9	90	[33] AUBERT	08BP	BABR	$e^+e^- \to \gamma\pi^+\pi^-(\pi^0)\ell^+\ell^-$

[32] Not independent of other values reported by LEES 11L.

[33] Not independent of other values reported by AUBERT 08BP.

$\Gamma(\Upsilon(1S)\pi^0)/\Gamma_{total}$ — Γ_9/Γ

VALUE (units 10^{-3})	CL%	DOCUMENT ID		TECN	COMMENT
<0.07	90	[34] HE	08A	CLEO	$e^+e^- \to \ell^+\ell^-\gamma\gamma$

[34] Authors assume B($\Upsilon(1S) \to e^+e^-$) + B($\Upsilon(1S) \to \mu^+\mu^-$) = 4.96%.

$\Gamma(h_b(1P)\pi^0)/\Gamma_{total}$ — Γ_{10}/Γ

VALUE	CL%	DOCUMENT ID		TECN	COMMENT
<1.2 × 10⁻³	90	[35] GE	11	CLEO	$\Upsilon(3S) \to \pi^0$ anything

[35] Assuming $M(h_b(1P))$ = 9900 MeV and $\Gamma(h_b(1P))$ = 0 MeV, and allowing B($h_b(1P) \to \gamma\eta_b(1S)$) to vary from 0–100%.

$\Gamma(h_b(1P)\pi^0 \to \gamma\eta_b(1S)\pi^0)/\Gamma_{total}$ — Γ_{11}/Γ

VALUE (units 10^{-4})	DOCUMENT ID		TECN	COMMENT
4.3±1.1±0.9	LEES	11K	BABR	$\Upsilon(3S) \to \eta_b\gamma\pi^0$

$\Gamma(h_b(1P)\pi^+\pi^-)/\Gamma_{total}$ — Γ_{12}/Γ

VALUE (units 10^{-4})	CL%	DOCUMENT ID		TECN	COMMENT
< 1.2	90	[36] LEES	11C	BABR	$e^+e^- \to \pi^+\pi^-X$
• • • We do not use the following data for averages, fits, limits, etc. • • •					
<18		[36] BUTLER	94B	CLE2	$e^+e^- \to \pi^+\pi^-X$
<15		[36] BROCK	91	CLEO	$e^+e^- \to \pi^+\pi^-X$

[36] For $M(h_b(1P))$ = 9900 MeV.

$\Gamma(\tau^+\tau^-)/\Gamma_{total}$ — Γ_{13}/Γ

VALUE (units 10^{-2})	EVTS	DOCUMENT ID		TECN	COMMENT
2.29±0.21±0.22	15k	[37] BESSON	07	CLEO	$e^+e^- \to \Upsilon(3S) \to \tau^+\tau^-$

[37] BESSON 07 reports [$\Gamma(\Upsilon(3S) \to \tau^+\tau^-)/\Gamma_{total}$] / [B($\Upsilon(3S) \to \mu^+\mu^-$)] = 1.05 ± 0.08 ± 0.05 which we multiply by our best value B($\Upsilon(3S) \to \mu^+\mu^-$) = (2.18 ± 0.21) × 10^{-2}. Our first error is their experiment's error and our second error is the systematic error from using our best value.

$\Gamma(\tau^+\tau^-)/\Gamma(\mu^+\mu^-)$ — Γ_{13}/Γ_{14}

VALUE	EVTS	DOCUMENT ID		TECN	COMMENT
0.968±0.016 OUR AVERAGE					
0.966±0.008±0.014	2.2M	LEES	20E	BABR	$e^+e^- \to \Upsilon(3S)$
1.05 ±0.08 ±0.05	15k	BESSON	07	CLEO	$e^+e^- \to \Upsilon(3S)$

Downloaded from https://academic.oup.com/ptep/article/2022/8/083C01/6651666 by KIT Library user on 27 September 2022

$\Gamma(\mu^+\mu^-)/\Gamma_{total}$ — Γ_{14}/Γ

VALUE	EVTS	DOCUMENT ID		TECN	COMMENT
0.0218±0.0021 OUR AVERAGE Error includes scale factor of 2.1. See the ideogram below.					
0.0239±0.0007±0.0010	81k	ADAMS	05	CLEO	$e^+e^- \to \mu^+\mu^-$
0.0202±0.0019±0.0033		CHEN	89B	CLEO	$e^+e^- \to \mu^+\mu^-$
0.0173±0.0015±0.0011		KAARSBERG	89	CSB2	$e^+e^- \to \mu^+\mu^-$
0.033 ±0.013 ±0.007	1096	ANDREWS	83	CLEO	$e^+e^- \to \mu^+\mu^-$

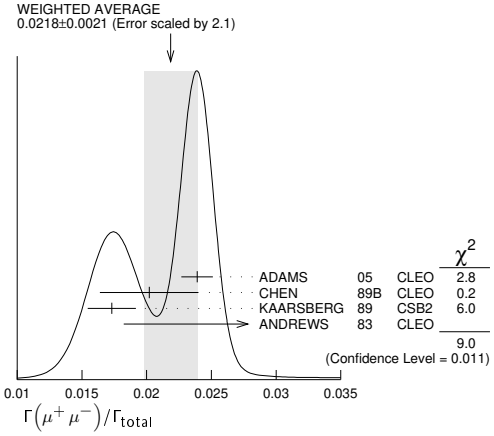

$\Gamma(ggg)/\Gamma_{total}$ — Γ_{17}/Γ

VALUE (units 10^{-2})	EVTS	DOCUMENT ID		TECN	COMMENT
35.7±2.6	3M	[38] BESSON	06A	CLEO	$\Upsilon(3S) \to$ hadrons

[38] Calculated using BESSON 06A value of $\Gamma(\gamma gg)/\Gamma(ggg) = (2.72 \pm 0.06 \pm 0.32 \pm 0.37)\%$ and the PDG 08 values of $B(\Upsilon(2S) + \text{anything}) = (10.6 \pm 0.8)\%$, $B(\pi^+\pi^-\Upsilon(1S)) = (4.40 \pm 0.10)\%$, $B(\pi^0\pi^0\Upsilon(1S)) = (2.20 \pm 0.13)\%$, $B(\gamma\chi_{b2}(2P)) = (13.1 \pm 1.6)\%$, $B(\gamma\chi_{b1}(2P)) = (12.6 \pm 1.2)\%$, $B(\gamma\chi_{b0}(2P)) = (5.9 \pm 0.6)\%$, $B(\gamma\chi_{b0}(1P)) = (0.30 \pm 0.11)\%$,$B(\mu^+\mu^-) = (2.18 \pm 0.21)\%$, and $R_{hadrons} = 3.51$. The statistical error is negligible and the systematic error is partially correlated with $\Gamma(\gamma gg)/\Gamma_{total}$ BESSON 06A value.

$\Gamma(\gamma gg)/\Gamma_{total}$ — Γ_{18}/Γ

VALUE (units 10^{-2})	EVTS	DOCUMENT ID		TECN	COMMENT
0.97±0.18	60k	[39] BESSON	06A	CLEO	$\Upsilon(3S) \to \gamma +$ hadrons

[39] Calculated using BESSON 06A values of $\Gamma(\gamma gg)/\Gamma(ggg) = (2.72 \pm 0.06 \pm 0.32 \pm 0.37)\%$ and $\Gamma(ggg)/\Gamma_{total}$. The statistical error is negligible and the systematic error is partially correlated with $\Gamma(ggg)/\Gamma_{total}$ BESSON 06A value.

$\Gamma(\gamma gg)/\Gamma(ggg)$ — Γ_{18}/Γ_{17}

VALUE (units 10^{-2})	EVTS	DOCUMENT ID		TECN	COMMENT
2.72±0.06±0.49	3M	BESSON	06A	CLEO	$\Upsilon(3S) \to (\gamma +)$ hadrons

$\Gamma(\overline{^2H}\text{ anything})/\Gamma_{total}$ — Γ_{19}/Γ

VALUE (units 10^{-5})	DOCUMENT ID		TECN	COMMENT
$2.33 \pm 0.15^{+0.31}_{-0.28}$	LEES	14G	BABR	$e^+e^- \to \overline{^2H}\,X$

$\Gamma(\gamma\chi_{b2}(2P))/\Gamma_{total}$ — Γ_{20}/Γ

VALUE	EVTS	DOCUMENT ID		TECN	COMMENT
0.131 ±0.016 OUR AVERAGE Error includes scale factor of 3.4. See the ideogram below.					
0.1579±0.0017±0.0073	568k	ARTUSO	05	CLEO	$e^+e^- \to \gamma X$
0.111 ±0.005 ±0.004	10319	[40] HEINTZ	92	CSB2	$e^+e^- \to \gamma X$
0.135 ±0.003 ±0.017	30741	MORRISON	91	CLE2	$e^+e^- \to \gamma X$

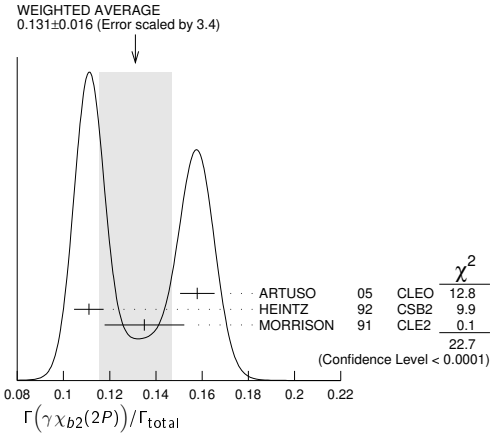

[40] Supersedes NARAIN 91.

$\Gamma(\gamma\chi_{b1}(2P))/\Gamma_{total}$ — Γ_{21}/Γ

VALUE	EVTS	DOCUMENT ID		TECN	COMMENT
0.126 ±0.012 OUR AVERAGE Error includes scale factor of 2.4. See the ideogram below.					
0.1454±0.0018±0.0073	537k	ARTUSO	05	CLEO	$e^+e^- \to \gamma X$
0.115 ±0.005 ±0.005	11147	[41] HEINTZ	92	CSB2	$e^+e^- \to \gamma X$
$0.105\ ^{+0.003}_{-0.002} \pm 0.013$	25759	MORRISON	91	CLE2	$e^+e^- \to \gamma X$

[41] Supersedes NARAIN 91.

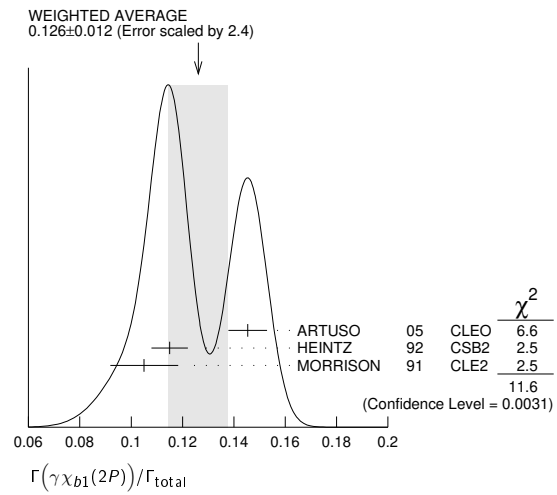

$\Gamma(\gamma\chi_{b0}(2P))/\Gamma_{total}$ — Γ_{22}/Γ

VALUE	EVTS	DOCUMENT ID		TECN	COMMENT
0.059 ±0.006 OUR AVERAGE Error includes scale factor of 1.4. See the ideogram below.					
0.0677±0.0020±0.0065	225k	ARTUSO	05	CLEO	$e^+e^- \to \gamma X$
0.060 ±0.004 ±0.006	4959	[42] HEINTZ	92	CSB2	$e^+e^- \to \gamma X$
$0.049\ ^{+0.003}_{-0.004} \pm 0.006$	9903	MORRISON	91	CLE2	$e^+e^- \to \gamma X$

[42] Supersedes NARAIN 91.

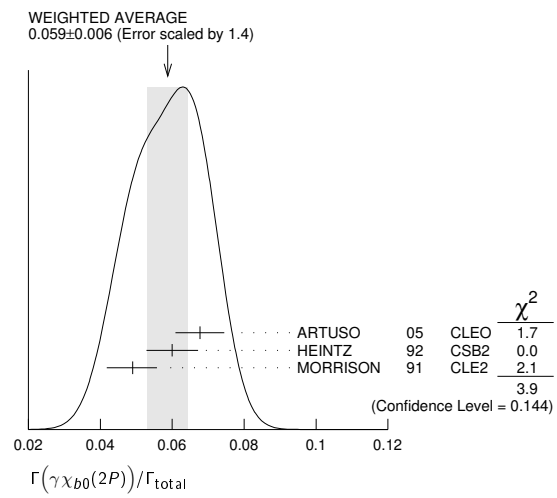

$\Gamma(\gamma\chi_{b2}(1P))/\Gamma_{total}$ — Γ_{23}/Γ

VALUE (units 10^{-3})	CL%	EVTS	DOCUMENT ID		TECN	COMMENT
10.0±1.0 OUR AVERAGE Error includes scale factor of 1.7.						
8.0±1.3±0.4		126	[43,44] KORNICER	11	CLEO	$e^+e^- \to \gamma\gamma\ell^+\ell^-$
$10.5 \pm 0.3^{+0.7}_{-0.6}$		9.7k	LEES	11J	BABR	$\Upsilon(3S) \to X\gamma$
• • • We do not use the following data for averages, fits, limits, etc. • • •						
<19	90		[45] ASNER	08A	CLEO	$\Upsilon(3S) \to \gamma +$ hadrons
seen			[46] HEINTZ	92	CSB2	$e^+e^- \to \gamma\gamma\ell^+\ell^-$

[43] Assuming $B(\Upsilon(1S) \to \ell^+\ell^-) = (2.48 \pm 0.05)\%$.

[44] KORNICER 11 reports $[\Gamma(\Upsilon(3S) \to \gamma\chi_{b2}(1P))/\Gamma_{total}] \times [B(\chi_{b2}(1P) \to \gamma\Upsilon(1S))] = (1.435 \pm 0.162 \pm 0.169) \times 10^{-3}$ which we divide by our best value $B(\chi_{b2}(1P) \to \gamma\Upsilon(1S)) = (18.0 \pm 1.0) \times 10^{-2}$. Our first error is their experiment's error and our second error is the systematic error from using our best value.

[45] ASNER 08A reports $[\Gamma(\Upsilon(3S) \to \gamma\chi_{b2}(1P))/\Gamma_{total}]$ / $[B(\Upsilon(2S) \to \gamma\chi_{b2}(1P))] < 27.1 \times 10^{-2}$ which we multiply by our best value $B(\Upsilon(2S) \to \gamma\chi_{b2}(1P)) = 7.15 \times 10^{-2}$.

Downloaded from https://academic.oup.com/ptep/article/2022/8/083C01/6651666 by KIT Library user on 27 September 2022

[46] HEINTZ 92, while unable to distinguish between different J states, measures $\sum_J B(\Upsilon(3S) \to \gamma\chi_{bJ}) \times B(\chi_{bJ} \to \gamma\Upsilon(1S)) = (1.7 \pm 0.4 \pm 0.6) \times 10^{-3}$ for J = 0,1,2 using inclusive $\Upsilon(1S)$ decays and $(1.2^{+0.4}_{-0.3} \pm 0.09) \times 10^{-3}$ for $J = 1,2$ using $\Upsilon(1S) \to \ell^+\ell^-$.

$\Gamma(\gamma\chi_{b1}(1P))/\Gamma_{total}$ — Γ_{24}/Γ

VALUE (units 10^{-3})	CL%	EVTS	DOCUMENT ID		TECN	COMMENT
0.9±0.5 OUR AVERAGE Error includes scale factor of 1.8.						
$1.5 \pm 0.4 \pm 0.1$	50		[47,48] KORNICER	11	CLEO	$e^+e^- \to \gamma\gamma\ell^+\ell^-$
$0.5 \pm 0.3^{+0.2}_{-0.1}$			LEES	11J	BABR	$\Upsilon(3S) \to X\gamma$
• • • We do not use the following data for averages, fits, limits, etc. • • •						
<1.7	90		[49] ASNER	08A	CLEO	$\Upsilon(3S) \to \gamma +$ hadrons
seen			[50] HEINTZ	92	CSB2	$e^+e^- \to \gamma\gamma\ell^+\ell^-$

[47] Assuming $B(\Upsilon(1S) \to \ell^+\ell^-) = (2.48 \pm 0.05)\%$.

[48] KORNICER 11 reports $[\Gamma(\Upsilon(3S) \to \gamma\chi_{b1}(1P))/\Gamma_{total}] \times [B(\chi_{b1}(1P) \to \gamma\Upsilon(1S))] = (5.38 \pm 1.20 \pm 0.95) \times 10^{-4}$ which we divide by our best value $B(\chi_{b1}(1P) \to \gamma\Upsilon(1S)) = (35.2 \pm 2.0) \times 10^{-2}$. Our first error is their experiment's error and our second error is the systematic error from using our best value.

[49] ASNER 08A reports $[\Gamma(\Upsilon(3S) \to \gamma\chi_{b1}(1P))/\Gamma_{total}]$ / $[B(\Upsilon(2S) \to \gamma\chi_{b1}(1P))] < 2.5 \times 10^{-2}$ which we multiply by our best value $B(\Upsilon(2S) \to \gamma\chi_{b1}(1P)) = 6.9 \times 10^{-2}$.

[50] HEINTZ 92, while unable to distinguish between different J states, measures $\sum_J B(\Upsilon(3S) \to \gamma\chi_{bJ}) \times B(\chi_{bJ} \to \gamma\Upsilon(1S)) = (1.7 \pm 0.4 \pm 0.6) \times 10^{-3}$ for J = 0,1,2 using inclusive $\Upsilon(1S)$ decays and $(1.2^{+0.4}_{-0.3} \pm 0.09) \times 10^{-3}$ for $J = 1,2$ using $\Upsilon(1S) \to \ell^+\ell^-$.

$\Gamma(\gamma\chi_{b0}(1P))/\Gamma_{total}$ — Γ_{25}/Γ

VALUE (units 10^{-2})	CL%	EVTS	DOCUMENT ID		TECN	COMMENT
0.27±0.04 OUR AVERAGE						
$0.27 \pm 0.04 \pm 0.02$		2.3k	LEES	11J	BABR	$\Upsilon(3S) \to X\gamma$
$0.30 \pm 0.04 \pm 0.10$		8.7k	ARTUSO	05	CLEO	$e^+e^- \to \gamma X$
• • • We do not use the following data for averages, fits, limits, etc. • • •						
<0.8	90		[51] ASNER	08A	CLEO	$\Upsilon(3S) \to \gamma +$ hadrons

[51] ASNER 08A reports $[\Gamma(\Upsilon(3S) \to \gamma\chi_{b0}(1P))/\Gamma_{total}]$ / $[B(\Upsilon(2S) \to \gamma\chi_{b0}(1P))] < 21.9 \times 10^{-2}$ which we multiply by our best value $B(\Upsilon(2S) \to \gamma\chi_{b0}(1P)) = 3.8 \times 10^{-2}$.

$\Gamma(\gamma\eta_b(2S))/\Gamma_{total}$ — Γ_{26}/Γ

VALUE (units 10^{-4})	CL%	DOCUMENT ID		TECN	COMMENT
< 6.2	90	ARTUSO	05	CLEO	$e^+e^- \to \gamma X$
• • • We do not use the following data for averages, fits, limits, etc. • • •					
<19	90	LEES	11J	BABR	$\Upsilon(3S) \to X\gamma$

$\Gamma(\gamma\eta_b(1S))/\Gamma_{total}$ — Γ_{27}/Γ

VALUE (units 10^{-4})	CL%	EVTS	DOCUMENT ID		TECN	COMMENT
5.1±0.7 OUR AVERAGE						
$7.1 \pm 1.8 \pm 1.3$		2.3±0.5k	[52] BONVICINI	10	CLEO	$\Upsilon(3S) \to \gamma X$
$4.8 \pm 0.5 \pm 0.6$		19 ± 3k	[52] AUBERT	09AQ	BABR	$\Upsilon(3S) \to \gamma X$
• • • We do not use the following data for averages, fits, limits, etc. • • •						
<8.5	90		LEES	11J	BABR	$\Upsilon(3S) \to X\gamma$
$4.8 \pm 0.5 \pm 1.2$		19 ± 3k	[52,53] AUBERT	08V	BABR	$\Upsilon(3S) \to \gamma X$
<4.3	90		[54] ARTUSO	05	CLEO	$e^+e^- \to \gamma X$

[52] Assuming $\Gamma_{\eta_b(1S)}$ = 10 MeV.

[53] Systematic error re-evaluated by AUBERT 09AQ.

[54] Superseded by BONVICINI 10.

$\Gamma(\gamma A^0 \to \gamma\text{hadrons})/\Gamma_{total}$ — Γ_{28}/Γ

(0.3 GeV < m_{A^0} < 7 GeV)

VALUE	CL%	DOCUMENT ID		TECN	COMMENT
<8 × 10^{-5}	90	[55] LEES	11H	BABR	$\Upsilon(3S) \to \gamma$ hadrons

[55] For a narrow scalar or pseudoscalar A^0, excluding known resonances, with mass in the range 0.3–7 GeV. Measured 90% CL limits as a function of m_{A^0} range from 1×10^{-6} to 8×10^{-5}.

$\Gamma(\gamma X \to \gamma + \geq 4 \text{ prongs})/\Gamma_{total}$ — Γ_{29}/Γ

(1.5 GeV < m_X < 5.0 GeV)

VALUE (units 10^{-4})	CL%	DOCUMENT ID		TECN	COMMENT
<2.2	95	ROSNER	07A	CLEO	$e^+e^- \to \gamma X$

$\Gamma(\gamma a_1^0 \to \gamma\mu^+\mu^-)/\Gamma_{total}$ — Γ_{30}/Γ

VALUE (units 10^{-6})	CL%	DOCUMENT ID		TECN	COMMENT
<5.5	90	[56] AUBERT	09Z	BABR	$e^+e^- \to \gamma a_1^0 \to \gamma\mu^+\mu^-$

[56] For a narrow scalar or pseudoscalar a_1^0 with mass in the range 212–9300 MeV, excluding J/ψ and $\psi(2S)$. Measured 90% CL limits as a function of $m_{a_1^0}$ range from 0.27–5.5 × 10^{-6}.

$\Gamma(\gamma a_1^0 \to \gamma\tau^+\tau^-)/\Gamma_{total}$ — Γ_{31}/Γ

VALUE	CL%	DOCUMENT ID		TECN	COMMENT
<1.6 × 10^{-4}	90	[57] AUBERT	09P	BABR	$e^+e^- \to \gamma a_1^0 \to \gamma\tau^+\tau^-$

[57] For a narrow scalar or pseudoscalar a_1^0 with $M(\tau^+\tau^-)$ in the ranges 4.03–9.52 and 9.61–10.10 GeV. Measured 90% CL limits as a function of $M(\tau^+\tau^-)$ range from 1.5–16 × 10^{-5}.

LEPTON FAMILY NUMBER (*LF*) VIOLATING MODES

$\Gamma(e^\pm\tau^\mp)/\Gamma_{total}$ — Γ_{32}/Γ

VALUE (units 10^{-6})	CL%	DOCUMENT ID		TECN	COMMENT
<4.2	90	LEES	10B	BABR	$e^+e^- \to e^\pm\tau^\mp$

$\Gamma(\mu^\pm\tau^\mp)/\Gamma_{total}$ — Γ_{33}/Γ

VALUE (units 10^{-6})	CL%	DOCUMENT ID		TECN	COMMENT
< 3.1	90	LEES	10B	BABR	$e^+e^- \to \mu^\pm\tau^\mp$
• • • We do not use the following data for averages, fits, limits, etc. • • •					
<20.3	95	LOVE	08A	CLEO	$e^+e^- \to \mu^\pm\tau^\mp$

$\Upsilon(3S)$ REFERENCES

LEES	20E	PRL 125 241801	J.P. Lees *et al.*	(BABAR Collab.)
LEES	14G	PR D89 111102	J.P. Lees *et al.*	(BABAR Collab.)
GE	11	PR D84 032008	J.Y. Ge *et al.*	(CLEO Collab.)
KORNICER	11	PR D83 054003	M. Kornicer *et al.*	(CLEO Collab.)
LEES	11C	PR D84 011104	J.P. Lees *et al.*	(BABAR Collab.)
LEES	11H	PRL 107 221803	J.P. Lees *et al.*	(BABAR Collab.)
LEES	11J	PR D84 072002	J.P. Lees *et al.*	(BABAR Collab.)
LEES	11K	PR D84 091101	J.P. Lees *et al.*	(BABAR Collab.)
LEES	11L	PR D84 092003	J.P. Lees *et al.*	(BABAR Collab.)
BONVICINI	10	PR D81 031104	G. Bonvicini *et al.*	(CLEO Collab.)
LEES	10B	PRL 104 151802	J.P. Lees *et al.*	(BABAR Collab.)
AUBERT	09AQ	PRL 103 161801	B. Aubert *et al.*	(BABAR Collab.)
AUBERT	09P	PRL 103 181801	B. Aubert *et al.*	(BABAR Collab.)
AUBERT	09Z	PRL 103 081803	B. Aubert *et al.*	(BABAR Collab.)
BHARI	09	PR D79 011103	S.R. Bhari *et al.*	(CLEO Collab.)
ASNER	08A	PR D78 091103	D.M. Asner *et al.*	(CLEO Collab.)
AUBERT	08BP	PR D78 112002	B. Aubert *et al.*	(BABAR Collab.)
AUBERT	08V	PRL 101 071801	B. Aubert *et al.*	(BABAR Collab.)
HE	08A	PRL 101 192001	Q. He *et al.*	(CLEO Collab.)
LOVE	08A	PRL 101 201601	W. Love *et al.*	(CLEO Collab.)
PDG	08	PL B667 1	C. Amsler *et al.*	(PDG Collab.)
BESSON	07	PRL 98 052002	D. Besson *et al.*	(CLEO Collab.)
ROSNER	07A	PR D76 117102	J.L. Rosner *et al.*	(CLEO Collab.)
BESSON	06A	PR D74 012003	D. Besson *et al.*	(CLEO Collab.)
ROSNER	06	PRL 96 092003	J.L. Rosner *et al.*	(CLEO Collab.)
ADAMS	05	PRL 94 012001	G.S. Adams *et al.*	(CLEO Collab.)
ARTUSO	05	PRL 94 032001	M. Artuso *et al.*	(CLEO Collab.)
ARTAMONOV	00	PL B474 427	A.S. Artamonov *et al.*	
BUTLER	94B	PR D49 40	F. Butler *et al.*	(CLEO Collab.)
WU	93	PL B301 307	Q.W. Wu *et al.*	(CUSB Collab.)
HEINTZ	92	PR D46 1928	U. Heintz *et al.*	(CUSB II Collab.)
BROCK	91	PR D43 1448	I.C. Brock *et al.*	(CLEO Collab.)
HEINTZ	91	PRL 66 1563	U. Heintz *et al.*	(CUSB Collab.)
MORRISON	91	PRL 67 1696	R.J. Morrison *et al.*	(CLEO Collab.)
NARAIN	91	PRL 66 3113	M. Narain *et al.*	(CUSB Collab.)
CHEN	89B	PR D39 3528	W.Y. Chen *et al.*	(CLEO Collab.)
KAARSBERG	89	PRL 62 2077	T.M. Kaarsberg *et al.*	(CUSB Collab.)
BUCHMUEL...	88	HE e^+e^- Physics 412 Editors: A. Ali and P. Soeding, World Scientific, Singapore	W. Buchmueller, S. Cooper	(HANN, DESY, MIT)
COHEN	87	RMP 59 1121	E.R. Cohen, B.N. Taylor	(RISC, NBS)
BARU	86B	ZPHY C32 622 (erratum)	S.E. Baru *et al.*	(NOVO)
KURAEV	85	SJNP 41 466 Translated from YAF 41 733.	E.A. Kuraev, V.S. Fadin	(NOVO)
ARTAMONOV	84	PL 137B 272	A.S. Artamonov *et al.*	(NOVO)
GILES	84B	PR D29 1285	R. Giles *et al.*	(CLEO Collab.)
ANDREWS	83	PRL 50 807	D.E. Andrews *et al.*	(CLEO Collab.)
GREEN	82	PRL 49 617	J. Green *et al.*	(CLEO Collab.)
MAGERAS	82	PL 118B 453	G. Mageras *et al.*	(COLU, CORN, LSU+)

$\chi_{b1}(3P)$

$I^G(J^{PC}) = 0^+(1^{++})$

Observed in the radiative decay to $\Upsilon(1S, 2S, 3S)$, therefore $C = +$.
J needs confirmation.

$\chi_{b1}(3P)$ MASS

VALUE (MeV)	EVTS	DOCUMENT ID		TECN	COMMENT
10513.42± 0.41± 0.53		[1] SIRUNYAN	18N	CMS	$pp \to \gamma\mu^+\mu^- X$
• • • We do not use the following data for averages, fits, limits, etc. • • •					
$10515.7^{+2.2}_{-3.9} \pm 1.5$	169	[2] AAIJ	14BG	LHCB	$pp \to \gamma\mu^+\mu^- X$
$10512.1 \pm 2.1 \pm 0.9$	351	[3] AAIJ	14BG	LHCB	$pp \to \gamma\mu^+\mu^- X$
$10511.3 \pm 1.7 \pm 2.5$	182	[4] AAIJ	14BI	LHCB	$pp \to \gamma\mu^+\mu^- X$
$10530 \pm 5 \pm 9$		[5] AAD	12A	ATLS	$pp \to \gamma\mu^+\mu^- X$
$10551 \pm 14 \pm 17$		[5] ABAZOV	12Q	D0	$p\overline{p} \to \gamma\mu^+\mu^- X$

[1] Systematic error includes an additional 0.5 MeV for the uncertainty on the $\Upsilon(3S)$ mass. Also measures $m_{\chi_{b2}(3P)} - m_{\chi_{b1}(3P)} = 10.60 \pm 0.64 \pm 0.17$ MeV. A total of 372 $\chi_{b1}(3P)$ and $\chi_{b2}(3P)$ events was observed.

[2] From $\chi_{b1}(3P) \to \Upsilon(1S, 2S)\gamma$ transitions assuming $m_{\chi_{b2}(3P)} - m_{\chi_{b1}(3P)} = 10.5 \pm 1.5$ MeV and allowing for ±30% variation in the $\chi_{b2}(3P)$ production rate relative to that of $\chi_{b1}(3P)$.

[3] The mass of the $\chi_{b1}(3P)$ state obtained by combining the results of AAIJ 14BG with that of AAIJ 14BI. The first uncertainty is experimental and the second attributable to the unknown mass splitting, assumed to be $m_{\chi_{b2}(3P)} - m_{\chi_{b1}(3P)} = 10.5 \pm 1.5$ MeV.

[4] From $\chi_{b1}(3P) \to \Upsilon(3S)\gamma$ transition assuming $m_{\chi_{b2}(3P)} - m_{\chi_{b1}(3P)} = 10.5 \pm 1.5$ MeV.

[5] The mass barycenter of the merged lineshapes from the J = 1 and 2 states.

Downloaded from https://academic.oup.com/ptep/article/2022/8/083C01/6651666 by KIT Library user on 27 September 2022

$\chi_{b1}(3P)$ DECAY MODES

	Mode	Fraction (Γ_i/Γ)
Γ_1	$\Upsilon(1S)\gamma$	seen
Γ_2	$\Upsilon(2S)\gamma$	seen
Γ_3	$\Upsilon(3S)\gamma$	seen

$\chi_{b1}(3P)$ BRANCHING RATIOS

$\Gamma(\Upsilon(1S)\gamma)/\Gamma_{total}$ — Γ_1/Γ

VALUE	EVTS	DOCUMENT ID		TECN	COMMENT
seen	169	[1] AAIJ	14BG	LHCB	$pp \to \gamma\mu^+\mu^- X$
• • • We do not use the following data for averages, fits, limits, etc. • • •					
seen		AAD	12A	ATLS	$pp \to \gamma\mu^+\mu^- X$
seen		ABAZOV	12Q	D0	$p\overline{p} \to \gamma\mu^+\mu^- X$

[1] From $\chi_{b1}(3P) \to \Upsilon(1S,2S)\gamma$ transitions assuming $m_{\chi_{b2}(3P)} - m_{\chi_{b1}(3P)} = 10.5 \pm 1.5$ MeV and allowing for $\pm 30\%$ variation in the $\chi_{b2}(3P)$ production rate relative to that of $\chi_{b1}(3P)$.

$\Gamma(\Upsilon(2S)\gamma)/\Gamma_{total}$ — Γ_2/Γ

VALUE	EVTS	DOCUMENT ID		TECN	COMMENT
seen	169	[1] AAIJ	14BG	LHCB	$pp \to \gamma\mu^+\mu^- X$
• • • We do not use the following data for averages, fits, limits, etc. • • •					
seen		AAD	12A	ATLS	$pp \to \gamma\mu^+\mu^- X$

[1] From $\chi_{b1}(3P) \to \Upsilon(1S,2S)\gamma$ transitions assuming $m_{\chi_{b2}(3P)} - m_{\chi_{b1}(3P)} = 10.5 \pm 1.5$ MeV and allowing for $\pm 30\%$ variation in the $\chi_{b2}(3P)$ production rate relative to that of $\chi_{b1}(3P)$.

$\Gamma(\Upsilon(3S)\gamma)/\Gamma_{total}$ — Γ_3/Γ

VALUE	EVTS	DOCUMENT ID		TECN	COMMENT
seen		SIRUNYAN	18N	CMS	$pp \to \gamma\mu^+\mu^- X$
seen	182	AAIJ	14BI	LHCB	$pp \to \gamma\mu^+\mu^- X$

$\chi_{b1}(3P)$ REFERENCES

SIRUNYAN	18N	PRL 121 092002	A.M. Sirunyan *et al.*	(CMS Collab.)
AAIJ	14BG	JHEP 1410 088	R. Aaij *et al.*	(LHCb Collab.)
AAIJ	14BI	EPJ C74 3092	R. Aaij *et al.*	(LHCb Collab.)
AAD	12A	PRL 108 152001	G. Aad *et al.*	(ATLAS Collab.)
ABAZOV	12Q	PR D86 031103	V.M. Abazov *et al.*	(D0 Collab.)

$\chi_{b2}(3P)$

$I^G(J^{PC}) = 0^+(2^{++})$

Observed in the radiative decay to $\Upsilon(3S)$, therefore $C = +$. J needs confirmation.

$\chi_{b2}(3P)$ MASS

VALUE (MeV)	DOCUMENT ID		TECN	COMMENT
10524.02±0.57±0.53	[1] SIRUNYAN	18N	CMS	$pp \to \gamma\mu^+\mu^- X$
• • • We do not use the following data for averages, fits, limits, etc. • • •				
10530 ±5 ±9	[2] AAD	12A	ATLS	$pp \to \gamma\mu^+\mu^- X$

[1] Systematic error includes an additional 0.5 MeV for the uncertainty on the $\Upsilon(3S)$ mass. Also measures $m_{\chi_{b2}(3P)} - m_{\chi_{b1}(3P)} = 10.60 \pm 0.64 \pm 0.17$ MeV. A total of 372 $\chi_{b1}(3P)$ and $\chi_{b2}(3P)$ events was observed.
[2] The mass barycenter of the merged lineshapes from the $J = 1$ and 2 states.

$\chi_{b2}(3P)$ DECAY MODES

	Mode	Fraction (Γ_i/Γ)
Γ_1	$\Upsilon(3S)\gamma$	seen

$\chi_{b2}(3P)$ BRANCHING RATIOS

$\Gamma(\Upsilon(3S)\gamma)/\Gamma_{total}$ — Γ_1/Γ

VALUE	DOCUMENT ID		TECN	COMMENT
seen	SIRUNYAN	18N	CMS	$pp \to \gamma\mu^+\mu^- X$

$\chi_{b2}(3P)$ REFERENCES

SIRUNYAN	18N	PRL 121 092002	A.M. Sirunyan *et al.*	(CMS Collab.)
AAD	12A	PRL 108 152001	G. Aad *et al.*	(ATLAS Collab.)

$\Upsilon(4S)$

$I^G(J^{PC}) = 0^-(1^{--})$

also known as $\Upsilon(10580)$

$\Upsilon(4S)$ MASS

VALUE (MeV)	DOCUMENT ID		TECN	COMMENT
10579.4±1.2 OUR AVERAGE				
10579.3±0.4±1.2	AUBERT	05Q	BABR	$e^+e^- \to$ hadrons
10580.0±3.5	[1] BEBEK	87	CLEO	$e^+e^- \to$ hadrons
• • • We do not use the following data for averages, fits, limits, etc. • • •				
10577.4±1.0	[2] LOVELOCK	85	CUSB	$e^+e^- \to$ hadrons

[1] Reanalysis of BESSON 85.
[2] No systematic error given.

$\Upsilon(4S)$ WIDTH

VALUE (MeV)	DOCUMENT ID		TECN	COMMENT
20.5±2.5 OUR AVERAGE				
20.7±1.6±2.5	AUBERT	05Q	BABR	$e^+e^- \to$ hadrons
20 ±2 ±4	BESSON	85	CLEO	$e^+e^- \to$ hadrons
• • • We do not use the following data for averages, fits, limits, etc. • • •				
25 ±2.5	LOVELOCK	85	CUSB	$e^+e^- \to$ hadrons

$\Upsilon(4S)$ DECAY MODES

	Mode	Fraction (Γ_i/Γ)	Confidence level
Γ_1	$B\overline{B}$	> 96 %	95%
Γ_2	B^+B^-	(51.4 ±0.6) %	
Γ_3	D_s^+ anything + c.c.	(17.8 ±2.6) %	
Γ_4	$B^0\overline{B}^0$	(48.6 ±0.6) %	
Γ_5	$J/\psi K_S^0 + (J/\psi, \eta_c) K_S^0$	$< 4 \times 10^{-7}$	90%
Γ_6	non-$B\overline{B}$	< 4 %	95%
Γ_7	e^+e^-	$(1.57\pm0.08) \times 10^{-5}$	
Γ_8	$\rho^+\rho^-$	$< 5.7 \times 10^{-6}$	90%
Γ_9	$K^*(892)^0\overline{K}^0$	$< 2.0 \times 10^{-6}$	90%
Γ_{10}	$J/\psi(1S)$ anything	$< 1.9 \times 10^{-4}$	95%
Γ_{11}	D^{*+} anything + c.c.	< 7.4 %	90%
Γ_{12}	ϕ anything	(7.1 ±0.6) %	
Γ_{13}	$\phi\eta$	$< 1.8 \times 10^{-6}$	90%
Γ_{14}	$\phi\eta'$	$< 4.3 \times 10^{-6}$	90%
Γ_{15}	$\rho\eta$	$< 1.3 \times 10^{-6}$	90%
Γ_{16}	$\rho\eta'$	$< 2.5 \times 10^{-6}$	90%
Γ_{17}	$\Upsilon(1S)$ anything	$< 4 \times 10^{-3}$	90%
Γ_{18}	$\Upsilon(1S)\pi^+\pi^-$	$(8.2 \pm 0.4) \times 10^{-5}$	
Γ_{19}	$\Upsilon(1S)\eta$	$(1.81\pm0.18) \times 10^{-4}$	
Γ_{20}	$\Upsilon(1S)\eta'$	$(3.4 \pm 0.9) \times 10^{-5}$	
Γ_{21}	$\Upsilon(2S)\pi^+\pi^-$	$(8.2 \pm 0.8) \times 10^{-5}$	
Γ_{22}	$h_b(1P)\pi^+\pi^-$	not seen	
Γ_{23}	$h_b(1P)\eta$	$(2.18\pm0.21) \times 10^{-3}$	
Γ_{24}	$\eta_b(1S)\omega$	$< 1.8 \times 10^{-4}$	90%
Γ_{25}	^2H anything	$< 1.3 \times 10^{-5}$	90%
	Double Radiative Decays		
Γ_{26}	$\gamma\gamma\,\Upsilon(D) \to \gamma\gamma\eta\,\Upsilon(1S)$	$< 2.3 \times 10^{-5}$	90%

$\Upsilon(4S)$ PARTIAL WIDTHS

$\Gamma(e^+e^-)$ — Γ_7

VALUE (keV)	DOCUMENT ID		TECN	COMMENT
0.272±0.029 OUR AVERAGE	Error includes scale factor of 1.5. See the ideogram below.			
0.321±0.017±0.029	AUBERT	05Q	BABR	$e^+e^- \to$ hadrons
0.28 ±0.05 ±0.01	[1] ALBRECHT	95E	ARG	$e^+e^- \to$ hadrons
0.192±0.007±0.038	BESSON	85	CLEO	$e^+e^- \to$ hadrons
0.283±0.037	LOVELOCK	85	CUSB	$e^+e^- \to$ hadrons

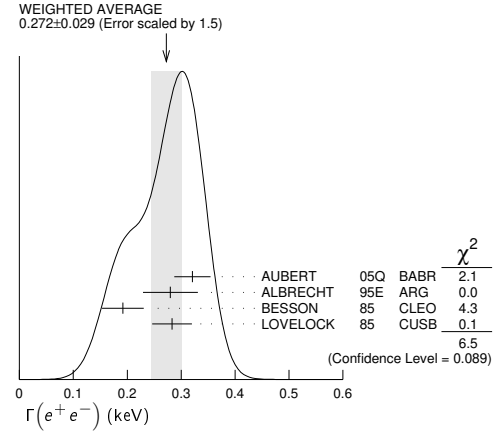

[1] Using LEYAOUANC 77 parametrization of $\Gamma(s)$.

Downloaded from https://academic.oup.com/ptep/article/2022/8/083C01/6651666 by KIT Library user on 27 September 2022

$\Upsilon(4S)$ BRANCHING RATIOS

$B\overline{B}$ DECAYS

The ratio of branching fraction to charged and neutral B mesons is often derived assuming isospin invariance in the decays, and relies on the knowledge of the B^+/B^0 lifetime ratio. "OUR EVALUATION" is obtained based on averages of rescaled data listed below. The average and rescaling were performed by the Heavy Flavor Averaging Group (HFLAV) and are described at https://hflav.web.cern.ch/. The averaging/rescaling procedure takes into account the common dependence of the measurement on the value of the lifetime ratio.

$\Gamma(B^+B^-)/\Gamma_{total}$ — Γ_2/Γ

VALUE	DOCUMENT ID
0.514±0.006 OUR EVALUATION	Assuming B($\Upsilon(4S) \to B\overline{B}$) = 1

$\Gamma(D_s^+$ anything + c.c.$)/\Gamma_{total}$ — Γ_3/Γ

VALUE	DOCUMENT ID		TECN	COMMENT
0.178±0.021±0.016	[1] ARTUSO	05B	CLE3	$e^+e^- \to D_X X$

[1] ARTUSO 05B reports $[\Gamma(\Upsilon(4S) \to D_s^+$ anything + c.c.$)/\Gamma_{total}] \times [B(D_s^+ \to \phi\pi^+)] = (8.0 \pm 0.2 \pm 0.9) \times 10^{-3}$ which we divide by our best value $B(D_s^+ \to \phi\pi^+) = (4.5 \pm 0.4) \times 10^{-2}$. Our first error is their experiment's error and our second error is the systematic error from using our best value.

$\Gamma(B^0\overline{B}^0)/\Gamma_{total}$ — Γ_4/Γ

VALUE	DOCUMENT ID		TECN	COMMENT
0.486±0.006 OUR EVALUATION	Assuming B($\Upsilon(4S) \to B\overline{B}$) = 1			
• • • We do not use the following data for averages, fits, limits, etc. • • •				
0.487±0.010±0.008	[1] AUBERT,B	05H	BABR	$\Upsilon(4S) \to \overline{B}B \to D^*\ell\nu_\ell$

[1] Direct measurement. This value is averaged with the value extracted from the $\Gamma(B^+B^-)$ / $\Gamma(B^0\overline{B}^0)$ measurements.

$\Gamma(B^+B^-)/\Gamma(B^0\overline{B}^0)$ — Γ_2/Γ_4

VALUE	DOCUMENT ID		TECN	COMMENT
1.058±0.024 OUR EVALUATION				
1.006±0.036±0.031	[1] AUBERT	04F	BABR	$\Upsilon(4S) \to B\overline{B} \to J/\psi K$
1.01 ±0.03 ±0.09	[1] HASTINGS	03	BELL	$\Upsilon(4S) \to B\overline{B} \to$ dileptons
1.058±0.084±0.136	[2] ATHAR	02	CLEO	$\Upsilon(4S) \to B\overline{B} \to D^*\ell\nu$
1.10 ±0.06 ±0.05	[3] AUBERT	02	BABR	$\Upsilon(4S) \to B\overline{B} \to (c\overline{c})K^*$
1.04 ±0.07 ±0.04	[4] ALEXANDER	01	CLEO	$\Upsilon(4S) \to B\overline{B} \to J/\psi K^*$

[1] HASTINGS 03 and AUBERT 04F assume $\tau(B^+)$ / $\tau(B^0) = 1.083 \pm 0.017$.
[2] ATHAR 02 assumes $\tau(B^+)$ / $\tau(B^0) = 1.074 \pm 0.028$. Supersedes BARISH 95.
[3] AUBERT 02 assumes $\tau(B^+)$ / $\tau(B^0) = 1.062 \pm 0.029$.
[4] ALEXANDER 01 assumes $\tau(B^+)$ / $\tau(B^0) = 1.066 \pm 0.024$.

$[\Gamma(J/\psi K_S^0) + \Gamma((J/\psi, \eta_c)K_S^0)]/\Gamma_{total}$ — Γ_5/Γ

Forbidden by CP invariance.

VALUE (units 10^{-7})	CL%	DOCUMENT ID		TECN	COMMENT
<4	90	[1] TAJIMA	07A	BELL	$\Upsilon(4S) \to B^0\overline{B}^0$

[1] $\Upsilon(4S)$ with $CP = +1$ decays to the final state with $CP = -1$.

non-$B\overline{B}$ DECAYS

Γ(non-$B\overline{B}$)$/\Gamma_{total}$ — Γ_6/Γ

VALUE	CL%	DOCUMENT ID		TECN	COMMENT
<0.04	95	BARISH	96B	CLEO	e^+e^-

$\Gamma(e^+e^-)/\Gamma_{total}$ — Γ_7/Γ

VALUE (units 10^{-5})	DOCUMENT ID		TECN	COMMENT
1.57±0.08 OUR AVERAGE				
1.55±0.04±0.07	AUBERT	05Q	BABR	$e^+e^- \to$ hadrons
2.77±0.50±0.49	[1] ALBRECHT	95E	ARG	$e^+e^- \to$ hadrons

[1] Using LEYAOUANC 77 parametrization of $\Gamma(s)$.

$\Gamma(\rho^+\rho^-)/\Gamma_{total}$ — Γ_8/Γ

VALUE	CL%	DOCUMENT ID		TECN	COMMENT
<5.7 × 10^{-6}	90	AUBERT	08BO	BABR	$e^+e^- \to \pi^+\pi^-2\pi^0$

$\Gamma(K^*(892)^0\overline{K}^0)/\Gamma_{total}$ — Γ_9/Γ

VALUE	CL%	DOCUMENT ID		TECN	COMMENT
<2.0 × 10^{-6}	90	SHEN	13A	BELL	$e^+e^- \to K^*(892)^0\overline{K}^0$

$\Gamma(J/\psi(1S)$ anything$)/\Gamma_{total}$ — Γ_{10}/Γ

VALUE (units 10^{-4})	CL%	DOCUMENT ID		TECN	COMMENT
<1.9	95	[1] ABE	02D	BELL	$e^+e^- \to J/\psi X \to \ell^+\ell^- X$
• • • We do not use the following data for averages, fits, limits, etc. • • •					
<4.7	90	[1] AUBERT	01C	BABR	$e^+e^- \to J/\psi X \to \ell^+\ell^- X$

[1] Uses $B(J/\psi \to e^+e^-) = 0.0593 \pm 0.0010$ and $B(J/\psi \to \mu^+\mu^-) = 0.0588 \pm 0.0010$.

$\Gamma(D^{*+}$ anything + c.c.$)/\Gamma_{total}$ — Γ_{11}/Γ

VALUE	CL%	DOCUMENT ID		TECN	COMMENT
<0.074	90	[1] ALEXANDER	90C	CLEO	e^+e^-

[1] For $x > 0.473$.

$\Gamma(\phi$ anything$)/\Gamma_{total}$ — Γ_{12}/Γ

VALUE (units 10^{-2})	CL%	DOCUMENT ID		TECN	COMMENT
7.1 ±0.1±0.6		HUANG	07	CLEO	$\Upsilon(4S) \to \phi X$
• • • We do not use the following data for averages, fits, limits, etc. • • •					
<0.23	90	[1] ALEXANDER	90C	CLEO	e^+e^-

[1] For $x > 0.52$.

$\Gamma(\phi\eta)/\Gamma_{total}$ — Γ_{13}/Γ

VALUE (units 10^{-6})	CL%	DOCUMENT ID		TECN	COMMENT
<1.8	90	[1] BELOUS	09	BELL	$e^+e^- \to \phi\eta$
• • • We do not use the following data for averages, fits, limits, etc. • • •					
<2.5	90	AUBERT,BE	06F	BABR	$e^+e^- \to \phi\eta$

[1] Using all intermedite branching fraction values from PDG 08.

$\Gamma(\phi\eta')/\Gamma_{total}$ — Γ_{14}/Γ

VALUE (units 10^{-6})	CL%	DOCUMENT ID		TECN	COMMENT
<4.3	90	[1] BELOUS	09	BELL	$e^+e^- \to \phi\eta'$

[1] Using all intermedite branching fraction values from PDG 08.

$\Gamma(\rho\eta)/\Gamma_{total}$ — Γ_{15}/Γ

VALUE (units 10^{-6})	CL%	DOCUMENT ID		TECN	COMMENT
<1.3	90	[1] BELOUS	09	BELL	$e^+e^- \to \rho\eta$

[1] Using all intermedite branching fraction values from PDG 08.

$\Gamma(\rho\eta')/\Gamma_{total}$ — Γ_{16}/Γ

VALUE (units 10^{-6})	CL%	DOCUMENT ID		TECN	COMMENT
<2.5	90	[1] BELOUS	09	BELL	$e^+e^- \to \rho\eta'$

[1] Using all intermedite branching fraction values from PDG 08.

$\Gamma(\Upsilon(1S)$ anything$)/\Gamma_{total}$ — Γ_{17}/Γ

VALUE	CL%	DOCUMENT ID		TECN	COMMENT
<0.004	90	ALEXANDER	90C	CLEO	e^+e^-

$\Gamma(\Upsilon(1S)\pi^+\pi^-)/\Gamma_{total}$ — Γ_{18}/Γ

VALUE (units 10^{-5})	CL%	EVTS	DOCUMENT ID		TECN	COMMENT
8.2 ±0.4 OUR AVERAGE						
8.2 ±0.5 ±0.4		515	GUIDO	17	BELL	$\Upsilon(4S) \to \pi^+\pi^-\mu^+\mu^-$
8.5 ±1.3 ±0.2		113 ± 16	[1] SOKOLOV	09	BELL	$e^+e^- \to \pi^+\pi^-\mu^+\mu^-$
8.00±0.64±0.27		430	[2] AUBERT	08BP	BABR	$\Upsilon(4S) \to \pi^+\pi^-\ell^+\ell^-$
• • • We do not use the following data for averages, fits, limits, etc. • • •						
17.8 ±4.0 ±0.3			[3,4] SOKOLOV	07	BELL	$e^+e^- \to \pi^+\pi^-\mu^+\mu^-$
9.0 ±1.5 ±0.2		167 ± 19	[5] AUBERT	06R	BABR	$e^+e^- \to \pi^+\pi^-\mu^+\mu^-$
<12	90		GLENN	99	CLE2	e^+e^-

[1] SOKOLOV 09 reports $[\Gamma(\Upsilon(4S) \to \Upsilon(1S)\pi^+\pi^-)/\Gamma_{total}] \times [B(\Upsilon(1S) \to \mu^+\mu^-)] = (0.211 \pm 0.030 \pm 0.014) \times 10^{-5}$ which we divide by our best value $B(\Upsilon(1S) \to \mu^+\mu^-) = (2.48 \pm 0.05) \times 10^{-2}$. Our first error is their experiment's error and our second error is the systematic error from using our best value.
[2] Using $B(\Upsilon(1S) \to e^+e^-) = (2.38 \pm 0.11)\%$ and $B(\Upsilon(1S) \to \mu^+\mu^-) = (2.48 \pm 0.05)\%$.
[3] SOKOLOV 07 reports $[\Gamma(\Upsilon(4S) \to \Upsilon(1S)\pi^+\pi^-)/\Gamma_{total}] \times [B(\Upsilon(1S) \to \mu^+\mu^-)] = (4.42 \pm 0.81 \pm 0.56) \times 10^{-6}$ which we divide by our best value $B(\Upsilon(1S) \to \mu^+\mu^-) = (2.48 \pm 0.05) \times 10^{-2}$. Our first error is their experiment's error and our second error is the systematic error from using our best value.
[4] According to the authors, systematic errors were underestimated.
[5] Superseded by AUBERT 08BP. AUBERT 06R reports $[\Gamma(\Upsilon(4S) \to \Upsilon(1S)\pi^+\pi^-)/\Gamma_{total}] \times [B(\Upsilon(1S) \to \mu^+\mu^-)] = (2.23 \pm 0.25 \pm 0.27) \times 10^{-6}$ which we divide by our best value $B(\Upsilon(1S) \to \mu^+\mu^-) = (2.48 \pm 0.05) \times 10^{-2}$. Our first error is their experiment's error and our second error is the systematic error from using our best value.

$\Gamma(\Upsilon(1S)\eta)/\Gamma_{total}$ — Γ_{19}/Γ

VALUE (units 10^{-4})	CL%	EVTS	DOCUMENT ID		TECN	COMMENT
1.81±0.18 OUR AVERAGE						
1.70±0.23±0.08		49	GUIDO	17	BELL	$\Upsilon(4S) \to \pi^+\pi^-\pi^0\mu^+\mu^-$
1.96±0.26±0.09		56	[1] AUBERT	08BP	BABR	$\Upsilon(4S) \to \pi^+\pi^-\pi^0\ell^+\ell^-$
• • • We do not use the following data for averages, fits, limits, etc. • • •						
<2.7	90		[2] TAMPONI	15	BELL	$e^+e^- \to \gamma\eta +$ hadrons

[1] Using $B(\Upsilon(1S) \to e^+e^-) = (2.38 \pm 0.11)\%$ and $B(\Upsilon(1S) \to \mu^+\mu^-) = (2.48 \pm 0.05)\%$.
[2] Using $B(\eta \to 2\gamma) = (39.41 \pm 0.20)\%$.

$\Gamma(\Upsilon(1S)\eta')/\Gamma_{total}$ — Γ_{20}/Γ

VALUE (units 10^{-5})	EVTS	DOCUMENT ID		TECN	COMMENT
3.43±0.88±0.21	27	GUIDO	18	BELL	$\Upsilon(4S) \to (\rho^0\gamma, \pi^+\pi^-\eta)\mu^+\mu^-$

Downloaded from https://academic.oup.com/ptep/article/2022/8/083C01/6651666 by KIT Library user on 27 September 2022

$\Gamma(\Upsilon(1S)\eta)/\Gamma(\Upsilon(1S)\pi^+\pi^-)$ — Γ_{19}/Γ_{18}

VALUE	EVTS	DOCUMENT ID		TECN	COMMENT
• • • We do not use the following data for averages, fits, limits, etc. • • •					
$2.41\pm0.40\pm0.12$	56	[1] AUBERT	08BP	BABR	$\Upsilon(4S)\to\pi^+\pi^-(\pi^0)\ell^+\ell^-$

[1] Not independent of other values reported by AUBERT 08BP.

$\Gamma(\Upsilon(2S)\pi^+\pi^-)/\Gamma_{total}$ — Γ_{21}/Γ

VALUE (units 10^{-5})	CL%	EVTS	DOCUMENT ID		TECN	COMMENT
8.2±0.8 OUR AVERAGE						
$7.9\pm1.0\pm0.4$		181	GUIDO	17	BELL	$\Upsilon(4S)\to\pi^+\pi^-\mu^+\mu^-$
$8.6\pm1.1\pm0.7$		220	[1] AUBERT	08BP	BABR	$\Upsilon(4S)\to\pi^+\pi^-\ell^+\ell^-$
• • • We do not use the following data for averages, fits, limits, etc. • • •						
$8.8\pm1.7\pm0.8$		97 ± 15	[2] AUBERT	06R	BABR	$e^+e^-\to\pi^+\pi^-\mu^+\mu^-$
<3.9	90		GLENN	99	CLE2	e^+e^-

[1] Using $B(\Upsilon(2S)\to e^+e^-)=(1.91\pm0.16)\%$ and $B(\Upsilon(2S)\to\mu^+\mu^-)=(1.93\pm0.17)\%$.
[2] Superseded by AUBERT 08BP. AUBERT 06R reports $[\Gamma(\Upsilon(4S)\to\Upsilon(2S)\pi^+\pi^-)/\Gamma_{total}]\times[B(\Upsilon(2S)\to\mu^+\mu^-)]=(1.69\pm0.26\pm0.20)\times10^{-6}$ which we divide by our best value $B(\Upsilon(2S)\to\mu^+\mu^-)=(1.93\pm0.17)\times10^{-2}$. Our first error is their experiment's error and our second error is the systematic error from using our best value.

$\Gamma(\Upsilon(2S)\pi^+\pi^-)/\Gamma(\Upsilon(1S)\pi^+\pi^-)$ — Γ_{21}/Γ_{18}

VALUE	EVTS	DOCUMENT ID		TECN	COMMENT
• • • We do not use the following data for averages, fits, limits, etc. • • •					
$1.16\pm0.16\pm0.14$	220	[1] AUBERT	08BP	BABR	$\Upsilon(4S)\to\pi^+\pi^-\ell^+\ell^-$

[1] Using $B(\Upsilon(1S)\to e^+e^-)=(2.38\pm0.11)\%$, $B(\Upsilon(1S)\to\mu^+\mu^-)=(2.48\pm0.05)\%$, $B(\Upsilon(2S)\to e^+e^-)=(1.91\pm0.16)\%$, and $B(\Upsilon(2S)\to\mu^+\mu^-)=(1.93\pm0.17)\%$. Not independent of other values reported by AUBERT 08BP.

$\Gamma(h_b(1P)\pi^+\pi^-)/\Gamma_{total}$ — Γ_{22}/Γ

VALUE	EVTS	DOCUMENT ID		TECN	COMMENT
not seen	(35^{+32}_{-26})k	[1] ADACHI	12	BELL	$10.58\ e^+e^-\to h_b(1P)\pi^+\pi^-$

[1] From the upper limit on the ratio of $\sigma(e^+e^-\to h_b(1P)\pi^+\pi^-)$ at the $\Upsilon(4S)$ to that at the $\Upsilon(5S)$ of 0.27.

$\Gamma(h_b(1P)\eta)/\Gamma_{total}$ — Γ_{23}/Γ

VALUE (units 10^{-3})	EVTS	DOCUMENT ID		TECN	COMMENT
$2.18\pm0.11\pm0.18$	112k	[1] TAMPONI	15	BELL	$e^+e^-\to h_b(1P)\eta$

[1] Using $B(\eta\to2\gamma)=(39.41\pm0.20)\%$.

$\Gamma(\eta_b(1S)\omega)/\Gamma_{total}$ — Γ_{24}/Γ

VALUE	CL%	DOCUMENT ID		TECN	COMMENT
$<1.8\times10^{-4}$	90	OSKIN	20	BELL	$e^+e^-\to\omega X$

$\Gamma(\eta_b(1S)\omega)/\Gamma(h_b(1P)\eta)$ — Γ_{24}/Γ_{23}

VALUE	CL%	DOCUMENT ID		TECN	COMMENT
$<8.4\times10^{-2}$	90	[1] OSKIN	20	BELL	$e^+e^-\to\omega X$

[1] Using $B(\Upsilon(4S)\to h_b(1P)\eta)=(2.18\pm0.11\pm0.18)\times10^{-3}$ from TAMPONI 15.

$\Gamma(\overline{2H}\text{ anything})/\Gamma_{total}$ — Γ_{25}/Γ

VALUE (units 10^{-5})	CL%	DOCUMENT ID		TECN	COMMENT
<1.3	90	ASNER	07	CLEO	$e^+e^-\to\overline{d}X$

Double Radiative Decays

$\Gamma(\gamma\gamma\Upsilon(D)\to\gamma\gamma\eta\Upsilon(1S))/\Gamma_{total}$ — Γ_{26}/Γ

VALUE	CL%	DOCUMENT ID		TECN	COMMENT
$<2.3\times10^{-5}$	90	GUIDO	17	BELL	$\Upsilon(4S)\to\gamma\gamma\pi^+\pi^-\pi^0\mu^+\mu^-$

$\Upsilon(4S)$ REFERENCES

OSKIN	20	PR D102 092011	P. Oskin et al.	(BELLE Collab.)
GUIDO	18	PRL 121 062001	E. Guido et al.	(BELLE Collab.)
GUIDO	17	PR D96 052005	E. Guido et al.	(BELLE Collab.)
TAMPONI	15	PRL 115 142001	U. Tamponi et al.	(BELLE Collab.)
SHEN	13A	PR D88 052019	C.P. Shen et al.	(BELLE Collab.)
ADACHI	12	PRL 108 032001	I. Adachi et al.	(BELLE Collab.)
BELOUS	09	PL B681 400	K. Belous et al.	(BELLE Collab.)
SOKOLOV	09	PR D79 051103	A. Sokolov et al.	(BELLE Collab.)
AUBERT	08BO	PR D78 071103	B. Aubert et al.	(BABAR Collab.)
AUBERT	08BP	PR D78 112002	B. Aubert et al.	(BABAR Collab.)
PDG	08	PL B667 1	C. Amsler et al.	(PDG Collab.)
ASNER	07	PR D75 012009	D.M. Asner et al.	(CLEO Collab.)
HUANG	07	PR D75 012002	G.S. Huang et al.	(CLEO Collab.)
SOKOLOV	07	PR D75 071103	A. Sokolov et al.	(BELLE Collab.)
TAJIMA	07A	PRL 99 211601	O. Tajima et al.	(BELLE Collab.)
AUBERT	06R	PRL 96 232001	B. Aubert et al.	(BABAR Collab.)
AUBERT,BE	06F	PR D74 111103	B. Aubert et al.	(BABAR Collab.)
ARTUSO	05B	PRL 95 261801	M. Artuso et al.	(CLEO Collab.)
AUBERT	05Q	PR D72 032005	B. Aubert et al.	(BABAR Collab.)
AUBERT,B	05H	PRL 95 042001	B. Aubert et al.	(BABAR Collab.)
AUBERT	04F	PR D69 071101	B.Aubert et al.	
HASTINGS	03	PR D67 052004	N.C. Hastings et al.	(BELLE Collab.)
ABE	02D	PRL 88 052001	K. Abe et al.	(BELLE Collab.)
ATHAR	02	PR D66 052003	S.B. Athar et al.	(CLEO Collab.)
AUBERT	02	PR D65 032001	B. Aubert et al.	(BABAR Collab.)
ALEXANDER	01	PRL 86 2737	J.P. Alexander et al.	(CLEO Collab.)
AUBERT	01C	PRL 87 162002	B. Aubert et al.	(BABAR Collab.)
GLENN	99	PR D59 052003	S. Glenn et al.	
BARISH	96B	PRL 76 1570	B.C. Barish et al.	(CLEO Collab.)
ALBRECHT	95E	ZPHY C65 619	H. Albrecht et al.	(ARGUS Collab.)
BARISH	95	PR D51 1014	B.C. Barish et al.	(CLEO Collab.)
ALEXANDER	90C	PRL 64 2226	J. Alexander et al.	(CLEO Collab.)
BEBEK	87	PR D36 1289	C. Bebek et al.	(CLEO Collab.)
BESSON	85	PRL 54 381	D. Besson et al.	(CLEO Collab.)
LOVELOCK	85	PRL 54 377	D.M.J. Lovelock et al.	(CUSB Collab.)
LEYAOUANC	77	PL B71 397	A. Le Yaouanc et al.	(ORSAY)

$Z_b(10610)$

$I^G(J^{PC}) = 1^+(1^{+-})$

was $X(10610)$

Properties incompatible with a $q\overline{q}$ structure (exotic state). See the review on non-$q\overline{q}$ states.

Observed by BONDAR 12 in $\Upsilon(5S)$ decays to $\Upsilon(nS)\pi^+\pi^-$ (n = 1, 2, 3) and $h_b(mP)\pi^+\pi^-$ (m = 1, 2). $J^P=1^+$ is favored from angular analyses.

$Z_b(10610)^\pm$ MASS

VALUE (MeV)	DOCUMENT ID		TECN	COMMENT
10607.2±2.0	[1] BONDAR	12	BELL	$e^+e^-\to$ hadrons
• • • We do not use the following data for averages, fits, limits, etc. • • •				
$10608.5\pm3.4^{+3.7}_{-1.4}$	[2] GARMASH	15	BELL	$e^+e^-\to\Upsilon(1S)\pi^+\pi^-$
$10608.1\pm1.2^{+1.5}_{-0.2}$	[2] GARMASH	15	BELL	$e^+e^-\to\Upsilon(2S)\pi^+\pi^-$
$10607.4\pm1.5^{+0.8}_{-0.2}$	[2] GARMASH	15	BELL	$e^+e^-\to\Upsilon(3S)\pi^+\pi^-$
$10611\ \pm4\ \pm3$	[3] BONDAR	12	BELL	$e^+e^-\to\Upsilon(1S)\pi^+\pi^-$
$10609\ \pm2\ \pm3$	[3] BONDAR	12	BELL	$e^+e^-\to\Upsilon(2S)\pi^+\pi^-$
$10608\ \pm2\ \pm3$	[3] BONDAR	12	BELL	$e^+e^-\to\Upsilon(3S)\pi^+\pi^-$
$10605\ \pm2\ ^{+3}_{-1}$	[3] BONDAR	12	BELL	$e^+e^-\to h_b(1P)\pi^+\pi^-$
$10599\ ^{+6}_{-3}\ ^{+5}_{-4}$	[3] BONDAR	12	BELL	$e^+e^-\to h_b(2P)\pi^+\pi^-$

[1] Average of the BONDAR 12 measurements in separate channels.
[2] Correlated with the corresponding result from BONDAR 12.
[3] Superseded by the average measurement of BONDAR 12.

$Z_b(10610)^0$ MASS

VALUE (MeV)	DOCUMENT ID		TECN	COMMENT
10609±4±4	[1] KROKOVNY	13	BELL	$e^+e^-\to\Upsilon(2S)/\Upsilon(3S)\pi^0\pi^0$

[1] From a simultaneous fit to the KROKOVNY 13 Dalitz analysis of $e^+e^-\to\Upsilon(2S)/\Upsilon(3S)\pi^0\pi^0$ decays with fixed width $\Gamma(Z_b(10610)^0)=18.4$ MeV.

$Z_b(10610)^\pm$ WIDTH

VALUE (MeV)	DOCUMENT ID		TECN	COMMENT
18.4± 2.4	[1] BONDAR	12	BELL	$e^+e^-\to$ hadrons
• • • We do not use the following data for averages, fits, limits, etc. • • •				
$18.5\pm\ 5.3^{+6.1}_{-2.3}$	[2] GARMASH	15	BELL	$e^+e^-\to\Upsilon(1S)\pi^+\pi^-$
$20.8\pm\ 2.5^{+0.3}_{-2.1}$	[2] GARMASH	15	BELL	$e^+e^-\to\Upsilon(2S)\pi^+\pi^-$
$18.7\pm\ 3.4^{+2.5}_{-1.3}$	[2] GARMASH	15	BELL	$e^+e^-\to\Upsilon(3S)\pi^+\pi^-$
$22.3\pm\ 7.7^{+3.0}_{-4.0}$	[3] BONDAR	12	BELL	$e^+e^-\to\Upsilon(1S)\pi^+\pi^-$
$24.2\pm\ 3.1^{+2.0}_{-3.0}$	[3] BONDAR	12	BELL	$e^+e^-\to\Upsilon(2S)\pi^+\pi^-$
$17.6\pm\ 3.0\pm3.0$	[3] BONDAR	12	BELL	$e^+e^-\to\Upsilon(3S)\pi^+\pi^-$
$11.4^{+\ 4.5}_{-\ 3.9}\ ^{+2.1}_{-1.2}$	[3] BONDAR	12	BELL	$e^+e^-\to h_b(1P)\pi^+\pi^-$
$13\ ^{+10}_{-\ 8}\ ^{+9}_{-\ 7}$	[3] BONDAR	12	BELL	$e^+e^-\to h_b(2P)\pi^+\pi^-$

[1] Average of the BONDAR 12 measurements in separate channels.
[2] Correlated with the corresponding result from BONDAR 12.
[3] Superseded by the average measurement of BONDAR 12.

$Z_b(10610)$ DECAY MODES

	Mode	Fraction (Γ_i/Γ)
Γ_1	$\Upsilon(1S)\pi^+$	$(5.4^{+1.9}_{-1.5})\times10^{-3}$
Γ_2	$\Upsilon(1S)\pi^0$	not seen
Γ_3	$\Upsilon(2S)\pi^+$	$(3.6^{+1.1}_{-0.8})$ %
Γ_4	$\Upsilon(2S)\pi^0$	seen
Γ_5	$\Upsilon(3S)\pi^+$	$(2.1^{+0.8}_{-0.6})$ %

Downloaded from https://academic.oup.com/ptep/article/2022/8/083C01/6651666 by KIT Library user on 27 September 2022

Γ_6	$\Upsilon(3S)\pi^0$	seen
Γ_7	$h_b(1P)\pi^+$	$(3.5^{+1.2}_{-0.9})$ %
Γ_8	$h_b(2P)\pi^+$	$(4.7^{+1.7}_{-1.3})$ %
Γ_9	$B^+\overline{B}^0$	not seen
Γ_{10}	$B^+\overline{B}^{*0} + B^{*+}\overline{B}^0$	$(85.6^{+2.1}_{-2.9})$ %

$Z_b(10610)$ BRANCHING RATIOS

$\Gamma(\Upsilon(1S)\pi^+)/\Gamma_{total}$ — Γ_1/Γ

VALUE (units 10^{-3})	DOCUMENT ID		TECN	COMMENT
$5.4^{+1.6+1.1}_{-1.3-0.8}$	[1] GARMASH	16	BELL	$e^+e^- \to \pi^-B^+\overline{B}^{*0}$, $\pi^-\overline{B}^0B^{*+}$
• • • We do not use the following data for averages, fits, limits, etc. • • •				
seen	GARMASH	15	BELL	$e^+e^- \to \Upsilon(1S)\pi^+\pi^-$
seen	BONDAR	12	BELL	$e^+e^- \to \Upsilon(1S)\pi^+\pi^-$

[1] Assuming the $Z_b(10610)$ decay width is saturated by the channels $\pi^+\Upsilon(1S,2S,3S)$, $\pi^+h_b(1P,2P)$, and $B^+\overline{B}^{*0} + \overline{B}^0B^{*+}$, and using the results from BONDAR 12 and MIZUK 16.

$\Gamma(\Upsilon(1S)\pi^0)/\Gamma_{total}$ — Γ_2/Γ

VALUE	DOCUMENT ID		TECN	COMMENT
not seen	KROKOVNY	13	BELL	$e^+e^- \to \Upsilon(1S)\pi^0\pi^0$

$\Gamma(\Upsilon(2S)\pi^+)/\Gamma_{total}$ — Γ_3/Γ

VALUE (units 10^{-2})	DOCUMENT ID		TECN	COMMENT
$3.62^{+0.76+0.79}_{-0.59-0.53}$	[1] GARMASH	16	BELL	$e^+e^- \to \pi^-B^+\overline{B}^{*0}$, $\pi^-\overline{B}^0B^{*+}$
• • • We do not use the following data for averages, fits, limits, etc. • • •				
seen	GARMASH	15	BELL	$e^+e^- \to \Upsilon(2S)\pi^+\pi^-$
seen	BONDAR	12	BELL	$e^+e^- \to \Upsilon(2S)\pi^+\pi^-$

[1] Assuming the $Z_b(10610)$ decay width is saturated by the channels $\pi^+\Upsilon(1S,2S,3S)$, $\pi^+h_b(1P,2P)$, and $B^+\overline{B}^{*0} + \overline{B}^0B^{*+}$, and using the results from BONDAR 12 and MIZUK 16.

$\Gamma(\Upsilon(2S)\pi^0)/\Gamma_{total}$ — Γ_4/Γ

VALUE	DOCUMENT ID		TECN	COMMENT
seen	[1] KROKOVNY	13	BELL	$e^+e^- \to \Upsilon(2S)\pi^0\pi^0$

[1] Combined significance in $e^+e^- \to \Upsilon(2S)/\Upsilon(3S)\pi^0\pi^0$, including systematics, of 6.5σ.

$\Gamma(\Upsilon(3S)\pi^+)/\Gamma_{total}$ — Γ_5/Γ

VALUE (units 10^{-2})	DOCUMENT ID		TECN	COMMENT
$2.15^{+0.55+0.60}_{-0.42-0.43}$	[1] GARMASH	16	BELL	$e^+e^- \to \pi^-B^+\overline{B}^{*0}$, $\pi^-\overline{B}^0B^{*+}$
• • • We do not use the following data for averages, fits, limits, etc. • • •				
seen	GARMASH	15	BELL	$e^+e^- \to \Upsilon(3S)\pi^+\pi^-$
seen	BONDAR	12	BELL	$e^+e^- \to \Upsilon(3S)\pi^+\pi^-$

[1] Assuming the $Z_b(10610)$ decay width is saturated by the channels $\pi^+\Upsilon(1S,2S,3S)$, $\pi^+h_b(1P,2P)$, and $B^+\overline{B}^{*0} + \overline{B}^0B^{*+}$, and using the results from BONDAR 12 and MIZUK 16.

$\Gamma(\Upsilon(3S)\pi^0)/\Gamma_{total}$ — Γ_6/Γ

VALUE	DOCUMENT ID		TECN	COMMENT
seen	[1] KROKOVNY	13	BELL	$e^+e^- \to \Upsilon(3S)\pi^0\pi^0$

[1] Combined significance in $e^+e^- \to \Upsilon(2S)/\Upsilon(3S)\pi^0\pi^0$, including systematics, of 6.5σ.

$\Gamma(h_b(1P)\pi^+)/\Gamma_{total}$ — Γ_7/Γ

VALUE (units 10^{-2})	DOCUMENT ID		TECN	COMMENT
$3.45^{+0.87+0.86}_{-0.71-0.63}$	[1] GARMASH	16	BELL	$e^+e^- \to \pi^-B^+\overline{B}^{*0}$, $\pi^-\overline{B}^0B^{*+}$
• • • We do not use the following data for averages, fits, limits, etc. • • •				
possibly seen	[2] MIZUK	16	BELL	$e^+e^- \to h_b(1P)\pi^+\pi^-$
seen	[3] BONDAR	12	BELL	$e^+e^- \to h_b(1P)\pi^+\pi^-$

[1] Assuming the $Z_b(10610)$ decay width is saturated by the channels $\pi^+\Upsilon(1S,2S,3S)$, $\pi^+h_b(1P,2P)$, and $B^+\overline{B}^{*0} + \overline{B}^0B^{*+}$, and using the results from BONDAR 12 and MIZUK 16.
[2] Using e^+e^- energies near the $\Upsilon(11020)$.
[3] Using e^+e^- energies near the $\Upsilon(10860)$.

$\Gamma(h_b(2P)\pi^+)/\Gamma_{total}$ — Γ_8/Γ

VALUE (units 10^{-2})	DOCUMENT ID		TECN	COMMENT
$4.67^{+1.24+1.18}_{-1.00-0.89}$	[1] GARMASH	16	BELL	$e^+e^- \to \pi^-B^+\overline{B}^{*0}$, $\pi^-\overline{B}^0B^{*+}$
• • • We do not use the following data for averages, fits, limits, etc. • • •				
possibly seen	[2] MIZUK	16	BELL	$e^+e^- \to h_b(2P)\pi^+\pi^-$
seen	[3] BONDAR	12	BELL	$e^+e^- \to h_b(2P)\pi^+\pi^-$

[1] Assuming the $Z_b(10610)$ decay width is saturated by the channels $\pi^+\Upsilon(1S,2S,3S)$, $\pi^+h_b(1P,2P)$, and $B^+\overline{B}^{*0} + \overline{B}^0B^{*+}$, and using the results from BONDAR 12 and MIZUK 16.
[2] Using e^+e^- energies near the $\Upsilon(11020)$.
[3] Using e^+e^- energies near the $\Upsilon(10860)$.

$\Gamma(B^+\overline{B}^0)/\Gamma_{total}$ — Γ_9/Γ

VALUE	DOCUMENT ID		TECN	COMMENT
not seen	GARMASH	16	BELL	$e^+e^- \to \pi^-B^+\overline{B}^0$

$[\Gamma(B^+\overline{B}^{*0}) + \Gamma(B^{*+}\overline{B}^0)]/\Gamma_{total}$ — Γ_{10}/Γ

VALUE (units 10^{-2})	EVTS	DOCUMENT ID		TECN	COMMENT
$85.6^{+1.5+1.5}_{-2.0-2.1}$	357	[1] GARMASH	16	BELL	$e^+e^- \to \pi^-B^+\overline{B}^{*0}$, $\pi^-B^{*+}\overline{B}^0$

[1] Assuming the $Z_b(10610)$ decay width is saturated by the channels $\pi^+\Upsilon(1S,2S,3S)$, $\pi^+h_b(1P,2P)$, and $B^+\overline{B}^{*0} + B^{*+}\overline{B}^0$, and using the results from BONDAR 12 and MIZUK 16. Using the mass and width of the $Z_b(10610)$ from BONDAR 12.

$[\Gamma(B^+\overline{B}^{*0}) + \Gamma(B^{*+}\overline{B}^0)]/[\Gamma(\Upsilon(1S)\pi^+) + \Gamma(\Upsilon(2S)\pi^+) + \Gamma(\Upsilon(3S)\pi^+) + \Gamma(h_b(1P)\pi^+) + \Gamma(h_b(2P)\pi^+)]$ — $\Gamma_{10}/(\Gamma_1+\Gamma_3+\Gamma_5+\Gamma_7+\Gamma_8)$

VALUE (units 10^{-2})	EVTS	DOCUMENT ID		TECN	COMMENT
• • • We do not use the following data for averages, fits, limits, etc. • • •					
$5.93^{+0.99+1.01}_{-0.69-0.73}$	357	[1] GARMASH	16	BELL	$e^+e^- \to \pi^-B^+\overline{B}^{*0}$, $\pi^-\overline{B}^0B^{*+}$

[1] Combined with the results of BONDAR 12 and MIZUK 16. Not independent from $Z_b(10610)$ branching fractions to $\pi^+\Upsilon(1S,2S,3S)$, $\pi^+h_b(1P,2P)$, and $B^+\overline{B}^{*0} + \overline{B}^0B^{*+}$.

$Z_b(10610)$ REFERENCES

GARMASH	16	PRL 116 212001	A. Garmash *et al.*	(BELLE Collab.)
MIZUK	16	PRL 117 142001	R. Mizuk *et al.*	(BELLE Collab.)
GARMASH	15	PR D91 072003	A. Garmash *et al.*	(BELLE Collab.)
KROKOVNY	13	PR D88 052016	P. Krokovny *et al.*	(BELLE Collab.)
BONDAR	12	PRL 108 122001	A. Bondar *et al.*	(BELLE Collab.)

$Z_b(10650)$

$I^G(J^{PC}) = 1^+(1^{+-})$
I, G, C need confirmation.

was $X(10650)^\pm$

Properties incompatible with a $q\overline{q}$ structure (exotic state). See the review on non-$q\overline{q}$ states.

Observed by BONDAR 12 in $\Upsilon(5S)$ decays to $\Upsilon(nS)\pi^+\pi^-$ (n = 1, 2, 3) and $h_b(mP)\pi^+\pi^-$ (m = 1, 2). $J^P = 1^+$ is favored from angular analyses.

$Z_b(10650)$ MASS

VALUE (MeV)	DOCUMENT ID		TECN	COMMENT
10652.2 ± 1.5	[1] BONDAR	12	BELL	$e^+e^- \to$ hadrons
• • • We do not use the following data for averages, fits, limits, etc. • • •				
$10656.7\pm5.0^{+1.1}_{-3.1}$	[2] GARMASH	15	BELL	$e^+e^- \to \Upsilon(1S)\pi^+\pi^-$
$10650.7\pm1.5^{+0.5}_{-0.2}$	[2] GARMASH	15	BELL	$e^+e^- \to \Upsilon(2S)\pi^+\pi^-$
$10651.2\pm1.0^{+0.4}_{-0.3}$	[2] GARMASH	15	BELL	$e^+e^- \to \Upsilon(3S)\pi^+\pi^-$
$10657 \pm6 \pm3$	[3] BONDAR	12	BELL	$e^+e^- \to \Upsilon(1S)\pi^+\pi^-$
$10651 \pm2 \pm3$	[3] BONDAR	12	BELL	$e^+e^- \to \Upsilon(2S)\pi^+\pi^-$
$10652 \pm1 \pm2$	[3] BONDAR	12	BELL	$e^+e^- \to \Upsilon(3S)\pi^+\pi^-$
$10654 \pm3 {}^{+1}_{-2}$	[3] BONDAR	12	BELL	$e^+e^- \to h_b(1P)\pi^+\pi^-$
$10651 {}^{+2}_{-3} {}^{+3}_{-2}$	[3] BONDAR	12	BELL	$e^+e^- \to h_b(2P)\pi^+\pi^-$

[1] Average of the BONDAR 12 measurements in separate channels.
[2] Correlated with the corresponding result from BONDAR 12.
[3] Superseded by the average measurement of BONDAR 12.

$Z_b(10650)$ WIDTH

VALUE (MeV)	DOCUMENT ID		TECN	COMMENT
11.5 ± 2.2	[4] BONDAR	12	BELL	$e^+e^- \to$ hadrons
• • • We do not use the following data for averages, fits, limits, etc. • • •				
$12.1^{+11.3}_{-4.8} \pm 2.7 \pm 0.6$	[5] GARMASH	15	BELL	$e^+e^- \to \Upsilon(1S)\pi^+\pi^-$
$14.2\pm 3.7^{+0.9}_{-0.4}$	[5] GARMASH	15	BELL	$e^+e^- \to \Upsilon(2S)\pi^+\pi^-$
$9.3\pm 2.2^{+0.3}_{-0.5}$	[5] GARMASH	15	BELL	$e^+e^- \to \Upsilon(3S)\pi^+\pi^-$
$16.3\pm 9.8^{+6.0}_{-2.0}$	[6] BONDAR	12	BELL	$e^+e^- \to \Upsilon(1S)\pi^+\pi^-$
$13.3\pm 3.3^{+4.0}_{-3.0}$	[6] BONDAR	12	BELL	$e^+e^- \to \Upsilon(2S)\pi^+\pi^-$
$8.4\pm 2.0\pm 2.0$	[6] BONDAR	12	BELL	$e^+e^- \to \Upsilon(3S)\pi^+\pi^-$
$20.9^{+5.4}_{-4.7} \pm 2.1 \pm 5.7$	[6] BONDAR	12	BELL	$e^+e^- \to h_b(1P)\pi^+\pi^-$
$19 \pm 7 {}^{+11}_{-7}$	[6] BONDAR	12	BELL	$e^+e^- \to h_b(2P)\pi^+\pi^-$

[4] Average of the BONDAR 12 measurements in separate channels.
[5] Correlated with the corresponding result from BONDAR 12.
[6] Superseded by the average measurement of BONDAR 12.

Downloaded from https://academic.oup.com/ptep/article/2022/8/083C01/6651666 by KIT Library user on 27 September 2022

$Z_b(10650)^+$ DECAY MODES

$Z_b(10650)^-$ decay modes are charge conjugates of the modes below.

	Mode	Fraction (Γ_i/Γ)
Γ_1	$\Upsilon(1S)\pi^+$	$(1.7^{+0.8}_{-0.6}) \times 10^{-3}$
Γ_2	$\Upsilon(2S)\pi^+$	$(1.4^{+0.6}_{-0.4})$ %
Γ_3	$\Upsilon(3S)\pi^+$	$(1.6^{+0.7}_{-0.5})$ %
Γ_4	$h_b(1P)\pi^+$	$(8.4^{+2.9}_{-2.4})$ %
Γ_5	$h_b(2P)\pi^+$	(15 ± 4) %
Γ_6	$B^+\overline{B}^0$	not seen
Γ_7	$B^+\overline{B}^{*0} + B^{*+}\overline{B}^0$	not seen
Γ_8	$B^{*+}\overline{B}^{*0}$	(74^{+4}_{-6}) %

$Z_b(10650)$ BRANCHING RATIOS

$\Gamma(\Upsilon(1S)\pi^+)/\Gamma_{total}$ — Γ_1/Γ

VALUE (units 10^{-3})	DOCUMENT ID		TECN	COMMENT
$1.7^{+0.7+0.3}_{-0.6-0.2}$	[7] GARMASH	16	BELL	$e^+e^- \to \pi^- B^{*+}\overline{B}^{*0}$
• • • We do not use the following data for averages, fits, limits, etc. • • •				
seen	GARMASH	15	BELL	$e^+e^- \to \Upsilon(1S)\pi^+\pi^-$
seen	BONDAR	12	BELL	$e^+e^- \to \Upsilon(1S)\pi^+\pi^-$

[7] Assuming the $Z_b(10650)$ decay width is saturated by the channels $\pi^+\Upsilon(1S,2S,3S)$, $\pi^+h_b(1P,2P)$, and $B^{*+}\overline{B}^{*0}$, and using the results from BONDAR 12 and MIZUK 16.

$\Gamma(\Upsilon(2S)\pi^+)/\Gamma_{total}$ — Γ_2/Γ

VALUE (units 10^{-2})	DOCUMENT ID		TECN	COMMENT
$1.39^{+0.48+0.34}_{-0.38-0.23}$	[8] GARMASH	16		$e^+e^- \to \pi^- B^{*+}\overline{B}^{*0}$
• • • We do not use the following data for averages, fits, limits, etc. • • •				
seen	GARMASH	15	BELL	$e^+e^- \to \Upsilon(2S)\pi^+\pi^-$
seen	BONDAR	12	BELL	$e^+e^- \to \Upsilon(2S)\pi^+\pi^-$

[8] Assuming the $Z_b(10650)$ decay width is saturated by the channels $\pi^+\Upsilon(1S,2S,3S)$, $\pi^+h_b(1P,2P)$, and $B^{*+}\overline{B}^{*0}$, and using the results from BONDAR 12 and MIZUK 16.

$\Gamma(\Upsilon(3S)\pi^+)/\Gamma_{total}$ — Γ_3/Γ

VALUE (units 10^{-2})	DOCUMENT ID		TECN	COMMENT
$1.63^{+0.53+0.39}_{-0.42-0.28}$	[9] GARMASH	16	BELL	$e^+e^- \to \pi^- B^{*+}\overline{B}^{*0}$
• • • We do not use the following data for averages, fits, limits, etc. • • •				
seen	GARMASH	15	BELL	$e^+e^- \to \Upsilon(3S)\pi^+\pi^-$
seen	BONDAR	12	BELL	$e^+e^- \to \Upsilon(3S)\pi^+\pi^-$

[9] Assuming the $Z_b(10650)$ decay width is saturated by the channels $\pi^+\Upsilon(1S,2S,3S)$, $\pi^+h_b(1P,2P)$, and $B^{*+}\overline{B}^{*0}$, and using the results from BONDAR 12 and MIZUK 16.

$\Gamma(h_b(1P)\pi^+)/\Gamma_{total}$ — Γ_4/Γ

VALUE (units 10^{-2})	DOCUMENT ID		TECN	COMMENT
$8.41^{+2.43+1.49}_{-2.12-1.06}$	[10] GARMASH	16	BELL	$e^+e^- \to \pi^- B^{*+}\overline{B}^{*0}$
• • • We do not use the following data for averages, fits, limits, etc. • • •				
seen	[11] MIZUK	16	BELL	$e^+e^- \to h_b(1P)\pi^+\pi^-$
seen	[12] BONDAR	12	BELL	$e^+e^- \to h_b(1P)\pi^+\pi^-$

[10] Assuming the $Z_b(10650)$ decay width is saturated by the channels $\pi^+\Upsilon(1S,2S,3S)$, $\pi^+h_b(1P,2P)$, and $B^{*+}\overline{B}^{*0}$, and using the results from BONDAR 12 and MIZUK 16.
[11] Using e^+e^- energies near the $\Upsilon(11020)$.
[12] Using e^+e^- energies near the $\Upsilon(10860)$.

$\Gamma(h_b(2P)\pi^+)/\Gamma_{total}$ — Γ_5/Γ

VALUE (units 10^{-2})	DOCUMENT ID		TECN	COMMENT
$14.7^{+3.2+2.8}_{-2.8-2.3}$	[13] GARMASH	16	BELL	$e^+e^- \to \pi^- B^{*+}\overline{B}^{*0}$
• • • We do not use the following data for averages, fits, limits, etc. • • •				
possibly seen	[14] MIZUK	16	BELL	$e^+e^- \to h_b(2P)\pi^+\pi^-$
seen	[15] BONDAR	12	BELL	$e^+e^- \to h_b(2P)\pi^+\pi^-$

[13] Assuming the $Z_b(10650)$ decay width is saturated by the channels $\pi^+\Upsilon(1S,2S,3S)$, $\pi^+h_b(1P,2P)$, and $B^{*+}\overline{B}^{*0}$, and using the results from BONDAR 12 and MIZUK 16.
[14] Using e^+e^- energies near the $\Upsilon(11020)$.
[15] Using e^+e^- energies near the $\Upsilon(10860)$.

$\Gamma(B^+\overline{B}^0)/\Gamma_{total}$ — Γ_6/Γ

VALUE	DOCUMENT ID		TECN	COMMENT
not seen	GARMASH	16	BELL	$e^+e^- \to \pi^- B^+\overline{B}^0$

$[\Gamma(B^+\overline{B}^{*0}) + \Gamma(B^{*+}\overline{B}^0)]/\Gamma_{total}$ — Γ_7/Γ

VALUE	DOCUMENT ID		TECN	COMMENT
not seen	GARMASH	16	BELL	$e^+e^- \to \pi^- B^+\overline{B}^{*0}$, $\pi^-\overline{B}^0 B^{*+}$

$\Gamma(B^{*+}\overline{B}^{*0})/\Gamma_{total}$ — Γ_8/Γ

VALUE (units 10^{-2})	EVTS	DOCUMENT ID		TECN	COMMENT
$73.7^{+3.4+2.7}_{-4.4-3.5}$	161	[16] GARMASH	16	BELL	$e^+e^- \to \pi^- B^{*+}\overline{B}^{*0}$

[16] Assuming the $Z_b(10650)$ decay width is saturated by the channels $\pi^+\Upsilon(1S,2S,3S)$, $\pi^+h_b(1P,2P)$, and $B^{*+}\overline{B}^{*0}$, and using the results from BONDAR 12 and MIZUK 16. Using the mass and width of the $Z_b(10650)$ from BONDAR 12.

$\Gamma(B^{*+}\overline{B}^{*0})/[\Gamma(\Upsilon(1S)\pi^+) + \Gamma(\Upsilon(2S)\pi^+) + \Gamma(\Upsilon(3S)\pi^+) + \Gamma(h_b(1P)\pi^+) + \Gamma(h_b(2P)\pi^+)]$ — $\Gamma_8/(\Gamma_1+\Gamma_2+\Gamma_3+\Gamma_4+\Gamma_5)$

VALUE (units 10^{-2})	EVTS	DOCUMENT ID		TECN	COMMENT
• • • We do not use the following data for averages, fits, limits, etc. • • •					
$2.80^{+0.69+0.54}_{-0.40-0.36}$	161	[17] GARMASH	16	BELL	$e^+e^- \to \pi^- B^{*+}\overline{B}^{*0}$

[17] Combined with the results of BONDAR 12 and MIZUK 16. Not independent from $Z_b(10650)$ branching fractions to $\pi^+\Upsilon(1S,2S,3S)$, $\pi^+h_b(1P,2P)$, and $B^{*+}\overline{B}^{*0}$.

$Z_b(10650)$ REFERENCES

GARMASH	16	PRL 116 212001	A. Garmash *et al.*	(BELLE Collab.)
MIZUK	16	PRL 117 142001	R. Mizuk *et al.*	(BELLE Collab.)
GARMASH	15	PR D91 072003	A. Garmash *et al.*	(BELLE Collab.)
BONDAR	12	PRL 108 122001	A. Bondar *et al.*	(BELLE Collab.)

$\Upsilon(10753)$

$I^G(J^{PC}) = ?^?(1^{--})$

OMITTED FROM SUMMARY TABLE

A candidate for $\Upsilon(3D)$ state or an exotic structure.

Seen by MIZUK 19 in $e^+e^- \to \Upsilon(nS)\pi^+\pi^-$ (n=1,2,3) with a significance of 5.2 σ.

$\Upsilon(10753)$ MASS

VALUE (MeV)	DOCUMENT ID		TECN	COMMENT
$10752.7 \pm 5.9^{+0.7}_{-1.1}$	[1] MIZUK	19	BELL	$e^+e^- \to \Upsilon(nS)\pi^+\pi^-$
• • • We do not use the following data for averages, fits, limits, etc. • • •				
10761 ± 2	[2] DONG	20A		$e^+e^- \to b\overline{b}$

[1] From a simultaneous fit to the $\Upsilon(nS)\pi^+\pi^-$, $n = 1, 2, 3$, cross sections at 28 energy points within $\sqrt{s} = 10.63$–11.02 GeV, including the initial-state radiation at $\Upsilon(10860)$.
[2] From a fit to the dressed cross sections of AUBERT 09E by BaBar and SANTEL 16 by Belle above 10.68 GeV with a coherent sum of a continuum amplitude and three Breit-Wigner functions with constant widths.

$\Upsilon(10753)$ WIDTH

VALUE (MeV)	DOCUMENT ID		TECN	COMMENT
$35.5^{+17.6+3.9}_{-11.3-3.3}$	[1] MIZUK	19	BELL	$e^+e^- \to \Upsilon(nS)\pi^+\pi^-$
• • • We do not use the following data for averages, fits, limits, etc. • • •				
48.5 ± 3.0	[2] DONG	20A		$e^+e^- \to b\overline{b}$

[1] From a simultaneous fit to the $\Upsilon(nS)\pi^+\pi^-$, $n = 1, 2, 3$, cross sections at 28 energy points within $\sqrt{s} = 10.63$–11.02 GeV, including the initial-state radiation at $\Upsilon(10860)$.
[2] From a fit to the dressed cross sections of AUBERT 09E by BaBar and SANTEL 16 by Belle above 10.68 GeV with a coherent sum of a continuum amplitude and three Breit-Wigner functions with constant widths.

$\Upsilon(10753)$ DECAY MODES

	Mode
Γ_1	$\Upsilon(1S)\pi^+\pi^-$
Γ_2	$\Upsilon(2S)\pi^+\pi^-$
Γ_3	$\Upsilon(3S)\pi^+\pi^-$
Γ_4	e^+e^-

$\Upsilon(10753)$ $\Gamma(i)\Gamma(e^+e^-)/\Gamma(total)$

$\Gamma(\Upsilon(1S)\pi^+\pi^-) \times \Gamma(e^+e^-)/\Gamma_{total}$ — $\Gamma_1\Gamma_4/\Gamma$

VALUE (eV)	DOCUMENT ID		TECN	COMMENT
• • • We do not use the following data for averages, fits, limits, etc. • • •				
0.295 ± 0.175	[1,2] MIZUK	19	BELL	$e^+e^- \to \Upsilon(nS)\pi^+\pi^-$

[1] From a simultaneous fit to the $\Upsilon(nS)\pi^+\pi^-$, $n = 1, 2, 3$, cross sections at 28 energy points within $\sqrt{s} = 10.63$–11.02 GeV, including the initial-state radiation at $\Upsilon(10860)$.
[2] Reported as the range 0.12–0.47 eV obtained from multiple solutions of an amplitude fit within a model composed as a sum of Breit-Wigner functions.

Downloaded from https://academic.oup.com/ptep/article/2022/8/083C01/6651666 by KIT Library user on 27 September 2022

$\Gamma(\Upsilon(2S)\pi^+\pi^-) \times \Gamma(e^+e^-)/\Gamma_{total}$ — $\Gamma_2\Gamma_4/\Gamma$

VALUE (eV)	DOCUMENT ID		TECN	COMMENT
• • • We do not use the following data for averages, fits, limits, etc. • • •				
0.875 ± 0.345	[1,2] MIZUK	19	BELL	$e^+e^- \to \Upsilon(nS)\pi^+\pi^-$

[1] From a simultaneous fit to the $\Upsilon(nS)\pi^+\pi^-$, $n = 1, 2, 3$, cross sections at 28 energy points within $\sqrt{s} = 10.63$–11.02 GeV, including the initial-state radiation at $\Upsilon(10860)$.

[2] Reported as the range 0.53–1.22 eV obtained from multiple solutions of an amplitude fit within a model composed as a sum of Breit-Wigner functions.

$\Gamma(\Upsilon(3S)\pi^+\pi^-) \times \Gamma(e^+e^-)/\Gamma_{total}$ — $\Gamma_3\Gamma_4/\Gamma$

VALUE (eV)	DOCUMENT ID		TECN	COMMENT
• • • We do not use the following data for averages, fits, limits, etc. • • •				
0.235 ± 0.025	[1,2] MIZUK	19	BELL	$e^+e^- \to \Upsilon(nS)\pi^+\pi^-$

[1] From a simultaneous fit to the $\Upsilon(nS)\pi^+\pi^-$, $n = 1, 2, 3$, cross sections at 28 energy points within $\sqrt{s} = 10.63$–11.02 GeV, including the initial-state radiation at $\Upsilon(10860)$.

[2] Reported as the range 0.21–0.26 eV obtained from multiple solutions of an amplitude fit within a model composed as a sum of Breit-Wigner functions.

$\Upsilon(10753)$ REFERENCES

DONG	20A	CP C44 083001	X.-K. Dong *et al.*	
MIZUK	19	JHEP 1910 220	R. Mizuk *et al.*	(BELLE Collab.)
SANTEL	16	PR D93 011101	D. Santel *et al.*	(BELLE Collab.)
AUBERT	09E	PRL 102 012001	B. Aubert *et al.*	(BABAR Collab.)

$\Upsilon(10860)$

$I^G(J^{PC}) = 0^-(1^{--})$

$\Upsilon(10860)$ MASS

VALUE (MeV)	DOCUMENT ID		TECN	COMMENT
$10885.2^{+2.6}_{-1.6}$ OUR AVERAGE				
$10885.3 \pm 1.5^{+2.2}_{-0.9}$	[1] MIZUK	19	BELL	$e^+e^- \to \Upsilon(nS)\pi^+\pi^-$
$10884.7^{+3.6+8.9}_{-3.4-1.0}$	[2] MIZUK	16	BELL	$e^+e^- \to h_b(1P,2P)\pi^+\pi^-$
• • • We do not use the following data for averages, fits, limits, etc. • • •				
10882 ± 1	[3] DONG	20A		$e^+e^- \to b\overline{b}$
$10881.8^{+1.0}_{-1.1} \pm 1.2$	[4,5] SANTEL	16	BELL	$e^+e^- \to$ hadrons
$10891.1 \pm 3.2^{+1.2}_{-2.0}$	[6,7] SANTEL	16	BELL	$e^+e^- \to \Upsilon(1S,2S,3S)\pi^+\pi^-$
10879 ± 3	[8,9] CHEN	10	BELL	$e^+e^- \to$ hadrons
$10888.4^{+2.7}_{-2.6} \pm 1.2$	[10] CHEN	10	BELL	$e^+e^- \to \Upsilon(1S,2S,3S)\pi^+\pi^-$
10876 ± 2	[8] AUBERT	09E	BABR	$e^+e^- \to$ hadrons
10869 ± 2	[11] AUBERT	09E	BABR	$e^+e^- \to$ hadrons
$10868 \pm 6 \pm 5$	[12] BESSON	85	CLEO	$e^+e^- \to$ hadrons
10845 ± 20	[13] LOVELOCK	85	CUSB	$e^+e^- \to$ hadrons

[1] From a simultaneous fit to the $\Upsilon(nS)\pi^+\pi^-$, $n = 1, 2, 3$, cross sections at 28 energy points within $\sqrt{s} = 10.6$–11.05 GeV, including the initial-state radiation at $\Upsilon(10860)$.

[2] From a simultaneous fit to the $h_b(nP)\pi^+\pi^-$, $n = 1, 2$ cross sections at 22 energy points within $\sqrt{s} = 10.77$–11.02 GeV to a pair of interfering Breit-Wigner amplitudes modified by phase space factors, with eight resonance parameters (a mass and width for each of $\Upsilon(10860)$ and $\Upsilon(11020)$, a single relative phase, a single relative amplitude, and two overall normalization factors, one for each n). The systematic error estimate is dominated by possible interference with a small nonresonant continuum amplitude.

[3] From a fit to the dressed cross sections of AUBERT 09E by BaBar and SANTEL 16 by Belle above 10.68 GeV with a coherent sum of a continuum amplitude and three Breit-Wigner functions with constant widths.

[4] From a fit to the total hadronic cross sections measured at 60 energy points within $\sqrt{s}$ = 10.82–11.05 GeV to a pair of interfering Breit-Wigner amplitudes and two floating continuum amplitudes with $1/\sqrt{s}$ dependence, one coherent with the resonances and one incoherent, with six resonance parameters (a mass, width, and an amplitude for each of $\Upsilon(10860)$ and $\Upsilon(11020)$, one relative phase, and one decoherence coefficient).

[5] Not including uncertain and potentially large systematic errors due to assumed continuum amplitude $1/\sqrt{s}$ dependence and related interference contributions.

[6] From a simultaneous fit to the $\Upsilon(nS)\pi^+\pi^-$, $n = 1, 2, 3$, cross sections at 25energy points within $\sqrt{s} = 10.6$–11.05 GeV to a pair of interfering Breit-Wigner amplitudesmodified by phase space factors, with fourteen resonance parameters (a mass, width, and threeamplitudes for each of $\Upsilon(10860)$ and $\Upsilon(11020)$, a single universal relativephase, and three decoherence coefficients, one for each n). Continuum contributions weremeasured (and therefore fixed) to be zero.

[7] Superseded by MIZUK 19.

[8] In a model where a flat non-resonant $b\overline{b}$-continuum is incoherently added to a second flat component interfering with two Breit-Wigner resonances. Systematic uncertainties not estimated.

[9] The parameters of the $\Upsilon(11020)$ are fixed to those in AUBERT 09E.

[10] In a model where a flat nonresonant $\Upsilon(1S,2S,3S)\pi^+\pi^-$ continuum interferes with a single Breit-Wigner resonance.

[11] In a model where a non-resonant $b\overline{b}$-continuum represented by a threshold function at $\sqrt{s}$=$2m_B$ is incoherently added to a flat component interfering with two Breit-Wigner resonances. Not independent of other AUBERT 09E results. Systematic uncertainties not estimated.

[12] Assuming four Gaussians with radiative tails and a single step in R.

[13] In a coupled-channel model with three resonances and a smooth step in R.

$\Upsilon(10860)$ WIDTH

VALUE (MeV)	DOCUMENT ID		TECN	COMMENT
37 ± 4 OUR AVERAGE				
$36.6^{+4.5+0.5}_{-3.9-1.1}$	[1] MIZUK	19	BELL	$e^+e^- \to \Upsilon(nS)\pi^+\pi^-$
$40.6^{+12.7+1.1}_{-8.0-19.1}$	[2] MIZUK	16	BELL	$e^+e^- \to h_b(1P,2P)\pi^+\pi^-$
• • • We do not use the following data for averages, fits, limits, etc. • • •				
49.5 ± 1.5	[3] DONG	20A		$e^+e^- \to b\overline{b}$
$48.5^{+1.9+2.0}_{-1.8-2.8}$	[4,5] SANTEL	16	BELL	$e^+e^- \to$ hadrons
$53.7^{+7.1+1.3}_{-5.6-5.4}$	[6,7] SANTEL	16	BELL	$e^+e^- \to \Upsilon(1S,2S,3S)\pi^+\pi^-$
46^{+9}_{-7}	[8,9] CHEN	10	BELL	$e^+e^- \to$ hadrons
$30.7^{+8.3}_{-7.0} \pm 3.1$	[10] CHEN	10	BELL	$e^+e^- \to \Upsilon(1S,2S,3S)\pi^+\pi^-$
43 ± 4	[8] AUBERT	09E	BABR	$e^+e^- \to$ hadrons
74 ± 4	[11] AUBERT	09E	BABR	$e^+e^- \to$ hadrons
$112 \pm 17 \pm 23$	[12] BESSON	85	CLEO	$e^+e^- \to$ hadrons
110 ± 15	[13] LOVELOCK	85	CUSB	$e^+e^- \to$ hadrons

[1] From a simultaneous fit to the $\Upsilon(nS)\pi^+\pi^-$, $n = 1, 2, 3$, cross sections at 28 energy points within $\sqrt{s} = 10.6$–11.05 GeV, including the initial-state radiation at $\Upsilon(10860)$.

[2] From a simultaneous fit to the $h_b(nP)\pi^+\pi^-$, $n = 1, 2$ cross sections at 22 energy points within $\sqrt{s} = 10.77$–11.02 GeV to a pair of interfering Breit-Wigner amplitudes modified by phase space factors, with eight resonance parameters (a mass and width for each of $\Upsilon(10860)$ and $\Upsilon(11020)$, a single relative phase, a single relative amplitude, and two overall normalization factors, one for each n). The systematic error estimate is dominated by possible interference with a small nonresonant continuum amplitude.

[3] From a fit to the dressed cross sections of AUBERT 09E by BaBar and SANTEL 16 by Belle above 10.68 GeV with a coherent sum of a continuum amplitude and three Breit-Wigner functions with constant widths.

[4] From a fit to the total hadronic cross sections measured at 60 energy points within $\sqrt{s}$ = 10.82–11.05 GeV to a pair of interfering Breit-Wigner amplitudes and two floating continuum amplitudes with $1/\sqrt{s}$ dependence, one coherent with the resonances and one incoherent, with six resonance parameters (a mass, width, and an amplitude for each of $\Upsilon(10860)$ and $\Upsilon(11020)$, one relative phase, and one decoherence coefficient).

[5] Not including uncertain and potentially large systematic errors due to assumed continuum amplitude $1/\sqrt{s}$ dependence and related interference contributions.

[6] From a simultaneous fit to the $\Upsilon(nS)\pi^+\pi^-$, $n = 1, 2, 3$, cross sections at 25energy points within $\sqrt{s} = 10.6$–11.05 GeV to a pair of interfering Breit-Wigner amplitudesmodified by phase space factors, with fourteen resonance parameters (a mass, width, and threeamplitudes for each of $\Upsilon(10860)$ and $\Upsilon(11020)$, a single universal relativephase, and three decoherence coefficients, one for each n). Continuum contributions weremeasured (and therefore fixed) to be zero.

[7] Superseded by MIZUK 19.

[8] In a model where a flat non-resonant $b\overline{b}$-continuum is incoherently added to a second flat component interfering with two Breit-Wigner resonances. Systematic uncertainties not estimated.

[9] The parameters of the $\Upsilon(11020)$ are fixed to those in AUBERT 09E.

[10] In a model where a flat nonresonant $\Upsilon(1S,2S,3S)\pi^+\pi^-$ continuum interferes with a single Breit-Wigner resonance.

[11] In a model where a non-resonant $b\overline{b}$-continuum represented by a threshold function at $\sqrt{s}$=$2m_B$ is incoherently added to a flat component interfering with two Breit-Wigner resonances. Not independent of other AUBERT 09E results. Systematic uncertainties not estimated.

[12] Assuming four Gaussians with radiative tails and a single step in R.

[13] In a coupled-channel model with three resonances and a smooth step in R.

$\Upsilon(10860)$ DECAY MODES

	Mode	Fraction (Γ_i/Γ)	Confidence level
Γ_1	$B\overline{B}X$	$(76.2^{+2.7}_{-4.0})$ %	
Γ_2	$B\overline{B}$	(5.5 ± 1.0) %	
Γ_3	$B\overline{B}^* +$ c.c.	(13.7 ± 1.6) %	
Γ_4	$B^*\overline{B}^*$	(38.1 ± 3.4) %	
Γ_5	$B\overline{B}^{(*)}\pi$	< 19.7 %	90%
Γ_6	$B\overline{B}\pi$	(0.0 ± 1.2) %	
Γ_7	$B^*\overline{B}\pi + B\overline{B}^*\pi$	(7.3 ± 2.3) %	
Γ_8	$B^*\overline{B}^*\pi$	(1.0 ± 1.4) %	
Γ_9	$B\overline{B}\pi\pi$	< 8.9 %	90%
Γ_{10}	$B_s^{(*)}\overline{B}_s^{(*)}$	(20.1 ± 3.1) %	
Γ_{11}	$B_s\overline{B}_s$	$(5 \pm 5) \times 10^{-3}$	
Γ_{12}	$B_s\overline{B}_s^* +$ c.c.	(1.35 ± 0.32) %	
Γ_{13}	$B_s^*\overline{B}_s^*$	(17.6 ± 2.7) %	
Γ_{14}	no open-bottom	$(3.8^{+5.0}_{-0.5})$ %	
Γ_{15}	e^+e^-	$(8.3 \pm 2.1) \times 10^{-6}$	
Γ_{16}	$K^*(892)^0\overline{K}^0$	$< 1.0 \times 10^{-5}$	90%
Γ_{17}	$\Upsilon(1S)\pi^+\pi^-$	$(5.3 \pm 0.6) \times 10^{-3}$	
Γ_{18}	$\Upsilon(1S)\eta$	$(8.5 \pm 1.7) \times 10^{-4}$	
Γ_{19}	$\Upsilon(1S)\eta'$	$< 6.9 \times 10^{-5}$	90%
Γ_{20}	$\Upsilon(2S)\pi^+\pi^-$	$(7.8 \pm 1.3) \times 10^{-3}$	
Γ_{21}	$\Upsilon(2S)\eta$	$(4.1 \pm 0.6) \times 10^{-3}$	

Downloaded from https://academic.oup.com/ptep/article/2022/8/083C01/6651666 by KIT Library user on 27 September 2022

Γ_{22}	$\Upsilon(3S)\pi^+\pi^-$	$(4.8\ ^{+1.9}_{-1.7})\times10^{-3}$	
Γ_{23}	$\Upsilon(1S)K^+K^-$	$(6.1\ \pm1.8)\times10^{-4}$	
Γ_{24}	$\eta\Upsilon_J(1D)$	$(4.8\ \pm1.1)\times10^{-3}$	
Γ_{25}	$h_b(1P)\pi^+\pi^-$	$(3.5\ ^{+1.0}_{-1.3})\times10^{-3}$	
Γ_{26}	$h_b(2P)\pi^+\pi^-$	$(5.7\ ^{+1.7}_{-2.1})\times10^{-3}$	
Γ_{27}	$\chi_{bJ}(1P)\pi^+\pi^-\pi^0$	$(2.5\ \pm2.3)\times10^{-3}$	
Γ_{28}	$\chi_{b0}(1P)\pi^+\pi^-\pi^0$	$<6.3\times10^{-3}$	90%
Γ_{29}	$\chi_{b0}(1P)\omega$	$<3.9\times10^{-3}$	90%
Γ_{30}	$\chi_{b0}(1P)(\pi^+\pi^-\pi^0)_{\text{non}-\omega}$	$<4.8\times10^{-3}$	90%
Γ_{31}	$\chi_{b1}(1P)\pi^+\pi^-\pi^0$	$(1.85\pm0.33)\times10^{-3}$	
Γ_{32}	$\chi_{b1}(1P)\omega$	$(1.57\pm0.30)\times10^{-3}$	
Γ_{33}	$\chi_{b1}(1P)(\pi^+\pi^-\pi^0)_{\text{non}-\omega}$	$(5.2\ \pm1.9)\times10^{-4}$	
Γ_{34}	$\chi_{b2}(1P)\pi^+\pi^-\pi^0$	$(1.17\pm0.30)\times10^{-3}$	
Γ_{35}	$\chi_{b2}(1P)\omega$	$(6.0\ \pm2.7)\times10^{-4}$	
Γ_{36}	$\chi_{b2}(1P)(\pi^+\pi^-\pi^0)_{\text{non}-\omega}$	$(6\ \pm4)\times10^{-4}$	
Γ_{37}	$\gamma X_b\to\gamma\Upsilon(1S)\omega$	$<3.8\times10^{-5}$	90%
Γ_{38}	$\eta_b(1S)\omega$	$<1.3\times10^{-3}$	90%
Γ_{39}	$\eta_b(2S)\omega$	$<5.6\times10^{-3}$	90%

Inclusive Decays.

These decay modes are submodes of one or more of the decay modes above.

Γ_{40}	ϕ anything	$(13.8\ ^{+2.4}_{-1.7})$ %
Γ_{41}	D^0 anything + c.c.	$(108\ \pm8)$ %
Γ_{42}	D_s anything + c.c.	$(46\ \pm6)$ %
Γ_{43}	J/ψ anything	(2.06 ± 0.21) %
Γ_{44}	B^0 anything + c.c.	$(77\ \pm8)$ %
Γ_{45}	B^+ anything + c.c.	$(72\ \pm6)$ %

$\Upsilon(10860)$ PARTIAL WIDTHS

$\Gamma(e^+e^-)$ — Γ_{15}

VALUE (keV)	DOCUMENT ID		TECN	COMMENT
0.31 ±0.07 OUR AVERAGE	Error includes scale factor of 1.3.			
0.22 ±0.05 ±0.07	BESSON	85	CLEO	$e^+e^-\to$ hadrons
0.365±0.070	LOVELOCK	85	CUSB	$e^+e^-\to$ hadrons

$\Gamma(e^+e^-)\times\Gamma(\Upsilon(1S)\pi^+\pi^-)/\Gamma_{\text{total}}$ — $\Gamma_{15}\Gamma_{17}/\Gamma$

VALUE (eV)	DOCUMENT ID		TECN	COMMENT
• • • We do not use the following data for averages, fits, limits, etc. • • •				
1.09±0.34	[1,2] MIZUK	19	BELL	$e^+e^-\to\Upsilon(nS)\pi^+\pi^-$

[1] From a simultaneous fit to the $\Upsilon(nS)\pi^+\pi^-$, n = 1, 2, 3, cross sections at 28 energy points within $\sqrt{s}$ = 10.6–11.05 GeV, including the initial-state radiation at $\Upsilon(10860)$.
[2] Reported as the range 0.75–1.43 eV obtained from multiple solutions of an amplitude fit within a model composed as a sum of Breit-Wigner functions.

$\Gamma(e^+e^-)\times\Gamma(\Upsilon(2S)\pi^+\pi^-)/\Gamma_{\text{total}}$ — $\Gamma_{15}\Gamma_{20}/\Gamma$

VALUE (eV)	DOCUMENT ID		TECN	COMMENT
• • • We do not use the following data for averages, fits, limits, etc. • • •				
2.58±1.22	[1,2] MIZUK	19	BELL	$e^+e^-\to\Upsilon(nS)\pi^+\pi^-$

[1] From a simultaneous fit to the $\Upsilon(nS)\pi^+\pi^-$, n = 1, 2, 3, cross sections at 28 energy points within $\sqrt{s}$ = 10.6–11.05 GeV, including the initial-state radiation at $\Upsilon(10860)$.
[2] Reported as the range 1.35–3.80 eV obtained from multiple solutions of an amplitude fit within a model composed as a sum of Breit-Wigner functions.

$\Gamma(e^+e^-)\times\Gamma(\Upsilon(3S)\pi^+\pi^-)/\Gamma_{\text{total}}$ — $\Gamma_{15}\Gamma_{22}/\Gamma$

VALUE (eV)	DOCUMENT ID		TECN	COMMENT
• • • We do not use the following data for averages, fits, limits, etc. • • •				
0.73±0.30	[1,2] MIZUK	19	BELL	$e^+e^-\to\Upsilon(nS)\pi^+\pi^-$

[1] From a simultaneous fit to the $\Upsilon(nS)\pi^+\pi^-$, n = 1, 2, 3, cross sections at 28 energy points within $\sqrt{s}$ = 10.6–11.05 GeV, including the initial-state radiation at $\Upsilon(10860)$.
[2] Reported as the range 0.43–1.03 eV obtained from multiple solutions of an amplitude fit within a model composed as a sum of Breit-Wigner functions.

$\Upsilon(10860)$ BRANCHING RATIOS

"OUR EVALUATION" is obtained based on averages of rescaled data listed below. The averages and rescaling were performed by the Heavy Flavor Averaging Group (HFLAV) and are described at https://hflav.web.cern.ch/.

$\Gamma(B\overline{B}X)/\Gamma_{\text{total}}$ — Γ_1/Γ

VALUE	EVTS	DOCUMENT ID		TECN	COMMENT
$0.762^{+0.027}_{-0.043}$ OUR EVALUATION					
0.71 ±0.06 OUR AVERAGE					
0.737±0.032±0.051	1063	[1] DRUTSKOY	10	BELL	$\Upsilon(5S)\to B^+X,\ B^0X$
0.589±0.100±0.092		[2] HUANG	07	CLEO	$\Upsilon(5S)\to$ hadrons

[1] Not independent of DRUTSKOY 10 values for $\Upsilon(5S)\to B^{\pm,0}$ anything.
[2] Using measurements or limits from AQUINES 06.

$\Gamma(B\overline{B})/\Gamma_{\text{total}}$ — Γ_2/Γ

VALUE (units 10^{-2})	CL%	DOCUMENT ID		TECN	COMMENT
$5.5^{+1.0}_{-0.9}\pm0.4$		[1] DRUTSKOY	10	BELL	$\Upsilon(5S)\to B^+X,\ B^0X$
• • • We do not use the following data for averages, fits, limits, etc. • • •					
<13.8	90	[2] HUANG	07	CLEO	$\Upsilon(5S)\to$ hadrons

[1] Assuming isospin conservation.
[2] Using measurements or limits from AQUINES 06.

$\Gamma(B\overline{B})/\Gamma(B\overline{B}X)$ — Γ_2/Γ_1

VALUE	CL%	DOCUMENT ID		TECN	COMMENT
<0.22	90	AQUINES	06	CLE3	$\Upsilon(5S)\to$ hadrons

$\Gamma(B\overline{B}^*+\text{c.c.})/\Gamma_{\text{total}}$ — Γ_3/Γ

VALUE	DOCUMENT ID		TECN	COMMENT
0.137±0.016 OUR AVERAGE				
0.137±0.013±0.011	[1] DRUTSKOY	10	BELL	$\Upsilon(5S)\to B^+X,\ B^0X$
0.143±0.053±0.027	[2] HUANG	07	CLEO	$\Upsilon(5S)\to$ hadrons

[1] Assuming isospin conservation.
[2] Using measurements or limits from AQUINES 06.

$\Gamma(B\overline{B}^*+\text{c.c.})/\Gamma(B\overline{B}X)$ — Γ_3/Γ_1

VALUE	EVTS	DOCUMENT ID		TECN	COMMENT
0.24±0.09±0.03	10	AQUINES	06	CLE3	$\Upsilon(5S)\to$ hadrons

$\Gamma(B^*\overline{B}^*)/\Gamma_{\text{total}}$ — Γ_4/Γ

VALUE	DOCUMENT ID		TECN	COMMENT
0.381±0.034 OUR AVERAGE				
$0.375^{+0.021}_{-0.019}\pm0.030$	[1] DRUTSKOY	10	BELL	$\Upsilon(5S)\to B^+X,\ B^0X$
0.436±0.083±0.072	[2] HUANG	07	CLEO	$\Upsilon(5S)\to$ hadrons

[1] Assuming isospin conservation.
[2] Using measurements or limits from AQUINES 06.

$\Gamma(B^*\overline{B}^*)/\Gamma(B\overline{B}X)$ — Γ_4/Γ_1

VALUE	EVTS	DOCUMENT ID		TECN	COMMENT
0.74±0.15±0.08	31	AQUINES	06	CLE3	$\Upsilon(5S)\to$ hadrons

$\Gamma(B\overline{B}^{(*)}\pi)/\Gamma_{\text{total}}$ — Γ_5/Γ

VALUE	CL%	DOCUMENT ID		TECN	COMMENT
<0.197	90	[1] HUANG	07	CLEO	$\Upsilon(5S)\to$ hadrons

[1] Using measurements or limits from AQUINES 06.

$\Gamma(B\overline{B}^{(*)}\pi)/\Gamma(B\overline{B}X)$ — Γ_5/Γ_1

VALUE	CL%	DOCUMENT ID		TECN	COMMENT
<0.32	90	AQUINES	06	CLE3	$\Upsilon(5S)\to$ hadrons

$\Gamma(B\overline{B}\pi)/\Gamma_{\text{total}}$ — Γ_6/Γ

VALUE (units 10^{-2})	EVTS	DOCUMENT ID		TECN	COMMENT
0.0±1.2±0.3	0	[1] DRUTSKOY	10	BELL	$\Upsilon(5S)\to B^{+,0}\pi^-X$

[1] Assuming isospin conservation.

$[\Gamma(B^*\overline{B}\pi)+\Gamma(B\overline{B}^*\pi)]/\Gamma_{\text{total}}$ — Γ_7/Γ

VALUE (units 10^{-2})	EVTS	DOCUMENT ID		TECN	COMMENT
$7.3^{+2.3}_{-2.1}\pm0.8$	38	[1] DRUTSKOY	10	BELL	$\Upsilon(5S)\to B^{+,0}\pi^-X$

[1] Assuming isospin conservation.

$\Gamma(B^*\overline{B}^*\pi)/\Gamma_{\text{total}}$ — Γ_8/Γ

VALUE (units 10^{-2})	EVTS	DOCUMENT ID		TECN	COMMENT
$1.0^{+1.4}_{-1.3}\pm0.4$	5	[1] DRUTSKOY	10	BELL	$\Upsilon(5S)\to B^{+,0}\pi^-X$

[1] Assuming isospin conservation.

$\Gamma(B\overline{B}\pi\pi)/\Gamma_{\text{total}}$ — Γ_9/Γ

VALUE	CL%	DOCUMENT ID		TECN	COMMENT
<0.089	90	[1] HUANG	07	CLEO	$\Upsilon(5S)\to$ hadrons

[1] Using measurements or limits from AQUINES 06.

$\Gamma(B\overline{B}\pi\pi)/\Gamma(B\overline{B}X)$ — Γ_9/Γ_1

VALUE	CL%	DOCUMENT ID		TECN	COMMENT
<0.14	90	AQUINES	06	CLE3	$\Upsilon(5S)\to$ hadrons

$\Gamma(B_s^{(*)}\overline{B}_s^{(*)})/\Gamma_{\text{total}}$ — $\Gamma_{10}/\Gamma=(\Gamma_{11}+\Gamma_{12}+\Gamma_{13})/\Gamma$

VALUE	DOCUMENT ID		TECN	COMMENT
$0.201^{+0.030}_{-0.031}$ OUR EVALUATION				
$0.189^{+0.027}_{-0.021}$ OUR AVERAGE				
0.172±0.030	[1] ESEN	13	BELL	$\Upsilon(5S)\to D^0X,\ D_sX$
$0.21\ ^{+0.06}_{-0.03}$	[2] HUANG	07	CLEO	$\Upsilon(5S)\to D_sX$
• • • We do not use the following data for averages, fits, limits, etc. • • •				
0.180±0.013±0.032	[3] DRUTSKOY	07	BELL	$\Upsilon(5S)\to D^0X,\ D_sX$
0.160±0.026±0.058	[4] ARTUSO	05B	CLEO	$e^+e^-\to D_sX$

Downloaded from https://academic.oup.com/ptep/article/2022/8/083C01/6651666 by KIT Library user on 27 September 2022

[1] Supersedes DRUTSKOY 07.
[2] Supersedes ARTUSO 05B. Combining inclusive ϕ, D_s, and B measurements. Using $B(D_s^+ \to \phi\pi^+) = 4.4 \pm 0.6\%$ from PDG 06.
[3] Using $B(D_s^+ \to \phi\pi^+) = (4.4 \pm 0.6)\%$ from PDG 06.
[4] Uses a model-dependent estimate $B(B_s \to D_s X) = (92 \pm 11)\%$.

$\Gamma(B_s^{(*)}\overline{B}_s^{(*)})/\Gamma(B\overline{B}X)$ — Γ_{10}/Γ_1

VALUE	DOCUMENT ID
$0.264^{+0.052}_{-0.045}$ **OUR EVALUATION**	

$\Gamma(B_s^*\overline{B}_s^*)/\Gamma(B_s^{(*)}\overline{B}_s^{(*)})$ — $\Gamma_{13}/\Gamma_{10} = \Gamma_{13}/(\Gamma_{11}+\Gamma_{12}+\Gamma_{13})$

VALUE (units 10^{-2})	EVTS	DOCUMENT ID		TECN	COMMENT
87.8±1.5 OUR AVERAGE					
87.0±1.7		[1,2] ESEN	13	BELL	$B_s^0 \to D_s^- \pi^+$
90.5±3.2±0.1	227	[2,3] LI	12	BELL	$B_s^0 \to J/\psi\eta^{(\prime)}$
• • • We do not use the following data for averages, fits, limits, etc. • • •					
$90.1^{+3.8}_{-4.0}\pm0.2$		[4] LOUVOT	09	BELL	10.86 $e^+e^- \to B_s^{(*)}\overline{B}_s^{(*)}$
$93^{+7}_{-9}\pm1$		[4] DRUTSKOY	07A	BELL	Superseded by LOUVOT 09

[1] Supersedes LOUVOT 09.
[2] With $N(B_s^{(*)}\overline{B}_s^{(*)}) = (7.11 \pm 1.30) \times 10^6$.
[3] The ratios $N(B_s^*\overline{B}_s^*)$ / $N(B_s^{(*)}\overline{B}_s^{(*)})$ and $N(B_s^*\overline{B}_s^0)$ / $N(B_s^{(*)}\overline{B}_s^{(*)})$ are measured with a correlation coefficient of −0.72.
[4] From a measurement of $\sigma(e^+e^- \to B_s^*\overline{B}_s^*)$ / $\sigma(e^+e^- \to B_s^{(*)}\overline{B}_s^{(*)})$ at $\sqrt{s} = 10.86$ GeV.

$\Gamma(B_s\overline{B}_s)/\Gamma(B_s^{(*)}\overline{B}_s^{(*)})$ — $\Gamma_{11}/\Gamma_{10} = \Gamma_{11}/(\Gamma_{11}+\Gamma_{12}+\Gamma_{13})$

VALUE (units 10^{-2})	DOCUMENT ID		TECN	COMMENT
$2.6^{+2.6}_{-2.5}$	LOUVOT	09	BELL	10.86 $e^+e^- \to B_s^{(*)}\overline{B}_s^{(*)}$

$\Gamma(B_s\overline{B}_s)/\Gamma(B_s^*\overline{B}_s^*)$ — Γ_{11}/Γ_{13}

VALUE	CL%	DOCUMENT ID		TECN	COMMENT
<0.16	90	BONVICINI	06	CLE3	e^+e^-

$\Gamma(B_s\overline{B}_s^* + \text{c.c.})/\Gamma(B_s^{(*)}\overline{B}_s^{(*)})$ — $\Gamma_{12}/\Gamma_{10} = \Gamma_{12}/(\Gamma_{11}+\Gamma_{12}+\Gamma_{13})$

VALUE (units 10^{-2})	EVTS	DOCUMENT ID		TECN	COMMENT
6.7±1.2 OUR AVERAGE					
7.3±1.4		[1,2] ESEN	13	BELL	$B_s^0 \to D_s^- \pi^+$
4.9±2.5±0.0	227	[2,3] LI	12	BELL	$B_s^0 \to J/\psi\eta^{(\prime)}$
• • • We do not use the following data for averages, fits, limits, etc. • • •					
$7.3^{+3.3}_{-3.0}\pm0.1$		LOUVOT	09	BELL	10.86 $e^+e^- \to B_s^{(*)}\overline{B}_s^{(*)}$

[1] Supersedes LOUVOT 09.
[2] With $N(B_s^{(*)}\overline{B}_s^{(*)}) = (7.11 \pm 1.30) \times 10^6$.
[3] The ratios $N(B_s^*\overline{B}_s^*)$ / $N(B_s^{(*)}\overline{B}_s^{(*)})$ and $N(B_s^*\overline{B}_s^0)$ / $N(B_s^{(*)}\overline{B}_s^{(*)})$ are measured with a correlation coefficient of −0.72.

$\Gamma(B_s\overline{B}_s^* + \text{c.c.})/\Gamma(B_s^*\overline{B}_s^*)$ — Γ_{12}/Γ_{13}

VALUE	CL%	DOCUMENT ID		TECN	COMMENT
<0.16	90	BONVICINI	06	CLE3	e^+e^-

$\Gamma(\text{no open-bottom})/\Gamma_{\text{total}}$ — Γ_{14}/Γ

VALUE	DOCUMENT ID
$0.038^{+0.051}_{-0.005}$ **OUR EVALUATION**	

$\Gamma(K^*(892)^0\overline{K}^0)/\Gamma_{\text{total}}$ — Γ_{16}/Γ

VALUE	CL%	DOCUMENT ID		TECN	COMMENT
$<1.0 \times 10^{-5}$	90	SHEN	13A	BELL	$e^+e^- \to K^*(892)^0\overline{K}^0$

$\Gamma(\eta\Upsilon_J(1D))/\Gamma_{\text{total}}$ — Γ_{24}/Γ

VALUE (units 10^{-3})	DOCUMENT ID		TECN	COMMENT
4.82±0.92±0.67	[1] TAMPONI	18	BELL	$e^+e^- \to \Upsilon(5S) \to \eta X$

[1] Mainly $J = 2$, assumes no continuum contribution under $\Upsilon(5S)$.

$\Gamma(\Upsilon(1S)\pi^+\pi^-)/\Gamma_{\text{total}}$ — Γ_{17}/Γ

VALUE (units 10^{-3})	EVTS	DOCUMENT ID		TECN	COMMENT
5.3±0.3±0.5	325	[1] CHEN	08	BELL	10.87 $e^+e^- \to \Upsilon(1S)\pi^+\pi^-$

[1] Assuming that the observed events are solely due to the $\Upsilon(5S)$ resonance.

$\Gamma(\Upsilon(1S)\eta)/\Gamma_{\text{total}}$ — Γ_{18}/Γ

VALUE (units 10^{-3})	DOCUMENT ID		TECN	COMMENT
0.85±0.15±0.08	[1,2] KOVALENKO	21	BELL	$e^+e^- \to \Upsilon(5S)$

[1] Assuming that the observed events are solely due to the $\Upsilon(5S)$ resonance.
[2] Using a data sample of 118.3 fb^{-1} of e^+e^- collisions at $\sqrt{s} = 10.866$ GeV.

$\Gamma(\Upsilon(1S)\eta')/\Gamma_{\text{total}}$ — Γ_{19}/Γ

VALUE	CL%	DOCUMENT ID		TECN	COMMENT
$<6.9 \times 10^{-5}$	90	[1,2] KOVALENKO	21	BELL	$e^+e^- \to \Upsilon(5S)$

[1] Assuming that the observed events are solely due to the $\Upsilon(5S)$ resonance.
[2] Using a data sample of 118.3 fb^{-1} of e^+e^- collisions at $\sqrt{s} = 10.866$ GeV.

$\Gamma(\Upsilon(2S)\pi^+\pi^-)/\Gamma_{\text{total}}$ — Γ_{20}/Γ

VALUE (units 10^{-3})	EVTS	DOCUMENT ID		TECN	COMMENT
7.8±0.6±1.1	186	[1] CHEN	08	BELL	10.87 $e^+e^- \to \Upsilon(2S)\pi^+\pi^-$

[1] Assuming that the observed events are solely due to the $\Upsilon(5S)$ resonance.

$\Gamma(\Upsilon(2S)\eta)/\Gamma_{\text{total}}$ — Γ_{21}/Γ

VALUE (units 10^{-3})	DOCUMENT ID		TECN	COMMENT
4.13±0.41±0.37	[1,2] KOVALENKO	21	BELL	$e^+e^- \to \Upsilon(5S)$

[1] Assuming that the observed events are solely due to the $\Upsilon(5S)$ resonance.
[2] Using a data sample of 118.3 fb^{-1} of e^+e^- collisions at $\sqrt{s} = 10.866$ GeV.

$\Gamma(\Upsilon(3S)\pi^+\pi^-)/\Gamma_{\text{total}}$ — Γ_{22}/Γ

VALUE (units 10^{-3})	EVTS	DOCUMENT ID		TECN	COMMENT
$4.8^{+1.8}_{-1.5}\pm0.7$	10	[1] CHEN	08	BELL	10.87 $e^+e^- \to \Upsilon(3S)\pi^+\pi^-$

[1] Assuming that the observed events are solely due to the $\Upsilon(5S)$ resonance.

$\Gamma(\Upsilon(1S)K^+K^-)/\Gamma_{\text{total}}$ — Γ_{23}/Γ

VALUE (units 10^{-4})	EVTS	DOCUMENT ID		TECN	COMMENT
$6.1^{+1.6}_{-1.4}\pm1.0$	20	[1] CHEN	08	BELL	10.87 $e^+e^- \to \Upsilon(1S)K^+K^-$

[1] Assuming that the observed events are solely due to the $\Upsilon(5S)$ resonance.

$\Gamma(h_b(1P)\pi^+\pi^-)/\Gamma(\Upsilon(2S)\pi^+\pi^-)$ — Γ_{25}/Γ_{20}

VALUE	DOCUMENT ID		TECN	COMMENT
$0.45\pm0.08^{+0.07}_{-0.12}$	ADACHI	12	BELL	10.86 $e^+e^- \to$ hadrons

$\Gamma(h_b(2P)\pi^+\pi^-)/\Gamma(\Upsilon(2S)\pi^+\pi^-)$ — Γ_{26}/Γ_{20}

VALUE	DOCUMENT ID		TECN	COMMENT
$0.77\pm0.08^{+0.22}_{-0.17}$	ADACHI	12	BELL	10.86 $e^+e^- \to$ hadrons

$\Gamma(h_b(1P)\pi^+\pi^-)/\Gamma(h_b(2P)\pi^+\pi^-)$ — Γ_{25}/Γ_{26}

VALUE	DOCUMENT ID		TECN	COMMENT
0.616±0.052±0.017	MIZUK	16	BELL	$e^+e^- \to h_b(1P,2P)\pi^+\pi^-$

$\Gamma(\chi_{bJ}(1P)\pi^+\pi^-\pi^0)/\Gamma_{\text{total}}$ — Γ_{27}/Γ

VALUE (units 10^{-3})	DOCUMENT ID		TECN	COMMENT
2.5±0.6±2.2	YIN	18	BELL	$e^+e^- \to$ hadrons

$\Gamma(\chi_{b0}(1P)\pi^+\pi^-\pi^0)/\Gamma_{\text{total}}$ — Γ_{28}/Γ

VALUE	CL%	DOCUMENT ID		TECN	COMMENT
$<6.3 \times 10^{-3}$	90	[1] HE	14	BELL	$\Upsilon(5S) \to \pi^+\pi^-\pi^0\gamma\Upsilon(1S)$

[1] Assuming that all the $b\overline{b}$ events are from $\Upsilon(5S)$ resonance decays and using $\sigma(e^+e^- \to b\overline{b}) = 0.340 \pm 0.016$ nb from ESEN 13. Correlated with other results from HE 14.

$\Gamma(\chi_{b0}(1P)\omega)/\Gamma_{\text{total}}$ — Γ_{29}/Γ

VALUE	CL%	DOCUMENT ID		TECN	COMMENT
$<3.9 \times 10^{-3}$	90	[1] HE	14	BELL	$\Upsilon(5S) \to \pi^+\pi^-\pi^0\gamma\Upsilon(1S)$

[1] Assuming that all the $b\overline{b}$ events are from $\Upsilon(5S)$ resonance decays and using $\sigma(e^+e^- \to b\overline{b}) = 0.340 \pm 0.016$ nb from ESEN 13. Correlated with other results from HE 14.

$\Gamma(\chi_{b0}(1P)(\pi^+\pi^-\pi^0)_{\text{non}-\omega})/\Gamma_{\text{total}}$ — Γ_{30}/Γ

VALUE	CL%	DOCUMENT ID		TECN	COMMENT
$<4.8 \times 10^{-3}$	90	[1] HE	14	BELL	$\Upsilon(5S) \to \pi^+\pi^-\pi^0\gamma\Upsilon(1S)$

[1] Assuming that all the $b\overline{b}$ events are from $\Upsilon(5S)$ resonance decays and using $\sigma(e^+e^- \to b\overline{b}) = 0.340 \pm 0.016$ nb from ESEN 13. Correlated with other results from HE 14.

$\Gamma(\chi_{b1}(1P)\pi^+\pi^-\pi^0)/\Gamma_{\text{total}}$ — Γ_{31}/Γ

VALUE (units 10^{-3})	EVTS	DOCUMENT ID		TECN	COMMENT
1.85±0.23±0.23	80	[1] HE	14	BELL	$\Upsilon(5S) \to \pi^+\pi^-\pi^0\gamma\Upsilon(1S)$

[1] Assuming that all the $b\overline{b}$ events are from $\Upsilon(5S)$ resonance decays and using $\sigma(e^+e^- \to b\overline{b}) = 0.340 \pm 0.016$ nb from ESEN 13. Correlated with other results from HE 14.

$\Gamma(\chi_{b1}(1P)\omega)/\Gamma_{\text{total}}$ — Γ_{32}/Γ

VALUE (units 10^{-3})	EVTS	DOCUMENT ID		TECN	COMMENT
1.57±0.22±0.21	60	[1] HE	14	BELL	$\Upsilon(5S) \to \pi^+\pi^-\pi^0\gamma\Upsilon(1S)$

[1] Assuming that all the $b\overline{b}$ events are from $\Upsilon(5S)$ resonance decays and using $\sigma(e^+e^- \to b\overline{b}) = 0.340 \pm 0.016$ nb from ESEN 13. Correlated with other results from HE 14.

Downloaded from https://academic.oup.com/ptep/article/2022/8/083C01/6651666 by KIT Library user on 27 September 2022

$\Gamma(\chi_{b1}(1P)(\pi^+\pi^-\pi^0)_{non-\omega})/\Gamma_{total}$ — Γ_{33}/Γ

VALUE (units 10^{-3})	EVTS	DOCUMENT ID		TECN	COMMENT
0.52±0.15±0.11	24	[1] HE	14	BELL	$\Upsilon(5S) \to \pi^+\pi^-\pi^0\gamma\Upsilon(1S)$

[1] Assuming that all the $b\overline{b}$ events are from $\Upsilon(5S)$ resonance decays and using $\sigma(e^+e^- \to b\overline{b}) = 0.340 \pm 0.016$ nb from ESEN 13. Correlated with other results from HE 14.

$\Gamma(\chi_{b2}(1P)\pi^+\pi^-\pi^0)/\Gamma_{total}$ — Γ_{34}/Γ

VALUE (units 10^{-3})	EVTS	DOCUMENT ID		TECN	COMMENT
1.17±0.27±0.14	29	[1] HE	14	BELL	$\Upsilon(5S) \to \pi^+\pi^-\pi^0\gamma\Upsilon(1S)$

[1] Assuming that all the $b\overline{b}$ events are from $\Upsilon(5S)$ resonance decays and using $\sigma(e^+e^- \to b\overline{b}) = 0.340 \pm 0.016$ nb from ESEN 13. Correlated with other results from HE 14.

$\Gamma(\chi_{b2}(1P)\omega)/\Gamma_{total}$ — Γ_{35}/Γ

VALUE (units 10^{-3})	EVTS	DOCUMENT ID		TECN	COMMENT
0.60±0.23±0.15	13	[1] HE	14	BELL	$\Upsilon(5S) \to \pi^+\pi^-\pi^0\gamma\Upsilon(1S)$

[1] Assuming that all the $b\overline{b}$ events are from $\Upsilon(5S)$ resonance decays and using $\sigma(e^+e^- \to b\overline{b}) = 0.340 \pm 0.016$ nb from ESEN 13. Correlated with other results from HE 14.

$\Gamma(\chi_{b2}(1P)\omega)/\Gamma(\chi_{b1}(1P)\omega)$ — Γ_{35}/Γ_{32}

VALUE	DOCUMENT ID		TECN	COMMENT
• • • We do not use the following data for averages, fits, limits, etc. • • •				
0.38±0.16±0.09	[1] HE	14	BELL	$\Upsilon(5S) \to \pi^+\pi^-\pi^0\gamma\Upsilon(1S)$

[1] Accounting for correlated systematics.

$\Gamma(\chi_{b2}(1P)(\pi^+\pi^-\pi^0)_{non-\omega})/\Gamma_{total}$ — Γ_{36}/Γ

VALUE (units 10^{-3})	EVTS	DOCUMENT ID		TECN	COMMENT
0.61±0.22±0.28	16	[1] HE	14	BELL	$\Upsilon(5S) \to \pi^+\pi^-\pi^0\gamma\Upsilon(1S)$

[1] Assuming that all the $b\overline{b}$ events are from $\Upsilon(5S)$ resonance decays and using $\sigma(e^+e^- \to b\overline{b}) = 0.340 \pm 0.016$ nb from ESEN 13. Correlated with other results from HE 14.

$\Gamma(\chi_{b2}(1P)(\pi^+\pi^-\pi^0)_{non-\omega})/\Gamma(\chi_{b1}(1P)(\pi^+\pi^-\pi^0)_{non-\omega})$ — Γ_{36}/Γ_{33}

VALUE	DOCUMENT ID		TECN	COMMENT
• • • We do not use the following data for averages, fits, limits, etc. • • •				
1.20±0.55±0.65	[1] HE	14	BELL	$\Upsilon(5S) \to \pi^+\pi^-\pi^0\gamma\Upsilon(1S)$

[1] Accounting for correlated systematics.

$\Gamma(\eta_b(1S)\omega)/\Gamma_{total}$ — Γ_{38}/Γ

VALUE	CL%	DOCUMENT ID		TECN	COMMENT
$<1.3 \times 10^{-3}$	90	[1] OSKIN	20	BELL	$e^+e^- \to \omega X$

[1] Using $\sigma_{b\overline{b}} = 0.340 \pm 0.016$ nb from TAMPONI 15.

$\Gamma(\eta_b(2S)\omega)/\Gamma_{total}$ — Γ_{39}/Γ

VALUE	CL%	DOCUMENT ID		TECN	COMMENT
$<5.6 \times 10^{-3}$	90	[1] OSKIN	20	BELL	$e^+e^- \to \omega X$

[1] Using $\sigma_{b\overline{b}} = 0.340 \pm 0.016$ nb from TAMPONI 15.

$\Gamma(\gamma X_b \to \gamma\Upsilon(1S)\omega)/\Gamma_{total}$ — Γ_{37}/Γ

VALUE	CL%	DOCUMENT ID		TECN	COMMENT
$<3.8 \times 10^{-5}$	90	[1] HE	14	BELL	$\Upsilon(5S) \to \pi^+\pi^-\pi^0\gamma\Upsilon(1S)$

[1] Assuming that all the $b\overline{b}$ events are from $\Upsilon(5S)$ resonance decays and using $\sigma(e^+e^- \to b\overline{b}) = 0.340 \pm 0.016$ nb from ESEN 13. Correlated with other results from HE 14. For a state X_b with mass between 10.55 GeV/c^2 and 10.65 GeV/c^2, the obtained 90% upper limit as a function of m_{X_b} varies from 2.6×10^{-5} to 3.8×10^{-5}.

$\Gamma(\phi \text{ anything})/\Gamma_{total}$ — Γ_{40}/Γ

VALUE	DOCUMENT ID		TECN	COMMENT
$0.138 \pm 0.007^{+0.023}_{-0.015}$	HUANG	07	CLEO	$\Upsilon(5S) \to \phi X$

$\Gamma(D^0 \text{ anything} + \text{c.c.})/\Gamma_{total}$ — Γ_{41}/Γ

VALUE	DOCUMENT ID		TECN	COMMENT
1.076±0.040±0.068	DRUTSKOY	07	BELL	$\Upsilon(5S) \to D^0 X$

$\Gamma(D_s \text{ anything} + \text{c.c.})/\Gamma_{total}$ — Γ_{42}/Γ

VALUE	DOCUMENT ID		TECN	COMMENT
0.46 ±0.06 OUR AVERAGE				
0.472±0.024±0.072	[1] DRUTSKOY	07	BELL	$\Upsilon(5S) \to D_s X$
0.44 ±0.09 ±0.04	[2] ARTUSO	05B	CLE3	$e^+e^- \to D_X X$

[1] Using $B(D_s^+ \to \phi\pi^+) = (4.4 \pm 0.6)\%$ from PDG 06.

[2] ARTUSO 05B reports $[\Gamma(\Upsilon(10860) \to D_s \text{ anything} + \text{c.c.})/\Gamma_{total}] \times [B(D_s^+ \to \phi\pi^+)] = 0.0198 \pm 0.0019 \pm 0.0038$ which we divide by our best value $B(D_s^+ \to \phi\pi^+) = (4.5 \pm 0.4) \times 10^{-2}$. Our first error is their experiment's error and our second error is the systematic error from using our best value.

$\Gamma(J/\psi \text{ anything})/\Gamma_{total}$ — Γ_{43}/Γ

VALUE (units 10^{-2})	DOCUMENT ID		TECN	COMMENT
2.060±0.160±0.134	DRUTSKOY	07	BELL	$\Upsilon(5S) \to J/\psi X$

$\Gamma(B^0 \text{ anything} + \text{c.c.})/\Gamma_{total}$ — Γ_{44}/Γ

VALUE	EVTS	DOCUMENT ID		TECN	COMMENT
$0.770^{+0.058}_{-0.056} \pm 0.061$	352	DRUTSKOY	10	BELL	$\Upsilon(5S) \to B^0 X$

$\Gamma(B^+ \text{ anything} + \text{c.c.})/\Gamma_{total}$ — Γ_{45}/Γ

VALUE	EVTS	DOCUMENT ID		TECN	COMMENT
$0.721^{+0.039}_{-0.038} \pm 0.050$	711	DRUTSKOY	10	BELL	$\Upsilon(5S) \to B^+ X$

$\Upsilon(10860)$ REFERENCES

KOVALENKO	21	PR D104 112006	E. Kovalenko *et al.*	(BELLE Collab.)
DONG	20A	CP C44 083001	X.-K. Dong *et al.*	
OSKIN	20	PR D102 092011	P. Oskin *et al.*	(BELLE Collab.)
MIZUK	19	JHEP 1910 220	R. Mizuk *et al.*	(BELLE Collab.)
TAMPONI	18	EPJ C78 633	U. Tamponi *et al.*	(BELLE Collab.)
YIN	18	PR D98 091102	J.H. Yin *et al.*	(BELLE Collab.)
MIZUK	16	PRL 117 142001	R. Mizuk *et al.*	(BELLE Collab.)
SANTEL	16	PR D93 011101	D. Santel *et al.*	(BELLE Collab.)
TAMPONI	15	PRL 115 142001	U. Tamponi *et al.*	(BELLE Collab.)
HE	14	PRL 113 142001	X.H. He *et al.*	(BELLE Collab.)
ESEN	13	PR D87 031101	S. Esen *et al.*	(BELLE Collab.)
SHEN	13A	PR D88 052019	C.P. Shen *et al.*	(BELLE Collab.)
ADACHI	12	PRL 108 032001	I. Adachi *et al.*	(BELLE Collab.)
LI	12	PRL 108 181808	J. Li *et al.*	(BELLE Collab.)
CHEN	10	PR D82 091106	K.-F. Chen *et al.*	(BELLE Collab.)
DRUTSKOY	10	PR D81 112003	A. Drutskoy *et al.*	(BELLE Collab.)
AUBERT	09E	PRL 102 012001	B. Aubert *et al.*	(BABAR Collab.)
LOUVOT	09	PRL 102 021801	R. Louvot *et al.*	(BELLE Collab.)
CHEN	08	PRL 100 112001	K.-F. Chen *et al.*	(BELLE Collab.)
DRUTSKOY	07	PRL 98 052001	A. Drutskoy *et al.*	(BELLE Collab.)
DRUTSKOY	07A	PR D76 012002	A. Drutskoy *et al.*	(BELLE Collab.)
HUANG	07	PR D75 012002	G.S. Huang *et al.*	(CLEO Collab.)
AQUINES	06	PRL 96 152001	O. Aquines *et al.*	(CLEO Collab.)
BONVICINI	06	PRL 96 022002	G. Bonvicini *et al.*	(CLEO Collab.)
PDG	06	JP G33 1	W.-M. Yao *et al.*	(PDG Collab.)
ARTUSO	05B	PRL 95 261801	M. Artuso *et al.*	(CLEO Collab.)
BESSON	85	PRL 54 381	D. Besson *et al.*	(CLEO Collab.)
LOVELOCK	85	PRL 54 377	D.M.J. Lovelock *et al.*	(CUSB Collab.)

$\Upsilon(11020)$

$I^G(J^{PC}) = 0^-(1^{--})$

$\Upsilon(11020)$ MASS

VALUE (MeV)	DOCUMENT ID		TECN	COMMENT
11000 ± 4 OUR AVERAGE				
$11000.0^{+4.0}_{-4.5}{}^{+1.0}_{-1.3}$	[1] MIZUK	19	BELL	$e^+e^- \to \Upsilon(1S,2S,3S)\pi^+\pi^-$
$10999.0^{+7.3}_{-7.8}{}^{+16.9}_{-1.0}$	[2] MIZUK	16	BELL	$e^+e^- \to h_b(1P,2P)\pi^+\pi^-$
• • • We do not use the following data for averages, fits, limits, etc. • • •				
11001 ± 1	[3] DONG	20A		$e^+e^- \to b\overline{b}$
$11003.0 \pm 1.1^{+0.9}_{-1.0}$	[4,5] SANTEL	16	BELL	$e^+e^- \to$ hadrons
$10987.5^{+6.4}_{-2.5}{}^{+9.1}_{-2.3}$	[6,7] SANTEL	16	BELL	$e^+e^- \to \Upsilon(1S,2S,3S)\pi^+\pi^-$
10996 ± 2	[8] AUBERT	09E	BABR	$e^+e^- \to$ hadrons
11019 ± 5 ± 7	BESSON	85	CLEO	$e^+e^- \to$ hadrons
11020 ±30	LOVELOCK	85	CUSB	$e^+e^- \to$ hadrons

[1] From a simultaneous fit to the $\Upsilon(nS)\pi^+\pi^-$, n = 1, 2, 3, cross sections at 28 energy points within $\sqrt{s}$ = 10.6–11.05 GeV, including the initial-state radiation at $\Upsilon(10860)$.

[2] From a simultaneous fit to the $h_b(nP)\pi^+\pi^-$, n = 1, 2 cross sections at 22 energy points within $\sqrt{s}$ = 10.77–11.02 GeV to a pair of interfering Breit-Wigner amplitudes modified by phase space factors, with eight resonance parameters (a mass and width for each of $\Upsilon(10860)$ and $\Upsilon(11020)$, a single relative phase, a single relative amplitude, and two overall normalization factors, one for each n). The systematic error estimate is dominated by possible interference with a small nonresonant continuum amplitude.

[3] From a fit to the dressed cross sections of AUBERT 09E by BaBar and SANTEL 16 by Belle above 10.68 GeV with a coherent sum of a continuum amplitude and three Breit-Wigner functions with constant widths.

[4] From a fit to the total hadronic cross sections measured at 60 energy points within $\sqrt{s}$ = 10.82–11.05 GeV to a pair of interfering Breit-Wigner amplitudes and two floating continuum amplitudes with $1/\sqrt{s}$ dependence, one coherent with the resonances and one incoherent, with six resonance parameters (a mass, width, and an amplitude for each of $\Upsilon(10860)$ and $\Upsilon(11020)$, one relative phase, and one decoherence coefficient).

[5] Not including uncertain and potentially large systematic errors due to assumed continuum amplitude $1/\sqrt{s}$ dependence and related interference contributions.

[6] From a simultaneous fit to the $\Upsilon(nS)\pi^+\pi^-$, n = 1, 2, 3, cross sections at 25energy points within $\sqrt{s}$ = 10.6–11.05 GeV to a pair of interfering Breit-Wigner amplitudesmodified by phase space factors, with fourteen resonance parameters (a mass, width, and threeamplitudes for each of $\Upsilon(10860)$ and $\Upsilon(11020)$, a single universal relativephase, and three decoherence coefficients, one for each n). Continuum contributions weremeasured (and therefore fixed) to be zero.

[7] Superseded by MIZUK 19.

[8] In a model where a flat non-resonant $b\overline{b}$-continuum is incoherently added to a second flat component interfering with two Breit-Wigner resonances. Systematic uncertainties not estimated.

$\Upsilon(11020)$ WIDTH

VALUE (MeV)	DOCUMENT ID		TECN	COMMENT
24^{+8}_{-6} OUR AVERAGE				
$23.8^{+8.0}_{-6.8}{}^{+0.7}_{-1.8}$	[1] MIZUK	19	BELL	$e^+e^- \to \Upsilon(nS)\pi^+\pi^-$
$27^{+27}_{-11}{}^{+5}_{-12}$	[2] MIZUK	16	BELL	$e^+e^- \to h_b(1P,2P)\pi^+\pi^-$

Downloaded from https://academic.oup.com/ptep/article/2022/8/083C01/6651666 by KIT Library user on 27 September 2022

• • • We do not use the following data for averages, fits, limits, etc. • • •

35.1 ± 1.2	[3] DONG	20A		$e^+e^- \to b\overline{b}$
$39.3^{+1.7}_{-1.6}{}^{+1.3}_{-2.4}$	[4,5] SANTEL	16	BELL	$e^+e^- \to$ hadrons
$61^{+9}_{-19}{}^{+2}_{-20}$	[6,7] SANTEL	16	BELL	$e^+e^- \to \Upsilon(1S,2S,3S)\pi^+\pi^-$
37 ± 3	[8] AUBERT	09E	BABR	$e^+e^- \to$ hadrons
$61 \pm 13 \pm 22$	BESSON	85	CLEO	$e^+e^- \to$ hadrons
90 ± 20	LOVELOCK	85	CUSB	$e^+e^- \to$ hadrons

[1] From a simultaneous fit to the $\Upsilon(nS)\pi^+\pi^-$, $n = 1, 2, 3$, cross sections at 28 energy points within $\sqrt{s} = 10.6$–11.05 GeV, including the initial-state radiation at $\Upsilon(10860)$.

[2] From a simultaneous fit to the $h_b(nP)\pi^+\pi^-$, $n = 1, 2$ cross sections at 22 energy points within $\sqrt{s} = 10.77$–11.02 GeV to a pair of interfering Breit-Wigner amplitudes modified by phase space factors, with eight resonance parameters (a mass and width for each of $\Upsilon(10860)$ and $\Upsilon(11020)$, a single relative phase, a single relative amplitude, and two overall normalization factors, one for each n). The systematic error estimate is dominated by possible interference with a small nonresonant continuum amplitude.

[3] From a fit to the dressed cross sections of AUBERT 09E by BaBar and SANTEL 16 by Belle above 10.68 GeV with a coherent sum of a continuum amplitude and three Breit-Wigner functions with constant widths.

[4] From a fit to the total hadronic cross sections measured at 60 energy points within $\sqrt{s} = 10.82$–11.05 GeV to a pair of interfering Breit-Wigner amplitudes and two floating continuum amplitudes with $1/\sqrt{s}$ dependence, one coherent with the resonances and one incoherent, with six resonance parameters (a mass, width, and an amplitude for each of $\Upsilon(10860)$ and $\Upsilon(11020)$, one relative phase, and one decoherence coefficient).

[5] Not including uncertain and potentially large systematic errors due to assumed continuum amplitude $1/\sqrt{s}$ dependence and related interference contributions.

[6] From a simultaneous fit to the $\Upsilon(nS)\pi^+\pi^-$, n=1, 2, 3, cross sections at 25energy points within $\sqrt{s} = 10.6$–11.05 GeV to a pair of interfering Breit-Wigner amplitudesmodified by phase space factors, with fourteen resonance parameters (a mass, width, and threeamplitudes for each of $\Upsilon(10860)$ and $\Upsilon(11020)$, a single universal relativephase, and three decoherence coefficients, one for each n). Continuum contributions weremeasured (and therefore fixed) to be zero.

[7] Superseded by MIZUK 19.

[8] In a model where a flat non-resonant $b\overline{b}$-continuum is incoherently added to a second flat component interfering with two Breit-Wigner resonances. Systematic uncertainties not estimated.

$\Upsilon(11020)$ DECAY MODES

	Mode	Fraction (Γ_i/Γ)
Γ_1	e^+e^-	$(5.4^{+1.9}_{-2.1}) \times 10^{-6}$
Γ_2	$\Upsilon(1S)\pi^+\pi^-$	
Γ_3	$\Upsilon(2S)\pi^+\pi^-$	
Γ_4	$\Upsilon(3S)\pi^+\pi^-$	
Γ_5	$\chi_{bJ}(1P)\pi^+\pi^-\pi^0$	$(9^{+9}_{-8}) \times 10^{-3}$
Γ_6	$\chi_{b1}(1P)\pi^+\pi^-\pi^0$	seen
Γ_7	$\chi_{b2}(1P)\pi^+\pi^-\pi^0$	seen

$\Upsilon(11020)$ PARTIAL WIDTHS

$\Gamma(e^+e^-)$ — Γ_1

VALUE (keV)	DOCUMENT ID		TECN	COMMENT
0.130±0.030 OUR AVERAGE				
$0.095 \pm 0.03 \pm 0.035$	BESSON	85	CLEO	$e^+e^- \to$ hadrons
0.156 ± 0.040	LOVELOCK	85	CUSB	$e^+e^- \to$ hadrons

$\Gamma(e^+e^-) \times \Gamma(\Upsilon(1S)\pi^+\pi^-)/\Gamma_{total}$ — $\Gamma_1\Gamma_2/\Gamma$

VALUE (eV)	DOCUMENT ID		TECN	COMMENT
• • • We do not use the following data for averages, fits, limits, etc. • • •				
0.46 ± 0.08	[1,2] MIZUK	19	BELL	$e^+e^- \to \Upsilon(nS)\pi^+\pi^-$

[1] From a simultaneous fit to the $\Upsilon(nS)\pi^+\pi^-$, $n = 1, 2, 3$, cross sections at 28 energy points within $\sqrt{s} = 10.6$–11.05 GeV, including the initial-state radiation at $\Upsilon(10860)$.

[2] Reported as the range 0.38–0.54 eV obtained from multiple solutions of an amplitude fit within a model composed as a sum of Breit-Wigner functions.

$\Gamma(e^+e^-) \times \Gamma(\Upsilon(2S)\pi^+\pi^-)/\Gamma_{total}$ — $\Gamma_1\Gamma_3/\Gamma$

VALUE (eV)	DOCUMENT ID		TECN	COMMENT
• • • We do not use the following data for averages, fits, limits, etc. • • •				
0.65 ± 0.52	[1,2] MIZUK	19	BELL	$e^+e^- \to \Upsilon(nS)\pi^+\pi^-$

[1] From a simultaneous fit to the $\Upsilon(nS)\pi^+\pi^-$, $n = 1, 2, 3$, cross sections at 28 energy points within $\sqrt{s} = 10.6$–11.05 GeV, including the initial-state radiation at $\Upsilon(10860)$.

[2] Reported as the range 0.13–1.16 eV obtained from multiple solutions of an amplitude fit within a model composed as a sum of Breit-Wigner functions.

$\Gamma(e^+e^-) \times \Gamma(\Upsilon(3S)\pi^+\pi^-)/\Gamma_{total}$ — $\Gamma_1\Gamma_4/\Gamma$

VALUE (eV)	DOCUMENT ID		TECN	COMMENT
• • • We do not use the following data for averages, fits, limits, etc. • • •				
0.33 ± 0.16	[1,2] MIZUK	19	BELL	$e^+e^- \to \Upsilon(nS)\pi^+\pi^-$

[1] From a simultaneous fit to the $\Upsilon(nS)\pi^+\pi^-$, $n = 1, 2, 3$, cross sections at 28 energy points within $\sqrt{s} = 10.6$–11.05 GeV, including the initial-state radiation at $\Upsilon(10860)$.

[2] Reported as the range 0.17–0.49 eV obtained from multiple solutions of an amplitude fit within a model composed as a sum of Breit-Wigner functions.

$\Gamma(\chi_{bJ}(1P)\pi^+\pi^-\pi^0)/\Gamma_{total}$ — Γ_5/Γ

VALUE (units 10^{-3})	DOCUMENT ID		TECN	COMMENT
$\mathbf{8.7 \pm 4.3^{+7.6}_{-6.6}}$	YIN	18	BELL	$e^+e^- \to$ hadrons

$\Gamma(\chi_{b1}(1P)\pi^+\pi^-\pi^0)/\Gamma_{total}$ — Γ_6/Γ

VALUE	DOCUMENT ID		TECN	COMMENT
seen	YIN	18	BELL	$e^+e^- \to$ hadrons

$\Gamma(\chi_{b2}(1P)\pi^+\pi^-\pi^0)/\Gamma_{total}$ — Γ_7/Γ

VALUE	DOCUMENT ID		TECN	COMMENT
seen	YIN	18	BELL	$e^+e^- \to$ hadrons

$\Gamma(\chi_{b2}(1P)\pi^+\pi^-\pi^0)/\Gamma(\chi_{b1}(1P)\pi^+\pi^-\pi^0)$ — Γ_7/Γ_6

VALUE	DOCUMENT ID		TECN	COMMENT
0.4±0.2	YIN	18	BELL	$e^+e^- \to$ hadrons

$\Upsilon(11020)$ REFERENCES

DONG	20A	CP C44 083001	X.-K. Dong *et al.*	
MIZUK	19	JHEP 1910 220	R. Mizuk *et al.*	(BELLE Collab.)
YIN	18	PR D98 091102	J.H. Yin *et al.*	(BELLE Collab.)
MIZUK	16	PRL 117 142001	R. Mizuk *et al.*	(BELLE Collab.)
SANTEL	16	PR D93 011101	D. Santel *et al.*	(BELLE Collab.)
AUBERT	09E	PRL 102 012001	B. Aubert *et al.*	(BABAR Collab.)
BESSON	85	PRL 54 381	D. Besson *et al.*	(CLEO Collab.)
LOVELOCK	85	PRL 54 377	D.M.J. Lovelock *et al.*	(CUSB Collab.)

Downloaded from https://academic.oup.com/ptep/article/2022/8/083C01/6651666 by KIT Library user on 27 September 2022

OTHER MESONS

Further States

OMITTED FROM SUMMARY TABLE

This section contains states observed by a single group or states poorly established that thus need confirmation.

QUANTUM NUMBERS, MASSES, WIDTHS, AND BRANCHING RATIOS

X(360) $I^G(J^{PC}) = ?^?(?^{?+})$

MASS (MeV)	WIDTH (MeV)	EVTS	DOCUMENT ID	TECN	COMMENT
$360 \pm 7 \pm 9$	64 ± 18	2.3k	[1] ABRAAMYAN 09	CNTR	2.75 $dC \to \gamma\gamma X$

[1] Not seen in $pC \to \gamma\gamma X$ at 5.5 GeV/c.

X(1070) $I^G(J^{PC}) = ?^?(0^{++})$

MASS (MeV)	WIDTH (MeV)	DOCUMENT ID	COMMENT
1072 ± 1	3.5 ± 0.5	[1] VLADIMIRSK...08	40 $\pi^- p \to K^0_S K^0_S n + m\pi^0$

[1] Supersedes GRIGOR'EV 05.

X(1110) $I^G(J^{PC}) = 0^+(\text{even}^{++})$

MASS (MeV)	WIDTH (MeV)	DOCUMENT ID		TECN	COMMENT
1107 ± 4	$111 \pm 8 \pm 15$	DAFTARI	87	DBC	0. $\overline{p} n \to \rho^- \pi^+ \pi^-$

f_0(1200–1600) $I^G(J^{PC}) = 0^+(0^{++})$

MASS (MeV)	WIDTH (MeV)	DOCUMENT ID		TECN	COMMENT
1323 ± 8	237 ± 20	VLADIMIRSK...06		SPEC	40 $\pi^- p \to K^0_S K^0_S n$
1480^{+100}_{-150}	1030^{+80}_{-170}	[1] ANISOVICH	03	SPEC	
1530^{+90}_{-250}	560 ± 40	[2] ANISOVICH	03	SPEC	

[1] K-matrix pole from combined analysis of $\pi^- p \to \pi^0 \pi^0 n$, $\pi^- p \to K\overline{K} n$, $\pi^+ \pi^- \to \pi^+ \pi^-$, $\overline{p} p \to \pi^0 \pi^0 \pi^0$, $\pi^0 \eta\eta$, $\pi^0 \pi^0 \eta$, $\pi^+ \pi^- \pi^0$, $K^+ K^- \pi^0$, $K^0_S K^0_S \pi^0$, $K^+ K^0_S \pi^-$ at rest, $\overline{p} n \to \pi^- \pi^- \pi^+$, $K^0_S K^- \pi^0$, $K^0_S K^0_S \pi^-$ at rest.

[2] K-matrix pole from combined analysis of $\pi^- p \to \pi^0 \pi^0 n$, $\pi^- p \to K\overline{K} n$, $\overline{p} p \to \pi^0 \pi^0 \pi^0$, $\pi^0 \eta\eta$, $\pi^0 \pi^0 \eta$ at rest.

X(1420) $I^G(J^{PC}) = 2^+(0^{++})$

MASS (MeV)	WIDTH (MeV)	DOCUMENT ID		TECN	COMMENT
1420 ± 20	160 ± 10	FILIPPI	00	OBLX	0 $\overline{n} p \to \pi^+ \pi^+ \pi^-$

X(1545) $I^G(J^{PC}) = ?^?(?^{++})$

MASS (MeV)	WIDTH (MeV)	DOCUMENT ID	COMMENT
1545 ± 3	6.0 ± 2.5	[1] VLADIMIRSK...08	40 $\pi^- p \to K^0_S K^0_S n + m\pi^0$

[1] Supersedes VLADIMIRSKII 00.

X(1575) $I^G(J^{PC}) = ?^?(1^{--})$

MASS (MeV)	WIDTH (MeV)	DOCUMENT ID		TECN	COMMENT
$1576^{+49}_{-55}{}^{+98}_{-91}$	$818^{+22}_{-23}{}^{+64}_{-133}$	[1] ABLIKIM	06S	BES	$J/\psi \to K^+ K^- \pi^0$

[1] A broad peak observed at $K^+ K^-$ invariant mass. Mass and width above are its pole position. The observed branching ratio is $B(J/\psi \to X\pi^0)\, B(X \to K^+ K^-) = (8.5 \pm 0.6^{+2.7}_{-3.6}) \times 10^{-4}$.

X(1600) $I^G(J^{PC}) = 2^+(2^{++})$

MASS (MeV)	WIDTH (MeV)	DOCUMENT ID		TECN	COMMENT
1600 ± 100	400 ± 200	[1] ALBRECHT	91F	ARG	10.2 $e^+ e^- \to e^+ e^- 2(\pi^+ \pi^-)$

[1] Our estimate.

X(1650) $I^G(J^{PC}) = 0^-(?^{?-})$

MASS (MeV)	WIDTH (MeV)	EVTS	DOCUMENT ID		TECN	COMMENT
1652 ± 7	<50	100	PROKOSHKIN	96	GAM2	32,38 $\pi p \to \omega\eta n$

a_0(1700) $I^G(J^{PC}) = 1^-(0^{++})$

MASS (MeV)	WIDTH (MeV)	DOCUMENT ID		COMMENT
$1704 \pm 5 \pm 2$	$110 \pm 15 \pm 11$	LEES	21A	$\eta_c(1S) \to \pi^+ \pi^- \eta$

X(1730) $I^G(J^{PC}) = ?^?(?^{?+})$

MASS (MeV)	WIDTH (MeV)	EVTS	DOCUMENT ID	TECN	COMMENT
$1731.0 \pm 1.2 \pm 2.0$	$3.2 \pm 0.8 \pm 1.3$	58	VLADIMIRSK...07	SPEC	40 $\pi^- p \to K^0_S K^0_S X$

f_2(1750) $I^G(J^{PC}) = 0^+(2^{++})$

MASS (MeV)	WIDTH (MeV)	EVTS	DOCUMENT ID		TECN	COMMENT
1755 ± 10	67 ± 12	870	[1] SCHEGELSKY	06A	RVUE	$\gamma\gamma \to K^0_S K^0_S$

$\Gamma(K\overline{K})$

VALUE (MeV)	EVTS	DOCUMENT ID		TECN	COMMENT
17 ± 5	870	[2] SCHEGELSKY	06A	RVUE	$\gamma\gamma \to K^0_S K^0_S$

$\Gamma(\gamma\gamma)$

VALUE (keV)	EVTS	DOCUMENT ID		TECN	COMMENT
0.13 ± 0.04	870	[2] SCHEGELSKY	06A	RVUE	$\gamma\gamma \to K^0_S K^0_S$

$\Gamma(\pi\pi)$

VALUE (MeV)	EVTS	DOCUMENT ID		TECN	COMMENT
1.3 ± 1.0	870	[2] SCHEGELSKY	06A	RVUE	$\gamma\gamma \to K^0_S K^0_S$

$\Gamma(\eta\eta)$

VALUE (MeV)	EVTS	DOCUMENT ID		TECN	COMMENT
2.0 ± 0.5	870	[2] SCHEGELSKY	06A	RVUE	$\gamma\gamma \to K^0_S K^0_S$

[1] From analysis of L3 data at 91 and 183–209 GeV.
[2] From analysis of L3 data at 91 and 183–209 GeV and using SU(3) relations.

X(1775) $I^G(J^{PC}) = 1^-(?^{-+})$

MASS (MeV)	WIDTH (MeV)	DOCUMENT ID		TECN	COMMENT
1763 ± 20	192 ± 60	CONDO	91	SHF	$\gamma p \to (p\pi^+)(\pi^+ \pi^- \pi^-)$
1787 ± 18	118 ± 60	CONDO	91	SHF	$\gamma p \to n\pi^+ \pi^+ \pi^-$

X(1850 - 3100) $I^G(J^{PC}) = ?^?(1^{--})$

$\Gamma(e^+e^-)\cdot B(X \to \text{hadrons})$ (eV)	CL%	DOCUMENT ID		TECN	COMMENT
<120	90	[1] ANASHIN	11	KEDR	$e^+ e^- \to$ hadrons

[1] This limit is center-of-mass energy dependent. We quote the most stringent one.

X(1855) $I^G(J^{PC}) = ?^?(?^{??})$

MASS (MeV)	WIDTH (MeV)	DOCUMENT ID		TECN	COMMENT
1856.6 ± 5	20 ± 5	BRIDGES	86D	SPEC	0. $\overline{p} d \to \pi\pi N$

X(1870) $I^G(J^{PC}) = ?^?(2^{??})$

MASS (MeV)	WIDTH (MeV)	DOCUMENT ID		TECN	COMMENT
1870 ± 40	250 ± 30	ALDE	86D	GAM4	100 $\pi^- p \to 2\eta X$

a_3(1875) $I^G(J^{PC}) = 1^-(3^{++})$

MASS (MeV)	WIDTH (MeV)	DOCUMENT ID		TECN	COMMENT
$1874 \pm 43 \pm 96$	$385 \pm 121 \pm 114$	CHUNG	02	B852	18.3 $\pi^- p \to \pi^+ \pi^- \pi^- p$

$B(a_3(1875) \to f_2(1270)\pi)/B(a_3(1875) \to \rho\pi)$

VALUE	DOCUMENT ID		TECN	COMMENT
0.8 ± 0.2	[1] CHUNG	02	B852	18.3 $\pi^- p \to \pi^+ \pi^- \pi^- p$

[1] Using the observable fractions of 50.0% $\rho\pi$, 56.5% $f_2\pi$, and 11.8% $\rho_3\pi$.

$B(a_3(1875) \to \rho_3(1690)\pi)/B(a_3(1875) \to \rho\pi)$

VALUE	DOCUMENT ID		TECN	COMMENT
0.9 ± 0.3	[1] CHUNG	02	B852	18.3 $\pi^- p \to \pi^+ \pi^- \pi^- p$

[1] Using the observable fractions of 50.0% $\rho\pi$, 56.5% $f_2\pi$, and 11.8% $\rho_3\pi$.

a_1(1930) $I^G(J^{PC}) = 1^-(1^{++})$

MASS (MeV)	WIDTH (MeV)	DOCUMENT ID		TECN	COMMENT
1930^{+30}_{-70}	155 ± 45	ANISOVICH	01F	SPEC	2.0 $\overline{p} p \to 3\pi^0, \pi^0 \eta, \pi^0 \eta'$

X(1935) $I^G(J^{PC}) = 1^+(1^{-?})$

MASS (MeV)	WIDTH (MeV)	DOCUMENT ID		TECN	COMMENT
1935 ± 20	215 ± 30	EVANGELIS...	79	OMEG	10,16 $\pi^- p \to \overline{p} p n$

ρ_2(1940) $I^G(J^{PC}) = 1^+(2^{--})$

MASS (MeV)	WIDTH (MeV)	DOCUMENT ID		TECN	COMMENT
1940 ± 40	155 ± 40	[1] ANISOVICH	02	SPEC	0.6–1.9 $p\overline{p} \to \omega\pi^0, \omega\eta\pi^0, \pi^+ \pi^-$

[1] From the combined analysis of ANISOVICH 00J, ANISOVICH 01D, ANISOVICH 01E, and ANISOVICH 02.

Downloaded from https://academic.oup.com/ptep/article/2022/8/083C01/6651666 by KIT Library user on 27 September 2022

$\omega_3(1945)$ $I^G(J^{PC}) = 0^-(3^{--})$

MASS (MeV)	WIDTH (MeV)	DOCUMENT ID		TECN	COMMENT
1945 ± 20	115 ± 22	[1] ANISOVICH	02B	SPEC	0.6–1.9 $p\overline{p} \to \omega\eta, \omega\pi^0\pi^0$

[1] From the combined analysis of ANISOVICH 00D, ANISOVICH 01C, and ANISOVICH 02B.

$a_2(1950)$ $I^G(J^{PC}) = 1^-(2^{++})$

MASS (MeV)	WIDTH (MeV)	DOCUMENT ID		TECN	COMMENT
1950^{+30}_{-70}	180^{+30}_{-70}	[1] ANISOVICH	01F	SPEC	1.96–2.41 $\overline{p}p$

[1] From the combined analysis of ANISOVICH 99C, ANISOVICH 99E, and ANISOVICH 01F.

$\omega(1960)$ $I^G(J^{PC}) = 0^-(1^{--})$

MASS (MeV)	WIDTH (MeV)	DOCUMENT ID		TECN	COMMENT
1960 ± 25	195 ± 60	[1] ANISOVICH	02B	SPEC	0.6–1.9 $p\overline{p} \to \omega\eta, \omega\pi^0\pi^0$

[1] From the combined analysis of ANISOVICH 00D, ANISOVICH 01C, and ANISOVICH 02B.

$b_1(1960)$ $I^G(J^{PC}) = 1^+(1^{+-})$

MASS (MeV)	WIDTH (MeV)	DOCUMENT ID		TECN	COMMENT
1960 ± 35	230 ± 50	[1] ANISOVICH	02	SPEC	0.6–1.9 $p\overline{p} \to \omega\pi^0$, $\omega\eta\pi^0$, $\pi^+\pi^-$

[1] From the combined analysis of ANISOVICH 00J, ANISOVICH 01D, ANISOVICH 01E, and ANISOVICH 02.

$h_1(1965)$ $I^G(J^{PC}) = 0^-(1^{+-})$

MASS (MeV)	WIDTH (MeV)	DOCUMENT ID		TECN	COMMENT
1965 ± 45	345 ± 75	[1] ANISOVICH	02B	SPEC	0.6–1.9 $p\overline{p} \to \omega\eta, \omega\pi^0\pi^0$

[1] From the combined analysis of ANISOVICH 00D, ANISOVICH 01C, and ANISOVICH 02B.

$f_1(1970)$ $I^G(J^{PC}) = 0^+(1^{++})$

MASS (MeV)	WIDTH (MeV)	DOCUMENT ID		TECN
1971 ± 15	240 ± 45	ANISOVICH	00J	SPEC

$X(1970)$ $I^G(J^{PC}) = ?^?(?^{??})$

MASS (MeV)	WIDTH (MeV)	DOCUMENT ID		TECN	COMMENT
1970 ± 10	40 ± 20	CHLIAPNIK...	80	HBC	32 $K^+p \to 2K^0_S 2\pi X$

$X(1975)$ $I^G(J^{PC}) = ?^?(?^{??})$

MASS (MeV)	WIDTH (MeV)	EVTS	DOCUMENT ID		TECN	COMMENT
1973 ± 15	80	30	CASO	70	HBC	11.2 $\pi^-p \to \rho 2\pi$

$\omega_2(1975)$ $I^G(J^{PC}) = 0^-(2^{--})$

MASS (MeV)	WIDTH (MeV)	DOCUMENT ID		TECN	COMMENT
1975 ± 20	175 ± 25	[1] ANISOVICH	02B	SPEC	0.6–1.9 $p\overline{p} \to \omega\eta, \omega\pi^0\pi^0$

[1] From the combined analysis of ANISOVICH 00D, ANISOVICH 01C, and ANISOVICH 02B.

$a_2(1990)$ $I^G(J^{PC}) = 1^-(2^{++})$

MASS (MeV)	WIDTH (MeV)	EVTS	DOCUMENT ID		TECN	COMMENT
2050 ± 10 ± 40	190 ± 22 ± 100	18k	[1] SCHEGELSKY	06	RVUE	$\gamma\gamma \to \pi^+\pi^-\pi^0$
2003 ± 10 ± 19	249 ± 23 ± 32		LU	05	B852	18 $\pi^-p \to \omega\pi^-\pi^0 p$

[1] From analysis of L3 data at 183–209 GeV.

$\Gamma(\gamma\gamma)\ \Gamma(\pi^+\pi^-\pi^0)\ /\ \Gamma(\text{total})$

VALUE (keV)	EVTS	DOCUMENT ID		TECN	COMMENT
0.11 ± 0.04 ± 0.05	18k	[1] SCHEGELSKY	06	RVUE	$\gamma\gamma \to \pi^+\pi^-\pi^0$

[1] From analysis of L3 data at 183–209 GeV.

$\rho(2000)$ $I^G(J^{PC}) = 1^+(1^{--})$

MASS (MeV)	WIDTH (MeV)	DOCUMENT ID		TECN	COMMENT
2000 ± 30	260 ± 45	[1] BUGG	04C	RVUE	Compilation
∼ 1988	∼ 244	HASAN	94	RVUE	$\overline{p}p \to \pi\pi$

[1] From the combined analysis of ANISOVICH 00J, ANISOVICH 01D, ANISOVICH 01E, and ANISOVICH 02.

$f_2(2000)$ $I^G(J^{PC}) = 0^+(2^{++})$

MASS (MeV)	WIDTH (MeV)	DOCUMENT ID		TECN	COMMENT
2001 ± 10	312 ± 32	ANISOVICH	00J	SPEC	
∼ 1996	∼ 134	HASAN	94	RVUE	$\overline{p}p \to \pi\pi$

$X(2000)$ $I^G(J^{PC}) = 1^-(?^{?+})$

MASS (MeV)	WIDTH (MeV)	DOCUMENT ID		TECN	CHG	COMMENT
1964 ± 35	225 ± 50	[1] ARMSTRONG	93D	E760		$\overline{p}p \to 3\pi^0 \to 6\gamma$
∼ 2100	∼ 500	[1] ANTIPOV	77	CIBS	−	25 $\pi^-p \to p\pi^-\rho_3$
2214 ± 15	355 ± 21	[2] BALTAY	77	HBC	0	15 $\pi^-p \to \Delta^{++}3\pi$
2080 ± 40	340 ± 80	KALELKAR	75	HBC	+	15 $\pi^+p \to p\pi^+\rho_3$

[1] Cannot determine spin to be 3.
[2] BALTAY 77 favors $J^P = ,3^+$.

$X(2000)$ $I^G(J^{PC}) = ?^?(4^{++})$

MASS (MeV)	WIDTH (MeV)	DOCUMENT ID		TECN	COMMENT
1998 ± 3 ± 5	<15	VLADIMIRSK...	03	SPEC	$\pi^-p \to K^0_S K^0_S MM$

$\eta(2010)$ $I^G(J^{PC}) = 0^+(0^{-+})$

MASS (MeV)	WIDTH (MeV)	DOCUMENT ID		TECN
2010^{+35}_{-60}	270 ± 60	ANISOVICH	00J	SPEC

$\pi_1(2015)$ $I^G(J^{PC}) = 1^-(1^{-+})$

MASS (MeV)	WIDTH (MeV)	EVTS	DOCUMENT ID		TECN	COMMENT
2014 ± 20 ± 16	230 ± 32 ± 73	145k	LU	05	B852	18 $\pi^-p \to \omega\pi^-\pi^0 p$
2001 ± 30 ± 92	333 ± 52 ± 49	69k	KUHN	04	B852	18 $\pi^-p \to \eta\pi^+\pi^-\pi^-p$

$a_0(2020)$ $I^G(J^{PC}) = 1^-(0^{++})$

MASS (MeV)	WIDTH (MeV)	DOCUMENT ID		TECN
2025 ± 30	330 ± 75	ANISOVICH	99C	SPEC

$X(2020)$ $I^G(J^{PC}) = ?^?(?^{??})$

MASS (MeV)	WIDTH (MeV)	DOCUMENT ID		TECN	COMMENT
2015 ± 3	10 ± 4	FERRER	99	RVUE	$\pi p \to pp\overline{p}\pi(\pi)$

$h_3(2025)$ $I^G(J^{PC}) = 0^-(3^{+-})$

MASS (MeV)	WIDTH (MeV)	DOCUMENT ID		TECN	COMMENT
2025 ± 20	145 ± 30	[1] ANISOVICH	02B	SPEC	0.6–1.9 $p\overline{p} \to \omega\eta, \omega\pi^0\pi^0$

[1] From the combined analysis of ANISOVICH 00D, ANISOVICH 01C, and ANISOVICH 02B.

$b_3(2030)$ $I^G(J^{PC}) = 1^+(3^{+-})$

MASS (MeV)	WIDTH (MeV)	DOCUMENT ID		TECN	COMMENT
2032 ± 12	117 ± 11	[1] ANISOVICH	02	SPEC	0.6–1.9 $p\overline{p} \to \omega\pi^0$, $\omega\eta\pi^0$, $\pi^+\pi^-$

[1] From the combined analysis of ANISOVICH 00J, ANISOVICH 01D, ANISOVICH 01E, and ANISOVICH 02.

$a_2(2030)$ $I^G(J^{PC}) = 1^-(2^{++})$

MASS (MeV)	WIDTH (MeV)	DOCUMENT ID		TECN	COMMENT
2030 ± 20	205 ± 30	[1] ANISOVICH	01F	SPEC	1.96–2.41 $\overline{p}p$

[1] From the combined analysis of ANISOVICH 99C, ANISOVICH 99E, and ANISOVICH 01F.

$a_3(2030)$ $I^G(J^{PC}) = 1^-(3^{++})$

MASS (MeV)	WIDTH (MeV)	DOCUMENT ID		TECN	COMMENT
2031 ± 12	150 ± 18	[1] ANISOVICH	01F	SPEC	1.96–2.41 $\overline{p}p$

[1] From the combined analysis of ANISOVICH 99C, ANISOVICH 99E, and ANISOVICH 01F.

$\eta_2(2030)$ $I^G(J^{PC}) = 0^+(2^{-+})$

MASS (MeV)	WIDTH (MeV)	DOCUMENT ID		TECN
2030 ± 5 ± 15	205 ± 10 ± 15	ANISOVICH	00E	SPEC

$B(a_2\pi)_{L=0}/B(a_2\pi)_{L=2}$

VALUE	DOCUMENT ID		TECN	COMMENT
0.05 ± 0.03	[1] ANISOVICH	11	SPEC	0.9–1.94 $p\overline{p}$

[1] Reanalysis of ADOMEIT 96 and ANISOVICH 00E.

$B(a_0\pi)/B(a_2\pi)_{L=2}$

VALUE	DOCUMENT ID		TECN	COMMENT
0.10 ± 0.08	[1] ANISOVICH	11	SPEC	0.9–1.94 $p\overline{p}$

[1] Reanalysis of ADOMEIT 96 and ANISOVICH 00E.

$B(f_2\eta)/B(a_2\pi)_{L=2}$

VALUE	DOCUMENT ID		TECN	COMMENT
0.13 ± 0.06	[1] ANISOVICH	11	SPEC	0.9–1.94 $p\overline{p}$

[1] Reanalysis of ADOMEIT 96 and ANISOVICH 00E.

Downloaded from https://academic.oup.com/ptep/article/2022/8/083C01/6651666 by KIT Library user on 27 September 2022

$f_3(2050)$ $I^G(J^{PC}) = 0^+(3^{++})$

MASS (MeV)	WIDTH (MeV)	DOCUMENT ID		TECN	COMMENT
2048±8	213 ± 34	ANISOVICH	00J	SPEC	2.0 $p\overline{p} \to \eta\pi^0\pi^0$

$f_0(2060)$ $I^G(J^{PC}) = 0^+(0^{++})$

MASS (MeV)	WIDTH (MeV)	DOCUMENT ID		TECN	COMMENT
~ 2050	~ 120	[1] OAKDEN	94	RVUE	0.36–1.55 $\overline{p}p \to \pi\pi$
~ 2060	~ 50	[1] OAKDEN	94	RVUE	0.36–1.55 $\overline{p}p \to \pi\pi$

[1] See SEMENOV 99 and KLOET 96.

$\pi(2070)$ $I^G(J^{PC}) = 1^-(0^{-+})$

MASS (MeV)	WIDTH (MeV)	DOCUMENT ID		TECN	COMMENT
2070±35	310^{+100}_{-50}	ANISOVICH	01F	SPEC	2.0 $\overline{p}p \to 3\pi^0, \pi^0\eta, \pi^0\eta'$

$X(2075)$ $I^G(J^{PC}) = ?^?(?^{??})$

MASS (MeV)	WIDTH (MeV)	DOCUMENT ID		TECN	COMMENT
2075±12±5	90 ± 35 ± 9	[1] ABLIKIM	04J	BES2	$J/\psi \to K^- p\overline{\Lambda}$

[1] From a fit in the region $M_{p\overline{\Lambda}} - M_p - M_\Lambda < 150$ MeV. S-wave in the $p\overline{\Lambda}$ system preferred.
A similar near-threshold enhancement in the $p\overline{\Lambda}$ system is observed in $B^+ \to p\overline{\Lambda}D^0$ by CHEN 11F.

$X(2080)$ $I^G(J^{PC}) = ?^?(?^{??})$

MASS (MeV)	WIDTH (MeV)	DOCUMENT ID		TECN	COMMENT
2080±10	110 ± 20	KREYMER	80	STRC	13 $\pi^- d \to p\overline{p}n(n_s)$

$X(2080)$ $I^G(J^{PC}) = ?^?(3^{-?})$

MASS (MeV)	WIDTH (MeV)	DOCUMENT ID		TECN	COMMENT
2080±10	190 ± 15	ROZANSKA	80	SPRK	18 $\pi^- p \to p\overline{p}n$

$a_1(2095)$ $I^G(J^{PC}) = 1^-(1^{++})$

MASS (MeV)	WIDTH (MeV)	EVTS	DOCUMENT ID		TECN	COMMENT
2096±17±121	451 ± 41 ± 81	69k	KUHN	04	B852	18 $\pi^- p \to \eta\pi^+\pi^-\pi^- p$

$B(a_1(2095) \to f_1(1285)\pi) / B(a_1(2095) \to a_1(1260))$

VALUE	EVTS	DOCUMENT ID		TECN	COMMENT
3.18±0.64	69k	KUHN	04	B852	18 $\pi^- p \to \eta\pi^+\pi^-\pi^- p$

$\eta(2100)$ $I^G(J^{PC}) = 0^+(0^{-+})$

MASS (MeV)	WIDTH (MeV)	EVTS	DOCUMENT ID		TECN	COMMENT
2050^{+30+75}_{-24-26}	$250^{+36+181}_{-30-164}$		[1] ABLIKIM	16N	BES3	$J/\psi \to \gamma K^+ K^- K^+ K^-$
2103±50	187 ± 75	586	[2] BISELLO	89B	DM2	$J/\psi \to 4\pi\gamma$

[1] From a partial wave analysis of $J/\psi \to \gamma\phi\phi$, for which the primary signal is $\eta(2225) \to \phi\phi$, and that also finds significant signals for for 0^{-+} phase space, $f_0(2100)$, $f_2(2010)$, $f_2(2300)$, $f_2(2340)$, and a previously unseen 0^{-+} state $X(2500)$ ($M = 2470^{+15+101}_{-19-23}$ MeV, $\Gamma = 230^{+64+56}_{-35-33}$ MeV).
[2] ASTON 81B sees no peak, has 850 events in Ajinenko+Barth bins. ARESTOV 80 sees no peak.

$X(2100)$ $I^G(J^{PC}) = ?^?(0^{??})$

MASS (MeV)	WIDTH (MeV)	DOCUMENT ID		TECN	COMMENT
2100±40	250 ± 40	ALDE	86D	GAM4	100 $\pi^- p \to 2\eta X$

$X(2110)$ $I^G(J^{PC}) = 1^+(3^{-?})$

MASS (MeV)	WIDTH (MeV)	DOCUMENT ID		TECN	COMMENT
2110±10	330 ± 20	EVANGELIS...	79	OMEG	10,16 $\pi^- p \to \overline{p}pn$

$f_2(2140)$ $I^G(J^{PC}) = 0^+(2^{++})$

MASS (MeV)	WIDTH (MeV)	EVTS	DOCUMENT ID		TECN	COMMENT
2141±12	49 ± 28	389	GREEN	86	MPSF	400 $pA \to 4KX$

$X(2150)$ $I^G(J^{PC}) = ?^?(2^{+?})$

MASS (MeV)	WIDTH (MeV)	DOCUMENT ID		TECN	COMMENT
2150±10	260 ± 10	ROZANSKA	80	SPRK	18 $\pi^- p \to p\overline{p}n$

$a_2(2175)$ $I^G(J^{PC}) = 1^-(2^{++})$

MASS (MeV)	WIDTH (MeV)	DOCUMENT ID		TECN	COMMENT
2175±40	310^{+90}_{-45}	ANISOVICH	01F	SPEC	2.0 $\overline{p}p \to 3\pi^0, \pi^0\eta, \pi^0\eta'$

$\eta(2190)$ $I^G(J^{PC}) = 0^+(0^{-+})$

MASS (MeV)	WIDTH (MeV)	DOCUMENT ID		TECN
2190±50	850 ± 100	BUGG	99	BES

$\omega_2(2195)$ $I^G(J^{PC}) = 0^-(2^{--})$

MASS (MeV)	WIDTH (MeV)	DOCUMENT ID		TECN	COMMENT
2195±30	225 ± 40	[1] ANISOVICH	02B	SPEC	0.6–1.9 $p\overline{p} \to \omega\eta, \omega\pi^0\pi^0$

[1] From the combined analysis of ANISOVICH 00D, ANISOVICH 01C, and ANISOVICH 02B.

$\omega(2205)$ $I^G(J^{PC}) = 0^-(1^{--})$

MASS (MeV)	WIDTH (MeV)	DOCUMENT ID		TECN	COMMENT
2205±30	350 ± 90	[1] ANISOVICH	02B	SPEC	0.6–1.9 $p\overline{p} \to \omega\eta, \omega\pi^0\pi^0$

[1] From the combined analysis of ANISOVICH 00D, ANISOVICH 01C, and ANISOVICH 02B.

$X(2210)$ $I^G(J^{PC}) = ?^?(?^{??})$

MASS (MeV)	WIDTH (MeV)	DOCUMENT ID		TECN	COMMENT
2210^{+79}_{-21}	203^{+437}_{-87}	EVANGELIS...	79B	OMEG	10 $\pi^- p \to K^+ K^- n$

$X(2210)$ $I^G(J^{PC}) = ?^?(?^{??})$

MASS (MeV)	WIDTH (MeV)	DOCUMENT ID		TECN	COMMENT
2207±22	130	CASO	70	HBC	11.2 $\pi^- p$

$h_1(2215)$ $I^G(J^{PC}) = 0^-(1^{+-})$

MASS (MeV)	WIDTH (MeV)	DOCUMENT ID		TECN	COMMENT
2215±40	325 ± 55	[1] ANISOVICH	02B	SPEC	0.6–1.9 $p\overline{p} \to \omega\eta, \omega\pi^0\pi^0$

[1] From the combined analysis of ANISOVICH 00D, ANISOVICH 01C, and ANISOVICH 02B.

$\rho_2(2225)$ $I^G(J^{PC}) = 1^+(2^{--})$

MASS (MeV)	WIDTH (MeV)	DOCUMENT ID		TECN	COMMENT
2225±35	335^{+100}_{-50}	[1] ANISOVICH	02	SPEC	0.6–1.9 $p\overline{p} \to \omega\pi^0, \omega\eta\pi^0, \pi^+\pi^-$

[1] From the combined analysis of ANISOVICH 00J, ANISOVICH 01D, ANISOVICH 01E, and ANISOVICH 02.

$\rho_4(2230)$ $I^G(J^{PC}) = 1^+(4^{--})$

MASS (MeV)	WIDTH (MeV)	DOCUMENT ID		TECN	COMMENT
2230±25	210 ± 30	[1] ANISOVICH	02	SPEC	0.6–1.9 $p\overline{p} \to \omega\pi^0, \omega\eta\pi^0, \pi^+\pi^-$

[1] From the combined analysis of ANISOVICH 00J, ANISOVICH 01D, ANISOVICH 01E, and ANISOVICH 02.

$b_1(2240)$ $I^G(J^{PC}) = 1^+(1^{+-})$

MASS (MeV)	WIDTH (MeV)	DOCUMENT ID		TECN	COMMENT
2240±35	320 ± 85	[1] ANISOVICH	02	SPEC	0.6–1.9 $p\overline{p} \to \omega\pi^0, \omega\eta\pi^0, \pi^+\pi^-$

[1] From the combined analysis of ANISOVICH 00J, ANISOVICH 01D, ANISOVICH 01E, and ANISOVICH 02.

$f_2(2240)$ $I^G(J^{PC}) = 0^+(2^{++})$

MASS (MeV)	WIDTH (MeV)	DOCUMENT ID		TECN	COMMENT
2240±15	241 ± 30	[1] ANISOVICH	00J	SPEC	1.92–2.41 $p\overline{p}$
• • • We do not use the following data for averages, fits, limits, etc. • • •					
~ 2226	~ 226	HASAN	94	RVUE	$p\overline{p} \to \pi\pi$

[1] From the combined analysis of ANISOVICH 99C, ANISOVICH 99F, ANISOVICH 99J, ANISOVICH 99K, and ANISOVICH 00B. See also ANISOVICH 12.

$b_3(2245)$ $I^G(J^{PC}) = 1^+(3^{+-})$

MASS (MeV)	WIDTH (MeV)	DOCUMENT ID		TECN
2245±50	320 ± 70	[1] BUGG	04C	RVUE

[1] From the combined analysis of ANISOVICH 00J, ANISOVICH 01D, ANISOVICH 01E, and ANISOVICH 02.

$\eta_2(2250)$ $I^G(J^{PC}) = 0^+(2^{-+})$

MASS (MeV)	WIDTH (MeV)	DOCUMENT ID		TECN
2248±20	280 ± 20	ANISOVICH	00I	SPEC
2267±14	290 ± 50	ANISOVICH	00J	SPEC

$\pi_4(2250)$ $I^G(J^{PC}) = 1^-(4^{-+})$

MASS (MeV)	WIDTH (MeV)	DOCUMENT ID		TECN	COMMENT
2250±15	215 ± 25	ANISOVICH	01F	SPEC	2.0 $\overline{p}p \to 3\pi^0, \pi^0\eta, \pi^0\eta'$

Downloaded from https://academic.oup.com/ptep/article/2022/8/083C01/6651666 by KIT Library user on 27 September 2022

$\omega_4(2250)$ $I^G(J^{PC}) = 0^-(4^{--})$

MASS (MeV)	WIDTH (MeV)	DOCUMENT ID		TECN	COMMENT
2250 ± 30	150 ± 50	[1] ANISOVICH	02B	SPEC	0.6–1.9 $p\overline{p} \to \omega\eta, \omega\pi^0\pi^0$

[1] From the combined analysis of ANISOVICH 00D, ANISOVICH 01C, and ANISOVICH 02B.

$\omega_5(2250)$ $I^G(J^{PC}) = 0^-(5^{--})$

MASS (MeV)	WIDTH (MeV)	DOCUMENT ID		TECN
2250 ± 70	320 ± 95	[1] BUGG	04	RVUE

[1] From the combined analysis of ANISOVICH 00D, ANISOVICH 01C, and ANISOVICH 02B.

$\omega_3(2255)$ $I^G(J^{PC}) = 0^-(3^{--})$

MASS (MeV)	WIDTH (MeV)	DOCUMENT ID		TECN	COMMENT
2255 ± 15	175 ± 30	[1] ANISOVICH	02B	SPEC	0.6–1.9 $p\overline{p} \to \omega\eta, \omega\pi^0\pi^0$

[1] From the combined analysis of ANISOVICH 00D, ANISOVICH 01C, and ANISOVICH 02B.

$a_4(2255)$ $I^G(J^{PC}) = 1^-(4^{++})$

MASS (MeV)	WIDTH (MeV)	DOCUMENT ID		TECN	COMMENT
2237 ± 5	291 ± 12	UMAN	06	E835	5.2 $\overline{p}p \to \eta\eta\pi^0$
2255 ± 40	330^{+110}_{-50}	[1] ANISOVICH	01F	SPEC	1.96–2.41 $\overline{p}p$

[1] From the combined analysis of ANISOVICH 99C, ANISOVICH 99E, and ANISOVICH 01F.

$a_2(2255)$ $I^G(J^{PC}) = 1^-(2^{++})$

MASS (MeV)	WIDTH (MeV)	DOCUMENT ID		TECN	COMMENT
2255 ± 20	230 ± 15	[1] ANISOVICH	01G	SPEC	1.96–2.41 $\overline{p}p$

[1] From the combined analysis of ANISOVICH 99C, ANISOVICH 99E, ANISOVICH 01F, and ANISOVICH 01G.

$X(2260)$ $I^G(J^{PC}) = 0^+(4^{+?})$

MASS (MeV)	WIDTH (MeV)	DOCUMENT ID		TECN	COMMENT
2260 ± 20	400 ± 100	EVANGELIS...	79	OMEG	10,16 $\pi^- p \to \overline{p}pn$

$\rho(2270)$ $I^G(J^{PC}) = 1^+(1^{--})$

MASS (MeV)	WIDTH (MeV)	DOCUMENT ID		TECN	COMMENT
2265 ± 40	325 ± 80	[1] ANISOVICH	02	SPEC	0.6–1.9 $p\overline{p} \to \omega\pi^0$, $\omega\eta\pi^0$, $\pi^+\pi^-$
2280 ± 50	440 ± 110	ATKINSON	85	OMEG	20–70 $\gamma p \to p\omega\pi^+\pi^-\pi^0$

[1] From the combined analysis of ANISOVICH 00J, ANISOVICH 01D, ANISOVICH 01E, and ANISOVICH 02.

$a_1(2270)$ $I^G(J^{PC}) = 1^-(1^{++})$

MASS (MeV)	WIDTH (MeV)	DOCUMENT ID		TECN	COMMENT
270^{+55}_{-40}	305^{+70}_{-40}	ANISOVICH	01F	SPEC	2.0 $\overline{p}p \to 3\pi^0, \pi^0\eta, \pi^0\eta'$

$h_3(2275)$ $I^G(J^{PC}) = 0^-(3^{+-})$

MASS (MeV)	WIDTH (MeV)	DOCUMENT ID		TECN	COMMENT
2275 ± 25	190 ± 45	[1] ANISOVICH	02B	SPEC	0.6–1.9 $p\overline{p} \to \omega\eta, \omega\pi^0\pi^0$

[1] From the combined analysis of ANISOVICH 00D, ANISOVICH 01C, and ANISOVICH 02B.

$a_3(2275)$ $I^G(J^{PC}) = 1^-(3^{++})$

MASS (MeV)	WIDTH (MeV)	DOCUMENT ID		TECN	COMMENT
2275 ± 35	350^{+100}_{-50}	[1] ANISOVICH	01G	SPEC	1.96–2.41 $\overline{p}p$

[1] From the combined analysis of ANISOVICH 99C, ANISOVICH 99E, ANISOVICH 01F, and ANISOVICH 01G.

$\pi_2(2285)$ $I^G(J^{PC}) = 1^-(2^{-+})$

MASS (MeV)	WIDTH (MeV)	DOCUMENT ID		TECN	COMMENT
2285 ± 20 ± 25	250 ± 20 ± 25	[1] ANISOVICH	11	SPEC	0.9–1.94 $p\overline{p}$

[1] Reanalysis of ADOMEIT 96 and ANISOVICH 00E.

$\omega_3(2285)$ $I^G(J^{PC}) = 0^-(3^{--})$

MASS (MeV)	WIDTH (MeV)	DOCUMENT ID		TECN	COMMENT
2278 ± 28	224 ± 50	[1] BUGG	04A	RVUE	
2285 ± 60	230 ± 40	[2] ANISOVICH	02B	SPEC	0.6–1.9 $p\overline{p} \to \omega\eta, \omega\pi^0\pi^0$

[1] Partial wave analysis of the data on $p\overline{p} \to \overline{\Lambda}\Lambda$ from BARNES 00.
[2] From the combined analysis of ANISOVICH 00D, ANISOVICH 01C, and ANISOVICH 02B.

$\omega(2290)$ $I^G(J^{PC}) = 0^-(1^{--})$

MASS (MeV)	WIDTH (MeV)	DOCUMENT ID		TECN
2290 ± 20	275 ± 35	[1] BUGG	04A	RVUE

[1] Partial wave analysis of the data on $p\overline{p} \to \overline{\Lambda}\Lambda$ from BARNES 00.

$f_2(2295)$ $I^G(J^{PC}) = 0^+(2^{++})$

MASS (MeV)	WIDTH (MeV)	DOCUMENT ID		TECN	COMMENT
2293 ± 13	216 ± 37	[1] ANISOVICH	00J	SPEC	1.92–2.41 $p\overline{p}$

[1] From the combined analysis of ANISOVICH 99C, ANISOVICH 99F, ANISOVICH 99J, ANISOVICH 99K, and ANISOVICH 00B. See also ANISOVICH 12.

$f_3(2300)$ $I^G(J^{PC}) = 0^+(3^{++})$

MASS (MeV)	WIDTH (MeV)	DOCUMENT ID		TECN
2334 ± 25	200 ± 20	[1] BUGG	04A	RVUE

[1] Partial wave analysis of the data on $p\overline{p} \to \overline{\Lambda}\Lambda$ from BARNES 00.

$f_1(2310)$ $I^G(J^{PC}) = 0^+(1^{++})$

MASS (MeV)	WIDTH (MeV)	DOCUMENT ID		TECN
2310 ± 60	255 ± 70	ANISOVICH	00J	SPEC

$\eta(2320)$ $I^G(J^{PC}) = 0^+(0^{-+})$

MASS (MeV)	WIDTH (MeV)	DOCUMENT ID		TECN
2320 ± 15	230 ± 35	[1] ANISOVICH	00M	SPEC

[1] From the combined analysis of $\overline{p}p \to \eta\eta\eta$ from ANISOVICH 00M and $\overline{p}p \to \eta\pi^0\pi^0$ from ANISOVICH 00J.

$\eta_4(2330)$ $I^G(J^{PC}) = 0^+(4^{-+})$

MASS (MeV)	WIDTH (MeV)	DOCUMENT ID		TECN	COMMENT
2328 ± 38	240 ± 90	ANISOVICH	00J	SPEC	2.0 $p\overline{p} \to \eta\pi^0\pi^0$

$\omega(2330)$ $I^G(J^{PC}) = 0^-(1^{--})$

MASS (MeV)	WIDTH (MeV)	DOCUMENT ID		TECN	COMMENT
2330 ± 30	435 ± 75	ATKINSON	88	OMEG	25–50 $\gamma p \to \rho^\pm\rho^0\pi^\mp$

$X(2340)$ $I^G(J^{PC}) = ?^?(?^{??})$

MASS (MeV)	WIDTH (MeV)	EVTS	DOCUMENT ID		TECN	COMMENT
2340 ± 20	180 ± 60	126	[1] BALTAY	75	HBC	15 $\pi^+ p \to p5\pi$

[1] Dominant decay into $\rho^0\rho^0\pi^+$. BALTAY 78 finds confirmation in $2\pi^+\pi^-2\pi^0$ events which contain $\rho^+\rho^0\pi^0$ and $2\rho^+\pi^-$.

$\pi(2360)$ $I^G(J^{PC}) = 1^-(0^{-+})$

MASS (MeV)	WIDTH (MeV)	DOCUMENT ID		TECN	COMMENT
2360 ± 25	300^{+100}_{-50}	ANISOVICH	01F	SPEC	2.0 $\overline{p}p \to 3\pi^0, \pi^0\eta, \pi^0\eta'$

$X(2360)$ $I^G(J^{PC}) = ?^?(4^{+?})$

MASS (MeV)	WIDTH (MeV)	DOCUMENT ID		TECN	COMMENT
2360 ± 10	430 ± 30	ROZANSKA	80	SPRK	18 $\pi^- p \to p\overline{p}n$

$X(2440)$ $I^G(J^{PC}) = ?^?(5^{-?})$

MASS (MeV)	WIDTH (MeV)	DOCUMENT ID		TECN	COMMENT
2440 ± 10	310 ± 20	ROZANSKA	80	SPRK	18 $\pi^- p \to p\overline{p}n$

$a_6(2450)$ $I^G(J^{PC}) = 1^-(6^{++})$

MASS (MeV)	WIDTH (MeV)	DOCUMENT ID		TECN	COMMENT
2450 ± 130	400 ± 250	CLELAND	82B	SPEC	50 $\pi p \to K^0_S K^\pm p$

$X(2540)$ $I^G(J^{PC}) = 0^+(0^{++})$

MASS (MeV)	WIDTH (MeV)	DOCUMENT ID		TECN	COMMENT
$2539 \pm 14^{+38}_{-14}$	$274^{+77+126}_{-61-163}$	UEHARA	13	BELL	$\gamma\gamma \to K^0_S K^0_S$

$\Gamma(\gamma\gamma) \times B(K\overline{K})$

VALUE (eV)	DOCUMENT ID		TECN	COMMENT
40^{+9+17}_{-7-40}	UEHARA	13	BELL	$\gamma\gamma \to K^0_S K^0_S$

$X(2632)$ $I^G(J^{PC}) = ?^?(?^{??})$

MASS (MeV)	WIDTH (MeV)	DOCUMENT ID		TECN	COMMENT
2635.2 ± 3.3		[1] EVDOKIMOV	04	SELX	$X(2632) \to D^+_s\eta$
2631.6 ± 2.1	< 17	[2] EVDOKIMOV	04	SELX	$X(2632) \to D^0K^+$

[1] From a mass difference to D^+_s of 666.9 ± 3.3 MeV.
[2] From a mass difference to D^0 of 767.0 ± 2.0 MeV.

Downloaded from https://academic.oup.com/ptep/article/2022/8/083C01/6651666 by KIT Library user on 27 September 2022

$B(X(2632) \to D^0 K^+)/B(X(2632) \to D_s^+ \eta)$

VALUE	DOCUMENT ID		TECN
0.14±0.06	[1] EVDOKIMOV	04	SELX

[1] Possible interpretation of this decay pattern is discussed by YASUI 07.

X(2680) $I^G(J^{PC}) = ?^?(?^{??})$

MASS (MeV)	WIDTH (MeV)	DOCUMENT ID		TECN	COMMENT
2676±27	150	CASO	70	HBC	$11.2\ \pi^- p \to \rho^- \pi^+ \pi^- p$

X(2710) $I^G(J^{PC}) = ?^?(6^{+?})$

MASS (MeV)	WIDTH (MeV)	DOCUMENT ID		TECN	COMMENT
2710±20	170 ± 40	ROZANSKA	80	SPRK	$18\ \pi^- p \to p \overline{p} n$

X(2750) $I^G(J^{PC}) = ?^?(7^{-?})$

MASS (MeV)	WIDTH (MeV)	DOCUMENT ID		TECN	COMMENT
2747±32	195 ± 75	DENNEY	83	LASS	$10\ \pi^+ p \to K^+ K^- \pi^+ p$

$f_6(3100)$ $I^G(J^{PC}) = 0^+(6^{++})$

MASS (MeV)	WIDTH (MeV)	DOCUMENT ID		TECN	COMMENT
3100±100	700 ± 130	BINON	05	GAMS	$33\ \pi^- p \to \eta \eta n$

X(3250) $I^G(J^{PC}) = ?^?(?^{??})$ 3-Body Decays

MASS (MeV)	WIDTH (MeV)	DOCUMENT ID		TECN	COMMENT
3250±8±20	45 ± 18	ALEEV	93	BIS2	$X(3250) \to \Lambda \overline{p} K^+$
3265±7±20	40 ± 18	ALEEV	93	BIS2	$X(3250) \to \overline{\Lambda} p K^-$

X(3250) $I^G(J^{PC}) = ?^?(?^{??})$ 4-Body Decays

MASS (MeV)	WIDTH (MeV)	DOCUMENT ID		TECN	COMMENT
3245±8±20	25 ± 11	ALEEV	93	BIS2	$X(3250) \to \Lambda \overline{p} K^+ \pi^\pm$
3250±9±20	50 ± 20	ALEEV	93	BIS2	$X(3250) \to \overline{\Lambda} p K^- \pi^\mp$
3270±8±20	25 ± 11	ALEEV	93	BIS2	$X(3250) \to K^0_S p \overline{p} K^\pm$

X(3350) $I^G(J^{PC}) = ?^?(?^{??})$

MASS (MeV)	WIDTH (MeV)	EVTS	DOCUMENT ID		TECN	COMMENT
$3350^{+10}_{-20}\pm20$	$70^{+40}_{-30} \pm 40$	50 ± 10	[1] GABYSHEV	06A	BELL	$B^- \to \Lambda_c^+ \overline{p} \pi^-$

[1] A similar enhancement in the $\Lambda_c^+ \overline{p}$ final state is also reported by BABAR collaboration in AUBERT 10H.

$Z_{cs}(4000)^+$ $I(J^P) = 1/2(1^+)$

MASS (MeV)	WIDTH (MeV)	DOCUMENT ID		TECN	COMMENT
$4003\ \pm6\ ^{+4}_{-14}$	131 ± 15 ± 26	[1,2] AAIJ	21E	LHCB	$B^+ \to J/\psi \phi K^+$
$3982.5^{+1.8}_{-2.6}\pm\ 2.1$	$12.8^{+5.3}_{-4.4} \pm 3.0$	[2,3] ABLIKIM	21G	BES3	$e^+e^- \to K^+(D_s^- D^{*0} + D_s^{*-} D^0)$

[1] From an amplitude analysis of the decay $B^+ \to J/\psi \phi K^+$ with a significance of 15 σ.
[2] Properties incompatible with a $q\overline{q}$ structure (exotic state). See the review on "Heavy Non-$q\overline{q}$ Mesons."
[3] Pole mass, width for a mass-,width-dependent Breit-Wigner fit to the mass, width spectrum recoiling against K^+ at center of mass energies between 4.628 and 4.698 GeV, with a significance of 5.3 σ.

$Z_{cs}(4220)^+$ $I(J^P) = 1/2(1^+)$

MASS (MeV)	WIDTH (MeV)	DOCUMENT ID		TECN	COMMENT
$4216\pm24^{+43}_{-30}$	$233 \pm 52^{+97}_{-73}$	[1,2] AAIJ	21E	LHCB	$B^+ \to J/\psi \phi K^+$

[1] From an amplitude analysis of the decay $B^+ \to J/\psi \phi K^+$ with a significance of 5.9 σ.
[2] Properties incompatible with a $q\overline{q}$ structure (exotic state). See the review on "Heavy Non-$q\overline{q}$ Mesons."

X(6900) $I^G(J^{PC}) = ?^?(?^{??})$

MASS (MeV)	WIDTH (MeV)	DOCUMENT ID		TECN	COMMENT
6886±11±11	168 ± 33 ± 69	[1] AAIJ	20AY	LHCB	$pp \to J/\psi J/\psi X$

[1] Assuming the interference of a Breit-Wigner shape with non-resonant single-parton scattering. Without interference, the mass and width are 6905±11±7 and 80±19±33 MeV. State incompatible with a $q\overline{q}$ structure. See the review on "Heavy Non-$q\overline{q}$ Mesons."

REFERENCES for Further States

AAIJ	21E	PRL 127 082001	R. Aaij et al.	(LHCb Collab.)
ABLIKIM	21G	PRL 126 102001	M. Ablikim et al.	(BESIII Collab.)
LEES	21A	PR D104 072002	J.P. Lees et al.	(BABAR Collab.)
AAIJ	20AY	SCIB 65 1983	R. Aaij et al.	(LHCb Collab.)
ABLIKIM	16N	PR D93 112011	M. Ablikim	(BESIII Collab.)
UEHARA	13	PTEP 2013 123C01	S. Uehara et al.	(BELLE Collab.)
ANISOVICH	12	PR D85 014001	A.V. Anisovich et al.	
ANASHIN	11	PL B703 543	V.V. Anashin et al.	(KEDR Collab.)
ANISOVICH	11	EPJ C71 1511	A.V. Anisovich et al.	(LOQM, RAL, PNPI)
CHEN	11F	PR D84 071501	P. Chen et al.	(BELLE Collab.)
AUBERT	10H	PR D82 031102	B. Aubert et al.	(BABAR Collab.)
ABRAAMYAN	09	PR C80 034001	Kh.U. Abraamyan et al.	
VLADIMIRSK...	08	PAN 71 2129	V.V. Vladimirsky et al.	(ITEP)
		Translated from YAF 71 2166.		
VLADIMIRSK...	07	PAN 70 1706	V. Vladimirsky et al.	
		Translated from YAF 70 1751.		
YASUI	07	PR D76 034009	S. Yasui, M. Oka	
ABLIKIM	06S	PRL 97 142002	M. Ablikim et al.	(BES Collab.)
GABYSHEV	06A	PRL 97 242001	N. Gabyshev et al.	(BELLE Collab.)
SCHEGELSKY	06	EPJ A27 199	V.A. Schegelsky et al.	
SCHEGELSKY	06A	EPJ A27 207	V.A. Schegelsky et al.	
UMAN	06	PR D73 052009	I. Uman et al.	(FNAL E835)
VLADIMIRSK...	06	PAN 69 493	V.V. Vladimirsky et al.	(ITEP, Moscow)
		Translated from YAF 69 515.		
BINON	05	PAN 68 960	F. Binon et al.	
		Translated from YAF 68 998.		
GRIGOR'EV	05	PAN 68 1271	V.K. Grigor'ev et al.	(ITEP)
		Translated from YAF 68 1324.		
LU	05	PRL 94 032002	M. Lu et al.	(BNL E852 Collab.)
ABLIKIM	04J	PRL 93 112002	M. Ablikim et al.	(BES Collab.)
BUGG	04	PL B595 556 (errat.)	D.V. Bugg	
BUGG	04A	EPJ C36 161	D.V. Bugg	
BUGG	04C	PRPL 397 257	D.V. Bugg	
EVDOKIMOV	04	PRL 93 242001	A.V. Evdokimov et al.	(SELEX Collab.)
KUHN	04	PL B595 109	J. Kuhn et al.	(BNL E852 Collab.)
ANISOVICH	03	EPJ A16 229	V.V. Anisovich et al.	
VLADIMIRSK...	03	PAN 66 700	V.V. Vladimirsky et al.	
		Translated from YAF 66 729.		
ANISOVICH	02	PL B542 8	A.V. Anisovich et al.	
ANISOVICH	02B	PL B542 19	A.V. Anisovich et al.	
CHUNG	02	PR D65 072001	S.U. Chung et al.	(BNL E852 Collab.)
ANISOVICH	01C	PL B507 23	A.V. Anisovich et al.	
ANISOVICH	01D	PL B508 6	A.V. Anisovich et al.	
ANISOVICH	01E	PL B513 281	A.V. Anisovich et al.	
ANISOVICH	01F	PL B517 261	A.V. Anisovich et al.	
ANISOVICH	01G	PL B517 273	A.V. Anisovich et al.	
ANISOVICH	00B	NP A662 319	A.V. Anisovich et al.	
ANISOVICH	00D	PL B476 15	A.V. Anisovich et al.	
ANISOVICH	00E	PL B477 19	A.V. Anisovich et al.	
ANISOVICH	00I	PL B491 40	A.V. Anisovich et al.	
ANISOVICH	00J	PL B491 47	A.V. Anisovich et al.	(RAL, LOQM, PNPI+)
ANISOVICH	00M	PL B496 145	A.V. Anisovich et al.	
BARNES	00	PR C62 055203	P.D. Barnes et al.	
FILIPPI	00	PL B495 284	A. Filippi et al.	(OBELIX Experiment)
VLADIMIRSKII	00	JETPL 72 486	V.V. Vladimirskii et al.	
		Translated from ZETFP 72 698.		
ANISOVICH	99C	PL B452 173	A.V. Anisovich et al.	
ANISOVICH	99E	PL B452 187	A.V. Anisovich et al.	
ANISOVICH	99F	NP A651 253	A.V. Anisovich et al.	
ANISOVICH	99J	PL B471 271	A.V. Anisovich et al.	
ANISOVICH	99K	PL B468 309	A.V. Anisovich et al.	
BUGG	99	PL B458 511	D.V. Bugg et al.	
FERRER	99	EPJ C10 249	A. Ferrer et al.	
SEMENOV	99	SPU 42 847	S.V. Semenov	
		Translated from UFN 42 937.		
ADOMEIT	96	ZPHY C71 227	J. Adomeit et al.	(Crystal Barrel Collab.)
KLOET	96	PR D53 6120	W.M. Kloet, F. Myhrer	(RUTG, NORD)
PROKOSHKIN	96	PD 41 247	Y.D. Prokoshkin, V.D. Samoilenko	(SERP)
		Translated from DANS 348 481.		
HASAN	94	PL B334 215	A. Hasan, D.V. Bugg	(LOQM)
OAKDEN	94	NP A574 731	M.N. Oakden, M.R. Pennington	(DURH)
ALEEV	93	PAN 56 1358	A.N. Aleev et al.	(BIS-2 Collab.)
		Translated from YAF 56 100.		
ARMSTRONG	93D	PL B307 399	T.A. Armstrong et al.	(FNAL, FERR, GENO+)
ALBRECHT	91F	ZPHY C50 1	H. Albrecht et al.	(ARGUS Collab.)
CONDO	91	PR D43 2787	G.T. Condo et al.	(SLAC Hybrid Collab.)
BISELLO	89B	PR D39 701	G. Busetto et al.	(DM2 Collab.)
ATKINSON	88	ZPHY C38 535	M. Atkinson et al.	(BONN, CERN, GLAS+)
DAFTARI	87	PRL 58 859	I.K. Daftari et al.	(SYRA)
ALDE	86D	NP B269 485	D.M. Alde et al.	(BELG, LAPP, SERP, CERN+)
BRIDGES	86D	PL B180 313	D.L. Bridges et al.	(SYRA, BNL, CASE+)
GREEN	86	PRL 56 1639	D.R. Green et al.	(FNAL, ARIZ, FSU+)
ATKINSON	85	ZPHY C29 333	M. Atkinson et al.	(BONN, CERN, GLAS+)
DENNEY	83	PR D28 2726	D.L. Denney et al.	(IOWA, MICH)
CLELAND	82B	NP B208 228	W.E. Cleland et al.	(DURH, GEVA, LAUS+)
ASTON	81B	NP B189 205	D. Aston et al.	(BONN, CERN, EPOL, GLAS+)
ARESTOV	80	IHEP 80-165	Y.I. Arestov et al.	(SERP)
CHLIAPNIK...	80	ZPHY C3 285	P.V. Chliapnikov et al.	(SERP, BRUX, MONS)
KREYMER	80	PR D22 36	A.E. Kreymer et al.	(IND, PURD, SLAC+)
ROZANSKA	80	NP B162 505	M. Rozanska et al.	(MPIM, CERN)
EVANGELIS...	79	NP B153 253	C. Evangelista et al.	(BARI, BONN, CERN+)
EVANGELIS...	79B	NP B154 381	C. Evangelista et al.	(BARI, BONN, CERN+)
BALTAY	78	PR D17 52	C. Baltay et al.	(COLU, BING)
ANTIPOV	77	NP B119 45	Y.M. Antipov et al.	(SERP, GEVA)
BALTAY	77	PRL 39 591	C. Baltay, C.V. Cautis, M. Kalelkar	(COLU)
BALTAY	75	PRL 35 891	C. Baltay et al.	(COLU, BING)
KALELKAR	75	Thesis Nevis 207	M.S. Kalelkar	(COLU)
CASO	70	LNC 3 707	C. Caso et al.	(GENO, HAMB, MILA, SACL)

Downloaded from https://academic.oup.com/ptep/article/2022/8/083C01/6651666 by KIT Library user on 27 September 2022

p 1987
n 1997
N resonances 2003

Δ resonances 2042

Λ 2065
Λ resonances 2068

Σ^+ 2090
Σ^0 2092
Σ^- 2093
Σ resonances 2095

Ξ^0 2121
Ξ^- 2123
Ξ resonances 2126

Ω^- 2133
Ω resonances 2135

Λ_c^+ 2136
$\Lambda_c(2595)^+$ 2143
$\Lambda_c(2625)^+$ 2143
$\Lambda_c(2765)^+$ aka $\Sigma_c(2765)$ 2144
$\Lambda_c(2860)^+$ 2144
$\Lambda_c(2880)^+$ 2144
$\Lambda_c(2940)^+$ 2145
$\Sigma_c(2455)$ 2145
$\Sigma_c(2520)$ 2146
$\Sigma_c(2800)$ 2147
Ξ_c^+ 2148
Ξ_c^0 2149
$\Xi_c^{\prime +}$ 2151
$\Xi_c^{\prime 0}$ 2151
$\Xi_c(2645)$ 2152
$\Xi_c(2790)$ 2152
$\Xi_c(2815)$ 2153
$\Xi_c(2923)$ 2153
$\Xi_c(2930)$ 2154
$\Xi_c(2970)$ was $\Xi_c(2980)$ 2154
$\Xi_c(3055)$ 2155
$\Xi_c(3080)$ 2155
$\Xi_c(3123)$ 2156
Ω_c^0 2156
$\Omega_c(2770)^0$ 2157
$\Omega_c(3000)^0$ 2157
$\Omega_c(3050)^0$ 2158
$\Omega_c(3065)^0$ 2158
$\Omega_c(3090)^0$ 2158
$\Omega_c(3120)^0$ 2159

Ξ_{cc}^+ 2160
Ξ_{cc}^{++} 2160

Λ_b^0 2161
$\Lambda_b(5912)^0$ 2169
$\Lambda_b(5920)^0$ 2169
$\Lambda_b(6070)^0$ 2170
$\Lambda_b(6146)^0$ 2170
$\Lambda_b(6152)^0$ 2170
Σ_b 2171
Σ_b^* 2171
$\Sigma_b(6097)^+$ 2172
$\Sigma_b(6097)^-$ 2172
Ξ_b^- 2172
Ξ_b^0 2174
$\Xi_b^{\prime}(5935)^-$ 2175
$\Xi_b(5945)^0$ 2176
$\Xi_b(5955)^-$ 2176
$\Xi_b(6227)^0$ 2177
$\Xi_b(6100)^-$ 2176
Ξ_{bc}^0 2177
Ω_b^- 2177
$\Omega_b(6316)^-$ 2178
$\Omega_b(6330)^-$ 2179
$\Omega_b(6340)^-$ 2179
$\Omega_b(6350)^-$ 2179
$\Xi_b(6227)^-$ 2176
b-baryon ADMIXTURE (Λ_b, Ξ_b, Ω_b) 2179

$P_c(4312)^+$ 2181
$P_c(4440)^+$ 2181
$P_c(4380)^+$ 2181
$P_c(4457)^+$ was $P_c(4450)$ 2181

Notes in the Listings

Radiative hyperon decays 2122
Ξ resonances 2126

Related Reviews in Volume 1

80. Baryon decay parameters 964
81. N and Δ resonances 965
82. Λ and Σ resonances (rev.) 970
83. Pole structure of the $\Lambda(1405)$ region (rev.) 973
84. Pentaquarks (rev.) 975

Downloaded from https://academic.oup.com/ptep/article/2022/8/083C01/6651666 by KIT Library user on 27 September 2022

Downloaded from https://academic.oup.com/ptep/article/2022/8/083C01/6651666 by KIT Library user on 27 September 2022

N BARYONS
($S = 0$, $I = 1/2$)

p, $N^+ = uud$; n, $N^0 = udd$

p

$I(J^P) = \frac{1}{2}(\frac{1}{2}^+)$ Status: ****

p MASS (atomic mass units u)

The mass is known more precisely in u (atomic mass units) than in MeV. See the next data block.

VALUE (u)	DOCUMENT ID		TECN	COMMENT
1.007276466621±0.000000000053 OUR EVALUATION		2018 CODATA		
1.007276466574±0.000000000010	[1] FINK	21	SPEC	Penning trap
1.007276466621±0.000000000053	[2] TIESINGA	21	RVUE	2018 CODATA value
• • • We do not use the following data for averages, fits, limits, etc. • • •				
1.007276466598±0.000000000033	[3] HEISSE	19	SPEC	Penning Trap
1.007276466583±0.000000000032	[4] HEISSE	17	SPEC	See HEISSE 19
1.007276466879±0.000000000091	MOHR	16	RVUE	2014 CODATA value
1.007276466812±0.000000000090	MOHR	12	RVUE	2010 CODATA value
1.00727646677 ±0.00000000010	MOHR	08	RVUE	2006 CODATA value
1.00727646688 ±0.00000000013	MOHR	05	RVUE	2002 CODATA value
1.00727646688 ±0.00000000013	MOHR	99	RVUE	1998 CODATA value
1.007276470 ±0.000000012	COHEN	87	RVUE	1986 CODATA value

[1] FINK 21 simultaneously measure the cyclotron frequencies of an H_2^+ ion and a deuteron in a coupled magnetron orbit. The proton mass is extracted using the precise deuteron mass value.

[2] The 2018 CODATA combination in TIESINGA 21 includes data from HEISSE 17, but does not include updates in HEISSE 19, which superseded HEISSE 17. Consequently, we do not average HEISSE 19 and TIESINGA 21. Updating the 2018 CODATA combination to use HEISSE 19 would shift the central value for the proton mass upwards by less than half a standard deviation. Therefore, we take the 2018 CODATA result in TIESINGA 21 as the recommended value for the proton mass.

[3] The value is an update of HEISSE 17; the result is shifted by 1.5×10^{-11} u, corresponding to 0.45 σ due to the corrected motional temperatures of the particles. The statistical and total systematic uncertainties are given as 16 and 29 in the last two digits.

[4] The statistical and systematic errors are 15 and 29 in the last two places of the value. Superseded by HEISSE 19.

p MASS (MeV)

The mass is known more precisely in u (atomic mass units) than in MeV. The conversion is: 1 u = 931.494 102 42(28) MeV/c^2 (2018 CODATA value, TIESINGA 21).

VALUE (MeV)	DOCUMENT ID		TECN	COMMENT
938.27208816±0.00000029 OUR EVALUATION		2018 CODATA		
938.27208812±0.00000029	[1] FINK	21	SPEC	Penning trap
938.27208816±0.00000029	TIESINGA	21	RVUE	2018 CODATA value
• • • We do not use the following data for averages, fits, limits, etc. • • •				
938.2720813 ±0.0000058	MOHR	16	RVUE	2014 CODATA value
938.272046 ±0.000021	MOHR	12	RVUE	2010 CODATA value
938.272013 ±0.000023	MOHR	08	RVUE	2006 CODATA value
938.272029 ±0.000080	MOHR	05	RVUE	2002 CODATA value
938.271998 ±0.000038	MOHR	99	RVUE	1998 CODATA value
938.27231 ±0.00028	COHEN	87	RVUE	1986 CODATA value
938.2796 ±0.0027	COHEN	73	RVUE	1973 CODATA value

[1] FINK 21 quote the more precise mass in atomic mass units.

$|m_p - m_{\overline{p}}|/m_p$

A test of CPT invariance. Note that the comparison of the $\overline{p}$ and p charge-to-mass ratio, given in the next data block, is much better determined.

VALUE	CL%	DOCUMENT ID		TECN	COMMENT
<7 $\times 10^{-10}$	90	[1] HORI	11	SPEC	$\overline{p}e^-$He atom
• • • We do not use the following data for averages, fits, limits, etc. • • •					
<2 $\times 10^{-9}$	90	[1] HORI	06	SPEC	$\overline{p}e^-$He atom
<1.0 $\times 10^{-8}$	90	[1] HORI	03	SPEC	$\overline{p}e^-$ ^{4}He, $\overline{p}e^-$ ^{3}He
<6 $\times 10^{-8}$	90	[1] HORI	01	SPEC	$\overline{p}e^-$He atom
<5 $\times 10^{-7}$		[2] TORII	99	SPEC	$\overline{p}e^-$He atom

[1] HORI 01, HORI 03, HORI 06, and HORI 11 use the more-precisely-known constraint on the $\overline{p}$ charge-to-mass ratio of GABRIELSE 99 (see below) to get their results. Their results are not independent of the HORI 01, HORI 03, HORI 06, and HORI 11 values for $|q_p + q_{\overline{p}}|/e$, below.

[2] TORII 99 uses the more-precisely-known constraint on the $\overline{p}$ charge-to-mass ratio of GABRIELSE 95 (see below) to get this result. This is not independent of the TORII 99 value for $|q_p + q_{\overline{p}}|/e$, below.

$\overline{p}/p$ CHARGE-TO-MASS RATIO, $|\frac{q_{\overline{p}}}{m_{\overline{p}}}|/(\frac{q_p}{m_p})$

A test of CPT invariance. Listed here are measurements involving the *inertial* masses. For a discussion of what may be inferred about the ratio of $\overline{p}$ and p *gravitational* masses, see ERICSON 90; they obtain an upper bound of 10^{-6}–10^{-7} for violation of the equivalence principle for $\overline{p}$s.

VALUE	DOCUMENT ID		TECN	COMMENT
1.000000000003±0.000000000016 OUR AVERAGE				
1.000000000003±0.000000000016	BORCHERT	22	TRAP	Penning trap
1.000000000001±0.000000000069	ULMER	15	TRAP	Penning trap
• • • We do not use the following data for averages, fits, limits, etc. • • •				
0.99999999991 ±0.00000000009	GABRIELSE	99	TRAP	Penning trap
1.0000000015 ±0.0000000011	[1] GABRIELSE	95	TRAP	Penning trap
1.000000023 ±0.000000042	[2] GABRIELSE	90	TRAP	Penning trap

[1] Equation (2) of GABRIELSE 95 should read $M(\overline{p})/M(p) = 0.999\,999\,998\underline{5}$ (11) (G. Gabrielse, private communication).

[2] GABRIELSE 90 also measures $m_{\overline{p}}/m_{e^-} = 1836.152660 \pm 0.000083$ and $m_p/m_{e^-} = 1836.152680 \pm 0.000088$. Both are completely consistent with the 1986 CODATA (COHEN 87) value for m_p/m_{e^-} of 1836.152701 ± 0.000037.

$(|\frac{q_{\overline{p}}}{m_{\overline{p}}}| - \frac{q_p}{m_p})/\frac{q_p}{m_p}$

A test of CPT invariance. Taken from the $\overline{p}/p$ charge-to-mass ratio, above.

VALUE	DOCUMENT ID
(0.1±6.9) $\times 10^{-11}$ OUR EVALUATION	

$|q_p + q_{\overline{p}}|/e$

A test of CPT invariance. Note that the comparison of the $\overline{p}$ and p charge-to-mass ratios given above is much better determined. See also a similar test involving the electron.

VALUE	CL%	DOCUMENT ID		TECN	COMMENT
<7 $\times 10^{-10}$	90	[1] HORI	11	SPEC	$\overline{p}e^-$He atom
• • • We do not use the following data for averages, fits, limits, etc. • • •					
<2 $\times 10^{-9}$	90	[1] HORI	06	SPEC	$\overline{p}e^-$He atom
<1.0 $\times 10^{-8}$	90	[1] HORI	03	SPEC	$\overline{p}e^-$ ^{4}He, $\overline{p}e^-$ ^{3}He
<6 $\times 10^{-8}$	90	[1] HORI	01	SPEC	$\overline{p}e^-$He atom
<5 $\times 10^{-7}$		[2] TORII	99	SPEC	$\overline{p}e^-$He atom
<2 $\times 10^{-5}$		[3] HUGHES	92	RVUE	

[1] HORI 01, HORI 03, HORI 06, and HORI 11 use the more-precisely-known constraint on the $\overline{p}$ charge-to-mass ratio of GABRIELSE 99 (see above) to get their results. Their results are not independent of the HORI 01, HORI 03, HORI 06, and HORI 11 values for $|m_p - m_{\overline{p}}|/m_p$, above.

[2] TORII 99 uses the more-precisely-known constraint on the $\overline{p}$ charge-to-mass ratio of GABRIELSE 95 (see above) to get this result. This is not independent of the TORII 99 value for $|m_p - m_{\overline{p}}|/m_p$, above.

[3] HUGHES 92 uses recent measurements of Rydberg-energy and cyclotron-frequency ratios.

$|q_p + q_e|/e$

See BRESSI 11 for a summary of experiments on the neutrality of matter. See also "n CHARGE" in the neutron Listings.

VALUE	DOCUMENT ID		COMMENT
<1 $\times 10^{-21}$	[1] BRESSI	11	Neutrality of SF_6
• • • We do not use the following data for averages, fits, limits, etc. • • •			
<3.2 $\times 10^{-20}$	[2] SENGUPTA	00	binary pulsar
<0.8 $\times 10^{-21}$	MARINELLI	84	Magnetic levitation
<1.0 $\times 10^{-21}$	[1] DYLLA	73	Neutrality of SF_6

[1] BRESSI 11 uses the method of DYLLA 73 but finds serious errors in that experiment that greatly reduce its accuracy. The BRESSI 11 limit assumes that $n \rightarrow p e^- \nu_e$ conserves charge. Thus the limit applies equally to the charge of the neutron.

[2] SENGUPTA 00 uses the difference between the observed rate of of rotational energy loss by the binary pulsar PSR B1913+16 and the rate predicted by general relativity to set this limit. See the paper for assumptions.

p MAGNETIC MOMENT

See the "Quark Model" review.

VALUE (μ_N)	DOCUMENT ID		TECN	COMMENT
2.79284734463±0.00000000082	TIESINGA	21	RVUE	2018 CODATA value
• • • We do not use the following data for averages, fits, limits, etc. • • •				
2.79284734462±0.00000000082	SCHNEIDER	17	TRAP	Double Penning trap
2.7928473508 ±0.0000000085	MOHR	16	RVUE	2014 CODATA value
2.792847356 ±0.000000023	MOHR	12	RVUE	2010 CODATA value
2.792847356 ±0.000000023	MOHR	08	RVUE	2006 CODATA value
2.792847351 ±0.000000028	MOHR	05	RVUE	2002 CODATA value
2.792847337 ±0.000000029	MOHR	99	RVUE	1998 CODATA value
2.792847386 ±0.000000063	COHEN	87	RVUE	1986 CODATA value

Downloaded from https://academic.oup.com/ptep/article/2022/8/083C01/6651666 by KIT Library user on 27 September 2022

$\overline{p}$ MAGNETIC MOMENT

A few early results have been omitted.

VALUE (μ_N)	DOCUMENT ID		TECN	COMMENT
−2.7928473441 ± 0.0000000042	SMORRA	17	TRAP	Hot/cold $\overline{p}$ frequencies, Penning traps
• • • We do not use the following data for averages, fits, limits, etc. • • •				
−2.7928465 ± 0.0000023	NAGAHAMA	17	TRAP	Single $\overline{p}$, Penning trap
−2.792845 ± 0.000012	DISCIACCA	13	TRAP	Single $\overline{p}$, Penning trap
−2.7862 ± 0.0083	PASK	09	CNTR	$\overline{p}$ He^+ hyperfine structure
−2.8005 ± 0.0090	KREISSL	88	CNTR	$\overline{p}$ ^{208}Pb 11→ 10 X-ray
−2.817 ± 0.048	ROBERTS	78	CNTR	
−2.791 ± 0.021	HU	75	CNTR	Exotic atoms

$(\mu_p + \mu_{\overline{p}}) / \mu_p$

A test of CPT invariance.

VALUE (units 10^{-6})	DOCUMENT ID		TECN	COMMENT
0.002 ± 0.004	SMORRA	17	TRAP	Hot/cold $\overline{p}$ frequencies, Penning traps
• • • We do not use the following data for averages, fits, limits, etc. • • •				
0.3 ± 0.8	NAGAHAMA	17	TRAP	Single $\overline{p}$, Penning trap
0 ± 5	DISCIACCA	13	TRAP	Single $\overline{p}$, Penning trap

p ELECTRIC DIPOLE MOMENT

A nonzero value is forbidden by both T invariance and P invariance.

VALUE (10^{-23} e cm)	DOCUMENT ID		TECN	COMMENT
< 0.021	[1] SAHOO	17		Theory plus ^{199}Hg atom EDM
• • • We do not use the following data for averages, fits, limits, etc. • • •				
< 0.54	[1] DMITRIEV	03		Theory plus ^{199}Hg atom EDM
− 3.7 ± 6.3	CHO	89	NMR	Tl F molecules
< 400	DZUBA	85	THEO	Uses ^{129}Xe moment
130 ± 200	[2] WILKENING	84		
900 ± 1400	[3] WILKENING	84		
700 ± 900	HARRISON	69	MBR	Molecular beam

[1] SAHOO 17 and DMITRIEV 03 are not direct measurements of the proton electric dipole moment. They use theory to calculate this limit from the limit on the electric dipole moment of the ^{199}Hg atom.

[2] This WILKENING 84 value includes a finite-size effect and a magnetic effect.

[3] This WILKENING 84 value is more cautious than the other and excludes the finite-size effect, which relies on uncertain nuclear integrals.

p ELECTRIC POLARIZABILITY α_p

For a very complete review of the "polarizability of the nucleon and Compton scattering," see SCHUMACHER 05, updated in SCHUMACHER 19.

VALUE (10^{-4} fm^3)	DOCUMENT ID		TECN	COMMENT
11.2 ± 0.4 OUR AVERAGE				
10.65 ± 0.35 ± 0.36	MCGOVERN	13	RVUE	χEFT + Compton scattering
12.1 ± 1.1 ± 0.5	[1] BEANE	03		EFT + γp
$11.82 \pm 0.98 ^{+0.52}_{-0.98}$	[2] BLANPIED	01	LEGS	$p(\vec{\gamma},\gamma)$, $p(\vec{\gamma},\pi^0)$, $p(\vec{\gamma},\pi^+)$
11.9 ± 0.5 ± 1.3	[3] OLMOSDEL...	01	CNTR	γp Compton scattering
12.1 ± 0.8 ± 0.5	[4] MACGIBBON	95	RVUE	global average
• • • We do not use the following data for averages, fits, limits, etc. • • •				
$12.03 ^{+0.48}_{-0.54}$	[5] PASQUINI	19		fit of RCS data sets
11.7 ± 0.8 ± 0.7	[6] BARANOV	01	RVUE	Global average
12.5 ± 0.6 ± 0.9	MACGIBBON	95	CNTR	γp Compton scattering
9.8 ± 0.4 ± 1.1	HALLIN	93	CNTR	γp Compton scattering
$10.62 ^{+1.25}_{-1.19} ^{+1.07}_{-1.03}$	ZIEGER	92	CNTR	γp Compton scattering
10.9 ± 2.2 ± 1.3	[7] FEDERSPIEL	91	CNTR	γp Compton scattering

[1] BEANE 03 uses effective field theory and low-energy γp and γd Compton-scattering data. It also gets for the isoscalar polarizabilities (see the erratum) $\alpha_N = (13.0 \pm 1.9 ^{+3.9}_{-1.5}) \times 10^{-4}$ fm^3 and $\beta_N = (-1.8 \pm 1.9 ^{+2.1}_{-0.9}) \times 10^{-4}$ fm^3.

[2] BLANPIED 01 gives $\alpha_p + \beta_p$ and $\alpha_p - \beta_p$. The separate α_p and β_p are provided to us by A. Sandorfi. The first error above is statistics plus systematics; the second is from the model.

[3] This OLMOSDELEON 01 result uses the TAPS data alone, and does not use the (re-evaluated) sum-rule constraint that $\alpha + \beta = (13.8 \pm 0.4) \times 10^{-4}$ fm^3. See the paper for a discussion.

[4] MACGIBBON 95 combine the results of ZIEGER 92, FEDERSPIEL 91, and their own experiment to get a "global average" in which model errors and systematic errors are treated in a consistent way. See MACGIBBON 95 for a discussion.

[5] PASQUINI 19 fit data sets for the unpolarized proton RCS cross section, using fixed-t subtracted dispersion relations and a bootstrap-based fitting technique.

[6] BARANOV 01 combines the results of 10 experiments from 1958 through 1995 to get a global average that takes into account both systematic and model errors and does not use the theoretical constraint on the sum $\alpha_p + \beta_p$.

[7] FEDERSPIEL 91 obtains for the (static) electric polarizability α_p, defined in terms of the induced electric dipole moment by $\mathbf{D} = 4\pi\epsilon_0\alpha_p\mathbf{E}$, the value $(7.0 \pm 2.2 \pm 1.3) \times 10^{-4}$ fm^3.

p MAGNETIC POLARIZABILITY β_p

The electric and magnetic polarizabilities are subject to a dispersion sum-rule constraint $\overline{\alpha} + \overline{\beta} = (14.2 \pm 0.5) \times 10^{-4}$ fm^3. Errors here are anticorrelated with those on $\overline{\alpha}_p$ due to this constraint.

VALUE (10^{-4} fm^3)	DOCUMENT ID		TECN	COMMENT
2.5 ± 0.4 OUR AVERAGE Error includes scale factor of 1.2.				
3.15 ± 0.35 ± 0.36	MCGOVERN	13	RVUE	χEFT + Compton scattering
3.4 ± 1.1 ± 0.1	[1] BEANE	03		EFT + γp
$1.43 \pm 0.98 ^{+0.52}_{-0.98}$	[2] BLANPIED	01	LEGS	$p(\vec{\gamma},\gamma)$, $p(\vec{\gamma},\pi^0)$, $p(\vec{\gamma},\pi^+)$
1.2 ± 0.7 ± 0.5	[3] OLMOSDEL...	01	CNTR	γp Compton scattering
2.1 ± 0.8 ± 0.5	[4] MACGIBBON	95	RVUE	global average
• • • We do not use the following data for averages, fits, limits, etc. • • •				
$1.77 ^{+0.52}_{-0.54}$	[5] PASQUINI	19		fit of RCS data sets
2.3 ± 0.9 ± 0.7	[6] BARANOV	01	RVUE	Global average
1.7 ± 0.6 ± 0.9	MACGIBBON	95	CNTR	γp Compton scattering
4.4 ± 0.4 ± 1.1	HALLIN	93	CNTR	γp Compton scattering
$3.58 ^{+1.19}_{-1.25} ^{+1.03}_{-1.07}$	ZIEGER	92	CNTR	γp Compton scattering
3.3 ± 2.2 ± 1.3	FEDERSPIEL	91	CNTR	γp Compton scattering

[1] BEANE 03 uses effective field theory and low-energy γp and γd Compton-scattering data. It also gets for the isoscalar polarizabilities (see the erratum) $\alpha_N = (13.0 \pm 1.9 ^{+3.9}_{-1.5}) \times 10^{-4}$ fm^3 and $\beta_N = (-1.8 \pm 1.9 ^{+2.1}_{-0.9}) \times 10^{-4}$ fm^3.

[2] BLANPIED 01 gives $\alpha_p + \beta_p$ and $\alpha_p - \beta_p$. The separate α_p and β_p are provided to us by A. Sandorfi. The first error above is statistics plus systematics; the second is from the model.

[3] This OLMOSDELEON 01 result uses the TAPS data alone, and does not use the (re-evaluated) sum-rule constraint that $\alpha + \beta = (13.8 \pm 0.4) \times 10^{-4}$ fm^3. See the paper for a discussion.

[4] MACGIBBON 95 combine the results of ZIEGER 92, FEDERSPIEL 91, and their own experiment to get a "global average" in which model errors and systematic errors are treated in a consistent way. See MACGIBBON 95 for a discussion.

[5] PASQUINI 19 fit data sets for the unpolarized proton RCS cross section, using fixed-t subtracted dispersion relations and a bootstrap-based fitting technique.

[6] BARANOV 01 combines the results of 10 experiments from 1958 through 1995 to get a global average that takes into account both systematic and model errors and does not use the theoretical constraint on the sum $\alpha_p + \beta_p$.

p CHARGE RADIUS

This is the rms electric charge radius, $\sqrt{\langle r_E^2 \rangle}$.

There are three kinds of measurements of the proton radius: via transitions in atomic hydrogen; via electron scattering off hydrogen; and via muonic hydrogen Lamb shift. Most measurements of the radius of the proton involve electron-proton interactions, the most recent of which is the electron scattering measurement $r_p = 0.831(14)$ fm (XIONG 19), and the atomic-hydrogen value, $r_p = 0.833(10)$ fm (BEZGINOV 19). These agree well with another recent atomic-hydrogen value $r_p = 0.8335(95)$ fm (BEYER 17), and with the best measurement using muonic hydrogen $r_p = 0.84087(39)$ fm (ANTOGNINI 13), that is far more precise.

The MOHR 16 value (2014 CODATA), obtained from the electronic results available at the time, was 0.8751(61) fm. This differs by 5.6 standard deviations from the muonic hydrogen value, leading to the so-called proton charge radius puzzle. See our 2018 edition (Physical Review **D98** 030001 (2018)) for a further discussion of interpretations of this puzzle. However, reflecting the new electronic measurements, the 2018 CODATA, TIESINGA 21, recommended value is 0.8414(19) fm, and the puzzle appears to be resolved.

See our 2014 edition (Chinese Physics **C38** 070001 (2014)) for values published before 2003.

VALUE (fm)	DOCUMENT ID		TECN	COMMENT
0.8409 ± 0.0004 OUR AVERAGE				
0.833 ± 0.010	[1] BEZGINOV	19	LASR	2S-2P transition in H
0.831 ± 0.007 ± 0.012	[2] XIONG	19	SPEC	$ep \to ep$ form factor
0.84087 ± 0.00026 ± 0.00029	ANTOGNINI	13	LASR	μp-atom Lamb shift
• • • We do not use the following data for averages, fits, limits, etc. • • •				
0.847 ± 0.008	[3] CUI	21	FIT	use existing ep data
0.878 ± 0.011 ± 0.031	[4] MIHOVILOVIC	21		ISR $ep \to ep$ reanalysis
0.877 ± 0.013	[5] FLEURBAEY	18	LASR	1S-3S transition in H
0.8335 ± 0.0095	[6] BEYER	17	LASR	2S-4P transition in H
0.8751 ± 0.0061	MOHR	16	RVUE	2014 CODATA value
0.895 ± 0.014 ± 0.014	[7] LEE	15	SPEC	Just 2010 Mainz data
0.916 ± 0.024	LEE	15	SPEC	World data, no Mainz
0.8775 ± 0.0051	MOHR	12	RVUE	2010 CODATA, ep data
0.875 ± 0.008 ± 0.006	ZHAN	11	SPEC	Recoil polarimetry

Downloaded from https://academic.oup.com/ptep/article/2022/8/083C01/6651666 by KIT Library user on 27 September 2022

0.879	±0.005	±0.006	BERNAUER	10	SPEC	$ep \to ep$ form factor
0.912	±0.009	±0.007	BORISYUK	10		reanalyzes old ep data
0.871	±0.009	±0.003	HILL	10		z-expansion reanalysis
0.84184	±0.00036	±0.00056	POHL	10	LASR	See ANTOGNINI 13
0.8768	±0.0069		MOHR	08	RVUE	2006 CODATA value
0.844	$^{+0.008}_{-0.004}$		BELUSHKIN	07		Dispersion analysis
0.897	±0.018		BLUNDEN	05		SICK 03 + 2γ correction
0.8750	±0.0068		MOHR	05	RVUE	2002 CODATA value
0.895	±0.010	±0.013	SICK	03		$ep \to ep$ reanalysis

[1] BEZGINOV 19 measures the $2S_{1/2}$ to $2P_{1/2}$ transition frequency in atomic hydrogen using the frequency-offset separated oscillatory field (FOSOF) technique. The result agrees well with the muonic hydrogen Lamb shift value.
[2] The XIONG 19 value from $ep \to ep$ scattering and supports the muonic hydrogen Lamb shift value.
[3] CUI 21 employ a new mathematical procedure (statistical SPM, Schlessinger point method) based on form-unbiased interpolations of existing ep scattering data.
[4] MIHOVILOVIC 21 reports a value of 0.878 ± 0.011 ± 0.031 ± 0.002 fm where the last uncertainty comes from the dependence on the model form factor function.
[5] FLEURBAEY 18 measures the 1S-3S transition frequency in hydrogen and in combination with the 1S-2S transition frequency deduces the proton radius and the Rydberg constant.
[6] The BEYER 17 result is 3.3 combined standard deviations below the MOHR 16 (2014 CODATA) value. The experiment measures the 2S-4P transition in hydrogen and gets the proton radius and the Rydberg constant.
[7] Authors also provide values for combinations of all available data.

p MAGNETIC RADIUS

This is the rms magnetic radius, $\sqrt{\langle r_M^2 \rangle}$.

VALUE (fm)	DOCUMENT ID		TECN	COMMENT
0.851±0.026	[1] LEE	15		Combination of world and Mainz data
• • • We do not use the following data for averages, fits, limits, etc. • • •				
0.817±0.027	[2] CUI	21B	FIT	use existing ep data
0.87 ±0.02	EPSTEIN	14		Using ep, en, $\pi\pi$ data
0.867±0.009±0.018	ZHAN	11	SPEC	Recoil polarimetry
0.777±0.013±0.010	BERNAUER	10	SPEC	$ep \to ep$ form factor
0.876±0.010±0.016	BORISYUK	10		Reanalyzes old $ep \to ep$ data
0.854±0.005	BELUSHKIN	07		Dispersion analysis

[1] In a consistent reanalysis LEE 2015 extract values separately for the Mainz 2010 data only (0.776+-0.034+-0.017) fm and for the world data without Mainz data (0.914+-0.035) fm. The quoted value is a simple combination of the two, which ignores possible discrepancies and unknown correlations and should be considered with caution.
[2] CUI 21B employ a new mathematical procedure (statistical SPM, Schlessinger point method) based on form-unbiased interpolations of existing ep scattering data.

p MEAN LIFE

A test of baryon conservation. See the "p Partial Mean Lives" section below for limits for identified final states. The limits here are to "anything" or are for "disappearance" modes of a bound proton (p) or (n). See also the 3ν modes in the "Partial Mean Lives" section. Table 1 of BACK 03 is a nice summary.

LIMIT (years)	PARTICLE	CL%	DOCUMENT ID		TECN	COMMENT
$>3.6 \times 10^{29}$	**p**	90	[1] ANDERSON	19A	SNO+	$p \to$ invisible
$>5.8 \times 10^{29}$	**n**	90	[2] ARAKI	06	KLND	$n \to$ invisible
• • • We do not use the following data for averages, fits, limits, etc. • • •						
$>2.5 \times 10^{29}$	n	90	[1] ANDERSON	19A	SNO+	$n \to$ invisible
$>2.1 \times 10^{29}$	p	90	[1] AHMED	04	SNO	$p \to$ invisible
$>1.9 \times 10^{29}$	n	90	[1] AHMED	04	SNO	$n \to$ invisible
$>1.8 \times 10^{25}$	n	90	[3] BACK	03	BORX	
$>1.1 \times 10^{26}$	p	90	[3] BACK	03	BORX	
$>3.5 \times 10^{28}$	p	90	[4] ZDESENKO	03		$p \to$ invisible
$>1 \times 10^{28}$	p	90	[5] AHMAD	02	SNO	$p \to$ invisible
$>4 \times 10^{23}$	p	95	TRETYAK	01		$d \to n +$?
$>1.9 \times 10^{24}$	p	90	[6] BERNABEI	00B	DAMA	
$>1.6 \times 10^{25}$	p, n		[7,8] EVANS	77		
$>3 \times 10^{23}$	p		[8] DIX	70	CNTR	
$>3 \times 10^{23}$	p, n		[8,9] FLEROV	58		

[1] AHMED 04 and ANDERSON 19A look for γ rays from the de-excitation of a residual $^{15}O^*$ or $^{15}N^*$ following the disappearance of a neutron or proton in ^{16}O.
[2] ARAKI 06 looks for signs of de-excitation of the residual nucleus after disappearance of a neutron from the s shell of ^{12}C.
[3] BACK 03 looks for decays of unstable nuclides left after N decays of parent ^{12}C, ^{13}C, ^{16}O nuclei. These are "invisible channel" limits.
[4] ZDESENKO 03 gets this limit on proton disappearance in deuterium by analyzing SNO data in AHMAD 02.
[5] AHMAD 02 (see its footnote 7) looks for neutrons left behind after the disappearance of the proton in deuterons.
[6] BERNABEI 00B looks for the decay of a $^{128}_{53}I$ nucleus following the disappearance of a proton in the otherwise-stable $^{129}_{54}Xe$ nucleus.
[7] EVANS 77 looks for the daughter nuclide ^{129}Xe from possible ^{130}Te decays in ancient Te ore samples.
[8] This mean-life limit has been obtained from a half-life limit by dividing the latter by ln(2) = 0.693.
[9] FLEROV 58 looks for the spontaneous fission of a ^{232}Th nucleus after the disappearance of one of its nucleons.

$\overline{p}$ MEAN LIFE

Of the two astrophysical limits here, that of GEER 00D involves considerably more refinements in its modeling. The other limits come from direct observations of stored antiprotons. See also "$\overline{p}$ Partial Mean Lives" after "p Partial Mean Lives," below, for exclusive-mode limits. The best (lifetime/branching fraction) limit there is 7×10^5 years, for $\overline{p} \to e^- \gamma$. We advance only the exclusive-mode limits to our Summary Tables.

LIMIT (years)	CL%	EVTS	DOCUMENT ID		TECN	COMMENT
• • • We do not use the following data for averages, fits, limits, etc. • • •						
>5.0	90		SELLNER	17	TRAP	Penning trap
$>8 \times 10^5$	90		[1] GEER	00D		$\overline{p}/p$ ratio, cosmic rays
>0.28			GABRIELSE	90	TRAP	Penning trap
>0.08	90	1	BELL	79	CNTR	Storage ring
$>1 \times 10^7$			GOLDEN	79	SPEC	$\overline{p}/p$ ratio, cosmic rays
$>3.7 \times 10^{-3}$			BREGMAN	78	CNTR	Storage ring

[1] GEER 00D uses agreement between a model of galactic $\overline{p}$ production and propagation and the observed $\overline{p}/p$ cosmic-ray spectrum to set this limit.

p DECAY MODES

See the "Note on Nucleon Decay" in our 1994 edition (Phys. Rev. **D50**, 1173) for a short review.

The "partial mean life" limits tabulated here are the limits on τ/B_i, where τ is the total mean life and B_i is the branching fraction for the mode in question. For N decays, p and n indicate proton and neutron partial lifetimes.

	Mode	Partial mean life (10^{30} years)	Confidence level
	Antilepton + meson		
τ_1	$N \to e^+ \pi$	>5300 (n), >16000 (p)	90%
τ_2	$N \to \mu^+ \pi$	>3500 (n), >7700 (p)	90%
τ_3	$N \to \nu \pi$	>1100 (n), >390 (p)	90%
τ_4	$p \to e^+ \eta$	>10000	90%
τ_5	$p \to \mu^+ \eta$	>4700	90%
τ_6	$n \to \nu \eta$	>158	90%
τ_7	$N \to e^+ \rho$	>217 (n), >720 (p)	90%
τ_8	$N \to \mu^+ \rho$	>228 (n), >570 (p)	90%
τ_9	$N \to \nu \rho$	>19 (n), >162 (p)	90%
τ_{10}	$p \to e^+ \omega$	>1600	90%
τ_{11}	$p \to \mu^+ \omega$	>2800	90%
τ_{12}	$n \to \nu \omega$	>108	90%
τ_{13}	$N \to e^+ K$	>17 (n), >1000 (p)	90%
τ_{14}	$p \to e^+ K^0_S$		
τ_{15}	$p \to e^+ K^0_L$		
τ_{16}	$N \to \mu^+ K$	>26 (n), >1600 (p)	90%
τ_{17}	$p \to \mu^+ K^0_S$		
τ_{18}	$p \to \mu^+ K^0_L$		
τ_{19}	$N \to \nu K$	>86 (n), >5900 (p)	90%
τ_{20}	$n \to \nu K^0_S$	>260	90%
τ_{21}	$p \to e^+ K^*(892)^0$	>84	90%
τ_{22}	$N \to \nu K^*(892)$	>78 (n), >51 (p)	90%
	Antilepton + mesons		
τ_{23}	$p \to e^+ \pi^+ \pi^-$	>82	90%
τ_{24}	$p \to e^+ \pi^0 \pi^0$	>147	90%
τ_{25}	$n \to e^+ \pi^- \pi^0$	>52	90%
τ_{26}	$p \to \mu^+ \pi^+ \pi^-$	>133	90%
τ_{27}	$p \to \mu^+ \pi^0 \pi^0$	>101	90%
τ_{28}	$n \to \mu^+ \pi^- \pi^0$	>74	90%
τ_{29}	$n \to e^+ K^0 \pi^-$	>18	90%
	Lepton + meson		
τ_{30}	$n \to e^- \pi^+$	>65	90%
τ_{31}	$n \to \mu^- \pi^+$	>49	90%
τ_{32}	$n \to e^- \rho^+$	>62	90%
τ_{33}	$n \to \mu^- \rho^+$	>7	90%
τ_{34}	$n \to e^- K^+$	>32	90%
τ_{35}	$n \to \mu^- K^+$	>57	90%
	Lepton + mesons		
τ_{36}	$p \to e^- \pi^+ \pi^+$	>30	90%
τ_{37}	$n \to e^- \pi^+ \pi^0$	>29	90%
τ_{38}	$p \to \mu^- \pi^+ \pi^+$	>17	90%

Downloaded from https://academic.oup.com/ptep/article/2022/8/083C01/6651666 by KIT Library user on 27 September 2022

τ_{39}	$n \to \mu^- \pi^+ \pi^0$	> 34	90%
τ_{40}	$p \to e^- \pi^+ K^+$	> 75	90%
τ_{41}	$p \to \mu^- \pi^+ K^+$	> 245	90%

Antilepton + photon(s)

τ_{42}	$p \to e^+ \gamma$	> 670	90%
τ_{43}	$p \to \mu^+ \gamma$	> 478	90%
τ_{44}	$n \to \nu \gamma$	> 550	90%
τ_{45}	$p \to e^+ \gamma \gamma$	> 100	90%
τ_{46}	$n \to \nu \gamma \gamma$	> 219	90%

Antilepton + single massless

τ_{47}	$p \to e^+ X$	> 790	90%
τ_{48}	$p \to \mu^+ X$	> 410	90%

Three (or more) leptons

τ_{49}	$p \to e^+ e^+ e^-$	> 793	90%
τ_{50}	$p \to e^+ \mu^+ \mu^-$	> 359	90%
τ_{51}	$p \to e^+ \nu \nu$	> 170	90%
τ_{52}	$n \to e^+ e^- \nu$	> 257	90%
τ_{53}	$n \to \mu^+ e^- \nu$	> 83	90%
τ_{54}	$n \to \mu^+ \mu^- \nu$	> 79	90%
τ_{55}	$p \to \mu^+ e^+ e^-$	> 529	90%
τ_{56}	$p \to \mu^- e^+ e^+$	$>1.90 \times 10^{34}$	
τ_{57}	$p \to \mu^+ \mu^+ \mu^-$	> 675	90%
τ_{58}	$p \to \mu^+ \nu \nu$	> 220	90%
τ_{59}	$p \to e^- \mu^+ \mu^+$	> 6	90%
τ_{60}	$n \to 3\nu$	$> 5 \times 10^{-4}$	90%
τ_{61}	$n \to 5\nu$		

Inclusive modes

τ_{62}	$N \to e^+$ anything	> 0.6 (n, p)	90%
τ_{63}	$N \to \mu^+$ anything	> 12 (n, p)	90%
τ_{64}	$N \to \nu$ anything		
τ_{65}	$N \to e^+ \pi^0$ anything	> 0.6 (n, p)	90%
τ_{66}	$N \to$ 2 bodies, ν-free		

$\Delta B = 2$ dinucleon modes

The following are lifetime limits per iron nucleus.

τ_{67}	$p p \to \pi^+ \pi^+$	> 72.2	90%
τ_{68}	$p n \to \pi^+ \pi^0$	> 170	90%
τ_{69}	$n n \to \pi^+ \pi^-$	> 0.7	90%
τ_{70}	$n n \to \pi^0 \pi^0$	> 404	90%
τ_{71}	$p p \to K^+ K^+$	> 170	90%
τ_{72}	$p p \to e^+ e^+$	> 5.8	90%
τ_{73}	$p p \to e^+ \mu^+$	> 3.6	90%
τ_{74}	$p p \to \mu^+ \mu^+$	> 1.7	90%
τ_{75}	$p n \to e^+ \overline{\nu}$	> 260	90%
τ_{76}	$p n \to \mu^+ \overline{\nu}$	> 200	90%
τ_{77}	$p n \to \tau^+ \overline{\nu}_\tau$	> 29	90%
τ_{78}	$n n \to \nu_e \overline{\nu}_e$	> 1.4	90%
τ_{79}	$n n \to \nu_\mu \overline{\nu}_\mu$	> 1.4	90%
τ_{80}	$p n \to$ invisible	$> 2.1 \times 10^{-5}$	90%
τ_{81}	$p p \to$ invisible	$> 5 \times 10^{-5}$	90%

$\overline{p}$ DECAY MODES

	Mode	Partial mean life (years)	Confidence level
τ_{82}	$\overline{p} \to e^- \gamma$	$> 7 \times 10^5$	90%
τ_{83}	$\overline{p} \to \mu^- \gamma$	$> 5 \times 10^4$	90%
τ_{84}	$\overline{p} \to e^- \pi^0$	$> 4 \times 10^5$	90%
τ_{85}	$\overline{p} \to \mu^- \pi^0$	$> 5 \times 10^4$	90%
τ_{86}	$\overline{p} \to e^- \eta$	$> 2 \times 10^4$	90%
τ_{87}	$\overline{p} \to \mu^- \eta$	$> 8 \times 10^3$	90%
τ_{88}	$\overline{p} \to e^- K^0_S$	> 900	90%
τ_{89}	$\overline{p} \to \mu^- K^0_S$	$> 4 \times 10^3$	90%
τ_{90}	$\overline{p} \to e^- K^0_L$	$> 9 \times 10^3$	90%
τ_{91}	$\overline{p} \to \mu^- K^0_L$	$> 7 \times 10^3$	90%
τ_{92}	$\overline{p} \to e^- \gamma \gamma$	$> 2 \times 10^4$	90%
τ_{93}	$\overline{p} \to \mu^- \gamma \gamma$	$> 2 \times 10^4$	90%
τ_{94}	$\overline{p} \to e^- \omega$	> 200	90%

p PARTIAL MEAN LIVES

The "partial mean life" limits tabulated here are the limits on τ/B_i, where τ is the total mean life for the proton and B_i is the branching fraction for the mode in question.

Decaying particle: p = proton, n = bound neutron. The same event may appear under more than one partial decay mode. Background estimates may be accurate to a factor of two.

Antilepton + meson

$\tau(N \to e^+ \pi)$ — τ_1

LIMIT (10^{30} years)	PARTICLE	CL%	EVTS	BKGD EST	DOCUMENT ID		TECN
>24000	***p***	**90**	**0**	**0.59**	[1] TAKENAKA	20	SKAM
> 5300	***n***	**90**	**0**	**0.41**	ABE	17D	SKAM
• • • We do not use the following data for averages, fits, limits, etc. • • •							
>16000	p	90	0	0.61	ABE	17	SKAM
> 2000	n	90	0	0.27	NISHINO	12	SKAM
> 8200	p	90	0	0.3	NISHINO	09	SKAM
> 540	p	90	0	0.2	MCGREW	99	IMB3
> 158	n	90	3	5	MCGREW	99	IMB3
> 1600	p	90	0	0.1	SHIOZAWA	98	SKAM
> 70	p	90	0	0.5	BERGER	91	FREJ
> 70	n	90	0	≤ 0.1	BERGER	91	FREJ
> 550	p	90	0	0.7	[2] BECKER-SZ...	90	IMB3
> 260	p	90	0	<0.04	HIRATA	89C	KAMI
> 130	n	90	0	<0.2	HIRATA	89C	KAMI
> 310	p	90	0	0.6	SEIDEL	88	IMB
> 100	n	90	0	1.6	SEIDEL	88	IMB
> 1.3	n	90	0		BARTELT	87	SOUD
> 1.3	p	90	0		BARTELT	87	SOUD
> 250	p	90	0	0.3	HAINES	86	IMB
> 31	n	90	8	9	HAINES	86	IMB
> 64	p	90	0	<0.4	ARISAKA	85	KAMI
> 26	n	90	0	<0.7	ARISAKA	85	KAMI
> 82	p (free)	90	0	0.2	BLEWITT	85	IMB
> 250	p	90	0	0.2	BLEWITT	85	IMB
> 25	n	90	4	4	PARK	85	IMB
> 15	p, n	90	0		BATTISTONI	84	NUSX
> 0.5	p	90	1	0.3	[3] BARTELT	83	SOUD
> 0.5	n	90	1	0.3	[3] BARTELT	83	SOUD
> 5.8	p	90	2		[4] KRISHNA...	82	KOLR
> 5.8	n	90	2		[4] KRISHNA...	82	KOLR
> 0.1	n	90			[5] GURR	67	CNTR

[1] TAKENAKA 20 includes data of ABE 17, and thus supersedes ABE 17.
[2] This BECKER-SZENDY 90 result includes data from SEIDEL 88.
[3] Limit based on zero events.
[4] We have calculated 90% CL limit from 1 confined event.
[5] We have converted half-life to 90% CL mean life.

$\tau(N \to \mu^+ \pi)$ — τ_2

LIMIT (10^{30} years)	PARTICLE	CL%	EVTS	BKGD EST	DOCUMENT ID		TECN
>16000	***p***	**90**	**1**	**0.94**	[1] TAKENAKA	20	SKAM
> 3500	***n***	**90**	**1**	**0.77**	ABE	17D	SKAM
• • • We do not use the following data for averages, fits, limits, etc. • • •							
> 7700	p	90	2	0.87	ABE	17	SKAM
> 1000	n	90	1	0.43	NISHINO	12	SKAM
> 6600	p	90	0	0.3	NISHINO	09	SKAM
> 473	p	90	0	0.6	MCGREW	99	IMB3
> 90	n	90	1	1.9	MCGREW	99	IMB3
> 81	p	90	0	0.2	BERGER	91	FREJ
> 35	n	90	1	1.0	BERGER	91	FREJ
> 230	p	90	0	<0.07	HIRATA	89C	KAMI
> 100	n	90	0	<0.2	HIRATA	89C	KAMI
> 270	p	90	0	0.5	SEIDEL	88	IMB
> 63	n	90	0	0.5	SEIDEL	88	IMB
> 76	p	90	2	1	HAINES	86	IMB
> 23	n	90	8	7	HAINES	86	IMB
> 46	p	90	0	<0.7	ARISAKA	85	KAMI
> 20	n	90	0	<0.4	ARISAKA	85	KAMI
> 59	p (free)	90	0	0.2	BLEWITT	85	IMB
> 100	p	90	1	0.4	BLEWITT	85	IMB
> 38	n	90	1	4	PARK	85	IMB
> 10	p, n	90	0		BATTISTONI	84	NUSX
> 1.3	p, n	90	0		ALEKSEEV	81	BAKS

[1] TAKENAKA 20 includes the data of ABE 17 and thus supersedes ABE 17.

$\tau(N \to \nu \pi)$ — τ_3

LIMIT (10^{30} years)	PARTICLE	CL%	EVTS	BKGD EST	DOCUMENT ID		TECN
> 390	***p***	**90**	**52.8**		ABE	14E	SKAM
>1100	***n***	**90**	**19.1**		ABE	14E	SKAM

Downloaded from https://academic.oup.com/ptep/article/2022/8/083C01/6651666 by KIT Library user on 27 September 2022

• • • We do not use the following data for averages, fits, limits, etc. • • •

> 16	p	90	6	6.7	WALL	00B	SOU2
> 39	n	90	4	3.8	WALL	00B	SOU2
> 10	p	90	15	20.3	MCGREW	99	IMB3
> 112	n	90	6	6.6	MCGREW	99	IMB3
> 13	n	90	1	1.2	BERGER	89	FREJ
> 10	p	90	11	14	BERGER	89	FREJ
> 25	p	90	32	32.8	[1] HIRATA	89C	KAMI
> 100	n	90	1	3	HIRATA	89C	KAMI
> 6	n	90	73	60	HAINES	86	IMB
> 2	p	90	16	13	KAJITA	86	KAMI
> 40	n	90	0	1	KAJITA	86	KAMI
> 7	n	90	28	19	PARK	85	IMB
> 7	n	90	0		BATTISTONI	84	NUSX
> 2	p	90	≤ 3		BATTISTONI	84	NUSX
> 5.8	p	90	1		[2] KRISHNA...	82	KOLR
> 0.3	p	90	2		[3] CHERRY	81	HOME
> 0.1	p	90			[4] GURR	67	CNTR

[1] In estimating the background, this HIRATA 89C limit (as opposed to the later limits of WALL 00B and MCGREW 99) does not take into account present understanding that the flux of ν_μ originating in the upper atmosphere is depleted. Doing so would reduce the background and thus also would reduce the limit here.
[2] We have calculated 90% CL limit from 1 confined event.
[3] We have converted 2 possible events to 90% CL limit.
[4] We have converted half-life to 90% CL mean life.

$\tau(p \to e^+ \eta)$ — τ_4

LIMIT (10^{30} years)	PARTICLE	CL%	EVTS	BKGD EST	DOCUMENT ID		TECN
>10000	**p**	**90**	**0**	**0.78**	ABE	17D	SKAM

• • • We do not use the following data for averages, fits, limits, etc. • • •

> 4200	p	90	0	0.44	NISHINO	12	SKAM
> 81	p	90	1	1.7	WALL	00B	SOU2
> 313	p	90	0	0.2	MCGREW	99	IMB3
> 44	p	90	0	0.1	BERGER	91	FREJ
> 140	p	90	0	<0.04	HIRATA	89C	KAMI
> 100	p	90	0	0.6	SEIDEL	88	IMB
> 200	p	90	5	3.3	HAINES	86	IMB
> 64	p	90	0	<0.8	ARISAKA	85	KAMI
> 64	p (free)	90	5	6.5	BLEWITT	85	IMB
> 200	p	90	5	4.7	BLEWITT	85	IMB
> 1.2	p	90	2		[1] CHERRY	81	HOME

[1] We have converted 2 possible events to 90% CL limit.

$\tau(p \to \mu^+ \eta)$ — τ_5

LIMIT (10^{30} years)	PARTICLE	CL%	EVTS	BKGD EST	DOCUMENT ID		TECN
>4700	**p**	**90**	**2**	**0.85**	ABE	17D	SKAM

• • • We do not use the following data for averages, fits, limits, etc. • • •

>1300	p	90	2	0.49	NISHINO	12	SKAM
> 89	p	90	0	1.6	WALL	00B	SOU2
> 126	p	90	3	2.8	MCGREW	99	IMB3
> 26	p	90	1	0.8	BERGER	91	FREJ
> 69	p	90	1	<0.08	HIRATA	89C	KAMI
> 1.3	p	90	0	0.7	PHILLIPS	89	HPW
> 34	p	90	1	1.5	SEIDEL	88	IMB
> 46	p	90	7	6	HAINES	86	IMB
> 26	p	90	1	<0.8	ARISAKA	85	KAMI
> 17	p (free)	90	6	6	BLEWITT	85	IMB
> 46	p	90	7	8	BLEWITT	85	IMB

$\tau(n \to \nu \eta)$ — τ_6

LIMIT (10^{30} years)	PARTICLE	CL%	EVTS	BKGD EST	DOCUMENT ID		TECN
>158	**n**	**90**	**0**	**1.2**	MCGREW	99	IMB3

• • • We do not use the following data for averages, fits, limits, etc. • • •

> 71	n	90	2	3.7	WALL	00B	SOU2
> 29	n	90	0	0.9	BERGER	89	FREJ
> 54	n	90	2	0.9	HIRATA	89C	KAMI
> 16	n	90	3	2.1	SEIDEL	88	IMB
> 25	n	90	7	6	HAINES	86	IMB
> 30	n	90	0	0.4	KAJITA	86	KAMI
> 18	n	90	4	3	PARK	85	IMB
> 0.6	n	90	2		[1] CHERRY	81	HOME

[1] We have converted 2 possible events to 90% CL limit.

$\tau(N \to e^+ \rho)$ — τ_7

LIMIT (10^{30} years)	PARTICLE	CL%	EVTS	BKGD EST	DOCUMENT ID		TECN
>720	**p**	**90**	**2**	**0.64**	ABE	17D	SKAM
>217	**n**	**90**	**4**	**4.8**	MCGREW	99	IMB3

• • • We do not use the following data for averages, fits, limits, etc. • • •

> 30	n	90	4	0.87	ABE	17D	SKAM
>710	p	90	0	0.35	NISHINO	12	SKAM
> 70	n	90	1	0.38	NISHINO	12	SKAM
> 29	p	90	0	2.2	BERGER	91	FREJ
> 41	n	90	0	1.4	BERGER	91	FREJ
> 75	p	90	2	2.7	HIRATA	89C	KAMI
> 58	n	90	0	1.9	HIRATA	89C	KAMI
> 38	n	90	2	4.1	SEIDEL	88	IMB
> 1.2	p	90	0		BARTELT	87	SOUD
> 1.5	n	90	0		BARTELT	87	SOUD
> 17	p	90	7	7	HAINES	86	IMB
> 14	n	90	9	4	HAINES	86	IMB
> 12	p	90	0	<1.2	ARISAKA	85	KAMI
> 6	n	90	2	<1	ARISAKA	85	KAMI
> 6.7	p (free)	90	6	6	BLEWITT	85	IMB
> 17	p	90	7	7	BLEWITT	85	IMB
> 12	n	90	4	2	PARK	85	IMB
> 0.6	n	90	1	0.3	[1] BARTELT	83	SOUD
> 0.5	p	90	1	0.3	[1] BARTELT	83	SOUD
> 9.8	p	90	1		[2] KRISHNA...	82	KOLR
> 0.8	p	90	2		[3] CHERRY	81	HOME

[1] Limit based on zero events.
[2] We have calculated 90% CL limit from 0 confined events.
[3] We have converted 2 possible events to 90% CL limit.

$\tau(N \to \mu^+ \rho)$ — τ_8

LIMIT (10^{30} years)	PARTICLE	CL%	EVTS	BKGD EST	DOCUMENT ID		TECN
>570	**p**	**90**	**1**	**1.30**	ABE	17D	SKAM
>228	**n**	**90**	**3**	**9.5**	MCGREW	99	IMB3

• • • We do not use the following data for averages, fits, limits, etc. • • •

> 60	n	90	1	0.96	ABE	17D	SKAM
>160	p	90	1	0.42	NISHINO	12	SKAM
> 36	n	90	0	0.29	NISHINO	12	SKAM
> 12	p	90	0	0.5	BERGER	91	FREJ
> 22	n	90	0	1.1	BERGER	91	FREJ
>110	p	90	0	1.7	HIRATA	89C	KAMI
> 23	n	90	1	1.8	HIRATA	89C	KAMI
> 4.3	p	90	0	0.7	PHILLIPS	89	HPW
> 30	p	90	0	0.5	SEIDEL	88	IMB
> 11	n	90	1	1.1	SEIDEL	88	IMB
> 16	p	90	4	4.5	HAINES	86	IMB
> 7	n	90	6	5	HAINES	86	IMB
> 12	p	90	0	<0.7	ARISAKA	85	KAMI
> 5	n	90	1	<1.2	ARISAKA	85	KAMI
> 5.5	p (free)	90	4	5	BLEWITT	85	IMB
> 16	p	90	4	5	BLEWITT	85	IMB
> 9	n	90	1	2	PARK	85	IMB

$\tau(N \to \nu \rho)$ — τ_9

LIMIT (10^{30} years)	PARTICLE	CL%	EVTS	BKGD EST	DOCUMENT ID		TECN
>162	**p**	**90**	**18**	**21.7**	MCGREW	99	IMB3
> 19	**n**	**90**	**0**	**0.5**	SEIDEL	88	IMB

• • • We do not use the following data for averages, fits, limits, etc. • • •

> 9	n	90	4	2.4	BERGER	89	FREJ
> 24	p	90	0	0.9	BERGER	89	FREJ
> 27	p	90	5	1.5	HIRATA	89C	KAMI
> 13	n	90	4	3.6	HIRATA	89C	KAMI
> 13	p	90	1	1.1	SEIDEL	88	IMB
> 8	p	90	6	5	HAINES	86	IMB
> 2	n	90	15	10	HAINES	86	IMB
> 11	p	90	2	1	KAJITA	86	KAMI
> 4	n	90	2	2	KAJITA	86	KAMI
> 4.1	p (free)	90	6	7	BLEWITT	85	IMB
> 8.4	p	90	6	5	BLEWITT	85	IMB
> 2	n	90	7	3	PARK	85	IMB
> 0.9	p	90	2		[1] CHERRY	81	HOME
> 0.6	n	90	2		[1] CHERRY	81	HOME

[1] We have converted 2 possible events to 90% CL limit.

$\tau(p \to e^+ \omega)$ — τ_{10}

LIMIT (10^{30} years)	PARTICLE	CL%	EVTS	BKGD EST	DOCUMENT ID		TECN
>1600	**p**	**90**	**1**	**1.35**	ABE	17D	SKAM

• • • We do not use the following data for averages, fits, limits, etc. • • •

> 320	p	90	1	0.53	NISHINO	12	SKAM
> 107	p	90	7	10.8	MCGREW	99	IMB3
> 17	p	90	0	1.1	BERGER	91	FREJ
> 45	p	90	2	1.45	HIRATA	89C	KAMI
> 26	p	90	1	1.0	SEIDEL	88	IMB
> 1.5	p	90	0		BARTELT	87	SOUD
> 37	p	90	6	5.3	HAINES	86	IMB
> 25	p	90	1	<1.4	ARISAKA	85	KAMI
> 12	p (free)	90	6	7.5	BLEWITT	85	IMB
> 37	p	90	6	5.7	BLEWITT	85	IMB
> 0.6	p	90	1	0.3	[1] BARTELT	83	SOUD
> 9.8	p	90	1		[2] KRISHNA...	82	KOLR
> 2.8	p	90	2		[3] CHERRY	81	HOME

[1] Limit based on zero events.
[2] We have calculated 90% CL limit from 0 confined events.
[3] We have converted 2 possible events to 90% CL limit.

Downloaded from https://academic.oup.com/ptep/article/2022/8/083C01/6651666 by KIT Library user on 27 September 2022

$\tau(p \to \mu^+ \omega)$ — τ_{11}

LIMIT (10^{30} years)	PARTICLE	CL%	EVTS	BKGD EST	DOCUMENT ID		TECN
>2800	**p**	**90**	**0**	**1.09**	ABE	17D	SKAM
• • • We do not use the following data for averages, fits, limits, etc. • • •							
> 780	p	90	0	0.48	NISHINO	12	SKAM
> 117	p	90	11	12.1	MCGREW	99	IMB3
> 11	p	90	0	1.0	BERGER	91	FREJ
> 57	p	90	2	1.9	HIRATA	89C	KAMI
> 4.4	p	90	0	0.7	PHILLIPS	89	HPW
> 10	p	90	2	1.3	SEIDEL	88	IMB
> 23	p	90	2	1	HAINES	86	IMB
> 6.5	p (free)	90	9	8.7	BLEWITT	85	IMB
> 23	p	90	8	7	BLEWITT	85	IMB

$\tau(n \to \nu \omega)$ — τ_{12}

LIMIT (10^{30} years)	PARTICLE	CL%	EVTS	BKGD EST	DOCUMENT ID		TECN
>108	**n**	**90**	**12**	**22.5**	MCGREW	99	IMB3
• • • We do not use the following data for averages, fits, limits, etc. • • •							
> 17	n	90	1	0.7	BERGER	89	FREJ
> 43	n	90	3	2.7	HIRATA	89C	KAMI
> 6	n	90	2	1.3	SEIDEL	88	IMB
> 12	n	90	6	6	HAINES	86	IMB
> 18	n	90	2	2	KAJITA	86	KAMI
> 16	n	90	1	2	PARK	85	IMB
> 2.0	n	90	2		[1] CHERRY	81	HOME

[1] We have converted 2 possible events to 90% CL limit.

$\tau(N \to e^+ K)$ — τ_{13}

LIMIT (10^{30} years)	PARTICLE	CL%	EVTS	BKGD EST	DOCUMENT ID		TECN
>1000	**p**	**90**	**6**	**4.7**	KOBAYASHI	05	SKAM
> 17	**n**	**90**	**35**	**29.4**	MCGREW	99	IMB3
• • • We do not use the following data for averages, fits, limits, etc. • • •							
> 85	p	90	3	4.9	WALL	00	SOU2
> 31	p	90	23	25.2	MCGREW	99	IMB3
> 60	p	90	0		BERGER	91	FREJ
> 150	p	90	0	<0.27	HIRATA	89C	KAMI
> 70	p	90	0	1.8	SEIDEL	88	IMB
> 77	p	90	5	4.5	HAINES	86	IMB
> 38	p	90	0	<0.8	ARISAKA	85	KAMI
> 24	p (free)	90	7	8.5	BLEWITT	85	IMB
> 77	p	90	5	4	BLEWITT	85	IMB
> 1.3	p	90	0		ALEKSEEV	81	BAKS
> 1.3	n	90	0		ALEKSEEV	81	BAKS

$\tau(p \to e^+ K^0_S)$ — τ_{14}

LIMIT (10^{30} years)	PARTICLE	CL%	EVTS	BKGD EST	DOCUMENT ID		TECN
• • • We do not use the following data for averages, fits, limits, etc. • • •							
>120	p	90	1	1.3	WALL	00	SOU2
> 76	p	90	0	0.5	BERGER	91	FREJ

$\tau(p \to e^+ K^0_L)$ — τ_{15}

LIMIT (10^{30} years)	PARTICLE	CL%	EVTS	BKGD EST	DOCUMENT ID		TECN
• • • We do not use the following data for averages, fits, limits, etc. • • •							
>51	p	90	2	3.5	WALL	00	SOU2
>44	p	90	0	$\leq$ 0.1	BERGER	91	FREJ

$\tau(N \to \mu^+ K)$ — τ_{16}

LIMIT (10^{30} years)	PARTICLE	CL%	EVTS	BKGD EST	DOCUMENT ID		TECN
>1600	**p**	**90**	**13**	**13.2**	REGIS	12	SKAM
> 26	**n**	**90**	**20**	**28.4**	MCGREW	99	IMB3
• • • We do not use the following data for averages, fits, limits, etc. • • •							
>1300	p	90	3	3.9	KOBAYASHI	05	SKAM
> 120	p	90	0	<1.2	WALL	00	SOU2
> 120	p	90	4	7.2	MCGREW	99	IMB3
> 54	p	90	0		BERGER	91	FREJ
> 120	p	90	1	0.4	HIRATA	89C	KAMI
> 3.0	p	90	0	0.7	PHILLIPS	89	HPW
> 19	p	90	3	2.5	SEIDEL	88	IMB
> 1.5	p	90	0		[1] BARTELT	87	SOUD
> 1.1	n	90	0		BARTELT	87	SOUD
> 40	p	90	7	6	HAINES	86	IMB
> 19	p	90	1	<1.1	ARISAKA	85	KAMI
> 6.7	p (free)	90	11	13	BLEWITT	85	IMB
> 40	p	90	7	8	BLEWITT	85	IMB
> 6	p	90	1		BATTISTONI	84	NUSX
> 0.6	p	90	0		[2] BARTELT	83	SOUD
> 0.4	n	90	0		[2] BARTELT	83	SOUD
> 5.8	p	90	2		[3] KRISHNA...	82	KOLR
> 2.0	p	90	0		CHERRY	81	HOME
> 0.2	n	90			[4] GURR	67	CNTR

[1] BARTELT 87 limit applies to $p \to \mu^+ K^0_S$.
[2] Limit based on zero events.
[3] We have calculated 90% CL limit from 1 confined event.
[4] We have converted half-life to 90% CL mean life.

$\tau(p \to \mu^+ K^0_S)$ — τ_{17}

LIMIT (10^{30} years)	PARTICLE	CL%	EVTS	BKGD EST	DOCUMENT ID		TECN
• • • We do not use the following data for averages, fits, limits, etc. • • •							
>150	p	90	0	<0.8	WALL	00	SOU2
> 64	p	90	0	1.2	BERGER	91	FREJ

$\tau(p \to \mu^+ K^0_L)$ — τ_{18}

LIMIT (10^{30} years)	PARTICLE	CL%	EVTS	BKGD EST	DOCUMENT ID		TECN
• • • We do not use the following data for averages, fits, limits, etc. • • •							
>83	p	90	0	0.4	WALL	00	SOU2
>44	p	90	0	$\leq$ 0.1	BERGER	91	FREJ

$\tau(N \to \nu K)$ — τ_{19}

LIMIT (10^{30} years)	PARTICLE	CL%	EVTS	BKGD EST	DOCUMENT ID		TECN
>5900	**p**	**90**	**0**	**1.0**	ABE	14G	SKAM
> 86	**n**	**90**	**0**	**2.4**	HIRATA	89C	KAMI
• • • We do not use the following data for averages, fits, limits, etc. • • •							
> 540	p	90	0	0.9	ASAKURA	15	KLND
>2300	p	90	0	1.3	KOBAYASHI	05	SKAM
> 26	n	90	16	9.1	WALL	00	SOU2
> 670	p	90			HAYATO	99	SKAM
> 151	p	90	15	21.4	MCGREW	99	IMB3
> 30	n	90	34	34.1	MCGREW	99	IMB3
> 43	p	90	1	1.54	[1] ALLISON	98	SOU2
> 15	n	90	1	1.8	BERGER	89	FREJ
> 15	p	90	1	1.8	BERGER	89	FREJ
> 100	p	90	9	7.3	HIRATA	89C	KAMI
> 0.28	p	90	0	0.7	PHILLIPS	89	HPW
> 0.3	p	90	0		BARTELT	87	SOUD
> 0.75	n	90	0		[2] BARTELT	87	SOUD
> 10	p	90	6	5	HAINES	86	IMB
> 15	n	90	3	5	HAINES	86	IMB
> 28	p	90	3	3	KAJITA	86	KAMI
> 32	n	90	0	1.4	KAJITA	86	KAMI
> 1.8	p (free)	90	6	11	BLEWITT	85	IMB
> 9.6	p	90	6	5	BLEWITT	85	IMB
> 10	n	90	2	2	PARK	85	IMB
> 5	n	90	0		BATTISTONI	84	NUSX
> 2	p	90	0		BATTISTONI	84	NUSX
> 0.3	n	90	0		[3] BARTELT	83	SOUD
> 0.1	p	90	0		[3] BARTELT	83	SOUD
> 5.8	p	90	1		[4] KRISHNA...	82	KOLR
> 0.3	n	90	2		[5] CHERRY	81	HOME

[1] This ALLISON 98 limit is with no background subtraction; with subtraction the limit becomes $> 46 \times 10^{30}$ years.
[2] BARTELT 87 limit applies to $n \to \nu K^0_S$.
[3] Limit based on zero events.
[4] We have calculated 90% CL limit from 1 confined event.
[5] We have converted 2 possible events to 90% CL limit.

$\tau(n \to \nu K^0_S)$ — τ_{20}

LIMIT (10^{30} years)	PARTICLE	CL%	EVTS	BKGD EST	DOCUMENT ID		TECN
>260	**n**	**90**	**34**	**30**	[1] KOBAYASHI	05	SKAM
• • • We do not use the following data for averages, fits, limits, etc. • • •							
> 51	n	90	16	9.1	WALL	00	SOU2

[1] We have doubled the $n \to \nu K^0$ limit given in KOBAYASHI 05 to obtain this $n \to \nu K^0_S$ limit.

$\tau(p \to e^+ K^*(892)^0)$ — τ_{21}

LIMIT (10^{30} years)	PARTICLE	CL%	EVTS	BKGD EST	DOCUMENT ID		TECN
>84	**p**	**90**	**38**	**52.0**	MCGREW	99	IMB3
• • • We do not use the following data for averages, fits, limits, etc. • • •							
>10	p	90	0	0.8	BERGER	91	FREJ
>52	p	90	2	1.55	HIRATA	89C	KAMI
>10	p	90	1	<1	ARISAKA	85	KAMI

$\tau(N \to \nu K^*(892))$ — τ_{22}

LIMIT (10^{30} years)	PARTICLE	CL%	EVTS	BKGD EST	DOCUMENT ID		TECN
>51	**p**	**90**	**7**	**9.1**	MCGREW	99	IMB3
>78	**n**	**90**	**40**	**50**	MCGREW	99	IMB3
• • • We do not use the following data for averages, fits, limits, etc. • • •							
>22	n	90	0	2.1	BERGER	89	FREJ
>17	p	90	0	2.4	BERGER	89	FREJ
>20	p	90	5	2.1	HIRATA	89C	KAMI
>21	n	90	4	2.4	HIRATA	89C	KAMI

Downloaded from https://academic.oup.com/ptep/article/2022/8/083C01/6651666 by KIT Library user on 27 September 2022

>10	p	90	7	6	HAINES	86	IMB
> 5	n	90	8	7	HAINES	86	IMB
> 8	p	90	3	2	KAJITA	86	KAMI
> 6	n	90	2	1.6	KAJITA	86	KAMI
> 5.8	p (free)	90	10	16	BLEWITT	85	IMB
> 9.6	p	90	7	6	BLEWITT	85	IMB
> 7	n	90	1	4	PARK	85	IMB
> 2.1	p	90	1		[1] BATTISTONI	82	NUSX

[1] We have converted 1 possible event to 90% CL limit.

Antilepton + mesons

$\tau(p \to e^+ \pi^+ \pi^-)$ — τ_{23}

LIMIT (10^{30} years)	PARTICLE	CL%	EVTS	BKGD EST	DOCUMENT ID		TECN
>82	**p**	**90**	**16**	**23.1**	MCGREW	99	IMB3
• • • We do not use the following data for averages, fits, limits, etc. • • •							
>21	p	90	0	2.2	BERGER	91	FREJ

$\tau(p \to e^+ \pi^0 \pi^0)$ — τ_{24}

LIMIT (10^{30} years)	PARTICLE	CL%	EVTS	BKGD EST	DOCUMENT ID		TECN
>147	**p**	**90**	**2**	**0.8**	MCGREW	99	IMB3
• • • We do not use the following data for averages, fits, limits, etc. • • •							
> 38	p	90	1	0.5	BERGER	91	FREJ

$\tau(n \to e^+ \pi^- \pi^0)$ — τ_{25}

LIMIT (10^{30} years)	PARTICLE	CL%	EVTS	BKGD EST	DOCUMENT ID		TECN
>52	**n**	**90**	**38**	**34.2**	MCGREW	99	IMB3
• • • We do not use the following data for averages, fits, limits, etc. • • •							
>32	n	90	1	0.8	BERGER	91	FREJ

$\tau(p \to \mu^+ \pi^+ \pi^-)$ — τ_{26}

LIMIT (10^{30} years)	PARTICLE	CL%	EVTS	BKGD EST	DOCUMENT ID		TECN
>133	**p**	**90**	**25**	**38.0**	MCGREW	99	IMB3
• • • We do not use the following data for averages, fits, limits, etc. • • •							
> 17	p	90	1	2.6	BERGER	91	FREJ
> 3.3	p	90	0	0.7	PHILLIPS	89	HPW

$\tau(p \to \mu^+ \pi^0 \pi^0)$ — τ_{27}

LIMIT (10^{30} years)	PARTICLE	CL%	EVTS	BKGD EST	DOCUMENT ID		TECN
>101	**p**	**90**	**3**	**1.6**	MCGREW	99	IMB3
• • • We do not use the following data for averages, fits, limits, etc. • • •							
> 33	p	90	1	0.9	BERGER	91	FREJ

$\tau(n \to \mu^+ \pi^- \pi^0)$ — τ_{28}

LIMIT (10^{30} years)	PARTICLE	CL%	EVTS	BKGD EST	DOCUMENT ID		TECN
>74	**n**	**90**	**17**	**20.8**	MCGREW	99	IMB3
• • • We do not use the following data for averages, fits, limits, etc. • • •							
>33	n	90	0	1.1	BERGER	91	FREJ

$\tau(n \to e^+ K^0 \pi^-)$ — τ_{29}

LIMIT (10^{30} years)	PARTICLE	CL%	EVTS	BKGD EST	DOCUMENT ID		TECN
>18	**n**	**90**	**1**	**0.2**	BERGER	91	FREJ

Lepton + meson

$\tau(n \to e^- \pi^+)$ — τ_{30}

LIMIT (10^{30} years)	PARTICLE	CL%	EVTS	BKGD EST	DOCUMENT ID		TECN
>65	**n**	**90**	**0**	**1.6**	SEIDEL	88	IMB
• • • We do not use the following data for averages, fits, limits, etc. • • •							
>55	n	90	0	1.09	BERGER	91B	FREJ
>16	n	90	9	7	HAINES	86	IMB
>25	n	90	2	4	PARK	85	IMB

$\tau(n \to \mu^- \pi^+)$ — τ_{31}

LIMIT (10^{30} years)	PARTICLE	CL%	EVTS	BKGD EST	DOCUMENT ID		TECN
>49	**n**	**90**	**0**	**0.5**	SEIDEL	88	IMB
• • • We do not use the following data for averages, fits, limits, etc. • • •							
>33	n	90	0	1.40	BERGER	91B	FREJ
> 2.7	n	90	0	0.7	PHILLIPS	89	HPW
>25	n	90	7	6	HAINES	86	IMB
>27	n	90	2	3	PARK	85	IMB

$\tau(n \to e^- \rho^+)$ — τ_{32}

LIMIT (10^{30} years)	PARTICLE	CL%	EVTS	BKGD EST	DOCUMENT ID		TECN
>62	**n**	**90**	**2**	**4.1**	SEIDEL	88	IMB
• • • We do not use the following data for averages, fits, limits, etc. • • •							
>12	n	90	13	6	HAINES	86	IMB
>12	n	90	5	3	PARK	85	IMB

$\tau(n \to \mu^- \rho^+)$ — τ_{33}

LIMIT (10^{30} years)	PARTICLE	CL%	EVTS	BKGD EST	DOCUMENT ID		TECN
>7	**n**	**90**	**1**	**1.1**	SEIDEL	88	IMB
• • • We do not use the following data for averages, fits, limits, etc. • • •							
>2.6	n	90	0	0.7	PHILLIPS	89	HPW
>9	n	90	7	5	HAINES	86	IMB
>9	n	90	2	2	PARK	85	IMB

$\tau(n \to e^- K^+)$ — τ_{34}

LIMIT (10^{30} years)	PARTICLE	CL%	EVTS	BKGD EST	DOCUMENT ID		TECN
>32	**n**	**90**	**3**	**2.96**	BERGER	91B	FREJ
• • • We do not use the following data for averages, fits, limits, etc. • • •							
> 0.23	n	90	0	0.7	PHILLIPS	89	HPW

$\tau(n \to \mu^- K^+)$ — τ_{35}

LIMIT (10^{30} years)	PARTICLE	CL%	EVTS	BKGD EST	DOCUMENT ID		TECN
>57	**n**	**90**	**0**	**2.18**	BERGER	91B	FREJ
• • • We do not use the following data for averages, fits, limits, etc. • • •							
> 4.7	n	90	0	0.7	PHILLIPS	89	HPW

Lepton + mesons

$\tau(p \to e^- \pi^+ \pi^+)$ — τ_{36}

LIMIT (10^{30} years)	PARTICLE	CL%	EVTS	BKGD EST	DOCUMENT ID		TECN
>30	**p**	**90**	**1**	**2.50**	BERGER	91B	FREJ
• • • We do not use the following data for averages, fits, limits, etc. • • •							
> 2.0	p	90	0	0.7	PHILLIPS	89	HPW

$\tau(n \to e^- \pi^+ \pi^0)$ — τ_{37}

LIMIT (10^{30} years)	PARTICLE	CL%	EVTS	BKGD EST	DOCUMENT ID		TECN
>29	**n**	**90**	**1**	**0.78**	BERGER	91B	FREJ

$\tau(p \to \mu^- \pi^+ \pi^+)$ — τ_{38}

LIMIT (10^{30} years)	PARTICLE	CL%	EVTS	BKGD EST	DOCUMENT ID		TECN
>17	**p**	**90**	**1**	**1.72**	BERGER	91B	FREJ
• • • We do not use the following data for averages, fits, limits, etc. • • •							
> 7.8	p	90	0	0.7	PHILLIPS	89	HPW

$\tau(n \to \mu^- \pi^+ \pi^0)$ — τ_{39}

LIMIT (10^{30} years)	PARTICLE	CL%	EVTS	BKGD EST	DOCUMENT ID		TECN
>34	**n**	**90**	**0**	**0.78**	BERGER	91B	FREJ

$\tau(p \to e^- \pi^+ K^+)$ — τ_{40}

LIMIT (10^{30} years)	PARTICLE	CL%	EVTS	BKGD EST	DOCUMENT ID		TECN
>75	**p**	**90**	**81**	**127.2**	MCGREW	99	IMB3
• • • We do not use the following data for averages, fits, limits, etc. • • •							
>20	p	90	3	2.50	BERGER	91B	FREJ

$\tau(p \to \mu^- \pi^+ K^+)$ — τ_{41}

LIMIT (10^{30} years)	PARTICLE	CL%	EVTS	BKGD EST	DOCUMENT ID		TECN
>245	**p**	**90**	**3**	**4.0**	MCGREW	99	IMB3
• • • We do not use the following data for averages, fits, limits, etc. • • •							
> 5	p	90	2	0.78	BERGER	91B	FREJ

Antilepton + photon(s)

$\tau(p \to e^+ \gamma)$ — τ_{42}

LIMIT (10^{30} years)	PARTICLE	CL%	EVTS	BKGD EST	DOCUMENT ID		TECN
>670	**p**	**90**	**0**	**0.1**	MCGREW	99	IMB3
• • • We do not use the following data for averages, fits, limits, etc. • • •							
>133	p	90	0	0.3	BERGER	91	FREJ
>460	p	90	0	0.6	SEIDEL	88	IMB
>360	p	90	0	0.3	HAINES	86	IMB
> 87	p (free)	90	0	0.2	BLEWITT	85	IMB
>360	p	90	0	0.2	BLEWITT	85	IMB
> 0.1	p	90			[1] GURR	67	CNTR

[1] We have converted half-life to 90% CL mean life.

$\tau(p \to \mu^+ \gamma)$ — τ_{43}

LIMIT (10^{30} years)	PARTICLE	CL%	EVTS	BKGD EST	DOCUMENT ID		TECN
>478	**p**	**90**	**0**	**0.1**	MCGREW	99	IMB3
• • • We do not use the following data for averages, fits, limits, etc. • • •							
>155	p	90	0	0.1	BERGER	91	FREJ
>380	p	90	0	0.5	SEIDEL	88	IMB
> 97	p	90	3	2	HAINES	86	IMB
> 61	p (free)	90	0	0.2	BLEWITT	85	IMB
>280	p	90	0	0.6	BLEWITT	85	IMB
> 0.3	p	90			[1] GURR	67	CNTR

[1] We have converted half-life to 90% CL mean life.

Downloaded from https://academic.oup.com/ptep/article/2022/8/083C01/6651666 by KIT Library user on 27 September 2022

$\tau(n \to \nu\gamma)$ — τ_{44}

LIMIT (10^{30} years)	PARTICLE	CL%	EVTS	BKGD EST	DOCUMENT ID		TECN
>550		**90**			TAKHISTOV	15	SKAM
• • • We do not use the following data for averages, fits, limits, etc. • • •							
> 28	*n*	90	163	144.7	MCGREW	99	IMB3
> 24	*n*	90	10	6.86	BERGER	91B	FREJ
> 9	*n*	90	73	60	HAINES	86	IMB
> 11	*n*	90	28	19	PARK	85	IMB

$\tau(p \to e^+\gamma\gamma)$ — τ_{45}

LIMIT (10^{30} years)	PARTICLE	CL%	EVTS	BKGD EST	DOCUMENT ID		TECN
>100	***p***	**90**	**1**	**0.8**	BERGER	91	FREJ

$\tau(n \to \nu\gamma\gamma)$ — τ_{46}

LIMIT (10^{30} years)	PARTICLE	CL%	EVTS	BKGD EST	DOCUMENT ID		TECN
>219	***n***	**90**	**5**	**7.5**	MCGREW	99	IMB3

Antilepton + single massless

$\tau(p \to e^+ X)$ — τ_{47}

VALUE (10^{30} years)	CL%	DOCUMENT ID		TECN
>790	90	TAKHISTOV	15	SKAM

$\tau(p \to \mu^+ X)$ — τ_{48}

VALUE (10^{30} years)	CL%	DOCUMENT ID		TECN
>410	90	TAKHISTOV	15	SKAM

Three (or more) leptons

$\tau(p \to e^+ e^+ e^-)$ — τ_{49}

LIMIT (10^{30} years)	PARTICLE	CL%	EVTS	BKGD EST	DOCUMENT ID		TECN
>34000	***p***	**90**	**0**	**0.58**	TANAKA	20	SKAM
• • • We do not use the following data for averages, fits, limits, etc. • • •							
> 793	*p*	90	0	0.5	MCGREW	99	IMB3
> 147	*p*	90	0	0.1	BERGER	91	FREJ
> 510	*p*	90	0	0.3	HAINES	86	IMB
> 89	*p* (free)	90	0	0.5	BLEWITT	85	IMB
> 510	*p*	90	0	0.7	BLEWITT	85	IMB

$\tau(p \to e^+ \mu^+ \mu^-)$ — τ_{50}

LIMIT (10^{30} years)	PARTICLE	CL%	EVTS	BKGD EST	DOCUMENT ID		TECN
>9200	***p***	**90**	**1**	**0.27**	TANAKA	20	SKAM
• • • We do not use the following data for averages, fits, limits, etc. • • •							
> 359	*p*	90	1	0.9	MCGREW	99	IMB3
> 81	*p*	90	0	0.16	BERGER	91	FREJ
> 5.0	*p*	90	0	0.7	PHILLIPS	89	HPW

$\tau(p \to e^+ \nu\nu)$ — τ_{51}

LIMIT (10^{30} years)	PARTICLE	CL%	EVTS	BKGD EST	DOCUMENT ID		TECN
>170	***p***	**90**			[1] TAKHISTOV	14	SKAM
• • • We do not use the following data for averages, fits, limits, etc. • • •							
> 17	*p*	90	152	153.7	MCGREW	99	IMB3
> 11	*p*	90	11	6.08	BERGER	91B	FREJ

[1] Allowed events at 90% CL are 459.

$\tau(n \to e^+ e^- \nu)$ — τ_{52}

LIMIT (10^{30} years)	PARTICLE	CL%	EVTS	BKGD EST	DOCUMENT ID		TECN
>257	***n***	**90**	**5**	**7.5**	MCGREW	99	IMB3
• • • We do not use the following data for averages, fits, limits, etc. • • •							
> 74	*n*	90	0	< 0.1	BERGER	91B	FREJ
> 45	*n*	90	5	5	HAINES	86	IMB
> 26	*n*	90	4	3	PARK	85	IMB

$\tau(n \to \mu^+ e^- \nu)$ — τ_{53}

LIMIT (10^{30} years)	PARTICLE	CL%	EVTS	BKGD EST	DOCUMENT ID		TECN
>83	***n***	**90**	**25**	**29.4**	MCGREW	99	IMB3
• • • We do not use the following data for averages, fits, limits, etc. • • •							
>47	*n*	90	0	< 0.1	BERGER	91B	FREJ

$\tau(n \to \mu^+ \mu^- \nu)$ — τ_{54}

LIMIT (10^{30} years)	PARTICLE	CL%	EVTS	BKGD EST	DOCUMENT ID		TECN
>79	***n***	**90**	**100**	**145**	MCGREW	99	IMB3
• • • We do not use the following data for averages, fits, limits, etc. • • •							
>42	*n*	90	0	1.4	BERGER	91B	FREJ
> 5.1	*n*	90	0	0.7	PHILLIPS	89	HPW
>16	*n*	90	14	7	HAINES	86	IMB
>19	*n*	90	4	7	PARK	85	IMB

$\tau(p \to \mu^+ e^+ e^-)$ — τ_{55}

LIMIT (10^{30} years)	PARTICLE	CL%	EVTS	BKGD EST	DOCUMENT ID		TECN
>23000	***p***	**90**	**0**	**0.5**	TANAKA	20	SKAM
• • • We do not use the following data for averages, fits, limits, etc. • • •							
> 529	*p*	90	0	1.0	MCGREW	99	IMB3
> 91	*p*	90	0	≤ 0.1	BERGER	91	FREJ

$\tau(p \to \mu^- e^+ e^+)$ — τ_{56}

LIMIT (10^{30} years)	PARTICLE	CL%	EVTS	BKGD EST	DOCUMENT ID		TECN
>19000	***p***	**90**	**0**	**0.5**	TANAKA	20	SKAM

$\tau(p \to \mu^+ \mu^+ \mu^-)$ — τ_{57}

LIMIT (10^{30} years)	PARTICLE	CL%	EVTS	BKGD EST	DOCUMENT ID		TECN
>10000	***p***	**90**	**1**	**0.4**	TANAKA	20	SKAM
• • • We do not use the following data for averages, fits, limits, etc. • • •							
> 675	*p*	90	0	0.3	MCGREW	99	IMB3
> 119	*p*	90	0	0.2	BERGER	91	FREJ
> 10.5	*p*	90	0	0.7	PHILLIPS	89	HPW
> 190	*p*	90	1	0.1	HAINES	86	IMB
> 44	*p* (free)	90	1	0.7	BLEWITT	85	IMB
> 190	*p*	90	1	0.9	BLEWITT	85	IMB
> 2.1	*p*	90	1		[1] BATTISTONI	82	NUSX

[1] We have converted 1 possible event to 90% CL limit.

$\tau(p \to \mu^+ \nu\nu)$ — τ_{58}

LIMIT (10^{30} years)	PARTICLE	CL%	EVTS	BKGD EST	DOCUMENT ID		TECN
>220	***p***	**90**			[1] TAKHISTOV	14	SKAM
• • • We do not use the following data for averages, fits, limits, etc. • • •							
> 21	*p*	90	7	11.23	BERGER	91B	FREJ

[1] Allowed events at 90% CL are 286.

$\tau(p \to e^- \mu^+ \mu^+)$ — τ_{59}

LIMIT (10^{30} years)	PARTICLE	CL%	EVTS	BKGD EST	DOCUMENT ID		TECN
>11000	***p***	**90**	**1**	**0.27**	TANAKA	20	SKAM
• • • We do not use the following data for averages, fits, limits, etc. • • •							
> 6.0	*p*	90	0	0.7	PHILLIPS	89	HPW

$\tau(n \to 3\nu)$ — τ_{60}

See also the "to anything" and "disappearance" limits for bound nucleons in the "*p* Mean Life" data block just in front of the list of possible *p* decay modes. Such modes could of course be to three (or five) neutrinos, and the limits are stronger, but we do not repeat them here.

LIMIT (10^{30} years)	PARTICLE	CL%	EVTS	BKGD EST	DOCUMENT ID		TECN
>0.00049	***n***	**90**	**2**	**2**	[1] SUZUKI	93B	KAMI
• • • We do not use the following data for averages, fits, limits, etc. • • •							
>0.0023	*n*	90			[2] GLICENSTEIN	97	KAMI
>0.00003	*n*	90	11	6.1	[3] BERGER	91B	FREJ
>0.00012	*n*	90	7	11.2	[3] BERGER	91B	FREJ
>0.0005	*n*	90	0		LEARNED	79	RVUE

[1] The SUZUKI 93B limit applies to any of $\nu_e \nu_e \overline{\nu}_e$, $\nu_\mu \nu_\mu \overline{\nu}_\mu$, or $\nu_\tau \nu_\tau \overline{\nu}_\tau$.

[2] GLICENSTEIN 97 uses Kamioka data and the idea that the disappearance of the neutron's magnetic moment should produce radiation.

[3] The first BERGER 91B limit is for $n \to \nu_e \nu_e \overline{\nu}_e$, the second is for $n \to \nu_\mu \nu_\mu \overline{\nu}_\mu$.

$\tau(n \to 5\nu)$ — τ_{61}

See the note on $\tau(n \to 3\nu)$ on the previous data block.

LIMIT (10^{30} years)	PARTICLE	CL%	EVTS	BKGD EST	DOCUMENT ID		TECN
• • • We do not use the following data for averages, fits, limits, etc. • • •							
>0.0017	*n*	90			[1] GLICENSTEIN	97	KAMI

[1] GLICENSTEIN 97 uses Kamioka data and the idea that the disappearance of the neutron's magnetic moment should produce radiation.

Inclusive modes

$\tau(N \to e^+ \text{anything})$ — τ_{62}

LIMIT (10^{30} years)	PARTICLE	CL%	EVTS	BKGD EST	DOCUMENT ID		TECN
>0.6	***p, n***	**90**			[1] LEARNED	79	RVUE

[1] The electron may be primary or secondary.

$\tau(N \to \mu^+ \text{anything})$ — τ_{63}

LIMIT (10^{30} years)	PARTICLE	CL%	EVTS	BKGD EST	DOCUMENT ID		TECN
>12	***p, n***	**90**	**2**		[1,2] CHERRY	81	HOME
• • • We do not use the following data for averages, fits, limits, etc. • • •							
> 1.8	*p, n*	90			[2] COWSIK	80	CNTR
> 6	*p, n*	90			[2] LEARNED	79	RVUE

[1] We have converted 2 possible events to 90% CL limit.

[2] The muon may be primary or secondary.

Downloaded from https://academic.oup.com/ptep/article/2022/8/083C01/6651666 by KIT Library user on 27 September 2022

$\tau(N \to \nu \text{anything})$ — τ_{64}

Anything = π, ρ, K, etc.

LIMIT (10^{30} years)	PARTICLE	CL%	EVTS	BKGD EST	DOCUMENT ID		TECN
• • • We do not use the following data for averages, fits, limits, etc. • • •							
>0.0002	p, n	90	0		LEARNED	79	RVUE

$\tau(N \to e^+ \pi^0 \text{anything})$ — τ_{65}

LIMIT (10^{30} years)	PARTICLE	CL%	EVTS	BKGD EST	DOCUMENT ID		TECN
>0.6	**p, n**	**90**	**0**		LEARNED	79	RVUE

$\tau(N \to 2 \text{ bodies}, \nu\text{-free})$ — τ_{66}

LIMIT (10^{30} years)	PARTICLE	CL%	EVTS	BKGD EST	DOCUMENT ID		TECN
• • • We do not use the following data for averages, fits, limits, etc. • • •							
>1.3	p, n	90	0		ALEKSEEV	81	BAKS

$\Delta B = 2$ dinucleon modes

$\tau(pp \to \pi^+ \pi^+)$ — τ_{67}

LIMIT (10^{30} years)	CL%	EVTS	BKGD EST	DOCUMENT ID		TECN	COMMENT
>72.2	**90**	**2**	**4.45**	GUSTAFSON	15	SKAM	per oxygen nucleus
• • • We do not use the following data for averages, fits, limits, etc. • • •							
> 0.7	90	4	2.34	BERGER	91B	FREJ	per iron nucleus

$\tau(pn \to \pi^+ \pi^0)$ — τ_{68}

LIMIT (10^{30} years)	CL%	EVTS	BKGD EST	DOCUMENT ID		TECN	COMMENT
>170	**90**			GUSTAFSON	15	SKAM	per oxygen nucleus
• • • We do not use the following data for averages, fits, limits, etc. • • •							
> 2.0	90	0	0.31	BERGER	91B	FREJ	per iron nucleus

$\tau(nn \to \pi^+ \pi^-)$ — τ_{69}

LIMIT (10^{30} years)	CL%	EVTS	BKGD EST	DOCUMENT ID		TECN	COMMENT
>0.7	**90**	**4**	**2.18**	BERGER	91B	FREJ	τ per iron nucleus

$\tau(nn \to \pi^0 \pi^0)$ — τ_{70}

LIMIT (10^{30} years)	CL%	EVTS	BKGD EST	DOCUMENT ID		TECN	COMMENT
>404	**90**			GUSTAFSON	15	SKAM	per oxygen nucleus
• • • We do not use the following data for averages, fits, limits, etc. • • •							
> 3.4	90	0	0.78	BERGER	91B	FREJ	per iron nucleus

$\tau(pp \to K^+ K^+)$ — τ_{71}

LIMIT (10^{30} years)	CL%	EVTS	BKGD EST	DOCUMENT ID		TECN	COMMENT
>170	**90**	**0**	**0.28**	LITOS	14	SKAM	τ per oxygen nucleus

$\tau(pp \to e^+ e^+)$ — τ_{72}

LIMIT (10^{30} years)	CL%	EVTS	BKGD EST	DOCUMENT ID		TECN	COMMENT
>5.8	**90**	**0**	**<0.1**	BERGER	91B	FREJ	τ per iron nucleus

$\tau(pp \to e^+ \mu^+)$ — τ_{73}

LIMIT (10^{30} years)	CL%	EVTS	BKGD EST	DOCUMENT ID		TECN	COMMENT
>3.6	**90**	**0**	**<0.1**	BERGER	91B	FREJ	τ per iron nucleus

$\tau(pp \to \mu^+ \mu^+)$ — τ_{74}

LIMIT (10^{30} years)	CL%	EVTS	BKGD EST	DOCUMENT ID		TECN	COMMENT
>1.7	**90**	**0**	**0.62**	BERGER	91B	FREJ	τ per iron nucleus

$\tau(pn \to e^+ \overline{\nu})$ — τ_{75}

LIMIT (10^{30} years)	CL%	EVTS	BKGD EST	DOCUMENT ID		TECN	COMMENT
>260	**90**			TAKHISTOV	15	SKAM	
• • • We do not use the following data for averages, fits, limits, etc. • • •							
> 2.8	90	5	9.67	BERGER	91B	FREJ	τ per iron nucleus

$\tau(pn \to \mu^+ \overline{\nu})$ — τ_{76}

LIMIT (10^{30} years)	CL%	EVTS	BKGD EST	DOCUMENT ID		TECN	COMMENT
>200	**90**			TAKHISTOV	15	SKAM	
• • • We do not use the following data for averages, fits, limits, etc. • • •							
> 1.6	90	4	4.37	BERGER	91B	FREJ	τ per iron nucleus

$\tau(pn \to \tau^+ \overline{\nu}_\tau)$ — τ_{77}

LIMIT (10^{30} years)	CL%	EVTS	BKGD EST	DOCUMENT ID		TECN
>29	**90**			TAKHISTOV	15	SKAM
• • • We do not use the following data for averages, fits, limits, etc. • • •						
> 1	90			[1] BRYMAN	14	CHER

[1] BRYMAN 14 uses a MCGREW 99 limit on the $p \to e^+ \nu\nu$ lifetime to extract this value.

$\tau(nn \to \nu_e \overline{\nu}_e)$ — τ_{78}

We include "invisible" modes here.

LIMIT (10^{30} years)	CL%	EVTS	BKGD EST	DOCUMENT ID		TECN	COMMENT
>1.4	**90**			[1] ARAKI	06	KLND	$nn \to$ invisible
• • • We do not use the following data for averages, fits, limits, etc. • • •							
>0.013	90			[2] ANDERSON	19A	SNO+	$nn \to$ invisible
>0.000042	90			[3] TRETYAK	04	CNTR	$nn \to$ invisible
>0.000049	90			[4] BACK	03	BORX	$nn \to$ invisible
>0.000012	90			[5] BERNABEI	00B	DAMA	$nn \to$ invisible
>0.000012	90	5	9.7	BERGER	91B	FREJ	τ per iron nucleus

[1] ARAKI 06 looks for signs of de-excitation of the residual nucleus after disappearance of two neutrons from the s shell of ^{12}C.
[2] ANDERSON 19A looks for γ rays from the de-excitation of a residual ^{14}O* following the disappearance of nn in ^{16}O.
[3] TRETYAK 04 uses data from an old Homestake-mine radiochemical experiment on limits for invisible decays of ^{39}K to ^{37}Ar.
[4] BACK 03 looks for decays of unstable nuclides left after NN decays of parent ^{12}C, ^{13}C, ^{16}O nuclei. These are "invisible channel" limits.
[5] BERNABEI 00B looks for the decay of a $^{127}_{54}$Xe nucleus following the disappearance of an nn pair in the otherwise-stable $^{129}_{54}$Xe nucleus. The limit here applies as well to $nn \to \nu_\mu \overline{\nu}_\mu$, $nn \to \nu_\tau \overline{\nu}_\tau$, or any "disappearance" mode.

$\tau(nn \to \nu_\mu \overline{\nu}_\mu)$ — τ_{79}

See the proceeding data block. "Invisible modes" would include any multi-neutrino mode.

LIMIT (10^{30} years)	CL%	EVTS	BKGD EST	DOCUMENT ID		TECN	COMMENT
> 1.4 (CL=90%) OUR LIMIT							
• • • We do not use the following data for averages, fits, limits, etc. • • •							
>0.000006	90	4	4.4	BERGER	91B	FREJ	τ per iron nucleus

$\tau(pn \to \text{invisible})$ — τ_{80}

This violates charge conservation as well as baryon number conservation.

VALUE (10^{30} years)	CL%	DOCUMENT ID		TECN
>0.026	90	[1] ANDERSON	19A	SNO+
>0.000021	90	[2] TRETYAK	04	CNTR

[1] ANDERSON 19A looks for γ rays from the de-excitation of a residual ^{14}N* following the disappearance of pn in ^{16}O.
[2] TRETYAK 04 uses data from an old Homestake-mine radiochemical experiment on limits for invisible decays of ^{39}K to ^{37}Ar.

$\tau(pp \to \text{invisible})$ — τ_{81}

This violates charge conservation as well as baryon number conservation.

LIMIT (10^{30} years)	CL%	EVTS	BKGD EST	DOCUMENT ID		TECN
>0.047	**90**			[1] ANDERSON	19A	SNO+
• • • We do not use the following data for averages, fits, limits, etc. • • •						
>0.00005	90			[2] BACK	03	BORX
>0.00000055	90			[3] BERNABEI	00B	DAMA

[1] ANDERSON 19A looks for γ rays from the de-excitation of a residual ^{14}C* following the disappearance of pp in ^{16}O.
[2] BACK 03 looks for decays of unstable nuclides left after NN decays of parent ^{12}C, ^{13}C, ^{16}O nuclei. These are "invisible channel" limits.
[3] BERNABEI 00B looks for the decay of a $^{127}_{52}$Te nucleus following the disappearance of a pp pair in the otherwise-stable $^{129}_{54}$Xe nucleus.

$\overline{p}$ PARTIAL MEAN LIVES

The "partial mean life" limits tabulated here are the limits on $\overline{\tau}/B_i$, where $\overline{\tau}$ is the total mean life for the antiproton and B_i is the branching fraction for the mode in question.

$\tau(\overline{p} \to e^- \gamma)$ — τ_{82}

VALUE (years)	CL%	DOCUMENT ID		TECN	COMMENT
> 7×10^5	90	GEER	00	APEX	8.9 GeV/c $\overline{p}$ beam
• • • We do not use the following data for averages, fits, limits, etc. • • •					
>1848	95	GEER	94	CALO	8.9 GeV/c $\overline{p}$ beam

$\tau(\overline{p} \to \mu^- \gamma)$ — τ_{83}

VALUE (years)	CL%	DOCUMENT ID		TECN	COMMENT
>5 $\times 10^4$	90	GEER	00	APEX	8.9 GeV/c $\overline{p}$ beam
• • • We do not use the following data for averages, fits, limits, etc. • • •					
>5.0 $\times 10^4$	90	HU	98B	APEX	8.9 GeV/c $\overline{p}$ beam

$\tau(\overline{p} \to e^- \pi^0)$ — τ_{84}

VALUE (years)	CL%	DOCUMENT ID		TECN	COMMENT
> 4×10^5	90	GEER	00	APEX	8.9 GeV/c $\overline{p}$ beam
• • • We do not use the following data for averages, fits, limits, etc. • • •					
>554	95	GEER	94	CALO	8.9 GeV/c $\overline{p}$ beam

$\tau(\overline{p} \to \mu^- \pi^0)$ — τ_{85}

VALUE (years)	CL%	DOCUMENT ID		TECN	COMMENT
>5 $\times 10^4$	90	GEER	00	APEX	8.9 GeV/c $\overline{p}$ beam
• • • We do not use the following data for averages, fits, limits, etc. • • •					
>4.8 $\times 10^4$	90	HU	98B	APEX	8.9 GeV/c $\overline{p}$ beam

Downloaded from https://academic.oup.com/ptep/article/2022/8/083C01/6651666 by KIT Library user on 27 September 2022

$\tau(\overline{p} \to e^- \eta)$ — τ_{86}

VALUE (years)	CL%	DOCUMENT ID		TECN	COMMENT
$> 2 \times 10^4$	90	GEER	00	APEX	8.9 GeV/c $\overline{p}$ beam
• • • We do not use the following data for averages, fits, limits, etc. • • •					
>171	95	GEER	94	CALO	8.9 GeV/c $\overline{p}$ beam

$\tau(\overline{p} \to \mu^- \eta)$ — τ_{87}

VALUE (years)	CL%	DOCUMENT ID		TECN	COMMENT
$>8 \times 10^3$	90	GEER	00	APEX	8.9 GeV/c $\overline{p}$ beam
• • • We do not use the following data for averages, fits, limits, etc. • • •					
$>7.9 \times 10^3$	90	HU	98B	APEX	8.9 GeV/c $\overline{p}$ beam

$\tau(\overline{p} \to e^- K^0_S)$ — τ_{88}

VALUE (years)	CL%	DOCUMENT ID		TECN	COMMENT
>900	90	GEER	00	APEX	8.9 GeV/c $\overline{p}$ beam
• • • We do not use the following data for averages, fits, limits, etc. • • •					
> 29	95	GEER	94	CALO	8.9 GeV/c $\overline{p}$ beam

$\tau(\overline{p} \to \mu^- K^0_S)$ — τ_{89}

VALUE (years)	CL%	DOCUMENT ID		TECN	COMMENT
$>4 \times 10^3$	90	GEER	00	APEX	8.9 GeV/c $\overline{p}$ beam
• • • We do not use the following data for averages, fits, limits, etc. • • •					
$>4.3 \times 10^3$	90	HU	98B	APEX	8.9 GeV/c $\overline{p}$ beam

$\tau(\overline{p} \to e^- K^0_L)$ — τ_{90}

VALUE (years)	CL%	DOCUMENT ID		TECN	COMMENT
$>9 \times 10^3$	90	GEER	00	APEX	8.9 GeV/c $\overline{p}$ beam
• • • We do not use the following data for averages, fits, limits, etc. • • •					
>9	95	GEER	94	CALO	8.9 GeV/c $\overline{p}$ beam

$\tau(\overline{p} \to \mu^- K^0_L)$ — τ_{91}

VALUE (years)	CL%	DOCUMENT ID		TECN	COMMENT
$>7 \times 10^3$	90	GEER	00	APEX	8.9 GeV/c $\overline{p}$ beam
• • • We do not use the following data for averages, fits, limits, etc. • • •					
$>6.5 \times 10^3$	90	HU	98B	APEX	8.9 GeV/c $\overline{p}$ beam

$\tau(\overline{p} \to e^- \gamma\gamma)$ — τ_{92}

VALUE (years)	CL%	DOCUMENT ID		TECN	COMMENT
$>2 \times 10^4$	90	GEER	00	APEX	8.9 GeV/c $\overline{p}$ beam

$\tau(\overline{p} \to \mu^- \gamma\gamma)$ — τ_{93}

VALUE (years)	CL%	DOCUMENT ID		TECN	COMMENT
$>2 \times 10^4$	90	GEER	00	APEX	8.9 GeV/c $\overline{p}$ beam
• • • We do not use the following data for averages, fits, limits, etc. • • •					
$>2.3 \times 10^4$	90	HU	98B	APEX	8.9 GeV/c $\overline{p}$ beam

$\tau(\overline{p} \to e^- \omega)$ — τ_{94}

VALUE (years)	CL%	DOCUMENT ID		TECN	COMMENT
>200	90	GEER	00	APEX	8.9 GeV/c $\overline{p}$ beam

p REFERENCES

BORCHERT	22	NAT 601 53	M.J. Borchert *et al.*	(BASE Collab.)
CUI	21	PRL 127 092001	Z.-F. Cui *et al.*	(NJU, ECT, HZDR)
CUI	21B	CPL 38 121401	Z.-F. Cui *et al.*	(NJU, ECT, HZDR)
FINK	21	PRL 127 243001	D.J. Fink, E.G. Myers	(FSU)
MIHOVILOVIC	21	EPJ A57 107	M. Mihovilovic *et al.*	(LJUB, MAINZ, MIT+)
TIESINGA	21	RMP 93 025010	E. Tiesinga *et al.*	(NIST)
TAKENAKA	20	PR D102 112011	A. Takenaka *et al.*	(Super-Kamiokande Collab.)
TANAKA	20	PR D101 052011	M. Tanaka *et al.*	(Super-Kamiokande Collab.)
ANDERSON	19A	PR D99 032008	M. Anderson *et al.*	(SNO+ Collab.)
BEZGINOV	19	SCI 365 1007	N. Bezginov *et al.*	(YORKC, TNTO)
HEISSE	19	PR A100 022518	F. Heisse *et al.*	(MPIK, GSI, MAINZ)
PASQUINI	19	JP G46 104001	B. Pasquini, P. Pedroni, S. Sconfietti	(PAVI)
SCHUMACHER	19	LHEP 4 4	M. Schumacher	(GOET)
XIONG	19	NAT 575 147	W. Xiong *et al.*	(PRad Collab.)
FLEURBAEY	18	PRL 120 183001	H. Fleurbaey *et al.*	(SORB)
PDG	18	PR D98 030001	M. Tanabashi *et al.*	(PDG Collab.)
ABE	17	PR D95 012004	K. Abe *et al.*	(Super-Kamiokande Collab.)
ABE	17D	PR D96 012003	K. Abe *et al.*	(Super-Kamiokande Collab.)
BEYER	17	SCI 358 79	A. Beyer *et al.*	(MPQG Collab.)
HEISSE	17	PRL 119 033001	F. Heisse *et al.*	(MPIK, GSI, MAINZ, RIKEN)
NAGAHAMA	17	NATC 8 14084	H. Nagahama *et al.*	(RIKEN, TOKY, CERN+)
SAHOO	17	PR D95 013002	B.K. Sahoo	(AHMEB)
SCHNEIDER	17	SCI 358 1081	G. Schneider *et al.*	(MAINZ, RIKEN, +)
SELLNER	17	NJP 19 083023	S. Sellner *et al.*	(RIKEN, MPIK, +)
SMORRA	17	NAT 550 371	C. Smorra *et al.*	(RIKEN, CERN, +)
MOHR	16	RMP 88 035009	P.J. Mohr, D.B. Newell, B.N. Taylor	(NIST)
ASAKURA	15	PR D92 052006	K. Asakura *et al.*	(KamLAND Collab.)
GUSTAFSON	15	PR D91 072009	J. Gustafson *et al.*	(Super-Kamiokande Collab.)
LEE	15	PR D92 013013	G. Lee, J.R. Arrington, R.J. Hill	(ANL, EFI+)
TAKHISTOV	15	PRL 115 121803	V. Takhistov *et al.*	(Super-Kamiokande Collab.)
ULMER	15	NAT 524 196	S. Ulmer *et al.*	(RIKEN, CERN, MPIK, +)
ABE	14E	PRL 113 121802	K. Abe *et al.*	(Super-Kamiokande Collab.)
ABE	14G	PR D90 072005	K. Abe *et al.*	(Super-Kamiokande Collab.)
BRYMAN	14	PL B733 190	D. Bryman	(BRCO)
EPSTEIN	14	PR D90 074027	Z. Epstein, G. Paz, J. Roy	(UMD, WAYN)
LITOS	14	PRL 112 131803	M. Litos *et al.*	(Super-Kamiokande Collab.)
PDG	14	CP C38 070001	K. Olive *et al.*	(PDG Collab.)
TAKHISTOV	14	PRL 113 101801	V. Takhistov *et al.*	(Super-Kamiokande Collab.)
ANTOGNINI	13	SCI 339 417	A. Antognini *et al.*	(MPIM, ETH, UPMC+)
DISCIACCA	13	PRL 110 130801	J. DiSciacca *et al.*	(ATRAP Collab.)
MCGOVERN	13	EPJ A49 12	J.A. McGovern, D.R. Phillips, H.W. Griesshammer	
MOHR	12	RMP 84 1527	P.J. Mohr, B.N. Taylor, D.B. Newell	(NIST)
NISHINO	12	PR D85 112001	H. Nishino *et al.*	(Super-Kamiokande Collab.)
REGIS	12	PR D86 012006	C. Regis *et al.*	(Super-Kamiokande Collab.)
BRESSI	11	PR A83 052101	G. Bressi *et al.*	(LEGN, PAVII, PADO, TRST+)
HORI	11	NAT 475 484	M. Hori *et al.*	(MPIQ, TOKY, BUDA, +)
ZHAN	11	PL B705 59	X. Zhan *et al.*	(JLAB-Hall A Collab.)
BERNAUER	10	PRL 105 242001	J.C. Bernauer *et al.*	(MAMI A1 Collab.)
Also		PR C90 015206	J.C. Bernauer *et al.*	(MAMI A1 Collab.)
BORISYUK	10	NP A843 59	D. Borisyuk	(KIEV)
HILL	10	PR D82 113005	R.J. Hill, G. Paz	(CHIC)
POHL	10	NAT 466 213	R. Pohl *et al.*	(MPIQ, ENSP, COIM, +)
NISHINO	09	PRL 102 141801	H. Nishino *et al.*	(Super-Kamiokande Collab.)
PASK	09	PL B678 55	T. Pask *et al.*	(Stefan Meyer Inst., Vienna, TOKY+)
MOHR	08	RMP 80 633	P.J. Mohr, B.N. Taylor, D.B. Newell	(NIST)
BELUSHKIN	07	PR C75 035202	M.A. Belushkin, H.W. Hammer, U.-G. Meissner	(BONN+)
ARAKI	06	PRL 96 101802	T. Araki *et al.*	(KamLAND Collab.)
HORI	06	PRL 96 243401	M. Hori *et al.*	(CERN, TOKYO+)
BLUNDEN	05	PR C72 057601	P.G. Blunden, I. Sick	(MANI, BASL)
KOBAYASHI	05	PR D72 052007	K. Kobayashi *et al.*	(Super-Kamiokande Collab.)
MOHR	05	RMP 77 1	P.J. Mohr, B.N. Taylor	(NIST)
SCHUMACHER	05	PPNP 55 567	M. Schumacher	(GOET)
AHMED	04	PRL 92 102004	S.N. Ahmed *et al.*	(SNO Collab.)
TRETYAK	04	JETPL 79 106	V.I. Tretyak, V.Yu. Denisov, Yu.G. Zdesenko	(KIEV)
		Translated from ZETFP 79 136.		
BACK	03	PL B563 23	H.O. Back *et al.*	(Borexino Collab.)
BEANE	03	PL B567 200	S.R. Beane *et al.*	
Also		PL B607 320 (errat.)	S.R. Beane *et al.*	
DMITRIEV	03	PRL 91 212303	V.F. Dmitriev, R.A. Senkov	(NOVO)
HORI	03	PRL 91 123401	M. Hori *et al.*	(CERN ASACUSA Collab.)
SICK	03	PL B576 62	I. Sick	(BASL)
ZDESENKO	03	PL B553 135	Yu.G. Zdesenko, V.I. Tretyak	(KIEV)
AHMAD	02	PRL 89 011301	Q.R. Ahmad *et al.*	(SNO Collab.)
BARANOV	01	PPN 32 376	P.S. Baranov *et al.*	
		Translated from FECAY 32 699.		
BLANPIED	01	PR C64 025203	G. Blanpied *et al.*	(BNL LEGS Collab.)
HORI	01	PRL 87 093401	M. Hori *et al.*	(CERN ASACUSA Collab.)
OLMOSDEL...	01	EPJ A10 207	V. Olmos de Leon *et al.*	(MAMI TAPS Collab.)
TRETYAK	01	PL B505 59	V.I. Tretyak, Yu.G. Zdesenko	(KIEV)
BERNABEI	00B	PL B493 12	R. Bernabei *et al.*	(Gran Sasso DAMA Collab.)
GEER	00	PRL 84 590	S. Geer *et al.*	(FNAL APEX Collab.)
Also		PR D62 052004	S. Geer *et al.*	(FNAL APEX Collab.)
Also		PRL 85 3546 (errat.)	S. Geer *et al.*	(FNAL APEX Collab.)
GEER	00D	APJ 532 648	S.H. Geer, D.C. Kennedy	
SENGUPTA	00	PL B484 275	S. Sengupta	
WALL	00	PR D61 072004	D. Wall *et al.*	(Soudan-2 Collab.)
WALL	00B	PR D62 092003	D. Wall *et al.*	(Soudan-2 Collab.)
GABRIELSE	99	PRL 82 3198	G. Gabrielse *et al.*	
HAYATO	99	PRL 83 1529	Y. Hayato *et al.*	(Super-Kamiokande Collab.)
MCGREW	99	PR D59 052004	C. McGrew *et al.*	(IMB-3 Collab.)
MOHR	99	JPCRD 28 1713	P.J. Mohr, B.N. Taylor	(NIST)
Also		RMP 72 351	P.J. Mohr, B.N. Taylor	(NIST)
TORII	99	PR A59 223	H.A. Torii *et al.*	(CERN PS-205 Collab.)
ALLISON	98	PL B427 217	W.W.M. Allison *et al.*	(Soudan-2 Collab.)
HU	98B	PR D58 111101	M. Hu *et al.*	(FNAL APEX Collab.)
SHIOZAWA	98	PRL 81 3319	M. Shiozawa *et al.*	(Super-Kamiokande Collab.)
GLICENSTEIN	97	PL B411 326	J.F. Glicenstein	(SACL)
GABRIELSE	95	PRL 74 3544	G. Gabrielse *et al.*	(HARV, MAINZ, SEOUL)
MACGIBBON	95	PR C52 2097	B.E. MacGibbon *et al.*	(ILL, SASK, INRM)
GEER	94	PRL 72 1596	S. Geer *et al.*	(FNAL, UCLA, PSU)
HALLIN	93	PR C48 1497	E.L. Hallin *et al.*	(SASK, BOST, ILL)
SUZUKI	93B	PL B311 357	Y. Suzuki *et al.*	(Kamiokande Collab.)
HUGHES	92	PRL 69 578	R.J. Hughes, B.I. Deutch	(LANL, AARH)
ZIEGER	92	PL B278 34	A. Zieger *et al.*	(MPCM)
Also		PL B281 417 (erratum)	A. Zieger *et al.*	(MPCM)
BERGER	91	ZPHY C50 385	C. Berger *et al.*	(FREJUS Collab.)
BERGER	91B	PL B269 227	C. Berger *et al.*	(FREJUS Collab.)
FEDERSPIEL	91	PRL 67 1511	F.J. Federspiel *et al.*	(ILL)
BECKER-SZ...	90	PR D42 2974	R.A. Becker-Szendy *et al.*	(IMB-3 Collab.)
ERICSON	90	EPL 11 295	T.E.O. Ericson, A. Richter	(CERN, DARM)
GABRIELSE	90	PRL 65 1317	G. Gabrielse *et al.*	(HARV, MAINZ, WASH+)
BERGER	89	NP B313 509	C. Berger *et al.*	(FREJUS Collab.)
CHO	89	PRL 63 2559	D. Cho, K. Sangster, E.A. Hinds	(YALE)
HIRATA	89C	PL B220 308	K.S. Hirata *et al.*	(Kamiokande Collab.)
PHILLIPS	89	PL B224 348	T.J. Phillips *et al.*	(HPW Collab.)
KREISSL	88	ZPHY C37 557	A. Kreissl *et al.*	(CERN PS176 Collab.)
SEIDEL	88	PRL 61 2522	S. Seidel *et al.*	(IMB Collab.)
BARTELT	87	PR D36 1990	J.E. Bartelt *et al.*	(Soudan Collab.)
Also		PR D40 1701 (erratum)	J.E. Bartelt *et al.*	(Soudan Collab.)
COHEN	87	RMP 59 1121	E.R. Cohen, B.N. Taylor	(RISC, NBS)
HAINES	86	PRL 57 1986	T.J. Haines *et al.*	(IMB Collab.)
KAJITA	86	JPSJ 55 711	T. Kajita *et al.*	(Kamiokande Collab.)
ARISAKA	85	JPSJ 54 3213	K. Arisaka *et al.*	(Kamiokande Collab.)
BLEWITT	85	PRL 55 2114	G.B. Blewitt *et al.*	(IMB Collab.)
DZUBA	85	PL 154B 93	V.A. Dzuba, V.V. Flambaum, P.G. Silvestrov	(NOVO)
PARK	85	PRL 54 22	H.S. Park *et al.*	(IMB Collab.)
BATTISTONI	84	PL 133B 454	G. Battistoni *et al.*	(NUSEX Collab.)
MARINELLI	84	PL 137B 439	M. Marinelli, G. Morpurgo	(GENO)
WILKENING	84	PR A29 425	D.A. Wilkening, N.F. Ramsey, D.J. Larson	(HARV+)
BARTELT	83	PRL 50 651	J.E. Bartelt *et al.*	(MINN, ANL)
BATTISTONI	82	PL 118B 461	G. Battistoni *et al.*	(NUSEX Collab.)
KRISHNA...	82	PL 115B 349	M.R. Krishnaswamy *et al.*	(TATA, OSKC+)
ALEKSEEV	81	JETPL 33 651	E.N. Alekseev *et al.*	(PNPI)
		Translated from ZETFP 33 664.		
CHERRY	81	PRL 47 1507	M.L. Cherry *et al.*	(PENN, BNL)
COWSIK	80	PR D22 2204	R. Cowsik, V.S. Narasimham	(TATA)
BELL	79	PL 86B 215	M. Bell *et al.*	(CERN)
GOLDEN	79	PRL 43 1196	R.L. Golden *et al.*	(NASA, PSLL)
LEARNED	79	PRL 43 907	J.G. Learned, F. Reines, A. Soni	(UCI)
BREGMAN	78	PL 78B 174	M. Bregman *et al.*	(CERN)
ROBERTS	78	PR D17 358	B.L. Roberts	(WILL, RHEL)
EVANS	77	SCI 197 989	J.C. Evans Jr., R.I. Steinberg	(BNL, PENN)
HU	75	NP A254 403	E. Hu *et al.*	(COLU, YALE)
COHEN	73	JPCRD 2 664	E.R. Cohen, B.N. Taylor	(RISC, NBS)
DYLLA	73	PR A7 1224	H.F. Dylla, J.G. King	(MIT)
DIX	70	Thesis Case	F.W. Dix	(CASE)
HARRISON	69	PRL 22 1263	G.E. Harrison, P.G.H. Sandars, S.J. Wright	(OXF)
GURR	67	PR 158 1321	H.S. Gurr *et al.*	(CASE, WITW)
FLEROV	58	DOKL 3 79	G.N. Flerov *et al.*	(ASCI)

Downloaded from https://academic.oup.com/ptep/article/2022/8/083C01/6651666 by KIT Library user on 27 September 2022

n

$I(J^P) = \frac{1}{2}(\frac{1}{2}^+)$ Status: ****

We have omitted some results that have been superseded by later experiments. See our earlier editions.

Anyone interested in the neutron should look at these two review articles: D. Dubbers and M.G. Schmidt, "The neutron and its role in cosmology and particle physics," Reviews of Modern Physics **83** 1111 (2011); and F.E. Wietfeldt and G.L. Greene, "The neutron lifetime," Reviews of Modern Physics **83** 1173 (2011).

n MASS (atomic mass units u)

The mass is known much more precisely in u (atomic mass units) than in MeV. See the next data block.

VALUE (u)	DOCUMENT ID		TECN	COMMENT
1.00866491595 ± 0.00000000049	TIESINGA	21	RVUE	2018 CODATA value
• • • We do not use the following data for averages, fits, limits, etc. • • •				
1.00866491588 ± 0.00000000049	MOHR	16	RVUE	2014 CODATA value
1.00866491600 ± 0.00000000043	MOHR	12	RVUE	2010 CODATA value
1.00866491597 ± 0.00000000043	MOHR	08	RVUE	2006 CODATA value
1.00866491560 ± 0.00000000055	MOHR	05	RVUE	2002 CODATA value
1.00866491578 ± 0.00000000055	MOHR	99	RVUE	1998 CODATA value
1.008665904 ± 0.000000014	COHEN	87	RVUE	1986 CODATA value

n MASS (MeV)

The mass is known more precisely in u (atomic mass units) than in MeV. The conversion is: 1 u = 931.494 102 42(28) MeV/c^2 (2018 CODATA value, TIESINGA 21).

VALUE (MeV)	DOCUMENT ID		TECN	COMMENT
939.56542052 ± 0.00000054	TIESINGA	21	RVUE	2018 CODATA value
• • • We do not use the following data for averages, fits, limits, etc. • • •				
939.5654133 ± 0.0000058	MOHR	16	RVUE	2014 CODATA value
939.565379 ± 0.000021	MOHR	12	RVUE	2010 CODATA value
939.565346 ± 0.000023	MOHR	08	RVUE	2006 CODATA value
939.565360 ± 0.000081	MOHR	05	RVUE	2002 CODATA value
939.565331 ± 0.000037	[1] KESSLER	99	SPEC	$np \to d\gamma$
939.565330 ± 0.000038	MOHR	99	RVUE	1998 CODATA value
939.56565 ± 0.00028	[2,3] DIFILIPPO	94	TRAP	Penning trap
939.56563 ± 0.00028	COHEN	87	RVUE	1986 CODATA value
939.56564 ± 0.00028	[3,4] GREENE	86	SPEC	$np \to d\gamma$
939.5731 ± 0.0027	[3] COHEN	73	RVUE	1973 CODATA value

[1] We use the 1998 CODATA u-to-MeV conversion factor (see the heading above) to get this mass in MeV from the much more precisely measured KESSLER 99 value of 1.00866491637 ± 0.00000000082 u.
[2] The mass is known much more precisely in u: m = 1.0086649235 ± 0.0000000023 u. We use the 1986 CODATA conversion factor to get the mass in MeV.
[3] These determinations are not independent of the $m_n - m_p$ measurements below.
[4] The mass is known much more precisely in u: m = 1.008664919 ± 0.000000014 u.

$\overline{n}$ MASS

VALUE (MeV)	EVTS	DOCUMENT ID		TECN	COMMENT
939.485 ± 0.051	59	[1] CRESTI	86	HBC	$\overline{p}p \to \overline{n}n$

[1] This is a corrected result (see the erratum). The error is statistical. The maximum systematic error is 0.029 MeV.

$(m_n - m_{\overline{n}})/m_n$

A test of CPT invariance. Calculated from the n and $\overline{n}$ masses, above.

VALUE	DOCUMENT ID
(9±6) × 10^{-5} OUR EVALUATION	

$m_n - m_p$

VALUE (MeV)	DOCUMENT ID		TECN	COMMENT
1.29333236 ± 0.00000046	[1] TIESINGA	21	RVUE	2018 CODATA value
• • • We do not use the following data for averages, fits, limits, etc. • • •				
1.29333205 ± 0.00000051	[2] MOHR	16	RVUE	2014 CODATA value
1.29333217 ± 0.00000042	[3] MOHR	12	RVUE	2010 CODATA value
1.29333214 ± 0.00000043	[4] MOHR	08	RVUE	2006 CODATA value
1.2933317 ± 0.0000005	[5] MOHR	05	RVUE	2002 CODATA value
1.2933318 ± 0.0000005	[6] MOHR	99	RVUE	1998 CODATA value
1.293318 ± 0.000009	[7] COHEN	87	RVUE	1986 CODATA value
1.2933328 ± 0.0000072	GREENE	86	SPEC	$np \to d\gamma$
1.293429 ± 0.000036	COHEN	73	RVUE	1973 CODATA value

[1] The 2018 CODATA mass difference in u is $m_n - m_p$ = 1.388 449 33(49) × $10^{-3}u$.
[2] The 2014 CODATA mass difference in u is $m_n - m_p$ = 1.388 449 00(51) × $10^{-3}u$.
[3] The 2010 CODATA mass difference in u is $m_n - m_p$ = 1.388 449 19(45) × $10^{-3}u$.
[4] Calculated by us from the MOHR 08 ratio m_n/m_p = 1.00137841918(46). In u, $m_n - m_p$ = 1.38844920(46) × 10^{-3} u.
[5] Calculated by us from the MOHR 05 ratio m_n/m_p = 1.00137841870 ± 0.00000000058. In u, $m_n - m_p$ = (1.3884487 ± 0.0000006) × 10^{-3} u.
[6] Calculated by us from the MOHR 99 ratio m_n/m_p = 1.00137841887 ± 0.00000000058. In u, $m_n - m_p$ = (1.3884489 ± 0.0000006) × 10^{-3} u.
[7] Calculated by us from the COHEN 87 ratio m_n/m_p = 1.001378404 ± 0.000000009. In u, $m_n - m_p$ = 0.001388434 ± 0.000000009 u.

n MEAN LIFE

Limits on lifetimes for *bound* neutrons are given in the section "p PARTIAL MEAN LIVES."

We average seven of the best eight measurements, those made with ultra-cold neutrons (UCN's). If we include the one in-beam measurement with a comparable error (YUE 13), we get 879.6 ± 0.8 s, where the scale factor is now 2.0.

For a recent discussion of the long-standing disagreement between in-beam and UCN results, see CZARNECKI 18 (Physical Review Letters **120** 202002 (2018)). For a full review of all matters concerning the neutron lifetime until about 2010, see WIETFELDT 11, F.E. Wietfeldt and G.L. Greene, "The neutron lifetime," Reviews of Modern Physics **83** 1173 (2011).

VALUE (s)	DOCUMENT ID		TECN	COMMENT
878.4 ± 0.5 OUR AVERAGE Error includes scale factor of 1.8. See the ideogram below.				
877.75 ± 0.28 $^{+0.22}_{-0.16}$	GONZALEZ	21	CNTR	UCN asym. magnetic trap
878.3 ± 1.6 ± 1.0	EZHOV	18	CNTR	UCN magneto-gravit. trap
877.7 ± 0.7 $^{+0.4}_{-0.2}$	[1] PATTIE	18	CNTR	UCN asym. magnetic trap
881.5 ± 0.7 ± 0.6	SEREBROV	18	CNTR	UCN gravitational trap
880.2 ± 1.2	[2] ARZUMANOV	15	CNTR	UCN double bottle
882.5 ± 1.4 ± 1.5	[3] STEYERL	12	CNTR	UCN material bottle
880.7 ± 1.3 ± 1.2	PICHLMAIER	10	CNTR	UCN material bottle
878.5 ± 0.7 ± 0.3	SEREBROV	05	CNTR	UCN gravitational trap
• • • We do not use the following data for averages, fits, limits, etc. • • •				
887 ± 14 $^{+7}_{-3}$	[4] WILSON	21	CNTR	space-based n rate
887.7 ± 1.2 ± 1.9	[5] YUE	13	CNTR	In-beam n, trapped p
881.6 ± 0.8 ± 1.9	[6] ARZUMANOV	12	CNTR	See ARZUMANOV 15
886.3 ± 1.2 ± 3.2	NICO	05	CNTR	See YUE 13
886.8 ± 1.2 ± 3.2	DEWEY	03	CNTR	See NICO 05
885.4 ± 0.9 ± 0.4	ARZUMANOV	00	CNTR	See ARZUMANOV 12
889.2 ± 3.0 ± 3.8	BYRNE	96	CNTR	Penning trap
882.6 ± 2.7	[7] MAMPE	93	CNTR	UCN material bottle
888.4 ± 3.1 ± 1.1	[8] NESVIZHEV...	92	CNTR	UCN material bottle
888.4 ± 2.9	ALFIMENKOV	90	CNTR	See NESVIZHEVSKII 92
893.6 ± 3.8 ± 3.7	BYRNE	90	CNTR	See BYRNE 96
878 ± 27 ± 14	KOSSAKOW...	89	TPC	Pulsed beam
887.6 ± 3.0	MAMPE	89	CNTR	See STEYERL 12
877 ± 10	PAUL	89	CNTR	Magnetic storage ring
876 ± 10 ± 19	LAST	88	SPEC	Pulsed beam
891 ± 9	SPIVAK	88	CNTR	Beam
903 ± 13	KOSVINTSEV	86	CNTR	UCN material bottle
937 ± 18	[9] BYRNE	80	CNTR	
875 ± 95	KOSVINTSEV	80	CNTR	
881 ± 8	BONDAREN...	78	CNTR	See SPIVAK 88
918 ± 14	CHRISTENSEN	72	CNTR	

[1] PATTIE 18 uses a new technique, with a semi-toroidal magneto-gravitational asymmetric trap and a novel in situ n-detector.
[2] ARZUMANOV 15 is a reanalysis of their 2008–2010 dataset, with improved systematic corrections of of ARZUMANOV 00 and ARZUMANOV 12.
[3] STEYERL 12 is a detailed reanalysis of neutron storage loss corrections to the raw data of MAMPE 89, and it replaces that value.
[4] WILSON 21 extract the value from the flux of n escaping the moon using data from the Lunar Prospector Neutron Spectrometer.
[5] YUE 13 differs from NICO 05 in that a different and better method was used to measure the neutron density in the fiducial volume. This shifted the lifetime by +1.4 seconds and reduced the previously largest source of systematic uncertainty by a factor of five.
[6] ARZUMANOV 12 reanalyzes its systematic corrections in ARZUMANOV 00 and obtains this corrected value.
[7] IGNATOVICH 95 calls into question some of the corrections and averaging procedures used by MAMPE 93. The response, BONDARENKO 96, denies the validity of the criticisms.
[8] The NESVIZHEVSKII 92 measurement has been withdrawn by A. Serebrov.
[9] The BYRNE 80 measurement has been withdrawn (J. Byrne, private communication, 1990).

Downloaded from https://academic.oup.com/ptep/article/2022/8/083C01/6651666 by KIT Library user on 27 September 2022

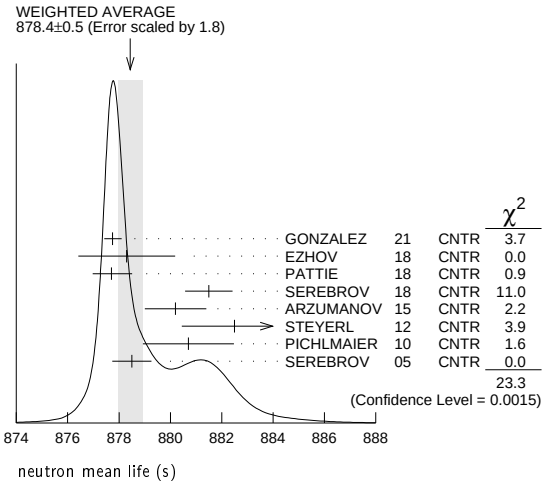

n MAGNETIC MOMENT

See the "Quark Model" review.

VALUE (μ_N)	DOCUMENT ID		TECN	COMMENT
−1.91304273±0.00000045	TIESINGA	21	RVUE	2018 CODATA value
• • • We do not use the following data for averages, fits, limits, etc. • • •				
−1.91304273±0.00000045	MOHR	16	RVUE	2014 CODATA value
−1.91304272±0.00000045	MOHR	12	RVUE	2010 CODATA value
−1.91304273±0.00000045	MOHR	08	RVUE	2006 CODATA value
−1.91304273±0.00000045	MOHR	05	RVUE	2002 CODATA value
−1.91304272±0.00000045	MOHR	99	RVUE	1998 CODATA value
−1.91304275±0.00000045	COHEN	87	RVUE	1986 CODATA value
−1.91304277±0.00000048	[1] GREENE	82	MRS	

[1] GREENE 82 measures the moment to be $(1.04187564 \pm 0.00000026) \times 10^{-3}$ Bohr magnetons. The value above is obtained by multiplying this by $m_p/m_e = 1836.152701 \pm 0.000037$ (the 1986 CODATA value from COHEN 87).

n ELECTRIC DIPOLE MOMENT

A nonzero value is forbidden by both T invariance and P invariance. A number of early results have been omitted. See RAMSEY 90, GOLUB 94, and LAMOREAUX 09 for reviews.

The results are upper limits on $|d_n|$.

VALUE (10^{-25} $e$cm)	CL%	DOCUMENT ID		TECN	COMMENT
< 0.18	90	[1] ABEL	20	MRS	UCN
• • • We do not use the following data for averages, fits, limits, etc. • • •					
< 0.22	95	[2] SAHOO	17		^{199}Hg atom EDM + theory
< 0.16	95	GRANER	16	MRS	^{199}Hg atom EDM + theory
< 0.30	90	[3] PENDLEBURY	15	MRS	Supersedes BAKER 06
< 0.55	90	SEREBROV	15	MRS	UCN's, $h\nu = 2\mu_n B \pm 2d_n E$
< 0.55	90	[4] SEREBROV	14	MRS	See SEREBROV 15
< 0.29	90	[5] BAKER	06	MRS	See PENDLEBURY 15
< 0.63	90	[6] HARRIS	99	MRS	$d = (-0.1 \pm 0.36) \times 10^{-25}$
< 0.97	90	ALTAREV	96	MRS	See SEREBROV 14
< 1.1	95	ALTAREV	92	MRS	See ALTAREV 96
< 1.2	95	SMITH	90	MRS	See HARRIS 99
< 2.6	95	ALTAREV	86	MRS	$d = (-1.4 \pm 0.6) \times 10^{-25}$
0.3 ±4.8		PENDLEBURY	84	MRS	Ultracold neutrons
< 6	90	ALTAREV	81	MRS	$d = (2.1 \pm 2.4) \times 10^{-25}$
<16	90	ALTAREV	79	MRS	$d = (4.0 \pm 7.5) \times 10^{-25}$

[1] ABEL 20 reports $d = (0.0 \pm 1.1 \pm 0.2) \times 10^{-26}$ e cm value corresponding to the listed limit.
[2] SAHOO 17 develops theory to calculate this limit from the measured limit by GRANER 16 of the ^{199}Hg atom EDM.
[3] PENDLEBURY 15 reports $d = (-0.21 \pm 1.82) \times 10^{-26}$ e cm value corresponding to the listed limit.
[4] SEREBROV 14 includes the data of ALTAREV 96.
[5] LAMOREAUX 07 faults BAKER 06 for not including in the estimate of systematic error an effect due to the Earth's rotation. BAKER 07 replies (1) that the effect was included implicitly in the analysis and (2) that further analysis confirms that the BAKER 06 limit is correct as is. See also SILENKO 07.
[6] This HARRIS 99 result includes the result of SMITH 90. However, the averaging of the results of these two experiments has been criticized by LAMOREAUX 00.

n MEAN-SQUARE CHARGE RADIUS

The mean-square charge radius of the neutron, $\langle r_n^2 \rangle$, is related to the neutron-electron scattering length b_{ne} by $\langle r_n^2 \rangle = 3(m_e a_0/m_n) b_{ne}$, where m_e and m_n are the masses of the electron and neutron, and a_0 is the Bohr radius. Numerically, $\langle r_n^2 \rangle = 86.34\ b_{ne}$, if we use a_0 for a nucleus with infinite mass.

VALUE (fm^2)	DOCUMENT ID		COMMENT
−0.1155±0.0017 OUR AVERAGE			
−0.115 ±0.002 ±0.003	KOPECKY	97	ne scattering (Pb)
−0.124 ±0.003 ±0.005	KOPECKY	97	ne scattering (Bi)
−0.114 ±0.003	KOESTER	95	ne scattering (Pb, Bi)
−0.115 ±0.003	[1] KROHN	73	ne scattering (Ne, Ar, Kr, Xe)
• • • We do not use the following data for averages, fits, limits, etc. • • •			
−0.1101±0.0089	[2] HEACOCK	21	n interferometry
$-0.106\ ^{+0.007}_{-0.005}$	[3] FILIN	20	chiral EFT analysis
$-0.117\ ^{+0.007}_{-0.011}$	BELUSHKIN	07	Dispersion analysis
−0.113 ±0.003 ±0.004	KOPECKY	95	ne scattering (Pb)
−0.134 ±0.009	ALEKSANDR...	86	ne scattering (Bi)
−0.114 ±0.003	KOESTER	86	ne scattering (Pb, Bi)
−0.118 ±0.002	KOESTER	76	ne scattering (Pb)
−0.120 ±0.002	KOESTER	76	ne scattering (Bi)
−0.116 ±0.003	KROHN	66	ne scattering (Ne, Ar, Kr, Xe)

[1] KROHN 73 measured -0.112 ± 0.003 fm^2. This value is as corrected by KOESTER 76.
[2] HEACOCK 21 extract the value from Pendelloesung interferometry to measure the neutron structure factors of silicon. This value is strongly anti-correlated with the mean-square thermal atomic displacement.
[3] FILIN 20 extract the value based on their chiral-EFT calculation of the deuteron structure radius and use as input the atomic data for the difference of the deuteron and proton charge radii.

n MAGNETIC RADIUS

This is the rms magnetic radius, $\sqrt{\langle r_M^2 \rangle}$.

VALUE (fm)	DOCUMENT ID		COMMENT
$0.864\ ^{+0.009}_{-0.008}$ OUR AVERAGE			
0.89 ±0.03	EPSTEIN	14	Using ep, en, $\pi\pi$ data
$0.862\ ^{+0.009}_{-0.008}$	BELUSHKIN	07	Dispersion analysis

n ELECTRIC POLARIZABILITY α_n

Following is the electric polarizability α_n defined in terms of the induced electric dipole moment by $\mathbf{D} = 4\pi\epsilon_0\alpha_n\mathbf{E}$. For a review, see SCHMIEDMAYER 89.

For a very complete reviews of the polarizability of the nucleon and Compton scattering, see SCHUMACHER 05, updated in SCHUMACHER 19, and GRIESSHAMMER 12.

VALUE (10^{-4} fm^3)	DOCUMENT ID		TECN	COMMENT
11.8 ± 1.1 OUR AVERAGE				
11.55± 1.25±0.8	MYERS	14	CNTR	$\gamma d \to \gamma d$
$12.5 \pm 1.8\ ^{+1.6}_{-1.3}$	[1] KOSSERT	03	CNTR	$\gamma d \to \gamma p n$
12.0 ± 1.5 ±2.0	SCHMIEDM...	91	CNTR	n Pb transmission
$10.7\ ^{+3.3}_{-10.7}$	ROSE	90B	CNTR	$\gamma d \to \gamma n p$
• • • We do not use the following data for averages, fits, limits, etc. • • •				
8.8 ± 2.4 ±3.0	[2] LUNDIN	03	CNTR	$\gamma d \to \gamma d$
13.6	[3] KOLB	00	CNTR	$\gamma d \to \gamma n p$
0.0 ± 5.0	[4] KOESTER	95	CNTR	n Pb, n Bi transmission
$11.7\ ^{+4.3}_{-11.7}$	ROSE	90	CNTR	See ROSE 90B
8 ±10	KOESTER	88	CNTR	n Pb, n Bi transmission
12 ±10	SCHMIEDM...	88	CNTR	n Pb, n C transmission

[1] KOSSERT 03 gets $\alpha_n - \beta_n = (9.8 \pm 3.6\ ^{+2.1}_{-1.1} \pm 2.2) \times 10^{-4}$ fm^3, and uses $\alpha_n + \beta_n = (15.2 \pm 0.5) \times 10^{-4}$ fm^3 from LEVCHUK 00. Thus the errors on α_n and β_n are anti-correlated.
[2] LUNDIN 03 measures $\alpha_N - \beta_N = (6.4 \pm 2.4) \times 10^{-4}$ fm^3 and uses accurate values for α_p and α_p and a precise sum-rule result for $\alpha_n + \beta_n$. The second error is a model uncertainty, and errors on α_n and β_n are anticorrelated. The data from this paper aer included in the analysis of MYERS 14.
[3] KOLB 00 obtains this value with a lower limit of 7.6×10^{-4} fm^3 but no upper limit from this experiment alone. Combined with results of ROSE 90, the 1-σ range is (7.6–14.0) $\times 10^{-4}$ fm^3.
[4] KOESTER 95 uses natural Pb and the isotopes 208, 207, and 206. See this paper for a discussion of methods used by various groups to extract α_n from data.

n MAGNETIC POLARIZABILITY β_n

VALUE (10^{-4} fm^3)	DOCUMENT ID		TECN	COMMENT
3.7 ±1.2 OUR AVERAGE				
3.65±1.25±0.8	MYERS	14	CNTR	$\gamma d \to \gamma d$
$2.7 \pm 1.8\ ^{+1.3}_{-1.6}$	[1] KOSSERT	03	CNTR	$\gamma d \to \gamma p n$
6.5 ±2.4 ±3.0	[2] LUNDIN	03	CNTR	$\gamma d \to \gamma d$
• • • We do not use the following data for averages, fits, limits, etc. • • •				
1.6	[3] KOLB	00	CNTR	$\gamma d \to \gamma n p$

Downloaded from https://academic.oup.com/ptep/article/2022/8/083C01/6651666 by KIT Library user on 27 September 2022

[1] KOSSERT 03 gets $\alpha_n - \beta_n = (9.8 \pm 3.6^{+2.1}_{-1.1} \pm 2.2) \times 10^{-4}$ fm^3, and uses $\alpha_n + \beta_n = (15.2 \pm 0.5) \times 10^{-4}$ fm^3 from LEVCHUK 00. Thus the errors on α_n and β_n are anti-correlated.

[2] LUNDIN 03 measures $\alpha_N - \beta_N = (6.4 \pm 2.4) \times 10^{-4}$ fm^3 and uses accurate values for α_p and α_p and a precise sum-rule result for $\alpha_n + \beta_n$. The second error is a model uncertainty, and errors on α_n and β_n are anticorrelated.

[3] KOLB 00 obtains this value with an upper limit of 7.6×10^{-4} fm^3 but no lower limit from this experiment alone. Combined with results of ROSE 90, the 1-σ range is (1.2–7.6) $\times 10^{-4}$ fm^3.

n CHARGE

See also "$|q_p + q_e|/e$" in the proton Listings.

VALUE (10^{-21} e)	DOCUMENT ID		TECN	COMMENT
− 0.2± 0.8 OUR AVERAGE				
− 0.1± 1.1	[1] BRESSI	11		Neutrality of SF_6
− 0.4± 1.1	[2] BAUMANN	88		Cold n deflection
• • • We do not use the following data for averages, fits, limits, etc. • • •				
−15 ±22	[3] GAEHLER	82	CNTR	Cold n deflection

[1] As a limit, this BRESSI 11 value is $< 1 \times 10^{-21}$ e.

[2] The BAUMANN 88 error ±1.1 gives the 68% CL limits about the the value −0.4.

[3] The GAEHLER 82 error ±22 gives the 90% CL limits about the the value −15.

LIMIT ON $n\overline{n}$ OSCILLATIONS

Mean Time for $n\overline{n}$ Transition

A test of ΔB=2 baryon number nonconservation. MOHAPATRA 80 and MOHAPATRA 89 discuss the theoretical motivations for looking for $n\overline{n}$ oscillations. DOVER 83 and DOVER 85 give phenomenological analyses. The best limits come from looking for the decay of neutrons bound in nuclei. However, these analyses require model-dependent corrections for nuclear effects. See KABIR 83, DOVER 89, ALBERICO 91, and GAL 00 for discussions. Direct searches for $n \to \overline{n}$ transitions using reactor neutrons are cleaner but give somewhat poorer limits. We include limits for both free and bound neutrons in the Summary Table. See MOHAPATRA 09 and PHILLIPS 16 for recent reviews.

VALUE (s)	CL%	DOCUMENT ID		TECN	COMMENT
>4.7 × 10^8	90	[1] ABE	21	CNTR	n bound in oxygen
>8.6 × 10^7	90	BALDO-...	94	CNTR	Reactor (free) neutrons
• • • We do not use the following data for averages, fits, limits, etc. • • •					
>1.37 × 10^8	90	[2] AHARMIM	17	SNO	n bound in deuteron
>2.7 × 10^8	90	ABE	15C	CNTR	n bound in oxygen
>1.3 × 10^8	90	CHUNG	02B	SOU2	n bound in iron
>1 × 10^7	90	BALDO-...	90	CNTR	See BALDO-CEOLIN 94
>1.2 × 10^8	90	BERGER	90	FREJ	n bound in iron
>4.9 × 10^5	90	BRESSI	90	CNTR	Reactor neutrons
>4.7 × 10^5	90	BRESSI	89	CNTR	See BRESSI 90
>1.2 × 10^8	90	TAKITA	86	CNTR	n bound in oxygen
>1 × 10^6	90	FIDECARO	85	CNTR	Reactor neutrons
>8.8 × 10^7	90	PARK	85B	CNTR	
>3 × 10^7		BATTISTONI	84	NUSX	
> 0.27–1.1 × 10^8		JONES	84	CNTR	
>2 × 10^7		CHERRY	83	CNTR	

[1] ABE 21 supersedes ABE 15C.

[2] The AHARMIM 17 value is an unbounded limit (it does not assume a positive lifetime). The bounded limit is 1.23 × 10^8 sec.

LIMIT ON nn' OSCILLATIONS

Lee and Yang (LEE 56) proposed the existence of mirror world in an attempt to restore global parity symmetry. A possible candidate for dark matter. Limits depend on assumptions about fields B and B'. See the papers for details. See BEREZHIANI 18 for a recent discussion.

VALUE (s)	CL%	DOCUMENT ID		TECN	COMMENT
>352	95	[1] ABEL	21	CNTR	UCN, scan of B field
>448	90	SEREBROV	09A	CNTR	Assumes $B' < 100$ nT
• • • We do not use the following data for averages, fits, limits, etc. • • •					
> 17	95	[2] BEREZHIANI	18	CNTR	UCN, scan of B field
> 12	95	[3] ALTAREV	09A	CNTR	UCN, scan $0 \le B \le 12.5$ μT
>414	90	SEREBROV	08	CNTR	UCN, B field on & off
>103	95	BAN	07	CNTR	UCN, B field on & off

[1] ABEL 21 determine several limits on the oscillation time as a function of the ratio mirror magnetic field B' to applied magnetic field B. The quoted limit of 352 s is for $B' = 0$. Lower limits on the oscillation time of 6 seconds are further obtained for any mirror field B' in the range 0.4–25.7 μT.

[2] The B field was set to (0.09, 0.12, 0.21) G. Limits on oscillation time are valid for any mirror field B' in (0.08–0.17) G, and for aligned fields B and B'. For larger values of B', the limits are significantly reduced.

[3] Losses of neutrons due to oscillations to mirror neutrons would be maximal when the magnetic fields B and B' in the two worlds were equal. Hence the scan over B by ALTAREV 09A: the limit applies for any B' over the given range. At $B' = 0$, the limit is 141 s (95% CL).

n DECAY MODES

	Mode		Fraction (Γ_i/Γ)	Confidence level
Γ_1	$p e^- \overline{\nu}_e$		100 %	
Γ_2	$p e^- \overline{\nu}_e \gamma$	[a]	(9.2±0.7) × 10^{-3}	
Γ_3	hydrogen-atom $\overline{\nu}_e$		< 2.7 × 10^{-3}	95%
	Charge conservation (Q) violating mode			
Γ_4	$p \nu_e \overline{\nu}_e$	Q	< 8 × 10^{-27}	68%
	Baryon number violating decay			
Γ_5	$e^+ e^-$ invisible			

[a] This limit is for γ energies between 0.4 and 782 keV.

n BRANCHING RATIOS

$\Gamma(p e^- \overline{\nu}_e \gamma)/\Gamma_{total}$ — Γ_2/Γ

VALUE (units 10^{-3})	CL%	DOCUMENT ID		TECN	COMMENT
9.17±0.24±0.64		[1] BALES	16	RDK2	Two different set-ups
• • • We do not use the following data for averages, fits, limits, etc. • • •					
3.09±0.11±0.30		[2] COOPER	10	CNTR	See BALES 16
3.13±0.11±0.33		NICO	06	CNTR	See COOPER 10
<6.9	90	[3] BECK	02	CNTR	γ, p, e^- coincidence

[1] BALES 16 gets a branching fraction of (5.82 ± 0.23 ± 0.62) × 10^{-3} for a photon energy range 0.4 to 14.0 keV, and with a different detector array, (3.35 ± 0.05 ± 0.15) × 10^{-3} for 14.1 to 782 keV. Our result above is the sum; the error on the sum is completely dominated by the error on the lower range.

[2] This COOPER 10 result is for γ energies between 15 and 340 keV.

[3] This BECK 02 limit is for γ energies between 35 and 100 keV.

$\Gamma(\text{hydrogen-atom } \overline{\nu}_e)/\Gamma_{total}$ — Γ_3/Γ

VALUE	CL%	DOCUMENT ID		TECN	COMMENT
<0.27 × 10^{-2}	95	[1] CZARNECKI	18		Lifetime analysis
• • • We do not use the following data for averages, fits, limits, etc. • • •					
<3 × 10^{-2}	95	[2] GREEN	90	RVUE	

[1] CZARNECKI 18 limit from an analysis of experimental discrepancies on the neutron lifetime and axial coupling applies as well to other possible exotic neutron decays.

[2] GREEN 90 infers that $\tau(\text{hydrogen-atom}\,\overline{\nu}_e) > 3 \times 10^4$ s by comparing neutron lifetime measurements made in storage experiments with those made in β-decay experiments. However, the result depends sensitively on the lifetime measurements, and does not of course take into account more recent measurements of same.

$\Gamma(p \nu_e \overline{\nu}_e)/\Gamma_{total}$ — Γ_4/Γ

Forbidden by charge conservation.

VALUE	CL%	DOCUMENT ID		TECN	COMMENT
<8 × 10^{-27}	68	[1] NORMAN	96	RVUE	^{71}Ga → ^{71}Ge neutrals
• • • We do not use the following data for averages, fits, limits, etc. • • •					
<9.7 × 10^{-18}	90	ROY	83	CNTR	^{113}Cd → ^{113m}In neut.
<7.9 × 10^{-21}		VAIDYA	83	CNTR	^{87}Rb → ^{87m}Sr neut.
<9 × 10^{-24}	90	BARABANOV	80	CNTR	^{71}Ga → ^{71}GeX
<3 × 10^{-19}		NORMAN	79	CNTR	^{87}Rb → ^{87m}Sr neut.

[1] NORMAN 96 gets this limit by attributing SAGE and GALLEX counting rates to the charge-nonconserving transition ^{71}Ga → ^{71}Ge+neutrals rather than to solar-neutrino reactions.

$\Gamma(e^+ e^- \text{invisible})/\Gamma_{total}$ — Γ_5/Γ

Baryon number violating decay

VALUE	CL%	DOCUMENT ID		TECN	COMMENT
• • • We do not use the following data for averages, fits, limits, etc. • • •					
<0.01	90	[1] KLOPF	19	CNTR	re-interpretation of MUND 13
<1 × 10^{-4}	90	[2] SUN	18	SPEC	Ultracold n, polarized

[1] KLOPF 19 value is for baryon number violating decay of neutron to electrons plus an invisible state, χ. The limit is valid for KE($e^+ e^-$) range between 32 keV and 664 keV, strengthening to few × 10^{-4} above approximately 100 keV.

[2] SUN 18 value is for baryon number violating decay of neutron to electrons plus an invisible state, χ. The limit is valid for 644 keV > KE($e^+ e^-$) > 100 keV. Assuming this decay $\chi e e$ is the only allowed χ decay channel, a 0.01 BR is ruled out for 644 keV > E($e^+ e^-$) > 100 keV at over 5σ.

See the related review(s):
Baryon Decay Parameters

Downloaded from https://academic.oup.com/ptep/article/2022/8/083C01/6651666 by KIT Library user on 27 September 2022

$n \to p e^- \overline{\nu}_e$ DECAY PARAMETERS

See the above "Note on Baryon Decay Parameters." For discussions of recent results, see the references cited at the beginning of the section on the neutron mean life. For discussions of the values of the weak coupling constants g_A and g_V obtained using the neutron lifetime and asymmetry parameter A, comparisons with other methods of obtaining these constants, and implications for particle physics and for astrophysics, see DUBBERS 91 and WOOLCOCK 91. For tests of the $V-A$ theory of neutron decay, see EROZOLIMSKII 91B, MOSTOVOI 96, NICO 05, SEVERIJNS 06, and ABELE 08.

$\lambda \equiv g_A / g_V$

VALUE	DOCUMENT ID		TECN	COMMENT
−1.2754 ±0.0013 OUR AVERAGE Error includes scale factor of 2.7. See the ideogram below.				
−1.2796 ±0.0062	[1] HASSAN	21	SPEC	Proton recoil spectrum
−1.2677 ±0.0028	[2] BECK	20	SPEC	Proton recoil spectrum
−1.27641 ±0.00045 ±0.00033	[3] MAERKISCH	19	SPEC	pulsed cold *n*, polarized
−1.2772 ±0.0020	[4] BROWN	18	UCNA	Ultracold *n*, polarized
−1.2748 ±0.0008 $^{+0.0010}_{-0.0011}$	[5] MUND	13	SPEC	Cold *n*, polarized
−1.275 ±0.006 ±0.015	SCHUMANN	08	CNTR	Cold *n*, polarized
−1.2686 ±0.0046 ±0.0007	[6] MOSTOVOI	01	CNTR	*A* and *B* × polarizations
−1.266 ±0.004	LIAUD	97	TPC	Cold *n*, polarized, *A*
−1.2594 ±0.0038	[7] YEROZLIM...	97	CNTR	Cold *n*, polarized, *A*
−1.262 ±0.005	BOPP	86	SPEC	Cold *n*, polarized, *A*
• • • We do not use the following data for averages, fits, limits, etc. • • •				
−1.27607 ±0.00068	[8] SAUL	20	SPEC	Cold *n*, polarized, *A*
−1.284 ±0.014	[9] DARIUS	17	SPEC	Cold *n*, unpolarized
−1.2755 ±0.0030	[10] MENDENHALL	13	UCNA	See BROWN 18
−1.27590 ±0.00239 $^{+0.00331}_{-0.00377}$	[11] PLASTER	12	UCNA	See MENDENHALL 13
−1.27590 $^{+0.00409}_{-0.00445}$	LIU	10	UCNA	See PLASTER 12
−1.2739 ±0.0019	[12] ABELE	02	SPEC	See MUND 13
−1.274 ±0.003	ABELE	97D	SPEC	Cold *n*, polarized, *A*
−1.266 ±0.004	SCHRECK...	95	TPC	See LIAUD 97
−1.2544 ±0.0036	EROZOLIM...	91	CNTR	See YEROZOLIMSKY 97
−1.226 ±0.042	MOSTOVOY	83	RVUE	
−1.261 ±0.012	EROZOLIM...	79	CNTR	Cold *n*, polarized, *A*
−1.259 ±0.017	[13] STRATOWA	78	CNTR	*p* recoil spectrum, *a*
−1.263 ±0.015	EROZOLIM...	77	CNTR	See EROZOLIMSKII 79
−1.250 ±0.036	[13] DOBROZE...	75	CNTR	See STRATOWA 78
−1.258 ±0.015	[14] KROHN	75	CNTR	Cold *n*, polarized, *A*
−1.263 ±0.016	[15] KROPF	74	RVUE	*n* decay alone
−1.250 ±0.009	[15] KROPF	74	RVUE	*n* decay + nuclear ft

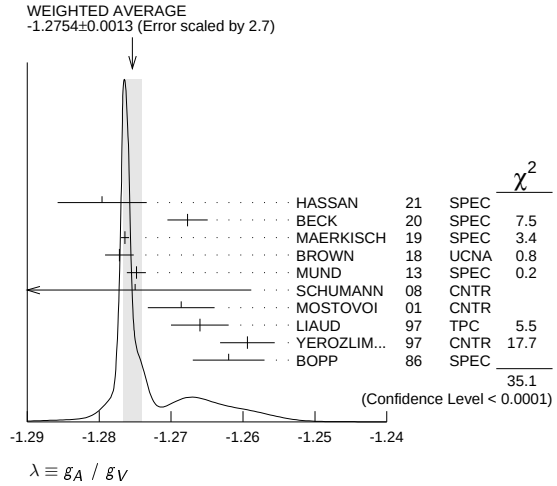

[1] HASSAN 21 include earlier data of DARIUS 17. The value is extracted from the angular correlation coefficient *a*.
[2] BECK 20 calculates this value from the measurement of the β-decay e–$\overline{\nu}_e$ angular correlation coefficient *a*.
[3] MAERKISCH 19 gets $A = -0.11985 \pm 0.00017 \pm 0.00012$.
[4] BROWN 18 gets $A = -0.12054 \pm 0.00044 \pm 0.00068$ and $\lambda = -1.2783 \pm 0.0022$. We quote the combined values that include the earlier UCNA measurements (MENDENHALL 13).
[5] This MUND 13 value includes earlier PERKEO II measurements (ABELE 02 and ABELE 97D).
[6] MOSTOVOI 01 measures the two *P*-odd correlations *A* and *B*, or rather *SA* and *SB*, where *S* is the *n* polarization, in free neutron decay.
[7] YEROZOLIMSKY 97 makes a correction to the EROZOLIMSKII 91 value.
[8] SAUL 20 quote this value of λ under the SM assumption of the Fierz term $b = 0$. In a combined fit authors extract a value of $\lambda = -1.2792 \pm 0.0060$.
[9] DARIUS 17 calculates this value from the measurement of the *a* parameter (see below). Data is included in HASSAN 21.
[10] MENDENHALL 13 gets $A = -0.11954 \pm 0.00055 \pm 0.00098$ and $\lambda = -1.2756 \pm 0.0030$. We quote the nearly identical values that include the earlier UCNA measurement (PLASTER 12), with a correction to that result.
[11] This PLASTER 12 value is identical with that given in LIU 10, but the experiment is now described in detail.
[12] This is the combined result of ABELE 02 and ABELE 97D.
[13] These experiments measure the absolute value of g_A/g_V only.
[14] KROHN 75 includes events of CHRISTENSEN 70.
[15] KROPF 74 reviews all data through 1972.

e^- ASYMMETRY PARAMETER *A*

This is the neutron-spin electron-momentum correlation coefficient. Unless otherwise noted, the values are corrected for radiative effects and weak magnetism. In the Standard Model, *A* is related to $\lambda \equiv g_A/g_V$ by $A = -2\lambda(\lambda+1)/(1+3\lambda^2)$; this assumes that g_A and g_V are real.

VALUE	DOCUMENT ID		TECN	COMMENT
−0.11958 ±0.00021 OUR AVERAGE Error includes scale factor of 1.2. See the ideogram below.				
−0.11985 ±0.00017 ±0.00012	[1] MAERKISCH	19	SPEC	pulsed cold *n*, polarized
−0.12015 ±0.00034 ±0.00063	[2] BROWN	18	UCNA	Ultracold *n*, polarized
−0.11926 ±0.00031 $^{+0.00036}_{-0.00042}$	[3] MUND	13	SPEC	Cold *n*, polarized
−0.1160 ±0.0009 ±0.0012	LIAUD	97	TPC	Cold *n*, polarized
−0.1135 ±0.0014	[4] YEROZLIM...	97	CNTR	Cold *n*, polarized
−0.1146 ±0.0019	BOPP	86	SPEC	Cold *n*, polarized
• • • We do not use the following data for averages, fits, limits, etc. • • •				
−0.11972 ±0.00025	[5] SAUL	20	SPEC	Cold *n*, polarized
−0.11952 ±0.00110	[6] MENDENHALL	13	UCNA	See BROWN 18
−0.11966 ±0.00089 $^{+0.00123}_{-0.00140}$	[7] PLASTER	12	UCNA	See MENDENHALL 13
−0.11966 ±0.00089 $^{+0.00123}_{-0.00140}$	LIU	10	UCNA	See PLASTER 12
−0.1138 ±0.0046 ±0.0021	PATTIE	09	SPEC	Ultracold *n*, polarized
−0.1189 ±0.0007	[8] ABELE	02	SPEC	See MUND 13
−0.1168 ±0.0017	[9] MOSTOVOI	01	CNTR	Inferred
−0.1189 ±0.0012	ABELE	97D	SPEC	Cold *n*, polarized
−0.1160 ±0.0009 ±0.0011	SCHRECK...	95	TPC	See LIAUD 97
−0.1116 ±0.0014	EROZOLIM...	91	CNTR	See YEROZOLIMSKY 97
−0.114 ±0.005	[10] EROZOLIM...	79	CNTR	Cold *n*, polarized
−0.113 ±0.006	[10] KROHN	75	CNTR	Cold *n*, polarized

[1] MAERKISCH 19 further derive a value for the CKM-element $|V_{ud}| = 0.97351 \pm 0.00060$, using $\tau_n = 879.7(8)$ sec and the relation from CZARNECKI 18.
[2] BROWN 18 gets $A = -0.12054 \pm 0.00044 \pm 0.00068$ and $\lambda = -1.2783 \pm 0.0022$. We quote the combined values that include the earlier UCNA measurements (MENDENHALL 13).
[3] This MUND 13 value includes earlier PERKEO II measurements (ABELE 02 and ABELE 97D), with a correction to those results.
[4] YEROZOLIMSKY 97 makes a correction to the EROZOLIMSKII 91 value.
[5] Under the SM assumption that the Fierz term $b = 0$, SAUL 20 obtain the quoted asymmetry parameter *A* and $\lambda = -1.27607 \pm 0.00068$. In a combined fit authors extract the values $A = -0.1209 \pm 0.0015$, $\lambda = -1.2792 \pm 0.0060$, and $b = 0.017 \pm 0.021$.
[6] MENDENHALL 13 gets $A = -0.11954 \pm 0.00055 \pm 0.00098$ and $\lambda = -1.2756 \pm 0.0030$. We quote the nearly identical values that include the earlier UCNA measurement (PLASTER 12), with a correction to that result.
[7] This PLASTER 12 value is identical with that given in LIU 10, but the experiment is now described in detail.
[8] This is the combined result of ABELE 02 and ABELE 97D.
[9] MOSTOVOI 01 calculates this from its measurement of $\lambda = g_A/g_V$ above.
[10] These results are not corrected for radiative effects and weak magnetism, but the corrections are small compared to the errors.

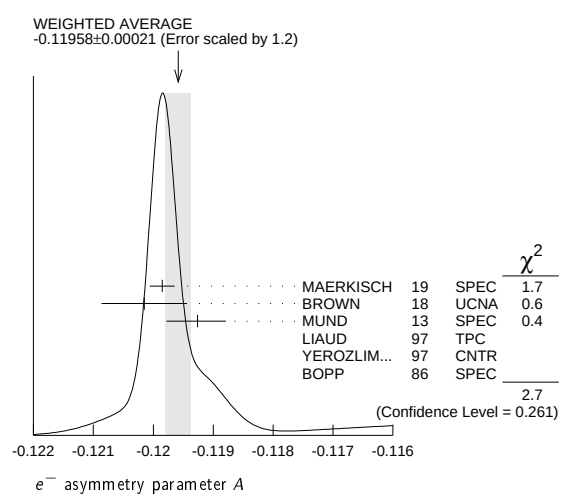

Downloaded from https://academic.oup.com/ptep/article/2022/8/083C01/6651666 by KIT Library user on 27 September 2022

$\overline{\nu}_e$ ASYMMETRY PARAMETER B

This is the neutron-spin antineutrino-momentum correlation coefficient. In the Standard Model, B is related to $\lambda \equiv g_A/g_V$ by $B = 2\lambda(\lambda - 1) / (1 + 3\lambda^2)$; this assumes that g_A and g_V are real.

VALUE	DOCUMENT ID		TECN	COMMENT
0.9807±0.0030 OUR AVERAGE	See the ideogram below.			
0.9802±0.0034±0.0036	SCHUMANN	07	CNTR	Cold n, polarized
0.967 ±0.006 ±0.010	KREUZ	05	CNTR	Cold n, polarized
0.9801±0.0046	SEREBROV	98	CNTR	Cold n, polarized
0.9894±0.0083	KUZNETSOV	95	CNTR	Cold n, polarized
1.00 ±0.05	CHRISTENSEN	70	CNTR	Cold n, polarized
0.995 ±0.034	EROZOLIM...	70C	CNTR	Cold n, polarized
• • • We do not use the following data for averages, fits, limits, etc. • • •				
0.9876±0.0004	[1] MOSTOVOI	01	CNTR	Inferred

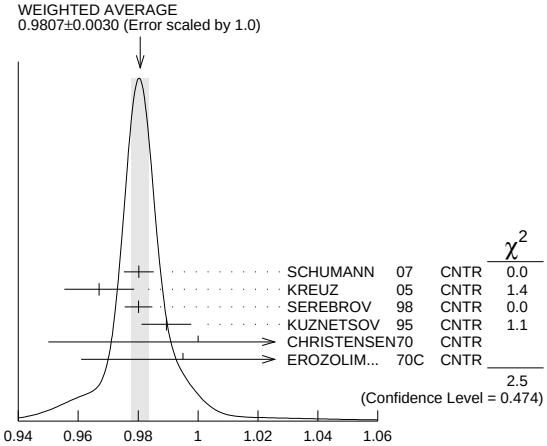

$\overline{\nu}_e$ ASYMMETRY PARAMETER B

[1] MOSTOVOI 01 calculates this from its measurement of $\lambda = g_A/g_V$ above.

PROTON ASYMMETRY PARAMETER C

Describes the correlation between the neutron spin and the proton momentum. In the Standard Model, C is related to $\lambda \equiv g_A/g_V$ by $C = -x_c\ (A + B) = x_c\ 4\lambda/(1 + 3\lambda^2)$, where $x_c = 0.27484$ is a kinematic factor; this assumes that g_A and g_V are real.

VALUE	DOCUMENT ID		TECN	COMMENT
−0.2377±0.0010±0.0024	SCHUMANN	08	CNTR	Cold n, polarized

e-$\overline{\nu}_e$ ANGULAR CORRELATION COEFFICIENT a

For a review of past experiments and plans for future measurements of the a parameter, see WIETFELDT 05. In the Standard Model, a is related to $\lambda \equiv g_A/g_V$ by $a = (1 - \lambda^2) / (1 + 3\lambda^2)$; this assumes that g_A and g_V are real.

VALUE	DOCUMENT ID		TECN	COMMENT
−0.1049 ±0.0013 OUR AVERAGE	Error includes scale factor of 1.8. See the ideogram below.			
−0.10782±0.00124±0.00133	[1] HASSAN	21	SPEC	Proton recoil spectrum
−0.10430±0.00084	BECK	20	SPEC	Proton recoil spectrum
−0.1054 ±0.0055	BYRNE	02	SPEC	Proton recoil spectrum
−0.1017 ±0.0051	STRATOWA	78	CNTR	Proton recoil spectrum
−0.091 ±0.039	GRIGOREV	68	SPEC	Proton recoil spectrum
• • • We do not use the following data for averages, fits, limits, etc. • • •				
−0.1090 ±0.0030 ±0.0028	[2] DARIUS	17	SPEC	Cold n, unpolarized
−0.1045 ±0.0014	[3] MOSTOVOI	01	CNTR	Inferred

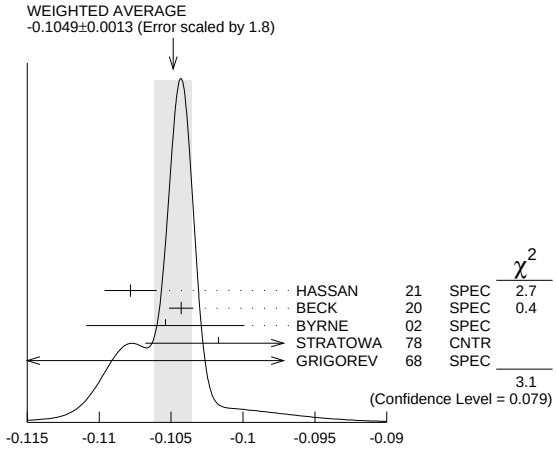

e-$\overline{\nu}_e$ Angular correlation coefficient a

[1] The result of HASSAN 21 includes the data of DARIUS 17, and thus supersedes those entries. HASSAN 21 uses the asymmetry in time-of-flight between the beta electron and recoil proton in delayed coincidence.

[2] DARIUS 17 exploits a "wishbone" correlation, where the p time of flight is correlated with the momentum of the electron in delayed coincidence. Data is included in HASSAN 21.

[3] MOSTOVOI 01 calculates this from its measurement of $\lambda = g_A/g_V$ above.

ϕ_{AV}, PHASE OF g_A RELATIVE TO g_V

Time reversal invariance requires this to be 0 or 180°. This is related to D given in the next data block and $\lambda \equiv g_A/g_V$ by $\sin(\phi_{AV}) \equiv D(1+3\lambda^2)/2|\lambda|$; this assumes that g_A and g_V are real.

VALUE (°)	CL%	DOCUMENT ID		TECN	COMMENT
180.017±0.026 OUR AVERAGE		See the ideogram below.			
180.012±0.028	68	CHUPP	12	CNTR	Cold n, polarized > 91%
180.04 ±0.09		SOLDNER	04	CNTR	Cold n, polarized
180.08 ±0.13		LISING	00	CNTR	Polarized > 93%
• • • We do not use the following data for averages, fits, limits, etc. • • •					
180.013±0.028		MUMM	11	CNTR	See CHUPP 12
179.71 ±0.39		EROZOLIM...	78	CNTR	Cold n, polarized
180.35 ±0.43		EROZOLIM...	74	CNTR	Cold n, polarized
181.1 ±1.3		[1] KROPF	74	RVUE	n decay
180.14 ±0.22		STEINBERG	74	CNTR	Cold n, polarized

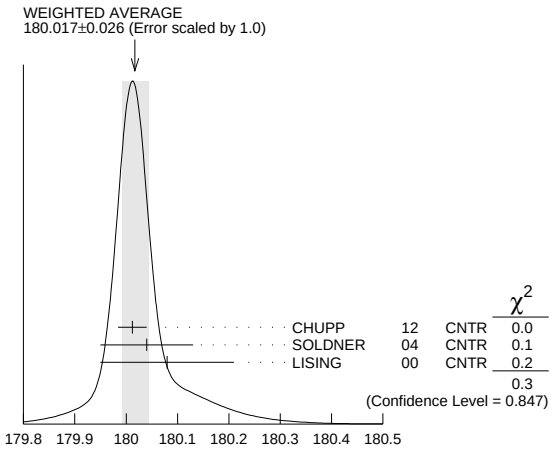

ϕ_{AV}, PHASE OF g_A RELATIVE TO g_V (°)

[1] KROPF 74 reviews all data through 1972.

TRIPLE CORRELATION COEFFICIENT D

These are measurements of the component of n spin perpendicular to the decay plane in β decay. Should be zero if T invariance is not violated.

VALUE (units 10^{-4})	DOCUMENT ID		TECN	COMMENT
− 1.2 ± 2.0 OUR AVERAGE	See the ideogram below.			
− 0.94± 1.89±0.97	CHUPP	12	CNTR	Cold n, polarized > 91%
− 2.8 ± 6.4 ±3.0	SOLDNER	04	CNTR	Cold n, polarized
− 6 ±12 ±5	LISING	00	CNTR	Polarized > 93%
• • • We do not use the following data for averages, fits, limits, etc. • • •				
− 0.96± 1.89±1.01	MUMM	11	CNTR	See CHUPP 12
+22 ±30	EROZOLIM...	78	CNTR	Cold n, polarized
−27 ±50	[1] EROZOLIM...	74	CNTR	Cold n, polarized
−11 ±17	STEINBERG	74	CNTR	Cold n, polarized

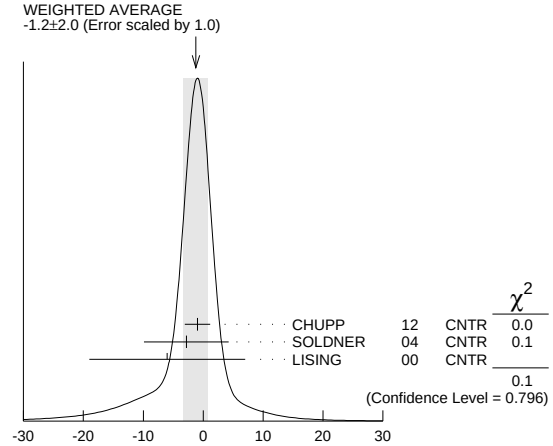

TRIPLE CORRELATION COEFFICIENT D (units 10^{-4})

Downloaded from https://academic.oup.com/ptep/article/2022/8/083C01/6651666 by KIT Library user on 27 September 2022

[1] EROZOLIMSKII 78 says asymmetric proton losses and nonuniform beam polarization may give a systematic error up to 30×10^{-4}, thus increasing the EROZOLIMSKII 74 error to 50×10^{-4}. STEINBERG 74 and STEINBERG 76 estimate these systematic errors to be insignificant in their experiment.

TRIPLE CORRELATION COEFFICIENT *R*

Another test of time-reversal invariance. *R* measures the polarization of the electron in the direction perpendicular to the plane defined by the neutron spin and the electron momentum. $R = 0$ for T invariance.

VALUE	*DOCUMENT ID*		*TECN*	*COMMENT*
+0.004±0.012±0.005	[1] KOZELA	12	CNTR	Mott polarimeter
• • • We do not use the following data for averages, fits, limits, etc. • • •				
+0.008±0.015±0.005	KOZELA	09	CNTR	See KOZELA 12

[1] KOZELA 12 also measures the polarization of the electron along the direction of the neutron spin. This is nonzero in the Standard Model; the correlation coefficient is $N = +0.067 \pm 0.011 \pm 0.004$.

FIERZ INTERFERENCE TERM *b*

The coefficient of the Fierz interference term, *b*, probes additional contributions to the differential decay rate of the neutron from scalar or tensor current interactions, beyond the Standard Model.

VALUE	*DOCUMENT ID*		*TECN*	*COMMENT*
0.017±0.020±0.003	[1] SAUL	20	SPEC	Cold *n*, polarized

[1] In a combined fit SAUL 20 extract this best fit value of the Fierz interference term *b* and the values $A = -0.1209 \pm 0.0015$ and $\lambda = -1.2792 \pm 0.0060$. For *b* it translates into a 90% CL region of $-0.018 \leq b \leq 0.052$ as a function of *A*.

n REFERENCES

We have omitted some papers that have been superseded by later experiments. See our earlier editions.

ABE 21 PR D103 012008 K. Abe *et al.* (Super-Kamiokande Collab.)
ABEL 21 PL B812 135993 C. Abel *et al.* (nEDM Collab.)
GONZALEZ 21 PRL 127 162501 F.M. Gonzalez *et al.* (UCNtau Collab.)
HASSAN 21 PR C103 045502 M.T. Hassan *et al.* (aCORN Collab)
HEACOCK 21 SCI 373 1239 B. Heacock *et al.* (NIST, RIKEN, NAGO+)
TIESINGA 21 RMP 93 025010 E. Tiesinga *et al.* (NIST)
WILSON 21 PR C104 045501 J.T. Wilson *et al.* (JHU, DURH)
ABEL 20 PRL 124 081803 C. Abel *et al.* (nEDM Collab.)
BECK 20 PR C101 055506 M. Beck *et al.* (aSPECT Collab.)
FILIN 20 PRL 124 082501 A.A. Filin *et al.*
SAUL 20 PRL 125 112501 H. Saul *et al.* (PERKEO III Collab.)
KLOPF 19 PRL 122 222503 M. Klopf *et al.* (PERKEO II Collab.)
MAERKISCH 19 PRL 122 242501 B. Maerkisch *et al.* (TUM, ILL, +)
SCHUMACHER 19 LHEP 4 4 M. Schumacher (GOET)
BEREZHIANI 18 EPJ C78 717 Z. Berezhiani *et al.* (AQUI, INFN, ILLG+)
BROWN 18 PR C97 035505 M.A.-P. Brown *et al.* (UCNA Collab.)
CZARNECKI 18 PRL 120 202002 A. Czarnecki, W.J. Marciano, A. Sirlin (ALBE+)
EZHOV 18 JETPL 107 671 V.F. Ezhov *et al.* (PNPI, LENSU, CAEN+)
PATTIE 18 SCI 360 627 R.W. Pattie Jr. *et al.* (LASL, IND, NCSU+)
SEREBROV 18 PR C97 055503 A.P. Serebrov *et al.* (PNPI, ILLG, RAL)
Also JETPL 106 623 A.P. Serebrov *et al.* (PNPI, ILLG, RAL)
SUN 18 PR C97 052501 X. Sun *et al.* (UCNA Collab.)
AHARMIM 17 PR D96 092005 B. Aharmim *et al.* (SNO Collab.)
DARIUS 17 PRL 119 042502 G. Darius *et al.* (aCORN at NIST)
SAHOO 17 PR D95 013002 B.K. Sahoo (AHMEB)
BALES 16 PRL 116 242501 M.J. Bales *et al.* (RDK II Collab.)
GRANER 16 PRL 116 161601 B. Graner *et al.* (WASH)
Also PRL 119 119901 (errat.) B. Graner *et al.* (WASH)
MOHR 16 RMP 88 035009 P.J. Mohr, D.B. Newell, B.N. Taylor (NIST)
PHILLIPS 16 PRPL 612 1 D.G. Phillips II *et al.*
ABE 15C PR D91 072006 K. Abe *et al.* (Super-Kamiokande Collab.)
ARZUMANOV 15 PL B745 79 S. Arzumanov *et al.* (ILLG, KIAE)
PENDLEBURY 15 PR D92 092003 J.M. Pendlebury *et al.* (ETHZ, PSI, SUSS)
SEREBROV 15 PR C92 055501 A.P. Serebrov *et al.* (PNPI, ILLG, IOFF)
EPSTEIN 14 PR D90 074027 Z. Epstein, G. Paz, J. Roy (UMD, WAYN)
MYERS 14 PRL 113 262506 L.S. Myers *et al.* (COMPTON/MAX-lab Collab.)
SEREBROV 14 JETPL 99 4 A.P. Serebrov *et al.* (PNPI, ILL, IOFF)
MENDENHALL 13 PR C87 032501 M.P. Mendenhall *et al.* (UCNA Collab.)
MUND 13 PRL 110 172502 D. Mund *et al.* (HEID, ILLG)
YUE 13 PRL 111 222501 A.T. Yue *et al.* (UMD, NIST, TENN, ORNL+)
ARZUMANOV 12 JETPL 95 224 S.S. Arzumanov *et al.* (KIAE)
Translated from ZETFP 95 248.
CHUPP 12 PR C86 035505 T.E. Chupp *et al.* (MICH, UCB, WASH+)
GRIESSHAM... 12 PPNP 67 841 H.W. Griesshammer *et al.* (GWU, MCHS+)
KOZELA 12 PR C85 045501 A. Kozela *et al.* (nTRV Collab.)
MOHR 12 RMP 84 1527 P.J. Mohr, B.N. Taylor, D.B. Newell (NIST)
PLASTER 12 PR C86 055501 B. Plaster *et al.* (UCNA Collab.)
STEYERL 12 PR C85 065503 A. Steyerl *et al.* (URI, SUSS)
BRESSI 11 PR A83 052101 G. Bressi *et al.* (LEGN, PAVII, PADO, TRST+)
DUBBERS 11 RMP 83 1111 D. Dubbers, M.G. Schmidt (HEID)
MUMM 11 PRL 107 102301 H.P. Mumm *et al.* (NIST, WASH, MICH, LBL+)
WIETFELDT 11 RMP 83 1173 F.E. Wietfeldt, G.L. Greene (TULA, TENN)
COOPER 10 PR C81 035503 R.L. Cooper *et al.* (MICH, NIST, TULA+)
LIU 10 PRL 105 181803 J. Liu *et al.* (UCNA Collab.)
Also PRL 105 219903 (errat.) J. Liu *et al.* (UCNA Collab.)
PICHLMAIER 10 PL B693 221 A. Pichlmaier *et al.* (TUM, PNPI, ILLG)
ALTAREV 09A PR D80 032003 I. Altarev *et al.* (TUM, RAL, CAEN+)
KOZELA 09 PRL 102 172301 A. Kozela *et al.* (JAGL, CRAC, PSI, CAEN+)
LAMOREAUX 09 JP G36 104002 S.K. Lamoreaux, R. Golub (YALE, NCSU)
MOHAPATRA 09 JP G36 104006 R.N. Mohapatra (UMD)
PATTIE 09 PRL 102 012301 R.W. Pattie Jr. *et al.* (Los Alamos UCNA Collab.)
SEREBROV 09A NIM A611 137 A.P. Serebrov *et al.* (PNPI, IOFF, ILLG+)
ABELE 08 PPNP 60 1 H. Abele (HEID)
MOHR 08 RMP 80 633 P.J. Mohr, B.N. Taylor, D.B. Newell (NIST)
SCHUMANN 08 PRL 100 151801 M. Schumann *et al.* (HEID, ILLG, KARL+)
SEREBROV 08 PL B663 181 A.P. Serebrov *et al.* (PNPI, IOFF, ILLG+)
BAKER 07 PRL 98 149102 C.A. Baker *et al.* (RAL, SUSS, ILLG)
BAN 07 PRL 99 161603 G. Ban *et al.* (CAEN, JAGL, PSI, JINR+)
BELUSHKIN 07 PR C75 035202 M.A. Belushkin, H.W. Hammer, U.-G. Meissner (BONN+)
LAMOREAUX 07 PRL 98 149101 S.K. Lamoreaux, R. Golub (YALE, NCSU)
SCHUMANN 07 PRL 99 191803 M. Schumann *et al.* (HEID, ILLG, KARL+)
SILENKO 07 PPNL 4 468 A.Ya. Silenko (Belarussian U.)
Translated from PFECAY 6 784.
BAKER 06 PRL 97 131801 C.A. Baker *et al.* (RAL, SUSS, ILLG)
NICO 06 NAT 444 1059 J.S. Nico *et al.* (NIST, TULN, MICH, UMD+)
SEVERIJNS 06 RMP 78 991 N. Severijns, M. Beck, O. Naviliat-Cuncic (LEUV+)
KREUZ 05 PL B619 263 M. Kreuz *et al.* (HEID, ILLG, MAINZ, KARL+)
MOHR 05 RMP 77 1 P.J. Mohr, B.N. Taylor (NIST)
NICO 05 PR C71 055502 J.S. Nico *et al.* (NIST, TULN, IND, TENN+)
SCHUMACHER 05 PPNP 55 567 M. Schumacher (GOET)
SEREBROV 05 PL B605 72 A.P. Serebrov *et al.* (PNPI, JINR, ILLG)
Also SPU 48 867 A.P. Serebrov *et al.* (PPNI, JINR, ILLG)
Translated from UFN 175 905.
WIETFELDT 05 MPL A20 1783 F.E. Wietfeldt (TULN)
SOLDNER 04 PL B581 49 T. Soldner *et al.* (ILLG, TUM)
DEWEY 03 PRL 91 152302 M.S. Dewey *et al.* (NIST, TULN, IND+)
KOSSERT 03 EPJ A16 259 K. Kossert *et al.* (Mainz MAMI Collab.)
Also PRL 88 162301 K. Kossert *et al.* (Mainz MAMI Collab.)
LUNDIN 03 PRL 90 192501 M. Lundin *et al.*
ABELE 02 PRL 88 211801 H. Abele *et al.* (PERKEO-II Collab.)
BECK 02 JETPL 76 332 M. Beck *et al.* (LEUV, SUSS, KIAE, PNPI)
Translated from ZETFP 76 392.
BYRNE 02 JP G28 1325 J. Byrne *et al.*
CHUNG 02B PR D66 032004 J. Chung *et al.* (SOUDAN-2 Collab.)
MOSTOVOI 01 PAN 64 1955 Yu.A. Mostovoi *et al.*
Translated from YAF 64 2040.
ARZUMANOV 00 PL B483 15 S. Arzumanov *et al.*
GAL 00 PR C61 028201 A. Gal
KOLB 00 PRL 85 1388 N.R. Kolb *et al.*
LAMOREAUX 00 PR D61 051301 S.K. Lamoreaux, R. Golub
LEVCHUK 00 NP A674 449 M.I. Levchuk, A.I. L'vov (BELA, LEBD)
LISING 00 PR C62 055501 L.J. Lising *et al.* (NIST emIT Collab.)
HARRIS 99 PRL 82 904 P.G. Harris *et al.*
KESSLER 99 PL A255 221 E.G. Kessler Jr *et al.*
MOHR 99 JPCRD 28 1713 P.J. Mohr, B.N. Taylor (NIST)
Also RMP 72 351 P.J. Mohr, B.N. Taylor (NIST)
SEREBROV 98 JETP 86 1074 A.P. Serebrov *et al.*
Translated from ZETF 113 1963.
ABELE 97D PL B407 212 H. Abele *et al.* (HEIDP, ILLG)
KOPECKY 97 PR C56 2229 S. Kopecky *et al.*
LIAUD 97 NP A612 53 P. Liaud *et al.* (ILLG, LAPP)
YEROZLIM... 97 PL B412 240 B.G. Erozolimsky *et al.* (HARV, PNPI, KIAE)
ALTAREV 96 PAN 59 1152 I.S. Altarev *et al.* (PNPI)
Translated from YAF 59 1204.
BONDAREN... 96 JETPL 64 416 L.N. Bondarenko *et al.* (KIAE)
Translated from ZETFP 64 382.
BYRNE 96 EPL 33 187 J. Byrne *et al.* (SUSS, ILLG)
MOSTOVOI 96 PAN 59 968 Y.A. Mostovoy (KIAE)
Translated from YAF 59 1013.
NORMAN 96 PR D53 4086 E.B. Norman, J.N. Bahcall, M. Goldhaber (LBL+)
IGNATOVICH 95 JETPL 62 1 V.K. Ignatovich (JINR)
Translated from ZETFP 62 3.
KOESTER 95 PR C51 3363 L. Koester *et al.* (TUM, JINR, LATV)
KOPECKY 95 PRL 74 2427 S. Kopecky *et al.*
KUZNETSOV 95 PRL 75 794 I.A. Kuznetsov *et al.* (PNPI, KIAE, HARV+)
SCHRECK... 95 PL B349 427 K. Schreckenbach *et al.* (TUM, ILLG, LAPP)
BALDO-... 94 ZPHY C63 409 M. Baldo-Ceolin *et al.* (HEID, ILLG, PADO+)
DIFILIPPO 94 PRL 73 1481 F. DiFilippo *et al.* (MIT)
Also PRL 71 1998 V. Natarajan *et al.* (MIT)
GOLUB 94 PRPL 237C 1 R. Golub, K. Lamoreaux (HAHN, WASH)
MAMPE 93 JETPL 57 82 B. Mampe *et al.* (KIAE)
Translated from ZETFP 57 77.
ALTAREV 92 PL B276 242 I.S. Altarev *et al.* (PNPI)
NESVIZHEV... 92 JETP 75 405 V.V. Nesvizhevsky *et al.* (PNPI, JINR)
Translated from ZETF 102 740.
ALBERICO 91 NP A523 488 W.M. Alberico, A. de Pace, M. Pignone (TORI)
DUBBERS 91 NP A527 239c D. Dubbers (ILLG)
Also EPL 11 195 D. Dubbers, W. Mampe, J. Dohner (ILLG, HEID)
EROZOLIM... 91 PL B263 33 B.G. Erozolimsky *et al.* (PNPI, KIAE)
Also SJNP 52 999 B.G. Erozolimsky *et al.* (PNPI, KIAE)
Translated from YAF 52 1583.
EROZOLIM... 91B SJNP 53 260 B.G. Erozolimsky, Y.A. Mostovoy (KIAE)
Translated from YAF 53 418.
SCHMIEDM... 91 PRL 66 1015 J. Schmiedmayer *et al.* (TUW, ORNL)
WOOLCOCK 91 MPL A6 2579 W.S. Woolcock (CANB)
ALFIMENKOV 90 JETPL 52 373 V.P. Alfimenkov *et al.* (PNPI, JINR)
Translated from ZETFP 52 984.
BALDO-... 90 PL B236 95 M. Baldo-Ceolin *et al.* (PADO, PAVI, HEIDP+)
BERGER 90 PL B240 237 C. Berger *et al.* (FREJUS Collab.)
BRESSI 90 NC 103A 731 G. Bressi *et al.* (PAVI, ROMA, MILA)
BYRNE 90 PRL 65 289 J. Byrne *et al.* (SUSS, NBS, SCOT, CBNM)
GREEN 90 JP G16 L75 K. Green, D. Thompson (RAL)
RAMSEY 90 ARNPS 40 1 N.F. Ramsey (HARV)
ROSE 90 PL B234 460 K.W. Rose *et al.* (GOET, MPCM, MAINZ)
ROSE 90B NP A514 621 K.W. Rose *et al.* (GOET, MPCM)
SMITH 90 PL B234 191 K.F. Smith *et al.* (SUSS, RAL, HARV+)
BRESSI 89 ZPHY C43 175 G. Bressi *et al.* (INFN, MILA, PAVI, ROMA)
DOVER 89 NIM A284 13 C.B. Dover, A. Gal, J.M. Richard (BNL, HEBR+)
KOSSAKOW... 89 NP A503 473 R. Kossakowski *et al.* (LAPP, SAVO, ISNG+)
MAMPE 89 PRL 63 593 W. Mampe *et al.* (ILLG, RISL, SUSS, URI)
MOHAPATRA 89 NIM A284 1 R.N. Mohapatra (UMD)
PAUL 89 ZPHY C45 25 W. Paul *et al.* (BONN, WUPP, MPIK, ILLG)
SCHMIEDM... 89 NIM A284 137 J. Schmiedmayer, H. Rauch, P. Riehs (WIEN)
BAUMANN 88 PR D37 3107 J. Baumann *et al.* (BAYR, MUNI, ILLG)
KOESTER 88 ZPHY A329 229 L. Koester, W. Waschkowski, J. Meier (MUNI, TUM)
LAST 88 PRL 60 995 I. Last *et al.* (HEIDP, ILLG, ANL)
SCHMIEDM... 88 PRL 61 1065 J. Schmiedmayer, H. Rauch, P. Riehs (TUW)
Also PRL 61 2509 (erratum) J. Schmiedmayer, H. Rauch, P. Riehs (TUW)
SPIVAK 88 JETP 67 1735 P.E. Spivak (KIAE)
Translated from ZETF 94 1.
COHEN 87 RMP 59 1121 E.R. Cohen, B.N. Taylor (RISC, NBS)
ALEKSANDR... 86 SJNP 44 900 Yu.A. Aleksandrov *et al.*
Translated from YAF 44 1384.
ALTAREV 86 JETPL 44 460 I.S. Altarev *et al.* (PNPI)
Translated from ZETFP 44 360.
BOPP 86 PRL 56 919 P. Bopp *et al.* (HEIDP, ANL, ILLG)
Also ZPHY C37 179 E. Klempt *et al.* (HEIDP, ANL, ILLG)
CRESTI 86 PL B177 206 M. Cresti *et al.* (PADO)
Also PL B200 587 (erratum) M. Cresti *et al.* (PADO)
GREENE 86 PRL 56 819 G.L. Greene *et al.* (NBS, ILLG)
KOESTER 86 Physica B137 282 L. Koester *et al.*
KOSVINTSEV 86 JETPL 44 571 Y.Y. Kosvintsev, V.I. Morozov, G.I. Terekhov (KIAE)
Translated from ZETFP 44 444.
TAKITA 86 PR D34 902 M. Takita *et al.* (KEK, TOKY+)
DOVER 85 PR C31 1423 C.B. Dover, A. Gal, J.M. Richard (BNL)
FIDECARO 85 PL 156B 122 G. Fidecaro *et al.* (CERN, ILLG, PADO+)
PARK 85B NP B252 261 H.S. Park *et al.* (IMB Collab.)
BATTISTONI 84 PL 133B 454 G. Battistoni *et al.* (NUSEX Collab.)
JONES 84 PRL 52 720 T.W. Jones *et al.* (IMB Collab.)
PENDLEBURY 84 PL 136B 327 J.M. Pendlebury *et al.* (SUSS, HARV, RAL+)
CHERRY 83 PRL 50 1354 M.L. Cherry *et al.* (PENN, BNL)
DOVER 83 PR D27 1090 C.B. Dover, A. Gal, J.M. Richard (BNL)
KABIR 83 PRL 51 231 P.K. Kabir (HARV)
MOSTOVOY 83 JETPL 37 196 Y.A. Mostovoy (KIAE)
Translated from ZETFP 37 162.

Downloaded from https://academic.oup.com/ptep/article/2022/8/083C01/6651666 by KIT Library user on 27 September 2022

ROY	83	PR D28 1770	A. Roy *et al.*	(TATA)
VAIDYA	83	PR D27 486	S.C. Vaidya *et al.*	(TATA)
GAEHLER	82	PR D25 2887	R. Gahler, J. Kalus, W. Mampe	(BAYR, ILLG)
GREENE	82	Metrologia 18 93	G.L. Greene *et al.*	(YALE, HARV, ILLG+)
ALTAREV	81	PL 102B 13	I.S. Altarev *et al.*	(PNPI)
BARABANOV	80	JETPL 32 359	I.R. Barabanov *et al.*	(PNPI)
		Translated from ZETFP 32 384.		
BYRNE	80	PL 92B 274	J. Byrne *et al.*	(SUSS, RL)
KOSVINTSEV	80	JETPL 31 236	Y.Y. Kosvintsev *et al.*	(JINR)
		Translated from ZETFP 31 257.		
MOHAPATRA	80	PRL 44 1316	R.N. Mohapatra, R.E. Marshak	(CUNY, VPI)
ALTAREV	79	JETPL 29 730	I.S. Altarev *et al.*	(PNPI)
		Translated from ZETFP 29 794.		
EROZOLIM...	79	SJNP 30 356	B.G. Erozolimsky *et al.*	(KIAE)
		Translated from YAF 30 692.		
NORMAN	79	PRL 43 1226	E.B. Norman, A.G. Seamster	(WASH)
BONDAREN...	78	JETPL 28 303	L.N. Bondarenko *et al.*	(KIAE)
		Translated from ZETFP 28 328.		
Also		Smolenice Conf.	P.G. Bondarenko	(KIAE)
EROZOLIM...	78	SJNP 28 48	B.G. Erozolimsky *et al.*	(KIAE)
		Translated from YAF 28 98.		
STRATOWA	78	PR D18 3970	C. Stratowa, R. Dobrozemsky, P. Weinzierl	(SEIB)
EROZOLIM...	77	JETPL 23 663	B.G. Erozolimsky *et al.*	(KIAE)
		Translated from ZETFP 23 720.		
KOESTER	76	PRL 36 1021	L. Koester *et al.*	
STEINBERG	76	PR D13 2469	R.I. Steinberg *et al.*	(YALE, ISNG)
DOBROZE...	75	PR D11 510	R. Dobrozemsky *et al.*	(SEIB)
KROHN	75	PL 55B 175	V.E. Krohn, G.R. Ringo	(ANL)
EROZOLIM...	74	JETPL 20 345	B.G. Erozolimsky *et al.*	
		Translated from ZETFP 20 745.		
KROPF	74	ZPHY 267 129	H. Kropf, E. Paul	(LINZ)
Also		NP A154 160	H. Paul	(VIEN)
STEINBERG	74	PRL 33 41	R.I. Steinberg *et al.*	(YALE, ISNG)
COHEN	73	JPCRD 2 664	E.R. Cohen, B.N. Taylor	(RISC, NBS)
KROHN	73	PR D8 1305	V.E. Krohn, G.R. Ringo	
CHRISTENSEN	72	PR D5 1628	C.J. Christensen *et al.*	(RISO)
CHRISTENSEN	70	PR C1 1693	C.J. Christensen, V.E. Krohn, G.R. Ringo	(ANL)
EROZOLIM...	70C	PL 33B 351	B.G. Erozolimsky *et al.*	(KIAE)
GRIGOREV	68	SJNP 6 239	V.K. Grigoriev *et al.*	(ITEP)
		Translated from YAF 6 329.		
KROHN	66	PR 148 1303	V.E. Krohn, G.R. Ringo	
LEE	56	PR 104 254	T.D. Lee, C.N. Yang	(COLU, BNL)

See the related review(s):
N and Δ Resonances

$N(1440)\ 1/2^+$

$I(J^P) = \frac{1}{2}(\frac{1}{2}^+)$ Status: ****

Older and obsolete values are listed and referenced in the 2014 edition, Chinese Physics **C38** 070001 (2014).

$N(1440)$ POLE POSITION

REAL PART

VALUE (MeV)	DOCUMENT ID		TECN	COMMENT
1360 to 1380 (≈ 1370) OUR ESTIMATE				
1369± 3	SOKHOYAN	15A	DPWA	Multichannel
1363± 2±2	[1] SVARC	14	L+P	$\pi N \to \pi N$
1375±30	CUTKOSKY	80	IPWA	$\pi N \to \pi N$
• • • We do not use the following data for averages, fits, limits, etc. • • •				
1360	HUNT	19	DPWA	Multichannel
1355	ROENCHEN	15A	DPWA	Multichannel
1386	SHKLYAR	13	DPWA	Multichannel
1370± 4	ANISOVICH	12A	DPWA	Multichannel
1363±11	BATINIC	10	DPWA	$\pi N \to N\pi,\ N\eta$
1359	ARNDT	06	DPWA	$\pi N \to \pi N,\ \eta N$
1383	VRANA	00	DPWA	Multichannel
1385	HOEHLER	93	SPED	$\pi N \to \pi N$

[1] Fit to the amplitudes of HOEHLER 79.

−2×IMAGINARY PART

VALUE (MeV)	DOCUMENT ID		TECN	COMMENT
160 to 190 (≈ 175) OUR ESTIMATE				
189± 5	SOKHOYAN	15A	DPWA	Multichannel
180± 4±5	[1] SVARC	14	L+P	$\pi N \to \pi N$
180±40	CUTKOSKY	80	IPWA	$\pi N \to \pi N$
• • • We do not use the following data for averages, fits, limits, etc. • • •				
186	HUNT	19	DPWA	Multichannel
215	ROENCHEN	15A	DPWA	Multichannel
277	SHKLYAR	13	DPWA	Multichannel
190± 7	ANISOVICH	12A	DPWA	Multichannel
151±13	BATINIC	10	DPWA	$\pi N \to N\pi,\ N\eta$
162	ARNDT	06	DPWA	$\pi N \to \pi N,\ \eta N$
316	VRANA	00	DPWA	Multichannel
164	HOEHLER	93	SPED	$\pi N \to \pi N$

[1] Fit to the amplitudes of HOEHLER 79.

$N(1440)$ ELASTIC POLE RESIDUE

MODULUS $|r|$

VALUE (MeV)	DOCUMENT ID		TECN	COMMENT
46 to 54 (≈ 50) OUR ESTIMATE				
49±3	SOKHOYAN	15A	DPWA	Multichannel
50±1±2	[1] SVARC	14	L+P	$\pi N \to \pi N$
52±5	CUTKOSKY	80	IPWA	$\pi N \to \pi N$
• • • We do not use the following data for averages, fits, limits, etc. • • •				
62	ROENCHEN	15A	DPWA	Multichannel
126	SHKLYAR	13	DPWA	Multichannel
48±3	ANISOVICH	12A	DPWA	Multichannel
44	BATINIC	10	DPWA	$\pi N \to N\pi,\ N\eta$
38	ARNDT	06	DPWA	$\pi N \to \pi N,\ \eta N$
40	HOEHLER	93	SPED	$\pi N \to \pi N$

[1] Fit to the amplitudes of HOEHLER 79.

PHASE θ

VALUE (°)	DOCUMENT ID		TECN	COMMENT
−100 to −80 (≈ −90) OUR ESTIMATE				
− 82± 5	SOKHOYAN	15A	DPWA	Multichannel
− 88± 1±2	[1] SVARC	14	L+P	$\pi N \to \pi N$
−100±35	CUTKOSKY	80	IPWA	$\pi N \to \pi N$
• • • We do not use the following data for averages, fits, limits, etc. • • •				
− 98	ROENCHEN	15A	DPWA	Multichannel
− 60	SHKLYAR	13	DPWA	Multichannel
− 78± 4	ANISOVICH	12A	DPWA	Multichannel
− 88	BATINIC	10	DPWA	$\pi N \to N\pi,\ N\eta$
− 98	ARNDT	06	DPWA	$\pi N \to \pi N,\ \eta N$

[1] Fit to the amplitudes of HOEHLER 79.

$N(1440)$ INELASTIC POLE RESIDUE

The "normalized residue" is the residue divided by $\Gamma_{pole}/2$.

Normalized residue in $N\pi \to N(1440) \to N\eta$

MODULUS	PHASE (°)	DOCUMENT ID		TECN	COMMENT
• • • We do not use the following data for averages, fits, limits, etc. • • •					
0.078	−27	ROENCHEN	15A	DPWA	Multichannel

Normalized residue in $N\pi \to N(1440) \to \Delta\pi$, P-wave

MODULUS	PHASE (°)	DOCUMENT ID		TECN	COMMENT
0.27±0.02	38 ± 5	SOKHOYAN	15A	DPWA	Multichannel
• • • We do not use the following data for averages, fits, limits, etc. • • •					
0.27±0.02	40 ± 5	ANISOVICH	12A	DPWA	Multichannel

Normalized residue in $N\pi \to N(1440) \to \Lambda K$

MODULUS	PHASE (°)	DOCUMENT ID		TECN	COMMENT
• • • We do not use the following data for averages, fits, limits, etc. • • •					
0.016	145	ROENCHEN	15A	DPWA	Multichannel

Normalized residue in $N\pi \to N(1440) \to \Sigma K$

MODULUS	PHASE (°)	DOCUMENT ID		TECN	COMMENT
• • • We do not use the following data for averages, fits, limits, etc. • • •					
0.027	113	ROENCHEN	15A	DPWA	Multichannel

Normalized residue in $N\pi \to N(1440) \to N\ (\pi\pi)^{I=0}_{S-wave}$

MODULUS	PHASE (°)	DOCUMENT ID		TECN	COMMENT
0.21±0.04	−136 ± 4	SOKHOYAN	15A	DPWA	Multichannel
• • • We do not use the following data for averages, fits, limits, etc. • • •					
0.21±0.05	−135 ± 7	ANISOVICH	12A	DPWA	Multichannel

$N(1440)$ BREIT-WIGNER MASS

VALUE (MeV)	DOCUMENT ID		TECN	COMMENT
1410 to 1470 (≈ 1440) OUR ESTIMATE				
1417 ± 4	[1] HUNT	19	DPWA	Multichannel
1430 ±10	SOKHOYAN	15A	DPWA	Multichannel
1515 ±15	[1] SHKLYAR	13	DPWA	Multichannel
1485.0± 1.2	[1] ARNDT	06	DPWA	$\pi N \to \pi N,\ \eta N$
1440 ±30	CUTKOSKY	80	IPWA	$\pi N \to \pi N$
1410 ±12	HOEHLER	79	IPWA	$\pi N \to \pi N$
• • • We do not use the following data for averages, fits, limits, etc. • • •				
1430 ± 8	ANISOVICH	12A	DPWA	Multichannel
1412 ± 2	[1] SHRESTHA	12A	DPWA	Multichannel
1439 ±19	BATINIC	10	DPWA	$\pi N \to N\pi,\ N\eta$
1518 ± 5	PENNER	02C	DPWA	Multichannel
1479 ±80	VRANA	00	DPWA	Multichannel

[1] Statistical error only.

$N(1440)$ BREIT-WIGNER WIDTH

VALUE (MeV)	DOCUMENT ID		TECN	COMMENT
250 to 450 (≈ 350) OUR ESTIMATE				
257± 11	[1] HUNT	19	DPWA	Multichannel
360± 30	SOKHOYAN	15A	DPWA	Multichannel
605± 90	[1] SHKLYAR	13	DPWA	Multichannel
284± 18	[1] ARNDT	06	DPWA	$\pi N \to \pi N,\ \eta N$
340± 70	CUTKOSKY	80	IPWA	$\pi N \to \pi N$
135± 10	HOEHLER	79	IPWA	$\pi N \to \pi N$

Downloaded from https://academic.oup.com/ptep/article/2022/8/083C01/6651666 by KIT Library user on 27 September 2022

• • • We do not use the following data for averages, fits, limits, etc. • • •

365 ± 35	ANISOVICH	12A	DPWA	Multichannel
248 ± 5	[1] SHRESTHA	12A	DPWA	Multichannel
437 ± 141	BATINIC	10	DPWA	$\pi N \to N\pi$, $N\eta$
668 ± 41	PENNER	02C	DPWA	Multichannel
490 ± 120	VRANA	00	DPWA	Multichannel

[1] Statistical error only.

$N(1440)$ DECAY MODES

The following branching fractions are our estimates, not fits or averages.

	Mode	Fraction (Γ_i/Γ)
Γ_1	$N\pi$	55–75 %
Γ_2	$N\eta$	<1 %
Γ_3	$N\pi\pi$	17–50 %
Γ_4	$\Delta(1232)\pi$, P-wave	6–27 %
Γ_5	$N\sigma$	11–23 %
Γ_6	$p\gamma$, helicity=1/2	0.035–0.048 %
Γ_7	$n\gamma$, helicity=1/2	0.02–0.04 %

$N(1440)$ BRANCHING RATIOS

$\Gamma(N\pi)/\Gamma_{total}$ — Γ_1/Γ

VALUE (%)	DOCUMENT ID		TECN	COMMENT
55 to 75 (≈ 65) OUR ESTIMATE				
59 ± 2	[1] HUNT	19	DPWA	Multichannel
63 ± 2	SOKHOYAN	15A	DPWA	Multichannel
56 ± 2	[1] SHKLYAR	13	DPWA	Multichannel
78.7 ± 1.6	[1] ARNDT	06	DPWA	$\pi N \to \pi N$, ηN
68 ± 4	CUTKOSKY	80	IPWA	$\pi N \to \pi N$
51 ± 5	HOEHLER	79	IPWA	$\pi N \to \pi N$
• • • We do not use the following data for averages, fits, limits, etc. • • •				
62 ± 3	ANISOVICH	12A	DPWA	Multichannel
64.8 ± 0.9	[1] SHRESTHA	12A	DPWA	Multichannel
62 ± 4	BATINIC	10	DPWA	$\pi N \to N\pi$, $N\eta$
57 ± 1	PENNER	02C	DPWA	Multichannel
72 ± 5	VRANA	00	DPWA	Multichannel

[1] Statistical error only.

$\Gamma(N\eta)/\Gamma_{total}$ — Γ_2/Γ

VALUE (%)	DOCUMENT ID		TECN	COMMENT
• • • We do not use the following data for averages, fits, limits, etc. • • •				
0 ± 1	VRANA	00	DPWA	Multichannel

$\Gamma(\Delta(1232)\pi, P\text{-wave})/\Gamma_{total}$ — Γ_4/Γ

VALUE (%)	DOCUMENT ID		TECN	COMMENT
6 to 27 (≈ 15) OUR ESTIMATE				
22 ± 4	[1] HUNT	19	DPWA	Multichannel
12^{+5}_{-3}	SHKLYAR	16	DPWA	Multichannel
20 ± 7	SOKHOYAN	15A	DPWA	Multichannel
• • • We do not use the following data for averages, fits, limits, etc. • • •				
21 ± 8	ANISOVICH	12A	DPWA	Multichannel
6.5 ± 0.8	[1] SHRESTHA	12A	DPWA	Multichannel
16 ± 1	VRANA	00	DPWA	Multichannel

[1] Statistical error only.

$\Gamma(N\sigma)/\Gamma_{total}$ — Γ_5/Γ

VALUE (%)	DOCUMENT ID		TECN	COMMENT
16 ± 3	[1] HUNT	19	DPWA	Multichannel
27^{+4}_{-9}	SHKLYAR	16	DPWA	Multichannel
17 ± 6	SOKHOYAN	15A	DPWA	Multichannel
• • • We do not use the following data for averages, fits, limits, etc. • • •				
17 ± 7	ANISOVICH	12A	DPWA	Multichannel
27 ± 1	[1] SHRESTHA	12A	DPWA	Multichannel
12 ± 1	VRANA	00	DPWA	Multichannel

[1] Statistical error only.

$N(1440)$ PHOTON DECAY AMPLITUDES AT THE POLE

$N(1440) \to p\gamma$, helicity-1/2 amplitude $A_{1/2}$

MODULUS (GeV$^{-1/2}$)	PHASE (°)	DOCUMENT ID		TECN	COMMENT
−0.044 ± 0.005	−40 ± 8	SOKHOYAN	15A	DPWA	Multichannel
$-0.054^{+0.004}_{-0.003}$	5^{+2}_{-5}	ROENCHEN	14	DPWA	
• • • We do not use the following data for averages, fits, limits, etc. • • •					
−0.060	−23	ROENCHEN	15A	DPWA	Multichannel

$N(1440)$ BREIT-WIGNER PHOTON DECAY AMPLITUDES

$N(1440) \to p\gamma$, helicity-1/2 amplitude $A_{1/2}$

VALUE (GeV$^{-1/2}$)	DOCUMENT ID		TECN	COMMENT
−0.080 to −0.050 (≈ −0.065) OUR ESTIMATE				
−0.091 ± 0.007	[1] HUNT	19	DPWA	Multichannel
−0.061 ± 0.006	SOKHOYAN	15A	DPWA	Multichannel
−0.085 ± 0.003	[1] SHKLYAR	13	DPWA	Multichannel
−0.056 ± 0.001	[1] WORKMAN	12A	DPWA	$\gamma N \to N\pi$
−0.051 ± 0.002	[1] DUGGER	07	DPWA	$\gamma N \to \pi N$
• • • We do not use the following data for averages, fits, limits, etc. • • •				
−0.061 ± 0.008	ANISOVICH	12A	DPWA	Multichannel
−0.084 ± 0.003	[1] SHRESTHA	12A	DPWA	Multichannel
−0.061	DRECHSEL	07	DPWA	$\gamma N \to \pi N$
−0.087	PENNER	02D	DPWA	Multichannel

[1] Statistical error only.

$N(1440) \to n\gamma$, helicity-1/2 amplitude $A_{1/2}$

VALUE (GeV$^{-1/2}$)	DOCUMENT ID		TECN	COMMENT
0.035 to 0.055 (≈ 0.045) OUR ESTIMATE				
0.013 ± 0.012	[1] HUNT	19	DPWA	Multichannel
0.043 ± 0.012	ANISOVICH	13B	DPWA	Multichannel
0.048 ± 0.004	[1] CHEN	12A	DPWA	$\gamma N \to \pi N$
• • • We do not use the following data for averages, fits, limits, etc. • • •				
0.040 ± 0.005	[1] SHRESTHA	12A	DPWA	Multichannel
0.054	DRECHSEL	07	DPWA	$\gamma N \to \pi N$
0.121	PENNER	02D	DPWA	Multichannel

[1] Statistical error only.

$N(1440)$ REFERENCES

For early references, see Physics Letters **111B** 1 (1982).

HUNT	19	PR C99 055205	B.C. Hunt, D.M. Manley	
SHKLYAR	16	PR C93 045206	V. Shklyar, H. Lenske, U. Mosel	(GIES)
ROENCHEN	15A	EPJ A51 70	D. Roenchen *et al.*	
SOKHOYAN	15A	EPJ A51 95	V. Sokhoyan *et al.*	(CBELSA/TAPS Collab.)
PDG	14	CP C38 070001	K. Olive *et al.*	(PDG Collab.)
ROENCHEN	14	EPJ A50 101	D. Roenchen *et al.*	
Also		EPJ A51 63 (errat.)	D. Roenchen *et al.*	
SVARC	14	PR C89 045205	A. Svarc *et al.*	(RBI Zagreb, UNI Tuzla)
ANISOVICH	13B	EPJ A49 67	A.V. Anisovich *et al.*	
SHKLYAR	13	PR C87 015201	V. Shklyar, H. Lenske, U. Mosel	(GIES)
ANISOVICH	12A	EPJ A48 15	A.V. Anisovich *et al.*	(BONN, PNPI)
CHEN	12A	PR C86 015206	W. Chen *et al.*	(DUKE, GWU, MSST, ITEP+)
SHRESTHA	12A	PR C86 055203	M. Shrestha, D.M. Manley	(KSU)
WORKMAN	12A	PR C86 015202	R. Workman *et al.*	(GWU)
BATINIC	10	PR C82 038203	M. Batinic *et al.*	(ZAGR)
DRECHSEL	07	EPJ A34 69	D. Drechsel, S.S. Kamalov, L. Tiator	(MAINZ, JINR)
DUGGER	07	PR C76 025211	M. Dugger *et al.*	(JLab CLAS Collab.)
ARNDT	06	PR C74 045205	R.A. Arndt *et al.*	(GWU)
PENNER	02C	PR C66 055211	G. Penner, U. Mosel	(GIES)
PENNER	02D	PR C66 055212	G. Penner, U. Mosel	(GIES)
VRANA	00	PRPL 328 181	T.P. Vrana, S.A. Dytman, T.-S.H. Lee	(PITT, ANL)
HOEHLER	93	πN Newsletter 9 1	G. Hohler	(KARL)
CUTKOSKY	80	Toronto Conf. 19	R.E. Cutkosky *et al.*	(CMU, LBL) IJP
Also		PR D20 2839	R.E. Cutkosky *et al.*	(CMU, LBL) IJP
HOEHLER	79	PDAT 12-1	G. Hohler *et al.*	(KARLT) IJP
Also		Toronto Conf. 3	R. Koch	(KARLT) IJP

$N(1520)\ 3/2^-$

$I(J^P) = \frac{1}{2}(\frac{3}{2}^-)$ Status: ****

Older and obsolete values are listed and referenced in the 2014 edition, Chinese Physics **C38** 070001 (2014).

$N(1520)$ POLE POSITION

REAL PART

VALUE (MeV)	DOCUMENT ID		TECN	COMMENT
1505 to 1515 (≈ 1510) OUR ESTIMATE				
1507 ± 2	SOKHOYAN	15A	DPWA	Multichannel
1506 ± 1 ± 1	[1] SVARC	14	L+P	$\pi N \to \pi N$
1510 ± 5	CUTKOSKY	80	IPWA	$\pi N \to \pi N$
• • • We do not use the following data for averages, fits, limits, etc. • • •				
1500	HUNT	19	DPWA	Multichannel
1512	ROENCHEN	15A	DPWA	Multichannel
1492	SHKLYAR	13	DPWA	Multichannel
1507 ± 3	ANISOVICH	12A	DPWA	Multichannel
1506 ± 9	BATINIC	10	DPWA	$\pi N \to N\pi$, $N\eta$
1515	ARNDT	06	DPWA	$\pi N \to \pi N$, ηN
1504	VRANA	00	DPWA	Multichannel
1510	HOEHLER	93	ARGD	$\pi N \to \pi N$

[1] Fit to the amplitudes of HOEHLER 79.

−2×IMAGINARY PART

VALUE (MeV)	DOCUMENT ID		TECN	COMMENT
105 to 120 (≈ 110) OUR ESTIMATE				
111 ± 3	SOKHOYAN	15A	DPWA	Multichannel
115 ± 2 ± 1	[1] SVARC	14	L+P	$\pi N \to \pi N$
114 ± 10	CUTKOSKY	80	IPWA	$\pi N \to \pi N$

Downloaded from https://academic.oup.com/ptep/article/2022/8/083C01/6651666 by KIT Library user on 27 September 2022

• • • We do not use the following data for averages, fits, limits, etc. • • •				
117	HUNT	19	DPWA	Multichannel
89	ROENCHEN	15A	DPWA	Multichannel
94	SHKLYAR	13	DPWA	Multichannel
111± 5	ANISOVICH	12A	DPWA	Multichannel
122± 9	BATINIC	10	DPWA	$\pi N \to N\pi$, $N\eta$
113	ARNDT	06	DPWA	$\pi N \to \pi N$, ηN
112	VRANA	00	DPWA	Multichannel
120	HOEHLER	93	ARGD	$\pi N \to \pi N$

[1] Fit to the amplitudes of HOEHLER 79.

N(1520) ELASTIC POLE RESIDUE

MODULUS |r|

VALUE (MeV)	DOCUMENT ID		TECN	COMMENT
32 to 38 (≈ 35) OUR ESTIMATE				
36±2	SOKHOYAN	15A	DPWA	Multichannel
33±1±1	[1] SVARC	14	L+P	$\pi N \to \pi N$
35±2	CUTKOSKY	80	IPWA	$\pi N \to \pi N$
• • • We do not use the following data for averages, fits, limits, etc. • • •				
37	ROENCHEN	15A	DPWA	Multichannel
27	SHKLYAR	13	DPWA	Multichannel
36±3	ANISOVICH	12A	DPWA	Multichannel
35	BATINIC	10	DPWA	$\pi N \to N\pi$, $N\eta$
38	ARNDT	06	DPWA	$\pi N \to \pi N$, ηN
32	HOEHLER	93	ARGD	$\pi N \to \pi N$

[1] Fit to the amplitudes of HOEHLER 79.

PHASE θ

VALUE (°)	DOCUMENT ID		TECN	COMMENT
−15 to −5 (≈ −10) OUR ESTIMATE				
−14±3	SOKHOYAN	15A	DPWA	Multichannel
−15±1±1	[1] SVARC	14	L+P	$\pi N \to \pi N$
−12±5	CUTKOSKY	80	IPWA	$\pi N \to \pi N$
• • • We do not use the following data for averages, fits, limits, etc. • • •				
− 6	ROENCHEN	15A	DPWA	Multichannel
−35	SHKLYAR	13	DPWA	Multichannel
−14±3	ANISOVICH	12A	DPWA	Multichannel
− 7	BATINIC	10	DPWA	$\pi N \to N\pi$, $N\eta$
− 5	ARNDT	06	DPWA	$\pi N \to \pi N$, ηN
− 8	HOEHLER	93	ARGD	$\pi N \to \pi N$

[1] Fit to the amplitudes of HOEHLER 79.

N(1520) INELASTIC POLE RESIDUE

The "normalized residue" is the residue divided by $\Gamma_{pole}/2$.

Normalized residue in $N\pi \to N(1520) \to \Delta\pi$, S-wave

MODULUS	PHASE (°)	DOCUMENT ID		TECN	COMMENT
0.33±0.04	155 ± 15	SOKHOYAN	15A	DPWA	Multichannel
• • • We do not use the following data for averages, fits, limits, etc. • • •					
0.33±0.05	150 ± 20	ANISOVICH	12A	DPWA	Multichannel

Normalized residue in $N\pi \to N(1520) \to \Delta\pi$, D-wave

MODULUS	PHASE (°)	DOCUMENT ID		TECN	COMMENT
0.25±0.03	105 ± 18	SOKHOYAN	15A	DPWA	Multichannel
• • • We do not use the following data for averages, fits, limits, etc. • • •					
0.25±0.03	100 ± 20	ANISOVICH	12A	DPWA	Multichannel

Normalized residue in $N\pi \to N(1520) \to N\eta$

MODULUS	PHASE (°)	DOCUMENT ID		TECN	COMMENT
• • • We do not use the following data for averages, fits, limits, etc. • • •					
0.026	95	ROENCHEN	15A	DPWA	Multichannel

Normalized residue in $N\pi \to N(1520) \to \Lambda K$

MODULUS	PHASE (°)	DOCUMENT ID		TECN	COMMENT
• • • We do not use the following data for averages, fits, limits, etc. • • •					
0.069	158	ROENCHEN	15A	DPWA	Multichannel

Normalized residue in $N\pi \to N(1520) \to \Sigma K$

MODULUS	PHASE (°)	DOCUMENT ID		TECN	COMMENT
• • • We do not use the following data for averages, fits, limits, etc. • • •					
0.049	−41	ROENCHEN	15A	DPWA	Multichannel

Normalized residue in $N\pi \to N(1520) \to N\sigma$

MODULUS	PHASE (°)	DOCUMENT ID		TECN	COMMENT
0.08±0.03	−45 ± 25	SOKHOYAN	15A	DPWA	Multichannel

N(1520) BREIT-WIGNER MASS

VALUE (MeV)	DOCUMENT ID		TECN	COMMENT
1510 to 1520 (≈ 1515) OUR ESTIMATE				
1512.0± 1.5	[1] HUNT	19	DPWA	Multichannel
1516 ± 2	SOKHOYAN	15A	DPWA	Multichannel
1505 ± 4	[1] SHKLYAR	13	DPWA	Multichannel
1514.5± 0.2	[1] ARNDT	06	DPWA	$\pi N \to \pi N$, ηN
1525 ±10	CUTKOSKY	80	IPWA	$\pi N \to \pi N$
1519 ± 4	HOEHLER	79	IPWA	$\pi N \to \pi N$
• • • We do not use the following data for averages, fits, limits, etc. • • •				
1517 ± 3	ANISOVICH	12A	DPWA	Multichannel
1512.6± 0.5	[1] SHRESTHA	12A	DPWA	Multichannel
1522 ± 8	BATINIC	10	DPWA	$\pi N \to N\pi$, $N\eta$
1509 ± 1	PENNER	02C	DPWA	Multichannel
1518 ± 3	VRANA	00	DPWA	Multichannel

[1] Statistical error only.

N(1520) BREIT-WIGNER WIDTH

VALUE (MeV)	DOCUMENT ID		TECN	COMMENT
100 to 120 (≈ 110) OUR ESTIMATE				
121 ± 3	[1] HUNT	19	DPWA	Multichannel
113 ± 4	SOKHOYAN	15A	DPWA	Multichannel
100 ± 2	[1] SHKLYAR	13	DPWA	Multichannel
103.6± 0.4	[1] ARNDT	06	DPWA	$\pi N \to \pi N$, ηN
120 ±15	CUTKOSKY	80	IPWA	$\pi N \to \pi N$
114 ± 7	HOEHLER	79	IPWA	$\pi N \to \pi N$
• • • We do not use the following data for averages, fits, limits, etc. • • •				
114 ± 5	ANISOVICH	12A	DPWA	Multichannel
117 ± 1	[1] SHRESTHA	12A	DPWA	Multichannel
132 ±11	BATINIC	10	DPWA	$\pi N \to N\pi$, $N\eta$
100 ± 2	PENNER	02C	DPWA	Multichannel
124 ± 4	VRANA	00	DPWA	Multichannel

[1] Statistical error only.

N(1520) DECAY MODES

The following branching fractions are our estimates, not fits or averages.

	Mode	Fraction (Γ_i/Γ)
Γ_1	$N\pi$	55–65 %
Γ_2	$N\eta$	0.07–0.09 %
Γ_3	$N\pi\pi$	25–35 %
Γ_4	$\Delta(1232)\pi$	22–34 %
Γ_5	$\Delta(1232)\pi$, S-wave	15–23 %
Γ_6	$\Delta(1232)\pi$, D-wave	7–11 %
Γ_7	$N\rho$	10–16 %
Γ_8	$N\rho$, S=3/2 , S-wave	10–16 %
Γ_9	$N\rho$, S=1/2 , D-wave	0.2–0.4 %
Γ_{10}	$N\sigma$	<10 %
Γ_{11}	$p\gamma$	0.31–0.52 %
Γ_{12}	$p\gamma$, helicity=1/2	0.01–0.02 %
Γ_{13}	$p\gamma$, helicity=3/2	0.30–0.50 %
Γ_{14}	$n\gamma$	0.30–0.53 %
Γ_{15}	$n\gamma$, helicity=1/2	0.04–0.10 %
Γ_{16}	$n\gamma$, helicity=3/2	0.25–0.45 %

N(1520) BRANCHING RATIOS

$\Gamma(N\pi)/\Gamma_{total}$ — Γ_1/Γ

VALUE (%)	DOCUMENT ID		TECN	COMMENT
55 to 65 (≈ 60) OUR ESTIMATE				
58.3±1.5	[1] HUNT	19	DPWA	Multichannel
61 ±2	SOKHOYAN	15A	DPWA	Multichannel
57 ±2	[1] SHKLYAR	13	DPWA	Multichannel
63.2±0.1	[1] ARNDT	06	DPWA	$\pi N \to \pi N$, ηN
58 ±3	CUTKOSKY	80	IPWA	$\pi N \to \pi N$
54 ±3	HOEHLER	79	IPWA	$\pi N \to \pi N$
• • • We do not use the following data for averages, fits, limits, etc. • • •				
62 ±3	ANISOVICH	12A	DPWA	Multichannel
62.7±0.5	[1] SHRESTHA	12A	DPWA	Multichannel
55 ±5	BATINIC	10	DPWA	$\pi N \to N\pi$, $N\eta$
56 ±1	PENNER	02C	DPWA	Multichannel
63 ±2	VRANA	00	DPWA	Multichannel

[1] Statistical error only.

Downloaded from https://academic.oup.com/ptep/article/2022/8/083C01/6651666 by KIT Library user on 27 September 2022

$\Gamma(N\eta)/\Gamma_{total}$ — Γ_2/Γ

VALUE (%)	DOCUMENT ID		TECN	COMMENT
<0.1	MUELLER	20	DPWA	Multichannel
0.03±0.01	[1] HUNT	19	DPWA	Multichannel
0.08±0.01	TIATOR	99	DPWA	$\gamma p \to p\eta$
• • • We do not use the following data for averages, fits, limits, etc. • • •				
<1	SHKLYAR	13	DPWA	Multichannel
0.1 ±0.1	BATINIC	10	DPWA	$\pi N \to N\pi$, $N\eta$
0.2 ±0.1	THOMA	08	DPWA	Multichannel
0.08 to 0.12	ARNDT	05	DPWA	Multichannel
0.23±0.04	PENNER	02C	DPWA	Multichannel
0 ±1	VRANA	00	DPWA	Multichannel

[1] Statistical error only.

$\Gamma(\Delta(1232)\pi, S\text{-wave})/\Gamma_{total}$ — Γ_5/Γ

VALUE (%)	DOCUMENT ID		TECN	COMMENT
12.1±2.1	ADAMCZEW...	20	DPWA	Multichannel
21 ±2	[1] HUNT	19	DPWA	Multichannel
19 ±4	SOKHOYAN	15A	DPWA	Multichannel
• • • We do not use the following data for averages, fits, limits, etc. • • •				
19 ±4	ANISOVICH	12A	DPWA	Multichannel
9.3±0.7	[1] SHRESTHA	12A	DPWA	Multichannel
15 ±2	VRANA	00	DPWA	Multichannel

[1] Statistical error only.

$\Gamma(\Delta(1232)\pi, D\text{-wave})/\Gamma_{total}$ — Γ_6/Γ

VALUE (%)	DOCUMENT ID		TECN	COMMENT
6 ±2	ADAMCZEW...	20	DPWA	Multichannel
6 ±1	[1] HUNT	19	DPWA	Multichannel
9 ±2	SOKHOYAN	15A	DPWA	Multichannel
• • • We do not use the following data for averages, fits, limits, etc. • • •				
9 ±2	ANISOVICH	12A	DPWA	Multichannel
6.3±0.5	[1] SHRESTHA	12A	DPWA	Multichannel
11 ±2	VRANA	00	DPWA	Multichannel

[1] Statistical error only.

$\Gamma(N\rho, S{=}3/2, S\text{-wave})/\Gamma_{total}$ — Γ_8/Γ

VALUE (%)	DOCUMENT ID		TECN	COMMENT
10–16 % OUR EVALUATION				
11.8±1.9	ADAMCZEW...	20	DPWA	Multichannel
14.1±1.5	[1] HUNT	19	DPWA	Multichannel

[1] Statistical error only

$\Gamma(N\rho, S{=}1/2, D\text{-wave})/\Gamma_{total}$ — Γ_9/Γ

VALUE (%)	DOCUMENT ID		TECN	COMMENT
0.2–0.4 % OUR EVALUATION				
0.4±0.2	ADAMCZEW...	20	DPWA	Multichannel

$\Gamma(N\sigma)/\Gamma_{total}$ — Γ_{10}/Γ

VALUE (%)	DOCUMENT ID		TECN	COMMENT
<10 % OUR ESTIMATE				
7 ±3	ADAMCZEW...	20	DPWA	Multichannel
<0.7	[1] HUNT	19	DPWA	Multichannel
<2	SOKHOYAN	15A	DPWA	Multichannel
• • • We do not use the following data for averages, fits, limits, etc. • • •				
<1	[1] SHRESTHA	12A	DPWA	Multichannel
<4	THOMA	08	DPWA	Multichannel
1 ±1	VRANA	00	DPWA	Multichannel

[1] Statistical error only.

$N(1520)$ PHOTON DECAY AMPLITUDES AT THE POLE

$N(1520) \to p\gamma$, helicity-1/2 amplitude $A_{1/2}$

MODULUS ($GeV^{-1/2}$)	PHASE (°)	DOCUMENT ID		TECN	COMMENT
−0.023±0.004	−6 ± 5	SOKHOYAN	15A	DPWA	Multichannel
$-0.024^{+0.008}_{-0.003}$	-17^{+16}_{-6}	ROENCHEN	14	DPWA	
• • • We do not use the following data for averages, fits, limits, etc. • • •					
−0.031	−17	ROENCHEN	15A	DPWA	Multichannel

$N(1520) \to p\gamma$, helicity-3/2 amplitude $A_{3/2}$

MODULUS ($GeV^{-1/2}$)	PHASE (°)	DOCUMENT ID		TECN	COMMENT
0.131±0.006	4 ± 4	SOKHOYAN	15A	DPWA	Multichannel
$0.117^{+0.006}_{-0.010}$	26 ± 2	ROENCHEN	14	DPWA	
• • • We do not use the following data for averages, fits, limits, etc. • • •					
0.075	1.7	ROENCHEN	15A	DPWA	Multichannel

$N(1520)$ BREIT-WIGNER PHOTON DECAY AMPLITUDES

$N(1520) \to p\gamma$, helicity-1/2 amplitude $A_{1/2}$

VALUE ($GeV^{-1/2}$)	DOCUMENT ID		TECN	COMMENT
−0.030 to −0.015 (≈ −0.025) OUR ESTIMATE				
−0.034±0.003	[1] HUNT	19	DPWA	Multichannel
−0.024±0.004	SOKHOYAN	15A	DPWA	Multichannel
−0.015±0.001	[1] SHKLYAR	13	DPWA	Multichannel
−0.019±0.002	[1] WORKMAN	12A	DPWA	$\gamma N \to N\pi$
−0.028±0.002	[1] DUGGER	07	DPWA	$\gamma N \to \pi N$
−0.038±0.003	[1] AHRENS	02	DPWA	$\gamma N \to \pi N$
• • • We do not use the following data for averages, fits, limits, etc. • • •				
−0.022±0.004	ANISOVICH	12A	DPWA	Multichannel
−0.034±0.001	[1] SHRESTHA	12A	DPWA	Multichannel
−0.027	DRECHSEL	07	DPWA	$\gamma N \to \pi N$
−0.003	PENNER	02D	DPWA	Multichannel
−0.052±0.010±0.007	[1] MUKHOPAD...	98		$\gamma p \to \eta p$

[1] Statistical error only.

$N(1520) \to p\gamma$, helicity-3/2 amplitude $A_{3/2}$

VALUE ($GeV^{-1/2}$)	DOCUMENT ID		TECN	COMMENT
0.135 to 0.145 (≈ 0.140) OUR ESTIMATE				
0.142±0.003	[1] HUNT	19	DPWA	Multichannel
0.130±0.006	SOKHOYAN	15A	DPWA	Multichannel
0.146±0.001	[1] SHKLYAR	13	DPWA	Multichannel
0.141±0.002	[1] WORKMAN	12A	DPWA	$\gamma N \to N\pi$
0.143±0.002	[1] DUGGER	07	DPWA	$\gamma N \to \pi N$
0.147±0.010	[1] AHRENS	02	DPWA	$\gamma N \to \pi N$
• • • We do not use the following data for averages, fits, limits, etc. • • •				
0.131±0.010	ANISOVICH	12A	DPWA	Multichannel
0.127±0.003	[1] SHRESTHA	12A	DPWA	Multichannel
0.161	DRECHSEL	07	DPWA	$\gamma N \to \pi N$
0.151	PENNER	02D	DPWA	Multichannel
0.130±0.020±0.015	[1] MUKHOPAD...	98		$\gamma p \to \eta p$

[1] Statistical error only.

$N(1520) \to n\gamma$, helicity-1/2 amplitude $A_{1/2}$

VALUE ($GeV^{-1/2}$)	DOCUMENT ID		TECN	COMMENT
−0.055 to −0.040 (≈ −0.050) OUR ESTIMATE				
−0.072±0.003	[1] HUNT	19	DPWA	Multichannel
−0.049±0.008	ANISOVICH	13B	DPWA	Multichannel
−0.046±0.006	[1] CHEN	12A	DPWA	$\gamma N \to \pi N$
• • • We do not use the following data for averages, fits, limits, etc. • • •				
−0.038±0.003	[1] SHRESTHA	12A	DPWA	Multichannel
−0.077	DRECHSEL	07	DPWA	$\gamma N \to \pi N$
−0.084	PENNER	02D	DPWA	Multichannel

[1] Statistical error only.

$N(1520) \to n\gamma$, helicity-3/2 amplitude $A_{3/2}$

VALUE ($GeV^{-1/2}$)	DOCUMENT ID		TECN	COMMENT
−0.120 to −0.100 (≈ −0.115) OUR ESTIMATE				
−0.123±0.006	[1] HUNT	19	DPWA	Multichannel
−0.113±0.012	ANISOVICH	13B	DPWA	Multichannel
−0.115±0.005	[1] CHEN	12A	DPWA	$\gamma N \to \pi N$
• • • We do not use the following data for averages, fits, limits, etc. • • •				
−0.101±0.004	[1] SHRESTHA	12A	DPWA	Multichannel
−0.154	DRECHSEL	07	DPWA	$\gamma N \to \pi N$
−0.159	PENNER	02D	DPWA	Multichannel

[1] Statistical error only.

$N(1520)$ REFERENCES

For early references, see Physics Letters **111B** 1 (1982). For very early references, see Reviews of Modern Physics **37** 633 (1965).

ADAMCZEW...	20	PR C102 024001	J. Adamczewski-Musch *et al.*	(HADES Collab.)
MUELLER	20	PL B803 135323	J. Mueller *et al.*	(CBELSA/TAPS Collab.)
HUNT	19	PR C99 055205	B.C. Hunt, D.M. Manley	
ROENCHEN	15A	EPJ A51 70	D. Roenchen *et al.*	
SOKHOYAN	15A	EPJ A51 95	V. Sokhoyan *et al.*	(CBELSA/TAPS Collab.)
PDG	14	CP C38 070001	K. Olive *et al.*	(PDG Collab.)
ROENCHEN	14	EPJ A50 101	D. Roenchen *et al.*	
Also		EPJ A51 63 (errat.)	D. Roenchen *et al.*	
SVARC	14	PR C89 045205	A. Svarc *et al.*	(RBI Zagreb, UNI Tuzla)
ANISOVICH	13B	EPJ A49 67	A.V. Anisovich *et al.*	
SHKLYAR	13	PR C87 015201	V. Shklyar, H. Lenske, U. Mosel	(GIES)
ANISOVICH	12A	EPJ A48 15	A.V. Anisovich *et al.*	(BONN, PNPI)
CHEN	12A	PR C86 015206	W. Chen *et al.*	(DUKE, GWU, MSST, ITEP+)
SHRESTHA	12A	PR C86 055203	M. Shrestha, D.M. Manley	(KSU)
WORKMAN	12A	PR C86 015202	R. Workman *et al.*	(GWU)
BATINIC	10	PR C82 038203	M. Batinic *et al.*	(ZAGR)
THOMA	08	PL B659 87	U. Thoma *et al.*	(CB-ELSA Collab.)
DRECHSEL	07	EPJ A34 69	D. Drechsel, S.S. Kamalov, L. Tiator	(MAINZ, JINR)
DUGGER	07	PR C76 025211	M. Dugger *et al.*	(JLab CLAS Collab.)
ARNDT	06	PR C74 045205	R.A. Arndt *et al.*	(GWU)
ARNDT	05	PR C72 045202	R.A. Arndt *et al.*	(GWU, PNPI)

Downloaded from https://academic.oup.com/ptep/article/2022/8/083C01/6651666 by KIT Library user on 27 September 2022

AHRENS	02	PRL 88 232002	J. Ahrens *et al.*	(Mainz MAMI GDH/A2 Collab.)
PENNER	02C	PR C66 055211	G. Penner, U. Mosel	(GIES)
PENNER	02D	PR C66 055212	G. Penner, U. Mosel	(GIES)
VRANA	00	PRPL 328 181	T.P. Vrana, S.A. Dytman, T.-S.H. Lee	(PITT, ANL)
TIATOR	99	PR C60 035210	L. Tiator *et al.*	
MUKHOPAD...	98	PL B444 7	N.C. Mukhopadhyay, N. Mathur	
HOEHLER	93	πN Newsletter 9 1	G. Hohler	(KARL)
CUTKOSKY	80	Toronto Conf. 19	R.E. Cutkosky *et al.*	(CMU, LBL) IJP
Also		PR D20 2839	R.E. Cutkosky *et al.*	(CMU, LBL) IJP
HOEHLER	79	PDAT 12-1	G. Hohler *et al.*	(KARLT) IJP
Also		Toronto Conf. 3	R. Koch	(KARLT) IJP

$N(1535)$ $1/2^-$

$I(J^P) = \frac{1}{2}(\frac{1}{2}^-)$ Status: ****

Older and obsolete values are listed and referenced in the 2014 edition, Chinese Physics **C38** 070001 (2014).

$N(1535)$ POLE POSITION

REAL PART

VALUE (MeV)	DOCUMENT ID		TECN	COMMENT
1500 to 1520 (≈ 1510) OUR ESTIMATE				
1496 ± 4	AFZAL	20	DPWA	Multichannel
1500 ± 4	SOKHOYAN	15A	DPWA	Multichannel
1509 ± 4 ± 2	[1] SVARC	14	L+P	$\pi N \to \pi N$
1510 ± 50	CUTKOSKY	80	IPWA	$\pi N \to \pi N$
• • • We do not use the following data for averages, fits, limits, etc. • • •				
1496	HUNT	19	DPWA	Multichannel
1499	ROENCHEN	15A	DPWA	Multichannel
1490	SHKLYAR	13	DPWA	Multichannel
1501 ± 4	ANISOVICH	12A	DPWA	Multichannel
1521 ± 14	BATINIC	10	DPWA	$\pi N \to N\pi$, $N\eta$
1502	ARNDT	06	DPWA	$\pi N \to \pi N$, ηN
1525	VRANA	00	DPWA	Multichannel
1487	HOEHLER	93	SPED	$\pi N \to \pi N$

[1] Fit to the amplitudes of HOEHLER 79.

−2×IMAGINARY PART

VALUE (MeV)	DOCUMENT ID		TECN	COMMENT
110 to 150 (≈ 130) OUR ESTIMATE				
125 ± 6	AFZAL	20	DPWA	Multichannel
128 ± 9	SOKHOYAN	15A	DPWA	Multichannel
118 ± 9 ± 2	[2] SVARC	14	L+P	$\pi N \to \pi N$
260 ± 80	CUTKOSKY	80	IPWA	$\pi N \to \pi N$
• • • We do not use the following data for averages, fits, limits, etc. • • •				
119	HUNT	19	DPWA	Multichannel
104	ROENCHEN	15A	DPWA	Multichannel
100	SHKLYAR	13	DPWA	Multichannel
134 ± 11	ANISOVICH	12A	DPWA	Multichannel
190 ± 28	BATINIC	10	DPWA	$\pi N \to N\pi$, $N\eta$
95	ARNDT	06	DPWA	$\pi N \to \pi N$, ηN
102	VRANA	00	DPWA	Multichannel

[2] Fit to the amplitudes of HOEHLER 79.

$N(1535)$ ELASTIC POLE RESIDUE

MODULUS $|r|$

VALUE (MeV)	DOCUMENT ID		TECN	COMMENT
15 to 35 (≈ 25) OUR ESTIMATE				
29 ± 4	SOKHOYAN	15A	DPWA	Multichannel
22 ± 2 ± 0.4	[3] SVARC	14	L+P	$\pi N \to \pi N$
120 ± 40	CUTKOSKY	80	IPWA	$\pi N \to \pi N$
• • • We do not use the following data for averages, fits, limits, etc. • • •				
22	ROENCHEN	15A	DPWA	Multichannel
15	SHKLYAR	13	DPWA	Multichannel
31 ± 4	ANISOVICH	12A	DPWA	Multichannel
68	BATINIC	10	DPWA	$\pi N \to N\pi$, $N\eta$
16	ARNDT	06	DPWA	$\pi N \to \pi N$, ηN

[3] Fit to the amplitudes of HOEHLER 79.

PHASE θ

VALUE (°)	DOCUMENT ID		TECN	COMMENT
−30 to 0 (≈ −15) OUR ESTIMATE				
−20 ± 10	SOKHOYAN	15A	DPWA	Multichannel
− 5 ± 5 ± 3	[4] SVARC	14	L+P	$\pi N \to \pi N$
+15 ± 45	CUTKOSKY	80	IPWA	$\pi N \to \pi N$
• • • We do not use the following data for averages, fits, limits, etc. • • •				
−46	ROENCHEN	15A	DPWA	Multichannel
−51	SHKLYAR	13	DPWA	Multichannel
−29 ± 5	ANISOVICH	12A	DPWA	Multichannel
12	BATINIC	10	DPWA	$\pi N \to N\pi$, $N\eta$
−16	ARNDT	06	DPWA	$\pi N \to \pi N$, ηN

[4] Fit to the amplitudes of HOEHLER 79.

$N(1535)$ INELASTIC POLE RESIDUE

The "normalized residue" is the residue divided by $\Gamma_{pole}/2$.

Normalized residue in $N\pi \to N(1535) \to N\eta$

MODULUS	PHASE (°)	DOCUMENT ID		TECN	COMMENT
0.43 ± 0.03	−76 ± 5	ANISOVICH	12A	DPWA	Multichannel
• • • We do not use the following data for averages, fits, limits, etc. • • •					
0.51	112	ROENCHEN	15A	DPWA	Multichannel

Normalized residue in $N\pi \to N(1535) \to \Lambda K$

MODULUS	PHASE (°)	DOCUMENT ID		TECN	COMMENT
• • • We do not use the following data for averages, fits, limits, etc. • • •					
0.05	32	ROENCHEN	15A	DPWA	Multichannel

Normalized residue in $N\pi \to N(1535) \to \Sigma K$

MODULUS	PHASE (°)	DOCUMENT ID		TECN	COMMENT
• • • We do not use the following data for averages, fits, limits, etc. • • •					
0.05	−69	ROENCHEN	15A	DPWA	Multichannel

Normalized residue in $N\pi \to N(1535) \to \Delta\pi$, D-wave

MODULUS	PHASE (°)	DOCUMENT ID		TECN	COMMENT
0.11 ± 0.02	160 ± 20	SOKHOYAN	15A	DPWA	Multichannel
• • • We do not use the following data for averages, fits, limits, etc. • • •					
0.12 ± 0.03	145 ± 17	ANISOVICH	12A	DPWA	Multichannel

Normalized residue in $N\pi \to N(1535) \to N\sigma$

MODULUS	PHASE (°)	DOCUMENT ID		TECN	COMMENT
0.16 ± 0.07	25 ± 40	SOKHOYAN	15A	DPWA	Multichannel

Normalized residue in $N\pi \to N(1535) \to N(1440)\pi$

MODULUS	PHASE (°)	DOCUMENT ID		TECN	COMMENT
0.21 ± 0.14	−45 ± 50	SOKHOYAN	15A	DPWA	Multichannel

$N(1535)$ BREIT-WIGNER MASS

VALUE (MeV)	DOCUMENT ID		TECN	COMMENT
1515 to 1545 (≈ 1530) OUR ESTIMATE				
1525 ± 2	[5] HUNT	19	DPWA	Multichannel
1528 ± 6	KASHEVAROV	17	DPWA	$\gamma p \to \eta p$, $\eta' p$
1517 ± 4	SOKHOYAN	15A	DPWA	Multichannel
1526 ± 2	[5] SHKLYAR	13	DPWA	Multichannel
1547.0 ± 0.7	[5] ARNDT	06	DPWA	$\pi N \to \pi N$, ηN
1550 ± 40	CUTKOSKY	80	IPWA	$\pi N \to \pi N$
1526 ± 7	HOEHLER	79	IPWA	$\pi N \to \pi N$
• • • We do not use the following data for averages, fits, limits, etc. • • •				
1519 ± 5	ANISOVICH	12A	DPWA	Multichannel
1538 ± 1	[5] SHRESTHA	12A	DPWA	Multichannel
1553 ± 8	BATINIC	10	DPWA	$\pi N \to N\pi$, $N\eta$
1546.7 ± 2.2	ARNDT	04	DPWA	$\pi N \to \pi N$, ηN
1526 ± 2	PENNER	02C	DPWA	Multichannel
1530 ± 10	BAI	01B	BES	$J/\psi \to p\overline{p}\eta$
1522 ± 11	THOMPSON	01	CLAS	$\gamma^* p \to p\eta$
1542 ± 3	VRANA	00	DPWA	Multichannel
1532 ± 5	ARMSTRONG	99B	DPWA	$\gamma^* p \to p\eta$

[5] Statistical error only.

$N(1535)$ BREIT-WIGNER WIDTH

VALUE (MeV)	DOCUMENT ID		TECN	COMMENT
125 to 175 (≈ 150) OUR ESTIMATE				
147 ± 5	[6] HUNT	19	DPWA	Multichannel
163 ± 25	KASHEVAROV	17	DPWA	$\gamma p \to \eta p$, $\eta' p$
120 ± 10	SOKHOYAN	15A	DPWA	Multichannel
131 ± 12	[6] SHKLYAR	13	DPWA	Multichannel
188.4 ± 3.8	[6] ARNDT	06	DPWA	$\pi N \to \pi N$, ηN
240 ± 80	CUTKOSKY	80	IPWA	$\pi N \to \pi N$
120 ± 20	HOEHLER	79	IPWA	$\pi N \to \pi N$
• • • We do not use the following data for averages, fits, limits, etc. • • •				
128 ± 14	ANISOVICH	12A	DPWA	Multichannel
141 ± 4	[6] SHRESTHA	12A	DPWA	Multichannel
182 ± 25	BATINIC	10	DPWA	$\pi N \to N\pi$, $N\eta$
129 ± 8	PENNER	02C	DPWA	Multichannel
95 ± 25	BAI	01B	BES	$J/\psi \to p\overline{p}\eta$
143 ± 18	THOMPSON	01	CLAS	$\gamma^* p \to p\eta$
112 ± 19	VRANA	00	DPWA	Multichannel
154 ± 20	ARMSTRONG	99B	DPWA	$\gamma^* p \to p\eta$

[6] Statistical error only.

Downloaded from https://academic.oup.com/ptep/article/2022/8/083C01/6651666 by KIT Library user on 27 September 2022

$N(1535)$ DECAY MODES

The following branching fractions are our estimates, not fits or averages.

	Mode	Fraction (Γ_i/Γ)
Γ_1	$N\pi$	32–52 %
Γ_2	$N\eta$	30–55 %
Γ_3	$N\pi\pi$	4–31 %
Γ_4	$\Delta(1232)\pi$, D-wave	1–4 %
Γ_5	$N\rho$	2–17 %
Γ_6	$N\rho$, $S=1/2$, S-wave	2–16 %
Γ_7	$N\rho$, $S=3/2$, D-wave	<1 %
Γ_8	$N\sigma$	2–10 %
Γ_9	$N(1440)\pi$	5–12 %
Γ_{10}	$p\gamma$, helicity=1/2	0.15–0.30 %
Γ_{11}	$n\gamma$, helicity=1/2	0.01–0.25 %

$N(1535)$ BRANCHING RATIOS

$\Gamma(N\pi)/\Gamma_{total}$ — Γ_1/Γ

VALUE (%)	DOCUMENT ID		TECN	COMMENT
32–52 % OUR ESTIMATE				
42 ± 2	[7] HUNT	19	DPWA	Multichannel
52 ± 5	SOKHOYAN	15A	DPWA	Multichannel
35 ± 3	[7] SHKLYAR	13	DPWA	Multichannel
35.5 ± 0.2	[7] ARNDT	06	DPWA	$\pi N \to \pi N$, ηN
50 ±10	CUTKOSKY	80	IPWA	$\pi N \to \pi N$
38 ± 4	HOEHLER	79	IPWA	$\pi N \to \pi N$
• • • We do not use the following data for averages, fits, limits, etc. • • •				
54 ± 5	ANISOVICH	12A	DPWA	Multichannel
37 ± 1	[7] SHRESTHA	12A	DPWA	Multichannel
46 ± 7	BATINIC	10	DPWA	$\pi N \to N\pi$, $N\eta$
36 ± 1	PENNER	02C	DPWA	Multichannel
35 ± 8	VRANA	00	DPWA	Multichannel

[7] Statistical error only.

$\Gamma(N\eta)/\Gamma_{total}$ — Γ_2/Γ

VALUE (%)	DOCUMENT ID		TECN	COMMENT
30–55 % OUR ESTIMATE				
41±4	MUELLER	20	DPWA	Multichannel
43±3	[8] HUNT	19	DPWA	Multichannel
41±4	[9] KASHEVAROV	17	DPWA	$\gamma p \to \eta p$, $\eta' p$
58±4	[8] SHKLYAR	13	DPWA	Multichannel
33±5	ANISOVICH	12A	DPWA	Multichannel
53±1	PENNER	02C	DPWA	Multichannel
51±5	VRANA	00	DPWA	Multichannel
• • • We do not use the following data for averages, fits, limits, etc. • • •				
41±2	[8] SHRESTHA	12A	DPWA	Multichannel
50±7	BATINIC	10	DPWA	$\pi N \to N\pi$, $N\eta$

[8] Statistical error only.
[9] Assuming $A_{1/2} = 0.115$ GeV$^{-1/2}$.

$\Gamma(N\eta)/\Gamma(N\pi)$ — Γ_2/Γ_1

VALUE	DOCUMENT ID		TECN	COMMENT
• • • We do not use the following data for averages, fits, limits, etc. • • •				
0.95±0.03	AZNAURYAN	09	CLAS	π, η electroproduction

$\Gamma(\Delta(1232)\pi, D\text{-wave})/\Gamma_{total}$ — Γ_4/Γ

VALUE (%)	DOCUMENT ID		TECN	COMMENT
1–4 % OUR ESTIMATE				
3 ±1	ADAMCZEW...	20	DPWA	Multichannel
<1.1	[10] HUNT	19	DPWA	Multichannel
2.5±1.5	SOKHOYAN	15A	DPWA	Multichannel
• • • We do not use the following data for averages, fits, limits, etc. • • •				
2.5±1.5	ANISOVICH	12A	DPWA	Multichannel
1.8±0.8	[10] SHRESTHA	12A	DPWA	Multichannel
1 ±1	VRANA	00	DPWA	Multichannel

[10] Statistical error only.

$\Gamma(N\rho, S=1/2, S\text{-wave})/\Gamma_{total}$ — Γ_6/Γ

VALUE (%)	DOCUMENT ID		TECN	COMMENT
2–16 % OUR ESTIMATE				
2.7±0.6	ADAMCZEW...	20	DPWA	Multichannel
14 ±2	[11] HUNT	19	DPWA	Multichannel

[11] Statistical error only.

$\Gamma(N\rho, S=3/2, D\text{-wave})/\Gamma_{total}$ — Γ_7/Γ

VALUE (%)	DOCUMENT ID		TECN	COMMENT
<1 % OUR ESTIMATE				
0.5±0.5	ADAMCZEW...	20	DPWA	Multichannel
<0.3	[12] HUNT	19	DPWA	Multichannel

[12] Statistical error only.

$\Gamma(N\sigma)/\Gamma_{total}$ — Γ_8/Γ

VALUE (%)	DOCUMENT ID		TECN	COMMENT
2–10 % OUR ESTIMATE				
<1	[13] HUNT	19	DPWA	Multichannel
6 ±4	SOKHOYAN	15A	DPWA	Multichannel
• • • We do not use the following data for averages, fits, limits, etc. • • •				
1.5±0.5	[13] SHRESTHA	12A	DPWA	Multichannel
2 ±1	VRANA	00	DPWA	Multichannel

[13] Statistical error only.

$\Gamma(N(1440)\pi)/\Gamma_{total}$ — Γ_9/Γ

VALUE (%)	DOCUMENT ID		TECN	COMMENT
5–12 % OUR ESTIMATE				
< 0.01	[14] HUNT	19	DPWA	Multichannel
12 ±8	SOKHOYAN	15A	DPWA	Multichannel
8 ±2	[14] STAROSTIN	03		$\pi^- p \to n 3\pi^0$
• • • We do not use the following data for averages, fits, limits, etc. • • •				
< 1	[14] SHRESTHA	12A	DPWA	Multichannel
10 ±9	VRANA	00	DPWA	Multichannel

[14] This value is an estimate made using simplest assumptions.

$N(1535)$ PHOTON DECAY AMPLITUDES AT THE POLE

$N(1535) \to p\gamma$, helicity-1/2 amplitude $A_{1/2}$

MODULUS (GeV$^{-1/2}$)	PHASE (°)	DOCUMENT ID		TECN	COMMENT
0.093±0.009	8 ± 4	ANISOVICH	17D	DPWA	Multichannel
0.050±0.004	-14^{+12}_{-10}	[15] ROENCHEN	14	DPWA	
• • • We do not use the following data for averages, fits, limits, etc. • • •					
0.114±0.008	10 ± 5	ANISOVICH	15A	DPWA	Multichannel
0.106	5.2	ROENCHEN	15A	DPWA	Multichannel
0.114±0.008	10 ± 5	SOKHOYAN	15A	DPWA	Multichannel

[15] T-Matrix amplitude

$N(1535) \to n\gamma$, helicity-1/2 amplitude $A_{1/2}$

MODULUS (GeV$^{-1/2}$)	PHASE (°)	DOCUMENT ID		TECN	COMMENT
−0.088±0.004	**5 ± 4**	ANISOVICH	17D	DPWA	Multichannel
• • • We do not use the following data for averages, fits, limits, etc. • • •					
−0.095±0.006	8 ± 5	ANISOVICH	15A	DPWA	Multichannel

$N(1535)$ BREIT-WIGNER PHOTON DECAY AMPLITUDES

$N(1535) \to p\gamma$, helicity-1/2 amplitude $A_{1/2}$

VALUE (GeV$^{-1/2}$)	DOCUMENT ID		TECN	COMMENT
0.090 to 0.120 (≈ 0.105) OUR ESTIMATE				
0.107±0.003	[16] HUNT	19	DPWA	Multichannel
0.101±0.007	SOKHOYAN	15A	DPWA	Multichannel
0.091±0.004	[16] SHKLYAR	13	DPWA	Multichannel
0.128±0.004	[16] WORKMAN	12A	DPWA	$\gamma N \to N\pi$
0.091±0.002	[16] DUGGER	07	DPWA	$\gamma N \to \pi N$
• • • We do not use the following data for averages, fits, limits, etc. • • •				
0.105±0.010	ANISOVICH	12A	DPWA	Multichannel
0.059±0.003	[16] SHRESTHA	12A	DPWA	Multichannel
0.066	DRECHSEL	07	DPWA	$\gamma N \to \pi N$
0.090	PENNER	02D	DPWA	Multichannel

[16] Statistical error only.

$N(1535) \to n\gamma$, helicity-1/2 amplitude $A_{1/2}$

VALUE (GeV$^{-1/2}$)	DOCUMENT ID		TECN	COMMENT
−0.095 to −0.055 (≈ −0.075) OUR ESTIMATE				
−0.055±0.006	[17] HUNT	19	DPWA	Multichannel
−0.093±0.011	ANISOVICH	13B	DPWA	Multichannel
−0.058±0.006	[17] CHEN	12A	DPWA	$\gamma N \to \pi N$
• • • We do not use the following data for averages, fits, limits, etc. • • •				
−0.049±0.003	[17] SHRESTHA	12A	DPWA	Multichannel
−0.051	DRECHSEL	07	DPWA	$\gamma N \to \pi N$
−0.024	PENNER	02D	DPWA	Multichannel

[17] Statistical error only.

$N(1535) \to N\gamma$, ratio $A^n_{1/2}/A^p_{1/2}$

VALUE (GeV$^{-1/2}$)	DOCUMENT ID		TECN
• • • We do not use the following data for averages, fits, limits, etc. • • •			
−0.84±0.15	MUKHOPAD...	95B	IPWA

$N(1535)$ REFERENCES

For early references, see Physics Letters **111B** 1 (1982).

ADAMCZEW... 20 PR C102 024001 J. Adamczewski-Musch *et al.* (HADES Collab.)
AFZAL 20 PRL 125 152002 F. Afzal *et al.* (CBELSA/TAPS Collab.)
MUELLER 20 PL B803 135323 J. Mueller *et al.* (CBELSA/TAPS Collab.)
HUNT 19 PR C99 055205 B.C. Hunt, D.M. Manley

Downloaded from https://academic.oup.com/ptep/article/2022/8/083C01/6651666 by KIT Library user on 27 September 2022

ANISOVICH	17D	PR C95 035211	A.V. Anisovich *et al.*	
KASHEVAROV	17	PRL 118 212001	V.L. Kashevarov *et al.*	(A2/MAMI Collab.)
ANISOVICH	15A	EPJ A51 72	A.V. Anisovich *et al.*	
ROENCHEN	15A	EPJ A51 70	D. Roenchen *et al.*	
SOKHOYAN	15A	EPJ A51 95	V. Sokhoyan *et al.*	(CBELSA/TAPS Collab.)
PDG	14	CP C38 070001	K. Olive *et al.*	(PDG Collab.)
ROENCHEN	14	EPJ A50 101	D. Roenchen *et al.*	
Also		EPJ A51 63 (errat.)	D. Roenchen *et al.*	
SVARC	14	PR C89 045205	A. Svarc *et al.*	(RBI Zagreb, UNI Tuzla)
ANISOVICH	13B	EPJ A49 67	A.V. Anisovich *et al.*	
SHKLYAR	13	PR C87 015201	V. Shklyar, H. Lenske, U. Mosel	(GIES)
ANISOVICH	12A	EPJ A48 15	A.V. Anisovich *et al.*	(BONN, PNPI)
CHEN	12A	PR C86 015206	W. Chen *et al.*	(DUKE, GWU, MSST, ITEP+)
SHRESTHA	12A	PR C86 055203	M. Shrestha, D.M. Manley	(KSU)
WORKMAN	12A	PR C86 015202	R. Workman *et al.*	(GWU)
BATINIC	10	PR C82 038203	M. Batinic *et al.*	(ZAGR)
AZNAURYAN	09	PR C80 055203	I.G. Aznauryan *et al.*	(JLab CLAS Collab.)
DRECHSEL	07	EPJ A34 69	D. Drechsel, S.S. Kamalov, L. Tiator	(MAINZ, JINR)
DUGGER	07	PR C76 025211	M. Dugger *et al.*	(JLab CLAS Collab.)
ARNDT	06	PR C74 045205	R.A. Arndt *et al.*	(GWU)
ARNDT	04	PR C69 035213	R.A. Arndt *et al.*	(GWU, TRIU)
STAROSTIN	03	PR C67 068201	A. Starostin *et al.*	(BNL Crystal Ball Collab.)
PENNER	02C	PR C66 055211	G. Penner, U. Mosel	(GIES)
PENNER	02D	PR C66 055212	G. Penner, U. Mosel	(GIES)
BAI	01B	PL B510 75	J.Z. Bai *et al.*	(BES Collab.)
THOMPSON	01	PRL 86 1702	R. Thompson *et al.*	(JLab CLAS Collab.)
VRANA	00	PRPL 328 181	T.P. Vrana, S.A. Dytman, T.-S.H. Lee	(PITT, ANL)
ARMSTRONG	99B	PR D60 052004	C.S. Armstrong *et al.*	
MUKHOPAD...	95B	PL B364 1	N.C. Mukhopadhyay, J.F. Zhang, M. Benmerrouche	
HOEHLER	93	πN Newsletter 9 1	G. Hohler	(KARL)
CUTKOSKY	80	Toronto Conf. 19	R.E. Cutkosky *et al.*	(CMU, LBL) IJP
Also		PR D20 2839	R.E. Cutkosky *et al.*	(CMU, LBL) IJP
HOEHLER	79	PDAT 12-1	G. Hohler *et al.*	(KARLT) IJP
Also		Toronto Conf. 3	R. Koch	(KARLT) IJP

$N(1650)$ $1/2^-$

$I(J^P) = \frac{1}{2}(\frac{1}{2}^-)$ Status: ****

Older and obsolete values are listed and referenced in the 2014 edition, Chinese Physics **C38** 070001 (2014).

$N(1650)$ POLE POSITION

REAL PART

VALUE (MeV)	DOCUMENT ID		TECN	COMMENT
1640 to 1670 (≈ 1655) OUR ESTIMATE				
1664 ± 4	AFZAL	20	DPWA	Multichannel
1658 ± 10	ANISOVICH	17A	DPWA	Multichannel
1660 ± 5	[1] ANISOVICH	17A	L+P	$\gamma p, \pi^- p \to K\Lambda$
1660 ± 3.5 ± 1	[2] SVARC	14	L+P	$\pi N \to \pi N$
1640 ± 20	CUTKOSKY	80	IPWA	$\pi N \to \pi N$
• • • We do not use the following data for averages, fits, limits, etc. • • •				
1656	HUNT	19	DPWA	Multichannel
1672	ROENCHEN	15A	DPWA	Multichannel
1652 ± 7	SOKHOYAN	15A	DPWA	Multichannel
1650	SHKLYAR	13	DPWA	Multichannel
1647 ± 6	ANISOVICH	12A	DPWA	Multichannel
1646 ± 8	BATINIC	10	DPWA	$\pi N \to N\pi, N\eta$
1648	ARNDT	06	DPWA	$\pi N \to \pi N, \eta N$
1663	VRANA	00	DPWA	Multichannel
1670	HOEHLER	93	ARGD	$\pi N \to \pi N$

[1] Statistical error only.
[2] Fit to the amplitudes of HOEHLER 79.

−2×IMAGINARY PART

VALUE (MeV)	DOCUMENT ID		TECN	COMMENT
100 to 170 (≈ 135) OUR ESTIMATE				
98 ± 6	AFZAL	20	DPWA	Multichannel
102 ± 8	ANISOVICH	17A	DPWA	Multichannel
59 ± 16	[1] ANISOVICH	17A	L+P	$\gamma p, \pi^- p \to K\Lambda$
167 ± 8 ± 2	[2] SVARC	14	L+P	$\pi N \to \pi N$
150 ± 30	CUTKOSKY	80	IPWA	$\pi N \to \pi N$
• • • We do not use the following data for averages, fits, limits, etc. • • •				
130	HUNT	19	DPWA	Multichannel
137	ROENCHEN	15A	DPWA	Multichannel
102 ± 8	SOKHOYAN	15A	DPWA	Multichannel
89	SHKLYAR	13	DPWA	Multichannel
103 ± 8	ANISOVICH	12A	DPWA	Multichannel
204 ± 17	BATINIC	10	DPWA	$\pi N \to N\pi, N\eta$
80	ARNDT	06	DPWA	$\pi N \to \pi N, \eta N$
240	VRANA	00	DPWA	Multichannel
163	HOEHLER	93	ARGD	$\pi N \to \pi N$

[1] Statistical error only.
[2] Fit to the amplitudes of HOEHLER 79.

$N(1650)$ ELASTIC POLE RESIDUE

MODULUS $|r|$

VALUE (MeV)	DOCUMENT ID		TECN	COMMENT
25 to 55 (≈ 45) OUR ESTIMATE				
27 ± 6	SOKHOYAN	15A	DPWA	Multichannel
47 ± 3 ± 1	[1] SVARC	14	L+P	$\pi N \to \pi N$
60 ± 10	CUTKOSKY	80	IPWA	$\pi N \to \pi N$
• • • We do not use the following data for averages, fits, limits, etc. • • •				
37	ROENCHEN	15A	DPWA	Multichannel
19	SHKLYAR	13	DPWA	Multichannel
24 ± 3	ANISOVICH	12A	DPWA	Multichannel
100	BATINIC	10	DPWA	$\pi N \to N\pi, N\eta$
14	ARNDT	06	DPWA	$\pi N \to \pi N, \eta N$
39	HOEHLER	93	ARGD	$\pi N \to \pi N$

[1] Fit to the amplitudes of HOEHLER 79.

PHASE θ

VALUE (°)	DOCUMENT ID		TECN	COMMENT
−80 to −50 (≈ −70) OUR ESTIMATE				
−60 ± 20	SOKHOYAN	15A	DPWA	Multichannel
−47 ± 3 ± 1	[1] SVARC	14	L+P	$\pi N \to \pi N$
−75 ± 25	CUTKOSKY	80	IPWA	$\pi N \to \pi N$
• • • We do not use the following data for averages, fits, limits, etc. • • •				
−59	ROENCHEN	15A	DPWA	Multichannel
−46	SHKLYAR	13	DPWA	Multichannel
−75 ± 12	ANISOVICH	12A	DPWA	Multichannel
−65	BATINIC	10	DPWA	$\pi N \to N\pi, N\eta$
−69	ARNDT	06	DPWA	$\pi N \to \pi N, \eta N$
−37	HOEHLER	93	ARGD	$\pi N \to \pi N$

[1] Fit to the amplitudes of HOEHLER 79.

$N(1650)$ INELASTIC POLE RESIDUE

The "normalized residue" is the residue divided by $\Gamma_{pole}/2$.

Normalized residue in $N\pi \to N(1650) \to N\eta$

MODULUS	PHASE (°)	DOCUMENT ID		TECN	COMMENT
0.29 ± 0.03	134 ± 10	ANISOVICH	12A	DPWA	Multichannel
• • • We do not use the following data for averages, fits, limits, etc. • • •					
0.21	48	ROENCHEN	15A	DPWA	Multichannel

Normalized residue in $N\pi \to N(1650) \to \Lambda K$

MODULUS	PHASE (°)	DOCUMENT ID		TECN	COMMENT
0.26 ± 0.10	110 ± 20	ANISOVICH	17A	DPWA	Multichannel
0.10 ± 0.10	95 ± 33	[1] ANISOVICH	17A	L+P	$\gamma p, \pi^- p \to K\Lambda$
• • • We do not use the following data for averages, fits, limits, etc. • • •					
0.20	−54	ROENCHEN	15A	DPWA	Multichannel
0.23 ± 0.09	85 ± 9	ANISOVICH	12A	DPWA	Multichannel

[1] Statistical error only.

Normalized residue in $N\pi \to N(1650) \to \Sigma K$

MODULUS	PHASE (°)	DOCUMENT ID		TECN	COMMENT
• • • We do not use the following data for averages, fits, limits, etc. • • •					
0.026	−74	ROENCHEN	15A	DPWA	Multichannel

Normalized residue in $N\pi \to N(1650) \to \Delta\pi$, D-wave

MODULUS	PHASE (°)	DOCUMENT ID		TECN	COMMENT
0.19 ± 0.06	−30 ± 20	SOKHOYAN	15A	DPWA	Multichannel
• • • We do not use the following data for averages, fits, limits, etc. • • •					
0.23 ± 0.04	−30 ± 20	ANISOVICH	12A	DPWA	Multichannel

Normalized residue in $N\pi \to N(1650) \to N\sigma$

MODULUS	PHASE (°)	DOCUMENT ID		TECN	COMMENT
0.20 ± 0.15	undefined	SOKHOYAN	15A	DPWA	Multichannel

Normalized residue in $N\pi \to N(1650) \to N(1440)\pi$

MODULUS	PHASE (°)	DOCUMENT ID		TECN	COMMENT
0.30 ± 0.17	undefined	SOKHOYAN	15A	DPWA	Multichannel

$N(1650)$ BREIT-WIGNER MASS

VALUE (MeV)	DOCUMENT ID		TECN	COMMENT
1635 to 1665 (≈ 1650) OUR ESTIMATE				
1657 ± 6	GOLOVATCH	19	DPWA	$\gamma p \to \pi^+\pi^- p$
1666 ± 3	[1] HUNT	19	DPWA	Multichannel
1634 ± 5	KASHEVAROV	17	DPWA	$\gamma p \to \eta p, \eta' p$
1654 ± 6	SOKHOYAN	15A	DPWA	Multichannel
1665 ± 2	[1] SHKLYAR	13	DPWA	Multichannel
1634.7 ± 1.1	[1] ARNDT	06	DPWA	$\pi N \to \pi N, \eta N$
1650 ± 30	CUTKOSKY	80	IPWA	$\pi N \to \pi N$
1670 ± 8	HOEHLER	79	IPWA	$\pi N \to \pi N$
• • • We do not use the following data for averages, fits, limits, etc. • • •				
1651 ± 6	ANISOVICH	12A	DPWA	Multichannel
1664 ± 2	[1] SHRESTHA	12A	DPWA	Multichannel
1652 ± 9	BATINIC	10	DPWA	$\pi N \to N\pi, N\eta$
1665 ± 2	PENNER	02C	DPWA	Multichannel
1647 ± 20	BAI	01B	BES	$J/\psi \to p\bar{p}\eta$
1689 ± 12	VRANA	00	DPWA	Multichannel

[1] Statistical error only.

Downloaded from https://academic.oup.com/ptep/article/2022/8/083C01/6651666 by KIT Library user on 27 September 2022

$N(1650)$ BREIT-WIGNER WIDTH

VALUE (MeV)	DOCUMENT ID		TECN	COMMENT
100 to 150 (≈ 125) OUR ESTIMATE				
154 ±28	GOLOVATCH	19	DPWA	$\gamma p \to \pi^+\pi^- p$
133 ± 7	[1] HUNT	19	DPWA	Multichannel
128 ±16	KASHEVAROV	17	DPWA	$\gamma p \to \eta p, \eta' p$
102 ± 8	SOKHOYAN	15A	DPWA	Multichannel
147 ±14	[1] SHKLYAR	13	DPWA	Multichannel
115.4 ± 2.8	[1] ARNDT	06	DPWA	$\pi N \to \pi N, \eta N$
150 ±40	CUTKOSKY	80	IPWA	$\pi N \to \pi N$
180 ±20	HOEHLER	79	IPWA	$\pi N \to \pi N$
• • • We do not use the following data for averages, fits, limits, etc. • • •				
104 ±10	ANISOVICH	12A	DPWA	Multichannel
126 ± 3	[1] SHRESTHA	12A	DPWA	Multichannel
202 ±16	BATINIC	10	DPWA	$\pi N \to N\pi, N\eta$
138 ± 7	PENNER	02C	DPWA	Multichannel
145 $^{+80}_{-45}$	BAI	01B	BES	$J/\psi \to p\overline{p}\eta$
202 ±40	VRANA	00	DPWA	Multichannel

[1] Statistical error only.

$N(1650)$ DECAY MODES

The following branching fractions are our estimates, not fits or averages.

	Mode	Fraction (Γ_i/Γ)
Γ_1	$N\pi$	50–70 %
Γ_2	$N\eta$	15–35 %
Γ_3	ΛK	5–15 %
Γ_4	$N\pi\pi$	20–58 %
Γ_5	$\Delta(1232)\pi$, D-wave	6–18 %
Γ_6	$N\rho$	12–22 %
Γ_7	$N\rho$, $S=1/2$, S-wave	<4 %
Γ_8	$N\rho$, $S=3/2$, D-wave	12–18 %
Γ_9	$N\sigma$	2–18 %
Γ_{10}	$N(1440)\pi$	6–26 %
Γ_{11}	$p\gamma$, helicity=1/2	0.04–0.20 %
Γ_{12}	$n\gamma$, helicity=1/2	0.003–0.17 %

$N(1650)$ BRANCHING RATIOS

$\Gamma(N\pi)/\Gamma_{total}$ — Γ_1/Γ

VALUE (%)	DOCUMENT ID		TECN	COMMENT
50 to 70 (≈ 60) OUR ESTIMATE				
64 ± 4	[1] HUNT	19	DPWA	Multichannel
51 ± 4	SOKHOYAN	15A	DPWA	Multichannel
74 ± 3	[1] SHKLYAR	13	DPWA	Multichannel
65 ±10	CUTKOSKY	80	IPWA	$\pi N \to \pi N$
61 ± 4	HOEHLER	79	IPWA	$\pi N \to \pi N$
• • • We do not use the following data for averages, fits, limits, etc. • • •				
51 ± 4	ANISOVICH	12A	DPWA	Multichannel
57 ± 2	[1] SHRESTHA	12A	DPWA	Multichannel
79 ± 6	BATINIC	10	DPWA	$\pi N \to N\pi, N\eta$
100	ARNDT	06	DPWA	$\pi N \to \pi N, \eta N$
65 ± 4	PENNER	02C	DPWA	Multichannel
74 ± 2	VRANA	00	DPWA	Multichannel

[1] Statistical error only.

$\Gamma(N\eta)/\Gamma_{total}$ — Γ_2/Γ

VALUE (%)	DOCUMENT ID		TECN	COMMENT
15 to 35 (≈ 25) OUR ESTIMATE				
33 ± 4	MUELLER	20	DPWA	Multichannel
0.8 ± 0.6	[1] HUNT	19	DPWA	Multichannel
28 ±11	[2] KASHEVAROV	17	DPWA	$\gamma p \to \eta p, \eta' p$
< 3	SHKLYAR	13	DPWA	Multichannel
18 ± 4	ANISOVICH	12A	DPWA	Multichannel
• • • We do not use the following data for averages, fits, limits, etc. • • •				
21 ± 2	[1] SHRESTHA	12A	DPWA	Multichannel
13 ± 5	BATINIC	10	DPWA	$\pi N \to N\pi, N\eta$
1.0 ± 0.6	PENNER	02C	DPWA	Multichannel
6 ± 1	VRANA	00	DPWA	Multichannel

[1] Statistical error only.
[2] Assuming $A_{1/2} = 0.045$ GeV$^{-1/2}$.

$\Gamma(\Lambda K)/\Gamma_{total}$ — Γ_3/Γ

VALUE (%)	DOCUMENT ID		TECN	COMMENT
5 to 15 (≈ 10) OUR ESTIMATE				
3.5 ± 0.2	[1] HUNT	19	DPWA	Multichannel
10 ±5	ANISOVICH	12A	DPWA	Multichannel
4 ±1	[1] SHKLYAR	05	DPWA	Multichannel
• • • We do not use the following data for averages, fits, limits, etc. • • •				
8 ±1	[1] SHRESTHA	12A	DPWA	Multichannel
2.7 ± 0.4	PENNER	02C	DPWA	Multichannel

[1] Statistical error only.

$\Gamma(N\pi\pi)/\Gamma_{total}$ — Γ_4/Γ

VALUE	DOCUMENT ID		TECN	COMMENT
0.12 ± 0.02	GOLOVATCH	19	DPWA	$\gamma p \to \pi^+\pi^- p$

$\Gamma(\Delta(1232)\pi, D\text{-wave})/\Gamma_{total}$ — Γ_5/Γ

VALUE (%)	DOCUMENT ID		TECN	COMMENT
< 0.2	[1] HUNT	19	DPWA	Multichannel
12 ± 6	SOKHOYAN	15A	DPWA	Multichannel
• • • We do not use the following data for averages, fits, limits, etc. • • •				
19 ± 9	ANISOVICH	12A	DPWA	Multichannel
7 ± 2	[1] SHRESTHA	12A	DPWA	Multichannel
2 ± 1	VRANA	00	DPWA	Multichannel

[1] Statistical error only.

$\Gamma(N\rho, S=1/2, S\text{-wave})/\Gamma_{total}$ — Γ_7/Γ

VALUE (%)	DOCUMENT ID		TECN	COMMENT
1.8 ± 1.7	[1] HUNT	19	DPWA	Multichannel

[1] Statistical error only.

$\Gamma(N\rho, S=3/2, D\text{-wave})/\Gamma_{total}$ — Γ_8/Γ

VALUE (%)	DOCUMENT ID		TECN	COMMENT
15 ± 3	[1] HUNT	19	DPWA	Multichannel

[1] Statistical error only.

$\Gamma(N\sigma)/\Gamma_{total}$ — Γ_9/Γ

VALUE (%)	DOCUMENT ID		TECN	COMMENT
12 ± 4	[1] HUNT	19	DPWA	Multichannel
10 ± 8	SOKHOYAN	15A	DPWA	Multichannel
• • • We do not use the following data for averages, fits, limits, etc. • • •				
< 1	[1] SHRESTHA	12A	DPWA	Multichannel
1 ± 1	VRANA	00	DPWA	Multichannel

[1] Statistical error only.

$\Gamma(N(1440)\pi)/\Gamma_{total}$ — Γ_{10}/Γ

VALUE (%)	DOCUMENT ID		TECN	COMMENT
2 ± 1	[1] HUNT	19	DPWA	Multichannel
16 ±10	SOKHOYAN	15A	DPWA	Multichannel
• • • We do not use the following data for averages, fits, limits, etc. • • •				
< 1	[1] SHRESTHA	12A	DPWA	Multichannel
3 ± 1	VRANA	00	DPWA	Multichannel

[1] Statistical error only.

$N(1650)$ PHOTON DECAY AMPLITUDES AT THE POLE

$N(1650) \to p\gamma$, helicity-1/2 amplitude $A_{1/2}$

MODULUS (GeV$^{-1/2}$)	PHASE (°)	DOCUMENT ID		TECN	COMMENT
0.032 ± 0.006	7 ± 7	ANISOVICH	17D	DPWA	Multichannel
0.023 $^{+0.003}_{-0.008}$	6 $^{+28}_{-15}$	ROENCHEN	14	DPWA	
• • • We do not use the following data for averages, fits, limits, etc. • • •					
0.032 ± 0.007	−2 ± 11	ANISOVICH	15A	DPWA	Multichannel
0.059	−14	ROENCHEN	15A	DPWA	Multichannel
0.032 ± 0.006	−2 ± 11	SOKHOYAN	15A	DPWA	Multichannel

$N(1650) \to n\gamma$, helicity-1/2 amplitude $A_{1/2}$

MODULUS (GeV$^{-1/2}$)	PHASE (°)	DOCUMENT ID		TECN	COMMENT
0.016 ± 0.004	−28 ± 10	ANISOVICH	17D	DPWA	Multichannel
• • • We do not use the following data for averages, fits, limits, etc. • • •					
0.019 ± 0.006	0 ± 15	ANISOVICH	15A	DPWA	Multichannel

$N(1650)$ BREIT-WIGNER PHOTON DECAY AMPLITUDES

$N(1650) \to p\gamma$, helicity-1/2 amplitude $A_{1/2}$

VALUE (GeV$^{-1/2}$)	DOCUMENT ID		TECN	COMMENT
0.035 to 0.055 (≈ 0.045) OUR ESTIMATE				
0.0605 ± 0.0077	GOLOVATCH	19	DPWA	$\gamma p \to \pi^+\pi^- p$
0.048 ± 0.003	[1] HUNT	19	DPWA	Multichannel
0.032 ± 0.006	SOKHOYAN	15A	DPWA	Multichannel
0.063 ± 0.006	[1] SHKLYAR	13	DPWA	Multichannel
0.055 ± 0.030	[1] WORKMAN	12A	DPWA	$\gamma N \to N\pi$
0.022 ± 0.007	[1] DUGGER	07	DPWA	$\gamma N \to \pi N$
• • • We do not use the following data for averages, fits, limits, etc. • • •				
0.033 ± 0.007	ANISOVICH	12A	DPWA	Multichannel
0.030 ± 0.003	[1] SHRESTHA	12A	DPWA	Multichannel
0.033	DRECHSEL	07	DPWA	$\gamma N \to \pi N$
0.049	PENNER	02D	DPWA	Multichannel

[1] Statistical error only.

Downloaded from https://academic.oup.com/ptep/article/2022/8/083C01/6651666 by KIT Library user on 27 September 2022

See key on page 1127

$N(1650) \to n\gamma$, helicity-1/2 amplitude $A_{1/2}$

VALUE ($GeV^{-1/2}$)	DOCUMENT ID		TECN	COMMENT
−0.040 to 0.030 (≈ −0.010) OUR ESTIMATE				
0.001±0.006	[1] HUNT	19	DPWA	Multichannel
0.025±0.020	ANISOVICH	13B	DPWA	Multichannel
−0.040±0.010	[1] CHEN	12A	DPWA	$\gamma N \to \pi N$
• • • We do not use the following data for averages, fits, limits, etc. • • •				
0.011±0.002	[1] SHRESTHA	12A	DPWA	Multichannel
0.009	DRECHSEL	07	DPWA	$\gamma N \to \pi N$
−0.011	PENNER	02D	DPWA	Multichannel

[1] Statistical error only.

$N(1650)$ REFERENCES

For early references, see Physics Letters **111B** 1 (1982).

AFZAL	20	PRL 125 152002	F. Afzal et al.	(CBELSA/TAPS Collab.)
MUELLER	20	PL B803 135323	J. Mueller et al.	(CBELSA/TAPS Collab.)
GOLOVATCH	19	PL B788 371	E. Golovatch et al.	(CLAS Collab.)
HUNT	19	PR C99 055205	B.C. Hunt, D.M. Manley	
ANISOVICH	17A	PRL 119 062004	A.V. Anisovich et al.	
ANISOVICH	17D	PR C95 035211	A.V. Anisovich et al.	
KASHEVAROV	17	PRL 118 212001	V.L. Kashevarov et al.	(A2/MAMI Collab.)
ANISOVICH	15A	EPJ A51 72	A.V. Anisovich et al.	
ROENCHEN	15A	EPJ A51 70	D. Roenchen et al.	
SOKHOYAN	15A	EPJ A51 95	V. Sokhoyan et al.	(CBELSA/TAPS Collab.)
PDG	14	CP C38 070001	K. Olive et al.	(PDG Collab.)
ROENCHEN	14	EPJ A50 101	D. Roenchen et al.	
Also		EPJ A51 63 (errat.)	D. Roenchen et al.	
SVARC	14	PR C89 045205	A. Svarc et al.	(RBI Zagreb, UNI Tuzla)
ANISOVICH	13B	EPJ A49 67	A.V. Anisovich et al.	
SHKLYAR	13	PR C87 015201	V. Shklyar, H. Lenske, U. Mosel	(GIES)
ANISOVICH	12A	EPJ A48 15	A.V. Anisovich et al.	(BONN, PNPI)
CHEN	12A	PR C86 015206	W. Chen et al.	(DUKE, GWU, MSST, ITEP+)
SHRESTHA	12A	PR C86 055203	M. Shrestha, D.M. Manley	(KSU)
WORKMAN	12A	PR C86 015202	R. Workman et al.	(GWU)
BATINIC	10	PR C82 038203	M. Batinic et al.	(ZAGR)
DRECHSEL	07	EPJ A34 69	D. Drechsel, S.S. Kamalov, L. Tiator	(MAINZ, JINR)
DUGGER	07	PR C76 025211	M. Dugger et al.	(JLab CLAS Collab.)
ARNDT	06	PR C74 045205	R.A. Arndt et al.	(GWU)
SHKLYAR	05	PR C72 015210	V. Shklyar, H. Lenske, U. Mosel	(GIES)
PENNER	02C	PR C66 055211	G. Penner, U. Mosel	(GIES)
PENNER	02D	PR C66 055212	G. Penner, U. Mosel	(GIES)
BAI	01B	PL B510 75	J.Z. Bai et al.	(BES Collab.)
VRANA	00	PRPL 328 181	T.P. Vrana, S.A. Dytman, T.-S.H. Lee	(PITT, ANL)
HOEHLER	93	πN Newsletter 9 1	G. Hohler	(KARL)
CUTKOSKY	80	Toronto Conf. 19	R.E. Cutkosky et al.	(CMU, LBL) IJP
Also		PR D20 2839	R.E. Cutkosky et al.	(CMU, LBL) IJP
HOEHLER	79	PDAT 12-1	G. Hohler et al.	(KARLT) IJP
Also		Toronto Conf. 3	R. Koch	(KARLT) IJP

$N(1675)\ 5/2^-$

$I(J^P) = \frac{1}{2}(\frac{5}{2}^-)$ Status: ****

Older and obsolete values are listed and referenced in the 2014 edition, Chinese Physics **C38** 070001 (2014).

$N(1675)$ POLE POSITION

REAL PART

VALUE (MeV)	DOCUMENT ID		TECN	COMMENT
1655 to 1665 (≈ 1660) OUR ESTIMATE				
1655± 4	SOKHOYAN	15A	DPWA	Multichannel
1654± 2	[1] SVARC	14	L+P	$\pi N \to \pi N$
1660±10	CUTKOSKY	80	IPWA	$\pi N \to \pi N$
• • • We do not use the following data for averages, fits, limits, etc. • • •				
1646	HUNT	19	DPWA	Multichannel
1646	ROENCHEN	15A	DPWA	Multichannel
1640	SHKLYAR	13	DPWA	Multichannel
1654± 4	ANISOVICH	12A	DPWA	Multichannel
1658± 9	BATINIC	10	DPWA	$\pi N \to N\pi$, $N\eta$
1657	ARNDT	06	DPWA	$\pi N \to \pi N$, ηN
1674	VRANA	00	DPWA	Multichannel
1656	HOEHLER	93	ARGD	$\pi N \to \pi N$

[1] Fit to the amplitudes of HOEHLER 79.

−2×IMAGINARY PART

VALUE (MeV)	DOCUMENT ID		TECN	COMMENT
125 to 150 (≈ 135) OUR ESTIMATE				
147± 5	SOKHOYAN	15A	DPWA	Multichannel
125± 3±1	[1] SVARC	14	L+P	$\pi N \to \pi N$
140±10	CUTKOSKY	80	IPWA	$\pi N \to \pi N$
• • • We do not use the following data for averages, fits, limits, etc. • • •				
146	HUNT	19	DPWA	Multichannel
125	ROENCHEN	15A	DPWA	Multichannel
108	SHKLYAR	13	DPWA	Multichannel
151± 5	ANISOVICH	12A	DPWA	Multichannel
137± 7	BATINIC	10	DPWA	$\pi N \to N\pi$, $N\eta$
139	ARNDT	06	DPWA	$\pi N \to \pi N$, ηN
120	VRANA	00	DPWA	Multichannel
126	HOEHLER	93	ARGD	$\pi N \to \pi N$

[1] Fit to the amplitudes of HOEHLER 79.

$N(1675)$ ELASTIC POLE RESIDUE

MODULUS $|r|$

VALUE (MeV)	DOCUMENT ID		TECN	COMMENT
23 to 33 (≈ 28) OUR ESTIMATE				
28±1	SOKHOYAN	15A	DPWA	Multichannel
23±1	[1] SVARC	14	L+P	$\pi N \to \pi N$
31±5	CUTKOSKY	80	IPWA	$\pi N \to \pi N$
• • • We do not use the following data for averages, fits, limits, etc. • • •				
24	ROENCHEN	15A	DPWA	Multichannel
20	SHKLYAR	13	DPWA	Multichannel
28±1	ANISOVICH	12A	DPWA	Multichannel
25	BATINIC	10	DPWA	$\pi N \to N\pi$, $N\eta$
27	ARNDT	06	DPWA	$\pi N \to \pi N$, ηN
23	HOEHLER	93	ARGD	$\pi N \to \pi N$

[1] Fit to the amplitudes of HOEHLER 79.

PHASE θ

VALUE (°)	DOCUMENT ID		TECN	COMMENT
−30 to −20 (≈ −25) OUR ESTIMATE				
−24± 4	SOKHOYAN	15A	DPWA	Multichannel
−25± 2	[1] SVARC	14	L+P	$\pi N \to \pi N$
−30±10	CUTKOSKY	80	IPWA	$\pi N \to \pi N$
• • • We do not use the following data for averages, fits, limits, etc. • • •				
−22	ROENCHEN	15A	DPWA	Multichannel
−49	SHKLYAR	13	DPWA	Multichannel
−26± 4	ANISOVICH	12A	DPWA	Multichannel
−16	BATINIC	10	DPWA	$\pi N \to N\pi$, $N\eta$
−21	ARNDT	06	DPWA	$\pi N \to \pi N$, ηN
−22	HOEHLER	93	ARGD	$\pi N \to \pi N$

[1] Fit to the amplitudes of HOEHLER 79.

$N(1675)$ INELASTIC POLE RESIDUE

The "normalized residue" is the residue divided by $\Gamma_{pole}/2$.

Normalized residue in $N\pi \to N(1675) \to \Delta\pi$, D-wave

MODULUS	PHASE (°)	DOCUMENT ID		TECN	COMMENT
0.33±0.04	90 ± 15	SOKHOYAN	15A	DPWA	Multichannel
• • • We do not use the following data for averages, fits, limits, etc. • • •					
0.33±0.05	82 ± 10	ANISOVICH	12A	DPWA	Multichannel

Normalized residue in $N\pi \to N(1675) \to N\eta$

MODULUS	PHASE (°)	DOCUMENT ID		TECN	COMMENT
• • • We do not use the following data for averages, fits, limits, etc. • • •					
0.044	−43	ROENCHEN	15A	DPWA	Multichannel

Normalized residue in $N\pi \to N(1675) \to \Lambda K$

MODULUS	PHASE (°)	DOCUMENT ID		TECN	COMMENT
• • • We do not use the following data for averages, fits, limits, etc. • • •					
0.001	100	ROENCHEN	15A	DPWA	Multichannel

Normalized residue in $N\pi \to N(1675) \to \Sigma K$

MODULUS	PHASE (°)	DOCUMENT ID		TECN	COMMENT
• • • We do not use the following data for averages, fits, limits, etc. • • •					
0.031	−175	ROENCHEN	15A	DPWA	Multichannel

Normalized residue in $N\pi \to N(1675) \to N\sigma$

MODULUS	PHASE (°)	DOCUMENT ID		TECN	COMMENT
0.13±0.03	125 ± 20	SOKHOYAN	15A	DPWA	Multichannel
• • • We do not use the following data for averages, fits, limits, etc. • • •					
0.15±0.04	132 ± 18	ANISOVICH	12A	DPWA	Multichannel

$N(1675)$ BREIT-WIGNER MASS

VALUE (MeV)	DOCUMENT ID		TECN	COMMENT
1665 to 1680 (≈ 1675) OUR ESTIMATE				
1669 ± 2	[1] HUNT	19	DPWA	Multichannel
1663 ± 4	SOKHOYAN	15A	DPWA	Multichannel
1666 ± 2	[1] SHKLYAR	13	DPWA	Multichannel
1674.1± 0.2	[1] ARNDT	06	DPWA	$\pi N \to \pi N$, ηN
1675 ±10	CUTKOSKY	80	IPWA	$\pi N \to \pi N$
1679 ± 8	HOEHLER	79	IPWA	$\pi N \to \pi N$
• • • We do not use the following data for averages, fits, limits, etc. • • •				
1664 ± 5	ANISOVICH	12A	DPWA	Multichannel
1679 ± 1	[1] SHRESTHA	12A	DPWA	Multichannel
1679 ± 9	BATINIC	10	DPWA	$\pi N \to N\pi$, $N\eta$
1685 ± 4	VRANA	00	DPWA	Multichannel

[1] Statistical error only.

Downloaded from https://academic.oup.com/ptep/article/2022/8/083C01/6651666 by KIT Library user on 27 September 2022

$N(1675)$ BREIT-WIGNER WIDTH

VALUE (MeV)	DOCUMENT ID		TECN	COMMENT
130 to 160 (≈ 145) OUR ESTIMATE				
161 ± 8	[1] HUNT	19	DPWA	Multichannel
146 ± 6	SOKHOYAN	15A	DPWA	Multichannel
148 ± 1	[1] SHKLYAR	13	DPWA	Multichannel
146.5 ± 1.0	[1] ARNDT	06	DPWA	$\pi N \to \pi N$, ηN
160 ±20	CUTKOSKY	80	IPWA	$\pi N \to \pi N$
120 ±15	HOEHLER	79	IPWA	$\pi N \to \pi N$
• • • We do not use the following data for averages, fits, limits, etc. • • •				
152 ± 7	ANISOVICH	12A	DPWA	Multichannel
145 ± 4	[1] SHRESTHA	12A	DPWA	Multichannel
152 ± 8	BATINIC	10	DPWA	$\pi N \to N\pi$, $N\eta$
131 ±10	VRANA	00	DPWA	Multichannel

[1] Statistical error only.

$N(1675)$ DECAY MODES

The following branching fractions are our estimates, not fits or averages.

	Mode	Fraction (Γ_i/Γ)
Γ_1	$N\pi$	38–42 %
Γ_2	$N\eta$	< 1 %
Γ_3	ΛK	<0.04 %
Γ_4	$N\pi\pi$	25–45 %
Γ_5	$\Delta(1232)\pi$, D-wave	23–37 %
Γ_6	$N\rho$	0.1–0.9 %
Γ_7	$N\rho$, $S=1/2$	<0.2 %
Γ_8	$N\rho$, $S=3/2$, D-wave	0.1–0.7 %
Γ_9	$N\sigma$	3–7 %
Γ_{10}	$p\gamma$	0–0.02 %
Γ_{11}	$p\gamma$, helicity=1/2	0–0.01 %
Γ_{12}	$p\gamma$, helicity=3/2	0–0.01 %
Γ_{13}	$n\gamma$	0–0.15 %
Γ_{14}	$n\gamma$, helicity=1/2	0–0.05 %
Γ_{15}	$n\gamma$, helicity=3/2	0–0.10 %

$N(1675)$ BRANCHING RATIOS

$\Gamma(N\pi)/\Gamma_{total}$ — Γ_1/Γ

VALUE (%)	DOCUMENT ID		TECN	COMMENT
38 to 42 (≈ 40) OUR ESTIMATE				
33 ±1	[1] HUNT	19	DPWA	Multichannel
41 ±2	SOKHOYAN	15A	DPWA	Multichannel
41 ±1	[1] SHKLYAR	13	DPWA	Multichannel
39.3±0.1	[1] ARNDT	06	DPWA	$\pi N \to \pi N$, ηN
38 ±5	CUTKOSKY	80	IPWA	$\pi N \to \pi N$
38 ±3	HOEHLER	79	IPWA	$\pi N \to \pi N$
• • • We do not use the following data for averages, fits, limits, etc. • • •				
40 ±3	ANISOVICH	12A	DPWA	Multichannel
38.6±0.6	[1] SHRESTHA	12A	DPWA	Multichannel
35 ±4	BATINIC	10	DPWA	$\pi N \to N\pi$, $N\eta$
35 ±1	VRANA	00	DPWA	Multichannel

[1] Statistical error only.

$\Gamma(N\eta)/\Gamma_{total}$ — Γ_2/Γ

VALUE (%)	DOCUMENT ID		TECN	COMMENT
0.5 ± 0.5	MUELLER	20	DPWA	Multichannel
2.0 ± 0.3	[1] HUNT	19	DPWA	Multichannel
<1	SHKLYAR	13	DPWA	Multichannel
• • • We do not use the following data for averages, fits, limits, etc. • • •				
<1	[1] SHRESTHA	12A	DPWA	Multichannel
0.1 ± 0.1	BATINIC	10	DPWA	$\pi N \to N\pi$, $N\eta$
3 ±3	THOMA	08	DPWA	Multichannel
0 ±1	VRANA	00	DPWA	Multichannel

[1] Statistical error only.

$\Gamma(\Lambda K)/\Gamma_{total}$ — Γ_3/Γ

VALUE (%)	DOCUMENT ID		TECN	COMMENT
<0.04 % OUR ESTIMATE				
<0.04	[1] HUNT	19	DPWA	Multichannel

[1] Statistical error only.

$\Gamma(\Delta(1232)\pi, D\text{-wave})/\Gamma_{total}$ — Γ_5/Γ

VALUE (%)	DOCUMENT ID		TECN	COMMENT
58.3±0.2	[1] HUNT	19	DPWA	Multichannel
30 ±7	SOKHOYAN	15A	DPWA	Multichannel
• • • We do not use the following data for averages, fits, limits, etc. • • •				
33 ±8	ANISOVICH	12A	DPWA	Multichannel
46 ±1	[1] SHRESTHA	12A	DPWA	Multichannel
63 ±2	VRANA	00	DPWA	Multichannel

[1] Statistical error only.

$\Gamma(N\rho, S=1/2)/\Gamma_{total}$ — Γ_7/Γ

VALUE (%)	DOCUMENT ID		TECN	COMMENT
<0.2 % OUR ESTIMATE				
<0.2	[1] HUNT	19	DPWA	Multichannel

[1] Statistical error only.

$\Gamma(N\rho, S=3/2, D\text{-wave})/\Gamma_{total}$ — Γ_8/Γ

VALUE (%)	DOCUMENT ID		TECN	COMMENT
0.1–0.7 % OUR ESTIMATE				
0.4±0.3	[1] HUNT	19	DPWA	Multichannel

[1] Statistical error only.

$\Gamma(N\sigma)/\Gamma_{total}$ — Γ_9/Γ

VALUE (%)	DOCUMENT ID		TECN	COMMENT
5±2	SOKHOYAN	15A	DPWA	Multichannel
• • • We do not use the following data for averages, fits, limits, etc. • • •				
7±3	ANISOVICH	12A	DPWA	Multichannel

$N(1675)$ PHOTON DECAY AMPLITUDES AT THE POLE

$N(1675) \to p\gamma$, helicity-1/2 amplitude $A_{1/2}$

MODULUS ($GeV^{-1/2}$)	PHASE (°)	DOCUMENT ID		TECN	COMMENT
0.022±0.003	−12 ± 7	SOKHOYAN	15A	DPWA	Multichannel
$0.022^{+0.004}_{-0.007}$	49^{+5}_{-2}	ROENCHEN	14	DPWA	
• • • We do not use the following data for averages, fits, limits, etc. • • •					
0.032	36	ROENCHEN	15A	DPWA	Multichannel

$N(1675) \to p\gamma$, helicity-3/2 amplitude $A_{3/2}$

MODULUS ($GeV^{-1/2}$)	PHASE (°)	DOCUMENT ID		TECN	COMMENT
0.028±0.006	−17 ± 6	SOKHOYAN	15A	DPWA	Multichannel
$0.036^{+0.004}_{-0.005}$	−30 ± 4	ROENCHEN	14	DPWA	
• • • We do not use the following data for averages, fits, limits, etc. • • •					
0.051	−9.3	ROENCHEN	15A	DPWA	Multichannel

$N(1675)$ BREIT-WIGNER PHOTON DECAY AMPLITUDES

$N(1675) \to p\gamma$, helicity-1/2 amplitude $A_{1/2}$

VALUE ($GeV^{-1/2}$)	DOCUMENT ID		TECN	COMMENT
0.010 to 0.025 (≈ 0.018) OUR ESTIMATE				
0.026±0.002	[1] HUNT	19	DPWA	Multichannel
0.022±0.003	SOKHOYAN	15A	DPWA	Multichannel
0.009±0.001	[1] SHKLYAR	13	DPWA	Multichannel
0.013±0.001	[1] WORKMAN	12A	DPWA	$\gamma N \to N\pi$
0.018±0.002	[1] DUGGER	07	DPWA	$\gamma N \to \pi N$
• • • We do not use the following data for averages, fits, limits, etc. • • •				
0.024±0.003	ANISOVICH	12A	DPWA	Multichannel
0.011±0.001	[1] SHRESTHA	12A	DPWA	Multichannel
0.015	DRECHSEL	07	DPWA	$\gamma N \to \pi N$

[1] Statistical error only.

$N(1675) \to p\gamma$, helicity-3/2 amplitude $A_{3/2}$

VALUE ($GeV^{-1/2}$)	DOCUMENT ID		TECN	COMMENT
0.015 to 0.030 (≈ 0.022) OUR ESTIMATE				
0.005±0.002	[1] HUNT	19	DPWA	Multichannel
0.027±0.006	SOKHOYAN	15A	DPWA	Multichannel
0.021±0.001	[1] SHKLYAR	13	DPWA	Multichannel
0.016±0.001	[1] WORKMAN	12A	DPWA	$\gamma N \to N\pi$
0.021±0.001	[1] DUGGER	07	DPWA	$\gamma N \to \pi N$
• • • We do not use the following data for averages, fits, limits, etc. • • •				
0.025±0.007	ANISOVICH	12A	DPWA	Multichannel
0.020±0.001	[1] SHRESTHA	12A	DPWA	Multichannel
0.022	DRECHSEL	07	DPWA	$\gamma N \to \pi N$

[1] Statistical error only.

$N(1675) \to n\gamma$, helicity-1/2 amplitude $A_{1/2}$

VALUE ($GeV^{-1/2}$)	DOCUMENT ID		TECN	COMMENT
−0.065 to −0.055 (≈ −0.060) OUR ESTIMATE				
−0.069±0.005	[1] HUNT	19	DPWA	Multichannel
−0.060±0.007	ANISOVICH	13B	DPWA	Multichannel
−0.058±0.002	[1] CHEN	12A	DPWA	$\gamma N \to \pi N$
• • • We do not use the following data for averages, fits, limits, etc. • • •				
−0.040±0.004	[1] SHRESTHA	12A	DPWA	Multichannel
−0.062	DRECHSEL	07	DPWA	$\gamma N \to \pi N$

[1] Statistical error only.

$N(1675) \to n\gamma$, helicity-3/2 amplitude $A_{3/2}$

VALUE ($GeV^{-1/2}$)	DOCUMENT ID		TECN	COMMENT
−0.095 to −0.075 (≈ −0.085) OUR ESTIMATE				
−0.031±0.005	[1] HUNT	19	DPWA	Multichannel
−0.088±0.010	ANISOVICH	13B	DPWA	Multichannel
−0.080±0.005	[1] CHEN	12A	DPWA	$\gamma N \to \pi N$

Downloaded from https://academic.oup.com/ptep/article/2022/8/083C01/6651666 by KIT Library user on 27 September 2022

• • • We do not use the following data for averages, fits, limits, etc. • • •

−0.068±0.004	[1] SHRESTHA	12A	DPWA	Multichannel
−0.084	DRECHSEL	07	DPWA	$\gamma N \to \pi N$

[1] Statistical error only.

$N(1675)$ REFERENCES

For early references, see Physics Letters **111B** 1 (1982).

MUELLER	20	PL B803 135323	J. Mueller *et al.*	(CBELSA/TAPS Collab.)
HUNT	19	PR C99 055205	B.C. Hunt, D.M. Manley	
ROENCHEN	15A	EPJ A51 70	D. Roenchen *et al.*	
SOKHOYAN	15A	EPJ A51 95	V. Sokhoyan *et al.*	(CBELSA/TAPS Collab.)
PDG	14	CP C38 070001	K. Olive *et al.*	(PDG Collab.)
ROENCHEN	14	EPJ A50 101	D. Roenchen *et al.*	
Also		EPJ A51 63 (errat.)	D. Roenchen *et al.*	
SVARC	14	PR C89 045205	A. Svarc *et al.*	(RBI Zagreb, UNI Tuzla)
ANISOVICH	13B	EPJ A49 67	A.V. Anisovich *et al.*	
SHKLYAR	13	PR C87 015201	V. Shklyar, H. Lenske, U. Mosel	(GIES)
ANISOVICH	12A	EPJ A48 15	A.V. Anisovich *et al.*	(BONN, PNPI)
CHEN	12A	PR C86 015206	W. Chen *et al.*	(DUKE, GWU, MSST, ITEP+)
SHRESTHA	12A	PR C86 055203	M. Shrestha, D.M. Manley	(KSU)
WORKMAN	12A	PR C86 015202	R. Workman *et al.*	(GWU)
BATINIC	10	PR C82 038203	M. Batinic *et al.*	(ZAGR)
THOMA	08	PL B659 87	U. Thoma *et al.*	(CB-ELSA Collab.)
DRECHSEL	07	EPJ A34 69	D. Drechsel, S.S. Kamalov, L. Tiator	(MAINZ, JINR)
DUGGER	07	PR C76 025211	M. Dugger *et al.*	(JLab CLAS Collab.)
ARNDT	06	PR C74 045205	R.A. Arndt *et al.*	(GWU)
VRANA	00	PRPL 328 181	T.P. Vrana, S.A. Dytman, T.-S.H. Lee	(PITT, ANL)
HOEHLER	93	πN Newsletter 9 1	G. Hohler	(KARL)
CUTKOSKY	80	Toronto Conf. 19	R.E. Cutkosky *et al.*	(CMU, LBL) IJP
Also		PR D20 2839	R.E. Cutkosky *et al.*	(CMU, LBL) IJP
HOEHLER	79	PDAT 12-1	G. Hohler *et al.*	(KARLT) IJP
Also		Toronto Conf. 3	R. Koch	(KARLT) IJP

$N(1680)$ $5/2^+$

$I(J^P) = \frac{1}{2}(\frac{5}{2}^+)$ Status: ****

Older and obsolete values are listed and referenced in the 2014 edition, Chinese Physics **C38** 070001 (2014).

$N(1680)$ POLE POSITION

REAL PART

VALUE (MeV)	DOCUMENT ID		TECN	COMMENT
1665 to 1680 (≈ 1675) OUR ESTIMATE				
1678±5	SOKHOYAN	15A	DPWA	Multichannel
1674±2±1	[1] SVARC	14	L+P	$\pi N \to \pi N$
1667±5	CUTKOSKY	80	IPWA	$\pi N \to \pi N$
• • • We do not use the following data for averages, fits, limits, etc. • • •				
1668	HUNT	19	DPWA	Multichannel
1669	ROENCHEN	15A	DPWA	Multichannel
1660	SHKLYAR	13	DPWA	Multichannel
1676±6	ANISOVICH	12A	DPWA	Multichannel
1666±8	BATINIC	10	DPWA	$\pi N \to N\pi,\ N\eta$
1674	ARNDT	06	DPWA	$\pi N \to \pi N,\ \eta N$
1667	VRANA	00	DPWA	Multichannel
1673	HOEHLER	93	ARGD	$\pi N \to \pi N$

[1] Fit to the amplitudes of HOEHLER 79.

−2×IMAGINARY PART

VALUE (MeV)	DOCUMENT ID		TECN	COMMENT
110 to 135 (≈ 120) OUR ESTIMATE				
113± 4	SOKHOYAN	15A	DPWA	Multichannel
129± 3±1	[1] SVARC	14	L+P	$\pi N \to \pi N$
110±10	CUTKOSKY	80	IPWA	$\pi N \to \pi N$
• • • We do not use the following data for averages, fits, limits, etc. • • •				
118	HUNT	19	DPWA	Multichannel
100	ROENCHEN	15A	DPWA	Multichannel
98	SHKLYAR	13	DPWA	Multichannel
113± 4	ANISOVICH	12A	DPWA	Multichannel
135± 6	BATINIC	10	DPWA	$\pi N \to N\pi,\ N\eta$
115	ARNDT	06	DPWA	$\pi N \to \pi N,\ \eta N$
122	VRANA	00	DPWA	Multichannel
135	HOEHLER	93	ARGD	$\pi N \to \pi N$

[1] Fit to the amplitudes of HOEHLER 79.

$N(1680)$ ELASTIC POLE RESIDUE

MODULUS $|r|$

VALUE (MeV)	DOCUMENT ID		TECN	COMMENT
35 to 45 (≈ 40) OUR ESTIMATE				
45±4	SOKHOYAN	15A	DPWA	Multichannel
44±1±1	[1] SVARC	14	L+P	$\pi N \to \pi N$
34±2	CUTKOSKY	80	IPWA	$\pi N \to \pi N$
• • • We do not use the following data for averages, fits, limits, etc. • • •				
34	ROENCHEN	15A	DPWA	Multichannel
33	SHKLYAR	13	DPWA	Multichannel
43±4	ANISOVICH	12A	DPWA	Multichannel
44	BATINIC	10	DPWA	$\pi N \to N\pi,\ N\eta$
42	ARNDT	06	DPWA	$\pi N \to \pi N,\ \eta N$
44	HOEHLER	93	ARGD	$\pi N \to \pi N$

[1] Fit to the amplitudes of HOEHLER 79.

PHASE θ

VALUE (°)	DOCUMENT ID		TECN	COMMENT
−20 to 10 (≈ −5) OUR ESTIMATE				
5±10	SOKHOYAN	15A	DPWA	Multichannel
−16± 1±1	[1] SVARC	14	L+P	$\pi N \to \pi N$
−25± 5	CUTKOSKY	80	IPWA	$\pi N \to \pi N$
• • • We do not use the following data for averages, fits, limits, etc. • • •				
−19	ROENCHEN	15A	DPWA	Multichannel
−32	SHKLYAR	13	DPWA	Multichannel
− 2±10	ANISOVICH	12A	DPWA	Multichannel
−19	BATINIC	10	DPWA	$\pi N \to N\pi,\ N\eta$
− 4	ARNDT	06	DPWA	$\pi N \to \pi N,\ \eta N$
−17	HOEHLER	93	ARGD	$\pi N \to \pi N$

[1] Fit to the amplitudes of HOEHLER 79.

$N(1680)$ INELASTIC POLE RESIDUE

The "normalized residue" is the residue divided by $\Gamma_{pole}/2$.

Normalized residue in $N\pi \to N(1680) \to \Delta\pi$, P-wave

MODULUS	PHASE (°)	DOCUMENT ID		TECN	COMMENT
0.15±0.03	−60 ± 30	SOKHOYAN	15A	DPWA	Multichannel
• • • We do not use the following data for averages, fits, limits, etc. • • •					
0.15±0.03	−70 ± 45	ANISOVICH	12A	DPWA	Multichannel

Normalized residue in $N\pi \to N(1680) \to \Delta\pi$, F-wave

MODULUS	PHASE (°)	DOCUMENT ID		TECN	COMMENT
0.23±0.04	90 ± 12	SOKHOYAN	15A	DPWA	Multichannel
• • • We do not use the following data for averages, fits, limits, etc. • • •					
0.23±0.04	85 ± 15	ANISOVICH	12A	DPWA	Multichannel

Normalized residue in $N\pi \to N(1680) \to N\eta$

MODULUS	PHASE (°)	DOCUMENT ID		TECN	COMMENT
• • • We do not use the following data for averages, fits, limits, etc. • • •					
0.027	136	ROENCHEN	15A	DPWA	Multichannel

Normalized residue in $N\pi \to N(1680) \to \Lambda K$

MODULUS	PHASE (°)	DOCUMENT ID		TECN	COMMENT
• • • We do not use the following data for averages, fits, limits, etc. • • •					
0.001	90	ROENCHEN	15A	DPWA	Multichannel

Normalized residue in $N\pi \to N(1680) \to \Sigma K$

MODULUS	PHASE (°)	DOCUMENT ID		TECN	COMMENT
• • • We do not use the following data for averages, fits, limits, etc. • • •					
0.004	148	ROENCHEN	15A	DPWA	Multichannel

Normalized residue in $N\pi \to N(1680) \to N\,(\pi\pi)^{I=0}_{S-wave}$

MODULUS	PHASE (°)	DOCUMENT ID		TECN	COMMENT
0.29±0.06	−45 ± 15	SOKHOYAN	15A	DPWA	Multichannel
• • • We do not use the following data for averages, fits, limits, etc. • • •					
0.26±0.04	−56 ± 15	ANISOVICH	12A	DPWA	Multichannel

$N(1680)$ BREIT-WIGNER MASS

VALUE (MeV)	DOCUMENT ID		TECN	COMMENT
1680 to 1690 (≈ 1685) OUR ESTIMATE				
1686 ± 5	GOLOVATCH	19	DPWA	$\gamma p \to \pi^+\pi^- p$
1681.0± 0.1	[1] HUNT	19	DPWA	Multichannel
1690 ± 5	SOKHOYAN	15A	DPWA	Multichannel
1676 ± 2	[1] SHKLYAR	13	DPWA	Multichannel
1680.1± 0.2	[1] ARNDT	06	DPWA	$\pi N \to \pi N,\ \eta N$
1680 ±10	CUTKOSKY	80	IPWA	$\pi N \to \pi N$
1684 ± 3	HOEHLER	79	IPWA	$\pi N \to \pi N$
• • • We do not use the following data for averages, fits, limits, etc. • • •				
1689 ± 6	ANISOVICH	12A	DPWA	Multichannel
1682.7± 0.5	[1] SHRESTHA	12A	DPWA	Multichannel
1680 ± 7	BATINIC	10	DPWA	$\pi N \to N\pi,\ N\eta$
1679 ± 3	VRANA	00	DPWA	Multichannel

[1] Statistical error only.

$N(1680)$ BREIT-WIGNER WIDTH

VALUE (MeV)	DOCUMENT ID		TECN	COMMENT
115 to 130 (≈ 120) OUR ESTIMATE				
118 ±20	GOLOVATCH	19	DPWA	$\gamma p \to \pi^+\pi^- p$
123 ± 3	[1] HUNT	19	DPWA	Multichannel
119 ± 4	SOKHOYAN	15A	DPWA	Multichannel
115 ± 1	[1] SHKLYAR	13	DPWA	Multichannel
128.0± 1.1	[1] ARNDT	06	DPWA	$\pi N \to \pi N,\ \eta N$
120 ±10	CUTKOSKY	80	IPWA	$\pi N \to \pi N$
128 ± 8	HOEHLER	79	IPWA	$\pi N \to \pi N$

Downloaded from https://academic.oup.com/ptep/article/2022/8/083C01/6651666 by KIT Library user on 27 September 2022

• • • We do not use the following data for averages, fits, limits, etc. • • •

118 ± 6	ANISOVICH	12A	DPWA	Multichannel
126 ± 1	[1] SHRESTHA	12A	DPWA	Multichannel
142 ± 7	BATINIC	10	DPWA	$\pi N \to N\pi$, $N\eta$
128 ± 9	VRANA	00	DPWA	Multichannel

[1] Statistical error only.

$N(1680)$ DECAY MODES

The following branching fractions are our estimates, not fits or averages.

	Mode	Fraction (Γ_i/Γ)
Γ_1	$N\pi$	60–70 %
Γ_2	$N\eta$	<1 %
Γ_3	$N\pi\pi$	28–53 %
Γ_4	$\Delta(1232)\pi$	11–23 %
Γ_5	$\Delta(1232)\pi$, P-wave	4–10 %
Γ_6	$\Delta(1232)\pi$, F-wave	1–13 %
Γ_7	$N\rho$	8–11 %
Γ_8	$N\rho$, $S=3/2$, P-wave	6–8 %
Γ_9	$N\rho$, $S=3/2$, F-wave	2–3 %
Γ_{10}	$N\sigma$	9–19 %
Γ_{11}	$p\gamma$	0.21–0.32 %
Γ_{12}	$p\gamma$, helicity=1/2	0.001–0.011 %
Γ_{13}	$p\gamma$, helicity=3/2	0.20–0.32 %
Γ_{14}	$n\gamma$	0.021–0.046 %
Γ_{15}	$n\gamma$, helicity=1/2	0.004–0.029 %
Γ_{16}	$n\gamma$, helicity=3/2	0.01–0.024 %

$N(1680)$ BRANCHING RATIOS

$\Gamma(N\pi)/\Gamma_{total}$ — Γ_1/Γ

VALUE (%)	DOCUMENT ID		TECN	COMMENT
60 to 70 (≈ 65) OUR ESTIMATE				
68.0±0.1	[1] HUNT	19	DPWA	Multichannel
62 ±4	SOKHOYAN	15A	DPWA	Multichannel
68 ±1	[1] SHKLYAR	13	DPWA	Multichannel
70.1±0.1	[1] ARNDT	06	DPWA	$\pi N \to \pi N$, ηN
62 ±5	CUTKOSKY	80	IPWA	$\pi N \to \pi N$
65 ±2	HOEHLER	79	IPWA	$\pi N \to \pi N$
• • • We do not use the following data for averages, fits, limits, etc. • • •				
64 ±5	ANISOVICH	12A	DPWA	Multichannel
68.0±0.5	[1] SHRESTHA	12A	DPWA	Multichannel
67 ±3	BATINIC	10	DPWA	$\pi N \to N\pi$, $N\eta$
69 ±2	VRANA	00	DPWA	Multichannel

[1] Statistical error only.

$\Gamma(N\eta)/\Gamma_{total}$ — Γ_2/Γ

VALUE (%)	DOCUMENT ID		TECN	COMMENT
0.2 ±0.1	MUELLER	20	DPWA	Multichannel
0.09±0.02	[1] HUNT	19	DPWA	Multichannel
<1	SHKLYAR	13	DPWA	Multichannel
$0.15^{+0.35}_{-0.10}$	TIATOR	99	DPWA	$\gamma p \to p\eta$
• • • We do not use the following data for averages, fits, limits, etc. • • •				
1.0 ±0.3	[1] SHRESTHA	12A	DPWA	Multichannel
0.4 ±0.2	BATINIC	10	DPWA	$\pi N \to N\pi$, $N\eta$
<1	THOMA	08	DPWA	Multichannel
0 ±1	VRANA	00	DPWA	Multichannel

[1] Statistical error only.

$\Gamma(N\pi\pi)/\Gamma_{total}$ — Γ_3/Γ

VALUE (%)	DOCUMENT ID		TECN	COMMENT
28–53 % OUR ESTIMATE				
24±4	GOLOVATCH	19	DPWA	$\gamma p \to \pi^+\pi^- p$

$\Gamma(\Delta(1232)\pi, P\text{-wave})/\Gamma_{total}$ — Γ_5/Γ

VALUE (%)	DOCUMENT ID		TECN	COMMENT
13 ±1	[1] HUNT	19	DPWA	Multichannel
7 ±3	SOKHOYAN	15A	DPWA	Multichannel
• • • We do not use the following data for averages, fits, limits, etc. • • •				
5 ±3	ANISOVICH	12A	DPWA	Multichannel
10.5±0.9	[1] SHRESTHA	12A	DPWA	Multichannel
14 ±3	VRANA	00	DPWA	Multichannel

[1] Statistical error only.

$\Gamma(\Delta(1232)\pi, F\text{-wave})/\Gamma_{total}$ — Γ_6/Γ

VALUE (%)	DOCUMENT ID		TECN	COMMENT
< 0.3	[1] HUNT	19	DPWA	Multichannel
10 ±3	SOKHOYAN	15A	DPWA	Multichannel
• • • We do not use the following data for averages, fits, limits, etc. • • •				
10 ±3	ANISOVICH	12A	DPWA	Multichannel
1.0±0.1	[1] SHRESTHA	12A	DPWA	Multichannel
1 ±1	VRANA	00	DPWA	Multichannel

[1] Statistical error only.

$\Gamma(N\rho, S=3/2, P\text{-wave})/\Gamma_{total}$ — Γ_8/Γ

VALUE (%)	DOCUMENT ID		TECN	COMMENT
6–8 % OUR ESTIMATE				
7±1	[1] HUNT	19	DPWA	Multichannel

[1] Statistical error only.

$\Gamma(N\rho, S=3/2, F\text{-wave})/\Gamma_{total}$ — Γ_9/Γ

VALUE (%)	DOCUMENT ID		TECN	COMMENT
2–3 % OUR ESTIMATE				
2.4±0.4	[1] HUNT	19	DPWA	Multichannel

[1] Statistical error only.

$\Gamma(N\sigma)/\Gamma_{total}$ — Γ_{10}/Γ

VALUE (%)	DOCUMENT ID		TECN	COMMENT
8.7±1.5	[1] HUNT	19	DPWA	Multichannel
14 ±5	SOKHOYAN	15A	DPWA	Multichannel
• • • We do not use the following data for averages, fits, limits, etc. • • •				
14 ±7	ANISOVICH	12A	DPWA	Multichannel
9.4±0.8	[1] SHRESTHA	12A	DPWA	Multichannel
9 ±1	VRANA	00	DPWA	Multichannel

[1] Statistical error only.

$N(1680)$ PHOTON DECAY AMPLITUDES AT THE POLE

$N(1680) \to p\gamma$, helicity-1/2 amplitude $A_{1/2}$

MODULUS ($GeV^{-1/2}$)	PHASE (°)	DOCUMENT ID		TECN	COMMENT
−0.013±0.003	−20 ± 17	SOKHOYAN	15A	DPWA	Multichannel
$-0.013^{+0.002}_{-0.005}$	-42^{+9}_{-18}	ROENCHEN	14	DPWA	
• • • We do not use the following data for averages, fits, limits, etc. • • •					
−0.022	−28	ROENCHEN	15A	DPWA	Multichannel

$N(1680) \to p\gamma$, helicity-3/2 amplitude $A_{3/2}$

MODULUS ($GeV^{-1/2}$)	PHASE (°)	DOCUMENT ID		TECN	COMMENT
0.135±0.005	1 ± 3	SOKHOYAN	15A	DPWA	Multichannel
$0.126^{+0.001}_{-0.002}$	-7^{+3}_{-2}	ROENCHEN	14	DPWA	
• • • We do not use the following data for averages, fits, limits, etc. • • •					
0.102	−11	ROENCHEN	15A	DPWA	Multichannel

$N(1680)$ BREIT-WIGNER PHOTON DECAY AMPLITUDES

$N(1680) \to p\gamma$, helicity-1/2 amplitude $A_{1/2}$

VALUE ($GeV^{-1/2}$)	DOCUMENT ID		TECN	COMMENT
−0.018 to −0.005 (≈ −0.010) OUR ESTIMATE				
−0.0278±0.0036	GOLOVATCH	19	DPWA	$\gamma p \to \pi^+\pi^- p$
−0.026 ±0.004	[1] HUNT	19	DPWA	Multichannel
−0.015 ±0.002	SOKHOYAN	15A	DPWA	Multichannel
0.003 ±0.001	[1] SHKLYAR	13	DPWA	Multichannel
−0.007 ±0.002	[1] WORKMAN	12A	DPWA	$\gamma N \to N\pi$
−0.017 ±0.001	[1] DUGGER	07	DPWA	$\gamma N \to \pi N$
• • • We do not use the following data for averages, fits, limits, etc. • • •				
−0.013 ±0.003	ANISOVICH	12A	DPWA	Multichannel
−0.017 ±0.001	[1] SHRESTHA	12A	DPWA	Multichannel
−0.025	DRECHSEL	07	DPWA	$\gamma N \to \pi N$

[1] Statistical error only.

$N(1680) \to p\gamma$, helicity-3/2 amplitude $A_{3/2}$

VALUE ($GeV^{-1/2}$)	DOCUMENT ID		TECN	COMMENT
0.130 to 0.140 (≈ 0.135) OUR ESTIMATE				
0.128±0.011	GOLOVATCH	19	DPWA	$\gamma p \to \pi^+\pi^- p$
0.112±0.005	[1] HUNT	19	DPWA	Multichannel
0.136±0.005	SOKHOYAN	15A	DPWA	Multichannel
0.116±0.001	[1] SHKLYAR	13	DPWA	Multichannel
0.140±0.002	[1] WORKMAN	12A	DPWA	$\gamma N \to N\pi$
0.134±0.002	[1] DUGGER	07	DPWA	$\gamma N \to \pi N$
• • • We do not use the following data for averages, fits, limits, etc. • • •				
0.135±0.006	ANISOVICH	12A	DPWA	Multichannel
0.136±0.001	[1] SHRESTHA	12A	DPWA	Multichannel
0.134	DRECHSEL	07	DPWA	$\gamma N \to \pi N$

[1] Statistical error only.

$N(1680) \to n\gamma$, helicity-1/2 amplitude $A_{1/2}$

VALUE ($GeV^{-1/2}$)	DOCUMENT ID		TECN	COMMENT
0.020 to 0.040 (≈ 0.030) OUR ESTIMATE				
0.005±0.004	[1] HUNT	19	DPWA	Multichannel
0.034±0.006	ANISOVICH	13B	DPWA	Multichannel
0.026±0.004	[1] CHEN	12A	DPWA	$\gamma N \to \pi N$

Downloaded from https://academic.oup.com/ptep/article/2022/8/083C01/6651666 by KIT Library user on 27 September 2022

• • • We do not use the following data for averages, fits, limits, etc. • • •

0.029±0.002	[1] SHRESTHA	12A	DPWA	Multichannel
0.028	DRECHSEL	07	DPWA	$\gamma N \to \pi N$

[1] Statistical error only.

$N(1680) \to n\gamma$, helicity-3/2 amplitude $A_{3/2}$

VALUE (GeV$^{-1/2}$)	DOCUMENT ID		TECN	COMMENT
−0.050 to −0.025 (≈ −0.035) OUR ESTIMATE				
−0.061±0.004	[1] HUNT	19	DPWA	Multichannel
−0.044±0.009	ANISOVICH	13B	DPWA	Multichannel
−0.029±0.002	[1] CHEN	12A	DPWA	$\gamma N \to \pi N$
• • • We do not use the following data for averages, fits, limits, etc. • • •				
−0.059±0.002	[1] SHRESTHA	12A	DPWA	Multichannel
−0.038	DRECHSEL	07	DPWA	$\gamma N \to \pi N$

[1] Statistical error only.

$N(1680)$ REFERENCES

For early references, see Physics Letters **111B** 1 (1982). For very early references, see Reviews of Modern Physics **37** 633 (1965).

MUELLER	20	PL B803 135323	J. Mueller *et al.*	(CBELSA/TAPS Collab.)
GOLOVATCH	19	PL B788 371	E. Golovatch *et al.*	(CLAS Collab.)
HUNT	19	PR C99 055205	B.C. Hunt, D.M. Manley	
ROENCHEN	15A	EPJ A51 70	D. Roenchen *et al.*	
SOKHOYAN	15A	EPJ A51 95	V. Sokhoyan *et al.*	(CBELSA/TAPS Collab.)
PDG	14	CP C38 070001	K. Olive *et al.*	(PDG Collab.)
ROENCHEN	14	EPJ A50 101	D. Roenchen *et al.*	
Also		EPJ A51 63 (errat.)	D. Roenchen *et al.*	
SVARC	14	PR C89 045205	A. Svarc *et al.*	(RBI Zagreb, UNI Tuzla)
ANISOVICH	13B	EPJ A49 67	A.V. Anisovich *et al.*	
SHKLYAR	13	PR C87 015201	V. Shklyar, H. Lenske, U. Mosel	(GIES)
ANISOVICH	12A	EPJ A48 15	A.V. Anisovich *et al.*	(BONN, PNPI)
CHEN	12A	PR C86 015206	W. Chen *et al.*	(DUKE, GWU, MSST, ITEP+)
SHRESTHA	12A	PR C86 055203	M. Shrestha, D.M. Manley	(KSU)
WORKMAN	12A	PR C86 015202	R. Workman *et al.*	(GWU)
BATINIC	10	PR C82 038203	M. Batinic *et al.*	(ZAGR)
THOMA	08	PL B659 87	U. Thoma *et al.*	(CB-ELSA Collab.)
DRECHSEL	07	EPJ A34 69	D. Drechsel, S.S. Kamalov, L. Tiator	(MAINZ, JINR)
DUGGER	07	PR C76 025211	M. Dugger *et al.*	(JLab CLAS Collab.)
ARNDT	06	PR C74 045205	R.A. Arndt *et al.*	(GWU)
VRANA	00	PRPL 328 181	T.P. Vrana, S.A. Dytman, T.-S.H. Lee	(PITT, ANL)
TIATOR	99	PR C60 035210	L. Tiator *et al.*	
HOEHLER	93	πN Newsletter 9 1	G. Hohler	(KARL)
CUTKOSKY	80	Toronto Conf. 19	R.E. Cutkosky *et al.*	(CMU, LBL) IJP
Also		PR D20 2839	R.E. Cutkosky *et al.*	(CMU, LBL) IJP
HOEHLER	79	PDAT 12-1	G. Hohler *et al.*	(KARLT) IJP
Also		Toronto Conf. 3	R. Koch	(KARLT) IJP

$N(1700)\ 3/2^-$

$I(J^P) = \frac{1}{2}(\frac{3}{2}^-)$ Status: ***

Older and obsolete values are listed and referenced in the 2014 edition, Chinese Physics **C38** 070001 (2014).

$N(1700)$ POLE POSITION

REAL PART

VALUE (MeV)	DOCUMENT ID		TECN	COMMENT
1650 to 1750 (≈ 1700) OUR ESTIMATE				
1780±35	SOKHOYAN	15A	DPWA	Multichannel
1757± 4±1	[1] SVARC	14	L+P	$\pi N \to \pi N$
1660±30	CUTKOSKY	80	IPWA	$\pi N \to \pi N$
• • • We do not use the following data for averages, fits, limits, etc. • • •				
1647	HUNT	19	DPWA	Multichannel
1770±40	ANISOVICH	12A	DPWA	Multichannel
1806±23	BATINIC	10	DPWA	$\pi N \to N\pi,\ N\eta$
1704	VRANA	00	DPWA	Multichannel
1700	HOEHLER	93	SPED	$\pi N \to \pi N$

[1] Fit to the amplitudes of HOEHLER 79.

−2×IMAGINARY PART

VALUE (MeV)	DOCUMENT ID		TECN	COMMENT
100 to 300 (≈ 200) OUR ESTIMATE				
420±140	SOKHOYAN	15A	DPWA	Multichannel
136± 7±4	[1] SVARC	14	L+P	$\pi N \to \pi N$
90± 40	CUTKOSKY	80	IPWA	$\pi N \to \pi N$
• • • We do not use the following data for averages, fits, limits, etc. • • •				
79	HUNT	19	DPWA	Multichannel
420±180	ANISOVICH	12A	DPWA	Multichannel
129± 33	BATINIC	10	DPWA	$\pi N \to N\pi,\ N\eta$
156	VRANA	00	DPWA	Multichannel
120	HOEHLER	93	SPED	$\pi N \to \pi N$

[1] Fit to the amplitudes of HOEHLER 79.

$N(1700)$ ELASTIC POLE RESIDUE

MODULUS $|r|$

VALUE (MeV)	DOCUMENT ID		TECN	COMMENT
5 to 50 (≈ 10) OUR ESTIMATE				
60±30	SOKHOYAN	15A	DPWA	Multichannel
7± 1±1	[1] SVARC	14	L+P	$\pi N \to \pi N$
6± 3	CUTKOSKY	80	IPWA	$\pi N \to \pi N$
• • • We do not use the following data for averages, fits, limits, etc. • • •				
50±40	ANISOVICH	12A	DPWA	Multichannel
7	BATINIC	10	DPWA	$\pi N \to N\pi,\ N\eta$
5	HOEHLER	93	SPED	$\pi N \to \pi N$

[1] Fit to the amplitudes of HOEHLER 79.

PHASE θ

VALUE (°)	DOCUMENT ID		TECN	COMMENT
−120 to 0 (≈ −90) OUR ESTIMATE				
−115±30	SOKHOYAN	15A	DPWA	Multichannel
−113± 4±2	[1] SVARC	14	L+P	$\pi N \to \pi N$
0±50	CUTKOSKY	80	IPWA	$\pi N \to \pi N$
• • • We do not use the following data for averages, fits, limits, etc. • • •				
−100±40	ANISOVICH	12A	DPWA	Multichannel
− 34	BATINIC	10	DPWA	$\pi N \to N\pi,\ N\eta$

[1] Fit to the amplitudes of HOEHLER 79.

$N(1700)$ INELASTIC POLE RESIDUE

The "normalized residue" is the residue divided by $\Gamma_{pole}/2$.

Normalized residue in $N\pi \to N(1700) \to \Delta\pi$, S-wave

MODULUS	PHASE (°)	DOCUMENT ID		TECN	COMMENT
0.33±0.10	−70 ± 25	SOKHOYAN	15A	DPWA	Multichannel
• • • We do not use the following data for averages, fits, limits, etc. • • •					
0.34±0.21	−60 ± 40	ANISOVICH	12A	DPWA	Multichannel

Normalized residue in $N\pi \to N(1700) \to \Delta\pi$, D-wave

MODULUS	PHASE (°)	DOCUMENT ID		TECN	COMMENT
0.10±0.06	75 ± 30	SOKHOYAN	15A	DPWA	Multichannel
• • • We do not use the following data for averages, fits, limits, etc. • • •					
0.08±0.06	90 ± 35	ANISOVICH	12A	DPWA	Multichannel

Normalized residue in $N\pi \to N(1700) \to N\sigma$

MODULUS	PHASE (°)	DOCUMENT ID		TECN	COMMENT
0.13±0.08	−100 ± 35	SOKHOYAN	15A	DPWA	Multichannel

Normalized residue in $N\pi \to N(1700) \to N(1440)\pi$

MODULUS	PHASE (°)	DOCUMENT ID		TECN	COMMENT
0.13±0.05	40 ± 35	SOKHOYAN	15A	DPWA	Multichannel

Normalized residue in $N\pi \to N(1700) \to N(1520)\pi$, P-wave

MODULUS	PHASE (°)	DOCUMENT ID		TECN	COMMENT
0.07±0.03	160 ± 45	SOKHOYAN	15A	DPWA	Multichannel

$N(1700)$ BREIT-WIGNER MASS

VALUE (MeV)	DOCUMENT ID		TECN	COMMENT
1650 to 1800 (≈ 1720) OUR ESTIMATE				
1653± 5	[1] HUNT	19	DPWA	Multichannel
1800±35	SOKHOYAN	15A	DPWA	Multichannel
1675±25	CUTKOSKY	80	IPWA	$\pi N \to \pi N$
1731±15	HOEHLER	79	IPWA	$\pi N \to \pi N$
• • • We do not use the following data for averages, fits, limits, etc. • • •				
1790±40	ANISOVICH	12A	DPWA	Multichannel
1665± 3	[1] SHRESTHA	12A	DPWA	Multichannel
1817±22	BATINIC	10	DPWA	$\pi N \to N\pi,\ N\eta$
1736±33	VRANA	00	DPWA	Multichannel

[1] Statistical error only.

$N(1700)$ BREIT-WIGNER WIDTH

VALUE (MeV)	DOCUMENT ID		TECN	COMMENT
100 to 300 (≈ 200) OUR ESTIMATE				
81± 13	[1] HUNT	19	DPWA	Multichannel
400±100	SOKHOYAN	15A	DPWA	Multichannel
90± 40	CUTKOSKY	80	IPWA	$\pi N \to \pi N$
110± 30	HOEHLER	79	IPWA	$\pi N \to \pi N$
• • • We do not use the following data for averages, fits, limits, etc. • • •				
390±140	ANISOVICH	12A	DPWA	Multichannel
56± 8	[1] SHRESTHA	12A	DPWA	Multichannel
134± 37	BATINIC	10	DPWA	$\pi N \to N\pi,\ N\eta$
175±133	VRANA	00	DPWA	Multichannel

[1] Statistical error only.

$N(1700)$ DECAY MODES

The following branching fractions are our estimates, not fits or averages.

	Mode	Fraction (Γ_i/Γ)
Γ_1	$N\pi$	7–17 %
Γ_2	$N\eta$	1–2 %

Downloaded from https://academic.oup.com/ptep/article/2022/8/083C01/6651666 by KIT Library user on 27 September 2022

Γ_3	$N\omega$	10–34 %
Γ_4	ΛK	1–2 %
Γ_5	$N\pi\pi$	>89 %
Γ_6	$\Delta(1232)\pi$	55–85 %
Γ_7	$\Delta(1232)\pi$, S-wave	50–80 %
Γ_8	$\Delta(1232)\pi$, D-wave	4–14 %
Γ_9	$N\rho$, $S=3/2$, S-wave	32–44 %
Γ_{10}	$N\sigma$	2–14 %
Γ_{11}	$N(1440)\pi$	3–11 %
Γ_{12}	$N(1520)\pi$	<4 %
Γ_{13}	$p\gamma$	0.01–0.05 %
Γ_{14}	$p\gamma$, helicity=1/2	0.0–0.024 %
Γ_{15}	$p\gamma$, helicity=3/2	0.002–0.026 %
Γ_{16}	$n\gamma$	0.01–0.13 %
Γ_{17}	$n\gamma$, helicity=1/2	0.0–0.09 %
Γ_{18}	$n\gamma$, helicity=3/2	0.01–0.05 %

$N(1700)$ BRANCHING RATIOS

$\Gamma(N\pi)/\Gamma_{total}$ — Γ_1/Γ

VALUE (%)	DOCUMENT ID		TECN	COMMENT
7 to 17 (≈ 12) OUR ESTIMATE				
3.7±0.1	[1] HUNT	19	DPWA	Multichannel
15 ±6	SOKHOYAN	15A	DPWA	Multichannel
11 ±5	CUTKOSKY	80	IPWA	$\pi N \to \pi N$
8 ±3	HOEHLER	79	IPWA	$\pi N \to \pi N$
• • • We do not use the following data for averages, fits, limits, etc. • • •				
12 ±5	ANISOVICH	12A	DPWA	Multichannel
2.8±0.5	[1] SHRESTHA	12A	DPWA	Multichannel
9 ±6	BATINIC	10	DPWA	$\pi N \to N\pi$, $N\eta$
4 ±2	VRANA	00	DPWA	Multichannel

[1] Statistical error only.

$\Gamma(N\eta)/\Gamma_{total}$ — Γ_2/Γ

VALUE (%)	DOCUMENT ID		TECN	COMMENT
1–2 % OUR ESTIMATE				
1 ±1	MUELLER	20	DPWA	Multichannel
1.1±0.6	[1] HUNT	19	DPWA	Multichannel
• • • We do not use the following data for averages, fits, limits, etc. • • •				
14 ±5	BATINIC	10	DPWA	$\pi N \to N\pi$, $N\eta$
10 ±5	THOMA	08	DPWA	Multichannel
0 ±1	VRANA	00	DPWA	Multichannel

[1] Statistical error only.

$\Gamma(N\omega)/\Gamma_{total}$ — Γ_3/Γ

VALUE (%)	DOCUMENT ID		TECN	COMMENT
22±12	DENISENKO	16	DPWA	Multichannel

$\Gamma(\Lambda K)/\Gamma_{total}$ — Γ_4/Γ

VALUE (%)	DOCUMENT ID		TECN	COMMENT
1–2 % OUR ESTIMATE				
1.3±0.7	[1] HUNT	19	DPWA	Multichannel

[1] Statistical error only.

$\Gamma(\Delta(1232)\pi, S\text{-wave})/\Gamma_{total}$ — Γ_7/Γ

VALUE (%)	DOCUMENT ID		TECN	COMMENT
11± 8	[1] HUNT	19	DPWA	Multichannel
65±15	SOKHOYAN	15A	DPWA	Multichannel
• • • We do not use the following data for averages, fits, limits, etc. • • •				
72±23	ANISOVICH	12A	DPWA	Multichannel
31± 9	[1] SHRESTHA	12A	DPWA	Multichannel
11± 1	VRANA	00	DPWA	Multichannel

[1] Statistical error only.

$\Gamma(\Delta(1232)\pi, D\text{-wave})/\Gamma_{total}$ — Γ_8/Γ

VALUE (%)	DOCUMENT ID		TECN	COMMENT
13± 5	[1] HUNT	19	DPWA	Multichannel
9± 5	SOKHOYAN	15A	DPWA	Multichannel
• • • We do not use the following data for averages, fits, limits, etc. • • •				
<10	ANISOVICH	12A	DPWA	Multichannel
3± 2	[1] SHRESTHA	12A	DPWA	Multichannel
79±56	VRANA	00	DPWA	Multichannel

[1] Statistical error only.

$\Gamma(N\rho, S=3/2, S\text{-wave})/\Gamma_{total}$ — Γ_9/Γ

VALUE (%)	DOCUMENT ID		TECN	COMMENT
7.5±3.6	[1] HUNT	19	DPWA	Multichannel
• • • We do not use the following data for averages, fits, limits, etc. • • •				
38 ±6	[1] SHRESTHA	12A	DPWA	Multichannel
7 ±1	VRANA	00	DPWA	Multichannel

[1] Statistical error only.

$\Gamma(N\sigma)/\Gamma_{total}$ — Γ_{10}/Γ

VALUE (%)	DOCUMENT ID		TECN	COMMENT
62± 9	[1] HUNT	19	DPWA	Multichannel
8± 6	SOKHOYAN	15A	DPWA	Multichannel
• • • We do not use the following data for averages, fits, limits, etc. • • •				
24± 6	[1] SHRESTHA	12A	DPWA	Multichannel
18±12	THOMA	08	DPWA	Multichannel
0± 1	VRANA	00	DPWA	Multichannel

[1] Statistical error only.

$\Gamma(N(1440)\pi)/\Gamma_{total}$ — Γ_{11}/Γ

VALUE (%)	DOCUMENT ID		TECN	COMMENT
7±4	SOKHOYAN	15A	DPWA	Multichannel

$\Gamma(N(1520)\pi)/\Gamma_{total}$ — Γ_{12}/Γ

VALUE (%)	DOCUMENT ID		TECN	COMMENT
<4	SOKHOYAN	15A	DPWA	Multichannel

$N(1700)$ PHOTON DECAY AMPLITUDES AT THE POLE

$N(1700) \to p\gamma$, helicity-1/2 amplitude $A_{1/2}$

MODULUS ($GeV^{-1/2}$)	PHASE (°)	DOCUMENT ID		TECN	COMMENT
0.047±0.016	75 ± 30	SOKHOYAN	15A	DPWA	Multichannel

$N(1700) \to p\gamma$, helicity-3/2 amplitude $A_{3/2}$

MODULUS ($GeV^{-1/2}$)	PHASE (°)	DOCUMENT ID		TECN	COMMENT
−0.041±0.014	0 ± 20	SOKHOYAN	15A	DPWA	Multichannel

$N(1700)$ BREIT-WIGNER PHOTON DECAY AMPLITUDES

$N(1700) \to p\gamma$, helicity-1/2 amplitude $A_{1/2}$

VALUE ($GeV^{-1/2}$)	DOCUMENT ID		TECN	COMMENT
0.032±0.005	[1] HUNT	19	DPWA	Multichannel
0.041±0.017	ANISOVICH	12A	DPWA	Multichannel
• • • We do not use the following data for averages, fits, limits, etc. • • •				
0.021±0.005	[1] SHRESTHA	12A	DPWA	Multichannel

[1] Statistical error only.

$N(1700) \to p\gamma$, helicity-3/2 amplitude $A_{3/2}$

VALUE ($GeV^{-1/2}$)	DOCUMENT ID		TECN	COMMENT
0.034±0.006	[1] HUNT	19	DPWA	Multichannel
−0.037±0.014	SOKHOYAN	15A	DPWA	Multichannel
• • • We do not use the following data for averages, fits, limits, etc. • • •				
−0.034±0.013	ANISOVICH	12A	DPWA	Multichannel
0.050±0.009	[1] SHRESTHA	12A	DPWA	Multichannel

[1] Statistical error only.

$N(1700) \to n\gamma$, helicity-1/2 amplitude $A_{1/2}$

VALUE ($GeV^{-1/2}$)	DOCUMENT ID		TECN	COMMENT
0.005±0.011	[1] HUNT	19	DPWA	Multichannel
0.025±0.010	ANISOVICH	13B	DPWA	Multichannel
• • • We do not use the following data for averages, fits, limits, etc. • • •				
−0.049±0.008	[1] SHRESTHA	12A	DPWA	Multichannel

[1] Statistical error only.

$N(1700) \to n\gamma$, helicity-3/2 amplitude $A_{3/2}$

VALUE ($GeV^{-1/2}$)	DOCUMENT ID		TECN	COMMENT
−0.094±0.017	[1] HUNT	19	DPWA	Multichannel
−0.032±0.018	ANISOVICH	13B	DPWA	Multichannel
• • • We do not use the following data for averages, fits, limits, etc. • • •				
−0.092±0.014	[1] SHRESTHA	12A	DPWA	Multichannel

[1] Statistical error only.

$N(1700)$ REFERENCES

For early references, see Physics Letters **111B** 1 (1982).

MUELLER	20	PL B803 135323	J. Mueller *et al.*	(CBELSA/TAPS Collab.)
HUNT	19	PR C99 055205	B.C. Hunt, D.M. Manley	
DENISENKO	16	PL B755 97	I. Denisenko *et al.*	
SOKHOYAN	15A	EPJ A51 95	V. Sokhoyan *et al.*	(CBELSA/TAPS Collab.)
PDG	14	CP C38 070001	K. Olive *et al.*	(PDG Collab.)
SVARC	14	PR C89 045205	A. Svarc *et al.*	(RBI Zagreb, UNI Tuzla)
ANISOVICH	13B	EPJ A49 67	A.V. Anisovich *et al.*	
ANISOVICH	12A	EPJ A48 15	A.V. Anisovich *et al.*	(BONN, PNPI)
SHRESTHA	12A	PR C86 055203	M. Shrestha, D.M. Manley	(KSU)
BATINIC	10	PR C82 038203	M. Batinic *et al.*	(ZAGR)
THOMA	08	PL B659 87	U. Thoma *et al.*	(CB-ELSA Collab.)
VRANA	00	PRPL 328 181	T.P. Vrana, S.A. Dytman, T.-S.H. Lee	(PITT, ANL)
HOEHLER	93	πN Newsletter 9 1	G. Hohler	(KARL)
CUTKOSKY	80	Toronto Conf. 19	R.E. Cutkosky *et al.*	(CMU, LBL) IJP
Also		PR D20 2839	R.E. Cutkosky *et al.*	(CMU, LBL) IJP
HOEHLER	79	PDAT 12-1	G. Hohler *et al.*	(KARLT) IJP
Also		Toronto Conf. 3	R. Koch	(KARLT) IJP

Downloaded from https://academic.oup.com/ptep/article/2022/8/083C01/6651666 by KIT Library user on 27 September 2022

N(1710) 1/2+

$I(J^P) = \frac{1}{2}(\frac{1}{2}^+)$ Status: ****

Older and obsolete values are listed and referenced in the 2014 edition, Chinese Physics **C38** 070001 (2014).

N(1710) POLE POSITION

REAL PART

VALUE (MeV)	DOCUMENT ID		TECN	COMMENT
1680 to 1720 (≈ 1700) OUR ESTIMATE				
1690±15	ANISOVICH	17A	DPWA	Multichannel
1697±23	[1] ANISOVICH	17A	L+P	γp, $\pi^- p \to K\Lambda$
1770± 5±2	[2] SVARC	14	L+P	$\pi N \to \pi N$
1690±20	CUTKOSKY	80	IPWA	$\pi N \to \pi N$
• • • We do not use the following data for averages, fits, limits, etc. • • •				
1615	HUNT	19	DPWA	Multichannel
1651	ROENCHEN	15A	DPWA	Multichannel
1690±15	SOKHOYAN	15A	DPWA	Multichannel
1690±15	GUTZ	14	DPWA	Multichannel
1670	SHKLYAR	13	DPWA	Multichannel
1687±17	ANISOVICH	12A	DPWA	Multichannel
1711±15	[3] BATINIC	10	DPWA	$\pi N \to N\pi$, $N\eta$
1679	VRANA	00	DPWA	Multichannel
1690	HOEHLER	93	SPED	$\pi N \to \pi N$
1698	CUTKOSKY	90	IPWA	$\pi N \to \pi N$

[1] Statistical error only.
[2] Fit to the amplitudes of HOEHLER 79.
[3] BATINIC 10 finds evidence for a second P_{11} state with all parameters except for the phase of the pole residue very similar to the parameters we give here.

−2×IMAGINARY PART

VALUE (MeV)	DOCUMENT ID		TECN	COMMENT
80 to 160 (≈ 120) OUR ESTIMATE				
155±25	ANISOVICH	17A	DPWA	Multichannel
84±34	[1] ANISOVICH	17A	L+P	γp, $\pi^- p \to K\Lambda$
98± 8±5	[2] SVARC	14	L+P	$\pi N \to \pi N$
80±20	CUTKOSKY	80	IPWA	$\pi N \to \pi N$
• • • We do not use the following data for averages, fits, limits, etc. • • •				
169	HUNT	19	DPWA	Multichannel
121	ROENCHEN	15A	DPWA	Multichannel
170±20	SOKHOYAN	15A	DPWA	Multichannel
170±20	GUTZ	14	DPWA	Multichannel
159	SHKLYAR	13	DPWA	Multichannel
200±25	ANISOVICH	12A	DPWA	Multichannel
174±16	[3] BATINIC	10	DPWA	$\pi N \to N\pi$, $N\eta$
132	VRANA	00	DPWA	Multichannel
200	HOEHLER	93	SPED	$\pi N \to \pi N$
88	CUTKOSKY	90	IPWA	$\pi N \to \pi N$

[1] Statistical error only.
[2] Fit to the amplitudes of HOEHLER 79.
[3] BATINIC 10 finds evidence for a second P_{11} state with all parameters except for the phase of the pole residue very similar to the parameters we give here.

N(1710) ELASTIC POLE RESIDUE

MODULUS |r|

VALUE (MeV)	DOCUMENT ID		TECN	COMMENT
4 to 10 (≈ 7) OUR ESTIMATE				
6 ±3	SOKHOYAN	15A	DPWA	Multichannel
5 ±1±1	[1] SVARC	14	L+P	$\pi N \to \pi N$
8 ±2	CUTKOSKY	80	IPWA	$\pi N \to \pi N$
• • • We do not use the following data for averages, fits, limits, etc. • • •				
3.2	ROENCHEN	15A	DPWA	Multichannel
6 ±3	GUTZ	14	DPWA	Multichannel
11	SHKLYAR	13	DPWA	Multichannel
6 ±4	ANISOVICH	12A	DPWA	Multichannel
24	[2] BATINIC	10	DPWA	$\pi N \to N\pi$, $N\eta$
15	HOEHLER	93	SPED	$\pi N \to \pi N$
9	CUTKOSKY	90	IPWA	$\pi N \to \pi N$

[1] Fit to the amplitudes of HOEHLER 79.
[2] BATINIC 10 finds evidence for a second P_{11} state with all parameters except for the phase of the pole residue very similar to the parameters we give here.

PHASE θ

VALUE (°)	DOCUMENT ID		TECN	COMMENT
120 to 260 (≈ 190) OUR ESTIMATE				
130±35	SOKHOYAN	15A	DPWA	Multichannel
−104± 7±3	[1] SVARC	14	L+P	$\pi N \to \pi N$
175±35	CUTKOSKY	80	IPWA	$\pi N \to \pi N$
• • • We do not use the following data for averages, fits, limits, etc. • • •				
55	ROENCHEN	15A	DPWA	Multichannel
120±45	GUTZ	14	DPWA	Multichannel
9	SHKLYAR	13	DPWA	Multichannel
120±70	ANISOVICH	12A	DPWA	Multichannel
20	[2] BATINIC	10	DPWA	$\pi N \to N\pi$, $N\eta$
−167	CUTKOSKY	90	IPWA	$\pi N \to \pi N$

[1] Fit to the amplitudes of HOEHLER 79.
[2] BATINIC 10 finds evidence for a second P_{11} state with all parameters except for the phase of the pole residue very similar to the parameters we give here.

N(1710) INELASTIC POLE RESIDUE

The "normalized residue" is the residue divided by $\Gamma_{pole}/2$.

Normalized residue in $N\pi \to N(1710) \to N\eta$

MODULUS	PHASE (°)	DOCUMENT ID		TECN	COMMENT
0.12±0.04	0 ± 45	ANISOVICH	12A	DPWA	Multichannel
• • • We do not use the following data for averages, fits, limits, etc. • • •					
0.16	−180	ROENCHEN	15A	DPWA	Multichannel

Normalized residue in $N\pi \to N(1710) \to \Lambda K$

MODULUS	PHASE (°)	DOCUMENT ID		TECN	COMMENT
0.16±0.05	−160 ± 25	ANISOVICH	17A	DPWA	Multichannel
$0.12^{+0.24}_{-0.12}$	−119 ± 83	[1] ANISOVICH	17A	L+P	γp, $\pi^- p \to K\Lambda$
• • • We do not use the following data for averages, fits, limits, etc. • • •					
0.12	−32	ROENCHEN	15A	DPWA	Multichannel
0.17±0.06	−110 ± 20	ANISOVICH	12A	DPWA	Multichannel

[1] Statistical error only.

Normalized residue in $N\pi \to N(1710) \to \Sigma K$

MODULUS	PHASE (°)	DOCUMENT ID		TECN	COMMENT
• • • We do not use the following data for averages, fits, limits, etc. • • •					
0.004	−43	ROENCHEN	15A	DPWA	Multichannel

Normalized residue in $N\pi \to N(1710) \to N(1535)\pi$

MODULUS	PHASE (°)	DOCUMENT ID		TECN	COMMENT
0.10±0.04	140 ± 40	GUTZ	14	DPWA	Multichannel

N(1710) BREIT-WIGNER MASS

VALUE (MeV)	DOCUMENT ID		TECN	COMMENT
1680 to 1740 (≈ 1710) OUR ESTIMATE				
1648±16	[1] HUNT	19	DPWA	Multichannel
1715±20	SOKHOYAN	15A	DPWA	Multichannel
1737±17	[1] SHKLYAR	13	DPWA	Multichannel
1700±50	CUTKOSKY	80	IPWA	$\pi N \to \pi N$
1723± 9	HOEHLER	79	IPWA	$\pi N \to \pi N$
• • • We do not use the following data for averages, fits, limits, etc. • • •				
1715±20	GUTZ	14	DPWA	Multichannel
1710±20	ANISOVICH	12A	DPWA	Multichannel
1662± 7	[1] SHRESTHA	12A	DPWA	Multichannel
1729±16	[2] BATINIC	10	DPWA	$\pi N \to N\pi$, $N\eta$
1752± 3	PENNER	02C	DPWA	Multichannel
1699±65	VRANA	00	DPWA	Multichannel

[1] Statistical error only.
[2] BATINIC 10 finds evidence for a second P_{11} state with all parameters except for the phase of the pole residue very similar to the parameters we give here.

N(1710) BREIT-WIGNER WIDTH

VALUE (MeV)	DOCUMENT ID		TECN	COMMENT
80 to 200 (≈ 140) OUR ESTIMATE				
195± 46	[1] HUNT	19	DPWA	Multichannel
175± 15	SOKHOYAN	15A	DPWA	Multichannel
368±120	[1] SHKLYAR	13	DPWA	Multichannel
93± 30	CUTKOSKY	90	IPWA	$\pi N \to \pi N$
90± 30	CUTKOSKY	80	IPWA	$\pi N \to \pi N$
120± 15	HOEHLER	79	IPWA	$\pi N \to \pi N$
• • • We do not use the following data for averages, fits, limits, etc. • • •				
175± 15	GUTZ	14	DPWA	Multichannel
200± 18	ANISOVICH	12A	DPWA	Multichannel
116± 17	[1] SHRESTHA	12A	DPWA	Multichannel
180± 17	[2] BATINIC	10	DPWA	$\pi N \to N\pi$, $N\eta$
386± 59	PENNER	02C	DPWA	Multichannel
143±100	VRANA	00	DPWA	Multichannel

[1] Statistical error only.
[2] BATINIC 10 finds evidence for a second P_{11} state with all parameters except for the phase of the pole residue very similar to the parameters we give here.

N(1710) DECAY MODES

The following branching fractions are our estimates, not fits or averages.

	Mode	Fraction (Γ_i/Γ)
Γ_1	$N\pi$	5–20 %
Γ_2	$N\eta$	10–50 %
Γ_3	$N\omega$	1–5 %
Γ_4	ΛK	5–25 %
Γ_5	ΣK	seen

Downloaded from https://academic.oup.com/ptep/article/2022/8/083C01/6651666 by KIT Library user on 27 September 2022

Γ_6	$N\pi\pi$	14–48 %
Γ_7	$\Delta(1232)\pi$, P-wave	3–9 %
Γ_8	$N\rho$, $S=1/2$, P-wave	11–23 %
Γ_9	$N\sigma$	<16 %
Γ_{10}	$N(1535)\pi$	9–21 %
Γ_{11}	$p\gamma$, helicity=1/2	0.002–0.08 %
Γ_{12}	$n\gamma$, helicity=1/2	0.0–0.02%

$N(1710)$ BRANCHING RATIOS

$\Gamma(N\pi)/\Gamma_{total}$ — Γ_1/Γ

VALUE (%)	DOCUMENT ID		TECN	COMMENT
5 to 20 (≈ 10) OUR ESTIMATE				
12± 6	[1] HUNT	19	DPWA	Multichannel
5± 3	SOKHOYAN	15A	DPWA	Multichannel
2± 2	[1] SHKLYAR	13	PWA	Multichannel
20± 4	CUTKOSKY	80	IPWA	$\pi N \to \pi N$
12± 4	HOEHLER	79	IPWA	$\pi N \to \pi N$
• • • We do not use the following data for averages, fits, limits, etc. • • •				
5± 3	GUTZ	14	DPWA	Multichannel
5± 4	ANISOVICH	12A	DPWA	Multichannel
15± 4	[1] SHRESTHA	12A	DPWA	Multichannel
22±24	[2] BATINIC	10	DPWA	$\pi N \to N\pi$, $N\eta$
14± 8	PENNER	02C	DPWA	Multichannel
27±13	VRANA	00	DPWA	Multichannel

[1] Statistical error only.
[2] BATINIC 10 finds evidence for a second P_{11} state with all parameters except for the phase of the pole residue very similar to the parameters we give here.

$\Gamma(N\eta)/\Gamma_{total}$ — Γ_2/Γ

VALUE (%)	DOCUMENT ID		TECN	COMMENT
10 to 50 (≈ 30) OUR ESTIMATE				
18±10	MUELLER	20	DPWA	Multichannel
17± 8	[1] HUNT	19	DPWA	Multichannel
45± 4	[1] SHKLYAR	13	DPWA	Multichannel
17±10	ANISOVICH	12A	DPWA	Multichannel
• • • We do not use the following data for averages, fits, limits, etc. • • •				
11± 7	[1] SHRESTHA	12A	DPWA	Multichannel
6± 8	[2] BATINIC	10	DPWA	$\pi N \to N\pi$, $N\eta$
36±11	PENNER	02C	DPWA	Multichannel
6± 1	VRANA	00	DPWA	Multichannel

[1] Statistical error only.
[2] BATINIC 10 finds evidence for a second P_{11} state with all parameters except for the phase of the pole residue very similar to the parameters we give here.

$\Gamma(N\omega)/\Gamma_{total}$ — Γ_3/Γ

VALUE (%)	DOCUMENT ID		TECN	COMMENT
1 to 5 (≈ 3) OUR ESTIMATE				
2±2	DENISENKO	16	DPWA	Multichannel
3±2	[1] SHKLYAR	13	DPWA	Multichannel
• • • We do not use the following data for averages, fits, limits, etc. • • •				
13±2	PENNER	02C	DPWA	Multichannel

[1] Statistical error only.

$\Gamma(\Lambda K)/\Gamma_{total}$ — Γ_4/Γ

VALUE (%)	DOCUMENT ID		TECN	COMMENT
5 to 25 (≈ 15) OUR ESTIMATE				
1.8± 1.5	[1] HUNT	19	DPWA	Multichannel
23 ± 7	ANISOVICH	12A	DPWA	Multichannel
5 ± 3	SHKLYAR	05	DPWA	Multichannel
• • • We do not use the following data for averages, fits, limits, etc. • • •				
8 ± 4	[1] SHRESTHA	12A	DPWA	Multichannel
5 ± 2	PENNER	02C	DPWA	Multichannel
10 ±10	VRANA	00	DPWA	Multichannel

[1] Statistical error only.

$\Gamma(\Sigma K)/\Gamma_{total}$ — Γ_5/Γ

VALUE (%)	DOCUMENT ID		TECN	COMMENT
• • • We do not use the following data for averages, fits, limits, etc. • • •				
7±7	PENNER	02C	DPWA	Multichannel

$\Gamma(\Delta(1232)\pi, P\text{-wave})/\Gamma_{total}$ — Γ_7/Γ

VALUE (%)	DOCUMENT ID		TECN	COMMENT
3–9 % OUR ESTIMATE				
28±9	[1] HUNT	19	DPWA	Multichannel
• • • We do not use the following data for averages, fits, limits, etc. • • •				
6±3	[1] SHRESTHA	12A	DPWA	Multichannel
39±8	VRANA	00	DPWA	Multichannel

[1] Statistical error only.

$\Gamma(N\rho, S=1/2, P\text{-wave})/\Gamma_{total}$ — Γ_8/Γ

VALUE (%)	DOCUMENT ID		TECN	COMMENT
11–23 % OUR ESTIMATE				
17±9	[1] HUNT	19	DPWA	Multichannel
• • • We do not use the following data for averages, fits, limits, etc. • • •				
17±6	[1] SHRESTHA	12A	DPWA	Multichannel
17±1	VRANA	00	DPWA	Multichannel

[1] Statistical error only.

$\Gamma(N\sigma)/\Gamma_{total}$ — Γ_9/Γ

VALUE (%)	DOCUMENT ID		TECN	COMMENT
<16 % OUR ESTIMATE				
<16	[1] HUNT	19	DPWA	Multichannel

[1] Statistical error only.

$\Gamma(N(1535)\pi)/\Gamma_{total}$ — Γ_{10}/Γ

VALUE (%)	DOCUMENT ID		TECN	COMMENT
15±6	GUTZ	14	DPWA	Multichannel

$N(1710)$ PHOTON DECAY AMPLITUDES AT THE POLE

$N(1710) \to p\gamma$, helicity-1/2 amplitude $A_{1/2}$

MODULUS ($GeV^{-1/2}$)	PHASE (°)	DOCUMENT ID		TECN	COMMENT
$0.028^{+0.009}_{-0.002}$	103^{+20}_{-6}	ROENCHEN	14	DPWA	
• • • We do not use the following data for averages, fits, limits, etc. • • •					
0.020	−83	ROENCHEN	15A	DPWA	Multichannel

$N(1710)$ BREIT-WIGNER PHOTON DECAY AMPLITUDES

$N(1710) \to p\gamma$, helicity-1/2 amplitude $A_{1/2}$

VALUE ($GeV^{-1/2}$)	DOCUMENT ID		TECN	COMMENT
0.014±0.008	[1] HUNT	19	DPWA	Multichannel
0.050±0.010	SOKHOYAN	15A	DPWA	Multichannel
−0.050±0.001	[1] SHKLYAR	13	DPWA	Multichannel
• • • We do not use the following data for averages, fits, limits, etc. • • •				
0.05 ±0.01	GUTZ	14	DPWA	Multichannel
0.052±0.015	ANISOVICH	12A	DPWA	Multichannel
−0.008±0.003	[1] SHRESTHA	12A	DPWA	Multichannel
0.044	PENNER	02D	DPWA	Multichannel

[1] Statistical error only.

$N(1710) \to n\gamma$, helicity-1/2 amplitude $A_{1/2}$

VALUE ($GeV^{-1/2}$)	DOCUMENT ID		TECN	COMMENT
0.0053±0.0003	[1] HUNT	19	DPWA	Multichannel
−0.040 ±0.020	ANISOVICH	13B	DPWA	Multichannel
• • • We do not use the following data for averages, fits, limits, etc. • • •				
0.017 ±0.003	[1] SHRESTHA	12A	DPWA	Multichannel
−0.024	PENNER	02D	DPWA	Multichannel

[1] Statistical error only.

$N(1710)$ REFERENCES

For early references, see Physics Letters **111B** 1 (1982).

MUELLER	20	PL B803 135323	J. Mueller *et al.*	(CBELSA/TAPS Collab.)
HUNT	19	PR C99 055205	B.C. Hunt, D.M. Manley	
ANISOVICH	17A	PRL 119 062004	A.V. Anisovich *et al.*	
DENISENKO	16	PL B755 97	I. Denisenko *et al.*	
ROENCHEN	15A	EPJ A51 70	D. Roenchen *et al.*	
SOKHOYAN	15A	EPJ A51 95	V. Sokhoyan *et al.*	(CBELSA/TAPS Collab.)
GUTZ	14	EPJ A50 74	E. Gutz *et al.*	(CBELSA/TAPS Collab.)
PDG	14	CP C38 070001	K. Olive *et al.*	(PDG Collab.)
ROENCHEN	14	EPJ A50 101	D. Roenchen *et al.*	
Also		EPJ A51 63 (errat.)	D. Roenchen *et al.*	
SVARC	14	PR C89 045205	A. Svarc *et al.*	(RBI Zagreb, UNI Tuzla)
ANISOVICH	13B	EPJ A49 67	A.V. Anisovich *et al.*	
SHKLYAR	13	PR C87 015201	V. Shklyar, H. Lenske, U. Mosel	(GIES)
ANISOVICH	12A	EPJ A48 15	A.V. Anisovich *et al.*	(BONN, PNPI)
SHRESTHA	12A	PR C86 055203	M. Shrestha, D.M. Manley	(KSU)
BATINIC	10	PR C82 038203	M. Batinic *et al.*	(ZAGR)
SHKLYAR	05	PR C72 015210	V. Shklyar, H. Lenske, U. Mosel	(GIES)
PENNER	02C	PR C66 055211	G. Penner, U. Mosel	(GIES)
PENNER	02D	PR C66 055212	G. Penner, U. Mosel	(GIES)
VRANA	00	PRPL 328 181	T.P. Vrana, S.A. Dytman, T.-S.H. Lee	(PITT, ANL)
HOEHLER	93	πN Newsletter 9 1	G. Hohler	(KARL)
CUTKOSKY	90	PR D42 235	R.E. Cutkosky, S. Wang	(CMU)
CUTKOSKY	80	Toronto Conf. 19	R.E. Cutkosky *et al.*	(CMU, LBL) IJP
Also		PR D20 2839	R.E. Cutkosky *et al.*	(CMU, LBL) IJP
HOEHLER	79	PDAT 12-1	G. Hohler *et al.*	(KARLT) IJP
Also		Toronto Conf. 3	R. Koch	(KARLT) IJP

$N(1720)\ 3/2^+$

$I(J^P) = \frac{1}{2}(\frac{3}{2}^+)$ Status: ****

Older and obsolete values are listed and referenced in the 2014 edition, Chinese Physics **C38** 070001 (2014).

$N(1720)$ POLE POSITION

REAL PART

VALUE (MeV)	DOCUMENT ID		TECN	COMMENT
1660 to 1690 (≈ 1675) OUR ESTIMATE				
1670±25	SOKHOYAN	15A	DPWA	Multichannel
1677± 4±1	[1] SVARC	14	L+P	$\pi N \to \pi N$
1680±30	CUTKOSKY	80	IPWA	$\pi N \to \pi N$

Downloaded from https://academic.oup.com/ptep/article/2022/8/083C01/6651666 by KIT Library user on 27 September 2022

• • • We do not use the following data for averages, fits, limits, etc. • • •

1654	HUNT	19	DPWA	Multichannel
1710	ROENCHEN	15A	DPWA	Multichannel
1670	SHKLYAR	13	DPWA	Multichannel
1660±30	ANISOVICH	12A	DPWA	Multichannel
1691±23	BATINIC	10	DPWA	$\pi N \to N\pi$, $N\eta$
1666	ARNDT	06	DPWA	$\pi N \to \pi N$, ηN
1692	VRANA	00	DPWA	Multichannel
1686	HOEHLER	93	SPED	$\pi N \to \pi N$

[1] Fit to the amplitudes of HOEHLER 79.

−2×IMAGINARY PART

VALUE (MeV)	DOCUMENT ID		TECN	COMMENT
150 to 400 (≈ 250) OUR ESTIMATE				
430±100	SOKHOYAN	15A	DPWA	Multichannel
184± 8±1	[1] SVARC	14	L+P	$\pi N \to \pi N$
120± 40	CUTKOSKY	80	IPWA	$\pi N \to \pi N$
• • • We do not use the following data for averages, fits, limits, etc. • • •				
100	HUNT	19	DPWA	Multichannel
219	ROENCHEN	15A	DPWA	Multichannel
118	SHKLYAR	13	DPWA	Multichannel
450±100	ANISOVICH	12A	DPWA	Multichannel
233± 23	BATINIC	10	DPWA	$\pi N \to N\pi$, $N\eta$
355	ARNDT	06	DPWA	$\pi N \to \pi N$, ηN
94	VRANA	00	DPWA	Multichannel
187	HOEHLER	93	SPED	$\pi N \to \pi N$

[1] Fit to the amplitudes of HOEHLER 79.

$N(1720)$ ELASTIC POLE RESIDUE

MODULUS $|r|$

VALUE (MeV)	DOCUMENT ID		TECN	COMMENT
10 to 25 (≈ 15) OUR ESTIMATE				
26 ±10	SOKHOYAN	15A	DPWA	Multichannel
13 ± 1	[1] SVARC	14	L+P	$\pi N \to \pi N$
8 ± 2	CUTKOSKY	80	IPWA	$\pi N \to \pi N$
• • • We do not use the following data for averages, fits, limits, etc. • • •				
4.2	ROENCHEN	15A	DPWA	Multichannel
12	SHKLYAR	13	DPWA	Multichannel
22 ± 8	ANISOVICH	12A	DPWA	Multichannel
20	BATINIC	10	DPWA	$\pi N \to N\pi$, $N\eta$
25	ARNDT	06	DPWA	$\pi N \to \pi N$, ηN
15	HOEHLER	93	SPED	$\pi N \to \pi N$

[1] Fit to the amplitudes of HOEHLER 79.

PHASE θ

VALUE (°)	DOCUMENT ID		TECN	COMMENT
−160 to −100 (≈ −130) OUR ESTIMATE				
−100±25	SOKHOYAN	15A	DPWA	Multichannel
−115± 3±2	[1] SVARC	14	L+P	$\pi N \to \pi N$
−160±30	CUTKOSKY	80	IPWA	$\pi N \to \pi N$
• • • We do not use the following data for averages, fits, limits, etc. • • •				
− 47	ROENCHEN	15A	DPWA	Multichannel
− 45	SHKLYAR	13	DPWA	Multichannel
−115±30	ANISOVICH	12A	DPWA	Multichannel
−109	BATINIC	10	DPWA	$\pi N \to N\pi$, $N\eta$
− 94	ARNDT	06	DPWA	$\pi N \to \pi N$, ηN

[1] Fit to the amplitudes of HOEHLER 79.

$N(1720)$ INELASTIC POLE RESIDUE

The "normalized residue" is the residue divided by $\Gamma_{pole}/2$.

Normalized residue in $N\pi \to N(1720) \to N\eta$

MODULUS	PHASE (°)	DOCUMENT ID		TECN	COMMENT
0.03 ±0.02		ANISOVICH	12A	DPWA	Multichannel
• • • We do not use the following data for averages, fits, limits, etc. • • •					
0.007	106	ROENCHEN	15A	DPWA	Multichannel

Normalized residue in $N\pi \to N(1720) \to \Lambda K$

MODULUS	PHASE (°)	DOCUMENT ID		TECN	COMMENT
0.06 ±0.04	−150 ± 45	ANISOVICH	12A	DPWA	Multichannel
• • • We do not use the following data for averages, fits, limits, etc. • • •					
0.011	−70	ROENCHEN	15A	DPWA	Multichannel

Normalized residue in $N\pi \to N(1720) \to \Sigma K$

MODULUS	PHASE (°)	DOCUMENT ID		TECN	COMMENT
• • • We do not use the following data for averages, fits, limits, etc. • • •					
0.002	79	ROENCHEN	15A	DPWA	Multichannel

Normalized residue in $N\pi \to N(1720) \to \Delta\pi$, P-wave

MODULUS	PHASE (°)	DOCUMENT ID		TECN	COMMENT
0.28±0.09	95 ± 30	SOKHOYAN	15A	DPWA	Multichannel
• • • We do not use the following data for averages, fits, limits, etc. • • •					
0.29±0.08	80 ± 40	ANISOVICH	12A	DPWA	Multichannel

Normalized residue in $N\pi \to N(1720) \to \Delta\pi$, F-wave

MODULUS	PHASE (°)	DOCUMENT ID		TECN	COMMENT
0.07±0.05		SOKHOYAN	15A	DPWA	Multichannel
• • • We do not use the following data for averages, fits, limits, etc. • • •					
0.03±0.03		ANISOVICH	12A	DPWA	Multichannel

Normalized residue in $N\pi \to N(1720) \to N\sigma$

MODULUS	PHASE (°)	DOCUMENT ID		TECN	COMMENT
0.08±0.04	−110 ± 35	SOKHOYAN	15A	DPWA	Multichannel

Normalized residue in $N\pi \to N(1720) \to N(1520)\pi$, S-wave

MODULUS	PHASE (°)	DOCUMENT ID		TECN	COMMENT
0.05±0.04	undefined	SOKHOYAN	15A	DPWA	Multichannel

$N(1720)$ BREIT-WIGNER MASS

VALUE (MeV)	DOCUMENT ID		TECN	COMMENT
1680 to 1750 (≈ 1720) OUR ESTIMATE				
1745 ± 6	GOLOVATCH	19	DPWA	$\gamma p \to \pi^+\pi^- p$
1711 ± 4	[1] HUNT	19	DPWA	Multichannel
1690 ± 30	SOKHOYAN	15A	DPWA	Multichannel
1700 ± 10	[1] SHKLYAR	13	DPWA	Multichannel
1763.8± 4.6	ARNDT	06	DPWA	$\pi N \to \pi N$, ηN
1700 ± 50	CUTKOSKY	80	IPWA	$\pi N \to \pi N$
1710 ± 20	HOEHLER	79	IPWA	$\pi N \to \pi N$
• • • We do not use the following data for averages, fits, limits, etc. • • •				
1748 ± 5	[2] MOKEEV	20	DPWA	$\gamma p \to \pi^+\pi^- p$
1725 ± 10	[3] MOKEEV	20	DPWA	$\gamma p \to \pi^+\pi^- p$
1690^{+70}_{-35}	ANISOVICH	12A	DPWA	Multichannel
1720 ± 5	[1] SHRESTHA	12A	DPWA	Multichannel
1720 ± 18	BATINIC	10	DPWA	$\pi N \to N\pi$, $N\eta$
1705 ± 10	PENNER	02C	DPWA	Multichannel
1716 ±112	VRANA	00	DPWA	Multichannel

[1] Statistical error only.
[2] State a) of two states seen by the CLAS collaboration.
[3] State b) of two states seen by the CLAS collaboration.

$N(1720)$ BREIT-WIGNER WIDTH

VALUE (MeV)	DOCUMENT ID		TECN	COMMENT
150 to 400 (≈ 250) OUR ESTIMATE				
116± 27	GOLOVATCH	19	DPWA	$\gamma p \to \pi^+\pi^- p$
229± 22	[1] HUNT	19	DPWA	Multichannel
420± 80	SOKHOYAN	15A	DPWA	Multichannel
152± 2	[1] SHKLYAR	13	DPWA	Multichannel
210± 22	ARNDT	06	DPWA	$\pi N \to \pi N$, ηN
125± 70	CUTKOSKY	80	IPWA	$\pi N \to \pi N$
190± 30	HOEHLER	79	IPWA	$\pi N \to \pi N$
• • • We do not use the following data for averages, fits, limits, etc. • • •				
114± 6	[2] MOKEEV	20	DPWA	$\gamma p \to \pi^+\pi^- p$
120± 6	[3] MOKEEV	20	DPWA	$\gamma p \to \pi^+\pi^- p$
420±100	ANISOVICH	12A	DPWA	Multichannel
200± 20	[1] SHRESTHA	12A	DPWA	Multichannel
244± 28	BATINIC	10	DPWA	$\pi N \to N\pi$, $N\eta$
237± 73	PENNER	02C	DPWA	Multichannel
121± 39	VRANA	00	DPWA	Multichannel

[1] Statistical error only.
[2] State a) of two states seen by the CLAS collaboration.
[3] State b) of two states seen by the CLAS collaboration.

$N(1720)$ DECAY MODES

The following branching fractions are our estimates, not fits or averages.

	Mode	Fraction (Γ_i/Γ)
Γ_1	$N\pi$	8–14 %
Γ_2	$N\eta$	1–5 %
Γ_3	$N\omega$	12–40 %
Γ_4	ΛK	4–19 %
Γ_5	$N\pi\pi$	>50 %
Γ_6	$\Delta(1232)\pi$	47–89 %
Γ_7	$\Delta(1232)\pi$, P-wave	47–77 %
Γ_8	$\Delta(1232)\pi$, F-wave	<12 %
Γ_9	$N\rho$	
Γ_{10}	$N\rho$, S=1/2, P-wave	1–2 %
Γ_{11}	$N\sigma$	2–14 %
Γ_{12}	$N(1440)\pi$	<2 %
Γ_{13}	$N(1520)\pi$, S-wave	1–5 %
Γ_{14}	$p\gamma$	0.05–0.25 %
Γ_{15}	$p\gamma$, helicity=1/2	0.05–0.15 %
Γ_{16}	$p\gamma$, helicity=3/2	0.002–0.16 %

Downloaded from https://academic.oup.com/ptep/article/2022/8/083C01/6651666 by KIT Library user on 27 September 2022

Γ_{17}	$n\gamma$	0.0–0.016 %
Γ_{18}	$n\gamma$, helicity=1/2	0.0–0.01 %
Γ_{19}	$n\gamma$, helicity=3/2	0.0–0.015 %

$N(1720)$ BRANCHING RATIOS

$\Gamma(N\pi)/\Gamma_{total}$ — Γ_1/Γ

VALUE (%)	DOCUMENT ID		TECN	COMMENT
8 to 14 (≈ 11) OUR ESTIMATE				
18 ±2	[1] HUNT	19	DPWA	Multichannel
11 ±4	SOKHOYAN	15A	DPWA	Multichannel
17 ±2	[1] SHKLYAR	13	DPWA	Multichannel
9.4±0.5	ARNDT	06	DPWA	$\pi N \to \pi N, \eta N$
10 ±4	CUTKOSKY	80	IPWA	$\pi N \to \pi N$
14 ±3	HOEHLER	79	IPWA	$\pi N \to \pi N$
• • • We do not use the following data for averages, fits, limits, etc. • • •				
10 ±5	ANISOVICH	12A	DPWA	Multichannel
13.6±0.6	[1] SHRESTHA	12A	DPWA	Multichannel
18 ±3	BATINIC	10	DPWA	$\pi N \to N\pi, N\eta$
17 ±2	PENNER	02C	DPWA	Multichannel
5 ±5	VRANA	00	DPWA	Multichannel

[1] Statistical error only.

$\Gamma(N\eta)/\Gamma_{total}$ — Γ_2/Γ

VALUE (%)	DOCUMENT ID		TECN	COMMENT
1 to 5 (≈ 3) OUR ESTIMATE				
3 ±2	MUELLER	20	DPWA	Multichannel
3.8±0.5	[1] HUNT	19	DPWA	Multichannel
< 1	SHKLYAR	13	DPWA	Multichannel
3 ±2	ANISOVICH	12A	DPWA	Multichannel
• • • We do not use the following data for averages, fits, limits, etc. • • •				
< 1	[1] SHRESTHA	12A	DPWA	Multichannel
0 ±1	BATINIC	10	DPWA	$\pi N \to N\pi, N\eta$
10 ±7	THOMA	08	DPWA	Multichannel
0.2±0.2	PENNER	02C	DPWA	Multichannel
4 ±1	VRANA	00	DPWA	Multichannel

[1] Statistical error only.

$\Gamma(N\omega)/\Gamma_{total}$ — Γ_3/Γ

VALUE (%)	DOCUMENT ID		TECN	COMMENT
26±14	DENISENKO	16	DPWA	Multichannel

$\Gamma(\Lambda K)/\Gamma_{total}$ — Γ_4/Γ

VALUE (%)	DOCUMENT ID		TECN	COMMENT
4–19 % OUR ESTIMATE				
16 ±3	[1] HUNT	19	DPWA	Multichannel
4.3±0.4	SHKLYAR	05	DPWA	Multichannel
• • • We do not use the following data for averages, fits, limits, etc. • • •				
2.8±0.4	[1] SHRESTHA	12A	DPWA	Multichannel
12 ±9	THOMA	08	DPWA	Multichannel
9 ±3	PENNER	02C	DPWA	Multichannel

[1] Statistical error only.

$\Gamma(N\pi\pi)/\Gamma_{total}$ — Γ_5/Γ

VALUE (%)	DOCUMENT ID		TECN	COMMENT
>50 % OUR ESTIMATE				
84±16	GOLOVATCH	19	DPWA	$\gamma p \to \pi^+\pi^- p$

$\Gamma(\Delta(1232)\pi)/\Gamma_{total}$ — Γ_6/Γ

VALUE (%)	DOCUMENT ID		TECN	COMMENT
• • • We do not use the following data for averages, fits, limits, etc. • • •				
45±8	[1] MOKEEV	20	DPWA	$\gamma p \to \pi^+\pi^- p$
54±8	[2] MOKEEV	20	DPWA	$\gamma p \to \pi^+\pi^- p$

[1] State a) of two states seen by the CLAS collaboration.
[2] State b) of two states seen by the CLAS collaboration.

$\Gamma(\Delta(1232)\pi, P\text{-wave})/\Gamma_{total}$ — Γ_7/Γ

VALUE (%)	DOCUMENT ID		TECN	COMMENT
62±15	SOKHOYAN	15A	DPWA	Multichannel
• • • We do not use the following data for averages, fits, limits, etc. • • •				
75±15	ANISOVICH	12A	DPWA	Multichannel

$\Gamma(\Delta(1232)\pi, F\text{-wave})/\Gamma_{total}$ — Γ_8/Γ

VALUE (%)	DOCUMENT ID		TECN	COMMENT
6±6	SOKHOYAN	15A	DPWA	Multichannel

$\Gamma(N\rho)/\Gamma_{total}$ — Γ_9/Γ

VALUE (%)	DOCUMENT ID		TECN	COMMENT
• • • We do not use the following data for averages, fits, limits, etc. • • •				
38±8	[1] MOKEEV	20	DPWA	$\gamma p \to \pi^+\pi^- p$
7±3	[2] MOKEEV	20	DPWA	$\gamma p \to \pi^+\pi^- p$

[1] State a) of two states seen by the CLAS collaboration.
[2] State b) of two states seen by the CLAS collaboration.

$\Gamma(N\rho, S{=}1/2, P\text{-wave})/\Gamma_{total}$ — Γ_{10}/Γ

VALUE (%)	DOCUMENT ID		TECN	COMMENT
1.4±0.5	[1] SHRESTHA	12A	DPWA	Multichannel
• • • We do not use the following data for averages, fits, limits, etc. • • •				
91 ±1	VRANA	00	DPWA	Multichannel

[1] Statistical error only.

$\Gamma(N\sigma)/\Gamma_{total}$ — Γ_{11}/Γ

VALUE (%)	DOCUMENT ID		TECN	COMMENT
8±6	SOKHOYAN	15A	DPWA	Multichannel

$\Gamma(N(1440)\pi)/\Gamma_{total}$ — Γ_{12}/Γ

VALUE (%)	DOCUMENT ID		TECN	COMMENT
<2	SOKHOYAN	15A	DPWA	Multichannel

$\Gamma(N(1520)\pi, S\text{-wave})/\Gamma_{total}$ — Γ_{13}/Γ

VALUE (%)	DOCUMENT ID		TECN	COMMENT
3±2	SOKHOYAN	15A	DPWA	Multichannel

$N(1720)$ PHOTON DECAY AMPLITUDES AT THE POLE

$N(1720) \to p\gamma$, helicity-1/2 amplitude $A_{1/2}$

MODULUS ($GeV^{-1/2}$)	PHASE (°)	DOCUMENT ID		TECN	COMMENT
0.115±0.045	0 ± 35	SOKHOYAN	15A	DPWA	Multichannel
$0.051^{+0.005}_{-0.004}$	57^{+9}_{-4}	ROENCHEN	14	DPWA	
• • • We do not use the following data for averages, fits, limits, etc. • • •					
0.039	5.3	ROENCHEN	15A	DPWA	Multichannel

$N(1720) \to p\gamma$, helicity-3/2 amplitude $A_{3/2}$

MODULUS ($GeV^{-1/2}$)	PHASE (°)	DOCUMENT ID		TECN	COMMENT
0.140±0.040	65 ± 35	SOKHOYAN	15A	DPWA	Multichannel
$0.014^{+0.009}_{-0.003}$	102^{+29}_{-59}	ROENCHEN	14	DPWA	
• • • We do not use the following data for averages, fits, limits, etc. • • •					
0.032	66	ROENCHEN	15A	DPWA	Multichannel

$N(1720)$ BREIT-WIGNER PHOTON DECAY AMPLITUDES

$N(1720) \to p\gamma$, helicity-1/2 amplitude $A_{1/2}$

VALUE ($GeV^{-1/2}$)	DOCUMENT ID		TECN	COMMENT
0.080 to 0.120 (≈ 0.100) OUR ESTIMATE				
0.0809±0.0115	GOLOVATCH	19	DPWA	$\gamma p \to \pi^+\pi^- p$
0.068 ±0.004	[1] HUNT	19	DPWA	Multichannel
0.115 ±0.045	SOKHOYAN	15A	DPWA	Multichannel
−0.065 ±0.002	[1] SHKLYAR	13	DPWA	Multichannel
0.095 ±0.002	WORKMAN	12A	DPWA	$\gamma N \to N\pi$
• • • We do not use the following data for averages, fits, limits, etc. • • •				
0.110 ±0.045	ANISOVICH	12A	DPWA	Multichannel
0.057 ±0.003	[1] SHRESTHA	12A	DPWA	Multichannel
0.073	DRECHSEL	07	DPWA	$\gamma N \to \pi N$
0.097 ±0.003	DUGGER	07	DPWA	$\gamma N \to \pi N$
−0.053	PENNER	02D	DPWA	Multichannel

[1] Statistical error only.

$N(1720) \to p\gamma$, helicity-3/2 amplitude $A_{3/2}$

VALUE ($GeV^{-1/2}$)	DOCUMENT ID		TECN	COMMENT
−0.034±0.0076	GOLOVATCH	19	DPWA	$\gamma p \to \pi^+\pi^- p$
0.028±0.003	[1] HUNT	19	DPWA	Multichannel
0.135±0.040	SOKHOYAN	15A	DPWA	Multichannel
0.035±0.002	[1] SHKLYAR	13	DPWA	Multichannel
−0.048±0.002	WORKMAN	12A	DPWA	$\gamma N \to N\pi$
• • • We do not use the following data for averages, fits, limits, etc. • • •				
0.150±0.030	ANISOVICH	12A	DPWA	Multichannel
−0.019±0.002	[1] SHRESTHA	12A	DPWA	Multichannel
−0.011	DRECHSEL	07	DPWA	$\gamma N \to \pi N$
−0.039±0.003	DUGGER	07	DPWA	$\gamma N \to \pi N$
0.027	PENNER	02D	DPWA	Multichannel

[1] Statistical error only.

$N(1720) \to n\gamma$, helicity-1/2 amplitude $A_{1/2}$

VALUE ($GeV^{-1/2}$)	DOCUMENT ID		TECN	COMMENT
−0.064±0.006	[1] HUNT	19	DPWA	Multichannel
−0.080±0.050	ANISOVICH	13B	DPWA	Multichannel
• • • We do not use the following data for averages, fits, limits, etc. • • •				
−0.002±0.001	[1] SHRESTHA	12A	DPWA	Multichannel
−0.003	DRECHSEL	07	DPWA	$\gamma N \to \pi N$
−0.004	PENNER	02D	DPWA	Multichannel

[1] Statistical error only.

$N(1720) \to n\gamma$, helicity-3/2 amplitude $A_{3/2}$

VALUE ($GeV^{-1/2}$)	DOCUMENT ID		TECN	COMMENT
−0.004±0.006	[1] HUNT	19	DPWA	Multichannel
−0.140±0.065	ANISOVICH	13B	DPWA	Multichannel

Downloaded from https://academic.oup.com/ptep/article/2022/8/083C01/6651666 by KIT Library user on 27 September 2022

• • • We do not use the following data for averages, fits, limits, etc. • • •

−0.001±0.002	[1] SHRESTHA	12A	DPWA	Multichannel
−0.031	DRECHSEL	07	DPWA	$\gamma N \to \pi N$
0.003	PENNER	02D	DPWA	Multichannel

[1] Statistical error only.

$N(1720)$ REFERENCES

For early references, see Physics Letters **111B** 1 (1982).

MOKEEV	20	PL B805 135457	V.I. Mokeev *et al.*	(CLAS Collab.)
MUELLER	20	PL B803 135323	J. Mueller *et al.*	(CBELSA/TAPS Collab.)
GOLOVATCH	19	PL B788 371	E. Golovatch *et al.*	(CLAS Collab.)
HUNT	19	PR C99 055205	B.C. Hunt, D.M. Manley	
DENISENKO	16	PL B755 97	I. Denisenko *et al.*	
ROENCHEN	15A	EPJ A51 70	D. Roenchen *et al.*	
SOKHOYAN	15A	EPJ A51 95	V. Sokhoyan *et al.*	(CBELSA/TAPS Collab.)
PDG	14	CP C38 070001	K. Olive *et al.*	(PDG Collab.)
ROENCHEN	14	EPJ A50 101	D. Roenchen *et al.*	
Also		EPJ A51 63 (errat.)	D. Roenchen *et al.*	
SVARC	14	PR C89 045205	A. Svarc *et al.*	(RBI Zagreb, UNI Tuzla)
ANISOVICH	13B	EPJ A49 67	A.V. Anisovich *et al.*	
SHKLYAR	13	PR C87 015201	V. Shklyar, H. Lenske, U. Mosel	(GIES)
ANISOVICH	12A	EPJ A48 15	A.V. Anisovich *et al.*	(BONN, PNPI)
SHRESTHA	12A	PR C86 055203	M. Shrestha, D.M. Manley	(KSU)
WORKMAN	12A	PR C86 015202	R. Workman *et al.*	(GWU)
BATINIC	10	PR C82 038203	M. Batinic *et al.*	(ZAGR)
THOMA	08	PL B659 87	U. Thoma *et al.*	(CB-ELSA Collab.)
DRECHSEL	07	EPJ A34 69	D. Drechsel, S.S. Kamalov, L. Tiator	(MAINZ, JINR)
DUGGER	07	PR C76 025211	M. Dugger *et al.*	(JLab CLAS Collab.)
ARNDT	06	PR C74 045205	R.A. Arndt *et al.*	(GWU)
SHKLYAR	05	PR C72 015210	V. Shklyar, H. Lenske, U. Mosel	(GIES)
PENNER	02C	PR C66 055211	G. Penner, U. Mosel	(GIES)
PENNER	02D	PR C66 055212	G. Penner, U. Mosel	(GIES)
VRANA	00	PRPL 328 181	T.P. Vrana, S.A. Dytman, T.-S.H. Lee	(PITT, ANL)
HOEHLER	93	πN Newsletter 9 1	G. Hohler	(KARL)
CUTKOSKY	80	Toronto Conf. 19	R.E. Cutkosky *et al.*	(CMU, LBL) IJP
Also		PR D20 2839	R.E. Cutkosky *et al.*	(CMU, LBL) IJP
HOEHLER	79	PDAT 12-1	G. Hohler *et al.*	(KARLT) IJP
Also		Toronto Conf. 3	R. Koch	(KARLT) IJP

$N(1860)\ 5/2^+$

$I(J^P) = \frac{1}{2}(\frac{5}{2}^+)$ Status: **

OMITTED FROM SUMMARY TABLE

Before the 2012 *Review*, all the evidence for a $J^P = 5/2^+$ state with a mass above 1800 MeV was filed under a two-star $N(2000)$. There is now some evidence from ANISOVICH 12A for two $5/2^+$ states in this region, so we have split the older data (according to mass) between two two-star $5/2^+$ states, an $N(1860)$ and an $N(2000)$.

$N(1860)$ POLE POSITION

REAL PART

VALUE (MeV)	DOCUMENT ID		TECN	COMMENT
1834± 19±6	[1] SVARC	14	L+P	$\pi N \to \pi N$
1830^{+120}_{-60}	ANISOVICH	12A	DPWA	Multichannel
• • • We do not use the following data for averages, fits, limits, etc. • • •				
1871	HUNT	19	DPWA	Multichannel
1807	ARNDT	06	DPWA	$\pi N \to \pi N, \eta N$

[1] Fit to the amplitudes of HOEHLER 79.

−2×IMAGINARY PART

VALUE (MeV)	DOCUMENT ID		TECN	COMMENT
122± 34±7	[2] SVARC	14	L+P	$\pi N \to \pi N$
250^{+150}_{-50}	ANISOVICH	12A	DPWA	Multichannel
• • • We do not use the following data for averages, fits, limits, etc. • • •				
337	HUNT	19	DPWA	Multichannel
109	ARNDT	06	DPWA	$\pi N \to \pi N, \eta N$

[2] Fit to the amplitudes of HOEHLER 79.

$N(1860)$ ELASTIC POLE RESIDUE

MODULUS $|r|$

VALUE (MeV)	DOCUMENT ID		TECN	COMMENT
4± 1±1	[3] SVARC	14	L+P	$\pi N \to \pi N$
50±20	ANISOVICH	12A	DPWA	Multichannel
• • • We do not use the following data for averages, fits, limits, etc. • • •				
60	ARNDT	06	DPWA	$\pi N \to \pi N, \eta N$

[3] Fit to the amplitudes of HOEHLER 79.

PHASE θ

VALUE (°)	DOCUMENT ID		TECN	COMMENT
−39±18±9	[4] SVARC	14	L+P	$\pi N \to \pi N$
−80±40	ANISOVICH	12A	DPWA	Multichannel
• • • We do not use the following data for averages, fits, limits, etc. • • •				
−67	ARNDT	06	DPWA	$\pi N \to \pi N, \eta N$

[4] Fit to the amplitudes of HOEHLER 79.

$N(1860)$ BREIT-WIGNER MASS

VALUE (MeV)	DOCUMENT ID		TECN	COMMENT
1928 ± 21	[5] HUNT	19	DPWA	Multichannel
1860^{+120}_{-60}	ANISOVICH	12A	DPWA	Multichannel
1882 ± 10	HOEHLER	79	IPWA	$\pi N \to \pi N$
• • • We do not use the following data for averages, fits, limits, etc. • • •				
1900 ± 7	[5] SHRESTHA	12A	DPWA	Multichannel
1817.7	ARNDT	06	DPWA	$\pi N \to \pi N, \eta N$

[5] Statistical error only.

$N(1860)$ BREIT-WIGNER WIDTH

VALUE (MeV)	DOCUMENT ID		TECN	COMMENT
376 ± 58	[6] HUNT	19	DPWA	Multichannel
270^{+140}_{-50}	ANISOVICH	12A	DPWA	Multichannel
95 ± 20	HOEHLER	79	IPWA	$\pi N \to \pi N$
• • • We do not use the following data for averages, fits, limits, etc. • • •				
219 ± 23	[6] SHRESTHA	12A	DPWA	Multichannel
117.6	ARNDT	06	DPWA	$\pi N \to \pi N, \eta N$

[6] Statistical error only.

$N(1860)$ DECAY MODES

	Mode	Fraction (Γ_i/Γ)
Γ_1	$N\pi$	4–20 %
Γ_2	$N\eta$	0–6 %
Γ_3	ΛK	<0.01 %
Γ_4	$N\pi\pi$	>61 %
Γ_5	$\Delta\pi$	20–54 %
Γ_6	$\Delta\pi$, P-wave	4–16 %
Γ_7	$\Delta\pi$, F-wave	16–38 %
Γ_8	$N\rho$	<8.6 %
Γ_9	$N\rho$, S=3/2 , P-wave	<8.5 %
Γ_{10}	$N\rho$, S=3/2 , F-wave	<0.1 %
Γ_{11}	$N\sigma$	41–61 %
Γ_{12}	$p\gamma$	
Γ_{13}	$p\gamma$, helicity=1/2	seen
Γ_{14}	$p\gamma$, helicity=3/2	seen
Γ_{15}	$n\gamma$	0.0017–0.062 %
Γ_{16}	$n\gamma$, helicity=1/2	0.0003–0.019 %
Γ_{17}	$n\gamma$, helicity=3/2	0.0014–0.043 %

$N(1860)$ BRANCHING RATIOS

$\Gamma(N\pi)/\Gamma_{total}$ — Γ_1/Γ

VALUE (%)	DOCUMENT ID		TECN	COMMENT
4–20 % OUR ESTIMATE				
8.0±0.1	[7] HUNT	19	DPWA	Multichannel
20 ±6	ANISOVICH	12A	DPWA	Multichannel
4 ±2	HOEHLER	79	IPWA	$\pi N \to \pi N$
• • • We do not use the following data for averages, fits, limits, etc. • • •				
17 ±1	[7] SHRESTHA	12A	DPWA	Multichannel
12.7	ARNDT	06	DPWA	$\pi N \to \pi N, \eta N$

[7] Statistical error only.

$\Gamma(N\eta)/\Gamma_{total}$ — Γ_2/Γ

VALUE (%)	DOCUMENT ID		TECN	COMMENT
0–6 % OUR ESTIMATE				
0.11±0.09	[8] HUNT	19	DPWA	Multichannel
• • • We do not use the following data for averages, fits, limits, etc. • • •				
4 ±2	[8] SHRESTHA	12A	DPWA	Multichannel

[8] Statistical error only.

$\Gamma(\Lambda K)/\Gamma_{total}$ — Γ_3/Γ

VALUE (%)	DOCUMENT ID		TECN	COMMENT
<0.01 % OUR ESTIMATE				
<0.01	[9] HUNT	19	DPWA	Multichannel

[9] Statistical error only.

$\Gamma(\Delta\pi, P\text{-wave})/\Gamma_{total}$ — Γ_6/Γ

VALUE (%)	DOCUMENT ID		TECN	COMMENT
4–16 % OUR ESTIMATE				
10±6	[10] HUNT	19	DPWA	Multichannel

[10] Statistical error only.

$\Gamma(\Delta\pi, F\text{-wave})/\Gamma_{total}$ — Γ_7/Γ

VALUE (%)	DOCUMENT ID		TECN	COMMENT
16–38 % OUR ESTIMATE				
27±11	[11] HUNT	19	DPWA	Multichannel

[11] Statistical error only.

Downloaded from https://academic.oup.com/ptep/article/2022/8/083C01/6651666 by KIT Library user on 27 September 2022

$\Gamma(N\rho, S{=}3/2, P\text{-wave})/\Gamma_{total}$ — Γ_9/Γ

VALUE (%)	DOCUMENT ID		TECN	COMMENT
<8.5 % OUR ESTIMATE				
<8.5	[12] HUNT	19	DPWA	Multichannel

[12] Statistical error only.

$\Gamma(N\rho, S{=}3/2, F\text{-wave})/\Gamma_{total}$ — Γ_{10}/Γ

VALUE (%)	DOCUMENT ID		TECN	COMMENT
<0.1 % OUR ESTIMATE				
<0.1	[13] HUNT	19	DPWA	Multichannel

[13] Statistical error only.

$\Gamma(N\sigma)/\Gamma_{total}$ — Γ_{11}/Γ

VALUE (%)	DOCUMENT ID		TECN	COMMENT
41–61 % OUR ESTIMATE				
51±10	[14] HUNT	19	DPWA	Multichannel
• • • We do not use the following data for averages, fits, limits, etc. • • •				
41± 6	[14] SHRESTHA	12A	DPWA	Multichannel

[14] Statistical error only.

$N(1860)$ BREIT-WIGNER PHOTON DECAY AMPLITUDES

$N(1860) \to p\gamma$, helicity-1/2 amplitude $A_{1/2}$

VALUE (GeV$^{-1/2}$)	DOCUMENT ID		TECN	COMMENT
−0.022±0.020	[15] HUNT	19	DPWA	Multichannel
• • • We do not use the following data for averages, fits, limits, etc. • • •				
−0.017±0.003	[15] SHRESTHA	12A	DPWA	Multichannel

[15] Statistical error only.

$N(1860) \to p\gamma$, helicity-3/2 amplitude $A_{3/2}$

VALUE	DOCUMENT ID		TECN	COMMENT
−0.032±0.034	[16] HUNT	19	DPWA	Multichannel
• • • We do not use the following data for averages, fits, limits, etc. • • •				
0.029±0.004	[16] SHRESTHA	12A	DPWA	Multichannel

[16] Statistical error only.

$N(1860) \to n\gamma$, helicity-1/2 amplitude $A_{1/2}$

VALUE (GeV$^{-1/2}$)	DOCUMENT ID		TECN	COMMENT
0.021±0.029	[17] HUNT	19	DPWA	Multichannel
0.021±0.013	ANISOVICH	13B	DPWA	Multichannel
• • • We do not use the following data for averages, fits, limits, etc. • • •				
0.010±0.005	[17] SHRESTHA	12A	DPWA	Multichannel

[17] Statistical error only.

$N(1860) \to n\gamma$, helicity-3/2 amplitude $A_{3/2}$

VALUE (GeV$^{-1/2}$)	DOCUMENT ID		TECN	COMMENT
0.070±0.035	[18] HUNT	19	DPWA	Multichannel
0.034±0.017	ANISOVICH	13B	DPWA	Multichannel
• • • We do not use the following data for averages, fits, limits, etc. • • •				
−0.009±0.005	[18] SHRESTHA	12A	DPWA	Multichannel

[18] Statistical error only.

$N(1860)$ REFERENCES

HUNT	19	PR C99 055205	B.C. Hunt, D.M. Manley	
SVARC	14	PR C89 045205	A. Svarc *et al.*	(RBI Zagreb, UNI Tuzla)
ANISOVICH	13B	EPJ A49 67	A.V. Anisovich *et al.*	
ANISOVICH	12A	EPJ A48 15	A.V. Anisovich *et al.*	(BONN, PNPI)
SHRESTHA	12A	PR C86 055203	M. Shrestha, D.M. Manley	(KSU)
ARNDT	06	PR C74 045205	R.A. Arndt *et al.*	(GWU)
HOEHLER	79	PDAT 12-1	G. Hohler *et al.*	(KARLT)

$N(1875)\ 3/2^-$

$I(J^P) = \frac{1}{2}(\frac{3}{2}^-)$ Status: ***

Before the 2012 *Review*, all the evidence for a $J^P = 3/2^-$ state with a mass above 1800 MeV was filed under a two-star $N(2080)$. There is now evidence from ANISOVICH 12A for two $3/2^-$ states in this region, so we have split the older data (according to mass) between a three-star $N(1875)$ and a two-star $N(2120)$.

$N(1875)$ POLE POSITION

REAL PART

VALUE (MeV)	DOCUMENT ID		TECN	COMMENT
1850 to 1950 (≈ 1900) OUR ESTIMATE				
1870± 20	SOKHOYAN	15A	DPWA	Multichannel
1880±100	CUTKOSKY	80	IPWA	$\pi N \to \pi N$ (lower m)
• • • We do not use the following data for averages, fits, limits, etc. • • •				
1993	HUNT	19	DPWA	Multichannel
1810	SHKLYAR	13	DPWA	Multichannel
1860± 25	ANISOVICH	12A	DPWA	Multichannel
1957± 49	BATINIC	10	DPWA	$\pi N \to N\pi$, $N\eta$
1824	VRANA	00	DPWA	Multichannel

−2×IMAGINARY PART

VALUE (MeV)	DOCUMENT ID		TECN	COMMENT
100 to 220 (≈ 160) OUR ESTIMATE				
200± 15	SOKHOYAN	15A	DPWA	Multichannel
160± 80	CUTKOSKY	80	IPWA	$\pi N \to \pi N$ (lower m)
• • • We do not use the following data for averages, fits, limits, etc. • • •				
319	HUNT	19	DPWA	Multichannel
98	SHKLYAR	13	DPWA	Multichannel
200± 20	ANISOVICH	12A	DPWA	Multichannel
467±106	BATINIC	10	DPWA	$\pi N \to N\pi$, $N\eta$
614	VRANA	00	DPWA	Multichannel

$N(1875)$ ELASTIC POLE RESIDUE

MODULUS $|r|$

VALUE (MeV)	DOCUMENT ID		TECN	COMMENT
3 to 12 (≈ 10) OUR ESTIMATE				
3 ±1.5	SOKHOYAN	15A	DPWA	Multichannel
10 ±5	CUTKOSKY	80	IPWA	$\pi N \to \pi N$ (lower m)
• • • We do not use the following data for averages, fits, limits, etc. • • •				
3	SHKLYAR	13	DPWA	Multichannel
2.5±1.0	ANISOVICH	12A	DPWA	Multichannel
53	BATINIC	10	DPWA	$\pi N \to N\pi$, $N\eta$

PHASE θ

VALUE (°)	DOCUMENT ID		TECN	COMMENT
50 to 200 (≈ 100) OUR ESTIMATE				
160±50	SOKHOYAN	15A	DPWA	Multichannel
100±80	CUTKOSKY	80	IPWA	$\pi N \to \pi N$ (lower m)
• • • We do not use the following data for averages, fits, limits, etc. • • •				
− 76	SHKLYAR	13	DPWA	Multichannel
− 65	BATINIC	10	DPWA	$\pi N \to N\pi$, $N\eta$

$N(1875)$ INELASTIC POLE RESIDUE

The "normalized residue" is the residue divided by $\Gamma_{pole}/2$.

Normalized residue in $N\pi \to N(1875) \to \Lambda K$

MODULUS	PHASE (°)	DOCUMENT ID		TECN	COMMENT
0.015±0.005		ANISOVICH	12A	DPWA	Multichannel

Normalized residue in $N\pi \to N(1875) \to \Sigma K$

MODULUS	PHASE (°)	DOCUMENT ID		TECN	COMMENT
0.04±0.02		ANISOVICH	12A	DPWA	Multichannel

Normalized residue in $N\pi \to N(1875) \to N\sigma$

MODULUS	PHASE (°)	DOCUMENT ID		TECN	COMMENT
0.09±0.03	−175 ± 45	SOKHOYAN	15A	DPWA	Multichannel
• • • We do not use the following data for averages, fits, limits, etc. • • •					
0.08±0.03	−170 ± 65	ANISOVICH	12A	DPWA	Multichannel

Normalized residue in $N\pi \to N(1875) \to \Delta(1232)\pi$, S-wave

MODULUS	PHASE (°)	DOCUMENT ID		TECN	COMMENT
0.05±0.03	undefined	SOKHOYAN	15A	DPWA	Multichannel

Normalized residue in $N\pi \to N(1875) \to \Delta(1232)\pi$, D-wave

MODULUS	PHASE (°)	DOCUMENT ID		TECN	COMMENT
0.04±0.02	undefined	SOKHOYAN	15A	DPWA	Multichannel

Normalized residue in $N\pi \to N(1875) \to N(1440)\pi$

MODULUS	PHASE (°)	DOCUMENT ID		TECN	COMMENT
0.03±0.02	undefined	SOKHOYAN	15A	DPWA	Multichannel

$N(1875)$ BREIT-WIGNER MASS

VALUE (MeV)	DOCUMENT ID		TECN	COMMENT
1850 to 1920 (≈ 1875) OUR ESTIMATE				
2005± 12	[1] HUNT	19	DPWA	Multichannel
1875± 20	SOKHOYAN	15A	DPWA	Multichannel
1934± 10	[1] SHKLYAR	13	DPWA	Multichannel
1880±100	CUTKOSKY	80	IPWA	$\pi N \to \pi N$
• • • We do not use the following data for averages, fits, limits, etc. • • •				
1880± 20	ANISOVICH	12A	DPWA	Multichannel
1951± 27	[1] SHRESTHA	12A	DPWA	Multichannel
2048± 65	BATINIC	10	DPWA	$\pi N \to N\pi$, $N\eta$
1946± 1	PENNER	02C	DPWA	Multichannel
1895	MART	00	DPWA	$\gamma p \to \Lambda K^+$
2003± 18	VRANA	00	DPWA	Multichannel

[1] Statistical error only.

$N(1875)$ BREIT-WIGNER WIDTH

VALUE (MeV)	DOCUMENT ID		TECN	COMMENT
120 to 250 (≈ 200) OUR ESTIMATE				
321± 21	[1] HUNT	19	DPWA	Multichannel
200± 25	SOKHOYAN	15A	DPWA	Multichannel
857±100	[1] SHKLYAR	13	DPWA	Multichannel
180± 60	CUTKOSKY	80	IPWA	$\pi N \to \pi N$ (lower m)

Downloaded from https://academic.oup.com/ptep/article/2022/8/083C01/6651666 by KIT Library user on 27 September 2022

See key on page 1127

• • • We do not use the following data for averages, fits, limits, etc. • • •

200± 25	ANISOVICH	12A	DPWA	Multichannel
500± 45	[1] SHRESTHA	12A	DPWA	Multichannel
529±128	BATINIC	10	DPWA	$\pi N \to N\pi$, $N\eta$
859± 7	PENNER	02C	DPWA	Multichannel
372	MART	00	DPWA	$\gamma p \to \Lambda K^+$
1070±858	VRANA	00	DPWA	Multichannel

[1] Statistical error only.

$N(1875)$ DECAY MODES

	Mode	Fraction (Γ_i/Γ)
Γ_1	$N\pi$	3–11 %
Γ_2	$N\eta$	3–16 %
Γ_3	$N\omega$	15–25 %
Γ_4	ΛK	1–2 %
Γ_5	ΣK	0.3–1.1 %
Γ_6	$N\pi\pi$	>56 %
Γ_7	$\Delta(1232)\pi$	4–44 %
Γ_8	$\Delta(1232)\pi$, S-wave	2–21 %
Γ_9	$\Delta(1232)\pi$, D-wave	2–23 %
Γ_{10}	$N\rho$, S=3/2, S-wave	36–56 %
Γ_{11}	$N\sigma$	16–60 %
Γ_{12}	$N(1440)\pi$	2–8 %
Γ_{13}	$N(1520)\pi$	<2 %
Γ_{14}	$\Lambda K^*(892)$	<0.2 %
Γ_{15}	$p\gamma$	0.001–0.025 %
Γ_{16}	$p\gamma$, helicity=1/2	0.001–0.021 %
Γ_{17}	$p\gamma$, helicity=3/2	<0.003 %
Γ_{18}	$n\gamma$	<0.040 %
Γ_{19}	$n\gamma$, helicity=1/2	<0.007 %
Γ_{20}	$n\gamma$, helicity=3/2	<0.033 %

$N(1875)$ BRANCHING RATIOS

$\Gamma(N\pi)/\Gamma_{total}$ — Γ_1/Γ

VALUE (%)	DOCUMENT ID		TECN	COMMENT
3 to 11 (≈ 7) OUR ESTIMATE				
7.5±0.1	[1] HUNT	19	DPWA	Multichannel
4 ±2	SOKHOYAN	15A	DPWA	Multichannel
11 ±1	[1] SHKLYAR	13	DPWA	Multichannel
10 ±4	CUTKOSKY	80	IPWA	$\pi N \to \pi N$ (lower m)
• • • We do not use the following data for averages, fits, limits, etc. • • •				
3 ±2	ANISOVICH	12A	DPWA	Multichannel
7 ±2	[1] SHRESTHA	12A	DPWA	Multichannel
17 ±7	BATINIC	10	DPWA	$\pi N \to N\pi$, $N\eta$
12 ±2	PENNER	02C	DPWA	Multichannel
13 ±3	VRANA	00	DPWA	Multichannel

[1] Statistical error only.

$\Gamma(N\eta)/\Gamma_{total}$ — Γ_2/Γ

VALUE (%)	DOCUMENT ID		TECN	COMMENT
3–16 % OUR ESTIMATE				
10 ±6	MUELLER	20	DPWA	Multichannel
3.3±0.8	[1] HUNT	19	DPWA	Multichannel
< 1	SHKLYAR	13	DPWA	Multichannel
• • • We do not use the following data for averages, fits, limits, etc. • • •				
8 ±3	BATINIC	10	DPWA	$\pi N \to N\pi$, $N\eta$
7 ±2	PENNER	02C	DPWA	Multichannel
0 ±2	VRANA	00	DPWA	Multichannel

[1] Statistical error only.

$\Gamma(N\omega)/\Gamma_{total}$ — Γ_3/Γ

VALUE (%)	DOCUMENT ID		TECN	COMMENT
13±7	DENISENKO	16	DPWA	Multichannel
20±5	[1] SHKLYAR	13	DPWA	Multichannel
• • • We do not use the following data for averages, fits, limits, etc. • • •				
21±7	PENNER	02C	DPWA	Multichannel

[1] Statistical error only.

$\Gamma(\Lambda K)/\Gamma_{total}$ — Γ_4/Γ

VALUE (%)	DOCUMENT ID		TECN	COMMENT
1–2 % OUR ESTIMATE				
1.1±0.4	[1] HUNT	19	DPWA	Multichannel
• • • We do not use the following data for averages, fits, limits, etc. • • •				
0.2±0.2	PENNER	02C	DPWA	Multichannel

[1] Statistical error only.

$\Gamma(\Sigma K)/\Gamma_{total}$ — Γ_5/Γ

VALUE (%)	DOCUMENT ID		TECN	COMMENT
0.3–1.1 % OUR ESTIMATE				
0.7±0.4	PENNER	02C	DPWA	Multichannel

$\Gamma(\Delta(1232)\pi, S\text{-wave})/\Gamma_{total}$ — Γ_8/Γ

VALUE (%)	DOCUMENT ID		TECN	COMMENT
2–21 % OUR ESTIMATE				
< 2	[1] HUNT	19	DPWA	Multichannel
14± 7	SOKHOYAN	15A	DPWA	Multichannel
• • • We do not use the following data for averages, fits, limits, etc. • • •				
87± 3	[1] SHRESTHA	12A	DPWA	Multichannel
40±10	VRANA	00	DPWA	Multichannel

[1] Statistical error only.

$\Gamma(\Delta(1232)\pi, D\text{-wave})/\Gamma_{total}$ — Γ_9/Γ

VALUE (%)	DOCUMENT ID		TECN	COMMENT
2–23 % OUR ESTIMATE				
17± 6	[1] HUNT	19	DPWA	Multichannel
7± 5	SOKHOYAN	15A	DPWA	Multichannel
• • • We do not use the following data for averages, fits, limits, etc. • • •				
< 6	[1] SHRESTHA	12A	DPWA	Multichannel
17±10	VRANA	00	DPWA	Multichannel

[1] Statistical error only.

$\Gamma(N\rho, S=3/2, S\text{-wave})/\Gamma_{total}$ — Γ_{10}/Γ

VALUE (%)	DOCUMENT ID		TECN	COMMENT
36–56 % OUR ESTIMATE				
46±10	[1] HUNT	19	DPWA	Multichannel
• • • We do not use the following data for averages, fits, limits, etc. • • •				
< 5	[1] SHRESTHA	12A	DPWA	Multichannel
6± 6	VRANA	00	DPWA	Multichannel

[1] Statistical error only.

$\Gamma(N\sigma)/\Gamma_{total}$ — Γ_{11}/Γ

VALUE (%)	DOCUMENT ID		TECN	COMMENT
16–60 % OUR ESTIMATE				
24.3± 8.6	[1] HUNT	19	DPWA	Multichannel
45 ±15	SOKHOYAN	15A	DPWA	Multichannel
• • • We do not use the following data for averages, fits, limits, etc. • • •				
< 4	[1] SHRESTHA	12A	DPWA	Multichannel
24 ±24	VRANA	00	DPWA	Multichannel

[1] Statistical error only.

$\Gamma(N(1440)\pi)/\Gamma_{total}$ — Γ_{12}/Γ

VALUE (%)	DOCUMENT ID		TECN	COMMENT
5±3	SOKHOYAN	15A	DPWA	Multichannel

$\Gamma(N(1520)\pi)/\Gamma_{total}$ — Γ_{13}/Γ

VALUE (%)	DOCUMENT ID		TECN	COMMENT
<2	SOKHOYAN	15A	DPWA	Multichannel

$\Gamma(\Lambda K^*(892))/\Gamma_{total}$ — Γ_{14}/Γ

VALUE (%)	DOCUMENT ID		TECN	COMMENT
<0.2 % OUR ESTIMATE				
<0.2	ANISOVICH	17B	DPWA	Multichannel

$N(1875)$ PHOTON DECAY AMPLITUDES AT THE POLE

$N(1875) \to p\gamma$, helicity-1/2 amplitude $A_{1/2}$

MODULUS ($GeV^{-1/2}$)	PHASE (°)	DOCUMENT ID		TECN	COMMENT
0.017±0.009	−110 ± 40	SOKHOYAN	15A	DPWA	Multichannel

$N(1875) \to p\gamma$, helicity-3/2 amplitude $A_{3/2}$

MODULUS ($GeV^{-1/2}$)	PHASE (°)	DOCUMENT ID		TECN	COMMENT
0.008±0.004	180 ± 40	SOKHOYAN	15A	DPWA	Multichannel

$N(1875)$ BREIT-WIGNER PHOTON DECAY AMPLITUDES

$N(1875) \to p\gamma$, helicity-1/2 amplitude $A_{1/2}$

VALUE ($GeV^{-1/2}$)	DOCUMENT ID		TECN	COMMENT
0.010 to 0.025 (≈ 0.015) OUR ESTIMATE				
−0.013±0.008	[1] HUNT	19	DPWA	Multichannel
0.011±0.001	[1] SHKLYAR	13	DPWA	Multichannel
0.018±0.010	ANISOVICH	12A	DPWA	Multichannel
• • • We do not use the following data for averages, fits, limits, etc. • • •				
0.007±0.008	[1] SHRESTHA	12A	DPWA	Multichannel
0.012	PENNER	02D	DPWA	Multichannel

[1] Statistical error only.

Downloaded from https://academic.oup.com/ptep/article/2022/8/083C01/6651666 by KIT Library user on 27 September 2022

$N(1875) \to p\gamma$, helicity-3/2 amplitude $A_{3/2}$

VALUE (GeV$^{-1/2}$)	DOCUMENT ID		TECN	COMMENT
−0.010 to 0.025 (≈ −0.005) OUR ESTIMATE				
−0.093±0.009	[1] HUNT	19	DPWA	Multichannel
−0.007±0.004	SOKHOYAN	15A	DPWA	Multichannel
0.026±0.001	[1] SHKLYAR	13	DPWA	Multichannel
• • • We do not use the following data for averages, fits, limits, etc. • • •				
−0.009±0.005	ANISOVICH	12A	DPWA	Multichannel
0.043±0.022	[1] SHRESTHA	12A	DPWA	Multichannel
−0.010	PENNER	02D	DPWA	Multichannel

[1] Statistical error only.

$N(1875) \to n\gamma$, helicity-1/2 amplitude $A_{1/2}$

VALUE (GeV$^{-1/2}$)	DOCUMENT ID		TECN	COMMENT
0.050±0.009	[1] HUNT	19	DPWA	Multichannel
0.010±0.006	ANISOVICH	13B	DPWA	Multichannel
• • • We do not use the following data for averages, fits, limits, etc. • • •				
0.055±0.021	[1] SHRESTHA	12A	DPWA	Multichannel
0.023	PENNER	02D	DPWA	Multichannel

[1] Statistical error only.

$N(1875) \to n\gamma$, helicity-3/2 amplitude $A_{3/2}$

VALUE (GeV$^{-1/2}$)	DOCUMENT ID		TECN	COMMENT
0.141±0.022	[1] HUNT	19	DPWA	Multichannel
−0.020±0.015	ANISOVICH	13B	DPWA	Multichannel
• • • We do not use the following data for averages, fits, limits, etc. • • •				
−0.085±0.031	[1] SHRESTHA	12A	DPWA	Multichannel
−0.009	PENNER	02D	DPWA	Multichannel

[1] Statistical error only.

$N(1875)$ REFERENCES

For early references, see Physics Letters **111B** 1 (1982).

MUELLER	20	PL B803 135323	J. Mueller *et al.*	(CBELSA/TAPS Collab.)
HUNT	19	PR C99 055205	B.C. Hunt, D.M. Manley	
ANISOVICH	17B	PL B771 142	A.V. Anisovich *et al.*	
DENISENKO	16	PL B755 97	I. Denisenko *et al.*	
SOKHOYAN	15A	EPJ A51 95	V. Sokhoyan *et al.*	(CBELSA/TAPS Collab.)
ANISOVICH	13B	EPJ A49 67	A.V. Anisovich *et al.*	
SHKLYAR	13	PR C87 015201	V. Shklyar, H. Lenske, U. Mosel	(GIES)
ANISOVICH	12A	EPJ A48 15	A.V. Anisovich *et al.*	(BONN, PNPI)
SHRESTHA	12A	PR C86 055203	M. Shrestha, D.M. Manley	(KSU)
BATINIC	10	PR C82 038203	M. Batinic *et al.*	(ZAGR)
PENNER	02C	PR C66 055211	G. Penner, U. Mosel	(GIES)
PENNER	02D	PR C66 055212	G. Penner, U. Mosel	(GIES)
MART	00	PR C61 012201	T. Mart, C. Bennhold	
VRANA	00	PRPL 328 181	T.P. Vrana, S.A. Dytman, T.-S.H. Lee	(PITT, ANL)
CUTKOSKY	80	Toronto Conf. 19	R.E. Cutkosky *et al.*	(CMU, LBL) IJP
Also		PR D20 2839	R.E. Cutkosky *et al.*	(CMU, LBL) IJP

$N(1880)\ 1/2^+$

$I(J^P) = \frac{1}{2}(\frac{1}{2}^+)$ Status: ***

$N(1880)$ POLE POSITION

REAL PART

VALUE (MeV)	DOCUMENT ID		TECN	COMMENT
1820 to 1900 (≈ 1860) OUR ESTIMATE				
1860±40	ANISOVICH	17A	DPWA	Multichannel
• • • We do not use the following data for averages, fits, limits, etc. • • •				
1880	HUNT	19	DPWA	Multichannel
1875±11	[1] ANISOVICH	17A	L+P	$\gamma p, \pi^- p \to K\Lambda$
1870±40	SOKHOYAN	15A	DPWA	Multichannel
1870±40	GUTZ	14	DPWA	Multichannel
1860±35	ANISOVICH	12A	DPWA	Multichannel

[1] Statistical error only.

−2×IMAGINARY PART

VALUE (MeV)	DOCUMENT ID		TECN	COMMENT
180 to 280 (≈ 230) OUR ESTIMATE				
230±50	ANISOVICH	17A	DPWA	Multichannel
• • • We do not use the following data for averages, fits, limits, etc. • • •				
429	HUNT	19	DPWA	Multichannel
33± 9	[2] ANISOVICH	17A	L+P	$\gamma p, \pi^- p \to K\Lambda$
220±50	SOKHOYAN	15A	DPWA	Multichannel
220±50	GUTZ	14	DPWA	Multichannel
250±70	ANISOVICH	12A	DPWA	Multichannel

[2] Statistical error only.

$N(1880)$ ELASTIC POLE RESIDUE

MODULUS $|r|$

VALUE (MeV)	DOCUMENT ID		TECN	COMMENT
6±4	SOKHOYAN	15A	DPWA	Multichannel
• • • We do not use the following data for averages, fits, limits, etc. • • •				
6±4	GUTZ	14	DPWA	Multichannel
6±4	ANISOVICH	12A	DPWA	Multichannel

PHASE θ

VALUE (°)	DOCUMENT ID		TECN	COMMENT
70±60	SOKHOYAN	15A	DPWA	Multichannel
• • • We do not use the following data for averages, fits, limits, etc. • • •				
70±60	GUTZ	14	DPWA	Multichannel
80±65	ANISOVICH	12A	DPWA	Multichannel

$N(1880)$ INELASTIC POLE RESIDUE

The "normalized residue" is the residue divided by $\Gamma_{pole}/2$.

Normalized residue in $N\pi \to N(1880) \to N\eta$

MODULUS	PHASE (°)	DOCUMENT ID		TECN	COMMENT
0.11±0.07	−75 ± 55	ANISOVICH	12A	DPWA	Multichannel

Normalized residue in $N\pi \to N(1880) \to \Lambda K$

MODULUS	PHASE (°)	DOCUMENT ID		TECN	COMMENT
0.05±0.02	27 ± 30	ANISOVICH	17A	DPWA	$\gamma p, \pi^- p \to K\Lambda$
• • • We do not use the following data for averages, fits, limits, etc. • • •					
0.3 ±0.1	82 ± 9	[3] ANISOVICH	17A	L+P	$\gamma p, \pi^- p \to K\Lambda$
0.03±0.02	40 ± 40	ANISOVICH	12A	DPWA	Multichannel

[3] Statistical error only.

Normalized residue in $N\pi \to N(1880) \to \Sigma K$

MODULUS	PHASE (°)	DOCUMENT ID		TECN	COMMENT
• • • We do not use the following data for averages, fits, limits, etc. • • •					
0.11±0.06	95 ± 40	ANISOVICH	12A	DPWA	Multichannel

Normalized residue in $N\pi \to N(1880) \to \Delta\pi$, P-wave

MODULUS	PHASE (°)	DOCUMENT ID		TECN	COMMENT
0.14±0.08	−150 ± 55	SOKHOYAN	15A	DPWA	Multichannel
• • • We do not use the following data for averages, fits, limits, etc. • • •					
0.20±0.08	−150 ± 50	ANISOVICH	12A	DPWA	Multichannel

Normalized residue in $N\pi \to N(1880) \to N(1535)\pi$

MODULUS	PHASE (°)	DOCUMENT ID		TECN	COMMENT
0.09±0.05	130 ± 60	GUTZ	14	DPWA	Multichannel

Normalized residue in $N\pi \to N(1880) \to N a_0(980)$

MODULUS	PHASE (°)	DOCUMENT ID		TECN	COMMENT
0.04±0.03	40 ± 65	GUTZ	14	DPWA	Multichannel

Normalized residue in $N\pi \to N(1880) \to N\sigma$

MODULUS	PHASE (°)	DOCUMENT ID		TECN	COMMENT
0.10±0.05	−140 ± 55	SOKHOYAN	15A	DPWA	Multichannel

$N(1880)$ BREIT-WIGNER MASS

VALUE (MeV)	DOCUMENT ID		TECN	COMMENT
1830 to 1930 (≈ 1880) OUR ESTIMATE				
1967±20	[4] HUNT	19	DPWA	Multichannel
1875±40	SOKHOYAN	15A	DPWA	Multichannel
• • • We do not use the following data for averages, fits, limits, etc. • • •				
1875±40	GUTZ	14	DPWA	Multichannel
1870±35	ANISOVICH	12A	DPWA	Multichannel
1900±36	[4] SHRESTHA	12A	DPWA	Multichannel

[4] Statistical error only.

$N(1880)$ BREIT-WIGNER WIDTH

VALUE (MeV)	DOCUMENT ID		TECN	COMMENT
200 to 400 (≈ 300) OUR ESTIMATE				
500± 77	[5] HUNT	19	DPWA	Multichannel
230± 50	SOKHOYAN	15A	DPWA	Multichannel
• • • We do not use the following data for averages, fits, limits, etc. • • •				
230± 50	GUTZ	14	DPWA	Multichannel
235± 65	ANISOVICH	12A	DPWA	Multichannel
485±142	[5] SHRESTHA	12A	DPWA	Multichannel

[5] Statistical error only.

$N(1880)$ DECAY MODES

	Mode	Fraction (Γ_i/Γ)
Γ_1	$N\pi$	3–31 %
Γ_2	$N\eta$	1–55 %
Γ_3	$N\omega$	12–28 %
Γ_4	ΛK	1–3 %
Γ_5	ΣK	10–24 %
Γ_6	$N\pi\pi$	>32 %
Γ_7	$\Delta(1232)\pi$	5–42 %
Γ_8	$N\rho$, $S=1/2$, P-wave	19–45 %

Downloaded from https://academic.oup.com/ptep/article/2022/8/083C01/6651666 by KIT Library user on 27 September 2022

See key on page 1127

Γ_9	$N\sigma$	8–40 %
Γ_{10}	$N(1535)\pi$	4–12 %
Γ_{11}	$N a_0(980)$	1–5 %
Γ_{12}	$\Lambda K^*(892)$	0.5–1.1 %
Γ_{13}	$p\gamma$, helicity=1/2	seen
Γ_{14}	$n\gamma$, helicity=1/2	0.002–0.63 %

$N(1880)$ BRANCHING RATIOS

$\Gamma(N\pi)/\Gamma_{total}$ — Γ_1/Γ

VALUE (%)	DOCUMENT ID		TECN	COMMENT
3–31 % OUR ESTIMATE				
25±6	[6] HUNT	19	DPWA	Multichannel
6±3	SOKHOYAN	15A	DPWA	Multichannel
• • • We do not use the following data for averages, fits, limits, etc. • • •				
6±3	GUTZ	14	DPWA	Multichannel
5±3	ANISOVICH	12A	DPWA	Multichannel
15±5	[6] SHRESTHA	12A	DPWA	Multichannel

[6] Statistical error only.

$\Gamma(N\eta)/\Gamma_{total}$ — Γ_2/Γ

VALUE (%)	DOCUMENT ID		TECN	COMMENT
1–55 % OUR ESTIMATE				
18± 8	MUELLER	20	DPWA	Multichannel
2± 1	[7] HUNT	19	DPWA	Multichannel
25^{+30}_{-20}	ANISOVICH	12A	DPWA	Multichannel
• • • We do not use the following data for averages, fits, limits, etc. • • •				
16± 7	[7] SHRESTHA	12A	DPWA	Multichannel

[7] Statistical error only.

$\Gamma(N\omega)/\Gamma_{total}$ — Γ_3/Γ

VALUE (%)	DOCUMENT ID		TECN	COMMENT
12–28 % OUR ESTIMATE				
20±8	DENISENKO	16	DPWA	Multichannel

$\Gamma(\Lambda K)/\Gamma_{total}$ — Γ_4/Γ

VALUE (%)	DOCUMENT ID		TECN	COMMENT
1–3 % OUR ESTIMATE				
2± 1	[8] HUNT	19	DPWA	Multichannel
2± 1	ANISOVICH	12A	DPWA	Multichannel
• • • We do not use the following data for averages, fits, limits, etc. • • •				
32±10	[8] SHRESTHA	12A	DPWA	Multichannel

[8] Statistical error only.

$\Gamma(\Sigma K)/\Gamma_{total}$ — Γ_5/Γ

VALUE (%)	DOCUMENT ID		TECN	COMMENT
10–24 % OUR ESTIMATE				
17±7	ANISOVICH	12A	DPWA	Multichannel

$\Gamma(\Delta(1232)\pi)/\Gamma_{total}$ — Γ_7/Γ

VALUE (%)	DOCUMENT ID		TECN	COMMENT
5–42 % OUR ESTIMATE				
11± 6	[9] HUNT	19	DPWA	Multichannel
30±12	SOKHOYAN	15A	DPWA	Multichannel
• • • We do not use the following data for averages, fits, limits, etc. • • •				
29±12	ANISOVICH	12A	DPWA	Multichannel
< 2	[9] SHRESTHA	12A	DPWA	Multichannel

[9] Statistical error only.

$\Gamma(N\rho, S{=}1/2, P\text{-wave})/\Gamma_{total}$ — Γ_8/Γ

VALUE (%)	DOCUMENT ID		TECN	COMMENT
19–45 % OUR ESTIMATE				
32±13	[10] HUNT	19	DPWA	Multichannel

[10] Statistical error only.

$\Gamma(N\sigma)/\Gamma_{total}$ — Γ_9/Γ

VALUE (%)	DOCUMENT ID		TECN	COMMENT
8–40 % OUR ESTIMATE				
< 9	[11] HUNT	19	DPWA	Multichannel
25±15	SOKHOYAN	15A	DPWA	Multichannel
• • • We do not use the following data for averages, fits, limits, etc. • • •				
8± 5	[11] SHRESTHA	12A	DPWA	Multichannel

[11] Statistical error only.

$\Gamma(N(1535)\pi)/\Gamma_{total}$ — Γ_{10}/Γ

VALUE (%)	DOCUMENT ID		TECN	COMMENT
4–12 % OUR ESTIMATE				
8±4	GUTZ	14	DPWA	Multichannel

$\Gamma(N a_0(980))/\Gamma_{total}$ — Γ_{11}/Γ

VALUE (%)	DOCUMENT ID		TECN	COMMENT
1–5 % OUR ESTIMATE				
3±2	GUTZ	14	DPWA	Multichannel

$\Gamma(\Lambda K^*(892))/\Gamma_{total}$ — Γ_{12}/Γ

VALUE (%)	DOCUMENT ID		TECN	COMMENT
0.5–1.1 % OUR ESTIMATE				
0.8±0.3	ANISOVICH	17B	DPWA	Multichannel

$N(1880)$ BREIT-WIGNER PHOTON DECAY AMPLITUDES

$N(1880) \to p\gamma$, helicity-1/2 amplitude $A_{1/2}$

VALUE (GeV$^{-1/2}$)	DOCUMENT ID		TECN	COMMENT
0.119±0.015	[12] HUNT	19	DPWA	Multichannel
• • • We do not use the following data for averages, fits, limits, etc. • • •				
0.021±0.006	[12] SHRESTHA	12A	DPWA	Multichannel

[12] Statistical error only.

$N(1880) \to n\gamma$, helicity-1/2 amplitude $A_{1/2}$

VALUE (GeV$^{-1/2}$)	DOCUMENT ID		TECN	COMMENT
0.016±0.010	[13] HUNT	19	DPWA	Multichannel
−0.060±0.050	ANISOVICH	13B	DPWA	Multichannel
• • • We do not use the following data for averages, fits, limits, etc. • • •				
0.014±0.007	[13] SHRESTHA	12A	DPWA	Multichannel

[13] Statistical error only.

$N(1880)$ REFERENCES

MUELLER	20	PL B803 135323	J. Mueller *et al.*	(CBELSA/TAPS Collab.)
HUNT	19	PR C99 055205	B.C. Hunt, D.M. Manley	
ANISOVICH	17A	PRL 119 062004	A.V. Anisovich *et al.*	
ANISOVICH	17B	PL B771 142	A.V. Anisovich *et al.*	
DENISENKO	16	PL B755 97	I. Denisenko *et al.*	
SOKHOYAN	15A	EPJ A51 95	V. Sokhoyan *et al.*	(CBELSA/TAPS Collab.)
GUTZ	14	EPJ A50 74	E. Gutz *et al.*	(CBELSA/TAPS Collab.)
ANISOVICH	13B	EPJ A49 67	A.V. Anisovich *et al.*	
ANISOVICH	12A	EPJ A48 15	A.V. Anisovich *et al.*	(BONN, PNPI)
SHRESTHA	12A	PR C86 055203	M. Shrestha, D.M. Manley	(KSU)

$N(1895)\ 1/2^-$

$I(J^P) = \frac{1}{2}(\frac{1}{2}^-)$ Status: ****

Before our 2012 *Review*, this state appeared in our Listings as the $N(2090)$. Any structure in the S_{11} wave above 1800 MeV is listed here. A few early results that are now obsolete have been omitted.

$N(1895)$ POLE POSITION

REAL PART

VALUE (MeV)	DOCUMENT ID		TECN	COMMENT
1890 to 1930 (≈ 1910) OUR ESTIMATE				
1907±10	AFZAL	20	DPWA	Multichannel
1895±15	ANISOVICH	17A	DPWA	Multichannel
1906±17	[1] ANISOVICH	17A	L+P	$\gamma p, \pi^- p \to K\Lambda$
1917±19±1	[2] SVARC	14	L+P	$\pi N \to \pi N$
• • • We do not use the following data for averages, fits, limits, etc. • • •				
1956	HUNT	19	DPWA	Multichannel
1907±10	ANISOVICH	17C	DPWA	Multichannel
1907±10	SOKHOYAN	15A	DPWA	Multichannel
1900±15	ANISOVICH	12A	DPWA	Multichannel
1797±26	BATINIC	10	DPWA	$\pi N \to N\pi, N\eta$
1795	VRANA	00	DPWA	Multichannel
2150±70	CUTKOSKY	80	IPWA	$\pi N \to \pi N$

[1] Statistical error only.
[2] Fit to the amplitudes of HOEHLER 79.

−2×IMAGINARY PART

VALUE (MeV)	DOCUMENT ID		TECN	COMMENT
80 to 140 (≈ 110) OUR ESTIMATE				
100^{+40}_{-10}	AFZAL	20	DPWA	Multichannel
132± 30	ANISOVICH	17A	DPWA	Multichannel
100± 10	[1] ANISOVICH	17A	L+P	$\gamma p, \pi^- p \to K\Lambda$
101± 36±1	[1,2] SVARC	14	L+P	$\pi N \to \pi N$
• • • We do not use the following data for averages, fits, limits, etc. • • •				
449	HUNT	19	DPWA	Multichannel
100^{+40}_{-10}	ANISOVICH	17C	DPWA	Multichannel
100^{+40}_{-15}	SOKHOYAN	15A	DPWA	Multichannel
90^{+30}_{-15}	ANISOVICH	12A	DPWA	Multichannel
420± 45	BATINIC	10	DPWA	$\pi N \to N\pi, N\eta$
220	VRANA	00	DPWA	Multichannel
350±100	CUTKOSKY	80	IPWA	$\pi N \to \pi N$

[1] Statistical error only.
[2] Fit to the amplitudes of HOEHLER 79.

Downloaded from https://academic.oup.com/ptep/article/2022/8/083C01/6651666 by KIT Library user on 27 September 2022

$N(1895)$ ELASTIC POLE RESIDUE

MODULUS $|r|$

VALUE (MeV)	DOCUMENT ID		TECN	COMMENT
1 to 5 ($\approx$ 3) OUR ESTIMATE				
3 ± 2	SOKHOYAN	15A	DPWA	Multichannel
3.1 ± 1.4	[1] SVARC	14	L+P	$\pi N \to \pi N$
• • • We do not use the following data for averages, fits, limits, etc. • • •				
1 ± 1	ANISOVICH	12A	DPWA	Multichannel
60	BATINIC	10	DPWA	$\pi N \to N\pi$, $N\eta$
40 ±20	CUTKOSKY	80	IPWA	$\pi N \to \pi N$

[1] Fit to the amplitudes of HOEHLER 79.

PHASE θ

VALUE (°)	DOCUMENT ID		TECN	COMMENT
125 ±45	SOKHOYAN	15A	DPWA	Multichannel
−107 ±23 ±2	[1] SVARC	14	L+P	$\pi N \to \pi N$
0 ±90	CUTKOSKY	80	IPWA	$\pi N \to \pi N$
• • • We do not use the following data for averages, fits, limits, etc. • • •				
−164	BATINIC	10	DPWA	$\pi N \to N\pi$, $N\eta$

[1] Fit to the amplitudes of HOEHLER 79.

$N(1895)$ INELASTIC POLE RESIDUE

The "normalized residue" is the residue divided by $\Gamma_{pole}/2$.

Normalized residue in $N\pi \to N(1895) \to \Lambda K$

MODULUS	PHASE (°)	DOCUMENT ID		TECN	COMMENT
0.09 ±0.03	8 ± 30	ANISOVICH	17A	DPWA	Multichannel
0.06 ±0.02	87 ± 27	[1] ANISOVICH	17A	L+P	γp, $\pi^- p \to K\Lambda$
• • • We do not use the following data for averages, fits, limits, etc. • • •					
0.05 ±0.02	−90 ± 30	ANISOVICH	12A	DPWA	Multichannel

[1] Statistical error only.

Normalized residue in $N\pi \to N(1895) \to \Sigma K$

MODULUS	PHASE (°)	DOCUMENT ID		TECN	COMMENT
0.06 ±0.02	40 ± 30	ANISOVICH	12A	DPWA	Multichannel

Normalized residue in $N\pi \to N(1895) \to \Delta(1232)\pi$

MODULUS	PHASE (°)	DOCUMENT ID		TECN	COMMENT
0.05 ±0.025	−100 ± 45	SOKHOYAN	15A	DPWA	Multichannel

Normalized residue in $N\pi \to N(1895) \to N(1440)\pi$

MODULUS	PHASE (°)	DOCUMENT ID		TECN	COMMENT
0.05 ±0.025	−100 ± 45	SOKHOYAN	15A	DPWA	Multichannel

$N(1895)$ BREIT-WIGNER MASS

VALUE (MeV)	DOCUMENT ID		TECN	COMMENT
1870 to 1920 ($\approx$ 1895) OUR ESTIMATE				
2000 ±29	[1] HUNT	19	DPWA	Multichannel
1890^{+9}_{-23}	KASHEVAROV	17	DPWA	$\gamma p \to \eta p$, $\eta' p$
1905 ±12	SOKHOYAN	15A	DPWA	Multichannel
1880 ±20	HOEHLER	79	IPWA	$\pi N \to \pi N$
• • • We do not use the following data for averages, fits, limits, etc. • • •				
1895 ±15	ANISOVICH	12A	DPWA	Multichannel
1910 ±15	[1] SHRESTHA	12A	DPWA	Multichannel
1812 ±25	BATINIC	10	DPWA	$\pi N \to N\pi$, $N\eta$
1822 ±43	VRANA	00	DPWA	Multichannel
2180 ±80	CUTKOSKY	80	IPWA	$\pi N \to \pi N$

[1] Statistical error only.

$N(1895)$ BREIT-WIGNER WIDTH

VALUE (MeV)	DOCUMENT ID		TECN	COMMENT
80 to 200 ($\approx$ 120) OUR ESTIMATE				
466 ± 72	[1] HUNT	19	DPWA	Multichannel
150 ± 57	KASHEVAROV	17	DPWA	$\gamma p \to \eta p$, $\eta' p$
100^{+30}_{-10}	SOKHOYAN	15A	DPWA	Multichannel
95 ± 30	HOEHLER	79	IPWA	$\pi N \to \pi N$
• • • We do not use the following data for averages, fits, limits, etc. • • •				
90^{+30}_{-15}	ANISOVICH	12A	DPWA	Multichannel
502 ± 47	[1] SHRESTHA	12A	DPWA	Multichannel
405 ± 40	BATINIC	10	DPWA	$\pi N \to N\pi$, $N\eta$
248 ±185	VRANA	00	DPWA	Multichannel
350 ±100	CUTKOSKY	80	IPWA	$\pi N \to \pi N$

[1] Statistical error only.

$N(1895)$ DECAY MODES

	Mode	Fraction (Γ_i/Γ)
Γ_1	$N\pi$	2–18 %
Γ_2	$N\eta$	15–45 %
Γ_3	$N\eta'$	10–40 %
Γ_4	$N\omega$	16–40 %
Γ_5	ΛK	3–23 %
Γ_6	ΣK	6–20 %
Γ_7	$N\pi\pi$	17–74 %
Γ_8	$\Delta(1232)\pi$, D-wave	3–11 %
Γ_9	$N\rho$	14–50 %
Γ_{10}	$N\rho$, S=1/2, S-wave	<18 %
Γ_{11}	$N\rho$, S=3/2, D-wave	14–32 %
Γ_{12}	$N\sigma$	<13 %
Γ_{13}	$N(1440)\pi$	2–12 %
Γ_{14}	$\Lambda K^*(892)$	4–9 %
Γ_{15}	$p\gamma$, helicity=1/2	0.01–0.06 %
Γ_{16}	$n\gamma$, helicity=1/2	0.003–0.05 %

$N(1895)$ BRANCHING RATIOS

$\Gamma(N\pi)/\Gamma_{total}$ — Γ_1/Γ

VALUE (%)	DOCUMENT ID		TECN	COMMENT
2–18 % OUR ESTIMATE				
8 ±4	[1] HUNT	19	DPWA	Multichannel
2.5 ±1.5	SOKHOYAN	15A	DPWA	Multichannel
9 ±5	HOEHLER	79	IPWA	$\pi N \to \pi N$
• • • We do not use the following data for averages, fits, limits, etc. • • •				
2 ±1	ANISOVICH	12A	DPWA	Multichannel
17 ±2	[1] SHRESTHA	12A	DPWA	Multichannel
32 ±6	BATINIC	10	DPWA	$\pi N \to N\pi$, $N\eta$
17 ±3	VRANA	00	DPWA	Multichannel
18 ±8	CUTKOSKY	80	IPWA	$\pi N \to \pi N$

[1] Statistical error only.

$\Gamma(N\eta)/\Gamma_{total}$ — Γ_2/Γ

VALUE (%)	DOCUMENT ID		TECN	COMMENT
15–45 % OUR ESTIMATE				
10 ± 5	MUELLER	20	DPWA	Multichannel
37 ± 9	[1] HUNT	19	DPWA	Multichannel
10 ± 5	ANISOVICH	17C	DPWA	Multichannel
20 ± 6	[2] KASHEVAROV	17	DPWA	$\gamma p \to \eta p$, $\eta' p$
• • • We do not use the following data for averages, fits, limits, etc. • • •				
21 ± 6	ANISOVICH	12A	DPWA	Multichannel
40 ± 4	[1] SHRESTHA	12A	DPWA	Multichannel
22 ±10	BATINIC	10	DPWA	$\pi N \to N\pi$, $N\eta$
41 ± 4	VRANA	00	DPWA	Multichannel

[1] Statistical error only.
[2] Assuming $A_{1/2} = -0.030$ GeV$^{-1/2}$.

$\Gamma(N\eta')/\Gamma_{total}$ — Γ_3/Γ

VALUE (%)	DOCUMENT ID		TECN	COMMENT
10–40 % OUR ESTIMATE				
13 ± 5	ANISOVICH	17C	DPWA	Multichannel
38 ±20	[1] KASHEVAROV	17	DPWA	$\gamma p \to \eta p$, $\eta' p$

[1] Assuming $A_{1/2} = -0.030$ GeV$^{-1/2}$.

$\Gamma(N\omega)/\Gamma_{total}$ — Γ_4/Γ

VALUE (%)	DOCUMENT ID		TECN	COMMENT
16–40 % OUR ESTIMATE				
28 ±12	DENISENKO	16	DPWA	Multichannel

$\Gamma(\Lambda K)/\Gamma_{total}$ — Γ_5/Γ

VALUE (%)	DOCUMENT ID		TECN	COMMENT
3–23 % OUR ESTIMATE				
7 ±4	[1] HUNT	19	DPWA	Multichannel
18 ±5	ANISOVICH	12A	DPWA	Multichannel
• • • We do not use the following data for averages, fits, limits, etc. • • •				
1.8 ±0.8	[1] SHRESTHA	12A	DPWA	Multichannel

[1] Statistical error only.

$\Gamma(\Sigma K)/\Gamma_{total}$ — Γ_6/Γ

VALUE (%)	DOCUMENT ID		TECN	COMMENT
6–20 % OUR ESTIMATE				
13 ±7	ANISOVICH	12A	DPWA	Multichannel

$\Gamma(\Delta(1232)\pi, D\text{-wave})/\Gamma_{total}$ — Γ_8/Γ

VALUE (%)	DOCUMENT ID		TECN	COMMENT
3–11 % OUR ESTIMATE				
<10	[1] HUNT	19	DPWA	Multichannel
7 ±4	SOKHOYAN	15A	DPWA	Multichannel

Downloaded from https://academic.oup.com/ptep/article/2022/8/083C01/6651666 by KIT Library user on 27 September 2022

• • • We do not use the following data for averages, fits, limits, etc. • • •

7±3	[1] SHRESTHA	12A	DPWA	Multichannel
1±1	VRANA	00	DPWA	Multichannel

[1] Statistical error only.

$\Gamma(N\rho, S=1/2, S\text{-wave})/\Gamma_{total}$ — Γ_{10}/Γ

VALUE (%)	DOCUMENT ID		TECN	COMMENT
<18 % OUR ESTIMATE				
<18	[1] HUNT	19	DPWA	Multichannel
• • • We do not use the following data for averages, fits, limits, etc. • • •				
< 2	[1] SHRESTHA	12A	DPWA	Multichannel
36±1	VRANA	00	DPWA	Multichannel

[1] Statistical error only.

$\Gamma(N\rho, S=3/2, D\text{-wave})/\Gamma_{total}$ — Γ_{11}/Γ

VALUE (%)	DOCUMENT ID		TECN	COMMENT
14–32 % OUR ESTIMATE				
23±9	[1] HUNT	19	DPWA	Multichannel
• • • We do not use the following data for averages, fits, limits, etc. • • •				
9±3	[1] SHRESTHA	12A	DPWA	Multichannel
1±1	VRANA	00	DPWA	Multichannel

[1] Statistical error only.

$\Gamma(N\sigma)/\Gamma_{total}$ — Γ_{12}/Γ

VALUE (%)	DOCUMENT ID		TECN	COMMENT
<13 % OUR ESTIMATE				
<13	[1] HUNT	19	DPWA	Multichannel
• • • We do not use the following data for averages, fits, limits, etc. • • •				
< 2	[1] SHRESTHA	12A	DPWA	Multichannel
2±1	VRANA	00	DPWA	Multichannel

[1] Statistical error only.

$\Gamma(N(1440)\pi)/\Gamma_{total}$ — Γ_{13}/Γ

VALUE (%)	DOCUMENT ID		TECN	COMMENT
2–12 % OUR ESTIMATE				
7 ±5	[1] HUNT	19	DPWA	Multichannel
2.5±1.5	SOKHOYAN	15A	DPWA	Multichannel
• • • We do not use the following data for averages, fits, limits, etc. • • •				
24 ±4	[1] SHRESTHA	12A	DPWA	Multichannel
2 ±1	VRANA	00	DPWA	Multichannel

[1] Statistical error only.

$\Gamma(\Lambda K^*(892))/\Gamma_{total}$ — Γ_{14}/Γ

VALUE (%)	DOCUMENT ID		TECN	COMMENT
4–9 % OUR ESTIMATE				
6.3±2.5	ANISOVICH	17B	DPWA	Multichannel

$N(1895)$ PHOTON DECAY AMPLITUDES AT THE POLE

$N(1895) \to p\gamma$, helicity-1/2 amplitude $A_{1/2}$

MODULUS ($GeV^{-1/2}$)	PHASE (°)	DOCUMENT ID		TECN	COMMENT
−0.015±0.006	−35 ± 35	ANISOVICH	17C	DPWA	Multichannel
• • • We do not use the following data for averages, fits, limits, etc. • • •					
0.015±0.006	145 ± 35	SOKHOYAN	15A	DPWA	Multichannel

$N(1895)$ BREIT-WIGNER PHOTON DECAY AMPLITUDES

$N(1895) \to p\gamma$, helicity-1/2 amplitude $A_{1/2}$

VALUE ($GeV^{-1/2}$)	DOCUMENT ID		TECN	COMMENT
0.017±0.005	[1] HUNT	19	DPWA	Multichannel
−0.016±0.006	SOKHOYAN	15A	DPWA	Multichannel
• • • We do not use the following data for averages, fits, limits, etc. • • •				
0.012±0.006	[1] SHRESTHA	12A	DPWA	Multichannel

[1] Statistical error only.

$N(1895) \to n\gamma$, helicity-1/2 amplitude $A_{1/2}$

VALUE ($GeV^{-1/2}$)	DOCUMENT ID		TECN	COMMENT
0.002±0.013	[1] HUNT	19	DPWA	Multichannel
0.013±0.006	ANISOVICH	13B	DPWA	Multichannel
• • • We do not use the following data for averages, fits, limits, etc. • • •				
0.003±0.007	[1] SHRESTHA	12A	DPWA	Multichannel

[1] Statistical error only.

$N(1895)$ REFERENCES

AFZAL	20	PRL 125 152002	F. Afzal et al.	(CBELSA/TAPS Collab.)
MUELLER	20	PL B803 135323	J. Mueller et al.	(CBELSA/TAPS Collab.)
HUNT	19	PR C99 055205	B.C. Hunt, D.M. Manley	
ANISOVICH	17A	PRL 119 062004	A.V. Anisovich et al.	
ANISOVICH	17B	PL B771 142	A.V. Anisovich et al.	
ANISOVICH	17C	PL B772 247	A.V. Anisovich et al.	
KASHEVAROV	17	PRL 118 212001	V.L. Kashevarov et al.	(A2/MAMI Collab.)
DENISENKO	16	PL B755 97	I. Denisenko et al.	
SOKHOYAN	15A	EPJ A51 95	V. Sokhoyan et al.	(CBELSA/TAPS Collab.)
SVARC	14	PR C89 045205	A. Svarc et al.	(RBI Zagreb, UNI Tuzla)
ANISOVICH	13B	EPJ A49 67	A.V. Anisovich et al.	
ANISOVICH	12A	EPJ A48 15	A.V. Anisovich et al.	(BONN, PNPI)
SHRESTHA	12A	PR C86 055203	M. Shrestha, D.M. Manley	(KSU)
BATINIC	10	PR C82 038203	M. Batinic et al.	(ZAGR)
VRANA	00	PRPL 328 181	T.P. Vrana, S.A. Dytman, T.-S.H. Lee	(PITT, ANL)
CUTKOSKY	80	Toronto Conf. 19	R.E. Cutkosky et al.	(CMU, LBL) IJP
Also		PR D20 2839	R.E. Cutkosky et al.	(CMU, LBL)
HOEHLER	79	PDAT 12-1	G. Hohler et al.	(KARLT) IJP
Also		Toronto Conf. 3	R. Koch	(KARLT) IJP

$N(1900)\ 3/2^+$

$I(J^P) = \frac{1}{2}(\frac{3}{2}^+)$ Status: ****

$N(1900)$ POLE POSITION

REAL PART

VALUE (MeV)	DOCUMENT ID		TECN	COMMENT
1900 to 1940 (≈ 1920) OUR ESTIMATE				
1945±35	ANISOVICH	17A	DPWA	Multichannel
1928±18±2	[1] SVARC	14	L+P	$\pi N \to \pi N$
• • • We do not use the following data for averages, fits, limits, etc. • • •				
1856	HUNT	19	DPWA	Multichannel
1912±30	[2] ANISOVICH	17A	L+P	$\gamma p, \pi^- p \to K\Lambda$
1910±30	SOKHOYAN	15A	DPWA	Multichannel
1910±30	GUTZ	14	DPWA	Multichannel
1910	SHKLYAR	13	DPWA	Multichannel
1900±30	ANISOVICH	12A	DPWA	Multichannel

[1] Fit to the amplitudes of HOEHLER 79.
[2] Statistical error only.

−2×IMAGINARY PART

VALUE (MeV)	DOCUMENT ID		TECN	COMMENT
100 to 200 (≈ 150) OUR ESTIMATE				
135^{+70}_{-30}	ANISOVICH	17A	DPWA	Multichannel
152± 40±9	[1] SVARC	14	L+P	$\pi N \to \pi N$
• • • We do not use the following data for averages, fits, limits, etc. • • •				
241	HUNT	19	DPWA	Multichannel
166± 30	[2] ANISOVICH	17A	L+P	$\gamma p, \pi^- p \to K\Lambda$
280± 50	SOKHOYAN	15A	DPWA	Multichannel
280± 50	GUTZ	14	DPWA	Multichannel
173	SHKLYAR	13	DPWA	Multichannel
200^{+100}_{-60}	ANISOVICH	12A	DPWA	Multichannel

[1] Fit to the amplitudes of HOEHLER 79.
[2] Statistical error only.

$N(1900)$ ELASTIC POLE RESIDUE

MODULUS $|r|$

VALUE (MeV)	DOCUMENT ID		TECN	COMMENT
2 to 6 (≈ 4) OUR ESTIMATE				
4±2	SOKHOYAN	15A	DPWA	Multichannel
4±1±1	[1] SVARC	14	L+P	$\pi N \to \pi N$
• • • We do not use the following data for averages, fits, limits, etc. • • •				
4±2	GUTZ	14	DPWA	Multichannel
10	SHKLYAR	13	DPWA	Multichannel
3±2	ANISOVICH	12A	DPWA	Multichannel

[1] Fit to the amplitudes of HOEHLER 79.

PHASE θ

VALUE (°)	DOCUMENT ID		TECN	COMMENT
−50 to 10 (≈ −20) OUR ESTIMATE				
−10±40	SOKHOYAN	15A	DPWA	Multichannel
−29±15±2	[1] SVARC	14	L+P	$\pi N \to \pi N$
• • • We do not use the following data for averages, fits, limits, etc. • • •				
−10±40	GUTZ	14	DPWA	Multichannel
−64	SHKLYAR	13	DPWA	Multichannel
10±35	ANISOVICH	12A	DPWA	Multichannel

[1] Fit to the amplitudes of HOEHLER 79.

$N(1900)$ INELASTIC POLE RESIDUE

The "normalized residue" is the residue divided by $\Gamma_{pole}/2$.

Normalized residue in $N\pi \to N(1900) \to N\eta$

MODULUS	PHASE (°)	DOCUMENT ID		TECN	COMMENT
0.05±0.02	70 ± 60	ANISOVICH	12A	DPWA	Multichannel

Normalized residue in $N\pi \to N(1900) \to \Lambda K$

MODULUS	PHASE (°)	DOCUMENT ID		TECN	COMMENT
0.03±0.02	90 ± 40	ANISOVICH	17A	DPWA	Multichannel
• • • We do not use the following data for averages, fits, limits, etc. • • •					
0.07±0.03	135 ± 25	ANISOVICH	12A	DPWA	Multichannel

Downloaded from https://academic.oup.com/ptep/article/2022/8/083C01/6651666 by KIT Library user on 27 September 2022

Normalized residue in $N\pi \to N(1900) \to \Sigma K$

MODULUS	PHASE (°)	DOCUMENT ID		TECN	COMMENT
0.04±0.02	110 ± 30	ANISOVICH	12A	DPWA	Multichannel

Normalized residue in $N\pi \to N(1900) \to N(1535)\pi$

MODULUS	PHASE (°)	DOCUMENT ID		TECN	COMMENT
0.04±0.01	170 ± 30	GUTZ	14	DPWA	Multichannel

Normalized residue in $N\pi \to N(1900) \to \Delta(1232)\pi$, P-wave

MODULUS	PHASE (°)	DOCUMENT ID		TECN	COMMENT
0.07±0.04	−65 ± 30	SOKHOYAN	15A	DPWA	Multichannel

Normalized residue in $N\pi \to N(1900) \to \Delta(1232)\pi$, F-wave

MODULUS	PHASE (°)	DOCUMENT ID		TECN	COMMENT
0.10±0.05	80 ± 30	SOKHOYAN	15A	DPWA	Multichannel

Normalized residue in $N\pi \to N(1900) \to N(1520)\pi$

MODULUS	PHASE (°)	DOCUMENT ID		TECN	COMMENT
0.07±0.04	−105 ± 35	SOKHOYAN	15A	DPWA	Multichannel

Normalized residue in $N\pi \to N(1900) \to N\sigma$

MODULUS	PHASE (°)	DOCUMENT ID		TECN	COMMENT
0.03±0.02	−110 ± 35	SOKHOYAN	15A	DPWA	Multichannel

$N(1900)$ BREIT-WIGNER MASS

VALUE (MeV)	DOCUMENT ID		TECN	COMMENT
1890 to 1950 (≈ 1920) OUR ESTIMATE				
1911± 6	[1] HUNT	19	DPWA	Multichannel
1910±30	SOKHOYAN	15A	DPWA	Multichannel
1998± 3	[1] SHKLYAR	13	DPWA	Multichannel
• • • We do not use the following data for averages, fits, limits, etc. • • •				
1910±30	GUTZ	14	DPWA	Multichannel
1905±30	ANISOVICH	12A	DPWA	Multichannel
1900± 8	[1] SHRESTHA	12A	DPWA	Multichannel
1951±53	PENNER	02C	DPWA	Multichannel

[1] Statistical error only.

$N(1900)$ BREIT-WIGNER WIDTH

VALUE (MeV)	DOCUMENT ID		TECN	COMMENT
100 to 320 (≈ 200) OUR ESTIMATE				
292± 16	[1] HUNT	19	DPWA	Multichannel
270± 50	SOKHOYAN	15A	DPWA	Multichannel
359± 10	[1] SHKLYAR	13	DPWA	Multichannel
• • • We do not use the following data for averages, fits, limits, etc. • • •				
270± 50	GUTZ	14	DPWA	Multichannel
250^{+120}_{-50}	ANISOVICH	12A	DPWA	Multichannel
101± 15	[1] SHRESTHA	12A	DPWA	Multichannel
622± 42	PENNER	02C	DPWA	Multichannel

[1] Statistical error only.

$N(1900)$ DECAY MODES

	Mode	Fraction (Γ_i/Γ)
Γ_1	$N\pi$	1–20 %
Γ_2	$N\eta$	2–14 %
Γ_3	$N\eta'$	4–8 %
Γ_4	$N\omega$	7–13 %
Γ_5	ΛK	2–20 %
Γ_6	ΣK	3–7 %
Γ_7	$N\pi\pi$	>56 %
Γ_8	$\Delta(1232)\pi$	30–70 %
Γ_9	$\Delta(1232)\pi$, P-wave	9–25 %
Γ_{10}	$\Delta(1232)\pi$, F-wave	21–45 %
Γ_{11}	$N\rho$, $S=1/2$	25–40 %
Γ_{12}	$N\sigma$	1–7 %
Γ_{13}	$N(1520)\pi$	7–23 %
Γ_{14}	$N(1535)\pi$	4–10 %
Γ_{15}	$\Lambda K^*(892)$	< 0.2 %
Γ_{16}	$p\gamma$	0.001–0.025 %
Γ_{17}	$p\gamma$, helicity=1/2	0.001–0.021 %
Γ_{18}	$p\gamma$, helicity=3/2	<0.003 %
Γ_{19}	$n\gamma$	<0.040 %
Γ_{20}	$n\gamma$, helicity=1/2	<0.007 %
Γ_{21}	$n\gamma$, helicity=3/2	<0.033 %

$N(1900)$ BRANCHING RATIOS

$\Gamma(N\pi)/\Gamma_{total}$ — Γ_1/Γ

VALUE (%)	DOCUMENT ID		TECN	COMMENT
1–20 % OUR ESTIMATE				
1.9±0.1	[1] HUNT	19	DPWA	Multichannel
3 ±2	SOKHOYAN	15A	DPWA	Multichannel
25 ±1	[1] SHKLYAR	13	DPWA	Multichannel
• • • We do not use the following data for averages, fits, limits, etc. • • •				
3 ±2	GUTZ	14	DPWA	Multichannel
3 ±2	ANISOVICH	12A	DPWA	Multichannel
7 ±4	[1] SHRESTHA	12A	DPWA	Multichannel
16 ±2	PENNER	02C	DPWA	Multichannel

[1] Statistical error only.

$\Gamma(N\eta)/\Gamma_{total}$ — Γ_2/Γ

VALUE (%)	DOCUMENT ID		TECN	COMMENT
2 ±2	MUELLER	20	DPWA	Multichannel
1.3±0.5	[1] HUNT	19	DPWA	Multichannel
2 ±2	[1] SHKLYAR	13	DPWA	Multichannel
10 ±4	ANISOVICH	12A	DPWA	Multichannel
• • • We do not use the following data for averages, fits, limits, etc. • • •				
< 1	[1] SHRESTHA	12A	DPWA	Multichannel
14 ±5	PENNER	02C	DPWA	Multichannel

[1] Statistical error only.

$\Gamma(N\eta')/\Gamma_{total}$ — Γ_3/Γ

VALUE (%)	DOCUMENT ID		TECN	COMMENT
4–8 % OUR ESTIMATE				
6±2	ANISOVICH	17C	DPWA	Multichannel

$\Gamma(N\omega)/\Gamma_{total}$ — Γ_4/Γ

VALUE (%)	DOCUMENT ID		TECN	COMMENT
15±8	DENISENKO	16	DPWA	Multichannel
10±3	[1] SHKLYAR	13	DPWA	Multichannel
• • • We do not use the following data for averages, fits, limits, etc. • • •				
39±9	PENNER	02C	DPWA	Multichannel

[1] Statistical error only.

$\Gamma(\Lambda K)/\Gamma_{total}$ — Γ_5/Γ

VALUE (%)	DOCUMENT ID		TECN	COMMENT
13.7±0.3	[1] HUNT	19	DPWA	Multichannel
16 ±5	ANISOVICH	12A	DPWA	Multichannel
2.4±0.3	[1] SHKLYAR	05	DPWA	Multichannel
• • • We do not use the following data for averages, fits, limits, etc. • • •				
14 ±5	[1] SHRESTHA	12A	DPWA	Multichannel
5 to 15	NIKONOV	08	DPWA	Multichannel
0.1±0.1	PENNER	02C	DPWA	Multichannel

[1] Statistical error only.

$\Gamma(\Sigma K)/\Gamma_{total}$ — Γ_6/Γ

VALUE (%)	DOCUMENT ID		TECN	COMMENT
5±2	ANISOVICH	12A	DPWA	Multichannel
• • • We do not use the following data for averages, fits, limits, etc. • • •				
1±1	PENNER	02C	DPWA	Multichannel

$\Gamma(\Delta(1232)\pi$, P-wave$)/\Gamma_{total}$ — Γ_9/Γ

VALUE (%)	DOCUMENT ID		TECN	COMMENT
17±8	SOKHOYAN	15A	DPWA	Multichannel

$\Gamma(\Delta(1232)\pi$, F-wave$)/\Gamma_{total}$ — Γ_{10}/Γ

VALUE (%)	DOCUMENT ID		TECN	COMMENT
33±12	SOKHOYAN	15A	DPWA	Multichannel

$\Gamma(N\rho, S=1/2)/\Gamma_{total}$ — Γ_{11}/Γ

VALUE (%)	DOCUMENT ID		TECN	COMMENT
25–40 % OUR ESTIMATE				
32±7	[1] HUNT	19	DPWA	Multichannel

[1] Statistical error only.

$\Gamma(N\sigma)/\Gamma_{total}$ — Γ_{12}/Γ

VALUE (%)	DOCUMENT ID		TECN	COMMENT
4±3	SOKHOYAN	15A	DPWA	Multichannel

$\Gamma(N(1520)\pi)/\Gamma_{total}$ — Γ_{13}/Γ

VALUE (%)	DOCUMENT ID		TECN	COMMENT
15±8	SOKHOYAN	15A	DPWA	Multichannel

$\Gamma(N(1535)\pi)/\Gamma_{total}$ — Γ_{14}/Γ

VALUE (%)	DOCUMENT ID		TECN	COMMENT
7±3	GUTZ	14	DPWA	Multichannel

Downloaded from https://academic.oup.com/ptep/article/2022/8/083C01/6651666 by KIT Library user on 27 September 2022

$\Gamma(\Lambda K^*(892))/\Gamma_{total}$ — Γ_{15}/Γ

VALUE (%)	DOCUMENT ID		TECN	COMMENT
< 0.2 % OUR ESTIMATE				
<0.2	ANISOVICH	17B	DPWA	Multichannel

$N(1900)$ PHOTON DECAY AMPLITUDES AT THE POLE

$N(1900) \to p\gamma$, helicity-1/2 amplitude $A_{1/2}$

MODULUS (GeV$^{-1/2}$)	PHASE (°)	DOCUMENT ID		TECN	COMMENT
0.026±0.014	60 ± 35	SOKHOYAN	15A	DPWA	Multichannel

$N(1900) \to p\gamma$, helicity-3/2 amplitude $A_{3/2}$

MODULUS (GeV$^{-1/2}$)	PHASE (°)	DOCUMENT ID		TECN	COMMENT
−0.070±0.030	70 ± 50	SOKHOYAN	15A	DPWA	Multichannel

$N(1900)$ BREIT-WIGNER PHOTON DECAY AMPLITUDES

$N(1900) \to p\gamma$, helicity-1/2 amplitude $A_{1/2}$

VALUE (GeV$^{-1/2}$)	DOCUMENT ID		TECN	COMMENT
0.040±0.004	[1] HUNT	19	DPWA	Multichannel
0.024±0.014	SOKHOYAN	15A	DPWA	Multichannel
−0.008±0.001	[1] SHKLYAR	13	DPWA	Multichannel
• • • We do not use the following data for averages, fits, limits, etc. • • •				
0.024±0.014	GUTZ	14	DPWA	Multichannel
0.026±0.015	ANISOVICH	12A	DPWA	Multichannel
0.041±0.008	[1] SHRESTHA	12A	DPWA	Multichannel
−0.017	PENNER	02D	DPWA	Multichannel

[1] Statistical error only.

$N(1900) \to p\gamma$, helicity-3/2 amplitude $A_{3/2}$

VALUE (GeV$^{-1/2}$)	DOCUMENT ID		TECN	COMMENT
−0.094±0.007	[1] HUNT	19	DPWA	Multichannel
−0.067±0.030	SOKHOYAN	15A	DPWA	Multichannel
< 0.001	SHKLYAR	13	DPWA	Multichannel
• • • We do not use the following data for averages, fits, limits, etc. • • •				
−0.067±0.030	GUTZ	14	DPWA	Multichannel
−0.065±0.030	ANISOVICH	12A	DPWA	Multichannel
−0.004±0.006	[1] SHRESTHA	12A	DPWA	Multichannel
0.031	PENNER	02D	DPWA	Multichannel

[1] Statistical error only.

$N(1900) \to n\gamma$, helicity-1/2 amplitude $A_{1/2}$

VALUE (GeV$^{-1/2}$)	DOCUMENT ID		TECN	COMMENT
0.007±0.014	[1] HUNT	19	DPWA	Multichannel
0.000±0.030	ANISOVICH	13B	DPWA	Multichannel
• • • We do not use the following data for averages, fits, limits, etc. • • •				
−0.010±0.004	[1] SHRESTHA	12A	DPWA	Multichannel
−0.016	PENNER	02D	DPWA	Multichannel

[1] Statistical error only.

$N(1900) \to n\gamma$, helicity-3/2 amplitude $A_{3/2}$

VALUE (GeV$^{-1/2}$)	DOCUMENT ID		TECN	COMMENT
0.007±0.011	[1] HUNT	19	DPWA	Multichannel
−0.060±0.045	ANISOVICH	13B	DPWA	Multichannel
• • • We do not use the following data for averages, fits, limits, etc. • • •				
−0.011±0.007	[1] SHRESTHA	12A	DPWA	Multichannel
−0.002	PENNER	02D	DPWA	Multichannel

[1] Statistical error only.

$N(1900)$ REFERENCES

MUELLER	20	PL B803 135323	J. Mueller et al.	(CBELSA/TAPS Collab.)
HUNT	19	PR C99 055205	B.C. Hunt, D.M. Manley	
ANISOVICH	17A	PRL 119 062004	A.V. Anisovich et al.	
ANISOVICH	17B	PL B771 142	A.V. Anisovich et al.	
ANISOVICH	17C	PL B772 247	A.V. Anisovich et al.	
DENISENKO	16	PL B755 97	I. Denisenko et al.	
SOKHOYAN	15A	EPJ A51 95	V. Sokhoyan et al.	(CBELSA/TAPS Collab.)
GUTZ	14	EPJ A50 74	E. Gutz et al.	(CBELSA/TAPS Collab.)
SVARC	14	PR C89 045205	A. Svarc et al.	(RBI Zagreb, UNI Tuzla)
ANISOVICH	13B	EPJ A49 67	A.V. Anisovich et al.	
SHKLYAR	13	PR C87 015201	V. Shklyar, H. Lenske, U. Mosel	(GIES)
ANISOVICH	12A	EPJ A48 15	A.V. Anisovich et al.	(BONN, PNPI)
SHRESTHA	12A	PR C86 055203	M. Shrestha, D.M. Manley	(KSU)
NIKONOV	08	PL B662 245	V.A. Nikonov et al.	(Bonn, Gatchina)
SHKLYAR	05	PR C72 015210	V. Shklyar, H. Lenske, U. Mosel	(GIES)
PENNER	02C	PR C66 055211	G. Penner, U. Mosel	(GIES)
PENNER	02D	PR C66 055212	G. Penner, U. Mosel	(GIES)
HOEHLER	79	PDAT 12-1	G. Hohler et al.	(KARLT)

$N(1990)$ $7/2^+$

$I(J^P) = \frac{1}{2}(\frac{7}{2}^+)$ Status: **

OMITTED FROM SUMMARY TABLE

Older and obsolete values are listed and referenced in the 2014 edition, Chinese Physics **C38** 070001 (2014).

$N(1990)$ POLE POSITION

REAL PART

VALUE (MeV)	DOCUMENT ID		TECN	COMMENT
2030±65	ANISOVICH	12A	DPWA	Multichannel
1900±30	CUTKOSKY	80	IPWA	$\pi N \to \pi N$
• • • We do not use the following data for averages, fits, limits, etc. • • •				
1913	HUNT	19	DPWA	Multichannel
1738	ROENCHEN	15A	DPWA	Multichannel
2301	VRANA	00	DPWA	Multichannel

−2×IMAGINARY PART

VALUE (MeV)	DOCUMENT ID		TECN	COMMENT
240±60	ANISOVICH	12A	DPWA	Multichannel
260±60	CUTKOSKY	80	IPWA	$\pi N \to \pi N$
• • • We do not use the following data for averages, fits, limits, etc. • • •				
163	HUNT	19	DPWA	Multichannel
188	ROENCHEN	15A	DPWA	Multichannel
202	VRANA	00	DPWA	Multichannel

$N(1990)$ ELASTIC POLE RESIDUE

MODULUS $|r|$

VALUE (MeV)	DOCUMENT ID		TECN	COMMENT
2 ±1	ANISOVICH	12A	DPWA	Multichannel
9 ±3	CUTKOSKY	80	IPWA	$\pi N \to \pi N$
• • • We do not use the following data for averages, fits, limits, etc. • • •				
4.3	ROENCHEN	15A	DPWA	Multichannel

PHASE θ

VALUE (°)	DOCUMENT ID		TECN	COMMENT
125±65	ANISOVICH	12A	DPWA	Multichannel
− 60±30	CUTKOSKY	80	IPWA	$\pi N \to \pi N$
• • • We do not use the following data for averages, fits, limits, etc. • • •				
− 70	ROENCHEN	15A	DPWA	Multichannel

$\Delta(1990)$ INELASTIC POLE RESIDUE

The "normalized residue" is the residue divided by $\Gamma_{pole}/2$.

Normalized residue in $N\pi \to N(1990) \to N\eta$

MODULUS	PHASE (°)	DOCUMENT ID		TECN	COMMENT
• • • We do not use the following data for averages, fits, limits, etc. • • •					
0.013	−82	ROENCHEN	15A	DPWA	Multichannel

Normalized residue in $N\pi \to N(1990) \to \Lambda K$

MODULUS	PHASE (°)	DOCUMENT ID		TECN	COMMENT
• • • We do not use the following data for averages, fits, limits, etc. • • •					
0.022	−111	ROENCHEN	15A	DPWA	Multichannel

Normalized residue in $N\pi \to N(1990) \to \Sigma K$

MODULUS	PHASE (°)	DOCUMENT ID		TECN	COMMENT
• • • We do not use the following data for averages, fits, limits, etc. • • •					
0.005	24	ROENCHEN	15A	DPWA	Multichannel

$N(1990)$ BREIT-WIGNER MASS

VALUE (MeV)	DOCUMENT ID		TECN	COMMENT
1950 to 2100 (≈ 2020) OUR ESTIMATE				
2028± 19	[1] HUNT	19	DPWA	Multichannel
2060± 65	ANISOVICH	12A	DPWA	Multichannel
1970± 50	CUTKOSKY	80	IPWA	$\pi N \to \pi N$
2005±150	HOEHLER	79	IPWA	$\pi N \to \pi N$
• • • We do not use the following data for averages, fits, limits, etc. • • •				
1990± 45	[1] SHRESTHA	12A	DPWA	Multichannel
2311± 16	VRANA	00	DPWA	Multichannel

[1] Statistical error only.

$N(1990)$ BREIT-WIGNER WIDTH

VALUE (MeV)	DOCUMENT ID		TECN	COMMENT
200 to 400 (≈ 300) OUR ESTIMATE				
490±110	[1] HUNT	19	DPWA	Multichannel
240± 50	ANISOVICH	12A	DPWA	Multichannel
350±120	CUTKOSKY	80	IPWA	$\pi N \to \pi N$
350±100	HOEHLER	79	IPWA	$\pi N \to \pi N$
• • • We do not use the following data for averages, fits, limits, etc. • • •				
203±161	[1] SHRESTHA	12A	DPWA	Multichannel
205± 72	VRANA	00	DPWA	Multichannel

[1] Statistical error only.

Downloaded from https://academic.oup.com/ptep/article/2022/8/083C01/6651666 by KIT Library user on 27 September 2022

$N(1990)$ DECAY MODES

	Mode	Fraction (Γ_i/Γ)
Γ_1	$N\pi$	2–6 %
Γ_2	$N\eta$	<3 %
Γ_3	ΛK	5.9–6.1 %
Γ_4	$p\gamma$	0.01–0.12%
Γ_5	$p\gamma$, helicity=1/2	0.003–0.042%
Γ_6	$p\gamma$, helicity=3/2	0.009–0.075 %
Γ_7	$n\gamma$	0.01–0.16 %
Γ_8	$n\gamma$, helicity=1/2	0.003–0.066 %
Γ_9	$n\gamma$, helicity=3/2	0.003–0.098 %

$N(1990)$ BRANCHING RATIOS

$\Gamma(N\pi)/\Gamma_{total}$ — Γ_1/Γ

VALUE (%)	DOCUMENT ID		TECN	COMMENT
2–6 % OUR ESTIMATE				
1.9± 0.4	[1] HUNT	19	DPWA	Multichannel
2 ± 1	ANISOVICH	12A	DPWA	Multichannel
6 ± 2	CUTKOSKY	80	IPWA	$\pi N \to \pi N$
4 ± 2	HOEHLER	79	IPWA	$\pi N \to \pi N$
• • • We do not use the following data for averages, fits, limits, etc. • • •				
2 ± 1	[1] SHRESTHA	12A	DPWA	Multichannel
22 ±11	VRANA	00	DPWA	Multichannel

[1] Statistical error only.

$\Gamma(N\eta)/\Gamma_{total}$ — Γ_2/Γ

VALUE (%)	DOCUMENT ID		TECN	COMMENT
<3 % OUR ESTIMATE				
1 ±1	MUELLER	20	DPWA	Multichannel
1.7±0.9	[1] HUNT	19	DPWA	Multichannel

[1] Statistical error only.

$\Gamma(\Lambda K)/\Gamma_{total}$ — Γ_3/Γ

VALUE (%)	DOCUMENT ID		TECN	COMMENT
5.9–6.1 % OUR ESTIMATE				
6.0±0.1	[1] HUNT	19	DPWA	Multichannel

[1] Statistical error only.

$N(1990)$ PHOTON DECAY AMPLITUDES AT THE POLE

$N(1990) \to p\gamma$, helicity-1/2 amplitude $A_{1/2}$

MODULUS ($GeV^{-1/2}$)	PHASE (°)	DOCUMENT ID		TECN	COMMENT
$0.010^{+0.011}_{-0.006}$	-103^{+108}_{-155}	ROENCHEN	14	DPWA	
• • • We do not use the following data for averages, fits, limits, etc. • • •					
0.029	67	ROENCHEN	15A	DPWA	Multichannel

$N(1990) \to p\gamma$, helicity-3/2 amplitude $A_{3/2}$

MODULUS ($GeV^{-1/2}$)	PHASE (°)	DOCUMENT ID		TECN	COMMENT
$0.053^{+0.023}_{-0.028}$	36^{+17}_{-4}	ROENCHEN	14	DPWA	
• • • We do not use the following data for averages, fits, limits, etc. • • •					
0.033	39	ROENCHEN	15A	DPWA	Multichannel

$N(1990)$ BREIT-WIGNER PHOTON DECAY AMPLITUDES

$N(1990) \to p\gamma$, helicity-1/2 amplitude $A_{1/2}$

VALUE ($GeV^{-1/2}$)	DOCUMENT ID		TECN	COMMENT
0.006±0.003	[1] HUNT	19	DPWA	Multichannel
0.040±0.012	ANISOVICH	12A	DPWA	Multichannel

[1] Statistical error only.

$N(1990) \to p\gamma$, helicity-3/2 amplitude $A_{3/2}$

VALUE ($GeV^{-1/2}$)	DOCUMENT ID		TECN	COMMENT
−0.055±0.008	[1] HUNT	19	DPWA	Multichannel
0.057±0.012	ANISOVICH	12A	DPWA	Multichannel

[1] Statistical error only.

$N(1990) \to n\gamma$, helicity-1/2 amplitude $A_{1/2}$

VALUE ($GeV^{-1/2}$)	DOCUMENT ID		TECN	COMMENT
−0.027±0.024	[1] HUNT	19	DPWA	Multichannel
−0.045±0.020	ANISOVICH	13B	DPWA	Multichannel

[1] Statistical error only.

$N(1990) \to n\gamma$, helicity-3/2 amplitude $A_{3/2}$

VALUE ($GeV^{-1/2}$)	DOCUMENT ID		TECN	COMMENT
0.051±0.020	[1] HUNT	19	DPWA	Multichannel
−0.052±0.027	ANISOVICH	13B	DPWA	Multichannel

[1] Statistical error only.

$N(1990)$ REFERENCES

For early references, see Physics Letters **111B** 1 (1982).

MUELLER	20	PL B803 135323	J. Mueller *et al.*	(CBELSA/TAPS Collab.)
HUNT	19	PR C99 055205	B.C. Hunt, D.M. Manley	
ROENCHEN	15A	EPJ A51 70	D. Roenchen *et al.*	
PDG	14	CP C38 070001	K. Olive *et al.*	(PDG Collab.)
ROENCHEN	14	EPJ A50 101	D. Roenchen *et al.*	
Also		EPJ A51 63 (errat.)	D. Roenchen *et al.*	
ANISOVICH	13B	EPJ A49 67	A.V. Anisovich *et al.*	
ANISOVICH	12A	EPJ A48 15	A.V. Anisovich *et al.*	(BONN, PNPI)
SHRESTHA	12A	PR C86 055203	M. Shrestha, D.M. Manley	(KSU)
VRANA	00	PRPL 328 181	T.P. Vrana, S.A. Dytman, T.-S.H. Lee	(PITT, ANL)
CUTKOSKY	80	Toronto Conf. 19	R.E. Cutkosky *et al.*	(CMU, LBL) IJP
Also		PR D20 2839	R.E. Cutkosky *et al.*	(CMU, LBL) IJP
HOEHLER	79	PDAT 12-1	G. Hohler *et al.*	(KARLT) IJP
Also		Toronto Conf. 3	R. Koch	(KARLT) IJP

$N(2000)\ 5/2^+$

$I(J^P) = \frac{1}{2}(\frac{5}{2}^+)$ Status: ∗∗

OMITTED FROM SUMMARY TABLE

Before the 2012 *Review*, all the evidence for a $J^P = 5/2^+$ state with a mass above 1800 MeV was filed under a two-star $N(2000)$. There is now some evidence from ANISOVICH 12A for two $5/2^+$ states in this region, so we have split the older data (according to mass) between two two-star $5/2^+$ states, an $N(1860)$ and an $N(2000)$.

$N(2000)$ POLE POSITION

REAL PART

VALUE (MeV)	DOCUMENT ID		TECN	COMMENT
2030± 40	SOKHOYAN	15A	DPWA	Multichannel
• • • We do not use the following data for averages, fits, limits, etc. • • •				
1900	SHKLYAR	13	DPWA	Multichannel
2030±110	ANISOVICH	12A	DPWA	Multichannel

−2×IMAGINARY PART

VALUE (MeV)	DOCUMENT ID		TECN	COMMENT
380± 60	SOKHOYAN	15A	DPWA	Multichannel
• • • We do not use the following data for averages, fits, limits, etc. • • •				
123	SHKLYAR	13	DPWA	Multichannel
480±100	ANISOVICH	12A	DPWA	Multichannel

$N(2000)$ ELASTIC POLE RESIDUE

MODULUS $|r|$

VALUE (MeV)	DOCUMENT ID		TECN	COMMENT
18± 8	SOKHOYAN	15A	DPWA	Multichannel
• • • We do not use the following data for averages, fits, limits, etc. • • •				
11	SHKLYAR	13	DPWA	Multichannel
35^{+80}_{-15}	ANISOVICH	12A	DPWA	Multichannel

PHASE θ

VALUE (°)	DOCUMENT ID		TECN	COMMENT
−150±40	SOKHOYAN	15A	DPWA	Multichannel
• • • We do not use the following data for averages, fits, limits, etc. • • •				
− 6	SHKLYAR	13	DPWA	Multichannel
−100±40	ANISOVICH	12A	DPWA	Multichannel

$N(2000)$ INELASTIC POLE RESIDUE

The "normalized residue" is the residue divided by $\Gamma_{pole}/2$.

Normalized residue in $N\pi \to N(2000) \to \Delta(1232)\pi$, P-wave

MODULUS	PHASE (°)	DOCUMENT ID		TECN	COMMENT
0.16±0.06	100 ± 50	SOKHOYAN	15A	DPWA	Multichannel

Normalized residue in $N\pi \to N(2000) \to \Delta(1232)\pi$, F-wave

MODULUS	PHASE (°)	DOCUMENT ID		TECN	COMMENT
0.20±0.10	−20 ± 45	SOKHOYAN	15A	DPWA	Multichannel

Normalized residue in $N\pi \to N(2000) \to N\sigma$

MODULUS	PHASE (°)	DOCUMENT ID		TECN	COMMENT
0.12±0.06	80 ± 40	SOKHOYAN	15A	DPWA	Multichannel

Normalized residue in $N\pi \to N(2000) \to N(1520)\pi$, D-wave

MODULUS	PHASE (°)	DOCUMENT ID		TECN	COMMENT
0.17±0.09	−60 ± 35	SOKHOYAN	15A	DPWA	Multichannel

$N(2000)$ BREIT-WIGNER MASS

VALUE (MeV)	DOCUMENT ID		TECN	COMMENT
2060± 30	SOKHOYAN	15A	DPWA	Multichannel
1946± 4	[1] SHKLYAR	13	DPWA	Multichannel

Downloaded from https://academic.oup.com/ptep/article/2022/8/083C01/6651666 by KIT Library user on 27 September 2022

• • • We do not use the following data for averages, fits, limits, etc. • • •

2090±120	ANISOVICH	12A	DPWA	Multichannel

[1] Statistical error only.

N(2000) BREIT-WIGNER WIDTH

VALUE (MeV)	DOCUMENT ID		TECN	COMMENT
390± 55	SOKHOYAN	15A	DPWA	Multichannel
198± 2	[2] SHKLYAR	13	DPWA	Multichannel
• • • We do not use the following data for averages, fits, limits, etc. • • •				
460±100	ANISOVICH	12A	DPWA	Multichannel

[2] Statistical error only.

N(2000) DECAY MODES

	Mode	Fraction (Γ_i/Γ)
Γ_1	$N\pi$	6–10 %
Γ_2	$N\eta$	<4 %
Γ_3	$N\omega$	<2 %
Γ_4	$N\pi\pi$	35–90 %
Γ_5	$\Delta(1232)\pi$	30–80 %
Γ_6	$\Delta(1232)\pi$, P-wave	12–32 %
Γ_7	$\Delta(1232)\pi$, F-wave	19–49 %
Γ_8	$N\sigma$	5–15 %
Γ_9	$N(1520)\pi$, D-wave	11–31 %
Γ_{10}	$N(1680)\pi$, P-wave	17–25 %
Γ_{11}	$\Lambda K^*(892)$	1–3 %
Γ_{12}	$p\gamma$	0.01–0.08 %
Γ_{13}	$p\gamma$, helicity=1/2	0.003–0.031 %
Γ_{14}	$p\gamma$, helicity=3/2	0.008–0.048 %
Γ_{15}	$n\gamma$	0.002–0.07 %
Γ_{16}	$n\gamma$, helicity=1/2	<0.017 %
Γ_{17}	$n\gamma$, helicity=3/2	0.001–0.056 %

N(2000) BRANCHING RATIOS

$\Gamma(N\pi)/\Gamma_{total}$ — Γ_1/Γ

VALUE (%)	DOCUMENT ID		TECN	COMMENT
6 to 10 (≈ 8) OUR ESTIMATE				
8±4	SOKHOYAN	15A	DPWA	Multichannel
10±1	[3] SHKLYAR	13	DPWA	Multichannel
• • • We do not use the following data for averages, fits, limits, etc. • • •				
9±4	ANISOVICH	12A	DPWA	Multichannel

[3] Statistical error only.

$\Gamma(N\eta)/\Gamma_{total}$ — Γ_2/Γ

VALUE (%)	DOCUMENT ID		TECN	COMMENT
2±2	MUELLER	20	DPWA	Multichannel
2±2	[4] SHKLYAR	13	DPWA	Multichannel

[4] Statistical error only.

$\Gamma(N\omega)/\Gamma_{total}$ — Γ_3/Γ

VALUE (%)	DOCUMENT ID		TECN	COMMENT
18±8	DENISENKO	16	DPWA	Multichannel
1±1	[5] SHKLYAR	13	DPWA	Multichannel

[5] Statistical error only.

$\Gamma(\Delta(1232)\pi, P\text{-wave})/\Gamma_{total}$ — Γ_6/Γ

VALUE (%)	DOCUMENT ID		TECN	COMMENT
22±10	SOKHOYAN	15A	DPWA	Multichannel

$\Gamma(\Delta(1232)\pi, F\text{-wave})/\Gamma_{total}$ — Γ_7/Γ

VALUE (%)	DOCUMENT ID		TECN	COMMENT
34±15	SOKHOYAN	15A	DPWA	Multichannel

$\Gamma(N\sigma)/\Gamma_{total}$ — Γ_8/Γ

VALUE (%)	DOCUMENT ID		TECN	COMMENT
10±5	SOKHOYAN	15A	DPWA	Multichannel

$\Gamma(N(1520)\pi, D\text{-wave})/\Gamma_{total}$ — Γ_9/Γ

VALUE (%)	DOCUMENT ID		TECN	COMMENT
21±10	SOKHOYAN	15A	DPWA	Multichannel

$\Gamma(N(1680)\pi, P\text{-wave})/\Gamma_{total}$ — Γ_{10}/Γ

VALUE (%)	DOCUMENT ID		TECN	COMMENT
16±9	SOKHOYAN	15A	DPWA	Multichannel

$\Gamma(\Lambda K^*(892))/\Gamma_{total}$ — Γ_{11}/Γ

VALUE (%)	DOCUMENT ID		TECN	COMMENT
1–3 % OUR EVALUATION				
2.2±1.0	ANISOVICH	17B	DPWA	Multichannel

N(2000) PHOTON DECAY AMPLITUDES AT THE POLE

$N(2000) \to p\gamma$, helicity-1/2 amplitude $A_{1/2}$

MODULUS ($GeV^{-1/2}$)	PHASE (°)	DOCUMENT ID		TECN	COMMENT
0.033±0.010	15 ± 25	SOKHOYAN	15A	DPWA	Multichannel

$N(2000) \to p\gamma$, helicity-3/2 amplitude $A_{3/2}$

MODULUS ($GeV^{-1/2}$)	PHASE (°)	DOCUMENT ID		TECN	COMMENT
0.045±0.008	−140 ± 25	SOKHOYAN	15A	DPWA	Multichannel

N(2000) BREIT-WIGNER PHOTON DECAY AMPLITUDES

$N(2000) \to p\gamma$, helicity-1/2 amplitude $A_{1/2}$

VALUE ($GeV^{-1/2}$)	DOCUMENT ID		TECN	COMMENT
0.031±0.010	SOKHOYAN	15A	DPWA	Multichannel
0.011±0.001	[6] SHKLYAR	13	DPWA	Multichannel

[6] Statistical error only.

$N(2000) \to p\gamma$, helicity-3/2 amplitude $A_{3/2}$

VALUE ($GeV^{-1/2}$)	DOCUMENT ID		TECN	COMMENT
−0.043±0.008	SOKHOYAN	15A	DPWA	Multichannel
0.025±0.001	[7] SHKLYAR	13	DPWA	Multichannel

[7] Statistical error only.

$N(2000) \to n\gamma$, helicity-1/2 amplitude $A_{1/2}$

VALUE ($GeV^{-1/2}$)	DOCUMENT ID		TECN	COMMENT
−0.018±0.012	ANISOVICH	13B	DPWA	Multichannel

$N(2000) \to n\gamma$, helicity-3/2 amplitude $A_{3/2}$

VALUE ($GeV^{-1/2}$)	DOCUMENT ID		TECN	COMMENT
−0.035±0.020	ANISOVICH	13B	DPWA	Multichannel

N(2000) REFERENCES

MUELLER	20	PL B803 135323	J. Mueller et al.	(CBELSA/TAPS Collab.)
ANISOVICH	17B	PL B771 142	A.V. Anisovich et al.	
DENISENKO	16	PL B755 97	I. Denisenko et al.	
SOKHOYAN	15A	EPJ A51 95	V. Sokhoyan et al.	(CBELSA/TAPS Collab.)
ANISOVICH	13B	EPJ A49 67	A.V. Anisovich et al.	
SHKLYAR	13	PR C87 015201	V. Shklyar, H. Lenske, U. Mosel	(GIES)
ANISOVICH	12A	EPJ A48 15	A.V. Anisovich et al.	(BONN, PNPI)

N(2040) 3/2+

$J^P = \frac{3}{2}^+$ Status: *

OMITTED FROM SUMMARY TABLE

N(2040) MASS

VALUE (MeV)	DOCUMENT ID		TECN	COMMENT
$2040^{+3}_{-4}\pm25$	ABLIKIM	09B	BES2	$J/\psi \to p\overline{p}\pi^0$
$2068\pm3^{+15}_{-40}$	ABLIKIM	06K	BES2	$J/\psi \to p\overline{n}\pi^-$, $n\overline{p}\pi^+$
• • • We do not use the following data for averages, fits, limits, etc. • • •				
2244±30	[1,2] HUNT	19	DPWA	Multichannel

[1] Statistical error only.
[2] We list here candidates for high-mass 3/2+ states.

N(2040) WIDTH

VALUE (MeV)	DOCUMENT ID		TECN	COMMENT
230± 8±52	ABLIKIM	09B	BES2	$J/\psi \to p\overline{p}\pi^0$
165±14±40	ABLIKIM	06K	BES2	$J/\psi \to p\overline{n}\pi^-$, $n\overline{p}\pi^+$
• • • We do not use the following data for averages, fits, limits, etc. • • •				
530±89	[3,4] HUNT	19	DPWA	Multichannel

[3] Statistical error only.
[4] We list here candidates for high-mass 3/2+ states.

N(2040) REFERENCES

HUNT	19	PR C99 055205	B.C. Hunt, D.M. Manley	
ABLIKIM	09B	PR D80 052004	M. Ablikim et al.	(BES II Collab.)
ABLIKIM	06K	PRL 97 062001	M. Ablikim et al.	(BES II Collab.)

Downloaded from https://academic.oup.com/ptep/article/2022/8/083C01/6651666 by KIT Library user on 27 September 2022

$N(2060)\ 5/2^-$

$I(J^P) = \frac{1}{2}(\frac{5}{2}^-)$ Status: ***

Before our 2012 *Review*, this state appeared in our Listings as the $N(2200)$.

$N(2060)$ POLE POSITION

REAL PART

VALUE (MeV)	DOCUMENT ID		TECN	COMMENT
2020 to 2130 (≈ 2070) OUR ESTIMATE				
2030±15	SOKHOYAN	15A	DPWA	Multichannel
2119±11±1	[1] SVARC	14	L+P	$\pi N \to \pi N$
2100±60	CUTKOSKY	80	IPWA	$\pi N \to \pi N$
• • • We do not use the following data for averages, fits, limits, etc. • • •				
2010	HUNT	19	DPWA	Multichannel
2040±15	ANISOVICH	12A	DPWA	Multichannel
2144±31	BATINIC	10	DPWA	$\pi N \to N\pi,\ N\eta$

[1] Fit to the amplitudes of HOEHLER 79.

−2×IMAGINARY PART

VALUE (MeV)	DOCUMENT ID		TECN	COMMENT
350 to 430 (≈ 400) OUR ESTIMATE				
400±35	SOKHOYAN	15A	DPWA	Multichannel
370±20±5	[1] SVARC	14	L+P	$\pi N \to \pi N$
360±80	CUTKOSKY	80	IPWA	$\pi N \to \pi N$
• • • We do not use the following data for averages, fits, limits, etc. • • •				
395	HUNT	19	DPWA	Multichannel
390±25	ANISOVICH	12A	DPWA	Multichannel
438±13	BATINIC	10	DPWA	$\pi N \to N\pi,\ N\eta$

[1] Fit to the amplitudes of HOEHLER 79.

$N(2060)$ ELASTIC POLE RESIDUE

MODULUS $|r|$

VALUE (MeV)	DOCUMENT ID		TECN	COMMENT
15 to 30 (≈ 20) OUR ESTIMATE				
25± 8	SOKHOYAN	15A	DPWA	Multichannel
19± 1±1	[1] SVARC	14	L+P	$\pi N \to \pi N$
20±10	CUTKOSKY	80	IPWA	$\pi N \to \pi N$
• • • We do not use the following data for averages, fits, limits, etc. • • •				
19± 5	ANISOVICH	12A	DPWA	Multichannel
26	BATINIC	10	DPWA	$\pi N \to N\pi,\ N\eta$

[1] Fit to the amplitudes of HOEHLER 79.

PHASE θ

VALUE (°)	DOCUMENT ID		TECN	COMMENT
−130 to −90 (≈ −110) OUR ESTIMATE				
−130±20	SOKHOYAN	15A	DPWA	Multichannel
− 94± 5±1	[1] SVARC	14	L+P	$\pi N \to \pi N$
− 90±50	CUTKOSKY	80	IPWA	$\pi N \to \pi N$
• • • We do not use the following data for averages, fits, limits, etc. • • •				
−125±20	ANISOVICH	12A	DPWA	Multichannel
− 71	BATINIC	10	DPWA	$\pi N \to N\pi,\ N\eta$

[1] Fit to the amplitudes of HOEHLER 79.

$N(2060)$ INELASTIC POLE RESIDUE

The "normalized residue" is the residue divided by $\Gamma_{pole}/2$.

Normalized residue in $N\pi \to N(2060) \to N\eta$

MODULUS	PHASE (°)	DOCUMENT ID		TECN	COMMENT
0.05±0.03	40 ± 25	ANISOVICH	12A	DPWA	Multichannel

Normalized residue in $N\pi \to N(2060) \to \Lambda K$

MODULUS	DOCUMENT ID		TECN	COMMENT
0.01±0.005	ANISOVICH	12A	DPWA	Multichannel

Normalized residue in $N\pi \to N(2060) \to \Sigma K$

MODULUS	PHASE (°)	DOCUMENT ID		TECN	COMMENT
0.04±0.02	−70 ± 30	ANISOVICH	12A	DPWA	Multichannel

Normalized residue in $N\pi \to N(2060) \to \Delta(1232)\pi$, D-wave

MODULUS	PHASE (°)	DOCUMENT ID		TECN	COMMENT
0.06±0.03	−90 ± 40	SOKHOYAN	15A	DPWA	Multichannel

Normalized residue in $N\pi \to N(2060) \to N\sigma$

MODULUS	PHASE (°)	DOCUMENT ID		TECN	COMMENT
0.12±0.06	80 ± 40	SOKHOYAN	15A	DPWA	Multichannel

Normalized residue in $N\pi \to N(2060) \to N(1440)\pi$

MODULUS	PHASE (°)	DOCUMENT ID		TECN	COMMENT
0.17±0.09	−60 ± 35	SOKHOYAN	15A	DPWA	Multichannel

Normalized residue in $N\pi \to N(2060) \to N(1520)\pi$, P-wave

MODULUS	PHASE (°)	DOCUMENT ID		TECN	COMMENT
0.14±0.06	−45 ± 15	SOKHOYAN	15A	DPWA	Multichannel

$N(2060)$ BREIT-WIGNER MASS

VALUE (MeV)	DOCUMENT ID		TECN	COMMENT
2030 to 2200 (≈ 2100) OUR ESTIMATE				
2111±17	[1] HUNT	19	DPWA	Multichannel
2045±15	SOKHOYAN	15A	DPWA	Multichannel
2180±80	CUTKOSKY	80	IPWA	$\pi N \to \pi N$
2228±30	HOEHLER	79	IPWA	$\pi N \to \pi N$
• • • We do not use the following data for averages, fits, limits, etc. • • •				
2060±15	ANISOVICH	12A	DPWA	Multichannel
2116±21	[1] SHRESTHA	12A	DPWA	Multichannel
2217±27	BATINIC	10	DPWA	$\pi N \to N\pi,\ N\eta$

[1] Statistical error only.

$N(2060)$ BREIT-WIGNER WIDTH

VALUE (MeV)	DOCUMENT ID		TECN	COMMENT
300 to 450 (≈ 400) OUR ESTIMATE				
499± 70	[1] HUNT	19	DPWA	Multichannel
420± 30	SOKHOYAN	15A	DPWA	Multichannel
400±100	CUTKOSKY	80	IPWA	$\pi N \to \pi N$
310± 50	HOEHLER	79	IPWA	$\pi N \to \pi N$
• • • We do not use the following data for averages, fits, limits, etc. • • •				
375± 25	ANISOVICH	12A	DPWA	Multichannel
307±112	[1] SHRESTHA	12A	DPWA	Multichannel
481± 17	BATINIC	10	DPWA	$\pi N \to N\pi,\ N\eta$

[1] Statistical error only.

$N(2060)$ DECAY MODES

	Mode	Fraction (Γ_i/Γ)
Γ_1	$N\pi$	7–12 %
Γ_2	$N\eta$	2–38 %
Γ_3	$N\omega$	1–7 %
Γ_4	ΛK	10–20 %
Γ_5	ΣK	1–5 %
Γ_6	$N\pi\pi$	12–52 %
Γ_7	$\Delta(1232)\pi$, D-wave	4–10 %
Γ_8	$N\rho$	5–33 %
Γ_9	$N\rho$, S=1/2, P-wave	<10 %
Γ_{10}	$N\rho$, S=3/2 , D-wave	5–23 %
Γ_{11}	$N\sigma$	3–9 %
Γ_{12}	$N(1440)\pi$	4–14 %
Γ_{13}	$N(1520)\pi$, P-wave	9–21 %
Γ_{14}	$N(1680)\pi$, S-wave	8–22 %
Γ_{15}	$\Lambda K^*(892)$	0.3–1.3 %
Γ_{16}	$p\gamma$	0.03–0.19 %
Γ_{17}	$p\gamma$, helicity=1/2	0.02–0.08 %
Γ_{18}	$p\gamma$, helicity=3/2	0.01–0.10 %
Γ_{19}	$n\gamma$	0.003–0.07 %
Γ_{20}	$n\gamma$, helicity=1/2	0.001–0.02 %
Γ_{21}	$n\gamma$, helicity=3/2	0.002–0.05 %

$N(2060)$ BRANCHING RATIOS

$\Gamma(N\pi)/\Gamma_{total}$ — Γ_1/Γ

VALUE (%)	DOCUMENT ID		TECN	COMMENT
7 to 12 (≈ 10) OUR ESTIMATE				
5.3±1.4	[1] HUNT	19	DPWA	Multichannel
11 ±2	SOKHOYAN	15A	DPWA	Multichannel
10 ±3	CUTKOSKY	80	IPWA	$\pi N \to \pi N$
7 ±2	HOEHLER	79	IPWA	$\pi N \to \pi N$
• • • We do not use the following data for averages, fits, limits, etc. • • •				
8 ±2	ANISOVICH	12A	DPWA	Multichannel
9 ±2	[1] SHRESTHA	12A	DPWA	Multichannel
13 ±4	BATINIC	10	DPWA	$\pi N \to N\pi,\ N\eta$

[1] Statistical error only.

$\Gamma(N\eta)/\Gamma_{total}$ — Γ_2/Γ

VALUE (%)	DOCUMENT ID		TECN	COMMENT
2–38 % OUR ESTIMATE				
6 ±2	MUELLER	20	DPWA	Multichannel
30 ±8	[1] HUNT	19	DPWA	Multichannel
4 ±2	ANISOVICH	12A	DPWA	Multichannel
• • • We do not use the following data for averages, fits, limits, etc. • • •				
< 1	[1] SHRESTHA	12A	DPWA	Multichannel
0.2±1.0	BATINIC	10	DPWA	$\pi N \to N\pi,\ N\eta$

[1] Statistical error only.

Downloaded from https://academic.oup.com/ptep/article/2022/8/083C01/6651666 by KIT Library user on 27 September 2022

$\Gamma(N\omega)/\Gamma_{total}$ — Γ_3/Γ

VALUE (%)	DOCUMENT ID		TECN	COMMENT
4±3	DENISENKO	16	DPWA	Multichannel

$\Gamma(\Lambda K)/\Gamma_{total}$ — Γ_4/Γ

VALUE (%)	DOCUMENT ID		TECN	COMMENT
10–20 % OUR ESTIMATE				
15±5	[1] HUNT	19	DPWA	Multichannel

[1] Statistical error only.

$\Gamma(\Sigma K)/\Gamma_{total}$ — Γ_5/Γ

VALUE (%)	DOCUMENT ID		TECN	COMMENT
3±2	ANISOVICH	12A	DPWA	Multichannel

$\Gamma(\Delta(1232)\pi, D\text{-wave})/\Gamma_{total}$ — Γ_7/Γ

VALUE (%)	DOCUMENT ID		TECN	COMMENT
4–10 % OUR ESTIMATE				
15± 6	[1] HUNT	19	DPWA	Multichannel
7± 3	SOKHOYAN	15A	DPWA	Multichannel
• • • We do not use the following data for averages, fits, limits, etc. • • •				
40±13	[1] SHRESTHA	12A	DPWA	Multichannel

[1] Statistical error only.

$\Gamma(N\rho, S=1/2, P\text{-wave})/\Gamma_{total}$ — Γ_9/Γ

VALUE (%)	DOCUMENT ID		TECN	COMMENT
<10 % OUR ESTIMATE				
<10	[1] HUNT	19	DPWA	Multichannel
• • • We do not use the following data for averages, fits, limits, etc. • • •				
21±15	[1] SHRESTHA	12A	DPWA	Multichannel

[1] Statistical error only.

$\Gamma(N\rho, S=3/2, D\text{-wave})/\Gamma_{total}$ — Γ_{10}/Γ

VALUE (%)	DOCUMENT ID		TECN	COMMENT
5–23 % OUR ESTIMATE				
14±9	[1] HUNT	19	DPWA	Multichannel

[1] Statistical error only.

$\Gamma(N\sigma)/\Gamma_{total}$ — Γ_{11}/Γ

VALUE (%)	DOCUMENT ID		TECN	COMMENT
6±3	SOKHOYAN	15A	DPWA	Multichannel

$\Gamma(N(1440)\pi)/\Gamma_{total}$ — Γ_{12}/Γ

VALUE (%)	DOCUMENT ID		TECN	COMMENT
9±5	SOKHOYAN	15A	DPWA	Multichannel

$\Gamma(N(1520)\pi, P\text{-wave})/\Gamma_{total}$ — Γ_{13}/Γ

VALUE (%)	DOCUMENT ID		TECN	COMMENT
15±6	SOKHOYAN	15A	DPWA	Multichannel

$\Gamma(N(1680)\pi, S\text{-wave})/\Gamma_{total}$ — Γ_{14}/Γ

VALUE (%)	DOCUMENT ID		TECN	COMMENT
15±7	SOKHOYAN	15A	DPWA	Multichannel

$\Gamma(\Lambda K^*(892))/\Gamma_{total}$ — Γ_{15}/Γ

VALUE (%)	DOCUMENT ID		TECN	COMMENT
0.3–1.3 % OUR ESTIMATE				
0.8±0.5	ANISOVICH	17B	DPWA	Multichannel

$N(2060)$ PHOTON DECAY AMPLITUDES AT THE POLE

$N(2060) \to p\gamma$, helicity-1/2 amplitude $A_{1/2}$

MODULUS ($GeV^{-1/2}$)	PHASE (°)	DOCUMENT ID		TECN	COMMENT
0.064±0.010	12 ± 8	SOKHOYAN	15A	DPWA	Multichannel

$N(2060) \to p\gamma$, helicity-3/2 amplitude $A_{3/2}$

MODULUS ($GeV^{-1/2}$)	PHASE (°)	DOCUMENT ID		TECN	COMMENT
0.060±0.020	13 ± 10	SOKHOYAN	15A	DPWA	Multichannel

$N(2060)$ BREIT-WIGNER PHOTON DECAY AMPLITUDES

$N(2060) \to p\gamma$, helicity-1/2 amplitude $A_{1/2}$

VALUE ($GeV^{-1/2}$)	DOCUMENT ID		TECN	COMMENT
−0.019±0.005	[1] HUNT	19	DPWA	Multichannel
0.062±0.010	SOKHOYAN	15A	DPWA	Multichannel
• • • We do not use the following data for averages, fits, limits, etc. • • •				
0.018±0.004	[1] SHRESTHA	12A	DPWA	Multichannel

[1] Statistical error only.

$N(2060) \to p\gamma$, helicity-3/2 amplitude $A_{3/2}$

VALUE ($GeV^{-1/2}$)	DOCUMENT ID		TECN	COMMENT
0.039±0.005	[1] HUNT	19	DPWA	Multichannel
0.062±0.020	SOKHOYAN	15A	DPWA	Multichannel
• • • We do not use the following data for averages, fits, limits, etc. • • •				
0.010±0.004	[1] SHRESTHA	12A	DPWA	Multichannel

[1] Statistical error only.

$N(2060) \to n\gamma$, helicity-1/2 amplitude $A_{1/2}$

VALUE ($GeV^{-1/2}$)	DOCUMENT ID		TECN	COMMENT
0.069±0.017	[1] HUNT	19	DPWA	Multichannel
0.025±0.011	ANISOVICH	13B	DPWA	Multichannel
• • • We do not use the following data for averages, fits, limits, etc. • • •				
−0.012±0.017	[1] SHRESTHA	12A	DPWA	Multichannel

[1] Statistical error only.

$N(2060) \to n\gamma$, helicity-3/2 amplitude $A_{3/2}$

VALUE ($GeV^{-1/2}$)	DOCUMENT ID		TECN	COMMENT
−0.023±0.020	[1] HUNT	19	DPWA	Multichannel
−0.037±0.017	ANISOVICH	13B	DPWA	Multichannel
• • • We do not use the following data for averages, fits, limits, etc. • • •				
−0.023±0.023	[1] SHRESTHA	12A	DPWA	Multichannel

[1] Statistical error only.

$N(2060)$ REFERENCES

MUELLER	20	PL B803 135323	J. Mueller *et al.*	(CBELSA/TAPS Collab.)
HUNT	19	PR C99 055205	B.C. Hunt, D.M. Manley	
ANISOVICH	17B	PL B771 142	A.V. Anisovich *et al.*	
DENISENKO	16	PL B755 97	I. Denisenko *et al.*	
SOKHOYAN	15A	EPJ A51 95	V. Sokhoyan *et al.*	(CBELSA/TAPS Collab.)
SVARC	14	PR C89 045205	A. Svarc *et al.*	(RBI Zagreb, UNI Tuzla)
ANISOVICH	13B	EPJ A49 67	A.V. Anisovich *et al.*	
ANISOVICH	12A	EPJ A48 15	A.V. Anisovich *et al.*	(BONN, PNPI)
SHRESTHA	12A	PR C86 055203	M. Shrestha, D.M. Manley	(KSU)
BATINIC	10	PR C82 038203	M. Batinic *et al.*	(ZAGR)
CUTKOSKY	80	Toronto Conf. 19	R.E. Cutkosky *et al.*	(CMU, LBL) IJP
Also		PR D20 2839	R.E. Cutkosky *et al.*	(CMU, LBL)
HOEHLER	79	PDAT 12-1	G. Hohler *et al.*	(KARLT) IJP
Also		Toronto Conf. 3	R. Koch	(KARLT) IJP

$N(2100)$ $1/2^+$

$I(J^P) = \frac{1}{2}(\frac{1}{2}^+)$ Status: ***

$N(2100)$ POLE POSITION

REAL PART

VALUE (MeV)	DOCUMENT ID		TECN	COMMENT
2050 to 2150 (≈ 2100) OUR ESTIMATE				
2120±25	SOKHOYAN	15A	DPWA	Multichannel
2052± 6±3	[1] SVARC	14	L+P	$\pi N \to \pi N$
2120±40	CUTKOSKY	80	IPWA	$\pi N \to \pi N$
• • • We do not use the following data for averages, fits, limits, etc. • • •				
2217	HUNT	19	DPWA	Multichannel
2120±47	BATINIC	10	DPWA	$\pi N \to N\pi$, $N\eta$
1810	VRANA	00	DPWA	Multichannel

[1] Fit to the amplitudes of HOEHLER 79.

−2×IMAGINARY PART

VALUE (MeV)	DOCUMENT ID		TECN	COMMENT
240 to 340 (≈ 300) OUR ESTIMATE				
290±30	SOKHOYAN	15A	DPWA	Multichannel
337±10±4	[1] SVARC	14	L+P	$\pi N \to \pi N$
240±80	CUTKOSKY	80	IPWA	$\pi N \to \pi N$
• • • We do not use the following data for averages, fits, limits, etc. • • •				
545	HUNT	19	DPWA	Multichannel
346±80	BATINIC	10	DPWA	$\pi N \to N\pi$, $N\eta$
622	VRANA	00	DPWA	Multichannel

[1] Fit to the amplitudes of HOEHLER 79.

$N(2100)$ ELASTIC POLE RESIDUE

MODULUS $|r|$

VALUE (MeV)	DOCUMENT ID		TECN	COMMENT
15 to 30 (≈ 20) OUR ESTIMATE				
23±5	SOKHOYAN	15A	DPWA	Multichannel
30±1±1	[1] SVARC	14	L+P	$\pi N \to \pi N$
14±7	CUTKOSKY	80	IPWA	$\pi N \to \pi N$
• • • We do not use the following data for averages, fits, limits, etc. • • •				
33	BATINIC	10	DPWA	$\pi N \to N\pi$, $N\eta$

[1] Fit to the amplitudes of HOEHLER 79.

PHASE θ

VALUE (°)	DOCUMENT ID		TECN	COMMENT
−100 to −60 (≈ −80) OUR ESTIMATE				
− 70±25	SOKHOYAN	15A	DPWA	Multichannel
− 92± 3±2	[1] SVARC	14	L+P	$\pi N \to \pi N$
35±25	CUTKOSKY	80	IPWA	$\pi N \to \pi N$
• • • We do not use the following data for averages, fits, limits, etc. • • •				
− 59	BATINIC	10	DPWA	$\pi N \to N\pi$, $N\eta$

[1] Fit to the amplitudes of HOEHLER 79.

Downloaded from https://academic.oup.com/ptep/article/2022/8/083C01/6651666 by KIT Library user on 27 September 2022

$N(2100)$ INELASTIC POLE RESIDUE

Normalized residue in $N\pi \to N(2100) \to \Delta(1232)\pi$

MODULUS	PHASE (°)	DOCUMENT ID		TECN	COMMENT
0.11±0.05	20 ± 60	SOKHOYAN	15A	DPWA	Multichannel

Normalized residue in $N\pi \to N(2100) \to N\sigma$

MODULUS	PHASE (°)	DOCUMENT ID		TECN	COMMENT
0.18±0.06	125 ± 25	SOKHOYAN	15A	DPWA	Multichannel

Normalized residue in $N\pi \to N(2100) \to N(1535)\pi$

MODULUS	PHASE (°)	DOCUMENT ID		TECN	COMMENT
0.22±0.06	−40 ± 25	SOKHOYAN	15A	DPWA	Multichannel

$N(2100)$ BREIT-WIGNER MASS

VALUE (MeV)	DOCUMENT ID		TECN	COMMENT
2050 to 2150 (≈ 2100) OUR ESTIMATE				
2221±92	[1] HUNT	19	DPWA	Multichannel
2115±20	SOKHOYAN	15A	DPWA	Multichannel
2125±75	CUTKOSKY	80	IPWA	$\pi N \to \pi N$
2050±20	HOEHLER	79	IPWA	$\pi N \to \pi N$
• • • We do not use the following data for averages, fits, limits, etc. • • •				
2157±42	BATINIC	10	DPWA	$\pi N \to N\pi$, $N\eta$
2068± 3^{+15}_{-40}	ABLIKIM	06K	BES2	$J/\psi \to (p\pi^-)\overline{n}$
2084±93	VRANA	00	DPWA	Multichannel

[1] Statistical error only.

$N(2100)$ BREIT-WIGNER WIDTH

VALUE (MeV)	DOCUMENT ID		TECN	COMMENT
200 to 320 (≈ 260) OUR ESTIMATE				
545±170	[1] HUNT	19	DPWA	Multichannel
290± 20	SOKHOYAN	15A	DPWA	Multichannel
260±100	CUTKOSKY	80	IPWA	$\pi N \to \pi N$
200± 30	HOEHLER	79	IPWA	$\pi N \to \pi N$
• • • We do not use the following data for averages, fits, limits, etc. • • •				
355± 88	BATINIC	10	DPWA	$\pi N \to N\pi$, $N\eta$
165± 14±40	ABLIKIM	06K	BES2	$J/\psi \to (p\pi^-)\overline{n}$
1077±643	VRANA	00	DPWA	Multichannel

[1] Statistical error only.

$N(2100)$ DECAY MODES

	Mode	Fraction (Γ_i/Γ)
Γ_1	$N\pi$	8–32 %
Γ_2	$N\eta$	5–45 %
Γ_3	$N\eta'$	5–11 %
Γ_4	$N\omega$	10–25 %
Γ_5	ΛK	<1.0 %
Γ_6	$N\pi\pi$	>55 %
Γ_7	$\Delta(1232)\pi$, P-wave	6–14 %
Γ_8	$N\rho$, S=1/2, P-wave	35–70
Γ_9	$N\sigma$	14–35 %
Γ_{10}	$N(1535)\pi$	26–34 %
Γ_{11}	$\Lambda K^*(892)$	3–11 %
Γ_{12}	$p\gamma$, helicity=1/2	0.001–0.13 %
Γ_{13}	$n\gamma$, helicity=1/2	0.004–0.09 %

$N(2100)$ BRANCHING RATIOS

$\Gamma(N\pi)/\Gamma_{total}$ — Γ_1/Γ

VALUE (%)	DOCUMENT ID		TECN	COMMENT
8–32 % OUR ESTIMATE				
21±11	[1] HUNT	19	DPWA	Multichannel
16± 5	SOKHOYAN	15A	DPWA	Multichannel
12± 3	CUTKOSKY	80	IPWA	$\pi N \to \pi N$
10± 4	HOEHLER	79	IPWA	$\pi N \to \pi N$
• • • We do not use the following data for averages, fits, limits, etc. • • •				
16± 5	BATINIC	10	DPWA	$\pi N \to N\pi$, $N\eta$
2± 5	VRANA	00	DPWA	Multichannel

[1] Statistical error only.

$\Gamma(N\eta)/\Gamma_{total}$ — Γ_2/Γ

VALUE (%)	DOCUMENT ID		TECN	COMMENT
5–45 % OUR ESTIMATE				
30 ±15	MUELLER	20	DPWA	Multichannel
< 4.7	[1] HUNT	19	DPWA	Multichannel
• • • We do not use the following data for averages, fits, limits, etc. • • •				
83 ± 5	BATINIC	10	DPWA	$\pi N \to N\pi$, $N\eta$
61 ±61	VRANA	00	DPWA	Multichannel

[1] Statistical error only.

$\Gamma(N\eta')/\Gamma_{total}$ — Γ_3/Γ

VALUE (%)	DOCUMENT ID		TECN	COMMENT
5–11 % OUR ESTIMATE				
8±3	ANISOVICH	17C	DPWA	Multichannel

$\Gamma(N\omega)/\Gamma_{total}$ — Γ_4/Γ

VALUE (%)	DOCUMENT ID		TECN	COMMENT
10–25 % OUR ESTIMATE				
15±10	DENISENKO	16	DPWA	Multichannel

$\Gamma(\Lambda K)/\Gamma_{total}$ — Γ_5/Γ

VALUE (%)	DOCUMENT ID		TECN	COMMENT
<1.0 % OUR ESTIMATE				
< 1.0	[1] HUNT	19	DPWA	Multichannel
• • • We do not use the following data for averages, fits, limits, etc. • • •				
21 ±20	VRANA	00	DPWA	Multichannel

[1] Statistical error only.

$\Gamma(\Delta(1232)\pi, P\text{-wave})/\Gamma_{total}$ — Γ_7/Γ

VALUE (%)	DOCUMENT ID		TECN	COMMENT
6–14 % OUR ESTIMATE				
< 7.5	[1] HUNT	19	DPWA	Multichannel
10 ±4	SOKHOYAN	15A	DPWA	Multichannel
• • • We do not use the following data for averages, fits, limits, etc. • • •				
2 ±1	VRANA	00	DPWA	Multichannel

[1] Statistical error only.

$\Gamma(N\rho, S{=}1/2, P\text{-wave})/\Gamma_{total}$ — Γ_8/Γ

VALUE (%)	DOCUMENT ID		TECN	COMMENT
35–70 OUR ESTIMATE				
52±19	[1] HUNT	19	DPWA	Multichannel
• • • We do not use the following data for averages, fits, limits, etc. • • •				
4± 1	VRANA	00	DPWA	Multichannel

[1] Statistical error only.

$\Gamma(\Lambda K^*(892))/\Gamma_{total}$ — Γ_{11}/Γ

VALUE (%)	DOCUMENT ID		TECN	COMMENT
3–11 % OUR ESTIMATE				
7±4	ANISOVICH	17B	DPWA	Multichannel

$\Gamma(N\sigma)/\Gamma_{total}$ — Γ_9/Γ

VALUE (%)	DOCUMENT ID		TECN	COMMENT
14–35 % OUR ESTIMATE				
<35	[1] HUNT	19	DPWA	Multichannel
20±6	SOKHOYAN	15A	DPWA	Multichannel
• • • We do not use the following data for averages, fits, limits, etc. • • •				
10±1	VRANA	00	DPWA	Multichannel

[1] Statistical error only.

$\Gamma(N(1535)\pi)/\Gamma_{total}$ — Γ_{10}/Γ

VALUE (%)	DOCUMENT ID		TECN	COMMENT
26–34 % OUR ESTIMATE				
30±4	SOKHOYAN	15A	DPWA	Multichannel

$N(2100)$ PHOTON DECAY AMPLITUDES AT THE POLE

$N(2100) \to p\gamma$, helicity-1/2 amplitude $A_{1/2}$

MODULUS ($GeV^{-1/2}$)	PHASE (°)	DOCUMENT ID		TECN	COMMENT
0.011±0.004	65 ± 30	SOKHOYAN	15A	DPWA	Multichannel

$N(2100)$ BREIT-WIGNER PHOTON DECAY AMPLITUDES

$N(2100) \to p\gamma$, helicity-1/2 amplitude $A_{1/2}$

VALUE ($GeV^{-1/2}$)	DOCUMENT ID		TECN	COMMENT
0.032±0.014	[1] HUNT	19	DPWA	Multichannel
0.010±0.004	SOKHOYAN	15A	DPWA	Multichannel

[1] Statistical error only.

$N(2100) \to n\gamma$, helicity-1/2 amplitude $A_{1/2}$

VALUE ($GeV^{-1/2}$)	DOCUMENT ID		TECN	COMMENT
0.026±0.013	[1] HUNT	19	DPWA	Multichannel

[1] Statistical error only.

$N(2100)$ REFERENCES

MUELLER 20 PL B803 135323 J. Mueller et al. (CBELSA/TAPS Collab.)
HUNT 19 PR C99 055205 B.C. Hunt, D.M. Manley
ANISOVICH 17B PL B771 142 A.V. Anisovich et al.
ANISOVICH 17C PL B772 247 A.V. Anisovich et al.
DENISENKO 16 PL B755 97 I. Denisenko et al.
SOKHOYAN 15A EPJ A51 95 V. Sokhoyan et al. (CBELSA/TAPS Collab.)
SVARC 14 PR C89 045205 A. Svarc et al. (RBI Zagreb, UNI Tuzla)
BATINIC 10 PR C82 038203 M. Batinic et al. (ZAGR)
ABLIKIM 06K PRL 97 062001 M. Ablikim et al. (BES II Collab.)
VRANA 00 PRPL 328 181 T.P. Vrana, S.A. Dytman, T.-S.H. Lee (PITT, ANL)
CUTKOSKY 80 Toronto Conf. 19 R.E. Cutkosky et al. (CMU, LBL) IJP
Also PR D20 2839 R.E. Cutkosky et al. (CMU, LBL)
HOEHLER 79 PDAT 12-1 G. Hohler et al. (KARLT) IJP
Also Toronto Conf. 3 R. Koch (KARLT) IJP

Downloaded from https://academic.oup.com/ptep/article/2022/8/083C01/6651666 by KIT Library user on 27 September 2022

N(2120) 3/2⁻

$I(J^P) = \frac{1}{2}(\frac{3}{2}^-)$ Status: ***

Before the 2012 *Review*, all the evidence for a $J^P = 3/2^-$ state with a mass above 1800 MeV was filed under a two-star N(2080). There is now evidence from ANISOVICH 12A for two $3/2^-$ states in this region, so we have split the older data (according to mass) between a three-star N(1875) and a two-star N(2120).

N(2120) POLE POSITION

REAL PART

VALUE (MeV)	DOCUMENT ID		TECN	COMMENT
2050 to 2150 (≈ 2100) OUR ESTIMATE				
2115±40	SOKHOYAN	15A	DPWA	Multichannel
2094± 7±11	SVARC	14	L+P	$\pi N \to \pi N$
2050±70	CUTKOSKY	80	IPWA	$\pi N \to \pi N$ (higher m)
• • • We do not use the following data for averages, fits, limits, etc. • • •				
2357	HUNT	19	DPWA	Multichannel
2115±40	GUTZ	14	DPWA	Multichannel
2110±50	ANISOVICH	12A	DPWA	Multichannel

−2×IMAGINARY PART

VALUE (MeV)	DOCUMENT ID		TECN	COMMENT
200 to 360 (≈ 280) OUR ESTIMATE				
345±35	SOKHOYAN	15A	DPWA	Multichannel
296±15±4	SVARC	14	L+P	$\pi N \to \pi N$
200±80	CUTKOSKY	80	IPWA	$\pi N \to \pi N$ (higher m)
• • • We do not use the following data for averages, fits, limits, etc. • • •				
503	HUNT	19	DPWA	Multichannel
345±35	GUTZ	14	DPWA	Multichannel
340±45	ANISOVICH	12A	DPWA	Multichannel

N(2120) ELASTIC POLE RESIDUE

MODULUS |r|

VALUE (MeV)	DOCUMENT ID		TECN	COMMENT
10 to 30 (≈ 20) OUR ESTIMATE				
11± 6	SOKHOYAN	15A	DPWA	Multichannel
13± 1±1	SVARC	14	L+P	$\pi N \to \pi N$
30±20	CUTKOSKY	80	IPWA	$\pi N \to \pi N$ (higher m)
• • • We do not use the following data for averages, fits, limits, etc. • • •				
11± 6	GUTZ	14	DPWA	Multichannel
13± 3	ANISOVICH	12A	DPWA	Multichannel

PHASE θ

VALUE (°)	DOCUMENT ID		TECN	COMMENT
−40 to 20 (≈ −10) OUR ESTIMATE				
−30± 20	SOKHOYAN	15A	DPWA	Multichannel
− 2± 4±9	SVARC	14	L+P	$\pi N \to \pi N$
0±100	CUTKOSKY	80	IPWA	$\pi N \to \pi N$ (higher m)
• • • We do not use the following data for averages, fits, limits, etc. • • •				
−30± 20	GUTZ	14	DPWA	Multichannel
−20± 10	ANISOVICH	12A	DPWA	Multichannel

N(2120) INELASTIC POLE RESIDUE

The "normalized residue" is the residue divided by $\Gamma_{pole}/2$.

Normalized residue in $N\pi \to N(2120) \to \Lambda K$

MODULUS	PHASE (°)	DOCUMENT ID		TECN	COMMENT
0.03±0.01	100 ± 30	ANISOVICH	12A	DPWA	Multichannel

Normalized residue in $N\pi \to N(2120) \to \Sigma K$

MODULUS	PHASE (°)	DOCUMENT ID		TECN	COMMENT
0.02±0.015	−50 ± 40	ANISOVICH	12A	DPWA	Multichannel

Normalized residue in $N\pi \to N(2120) \to N(1535)\pi$

MODULUS	PHASE (°)	DOCUMENT ID		TECN	COMMENT
0.15±0.08	−90 ± 40	GUTZ	14	DPWA	Multichannel

Normalized residue in $N\pi \to N(2120) \to \Delta(1232)\pi$, S-wave

MODULUS	PHASE (°)	DOCUMENT ID		TECN	COMMENT
0.25±0.10	undefined	SOKHOYAN	15A	DPWA	Multichannel

Normalized residue in $N\pi \to N(2120) \to \Delta(1232)\pi$, D-wave

MODULUS	PHASE (°)	DOCUMENT ID		TECN	COMMENT
0.15±0.06	−35 ± 30	SOKHOYAN	15A	DPWA	Multichannel

Normalized residue in $N\pi \to N(2120) \to N\sigma$

MODULUS	PHASE (°)	DOCUMENT ID		TECN	COMMENT
0.09±0.05	−80 ± 50	SOKHOYAN	15A	DPWA	Multichannel

N(2120) BREIT-WIGNER MASS

VALUE (MeV)	DOCUMENT ID		TECN	COMMENT
2060 to 2160 (≈ 2120) OUR ESTIMATE				
2353±29	[1] HUNT	19	DPWA	Multichannel
2120±45	SOKHOYAN	15A	DPWA	Multichannel
2060±80	CUTKOSKY	80	IPWA	$\pi N \to \pi N$
2081±20	HOEHLER	79	IPWA	$\pi N \to \pi N$
• • • We do not use the following data for averages, fits, limits, etc. • • •				
2120±35	GUTZ	14	DPWA	Multichannel
2150±60	ANISOVICH	12A	DPWA	Multichannel

[1] Statistical error only.

N(2120) BREIT-WIGNER WIDTH

VALUE (MeV)	DOCUMENT ID		TECN	COMMENT
260 to 360 (≈ 300) OUR ESTIMATE				
503± 62	[1] HUNT	19	DPWA	Multichannel
340± 35	SOKHOYAN	15A	DPWA	Multichannel
300±100	CUTKOSKY	80	IPWA	$\pi N \to \pi N$ (higher m)
265± 40	HOEHLER	79	IPWA	$\pi N \to \pi N$
• • • We do not use the following data for averages, fits, limits, etc. • • •				
340± 35	GUTZ	14	DPWA	Multichannel
330± 45	ANISOVICH	12A	DPWA	Multichannel

[1] Statistical error only.

N(2120) DECAY MODES

	Mode	Fraction (Γ_i/Γ)
Γ_1	$N\pi$	5–15 %
Γ_2	$N\eta$	1–5 %
Γ_3	$N\eta'$	2–6 %
Γ_4	$N\omega$	4–20 %
Γ_5	ΛK	6–11 %
Γ_6	$N\pi\pi$	>27 %
Γ_7	$\Delta(1232)\pi$	>23 %
Γ_8	$\Delta(1232)\pi$, S-wave	15–70 %
Γ_9	$\Delta(1232)\pi$, D-wave	8–45 %
Γ_{10}	$N\rho$, $S=3/2$, S-wave	< 3 %
Γ_{11}	$N\sigma$	4–15 %
Γ_{12}	$N(1535)\pi$	7–23 %
Γ_{13}	$\Lambda K^*(892)$	< 0.2 %
Γ_{14}	$p\gamma$	0.16–2.1 %
Γ_{15}	$p\gamma$, helicity=1/2	0.07–0.80 %
Γ_{16}	$p\gamma$, helicity=3/2	0.09–1.3 %
Γ_{17}	$n\gamma$	0.04–0.72 %
Γ_{18}	$n\gamma$, helicity=1/2	0.04–0.60 %
Γ_{19}	$n\gamma$, helicity=3/2	0.001–0.12 %

N(2120) BRANCHING RATIOS

$\Gamma(N\pi)/\Gamma_{total}$ — Γ_1/Γ

VALUE (%)	DOCUMENT ID		TECN	COMMENT
5–15 % OUR ESTIMATE				
19±2	[1] HUNT	19	DPWA	Multichannel
5±3	SOKHOYAN	15A	DPWA	Multichannel
14±7	CUTKOSKY	80	IPWA	$\pi N \to \pi N$ (higher m)
6±2	HOEHLER	79	IPWA	$\pi N \to \pi N$
• • • We do not use the following data for averages, fits, limits, etc. • • •				
5±3	GUTZ	14	DPWA	Multichannel
6±2	ANISOVICH	12A	DPWA	Multichannel

[1] Statistical error only.

$\Gamma(N\eta)/\Gamma_{total}$ — Γ_2/Γ

VALUE (%)	DOCUMENT ID		TECN	COMMENT
1–5 % OUR ESTIMATE				
<1	MUELLER	20	DPWA	Multichannel
3.1±2.4	[1] HUNT	19	DPWA	Multichannel

[1] Statistical error only.

$\Gamma(N\eta')/\Gamma_{total}$ — Γ_3/Γ

VALUE (%)	DOCUMENT ID		TECN	COMMENT
2–6 % OUR ESTIMATE				
4±2	ANISOVICH	17C	DPWA	Multichannel

$\Gamma(N\omega)/\Gamma_{total}$ — Γ_4/Γ

VALUE (%)	DOCUMENT ID		TECN	COMMENT
4–20 % OUR ESTIMATE				
12±8	DENISENKO	16	DPWA	Multichannel

Downloaded from https://academic.oup.com/ptep/article/2022/8/083C01/6651666 by KIT Library user on 27 September 2022

$\Gamma(\Lambda K)/\Gamma_{total}$ — Γ_5/Γ

VALUE (%)	DOCUMENT ID		TECN	COMMENT
6–11 % OUR ESTIMATE				
8.5 ± 2.5	[1] HUNT	19	DPWA	Multichannel

[1] Statistical error only.

$\Gamma(\Delta(1232)\pi, S\text{-wave})/\Gamma_{total}$ — Γ_8/Γ

VALUE (%)	DOCUMENT ID		TECN	COMMENT
15–70 % OUR ESTIMATE				
25 ± 11	[1] HUNT	19	DPWA	Multichannel
50 ± 20	SOKHOYAN	15A	DPWA	Multichannel

[1] Statistical error only.

$\Gamma(\Delta(1232)\pi, D\text{-wave})/\Gamma_{total}$ — Γ_9/Γ

VALUE (%)	DOCUMENT ID		TECN	COMMENT
8–45 % OUR ESTIMATE				
34 ± 11	[1] HUNT	19	DPWA	Multichannel
20 ± 12	SOKHOYAN	15A	DPWA	Multichannel

[1] Statistical error only.

$\Gamma(N\rho, S{=}3/2, S\text{-wave})/\Gamma_{total}$ — Γ_{10}/Γ

VALUE (%)	DOCUMENT ID		TECN	COMMENT
< 3 % OUR ESTIMATE				
<3	[1] HUNT	19	DPWA	Multichannel

[1] Statistical error only.

$\Gamma(N\sigma)/\Gamma_{total}$ — Γ_{11}/Γ

VALUE (%)	DOCUMENT ID		TECN	COMMENT
4–15 % OUR ESTIMATE				
9 ± 5	[1] HUNT	19	DPWA	Multichannel
11 ± 4	SOKHOYAN	15A	DPWA	Multichannel

[1] Statistical error only.

$\Gamma(N(1535)\pi)/\Gamma_{total}$ — Γ_{12}/Γ

VALUE (%)	DOCUMENT ID		TECN	COMMENT
7–23 % OUR ESTIMATE				
15 ± 8	GUTZ	14	DPWA	Multichannel

$\Gamma(\Lambda K^*(892))/\Gamma_{total}$ — Γ_{13}/Γ

VALUE (%)	DOCUMENT ID		TECN	COMMENT
< 0.2 % OUR ESTIMATE				
<0.2	ANISOVICH	17B	DPWA	Multichannel

$N(2120)$ PHOTON DECAY AMPLITUDES AT THE POLE

$N(2120) \to p\gamma$, helicity-1/2 amplitude $A_{1/2}$

MODULUS ($GeV^{-1/2}$)	PHASE (°)	DOCUMENT ID		TECN	COMMENT
0.130 ± 0.045	−40 ± 25	SOKHOYAN	15A	DPWA	Multichannel

$N(2120) \to p\gamma$, helicity-3/2 amplitude $A_{3/2}$

MODULUS ($GeV^{-1/2}$)	PHASE (°)	DOCUMENT ID		TECN	COMMENT
0.160 ± 0.060	−30 ± 15	SOKHOYAN	15A	DPWA	Multichannel

$N(2120)$ BREIT-WIGNER PHOTON DECAY AMPLITUDES

$N(2120) \to p\gamma$, helicity-1/2 amplitude $A_{1/2}$

VALUE ($GeV^{-1/2}$)	DOCUMENT ID		TECN	COMMENT
0.047 ± 0.009	[1] HUNT	19	DPWA	Multichannel
0.130 ± 0.050	SOKHOYAN	15A	DPWA	Multichannel
• • • We do not use the following data for averages, fits, limits, etc. • • •				
0.130 ± 0.050	GUTZ	14	DPWA	Multichannel

[1] Statistical error only.

$N(2120) \to p\gamma$, helicity-3/2 amplitude $A_{3/2}$

VALUE ($GeV^{-1/2}$)	DOCUMENT ID		TECN	COMMENT
0.001 ± 0.007	[1] HUNT	19	DPWA	Multichannel
0.160 ± 0.065	SOKHOYAN	15A	DPWA	Multichannel
• • • We do not use the following data for averages, fits, limits, etc. • • •				
0.160 ± 0.065	GUTZ	14	DPWA	Multichannel

[1] Statistical error only.

$N(2120) \to n\gamma$, helicity-1/2 amplitude $A_{1/2}$

VALUE ($GeV^{-1/2}$)	DOCUMENT ID		TECN	COMMENT
−0.020 ± 0.013	[1] HUNT	19	DPWA	Multichannel
0.110 ± 0.045	ANISOVICH	13B	DPWA	Multichannel

[1] Statistical error only.

$N(2120) \to n\gamma$, helicity-3/2 amplitude $A_{3/2}$

VALUE ($GeV^{-1/2}$)	DOCUMENT ID		TECN	COMMENT
−0.00 ± 0.02	[1] HUNT	19	DPWA	Multichannel
0.040 ± 0.030	ANISOVICH	13B	DPWA	Multichannel

[1] Statistical error only.

$N(2120)$ REFERENCES

MUELLER	20	PL B803 135323	J. Mueller *et al.*	(CBELSA/TAPS Collab.)
HUNT	19	PR C99 055205	B.C. Hunt, D.M. Manley	
ANISOVICH	17B	PL B771 142	A.V. Anisovich *et al.*	
ANISOVICH	17C	PL B772 247	A.V. Anisovich *et al.*	
DENISENKO	16	PL B755 97	I. Denisenko *et al.*	
SOKHOYAN	15A	EPJ A51 95	V. Sokhoyan *et al.*	(CBELSA/TAPS Collab.)
GUTZ	14	EPJ A50 74	E. Gutz *et al.*	(CBELSA/TAPS Collab.)
SVARC	14	PR C89 045205	A. Svarc *et al.*	(RBI Zagreb, UNI Tuzla)
ANISOVICH	13B	EPJ A49 67	A.V. Anisovich *et al.*	
ANISOVICH	12A	EPJ A48 15	A.V. Anisovich *et al.*	(BONN, PNPI)
CUTKOSKY	80	Toronto Conf. 19	R.E. Cutkosky *et al.*	(CMU, LBL)
HOEHLER	79	PDAT 12-1	G. Hohler *et al.*	(KARLT)

$N(2190)\ 7/2^-$

$I(J^P) = \frac{1}{2}(\frac{7}{2}^-)$ Status: ****

Older and obsolete values are listed and referenced in the 2014 edition, Chinese Physics **C38** 070001 (2014).

$N(2190)$ POLE POSITION

REAL PART

VALUE (MeV)	DOCUMENT ID		TECN	COMMENT
2050 to 2150 (≈ 2100) OUR ESTIMATE				
2140 ± 20	AFZAL	20	DPWA	Multichannel
2150 ± 25	SOKHOYAN	15A	DPWA	Multichannel
2079 ± 4 ± 9	[1] SVARC	14	L+P	$\pi N \to \pi N$
2100 ± 50	CUTKOSKY	80	IPWA	$\pi N \to \pi N$
• • • We do not use the following data for averages, fits, limits, etc. • • •				
2162	HUNT	19	DPWA	Multichannel
2074	ROENCHEN	15A	DPWA	Multichannel
2150 ± 25	ANISOVICH	12A	DPWA	Multichannel
2063 ± 32	BATINIC	10	DPWA	$\pi N \to N\pi, N\eta$
2070	ARNDT	06	DPWA	$\pi N \to \pi N, \eta N$
2107	VRANA	00	DPWA	Multichannel
2042	HOEHLER	93	SPED	$\pi N \to \pi N$

[1] Fit to the amplitudes of HOEHLER 79.

−2×IMAGINARY PART

VALUE (MeV)	DOCUMENT ID		TECN	COMMENT
300 to 500 (≈ 400) OUR ESTIMATE				
420^{+120}_{-40}	AFZAL	20	DPWA	Multichannel
325 ± 25	SOKHOYAN	15A	DPWA	Multichannel
509 ± 7 ± 16	[1] SVARC	14	L+P	$\pi N \to \pi N$
400 ± 160	CUTKOSKY	80	IPWA	$\pi N \to \pi N$
• • • We do not use the following data for averages, fits, limits, etc. • • •				
407	HUNT	19	DPWA	Multichannel
327	ROENCHEN	15A	DPWA	Multichannel
330 ± 30	ANISOVICH	12A	DPWA	Multichannel
330 ± 101	BATINIC	10	DPWA	$\pi N \to N\pi, N\eta$
520	ARNDT	06	DPWA	$\pi N \to \pi N, \eta N$
380	VRANA	00	DPWA	Multichannel
482	HOEHLER	93	SPED	$\pi N \to \pi N$

[1] Fit to the amplitudes of HOEHLER 79.

$N(2190)$ ELASTIC POLE RESIDUE

MODULUS $|r|$

VALUE (MeV)	DOCUMENT ID		TECN	COMMENT
25 to 70 (≈ 50) OUR ESTIMATE				
30 ± 4	SOKHOYAN	15A	DPWA	Multichannel
54 ± 1 ± 3	[1] SVARC	14	L+P	$\pi N \to \pi N$
25 ± 10	CUTKOSKY	80	IPWA	$\pi N \to \pi N$
• • • We do not use the following data for averages, fits, limits, etc. • • •				
35	ROENCHEN	15A	DPWA	Multichannel
30 ± 5	ANISOVICH	12A	DPWA	Multichannel
34	BATINIC	10	DPWA	$\pi N \to N\pi, N\eta$
72	ARNDT	06	DPWA	$\pi N \to \pi N, \eta N$
45	HOEHLER	93	SPED	$\pi N \to \pi N$

[1] Fit to the amplitudes of HOEHLER 79.

PHASE θ

VALUE (°)	DOCUMENT ID		TECN	COMMENT
−30 to 30 (≈ 0) OUR ESTIMATE				
28 ± 10	SOKHOYAN	15A	DPWA	Multichannel
−18 ± 1 ± 3	[1] SVARC	14	L+P	$\pi N \to \pi N$
−30 ± 50	CUTKOSKY	80	IPWA	$\pi N \to \pi N$
• • • We do not use the following data for averages, fits, limits, etc. • • •				
−40	ROENCHEN	15A	DPWA	Multichannel
30 ± 10	ANISOVICH	12A	DPWA	Multichannel
−19	BATINIC	10	DPWA	$\pi N \to N\pi, N\eta$
−32	ARNDT	06	DPWA	$\pi N \to \pi N, \eta N$

[1] Fit to the amplitudes of HOEHLER 79.

Downloaded from https://academic.oup.com/ptep/article/2022/8/083C01/6651666 by KIT Library user on 27 September 2022

N(2190) INELASTIC POLE RESIDUE

The "normalized residue" is the residue divided by $\Gamma_{pole}/2$.

Normalized residue in $N\pi \to N(2190) \to \Lambda K$

MODULUS	PHASE (°)	DOCUMENT ID		TECN	COMMENT
0.03 ±0.01	20 ± 15	ANISOVICH	12A	DPWA	Multichannel
• • • We do not use the following data for averages, fits, limits, etc. • • •					
0.005	−51	ROENCHEN	15A	DPWA	Multichannel

Normalized residue in $N\pi \to N(2190) \to \Sigma K$

MODULUS	PHASE (°)	DOCUMENT ID		TECN	COMMENT
• • • We do not use the following data for averages, fits, limits, etc. • • •					
0.013	−69	ROENCHEN	15A	DPWA	Multichannel

Normalized residue in $N\pi \to N(2190) \to N\eta$

MODULUS	PHASE (°)	DOCUMENT ID		TECN	COMMENT
• • • We do not use the following data for averages, fits, limits, etc. • • •					
0.016	129	ROENCHEN	15A	DPWA	Multichannel

Normalized residue in $N\pi \to N(2190) \to \Delta(1232)\pi$, D-wave

MODULUS	PHASE (°)	DOCUMENT ID		TECN	COMMENT
0.27±0.04	−165 ± 20	SOKHOYAN	15A	DPWA	Multichannel

Normalized residue in $N\pi \to N(2190) \to N\sigma$

MODULUS	PHASE (°)	DOCUMENT ID		TECN	COMMENT
0.13±0.05	50 ± 15	SOKHOYAN	15A	DPWA	Multichannel

N(2190) BREIT-WIGNER MASS

VALUE (MeV)	DOCUMENT ID		TECN	COMMENT
2140 to 2220 (≈ 2180) OUR ESTIMATE				
2222 ±15	[1] HUNT	19	DPWA	Multichannel
2205 ±18	SOKHOYAN	15A	DPWA	Multichannel
2152.4± 1.4	[1] ARNDT	06	DPWA	$\pi N \to \pi N$, ηN
2200 ±70	CUTKOSKY	80	IPWA	$\pi N \to \pi N$
2140 ±12	HOEHLER	79	IPWA	$\pi N \to \pi N$
• • • We do not use the following data for averages, fits, limits, etc. • • •				
2180 ±20	ANISOVICH	12A	DPWA	Multichannel
2150 ±26	[1] SHRESTHA	12A	DPWA	Multichannel
2125 ±61	BATINIC	10	DPWA	$\pi N \to N\pi$, $N\eta$
2168 ±18	VRANA	00	DPWA	Multichannel

[1] Statistical error only.

N(2190) BREIT-WIGNER WIDTH

VALUE (MeV)	DOCUMENT ID		TECN	COMMENT
300 to 500 (≈ 400) OUR ESTIMATE				
442± 40	[1] HUNT	19	DPWA	Multichannel
355± 30	SOKHOYAN	15A	DPWA	Multichannel
484± 13	[1] ARNDT	06	DPWA	$\pi N \to \pi N$, ηN
500±150	CUTKOSKY	80	IPWA	$\pi N \to \pi N$
390± 30	HOEHLER	79	IPWA	$\pi N \to \pi N$
• • • We do not use the following data for averages, fits, limits, etc. • • •				
335± 40	ANISOVICH	12A	DPWA	Multichannel
500± 74	[1] SHRESTHA	12A	DPWA	Multichannel
381±160	BATINIC	10	DPWA	$\pi N \to N\pi$, $N\eta$
453±101	VRANA	00	DPWA	Multichannel

[1] Statistical error only.

N(2190) DECAY MODES

The following branching fractions are our estimates, not fits or averages.

	Mode	Fraction (Γ_i/Γ)
Γ_1	$N\pi$	10–20 %
Γ_2	$N\eta$	1–5 %
Γ_3	$N\omega$	8–20 %
Γ_4	ΛK	0.2–0.8 %
Γ_5	$N\pi\pi$	22–51 %
Γ_6	$\Delta(1232)\pi$, D-wave	19–31 %
Γ_7	$N\rho$, S=3/2, D-wave	<11 %
Γ_8	$N\sigma$	3–9 %
Γ_9	$\Lambda K^*(892)$	0.2–0.8 %
Γ_{10}	$p\gamma$	<0.08 %
Γ_{11}	$p\gamma$, helicity=1/2	<0.06 %
Γ_{12}	$p\gamma$, helicity=3/2	<0.02 %
Γ_{13}	$n\gamma$	<0.04 %
Γ_{14}	$n\gamma$, helicity=1/2	<0.01 %
Γ_{15}	$n\gamma$, helicity=3/2	<0.03 %

N(2190) BRANCHING RATIOS

$\Gamma(N\pi)/\Gamma_{total}$ — Γ_1/Γ

VALUE (%)	DOCUMENT ID		TECN	COMMENT
10–20 % OUR ESTIMATE				
22.9± 0.6	[1] HUNT	19	DPWA	Multichannel
16 ± 2	SOKHOYAN	15A	DPWA	Multichannel
23.8± 0.1	[1] ARNDT	06	DPWA	$\pi N \to \pi N$, ηN
12 ± 6	CUTKOSKY	80	IPWA	$\pi N \to \pi N$
14 ± 2	HOEHLER	79	IPWA	$\pi N \to \pi N$
• • • We do not use the following data for averages, fits, limits, etc. • • •				
16 ± 2	ANISOVICH	12A	DPWA	Multichannel
20 ± 1	[1] SHRESTHA	12A	DPWA	Multichannel
18 ±12	BATINIC	10	DPWA	$\pi N \to N\pi$, $N\eta$
20 ± 4	VRANA	00	DPWA	Multichannel

[1] Statistical error only.

$\Gamma(N\eta)/\Gamma_{total}$ — Γ_2/Γ

VALUE (%)	DOCUMENT ID		TECN	COMMENT
1–5 % OUR ESTIMATE				
4 ±2	MUELLER	20	DPWA	Multichannel
2.7±2.2	[1] HUNT	19	DPWA	Multichannel
• • • We do not use the following data for averages, fits, limits, etc. • • •				
2 ±1	[1] SHRESTHA	12A	DPWA	Multichannel
0.1±0.3	BATINIC	10	DPWA	$\pi N \to N\pi$, $N\eta$
0 ±1	VRANA	00	DPWA	Multichannel

[1] Statistical error only.

$\Gamma(N\omega)/\Gamma_{total}$ — Γ_3/Γ

VALUE (%)	DOCUMENT ID		TECN	COMMENT
8–20 % OUR ESTIMATE				
14±6	DENISENKO	16	DPWA	Multichannel
• • • We do not use the following data for averages, fits, limits, etc. • • •				
seen	WILLIAMS	09	IPWA	$\gamma p \to p\omega$

$\Gamma(\Lambda K)/\Gamma_{total}$ — Γ_4/Γ

VALUE (%)	DOCUMENT ID		TECN	COMMENT
0.2–0.8 % OUR ESTIMATE				
0.6±0.1	[1] HUNT	19	DPWA	Multichannel
0.5±0.3	ANISOVICH	12A	DPWA	Multichannel
• • • We do not use the following data for averages, fits, limits, etc. • • •				
<1	[1] SHRESTHA	12A	DPWA	Multichannel

[1] Statistical error only.

$\Gamma(\Delta(1232)\pi, D\text{-wave})/\Gamma_{total}$ — Γ_6/Γ

VALUE (%)	DOCUMENT ID		TECN	COMMENT
19–31 % OUR ESTIMATE				
25±6	SOKHOYAN	15A	DPWA	Multichannel

$\Gamma(N\rho, S=3/2, D\text{-wave})/\Gamma_{total}$ — Γ_7/Γ

VALUE (%)	DOCUMENT ID		TECN	COMMENT
<11 % OUR ESTIMATE				
<11	[1] HUNT	19	DPWA	Multichannel
• • • We do not use the following data for averages, fits, limits, etc. • • •				
29±28	VRANA	00	DPWA	Multichannel

[1] Statistical error only.

$\Gamma(N\sigma)/\Gamma_{total}$ — Γ_8/Γ

VALUE (%)	DOCUMENT ID		TECN	COMMENT
3–9 % OUR ESTIMATE				
6±3	SOKHOYAN	15A	DPWA	Multichannel

$\Gamma(\Lambda K^*(892))/\Gamma_{total}$ — Γ_9/Γ

VALUE (%)	DOCUMENT ID		TECN	COMMENT
0.2–0.8 % OUR ESTIMATE				
0.5±0.3	ANISOVICH	17B	DPWA	Multichannel

N(2190) PHOTON DECAY AMPLITUDES AT THE POLE

$N(2190) \to p\gamma$, helicity-1/2 amplitude $A_{1/2}$

MODULUS ($GeV^{-1/2}$)	PHASE (°)	DOCUMENT ID		TECN	COMMENT
0.068±0.005	−170 ± 12	SOKHOYAN	15A	DPWA	Multichannel
$-0.083^{+0.007}_{-0.003}$	-11^{+6}_{-2}	ROENCHEN	14	DPWA	
• • • We do not use the following data for averages, fits, limits, etc. • • •					
−0.041	−21	ROENCHEN	15A	DPWA	Multichannel

$N(2190) \to p\gamma$, helicity-3/2 amplitude $A_{3/2}$

MODULUS ($GeV^{-1/2}$)	PHASE (°)	DOCUMENT ID		TECN	COMMENT
0.025±0.010	22 ± 10	SOKHOYAN	15A	DPWA	Multichannel
$0.095^{+0.013}_{-0.010}$	-3^{+3}_{-5}	ROENCHEN	14	DPWA	
• • • We do not use the following data for averages, fits, limits, etc. • • •					
0.085	−22	ROENCHEN	15A	DPWA	Multichannel

Downloaded from https://academic.oup.com/ptep/article/2022/8/083C01/6651666 by KIT Library user on 27 September 2022

$N(2190)$ BREIT-WIGNER PHOTON DECAY AMPLITUDES

$N(2190) \to p\gamma$, helicity-1/2 amplitude $A_{1/2}$

VALUE (GeV$^{-1/2}$)	DOCUMENT ID		TECN	COMMENT
0.001 ± 0.002	[1] HUNT	19	DPWA	Multichannel
−0.071 ± 0.006	SOKHOYAN	15A	DPWA	Multichannel
• • • We do not use the following data for averages, fits, limits, etc. • • •				
−0.065 ± 0.008	ANISOVICH	12A	DPWA	Multichannel

[1] Statistical error only.

$N(2190) \to p\gamma$, helicity-3/2 amplitude $A_{3/2}$

VALUE (GeV$^{-1/2}$)	DOCUMENT ID		TECN	COMMENT
0.015 ± 0.003	[1] HUNT	19	DPWA	Multichannel
0.027 ± 0.010	SOKHOYAN	15A	DPWA	Multichannel
• • • We do not use the following data for averages, fits, limits, etc. • • •				
0.035 ± 0.017	ANISOVICH	12A	DPWA	Multichannel

[1] Statistical error only.

$N(2190) \to p\gamma$, ratio of helicity amplitudes $A_{3/2}/A_{1/2}$

VALUE	DOCUMENT ID		TECN	COMMENT
• • • We do not use the following data for averages, fits, limits, etc. • • •				
−0.17 ± 0.15	WILLIAMS	09	IPWA	$\gamma p \to p\omega$

$N(2190) \to n\gamma$, helicity-1/2 amplitude $A_{1/2}$

VALUE (GeV$^{-1/2}$)	DOCUMENT ID		TECN	COMMENT
−0.01 ± 0.02	[1] HUNT	19	DPWA	Multichannel
−0.015 ± 0.013	ANISOVICH	13B	DPWA	Multichannel

[1] Statistical error only.

$N(2190) \to n\gamma$, helicity-3/2 amplitude $A_{3/2}$

VALUE (GeV$^{-1/2}$)	DOCUMENT ID		TECN	COMMENT
−0.023 ± 0.022	[1] HUNT	19	DPWA	Multichannel
−0.034 ± 0.022	ANISOVICH	13B	DPWA	Multichannel

[1] Statistical error only.

$N(2190)$ REFERENCES

For early references, see Physics Letters **111B** 1 (1982).

AFZAL	20	PRL 125 152002	F. Afzal *et al.*	(CBELSA/TAPS Collab.)
MUELLER	20	PL B803 135323	J. Mueller *et al.*	(CBELSA/TAPS Collab.)
HUNT	19	PR C99 055205	B.C. Hunt, D.M. Manley	
ANISOVICH	17B	PL B771 142	A.V. Anisovich *et al.*	
DENISENKO	16	PL B755 97	I. Denisenko *et al.*	
ROENCHEN	15A	EPJ A51 70	D. Roenchen *et al.*	
SOKHOYAN	15A	EPJ A51 95	V. Sokhoyan *et al.*	(CBELSA/TAPS Collab.)
PDG	14	CP C38 070001	K. Olive *et al.*	(PDG Collab.)
ROENCHEN	14	EPJ A50 101	D. Roenchen *et al.*	
Also		EPJ A51 63 (errat.)	D. Roenchen *et al.*	
SVARC	14	PR C89 045205	A. Svarc *et al.*	(RBI Zagreb, UNI Tuzla)
ANISOVICH	13B	EPJ A49 67	A.V. Anisovich *et al.*	
ANISOVICH	12A	EPJ A48 15	A.V. Anisovich *et al.*	(BONN, PNPI)
SHRESTHA	12A	PR C86 055203	M. Shrestha, D.M. Manley	(KSU)
BATINIC	10	PR C82 038203	M. Batinic *et al.*	(ZAGR)
WILLIAMS	09	PR C80 065209	M. Williams *et al.*	(JLab CLAS Collab.)
ARNDT	06	PR C74 045205	R.A. Arndt *et al.*	(GWU)
VRANA	00	PRPL 328 181	T.P. Vrana, S.A. Dytman, T.-S.H. Lee	(PITT, ANL)
HOEHLER	93	πN Newsletter 9 1	G. Hohler	(KARL)
CUTKOSKY	80	Toronto Conf. 19	R.E. Cutkosky *et al.*	(CMU, LBL) IJP
Also		PR D20 2839	R.E. Cutkosky *et al.*	(CMU, LBL) IJP
HOEHLER	79	PDAT 12-1	G. Hohler *et al.*	(KARLT) IJP
Also		Toronto Conf. 3	R. Koch	(KARLT) IJP

$N(2220)$ $9/2^+$

$I(J^P) = \frac{1}{2}(\frac{9}{2}^+)$ Status: ****

Older and obsolete values are listed and referenced in the 2014 edition, Chinese Physics **C38** 070001 (2014).

$N(2220)$ POLE POSITION

REAL PART

VALUE (MeV)	DOCUMENT ID		TECN	COMMENT
2130 to 2200 (≈ 2170) OUR ESTIMATE				
2127 ± 3 ± 24	[1] SVARC	14	L+P	$\pi N \to \pi N$
2150 ± 35	ANISOVICH	12A	DPWA	Multichannel
2160 ± 80	CUTKOSKY	80	IPWA	$\pi N \to \pi N$
• • • We do not use the following data for averages, fits, limits, etc. • • •				
2171	ROENCHEN	15A	DPWA	Multichannel
2199	ARNDT	06	DPWA	$\pi N \to \pi N, \eta N$
2135	HOEHLER	93	ARGD	$\pi N \to \pi N$

[1] Fit to the amplitudes of HOEHLER 79.

−2×IMAGINARY PART

VALUE (MeV)	DOCUMENT ID		TECN	COMMENT
360 to 480 (≈ 400) OUR ESTIMATE				
380 ± 7 ± 22	[1] SVARC	14	L+P	$\pi N \to \pi N$
440 ± 40	ANISOVICH	12A	DPWA	Multichannel
480 ± 100	CUTKOSKY	80	IPWA	$\pi N \to \pi N$
• • • We do not use the following data for averages, fits, limits, etc. • • •				
593	ROENCHEN	15A	DPWA	Multichannel
372	ARNDT	06	DPWA	$\pi N \to \pi N, \eta N$
400	HOEHLER	93	ARGD	$\pi N \to \pi N$

[1] Fit to the amplitudes of HOEHLER 79.

$N(2220)$ ELASTIC POLE RESIDUE

MODULUS $|r|$

VALUE (MeV)	DOCUMENT ID		TECN	COMMENT
35 to 60 (≈ 45) OUR ESTIMATE				
38 ± 1 ± 5	[1] SVARC	14	L+P	$\pi N \to \pi N$
60 ± 12	ANISOVICH	12A	DPWA	Multichannel
45 ± 20	CUTKOSKY	80	IPWA	$\pi N \to \pi N$
• • • We do not use the following data for averages, fits, limits, etc. • • •				
62	ROENCHEN	15A	DPWA	Multichannel
33	ARNDT	06	DPWA	$\pi N \to \pi N, \eta N$
40	HOEHLER	93	ARGD	$\pi N \to \pi N$

[1] Fit to the amplitudes of HOEHLER 79.

PHASE θ

VALUE (°)	DOCUMENT ID		TECN	COMMENT
−60 to −30 (≈ −50) OUR ESTIMATE				
−52 ± 1 ± 14	[1] SVARC	14	L+P	$\pi N \to \pi N$
−58 ± 12	ANISOVICH	12A	DPWA	Multichannel
−45 ± 25	CUTKOSKY	80	IPWA	$\pi N \to \pi N$
• • • We do not use the following data for averages, fits, limits, etc. • • •				
−59	ROENCHEN	15A	DPWA	Multichannel
−33	ARNDT	06	DPWA	$\pi N \to \pi N, \eta N$
−50	HOEHLER	93	ARGD	$\pi N \to \pi N$

[1] Fit to the amplitudes of HOEHLER 79.

$N(2220)$ INELASTIC POLE RESIDUE

The "normalized residue" is the residue divided by $\Gamma_{pole}/2$.

Normalized residue in $N\pi \to N(2220) \to N\eta$

MODULUS	PHASE (°)	DOCUMENT ID		TECN	COMMENT
• • • We do not use the following data for averages, fits, limits, etc. • • •					
0.004	−101	ROENCHEN	15A	DPWA	Multichannel

Normalized residue in $N\pi \to N(2220) \to \Lambda K$

MODULUS	PHASE (°)	DOCUMENT ID		TECN	COMMENT
• • • We do not use the following data for averages, fits, limits, etc. • • •					
0.007	62	ROENCHEN	15A	DPWA	Multichannel

Normalized residue in $N\pi \to N(2220) \to \Sigma K$

MODULUS	PHASE (°)	DOCUMENT ID		TECN	COMMENT
• • • We do not use the following data for averages, fits, limits, etc. • • •					
0.009	−128	ROENCHEN	15A	DPWA	Multichannel

$N(2220)$ BREIT-WIGNER MASS

VALUE (MeV)	DOCUMENT ID		TECN	COMMENT
2200 to 2300 (≈ 2250) OUR ESTIMATE				
2316.3 ± 2.9	[1] ARNDT	06	DPWA	$\pi N \to \pi N, \eta N$
2230 ± 80	CUTKOSKY	80	IPWA	$\pi N \to \pi N$
2205 ± 10	HOEHLER	79	IPWA	$\pi N \to \pi N$

[1] Statistical error only.

$N(2220)$ BREIT-WIGNER WIDTH

VALUE (MeV)	DOCUMENT ID		TECN	COMMENT
350 to 500 (≈ 400) OUR ESTIMATE				
633 ± 17	[1] ARNDT	06	DPWA	$\pi N \to \pi N, \eta N$
500 ± 150	CUTKOSKY	80	IPWA	$\pi N \to \pi N$
365 ± 30	HOEHLER	79	IPWA	$\pi N \to \pi N$

[1] Statistical error only.

$N(2220)$ DECAY MODES

The following branching fractions are our estimates, not fits or averages.

	Mode	Fraction (Γ_i/Γ)
Γ_1	$N\pi$	15–30 %

$N(2220)$ BRANCHING RATIOS

$\Gamma(N\pi)/\Gamma_{total}$ — Γ_1/Γ

VALUE (%)	DOCUMENT ID		TECN	COMMENT
15 to 30 (≈ 25) OUR ESTIMATE				
24 ± 5	ANISOVICH	12A	DPWA	Multichannel
24.6 ± 0.1	[1] ARNDT	06	DPWA	$\pi N \to \pi N, \eta N$
15 ± 3	CUTKOSKY	80	IPWA	$\pi N \to \pi N$
18.0 ± 1.5	HOEHLER	79	IPWA	$\pi N \to \pi N$

[1] Statistical error only.

Downloaded from https://academic.oup.com/ptep/article/2022/8/083C01/6651666 by KIT Library user on 27 September 2022

$N(2220)$ PHOTON DECAY AMPLITUDES AT THE POLE

$N(2220) \to p\gamma$, helicity-1/2 amplitude $A_{1/2}$

MODULUS ($GeV^{-1/2}$)	PHASE (°)	DOCUMENT ID		TECN	COMMENT
$-0.233^{+0.084}_{-0.044}$	-47^{+10}_{-6}	ROENCHEN	14	DPWA	
• • • We do not use the following data for averages, fits, limits, etc. • • •					
0.135	114	ROENCHEN	15A	DPWA	Multichannel

$N(2220) \to p\gamma$, helicity-3/2 amplitude $A_{3/2}$

MODULUS ($GeV^{-1/2}$)	PHASE (°)	DOCUMENT ID		TECN	COMMENT
$0.162^{+0.041}_{-0.038}$	-27^{+26}_{-13}	ROENCHEN	14	DPWA	
• • • We do not use the following data for averages, fits, limits, etc. • • •					
0.082	−41	ROENCHEN	15A	DPWA	Multichannel

$N(2220)$ REFERENCES

For early references, see Physics Letters **111B** 1 (1982).

ROENCHEN	15A	EPJ A51 70	D. Roenchen *et al.*	
PDG	14	CP C38 070001	K. Olive *et al.*	(PDG Collab.)
ROENCHEN	14	EPJ A50 101	D. Roenchen *et al.*	
Also		EPJ A51 63 (errat.)	D. Roenchen *et al.*	
SVARC	14	PR C89 045205	A. Svarc *et al.*	(RBI Zagreb, UNI Tuzla)
ANISOVICH	12A	EPJ A48 15	A.V. Anisovich *et al.*	(BONN, PNPI)
ARNDT	06	PR C74 045205	R.A. Arndt *et al.*	(GWU)
HOEHLER	93	πN Newsletter 9 1	G. Hohler	(KARL)
CUTKOSKY	80	Toronto Conf. 19	R.E. Cutkosky *et al.*	(CMU, LBL) IJP
Also		PR D20 2839	R.E. Cutkosky *et al.*	(CMU, LBL) IJP
HOEHLER	79	PDAT 12-1	G. Hohler *et al.*	(KARLT) IJP
Also		Toronto Conf. 3	R. Koch	(KARLT) IJP

$N(2250)$ $9/2^-$

$I(J^P) = \frac{1}{2}(\frac{9}{2}^-)$ Status: ****

Older and obsolete values are listed and referenced in the 2014 edition, Chinese Physics **C38** 070001 (2014).

$N(2250)$ POLE POSITION

REAL PART

VALUE (MeV)	DOCUMENT ID		TECN	COMMENT
2150 to 2250 (≈ 2200) OUR ESTIMATE				
2195 ± 45	AFZAL	20	DPWA	Multichannel
2157 ± 3 ± 14	[1] SVARC	14	L+P	$\pi N \to \pi N$
2195 ± 45	ANISOVICH	12A	DPWA	Multichannel
2150 ± 50	CUTKOSKY	80	IPWA	$\pi N \to \pi N$
• • • We do not use the following data for averages, fits, limits, etc. • • •				
2127	HUNT	19	DPWA	Multichannel
2062	ROENCHEN	15A	DPWA	Multichannel
2217	ARNDT	06	DPWA	$\pi N \to \pi N, \eta N$
2187	HOEHLER	93	SPED	$\pi N \to \pi N$

[1] Fit to the amplitudes of HOEHLER 79.

−2×IMAGINARY PART

VALUE (MeV)	DOCUMENT ID		TECN	COMMENT
350 to 500 (≈ 420) OUR ESTIMATE				
470 ± 50	AFZAL	20	DPWA	Multichannel
412 ± 7 ± 44	[1] SVARC	14	L+P	$\pi N \to \pi N$
470 ± 50	ANISOVICH	12A	DPWA	Multichannel
360 ± 100	CUTKOSKY	80	IPWA	$\pi N \to \pi N$
• • • We do not use the following data for averages, fits, limits, etc. • • •				
262	HUNT	19	DPWA	Multichannel
403	ROENCHEN	15A	DPWA	Multichannel
431	ARNDT	06	DPWA	$\pi N \to \pi N, \eta N$
388	HOEHLER	93	SPED	$\pi N \to \pi N$

[1] Fit to the amplitudes of HOEHLER 79.

$N(2250)$ ELASTIC POLE RESIDUE

MODULUS $|r|$

VALUE (MeV)	DOCUMENT ID		TECN	COMMENT
20 to 30 (≈ 25) OUR ESTIMATE				
24 ± 1 ± 5	[1] SVARC	14	L+P	$\pi N \to \pi N$
26 ± 5	ANISOVICH	12A	DPWA	Multichannel
20 ± 6	CUTKOSKY	80	IPWA	$\pi N \to \pi N$
• • • We do not use the following data for averages, fits, limits, etc. • • •				
8.2	ROENCHEN	15A	DPWA	Multichannel
21	ARNDT	06	DPWA	$\pi N \to \pi N, \eta N$
21	HOEHLER	93	SPED	$\pi N \to \pi N$

[1] Fit to the amplitudes of HOEHLER 79.

PHASE θ

VALUE (°)	DOCUMENT ID		TECN	COMMENT
−60 to −20 (≈ −40) OUR ESTIMATE				
−62 ± 1 ± 11	[1] SVARC	14	L+P	$\pi N \to \pi N$
−38 ± 25	ANISOVICH	12A	DPWA	Multichannel
−50 ± 20	CUTKOSKY	80	IPWA	$\pi N \to \pi N$
• • • We do not use the following data for averages, fits, limits, etc. • • •				
−64	ROENCHEN	15A	DPWA	Multichannel
−20	ARNDT	06	DPWA	$\pi N \to \pi N, \eta N$

[1] Fit to the amplitudes of HOEHLER 79.

$N(2250)$ INELASTIC POLE RESIDUE

The "normalized residue" is the residue divided by $\Gamma_{pole}/2$.

Normalized residue in $N\pi \to N(2250) \to N\eta$

MODULUS	PHASE (°)	DOCUMENT ID		TECN	COMMENT
• • • We do not use the following data for averages, fits, limits, etc. • • •					
0.017	−89	ROENCHEN	15A	DPWA	Multichannel

Normalized residue in $N\pi \to N(2250) \to \Lambda K$

MODULUS	PHASE (°)	DOCUMENT ID		TECN	COMMENT
• • • We do not use the following data for averages, fits, limits, etc. • • •					
0.006	−101	ROENCHEN	15A	DPWA	Multichannel

Normalized residue in $N\pi \to N(2250) \to \Sigma K$

MODULUS	PHASE (°)	DOCUMENT ID		TECN	COMMENT
• • • We do not use the following data for averages, fits, limits, etc. • • •					
0.002	70	ROENCHEN	15A	DPWA	Multichannel

$N(2250)$ BREIT-WIGNER MASS

VALUE (MeV)	DOCUMENT ID		TECN	COMMENT
2250 to 2320 (≈ 2280) OUR ESTIMATE				
2200 ± 10	[1] HUNT	19	DPWA	Multichannel
2280 ± 40	ANISOVICH	12A	DPWA	Multichannel
2302 ± 6	[1] ARNDT	06	DPWA	$\pi N \to \pi N, \eta N$
2250 ± 80	CUTKOSKY	80	IPWA	$\pi N \to \pi N$
2268 ± 15	HOEHLER	79	IPWA	$\pi N \to \pi N$

[1] Statistical error only.

$N(2250)$ BREIT-WIGNER WIDTH

VALUE (MeV)	DOCUMENT ID		TECN	COMMENT
300 to 600 (≈ 500) OUR ESTIMATE				
343 ± 51	[1] HUNT	19	DPWA	Multichannel
520 ± 50	ANISOVICH	12A	DPWA	Multichannel
628 ± 28	[1] ARNDT	06	DPWA	$\pi N \to \pi N, \eta N$
480 ± 120	CUTKOSKY	80	IPWA	$\pi N \to \pi N$
300 ± 40	HOEHLER	79	IPWA	$\pi N \to \pi N$

[1] Statistical error only.

$N(2250)$ DECAY MODES

The following branching fractions are our estimates, not fits or averages.

	Mode	Fraction (Γ_i/Γ)
Γ_1	$N\pi$	5–15 %
Γ_2	$N\eta$	<5 %
Γ_3	ΛK	1–3 %

$N(2250)$ BRANCHING RATIOS

$\Gamma(N\pi)/\Gamma_{total}$ — Γ_1/Γ

VALUE (%)	DOCUMENT ID		TECN	COMMENT
5–15 % OUR ESTIMATE				
8.5 ± 0.4	[1] HUNT	19	DPWA	Multichannel
12 ± 4	ANISOVICH	12A	DPWA	Multichannel
8.9 ± 0.1	[1] ARNDT	06	DPWA	$\pi N \to \pi N, \eta N$
10 ± 2	CUTKOSKY	80	IPWA	$\pi N \to \pi N$
10 ± 2	HOEHLER	79	IPWA	$\pi N \to \pi N$

[1] Statistical error only.

$\Gamma(N\eta)/\Gamma_{total}$ — Γ_2/Γ

VALUE (%)	DOCUMENT ID		TECN	COMMENT
<5 % OUR ESTIMATE				
<5	[1] HUNT	19	DPWA	Multichannel

[1] Statistical error only.

Downloaded from https://academic.oup.com/ptep/article/2022/8/083C01/6651666 by KIT Library user on 27 September 2022

$\Gamma(\Lambda K)/\Gamma_{total}$ — Γ_3/Γ

VALUE (%)	DOCUMENT ID		TECN	COMMENT
1–3 % OUR ESTIMATE				
2.0 ± 0.6	[1] HUNT	19	DPWA	Multichannel

[1] Statistical error only.

$N(2250)$ PHOTON DECAY AMPLITUDES AT THE POLE

$N(2250) \to p\gamma$, helicity-1/2 amplitude $A_{1/2}$

MODULUS ($GeV^{-1/2}$)	PHASE (°)	DOCUMENT ID		TECN	COMMENT
$-0.090^{+0.025}_{-0.022}$	-49^{+17}_{-11}	ROENCHEN	14	DPWA	
• • • We do not use the following data for averages, fits, limits, etc. • • •					
0.026	-26	ROENCHEN	15A	DPWA	Multichannel

$N(2250) \to p\gamma$, helicity-3/2 amplitude $A_{3/2}$

MODULUS ($GeV^{-1/2}$)	PHASE (°)	DOCUMENT ID		TECN	COMMENT
$0.049^{+0.031}_{-0.019}$	171^{+36}_{-43}	ROENCHEN	14	DPWA	
• • • We do not use the following data for averages, fits, limits, etc. • • •					
0.119	-42	ROENCHEN	15A	DPWA	Multichannel

$N(2250)$ BREIT-WIGNER PHOTON DECAY AMPLITUDES

$N(2250) \to p\gamma$, helicity-1/2 amplitude $A_{1/2}$

VALUE ($GeV^{-1/2}$)	DOCUMENT ID		TECN	COMMENT
0.0006 ± 0.0037	[1] HUNT	19	DPWA	Multichannel

[1] Statistical error only.

$N(2250) \to p\gamma$, helicity-3/2 amplitude $A_{3/2}$

VALUE ($GeV^{-1/2}$)	DOCUMENT ID		TECN	COMMENT
0.013 ± 0.004	[1] HUNT	19	DPWA	Multichannel

[1] Statistical error only.

$N(2250)$ REFERENCES

AFZAL	20	PRL 125 152002	F. Afzal *et al.*	(CBELSA/TAPS Collab.)
HUNT	19	PR C99 055205	B.C. Hunt, D.M. Manley	
ROENCHEN	15A	EPJ A51 70	D. Roenchen *et al.*	
PDG	14	CP C38 070001	K. Olive *et al.*	(PDG Collab.)
ROENCHEN	14	EPJ A50 101	D. Roenchen *et al.*	
Also		EPJ A51 63 (errat.)	D. Roenchen *et al.*	
SVARC	14	PR C89 045205	A. Svarc *et al.*	(RBI Zagreb, UNI Tuzla)
ANISOVICH	12A	EPJ A48 15	A.V. Anisovich *et al.*	(BONN, PNPI)
ARNDT	06	PR C74 045205	R.A. Arndt *et al.*	(GWU)
HOEHLER	93	πN Newsletter 9 1	G. Hohler	(KARL)
CUTKOSKY	80	Toronto Conf. 19	R.E. Cutkosky *et al.*	(CMU, LBL) IJP
Also		PR D20 2839	R.E. Cutkosky *et al.*	(CMU, LBL) IJP
HOEHLER	79	PDAT 12-1	G. Hohler *et al.*	(KARLT) IJP
Also		Toronto Conf. 3	R. Koch	(KARLT) IJP

$N(2300)\ 1/2^+$

$I(J^P) = \frac{1}{2}(\frac{1}{2}^+)$ Status: **

OMITTED FROM SUMMARY TABLE

$N(2300)$ MASS

VALUE (MeV)	DOCUMENT ID		TECN	COMMENT
$2300^{+40+109}_{-30-0}$	ABLIKIM	13A	BES3	$\psi(2S) \to p\overline{p}\pi^0$

$N(2300)$ WIDTH

VALUE (MeV)	DOCUMENT ID		TECN	COMMENT
$340 \pm 30^{+110}_{-58}$	ABLIKIM	13A	BES3	$\psi(2S) \to p\overline{p}\pi^0$

$N(2300)$ REFERENCES

ABLIKIM	13A	PRL 110 022001	M. Ablikim *et al.*	(BESIII Collab.)

$N(2570)\ 5/2^-$

$I(J^P) = \frac{1}{2}(\frac{5}{2}^-)$ Status: **

OMITTED FROM SUMMARY TABLE

$N(2570)$ MASS

VALUE (MeV)	DOCUMENT ID		TECN	COMMENT
2570^{+19+34}_{-10-10}	ABLIKIM	13A	BES3	$\psi(2S) \to p\overline{p}\pi^0$

$N(2570)$ WIDTH

VALUE (MeV)	DOCUMENT ID		TECN	COMMENT
250^{+14+69}_{-24-21}	ABLIKIM	13A	BES3	$\psi(2S) \to p\overline{p}\pi^0$

$N(2570)$ REFERENCES

ABLIKIM	13A	PRL 110 022001	M. Ablikim *et al.*	(BESIII Collab.)

$N(2600)\ 11/2^-$

$I(J^P) = \frac{1}{2}(\frac{11}{2}^-)$ Status: ***

$N(2600)$ BREIT-WIGNER MASS

VALUE (MeV)	DOCUMENT ID		TECN	COMMENT
2550 to 2750 (≈ 2600) OUR ESTIMATE				
2623 ± 197	ARNDT	06	DPWA	$\pi N \to \pi N, \eta N$
2577 ± 50	HOEHLER	79	IPWA	$\pi N \to \pi N$

$N(2600)$ BREIT-WIGNER WIDTH

VALUE (MeV)	DOCUMENT ID		TECN	COMMENT
500 to 800 (≈ 650) OUR ESTIMATE				
1311 ± 996	ARNDT	06	DPWA	$\pi N \to \pi N, \eta N$
400 ± 100	HOEHLER	79	IPWA	$\pi N \to \pi N$

$N(2600)$ DECAY MODES

	Mode	Fraction (Γ_i/Γ)
Γ_1	$N\pi$	3–8 %

$N(2600)$ BRANCHING RATIOS

$\Gamma(N\pi)/\Gamma_{total}$ — Γ_1/Γ

VALUE (%)	DOCUMENT ID		TECN	COMMENT
3 to 8 (≈ 5) OUR ESTIMATE				
5.0 ± 1.8	ARNDT	06	DPWA	$\pi N \to \pi N, \eta N$
5 ± 1	HOEHLER	79	IPWA	$\pi N \to \pi N$

$N(2600)$ REFERENCES

ARNDT	06	PR C74 045205	R.A. Arndt *et al.*	(GWU)
HOEHLER	79	PDAT 12-1	G. Hohler *et al.*	(KARLT) IJP
Also		Toronto Conf. 3	R. Koch	(KARLT) IJP

$N(2700)\ 13/2^+$

$I(J^P) = \frac{1}{2}(\frac{13}{2}^+)$ Status: **

OMITTED FROM SUMMARY TABLE

$N(2700)$ BREIT-WIGNER MASS

VALUE (MeV)	DOCUMENT ID		TECN	COMMENT
2612 ± 45	HOEHLER	79	IPWA	$\pi N \to \pi N$

$N(2700)$ BREIT-WIGNER WIDTH

VALUE (MeV)	DOCUMENT ID		TECN	COMMENT
350 ± 50	HOEHLER	79	IPWA	$\pi N \to \pi N$

$N(2700)$ DECAY MODES

	Mode	Fraction (Γ_i/Γ)
Γ_1	$N\pi$	3–5 %

$N(2700)$ BRANCHING RATIOS

$\Gamma(N\pi)/\Gamma_{total}$ — Γ_1/Γ

VALUE (%)	DOCUMENT ID		TECN	COMMENT
4 ± 1	HOEHLER	79	IPWA	$\pi N \to \pi N$

$N(2700)$ REFERENCES

HOEHLER	79	PDAT 12-1	G. Hohler *et al.*	(KARLT) IJP
Also		Toronto Conf. 3	R. Koch	(KARLT) IJP

Downloaded from https://academic.oup.com/ptep/article/2022/8/083C01/6651666 by KIT Library user on 27 September 2022

$N(\sim 3000$ Region) Partial-Wave Analyses

OMITTED FROM SUMMARY TABLE

We list here miscellaneous high-mass candidates for isospin-1/2 resonances found in partial-wave analyses.

Our 1982 edition had an $N(3245)$, an $N(3690)$, and an $N(3755)$, each a narrow peak seen in a production experiment. Since nothing has been heard from them since the 1960's, we declare them to be dead. There was also an $N(3030)$, deduced from total cross-section and 180° elastic cross-section measurements; it is the KOCH 80 $L_{1,15}$ state below.

$N(\sim 3000)$ BREIT-WIGNER MASS

VALUE (MeV)	DOCUMENT ID		TECN	COMMENT
≈ 3000 OUR ESTIMATE				
2600	KOCH	80	IPWA	$\pi N \to \pi N$ D_{13}
3100	KOCH	80	IPWA	$\pi N \to \pi N$ $L_{1,15}$ wave
3500	KOCH	80	IPWA	$\pi N \to \pi N$ $M_{1,17}$ wave
3500 to 4000	KOCH	80	IPWA	$\pi N \to \pi N$ $N_{1,19}$ wave
3500±200	HENDRY	78	MPWA	$\pi N \to \pi N$ $L_{1,15}$ wave
3800±200	HENDRY	78	MPWA	$\pi N \to \pi N$ $M_{1,17}$ wave
4100±200	HENDRY	78	MPWA	$\pi N \to \pi N$ $N_{1,19}$ wave

$N(\sim 3000)$ BREIT-WIGNER WIDTH

VALUE (MeV)	DOCUMENT ID		TECN	COMMENT
1300±200	HENDRY	78	MPWA	$\pi N \to \pi N$ $L_{1,15}$ wave
1600±200	HENDRY	78	MPWA	$\pi N \to \pi N$ $M_{1,17}$ wave
1900±300	HENDRY	78	MPWA	$\pi N \to \pi N$ $N_{1,19}$ wave

$N(\sim 3000)$ DECAY MODES

	Mode	Fraction (Γ_i/Γ)
Γ_1	$N\pi$	2–8 %

$N(\sim 3000)$ BRANCHING RATIOS

$\Gamma(N\pi)/\Gamma_{total}$				Γ_1/Γ
VALUE (%)	DOCUMENT ID		TECN	COMMENT
2–8 % OUR ESTIMATE				
6 ±2	HENDRY	78	MPWA	$\pi N \to \pi N$ $L_{1,15}$ wave
4.0±1.5	HENDRY	78	MPWA	$\pi N \to \pi N$ $M_{1,17}$ wave
3.0±1.5	HENDRY	78	MPWA	$\pi N \to \pi N$ $N_{1,19}$ wave

$N(\sim 3000)$ REFERENCES

KOCH	80	Toronto Conf. 3	R. Koch	(KARLT) IJP
HENDRY	78	PRL 41 222	A.W. Hendry	(IND, LBL) IJP
Also		ANP 136 1	A.W. Hendry	(IND) IJP

Downloaded from https://academic.oup.com/ptep/article/2022/8/083C01/6651666 by KIT Library user on 27 September 2022

Δ BARYONS
($S = 0$, $I = 3/2$)

$\Delta^{++} = uuu$, $\Delta^{+} = uud$, $\Delta^{0} = udd$, $\Delta^{-} = ddd$

$\Delta(1232)\ 3/2^+$

$I(J^P) = \frac{3}{2}(\frac{3}{2}^+)$ Status: ****

Older and obsolete values are listed and referenced in the 2014 edition, Chinese Physics **C38** 070001 (2014).

$\Delta(1232)$ POLE POSITIONS

REAL PART, MIXED CHARGES

VALUE (MeV)	DOCUMENT ID		TECN	COMMENT
1209 to 1211 (≈ 1210) OUR ESTIMATE				
1211 ±1 ±1	[1] SVARC	14	L+P	$\pi N \to \pi N$
1210.5 ±1.0	ANISOVICH	12A	DPWA	Multichannel
1210 ±1	CUTKOSKY	80	IPWA	$\pi N \to \pi N$
• • • We do not use the following data for averages, fits, limits, etc. • • •				
1212.4	HUNT	19	DPWA	Multichannel
1218	ROENCHEN	15A	DPWA	Multichannel
1211 ±1	ANISOVICH	10	DPWA	Multichannel
1211	ARNDT	06	DPWA	$\pi N \to \pi N, \eta N$
1210	ARNDT	04	DPWA	$\pi N \to \pi N, \eta N$
1209	[2] HOEHLER	93	ARGD	$\pi N \to \pi N$

[1] Fit to the amplitudes of HOEHLER 79.
[2] See HOEHLER 93 for a detailed discussion of the evidence for and the pole parameters of N and Δ resonances as determined from Argand diagrams of πN elastic partial-wave amplitudes and from plots of the speeds with which the amplitudes traverse the diagrams.

−2×IMAGINARY PART, MIXED CHARGES

VALUE (MeV)	DOCUMENT ID		TECN	COMMENT
98 to 102 (≈ 100) OUR ESTIMATE				
98 ±2±1	[1] SVARC	14	L+P	$\pi N \to \pi N$
99 ±2	ANISOVICH	12A	DPWA	Multichannel
100 ±2	CUTKOSKY	80	IPWA	$\pi N \to \pi N$
• • • We do not use the following data for averages, fits, limits, etc. • • •				
96.8	HUNT	19	DPWA	Multichannel
92	ROENCHEN	15A	DPWA	Multichannel
100 ±2	ANISOVICH	10	DPWA	Multichannel
99	ARNDT	06	DPWA	$\pi N \to \pi N, \eta N$
100	ARNDT	04	DPWA	$\pi N \to \pi N, \eta N$
100	[2] HOEHLER	93	ARGD	$\pi N \to \pi N$

[1] Fit to the amplitudes of HOEHLER 79.
[2] See HOEHLER 93 for a detailed discussion of the evidence for and the pole parameters of N and Δ resonances as determined from Argand diagrams of πN elastic partial-wave amplitudes and from plots of the speeds with which the amplitudes traverse the diagrams.

REAL PART, $\Delta(1232)^{++}$

VALUE (MeV)	DOCUMENT ID		COMMENT
• • • We do not use the following data for averages, fits, limits, etc. • • •			
1212.50 ±0.24	BERNICHA	96	Fit to PEDRONI 78

−2×IMAGINARY PART, $\Delta(1232)^{++}$

VALUE (MeV)	DOCUMENT ID		COMMENT
• • • We do not use the following data for averages, fits, limits, etc. • • •			
97.37 ±0.42	BERNICHA	96	Fit to PEDRONI 78

REAL PART, $\Delta(1232)^{+}$

VALUE (MeV)	DOCUMENT ID		TECN	COMMENT
• • • We do not use the following data for averages, fits, limits, etc. • • •				
1211 ±1 to 1212 ± 1	HANSTEIN	96	DPWA	$\gamma N \to \pi N$
1206.9 ±0.9 to 1210.5 ± 1.8	MIROSHNIC...	79		Fit photoproduction

−2×IMAGINARY PART, $\Delta(1232)^{+}$

VALUE (MeV)	DOCUMENT ID		TECN	COMMENT
• • • We do not use the following data for averages, fits, limits, etc. • • •				
102 ±2 to 99 ± 2	[1] HANSTEIN	96	DPWA	$\gamma N \to \pi N$
111.2 ±2.0 to 116.6 ± 2.2	MIROSHNIC...	79		Fit photoproduction

[1] The second (lower) value of HANSTEIN 96 here goes with the second (higher) value of the real part in the preceding data block.

REAL PART, $\Delta(1232)^{0}$

VALUE (MeV)	DOCUMENT ID		COMMENT
• • • We do not use the following data for averages, fits, limits, etc. • • •			
1213.20 ±0.66	BERNICHA	96	Fit to PEDRONI 78

−2×IMAGINARY PART, $\Delta(1232)^{0}$

VALUE (MeV)	DOCUMENT ID		COMMENT
• • • We do not use the following data for averages, fits, limits, etc. • • •			
104.10 ±1.01	BERNICHA	96	Fit to PEDRONI 78

$\Delta(1232)$ ELASTIC POLE RESIDUES

ABSOLUTE VALUE, MIXED CHARGES

VALUE (MeV)	DOCUMENT ID		TECN	COMMENT
49 to 52 (≈ 50) OUR ESTIMATE				
50 ±1 ±1	[1] SVARC	14	L+P	$\pi N \to \pi N$
51.6 ±0.6	ANISOVICH	12A	DPWA	Multichannel
53 ±2	CUTKOSKY	80	IPWA	$\pi N \to \pi N$
• • • We do not use the following data for averages, fits, limits, etc. • • •				
46	ROENCHEN	15A	DPWA	Multichannel
52	ARNDT	06	DPWA	$\pi N \to \pi N, \eta N$
53	ARNDT	04	DPWA	$\pi N \to \pi N, \eta N$
50	HOEHLER	93	ARGD	$\pi N \to \pi N$

PHASE, MIXED CHARGES

VALUE (°)	DOCUMENT ID		TECN	COMMENT
−48 to −45 (≈ −46) OUR ESTIMATE				
−46 ±1 ±1	[1] SVARC	14	L+P	$\pi N \to \pi N$
−46 ±1	ANISOVICH	12A	DPWA	Multichannel
−47 ±1	CUTKOSKY	80	IPWA	$\pi N \to \pi N$
• • • We do not use the following data for averages, fits, limits, etc. • • •				
−36	ROENCHEN	15A	DPWA	Multichannel
−47	ARNDT	06	DPWA	$\pi N \to \pi N, \eta N$
−47	ARNDT	04	DPWA	$\pi N \to \pi N, \eta N$
−48	HOEHLER	93	ARGD	$\pi N \to \pi N$

[1] Fit to the amplitudes of HOEHLER 79.

$\Delta(1232)$ BREIT-WIGNER MASSES

MIXED CHARGES

VALUE (MeV)	DOCUMENT ID		TECN	COMMENT
1230 to 1234 (≈ 1232) OUR ESTIMATE				
1230.8 ±0.4	[1] HUNT	19	DPWA	Multichannel
1228 ±2	ANISOVICH	12A	DPWA	Multichannel
1233.4 ±0.4	[1] ARNDT	06	DPWA	$\pi N \to \pi N, \eta N$
1232 ±3	CUTKOSKY	80	IPWA	$\pi N \to \pi N$
1233 ±2	HOEHLER	79	IPWA	$\pi N \to \pi N$
• • • We do not use the following data for averages, fits, limits, etc. • • •				
1231.1 ±0.2	[1] SHRESTHA	12A	DPWA	Multichannel
1230 ±2	ANISOVICH	10	DPWA	Multichannel
1232.9 ±1.2	ARNDT	04	DPWA	$\pi N \to \pi N, \eta N$
1228 ±1	PENNER	02C	DPWA	Multichannel

[1] Statistical error only.

$\Delta(1232)^{++}$ MASS

VALUE (MeV)	DOCUMENT ID		TECN	COMMENT
• • • We do not use the following data for averages, fits, limits, etc. • • •				
1230.55 ±0.20	GRIDNEV	06	DPWA	$\pi N \to \pi N$
1231.88 ±0.29	BERNICHA	96		Fit to PEDRONI 78
1230.5 ±0.2	ABAEV	95	IPWA	$\pi N \to \pi N$
1230.9 ±0.3	KOCH	80B	IPWA	$\pi N \to \pi N$
1231.1 ±0.2	PEDRONI	78		$\pi N \to \pi N$ 70–370 MeV

$\Delta(1232)^{+}$ MASS

VALUE (MeV)	DOCUMENT ID		COMMENT
• • • We do not use the following data for averages, fits, limits, etc. • • •			
1234.9 ±1.4	MIROSHNIC...	79	Fit photoproduction

$\Delta(1232)^{0}$ MASS

VALUE (MeV)	DOCUMENT ID		TECN	COMMENT
• • • We do not use the following data for averages, fits, limits, etc. • • •				
1231.3 ±0.6	BREITSCHOP...	06	CNTR	Using new CHEX data
1233.40 ±0.22	GRIDNEV	06	DPWA	$\pi N \to \pi N$
1234.35 ±0.75	BERNICHA	96		Fit to PEDRONI 78
1233.1 ±0.3	ABAEV	95	IPWA	$\pi N \to \pi N$
1233.6 ±0.5	KOCH	80B	IPWA	$\pi N \to \pi N$
1233.8 ±0.2	PEDRONI	78		$\pi N \to \pi N$ 70–370 MeV

$m_{\Delta^0} - m_{\Delta^{++}}$

VALUE (MeV)	DOCUMENT ID		TECN	COMMENT
• • • We do not use the following data for averages, fits, limits, etc. • • •				
2.86 ±0.30	GRIDNEV	06	DPWA	$\pi N \to \pi N$
2.25 ±0.68	BERNICHA	96		Fit to PEDRONI 78
2.6 ±0.4	ABAEV	95	IPWA	$\pi N \to \pi N$
2.7 ±0.3	[1] PEDRONI	78		See the masses

[1] Using $\pi^{\pm}d$ as well, PEDRONI 78 determine $(M^- - M^{++}) + (M^0 - M^+)/3 = 4.6 \pm 0.2$ MeV.

Downloaded from https://academic.oup.com/ptep/article/2022/8/083C01/6651666 by KIT Library user on 27 September 2022

$\Delta(1232)$ BREIT-WIGNER WIDTHS

MIXED CHARGES

VALUE (MeV)	DOCUMENT ID		TECN	COMMENT
114 to 120 ($\approx$ 117) OUR ESTIMATE				
110.9±0.8	[1] HUNT	19	DPWA	Multichannel
110 ±3	ANISOVICH	12A	DPWA	Multichannel
118.7±0.6	[1] ARNDT	06	DPWA	$\pi N \to \pi N, \eta N$
120 ±5	CUTKOSKY	80	IPWA	$\pi N \to \pi N$
116 ±5	HOEHLER	79	IPWA	$\pi N \to \pi N$
• • • We do not use the following data for averages, fits, limits, etc. • • •				
113.0±0.5	[1] SHRESTHA	12A	DPWA	Multichannel
112 ±4	ANISOVICH	10	DPWA	Multichannel
118.0±2.2	ARNDT	04	DPWA	$\pi N \to \pi N, \eta N$
106 ±1	PENNER	02C	DPWA	Multichannel

[1] Statistical error only.

$\Delta(1232)^{++}$ WIDTH

VALUE (MeV)	DOCUMENT ID		TECN	COMMENT
• • • We do not use the following data for averages, fits, limits, etc. • • •				
112.2 ±0.7	GRIDNEV	06	DPWA	$\pi N \to \pi N$
109.07±0.48	BERNICHA	96		Fit to PEDRONI 78
111.0 ±1.0	KOCH	80B	IPWA	$\pi N \to \pi N$
111.3 ±0.5	PEDRONI	78		$\pi N \to \pi N$ 70–370 MeV

$\Delta(1232)^{+}$ WIDTH

VALUE (MeV)	DOCUMENT ID		COMMENT
• • • We do not use the following data for averages, fits, limits, etc. • • •			
131.1±2.4	MIROSHNIC...	79	Fit photoproduction

$\Delta(1232)^{0}$ WIDTH

VALUE (MeV)	DOCUMENT ID		TECN	COMMENT
• • • We do not use the following data for averages, fits, limits, etc. • • •				
112.5 ±1.9	BREITSCHOP...	06	CNTR	Using new CHEX data
116.9 ±0.7	GRIDNEV	06	DPWA	$\pi N \to \pi N$
117.58±1.16	BERNICHA	96		Fit to PEDRONI 78
113.0 ±1.5	KOCH	80B	IPWA	$\pi N \to \pi N$
117.9 ±0.9	PEDRONI	78		$\pi N \to \pi N$ 70–370 MeV

Δ^0-Δ^{++} WIDTH DIFFERENCE

VALUE (MeV)	DOCUMENT ID		TECN	COMMENT
• • • We do not use the following data for averages, fits, limits, etc. • • •				
4.66±1.0	GRIDNEV	06	DPWA	$\pi N \to \pi N$
8.45±1.11	BERNICHA	96		Fit to PEDRONI 78
5.1 ±1.0	ABAEV	95	IPWA	$\pi N \to \pi N$
6.6 ±1.0	PEDRONI	78		See the widths

$\Delta(1232)$ DECAY MODES

The following branching fractions are our estimates, not fits or averages.

	Mode	Fraction (Γ_i/Γ)
Γ_1	$N\pi$	99.4 %
Γ_2	$N\gamma$	0.55–0.65 %
Γ_3	$N\gamma$, helicity=1/2	0.11–0.13 %
Γ_4	$N\gamma$, helicity=3/2	0.44–0.52 %
Γ_5	$p e^+ e^-$	$(4.2\pm0.7)\times10^{-5}$

$\Delta(1232)$ BRANCHING RATIOS

$\Gamma(N\pi)/\Gamma_{total}$ — Γ_1/Γ

VALUE	DOCUMENT ID		TECN	COMMENT
0.994 OUR ESTIMATE				
0.9939±0.0001	[1] HUNT	19	DPWA	Multichannel
1.00	ARNDT	06	DPWA	$\pi N \to \pi N, \eta N$
1.0	CUTKOSKY	80	IPWA	$\pi N \to \pi N$
1.0	HOEHLER	79	IPWA	$\pi N \to \pi N$
• • • We do not use the following data for averages, fits, limits, etc. • • •				
0.994	SHRESTHA	12A	DPWA	Multichannel
1.0	ANISOVICH	10	DPWA	Multichannel
1.000	ARNDT	04	DPWA	$\pi N \to \pi N, \eta N$
1.00	PENNER	02C	DPWA	Multichannel

[1] Statistical error only.

$\Gamma(p e^+ e^-)/\Gamma_{total}$ — Γ_5/Γ

VALUE (units 10^{-5})	DOCUMENT ID	
4.19±0.34±0.62	[1] ADAMCZEW...	17

[1] The systematic uncertainty includes the model dependence.

$\Delta(1232)$ PHOTON DECAY AMPLITUDES AT THE POLE

$\Delta(1232) \to N\gamma$, helicity-1/2 amplitude $A_{1/2}$

MODULUS ($GeV^{-1/2}$)	PHASE (°)	DOCUMENT ID		TECN	COMMENT
$-0.114^{+0.010}_{-0.003}$	-9^{+4}_{-2}	ROENCHEN	14	DPWA	
• • • We do not use the following data for averages, fits, limits, etc. • • •					
−0.117	−6.6	ROENCHEN	15A	DPWA	Multichannel

$\Delta(1232) \to N\gamma$, helicity-3/2 amplitude $A_{3/2}$

MODULUS ($GeV^{-1/2}$)	PHASE (°)	DOCUMENT ID		TECN	COMMENT
$-0.229^{+0.003}_{-0.004}$	$3^{+0.3}_{-0.4}$	ROENCHEN	14	DPWA	
• • • We do not use the following data for averages, fits, limits, etc. • • •					
−0.226	2.8	ROENCHEN	15A	DPWA	Multichannel

$\Delta(1232)$ BREIT-WIGNER PHOTON DECAY AMPLITUDES

Papers on γN amplitudes predating 1981 may be found in our 2006 edition, Journal of Physics **G33** 1 (2006).

$\Delta(1232) \to N\gamma$, helicity-1/2 amplitude $A_{1/2}$

VALUE ($GeV^{-1/2}$)	DOCUMENT ID		TECN	COMMENT
−0.142 to −0.129 ($\approx$ −0.135) OUR ESTIMATE				
−0.146 ±0.002	[1] HUNT	19	DPWA	Multichannel
−0.131 ±0.004	ANISOVICH	12A	DPWA	Multichannel
−0.139 ±0.002	[1] WORKMAN	12A	DPWA	$\gamma N \to N\pi$
−0.139 ±0.004	[1] DUGGER	07	DPWA	$\gamma N \to \pi N$
−0.137 ±0.005	AHRENS	04A	DPWA	$\vec{\gamma}\vec{p} \to N\pi$
−0.1357±0.0013±0.0037	BLANPIED	01	LEGS	$\gamma p \to p\gamma, p\pi^0, n\pi^+$
−0.131 ±0.001	[1] BECK	00	IPWA	$\vec{\gamma}p \to p\pi^0, n\pi^+$
−0.140 ±0.005	KAMALOV	99	DPWA	$\gamma N \to \pi N$
−0.1294±0.0013	HANSTEIN	98	IPWA	$\gamma N \to \pi N$
−0.1278±0.0012	DAVIDSON	97	DPWA	$\gamma N \to \pi N$
• • • We do not use the following data for averages, fits, limits, etc. • • •				
−0.137 ±0.001	[1] SHRESTHA	12A	DPWA	Multichannel
−0.136 ±0.005	ANISOVICH	10	DPWA	Multichannel
−0.140	DRECHSEL	07	DPWA	$\gamma N \to \pi N$
−0.129 ±0.001	ARNDT	02	DPWA	$\gamma p \to N\pi$
−0.128	PENNER	02D	DPWA	Multichannel
−0.1312	HANSTEIN	98	DPWA	$\gamma N \to \pi N$

[1] Statistical error only.

$\Delta(1232) \to N\gamma$, helicity-3/2 amplitude $A_{3/2}$

VALUE ($GeV^{-1/2}$)	DOCUMENT ID		TECN	COMMENT
−0.262 to −0.248 ($\approx$ −0.255) OUR ESTIMATE				
−0.250 ±0.002	[1] HUNT	19	DPWA	Multichannel
−0.254 ±0.005	ANISOVICH	12A	DPWA	Multichannel
−0.262 ±0.003	WORKMAN	12A	DPWA	$\gamma N \to N\pi$
−0.258 ±0.005	DUGGER	07	DPWA	$\gamma N \to \pi N$
−0.256 ±0.003	AHRENS	04A	DPWA	$\vec{\gamma}\vec{p} \to N\pi$
−0.2669±0.0016±0.0078	BLANPIED	01	LEGS	$\gamma p \to p\gamma, p\pi^0, n\pi^+$
−0.251 ±0.001	BECK	00	IPWA	$\vec{\gamma}p \to p\pi^0, n\pi^+$
−0.258 ±0.006	KAMALOV	99	DPWA	$\gamma N \to \pi N$
−0.2466±0.0013	HANSTEIN	98	IPWA	$\gamma N \to \pi N$
−0.2524±0.0013	DAVIDSON	97	DPWA	$\gamma N \to \pi N$
• • • We do not use the following data for averages, fits, limits, etc. • • •				
−0.251 ±0.001	[1] SHRESTHA	12A	DPWA	Multichannel
−0.267 ±0.008	ANISOVICH	10	DPWA	Multichannel
−0.265	DRECHSEL	07	DPWA	$\gamma N \to \pi N$
−0.243 ±0.001	ARNDT	02	DPWA	$\gamma p \to N\pi$
−0.247	PENNER	02D	DPWA	Multichannel
−0.2522	HANSTEIN	98	DPWA	$\gamma N \to \pi N$

[1] Statistical error only.

$\Delta(1232) \to N\gamma$, E_2/M_1 ratio

VALUE	DOCUMENT ID		TECN	COMMENT
−0.030 to −0.020 ($\approx$ −0.025) OUR ESTIMATE				
−0.0274±0.0003±0.0030	AHRENS	04A	DPWA	$\vec{\gamma}\vec{p} \to N\pi$
−0.020 ±0.002	ARNDT	02	DPWA	$\gamma p \to N\pi$
−0.0307±0.0026±0.0024	BLANPIED	01	LEGS	$\gamma p \to p\gamma, p\pi^0, n\pi^+$
−0.016 ±0.004 ±0.002	GALLER	01	DPWA	$\gamma p \to \gamma p$
−0.025 ±0.001 ±0.002	BECK	00	IPWA	$\vec{\gamma}p \to p\pi^0, n\pi^+$
−0.0233±0.0017	HANSTEIN	98	IPWA	$\gamma N \to \pi N$
−0.015 ±0.005	[1] ARNDT	97	IPWA	$\gamma N \to \pi N$
−0.0319±0.0024	DAVIDSON	97	DPWA	$\gamma N \to \pi N$
• • • We do not use the following data for averages, fits, limits, etc. • • •				
−0.022	DRECHSEL	07	DPWA	$\gamma N \to \pi N$
−0.026	PENNER	02D	DPWA	Multichannel
−0.0254±0.0010	HANSTEIN	98	DPWA	$\gamma N \to \pi N$
−0.025 ±0.002 ±0.002	BECK	97	IPWA	$\gamma N \to \pi N$
−0.030 ±0.003 ±0.002	BLANPIED	97	DPWA	$\gamma N \to \pi N, \gamma N$

[1] This ARNDT 97 value is very sensitive to the database being fitted. The result is from a fit to the full pion photoproduction database, apart from the BLANPIED 97 cross-section measurements.

Downloaded from https://academic.oup.com/ptep/article/2022/8/083C01/6651666 by KIT Library user on 27 September 2022

$\Delta(1232) \to N\gamma$, absolute value of E_2/M_1 ratio at pole

VALUE	DOCUMENT ID		TECN	COMMENT
• • • We do not use the following data for averages, fits, limits, etc. • • •				
0.065±0.007	ARNDT	97	DPWA	$\gamma N \to \pi N$
0.058	HANSTEIN	96	DPWA	$\gamma N \to \pi N$

$\Delta(1232) \to N\gamma$, phase of E_2/M_1 ratio at pole

VALUE	DOCUMENT ID		TECN	COMMENT
• • • We do not use the following data for averages, fits, limits, etc. • • •				
−122 ±5	ARNDT	97	DPWA	$\gamma N \to \pi N$
−127.2	HANSTEIN	96	DPWA	$\gamma N \to \pi N$

$\Delta(1232)$ MAGNETIC MOMENTS

$\Delta(1232)^{++}$ MAGNETIC MOMENT

The values are extracted from UCLA and SIN data on $\pi^+ p$ bremsstrahlung using a variety of different theoretical approximations and methods. Our estimate is *only* a rough guess of the range we expect the moment to lie within.

VALUE (μ_N)	DOCUMENT ID		TECN	COMMENT
• • • We do not use the following data for averages, fits, limits, etc. • • •				
6.14±0.51	LOPEZCAST...	01	DPWA	$\pi^+ p \to \pi^+ p\gamma$
4.52±0.50±0.45	BOSSHARD	91		$\pi^+ p \to \pi^+ p\gamma$ (SIN data)
3.7 to 4.2	LIN	91B		$\pi^+ p \to \pi^+ p\gamma$ (from UCLA data)
4.6 to 4.9	LIN	91B		$\pi^+ p \to \pi^+ p\gamma$ (from SIN data)
5.6 to 7.5	WITTMAN	88		$\pi^+ p \to \pi^+ p\gamma$ (from UCLA data)
6.9 to 9.8	HELLER	87		$\pi^+ p \to \pi^+ p\gamma$ (from UCLA data)
4.7 to 6.7	NEFKENS	78		$\pi^+ p \to \pi^+ p\gamma$ (UCLA data)

$\Delta(1232)^{+}$ MAGNETIC MOMENT

VALUE (μ_N)	DOCUMENT ID		COMMENT
• • • We do not use the following data for averages, fits, limits, etc. • • •			
$2.7^{+1.0}_{-1.3} \pm 1.5 \pm 3$	[1] KOTULLA	02	$\gamma p \to p\pi^0\gamma'$

[1] The second error is systematic, the third is an estimate of theoretical uncertainties.

$\Delta(1232)$ REFERENCES

For early references, see Physics Letters **111B** 1 (1982).

HUNT	19	PR C99 055205	B.C. Hunt, D.M. Manley	
ADAMCZEW...	17	PR C95 065205	J. Adamczewski-Musch *et al.*	(HADES Collab.)
ROENCHEN	15A	EPJ A51 70	D. Roenchen *et al.*	
PDG	14	CP C38 070001	K. Olive *et al.*	(PDG Collab.)
ROENCHEN	14	EPJ A50 101	D. Roenchen *et al.*	
Also		EPJ A51 63 (errat.)	D. Roenchen *et al.*	
SVARC	14	PR C89 045205	A. Svarc *et al.*	(RBI Zagreb, UNI Tuzla)
ANISOVICH	12A	EPJ A48 15	A.V. Anisovich *et al.*	(BONN, PNPI)
SHRESTHA	12A	PR C86 055203	M. Shrestha, D.M. Manley	(KSU)
WORKMAN	12A	PR C86 015202	R. Workman *et al.*	(GWU)
ANISOVICH	10	EPJ A44 203	A.V. Anisovich *et al.*	(BONN, PNPI)
DRECHSEL	07	EPJ A34 69	D. Drechsel, S.S. Kamalov, L. Tiator	(MAINZ, JINR)
DUGGER	07	PR C76 025211	M. Dugger *et al.*	(JLab CLAS Collab.)
ARNDT	06	PR C74 045205	R.A. Arndt *et al.*	(GWU)
BREITSCHOP...	06	PL B639 424	J. Breitschopf *et al.*	(TUBIN, HEBR, CSUS)
GRIDNEV	06	PAN 69 1542	A.B. Gridnev *et al.*	(PNPI, BONN, GWU)
PDG	06	JP G33 1	W.-M. Yao *et al.*	(PDG Collab.)
AHRENS	04A	EPJ A21 323	J. Ahrens *et al.*	(A2 Collab.)
ARNDT	04	PR C69 035213	R.A. Arndt *et al.*	(GWU, TRIU)
ARNDT	02	PR C66 055213	R. A. Arndt *et al.*	(GWU)
KOTULLA	02	PRL 89 272001	M. Kotulla *et al.*	(MAMI TAPS Collab.)
PENNER	02C	PR C66 055211	G. Penner, U. Mosel	(GIES)
PENNER	02D	PR C66 055212	G. Penner, U. Mosel	(GIES)
BLANPIED	01	PR C64 025203	G. Blanpied *et al.*	(BNL LEGS Collab.)
GALLER	01	PL B503 245	G. Galler *et al.*	(Mainz LARA Collab.)
LOPEZCAST...	01	PL B517 339	G. Lopez Castro, A. Mariano	
Also		NP A697 440	G. Lopez Castro, A. Mariano	
BECK	00	PR C61 035204	R. Beck *et al.*	(Mainz Microtron DAPHNE Col.)
KAMALOV	99	PRL 83 4494	S.S. Kamalov, S.N. Yang	(Taiwan U.)
HANSTEIN	98	NP A632 561	O. Hanstein, D. Drechsel, L. Tiator	
ARNDT	97	PR C56 577	R.A. Arndt, I.I. Strakovsky, R.L. Workman	(VPI)
BECK	97	PRL 78 606	R. Beck *et al.*	(MAINZ, SACL, PAVI, GLAS)
Also		PRL 79 4510	R.L. Beck, H.P. Krahn	(MAINZ)
Also		PRL 79 4512	R.L. Beck, H.P. Krahn	(MAINZ)
Also		PRL 79 4515 (erratum)	R.L. Beck *et al.*	(MAINZ, SACL, PAVI, GLAS)
BLANPIED	97	PRL 79 4337	G.S. Blanpied *et al.*	(LEGS Collab.)
DAVIDSON	97	PRL 79 4509	R.M. Davidson, N.C.A. Mukhopadhyay	(RPI)
BERNICHA	96	NP A597 623	A. Bernicha, G. Lopez Castro, J. Pestieau	(LOUV+)
HANSTEIN	96	PL B385 45	O. Hanstein, D. Drechsel, L. Tiator	(MAINZ)
ABAEV	95	ZPHY A352 85	V.V. Abaev, S.P. Kruglov	(PNPI)
HOEHLER	93	πN Newsletter 9 1	G. Hohler	(KARL)
BOSSHARD	91	PR D44 1962	A. Bosshard *et al.*	(ZURI, LBL, VILL+)
Also		PRL 64 2619	A. Bosshard *et al.*	(CATH, LAUS, LBL+)
LIN	91B	PR C44 1819	D.H. Lin, M.K. Liou, Z.M. Ding	(CUNY, CSOK)
Also		PR C43 R930	D. Lin, M.K. Liou	(CUNY)
WITTMAN	88	PR C37 2075	R. Wittman	(TRIU)
HELLER	87	PR C35 718	L. Heller *et al.*	(LANL, MIT, ILL)
CUTKOSKY	80	Toronto Conf. 19	R.E. Cutkosky *et al.*	(CMU, LBL) IJP
Also		PR D20 2839	R.E. Cutkosky *et al.*	(CMU, LBL)
KOCH	80B	NP A336 331	R. Koch, E. Pietarinen	(KARLT) IJP
HOEHLER	79	PDAT 12-1	G. Hohler *et al.*	(KARLT) IJP
Also		Toronto Conf. 3	R. Koch	(KARLT) IJP
MIROSHNIC...	79	SJNP 29 94	I.I. Miroshnichenko *et al.*	(KFTI) IJP
		Translated from YAF 29 188.		
NEFKENS	78	PR D18 3911	B.M.K. Nefkens *et al.*	(UCLA, CATH) IJP
PEDRONI	78	NP A300 321	E. Pedroni *et al.*	(SIN, ISNG, KARLE+) IJP

$\Delta(1600)\ 3/2^+$

$I(J^P) = \frac{3}{2}(\frac{3}{2}^+)$ Status: ****

Older and obsolete values are listed and referenced in the 2014 edition, Chinese Physics **C38** 070001 (2014).

$\Delta(1600)$ POLE POSITION

REAL PART

VALUE (MeV)	DOCUMENT ID		TECN	COMMENT
1460 to 1560 (≈ 1510) OUR ESTIMATE				
1515±20	SOKHOYAN	15A	DPWA	Multichannel
1469±10±5	[1] SVARC	14	L+P	$\pi N \to \pi N$
1550±40	CUTKOSKY	80	IPWA	$\pi N \to \pi N$
• • • We do not use the following data for averages, fits, limits, etc. • • •				
1619	HUNT	19	DPWA	Multichannel
1552	ROENCHEN	15A	DPWA	Multichannel
1498±25	ANISOVICH	12A	DPWA	Multichannel
1457	ARNDT	06	DPWA	$\pi N \to \pi N, \eta N$
1599	VRANA	00	DPWA	Multichannel
1550	HOEHLER	93	SPED	$\pi N \to \pi N$

[1] Fit to the amplitudes of HOEHLER 79.

−2×IMAGINARY PART

VALUE (MeV)	DOCUMENT ID		TECN	COMMENT
200 to 340 (≈ 270) OUR ESTIMATE				
250±30	SOKHOYAN	15A	DPWA	Multichannel
314±18±8	[1] SVARC	14	L+P	$\pi N \to \pi N$
200±60	CUTKOSKY	80	IPWA	$\pi N \to \pi N$
• • • We do not use the following data for averages, fits, limits, etc. • • •				
295	HUNT	19	DPWA	Multichannel
350	ROENCHEN	15A	DPWA	Multichannel
230±50	ANISOVICH	12A	DPWA	Multichannel
400	ARNDT	06	DPWA	$\pi N \to \pi N, \eta N$
312	VRANA	00	DPWA	Multichannel

[1] Fit to the amplitudes of HOEHLER 79.

$\Delta(1600)$ ELASTIC POLE RESIDUE

MODULUS $|r|$

VALUE (MeV)	DOCUMENT ID		TECN	COMMENT
10 to 40 (≈ 25) OUR ESTIMATE				
13±3	SOKHOYAN	15A	DPWA	Multichannel
38±2±2	[1] SVARC	14	L+P	$\pi N \to \pi N$
17±4	CUTKOSKY	80	IPWA	$\pi N \to \pi N$
• • • We do not use the following data for averages, fits, limits, etc. • • •				
23	ROENCHEN	15A	DPWA	Multichannel
11±6	ANISOVICH	12A	DPWA	Multichannel
44	ARNDT	06	DPWA	$\pi N \to \pi N, \eta N$

[1] Fit to the amplitudes of HOEHLER 79.

PHASE θ

VALUE (°)	DOCUMENT ID		TECN	COMMENT
150 to 210 (≈ 180) OUR ESTIMATE				
−155±20	SOKHOYAN	15A	DPWA	Multichannel
173± 5±5	[1] SVARC	14	L+P	$\pi N \to \pi N$
−150±30	CUTKOSKY	80	IPWA	$\pi N \to \pi N$
• • • We do not use the following data for averages, fits, limits, etc. • • •				
−155	ROENCHEN	15A	DPWA	Multichannel
−160±33	ANISOVICH	12A	DPWA	Multichannel
+147	ARNDT	06	DPWA	$\pi N \to \pi N, \eta N$

[1] Fit to the amplitudes of HOEHLER 79.

$\Delta(1600)$ INELASTIC POLE RESIDUE

The "normalized residue" is the residue divided by $\Gamma_{pole}/2$.

Normalized residue in $N\pi \to \Delta(1600) \to \Delta\pi$, P-wave

MODULUS	PHASE (°)	DOCUMENT ID		TECN	COMMENT
0.15±0.04	30 ± 35	SOKHOYAN	15A	DPWA	Multichannel
• • • We do not use the following data for averages, fits, limits, etc. • • •					
0.31	31	ROENCHEN	15A	DPWA	Multichannel
0.14±0.10	154 ± 40	ANISOVICH	12A	DPWA	Multichannel

Normalized residue in $N\pi \to \Delta(1600) \to \Delta\pi$, F-wave

MODULUS	PHASE (°)	DOCUMENT ID		TECN	COMMENT
0.010±0.005		SOKHOYAN	15A	DPWA	Multichannel
• • • We do not use the following data for averages, fits, limits, etc. • • •					
0.013	29	ROENCHEN	15A	DPWA	Multichannel
0.010±0.005		ANISOVICH	12A	DPWA	Multichannel

Downloaded from https://academic.oup.com/ptep/article/2022/8/083C01/6651666 by KIT Library user on 27 September 2022

Normalized residue in $N\pi \to \Delta(1600) \to \Sigma K$

MODULUS	PHASE (°)	DOCUMENT ID		TECN	COMMENT
• • • We do not use the following data for averages, fits, limits, etc. • • •					
0.13	−5.6	ROENCHEN	15A	DPWA	Multichannel

$\Delta(1600)$ BREIT-WIGNER MASS

VALUE (MeV)	DOCUMENT ID		TECN	COMMENT
1500 to 1640 (≈ 1570) OUR ESTIMATE				
1664±16	[1] HUNT	19	DPWA	Multichannel
1520±20	SOKHOYAN	15A	DPWA	Multichannel
1600±50	CUTKOSKY	80	IPWA	$\pi N \to \pi N$
1522±13	HOEHLER	79	IPWA	$\pi N \to \pi N$
• • • We do not use the following data for averages, fits, limits, etc. • • •				
1510±20	ANISOVICH	12A	DPWA	Multichannel
1626± 8	[1] SHRESTHA	12A	DPWA	Multichannel
1667± 1	PENNER	02C	DPWA	Multichannel
1687±44	VRANA	00	DPWA	Multichannel

[1] Statistical error only.

$\Delta(1600)$ BREIT-WIGNER WIDTH

VALUE (MeV)	DOCUMENT ID		TECN	COMMENT
200 to 300 (≈ 250) OUR ESTIMATE				
322± 46	[1] HUNT	19	DPWA	Multichannel
235± 30	SOKHOYAN	15A	DPWA	Multichannel
300±100	CUTKOSKY	80	IPWA	$\pi N \to \pi N$
220± 40	HOEHLER	79	IPWA	$\pi N \to \pi N$
• • • We do not use the following data for averages, fits, limits, etc. • • •				
220± 45	ANISOVICH	12A	DPWA	Multichannel
225± 18	[1] SHRESTHA	12A	DPWA	Multichannel
397± 10	PENNER	02C	DPWA	Multichannel
493± 75	VRANA	00	DPWA	Multichannel

[1] Statistical error only.

$\Delta(1600)$ DECAY MODES

The following branching fractions are our estimates, not fits or averages.

	Mode	Fraction (Γ_i/Γ)
Γ_1	$N\pi$	8–24%
Γ_2	$N\pi\pi$	58–84 %
Γ_3	$\Delta(1232)\pi$	58–82 %
Γ_4	$\Delta(1232)\pi$, P-wave	72–82%
Γ_5	$\Delta(1232)\pi$, F-wave	<2%
Γ_6	$N(1440)\pi$	17–27%
Γ_7	$N\gamma$	0.001–0.035 %
Γ_8	$N\gamma$, helicity=1/2	0.0–0.02 %
Γ_9	$N\gamma$, helicity=3/2	0.001–0.015 %

$\Delta(1600)$ BRANCHING RATIOS

$\Gamma(N\pi)/\Gamma_{total}$ — Γ_1/Γ

VALUE (%)	DOCUMENT ID		TECN	COMMENT
8–24% OUR ESTIMATE				
10.7±1.9	[1] HUNT	19	DPWA	Multichannel
14 ±4	SOKHOYAN	15A	DPWA	Multichannel
18 ±4	CUTKOSKY	80	IPWA	$\pi N \to \pi N$
21 ±6	HOEHLER	79	IPWA	$\pi N \to \pi N$
• • • We do not use the following data for averages, fits, limits, etc. • • •				
12 ±5	ANISOVICH	12A	DPWA	Multichannel
8 ±2	[1] SHRESTHA	12A	DPWA	Multichannel
13 ±1	PENNER	02C	DPWA	Multichannel
28 ±5	VRANA	00	DPWA	Multichannel

[1] Statistical error only.

$\Gamma(\Delta(1232)\pi, P\text{-wave})/\Gamma_{total}$ — Γ_4/Γ

VALUE (%)	DOCUMENT ID		TECN	COMMENT
72–82% OUR ESTIMATE				
64± 6	[1] HUNT	19	DPWA	Multichannel
77± 5	SOKHOYAN	15A	DPWA	Multichannel
• • • We do not use the following data for averages, fits, limits, etc. • • •				
78± 6	ANISOVICH	12A	DPWA	Multichannel
70± 3	[1] SHRESTHA	12A	DPWA	Multichannel
59±10	VRANA	00	DPWA	Multichannel

[1] Statistical error only.

$\Gamma(\Delta(1232)\pi, F\text{-wave})/\Gamma_{total}$ — Γ_5/Γ

VALUE (%)	DOCUMENT ID		TECN	COMMENT
<2% OUR ESTIMATE				
<2	SOKHOYAN	15A	DPWA	Multichannel

$\Gamma(N(1440)\pi)/\Gamma_{total}$ — Γ_6/Γ

VALUE (%)	DOCUMENT ID		TECN	COMMENT
17–27% OUR ESTIMATE				
22±5	[1] HUNT	19	DPWA	Multichannel
• • • We do not use the following data for averages, fits, limits, etc. • • •				
22±3	[1] SHRESTHA	12A	DPWA	Multichannel
13±4	VRANA	00	DPWA	Multichannel

[1] Statistical error only.

$\Delta(1600)$ PHOTON DECAY AMPLITUDES AT THE POLE

$\Delta(1600) \to N\gamma$, helicity-1/2 amplitude $A_{1/2}$

MODULUS ($GeV^{-1/2}$)	PHASE (°)	DOCUMENT ID		TECN	COMMENT
0.053±0.010	130 ± 15	SOKHOYAN	15A	DPWA	Multichannel
$0.193^{+0.023}_{-0.024}$	151^{+9}_{-15}	ROENCHEN	14	DPWA	
• • • We do not use the following data for averages, fits, limits, etc. • • •					
−0.230	−42	ROENCHEN	15A	DPWA	Multichannel

$\Delta(1600) \to N\gamma$, helicity-3/2 amplitude $A_{3/2}$

MODULUS ($GeV^{-1/2}$)	PHASE (°)	DOCUMENT ID		TECN	COMMENT
0.055±0.010	152 ± 15	SOKHOYAN	15A	DPWA	Multichannel
$-0.254^{+0.085}_{-0.086}$	110^{+10}_{-6}	ROENCHEN	14	DPWA	
• • • We do not use the following data for averages, fits, limits, etc. • • •					
0.332	−71	ROENCHEN	15A	DPWA	Multichannel

$\Delta(1600)$ BREIT-WIGNER PHOTON DECAY AMPLITUDES

$\Delta(1600) \to N\gamma$, helicity-1/2 amplitude $A_{1/2}$

VALUE ($GeV^{-1/2}$)	DOCUMENT ID		TECN	COMMENT
−0.060 to −0.030 (≈ −0.045) OUR ESTIMATE				
0.0082±0.0014	[1] HUNT	19	DPWA	Multichannel
−0.051 ±0.010	SOKHOYAN	15A	DPWA	Multichannel
−0.018 ±0.015	[1] ARNDT	96	IPWA	$\gamma N \to \pi N$
• • • We do not use the following data for averages, fits, limits, etc. • • •				
−0.050 ±0.009	ANISOVICH	12A	DPWA	Multichannel
0.006 ±0.005	[1] SHRESTHA	12A	DPWA	Multichannel
0.0	PENNER	02D	DPWA	Multichannel

[1] Statistical error only.

$\Delta(1600) \to N\gamma$, helicity-3/2 amplitude $A_{3/2}$

VALUE ($GeV^{-1/2}$)	DOCUMENT ID		TECN	COMMENT
−0.050 to −0.020 (≈ −0.035) OUR ESTIMATE				
0.048±0.014	[1] HUNT	19	DPWA	Multichannel
−0.055±0.010	SOKHOYAN	15A	DPWA	Multichannel
−0.025±0.015	[1] ARNDT	96	IPWA	$\gamma N \to \pi N$
• • • We do not use the following data for averages, fits, limits, etc. • • •				
−0.040±0.012	ANISOVICH	12A	DPWA	Multichannel
0.052±0.008	[1] SHRESTHA	12A	DPWA	Multichannel
−0.024	PENNER	02D	DPWA	Multichannel

[1] Statistical error only.

$\Delta(1600)$ REFERENCES

For early references, see Physics Letters **111B** 1 (1982).

HUNT	19	PR C99 055205	B.C. Hunt, D.M. Manley	
ROENCHEN	15A	EPJ A51 70	D. Roenchen *et al.*	
SOKHOYAN	15A	EPJ A51 95	V. Sokhoyan *et al.*	(CBELSA/TAPS Collab.)
PDG	14	CP C38 070001	K. Olive *et al.*	(PDG Collab.)
ROENCHEN	14	EPJ A50 101	D. Roenchen *et al.*	
Also		EPJ A51 63 (errat.)	D. Roenchen *et al.*	
SVARC	14	PR C89 045205	A. Svarc *et al.*	(RBI Zagreb, UNI Tuzla)
ANISOVICH	12A	EPJ A48 15	A.V. Anisovich *et al.*	(BONN, PNPI)
SHRESTHA	12A	PR C86 055203	M. Shrestha, D.M. Manley	(KSU)
ARNDT	06	PR C74 045205	R.A. Arndt *et al.*	(GWU)
PENNER	02C	PR C66 055211	G. Penner, U. Mosel	(GIES)
PENNER	02D	PR C66 055212	G. Penner, U. Mosel	(GIES)
VRANA	00	PRPL 328 181	T.P. Vrana, S.A. Dytman, T.-S.H. Lee	(PITT, ANL)
ARNDT	96	PR C53 430	R.A. Arndt, I.I. Strakovsky, R.L. Workman	(VPI)
HOEHLER	93	πN Newsletter 9 1	G. Hohler	(KARL)
CUTKOSKY	80	Toronto Conf. 19	R.E. Cutkosky *et al.*	(CMU, LBL) IJP
Also		PR D20 2839	R.E. Cutkosky *et al.*	(CMU, LBL) IJP
HOEHLER	79	PDAT 12-1	G. Hohler *et al.*	(KARLT) IJP
Also		Toronto Conf. 3	R. Koch	(KARLT) IJP

$\Delta(1620)\ 1/2^-$

$I(J^P) = \frac{3}{2}(\frac{1}{2}^-)$ Status: ****

Older and obsolete values are listed and referenced in the 2014 edition, Chinese Physics **C38** 070001 (2014).

$\Delta(1620)$ POLE POSITION

REAL PART

VALUE (MeV)	DOCUMENT ID		TECN	COMMENT
1590 to 1610 (≈ 1600) OUR ESTIMATE				
1597± 5	SOKHOYAN	15A	DPWA	Multichannel
1603± 7±2	[1] SVARC	14	L+P	$\pi N \to \pi N$
1600±15	CUTKOSKY	80	IPWA	$\pi N \to \pi N$

Downloaded from https://academic.oup.com/ptep/article/2022/8/083C01/6651666 by KIT Library user on 27 September 2022

• • • We do not use the following data for averages, fits, limits, etc. • • •

1577	HUNT	19	DPWA	Multichannel
1600	ROENCHEN	15A	DPWA	Multichannel
1597± 4	ANISOVICH	12A	DPWA	Multichannel
1595	ARNDT	06	DPWA	$\pi N \to \pi N, \eta N$
1607	VRANA	00	DPWA	Multichannel
1608	HOEHLER	93	SPED	$\pi N \to \pi N$

[1] Fit to the amplitudes of HOEHLER 79.

−2×IMAGINARY PART

VALUE (MeV)	DOCUMENT ID		TECN	COMMENT
100 to 140 (≈ 120) OUR ESTIMATE				
134± 8	SOKHOYAN	15A	DPWA	Multichannel
114±12±4	[1] SVARC	14	L+P	$\pi N \to \pi N$
120±20	CUTKOSKY	80	IPWA	$\pi N \to \pi N$
• • • We do not use the following data for averages, fits, limits, etc. • • •				
101	HUNT	19	DPWA	Multichannel
65	ROENCHEN	15A	DPWA	Multichannel
130± 9	ANISOVICH	12A	DPWA	Multichannel
135	ARNDT	06	DPWA	$\pi N \to \pi N, \eta N$
148	VRANA	00	DPWA	Multichannel
116	HOEHLER	93	SPED	$\pi N \to \pi N$

[1] Fit to the amplitudes of HOEHLER 79.

$\Delta(1620)$ ELASTIC POLE RESIDUE

MODULUS $|r|$

VALUE (MeV)	DOCUMENT ID		TECN	COMMENT
15 to 20 (≈ 17) OUR ESTIMATE				
20±3	SOKHOYAN	15A	DPWA	Multichannel
17±2±1	[1] SVARC	14	L+P	$\pi N \to \pi N$
15±2	CUTKOSKY	80	IPWA	$\pi N \to \pi N$
• • • We do not use the following data for averages, fits, limits, etc. • • •				
16	ROENCHEN	15A	DPWA	Multichannel
18±2	ANISOVICH	12A	DPWA	Multichannel
15	ARNDT	06	DPWA	$\pi N \to \pi N, \eta N$
19	HOEHLER	93	SPED	$\pi N \to \pi N$

[1] Fit to the amplitudes of HOEHLER 79.

PHASE θ

VALUE (°)	DOCUMENT ID		TECN	COMMENT
−120 to −80 (≈ −100) OUR ESTIMATE				
− 90±15	SOKHOYAN	15A	DPWA	Multichannel
−106±10±4	[1] SVARC	14	L+P	$\pi N \to \pi N$
−110±20	CUTKOSKY	80	IPWA	$\pi N \to \pi N$
• • • We do not use the following data for averages, fits, limits, etc. • • •				
−104	ROENCHEN	15A	DPWA	Multichannel
−100± 5	ANISOVICH	12A	DPWA	Multichannel
− 92	ARNDT	06	DPWA	$\pi N \to \pi N, \eta N$
− 95	HOEHLER	93	SPED	$\pi N \to \pi N$

[1] Fit to the amplitudes of HOEHLER 79.

$\Delta(1620)$ INELASTIC POLE RESIDUE

The "normalized residue" is the residue divided by $\Gamma_{pole}/2$.

Normalized residue in $N\pi \to \Delta(1620) \to \Delta\pi$, D-wave

MODULUS	PHASE (°)	DOCUMENT ID		TECN	COMMENT
0.42±0.06	−90 ± 20	SOKHOYAN	15A	DPWA	Multichannel
• • • We do not use the following data for averages, fits, limits, etc. • • •					
0.57	105	ROENCHEN	15A	DPWA	Multichannel
0.38±0.09	−85 ± 30	ANISOVICH	12A	DPWA	Multichannel

Normalized residue in $N\pi \to \Delta(1620) \to \Sigma K$

MODULUS	PHASE (°)	DOCUMENT ID		TECN	COMMENT
• • • We do not use the following data for averages, fits, limits, etc. • • •					
0.22	−105	ROENCHEN	15A	DPWA	Multichannel

Normalized residue in $N\pi \to \Delta(1620) \to N(1440)\pi$

MODULUS	PHASE (°)	DOCUMENT ID		TECN	COMMENT
0.10±0.06	−65 ± 30	SOKHOYAN	15A	DPWA	Multichannel

$\Delta(1620)$ BREIT-WIGNER MASS

VALUE (MeV)	DOCUMENT ID		TECN	COMMENT
1590 to 1630 (≈ 1610) OUR ESTIMATE				
1635 ± 8	GOLOVATCH	19	DPWA	$\gamma p \to \pi^+\pi^- p$
1589 ± 3	[1] HUNT	19	DPWA	Multichannel
1595 ± 8	SOKHOYAN	15A	DPWA	Multichannel
1615.2± 0.4	[1] ARNDT	06	DPWA	$\pi N \to \pi N, \eta N$
1620 ±20	CUTKOSKY	80	IPWA	$\pi N \to \pi N$
1610 ± 7	HOEHLER	79	IPWA	$\pi N \to \pi N$
• • • We do not use the following data for averages, fits, limits, etc. • • •				
1600 ± 8	ANISOVICH	12A	DPWA	Multichannel
1600 ± 1	[1] SHRESTHA	12A	DPWA	Multichannel
1612 ± 2	PENNER	02C	DPWA	Multichannel
1617 ±15	VRANA	00	DPWA	Multichannel

[1] Statistical error only.

$\Delta(1620)$ BREIT-WIGNER WIDTH

VALUE (MeV)	DOCUMENT ID		TECN	COMMENT
110 to 150 (≈ 130) OUR ESTIMATE				
144 ±16	GOLOVATCH	19	DPWA	$\gamma p \to \pi^+\pi^- p$
107 ± 7	[1] HUNT	19	DPWA	Multichannel
135 ± 9	SOKHOYAN	15A	DPWA	Multichannel
146.9± 1.9	[1] ARNDT	06	DPWA	$\pi N \to \pi N, \eta N$
140 ±20	CUTKOSKY	80	IPWA	$\pi N \to \pi N$
139 ±18	HOEHLER	79	IPWA	$\pi N \to \pi N$
• • • We do not use the following data for averages, fits, limits, etc. • • •				
130 ±11	ANISOVICH	12A	DPWA	Multichannel
112 ± 2	[1] SHRESTHA	12A	DPWA	Multichannel
202 ± 7	PENNER	02C	DPWA	Multichannel
143 ±42	VRANA	00	DPWA	Multichannel

[1] Statistical error only.

$\Delta(1620)$ DECAY MODES

The following branching fractions are our estimates, not fits or averages.

	Mode	Fraction (Γ_i/Γ)
Γ_1	$N\pi$	25–35 %
Γ_2	$N\pi\pi$	>67 %
Γ_3	$\Delta(1232)\pi$, D-wave	44–72 %
Γ_4	$N\rho$	23–32%
Γ_5	$N\rho$, S=1/2, S-wave	23–32%
Γ_6	$N\rho$, S=3/2, D-wave	<0.04%
Γ_7	$N(1440)\pi$	<9 %
Γ_8	$N\gamma$, helicity=1/2	0.03–0.10 %

$\Delta(1620)$ BRANCHING RATIOS

$\Gamma(N\pi)/\Gamma_{total}$ — Γ_1/Γ

VALUE (%)	DOCUMENT ID		TECN	COMMENT
25 to 35 (≈ 30) OUR ESTIMATE				
24 ±2	[1] HUNT	19	DPWA	Multichannel
28 ±3	SOKHOYAN	15A	DPWA	Multichannel
31.5±0.1	[1] ARNDT	06	DPWA	$\pi N \to \pi N, \eta N$
25 ±3	CUTKOSKY	80	IPWA	$\pi N \to \pi N$
35 ±6	HOEHLER	79	IPWA	$\pi N \to \pi N$
• • • We do not use the following data for averages, fits, limits, etc. • • •				
28 ±3	ANISOVICH	12A	DPWA	Multichannel
33 ±2	[1] SHRESTHA	12A	DPWA	Multichannel
34 ±1	PENNER	02C	DPWA	Multichannel
45 ±5	VRANA	00	DPWA	Multichannel

[1] Statistical error only.

$\Gamma(N\pi\pi)/\Gamma_{total}$ — Γ_2/Γ

VALUE	DOCUMENT ID		TECN	COMMENT
0.90±0.10	GOLOVATCH	19	DPWA	$\gamma p \to \pi^+\pi^- p$

$\Gamma(\Delta(1232)\pi, D\text{-wave})/\Gamma_{total}$ — Γ_3/Γ

VALUE (%)	DOCUMENT ID		TECN	COMMENT
48± 4	[1] HUNT	19	DPWA	Multichannel
62±10	SOKHOYAN	15A	DPWA	Multichannel
• • • We do not use the following data for averages, fits, limits, etc. • • •				
60±17	ANISOVICH	12A	DPWA	Multichannel
32± 2	[1] SHRESTHA	12A	DPWA	Multichannel
39± 2	VRANA	00	DPWA	Multichannel

[1] Statistical error only.

$\Gamma(N\rho, S{=}1/2, S\text{-wave})/\Gamma_{total}$ — Γ_5/Γ

VALUE (%)	DOCUMENT ID		TECN	COMMENT
27±4	[1] HUNT	19	DPWA	Multichannel
• • • We do not use the following data for averages, fits, limits, etc. • • •				
26±2	[1] SHRESTHA	12A	DPWA	Multichannel
14±3	VRANA	00	DPWA	Multichannel

[1] Statistical error only.

Downloaded from https://academic.oup.com/ptep/article/2022/8/083C01/6651666 by KIT Library user on 27 September 2022

$\Gamma(N\rho, S=3/2, D\text{-wave})/\Gamma_{total}$ — Γ_6/Γ

VALUE (%)	DOCUMENT ID		TECN	COMMENT
<0.04	[1] HUNT	19	DPWA	Multichannel
• • • We do not use the following data for averages, fits, limits, etc. • • •				
2 ±1	VRANA	00	DPWA	Multichannel

[1] Statistical error only.

$\Gamma(N(1440)\pi)/\Gamma_{total}$ — Γ_7/Γ

VALUE (%)	DOCUMENT ID		TECN	COMMENT
<0.02	[1] HUNT	19	DPWA	Multichannel
6 ±3	SOKHOYAN	15A	DPWA	Multichannel
• • • We do not use the following data for averages, fits, limits, etc. • • •				
9 ±1	[1] SHRESTHA	12A	DPWA	Multichannel
0 ±1	VRANA	00	DPWA	Multichannel

[1] Statistical error only.

$\Delta(1620)$ PHOTON DECAY AMPLITUDES AT THE POLE

$\Delta(1620) \to N\gamma$, helicity-1/2 amplitude $A_{1/2}$

MODULUS (GeV$^{-1/2}$)	PHASE (°)	DOCUMENT ID		TECN	COMMENT
0.054±0.007	−6 ± 7	SOKHOYAN	15A	DPWA	Multichannel
$-0.028^{+0.006}_{-0.002}$	-166^{+1}_{-4}	ROENCHEN	14	DPWA	
• • • We do not use the following data for averages, fits, limits, etc. • • •					
0.014	26	ROENCHEN	15A	DPWA	Multichannel

$\Delta(1620)$ BREIT-WIGNER PHOTON DECAY AMPLITUDES

$\Delta(1620) \to N\gamma$, helicity-1/2 amplitude $A_{1/2}$

VALUE (GeV$^{-1/2}$)	DOCUMENT ID		TECN	COMMENT
0.030 to 0.060 (≈ 0.050) OUR ESTIMATE				
0.029 ±0.0062	GOLOVATCH	19	DPWA	$\gamma p \to \pi^+\pi^- p$
0.0124±0.0007	[1] HUNT	19	DPWA	Multichannel
0.055 ±0.007	SOKHOYAN	15A	DPWA	Multichannel
0.029 ±0.003	[1] WORKMAN	12A	DPWA	$\gamma N \to N\pi$
0.050 ±0.002	[1] DUGGER	07	DPWA	$\gamma N \to \pi N$
• • • We do not use the following data for averages, fits, limits, etc. • • •				
0.052 ±0.005	ANISOVICH	12A	DPWA	Multichannel
−0.003 ±0.003	[1] SHRESTHA	12A	DPWA	Multichannel
0.066	DRECHSEL	07	DPWA	$\gamma N \to \pi N$
−0.050	PENNER	02D	DPWA	Multichannel

[1] Statistical error only.

$\Delta(1620)$ REFERENCES

For early references, see Physics Letters **111B** 1 (1982).

GOLOVATCH	19	PL B788 371	E. Golovatch *et al.*	(CLAS Collab.)
HUNT	19	PR C99 055205	B.C. Hunt, D.M. Manley	
ROENCHEN	15A	EPJ A51 70	D. Roenchen *et al.*	
SOKHOYAN	15A	EPJ A51 95	V. Sokhoyan *et al.*	(CBELSA/TAPS Collab.)
PDG	14	CP C38 070001	K. Olive *et al.*	(PDG Collab.)
ROENCHEN	14	EPJ A50 101	D. Roenchen *et al.*	
Also		EPJ A51 63 (errat.)	D. Roenchen *et al.*	
SVARC	14	PR C89 045205	A. Svarc *et al.*	(RBI Zagreb, UNI Tuzla)
ANISOVICH	12A	EPJ A48 15	A.V. Anisovich *et al.*	(BONN, PNPI)
SHRESTHA	12A	PR C86 055203	M. Shrestha, D.M. Manley	(KSU)
WORKMAN	12A	PR C86 015202	R. Workman *et al.*	(GWU)
DRECHSEL	07	EPJ A34 69	D. Drechsel, S.S. Kamalov, L. Tiator	(MAINZ, JINR)
DUGGER	07	PR C76 025211	M. Dugger *et al.*	(JLab CLAS Collab.)
ARNDT	06	PR C74 045205	R.A. Arndt *et al.*	(GWU)
PENNER	02C	PR C66 055211	G. Penner, U. Mosel	(GIES)
PENNER	02D	PR C66 055212	G. Penner, U. Mosel	(GIES)
VRANA	00	PRPL 328 181	T.P. Vrana, S.A. Dytman, T.-S.H. Lee	(PITT, ANL)
HOEHLER	93	πN Newsletter 9 1	G. Hohler	(KARL)
CUTKOSKY	80	Toronto Conf. 19	R.E. Cutkosky *et al.*	(CMU, LBL) IJP
Also		PR D20 2839	R.E. Cutkosky *et al.*	(CMU, LBL) IJP
HOEHLER	79	PDAT 12-1	G. Hohler *et al.*	(KARLT) IJP
Also		Toronto Conf. 3	R. Koch	(KARLT) IJP

$\Delta(1700)\ 3/2^-$

$I(J^P) = \frac{3}{2}(\frac{3}{2}^-)$ Status: ****

Older and obsolete values are listed and referenced in the 2014 edition, Chinese Physics **C38** 070001 (2014).

$\Delta(1700)$ POLE POSITION

REAL PART

VALUE (MeV)	DOCUMENT ID		TECN	COMMENT
1640 to 1690 (≈ 1665) OUR ESTIMATE				
1685±10	SOKHOYAN	15A	DPWA	Multichannel
1643± 6±3	[1] SVARC	14	L+P	$\pi N \to \pi N$
1675±25	CUTKOSKY	80	IPWA	$\pi N \to \pi N$
• • • We do not use the following data for averages, fits, limits, etc. • • •				
1693	HUNT	19	DPWA	Multichannel
1677	ROENCHEN	15A	DPWA	Multichannel
1685±10	GUTZ	14	DPWA	Multichannel
1680±10	ANISOVICH	12A	DPWA	Multichannel
1632	ARNDT	06	DPWA	$\pi N \to \pi N, \eta N$
1726	VRANA	00	DPWA	Multichannel
1651	HOEHLER	93	SPED	$\pi N \to \pi N$

[1] Fit to the amplitudes of HOEHLER 79.

−2×IMAGINARY PART

VALUE (MeV)	DOCUMENT ID		TECN	COMMENT
200 to 300 (≈ 250) OUR ESTIMATE				
300±15	SOKHOYAN	15A	DPWA	Multichannel
217±10±8	[1] SVARC	14	L+P	$\pi N \to \pi N$
220±40	CUTKOSKY	80	IPWA	$\pi N \to \pi N$
• • • We do not use the following data for averages, fits, limits, etc. • • •				
213	HUNT	19	DPWA	Multichannel
305	ROENCHEN	15A	DPWA	Multichannel
300±15	GUTZ	14	DPWA	Multichannel
305±15	ANISOVICH	12A	DPWA	Multichannel
253	ARNDT	06	DPWA	$\pi N \to \pi N, \eta N$
118	VRANA	00	DPWA	Multichannel
159	HOEHLER	93	SPED	$\pi N \to \pi N$

[1] Fit to the amplitudes of HOEHLER 79.

$\Delta(1700)$ ELASTIC POLE RESIDUE

MODULUS $|r|$

VALUE (MeV)	DOCUMENT ID		TECN	COMMENT
10 to 40 (≈ 25) OUR ESTIMATE				
40±6	SOKHOYAN	15A	DPWA	Multichannel
13±1±1	[1] SVARC	14	L+P	$\pi N \to \pi N$
13±3	CUTKOSKY	80	IPWA	$\pi N \to \pi N$
• • • We do not use the following data for averages, fits, limits, etc. • • •				
24	ROENCHEN	15A	DPWA	Multichannel
40±6	GUTZ	14	DPWA	Multichannel
42±7	ANISOVICH	12A	DPWA	Multichannel
18	ARNDT	06	DPWA	$\pi N \to \pi N, \eta N$
10	HOEHLER	93	SPED	$\pi N \to \pi N$

[1] Fit to the amplitudes of HOEHLER 79.

PHASE θ

VALUE (°)	DOCUMENT ID		TECN	COMMENT
−40 to 0 (≈ −20) OUR ESTIMATE				
− 1 ±10	SOKHOYAN	15A	DPWA	Multichannel
−30 ± 4±3	[1] SVARC	14	L+P	$\pi N \to \pi N$
−40	ARNDT	06	DPWA	$\pi N \to \pi N, \eta N$
−20 ±25	CUTKOSKY	80	IPWA	$\pi N \to \pi N$
• • • We do not use the following data for averages, fits, limits, etc. • • •				
− 7.3	ROENCHEN	15A	DPWA	Multichannel
− 1 ±10	GUTZ	14	DPWA	Multichannel
− 3 ±15	ANISOVICH	12A	DPWA	Multichannel

[1] Fit to the amplitudes of HOEHLER 79.

$\Delta(1700)$ INELASTIC POLE RESIDUE

The "normalized residue" is the residue divided by $\Gamma_{pole}/2$.

Normalized residue in $N\pi \to \Delta(1700) \to \Delta\eta$

MODULUS	PHASE (°)	DOCUMENT ID		TECN	COMMENT
0.12±0.02	−60 ± 12	GUTZ	14	DPWA	Multichannel
• • • We do not use the following data for averages, fits, limits, etc. • • •					
0.12±0.03	−60 ± 15	ANISOVICH	12A	DPWA	Multichannel

Normalized residue in $N\pi \to \Delta(1700) \to \Sigma K$

MODULUS	PHASE (°)	DOCUMENT ID		TECN	COMMENT
• • • We do not use the following data for averages, fits, limits, etc. • • •					
0.011	−147	ROENCHEN	15A	DPWA	Multichannel

Normalized residue in $N\pi \to \Delta(1700) \to N(1535)\pi$

MODULUS	PHASE (°)	DOCUMENT ID		TECN	COMMENT
0.035±0.015	−75 ± 30	GUTZ	14	DPWA	Multichannel

Normalized residue in $N\pi \to \Delta(1700) \to \Delta(1232)\pi$, S-wave

MODULUS	PHASE (°)	DOCUMENT ID		TECN	COMMENT
0.25±0.12	135 ± 45	SOKHOYAN	15A	DPWA	Multichannel
• • • We do not use the following data for averages, fits, limits, etc. • • •					
0.39	151	ROENCHEN	15A	DPWA	Multichannel

Normalized residue in $N\pi \to \Delta(1700) \to \Delta(1232)\pi$, D-wave

MODULUS	PHASE (°)	DOCUMENT ID		TECN	COMMENT
0.12 ±0.06	−160 ± 30	SOKHOYAN	15A	DPWA	Multichannel
• • • We do not use the following data for averages, fits, limits, etc. • • •					
0.054	166	ROENCHEN	15A	DPWA	Multichannel

Downloaded from https://academic.oup.com/ptep/article/2022/8/083C01/6651666 by KIT Library user on 27 September 2022

Normalized residue in $N\pi \to \Delta(1700) \to N(1520)\pi$, P-wave

MODULUS	PHASE (°)	DOCUMENT ID		TECN	COMMENT
0.10±0.03	−10 ± 20	SOKHOYAN	15A	DPWA	Multichannel

$\Delta(1700)$ BREIT-WIGNER MASS

VALUE (MeV)	DOCUMENT ID		TECN	COMMENT
1690 to 1730 (≈ 1710) OUR ESTIMATE				
1704 ± 8	GOLOVATCH	19	DPWA	$\gamma p \to \pi^+\pi^- p$
1720 ± 5	[1] HUNT	19	DPWA	Multichannel
1715 ±20	SOKHOYAN	15A	DPWA	Multichannel
1695.0± 1.3	[1] ARNDT	06	DPWA	$\pi N \to \pi N, \eta N$
1710 ±30	CUTKOSKY	80	IPWA	$\pi N \to \pi N$
1680 ±70	HOEHLER	79	IPWA	$\pi N \to \pi N$
• • • We do not use the following data for averages, fits, limits, etc. • • •				
1715 ±20	GUTZ	14	DPWA	Multichannel
1715 $^{+30}_{-15}$	ANISOVICH	12A	DPWA	Multichannel
1691 ± 4	[1] SHRESTHA	12A	DPWA	Multichannel
1678 ± 1	PENNER	02C	DPWA	Multichannel
1732 ±23	VRANA	00	DPWA	Multichannel

[1] Statistical error only.

$\Delta(1700)$ BREIT-WIGNER WIDTH

VALUE (MeV)	DOCUMENT ID		TECN	COMMENT
220 to 380 (≈ 300) OUR ESTIMATE				
295 ±35	GOLOVATCH	19	DPWA	$\gamma p \to \pi^+\pi^- p$
226 ±14	[1] HUNT	19	DPWA	Multichannel
300 ±25	SOKHOYAN	15A	DPWA	Multichannel
375.5± 7.0	[1] ARNDT	06	DPWA	$\pi N \to \pi N, \eta N$
280 ±80	CUTKOSKY	80	IPWA	$\pi N \to \pi N$
230 ±80	HOEHLER	79	IPWA	$\pi N \to \pi N$
• • • We do not use the following data for averages, fits, limits, etc. • • •				
300 ±25	GUTZ	14	DPWA	Multichannel
310 $^{+40}_{-15}$	ANISOVICH	12A	DPWA	Multichannel
248 ± 9	[1] SHRESTHA	12A	DPWA	Multichannel
606 ±15	PENNER	02C	DPWA	Multichannel
119 ±70	VRANA	00	DPWA	Multichannel

[1] Statistical error only.

$\Delta(1700)$ DECAY MODES

The following branching fractions are our estimates, not fits or averages.

	Mode	Fraction (Γ_i/Γ)
Γ_1	$N\pi$	10–20 %
Γ_2	$N\pi\pi$	>31 %
Γ_3	$\Delta(1232)\pi$	9–70 %
Γ_4	$\Delta(1232)\pi$, S-wave	5–54 %
Γ_5	$\Delta(1232)\pi$, D-wave	4–16 %
Γ_6	$N\rho$, S=3/2, S-wave	22–32%
Γ_7	$N(1520)\pi$, P-wave	1–5 %
Γ_8	$N(1535)\pi$	0.5–1.5 %
Γ_9	$\Delta(1232)\eta$	3–7 %
Γ_{10}	$N\gamma$	0.22–0.60 %
Γ_{11}	$N\gamma$, helicity=1/2	0.12–0.30 %
Γ_{12}	$N\gamma$, helicity=3/2	0.10–0.30 %

$\Delta(1700)$ BRANCHING RATIOS

$\Gamma(N\pi)/\Gamma_{total}$ — Γ_1/Γ

VALUE (%)	DOCUMENT ID		TECN	COMMENT
10 to 20 OUR ESTIMATE				
15 ±2	[1] HUNT	19	DPWA	Multichannel
22 ±4	SOKHOYAN	15A	DPWA	Multichannel
15.6±0.1	[1] ARNDT	06	DPWA	$\pi N \to \pi N, \eta N$
12 ±3	CUTKOSKY	80	IPWA	$\pi N \to \pi N$
20 ±3	HOEHLER	79	IPWA	$\pi N \to \pi N$
• • • We do not use the following data for averages, fits, limits, etc. • • •				
22 ±4	GUTZ	14	DPWA	Multichannel
22 ±4	ANISOVICH	12A	DPWA	Multichannel
14 ±1	[1] SHRESTHA	12A	DPWA	Multichannel
14 ±1	PENNER	02C	DPWA	Multichannel
5 ±1	VRANA	00	DPWA	Multichannel

[1] Statistical error only.

$\Gamma(N\pi\pi)/\Gamma_{total}$ — Γ_2/Γ

VALUE	DOCUMENT ID		TECN	COMMENT
0.89±0.11	GOLOVATCH	19	DPWA	$\gamma p \to \pi^+\pi^- p$

$\Gamma(\Delta(1232)\pi, S\text{-wave})/\Gamma_{total}$ — Γ_4/Γ

VALUE (%)	DOCUMENT ID		TECN	COMMENT
49± 5	[1] HUNT	19	DPWA	Multichannel
20±15	SOKHOYAN	15A	DPWA	Multichannel
• • • We do not use the following data for averages, fits, limits, etc. • • •				
20 $^{+25}_{-13}$	ANISOVICH	12A	DPWA	Multichannel
54± 3	[1] SHRESTHA	12A	DPWA	Multichannel
90± 2	VRANA	00	DPWA	Multichannel

[1] Statistical error only.

$\Gamma(\Delta(1232)\pi, D\text{-wave})/\Gamma_{total}$ — Γ_5/Γ

VALUE (%)	DOCUMENT ID		TECN	COMMENT
7.6± 0.3	[1] HUNT	19	DPWA	Multichannel
10 ± 6	SOKHOYAN	15A	DPWA	Multichannel
• • • We do not use the following data for averages, fits, limits, etc. • • •				
12 $^{+14}_{-7}$	ANISOVICH	12A	DPWA	Multichannel
1 ± 1	[1] SHRESTHA	12A	DPWA	Multichannel
4 ± 1	VRANA	00	DPWA	Multichannel

[1] Statistical error only.

$\Gamma(N\rho, S=3/2, S\text{-wave})/\Gamma_{total}$ — Γ_6/Γ

VALUE (%)	DOCUMENT ID		TECN	COMMENT
27±5	[1] HUNT	19	DPWA	Multichannel
• • • We do not use the following data for averages, fits, limits, etc. • • •				
30±3	[1] SHRESTHA	12A	DPWA	Multichannel
1±1	VRANA	00	DPWA	Multichannel

[1] Statistical error only.

$\Gamma(N(1520)\pi, P\text{-wave})/\Gamma_{total}$ — Γ_7/Γ

VALUE (%)	DOCUMENT ID		TECN	COMMENT
3±2	SOKHOYAN	15A	DPWA	Multichannel

$\Gamma(N(1535)\pi)/\Gamma_{total}$ — Γ_8/Γ

VALUE (%)	DOCUMENT ID		TECN	COMMENT
1.0±0.5	GUTZ	14	DPWA	Multichannel
• • • We do not use the following data for averages, fits, limits, etc. • • •				
4 ±2	HORN	08A	DPWA	Multichannel

$\Gamma(\Delta(1232)\eta)/\Gamma_{total}$ — Γ_9/Γ

VALUE (%)	DOCUMENT ID		TECN	COMMENT
5±2	GUTZ	14	DPWA	Multichannel
• • • We do not use the following data for averages, fits, limits, etc. • • •				
5±2	ANISOVICH	12A	DPWA	Multichannel

$\Gamma(N(1535)\pi)/\Gamma(\Delta(1232)\eta)$ — Γ_8/Γ_9

VALUE	DOCUMENT ID		TECN	COMMENT
• • • We do not use the following data for averages, fits, limits, etc. • • •				
0.67	KASHEVAROV	09	CBAL	$\gamma p \to p\pi^0\eta$

$\Delta(1700)$ PHOTON DECAY AMPLITUDES AT THE POLE

$\Delta(1700) \to N\gamma$, helicity-1/2 amplitude $A_{1/2}$

MODULUS (GeV$^{-1/2}$)	PHASE (°)	DOCUMENT ID		TECN	COMMENT
0.175±0.020	50 ± 10	SOKHOYAN	15A	DPWA	Multichannel
0.109±0.010	−21 $^{+12}_{-6}$	ROENCHEN	14	DPWA	
• • • We do not use the following data for averages, fits, limits, etc. • • •					
0.123	1.1	ROENCHEN	15A	DPWA	Multichannel

$\Delta(1700) \to N\gamma$, helicity-3/2 amplitude $A_{3/2}$

MODULUS (GeV$^{-1/2}$)	PHASE (°)	DOCUMENT ID		TECN	COMMENT
0.180±0.020	45 ± 10	SOKHOYAN	15A	DPWA	Multichannel
0.111 $^{+0.027}_{-0.006}$	12 $^{+9}_{-11}$	ROENCHEN	14	DPWA	
• • • We do not use the following data for averages, fits, limits, etc. • • •					
0.124	22	ROENCHEN	15A	DPWA	Multichannel

$\Delta(1700)$ BREIT-WIGNER PHOTON DECAY AMPLITUDES

$\Delta(1700) \to N\gamma$, helicity-1/2 amplitude $A_{1/2}$

VALUE (GeV$^{-1/2}$)	DOCUMENT ID		TECN	COMMENT
0.100 to 0.160 (≈ 0.130) OUR ESTIMATE				
0.0872±0.0189	GOLOVATCH	19	DPWA	$\gamma p \to \pi^+\pi^- p$
0.156 ±0.017	[1] HUNT	19	DPWA	Multichannel
0.165 ±0.020	SOKHOYAN	15A	DPWA	Multichannel
0.132 ±0.005	[1] DUGGER	13	DPWA	$\gamma N \to \pi N$
0.105 ±0.005	[1] WORKMAN	12A	DPWA	$\gamma N \to \pi N$
• • • We do not use the following data for averages, fits, limits, etc. • • •				
0.165 ±0.020	GUTZ	14	DPWA	Multichannel
0.160 ±0.020	ANISOVICH	12A	DPWA	Multichannel
0.058 ±0.010	[1] SHRESTHA	12A	DPWA	Multichannel
0.226	DRECHSEL	07	DPWA	$\gamma N \to \pi N$
0.125 ±0.003	DUGGER	07	DPWA	$\gamma N \to \pi N$
0.096	PENNER	02D	DPWA	Multichannel

[1] Statistical error only.

Downloaded from https://academic.oup.com/ptep/article/2022/8/083C01/6651666 by KIT Library user on 27 September 2022

$\Delta(1700) \to N\gamma$, helicity-3/2 amplitude $A_{3/2}$

VALUE (GeV$^{-1/2}$)	DOCUMENT ID		TECN	COMMENT
0.090 to 0.170 (≈ 0.130) OUR ESTIMATE				
0.0872 ± 0.0164	GOLOVATCH	19	DPWA	$\gamma p \to \pi^+ \pi^- p$
0.0125 ± 0.0016	[1] HUNT	19	DPWA	Multichannel
0.170 ± 0.025	SOKHOYAN	15A	DPWA	Multichannel
0.108 ± 0.005	[1] DUGGER	13	DPWA	$\gamma N \to \pi N$
0.092 ± 0.004	[1] WORKMAN	12A	DPWA	$\gamma N \to \pi N$
• • • We do not use the following data for averages, fits, limits, etc. • • •				
0.170 ± 0.025	GUTZ	14	DPWA	Multichannel
0.165 ± 0.025	ANISOVICH	12A	DPWA	Multichannel
0.097 ± 0.008	[1] SHRESTHA	12A	DPWA	Multichannel
0.210	DRECHSEL	07	DPWA	$\gamma N \to \pi N$
0.105 ± 0.003	DUGGER	07	DPWA	$\gamma N \to \pi N$
0.154	PENNER	02D	DPWA	Multichannel

[1] Statistical error only.

$\Delta(1700)$ REFERENCES

For early references, see Physics Letters **111B** 1 (1982).

GOLOVATCH	19	PL B788 371	E. Golovatch *et al.*	(CLAS Collab.)
HUNT	19	PR C99 055205	B.C. Hunt, D.M. Manley	
ROENCHEN	15A	EPJ A51 70	D. Roenchen *et al.*	
SOKHOYAN	15A	EPJ A51 95	V. Sokhoyan *et al.*	(CBELSA/TAPS Collab.)
GUTZ	14	EPJ A50 74	E. Gutz *et al.*	(CBELSA/TAPS Collab.)
PDG	14	CP C38 070001	K. Olive *et al.*	(PDG Collab.)
ROENCHEN	14	EPJ A50 101	D. Roenchen *et al.*	
Also		EPJ A51 63 (errat.)	D. Roenchen *et al.*	
SVARC	14	PR C89 045205	A. Svarc *et al.*	(RBI Zagreb, UNI Tuzla)
DUGGER	13	PR C88 065203	M. Dugger *et al.*	(JLab CLAS Collab.)
ANISOVICH	12A	EPJ A48 15	A.V. Anisovich *et al.*	(BONN, PNPI)
SHRESTHA	12A	PR C86 055203	M. Shrestha, D.M. Manley	(KSU)
WORKMAN	12A	PR C86 015202	R. Workman *et al.*	(GWU)
KASHEVAROV	09	EPJ A42 141	V.L. Kashevarov *et al.*	(MAMI Crystal Ball/TAPS)
HORN	08A	EPJ A38 173	I. Horn *et al.*	(CB-ELSA Collab.)
Also		PRL 101 202002	I. Horn *et al.*	(CB-ELSA Collab.)
DRECHSEL	07	EPJ A34 69	D. Drechsel, S.S. Kamalov, L. Tiator	(MAINZ, JINR)
DUGGER	07	PR C76 025211	M. Dugger *et al.*	(JLab CLAS Collab.)
ARNDT	06	PR C74 045205	R.A. Arndt *et al.*	(GWU)
PENNER	02C	PR C66 055211	G. Penner, U. Mosel	(GIES)
PENNER	02D	PR C66 055212	G. Penner, U. Mosel	(GIES)
VRANA	00	PRPL 328 181	T.P. Vrana, S.A. Dytman, T.-S.H. Lee	(PITT, ANL)
HOEHLER	93	πN Newsletter 9 1	G. Hohler	(KARL)
CUTKOSKY	80	Toronto Conf. 19	R.E. Cutkosky *et al.*	(CMU, LBL) IJP
Also		PR D20 2839	R.E. Cutkosky *et al.*	(CMU, LBL) IJP
HOEHLER	79	PDAT 12-1	G. Hohler *et al.*	(KARLT) IJP
Also		Toronto Conf. 3	R. Koch	(KARLT) IJP

$\Delta(1750)\ 1/2^+$

$I(J^P) = \frac{3}{2}(\frac{1}{2}^+)$ Status: *

OMITTED FROM SUMMARY TABLE

$\Delta(1750)$ POLE POSITION

REAL PART

VALUE (MeV)	DOCUMENT ID		TECN	COMMENT
• • • We do not use the following data for averages, fits, limits, etc. • • •				
1748	ARNDT	04	DPWA	$\pi N \to \pi N, \eta N$
1714	VRANA	00	DPWA	Multichannel

−2×IMAGINARY PART

VALUE (MeV)	DOCUMENT ID		TECN	COMMENT
• • • We do not use the following data for averages, fits, limits, etc. • • •				
524	ARNDT	04	DPWA	$\pi N \to \pi N, \eta N$
68	VRANA	00	DPWA	Multichannel

$\Delta(1750)$ ELASTIC POLE RESIDUE

MODULUS $|r|$

VALUE (MeV)	DOCUMENT ID		TECN	COMMENT
• • • We do not use the following data for averages, fits, limits, etc. • • •				
48	ARNDT	04	DPWA	$\pi N \to \pi N, \eta N$

PHASE θ

VALUE (°)	DOCUMENT ID		TECN	COMMENT
• • • We do not use the following data for averages, fits, limits, etc. • • •				
158	ARNDT	04	DPWA	$\pi N \to \pi N, \eta N$

$\Delta(1750)$ BREIT-WIGNER MASS

VALUE (MeV)	DOCUMENT ID		TECN	COMMENT
• • • We do not use the following data for averages, fits, limits, etc. • • •				
1712 ± 1	PENNER	02C	DPWA	Multichannel
1721 ± 61	VRANA	00	DPWA	Multichannel

$\Delta(1750)$ BREIT-WIGNER WIDTH

VALUE (MeV)	DOCUMENT ID		TECN	COMMENT
• • • We do not use the following data for averages, fits, limits, etc. • • •				
643 ± 17	PENNER	02C	DPWA	Multichannel
70 ± 50	VRANA	00	DPWA	Multichannel

$\Delta(1750)$ DECAY MODES

	Mode	Fraction (Γ_i/Γ)
Γ_1	$N\pi$	seen
Γ_2	$N(1440)\pi$	seen
Γ_3	ΣK	seen

$\Delta(1750)$ BRANCHING RATIOS

$\Gamma(N\pi)/\Gamma_{total}$ — Γ_1/Γ

VALUE (%)	DOCUMENT ID		TECN	COMMENT
• • • We do not use the following data for averages, fits, limits, etc. • • •				
1 ± 1	PENNER	02C	DPWA	Multichannel
6 ± 9	VRANA	00	DPWA	Multichannel

$\Gamma(N(1440)\pi)/\Gamma_{total}$ — Γ_2/Γ

VALUE (%)	DOCUMENT ID		TECN	COMMENT
• • • We do not use the following data for averages, fits, limits, etc. • • •				
83 ± 1	VRANA	00	DPWA	Multichannel

$\Gamma(\Sigma K)/\Gamma_{total}$ — Γ_3/Γ

VALUE (%)	DOCUMENT ID		TECN	COMMENT
• • • We do not use the following data for averages, fits, limits, etc. • • •				
0.1 ± 0.1	PENNER	02C	DPWA	Multichannel

$\Delta(1750)$ BREIT-WIGNER PHOTON DECAY AMPLITUDES

Papers on γN amplitudes predating 1981 may be found in our 2006 edition, Journal of Physics **G33** 1 (2006).

$\Delta(1750) \to N\gamma$, helicity-1/2 amplitude $A_{1/2}$

VALUE (GeV$^{-1/2}$)	DOCUMENT ID		TECN	COMMENT
• • • We do not use the following data for averages, fits, limits, etc. • • •				
0.053	PENNER	02D	DPWA	Multichannel

$\Delta(1750)$ REFERENCES

PDG	06	JP G33 1	W.-M. Yao *et al.*	(PDG Collab.)
ARNDT	04	PR C69 035213	R.A. Arndt *et al.*	(GWU, TRIU)
PENNER	02C	PR C66 055211	G. Penner, U. Mosel	(GIES)
PENNER	02D	PR C66 055212	G. Penner, U. Mosel	(GIES)
VRANA	00	PRPL 328 181	T.P. Vrana, S.A. Dytman, T.-S.H. Lee	(PITT, ANL)

$\Delta(1900)\ 1/2^-$

$I(J^P) = \frac{3}{2}(\frac{1}{2}^-)$ Status: ***

Older and obsolete values are listed and referenced in the 2014 edition, Chinese Physics **C38** 070001 (2014).

$\Delta(1900)$ POLE POSITION

REAL PART

VALUE (MeV)	DOCUMENT ID		TECN	COMMENT
1830 to 1900 (≈ 1865) OUR ESTIMATE				
1845 ± 20	SOKHOYAN	15A	DPWA	Multichannel
1865 ± 35 ± 19	[1] SVARC	14	L+P	$\pi N \to \pi N$
1870 ± 40	CUTKOSKY	80	IPWA	$\pi N \to \pi N$
• • • We do not use the following data for averages, fits, limits, etc. • • •				
1957	HUNT	19	DPWA	Multichannel
1845 ± 20	GUTZ	14	DPWA	Multichannel
1845 ± 25	ANISOVICH	12A	DPWA	Multichannel
1795	VRANA	00	DPWA	Multichannel
1780	HOEHLER	93	SPED	$\pi N \to \pi N$

[1] Fit to the amplitudes of HOEHLER 79.

−2×IMAGINARY PART

VALUE (MeV)	DOCUMENT ID		TECN	COMMENT
180 to 300 (≈ 240) OUR ESTIMATE				
295 ± 35	SOKHOYAN	15A	DPWA	Multichannel
187 ± 50 ± 19	[1] SVARC	14	L+P	$\pi N \to \pi N$
180 ± 50	CUTKOSKY	80	IPWA	$\pi N \to \pi N$
• • • We do not use the following data for averages, fits, limits, etc. • • •				
447	HUNT	19	DPWA	Multichannel
295 ± 35	GUTZ	14	DPWA	Multichannel
300 ± 45	ANISOVICH	12A	DPWA	Multichannel
58	VRANA	00	DPWA	Multichannel

[1] Fit to the amplitudes of HOEHLER 79.

$\Delta(1900)$ ELASTIC POLE RESIDUE

MODULUS $|r|$

VALUE (MeV)	DOCUMENT ID		TECN	COMMENT
8 to 14 (≈ 11) OUR ESTIMATE				
11 ± 2	SOKHOYAN	15A	DPWA	Multichannel
11 ± 4 ± 2	[1] SVARC	14	L+P	$\pi N \to \pi N$
10 ± 3	CUTKOSKY	80	IPWA	$\pi N \to \pi N$

Downloaded from https://academic.oup.com/ptep/article/2022/8/083C01/6651666 by KIT Library user on 27 September 2022

• • • We do not use the following data for averages, fits, limits, etc. • • •

11±2	GUTZ	14	DPWA	Multichannel
10±3	ANISOVICH	12A	DPWA	Multichannel

[1] Fit to the amplitudes of HOEHLER 79.

PHASE θ

VALUE (°)	DOCUMENT ID		TECN	COMMENT
−115±20	SOKHOYAN	15A	DPWA	Multichannel
20±27±19	[1] SVARC	14	L+P	$\pi N \to \pi N$
+ 20±40	CUTKOSKY	80	IPWA	$\pi N \to \pi N$
• • • We do not use the following data for averages, fits, limits, etc. • • •				
−115±20	GUTZ	14	DPWA	Multichannel
−125±20	ANISOVICH	12A	DPWA	Multichannel

[1] Fit to the amplitudes of HOEHLER 79.

$\Delta(1900)$ INELASTIC POLE RESIDUE

The "normalized residue" is the residue divided by $\Gamma_{pole}/2$.

Normalized residue in $N\pi \to \Delta(1900) \to \Sigma K$

MODULUS	PHASE (°)	DOCUMENT ID		TECN	COMMENT
0.07±0.02	−50 ± 30	ANISOVICH	12A	DPWA	Multichannel

Normalized residue in $N\pi \to \Delta(1900) \to \Delta\pi$, D-wave

MODULUS	PHASE (°)	DOCUMENT ID		TECN	COMMENT
0.18±0.10	105 ± 25	SOKHOYAN	15A	DPWA	Multichannel
• • • We do not use the following data for averages, fits, limits, etc. • • •					
$0.12^{+0.08}_{-0.05}$	110 ± 20	ANISOVICH	12A	DPWA	Multichannel

Normalized residue in $N\pi \to \Delta(1900) \to \Delta(1232)\eta$

MODULUS	PHASE (°)	DOCUMENT ID		TECN	COMMENT
0.013±0.006	undefined	GUTZ	14	DPWA	Multichannel

Normalized residue in $N\pi \to \Delta(1900) \to N(1440)\pi$

MODULUS	PHASE (°)	DOCUMENT ID		TECN	COMMENT
0.11±0.06	115 ± 30	SOKHOYAN	15A	DPWA	Multichannel

Normalized residue in $N\pi \to \Delta(1900) \to N(1520)\pi$

MODULUS	PHASE (°)	DOCUMENT ID		TECN	COMMENT
0.06±0.03	undefined	SOKHOYAN	15A	DPWA	Multichannel

$\Delta(1900)$ BREIT-WIGNER MASS

VALUE (MeV)	DOCUMENT ID		TECN	COMMENT
1840 to 1920 (≈ 1860) OUR ESTIMATE				
1989±22	[1] HUNT	19	DPWA	Multichannel
1840±20	SOKHOYAN	15A	DPWA	Multichannel
1890±50	CUTKOSKY	80	IPWA	$\pi N \to \pi N$
1908±30	HOEHLER	79	IPWA	$\pi N \to \pi N$
• • • We do not use the following data for averages, fits, limits, etc. • • •				
1840±20	GUTZ	14	DPWA	Multichannel
1840±30	ANISOVICH	12A	DPWA	Multichannel
1868±12	[1] SHRESTHA	12A	DPWA	Multichannel
1802±87	VRANA	00	DPWA	Multichannel

[1] Statistical error only.

$\Delta(1900)$ BREIT-WIGNER WIDTH

VALUE (MeV)	DOCUMENT ID		TECN	COMMENT
180 to 320 (≈ 250) OUR ESTIMATE				
457±60	[1] HUNT	19	DPWA	Multichannel
295±30	SOKHOYAN	15A	DPWA	Multichannel
170±50	CUTKOSKY	80	IPWA	$\pi N \to \pi N$
140±40	HOEHLER	79	IPWA	$\pi N \to \pi N$
• • • We do not use the following data for averages, fits, limits, etc. • • •				
295±30	GUTZ	14	DPWA	Multichannel
300±45	ANISOVICH	12A	DPWA	Multichannel
234±27	[1] SHRESTHA	12A	DPWA	Multichannel
48±45	VRANA	00	DPWA	Multichannel

[1] Statistical error only.

$\Delta(1900)$ DECAY MODES

The following branching fractions are our estimates, not fits or averages.

	Mode	Fraction (Γ_i/Γ)
Γ_1	$N\pi$	4–12%
Γ_2	ΣK	seen
Γ_3	$N\pi\pi$	> 52%
Γ_4	$\Delta(1232)\pi$, D-wave	30–70%
Γ_5	$N\rho$	22–60 %
Γ_6	$N\rho$, S=1/2, S-wave	11–35%
Γ_7	$N\rho$, S=3/2, D-wave	11–25%
Γ_8	$N(1440)\pi$	3–32%
Γ_9	$N(1520)\pi$	2–10%
Γ_{10}	$\Delta(1232)\eta$	< 2%
Γ_{11}	$N\gamma$, helicity=1/2	0.06–0.43 %

$\Delta(1900)$ BRANCHING RATIOS

$\Gamma(N\pi)/\Gamma_{total}$ — Γ_1/Γ

VALUE (%)	DOCUMENT ID		TECN	COMMENT
4–12% OUR ESTIMATE				
3.7± 0.8	[1] HUNT	19	DPWA	Multichannel
7 ± 2	SOKHOYAN	15A	DPWA	Multichannel
10 ± 3	CUTKOSKY	80	IPWA	$\pi N \to \pi N$
8 ± 4	HOEHLER	79	IPWA	$\pi N \to \pi N$
• • • We do not use the following data for averages, fits, limits, etc. • • •				
7 ± 2	GUTZ	14	DPWA	Multichannel
7 ± 3	ANISOVICH	12A	DPWA	Multichannel
8 ± 1	[1] SHRESTHA	12A	DPWA	Multichannel
33 ±10	VRANA	00	DPWA	Multichannel

[1] Statistical error only.

$\Gamma(\Delta(1232)\pi, D\text{-wave})/\Gamma_{total}$ — Γ_4/Γ

VALUE (%)	DOCUMENT ID		TECN	COMMENT
30–70% OUR ESTIMATE				
42± 8	[1] HUNT	19	DPWA	Multichannel
50±20	SOKHOYAN	15A	DPWA	Multichannel
• • • We do not use the following data for averages, fits, limits, etc. • • •				
15^{+50}_{-10}	ANISOVICH	12A	DPWA	Multichannel
56± 6	[1] SHRESTHA	12A	DPWA	Multichannel
28± 1	VRANA	00	DPWA	Multichannel

[1] Statistical error only.

$\Gamma(N\rho, S=1/2, S\text{-wave})/\Gamma_{total}$ — Γ_6/Γ

VALUE (%)	DOCUMENT ID		TECN	COMMENT
11–35% OUR ESTIMATE				
23±12	[1] HUNT	19	DPWA	Multichannel
• • • We do not use the following data for averages, fits, limits, etc. • • •				
12± 4	[1] SHRESTHA	12A	DPWA	Multichannel
30± 2	VRANA	00	DPWA	Multichannel

[1] Statistical error only.

$\Gamma(N\rho, S=3/2, D\text{-wave})/\Gamma_{total}$ — Γ_7/Γ

VALUE (%)	DOCUMENT ID		TECN	COMMENT
11–25% OUR ESTIMATE				
18±7	[1] HUNT	19	DPWA	Multichannel
• • • We do not use the following data for averages, fits, limits, etc. • • •				
23±5	[1] SHRESTHA	12A	DPWA	Multichannel
5±1	VRANA	00	DPWA	Multichannel

[1] Statistical error only.

$\Gamma(N(1440)\pi)/\Gamma_{total}$ — Γ_8/Γ

VALUE (%)	DOCUMENT ID		TECN	COMMENT
3–32% OUR ESTIMATE				
12± 9	[1] HUNT	19	DPWA	Multichannel
20±12	SOKHOYAN	15A	DPWA	Multichannel
• • • We do not use the following data for averages, fits, limits, etc. • • •				
< 1	[1] SHRESTHA	12A	DPWA	Multichannel
4± 1	VRANA	00	DPWA	Multichannel

[1] Statistical error only.

$\Gamma(N(1520)\pi)/\Gamma_{total}$ — Γ_9/Γ

VALUE (%)	DOCUMENT ID		TECN	COMMENT
2–10% OUR ESTIMATE				
6±4	SOKHOYAN	15A	DPWA	Multichannel

$\Gamma(\Delta(1232)\eta)/\Gamma_{total}$ — Γ_{10}/Γ

VALUE (%)	DOCUMENT ID		TECN	COMMENT
< 2% OUR ESTIMATE				
1±1	GUTZ	14	DPWA	Multichannel

$\Delta(1900)$ PHOTON DECAY AMPLITUDES AT THE POLE

$\Delta(1900) \to N\gamma$, helicity-1/2 amplitude $A_{1/2}$

MODULUS ($GeV^{-1/2}$)	PHASE (°)	DOCUMENT ID		TECN	COMMENT
0.064±0.015	60 ± 20	SOKHOYAN	15A	DPWA	Multichannel

Downloaded from https://academic.oup.com/ptep/article/2022/8/083C01/6651666 by KIT Library user on 27 September 2022

$\Delta(1900)$ BREIT-WIGNER PHOTON DECAY AMPLITUDES

$\Delta(1900) \to N\gamma$, helicity-1/2 amplitude $A_{1/2}$

VALUE (GeV$^{-1/2}$)	DOCUMENT ID		TECN	COMMENT
0.212±0.029	[1] HUNT	19	DPWA	Multichannel
0.065±0.015	SOKHOYAN	15A	DPWA	Multichannel
• • • We do not use the following data for averages, fits, limits, etc. • • •				
0.057±0.014	GUTZ	14	DPWA	Multichannel
−0.082±0.009	[1] SHRESTHA	12A	DPWA	Multichannel

[1] Statistical error only.

$\Delta(1900)$ REFERENCES

For early references, see Physics Letters **111B** 1 (1982).

HUNT	19	PR C99 055205	B.C. Hunt, D.M. Manley	
SOKHOYAN	15A	EPJ A51 95	V. Sokhoyan *et al.*	(CBELSA/TAPS Collab.)
GUTZ	14	EPJ A50 74	E. Gutz *et al.*	(CBELSA/TAPS Collab.)
PDG	14	CP C38 070001	K. Olive *et al.*	(PDG Collab.)
SVARC	14	PR C89 045205	A. Svarc *et al.*	(RBI Zagreb, UNI Tuzla)
ANISOVICH	12A	EPJ A48 15	A.V. Anisovich *et al.*	(BONN, PNPI)
SHRESTHA	12A	PR C86 055203	M. Shrestha, D.M. Manley	(KSU)
VRANA	00	PRPL 328 181	T.P. Vrana, S.A. Dytman, T.-S.H. Lee	(PITT, ANL)
HOEHLER	93	πN Newsletter 9 1	G. Hohler	(KARL)
CUTKOSKY	80	Toronto Conf. 19	R.E. Cutkosky *et al.*	(CMU, LBL) IJP
Also		PR D20 2839	R.E. Cutkosky *et al.*	(CMU, LBL) IJP
HOEHLER	79	PDAT 12-1	G. Hohler *et al.*	(KARLT) IJP
Also		Toronto Conf. 3	R. Koch	(KARLT) IJP

$\Delta(1905)\ 5/2^+$

$I(J^P) = \frac{3}{2}(\frac{5}{2}^+)$ Status: ****

Older and obsolete values are listed and referenced in the 2014 edition, Chinese Physics **C38** 070001 (2014).

$\Delta(1905)$ POLE POSITION

REAL PART

VALUE (MeV)	DOCUMENT ID		TECN	COMMENT
1770 to 1830 (≈ 1800) OUR ESTIMATE				
1800± 6	SOKHOYAN	15A	DPWA	Multichannel
1752± 3±2	[1] SVARC	14	L+P	$\pi N \to \pi N$
1830±40	CUTKOSKY	80	IPWA	$\pi N \to \pi N$
• • • We do not use the following data for averages, fits, limits, etc. • • •				
1819	HUNT	19	DPWA	Multichannel
1795	ROENCHEN	15A	DPWA	Multichannel
1800± 6	GUTZ	14	DPWA	Multichannel
1805±10	ANISOVICH	12A	DPWA	Multichannel
1819	ARNDT	06	DPWA	$\pi N \to \pi N, \eta N$
1793	VRANA	00	DPWA	Multichannel
1829	HOEHLER	93	SPED	$\pi N \to \pi N$

[1] Fit to the amplitudes of HOEHLER 79.

−2×IMAGINARY PART

VALUE (MeV)	DOCUMENT ID		TECN	COMMENT
260 to 340 (≈ 300) OUR ESTIMATE				
290±15	SOKHOYAN	15A	DPWA	Multichannel
346± 6±2	[1] SVARC	14	L+P	$\pi N \to \pi N$
280±60	CUTKOSKY	80	IPWA	$\pi N \to \pi N$
• • • We do not use the following data for averages, fits, limits, etc. • • •				
253	HUNT	19	DPWA	Multichannel
247	ROENCHEN	15A	DPWA	Multichannel
290±15	GUTZ	14	DPWA	Multichannel
300±15	ANISOVICH	12A	DPWA	Multichannel
247	ARNDT	06	DPWA	$\pi N \to \pi N, \eta N$
302	VRANA	00	DPWA	Multichannel
303	HOEHLER	93	SPED	$\pi N \to \pi N$

[1] Fit to the amplitudes of HOEHLER 79.

$\Delta(1905)$ ELASTIC POLE RESIDUE

MODULUS $|r|$

VALUE (MeV)	DOCUMENT ID		TECN	COMMENT
15 to 25 (≈ 20) OUR ESTIMATE				
19 ±2	SOKHOYAN	15A	DPWA	Multichannel
24 ±1±1	[1] SVARC	14	L+P	$\pi N \to \pi N$
25 ±8	CUTKOSKY	80	IPWA	$\pi N \to \pi N$
• • • We do not use the following data for averages, fits, limits, etc. • • •				
5.3	ROENCHEN	15A	DPWA	Multichannel
19 ±2	GUTZ	14	DPWA	Multichannel
20 ±2	ANISOVICH	12A	DPWA	Multichannel
15	ARNDT	06	DPWA	$\pi N \to \pi N, \eta N$
25	HOEHLER	93	SPED	$\pi N \to \pi N$

[1] Fit to the amplitudes of HOEHLER 79.

PHASE θ

VALUE (°)	DOCUMENT ID		TECN	COMMENT
−120 to −30 (≈ −50) OUR ESTIMATE				
− 45± 4	SOKHOYAN	15A	DPWA	Multichannel
−114± 1±2	[1] SVARC	14	L+P	$\pi N \to \pi N$
− 50±20	CUTKOSKY	80	IPWA	$\pi N \to \pi N$
• • • We do not use the following data for averages, fits, limits, etc. • • •				
− 89	ROENCHEN	15A	DPWA	Multichannel
− 45± 4	GUTZ	14	DPWA	Multichannel
− 44± 5	ANISOVICH	12A	DPWA	Multichannel
− 30	ARNDT	06	DPWA	$\pi N \to \pi N, \eta N$

[1] Fit to the amplitudes of HOEHLER 79.

$\Delta(1905)$ INELASTIC POLE RESIDUE

The "normalized residue" is the residue divided by $\Gamma_{pole}/2$.

Normalized residue in $N\pi \to \Delta(1905) \to \Delta\pi$, P-wave

MODULUS	PHASE (°)	DOCUMENT ID		TECN	COMMENT
0.19 ±0.07	10 ± 30	SOKHOYAN	15A	DPWA	Multichannel
• • • We do not use the following data for averages, fits, limits, etc. • • •					
0.0870	72	ROENCHEN	15A	DPWA	Multichannel
0.25 ±0.06	0 ± 15	ANISOVICH	12A	DPWA	Multichannel

Normalized residue in $N\pi \to \Delta(1905) \to \Delta\pi$, F-wave

MODULUS	PHASE (°)	DOCUMENT ID		TECN	COMMENT
• • • We do not use the following data for averages, fits, limits, etc. • • •					
0.009	64	ROENCHEN	15A	DPWA	Multichannel

Normalized residue in $N\pi \to \Delta(1905) \to \Sigma K$

MODULUS	PHASE (°)	DOCUMENT ID		TECN	COMMENT
• • • We do not use the following data for averages, fits, limits, etc. • • •					
0.001	−155	ROENCHEN	15A	DPWA	Multichannel

Normalized residue in $N\pi \to \Delta(1905) \to N(1535)\pi$

MODULUS	PHASE (°)	DOCUMENT ID		TECN	COMMENT
0.025±0.010	130 ± 35	GUTZ	14	DPWA	Multichannel

Normalized residue in $N\pi \to \Delta(1905) \to \Delta(1232)\eta$

MODULUS	PHASE (°)	DOCUMENT ID		TECN	COMMENT
0.07±0.02	40 ± 20	GUTZ	14	DPWA	Multichannel

$\Delta(1905)$ BREIT-WIGNER MASS

VALUE (MeV)	DOCUMENT ID		TECN	COMMENT
1855 to 1910 (≈ 1880) OUR ESTIMATE				
1883 ±19	GOLOVATCH	19	DPWA	$\gamma p \to \pi^+\pi^- p$
1866 ± 9	[1] HUNT	19	DPWA	Multichannel
1856 ± 6	SOKHOYAN	15A	DPWA	Multichannel
1857.8± 1.6	[1] ARNDT	06	DPWA	$\pi N \to \pi N, \eta N$
1910 ±30	CUTKOSKY	80	IPWA	$\pi N \to \pi N$
1905 ±20	HOEHLER	79	IPWA	$\pi N \to \pi N$
• • • We do not use the following data for averages, fits, limits, etc. • • •				
1856 ± 6	GUTZ	14	DPWA	Multichannel
1861 ± 6	ANISOVICH	12A	DPWA	Multichannel
1818 ± 8	[1] SHRESTHA	12A	DPWA	Multichannel
1873 ±77	VRANA	00	DPWA	Multichannel

[1] Statistical error only.

$\Delta(1905)$ BREIT-WIGNER WIDTH

VALUE (MeV)	DOCUMENT ID		TECN	COMMENT
270 to 400 (≈ 330) OUR ESTIMATE				
327 ± 69	GOLOVATCH	19	DPWA	$\gamma p \to \pi^+\pi^- p$
289 ± 20	[1] HUNT	19	DPWA	Multichannel
325 ± 15	SOKHOYAN	15A	DPWA	Multichannel
320.6± 8.6	[1] ARNDT	06	DPWA	$\pi N \to \pi N, \eta N$
400 ±100	CUTKOSKY	80	IPWA	$\pi N \to \pi N$
260 ± 20	HOEHLER	79	IPWA	$\pi N \to \pi N$
• • • We do not use the following data for averages, fits, limits, etc. • • •				
325 ± 15	GUTZ	14	DPWA	Multichannel
335 ± 18	ANISOVICH	12A	DPWA	Multichannel
278 ± 18	[1] SHRESTHA	12A	DPWA	Multichannel
461 ±111	VRANA	00	DPWA	Multichannel

[1] Statistical error only.

$\Delta(1905)$ DECAY MODES

The following branching fractions are our estimates, not fits or averages.

	Mode	Fraction (Γ_i/Γ)
Γ_1	$N\pi$	9–15%
Γ_2	$N\pi\pi$	>65%
Γ_3	$\Delta(1232)\pi$	>48%
Γ_4	$\Delta(1232)\pi$, P-wave	8–43%
Γ_5	$\Delta(1232)\pi$, F-wave	40–58%
Γ_6	$N\rho$, $S=3/2$, P-wave	17–35%
Γ_7	$N(1535)\pi$	< 1 %
Γ_8	$N(1680)\pi$, P-wave	5–15%

Downloaded from https://academic.oup.com/ptep/article/2022/8/083C01/6651666 by KIT Library user on 27 September 2022

Γ_9	$\Delta(1232)\eta$	2–6%
Γ_{10}	$N\gamma$	0.012–0.036 %
Γ_{11}	$N\gamma$, helicity=1/2	0.002–0.006 %
Γ_{12}	$N\gamma$, helicity=3/2	0.01–0.03 %

$\Delta(1905)$ BRANCHING RATIOS

$\Gamma(N\pi)/\Gamma_{total}$ — Γ_1/Γ

VALUE (%)	DOCUMENT ID		TECN	COMMENT
9–15% OUR ESTIMATE				
17 ±1	[1] HUNT	19	DPWA	Multichannel
13 ±2	SOKHOYAN	15A	DPWA	Multichannel
12.2±0.1	[1] ARNDT	06	DPWA	$\pi N \to \pi N, \eta N$
8 ±3	CUTKOSKY	80	IPWA	$\pi N \to \pi N$
15 ±2	HOEHLER	79	IPWA	$\pi N \to \pi N$
• • • We do not use the following data for averages, fits, limits, etc. • • •				
13 ±2	GUTZ	14	DPWA	Multichannel
13 ±2	ANISOVICH	12A	DPWA	Multichannel
6 ±1	[1] SHRESTHA	12A	DPWA	Multichannel
9 ±1	VRANA	00	DPWA	Multichannel

[1] Statistical error only.

$\Gamma(N\pi\pi)/\Gamma_{total}$ — Γ_2/Γ

VALUE	DOCUMENT ID		TECN	COMMENT
>65% OUR ESTIMATE				
0.85±0.15	GOLOVATCH	19	DPWA	$\gamma p \to \pi^+\pi^- p$

$\Gamma(\Delta(1232)\pi, P\text{-wave})/\Gamma_{total}$ — Γ_4/Γ

VALUE (%)	DOCUMENT ID		TECN	COMMENT
8–43% OUR ESTIMATE				
8.4± 0.5	[1] HUNT	19	DPWA	Multichannel
33 ±10	SOKHOYAN	15A	DPWA	Multichannel
• • • We do not use the following data for averages, fits, limits, etc. • • •				
45 ±14	ANISOVICH	12A	DPWA	Multichannel
28 ± 7	[1] SHRESTHA	12A	DPWA	Multichannel
23 ± 1	VRANA	00	DPWA	Multichannel

[1] Statistical error only.

$\Gamma(\Delta(1232)\pi, F\text{-wave})/\Gamma_{total}$ — Γ_5/Γ

VALUE (%)	DOCUMENT ID		TECN	COMMENT
40–58% OUR ESTIMATE				
49±9	[1] HUNT	19	DPWA	Multichannel
• • • We do not use the following data for averages, fits, limits, etc. • • •				
64±8	[1] SHRESTHA	12A	DPWA	Multichannel
44±1	VRANA	00	DPWA	Multichannel

[1] Statistical error only.

$\Gamma(N\rho, S=3/2, P\text{-wave})/\Gamma_{total}$ — Γ_6/Γ

VALUE (%)	DOCUMENT ID		TECN	COMMENT
17–35% OUR ESTIMATE				
26±9	[1] HUNT	19	DPWA	Multichannel
• • • We do not use the following data for averages, fits, limits, etc. • • •				
< 6	[1] SHRESTHA	12A	DPWA	Multichannel
24±1	VRANA	00	DPWA	Multichannel

[1] Statistical error only.

$\Gamma(N(1535)\pi)/\Gamma_{total}$ — Γ_7/Γ

VALUE (%)	DOCUMENT ID		TECN	COMMENT
< 1 % OUR ESTIMATE				
<1	GUTZ	14	DPWA	Multichannel

$\Gamma(N(1680)\pi, P\text{-wave})/\Gamma_{total}$ — Γ_8/Γ

VALUE (%)	DOCUMENT ID		TECN	COMMENT
5–15% OUR ESTIMATE				
10±5	SOKHOYAN	15A	DPWA	Multichannel

$\Gamma(\Delta(1232)\eta)/\Gamma_{total}$ — Γ_9/Γ

VALUE (%)	DOCUMENT ID		TECN	COMMENT
2–6% OUR ESTIMATE				
4±2	GUTZ	14	DPWA	Multichannel

$\Delta(1905)$ PHOTON DECAY AMPLITUDES AT THE POLE

$\Delta(1905) \to N\gamma$, helicity-1/2 amplitude $A_{1/2}$

MODULUS ($GeV^{-1/2}$)	PHASE (°)	DOCUMENT ID		TECN	COMMENT
0.025±0.005	−28 ± 12	SOKHOYAN	15A	DPWA	Multichannel
$0.013^{+0.013}_{-0.005}$	64^{+72}_{-36}	ROENCHEN	14	DPWA	
• • • We do not use the following data for averages, fits, limits, etc. • • •					
0.053	89	ROENCHEN	15A	DPWA	Multichannel

$\Delta(1905) \to N\gamma$, helicity-3/2 amplitude $A_{3/2}$

MODULUS ($GeV^{-1/2}$)	PHASE (°)	DOCUMENT ID		TECN	COMMENT
−0.050±0.004	5 ± 10	SOKHOYAN	15A	DPWA	Multichannel
0.072±0.016	113^{+13}_{-7}	ROENCHEN	14	DPWA	
• • • We do not use the following data for averages, fits, limits, etc. • • •					
−0.030	80	ROENCHEN	15A	DPWA	Multichannel

$\Delta(1905)$ BREIT-WIGNER PHOTON DECAY AMPLITUDES

$\Delta(1905) \to N\gamma$, helicity-1/2 amplitude $A_{1/2}$

VALUE ($GeV^{-1/2}$)	DOCUMENT ID		TECN	COMMENT
0.017 to 0.027 (≈ 0.022) OUR ESTIMATE				
0.019±0.0076	GOLOVATCH	19	DPWA	$\gamma p \to \pi^+\pi^- p$
0.077±0.010	[1] HUNT	19	DPWA	Multichannel
0.025±0.005	SOKHOYAN	15A	DPWA	Multichannel
0.020±0.002	[1] DUGGER	13	DPWA	$\gamma N \to \pi N$
0.019±0.002	[1] WORKMAN	12A	DPWA	$\gamma N \to \pi N$
• • • We do not use the following data for averages, fits, limits, etc. • • •				
0.025±0.005	GUTZ	14	DPWA	Multichannel
0.025±0.004	ANISOVICH	12A	DPWA	Multichannel
0.066±0.018	[1] SHRESTHA	12A	DPWA	Multichannel
0.018	DRECHSEL	07	DPWA	$\gamma N \to \pi N$

[1] Statistical error only.

$\Delta(1905) \to N\gamma$, helicity-3/2 amplitude $A_{3/2}$

VALUE ($GeV^{-1/2}$)	DOCUMENT ID		TECN	COMMENT
−0.055 to −0.035 (≈ −0.045) OUR ESTIMATE				
−0.0432±0.0173	GOLOVATCH	19	DPWA	$\gamma p \to \pi^+\pi^- p$
−0.053 ±0.029	[1] HUNT	19	DPWA	Multichannel
−0.050 ±0.005	SOKHOYAN	15A	DPWA	Multichannel
−0.049 ±0.005	[1] DUGGER	13	DPWA	$\gamma N \to \pi N$
−0.038 ±0.004	WORKMAN	12A	DPWA	$\gamma N \to \pi N$
• • • We do not use the following data for averages, fits, limits, etc. • • •				
−0.050 ±0.005	GUTZ	14	DPWA	Multichannel
−0.049 ±0.004	ANISOVICH	12A	DPWA	Multichannel
−0.223 ±0.029	[1] SHRESTHA	12A	DPWA	Multichannel
−0.028	DRECHSEL	07	DPWA	$\gamma N \to \pi N$

[1] Statistical error only.

$\Delta(1905)$ REFERENCES

For early references, see Physics Letters **111B** 1 (1982).

GOLOVATCH	19	PL B788 371	E. Golovatch *et al.*	(CLAS Collab.)
HUNT	19	PR C99 055205	B.C. Hunt, D.M. Manley	
ROENCHEN	15A	EPJ A51 70	D. Roenchen *et al.*	
SOKHOYAN	15A	EPJ A51 95	V. Sokhoyan *et al.*	(CBELSA/TAPS Collab.)
GUTZ	14	EPJ A50 74	E. Gutz *et al.*	(CBELSA/TAPS Collab.)
PDG	14	CP C38 070001	K. Olive *et al.*	(PDG Collab.)
ROENCHEN	14	EPJ A50 101	D. Roenchen *et al.*	
Also		EPJ A51 63 (errat.)	D. Roenchen *et al.*	
SVARC	14	PR C89 045205	A. Svarc *et al.*	(RBI Zagreb, UNI Tuzla)
DUGGER	13	PR C88 065203	M. Dugger *et al.*	(JLab CLAS Collab.)
ANISOVICH	12A	EPJ A48 15	A.V. Anisovich *et al.*	(BONN, PNPI)
SHRESTHA	12A	PR C86 055203	M. Shrestha, D.M. Manley	(KSU)
WORKMAN	12A	PR C86 015202	R. Workman *et al.*	(GWU)
DRECHSEL	07	EPJ A34 69	D. Drechsel, S.S. Kamalov, L. Tiator	(MAINZ, JINR)
ARNDT	06	PR C74 045205	R.A. Arndt *et al.*	(GWU)
VRANA	00	PRPL 328 181	T.P. Vrana, S.A. Dytman, T.-S.H. Lee	(PITT, ANL)
HOEHLER	93	πN Newsletter 9 1	G. Hohler	(KARL)
CUTKOSKY	80	Toronto Conf. 19	R.E. Cutkosky *et al.*	(CMU, LBL) IJP
Also		PR D20 2839	R.E. Cutkosky *et al.*	(CMU, LBL) IJP
HOEHLER	79	PDAT 12-1	G. Hohler *et al.*	(KARLT) IJP
Also		Toronto Conf. 3	R. Koch	(KARLT) IJP

$\Delta(1910)\ 1/2^+$

$I(J^P) = \frac{3}{2}(\frac{1}{2}^+)$ Status: ****

Older and obsolete values are listed and referenced in the 2014 edition, Chinese Physics **C38** 070001 (2014).

$\Delta(1910)$ POLE POSITION

REAL PART

VALUE (MeV)	DOCUMENT ID		TECN	COMMENT
1830 to 1890 (≈ 1860) OUR ESTIMATE				
1840±40	SOKHOYAN	15A	DPWA	Multichannel
1896±11	[1] SVARC	14	L+P	$\pi N \to \pi N$
1880±30	CUTKOSKY	80	IPWA	$\pi N \to \pi N$
• • • We do not use the following data for averages, fits, limits, etc. • • •				
1801	HUNT	19	DPWA	Multichannel
1799	ROENCHEN	15A	DPWA	Multichannel
1840±40	GUTZ	14	DPWA	Multichannel
1850±40	ANISOVICH	12A	DPWA	Multichannel
1771	ARNDT	06	DPWA	$\pi N \to \pi N, \eta N$
1880	VRANA	00	DPWA	Multichannel
1874	HOEHLER	93	SPED	$\pi N \to \pi N$

[1] Fit to the amplitudes of HOEHLER 79.

Downloaded from https://academic.oup.com/ptep/article/2022/8/083C01/6651666 by KIT Library user on 27 September 2022

−2×IMAGINARY PART

VALUE (MeV)	DOCUMENT ID		TECN	COMMENT
200 to 400 (≈ 300) OUR ESTIMATE				
370±60	SOKHOYAN	15A	DPWA	Multichannel
302±22	[1] SVARC	14	L+P	$\pi N \to \pi N$
200±40	CUTKOSKY	80	IPWA	$\pi N \to \pi N$
• • • We do not use the following data for averages, fits, limits, etc. • • •				
224	HUNT	19	DPWA	Multichannel
648	ROENCHEN	15A	DPWA	Multichannel
370±60	GUTZ	14	DPWA	Multichannel
350±45	ANISOVICH	12A	DPWA	Multichannel
479	ARNDT	06	DPWA	$\pi N \to \pi N, \eta N$
496	VRANA	00	DPWA	Multichannel
283	HOEHLER	93	SPED	$\pi N \to \pi N$

[1] Fit to the amplitudes of HOEHLER 79.

$\Delta(1910)$ ELASTIC POLE RESIDUE

MODULUS $|r|$

VALUE (MeV)	DOCUMENT ID		TECN	COMMENT
20 to 30 (≈ 25) OUR ESTIMATE				
25±6	SOKHOYAN	15A	DPWA	Multichannel
29±2	[1] SVARC	14	L+P	$\pi N \to \pi N$
20±4	CUTKOSKY	80	IPWA	$\pi N \to \pi N$
• • • We do not use the following data for averages, fits, limits, etc. • • •				
90	ROENCHEN	15A	DPWA	Multichannel
25±6	GUTZ	14	DPWA	Multichannel
24±6	ANISOVICH	12A	DPWA	Multichannel
45	ARNDT	06	DPWA	$\pi N \to \pi N, \eta N$
38	HOEHLER	93	SPED	$\pi N \to \pi N$

[1] Fit to the amplitudes of HOEHLER 79.

PHASE θ

VALUE (°)	DOCUMENT ID		TECN	COMMENT
−180 to −80 (≈ −130) OUR ESTIMATE				
−155±30	SOKHOYAN	15A	DPWA	Multichannel
−83± 4±1	[1] SVARC	14	L+P	$\pi N \to \pi N$
−90±30	CUTKOSKY	80	IPWA	$\pi N \to \pi N$
• • • We do not use the following data for averages, fits, limits, etc. • • •				
−83	ROENCHEN	15A	DPWA	Multichannel
−155±30	GUTZ	14	DPWA	Multichannel
−145±30	ANISOVICH	12A	DPWA	Multichannel
+172	ARNDT	06	DPWA	$\pi N \to \pi N, \eta N$

[1] Fit to the amplitudes of HOEHLER 79.

$\Delta(1910)$ INELASTIC POLE RESIDUE

The "normalized residue" is the residue divided by $\Gamma_{pole}/2$.

Normalized residue in $N\pi \to \Delta(1910) \to \Sigma K$

MODULUS	PHASE (°)	DOCUMENT ID		TECN	COMMENT
0.07 ±0.02	−110 ± 30	ANISOVICH	12A	DPWA	Multichannel
• • • We do not use the following data for averages, fits, limits, etc. • • •					
0.019	−123	ROENCHEN	15A	DPWA	Multichannel

Normalized residue in $N\pi \to \Delta(1910) \to \Delta\pi$, P-wave

MODULUS	PHASE (°)	DOCUMENT ID		TECN	COMMENT
0.24±0.10	85 ± 35	SOKHOYAN	15A	DPWA	Multichannel
• • • We do not use the following data for averages, fits, limits, etc. • • •					
0.58	131	ROENCHEN	15A	DPWA	Multichannel
0.16±0.09	95 ± 40	ANISOVICH	12A	DPWA	Multichannel

Normalized residue in $N\pi \to \Delta(1910) \to \Delta(1232)\eta$

MODULUS	PHASE (°)	DOCUMENT ID		TECN	COMMENT
0.11±0.04	−150 ± 50	GUTZ	14	DPWA	Multichannel

Normalized residue in $N\pi \to \Delta(1910) \to N(1440)\pi$

MODULUS	PHASE (°)	DOCUMENT ID		TECN	COMMENT
0.06±0.03	170 ± 45	SOKHOYAN	15A	DPWA	Multichannel

$\Delta(1910)$ BREIT-WIGNER MASS

VALUE (MeV)	DOCUMENT ID		TECN	COMMENT
1850 to 1950 (≈ 1900) OUR ESTIMATE				
1846 ±18	[1] HUNT	19	DPWA	Multichannel
1845 ±40	SOKHOYAN	15A	DPWA	Multichannel
2067.9± 1.7	[1] ARNDT	06	DPWA	$\pi N \to \pi N, \eta N$
1910 ±40	CUTKOSKY	80	IPWA	$\pi N \to \pi N$
1888 ±20	HOEHLER	79	IPWA	$\pi N \to \pi N$
• • • We do not use the following data for averages, fits, limits, etc. • • •				
1845 ±40	GUTZ	14	DPWA	Multichannel
1860 ±40	ANISOVICH	12A	DPWA	Multichannel
1934 ± 5	[1] SHRESTHA	12A	DPWA	Multichannel
1995 ±12	VRANA	00	DPWA	Multichannel

[1] Statistical error only.

$\Delta(1910)$ BREIT-WIGNER WIDTH

VALUE (MeV)	DOCUMENT ID		TECN	COMMENT
200 to 400 (≈ 300) OUR ESTIMATE				
260± 57	[1] HUNT	19	DPWA	Multichannel
360± 60	SOKHOYAN	15A	DPWA	Multichannel
543± 10	[1] ARNDT	06	DPWA	$\pi N \to \pi N, \eta N$
225± 50	CUTKOSKY	80	IPWA	$\pi N \to \pi N$
280± 50	HOEHLER	79	IPWA	$\pi N \to \pi N$
• • • We do not use the following data for averages, fits, limits, etc. • • •				
360± 60	GUTZ	14	DPWA	Multichannel
350± 55	ANISOVICH	12A	DPWA	Multichannel
211± 11	[1] SHRESTHA	12A	DPWA	Multichannel
713±465	VRANA	00	DPWA	Multichannel

[1] Statistical error only.

$\Delta(1910)$ DECAY MODES

The following branching fractions are our estimates, not fits or averages.

	Mode	Fraction (Γ_i/Γ)
Γ_1	$N\pi$	10–30%
Γ_2	ΣK	4–14%
Γ_3	$\Delta(1232)\pi$	34–66%
Γ_4	$N(1440)\pi$	3–45%
Γ_5	$\Delta(1232)\eta$	5–13%
Γ_6	$N\gamma$, helicity=1/2	0.0–0.02 %

$\Delta(1910)$ BRANCHING RATIOS

$\Gamma(N\pi)/\Gamma_{total}$ — Γ_1/Γ

VALUE (%)	DOCUMENT ID		TECN	COMMENT
10–30% OUR ESTIMATE				
13 ± 3	[1] HUNT	19	DPWA	Multichannel
12 ± 3	SOKHOYAN	15A	DPWA	Multichannel
23.9± 0.1	[1] ARNDT	06	DPWA	$\pi N \to \pi N, \eta N$
19 ± 3	CUTKOSKY	80	IPWA	$\pi N \to \pi N$
24 ± 6	HOEHLER	79	IPWA	$\pi N \to \pi N$
• • • We do not use the following data for averages, fits, limits, etc. • • •				
12 ± 3	GUTZ	14	DPWA	Multichannel
12 ± 3	ANISOVICH	12A	DPWA	Multichannel
17 ± 1	[1] SHRESTHA	12A	DPWA	Multichannel
29 ±21	VRANA	00	DPWA	Multichannel

[1] Statistical error only.

$\Gamma(\Sigma K)/\Gamma_{total}$ — Γ_2/Γ

VALUE (%)	DOCUMENT ID		TECN	COMMENT
4–14% OUR ESTIMATE				
9±5	ANISOVICH	12A	DPWA	Multichannel

$\Gamma(\Delta(1232)\pi)/\Gamma_{total}$ — Γ_3/Γ

VALUE (%)	DOCUMENT ID		TECN	COMMENT
34–66% OUR ESTIMATE				
50±16	SOKHOYAN	15A	DPWA	Multichannel
• • • We do not use the following data for averages, fits, limits, etc. • • •				
60±28	ANISOVICH	12A	DPWA	Multichannel

$\Gamma(N(1440)\pi)/\Gamma_{total}$ — Γ_4/Γ

VALUE (%)	DOCUMENT ID		TECN	COMMENT
3–45% OUR ESTIMATE				
33±12	[1] HUNT	19	DPWA	Multichannel
6± 3	SOKHOYAN	15A	DPWA	Multichannel
• • • We do not use the following data for averages, fits, limits, etc. • • •				
47± 6	[1] SHRESTHA	12A	DPWA	Multichannel
56± 7	VRANA	00	DPWA	Multichannel

[1] Statistical error only.

$\Gamma(\Delta(1232)\eta)/\Gamma_{total}$ — Γ_5/Γ

VALUE (%)	DOCUMENT ID		TECN	COMMENT
5–13% OUR ESTIMATE				
9±4	GUTZ	14	DPWA	Multichannel

$\Delta(1910)$ PHOTON DECAY AMPLITUDES AT THE POLE

$\Delta(1910) \to N\gamma$, helicity-1/2 amplitude $A_{1/2}$

MODULUS ($GeV^{-1/2}$)	PHASE (°)	DOCUMENT ID		TECN	COMMENT
0.027±0.009	−30 ± 60	SOKHOYAN	15A	DPWA	Multichannel
$-0.246^{+0.024}_{-0.047}$	159^{+9}_{-4}	ROENCHEN	14	DPWA	

Downloaded from https://academic.oup.com/ptep/article/2022/8/083C01/6651666 by KIT Library user on 27 September 2022

• • • We do not use the following data for averages, fits, limits, etc. • • •					
0.321	39	ROENCHEN	15A	DPWA	Multichannel

$\Delta(1910)$ BREIT-WIGNER PHOTON DECAY AMPLITUDES

$\Delta(1910) \to N\gamma$, helicity-1/2 amplitude $A_{1/2}$

VALUE (GeV$^{-1/2}$)	DOCUMENT ID		TECN	COMMENT
0.010 to 0.030 (≈ 0.020) OUR ESTIMATE				
0.203±0.056	[1] HUNT	19	DPWA	Multichannel
0.026±0.008	SOKHOYAN	15A	DPWA	Multichannel
−0.002±0.008	[1] ARNDT	96	IPWA	$\gamma N \to \pi N$
• • • We do not use the following data for averages, fits, limits, etc. • • •				
0.026±0.008	GUTZ	14	DPWA	Multichannel
0.022±0.009	ANISOVICH	12A	DPWA	Multichannel
0.030±0.002	[1] SHRESTHA	12A	DPWA	Multichannel

[1] Statistical error only.

$\Delta(1910)$ REFERENCES

For early references, see Physics Letters **111B** 1 (1982).

HUNT	19	PR C99 055205	B.C. Hunt, D.M. Manley	
ROENCHEN	15A	EPJ A51 70	D. Roenchen *et al.*	
SOKHOYAN	15A	EPJ A51 95	V. Sokhoyan *et al.*	(CBELSA/TAPS Collab.)
GUTZ	14	EPJ A50 74	E. Gutz *et al.*	(CBELSA/TAPS Collab.)
PDG	14	CP C38 070001	K. Olive *et al.*	(PDG Collab.)
ROENCHEN	14	EPJ A50 101	D. Roenchen *et al.*	
Also		EPJ A51 63 (errat.)	D. Roenchen *et al.*	
SVARC	14	PR C89 045205	A. Svarc *et al.*	(RBI Zagreb, UNI Tuzla)
ANISOVICH	12A	EPJ A48 15	A.V. Anisovich *et al.*	(BONN, PNPI)
SHRESTHA	12A	PR C86 055203	M. Shrestha, D.M. Manley	(KSU)
ARNDT	06	PR C74 045205	R.A. Arndt *et al.*	(GWU)
VRANA	00	PRPL 328 181	T.P. Vrana, S.A. Dytman, T.-S.H. Lee	(PITT, ANL)
ARNDT	96	PR C53 430	R.A. Arndt, I.I. Strakovsky, R.L. Workman	(VPI)
HOEHLER	93	πN Newsletter 9 1	G. Hohler	(KARL)
CUTKOSKY	80	Toronto Conf. 19	R.E. Cutkosky *et al.*	(CMU, LBL) IJP
Also		PR D20 2839	R.E. Cutkosky *et al.*	(CMU, LBL) IJP
HOEHLER	79	PDAT 12-1	G. Hohler *et al.*	(KARLT) IJP
Also		Toronto Conf. 3	R. Koch	(KARLT) IJP

$\Delta(1920)\ 3/2^+$

$I(J^P) = \frac{3}{2}(\frac{3}{2}^+)$ Status: ***

Older and obsolete values are listed and referenced in the 2014 edition, Chinese Physics **C38** 070001 (2014).

$\Delta(1920)$ POLE POSITION

REAL PART

VALUE (MeV)	DOCUMENT ID		TECN	COMMENT
1850 to 1950 (≈ 1900) OUR ESTIMATE				
1875±30	SOKHOYAN	15A	DPWA	Multichannel
1906±10±2	[1] SVARC	14	L+P	$\pi N \to \pi N$
1900±80	CUTKOSKY	80	IPWA	$\pi N \to \pi N$
• • • We do not use the following data for averages, fits, limits, etc. • • •				
1910	HUNT	19	DPWA	Multichannel
1715	ROENCHEN	15A	DPWA	Multichannel
1875±30	GUTZ	14	DPWA	Multichannel
1890±30	ANISOVICH	12A	DPWA	Multichannel
1880	VRANA	00	DPWA	Multichannel
1900	HOEHLER	93	SPED	$\pi N \to \pi N$

[1] Fit to the amplitudes of HOEHLER 79.

−2×IMAGINARY PART

VALUE (MeV)	DOCUMENT ID		TECN	COMMENT
200 to 400 (≈ 300) OUR ESTIMATE				
300± 40	SOKHOYAN	15A	DPWA	Multichannel
310± 20±11	[1] SVARC	14	L+P	$\pi N \to \pi N$
300±100	CUTKOSKY	80	IPWA	$\pi N \to \pi N$
• • • We do not use the following data for averages, fits, limits, etc. • • •				
472	HUNT	19	DPWA	Multichannel
882	ROENCHEN	15A	DPWA	Multichannel
300± 40	GUTZ	14	DPWA	Multichannel
300± 60	ANISOVICH	12A	DPWA	Multichannel
120	VRANA	00	DPWA	Multichannel

[1] Fit to the amplitudes of HOEHLER 79.

$\Delta(1920)$ ELASTIC POLE RESIDUE

MODULUS $|r|$

VALUE (MeV)	DOCUMENT ID		TECN	COMMENT
8 to 24 (≈ 16) OUR ESTIMATE				
16±6	SOKHOYAN	15A	DPWA	Multichannel
26±3±2	[1] SVARC	14	L+P	$\pi N \to \pi N$
24±4	CUTKOSKY	80	IPWA	$\pi N \to \pi N$
• • • We do not use the following data for averages, fits, limits, etc. • • •				
38	ROENCHEN	15A	DPWA	Multichannel
16±6	GUTZ	14	DPWA	Multichannel
17±8	ANISOVICH	12A	DPWA	Multichannel

[1] Fit to the amplitudes of HOEHLER 79.

PHASE θ

VALUE (°)	DOCUMENT ID		TECN	COMMENT
−150 to −50 (≈ −100) OUR ESTIMATE				
− 50±25	SOKHOYAN	15A	DPWA	Multichannel
−130± 5±3	[1] SVARC	14	L+P	$\pi N \to \pi N$
−150±30	CUTKOSKY	80	IPWA	$\pi N \to \pi N$
• • • We do not use the following data for averages, fits, limits, etc. • • •				
146	ROENCHEN	15A	DPWA	Multichannel
− 50±25	GUTZ	14	DPWA	Multichannel
− 40±20	ANISOVICH	12A	DPWA	Multichannel

[1] Fit to the amplitudes of HOEHLER 79.

$\Delta(1920)$ INELASTIC POLE RESIDUE

The "normalized residue" is the residue divided by $\Gamma_{pole}/2$.

Normalized residue in $N\pi \to \Delta(1920) \to \Delta\eta$

MODULUS	PHASE (°)	DOCUMENT ID		TECN	COMMENT
0.15±0.04	70 ± 20	GUTZ	14	DPWA	Multichannel
• • • We do not use the following data for averages, fits, limits, etc. • • •					
0.17±0.08	70 ± 20	ANISOVICH	12A	DPWA	Multichannel

Normalized residue in $N\pi \to \Delta(1920) \to \Sigma K$

MODULUS	PHASE (°)	DOCUMENT ID		TECN	COMMENT
0.09±0.03	80 ± 40	ANISOVICH	12A	DPWA	Multichannel
• • • We do not use the following data for averages, fits, limits, etc. • • •					
0.17	−35	ROENCHEN	15A	DPWA	Multichannel

Normalized residue in $N\pi \to \Delta(1920) \to \Delta\pi$, P-wave

MODULUS	PHASE (°)	DOCUMENT ID		TECN	COMMENT
0.20 ±0.08	−105 ± 25	SOKHOYAN	15A	DPWA	Multichannel
• • • We do not use the following data for averages, fits, limits, etc. • • •					
0.069	131	ROENCHEN	15A	DPWA	Multichannel
0.20 ±0.12	−120 ± 30	ANISOVICH	12A	DPWA	Multichannel

Normalized residue in $N\pi \to \Delta(1920) \to \Delta\pi$, F-wave

MODULUS	PHASE (°)	DOCUMENT ID		TECN	COMMENT
0.37 ±0.10	−90 ± 20	SOKHOYAN	15A	DPWA	Multichannel
• • • We do not use the following data for averages, fits, limits, etc. • • •					
0.013	−115	ROENCHEN	15A	DPWA	Multichannel
0.28 ±0.07	−95 ± 35	ANISOVICH	12A	DPWA	Multichannel

Normalized residue in $N\pi \to \Delta(1920) \to N(1535)\pi$

MODULUS	PHASE (°)	DOCUMENT ID		TECN	COMMENT
0.03±0.02	35 ± 45	GUTZ	14	DPWA	Multichannel

Normalized residue in $N\pi \to \Delta(1920) \to N a_0(980)$

MODULUS	PHASE (°)	DOCUMENT ID		TECN	COMMENT
0.03±0.02	−85 ± 45	GUTZ	14	DPWA	Multichannel

Normalized residue in $N\pi \to \Delta(1920) \to N(1440)\pi$

MODULUS	PHASE (°)	DOCUMENT ID		TECN	COMMENT
0.04±0.03	undefined	SOKHOYAN	15A	DPWA	Multichannel

Normalized residue in $N\pi \to \Delta(1920) \to N(1520)\pi$, S-wave

MODULUS	PHASE (°)	DOCUMENT ID		TECN	COMMENT
0.05±0.05	undefined	SOKHOYAN	15A	DPWA	Multichannel

$\Delta(1920)$ BREIT-WIGNER MASS

VALUE (MeV)	DOCUMENT ID		TECN	COMMENT
1870 to 1970 (≈ 1920) OUR ESTIMATE				
1976± 49	HUNT	19	DPWA	Multichannel
1880± 30	SOKHOYAN	15A	DPWA	Multichannel
2146± 32	[1] SHRESTHA	12A	DPWA	Multichannel
1920± 80	CUTKOSKY	80	IPWA	$\pi N \to \pi N$
1868± 10	HOEHLER	79	IPWA	$\pi N \to \pi N$
• • • We do not use the following data for averages, fits, limits, etc. • • •				
1880± 30	GUTZ	14	DPWA	Multichannel
1900± 30	ANISOVICH	12A	DPWA	Multichannel
2057± 1	PENNER	02C	DPWA	Multichannel
1889±100	VRANA	00	DPWA	Multichannel

[1] Statistical error only.

$\Delta(1920)$ BREIT-WIGNER WIDTH

VALUE (MeV)	DOCUMENT ID		TECN	COMMENT
240 to 360 (≈ 300) OUR ESTIMATE				
509±170	HUNT	19	DPWA	Multichannel
300± 40	SOKHOYAN	15A	DPWA	Multichannel
400± 80	[1] SHRESTHA	12A	DPWA	Multichannel
300±100	CUTKOSKY	80	IPWA	$\pi N \to \pi N$
220± 80	HOEHLER	79	IPWA	$\pi N \to \pi N$

Downloaded from https://academic.oup.com/ptep/article/2022/8/083C01/6651666 by KIT Library user on 27 September 2022

• • • We do not use the following data for averages, fits, limits, etc. • • •

300 ± 40	GUTZ	14	DPWA	Multichannel
310 ± 60	ANISOVICH	12A	DPWA	Multichannel
525 ± 32	PENNER	02C	DPWA	Multichannel
123 ± 53	VRANA	00	DPWA	Multichannel

[1] Statistical error only.

$\Delta(1920)$ DECAY MODES

The following branching fractions are our estimates, not fits or averages.

	Mode	Fraction (Γ_i/Γ)
Γ_1	$N\pi$	5–20 %
Γ_2	ΣK	2–6 %
Γ_3	$N\pi\pi$	>46 %
Γ_4	$\Delta(1232)\pi$	>46 %
Γ_5	$\Delta(1232)\pi$, P-wave	2–28 %
Γ_6	$\Delta(1232)\pi$, F-wave	44–72 %
Γ_7	$N(1440)\pi$, P-wave	4–86 %
Γ_8	$N(1520)\pi$, S-wave	<5 %
Γ_9	$N(1535)\pi$	<2 %
Γ_{10}	$N a_0(980)$	seen
Γ_{11}	$\Delta(1232)\eta$	5–17 %
Γ_{12}	$N\gamma$	0.01–0.84 %
Γ_{13}	$N\gamma$, helicity=1/2	0.0–0.42 %
Γ_{14}	$N\gamma$, helicity=3/2	0.01–0.42 %

$\Delta(1920)$ BRANCHING RATIOS

$\Gamma(N\pi)/\Gamma_{total}$ — Γ_1/Γ

VALUE (%)	DOCUMENT ID		TECN	COMMENT
5–20 % OUR ESTIMATE				
10.5 ± 3.0	[1] HUNT	19	DPWA	Multichannel
8 ± 4	SOKHOYAN	15A	DPWA	Multichannel
20 ± 5	CUTKOSKY	80	IPWA	$\pi N \to \pi N$
14 ± 4	HOEHLER	79	IPWA	$\pi N \to \pi N$
• • • We do not use the following data for averages, fits, limits, etc. • • •				
8 ± 4	GUTZ	14	DPWA	Multichannel
8 ± 4	ANISOVICH	12A	DPWA	Multichannel
16 ± 4	[1] SHRESTHA	12A	DPWA	Multichannel
15 ± 1	PENNER	02C	DPWA	Multichannel
5 ± 4	VRANA	00	DPWA	Multichannel

[1] Statistical error only.

$\Gamma(\Sigma K)/\Gamma_{total}$ — Γ_2/Γ

VALUE (%)	DOCUMENT ID		TECN	COMMENT
2–6 % OUR ESTIMATE				
4 ± 2	ANISOVICH	12A	DPWA	Multichannel
• • • We do not use the following data for averages, fits, limits, etc. • • •				
2.1 ± 0.3	PENNER	02C	DPWA	Multichannel

$\Gamma(\Delta(1232)\pi, P\text{-wave})/\Gamma_{total}$ — Γ_5/Γ

VALUE (%)	DOCUMENT ID		TECN	COMMENT
2–28 % OUR ESTIMATE				
< 1.6	[1] HUNT	19	DPWA	Multichannel
18 ± 10	SOKHOYAN	15A	DPWA	Multichannel
• • • We do not use the following data for averages, fits, limits, etc. • • •				
22 ± 12	ANISOVICH	12A	DPWA	Multichannel
7 ± 5	[1] SHRESTHA	12A	DPWA	Multichannel
41 ± 3	VRANA	00	DPWA	Multichannel

[1] Statistical error only.

$\Gamma(\Delta(1232)\pi, F\text{-wave})/\Gamma_{total}$ — Γ_6/Γ

VALUE (%)	DOCUMENT ID		TECN	COMMENT
44–72 % OUR ESTIMATE				
58 ± 14	SOKHOYAN	15A	DPWA	Multichannel
• • • We do not use the following data for averages, fits, limits, etc. • • •				
45 ± 20	ANISOVICH	12A	DPWA	Multichannel

$\Gamma(N(1440)\pi, P\text{-wave})/\Gamma_{total}$ — Γ_7/Γ

VALUE (%)	DOCUMENT ID		TECN	COMMENT
4–86 % OUR ESTIMATE				
77 ± 9	[1] HUNT	19	DPWA	Multichannel
< 4	SOKHOYAN	15A	DPWA	Multichannel
• • • We do not use the following data for averages, fits, limits, etc. • • •				
<20	[1] SHRESTHA	12A	DPWA	Multichannel
53 ± 8	VRANA	00	DPWA	Multichannel

[1] Statistical error only.

$\Gamma(N(1520)\pi, S\text{-wave})/\Gamma_{total}$ — Γ_8/Γ

VALUE (%)	DOCUMENT ID		TECN	COMMENT
<5 OUR ESTIMATE				
<5	SOKHOYAN	15A	DPWA	Multichannel

$\Gamma(N(1535)\pi)/\Gamma_{total}$ — Γ_9/Γ

VALUE (%)	DOCUMENT ID		TECN	COMMENT
<2 OUR ESTIMATE				
<2	GUTZ	14	DPWA	Multichannel

$\Gamma(N a_0(980))/\Gamma_{total}$ — Γ_{10}/Γ

VALUE (%)	DOCUMENT ID		TECN	COMMENT
seen OUR ESTIMATE				
• • • We do not use the following data for averages, fits, limits, etc. • • •				
4 ± 2	HORN	08A	DPWA	Multichannel

$\Gamma(\Delta(1232)\eta)/\Gamma_{total}$ — Γ_{11}/Γ

VALUE (%)	DOCUMENT ID		TECN	COMMENT
5–17 % OUR ESTIMATE				
11 ± 6	GUTZ	14	DPWA	Multichannel
• • • We do not use the following data for averages, fits, limits, etc. • • •				
15 ± 8	ANISOVICH	12A	DPWA	Multichannel

$\Delta(1920)$ PHOTON DECAY AMPLITUDES AT THE POLE

$\Delta(1920) \to N\gamma$, helicity-1/2 amplitude $A_{1/2}$

MODULUS ($GeV^{-1/2}$)	PHASE (°)	DOCUMENT ID		TECN	COMMENT
0.110 ± 0.030	−50 ± 20	SOKHOYAN	15A	DPWA	Multichannel
$0.190^{+0.050}_{-0.022}$	-160^{+24}_{-11}	ROENCHEN	14	DPWA	
• • • We do not use the following data for averages, fits, limits, etc. • • •					
−0.192	46	ROENCHEN	15A	DPWA	Multichannel

$\Delta(1920) \to N\gamma$, helicity-3/2 amplitude $A_{3/2}$

MODULUS ($GeV^{-1/2}$)	PHASE (°)	DOCUMENT ID		TECN	COMMENT
−0.100 ± 0.040	0 ± 20	SOKHOYAN	15A	DPWA	Multichannel
$-0.398^{+0.070}_{-0.067}$	-110^{+4}_{-5}	ROENCHEN	14	DPWA	
• • • We do not use the following data for averages, fits, limits, etc. • • •					
0.522	67	ROENCHEN	15A	DPWA	Multichannel

$\Delta(1920)$ BREIT-WIGNER PHOTON DECAY AMPLITUDES

$\Delta(1920) \to N\gamma$, helicity-1/2 amplitude $A_{1/2}$

VALUE ($GeV^{-1/2}$)	DOCUMENT ID		TECN	COMMENT
−0.028 ± 0.010	[1] HUNT	19	DPWA	Multichannel
0.110 ± 0.030	SOKHOYAN	15A	DPWA	Multichannel
• • • We do not use the following data for averages, fits, limits, etc. • • •				
0.110 ± 0.030	GUTZ	14	DPWA	Multichannel
$0.130^{+0.030}_{-0.060}$	ANISOVICH	12A	DPWA	Multichannel
0.051 ± 0.010	[1] SHRESTHA	12A	DPWA	Multichannel
−0.007	PENNER	02D	DPWA	Multichannel

[1] Statistical error only.

$\Delta(1920) \to N\gamma$, helicity-3/2 amplitude $A_{3/2}$

VALUE ($GeV^{-1/2}$)	DOCUMENT ID		TECN	COMMENT
−0.043 ± 0.014	[1] HUNT	19	DPWA	Multichannel
−0.105 ± 0.035	SOKHOYAN	15A	DPWA	Multichannel
• • • We do not use the following data for averages, fits, limits, etc. • • •				
−0.105 ± 0.035	GUTZ	14	DPWA	Multichannel
$-0.115^{+0.025}_{-0.050}$	ANISOVICH	12A	DPWA	Multichannel
0.017 ± 0.015	[1] SHRESTHA	12A	DPWA	Multichannel
−0.001	PENNER	02D	DPWA	Multichannel

[1] Statistical error only.

$\Delta(1920)$ REFERENCES

For early references, see Physics Letters **111B** 1 (1982).

HUNT	19	PR C99 055205	B.C. Hunt, D.M. Manley	
ROENCHEN	15A	EPJ A51 70	D. Roenchen *et al.*	
SOKHOYAN	15A	EPJ A51 95	V. Sokhoyan *et al.*	(CBELSA/TAPS Collab.)
GUTZ	14	EPJ A50 74	E. Gutz *et al.*	(CBELSA/TAPS Collab.)
PDG	14	CP C38 070001	K. Olive *et al.*	(PDG Collab.)
ROENCHEN	14	EPJ A50 101	D. Roenchen *et al.*	
Also		EPJ A51 63 (errat.)	D. Roenchen *et al.*	
SVARC	14	PR C89 045205	A. Svarc *et al.*	(RBI Zagreb, UNI Tuzla)
ANISOVICH	12A	EPJ A48 15	A.V. Anisovich *et al.*	(BONN, PNPI)
SHRESTHA	12A	PR C86 055203	M. Shrestha, D.M. Manley	(KSU)
HORN	08A	EPJ A38 173	I. Horn *et al.*	(CB-ELSA Collab.)
Also		PRL 101 202002	I. Horn *et al.*	(CB-ELSA Collab.)
PENNER	02C	PR C66 055211	G. Penner, U. Mosel	(GIES)
PENNER	02D	PR C66 055212	G. Penner, U. Mosel	(GIES)
VRANA	00	PRPL 328 181	T.P. Vrana, S.A. Dytman, T.-S.H. Lee	(PITT, ANL)
HOEHLER	93	πN Newsletter 9 1	G. Hohler	(KARL)
CUTKOSKY	80	Toronto Conf. 19	R.E. Cutkosky *et al.*	(CMU, LBL) IJP
Also		PR D20 2839	R.E. Cutkosky *et al.*	(CMU, LBL) IJP
HOEHLER	79	PDAT 12-1	G. Hohler *et al.*	(KARLT) IJP
Also		Toronto Conf. 3	R. Koch	(KARLT) IJP

Downloaded from https://academic.oup.com/ptep/article/2022/8/083C01/6651666 by KIT Library user on 27 September 2022

$\Delta(1930)\ 5/2^-$

$I(J^P) = \frac{3}{2}(\frac{5}{2}^-)$ Status: ***

Older and obsolete values are listed and referenced in the 2014 edition, Chinese Physics **C38** 070001 (2014).

$\Delta(1930)$ POLE POSITION

REAL PART

VALUE (MeV)	DOCUMENT ID		TECN	COMMENT
1840 to 1920 (≈ 1880) OUR ESTIMATE				
1848± 9±19	[1] SVARC	14	L+P	$\pi N \to \pi N$
1890±50	CUTKOSKY	80	IPWA	$\pi N \to \pi N$
• • • We do not use the following data for averages, fits, limits, etc. • • •				
1863	HUNT	19	DPWA	Multichannel
1836	ROENCHEN	15A	DPWA	Multichannel
2001	ARNDT	06	DPWA	$\pi N \to \pi N, \eta N$
1883	VRANA	00	DPWA	Multichannel
1850	HOEHLER	93	SPED	$\pi N \to \pi N$

[1] Fit to the amplitudes of HOEHLER 79.

−2×IMAGINARY PART

VALUE (MeV)	DOCUMENT ID		TECN	COMMENT
230 to 330 (≈ 280) OUR ESTIMATE				
321±17±7	[1] SVARC	14	L+P	$\pi N \to \pi N$
260±60	CUTKOSKY	80	IPWA	$\pi N \to \pi N$
• • • We do not use the following data for averages, fits, limits, etc. • • •				
260	HUNT	19	DPWA	Multichannel
724	ROENCHEN	15A	DPWA	Multichannel
387	ARNDT	06	DPWA	$\pi N \to \pi N, \eta N$
250	VRANA	00	DPWA	Multichannel
180	HOEHLER	93	SPED	$\pi N \to \pi N$

[1] Fit to the amplitudes of HOEHLER 79.

$\Delta(1930)$ ELASTIC POLE RESIDUE

MODULUS $|r|$

VALUE (MeV)	DOCUMENT ID		TECN	COMMENT
8 to 20 (≈ 14) OUR ESTIMATE				
9±1±1	[1] SVARC	14	L+P	$\pi N \to \pi N$
18±6	CUTKOSKY	80	IPWA	$\pi N \to \pi N$
• • • We do not use the following data for averages, fits, limits, etc. • • •				
34	ROENCHEN	15A	DPWA	Multichannel
7	ARNDT	06	DPWA	$\pi N \to \pi N, \eta N$
20	HOEHLER	93	SPED	$\pi N \to \pi N$

[1] Fit to the amplitudes of HOEHLER 79.

PHASE θ

VALUE (°)	DOCUMENT ID		TECN	COMMENT
− 40 to −10 (≈ − 30) OUR ESTIMATE				
− 37± 3±7	[1] SVARC	14	L+P	$\pi N \to \pi N$
− 20±40	CUTKOSKY	80	IPWA	$\pi N \to \pi N$
• • • We do not use the following data for averages, fits, limits, etc. • • •				
−155	ROENCHEN	15A	DPWA	Multichannel
− 12	ARNDT	06	DPWA	$\pi N \to \pi N, \eta N$

[1] Fit to the amplitudes of HOEHLER 79.

$\Delta(1930)$ INELASTIC POLE RESIDUE

The "normalized residue" is the residue divided by $\Gamma_{pole}/2$.

Normalized residue in $N\pi \to \Delta(1930) \to \Sigma K$

MODULUS	PHASE (°)	DOCUMENT ID		TECN	COMMENT
• • • We do not use the following data for averages, fits, limits, etc. • • •					
0.043	−0.5	ROENCHEN	15A	DPWA	Multichannel

Normalized residue in $N\pi \to \Delta(1930) \to \Delta\pi$, D-wave

MODULUS	PHASE (°)	DOCUMENT ID		TECN	COMMENT
• • • We do not use the following data for averages, fits, limits, etc. • • •					
0.15	30	ROENCHEN	15A	DPWA	Multichannel

Normalized residue in $N\pi \to \Delta(1930) \to \Delta\pi$, G-wave

MODULUS	PHASE (°)	DOCUMENT ID		TECN	COMMENT
• • • We do not use the following data for averages, fits, limits, etc. • • •					
0.009	121	ROENCHEN	15A	DPWA	Multichannel

$\Delta(1930)$ BREIT-WIGNER MASS

VALUE (MeV)	DOCUMENT ID		TECN	COMMENT
1900 to 2000 (≈ 1950) OUR ESTIMATE				
1988± 32	[1] HUNT	19	DPWA	Multichannel
2233± 53	[1] ARNDT	06	DPWA	$\pi N \to \pi N, \eta N$
1940± 30	CUTKOSKY	80	IPWA	$\pi N \to \pi N$
1901± 15	HOEHLER	79	IPWA	$\pi N \to \pi N$
• • • We do not use the following data for averages, fits, limits, etc. • • •				
1930± 12	[1] SHRESTHA	12A	DPWA	Multichannel
1932±100	VRANA	00	DPWA	Multichannel

[1] Statistical error only.

$\Delta(1930)$ BREIT-WIGNER WIDTH

VALUE (MeV)	DOCUMENT ID		TECN	COMMENT
200 to 400 (≈ 300) OUR ESTIMATE				
500±160	[1] HUNT	19	DPWA	Multichannel
773±187	ARNDT	06	DPWA	$\pi N \to \pi N, \eta N$
320± 60	CUTKOSKY	80	IPWA	$\pi N \to \pi N$
195± 60	HOEHLER	79	IPWA	$\pi N \to \pi N$
• • • We do not use the following data for averages, fits, limits, etc. • • •				
235± 39	[1] SHRESTHA	12A	DPWA	Multichannel
316±237	VRANA	00	DPWA	Multichannel

[1] Statistical error only.

$\Delta(1930)$ DECAY MODES

The following branching fractions are our estimates, not fits or averages.

	Mode	Fraction (Γ_i/Γ)
Γ_1	$N\pi$	5–15 %
Γ_2	$N\gamma$	0.0–0.01 %
Γ_3	$N\gamma$, helicity=1/2	0.0–0.005 %
Γ_4	$N\gamma$, helicity=3/2	0.0–0.004 %

$\Delta(1930)$ BRANCHING RATIOS

$\Gamma(N\pi)/\Gamma_{total}$ — Γ_1/Γ

VALUE (%)	DOCUMENT ID		TECN	COMMENT
5 to 15 (≈ 10) OUR ESTIMATE				
9.5±0.1	[1] HUNT	19	DPWA	Multichannel
8.1±1.2	[1] ARNDT	06	DPWA	$\pi N \to \pi N, \eta N$
14 ±4	CUTKOSKY	80	IPWA	$\pi N \to \pi N$
4 ±3	HOEHLER	79	IPWA	$\pi N \to \pi N$
• • • We do not use the following data for averages, fits, limits, etc. • • •				
7.9±0.4	[1] SHRESTHA	12A	DPWA	Multichannel
9 ±8	VRANA	00	DPWA	Multichannel

[1] Statistical error only.

$\Delta(1930)$ PHOTON DECAY AMPLITUDES AT THE POLE

$\Delta(1930) \to N\gamma$, helicity-1/2 amplitude $A_{1/2}$

MODULUS ($GeV^{-1/2}$)	PHASE (°)	DOCUMENT ID		TECN	COMMENT
$0.130^{+0.073}_{-0.096}$	-50^{+77}_{-26}	ROENCHEN	14	DPWA	
• • • We do not use the following data for averages, fits, limits, etc. • • •					
−0.270	33	ROENCHEN	15A	DPWA	Multichannel

$\Delta(1930) \to N\gamma$, helicity-3/2 amplitude $A_{3/2}$

MODULUS ($GeV^{-1/2}$)	PHASE (°)	DOCUMENT ID		TECN	COMMENT
$-0.056^{+0.003}_{-0.151}$	168^{+72}_{-76}	ROENCHEN	14	DPWA	
• • • We do not use the following data for averages, fits, limits, etc. • • •					
0.153	81	ROENCHEN	15A	DPWA	Multichannel

$\Delta(1930)$ BREIT-WIGNER PHOTON DECAY AMPLITUDES

$\Delta(1930) \to N\gamma$, helicity-1/2 amplitude $A_{1/2}$

VALUE ($GeV^{-1/2}$)	DOCUMENT ID		TECN	COMMENT
−0.043±0.008	[1] HUNT	19	DPWA	Multichannel
−0.007±0.010	[1] ARNDT	96	IPWA	$\gamma N \to \pi N$
• • • We do not use the following data for averages, fits, limits, etc. • • •				
0.011±0.003	[1] SHRESTHA	12A	DPWA	Multichannel

[1] Statistical error only.

$\Delta(1930) \to N\gamma$, helicity-3/2 amplitude $A_{3/2}$

VALUE ($GeV^{-1/2}$)	DOCUMENT ID		TECN	COMMENT
−0.020±0.017	[1] HUNT	19	DPWA	Multichannel
0.005±0.010	[1] ARNDT	96	IPWA	$\gamma N \to \pi N$
• • • We do not use the following data for averages, fits, limits, etc. • • •				
0.002±0.002	[1] SHRESTHA	12A	DPWA	Multichannel

[1] Statistical error only.

$\Delta(1930)$ REFERENCES

For early references, see Physics Letters **111B** 1 (1982).

HUNT	19	PR C99 055205	B.C. Hunt, D.M. Manley	
ROENCHEN	15A	EPJ A51 70	D. Roenchen *et al.*	
PDG	14	CP C38 070001	K. Olive *et al.*	(PDG Collab.)
ROENCHEN	14	EPJ A50 101	D. Roenchen *et al.*	
Also		EPJ A51 63 (errat.)	D. Roenchen *et al.*	
SVARC	14	PR C89 045205	A. Svarc *et al.*	(RBI Zagreb, UNI Tuzla)
SHRESTHA	12A	PR C86 055203	M. Shrestha, D.M. Manley	(KSU)

Downloaded from https://academic.oup.com/ptep/article/2022/8/083C01/6651666 by KIT Library user on 27 September 2022

ARNDT	06	PR C74 045205	R.A. Arndt *et al.*	(GWU)
VRANA	00	PRPL 328 181	T.P. Vrana, S.A. Dytman, T.-S.H. Lee	(PITT, ANL)
ARNDT	96	PR C53 430	R.A. Arndt, I.I. Strakovsky, R.L. Workman	(VPI)
HOEHLER	93	πN Newsletter 9 1	G. Hohler	(KARL)
CUTKOSKY	80	Toronto Conf. 19	R.E. Cutkosky *et al.*	(CMU, LBL) IJP
Also		PR D20 2839	R.E. Cutkosky *et al.*	(CMU, LBL) IJP
HOEHLER	79	PDAT 12-1	G. Hohler *et al.*	(KARLT) IJP
Also		Toronto Conf. 3	R. Koch	(KARLT) IJP

$\Delta(1940)\ 3/2^-$

$I(J^P) = \frac{3}{2}(\frac{3}{2}^-)$ Status: **

OMITTED FROM SUMMARY TABLE

$\Delta(1940)$ POLE POSITION

REAL PART

VALUE (MeV)	DOCUMENT ID		TECN	COMMENT
1850 to 2050 (≈ 1950) OUR ESTIMATE				
2040± 50	SOKHOYAN	15A	DPWA	Multichannel
1878± 11±5.5	[1] SVARC	14	L+P	$\pi N \to \pi N$
1900±100	CUTKOSKY	80	IPWA	$\pi N \to \pi N$
• • • We do not use the following data for averages, fits, limits, etc. • • •				
2139	HUNT	19	DPWA	Multichannel
2040± 50	GUTZ	14	DPWA	Multichannel
1990^{+100}_{-50}	ANISOVICH	12A	DPWA	Multichannel

[1] Fit to the amplitudes of HOEHLER 79.

−2×IMAGINARY PART

VALUE (MeV)	DOCUMENT ID		TECN	COMMENT
200 to 500 (≈ 350) OUR ESTIMATE				
450±90	SOKHOYAN	15A	DPWA	Multichannel
212±21±6	[1] SVARC	14	L+P	$\pi N \to \pi N$
200±60	CUTKOSKY	80	IPWA	$\pi N \to \pi N$
• • • We do not use the following data for averages, fits, limits, etc. • • •				
400	HUNT	19	DPWA	Multichannel
450±90	GUTZ	14	DPWA	Multichannel
450±90	ANISOVICH	12A	DPWA	Multichannel

[1] Fit to the amplitudes of HOEHLER 79.

$\Delta(1940)$ ELASTIC POLE RESIDUE

MODULUS $|r|$

VALUE (MeV)	DOCUMENT ID		TECN	COMMENT
4 to 10 (≈ 7) OUR ESTIMATE				
6±3	SOKHOYAN	15A	DPWA	Multichannel
9±1±1	[1] SVARC	14	L+P	$\pi N \to \pi N$
8±3	CUTKOSKY	80	IPWA	$\pi N \to \pi N$
• • • We do not use the following data for averages, fits, limits, etc. • • •				
4±3	GUTZ	14	DPWA	Multichannel
4±4	ANISOVICH	12A	DPWA	Multichannel

[1] Fit to the amplitudes of HOEHLER 79.

PHASE θ

VALUE (°)	DOCUMENT ID		TECN	COMMENT
150 to 250 (≈ 200) OUR ESTIMATE				
− 90±35	SOKHOYAN	15A	DPWA	Multichannel
140± 7±7	[1] SVARC	14	L+P	$\pi N \to \pi N$
135±45	CUTKOSKY	80	IPWA	$\pi N \to \pi N$
• • • We do not use the following data for averages, fits, limits, etc. • • •				
− 50±35	GUTZ	14	DPWA	Multichannel

[1] Fit to the amplitudes of HOEHLER 79.

$\Delta(1940)$ INELASTIC POLE RESIDUE

The "normalized residue" is the residue divided by $\Gamma_{pole}/2$.

Normalized residue in $N\pi \to \Delta(1940) \to \Delta(1232)\eta$

MODULUS	PHASE (°)	DOCUMENT ID		TECN	COMMENT
<0.01	undefined	GUTZ	14	DPWA	Multichannel

Normalized residue in $N\pi \to \Delta(1940) \to N(1535)\pi$

MODULUS	PHASE (°)	DOCUMENT ID		TECN	COMMENT
<0.03	undefined	GUTZ	14	DPWA	Multichannel

Normalized residue in $N\pi \to \Delta(1940) \to \Delta(1232)\pi$, S-wave

MODULUS	PHASE (°)	DOCUMENT ID		TECN	COMMENT
0.12±0.06	120 ± 45	SOKHOYAN	15A	DPWA	Multichannel

Normalized residue in $N\pi \to \Delta(1940) \to \Delta(1232)\pi$, D-wave

MODULUS	PHASE (°)	DOCUMENT ID		TECN	COMMENT
0.06±0.04	− 80 ± 35	SOKHOYAN	15A	DPWA	Multichannel

$\Delta(1940)$ BREIT-WIGNER MASS

VALUE (MeV)	DOCUMENT ID		TECN	COMMENT
1940 to 2060 (≈ 2000) OUR ESTIMATE				
2137± 13	[1] HUNT	19	DPWA	Multichannel
2050± 40	SOKHOYAN	15A	DPWA	Multichannel
1940±100	CUTKOSKY	80	IPWA	$\pi N \to \pi N$
• • • We do not use the following data for averages, fits, limits, etc. • • •				
2050± 40	GUTZ	14	DPWA	Multichannel
1995^{+105}_{-60}	ANISOVICH	12A	DPWA	Multichannel

[1] Statistical error only.

$\Delta(1940)$ BREIT-WIGNER WIDTH

VALUE (MeV)	DOCUMENT ID		TECN	COMMENT
300 to 500 (≈ 400) OUR ESTIMATE				
400± 43	[1] HUNT	19	DPWA	Multichannel
450± 70	SOKHOYAN	15A	DPWA	Multichannel
200±100	CUTKOSKY	80	IPWA	$\pi N \to \pi N$
• • • We do not use the following data for averages, fits, limits, etc. • • •				
450± 70	GUTZ	14	DPWA	Multichannel
450±100	ANISOVICH	12A	DPWA	Multichannel

[1] Statistical error only.

$\Delta(1940)$ DECAY MODES

	Mode	Fraction (Γ_i/Γ)
Γ_1	$N\pi$	1–20 %
Γ_2	$N\pi\pi$	>81 %
Γ_3	$\Delta(1232)\pi$	6–85 %
Γ_4	$\Delta(1232)\pi$, S-wave	1–65 %
Γ_5	$\Delta(1232)\pi$, D-wave	5–20 %
Γ_6	$N\rho$, $S=3/2$, S-wave	75–85 %
Γ_7	$N(1535)\pi$	2–14 %
Γ_8	$N a_0(980)$	seen
Γ_9	$\Delta(1232)\eta$	4–16 %
Γ_{10}	$N\gamma$	0.06–2.53 %
Γ_{11}	$N\gamma$, helicity=1/2	0.06–1.51 %
Γ_{12}	$N\gamma$, helicity=3/2	0–1.02 %

$\Delta(1940)$ BRANCHING RATIOS

$\Gamma(N\pi)/\Gamma_{total}$ — Γ_1/Γ

VALUE (%)	DOCUMENT ID		TECN	COMMENT
1–20 % OUR ESTIMATE				
16±4	[1] HUNT	19	DPWA	Multichannel
2±1	SOKHOYAN	15A	DPWA	Multichannel
5±2	CUTKOSKY	80	IPWA	$\pi N \to \pi N$
• • • We do not use the following data for averages, fits, limits, etc. • • •				
2±1	GUTZ	14	DPWA	Multichannel

[1] Statistical error only.

$\Gamma(\Delta(1232)\pi, S\text{-wave})/\Gamma_{total}$ — Γ_4/Γ

VALUE (%)	DOCUMENT ID		TECN	COMMENT
1–65 % OUR ESTIMATE				
< 0.9	[1] HUNT	19	DPWA	Multichannel
46 ±20	SOKHOYAN	15A	DPWA	Multichannel

[1] Statistical error only.

$\Gamma(\Delta(1232)\pi, D\text{-wave})/\Gamma_{total}$ — Γ_5/Γ

VALUE (%)	DOCUMENT ID		TECN	COMMENT
5–20 % OUR ESTIMATE				
< 6.3	[1] HUNT	19	DPWA	Multichannel
12 ±7	SOKHOYAN	15A	DPWA	Multichannel

[1] Statistical error only.

$\Gamma(N\rho, S=3/2, S\text{-wave})/\Gamma_{total}$ — Γ_6/Γ

VALUE (%)	DOCUMENT ID		TECN	COMMENT
75–85 % OUR ESTIMATE				
80±5	[1] HUNT	19	DPWA	Multichannel

[1] Statistical error only.

$\Gamma(N(1535)\pi)/\Gamma_{total}$ — Γ_7/Γ

VALUE (%)	DOCUMENT ID		TECN	COMMENT
2–14 % OUR ESTIMATE				
8±6	GUTZ	14	DPWA	Multichannel
• • • We do not use the following data for averages, fits, limits, etc. • • •				
2±1	HORN	08A	DPWA	Multichannel

Downloaded from https://academic.oup.com/ptep/article/2022/8/083C01/6651666 by KIT Library user on 27 September 2022

$\Gamma(Na_0(980))/\Gamma_{total}$ — Γ_8/Γ

VALUE (%)	DOCUMENT ID		TECN	COMMENT
seen OUR ESTIMATE				
• • • We do not use the following data for averages, fits, limits, etc. • • •				
2±1	HORN	08A	DPWA	Multichannel

$\Gamma(\Delta(1232)\eta)/\Gamma_{total}$ — Γ_9/Γ

VALUE (%)	DOCUMENT ID		TECN	COMMENT
4–16 % OUR ESTIMATE				
10±6	GUTZ	14	DPWA	Multichannel
• • • We do not use the following data for averages, fits, limits, etc. • • •				
4±2	HORN	08A	DPWA	Multichannel

$\Delta(1940)$ PHOTON DECAY AMPLITUDES AT THE POLE

$\Delta(1940) \to N\gamma$, helicity-1/2 amplitude $A_{1/2}$

MODULUS (GeV$^{-1/2}$)	PHASE (°)	DOCUMENT ID		TECN	COMMENT
$0.170^{+0.120}_{-0.100}$	−10 ± 30	SOKHOYAN	15A	DPWA	Multichannel

$\Delta(1940) \to N\gamma$, helicity-3/2 amplitude $A_{3/2}$

MODULUS (GeV$^{-1/2}$)	PHASE (°)	DOCUMENT ID		TECN	COMMENT
0.150±0.080	−10 ± 30	SOKHOYAN	15A	DPWA	Multichannel

$\Delta(1940)$ BREIT-WIGNER PHOTON DECAY AMPLITUDES

$\Delta(1940) \to N\gamma$, helicity-1/2 amplitude $A_{1/2}$

VALUE (GeV$^{-1/2}$)	DOCUMENT ID		TECN	COMMENT
0.1614±0.0031	[1] HUNT	19	DPWA	Multichannel
$0.170^{+0.110}_{-0.080}$	SOKHOYAN	15A	DPWA	Multichannel
• • • We do not use the following data for averages, fits, limits, etc. • • •				
$0.170^{+0.110}_{-0.080}$	GUTZ	14	DPWA	Multichannel

[1] Statistical error only.

$\Delta(1940) \to N\gamma$, helicity-3/2 amplitude $A_{3/2}$

VALUE (GeV$^{-1/2}$)	DOCUMENT ID		TECN	COMMENT
−0.209±0.023	[1] HUNT	19	DPWA	Multichannel
0.150±0.080	SOKHOYAN	15A	DPWA	Multichannel
• • • We do not use the following data for averages, fits, limits, etc. • • •				
0.150±0.080	GUTZ	14	DPWA	Multichannel

[1] Statistical error only.

$\Delta(1940)$ REFERENCES

HUNT	19	PR C99 055205	B.C. Hunt, D.M. Manley	
SOKHOYAN	15A	EPJ A51 95	V. Sokhoyan *et al.*	(CBELSA/TAPS Collab.)
GUTZ	14	EPJ A50 74	E. Gutz *et al.*	(CBELSA/TAPS Collab.)
SVARC	14	PR C89 045205	A. Svarc *et al.*	(RBI Zagreb, UNI Tuzla)
ANISOVICH	12A	EPJ A48 15	A.V. Anisovich *et al.*	(BONN, PNPI)
HORN	08A	EPJ A38 173	I. Horn *et al.*	(CB-ELSA Collab.)
Also		PRL 101 202002	I. Horn *et al.*	(CB-ELSA Collab.)
CUTKOSKY	80	Toronto Conf. 19	R.E. Cutkosky *et al.*	(CMU, LBL) IJP
Also		PR D20 2839	R.E. Cutkosky *et al.*	(CMU, LBL)
HOEHLER	79	PDAT 12-1	G. Hohler *et al.*	(KARLT)

$\Delta(1950)\ 7/2^+$

$I(J^P) = \frac{3}{2}(\frac{7}{2}^+)$ Status: ****

Older and obsolete values are listed and referenced in the 2014 edition, Chinese Physics **C38** 070001 (2014).

$\Delta(1950)$ POLE POSITION

REAL PART

VALUE (MeV)	DOCUMENT ID		TECN	COMMENT
1870 to 1890 (≈ 1880) OUR ESTIMATE				
1888± 4	SOKHOYAN	15A	DPWA	Multichannel
1877± 2±1	[1] SVARC	14	L+P	$\pi N \to \pi N$
1890±15	CUTKOSKY	80	IPWA	$\pi N \to \pi N$
• • • We do not use the following data for averages, fits, limits, etc. • • •				
1871	HUNT	19	DPWA	Multichannel
1874	ROENCHEN	15A	DPWA	Multichannel
1888± 4	GUTZ	14	DPWA	Multichannel
1890± 4	ANISOVICH	12A	DPWA	Multichannel
1876	ARNDT	06	DPWA	$\pi N \to \pi N, \eta N$
1910	VRANA	00	DPWA	Multichannel
1878	HOEHLER	93	ARGD	$\pi N \to \pi N$

[1] Fit to the amplitudes of HOEHLER 79.

−2×IMAGINARY PART

VALUE (MeV)	DOCUMENT ID		TECN	COMMENT
220 to 260 (≈ 240) OUR ESTIMATE				
245± 8	SOKHOYAN	15A	DPWA	Multichannel
223± 4±1	[1] SVARC	14	L+P	$\pi N \to \pi N$
260±40	CUTKOSKY	80	IPWA	$\pi N \to \pi N$
• • • We do not use the following data for averages, fits, limits, etc. • • •				
206	HUNT	19	DPWA	Multichannel
239	ROENCHEN	15A	DPWA	Multichannel
245± 8	GUTZ	14	DPWA	Multichannel
243± 8	ANISOVICH	12A	DPWA	Multichannel
227	ARNDT	06	DPWA	$\pi N \to \pi N, \eta N$
230	VRANA	00	DPWA	Multichannel
230	HOEHLER	93	ARGD	$\pi N \to \pi N$

[1] Fit to the amplitudes of HOEHLER 79.

$\Delta(1950)$ ELASTIC POLE RESIDUE

MODULUS $|r|$

VALUE (MeV)	DOCUMENT ID		TECN	COMMENT
44 to 60 (≈ 52) OUR ESTIMATE				
58±2	SOKHOYAN	15A	DPWA	Multichannel
44±1	[1] SVARC	14	L+P	$\pi N \to \pi N$
50±7	CUTKOSKY	80	IPWA	$\pi N \to \pi N$
• • • We do not use the following data for averages, fits, limits, etc. • • •				
56	ROENCHEN	15A	DPWA	Multichannel
58±2	GUTZ	14	DPWA	Multichannel
58±2	ANISOVICH	12A	DPWA	Multichannel
53	ARNDT	06	DPWA	$\pi N \to \pi N, \eta N$
47	HOEHLER	93	ARGD	$\pi N \to \pi N$

[1] Fit to the amplitudes of HOEHLER 79.

PHASE θ

VALUE (°)	DOCUMENT ID		TECN	COMMENT
−40 to −24 (≈ −32) OUR ESTIMATE				
−24±3	SOKHOYAN	15A	DPWA	Multichannel
−39±1±1	[1] SVARC	14	L+P	$\pi N \to \pi N$
−33±8	CUTKOSKY	80	IPWA	$\pi N \to \pi N$
• • • We do not use the following data for averages, fits, limits, etc. • • •				
−33	ROENCHEN	15A	DPWA	Multichannel
−24±3	GUTZ	14	DPWA	Multichannel
−24±3	ANISOVICH	12A	DPWA	Multichannel
−31	ARNDT	06	DPWA	$\pi N \to \pi N, \eta N$
−32	HOEHLER	93	ARGD	$\pi N \to \pi N$

[1] Fit to the amplitudes of HOEHLER 79.

$\Delta(1950)$ INELASTIC POLE RESIDUE

The "normalized residue" is the residue divided by $\Gamma_{pole}/2$.

Normalized residue in $N\pi \to \Delta(1950) \to \Sigma K$

MODULUS	PHASE (°)	DOCUMENT ID		TECN	COMMENT
0.05 ±0.01	−65 ± 25	ANISOVICH	12A	DPWA	Multichannel
• • • We do not use the following data for averages, fits, limits, etc. • • •					
0.031	−87	ROENCHEN	15A	DPWA	Multichannel

Normalized residue in $N\pi \to \Delta(1950) \to \Delta\pi$, F-wave

MODULUS	PHASE (°)	DOCUMENT ID		TECN	COMMENT
0.12±0.04	undefined	SOKHOYAN	15A	DPWA	Multichannel
• • • We do not use the following data for averages, fits, limits, etc. • • •					
0.54	131	ROENCHEN	15A	DPWA	Multichannel
0.12±0.04	12 ± 10	ANISOVICH	12A	DPWA	Multichannel

Normalized residue in $N\pi \to \Delta(1950) \to \Delta\pi$, H-wave

MODULUS	PHASE (°)	DOCUMENT ID		TECN	COMMENT
• • • We do not use the following data for averages, fits, limits, etc. • • •					
0.033	−97	ROENCHEN	15A	DPWA	Multichannel

Normalized residue in $N\pi \to \Delta(1950) \to \Delta(1232)\eta$

MODULUS	PHASE (°)	DOCUMENT ID		TECN	COMMENT
0.035±0.005	90 ± 25	GUTZ	14	DPWA	Multichannel

$\Delta(1950)$ BREIT-WIGNER MASS

VALUE (MeV)	DOCUMENT ID		TECN	COMMENT
1915 to 1950 (≈ 1930) OUR ESTIMATE				
1943 ±18	GOLOVATCH	19	DPWA	$\gamma p \to \pi^+\pi^- p$
1913 ± 4	[1] HUNT	19	DPWA	Multichannel
1917 ± 4	ANISOVICH	17	DPWA	Multichannel
1921.3± 0.2	[1] ARNDT	06	DPWA	$\pi N \to \pi N, \eta N$
1950 ±15	CUTKOSKY	80	IPWA	$\pi N \to \pi N$
1913 ± 8	HOEHLER	79	IPWA	$\pi N \to \pi N$
• • • We do not use the following data for averages, fits, limits, etc. • • •				
1917 ± 4	SOKHOYAN	15A	DPWA	Multichannel
1917 ± 4	GUTZ	14	DPWA	Multichannel
1915 ± 6	ANISOVICH	12A	DPWA	Multichannel
1918 ± 1	[1] SHRESTHA	12A	DPWA	Multichannel
1936 ± 5	VRANA	00	DPWA	Multichannel

Downloaded from https://academic.oup.com/ptep/article/2022/8/083C01/6651666 by KIT Library user on 27 September 2022

[1] Statistical error only.

$\Delta(1950)$ BREIT-WIGNER WIDTH

VALUE (MeV)	DOCUMENT ID		TECN	COMMENT
235 to 335 (≈ 285) OUR ESTIMATE				
230 ±88	GOLOVATCH	19	DPWA	$\gamma p \to \pi^+\pi^- p$
241 ±10	[1] HUNT	19	DPWA	Multichannel
251 ± 8	ANISOVICH	17	DPWA	Multichannel
271.1 ± 1.1	[1] ARNDT	06	DPWA	$\pi N \to \pi N, \eta N$
340 ±50	CUTKOSKY	80	IPWA	$\pi N \to \pi N$
224 ±10	HOEHLER	79	IPWA	$\pi N \to \pi N$
• • • We do not use the following data for averages, fits, limits, etc. • • •				
251 ± 8	SOKHOYAN	15A	DPWA	Multichannel
251 ± 8	GUTZ	14	DPWA	Multichannel
246 ±10	ANISOVICH	12A	DPWA	Multichannel
259 ± 4	[1] SHRESTHA	12A	DPWA	Multichannel
245 ±12	VRANA	00	DPWA	Multichannel

[1] Statistical error only.

$\Delta(1950)$ DECAY MODES

The following branching fractions are our estimates, not fits or averages.

	Mode	Fraction (Γ_i/Γ)
Γ_1	$N\pi$	35–45 %
Γ_2	ΣK	0.3–0.5 %
Γ_3	$N\pi\pi$	37–77 %
Γ_4	$\Delta(1232)\pi$, F-wave	1–9 %
Γ_5	$N(1680)\pi$, P-wave	3–9 %
Γ_6	$\Delta(1232)\eta$	< 0.6 %
Γ_7	$N\gamma$	0.06–0.14 %
Γ_8	$N\gamma$, helicity=1/2	0.03–0.05 %
Γ_9	$N\gamma$, helicity=3/2	0.04–0.09 %

$\Delta(1950)$ BRANCHING RATIOS

$\Gamma(N\pi)/\Gamma_{total}$ — Γ_1/Γ

VALUE (%)	DOCUMENT ID		TECN	COMMENT
35–45 % OUR ESTIMATE				
38 ±2	[1] HUNT	19	DPWA	Multichannel
46 ±2	ANISOVICH	17	DPWA	Multichannel
47.1 ±0.1	[1] ARNDT	06	DPWA	$\pi N \to \pi N, \eta N$
39 ±4	CUTKOSKY	80	IPWA	$\pi N \to \pi N$
38 ±2	HOEHLER	79	IPWA	$\pi N \to \pi N$
• • • We do not use the following data for averages, fits, limits, etc. • • •				
0.046±0.002	SOKHOYAN	15A	DPWA	Multichannel
46 ±2	GUTZ	14	DPWA	Multichannel
45 ±2	ANISOVICH	12A	DPWA	Multichannel
45.6 ±0.4	[1] SHRESTHA	12A	DPWA	Multichannel
44 ±1	VRANA	00	DPWA	Multichannel

[1] Statistical error only.

$\Gamma(N\pi\pi)/\Gamma_{total}$ — Γ_3/Γ

VALUE (%)	DOCUMENT ID		TECN	COMMENT
57±20	GOLOVATCH	19	DPWA	$\gamma p \to \pi^+\pi^- p$

$\Gamma(\Sigma K)/\Gamma_{total}$ — Γ_2/Γ

VALUE (%)	DOCUMENT ID		TECN	COMMENT
0.6±0.2	ANISOVICH	17	DPWA	Multichannel
• • • We do not use the following data for averages, fits, limits, etc. • • •				
0.4±0.1	ANISOVICH	12A	DPWA	Multichannel

$\Gamma(\Delta(1232)\pi, F\text{-wave})/\Gamma_{total}$ — Γ_4/Γ

VALUE (%)	DOCUMENT ID		TECN	COMMENT
5 ±3	ANISOVICH	17	DPWA	Multichannel
8 ±1	[1] SHRESTHA	12A	DPWA	Multichannel
• • • We do not use the following data for averages, fits, limits, etc. • • •				
5 ±4	SOKHOYAN	15A	DPWA	Multichannel
2.8±1.4	ANISOVICH	12A	DPWA	Multichannel
36 ±1	VRANA	00	DPWA	Multichannel

[1] Statistical error only.

$\Gamma(N(1680)\pi, P\text{-wave})/\Gamma_{total}$ — Γ_5/Γ

VALUE (%)	DOCUMENT ID		TECN	COMMENT
6±3	SOKHOYAN	15A	DPWA	Multichannel

$\Gamma(\Delta(1232)\eta)/\Gamma_{total}$ — Γ_6/Γ

VALUE (%)	DOCUMENT ID		TECN	COMMENT
0.3±0.3	ANISOVICH	17	DPWA	Multichannel
• • • We do not use the following data for averages, fits, limits, etc. • • •				
<1	GUTZ	14	DPWA	Multichannel

$\Delta(1950)$ PHOTON DECAY AMPLITUDES AT THE POLE

$\Delta(1950) \to N\gamma$, helicity-1/2 amplitude $A_{1/2}$

MODULUS ($GeV^{-1/2}$)	PHASE (°)	DOCUMENT ID		TECN	COMMENT
−0.067±0.004	−10 ± 5	SOKHOYAN	15A	DPWA	Multichannel
−0.071±0.004	-14^{+2}_{-4}	ROENCHEN	14	DPWA	
• • • We do not use the following data for averages, fits, limits, etc. • • •					
−0.068	−19	ROENCHEN	15A	DPWA	Multichannel

$\Delta(1950) \to N\gamma$, helicity-3/2 amplitude $A_{3/2}$

MODULUS ($GeV^{-1/2}$)	PHASE (°)	DOCUMENT ID		TECN	COMMENT
−0.095±0.004	−10 ± 5	SOKHOYAN	15A	DPWA	Multichannel
$-0.089^{+0.008}_{-0.007}$	-10^{+3}_{-1}	ROENCHEN	14	DPWA	
• • • We do not use the following data for averages, fits, limits, etc. • • •					
−0.084	−19	ROENCHEN	15A	DPWA	Multichannel

$\Delta(1950)$ BREIT-WIGNER PHOTON DECAY AMPLITUDES

$\Delta(1950) \to N\gamma$, helicity-1/2 amplitude $A_{1/2}$

VALUE ($GeV^{-1/2}$)	DOCUMENT ID		TECN	COMMENT
−0.075 to −0.065 (≈ −0.070) OUR ESTIMATE				
−0.0698±0.0141	GOLOVATCH	19	DPWA	$\gamma p \to \pi^+\pi^- p$
−0.047 ±0.002	[1] HUNT	19	DPWA	Multichannel
−0.067 ±0.005	ANISOVICH	17	DPWA	Multichannel
−0.083 ±0.004	WORKMAN	12A	DPWA	$\gamma N \to N\pi$
• • • We do not use the following data for averages, fits, limits, etc. • • •				
−0.067 ±0.005	SOKHOYAN	15A	DPWA	Multichannel
−0.067 ±0.005	GUTZ	14	DPWA	Multichannel
−0.071 ±0.004	ANISOVICH	12A	DPWA	Multichannel
−0.065 ±0.001	[1] SHRESTHA	12A	DPWA	Multichannel
−0.094	DRECHSEL	07	DPWA	$\gamma N \to \pi N$

[1] Statistical error only.

$\Delta(1950) \to N\gamma$, helicity-3/2 amplitude $A_{3/2}$

VALUE ($GeV^{-1/2}$)	DOCUMENT ID		TECN	COMMENT
−0.100 to −0.080 (≈ −0.090) OUR ESTIMATE				
−0.1181±0.0193	GOLOVATCH	19	DPWA	$\gamma p \to \pi^+\pi^- p$
−0.074 ±0.002	[1] HUNT	19	DPWA	Multichannel
−0.094 ±0.004	ANISOVICH	17	DPWA	Multichannel
−0.096 ±0.004	WORKMAN	12A	DPWA	$\gamma N \to N\pi$
• • • We do not use the following data for averages, fits, limits, etc. • • •				
−0.094 ±0.004	SOKHOYAN	15A	DPWA	Multichannel
−0.094 ±0.004	GUTZ	14	DPWA	Multichannel
−0.094 ±0.005	ANISOVICH	12A	DPWA	Multichannel
−0.083 ±0.001	[1] SHRESTHA	12A	DPWA	Multichannel
−0.121	DRECHSEL	07	DPWA	$\gamma N \to \pi N$

[1] Statistical error only.

$\Delta(1950)$ REFERENCES

GOLOVATCH	19	PL B788 371	E. Golovatch *et al.*	(CLAS Collab.)
HUNT	19	PR C99 055205	B.C. Hunt, D.M. Manley	
ANISOVICH	17	PL B766 357	A.V. Anisovich *et al.*	
ROENCHEN	15A	EPJ A51 70	D. Roenchen *et al.*	
SOKHOYAN	15A	EPJ A51 95	V. Sokhoyan *et al.*	(CBELSA/TAPS Collab.)
GUTZ	14	EPJ A50 74	E. Gutz *et al.*	(CBELSA/TAPS Collab.)
PDG	14	CP C38 070001	K. Olive *et al.*	(PDG Collab.)
ROENCHEN	14	EPJ A50 101	D. Roenchen *et al.*	
Also		EPJ A51 63 (errat.)	D. Roenchen *et al.*	
SVARC	14	PR C89 045205	A. Svarc *et al.*	(RBI Zagreb, UNI Tuzla)
ANISOVICH	12A	EPJ A48 15	A.V. Anisovich *et al.*	(BONN, PNPI)
SHRESTHA	12A	PR C86 055203	M. Shrestha, D.M. Manley	(KSU)
WORKMAN	12A	PR C86 015202	R. Workman *et al.*	(GWU)
DRECHSEL	07	EPJ A34 69	D. Drechsel, S.S. Kamalov, L. Tiator	(MAINZ, JINR)
ARNDT	06	PR C74 045205	R.A. Arndt *et al.*	(GWU)
VRANA	00	PRPL 328 181	T.P. Vrana, S.A. Dytman, T.-S.H. Lee	(PITT, ANL)
HOEHLER	93	πN Newsletter 9 1	G. Hohler	(KARL)
CUTKOSKY	80	Toronto Conf. 19	R.E. Cutkosky *et al.*	(CMU, LBL) IJP
Also		PR D20 2839	R.E. Cutkosky *et al.*	(CMU, LBL) IJP
HOEHLER	79	PDAT 12-1	G. Hohler *et al.*	(KARLT) IJP
Also		Toronto Conf. 3	R. Koch	(KARLT) IJP

$\Delta(2000)\ 5/2^+$

$I(J^P) = \frac{3}{2}(\frac{5}{2}^+)$ Status: **

OMITTED FROM SUMMARY TABLE

$\Delta(2000)$ POLE POSITION

REAL PART

VALUE (MeV)	DOCUMENT ID		TECN	COMMENT
1998± 4±4	[1] SVARC	14	L+P	$\pi N \to \pi N$
1976	SHRESTHA	12A	DPWA	Multichannel
2150±100	CUTKOSKY	80	IPWA	$\pi N \to \pi N$
• • • We do not use the following data for averages, fits, limits, etc. • • •				
1697	VRANA	00	DPWA	Multichannel

[1] Fit to the amplitudes of HOEHLER 79.

Downloaded from https://academic.oup.com/ptep/article/2022/8/083C01/6651666 by KIT Library user on 27 September 2022

−2×IMAGINARY PART

VALUE (MeV)	DOCUMENT ID		TECN	COMMENT
404± 10±4	[1] SVARC	14	L+P	$\pi N \to \pi N$
350±100	CUTKOSKY	80	IPWA	$\pi N \to \pi N$
• • • We do not use the following data for averages, fits, limits, etc. • • •				
488	SHRESTHA	12A	DPWA	Multichannel
112	VRANA	00	DPWA	Multichannel

[1] Fit to the amplitudes of HOEHLER 79.

$\Delta(2000)$ ELASTIC POLE RESIDUE

MODULUS $|r|$

VALUE (MeV)	DOCUMENT ID		TECN	COMMENT
34±1±1	[1] SVARC	14	L+P	$\pi N \to \pi N$
16±5	CUTKOSKY	80	IPWA	$\pi N \to \pi N$

[1] Fit to the amplitudes of HOEHLER 79.

PHASE θ

VALUE (°)	DOCUMENT ID		TECN	COMMENT
110± 1±3	[1] SVARC	14	L+P	$\pi N \to \pi N$
150±90	CUTKOSKY	80	IPWA	$\pi N \to \pi N$

[1] Fit to the amplitudes of HOEHLER 79.

$\Delta(2000)$ BREIT-WIGNER MASS

VALUE (MeV)	DOCUMENT ID		TECN	COMMENT
2015± 24	[1] SHRESTHA	12A	DPWA	Multichannel
2200±125	CUTKOSKY	80	IPWA	$\pi N \to \pi N$
• • • We do not use the following data for averages, fits, limits, etc. • • •				
1724± 61	VRANA	00	DPWA	Multichannel
1752± 32	MANLEY	92	IPWA	$\pi N \to \pi N$ & $N\pi\pi$

[1] Statistical error only.

$\Delta(2000)$ BREIT-WIGNER WIDTH

VALUE (MeV)	DOCUMENT ID		TECN	COMMENT
500± 52	[1] SHRESTHA	12A	DPWA	Multichannel
400±125	CUTKOSKY	80	IPWA	$\pi N \to \pi N$
• • • We do not use the following data for averages, fits, limits, etc. • • •				
138± 68	VRANA	00	DPWA	Multichannel
251± 93	MANLEY	92	IPWA	$\pi N \to \pi N$ & $N\pi\pi$

[1] Statistical error only.

$\Delta(2000)$ DECAY MODES

	Mode	Fraction (Γ_i/Γ)
Γ_1	$N\pi$	3–11 %
Γ_2	$N\pi\pi$	>87 %
Γ_3	$\Delta(1232)\pi$	<9 %
Γ_4	$\Delta(1232)\pi$, P-wave	<6 %
Γ_5	$\Delta(1232)\pi$, F-wave	<3 %
Γ_6	$N\rho$, S=3/2, P-wave	seen
Γ_7	$N\gamma$	
Γ_8	$N\gamma$, helicity=1/2	seen
Γ_9	$N\gamma$, helicity=3/2	seen

$\Delta(2000)$ BRANCHING RATIOS

$\Gamma(N\pi)/\Gamma_{total}$ — Γ_1/Γ

VALUE (%)	DOCUMENT ID		TECN	COMMENT
7±1	[1] SHRESTHA	12A	DPWA	Multichannel
7±4	CUTKOSKY	80	IPWA	$\pi N \to \pi N$
• • • We do not use the following data for averages, fits, limits, etc. • • •				
0±1	VRANA	00	DPWA	Multichannel
2±1	MANLEY	92	IPWA	$\pi N \to \pi N$ & $N\pi\pi$

[1] Statistical error only.

$\Gamma(\Delta(1232)\pi, P\text{-wave})/\Gamma_{total}$ — Γ_4/Γ

VALUE (%)	DOCUMENT ID		TECN	COMMENT
3±3	[1] SHRESTHA	12A	DPWA	Multichannel
• • • We do not use the following data for averages, fits, limits, etc. • • •				
0±1	VRANA	00	DPWA	Multichannel

[1] Statistical error only.

$\Gamma(\Delta(1232)\pi, F\text{-wave})/\Gamma_{total}$ — Γ_5/Γ

VALUE (%)	DOCUMENT ID		TECN	COMMENT
< 3	SHRESTHA	12A	DPWA	Multichannel
• • • We do not use the following data for averages, fits, limits, etc. • • •				
40±1	VRANA	00	DPWA	Multichannel

$\Gamma(N\rho, S=3/2, P\text{-wave})/\Gamma_{total}$ — Γ_6/Γ

VALUE (%)	DOCUMENT ID		TECN	COMMENT
90± 3	[1] SHRESTHA	12A	DPWA	Multichannel
• • • We do not use the following data for averages, fits, limits, etc. • • •				
60±60	VRANA	00	DPWA	Multichannel

[1] Statistical error only.

$\Delta(2000)$ BREIT-WIGNER PHOTON DECAY AMPLITUDES

$\Delta(2000) \to p\gamma$, helicity-1/2 amplitude $A_{1/2}$

VALUE (GeV$^{-1/2}$)	DOCUMENT ID		TECN	COMMENT
• • • We do not use the following data for averages, fits, limits, etc. • • •				
−0.061±0.018	[1] SHRESTHA	12A	DPWA	Multichannel

[1] Statistical error only.

$\Delta(2000) \to p\gamma$, helicity-3/2 amplitude $A_{3/2}$

VALUE (GeV$^{-1/2}$)	DOCUMENT ID		TECN	COMMENT
• • • We do not use the following data for averages, fits, limits, etc. • • •				
0.158±0.032	[1] SHRESTHA	12A	DPWA	Multichannel

[1] Statistical error only.

$\Delta(2000)$ REFERENCES

SVARC	14	PR C89 045205	A. Svarc *et al.*	(RBI Zagreb, UNI Tuzla)
SHRESTHA	12A	PR C86 055203	M. Shrestha, D.M. Manley	(KSU)
VRANA	00	PRPL 328 181	T.P. Vrana, S.A. Dytman, T.-S.H. Lee	(PITT, ANL)
MANLEY	92	PR D45 4002	D.M. Manley, E.M. Saleski	(KSA) IJP
Also		PR D30 904	D.M. Manley *et al.*	(VPI)
CUTKOSKY	80	Toronto Conf. 19	R.E. Cutkosky *et al.*	(CMU, LBL)
Also		PR D20 2839	R.E. Cutkosky *et al.*	(CMU, LBL)
HOEHLER	79	PDAT 12-1	G. Hohler *et al.*	(KARLT)

$\Delta(2150)$ $1/2^-$

$I(J^P) = \frac{3}{2}(\frac{1}{2}^-)$ Status: *

OMITTED FROM SUMMARY TABLE

$\Delta(2150)$ POLE POSITION

REAL PART

VALUE (MeV)	DOCUMENT ID		TECN	COMMENT
2140±80	CUTKOSKY	80	IPWA	$\pi N \to \pi N$

−2×IMAGINARY PART

VALUE (MeV)	DOCUMENT ID		TECN	COMMENT
200±80	CUTKOSKY	80	IPWA	$\pi N \to \pi N$

$\Delta(2150)$ ELASTIC POLE RESIDUE

MODULUS $|r|$

VALUE (MeV)	DOCUMENT ID		TECN	COMMENT
7±2	CUTKOSKY	80	IPWA	$\pi N \to \pi N$

PHASE θ

VALUE (°)	DOCUMENT ID		TECN	COMMENT
−60±90	CUTKOSKY	80	IPWA	$\pi N \to \pi N$

$\Delta(2150)$ BREIT-WIGNER MASS

VALUE (MeV)	DOCUMENT ID		TECN	COMMENT
2150±100	CUTKOSKY	80	IPWA	$\pi N \to \pi N$

$\Delta(2150)$ BREIT-WIGNER WIDTH

VALUE (MeV)	DOCUMENT ID		TECN	COMMENT
200±100	CUTKOSKY	80	IPWA	$\pi N \to \pi N$

$\Delta(2150)$ DECAY MODES

	Mode	Fraction (Γ_i/Γ)
Γ_1	$N\pi$	6–10 %

$\Delta(2150)$ BRANCHING RATIOS

$\Gamma(N\pi)/\Gamma_{total}$ — Γ_1/Γ

VALUE (%)	DOCUMENT ID		TECN	COMMENT
8±2	CUTKOSKY	80	IPWA	$\pi N \to \pi N$

$\Delta(2150)$ REFERENCES

CUTKOSKY	80	Toronto Conf. 19	R.E. Cutkosky *et al.*	(CMU, LBL) IJP
Also		PR D20 2839	R.E. Cutkosky *et al.*	(CMU, LBL)

Downloaded from https://academic.oup.com/ptep/article/2022/8/083C01/6651666 by KIT Library user on 27 September 2022

Δ(2200) 7/2⁻

$I(J^P) = \frac{3}{2}(\frac{7}{2}^-)$ Status: ***

Δ(2200) POLE POSITION

REAL PART

VALUE (MeV)	DOCUMENT ID		TECN	COMMENT
2050 to 2150 (≈ 2100) OUR ESTIMATE				
2100±50	CUTKOSKY	80	IPWA	$\pi N \to \pi N$
• • • We do not use the following data for averages, fits, limits, etc. • • •				
2142	ROENCHEN	15A	DPWA	Multichannel

−2×IMAGINARY PART

VALUE (MeV)	DOCUMENT ID		TECN	COMMENT
260 to 420 (≈ 340) OUR ESTIMATE				
340±80	CUTKOSKY	80	IPWA	$\pi N \to \pi N$
• • • We do not use the following data for averages, fits, limits, etc. • • •				
486	ROENCHEN	15A	DPWA	Multichannel

Δ(2200) ELASTIC POLE RESIDUE

MODULUS |r|

VALUE (MeV)	DOCUMENT ID		TECN	COMMENT
8±3	CUTKOSKY	80	IPWA	$\pi N \to \pi N$
• • • We do not use the following data for averages, fits, limits, etc. • • •				
17	ROENCHEN	15A	DPWA	Multichannel

PHASE θ

VALUE (°)	DOCUMENT ID		TECN	COMMENT
−70±40	CUTKOSKY	80	IPWA	$\pi N \to \pi N$
• • • We do not use the following data for averages, fits, limits, etc. • • •				
−56	ROENCHEN	15A	DPWA	Multichannel

Δ(2200) INELASTIC POLE RESIDUE

The "normalized residue" is the residue divided by $\Gamma_{pole}/2$.

Normalized residue in $N\pi \to \Delta(2200) \to \Sigma K$

MODULUS	PHASE (°)	DOCUMENT ID		TECN	COMMENT
• • • We do not use the following data for averages, fits, limits, etc. • • •					
0.005	−103	ROENCHEN	15A	DPWA	Multichannel

Normalized residue in $N\pi \to \Delta(2200) \to \Delta\pi$, D-wave

MODULUS	PHASE (°)	DOCUMENT ID		TECN	COMMENT
• • • We do not use the following data for averages, fits, limits, etc. • • •					
0.23	107	ROENCHEN	15A	DPWA	Multichannel

Normalized residue in $N\pi \to \Delta(2200) \to \Delta\pi$, G-wave

MODULUS	PHASE (°)	DOCUMENT ID		TECN	COMMENT
• • • We do not use the following data for averages, fits, limits, etc. • • •					
0.022	−151	ROENCHEN	15A	DPWA	Multichannel

Δ(2200) BREIT-WIGNER MASS

VALUE (MeV)	DOCUMENT ID		TECN	COMMENT
2150 to 2250 (≈ 2200) OUR ESTIMATE				
2176±40	ANISOVICH	17	DPWA	Multichannel
2200±80	CUTKOSKY	80	IPWA	$\pi N \to \pi N$
2215±60	HOEHLER	79	IPWA	$\pi N \to \pi N$

Δ(2200) BREIT-WIGNER WIDTH

VALUE (MeV)	DOCUMENT ID		TECN	COMMENT
200 to 500 (≈ 350) OUR ESTIMATE				
210± 70	ANISOVICH	17	DPWA	Multichannel
450±100	CUTKOSKY	80	IPWA	$\pi N \to \pi N$
400±100	HOEHLER	79	IPWA	$\pi N \to \pi N$

Δ(2200) DECAY MODES

	Mode	Fraction (Γ_i/Γ)
Γ_1	$N\pi$	2–8 %
Γ_2	ΣK	1–7 %
Γ_3	$N\pi\pi$	>45 %
Γ_4	$\Delta\pi$	>45 %
Γ_5	$\Delta\pi$, D-wave	>40 %
Γ_6	$\Delta\pi$, G-wave	5–25 %
Γ_7	$\Delta\eta$	
Γ_8	$\Delta\eta$, D-wave	seen

Δ(2200) BRANCHING RATIOS

$\Gamma(N\pi)/\Gamma_{total}$ — Γ_1/Γ

VALUE (%)	DOCUMENT ID		TECN	COMMENT
2–8 % OUR ESTIMATE				
3.5±1.5	ANISOVICH	17	DPWA	Multichannel
6 ±2	CUTKOSKY	80	IPWA	$\pi N \to \pi N$
5 ±2	HOEHLER	79	IPWA	$\pi N \to \pi N$

$\Gamma(\Sigma K)/\Gamma_{total}$ — Γ_2/Γ

VALUE	DOCUMENT ID		TECN	COMMENT
0.04±0.03	ANISOVICH	17	DPWA	Multichannel

$\Gamma(\Delta\pi, D\text{-wave})/\Gamma_{total}$ — Γ_5/Γ

VALUE	DOCUMENT ID		TECN	COMMENT
>40 % OUR ESTIMATE				
0.70±0.30	ANISOVICH	17	DPWA	Multichannel

$\Gamma(\Delta\pi, G\text{-wave})/\Gamma_{total}$ — Γ_6/Γ

VALUE	DOCUMENT ID		TECN	COMMENT
0.15±0.10	ANISOVICH	17	DPWA	Multichannel

$\Gamma(\Delta\eta, D\text{-wave})/\Gamma_{total}$ — Γ_8/Γ

VALUE	DOCUMENT ID		TECN	COMMENT
∼ 0.01	ANISOVICH	17	DPWA	Multichannel

Δ(2200) PHOTON DECAY AMPLITUDES AT THE POLE

$\Delta(2200) \to N\gamma$, helicity-1/2 amplitude $A_{1/2}$

MODULUS ($GeV^{-1/2}$)	PHASE (°)	DOCUMENT ID		TECN	COMMENT
$0.107^{+0.011}_{-0.020}$	−36 ± 5	ROENCHEN	14	DPWA	
• • • We do not use the following data for averages, fits, limits, etc. • • •					
0.106	−23	ROENCHEN	15A	DPWA	Multichannel

$\Delta(2200) \to N\gamma$, helicity-3/2 amplitude $A_{3/2}$

MODULUS ($GeV^{-1/2}$)	PHASE (°)	DOCUMENT ID		TECN	COMMENT
$-0.131^{+0.024}_{-0.009}$	113^{+9}_{-5}	ROENCHEN	14	DPWA	
• • • We do not use the following data for averages, fits, limits, etc. • • •					
0.157	−60	ROENCHEN	15A	DPWA	Multichannel

Δ(2200) REFERENCES

ANISOVICH	17	PL B766 357	A.V. Anisovich *et al.*	
ROENCHEN	15A	EPJ A51 70	D. Roenchen *et al.*	
ROENCHEN	14	EPJ A50 101	D. Roenchen *et al.*	
Also		EPJ A51 63 (errat.)	D. Roenchen *et al.*	
CUTKOSKY	80	Toronto Conf. 19	R.E. Cutkosky *et al.*	(CMU, LBL) IJP
Also		PR D20 2839	R.E. Cutkosky *et al.*	(CMU, LBL) IJP
HOEHLER	79	PDAT 12-1	G. Höhler *et al.*	(KARLT) IJP
Also		Toronto Conf. 3	R. Koch	(KARLT) IJP

Δ(2300) 9/2⁺

$I(J^P) = \frac{3}{2}(\frac{9}{2}^+)$ Status: **

OMITTED FROM SUMMARY TABLE

Δ(2300) POLE POSITION

REAL PART

VALUE (MeV)	DOCUMENT ID		TECN	COMMENT
2370±80	CUTKOSKY	80	IPWA	$\pi N \to \pi N$

−2×IMAGINARY PART

VALUE (MeV)	DOCUMENT ID		TECN	COMMENT
420±160	CUTKOSKY	80	IPWA	$\pi N \to \pi N$

Δ(2300) ELASTIC POLE RESIDUE

MODULUS |r|

VALUE (MeV)	DOCUMENT ID		TECN	COMMENT
10±4	CUTKOSKY	80	IPWA	$\pi N \to \pi N$

PHASE θ

VALUE (°)	DOCUMENT ID		TECN	COMMENT
−20±30	CUTKOSKY	80	IPWA	$\pi N \to \pi N$

Δ(2300) BREIT-WIGNER MASS

VALUE (MeV)	DOCUMENT ID		TECN	COMMENT
2400±125	CUTKOSKY	80	IPWA	$\pi N \to \pi N$
2217± 80	HOEHLER	79	IPWA	$\pi N \to \pi N$

Δ(2300) BREIT-WIGNER WIDTH

VALUE (MeV)	DOCUMENT ID		TECN	COMMENT
425±150	CUTKOSKY	80	IPWA	$\pi N \to \pi N$
300±100	HOEHLER	79	IPWA	$\pi N \to \pi N$

Downloaded from https://academic.oup.com/ptep/article/2022/8/083C01/6651666 by KIT Library user on 27 September 2022

$\Delta(2300)$ DECAY MODES

	Mode	Fraction (Γ_i/Γ)
Γ_1	$N\pi$	1–8 %

$\Delta(2300)$ BRANCHING RATIOS

$\Gamma(N\pi)/\Gamma_{total}$ — Γ_1/Γ

VALUE (%)	DOCUMENT ID		TECN	COMMENT
6±2	CUTKOSKY	80	IPWA	$\pi N \to \pi N$
3±2	HOEHLER	79	IPWA	$\pi N \to \pi N$

$\Delta(2300)$ REFERENCES

CUTKOSKY 80	Toronto Conf. 19	R.E. Cutkosky *et al.*	(CMU, LBL) IJP
Also	PR D20 2839	R.E. Cutkosky *et al.*	(CMU, LBL)
HOEHLER 79	PDAT 12-1	G. Hohler *et al.*	(KARLT) IJP
Also	Toronto Conf. 3	R. Koch	(KARLT) IJP

$\Delta(2350)\ 5/2^-$

$I(J^P) = \frac{3}{2}(\frac{5}{2}^-)$ Status: *

OMITTED FROM SUMMARY TABLE

$\Delta(2350)$ POLE POSITION

REAL PART

VALUE (MeV)	DOCUMENT ID		TECN	COMMENT
2400±125	CUTKOSKY	80	IPWA	$\pi N \to \pi N$
• • • We do not use the following data for averages, fits, limits, etc. • • •				
2427	VRANA	00	DPWA	Multichannel

−2×IMAGINARY PART

VALUE (MeV)	DOCUMENT ID		TECN	COMMENT
400±150	CUTKOSKY	80	IPWA	$\pi N \to \pi N$
• • • We do not use the following data for averages, fits, limits, etc. • • •				
458	VRANA	00	DPWA	Multichannel

$\Delta(2350)$ ELASTIC POLE RESIDUE

MODULUS $|r|$

VALUE (MeV)	DOCUMENT ID		TECN	COMMENT
15±8	CUTKOSKY	80	IPWA	$\pi N \to \pi N$

PHASE θ

VALUE (°)	DOCUMENT ID		TECN	COMMENT
−70±70	CUTKOSKY	80	IPWA	$\pi N \to \pi N$

$\Delta(2350)$ BREIT-WIGNER MASS

VALUE (MeV)	DOCUMENT ID		TECN	COMMENT
2400±125	CUTKOSKY	80	IPWA	$\pi N \to \pi N$
2305± 26	HOEHLER	79	IPWA	$\pi N \to \pi N$
• • • We do not use the following data for averages, fits, limits, etc. • • •				
2459±100	VRANA	00	DPWA	Multichannel

$\Delta(2350)$ BREIT-WIGNER WIDTH

VALUE (MeV)	DOCUMENT ID		TECN	COMMENT
400±150	CUTKOSKY	80	IPWA	$\pi N \to \pi N$
300± 70	HOEHLER	79	IPWA	$\pi N \to \pi N$
• • • We do not use the following data for averages, fits, limits, etc. • • •				
480±360	VRANA	00	DPWA	Multichannel

$\Delta(2350)$ DECAY MODES

	Mode	Fraction (Γ_i/Γ)
Γ_1	$N\pi$	4–30 %

$\Delta(2350)$ BRANCHING RATIOS

$\Gamma(N\pi)/\Gamma_{total}$ — Γ_1/Γ

VALUE (%)	DOCUMENT ID		TECN	COMMENT
20±10	CUTKOSKY	80	IPWA	$\pi N \to \pi N$
4± 2	HOEHLER	79	IPWA	$\pi N \to \pi N$
• • • We do not use the following data for averages, fits, limits, etc. • • •				
7±14	VRANA	00	DPWA	Multichannel

$\Delta(2350)$ REFERENCES

VRANA 00	PRPL 328 181	T.P. Vrana, S.A. Dytman, T.-S.H. Lee	(PITT, ANL)
CUTKOSKY 80	Toronto Conf. 19	R.E. Cutkosky *et al.*	(CMU, LBL) IJP
Also	PR D20 2839	R.E. Cutkosky *et al.*	(CMU, LBL)
HOEHLER 79	PDAT 12-1	G. Hohler *et al.*	(KARLT) IJP
Also	Toronto Conf. 3	R. Koch	(KARLT) IJP

$\Delta(2390)\ 7/2^+$

$I(J^P) = \frac{3}{2}(\frac{7}{2}^+)$ Status: *

OMITTED FROM SUMMARY TABLE

$\Delta(2390)$ POLE POSITION

REAL PART

VALUE (MeV)		DOCUMENT ID		TECN	COMMENT
2223± 15±19	[1]	SVARC	14	L+P	$\pi N \to \pi N$
2350±100		CUTKOSKY	80	IPWA	$\pi N \to \pi N$

−2×IMAGINARY PART

VALUE (MeV)		DOCUMENT ID		TECN	COMMENT
431± 26±7	[1]	SVARC	14	L+P	$\pi N \to \pi N$
260±100		CUTKOSKY	80	IPWA	$\pi N \to \pi N$

$\Delta(2390)$ ELASTIC POLE RESIDUE

MODULUS $|r|$

VALUE (MeV)		DOCUMENT ID		TECN	COMMENT
26±2±1	[1]	SVARC	14	L+P	$\pi N \to \pi N$
12±6		CUTKOSKY	80	IPWA	$\pi N \to \pi N$

PHASE θ

VALUE (°)		DOCUMENT ID		TECN	COMMENT
−160± 5±11	[1]	SVARC	14	L+P	$\pi N \to \pi N$
− 90±60		CUTKOSKY	80	IPWA	$\pi N \to \pi N$

$\Delta(2390)$ BREIT-WIGNER MASS

VALUE (MeV)	DOCUMENT ID		TECN	COMMENT
2350±100	CUTKOSKY	80	IPWA	$\pi N \to \pi N$
2425± 60	HOEHLER	79	IPWA	$\pi N \to \pi N$

$\Delta(2390)$ BREIT-WIGNER WIDTH

VALUE (MeV)	DOCUMENT ID		TECN	COMMENT
300±100	CUTKOSKY	80	IPWA	$\pi N \to \pi N$
300± 80	HOEHLER	79	IPWA	$\pi N \to \pi N$

$\Delta(2390)$ DECAY MODES

	Mode	Fraction (Γ_i/Γ)
Γ_1	$N\pi$	3–12 %

$\Delta(2390)$ BRANCHING RATIOS

$\Gamma(N\pi)/\Gamma_{total}$ — Γ_1/Γ

VALUE (%)	DOCUMENT ID		TECN	COMMENT
8±4	CUTKOSKY	80	IPWA	$\pi N \to \pi N$
7±4	HOEHLER	79	IPWA	$\pi N \to \pi N$

$\Delta(2390)$ FOOTNOTES

[1] Fit to the amplitudes of HOEHLER 79.

$\Delta(2390)$ REFERENCES

SVARC 14	PR C89 045205	A. Svarc *et al.*	(RBI Zagreb, UNI Tuzla)
CUTKOSKY 80	Toronto Conf. 19	R.E. Cutkosky *et al.*	(CMU, LBL) IJP
Also	PR D20 2839	R.E. Cutkosky *et al.*	(CMU, LBL)
HOEHLER 79	PDAT 12-1	G. Hohler *et al.*	(KARLT) IJP
Also	Toronto Conf. 3	R. Koch	(KARLT) IJP

$\Delta(2400)\ 9/2^-$

$I(J^P) = \frac{3}{2}(\frac{9}{2}^-)$ Status: **

OMITTED FROM SUMMARY TABLE

$\Delta(2400)$ POLE POSITION

REAL PART

VALUE (MeV)	DOCUMENT ID		TECN	COMMENT
2260±60	CUTKOSKY	80	IPWA	$\pi N \to \pi N$
• • • We do not use the following data for averages, fits, limits, etc. • • •				
1931	ROENCHEN	15A	DPWA	Multichannel
1983	ARNDT	06	DPWA	$\pi N \to \pi N, \eta N$

−2×IMAGINARY PART

VALUE (MeV)	DOCUMENT ID		TECN	COMMENT
320±160	CUTKOSKY	80	IPWA	$\pi N \to \pi N$
• • • We do not use the following data for averages, fits, limits, etc. • • •				
442	ROENCHEN	15A	DPWA	Multichannel
878	ARNDT	06	DPWA	$\pi N \to \pi N, \eta N$

Downloaded from https://academic.oup.com/ptep/article/2022/8/083C01/6651666 by KIT Library user on 27 September 2022

$\Delta(2400)$ ELASTIC POLE RESIDUE

MODULUS $|r|$

VALUE (MeV)	DOCUMENT ID		TECN	COMMENT
8±4	CUTKOSKY	80	IPWA	$\pi N \to \pi N$
• • • We do not use the following data for averages, fits, limits, etc. • • •				
13	ROENCHEN	15A	DPWA	Multichannel
24	ARNDT	06	DPWA	$\pi N \to \pi N, \eta N$

PHASE θ

VALUE (°)	DOCUMENT ID		TECN	COMMENT
− 25±15	CUTKOSKY	80	IPWA	$\pi N \to \pi N$
• • • We do not use the following data for averages, fits, limits, etc. • • •				
− 96	ROENCHEN	15A	DPWA	Multichannel
−139	ARNDT	06	DPWA	$\pi N \to \pi N, \eta N$

$\Delta(2400)$ INELASTIC POLE RESIDUE

The "normalized residue" is the residue divided by $\Gamma_{pole}/2$.

Normalized residue in $N\pi \to \Delta(2400) \to \Sigma K$

MODULUS	PHASE (°)	DOCUMENT ID		TECN	COMMENT
• • • We do not use the following data for averages, fits, limits, etc. • • •					
0.009	25	ROENCHEN	15A	DPWA	Multichannel

Normalized residue in $N\pi \to \Delta(2400) \to \Delta\pi$, G-wave

MODULUS	PHASE (°)	DOCUMENT ID		TECN	COMMENT
• • • We do not use the following data for averages, fits, limits, etc. • • •					
0.18	−110	ROENCHEN	15A	DPWA	Multichannel

Normalized residue in $N\pi \to \Delta(2400) \to \Delta\pi$, I-wave

MODULUS	PHASE (°)	DOCUMENT ID		TECN	COMMENT
• • • We do not use the following data for averages, fits, limits, etc. • • •					
0.012	−1.0	ROENCHEN	15A	DPWA	Multichannel

$\Delta(2400)$ BREIT-WIGNER MASS

VALUE (MeV)	DOCUMENT ID		TECN	COMMENT
2643±141	[1] ARNDT	06	DPWA	$\pi N \to \pi N, \eta N$
2300±100	CUTKOSKY	80	IPWA	$\pi N \to \pi N$
2468± 50	HOEHLER	79	IPWA	$\pi N \to \pi N$

[1] Statistical error only.

$\Delta(2400)$ BREIT-WIGNER WIDTH

VALUE (MeV)	DOCUMENT ID		TECN	COMMENT
895±432	[2] ARNDT	06	DPWA	$\pi N \to \pi N, \eta N$
330±100	CUTKOSKY	80	IPWA	$\pi N \to \pi N$
480±100	HOEHLER	79	IPWA	$\pi N \to \pi N$

[2] Statistical error only.

$\Delta(2400)$ DECAY MODES

	Mode	Fraction (Γ_i/Γ)
Γ_1	$N\pi$	3–9 %

$\Delta(2400)$ BRANCHING RATIOS

$\Gamma(N\pi)/\Gamma_{total}$ — Γ_1/Γ

VALUE (%)	DOCUMENT ID		TECN	COMMENT
6.4±2.2	[3] ARNDT	06	DPWA	$\pi N \to \pi N, \eta N$
5 ±2	CUTKOSKY	80	IPWA	$\pi N \to \pi N$
6 ±3	HOEHLER	79	IPWA	$\pi N \to \pi N$

[3] Statistical error only.

$\Delta(2400)$ PHOTON DECAY AMPLITUDES AT THE POLE

$\Delta(2400) \to N\gamma$, helicity-1/2 amplitude $A_{1/2}$

MODULUS (GeV$^{-1/2}$)	PHASE (°)	DOCUMENT ID		TECN	COMMENT
$-0.128^{+0.046}_{-0.012}$	118^{+24}_{-3}	ROENCHEN	14	DPWA	
• • • We do not use the following data for averages, fits, limits, etc. • • •					
−0.034	63	ROENCHEN	15A	DPWA	Multichannel

$\Delta(2400) \to N\gamma$, helicity-3/2 amplitude $A_{3/2}$

MODULUS (GeV$^{-1/2}$)	PHASE (°)	DOCUMENT ID		TECN	COMMENT
$-0.115^{+0.042}_{-0.024}$	140^{+17}_{-28}	ROENCHEN	14	DPWA	
• • • We do not use the following data for averages, fits, limits, etc. • • •					
0.054	−75	ROENCHEN	15A	DPWA	Multichannel

$\Delta(2400)$ REFERENCES

ROENCHEN	15A	EPJ A51 70	D. Roenchen *et al.*	
ROENCHEN	14	EPJ A50 101	D. Roenchen *et al.*	
Also		EPJ A51 63 (errat.)	D. Roenchen *et al.*	
ARNDT	06	PR C74 045205	R.A. Arndt *et al.*	(GWU)
CUTKOSKY	80	Toronto Conf. 19	R.E. Cutkosky *et al.*	(CMU, LBL) IJP
Also		PR D20 2839	R.E. Cutkosky *et al.*	(CMU, LBL)
HOEHLER	79	PDAT 12-1	G. Hohler *et al.*	(KARLT) IJP
Also		Toronto Conf. 3	R. Koch	(KARLT) IJP

$\Delta(2420)\ 11/2^+$

$I(J^P) = \frac{3}{2}(\frac{11}{2}^+)$ Status: ****

Older and obsolete values are listed and referenced in the 2014 edition, Chinese Physics **C38** 070001 (2014).

$\Delta(2420)$ POLE POSITION

REAL PART

VALUE (MeV)	DOCUMENT ID		TECN	COMMENT
2300 to 2500 (≈ 2400) OUR ESTIMATE				
2454± 4±11	[1] SVARC	14	L+P	$\pi N \to \pi N$
2360±100	CUTKOSKY	80	IPWA	$\pi N \to \pi N$
• • • We do not use the following data for averages, fits, limits, etc. • • •				
2529	ARNDT	06	DPWA	$\pi N \to \pi N, \eta N$
2300	HOEHLER	93	ARGD	$\pi N \to \pi N$

[1] Fit to the amplitudes of HOEHLER 79.

−2×IMAGINARY PART

VALUE (MeV)	DOCUMENT ID		TECN	COMMENT
350 to 550 (≈ 450) OUR ESTIMATE				
462± 8±50	[1] SVARC	14	L+P	$\pi N \to \pi N$
420±100	CUTKOSKY	80	IPWA	$\pi N \to \pi N$
• • • We do not use the following data for averages, fits, limits, etc. • • •				
621	ARNDT	06	DPWA	$\pi N \to \pi N, \eta N$
620	HOEHLER	93	ARGD	$\pi N \to \pi N$

[1] Fit to the amplitudes of HOEHLER 79.

$\Delta(2420)$ ELASTIC POLE RESIDUE

MODULUS $|r|$

VALUE (MeV)	DOCUMENT ID		TECN	COMMENT
20 to 40 (≈ 30) OUR ESTIMATE				
30±1±7	[1] SVARC	14	L+P	$\pi N \to \pi N$
18±6	CUTKOSKY	80	IPWA	$\pi N \to \pi N$
• • • We do not use the following data for averages, fits, limits, etc. • • •				
33	ARNDT	06	DPWA	$\pi N \to \pi N, \eta N$
39	HOEHLER	93	ARGD	$\pi N \to \pi N$

[1] Fit to the amplitudes of HOEHLER 79.

PHASE θ

VALUE (°)	DOCUMENT ID		TECN	COMMENT
−60 to 20 (≈ − 20) OUR ESTIMATE				
11± 1±8	[1] SVARC	14	L+P	$\pi N \to \pi N$
−30±40	CUTKOSKY	80	IPWA	$\pi N \to \pi N$
• • • We do not use the following data for averages, fits, limits, etc. • • •				
−45	ARNDT	06	DPWA	$\pi N \to \pi N, \eta N$
−60	HOEHLER	93	ARGD	$\pi N \to \pi N$

[1] Fit to the amplitudes of HOEHLER 79.

$\Delta(2420)$ BREIT-WIGNER MASS

VALUE (MeV)	DOCUMENT ID		TECN	COMMENT
2300 to 2600 (≈ 2450) OUR ESTIMATE				
2633± 29	[1] ARNDT	06	DPWA	$\pi N \to \pi N, \eta N$
2400±125	CUTKOSKY	80	IPWA	$\pi N \to \pi N$
2416± 17	HOEHLER	79	IPWA	$\pi N \to \pi N$

[1] Statistical error only.

$\Delta(2420)$ BREIT-WIGNER WIDTH

VALUE (MeV)	DOCUMENT ID		TECN	COMMENT
300 to 700 (≈ 500) OUR ESTIMATE				
692± 47	[1] ARNDT	06	DPWA	$\pi N \to \pi N, \eta N$
450±150	CUTKOSKY	80	IPWA	$\pi N \to \pi N$
340± 28	HOEHLER	79	IPWA	$\pi N \to \pi N$

[1] Statistical error only.

$\Delta(2420)$ DECAY MODES

The following branching fractions are our estimates, not fits or averages.

	Mode	Fraction (Γ_i/Γ)
Γ_1	$N\pi$	5–10 %

Downloaded from https://academic.oup.com/ptep/article/2022/8/083C01/6651666 by KIT Library user on 27 September 2022

$\Delta(2420)$ BRANCHING RATIOS

$\Gamma(N\pi)/\Gamma_{total}$ — Γ_1/Γ

VALUE (%)	DOCUMENT ID		TECN	COMMENT
5 to 10 (≈ 8) OUR ESTIMATE				
8.5 ± 0.8	[1] ARNDT	06	DPWA	$\pi N \to \pi N, \eta N$
8 ± 3	CUTKOSKY	80	IPWA	$\pi N \to \pi N$
8.0 ± 1.5	HOEHLER	79	IPWA	$\pi N \to \pi N$

[1] Statistical error only.

$\Delta(2420)$ REFERENCES

PDG	14	CP C38 070001	K. Olive *et al.*	(PDG Collab.)
SVARC	14	PR C89 045205	A. Svarc *et al.*	(RBI Zagreb, UNI Tuzla)
ARNDT	06	PR C74 045205	R.A. Arndt *et al.*	(GWU)
HOEHLER	93	πN Newsletter 9 1	G. Hohler	(KARL)
CUTKOSKY	80	Toronto Conf. 19	R.E. Cutkosky *et al.*	(CMU, LBL) IJP
Also		PR D20 2839	R.E. Cutkosky *et al.*	(CMU, LBL)
HOEHLER	79	PDAT 12-1	G. Hohler *et al.*	(KARLT) IJP
Also		Toronto Conf. 3	R. Koch	(KARLT) IJP

$\Delta(2750)\ 13/2^-$

$I(J^P) = \frac{3}{2}(\frac{13}{2}^-)$ Status: **

OMITTED FROM SUMMARY TABLE

$\Delta(2750)$ BREIT-WIGNER MASS

VALUE (MeV)	DOCUMENT ID		TECN	COMMENT
2794 ± 80	HOEHLER	79	IPWA	$\pi N \to \pi N$

$\Delta(2750)$ BREIT-WIGNER WIDTH

VALUE (MeV)	DOCUMENT ID		TECN	COMMENT
350 ± 100	HOEHLER	79	IPWA	$\pi N \to \pi N$

$\Delta(2750)$ DECAY MODES

	Mode	Fraction (Γ_i/Γ)
Γ_1	$N\pi$	2–6 %

$\Delta(2750)$ BRANCHING RATIOS

$\Gamma(N\pi)/\Gamma_{total}$ — Γ_1/Γ

VALUE (%)	DOCUMENT ID		TECN	COMMENT
4.0 ± 1.5	HOEHLER	79	IPWA	$\pi N \to \pi N$

$\Delta(2750)$ REFERENCES

HOEHLER	79	PDAT 12-1	G. Hohler *et al.*	(KARLT) IJP
Also		Toronto Conf. 3	R. Koch	(KARLT) IJP

$\Delta(2950)\ 15/2^+$

$I(J^P) = \frac{3}{2}(\frac{15}{2}^+)$ Status: **

OMITTED FROM SUMMARY TABLE

$\Delta(2950)$ BREIT-WIGNER MASS

VALUE (MeV)	DOCUMENT ID		TECN	COMMENT
2990 ± 100	HOEHLER	79	IPWA	$\pi N \to \pi N$

$\Delta(2950)$ BREIT-WIGNER WIDTH

VALUE (MeV)	DOCUMENT ID		TECN	COMMENT
330 ± 100	HOEHLER	79	IPWA	$\pi N \to \pi N$

$\Delta(2950)$ DECAY MODES

	Mode	Fraction (Γ_i/Γ)
Γ_1	$N\pi$	2–6 %

$\Delta(2950)$ BRANCHING RATIOS

$\Gamma(N\pi)/\Gamma_{total}$ — Γ_1/Γ

VALUE (%)	DOCUMENT ID		TECN	COMMENT
4 ± 2	HOEHLER	79	IPWA	$\pi N \to \pi N$

$\Delta(2950)$ REFERENCES

HOEHLER	79	PDAT 12-1	G. Hohler *et al.*	(KARLT) IJP
Also		Toronto Conf. 3	R. Koch	(KARLT) IJP

$\Delta(\sim 3000$ Region) Partial-Wave Analyses

OMITTED FROM SUMMARY TABLE

We list here miscellaneous high-mass candidates for isospin-3/2 resonances found in partial-wave analyses.

Our 1982 edition also had a $\Delta(2850)$ and a $\Delta(3230)$. The evidence for them was deduced from total cross-section and 180° elastic cross-section measurements. The $\Delta(2850)$ has been resolved into the $\Delta(2750)$ $I_{3,13}$ and $\Delta(2950)$ $K_{3,15}$. The $\Delta(3230)$ is perhaps related to the $K_{3,13}$ of HENDRY 78 and to the $L_{3,17}$ of KOCH 80.

$\Delta(\sim 3000)$ BREIT-WIGNER MASS

VALUE (MeV)	DOCUMENT ID		TECN	COMMENT
3300	[1] KOCH	80	IPWA	$\pi N \to \pi N$ $L_{3,17}$ wave
3500	[1] KOCH	80	IPWA	$\pi N \to \pi N$ $M_{3,19}$ wave
2850 ± 150	HENDRY	78	MPWA	$\pi N \to \pi N$ $I_{3,11}$ wave
3200 ± 200	HENDRY	78	MPWA	$\pi N \to \pi N$ $K_{3,13}$ wave
3300 ± 200	HENDRY	78	MPWA	$\pi N \to \pi N$ $L_{3,17}$ wave
3700 ± 200	HENDRY	78	MPWA	$\pi N \to \pi N$ $M_{3,19}$ wave
4100 ± 300	HENDRY	78	MPWA	$\pi N \to \pi N$ $N_{3,21}$ wave

$\Delta(\sim 3000)$ BREIT-WIGNER WIDTH

VALUE (MeV)	DOCUMENT ID		TECN	COMMENT
700 ± 200	HENDRY	78	MPWA	$\pi N \to \pi N$ $I_{3,11}$ wave
1000 ± 300	HENDRY	78	MPWA	$\pi N \to \pi N$ $K_{3,13}$ wave
1100 ± 300	HENDRY	78	MPWA	$\pi N \to \pi N$ $L_{3,17}$ wave
1300 ± 400	HENDRY	78	MPWA	$\pi N \to \pi N$ $M_{3,19}$ wave
1600 ± 500	HENDRY	78	MPWA	$\pi N \to \pi N$ $N_{3,21}$ wave

$\Delta(\sim 3000)$ DECAY MODES

	Mode	Fraction (Γ_i/Γ)
Γ_1	$N\pi$	1–8%

$\Delta(\sim 3000)$ BRANCHING RATIOS

$\Gamma(N\pi)/\Gamma_{total}$ — Γ_1/Γ

VALUE (%)	DOCUMENT ID		TECN	COMMENT
1–8% OUR ESTIMATE				
6 ± 2	HENDRY	78	MPWA	$\pi N \to \pi N$ $I_{3,11}$ wave
5 ± 2	HENDRY	78	MPWA	$\pi N \to \pi N$ $K_{3,13}$ wave
3 ± 1	HENDRY	78	MPWA	$\pi N \to \pi N$ $L_{3,17}$ wave
3 ± 1	HENDRY	78	MPWA	$\pi N \to \pi N$ $M_{3,19}$ wave
2 ± 1	HENDRY	78	MPWA	$\pi N \to \pi N$ $N_{3,21}$ wave

$\Delta(\sim 3000)$ FOOTNOTES

[1] In addition, KOCH 80 reports some evidence for an S_{31} $\Delta(2700)$ and a P_{33} $\Delta(2800)$.

$\Delta(\sim 3000)$ REFERENCES

KOCH	80	Toronto Conf. 3	R. Koch	(KARLT) IJP
HENDRY	78	PRL 41 222	A.W. Hendry	(IND, LBL) IJP
Also		ANP 136 1	A.W. Hendry	(IND)

Downloaded from https://academic.oup.com/ptep/article/2022/8/083C01/6651666 by KIT Library user on 27 September 2022

Λ BARYONS
($S = -1$, $I = 0$)

$\Lambda^0 = uds$

Λ

$I(J^P) = 0(\frac{1}{2}^+)$ Status: ****

We have omitted some results that have been superseded by later experiments. See our earlier editions.

Λ MASS

The fit uses Λ, Σ^+, Σ^0, Σ^- mass and mass-difference measurements.

VALUE (MeV)	EVTS	DOCUMENT ID		TECN	COMMENT
1115.683±0.006 OUR FIT					
1115.683±0.006 OUR AVERAGE					
1115.678±0.006±0.006	20k	HARTOUNI	94	SPEC	pp 27.5 GeV/c
1115.690±0.008±0.006	18k	[1] HARTOUNI	94	SPEC	pp 27.5 GeV/c
• • • We do not use the following data for averages, fits, limits, etc. • • •					
1115.59 ±0.08	935	HYMAN	72	HEBC	
1115.39 ±0.12	195	MAYEUR	67	EMUL	
1115.6 ±0.4		LONDON	66	HBC	
1115.65 ±0.07	488	[2] SCHMIDT	65	HBC	
1115.44 ±0.12		[3] BHOWMIK	63	RVUE	

[1] We assume CPT invariance: this is the $\overline{\Lambda}$ mass as measured by HARTOUNI 94. See below for the fractional mass difference, testing CPT.
[2] The SCHMIDT 65 masses have been reevaluated using our April 1973 proton and $K^\pm$ and $\pi^\pm$ masses. P. Schmidt, private communication (1974).
[3] The mass has been raised 35 keV to take into account a 46 keV increase in the proton mass and an 11 keV decrease in the $\pi^\pm$ mass (note added Reviews of Modern Physics **39** 1 (1967)).

$(m_\Lambda - m_{\overline{\Lambda}}) / m_\Lambda$

A test of CPT invariance.

VALUE (units 10^{-5})	EVTS	DOCUMENT ID		TECN	COMMENT
− 0.1 ± 1.1 OUR AVERAGE	Error includes scale factor of 1.6.				
+ 1.3 ± 1.2	31k	[1] RYBICKI	96	NA32	π^- Cu, 230 GeV
− 1.08 ± 0.90		HARTOUNI	94	SPEC	pp 27.5 GeV/c
4.5 ± 5.4		CHIEN	66	HBC	6.9 GeV/c $\overline{p}p$
• • • We do not use the following data for averages, fits, limits, etc. • • •					
−26 ±13		BADIER	67	HBC	2.4 GeV/c $\overline{p}p$

[1] RYBICKI 96 is an analysis of old ACCMOR (NA32) data.

Λ MEAN LIFE

Measurements with an error $\geq 0.1 \times 10^{-10}$ s have been omitted altogether, and only the latest high-statistics measurements are used for the average.

VALUE (10^{-10} s)	EVTS	DOCUMENT ID		TECN	COMMENT
2.632±0.020 OUR AVERAGE	Error includes scale factor of 1.6.				See the ideogram below.
2.69 ±0.03	53k	ZECH	77	SPEC	Neutral hyperon beam
2.611±0.020	34k	CLAYTON	75	HBC	0.96–1.4 GeV/c K^-p
2.626±0.020	36k	POULARD	73	HBC	0.4–2.3 GeV/c K^-p
• • • We do not use the following data for averages, fits, limits, etc. • • •					
2.69 ±0.05	6582	ALTHOFF	73B	OSPK	$\pi^+ n \to \Lambda K^+$
2.54 ±0.04	4572	BALTAY	71B	HBC	K^-p at rest
2.535±0.035	8342	GRIMM	68	HBC	
2.47 ±0.08	2600	HEPP	68	HBC	
2.35 ±0.09	916	BURAN	66	HLBC	
$2.452^{+0.056}_{-0.054}$	2213	ENGELMANN	66	HBC	
2.59 ±0.09	794	HUBBARD	64	HBC	
2.59 ±0.07	1378	SCHWARTZ	64	HBC	
2.36 ±0.06	2239	BLOCK	63	HEBC	

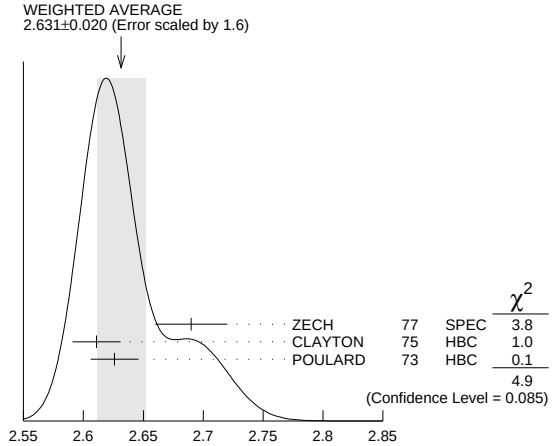

$(\tau_\Lambda - \tau_{\overline{\Lambda}}) / \tau_\Lambda$

A test of CPT invariance.

VALUE	DOCUMENT ID		TECN	COMMENT
−0.001 ±0.009 OUR AVERAGE				
−0.0018±0.0066±0.0056	BARNES	96	CNTR	LEAR $\overline{p}p \to \overline{\Lambda}\Lambda$
0.044 ±0.085	BADIER	67	HBC	2.4 GeV/c $\overline{p}p$

Λ MAGNETIC MOMENT

See the "Quark Model" review. Measurements with an error $\geq 0.15\ \mu_N$ have been omitted.

VALUE (μ_N)	EVTS	DOCUMENT ID		TECN	COMMENT
−0.613 ±0.004 OUR AVERAGE					
−0.606 ±0.015	200k	COX	81	SPEC	
−0.6138±0.0047	3M	SCHACHIN...	78	SPEC	
−0.59 ±0.07	350k	HELLER	77	SPEC	
−0.57 ±0.05	1.2M	BUNCE	76	SPEC	
−0.66 ±0.07	1300	DAHL-JENSEN	71	EMUL	200 kG field

Λ ELECTRIC DIPOLE MOMENT

A nonzero value is forbidden by both T invariance and P invariance.

VALUE (10^{-16} ecm)	CL%	DOCUMENT ID		TECN
< 1.5	95	[1] PONDROM	81	SPEC
• • • We do not use the following data for averages, fits, limits, etc. • • •				
<100	95	[2] BARONI	71	EMUL
<500	95	GIBSON	66	EMUL

[1] PONDROM 81 measures $(-3.0 \pm 7.4) \times 10^{-17}$ e-cm.
[2] BARONI 71 measures $(-5.9 \pm 2.9) \times 10^{-15}$ e-cm.

Λ DECAY MODES

	Mode		Fraction (Γ_i/Γ)	Confidence level
Γ_1	$p\pi^-$		(63.9 ±0.5) %	
Γ_2	$n\pi^0$		(35.8 ±0.5) %	
Γ_3	$n\gamma$		(1.75±0.15) $\times 10^{-3}$	
Γ_4	$p\pi^-\gamma$	[a]	(8.4 ±1.4) $\times 10^{-4}$	
Γ_5	$pe^-\overline{\nu}_e$		(8.32±0.14) $\times 10^{-4}$	
Γ_6	$p\mu^-\overline{\nu}_\mu$		(1.57±0.35) $\times 10^{-4}$	
	Lepton (L) and/or Baryon (B) number violating decay modes			
Γ_7	π^+e^-	L,B	< 6 $\times 10^{-7}$	90%
Γ_8	$\pi^+\mu^-$	L,B	< 6 $\times 10^{-7}$	90%
Γ_9	π^-e^+	L,B	< 4 $\times 10^{-7}$	90%
Γ_{10}	$\pi^-\mu^+$	L,B	< 6 $\times 10^{-7}$	90%
Γ_{11}	K^+e^-	L,B	< 2 $\times 10^{-6}$	90%
Γ_{12}	$K^+\mu^-$	L,B	< 3 $\times 10^{-6}$	90%
Γ_{13}	K^-e^+	L,B	< 2 $\times 10^{-6}$	90%
Γ_{14}	$K^-\mu^+$	L,B	< 3 $\times 10^{-6}$	90%
Γ_{15}	$K^0_S\nu$	L,B	< 2 $\times 10^{-5}$	90%
Γ_{16}	$\overline{p}\pi^+$	B	< 9 $\times 10^{-7}$	90%

[a] See the Listings below for the pion momentum range used in this measurement.

Downloaded from https://academic.oup.com/ptep/article/2022/8/083C01/6651666 by KIT Library user on 27 September 2022

CONSTRAINED FIT INFORMATION

An overall fit to 5 branching ratios uses 20 measurements and one constraint to determine 5 parameters. The overall fit has a $\chi^2 = 10.5$ for 16 degrees of freedom.

The following *off-diagonal* array elements are the correlation coefficients $\langle \delta x_i \delta x_j \rangle / (\delta x_i \cdot \delta x_j)$, in percent, from the fit to the branching fractions, $x_i \equiv \Gamma_i/\Gamma_{total}$. The fit constrains the x_i whose labels appear in array to sum to one.

	x_1	x_2	x_3	x_5
x_2	−100			
x_3	−2	−1		
x_5	46	−46	−1	
x_6	0	0	0	0

Λ BRANCHING RATIOS

$\Gamma(p\pi^-)/\Gamma(N\pi)$ — $\Gamma_1/(\Gamma_1+\Gamma_2)$

VALUE	EVTS	DOCUMENT ID		TECN	COMMENT
0.641±0.005 OUR FIT					
0.640±0.005 OUR AVERAGE					
0.646±0.008	4572	BALTAY	71B	HBC	K^-p at rest
0.635±0.007	6736	DOYLE	69	HBC	$\pi^-p \to \Lambda K^0$
0.643±0.016	903	HUMPHREY	62	HBC	
0.624±0.030		CRAWFORD	59B	HBC	$\pi^-p \to \Lambda K^0$

$\Gamma(n\pi^0)/\Gamma(N\pi)$ — $\Gamma_2/(\Gamma_1+\Gamma_2)$

VALUE	EVTS	DOCUMENT ID		TECN
0.359±0.005 OUR FIT				
0.310±0.028 OUR AVERAGE				
0.35 ±0.05		BROWN	63	HLBC
0.291±0.034	75	CHRETIEN	63	HLBC

$\Gamma(n\gamma)/\Gamma_{total}$ — Γ_3/Γ

VALUE (units 10^{-3})	EVTS	DOCUMENT ID		TECN	COMMENT
1.75±0.15 OUR FIT					
1.75±0.15	1816	LARSON	93	SPEC	K^-p at rest
• • • We do not use the following data for averages, fits, limits, etc. • • •					
$1.78 \pm 0.24 {}^{+0.14}_{-0.16}$	287	NOBLE	92	SPEC	See LARSON 93

$\Gamma(n\gamma)/\Gamma(n\pi^0)$ — Γ_3/Γ_2

VALUE (units 10^{-3})	EVTS	DOCUMENT ID		TECN	COMMENT
• • • We do not use the following data for averages, fits, limits, etc. • • •					
2.86±0.74±0.57	24	BIAGI	86	SPEC	SPS hyperon beam

$\Gamma(p\pi^-\gamma)/\Gamma(p\pi^-)$ — Γ_4/Γ_1

VALUE (units 10^{-3})	EVTS	DOCUMENT ID		TECN	COMMENT
1.32±0.22	72	BAGGETT	72C	HBC	$\pi^- < 95$ MeV/c

$\Gamma(pe^-\overline{\nu}_e)/\Gamma(p\pi^-)$ — Γ_5/Γ_1

VALUE (units 10^{-3})	EVTS	DOCUMENT ID		TECN	COMMENT
1.301±0.019 OUR FIT					
1.301±0.019 OUR AVERAGE					
1.335±0.056	7111	BOURQUIN	83	SPEC	SPS hyperon beam
1.313±0.024	10k	WISE	80	SPEC	
1.23 ±0.11	544	LINDQUIST	77	SPEC	$\pi^-p \to K^0\Lambda$
1.27 ±0.07	1089	KATZ	73	HBC	
1.31 ±0.06	1078	ALTHOFF	71	OSPK	
1.17 ±0.13	86	[1] CANTER	71	HBC	K^-p at rest
1.20 ±0.12	143	[2] MALONEY	69	HBC	
1.17 ±0.18	120	[2] BAGLIN	64	FBC	K^- freon 1.45 GeV/c
1.23 ±0.20	150	[2] ELY	63	FBC	
• • • We do not use the following data for averages, fits, limits, etc. • • •					
1.32 ±0.15	218	[1] LINDQUIST	71	OSPK	See LINDQUIST 77

[1] Changed by us from $\Gamma(pe^-\overline{\nu}_e)/\Gamma(N\pi)$ assuming the authors used $\Gamma(\Lambda \to p\pi^-)/\Gamma(\text{total}) = 2/3$.
[2] Changed by us from $\Gamma(pe^-\overline{\nu}_e)/\Gamma(N\pi)$ because $\Gamma(pe^-\nu)/\Gamma(p\pi^-)$ is the directly measured quantity.

$\Gamma(p\mu^-\overline{\nu}_\mu)/\Gamma_{total}$ — Γ_6/Γ

VALUE (units 10^{-4})	EVTS	DOCUMENT ID		TECN	COMMENT
1.48±0.21±0.08	64	[1] ABLIKIM	21AG	BES3	$J/\psi \to \Lambda\overline{\Lambda}$

[1] ABLIKIM 21AG use $\overline{\Lambda} \to \overline{p}\pi^+$ decay mode as the double tag identifier and thus as indirect normalization.

$\Gamma(p\mu^-\overline{\nu}_\mu)/\Gamma(N\pi)$ — $\Gamma_6/(\Gamma_1+\Gamma_2)$

VALUE (units 10^{-4})	EVTS	DOCUMENT ID		TECN	COMMENT
1.57±0.35 OUR FIT					
1.57±0.35 OUR AVERAGE					
1.4 ±0.5	14	BAGGETT	72B	HBC	K^-p at rest
2.4 ±0.8	9	CANTER	71B	HBC	K^-p at rest
1.3 ±0.7	3	LIND	64	RVUE	
1.5 ±1.2	2	RONNE	64	FBC	

Lepton (L) and/or Baryon (B) number violating decay modes

$\Gamma(\pi^+e^-)/\Gamma_{total}$ — Γ_7/Γ

VALUE	CL%	DOCUMENT ID		TECN	COMMENT
$<6\times10^{-7}$	90	[1] MCCRACKEN	15	CLAS	$\gamma p \to K^+\Lambda$

[1] Uses $B(\Lambda \to p\pi^-) = (63.9 \pm 0.5)\%$ for normalization mode.

$\Gamma(\pi^+\mu^-)/\Gamma_{total}$ — Γ_8/Γ

VALUE	CL%	DOCUMENT ID		TECN	COMMENT
$<6\times10^{-7}$	90	[1] MCCRACKEN	15	CLAS	$\gamma p \to K^+\Lambda$

[1] Uses $B(\Lambda \to p\pi^-) = (63.9 \pm 0.5)\%$ for normalization mode.

$\Gamma(\pi^-e^+)/\Gamma_{total}$ — Γ_9/Γ

VALUE	CL%	DOCUMENT ID		TECN	COMMENT
$<4\times10^{-7}$	90	[1] MCCRACKEN	15	CLAS	$\gamma p \to K^+\Lambda$

[1] Uses $B(\Lambda \to p\pi^-) = (63.9 \pm 0.5)\%$ for normalization mode.

$\Gamma(\pi^-\mu^+)/\Gamma_{total}$ — Γ_{10}/Γ

VALUE	CL%	DOCUMENT ID		TECN	COMMENT
$<6\times10^{-7}$	90	[1] MCCRACKEN	15	CLAS	$\gamma p \to K^+\Lambda$

[1] Uses $B(\Lambda \to p\pi^-) = (63.9 \pm 0.5)\%$ for normalization mode.

$\Gamma(K^+e^-)/\Gamma_{total}$ — Γ_{11}/Γ

VALUE	CL%	DOCUMENT ID		TECN	COMMENT
$<2\times10^{-6}$	90	[1] MCCRACKEN	15	CLAS	$\gamma p \to K^+\Lambda$

[1] Uses $B(\Lambda \to p\pi^-) = (63.9 \pm 0.5)\%$ for normalization mode.

$\Gamma(K^+\mu^-)/\Gamma_{total}$ — Γ_{12}/Γ

VALUE	CL%	DOCUMENT ID		TECN	COMMENT
$<3\times10^{-6}$	90	[1] MCCRACKEN	15	CLAS	$\gamma p \to K^+\Lambda$

[1] Uses $B(\Lambda \to p\pi^-) = (63.9 \pm 0.5)\%$ for normalization mode.

$\Gamma(K^-e^+)/\Gamma_{total}$ — Γ_{13}/Γ

VALUE	CL%	DOCUMENT ID		TECN	COMMENT
$<2\times10^{-6}$	90	[1] MCCRACKEN	15	CLAS	$\gamma p \to K^+\Lambda$

[1] Uses $B(\Lambda \to p\pi^-) = (63.9 \pm 0.5)\%$ for normalization mode.

$\Gamma(K^-\mu^+)/\Gamma_{total}$ — Γ_{14}/Γ

VALUE	CL%	DOCUMENT ID		TECN	COMMENT
$<3\times10^{-6}$	90	[1] MCCRACKEN	15	CLAS	$\gamma p \to K^+\Lambda$

[1] Uses $B(\Lambda \to p\pi^-) = (63.9 \pm 0.5)\%$ for normalization mode.

$\Gamma(K^0_S\nu)/\Gamma_{total}$ — Γ_{15}/Γ

VALUE	CL%	DOCUMENT ID		TECN	COMMENT
$<2\times10^{-5}$	90	[1] MCCRACKEN	15	CLAS	$\gamma p \to K^+\Lambda$

[1] Uses $B(\Lambda \to p\pi^-) = (63.9 \pm 0.5)\%$ for normalization mode.

$\Gamma(\overline{p}\pi^+)/\Gamma_{total}$ — Γ_{16}/Γ

VALUE	CL%	DOCUMENT ID		TECN	COMMENT
$<9\times10^{-7}$	90	[1] MCCRACKEN	15	CLAS	$\gamma p \to K^+\Lambda$

[1] Uses $B(\Lambda \to p\pi^-) = (63.9 \pm 0.5)\%$ for normalization mode.

Λ CP-violating decay-rate asymmetries

This is the difference between Λ and $\overline{\Lambda}$ decay rates to state f and $\overline{f}$ divided by the sum of the rates:
$A_{CP}(f) = [(B(\Lambda \to f)) - (B(\overline{\Lambda} \to \overline{f}))]/\text{Sum}$.

$A_{CP}(p\mu^-\overline{\nu}_\mu)$ in $\Lambda \to p\mu^-\overline{\nu}_\mu, \overline{\Lambda} \to \overline{p}\mu^+\nu_\mu$

VALUE	DOCUMENT ID		TECN	COMMENT
0.02±0.14±0.02	ABLIKIM	21AG	BES3	$J/\psi \to \Lambda\overline{\Lambda}$

Λ DECAY PARAMETERS

See the "Note on Baryon Decay Parameters" in the neutron Listings. Some early results have been omitted.

α_- FOR $\Lambda \to p\pi^-$

VALUE	EVTS	DOCUMENT ID		TECN	COMMENT
0.732±0.014 OUR AVERAGE		Error includes scale factor of 2.3.			
0.750±0.009±0.004	420k	ABLIKIM	19BJ	BES3	J/ψ to $\Lambda\overline{\Lambda}$
0.721±0.006±0.005		[1] IRELAND	19	CLAS	K production
• • • We do not use the following data for averages, fits, limits, etc. • • •					
$0.74 {}^{+0.04}_{-0.03}$		AAIJ	20O	LHCB	$\Lambda_b \to J/\psi\Lambda$
0.584±0.046	8500	ASTBURY	75	SPEC	
0.649±0.023	10325	CLELAND	72	OSPK	
0.67 ±0.06	3520	DAUBER	69	HBC	From Ξ decay
0.645±0.017	10130	OVERSETH	67	OSPK	Λ from π^-p
0.62 ±0.07	1156	CRONIN	63	CNTR	Λ from π^-p

[1] This is a new analysis based on existing kaon photoproduction data of the CLAS collaboration and using spin algebra constraints.

Downloaded from https://academic.oup.com/ptep/article/2022/8/083C01/6651666 by KIT Library user on 27 September 2022

α_+ FOR $\overline{\Lambda} \to \overline{p}\pi^+$

VALUE	EVTS	DOCUMENT ID		TECN	COMMENT
−0.758±0.010±0.007	420k	ABLIKIM	19BJ	BES3	J/ψ to $\Lambda\overline{\Lambda}$
• • • We do not use the following data for averages, fits, limits, etc. • • •					
−0.755±0.083±0.063	≈ 8.7k	ABLIKIM	10	BES	$J/\psi \to \Lambda\overline{\Lambda}$
−0.63 ±0.13	770	TIXIER	88	DM2	$J/\psi \to \Lambda\overline{\Lambda}$

$\overline{\alpha}_0$ FOR $\overline{\Lambda} \to \overline{n}\pi^0$

VALUE	EVTS	DOCUMENT ID		TECN	COMMENT
−0.692±0.016±0.006	47k	ABLIKIM	19BJ	BES3	J/ψ to $\Lambda\overline{\Lambda}$

ϕ ANGLE FOR $\Lambda \to p\pi^-$ ($\tan\phi = \beta / \gamma$)

VALUE (°)	EVTS	DOCUMENT ID		TECN	COMMENT
− 6.5± 3.5 OUR AVERAGE					
− 7.0± 4.5	10325	CLELAND	72	OSPK	Λ from $\pi^- p$
− 8.0± 6.0	10130	OVERSETH	67	OSPK	Λ from $\pi^- p$
13.0±17.0	1156	CRONIN	63	OSPK	Λ from $\pi^- p$

$\alpha_0 / \alpha_- = \alpha(\Lambda \to n\pi^0) / \alpha(\Lambda \to p\pi^-)$

VALUE	EVTS	DOCUMENT ID		TECN	COMMENT
1.01 ±0.07 OUR AVERAGE					
1.000±0.068	4760	[1] OLSEN	70	OSPK	$\pi^+ n \to \Lambda K^+$
1.10 ±0.27		CORK	60	CNTR	

[1] OLSEN 70 compares proton and neutron distributions from Λ decay.

$\overline{\alpha}_0 / \alpha_+$ in $\overline{\Lambda} \to \overline{n}\pi^0, \overline{\Lambda} \to \overline{p}\pi^+$

VALUE	EVTS	DOCUMENT ID		TECN	COMMENT
0.913±0.028±0.012	47k	ABLIKIM	19BJ	BES3	J/ψ to $\Lambda\overline{\Lambda}$

$(\alpha + \overline{\alpha})/(\alpha - \overline{\alpha})$ in $\Lambda \to p\pi^-, \overline{\Lambda} \to \overline{p}\pi^+$

Zero if CP is conserved; α_- and α_+ are the asymmetry parameters for $\Lambda \to p\pi^-$ and $\overline{\Lambda} \to \overline{p}\pi^+$ decay. See also the Ξ^- for a similar test involving the decay chain $\Xi^- \to \Lambda\pi^-$, $\Lambda \to p\pi^-$ and the corresponding antiparticle chain.

VALUE	EVTS	DOCUMENT ID		TECN	COMMENT
−0.002±0.012 OUR AVERAGE					
−0.006±0.012±0.007	420k	ABLIKIM	19BJ	BES3	J/ψ to $\Lambda\overline{\Lambda}$
−0.081±0.055±0.059	≈ 8.7k	ABLIKIM	10	BES	$J/\psi \to \Lambda\overline{\Lambda}$
+0.013±0.022	96k	BARNES	96	CNTR	LEAR $\overline{p}p \to \overline{\Lambda}\Lambda$
+0.01 ±0.10	770	TIXIER	88	DM2	$J/\psi \to \Lambda\overline{\Lambda}$
−0.02 ±0.14	10k	[1] CHAUVAT	85	CNTR	$pp, \overline{p}p$ ISR
• • • We do not use the following data for averages, fits, limits, etc. • • •					
−0.07 ±0.09	4063	BARNES	87	CNTR	See BARNES 96

[1] CHAUVAT 85 actually gives $\alpha_+(\overline{\Lambda})/\alpha_-(\Lambda) = -1.04 \pm 0.29$. Assumes polarization is same in $\overline{p}p \to \overline{\Lambda}X$ and $pp \to \Lambda X$. Tests of this assumption, based on C-invariance and fragmentation, are satisfied by the data.

R = $|G_E/G_M|$ in $\Lambda \to p\pi^-, \overline{\Lambda} \to \overline{p}\pi^+$

VALUE	DOCUMENT ID		TECN	COMMENT
0.96±0.14±0.02	[1] ABLIKIM	19BF	BES3	$e^+e^- \to \overline{\Lambda}\Lambda$ at $\sqrt{s}$ = 2.396 GeV

[1] Determined using the latest BES-III value on the asymmetry parameter $\alpha = 0.750 \pm 0.010$.

$\Delta\Phi = \Phi_E - \Phi_M$ in $\Lambda \to p\pi^-, \overline{\Lambda} \to \overline{p}\pi^+$

VALUE (degrees)	DOCUMENT ID		TECN	COMMENT
37±12±6	[1] ABLIKIM	19BF	BES3	$e^+e^- \to \overline{\Lambda}\Lambda$ at $\sqrt{s}$ = 2.396 GeV

[1] Relative phase between GE and GM, determined using the latest BES-III value on the asymmetry parameter $\alpha = 0.750 \pm 0.010$.

g_A / g_V FOR $\Lambda \to pe^-\overline{\nu}_e$

Measurements with fewer than 500 events have been omitted. Where necessary, signs have been changed to agree with our conventions, which are given in the "Note on Baryon Decay Parameters" in the neutron Listings. The measurements all assume that the form factor $g_2 = 0$. See also the footnote on DWORKIN 90.

VALUE	EVTS	DOCUMENT ID		TECN	COMMENT
−0.718±0.015 OUR AVERAGE					
−0.719±0.016±0.012	37k	[1] DWORKIN	90	SPEC	$e\nu$ angular corr.
−0.70 ±0.03	7111	BOURQUIN	83	SPEC	$\Xi \to \Lambda\pi^-$
−0.734±0.031	10k	[2] WISE	81	SPEC	$e\nu$ angular correl.
• • • We do not use the following data for averages, fits, limits, etc. • • •					
−0.63 ±0.06	817	ALTHOFF	73	OSPK	Polarized Λ

[1] The tabulated result assumes the weak-magnetism coupling $w \equiv g_W(0)/g_V(0)$ to be 0.97, as given by the CVC hypothesis and as assumed by the other listed measurements. However, DWORKIN 90 *measures* w to be 0.15 ± 0.30, and then $g_A/g_V = -0.731 \pm 0.016$.

[2] This experiment measures only the absolute value of g_A/g_V.

Λ REFERENCES

We have omitted some papers that have been superseded by later experiments. See our earlier editions.

ABLIKIM	21AG	PRL 127 121802	M. Ablikim *et al.*	(BESIII Collab.)
AAIJ	20O	JHEP 2006 110	R. Aaij *et al.*	(LHCb Collab.)
ABLIKIM	19BF	PRL 123 122003	M. Ablikim *et al.*	(BESIII Collab.)
ABLIKIM	19BJ	NATP 15 631	M. Ablikim *et al.*	(BESIII Collab.)
IRELAND	19	PRL 123 182301	D.G. Ireland *et al.*	(GLAS, GWU, JULI+)
MCCRACKEN	15	PR D92 072002	M.E. McCracken *et al.*	(JLab CLAS Collab.)
ABLIKIM	10	PR D81 012003	M. Ablikim *et al.*	(BES Collab.)
BARNES	96	PR C54 1877	P.D. Barnes *et al.*	(CERN PS-185 Collab.)
RYBICKI	96	APP B27 2155	K. Rybicki	
HARTOUNI	94	PRL 72 1322	E.P. Hartouni *et al.*	(BNL E766 Collab.)
Also		PRL 72 2821 (erratum)	E.P. Hartouni *et al.*	(BNL E766 Collab.)
LARSON	93	PR D47 799	K.D. Larson *et al.*	(BNL-811 Collab.)
NOBLE	92	PRL 69 414	A.J. Noble *et al.*	(BIRM, BOST, BRCO+)
DWORKIN	90	PR D41 780	J. Dworkin *et al.*	(MICH, WISC, RUTG+)
TIXIER	88	PL B212 523	M.H. Tixier *et al.*	(DM2 Collab.)
BARNES	87	PL B199 147	P.D. Barnes *et al.*	(CMU, SACL, LANL+)
BIAGI	86	ZPHY C30 201	S.F. Biagi *et al.*	(BRIS, CERN, GEVA+)
CHAUVAT	85	PL 163B 273	P. Chauvat *et al.*	(CERN, CLER, UCLA+)
BOURQUIN	83	ZPHY C21 1	M.H. Bourquin *et al.*	(BRIS, GEVA, HEIDP+)
COX	81	PRL 46 877	P.T. Cox *et al.*	(MICH, WISC, RUTG, MINN+)
PONDROM	81	PR D23 814	L. Pondrom *et al.*	(WISC, MICH, RUTG+)
WISE	81	PL 98B 123	J.E. Wise *et al.*	(MASA, BNL)
WISE	80	PL 91B 165	J.E. Wise *et al.*	(MASA, BNL)
SCHACHIN...	78	PRL 41 1348	L. Schachinger *et al.*	(MICH, RUTG, WISC)
HELLER	77	PL 68B 480	K. Heller *et al.*	(MICH, WISC, HEIDH)
LINDQUIST	77	PR D16 2104	J. Lindquist *et al.*	(EFI, OSU, ANL)
Also		JP G2 L211	J. Lindquist *et al.*	(EFI, WUSL, OSU+)
ZECH	77	NP B124 413	G. Zech *et al.*	(SIEG, CERN, DORT, HEIDH)
BUNCE	76	PRL 36 1113	G.R.M. Bunce *et al.*	(WISC, MICH, RUTG)
ASTBURY	75	NP B99 30	P. Astbury *et al.*	(LOIC, CERN, ETH+)
CLAYTON	75	NP B95 130	E.F. Clayton *et al.*	(LOIC, RHEL)
ALTHOFF	73	PL 43B 237	K.H. Althoff *et al.*	(CERN, HEID)
ALTHOFF	73B	NP B66 29	K.H. Althoff *et al.*	(CERN, HEID)
KATZ	73	Thesis MDDP-TR-74-044	C.N. Katz	(UMD)
POULARD	73	PL 46B 135	G. Poulard, A. Givernaud, A.C. Borg	(SACL)
BAGGETT	72B	ZPHY 252 362	M.J. Baggett *et al.*	(HEID)
BAGGETT	72C	PL 42B 379	M.J. Baggett *et al.*	(HEID)
CLELAND	72	NP B40 221	W.E. Cleland *et al.*	(CERN, GEVA, LUND)
HYMAN	72	PR D5 1063	L.G. Hyman *et al.*	(ANL, CMU)
ALTHOFF	71	PL 37B 531	K.H. Althoff *et al.*	(CERN, HEID)
BALTAY	71B	PR D4 670	C. Baltay *et al.*	(COLU, BING)
BARONI	71	LNC 2 1256	G. Baroni, S. Petrera, G. Romano	(ROMA)
CANTER	71	PRL 26 868	J. Canter *et al.*	(STON, COLU)
CANTER	71B	PRL 27 59	J. Canter *et al.*	(STON, COLU)
DAHL-JENSEN	71	NC 3A 1	E. Dahl-Jensen *et al.*	(CERN, ANKA, LAUS+)
LINDQUIST	71	PRL 27 612	J. Lindquist *et al.*	(EFI, WUSL, OSU+)
OLSEN	70	PRL 24 843	S.L. Olsen *et al.*	(WISC, MICH)
DAUBER	69	PR 179 1262	P.M. Dauber *et al.*	(LRL)
DOYLE	69	Thesis UCRL 18139	J.C. Doyle	(LRL)
MALONEY	69	PRL 23 425	J.E. Maloney, B. Sechi-Zorn	(UMD)
GRIMM	68	NC 54A 187	H.J. Grimm	(HEID)
HEPP	68	ZPHY 214 71	V. Hepp, H. Schleich	(HEID)
BADIER	67	PL 25B 152	J. Badier *et al.*	(EPOL)
MAYEUR	67	U.Libr.Brux.Bul. 32	C. Mayeur, E. Tompa, J.H. Wickens	(BELG, LOUC)
OVERSETH	67	PRL 19 391	O.E. Overseth, R.F. Roth	(MICH, PRIN)
PDG	67	RMP 39 1	A.H. Rosenfeld *et al.*	(LRL, CERN, YALE)
BURAN	66	PL 20 318	T. Buran *et al.*	(OSLO)
CHIEN	66	PR 152 1171	C.Y. Chien *et al.*	(YALE, BNL)
ENGELMANN	66	NC 45A 1038	R. Engelmann *et al.*	(HEID, REHO)
GIBSON	66	NC 45A 882	W.M. Gibson, K. Green	(BRIS)
LONDON	66	PR 143 1034	G.W. London *et al.*	(BNL, SYRA)
SCHMIDT	65	PR 140 B1328	P. Schmidt	(COLU)
BAGLIN	64	NC 35 977	C. Baglin *et al.*	(EPOL, CERN, LOUC, RHEL+)
HUBBARD	64	PR 135 B183	J.R. Hubbard *et al.*	(LRL)
LIND	64	PR 135 B1483	V.G. Lind *et al.*	(WISC)
RONNE	64	PL 11 357	B.E. Ronne *et al.*	(CERN, EPOL, LOUC+)
SCHWARTZ	64	Thesis UCRL 11360	J.A. Schwartz	(LRL)
BHOWMIK	63	NC 28 1494	B. Bhowmik, D.P. Goyal	(DELH)
BLOCK	63	PR 130 766	M.M. Block *et al.*	(NWES, BGNA, SYRA+)
BROWN	63	PR 130 769	J.L. Brown *et al.*	(LRL, MICH)
CHRETIEN	63	PR 131 2208	M. Chretien *et al.*	(BRAN, BROW, HARV+)
CRONIN	63	PR 129 1795	J.W. Cronin, O.E. Overseth	(PRIN)
ELY	63	PR 131 868	R.P. Ely *et al.*	(LRL)
HUMPHREY	62	PR 127 1305	W.E. Humphrey, R.R. Ross	(LRL)
CORK	60	PR 120 1000	B. Cork *et al.*	(LRL, PRIN, BNL)
CRAWFORD	59B	PRL 2 266	F.S. Crawford *et al.*	(LRL)

See the related review(s):
Λ and Σ Resonances

$\Lambda(1380)$ $1/2^-$

$J^P = \frac{1}{2}^-$ Status: **

OMITTED FROM SUMMARY TABLE

See the related review on "Pole Structure of the $\Lambda(1405)$ Region."

$\Lambda(1380)$ POLE POSITION

REAL PART

VALUE (MeV)	DOCUMENT ID		TECN
• • • We do not use the following data for averages, fits, limits, etc. • • •			
1325±15	[1] MAI	15	DPWA
1330^{+4}_{-5}	[2] MAI	15	DPWA
1388± 9	GUO	13	DPWA
1381^{+18}_{-6}	IKEDA	12	DPWA

[1] Solution number 4.
[2] Solution number 2.

−2×IMAGINARY PART

VALUE (MeV)	DOCUMENT ID		TECN
• • • We do not use the following data for averages, fits, limits, etc. • • •			
180^{+24}_{-36}	[1] MAI	15	DPWA
112^{+34}_{-22}	[2] MAI	15	DPWA
228^{+48}_{-50}	GUO	13	DPWA
162^{+38}_{-16}	IKEDA	12	DPWA

[1] Solution number 4.
[2] Solution number 2.

Downloaded from https://academic.oup.com/ptep/article/2022/8/083C01/6651666 by KIT Library user on 27 September 2022

$\Lambda(1380)$ REFERENCES

MAI	15	EPJ A51 30	M. Mai, U.-G. Meissner	(BONN, JULI)
GUO	13	PR C87 035202	Z.-H. Guo, J. Oller	
IKEDA	12	NP A881 98	Y. Ikeda, T. Hyodo, W. Weise	(TUM, RIKEN, TINT)

$\Lambda(1405)\ 1/2^-$

$I(J^P) = 0(\frac{1}{2}^-)$ Status: ****

In the 1998 Note on the $\Lambda(1405)$ in PDG 98, R.H. Dalitz discussed the S-shaped cusp behavior of the intensity at the N-$\overline{K}$ threshold observed in THOMAS 73 and HEMINGWAY 85. He commented that this behavior "is characteristic of S-wave coupling; the other below threshold hyperon, the $\Sigma(1385)$, has no such threshold distortion because its N-$\overline{K}$ coupling is P-wave. For $\Lambda(1405)$ this asymmetry is the sole direct evidence that $J^P = 1/2^-$."

A recent measurement by the CLAS collaboration, MORIYA 14, definitively established the long-assumed $J^P = 1/2^-$ spin-parity assignment of the $\Lambda(1405)$. The experiment produced the $\Lambda(1405)$ spin-polarized in the photoproduction process $\gamma p \rightarrow K^+\Lambda(1405)$ and measured the decay of the $\Lambda(1405)$(polarized) $\rightarrow \Sigma^+$(polarized)π^-. The observed isotropic decay of $\Lambda(1405)$ is consistent with spin $J = 1/2$. The polarization transfer to the Σ^+(polarized) direction revealed negative parity, and thus established $J^P = 1/2^-$.

See the related review(s):
Pole Structure of the $\Lambda(1405)$ Region

$\Lambda(1405)$ POLE POSITION

REAL PART

VALUE (MeV)	DOCUMENT ID		TECN
• • • We do not use the following data for averages, fits, limits, etc. • • •			
1429^{+8}_{-7}	[1] MAI	15	DPWA
1434 ± 2	[2] MAI	15	DPWA
1421^{+3}_{-2}	GUO	13	DPWA
1424^{+7}_{-23}	IKEDA	12	DPWA

[1] Solution number 4.
[2] Solution number 2.

$-2\times$IMAGINARY PART

VALUE (MeV)	DOCUMENT ID		TECN
• • • We do not use the following data for averages, fits, limits, etc. • • •			
24^{+4}_{-6}	[1] MAI	15	DPWA
20^{+4}_{-2}	[2] MAI	15	DPWA
38^{+16}_{-10}	GUO	13	DPWA
52^{+6}_{-28}	IKEDA	12	DPWA

[1] Solution number 4.
[2] Solution number 2.

$\Lambda(1405)$ MASS

PRODUCTION EXPERIMENTS

VALUE (MeV)	EVTS	DOCUMENT ID		TECN	COMMENT
$1405.1^{+1.3}_{-1.0}$ OUR AVERAGE					
1405^{+11}_{-9}		HASSANVAND	13	SPEC	$pp \rightarrow p\Lambda(1405)K^+$
$1405^{+1.4}_{-1.0}$		ESMAILI	10	RVUE	^{4}He $K^- \rightarrow \Sigma^\pm\pi^\mp X$ at rest
1406.5 ± 4.0		[1] DALITZ	91		M-matrix fit
• • • We do not use the following data for averages, fits, limits, etc. • • •					
1391 ± 1	700	[1] HEMINGWAY	85	HBC	K^-p 4.2 GeV/c
~ 1405	400	[2] THOMAS	73	HBC	π^-p 1.69 GeV/c
1405	120	BARBARO-...	68B	DBC	K^-d 2.1–2.7 GeV/c
1400 ± 5	67	BIRMINGHAM	66	HBC	K^-p 3.5 GeV/c
1382 ± 8		ENGLER	65	HDBC	π^-p, π^+d 1.68 GeV/c
1400 ± 24		MUSGRAVE	65	HBC	$\overline{p}p$ 3–4 GeV/c
1410		ALEXANDER	62	HBC	π^-p 2.1 GeV/c
1405		ALSTON	62	HBC	K^-p 1.2–0.5 GeV/c
1405		ALSTON	61B	HBC	K^-p 1.15 GeV/c

[1] DALITZ 91 fits the HEMINGWAY 85 data.
[2] THOMAS 73 data is fit by CHAO 73 (see next section).

EXTRAPOLATIONS BELOW $N\overline{K}$ THRESHOLD

VALUE (MeV)	DOCUMENT ID		TECN	COMMENT
• • • We do not use the following data for averages, fits, limits, etc. • • •				
1407.56 or 1407.50	[1] KIMURA	00		potential model
1411	[2] MARTIN	81		K-matrix fit
1406	[3] CHAO	73	DPWA	0–range fit (sol. B)
1421	MARTIN	70	RVUE	Constant K-matrix
1416 ± 4	MARTIN	69	HBC	Constant K-matrix
1403 ± 3	KIM	67	HBC	K-matrix fit
1407.5 ± 1.2	[4] KITTEL	66	HBC	0–effective-range fit
1410.7 ± 1.0	KIM	65	HBC	0–effective-range fit
1409.6 ± 1.7	[4] SAKITT	65	HBC	0–effective-range fit

[1] The KIMURA 00 values are from fits A and B from a coupled-channel potential model using low-energy $\overline{K}N$ and $\Sigma\pi$ data, kaonic-hydrogen x-ray measurements, and our $\Lambda(1405)$ mass and width. The results bear mainly on the *nature* of the $\Lambda(1405)$: three-quark state or $\overline{K}N$ bound state.
[2] The MARTIN 81 fit includes the $K^\pm p$ forward scattering amplitudes and the dispersion relations they must satisfy.
[3] See also the accompanying paper of THOMAS 73.
[4] Data of SAKITT 65 are used in the fit by KITTEL 66.

$\Lambda(1405)$ WIDTH

PRODUCTION EXPERIMENTS

VALUE (MeV)	EVTS	DOCUMENT ID		TECN	COMMENT
50.5 ± 2.0 OUR AVERAGE					
62 ± 10		HASSANVAND	13	SPEC	$pp \rightarrow p\Lambda(1405)K^+$
50 ± 2		[1] DALITZ	91		M-matrix fit
• • • We do not use the following data for averages, fits, limits, etc. • • •					
24^{+4}_{-3}		ESMAILI	10	RVUE	^{4}He $K^- \rightarrow \Sigma^\pm\pi^\mp X$ at rest
32 ± 1	700	[1] HEMINGWAY	85	HBC	K^-p 4.2 GeV/c
45 to 55	400	[2] THOMAS	73	HBC	π^-p 1.69 GeV/c
35	120	BARBARO-...	68B	DBC	K^-d 2.1–2.7 GeV/c
50 ± 10	67	BIRMINGHAM	66	HBC	K^-p 3.5 GeV/c
89 ± 20		ENGLER	65	HDBC	
60 ± 20		MUSGRAVE	65	HBC	
35 ± 5		ALEXANDER	62	HBC	
50		ALSTON	62	HBC	
20		ALSTON	61B	HBC	

[1] DALITZ 91 fits the HEMINGWAY 85 data.
[2] THOMAS 73 data is fit by CHAO 73 (see next section).

EXTRAPOLATIONS BELOW $N\overline{K}$ THRESHOLD

VALUE (MeV)	DOCUMENT ID		TECN	COMMENT
• • • We do not use the following data for averages, fits, limits, etc. • • •				
50.24 or 50.26	[1] KIMURA	00		potential model
30	[2] MARTIN	81		K-matrix fit
55	[3,4] CHAO	73	DPWA	0–range fit (sol. B)
20	MARTIN	70	RVUE	Constant K-matrix
29 ± 6	MARTIN	69	HBC	Constant K-matrix
50 ± 5	KIM	67	HBC	K-matrix fit
34.1 ± 4.1	[5] KITTEL	66	HBC	
37.0 ± 3.2	KIM	65	HBC	
28.2 ± 4.1	[5] SAKITT	65	HBC	

[1] The KIMURA 00 values are from fits A and B from a coupled-channel potential model using low-energy $\overline{K}N$ and $\Sigma\pi$ data, kaonic-hydrogen x-ray measurements, and our $\Lambda(1405)$ mass and width. The results bear mainly on the *nature* of the $\Lambda(1405)$: three-quark state or $\overline{K}N$ bound state.
[2] The MARTIN 81 fit includes the $K^\pm p$ forward scattering amplitudes and the dispersion relations they must satisfy.
[3] An asymmetric shape, with $\Gamma/2 = 41$ MeV below resonance, 14 MeV above.
[4] See also the accompanying paper of THOMAS 73.
[5] Data of SAKITT 65 are used in the fit by KITTEL 66.

$\Lambda(1405)$ DECAY MODES

	Mode	Fraction (Γ_i/Γ)
Γ_1	$\Sigma\pi$	100 %
Γ_2	$\Lambda\gamma$	
Γ_3	$\Sigma^0\gamma$	
Γ_4	$N\overline{K}$	

$\Lambda(1405)$ PARTIAL WIDTHS

$\Gamma(\Lambda\gamma)$ — Γ_2

VALUE (keV)	DOCUMENT ID	COMMENT
• • • We do not use the following data for averages, fits, limits, etc. • • •		
27 ± 8	BURKHARDT 91	Isobar model fit

$\Gamma(\Sigma^0\gamma)$ — Γ_3

VALUE (keV)	DOCUMENT ID	COMMENT
• • • We do not use the following data for averages, fits, limits, etc. • • •		
10 ± 4 or 23 ± 7	BURKHARDT 91	Isobar model fit

$\Lambda(1405)$ BRANCHING RATIOS

$\Gamma(N\overline{K})/\Gamma(\Sigma\pi)$ — Γ_4/Γ_1

VALUE	CL%	DOCUMENT ID		TECN	COMMENT
• • • We do not use the following data for averages, fits, limits, etc. • • •					
<3	95	HEMINGWAY	85	HBC	K^-p 4.2 GeV/c

Downloaded from https://academic.oup.com/ptep/article/2022/8/083C01/6651666 by KIT Library user on 27 September 2022

$\Lambda(1405)$ REFERENCES

MAI	15	EPJ A51 30	M. Mai, U.-G. Meissner	(BONN, JULI)
MORIYA	14	PRL 112 082004	K. Moriya *et al.*	(CLAS Collab.) JP
GUO	13	PR C87 035202	Z.-H. Guo, J. Oller	
HASSANVAND	13	PR C87 055202	M. Hassanvand *et al.*	
Also		PR C88 019905 (errat.)	M. Hassanvand *et al.*	
IKEDA	12	NP A881 98	Y. Ikeda, T. Hyodo, W. Weise	(TUM, RIKEN, TINT)
ESMAILI	10	PL B686 23	J. Esmaili, Y. Akaishi, T. Yamazaki	(RIKEN, ISUT+)
KIMURA	00	PR C62 015206	M. Kimura *et al.*	
PDG	98	EPJ C3 1	C. Caso *et al.*	(PDG Collab.)
BURKHARDT	91	PR C44 607	H. Burkhardt, J. Lowe	(NOTT, UNM, BIRM)
DALITZ	91	JP G17 289	R.H. Dalitz, A. Deloff	(OXFTP, WINR)
HEMINGWAY	85	NP B253 742	R.J. Hemingway	(CERN) J
MARTIN	81	NP B179 33	A.D. Martin	(DURH)
CHAO	73	NP B56 46	Y.A. Chao *et al.*	(RHEL, CMU, LOUC)
THOMAS	73	NP B56 15	D.W. Thomas *et al.*	(CMU) J
MARTIN	70	NP B16 479	A.D. Martin, G.G. Ross	(DURH)
MARTIN	69	PR 183 1352	B.R. Martin, M. Sakitt	(LOUC, BNL)
Also		PR 183 1345	B.R. Martin, M. Sakitt	(LOUC, BNL)
BARBARO-...	68B	PRL 21 573	A. Barbaro-Galtieri *et al.*	(LRL, SLAC)
KIM	67	PRL 19 1074	J.K. Kim	(YALE)
BIRMINGHAM	66	PR 152 1148	M. Haque *et al.*	(BIRM, GLAS, LOIC, OXF+)
KITTEL	66	PL 21 349	W. Kittel, G. Otter, I. Wacek	(VIEN)
ENGLER	65	PRL 15 224	A. Engler *et al.*	(CMU, BNL) IJ
KIM	65	PRL 14 29	J.K. Kim	(COLU)
MUSGRAVE	65	NC 35 735	B. Musgrave *et al.*	(BIRM, CERN, EPOL+)
SAKITT	65	PR 139 B719	M. Sakitt *et al.*	(UMD, LRL)
ALEXANDER	62	PRL 8 447	G. Alexander *et al.*	(LRL) I
ALSTON	62	CERN Conf. 311	M.H. Alston *et al.*	(LRL) I
ALSTON	61B	PRL 6 698	M.H. Alston *et al.*	(LRL) I

OTHER RELATED PAPERS

IWASAKI	97	PRL 78 3067	M. Iwasaki *et al.*	(KEK 228 Collab.)
FINK	90	PR C41 2720	P.J.Jr. Fink *et al.*	(IBMY, ORST, ANSM)
LEINWEBER	90	ANP 198 203	D.B. Leinweber	(MCMS)
MUELLER-GR...	90	NP A513 557	A. Mueller-Groeling, K. Holinde, J. Speth	(JULI)
BARRETT	89	NC 102A 179	R.C. Barrett	(SURR)
BATTY	89	NC 102A 255	C.J. Batty, A. Gal	(RAL, HEBR)
CAPSTICK	89	Excited Baryons 88, p.32	S. Capstick	(GUEL)
LOWE	89	NC 102A 167	J. Lowe	(BIRM)
WHITEHOUSE	89	PRL 63 1352	D.A. Whitehouse *et al.*	(BIRM, BOST, BRCO+)
SIEGEL	88	PR C38 2221	P.B. Siegel, W. Weise	(REGE)
WORKMAN	88	PR D37 3117	R.L. Workman, H.W. Fearing	(TRIU)
SCHNICK	87	PRL 58 1719	J. Schnick, R.H. Landau	(ORST)
CAPSTICK	86	PR D34 2809	S. Capstick, N. Isgur	(TNTO)
JENNINGS	86	PL B176 229	B.K. Jennings	(TRIU)
MALTMAN	86	PR D34 1372	K. Maltman, N. Isgur	(LANL, TNTO)
ZHONG	86	PL B171 471	Y.S. Zhong *et al.*	(ADLD, TRIU, SURR)
BURKHARDT	85	NP A440 653	H. Burkhardt, J. Lowe, A.S. Rosenthal	(NOTT+)
DAREWYCH	85	PR D32 1765	J.W. Darewych, R. Koniuk, N. Isgur	(YORKC, TNTO)
VEIT	85	PR D31 1033	E.A. Veit *et al.*	(TRIU, ADLD, SURR)
KIANG	84	PR C30 1638	D. Kiang *et al.*	(DALH, MCMS)
MILLER	84	Conference paper	D.J. Miller	(LOUC)
Conf. Intersections between Particle and Nuclear Physics, p. 783				
VANDIJK	84	PR D30 937	W. van Dijk	(MCMS)
VEIT	84	PL 137B 415	E.A. Veit *et al.*	(TRIU, SURR, CERN)
DALITZ	82	Heid. Conf.	R.H. Dalitz *et al.*	(OXFTP)
Heidelberg Conf., p. 201				
DALITZ	81	Kaon Conf.	R.H. Dalitz, J.G. McGinley	(OXFTP)
Low and Intermediate Energy Kaon-Nucleon Physics, p.381				
MARTIN	81B	Kaon Conf.	A.D. Martin	(DURH)
Low and Intermediate Energy Kaon-Nucelon Physics, p. 97				
OADES	77	NC 42A 462	G.C. Oades, G. Rasche	(AARH, ZURI)
SHAW	73	Purdue Conf. 417	G.L. Shaw	(UCI)
BARBARO-...	72	LBL-555	A. Barbaro-Galtieri	(LBL)
DOBSON	72	PR D6 3256	P.N. Dobson, R. McElhaney	(HAWA)
RAJASEKA...	72	PR D5 610	G. Rajasekaran	(TATA)
Earlier papers also cited in RAJASEKARAN 72.				
CLINE	71	PRL 26 1194	D. Cline, R. Laumann, J. Mapp	(WISC)
MARTIN	71	PL 35B 62	A.D. Martin, A.D. Martin, G.G. Ross	(DURH, LOUC+)
DALITZ	67	PR 153 1617	R.H. Dalitz, T.C. Wong, G. Rajasekaran	(OXFTP+)
DONALD	66	PL 22 711	R.A. Donald *et al.*	(LIVP)
KADYK	66	PRL 17 599	J.A. Kadyk *et al.*	(LRL)
ABRAMS	65	PR 139 B454	G.S. Abrams, B. Sechi-Zorn	(UMD)

$\Lambda(1520)\ 3/2^-$

$I(J^P) = 0(\frac{3}{2}^-)$ Status: ****

Discovered by FERRO-LUZZI 62; the elaboration in WATSON 63 is the classic paper on the Breit-Wigner analysis of a multichannel resonance.

The measurements of the mass, width, and elasticity published before 1975 are now obsolete and have been omitted. They were last listed in our 1982 edition Physics Letters **111B** 1 (1982).

Production and formation experiments agree quite well, so they are listed together here.

$\Lambda(1520)$ POLE POSITION

REAL PART

VALUE (MeV)	DOCUMENT ID		TECN	COMMENT
1517 to 1518 (≈ 1517.5) OUR ESTIMATE				
1517.5 ± 0.4 OUR AVERAGE				
1517.5 ± 0.4	SARANTSEV	19	DPWA	$\overline{K}N$ multichannel
1517 $^{+4}_{-4}$	[1] KAMANO	15	DPWA	$\overline{K}N$ multichannel
• • • We do not use the following data for averages, fits, limits, etc. • • •				
1518	ZHANG	13A	DPWA	$\overline{K}N$ multichannel
1518.8	QIANG	10	SPEC	$ep \to e'K^+X$ (fit to X)

[1] From the preferred solution A in KAMANO 15.

$-2\times$IMAGINARY PART

VALUE (MeV)	DOCUMENT ID		TECN	COMMENT
14 to 18 (≈ 16) OUR ESTIMATE				
15.3 ± 0.9 OUR AVERAGE				
15.3 ± 0.9	SARANTSEV	19	DPWA	$\overline{K}N$ multichannel
15 $^{+10}_{-8}$	[1] KAMANO	15	DPWA	$\overline{K}N$ multichannel
• • • We do not use the following data for averages, fits, limits, etc. • • •				
16	ZHANG	13A	DPWA	$\overline{K}N$ multichannel
17.2	QIANG	10	SPEC	$ep \to e'K^+X$ (fit to X)

[1] From the preferred solution A in KAMANO 15.

$\Lambda(1520)$ POLE RESIDUES

The normalized residue is the residue divided by $\Gamma_{pole}/2$.

Normalized residue in $N\overline{K} \to \Lambda(1520) \to N\overline{K}$

MODULUS	PHASE (°)	DOCUMENT ID		TECN	COMMENT
0.45 ± 0.01	**−10 ± 3**	SARANTSEV	19	DPWA	$\overline{K}N$ multichannel
• • • We do not use the following data for averages, fits, limits, etc. • • •					
0.431	−11	[1] KAMANO	15	DPWA	$\overline{K}N$ multichannel

[1] From the preferred solution A in KAMANO 15.

Normalized residue in $N\overline{K} \to \Lambda(1520) \to \Sigma\pi$

MODULUS	PHASE (°)	DOCUMENT ID		TECN	COMMENT
0.44 ± 0.01	**−15 ± 3**	SARANTSEV	19	DPWA	$\overline{K}N$ multichannel
• • • We do not use the following data for averages, fits, limits, etc. • • •					
0.435	−10	[1] KAMANO	15	DPWA	$\overline{K}N$ multichannel

[1] From the preferred solution A in KAMANO 15.

Normalized residue in $N\overline{K} \to \Lambda(1520) \to \Lambda\eta$

MODULUS	PHASE (°)	DOCUMENT ID		TECN	COMMENT
0.013 ± 0.003	**116 ± 3**	SARANTSEV	19	DPWA	$\overline{K}N$ multichannel

Normalized residue in $N\overline{K} \to \Lambda(1520) \to \Sigma(1385)\pi$, S-wave

MODULUS	PHASE (°)	DOCUMENT ID		TECN	COMMENT
• • • We do not use the following data for averages, fits, limits, etc. • • •					
0.431	−123	[1] KAMANO	15	DPWA	$\overline{K}N$ multichannel

[1] From the preferred solution A in KAMANO 15.

Normalized residue in $N\overline{K} \to \Lambda(1520) \to \Sigma(1385)\pi$, D-wave

MODULUS	PHASE (°)	DOCUMENT ID		TECN	COMMENT
• • • We do not use the following data for averages, fits, limits, etc. • • •					
0.0141	122	[1] KAMANO	15	DPWA	$\overline{K}N$ multichannel

[1] From the preferred solution A in KAMANO 15.

$\Lambda(1520)$ MASS

VALUE (MeV)	EVTS	DOCUMENT ID		TECN	COMMENT
1518 to 1520 (≈ 1519) OUR ESTIMATE					
1519.42 ± 0.19 OUR AVERAGE Error includes scale factor of 1.1.					
1518.5 ± 0.5		SARANTSEV	19	DPWA	$\overline{K}N$ multichannel
1519.6 ± 0.5		ZHANG	13A	DPWA	$\overline{K}N$ multichannel
1520.4 ± 0.6 ± 1.5		QIANG	10	SPEC	$ep \to e'K^+X$ (fit to X)
1517.3 ± 1.5	300	BARBER	80D	SPEC	$\gamma p \to \Lambda(1520)K^+$
1517.8 ± 1.2	5k	BARLAG	79	HBC	K^-p 4.2 GeV/c
1520.0 ± 0.5		ALSTON-...	78	DPWA	$\overline{K}N \to \overline{K}N$
1519.7 ± 0.3	4k	CAMERON	77	HBC	K^-p 0.96–1.36 GeV/c
1519 ± 1		GOPAL	77	DPWA	$\overline{K}N$ multichannel
1519.4 ± 0.3	2000	CORDEN	75	DBC	K^-d 1.4–1.8 GeV/c

$\Lambda(1520)$ WIDTH

VALUE (MeV)	EVTS	DOCUMENT ID		TECN	COMMENT
15 to 17 (≈ 16) OUR ESTIMATE					
15.73 ± 0.26 OUR AVERAGE					
15.7 ± 1.0		SARANTSEV	19	DPWA	$\overline{K}N$ multichannel
17 ± 1		ZHANG	13A	DPWA	$\overline{K}N$ multichannel
18.6 ± 1.9 ± 1.0		QIANG	10	SPEC	$ep \to e'K^+X$ (fit to X)
16.3 ± 3.3	300	BARBER	80D	SPEC	$\gamma p \to \Lambda(1520)K^+$
16 ± 1		GOPAL	80	DPWA	$\overline{K}N \to \overline{K}N$
14 ± 3	677	[1] BARLAG	79	HBC	K^-p 4.2 GeV/c
15.4 ± 0.5		ALSTON-...	78	DPWA	$\overline{K}N \to \overline{K}N$
16.3 ± 0.5	4k	CAMERON	77	HBC	K^-p 0.96–1.36 GeV/c
15.0 ± 0.5		GOPAL	77	DPWA	$\overline{K}N$ multichannel
15.5 ± 1.6	2000	CORDEN	75	DBC	K^-d 1.4–1.8 GeV/c

[1] From the best-resolution sample of $\Lambda\pi\pi$ events only.

Downloaded from https://academic.oup.com/ptep/article/2022/8/083C01/6651666 by KIT Library user on 27 September 2022

$\Lambda(1520)$ DECAY MODES

	Mode	Fraction (Γ_i/Γ)
Γ_1	$N\overline{K}$	(45 ±1) %
Γ_2	$\Sigma\pi$	(42 ±1) %
Γ_3	$\Lambda\pi\pi$	(10 ±1) %
Γ_4	$\Sigma(1385)\pi$, S-wave	
Γ_5	$\Sigma(1385)\pi$, D-wave	
Γ_6	$\Sigma(1385)\pi$	
Γ_7	$\Sigma(1385)\pi(\rightarrow \Lambda\pi\pi)$	
Γ_8	$\Lambda(\pi\pi)_{S\text{-wave}}$	
Γ_9	$\Sigma\pi\pi$	(0.9 ±0.1) %
Γ_{10}	$\Lambda\gamma$	(0.85±0.15) %
Γ_{11}	$\Sigma^0\gamma$	

$\Lambda(1520)$ BRANCHING RATIOS

See "Sign conventions for resonance couplings" in the Note on Λ and Σ Resonances.

$\Gamma(N\overline{K})/\Gamma_{total}$ — Γ_1/Γ

VALUE	DOCUMENT ID		TECN	COMMENT
0.45 to 0.47 OUR ESTIMATE				
0.45 ±0.01	SARANTSEV	19	DPWA	$\overline{K}N$ multichannel
0.47 ±0.04	ZHANG	13A	DPWA	$\overline{K}N$ multichannel
0.47 ±0.02	GOPAL	80	DPWA	$\overline{K}N \rightarrow \overline{K}N$
0.45 ±0.03	ALSTON-...	78	DPWA	$\overline{K}N \rightarrow \overline{K}N$
0.448±0.014	CORDEN	75	DBC	$K^- d$ 1.4–1.8 GeV/c
• • • We do not use the following data for averages, fits, limits, etc. • • •				
0.43	[1] KAMANO	15	DPWA	$\overline{K}N$ multichannel
0.47 ±0.01	GOPAL	77	DPWA	See GOPAL 80
0.42	MAST	76	HBC	$K^- p \rightarrow \overline{K}^0 n$

[1] From the preferred solution A in KAMANO 15.

$\Gamma(\Sigma\pi)/\Gamma_{total}$ — Γ_2/Γ

VALUE	DOCUMENT ID		TECN	COMMENT
0.42 to 0.46 OUR ESTIMATE				
0.43 ±0.01	SARANTSEV	19	DPWA	$\overline{K}N$ multichannel
0.47 ±0.05	ZHANG	13A	DPWA	$\overline{K}N$ multichannel
0.426±0.014	CORDEN	75	DBC	$K^- d$ 1.4–1.8 GeV/c
0.418±0.017	BARBARO-...	69B	HBC	$K^- p$ 0.28–0.45 GeV/c
• • • We do not use the following data for averages, fits, limits, etc. • • •				
0.446	[1] KAMANO	15	DPWA	$\overline{K}N$ multichannel
0.46	KIM	71	DPWA	K-matrix analysis

[1] From the preferred solution A in KAMANO 15.

$\Gamma(\Sigma\pi)/\Gamma(N\overline{K})$ — Γ_2/Γ_1

VALUE	DOCUMENT ID		TECN	COMMENT
0.9 to 1.0 OUR ESTIMATE				
0.98±0.03	[1] GOPAL	77	DPWA	$\overline{K}N$ multichannel
0.82±0.08	BURKHARDT	69	HBC	$K^- p$ 0.8–1.2 GeV/c
1.06±0.14	SCHEUER	68	DBC	$K^- N$ 3 GeV/c
0.96±0.20	DAHL	67	HBC	$\pi^- p$ 1.6–4 GeV/c
0.73±0.11	DAUBER	67	HBC	$K^- p$ 2 GeV/c
• • • We do not use the following data for averages, fits, limits, etc. • • •				
1.06±0.12	BERTHON	74	HBC	Quasi-2-body σ
1.72±0.78	MUSGRAVE	65	HBC	

[1] The $\overline{K}N \rightarrow \Sigma\pi$ amplitude at resonance is +0.46 ± 0.01.

$\Gamma(\Lambda\pi\pi)/\Gamma_{total}$ — Γ_3/Γ

VALUE	DOCUMENT ID		TECN	COMMENT
0.09 to 0.11 OUR ESTIMATE				
0.091±0.006	CORDEN	75	DBC	$K^- d$ 1.4–1.8 GeV/c
0.11 ±0.01	[1] MAST	73B	IPWA	$K^- p \rightarrow \Lambda\pi\pi$

[1] Assumes $\Gamma(N\overline{K})/\Gamma_{total} = 0.46 \pm 0.02$.

$\Gamma(\Lambda\pi\pi)/\Gamma(N\overline{K})$ — Γ_3/Γ_1

VALUE	DOCUMENT ID		TECN	COMMENT
0.18 to 0.22 OUR ESTIMATE				
0.22±0.03	BURKHARDT	69	HBC	$K^- p$ 0.8–1.2 GeV/c
0.19±0.04	SCHEUER	68	DBC	$K^- N$ 3 GeV/c
0.17±0.05	DAHL	67	HBC	$\pi^- p$ 1.6–4 GeV/c
0.21±0.18	DAUBER	67	HBC	$K^- p$ 2 GeV/c
• • • We do not use the following data for averages, fits, limits, etc. • • •				
0.27±0.13	BERTHON	74	HBC	Quasi-2-body σ
0.2	KIM	71	DPWA	K-matrix analysis

$\Gamma(\Sigma\pi)/\Gamma(\Lambda\pi\pi)$ — Γ_2/Γ_3

VALUE	DOCUMENT ID		TECN	COMMENT
3.4 to 4.4 OUR ESTIMATE				
3.9±1.0	UHLIG	67	HBC	$K^- p$ 0.9–1.0 GeV/c
3.3±1.1	BIRMINGHAM	66	HBC	$K^- p$ 3.5 GeV/c
4.5±1.0	ARMENTEROS	65C	HBC	

$\Gamma(\Sigma(1385)\pi, S\text{-wave})/\Gamma_{total}$ — Γ_4/Γ

VALUE	DOCUMENT ID		TECN	COMMENT
• • • We do not use the following data for averages, fits, limits, etc. • • •				
0.121	[1] KAMANO	15	DPWA	$\overline{K}N$ multichannel

[1] From the preferred solution A in KAMANO 15.

$\Gamma(\Sigma(1385)\pi, D\text{-wave})/\Gamma_{total}$ — Γ_5/Γ

VALUE	DOCUMENT ID		TECN	COMMENT
• • • We do not use the following data for averages, fits, limits, etc. • • •				
0.003	[1] KAMANO	15	DPWA	Multichannel

[1] From the preferred solution A in KAMANO 15.

$\Gamma(\Sigma(1385)\pi)/\Gamma_{total}$ — Γ_6/Γ

VALUE	DOCUMENT ID		TECN	COMMENT
0.041±0.005	CHAN	72	HBC	$K^- p \rightarrow \Lambda\pi\pi$

$\Gamma(\Sigma(1385)\pi(\rightarrow \Lambda\pi\pi))/\Gamma(\Lambda\pi\pi)$ — Γ_7/Γ_3

The $\Lambda\pi\pi$ mode is largely due to $\Sigma(1385)\pi$. Only the values of $(\Sigma(1385)\pi)$ / $(\Lambda 2\pi)$ given by MAST 73B and CORDEN 75 are based on real 3-body partial-wave analyses. The discrepancy between the two results is essentially due to the different hypotheses made concerning the shape of the $(\pi\pi)_{S\text{-wave}}$ state.

VALUE	CL%	DOCUMENT ID		TECN	COMMENT
0.58±0.22		CORDEN	75	DBC	$K^- d$ 1.4–1.8 GeV/c
0.82±0.10		[1] MAST	73B	IPWA	$K^- p \rightarrow \Lambda\pi\pi$
• • • We do not use the following data for averages, fits, limits, etc. • • •					
<0.44	90	WIELAND	11	SPHR	$\gamma p \rightarrow K^+\Lambda(1520)$
0.39±0.10		[2] BURKHARDT	71	HBC	$K^- p \rightarrow (\Lambda\pi\pi)\pi$

[1] Both $\Sigma(1385)\pi$ DS_{03} and $\Sigma(\pi\pi)$ DP_{03} contribute.

[2] The central bin (1514–1524 MeV) gives 0.74 ± 0.10; other bins are lower by 2-to-5 standard deviations.

$\Gamma(\Lambda(\pi\pi)_{S\text{-wave}})/\Gamma(\Lambda\pi\pi)$ — Γ_8/Γ_3

VALUE	DOCUMENT ID		TECN	COMMENT
0.20±0.08	CORDEN	75	DBC	$K^- d$ 1.4–1.8 GeV/c

$\Gamma(\Sigma\pi\pi)/\Gamma_{total}$ — Γ_9/Γ

VALUE	DOCUMENT ID		TECN	COMMENT
0.007 to 0.011 OUR ESTIMATE				
0.007 ±0.002	[1] CORDEN	75	DBC	$K^- d$ 1.4–1.8 GeV/c
0.0085±0.0006	[2] MAST	73	MPWA	$K^- p \rightarrow \Sigma\pi\pi$
0.010 ±0.0015	BARBARO-...	69B	HBC	$K^- p$ 0.28–0.45 GeV/c

[1] Much of the $\Sigma\pi\pi$ decay proceeds via $\Sigma(1385)\pi$.

[2] Assumes $\Gamma(N\overline{K})/\Gamma_{total} = 0.46$.

$\Gamma(\Lambda\gamma)/\Gamma_{total}$ — Γ_{10}/Γ

VALUE (units 10^{-3})	EVTS	DOCUMENT ID		TECN	COMMENT
7 to 11 OUR ESTIMATE					
$10.7\pm2.9^{+1.5}_{-0.4}$	32	TAYLOR	05	CLAS	$\gamma p \rightarrow K^+\Lambda\gamma$
10.2±2.1±1.5	290	ANTIPOV	04A	SPNX	$p N(C) \rightarrow \Lambda(1520) K^+ N(C)$
8.0±1.4	238	MAST	68B	HBC	Using $\Gamma(N\overline{K})/\Gamma_{total} = 0.45$

$\Gamma(\Sigma^0\gamma)/\Gamma_{total}$ — Γ_{11}/Γ

VALUE	DOCUMENT ID		TECN	COMMENT
0.02±0.0035	[1] MAST	68B	HBC	Not measured; see note

[1] Calculated from $\Gamma(\Lambda\gamma)/\Gamma_{total}$, assuming SU(3). Needed to constrain the sum of all the branching ratios to be unity.

$\Lambda(1520)$ REFERENCES

SARANTSEV	19	EPJ A55 180	A.V. Sarantsev *et al.*	(BONN, PNPI)
KAMANO	15	PR C92 025205	H. Kamano *et al.*	(ANL, OSAK)
ZHANG	13A	PR C88 035205	H. Zhang *et al.*	(KSU)
WIELAND	11	EPJ A47 47	F. Wieland *et al.*	(ELSA SAPHIR Collab.)
QIANG	10	PL B694 123	Y. Qiang *et al.*	(DUKE, JEFF, PNPI, GWU+)
TAYLOR	05	PR C71 054609	S. Taylor *et al.*	(JLab CLAS Collab.)
Also		PR C72 039902 (errat.)	S. Taylor *et al.*	(JLab CLAS Collab.)
ANTIPOV	04A	PL B604 22	Yu.M. Antipov *et al.*	(IHEP SPHINX Collab.)
PDG	82	PL 111B 1	M. Roos *et al.*	(HELS, CIT, CERN)
BARBER	80D	ZPHY C7 17	D.P. Barber *et al.*	(DARE, LANC, SHEF)
GOPAL	80	Toronto Conf. 159	G.P. Gopal	(RHEL) IJP
BARLAG	79	NP B149 220	S.J.M. Barlag *et al.*	(AMST, CERN, NIJM+)
ALSTON-...	78	PR D18 182	M. Alston-Garnjost *et al.*	(LBL, MTHO+) IJP
Also		PRL 38 1007	M. Alston-Garnjost *et al.*	(LBL, MTHO+) IJP
CAMERON	77	NP B131 399	W. Cameron *et al.*	(RHEL, LOIC) IJP
GOPAL	77	NP B119 362	G.P. Gopal *et al.*	(LOIC, RHEL) IJP
MAST	76	PR D14 13	T.S. Mast *et al.*	(LBL)
CORDEN	75	NP B84 306	M.J. Corden *et al.*	(BIRM)
BERTHON	74	NC 21A 146	A. Berthon *et al.*	(CDEF, RHEL, SACL+)
MAST	73	PR D7 3212	T.S. Mast *et al.*	(LBL) IJP
MAST	73B	PR D7 5	T.S. Mast *et al.*	(LBL) IJP
CHAN	72	PRL 28 256	S.B. Chan *et al.*	(MASA, YALE)
BURKHARDT	71	NP B27 64	E. Burkhardt *et al.*	(HEID, CERN, SACL)
KIM	71	PRL 27 356	J.K. Kim	(HARV) IJP
Also		Duke Conf. 161	J.K. Kim	(HARV) IJP
Hyperon Resonances, 1970				
BARBARO-...	69B	Lund Conf. 352	A. Barbaro-Galtieri *et al.*	(LRL)
Also		Duke Conf. 95	R.D. Tripp	(LRL)
Hyperon Resonances 1970				
BURKHARDT	69	NP B14 106	E. Burkhardt *et al.*	(HEID, EFI, CERN+)
MAST	68B	PRL 21 1715	T.S. Mast *et al.*	(LRL)
SCHEUER	68	NP B8 503	J.C. Scheuer *et al.*	(SABRE Collab.)
DAHL	67	PR 163 1377	O.I. Dahl *et al.*	(LRL)
DAUBER	67	PL 24B 525	P.M. Dauber *et al.*	(UCLA)

Downloaded from https://academic.oup.com/ptep/article/2022/8/083C01/6651666 by KIT Library user on 27 September 2022

UHLIG	67	PR 155 1448	R.P. Uhlig *et al.*	(UMD, NRL)
BIRMINGHAM	66	PR 152 1148	M. Haque *et al.*	(BIRM, GLAS, LOIC, OXF+)
ARMENTEROS	65C	PL 19 338	R. Armenteros *et al.*	(CERN, HEID, SACL)
MUSGRAVE	65	NC 35 735	B. Musgrave *et al.*	(BIRM, CERN, EPOL+)
WATSON	63	PR 131 2248	M.B. Watson, M. Ferro-Luzzi, R.D. Tripp	(LRL) IJP
FERRO-LUZZI	62	PRL 8 28	M. Ferro-Luzzi, R.D. Tripp, M.B. Watson	(LRL) IJP

$\Lambda(1600)\ 1/2^+$

$I(J^P) = 0(\frac{1}{2}^+)$ Status: ****

$\Lambda(1600)$ POLE POSITION

REAL PART

VALUE (MeV)	DOCUMENT ID		TECN	COMMENT
1540 to 1560 (≈ 1550) OUR ESTIMATE				
1546±6 OUR AVERAGE Error includes scale factor of 2.1.				
1562±8	SARANTSEV	19	DPWA	$\overline{K}N$ multichannel
1544^{+3}_{-3}	[1] KAMANO	15	DPWA	Multichannel
• • • We do not use the following data for averages, fits, limits, etc. • • •				
1572	ZHANG	13A	DPWA	Multichannel

[1] From the preferred solution A in KAMANO 15.

−2×IMAGINARY PART

VALUE (MeV)	DOCUMENT ID		TECN	COMMENT
120 to 240 (≈ 180) OUR ESTIMATE				
$\mathbf{159^{+60}_{-12}}$ **OUR AVERAGE** Error includes scale factor of 6.2.				
232±15	SARANTSEV	19	DPWA	$\overline{K}N$ multichannel
112^{+12}_{-2}	[1] KAMANO	15	DPWA	Multichannel
• • • We do not use the following data for averages, fits, limits, etc. • • •				
138	ZHANG	13A	DPWA	Multichannel

[1] From the preferred solution A in KAMANO 15.

$\Lambda(1600)$ POLE RESIDUES

The normalized residue is the residue divided by $\Gamma_{pole}/2$.

Normalized residue in $N\overline{K} \to \Lambda(1600) \to N\overline{K}$

MODULUS	PHASE (°)	DOCUMENT ID		TECN	COMMENT
0.36 ±0.07	**−63 ± 10**	SARANTSEV	19	DPWA	$\overline{K}N$ multichannel
• • • We do not use the following data for averages, fits, limits, etc. • • •					
0.105	−80	[1] KAMANO	15	DPWA	Multichannel

[1] From the preferred solution A in KAMANO 15.

Normalized residue in $N\overline{K} \to \Lambda(1600) \to \Sigma\pi$

MODULUS	PHASE (°)	DOCUMENT ID		TECN	COMMENT
0.39 ±0.08	**148 ± 10**	SARANTSEV	19	DPWA	$\overline{K}N$ multichannel
• • • We do not use the following data for averages, fits, limits, etc. • • •					
0.232	108	[1] KAMANO	15	DPWA	Multichannel

[1] From the preferred solution A in KAMANO 15.

Normalized residue in $N\overline{K} \to \Lambda(1600) \to \Lambda\eta$

MODULUS	PHASE (°)	DOCUMENT ID		TECN	COMMENT
0.22±0.13	**180 ± 20**	SARANTSEV	19	DPWA	$\overline{K}N$ multichannel

Normalized residue in $N\overline{K} \to \Lambda(1600) \to \Lambda\sigma$

MODULUS	PHASE (°)	DOCUMENT ID		TECN	COMMENT
0.30±0.06	**−70 ± 10**	SARANTSEV	19	DPWA	$\overline{K}N$ multichannel

Normalized residue in $N\overline{K} \to \Lambda(1600) \to \Sigma(1385)\pi$

MODULUS	PHASE (°)	DOCUMENT ID		TECN	COMMENT
0.37 ±0.07	**103 ± 12**	SARANTSEV	19	DPWA	$\overline{K}N$ multichannel
• • • We do not use the following data for averages, fits, limits, etc. • • •					
0.183	77	[1] KAMANO	15	DPWA	Multichannel

[1] From the preferred solution A in KAMANO 15.

Normalized residue in $N\overline{K} \to \Lambda(1600) \to N\overline{K}^*(892)$, S=1/2, P-wave

MODULUS	PHASE (°)	DOCUMENT ID		TECN	COMMENT
0.02±0.01	**126 ± 45**	SARANTSEV	19	DPWA	$\overline{K}N$ multichannel

Normalized residue in $N\overline{K} \to \Lambda(1600) \to N\overline{K}^*(892)$, S=3/2, P-wave

MODULUS	PHASE (°)	DOCUMENT ID		TECN	COMMENT
0.02±0.01	**−135 ± 45**	SARANTSEV	19	DPWA	$\overline{K}N$ multichannel

$\Lambda(1600)$ MASS

VALUE (MeV)	DOCUMENT ID		TECN	COMMENT
1570 to 1630 (≈ 1600) OUR ESTIMATE				
1605± 8	SARANTSEV	19	DPWA	$\overline{K}N$ multichannel
1592± 10	ZHANG	13A	DPWA	Multichannel
1568± 20	GOPAL	80	DPWA	$\overline{K}N \to \overline{K}N$
1703±100	ALSTON-...	78	DPWA	$\overline{K}N \to \overline{K}N$
1573± 25	GOPAL	77	DPWA	$\overline{K}N$ multichannel
1596± 6	KANE	74	DPWA	$K^-p \to \Sigma\pi$
1620± 10	LANGBEIN	72	IPWA	$\overline{K}N$ multichannel
• • • We do not use the following data for averages, fits, limits, etc. • • •				
1572 or 1617	[1] MARTIN	77	DPWA	$\overline{K}N$ multichannel
1646± 7	[2] CARROLL	76	DPWA	Isospin-0 total σ
1570	KIM	71	DPWA	K-matrix analysis

[1] The two MARTIN 77 values are from a T-matrix pole and from a Breit-Wigner fit.
[2] A total cross-section bump with $(J+1/2)\ \Gamma_{el}\ /\ \Gamma_{total} = 0.04$.

$\Lambda(1600)$ WIDTH

VALUE (MeV)	DOCUMENT ID		TECN	COMMENT
150 to 250 (≈ 200) OUR ESTIMATE				
245± 15	SARANTSEV	19	DPWA	$\overline{K}N$ multichannel
150± 28	ZHANG	13A	DPWA	Multichannel
116± 20	GOPAL	80	DPWA	$\overline{K}N \to \overline{K}N$
593±200	ALSTON-...	78	DPWA	$\overline{K}N \to \overline{K}N$
147± 50	GOPAL	77	DPWA	$\overline{K}N$ multichannel
175± 20	KANE	74	DPWA	$K^-p \to \Sigma\pi$
60± 10	LANGBEIN	72	IPWA	$\overline{K}N$ multichannel
• • • We do not use the following data for averages, fits, limits, etc. • • •				
247 or 271	[1] MARTIN	77	DPWA	$\overline{K}N$ multichannel
20	[2] CARROLL	76	DPWA	Isospin-0 total σ
50	KIM	71	DPWA	K-matrix analysis

[1] The two MARTIN 77 values are from a T-matrix pole and from a Breit-Wigner fit.
[2] A total cross-section bump with $(J+1/2)\ \Gamma_{el}\ /\ \Gamma_{total} = 0.04$.

$\Lambda(1600)$ DECAY MODES

	Mode	Fraction (Γ_i/Γ)
Γ_1	$N\overline{K}$	15–30 %
Γ_2	$\Sigma\pi$	10–60 %
Γ_3	$\Lambda\sigma$	(19±4) %
Γ_4	$\Sigma(1385)\pi$	(9±4) %

$\Lambda(1600)$ BRANCHING RATIOS

See "Sign conventions for resonance couplings" in the Note on Λ and Σ Resonances.

$\Gamma(N\overline{K})/\Gamma_{total}$ — Γ_1/Γ

VALUE	DOCUMENT ID		TECN	COMMENT
0.14 to 0.28 OUR ESTIMATE				
0.29 ±0.06	SARANTSEV	19	DPWA	$\overline{K}N$ multichannel
0.14 ±0.04	ZHANG	13A	DPWA	Multichannel
0.23 ±0.04	GOPAL	80	DPWA	$\overline{K}N \to \overline{K}N$
0.14 ±0.05	ALSTON-...	78	DPWA	$\overline{K}N \to \overline{K}N$
0.25 ±0.15	LANGBEIN	72	IPWA	$\overline{K}N$ multichannel
• • • We do not use the following data for averages, fits, limits, etc. • • •				
0.064	[1] KAMANO	15	DPWA	Multichannel
0.24 ±0.04	GOPAL	77	DPWA	See GOPAL 80
0.30 or 0.29	[2] MARTIN	77	DPWA	$\overline{K}N$ multichannel

[1] From the preferred solution A in KAMANO 15.
[2] The two MARTIN 77 values are from a T-matrix pole and from a Breit-Wigner fit.

$\Gamma(\Sigma\pi)/\Gamma_{total}$ — Γ_2/Γ

VALUE	DOCUMENT ID		TECN	COMMENT
0.37 ±0.07	SARANTSEV	19	DPWA	$\overline{K}N$ multichannel
• • • We do not use the following data for averages, fits, limits, etc. • • •				
0.851	[1] KAMANO	15	DPWA	Multichannel

[1] From the preferred solution A in KAMANO 15.

$\Gamma(\Lambda\sigma)/\Gamma_{total}$ — Γ_3/Γ

VALUE	DOCUMENT ID		TECN	COMMENT
0.19±0.04	SARANTSEV	19	DPWA	$\overline{K}N$ multichannel

$\Gamma(\Sigma(1385)\pi)/\Gamma_{total}$ — Γ_4/Γ

VALUE	DOCUMENT ID		TECN	COMMENT
0.09 ±0.04	SARANTSEV	19	DPWA	$\overline{K}N$ multichannel
• • • We do not use the following data for averages, fits, limits, etc. • • •				
0.085	[1] KAMANO	15	DPWA	Multichannel

[1] From the preferred solution A in KAMANO 15.

$(\Gamma_i\Gamma_f)^{1/2}/\Gamma_{total}$ in $N\overline{K} \to \Lambda(1600) \to \Sigma\pi$ — $(\Gamma_1\Gamma_2)^{1/2}/\Gamma$

VALUE	DOCUMENT ID		TECN	COMMENT
−0.23±0.03	ZHANG	13A	DPWA	Multichannel
−0.16±0.04	GOPAL	77	DPWA	$\overline{K}N$ multichannel
−0.33±0.11	KANE	74	DPWA	$K^-p \to \Sigma\pi$
0.28±0.09	LANGBEIN	72	IPWA	$\overline{K}N$ multichannel
• • • We do not use the following data for averages, fits, limits, etc. • • •				
−0.39 or −0.39	[1] MARTIN	77	DPWA	$\overline{K}N$ multichannel
not seen	HEPP	76B	DPWA	$K^-N \to \Sigma\pi$

[1] The two MARTIN 77 values are from a T-matrix pole and from a Breit-Wigner fit.

Downloaded from https://academic.oup.com/ptep/article/2022/8/083C01/6651666 by KIT Library user on 27 September 2022

$\Lambda(1600)$ REFERENCES

SARANTSEV	19	EPJ A55 180	A.V. Sarantsev *et al.*	(BONN, PNPI)
KAMANO	15	PR C92 025205	H. Kamano *et al.*	(ANL, OSAK)
ZHANG	13A	PR C88 035205	H. Zhang *et al.*	(KSU)
GOPAL	80	Toronto Conf. 159	G.P. Gopal	(RHEL) IJP
ALSTON-...	78	PR D18 182	M. Alston-Garnjost *et al.*	(LBL, MTHO+) IJP
Also		PRL 38 1007	M. Alston-Garnjost *et al.*	(LBL, MTHO+) IJP
GOPAL	77	NP B119 362	G.P. Gopal *et al.*	(LOIC, RHEL) IJP
MARTIN	77	NP B127 349	B.R. Martin, M.K. Pidcock, R.G. Moorhouse	(LOUC+) IJP
Also		NP B126 266	B.R. Martin, M.K. Pidcock	(LOUC)
Also		NP B126 285	B.R. Martin, M.K. Pidcock	(LOUC) IJP
CARROLL	76	PRL 37 806	A.S. Carroll *et al.*	(BNL) I
HEPP	76B	PL 65B 487	V. Hepp *et al.*	(CERN, HEIDH, MPIM) IJP
KANE	74	LBL-2452	D.F. Kane	(LBL) IJP
LANGBEIN	72	NP B47 477	W. Langbein, F. Wagner	(MPIM) IJP
KIM	71	PRL 27 356	J.K. Kim	(HARV) IJP

$\Lambda(1670)$ $1/2^-$

$I(J^P) = 0(\frac{1}{2}^-)$ Status: ****

The measurements of the mass, width, and elasticity published before 1974 are now obsolete and have been omitted. They were last listed in our 1982 edition Physics Letters **111B** 1 (1982).

$\Lambda(1670)$ POLE POSITIONS

REAL PART

VALUE (MeV)	DOCUMENT ID		TECN	COMMENT
1670 to 1678 (≈ 1674) OUR ESTIMATE				
1676 ±2	SARANTSEV	19	DPWA	$\overline{K}N$ multichannel
1669 $^{+3}_{-8}$	[1] KAMANO	15	DPWA	$\overline{K}N$ multichannel
1677.5 ±0.8	GARCIA-REC...	03	DPWA	$\overline{K}N$ multichannel
• • • We do not use the following data for averages, fits, limits, etc. • • •				
1667	ZHANG	13A	DPWA	$\overline{K}N$ multichannel

[1] From the preferred solution A in KAMANO 15.

−2×IMAGINARY PART

VALUE (MeV)	DOCUMENT ID		TECN	COMMENT
28 to 36 (≈ 32) OUR ESTIMATE				
33 ± 4	SARANTSEV	19	DPWA	$\overline{K}N$ multichannel
19 $^{+18}_{-2}$	[1] KAMANO	15	DPWA	$\overline{K}N$ multichannel
29.2± 1.4	GARCIA-REC...	03	DPWA	$\overline{K}N$ multichannel
• • • We do not use the following data for averages, fits, limits, etc. • • •				
26	ZHANG	13A	DPWA	$\overline{K}N$ multichannel

[1] From the preferred solution A in KAMANO 15.

$\Lambda(1670)$ POLE RESIDUES

The normalized residue is the residue divided by $\Gamma_{pole}/2$.

Normalized residue in $\overline{K}N \to \Lambda(1670) \to \overline{K}N$

MODULUS	PHASE (°)	DOCUMENT ID		TECN	COMMENT
0.30 ±0.06	**−145 ± 11**	SARANTSEV	19	DPWA	$\overline{K}N$ multichannel
• • • We do not use the following data for averages, fits, limits, etc. • • •					
0.351	164	[1] KAMANO	15	DPWA	$\overline{K}N$ multichannel

[1] From the preferred solution A in KAMANO 15.

Normalized residue in $N\overline{K} \to \Lambda(1670) \to \Sigma\pi$

MODULUS	PHASE (°)	DOCUMENT ID		TECN	COMMENT
0.19 ±0.06	**145 ± 14**	SARANTSEV	19	DPWA	$\overline{K}N$ multichannel
• • • We do not use the following data for averages, fits, limits, etc. • • •					
0.327	125	[1] KAMANO	15	DPWA	$\overline{K}N$ multichannel

[1] From the preferred solution A in KAMANO 15.

Normalized residue in $N\overline{K} \to \Lambda(1670) \to \Lambda\eta$

MODULUS	PHASE (°)	DOCUMENT ID		TECN	COMMENT
0.26 ±0.09	**104 ± 14**	SARANTSEV	19	DPWA	$\overline{K}N$ multichannel
• • • We do not use the following data for averages, fits, limits, etc. • • •					
0.474	59	[1] KAMANO	15	DPWA	Multichannel

[1] From the preferred solution A in KAMANO 15.

Normalized residue in $N\overline{K} \to \Lambda(1670) \to \Xi K$

MODULUS	PHASE (°)	DOCUMENT ID		TECN	COMMENT
0.02±0.02	**100 ± 25**	SARANTSEV	19	DPWA	$\overline{K}N$ multichannel

Normalized residue in $N\overline{K} \to \Lambda(1670) \to \Lambda\omega$, S=1/2, S-wave

MODULUS	PHASE (°)	DOCUMENT ID		TECN	COMMENT
0.09±0.04	**−60 ± 35**	SARANTSEV	19	DPWA	$\overline{K}N$ multichannel

Normalized residue in $N\overline{K} \to \Lambda(1670) \to \Lambda\omega$, S=3/2, D-wave

MODULUS	PHASE (°)	DOCUMENT ID		TECN	COMMENT
0.05±0.04		SARANTSEV	19	DPWA	$\overline{K}N$ multichannel

Normalized residue in $N\overline{K} \to \Lambda(1670) \to N\overline{K}^*(892)$, S=1/2, S-wave

MODULUS	PHASE (°)	DOCUMENT ID		TECN	COMMENT
0.31±0.14	**100 ± 45**	SARANTSEV	19	DPWA	$\overline{K}N$ multichannel

Normalized residue in $N\overline{K} \to \Lambda(1670) \to N\overline{K}^*(892)$, S=3/2, D-wave

MODULUS	PHASE (°)	DOCUMENT ID		TECN	COMMENT
0.06±0.03	**−85 ± 40**	SARANTSEV	19	DPWA	$\overline{K}N$ multichannel

Normalized residue in $N\overline{K} \to \Lambda(1670) \to \Lambda\sigma$

MODULUS	PHASE (°)	DOCUMENT ID		TECN	COMMENT
0.25±0.08	**160 ± 15**	SARANTSEV	19	DPWA	$\overline{K}N$ multichannel

Normalized residue in $N\overline{K} \to \Lambda(1670) \to \Sigma(1385)\pi$

MODULUS	PHASE (°)	DOCUMENT ID		TECN	COMMENT
0.13 ±0.06	**110 ± 12**	SARANTSEV	19	DPWA	$\overline{K}N$ multichannel
• • • We do not use the following data for averages, fits, limits, etc. • • •					
0.0988	−104	[1] KAMANO	15	DPWA	Multichannel

[1] From the preferred solution A in KAMANO 15.

$\Lambda(1670)$ MASS

VALUE (MeV)	DOCUMENT ID		TECN	COMMENT
1670 to 1678 (≈ 1674) OUR ESTIMATE				
1674.3±0.8±4.9	LEE	21A	BELL	$\Lambda_c^+ \to \Lambda(1670)\pi^+$
1677 ±2	SARANTSEV	19	DPWA	$\overline{K}N$ multichannel
1672 ±3	ZHANG	13A	DPWA	Multichannel
1670.8±1.7	KOISO	85	DPWA	$K^-p \to \Sigma\pi$
1667 ±5	GOPAL	80	DPWA	$\overline{K}N \to \overline{K}N$
1671 ±3	ALSTON-...	78	DPWA	$\overline{K}N \to \overline{K}N$
1675 ±2	HEPP	76B	DPWA	$K^-N \to \Sigma\pi$
1679 ±1	KANE	74	DPWA	$K^-p \to \Sigma\pi$
1665 ±5	PREVOST	74	DPWA	$K^-N \to \Sigma(1385)\pi$
• • • We do not use the following data for averages, fits, limits, etc. • • •				
1673 ±2	MANLEY	02	DPWA	$\overline{K}N$ multichannel
1668.9±2.0	ABAEV	96	DPWA	$K^-p \to \Lambda\eta$
1670 ±5	GOPAL	77	DPWA	$\overline{K}N$ multichannel
1664	[1] MARTIN	77	DPWA	$\overline{K}N$ multichannel

[1] MARTIN 77 obtains identical resonance parameters from a T-matrix pole and from a Breit-Wigner fit.

$\Lambda(1670)$ WIDTH

VALUE (MeV)	DOCUMENT ID		TECN	COMMENT
25 to 35 (≈ 30) OUR ESTIMATE				
36.1± 2.4±4.8	LEE	21A	BELL	$\Lambda_c^+ \to \Lambda(1670)\pi^+$
33 ± 4	SARANTSEV	19	DPWA	$\overline{K}N$ multichannel
29 ± 5	ZHANG	13A	DPWA	$\overline{K}N$ multichannel
34.1± 3.7	KOISO	85	DPWA	$K^-p \to \Sigma\pi$
29 ± 5	GOPAL	80	DPWA	$\overline{K}N \to \overline{K}N$
29 ± 5	ALSTON-...	78	DPWA	$\overline{K}N \to \overline{K}N$
46 ± 5	HEPP	76B	DPWA	$K^-N \to \Sigma\pi$
40 ± 3	KANE	74	DPWA	$K^-p \to \Sigma\pi$
19 ± 5	PREVOST	74	DPWA	$K^-N \to \Sigma(1385)\pi$
• • • We do not use the following data for averages, fits, limits, etc. • • •				
23 ± 6	MANLEY	02	DPWA	$\overline{K}N$ multichannel
21.1± 3.6	ABAEV	96	DPWA	$K^-p \to \Lambda\eta$
45 ±10	GOPAL	77	DPWA	$\overline{K}N$ multichannel
12	[1] MARTIN	77	DPWA	$\overline{K}N$ multichannel

[1] MARTIN 77 obtains identical resonance parameters from a T-matrix pole and from a Breit-Wigner fit.

$\Lambda(1670)$ DECAY MODES

	Mode	Fraction (Γ_i/Γ)
Γ_1	$N\overline{K}$	20–30 %
Γ_2	$\Sigma\pi$	25–55 %
Γ_3	$\Lambda\eta$	10–25 %
Γ_4	$\Sigma(1385)\pi$, D-wave	(6.0±2.0) %
Γ_5	$N\overline{K}^*(892)$, S=1/2, S-wave	
Γ_6	$N\overline{K}^*(892)$, S=3/2, D-wave	(5 ±4) %
Γ_7	$\Lambda\sigma$	(20 ±8) %

$\Lambda(1670)$ BRANCHING RATIOS

See "Sign conventions for resonance couplings" in the Note on Λ and Σ Resonances.

$\Gamma(N\overline{K})/\Gamma_{total}$ — Γ_1/Γ

VALUE	DOCUMENT ID		TECN	COMMENT
0.20 to 0.30 OUR ESTIMATE				
0.33 ±0.07	SARANTSEV	19	DPWA	$\overline{K}N$ multichannel
0.26 ±0.25	ZHANG	13A	DPWA	$\overline{K}N$ multichannel
0.18 ±0.03	GOPAL	80	DPWA	$\overline{K}N \to \overline{K}N$
0.17 ±0.03	ALSTON-...	78	DPWA	$\overline{K}N \to \overline{K}N$

Downloaded from https://academic.oup.com/ptep/article/2022/8/083C01/6651666 by KIT Library user on 27 September 2022

• • • We do not use the following data for averages, fits, limits, etc. • • •

0.318	[1] KAMANO	15	DPWA	$\overline{K}N$ multichannel
0.37 ±0.07	MANLEY	02	DPWA	$\overline{K}N$ multichannel
0.20 ±0.03	GOPAL	77	DPWA	See GOPAL 80
0.15	[2] MARTIN	77	DPWA	$\overline{K}N$ multichannel

[1] From the preferred solution A in KAMANO 15.
[2] MARTIN 77 obtains identical resonance parameters from a T-matrix pole and from a Breit-Wigner fit.

$\Gamma(\Sigma\pi)/\Gamma_{total}$ — Γ_2/Γ

VALUE	DOCUMENT ID		TECN	COMMENT
0.12 ±0.03	SARANTSEV	19	DPWA	$\overline{K}N$ multichannel
• • • We do not use the following data for averages, fits, limits, etc. • • •				
0.289	[1] KAMANO	15	DPWA	Multichannel

[1] From the preferred solution A in KAMANO 15.

$\Gamma(\Lambda\eta)/\Gamma_{total}$ — Γ_3/Γ

VALUE	DOCUMENT ID		TECN	COMMENT
0.20 ±0.08	SARANTSEV	19	DPWA	$\overline{K}N$ multichannel
• • • We do not use the following data for averages, fits, limits, etc. • • •				
0.373	KAMANO	15	DPWA	Multichannel
0.30 ±0.08	ABAEV	96	DPWA	$K^-p \to \Lambda\eta$

$\Gamma(\Sigma(1385)\pi, D\text{-wave})/\Gamma_{total}$ — Γ_4/Γ

VALUE	DOCUMENT ID		TECN	COMMENT
0.06 ±0.02	SARANTSEV	19	DPWA	$\overline{K}N$ multichannel
• • • We do not use the following data for averages, fits, limits, etc. • • •				
0.019	KAMANO	15	DPWA	Multi-channel

$\Gamma(\Lambda\sigma)/\Gamma_{total}$ — Γ_7/Γ

VALUE	DOCUMENT ID		TECN	COMMENT
0.20±0.08	SARANTSEV	19	DPWA	$\overline{K}N$ multichannel

$\Gamma(N\overline{K}^*(892), S=1/2, S\text{-wave})/\Gamma_{total}$ — Γ_5/Γ

VALUE	DOCUMENT ID		TECN	COMMENT
• • • We do not use the following data for averages, fits, limits, etc. • • •				
not seen	[1] KAMANO	15	DPWA	Multichannel

[1] Not seen in the preferred solution A in KAMANO 15.

$\Gamma(N\overline{K}^*(892), S=3/2, D\text{-wave})/\Gamma_{total}$ — Γ_6/Γ

VALUE	DOCUMENT ID		TECN	COMMENT
0.05±0.04	ZHANG	13A	DPWA	Multichannel
• • • We do not use the following data for averages, fits, limits, etc. • • •				
not seen	[1] KAMANO	15	DPWA	Multichannel

[1] Not seen in the preferred solution A in KAMANO 15.

$(\Gamma_i\Gamma_f)^{1/2}/\Gamma_{total}$ in $N\overline{K} \to \Lambda(1670) \to \Sigma\pi$ — $(\Gamma_1\Gamma_2)^{1/2}/\Gamma$

VALUE	DOCUMENT ID		TECN	COMMENT
−0.29±0.06	ZHANG	13A	DPWA	Multichannel
−0.26±0.02	KOISO	85	DPWA	$K^-p \to \Sigma\pi$
−0.31±0.03	GOPAL	77	DPWA	$\overline{K}N$ multichannel
−0.29±0.03	HEPP	76B	DPWA	$K^-N \to \Sigma\pi$
−0.23±0.03	LONDON	75	HLBC	$K^-p \to \Sigma^0\pi^0$
−0.27±0.02	KANE	74	DPWA	$K^-p \to \Sigma\pi$
• • • We do not use the following data for averages, fits, limits, etc. • • •				
−0.38±0.03	MANLEY	02	DPWA	$\overline{K}N$ multichannel
−0.13	[1] MARTIN	77	DPWA	$\overline{K}N$ multichannel

[1] MARTIN 77 obtains identical resonance parameters from a T-matrix pole and from a Breit-Wigner fit.

$(\Gamma_i\Gamma_f)^{1/2}/\Gamma_{total}$ in $N\overline{K} \to \Lambda(1670) \to \Lambda\eta$ — $(\Gamma_1\Gamma_3)^{1/2}/\Gamma$

VALUE	DOCUMENT ID		TECN	COMMENT
−0.30±0.10	ZHANG	13A	DPWA	Multichannel
+0.20±0.05	BAXTER	73	DPWA	$K^-p \to$ neutrals
• • • We do not use the following data for averages, fits, limits, etc. • • •				
+0.24±0.04	MANLEY	02	DPWA	$\overline{K}N$ multichannel
0.24	KIM	71	DPWA	K-matrix analysis
0.26	ARMENTEROS	69C	HBC	
0.20 or 0.23	BERLEY	65	HBC	

$(\Gamma_i\Gamma_f)^{1/2}/\Gamma_{total}$ in $N\overline{K} \to \Lambda(1670) \to \Sigma(1385)\pi$, D-wave — $(\Gamma_1\Gamma_4)^{1/2}/\Gamma$

VALUE	DOCUMENT ID		TECN	COMMENT
−0.17±0.06	MANLEY	02	DPWA	$\overline{K}N$ multichannel
−0.18±0.05	PREVOST	74	DPWA	$K^-N \to \Sigma(1385)\pi$

$\Lambda(1670)$ REFERENCES

LEE	21A	PR D103 052005	J.Y. Lee *et al.*	(BELLE Collab.)
SARANTSEV	19	EPJ A55 180	A.V. Sarantsev *et al.*	(BONN, PNPI)
KAMANO	15	PR C92 025205	H. Kamano *et al.*	(ANL, OSAK)
ZHANG	13A	PR C88 035205	H. Zhang *et al.*	(KSU)
GARCIA-REC...	03	PR D67 076009	C. Garcia-Recio *et al.*	(GRAN, VALE)
MANLEY	02	PRL 88 012002	D.M. Manley *et al.*	(BNL Crystal Ball Collab.)
ABAEV	96	PR C53 385	V.V. Abaev, B.M.K. Nefkens	(UCLA)
KOISO	85	NP A433 619	H. Koiso *et al.*	(TOKY, MASA)
PDG	82	PL 111B 1	M. Roos *et al.*	(HELS, CIT, CERN)
GOPAL	80	Toronto Conf. 159	G.P. Gopal	(RHEL) IJP
ALSTON-...	78	PR D18 182	M. Alston-Garnjost *et al.*	(LBL, MTHO+) IJP
Also		PRL 38 1007	M. Alston-Garnjost *et al.*	(LBL, MTHO+) IJP
GOPAL	77	NP B119 362	G.P. Gopal *et al.*	(LOIC, RHEL) IJP
MARTIN	77	NP B127 349	B.R. Martin, M.K. Pidcock, R.G. Moorhouse	(LOUC+) IJP
Also		NP B126 266	B.R. Martin, M.K. Pidcock	(LOUC)
Also		NP B126 285	B.R. Martin, M.K. Pidcock	(LOUC) IJP
HEPP	76B	PL 65B 487	V. Hepp *et al.*	(CERN, HEIDH, MPIM) IJP
LONDON	75	NP B85 289	G.W. London *et al.*	(BNL, CERN, EPOL+)
KANE	74	LBL-2452	D.F. Kane	(LBL) IJP
PREVOST	74	NP B69 246	J. Prevost *et al.*	(SACL, CERN, HEID)
BAXTER	73	NP B67 125	D.F. Baxter *et al.*	(OXF) IJP
KIM	71	PRL 27 356	J.K. Kim	(HARV) IJP
Also		Duke Conf. 161 Hyperon Resonances, 1970	J.K. Kim	(HARV) IJP
ARMENTEROS	69C	Lund Paper 229 Values are quoted in LEVI-SETTI 69.	R. Armenteros *et al.*	(CERN, HEID, SACL) IJP
BERLEY	65	PRL 15 641	D. Berley *et al.*	(BNL) IJP

$\Lambda(1690)\ 3/2^-$

$I(J^P) = 0(\frac{3}{2}^-)$ Status: ****

The measurements of the mass, width, and elasticity published before 1974 are now obsolete and have been omitted. They were last listed in our 1982 edition Physics Letters **111B** 1 (1982).

$\Lambda(1690)$ POLE POSITION

REAL PART

VALUE (MeV)	DOCUMENT ID		TECN	COMMENT
1680 to 1700 (≈ 1690) OUR ESTIMATE				
1683±3	SARANTSEV	19	DPWA	$\overline{K}N$ multichannel
1697^{+6}_{-6}	[1] KAMANO	15	DPWA	$\overline{K}N$ multichannel
• • • We do not use the following data for averages, fits, limits, etc. • • •				
1689	ZHANG	13A	DPWA	$\overline{K}N$ multichannel

[1] From the preferred solution A in KAMANO 15.

−2×IMAGINARY PART

VALUE (MeV)	DOCUMENT ID		TECN	COMMENT
60 to 80 (≈ 70) OUR ESTIMATE				
72± 5	SARANTSEV	19	DPWA	$\overline{K}N$ multichannel
65±14	[1] KAMANO	15	DPWA	$\overline{K}N$ multichannel
• • • We do not use the following data for averages, fits, limits, etc. • • •				
53	ZHANG	13A	DPWA	$\overline{K}N$ multichannel

[1] From the preferred solution A in KAMANO 15.

$\Lambda(1690)$ POLE RESIDUES

The normalized residue is the residue divided by $\Gamma_{pole}/2$.

Normalized residue in $N\overline{K} \to \Lambda(1690) \to N\overline{K}$

MODULUS	PHASE (°)	DOCUMENT ID		TECN	COMMENT
0.24 ±0.05	**−28 ± 5**	SARANTSEV	19	DPWA	$\overline{K}N$ multichannel
• • • We do not use the following data for averages, fits, limits, etc. • • •					
0.251	3	[1] KAMANO	15	DPWA	Multichannel

[1] From the preferred solution A in KAMANO 15.

Normalized residue in $N\overline{K} \to \Lambda(1690) \to \Sigma\pi$

MODULUS	PHASE (°)	DOCUMENT ID		TECN	COMMENT
0.35 ±0.07	**175 ± 6**	SARANTSEV	19	DPWA	$\overline{K}N$ multichannel
• • • We do not use the following data for averages, fits, limits, etc. • • •					
0.315	−173	[1] KAMANO	15	DPWA	$\overline{K}N$ multichannel

[1] From the preferred solution A in KAMANO 15.

Normalized residue in $N\overline{K} \to \Lambda(1690) \to \Lambda\eta$

MODULUS	PHASE (°)	DOCUMENT ID		TECN	COMMENT
0.05 ±0.02	**88 ± 8**	SARANTSEV	19	DPWA	$\overline{K}N$ multichannel
• • • We do not use the following data for averages, fits, limits, etc. • • •					
0.00567	81	[1] KAMANO	15	DPWA	Multichannel

[1] From the preferred solution A in KAMANO 15.

Normalized residue in $N\overline{K} \to \Lambda(1690) \to \Lambda\sigma$

MODULUS	PHASE (°)	DOCUMENT ID		TECN	COMMENT
0.08±0.02	**−10 ± 6**	SARANTSEV	19	DPWA	$\overline{K}N$ multichannel

Normalized residue in $N\overline{K} \to \Lambda(1690) \to \Sigma(1385)\pi$, S-wave

MODULUS	PHASE (°)	DOCUMENT ID		TECN	COMMENT
0.11 ±0.06	**170 ± 70**	SARANTSEV	19	DPWA	$\overline{K}N$ multichannel
• • • We do not use the following data for averages, fits, limits, etc. • • •					
0.134	168	[1] KAMANO	15	DPWA	$\overline{K}N$ multichannel

[1] From the preferred solution A in KAMANO 15.

Normalized residue in $N\overline{K} \to \Lambda(1690) \to \Sigma(1385)\pi$, D-wave

MODULUS	PHASE (°)	DOCUMENT ID		TECN	COMMENT
0.06 ±0.04	**164 ± 15**	SARANTSEV	19	DPWA	$\overline{K}N$ multichannel
• • • We do not use the following data for averages, fits, limits, etc. • • •					
0.319	−22	[1] KAMANO	15	DPWA	$\overline{K}N$ multichannel

[1] From the preferred solution A in KAMANO 15.

Downloaded from https://academic.oup.com/ptep/article/2022/8/083C01/6651666 by KIT Library user on 27 September 2022

Normalized residue in $N\overline{K} \to \Lambda(1690) \to N\overline{K}^*(892)$, S-wave

VALUE	DOCUMENT ID		TECN	COMMENT
0.05±0.04	SARANTSEV	19	DPWA	$\overline{K}N$ multichannel

Normalized residue in $N\overline{K} \to \Lambda(1690) \to N\overline{K}^*(892)$, D-wave

VALUE	DOCUMENT ID		TECN	COMMENT
0.18+-0.05@-110+-45	SARANTSEV	19	DPWA	$\overline{K}N$ multichannel

$\Lambda(1690)$ MASS

VALUE (MeV)	DOCUMENT ID		TECN	COMMENT
1685 to 1695 (≈ 1690) OUR ESTIMATE				
1689 ±3	SARANTSEV	19	DPWA	$\overline{K}N$ multichannel
1691 ±3	ZHANG	13A	DPWA	$\overline{K}N$ multichannel
1695.7±2.6	KOISO	85	DPWA	$K^-p \to \Sigma\pi$
1690 ±5	GOPAL	80	DPWA	$\overline{K}N \to \overline{K}N$
1692 ±5	ALSTON-...	78	DPWA	$\overline{K}N \to \overline{K}N$
1690 ±3	HEPP	76B	DPWA	$K^-N \to \Sigma\pi$
1689 ±1	KANE	74	DPWA	$K^-p \to \Sigma\pi$
• • • We do not use the following data for averages, fits, limits, etc. • • •				
1690 ±5	GOPAL	77	DPWA	$\overline{K}N$ multichannel
1687 or 1689	[1] MARTIN	77	DPWA	$\overline{K}N$ multichannel
1692 ±4	CARROLL	76	DPWA	Isospin-0 total σ

[1] The two MARTIN 77 values are from a T-matrix pole and from a Breit-Wigner fit. Another D_{03} Λ at 1966 MeV is also suggested by MARTIN 77, but is very uncertain.

$\Lambda(1690)$ WIDTH

VALUE (MeV)	DOCUMENT ID		TECN	COMMENT
60 to 80 (≈ 70) OUR ESTIMATE				
75 ± 5	SARANTSEV	19	DPWA	$\overline{K}N$ multichannel
54 ± 5	ZHANG	13A	DPWA	$\overline{K}N$ multichannel
67.2± 5.6	KOISO	85	DPWA	$K^-p \to \Sigma\pi$
61 ± 5	GOPAL	80	DPWA	$\overline{K}N \to \overline{K}N$
64 ±10	ALSTON-...	78	DPWA	$\overline{K}N \to \overline{K}N$
82 ± 8	HEPP	76B	DPWA	$K^-N \to \Sigma\pi$
60 ± 4	KANE	74	DPWA	$K^-p \to \Sigma\pi$
• • • We do not use the following data for averages, fits, limits, etc. • • •				
60 ± 5	GOPAL	77	DPWA	$\overline{K}N$ multichannel
62 or 62	[1] MARTIN	77	DPWA	$\overline{K}N$ multichannel
38	CARROLL	76	DPWA	Isospin-0 total σ

[1] The two MARTIN 77 values are from a T-matrix pole and from a Breit-Wigner fit. Another D_{03} Λ at 1966 MeV is also suggested by MARTIN 77, but is very uncertain.

$\Lambda(1690)$ DECAY MODES

	Mode	Fraction (Γ_i/Γ)
Γ_1	$N\overline{K}$	20–30 %
Γ_2	$\Sigma\pi$	20–40 %
Γ_3	$\Lambda\sigma$	(5.0±2.0) %
Γ_4	$\Lambda\pi\pi$	∼ 25 %
Γ_5	$\Sigma\pi\pi$	∼ 20 %
Γ_6	$\Lambda\eta$	
Γ_7	$\Sigma(1385)\pi$, S-wave	(9 ±5) %
Γ_8	$\Sigma(1385)\pi$, D-wave	(3.0±2.0) %
Γ_9	$N\overline{K}^*(892)$, S=1/2, D-wave	
Γ_{10}	$N\overline{K}^*(892)$, S=3/2, S-wave	
Γ_{11}	$N\overline{K}^*(892)$, S=3/2, D-wave	

$\Lambda(1690)$ BRANCHING RATIOS

$\Gamma(N\overline{K})/\Gamma_{total}$ — Γ_1/Γ

VALUE	DOCUMENT ID		TECN	COMMENT
0.20 to 0.28 OUR ESTIMATE				
0.23 ±0.05	SARANTSEV	19	DPWA	$\overline{K}N$ multichannel
0.25 ±0.04	ZHANG	13A	DPWA	$\overline{K}N$ multichannel
0.23 ±0.03	GOPAL	80	DPWA	$\overline{K}N \to \overline{K}N$
0.22 ±0.03	ALSTON-...	78	DPWA	$\overline{K}N \to \overline{K}N$
• • • We do not use the following data for averages, fits, limits, etc. • • •				
0.239	[1] KAMANO	15	DPWA	$\overline{K}N$ multichannel
0.24 ±0.03	GOPAL	77	DPWA	See GOPAL 80
0.28 or 0.26	[2] MARTIN	77	DPWA	$\overline{K}N$ multichannel

[1] From the preferred solution A in KAMANO 15.
[2] The two MARTIN 77 values are from a T-matrix pole and from a Breit-Wigner fit. Another D_{03} Λ at 1966 MeV is also suggested by MARTIN 77, but is very uncertain.

$\Gamma(\Sigma\pi)/\Gamma_{total}$ — Γ_2/Γ

VALUE	DOCUMENT ID		TECN	COMMENT
0.50 ±0.10	SARANTSEV	19	DPWA	$\overline{K}N$ multichannel
• • • We do not use the following data for averages, fits, limits, etc. • • •				
0.387	[1] KAMANO	15	DPWA	$\overline{K}N$ multichannel

[1] From the preferred solution A in KAMANO 15.

$\Gamma(\Lambda\eta)/\Gamma_{total}$ — Γ_6/Γ

VALUE	DOCUMENT ID		TECN	COMMENT
∼ 0.01	SARANTSEV	19	DPWA	$\overline{K}N$ multichannel
• • • We do not use the following data for averages, fits, limits, etc. • • •				
not seen	[1] KAMANO	15	DPWA	Multichannel

[1] From the preferred solution A in KAMANO 15.

$\Gamma(\Lambda\sigma)/\Gamma_{total}$ — Γ_3/Γ

VALUE	DOCUMENT ID		TECN	COMMENT
0.05±0.02	SARANTSEV	19	DPWA	$\overline{K}N$ multichannel

$\Gamma(\Sigma(1385)\pi, S\text{-wave})/\Gamma_{total}$ — Γ_7/Γ

VALUE	DOCUMENT ID		TECN	COMMENT
0.09 ±0.05	SARANTSEV	19	DPWA	$\overline{K}N$ multichannel
• • • We do not use the following data for averages, fits, limits, etc. • • •				
0.062	[1] KAMANO	15	DPWA	$\overline{K}N$ multichannel

[1] From the preferred solution A in KAMANO 15.

$\Gamma(\Sigma(1385)\pi, D\text{-wave})/\Gamma_{total}$ — Γ_8/Γ

VALUE	DOCUMENT ID		TECN	COMMENT
0.03 ±0.02	SARANTSEV	19	DPWA	$\overline{K}N$ multichannel
• • • We do not use the following data for averages, fits, limits, etc. • • •				
0.308	[1] KAMANO	15	DPWA	$\overline{K}N$ multichannel

[1] From the preferred solution A in KAMANO 15.

$\Gamma(N\overline{K}^*(892), S=1/2, D\text{-wave})/\Gamma_{total}$ — Γ_9/Γ

VALUE	DOCUMENT ID		TECN	COMMENT
• • • We do not use the following data for averages, fits, limits, etc. • • •				
not seen	SARANTSEV	19	DPWA	$\overline{K}N$ multichannel
not seen	[1] KAMANO	15	DPWA	$\overline{K}N$ multichannel

[1] From the preferred solution A in KAMANO 15.

$\Gamma(N\overline{K}^*(892), S=3/2, S\text{-wave})/\Gamma_{total}$ — Γ_{10}/Γ

VALUE	DOCUMENT ID		TECN	COMMENT
• • • We do not use the following data for averages, fits, limits, etc. • • •				
0.003	KAMANO	15	DPWA	Multichannel

$\Gamma(N\overline{K}^*(892), S=3/2, D\text{-wave})/\Gamma_{total}$ — Γ_{11}/Γ

VALUE	DOCUMENT ID		TECN	COMMENT
• • • We do not use the following data for averages, fits, limits, etc. • • •				
not seen	[1] KAMANO	15	DPWA	Multichannel

[1] From the preferred solution A in KAMANO 15.

$(\Gamma_i\Gamma_f)^{1/2}/\Gamma_{total}$ in $N\overline{K} \to \Lambda(1690) \to \Sigma\pi$ — $(\Gamma_1\Gamma_2)^{1/2}/\Gamma$

VALUE	DOCUMENT ID		TECN	COMMENT
−0.27±0.03	ZHANG	13A	DPWA	Multichannel
−0.34±0.02	KOISO	85	DPWA	$K^-p \to \Sigma\pi$
−0.25±0.03	GOPAL	77	DPWA	$\overline{K}N$ multichannel
−0.29±0.03	HEPP	76B	DPWA	$K^-N \to \Sigma\pi$
−0.28±0.03	LONDON	75	HLBC	$K^-p \to \Sigma^0\pi^0$
−0.28±0.02	KANE	74	DPWA	$K^-p \to \Sigma\pi$
• • • We do not use the following data for averages, fits, limits, etc. • • •				
−0.30 or −0.28	[1] MARTIN	77	DPWA	$\overline{K}N$ multichannel

[1] The two MARTIN 77 values are from a T-matrix pole and from a Breit-Wigner fit. Another D_{03} Λ at 1966 MeV is also suggested by MARTIN 77, but is very uncertain.

$(\Gamma_i\Gamma_f)^{1/2}/\Gamma_{total}$ in $N\overline{K} \to \Lambda(1690) \to \Lambda\pi\pi$ — $(\Gamma_1\Gamma_4)^{1/2}/\Gamma$

VALUE	DOCUMENT ID		TECN	COMMENT
• • • We do not use the following data for averages, fits, limits, etc. • • •				
0.25±0.02	[1] BARTLEY	68	HDBC	$K^-p \to \Lambda\pi\pi$

[1] BARTLEY 68 uses only cross-section data. The enhancement is not seen by PREVOST 71.

$(\Gamma_i\Gamma_f)^{1/2}/\Gamma_{total}$ in $N\overline{K} \to \Lambda(1690) \to \Sigma\pi\pi$ — $(\Gamma_1\Gamma_5)^{1/2}/\Gamma$

VALUE	DOCUMENT ID		TECN	COMMENT
0.21	ARMENTEROS	68C	HDBC	$K^-N \to \Sigma\pi\pi$

$(\Gamma_i\Gamma_f)^{1/2}/\Gamma_{total}$ in $N\overline{K} \to \Lambda(1690) \to \Lambda\eta$ — $(\Gamma_1\Gamma_6)^{1/2}/\Gamma$

VALUE	DOCUMENT ID		TECN	COMMENT
0.00±0.03	BAXTER	73	DPWA	$K^-p \to$ neutrals

$(\Gamma_i\Gamma_f)^{1/2}/\Gamma_{total}$ in $N\overline{K} \to \Lambda(1690) \to \Sigma(1385)\pi$, S-wave — $(\Gamma_1\Gamma_7)^{1/2}/\Gamma$

VALUE	DOCUMENT ID		TECN	COMMENT
−0.28±0.06	ZHANG	13A	DPWA	Multichannel
+0.27±0.04	PREVOST	74	DPWA	$K^-N \to \Sigma(1385)\pi$

$\Lambda(1690)$ REFERENCES

SARANTSEV	19	EPJ A55 180	A.V. Sarantsev *et al.*	(BONN, PNPI)
KAMANO	15	PR C92 025205	H. Kamano *et al.*	(ANL, OSAK)
ZHANG	13A	PR C88 035205	H. Zhang *et al.*	(KSU)
KOISO	85	NP A433 619	H. Koiso *et al.*	(TOKY, MASA)
PDG	82	PL 111B 1	M. Roos *et al.*	(HELS, CIT, CERN)
GOPAL	80	Toronto Conf. 159	G.P. Gopal	(RHEL) IJP

Downloaded from https://academic.oup.com/ptep/article/2022/8/083C01/6651666 by KIT Library user on 27 September 2022

ALSTON-...	78	PR D18 182	M. Alston-Garnjost *et al.*	(LBL, MTHO+) IJP
Also		PRL 38 1007	M. Alston-Garnjost *et al.*	(LBL, MTHO+) IJP
GOPAL	77	NP B119 362	G.P. Gopal *et al.*	(LOIC, RHEL) IJP
MARTIN	77	NP B127 349	B.R. Martin, M.K. Pidcock, R.G. Moorhouse	(LOUC+) IJP
Also		NP B126 266	B.R. Martin, M.K. Pidcock	(LOUC)
Also		NP B126 285	B.R. Martin, M.K. Pidcock	(LOUC) IJP
CARROLL	76	PRL 37 806	A.S. Carroll *et al.*	(BNL) I
HEPP	76B	PL 65B 487	V. Hepp *et al.*	(CERN, HEIDH, MPIM) IJP
LONDON	75	NP B85 289	G.W. London *et al.*	(BNL, CERN, EPOL+)
KANE	74	LBL-2452	D.F. Kane	(LBL) IJP
PREVOST	74	NP B69 246	J. Prevost *et al.*	(SACL, CERN, HEID)
BAXTER	73	NP B67 125	D.F. Baxter *et al.*	(OXF) IJP
PREVOST	71	Amsterdam Conf.	J. Prevost	(CERN, HEID, SACL)
ARMENTEROS	68C	NP B8 216	R. Armenteros *et al.*	(CERN, HEID, SACL) I
BARTLEY	68	PRL 21 1111	J.H. Bartley *et al.*	(TUFTS, FSU, BRAN) I

$\Lambda(1710)\ 1/2^+$

$I(J^P) = 0(\frac{1}{2}^+)$ Status: *

OMITTED FROM SUMMARY TABLE

$\Lambda(1710)$ MASS

VALUE (MeV)	DOCUMENT ID		TECN	COMMENT
1713±13	ZHANG	13A	DPWA	Multichannel

$\Lambda(1710)$ WIDTH

VALUE (MeV)	DOCUMENT ID		TECN	COMMENT
180±42	ZHANG	13A	DPWA	Multichannel

$\Lambda(1710)$ DECAY MODES

	Mode	Fraction (Γ_i/Γ)
Γ_1	$N\overline{K}$	(43±4) %
Γ_2	$\Sigma\pi$	(21±5) %
Γ_3	$\Sigma^*(1385)\pi$, P-wave	(20±8) %
Γ_4	$N\overline{K}^*(892)$	
Γ_5	$N\overline{K}^*(892)$, S=1/2	(5±4) %
Γ_6	$N\overline{K}^*(892)$, S=3/2, P-wave	(10±8) %

$\Lambda(1710)$ BRANCHING RATIOS

$\Gamma(N\overline{K})/\Gamma_{total}$ — Γ_1/Γ

VALUE	DOCUMENT ID		TECN	COMMENT
0.43±0.04	ZHANG	13A	DPWA	Multichannel

$\Gamma(\Sigma\pi)/\Gamma_{total}$ — Γ_2/Γ

VALUE	DOCUMENT ID		TECN	COMMENT
0.21±0.05	ZHANG	13A	DPWA	Multichannel

$\Gamma(\Sigma^*(1385)\pi, P\text{-wave})/\Gamma_{total}$ — Γ_3/Γ

VALUE	DOCUMENT ID		TECN	COMMENT
0.20±0.08	ZHANG	13A	DPWA	Multichannel

$\Gamma(N\overline{K}^*(892), S=1/2)/\Gamma_{total}$ — Γ_5/Γ

VALUE	DOCUMENT ID		TECN	COMMENT
0.05±0.04	ZHANG	13A	DPWA	Multichannel

$\Gamma(N\overline{K}^*(892), S=3/2, P\text{-wave})/\Gamma_{total}$ — Γ_6/Γ

VALUE	DOCUMENT ID		TECN	COMMENT
0.10±0.08	ZHANG	13A	DPWA	Multichannel

$\Lambda(1710)$ REFERENCES

ZHANG 13A PR C88 035205 H. Zhang *et al.* (KSU)

$\Lambda(1800)\ 1/2^-$

$I(J^P) = 0(\frac{1}{2}^-)$ Status: ***

$\Lambda(1800)$ POLE POSITION

REAL PART

VALUE (MeV)	DOCUMENT ID		TECN	COMMENT
1809±9	SARANTSEV	19	DPWA	$\overline{K}N$ multichannel
• • • We do not use the following data for averages, fits, limits, etc. • • •				
1729	ZHANG	13A	DPWA	Multichannel

−2×IMAGINARY PART

VALUE (MeV)	DOCUMENT ID		TECN	COMMENT
205±16	SARANTSEV	19	DPWA	$\overline{K}N$ multichannel
• • • We do not use the following data for averages, fits, limits, etc. • • •				
198	ZHANG	13A	DPWA	Multichannel

$\Lambda(1800)$ POLE RESIDUES

The normalized residue is the residue divided by $\Gamma_{pole}/2$.

Normalized residue in $N\overline{K} \to \Lambda(1800) \to N\overline{K}$

MODULUS	PHASE (°)	DOCUMENT ID		TECN	COMMENT
0.34±0.07	**103 ± 8**	SARANTSEV	19	DPWA	$\overline{K}N$ multichannel

Normalized residue in $N\overline{K} \to \Lambda(1800) \to \Sigma\pi$

MODULUS	PHASE (°)	DOCUMENT ID		TECN	COMMENT
0.30±0.06	**−123 ± 8**	SARANTSEV	19	DPWA	$\overline{K}N$ multichannel

Normalized residue in $N\overline{K} \to \Lambda(1800) \to \Lambda\eta$

MODULUS	PHASE (°)	DOCUMENT ID		TECN	COMMENT
0.06±0.03	**75 ± 10**	SARANTSEV	19	DPWA	$\overline{K}N$ multichannel

Normalized residue in $N\overline{K} \to \Lambda(1800) \to \Lambda\sigma$

MODULUS	PHASE (°)	DOCUMENT ID		TECN	COMMENT
0.24±0.05	**25 ± 10**	SARANTSEV	19	DPWA	$\overline{K}N$ multichannel

Normalized residue in $N\overline{K} \to \Lambda(1800) \to \Lambda\omega$, S=1/2, S-wave

MODULUS	PHASE (°)	DOCUMENT ID		TECN	COMMENT
0.12±0.04	**−114 ± 30**	SARANTSEV	19	DPWA	$\overline{K}N$ multichannel

Normalized residue in $N\overline{K} \to \Lambda(1800) \to \Lambda\omega$, S=3/2, D-wave

MODULUS	PHASE (°)	DOCUMENT ID		TECN	COMMENT
0.08±0.03	**−90 ± 17**	SARANTSEV	19	DPWA	$\overline{K}N$ multichannel

Normalized residue in $N\overline{K} \to \Lambda(1800) \to \Sigma(1385)\pi$

MODULUS	PHASE (°)	DOCUMENT ID		TECN	COMMENT
0.16±0.06	**−140 ± 35**	SARANTSEV	19	DPWA	$\overline{K}N$ multichannel

Normalized residue in $N\overline{K} \to \Lambda(1800) \to N\overline{K}^*(892)$, S=1/2, S-wave

MODULUS	PHASE (°)	DOCUMENT ID		TECN	COMMENT
0.18±0.06	**65 ± 40**	SARANTSEV	19	DPWA	$\overline{K}N$ multichannel

Normalized residue in $N\overline{K} \to \Lambda(1800) \to N\overline{K}^*(892)$, S=3/2, D-wave

MODULUS	PHASE (°)	DOCUMENT ID		TECN	COMMENT
0.09±0.07		SARANTSEV	19	DPWA	$\overline{K}N$ multichannel

$\Lambda(1800)$ MASS

VALUE (MeV)	DOCUMENT ID		TECN	COMMENT
1750 to 1850 (≈ 1800) OUR ESTIMATE				
1811±10	SARANTSEV	19	DPWA	$\overline{K}N$ multichannel
1783±19	ZHANG	13A	DPWA	$\overline{K}N$ multichannel
1841±10	GOPAL	80	DPWA	$\overline{K}N \to \overline{K}N$
1725±20	ALSTON-...	78	DPWA	$\overline{K}N \to \overline{K}N$
1830±20	LANGBEIN	72	IPWA	$\overline{K}N$ multichannel
• • • We do not use the following data for averages, fits, limits, etc. • • •				
1845±10	MANLEY	02	DPWA	$\overline{K}N$ multichannel
1825±20	GOPAL	77	DPWA	$\overline{K}N$ multichannel
1767 or 1842 [1]	MARTIN	77	DPWA	$\overline{K}N$ multichannel
1780	KIM	71	DPWA	K-matrix analysis
1872±10	BRICMAN	70B	DPWA	$\overline{K}N \to \overline{K}N$

$\Lambda(1800)$ WIDTH

VALUE (MeV)	DOCUMENT ID		TECN	COMMENT
150 to 250 (≈ 200) OUR ESTIMATE				
209±18	SARANTSEV	19	DPWA	$\overline{K}N$ multichannel
256±35	ZHANG	13A	DPWA	$\overline{K}N$ multichannel
228±20	GOPAL	80	DPWA	$\overline{K}N \to \overline{K}N$
185±20	ALSTON-...	78	DPWA	$\overline{K}N \to \overline{K}N$
70±15	LANGBEIN	72	IPWA	$\overline{K}N$ multichannel
• • • We do not use the following data for averages, fits, limits, etc. • • •				
518±84	MANLEY	02	DPWA	$\overline{K}N$ multichannel
230±20	GOPAL	77	DPWA	$\overline{K}N$ multichannel
435 or 473 [1]	MARTIN	77	DPWA	$\overline{K}N$ multichannel
40	KIM	71	DPWA	K-matrix analysis
100±20	BRICMAN	70B	DPWA	$\overline{K}N \to \overline{K}N$

$\Lambda(1800)$ DECAY MODES

	Mode	Fraction (Γ_i/Γ)
Γ_1	$N\overline{K}$	25–40 %
Γ_2	$\Sigma\pi$	seen
Γ_3	$\Lambda\sigma$	(15 ±4) %
Γ_4	$\Sigma(1385)\pi$	seen
Γ_5	$\Lambda\eta$	0.01 to 0.10
Γ_6	$N\overline{K}^*(892)$	seen
Γ_7	$N\overline{K}^*(892)$, S=1/2, S-wave	
Γ_8	$N\overline{K}^*(892)$, S=3/2, D-wave	

Downloaded from https://academic.oup.com/ptep/article/2022/8/083C01/6651666 by KIT Library user on 27 September 2022

$\Lambda(1800)$ BRANCHING RATIOS

See "Sign conventions for resonance couplings" in the Note on Λ and Σ Resonances.

$\Gamma(N\overline{K})/\Gamma_{total}$ — Γ_1/Γ

VALUE	DOCUMENT ID		TECN	COMMENT
0.25 to 0.40 OUR ESTIMATE				
0.35±0.07	SARANTSEV	19	DPWA	$\overline{K}N$ multichannel
0.13±0.06	ZHANG	13A	DPWA	$\overline{K}N$ multichannel
0.36±0.04	GOPAL	80	DPWA	$\overline{K}N \to \overline{K}N$
0.28±0.05	ALSTON-...	78	DPWA	$\overline{K}N \to \overline{K}N$
0.35±0.15	LANGBEIN	72	IPWA	$\overline{K}N$ multichannel
• • • We do not use the following data for averages, fits, limits, etc. • • •				
0.24±0.10	MANLEY	02	DPWA	$\overline{K}N$ multichannel
0.37±0.05	GOPAL	77	DPWA	See GOPAL 80
1.21 or 0.70	[1] MARTIN	77	DPWA	$\overline{K}N$ multichannel
0.80	KIM	71	DPWA	K-matrix analysis
0.18±0.02	BRICMAN	70B	DPWA	$\overline{K}N \to \overline{K}N$

$\Gamma(\Sigma\pi)/\Gamma_{total}$ — Γ_2/Γ

VALUE	DOCUMENT ID		TECN	COMMENT
0.27±0.06	SARANTSEV	19	DPWA	$\overline{K}N$ multichannel

$\Gamma(\Lambda\sigma)/\Gamma_{total}$ — Γ_3/Γ

VALUE	DOCUMENT ID		TECN	COMMENT
0.15±0.04	SARANTSEV	19	DPWA	$\overline{K}N$ multichannel

$\Gamma(\Sigma(1385)\pi)/\Gamma_{total}$ — Γ_4/Γ

VALUE	DOCUMENT ID		TECN	COMMENT
0.09±0.04	SARANTSEV	19	DPWA	$\overline{K}N$ multichannel

$\Gamma(\Lambda\eta)/\Gamma_{total}$ — Γ_5/Γ

VALUE	DOCUMENT ID		TECN	COMMENT
0.01 to 0.10 OUR ESTIMATE				
0.010±0.005	SARANTSEV	19	DPWA	$\overline{K}N$ multichannel
0.06 ±0.05	ZHANG	13A	DPWA	Multichannel

$(\Gamma_i\Gamma_f)^{1/2}/\Gamma_{total}$ in $N\overline{K} \to \Lambda(1800) \to \Sigma\pi$ — $(\Gamma_1\Gamma_2)^{1/2}/\Gamma$

VALUE	DOCUMENT ID		TECN	COMMENT
−0.07±0.02	ZHANG	13A	DPWA	Multichannel
−0.08±0.05	GOPAL	77	DPWA	$\overline{K}N$ multichannel
• • • We do not use the following data for averages, fits, limits, etc. • • •				
−0.74 or −0.43	[1] MARTIN	77	DPWA	$\overline{K}N$ multichannel
0.24	KIM	71	DPWA	K-matrix analysis

$(\Gamma_i\Gamma_f)^{1/2}/\Gamma_{total}$ in $N\overline{K} \to \Lambda(1800) \to \Sigma(1385)\pi$ — $(\Gamma_1\Gamma_4)^{1/2}/\Gamma$

VALUE	DOCUMENT ID		TECN	COMMENT
−0.09 ±0.05	ZHANG	13A	DPWA	Multichannel
+0.056±0.028	[2] CAMERON	78	DPWA	$K^-p \to \Sigma(1385)\pi$

$(\Gamma_i\Gamma_f)^{1/2}/\Gamma_{total}$ in $N\overline{K} \to \Lambda(1800) \to N\overline{K}^*(892)$, S=1/2, S-wave — $(\Gamma_1\Gamma_7)^{1/2}/\Gamma$

VALUE	DOCUMENT ID		TECN	COMMENT
−0.13±0.02	ZHANG	13A	DPWA	Multichannel
−0.17±0.03	[2] CAMERON	78B	DPWA	$K^-p \to N\overline{K}^*$

$(\Gamma_i\Gamma_f)^{1/2}/\Gamma_{total}$ in $N\overline{K} \to \Lambda(1800) \to N\overline{K}^*(892)$, S=3/2, D-wave — $(\Gamma_1\Gamma_8)^{1/2}/\Gamma$

VALUE	DOCUMENT ID		TECN	COMMENT
−0.13±0.04	CAMERON	78B	DPWA	$K^-p \to N\overline{K}^*$

$\Lambda(1800)$ FOOTNOTES

[1] The two MARTIN 77 values are from a T-matrix pole and from a Breit-Wigner fit.
[2] The published sign has been changed to be in accord with the baryon-first convention.

$\Lambda(1800)$ REFERENCES

SARANTSEV	19	EPJ A55 180	A.V. Sarantsev *et al.*	(BONN, PNPI)
ZHANG	13A	PR C88 035205	H. Zhang *et al.*	(KSU)
MANLEY	02	PRL 88 012002	D.M. Manley *et al.*	(BNL Crystal Ball Collab.)
GOPAL	80	Toronto Conf. 159	G.P. Gopal	(RHEL) IJP
ALSTON-...	78	PR D18 182	M. Alston-Garnjost *et al.*	(LBL, MTHO+) IJP
Also		PRL 38 1007	M. Alston-Garnjost *et al.*	(LBL, MTHO+) IJP
CAMERON	78	NP B143 189	W. Cameron *et al.*	(RHEL, LOIC) IJP
CAMERON	78B	NP B146 327	W. Cameron *et al.*	(RHEL, LOIC) IJP
GOPAL	77	NP B119 362	G.P. Gopal *et al.*	(LOIC, RHEL) IJP
MARTIN	77	NP B127 349	B.R. Martin, M.K. Pidcock, R.G. Moorhouse	(LOUC+) IJP
Also		NP B126 266	B.R. Martin, M.K. Pidcock	(LOUC)
Also		NP B126 285	B.R. Martin, M.K. Pidcock	(LOUC) IJP
LANGBEIN	72	NP B47 477	W. Langbein, F. Wagner	(MPIM) IJP
KIM	71	PRL 27 356	J.K. Kim	(HARV) IJP
Also		Duke Conf. 161	J.K. Kim	(HARV) IJP
Hyperon Resonances, 1970				
BRICMAN	70B	PL 33B 511	C. Bricman, M. Ferro-Luzzi, J.P. Lagnaux	(CERN) IJP

$\Lambda(1810)$ $1/2^+$

$I(J^P) = 0(\frac{1}{2}^+)$ Status: ***

$\Lambda(1810)$ POLE POSITION

REAL PART

VALUE (MeV)	DOCUMENT ID		TECN	COMMENT
1773± 7	SARANTSEV	19	DPWA	$\overline{K}N$ multichannel
• • • We do not use the following data for averages, fits, limits, etc. • • •				
2097^{+40}_{-1}	[1] KAMANO	15	DPWA	Multichannel
1780	ZHANG	13A	DPWA	Multichannel

[1] From the preferred solution A in KAMANO 15. Solution B reports M = 1841^{+3}_{-4} MeV.

−2×IMAGINARY PART

VALUE (MeV)	DOCUMENT ID		TECN	COMMENT
38±14	SARANTSEV	19	DPWA	$\overline{K}N$ multichannel
• • • We do not use the following data for averages, fits, limits, etc. • • •				
166^{+64}_{-12}	[1] KAMANO	15	DPWA	Multichannel
64	ZHANG	13A	DPWA	Multichannel

[1] From the preferred solution A in KAMANO 15. Solution B Reports Γ = 62^{+6}_{-4} MeV.

$\Lambda(1810)$ POLE RESIDUES

The normalized residue is the residue divided by $\Gamma_{pole}/2$.

Normalized residue in $N\overline{K} \to \Lambda(1810) \to N\overline{K}$

MODULUS	PHASE (°)	DOCUMENT ID		TECN	COMMENT
0.018±0.008	**65 ± 26**	SARANTSEV	19	DPWA	$\overline{K}N$ multichannel
• • • We do not use the following data for averages, fits, limits, etc. • • •					
0.205	−63	[1] KAMANO	15	DPWA	Multichannel

[1] From the preferred solution A in KAMANO 15.

Normalized residue in $N\overline{K} \to \Lambda(1810) \to \Sigma\pi$

MODULUS	PHASE (°)	DOCUMENT ID		TECN	COMMENT
0.045 ±0.020	**−143 ± 24**	SARANTSEV	19	DPWA	$\overline{K}N$ multichannel
• • • We do not use the following data for averages, fits, limits, etc. • • •					
0.0325	29	[1] KAMANO	15	DPWA	Multichannel

[1] From the preferred solution A in KAMANO 15.

Normalized residue in $N\overline{K} \to \Lambda(1810) \to \Lambda\eta$

MODULUS	PHASE (°)	DOCUMENT ID		TECN	COMMENT
• • • We do not use the following data for averages, fits, limits, etc. • • •					
0.155	165	[1] KAMANO	15	DPWA	Multichannel

[1] From the preferred solution A in KAMANO 15.

Normalized residue in $N\overline{K} \to \Lambda(1810) \to \Lambda\sigma$

MODULUS	PHASE (°)	DOCUMENT ID		TECN	COMMENT
0.055±0.020	**30 ± 16**	SARANTSEV	19	DPWA	$\overline{K}N$ multichannel

Normalized residue in $N\overline{K} \to \Lambda(1810) \to \Xi K$

MODULUS	PHASE (°)	DOCUMENT ID		TECN	COMMENT
• • • We do not use the following data for averages, fits, limits, etc. • • •					
0.0937	−64	[1] KAMANO	15	DPWA	Multichannel

[1] From the preferred solution A in KAMANO 15.

Normalized residue in $N\overline{K} \to \Lambda(1810) \to \Sigma(1385)\pi$

MODULUS	PHASE (°)	DOCUMENT ID		TECN	COMMENT
0.08 ±0.03	**−50 ± 30**	SARANTSEV	19	DPWA	$\overline{K}N$ multichannel
• • • We do not use the following data for averages, fits, limits, etc. • • •					
0.244	−10	[1] KAMANO	15	DPWA	Multichannel

[1] From the preferred solution A in KAMANO 15.

Normalized residue in $N\overline{K} \to \Lambda(1810) \to N\overline{K}^*(892)$, S=1/2, P-wave

MODULUS	PHASE (°)	DOCUMENT ID		TECN	COMMENT
0.03 ±0.03		SARANTSEV	19	DPWA	$\overline{K}N$ multichannel
• • • We do not use the following data for averages, fits, limits, etc. • • •					
0.159	−97	[1] KAMANO	15	DPWA	Multichannel

[1] From the preferred solution A in KAMANO 15.

Normalized residue in $N\overline{K} \to \Lambda(1810) \to N\overline{K}^*(892)$, S=3/2, P-wave

MODULUS	PHASE (°)	DOCUMENT ID		TECN	COMMENT
0.05 ±0.04		SARANTSEV	19	DPWA	$\overline{K}N$ multichannel
• • • We do not use the following data for averages, fits, limits, etc. • • •					
0.0497	2	[1] KAMANO	15	DPWA	Multichannel

[1] From the preferred solution A in KAMANO 15.

$\Lambda(1810)$ MASS

VALUE (MeV)	DOCUMENT ID		TECN	COMMENT
1740 to 1840 (≈ 1790) OUR ESTIMATE				
1773± 7	SARANTSEV	19	DPWA	$\overline{K}N$ multichannel
1821±10	ZHANG	13A	DPWA	Multichannel
1841±20	GOPAL	80	DPWA	$\overline{K}N \to \overline{K}N$
1735± 5	CARROLL	76	DPWA	Isospin-0 total σ
1746±10	PREVOST	74	DPWA	$K^-N \to \Sigma(1385)\pi$
1780±20	LANGBEIN	72	IPWA	$\overline{K}N$ multichannel

Downloaded from https://academic.oup.com/ptep/article/2022/8/083C01/6651666 by KIT Library user on 27 September 2022

• • • We do not use the following data for averages, fits, limits, etc. • • •

1853±20	GOPAL	77	DPWA	$\overline{K}N$ multichannel
1861 or 1953	[1] MARTIN	77	DPWA	$\overline{K}N$ multichannel
1755	KIM	71	DPWA	K-matrix analysis
1800	ARMENTEROS	70	HBC	$\overline{K}N \to \overline{K}N$
1750	ARMENTEROS	70	HBC	$\overline{K}N \to \Sigma\pi$
1690±10	BARBARO-...	70	HBC	$\overline{K}N \to \Sigma\pi$
1740	BAILEY	69	DPWA	$\overline{K}N \to \overline{K}N$
1745	ARMENTEROS	68B	HBC	$\overline{K}N \to \overline{K}N$

[1] The two MARTIN 77 values are from a T-matrix pole and from a Breit-Wigner fit.

$\Lambda(1810)$ WIDTH

VALUE (MeV)	DOCUMENT ID		TECN	COMMENT
50 to 170 (≈ 110) OUR ESTIMATE				
39±15	SARANTSEV	19	DPWA	$\overline{K}N$ multichannel
174±50	ZHANG	13A	DPWA	Multichannel
164±20	GOPAL	80	DPWA	$\overline{K}N \to \overline{K}N$
90±20	CAMERON	78B	DPWA	$K^-p \to N\overline{K}^*$
46±20	PREVOST	74	DPWA	$K^-N \to \Sigma(1385)\pi$
120±10	LANGBEIN	72	IPWA	$\overline{K}N$ multichannel
• • • We do not use the following data for averages, fits, limits, etc. • • •				
166±20	GOPAL	77	DPWA	$\overline{K}N$ multichannel
535 or 585	[1] MARTIN	77	DPWA	$\overline{K}N$ multichannel
28	CARROLL	76	DPWA	Isospin-0 total σ
35	KIM	71	DPWA	K-matrix analysis
30	ARMENTEROS	70	HBC	$\overline{K}N \to \overline{K}N$
70	ARMENTEROS	70	HBC	$\overline{K}N \to \Sigma\pi$
22	BARBARO-...	70	HBC	$\overline{K}N \to \Sigma\pi$
300	BAILEY	69	DPWA	$\overline{K}N \to \overline{K}N$
147	ARMENTEROS	68B	HBC	

[1] The two MARTIN 77 values are from a T-matrix pole and from a Breit-Wigner fit.

$\Lambda(1810)$ DECAY MODES

	Mode	Fraction (Γ_i/Γ)
Γ_1	$N\overline{K}$	0.05 to 0.35
Γ_2	$\Sigma\pi$	(16 ± 5) %
Γ_3	$\Lambda\eta$	
Γ_4	ΞK	
Γ_5	$\Sigma(1385)\pi$	(40 ±15) %
Γ_6	$N\overline{K}^*(892)$	30–60 %
Γ_7	$N\overline{K}^*(892)$, $S=1/2$, P-wave	
Γ_8	$N\overline{K}^*(892)$, $S=3/2$, P-wave	

$\Lambda(1810)$ BRANCHING RATIOS

$\Gamma(N\overline{K})/\Gamma_{total}$ — Γ_1/Γ

VALUE	DOCUMENT ID		TECN	COMMENT
0.05 to 0.35 OUR ESTIMATE				
0.025±0.013	SARANTSEV	19	DPWA	$\overline{K}N$ multichannel
0.19 ±0.08	ZHANG	13A	DPWA	$\overline{K}N$ multichannel
0.24 ±0.04	GOPAL	80	DPWA	$\overline{K}N \to \overline{K}N$
0.36 ±0.05	LANGBEIN	72	IPWA	$\overline{K}N$ multichannel
• • • We do not use the following data for averages, fits, limits, etc. • • •				
0.225	[1] KAMANO	15	DPWA	$\overline{K}N$ multichannel
0.21 ±0.04	GOPAL	77	DPWA	See GOPAL 80
0.52 or 0.49	[2] MARTIN	77	DPWA	$\overline{K}N$ multichannel
0.30	KIM	71	DPWA	K-matrix analysis
0.15	ARMENTEROS	70	DPWA	$\overline{K}N \to \overline{K}N$
0.55	BAILEY	69	DPWA	$\overline{K}N \to \overline{K}N$
0.4	ARMENTEROS	68B	DPWA	$\overline{K}N \to \overline{K}N$

[1] From the preferred solution A in KAMANO 15.
[2] The two MARTIN 77 values are from a T-matrix pole and from a Breit-Wigner fit.

$\Gamma(\Sigma\pi)/\Gamma_{total}$ — Γ_2/Γ

VALUE	DOCUMENT ID		TECN	COMMENT
0.16 ±0.05	SARANTSEV	19	DPWA	$\overline{K}N$ multichannel
• • • We do not use the following data for averages, fits, limits, etc. • • •				
0.009	[1] KAMANO	15	DPWA	Multichannel

[1] From the preferred solution A in KAMANO 15.

$\Gamma(\Lambda\eta)/\Gamma_{total}$ — Γ_3/Γ

VALUE	DOCUMENT ID		TECN	COMMENT
• • • We do not use the following data for averages, fits, limits, etc. • • •				
0.111	[1] KAMANO	15	DPWA	Multichannel

[1] From the preferred solution A in KAMANO 15.

$\Gamma(\Xi K)/\Gamma_{total}$ — Γ_4/Γ

VALUE	DOCUMENT ID		TECN	COMMENT
• • • We do not use the following data for averages, fits, limits, etc. • • •				
0.051	[1] KAMANO	15	DPWA	Multichannel

[1] From the preferred solution A in KAMANO 15.

$\Gamma(\Sigma(1385)\pi)/\Gamma_{total}$ — Γ_5/Γ

VALUE	DOCUMENT ID		TECN	COMMENT
0.40 ±0.15	SARANTSEV	19	DPWA	$\overline{K}N$ multichannel
• • • We do not use the following data for averages, fits, limits, etc. • • •				
0.600	[1] KAMANO	15	DPWA	Multichannel

[1] From the preferred solution A in KAMANO 15.

$\Gamma(N\overline{K}^*(892), S=1/2, P\text{-wave})/\Gamma_{total}$ — Γ_7/Γ

VALUE	DOCUMENT ID		TECN	COMMENT
• • • We do not use the following data for averages, fits, limits, etc. • • •				
0.003	[1] KAMANO	15	DPWA	Multichannel

[1] From the preferred solution A in KAMANO 15.

$(\Gamma_i\Gamma_f)^{1/2}/\Gamma_{total}$ in $N\overline{K} \to \Lambda(1810) \to \Sigma\pi$ — $(\Gamma_1\Gamma_2)^{1/2}/\Gamma$

VALUE	DOCUMENT ID		TECN	COMMENT
−0.08±0.05	ZHANG	13A	DPWA	Multichannel
−0.24±0.04	GOPAL	77	DPWA	$\overline{K}N$ multichannel
• • • We do not use the following data for averages, fits, limits, etc. • • •				
+0.25 or +0.23	[1] MARTIN	77	DPWA	$\overline{K}N$ multichannel
< 0.01	LANGBEIN	72	IPWA	$\overline{K}N$ multichannel
0.17	KIM	71	DPWA	K-matrix analysis
+0.20	[2] ARMENTEROS	70	DPWA	$\overline{K}N \to \Sigma\pi$
−0.13±0.03	BARBARO-...	70	DPWA	$\overline{K}N \to \Sigma\pi$

[1] The two MARTIN 77 values are from a T-matrix pole and from a Breit-Wigner fit.
[2] The published sign has been changed to be in accord with the baryon-first convention.

$(\Gamma_i\Gamma_f)^{1/2}/\Gamma_{total}$ in $N\overline{K} \to \Lambda(1810) \to \Sigma(1385)\pi$ — $(\Gamma_1\Gamma_5)^{1/2}/\Gamma$

VALUE	DOCUMENT ID		TECN	COMMENT
+0.18±0.10	PREVOST	74	DPWA	$K^-N \to \Sigma(1385)\pi$

$(\Gamma_i\Gamma_f)^{1/2}/\Gamma_{total}$ in $N\overline{K} \to \Lambda(1810) \to N\overline{K}^*(892)$, $S=1/2$, P-wave — $(\Gamma_1\Gamma_7)^{1/2}/\Gamma$

VALUE	DOCUMENT ID		TECN	COMMENT
−0.14±0.03	[1] CAMERON	78B	DPWA	$K^-p \to N\overline{K}^*$

[1] The published sign has been changed to be in accord with the baryon-first convention.

$(\Gamma_i\Gamma_f)^{1/2}/\Gamma_{total}$ in $N\overline{K} \to \Lambda(1810) \to N\overline{K}^*(892)$, $S=3/2$, P-wave — $(\Gamma_1\Gamma_8)^{1/2}/\Gamma$

VALUE	DOCUMENT ID		TECN	COMMENT
+0.38±0.06	ZHANG	13A	DPWA	Multichannel
+0.35±0.06	CAMERON	78B	DPWA	$K^-p \to N\overline{K}^*$

$\Lambda(1810)$ REFERENCES

SARANTSEV	19	EPJ A55 180	A.V. Sarantsev *et al.*	(BONN, PNPI)
KAMANO	15	PR C92 025205	H. Kamano *et al.*	(ANL, OSAK)
ZHANG	13A	PR C88 035205	H. Zhang *et al.*	(KSU)
GOPAL	80	Toronto Conf. 159	G.P. Gopal	(RHEL) IJP
CAMERON	78B	NP B146 327	W. Cameron *et al.*	(RHEL, LOIC) IJP
GOPAL	77	NP B119 362	G.P. Gopal *et al.*	(LOIC, RHEL) IJP
MARTIN	77	NP B127 349	B.R. Martin, M.K. Pidcock, R.G. Moorhouse	(LOUC+) IJP
Also		NP B126 266	B.R. Martin, M.K. Pidcock	(LOUC)
Also		NP B126 285	B.R. Martin, M.K. Pidcock	(LOUC) IJP
CARROLL	76	PRL 37 806	A.S. Carroll *et al.*	(BNL) I
PREVOST	74	NP B69 246	J. Prevost *et al.*	(SACL, CERN, HEID)
LANGBEIN	72	NP B47 477	W. Langbein, F. Wagner	(MPIM) IJP
KIM	71	PRL 27 356	J.K. Kim	(HARV) IJP
Also		Duke Conf. 161 Hyperon Resonances, 1970	J.K. Kim	(HARV) IJP
ARMENTEROS	70	Duke Conf. 123 Hyperon Resonances, 1970	R. Armenteros *et al.*	(CERN, HEID, SACL) IJP
BARBARO-...	70	Duke Conf. 173 Hyperon Resonances, 1970	A. Barbaro-Galtieri	(LRL) IJP
BAILEY	69	Thesis UCRL 50617	J.M. Bailey	(LLL) IJP
ARMENTEROS	68B	NP B8 195	R. Armenteros *et al.*	(CERN, HEID, SACL) IJP

$\Lambda(1820)\ 5/2^+$

$I(J^P) = 0(\frac{5}{2}^+)$ Status: ****

This resonance is the cornerstone for all partial-wave analyses in this region. Most of the results published before 1973 are now obsolete and have been omitted. They may be found in our 1982 edition Physics Letters **111B** 1 (1982).

$\Lambda(1820)$ POLE POSITION

REAL PART

VALUE (MeV)	DOCUMENT ID		TECN	COMMENT
1812 to 1825 (≈ 1818) OUR ESTIMATE				
1813±3	SARANTSEV	19	DPWA	$\overline{K}N$ multichannel
1824^{+2}_{-1}	[1] KAMANO	15	DPWA	$\overline{K}N$ multichannel
• • • We do not use the following data for averages, fits, limits, etc. • • •				
1814	ZHANG	13A	DPWA	$\overline{K}N$ multichannel

[1] From the preferred solution A in KAMANO 15.

−2×IMAGINARY PART

VALUE (MeV)	DOCUMENT ID		TECN	COMMENT
75 to 80 (≈ 77) OUR ESTIMATE				
78±7	SARANTSEV	19	DPWA	$\overline{K}N$ multichannel
77±2	[1] KAMANO	15	DPWA	$\overline{K}N$ multichannel

Downloaded from https://academic.oup.com/ptep/article/2022/8/083C01/6651666 by KIT Library user on 27 September 2022

• • • We do not use the following data for averages, fits, limits, etc. • • •

85	ZHANG	13A	DPWA	$\overline{K}N$ multichannel

[1] From the preferred solution A in KAMANO 15.

$\Lambda(1820)$ POLE RESIDUES

The normalized residue is the residue divided by $\Gamma_{pole}/2$.

Normalized residue in $N\overline{K} \to \Lambda(1820) \to N\overline{K}$

MODULUS	PHASE (°)	DOCUMENT ID		TECN	COMMENT
0.60 ±0.12	**−22 ± 5**	SARANTSEV	19	DPWA	$\overline{K}N$ multichannel
• • • We do not use the following data for averages, fits, limits, etc. • • •					
0.558	−13	[1] KAMANO	15	DPWA	$\overline{K}N$ multichannel

[1] From the preferred solution A in KAMANO 15.

Normalized residue in $N\overline{K} \to \Lambda(1820) \to \Sigma\pi$

MODULUS	PHASE (°)	DOCUMENT ID		TECN	COMMENT
0.34 ±0.07	**174 ± 5**	SARANTSEV	19	DPWA	$\overline{K}N$ multichannel
• • • We do not use the following data for averages, fits, limits, etc. • • •					
0.357	168	[1] KAMANO	15	DPWA	$\overline{K}N$ multichannel

[1] From the preferred solution A in KAMANO 15.

Normalized residue in $N\overline{K} \to \Lambda(1820) \to \Lambda\eta$

MODULUS	PHASE (°)	DOCUMENT ID		TECN	COMMENT
• • • We do not use the following data for averages, fits, limits, etc. • • •					
0.0184	−3	[1] KAMANO	15	DPWA	$\overline{K}N$ multichannel

[1] From the preferred solution A in KAMANO 15.

Normalized residue in $N\overline{K} \to \Lambda(1820) \to \Xi K$

MODULUS	PHASE (°)	DOCUMENT ID		TECN	COMMENT
∼ 0		SARANTSEV	19	DPWA	$\overline{K}N$ multichannel
• • • We do not use the following data for averages, fits, limits, etc. • • •					
0.00111	70	[1] KAMANO	15	DPWA	$\overline{K}N$ multichannel

[1] From the preferred solution A in KAMANO 15.

Normalized residue in $N\overline{K} \to \Lambda(1820) \to \Sigma(1385)\pi$, P-wave

MODULUS	PHASE (°)	DOCUMENT ID		TECN	COMMENT
0.07 ±0.02	**−60 ± 50**	SARANTSEV	19	DPWA	$\overline{K}N$ multichannel
• • • We do not use the following data for averages, fits, limits, etc. • • •					
0.340	161	[1] KAMANO	15	DPWA	$\overline{K}N$ multichannel

[1] From the preferred solution A in KAMANO 15.

Normalized residue in $N\overline{K} \to \Lambda(1820) \to \Sigma(1385)\pi$, F-wave

MODULUS	PHASE (°)	DOCUMENT ID		TECN	COMMENT
0.11 ±0.04	**5 ± 45**	SARANTSEV	19	DPWA	$\overline{K}N$ multichannel
• • • We do not use the following data for averages, fits, limits, etc. • • •					
0.201	151	[1] KAMANO	15	DPWA	$\overline{K}N$ multichannel

[1] From the preferred solution A in KAMANO 15.

Normalized residue in $N\overline{K} \to \Lambda(1820) \to N\overline{K}^*(892)$, S=1/2 , F-wave

MODULUS	PHASE (°)	DOCUMENT ID		TECN	COMMENT
0.02 ±0.02		SARANTSEV	19	DPWA	$\overline{K}N$ multichannel
• • • We do not use the following data for averages, fits, limits, etc. • • •					
0.00750	41	[1] KAMANO	15	DPWA	$\overline{K}N$ multichannel

[1] From the preferred solution A in KAMANO 15.

Normalized residue in $N\overline{K} \to \Lambda(1820) \to N\overline{K}^*(892)$, S=3/2 , P-wave

MODULUS	PHASE (°)	DOCUMENT ID		TECN	COMMENT
0.35 ±0.15	**−30 ± 45**	SARANTSEV	19	DPWA	$\overline{K}N$ multichannel
• • • We do not use the following data for averages, fits, limits, etc. • • •					
0.171	−139	[1] KAMANO	15	DPWA	$\overline{K}N$ multichannel

[1] From the preferred solution A in KAMANO 15.

Normalized residue in $N\overline{K} \to \Lambda(1820) \to N\overline{K}^*(892)$, S=3/2 , F-wave

MODULUS	PHASE (°)	DOCUMENT ID		TECN	COMMENT
0.02 ±0.02		SARANTSEV	19	DPWA	$\overline{K}N$ multichannel
• • • We do not use the following data for averages, fits, limits, etc. • • •					
0.000517	161	[1] KAMANO	15	DPWA	$\overline{K}N$ multichannel

[1] From the preferred solution A in KAMANO 15.

$\Lambda(1820)$ MASS

VALUE (MeV)	DOCUMENT ID		TECN	COMMENT
1815 to 1825 (≈ 1820) OUR ESTIMATE				
1822 ±4	SARANTSEV	19	DPWA	$\overline{K}N$ multichannel
1823.5 ± 0.8	ZHANG	13A	DPWA	$\overline{K}N$ multichannel
1823 ±3	GOPAL	80	DPWA	$\overline{K}N \to \overline{K}N$
1819 ±2	ALSTON-...	78	DPWA	$\overline{K}N \to \overline{K}N$
1821 ±2	KANE	74	DPWA	$K^-p \to \Sigma\pi$
• • • We do not use the following data for averages, fits, limits, etc. • • •				
1830	DECLAIS	77	DPWA	$\overline{K}N \to \overline{K}N$
1822 ±2	GOPAL	77	DPWA	$\overline{K}N$ multichannel
1817 or 1819	[1] MARTIN	77	DPWA	$\overline{K}N$ multichannel

[1] The two MARTIN 77 values are from a T-matrix pole and from a Breit-Wigner fit.

$\Lambda(1820)$ WIDTH

VALUE (MeV)	DOCUMENT ID		TECN	COMMENT
70 to 90 (≈ 80) OUR ESTIMATE				
80 ±8	SARANTSEV	19	DPWA	$\overline{K}N$ multichannel
89 ±2	ZHANG	13A	DPWA	$\overline{K}N$ multichannel
77 ±5	GOPAL	80	DPWA	$\overline{K}N \to \overline{K}N$
72 ±5	ALSTON-...	78	DPWA	$\overline{K}N \to \overline{K}N$
87 ±3	KANE	74	DPWA	$K^-p \to \Sigma\pi$
• • • We do not use the following data for averages, fits, limits, etc. • • •				
82	DECLAIS	77	DPWA	$\overline{K}N \to \overline{K}N$
81 ±5	GOPAL	77	DPWA	$\overline{K}N$ multichannel
76 or 76	[1] MARTIN	77	DPWA	$\overline{K}N$ multichannel

[1] The two MARTIN 77 values are from a T-matrix pole and from a Breit-Wigner fit.

$\Lambda(1820)$ DECAY MODES

	Mode	Fraction (Γ_i/Γ)
Γ_1	$N\overline{K}$	55–65 %
Γ_2	$\Sigma\pi$	8–14 %
Γ_3	$\Sigma(1385)\pi$	5–10 %
Γ_4	$\Sigma(1385)\pi$, P-wave	
Γ_5	$\Sigma(1385)\pi$, F-wave	(2.0±1.0) %
Γ_6	$\Lambda\eta$	
Γ_7	ΞK	
Γ_8	$\Sigma\pi\pi$	
Γ_9	$N\overline{K}^*(892)$, S=1/2, F-wave	
Γ_{10}	$N\overline{K}^*(892)$, S=3/2, P-wave	(3.0±1.0) %
Γ_{11}	$N\overline{K}^*(892)$, S=3/2, F-wave	

$\Lambda(1820)$ BRANCHING RATIOS

Errors quoted do not include uncertainties in the parametrizations used in the partial-wave analyses and are thus too small. See also "Sign conventions for resonance couplings" in the Note on Λ and Σ Resonances.

$\Gamma(N\overline{K})/\Gamma_{total}$ — Γ_1/Γ

VALUE	DOCUMENT ID		TECN	COMMENT
0.55 to 0.65 OUR ESTIMATE				
0.58 ±0.12	SARANTSEV	19	DPWA	$\overline{K}N$ multichannel
0.54 ±0.01	ZHANG	13A	DPWA	$\overline{K}N$ multichannel
0.58 ±0.02	GOPAL	80	DPWA	$\overline{K}N \to \overline{K}N$
0.60 ±0.03	ALSTON-...	78	DPWA	$\overline{K}N \to \overline{K}N$
• • • We do not use the following data for averages, fits, limits, etc. • • •				
0.547	[1] KAMANO	15	DPWA	$\overline{K}N$ multichannel
0.51	DECLAIS	77	DPWA	$\overline{K}N \to \overline{K}N$
0.57 ±0.02	GOPAL	77	DPWA	See GOPAL 80
0.59 or 0.58	[2] MARTIN	77	DPWA	$\overline{K}N$ multichannel

[1] From the preferred solution A in KAMANO 15.
[2] The two MARTIN 77 values are from a T-matrix pole and from a Breit-Wigner fit.

$\Gamma(\Sigma\pi)/\Gamma_{total}$ — Γ_2/Γ

VALUE	DOCUMENT ID		TECN	COMMENT
0.19 ±0.04	SARANTSEV	19	DPWA	$\overline{K}N$ multichannel
• • • We do not use the following data for averages, fits, limits, etc. • • •				
0.218	[1] KAMANO	15	DPWA	$\overline{K}N$ multichannel

[1] From the preferred solution A in KAMANO 15.

$\Gamma(\Sigma(1385)\pi, P\text{-wave})/\Gamma_{total}$ — Γ_4/Γ

VALUE	DOCUMENT ID		TECN	COMMENT
∼ 0.01	SARANTSEV	19	DPWA	$\overline{K}N$ multichannel
• • • We do not use the following data for averages, fits, limits, etc. • • •				
0.173	[1] KAMANO	15	DPWA	$\overline{K}N$ multichannel

[1] From the preferred solution A in KAMANO 15.

$\Gamma(\Sigma(1385)\pi, F\text{-wave})/\Gamma_{total}$ — Γ_5/Γ

VALUE	DOCUMENT ID		TECN	COMMENT
0.02 ±0.01	SARANTSEV	19	DPWA	$\overline{K}N$ multichannel
• • • We do not use the following data for averages, fits, limits, etc. • • •				
0.055	[1] KAMANO	15	DPWA	$\overline{K}N$ multichannel

[1] From the preferred solution A in KAMANO 15.

$\Gamma(\Lambda\eta)/\Gamma_{total}$ — Γ_6/Γ

VALUE	DOCUMENT ID		TECN	COMMENT
• • • We do not use the following data for averages, fits, limits, etc. • • •				
0.001	[1] KAMANO	15	DPWA	Multichannel

[1] From the preferred solution A in KAMANO 15.

Downloaded from https://academic.oup.com/ptep/article/2022/8/083C01/6651666 by KIT Library user on 27 September 2022

$\Gamma(\Xi K)/\Gamma_{total}$ — Γ_7/Γ

VALUE	DOCUMENT ID		TECN	COMMENT
• • • We do not use the following data for averages, fits, limits, etc. • • •				
not seen	[1] KAMANO	15	DPWA	Multichannel

[1] From the preferred solution A in KAMANO 15.

$\Gamma(\Sigma\pi\pi)/\Gamma_{total}$ — Γ_8/Γ

VALUE	DOCUMENT ID		TECN	COMMENT
no clear signal	[1] ARMENTEROS	68C	HDBC	$K^- N \to \Sigma\pi\pi$

[1] There is a suggestion of a bump, enough to be consistent with what is expected from $\Sigma(1385) \to \Sigma\pi$ decay.

$\Gamma(N\overline{K}^*(892), S=1/2, P\text{-wave})/\Gamma_{total}$ — Γ_9/Γ

VALUE	DOCUMENT ID		TECN	COMMENT
• • • We do not use the following data for averages, fits, limits, etc. • • •				
not seen	[1] KAMANO	15	DPWA	Multichannel

[1] From the preferred solution A in KAMANO 15.

$\Gamma(N\overline{K}^*(892), S=3/2, P\text{-wave})/\Gamma_{total}$ — Γ_{10}/Γ

VALUE	DOCUMENT ID		TECN	COMMENT
0.03 ±0.01	ZHANG	13A	DPWA	Multichannel
• • • We do not use the following data for averages, fits, limits, etc. • • •				
0.006	[1] KAMANO	15	DPWA	Multichannel

[1] From the preferred solution A in KAMANO 15.

$\Gamma(N\overline{K}^*(892), S=3/2, F\text{-wave})/\Gamma_{total}$ — Γ_{11}/Γ

VALUE	DOCUMENT ID		TECN	COMMENT
• • • We do not use the following data for averages, fits, limits, etc. • • •				
not seen	[1] KAMANO	15	DPWA	Multichannel

[1] From the preferred solution A in KAMANO 15.

$(\Gamma_i\Gamma_f)^{1/2}/\Gamma_{total}$ in $N\overline{K} \to \Lambda(1820) \to \Sigma\pi$ — $(\Gamma_1\Gamma_2)^{1/2}/\Gamma$

VALUE	DOCUMENT ID		TECN	COMMENT
−0.28±0.01	ZHANG	13A	DPWA	Multichannel
−0.28±0.03	GOPAL	77	DPWA	$\overline{K}N$ multichannel
−0.28±0.01	KANE	74	DPWA	$K^- p \to \Sigma\pi$
• • • We do not use the following data for averages, fits, limits, etc. • • •				
−0.25 or −0.25	[1] MARTIN	77	DPWA	$\overline{K}N$ multichannel

[1] The two MARTIN 77 values are from a T-matrix pole and from a Breit-Wigner fit.

$(\Gamma_i\Gamma_f)^{1/2}/\Gamma_{total}$ in $N\overline{K} \to \Lambda(1820) \to \Sigma(1385)\pi$, P-wave — $(\Gamma_1\Gamma_4)^{1/2}/\Gamma$

VALUE	DOCUMENT ID		TECN	COMMENT
−0.20 ±0.02	ZHANG	13A	DPWA	Multichannel
−0.167±0.054	[1] CAMERON	78	DPWA	$K^- p \to \Sigma(1385)\pi$
+0.27 ±0.03	PREVOST	74	DPWA	$K^- N \to \Sigma(1385)\pi$

[1] The published sign has been changed to be in accord with the baryon-first convention.

$(\Gamma_i\Gamma_f)^{1/2}/\Gamma_{total}$ in $N\overline{K} \to \Lambda(1820) \to \Sigma(1385)\pi$, F-wave — $(\Gamma_1\Gamma_5)^{1/2}/\Gamma$

VALUE	DOCUMENT ID		TECN	COMMENT
+0.065±0.029	[1] CAMERON	78	DPWA	$K^- p \to \Sigma(1385)\pi$

[1] The published sign has been changed to be in accord with the baryon-first convention.

$(\Gamma_i\Gamma_f)^{1/2}/\Gamma_{total}$ in $N\overline{K} \to \Lambda(1820) \to \Lambda\eta$ — $(\Gamma_1\Gamma_6)^{1/2}/\Gamma$

VALUE	DOCUMENT ID		TECN
$-0.096^{+0.040}_{-0.020}$	RADER	73	MPWA

$\Lambda(1820)$ REFERENCES

SARANTSEV	19	EPJ A55 180	A.V. Sarantsev *et al.*	(BONN, PNPI)
KAMANO	15	PR C92 025205	H. Kamano *et al.*	(ANL, OSAK)
ZHANG	13A	PR C88 035205	H. Zhang *et al.*	(KSU)
PDG	82	PL 111B 1	M. Roos *et al.*	(HELS, CIT, CERN)
GOPAL	80	Toronto Conf. 159	G.P. Gopal	(RHEL) IJP
ALSTON-...	78	PR D18 182	M. Alston-Garnjost *et al.*	(LBL, MTHO+) IJP
Also		PRL 38 1007	M. Alston-Garnjost *et al.*	(LBL, MTHO+) IJP
CAMERON	78	NP B143 189	W. Cameron *et al.*	(RHEL, LOIC) IJP
DECLAIS	77	CERN 77-16	Y. Declais *et al.*	(CAEN, CERN) IJP
GOPAL	77	NP B119 362	G.P. Gopal *et al.*	(LOIC, RHEL) IJP
MARTIN	77	NP B127 349	B.R. Martin, M.K. Pidcock, R.G. Moorhouse	(LOUC+) IJP
Also		NP B126 266	B.R. Martin, M.K. Pidcock	(LOUC)
Also		NP B126 285	B.R. Martin, M.K. Pidcock	(LOUC) IJP
KANE	74	LBL-2452	D.F. Kane	(LBL) IJP
PREVOST	74	NP B69 246	J. Prevost *et al.*	(SACL, CERN, HEID)
RADER	73	NC 16A 178	R.K. Rader *et al.*	(SACL, HEID, CERN+)
ARMENTEROS	68C	NP B8 216	R. Armenteros *et al.*	(CERN, HEID, SACL) I

$\Lambda(1830)\ 5/2^-$

$I(J^P) = 0(\frac{5}{2}^-)$ Status: ****

For results published before 1973 (they are now obsolete), see our 1982 edition Physics Letters **111B** 1 (1982).

The best evidence for this resonance is in the $\Sigma\pi$ channel.

$\Lambda(1830)$ POLE POSITION

REAL PART

VALUE (MeV)	DOCUMENT ID		TECN	COMMENT
1800 to 1860 (≈ 1830) OUR ESTIMATE				
1819.5± 3.0	SARANTSEV	19	DPWA	$\overline{K}N$ multichannel
1899^{+35}_{-37}	[1] KAMANO	15	DPWA	Multichannel
• • • We do not use the following data for averages, fits, limits, etc. • • •				
1766^{+37}_{-34}	[2] KAMANO	15	DPWA	Multichannel
1809	ZHANG	13A	DPWA	Multichannel

[1] The preferred solution A in KAMANO 15 reports two poles. This entry is from the preferred solution A.
[2] From the preferred solution A in KAMANO 15. Not seen in solution B.

−2×IMAGINARY PART

VALUE (MeV)	DOCUMENT ID		TECN	COMMENT
50 to 80 (≈ 65) OUR ESTIMATE				
62± 5	SARANTSEV	19	DPWA	$\overline{K}N$ multichannel
80^{+100}_{-34}	[1] KAMANO	15	DPWA	Multichannel
• • • We do not use the following data for averages, fits, limits, etc. • • •				
212^{+94}_{-62}	[2] KAMANO	15	DPWA	Multichannel
109	ZHANG	13A	DPWA	Multichannel

[1] The preferred solution A in KAMANO 15 reports two poles. This entry is from the preferred solution A.
[2] From the preferred solution A in KAMANO 15. Not seen in solution B.

$\Lambda(1830)$ POLE RESIDUES

The normalized residue is the residue divided by $\Gamma_{pole}/2$.

Normalized residue in $N\overline{K} \to \Lambda(1830) \to N\overline{K}$

MODULUS	PHASE (°)	DOCUMENT ID		TECN	COMMENT
0.055 ±0.010	**20 ± 14**	SARANTSEV	19	DPWA	$\overline{K}N$ multichannel
• • • We do not use the following data for averages, fits, limits, etc. • • •					
0.00502	−80	[1] KAMANO	15	DPWA	Multichannel

[1] From the preferred solution A in KAMANO 15.

Normalized residue in $N\overline{K} \to \Lambda(1830) \to \Sigma\pi$

MODULUS	PHASE (°)	DOCUMENT ID		TECN	COMMENT
0.15 ±0.03	**180 ± 10**	SARANTSEV	19	DPWA	$\overline{K}N$ multichannel
• • • We do not use the following data for averages, fits, limits, etc. • • •					
0.00581	179	[1] KAMANO	15	DPWA	Multichannel

[1] From the preferred solution A in KAMANO 15.

Normalized residue in $N\overline{K} \to \Lambda(1830) \to \Lambda\eta$

MODULUS	PHASE (°)	DOCUMENT ID		TECN	COMMENT
• • • We do not use the following data for averages, fits, limits, etc. • • •					
0.00941	−65	[1] KAMANO	15	DPWA	Multichannel

[1] From the preferred solution A in KAMANO 15.

Normalized residue in $N\overline{K} \to \Lambda(1830) \to \Xi K$

MODULUS	PHASE (°)	DOCUMENT ID		TECN	COMMENT
0.010 ±0.005	**65 ± 20**	SARANTSEV	19	DPWA	$\overline{K}N$ multichannel
• • • We do not use the following data for averages, fits, limits, etc. • • •					
0.0477	94	[1] KAMANO	15	DPWA	Multichannel

[1] From the preferred solution A in KAMANO 15.

Normalized residue in $N\overline{K} \to \Lambda(1830) \to \Sigma(1385)\pi$, D-wave

MODULUS	PHASE (°)	DOCUMENT ID		TECN	COMMENT
0.10 ±0.04	**10 ± 25**	SARANTSEV	19	DPWA	$\overline{K}N$ multichannel
• • • We do not use the following data for averages, fits, limits, etc. • • •					
0.0237	113	[1] KAMANO	15	DPWA	Multichannel

[1] From the preferred solution A in KAMANO 15.

Normalized residue in $N\overline{K} \to \Lambda(1830) \to \Sigma(1385)\pi$, G-wave

MODULUS	PHASE (°)	DOCUMENT ID		TECN	COMMENT
0.03 ±0.02		SARANTSEV	19	DPWA	$\overline{K}N$ multichannel
• • • We do not use the following data for averages, fits, limits, etc. • • •					
0.000726	127	[1] KAMANO	15	DPWA	Multichannel

[1] From the preferred solution A in KAMANO 15.

Normalized residue in $N\overline{K} \to \Lambda(1830) \to N\overline{K}^*(892)$, $S=1/2$, D-wave

MODULUS	PHASE (°)	DOCUMENT ID		TECN	COMMENT
• • • We do not use the following data for averages, fits, limits, etc. • • •					
0.0278	−177	[1] KAMANO	15	DPWA	Multichannel

[1] From the preferred solution A in KAMANO 15.

Downloaded from https://academic.oup.com/ptep/article/2022/8/083C01/6651666 by KIT Library user on 27 September 2022

Normalized residue in $N\overline{K} \to \Lambda(1830) \to N\overline{K}^*(892)$, $S=3/2$, D-wave

MODULUS	PHASE (°)	DOCUMENT ID		TECN	COMMENT
• • • We do not use the following data for averages, fits, limits, etc. • • •					
0.0255	3	[1] KAMANO	15	DPWA	Multichannel

[1] From the preferred solution A in KAMANO 15.

Normalized residue in $N\overline{K} \to \Lambda(1830) \to N\overline{K}^*(892)$, $S=3/2$, G-wave

MODULUS	PHASE (°)	DOCUMENT ID		TECN	COMMENT
• • • We do not use the following data for averages, fits, limits, etc. • • •					
0.00773	−17	[1] KAMANO	15	DPWA	Multichannel

[1] From the preferred solution A in KAMANO 15.

Normalized residue in $N\overline{K} \to \Lambda(1830) \to \Lambda\omega$, $S=1/2$, D-wave

MODULUS	PHASE (°)	DOCUMENT ID		TECN	COMMENT
0.04±0.03		SARANTSEV	19	DPWA	$\overline{K}N$ multichannel

Normalized residue in $N\overline{K} \to \Lambda(1830) \to \Lambda\omega$, $S=3/2$, D-wave

MODULUS	PHASE (°)	DOCUMENT ID		TECN	COMMENT
0.05±0.03	**−110 ± 35**	SARANTSEV	19	DPWA	$\overline{K}N$ multichannel

$\Lambda(1830)$ MASS

VALUE (MeV)	DOCUMENT ID		TECN	COMMENT
1820 to 1830 (≈ 1825) OUR ESTIMATE				
1821± 3	SARANTSEV	19	DPWA	$\overline{K}N$ multichannel
1820± 4	ZHANG	13A	DPWA	Multichannel
1831±10	GOPAL	80	DPWA	$\overline{K}N \to \overline{K}N$
1825±10	GOPAL	77	DPWA	$\overline{K}N$ multichannel
1825± 1	KANE	74	DPWA	$K^-p \to \Sigma\pi$
• • • We do not use the following data for averages, fits, limits, etc. • • •				
1817 or 1818	[1] MARTIN	77	DPWA	$\overline{K}N$ multichannel

[1] The two MARTIN 77 values are from a T-matrix pole and from a Breit-Wigner fit.

$\Lambda(1830)$ WIDTH

VALUE (MeV)	DOCUMENT ID		TECN	COMMENT
60 to 120 (≈ 90) OUR ESTIMATE				
64± 7	SARANTSEV	19	DPWA	$\overline{K}N$ multichannel
114±10	ZHANG	13A	DPWA	Multichannel
100±10	GOPAL	80	DPWA	$\overline{K}N \to \overline{K}N$
94±10	GOPAL	77	DPWA	$\overline{K}N$ multichannel
119± 3	KANE	74	DPWA	$K^-p \to \Sigma\pi$
• • • We do not use the following data for averages, fits, limits, etc. • • •				
56 or 56	[1] MARTIN	77	DPWA	$\overline{K}N$ multichannel

[1] The two MARTIN 77 values are from a T-matrix pole and from a Breit-Wigner fit.

$\Lambda(1830)$ DECAY MODES

	Mode	Fraction (Γ_i/Γ)	Scale factor
Γ_1	$N\overline{K}$	0.04 to 0.08	
Γ_2	$\Sigma\pi$	35–75 %	
Γ_3	ΞK		
Γ_4	$\Sigma(1385)\pi$	>15 %	
Γ_5	$\Sigma(1385)\pi$, D-wave	(40 ±15) %	3.2
Γ_6	$\Sigma(1385)\pi$, G-wave		
Γ_7	$\Lambda\eta$		
Γ_8	$N\overline{K}^*(892)$, $S=1/2$, D-wave		
Γ_9	$N\overline{K}^*(892)$, $S=3/2$, D-wave		
Γ_{10}	$N\overline{K}^*(892)$, $S=3/2$, G-wave		

$\Lambda(1830)$ BRANCHING RATIOS

See "Sign conventions for resonance couplings" in the Note on Λ and Σ Resonances.

$\Gamma(N\overline{K})/\Gamma_{total}$ — Γ_1/Γ

VALUE	DOCUMENT ID		TECN	COMMENT
0.04 to 0.08 OUR ESTIMATE				
0.055±0.010	SARANTSEV	19	DPWA	$\overline{K}N$ multichannel
0.041±0.005	ZHANG	13A	DPWA	Multichannel
0.08 ±0.03	GOPAL	80	DPWA	$\overline{K}N \to \overline{K}N$
0.02 ±0.02	ALSTON-...	78	DPWA	$\overline{K}N \to \overline{K}N$
• • • We do not use the following data for averages, fits, limits, etc. • • •				
0.006	[1] KAMANO	15	DPWA	Multichannel
0.04 ±0.03	GOPAL	77	DPWA	See GOPAL 80
0.04 or 0.04	[2] MARTIN	77	DPWA	$\overline{K}N$ multichannel

[1] From the preferred solution A in KAMANO 15.
[2] The two MARTIN 77 values are from a T-matrix pole and from a Breit-Wigner fit.

$\Gamma(\Sigma\pi)/\Gamma_{total}$ — Γ_2/Γ

VALUE	DOCUMENT ID		TECN	COMMENT
0.42 ±0.08	SARANTSEV	19	DPWA	$\overline{K}N$ multichannel
• • • We do not use the following data for averages, fits, limits, etc. • • •				
0.017	[1] KAMANO	15	DPWA	Multichannel

[1] From the preferred solution A in KAMANO 15.

$\Gamma(\Xi K)/\Gamma_{total}$ — Γ_3/Γ

VALUE	DOCUMENT ID		TECN	COMMENT
• • • We do not use the following data for averages, fits, limits, etc. • • •				
0.562	[1] KAMANO	15	DPWA	Multichannel

[1] From the preferred solution A in KAMANO 15.

$\Gamma(\Sigma(1385)\pi$, D-wave$)/\Gamma_{total}$ — Γ_5/Γ

VALUE	DOCUMENT ID		TECN	COMMENT
0.40 ±0.15 OUR AVERAGE Error includes scale factor of 3.2.				
0.20 ±0.08	SARANTSEV	19	DPWA	$\overline{K}N$ multichannel
0.52 ±0.06	ZHANG	13A	DPWA	Multichannel
• • • We do not use the following data for averages, fits, limits, etc. • • •				
0.134	[1] KAMANO	15	DPWA	Multichannel

[1] From the preferred solution A in KAMANO 15.

$\Gamma(\Sigma(1385)\pi$, G-wave$)/\Gamma_{total}$ — Γ_6/Γ

VALUE	DOCUMENT ID		TECN	COMMENT
0.020±0.015	SARANTSEV	19	DPWA	$\overline{K}N$ multichannel

$\Gamma(\Lambda\eta)/\Gamma_{total}$ — Γ_7/Γ

VALUE	DOCUMENT ID		TECN	COMMENT
• • • We do not use the following data for averages, fits, limits, etc. • • •				
0.024	[1] KAMANO	15	DPWA	Multichannel

[1] From the preferred solution A in KAMANO 15.

$\Gamma(N\overline{K}^*(892), S=1/2, D\text{-wave})/\Gamma_{total}$ — Γ_8/Γ

VALUE	DOCUMENT ID		TECN	COMMENT
• • • We do not use the following data for averages, fits, limits, etc. • • •				
0.134	[1] KAMANO	15	DPWA	Multichannel

[1] From the preferred solution A in KAMANO 15.

$\Gamma(N\overline{K}^*(892), S=3/2, D\text{-wave})/\Gamma_{total}$ — Γ_9/Γ

VALUE	DOCUMENT ID		TECN	COMMENT
• • • We do not use the following data for averages, fits, limits, etc. • • •				
0.115	[1] KAMANO	15	DPWA	Multichannel

[1] From the preferred solution A in KAMANO 15.

$\Gamma(N\overline{K}^*(892), S=3/2, G\text{-wave})/\Gamma_{total}$ — Γ_{10}/Γ

VALUE	DOCUMENT ID		TECN	COMMENT
• • • We do not use the following data for averages, fits, limits, etc. • • •				
0.009	[1] KAMANO	15	DPWA	Multichannel

[1] From the preferred solution A in KAMANO 15.

$(\Gamma_i\Gamma_f)^{1/2}/\Gamma_{total}$ in $N\overline{K} \to \Lambda(1830) \to \Sigma\pi$ — $(\Gamma_1\Gamma_2)^{1/2}/\Gamma$

VALUE	DOCUMENT ID		TECN	COMMENT
−0.13±0.01	ZHANG	13A	DPWA	Multichannel
−0.17±0.03	GOPAL	77	DPWA	$\overline{K}N$ multichannel
−0.15±0.01	KANE	74	DPWA	$K^-p \to \Sigma\pi$
• • • We do not use the following data for averages, fits, limits, etc. • • •				
−0.17 or −0.17	[1] MARTIN	77	DPWA	$\overline{K}N$ multichannel

[1] The two MARTIN 77 values are from a T-matrix pole and from a Breit-Wigner fit.

$(\Gamma_i\Gamma_f)^{1/2}/\Gamma_{total}$ in $N\overline{K} \to \Lambda(1830) \to \Sigma(1385)\pi$ — $(\Gamma_1\Gamma_4)^{1/2}/\Gamma$

VALUE	DOCUMENT ID		TECN	COMMENT
0.20 to 0.50 OUR ESTIMATE				
+0.141±0.014	[1] CAMERON	78	DPWA	$K^-p \to \Sigma(1385)\pi$
+0.13 ±0.03	PREVOST	74	DPWA	$K^-N \to \Sigma(1385)\pi$

[1] The CAMERON 78 upper limit on G-wave decay is 0.03. The published sign has been changed to be in accord with the baryon-first convention.

$(\Gamma_i\Gamma_f)^{1/2}/\Gamma_{total}$ in $N\overline{K} \to \Lambda(1830) \to \Lambda\eta$ — $(\Gamma_1\Gamma_7)^{1/2}/\Gamma$

VALUE	DOCUMENT ID		TECN
−0.044±0.020	RADER	73	MPWA

$\Lambda(1830)$ REFERENCES

SARANTSEV	19	EPJ A55 180	A.V. Sarantsev *et al.*	(BONN, PNPI)
KAMANO	15	PR C92 025205	H. Kamano *et al.*	(ANL, OSAK)
ZHANG	13A	PR C88 035205	H. Zhang *et al.*	(KSU)
PDG	82	PL 111B 1	M. Roos *et al.*	(HELS, CIT, CERN)
GOPAL	80	Toronto Conf. 159	G.P. Gopal	(RHEL) IJP
ALSTON-...	78	PR D18 182	M. Alston-Garnjost *et al.*	(LBL, MTHO+) IJP
Also		PRL 38 1007	M. Alston-Garnjost *et al.*	(LBL, MTHO+) IJP
CAMERON	78	NP B143 189	W. Cameron *et al.*	(RHEL, LOIC) IJP
GOPAL	77	NP B119 362	G.P. Gopal *et al.*	(LOIC, RHEL) IJP
MARTIN	77	NP B127 349	B.R. Martin, M.K. Pidcock, R.G. Moorhouse	(LOUC+) IJP
Also		NP B126 266	B.R. Martin, M.K. Pidcock	(LOUC)
Also		NP B126 285	B.R. Martin, M.K. Pidcock	(LOUC) IJP
KANE	74	LBL-2452	D.F. Kane	(LBL) IJP
PREVOST	74	NP B69 246	J. Prevost *et al.*	(SACL, CERN, HEID)
RADER	73	NC 16A 178	R.K. Rader *et al.*	(SACL, HEID, CERN+)

Downloaded from https://academic.oup.com/ptep/article/2022/8/083C01/6651666 by KIT Library user on 27 September 2022

$\Lambda(1890)\ 3/2^+$

$I(J^P) = 0(\frac{3}{2}^+)$ Status: ****

For results published before 1974 (they are now obsolete), see our 1982 edition Physics Letters **111B** 1 (1982).

$\Lambda(1890)$ POLE POSITION

REAL PART

VALUE (MeV)	DOCUMENT ID		TECN	COMMENT
1872±5	SARANTSEV	19	DPWA	$\overline{K}N$ multichannel
• • • We do not use the following data for averages, fits, limits, etc. • • •				
1859^{+5}_{-7}	[1] KAMANO	15	DPWA	Multichannel
1876	ZHANG	13A	DPWA	Multichannel

[1] From the preferred solution A in KAMANO 15, incompatible with solution B.

−2×IMAGINARY PART

VALUE (MeV)	DOCUMENT ID		TECN	COMMENT
101±10	SARANTSEV	19	DPWA	$\overline{K}N$ multichannel
• • • We do not use the following data for averages, fits, limits, etc. • • •				
113^{+20}_{-4}	[1] KAMANO	15	DPWA	$\overline{K}N$ multichannel
145	ZHANG	13A	DPWA	$\overline{K}N$ multichannel

[1] From the preferred solution A in KAMANO 15, incompatible with solution B.

$\Lambda(1890)$ POLE RESIDUE

The "normalized residue" is the residue divided by $\Gamma_{pole}/2$.

Normalized residue in $KN \to \Lambda(1890) \to KN$

MODULUS	PHASE (°)	DOCUMENT ID		TECN	COMMENT
0.30 ±0.06	**0 ± 10**	SARANTSEV	19	DPWA	$\overline{K}N$ multichannel
• • • We do not use the following data for averages, fits, limits, etc. • • •					
0.241	−23	[1] KAMANO	15	DPWA	$\overline{K}N$ multichannel

[1] From the preferred solution A in KAMANO 15.

Normalized residue in $N\overline{K} \to \Lambda(1890) \to \Sigma\pi$

MODULUS	PHASE (°)	DOCUMENT ID		TECN	COMMENT
0.14 ±0.05	**148 ± 12**	SARANTSEV	19	DPWA	$\overline{K}N$ multichannel
• • • We do not use the following data for averages, fits, limits, etc. • • •					
0.101	104	[1] KAMANO	15	DPWA	$\overline{K}N$ multichannel

[1] From the preferred solution A in KAMANO 15.

Normalized residue in $N\overline{K} \to \Lambda(1890) \to \Lambda\eta$

MODULUS	PHASE (°)	DOCUMENT ID		TECN	COMMENT
• • • We do not use the following data for averages, fits, limits, etc. • • •					
0.0485	−54	[1] KAMANO	15	DPWA	Multichannel

[1] From the preferred solution A in KAMANO 15.

Normalized residue in $N\overline{K} \to \Lambda(1890) \to \Xi K$

MODULUS	PHASE (°)	DOCUMENT ID		TECN	COMMENT
0.065 ±0.020	**160 ± 30**	SARANTSEV	19	DPWA	$\overline{K}N$ multichannel
• • • We do not use the following data for averages, fits, limits, etc. • • •					
0.0562	−85	[1] KAMANO	15	DPWA	$\overline{K}N$ multichannel

[1] From the preferred solution A in KAMANO 15.

Normalized residue in $N\overline{K} \to \Lambda(1890) \to \Sigma(1385)\pi$, P-wave

MODULUS	PHASE (°)	DOCUMENT ID		TECN	COMMENT
0.11 ±0.05	**−160 ± 45**	SARANTSEV	19	DPWA	$\overline{K}N$ multichannel
• • • We do not use the following data for averages, fits, limits, etc. • • •					
0.295	−40	[1] KAMANO	15	DPWA	$\overline{K}N$ multichannel

[1] From the preferred solution A in KAMANO 15.

Normalized residue in $N\overline{K} \to \Lambda(1890) \to \Sigma(1385)\pi$, F-wave

MODULUS	PHASE (°)	DOCUMENT ID		TECN	COMMENT
0.10 ±0.04	**10 ± 50**	SARANTSEV	19	DPWA	$\overline{K}N$ multichannel
• • • We do not use the following data for averages, fits, limits, etc. • • •					
0.064	127	[1] KAMANO	15	DPWA	$\overline{K}N$ multichannel

[1] From the preferred solution A in KAMANO 15.

Normalized residue in $N\overline{K} \to \Lambda(1890) \to N\overline{K}^*(892)$, S=1/2 , P-wave

MODULUS	PHASE (°)	DOCUMENT ID		TECN	COMMENT
0.03 ±0.03		SARANTSEV	19	DPWA	$\overline{K}N$ multichannel
• • • We do not use the following data for averages, fits, limits, etc. • • •					
0.188	−160	[1] KAMANO	15	DPWA	$\overline{K}N$ multichannel

[1] From the preferred solution A in KAMANO 15.

Normalized residue in $N\overline{K} \to \Lambda(1890) \to N\overline{K}^*(892)$, S=3/2 , P-wave

MODULUS	PHASE (°)	DOCUMENT ID		TECN	COMMENT
0.05 ±0.03	**180 ± 40**	SARANTSEV	19	DPWA	$\overline{K}N$ multichannel
• • • We do not use the following data for averages, fits, limits, etc. • • •					
0.209	15	[1] KAMANO	15	DPWA	$\overline{K}N$ multichannel

[1] From the preferred solution A in KAMANO 15.

Normalized residue in $N\overline{K} \to \Lambda(1890) \to N\overline{K}^*(892)$, S=3/2, F-wave

MODULUS	PHASE (°)	DOCUMENT ID		TECN	COMMENT
• • • We do not use the following data for averages, fits, limits, etc. • • •					
0.0141	129	[1] KAMANO	15	DPWA	Multichannel

[1] From the preferred solution A in KAMANO 15.

Normalized residue in $N\overline{K} \to \Lambda(1890) \to \Lambda\omega$, S=1/2 , P-wave

MODULUS	PHASE (°)	DOCUMENT ID		TECN	COMMENT
0.24±0.06	**15 ± 20**	SARANTSEV	19	DPWA	$\overline{K}N$ multichannel

Normalized residue in $N\overline{K} \to \Lambda(1890) \to \Lambda\omega$, S=3/2 , P-wave

MODULUS	PHASE (°)	DOCUMENT ID		TECN	COMMENT
0.15±0.08	**−165 ± 20**	SARANTSEV	19	DPWA	$\overline{K}N$ multichannel

$\Lambda(1890)$ MASS

VALUE (MeV)	DOCUMENT ID		TECN	COMMENT
1870 to 1910 (≈ 1890) OUR ESTIMATE				
1873± 5	SARANTSEV	19	DPWA	$\overline{K}N$ multichannel
1900± 5	ZHANG	13A	DPWA	$\overline{K}N$ multichannel
1897± 5	GOPAL	80	DPWA	$\overline{K}N \to \overline{K}N$
1908±10	ALSTON-...	78	DPWA	$\overline{K}N \to \overline{K}N$
1894±10	HEMINGWAY	75	DPWA	$K^-p \to \overline{K}N$
• • • We do not use the following data for averages, fits, limits, etc. • • •				
1900± 5	GOPAL	77	DPWA	$\overline{K}N$ multichannel
1856 or 1868	[1] MARTIN	77	DPWA	$\overline{K}N$ multichannel
1900	[2] NAKKASYAN	75	DPWA	$K^-p \to \Lambda\omega$

[1] The two MARTIN 77 values are from a T-matrix pole and from a Breit-Wigner fit.
[2] Found in one of two best solutions.

$\Lambda(1890)$ WIDTH

VALUE (MeV)	DOCUMENT ID		TECN	COMMENT
80 to 160 (≈ 120) OUR ESTIMATE				
103±10	SARANTSEV	19	DPWA	$\overline{K}N$ multichannel
161±15	ZHANG	13A	DPWA	$\overline{K}N$ multichannel
74±10	GOPAL	80	DPWA	$\overline{K}N \to \overline{K}N$
119±20	ALSTON-...	78	DPWA	$\overline{K}N \to \overline{K}N$
107±10	HEMINGWAY	75	DPWA	$K^-p \to \overline{K}N$
• • • We do not use the following data for averages, fits, limits, etc. • • •				
72±10	GOPAL	77	DPWA	$\overline{K}N$ multichannel
191 or 193	[1] MARTIN	77	DPWA	$\overline{K}N$ multichannel
100	[2] NAKKASYAN	75	DPWA	$K^-p \to \Lambda\omega$

[1] The two MARTIN 77 values are from a T-matrix pole and from a Breit-Wigner fit.
[2] Found in one of two best solutions.

$\Lambda(1890)$ DECAY MODES

	Mode	Fraction (Γ_i/Γ)
Γ_1	$N\overline{K}$	0.24 to 0.36
Γ_2	$\Sigma\pi$	3–10 %
Γ_3	$\Lambda\eta$	
Γ_4	ΞK	
Γ_5	$\Sigma(1385)\pi$	seen
Γ_6	$\Sigma(1385)\pi$, P-wave	(6.0 ±3.0) %
Γ_7	$\Sigma(1385)\pi$, F-wave	(4.0 ±2.0) %
Γ_8	$N\overline{K}^*(892)$	seen
Γ_9	$N\overline{K}^*(892)$, S=1/2	
Γ_{10}	$N\overline{K}^*(892)$, S=1/2, P-wave	
Γ_{11}	$N\overline{K}^*(892)$, S=3/2, P-wave	
Γ_{12}	$N\overline{K}^*(892)$, S=3/2, F-wave	
Γ_{13}	$\Lambda\omega$	

$\Lambda(1890)$ BRANCHING RATIOS

See "Sign conventions for resonance couplings" in the Note on Λ and Σ Resonances.

$\Gamma(N\overline{K})/\Gamma_{total}$ — Γ_1/Γ

VALUE	DOCUMENT ID		TECN	COMMENT
0.24 to 0.36 OUR ESTIMATE				
0.30 ±0.06	SARANTSEV	19	DPWA	$\overline{K}N$ multichannel
0.37 ±0.03	ZHANG	13A	DPWA	$\overline{K}N$ multichannel
0.20 ±0.02	GOPAL	80	DPWA	$\overline{K}N \to \overline{K}N$
0.34 ±0.05	ALSTON-...	78	DPWA	$\overline{K}N \to \overline{K}N$
0.24 ±0.04	HEMINGWAY	75	DPWA	$K^-p \to \overline{K}N$

Downloaded from https://academic.oup.com/ptep/article/2022/8/083C01/6651666 by KIT Library user on 27 September 2022

• • • We do not use the following data for averages, fits, limits, etc. • • •

0.305	[1] KAMANO	15	DPWA	$\overline{K}N$ multichannel
0.18 ±0.02	GOPAL	77	DPWA	See GOPAL 80
0.36 or 0.34	[2] MARTIN	77	DPWA	$\overline{K}N$ multichannel

[1] From the preferred solution A in KAMANO 15.
[2] The two MARTIN 77 values are from a T-matrix pole and from a Breit-Wigner fit.

$\Gamma(\Sigma\pi)/\Gamma_{total}$ — Γ_2/Γ

VALUE	DOCUMENT ID		TECN	COMMENT
6 ±2	SARANTSEV	19	DPWA	$\overline{K}N$ multichannel
<0.03	LANGBEIN	72	IPWA	$\overline{K}N$ multichannel

• • • We do not use the following data for averages, fits, limits, etc. • • •

0.04	[1] KAMANO	15	DPWA	$\overline{K}N$ multichannel

[1] From the preferred solution A in KAMANO 15.

$\Gamma(\Lambda\eta)/\Gamma_{total}$ — Γ_3/Γ

VALUE	DOCUMENT ID	TECN	COMMENT

• • • We do not use the following data for averages, fits, limits, etc. • • •

0.012	[1] KAMANO	15	DPWA	$\overline{K}N$ multichannel

[1] From the preferred solution A in KAMANO 15.

$\Gamma(\Xi K)/\Gamma_{total}$ — Γ_4/Γ

VALUE	DOCUMENT ID		TECN	COMMENT
~ 0.01	SARANTSEV	19	DPWA	$\overline{K}N$ multichannel

• • • We do not use the following data for averages, fits, limits, etc. • • •

0.009	[1] KAMANO	15	DPWA	$\overline{K}N$ multichannel

[1] From the preferred solution A in KAMANO 15.

$\Gamma(\Sigma(1385)\pi$, P-wave$)/\Gamma_{total}$ — Γ_6/Γ

VALUE	DOCUMENT ID		TECN	COMMENT
0.06 ±0.03	SARANTSEV	19	DPWA	$\overline{K}N$ multichannel

• • • We do not use the following data for averages, fits, limits, etc. • • •

0.453	[1] KAMANO	15	DPWA	$\overline{K}N$ multichannel

[1] From the preferred solution A in KAMANO 15.

$\Gamma(\Sigma(1385)\pi$, F-wave$)/\Gamma_{total}$ — Γ_7/Γ

VALUE	DOCUMENT ID		TECN	COMMENT
0.04 ±0.02	SARANTSEV	19	DPWA	$\overline{K}N$ multichannel

• • • We do not use the following data for averages, fits, limits, etc. • • •

0.019	[1] KAMANO	15	DPWA	$\overline{K}N$ multichannel

[1] From the preferred solution A in KAMANO 15.

$\Gamma(N\overline{K}^*(892), S=1/2, P$-wave$)/\Gamma_{total}$ — Γ_{10}/Γ

VALUE	DOCUMENT ID		TECN	COMMENT
<0.01	SARANTSEV	19	DPWA	$\overline{K}N$ multichannel

• • • We do not use the following data for averages, fits, limits, etc. • • •

0.073	[1] KAMANO	15	DPWA	$\overline{K}N$ multichannel

[1] From the preferred solution A in KAMANO 15.

$\Gamma(N\overline{K}^*(892), S=3/2, P$-wave$)/\Gamma_{total}$ — Γ_{11}/Γ

VALUE	DOCUMENT ID		TECN	COMMENT
~ 0.01	SARANTSEV	19	DPWA	$\overline{K}N$ multichannel

• • • We do not use the following data for averages, fits, limits, etc. • • •

0.088	[1] KAMANO	15	DPWA	$\overline{K}N$ multichannel

[1] From the preferred solution A in KAMANO 15.

$\Gamma(N\overline{K}^*(892), S=3/2, F$-wave$)/\Gamma_{total}$ — Γ_{12}/Γ

VALUE	DOCUMENT ID	TECN	COMMENT

• • • We do not use the following data for averages, fits, limits, etc. • • •

0.001	[1] KAMANO	15	DPWA	$\overline{K}N$ multichannel

[1] From the preferred solution A in KAMANO 15.

$(\Gamma_i\Gamma_f)^{1/2}/\Gamma_{total}$ in $N\overline{K}\to\Lambda(1890)\to\Sigma\pi$ — $(\Gamma_1\Gamma_2)^{1/2}/\Gamma$

VALUE	DOCUMENT ID		TECN	COMMENT
−0.09±0.02	ZHANG	13A	DPWA	$\overline{K}N$ multichannel
−0.09±0.03	GOPAL	77	DPWA	$\overline{K}N$ multichannel

• • • We do not use the following data for averages, fits, limits, etc. • • •

+0.15 or +0.14	[1] MARTIN	77	DPWA	$\overline{K}N$ multichannel

[1] The two MARTIN 77 values are from a T-matrix pole and from a Breit-Wigner fit.

$(\Gamma_i\Gamma_f)^{1/2}/\Gamma_{total}$ in $N\overline{K}\to\Lambda(1890)\to\Sigma(1385)\pi$, P-wave — $(\Gamma_1\Gamma_6)^{1/2}/\Gamma$

VALUE	DOCUMENT ID	TECN	COMMENT
<0.03	CAMERON 78	DPWA	$K^-p\to\Sigma(1385)\pi$

$(\Gamma_i\Gamma_f)^{1/2}/\Gamma_{total}$ in $N\overline{K}\to\Lambda(1890)\to\Sigma(1385)\pi$, F-wave — $(\Gamma_1\Gamma_7)^{1/2}/\Gamma$

VALUE	DOCUMENT ID		TECN	COMMENT
−0.31 ±0.04	ZHANG	13A	DPWA	$\overline{K}N$ multichannel
−0.126±0.055	[1] CAMERON	78	DPWA	$K^-p\to\Sigma(1385)\pi$

[1] The published sign has been changed to be in accord with the baryon-first convention.

$(\Gamma_i\Gamma_f)^{1/2}/\Gamma_{total}$ in $N\overline{K}\to\Lambda(1890)\to N\overline{K}^*(892)$, $S=1/2$ — $(\Gamma_1\Gamma_9)^{1/2}/\Gamma$

VALUE	DOCUMENT ID		TECN	COMMENT
−0.17±0.05	ZHANG	13A	DPWA	$\overline{K}N$ multichannel
−0.07±0.03	[1,2] CAMERON	78B	DPWA	$K^-p\to N\overline{K}^*$

[1] Upper limits on the P_3 and F_3 waves are each 0.03.
[2] The published sign has been changed to be in accord with the baryon-first convention.

$(\Gamma_i\Gamma_f)^{1/2}/\Gamma_{total}$ in $N\overline{K}\to\Lambda(1890)\to N\overline{K}^*(892)$, $S=3/2$, F-wave — $(\Gamma_1\Gamma_{12})^{1/2}/\Gamma$

VALUE	DOCUMENT ID		TECN	COMMENT
−0.11±0.03	ZHANG	13A	DPWA	$\overline{K}N$ multichannel

$(\Gamma_i\Gamma_f)^{1/2}/\Gamma_{total}$ in $N\overline{K}\to\Lambda(1890)\to\Lambda\omega$ — $(\Gamma_1\Gamma_{13})^{1/2}/\Gamma$

VALUE	DOCUMENT ID		TECN	COMMENT
seen	BACCARI	77	IPWA	$K^-p\to\Lambda\omega$
0.032	[1] NAKKASYAN	75	DPWA	$K^-p\to\Lambda\omega$

[1] Found in one of two best solutions.

$\Lambda(1890)$ REFERENCES

SARANTSEV	19	EPJ A55 180	A.V. Sarantsev *et al.*	(BONN, PNPI)
KAMANO	15	PR C92 025205	H. Kamano *et al.*	(ANL, OSAK)
ZHANG	13A	PR C88 035205	H. Zhang *et al.*	(KSU)
PDG	82	PL 111B 1	M. Roos *et al.*	(HELS, CIT, CERN)
GOPAL	80	Toronto Conf. 159	G.P. Gopal	(RHEL) IJP
ALSTON-...	78	PR D18 182	M. Alston-Garnjost *et al.*	(LBL, MTHO+) IJP
Also		PRL 38 1007	M. Alston-Garnjost *et al.*	(LBL, MTHO+) IJP
CAMERON	78	NP B143 189	W. Cameron *et al.*	(RHEL, LOIC) IJP
CAMERON	78B	NP B146 327	W. Cameron *et al.*	(RHEL, LOIC) IJP
BACCARI	77	NC 41A 96	B. Baccari *et al.*	(SACL, CDEF) IJP
GOPAL	77	NP B119 362	G.P. Gopal *et al.*	(LOIC, RHEL) IJP
MARTIN	77	NP B127 349	B.R. Martin, M.K. Pidcock, R.G. Moorhouse	(LOUC+) IJP
Also		NP B126 266	B.R. Martin, M.K. Pidcock	(LOUC)
Also		NP B126 285	B.R. Martin, M.K. Pidcock	(LOUC) IJP
HEMINGWAY	75	NP B91 12	R.J. Hemingway *et al.*	(CERN, HEIDH, MPIM) IJP
NAKKASYAN	75	NP B93 85	A. Nakkasyan	(CERN) IJP
LANGBEIN	72	NP B47 477	W. Langbein, F. Wagner	(MPIM) IJP

$\Lambda(2000)$ $1/2^-$

$I(J^P) = 0(\frac{1}{2}^-)$ Status: *

OMITTED FROM SUMMARY TABLE

BARBARO-GALTIERI 70 (in $\Sigma\pi$) and BRANDSTETTER 72 (in $\Lambda\omega$) proposed a state at about this mass. Those analyses are considered to be obsolete, see NAKKASYAN 75 and PDG 18.

$\Lambda(2000)$ MASS

VALUE (MeV)	DOCUMENT ID		TECN	COMMENT
≈ 2000 OUR ESTIMATE				
2020±16	ZHANG	13A	DPWA	Multichannel
2030±30	CAMERON	78B	DPWA	$K^-p\to N\overline{K}^*$

$\Lambda(2000)$ WIDTH

VALUE (MeV)	DOCUMENT ID		TECN	COMMENT
255±63	ZHANG	13A	DPWA	Multichannel
125±25	CAMERON	78B	DPWA	$K^-p\to N\overline{K}^*$

$\Lambda(2000)$ DECAY MODES

	Mode	Fraction (Γ_i/Γ)
Γ_1	$N\overline{K}$	(27±6) %
Γ_2	$\Sigma\pi$	
Γ_3	$\Lambda\eta$	(16±7) %
Γ_4	$N\overline{K}^*(892)$, $S=1/2$, S-wave	
Γ_5	$N\overline{K}^*(892)$, $S=3/2$, D-wave	

$\Lambda(2000)$ BRANCHING RATIOS

See "Sign conventions for resonance couplings" in the Note on Λ and Σ Resonances.

$\Gamma(N\overline{K})/\Gamma_{total}$ — Γ_1/Γ

VALUE	DOCUMENT ID		TECN	COMMENT
0.27±0.06	ZHANG	13A	DPWA	Multichannel

$(\Gamma_i\Gamma_f)^{1/2}/\Gamma_{total}$ in $N\overline{K}\to\Lambda(2000)\to\Sigma\pi$ — $(\Gamma_1\Gamma_2)^{1/2}/\Gamma$

VALUE	DOCUMENT ID		TECN	COMMENT
−0.07±0.03	ZHANG	13A	DPWA	Multichannel

$\Gamma(\Lambda\eta)/\Gamma_{total}$ — Γ_3/Γ

VALUE	DOCUMENT ID		TECN	COMMENT
0.16±0.07	ZHANG	13A	DPWA	Multichannel

Downloaded from https://academic.oup.com/ptep/article/2022/8/083C01/6651666 by KIT Library user on 27 September 2022

$(\Gamma_i\Gamma_f)^{1/2}/\Gamma_{total}$ in $N\overline{K} \to \Lambda(2000) \to N\overline{K}^*(892)$, $S=1/2$, S-wave $(\Gamma_1\Gamma_4)^{1/2}/\Gamma$

VALUE	DOCUMENT ID		TECN	COMMENT
-0.12 ± 0.03	[1] CAMERON	78B	DPWA	$K^-p \to N\overline{K}^*$

[1] The published sign has been changed to be in accord with the baryon-first convention.

$(\Gamma_i\Gamma_f)^{1/2}/\Gamma_{total}$ in $N\overline{K} \to \Lambda(2000) \to N\overline{K}^*(892)$, $S=3/2$, D-wave $(\Gamma_1\Gamma_5)^{1/2}/\Gamma$

VALUE	DOCUMENT ID		TECN	COMMENT
$+0.34\pm0.05$	ZHANG	13A	DPWA	Multichannel
$+0.09\pm0.03$	CAMERON	78B	DPWA	$K^-p \to N\overline{K}^*$

$\Lambda(2000)$ REFERENCES

PDG	18	PR D98 030001	M. Tanabashi *et al.*	(PDG Collab.)
ZHANG	13A	PR C88 035205	H. Zhang *et al.*	(KSU)
CAMERON	78B	NP B146 327	W. Cameron *et al.*	(RHEL, LOIC) IJP
NAKKASYAN	75	NP B93 85	A. Nakkasyan	(CERN) IJP
BRANDSTET...	72	NP B39 13	A.A. Brandstetter *et al.*	(RHEL, CDEF+)
BARBARO-...	70	Duke Conf. 173 Hyperon Resonances, 1970	A. Barbaro-Galtieri	(LRL) IJP

$\Lambda(2050)\ 3/2^-$

$I(J^P) = 0(\frac{3}{2}^-)$ Status: *

OMITTED FROM SUMMARY TABLE

$\Lambda(2050)$ MASS

VALUE (MeV)	DOCUMENT ID		TECN	COMMENT
2056±22	ZHANG	13A	DPWA	Multichannel

$\Lambda(2050)$ WIDTH

VALUE (MeV)	DOCUMENT ID		TECN	COMMENT
493±61	ZHANG	13A	DPWA	Multichannel

$\Lambda(2050)$ DECAY MODES

	Mode	Fraction (Γ_i/Γ)
Γ_1	$N\overline{K}$	(19 ±4) %
Γ_2	$\Sigma\pi$	(6.0±3.0) %
Γ_3	$\Sigma^*(1385)\pi$, S-wave	(8 ±6) %
Γ_4	$\Sigma^*(1385)\pi$, D-wave	(4.0±3.0) %
Γ_5	$N\overline{K}^*(892)$, $S=1/2$	(23 ±7) %

$\Lambda(2050)$ BRANCHING RATIOS

$\Gamma(N\overline{K})/\Gamma_{total}$ — Γ_1/Γ

VALUE	DOCUMENT ID		TECN	COMMENT
0.19±0.04	ZHANG	13A	DPWA	Multichannel

$\Gamma(\Sigma\pi)/\Gamma_{total}$ — Γ_2/Γ

VALUE	DOCUMENT ID		TECN	COMMENT
0.06±0.03	ZHANG	13A	DPWA	Multichannel

$\Gamma(\Sigma^*(1385)\pi, S\text{-wave})/\Gamma_{total}$ — Γ_3/Γ

VALUE	DOCUMENT ID		TECN	COMMENT
0.08±0.06	ZHANG	13A	DPWA	Multichannel

$\Gamma(\Sigma^*(1385)\pi, D\text{-wave})/\Gamma_{total}$ — Γ_4/Γ

VALUE	DOCUMENT ID		TECN	COMMENT
0.04±0.03	ZHANG	13A	DPWA	Multichannel

$\Gamma(N\overline{K}^*(892), S=1/2)/\Gamma_{total}$ — Γ_5/Γ

VALUE	DOCUMENT ID		TECN	COMMENT
0.23±0.07	ZHANG	13A	DPWA	Multichannel

$\Lambda(2050)$ REFERENCES

ZHANG	13A	PR C88 035205	H. Zhang *et al.*	(KSU)

$\Lambda(2070)\ 3/2^+$

$J^P = \frac{3}{2}^+$ Status: *

OMITTED FROM SUMMARY TABLE

$\Lambda(2070)$ POLE POSITION

REAL PART

VALUE (MeV)	DOCUMENT ID		TECN	COMMENT
2044±20	SARANTSEV	19	DPWA	$\overline{K}N$ multichannel

$-2\times$IMAGINARY PART

VALUE (MeV)	DOCUMENT ID		TECN	COMMENT
360±45	SARANTSEV	19	DPWA	$\overline{K}N$ multichannel

$\Lambda(2070)$ POLE RESIDUES

Normalized residue in $N\overline{K} \to \Lambda(2070) \to N\overline{K}$

MODULUS	PHASE (°)	DOCUMENT ID		TECN	COMMENT
0.15±0.05	**−37 ± 10**	SARANTSEV	19	DPWA	$\overline{K}N$ multichannel

Normalized residue in $N\overline{K} \to \Lambda(2070) \to \Sigma\pi$

MODULUS	PHASE (°)	DOCUMENT ID		TECN	COMMENT
0.10±0.03	**−47 ± 8**	SARANTSEV	19	DPWA	$\overline{K}N$ multichannel

Normalized residue in $N\overline{K} \to \Lambda(2070) \to \Xi K$

MODULUS	PHASE (°)	DOCUMENT ID		TECN	COMMENT
0.11±0.03	**0 ± 25**	SARANTSEV	19	DPWA	$\overline{K}N$ multichannel

Normalized residue in $N\overline{K} \to \Lambda(2070) \to \Lambda\omega$, S=1/2 , P-wave

MODULUS	PHASE (°)	DOCUMENT ID		TECN	COMMENT
0.10±0.04	**150 ± 17**	SARANTSEV	19	DPWA	$\overline{K}N$ multichannel

Normalized residue in $N\overline{K} \to \Lambda(2070) \to \Lambda\omega$, S=3/2 , P-wave

MODULUS	PHASE (°)	DOCUMENT ID		TECN	COMMENT
0.08±0.04	**20 ± 30**	SARANTSEV	19	DPWA	$\overline{K}N$ multichannel

Normalized residue in $N\overline{K} \to \Lambda(2070) \to \Lambda\omega$, S=3/2 , F-wave

MODULUS	PHASE (°)	DOCUMENT ID		TECN	COMMENT
0.04±0.02	**−175 ± 35**	SARANTSEV	19	DPWA	$\overline{K}N$ multichannel

Normalized residue in $N\overline{K} \to \Lambda(2070) \to \Sigma(1385)\pi$, P-wave

MODULUS	PHASE (°)	DOCUMENT ID		TECN	COMMENT
0.12±0.07	**−160 ± 55**	SARANTSEV	19	DPWA	$\overline{K}N$ multichannel

Normalized residue in $N\overline{K} \to \Lambda(2070) \to \Sigma(1385)\pi$, F-wave

MODULUS	PHASE (°)	DOCUMENT ID		TECN	COMMENT
0.07±0.04	**−145 ± 50**	SARANTSEV	19	DPWA	$\overline{K}N$ multichannel

Normalized residue in $N\overline{K} \to \Lambda(2070) \to N\overline{K}^*(892)$, S=1/2 , P-wave

MODULUS	PHASE (°)	DOCUMENT ID		TECN	COMMENT
0.36±0.07	**−45 ± 30**	SARANTSEV	19	DPWA	$\overline{K}N$ multichannel

Normalized residue in $N\overline{K} \to \Lambda(2070) \to N\overline{K}^*(892)$, S=3/2 , P-wave

MODULUS	PHASE (°)	DOCUMENT ID		TECN	COMMENT
0.16±0.05	**150 ± 35**	SARANTSEV	19	DPWA	$\overline{K}N$ multichannel

Normalized residue in $N\overline{K} \to \Lambda(2070) \to N\overline{K}^*(892)$, S=3/2 , F-wave

MODULUS	PHASE (°)	DOCUMENT ID		TECN	COMMENT
0.14±0.08	**−50 ± 30**	SARANTSEV	19	DPWA	$\overline{K}N$ multichannel

$\Lambda(2070)$ MASS

VALUE (MeV)	DOCUMENT ID		TECN	COMMENT
2070±24	SARANTSEV	19	DPWA	$\overline{K}N$ multichannel

$\Lambda(2070)$ WIDTH

VALUE (MeV)	DOCUMENT ID		TECN	COMMENT
370±50	SARANTSEV	19	DPWA	$\overline{K}N$ multichannel

$\Lambda(2070)$ DECAY MODES

	Mode	Fraction (Γ_i/Γ)
Γ_1	$N\overline{K}$	(12 ±5) %
Γ_2	$\Sigma\pi$	(7.0±3.0) %
Γ_3	ΞK	(7.0±3.0) %
Γ_4	$\Lambda\omega$, S=1/2 , P-wave	(7 ±4) %
Γ_5	$\Lambda\omega$, S=3/2 , P-wave	(3.0±2.0) %
Γ_6	$\Lambda\omega$, S=3/2 , F-wave	(1.0±1.0) %
Γ_7	$\Sigma(1385)\pi$, P-wave	(10 ±5) %
Γ_8	$\Sigma(1385)\pi$, F-wave	(2.0±2.0) %
Γ_9	$N\overline{K}^*(892)$, S=1/2 , P-wave	(42 ±8) %
Γ_{10}	$N\overline{K}^*(892)$, S=3/2 , P-wave	(14 ±6) %
Γ_{11}	$N\overline{K}^*(892)$, S=3/2 , F-wave	(10 ±6) %

$\Lambda(2070)$ BRANCHING RATIOS

$\Gamma(N\overline{K})/\Gamma_{total}$ — Γ_1/Γ

VALUE	DOCUMENT ID		TECN	COMMENT
0.12±0.05	SARANTSEV	19	DPWA	$\overline{K}N$ multichannel

Downloaded from https://academic.oup.com/ptep/article/2022/8/083C01/6651666 by KIT Library user on 27 September 2022

$\Gamma(\Sigma\pi)/\Gamma_{total}$ — Γ_2/Γ

VALUE	DOCUMENT ID	TECN	COMMENT
0.07±0.03	SARANTSEV 19	DPWA	$\overline{K}N$ multichannel

$\Gamma(\Xi K)/\Gamma_{total}$ — Γ_3/Γ

VALUE	DOCUMENT ID	TECN	COMMENT
0.07±0.03	SARANTSEV 19	DPWA	$\overline{K}N$ multichannel

$\Gamma(\Lambda\omega, S=1/2, P\text{-wave})/\Gamma_{total}$ — Γ_4/Γ

VALUE	DOCUMENT ID	TECN	COMMENT
0.07±0.04	SARANTSEV 19	DPWA	$\overline{K}N$ multichannel

$\Gamma(\Lambda\omega, S=3/2, P\text{-wave})/\Gamma_{total}$ — Γ_5/Γ

VALUE	DOCUMENT ID	TECN	COMMENT
0.03±0.02	SARANTSEV 19	DPWA	$\overline{K}N$ multichannel

$\Gamma(\Lambda\omega, S=3/2, F\text{-wave})/\Gamma_{total}$ — Γ_6/Γ

VALUE	DOCUMENT ID	TECN	COMMENT
0.01±0.01	SARANTSEV 19	DPWA	$\overline{K}N$ multichannel

$\Gamma(\Sigma(1385)\pi, P\text{-wave})/\Gamma_{total}$ — Γ_7/Γ

VALUE	DOCUMENT ID	TECN	COMMENT
0.10±0.05	SARANTSEV 19	DPWA	$\overline{K}N$ multichannel

$\Gamma(\Sigma(1385)\pi, F\text{-wave})/\Gamma_{total}$ — Γ_8/Γ

VALUE	DOCUMENT ID	TECN	COMMENT
0.02±0.02	SARANTSEV 19	DPWA	$\overline{K}N$ multichannel

$\Gamma(N\overline{K}^*(892), S=1/2, P\text{-wave})/\Gamma_{total}$ — Γ_9/Γ

VALUE	DOCUMENT ID	TECN	COMMENT
0.42±0.08	SARANTSEV 19	DPWA	$\overline{K}N$ multichannel

$\Gamma(N\overline{K}^*(892), S=3/2, P\text{-wave})/\Gamma_{total}$ — Γ_{10}/Γ

VALUE	DOCUMENT ID	TECN	COMMENT
0.14±0.06	SARANTSEV 19	DPWA	$\overline{K}N$ multichannel

$\Gamma(N\overline{K}^*(892), S=3/2, F\text{-wave})/\Gamma_{total}$ — Γ_{11}/Γ

VALUE	DOCUMENT ID	TECN	COMMENT
0.10±0.06	SARANTSEV 19	DPWA	$\overline{K}N$ multichannel

$\Lambda(2070)$ REFERENCES

SARANTSEV 19 EPJ A55 180 A.V. Sarantsev *et al.* (BONN, PNPI)

$\Lambda(2080)$ $5/2^-$

$J^P = \frac{5}{2}^-$ Status: *

OMITTED FROM SUMMARY TABLE

$\Lambda(2080)$ POLE POSITION

REAL PART

VALUE (MeV)	DOCUMENT ID	TECN	COMMENT
2070±15	SARANTSEV 19	DPWA	$\overline{K}N$ multichannel

$-2\times$IMAGINARY PART

VALUE (MeV)	DOCUMENT ID	TECN	COMMENT
172±28	SARANTSEV 19	DPWA	$\overline{K}N$ multichannel

$\Lambda(2080)$ POLE RESIDUES

Normalized residue in $N\overline{K} \to \Lambda(2080) \to N\overline{K}$

MODULUS	PHASE (°)	DOCUMENT ID	TECN	COMMENT
0.12±0.03	−35 ± 22	SARANTSEV 19	DPWA	$\overline{K}N$ multichannel

Normalized residue in $N\overline{K} \to \Lambda(2080) \to \Sigma\pi$

MODULUS	PHASE (°)	DOCUMENT ID	TECN	COMMENT
0.07±0.03	11 ± 16	SARANTSEV 19	DPWA	$\overline{K}N$ multichannel

Normalized residue in $N\overline{K} \to \Lambda(2080) \to \Xi K$

MODULUS	PHASE (°)	DOCUMENT ID	TECN	COMMENT
0.06±0.02	115 ± 20	SARANTSEV 19	DPWA	$\overline{K}N$ multichannel

Normalized residue in $N\overline{K} \to \Lambda(2080) \to \Lambda\omega$, S=1/2, D-wave

MODULUS	PHASE (°)	DOCUMENT ID	TECN	COMMENT
0.06±0.03	115 ± 25	SARANTSEV 19	DPWA	$\overline{K}N$ multichannel

Normalized residue in $N\overline{K} \to \Lambda(2080) \to \Lambda\omega$, S=3/2 , D-wave

MODULUS	PHASE (°)	DOCUMENT ID	TECN	COMMENT
0.09±0.03	−10 ± 35	SARANTSEV 19	DPWA	$\overline{K}N$ multichannel

Normalized residue in $N\overline{K} \to \Lambda(2080) \to \Sigma(1385)\pi$, D-wave

MODULUS	PHASE (°)	DOCUMENT ID	TECN	COMMENT
0.14±0.04	155 ± 45	SARANTSEV 19	DPWA	$\overline{K}N$ multichannel

Normalized residue in $N\overline{K} \to \Lambda(2080) \to \Sigma(1385)\pi$, G-wave

MODULUS	PHASE (°)	DOCUMENT ID	COMMENT
0.05±0.03	30 ± 45	SARANTSEV 19	$\overline{K}N$ multichannel

Normalized residue in $N\overline{K} \to \Lambda(2080) \to N\overline{K}^*(892)$, S=1/2 , D-wave

MODULUS	PHASE (°)	DOCUMENT ID	TECN	COMMENT
0.16±0.08	−120 ± 50	SARANTSEV 19	DPWA	$\overline{K}N$ multichannel

Normalized residue in $N\overline{K} \to \Lambda(2080) \to N\overline{K}^*(892)$, S=3/2 , D-wave

MODULUS	PHASE (°)	DOCUMENT ID	TECN	COMMENT
0.20±0.14	60 ± 50	SARANTSEV 19	DPWA	$\overline{K}N$ multichannel

$\Lambda(2080)$ MASS

VALUE (MeV)	DOCUMENT ID	TECN	COMMENT
2082±13	SARANTSEV 19	DPWA	$\overline{K}N$ multichannel

$\Lambda(2080)$ WIDTH

VALUE (MeV)	DOCUMENT ID	TECN	COMMENT
181±29	SARANTSEV 19	DPWA	$\overline{K}N$ multichannel

$\Lambda(2080)$ DECAY MODES

	Mode	Fraction (Γ_i/Γ)
Γ_1	$N\overline{K}$	(11.0± 3.0) %
Γ_2	$\Sigma\pi$	(5.0± 2.0) %
Γ_3	ΞK	(4.0± 1.0) %
Γ_4	$\Lambda\omega$, S=1/2, D-wave	(4.0± 2.0) %
Γ_5	$\Lambda\omega$, S=3/2, D-wave	(8.0± 3.0) %
Γ_6	$\Sigma(1385)\pi$, D-wave	(15 ± 5) %
Γ_7	$\Sigma(1385)\pi$, G-wave	(3.0± 2.0) %
Γ_8	$N\overline{K}^*(892)$, S=1/2, D-wave	(17 ± 9) %
Γ_9	$N\overline{K}^*(892)$, S=3/2, D-wave	(25 ±16) %

$\Lambda(2080)$ BRANCHING RATIOS

$\Gamma(N\overline{K})/\Gamma_{total}$ — Γ_1/Γ

VALUE	DOCUMENT ID	TECN	COMMENT
0.11±0.03	SARANTSEV 19	DPWA	$\overline{K}N$ multichannel

$\Gamma(\Sigma\pi)/\Gamma_{total}$ — Γ_2/Γ

VALUE	DOCUMENT ID	TECN	COMMENT
0.05±0.02	SARANTSEV 19	DPWA	$\overline{K}N$ multichannel

$\Gamma(\Xi K)/\Gamma_{total}$ — Γ_3/Γ

VALUE	DOCUMENT ID	TECN	COMMENT
0.04±0.01	SARANTSEV 19	DPWA	$\overline{K}N$ multichannel

$\Gamma(\Lambda\omega, S=1/2, D\text{-wave})/\Gamma_{total}$ — Γ_4/Γ

VALUE	DOCUMENT ID	TECN	COMMENT
0.04±0.02	SARANTSEV 19	DPWA	$\overline{K}N$ multichannel

$\Gamma(\Lambda\omega, S=3/2, D\text{-wave})/\Gamma_{total}$ — Γ_5/Γ

VALUE	DOCUMENT ID	TECN	COMMENT
0.08±0.03	SARANTSEV 19	DPWA	$\overline{K}N$ multichannel

$\Gamma(\Sigma(1385)\pi, D\text{-wave})/\Gamma_{total}$ — Γ_6/Γ

VALUE	DOCUMENT ID	TECN	COMMENT
0.15±0.05	SARANTSEV 19	DPWA	$\overline{K}N$ multichannel

$\Gamma(\Sigma(1385)\pi, G\text{-wave})/\Gamma_{total}$ — Γ_7/Γ

VALUE	DOCUMENT ID	TECN	COMMENT
0.03±0.02	SARANTSEV 19	DPWA	$\overline{K}N$ multichannel

$\Gamma(N\overline{K}^*(892), S=1/2, D\text{-wave})/\Gamma_{total}$ — Γ_8/Γ

VALUE	DOCUMENT ID	TECN	COMMENT
0.17±0.09	SARANTSEV 19	DPWA	$\overline{K}N$ multichannel

$\Gamma(N\overline{K}^*(892), S=3/2, D\text{-wave})/\Gamma_{total}$ — Γ_9/Γ

VALUE	DOCUMENT ID	TECN	COMMENT
0.25±0.16	SARANTSEV 19	DPWA	$\overline{K}N$ multichannel

$\Lambda(2080)$ REFERENCES

SARANTSEV 19 EPJ A55 180 A.V. Sarantsev *et al.* (BONN, PNPI)

Downloaded from https://academic.oup.com/ptep/article/2022/8/083C01/6651666 by KIT Library user on 27 September 2022

Λ(2085) 7/2+

$I(J^P) = 0(\frac{7}{2}^+)$ Status: **

OMITTED FROM SUMMARY TABLE
was Λ(2020)

In LITCHFIELD 71, need for the state rests solely on a possibly inconsistent polarization measurement at 1.784 GeV/c. HEMINGWAY 75 does not require this state. GOPAL 77 does not need it in either $N\overline{K}$ or $\Sigma\pi$. With new K^-n angular distributions included, DECLAIS 77 sees it. However, this and other new data are included in GOPAL 80 and the state is not required. BACCARI 77 weakly supports it.

Λ(2085) POLE POSITION

REAL PART

VALUE	DOCUMENT ID		TECN	COMMENT
• • • We do not use the following data for averages, fits, limits, etc. • • •				
1757	[1] KAMANO	15	DPWA	Multichannel

[1] From the preferred solution A in KAMANO 15. Solution B reports $M = 2041^{+80}_{-82}$ MeV.

−2×IMAGINARY PART

VALUE	DOCUMENT ID		TECN	COMMENT
• • • We do not use the following data for averages, fits, limits, etc. • • •				
146	[1] KAMANO	15	DPWA	Multichannel

[1] From the preferred solution A in KAMANO 15. Solution B reports $M = 238^{+114}_{-34}$ MeV.

Λ(2085) POLE RESIDUES

The normalized residue is the residue divided by $\Gamma_{pole}/2$.

Normalized residue in $N\overline{K} \to \Lambda(2085) \to N\overline{K}$

MODULUS	PHASE (°)	DOCUMENT ID		TECN	COMMENT
• • • We do not use the following data for averages, fits, limits, etc. • • •					
0.000145	−77	[1] KAMANO	15	DPWA	Multichannel

[1] From the preferred solution A in KAMANO 15.

Normalized residue in $N\overline{K} \to \Lambda(2085) \to \Sigma\pi$

MODULUS	PHASE (°)	DOCUMENT ID		TECN	COMMENT
• • • We do not use the following data for averages, fits, limits, etc. • • •					
0.0112	120	[1] KAMANO	15	DPWA	Multichannel

[1] From the preferred solution A in KAMANO 15.

Normalized residue in $N\overline{K} \to \Lambda(2085) \to \Lambda\eta$

MODULUS	PHASE (°)	DOCUMENT ID		TECN	COMMENT
• • • We do not use the following data for averages, fits, limits, etc. • • •					
0.000786	−100	[1] KAMANO	15	DPWA	Multichannel

[1] From the preferred solution A in KAMANO 15.

Normalized residue in $N\overline{K} \to \Lambda(2085) \to \Sigma(1385)\pi$, F-wave

MODULUS	PHASE (°)	DOCUMENT ID		TECN	COMMENT
• • • We do not use the following data for averages, fits, limits, etc. • • •					
0.00451	−82	[1] KAMANO	15	DPWA	Multichannel

[1] From the preferred solution A in KAMANO 15.

Normalized residue in $N\overline{K} \to \Lambda(2085) \to \Sigma(1385)\pi$, H-wave

MODULUS	PHASE (°)	DOCUMENT ID		TECN	COMMENT
• • • We do not use the following data for averages, fits, limits, etc. • • •					
0.0000298	−128	[1] KAMANO	15	DPWA	Multichannel

[1] From the preferred solution A in KAMANO 15.

Λ(2085) MASS

VALUE (MeV)	DOCUMENT ID		TECN	COMMENT
≈ 2020 OUR ESTIMATE				
2043±22	ZHANG	13A	DPWA	Multichannel
2140	BACCARI	77	DPWA	$K^-p \to \Lambda\omega$
2117	DECLAIS	77	DPWA	$\overline{K}N \to \overline{K}N$
2100±30	LITCHFIELD	71	DPWA	$K^-p \to \overline{K}N$
2020±20	BARBARO-...	70	DPWA	$K^-p \to \Sigma\pi$

Λ(2085) WIDTH

VALUE (MeV)	DOCUMENT ID		TECN	COMMENT
200±75	ZHANG	13A	DPWA	Multichannel
128	BACCARI	77	DPWA	$K^-p \to \Lambda\omega$
167	DECLAIS	77	DPWA	$\overline{K}N \to \overline{K}N$
120±30	LITCHFIELD	71	DPWA	$K^-p \to \overline{K}N$
160±30	BARBARO-...	70	DPWA	$K^-p \to \Sigma\pi$

Λ(2085) DECAY MODES

	Mode	Fraction (Γ_i/Γ)
Γ_1	$N\overline{K}$	
Γ_2	$\Sigma\pi$	
Γ_3	$\Lambda\eta$	
Γ_4	$\Sigma(1385)\pi$, F-wave	
Γ_5	$\Sigma(1385)\pi$, H-wave	
Γ_6	$N\overline{K}^*(892)$, S=1/2	(30±9) %
Γ_7	$N\overline{K}^*(892)$, S=1/2, F-wave	
Γ_8	$N\overline{K}^*(892)$, S=3/2, F-wave	
Γ_9	$N\overline{K}^*(892)$, S=3/2, H-wave	
Γ_{10}	$\Lambda\omega$	

Λ(2085) BRANCHING RATIOS

See "Sign conventions for resonance couplings" in the Note on Λ and Σ Resonances.

$\Gamma(N\overline{K})/\Gamma_{total}$ — Γ_1/Γ

VALUE	DOCUMENT ID		TECN	COMMENT
0.028±0.005	ZHANG	13A	DPWA	Multichannel
0.05	DECLAIS	77	DPWA	$\overline{K}N \to \overline{K}N$
0.05 ±0.02	LITCHFIELD	71	DPWA	$K^-p \to \overline{K}N$
• • • We do not use the following data for averages, fits, limits, etc. • • •				
not seen	[1] KAMANO	15	DPWA	Multichannel

[1] From the preferred solution A in KAMANO 15.

$\Gamma(\Sigma\pi)/\Gamma_{total}$ — Γ_2/Γ

VALUE	DOCUMENT ID		TECN	COMMENT
• • • We do not use the following data for averages, fits, limits, etc. • • •				
0.891	[1] KAMANO	15	DPWA	Multichannel

[1] From the preferred solution A in KAMANO 15.

$\Gamma(\Lambda\eta)/\Gamma_{total}$ — Γ_3/Γ

VALUE	DOCUMENT ID		TECN	COMMENT
• • • We do not use the following data for averages, fits, limits, etc. • • •				
0.002	[1] KAMANO	15	DPWA	Multichannel

[1] From the preferred solution A in KAMANO 15.

$\Gamma(\Sigma(1385)\pi$, F-wave$)/\Gamma_{total}$ — Γ_4/Γ

VALUE	DOCUMENT ID		TECN	COMMENT
• • • We do not use the following data for averages, fits, limits, etc. • • •				
0.105	[1] KAMANO	15	DPWA	Multichannel

[1] From the preferred solution A in KAMANO 15.

$\Gamma(\Sigma(1385)\pi$, H-wave$)/\Gamma_{total}$ — Γ_5/Γ

VALUE	DOCUMENT ID		TECN	COMMENT
• • • We do not use the following data for averages, fits, limits, etc. • • •				
not seen	[1] KAMANO	15	DPWA	Multichannel

[1] From the preferred solution A in KAMANO 15.

$\Gamma(N\overline{K}^*(892)$, S=1/2, F-wave$)/\Gamma_{total}$ — Γ_7/Γ

VALUE	DOCUMENT ID		TECN	COMMENT
• • • We do not use the following data for averages, fits, limits, etc. • • •				
not seen	[1] KAMANO	15	DPWA	Multichannel

[1] From the preferred solution A in KAMANO 15.

$\Gamma(N\overline{K}^*(892)$, S=3/2, F-wave$)/\Gamma_{total}$ — Γ_8/Γ

VALUE	DOCUMENT ID		TECN	COMMENT
• • • We do not use the following data for averages, fits, limits, etc. • • •				
0.001	[1] KAMANO	15	DPWA	Multichannel

[1] From the preferred solution A in KAMANO 15.

$\Gamma(N\overline{K}^*(892)$, S=3/2, H-wave$)/\Gamma_{total}$ — Γ_9/Γ

VALUE	DOCUMENT ID		TECN	COMMENT
• • • We do not use the following data for averages, fits, limits, etc. • • •				
not seen	[1] KAMANO	15	DPWA	Multichannel

[1] From the preferred solution A in KAMANO 15.

$\Gamma(N\overline{K}^*(892)$, S=1/2$)/\Gamma_{total}$ — Γ_6/Γ

VALUE	DOCUMENT ID		TECN	COMMENT
0.30±0.09	ZHANG	13A	DPWA	Multichannel

$(\Gamma_i\Gamma_f)^{1/2}/\Gamma_{total}$ in $N\overline{K} \to \Lambda(2085) \to \Sigma\pi$ — $(\Gamma_1\Gamma_2)^{1/2}/\Gamma$

VALUE	DOCUMENT ID		TECN	COMMENT
+0.02±0.01	ZHANG	13A	DPWA	Multichannel
−0.15±0.02	BARBARO-...	70	DPWA	$K^-p \to \Sigma\pi$

Downloaded from https://academic.oup.com/ptep/article/2022/8/083C01/6651666 by KIT Library user on 27 September 2022

$(\Gamma_i\Gamma_f)^{1/2}/\Gamma_{total}$ in $N\overline{K} \to \Lambda(2085) \to \Lambda\omega$ — $(\Gamma_1\Gamma_{10})^{1/2}/\Gamma$

VALUE	DOCUMENT ID		TECN	COMMENT
<0.05	BACCARI	77	DPWA	$K^-p \to \Lambda\omega$

$\Lambda(2085)$ REFERENCES

KAMANO	15	PR C92 025205	H. Kamano *et al.*	(ANL, OSAK)
ZHANG	13A	PR C88 035205	H. Zhang *et al.*	(KSU)
GOPAL	80	Toronto Conf. 159	G.P. Gopal	(RHEL)
BACCARI	77	NC 41A 96	B. Baccari *et al.*	(SACL, CDEF) IJP
DECLAIS	77	CERN 77-16	Y. Declais *et al.*	(CAEN, CERN) IJP
GOPAL	77	NP B119 362	G.P. Gopal *et al.*	(LOIC, RHEL)
HEMINGWAY	75	NP B91 12	R.J. Hemingway *et al.*	(CERN, HEIDH, MPIM) IJP
LITCHFIELD	71	NP B30 125	P.J. Litchfield *et al.*	(RHEL, CDEF, SACL) IJP
BARBARO-...	70	Duke Conf. 173 Hyperon Resonances, 1970	A. Barbaro-Galtieri	(LRL) IJP

$\Lambda(2100)\ 7/2^-$

$I(J^P) = 0(\frac{7}{2}^-)$ Status: ****

Most of the results published before 1973 are now obsolete and have been omitted. They may be found in our 1982 edition Physics Letters **111B** 1 (1982).

This entry only includes results from partial-wave analyses. Parameters of peaks seen in cross sections and in invariant-mass distributions around 2100 MeV used to be listed in a separate entry immediately following. It may be found in our 1986 edition Physics Letters **170B** 1 (1986).

$\Lambda(2100)$ POLE POSITION

REAL PART

VALUE (MeV)	DOCUMENT ID		TECN	COMMENT
2040±14	SARANTSEV	19	DPWA	$\overline{K}N$ multichannel
• • • We do not use the following data for averages, fits, limits, etc. • • •				
2023	ZHANG	13A	DPWA	Multichannel

−2×IMAGINARY PART

VALUE (MeV)	DOCUMENT ID		TECN	COMMENT
215±29	SARANTSEV	19	DPWA	$\overline{K}N$ multichannel
• • • We do not use the following data for averages, fits, limits, etc. • • •				
239	ZHANG	13A	DPWA	Multichannel

$\Lambda(2100)$ POLE RESIDUE

The "normalized residue" is the residue divided by $\Gamma_{pole}/2$.

Normalized residue in $N\overline{K} \to \Lambda(2100) \to N\overline{K}$

MODULUS	PHASE (°)	DOCUMENT ID		TECN	COMMENT
0.28±0.06	**−40 ± 10**	SARANTSEV	19	DPWA	$\overline{K}N$ multichannel

Normalized residue in $N\overline{K} \to \Lambda(2100) \to \Sigma\pi$

MODULUS	PHASE (°)	DOCUMENT ID		TECN	COMMENT
0.09±0.02	**−35 ± 15**	SARANTSEV	19	DPWA	$\overline{K}N$ multichannel

Normalized residue in $N\overline{K} \to \Lambda(2100) \to \Sigma(1385)\pi$, D-wave

MODULUS	PHASE (°)	DOCUMENT ID		TECN	COMMENT
0.04±0.03		SARANTSEV	19	DPWA	$\overline{K}N$ multichannel

Normalized residue in $N\overline{K} \to \Lambda(2100) \to \Sigma(1385)\pi$, G-wave

MODULUS	PHASE (°)	DOCUMENT ID		TECN	COMMENT
0.06±0.03	**−45 ± 15**	SARANTSEV	19	DPWA	$\overline{K}N$ multichannel

Normalized residue in $N\overline{K} \to \Lambda(2100) \to N\overline{K}^*(892)$, S=3/2, D-wave

MODULUS	PHASE (°)	DOCUMENT ID		TECN	COMMENT
0.11±0.06	**−30 ± 30**	SARANTSEV	19	DPWA	$\overline{K}N$ multichannel

$\Lambda(2100)$ MASS

VALUE (MeV)	DOCUMENT ID		TECN	COMMENT
2090 to 2110 (≈ 2100) OUR ESTIMATE				
2090±15	SARANTSEV	19	DPWA	$\overline{K}N$ multichannel
2086± 6	ZHANG	13A	DPWA	Multichannel
2104±10	GOPAL	80	DPWA	$\overline{K}N \to \overline{K}N$
2106±30	DEBELLEFON	78	DPWA	$\overline{K}N \to \overline{K}N$
2110±10	GOPAL	77	DPWA	$\overline{K}N$ multichannel
2105±10	HEMINGWAY	75	DPWA	$K^-p \to \overline{K}N$
2115±10	KANE	74	DPWA	$K^-p \to \Sigma\pi$
• • • We do not use the following data for averages, fits, limits, etc. • • •				
2094	BACCARI	77	DPWA	$K^-p \to \Lambda\omega$
2094	DECLAIS	77	DPWA	$\overline{K}N \to \overline{K}N$
2110 or 2089	[1] NAKKASYAN	75	DPWA	$K^-p \to \Lambda\omega$

$\Lambda(2100)$ WIDTH

VALUE (MeV)	DOCUMENT ID		TECN	COMMENT
100 to 250 (≈ 200) OUR ESTIMATE				
290±30	SARANTSEV	19	DPWA	$\overline{K}N$ multichannel
305±16	ZHANG	13A	DPWA	Multichannel
157±40	DEBELLEFON	78	DPWA	$\overline{K}N \to \overline{K}N$
250±30	GOPAL	77	DPWA	$\overline{K}N$ multichannel
241±30	HEMINGWAY	75	DPWA	$K^-p \to \overline{K}N$
152±15	KANE	74	DPWA	$K^-p \to \Sigma\pi$
• • • We do not use the following data for averages, fits, limits, etc. • • •				
98	BACCARI	77	DPWA	$K^-p \to \Lambda\omega$
250	DECLAIS	77	DPWA	$\overline{K}N \to \overline{K}N$
244 or 302	[1] NAKKASYAN	75	DPWA	$K^-p \to \Lambda\omega$

$\Lambda(2100)$ DECAY MODES

	Mode	Fraction (Γ_i/Γ)
Γ_1	$N\overline{K}$	25–35 %
Γ_2	$\Sigma\pi$	∼ 5 %
Γ_3	$\Lambda\eta$	<3 %
Γ_4	ΞK	<3 %
Γ_5	$\Lambda\omega$	<8 %
Γ_6	$\Sigma(1385)\pi$, D-wave	
Γ_7	$\Sigma(1385)\pi$, G-wave	(1.0±1.0) %
Γ_8	$N\overline{K}^*(892)$	10–20 %
Γ_9	$N\overline{K}^*(892)$, S=3/2, D-wave	(4.0±2.0) %
Γ_{10}	$N\overline{K}^*(892)$, S=1/2, G-wave	
Γ_{11}	$N\overline{K}^*(892)$, S=3/2, G-wave	

$\Lambda(2100)$ BRANCHING RATIOS

See "Sign conventions for resonance couplings" in the Note on Λ and Σ Resonances.

$\Gamma(N\overline{K})/\Gamma_{total}$ — Γ_1/Γ

VALUE	DOCUMENT ID		TECN	COMMENT
0.25 to 0.35 (≈ 0.30) OUR ESTIMATE				
0.24±0.05	SARANTSEV	19	DPWA	$\overline{K}N$ multichannel
0.23±0.01	ZHANG	13A	DPWA	Multichannel
0.34±0.03	GOPAL	80	DPWA	$\overline{K}N \to \overline{K}N$
0.24±0.06	DEBELLEFON	78	DPWA	$\overline{K}N \to \overline{K}N$
0.31±0.03	HEMINGWAY	75	DPWA	$K^-p \to \overline{K}N$
• • • We do not use the following data for averages, fits, limits, etc. • • •				
0.29	DECLAIS	77	DPWA	$\overline{K}N \to \overline{K}N$
0.30±0.03	GOPAL	77	DPWA	See GOPAL 80

$\Gamma(\Sigma\pi)/\Gamma_{total}$ — Γ_2/Γ

VALUE	DOCUMENT ID		TECN	COMMENT
0.030±0.015	SARANTSEV	19	DPWA	$\overline{K}N$ multichannel

$\Gamma(\Sigma(1385)\pi, D\text{-wave})/\Gamma_{total}$ — Γ_6/Γ

VALUE	DOCUMENT ID		TECN	COMMENT
<0.01	SARANTSEV	19	DPWA	$\overline{K}N$ multichannel

$\Gamma(\Sigma(1385)\pi, G\text{-wave})/\Gamma_{total}$ — Γ_7/Γ

VALUE	DOCUMENT ID		TECN	COMMENT
0.01±0.01	SARANTSEV	19	DPWA	$\overline{K}N$ multichannel

$\Gamma(N\overline{K}^*(892), S=3/2, D\text{-wave})/\Gamma_{total}$ — Γ_9/Γ

VALUE	DOCUMENT ID		TECN	COMMENT
0.04±0.02	SARANTSEV	19	DPWA	$\overline{K}N$ multichannel

$(\Gamma_i\Gamma_f)^{1/2}/\Gamma_{total}$ in $N\overline{K} \to \Lambda(2100) \to \Sigma\pi$ — $(\Gamma_1\Gamma_2)^{1/2}/\Gamma$

VALUE	DOCUMENT ID		TECN	COMMENT
+0.03±0.01	ZHANG	13A	DPWA	Multichannel
+0.12±0.04	GOPAL	77	DPWA	$\overline{K}N$ multichannel
+0.11±0.01	KANE	74	DPWA	$K^-p \to \Sigma\pi$

$(\Gamma_i\Gamma_f)^{1/2}/\Gamma_{total}$ in $N\overline{K} \to \Lambda(2100) \to \Lambda\eta$ — $(\Gamma_1\Gamma_3)^{1/2}/\Gamma$

VALUE	DOCUMENT ID		TECN	COMMENT
−0.050±0.020	RADER	73	MPWA	$K^-p \to \Lambda\eta$

$(\Gamma_i\Gamma_f)^{1/2}/\Gamma_{total}$ in $N\overline{K} \to \Lambda(2100) \to \Xi K$ — $(\Gamma_1\Gamma_4)^{1/2}/\Gamma$

VALUE	DOCUMENT ID		TECN	COMMENT
0.035±0.018	LITCHFIELD	71	DPWA	$K^-p \to \Xi K$
• • • We do not use the following data for averages, fits, limits, etc. • • •				
0.003	MULLER	69B	DPWA	$K^-p \to \Xi K$
0.05	TRIPP	67	RVUE	$K^-p \to \Xi K$

Downloaded from https://academic.oup.com/ptep/article/2022/8/083C01/6651666 by KIT Library user on 27 September 2022

$(\Gamma_i\Gamma_f)^{1/2}/\Gamma_{total}$ in $N\overline{K} \to \Lambda(2100) \to \Lambda\omega$ $(\Gamma_1\Gamma_5)^{1/2}/\Gamma$

VALUE	DOCUMENT ID		TECN	COMMENT
−0.070	[2] BACCARI	77	DPWA	GD_{37} wave
+0.011	[2] BACCARI	77	DPWA	GG_{17} wave
+0.008	[2] BACCARI	77	DPWA	GG_{37} wave
0.122 or 0.154	[1] NAKKASYAN	75	DPWA	$K^-p \to \Lambda\omega$

$(\Gamma_i\Gamma_f)^{1/2}/\Gamma_{total}$ in $N\overline{K} \to \Lambda(2100) \to N\overline{K}^*(892)$, S=3/2, D-wave $(\Gamma_1\Gamma_9)^{1/2}/\Gamma$

VALUE	DOCUMENT ID		TECN	COMMENT
+0.16±0.02	ZHANG	13A	DPWA	Multichannel
+0.21±0.04	CAMERON	78B	DPWA	$K^-p \to N\overline{K}^*$

$(\Gamma_i\Gamma_f)^{1/2}/\Gamma_{total}$ in $N\overline{K} \to \Lambda(2100) \to N\overline{K}^*(892)$, S=1/2, G-wave $(\Gamma_1\Gamma_{10})^{1/2}/\Gamma$

VALUE	DOCUMENT ID		TECN	COMMENT
−0.03±0.02	ZHANG	13A	DPWA	Multichannel
−0.04±0.03	[3] CAMERON	78B	DPWA	$K^-p \to N\overline{K}^*$

$(\Gamma_i\Gamma_f)^{1/2}/\Gamma_{total}$ in $N\overline{K} \to \Lambda(2100) \to N\overline{K}^*(892)$, S=3/2, G-wave $(\Gamma_1\Gamma_{11})^{1/2}/\Gamma$

VALUE	DOCUMENT ID		TECN	COMMENT
+0.08±0.02	ZHANG	13A	DPWA	Multichannel

$\Lambda(2100)$ FOOTNOTES

[1] The NAKKASYAN 75 values are from the two best solutions found. Each has the $\Lambda(2100)$ and one additional resonance (P_3 or F_5).

[2] Note that the three for BACCARI 77 entries are for three different waves.

[3] The published sign has been changed to be in accord with the baryon-first convention. The upper limit on the G_3 wave is 0.03.

$\Lambda(2100)$ REFERENCES

SARANTSEV	19	EPJ A55 180	A.V. Sarantsev *et al.*	(BONN, PNPI)
ZHANG	13A	PR C88 035205	H. Zhang *et al.*	(KSU)
PDG	86	PL 170B 1	M. Aguilar-Benitez *et al.*	(CERN, CIT+)
PDG	82	PL 111B 1	M. Roos *et al.*	(HELS, CIT, CERN)
GOPAL	80	Toronto Conf. 159	G.P. Gopal	(RHEL) IJP
CAMERON	78B	NP B146 327	W. Cameron *et al.*	(RHEL, LOIC) IJP
DEBELLEFON	78	NC 42A 403	A. de Bellefon *et al.*	(CDEF, SACL) IJP
BACCARI	77	NC 41A 96	B. Baccari *et al.*	(SACL, CDEF) IJP
DECLAIS	77	CERN 77-16	Y. Declais *et al.*	(CAEN, CERN) IJP
GOPAL	77	NP B119 362	G.P. Gopal *et al.*	(LOIC, RHEL) IJP
HEMINGWAY	75	NP B91 12	R.J. Hemingway *et al.*	(CERN, HEIDH, MPIM) IJP
NAKKASYAN	75	NP B93 85	A. Nakkasyan	(CERN) IJP
KANE	74	LBL-2452	D.F. Kane	(LBL) IJP
RADER	73	NC 16A 178	R.K. Rader *et al.*	(SACL, HEID, CERN+)
LITCHFIELD	71	NP B30 125	P.J. Litchfield *et al.*	(RHEL, CDEF, SACL) IJP
MULLER	69B	Thesis UCRL 19372	R.A. Muller	(LRL)
TRIPP	67	NP B3 10	R.D. Tripp *et al.*	(LRL, SLAC, CERN+)

$\Lambda(2110)\ 5/2^+$

$I(J^P) = 0(\frac{5}{2}^+)$ Status: ***

For results published before 1974 (they are now obsolete), see our 1982 edition Physics Letters **111B** 1 (1982). All the references have been retained.

This resonance is in the Baryon Summary Table, but the evidence for it could be better.

$\Lambda(2110)$ POLE POSITION

REAL PART

VALUE (MeV)	DOCUMENT ID		TECN	COMMENT
2048±10	SARANTSEV	19	DPWA	$\overline{K}N$ multichannel
• • • We do not use the following data for averages, fits, limits, etc. • • •				
1970	ZHANG	13A	DPWA	$\overline{K}N$ multichannel

−2×IMAGINARY PART

VALUE (MeV)	DOCUMENT ID		TECN	COMMENT
255±20	SARANTSEV	19	DPWA	$\overline{K}N$ multichannel
• • • We do not use the following data for averages, fits, limits, etc. • • •				
350	ZHANG	13A	DPWA	$\overline{K}N$ multichannel

$\Lambda(2110)$ POLE RESIDUE

The "normalized residue" is the residue divided by $\Gamma_{pole}/2$.

Normalized residue in $N\overline{K} \to \Lambda(2110) \to N\overline{K}$

MODULUS	PHASE (°)	DOCUMENT ID		TECN	COMMENT
0.020±0.005	**5 ± 15**	SARANTSEV	19	DPWA	$\overline{K}N$ multichannel

Normalized residue in $N\overline{K} \to \Lambda(2110) \to \Sigma\pi$

MODULUS	PHASE (°)	DOCUMENT ID		TECN	COMMENT
0.13±0.03	**0 ± 15**	SARANTSEV	19	DPWA	$\overline{K}N$ multichannel

Normalized residue in $N\overline{K} \to \Lambda(2110) \to \Xi K$

MODULUS	PHASE (°)	DOCUMENT ID		TECN	COMMENT
0.005±0.005		SARANTSEV	19	DPWA	$\overline{K}N$ multichannel

Normalized residue in $N\overline{K} \to \Lambda(2110) \to \Lambda\omega$, S=1/2, P-wave

MODULUS	PHASE (°)	DOCUMENT ID		TECN	COMMENT
0.01±0.01		SARANTSEV	19	DPWA	$\overline{K}N$ multichannel

Normalized residue in $N\overline{K} \to \Lambda(2110) \to \Lambda\omega$, S=3/2, P-wave

MODULUS	PHASE (°)	DOCUMENT ID		TECN	COMMENT
0.03±0.01	**−7 ± 16**	SARANTSEV	19	DPWA	$\overline{K}N$ multichannel

Normalized residue in $N\overline{K} \to \Lambda(2110) \to \Lambda\omega$, S=3/2, F-wave

MODULUS	PHASE (°)	DOCUMENT ID		TECN	COMMENT
0.01±0.01		SARANTSEV	19	DPWA	$\overline{K}N$ multichannel

$\Lambda(2110)$ MASS

VALUE (MeV)	DOCUMENT ID		TECN	COMMENT
2050 to 2130 (≈ 2090) OUR ESTIMATE				
2086±12	SARANTSEV	19	DPWA	$\overline{K}N$ multichannel
2036±13	ZHANG	13A	DPWA	$\overline{K}N$ multichannel
2092±25	GOPAL	80	DPWA	$\overline{K}N \to \overline{K}N$
2125±25	CAMERON	78B	DPWA	$K^-p \to N\overline{K}^*$
2106±50	DEBELLEFON	78	DPWA	$\overline{K}N \to \overline{K}N$
2140±20	DEBELLEFON	77	DPWA	$K^-p \to \Sigma\pi$
2100±50	GOPAL	77	DPWA	$\overline{K}N$ multichannel
2112± 7	KANE	74	DPWA	$K^-p \to \Sigma\pi$
• • • We do not use the following data for averages, fits, limits, etc. • • •				
2137	BACCARI	77	DPWA	$K^-p \to \Lambda\omega$
2103	[1] NAKKASYAN	75	DPWA	$K^-p \to \Lambda\omega$

$\Lambda(2110)$ WIDTH

VALUE (MeV)	DOCUMENT ID		TECN	COMMENT
200 to 300 (≈ 250) OUR ESTIMATE				
274±25	SARANTSEV	19	DPWA	$\overline{K}N$ multichannel
400±38	ZHANG	13A	DPWA	$\overline{K}N$ multichannel
245±25	GOPAL	80	DPWA	$\overline{K}N \to \overline{K}N$
160±30	CAMERON	78B	DPWA	$K^-p \to N\overline{K}^*$
251±50	DEBELLEFON	78	DPWA	$\overline{K}N \to \overline{K}N$
140±20	DEBELLEFON	77	DPWA	$K^-p \to \Sigma\pi$
200±50	GOPAL	77	DPWA	$\overline{K}N$ multichannel
190±30	KANE	74	DPWA	$K^-p \to \Sigma\pi$
• • • We do not use the following data for averages, fits, limits, etc. • • •				
132	BACCARI	77	DPWA	$K^-p \to \Lambda\omega$
391	[1] NAKKASYAN	75	DPWA	$K^-p \to \Lambda\omega$

$\Lambda(2110)$ DECAY MODES

	Mode	Fraction (Γ_i/Γ)
Γ_1	$N\overline{K}$	5–25 %
Γ_2	$\Sigma\pi$	10–40 %
Γ_3	$\Lambda\omega$	seen
Γ_4	$\Lambda\omega$, S=1/2, P-wave	
Γ_5	$\Lambda\omega$, S=3/2, P-wave	(5.0±2.0) %
Γ_6	$\Lambda\omega$, S=3/2, F-wave	
Γ_7	ΞK	
Γ_8	$\Sigma(1385)\pi$	seen
Γ_9	$\Sigma(1385)\pi$, P-wave	
Γ_{10}	$N\overline{K}^*(892)$	10–60 %
Γ_{11}	$N\overline{K}^*(892)$, S=1/2	
Γ_{12}	$N\overline{K}^*(892)$, S=3/2, P-wave	

$\Lambda(2110)$ BRANCHING RATIOS

See "Sign conventions for resonance couplings" in the Note on Λ and Σ Resonances.

$\Gamma(N\overline{K})/\Gamma_{total}$ Γ_1/Γ

VALUE	DOCUMENT ID		TECN	COMMENT
0.05 to 0.25 OUR ESTIMATE				
0.020±0.005	SARANTSEV	19	DPWA	$\overline{K}N$ multichannel
0.083±0.005	ZHANG	13A	DPWA	$\overline{K}N$ multichannel
0.07 ±0.03	GOPAL	80	DPWA	$\overline{K}N \to \overline{K}N$
0.27 ±0.06	[2] DEBELLEFON	78	DPWA	$\overline{K}N \to \overline{K}N$
• • • We do not use the following data for averages, fits, limits, etc. • • •				
0.07 ±0.03	GOPAL	77	DPWA	See GOPAL 80

$\Gamma(\Sigma\pi)/\Gamma_{total}$ Γ_2/Γ

VALUE	DOCUMENT ID		TECN	COMMENT
0.88±0.20	SARANTSEV	19	DPWA	$\overline{K}N$ multichannel

Downloaded from https://academic.oup.com/ptep/article/2022/8/083C01/6651666 by KIT Library user on 27 September 2022

$\Gamma(\Lambda\omega, S=1/2, P\text{-wave})/\Gamma_{total}$ — Γ_4/Γ

VALUE	DOCUMENT ID		TECN	COMMENT
<0.01	SARANTSEV	19	DPWA	$\overline{K}N$ multichannel

$\Gamma(\Lambda\omega, S=3/2, P\text{-wave})/\Gamma_{total}$ — Γ_5/Γ

VALUE	DOCUMENT ID		TECN	COMMENT
0.05 ± 0.02	SARANTSEV	19	DPWA	$\overline{K}N$ multichannel

$\Gamma(\Lambda\omega, S=3/2, F\text{-wave})/\Gamma_{total}$ — Γ_6/Γ

VALUE	DOCUMENT ID		TECN	COMMENT
<0.01	SARANTSEV	19	DPWA	$\overline{K}N$ multichannel

$\Gamma(\Xi K)/\Gamma_{total}$ — Γ_7/Γ

VALUE	DOCUMENT ID		TECN	COMMENT
~ 0	SARANTSEV	19	DPWA	$\overline{K}N$ multichannel

$(\Gamma_i\Gamma_f)^{1/2}/\Gamma_{total}$ in $N\overline{K}\to\Lambda(2110)\to\Sigma\pi$ — $(\Gamma_1\Gamma_2)^{1/2}/\Gamma$

VALUE	DOCUMENT ID		TECN	COMMENT
$+0.04\pm0.01$	ZHANG	13A	DPWA	Multichannel
$+0.14\pm0.01$	DEBELLEFON	77	DPWA	$K^-p\to\Sigma\pi$
$+0.20\pm0.03$	KANE	74	DPWA	$K^-p\to\Sigma\pi$
• • • We do not use the following data for averages, fits, limits, etc. • • •				
$+0.10\pm0.03$	GOPAL	77	DPWA	$\overline{K}N$ multichannel

$(\Gamma_i\Gamma_f)^{1/2}/\Gamma_{total}$ in $N\overline{K}\to\Lambda(2110)\to\Lambda\omega$ — $(\Gamma_1\Gamma_3)^{1/2}/\Gamma$

VALUE	DOCUMENT ID		TECN	COMMENT
<0.05	BACCARI	77	DPWA	$K^-p\to\Lambda\omega$
0.112	[1] NAKKASYAN	75	DPWA	$K^-p\to\Lambda\omega$

$(\Gamma_i\Gamma_f)^{1/2}/\Gamma_{total}$ in $N\overline{K}\to\Lambda(2110)\to\Sigma(1385)\pi$, P-wave — $(\Gamma_1\Gamma_9)^{1/2}/\Gamma$

VALUE	DOCUMENT ID		TECN	COMMENT
$+0.04\ \pm0.01$	ZHANG	13A	DPWA	Multichannel
$+0.071\pm0.025$	[3] CAMERON	78	DPWA	$K^-p\to\Sigma(1385)\pi$

$(\Gamma_i\Gamma_f)^{1/2}/\Gamma_{total}$ in $N\overline{K}\to\Lambda(2110)\to N\overline{K}^*(892)$, $S=1/2$ — $(\Gamma_1\Gamma_{11})^{1/2}/\Gamma$

VALUE	DOCUMENT ID		TECN	COMMENT
-0.09 ± 0.01	ZHANG	13A	DPWA	Multichannel
-0.17 ± 0.04	[4] CAMERON	78B	DPWA	$K^-p\to N\overline{K}^*$

$(\Gamma_i\Gamma_f)^{1/2}/\Gamma_{total}$ in $N\overline{K}\to\Lambda(2110)\to N\overline{K}^*(892)$, $S=3/2$, P-wave — $(\Gamma_1\Gamma_{12})^{1/2}/\Gamma$

VALUE	DOCUMENT ID		TECN	COMMENT
0.24 ± 0.01	ZHANG	13A	DPWA	Multichannel

$\Lambda(2110)$ FOOTNOTES

[1] Found in one of two best solutions.
[2] The published error of 0.6 was a misprint.
[3] The CAMERON 78 upper limit on F-wave decay is 0.03. The sign here has been changed to be in accord with the baryon-first convention.
[4] The published sign has been changed to be in accord with the baryon-first convention. The CAMERON 78B upper limits on the P_3 and F_3 waves are each 0.03.

$\Lambda(2110)$ REFERENCES

SARANTSEV	19	EPJ A55 180	A.V. Sarantsev *et al.*	(BONN, PNPI)
ZHANG	13A	PR C88 035205	H. Zhang *et al.*	(KSU)
PDG	82	PL 111B 1	M. Roos *et al.*	(HELS, CIT, CERN)
GOPAL	80	Toronto Conf. 159	G.P. Gopal	(RHEL) IJP
CAMERON	78	NP B143 189	W. Cameron *et al.*	(RHEL, LOIC) IJP
CAMERON	78B	NP B146 327	W. Cameron *et al.*	(RHEL, LOIC) IJP
DEBELLEFON	78	NC 42A 403	A. de Bellefon *et al.*	(CDEF, SACL) IJP
BACCARI	77	NC 41A 96	B. Baccari *et al.*	(SACL, CDEF) IJP
DEBELLEFON	77	NC 37A 175	A. de Bellefon *et al.*	(CDEF, SACL) IJP
GOPAL	77	NP B119 362	G.P. Gopal *et al.*	(LOIC, RHEL) IJP
NAKKASYAN	75	NP B93 85	A. Nakkasyan	(CERN) IJP
KANE	74	LBL-2452	D.F. Kane	(LBL) IJP

$\Lambda(2325)\ 3/2^-$

$I(J^P) = 0(\frac{3}{2}^-)$ Status: *

OMITTED FROM SUMMARY TABLE

BACCARI 77 finds this state with either $J^P = 3/2^-$ or $3/2^+$ in a energy-dependent partial-wave analyses of $K^-p\to\Lambda\omega$ from 2070 to 2436 MeV. A subsequent semi-energy-independent analysis from threshold to 2436 MeV selects $3/2^-$. DEBELLEFON 78 (same group) also sees this state in an energy-dependent partial-wave analysis of $K^-p\to\overline{K}N$ data, and finds $J^P = 3/2^-$ or $3/2^+$. They again prefer $J^P = 3/2^-$, but only on the basis of model-dependent considerations.

$\Lambda(2325)$ MASS

VALUE (MeV)	DOCUMENT ID		TECN	COMMENT
≈ 2325 OUR ESTIMATE				
2342 ± 30	DEBELLEFON	78	DPWA	$\overline{K}N\to\overline{K}N$
2327 ± 20	BACCARI	77	DPWA	$K^-p\to\Lambda\omega$

$\Lambda(2325)$ WIDTH

VALUE (MeV)	DOCUMENT ID		TECN	COMMENT
177 ± 40	DEBELLEFON	78	DPWA	$\overline{K}N\to\overline{K}N$
160 ± 40	BACCARI	77	IPWA	$K^-p\to\Lambda\omega$

$\Lambda(2325)$ DECAY MODES

	Mode
Γ_1	$N\overline{K}$
Γ_2	$\Lambda\omega$

$\Lambda(2325)$ BRANCHING RATIOS

$\Gamma(N\overline{K})/\Gamma_{total}$ — Γ_1/Γ

VALUE	DOCUMENT ID		TECN	COMMENT
0.19 ± 0.06	DEBELLEFON	78	DPWA	$\overline{K}N\to\overline{K}N$

$(\Gamma_i\Gamma_f)^{1/2}/\Gamma_{total}$ in $N\overline{K}\to\Lambda(2325)\to\Lambda\omega$ — $(\Gamma_1\Gamma_2)^{1/2}/\Gamma$

VALUE	DOCUMENT ID		TECN	COMMENT
0.06 ± 0.02	[1] BACCARI	77	IPWA	DS_{33} wave
0.05 ± 0.02	[1] BACCARI	77	DPWA	DD_{13} wave
0.08 ± 0.03	[1] BACCARI	77	DPWA	DD_{33} wave

$\Lambda(2325)$ FOOTNOTES

[1] Note that the three BACCARI 77 entries are for three different waves.

$\Lambda(2325)$ REFERENCES

DEBELLEFON	78	NC 42A 403	A. de Bellefon *et al.*	(CDEF, SACL) IJP
BACCARI	77	NC 41A 96	B. Baccari *et al.*	(SACL, CDEF) IJP

$\Lambda(2350)\ 9/2^+$

$I(J^P) = 0(\frac{9}{2}^+)$ Status: ***

DAUM 68 favors $J^P = 7/2^-$ or $9/2^+$. BRICMAN 70 favors $9/2^+$. LASINSKI 71 suggests three states in this region using a Pomeron + resonances model. There are now also three formation experiments from the College de France-Saclay group, DEBELLEFON 77, BACCARI 77, and DEBELLEFON 78, which find $9/2^+$ in energy-dependent partial-wave analyses of $\overline{K}N\to\Sigma\pi$, $\Lambda\omega$, and $N\overline{K}$.

$\Lambda(2350)$ MASS

VALUE (MeV)	DOCUMENT ID		TECN	COMMENT
2340 to 2370 (≈ 2350) OUR ESTIMATE				
2370 ± 50	DEBELLEFON	78	DPWA	$\overline{K}N\to\overline{K}N$
2365 ± 20	DEBELLEFON	77	DPWA	$K^-p\to\Sigma\pi$
$2358\pm\ 6$	BRICMAN	70	CNTR	Total, charge exchange
• • • We do not use the following data for averages, fits, limits, etc. • • •				
2372	BACCARI	77	DPWA	$K^-p\to\Lambda\omega$
2344 ± 15	COOL	70	CNTR	K^-p, K^-d total
2360 ± 20	LU	70	CNTR	$\gamma p\to K^+Y^*$
$2340\pm\ 7$	BUGG	68	CNTR	K^-p, K^-d total

$\Lambda(2350)$ WIDTH

VALUE (MeV)	DOCUMENT ID		TECN	COMMENT
100 to 250 (≈ 150) OUR ESTIMATE				
204 ± 50	DEBELLEFON	78	DPWA	$\overline{K}N\to\overline{K}N$
110 ± 20	DEBELLEFON	77	DPWA	$K^-p\to\Sigma\pi$
324 ± 30	BRICMAN	70	CNTR	Total, charge exchange
• • • We do not use the following data for averages, fits, limits, etc. • • •				
257	BACCARI	77	DPWA	$K^-p\to\Lambda\omega$
190	COOL	70	CNTR	K^-p, K^-d total
55	LU	70	CNTR	$\gamma p\to K^+Y^*$
140 ± 20	BUGG	68	CNTR	K^-p, K^-d total

$\Lambda(2350)$ DECAY MODES

	Mode	Fraction (Γ_i/Γ)
Γ_1	$N\overline{K}$	~ 12 %
Γ_2	$\Sigma\pi$	~ 10 %
Γ_3	$\Lambda\omega$	

$\Lambda(2350)$ BRANCHING RATIOS

See "Sign conventions for resonance couplings" in the Note on Λ and Σ Resonances.

$\Gamma(N\overline{K})/\Gamma_{total}$ — Γ_1/Γ

VALUE	DOCUMENT ID		TECN	COMMENT
~ 0.12 OUR ESTIMATE				
0.12 ± 0.04	DEBELLEFON	78	DPWA	$\overline{K}N\to\overline{K}N$

Downloaded from https://academic.oup.com/ptep/article/2022/8/083C01/6651666 by KIT Library user on 27 September 2022

$(\Gamma_i\Gamma_f)^{1/2}/\Gamma_{total}$ in $N\overline{K} \to \Lambda(2350) \to \Sigma\pi$ **$(\Gamma_1\Gamma_2)^{1/2}/\Gamma$**

VALUE	DOCUMENT ID		TECN	COMMENT
-0.11 ± 0.02	DEBELLEFON	77	DPWA	$K^- p \to \Sigma\pi$

$(\Gamma_i\Gamma_f)^{1/2}/\Gamma_{total}$ in $N\overline{K} \to \Lambda(2350) \to \Lambda\omega$ **$(\Gamma_1\Gamma_3)^{1/2}/\Gamma$**

VALUE	DOCUMENT ID		TECN	COMMENT
<0.05	BACCARI	77	DPWA	$K^- p \to \Lambda\omega$

$\Lambda(2350)$ REFERENCES

DEBELLEFON	78	NC 42A 403	A. de Bellefon *et al.*	(CDEF, SACL) IJP
BACCARI	77	NC 41A 96	B. Baccari *et al.*	(SACL, CDEF) IJP
DEBELLEFON	77	NC 37A 175	A. de Bellefon *et al.*	(CDEF, SACL) IJP
LASINSKI	71	NP B29 125	T.A. Lasinski	(EFI) IJP
BRICMAN	70	PL 31B 152	C. Bricman *et al.*	(CERN, CAEN, SACL)
COOL	70	PR D1 1887	R.L. Cool *et al.*	(BNL) I
Also		PRL 16 1228	R.L. Cool *et al.*	(BNL) I
LU	70	PR D2 1846	D.C. Lu *et al.*	(YALE)
BUGG	68	PR 168 1466	D.V. Bugg *et al.*	(RHEL, BIRM, CAVE) I
DAUM	68	NP B7 19	C. Daum *et al.*	(CERN) JP

$\Lambda(2585)$ Bumps

$I(J^P) = 0(?^?)$ Status: *

OMITTED FROM SUMMARY TABLE

$\Lambda(2585)$ MASS (BUMPS)

VALUE (MeV)	DOCUMENT ID		TECN	COMMENT
≈ 2585 OUR ESTIMATE				
2585 ± 45	ABRAMS	70	CNTR	$K^- p$, $K^- d$ total
2530 ± 25	LU	70	CNTR	$\gamma p \to K^+ Y^*$

$\Lambda(2585)$ WIDTH (BUMPS)

VALUE (MeV)	DOCUMENT ID		TECN	COMMENT
300	ABRAMS	70	CNTR	$K^- p$, $K^- d$ total
150	LU	70	CNTR	$\gamma p \to K^+ Y^*$

$\Lambda(2585)$ DECAY MODES (BUMPS)

	Mode
Γ_1	$N\overline{K}$

$\Lambda(2585)$ BRANCHING RATIOS (BUMPS)

$(J+\frac{1}{2})\times\Gamma(N\overline{K})/\Gamma_{total}$ **Γ_1/Γ**

J is not known, so only $(J+\frac{1}{2}) \times \Gamma(N\overline{K})/\Gamma_{total}$ can be given.

VALUE	DOCUMENT ID		TECN	COMMENT
1	ABRAMS	70	CNTR	$K^- p$, $K^- d$ total
0.12 ± 0.12	[1] BRICMAN	70	CNTR	Total, charge exchange

$\Lambda(2585)$ FOOTNOTES (BUMPS)

[1] The resonance is at the end of the region analyzed — no clear signal.

$\Lambda(2585)$ REFERENCES (BUMPS)

ABRAMS	70	PR D1 1917	R.J. Abrams *et al.*	(BNL) I
Also		PRL 16 1228	R.L. Cool *et al.*	(BNL) I
BRICMAN	70	PL 31B 152	C. Bricman *et al.*	(CERN, CAEN, SACL)
LU	70	PR D2 1846	D.C. Lu *et al.*	(YALE)

Downloaded from https://academic.oup.com/ptep/article/2022/8/083C01/6651666 by KIT Library user on 27 September 2022

Σ BARYONS
($S = -1$, $I = 1$)

$\Sigma^+ = uus$, $\Sigma^0 = uds$, $\Sigma^- = dds$

Σ^+

$I(J^P) = 1(\frac{1}{2}^+)$ Status: ****

We have omitted some results that have been superseded by later experiments. See our earlier editions.

Σ^+ MASS

The fit uses Σ^+, Σ^0, Σ^-, and Λ mass and mass-difference measurements.

VALUE (MeV)	EVTS	DOCUMENT ID		TECN	COMMENT
1189.37±0.07 OUR FIT	Error includes scale factor of 2.2.				
1189.37±0.06 OUR AVERAGE	Error includes scale factor of 1.8. See the ideogram below.				
1189.33±0.04	607	[1] BOHM	72	EMUL	
1189.16±0.12		HYMAN	67	HEBC	
1189.61±0.08	4205	SCHMIDT	65	HBC	See note with Λ mass
1189.48±0.22	58	[2] BHOWMIK	64	EMUL	
1189.38±0.15	144	[2] BARKAS	63	EMUL	

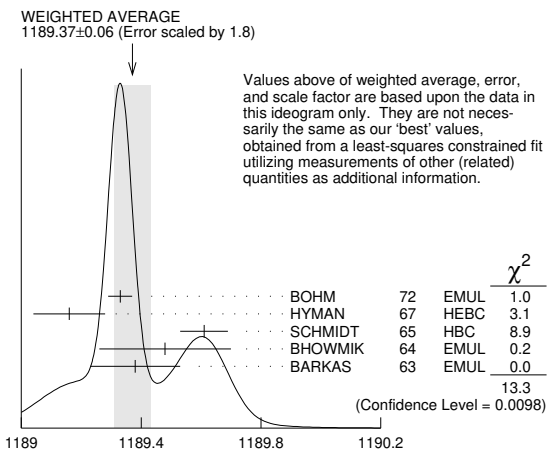

[1] BOHM 72 is updated with our 1973 K^-, π^-, and π^0 masses (Reviews of Modern Physics **45** S1 (1973)).

[2] These masses have been raised 30 keV to take into account a 46 keV increase in the proton mass and a 21 keV decrease in the π^0 mass (note added 1967 edition, Reviews of Modern Physics **39** 1 (1967)).

Σ^+ MEAN LIFE

Measurements with fewer than 1000 events have been omitted.

VALUE (10^{-10} s)	EVTS	DOCUMENT ID		TECN	COMMENT
0.8018±0.0026 OUR AVERAGE					
0.8038±0.0040±0.0014		BARBOSA	00	E761	hyperons, 375 GeV
0.8043±0.0080±0.0014		[1] BARBOSA	00	E761	hyperons, 375 GeV
0.798 ±0.005	30k	MARRAFFINO	80	HBC	K^-p 0.42–0.5 GeV/c
0.807 ±0.013	5719	CONFORTO	76	HBC	K^-p 1–1.4 GeV/c
0.795 ±0.010	20k	EISELE	70	HBC	K^-p at rest
0.803 ±0.008	10664	BARLOUTAUD	69	HBC	K^-p 0.4–1.2 GeV/c
0.83 ±0.032	1300	[2] CHANG	66	HBC	

[1] This is a measurement of the $\overline{\Sigma}^-$ lifetime. Here we assume CPT invariance; see below for the fractional Σ^+-$\overline{\Sigma}^-$ lifetime difference obtained by BARBOSA 00.

[2] We have increased the CHANG 66 error of 0.018; see our 1970 edition, Reviews of Modern Physics **42** 87 (1970).

$(\tau_{\Sigma^+} - \tau_{\overline{\Sigma}^-}) / \tau_{\Sigma^+}$

A test of CPT invariance.

VALUE	DOCUMENT ID		TECN	COMMENT
$(-6\pm12)\times10^{-4}$	BARBOSA	00	E761	hyperons, 375 GeV

Σ^+ MAGNETIC MOMENT

See the "Quark Model" review. Measurements with an error $\geq 0.1\ \mu_N$ have been omitted.

VALUE (μ_N)	EVTS	DOCUMENT ID		TECN	COMMENT
2.458 ±0.010 OUR AVERAGE	Error includes scale factor of 2.1. See the ideogram below.				
2.4613±0.0034±0.0040	250k	MORELOS	93	SPEC	pCu 800 GeV
2.428 ±0.036 ±0.007	12k	[1] MORELOS	93	SPEC	pCu 800 GeV
2.479 ±0.012 ±0.022	137k	WILKINSON	87	SPEC	pBe 400 GeV
2.4040±0.0198	44k	[2] ANKENBRA...	83	CNTR	pCu 400 GeV

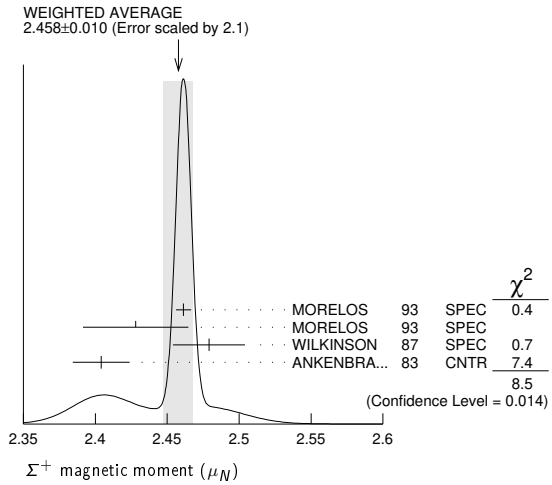

[1] We assume CPT invariance: this is (minus) the $\overline{\Sigma}^-$ magnetic moment as measured by MORELOS 93. See below for the moment difference testing CPT.

[2] ANKENBRANDT 83 gives the value 2.38 ± 0.02μ_N. MORELOS 93 uses the same hyperon magnet and channel and claims to determine the field integral better, leading to the revised value given here.

$(\mu_{\Sigma^+} + \mu_{\overline{\Sigma}^-}) / \mu_{\Sigma^+}$

A test of CPT invariance.

VALUE	DOCUMENT ID		TECN	COMMENT
0.014±0.015	[1] MORELOS	93	SPEC	pCu 800 GeV

[1] This is our calculation from the MORELOS 93 measurements of the Σ^+ and $\overline{\Sigma}^-$ magnetic moments given above. The statistical error on $\mu_{\overline{\Sigma}^-}$ dominates the error here.

Σ^+ DECAY MODES

	Mode		Fraction (Γ_i/Γ)	Confidence level
Γ_1	$p\pi^0$		(51.57±0.30) %	
Γ_2	$n\pi^+$		(48.31±0.30) %	
Γ_3	$p\gamma$		$(1.23\pm0.05)\times10^{-3}$	
Γ_4	$n\pi^+\gamma$	[a]	$(4.5\pm0.5)\times10^{-4}$	
Γ_5	$\Lambda e^+\nu_e$		$(2.0\pm0.5)\times10^{-5}$	
	$\Delta S = \Delta Q$ (SQ) violating modes or $\Delta S = 1$ weak neutral current ($S1$) modes			
Γ_6	$n e^+\nu_e$	SQ	$< 5\times10^{-6}$	90%
Γ_7	$n\mu^+\nu_\mu$	SQ	$< 3.0\times10^{-5}$	90%
Γ_8	$p e^+ e^-$	$S1$	$< 7\times10^{-6}$	
Γ_9	$p\mu^+\mu^-$	$S1$	$(2.4\ ^{+1.7}_{-1.3})\times10^{-8}$	

[a] See the Listings below for the pion momentum range used in this measurement.

CONSTRAINED FIT INFORMATION

An overall fit to 2 branching ratios uses 14 measurements and one constraint to determine 3 parameters. The overall fit has $\chi^2 = 7.7$ for 12 degrees of freedom.

The following *off-diagonal* array elements are the correlation coefficients $\langle \delta x_i \delta x_j \rangle / (\delta x_i \cdot \delta x_j)$, in percent, from the fit to the branching fractions, $x_i \equiv \Gamma_i/\Gamma_{total}$. The fit constrains the x_i whose labels appear in this array to sum to one.

x_2	−100	
x_3	12	−14
	x_1	x_2

Downloaded from https://academic.oup.com/ptep/article/2022/8/083C01/6651666 by KIT Library user on 27 September 2022

Σ^+ BRANCHING RATIOS

$\Gamma(n\pi^+)/\Gamma(N\pi)$ — $\Gamma_2/(\Gamma_1+\Gamma_2)$

VALUE	EVTS	DOCUMENT ID		TECN	COMMENT
0.4836±0.0030 OUR FIT					
0.4836±0.0030 OUR AVERAGE					
0.4828±0.0036	10k	[1] MARRAFFINO	80	HBC	K^-p 0.42–0.5 GeV/c
0.488 ±0.008	1861	NOWAK	78	HBC	
0.484 ±0.015	537	TOVEE	71	EMUL	
0.488 ±0.010	1331	BARLOUTAUD	69	HBC	K^-p 0.4–1.2 GeV/c
0.46 ±0.02	534	CHANG	66	HBC	
0.490 ±0.024	308	HUMPHREY	62	HBC	

[1] MARRAFFINO 80 actually gives $\Gamma(p\pi^0)/\Gamma(\text{total}) = 0.5172 \pm 0.0036$.

$\Gamma(p\gamma)/\Gamma(p\pi^0)$ — Γ_3/Γ_1

VALUE (units 10^{-3})	EVTS	DOCUMENT ID		TECN	COMMENT
2.38±0.10 OUR FIT					
2.38±0.10 OUR AVERAGE					
2.32±0.11±0.10	32k	TIMM	95	E761	Σ^+ 375 GeV
$2.81\pm0.39^{+0.21}_{-0.43}$	408	HESSEY	89	CNTR	$K^-p \to \Sigma^+\pi^-$ at rest
2.52±0.28	190	[1] KOBAYASHI	87	CNTR	$\pi^+p \to \Sigma^+K^+$
$2.46^{+0.30}_{-0.35}$	155	BIAGI	85	CNTR	CERN hyperon beam
2.11±0.38	46	MANZ	80	HBC	$K^-p \to \Sigma^+\pi^-$
2.1 ±0.3	45	ANG	69B	HBC	K^-p at rest
2.76±0.51	31	GERSHWIN	69B	HBC	$K^-p \to \Sigma^+\pi^-$
3.7 ±0.8	24	BAZIN	65	HBC	K^-p at rest

[1] KOBAYASHI 87 actually gives $\Gamma(p\gamma)/\Gamma(\text{total}) = (1.30 \pm 0.15) \times 10^{-3}$.

$\Gamma(n\pi^+\gamma)/\Gamma(n\pi^+)$ — Γ_4/Γ_2

The π^+ momentum cuts differ, so we do not average the results but simply use the latest value in the Summary Table.

VALUE (units 10^{-3})	EVTS	DOCUMENT ID		TECN	COMMENT
0.93±0.10	180	EBENHOH	73	HBC	$\pi^+ < 150$ MeV/c
• • • We do not use the following data for averages, fits, limits, etc. • • •					
0.27±0.05	29	ANG	69B	HBC	$\pi^+ < 110$ MeV/c
∼ 1.8		BAZIN	65B	HBC	$\pi^+ < 116$ MeV/c

$\Gamma(\Lambda e^+\nu_e)/\Gamma_{total}$ — Γ_5/Γ

VALUE (units 10^{-5})	EVTS	DOCUMENT ID		TECN	COMMENT
2.0±0.5 OUR AVERAGE					
1.6±0.7	5	BALTAY	69	HBC	K^-p at rest
2.9±1.0	10	EISELE	69	HBC	K^-p at rest
2.0±0.8	6	BARASH	67	HBC	K^-p at rest

$\Gamma(ne^+\nu_e)/\Gamma(n\pi^+)$ — Γ_6/Γ_2

Test of $\Delta S = \Delta Q$ rule. Experiments with an effective denominator less than 100,000 have been omitted.

EFFECTIVE DENOM.	EVTS	DOCUMENT ID		TECN	COMMENT
$< 1.1 \times 10^{-5}$ OUR LIMIT Our 90% CL limit = (2.3 events)/(effective denominator sum). [Number of events increased to 2.3 for a 90% confidence level.]					
111000	0	[1] EBENHOH	74	HBC	K^-p at rest
105000	0	[1] SECHI-ZORN	73	HBC	K^-p at rest

[1] Effective denominator calculated by us.

$\Gamma(n\mu^+\nu_\mu)/\Gamma(n\pi^+)$ — Γ_7/Γ_2

Test of $\Delta S = \Delta Q$ rule.

EFFECTIVE DENOM.	EVTS	DOCUMENT ID		TECN
$< 6.2 \times 10^{-5}$ OUR LIMIT Our 90% CL limit = (6.7 events)/(effective denominator sum). [Number of events increased to 6.7 for a 90% confidence level.]				
33800	0	BAGGETT	69B	HBC
62000	2	[1] EISELE	69B	HBC
10150	0	[2] COURANT	64	HBC
1710	0	[2] NAUENBERG	64	HBC
120	1	GALTIERI	62	EMUL

[1] Effective denominator calculated by us.
[2] Effective denominator taken from EISELE 67.

$\Gamma(pe^+e^-)/\Gamma_{total}$ — Γ_8/Γ

VALUE (units 10^{-6})	DOCUMENT ID		TECN	COMMENT
<7	[1] ANG	69B	HBC	K^-p at rest

[1] ANG 69B found three pe^+e^- events in agreement with $\gamma \to e^+e^-$ conversion from $\Sigma^+ \to p\gamma$. The limit given here is for neutral currents.

$\Gamma(p\mu^+\mu^-)/\Gamma_{total}$ — Γ_9/Γ

A test for a $\Delta S = 1$ weak neutral current, but also allowed by higher-order electroweak interactions.

VALUE (units 10^{-8})	EVTS	DOCUMENT ID		TECN	COMMENT
$2.4^{+1.7}_{-1.3}$ OUR AVERAGE					
$2.2^{+0.9}_{-0.8}{}^{+1.5}_{-1.1}$	10.2	[1] AAIJ	18E	LHCB	pp at 7, 8 TeV
$8.6^{+6.6}_{-5.4}\pm5.5$	3	[2] PARK	05	HYCP	p Cu, 800 GeV

[1] AAIJ 18E sees no structure in the dimuon mass distribution, contrary to PARK 05.
[2] The masses of the three dimuons of PARK 05 are within 1 MeV of one another, perhaps indicating the existence of a new state P^0 with mass 214.3 ± 0.5 MeV. In that case, the decay is $\Sigma^+ \to pP^0$, $P^0 \to \mu^+\mu^-$, with a branching fraction of $(3.1^{+2.4}_{-1.9} \pm 1.5) \times 10^{-8}$.

$\Gamma(\Sigma^+ \to ne^+\nu_e)/\Gamma(\Sigma^- \to ne^-\overline{\nu}_e)$ — $\Gamma_6/\Gamma_3^{\Sigma^-}$

VALUE	CL%	EVTS	DOCUMENT ID		TECN	COMMENT
<0.009 OUR LIMIT Our 90% CL limit, using $\Gamma(ne^+\nu_e)/\Gamma(n\pi^+)$ above.						
• • • We do not use the following data for averages, fits, limits, etc. • • •						
<0.019	90	0	EBENHOH	74	HBC	K^-p at rest
<0.018	90	0	SECHI-ZORN	73	HBC	K^-p at rest
<0.12	95	0	COLE	71	HBC	K^-p at rest
<0.03	90	0	EISELE	69B	HBC	See EBENHOH 74

$\Gamma(\Sigma^+ \to n\mu^+\nu_\mu)/\Gamma(\Sigma^- \to n\mu^-\overline{\nu}_\mu)$ — $\Gamma_7/\Gamma_4^{\Sigma^-}$

VALUE	EVTS	DOCUMENT ID		TECN	COMMENT
<0.12 OUR LIMIT Our 90% CL limit, using $\Gamma(n\mu^+\nu_\mu)/\Gamma(n\pi^+)$ above.					
• • • We do not use the following data for averages, fits, limits, etc. • • •					
$0.06^{+0.045}_{-0.03}$	2	EISELE	69B	HBC	K^-p at rest

$\Gamma(\Sigma^+ \to n\ell^+\nu)/\Gamma(\Sigma^- \to n\ell^-\overline{\nu}_\ell)$ — $(\Gamma_6+\Gamma_7)/(\Gamma_3^{\Sigma^-}+\Gamma_4^{\Sigma^-})$

Test of $\Delta S = \Delta Q$ rule.

VALUE	EVTS	DOCUMENT ID		TECN
<0.043 OUR LIMIT Our 90% CL limit, using $[\Gamma(\Sigma^+ \to n\mu^+\nu_\mu) + \Gamma(\Sigma^+ \to ne^+\nu_e)]/\Gamma(\Sigma^+ \to n\pi^+)$.				
• • • We do not use the following data for averages, fits, limits, etc. • • •				
<0.08	1	NORTON	69	HBC
<0.034	0	BAGGETT	67	HBC

Σ^+ DECAY PARAMETERS

See the "Note on Baryon Decay Parameters" in the neutron Listings. A few early results have been omitted.

α_0 FOR $\Sigma^+ \to p\pi^0$

VALUE	EVTS	DOCUMENT ID		TECN	COMMENT
−0.982±0.014 OUR FIT					
$-0.982^{+0.016}_{-0.013}$ OUR AVERAGE					
−0.998±0.037±0.009	93k	[1] ABLIKIM	20X	BES3	$J/\psi/\psi(2S) \to \Sigma^+\overline{\Sigma}^-$
$-0.945^{+0.055}_{-0.042}$	1259	[2] LIPMAN	73	OSPK	$\pi^+p \to \Sigma^+$
−0.940±0.045	16k	BELLAMY	72	ASPK	$\pi^+p \to \Sigma^+K^+$
$-0.98^{+0.05}_{-0.02}$	1335	[3] HARRIS	70	OSPK	$\pi^+p \to \Sigma^+K^+$
−0.999±0.022	32k	BANGERTER	69	HBC	K^-p 0.4 GeV/c

[1] ABLIKIM 20X uses production through $e^+e \to J/\psi \to \Sigma^+\overline{\Sigma}^-$ and $e^+e \to \psi(2S) \to \Sigma^+\overline{\Sigma}^-$, with 87,815 and 5,327 events, respectively. Note that the reported values of decay parameters α_0 of Σ^+ and $\overline{\alpha}_0$ of $\overline{\Sigma}^-$ are correlated.
[2] Decay protons scattered off aluminum.
[3] Decay protons scattered off carbon.

$\overline{\alpha}_0$ FOR $\overline{\Sigma}^- \to \overline{p}\pi^0$

VALUE	EVTS	DOCUMENT ID		TECN	COMMENT
0.990±0.037±0.011	93k	[1] ABLIKIM	20X	BES3	$J/\psi/\psi(2S) \to \Sigma^+\overline{\Sigma}^-$

[1] ABLIKIM 20X uses production through $e^+e \to J/\psi \to \Sigma^+\overline{\Sigma}^-$ and $e^+e \to \psi(2S) \to \Sigma^+\overline{\Sigma}^-$, with 87,815 and 5,327 events, respectively. Note that the reported values of decay parameters α_0 of Σ^+ and $\overline{\alpha}_0$ of $\overline{\Sigma}^-$ are correlated.

$(\alpha_0 + \overline{\alpha}_0) / (\alpha_0 - \overline{\alpha}_0)$

VALUE	EVTS	DOCUMENT ID		TECN	COMMENT
0.004±0.037±0.010	93k	[1] ABLIKIM	20X	BES3	$J/\psi/\psi(2S) \to \Sigma^+\overline{\Sigma}^-$

[1] ABLIKIM 20X uses production through $e^+e \to J/\psi \to \Sigma^+\overline{\Sigma}^-$ and $e^+e \to \psi(2S) \to \Sigma^+\overline{\Sigma}^-$, with 87,815 and 5,327 events, respectively. Note that the reported values of decay parameters α_0 of Σ^+ and $\overline{\alpha}_0$ of $\overline{\Sigma}^-$ are correlated.

ϕ_0 ANGLE FOR $\Sigma^+ \to p\pi^0$ — $(\tan\phi_0 = \beta/\gamma)$

VALUE (°)	EVTS	DOCUMENT ID		TECN	COMMENT
36 ±34 OUR AVERAGE					
$38.1^{+35.7}_{-37.1}$	1259	[1] LIPMAN	73	OSPK	$\pi^+p \to \Sigma^+K^+$
22 ±90		[2] HARRIS	70	OSPK	$\pi^+p \to \Sigma^+K^+$

[1] Decay proton scattered off aluminum.
[2] Decay protons scattered off carbon.

α_+ / α_0

Older results have been omitted.

VALUE	EVTS	DOCUMENT ID		TECN	COMMENT
−0.069±0.013 OUR FIT					
−0.073±0.021	23k	MARRAFFINO	80	HBC	K^-p 0.42–0.5 GeV/c

Downloaded from https://academic.oup.com/ptep/article/2022/8/083C01/6651666 by KIT Library user on 27 September 2022

α_+ FOR $\Sigma^+ \to n\pi^+$

VALUE	EVTS	DOCUMENT ID		TECN	COMMENT
0.068±0.013 OUR FIT					
0.066±0.016 OUR AVERAGE					
0.037±0.049	4101	BERLEY	70B	HBC	
0.069±0.017	35k	BANGERTER	69	HBC	$K^- p$ 0.4 GeV/c

ϕ_+ ANGLE FOR $\Sigma^+ \to n\pi^+$ $(\tan\phi_+ = \beta/\gamma)$

VALUE (°)	EVTS	DOCUMENT ID		TECN	COMMENT
167±20 OUR AVERAGE Error includes scale factor of 1.1.					
184±24	1054	[1] BERLEY	70B	HBC	
143±29	560	BANGERTER	69B	HBC	$K^- p$ 0.4 GeV/c

[1] Changed from 176 to 184° to agree with our sign convention.

α_γ FOR $\Sigma^+ \to p\gamma$

VALUE	EVTS	DOCUMENT ID		TECN	COMMENT
−0.76 ±0.08 OUR AVERAGE					
−0.720±0.086±0.045	35k	[1] FOUCHER	92	SPEC	Σ^+ 375 GeV
−0.86 ±0.13 ±0.04	190	KOBAYASHI	87	CNTR	$\pi^+ p \to \Sigma^+ K^+$
$-0.53\ ^{+0.38}_{-0.36}$	46	MANZ	80	HBC	$K^- p \to \Sigma^+ \pi^-$
$-1.03\ ^{+0.52}_{-0.42}$	61	GERSHWIN	69B	HBC	$K^- p \to \Sigma^+ \pi^-$

[1] See TIMM 95 for a detailed description of the analysis.

Σ^+ REFERENCES

We have omitted some papers that have been superseded by later experiments. See our earlier editions.

ABLIKIM	20X	PRL 125 052004	M. Ablikim et al.	(BESIII Collab.)
AAIJ	18E	PRL 120 221803	R. Aaij et al.	(LHCb Collab.)
PARK	05	PRL 94 021801	H.K. Park et al.	(FNAL HyperCP Collab.)
BARBOSA	00	PR D61 031101	R.F. Barbosa et al.	(FNAL E761 Collab.)
TIMM	95	PR D51 4638	S. Timm et al.	(FNAL E761 Collab.)
MORELOS	93	PRL 71 3417	A. Morelos et al.	(FNAL E761 Collab.)
FOUCHER	92	PRL 68 3004	M. Foucher et al.	(FNAL E761 Collab.)
HESSEY	89	ZPHY C42 175	N.P. Hessey et al.	(BNL-811 Collab.)
KOBAYASHI	87	PRL 59 868	M. Kobayashi et al.	(KYOT)
WILKINSON	87	PRL 58 855	C.A. Wilkinson et al.	(WISC, MICH, RUTG+)
BIAGI	85	ZPHY C28 495	S.F. Biagi et al.	(CERN WA62 Collab.)
ANKENBRA...	83	PRL 51 863	C.M. Ankenbrandt et al.	(FNAL, IOWA, ISU+)
MANZ	80	PL 96B 217	A. Manz et al.	(MPIM, VAND)
MARRAFFINO	80	PR D21 2501	J. Marraffino et al.	(VAND, MPIM)
NOWAK	78	NP B139 61	R.J. Nowak et al.	(LOUC, BELG, DURH+)
CONFORTO	76	NP B105 189	B. Conforto et al.	(RHEL, LOIC)
EBENHOH	74	ZPHY 266 367	H. Ebenhoh et al.	(HEIDT)
EBENHOH	73	ZPHY 264 413	W. Ebenhoh et al.	(HEIDT)
LIPMAN	73	PL 43B 89	N.H. Lipman et al.	(RHEL, SUSS, LOWC)
PDG	73	RMP 45 S1	T.A. Lasinski et al.	(LBL, BRAN, CERN+)
SECHI-ZORN	73	PR D8 12	B. Sechi-Zorn, G.A. Snow	(UMD)
BELLAMY	72	PL 39B 299	E.H. Bellamy et al.	(LOWC, RHEL, SUSS)
BOHM	72	NP B48 1	G. Bohm et al.	(BERL, KIDR, BRUX, IASD+)
Also		IIHE-73.2 Nov	G. Bohm	(BERL, KIDR, BRUX, IASD, DUUC+)
COLE	71	PR D4 631	J. Cole et al.	(STON, COLU)
TOVEE	71	NP B33 493	D.N. Tovee et al.	(LOUC, KIDR, BERL+)
BERLEY	70B	PR D1 2015	D. Berley et al.	(BNL, MASA, YALE)
EISELE	70	ZPHY 238 372	F. Eisele et al.	(HEID)
HARRIS	70	PRL 24 165	F. Harris et al.	(MICH, WISC)
PDG	70	RMP 42 87	A. Barbaro-Galtieri et al.	(LRL, BRAN+)
ANG	69B	ZPHY 228 151	G. Ang et al.	(HEID)
BAGGETT	69B	Thesis MDDP-TR-973	N.V. Baggett	(UMD)
BALTAY	69	PRL 22 615	C. Baltay et al.	(COLU, STON)
BANGERTER	69	Thesis UCRL 19244	R.O. Bangerter	(LRL)
BANGERTER	69B	PR 187 1821	R.O. Bangerter et al.	(LRL)
BARLOUTAUD	69	NP B14 153	R. Barloutaud et al.	(SACL, CERN, HEID)
EISELE	69	ZPHY 221 1	F. Eisele et al.	(HEID)
Also		PRL 13 291	W. Willis et al.	(BNL, CERN, HEID, UMD)
EISELE	69B	ZPHY 221 401	F. Eisele et al.	(HEID)
GERSHWIN	69B	PR 188 2077	L.K. Gershwin et al.	(LRL)
Also		Thesis UCRL 19246	L.K. Gershwin	(LRL)
NORTON	69	Thesis Nevis 175	H. Norton	(COLU)
BAGGETT	67	PRL 19 1458	N. Baggett et al.	(UMD)
Also		Vienna Abs. 374	N.V. Baggett, B. Kehoe	(UMD)
Also		Private Comm.	N.V. Baggett	(UMD)
BARASH	67	PRL 19 181	N. Barash et al.	(UMD)
EISELE	67	ZPHY 205 409	F. Eisele et al.	(HEID)
HYMAN	67	PL 25B 376	L.G. Hyman et al.	(ANL, CMU, NWES)
PDG	67	RMP 39 1	A.H. Rosenfeld et al.	(LRL, CERN, YALE)
CHANG	66	PR 151 1081	C.Y. Chang	(COLU)
Also		Thesis Nevis 145	C.Y. Chang	(COLU)
BAZIN	65	PRL 14 154	M. Bazin et al.	(PRIN, COLU)
BAZIN	65B	PR 140 B1358	M. Bazin et al.	(PRIN, RUTG, COLU)
SCHMIDT	65	PR 140 B1328	P. Schmidt	(COLU)
BHOWMIK	64	NP 53 22	B. Bhowmik et al.	(DELH)
COURANT	64	PR 136 B1791	H. Courant et al.	(CERN, HEID, UMD+)
NAUENBERG	64	PRL 12 679	U. Nauenberg et al.	(COLU, RUTG, PRIN)
BARKAS	63	PRL 11 26	W.H. Barkas, J.N. Dyer, H.H. Heckman	(LRL)
Also		Thesis UCRL 9450	J.N. Dyer	(LRL)
GALTIERI	62	PRL 9 26	A. Barbaro-Galtieri et al.	(LRL)
HUMPHREY	62	PR 127 1305	W.E. Humphrey, R.R. Ross	(LRL)

Σ^0

$I(J^P) = 1(\frac{1}{2}^+)$ Status: ****

COURANT 63 and ALFF 65, using $\Sigma^0 \to \Lambda e^+ e^-$ decays (Dalitz decays), determined the Σ^0 parity to be positive, given that $J = 1/2$ and that certain very reasonable assumptions about form factors are true. The results of experiments involving the Primakoff effect, from which the Σ^0 mean life and $\Sigma^0 \to \Lambda$ transition magnetic moment come (see below), strongly support $J = 1/2$.

Σ^0 MASS

The fit uses Σ^+, Σ^0, Σ^-, and Λ mass and mass-difference measurements.

VALUE (MeV)	EVTS	DOCUMENT ID		TECN	COMMENT
1192.642±0.024 OUR FIT					
• • • We do not use the following data for averages, fits, limits, etc. • • •					
1192.65 ±0.020±0.014	3327	[1] WANG	97	SPEC	$\Sigma^0 \to \Lambda\gamma \to (p\pi^-)(e^+e^-)$

[1] This WANG 97 result is redundant with the Σ^0-Λ mass-difference measurement below.

$m_{\Sigma^-} - m_{\Sigma^0}$

VALUE (MeV)	EVTS	DOCUMENT ID		TECN	COMMENT
4.807±0.035 OUR FIT Error includes scale factor of 1.1.					
4.86 ±0.08 OUR AVERAGE Error includes scale factor of 1.2.					
4.87 ±0.12	37	DOSCH	65	HBC	
5.01 ±0.12	12	SCHMIDT	65	HBC	See note with Λ mass
4.75 ±0.1	18	BURNSTEIN	64	HBC	

$m_{\Sigma^0} - m_\Lambda$

VALUE (MeV)	EVTS	DOCUMENT ID		TECN	COMMENT
76.959±0.023 OUR FIT					
76.966±0.020±0.013	3327	WANG	97	SPEC	$\Sigma^0 \to \Lambda\gamma \to (p\pi^-)(e^+e^-)$
• • • We do not use the following data for averages, fits, limits, etc. • • •					
76.23 ±0.55	109	COLAS	75	HLBC	$\Sigma^0 \to \Lambda\gamma$
76.63 ±0.28	208	SCHMIDT	65	HBC	See note with Λ mass

Σ^0 MEAN LIFE

These lifetimes are deduced from measurements of the cross sections for the Primakoff process $\Lambda \to \Sigma^0$ in nuclear Coulomb fields. An alternative expression of the same information is the Σ^0-Λ transition magnetic moment given in the following section. The relation is $(\mu_{\Sigma\Lambda}/\mu_N)^2\ \tau = 1.92951 \times 10^{-19}$ s (see DEVLIN 86).

VALUE (10^{-20} s)	DOCUMENT ID		TECN	COMMENT
7.4±0.7 OUR EVALUATION Using $\mu_{\Sigma\Lambda}$ (see the above note).				
$6.5\ ^{+1.7}_{-1.1}$	[2] DEVLIN	86	SPEC	Primakoff effect
7.6±0.5±0.7	[3] PETERSEN	86	SPEC	Primakoff effect
• • • We do not use the following data for averages, fits, limits, etc. • • •				
5.8±1.3	[2] DYDAK	77	SPEC	See DEVLIN 86

[2] DEVLIN 86 is a recalculation of the results of DYDAK 77 removing a numerical approximation made in that work.
[3] An additional uncertainty of the Primakoff formalism is estimated to be < 5%.

$|\mu(\Sigma^0 \to \Lambda)|$ TRANSITION MAGNETIC MOMENT

See the note in the Σ^0 mean-life section above. Also, See the "Quark Model" review.

VALUE (μ_N)	DOCUMENT ID		TECN	COMMENT
1.61±0.08 OUR AVERAGE				
$1.72\ ^{+0.17}_{-0.19}$	[4] DEVLIN	86	SPEC	Primakoff effect
1.59±0.05±0.07	[5] PETERSEN	86	SPEC	Primakoff effect
• • • We do not use the following data for averages, fits, limits, etc. • • •				
$1.82\ ^{+0.25}_{-0.18}$	[4] DYDAK	77	SPEC	See DEVLIN 86

[4] DEVLIN 86 is a recalculation of the results of DYDAK 77 removing a numerical approximation made in that work.
[5] An additional uncertainty of the Primakoff formalism is estimated to be < 2.5%.

Σ^0 DECAY MODES

	Mode	Fraction (Γ_i/Γ)	Confidence level
Γ_1	$\Lambda\gamma$	100 %	
Γ_2	$\Lambda\gamma\gamma$	< 3 %	90%
Γ_3	$\Lambda e^+ e^-$	[a] 5×10^{-3}	

[a] A theoretical value using QED.

Σ^0 BRANCHING RATIOS

$\Gamma(\Lambda\gamma\gamma)/\Gamma_{total}$ — Γ_2/Γ

VALUE	CL%	DOCUMENT ID		TECN
<0.03	90	COLAS	75	HLBC

Downloaded from https://academic.oup.com/ptep/article/2022/8/083C01/6651666 by KIT Library user on 27 September 2022

$\Gamma(\Lambda e^+ e^-)/\Gamma_{total}$ — Γ_3/Γ

See COURANT 63 and ALFF 65 for measurements of the invariant-mass spectrum of the Dalitz pairs.

VALUE	DOCUMENT ID		COMMENT
0.00545	FEINBERG	58	Theoretical QED calculation

Σ^0 REFERENCES

WANG	97	PR D56 2544	M.H.L.S. Wang *et al.*	(BNL-E766 Collab.)
DEVLIN	86	PR D34 1626	T. Devlin, P.C. Petersen, A. Beretvas	(RUTG)
PETERSEN	86	PRL 57 949	P.C. Petersen *et al.*	(RUTG, WISC, MICH+)
DYDAK	77	NP B118 1	F. Dydak *et al.*	(CERN, DORT, HEIDH)
COLAS	75	NP B91 253	J. Colas *et al.*	(ORSAY)
ALFF	65	PR 137 B1105	C. Alff *et al.*	(COLU, RUTG, BNL) P
DOSCH	65	PL 14 239	H.C. Dosch *et al.*	(HEID)
SCHMIDT	65	PR 140 B1328	P. Schmidt	(COLU)
BURNSTEIN	64	PRL 13 66	R.A. Burnstein *et al.*	(UMD)
COURANT	63	PRL 10 409	H. Courant *et al.*	(CERN, UMD) P
FEINBERG	58	PR 109 1019	G. Feinberg	(BNL)

Σ^-

$I(J^P) = 1(\frac{1}{2}^+)$ Status: ****

We have omitted some results that have been superseded by later experiments. See our earlier editions.

Σ^- MASS

The fit uses Σ^+, Σ^0, Σ^-, and Λ mass and mass-difference measurements.

VALUE (MeV)	EVTS	DOCUMENT ID		TECN	COMMENT
1197.449±0.030 OUR FIT		Error includes scale factor of 1.2.			
1197.45 ±0.04 OUR AVERAGE		Error includes scale factor of 1.2.			
1197.417±0.040		GUREV	93	SPEC	Σ^- C atom, crystal diff.
1197.532±0.057		GALL	88	CNTR	Σ^- Pb, Σ^- W atoms
1197.43 ±0.08	3000	SCHMIDT	65	HBC	See note with Λ mass
• • • We do not use the following data for averages, fits, limits, etc. • • •					
1197.24 ±0.15		[1] DUGAN	75	CNTR	Exotic atoms

[1] GALL 88 concludes that the DUGAN 75 mass needs to be reevaluated.

$m_{\Sigma^-} - m_{\Sigma^+}$

VALUE (MeV)	EVTS	DOCUMENT ID		TECN
8.08±0.08 OUR FIT	Error includes scale factor of 1.9.			
8.09±0.16 OUR AVERAGE				
7.91±0.23	86	BOHM	72	EMUL
8.25±0.25	2500	DOSCH	65	HBC
8.25±0.40	87	BARKAS	63	EMUL

$m_{\Sigma^-} - m_{\Lambda}$

VALUE (MeV)	EVTS	DOCUMENT ID		TECN	COMMENT
81.766±0.030 OUR FIT		Error includes scale factor of 1.2.			
81.69 ±0.07 OUR AVERAGE					
81.64 ±0.09	2279	HEPP	68	HBC	
81.80 ±0.13	85	SCHMIDT	65	HBC	See note with Λ mass
81.70 ±0.19		BURNSTEIN	64	HBC	

Σ^- MEAN LIFE

Measurements with an error $\geq 0.2 \times 10^{-10}$ s have been omitted.

VALUE (10^{-10} s)	EVTS	DOCUMENT ID		TECN	COMMENT
1.479±0.011 OUR AVERAGE		Error includes scale factor of 1.3.			See the ideogram below.
1.480±0.014	16k	MARRAFFINO	80	HBC	$K^- p$ 0.42–0.5 GeV/c
1.49 ±0.03	8437	CONFORTO	76	HBC	$K^- p$ 1–1.4 GeV/c
1.463±0.039	2400	ROBERTSON	72	HBC	$K^- p$ 0.25 GeV/c
1.42 ±0.05	1383	BAKKER	71	DBC	$K^- N \to \Sigma^- \pi\pi$
$1.41 \; {}^{+0.09}_{-0.08}$		TOVEE	71	EMUL	
1.485±0.022	100k	EISELE	70	HBC	$K^- p$ at rest
1.472±0.016	10k	BARLOUTAUD	69	HBC	$K^- p$ 0.4–1.2 GeV/c
1.38 ±0.07	506	WHITESIDE	68	HBC	$K^- p$ at rest
1.666±0.075	3267	[1] CHANG	66	HBC	$K^- p$ at rest
1.58 ±0.06	1208	HUMPHREY	62	HBC	$K^- p$ at rest

[1] We have increased the CHANG 66 error of 0.026; see our 1970 edition, Reviews of Modern Physics **42** 87 (1970).

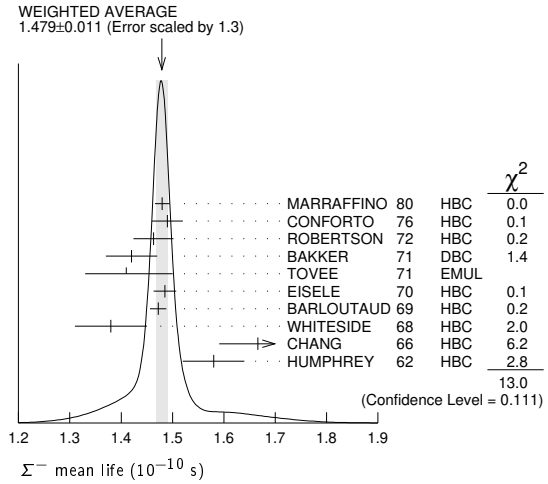

Σ^- MAGNETIC MOMENT

See the "Quark Model" review. Measurements with an error $\geq 0.3\ \mu_N$ have been omitted.

VALUE (μ_N)	EVTS	DOCUMENT ID		TECN	COMMENT
−1.160±0.025 OUR AVERAGE		Error includes scale factor of 1.7. See the ideogram below.			
−1.105±0.029±0.010		HERTZOG	88	CNTR	Σ^- Pb, Σ^- W atoms
−1.166±0.014±0.010	671k	ZAPALAC	86	SPEC	$ne^-\nu$, $n\pi^-$ decays
−1.23 ±0.03 ±0.03		WAH	85	CNTR	pCu $\to \Sigma^- X$
• • • We do not use the following data for averages, fits, limits, etc. • • •					
−0.89 ±0.14	516k	DECK	83	SPEC	pBe $\to \Sigma^- X$

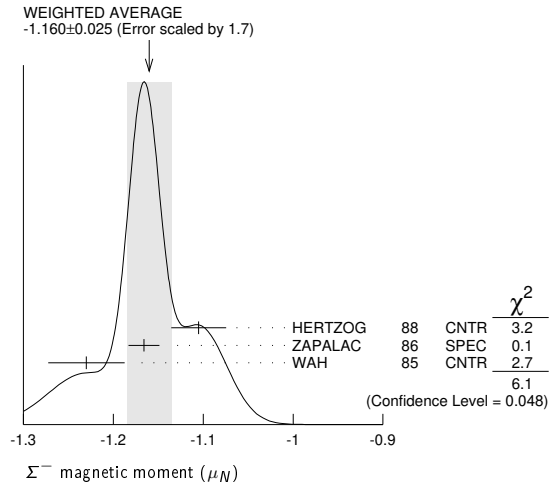

Σ^- CHARGE RADIUS

VALUE (fm)	DOCUMENT ID		TECN	COMMENT
0.780±0.080±0.060	[1] ESCHRICH	01	SELX	$\Sigma^- e \to \Sigma^- e$

[1] ESCHRICH 01 actually gives $\langle r^2 \rangle = (0.61 \pm 0.12 \pm 0.09)$ fm^2.

Σ^- DECAY MODES

	Mode		Fraction (Γ_i/Γ)	Confidence level
Γ_1	$n\pi^-$		(99.848±0.005) %	
Γ_2	$n\pi^-\gamma$	[a]	$(4.6 \pm 0.6) \times 10^{-4}$	
Γ_3	$ne^-\overline{\nu}_e$		$(1.017 \pm 0.034) \times 10^{-3}$	
Γ_4	$n\mu^-\overline{\nu}_\mu$		$(4.5 \pm 0.4) \times 10^{-4}$	
Γ_5	$\Lambda e^-\overline{\nu}_e$		$(5.73 \pm 0.27) \times 10^{-5}$	
Γ_6	$\Sigma^+ X$		$< 1.2 \times 10^{-4}$	90%
	Lepton number (L) violating modes			
Γ_7	pe^-e^-	L	$< 6.7 \times 10^{-5}$	90%

[a] See the Listings below for the pion momentum range used in this measurement.

Downloaded from https://academic.oup.com/ptep/article/2022/8/083C01/6651666 by KIT Library user on 27 September 2022

CONSTRAINED FIT INFORMATION

An overall fit to 3 branching ratios uses 16 measurements and one constraint to determine 4 parameters. The overall fit has a $\chi^2 =$ 8.7 for 13 degrees of freedom.

The following *off-diagonal* array elements are the correlation coefficients $\langle \delta x_i \delta x_j \rangle / (\delta x_i \cdot \delta x_j)$, in percent, from the fit to the branching fractions, $x_i \equiv \Gamma_i/\Gamma_{total}$. The fit constrains the x_i whose labels appear in this array to sum to one.

x_3	−64		
x_4	−77	0	
x_5	−5	0	0
	x_1	x_3	x_4

Σ^- BRANCHING RATIOS

$\Gamma(n\pi^-\gamma)/\Gamma(n\pi^-)$ — Γ_2/Γ_1

The π^+ momentum cuts differ, so we do not average the results but simply use the latest value for the Summary Table.

VALUE (units 10^{-3})	EVTS	DOCUMENT ID		TECN	COMMENT
0.46±0.06	292	EBENHOH	73	HBC	π^+ < 150 MeV/c
• • • We do not use the following data for averages, fits, limits, etc. • • •					
0.10±0.02	23	ANG	69B	HBC	π^- < 110 MeV/c
∼ 1.1		BAZIN	65B	HBC	π^- < 166 MeV/c

$\Gamma(ne^-\overline{\nu}_e)/\Gamma(n\pi^-)$ — Γ_3/Γ_1

Measurements with an error $\geq 0.2 \times 10^{-3}$ have been omitted.

VALUE (units 10^{-3})	EVTS	DOCUMENT ID		TECN	COMMENT
1.019±0.035 OUR FIT					
$1.019^{+0.031}_{-0.040}$ OUR AVERAGE					
0.96 ±0.05	2847	BOURQUIN	83C	SPEC	SPS hyperon beam
$1.09\ ^{+0.06}_{-0.08}$	601	[1] EBENHOH	74	HBC	K^-p at rest
$1.05\ ^{+0.07}_{-0.13}$	455	[1] SECHI-ZORN	73	HBC	K^-p at rest
0.97 ±0.15	57	COLE	71	HBC	K^-p at rest
1.11 ±0.09	180	BIERMAN	68	HBC	

[1] An additional negative systematic error is included for internal radiative corrections and latest form factors; see BOURQUIN 83C.

$\Gamma(n\mu^-\overline{\nu}_\mu)/\Gamma(n\pi^-)$ — Γ_4/Γ_1

VALUE (units 10^{-3})	EVTS	DOCUMENT ID		TECN	COMMENT
0.45±0.04 OUR FIT					
0.45±0.04 OUR AVERAGE					
0.38±0.11	13	COLE	71	HBC	K^-p at rest
0.43±0.06	72	ANG	69	HBC	K^-p at rest
0.43±0.09	56	BAGGETT	69	HBC	K^-p at rest
0.56±0.20	11	BAZIN	65B	HBC	K^-p at rest
0.66±0.15	22	COURANT	64	HBC	

$\Gamma(\Lambda e^-\overline{\nu}_e)/\Gamma(n\pi^-)$ — Γ_5/Γ_1

VALUE (units 10^{-4})	EVTS	DOCUMENT ID		TECN	COMMENT
0.574±0.027 OUR FIT					
0.574±0.027 OUR AVERAGE					
0.561±0.031	1620	[1] BOURQUIN	82	SPEC	SPS hyperon beam
0.63 ±0.11	114	THOMPSON	80	ASPK	Hyperon beam
0.52 ±0.09	31	BALTAY	69	HBC	K^-p at rest
0.69 ±0.12	31	EISELE	69	HBC	K^-p at rest
0.64 ±0.12	35	BARASH	67	HBC	K^-p at rest
0.75 ±0.28	11	COURANT	64	HBC	K^-p at rest

[1] The value is from BOURQUIN 83B, and includes radiation corrections and new acceptance.

$\Gamma(\Sigma^+X)/\Gamma_{total}$ — Γ_6/Γ

Here mode X can be any particle combination.

VALUE	CL%	DOCUMENT ID		TECN	COMMENT
$<1.2 \times 10^{-4}$	90	ABLIKIM	21F	BES	1,311 M J/ψ decays

Lepton number (L) violating modes

$\Gamma(pe^-e^-)/\Gamma_{total}$ — Γ_7/Γ

This decay violates lepton number conservation with $\Delta Q = \Delta L = 2$.

VALUE	CL%	DOCUMENT ID		TECN	COMMENT
$<6.7 \times 10^{-5}$	90	ABLIKIM	21F	BES	1,311 M J/ψ decays

Σ^- DECAY PARAMETERS

See the "Note on Baryon Decay Parameters" in the neutron Listings. Older, outdated results have been omitted.

α_- FOR $\Sigma^- \to n\pi^-$

VALUE	EVTS	DOCUMENT ID		TECN	COMMENT
−0.068±0.008 OUR AVERAGE					
−0.062±0.024	28k	HANSL	78	HBC	$K^-p \to \Sigma^-\pi^+$
−0.067±0.011	60k	BOGERT	70	HBC	K^-p 0.4 GeV/c
−0.071±0.012	51k	BANGERTER	69	HBC	K^-p 0.4 GeV/c

ϕ ANGLE FOR $\Sigma^- \to n\pi^-$ — ($\tan\phi = \beta / \gamma$)

VALUE (°)	EVTS	DOCUMENT ID		TECN	COMMENT
10±15 OUR AVERAGE					
+ 5±23	1092	[1] BERLEY	70B	HBC	n rescattering
14±19	1385	BANGERTER	69B	HBC	K^-p 0.4 GeV/c

[1] BERLEY 70B changed from −5 to +5° to agree with our sign convention.

g_A/g_V FOR $\Sigma^- \to ne^-\overline{\nu}_e$

Measurements with fewer than 500 events have been omitted. Where necessary, signs have been changed to agree with our conventions, which are given in the "Note on Baryon Decay Parameters" in the neutron Listings. What is actually listed is $|g_1/f_1 - 0.237 g_2/f_1|$. This reduces to $g_A/g_V \equiv g_1(0)/f_1(0)$ on making the usual assumption that $g_2 = 0$. See also the note on HSUEH 88.

VALUE	EVTS	DOCUMENT ID		TECN	COMMENT
0.340±0.017 OUR AVERAGE					
+0.327±0.007±0.019	50k	[1] HSUEH	88	SPEC	Σ^- 250 GeV
+0.34 ±0.05	4456	[2] BOURQUIN	83C	SPEC	SPS hyperon beam
0.385±0.037	3507	[3] TANENBAUM	74	ASPK	
• • • We do not use the following data for averages, fits, limits, etc. • • •					
0.29 ±0.07	25k	HSUEH	85	SPEC	See HSUEH 88
$0.17\ ^{+0.07}_{-0.09}$	519	DECAMP	77	ELEC	Hyperon beam

[1] The sign is, *with our conventions*, unambiguously positive. The value assumes, as usual, that $g_2 = 0$. If g_2 is included in the fit, than (with our sign convention) $g_2 = -0.56 \pm 0.37$, with a corresponding reduction of g_A/g_V to $+0.20 \pm 0.08$.

[2] BOURQUIN 83C favors the positive sign by at least 2.6 standard deviations.

[3] TANENBAUM 74 gives 0.435 ± 0.035, assuming no q^2 dependence in g_A and g_V. The listed result allows q^2 dependence, and is taken from HSUEH 88.

$f_2(0)/f_1(0)$ FOR $\Sigma^- \to ne^-\overline{\nu}_e$

The signs have been changed to be in accord with our conventions, given in the "Note on Baryon Decay Parameters" in the neutron Listings.

VALUE	EVTS	DOCUMENT ID		TECN	COMMENT
0.97±0.14 OUR AVERAGE					
+0.96±0.07±0.13	50k	HSUEH	88	SPEC	Σ^- 250 GeV
+1.02±0.34	4456	BOURQUIN	83C	SPEC	SPS hyperon beam

TRIPLE CORRELATION COEFFICIENT D for $\Sigma^- \to ne^-\overline{\nu}_e$

The coefficient D of the term $D\ \mathbf{P}\cdot(\hat{\mathbf{p}}_e \times \hat{\mathbf{p}}_\nu)$ in the $\Sigma^- \to ne^-\overline{\nu}$ decay angular distribution. A nonzero value would indicate a violation of time-reversal invariance.

VALUE	EVTS	DOCUMENT ID		TECN	COMMENT
0.11±0.10	50k	HSUEH	88	SPEC	Σ^- 250 GeV

g_V/g_A FOR $\Sigma^- \to \Lambda e^-\overline{\nu}_e$

For the sign convention, see the "Note on Baryon Decay Parameters" in the neutron Listings. The value is predicted to be zero by conserved vector current theory. The values averaged assume CVC-SU(3) weak magnetism term.

VALUE	EVTS	DOCUMENT ID		TECN	COMMENT
0.01 ±0.10 OUR AVERAGE Error includes scale factor of 1.5. See the ideogram below.					
−0.034±0.080	1620	[1] BOURQUIN	82	SPEC	SPS hyperon beam
−0.29 ±0.29	114	THOMPSON	80	ASPK	BNL hyperon beam
−0.17 ±0.35	55	TANENBAUM	75B	SPEC	BNL hyperon beam
+0.45 ±0.20	186	[1,2] FRANZINI	72	HBC	

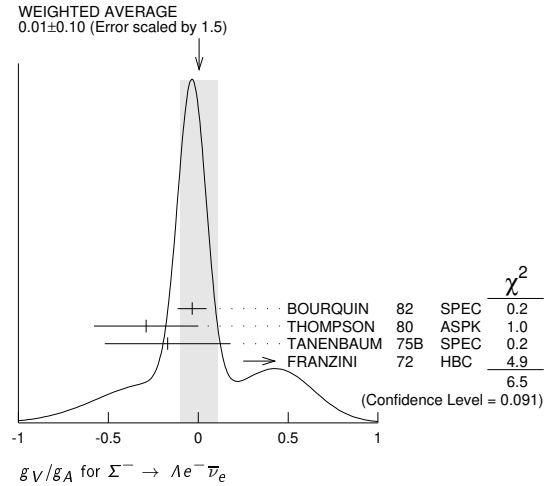

g_V/g_A for $\Sigma^- \to \Lambda e^-\overline{\nu}_e$

[1] The sign has been changed to agree with our convention.

Downloaded from https://academic.oup.com/ptep/article/2022/8/083C01/6651666 by KIT Library user on 27 September 2022

[2] The FRANZINI 72 value includes the events of earlier papers.

g_{WM}/g_A FOR $\Sigma^- \to \Lambda e^- \bar{\nu}_e$

The values quoted assume the CVC prediction $g_V = 0$.

VALUE	EVTS	DOCUMENT ID		TECN	COMMENT
2.4 ±1.7 OUR AVERAGE					
1.75±3.5	114	THOMPSON	80	ASPK	BNL hyperon beam
3.5 ±4.5	55	TANENBAUM	75B	SPEC	BNL hyperon beam
2.4 ±2.1	186	FRANZINI	72	HBC	

Σ^- REFERENCES

We have omitted some papers that have been superseded by later experiments. See our earlier editions.

ABLIKIM	21F	PR D103 052011	M. Ablikim et al.	(BESIII Collab.)
ESCHRICH	01	PL B522 233	I. Eschrich et al.	(FNAL SELEX Collab.)
GUREV	93	JETPL 57 400 Translated from ZETFP 57 389.	M.P. Gurev et al.	(PNPI)
GALL	88	PRL 60 186	K.P. Gall et al.	(BOST, MIT, WILL, CIT+)
HERTZOG	88	PR D37 1142	D.W. Hertzog et al.	(WILL, BOST, MIT+)
HSUEH	88	PR D38 2056	S.Y. Hsueh et al.	(CHIC, ELMT, FNAL+)
ZAPALAC	86	PRL 57 1526	G. Zapalac et al.	(EFI, ELMT, FNAL+)
HSUEH	85	PRL 54 2399	S.Y. Hsueh et al.	(CHIC, ELMT, FNAL+)
WAH	85	PRL 55 2551	Y.W. Wah et al.	(FNAL, IOWA, ISU)
BOURQUIN	83B	ZPHY C21 27	M.H. Bourquin et al.	(BRIS, GEVA, HEIDP+)
BOURQUIN	83C	ZPHY C21 17	M.H. Bourquin et al.	(BRIS, GEVA, HEIDP+)
DECK	83	PR D28 1	L. Deck et al.	(RUTG, WISC, MICH, MINN)
BOURQUIN	82	ZPHY C12 307	M.H. Bourquin et al.	(BRIS, GEVA, HEIDP+)
MARRAFFINO	80	PR D21 2501	J. Marraffino et al.	(VAND, MPIM)
THOMPSON	80	PR D21 25	J.A. Thompson et al.	(PITT, BNL)
HANSL	78	NP B132 45	T. Hansl et al.	(MPIM, VAND)
DECAMP	77	PL 66B 295	D. Decamp et al.	(LALO, EPOL)
CONFORTO	76	NP B105 189	B. Conforto et al.	(RHEL, LOIC)
DUGAN	75	NP A254 396	G. Dugan et al.	(COLU, YALE)
TANENBAUM	75B	PR D12 1871	W. Tanenbaum et al.	(YALE, FNAL, BNL)
EBENHOH	74	ZPHY 266 367	H. Ebenhoh et al.	(HEIDT)
TANENBAUM	74	PRL 33 175	W. Tanenbaum et al.	(YALE, FNAL, BNL)
EBENHOH	73	ZPHY 264 413	W. Ebenhoh et al.	(HEIDT)
SECHI-ZORN	73	PR D8 12	B. Sechi-Zorn, G.A. Snow	(UMD)
BOHM	72	NP B48 1	G. Bohm et al.	(BERL, KIDR, BRUX, IASD+)
FRANZINI	72	PR D6 2417	P. Franzini et al.	(COLU, HEID, UMD+)
ROBERTSON	72	Thesis UMI 78-00877	R.M. Robertson	(IIT)
BAKKER	71	LNC 1 37	A.M. Bakker et al.	(SABRE Collab.)
COLE	71	PR D4 631	J. Cole et al.	(STON, COLU)
Also		Thesis Nevis 175	H. Norton	(COLU)
TOVEE	71	NP B33 493	D.N. Tovee et al.	(LOUC, KIDR, BERL+)
BERLEY	70B	PR D1 2015	D. Berley et al.	(BNL, MASA, YALE)
BOGERT	70	PR D2 6	D.V. Bogert et al.	(BNL, MASA, YALE)
EISELE	70	ZPHY 238 372	F. Eisele et al.	(HEID)
PDG	70	RMP 42 87	A. Barbaro-Galtieri et al.	(LRL, BRAN+)
ANG	69	ZPHY 223 103	G. Ang et al.	(HEID)
ANG	69B	ZPHY 228 151	G. Ang et al.	(HEID)
BAGGETT	69	PRL 23 249	N.V. Baggett, B. Kehoe, G.A. Snow	(UMD)
BALTAY	69	PRL 22 615	C. Baltay et al.	(COLU, STON)
BANGERTER	69	Thesis UCRL 19244	R.O. Bangerter	(LRL)
BANGERTER	69B	PR 187 1821	R.O. Bangerter et al.	(LRL)
BARLOUTAUD	69	NP B14 153	R. Barloutaud et al.	(SACL, CERN, HEID)
EISELE	69	ZPHY 221 1	F. Eisele et al.	(HEID)
BIERMAN	68	PRL 20 1459	E. Bierman et al.	(PRIN)
HEPP	68	ZPHY 214 71	V. Hepp, H. Schleich	(HEID)
WHITESIDE	68	NC 54A 537	H. Whiteside, J. Gollub	(OBER)
BARASH	67	PRL 19 181	N. Barash et al.	(UMD)
CHANG	66	PR 151 1081	C.Y. Chang	(COLU)
BAZIN	65B	PR 140 B1358	M. Bazin et al.	(PRIN, RUTG, COLU)
DOSCH	65	PL 14 239	H.C. Dosch et al.	(HEID)
Also		PR 151 1081	C.Y. Chang	(COLU)
SCHMIDT	65	PR 140 B1328	P. Schmidt	(COLU)
BURNSTEIN	64	PRL 13 66	R.A. Burnstein et al.	(UMD)
COURANT	64	PR 136 B1791	H. Courant et al.	(CERN, HEID, UMD+)
BARKAS	63	PRL 11 26	W.H. Barkas, J.N. Dyer, H.H. Heckman	(LRL)
HUMPHREY	62	PR 127 1305	W.E. Humphrey, R.R. Ross	(LRL)

$\Sigma(1385)\ 3/2^+$

$I(J^P) = 1(\frac{3}{2}^+)$ Status: ****

Discovered by ALSTON 60. Early measurements of the mass and width for combined charge states have been omitted. They may be found in our 1984 edition Reviews of Modern Physics **56** S1 (1984).

We average only the most significant determinations. We do not average results from inclusive experiments with large backgrounds or results which are not accompanied by some discussion of experimental resolution. Nevertheless systematic differences between experiments remain. (See the ideograms in the Listings below.) These differences could arise from interference effects that change with production mechanism and/or beam momentum. They can also be accounted for in part by differences in the parametrizations employed. (See BORENSTEIN 74 for a discussion on this point.) Thus BORENSTEIN 74 uses a Breit-Wigner with energy-independent width, since a P-wave was found to give unsatisfactory fits. CAMERON 78 uses the same form. On the other hand HOLMGREN 77 obtains a good fit to their $\Lambda\pi$ spectrum with a P-wave Breit-Wigner, but includes the partial width for the $\Sigma\pi$ decay mode in the parametrization. AGUILAR-BENITEZ 81D gives masses and widths for five different Breit-Wigner shapes. The results vary considerably. Only the best-fit S-wave results are given here.

$\Sigma(1385)$ POLE POSITIONS

$\Sigma(1385)^+$ REAL PART

VALUE	DOCUMENT ID	COMMENT
1379±1	LICHTENBERG74	Extrapolates HABIBI 73

$\Sigma(1385)^+$ −IMAGINARY PART

VALUE	DOCUMENT ID	COMMENT
17.5±1.5	LICHTENBERG74	Extrapolates HABIBI 73

$\Sigma(1385)^-$ REAL PART

VALUE	DOCUMENT ID	COMMENT
1383±1	LICHTENBERG74	Extrapolates HABIBI 73

$\Sigma(1385)^-$ −IMAGINARY PART

VALUE	DOCUMENT ID	COMMENT
22.5±1.5	LICHTENBERG74	Extrapolates HABIBI 73

$\Sigma(1385)$ MASSES

$\Sigma(1385)^+$ MASS

VALUE (MeV)	EVTS	DOCUMENT ID		TECN	COMMENT
1382.83±0.34 OUR AVERAGE		Error includes scale factor of 1.9. See the ideogram below.			
1384.8 ±0.3 ±1.4		LEE	21A	BELL	$\Lambda_c^+ \to \eta\Sigma(1385)^+$
1383.2 ±0.9 $^{+0.1}_{-1.5}$		AGAKISHIEV	12	SPEC	$pp \to \Sigma(1385)^+ K^+ n$, 3.5 GeV
1384.1 ±0.7	1897	BAUBILLIER	84	HBC	$K^- p$ 8.25 GeV/c
1384.5 ±0.5	5256	AGUILAR-...	81D	HBC	$K^- p \to \Lambda\pi\pi$ 4.2 GeV/c
1383.0 ±0.4	9361	AGUILAR-...	81D	HBC	$K^- p \to \Lambda 3\pi$ 4.2 GeV/c
1381.9 ±0.3	6900	CAMERON	78	HBC	$K^- p$ 0.96–1.36 GeV/c
1381 ±1	6846	BORENSTEIN	74	HBC	$K^- p$ 2.18 GeV/c
1383.5 ±0.85	2300	HABIBI	73	HBC	$K^- p \to \Lambda\pi\pi$
1382 ±2	400	AGUILAR-...	72B	HBC	$K^- p \to \Lambda\pi$'s
1384.4 ±1.0	1260	SIEGEL	67	HBC	$K^- p$ 2.1 GeV/c
1382 ±1	750	ARMENTEROS	65B	HBC	$K^- p$ 0.9–1.2 GeV/c
1381.0 ±1.6	859	HUWE	64	HBC	$K^- p$ 1.22 GeV/c
• • • We do not use the following data for averages, fits, limits, etc. • • •					
1385.1 ±1.2	600	BAKER	80	HYBR	$\pi^+ p$ 7 GeV/c
1383.2 ±1.0	750	BAKER	80	HYBR	$K^- p$ 7 GeV/c
1381 ±2	7k	[1] BAUBILLIER	79B	HBC	$K^- p$ 8.25 GeV/c
1391 ±2	2k	CAUTIS	79	HYBR	$\pi^+ p/K^- p$ 11.5 GeV
1390 ±2	100	[1] SUGAHARA	79B	HBC	$\pi^- p$ 6 GeV/c
1385 ±3	22k	[1,2] BARREIRO	77B	HBC	$K^- p$ 4.2 GeV/c
1385 ±1	2594	HOLMGREN	77	HBC	See AGUILAR-BENITEZ 81D
1380 ±2		[1] BARDADIN-...	75	HBC	$K^- p$ 14.3 GeV/c
1382 ±1	3740	[3] BERTHON	74	HBC	$K^- p$ 1263–1843 MeV/c
1390 ±6	46	AGUILAR-...	70B	HBC	$K^- p \to \Sigma\pi$'s 4 GeV/c
1383 ±8	62	[4] BIRMINGHAM	66	HBC	$K^- p$ 3.5 GeV/c
1378 ±5	135	LONDON	66	HBC	$K^- p$ 2.24 GeV/c
1384.3 ±1.9	250	[4] SMITH	65	HBC	$K^- p$ 1.8 GeV/c
1382.6 ±2.1	250	[4] SMITH	65	HBC	$K^- p$ 1.95 GeV/c
1375.0 ±3.9	170	COOPER	64	HBC	$K^- p$ 1.45 GeV/c
1376.0 ±3.9	154	[4] ELY	61	HLBC	$K^- p$ 1.11 GeV/c

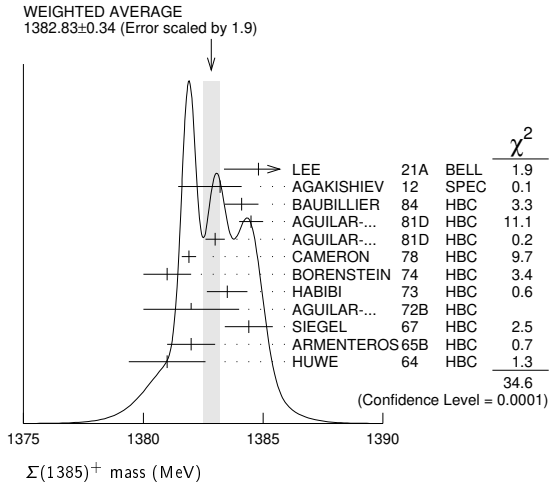

$\Sigma(1385)^0$ MASS

VALUE (MeV)	EVTS	DOCUMENT ID		TECN	COMMENT
1383.7±1.0 OUR AVERAGE		Error includes scale factor of 1.4. See the ideogram below.			
1384.1±0.8	5722	AGUILAR-...	81D	HBC	$K^- p \to \Lambda 3\pi$ 4.2 GeV/c
1380 ±2	3100	[5] BORENSTEIN	74	HBC	$K^- p \to \Lambda 3\pi$ 2.18 GeV/c
1385.1±2.5	240	[4] THOMAS	73	HBC	$\pi^- p \to \Lambda\pi^0 K^0$
• • • We do not use the following data for averages, fits, limits, etc. • • •					
1389 ±3	500	[6] BAUBILLIER	79B	HBC	$K^- p$ 8.25 GeV/c

Downloaded from https://academic.oup.com/ptep/article/2022/8/083C01/6651666 by KIT Library user on 27 September 2022

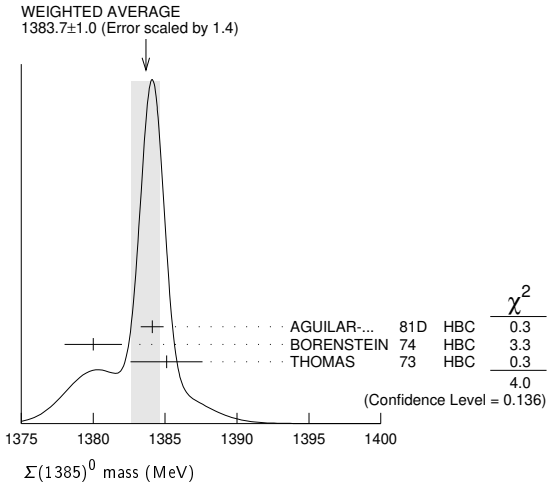

$\Sigma(1385)^-$ MASS

VALUE (MeV)	EVTS	DOCUMENT ID		TECN	COMMENT
1387.2±0.5 OUR AVERAGE		Error includes scale factor of 2.2. See the ideogram below.			
1388.3±1.7	620	AGUILAR-...	81D	HBC	$K^- p \to \Lambda \pi\pi$ 4.2 GeV/c
1384.9±0.8	3346	AGUILAR-...	81D	HBC	$K^- p \to \Lambda 3\pi$ 4.2 GeV/c
1387.6±0.3	9720	CAMERON	78	HBC	$K^- p$ 0.96–1.36 GeV/c
1383 ±2	2303	BORENSTEIN	74	HBC	$K^- p$ 2.18 GeV/c
1390.7±1.2	1900	HABIBI	73	HBC	$K^- p \to \Lambda \pi\pi$
1387.1±1.9	630	[4] THOMAS	73	HBC	$\pi^- p \to \Lambda \pi^- K^+$
1390.7±2.0	370	SIEGEL	67	HBC	$K^- p$ 2.1 GeV/c
1384 ±1	1380	ARMENTEROS	65B	HBC	$K^- p$ 0.9–1.2 GeV/c
1385.3±1.9	1086	[4] HUWE	64	HBC	$K^- p$ 1.15–1.30 GeV/c
• • • We do not use the following data for averages, fits, limits, etc. • • •					
1383 ±1	4.5k	[1] BAUBILLIER	79B	HBC	$K^- p$ 8.25 GeV/c
1380 ±6	150	[1] SUGAHARA	79B	HBC	$\pi^- p$ 6 GeV/c
1387 ±3	12k	[1,2] BARREIRO	77B	HBC	$K^- p$ 4.2 GeV/c
1391 ±3	193	HOLMGREN	77	HBC	See AGUILAR-BENITEZ 81D
1383 ±2		[1] BARDADIN-...	75	HBC	$K^- p$ 14.3 GeV/c
1389 ±1	3060	[3] BERTHON	74	HBC	$K^- p$ 1263–1843 MeV/c
1389 ±9	15	LONDON	66	HBC	$K^- p$ 2.24 GeV/c
1391.5±2.6	120	[4] SMITH	65	HBC	$K^- p$ 1.8 GeV/c
1399.8±2.2	58	[4] SMITH	65	HBC	$K^- p$ 1.95 GeV/c
1392.0±6.2	200	COOPER	64	HBC	$K^- p$ 1.45 GeV/c
1382 ±3	93	DAHL	61	DBC	$K^- d$ 0.45 GeV/c
1376.0±4.4	224	[4] ELY	61	HLBC	$K^- p$ 1.11 GeV/c

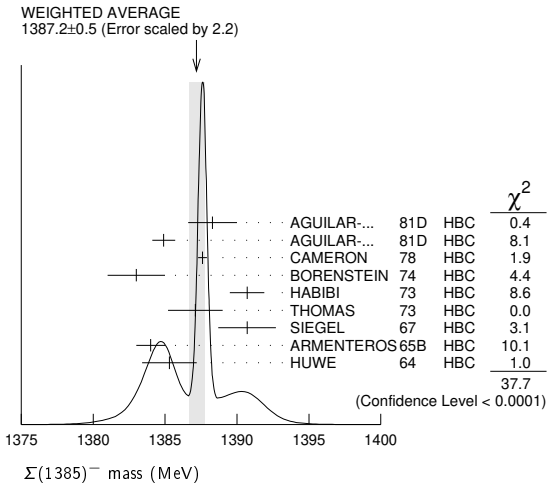

$m_{\Sigma(1385)^-} - m_{\Sigma(1385)^+}$

VALUE (MeV)	CL%	DOCUMENT ID		TECN	COMMENT
• • • We do not use the following data for averages, fits, limits, etc. • • •					
−2 to +6	95	[7] BORENSTEIN	74	HBC	$K^- p$ 2.18 GeV/c
7.2±1.4		[7] HABIBI	73	HBC	$K^- p \to \Lambda \pi\pi$
6.3±2.0		[7] SIEGEL	67	HBC	$K^- p$ 2.1 GeV/c
11 ±9		[7] LONDON	66	HBC	$K^- p$ 2.24 GeV/c
9 ±6		LONDON	66	HBC	$\Lambda 3\pi$ events
2.0±1.5		[7] ARMENTEROS	65B	HBC	$K^- p$ 0.9–1.2 GeV/c
7.2±2.1		[7] SMITH	65	HBC	$K^- p$ 1.8 GeV/c
17.2±2.0		[7] SMITH	65	HBC	$K^- p$ 1.95 GeV/c
17 ±7		[7] COOPER	64	HBC	$K^- p$ 1.45 GeV/c
4.3±2.2		[7] HUWE	64	HBC	$K^- p$ 1.22 GeV/c
0.0±4.2		[7] ELY	61	HLBC	$K^- p$ 1.11 GeV/c

$m_{\Sigma(1385)^0} - m_{\Sigma(1385)^+}$

VALUE (MeV)	CL%	DOCUMENT ID		TECN	COMMENT
• • • We do not use the following data for averages, fits, limits, etc. • • •					
−4 to +4	95	[7] BORENSTEIN	74	HBC	$K^- p$ 2.18 GeV/c

$m_{\Sigma(1385)^-} - m_{\Sigma(1385)^0}$

VALUE (MeV)	DOCUMENT ID		TECN	COMMENT
• • • We do not use the following data for averages, fits, limits, etc. • • •				
2.0±2.4	[7] THOMAS	73	HBC	$\pi^- p \to \Lambda \pi^- K^+$

$\Sigma(1385)$ WIDTHS

$\Sigma(1385)^+$ WIDTH

VALUE (MeV)	EVTS	DOCUMENT ID		TECN	COMMENT
36.2± 0.7 OUR AVERAGE					
38.1± 1.5±2.1		LEE	21A	BELL	$\Lambda_c^+ \to \eta \Sigma(1385)^+$
40.2± $2.1^{+1.2}_{-2.8}$		AGAKISHIEV	12	SPEC	$pp \to \Sigma(1385)^+ K^+ n$, 3.5 GeV
37.2± 2.0	1897	BAUBILLIER	84	HBC	$K^- p$ 8.25 GeV/c
35.1± 1.7	5256	AGUILAR-...	81D	HBC	$K^- p \to \Lambda \pi\pi$ 4.2 GeV/c
37.5± 2.0	9361	AGUILAR-...	81D	HBC	$K^- p \to \Lambda 3\pi$ 4.2 GeV/c
35.5± 1.9	6900	CAMERON	78	HBC	$K^- p$ 0.96–1.36 GeV/c
34.0± 1.6	6846	[8] BORENSTEIN	74	HBC	$K^- p$ 2.18 GeV/c
38.3± 3.2	2300	[9] HABIBI	73	HBC	$K^- p \to \Lambda \pi\pi$
32.5± 6.0	400	AGUILAR-...	72B	HBC	$K^- p \to \Lambda \pi$'s
36 ± 4	1260	[9] SIEGEL	67	HBC	$K^- p$ 2.1 GeV/c
32.0± 4.7	750	[9] ARMENTEROS	65B	HBC	$K^- p$ 0.95–1.20 GeV/c
46.5± 6.4	859	[9] HUWE	64	HBC	$K^- p$ 1.15–1.30 GeV/c
• • • We do not use the following data for averages, fits, limits, etc. • • •					
40 ± 3	600	BAKER	80	HYBR	$\pi^+ p$ 7 GeV/c
37 ± 2	750	BAKER	80	HYBR	$K^- p$ 7 GeV/c
37 ± 2	7k	[1] BAUBILLIER	79B	HBC	$K^- p$ 8.25 GeV/c
30 ± 4	2k	CAUTIS	79	HYBR	$\pi^+ p / K^- p$ 11.5 GeV
30 ± 6	100	[1] SUGAHARA	79B	HBC	$\pi^- p$ 6 GeV/c
43 ± 5	22k	[1,2] BARREIRO	77B	HBC	$K^- p$ 4.2 GeV/c
34 ± 2	2594	HOLMGREN	77	HBC	See AGUILAR-BENITEZ 81D
40.0± 3.2		[1] BARDADIN-...	75	HBC	$K^- p$ 14.3 GeV/c
48 ± 3	3740	[3] BERTHON	74	HBC	$K^- p$ 1263–1843 MeV/c
33 ±20	46	[9] AGUILAR-...	70B	HBC	$K^- p \to \Sigma \pi$'s 4 GeV/c
25 ±32	62	[9] BIRMINGHAM	66	HBC	$K^- p$ 3.5 GeV/c
30.3± 7.5	250	[9] SMITH	65	HBC	$K^- p$ 1.8 GeV/c
33.1± 8.3	250	[9] SMITH	65	HBC	$K^- p$ 1.95 GeV/c
51 ±16	170	[9] COOPER	64	HBC	$K^- p$ 1.45 GeV/c
48 ±16	154	[9] ELY	61	HLBC	$K^- p$ 1.11 GeV/c

$\Sigma(1385)^0$ WIDTH

VALUE (MeV)	EVTS	DOCUMENT ID		TECN	COMMENT
36 ± 5 OUR AVERAGE					
34.8± 5.6	5722	AGUILAR-...	81D	HBC	$K^- p \to \Lambda 3\pi$ 4.2 GeV/c
39.3±10.2	240	[9] THOMAS	73	HBC	$\pi^- p \to \Lambda \pi^0 K^0$
• • • We do not use the following data for averages, fits, limits, etc. • • •					
53 ± 8	3100	[10] BORENSTEIN	74	HBC	$K^- p \to \Lambda 3\pi$ 2.18 GeV/c
30 ± 9	106	CURTIS	63	OSPK	$\pi^- p$ 1.5 GeV/c

$\Sigma(1385)^-$ WIDTH

VALUE (MeV)	EVTS	DOCUMENT ID		TECN	COMMENT
39.4± 2.1 OUR AVERAGE		Error includes scale factor of 1.7. See the ideogram below.			
38.4±10.7	620	AGUILAR-...	81D	HBC	$K^- p \to \Lambda \pi\pi$ 4.2 GeV/c
34.6± 4.2	3346	AGUILAR-...	81D	HBC	$K^- p \to \Lambda 3\pi$ 4.2 GeV/c
39.2± 1.7	9720	CAMERON	78	HBC	$K^- p$ 0.96–1.36 GeV/c
35 ± 3	2303	[8] BORENSTEIN	74	HBC	$K^- p$ 2.18 GeV/c
51.9± 4.8	1900	[9] HABIBI	73	HBC	$K^- p \to \Lambda \pi\pi$
48.2± 7.7	630	[9] THOMAS	73	HBC	$\pi^- p \to \Lambda \pi^- K^0$
31.0± 6.5	370	[9] SIEGEL	67	HBC	$K^- p$ 2.1 GeV/c
38.0± 4.1	1382	[9] ARMENTEROS	65B	HBC	$K^- p$ 0.95–1.20 GeV/c
62 ± 7	1086	HUWE	64	HBC	$K^- p$ 1.15–1.30 GeV/c
• • • We do not use the following data for averages, fits, limits, etc. • • •					
44 ± 4	4.5k	[1] BAUBILLIER	79B	HBC	$K^- p$ 8.25 GeV/c
58 ± 4	150	[1] SUGAHARA	79B	HBC	$\pi^- p$ 6 GeV/c
45 ± 5	12k	[1,2] BARREIRO	77B	HBC	$K^- p$ 4.2 GeV/c
35 ±10	193	HOLMGREN	77	HBC	See AGUILAR-BENITEZ 81D
47 ± 6		[1] BARDADIN-...	75	HBC	$K^- p$ 14.3 GeV/c
40 ± 3	3060	[3] BERTHON	74	HBC	$K^- p$ 1263–1843 MeV/c

Downloaded from https://academic.oup.com/ptep/article/2022/8/083C01/6651666 by KIT Library user on 27 September 2022

29.2±10.6	120	[9] SMITH	65	HBC	$K^- p$ 1.80 GeV/c
17.1± 8.9	58	[9] SMITH	65	HBC	$K^- p$ 1.95 GeV/c
88 ±24	200	[9] COOPER	64	HBC	$K^- p$ 1.45 GeV/c
40		DAHL	61	DBC	$K^- d$ 0.45 GeV/c
66 ±18	224	[9] ELY	61	HLBC	$K^- p$ 1.11 GeV/c

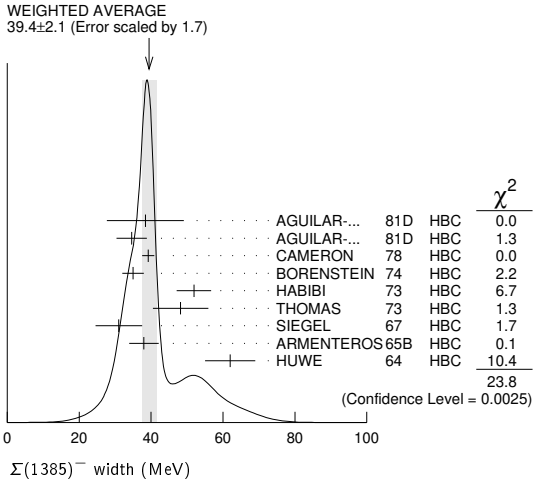

$\Sigma(1385)$ DECAY MODES

	Mode	Fraction (Γ_i/Γ)	Confidence level
Γ_1	$\Lambda\pi$	(87.0 ±1.5) %	
Γ_2	$\Sigma\pi$	(11.7 ±1.5) %	
Γ_3	$\Lambda\gamma$	($1.25^{+0.13}_{-0.12}$) %	
Γ_4	$\Sigma^+\gamma$	(7.0 ±1.7) $\times 10^{-3}$	
Γ_5	$\Sigma^-\gamma$	< 2.4 $\times 10^{-4}$	90%
Γ_6	$N\overline{K}$		

$\Sigma(1385)$ BRANCHING RATIOS

$\Gamma(\Sigma\pi)/\Gamma(\Lambda\pi)$ — Γ_2/Γ_1

VALUE	DOCUMENT ID		TECN	CHG	COMMENT
0.135±0.011 OUR AVERAGE					
0.20 ±0.06	DIONISI	78B	HBC	±	$K^- p \to Y^* K\overline{K}$
0.16 ±0.03	BERTHON	74	HBC	+	$K^- p$ 1.26–1.84 GeV/c
0.11 ±0.02	BERTHON	74	HBC	−	$K^- p$ 1.26–1.84 GeV/c
0.21 ±0.05	BORENSTEIN	74	HBC	+	$K^- p \to \Lambda\pi^+\pi^-$, $\Sigma^0\pi^+\pi^-$
0.18 ±0.04	MAST	73	MPWA	±	$K^- p \to \Lambda\pi^+\pi^-$, $\Sigma^0\pi^+\pi^-$
0.10 ±0.05	THOMAS	73	HBC	−	$\pi^- p \to \Lambda K\pi$, $\Sigma K\pi$
0.16 ±0.07	AGUILAR-...	72B	HBC	+	$K^- p$ 3.9, 4.6 GeV/c
0.13 ±0.04	COLLEY	71B	DBC	−0	$K^- N$ 1.5 GeV/c
0.13 ±0.04	PAN	69	HBC	+	$\pi^+ p \to \Lambda K\pi$, $\Sigma K\pi$
0.08 ±0.06	LONDON	66	HBC	+	$K^- p$ 2.24 GeV/c
0.163±0.041	ARMENTEROS	65B	HBC	±	$K^- p$ 0.95–1.20 GeV/c
0.09 ±0.04	HUWE	64	HBC	±	$K^- p$ 1.2–1.7 GeV
• • • We do not use the following data for averages, fits, limits, etc. • • •					
<0.04	ALSTON	62	HBC	±0	$K^- p$ 1.15 GeV/c
0.04 ±0.04	BASTIEN	61	HBC	±	

$\Gamma(\Lambda\gamma)/\Gamma(\Lambda\pi)$ — Γ_3/Γ_1

This ratio is of course for $\Sigma(1385)^0 \to \Lambda\gamma$ and $\Lambda\pi^0$.

VALUE (units 10^{-2})	EVTS	DOCUMENT ID		TECN	COMMENT
$1.43^{+0.15}_{-0.13}$ OUR AVERAGE					
$1.42\pm0.12^{+0.11}_{-0.07}$	624 ± 25	KELLER	11	CLAS	$\gamma p \to K^+\Lambda\gamma$, E_γ 1.6–3.8 GeV
$1.53\pm0.39^{+0.15}_{-0.24}$	61	TAYLOR	05	CLAS	$\gamma p \to K^+\Lambda\gamma$

$\Gamma(\Sigma^+\gamma)/\Gamma(\Sigma\pi)$ — Γ_4/Γ_2

This ratio is for $\Sigma(1385)^+ \to \Sigma^+\gamma$ over $\Sigma(1385)^+ \to \Sigma\pi$.

VALUE (%)	DOCUMENT ID		TECN	COMMENT
$5.98\pm1.11^{+0.27}_{-0.61}$	[11] KELLER	12	CLAS	$\gamma p \to K^0\Sigma(1385)^+$

$\Gamma(\Sigma^-\gamma)/\Gamma_{total}$ — Γ_5/Γ

VALUE	CL%	DOCUMENT ID		TECN	CHG	COMMENT
$<2.4\times10^{-4}$	90	[12] MOLCHANOV	04	SELX	−	$\Sigma^- Pb \to \Sigma(1385)^- Pb$, 600 GeV
• • • We do not use the following data for averages, fits, limits, etc. • • •						
$<6.1\times10^{-4}$	90	[13] ARIK	77	SPEC	−	$\Sigma^- Pb \to \Sigma(1385)^- Pb$, 23 GeV

$(\Gamma_i\Gamma_f)^{1/2}/\Gamma_{total}$ in $N\overline{K} \to \Sigma(1385) \to \Lambda\pi$ — $(\Gamma_6\Gamma_1)^{1/2}/\Gamma$

VALUE	DOCUMENT ID		CHG	COMMENT
+0.586±0.319	[14] DEVENISH	74B	0	Fixed-t dispersion rel.

$\Sigma(1385)$ FOOTNOTES

[1] From fit to inclusive $\Lambda\pi$ spectrum.
[2] Includes data of HOLMGREN 77.
[3] The errors are statistical only. The resolution is not unfolded.
[4] The error is enlarged to $\Gamma/\sqrt{N}$. See the note on the $K^*(892)$ mass in the 1984 edition.
[5] From a fit to $\Lambda\pi^0$ with the width fixed at 34 MeV.
[6] From fit to inclusive $\Lambda\pi^0$ spectrum with the width fixed at 40 MeV.
[7] Redundant with data in the mass Listings.
[8] Results from $\Lambda\pi^+\pi^-$ and $\Lambda\pi^+\pi^-\pi^0$ combined by us.
[9] The error is enlarged to $4\Gamma/\sqrt{N}$. See the note on the $K^*(892)$ mass in the 1984 edition.
[10] Consistent with +, 0, and − widths equal.
[11] KELLER 12 gives $\Gamma(\Sigma^+\gamma)/\Gamma(\Sigma^+\pi^0) = (11.95 \pm 2.21^{+0.53}_{-1.21})$%, using 1/2 our total $\Sigma(1385) \to \Sigma\pi$ fraction for $\Sigma^+\pi^0$. We divide the KELLER 12 value by two.
[12] We calculate this from the MOLCHANOV 04 upper limit of 9.5 keV on the $\Sigma^-\gamma$ width.
[13] We calculate this from the ARIK 77 upper limit of 24 keV on the $\Sigma^-\gamma$ width.
[14] An extrapolation of the parametrized amplitude below threshold.

$\Sigma(1385)$ REFERENCES

LEE	21A	PR D103 052005	J.Y. Lee *et al.*	(BELLE Collab.)
AGAKISHIEV	12	PR C85 035203	G. Agakishiev *et al.*	(HADES Collab.)
KELLER	12	PR D85 052004	D. Keller *et al.*	(JLab CLAS Collab.)
KELLER	11	PR D83 072004	D. Keller *et al.*	(JLab CLAS Collab.)
TAYLOR	05	PR C71 054609	S. Taylor *et al.*	(JLab CLAS Collab.)
Also		PR C72 039902 (errat.)	S. Taylor *et al.*	(JLab CLAS Collab.)
MOLCHANOV	04	PL B590 161	V.V. Molchanov *et al.*	(FNAL SELEX Collab.)
BAUBILLIER	84	ZPHY C23 213	M. Baubillier *et al.*	(BIRM, CERN, GLAS+)
PDG	84	RMP 56 S1	C.G. Wohl *et al.*	(LBL, CIT, CERN)
AGUILAR-...	81D	AFIS A77 144	M. Aguilar-Benitez, J. Salicio	(MADR)
BAKER	80	NP B166 207	P.A. Baker *et al.*	(LOIC)
BAUBILLIER	79B	NP B148 18	M. Baubillier *et al.*	(BIRM, CERN, GLAS+)
CAUTIS	79	NP B156 507	C.V. Cautis *et al.*	(SLAC)
SUGAHARA	79B	NP B156 237	R. Sugahara *et al.*	(KEK, OSKC, KINK)
CAMERON	78	NP B143 189	W. Cameron *et al.*	(RHEL, LOIC)
DIONISI	78B	PL 78B 154	C. Dionisi, R. Armenteros, J. Diaz	(CERN, AMST+)
ARIK	77	PRL 38 1000	E. Arik *et al.*	(PITT, BNL, MASA)
BARREIRO	77B	NP B126 319	F. Barreiro *et al.*	(CERN, AMST, NIJM)
HOLMGREN	77	NP B119 261	S.O. Holmgren *et al.*	(CERN, AMST, NIJM)
BARDADIN-...	75	NP B98 418	M. Bardadin-Otwinowska *et al.*	(SACL, EPOL+)
BERTHON	74	NC 21A 146	A. Berthon *et al.*	(CDEF, RHEL, SACL+)
BORENSTEIN	74	PR D9 3006	S.R. Borenstein *et al.*	(BNL, MICH)
DEVENISH	74B	NP B81 330	R.C.E. Devenish, C.D. Froggatt, B.R. Martin	(DESY+)
LICHTENBERG	74	PR D10 3865	D.B. Lichtenberg	(IND)
Also		Private Comm.	D.B. Lichtenberg	(IND)
HABIBI	73	Thesis Nevis 199	M. Habibi	(COLU)
Also		Purdue Conf. 387	C. Baltay *et al.*	(COLU, BING)
MAST	73	PR D7 3212	T.S. Mast *et al.*	(LBL) IJP
Also		PR D7 5	T.S. Mast *et al.*	(LBL) IJP
THOMAS	73	NP B56 15	D.W. Thomas *et al.*	(CMU) JP
AGUILAR-...	72B	PR D6 29	M. Aguilar-Benitez *et al.*	(BNL)
COLLEY	71B	NP B31 61	D.C. Colley *et al.*	(BIRM, EDIN, GLAS+)
AGUILAR-...	70B	PRL 25 58	M. Aguilar-Benitez *et al.*	(BNL, SYRA)
PAN	69	PRL 23 808	Y.L. Pan, F.L. Forman	(PENN) I
SIEGEL	67	Thesis UCRL 18041	D.M. Siegel	(LRL)
BIRMINGHAM	66	PR 152 1148	M. Haque *et al.*	(BIRM, GLAS, LOIC, OXF+)
LONDON	66	PR 143 1034	G.W. London *et al.*	(BNL, SYRA) J
ARMENTEROS	65B	PL 19 75	R. Armenteros *et al.*	(CERN, HEID, SACL)
SMITH	65	Thesis UCLA	L.T. Smith	(UCLA)
COOPER	64	PL 8 365	W.A. Cooper *et al.*	(CERN, AMST)
HUWE	64	Thesis UCRL 11291	D.O. Huwe	(LRL) JP
Also		PR 181 1824	D.O. Huwe	(LRL)
CURTIS	63	PR 132 1771	L.J. Curtis *et al.*	(MICH) J
ALSTON	62	CERN Conf. 311	M.H. Alston *et al.*	(LRL)
BASTIEN	61	PRL 6 702	P.L. Bastien, M. Ferro-Luzzi, A.H. Rosenfeld	(LRL)
DAHL	61	PRL 6 142	O.I. Dahl *et al.*	(LRL)
ELY	61	PRL 7 461	R.P. Ely *et al.*	(LRL) J
ALSTON	60	PRL 5 520	M.H. Alston *et al.*	(LRL) I

$\Sigma(1580)\ 3/2^-$

$I(J^P) = 1(\frac{3}{2}^-)$ Status: *

OMITTED FROM SUMMARY TABLE

Seen in the isospin-1 $\overline{K}N$ cross section at BNL (LI 73, CARROLL 76) and in a partial-wave analysis of $K^- p \to \Lambda\pi^0$ for c.m. energies 1560–1600 MeV by LITCHFIELD 74. LITCHFIELD 74 finds $J^P = 3/2^-$. Not seen by ENGLER 78, CAMERON 78C, OLMSTED 04, nor by PRAKHOV 04.

Neither ZHANG 13A nor SARANTSEV 19 see any evidence for this state.

$\Sigma(1580)$ POLE POSITION

REAL PART

VALUE (MeV)	DOCUMENT ID		TECN	COMMENT
• • • We do not use the following data for averages, fits, limits, etc. • • •				
1607^{+13}_{-11}	[1] KAMANO	15	DPWA	Multichannel

[1] From the preferred solution A in KAMANO 15. Solution B reports M = 1492^{+4}_{-7} MeV.

−2×IMAGINARY PART

VALUE (MeV)	DOCUMENT ID		TECN	COMMENT
• • • We do not use the following data for averages, fits, limits, etc. • • •				
253^{+30}_{-18}	[2] KAMANO	15	DPWA	Multichannel

[2] From the preferred solution A in KAMANO 15. Solution B reports M = 138^{+8}_{-14} MeV.

Downloaded from https://academic.oup.com/ptep/article/2022/8/083C01/6651666 by KIT Library user on 27 September 2022

$\Sigma(1580)$ POLE RESIDUES

The "normalized residue" is the residue divided by $\Gamma_{pole}/2$.

Normalized residue in $N\overline{K} \to \Sigma(1580) \to N\overline{K}$

MODULUS	PHASE (°)	DOCUMENT ID		TECN	COMMENT
• • • We do not use the following data for averages, fits, limits, etc. • • •					
0.00778	51	[3] KAMANO	15	DPWA	Multichannel

[3] From the preferred solution A in KAMANO 15.

Normalized residue in $N\overline{K} \to \Sigma(1580) \to \Sigma\pi$

MODULUS	PHASE (°)	DOCUMENT ID		TECN	COMMENT
• • • We do not use the following data for averages, fits, limits, etc. • • •					
0.0625	−6	[4] KAMANO	15	DPWA	Multichannel

[4] From the preferred solution A in KAMANO 15.

Normalized residue in $N\overline{K} \to \Sigma(1580) \to \Lambda\pi$

MODULUS	PHASE (°)	DOCUMENT ID		TECN	COMMENT
• • • We do not use the following data for averages, fits, limits, etc. • • •					
0.059	156	[5] KAMANO	15	DPWA	Multichannel

[5] From the preferred solution A in KAMANO 15.

Normalized residue in $N\overline{K} \to \Sigma(1580) \to \Sigma(1385)\pi$, S-wave

MODULUS	PHASE (°)	DOCUMENT ID		TECN	COMMENT
• • • We do not use the following data for averages, fits, limits, etc. • • •					
0.0368	−18	[6] KAMANO	15	DPWA	Multichannel

[6] From the preferred solution A in KAMANO 15.

Normalized residue in $N\overline{K} \to \Sigma(1580) \to \Sigma(1385)\pi$, D-wave

MODULUS	PHASE (°)	DOCUMENT ID		TECN	COMMENT
• • • We do not use the following data for averages, fits, limits, etc. • • •					
0.0103	123	[7] KAMANO	15	DPWA	Multichannel

[7] From the preferred solution A in KAMANO 15.

$\Sigma(1580)$ MASS

VALUE (MeV)	DOCUMENT ID		TECN	COMMENT
≈ 1580 OUR ESTIMATE				
1583±4	[8] CARROLL	76	DPWA	Isospin-1 total σ
1582±4	[9] LITCHFIELD	74	DPWA	$K^- p \to \Lambda\pi^0$

[8] CARROLL 76 sees a total-cross-section bump with $(J+1/2)\ \Gamma_{el}\ /\ \Gamma_{total} = 0.06$.

[9] The main effect observed by LITCHFIELD 74 is in the $\Lambda\pi$ final state; the $\overline{K}N$ and $\Sigma\pi$ couplings are estimated from a multichannel fit including total-cross-section data of LI 73.

$\Sigma(1580)$ WIDTH

VALUE (MeV)	DOCUMENT ID		TECN	COMMENT
15	[10] CARROLL	76	DPWA	Isospin-1 total σ
11±4	[11] LITCHFIELD	74	DPWA	$K^- p \to \Lambda\pi^0$

[10] CARROLL 76 sees a total-cross-section bump with $(J+1/2)\ \Gamma_{el}\ /\ \Gamma_{total} = 0.06$.

[11] The main effect observed by LITCHFIELD 74 is in the $\Lambda\pi$ final state; the $\overline{K}N$ and $\Sigma\pi$ couplings are estimated from a multichannel fit including total-cross-section data of LI 73.

$\Sigma(1580)$ DECAY MODES

	Mode
Γ_1	$N\overline{K}$
Γ_2	$\Lambda\pi$
Γ_3	$\Sigma\pi$
Γ_4	$\Sigma(1385)\pi$, S-wave
Γ_5	$\Sigma(1385)\pi$, D-wave
Γ_6	$N\overline{K}^*(892)$, S=1/2, D-wave
Γ_7	$N\overline{K}^*(892)$, S=3/2, S-wave
Γ_8	$N\overline{K}^*(892)$, S=3/2, D-wave

$\Sigma(1580)$ BRANCHING RATIOS

See "Sign conventions for resonance couplings" in the Note on Λ and Σ Resonances.

$\Gamma(N\overline{K})/\Gamma_{total}$ — Γ_1/Γ

VALUE	DOCUMENT ID		TECN	COMMENT
+0.03 ±0.01	[12] LITCHFIELD	74	DPWA	$\overline{K}N$ multichannel
• • • We do not use the following data for averages, fits, limits, etc. • • •				
0.003	[13] KAMANO	15	DPWA	Multichannel

[12] The main effect observed by LITCHFIELD 74 is in the $\Lambda\pi$ final state; the $\overline{K}N$ and $\Sigma\pi$ couplings are estimated from a multichannel fit including total-cross-section data of LI 73.

[13] From the preferred solution A in KAMANO 15.

$\Gamma(\Lambda\pi)/\Gamma_{total}$ — Γ_2/Γ

VALUE	DOCUMENT ID		TECN	COMMENT
• • • We do not use the following data for averages, fits, limits, etc. • • •				
0.490	[14] KAMANO	15	DPWA	Multichannel

[14] From the preferred solution A in KAMANO 15.

$\Gamma(\Sigma\pi)/\Gamma_{total}$ — Γ_3/Γ

VALUE	DOCUMENT ID		TECN	COMMENT
• • • We do not use the following data for averages, fits, limits, etc. • • •				
0.387	[15] KAMANO	15	DPWA	Multichannel

[15] From the preferred solution A in KAMANO 15.

$\Gamma(\Sigma(1385)\pi, S\text{-wave})/\Gamma_{total}$ — Γ_4/Γ

VALUE	DOCUMENT ID		TECN	COMMENT
• • • We do not use the following data for averages, fits, limits, etc. • • •				
0.12	[16] KAMANO	15	DPWA	Multichannel

[16] From the preferred solution A in KAMANO 15.

$\Gamma(\Sigma(1385)\pi, D\text{-wave})/\Gamma_{total}$ — Γ_5/Γ

VALUE	DOCUMENT ID		TECN	COMMENT
• • • We do not use the following data for averages, fits, limits, etc. • • •				
0.001	[17] KAMANO	15	DPWA	Multichannel

[17] From the preferred solution A in KAMANO 15.

$\Gamma(N\overline{K}^*(892), S=1/2, D\text{-wave})/\Gamma_{total}$ — Γ_6/Γ

VALUE	DOCUMENT ID		TECN	COMMENT
• • • We do not use the following data for averages, fits, limits, etc. • • •				
not seen	[18] KAMANO	15	DPWA	Multichannel

[18] From the preferred solution A in KAMANO 15.

$\Gamma(N\overline{K}^*(892), S=3/2, S\text{-wave})/\Gamma_{total}$ — Γ_7/Γ

VALUE	DOCUMENT ID		TECN	COMMENT
• • • We do not use the following data for averages, fits, limits, etc. • • •				
not seen	[19] KAMANO	15	DPWA	Multichannel

[19] From the preferred solution A in KAMANO 15.

$\Gamma(N\overline{K}^*(892), S=3/2, D\text{-wave})/\Gamma_{total}$ — Γ_8/Γ

VALUE	DOCUMENT ID		TECN	COMMENT
• • • We do not use the following data for averages, fits, limits, etc. • • •				
not seen	[20] KAMANO	15	DPWA	Multichannel

[20] From the preferred solution A in KAMANO 15.

$(\Gamma_i\Gamma_f)^{1/2}/\Gamma_{total}$ in $N\overline{K} \to \Sigma(1580) \to \Lambda\pi$ — $(\Gamma_1\Gamma_2)^{1/2}/\Gamma$

VALUE	DOCUMENT ID		TECN	COMMENT
not seen	CAMERON	78C	HBC	$K^0_L p \to \Lambda\pi^+$
not seen	ENGLER	78	HBC	$K^0_L p \to \Lambda\pi^+$
+0.10±0.02	[21] LITCHFIELD	74	DPWA	$K^- p \to \Lambda\pi^0$

[21] The main effect observed by LITCHFIELD 74 is in the $\Lambda\pi$ final state; the $\overline{K}N$ and $\Sigma\pi$ couplings are estimated from a multichannel fit including total-cross-section data of LI 73.

$(\Gamma_i\Gamma_f)^{1/2}/\Gamma_{total}$ in $N\overline{K} \to \Sigma(1580) \to \Sigma\pi$ — $(\Gamma_1\Gamma_3)^{1/2}/\Gamma$

VALUE	DOCUMENT ID		TECN	COMMENT
not seen	CAMERON	78C	HBC	$K^0_L p \to \Sigma^0\pi^+$
not seen	ENGLER	78	HBC	$K^0_L p \to \Sigma^0\pi^+$
+0.03±0.04	[22] LITCHFIELD	74	DPWA	$\overline{K}N$ multichannel

[22] The main effect observed by LITCHFIELD 74 is in the $\Lambda\pi$ final state; the $\overline{K}N$ and $\Sigma\pi$ couplings are estimated from a multichannel fit including total-cross-section data of LI 73.

$\Sigma(1580)$ REFERENCES

SARANTSEV	19	EPJ A55 180	A.V. Sarantsev *et al.*	(BONN, PNPI)
KAMANO	15	PR C92 025205	H. Kamano *et al.*	(ANL, OSAK)
ZHANG	13A	PR C88 035205	H. Zhang *et al.*	(KSU)
OLMSTED	04	PL B588 29	J. Olmsted *et al.*	(BNL Crystal Ball Collab.)
PRAKHOV	04	PR C69 042202	S. Prakhov *et al.*	(BNL Crystal Ball Collab.)
CAMERON	78C	NP B132 189	W. Cameron *et al.*	(BGNA, EDIN, GLAS+) I
ENGLER	78	PR D18 3061	A. Engler *et al.*	(CMU, ANL)
CARROLL	76	PRL 37 806	A.S. Carroll *et al.*	(BNL) I
LITCHFIELD	74	PL 51B 509	P.J. Litchfield	(CERN) IJP
LI	73	Purdue Conf. 283	K.K. Li	(BNL) I

$\Sigma(1620)\ 1/2^-$

$I(J^P) = 1(\frac{1}{2}^-)$ Status: *

OMITTED FROM SUMMARY TABLE

The S_{11} state at 1697 MeV reported by VANHORN 75 is tentatively listed under the $\Sigma(1750)$. CARROLL 76 sees two bumps in the isospin-1 total cross section near this mass. GAO 12 sees no evidence for this resonance.

Production experiments are listed separately in the next entry.

Downloaded from https://academic.oup.com/ptep/article/2022/8/083C01/6651666 by KIT Library user on 27 September 2022

$\Sigma(1620)$ POLE POSITION

REAL PART

VALUE (MeV)	DOCUMENT ID		TECN	COMMENT
1680±8	SARANTSEV	19	DPWA	$\overline{K}N$ multichannel
• • • We do not use the following data for averages, fits, limits, etc. • • •				
1501	ZHANG	13A	DPWA	$\overline{K}N$ multichannel

−2×IMAGINARY PART

VALUE (MeV)	DOCUMENT ID		TECN	COMMENT
39±11	SARANTSEV	19	DPWA	$\overline{K}N$ multichannel
• • • We do not use the following data for averages, fits, limits, etc. • • •				
171	ZHANG	13A	DPWA	$\overline{K}N$ multichannel

$\Sigma(1620)$ POLE RESIDUE

The "normalized residue" is the residue divided by $\Gamma_{pole}/2$.

Normalized residue in $N\overline{K} \to \Sigma(1620) \to \Sigma\pi$

MODULUS	PHASE (°)	DOCUMENT ID		TECN	COMMENT
0.14±0.03	**−90 ± 25**	SARANTSEV	19	DPWA	$\overline{K}N$ multichannel

Normalized residue in $N\overline{K} \to \Sigma(1620) \to \Lambda\pi$

MODULUS	PHASE (°)	DOCUMENT ID		TECN	COMMENT
0.10±0.03	**75 ± 20**	SARANTSEV	19	DPWA	$\overline{K}N$ multichannel

Normalized residue in $N\overline{K} \to \Sigma(1620) \to \Xi K$

MODULUS	PHASE (°)	DOCUMENT ID		TECN	COMMENT
0.02±0.01	**120 ± 20**	SARANTSEV	19	DPWA	$\overline{K}N$ multichannel

Normalized residue in $N\overline{K} \to \Sigma(1620) \to \Lambda(1520)\pi$

MODULUS	PHASE (°)	DOCUMENT ID		TECN	COMMENT
0.12±0.05	**140 ± 40**	SARANTSEV	19	DPWA	$\overline{K}N$ multichannel

Normalized residue in $N\overline{K} \to \Sigma(1620) \to \Sigma(1385)\pi$

MODULUS	PHASE (°)	DOCUMENT ID		TECN	COMMENT
0.015±0.010	**155 ± 40**	SARANTSEV	19	DPWA	$\overline{K}N$ multichannel

Normalized residue in $N\overline{K} \to \Sigma(1620) \to N\overline{K}^*(892)$, S-wave

MODULUS	PHASE (°)	DOCUMENT ID		TECN	COMMENT
0.05±0.04		SARANTSEV	19	DPWA	$\overline{K}N$ multichannel

Normalized residue in $N\overline{K} \to \Sigma(1620) \to N\overline{K}^*(892)$, D-wave

MODULUS	PHASE (°)	DOCUMENT ID		TECN	COMMENT
0.01±0.01		SARANTSEV	19	DPWA	$\overline{K}N$ multichannel

Normalized residue in $N\overline{K} \to \Sigma(1620) \to N\overline{K}$

VALUE	DOCUMENT ID		TECN	COMMENT
0.11+-0.03@43+-20	SARANTSEV	19	DPWA	$\overline{K}N$ multichannel

$\Sigma(1620)$ MASS

VALUE (MeV)	DOCUMENT ID		TECN	COMMENT
1600 to 1650 (≈ 1620) OUR ESTIMATE				
1681± 6	SARANTSEV	19	DPWA	$\overline{K}N$ multichannel
1600±15	ZHANG	13A	DPWA	$\overline{K}N$ multichannel
1600± 6	[1] MORRIS	78	DPWA	$K^-n \to \Lambda\pi^-$
1608± 5	[2] CARROLL	76	DPWA	Isospin-1 total σ
1630±10	LANGBEIN	72	IPWA	$\overline{K}N$ multichannel
1620	KIM	71	DPWA	K-matrix analysis
• • • We do not use the following data for averages, fits, limits, etc. • • •				
1633±10	[3] CARROLL	76	DPWA	Isospin-1 total σ

$\Sigma(1620)$ WIDTH

VALUE (MeV)	DOCUMENT ID		TECN	COMMENT
40 to 100 (≈ 70) OUR ESTIMATE				
40± 12	SARANTSEV	19	DPWA	$\overline{K}N$ multichannel
400±152	ZHANG	13A	DPWA	$\overline{K}N$ multichannel
87± 19	[1] MORRIS	78	DPWA	$K^-n \to \Lambda\pi^-$
15	[2] CARROLL	76	DPWA	Isospin-1 total σ
65± 20	LANGBEIN	72	IPWA	$\overline{K}N$ multichannel
40	KIM	71	DPWA	K-matrix analysis
• • • We do not use the following data for averages, fits, limits, etc. • • •				
10	[3] CARROLL	76	DPWA	Isospin-1 total σ

$\Sigma(1620)$ DECAY MODES

	Mode	Fraction (Γ_i/Γ)
Γ_1	$N\overline{K}$	0.10 to 0.60
Γ_2	$\Lambda\pi$	(9.0 ±3.0) %
Γ_3	$\Sigma\pi$	(17 ±5) %
Γ_4	ΞK	
Γ_5	$\Lambda(1520)\pi$	(10 ±5) %
Γ_6	$\Sigma(1385)\pi$	

$\Sigma(1620)$ BRANCHING RATIOS

$\Gamma(N\overline{K})/\Gamma_{total}$ — Γ_1/Γ

VALUE	DOCUMENT ID		TECN	COMMENT
0.10 to 0.60 OUR ESTIMATE				
0.11±0.03	SARANTSEV	19	DPWA	$\overline{K}N$ multichannel
0.59±0.10	ZHANG	13A	DPWA	$\overline{K}N$ multichannel
0.22±0.02	LANGBEIN	72	IPWA	$\overline{K}N$ multichannel
0.05	KIM	71	DPWA	K-matrix analysis

$\Gamma(\Sigma\pi)/\Gamma_{total}$ — Γ_3/Γ

VALUE	DOCUMENT ID		TECN	COMMENT
0.17±0.05	SARANTSEV	19	DPWA	$\overline{K}N$ multichannel

$\Gamma(\Lambda\pi)/\Gamma_{total}$ — Γ_2/Γ

VALUE	DOCUMENT ID		TECN	COMMENT
0.09±0.03	SARANTSEV	19	DPWA	$\overline{K}N$ multichannel

$\Gamma(\Xi K)/\Gamma_{total}$ — Γ_4/Γ

VALUE	DOCUMENT ID		TECN	COMMENT
~ 0	SARANTSEV	19	DPWA	$\overline{K}N$ multichannel

$\Gamma(\Lambda(1520)\pi)/\Gamma_{total}$ — Γ_5/Γ

VALUE	DOCUMENT ID		TECN	COMMENT
0.10±0.05	SARANTSEV	19	DPWA	$\overline{K}N$ multichannel

$\Gamma(\Sigma(1385)\pi)/\Gamma_{total}$ — Γ_6/Γ

VALUE	DOCUMENT ID		TECN	COMMENT
<0.01	SARANTSEV	19	DPWA	$\overline{K}N$ multichannel

$(\Gamma_i\Gamma_f)^{1/2}/\Gamma_{total}$ in $N\overline{K} \to \Sigma(1620) \to \Lambda\pi$ — $(\Gamma_1\Gamma_2)^{1/2}/\Gamma$

VALUE	DOCUMENT ID		TECN	COMMENT
0.12±0.02	[1] MORRIS	78	DPWA	$K^-n \to \Lambda\pi^-$
not seen	BAILLON	75	IPWA	$\overline{K}N \to \Lambda\pi$
0.15	KIM	71	DPWA	K-matrix analysis

$(\Gamma_i\Gamma_f)^{1/2}/\Gamma_{total}$ in $N\overline{K} \to \Sigma(1620) \to \Sigma\pi$ — $(\Gamma_1\Gamma_3)^{1/2}/\Gamma$

VALUE	DOCUMENT ID		TECN	COMMENT
+0.32±0.03	ZHANG	13A	DPWA	Multichannel
not seen	HEPP	76B	DPWA	$K^-N \to \Sigma\pi$
+0.40±0.06	LANGBEIN	72	IPWA	$\overline{K}N$ multichannel
+0.08	KIM	71	DPWA	K-matrix analysis

$\Sigma(1620)$ FOOTNOTES

[1] MORRIS 78 obtains an equally good fit without including this resonance.
[2] Total cross-section bump with (J+1/2) Γ_{el} / Γ_{total} is 0.06 seen by CARROLL 76.
[3] Total cross-section bump with (J+1/2) Γ_{el} / Γ_{total} is 0.04 seen by CARROLL 76.

$\Sigma(1620)$ REFERENCES

SARANTSEV	19	EPJ A55 180	A.V. Sarantsev *et al.*	(BONN, PNPI)
ZHANG	13A	PR C88 035205	H. Zhang *et al.*	(KSU)
GAO	12	PR C86 025201	P. Gao, J. Shi, B.S. Zou	(BHEP, BEIJT)
Also		NP A867 41	P. Gao, B.S. Zou, A. Sibirtsev	(BHEP, BEIJT+)
MORRIS	78	PR D17 55	W.A. Morris *et al.*	(FSU) IJP
CARROLL	76	PRL 37 806	A.S. Carroll *et al.*	(BNL) I
HEPP	76B	PL 65B 487	V. Hepp *et al.*	(CERN, HEIDH, MPIM) IJP
BAILLON	75	NP B94 39	P.H. Baillon, P.J. Litchfield	(CERN, RHEL) IJP
VANHORN	75	NP B87 145	A.J. van Horn	(LBL) IJP
Also		NP B87 157	A.J. van Horn	(LBL) IJP
LANGBEIN	72	NP B47 477	W. Langbein, F. Wagner	(MPIM) IJP
KIM	71	PRL 27 356	J.K. Kim	(HARV) IJP
Also		Duke Conf. 161 Hyperon Resonances, 1970	J.K. Kim	(HARV) IJP

$\Sigma(1660)$ $1/2^+$

$I(J^P) = 1(\frac{1}{2}^+)$ Status: ***

For results published before 1974 (they are now obsolete), see our 1982 edition Physics Letters **111B** 1 (1982).

$\Sigma(1660)$ POLE POSITION

REAL PART

VALUE (MeV)	DOCUMENT ID		TECN	COMMENT
1585± 20	SARANTSEV	19	DPWA	$\overline{K}N$ multichannel
• • • We do not use the following data for averages, fits, limits, etc. • • •				
1547^{+111}_{-59}	[1] KAMANO	15	DPWA	$\overline{K}N$ multichannel

[1] From the preferred solution A in KAMANO 15. Solution B reports M = 1457^{+5}_{-1} MeV.

−2×IMAGINARY PART

VALUE (MeV)	DOCUMENT ID		TECN	COMMENT
290^{+140}_{-40}	SARANTSEV	19	DPWA	$\overline{K}N$ multichannel
• • • We do not use the following data for averages, fits, limits, etc. • • •				
183^{+86}_{-78}	[1] KAMANO	15	DPWA	$\overline{K}N$ multichannel

[1] From the preferred solution A in KAMANO 15. Solution B reports Γ = 78^{+2}_{-8} MeV.

Downloaded from https://academic.oup.com/ptep/article/2022/8/083C01/6651666 by KIT Library user on 27 September 2022

$\Sigma(1660)$ POLE RESIDUES

The normalized residue is the residue divided by $\Gamma_{pole}/2$.

Normalized residue in $N\overline{K} \to \Sigma(1660) \to N\overline{K}$

MODULUS	PHASE (°)	DOCUMENT ID		TECN	COMMENT
0.07 ±0.03	**−165 ± 35**	SARANTSEV	19	DPWA	$\overline{K}N$ multichannel
• • • We do not use the following data for averages, fits, limits, etc. • • •					
0.0247	168	[1] KAMANO	15	DPWA	$\overline{K}N$ multichannel

[1] From the preferred solution A in KAMANO 15.

Normalized residue in $N\overline{K} \to \Sigma(1660) \to \Sigma\pi$

MODULUS	PHASE (°)	DOCUMENT ID		TECN	COMMENT
0.17±0.04	**150 ± 20**	SARANTSEV	19	DPWA	$\overline{K}N$ multichannel
• • • We do not use the following data for averages, fits, limits, etc. • • •					
0.16	78	[1] KAMANO	15	DPWA	$\overline{K}N$ multichannel

[1] From the preferred solution A in KAMANO 15.

Normalized residue in $N\overline{K} \to \Sigma(1660) \to \Lambda\pi$

MODULUS	PHASE (°)	DOCUMENT ID		TECN	COMMENT
0.16 ±0.05	**0 ± 25**	SARANTSEV	19	DPWA	$\overline{K}N$ multichannel
• • • We do not use the following data for averages, fits, limits, etc. • • •					
0.0614	−84	[1] KAMANO	15	DPWA	$\overline{K}N$ multichannel

[1] From the preferred solution A in KAMANO 15.

Normalized residue in $N\overline{K} \to \Sigma(1660) \to \Sigma\sigma$

MODULUS	PHASE (°)	DOCUMENT ID		TECN	COMMENT
0.14±0.06	**−150 ± 30**	SARANTSEV	19	DPWA	$\overline{K}N$ multichannel

Normalized residue in $N\overline{K} \to \Sigma(1660) \to \Sigma(1385)\pi$

MODULUS	PHASE (°)	DOCUMENT ID		TECN	COMMENT
• • • We do not use the following data for averages, fits, limits, etc. • • •					
0.0513	−44	[1] KAMANO	15	DPWA	Multichannel

[1] From the preferred solution A in KAMANO 15.

Normalized residue in $N\overline{K} \to \Sigma(1660) \to \Lambda(1405)\pi$

MODULUS	PHASE (°)	DOCUMENT ID		TECN	COMMENT
0.06±0.03	**−90 ± 25**	SARANTSEV	19	DPWA	$\overline{K}N$ multichannel

Normalized residue in $N\overline{K} \to \Sigma(1660) \to \Lambda(1520)\pi$

MODULUS	PHASE (°)	DOCUMENT ID		TECN	COMMENT
0.04±0.02	**5 ± 20**	SARANTSEV	19	DPWA	$\overline{K}N$ multichannel

$\Sigma(1660)$ MASS

VALUE (MeV)	DOCUMENT ID		TECN	COMMENT
1640 to 1680 (≈ 1660) OUR ESTIMATE				
1665 ±20	SARANTSEV	19	DPWA	$\overline{K}N$ multichannel
1633 ± 3	GAO	12	DPWA	$\overline{K}N \to \Lambda\pi$
1665.1±11.2	[1] KOISO	85	DPWA	$K^-p \to \Sigma\pi$
1670 ±10	GOPAL	80	DPWA	$\overline{K}N \to \overline{K}N$
1679 ±10	ALSTON-...	78	DPWA	$\overline{K}N \to \overline{K}N$
1668 ±25	VANHORN	75	DPWA	$K^-p \to \Lambda\pi^0$
1670 ±20	KANE	74	DPWA	$K^-p \to \Sigma\pi$
• • • We do not use the following data for averages, fits, limits, etc. • • •				
1676 ±15	GOPAL	77	DPWA	$\overline{K}N$ multichannel
1565 or 1597	[2] MARTIN	77	DPWA	$\overline{K}N$ multichannel
1660 ±30	[3] BAILLON	75	IPWA	$\overline{K}N \to \Lambda\pi$
1671 ± 2	[4] PONTE	75	DPWA	$K^-p \to \Lambda\pi^0$

[1] The evidence of KOISO 85 is weak.
[2] The two MARTIN 77 values are from a T-matrix pole and from a Breit-Wigner fit.
[3] From solution 1 of BAILLON 75; not present in solution 2.
[4] From solution 2 of PONTE 75; not present in solution 1.

$\Sigma(1660)$ WIDTH

VALUE (MeV)	DOCUMENT ID		TECN	COMMENT
100 to 300 (≈ 200) OUR ESTIMATE				
300^{+140}_{-40}	SARANTSEV	19	DPWA	$\overline{K}N$ multichannel
121^{+4}_{-7}	GAO	12	DPWA	$\overline{K}N \to \Lambda\pi$
81.5± 22.2	[1] KOISO	85	DPWA	$K^-p \to \Sigma\pi$
152 ± 20	GOPAL	80	DPWA	$\overline{K}N \to \overline{K}N$
38 ± 10	ALSTON-...	78	DPWA	$\overline{K}N \to \overline{K}N$
230^{+165}_{-60}	VANHORN	75	DPWA	$K^-p \to \Lambda\pi^0$
250 ±110	KANE	74	DPWA	$K^-p \to \Sigma\pi$
• • • We do not use the following data for averages, fits, limits, etc. • • •				
120 ± 20	GOPAL	77	DPWA	$\overline{K}N$ multichannel
202 or 217	[2] MARTIN	77	DPWA	$\overline{K}N$ multichannel
80 ± 40	[3] BAILLON	75	IPWA	$\overline{K}N \to \Lambda\pi$
81 ± 10	[4] PONTE	75	DPWA	$K^-p \to \Lambda\pi^0$

[1] The evidence of KOISO 85 is weak.
[2] The two MARTIN 77 values are from a T-matrix pole and from a Breit-Wigner fit.
[3] From solution 1 of BAILLON 75; not present in solution 2.
[4] From solution 2 of PONTE 75; not present in solution 1.

$\Sigma(1660)$ DECAY MODES

	Mode	Fraction (Γ_i/Γ)
Γ_1	$N\overline{K}$	0.05 to 0.15 (≈ 010)
Γ_2	$\Lambda\pi$	(35 ±12) %
Γ_3	$\Sigma\pi$	(37 ±10) %
Γ_4	$\Sigma\sigma$	(20 ± 8) %
Γ_5	$\Sigma(1385)\pi$	
Γ_6	$\Lambda(1405)\pi$	(4.0 ± 2.0) %
Γ_7	$\Lambda(1520)\pi$	

$\Sigma(1660)$ BRANCHING RATIOS

See "Sign conventions for resonance couplings" in the Note on Λ and Σ Resonances.

$\Gamma(N\overline{K})/\Gamma_{total}$ — Γ_1/Γ

VALUE	DOCUMENT ID		TECN	COMMENT
0.05 to 0.15 (≈ 010) OUR ESTIMATE				
0.07 ±0.03	SARANTSEV	19	DPWA	$\overline{K}N$ multichannel
0.12 ±0.03	GOPAL	80	DPWA	$\overline{K}N \to \overline{K}N$
0.10 ±0.05	ALSTON-...	78	DPWA	$\overline{K}N \to \overline{K}N$
• • • We do not use the following data for averages, fits, limits, etc. • • •				
0.005	[1] KAMANO	15	DPWA	$\overline{K}N$ multichannel
<0.04	GOPAL	77	DPWA	See GOPAL 80
0.27 or 0.29	[2] MARTIN	77	DPWA	$\overline{K}N$ multichannel

[1] From the preferred solution A in KAMANO 15.
[2] The two MARTIN 77 values are from a T-matrix pole and from a Breit-Wigner fit.

$\Gamma(\Lambda\pi)/\Gamma_{total}$ — Γ_2/Γ

VALUE	DOCUMENT ID		TECN	COMMENT
0.35 ±0.12	SARANTSEV	19	DPWA	$\overline{K}N$ multichannel
• • • We do not use the following data for averages, fits, limits, etc. • • •				
0.128	[1] KAMANO	15	DPWA	$\overline{K}N$ multichannel

[1] From the preferred solution A in KAMANO 15.

$\Gamma(\Sigma\pi)/\Gamma_{total}$ — Γ_3/Γ

VALUE	DOCUMENT ID		TECN	COMMENT
0.37 ±0.10	SARANTSEV	19	DPWA	$\overline{K}N$ multichannel
• • • We do not use the following data for averages, fits, limits, etc. • • •				
0.865	[1] KAMANO	15	DPWA	$\overline{K}N$ multichannel

[1] From the preferred solution A in KAMANO 15.

$\Gamma(\Sigma\sigma)/\Gamma_{total}$ — Γ_4/Γ

VALUE	DOCUMENT ID		TECN	COMMENT
0.20±0.08	SARANTSEV	19	DPWA	$\overline{K}N$ multichannel

$\Gamma(\Sigma(1385)\pi)/\Gamma_{total}$ — Γ_5/Γ

VALUE	DOCUMENT ID		TECN	COMMENT
• • • We do not use the following data for averages, fits, limits, etc. • • •				
0.001	[1] KAMANO	15	DPWA	Multichannel

[1] From the preferred solution A in KAMANO 15.

$\Gamma(\Lambda(1405)\pi)/\Gamma_{total}$ — Γ_6/Γ

VALUE	DOCUMENT ID		TECN	COMMENT
0.04±0.02	SARANTSEV	19	DPWA	$\overline{K}N$ multichannel

$\Gamma(\Lambda(1520)\pi)/\Gamma_{total}$ — Γ_7/Γ

VALUE	DOCUMENT ID		TECN	COMMENT
<0.01	SARANTSEV	19	DPWA	$\overline{K}N$ multichannel

$(\Gamma_i\Gamma_f)^{1/2}/\Gamma_{total}$ in $N\overline{K} \to \Sigma(1660) \to \Lambda\pi$ — $(\Gamma_1\Gamma_2)^{1/2}/\Gamma$

VALUE	DOCUMENT ID		TECN	COMMENT
$-0.064^{+0.005}_{-0.003}$	GAO	12	DPWA	$\overline{K}N \to \Lambda\pi$
< 0.04	GOPAL	77	DPWA	$\overline{K}N$ multichannel
$0.12^{+0.12}_{-0.04}$	VANHORN	75	DPWA	$K^-p \to \Lambda\pi^0$
• • • We do not use the following data for averages, fits, limits, etc. • • •				
−0.10 or −0.11	[1] MARTIN	77	DPWA	$\overline{K}N$ multichannel
−0.04 ±0.02	[2] BAILLON	75	IPWA	$\overline{K}N \to \Lambda\pi$
+0.16 ±0.01	[3] PONTE	75	DPWA	$K^-p \to \Lambda\pi^0$

[1] The two MARTIN 77 values are from a T-matrix pole and from a Breit-Wigner fit.
[2] From solution 1 of BAILLON 75; not present in solution 2.
[3] From solution 2 of PONTE 75; not present in solution 1.

$(\Gamma_i\Gamma_f)^{1/2}/\Gamma_{total}$ in $N\overline{K} \to \Sigma(1660) \to \Sigma\pi$ — $(\Gamma_1\Gamma_3)^{1/2}/\Gamma$

VALUE	DOCUMENT ID		TECN	COMMENT
−0.13±0.04	[1] KOISO	85	DPWA	$K^-p \to \Sigma\pi$
−0.16±0.03	GOPAL	77	DPWA	$\overline{K}N$ multichannel
−0.11±0.01	KANE	74	DPWA	$K^-p \to \Sigma\pi$
• • • We do not use the following data for averages, fits, limits, etc. • • •				
−0.34 or −0.37	[2] MARTIN	77	DPWA	$\overline{K}N$ multichannel
not seen	HEPP	76B	DPWA	$K^-N \to \Sigma\pi$

[1] The evidence of KOISO 85 is weak.
[2] The two MARTIN 77 values are from a T-matrix pole and from a Breit-Wigner fit.

Downloaded from https://academic.oup.com/ptep/article/2022/8/083C01/6651666 by KIT Library user on 27 September 2022

$\Sigma(1660)$ REFERENCES

SARANTSEV	19	EPJ A55 180	A.V. Sarantsev *et al.*	(BONN, PNPI)
KAMANO	15	PR C92 025205	H. Kamano *et al.*	(ANL, OSAK)
GAO	12	PR C86 025201	P. Gao, J. Shi, B.S. Zou	(BHEP, BEIJT)
Also		NP A867 41	P. Gao, B.S. Zou, A. Sibirtsev	(BHEP, BEIJT+)
KOISO	85	NP A433 619	H. Koiso *et al.*	(TOKY, MASA)
PDG	82	PL 111B 1	M. Roos *et al.*	(HELS, CIT, CERN)
GOPAL	80	Toronto Conf. 159	G.P. Gopal	(RHEL) IJP
ALSTON-...	78	PR D18 182	M. Alston-Garnjost *et al.*	(LBL, MTHO+) IJP
Also		PRL 38 1007	M. Alston-Garnjost *et al.*	(LBL, MTHO+) IJP
GOPAL	77	NP B119 362	G.P. Gopal *et al.*	(LOIC, RHEL) IJP
MARTIN	77	NP B127 349	B.R. Martin, M.K. Pidcock, R.G. Moorhouse	(LOUC+) IJP
Also		NP B126 266	B.R. Martin, M.K. Pidcock	(LOUC)
Also		NP B126 285	B.R. Martin, M.K. Pidcock	(LOUC) IJP
HEPP	76B	PL 65B 487	V. Hepp *et al.*	(CERN, HEIDH, MPIM) IJP
BAILLON	75	NP B94 39	P.H. Baillon, P.J. Litchfield	(CERN, RHEL) IJP
PONTE	75	PR D12 2597	R.A. Ponte *et al.*	(MASA, TENN, UCR) IJP
VANHORN	75	NP B87 145	A.J. van Horn	(LBL) IJP
Also		NP B87 157	A.J. van Horn	(LBL) IJP
KANE	74	LBL-2452	D.F. Kane	(LBL) IJP

$\Sigma(1670)$ $3/2^-$

$I(J^P) = 1(\frac{3}{2}^-)$ Status: ****

For most results published before 1974 (they are now obsolete), see our 1982 edition Physics Letters **111B** 1 (1982).

Results from production experiments are listed separately in the next entry.

$\Sigma(1670)$ POLE POSITION

REAL PART

VALUE (MeV)	DOCUMENT ID		TECN	COMMENT
1655 to 1675 (≈ 1662) OUR ESTIMATE				
1661 ± 3	SARANTSEV	19	DPWA	$\overline{K}N$ multichannel
1669^{+7}_{-7}	[1] KAMANO	15	DPWA	$\overline{K}N$ multichannel
• • • We do not use the following data for averages, fits, limits, etc. • • •				
1674	ZHANG	13A	DPWA	$\overline{K}N$ multichannel

[1] From the preferred solution A in KAMANO 15.

−2×IMAGINARY PART

VALUE (MeV)	DOCUMENT ID		TECN	COMMENT
45 to 65 (≈ 55) OUR ESTIMATE				
52 ± 6	SARANTSEV	19	DPWA	$\overline{K}N$ multichannel
64^{+10}_{-14}	[1] KAMANO	15	DPWA	$\overline{K}N$ multichannel
• • • We do not use the following data for averages, fits, limits, etc. • • •				
54	ZHANG	13A	DPWA	$\overline{K}N$ multichannel

[1] From the preferred solution A in KAMANO 15.

$\Sigma(1670)$ POLE RESIDUES

The normalized residue is the residue divided by $\Gamma_{pole}/2$.

Normalized residue in $N\overline{K} \to \Sigma(1670) \to N\overline{K}$

MODULUS	PHASE (°)	DOCUMENT ID		TECN	COMMENT
0.10 ±0.02	**−31 ± 12**	SARANTSEV	19	DPWA	$\overline{K}N$ multichannel
• • • We do not use the following data for averages, fits, limits, etc. • • •					
0.129	−20	[1] KAMANO	15	DPWA	$\overline{K}N$ multichannel

[1] From the preferred solution A in KAMANO 15.

Normalized residue in $N\overline{K} \to \Sigma(1670) \to \Sigma\pi$

MODULUS	PHASE (°)	DOCUMENT ID		TECN	COMMENT
0.25 ±0.05	**−25 ± 10**	SARANTSEV	19	DPWA	$\overline{K}N$ multichannel
• • • We do not use the following data for averages, fits, limits, etc. • • •					
0.249	−21	[1] KAMANO	15	DPWA	$\overline{K}N$ multichannel

[1] From the preferred solution A in KAMANO 15.

Normalized residue in $N\overline{K} \to \Sigma(1670) \to \Lambda\pi$

MODULUS	PHASE (°)	DOCUMENT ID		TECN	COMMENT
0.09 ±0.03	**−52 ± 12**	SARANTSEV	19	DPWA	$\overline{K}N$ multichannel
• • • We do not use the following data for averages, fits, limits, etc. • • •					
0.0818	−7	[1] KAMANO	15	DPWA	$\overline{K}N$ multichannel

[1] From the preferred solution A in KAMANO 15.

Normalized residue in $N\overline{K} \to \Sigma(1670) \to \Xi K$

MODULUS	PHASE (°)	DOCUMENT ID		TECN	COMMENT
0.02±0.01	**160 ± 20**	SARANTSEV	19	DPWA	$\overline{K}N$ multichannel

Normalized residue in $N\overline{K} \to \Sigma(1670) \to \Sigma\sigma$

MODULUS	PHASE (°)	DOCUMENT ID		TECN	COMMENT
0.08±0.03	**−25 ± 15**	SARANTSEV	19	DPWA	$\overline{K}N$ multichannel

Normalized residue in $N\overline{K} \to \Sigma(1670) \to \Sigma(1385)\pi$, S-wave

MODULUS	PHASE (°)	DOCUMENT ID		TECN	COMMENT
• • • We do not use the following data for averages, fits, limits, etc. • • •					
0.228	167	[1] KAMANO	15	DPWA	$\overline{K}N$ multichannel

[1] From the preferred solution A in KAMANO 15.

Normalized residue in $N\overline{K} \to \Sigma(1670) \to \Sigma(1385)\pi$, D-wave

MODULUS	PHASE (°)	DOCUMENT ID		TECN	COMMENT
• • • We do not use the following data for averages, fits, limits, etc. • • •					
0.0915	141	KAMANO	15	DPWA	$\overline{K}N$ multichannel

Normalized residue in $N\overline{K} \to \Sigma(1670) \to \Lambda(1405)\pi$

MODULUS	PHASE (°)	DOCUMENT ID		TECN	COMMENT
0.03±0.02	**160 ± 15**	SARANTSEV	19	DPWA	$\overline{K}N$ multichannel

Normalized residue in $N\overline{K} \to \Sigma(1670) \to \Lambda(1520)\pi$, P-wave

MODULUS	PHASE (°)	DOCUMENT ID		TECN	COMMENT
0.04±0.02	**120 ± 20**	SARANTSEV	19	DPWA	$\overline{K}N$ multichannel

Normalized residue in $N\overline{K} \to \Sigma(1670) \to \Lambda(1520)\pi$, F-wave

MODULUS	PHASE (°)	DOCUMENT ID		TECN	COMMENT
0.01±0.01		SARANTSEV	19	DPWA	$\overline{K}N$ multichannel

Normalized residue in $N\overline{K} \to \Sigma(1670) \to \Delta\overline{K}$, S-wave

MODULUS	PHASE (°)	DOCUMENT ID		TECN	COMMENT
0.01±0.01		SARANTSEV	19	DPWA	$\overline{K}N$ multichannel

Normalized residue in $N\overline{K} \to \Sigma(1670) \to N\overline{K}^*(892)$, S=3/2, S-wave

VALUE	DOCUMENT ID		TECN	COMMENT
0.05+-0.03@50+-60	SARANTSEV	19	DPWA	$\overline{K}N$ multichannel

Normalized residue in $N\overline{K} \to \Sigma(1670) \to N\overline{K}^*(892)$, S=3/2, D-wave

MODULUS	PHASE (°)	DOCUMENT ID		TECN	COMMENT
0.01±0.01		SARANTSEV	19	DPWA	$\overline{K}N$ multichannel

Normalized residue in $N\overline{K} \to \Sigma(1670) \to N\overline{K}^*(892)$, S=1/2, D-wave

MODULUS	PHASE (°)	DOCUMENT ID		TECN	COMMENT
0.03±0.02		SARANTSEV	19	DPWA	$\overline{K}N$ multichannel

$\Sigma(1670)$ MASS

VALUE (MeV)	DOCUMENT ID		TECN	COMMENT
1665 to 1685 (≈ 1675) OUR ESTIMATE				
1665 ± 3	SARANTSEV	19	DPWA	$\overline{K}N$ multichannel
1678 ± 2	ZHANG	13A	DPWA	$\overline{K}N$ multichannel
1673 ± 1	GAO	12	DPWA	$\overline{K}N \to \Lambda\pi$
1665.1 ± 4.1	KOISO	85	DPWA	$K^-p \to \Sigma\pi$
1682 ± 5	GOPAL	80	DPWA	$\overline{K}N \to \overline{K}N$
1679 ±10	ALSTON-...	78	DPWA	$\overline{K}N \to \overline{K}N$
1670 ± 5	GOPAL	77	DPWA	$\overline{K}N$ multichannel
1670 ± 6	HEPP	76B	DPWA	$K^-N \to \Sigma\pi$
1685 ±20	BAILLON	75	IPWA	$\overline{K}N \to \Lambda\pi$
1659^{+12}_{-5}	VANHORN	75	DPWA	$K^-p \to \Lambda\pi^0$
1670 ± 2	KANE	74	DPWA	$K^-p \to \Sigma\pi$
• • • We do not use the following data for averages, fits, limits, etc. • • •				
1667 or 1668	[1] MARTIN	77	DPWA	$\overline{K}N$ multichannel
1650	DEBELLEFON	76	IPWA	$K^-p \to \Lambda\pi^0$
1671 ± 3	PONTE	75	DPWA	$K^-p \to \Lambda\pi^0$ (sol. 1)
1655 ± 2	PONTE	75	DPWA	$K^-p \to \Lambda\pi^0$ (sol. 2)

[1] The two MARTIN 77 values are from a T-matrix pole and from a Breit-Wigner fit.

$\Sigma(1670)$ WIDTH

VALUE (MeV)	DOCUMENT ID		TECN	COMMENT
40 to 100 (≈ 70) OUR ESTIMATE				
54 ± 6	SARANTSEV	19	DPWA	$\overline{K}N$ multichannel
55 ± 4	ZHANG	13A	DPWA	$\overline{K}N$ multichannel
52^{+5}_{-2}	GAO	12	DPWA	$\overline{K}N \to \Lambda\pi$
65.0 ± 7.3	KOISO	85	DPWA	$K^-p \to \Sigma\pi$
79 ±10	GOPAL	80	DPWA	$\overline{K}N \to \overline{K}N$
56 ±20	ALSTON-...	78	DPWA	$\overline{K}N \to \overline{K}N$
50 ± 5	GOPAL	77	DPWA	$\overline{K}N$ multichannel
56 ± 3	HEPP	76B	DPWA	$K^-N \to \Sigma\pi$
85 ±25	BAILLON	75	IPWA	$\overline{K}N \to \Lambda\pi$
32 ±11	VANHORN	75	DPWA	$K^-p \to \Lambda\pi^0$
79 ± 6	KANE	74	DPWA	$K^-p \to \Sigma\pi$
• • • We do not use the following data for averages, fits, limits, etc. • • •				
46 or 46	[1] MARTIN	77	DPWA	$\overline{K}N$ multichannel
80	DEBELLEFON	76	IPWA	$K^-p \to \Lambda\pi^0$
44 ±11	PONTE	75	DPWA	$K^-p \to \Lambda\pi^0$ (sol. 1)
76 ± 5	PONTE	75	DPWA	$K^-p \to \Lambda\pi^0$ (sol. 2)

[1] The two MARTIN 77 values are from a T-matrix pole and from a Breit-Wigner fit.

$\Sigma(1670)$ DECAY MODES

	Mode	Fraction (Γ_i/Γ)
Γ_1	$N\overline{K}$	0.06 to 0.12
Γ_2	$\Lambda\pi$	5–15 %

Downloaded from https://academic.oup.com/ptep/article/2022/8/083C01/6651666 by KIT Library user on 27 September 2022

Γ_3	$\Sigma\pi$	30–60 %
Γ_4	$\Lambda\pi\pi$	
Γ_5	$\Sigma\pi\pi$	
Γ_6	$\Sigma\sigma$	(7.0 ±3.0) %
Γ_7	$\Sigma(1385)\pi$	
Γ_8	$\Sigma(1385)\pi$, S-wave	
Γ_9	$\Sigma(1385)\pi$, D-wave	
Γ_{10}	$N\overline{K}^*(892)$, S=1/2, D-wave	
Γ_{11}	$N\overline{K}^*(892)$, S=3/2, S-wave	
Γ_{12}	$N\overline{K}^*(892)$, S=3/2, D-wave	
Γ_{13}	$\Lambda(1405)\pi$	
Γ_{14}	$\Lambda(1520)\pi$	

$\Sigma(1670)$ BRANCHING RATIOS

See "Sign conventions for resonance couplings" in the Note on Λ and Σ Resonances.

$\Gamma(N\overline{K})/\Gamma_{total}$ — Γ_1/Γ

VALUE	DOCUMENT ID		TECN	COMMENT
0.06 to 0.12 OUR ESTIMATE				
0.10 ±0.02	SARANTSEV	19	DPWA	$\overline{K}N$ multichannel
0.062±0.007	ZHANG	13A	DPWA	$\overline{K}N$ multichannel
0.10 ±0.03	GOPAL	80	DPWA	$\overline{K}N \to \overline{K}N$
0.11 ±0.03	ALSTON-...	78	DPWA	$\overline{K}N \to \overline{K}N$
• • • We do not use the following data for averages, fits, limits, etc. • • •				
0.121	[1] KAMANO	15	DPWA	$\overline{K}N$ multichannel
0.08 ±0.03	GOPAL	77	DPWA	See GOPAL 80
0.07 or 0.07	[2] MARTIN	77	DPWA	$\overline{K}N$ multichannel

[1] From the preferred solution A in KAMANO 15.
[2] The two MARTIN 77 values are from a T-matrix pole and from a Breit-Wigner fit.

$\Gamma(\Lambda\pi)/\Gamma_{total}$ — Γ_2/Γ

VALUE	DOCUMENT ID		TECN	COMMENT
0.09 ±0.02	SARANTSEV	19	DPWA	$\overline{K}N$ multichannel
• • • We do not use the following data for averages, fits, limits, etc. • • •				
0.058	[1] KAMANO	15	DPWA	$\overline{K}N$ multichannel

[1] From the preferred solution A in KAMANO 15.

$\Gamma(\Sigma\pi)/\Gamma_{total}$ — Γ_3/Γ

VALUE	DOCUMENT ID		TECN	COMMENT
0.70 ±0.15	SARANTSEV	19	DPWA	$\overline{K}N$ multichannel
• • • We do not use the following data for averages, fits, limits, etc. • • •				
0.465	[1] KAMANO	15	DPWA	$\overline{K}N$ multichannel

[1] From the preferred solution A in KAMANO 15.

$\Gamma(\Lambda\pi\pi)/\Gamma_{total}$ — Γ_4/Γ

VALUE	DOCUMENT ID		TECN	COMMENT
• • • We do not use the following data for averages, fits, limits, etc. • • •				
<0.11	ARMENTEROS	68E	HBC	K^-p (Γ_1=0.09)

$\Gamma(\Sigma\pi\pi)/\Gamma_{total}$ — Γ_5/Γ

VALUE	DOCUMENT ID		TECN	COMMENT
• • • We do not use the following data for averages, fits, limits, etc. • • •				
<0.14	[1] ARMENTEROS	68E	HBC	K^-p, K^-d (Γ_1=0.09)

[1] Ratio only for $\Sigma 2\pi$ system in $I = 1$, which cannot be $\Sigma(1385)$.

$\Gamma(\Sigma\sigma)/\Gamma_{total}$ — Γ_6/Γ

VALUE	DOCUMENT ID		TECN	COMMENT
0.07±0.03	SARANTSEV	19	DPWA	$\overline{K}N$ multichannel

$\Gamma(\Sigma(1385)\pi, S\text{-wave})/\Gamma_{total}$ — Γ_8/Γ

VALUE	DOCUMENT ID		TECN	COMMENT
• • • We do not use the following data for averages, fits, limits, etc. • • •				
0.309	[1] KAMANO	15	DPWA	Multichannel

[1] From the preferred solution A in KAMANO 15.

$\Gamma(\Sigma(1385)\pi, D\text{-wave})/\Gamma_{total}$ — Γ_9/Γ

VALUE	DOCUMENT ID		TECN	COMMENT
• • • We do not use the following data for averages, fits, limits, etc. • • •				
0.044	[1] KAMANO	15	DPWA	Multichannel

[1] From the preferred solution A in KAMANO 15.

$\Gamma(N\overline{K}^*(892), S$=1/2, D-wave$)/\Gamma_{total}$ — Γ_{10}/Γ

VALUE	DOCUMENT ID		TECN	COMMENT
• • • We do not use the following data for averages, fits, limits, etc. • • •				
0.001	[1] KAMANO	15	DPWA	Multichannel

[1] From the preferred solution A in KAMANO 15.

$\Gamma(N\overline{K}^*(892), S$=3/2, S-wave$)/\Gamma_{total}$ — Γ_{11}/Γ

VALUE	DOCUMENT ID		TECN	COMMENT
• • • We do not use the following data for averages, fits, limits, etc. • • •				
0.002	[1] KAMANO	15	DPWA	Multichannel

[1] From the preferred solution A in KAMANO 15.

$\Gamma(N\overline{K}^*(892), S$=3/2, D-wave$)/\Gamma_{total}$ — Γ_{12}/Γ

VALUE	DOCUMENT ID		TECN	COMMENT
• • • We do not use the following data for averages, fits, limits, etc. • • •				
0.001	[1] KAMANO	15	DPWA	Multichannel

[1] From the preferred solution A in KAMANO 15.

$\Gamma(\Lambda(1405)\pi)/\Gamma_{total}$ — Γ_{13}/Γ

VALUE	DOCUMENT ID		TECN	COMMENT
0.01±0.01	SARANTSEV	19	DPWA	$\overline{K}N$ multichannel
• • • We do not use the following data for averages, fits, limits, etc. • • •				
<0.06	ARMENTEROS	68E	HBC	K^-p, K^-d (Γ_1=0.09)

$\Gamma(\Lambda(1405)\pi)/\Gamma(\Sigma(1385)\pi)$ — Γ_{13}/Γ_7

VALUE	DOCUMENT ID		TECN	COMMENT
0.23±0.08	BRUCKER	70	DBC	$K^-N \to \Sigma\pi\pi$

$(\Gamma_i\Gamma_f)^{1/2}/\Gamma_{total}$ in $N\overline{K} \to \Sigma(1670) \to \Lambda\pi$ — $(\Gamma_1\Gamma_2)^{1/2}/\Gamma$

VALUE	DOCUMENT ID		TECN	COMMENT
+0.08 ±0.01	ZHANG	13A	DPWA	Multichannel
$+0.081^{+0.002}_{-0.004}$	GAO	12	DPWA	$\overline{K}N \to \Lambda\pi$
+0.17 ±0.03	[1] MORRIS	78	DPWA	$K^-n \to \Lambda\pi^-$
+0.13 ±0.02	[1] MORRIS	78	DPWA	$K^-n \to \Lambda\pi^-$
+0.10 ±0.02	GOPAL	77	DPWA	$\overline{K}N$ multichannel
+0.06 ±0.02	BAILLON	75	IPWA	$\overline{K}N \to \Lambda\pi$
+0.09 ±0.02	VANHORN	75	DPWA	$K^-p \to \Lambda\pi^0$
+0.018±0.060	DEVENISH	74B		Fixed-t dispersion rel.
• • • We do not use the following data for averages, fits, limits, etc. • • •				
+0.08 or +0.08	[2] MARTIN	77	DPWA	$\overline{K}N$ multichannel
+0.05	DEBELLEFON	76	IPWA	$K^-p \to \Lambda\pi^0$
+0.08 ±0.01	PONTE	75	DPWA	$K^-p \to \Lambda\pi^0$ (sol. 1)
+0.17 ±0.01	PONTE	75	DPWA	$K^-p \to \Lambda\pi^0$ (sol. 2)

[1] Results are with and without an S_{11} $\Sigma(1620)$ in the fit.
[2] The two MARTIN 77 values are from a T-matrix pole and from a Breit-Wigner fit.

$(\Gamma_i\Gamma_f)^{1/2}/\Gamma_{total}$ in $N\overline{K} \to \Sigma(1670) \to \Sigma\pi$ — $(\Gamma_1\Gamma_3)^{1/2}/\Gamma$

VALUE	DOCUMENT ID		TECN	COMMENT
+0.20±0.01	ZHANG	13A	DPWA	Multichannel
+0.20±0.02	KOISO	85	DPWA	$K^-p \to \Sigma\pi$
+0.21±0.02	GOPAL	77	DPWA	$\overline{K}N$ multichannel
+0.20±0.01	HEPP	76B	DPWA	$K^-N \to \Sigma\pi$
+0.21±0.03	KANE	74	DPWA	$K^-p \to \Sigma\pi$
• • • We do not use the following data for averages, fits, limits, etc. • • •				
+0.18 or +0.17	[1] MARTIN	77	DPWA	$\overline{K}N$ multichannel

[1] The two MARTIN 77 values are from a T-matrix pole and from a Breit-Wigner fit.

$(\Gamma_i\Gamma_f)^{1/2}/\Gamma_{total}$ in $N\overline{K} \to \Sigma(1670) \to \Sigma(1385)\pi$, S-wave — $(\Gamma_1\Gamma_8)^{1/2}/\Gamma$

VALUE	DOCUMENT ID		TECN	COMMENT
+0.11±0.03	PREVOST	74	DPWA	$K^-N \to \Sigma(1385)\pi$
• • • We do not use the following data for averages, fits, limits, etc. • • •				
0.17±0.02	[1] SIMS	68	DBC	$K^-N \to \Lambda\pi\pi$

[1] SIMS 68 uses only cross-section data. Result used as upper limit only.

$\Gamma_i\Gamma_f/\Gamma^2_{total}$ in $N\overline{K} \to \Sigma(1670) \to \Lambda(1405)\pi$ — $\Gamma_1\Gamma_{13}/\Gamma^2$

VALUE	DOCUMENT ID		TECN	COMMENT
0.007±0.002	[1] BRUCKER	70	DBC	$K^-N \to \Sigma\pi\pi$
• • • We do not use the following data for averages, fits, limits, etc. • • •				
<0.03	BERLEY	69	HBC	K^-p 0.6–0.82 GeV/c

[1] Assuming the $\Lambda(1405)\pi$ cross-section bump is due only to $3/2^-$ resonance.

$(\Gamma_i\Gamma_f)^{1/2}/\Gamma_{total}$ in $N\overline{K} \to \Sigma(1670) \to \Lambda(1520)\pi$ — $(\Gamma_1\Gamma_{14})^{1/2}/\Gamma$

VALUE	DOCUMENT ID		TECN	COMMENT
0.081±0.016	[1] CAMERON	77	DPWA	P-wave decay

[1] The CAMERON 77 upper limit on F-wave decay is 0.03.

$\Sigma(1670)$ REFERENCES

SARANTSEV	19	EPJ A55 180	A.V. Sarantsev *et al.*	(BONN, PNPI)
KAMANO	15	PR C92 025205	H. Kamano *et al.*	(ANL, OSAK)
ZHANG	13A	PR C88 035205	H. Zhang *et al.*	(KSU)
GAO	12	PR C86 025201	P. Gao, J. Shi, B.S. Zou	(BHEP, BEIJT)
Also		NP A867 41	P. Gao, B.S. Zou, A. Sibirtsev	(BHEP, BEIJT+)
KOISO	85	NP A433 619	H. Koiso *et al.*	(TOKY, MASA)
PDG	82	PL 111B 1	M. Roos *et al.*	(HELS, CIT, CERN)
GOPAL	80	Toronto Conf. 159	G.P. Gopal	(RHEL) IJP
ALSTON-...	78	PR D18 182	M. Alston-Garnjost *et al.*	(LBL, MTHO+) IJP
Also		PRL 38 1007	M. Alston-Garnjost *et al.*	(LBL, MTHO+) IJP
MORRIS	78	PR D17 55	W.A. Morris *et al.*	(FSU) IJP
CAMERON	77	NP B131 399	W. Cameron *et al.*	(RHEL, LOIC) IJP
GOPAL	77	NP B119 362	G.P. Gopal *et al.*	(LOIC, RHEL) IJP

Downloaded from https://academic.oup.com/ptep/article/2022/8/083C01/6651666 by KIT Library user on 27 September 2022

MARTIN	77	NP B127 349	B.R. Martin, M.K. Pidcock, R.G. Moorhouse	(LOUC+) IJP
Also		NP B126 266	B.R. Martin, M.K. Pidcock	(LOUC)
Also		NP B126 285	B.R. Martin, M.K. Pidcock	(LOUC) IJP
DEBELLEFON	76	NP B109 129	A. de Bellefon, A. Berthon	(CDEF) IJP
HEPP	76B	PL 65B 487	V. Hepp *et al.*	(CERN, HEIDH, MPIM) IJP
BAILLON	75	NP B94 39	P.H. Baillon, P.J. Litchfield	(CERN, RHEL) IJP
PONTE	75	PR D12 2597	R.A. Ponte *et al.*	(MASA, TENN, UCR) IJP
VANHORN	75	NP B87 145	A.J. van Horn	(LBL) IJP
Also		NP B87 157	A.J. van Horn	(LBL) IJP
DEVENISH	74B	NP B81 330	R.C.E. Devenish, C.D. Froggatt, B.R. Martin	(DESY+)
KANE	74	LBL-2452	D.F. Kane	(LBL) IJP
PREVOST	74	NP B69 246	J. Prevost *et al.*	(SACL, CERN, HEID)
BRUCKER	70	Duke Conf. 155 Hyperon Resonances, 1970	E.B. Brucker *et al.*	(FSU) I
BERLEY	69	PL 30B 430	D. Berley *et al.*	(BNL)
ARMENTEROS	68E	PL 28B 521	R. Armenteros *et al.*	(CERN, HEID, SACL) I
SIMS	68	PRL 21 1413	W.H. Sims *et al.*	(FSU, TUFTS, BRAN)

$\Sigma(1750)\ 1/2^-$

$I(J^P) = 1(\frac{1}{2}^-)$ Status: ***

For most results published before 1974 (they are now obsolete), see our 1982 edition Physics Letters **111B** 1 (1982).

There is evidence for this state in many partial-wave analyses, but with wide variations in the mass, width, and couplings. The latest analyses indicated significant couplings to $N\overline{K}$ and $\Lambda\pi$, as well as to $\Sigma\eta$ whose threshold is at 1746 MeV (JONES 74).

$\Sigma(1750)$ POLE POSITION

REAL PART

VALUE (MeV)	DOCUMENT ID		TECN	COMMENT
1689±11	SARANTSEV	19	DPWA	$\overline{K}N$ multichannel
• • • We do not use the following data for averages, fits, limits, etc. • • •				
1704^{+3}_{-6}	[1] KAMANO	15	DPWA	$\overline{K}N$ multichannel
1708	ZHANG	13A	DPWA	$\overline{K}N$ multichannel

[1] From the preferred solution A in KAMANO 15. Solution B reports two poles at M = 1551^{+2}_{-9} MeV and 1940^{+2}_{-2} MeV.

−2×IMAGINARY PART

VALUE (MeV)	DOCUMENT ID		TECN	COMMENT
206±18	SARANTSEV	19	DPWA	$\overline{K}N$ multichannel
• • • We do not use the following data for averages, fits, limits, etc. • • •				
86^{+14}_{-4}	[1] KAMANO	15	DPWA	$\overline{K}N$ multichannel
158	ZHANG	13A	DPWA	$\overline{K}N$ multichannel

[1] From the preferred solution A in KAMANO 15. Solution B Reports two poles with Γ = 376^{+12}_{-2} and 172^{+4}_{-4} MeV.

$\Sigma(1750)$ POLE RESIDUES

The normalized residue is the residue divided by $\Gamma_{pole}/2$.

Normalized residue in $N\overline{K} \to \Sigma(1750) \to N\overline{K}$

MODULUS	PHASE (°)	DOCUMENT ID		TECN	COMMENT
0.46 ±0.09	**−144 ± 15**	SARANTSEV	19	DPWA	$\overline{K}N$ multichannel
• • • We do not use the following data for averages, fits, limits, etc. • • •					
0.0982	178	[1] KAMANO	15	DPWA	$\overline{K}N$ multichannel

[1] From the preferred solution A in KAMANO 15.

Normalized residue in $N\overline{K} \to \Sigma(1750) \to \Sigma\pi$

MODULUS	PHASE (°)	DOCUMENT ID		TECN	COMMENT
0.27 ±0.05	**100 ± 18**	SARANTSEV	19	DPWA	$\overline{K}N$ multichannel
• • • We do not use the following data for averages, fits, limits, etc. • • •					
0.192	137	[1] KAMANO	15	DPWA	Multichannel

[1] From the preferred solution A in KAMANO 15.

Normalized residue in $N\overline{K} \to \Sigma(1750) \to \Sigma\eta$

MODULUS	PHASE (°)	DOCUMENT ID		TECN	COMMENT
0.05±0.03		SARANTSEV	19	DPWA	$\overline{K}N$ multichannel

Normalized residue in $N\overline{K} \to \Sigma(1750) \to \Lambda\pi$

MODULUS	PHASE (°)	DOCUMENT ID		TECN	COMMENT
0.26 ±0.06	**115 ± 15**	SARANTSEV	19	DPWA	$\overline{K}N$ multichannel
• • • We do not use the following data for averages, fits, limits, etc. • • •					
0.207	169	[1] KAMANO	15	DPWA	$\overline{K}N$ multichannel

[1] From the preferred solution A in KAMANO 15.

Normalized residue in $N\overline{K} \to \Sigma(1750) \to \Xi K$

MODULUS	PHASE (°)	DOCUMENT ID		TECN	COMMENT
0.02±0.02		SARANTSEV	19	DPWA	$\overline{K}N$ multichannel

Normalized residue in $N\overline{K} \to \Sigma(1750) \to \Sigma(1385)\pi$, D-wave

MODULUS	PHASE (°)	DOCUMENT ID		TECN	COMMENT
0.04 ±0.03		SARANTSEV	19	DPWA	$\overline{K}N$ multichannel
• • • We do not use the following data for averages, fits, limits, etc. • • •					
0.0536	73	[1] KAMANO	15	DPWA	$\overline{K}N$ multichannel

[1] From the preferred solution A in KAMANO 15.

Normalized residue in $N\overline{K} \to \Sigma(1750) \to \Lambda(1520)\pi$

MODULUS	PHASE (°)	DOCUMENT ID		TECN	COMMENT
0.15±0.07	**−25 ± 40**	SARANTSEV	19	DPWA	$\overline{K}N$ multichannel

Normalized residue in $N\overline{K} \to \Sigma(1750) \to N\overline{K}^*(892)$, S=1/2, S-wave

MODULUS	PHASE (°)	DOCUMENT ID		TECN	COMMENT
0.05±0.03	**−100 ± 35**	SARANTSEV	19	DPWA	$\overline{K}N$ multichannel

$\Sigma(1750)$ MASS

VALUE (MeV)	DOCUMENT ID		TECN	COMMENT
1700 to 1800 (≈ 1750) OUR ESTIMATE				
1692±11	SARANTSEV	19	DPWA	$\overline{K}N$ multichannel
1739± 8	ZHANG	13A	DPWA	$\overline{K}N$ multichannel
1756±10	GOPAL	80	DPWA	$\overline{K}N \to \overline{K}N$
1770±10	ALSTON-...	78	DPWA	$\overline{K}N \to \overline{K}N$
• • • We do not use the following data for averages, fits, limits, etc. • • •				
1770±15	GOPAL	77	DPWA	$\overline{K}N$ multichannel
1800 or 1813	[1] MARTIN	77	DPWA	$\overline{K}N$ multichannel
1715±10	[2] CARROLL	76	DPWA	Isospin-1 total σ
1730	DEBELLEFON	76	IPWA	$K^-p \to \Lambda\pi^0$
1780±30	BAILLON	75	IPWA	$\overline{K}N \to \Lambda\pi$ (sol. 1)
1700±30	BAILLON	75	IPWA	$\overline{K}N \to \Lambda\pi$ (sol. 2)
1697^{+20}_{-10}	VANHORN	75	DPWA	$K^-p \to \Lambda\pi^0$
1785±12	CHU	74	DBC	Fits $\sigma(K^-n \to \Sigma^-\eta)$
1760± 5	[3] JONES	74	HBC	Fits $\sigma(K^-p \to \Sigma^0\eta)$
1739±10	PREVOST	74	DPWA	$K^-N \to \Sigma(1385)\pi$

[1] The two MARTIN 77 values are from a T-matrix pole and from a Breit-Wigner fit.
[2] A total cross-section bump with $(J+1/2)\ \Gamma_{el}\ /\ \Gamma_{total} = 0.30$.
[3] An S-wave Breit-Wigner fit to the threshold cross section with no background and errors statistical only.

$\Sigma(1750)$ WIDTH

VALUE (MeV)	DOCUMENT ID		TECN	COMMENT
100 to 200 (≈ 150) OUR ESTIMATE				
208±18	SARANTSEV	19	DPWA	$\overline{K}N$ multichannel
182±60	ZHANG	13A	DPWA	$\overline{K}N$ multichannel
64±10	GOPAL	80	DPWA	$\overline{K}N \to \overline{K}N$
161±20	ALSTON-...	78	DPWA	$\overline{K}N \to \overline{K}N$
• • • We do not use the following data for averages, fits, limits, etc. • • •				
60±10	GOPAL	77	DPWA	$\overline{K}N$ multichannel
117 or 119	[1] MARTIN	77	DPWA	$\overline{K}N$ multichannel
10	[2] CARROLL	76	DPWA	Isospin-1 total σ
110	DEBELLEFON	76	IPWA	$K^-p \to \Lambda\pi^0$
140±30	BAILLON	75	IPWA	$\overline{K}N \to \Lambda\pi$ (sol. 1)
160±50	BAILLON	75	IPWA	$\overline{K}N \to \Lambda\pi$ (sol. 2)
66^{+14}_{-12}	VANHORN	75	DPWA	$K^-p \to \Lambda\pi^0$
89±33	CHU	74	DBC	Fits $\sigma(K^-n \to \Sigma^-\eta)$
92± 7	[3] JONES	74	HBC	Fits $\sigma(K^-p \to \Sigma^0\eta)$
108±20	PREVOST	74	DPWA	$K^-N \to \Sigma(1385)\pi$

[1] The two MARTIN 77 values are from a T-matrix pole and from a Breit-Wigner fit.
[2] A total cross-section bump with $(J+1/2)\ \Gamma_{el}\ /\ \Gamma_{total} = 0.30$.
[3] An S-wave Breit-Wigner fit to the threshold cross section with no background and errors statistical only.

$\Sigma(1750)$ DECAY MODES

	Mode	Fraction (Γ_i/Γ)
Γ_1	$N\overline{K}$	0.06 to 0.12
Γ_2	$\Lambda\pi$	(14 ±5) %
Γ_3	$\Sigma\pi$	(16 ±4) %
Γ_4	$\Sigma\eta$	15–55 %
Γ_5	$\Sigma(1385)\pi$, D-wave	< 1 %
Γ_6	$\Lambda(1520)\pi$	(2.0 ±1.0) %
Γ_7	$N\overline{K}^*(892)$, S=1/2	(8 ±4) %
Γ_8	$N\overline{K}^*(892)$, S=3/2, D-wave	

$\Sigma(1750)$ BRANCHING RATIOS

See "Sign conventions for resonance couplings" in the Note on Λ and Σ Resonances.

$\Gamma(N\overline{K})/\Gamma_{total}$ — Γ_1/Γ

VALUE	DOCUMENT ID		TECN	COMMENT
0.06 to 0.12 OUR ESTIMATE				
0.46 ±0.09	SARANTSEV	19	DPWA	$\overline{K}N$ multichannel
0.09 ±0.07	ZHANG	13A	DPWA	Multichannel
0.14 ±0.03	GOPAL	80	DPWA	$\overline{K}N \to \overline{K}N$
0.33 ±0.05	ALSTON-...	78	DPWA	$\overline{K}N \to \overline{K}N$

Downloaded from https://academic.oup.com/ptep/article/2022/8/083C01/6651666 by KIT Library user on 27 September 2022

• • • We do not use the following data for averages, fits, limits, etc. • • •

0.154	[1] KAMANO	15	DPWA	Multichannel
0.15 ±0.03	GOPAL	77	DPWA	See GOPAL 80
0.06 or 0.05	[2] MARTIN	77	DPWA	$\overline{K}N$ multichannel

[1] From the preferred solution A in KAMANO 15.
[2] The two MARTIN 77 values are from a T-matrix pole and from a Breit-Wigner fit.

$\Gamma(\Lambda\pi)/\Gamma_{total}$ — Γ_2/Γ

VALUE	DOCUMENT ID		TECN	COMMENT
0.14 ±0.05	SARANTSEV	19	DPWA	$\overline{K}N$ multichannel
• • • We do not use the following data for averages, fits, limits, etc. • • •				
0.435	[1] KAMANO	15	DPWA	$\overline{K}N$ multichannel

[1] From the preferred solution A in KAMANO 15.

$\Gamma(\Sigma\pi)/\Gamma_{total}$ — Γ_3/Γ

VALUE	DOCUMENT ID		TECN	COMMENT
0.16 ±0.04	SARANTSEV	19	DPWA	$\overline{K}N$ multichannel
• • • We do not use the following data for averages, fits, limits, etc. • • •				
0.373	[1] KAMANO	15	DPWA	$\overline{K}N$ multichannel

[1] From the preferred solution A in KAMANO 15.

$\Gamma(\Lambda(1520)\pi)/\Gamma_{total}$ — Γ_6/Γ

VALUE	DOCUMENT ID		TECN	COMMENT
0.02±0.01	SARANTSEV	19	DPWA	$\overline{K}N$ multichannel

$\Gamma(\Sigma(1385)\pi, D\text{-wave})/\Gamma_{total}$ — Γ_5/Γ

VALUE	DOCUMENT ID		TECN	COMMENT
<0.01	SARANTSEV	19	DPWA	$\overline{K}N$ multichannel
• • • We do not use the following data for averages, fits, limits, etc. • • •				
0.024	[1] KAMANO	15	DPWA	$\overline{K}N$ multichannel

[1] From the preferred solution A in KAMANO 15.

$\Gamma(N\overline{K}^*(892), S=1/2)/\Gamma_{total}$ — Γ_7/Γ

VALUE	DOCUMENT ID		TECN	COMMENT
∼ 0	SARANTSEV	19	DPWA	$\overline{K}N$ multichannel
0.08 ±0.04	ZHANG	13A	DPWA	$\overline{K}N$ multichannel
• • • We do not use the following data for averages, fits, limits, etc. • • •				
0.004	[1] KAMANO	15	DPWA	$\overline{K}N$ multichannel

[1] From the preferred solution A in KAMANO 15.

$\Gamma(N\overline{K}^*(892), S=3/2, D\text{-wave})/\Gamma_{total}$ — Γ_8/Γ

VALUE	DOCUMENT ID		TECN	COMMENT
• • • We do not use the following data for averages, fits, limits, etc. • • •				
0.01	[1] KAMANO	15	DPWA	Multichannel

[1] From the preferred solution A in KAMANO 15.

$(\Gamma_i\Gamma_f)^{1/2}/\Gamma_{total}$ in $N\overline{K}\to\Sigma(1750)\to\Lambda\pi$ — $(\Gamma_1\Gamma_2)^{1/2}/\Gamma$

VALUE	DOCUMENT ID		TECN	COMMENT
+0.10 ±0.04	ZHANG	13A	DPWA	Multichannel
0.04 ±0.03	GOPAL	77	DPWA	$\overline{K}N$ multichannel
• • • We do not use the following data for averages, fits, limits, etc. • • •				
−0.10 or −0.09	[1] MARTIN	77	DPWA	$\overline{K}N$ multichannel
−0.12	DEBELLEFON	76	IPWA	$K^-p\to\Lambda\pi^0$
−0.12 ±0.02	BAILLON	75	IPWA	$\overline{K}N\to\Lambda\pi$ (sol. 1)
−0.13 ±0.03	BAILLON	75	IPWA	$\overline{K}N\to\Lambda\pi$ (sol. 2)
−0.13 ±0.04	VANHORN	75	DPWA	$K^-p\to\Lambda\pi^0$
−0.120±0.077	DEVENISH	74B		Fixed-t dispersion rel.

[1] The two MARTIN 77 values are from a T-matrix pole and from a Breit-Wigner fit.

$(\Gamma_i\Gamma_f)^{1/2}/\Gamma_{total}$ in $N\overline{K}\to\Sigma(1750)\to\Sigma\pi$ — $(\Gamma_1\Gamma_3)^{1/2}/\Gamma$

VALUE	DOCUMENT ID		TECN	COMMENT
+0.17±0.07	ZHANG	13A	DPWA	Multichannel
−0.09±0.05	GOPAL	77	DPWA	$\overline{K}N$ multichannel
• • • We do not use the following data for averages, fits, limits, etc. • • •				
+0.06 or +0.06	[1] MARTIN	77	DPWA	$\overline{K}N$ multichannel
0.13±0.02	LANGBEIN	72	IPWA	$\overline{K}N$ multichannel

[1] The two MARTIN 77 values are from a T-matrix pole and from a Breit-Wigner fit.

$(\Gamma_i\Gamma_f)^{1/2}/\Gamma_{total}$ in $N\overline{K}\to\Sigma(1750)\to\Sigma\eta$ — $(\Gamma_1\Gamma_4)^{1/2}/\Gamma$

VALUE	DOCUMENT ID		TECN	COMMENT
0.23±0.01	[1] JONES	74	HBC	Fits $\sigma(K^-p\to\Sigma^0\eta)$
• • • We do not use the following data for averages, fits, limits, etc. • • •				
seen	CLINE	69	DBC	Threshold bump

[1] An S-wave Breit-Wigner fit to the threshold cross section with no background and errors statistical only.

$(\Gamma_i\Gamma_f)^{1/2}/\Gamma_{total}$ in $N\overline{K}\to\Sigma(1750)\to\Sigma(1385)\pi$, D-wave — $(\Gamma_1\Gamma_5)^{1/2}/\Gamma$

VALUE	DOCUMENT ID		TECN	COMMENT
+0.17±0.07	ZHANG	13A	DPWA	Multichannel
+0.18±0.15	PREVOST	74	DPWA	$K^-N\to\Sigma(1385)\pi$

$(\Gamma_i\Gamma_f)^{1/2}/\Gamma_{total}$ in $N\overline{K}\to\Sigma(1750)\to\Lambda(1520)\pi$ — $(\Gamma_1\Gamma_6)^{1/2}/\Gamma$

VALUE	DOCUMENT ID		TECN	COMMENT
• • • We do not use the following data for averages, fits, limits, etc. • • •				
0.032±0.021	CAMERON	77	DPWA	P-wave decay

$\Sigma(1750)$ REFERENCES

SARANTSEV	19	EPJ A55 180	A.V. Sarantsev *et al.*	(BONN, PNPI)
KAMANO	15	PR C92 025205	H. Kamano *et al.*	(ANL, OSAK)
ZHANG	13A	PR C88 035205	H. Zhang *et al.*	(KSU)
PDG	82	PL 111B 1	M. Roos *et al.*	(HELS, CIT, CERN)
GOPAL	80	Toronto Conf. 159	G.P. Gopal	(RHEL) IJP
ALSTON-...	78	PR D18 182	M. Alston-Garnjost *et al.*	(LBL, MTHO+) IJP
Also		PRL 38 1007	M. Alston-Garnjost *et al.*	(LBL, MTHO+) IJP
CAMERON	77	NP B131 399	W. Cameron *et al.*	(RHEL, LOIC) IJP
GOPAL	77	NP B119 362	G.P. Gopal *et al.*	(LOIC, RHEL) IJP
MARTIN	77	NP B127 349	B.R. Martin, M.K. Pidcock, R.G. Moorhouse	(LOUC+) IJP
Also		NP B126 266	B.R. Martin, M.K. Pidcock	(LOUC)
Also		NP B126 285	B.R. Martin, M.K. Pidcock	(LOUC) IJP
CARROLL	76	PRL 37 806	A.S. Carroll *et al.*	(BNL) I
DEBELLEFON	76	NP B109 129	A. de Bellefon, A. Berthon	(CDEF) IJP
BAILLON	75	NP B94 39	P.H. Baillon, P.J. Litchfield	(CERN, RHEL) IJP
VANHORN	75	NP B87 145	A.J. van Horn	(LBL) IJP
Also		NP B87 157	A.J. van Horn	(LBL) IJP
CHU	74	NC 20A 35	R.Y.L. Chu *et al.*	(PLAT, TUFTS, BRAN) IJP
DEVENISH	74B	NP B81 330	R.C.E. Devenish, C.D. Froggatt, B.R. Martin	(DESY+)
JONES	74	NP B73 141	M.D. Jones	(CHIC) IJP
PREVOST	74	NP B69 246	J. Prevost *et al.*	(SACL, CERN, HEID)
LANGBEIN	72	NP B47 477	W. Langbein, F. Wagner	(MPIM) IJP
CLINE	69	LNC 2 407	D. Cline, R. Laumann, J. Mapp	(WISC)

$\Sigma(1775)\ 5/2^-$

$I(J^P) = 1(\frac{5}{2}^-)$ Status: ****

Discovered by GALTIERI 63, this resonance plays the same role as cornerstone for isospin-1 analyses in this region as the $\Lambda(1820)F_{05}$ does in the isospin-0 channel.

For most results published before 1974 (they are now obsolete), see our 1982 edition Physics Letters **111B** 1 (1982).

$\Sigma(1775)$ POLE POSITION

REAL PART

VALUE (MeV)	DOCUMENT ID		TECN	COMMENT
1760 to 1780 (≈ 1770) OUR ESTIMATE				
1767±4	SARANTSEV	19	DPWA	$\overline{K}N$ multichannel
1767^{+2}_{-2}	[1] KAMANO	15	DPWA	$\overline{K}N$ multichannel
• • • We do not use the following data for averages, fits, limits, etc. • • •				
1759	ZHANG	13A	DPWA	$\overline{K}N$ multichannel

[1] From the preferred solution A in KAMANO 15.

−2×IMAGINARY PART

VALUE (MeV)	DOCUMENT ID		TECN	COMMENT
45 to 65 (≈ 55) OUR ESTIMATE				
122±8	SARANTSEV	19	DPWA	$\overline{K}N$ multichannel
128^{+4}_{-2}	[1] KAMANO	15	DPWA	$\overline{K}N$ multichannel
• • • We do not use the following data for averages, fits, limits, etc. • • •				
118	ZHANG	13A	DPWA	$\overline{K}N$ multichannel

[1] From the preferred solution A in KAMANO 15.

$\Sigma(1775)$ POLE RESIDUES

The normalized residue is the residue divided by $\Gamma_{pole}/2$.

Normalized residue in $N\overline{K}\to\Sigma(1775)\to N\overline{K}$

MODULUS	PHASE (°)	DOCUMENT ID		TECN	COMMENT
0.44 ±0.09	−17 ± 10	SARANTSEV	19	DPWA	$\overline{K}N$ multichannel
• • • We do not use the following data for averages, fits, limits, etc. • • •					
0.371	−32	[1] KAMANO	15	DPWA	$\overline{K}N$ multichannel

[1] From the preferred solution A in KAMANO 15.

Normalized residue in $N\overline{K}\to\Sigma(1775)\to\Sigma\pi$

MODULUS	PHASE (°)	DOCUMENT ID		TECN	COMMENT
0.13 ±0.03	10 ± 12	SARANTSEV	19	DPWA	$\overline{K}N$ multichannel
• • • We do not use the following data for averages, fits, limits, etc. • • •					
0.115	−24	[1] KAMANO	15	DPWA	$\overline{K}N$ multichannel

[1] From the preferred solution A in KAMANO 15.

Normalized residue in $N\overline{K}\to\Sigma(1775)\to\Lambda\pi$

MODULUS	PHASE (°)	DOCUMENT ID		TECN	COMMENT
0.47 ±0.10	130 ± 15	SARANTSEV	19	DPWA	$\overline{K}N$ multichannel
• • • We do not use the following data for averages, fits, limits, etc. • • •					
0.325	157	[1] KAMANO	15	DPWA	$\overline{K}N$ multichannel

[1] From the preferred solution A in KAMANO 15.

Downloaded from https://academic.oup.com/ptep/article/2022/8/083C01/6651666 by KIT Library user on 27 September 2022

Normalized residue in $N\overline{K} \to \Sigma(1775) \to \Sigma(1385)\pi$, D-wave

MODULUS	PHASE (°)	DOCUMENT ID		TECN	COMMENT
• • • We do not use the following data for averages, fits, limits, etc. • • •					
0.391	137	[1] KAMANO	15	DPWA	$\overline{K}N$ multichannel

[1] From the preferred solution A in KAMANO 15.

Normalized residue in $N\overline{K} \to \Sigma(1775) \to \Sigma(1385)\pi$, G-wave

MODULUS	PHASE (°)	DOCUMENT ID		TECN	COMMENT
• • • We do not use the following data for averages, fits, limits, etc. • • •					
0.0129	−58	[1] KAMANO	15	DPWA	$\overline{K}N$ multichannel

[1] From the preferred solution A in KAMANO 15.

Normalized residue in $N\overline{K} \to \Sigma(1775) \to N\overline{K}^*(892)$, S=1/2, D-wave

MODULUS	PHASE (°)	DOCUMENT ID		TECN	COMMENT
0.04±0.02	−100 ± 60	SARANTSEV	19	DPWA	$\overline{K}N$ multichannel

Normalized residue in $N\overline{K} \to \Sigma(1775) \to N\overline{K}^*(892)$, S=3/2, D-wave

MODULUS	PHASE (°)	DOCUMENT ID		TECN	COMMENT
0.09±0.06	10 ± 50	SARANTSEV	19	DPWA	$\overline{K}N$ multichannel

Normalized residue in $N\overline{K} \to \Sigma(1775) \to N\overline{K}^*(892)$, S=3/2, G-wave

MODULUS	PHASE (°)	DOCUMENT ID		TECN	COMMENT
0.04±0.02	−100 ± 60	SARANTSEV	19	DPWA	$\overline{K}N$ multichannel

Normalized residue in $N\overline{K} \to \Sigma(1775) \to \Xi K$

MODULUS	PHASE (°)	DOCUMENT ID		TECN	COMMENT
0.02±0.01	−90 ± 35	SARANTSEV	19	DPWA	$\overline{K}N$ multichannel

Normalized residue in $N\overline{K} \to \Sigma(1775) \to \Lambda(1520)\pi$, P-wave

MODULUS	PHASE (°)	DOCUMENT ID		TECN	COMMENT
0.09±0.03	10 ± 30	SARANTSEV	19	DPWA	$\overline{K}N$ multichannel

Normalized residue in $N\overline{K} \to \Sigma(1775) \to \Lambda(1520)\pi$, F-wave

VALUE	DOCUMENT ID		TECN	COMMENT
0.01±0.01	SARANTSEV	19	DPWA	$\overline{K}N$ multichannel

Normalized residue in $N\overline{K} \to \Sigma(1775) \to \Delta\overline{K}$, D-wave

VALUE	DOCUMENT ID		TECN	COMMENT
0.02±0.02	SARANTSEV	19	DPWA	$\overline{K}N$ multichannel

$\Sigma(1775)$ MASS

VALUE (MeV)	DOCUMENT ID		TECN	COMMENT
1770 to 1780 (≈ 1775) OUR ESTIMATE				
1776± 4	SARANTSEV	19	DPWA	$\overline{K}N$ multichannel
1778± 1	ZHANG	13A	DPWA	$\overline{K}N$ multichannel
1778± 5	GOPAL	80	DPWA	$\overline{K}N \to \overline{K}N$
1777± 5	ALSTON-...	78	DPWA	$\overline{K}N \to \overline{K}N$
1775±10	BAILLON	75	IPWA	$\overline{K}N \to \Lambda\pi$
1774±10	VANHORN	75	DPWA	$K^-p \to \Lambda\pi^0$
1772± 6	KANE	74	DPWA	$K^-p \to \Sigma\pi$
• • • We do not use the following data for averages, fits, limits, etc. • • •				
1774± 5	GOPAL	77	DPWA	$\overline{K}N$ multichannel
1772 or 1777	[1] MARTIN	77	DPWA	$\overline{K}N$ multichannel
1765	DEBELLEFON	76	IPWA	$K^-p \to \Lambda\pi^0$

[1] The two MARTIN 77 values are from a T-matrix pole and from a Breit-Wigner fit.

$\Sigma(1775)$ WIDTH

VALUE (MeV)	DOCUMENT ID		TECN	COMMENT
105 to 135 (≈ 120) OUR ESTIMATE				
124± 8	SARANTSEV	19	DPWA	$\overline{K}N$ multichannel
131± 3	ZHANG	13A	DPWA	$\overline{K}N$ multichannel
137±10	GOPAL	80	DPWA	$\overline{K}N \to \overline{K}N$
116±10	ALSTON-...	78	DPWA	$\overline{K}N \to \overline{K}N$
125±15	BAILLON	75	IPWA	$\overline{K}N \to \Lambda\pi$
146±18	VANHORN	75	DPWA	$K^-p \to \Lambda\pi^0$
154±10	KANE	74	DPWA	$K^-p \to \Sigma\pi$
• • • We do not use the following data for averages, fits, limits, etc. • • •				
130±10	GOPAL	77	DPWA	$\overline{K}N$ multichannel
102 or 103	[1] MARTIN	77	DPWA	$\overline{K}N$ multichannel
120	DEBELLEFON	76	IPWA	$K^-p \to \Lambda\pi^0$

[1] The two MARTIN 77 values are from a T-matrix pole and from a Breit-Wigner fit.

$\Sigma(1775)$ DECAY MODES

	Mode	Fraction (Γ_i/Γ)
Γ_1	$N\overline{K}$	37–43%
Γ_2	$\Lambda\pi$	14–20%
Γ_3	$\Sigma\pi$	2–5%
Γ_4	$\Sigma(1385)\pi$	8–12%
Γ_5	$\Sigma(1385)\pi$, D-wave	
Γ_6	$\Sigma(1385)\pi$, G-wave	
Γ_7	$\Lambda(1520)\pi$, P-wave	17–23%
Γ_8	$\Sigma\pi\pi$	
Γ_9	$\Delta(1232)\overline{K}$, D-wave	
Γ_{10}	$N\overline{K}^*(892)$, S=1/2	
Γ_{11}	$N\overline{K}^*(892)$, S=1/2, D-wave	
Γ_{12}	$N\overline{K}^*(892)$, S=3/2, D-wave	
Γ_{13}	$N\overline{K}^*(892)$, S=3/2, G-wave	

$\Sigma(1775)$ BRANCHING RATIOS

See "Sign conventions for resonance couplings" in the Note on Λ and Σ Resonances. Also, the errors quoted do not include uncertainties due to the parametrization used in the partial-wave analyses and are thus too small.

$\Gamma(N\overline{K})/\Gamma_{total}$ — Γ_1/Γ

VALUE	DOCUMENT ID		TECN	COMMENT
0.37 to 0.43 OUR ESTIMATE				
0.43 ±0.09	SARANTSEV	19	DPWA	$\overline{K}N$ multichannel
0.40 ±0.01	ZHANG	13A	DPWA	$\overline{K}N$ multichannel
0.40 ±0.02	GOPAL	80	DPWA	$\overline{K}N \to \overline{K}N$
0.37 ±0.03	ALSTON-...	78	DPWA	$\overline{K}N \to \overline{K}N$
• • • We do not use the following data for averages, fits, limits, etc. • • •				
0.402	[1] KAMANO	15	DPWA	Multichannel
0.41 ±0.03	GOPAL	77	DPWA	See GOPAL 80
0.37 or 0.36	[2] MARTIN	77	DPWA	$\overline{K}N$ multichannel

[1] From the preferred solution A in KAMANO 15.
[2] The two MARTIN 77 values are from a T-matrix pole and from a Breit-Wigner fit.

$\Gamma(\Lambda\pi)/\Gamma_{total}$ — Γ_2/Γ

VALUE	DOCUMENT ID		TECN	COMMENT
0.49 ±0.10	SARANTSEV	19	DPWA	$\overline{K}N$ multichannel
• • • We do not use the following data for averages, fits, limits, etc. • • •				
0.244	[1] KAMANO	15	DPWA	$\overline{K}N$ multichannel

[1] From the preferred solution A in KAMANO 15.

$\Gamma(\Lambda\pi)/\Gamma(N\overline{K})$ — Γ_2/Γ_1

VALUE	DOCUMENT ID		TECN	COMMENT
0.33±0.05	UHLIG	67	HBC	K^-p 0.9 GeV/c

$\Gamma(\Sigma\pi)/\Gamma_{total}$ — Γ_3/Γ

VALUE	DOCUMENT ID		TECN	COMMENT
0.035±0.010	SARANTSEV	19	DPWA	$\overline{K}N$ multichannel
• • • We do not use the following data for averages, fits, limits, etc. • • •				
0.042	[1] KAMANO	15	DPWA	$\overline{K}N$ multichannel

[1] From the preferred solution A in KAMANO 15.

$\Gamma(\Sigma(1385)\pi)/\Gamma(N\overline{K})$ — Γ_4/Γ_1

VALUE	DOCUMENT ID		TECN	COMMENT
0.25±0.09	UHLIG	67	HBC	K^-p 0.9 GeV/c

$\Gamma(\Sigma(1385)\pi$, D-wave$)/\Gamma_{total}$ — Γ_5/Γ

VALUE	DOCUMENT ID		TECN	COMMENT
• • • We do not use the following data for averages, fits, limits, etc. • • •				
0.309	[1] KAMANO	15	DPWA	Multichannel

[1] From the preferred solution A in KAMANO 15.

$\Gamma(\Sigma(1385)\pi$, G-wave$)/\Gamma_{total}$ — Γ_6/Γ

VALUE	DOCUMENT ID		TECN	COMMENT
• • • We do not use the following data for averages, fits, limits, etc. • • •				
not seen	[1] KAMANO	15	DPWA	Multichannel

[1] From the preferred solution A in KAMANO 15.

$\Gamma(\Lambda(1520)\pi$, P-wave$)/\Gamma_{total}$ — Γ_7/Γ

VALUE	DOCUMENT ID		TECN	COMMENT
0.02±0.01	SARANTSEV	19	DPWA	$\overline{K}N$ multichannel

$\Gamma(\Lambda(1520)\pi$, P-wave$)/\Gamma(N\overline{K})$ — Γ_7/Γ_1

VALUE	DOCUMENT ID		TECN	COMMENT
0.28±0.05	UHLIG	67	HBC	K^-p 0.9 GeV/c

$\Gamma(\Sigma\pi\pi)/\Gamma_{total}$ — Γ_8/Γ

VALUE	DOCUMENT ID		TECN	COMMENT
• • • We do not use the following data for averages, fits, limits, etc. • • •				
0.12	[1] ARMENTEROS68C		HDBC	$K^-N \to \Sigma\pi\pi$

[1] For about 3/4 of this, the $\Sigma\pi$ system has $I = 0$ and is almost entirely $\Lambda(1520)$. For the rest, the $\Sigma\pi$ has $I = 1$, which is about what is expected from the known $\Sigma(1775) \to \Sigma(1385)\pi$ rate, as seen in $\Lambda\pi\pi$.

$\Gamma(N\overline{K}^*(892)$, S=1/2, D-wave$)/\Gamma_{total}$ — Γ_{11}/Γ

VALUE	DOCUMENT ID		TECN	COMMENT
• • • We do not use the following data for averages, fits, limits, etc. • • •				
not seen	[1] KAMANO	15	DPWA	Multichannel

[1] From the preferred solution A in KAMANO 15.

Downloaded from https://academic.oup.com/ptep/article/2022/8/083C01/6651666 by KIT Library user on 27 September 2022

$\Gamma(N\overline{K}^*(892), S=3/2, D\text{-wave})/\Gamma_{total}$ — Γ_{12}/Γ

VALUE	DOCUMENT ID		TECN	COMMENT
• • • We do not use the following data for averages, fits, limits, etc. • • •				
0.003	[1] KAMANO	15	DPWA	Multichannel

[1] From the preferred solution A in KAMANO 15.

$\Gamma(N\overline{K}^*(892), S=3/2, G\text{-wave})/\Gamma_{total}$ — Γ_{13}/Γ

VALUE	DOCUMENT ID		TECN	COMMENT
• • • We do not use the following data for averages, fits, limits, etc. • • •				
not seen	[1] KAMANO	15	DPWA	Multichannel

[1] From the preferred solution A in KAMANO 15.

$(\Gamma_i\Gamma_f)^{1/2}/\Gamma_{total}$ in $N\overline{K} \to \Sigma(1775) \to \Lambda\pi$ — $(\Gamma_1\Gamma_2)^{1/2}/\Gamma$

VALUE	DOCUMENT ID		TECN	COMMENT
-0.31 ± 0.01	ZHANG	13A	DPWA	Multichannel
-0.28 ± 0.03	GOPAL	77	DPWA	$\overline{K}N$ multichannel
-0.25 ± 0.02	BAILLON	75	IPWA	$\overline{K}N \to \Lambda\pi$
$-0.28\ ^{+0.04}_{-0.05}$	VANHORN	75	DPWA	$K^-p \to \Lambda\pi^0$
-0.259 ± 0.048	DEVENISH	74B		Fixed-t dispersion rel.
• • • We do not use the following data for averages, fits, limits, etc. • • •				
-0.29 or -0.28	[1] MARTIN	77	DPWA	$\overline{K}N$ multichannel
-0.30	DEBELLEFON	76	IPWA	$K^-p \to \Lambda\pi^0$

[1] The two MARTIN 77 values are from a T-matrix pole and from a Breit-Wigner fit.

$(\Gamma_i\Gamma_f)^{1/2}/\Gamma_{total}$ in $N\overline{K} \to \Sigma(1775) \to \Sigma\pi$ — $(\Gamma_1\Gamma_3)^{1/2}/\Gamma$

VALUE	DOCUMENT ID		TECN	COMMENT
$+0.08 \pm 0.01$	ZHANG	13A	DPWA	Multichannel
$+0.13 \pm 0.02$	GOPAL	77	DPWA	$\overline{K}N$ multichannel
0.09 ± 0.01	KANE	74	DPWA	$K^-p \to \Sigma\pi$
• • • We do not use the following data for averages, fits, limits, etc. • • •				
$+0.08$ or $+0.08$	[1] MARTIN	77	DPWA	$\overline{K}N$ multichannel

[1] The two MARTIN 77 values are from a T-matrix pole and from a Breit-Wigner fit.

$(\Gamma_i\Gamma_f)^{1/2}/\Gamma_{total}$ in $N\overline{K} \to \Sigma(1775) \to \Sigma(1385)\pi$, D-wave — $(\Gamma_1\Gamma_5)^{1/2}/\Gamma$

VALUE	DOCUMENT ID		TECN	COMMENT
-0.12 ± 0.01	ZHANG	13A	DPWA	Multichannel
-0.184 ± 0.011	[1] CAMERON	78	DPWA	$K^-p \to \Sigma(1385)\pi$
$+0.20 \pm 0.02$	PREVOST	74	DPWA	$K^-N \to \Sigma(1385)\pi$
• • • We do not use the following data for averages, fits, limits, etc. • • •				
0.32 ± 0.06	SIMS	68	DBC	$K^-N \to \Lambda\pi\pi$
0.24 ± 0.03	ARMENTEROS	67C	HBC	$K^-p \to \Lambda\pi\pi$

[1] The CAMERON 78 upper limit on G-wave decay is 0.03.

$(\Gamma_i\Gamma_f)^{1/2}/\Gamma_{total}$ in $N\overline{K} \to \Sigma(1775) \to \Lambda(1520)\pi$, P-wave — $(\Gamma_1\Gamma_7)^{1/2}/\Gamma$

VALUE	DOCUMENT ID		TECN	COMMENT
-0.06 ± 0.01	ZHANG	13A	DPWA	Multichannel
-0.305 ± 0.010	[1] CAMERON	77	DPWA	$K^-p \to \Lambda(1520)\pi^0$
0.31 ± 0.02	BARLETTA	72	DPWA	$K^-p \to \Lambda(1520)\pi^0$
0.27 ± 0.03	ARMENTEROS	65C	HBC	$K^-p \to \Lambda(1520)\pi^0$

[1] This rate combines P-wave- and F-wave decays. The CAMERON 77 results for the separate P-wave- and F-wave decays are -0.303 ± 0.010 and -0.037 ± 0.014. The published signs have been changed here to be in accord with the baryon-first convention.

$(\Gamma_i\Gamma_f)^{1/2}/\Gamma_{total}$ in $N\overline{K} \to \Sigma(1775) \to \Delta(1232)\overline{K}$, D-wave — $(\Gamma_1\Gamma_9)^{1/2}/\Gamma$

VALUE	DOCUMENT ID		TECN	COMMENT
$+0.06 \pm 0.03$	ZHANG	13A	DPWA	Multichannel

$(\Gamma_i\Gamma_f)^{1/2}/\Gamma_{total}$ in $N\overline{K} \to \Sigma(1775) \to N\overline{K}^*(892)$, $S=1/2$ — $(\Gamma_1\Gamma_{10})^{1/2}/\Gamma$

VALUE	DOCUMENT ID		TECN	COMMENT
$+0.04 \pm 0.01$	ZHANG	13A	DPWA	Multichannel

$(\Gamma_i\Gamma_f)^{1/2}/\Gamma_{total}$ in $N\overline{K} \to \Sigma(1775) \to N\overline{K}^*(892)$, $S=3/2$, D-wave — $(\Gamma_1\Gamma_{12})^{1/2}/\Gamma$

VALUE	DOCUMENT ID		TECN	COMMENT
$+0.04 \pm 0.01$	ZHANG	13A	DPWA	Multichannel

$\Sigma(1775)$ REFERENCES

SARANTSEV	19	EPJ A55 180	A.V. Sarantsev *et al.*	(BONN, PNPI)
KAMANO	15	PR C92 025205	H. Kamano *et al.*	(ANL, OSAK)
ZHANG	13A	PR C88 035205	H. Zhang *et al.*	(KSU)
PDG	82	PL 111B 1	M. Roos *et al.*	(HELS, CIT, CERN)
GOPAL	80	Toronto Conf. 159	G.P. Gopal	(RHEL) IJP
ALSTON-...	78	PR D18 182	M. Alston-Garnjost *et al.*	(LBL, MTHO+) IJP
Also		PRL 38 1007	M. Alston-Garnjost *et al.*	(LBL, MTHO+) IJP
CAMERON	78	NP B143 189	W. Cameron *et al.*	(RHEL, LOIC) IJP
CAMERON	77	NP B131 399	W. Cameron *et al.*	(RHEL, LOIC) IJP
GOPAL	77	NP B119 362	G.P. Gopal *et al.*	(LOIC, RHEL) IJP
MARTIN	77	NP B127 349	B.R. Martin, M.K. Pidcock, R.G. Moorhouse	(LOUC+) IJP
Also		NP B126 266	B.R. Martin, M.K. Pidcock	(LOUC)
Also		NP B126 285	B.R. Martin, M.K. Pidcock	(LOUC) IJP
DEBELLEFON	76	NP B109 129	A. de Bellefon, A. Berthon	(CDEF) IJP
BAILLON	75	NP B94 39	P.H. Baillon, P.J. Litchfield	(CERN, RHEL) IJP
VANHORN	75	NP B87 145	A.J. van Horn	(LBL) IJP
Also		NP B87 157	A.J. van Horn	(LBL) IJP
DEVENISH	74B	NP B81 330	R.C.E. Devenish, C.D. Froggatt, B.R. Martin	(DESY+)
KANE	74	LBL-2452	D.F. Kane	(LBL) IJP
PREVOST	74	NP B69 246	J. Prevost *et al.*	(SACL, CERN, HEID)
BARLETTA	72	NP B40 45	W.A. Barletta	(EFI) IJP
Also		PRL 17 841	S. Fenster *et al.*	(CHIC, ANL, CERN) IJP
ARMENTEROS	68C	NP B8 216	R. Armenteros *et al.*	(CERN, HEID, SACL) I
SIMS	68	PRL 21 1413	W.H. Sims *et al.*	(FSU, TUFTS, BRAN)
ARMENTEROS	67C	ZPHY 202 486	R. Armenteros *et al.*	(CERN, HEID, SACL)
UHLIG	67	PR 155 1448	R.P. Uhlig *et al.*	(UMD, NRL)
ARMENTEROS	65C	PL 19 338	R. Armenteros *et al.*	(CERN, HEID, SACL) IJP
GALTIERI	63	PL 6 296	A. Galtieri, A. Hussain, R. Tripp	(LRL) IJ

$\Sigma(1780)\ 3/2^+$

$I(J^P) = 1(\frac{3}{2}^+)$ Status: *

OMITTED FROM SUMMARY TABLE
was $\Sigma(1730)$

$\Sigma(1780)$ MASS

VALUE (MeV)	DOCUMENT ID		TECN	COMMENT
1730 to 1830 (≈ 1780) OUR ESTIMATE				
1727 ± 27	ZHANG	13A	DPWA	Multichannel
1798 or 1802	[1] MARTIN	77	DPWA	$\overline{K}N$ multichannel
1720 ± 30	[2] BAILLON	75	IPWA	$\overline{K}N \to \Lambda\pi$
1840 ± 10	LANGBEIN	72	IPWA	$\overline{K}N$ multichannel

[1] The two MARTIN 77 values are from a T-matrix pole and from a Breit-Wigner fit.
[2] From solution 1 of BAILLON 75; not present in solution 2.

$\Sigma(1780)$ WIDTH

VALUE (MeV)	DOCUMENT ID		TECN	COMMENT
100 to 300 (≈ 200) OUR ESTIMATE				
276 ± 87	ZHANG	13A	DPWA	Multichannel
93 or 93	[1] MARTIN	77	DPWA	$\overline{K}N$ multichannel
120 ± 30	[2] BAILLON	75	IPWA	$\overline{K}N \to \Lambda\pi$
120 ± 10	LANGBEIN	72	IPWA	$\overline{K}N$ multichannel

[1] The two MARTIN 77 values are from a T-matrix pole and from a Breit-Wigner fit.
[2] From solution 1 of BAILLON 75; not present in solution 2.

$\Sigma(1780)$ DECAY MODES

	Mode	Fraction (Γ_i/Γ)
Γ_1	$N\overline{K}$	(2.0 ± 1.0) %
Γ_2	$\Lambda\pi$	(70 ± 17) %
Γ_3	$\Sigma\pi$	(12 ± 6) %

$\Sigma(1780)$ BRANCHING RATIOS

$\Gamma(N\overline{K})/\Gamma_{total}$ — Γ_1/Γ

VALUE	DOCUMENT ID		TECN	COMMENT
0.02±0.01	ZHANG	13A	DPWA	Multichannel

$\Gamma(\Lambda\pi)/\Gamma_{total}$ — Γ_2/Γ

VALUE	DOCUMENT ID		TECN	COMMENT
0.70±0.17	ZHANG	13A	DPWA	Multichannel

$\Gamma(\Sigma\pi)/\Gamma_{total}$ — Γ_3/Γ

VALUE	DOCUMENT ID		TECN	COMMENT
0.12±0.06	ZHANG	13A	DPWA	Multichannel

$\Sigma(1780)$ REFERENCES

ZHANG	13A	PR C88 035205	H. Zhang *et al.*	(KSU)
MARTIN	77	NP B127 349	B.R. Martin, M.K. Pidcock, R.G. Moorhouse	(LOUC+)
BAILLON	75	NP B94 39	P.H. Baillon, P.J. Litchfield	(CERN, RHEL)
LANGBEIN	72	NP B47 477	W. Langbein, F. Wagner	(MPIM)

$\Sigma(1880)\ 1/2^+$

$I(J^P) = 1(\frac{1}{2}^+)$ Status: **

OMITTED FROM SUMMARY TABLE

A P_{11} resonance is suggested by several partial-wave analyses, but with wide variations in the mass and other parameters. We list here all claims which lie well above the P_{11} $\Sigma(1770)$.

$\Sigma(1880)$ POLE POSITION

REAL PART

VALUE (MeV)	DOCUMENT ID		TECN	COMMENT
• • • We do not use the following data for averages, fits, limits, etc. • • •				
1776	ZHANG	13A	DPWA	Multichannel

Downloaded from https://academic.oup.com/ptep/article/2022/8/083C01/6651666 by KIT Library user on 27 September 2022

$-2\times$IMAGINARY PART

VALUE (MeV)	DOCUMENT ID		TECN	COMMENT
• • • We do not use the following data for averages, fits, limits, etc. • • •				
270	ZHANG	13A	DPWA	Multichannel

$\Sigma(1880)$ MASS

VALUE (MeV)	DOCUMENT ID		TECN	COMMENT
1820 to 1940 (≈ 1880) OUR ESTIMATE				
1821±17	ZHANG	13A	DPWA	Multichannel
1826±20	GOPAL	80	DPWA	$\overline{K}N \to \overline{K}N$
1870±10	CAMERON	78B	DPWA	$K^-p \to N\overline{K}^*$
1847 or 1863	[1] MARTIN	77	DPWA	$\overline{K}N$ multichannel
1960±30	[2] BAILLON	75	IPWA	$\overline{K}N \to \Lambda\pi$
1985±50	VANHORN	75	DPWA	$K^-p \to \Lambda\pi^0$
1898	[3] LEA	73	DPWA	Multichannel K-matrix
∼ 1850	ARMENTEROS	70	IPWA	$\overline{K}N \to \overline{K}N$
1950±50	BARBARO-...	70	DPWA	$K^-N \to \Lambda\pi$
1920±30	LITCHFIELD	70	DPWA	$K^-N \to \Lambda\pi$
1850	BAILEY	69	DPWA	$\overline{K}N \to \overline{K}N$
1882±40	SMART	68	DPWA	$K^-N \to \Lambda\pi$

$\Sigma(1880)$ WIDTH

VALUE (MeV)	DOCUMENT ID		TECN	COMMENT
100 to 300 (≈ 200) OUR ESTIMATE				
300± 59	ZHANG	13A	DPWA	Multichannel
86± 15	GOPAL	80	DPWA	$\overline{K}N \to \overline{K}N$
80± 10	CAMERON	78B	DPWA	$K^-p \to N\overline{K}^*$
216 or 220	[1] MARTIN	77	DPWA	$\overline{K}N$ multichannel
260± 40	[2] BAILLON	75	IPWA	$\overline{K}N \to \Lambda\pi$
220±140	VANHORN	75	DPWA	$K^-p \to \Lambda\pi^0$
222	[3] LEA	73	DPWA	Multichannel K-matrix
∼ 30	ARMENTEROS	70	IPWA	$\overline{K}N \to \overline{K}N$
200± 50	BARBARO-...	70	DPWA	$K^-N \to \Lambda\pi$
170± 40	LITCHFIELD	70	DPWA	$K^-N \to \Lambda\pi$
200	BAILEY	69	DPWA	$\overline{K}N \to \overline{K}N$
222±150	SMART	68	DPWA	$K^-N \to \Lambda\pi$

$\Sigma(1880)$ DECAY MODES

	Mode	Fraction (Γ_i/Γ)
Γ_1	$N\overline{K}$	0.10 to 0.30 (≈ 0.20)
Γ_2	$\Lambda\pi$	
Γ_3	$\Sigma\pi$	
Γ_4	$\Lambda(1520)\pi$, D-wave	(2.0 ±1.0) %
Γ_5	$N\overline{K}^*(892)$, S=1/2, P-wave	
Γ_6	$N\overline{K}^*(892)$, S=3/2, P-wave	
Γ_7	$\Delta(1232)\overline{K}$, P-wave	(39 ±8) %

$\Sigma(1880)$ BRANCHING RATIOS

See "Sign conventions for resonance couplings" in the Note on Λ and Σ Resonances.

$\Gamma(N\overline{K})/\Gamma_{total}$ — Γ_1/Γ

VALUE	DOCUMENT ID		TECN	COMMENT
0.10 to 0.30 (≈ 0.20) OUR ESTIMATE				
0.10±0.03	ZHANG	13A	DPWA	Multichannel
0.06±0.02	GOPAL	80	DPWA	$\overline{K}N \to \overline{K}N$
0.27 or 0.27	[1] MARTIN	77	DPWA	$\overline{K}N$ multichannel
0.31	[3] LEA	73	DPWA	Multichannel K-matrix
0.20	ARMENTEROS	70	IPWA	$\overline{K}N \to \overline{K}N$
0.22	BAILEY	69	DPWA	$\overline{K}N \to \overline{K}N$

$(\Gamma_i\Gamma_f)^{1/2}/\Gamma_{total}$ in $N\overline{K} \to \Sigma(1880) \to \Lambda\pi$ — $(\Gamma_1\Gamma_2)^{1/2}/\Gamma$

VALUE	DOCUMENT ID		TECN	COMMENT
−0.24 or −0.24	[1] MARTIN	77	DPWA	$\overline{K}N$ multichannel
−0.12 ±0.02	[2] BAILLON	75	IPWA	$\overline{K}N \to \Lambda\pi$
$+0.05\ ^{+0.07}_{-0.02}$	VANHORN	75	DPWA	$K^-p \to \Lambda\pi^0$
−0.169±0.119	DEVENISH	74B		Fixed-t dispersion rel.
−0.30	[3] LEA	73	DPWA	Multichannel K-matrix
−0.09 ±0.04	BARBARO-...	70	DPWA	$K^-N \to \Lambda\pi$
−0.14 ±0.03	LITCHFIELD	70	DPWA	$K^-N \to \Lambda\pi$
−0.11 ±0.03	SMART	68	DPWA	$K^-N \to \Lambda\pi$

$(\Gamma_i\Gamma_f)^{1/2}/\Gamma_{total}$ in $N\overline{K} \to \Sigma(1880) \to \Sigma\pi$ — $(\Gamma_1\Gamma_3)^{1/2}/\Gamma$

VALUE	DOCUMENT ID		TECN	COMMENT
+0.30 or +0.29	[1] MARTIN	77	DPWA	$\overline{K}N$ multichannel
not seen	[3] LEA	73	DPWA	Multichannel K-matrix

$\Gamma(\Lambda(1520)\pi, D\text{-wave})/\Gamma_{total}$ — Γ_4/Γ

VALUE	DOCUMENT ID		TECN	COMMENT
0.02±0.01	ZHANG	13A	DPWA	Multichannel

$(\Gamma_i\Gamma_f)^{1/2}/\Gamma_{total}$ in $N\overline{K} \to \Sigma(1880) \to N\overline{K}^*(892)$, S=1/2, P-wave — $(\Gamma_1\Gamma_5)^{1/2}/\Gamma$

VALUE	DOCUMENT ID		TECN	COMMENT
−0.05±0.03	[4] CAMERON	78B	DPWA	$K^-p \to N\overline{K}^*$

$(\Gamma_i\Gamma_f)^{1/2}/\Gamma_{total}$ in $N\overline{K} \to \Sigma(1880) \to N\overline{K}^*(892)$, S=3/2, P-wave — $(\Gamma_1\Gamma_6)^{1/2}/\Gamma$

VALUE	DOCUMENT ID		TECN	COMMENT
+0.11±0.03	CAMERON	78B	DPWA	$K^-p \to N\overline{K}^*$

$\Gamma(\Delta(1232)\overline{K}, P\text{-wave})/\Gamma_{total}$ — Γ_7/Γ

VALUE	DOCUMENT ID		TECN	COMMENT
0.39±0.08	ZHANG	13A	DPWA	Multichannel

$\Sigma(1880)$ FOOTNOTES

[1] The two MARTIN 77 values are from a T-matrix pole and from a Breit-Wigner fit.
[2] From solution 1 of BAILLON 75; not present in solution 2.
[3] Only unconstrained states from table 1 of LEA 73 are listed.
[4] The published sign has been changed to be in accord with the baryon-first convention.

$\Sigma(1880)$ REFERENCES

ZHANG	13A	PR C88 035205	H. Zhang *et al.*	(KSU)
GOPAL	80	Toronto Conf. 159	G.P. Gopal	(RHEL) IJP
CAMERON	78B	NP B146 327	W. Cameron *et al.*	(RHEL, LOIC) IJP
MARTIN	77	NP B127 349	B.R. Martin, M.K. Pidcock, R.G. Moorhouse	(LOUC+) IJP
Also		NP B126 266	B.R. Martin, M.K. Pidcock	(LOUC)
Also		NP B126 285	B.R. Martin, M.K. Pidcock	(LOUC) IJP
BAILLON	75	NP B94 39	P.H. Baillon, P.J. Litchfield	(CERN, RHEL) IJP
VANHORN	75	NP B87 145	A.J. van Horn	(LBL) IJP
Also		NP B87 157	A.J. van Horn	(LBL) IJP
DEVENISH	74B	NP B81 330	R.C.E. Devenish, C.D. Froggatt, B.R. Martin	(DESY+)
LEA	73	NP B56 77	A.T. Lea *et al.*	(RHEL, LOUC, GLAS, AARH) IJP
ARMENTEROS	70	Duke Conf. 123 Hyperon Resonances, 1970	R. Armenteros *et al.*	(CERN, HEID, SACL) IJP
BARBARO-...	70	Duke Conf. 173 Hyperon Resonances, 1970	A. Barbaro-Galtieri	(LRL) IJP
LITCHFIELD	70	NP B22 269	P.J. Litchfield	(RHEL) IJP
BAILEY	69	Thesis UCRL 50617	J.M. Bailey	(LLL) IJP
SMART	68	PR 169 1330	W.M. Smart	(LRL) IJP

$\Sigma(1900)$ $1/2^-$

$I(J^P) = 1(\frac{1}{2}^-)$ Status: **

OMITTED FROM SUMMARY TABLE

$\Sigma(1900)$ POLE POSITION

REAL PART

VALUE	DOCUMENT ID		TECN	COMMENT
1936±10	SARANTSEV	19	DPWA	$\overline{K}N$ multichannel

$-2\times$IMAGINARY PART

VALUE	DOCUMENT ID		TECN	COMMENT
150±25	SARANTSEV	19	DPWA	$\overline{K}N$ multichannel

$\Sigma(1900)$ POLE RESIDUES

The normalized residue is the residue divided by $\Gamma_{pole}/2$.

Normalized residue in $N\overline{K} \to \Sigma(1900) \to N\overline{K}$

MODULUS	PHASE (°)	DOCUMENT ID		TECN	COMMENT
0.45±0.09	**90 ± 25**	SARANTSEV	19	DPWA	$\overline{K}N$ multichannel

Normalized residue in $N\overline{K} \to \Sigma(1900) \to \Sigma\pi$

MODULUS	PHASE (°)	DOCUMENT ID		TECN	COMMENT
0.38±0.08	**95 ± 20**	SARANTSEV	19	DPWA	$\overline{K}N$ multichannel

Normalized residue in $N\overline{K} \to \Sigma(1900) \to \Sigma\eta$

MODULUS	PHASE (°)	DOCUMENT ID		TECN	COMMENT
0.03±0.01	**20 ± 20**	SARANTSEV	19	DPWA	$\overline{K}N$ multichannel

Normalized residue in $N\overline{K} \to \Sigma(1900) \to \Lambda\pi$

MODULUS	PHASE (°)	DOCUMENT ID		TECN	COMMENT
0.14±0.05	**−160 ± 50**	SARANTSEV	19	DPWA	$\overline{K}N$ multichannel

Normalized residue in $N\overline{K} \to \Sigma(1900) \to \Xi K$

MODULUS	PHASE (°)	DOCUMENT ID		TECN	COMMENT
0.08±0.05	**75 ± 25**	SARANTSEV	19	DPWA	$\overline{K}N$ multichannel

Normalized residue in $N\overline{K} \to \Sigma(1900) \to \Sigma(1385)\pi$

MODULUS	PHASE (°)	DOCUMENT ID		TECN	COMMENT
0.16±0.05	**40 ± 30**	SARANTSEV	19	DPWA	$\overline{K}N$ multichannel

Normalized residue in $N\overline{K} \to \Sigma(1900) \to \Lambda(1520)\pi$

MODULUS	PHASE (°)	DOCUMENT ID		TECN	COMMENT
0.04±0.02	**−25 ± 40**	SARANTSEV	19	DPWA	$\overline{K}N$ multichannel

Downloaded from https://academic.oup.com/ptep/article/2022/8/083C01/6651666 by KIT Library user on 27 September 2022

Normalized residue in $N\overline{K} \rightarrow \Sigma(1900) \rightarrow \Delta\overline{K}$

MODULUS	PHASE (°)	DOCUMENT ID		TECN	COMMENT
0.11±0.04	**60 ± 30**	SARANTSEV	19	DPWA	$\overline{K}N$ multichannel

Normalized residue in $N\overline{K} \rightarrow \Sigma(1900) \rightarrow N\overline{K}^*(892)$, S=1/2, S-wave

MODULUS	PHASE (°)	DOCUMENT ID		TECN	COMMENT
0.17±0.06	**50 ± 50**	SARANTSEV	19	DPWA	$\overline{K}N$ multichannel

Normalized residue in $N\overline{K} \rightarrow \Sigma(1900) \rightarrow N\overline{K}^*(892)$, S=3/2, D-wave

MODULUS	PHASE (°)	DOCUMENT ID		TECN	COMMENT
0.05±0.04		SARANTSEV	19	DPWA	$\overline{K}N$ multichannel

$\Sigma(1900)$ MASS

VALUE (MeV)	DOCUMENT ID		TECN	COMMENT
1900 to 1950 (≈ 1925) OUR ESTIMATE				
1938±12	SARANTSEV	19	DPWA	$\overline{K}N$ multichannel
1900±21	ZHANG	13A	DPWA	$\overline{K}N$ multichannel
1944±15	GOPAL	80	DPWA	$\overline{K}N \rightarrow \overline{K}N$
1755 or 1834	[1] MARTIN	77	DPWA	$\overline{K}N$ multichannel
2004±40	VANHORN	75	DPWA	$K^-p \rightarrow \Lambda\pi^0$
• • • We do not use the following data for averages, fits, limits, etc. • • •				
1955±15	GOPAL	77	DPWA	$\overline{K}N$ multichannel

[1] The two MARTIN 77 values are from a T-matrix pole and from a Breit-Wigner fit.

$\Sigma(1900)$ WIDTH

VALUE (MeV)	DOCUMENT ID		TECN	COMMENT
140 to 190 (≈ 165) OUR ESTIMATE				
155±30	SARANTSEV	19	DPWA	$\overline{K}N$ multichannel
191±47	ZHANG	13A	DPWA	$\overline{K}N$ multichannel
215±25	GOPAL	80	DPWA	$\overline{K}N \rightarrow \overline{K}N$
413 or 450	[1] MARTIN	77	DPWA	$\overline{K}N$ multichannel
116±40	VANHORN	75	DPWA	$K^-p \rightarrow \Lambda\pi^0$
• • • We do not use the following data for averages, fits, limits, etc. • • •				
170±40	GOPAL	77	DPWA	$\overline{K}N$ multichannel

[1] The two MARTIN 77 values are from a T-matrix pole and from a Breit-Wigner fit.

$\Sigma(1900)$ DECAY MODES

	Mode	Fraction (Γ_i/Γ)
Γ_1	$N\overline{K}$	0.40 to 0.70 (≈ 0.55)
Γ_2	$\Sigma\pi$	0.10 to 0.40 (≈ 0.25)
Γ_3	$\Sigma\eta$	(1.0 ±1.0) %
Γ_4	$\Lambda\pi$	(6.0 ±2.0) %
Γ_5	ΞK	(3.0 ±2.0) %
Γ_6	$\Sigma(1385)\pi$	(7.0 ±3.0) %
Γ_7	$\Lambda(1520)\pi$	
Γ_8	$\Delta\overline{K}$	(2.5 ±1.0) %
Γ_9	$N\overline{K}^*(892)$, S=1/2, S-wave	(7.0 ±3.0) %
Γ_{10}	$N\overline{K}^*(892)$, S=3/2, D-wave	

$\Sigma(1900)$ BRANCHING RATIOS

$\Gamma(N\overline{K})/\Gamma_{total}$ — Γ_1/Γ

VALUE	DOCUMENT ID		TECN	COMMENT
0.40 to 0.70 (≈ 0.55) OUR ESTIMATE				
0.45±0.09	SARANTSEV	19	DPWA	$\overline{K}N$ multichannel
0.67±0.17	ZHANG	13A	DPWA	$\overline{K}N$ multichannel

$\Gamma(\Sigma\pi)/\Gamma_{total}$ — Γ_2/Γ

VALUE	DOCUMENT ID		TECN	COMMENT
0.10 to 0.40 (≈ 0.25) OUR ESTIMATE				
0.33±0.07	SARANTSEV	19	DPWA	$\overline{K}N$ multichannel
0.10±0.05	ZHANG	13A	DPWA	$\overline{K}N$ multichannel

$\Gamma(\Sigma\eta)/\Gamma_{total}$ — Γ_3/Γ

VALUE	DOCUMENT ID		TECN	COMMENT
0.01±0.01	SARANTSEV	19	DPWA	$\overline{K}N$ multichannel

$\Gamma(\Lambda\pi)/\Gamma_{total}$ — Γ_4/Γ

VALUE	DOCUMENT ID		TECN	COMMENT
0.06±0.02	SARANTSEV	19	DPWA	$\overline{K}N$ multichannel

$\Gamma(\Xi K)/\Gamma_{total}$ — Γ_5/Γ

VALUE	DOCUMENT ID		TECN	COMMENT
0.03±0.02	SARANTSEV	19	DPWA	$\overline{K}N$ multichannel

$\Gamma(\Sigma(1385)\pi)/\Gamma_{total}$ — Γ_6/Γ

VALUE	DOCUMENT ID		TECN	COMMENT
0.07±0.03	SARANTSEV	19	DPWA	$\overline{K}N$ multichannel

$\Gamma(\Lambda(1520)\pi)/\Gamma_{total}$ — Γ_7/Γ

VALUE	DOCUMENT ID		TECN	COMMENT
<0.01	SARANTSEV	19	DPWA	$\overline{K}N$ multichannel

$\Gamma(\Delta\overline{K})/\Gamma_{total}$ — Γ_8/Γ

VALUE	DOCUMENT ID		TECN	COMMENT
0.025±0.010	SARANTSEV	19	DPWA	$\overline{K}N$ multichannel

$\Gamma(N\overline{K}^*(892), S=1/2, S\text{-wave})/\Gamma_{total}$ — Γ_9/Γ

VALUE	DOCUMENT ID		TECN	COMMENT
0.07±0.03	SARANTSEV	19	DPWA	$\overline{K}N$ multichannel

$\Gamma(N\overline{K}^*(892), S=3/2, D\text{-wave})/\Gamma_{total}$ — Γ_{10}/Γ

VALUE	DOCUMENT ID		TECN	COMMENT
<0.01	SARANTSEV	19	DPWA	$\overline{K}N$ multichannel

$\Sigma(1900)$ REFERENCES

SARANTSEV	19	EPJ A55 180	A.V. Sarantsev *et al.*	(BONN, PNPI)
ZHANG	13A	PR C88 035205	H. Zhang *et al.*	(KSU)
GOPAL	80	Toronto Conf. 159	G.P. Gopal	(RHEL)
GOPAL	77	NP B119 362	G.P. Gopal *et al.*	(LOIC, RHEL)
MARTIN	77	NP B127 349	B.R. Martin, M.K. Pidcock, R.G. Moorhouse	(LOUC+)
VANHORN	75	NP B87 145	A.J. van Horn	(LBL)

$\Sigma(1910)\ 3/2^-$

$I(J^P) = 1(\frac{3}{2}^-)$ Status: ***

was $\Sigma(1940)$

For results published before 1974 (they are now obsolete), see our 1982 edition Physics Letters **111B** 1 (1982).

Not all analyses require this state. It is not required by the GOYAL 77 analysis of $K^-n \rightarrow (\Sigma\pi)^-$ nor by the GOPAL 80 analysis of $K^-n \rightarrow K^-n$. See also HEMINGWAY 75.

$\Sigma(1910)$ POLE RESIDUES

The normalized residue is the residue divided by $\Gamma_{pole}/2$.

Normalized residue in $N\overline{K} \rightarrow \Sigma(1910) \rightarrow N\overline{K}$

MODULUS	PHASE (°)	DOCUMENT ID		TECN	COMMENT
0.03±0.02	**−95 ± 60**	SARANTSEV	19	DPWA	$\overline{K}N$ multichannel

Normalized residue in $N\overline{K} \rightarrow \Sigma(1910) \rightarrow \Sigma\pi$

MODULUS	PHASE (°)	DOCUMENT ID		TECN	COMMENT
0.16±0.04	**−160 ± 15**	SARANTSEV	19	DPWA	$\overline{K}N$ multichannel

Normalized residue in $N\overline{K} \rightarrow \Sigma(1910) \rightarrow \Lambda\pi$

MODULUS	PHASE (°)	DOCUMENT ID		TECN	COMMENT
0.04±0.03	**25 ± 25**	SARANTSEV	19	DPWA	$\overline{K}N$ multichannel

Normalized residue in $N\overline{K} \rightarrow \Sigma(1910) \rightarrow \Xi\pi$

MODULUS	PHASE (°)	DOCUMENT ID		TECN	COMMENT
0.01±0.01		SARANTSEV	19	DPWA	$\overline{K}N$ multichannel

Normalized residue in $N\overline{K} \rightarrow \Sigma(1910) \rightarrow \Lambda(1520)\pi$, P-wave

MODULUS	PHASE (°)	DOCUMENT ID		TECN	COMMENT
0.01±0.01		SARANTSEV	19	DPWA	$\overline{K}N$ multichannel

Normalized residue in $N\overline{K} \rightarrow \Sigma(1910) \rightarrow \Lambda(1520)\pi$, F-wave

MODULUS	PHASE (°)	DOCUMENT ID		TECN	COMMENT
∼ 0		SARANTSEV	19	DPWA	$\overline{K}N$ multichannel

Normalized residue in $N\overline{K} \rightarrow \Sigma(1910) \rightarrow \Delta\overline{K}$, S-wave

MODULUS	PHASE (°)	DOCUMENT ID		TECN	COMMENT
0.03±0.01	**120 ± 20**	SARANTSEV	19	DPWA	$\overline{K}N$ multichannel

Normalized residue in $N\overline{K} \rightarrow \Sigma(1910) \rightarrow N\overline{K}^*(892)$, S=3/2, S-wave

MODULUS	PHASE (°)	DOCUMENT ID		TECN	COMMENT
0.03±0.02	**20 ± 35**	SARANTSEV	19	DPWA	$\overline{K}N$ multichannel

Normalized residue in $N\overline{K} \rightarrow \Sigma(1910) \rightarrow N\overline{K}^*(892)$, S=1/2, D-wave

MODULUS	PHASE (°)	DOCUMENT ID		TECN	COMMENT
0.02±0.01		SARANTSEV	19	DPWA	$\overline{K}N$ multichannel

Normalized residue in $N\overline{K} \rightarrow \Sigma(1910) \rightarrow N\overline{K}^*(892)$, S=3/2, D-wave

MODULUS	PHASE (°)	DOCUMENT ID		TECN	COMMENT
0.01±0.01		SARANTSEV	19	DPWA	$\overline{K}N$ multichannel

$\Sigma(1910)$ MASS

VALUE (MeV)	DOCUMENT ID		TECN	COMMENT
1870 to 1950 (≈ 1910) OUR ESTIMATE				
1878±12	SARANTSEV	19	DPWA	$\overline{K}N$ multichannel
1920±50	GOPAL	77	DPWA	$\overline{K}N$ multichannel
1950±30	BAILLON	75	IPWA	$\overline{K}N \rightarrow \Lambda\pi$

Downloaded from https://academic.oup.com/ptep/article/2022/8/083C01/6651666 by KIT Library user on 27 September 2022

1949^{+40}_{-60}	VANHORN	75	DPWA	$K^- p \to \Lambda \pi^0$
1935 ± 80	KANE	74	DPWA	$K^- p \to \Sigma \pi$
1940 ± 20	LITCHFIELD	74B	DPWA	$K^- p \to \Lambda(1520) \pi^0$
1950 ± 20	LITCHFIELD	74C	DPWA	$K^- p \to \Delta(1232) \overline{K}$
• • • We do not use the following data for averages, fits, limits, etc. • • •				
1886 or 1893	[1] MARTIN	77	DPWA	$\overline{K} N$ multichannel
1940	DEBELLEFON	76	IPWA	$K^- p \to \Lambda \pi^0$, F_{17} wave

$\Sigma(1910)$ WIDTH

VALUE (MeV)	DOCUMENT ID		TECN	COMMENT
150 to 300 ($\approx$ 220) OUR ESTIMATE				
224 ± 25	SARANTSEV	19	DPWA	$\overline{K} N$ multichannel
170 ± 25	CAMERON	78B	DPWA	$K^- p \to N \overline{K}^*$
300 ± 80	GOPAL	77	DPWA	$\overline{K} N$ multichannel
150 ± 75	BAILLON	75	IPWA	$\overline{K} N \to \Lambda \pi$
160^{+70}_{-40}	VANHORN	75	DPWA	$K^- p \to \Lambda \pi^0$
330 ± 80	KANE	74	DPWA	$K^- p \to \Sigma \pi$
60 ± 20	LITCHFIELD	74B	DPWA	$K^- p \to \Lambda(1520) \pi^0$
70^{+30}_{-20}	LITCHFIELD	74C	DPWA	$K^- p \to \Delta(1232) \overline{K}$
• • • We do not use the following data for averages, fits, limits, etc. • • •				
157 or 159	[1] MARTIN	77	DPWA	$\overline{K} N$ multichannel

$\Sigma(1910)$ DECAY MODES

	Mode	Fraction (Γ_i/Γ)
Γ_1	$N \overline{K}$	0.01 to 0.05 ($\approx$ 0.02)
Γ_2	$\Lambda \pi$	(6 $\pm$ 4) %
Γ_3	$\Sigma \pi$	(86 $\pm$21) %
Γ_4	ΞK	
Γ_5	$\Sigma(1385) \pi$	seen
Γ_6	$\Sigma(1385) \pi$, S-wave	
Γ_7	$\Lambda(1520) \pi$	seen
Γ_8	$\Lambda(1520) \pi$, P-wave	
Γ_9	$\Lambda(1520) \pi$, F-wave	
Γ_{10}	$\Delta(1232) \overline{K}$	(3.0 $\pm$ 1.0) %
Γ_{11}	$\Delta(1232) \overline{K}$, S-wave	
Γ_{12}	$\Delta(1232) \overline{K}$, D-wave	
Γ_{13}	$N \overline{K}^*(892)$	seen
Γ_{14}	$N \overline{K}^*(892)$, S=3/2, S-wave	
Γ_{15}	$N \overline{K}^*(892)$, S=1/2 , D-wave	(1.0 $\pm$ 1.0) %
Γ_{16}	$N \overline{K}^*(892)$, S=3/2 , D-wave	

$\Sigma(1910)$ BRANCHING RATIOS

See "Sign conventions for resonance couplings" in the Note on Λ and Σ Resonances.

$\Gamma(N\overline{K})/\Gamma_{total}$ — Γ_1/Γ

VALUE	DOCUMENT ID		TECN	COMMENT
0.01 to 0.05 ($\approx$ 0.02) OUR ESTIMATE				
0.03 ± 0.02	SARANTSEV	19	DPWA	$\overline{K} N$ multichannel
<0.04	GOPAL	77	DPWA	$\overline{K} N$ multichannel
0.14 or 0.13	[1] MARTIN	77	DPWA	$\overline{K} N$ multichannel

$\Gamma(\Lambda\pi)/\Gamma_{total}$ — Γ_2/Γ

VALUE	DOCUMENT ID		TECN	COMMENT
0.06 ± 0.04	SARANTSEV	19	DPWA	$\overline{K} N$ multichannel

$\Gamma(\Sigma\pi)/\Gamma_{total}$ — Γ_3/Γ

VALUE	DOCUMENT ID		TECN	COMMENT
0.86 ± 0.21	SARANTSEV	19	DPWA	$\overline{K} N$ multichannel

$\Gamma(\Xi K)/\Gamma_{total}$ — Γ_4/Γ

VALUE	DOCUMENT ID		TECN	COMMENT
~ 0	SARANTSEV	19	DPWA	$\overline{K} N$ multichannel

$\Gamma(\Lambda(1520)\pi, P\text{-wave})/\Gamma_{total}$ — Γ_8/Γ

VALUE	DOCUMENT ID		TECN	COMMENT
~ 0	SARANTSEV	19	DPWA	$\overline{K} N$ multichannel

$\Gamma(\Lambda(1520)\pi, F\text{-wave})/\Gamma_{total}$ — Γ_9/Γ

VALUE	DOCUMENT ID		TECN	COMMENT
~ 0	SARANTSEV	19	DPWA	$\overline{K} N$ multichannel

$\Gamma(\Delta(1232)\overline{K})/\Gamma_{total}$ — Γ_{10}/Γ

VALUE	DOCUMENT ID		TECN	COMMENT
0.03 ± 0.01	SARANTSEV	19	DPWA	$\overline{K} N$ multichannel

$\Gamma(N\overline{K}^*(892))/\Gamma_{total}$ — Γ_{13}/Γ

VALUE	DOCUMENT ID		TECN	COMMENT
0.03 ± 0.02	SARANTSEV	19	DPWA	$\overline{K} N$ multichannel

$\Gamma(N\overline{K}^*(892), S=1/2, D\text{-wave})/\Gamma_{total}$ — Γ_{15}/Γ

VALUE	DOCUMENT ID		TECN	COMMENT
0.01 ± 0.01	SARANTSEV	19	DPWA	$\overline{K} N$ multichannel

$\Gamma(N\overline{K}^*(892), S=3/2, D\text{-wave})/\Gamma_{total}$ — Γ_{16}/Γ

VALUE	DOCUMENT ID		TECN	COMMENT
~ 0	SARANTSEV	19	DPWA	$\overline{K} N$ multichannel

$(\Gamma_i\Gamma_f)^{1/2}/\Gamma_{total}$ in $N\overline{K} \to \Sigma(1910) \to \Lambda\pi$ — $(\Gamma_1\Gamma_2)^{1/2}/\Gamma$

VALUE	DOCUMENT ID		TECN	COMMENT
-0.06 ± 0.03	GOPAL	77	DPWA	$\overline{K} N$ multichannel
-0.04 ± 0.02	BAILLON	75	IPWA	$\overline{K} N \to \Lambda \pi$
$-0.05\ ^{+0.03}_{-0.02}$	VANHORN	75	DPWA	$K^- p \to \Lambda \pi^0$
-0.153 ± 0.070	DEVENISH	74B		Fixed-t dispersion rel.
• • • We do not use the following data for averages, fits, limits, etc. • • •				
-0.15 or -0.14	[1] MARTIN	77	DPWA	$\overline{K} N$ multichannel

$(\Gamma_i\Gamma_f)^{1/2}/\Gamma_{total}$ in $N\overline{K} \to \Sigma(1910) \to \Sigma\pi$ — $(\Gamma_1\Gamma_3)^{1/2}/\Gamma$

VALUE	DOCUMENT ID		TECN	COMMENT
-0.08 ± 0.04	GOPAL	77	DPWA	$\overline{K} N$ multichannel
-0.14 ± 0.04	KANE	74	DPWA	$K^- p \to \Sigma \pi$
• • • We do not use the following data for averages, fits, limits, etc. • • •				
$+0.16$ or $+0.16$	[1] MARTIN	77	DPWA	$\overline{K} N$ multichannel

$(\Gamma_i\Gamma_f)^{1/2}/\Gamma_{total}$ in $N\overline{K} \to \Sigma(1910) \to \Sigma(1385)\pi$ — $(\Gamma_1\Gamma_5)^{1/2}/\Gamma$

VALUE	DOCUMENT ID		TECN	COMMENT
$+0.066 \pm 0.025$	[2] CAMERON	78	DPWA	$K^- p \to \Sigma(1385) \pi$

$(\Gamma_i\Gamma_f)^{1/2}/\Gamma_{total}$ in $N\overline{K} \to \Sigma(1910) \to \Lambda(1520)\pi$, P-wave — $(\Gamma_1\Gamma_8)^{1/2}/\Gamma$

VALUE	DOCUMENT ID		TECN	COMMENT
< 0.03	CAMERON	77	DPWA	$K^- p \to \Lambda(1520) \pi^0$
-0.11 ± 0.04	LITCHFIELD	74B	DPWA	$K^- p \to \Lambda(1520) \pi^0$

$(\Gamma_i\Gamma_f)^{1/2}/\Gamma_{total}$ in $N\overline{K} \to \Sigma(1910) \to \Lambda(1520)\pi$, F-wave — $(\Gamma_1\Gamma_9)^{1/2}/\Gamma$

VALUE	DOCUMENT ID		TECN	COMMENT
0.062 ± 0.021	CAMERON	77	DPWA	$K^- p \to \Lambda(1520) \pi^0$
-0.08 ± 0.04	LITCHFIELD	74B	DPWA	$K^- p \to \Lambda(1520) \pi^0$

$(\Gamma_i\Gamma_f)^{1/2}/\Gamma_{total}$ in $N\overline{K} \to \Sigma(1910) \to \Delta(1232)\overline{K}$, S-wave — $(\Gamma_1\Gamma_{11})^{1/2}/\Gamma$

VALUE	DOCUMENT ID		TECN	COMMENT
-0.16 ± 0.05	LITCHFIELD	74C	DPWA	$K^- p \to \Delta(1232) \overline{K}$

$(\Gamma_i\Gamma_f)^{1/2}/\Gamma_{total}$ in $N\overline{K} \to \Sigma(1910) \to \Delta(1232)\overline{K}$, D-wave — $(\Gamma_1\Gamma_{12})^{1/2}/\Gamma$

VALUE	DOCUMENT ID		TECN	COMMENT
-0.14 ± 0.05	LITCHFIELD	74C	DPWA	$K^- p \to \Delta(1232) \overline{K}$

$(\Gamma_i\Gamma_f)^{1/2}/\Gamma_{total}$ in $N\overline{K} \to \Sigma(1910) \to N\overline{K}^*(892)$ — $(\Gamma_1\Gamma_{13})^{1/2}/\Gamma$

VALUE	DOCUMENT ID		TECN	COMMENT
-0.09 ± 0.02	[3] CAMERON	78B	DPWA	$K^- p \to N \overline{K}^*$

$\Sigma(1910)$ FOOTNOTES

[1] The two MARTIN 77 values are from a T-matrix pole and from a Breit-Wigner fit.
[2] The published sign has been changed to be in accord with the baryon-first convention.
[3] Upper limits on the D_1 and D_3 waves are each 0.03.

$\Sigma(1910)$ REFERENCES

SARANTSEV	19	EPJ A55 180	A.V. Sarantsev *et al.*	(BONN, PNPI)
PDG	82	PL 111B 1	M. Roos *et al.*	(HELS, CIT, CERN)
GOPAL	80	Toronto Conf. 159	G.P. Gopal	(RHEL)
CAMERON	78	NP B143 189	W. Cameron *et al.*	(RHEL, LOIC) IJP
CAMERON	78B	NP B146 327	W. Cameron *et al.*	(RHEL, LOIC) IJP
CAMERON	77	NP B131 399	W. Cameron *et al.*	(RHEL, LOIC) IJP
GOPAL	77	NP B119 362	G.P. Gopal *et al.*	(LOIC, RHEL) IJP
GOYAL	77	PR D16 2746	D.P. Goyal, A.V. Sodhi	(DELH)
MARTIN	77	NP B127 349	B.R. Martin, M.K. Pidcock, R.G. Moorhouse	(LOUC+) IJP
Also		NP B126 266	B.R. Martin, M.K. Pidcock	(LOUC)
Also		NP B126 285	B.R. Martin, M.K. Pidcock	(LOUC) IJP
DEBELLEFON	76	NP B109 129	A. de Bellefon, A. Berthon	(CDEF) IJP
BAILLON	75	NP B94 39	P.H. Baillon, P.J. Litchfield	(CERN, RHEL) IJP
HEMINGWAY	75	NP B91 12	R.J. Hemingway *et al.*	(CERN, HEIDH, MPIM) IJP
VANHORN	75	NP B87 145	A.J. van Horn	(LBL) IJP
Also		NP B87 157	A.J. van Horn	(LBL) IJP
DEVENISH	74B	NP B81 330	R.C.E. Devenish, C.D. Froggatt, B.R. Martin	(DESY+)
KANE	74	LBL-2452	D.F. Kane	(LBL) IJP
LITCHFIELD	74B	NP B74 19	P.J. Litchfield *et al.*	(CERN, HEIDH) IJP
LITCHFIELD	74C	NP B74 39	P.J. Litchfield *et al.*	(CERN, HEIDH) IJP

Downloaded from https://academic.oup.com/ptep/article/2022/8/083C01/6651666 by KIT Library user on 27 September 2022

$\Sigma(1915)\ 5/2^+$

$I(J^P) = 1(\frac{5}{2}^+)$ Status: ****

Discovered by COOL 66. For results published before 1974 (they are now obsolete), see our 1982 edition Physics Letters **111B** 1 (1982).

This entry only includes results from partial-wave analyses. Parameters of peaks seen in cross sections and invariant-mass distributions in this region used to be listed in in a separate entry immediately following. They may be found in our 1986 edition Physics Letters **170B** 1 (1986).

$\Sigma(1915)$ POLE POSITION

REAL PART

VALUE (MeV)	DOCUMENT ID		TECN	COMMENT
1885 to 1915 (≈ 1900) OUR ESTIMATE				
1908 ± 7	SARANTSEV	19	DPWA	$\overline{K}N$ multichannel
1890^{+3}_{-2}	[1] KAMANO	15	DPWA	$\overline{K}N$ multichannel
• • • We do not use the following data for averages, fits, limits, etc. • • •				
1897	ZHANG	13A	DPWA	$\overline{K}N$ multichannel

[1] From the preferred solution A in KAMANO 15.

−2×IMAGINARY PART

VALUE (MeV)	DOCUMENT ID		TECN	COMMENT
90 to 110 (≈ 100) OUR ESTIMATE				
98 ± 12	SARANTSEV	19	DPWA	$\overline{K}N$ multichannel
97^{+4}_{-6}	[1] KAMANO	15	DPWA	$\overline{K}N$ multichannel
• • • We do not use the following data for averages, fits, limits, etc. • • •				
133	ZHANG	13A	DPWA	$\overline{K}N$ multichannel

[1] From the preferred solution A in KAMANO 15.

$\Sigma(1915)$ POLE RESIDUES

The normalized residue is the residue divided by $\Gamma_{pole}/2$.

Normalized residue in $N\overline{K} \to \Sigma(1915) \to N\overline{K}$

MODULUS	PHASE (°)	DOCUMENT ID		TECN	COMMENT
0.08 ± 0.02	**−33 ± 15**	SARANTSEV	19	DPWA	$\overline{K}N$ multichannel
• • • We do not use the following data for averages, fits, limits, etc. • • •					
0.0391	−15	[1] KAMANO	15	DPWA	$\overline{K}N$ multichannel

[1] From the preferred solution A in KAMANO 15.

Normalized residue in $N\overline{K} \to \Sigma(1915) \to \Sigma\pi$

MODULUS	PHASE (°)	DOCUMENT ID		TECN	COMMENT
0.09 ± 0.02	**180 ± 12**	SARANTSEV	19	DPWA	$\overline{K}N$ multichannel
• • • We do not use the following data for averages, fits, limits, etc. • • •					
0.157	157	[1] KAMANO	15	DPWA	$\overline{K}N$ multichannel

[1] From the preferred solution A in KAMANO 15.

Normalized residue in $N\overline{K} \to \Sigma(1915) \to \Lambda\pi$

MODULUS	PHASE (°)	DOCUMENT ID		TECN	COMMENT
0.07 ± 0.02	**−170 ± 20**	SARANTSEV	19	DPWA	$\overline{K}N$ multichannel
• • • We do not use the following data for averages, fits, limits, etc. • • •					
0.0757	166	[1] KAMANO	15	DPWA	$\overline{K}N$ multichannel

[1] From the preferred solution A in KAMANO 15.

Normalized residue in $N\overline{K} \to \Sigma(1915) \to \Xi K$

MODULUS	PHASE (°)	DOCUMENT ID		TECN	COMMENT
0.02 ± 0.01	**−65 ± 35**	SARANTSEV	19	DPWA	$\overline{K}N$ multichannel
• • • We do not use the following data for averages, fits, limits, etc. • • •					
0.002	−88	[1] KAMANO	15	DPWA	$\overline{K}N$ multichannel

[1] From the preferred solution A in KAMANO 15.

Normalized residue in $N\overline{K} \to \Lambda(1915) \to \Sigma(1385)\pi$, P-wave

MODULUS	PHASE (°)	DOCUMENT ID		TECN	COMMENT
0.02 ± 0.02		SARANTSEV	19	DPWA	$\overline{K}N$ multichannel
• • • We do not use the following data for averages, fits, limits, etc. • • •					
0.0724	161	[1] KAMANO	15	DPWA	$\overline{K}N$ multichannel

[1] From the preferred solution A in KAMANO 15.

Normalized residue in $N\overline{K} \to \Lambda(1915) \to \Sigma(1385)\pi$, F-wave

MODULUS	PHASE (°)	DOCUMENT ID		TECN	COMMENT
0.05 ± 0.03	**−30 ± 50**	SARANTSEV	19	DPWA	$\overline{K}N$ multichannel
• • • We do not use the following data for averages, fits, limits, etc. • • •					
0.0162	−163	[1] KAMANO	15	DPWA	$\overline{K}N$ multichannel

[1] From the preferred solution A in KAMANO 15.

Normalized residue in $N\overline{K} \to \Sigma(1915) \to \Lambda(1520)\pi$, D-wave

MODULUS	PHASE (°)	DOCUMENT ID		TECN	COMMENT
0.08 ± 0.02	**−105 ± 50**	SARANTSEV	19	DPWA	$\overline{K}N$ multichannel

Normalized residue in $N\overline{K} \to \Sigma(1915) \to \Delta\overline{K}$, P-wave

MODULUS	PHASE (°)	DOCUMENT ID		TECN	COMMENT
0.12 ± 0.03	**−10 ± 20**	SARANTSEV	19	DPWA	$\overline{K}N$ multichannel

Normalized residue in $N\overline{K} \to \Sigma(1915) \to \Delta\overline{K}$, F-wave

MODULUS	PHASE (°)	DOCUMENT ID		TECN	COMMENT
0.07 ± 0.02	**−35 ± 25**	SARANTSEV	19	DPWA	$\overline{K}N$ multichannel

Normalized residue in $N\overline{K} \to \Sigma(1915) \to \Lambda(1520)\pi$, G-wave

MODULUS	PHASE (°)	DOCUMENT ID		TECN	COMMENT
0.01 ± 0.01		SARANTSEV	19	DPWA	$\overline{K}N$ multichannel

Normalized residue in $N\overline{K} \to \Sigma(1915) \to N\overline{K}^*(892)$, S=1/2 , F-wave

MODULUS	PHASE (°)	DOCUMENT ID		TECN	COMMENT
0.07 ± 0.04	**−60 ± 45**	SARANTSEV	19	DPWA	$\overline{K}N$ multichannel
• • • We do not use the following data for averages, fits, limits, etc. • • •					
0.00476	4	[1] KAMANO	15	DPWA	$\overline{K}N$ multichannel

[1] From the preferred solution A in KAMANO 15.

Normalized residue in $N\overline{K} \to \Sigma(1915) \to N\overline{K}^*(892)$, S=3/2 , P-wave

MODULUS	PHASE (°)	DOCUMENT ID		TECN	COMMENT
• • • We do not use the following data for averages, fits, limits, etc. • • •					
0.0494	51	[1] KAMANO	15	DPWA	$\overline{K}N$ multichannel

[1] From the preferred solution A in KAMANO 15.

Normalized residue in $N\overline{K} \to \Sigma(1915) \to N\overline{K}^*(892)$, S=3/2 , F-wave

MODULUS	PHASE (°)	DOCUMENT ID		TECN	COMMENT
0.07 ± 0.03	**−40 ± 45**	SARANTSEV	19	DPWA	$\overline{K}N$ multichannel
• • • We do not use the following data for averages, fits, limits, etc. • • •					
0.000314	16	[1] KAMANO	15	DPWA	$\overline{K}N$ multichannel

[1] From the preferred solution A in KAMANO 15.

$\Sigma(1915)$ MASS

VALUE (MeV)	DOCUMENT ID		TECN	COMMENT
1900 to 1935 (≈ 1915) OUR ESTIMATE				
1918 ± 6	SARANTSEV	19	DPWA	$\overline{K}N$ multichannel
1920 ± 7	ZHANG	13A	DPWA	$\overline{K}N$ multichannel
1937 ± 20	ALSTON-...	78	DPWA	$\overline{K}N \to \overline{K}N$
1894 ± 5	[1] CORDEN	77C		$K^-n \to \Sigma\pi$
1909 ± 5	[1] CORDEN	77C		$K^-n \to \Sigma\pi$
1920 ± 10	GOPAL	77	DPWA	$\overline{K}N$ multichannel
1920 ± 30	BAILLON	75	IPWA	$\overline{K}N \to \Lambda\pi$
1914 ± 10	HEMINGWAY	75	DPWA	$K^-p \to \overline{K}N$
1920^{+15}_{-20}	VANHORN	75	DPWA	$K^-p \to \Lambda\pi^0$
1920 ± 5	KANE	74	DPWA	$K^-p \to \Sigma\pi$
• • • We do not use the following data for averages, fits, limits, etc. • • •				
not seen	DECLAIS	77	DPWA	$\overline{K}N \to \overline{K}N$
1925 or 1933	[2] MARTIN	77	DPWA	$\overline{K}N$ multichannel
1900 ± 4	[3] CORDEN	76	DPWA	$K^-n \to \Lambda\pi^-$
1915	DEBELLEFON	76	IPWA	$K^-p \to \Lambda\pi^0$

[1] The two entries for CORDEN 77C are from two different acceptable solutions.
[2] The two MARTIN 77 values are from a T-matrix pole and from a Breit-Wigner fit.
[3] Preferred solution 3; see CORDEN 76 for other possibilities.

$\Sigma(1915)$ WIDTH

VALUE (MeV)	DOCUMENT ID		TECN	COMMENT
80 to 160 (≈ 120) OUR ESTIMATE				
102 ± 12	SARANTSEV	19	DPWA	$\overline{K}N$ multichannel
149 ± 17	ZHANG	13A	DPWA	Multichannel
161 ± 20	ALSTON-...	78	DPWA	$\overline{K}N \to \overline{K}N$
107 ± 14	[1] CORDEN	77C		$K^-n \to \Sigma\pi$
85 ± 13	[1] CORDEN	77C		$K^-n \to \Sigma\pi$
130 ± 10	GOPAL	77	DPWA	$\overline{K}N$ multichannel
70 ± 20	BAILLON	75	IPWA	$\overline{K}N \to \Lambda\pi$
85 ± 15	HEMINGWAY	75	DPWA	$K^-p \to \overline{K}N$
102 ± 18	VANHORN	75	DPWA	$K^-p \to \Lambda\pi^0$
162 ± 25	KANE	74	DPWA	$K^-p \to \Sigma\pi$
• • • We do not use the following data for averages, fits, limits, etc. • • •				
171 or 173	[2] MARTIN	77	DPWA	$\overline{K}N$ multichannel
75 ± 14	[3] CORDEN	76	DPWA	$K^-n \to \Lambda\pi^-$
60	DEBELLEFON	76	IPWA	$K^-p \to \Lambda\pi^0$

[1] The two entries for CORDEN 77C are from two different acceptable solutions.
[2] The two MARTIN 77 values are from a T-matrix pole and from a Breit-Wigner fit.
[3] Preferred solution 3; see CORDEN 76 for other possibilities.

$\Sigma(1915)$ DECAY MODES

	Mode	Fraction (Γ_i/Γ)
Γ_1	$N\overline{K}$	0.05 to 0.15
Γ_2	$\Lambda\pi$	(6.0 ± 2.0) %

Downloaded from https://academic.oup.com/ptep/article/2022/8/083C01/6651666 by KIT Library user on 27 September 2022

Γ_3	$\Sigma\pi$	(10.0 ±2.0) %
Γ_4	ΞK	
Γ_5	$\Sigma(1385)\pi$	
Γ_6	$\Sigma(1385)\pi$, P-wave	(2.0 ±2.0) %
Γ_7	$\Sigma(1385)\pi$, F-wave	(4.0 ±2.0) %
Γ_8	$\Lambda(1520)\pi$, D-wave	(8.0 ±2.0) %
Γ_9	$\Lambda(1520)\pi$, G-wave	
Γ_{10}	$N\overline{K}^*(892)$, S=1/2, F-wave	(5.0 ±3.0) %
Γ_{11}	$N\overline{K}^*(892)$, S=3/2, P-wave	
Γ_{12}	$N\overline{K}^*(892)$, S=3/2, F-wave	(5.0 ±2.0) %
Γ_{13}	$\Delta\overline{K}$, P-wave	(16 ±5) %
Γ_{14}	$\Delta\overline{K}$, F-wave	(5.0 ±3.0) %

$\Sigma(1915)$ BRANCHING RATIOS

See "Sign conventions for resonance couplings" in the Note on Λ and Σ Resonances.

$\Gamma(N\overline{K})/\Gamma_{total}$ — Γ_1/Γ

VALUE	DOCUMENT ID		TECN	COMMENT
0.05 to 0.15 OUR ESTIMATE				
0.08 ±0.02	SARANTSEV	19	DPWA	$\overline{K}N$ multichannel
0.026±0.004	ZHANG	13A	DPWA	$\overline{K}N$ multichannel
0.03 ±0.02	[1] GOPAL	80	DPWA	$\overline{K}N \to \overline{K}N$
0.14 ±0.05	ALSTON-...	78	DPWA	$\overline{K}N \to \overline{K}N$
0.11 ±0.04	HEMINGWAY	75	DPWA	$K^-p \to \overline{K}N$
• • • We do not use the following data for averages, fits, limits, etc. • • •				
0.036	[2] KAMANO	15	DPWA	$\overline{K}N$ multichannel
0.05 ±0.03	GOPAL	77	DPWA	See GOPAL 80
0.08 or 0.08	[3] MARTIN	77	DPWA	$\overline{K}N$ multichannel

[1] The mass and width are fixed to the GOPAL 77 values due to the low elasticity.
[2] From the preferred solution A in KAMANO 15.
[3] The two MARTIN 77 values are from a T-matrix pole and from a Breit-Wigner fit.

$\Gamma(\Lambda\pi)/\Gamma_{total}$ — Γ_2/Γ

VALUE	DOCUMENT ID		TECN	COMMENT
0.06 ±0.02	SARANTSEV	19	DPWA	$\overline{K}N$ multichannel
• • • We do not use the following data for averages, fits, limits, etc. • • •				
0.127	[1] KAMANO	15	DPWA	$\overline{K}N$ multichannel

[1] From the preferred solution A in KAMANO 15.

$\Gamma(\Sigma\pi)/\Gamma_{total}$ — Γ_3/Γ

VALUE	DOCUMENT ID		TECN	COMMENT
0.10 ±0.02	SARANTSEV	19	DPWA	$\overline{K}N$ multichannel
• • • We do not use the following data for averages, fits, limits, etc. • • •				
0.678	[1] KAMANO	15	DPWA	$\overline{K}N$ multichannel

[1] From the preferred solution A in KAMANO 15.

$\Gamma(\Xi K)/\Gamma_{total}$ — Γ_4/Γ

VALUE	DOCUMENT ID		TECN	COMMENT
<0.01	SARANTSEV	19	DPWA	$\overline{K}N$ multichannel
• • • We do not use the following data for averages, fits, limits, etc. • • •				
not seen	[1] KAMANO	15	DPWA	Multichannel

[1] From the preferred solution A in KAMANO 15.

$\Gamma(\Sigma(1385)\pi, P\text{-wave})/\Gamma_{total}$ — Γ_6/Γ

VALUE	DOCUMENT ID		TECN	COMMENT
0.02 ±0.02	SARANTSEV	19	DPWA	$\overline{K}N$ multichannel
• • • We do not use the following data for averages, fits, limits, etc. • • •				
0.112	[1] KAMANO	15	DPWA	$\overline{K}N$ multichannel

[1] From the preferred solution A in KAMANO 15.

$\Gamma(\Sigma(1385)\pi, F\text{-wave})/\Gamma_{total}$ — Γ_7/Γ

VALUE	DOCUMENT ID		TECN	COMMENT
0.04 ±0.02	SARANTSEV	19	DPWA	$\overline{K}N$ multichannel
• • • We do not use the following data for averages, fits, limits, etc. • • •				
0.004	[1] KAMANO	15	DPWA	$\overline{K}N$ multichannel

[1] From the preferred solution A in KAMANO 15.

$\Gamma(\Lambda(1520)\pi, D\text{-wave})/\Gamma_{total}$ — Γ_8/Γ

VALUE	DOCUMENT ID		TECN	COMMENT
0.08±0.02	SARANTSEV	19	DPWA	$\overline{K}N$ multichannel

$\Gamma(\Lambda(1520)\pi, G\text{-wave})/\Gamma_{total}$ — Γ_9/Γ

VALUE	DOCUMENT ID		TECN	COMMENT
def 0	SARANTSEV	19	DPWA	$\overline{K}N$ multichannel

$\Gamma(N\overline{K}^*(892), S=1/2, F\text{-wave})/\Gamma_{total}$ — Γ_{10}/Γ

VALUE	DOCUMENT ID		TECN	COMMENT
0.05 ±0.03	SARANTSEV	19	DPWA	$\overline{K}N$ multichannel
• • • We do not use the following data for averages, fits, limits, etc. • • •				
0.001	[1] KAMANO	15	DPWA	Multichannel

[1] From the preferred solution A in KAMANO 15.

$\Gamma(N\overline{K}^*(892), S=3/2, P\text{-wave})/\Gamma_{total}$ — Γ_{11}/Γ

VALUE	DOCUMENT ID		TECN	COMMENT
• • • We do not use the following data for averages, fits, limits, etc. • • •				
0.042	[1] KAMANO	15	DPWA	Multichannel

[1] From the preferred solution A in KAMANO 15.

$\Gamma(N\overline{K}^*(892), S=3/2, F\text{-wave})/\Gamma_{total}$ — Γ_{12}/Γ

VALUE	DOCUMENT ID		TECN	COMMENT
0.05±0.02	SARANTSEV	19	DPWA	$\overline{K}N$ multichannel
• • • We do not use the following data for averages, fits, limits, etc. • • •				
not seen	[1] KAMANO	15	DPWA	Multichannel

[1] From the preferred solution A in KAMANO 15.

$\Gamma(\Delta\overline{K}, P\text{-wave})/\Gamma_{total}$ — Γ_{13}/Γ

VALUE	DOCUMENT ID		TECN	COMMENT
0.16±0.05	SARANTSEV	19	DPWA	$\overline{K}N$ multichannel

$\Gamma(\Delta\overline{K}, F\text{-wave})/\Gamma_{total}$ — Γ_{14}/Γ

VALUE	DOCUMENT ID		TECN	COMMENT
0.05±0.03	SARANTSEV	19	DPWA	$\overline{K}N$ multichannel

$(\Gamma_i\Gamma_f)^{1/2}/\Gamma_{total}$ in $N\overline{K} \to \Sigma(1915) \to \Lambda\pi$ — $(\Gamma_1\Gamma_2)^{1/2}/\Gamma$

VALUE	DOCUMENT ID		TECN	COMMENT
−0.09 ±0.03	GOPAL	77	DPWA	$\overline{K}N$ multichannel
−0.10 ±0.01	[1] CORDEN	76	DPWA	$K^-n \to \Lambda\pi^-$
−0.06 ±0.02	BAILLON	75	IPWA	$\overline{K}N \to \Lambda\pi$
−0.09 ±0.02	VANHORN	75	DPWA	$K^-p \to \Lambda\pi^0$
−0.087±0.056	DEVENISH	74B		Fixed-t dispersion rel.
• • • We do not use the following data for averages, fits, limits, etc. • • •				
−0.09 or −0.09	[2] MARTIN	77	DPWA	$\overline{K}N$ multichannel
−0.10	DEBELLEFON	76	IPWA	$K^-p \to \Lambda\pi^0$

[1] Preferred solution 3; see CORDEN 76 for other possibilities.
[2] The two MARTIN 77 values are from a T-matrix pole and from a Breit-Wigner fit.

$(\Gamma_i\Gamma_f)^{1/2}/\Gamma_{total}$ in $N\overline{K} \to \Sigma(1915) \to \Sigma\pi$ — $(\Gamma_1\Gamma_3)^{1/2}/\Gamma$

VALUE	DOCUMENT ID		TECN	COMMENT
−0.14±0.01	ZHANG	13A	DPWA	Multichannel
−0.17±0.01	[1] CORDEN	77C		$K^-n \to \Sigma\pi$
−0.15±0.02	[1] CORDEN	77C		$K^-n \to \Sigma\pi$
−0.19±0.03	GOPAL	77	DPWA	$\overline{K}N$ multichannel
−0.16±0.03	KANE	74	DPWA	$K^-p \to \Sigma\pi$
• • • We do not use the following data for averages, fits, limits, etc. • • •				
−0.05 or −0.05	[2] MARTIN	77	DPWA	$\overline{K}N$ multichannel

[1] The two entries for CORDEN 77C are from two different acceptable solutions.
[2] The two MARTIN 77 values are from a T-matrix pole and from a Breit-Wigner fit.

$(\Gamma_i\Gamma_f)^{1/2}/\Gamma_{total}$ in $N\overline{K} \to \Sigma(1915) \to \Sigma(1385)\pi$, P-wave — $(\Gamma_1\Gamma_6)^{1/2}/\Gamma$

VALUE	DOCUMENT ID		TECN	COMMENT
<0.01	CAMERON	78	DPWA	$K^-p \to \Sigma(1385)\pi$

$(\Gamma_i\Gamma_f)^{1/2}/\Gamma_{total}$ in $N\overline{K} \to \Sigma(1915) \to \Sigma(1385)\pi$, F-wave — $(\Gamma_1\Gamma_7)^{1/2}/\Gamma$

VALUE	DOCUMENT ID		TECN	COMMENT
+0.06 ±0.02	ZHANG	13A	DPWA	Multichannel
+0.039±0.009	[1] CAMERON	78	DPWA	$K^-p \to \Sigma(1385)\pi$

[1] The published sign has been changed to be in accord with the baryon-first convention.

$\Sigma(1915)$ REFERENCES

SARANTSEV	19	EPJ A55 180	A.V. Sarantsev *et al.*	(BONN, PNPI)
KAMANO	15	PR C92 025205	H. Kamano *et al.*	(ANL, OSAK)
ZHANG	13A	PR C88 035205	H. Zhang *et al.*	(KSU)
PDG	86	PL 170B 1	M. Aguilar-Benitez *et al.*	(CERN, CIT+)
PDG	82	PL 111B 1	M. Roos *et al.*	(HELS, CIT, CERN)
GOPAL	80	Toronto Conf. 159	G.P. Gopal	(RHEL) IJP
ALSTON-...	78	PR D18 182	M. Alston-Garnjost *et al.*	(LBL, MTHO+) IJP
Also		PRL 38 1007	M. Alston-Garnjost *et al.*	(LBL, MTHO+) IJP
CAMERON	78	NP B143 189	W. Cameron *et al.*	(RHEL, LOIC) IJP
CORDEN	77C	NP B125 61	M.J. Corden *et al.*	(BIRM) IJP
DECLAIS	77	CERN 77-16	Y. Declais *et al.*	(CAEN, CERN) IJP
GOPAL	77	NP B119 362	G.P. Gopal *et al.*	(LOIC, RHEL) IJP
MARTIN	77	NP B127 349	B.R. Martin, M.K. Pidcock, R.G. Moorhouse	(LOUC+) IJP
Also		NP B126 266	B.R. Martin, M.K. Pidcock	(LOUC)
Also		NP B126 285	B.R. Martin, M.K. Pidcock	(LOUC) IJP
CORDEN	76	NP B104 382	M.J. Corden *et al.*	(BIRM) IJP
DEBELLEFON	76	NP B109 129	A. de Bellefon, A. Berthon	(CDEF) IJP
BAILLON	75	NP B94 39	P.H. Baillon, P.J. Litchfield	(CERN, RHEL) IJP
HEMINGWAY	75	NP B91 12	R.J. Hemingway *et al.*	(CERN, HEIDH, MPIM) IJP
VANHORN	75	NP B87 145	A.J. van Horn	(LBL) IJP
Also		NP B87 157	A.J. van Horn	(LBL) IJP
DEVENISH	74B	NP B81 330	R.C.E. Devenish, C.D. Froggatt, B.R. Martin	(DESY+)
KANE	74	LBL-2452	D.F. Kane	(LBL) IJP
COOL	66	PRL 16 1228	R.L. Cool *et al.*	(BNL)

Downloaded from https://academic.oup.com/ptep/article/2022/8/083C01/6651666 by KIT Library user on 27 September 2022

$\Sigma(1940)\ 3/2^+$

$I(J^P) = 1(\frac{3}{2}^+)$ Status: *

OMITTED FROM SUMMARY TABLE

$\Sigma(1940)$ MASS

VALUE (MeV)	DOCUMENT ID		TECN	COMMENT
1920 to 1960 (≈ 1940) OUR ESTIMATE				
1941 ± 18	ZHANG	13A	DPWA	$\overline{K}N$ multichannel
1925 ± 200	VANHORN	75	DPWA	$K^- p \to \Lambda\pi^0$

$\Sigma(1940)$ WIDTH

VALUE (MeV)	DOCUMENT ID		TECN	COMMENT
100 to 400 (≈ 250) OUR ESTIMATE				
400 ± 49	ZHANG	13A	DPWA	$\overline{K}N$ multichannel
65^{+50}_{-20}	VANHORN	75	DPWA	$K^- p \to \Lambda\pi^0$

$\Sigma(1940)$ DECAY MODES

	Mode	Fraction (Γ_i/Γ)
Γ_1	$N\overline{K}$	(13.0 ± 2.0) %
Γ_2	$\Sigma\pi$	(4.0 ± 2.0) %
Γ_3	$\Sigma(1385)\pi$, P-wave	(22 ± 7) %
Γ_4	$\Lambda(1520)\pi$, S-wave	(5.0 ± 2.0) %

$\Sigma(1940)$ BRANCHING RATIOS

$\Gamma(N\overline{K})/\Gamma_{total}$ — Γ_1/Γ

VALUE	DOCUMENT ID		TECN	COMMENT
0.13 ± 0.02	ZHANG	13A	DPWA	$\overline{K}N$ multichannel

$\Gamma(\Sigma\pi)/\Gamma_{total}$ — Γ_2/Γ

VALUE	DOCUMENT ID		TECN	COMMENT
0.04 ± 0.02	ZHANG	13A	DPWA	$\overline{K}N$ multichannel

$\Gamma(\Sigma(1385)\pi$, P-wave$)/\Gamma_{total}$ — Γ_3/Γ

VALUE	DOCUMENT ID		TECN	COMMENT
0.22 ± 0.07	ZHANG	13A	DPWA	$\overline{K}N$ multichannel

$\Gamma(\Lambda(1520)\pi$, S-wave$)/\Gamma_{total}$ — Γ_4/Γ

VALUE	DOCUMENT ID		TECN	COMMENT
0.05 ± 0.02	ZHANG	13A	DPWA	$\overline{K}N$ multichannel

$\Sigma(1940)$ REFERENCES

ZHANG 13A PR C88 035205 H. Zhang et al. (KSU)
VANHORN 75 NP B87 145 A.J. van Horn (LBL)

$\Sigma(2010)\ 3/2^-$

$I(J^P) = 1(\frac{3}{2}^-)$ Status: *

OMITTED FROM SUMMARY TABLE

$\Sigma(2010)$ POLE POSITION

REAL PART

VALUE (MeV)	DOCUMENT ID		TECN	COMMENT
1995 ± 12	SARANTSEV	19	DPWA	$\overline{K}N$ multichannel

−2×IMAGINARY PART

VALUE (MeV)	DOCUMENT ID		TECN	COMMENT
175 ± 24	SARANTSEV	19	DPWA	$\overline{K}N$ multichannel

$\Sigma(2010)$ POLE RESIDUES

The normalized residue is the residue divided by $\Gamma_{pole}/2$.

Normalized residue in $N\overline{K} \to \Sigma(2010) \to N\overline{K}$

MODULUS	PHASE (°)	DOCUMENT ID		TECN	COMMENT
0.07 ± 0.03	**−115 ± 25**	SARANTSEV	19	DPWA	$\overline{K}N$ multichannel

Normalized residue in $N\overline{K} \to \Sigma(2010) \to \Sigma\pi$

MODULUS	PHASE (°)	DOCUMENT ID		TECN	COMMENT
0.04 ± 0.02	**130 ± 22**	SARANTSEV	19	DPWA	$\overline{K}N$ multichannel

Normalized residue in $N\overline{K} \to \Sigma(2010) \to \Lambda\pi$

MODULUS	PHASE (°)	DOCUMENT ID		TECN	COMMENT
0.06 ± 0.03	**170 ± 25**	SARANTSEV	19	DPWA	$\overline{K}N$ multichannel

Normalized residue in $N\overline{K} \to \Sigma(2010) \to \Xi K$

MODULUS	PHASE (°)	DOCUMENT ID		TECN	COMMENT
0.04 ± 0.02	**−120 ± 45**	SARANTSEV	19	DPWA	$\overline{K}N$ multichannel

Normalized residue in $N\overline{K} \to \Sigma(2010) \to \Lambda(1520)\pi$, P-wave

MODULUS	PHASE (°)	DOCUMENT ID		TECN	COMMENT
0.03 ± 0.02	**80 ± 35**	SARANTSEV	19	DPWA	$\overline{K}N$ multichannel

Normalized residue in $N\overline{K} \to \Sigma(2010) \to \Lambda(1520)\pi$, F-wave

MODULUS	PHASE (°)	DOCUMENT ID		TECN	COMMENT
0.08 ± 0.05	**150 ± 65**	SARANTSEV	19	DPWA	$\overline{K}N$ multichannel

Normalized residue in $N\overline{K} \to \Sigma(2010) \to \Sigma(1385)\pi$, P-wave

VALUE	DOCUMENT ID		TECN	COMMENT
0.04+-0.02025+-45	SARANTSEV	19	DPWA	$\overline{K}N$ multichannel

Normalized residue in $N\overline{K} \to \Sigma(2010) \to \Sigma(1385)\pi$, F-wave

VALUE	DOCUMENT ID		TECN	COMMENT
0.02 ± 0.02	SARANTSEV	19	DPWA	$\overline{K}N$ multichannel

Normalized residue in $N\overline{K} \to \Sigma(2010) \to \Delta\overline{K}$, S-wave

MODULUS	PHASE (°)	DOCUMENT ID		TECN	COMMENT
0.08 ± 0.04	**0 ± 30**	SARANTSEV	19	DPWA	$\overline{K}N$ multichannel

Normalized residue in $N\overline{K} \to \Sigma(2010) \to \Delta\overline{K}$, D-wave

MODULUS	PHASE (°)	DOCUMENT ID		TECN	COMMENT
0.02 ± 0.02		SARANTSEV	19	DPWA	$\overline{K}N$ multichannel

Normalized residue in $N\overline{K} \to \Sigma(2010) \to N\overline{K}^*(892)$, S-wave

VALUE	DOCUMENT ID		TECN	COMMENT
0.12+-0.0360+-60	SARANTSEV	19	DPWA	$\overline{K}N$ multichannel

Normalized residue in $N\overline{K} \to \Sigma(2010) \to N\overline{K}^*(892)$, S=1/2 , D-wave

MODULUS	PHASE (°)	DOCUMENT ID		TECN	COMMENT
0.08 ± 0.04	**55 ± 60**	SARANTSEV	19	DPWA	$\overline{K}N$ multichannel

Normalized residue in $N\overline{K} \to \Sigma(2010) \to N\overline{K}^*(892)$, S=3/2 , D-wave

MODULUS	PHASE (°)	DOCUMENT ID		TECN	COMMENT
0.08 ± 0.04	**15 ± 60**	SARANTSEV	19	DPWA	$\overline{K}N$ multichannel

$\Sigma(2010)$ MASS

VALUE (MeV)	DOCUMENT ID		TECN	COMMENT
2005 ± 14	SARANTSEV	19	DPWA	$\overline{K}N$ multichannel

$\Sigma(2010)$ WIDTH

VALUE (MeV)	DOCUMENT ID		TECN	COMMENT
178 ± 23	SARANTSEV	19	DPWA	$\overline{K}N$ multichannel

$\Sigma(2010)$ DECAY MODES

	Mode	Fraction (Γ_i/Γ)
Γ_1	$N\overline{K}$	(7.0 ± 3.0) %
Γ_2	$\Lambda\pi$	(5.0 ± 2.0) %
Γ_3	$\Sigma\pi$	(3.0 ± 2.0) %
Γ_4	ΞK	(3.0 ± 2.0) %
Γ_5	$\Sigma(1385)\pi$, P-wave	(3.0 ± 2.0) %
Γ_6	$\Sigma(1385)\pi$, F-wave	(2.0 ± 2.0) %
Γ_7	$\Lambda(1520)\pi$, P-wave	(2.0 ± 2.0) %
Γ_8	$\Lambda(1520)\pi$, F-wave	(12 ± 6) %
Γ_9	$\Delta\overline{K}$, S-wave	(11 ± 5) %
Γ_{10}	$\Delta\overline{K}$, D-wave	(1.0 ± 1.0) %
Γ_{11}	$N\overline{K}^*(892)$, S=1/2, S-wave	(27 ± 7) %
Γ_{12}	$N\overline{K}^*(892)$, S=1/2 , D-wave	(13 ± 6) %
Γ_{13}	$N\overline{K}^*(892)$, S=3/2, D-wave	(13 ± 6) %

$\Sigma(2010)$ BRANCHING RATIOS

See "Sign conventions for resonance couplings" in the Note on Λ and Σ Resonances.

$\Gamma(N\overline{K})/\Gamma_{total}$ — Γ_1/Γ

VALUE	DOCUMENT ID		TECN	COMMENT
0.07 ± 0.03	SARANTSEV	19	DPWA	$\overline{K}N$ multichannel

$\Gamma(\Lambda\pi)/\Gamma_{total}$ — Γ_2/Γ

VALUE	DOCUMENT ID		TECN	COMMENT
0.05 ± 0.02	SARANTSEV	19	DPWA	$\overline{K}N$ multichannel

$\Gamma(\Sigma\pi)/\Gamma_{total}$ — Γ_3/Γ

VALUE	DOCUMENT ID		TECN	COMMENT
0.03 ± 0.02	SARANTSEV	19	DPWA	$\overline{K}N$ multichannel

Downloaded from https://academic.oup.com/ptep/article/2022/8/083C01/6651666 by KIT Library user on 27 September 2022

$\Gamma(\Xi K)/\Gamma_{total}$ — Γ_4/Γ

VALUE	DOCUMENT ID		TECN	COMMENT
0.03±0.02	SARANTSEV	19	DPWA	$\overline{K}N$ multichannel

$\Gamma(\Sigma(1385)\pi, P\text{-wave})/\Gamma_{total}$ — Γ_5/Γ

VALUE	DOCUMENT ID		TECN	COMMENT
0.03±0.02	SARANTSEV	19	DPWA	$\overline{K}N$ multichannel

$\Gamma(\Sigma(1385)\pi, F\text{-wave})/\Gamma_{total}$ — Γ_6/Γ

VALUE	DOCUMENT ID		TECN	COMMENT
0.02±0.02	SARANTSEV	19	DPWA	$\overline{K}N$ multichannel

$\Gamma(\Lambda(1520)\pi, P\text{-wave})/\Gamma_{total}$ — Γ_7/Γ

VALUE	DOCUMENT ID		TECN	COMMENT
0.02±0.02	SARANTSEV	19	DPWA	$\overline{K}N$ multichannel

$\Gamma(\Lambda(1520)\pi, F\text{-wave})/\Gamma_{total}$ — Γ_8/Γ

VALUE	DOCUMENT ID		TECN	COMMENT
0.12±0.06	SARANTSEV	19	DPWA	$\overline{K}N$ multichannel

$\Gamma(\Delta\overline{K}, S\text{-wave})/\Gamma_{total}$ — Γ_9/Γ

VALUE	DOCUMENT ID		TECN	COMMENT
0.11±0.05	SARANTSEV	19	DPWA	$\overline{K}N$ multichannel

$\Gamma(\Delta\overline{K}, D\text{-wave})/\Gamma_{total}$ — Γ_{10}/Γ

VALUE	DOCUMENT ID		TECN	COMMENT
0.01±0.01	SARANTSEV	19	DPWA	$\overline{K}N$ multichannel

$\Gamma(N\overline{K}^*(892), S=1/2, S\text{-wave})/\Gamma_{total}$ — Γ_{11}/Γ

VALUE	DOCUMENT ID		TECN	COMMENT
0.27±0.07	SARANTSEV	19	DPWA	$\overline{K}N$ multichannel

$\Gamma(N\overline{K}^*(892), S=1/2, D\text{-wave})/\Gamma_{total}$ — Γ_{12}/Γ

VALUE	DOCUMENT ID		TECN	COMMENT
0.13±0.06	SARANTSEV	19	DPWA	$\overline{K}N$ multichannel

$\Gamma(N\overline{K}^*(892), S=3/2, D\text{-wave})/\Gamma_{total}$ — Γ_{13}/Γ

VALUE	DOCUMENT ID		TECN	COMMENT
0.13±0.06	SARANTSEV	19	DPWA	$\overline{K}N$ multichannel

$\Sigma(2010)$ REFERENCES

SARANTSEV 19 EPJ A55 180 A.V. Sarantsev *et al.* (BONN, PNPI)

$\Sigma(2030)\ 7/2^+$

$I(J^P) = 1(\frac{7}{2}^+)$ Status: ****

Discovered by COOL 66 and by WOHL 66. For most results published before 1974 (they are now obsolete), see our 1982 edition Physics Letters **111B** 1 (1982).

This entry only includes results from partial-wave analyses. Parameters of peaks seen in cross sections and invariant-mass distributions around 2030 MeV may be found in our 1984 edition, Reviews of Modern Physics **56** S1 (1984).

$\Sigma(2030)$ POLE POSITION

REAL PART

VALUE (MeV)	DOCUMENT ID		TECN	COMMENT
2010 to 2030 (≈ 2020) OUR ESTIMATE				
2014 ± 6	SARANTSEV	19	DPWA	$\overline{K}N$ multichannel
2025^{+10}_{-5}	[1] KAMANO	15	DPWA	$\overline{K}N$ multichannel
• • • We do not use the following data for averages, fits, limits, etc. • • •				
1993	ZHANG	13A	DPWA	$\overline{K}N$ multichannel

[1] From the preferred solution A in KAMANO 15.

−2×IMAGINARY PART

VALUE (MeV)	DOCUMENT ID		TECN	COMMENT
130 to 190 (≈ 160) OUR ESTIMATE				
172±12	SARANTSEV	19	DPWA	$\overline{K}N$ multichannel
130^{+6}_{-24}	[1] KAMANO	15	DPWA	$\overline{K}N$ multichannel
• • • We do not use the following data for averages, fits, limits, etc. • • •				
176	ZHANG	13A	DPWA	$\overline{K}N$ multichannel

[1] From the preferred solution A in KAMANO 15.

$\Sigma(2030)$ POLE RESIDUES

The normalized residue is the residue divided by $\Gamma_{pole}/2$.

Normalized residue in $N\overline{K} \to \Sigma(2030) \to N\overline{K}$

MODULUS	PHASE (°)	DOCUMENT ID		TECN	COMMENT
0.20 ±0.04	**−38 ± 8**	SARANTSEV	19	DPWA	$\overline{K}N$ multichannel
• • • We do not use the following data for averages, fits, limits, etc. • • •					
0.220	−38	[1] KAMANO	15	DPWA	$\overline{K}N$ multichannel

[1] From the preferred solution A in KAMANO 15.

Normalized residue in $N\overline{K} \to \Sigma(2030) \to \Sigma\pi$

MODULUS	PHASE (°)	DOCUMENT ID		TECN	COMMENT
0.07 ±0.02	**165 ± 12**	SARANTSEV	19	DPWA	$\overline{K}N$ multichannel
• • • We do not use the following data for averages, fits, limits, etc. • • •					
0.0807	135	[1] KAMANO	15	DPWA	$\overline{K}N$ multichannel

[1] From the preferred solution A in KAMANO 15.

Normalized residue in $N\overline{K} \to \Sigma(2030) \to \Lambda\pi$

MODULUS	PHASE (°)	DOCUMENT ID		TECN	COMMENT
0.18 ±0.04	**−22 ± 12**	SARANTSEV	19	DPWA	$\overline{K}N$ multichannel
• • • We do not use the following data for averages, fits, limits, etc. • • •					
0.138	−24	[1] KAMANO	15	DPWA	$\overline{K}N$ multichannel

[1] From the preferred solution A in KAMANO 15.

Normalized residue in $N\overline{K} \to \Sigma(2030) \to \Xi K$

MODULUS	PHASE (°)	DOCUMENT ID		TECN	COMMENT
0.01 ±0.01		SARANTSEV	19	DPWA	$\overline{K}N$ multichannel
• • • We do not use the following data for averages, fits, limits, etc. • • •					
0.0348	129	[1] KAMANO	15	DPWA	$\overline{K}N$ multichannel

[1] From the preferred solution A in KAMANO 15.

Normalized residue in $N\overline{K} \to \Sigma(2030) \to \Sigma(1385)\pi$, F-wave

MODULUS	PHASE (°)	DOCUMENT ID		TECN	COMMENT
0.04 ±0.03		SARANTSEV	19	DPWA	$\overline{K}N$ multichannel
• • • We do not use the following data for averages, fits, limits, etc. • • •					
0.089	−23	[1] KAMANO	15	DPWA	$\overline{K}N$ multichannel

[1] From the preferred solution A in KAMANO 15.

Normalized residue in $N\overline{K} \to \Sigma(2030) \to \Sigma(1385)\pi$, H-wave

MODULUS	PHASE (°)	DOCUMENT ID		TECN	COMMENT
• • • We do not use the following data for averages, fits, limits, etc. • • •					
0.0245	132	[1] KAMANO	15	DPWA	Multichannel

[1] From the preferred solution A in KAMANO 15.

Normalized residue in $N\overline{K} \to \Sigma(2030) \to \Lambda(1520)\pi$, D-wave

MODULUS	PHASE (°)	DOCUMENT ID		TECN	COMMENT
0.03±0.02	**−100 ± 40**	SARANTSEV	19	DPWA	$\overline{K}N$ multichannel

Normalized residue in $N\overline{K} \to \Sigma(2030) \to \Lambda(1520)\pi$, G-wave

MODULUS	PHASE (°)	DOCUMENT ID		TECN	COMMENT
0.02±0.02		SARANTSEV	19	DPWA	$\overline{K}N$ multichannel

Normalized residue in $N\overline{K} \to \Sigma(2030) \to \Delta\overline{K}$, F-wave

MODULUS	PHASE (°)	DOCUMENT ID		TECN	COMMENT
0.16±0.06	**−130 ± 20**	SARANTSEV	19	DPWA	$\overline{K}N$ multichannel

Normalized residue in $N\overline{K} \to \Sigma(2030) \to \Delta\overline{K}$, H-wave

MODULUS	PHASE (°)	DOCUMENT ID		TECN	COMMENT
0.04±0.02	**−130 ± 35**	SARANTSEV	19	DPWA	$\overline{K}N$ multichannel

Normalized residue in $N\overline{K} \to \Sigma(2030) \to N\overline{K}^*(892)$, $S=1/2$, F-wave

MODULUS	PHASE (°)	DOCUMENT ID		TECN	COMMENT
0.02 ±0.02		SARANTSEV	19	DPWA	$\overline{K}N$ multichannel
• • • We do not use the following data for averages, fits, limits, etc. • • •					
0.193	38	[1] KAMANO	15	DPWA	$\overline{K}N$ multichannel

[1] From the preferred solution A in KAMANO 15.

Normalized residue in $N\overline{K} \to \Sigma(2030) \to N\overline{K}^*(892)$, $S=3/2$, F-wave

MODULUS	PHASE (°)	DOCUMENT ID		TECN	COMMENT
0.16 ±0.09	**−160 ± 40**	SARANTSEV	19	DPWA	$\overline{K}N$ multichannel
• • • We do not use the following data for averages, fits, limits, etc. • • •					
0.320	37	[1] KAMANO	15	DPWA	$\overline{K}N$ multichannel

[1] From the preferred solution A in KAMANO 15.

Normalized residue in $N\overline{K} \to \Sigma(2030) \to N\overline{K}^*(892)$, $S=3/2$, H-wave

MODULUS	PHASE (°)	DOCUMENT ID		TECN	COMMENT
• • • We do not use the following data for averages, fits, limits, etc. • • •					
0.00358	22	[1] KAMANO	15	DPWA	Multichannel

[1] From the preferred solution A in KAMANO 15.

$\Sigma(2030)$ MASS

VALUE (MeV)	DOCUMENT ID		TECN	COMMENT
2025 to 2040 (≈ 2030) OUR ESTIMATE				
2032 ± 6	SARANTSEV	19	DPWA	$\overline{K}N$ multichannel
2030 ± 5	ZHANG	13A	DPWA	$\overline{K}N$ multichannel
2036 ± 5	GOPAL	80	DPWA	$\overline{K}N \to \overline{K}N$
2038±10	CORDEN	77B		$K^-N \to N\overline{K}^*$
2030 ± 3	[1] CORDEN	76	DPWA	$K^-n \to \Lambda\pi^-$
2035±15	BAILLON	75	IPWA	$\overline{K}N \to \Lambda\pi$
2038±10	HEMINGWAY	75	DPWA	$K^-p \to \overline{K}N$
2042±11	VANHORN	75	DPWA	$K^-p \to \Lambda\pi^0$
2020 ± 6	KANE	74	DPWA	$K^-p \to \Sigma\pi$
2035±10	LITCHFIELD	74B	DPWA	$K^-p \to \Lambda(1520)\pi^0$
2020±30	LITCHFIELD	74C	DPWA	$K^-p \to \Delta(1232)\overline{K}$
2025±10	LITCHFIELD	74D	DPWA	$K^-p \to \Lambda(1820)\pi^0$

Downloaded from https://academic.oup.com/ptep/article/2022/8/083C01/6651666 by KIT Library user on 27 September 2022

• • • We do not use the following data for averages, fits, limits, etc. • • •

2040 ± 5	GOPAL	77	DPWA	$\overline{K}N$ multichannel
2027 to 2057	GOYAL	77	DPWA	$K^- N \to \Sigma\pi$
2030	DEBELLEFON	76	IPWA	$K^- p \to \Lambda\pi^0$

[1] Preferred solution 3; see CORDEN 76 for other possibilities.

$\Sigma(2030)$ WIDTH

VALUE (MeV)	DOCUMENT ID		TECN	COMMENT
150 to 200 (≈ 180) OUR ESTIMATE				
177±12	SARANTSEV	19	DPWA	$\overline{K}N$ multichannel
207±17	ZHANG	13A	DPWA	$\overline{K}N$ multichannel
172±10	GOPAL	80	DPWA	$\overline{K}N \to \overline{K}N$
137±40	CORDEN	77B		$K^- N \to N\overline{K}^*$
201± 9	[1] CORDEN	76	DPWA	$K^- n \to \Lambda\pi^-$
180±20	BAILLON	75	IPWA	$\overline{K}N \to \Lambda\pi$
172±15	HEMINGWAY	75	DPWA	$K^- p \to \overline{K}N$
178±13	VANHORN	75	DPWA	$K^- p \to \Lambda\pi^0$
111± 5	KANE	74	DPWA	$K^- p \to \Sigma\pi$
160±20	LITCHFIELD	74B	DPWA	$K^- p \to \Lambda(1520)\pi^0$
200±30	LITCHFIELD	74C	DPWA	$K^- p \to \Delta(1232)\overline{K}$
• • • We do not use the following data for averages, fits, limits, etc. • • •				
260	DECLAIS	77	DPWA	$\overline{K}N \to \overline{K}N$
190±10	GOPAL	77	DPWA	$\overline{K}N$ multichannel
126 to 195	GOYAL	77	DPWA	$K^- N \to \Sigma\pi$
160	DEBELLEFON	76	IPWA	$K^- p \to \Lambda\pi^0$
70 to 125	LITCHFIELD	74D	DPWA	$K^- p \to \Lambda(1820)\pi^0$

[1] Preferred solution 3; see CORDEN 76 for other possibilities.

$\Sigma(2030)$ DECAY MODES

	Mode	Fraction (Γ_i/Γ)
Γ_1	$N\overline{K}$	17–23 %
Γ_2	$\Lambda\pi$	17–23 %
Γ_3	$\Sigma\pi$	5–10 %
Γ_4	ΞK	<2 %
Γ_5	$\Sigma(1385)\pi$	5–15 %
Γ_6	$\Sigma(1385)\pi$, F-wave	(1.0±1.0) %
Γ_7	$\Sigma(1385)\pi$, H-wave	
Γ_8	$\Lambda(1520)\pi$	10–20 %
Γ_9	$\Lambda(1520)\pi$, D-wave	
Γ_{10}	$\Lambda(1520)\pi$, G-wave	
Γ_{11}	$\Delta(1232)\overline{K}$	10–20 %
Γ_{12}	$\Delta(1232)\overline{K}$, F-wave	(15 ±5) %
Γ_{13}	$\Delta(1232)\overline{K}$, H-wave	(1.0±1.0) %
Γ_{14}	$N\overline{K}^*(892)$	
Γ_{15}	$N\overline{K}^*(892)$, S=1/2, F-wave	
Γ_{16}	$N\overline{K}^*(892)$, S=3/2, F-wave	(14 ±8) %
Γ_{17}	$N\overline{K}^*(892)$, S=3/2, H-wave	
Γ_{18}	$\Lambda(1820)\pi$, P-wave	

$\Sigma(2030)$ BRANCHING RATIOS

See "Sign conventions for resonance couplings" in the Note on Λ and Σ Resonances.

$\Gamma(N\overline{K})/\Gamma_{total}$ — Γ_1/Γ

VALUE	DOCUMENT ID		TECN	COMMENT
0.17 to 0.23 OUR ESTIMATE				
0.20 ±0.04	SARANTSEV	19	DPWA	$\overline{K}N$ multichannel
0.13 ±0.01	ZHANG	13A	DPWA	$\overline{K}N$ multichannel
0.19 ±0.03	GOPAL	80	DPWA	$\overline{K}N \to \overline{K}N$
0.18 ±0.03	HEMINGWAY	75	DPWA	$K^- p \to \overline{K}N$
• • • We do not use the following data for averages, fits, limits, etc. • • •				
0.269	[1] KAMANO	15	DPWA	Multichannel
0.15	DECLAIS	77	DPWA	$\overline{K}N \to \overline{K}N$
0.24 ±0.02	GOPAL	77	DPWA	See GOPAL 80

[1] From the preferred solution A in KAMANO 15.

$\Gamma(\Lambda\pi)/\Gamma_{total}$ — Γ_2/Γ

VALUE	DOCUMENT ID		TECN	COMMENT
0.17 ±0.04	SARANTSEV	19	DPWA	$\overline{K}N$ multichannel
• • • We do not use the following data for averages, fits, limits, etc. • • •				
0.080	[1] KAMANO	15	DPWA	$\overline{K}N$ multichannel

[1] From the preferred solution A in KAMANO 15.

$\Gamma(\Sigma\pi)/\Gamma_{total}$ — Γ_3/Γ

VALUE	DOCUMENT ID		TECN	COMMENT
0.025±0.008	SARANTSEV	19	DPWA	$\overline{K}N$ multichannel
• • • We do not use the following data for averages, fits, limits, etc. • • •				
0.037	[1] KAMANO	15	DPWA	$\overline{K}N$ multichannel

[1] From the preferred solution A in KAMANO 15.

$\Gamma(\Xi K)/\Gamma_{total}$ — Γ_4/Γ

VALUE	DOCUMENT ID		TECN	COMMENT
<0.01	SARANTSEV	19	DPWA	$\overline{K}N$ multichannel
• • • We do not use the following data for averages, fits, limits, etc. • • •				
0.006	[1] KAMANO	15	DPWA	$\overline{K}N$ multichannel

[1] From the preferred solution A in KAMANO 15.

$\Gamma(\Lambda(1520)\pi, D\text{-wave})/\Gamma_{total}$ — Γ_9/Γ

VALUE	DOCUMENT ID		TECN	COMMENT
~ 0.01	SARANTSEV	19	DPWA	$\overline{K}N$ multichannel

$\Gamma(\Lambda(1520)\pi, G\text{-wave})/\Gamma_{total}$ — Γ_{10}/Γ

VALUE	DOCUMENT ID		TECN	COMMENT
<0.01	SARANTSEV	19	DPWA	$\overline{K}N$ multichannel

$\Gamma(\Sigma(1385)\pi, F\text{-wave})/\Gamma_{total}$ — Γ_6/Γ

VALUE	DOCUMENT ID		TECN	COMMENT
0.01 ±0.01	SARANTSEV	19	DPWA	$\overline{K}N$ multichannel
• • • We do not use the following data for averages, fits, limits, etc. • • •				
0.030	[1] KAMANO	15	DPWA	$\overline{K}N$ multichannel

[1] From the preferred solution A in KAMANO 15.

$\Gamma(\Sigma(1385)\pi, H\text{-wave})/\Gamma_{total}$ — Γ_7/Γ

VALUE	DOCUMENT ID		TECN	COMMENT
• • • We do not use the following data for averages, fits, limits, etc. • • •				
0.003	[1] KAMANO	15	DPWA	Multichannel

[1] From the preferred solution A in KAMANO 15.

$\Gamma(\Delta(1232)\overline{K}, F\text{-wave})/\Gamma_{total}$ — Γ_{12}/Γ

VALUE	DOCUMENT ID		TECN	COMMENT
0.15±0.05	SARANTSEV	19	DPWA	$\overline{K}N$ multichannel

$\Gamma(\Delta(1232)\overline{K}, H\text{-wave})/\Gamma_{total}$ — Γ_{13}/Γ

VALUE	DOCUMENT ID		TECN	COMMENT
0.01±0.01	SARANTSEV	19	DPWA	$\overline{K}N$ multichannel

$\Gamma(N\overline{K}^*(892), S=1/2, F\text{-wave})/\Gamma_{total}$ — Γ_{15}/Γ

VALUE	DOCUMENT ID		TECN	COMMENT
<0.01	SARANTSEV	19	DPWA	$\overline{K}N$ multichannel
• • • We do not use the following data for averages, fits, limits, etc. • • •				
0.154	[1] KAMANO	15	DPWA	$\overline{K}N$ multichannel

[1] From the preferred solution A in KAMANO 15.

$\Gamma(N\overline{K}^*(892), S=3/2, F\text{-wave})/\Gamma_{total}$ — Γ_{16}/Γ

VALUE	DOCUMENT ID		TECN	COMMENT
0.14 ±0.08	SARANTSEV	19	DPWA	$\overline{K}N$ multichannel
• • • We do not use the following data for averages, fits, limits, etc. • • •				
0.422	[1] KAMANO	15	DPWA	$\overline{K}N$ multichannel

[1] From the preferred solution A in KAMANO 15.

$\Gamma(N\overline{K}^*(892), S=3/2, H\text{-wave})/\Gamma_{total}$ — Γ_{17}/Γ

VALUE	DOCUMENT ID		TECN	COMMENT
• • • We do not use the following data for averages, fits, limits, etc. • • •				
not seen	[1] KAMANO	15	DPWA	$\overline{K}N$ multichannel

[1] From the preferred solution A in KAMANO 15.

$(\Gamma_i\Gamma_f)^{1/2}/\Gamma_{total}$ in $N\overline{K} \to \Sigma(2030) \to \Lambda\pi$ — $(\Gamma_1\Gamma_2)^{1/2}/\Gamma$

VALUE	DOCUMENT ID		TECN	COMMENT
+0.15 ±0.01	ZHANG	13A	DPWA	Multichannel
+0.18 ±0.02	GOPAL	77	DPWA	$\overline{K}N$ multichannel
+0.20 ±0.01	[1] CORDEN	76	DPWA	$K^- n \to \Lambda\pi^-$
+0.18 ±0.02	BAILLON	75	IPWA	$\overline{K}N \to \Lambda\pi$
+0.20 ±0.01	VANHORN	75	DPWA	$K^- p \to \Lambda\pi^0$
+0.195±0.053	DEVENISH	74B		Fixed-t dispersion rel.
• • • We do not use the following data for averages, fits, limits, etc. • • •				
0.20	DEBELLEFON	76	IPWA	$K^- p \to \Lambda\pi^0$

[1] Preferred solution 3; see CORDEN 76 for other possibilities.

$(\Gamma_i\Gamma_f)^{1/2}/\Gamma_{total}$ in $N\overline{K} \to \Sigma(2030) \to \Sigma\pi$ — $(\Gamma_1\Gamma_3)^{1/2}/\Gamma$

VALUE	DOCUMENT ID		TECN	COMMENT
−0.08 ±0.01	ZHANG	13A	DPWA	Multichannel
−0.09 ±0.01	[1] CORDEN	77C		$K^- n \to \Sigma\pi$
−0.06 ±0.01	[1] CORDEN	77C		$K^- n \to \Sigma\pi$
−0.15 ±0.03	GOPAL	77	DPWA	$\overline{K}N$ multichannel
−0.10 ±0.01	KANE	74	DPWA	$K^- p \to \Sigma\pi$
• • • We do not use the following data for averages, fits, limits, etc. • • •				
−0.085±0.02	[2] GOYAL	77	DPWA	$K^- N \to \Sigma\pi$

[1] The two entries for CORDEN 77C are from two different acceptable solutions.
[2] This coupling is extracted from unnormalized data.

Downloaded from https://academic.oup.com/ptep/article/2022/8/083C01/6651666 by KIT Library user on 27 September 2022

$(\Gamma_i\Gamma_f)^{1/2}/\Gamma_{total}$ in $N\overline{K} \to \Sigma(2030) \to \Xi K$ — $(\Gamma_1\Gamma_4)^{1/2}/\Gamma$

VALUE	DOCUMENT ID		TECN	COMMENT
0.023	MULLER	69B	DPWA	$K^-p \to \Xi K$
<0.05	BURGUN	68	DPWA	$K^-p \to \Xi K$
<0.05	TRIPP	67	RVUE	$K^-p \to \Xi K$

$(\Gamma_i\Gamma_f)^{1/2}/\Gamma_{total}$ in $N\overline{K} \to \Sigma(2030) \to \Sigma(1385)\pi$, F-wave — $(\Gamma_1\Gamma_6)^{1/2}/\Gamma$

VALUE	DOCUMENT ID		TECN	COMMENT
+0.16 ±0.01	ZHANG	13A	DPWA	Multichannel
+0.153±0.026	[1] CAMERON	78	DPWA	$K^-p \to \Sigma(1385)\pi$

[1] The published sign has been changed to be in accord with the baryon-first convention.

$(\Gamma_i\Gamma_f)^{1/2}/\Gamma_{total}$ in $N\overline{K} \to \Sigma(2030) \to \Lambda(1520)\pi$, D-wave — $(\Gamma_1\Gamma_9)^{1/2}/\Gamma$

VALUE	DOCUMENT ID		TECN	COMMENT
+0.114±0.010	[1] CAMERON	77	DPWA	$K^-p \to \Lambda(1520)\pi^0$
0.14 ±0.03	LITCHFIELD	74B	DPWA	$K^-p \to \Lambda(1520)\pi^0$
• • • We do not use the following data for averages, fits, limits, etc. • • •				
0.10 ±0.03	[2] CORDEN	75B	DBC	$K^-n \to N\overline{K}\pi^-$

[1] The published sign has been changed to be in accord with the baryon-first convention.
[2] An upper limit.

$(\Gamma_i\Gamma_f)^{1/2}/\Gamma_{total}$ in $N\overline{K} \to \Sigma(2030) \to \Lambda(1520)\pi$, G-wave — $(\Gamma_1\Gamma_{10})^{1/2}/\Gamma$

VALUE	DOCUMENT ID		TECN	COMMENT
+0.146±0.010	[1] CAMERON	77	DPWA	$K^-p \to \Lambda(1520)\pi^0$
0.02 ±0.02	LITCHFIELD	74B	DPWA	$K^-p \to \Lambda(1520)\pi^0$

[1] The published sign has been changed to be in accord with the baryon-first convention.

$(\Gamma_i\Gamma_f)^{1/2}/\Gamma_{total}$ in $N\overline{K} \to \Sigma(2030) \to \Delta(1232)\overline{K}$, F-wave — $(\Gamma_1\Gamma_{12})^{1/2}/\Gamma$

VALUE	DOCUMENT ID		TECN	COMMENT
+0.12±0.02	ZHANG	13A	DPWA	Multichannel
0.16±0.03	LITCHFIELD	74C	DPWA	$K^-p \to \Delta(1232)\overline{K}$
• • • We do not use the following data for averages, fits, limits, etc. • • •				
0.17±0.03	[1] CORDEN	75B	DBC	$K^-n \to N\overline{K}\pi^-$

[1] An upper limit.

$(\Gamma_i\Gamma_f)^{1/2}/\Gamma_{total}$ in $N\overline{K} \to \Sigma(2030) \to \Delta(1232)\overline{K}$, H-wave — $(\Gamma_1\Gamma_{13})^{1/2}/\Gamma$

VALUE	DOCUMENT ID		TECN	COMMENT
0.00±0.02	LITCHFIELD	74C	DPWA	$K^-p \to \Delta(1232)\overline{K}$

$(\Gamma_i\Gamma_f)^{1/2}/\Gamma_{total}$ in $N\overline{K} \to \Sigma(2030) \to N\overline{K}^*(892)$, $S=1/2$, F-wave — $(\Gamma_1\Gamma_{15})^{1/2}/\Gamma$

VALUE	DOCUMENT ID		TECN	COMMENT
+0.06±0.02	ZHANG	13A	DPWA	Multichannel
+0.06±0.03	[1] CAMERON	78B	DPWA	$K^-p \to N\overline{K}^*$
−0.02±0.01	CORDEN	77B		$K^-d \to NN\overline{K}^*$

[1] The published sign has been changed to be in accord with the baryon-first convention.

$(\Gamma_i\Gamma_f)^{1/2}/\Gamma_{total}$ in $N\overline{K} \to \Sigma(2030) \to N\overline{K}^*(892)$, $S=3/2$, F-wave — $(\Gamma_1\Gamma_{16})^{1/2}/\Gamma$

VALUE	DOCUMENT ID		TECN	COMMENT
+0.05±0.01	ZHANG	13A	DPWA	Multichannel
+0.04±0.03	[1] CAMERON	78B	DPWA	$K^-p \to N\overline{K}^*$
−0.12±0.02	CORDEN	77B		$K^-d \to NN\overline{K}^*$

[1] The upper limit on the G_3 wave is 0.03.

$(\Gamma_i\Gamma_f)^{1/2}/\Gamma_{total}$ in $N\overline{K} \to \Sigma(2030) \to \Lambda(1820)\pi$, P-wave — $(\Gamma_1\Gamma_{18})^{1/2}/\Gamma$

VALUE	DOCUMENT ID		TECN	COMMENT
0.14±0.02	CORDEN	75B	DBC	$K^-n \to N\overline{K}\pi^-$
0.18±0.04	LITCHFIELD	74D	DPWA	$K^-p \to \Lambda(1820)\pi^0$

$\Sigma(2030)$ REFERENCES

SARANTSEV	19	EPJ A55 180	A.V. Sarantsev *et al.*	(BONN, PNPI)
KAMANO	15	PR C92 025205	H. Kamano *et al.*	(ANL, OSAK)
ZHANG	13A	PR C88 035205	H. Zhang *et al.*	(KSU)
PDG	84	RMP 56 S1	C.G. Wohl *et al.*	(LBL, CIT, CERN)
PDG	82	PL 111B 1	M. Roos *et al.*	(HELS, CIT, CERN)
GOPAL	80	Toronto Conf. 159	G.P. Gopal	(RHEL) IJP
CAMERON	78	NP B143 189	W. Cameron *et al.*	(RHEL, LOIC) IJP
CAMERON	78B	NP B146 327	W. Cameron *et al.*	(RHEL, LOIC) IJP
CAMERON	77	NP B131 399	W. Cameron *et al.*	(RHEL, LOIC) IJP
CORDEN	77B	NP B121 365	M.J. Corden *et al.*	(BIRM) IJP
CORDEN	77C	NP B125 61	M.J. Corden *et al.*	(BIRM) IJP
DECLAIS	77	CERN 77-16	Y. Declais *et al.*	(CAEN, CERN) IJP
GOPAL	77	NP B119 362	G.P. Gopal *et al.*	(LOIC, RHEL) IJP
GOYAL	77	PR D16 2746	D.P. Goyal, A.V. Sodhi	(DELH) IJP
CORDEN	76	NP B104 382	M.J. Corden *et al.*	(BIRM) IJP
DEBELLEFON	76	NP B109 129	A. de Bellefon, A. Berthon	(CDEF) IJP
BAILLON	75	NP B94 39	P.H. Baillon, P.J. Litchfield	(CERN, RHEL) IJP
CORDEN	75B	NP B92 365	M.J. Corden *et al.*	(BIRM) IJP
HEMINGWAY	75	NP B91 12	R.J. Hemingway *et al.*	(CERN, HEIDH, MPIM) IJP
VANHORN	75	NP B87 145	A.J. van Horn	(LBL) IJP
Also		NP B87 157	A.J. van Horn	(LBL) IJP
DEVENISH	74B	NP B81 330	R.C.E. Devenish, C.D. Froggatt, B.R. Martin	(DESY+)
KANE	74	LBL-2452	D.F. Kane	(LBL) IJP
LITCHFIELD	74B	NP B74 19	P.J. Litchfield *et al.*	(CERN, HEIDH) IJP
LITCHFIELD	74C	NP B74 39	P.J. Litchfield *et al.*	(CERN, HEIDH) IJP
LITCHFIELD	74D	NP B74 12	P.J. Litchfield *et al.*	(CERN, HEIDH) IJP
MULLER	69B	Thesis UCRL 19372	R.A. Muller	(LRL)
BURGUN	68	NP B8 447	G. Burgun *et al.*	(SACL, CDEF, RHEL)
TRIPP	67	NP B3 10	R.D. Tripp *et al.*	(LRL, SLAC, CERN+)
COOL	66	PRL 16 1228	R.L. Cool *et al.*	(BNL)
WOHL	66	PRL 17 107	C.G. Wohl, F.T. Solmitz, M.L. Stevenson	(LRL) IJP

$\Sigma(2070)\ 5/2^+$

$I(J^P) = 1(\frac{5}{2}^+)$ Status: *

OMITTED FROM SUMMARY TABLE

This state suggested by BERTHON 70B finds support in GOPAL 80 with new K^-p polarization and K^-n angular distributions. The very broad state seen in KANE 72 is not required in the later (KANE 74) analysis of $\overline{K}N \to \Sigma\pi$.

$\Sigma(2070)$ MASS

VALUE (MeV)	DOCUMENT ID		TECN	COMMENT
2020 to 2100 (≈ 2060) OUR ESTIMATE				
2051±25	GOPAL	80	DPWA	$\overline{K}N \to \overline{K}N$
2070±10	BERTHON	70B	DPWA	$K^-p \to \Sigma\pi$
• • • We do not use the following data for averages, fits, limits, etc. • • •				
2057	KANE	72	DPWA	$K^-p \to \Sigma\pi$

$\Sigma(2070)$ WIDTH

VALUE (MeV)	DOCUMENT ID		TECN	COMMENT
100 to 300 (≈ 200) OUR ESTIMATE				
300±30	GOPAL	80	DPWA	$\overline{K}N \to \overline{K}N$
140±20	BERTHON	70B	DPWA	$K^-p \to \Sigma\pi$
• • • We do not use the following data for averages, fits, limits, etc. • • •				
906	KANE	72	DPWA	$K^-p \to \Sigma\pi$

$\Sigma(2070)$ DECAY MODES

	Mode
Γ_1	$N\overline{K}$
Γ_2	$\Sigma\pi$

$\Sigma(2070)$ BRANCHING RATIOS

See "Sign conventions for resonance couplings" in the Note on Λ and Σ Resonances.

$\Gamma(N\overline{K})/\Gamma_{total}$ — Γ_1/Γ

VALUE	DOCUMENT ID		TECN	COMMENT
0.08±0.03	GOPAL	80	DPWA	$\overline{K}N \to \overline{K}N$

$(\Gamma_i\Gamma_f)^{1/2}/\Gamma_{total}$ in $N\overline{K} \to \Sigma(2070) \to \Sigma\pi$ — $(\Gamma_1\Gamma_2)^{1/2}/\Gamma$

VALUE	DOCUMENT ID		TECN	COMMENT
0.12 ±0.02	BERTHON	70B	DPWA	$K^-p \to \Sigma\pi$
• • • We do not use the following data for averages, fits, limits, etc. • • •				
0.104	KANE	72	DPWA	$K^-p \to \Sigma\pi$

$\Sigma(2070)$ REFERENCES

GOPAL	80	Toronto Conf. 159	G.P. Gopal	(RHEL) IJP
KANE	74	LBL-2452	D.F. Kane	(LBL)
KANE	72	PR D5 1583	D.F.J. Kane	(LBL)
BERTHON	70B	NP B24 417	A. Berthon *et al.*	(CDEF, RHEL, SACL) IJP

$\Sigma(2080)\ 3/2^+$

$I(J^P) = 1(\frac{3}{2}^+)$ Status: *

OMITTED FROM SUMMARY TABLE

Suggested by some but not all partial-wave analyses across this region.

$\Sigma(2080)$ MASS

VALUE (MeV)	DOCUMENT ID		TECN	COMMENT
2060 to 2120 (≈ 2090) OUR ESTIMATE				
2091± 7	[1] CORDEN	76	DPWA	$K^-n \to \Lambda\pi^-$
2070 to 2120	DEBELLEFON	76	IPWA	$K^-p \to \Lambda\pi^0$
2120±40	BAILLON	75	IPWA	$\overline{K}N \to \Lambda\pi$ (sol. 1)
2140±40	BAILLON	75	IPWA	$\overline{K}N \to \Lambda\pi$ (sol. 2)
2082± 4	COX	70	DPWA	See CORDEN 76
2070±30	LITCHFIELD	70	DPWA	$K^-N \to \Lambda\pi$

Downloaded from https://academic.oup.com/ptep/article/2022/8/083C01/6651666 by KIT Library user on 27 September 2022

$\Sigma(2080)$ WIDTH

VALUE (MeV)	DOCUMENT ID		TECN	COMMENT
100 to 240 (≈ 170) OUR ESTIMATE				
186±48	[1] CORDEN	76	DPWA	$K^- n \to \Lambda\pi^-$
100	DEBELLEFON	76	IPWA	$K^- p \to \Lambda\pi^0$
240±50	BAILLON	75	IPWA	$\overline{K}N \to \Lambda\pi$ (sol. 1)
200±50	BAILLON	75	IPWA	$\overline{K}N \to \Lambda\pi$ (sol. 2)
87±20	COX	70	DPWA	See CORDEN 76
250±40	LITCHFIELD	70	DPWA	$K^- N \to \Lambda\pi$

$\Sigma(2080)$ DECAY MODES

	Mode
Γ_1	$N\overline{K}$
Γ_2	$\Lambda\pi$

$\Sigma(2080)$ BRANCHING RATIOS

See "Sign conventions for resonance couplings" in the Note on Λ and Σ Resonances.

$(\Gamma_i\Gamma_f)^{1/2}/\Gamma_{total}$ in $N\overline{K} \to \Sigma(2080) \to \Lambda\pi$ — **$(\Gamma_1\Gamma_2)^{1/2}/\Gamma$**

VALUE	DOCUMENT ID		TECN	COMMENT
−0.10±0.03	[1] CORDEN	76	DPWA	$K^- n \to \Lambda\pi^-$
−0.10	DEBELLEFON	76	IPWA	$K^- p \to \Lambda\pi^0$
−0.13±0.04	BAILLON	75	IPWA	$\overline{K}N \to \Lambda\pi$ (sol. 1 and 2)
−0.16±0.03	COX	70	DPWA	See CORDEN 76
−0.09±0.03	LITCHFIELD	70	DPWA	$K^- N \to \Lambda\pi$

$\Sigma(2080)$ FOOTNOTES

[1] Preferred solution 3; see CORDEN 76 for other possibilities, including a D_{15} at this mass.

$\Sigma(2080)$ REFERENCES

CORDEN	76	NP B104 382	M.J. Corden *et al.*	(BIRM) IJP
DEBELLEFON	76	NP B109 129	A. de Bellefon, A. Berthon	(CDEF) IJP
Also		NP B90 1	A. de Bellefon *et al.*	(CDEF, SACL) IJP
BAILLON	75	NP B94 39	P.H. Baillon, P.J. Litchfield	(CERN, RHEL) IJP
COX	70	NP B19 61	G.F. Cox *et al.*	(BIRM, EDIN, GLAS, LOIC) IJP
LITCHFIELD	70	NP B22 269	P.J. Litchfield	(RHEL) IJP

$\Sigma(2100)\ 7/2^-$

$I(J^P) = 1(\frac{7}{2}^-)$ Status: *

OMITTED FROM SUMMARY TABLE

$\Sigma(2100)$ POLE POSITION

REAL PART

VALUE (MeV)	DOCUMENT ID		TECN	COMMENT
2093±16	SARANTSEV	19	DPWA	$\overline{K}N$ multichannel

−2×IMAGINARY PART

VALUE (MeV)	DOCUMENT ID		TECN	COMMENT
210±35	SARANTSEV	19	DPWA	$\overline{K}N$ multichannel

$\Sigma(2100)$ POLE RESIDUES

Normalized residue in $N\overline{K} \to \Sigma(2100) \to N\overline{K}$

MODULUS	PHASE (°)	DOCUMENT ID		TECN	COMMENT
0.09±0.02	**−110 ± 15**	SARANTSEV	19	DPWA	$\overline{K}N$ multichannel

Normalized residue in $N\overline{K} \to \Sigma(2100) \to \Sigma\pi$

MODULUS	PHASE (°)	DOCUMENT ID		TECN	COMMENT
0.04±0.02	**−50 ± 20**	SARANTSEV	19	DPWA	$\overline{K}N$ multichannel

Normalized residue in $N\overline{K} \to \Sigma(2100) \to \Lambda\pi$

MODULUS	PHASE (°)	DOCUMENT ID		TECN	COMMENT
0.03±0.02	**−100 ± 25**	SARANTSEV	19	DPWA	$\overline{K}N$ multichannel

Normalized residue in $N\overline{K} \to \Sigma(2100) \to \Xi K$

MODULUS	PHASE (°)	DOCUMENT ID		TECN	COMMENT
0.010±0.005	**−120 ± 35**	SARANTSEV	19	DPWA	$\overline{K}N$ multichannel

Normalized residue in $N\overline{K} \to \Sigma(2100) \to \Lambda(1520)\pi$, F-wave

MODULUS	PHASE (°)	DOCUMENT ID		TECN	COMMENT
0.02±0.01	**−100 ± 30**	SARANTSEV	19	DPWA	$\overline{K}N$ multichannel

Normalized residue in $N\overline{K} \to \Sigma(2100) \to \Lambda(1520)\pi$, H-wave

MODULUS	PHASE (°)	DOCUMENT ID		TECN	COMMENT
0.01±0.01		SARANTSEV	19	DPWA	$\overline{K}N$ multichannel

Normalized residue in $N\overline{K} \to \Sigma(2100) \to \Sigma(1385)\pi$, D-wave

MODULUS	PHASE (°)	DOCUMENT ID		TECN	COMMENT
0.10±0.03	**−60 ± 30**	SARANTSEV	19	DPWA	$\overline{K}N$ multichannel

Normalized residue in $N\overline{K} \to \Sigma(2100) \to \Sigma(1385)\pi$, G-wave

MODULUS	PHASE (°)	DOCUMENT ID		TECN	COMMENT
0.03±0.01	**−50 ± 30**	SARANTSEV	19	DPWA	$\overline{K}N$ multichannel

Normalized residue in $N\overline{K} \to \Sigma(2100) \to \Delta\overline{K}$, G-wave

MODULUS	PHASE (°)	DOCUMENT ID		TECN	COMMENT
0.04±0.02	**75 ± 35**	SARANTSEV	19	DPWA	$\overline{K}N$ multichannel

Normalized residue in $N\overline{K} \to \Sigma(2100) \to N\overline{K}^*(892)$, S=3/2, D-wave

MODULUS	PHASE (°)	DOCUMENT ID		TECN	COMMENT
0.08±0.04	**20 ± 50**	SARANTSEV	19	DPWA	$\overline{K}N$ multichannel

$\Sigma(2100)$ MASS

VALUE (MeV)	DOCUMENT ID		TECN	COMMENT
≈ 2100 OUR ESTIMATE				
2146±17	SARANTSEV	19	DPWA	$\overline{K}N$ multichannel
2060±20	BARBARO-...	70	DPWA	$K^- p \to \Lambda\pi^0$
2120±30	BARBARO-...	70	DPWA	$K^- p \to \Sigma\pi$

$\Sigma(2100)$ WIDTH

VALUE (MeV)	DOCUMENT ID		TECN	COMMENT
260±40	SARANTSEV	19	DPWA	$\overline{K}N$ multichannel
70±30	BARBARO-...	70	DPWA	$K^- p \to \Lambda\pi^0$
135±30	BARBARO-...	70	DPWA	$K^- p \to \Sigma\pi$

$\Sigma(2100)$ DECAY MODES

	Mode	Fraction (Γ_i/Γ)
Γ_1	$N\overline{K}$	(8.0±2.0) %
Γ_2	$\Lambda\pi$	(1.5±1.0) %
Γ_3	$\Sigma\pi$	(2.0±1.0) %
Γ_4	ΞK	
Γ_5	$\Sigma(1385)\pi$, D-wave	(12 ±6) %
Γ_6	$\Sigma(1385)\pi$, G-wave	
Γ_7	$\Lambda(1520)\pi$, F-wave	(1.0±1.0) %
Γ_8	$\Lambda(1520)\pi$, H-wave	
Γ_9	$N\overline{K}^*(892)$, S=3/2 , D-wave	(6.0±3.0) %
Γ_{10}	$\Delta\overline{K}$, G-wave	(1.0±1.0) %

$\Sigma(2100)$ BRANCHING RATIOS

See "Sign conventions for resonance couplings" in the Note on Λ and Σ Resonances.

$(\Gamma_i\Gamma_f)^{1/2}/\Gamma_{total}$ in $N\overline{K} \to \Sigma(2100) \to \Lambda\pi$ — **$(\Gamma_1\Gamma_2)^{1/2}/\Gamma$**

VALUE	DOCUMENT ID		TECN	COMMENT
−0.07±0.02	BARBARO-...	70	DPWA	$K^- p \to \Lambda\pi^0$

$(\Gamma_i\Gamma_f)^{1/2}/\Gamma_{total}$ in $N\overline{K} \to \Sigma(2100) \to \Sigma\pi$ — **$(\Gamma_1\Gamma_3)^{1/2}/\Gamma$**

VALUE	DOCUMENT ID		TECN	COMMENT
+0.13±0.02	BARBARO-...	70	DPWA	$K^- p \to \Sigma\pi$

$\Gamma(N\overline{K})/\Gamma_{total}$ — **Γ_1/Γ**

VALUE	DOCUMENT ID		TECN	COMMENT
0.08±0.02	SARANTSEV	19	DPWA	$\overline{K}N$ multichannel

$\Gamma(\Lambda\pi)/\Gamma_{total}$ — **Γ_2/Γ**

VALUE	DOCUMENT ID		TECN	COMMENT
0.015±0.01	SARANTSEV	19	DPWA	$\overline{K}N$ multichannel

$\Gamma(\Sigma\pi)/\Gamma_{total}$ — **Γ_3/Γ**

VALUE	DOCUMENT ID		TECN	COMMENT
0.02±0.01	SARANTSEV	19	DPWA	$\overline{K}N$ multichannel

$\Gamma(\Xi K)/\Gamma_{total}$ — **Γ_4/Γ**

VALUE	DOCUMENT ID		TECN	COMMENT
<0.01	SARANTSEV	19	DPWA	$\overline{K}N$ multichannel

$\Gamma(\Sigma(1385)\pi$, D-wave$)/\Gamma_{total}$ — **Γ_5/Γ**

VALUE	DOCUMENT ID		TECN	COMMENT
0.12±0.06	SARANTSEV	19	DPWA	$\overline{K}N$ multichannel

$\Gamma(\Sigma(1385)\pi$, G-wave$)/\Gamma_{total}$ — **Γ_6/Γ**

VALUE	DOCUMENT ID		TECN	COMMENT
∼ 0.01	SARANTSEV	19	DPWA	$\overline{K}N$ multichannel

Downloaded from https://academic.oup.com/ptep/article/2022/8/083C01/6651666 by KIT Library user on 27 September 2022

$\Gamma(\Lambda(1520)\pi, F\text{-wave})/\Gamma_{total}$ — Γ_7/Γ

VALUE	DOCUMENT ID		TECN	COMMENT
0.01±0.01	SARANTSEV	19	DPWA	$\overline{K}N$ multichannel

$\Gamma(\Lambda(1520)\pi, H\text{-wave})/\Gamma_{total}$ — Γ_8/Γ

VALUE	DOCUMENT ID		TECN	COMMENT
~ 0	SARANTSEV	19	DPWA	$\overline{K}N$ multichannel

$\Gamma(N\overline{K}^*(892), S=3/2, D\text{-wave})/\Gamma_{total}$ — Γ_9/Γ

VALUE	DOCUMENT ID		TECN	COMMENT
0.06±0.03	SARANTSEV	19	DPWA	$\overline{K}N$ multichannel

$\Gamma(\Delta\overline{K}, G\text{-wave})/\Gamma_{total}$ — Γ_{10}/Γ

VALUE	DOCUMENT ID		TECN	COMMENT
0.01±0.01	SARANTSEV	19	DPWA	$\overline{K}N$ multichannel

$\Sigma(2100)$ REFERENCES

SARANTSEV 19 EPJ A55 180 A.V. Sarantsev et al. (BONN, PNPI)
BARBARO-... 70 Duke Conf. 173 A. Barbaro-Galtieri (LRL) IJP
Hyperon Resonances, 1970

$\Sigma(2110)\ 1/2^-$

$I(J^P) = 1(\frac{1}{2}^-)$ Status: *

OMITTED FROM SUMMARY TABLE
was $\Sigma(2160)$

$\Sigma(2110)$ POLE POSITION

REAL PART

VALUE (MeV)	DOCUMENT ID		TECN	COMMENT
2158±25	SARANTSEV	19	DPWA	$\overline{K}N$ multichannel

−2×IMAGINARY PART

VALUE (MeV)	DOCUMENT ID		TECN	COMMENT
300^{+300}_{-60}	SARANTSEV	19	DPWA	$\overline{K}N$ multichannel

$\Sigma(2110)$ POLE RESIDUES

Normalized residue in $N\overline{K} \to \Sigma(2110) \to N\overline{K}$

MODULUS	PHASE (°)	DOCUMENT ID		TECN	COMMENT
0.29±0.08	**−20 ± 35**	SARANTSEV	19	DPWA	$\overline{K}N$ multichannel

Normalized residue in $N\overline{K} \to \Sigma(2110) \to \Sigma\pi$

MODULUS	PHASE (°)	DOCUMENT ID		TECN	COMMENT
0.14±0.04	**−5 ± 35**	SARANTSEV	19	DPWA	$\overline{K}N$ multichannel

Normalized residue in $N\overline{K} \to \Sigma(2110) \to \Lambda\pi$

MODULUS	PHASE (°)	DOCUMENT ID		TECN	COMMENT
0.39±0.08	**85 ± 25**	SARANTSEV	19	DPWA	$\overline{K}N$ multichannel

Normalized residue in $N\overline{K} \to \Sigma(2110) \to \Xi K$

MODULUS	PHASE (°)	DOCUMENT ID		TECN	COMMENT
0.05±0.02	**−85 ± 35**	SARANTSEV	19	DPWA	$\overline{K}N$ multichannel

Normalized residue in $N\overline{K} \to \Sigma(2110) \to \Lambda(1520)\pi$

MODULUS	PHASE (°)	DOCUMENT ID		TECN	COMMENT
0.025±0.015		SARANTSEV	19	DPWA	$\overline{K}N$ multichannel

Normalized residue in $N\overline{K} \to \Sigma(2110) \to \Sigma(1385)\pi$

MODULUS	PHASE (°)	DOCUMENT ID		TECN	COMMENT
0.03±0.02		SARANTSEV	19	DPWA	$\overline{K}N$ multichannel

Normalized residue in $N\overline{K} \to \Sigma(2110) \to \Delta\overline{K}$

MODULUS	PHASE (°)	DOCUMENT ID		TECN	COMMENT
0.035±0.02	**−30 ± 40**	SARANTSEV	19	DPWA	$\overline{K}N$ multichannel

Normalized residue in $N\overline{K} \to \Sigma(2110) \to N\overline{K}^*(892)$, S-wave

MODULUS	PHASE (°)	DOCUMENT ID		TECN	COMMENT
0.09±0.03	**−40 ± 50**	SARANTSEV	19	DPWA	$\overline{K}N$ multichannel

Normalized residue in $N\overline{K} \to \Sigma(2110) \to N\overline{K}^*(892)$, D-wave

MODULUS	PHASE (°)	DOCUMENT ID		TECN	COMMENT
0.04±0.03		SARANTSEV	19	DPWA	$\overline{K}N$ multichannel

$\Sigma(2110)$ MASS

VALUE (MeV)	DOCUMENT ID		TECN	COMMENT
2105±50 OUR AVERAGE Error includes scale factor of 3.4.				
2165 ± 23	SARANTSEV	19	DPWA	$\overline{K}N$ multichannel
2060 ± 20	ZHANG	13A	DPWA	$\overline{K}N$ multichannel

$\Sigma(2110)$ WIDTH

VALUE (MeV)	DOCUMENT ID		TECN	COMMENT
313^{+120}_{-50} OUR AVERAGE				
320^{+300}_{-60}	SARANTSEV	19	DPWA	$\overline{K}N$ multichannel
300±134	ZHANG	13A	DPWA	$\overline{K}N$ multichannel

$\Sigma(2110)$ DECAY MODES

	Mode	Fraction (Γ_i/Γ)
Γ_1	$N\overline{K}$	(29 ± 7) %
Γ_2	$\Sigma\pi$	(7.0± 2.0) %
Γ_3	$\Lambda\pi$	(54 ±12) %
Γ_4	$N\overline{K}^*(892)$, S-wave	(3.0± 1.0) %
Γ_5	$N\overline{K}^*(892)$, D-wave	

$\Sigma(2110)$ BRANCHING RATIOS

$\Gamma(N\overline{K})/\Gamma_{total}$ — Γ_1/Γ

VALUE	DOCUMENT ID		TECN	COMMENT
0.29±0.07	SARANTSEV	19	DPWA	$\overline{K}N$ multichannel

$\Gamma(\Sigma\pi)/\Gamma_{total}$ — Γ_2/Γ

VALUE	DOCUMENT ID		TECN	COMMENT
0.07±0.02	SARANTSEV	19	DPWA	$\overline{K}N$ multichannel

$\Gamma(\Lambda\pi)/\Gamma_{total}$ — Γ_3/Γ

VALUE	DOCUMENT ID		TECN	COMMENT
0.54±0.12	SARANTSEV	19	DPWA	$\overline{K}N$ multichannel

$\Gamma(N\overline{K}^*(892), S\text{-wave})/\Gamma_{total}$ — Γ_4/Γ

VALUE	DOCUMENT ID		TECN	COMMENT
0.03±0.01	SARANTSEV	19	DPWA	$\overline{K}N$ multichannel

$\Gamma(N\overline{K}^*(892), D\text{-wave})/\Gamma_{total}$ — Γ_5/Γ

VALUE	DOCUMENT ID		TECN	COMMENT
• • • We do not use the following data for averages, fits, limits, etc. • • •				
~ 0.01	SARANTSEV	19	DPWA	$\overline{K}N$ multichannel

$\Sigma(2110)$ REFERENCES

SARANTSEV 19 EPJ A55 180 A.V. Sarantsev et al. (BONN, PNPI)
ZHANG 13A PR C88 035205 H. Zhang et al. (KSU)

$\Sigma(2230)\ 3/2^+$

$I(J^P) = 1(\frac{3}{2}^+)$ Status: *

OMITTED FROM SUMMARY TABLE

$\Sigma(2230)$ POLE POSITION

REAL PART

VALUE (MeV)	DOCUMENT ID		TECN	COMMENT
2234±25	SARANTSEV	19	DPWA	$\overline{K}N$ multichannel

−2×IMAGINARY PART

VALUE (MeV)	DOCUMENT ID		TECN	COMMENT
340±45	SARANTSEV	19	DPWA	$\overline{K}N$ multichannel

$\Sigma(2230)$ POLE RESIDUES

Normalized residue in $N\overline{K} \to \Sigma(2230) \to N\overline{K}$

MODULUS	PHASE (°)	DOCUMENT ID		TECN	COMMENT
0.07±0.02	**25 ± 15**	SARANTSEV	19	DPWA	$\overline{K}N$ multichannel

Normalized residue in $N\overline{K} \to \Sigma(2230) \to \Sigma\pi$

MODULUS	PHASE (°)	DOCUMENT ID		TECN	COMMENT
0.03±0.02	**180 ± 25**	SARANTSEV	19	DPWA	$\overline{K}N$ multichannel

Normalized residue is $N\overline{K} \to \Sigma(2030) \to \Lambda\pi$

MODULUS	PHASE (°)	DOCUMENT ID		TECN	COMMENT
0.11±0.05	**−16 ± 10**	SARANTSEV	19	DPWA	$\overline{K}N$ multichannel

Normalized residue in $N\overline{K} \to \Sigma(2230) \to \Xi K$

MODULUS	PHASE (°)	DOCUMENT ID		TECN	COMMENT
0.04±0.02	**155 ± 20**	SARANTSEV	19	DPWA	$\overline{K}N$ multichannel

Normalized residue in $N\overline{K} \to \Sigma(2230) \to \Lambda(1520)\pi$, S-wave

MODULUS	PHASE (°)	DOCUMENT ID		TECN	COMMENT
0.12±0.05	**−80 ± 25**	SARANTSEV	19	DPWA	$\overline{K}N$ multichannel

Downloaded from https://academic.oup.com/ptep/article/2022/8/083C01/6651666 by KIT Library user on 27 September 2022

Normalized residue in $N\overline{K} \rightarrow \Sigma(2230) \rightarrow \Lambda(1520)\pi$, D-wave

MODULUS	PHASE (°)	DOCUMENT ID		TECN	COMMENT
0.03±0.02	160 ± 30	SARANTSEV	19	DPWA	$\overline{K}N$ multichannel

Normalized residue in $N\overline{K} \rightarrow \Sigma(2230) \rightarrow \Sigma(1385)\pi$, P-wave

MODULUS	PHASE (°)	DOCUMENT ID		TECN	COMMENT
0.05±0.02	60 ± 25	SARANTSEV	19	DPWA	$\overline{K}N$ multichannel

Normalized residue in $N\overline{K} \rightarrow \Sigma(2230) \rightarrow \Sigma(1385)\pi$, F-wave

MODULUS	PHASE (°)	DOCUMENT ID		TECN	COMMENT
0.05±0.03	−70 ± 20	SARANTSEV	19	DPWA	$\overline{K}N$ multichannel

Normalized residue in $N\overline{K} \rightarrow \Sigma(2230) \rightarrow \Delta\overline{K}$, P-wave

MODULUS	PHASE (°)	DOCUMENT ID		TECN	COMMENT
0.11±0.04	60 ± 15	SARANTSEV	19	DPWA	$\overline{K}N$ multichannel

Normalized residue in $N\overline{K} \rightarrow \Sigma(2230) \rightarrow \Delta\overline{K}$, F-wave

MODULUS	PHASE (°)	DOCUMENT ID		TECN	COMMENT
0.07±0.03	90 ± 25	SARANTSEV	19	DPWA	$\overline{K}N$ multichannel

Normalized residue in $N\overline{K} \rightarrow \Sigma(2230) \rightarrow N\overline{K}^*(892)$, S=1/2 , P-wave

MODULUS	PHASE (°)	DOCUMENT ID		TECN	COMMENT
0.08±0.04	40 ± 45	SARANTSEV	19	DPWA	$\overline{K}N$ multichannel

Normalized residue in $N\overline{K} \rightarrow \Sigma(2230) \rightarrow N\overline{K}^*(892)$, S=3/2 , P-wave

MODULUS	PHASE (°)	DOCUMENT ID		TECN	COMMENT
0.14±0.03	−40 ± 45	SARANTSEV	19	DPWA	$\overline{K}N$ multichannel

Normalized residue in $N\overline{K} \rightarrow \Sigma(2230) \rightarrow N\overline{K}^*(892)$, S=3/2 , F-wave

MODULUS	PHASE (°)	DOCUMENT ID		TECN	COMMENT
0.05±0.03	35 ± 30	SARANTSEV	19	DPWA	$\overline{K}N$ multichannel

$\Sigma(2230)$ MASS

VALUE (MeV)	DOCUMENT ID		TECN	COMMENT
2240±27	SARANTSEV	19	DPWA	$\overline{K}N$ multichannel

$\Sigma(2230)$ WIDTH

VALUE (MeV)	DOCUMENT ID		TECN	COMMENT
345±50	SARANTSEV	19	DPWA	$\overline{K}N$ multichannel

$\Sigma(2230)$ DECAY MODES

	Mode	Fraction (Γ_i/Γ)
Γ_1	$N\overline{K}$	(6.0±2.0) %
Γ_2	$\Sigma\pi$	(2.0±1.0) %
Γ_3	$\Lambda\pi$	(12 ±6) %
Γ_4	ΞK	(2.0±1.0) %
Γ_5	$\Lambda(1520)\pi$, S-wave	(14 ±5) %
Γ_6	$\Lambda(1520)\pi$, D-wave	
Γ_7	$\Sigma(1385)\pi$, P-wave	(4 ±4) %
Γ_8	$\Sigma(1385)\pi$, F-wave	(3.0±2.0) %
Γ_9	$\Delta\overline{K}$, P-wave	(14 ±5) %
Γ_{10}	$\Delta\overline{K}$, F-wave	(8.0±2.0) %
Γ_{11}	$N\overline{K}^*(892)$, S=1/2 , F-wave	(8.0±3.0) %
Γ_{12}	$N\overline{K}^*(892)$, S=3/2 , F-wave	(26 ±5) %

$\Sigma(2230)$ BRANCHING RATIOS

$\Gamma(N\overline{K})/\Gamma_{total}$ — Γ_1/Γ

VALUE	DOCUMENT ID		TECN	COMMENT
0.06±0.02	SARANTSEV	19	DPWA	$\overline{K}N$ multichannel

$\Gamma(\Sigma\pi)/\Gamma_{total}$ — Γ_2/Γ

VALUE	DOCUMENT ID		TECN	COMMENT
0.02±0.01	SARANTSEV	19	DPWA	$\overline{K}N$ multichannel

$\Gamma(\Lambda\pi)/\Gamma_{total}$ — Γ_3/Γ

VALUE	DOCUMENT ID		TECN	COMMENT
0.12±0.06	SARANTSEV	19	DPWA	$\overline{K}N$ multichannel

$\Gamma(\Xi K)/\Gamma_{total}$ — Γ_4/Γ

VALUE	DOCUMENT ID		TECN	COMMENT
0.02±0.01	SARANTSEV	19	DPWA	$\overline{K}N$ multichannel

$\Gamma(\Lambda(1520)\pi, S\text{-wave})/\Gamma_{total}$ — Γ_5/Γ

VALUE	DOCUMENT ID		TECN	COMMENT
0.14±0.05	SARANTSEV	19	DPWA	$\overline{K}N$ multichannel

$\Gamma(\Lambda(1520)\pi, D\text{-wave})/\Gamma_{total}$ — Γ_6/Γ

VALUE	DOCUMENT ID		TECN	COMMENT
• • • We do not use the following data for averages, fits, limits, etc. • • •				
∼ 1	SARANTSEV	19	DPWA	$\overline{K}N$ multichannel

$\Gamma(\Sigma(1385)\pi, P\text{-wave})/\Gamma_{total}$ — Γ_7/Γ

VALUE	DOCUMENT ID		TECN	COMMENT
0.04±0.04	SARANTSEV	19	DPWA	$\overline{K}N$ multichannel

$\Gamma(\Sigma(1385)\pi, F\text{-wave})/\Gamma_{total}$ — Γ_8/Γ

VALUE	DOCUMENT ID		TECN	COMMENT
0.03±0.02	SARANTSEV	19	DPWA	$\overline{K}N$ multichannel

$\Gamma(\Delta\overline{K}, P\text{-wave})/\Gamma_{total}$ — Γ_9/Γ

VALUE	DOCUMENT ID		TECN	COMMENT
0.14±0.05	SARANTSEV	19	DPWA	$\overline{K}N$ multichannel

$\Gamma(\Delta\overline{K}, F\text{-wave})/\Gamma_{total}$ — Γ_{10}/Γ

VALUE	DOCUMENT ID		TECN	COMMENT
0.08±0.02	SARANTSEV	19	DPWA	$\overline{K}N$ multichannel

$\Gamma(N\overline{K}^*(892), S=1/2, F\text{-wave})/\Gamma_{total}$ — Γ_{11}/Γ

VALUE	DOCUMENT ID		TECN	COMMENT
0.08±0.03	SARANTSEV	19	DPWA	$\overline{K}N$ multichannel

$\Gamma(N\overline{K}^*(892), S=3/2, F\text{-wave})/\Gamma_{total}$ — Γ_{12}/Γ

VALUE	DOCUMENT ID		TECN	COMMENT
0.26±0.05	SARANTSEV	19	DPWA	$\overline{K}N$ multichannel

$\Sigma(2230)$ REFERENCES

SARANTSEV 19 EPJ A55 180 A.V. Sarantsev *et al.* (BONN, PNPI)

$\Sigma(2250)$

$I(J^P) = 1(?^?)$ Status: ∗∗

OMITTED FROM SUMMARY TABLE

Results from partial-wave analyses are too weak to warrant separating them from the production and cross-section experiments. LASINSKI 71 in $\overline{K}N$ using a Pomeron + resonances model, and DEBELLEFON 76, DEBELLEFON 77, and DEBELLEFON 78 in energy-dependent partial-wave analyses of $\overline{K}N \rightarrow \Lambda\pi$, $\Sigma\pi$, and $N\overline{K}$, respectively, suggest two resonances around this mass.

$\Sigma(2250)$ MASS

VALUE (MeV)	DOCUMENT ID		TECN	COMMENT
2210 to 2280 (≈ 2250) OUR ESTIMATE				
2270±50	DEBELLEFON	78	DPWA	D_5 wave
2210±30	DEBELLEFON	78	DPWA	G_9 wave
2275±20	DEBELLEFON	77	DPWA	D_5 wave
2215±20	DEBELLEFON	77	DPWA	G_9 wave
2300±30	[1] DEBELLEFON	75B	HBC	$K^-p \rightarrow \Xi^{*0}K^0$
2251^{+30}_{-20}	VANHORN	75	DPWA	$K^-p \rightarrow \Lambda\pi^0$, F_5 wave
2280±14	AGUILAR-...	70B	HBC	K^-p 3.9, 4.6 GeV/c
2237±11	BRICMAN	70	CNTR	Total, charge exchange
2255±10	COOL	70	CNTR	K^-p, K^-d total
2250± 7	BUGG	68	CNTR	K^-p, K^-d total
• • • We do not use the following data for averages, fits, limits, etc. • • •				
2260	DEBELLEFON	76	IPWA	D_5 wave
2215	DEBELLEFON	76	IPWA	G_9 wave
2250±20	LU	70	CNTR	$\gamma p \rightarrow K^+Y^*$
2245	BLANPIED	65	CNTR	$\gamma p \rightarrow K^+Y^*$
2299± 6	BOCK	65	HBC	$\overline{p}p$ 5.7 GeV/c

$\Sigma(2250)$ WIDTH

VALUE (MeV)	DOCUMENT ID		TECN	COMMENT
60 to 150 (≈ 100) OUR ESTIMATE				
120±40	DEBELLEFON	78	DPWA	D_5 wave
80±20	DEBELLEFON	78	DPWA	G_9 wave
70±20	DEBELLEFON	77	DPWA	D_5 wave
60±20	DEBELLEFON	77	DPWA	G_9 wave
130±20	[1] DEBELLEFON	75B	HBC	$K^-p \rightarrow \Xi^{*0}K^0$
192±30	VANHORN	75	DPWA	$K^-p \rightarrow \Lambda\pi^0$, F_5 wave
100±20	AGUILAR-...	70B	HBC	K^-p 3.9, 4.6 GeV/c
164±50	BRICMAN	70	CNTR	Total, charge exchange
230±20	BUGG	68	CNTR	K^-p, K^-d total

Downloaded from https://academic.oup.com/ptep/article/2022/8/083C01/6651666 by KIT Library user on 27 September 2022

• • • We do not use the following data for averages, fits, limits, etc. • • •

100	DEBELLEFON	76	IPWA	D_5 wave
140	DEBELLEFON	76	IPWA	G_9 wave
170	COOL	70	CNTR	$K^- p$, $K^- d$ total
125	LU	70	CNTR	$\gamma p \to K^+ Y^*$
150	BLANPIED	65	CNTR	$\gamma p \to K^+ Y^*$
21^{+17}_{-21}	BOCK	65	HBC	$\overline{p} p$ 5.7 GeV/c

$\Sigma(2250)$ DECAY MODES

	Mode	Fraction (Γ_i/Γ)
Γ_1	$N\overline{K}$	<10 %
Γ_2	$\Lambda\pi$	seen
Γ_3	$\Sigma\pi$	seen
Γ_4	$\Xi(1530)K$	

$\Sigma(2250)$ BRANCHING RATIOS

See "Sign conventions for resonance couplings" in the Note on Λ and Σ Resonances.

$\Gamma(N\overline{K})/\Gamma_{total}$ — Γ_1/Γ

VALUE	DOCUMENT ID		TECN	COMMENT
<0.1 OUR ESTIMATE				
0.08±0.02	DEBELLEFON	78	DPWA	D_5 wave
0.02±0.01	DEBELLEFON	78	DPWA	G_9 wave

$(J+\frac{1}{2})\times\Gamma(N\overline{K})/\Gamma_{total}$ — Γ_1/Γ

VALUE	DOCUMENT ID		TECN	COMMENT
• • • We do not use the following data for averages, fits, limits, etc. • • •				
0.16±0.12	BRICMAN	70	CNTR	Total, charge exchange
0.42	COOL	70	CNTR	$K^- p$, $K^- d$ total
0.47	BUGG	68	CNTR	

$(\Gamma_i\Gamma_f)^{1/2}/\Gamma_{total}$ in $N\overline{K}\to\Sigma(2250)\to\Lambda\pi$ — $(\Gamma_1\Gamma_2)^{1/2}/\Gamma$

VALUE	DOCUMENT ID		TECN	COMMENT
−0.16±0.03	VANHORN	75	DPWA	$K^- p \to \Lambda\pi^0$, F_5 wave
• • • We do not use the following data for averages, fits, limits, etc. • • •				
+0.11	DEBELLEFON	76	IPWA	D_5 wave
−0.10	DEBELLEFON	76	IPWA	G_9 wave
−0.18	BARBARO-...	70	DPWA	$K^- p \to \Lambda\pi^0$, G_9 wave

$(\Gamma_i\Gamma_f)^{1/2}/\Gamma_{total}$ in $N\overline{K}\to\Sigma(2250)\to\Sigma\pi$ — $(\Gamma_1\Gamma_3)^{1/2}/\Gamma$

VALUE	DOCUMENT ID		TECN	COMMENT
+0.06±0.02	DEBELLEFON	77	DPWA	D_5 wave
−0.03±0.02	DEBELLEFON	77	DPWA	G_9 wave
+0.07	BARBARO-...	70	DPWA	$K^- p \to \Sigma\pi$, G_9 wave

$\Gamma(N\overline{K})/\Gamma(\Sigma\pi)$ — Γ_1/Γ_3

VALUE	DOCUMENT ID		TECN	COMMENT
• • • We do not use the following data for averages, fits, limits, etc. • • •				
<0.18	BARNES	69	HBC	1 standard dev. limit

$\Gamma(\Lambda\pi)/\Gamma(\Sigma\pi)$ — Γ_2/Γ_3

VALUE	DOCUMENT ID		TECN	COMMENT
• • • We do not use the following data for averages, fits, limits, etc. • • •				
<0.18	BARNES	69	HBC	1 standard dev. limit

$(\Gamma_i\Gamma_f)^{1/2}/\Gamma_{total}$ in $N\overline{K}\to\Sigma(2250)\to\Xi(1530)K$ — $(\Gamma_1\Gamma_4)^{1/2}/\Gamma$

VALUE	DOCUMENT ID		TECN	COMMENT
0.18±0.04	[1] DEBELLEFON	75B	HBC	$K^- p \to \Xi^{*0} K^0$

$\Sigma(2250)$ FOOTNOTES

[1] Seen in the (initial and final state) D_5 wave. Isospin not determined.

$\Sigma(2250)$ REFERENCES

DEBELLEFON	78	NC 42A 403	A. de Bellefon *et al.*	(CDEF, SACL) IJP
DEBELLEFON	77	NC 37A 175	A. de Bellefon *et al.*	(CDEF, SACL) IJP
DEBELLEFON	76	NP B109 129	A. de Bellefon, A. Berthon	(CDEF) IJP
Also		NP B90 1	A. de Bellefon *et al.*	(CDEF, SACL) IJP
DEBELLEFON	75B	NC 28A 289	A. de Bellefon *et al.*	(CDEF, SACL)
VANHORN	75	NP B87 145	A.J. van Horn	(LBL) IJP
Also		NP B87 157	A.J. van Horn	(LBL) IJP
LASINSKI	71	NP B29 125	T.A. Lasinski	(EFI) IJP
AGUILAR-...	70B	PRL 25 58	M. Aguilar-Benitez *et al.*	(BNL, SYRA)
BARBARO-...	70	Duke Conf. 173 Hyperon Resonances, 1970	A. Barbaro-Galtieri	(LRL) IJP
BRICMAN	70	PL 31B 152	C. Bricman *et al.*	(CERN, CAEN, SACL)
COOL	70	PR D1 1887	R.L. Cool *et al.*	(BNL) I
Also		PRL 16 1228	R.L. Cool *et al.*	(BNL) I
LU	70	PR D2 1846	D.C. Lu *et al.*	(YALE)
BARNES	69	PRL 22 479	V.E. Barnes *et al.*	(BNL, SYRA)
BUGG	68	PR 168 1466	D.V. Bugg *et al.*	(RHEL, BIRM, CAVE) I
BLANPIED	65	PRL 14 741	W.A. Blanpied *et al.*	(YALE, CEA)
BOCK	65	PL 17 166	R.K. Bock *et al.*	(CERN, SACL)

$\Sigma(2455)$ Bumps

$I(J^P) = 1(?^?)$ Status: *

OMITTED FROM SUMMARY TABLE

There is also some slight evidence for Y^* states in this mass region from the reaction $\gamma p \to K^+ X$ — see GREENBERG 68.

$\Sigma(2455)$ MASS

VALUE (MeV)	DOCUMENT ID		TECN	COMMENT
≈ 2455 OUR ESTIMATE				
2455±10	ABRAMS	70	CNTR	$K^- p$, $K^- d$ total
2455± 7	BUGG	68	CNTR	$K^- p$, $K^- d$ total

$\Sigma(2455)$ WIDTH

VALUE (MeV)	DOCUMENT ID		TECN	COMMENT
140	ABRAMS	70	CNTR	$K^- p$, $K^- d$ total
100±20	BUGG	68	CNTR	

$\Sigma(2455)$ DECAY MODES

	Mode
Γ_1	$N\overline{K}$

$\Sigma(2455)$ BRANCHING RATIOS

$(J+\frac{1}{2})\times\Gamma(N\overline{K})/\Gamma_{total}$ — Γ_1/Γ

VALUE	DOCUMENT ID		TECN	COMMENT
0.39	ABRAMS	70	CNTR	$K^- p$, $K^- d$ total
0.05±0.05	[1] BRICMAN	70	CNTR	Total, charge exchange
0.3	BUGG	68	CNTR	

$\Sigma(2455)$ FOOTNOTES

[1] Fit of total cross section given by BRICMAN 70 is poor in this region.

$\Sigma(2455)$ REFERENCES

ABRAMS	70	PR D1 1917	R.J. Abrams *et al.*	(BNL) I
Also		PRL 19 678	R.J. Abrams *et al.*	(BNL)
BRICMAN	70	PL 31B 152	C. Bricman *et al.*	(CERN, CAEN, SACL)
BUGG	68	PR 168 1466	D.V. Bugg *et al.*	(RHEL, BIRM, CAVE) I
GREENBERG	68	PRL 20 221	J.S. Greenberg *et al.*	(YALE)

$\Sigma(2620)$ Bumps

$I(J^P) = 1(?^?)$ Status: *

OMITTED FROM SUMMARY TABLE

$\Sigma(2620)$ MASS

VALUE (MeV)	DOCUMENT ID		TECN	COMMENT
≈ 2620 OUR ESTIMATE				
2542±22	DIBIANCA	75	DBC	$K^- N \to \Xi K\pi$
2620±15	ABRAMS	70	CNTR	$K^- p$, $K^- d$ total

$\Sigma(2620)$ WIDTH

VALUE (MeV)	DOCUMENT ID		TECN	COMMENT
221±81	DIBIANCA	75	DBC	$K^- N \to \Xi K\pi$
175	ABRAMS	70	CNTR	$K^- p$, $K^- d$ total

$\Sigma(2620)$ DECAY MODES

	Mode
Γ_1	$N\overline{K}$

$\Sigma(2620)$ BRANCHING RATIOS

$(J+\frac{1}{2})\times\Gamma(N\overline{K})/\Gamma_{total}$ — Γ_1/Γ

VALUE	DOCUMENT ID		TECN	COMMENT
0.32	ABRAMS	70	CNTR	$K^- p$, $K^- d$ total
0.36±0.12	BRICMAN	70	CNTR	Total, charge exchange

$\Sigma(2620)$ REFERENCES

DIBIANCA	75	NP B98 137	F.A. Dibianca, R.J. Endorf	(CMU)
ABRAMS	70	PR D1 1917	R.J. Abrams *et al.*	(BNL) I
Also		PRL 19 678	R.J. Abrams *et al.*	(BNL)
BRICMAN	70	PL 31B 152	C. Bricman *et al.*	(CERN, CAEN, SACL)

Downloaded from https://academic.oup.com/ptep/article/2022/8/083C01/6651666 by KIT Library user on 27 September 2022

$\Sigma(3000)$ Bumps

$I(J^P) = 1(?^?)$ Status: *

OMITTED FROM SUMMARY TABLE

Seen as an enhancement in $\Lambda\pi$ and $\overline{K}N$ invariant mass spectra and in the missing mass of neutrals recoiling against a K^0.

$\Sigma(3000)$ MASS

VALUE (MeV)	DOCUMENT ID		TECN	CHG	COMMENT
≈ 3000 OUR ESTIMATE					
3000	EHRLICH	66	HBC	0	$\pi^- p$ 7.91 GeV/c

$\Sigma(3000)$ DECAY MODES

	Mode
Γ_1	$N\overline{K}$
Γ_2	$\Lambda\pi$

$\Sigma(3000)$ REFERENCES

EHRLICH 66 PR 152 1194 R. Ehrlich, W. Selove, H. Yuta (PENN)I

$\Sigma(3170)$ Bumps

$I(J^P) = 1(?^?)$ Status: *

OMITTED FROM SUMMARY TABLE

Seen by AMIRZADEH 79 as a narrow 6.5-standard-deviation enhancement in the reaction $K^- p \rightarrow Y^{*+}\pi^-$ using data from independent high statistics bubble chamber experiments at 8.25 and 6.5 GeV/c. The dominant decay modes are multibody, multistrange final states and the production is via isospin-3/2 baryon exchange. Isospin 1 is favored.

Not seen in a $K^- p$ experiment in LASS at 11 GeV/c (ASTON 85B).

$\Sigma(3170)$ MASS (PRODUCTION EXPERIMENTS)

VALUE (MeV)	EVTS	DOCUMENT ID		TECN	COMMENT
≈ 3170 OUR ESTIMATE					
3170±5	35	AMIRZADEH	79	HBC	$K^- p \rightarrow Y^{*+}\pi^-$

$\Sigma(3170)$ WIDTH (PRODUCTION EXPERIMENTS)

VALUE (MeV)	EVTS	DOCUMENT ID		TECN	COMMENT
<20	35	[1] AMIRZADEH	79	HBC	$K^- p \rightarrow Y^{*+}\pi^-$

$\Sigma(3170)$ DECAY MODES (PRODUCTION EXPERIMENTS)

	Mode	Fraction (Γ_i/Γ)
Γ_1	$\Lambda K\overline{K}\pi$'s	seen
Γ_2	$\Sigma K\overline{K}\pi$'s	seen
Γ_3	$\Xi K\pi$'s	seen

$\Sigma(3170)$ BRANCHING RATIOS (PRODUCTION EXPERIMENTS)

$\Gamma(\Lambda K\overline{K}\pi\text{'s})/\Gamma_{total}$ — **Γ_1/Γ**

VALUE	DOCUMENT ID		TECN	COMMENT
seen	AMIRZADEH	79	HBC	$K^- p \rightarrow Y^{*+}\pi^-$

$\Gamma(\Sigma K\overline{K}\pi\text{'s})/\Gamma_{total}$ — **Γ_2/Γ**

VALUE	DOCUMENT ID		TECN	COMMENT
seen	AMIRZADEH	79	HBC	$K^- p \rightarrow Y^{*+}\pi^-$

$\Gamma(\Xi K\pi\text{'s})/\Gamma_{total}$ — **Γ_3/Γ**

VALUE	DOCUMENT ID		TECN	COMMENT
seen	AMIRZADEH	79	HBC	$K^- p \rightarrow Y^{*+}\pi^-$

$\Sigma(3170)$ FOOTNOTES (PRODUCTION EXPERIMENTS)

[1] Observed width consistent with experimental resolution.

$\Sigma(3170)$ REFERENCES (PRODUCTION EXPERIMENTS)

ASTON 85B PR D32 2270 D. Aston et al. (SLAC, CARL, CNRC, CINC)
AMIRZADEH 79 PL 89B 125 J. Amirzadeh et al. (BIRM, CERN, GLAS+)I
Also Toronto Conf. 263 J.B. Kinson et al. (BIRM, CERN, GLAS+)I

Downloaded from https://academic.oup.com/ptep/article/2022/8/083C01/6651666 by KIT Library user on 27 September 2022

Ξ BARYONS
($S = -2$, $I = 1/2$)

$\Xi^0 = uss$, $\Xi^- = dss$

Ξ^0

$I(J^P) = \frac{1}{2}(\frac{1}{2}^+)$ Status: ****

The parity has not actually been measured, but + is of course expected.

Ξ^0 MASS

The fit uses the Ξ^0, Ξ^-, and $\overline{\Xi}^+$ masses and the $\Xi^- - \Xi^0$ mass difference. It assumes that the Ξ^- and $\overline{\Xi}^+$ masses are the same.

VALUE (MeV)	EVTS	DOCUMENT ID		TECN	COMMENT
1314.86±0.20 OUR FIT					
1314.82±0.06±0.20	3120	FANTI	00	NA48	p Be, 450 GeV
• • • We do not use the following data for averages, fits, limits, etc. • • •					
1315.2 ±0.92	49	WILQUET	72	HLBC	
1313.4 ±1.8	1	PALMER	68	HBC	

$m_{\Xi^-} - m_{\Xi^0}$

The fit uses the Ξ^0, Ξ^-, and $\overline{\Xi}^+$ masses and the $\Xi^- - \Xi^0$ mass difference. It assumes that the Ξ^- and $\overline{\Xi}^+$ masses are the same.

VALUE (MeV)	EVTS	DOCUMENT ID		TECN	COMMENT
6.85±0.21 OUR FIT					
6.3 ±0.7 OUR AVERAGE					
6.9 ±2.2	29	LONDON	66	HBC	
6.1 ±0.9	88	PJERROU	65B	HBC	
6.8 ±1.6	23	JAUNEAU	63	FBC	
• • • We do not use the following data for averages, fits, limits, etc. • • •					
6.1 ±1.6	45	CARMONY	64B	HBC	See PJERROU 65B

Ξ^0 MEAN LIFE

VALUE (10^{-10} s)	EVTS	DOCUMENT ID		TECN	COMMENT
2.90±0.09 OUR AVERAGE					
2.83±0.16	6300	[1] ZECH	77	SPEC	Neutral hyperon beam
$2.88^{+0.21}_{-0.19}$	652	BALTAY	74	HBC	1.75 GeV/c K^-p
$2.90^{+0.32}_{-0.27}$	157	[2] MAYEUR	72	HLBC	2.1 GeV/c K^-
$3.07^{+0.22}_{-0.20}$	340	DAUBER	69	HBC	
3.0 ±0.5	80	PJERROU	65B	HBC	
$2.5^{+0.4}_{-0.3}$	101	HUBBARD	64	HBC	
$3.9^{+1.4}_{-0.8}$	24	JAUNEAU	63	FBC	
• • • We do not use the following data for averages, fits, limits, etc. • • •					
$3.5^{+1.0}_{-0.8}$	45	CARMONY	64B	HBC	See PJERROU 65B

[1] The ZECH 77 result is $\tau_{\Xi^0} = [2.77-(\tau_\Lambda - 2.69)] \times 10^{-10}$ s, in which we use $\tau_\Lambda = 2.63 \times 10^{-10}$ s.
[2] The MAYEUR 72 value is modified by the erratum.

Ξ^0 MAGNETIC MOMENT

See the "Quark Model" review.

VALUE (μ_N)	EVTS	DOCUMENT ID		TECN
−1.250±0.014 OUR AVERAGE				
−1.253±0.014	270k	COX	81	SPEC
−1.20 ±0.06	42k	BUNCE	79	SPEC

Ξ^0 DECAY MODES

	Mode	Fraction (Γ_i/Γ)	Confidence level
Γ_1	$\Lambda\pi^0$	(99.524±0.012) %	
Γ_2	$\Lambda\gamma$	(1.17 ±0.07) $\times 10^{-3}$	
Γ_3	$\Lambda e^+ e^-$	(7.6 ±0.6) $\times 10^{-6}$	
Γ_4	$\Sigma^0\gamma$	(3.33 ±0.10) $\times 10^{-3}$	
Γ_5	$\Sigma^+ e^- \overline{\nu}_e$	(2.52 ±0.08) $\times 10^{-4}$	
Γ_6	$\Sigma^+ \mu^- \overline{\nu}_\mu$	(2.33 ±0.35) $\times 10^{-6}$	

$\Delta S = \Delta Q$ (SQ) violating modes or $\Delta S = 2$ forbidden ($S2$) modes

Γ_7	$\Sigma^- e^+ \nu_e$	SQ	< 9	$\times 10^{-4}$	90%
Γ_8	$\Sigma^- \mu^+ \nu_\mu$	SQ	< 9	$\times 10^{-4}$	90%
Γ_9	$p\pi^-$	$S2$	< 8	$\times 10^{-6}$	90%
Γ_{10}	$p e^- \overline{\nu}_e$	$S2$	< 1.3	$\times 10^{-3}$	
Γ_{11}	$p \mu^- \overline{\nu}_\mu$	$S2$	< 1.3	$\times 10^{-3}$	

CONSTRAINED FIT INFORMATION

An overall fit to 5 branching ratios uses 11 measurements and one constraint to determine 5 parameters. The overall fit has a $\chi^2 = 7.5$ for 7 degrees of freedom.

The following *off-diagonal* array elements are the correlation coefficients $\langle \delta x_i \delta x_j \rangle / (\delta x_i \cdot \delta x_j)$, in percent, from the fit to the branching fractions, $x_i \equiv \Gamma_i/\Gamma_{total}$. The fit constrains the x_i whose labels appear in this array to sum to one.

	x_1	x_2	x_4	x_5
x_2	−57			
x_4	−82	0		
x_5	−7	0	0	
x_6	0	0	0	1

Ξ^0 BRANCHING RATIOS

$\Gamma(\Lambda\gamma)/\Gamma(\Lambda\pi^0)$ — Γ_2/Γ_1

VALUE (units 10^{-3})	EVTS	DOCUMENT ID		TECN	COMMENT
1.17±0.07 OUR FIT					
1.17±0.07 OUR AVERAGE					
1.17±0.05±0.06	672	[3] LAI	04A	NA48	p Be, 450 GeV
1.91±0.34±0.19	31	[4] FANTI	00	NA48	p Be, 450 GeV
1.06±0.12±0.11	116	JAMES	90	SPEC	FNAL hyperons

[3] LAI 04A used our 2002 value of 99.5% for the $\Xi^0 \to \Lambda\pi^0$ branching fraction to get $\Gamma(\Xi^0 \to \Lambda\gamma)/\Gamma_{total} = (1.16 \pm 0.05 \pm 0.06) \times 10^{-3}$. We adjust slightly to go back to what was directly measured.
[4] FANTI 00 used our 1998 value of 99.5% for the $\Xi^0 \to \Lambda\pi^0$ branching fraction to get $\Gamma(\Xi^0 \to \Lambda\gamma)/\Gamma_{total} = (1.90 \pm 0.34 \pm 0.19) \times 10^{-3}$. We adjust slightly to go back to what was directly measured.

$\Gamma(\Lambda e^+ e^-)/\Gamma_{total}$ — Γ_3/Γ

VALUE (units 10^{-6})	EVTS	DOCUMENT ID		TECN	COMMENT
7.6±0.4±0.5	397 ± 21	[5] BATLEY	07C	NA48	p Be, 400 GeV

[5] This BATLEY 07C result is consistent with internal bremsstrahlung.

$\Gamma(\Sigma^0\gamma)/\Gamma(\Lambda\pi^0)$ — Γ_4/Γ_1

VALUE (units 10^{-3})	EVTS	DOCUMENT ID		TECN	COMMENT
3.35±0.10 OUR FIT					
3.35±0.10 OUR AVERAGE					
3.34±0.05±0.09	4045	ALAVI-HARATI	01C	KTEV	p nucleus, 800 GeV
3.16±0.76±0.32	17	[6] FANTI	00	NA48	p Be, 450 GeV
3.56±0.42±0.10	85	TEIGE	89	SPEC	FNAL hyperons

[6] FANTI 00 used our 1998 value of 99.5% for the $\Xi^0 \to \Lambda\pi^0$ branching fraction to get $\Gamma(\Xi^0 \to \Sigma^0\gamma)/\Gamma_{total} = (3.14 \pm 0.76 \pm 0.32) \times 10^{-3}$. We adjust slightly to go back to what was directly measured.

$\Gamma(\Sigma^+ e^- \overline{\nu}_e)/\Gamma_{total}$ — Γ_5/Γ

VALUE (units 10^{-4})	EVTS	DOCUMENT ID		TECN	COMMENT
2.52±0.08 OUR FIT					
2.53±0.08 OUR AVERAGE					
2.51±0.03±0.09	6101	BATLEY	07	NA48	p Be, 400 GeV
2.55±0.14±0.10	419	[7] BATLEY	07	NA48	p Be, 400 GeV
2.71±0.22±0.31	176	AFFOLDER	99	KTEV	p nucleus, 800 GeV

[7] This BATLEY 07 result is for $\overline{\Xi}^0 \to \overline{\Sigma}^- e^+ \nu_e$ events.

$\Gamma(\Sigma^+ \mu^- \overline{\nu}_\mu)/\Gamma_{total}$ — Γ_6/Γ

VALUE (units 10^{-6})	EVTS	DOCUMENT ID		TECN	COMMENT
2.3 ±0.4 OUR FIT					
2.17±0.32±0.17	66	[8] BATLEY	13	NA48	p Be, 400 GeV

[8] BATLEY 13 used $\Xi^0 \to \Sigma^+ e^- \overline{\nu}_e$ decay as a normalization mode and its branching fraction value of $(2.51 \pm 0.03 \pm 0.09) \times 10^{-4}$ from BATLEY 07.

$\Gamma(\Sigma^+ \mu^- \overline{\nu}_\mu)/\Gamma(\Sigma^+ e^- \overline{\nu}_e)$ — Γ_6/Γ_5

VALUE	EVTS	DOCUMENT ID		TECN	COMMENT
0.0092±0.0015 OUR FIT					
$0.018^{+0.007}_{-0.005}$ ±0.002	9	ABOUZAID	05	KTEV	p nucleus 800 GeV

Downloaded from https://academic.oup.com/ptep/article/2022/8/083C01/6651666 by KIT Library user on 27 September 2022

$\Gamma(\Sigma^- e^+ \nu_e)/\Gamma(\Lambda\pi^0)$ — Γ_7/Γ_1

Test of $\Delta S = \Delta Q$ rule.

VALUE (units 10^{-3})	CL%	EVTS	DOCUMENT ID		TECN	COMMENT
<0.9	90	0	YEH	74	HBC	Effective denom.=2500
• • • We do not use the following data for averages, fits, limits, etc. • • •						
<1.5			DAUBER	69	HBC	
<6			HUBBARD	66	HBC	

$\Gamma(\Sigma^- \mu^+ \nu_\mu)/\Gamma(\Lambda\pi^0)$ — Γ_8/Γ_1

Test of $\Delta S = \Delta Q$ rule.

VALUE (units 10^{-3})	CL%	EVTS	DOCUMENT ID		TECN	COMMENT
<0.9	90	0	YEH	74	HBC	Effective denom.=2500
• • • We do not use the following data for averages, fits, limits, etc. • • •						
<1.5			DAUBER	69	HBC	
<6			HUBBARD	66	HBC	

$\Gamma(p\pi^-)/\Gamma(\Lambda\pi^0)$ — Γ_9/Γ_1

ΔS=2. Forbidden in first-order weak interaction.

VALUE (units 10^{-6})	CL%	EVTS	DOCUMENT ID		TECN	COMMENT
< 8.2	90		WHITE	05	HYCP	p Cu, 800 GeV
• • • We do not use the following data for averages, fits, limits, etc. • • •						
< 36	90		GEWENIGER	75	SPEC	
<1800	90	0	YEH	74	HBC	Effective denom.=1300
< 900			DAUBER	69	HBC	
<5000			HUBBARD	66	HBC	

$\Gamma(pe^-\overline{\nu}_e)/\Gamma(\Lambda\pi^0)$ — Γ_{10}/Γ_1

ΔS=2. Forbidden in first-order weak interaction.

VALUE (units 10^{-3})	CL%	EVTS	DOCUMENT ID		TECN	COMMENT
<1.3			DAUBER	69	HBC	
• • • We do not use the following data for averages, fits, limits, etc. • • •						
<3.4	90	0	YEH	74	HBC	Effective denom.=670
<6			HUBBARD	66	HBC	

$\Gamma(p\mu^-\overline{\nu}_\mu)/\Gamma(\Lambda\pi^0)$ — Γ_{11}/Γ_1

ΔS=2. Forbidden in first-order weak interaction.

VALUE (units 10^{-3})	CL%	EVTS	DOCUMENT ID		TECN	COMMENT
<1.3			DAUBER	69	HBC	
• • • We do not use the following data for averages, fits, limits, etc. • • •						
<3.5	90	0	YEH	74	HBC	Effective denom.=664
<6			HUBBARD	66	HBC	

Ξ^0 DECAY PARAMETERS

See the "Note on Baryon Decay Parameters" in the neutron Listings.

$\alpha(\Xi^0)\ \alpha_-(\Lambda)$

This is a product of the $\Xi^0 \to \Lambda\pi^0$ and $\Lambda \to p\pi^-$ asymmetries.

VALUE	EVTS	DOCUMENT ID		TECN	COMMENT
−0.261±0.006 OUR AVERAGE					
−0.276±0.001±0.035	4M	BATLEY	10B	NA48	p Be, 400 GeV
−0.260±0.004±0.005	300k	HANDLER	82	SPEC	FNAL hyperons
• • • We do not use the following data for averages, fits, limits, etc. • • •					
−0.317±0.027	6075	BUNCE	78	SPEC	FNAL hyperons
−0.35 ±0.06	505	BALTAY	74	HBC	$K^- p$ 1.75 GeV/c
−0.28 ±0.06	739	DAUBER	69	HBC	$K^- p$ 1.7–2.6 GeV/c

α FOR $\Xi^0 \to \Lambda\pi^0$

The above average, $\alpha(\Xi^0)\alpha_-(\Lambda) = -0.261 \pm 0.006$, divided by our current average $\alpha_-(\Lambda) = 0.732 \pm 0.014$, gives the following value for $\alpha(\Xi^0)$:

VALUE	DOCUMENT ID
−0.356±0.011 OUR EVALUATION	

ϕ ANGLE FOR $\Xi^0 \to \Lambda\pi^0$ — ($\tan\phi = \beta/\gamma$)

VALUE (°)	EVTS	DOCUMENT ID		TECN	COMMENT
21±12 OUR AVERAGE					
16±17	652	BALTAY	74	HBC	1.75 GeV/c $K^- p$
38±19	739	[9] DAUBER	69	HBC	
− 8±30	146	[10] BERGE	66	HBC	

[9] DAUBER 69 uses $\alpha_\Lambda = 0.647 \pm 0.020$.

[10] The errors have been multiplied by 1.2 due to approximations used for the Ξ polarization; see DAUBER 69 for a discussion.

RADIATIVE HYPERON DECAYS

Revised July 2011 by J.D. Jackson (LBNL).

The weak radiative decays of spin-1/2 hyperons, $B_i \to B_f\gamma$, yield information about matrix elements (form factors) similar to that gained from weak hadronic decays. For a polarized spin-1/2 hyperon decaying radiatively via a $\Delta Q = 0$, $\Delta S = 1$ transition, the angular distribution of the direction $\hat{\mathbf{p}}$ of the final spin-1/2 baryon in the hyperon rest frame is

$$\frac{dN}{d\Omega} = \frac{N}{4\pi}\,(1 + \alpha_\gamma\,\mathbf{P}_i\cdot\hat{\mathbf{p}})\ . \qquad (1)$$

Here $\mathbf{P}_i$ is the polarization of the decaying hyperon, and α_γ is the asymmetry parameter. In terms of the form factors $F_1(q^2)$, $F_2(q^2)$, and $G(q^2)$ of the effective hadronic weak electromagnetic vertex,

$$F_1(q^2)\gamma_\lambda + iF_2(q^2)\sigma_{\lambda\mu}q^\mu + G(q^2)\gamma_\lambda\gamma_5\ ,$$

α_γ is

$$\alpha_\gamma = \frac{2\,\mathrm{Re}[G(0)F_M^*(0)]}{|G(0)|^2 + |F_M(0)|^2}\ , \qquad (2)$$

where $F_M = (m_i - m_f)[F_2 - F_1/(m_i + m_f)]$. If the decaying hyperon is unpolarized, the decay baryon has a longitudinal polarization given by $P_f = -\alpha_\gamma$ [1].

The angular distribution for the weak hadronic decay, $B_i \to B_f\pi$, has the same form as Eq. (1), but of course with a different asymmetry parameter, α_π. Now, however, if the decaying hyperon is unpolarized, the decay baryon has a longitudinal polarization given by $P_f = +\alpha_\pi$ [2,3]. The difference of sign is because the spins of the pion and photon are different.

$\Xi^0 \to \Lambda\gamma$ *decay*—The radiative decay $\Xi^0 \to \Lambda\gamma$ of an unpolarized Ξ^0 uses the hadronic decay $\Lambda \to p\pi^-$ as the analyzer. As noted above, the longitudinal polarization of the Λ will be $P_\Lambda = -\alpha_{\Xi\Lambda\gamma}$. Let α_- be the $\Lambda \to p\pi^-$ asymmetry parameter and $\theta_{\Lambda p}$ be the angle, as seen in the Λ rest frame, between the Λ line of flight and the proton momentum. Then the hadronic version of Eq. (1) applied to the $\Lambda \to p\pi^-$ decay gives

$$\frac{dN}{d\cos\theta_{\Lambda p}} = \frac{N}{2}\,(1 - \alpha_{\Xi\Lambda\gamma}\,\alpha_-\cos\theta_{\Lambda p}) \qquad (3)$$

for the angular distribution of the proton in the Λ frame. Our current value, from the CERN NA48/1 experiment [4], is $\alpha_{\Xi\Lambda\gamma} = -0.704 \pm 0.019 \pm 0.064$.

$\Xi^0 \to \Sigma^0\gamma$ *decay*—The asymmetry parameter here, $\alpha_{\Xi\Sigma\gamma}$, is measured by following the decay chain $\Xi^0 \to \Sigma^0\gamma$, $\Sigma^0 \to \Lambda\gamma$, $\Lambda \to p\pi^-$. Again, for an unpolarized Ξ^0, the longitudinal polarization of the Σ^0 will be $P_\Sigma = -\alpha_{\Xi\Sigma\gamma}$. In the $\Sigma^0 \to \Lambda\gamma$ decay, a parity-conserving magnetic-dipole transition, the polarization of the Σ^0 is transferred to the Λ, as may be seen as follows. Let $\theta_{\Sigma\Lambda}$ be the angle seen in the Σ^0 rest frame between the Σ^0 line of flight and the Λ momentum. For Σ^0 helicity $+1/2$, the probability amplitudes for positive and negative spin states of the Σ^0 *along the* Λ *momentum* are $\cos(\theta_{\Sigma\Lambda}/2)$ and $\sin(\theta_{\Sigma\Lambda}/2)$. Then the amplitude for a negative helicity photon and a negative helicity Λ is $\cos(\theta_{\Sigma\Lambda}/2)$, while the amplitude for positive helicities for the photon and Λ is $\sin(\theta_{\Sigma\Lambda}/2)$. For Σ^0 helicity $-1/2$, the amplitudes are interchanged. If the Σ^0 has longitudinal polarization P_Σ, the probabilities for Λ helicities $\pm 1/2$ are therefore

$$p(\pm 1/2) = \frac{1}{2}(1 \mp P_\Sigma)\cos^2(\theta_{\Sigma\Lambda}/2) + \frac{1}{2}(1 \pm P_\Sigma)\sin^2(\theta_{\Sigma\Lambda}/2)\ , \qquad (4)$$

Downloaded from https://academic.oup.com/ptep/article/2022/8/083C01/6651666 by KIT Library user on 27 September 2022

and the longitudinal polarization of the Λ is

$$P_\Lambda = -P_\Sigma \cos\theta_{\Sigma\Lambda} = +\alpha_{\Xi\Sigma\gamma} \cos\theta_{\Sigma\Lambda} \ . \qquad (5)$$

Using Eq. (1) for the $\Lambda \to p\pi^-$ decay again, we get for the joint angular distribution of the $\Sigma^0 \to \Lambda\gamma$, $\Lambda \to p\pi^-$ chain,

$$\frac{d^2N}{d\cos\theta_{\Sigma\Lambda}\, d\cos\theta_{\Lambda p}} = \frac{N}{4}\left(1 + \alpha_{\Xi\Sigma\gamma} \cos\theta_{\Sigma\Lambda}\, \alpha_- \cos\theta_{\Lambda p}\right) \ . \qquad (6)$$

Our current average for $\alpha_{\Xi\Sigma\gamma}$ is -0.69 ± 0.06 [4,5].

References

1. R.E. Behrends, Phys. Rev. **111**, 1691 (1958); see Eq. (7) or (8).
2. In ancient times, the signs of the asymmetry term in the angular distributions of radiative and hadronic decays of polarized hyperons were sometimes opposite. For roughly 50 years, however, the overwhelming convention has been to make them the same. The aim, not always achieved, is to remove ambiguities.
3. For the definition of α_π, see the note on "Baryon Decay Parameters" in the Neutron Listings.
4. J.R. Batley *et al.*, Phys. Lett. **B693**, 241 (2010).
5. A. Alavi-Harati *et al.*, Phys. Rev. Lett. **86**, 3239 (2001).

α FOR $\Xi^0 \to \Lambda\gamma$

See the note above on "Radiative Hyperon Decays."

VALUE	EVTS	DOCUMENT ID		TECN	COMMENT
$-0.704 \pm 0.019 \pm 0.064$	52k	[11] BATLEY	10B	NA48	p Be, 400 GeV
• • • We do not use the following data for averages, fits, limits, etc. • • •					
$-0.78 \pm 0.18 \pm 0.06$	672	LAI	04A	NA48	See BATLEY 10B
-0.43 ± 0.44	87	[12] JAMES	90	SPEC	FNAL hyperons

[11] BATLEY 10B also measured the $\overline{\Xi}^0 \to \overline{\Lambda}\gamma$ asymmetry to be -0.798 ± 0.064 (no systematic error given) with 4769 events.
[12] The sign has been changed; see the erratum, JAMES 02.

α FOR $\Xi^0 \to \Lambda e^+ e^-$

VALUE	EVTS	DOCUMENT ID		TECN	COMMENT
-0.8 ± 0.2	397 ± 21	[13] BATLEY	07C	NA48	p Be, 400 GeV

[13] This BATLEY 07C result is consistent with the asymmetry α for $\Xi^0 \to \Lambda\gamma$, as expected if the mechanism is internal bremsstrahlung.

α FOR $\Xi^0 \to \Sigma^0\gamma$

See the note above on "Radiative Hyperon Decays."

VALUE	EVTS	DOCUMENT ID		TECN	COMMENT
-0.69 ± 0.06 OUR AVERAGE					
$-0.729 \pm 0.030 \pm 0.076$	15k	[14] BATLEY	10B	NA48	p Be, 400 GeV
$-0.63 \pm 0.08 \pm 0.05$	4045	ALAVI-HARATI	01C	KTEV	p nucleus, 800 GeV
• • • We do not use the following data for averages, fits, limits, etc. • • •					
$+0.20 \pm 0.32 \pm 0.05$	85	[15] TEIGE	89	SPEC	FNAL hyperons

[14] BATLEY 10B also measured the $\overline{\Xi}^0 \to \overline{\Sigma}^0\gamma$ asymmetry to be -0.786 ± 0.104 (no systematic error given) with 1404 events.
[15] This result has been withdrawn, due to an error. See the erratum, TEIGE 02.

$g_1(0)/f_1(0)$ FOR $\Xi^0 \to \Sigma^+ e^- \overline{\nu}_e$

VALUE	EVTS	DOCUMENT ID		TECN	COMMENT
1.22 ± 0.05 OUR AVERAGE					
1.21 ± 0.05		BATLEY	13	NA48	p Be, 400 GeV
$1.32^{+0.21}_{-0.17} \pm 0.05$	487	[16] ALAVI-HARATI	01I	KTEV	p nucleus, 800 GeV
• • • We do not use the following data for averages, fits, limits, etc. • • •					
$1.20 \pm 0.04 \pm 0.03$	6520	[17] BATLEY	07	NA48	See BATLEY 13

[16] ALAVI-HARATI 01I assumes here that the second-class current is zero and that the weak-magnetism term takes its exact SU(3) value.
[17] This BATLEY 07 result uses our 2006 value of V_{us} from semileptonic kaon decays as input.

$g_2(0)/f_1(0))$ FOR $\Xi^0 \to \Sigma^+ e^- \overline{\nu}_e$

VALUE	EVTS	DOCUMENT ID		TECN	COMMENT
$-1.7^{+2.1}_{-2.0} \pm 0.5$	487	[18] ALAVI-HARATI	01I	KTEV	p nucleus, 800 GeV

[18] ALAVI-HARATI 01I thus assumes that $g_2 = 0$ in calculating g_1/f_1, above.

$f_2(0)/f_1(0)$ FOR $\Xi^0 \to \Sigma^+ e^- \overline{\nu}_e$

VALUE	EVTS	DOCUMENT ID		TECN	COMMENT
2.0 ± 0.9 OUR AVERAGE					
2.0 ± 1.3		BATLEY	13	NA48	p Be, 400 GeV
$2.0 \pm 1.2 \pm 0.5$	487	ALAVI-HARATI	01I	KTEV	p nucleus, 800 GeV

Ξ^0 REFERENCES

BATLEY	13	PL B720 105	J.R. Batley *et al.*	(CERN NA48/1 Collab.)
BATLEY	10B	PL B693 241	J.R. Batley *et al.*	(CERN NA48/1 Collab.)
BATLEY	07	PL B645 36	J.R. Batley *et al.*	(CERN NA48/1 Collab.)
BATLEY	07C	PL B650 1	J.R. Batley *et al.*	(CERN NA48 Collab.)
ABOUZAID	05	PRL 95 081801	E. Abouzaid *et al.*	(FNAL KTeV Collab.)
WHITE	05	PRL 94 101804	C.G. White *et al.*	(FNAL HyperCP Collab.)
LAI	04A	PL B584 251	A. Lai *et al.*	(CERN NA48 Collab.)
JAMES	02	PRL 89 169901 (errat.)	C. James *et al.*	(MINN, MICH, WISC, RUTG)
TEIGE	02	PRL 89 169902 (errat.)	S. Teige *et al.*	(RUTG, MICH, MINN)
ALAVI-HARATI	01C	PRL 86 3239	A. Alavi-Harati *et al.*	(FNAL KTeV Collab.)
ALAVI-HARATI	01I	PRL 87 132001	A. Alavi-Harati *et al.*	(FNAL KTeV Collab.)
FANTI	00	EPJ C12 69	V. Fanti *et al.*	(CERN NA48 Collab.)
AFFOLDER	99	PRL 82 3751	A. Affolder *et al.*	(FNAL KTeV Collab.)
JAMES	90	PRL 64 843	C. James *et al.*	(MINN, MICH, WISC, RUTG)
TEIGE	89	PRL 63 2717	S. Teige *et al.*	(RUTG, MICH, MINN)
HANDLER	82	PR D25 639	R. Handler *et al.*	(WISC, MICH, MINN+)
COX	81	PRL 46 877	P.T. Cox *et al.*	(MICH, WISC, RUTG, MINN+)
BUNCE	79	PL 86B 386	G.R.M. Bunce *et al.*	(BNL, MICH, RUTG+)
BUNCE	78	PR D18 633	G.R.M. Bunce *et al.*	(WISC, MICH, RUTG)
ZECH	77	NP B124 413	G. Zech *et al.*	(SIEG, CERN, DORT, HEIDH)
GEWENIGER	75	PL 57B 193	C. Geweniger *et al.*	(CERN, HEIDH)
BALTAY	74	PR D9 49	C. Baltay *et al.*	(COLU, BING) J
YEH	74	PR D10 3545	N. Yeh *et al.*	(BING, COLU)
MAYEUR	72	NP B47 333	C. Mayeur *et al.*	(BRUX, CERN, TUFTS, LOUC)
Also		NP B53 268 (erratum)	C. Mayeur	
WILQUET	72	PL 42B 372	G. Wilquet *et al.*	(BRUX, CERN, TUFTS+)
DAUBER	69	PR 179 1262	P.M. Dauber *et al.*	(LRL)
PALMER	68	PL 26B 323	R.B. Palmer *et al.*	(BNL, SYRA)
BERGE	66	PR 147 945	J.P. Berge *et al.*	(LRL)
HUBBARD	66	Thesis UCRL 11510	J.R. Hubbard	(LRL)
LONDON	66	PR 143 1034	G.W. London *et al.*	(BNL, SYRA)
PJERROU	65B	PRL 14 275	G.M. Pjerrou *et al.*	(UCLA)
Also		Thesis	G.M. Pjerrou	(UCLA)
CARMONY	64B	PRL 12 482	D.D. Carmony *et al.*	(UCLA)
HUBBARD	64	PR 135 B183	J.R. Hubbard *et al.*	(LRL)
JAUNEAU	63	PL 4 49	L. Jauneau *et al.*	(EPOL, CERN, LOUC+)
Also		Siena Conf. 1 1	L. Jauneau *et al.*	(EPOL, CERN, LOUC+)

Ξ^-

$I(J^P) = \frac{1}{2}(\frac{1}{2}^+)$ Status: ****

The parity has not actually been measured, but + is of course expected.

We have omitted some results that have been superseded by later experiments. See our earlier editions.

Ξ^- MASS

The fit uses the Ξ^-, $\overline{\Xi}^+$, and Ξ^0 masses and the $\Xi - \overline{\Xi}^+$ mass difference. It assumes that the Ξ^- and $\overline{\Xi}^+$ masses are the same.

VALUE (MeV)	EVTS	DOCUMENT ID		TECN	COMMENT
1321.71 ± 0.07 OUR FIT					
$1321.70 \pm 0.08 \pm 0.05$	2478 ± 68	ABDALLAH	06E	DLPH	from Z decays
• • • We do not use the following data for averages, fits, limits, etc. • • •					
1321.46 ± 0.34	632	DIBIANCA	75	DBC	4.9 GeV/c $K^- d$
1321.12 ± 0.41	268	WILQUET	72	HLBC	
1321.87 ± 0.51	195	[1] GOLDWASSER	70	HBC	5.5 GeV/c $K^- p$
1321.67 ± 0.52	6	CHIEN	66	HBC	6.9 GeV/c $\overline{p}p$
1321.4 ± 1.1	299	LONDON	66	HBC	
1321.3 ± 0.4	149	PJERROU	65B	HBC	
1321.1 ± 0.3	241	[2] BADIER	64	HBC	
1321.4 ± 0.4	517	[2] JAUNEAU	63D	FBC	
1321.1 ± 0.65	62	[2] SCHNEIDER	63	HBC	

[1] GOLDWASSER 70 uses $m_\Lambda = 1115.58$ MeV.
[2] These masses have been increased 0.09 MeV because the Λ mass increased.

$\overline{\Xi}^+$ MASS

The fit uses the Ξ^-, $\overline{\Xi}^+$, and Ξ^0 masses and the $\Xi^- - \overline{\Xi}^+$ mass difference. It assumes that the Ξ^- and $\overline{\Xi}^+$ masses are the same.

VALUE (MeV)	EVTS	DOCUMENT ID		TECN	COMMENT
1321.71 ± 0.07 OUR FIT					
$1321.73 \pm 0.08 \pm 0.05$	2256 ± 63	ABDALLAH	06E	DLPH	from Z decays
• • • We do not use the following data for averages, fits, limits, etc. • • •					
1321.6 ± 0.8	35	VOTRUBA	72	HBC	10 GeV/c $K^+ p$
1321.2 ± 0.4	34	STONE	70	HBC	
1320.69 ± 0.93	5	CHIEN	66	HBC	6.9 GeV/c $\overline{p}p$

$(m_{\Xi^-} - m_{\overline{\Xi}^+}) / m_{\Xi^-}$

A test of CPT invariance.

VALUE	DOCUMENT ID		TECN	COMMENT
$(-2.5 \pm 8.7) \times 10^{-5}$	ABDALLAH	06E	DLPH	from Z decays

Ξ^- MEAN LIFE

Measurements with an error $> 0.2 \times 10^{-10}$ s or with systematic errors not included have been omitted.

VALUE (10^{-10} s)	EVTS	DOCUMENT ID		TECN	COMMENT
1.639 ± 0.015 OUR AVERAGE					
$1.65 \pm 0.07 \pm 0.12$	2478 ± 68	ABDALLAH	06E	DLPH	from Z decays
1.652 ± 0.051	32k	BOURQUIN	84	SPEC	Hyperon beam

Downloaded from https://academic.oup.com/ptep/article/2022/8/083C01/6651666 by KIT Library user on 27 September 2022

1.665 ± 0.065	41k	BOURQUIN	79	SPEC	Hyperon beam
1.609 ± 0.028	4286	HEMINGWAY	78	HBC	4.2 GeV/c $K^- p$
1.67 ± 0.08		DIBIANCA	75	DBC	4.9 GeV/c $K^- d$
1.63 ± 0.03	4303	BALTAY	74	HBC	1.75 GeV/c $K^- p$
$1.73 {}^{+0.08}_{-0.07}$	680	MAYEUR	72	HLBC	2.1 GeV/c K^-
1.61 ± 0.04	2610	DAUBER	69	HBC	
1.80 ± 0.16	299	LONDON	66	HBC	
1.70 ± 0.12	246	PJERROU	65B	HBC	
1.69 ± 0.07	794	HUBBARD	64	HBC	
$1.86 {}^{+0.15}_{-0.14}$	517	JAUNEAU	63D	FBC	

$\overline{\Xi}^+$ MEAN LIFE

VALUE (10^{-10} s)	EVTS	DOCUMENT ID		TECN	COMMENT
$1.70 \pm 0.08 \pm 0.12$	2256 ± 63	ABDALLAH	06E	DLPH	from Z decays
• • • We do not use the following data for averages, fits, limits, etc. • • •					
$1.55 {}^{+0.35}_{-0.20}$	35	[3] VOTRUBA	72	HBC	10 GeV/c $K^+ p$
1.6 ± 0.3	34	STONE	70	HBC	
$1.9 {}^{+0.7}_{-0.5}$	12	[3] SHEN	67	HBC	
1.51 ± 0.55	5	[3] CHIEN	66	HBC	6.9 GeV/c $\overline{p}p$

[3] The error is statistical only.

$(\tau_{\Xi^-} - \tau_{\overline{\Xi}^+}) / \tau_{\Xi^-}$

A test of CPT invariance.

VALUE	DOCUMENT ID		TECN	COMMENT
-0.01 ± 0.07	ABDALLAH	06E	DLPH	from Z decays

Ξ^- MAGNETIC MOMENT

See the "Quark Model" review.

VALUE (μ_N)	EVTS	DOCUMENT ID		TECN	COMMENT
-0.6507 ± 0.0025 OUR AVERAGE					
-0.6505 ± 0.0025	4.36M	DURYEA	92	SPEC	800 GeV p Be
$-0.661 \pm 0.036 \pm 0.036$	44k	TROST	89	SPEC	Ξ^- ~ 250 GeV
-0.69 ± 0.04	218k	RAMEIKA	84	SPEC	400 GeV pBe
• • • We do not use the following data for averages, fits, limits, etc. • • •					
$-0.674 \pm 0.021 \pm 0.020$	122k	HO	90	SPEC	See DURYEA 92
-2.1 ± 0.8	2436	COOL	74	OSPK	1.8 GeV/c $K^- p$
-0.1 ± 2.1	2724	BINGHAM	70B	OSPK	1.8 GeV/c $K^- p$

$\overline{\Xi}^+$ MAGNETIC MOMENT

See the "Quark Model" review.

VALUE (μ_N)	EVTS	DOCUMENT ID		TECN	COMMENT
$+0.657 \pm 0.028 \pm 0.020$	70k	HO	90	SPEC	800 GeV pBe

$(\mu_{\Xi^-} + \mu_{\overline{\Xi}^+}) / |\mu_{\Xi^-}|$

A test of CPT invariance. We calculate this from the Ξ^- and $\overline{\Xi}^+$ magnetic moments above.

VALUE	DOCUMENT ID
$+0.01 \pm 0.05$ OUR EVALUATION	

Ξ^- DECAY MODES

	Mode	Fraction (Γ_i/Γ)	Confidence level
Γ_1	$\Lambda\pi^-$	(99.887 ± 0.035) %	
Γ_2	$\Sigma^-\gamma$	$(1.27 \pm 0.23) \times 10^{-4}$	
Γ_3	$\Lambda e^-\overline{\nu}_e$	$(5.63 \pm 0.31) \times 10^{-4}$	
Γ_4	$\Lambda\mu^-\overline{\nu}_\mu$	$(3.5 {}^{+3.5}_{-2.2}) \times 10^{-4}$	
Γ_5	$\Sigma^0 e^-\overline{\nu}_e$	$(8.7 \pm 1.7) \times 10^{-5}$	
Γ_6	$\Sigma^0\mu^-\overline{\nu}_\mu$	$< 8 \times 10^{-4}$	90%
Γ_7	$\Xi^0 e^-\overline{\nu}_e$	$< 2.59 \times 10^{-4}$	90%
	$\Delta S = 2$ forbidden ($S2$) modes		
Γ_8	$n\pi^-$	$S2$ $< 1.9 \times 10^{-5}$	90%
Γ_9	$n e^-\overline{\nu}_e$	$S2$ $< 3.2 \times 10^{-3}$	90%
Γ_{10}	$n\mu^-\overline{\nu}_\mu$	$S2$ < 1.5 %	90%
Γ_{11}	$p\pi^-\pi^-$	$S2$ $< 4 \times 10^{-4}$	90%
Γ_{12}	$p\pi^- e^-\overline{\nu}_e$	$S2$ $< 4 \times 10^{-4}$	90%
Γ_{13}	$p\pi^-\mu^-\overline{\nu}_\mu$	$S2$ $< 4 \times 10^{-4}$	90%
Γ_{14}	$p\mu^-\mu^-$	L $< 4 \times 10^{-8}$	90%

CONSTRAINED FIT INFORMATION

An overall fit to 4 branching ratios uses 5 measurements and one constraint to determine 5 parameters. The overall fit has a $\chi^2 = 1.0$ for 1 degrees of freedom.

The following *off-diagonal* array elements are the correlation coefficients $\langle \delta x_i \delta x_j \rangle / (\delta x_i \cdot \delta x_j)$, in percent, from the fit to the branching fractions, $x_i \equiv \Gamma_i/\Gamma_{\rm total}$. The fit constrains the x_i whose labels appear in this array to sum to one.

	x_1	x_2	x_3	x_4
x_2	-6			
x_3	-8	0		
x_4	-99	0	-1	
x_5	-5	0	0	0

Ξ^- BRANCHING RATIOS

A number of early results have been omitted.

$\Gamma(\Sigma^-\gamma)/\Gamma(\Lambda\pi^-)$ — Γ_2/Γ_1

VALUE (units 10^{-4})	EVTS	DOCUMENT ID		TECN	COMMENT
1.27 ± 0.24 OUR FIT					
1.27 ± 0.23 OUR AVERAGE					
$1.22 \pm 0.23 \pm 0.06$	211	[4] DUBBS	94	E761	Ξ^- 375 GeV
2.27 ± 1.02	9	BIAGI	87B	SPEC	SPS hyperon beam

[4] DUBBS 94 also finds weak evidence that the asymmetry parameter α_γ is positive ($\alpha_\gamma = 1.0 \pm 1.3$).

$\Gamma(\Lambda e^-\overline{\nu}_e)/\Gamma(\Lambda\pi^-)$ — Γ_3/Γ_1

VALUE (units 10^{-3})	EVTS	DOCUMENT ID		TECN	COMMENT
0.564 ± 0.031 OUR FIT					
0.564 ± 0.031	2857	BOURQUIN	83	SPEC	SPS hyperon beam
• • • We do not use the following data for averages, fits, limits, etc. • • •					
0.30 ± 0.13	11	THOMPSON	80	ASPK	Hyperon beam

$\Gamma(\Lambda\mu^-\overline{\nu}_\mu)/\Gamma(\Lambda\pi^-)$ — Γ_4/Γ_1

VALUE (units 10^{-3})	CL%	EVTS	DOCUMENT ID		TECN	COMMENT
$0.35 {}^{+0.35}_{-0.22}$ OUR FIT						
0.35 ± 0.35		1	YEH	74	HBC	Effective denom.=2859
• • • We do not use the following data for averages, fits, limits, etc. • • •						
< 2.3	90	0	THOMPSON	80	ASPK	Effective denom.=1017
< 1.3			DAUBER	69	HBC	
<12			BERGE	66	HBC	

$\Gamma(\Sigma^0 e^-\overline{\nu}_e)/\Gamma(\Lambda\pi^-)$ — Γ_5/Γ_1

VALUE (units 10^{-3})	EVTS	DOCUMENT ID		TECN	COMMENT
0.087 ± 0.017 OUR FIT					
0.087 ± 0.017	154	BOURQUIN	83	SPEC	SPS hyperon beam

$[\Gamma(\Lambda e^-\overline{\nu}_e) + \Gamma(\Sigma^0 e^-\overline{\nu}_e)]/\Gamma(\Lambda\pi^-)$ — $(\Gamma_3+\Gamma_5)/\Gamma_1$

VALUE (units 10^{-3})	EVTS	DOCUMENT ID		TECN	COMMENT
• • • We do not use the following data for averages, fits, limits, etc. • • •					
0.651 ± 0.031	3011	[5] BOURQUIN	83	SPEC	SPS hyperon beam
0.68 ± 0.22	17	[6] DUCLOS	71	OSPK	

[5] See the separate BOURQUIN 83 values for $\Gamma(\Lambda e^-\overline{\nu}_e)/\Gamma(\Lambda\pi^-)$ and $\Gamma(\Sigma^0 e^-\overline{\nu}_e)/\Gamma(\Lambda\pi^-)$ above.

[6] DUCLOS 71 cannot distinguish Σ^0's from Λ's. The Cabibbo theory predicts the Σ^0 rate is about a factor 6 smaller than the Λ rate.

$\Gamma(\Sigma^0\mu^-\overline{\nu}_\mu)/\Gamma(\Lambda\pi^-)$ — Γ_6/Γ_1

VALUE (units 10^{-3})	CL%	EVTS	DOCUMENT ID		TECN	COMMENT
<0.76	90	0	YEH	74	HBC	Effective denom.=3026
• • • We do not use the following data for averages, fits, limits, etc. • • •						
<5			BERGE	66	HBC	

$\Gamma(\Xi^0 e^-\overline{\nu}_e)/\Gamma_{\rm total}$ — Γ_7/Γ

VALUE	CL%	DOCUMENT ID		TECN	COMMENT
$<2.59 \times 10^{-4}$	90	ABLIKIM	21AH	BES3	$J/\psi \to \Xi\overline{\Xi}$

$\Gamma(\Xi^0 e^-\overline{\nu}_e)/\Gamma(\Lambda\pi^-)$ — Γ_7/Γ_1

VALUE	CL%	DOCUMENT ID		TECN	COMMENT
• • • We do not use the following data for averages, fits, limits, etc. • • •					
$<2.3 \times 10^{-3}$	90	YEH	74	HBC	Effective denom.=1000

$\Gamma(n\pi^-)/\Gamma(\Lambda\pi^-)$ — Γ_8/Γ_1

ΔS=2. Forbidden in first-order weak interaction.

VALUE (units 10^{-3})	CL%	EVTS	DOCUMENT ID		TECN	COMMENT
<0.019	90		BIAGI	82B	SPEC	SPS hyperon beam
• • • We do not use the following data for averages, fits, limits, etc. • • •						
<3.0	90	0	YEH	74	HBC	Effective denom.=760
<1.1			DAUBER	69	HBC	
<5.0			FERRO-LUZZI	63	HBC	

Downloaded from https://academic.oup.com/ptep/article/2022/8/083C01/6651666 by KIT Library user on 27 September 2022

$\Gamma(ne^-\overline{\nu}_e)/\Gamma(\Lambda\pi^-)$ — Γ_9/Γ_1

ΔS=2. Forbidden in first-order weak interaction.

VALUE (units 10^{-3})	CL%	EVTS	DOCUMENT ID		TECN	COMMENT
< 3.2	90	0	YEH	74	HBC	Effective denom.=715
• • • We do not use the following data for averages, fits, limits, etc. • • •						
<10	90		BINGHAM	65	RVUE	

$\Gamma(n\mu^-\overline{\nu}_\mu)/\Gamma(\Lambda\pi^-)$ — Γ_{10}/Γ_1

ΔS=2. Forbidden in first-order weak interaction.

VALUE (units 10^{-3})	CL%	EVTS	DOCUMENT ID		TECN	COMMENT
<15.3	90	0	YEH	74	HBC	Effective denom.=150

$\Gamma(p\pi^-\pi^-)/\Gamma(\Lambda\pi^-)$ — Γ_{11}/Γ_1

ΔS=2. Forbidden in first-order weak interaction.

VALUE (units 10^{-4})	CL%	EVTS	DOCUMENT ID		TECN	COMMENT
<3.7	90	0	YEH	74	HBC	Effective denom.=6200

$\Gamma(p\pi^-e^-\overline{\nu}_e)/\Gamma(\Lambda\pi^-)$ — Γ_{12}/Γ_1

ΔS=2. Forbidden in first-order weak interaction.

VALUE (units 10^{-4})	CL%	EVTS	DOCUMENT ID		TECN	COMMENT
<3.7	90	0	YEH	74	HBC	Effective denom.=6200

$\Gamma(p\pi^-\mu^-\overline{\nu}_\mu)/\Gamma(\Lambda\pi^-)$ — Γ_{13}/Γ_1

ΔS=2. Forbidden in first-order weak interaction.

VALUE (units 10^{-4})	CL%	EVTS	DOCUMENT ID		TECN	COMMENT
<3.7	90	0	YEH	74	HBC	Effective denom.=6200

$\Gamma(p\mu^-\mu^-)/\Gamma(\Lambda\pi^-)$ — Γ_{14}/Γ_1

A ΔL=2 decay, forbidden by total lepton number conservation.

VALUE (units 10^{-8})	CL%	DOCUMENT ID		TECN	COMMENT
<4.0	90	RAJARAM	05	HYCP	p Cu, 800 GeV
• • • We do not use the following data for averages, fits, limits, etc. • • •					
$<3.7\times10^4$	90	[7] LITTENBERG	92B	HBC	Uses YEH 74 data

[7] This LITTENBERG 92B limit and the identical YEH 74 limits for the preceding three modes all result from nonobservance of any 3-prong decays of the Ξ^-. One could as well apply the limit to the *sum* of the four modes.

Ξ^- DECAY PARAMETERS

See the "Note on Baryon Decay Parameters" in the neutron Listings.

$\alpha(\Xi^-)\alpha_-(\Lambda)$

VALUE	EVTS	DOCUMENT ID		TECN	COMMENT
−0.294 ±0.005 OUR AVERAGE		Error includes scale factor of 1.7. See the ideogram below.			
−0.2963±0.0042	189k	LUK	00	E756	p Be, 800 GeV
−0.2894±0.0073	63k	[8] LUK	00	E756	p Be, 800 GeV
−0.303 ±0.004 ±0.004	192k	RAMEIKA	86	SPEC	400 GeV pBe
−0.257 ±0.020	11k	ASTON	85B	LASS	11 GeV/c K^-p
−0.260 ±0.017	21k	BENSINGER	85	MPS	5 GeV/c K^-p
−0.299 ±0.007	150k	BIAGI	82	SPEC	SPS hyperon beam
−0.315 ±0.026	9046	CLELAND	80C	ASPK	BNL hyperon beam
−0.239 ±0.021	6599	HEMINGWAY	78	HBC	4.2 GeV/c K^-p
−0.243 ±0.025	4303	BALTAY	74	HBC	1.75 GeV/c K^-p
−0.252 ±0.032	2436	COOL	74	OSPK	1.8 GeV/c K^-p
−0.253 ±0.028	2781	DAUBER	69	HBC	

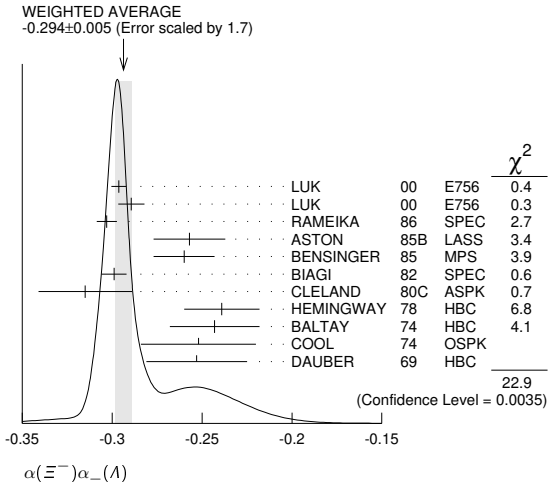

[8] This LUK 00 value is for $\alpha(\overline{\Xi}^+)\ \alpha_+(\overline{\Lambda})$. We assume *CP* conservation here by including it in the average for $\alpha(\Xi^-)\ \alpha_-(\Lambda)$. But see the second data block below for the *CP* test.

α FOR $\Xi^- \to \Lambda\pi^-$

The above average, $\alpha(\Xi^-)\ \alpha_-(\Lambda) = -0.294 \pm 0.005$, divided by our current average $\alpha_-(\Lambda) = 0.732 \pm 0.014$, gives the following value for $\alpha(\Xi^-)$:

VALUE	DOCUMENT ID
−0.401±0.010 OUR EVALUATION	

$\dfrac{[\alpha(\Xi^-)\alpha_-(\Lambda)-\alpha(\overline{\Xi}^+)\alpha_+(\overline{\Lambda})]}{[\alpha(\Xi^-)\alpha_-(\Lambda)+\alpha(\overline{\Xi}^+)\alpha_+(\overline{\Lambda})]}$

This is zero if *CP* is conserved. The α's are the decay-asymmetry parameters for $\Xi^- \to \Lambda\pi^-$ and $\Lambda \to p\pi^-$ and for $\overline{\Xi}^+ \to \overline{\Lambda}\pi^+$ and $\overline{\Lambda} \to \overline{p}\pi^+$.

VALUE (units 10^{-4})	EVTS	DOCUMENT ID		TECN	COMMENT
0.0± 5.1±4.4	158M	HOLMSTROM	04	HYCP	p Cu, 800 GeV
• • • We do not use the following data for averages, fits, limits, etc. • • •					
+120 ±140	252k	LUK	00	E756	p Be, 800 GeV

ϕ ANGLE FOR $\Xi^- \to \Lambda\pi^-$ — $(\tan\phi = \beta/\gamma)$

VALUE (°)	EVTS	DOCUMENT ID		TECN	COMMENT
− 2.1 ± 0.8 OUR AVERAGE					
− 2.39± 0.64±0.64	144M	[9] HUANG	04	HYCP	p Cu, 800 GeV
− 1.61± 2.66±0.37	1.35M	[10] CHAKRAVO...	03	E756	p Be, 800 GeV
5 ±10	11k	ASTON	85B	LASS	K^-p
14.7 ±16.0	21k	[11] BENSINGER	85	MPS	5 GeV/c K^-p
11 ± 9	4303	BALTAY	74	HBC	1.75 GeV/c K^-p
5 ±16	2436	COOL	74	OSPK	1.8 GeV/c K^-p
−14 ±11	2781	DAUBER	69	HBC	Uses $\alpha_\Lambda = 0.647\pm0.020$
0 ±12	1004	[12] BERGE	66	HBC	
• • • We do not use the following data for averages, fits, limits, etc. • • •					
−26 ±30	2724	BINGHAM	70B	OSPK	
0 ±20.4	364	[12] LONDON	66	HBC	Using α_Λ=0.62
54 ±30	356	[12] CARMONY	64B	HBC	

[9] From this result and α_Ξ, HUANG 04 gets $\beta_\Xi = -0.037 \pm 0.011 \pm 0.010$ and $\gamma_\Xi = 0.888 \pm 0.0004 \pm 0.006$. And the strong p–s phase difference for $\Lambda\pi^-$ scattering is $(4.6 \pm 1.4 \pm 1.2)^\circ$.

[10] From this result and α_Ξ, CHAKRAVORTY 03 obtains $\beta_\Xi = -0.025 \pm 0.042 \pm 0.006$ and $\gamma_\Xi = 0.889\pm0.001\pm0.007$. And the strong p–s phase difference for $\Lambda\pi^-$ scattering is $(3.17 \pm 5.28 \pm 0.73)^\circ$.

[11] BENSINGER 85 used $\alpha_\Lambda = 0.642 \pm 0.013$.

[12] The errors have been multiplied by 1.2 due to approximations used for the Ξ polarization; see DAUBER 69 for a discussion.

$g_A\ /\ g_V$ FOR $\Xi^- \to \Lambda e^-\overline{\nu}_e$

VALUE	EVTS	DOCUMENT ID		TECN	COMMENT
−0.25±0.05	1992	[13] BOURQUIN	83	SPEC	SPS hyperon beam

[13] BOURQUIN 83 assumes that $g_2 = 0$. Also, the sign has been changed to agree with our conventions, given in the "Note on Baryon Decay Parameters" in the neutron Listings.

Ξ^- REFERENCES

We have omitted some papers that have been superseded by later experiments. See our earlier editions.

ABLIKIM	21AH	PR D104 072007	M. Ablikim *et al.*	(BESIII Collab.)
ABDALLAH	06E	PL B639 179	J. Abdallah *et al.*	(DELPHI Collab.)
RAJARAM	05	PRL 94 181801	D. Rajaram *et al.*	(FNAL HyperCP Collab.)
HOLMSTROM	04	PRL 93 262001	T. Holmstrom *et al.*	(FNAL HyperCP Collab.)
HUANG	04	PRL 93 011802	M. Huang *et al.*	(FNAL HyperCP Collab.)
CHAKRAVO...	03	PRL 91 031601	A. Chakravorty *et al.*	(FNAL E756 Collab.)
LUK	00	PRL 85 4860	K.B. Luk *et al.*	(FNAL E756 Collab.)
DUBBS	94	PRL 72 808	T. Dubbs *et al.*	(FNAL E761 Collab.)
DURYEA	92	PRL 68 768	J. Duryea *et al.*	(MINN, FNAL, MICH, RUTG)
LITTENBERG	92B	PR D46 892	L.S. Littenberg, R.E. Shrock	(BNL, STON)
HO	90	PRL 65 1713	P.M. Ho *et al.*	(MICH, FNAL, MINN, RUTG)
Also		PR D44 3402	P.M. Ho *et al.*	(MICH, FNAL, MINN, RUTG)
TROST	89	PR D40 1703	L.H. Trost *et al.*	(FNAL-715 Collab.)
BIAGI	87B	ZPHY C35 143	S.F. Biagi *et al.*	(BRIS, CERN, GEVA+)
RAMEIKA	86	PR D33 3172	R. Rameika *et al.*	(RUTG, MICH, WISC+)
ASTON	85B	PR D32 2270	D. Aston *et al.*	(SLAC, CARL, CNRC, CINC)
BENSINGER	85	NP B252 561	J.R. Bensinger *et al.*	(CHIC, ELMT, FNAL+)
BOURQUIN	84	NP B241 1	M.H. Bourquin *et al.*	(BRIS, GEVA, HEIDP+)
RAMEIKA	84	PRL 52 581	R. Rameika *et al.*	(RUTG, MICH, WISC+)
BOURQUIN	83	ZPHY C21 1	M.H. Bourquin *et al.*	(BRIS, GEVA, HEIDP+)
BIAGI	82	PL 112B 265	S.F. Biagi *et al.*	(BRIS, CAVE, GEVA+)
BIAGI	82B	PL 112B 277	S.F. Biagi *et al.*	(LOQM, GEVA, RL+)
CLELAND	80C	PR D21 12	W.E. Cleland *et al.*	(PITT, BNL)
THOMPSON	80	PR D21 25	J.A. Thompson *et al.*	(PITT, BNL)
BOURQUIN	79	PL 87B 297	M.H. Bourquin *et al.*	(BRIS, GEVA, HEIDP+)
HEMINGWAY	78	NP B142 205	R.J. Hemingway *et al.*	(CERN, ZEEM, NIJM+)
DIBIANCA	75	NP B98 137	F.A. Dibianca, R.J. Endorf	(CMU)
BALTAY	74	PR D9 49	C. Baltay *et al.*	(COLU, BING) J
COOL	74	PR D10 792	R.L. Cool *et al.*	(BNL)
Also		PRL 29 1630	R.L. Cool *et al.*	(BNL)
YEH	74	PR D10 3545	N. Yeh *et al.*	(BING, COLU)
MAYEUR	72	NP B47 333	C. Mayeur *et al.*	(BRUX, CERN, TUFTS, LOUC)
VOTRUBA	72	NP B45 77	M.F. Votruba, A. Safder, T.M. Ratcliffe	(BIRM+)
WILQUET	72	PL 42B 372	G. Wilquet *et al.*	(BRUX, CERN, TUFTS+)
DUCLOS	71	NP B32 493	J. Duclos *et al.*	(CERN)
BINGHAM	70B	PR D1 3010	G.M. Bingham *et al.*	(UCSD, WASH)
GOLDWASSER	70	PR D1 1960	E.L. Goldwasser, P.F. Schultz	(ILL)
STONE	70	PL 32B 515	S.L. Stone *et al.*	(ROCH)
DAUBER	69	PR 179 1262	P.M. Dauber *et al.*	(LRL) J
SHEN	67	PL 25B 443	B.C. Shen, A. Firestone, G. Goldhaber	(UCB+)
BERGE	66	PR 147 945	J.P. Berge *et al.*	(LRL)
CHIEN	66	PR 152 1171	C.Y. Chien *et al.*	(YALE, BNL)
LONDON	66	PR 143 1034	G.W. London *et al.*	(BNL, SYRA)
BINGHAM	65	PRSL 285 202	H.H. Bingham	(CERN)
PJERROU	65B	PRL 14 275	G.M. Pjerrou *et al.*	(UCLA)
Also		Thesis	G.M. Pjerrou	(UCLA)

Downloaded from https://academic.oup.com/ptep/article/2022/8/083C01/6651666 by KIT Library user on 27 September 2022

BADIER	64	Dubna Conf. 1 593	J. Badier *et al.*	(EPOL, SACL, ZEEM)
CARMONY	64B	PRL 12 482	D.D. Carmony *et al.*	(UCLA) J
HUBBARD	64	PR 135 B183	J.R. Hubbard *et al.*	(LRL)
FERRO-LUZZI	63	PR 130 1568	M. Ferro-Luzzi *et al.*	(LRL)
JAUNEAU	63D	Siena Conf. 4	L. Jauneau *et al.*	(EPOL, CERN, LOUC+)
Also		PL 5 261	L. Jauneau *et al.*	(EPOL, CERN, LOUC+)
SCHNEIDER	63	PL 4 360	J. Schneider	(CERN)

Ξ RESONANCES

Revised 2004 by C.G. Wohl, (LBNL).

The accompanying table gives our evaluation of the present status of the Ξ resonances. Not much is known about Ξ resonances. This is because (1) they can only be produced as a part of a final state, and so the analysis is more complicated than if direct formation were possible, (2) the production cross sections are small (typically a few μb), and (3) the final states are topologically complicated and difficult to study with electronic techniques. Thus early information about Ξ resonances came entirely from bubble chamber experiments, where the numbers of events are small, and only in the 1980's did electronic experiments make any significant contributions. However, nothing of significance on Ξ resonances has been added since our 1988 edition.

For a detailed earlier review, see Meadows [1].

Table 1. The status of the Ξ resonances. Only those with an overall status of *** or **** are included in the Baryon Summary Table.

			Status as seen in —				
Particle	J^P	Overall status	$\Xi\pi$	ΛK	ΣK	$\Xi(1530)\pi$	Other channels
Ξ(1318)	1/2+	****					Decays weakly
Ξ(1530)	3/2+	****	****				
Ξ(1620)		*	*				
Ξ(1690)		***		***	**		
Ξ(1820)	3/2−	***	**	***	**	**	
Ξ(1950)		***	**	**		*	
Ξ(2030)		***		**	***		
Ξ(2120)		*		*			
Ξ(2250)		**					3-body decays
Ξ(2370)		**					3-body decays
Ξ(2500)		*		*	*		3-body decays

**** Existence is certain, and properties are at least fairly well explored.
*** Existence ranges from very likely to certain, but further confirmation is desirable and/or quantum numbers, branching fractions, *etc.* are not well determined.
** Evidence of existence is only fair.
* Evidence of existence is poor.

Reference

1. B.T. Meadows, in *Proceedings of the IVth International Conference on Baryon Resonances* (Toronto, 1980), ed. N. Isgur, p. 283.

$\Xi(1530)\ 3/2^+$

$I(J^P) = \frac{1}{2}(\frac{3}{2}^+)$ Status: ****

This is the only Ξ resonance whose properties are all reasonably well known. Assuming that the Λ_c^+ has $J^P = 1/2^+$, AUBERT 08AK, in a study of $\Lambda_c^+ \to \Xi^-\pi^+K^+$, finds conclusively that the spin of the $\Xi(1530)^0$ is 3/2. In conjunction with SCHLEIN 63B and BUTTON-SHAFER 66, this proves also that the parity is +.

We use only those determinations of the mass and width that are accompanied by some discussion of systematics and resolution.

Ξ(1530) POLE POSITIONS

$\Xi(1530)^0$ REAL PART

VALUE	DOCUMENT ID	COMMENT
1531.6±0.4	LICHTENBERG74	Using HABIBI 73

$\Xi(1530)^0$ IMAGINARY PART

VALUE	DOCUMENT ID	COMMENT
4.45±0.35	LICHTENBERG74	Using HABIBI 73

$\Xi(1530)^-$ REAL PART

VALUE	DOCUMENT ID	COMMENT
1534.4±1.1	LICHTENBERG74	Using HABIBI 73

$\Xi(1530)^-$ IMAGINARY PART

VALUE	DOCUMENT ID	COMMENT
$3.9^{+1.75}_{-3.9}$	LICHTENBERG74	Using HABIBI 73

Ξ(1530) MASSES

$\Xi(1530)^0$ MASS

VALUE (MeV)	EVTS	DOCUMENT ID		TECN	COMMENT
1531.80±0.32 OUR FIT Error includes scale factor of 1.3.					
1531.78±0.34 OUR AVERAGE Error includes scale factor of 1.4. See the ideogram below.					
1532.2 ±0.7		DEBELLEFON	75B	HBC	$K^-p \to \Xi^-\overline{K}\pi$
1533 ±1		ROSS	73B	HBC	$K^-p \to \Xi\overline{K}\pi(\pi)$
1531.4 ±0.8	59	BADIER	72	HBC	K^-p 3.95 GeV/c
1532.0 ±0.4	1262	BALTAY	72	HBC	K^-p 1.75 GeV/c
1531.3 ±0.6	324	BORENSTEIN	72	HBC	K^-p 2.2 GeV/c
1532.3 ±0.7	286	KIRSCH	72	HBC	K^-p 2.87 GeV/c
1528.7 ±1.1	76	LONDON	66	HBC	K^-p 2.24 GeV/c
• • • We do not use the following data for averages, fits, limits, etc. • • •					
1532.1 ±0.4	1244	ASTON	85B	LASS	K^-p 11 GeV/c
1532.1 ±0.6	2700	[1] BAUBILLIER	81B	HBC	K^-p 8.25 GeV/c
1530 ±1	450	BIAGI	81	SPEC	SPS hyperon beam
1527 ±6	80	SIXEL	79	HBC	K^-p 10 GeV/c
1535 ±4	100	SIXEL	79	HBC	K^-p 16 GeV/c
1533.6 ±1.4	97	BERTHON	74	HBC	Quasi-2-body σ

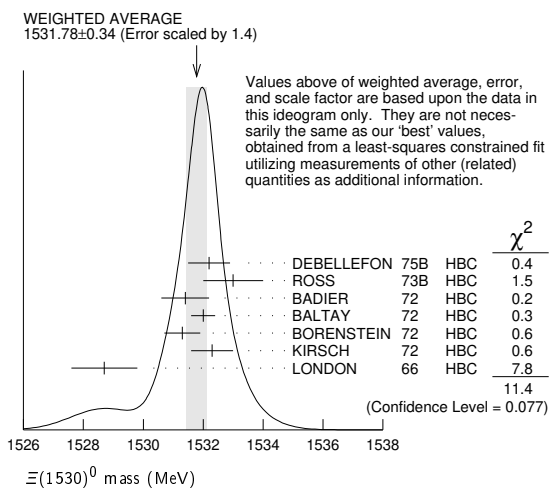

$\Xi(1530)^-$ MASS

VALUE (MeV)	EVTS	DOCUMENT ID		TECN	COMMENT
1535.0±0.6 OUR FIT					
1535.2±0.8 OUR AVERAGE					
1534.5±1.2		DEBELLEFON	75B	HBC	$K^-p \to \Xi^-\overline{K}\pi$
1535.3±2.0		ROSS	73B	HBC	$K^-p \to \Xi\overline{K}\pi(\pi)$
1536.2±1.6	185	KIRSCH	72	HBC	K^-p 2.87 GeV/c
1535.7±3.2	38	LONDON	66	HBC	K^-p 2.24 GeV/c
• • • We do not use the following data for averages, fits, limits, etc. • • •					
1540 ±3	48	BERTHON	74	HBC	Quasi-2-body σ
1534.7±1.1	334	BALTAY	72	HBC	K^-p 1.75 GeV/c

$m_{\Xi(1530)^-} - m_{\Xi(1530)}$

VALUE (MeV)	DOCUMENT ID		TECN	COMMENT
3.2±0.6 OUR FIT				
2.9±0.9 OUR AVERAGE				
2.7±1.0	BALTAY	72	HBC	K^-p 1.75 GeV/c
2.0±3.2	MERRILL	66	HBC	K^-p 1.7–2.7 GeV/c
5.7±3.0	PJERROU	65B	HBC	K^-p 1.8–1.95 GeV/c
• • • We do not use the following data for averages, fits, limits, etc. • • •				
3.9±1.8	[2] KIRSCH	72	HBC	K^-p 2.87 GeV/c
7 ±4	[2] LONDON	66	HBC	K^-p 2.24 GeV/c

Ξ(1530) WIDTHS

Downloaded from https://academic.oup.com/ptep/article/2022/8/083C01/6651666 by KIT Library user on 27 September 2022

$\Xi(1530)^0$ WIDTH

VALUE (MeV)	EVTS	DOCUMENT ID		TECN	COMMENT
9.1±0.5 OUR AVERAGE					
9.5±1.2		DEBELLEFON	75B	HBC	$K^- p \to \Xi^- \overline{K} \pi$
9.1±2.4		ROSS	73B	HBC	$K^- p \to \Xi \overline{K} \pi(\pi)$
11 ±2		BADIER	72	HBC	$K^- p$ 3.95 GeV/c
9.0±0.7		BALTAY	72	HBC	$K^- p$ 1.75 GeV/c
8.4±1.4		BORENSTEIN	72	HBC	$\Xi^- \pi^+$
11.0±1.8		KIRSCH	72	HBC	$\Xi^- \pi^+$
7 ±7		BERGE	66	HBC	$K^- p$ 1.5–1.7 GeV/c
8.5±3.5		LONDON	66	HBC	$K^- p$ 2.24 GeV/c
7 ±2		SCHLEIN	63B	HBC	$K^- p$ 1.8, 1.95 GeV/c
• • • We do not use the following data for averages, fits, limits, etc. • • •					
12.8±1.0	2700	[1] BAUBILLIER	81B	HBC	$K^- p$ 8.25 GeV/c
19 ±6	80	[3] SIXEL	79	HBC	$K^- p$ 10 GeV/c
14 ±5	100	[3] SIXEL	79	HBC	$K^- p$ 16 GeV/c

$\Xi(1530)^-$ WIDTH

VALUE (MeV)	DOCUMENT ID		TECN	COMMENT
$9.9^{+1.7}_{-1.9}$ OUR AVERAGE				
9.6±2.8	DEBELLEFON	75B	HBC	$K^- p \to \Xi^- \overline{K} \pi$
8.3±3.6	ROSS	73B	HBC	$K^- p \to \Xi \overline{K} \pi(\pi)$
$7.8^{+3.5}_{-7.8}$	BALTAY	72	HBC	$K^- p$ 1.75 GeV/c
16.2±4.6	KIRSCH	72	HBC	$\Xi^- \pi^0$, $\Xi^0 \pi^-$

$\Xi(1530)$ DECAY MODES

	Mode	Fraction (Γ_i/Γ)	Confidence level
Γ_1	$\Xi \pi$	100 %	
Γ_2	$\Xi \gamma$	<3.7 %	90%

$\Xi(1530)$ BRANCHING RATIOS

$\Gamma(\Xi\gamma)/\Gamma_{total}$ — Γ_2/Γ

VALUE	CL%	DOCUMENT ID		TECN	COMMENT
<0.037	90	ABLIKIM	20	BES3	$J/\psi \to \Xi(1530)^- \overline{\Xi}^+$
• • • We do not use the following data for averages, fits, limits, etc. • • •					
<0.04	90	KALBFLEISCH	75	HBC	$K^- p$ 2.18 GeV/c

$\Xi(1530)$ FOOTNOTES

[1] BAUBILLIER 81B is a fit to the inclusive spectrum. The resolution (5 MeV) is not unfolded.

[2] Redundant with data in the mass Listings.

[3] SIXEL 79 doesn't unfold the experimental resolution of 15 MeV.

$\Xi(1530)$ REFERENCES

ABLIKIM	20	PR D101 012004	M. Ablikim *et al.*	(BESIII Collab.)
AUBERT	08AK	PR D78 034008	B. Aubert *et al.*	(BABAR Collab.)
ASTON	85B	PR D32 2270	D. Aston *et al.*	(SLAC, CARL, CNRC, CINC)
BAUBILLIER	81B	NP B192 1	M. Baubillier *et al.*	(BIRM, CERN, GLAS+)
BIAGI	81	ZPHY C9 305	S.F. Biagi *et al.*	(BRIS, CAVE, GEVA+)
SIXEL	79	NP B159 125	P. Sixel *et al.*	(AACH3, BERL, CERN, LOIC+)
DEBELLEFON	75B	NC 28A 289	A. de Bellefon *et al.*	(CDEF, SACL)
KALBFLEISCH	75	PR D11 987	G.R. Kalbfleisch, R.C. Strand, J.W. Chapman	(BNL+)
BERTHON	74	NC 21A 146	A. Berthon *et al.*	(CDEF, RHEL, SACL+)
LICHTENBERG	74	PR D10 3865	D.B. Lichtenberg	(IND)
Also		Private Comm.	D.B. Lichtenberg	(IND)
HABIBI	73	Thesis Nevis 199	M. Habibi	(COLU)
ROSS	73B	Purdue Conf. 355	R.T. Ross, J.L. Lloyd, D. Radojicic	(OXF)
BADIER	72	NP B37 429	J. Badier *et al.*	(EPOL)
BALTAY	72	PL 42B 129	C. Baltay *et al.*	(COLU, BING)
BORENSTEIN	72	PR D5 1559	S.R. Borenstein *et al.*	(BNL, MICH) I
KIRSCH	72	NP B40 349	L.E. Kirsch *et al.*	(BRAN, UMD, SYRA+) I
BERGE	66	PR 147 945	J.P. Berge *et al.*	(LRL) I
BUTTON-...	66	PR 142 883	J. Button-Shafer *et al.*	(LRL) JP
LONDON	66	PR 143 1034	G.W. London *et al.*	(BNL, SYRA) IJ
MERRILL	66	Thesis UCRL 16455	D.W. Merrill	(LRL) JP
PJERROU	65B	PRL 14 275	G.M. Pjerrou *et al.*	(UCLA)
SCHLEIN	63B	PRL 11 167	P.E. Schlein *et al.*	(UCLA) IJP

OTHER RELATED PAPERS

MAZZUCATO	81	NP B178 1	M. Mazzucato *et al.*	(AMST, CERN, NIJM+)
BRIEFEL	77	PR D16 2706	E. Briefel *et al.*	(BRAN, UMD, SYRA+)
BRIEFEL	75	PR D12 1859	E. Briefel *et al.*	(BRAN, UMD, SYRA+)
HUNGERBU...	74	PR D10 2051	V. Hungerbuhler *et al.*	(YALE, FNAL, BNL+)
BUTTON-...	66	PR 142 883	J. Button-Shafer *et al.*	(LRL) JP

$\Xi(1620)$

$I(J^P) = \frac{1}{2}(?^?)$ Status: *

J, P need confirmation.

OMITTED FROM SUMMARY TABLE

What little evidence there is consists of weak signals in the $\Xi\pi$ channel. A number of other experiments (e.g., BORENSTEIN 72 and HASSALL 81) have looked for but not seen any effect.

$\Xi(1620)$ MASS

VALUE (MeV)	EVTS	DOCUMENT ID		TECN	COMMENT
≈ 1620 OUR ESTIMATE					
1624± 3	31	BRIEFEL	77	HBC	$K^- p$ 2.87 GeV/c
1633±12	34	DEBELLEFON	75B	HBC	$K^- p \to \Xi^- \overline{K} \pi$
1606± 6	29	ROSS	72	HBC	$K^- p$ 3.1–3.7 GeV/c

$\Xi(1620)$ WIDTH

VALUE (MeV)	EVTS	DOCUMENT ID		TECN	COMMENT
22.5	31	[1] BRIEFEL	77	HBC	$K^- p$ 2.87 GeV/c
40 ±15	34	DEBELLEFON	75B	HBC	$K^- p \to \Xi^- \overline{K} \pi$
21 ± 7	29	ROSS	72	HBC	$K^- p \to \Xi^- \pi^+ K^{*0}(892)$

$\Xi(1620)$ DECAY MODES

	Mode
Γ_1	$\Xi \pi$

$\Xi(1620)$ FOOTNOTES

[1] The fit is insensitive to values between 15 and 30 MeV.

$\Xi(1620)$ REFERENCES

HASSALL	81	NP B189 397	J.K. Hassall *et al.*	(CAVE, MSU)
BRIEFEL	77	PR D16 2706	E. Briefel *et al.*	(BRAN, UMD, SYRA+)
Also		Duke Conf. 317 Hyperon Resonances, 1970	E. Briefel *et al.*	(BRAN, UMD, SYRA+)
Also		PR D12 1859	E. Briefel *et al.*	(BRAN, UMD, SYRA+)
DEBELLEFON	75B	NC 28A 289	A. de Bellefon *et al.*	(CDEF, SACL)
BORENSTEIN	72	PR D5 1559	S.R. Borenstein *et al.*	(BNL, MICH) I
ROSS	72	PL 38B 177	R.T. Ross *et al.*	(OXF) I

OTHER RELATED PAPERS

HUNGERBU...	74	PR D10 2051	V. Hungerbuhler *et al.*	(YALE, FNAL, BNL+)
SCHMIDT	73	Purdue Conf. 363	P.E. Schmidt	(BRAN)
KALBFLEISCH	70	Duke Conf. 331 Hyperon Resonances 1970	G.R. Kalbfleisch	(BNL) I
APSELL	69	PRL 23 884	S.P. Apsell *et al.*	(BRAN, UMD, SYRA+)
BARTSCH	69	PL 28B 439	J. Bartsch *et al.*	(AACH, BERL, CERN+)

$\Xi(1690)$

$I(J^P) = \frac{1}{2}(?^?)$ Status: ***

AUBERT 08AK, in a study of $\Lambda_c^+ \to \Xi^- \pi^+ K^+$, finds some evidence that the $\Xi(1690)$ has $J^P = 1/2^-$.

DIONISI 78 sees a threshold enhancement in both the neutral and negatively charged $\Sigma\overline{K}$ mass spectra in $K^- p \to (\Sigma\overline{K}) K\pi$ at 4.2 GeV/c. The data from the $\Sigma\overline{K}$ channels alone cannot distinguish between a resonance and a large scattering length. Weaker evidence at the same mass is seen in the corresponding $\Lambda\overline{K}$ channels, and a coupled-channel analysis yields results consistent with a new Ξ.

BIAGI 81 sees an enhancement at 1700 MeV in the diffractively produced ΛK^- system. A peak is also observed in the $\Lambda\overline{K}^0$ mass spectrum at 1660 MeV that is consistent with a 1720 MeV resonance decaying to $\Sigma^0\overline{K}^0$, with the γ from the Σ^0 decay not detected.

BIAGI 87 provides further confirmation of this state in diffractive dissociation of Ξ^- into ΛK^-. The significance claimed is 6.7 standard deviations.

ADAMOVICH 98 sees a peak of 1400 ± 300 events in the $\Xi^-\pi^+$ spectrum produced by 345 GeV/c Σ^--nucleus interactions.

$\Xi(1690)$ MASSES

MIXED CHARGES

VALUE (MeV)	DOCUMENT ID
1690±10 OUR ESTIMATE This is only an educated guess; the error given is larger than the error on the average of the published values.	

$\Xi(1690)^0$ MASS

VALUE (MeV)	EVTS	DOCUMENT ID		TECN	COMMENT
1686±4	1400	ADAMOVICH	98	WA89	Σ^- nucleus, 345 GeV/c
1699±5	175	[1] DIONISI	78	HBC	$K^- p$ 4.2 GeV/c
1684±5	183	[2] DIONISI	78	HBC	$K^- p$ 4.2 GeV/c

$\Xi(1690)^-$ MASS

VALUE (MeV)	EVTS	DOCUMENT ID		TECN	COMMENT
1691.1± 1.9±2.0	104	BIAGI	87	SPEC	Ξ^- Be 116 GeV
1700 ±10	150	[3] BIAGI	81	SPEC	Ξ^- H 100, 135 GeV
1694 ± 6	45	[4] DIONISI	78	HBC	$K^- p$ 4.2 GeV/c

Downloaded from https://academic.oup.com/ptep/article/2022/8/083C01/6651666 by KIT Library user on 27 September 2022

$\Xi(1690)$ WIDTHS

MIXED CHARGES

VALUE (MeV)	DOCUMENT ID
20±15 OUR ESTIMATE	

$\Xi(1690)^0$ WIDTH

VALUE (MeV)	EVTS	DOCUMENT ID		TECN	COMMENT
10± 6	1400	ADAMOVICH	98	WA89	Σ^- nucleus, 345 GeV/c
44±23	175	[1] DIONISI	78	HBC	$K^- p$ 4.2 GeV/c
20± 4	183	[2] DIONISI	78	HBC	$K^- p$ 4.2 GeV/c

$\Xi(1690)^-$ WIDTH

VALUE (MeV)	CL%	EVTS	DOCUMENT ID		TECN	COMMENT
< 8	90	104	BIAGI	87	SPEC	Ξ^-Be 116 GeV
47±14		150	[3] BIAGI	81	SPEC	Ξ^-H 100, 135 GeV
26± 6		45	[4] DIONISI	78	HBC	$K^- p$ 4.2 GeV/c

$\Xi(1690)$ DECAY MODES

	Mode	Fraction (Γ_i/Γ)
Γ_1	$\Lambda\overline{K}$	seen
Γ_2	$\Sigma\overline{K}$	seen
Γ_3	$\Xi\pi$	seen
Γ_4	$\Xi^-\pi^+\pi^0$	
Γ_5	$\Xi^-\pi^+\pi^-$	possibly seen
Γ_6	$\Xi(1530)\pi$	

$\Xi(1690)$ BRANCHING RATIOS

$\Gamma(\Lambda\overline{K})/\Gamma_{total}$ — Γ_1/Γ

VALUE	EVTS	DOCUMENT ID		TECN	CHG	COMMENT
seen	104	BIAGI	87	SPEC	–	Ξ^-Be 116 GeV

$\Gamma(\Sigma\overline{K})/\Gamma(\Lambda\overline{K})$ — Γ_2/Γ_1

VALUE	EVTS	DOCUMENT ID		TECN	CHG	COMMENT
0.75±0.39	75	ABE	02C	BELL		$e^+e^- \approx \Upsilon(4S)$
2.7 ±0.9		DIONISI	78	HBC	0	$K^- p$ 4.2 GeV/c
3.1 ±1.4		DIONISI	78	HBC	–	$K^- p$ 4.2 GeV/c

$\Gamma(\Xi\pi)/\Gamma(\Sigma\overline{K})$ — Γ_3/Γ_2

VALUE	DOCUMENT ID		TECN	CHG	COMMENT
<0.09	DIONISI	78	HBC	0	$K^- p$ 4.2 GeV/c

$\Gamma(\Xi\pi)/\Gamma_{total}$ — Γ_3/Γ

VALUE	DOCUMENT ID		TECN	COMMENT
seen	ADAMOVICH	98	WA89	Σ^- nucleus, 345 GeV/c

$\Gamma(\Xi^-\pi^+\pi^0)/\Gamma(\Sigma\overline{K})$ — Γ_4/Γ_2

VALUE	DOCUMENT ID		TECN	CHG	COMMENT
<0.04	DIONISI	78	HBC	0	$K^- p$ 4.2 GeV/c

$\Gamma(\Xi^-\pi^+\pi^-)/\Gamma_{total}$ — Γ_5/Γ

VALUE	EVTS	DOCUMENT ID		TECN	CHG	COMMENT
possibly seen	4	BIAGI	87	SPEC	–	Ξ^-Be 116 GeV

$\Gamma(\Xi^-\pi^+\pi^-)/\Gamma(\Sigma\overline{K})$ — Γ_5/Γ_2

VALUE	DOCUMENT ID		TECN	CHG	COMMENT
<0.03	DIONISI	78	HBC	–	$K^- p$ 4.2 GeV/c

$\Gamma(\Xi(1530)\pi)/\Gamma(\Sigma\overline{K})$ — Γ_6/Γ_2

VALUE	DOCUMENT ID		TECN	CHG	COMMENT
<0.06	DIONISI	78	HBC	–	$K^- p$ 4.2 GeV/c

$\Xi(1690)$ FOOTNOTES

[1] From a fit to the $\Sigma^+ K^-$ spectrum.
[2] From a coupled-channel analysis of the $\Sigma^+ K^-$ and $\Lambda\overline{K}^0$ spectra.
[3] A fit to the inclusive spectrum from $\Xi^- N \to \Lambda K^- X$.
[4] From a coupled-channel analysis of the $\Sigma^0 K^-$ and ΛK^- spectra.

$\Xi(1690)$ REFERENCES

AUBERT	08AK	PR D78 034008	B. Aubert *et al.*	(BABAR Collab.)
ABE	02C	PL B524 33	K. Abe *et al.*	(KEK BELLE Collab.)
ADAMOVICH	98	EPJ C5 621	M.I. Adamovich *et al.*	(CERN WA89 Collab.)
BIAGI	87	ZPHY C34 15	S.F. Biagi *et al.*	(BRIS, CERN, GEVA+) I
BIAGI	81	ZPHY C9 305	S.F. Biagi *et al.*	(BRIS, CAVE, GEVA+)
DIONISI	78	PL 80B 145	C. Dionisi *et al.*	(CERN, AMST, NIJM+) I

$\Xi(1820)\ 3/2^-$

$I(J^P) = \frac{1}{2}(\frac{3}{2}^-)$ Status: ***

The clearest evidence is an 8-standard-deviation peak in ΛK^- seen by GAY 76C. TEODORO 78 favors $J = 3/2$, but cannot make a parity discrimination. BIAGI 87C is consistent with $J = 3/2$ and favors negative parity for this J value.

$\Xi(1820)$ MASS

We only average the measurements that appear to us to be most significant and best determined.

VALUE (MeV)	EVTS	DOCUMENT ID		TECN	CHG	COMMENT
1823 ± 5 OUR ESTIMATE						
1823.5± 1.4 OUR AVERAGE						
1825.5± 4.7±4.7	288	ABLIKIM	20C	BES3	–	$e^+e^- \to \Xi(1820)^-\overline{\Xi}^+$
1819.4± 3.1±2.0	280	[1] BIAGI	87	SPEC	0	Ξ^-Be $\to (\Lambda K^-)$ X
1826 ± 3 ±1	54	BIAGI	87C	SPEC	0	Ξ^-Be $\to (\Lambda\overline{K}^0)$ X
1822 ± 6		JENKINS	83	MPS	–	$K^- p \to K^+$ (MM)
1830 ± 6	300	BIAGI	81	SPEC	–	SPS hyperon beam
1823 ± 2	130	GAY	76C	HBC	–	$K^- p$ 4.2 GeV/c
• • • We do not use the following data for averages, fits, limits, etc. • • •						
1817 ± 3		ADAMOVICH	99B	WA89		Σ^- nucleus, 345 GeV
1797 ±19	74	BRIEFEL	77	HBC	0	$K^- p$ 2.87 GeV/c
1829 ± 9	68	BRIEFEL	77	HBC	–0	$\Xi(1530)\pi$
1860 ±14	39	BRIEFEL	77	HBC	–	$\Sigma^-\overline{K}^0$
1870 ± 9	44	BRIEFEL	77	HBC	0	$\Lambda\overline{K}^0$
1813 ± 4	57	BRIEFEL	77	HBC	–	ΛK^-
1807 ±27		DIBIANCA	75	DBC	–0	$\Xi\pi\pi$, $\Xi^*\pi$
1762 ± 8	28	[2] BADIER	72	HBC	–0	$\Xi\pi$, $\Xi\pi\pi$, $Y K$
1838 ± 5	38	[2] BADIER	72	HBC	–0	$\Xi\pi$, $\Xi\pi\pi$, $Y K$
1830 ±10	25	[3] CRENNELL	70B	DBC	–0	3.6, 3.9 GeV/c
1826 ±12		[4] CRENNELL	70B	DBC	–0	3.6, 3.9 GeV/c
1830 ±10	40	ALITTI	69	HBC	–	Λ, $\Sigma\overline{K}$
1814 ± 4	30	BADIER	65	HBC	0	$\Lambda\overline{K}^0$
1817 ± 7	29	SMITH	65C	HBC	–0	$\Lambda\overline{K}^0$, ΛK^-
1770		HALSTEINSLID	63	FBC	–0	K^- freon 3.5 GeV/c

$\Xi(1820)$ WIDTH

VALUE (MeV)	EVTS	DOCUMENT ID		TECN	CHG	COMMENT
$^{+15}_{-10}$ OUR ESTIMATE						
24 ± 5 OUR AVERAGE Error includes scale factor of 1.3. See the ideogram below.						
17.0±15.0±7.9	288	ABLIKIM	20C	BES3	–	$e^+e^- \to \Xi(1820)^-\overline{\Xi}^+$
24.6± 5.3	280	[1] BIAGI	87	SPEC	0	Ξ^-Be $\to (\Lambda K^-)$ X
12 ±14 ±1.7	54	BIAGI	87C	SPEC	0	Ξ^-Be $\to (\Lambda\overline{K}^0)$ X
72 ±20	300	BIAGI	81	SPEC	–	SPS hyperon beam
21 ± 7	130	GAY	76C	HBC	–	$K^- p$ 4.2 GeV/c
• • • We do not use the following data for averages, fits, limits, etc. • • •						
23 ±13		ADAMOVICH	99B	WA89		Σ^- nucleus, 345 GeV
99 ±57	74	BRIEFEL	77	HBC	0	$K^- p$ 2.87 GeV/c
52 ±34	68	BRIEFEL	77	HBC	–0	$\Xi(1530)\pi$
72 ±17	39	BRIEFEL	77	HBC	–	$\Sigma^-\overline{K}^0$
44 ±11	44	BRIEFEL	77	HBC	0	$\Lambda\overline{K}^0$
26 ±11	57	BRIEFEL	77	HBC	–	ΛK^-
85 ±58		DIBIANCA	75	DBC	–0	$\Xi\pi\pi$, $\Xi^*\pi$
51 ±13		[2] BADIER	72	HBC	–0	Lower mass
58 ±13		[2] BADIER	72	HBC	–0	Higher mass
103 $^{+38}_{-24}$		[3] CRENNELL	70B	DBC	–0	3.6, 3.9 GeV/c
48 $^{+36}_{-19}$		[4] CRENNELL	70B	DBC	–0	3.6, 3.9 GeV/c
55 $^{+40}_{-20}$		ALITTI	69	HBC	–	Λ, $\Sigma\overline{K}$
12 ± 4		BADIER	65	HBC	0	$\Lambda\overline{K}^0$
30 ± 7		SMITH	65B	HBC	–0	$\Lambda\overline{K}$
<80		HALSTEINSLID	63	FBC	–0	K^- freon 3.5 GeV/c

Downloaded from https://academic.oup.com/ptep/article/2022/8/083C01/6651666 by KIT Library user on 27 September 2022

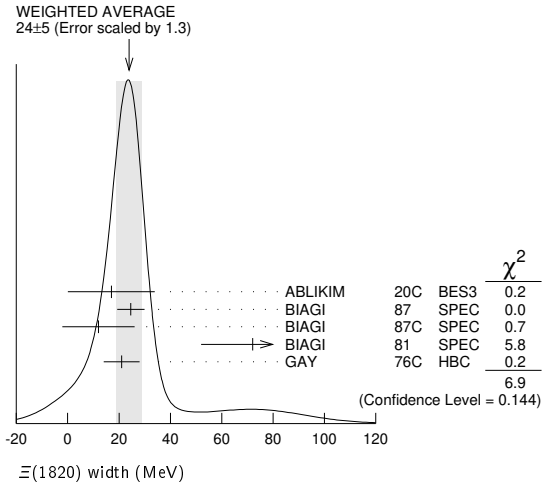

$\Xi(1820)$ DECAY MODES

	Mode	Fraction (Γ_i/Γ)
Γ_1	$\Lambda\overline{K}$	large
Γ_2	$\Sigma\overline{K}$	small
Γ_3	$\Xi\pi$	small
Γ_4	$\Xi(1530)\pi$	small
Γ_5	$\Xi\pi\pi$(not $\Xi(1530)\pi$)	

$\Xi(1820)$ BRANCHING RATIOS

The dominant modes seem to be $\Lambda\overline{K}$ and (perhaps) $\Xi(1530)\pi$, but the branching fractions are very poorly determined.

$\Gamma(\Lambda\overline{K})/\Gamma_{total}$ — Γ_1/Γ

VALUE	DOCUMENT ID		TECN	CHG	COMMENT
0.25±0.05 OUR AVERAGE					
0.24±0.05	ANISOVICH	12A	DPWA		Multichannel
0.30±0.15	ALITTI	69	HBC	−	K^-p 3.9–5 GeV/c

$\Gamma(\Xi\pi)/\Gamma_{total}$ — Γ_3/Γ

VALUE	DOCUMENT ID		TECN	CHG	COMMENT
0.10±0.10	ALITTI	69	HBC	−	K^-p 3.9–5 GeV/c

$\Gamma(\Xi\pi)/\Gamma(\Lambda\overline{K})$ — Γ_3/Γ_1

VALUE	CL%	DOCUMENT ID		TECN	CHG	COMMENT
<0.36	95	GAY	76C	HBC	−	K^-p 4.2 GeV/c
0.20±0.20		BADIER	65	HBC	0	K^-p 3 GeV/c

$\Gamma(\Xi\pi)/\Gamma(\Xi(1530)\pi)$ — Γ_3/Γ_4

VALUE	DOCUMENT ID		TECN	CHG	COMMENT
$1.5^{+0.6}_{-0.4}$	APSELL	70	HBC	0	K^-p 2.87 GeV/c

$\Gamma(\Sigma\overline{K})/\Gamma_{total}$ — Γ_2/Γ

VALUE	DOCUMENT ID		TECN	CHG	COMMENT
0.30±0.15	ALITTI	69	HBC	−	K^-p 3.9–5 GeV/c
• • • We do not use the following data for averages, fits, limits, etc. • • •					
<0.02	TRIPP	67	RVUE		Use SMITH 65C

$\Gamma(\Sigma\overline{K})/\Gamma(\Lambda\overline{K})$ — Γ_2/Γ_1

VALUE	DOCUMENT ID		TECN	CHG	COMMENT
0.24±0.10	GAY	76C	HBC	−	K^-p 4.2 GeV/c

$\Gamma(\Xi(1530)\pi)/\Gamma_{total}$ — Γ_4/Γ

VALUE	DOCUMENT ID		TECN	CHG	COMMENT
0.30±0.15	ALITTI	69	HBC	−	K^-p 3.9–5 GeV/c
• • • We do not use the following data for averages, fits, limits, etc. • • •					
seen	ASTON	85B	LASS		K^-p 11 GeV/c
not seen	[5] HASSALL	81	HBC		K^-p 6.5 GeV/c
<0.25	[6] DAUBER	69	HBC		K^-p 2.7 GeV/c

$\Gamma(\Xi(1530)\pi)/\Gamma(\Lambda\overline{K})$ — Γ_4/Γ_1

VALUE	DOCUMENT ID		TECN	CHG	COMMENT
0.38±0.27 OUR AVERAGE	Error includes scale factor of 2.3.				
1.0 ±0.3	GAY	76C	HBC	−	K^-p 4.2 GeV/c
0.26±0.13	SMITH	65C	HBC	−0	K^-p 2.45–2.7 GeV/c

$\Gamma(\Xi\pi\pi(\text{not }\Xi(1530)\pi))/\Gamma(\Lambda\overline{K})$ — Γ_5/Γ_1

VALUE	DOCUMENT ID		TECN	CHG	COMMENT
0.30±0.20	BIAGI	87	SPEC	−	Ξ^-Be 116 GeV
• • • We do not use the following data for averages, fits, limits, etc. • • •					
<0.14	[7] BADIER	65	HBC	0	1 st. dev. limit
>0.1	SMITH	65C	HBC	−0	K^-p 2.45–2.7 GeV/c

$\Gamma(\Xi\pi\pi(\text{not }\Xi(1530)\pi))/\Gamma(\Xi(1530)\pi)$ — Γ_5/Γ_4

VALUE	DOCUMENT ID		TECN	CHG	COMMENT
consistent with zero	GAY	76C	HBC	−	K^-p 4.2 GeV/c
• • • We do not use the following data for averages, fits, limits, etc. • • •					
0.3±0.5	[8] APSELL	70	HBC	0	K^-p 2.87 GeV/c

$\Xi(1820)$ FOOTNOTES

[1] BIAGI 87 also sees weak signals in the in the $\Xi^-\pi^+\pi^-$ channel at 1782.6 ± 1.4 MeV (Γ = 6.0 ± 1.5 MeV) and 1831.9 ± 2.8 MeV (Γ = 9.6 ± 9.9 MeV).
[2] BADIER 72 adds all channels and divides the peak into lower and higher mass regions. The data can also be fitted with a single Breit-Wigner of mass 1800 MeV and width 150 MeV.
[3] From a fit to inclusive $\Xi\pi$, $\Xi\pi\pi$, and ΛK^- spectra.
[4] From a fit to inclusive $\Xi\pi$ and $\Xi\pi\pi$ spectra only.
[5] Including $\Xi\pi\pi$.
[6] DAUBER 69 uses in part the same data as SMITH 65C.
[7] For the decay mode $\Xi^-\pi^+\pi^0$ only. This limit includes $\Xi(1530)\pi$.
[8] Or less. Upper limit for the 3-body decay.

$\Xi(1820)$ REFERENCES

ABLIKIM	20C	PRL 124 032002	M. Ablikim *et al.*	(BESIII Collab.)
ANISOVICH	12A	EPJ A48 15	A.V. Anisovich *et al.*	(BONN, PNPI)
ADAMOVICH	99B	EPJ C11 271	M.I. Adamovich *et al.*	(CERN WA89 Collab.)
BIAGI	87	ZPHY C34 15	S.F. Biagi *et al.*	(BRIS, CERN, GEVA+)
BIAGI	87C	ZPHY C34 175	S.F. Biagi *et al.*	(BRIS, CERN, GEVA+) JP
ASTON	85B	PR D32 2270	D. Aston *et al.*	(SLAC, CARL, CNRC, CINC)
JENKINS	83	PRL 51 951	C.M. Jenkins *et al.*	(FSU, BRAN, LBL+)
BIAGI	81	ZPHY C9 305	S.F. Biagi *et al.*	(BRIS, CAVE, GEVA+)
HASSALL	81	NP B189 397	J.K. Hassall *et al.*	(CAVE, MSU)
TEODORO	78	PL 77B 451	D. Teodoro *et al.*	(AMST, CERN, NIJM+) JP
BRIEFEL	77	PR D16 2706	E. Briefel *et al.*	(BRAN, UMD, SYRA+)
Also		PRL 23 884	S.P. Apsell *et al.*	(BRAN, UMD, SYRA+)
GAY	76C	PL 62B 477	J.B. Gay *et al.*	(AMST, CERN, NIJM) IJ
DIBIANCA	75	NP B98 137	F.A. Dibianca, R.J. Endorf	(CMU)
BADIER	72	NP B37 429	J. Badier *et al.*	(EPOL)
APSELL	70	PRL 24 777	S.P. Apsell *et al.*	(BRAN, UMD, SYRA+) I
CRENNELL	70B	PR D1 847	D.J. Crennell *et al.*	(BNL)
ALITTI	69	PRL 22 79	J. Alitti *et al.*	(BNL, SYRA) I
DAUBER	69	PR 179 1262	P.M. Dauber *et al.*	(LRL)
TRIPP	67	NP B3 10	R.D. Tripp *et al.*	(LRL, SLAC, CERN+)
BADIER	65	PL 16 171	J. Badier *et al.*	(EPOL, SACL, AMST) I
SMITH	65B	Athens Conf. 251	G.A. Smith, J.S. Lindsey	(LRL)
SMITH	65C	PRL 14 25	G.A. Smith *et al.*	(LRL) IJP
HALSTEINSLID	63	Siena Conf. 1 73	A. Halsteinslid *et al.*	(BERG, CERN, EPOL+) I

OTHER RELATED PAPERS

TEODORO	78	PL 77B 451	D. Teodoro *et al.*	(AMST, CERN, NIJM+) JP
BRIEFEL	75	PR D12 1859	E. Briefel *et al.*	(BRAN, UMD, SYRA+)
SCHMIDT	73	Purdue Conf. 363	P.E. Schmidt	(BRAN)
MERRILL	68	PR 167 1202	D.W. Merrill, J. Button-Shafer	(LRL)
SMITH	64	PRL 13 61	G.A. Smith *et al.*	(LRL) IJP

$\Xi(1950)$

$I(J^P) = \frac{1}{2}(?^?)$ Status: ***

We list here everything reported between 1875 and 2000 MeV. The accumulated evidence for a Ξ near 1950 MeV seems strong enough to include a $\Xi(1950)$ in the main Baryon Table, but not much can be said about its properties. In fact, there may be more than one Ξ near this mass.

$\Xi(1950)$ MASS

VALUE (MeV)	EVTS	DOCUMENT ID		TECN	COMMENT
1950±15 OUR ESTIMATE					
1955± 6		ADAMOVICH	99B	WA89	Σ^- nucleus, 345 GeV
1944± 9	129	BIAGI	87	SPEC	Ξ^-Be → ($\Xi^-\pi^+$)π^-X
1963± 5±2	63	BIAGI	87C	SPEC	Ξ^-Be → ($\Lambda\overline{K}^0$) X
1937± 7	150	BIAGI	81	SPEC	SPS hyperon beam
1961±18	139	BRIEFEL	77	HBC	2.87 K^-p → $\Xi^-\pi^+$X
1936±22	44	BRIEFEL	77	HBC	2.87 K^-p → $\Xi^0\pi^-$X
1964±10	56	BRIEFEL	77	HBC	$\Xi(1530)\pi$
1900±12		DIBIANCA	75	DBC	$\Xi\pi$
1952±11	25	ROSS	73C		$(\Xi\pi)^-$
1956± 6	29	BADIER	72	HBC	$\Xi\pi$, $\Xi\pi\pi$, YK
1955±14	21	GOLDWASSER	70	HBC	$\Xi\pi$
1894±18	66	DAUBER	69	HBC	$\Xi\pi$
1930±20	27	ALITTI	68	HBC	$\Xi^-\pi^+$
1933±16	35	BADIER	65	HBC	$\Xi^-\pi^+$

Downloaded from https://academic.oup.com/ptep/article/2022/8/083C01/6651666 by KIT Library user on 27 September 2022

$\Xi(1950)$ WIDTH

VALUE (MeV)	EVTS	DOCUMENT ID		TECN	COMMENT
60±20 OUR ESTIMATE					
68±22		ADAMOVICH	99B	WA89	Σ^- nucleus, 345 GeV
100±31	129	BIAGI	87	SPEC	$\Xi^- Be \to (\Xi^- \pi^+) \pi^- X$
25±15±1.2	63	BIAGI	87C	SPEC	$\Xi^- Be \to (\Lambda \overline{K}^0) X$
60± 8	150	BIAGI	81	SPEC	SPS hyperon beam
159±57	139	BRIEFEL	77	HBC	2.87 $K^- p \to \Xi^- \pi^+ X$
87±26	44	BRIEFEL	77	HBC	2.87 $K^- p \to \Xi^0 \pi^- X$
60±39	56	BRIEFEL	77	HBC	$\Xi(1530)\pi$
63±78		DIBIANCA	75	DBC	$\Xi\pi$
38±10		ROSS	73C		$(\Xi\pi)^-$
35±11	29	BADIER	72	HBC	$\Xi\pi$, $\Xi\pi\pi$, YK
56±26	21	GOLDWASSER	70	HBC	$\Xi\pi$
98±23	66	DAUBER	69	HBC	$\Xi\pi$
80±40	27	ALITTI	68	HBC	$\Xi^-\pi^+$
140±35	35	BADIER	65	HBC	$\Xi^-\pi^+$

$\Xi(1950)$ DECAY MODES

	Mode	Fraction (Γ_i/Γ)
Γ_1	$\Lambda\overline{K}$	seen
Γ_2	$\Sigma\overline{K}$	possibly seen
Γ_3	$\Xi\pi$	seen
Γ_4	$\Xi(1530)\pi$	
Γ_5	$\Xi\pi\pi$(not $\Xi(1530)\pi$)	

$\Xi(1950)$ BRANCHING RATIOS

$\Gamma(\Sigma\overline{K})/\Gamma(\Lambda\overline{K})$ — Γ_2/Γ_1

VALUE	CL%	EVTS	DOCUMENT ID		TECN	COMMENT
<2.3	90	0	BIAGI	87C	SPEC	Ξ^- Be 116 GeV

$\Gamma(\Sigma\overline{K})/\Gamma_{total}$ — Γ_2/Γ

VALUE	EVTS	DOCUMENT ID		TECN	COMMENT
possibly seen	17	HASSALL	81	HBC	$K^- p$ 6.5 GeV/c

$\Gamma(\Xi\pi)/\Gamma(\Xi(1530)\pi)$ — Γ_3/Γ_4

VALUE	DOCUMENT ID		TECN
$2.8^{+0.7}_{-0.6}$	APSELL	70	HBC

$\Gamma(\Xi\pi\pi(\text{not } \Xi(1530)\pi))/\Gamma(\Xi(1530)\pi)$ — Γ_5/Γ_4

VALUE	DOCUMENT ID		TECN
0.0±0.3	APSELL	70	HBC

$\Xi(1950)$ REFERENCES

ADAMOVICH	99B	EPJ C11 271	M.I. Adamovich *et al.*	(CERN WA89 Collab.)
BIAGI	87	ZPHY C34 15	S.F. Biagi *et al.*	(BRIS, CERN, GEVA+)
BIAGI	87C	ZPHY C34 175	S.F. Biagi *et al.*	(BRIS, CERN, GEVA+)
BIAGI	81	ZPHY C9 305	S.F. Biagi *et al.*	(BRIS, CAVE, GEVA+)
HASSALL	81	NP B189 397	J.K. Hassall *et al.*	(CAVE, MSU)
BRIEFEL	77	PR D16 2706	E. Briefel *et al.*	(BRAN, UMD, SYRA+)
Also		Duke Conf. 317 Hyperon Resonances, 1970	E. Briefel *et al.*	(BRAN, UMD, SYRA+)
DIBIANCA	75	NP B98 137	F.A. Dibianca, R.J. Endorf	(CMU)
ROSS	73C	Purdue Conf. 345	R.T. Ross, J.L. Lloyd, D. Radojicic	(OXF)
BADIER	72	NP B37 429	J. Badier *et al.*	(EPOL)
APSELL	70	PRL 24 777	S.P. Apsell *et al.*	(BRAN, UMD, SYRA+) I
GOLDWASSER	70	PR D1 1960	E.L. Goldwasser, P.F. Schultz	(ILL)
DAUBER	69	PR 179 1262	P.M. Dauber *et al.*	(LRL) I
ALITTI	68	PRL 21 1119	J. Alitti *et al.*	(BNL, SYRA) I
BADIER	65	PL 16 171	J. Badier *et al.*	(EPOL, SACL, AMST) I

$\Xi(2030)$

$I(J^P) = \frac{1}{2}(\geq \frac{5}{2}^?)$ Status: ***

The evidence for this state has been much improved by HEMINGWAY 77, who see an eight standard deviation enhancement in $\Sigma\overline{K}$ and a weaker coupling to $\Lambda\overline{K}$. ALITTI 68 and HEMINGWAY 77 observe no signals in the $\Xi\pi\pi$ (or $\Xi(1530)\pi$) channel, in contrast to DIBIANCA 75. The decay $(\Lambda/\Sigma)\overline{K}\pi$ reported by BARTSCH 69 is also not confirmed by HEMINGWAY 77.

A moments analysis of the HEMINGWAY 77 data indicates at a level of three standard deviations that $J \geq 5/2$.

$\Xi(2030)$ MASS

VALUE (MeV)	EVTS	DOCUMENT ID		TECN	CHG	COMMENT
2025 ± 5 OUR ESTIMATE						
2025.1± 2.4 OUR AVERAGE		Error includes scale factor of 1.3. See the ideogram below.				
2022 ± 7		JENKINS	83	MPS	–	$K^- p \to K^+$ MM
2024 ± 2	200	HEMINGWAY	77	HBC	–	$K^- p$ 4.2 GeV/c
2044 ± 8		DIBIANCA	75	DBC	−0	$\Xi\pi\pi$, $\Xi^*\pi$
2019 ± 7	15	ROSS	73C	HBC	−0	$\Sigma\overline{K}$
2030 ±10	42	ALITTI	69	HBC	–	$K^- p$ 3.9–5 GeV/c
2058 ±17	40	BARTSCH	69	HBC	−0	$K^- p$ 10 GeV/c

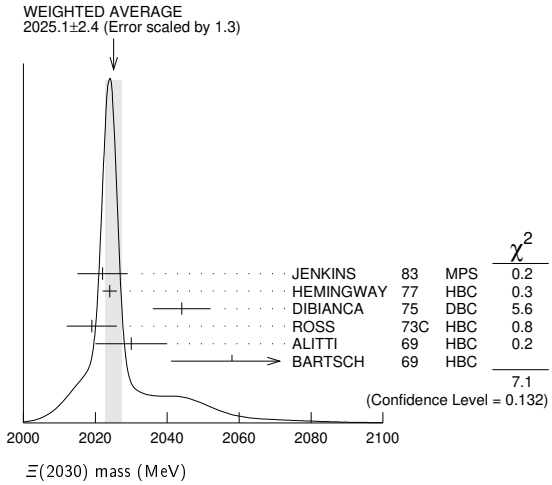

$\Xi(2030)$ WIDTH

VALUE (MeV)	EVTS	DOCUMENT ID		TECN	CHG	COMMENT
20^{+15}_{-5} OUR ESTIMATE						
21± 6 OUR AVERAGE		Error includes scale factor of 1.3. See the ideogram below.				
16± 5	200	HEMINGWAY	77	HBC	–	$K^- p$ 4.2 GeV/c
60±24		DIBIANCA	75	DBC	−0	$\Xi\pi\pi$, $\Xi^*\pi$
33±17	15	ROSS	73C	HBC	−0	$\Sigma\overline{K}$
45^{+40}_{-20}		ALITTI	69	HBC	–	$K^- p$ 3.9–5 GeV/c
57±30		BARTSCH	69	HBC	−0	$K^- p$ 10 GeV/c

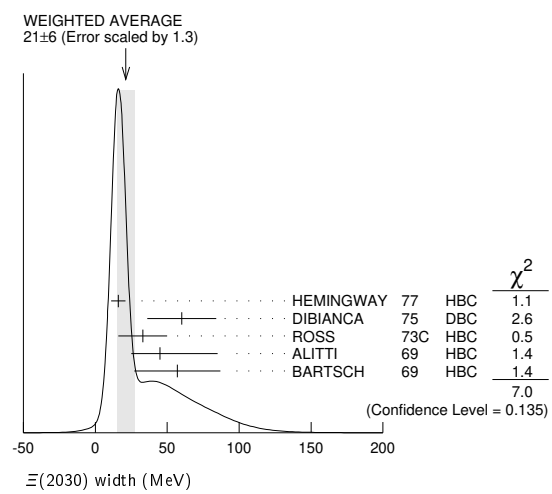

$\Xi(2030)$ DECAY MODES

	Mode	Fraction (Γ_i/Γ)
Γ_1	$\Lambda\overline{K}$	~ 20 %
Γ_2	$\Sigma\overline{K}$	~ 80 %
Γ_3	$\Xi\pi$	small
Γ_4	$\Xi(1530)\pi$	small
Γ_5	$\Xi\pi\pi$(not $\Xi(1530)\pi$)	small
Γ_6	$\Lambda\overline{K}\pi$	small
Γ_7	$\Sigma\overline{K}\pi$	small

$\Xi(2030)$ BRANCHING RATIOS

$\Gamma(\Xi\pi)/[\Gamma(\Lambda\overline{K})+\Gamma(\Sigma\overline{K})+\Gamma(\Xi\pi)+\Gamma(\Xi(1530)\pi)]$ — $\Gamma_3/(\Gamma_1+\Gamma_2+\Gamma_3+\Gamma_4)$

VALUE	DOCUMENT ID		TECN	CHG	COMMENT
• • • We do not use the following data for averages, fits, limits, etc. • • •					
<0.30	ALITTI	69	HBC	–	1 standard dev. limit

Downloaded from https://academic.oup.com/ptep/article/2022/8/083C01/6651666 by KIT Library user on 27 September 2022

$\Gamma(\Xi\pi)/\Gamma(\Sigma\overline{K})$ — Γ_3/Γ_2

VALUE	CL%	DOCUMENT ID		TECN	CHG	COMMENT
<0.19	95	HEMINGWAY	77	HBC	–	K^-p 4.2 GeV/c

$\Gamma(\Lambda\overline{K})/[\Gamma(\Lambda\overline{K})+\Gamma(\Sigma\overline{K})+\Gamma(\Xi\pi)+\Gamma(\Xi(1530)\pi)]$ — $\Gamma_1/(\Gamma_1+\Gamma_2+\Gamma_3+\Gamma_4)$

VALUE	DOCUMENT ID		TECN	CHG	COMMENT
0.25±0.15	ALITTI	69	HBC	–	K^-p 3.9–5 GeV/c

$\Gamma(\Lambda\overline{K})/\Gamma(\Sigma\overline{K})$ — Γ_1/Γ_2

VALUE	DOCUMENT ID		TECN	CHG	COMMENT
0.22±0.09	HEMINGWAY	77	HBC	–	K^-p 4.2 GeV/c

$\Gamma(\Sigma\overline{K})/[\Gamma(\Lambda\overline{K})+\Gamma(\Sigma\overline{K})+\Gamma(\Xi\pi)+\Gamma(\Xi(1530)\pi)]$ — $\Gamma_2/(\Gamma_1+\Gamma_2+\Gamma_3+\Gamma_4)$

VALUE	DOCUMENT ID		TECN	CHG	COMMENT
0.75±0.20	ALITTI	69	HBC	–	K^-p 3.9–5 GeV/c

$\Gamma(\Xi(1530)\pi)/[\Gamma(\Lambda\overline{K})+\Gamma(\Sigma\overline{K})+\Gamma(\Xi\pi)+\Gamma(\Xi(1530)\pi)]$ — $\Gamma_4/(\Gamma_1+\Gamma_2+\Gamma_3+\Gamma_4)$

VALUE	DOCUMENT ID		TECN	CHG	COMMENT
• • • We do not use the following data for averages, fits, limits, etc. • • •					
<0.15	ALITTI	69	HBC	–	1 standard dev. limit

$[\Gamma(\Xi(1530)\pi)+\Gamma(\Xi\pi\pi(\text{not }\Xi(1530)\pi))]/\Gamma(\Sigma\overline{K})$ — $(\Gamma_4+\Gamma_5)/\Gamma_2$

VALUE	CL%	DOCUMENT ID		TECN	CHG	COMMENT
<0.11	95	[1] HEMINGWAY	77	HBC	–	K^-p 4.2 GeV/c

$\Gamma(\Lambda\overline{K}\pi)/\Gamma_{total}$ — Γ_6/Γ

VALUE	DOCUMENT ID		TECN	COMMENT
• • • We do not use the following data for averages, fits, limits, etc. • • •				
seen	BARTSCH	69	HBC	K^-p 10 GeV

$\Gamma(\Lambda\overline{K}\pi)/\Gamma(\Sigma\overline{K})$ — Γ_6/Γ_2

VALUE	CL%	DOCUMENT ID		TECN	CHG	COMMENT
<0.32	95	HEMINGWAY	77	HBC	–	K^-p 4.2 GeV/c

$\Gamma(\Sigma\overline{K}\pi)/\Gamma_{total}$ — Γ_7/Γ

VALUE	DOCUMENT ID		TECN	COMMENT
• • • We do not use the following data for averages, fits, limits, etc. • • •				
seen	BARTSCH	69	HBC	K^-p 10 GeV

$\Gamma(\Sigma\overline{K}\pi)/\Gamma(\Sigma\overline{K})$ — Γ_7/Γ_2

VALUE	CL%	DOCUMENT ID		TECN	CHG	COMMENT
<0.04	95	[2] HEMINGWAY	77	HBC	–	K^-p 4.2 GeV/c

$\Xi(2030)$ FOOTNOTES

[1] For the decay mode $\Xi^-\pi^+\pi^-$ only.
[2] For the decay mode $\Sigma^\pm K^-\pi^\mp$ only.

$\Xi(2030)$ REFERENCES

JENKINS	83	PRL 51 951	C.M. Jenkins *et al.*	(FSU, BRAN, LBL+)
HEMINGWAY	77	PL 68B 197	R.J. Hemingway *et al.*	(AMST, CERN, NIJM+) IJ
Also		PL 62B 477	J.B. Gay *et al.*	(AMST, CERN, NIJM)
DIBIANCA	75	NP B98 137	F.A. Dibianca, R.J. Endorf	(CMU)
ROSS	73C	Purdue Conf. 345	R.T. Ross, J.L. Lloyd, D. Radojicic	(OXF)
ALITTI	69	PRL 22 79	J. Alitti *et al.*	(BNL, SYRA) I
BARTSCH	69	PL 28B 439	J. Bartsch *et al.*	(AACH, BERL, CERN+)
ALITTI	68	PRL 21 1119	J. Alitti *et al.*	(BNL, SYRA)

$\Xi(2120)$

$I(J^P) = \frac{1}{2}(?^?)$ Status: *
J, P need confirmation.

OMITTED FROM SUMMARY TABLE

$\Xi(2120)$ MASS

VALUE (MeV)	EVTS	DOCUMENT ID		TECN	COMMENT
≈ 2120 OUR ESTIMATE					
2137±4	18	[1] CHLIAPNIK...	79	HBC	K^+p 32 GeV/c
2123±7		[2] GAY	76C	HBC	K^-p 4.2 GeV/c

$\Xi(2120)$ WIDTH

VALUE (MeV)	EVTS	DOCUMENT ID		TECN	COMMENT
<20	18	[1] CHLIAPNIK...	79	HBC	K^+p 32 GeV/c
25±12		[2] GAY	76C	HBC	K^-p 4.2 GeV/c

$\Xi(2120)$ DECAY MODES

	Mode	Fraction (Γ_i/Γ)
Γ_1	$\Lambda\overline{K}$	seen

$\Xi(2120)$ BRANCHING RATIOS

$\Gamma(\Lambda\overline{K})/\Gamma_{total}$ — Γ_1/Γ

VALUE	DOCUMENT ID		TECN	COMMENT
seen	[1] CHLIAPNIK...	79	HBC	$K^+p \to (\overline{\Lambda}K^+)$ X
seen	[2] GAY	76C	HBC	K^-p 4.2 GeV/c

$\Xi(2120)$ FOOTNOTES

[1] CHLIAPNIKOV 79 does not uniquely identify the K^+ in the $(\overline{\Lambda}K^+)$ X final state. It also reports bumps with fewer events at 2240, 2540, and 2830 MeV.
[2] GAY 76C sees a 4-standard deviation signal. However, HEMINGWAY 77, with more events from the same experiment points out that the signal is greatly reduced if a cut is made on the 4-momentum u. This suggests an anomalous production mechanism if the $\Xi(2120)$ is real.

$\Xi(2120)$ REFERENCES

CHLIAPNIK...	79	NP B158 253	P.V. Chliapnikov *et al.*	(CERN, BELG, MONS)
HEMINGWAY	77	PL 68B 197	R.J. Hemingway *et al.*	(AMST, CERN, NIJM+)
GAY	76C	PL 62B 477	J.B. Gay *et al.*	(AMST, CERN, NIJM)

$\Xi(2250)$

$I(J^P) = \frac{1}{2}(?^?)$ Status: **
J, P need confirmation.

OMITTED FROM SUMMARY TABLE

The evidence for this state is mixed. BARTSCH 69 sees a bump of not much statistical significance in $\Lambda\overline{K}\pi$, $\Sigma\overline{K}\pi$, and $\Xi\pi\pi$ mass spectra. GOLDWASSER 70 sees a narrower bump in $\Xi\pi\pi$ at a higher mass. Not seen by HASSALL 81 with 45 events/μb at 6.5 GeV/c. Seen by JENKINS 83. Perhaps seen by BIAGI 87.

$\Xi(2250)$ MASS

VALUE (MeV)	EVTS	DOCUMENT ID		TECN	CHG	COMMENT
≈ 2250 OUR ESTIMATE						
2189± 7	66	BIAGI	87	SPEC	–	Ξ^-Be → ($\Xi^-\pi^+\pi^-$) X
2214± 5		JENKINS	83	MPS	–	$K^-p \to K^+$ MM
2295±15	18	GOLDWASSER	70	HBC	–	K^-p 5.5 GeV/c
2244±52	35	BARTSCH	69	HBC		K^-p 10 GeV/c

$\Xi(2250)$ WIDTH

VALUE (MeV)	EVTS	DOCUMENT ID		TECN	CHG	COMMENT
46±27	66	BIAGI	87	SPEC	–	Ξ^-Be → ($\Xi^-\pi^+\pi^-$) X
< 30		GOLDWASSER	70	HBC	–	K^-p 5.5 GeV/c
130±80		BARTSCH	69	HBC		

$\Xi(2250)$ DECAY MODES

	Mode
Γ_1	$\Xi\pi\pi$
Γ_2	$\Lambda\overline{K}\pi$
Γ_3	$\Sigma\overline{K}\pi$

$\Xi(2250)$ REFERENCES

BIAGI	87	ZPHY C34 15	S.F. Biagi *et al.*	(BRIS, CERN, GEVA+)
JENKINS	83	PRL 51 951	C.M. Jenkins *et al.*	(FSU, BRAN, LBL+)
HASSALL	81	NP B189 397	J.K. Hassall *et al.*	(CAVE, MSU)
GOLDWASSER	70	PR D1 1960	E.L. Goldwasser, P.F. Schultz	(ILL)
BARTSCH	69	PL 28B 439	J. Bartsch *et al.*	(AACH, BERL, CERN+)

$\Xi(2370)$

$I(J^P) = \frac{1}{2}(?^?)$ Status: **
J, P need confirmation.

OMITTED FROM SUMMARY TABLE

$\Xi(2370)$ MASS

VALUE (MeV)	EVTS	DOCUMENT ID		TECN	CHG	COMMENT
≈ 2370 OUR ESTIMATE						
2356±10		JENKINS	83	MPS	–	$K^-p \to K^+$ MM
2370	50	HASSALL	81	HBC	–0	K^-p 6.5 GeV/c
2373± 8	94	AMIRZADEH	80	HBC	–0	K^-p 8.25 GeV/c
2392±27		DIBIANCA	75	DBC		$\Xi 2\pi$

$\Xi(2370)$ WIDTH

VALUE (MeV)	EVTS	DOCUMENT ID		TECN	CHG	COMMENT
80	50	HASSALL	81	HBC	–0	K^-p 6.5 GeV/c
80±25	94	AMIRZADEH	80	HBC	–0	K^-p 8.25 GeV/c
75±69		DIBIANCA	75	DBC		$\Xi 2\pi$

Downloaded from https://academic.oup.com/ptep/article/2022/8/083C01/6651666 by KIT Library user on 27 September 2022

$\Xi(2370)$ DECAY MODES

	Mode	Fraction (Γ_i/Γ)
Γ_1	$\Lambda\overline{K}\pi$ Includes $\Gamma_4+\Gamma_6$.	seen
Γ_2	$\Sigma\overline{K}\pi$ Includes $\Gamma_5+\Gamma_6$.	seen
Γ_3	Ω^-K	
Γ_4	$\Lambda\overline{K}^*(892)$	
Γ_5	$\Sigma\overline{K}^*(892)$	
Γ_6	$\Sigma(1385)\overline{K}$	

$\Xi(2370)$ BRANCHING RATIOS

$\Gamma(\Lambda\overline{K}\pi)/\Gamma_{total}$ — Γ_1/Γ

VALUE	DOCUMENT ID		TECN	CHG	COMMENT
seen	AMIRZADEH	80	HBC	−0	K^-p 8.25 GeV/c

$\Gamma(\Sigma\overline{K}\pi)/\Gamma_{total}$ — Γ_2/Γ

VALUE	DOCUMENT ID		TECN	CHG	COMMENT
seen	AMIRZADEH	80	HBC	−0	K^-p 8.25 GeV/c

$[\Gamma(\Lambda\overline{K}\pi)+\Gamma(\Sigma\overline{K}\pi)]/\Gamma_{total}$ — $(\Gamma_1+\Gamma_2)/\Gamma$

VALUE	EVTS	DOCUMENT ID		TECN	CHG	COMMENT
seen	50	HASSALL	81	HBC	−0	K^-p 6.5 GeV/c

$\Gamma(\Omega^-K)/\Gamma_{total}$ — Γ_3/Γ

VALUE	DOCUMENT ID		TECN	CHG	COMMENT
0.09±0.04	[1] KINSON	80	HBC	−	K^-p 8.25 GeV/c

$[\Gamma(\Lambda\overline{K}^*(892))+\Gamma(\Sigma\overline{K}^*(892))]/\Gamma_{total}$ — $(\Gamma_4+\Gamma_5)/\Gamma$

VALUE	DOCUMENT ID		TECN	CHG	COMMENT
0.22±0.13	[1] KINSON	80	HBC	−	K^-p 8.25 GeV/c

$\Gamma(\Sigma(1385)\overline{K})/\Gamma_{total}$ — Γ_6/Γ

VALUE	DOCUMENT ID		TECN	CHG	COMMENT
0.12±0.08	[1] KINSON	80	HBC	−	K^-p 8.25 GeV/c

$\Xi(2370)$ FOOTNOTES

vglue.1in

[1] KINSON 80 is a reanalysis of AMIRZADEH 80 with 50% more events.

$\Xi(2370)$ REFERENCES

JENKINS	83	PRL 51 951	C.M. Jenkins *et al.*	(FSU, BRAN, LBL+)
HASSALL	81	NP B189 397	J.K. Hassall *et al.*	(CAVE, MSU)
AMIRZADEH	80	PL 90B 324	J. Amirzadeh *et al.*	(BIRM, CERN, GLAS+) I
KINSON	80	Toronto Conf. 263	J.B. Kinson *et al.*	(BIRM, CERN, GLAS+) I
DIBIANCA	75	NP B98 137	F.A. Dibianca, R.J. Endorf	(CMU)

$\Xi(2500)$

$I(J^P) = \frac{1}{2}(?^?)$ Status: $*$
J, P need confirmation.

OMITTED FROM SUMMARY TABLE

The ALITTI 69 peak might be instead the $\Xi(2370)$ or might be neither the $\Xi(2370)$ nor the $\Xi(2500)$.

$\Xi(2500)$ MASS

VALUE (MeV)	EVTS	DOCUMENT ID		TECN	CHG	COMMENT
≈ 2500 OUR ESTIMATE						
2505±10		JENKINS	83	MPS	−	$K^-p \to K^+$ MM
2430±20	30	ALITTI	69	HBC	−	K^-p 4.6–5 GeV/c
2500±10	45	BARTSCH	69	HBC	−0	K^-p 10 GeV/c

$\Xi(2500)$ WIDTH

VALUE (MeV)	DOCUMENT ID		TECN	CHG
150^{+60}_{-40}	ALITTI	69	HBC	−
59±27	BARTSCH	69	HBC	−0

$\Xi(2500)$ DECAY MODES

	Mode	Fraction (Γ_i/Γ)
Γ_1	$\Xi\pi$	
Γ_2	$\Lambda\overline{K}$	
Γ_3	$\Sigma\overline{K}$	
Γ_4	$\Xi\pi\pi$	seen
Γ_5	$\Xi(1530)\pi$	
Γ_6	$\Lambda\overline{K}\pi + \Sigma\overline{K}\pi$	seen

$\Xi(2500)$ BRANCHING RATIOS

$\Gamma(\Xi\pi)/[\Gamma(\Xi\pi)+\Gamma(\Lambda\overline{K})+\Gamma(\Sigma\overline{K})+\Gamma(\Xi(1530)\pi)]$ — $\Gamma_1/(\Gamma_1+\Gamma_2+\Gamma_3+\Gamma_5)$

VALUE	DOCUMENT ID		TECN	COMMENT
<0.5	ALITTI	69	HBC	1 standard dev. limit

$\Gamma(\Lambda\overline{K})/[\Gamma(\Xi\pi)+\Gamma(\Lambda\overline{K})+\Gamma(\Sigma\overline{K})+\Gamma(\Xi(1530)\pi)]$ — $\Gamma_2/(\Gamma_1+\Gamma_2+\Gamma_3+\Gamma_5)$

VALUE	DOCUMENT ID		TECN	CHG
0.5±0.2	ALITTI	69	HBC	−

$\Gamma(\Sigma\overline{K})/[\Gamma(\Xi\pi)+\Gamma(\Lambda\overline{K})+\Gamma(\Sigma\overline{K})+\Gamma(\Xi(1530)\pi)]$ — $\Gamma_3/(\Gamma_1+\Gamma_2+\Gamma_3+\Gamma_5)$

VALUE	DOCUMENT ID		TECN	CHG
0.5±0.2	ALITTI	69	HBC	−

$\Gamma(\Xi(1530)\pi)/[\Gamma(\Xi\pi)+\Gamma(\Lambda\overline{K})+\Gamma(\Sigma\overline{K})+\Gamma(\Xi(1530)\pi)]$ — $\Gamma_5/(\Gamma_1+\Gamma_2+\Gamma_3+\Gamma_5)$

VALUE	DOCUMENT ID		TECN	COMMENT
<0.2	ALITTI	69	HBC	1 standard dev. limit

$\Gamma(\Xi\pi\pi)/\Gamma_{total}$ — Γ_4/Γ

VALUE	DOCUMENT ID		TECN	CHG
seen	BARTSCH	69	HBC	−0

$[\Gamma(\Lambda\overline{K}\pi)+\Gamma(\Sigma\overline{K}\pi)]/\Gamma_{total}$ — Γ_6/Γ

VALUE	DOCUMENT ID		TECN	CHG
seen	BARTSCH	69	HBC	−0

$\Xi(2500)$ REFERENCES

JENKINS	83	PRL 51 951	C.M. Jenkins *et al.*	(FSU, BRAN, LBL+)
ALITTI	69	PRL 22 79	J. Alitti *et al.*	(BNL, SYRA) I
BARTSCH	69	PL 28B 439	J. Bartsch *et al.*	(AACH, BERL, CERN+)

Downloaded from https://academic.oup.com/ptep/article/2022/8/083C01/6651666 by KIT Library user on 27 September 2022

Ω BARYONS
($S = -3$, $I = 0$)

$\Omega^- = sss$

Ω^-

$I(J^P) = 0(\frac{3}{2}^+)$ Status: ****

The unambiguous discovery in both production and decay was by BARNES 64. The quantum numbers follow from the assignment of the particle to the baryon decuplet. DEUTSCHMANN 78 and BAUBILLIER 78 rule out $J = 1/2$ and find consistency with $J = 3/2$. AUBERT,BE 06 finds from the decay angular distributions of $\Xi_c^0 \to \Omega^- K^+$ and $\Omega_c^0 \to \Omega^- K^+$ that $J = 3/2$; this depends on the spins of the Ξ_c^0 and Ω_c^0 being $J = 1/2$, their supposed values. ABLIKIM 21E determines the Ω^- spin to be $J = 3/2$ from the decay angular distributions of the complete decay chain $\psi(3686) \to \Omega^- \overline{\Omega}^+$, with subsequent decays $\Omega^- \to K^- \Lambda$ and $\overline{\Omega}^+ \to K^+ \overline{\Lambda}$.

We have omitted some results that have been superseded by later experiments. See our earlier editions.

Ω^- MASS

The fit assumes the Ω^- and $\overline{\Omega}^+$ masses are the same, and averages them together.

VALUE (MeV)	EVTS	DOCUMENT ID		TECN	COMMENT
1672.45±0.29 OUR FIT					
1672.43±0.32 OUR AVERAGE					
1673 ±1	100	HARTOUNI	85	SPEC	80–280 GeV K_L^0 C
1673.0 ±0.8	41	BAUBILLIER	78	HBC	8.25 GeV/c $K^- p$
1671.7 ±0.6	27	HEMINGWAY	78	HBC	4.2 GeV/c $K^- p$
1673.4 ±1.7	4	[1] DIBIANCA	75	DBC	4.9 GeV/c $K^- d$
1673.3 ±1.0	3	PALMER	68	HBC	$K^- p$ 4.6, 5 GeV/c
1671.8 ±0.8	3	SCHULTZ	68	HBC	$K^- p$ 5.5 GeV/c
1674.2 ±1.6	5	SCOTTER	68	HBC	$K^- p$ 6 GeV/c
1672.1 ±1.0	1	[2] FRY	55	EMUL	
• • • We do not use the following data for averages, fits, limits, etc. • • •					
1671.43±0.78	13	[3] DEUTSCH...	73	HBC	$K^- p$ 10 GeV/c
1671.9 ±1.2	6	[3] SPETH	69	HBC	See DEUTSCHMANN 73
1673.0 ±8.0	1	ABRAMS	64	HBC	$\to \Xi^- \pi^0$
1670.6 ±1.0	1	[2] FRY	55B	EMUL	
1615	1	[4] EISENBERG	54	EMUL	

[1] DIBIANCA 75 gives a mass for each event. We quote the average.
[2] The FRY 55 and FRY 55B events were identified as Ω^- by ALVAREZ 73. The masses assume decay to ΛK^- at rest. For FRY 55B, decay from an atomic orbit could Doppler shift the K^- energy and the resulting Ω^- mass by several MeV. This shift is negligible for FRY 55 because the Ω decay is approximately perpendicular to its orbital velocity, as is known because the Λ strikes the nucleus (L.Alvarez, private communication 1973). We have calculated the error assuming that the orbital n is 4 or larger.
[3] Excluded from the average; the Ω^- lifetimes measured by the experiments differ significantly from other measurements.
[4] The EISENBERG 54 mass was calculated for decay in flight. ALVAREZ 73 has shown that the Ω interacted with an Ag nucleus to give $K^- \Xi$Ag.

$\overline{\Omega}^+$ MASS

The fit assumes the Ω^- and $\overline{\Omega}^+$ masses are the same, and averages them together.

VALUE (MeV)	EVTS	DOCUMENT ID		TECN	COMMENT
1672.45±0.29 OUR FIT					
1672.5 ±0.7 OUR AVERAGE					
1672 ±1	72	HARTOUNI	85	SPEC	80–280 GeV K_L^0 C
1673.1 ±1.0	1	FIRESTONE	71B	HBC	12 GeV/c $K^+ d$

$(m_{\Omega^-} - m_{\overline{\Omega}^+}) / m_{\Omega^-}$

A test of CPT invariance.

VALUE	DOCUMENT ID		TECN	COMMENT
$(-1.44\pm7.98)\times10^{-5}$	CHAN	98	E756	p Be, 800 GeV

Ω^- MEAN LIFE

Measurements with an error $> 0.1\times10^{-10}$ s have been omitted. The fit assumes the Ω^- and $\overline{\Omega}^+$ mean lives are the same, and averages them together.

VALUE (10^{-10} s)	EVTS	DOCUMENT ID		TECN	COMMENT
0.821±0.011 OUR FIT					
0.821±0.011 OUR AVERAGE					
0.817±0.013±0.018	6934	CHAN	98	E756	p Be, 800 GeV
0.811±0.037	1096	LUK	88	SPEC	pBe 400 GeV
0.823±0.013	12k	BOURQUIN	84	SPEC	SPS hyperon beam
• • • We do not use the following data for averages, fits, limits, etc. • • •					
0.822±0.028	2437	BOURQUIN	79B	SPEC	See BOURQUIN 84

$\overline{\Omega}^+$ MEAN LIFE

The fit assumes the Ω^- and $\overline{\Omega}^+$ mean lives are the same, and averages them together.

VALUE (10^{-10} s)	EVTS	DOCUMENT ID		TECN	COMMENT
0.821±0.011 OUR FIT					
0.823±0.031±0.022	1801	CHAN	98	E756	p Be, 800 GeV

$(\tau_{\Omega^-} - \tau_{\overline{\Omega}^+}) / \tau_{\Omega^-}$

A test of CPT invariance. Our calculation, from the averages in the preceding two data blocks.

VALUE	DOCUMENT ID
0.00±0.05 OUR ESTIMATE	

Ω^- MAGNETIC MOMENT

VALUE (μ_N)	EVTS	DOCUMENT ID		TECN	COMMENT
−2.02 ±0.05 OUR AVERAGE					
−2.024±0.056	235k	WALLACE	95	SPEC	Ω^- 300–550 GeV
−1.94 ±0.17 ±0.14	25k	DIEHL	91	SPEC	Spin-transfer production

Ω^- DECAY MODES

	Mode		Fraction (Γ_i/Γ)	Confidence level
Γ_1	ΛK^-		(67.8±0.7) %	
Γ_2	$\Xi^0 \pi^-$		(23.6±0.7) %	
Γ_3	$\Xi^- \pi^0$		(8.6±0.4) %	
Γ_4	$\Xi^- \pi^+ \pi^-$		$(3.7^{+0.7}_{-0.6})\times10^{-4}$	
Γ_5	$\Xi(1530)^0 \pi^-$		$< 7 \times10^{-5}$	90%
Γ_6	$\Xi^0 e^- \overline{\nu}_e$		$(5.6\pm2.8)\times10^{-3}$	
Γ_7	$\Xi^- \gamma$		$< 4.6 \times10^{-4}$	90%
	$\Delta S = 2$ forbidden ($S2$) modes			
Γ_8	$\Lambda \pi^-$	$S2$	$< 2.9 \times10^{-6}$	90%

Ω^- BRANCHING RATIOS

The BOURQUIN 84 values (which include results of BOURQUIN 79B, a separate experiment) are much more accurate than any other results, and so the other results have been omitted.

$\Gamma(\Lambda K^-)/\Gamma_{total}$ — Γ_1/Γ

VALUE	EVTS	DOCUMENT ID		TECN	COMMENT
0.678±0.007	14k	BOURQUIN	84	SPEC	SPS hyperon beam
• • • We do not use the following data for averages, fits, limits, etc. • • •					
0.686±0.013	1920	BOURQUIN	79B	SPEC	See BOURQUIN 84

$\Gamma(\Xi^0 \pi^-)/\Gamma_{total}$ — Γ_2/Γ

VALUE	EVTS	DOCUMENT ID		TECN	COMMENT
0.236±0.007	1947	BOURQUIN	84	SPEC	SPS hyperon beam
• • • We do not use the following data for averages, fits, limits, etc. • • •					
0.234±0.013	317	BOURQUIN	79B	SPEC	See BOURQUIN 84

$\Gamma(\Xi^- \pi^0)/\Gamma_{total}$ — Γ_3/Γ

VALUE	EVTS	DOCUMENT ID		TECN	COMMENT
0.086±0.004	759	BOURQUIN	84	SPEC	SPS hyperon beam
• • • We do not use the following data for averages, fits, limits, etc. • • •					
0.080±0.008	145	BOURQUIN	79B	SPEC	See BOURQUIN 84

$\Gamma(\Xi^- \pi^+ \pi^-)/\Gamma_{total}$ — Γ_4/Γ

VALUE (units 10^{-4})	EVTS	DOCUMENT ID		TECN	COMMENT
$3.74^{+0.67}_{-0.56}$	100	[5] KAMAEV	10	HYCP	p Cu, 800 GeV
• • • We do not use the following data for averages, fits, limits, etc. • • •					
$4.3^{+3.4}_{-1.3}$	4	BOURQUIN	84	SPEC	SPS hyperon beam

[5] This KAMAEV 10 value uses 76 $\Omega^- \to \Xi^- \pi^+ \pi^-$ and 24 $\overline{\Omega}^+ \to \overline{\Xi}^+ \pi^- \pi^+$ decays. The Ω^- and $\overline{\Omega}^+$ branching fractions measurements are statistically equal. The errors given combine statistical and systematic contributions. The CP branching-fraction asymmetry, $(\Omega^- - \overline{\Omega}^+)$/sum, is $+0.12 \pm 0.20$.

$\Gamma(\Xi(1530)^0 \pi^-)/\Gamma_{total}$ — Γ_5/Γ

VALUE (units 10^{-4})	CL%	EVTS	DOCUMENT ID		TECN	COMMENT
<0.7	90		KAMAEV	10	HYCP	p Cu, 800 GeV

Downloaded from https://academic.oup.com/ptep/article/2022/8/083C01/6651666 by KIT Library user on 27 September 2022

• • • We do not use the following data for averages, fits, limits, etc. • • •

$6.4^{+5.1}_{-2.0}$	4	[6] BOURQUIN	84	SPEC	SPS hyperon beam

[6] The same 4 events as in the previous mode, with the isospin factor to take into account $\Xi(1530)^0 \to \Xi^0\pi^0$ decays included. BOURQUIN 84 adopted a theoretical assumption that $\Xi(1530)^0\pi^-$ would dominate $\Xi^-\pi^+\pi^-$ decay.

$\Gamma(\Xi^0 e^-\overline{\nu}_e)/\Gamma_{total}$ — Γ_6/Γ

VALUE (units 10^{-3})	EVTS	DOCUMENT ID		TECN	COMMENT
5.6±2.8	14	BOURQUIN	84	SPEC	SPS hyperon beam

• • • We do not use the following data for averages, fits, limits, etc. • • •

~ 10	3	BOURQUIN	79B	SPEC	See BOURQUIN 84

$\Gamma(\Xi^-\gamma)/\Gamma_{total}$ — Γ_7/Γ

VALUE (units 10^{-4})	CL%	EVTS	DOCUMENT ID		TECN	COMMENT
< 4.6	90	0	ALBUQUERQ...	94	E761	Ω^- 375 GeV

• • • We do not use the following data for averages, fits, limits, etc. • • •

<22	90	9	BOURQUIN	84	SPEC	SPS hyperon beam
<31	90	0	BOURQUIN	79B	SPEC	See BOURQUIN 84

$\Gamma(\Lambda\pi^-)/\Gamma_{total}$ — Γ_8/Γ

ΔS=2. Forbidden in first-order weak interaction.

VALUE (units 10^{-6})	CL%	DOCUMENT ID		TECN	COMMENT
< 2.9	90	WHITE	05	HYCP	p Cu, 800 GeV

• • • We do not use the following data for averages, fits, limits, etc. • • •

< 190	90	BOURQUIN	84	SPEC	SPS hyperon beam
<1300	90	BOURQUIN	79B	SPEC	See BOURQUIN 84

Ω^- DECAY PARAMETERS

$\alpha(\Omega^-)\ \alpha_-(\Lambda)$ FOR $\Omega^- \to \Lambda K^-$

Some early results have been omitted.

VALUE	EVTS	DOCUMENT ID		TECN	COMMENT
0.0115±0.0015 OUR AVERAGE					
0.0133±0.0033±0.0052	960k	[7] CHEN	05	HYCP	p Cu, 800 GeV
0.0114±0.0012±0.0010	4.5M	[7] LU	05A	HYCP	p Cu, 800 GeV

• • • We do not use the following data for averages, fits, limits, etc. • • •

−0.018 ±0.030	6953	CHAN	98	E756	p Be, 800 GeV
−0.022 ±0.051	1743	LUK	88	SPEC	p Be 400 GeV
−0.016 ±0.018	12k	BOURQUIN	84	SPEC	SPS hyperon beam

[7] The results of CHEN 05 and LU 05A are from different experimental runs.

α FOR $\Omega^- \to \Lambda K^-$

The above average, $\alpha(\Omega^-)\alpha_-(\Lambda) = 0.0115 \pm 0.0015$, divided by our current average $\alpha_-(\Lambda) = 0.732 \pm 0.014$ gives $\alpha(\Omega^-)$:

VALUE	DOCUMENT ID
0.0157±0.0021 OUR EVALUATION	

$\overline{\alpha}$ FOR $\overline{\Omega}^+ \to \overline{\Lambda}K^+$

VALUE	EVTS	DOCUMENT ID		TECN	COMMENT
−0.0181±0.0028±0.0026	1.89M	LU	06	HYCP	p Cu, 800 GeV

• • • We do not use the following data for averages, fits, limits, etc. • • •

+0.017 ±0.077	1823	CHAN	98	E756	p Be, 800 GeV

$(\alpha+\overline{\alpha})/(\alpha-\overline{\alpha})$ in $\Omega^- \to \Lambda K^-, \overline{\Omega}^+ \to \overline{\Lambda}K^+$

Zero if CP is conserved.

VALUE	DOCUMENT ID		TECN	COMMENT
−0.016±0.092±0.089	[8] LU	06	HYCP	p Cu, 800 GeV

[8] This value uses the results of CHEN 05, LU 05A, and LU 06.

α FOR $\Omega^- \to \Xi^0\pi^-$

VALUE	EVTS	DOCUMENT ID		TECN	COMMENT
+0.09±0.14	1630	BOURQUIN	84	SPEC	SPS hyperon beam

α FOR $\Omega^- \to \Xi^-\pi^0$

VALUE	EVTS	DOCUMENT ID		TECN	COMMENT
+0.05±0.21	614	BOURQUIN	84	SPEC	SPS hyperon beam

Ω^- REFERENCES

We have omitted some papers that have been superseded by later experiments. See our earlier editions.

ABLIKIM	21E	PRL 126 092002	M. Ablikim et al.	(BESIII Collab.)
KAMAEV	10	PL B693 236	O. Kamaev et al.	(FNAL HyperCP Collab.)
AUBERT,BE	06	PRL 97 112001	B. Aubert et al.	(BABAR Collab.)
LU	06	PRL 96 242001	L.C. Lu et al.	(FNAL HyperCP Collab.)
CHEN	05	PR D71 051102	Y.C. Chen et al.	(FNAL HyperCP Collab.)
LU	05A	PL B617 11	L.C. Lu et al.	(FNAL HyperCP Collab.)
WHITE	05	PRL 94 101804	C.G. White et al.	(FNAL HyperCP Collab.)
CHAN	98	PR D58 072002	A.W. Chan et al.	(FNAL E756 Collab.)
WALLACE	95	PRL 74 3732	N.B. Wallace et al.	(MINN, ARIZ, MICH+)
ALBUQUERQ...	94	PR D50 18	I.F. Albuquerque et al.	(FNAL E761 Collab.)
DIEHL	91	PRL 67 804	H.T. Diehl et al.	(RUTG, FNAL, MICH+)
LUK	88	PR D38 19	K.B. Luk et al.	(RUTG, WISC, MICH, MINN)
HARTOUNI	85	PRL 54 628	E.P. Hartouni et al.	(COLU, ILL, FNAL)
BOURQUIN	84	NP B241 1	M.H. Bourquin et al.	(BRIS, GEVA, HEIDP+)
Also		PL 87B 297	M.H. Bourquin et al.	(BRIS, GEVA, HEIDP+)
BOURQUIN	79B	PL 88B 192	M.H. Bourquin et al.	(BRIS, GEVA, HEIDP+)
BAUBILLIER	78	PL 78B 342	M. Baubillier et al.	(BIRM, CERN, GLAS+) J
DEUTSCH...	78	PL 73B 96	M. Deutschmann et al.	(AACH3, BERL, CERN+) J
HEMINGWAY	78	NP B142 205	R.J. Hemingway et al.	(CERN, ZEEM, NIJM+)
DIBIANCA	75	NP B98 137	F.A. Dibianca, R.J. Endorf	(CMU)
ALVAREZ	73	PR D8 702	L.W. Alvarez	(LBL)
DEUTSCH...	73	NP B61 102	M. Deutschmann et al.	(ABCLV Collab.)
FIRESTONE	71B	PRL 26 410	I. Firestone et al.	(LRL)
SPETH	69	PL 29B 252	R. Speth et al.	(AACH, BERL, CERN, LOIC+)
PALMER	68	PL 26B 323	R.B. Palmer et al.	(BNL, SYRA)
SCHULTZ	68	PR 168 1509	P.F. Schultz et al.	(ILL, ANL, NWES+)
SCOTTER	68	PL 26B 474	D. Scotter et al.	(BIRM, GLAS, LOIC+)
ABRAMS	64	PRL 13 670	G.S. Abrams et al.	(UMD, NRL)
BARNES	64	PRL 12 204	V.E. Barnes et al.	(BNL)
FRY	55	PR 97 1189	W.F. Fry, J. Schneps, M.S. Swami	(WISC)
FRY	55B	NC 2 346	W.F. Fry, J. Schneps, M.S. Swami	(WISC)
EISENBERG	54	PR 96 541	Y. Eisenberg	(CORN)

$\Omega(2012)^-$

$I(J^P) = 0(?^-)$ Status: ***

Seen in $\Xi^0 K^-$ and $\Xi^- K^0_S$ decays with a combined significance of 8.3 standard deviations.

$\Omega(2012)^-$ MASS

VALUE (MeV)	EVTS	DOCUMENT ID		TECN	COMMENT
2012.4±0.7±0.6	520	YELTON	18A	BELL	In $\Upsilon(1S)$, $\Upsilon(2S)$, $\Upsilon(3S)$

$\Omega(2012)^-$ WIDTH

VALUE (MeV)	EVTS	DOCUMENT ID		TECN	COMMENT
$6.4^{+2.5}_{-2.0}$±1.6	520	YELTON	18A	BELL	In $\Upsilon(1S)$, $\Upsilon(2S)$, $\Upsilon(3S)$

$\Omega(2012)^-$ DECAY MODES

Branching fractions are given relative to the one **DEFINED AS 1**.

	Mode	Fraction (Γ_i/Γ)	Confidence level
Γ_1	ΞK		
Γ_2	$(\Xi\pi)K$		
Γ_3	$\Xi^0 K^-$	**DEFINED AS 1**	
Γ_4	$\Xi^-\overline{K}^0$	0.83±0.21	
Γ_5	$\Xi^0\pi^0 K^-$	<0.30	90%
Γ_6	$\Xi^0\pi^-\overline{K}^0$	<0.21	90%
Γ_7	$\Xi^-\pi^0\overline{K}^0$	<0.7	90%
Γ_8	$\Xi^-\pi^+ K^-$	<0.08	90%

$\Omega(2012)^-$ BRANCHING RATIOS

$\Gamma((\Xi\pi)K)/\Gamma(\Xi K)$ — Γ_2/Γ_1

VALUE	CL%	DOCUMENT ID		TECN	COMMENT
<0.119	90	JIA	19	BELL	In $\Upsilon(1S,2S,3S)$

$\Gamma(\Xi^0 K^-)/\Gamma(\Xi^-\overline{K}^0)$ — Γ_3/Γ_4

VALUE	DOCUMENT ID		TECN	COMMENT
1.2±0.3	YELTON	18A	BELL	In $\Upsilon(1S,2S,3S)$

$\Gamma(\Xi^0\pi^0 K^-)/\Gamma(\Xi^0 K^-)$ — Γ_5/Γ_3

VALUE	CL%	DOCUMENT ID		TECN	COMMENT
<0.304	90	JIA	19	BELL	In $\Upsilon(1S,2S,3S)$

$\Gamma(\Xi^0\pi^-\overline{K}^0)/\Gamma(\Xi^0 K^-)$ — Γ_6/Γ_3

VALUE	CL%	DOCUMENT ID		TECN	COMMENT
<0.213	90	JIA	19	BELL	In $\Upsilon(1S,2S,3S)$

$\Gamma(\Xi^0\pi^-\overline{K}^0)/\Gamma(\Xi^-\overline{K}^0)$ — Γ_6/Γ_4

VALUE	CL%	DOCUMENT ID		TECN	COMMENT
<0.256	90	JIA	19	BELL	In $\Upsilon(1S,2S,3S)$

$\Gamma(\Xi^-\pi^0\overline{K}^0)/\Gamma(\Xi^-\overline{K}^0)$ — Γ_7/Γ_4

VALUE	CL%	DOCUMENT ID		TECN	COMMENT
<0.811	90	JIA	19	BELL	In $\Upsilon(1S,2S,3S)$

$\Gamma(\Xi^-\pi^+ K^-)/\Gamma(\Xi^0 K^-)$ — Γ_8/Γ_3

VALUE	CL%	DOCUMENT ID		TECN	COMMENT
<0.078	90	JIA	19	BELL	In $\Upsilon(1S,2S,3S)$

$\Gamma(\Xi^-\pi^+ K^-)/\Gamma(\Xi^-\overline{K}^0)$ — Γ_8/Γ_4

VALUE	CL%	DOCUMENT ID		TECN	COMMENT
<0.093	90	JIA	19	BELL	In $\Upsilon(1S,2S,3S)$

$\Omega(2012)^-$ REFERENCES

JIA	19	PR D100 032006	S. Jia et al.	(BELLE Collab.)
YELTON	18A	PRL 121 052003	J. Yelton et al.	(BELLE Collab.)

Downloaded from https://academic.oup.com/ptep/article/2022/8/083C01/6651666 by KIT Library user on 27 September 2022

$\Omega(2250)^-$

$I(J^P) = 0(?^?)$ Status: ***

$\Omega(2250)^-$ MASS

VALUE (MeV)	EVTS	DOCUMENT ID		TECN	COMMENT
2252± 9 OUR AVERAGE					
2253±13	44	ASTON	87B	LASS	$K^- p$ 11 GeV/c
2251± 9±8	78	BIAGI	86B	SPEC	SPS Ξ^- beam

$\Omega(2250)^-$ WIDTH

VALUE (MeV)	EVTS	DOCUMENT ID		TECN	COMMENT
55±18 OUR AVERAGE					
81±38	44	ASTON	87B	LASS	$K^- p$ 11 GeV/c
48±20	78	BIAGI	86B	SPEC	SPS Ξ^- beam

$\Omega(2250)^-$ DECAY MODES

	Mode	Fraction (Γ_i/Γ)
Γ_1	$\Xi^-\pi^+K^-$	seen
Γ_2	$\Xi(1530)^0K^-$	seen

$\Omega(2250)^-$ BRANCHING RATIOS

$\Gamma(\Xi(1530)^0K^-)/\Gamma(\Xi^-\pi^+K^-)$ Γ_2/Γ_1

VALUE	EVTS	DOCUMENT ID		TECN	COMMENT
~1.0	44	ASTON	87B	LASS	$K^- p$ 11 GeV/c
0.70±0.20	49	BIAGI	86B	SPEC	Ξ^- Be 116 GeV/c

$\Omega(2250)^-$ REFERENCES

ASTON 87B PL B194 579 D. Aston et al. (SLAC, NAGO, CINC, INUS)
BIAGI 86B ZPHY C31 33 S.F. Biagi et al. (LOQM, GEVA, RAL+)

$\Omega(2380)^-$

Status: **

OMITTED FROM SUMMARY TABLE

$\Omega(2380)^-$ MASS

VALUE (MeV)	EVTS	DOCUMENT ID		TECN	COMMENT
≈ 2380 OUR ESTIMATE					
2384±9±8	45	BIAGI	86B	SPEC	SPS Ξ^- beam

$\Omega(2380)^-$ WIDTH

VALUE (MeV)	EVTS	DOCUMENT ID		TECN	COMMENT
26±23	45	BIAGI	86B	SPEC	SPS Ξ^- beam

$\Omega(2380)^-$ DECAY MODES

	Mode	Fraction (Γ_i/Γ)
Γ_1	$\Xi^-\pi^+K^-$	
Γ_2	$\Xi(1530)^0K^-$	seen
Γ_3	$\Xi^-\overline{K}^*(892)^0$	

$\Omega(2380)^-$ BRANCHING RATIOS

$\Gamma(\Xi(1530)^0K^-)/\Gamma(\Xi^-\pi^+K^-)$ Γ_2/Γ_1

VALUE	CL%	EVTS	DOCUMENT ID		TECN	COMMENT
<0.44	90	9	BIAGI	86B	SPEC	Ξ^- Be 116 GeV/c

$\Gamma(\Xi^-\overline{K}^*(892)^0)/\Gamma(\Xi^-\pi^+K^-)$ Γ_3/Γ_1

VALUE	EVTS	DOCUMENT ID		TECN	COMMENT
0.5±0.3	21	BIAGI	86B	SPEC	Ξ^- Be 116 GeV/c

$\Omega(2380)^-$ REFERENCES

BIAGI 86B ZPHY C31 33 S.F. Biagi et al. (LOQM, GEVA, RAL+)

$\Omega(2470)^-$

Status: **

OMITTED FROM SUMMARY TABLE

A peak in the $\Omega^-\pi^+\pi^-$ mass spectrum with a signal significance claimed to be at least 5.5 standard deviations. There is no reason to seriously doubt the existence of this state, but unless the evidence is overwhelming we usually wait for confirmation from a second experiment before elevating peaks to the Summary Table.

$\Omega(2470)^-$ MASS

VALUE (MeV)	EVTS	DOCUMENT ID		TECN	COMMENT
2474±12	59	ASTON	88G	LASS	$K^- p$ 11 GeV/c

$\Omega(2470)^-$ WIDTH

VALUE (MeV)	EVTS	DOCUMENT ID		TECN	COMMENT
72±33	59	ASTON	88G	LASS	$K^- p$ 11 GeV/c

$\Omega(2470)^-$ DECAY MODES

	Mode
Γ_1	$\Omega^-\pi^+\pi^-$

$\Omega(2470)^-$ REFERENCES

ASTON 88G PL B215 799 D. Aston et al. (SLAC, NAGO, CINC, INUS)

Downloaded from https://academic.oup.com/ptep/article/2022/8/083C01/6651666 by KIT Library user on 27 September 2022

CHARMED BARYONS
($C = +1$)

$\Lambda_c^+ = udc$, $\Sigma_c^{++} = uuc$, $\Sigma_c^+ = udc$, $\Sigma_c^0 = ddc$,
$\Xi_c^+ = usc$, $\Xi_c^0 = dsc$, $\Omega_c^0 = ssc$

Λ_c^+

$I(J^P) = 0(\frac{1}{2}^+)$ Status: ****

The parity of the Λ_c^+ is defined to be positive (as are the parities of the proton, neutron, and Λ). The quark content is udc. Results of an analysis of $pK^-\pi^+$ decays (JEZABEK 92) are consistent with $J = 1/2$. ABLIKIM 21N determines the Λ_c^+ spin to be $J = 1/2$, from an angular analysis of various 2-body Λ_c^+ decays in $e^+e^- \to \Lambda_c^+\overline{\Lambda}_c^-$.

We have omitted some results that have been superseded by later experiments. The omitted results may be found in earlier editions.

Λ_c^+ MASS

Our value in 2004, 2284.9 ± 0.6 MeV, was the average of the measurements now filed below as "not used." The BABAR measurement is so much better that we use it alone. Note that it is about 2.6 (old) standard deviations above the 2004 value.

The fit also includes Σ_c–Λ_c^+ and Λ_c^{*+}–Λ_c^+ mass-difference measurements, but this doesn't affect the Λ_c^+ mass. The new (in 2006) Λ_c^+ mass simply pushes all those other masses higher.

VALUE (MeV)	EVTS	DOCUMENT ID		TECN	COMMENT
2286.46±0.14 OUR FIT					
2286.46±0.14	4891	[1] AUBERT,B	05S	BABR	$\Lambda K_S^0 K^+$ and $\Sigma^0 K_S^0 K^+$
• • • We do not use the following data for averages, fits, limits, etc. • • •					
2284.7 ±0.6 ±0.7	1134	AVERY	91	CLEO	Six modes
2281.7 ±2.7 ±2.6	29	ALVAREZ	90B	NA14	$pK^-\pi^+$
2285.8 ±0.6 ±1.2	101	BARLAG	89	NA32	$pK^-\pi^+$
2284.7 ±2.3 ±0.5	5	AGUILAR-...	88B	LEBC	$pK^-\pi^+$
2283.1 ±1.7 ±2.0	628	ALBRECHT	88C	ARG	$pK^-\pi^+$, $p\overline{K}^0$, $\Lambda 3\pi$
2286.2 ±1.7 ±0.7	97	ANJOS	88B	E691	$pK^-\pi^+$
2281 ±3	2	JONES	87	HBC	$pK^-\pi^+$
2283 ±3	3	BOSETTI	82	HBC	$pK^-\pi^+$
2290 ±3	1	CALICCHIO	80	HYBR	$pK^-\pi^+$

[1] AUBERT,B 05S uses low-Q $\Lambda K_S^0 K^+$ and $\Sigma^0 K_S^0 K^+$ decays to minimize systematic errors. The error above includes systematic as well as statistical errors. Many cross checks and adjustments to properties of the BABAR detector, as well as the large number of clean events, make this by far the best measurement of the Λ_c^+ mass.

Λ_c^+ MEAN LIFE

Measurements with an error $\geq 100 \times 10^{-15}$ s or with fewer than 20 events have been omitted from the Listings.

VALUE (10^{-15} s)	EVTS	DOCUMENT ID		TECN	COMMENT
201.5± 2.7 OUR AVERAGE Error includes scale factor of 1.6. See the ideogram below.					
202.1± 1.7± 0.9	304k	[1] AAIJ	19AG	LHCB	$\Lambda_c^+ \to pK^-\pi^+$
204.6± 3.4± 2.5	8034	LINK	02C	FOCS	$\Lambda_c^+ \to pK^-\pi^+$
198.1± 7.0± 5.6	1630	KUSHNIR...	01	SELX	$\Lambda_c^+ \to pK^-\pi^+$
179.6± 6.9± 4.4	4749	MAHMOOD	01	CLE2	$e^+e^- \approx \Upsilon(4S)$
215 ±16 ± 8	1340	FRABETTI	93D	E687	γBe, $\Lambda_c^+ \to pK^-\pi^+$
• • • We do not use the following data for averages, fits, limits, etc. • • •					
180 ±30 ±30	29	ALVAREZ	90	NA14	γ, $\Lambda_c^+ \to pK^-\pi^+$
200 ±30 ±30	90	FRABETTI	90	E687	γBe, $\Lambda_c^+ \to pK^-\pi^+$
196 $^{+23}_{-20}$	101	BARLAG	89	NA32	$pK^-\pi^+$ + c.c.
220 ±30 ±20	97	ANJOS	88B	E691	$pK^-\pi^+$ + c.c.

[1] AAIJ 19AG reports [Λ_c^+ MEAN LIFE] / [$D^\pm$ MEAN LIFE] = 0.1956 ± 0.0010 ± 0.0013 which we multiply by our best value $D^\pm$ MEAN LIFE = (1.033 ± 0.005) × 10^{-12} s. Our first error is their experiment's error and our second error is the systematic error from using our best value.

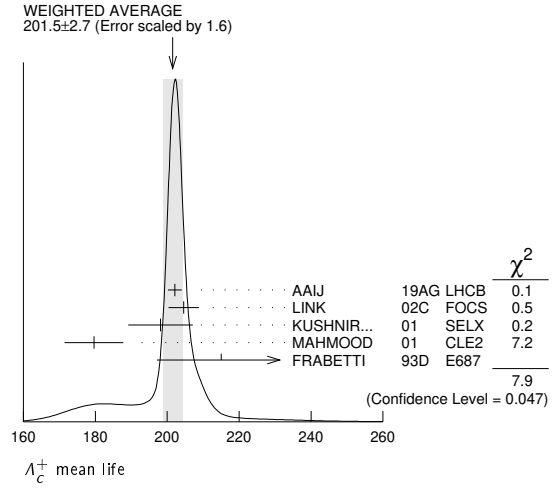

Λ_c^+ DECAY MODES

Branching fractions marked with a footnote, e.g. [a], have been corrected for decay modes not observed in the experiments. For example, the submode fraction $\Lambda_c^+ \to p\overline{K}^*(892)^0$ seen in $\Lambda_c^+ \to pK^-\pi^+$ has been multiplied up to include $\overline{K}^*(892)^0 \to \overline{K}^0\pi^0$ decays.

	Mode		Fraction (Γ_i/Γ)	Scale factor / Confidence level
	Hadronic modes with a p or n: $S = -1$ final states			
Γ_1	pK_S^0		(1.59± 0.08) %	S=1.1
Γ_2	$pK^-\pi^+$		(6.28± 0.32) %	S=1.4
Γ_3	$p\overline{K}^*(892)^0$	[a]	(1.96± 0.27) %	
Γ_4	$\Delta(1232)^{++}K^-$		(1.08± 0.25) %	
Γ_5	$\Lambda(1520)\pi^+$	[a]	(2.2 ± 0.5) %	
Γ_6	$pK^-\pi^+$ nonresonant		(3.5 ± 0.4) %	
Γ_7	$pK_S^0\pi^0$		(1.97± 0.13) %	S=1.1
Γ_8	$nK_S^0\pi^+$		(1.82± 0.25) %	
Γ_9	$p\overline{K}^0\eta$		(8.3 ± 1.8) × 10^{-3}	
Γ_{10}	$pK_S^0\pi^+\pi^-$		(1.60± 0.12) %	S=1.1
Γ_{11}	$pK^-\pi^+\pi^0$		(4.46± 0.30) %	S=1.5
Γ_{12}	$pK^*(892)^-\pi^+$	[a]	(1.4 ± 0.5) %	
Γ_{13}	$p(K^-\pi^+)_{\text{nonresonant}}\pi^0$		(4.6 ± 0.8) %	
Γ_{14}	$\Delta(1232)\overline{K}^*(892)$		seen	
Γ_{15}	$pK^-2\pi^+\pi^-$		(1.4 ± 0.9) × 10^{-3}	
Γ_{16}	$pK^-\pi^+2\pi^0$		(1.0 ± 0.5) %	
	Hadronic modes with a p: $S = 0$ final states			
Γ_{17}	$p\pi^0$		< 8 × 10^{-5}	CL=90%
Γ_{18}	$p\eta$		(1.42± 0.12) × 10^{-3}	
Γ_{19}	$p\omega(782)^0$		(8.3 ± 1.1) × 10^{-4}	
Γ_{20}	$p\pi^+\pi^-$		(4.61± 0.28) × 10^{-3}	
Γ_{21}	$pf_0(980)$	[a]	(3.5 ± 2.3) × 10^{-3}	
Γ_{22}	$p2\pi^+2\pi^-$		(2.3 ± 1.4) × 10^{-3}	
Γ_{23}	pK^+K^-		(1.06± 0.06) × 10^{-3}	
Γ_{24}	$p\phi$	[a]	(1.06± 0.14) × 10^{-3}	
Γ_{25}	pK^+K^- non-ϕ		(5.3 ± 1.2) × 10^{-4}	
Γ_{26}	$p\phi\pi^0$		(10 ± 4) × 10^{-5}	
Γ_{27}	$pK^+K^-\pi^0$ nonresonant		< 6.3 × 10^{-5}	CL=90%
	Hadronic modes with a hyperon: $S = -1$ final states			
Γ_{28}	$\Lambda\pi^+$		(1.30± 0.07) %	S=1.1
Γ_{29}	$\Lambda(1670)\pi^+$, $\Lambda(1670) \to \eta\Lambda$		(3.5 ± 0.5) × 10^{-3}	
Γ_{30}	$\Lambda\pi^+\pi^0$		(7.1 ± 0.4) %	S=1.1
Γ_{31}	$\Lambda\rho^+$		< 6 %	CL=95%
Γ_{32}	$\Lambda\pi^-2\pi^+$		(3.64± 0.29) %	S=1.4
Γ_{33}	$\Sigma(1385)^+\pi^+\pi^-$, $\Sigma^{*+} \to \Lambda\pi^+$		(1.0 ± 0.5) %	
Γ_{34}	$\Sigma(1385)^-2\pi^+$, $\Sigma^{*-} \to \Lambda\pi^-$		(7.6 ± 1.4) × 10^{-3}	
Γ_{35}	$\Lambda\pi^+\rho^0$		(1.5 ± 0.6) %	
Γ_{36}	$\Sigma(1385)^+\rho^0$, $\Sigma^{*+} \to \Lambda\pi^+$		(5 ± 4) × 10^{-3}	
Γ_{37}	$\Lambda\pi^-2\pi^+$ nonresonant		< 1.1 %	CL=90%
Γ_{38}	$\Lambda\pi^-\pi^02\pi^+$ total		(2.3 ± 0.8) %	
Γ_{39}	$\Lambda\pi^+\eta$	[a]	(1.84± 0.26) %	
Γ_{40}	$\Sigma(1385)^+\eta$	[a]	(9.1 ± 2.0) × 10^{-3}	
Γ_{41}	$\Lambda\pi^+\omega$	[a]	(1.5 ± 0.5) %	

Downloaded from https://academic.oup.com/ptep/article/2022/8/083C01/6651666 by KIT Library user on 27 September 2022

Γ_{42}	$\Lambda\pi^-\pi^0 2\pi^+$, no η or ω		$< 8 \times 10^{-3}$	CL=90%
Γ_{43}	$\Lambda K^+\overline{K}^0$		$(5.7 \pm 1.1) \times 10^{-3}$	S=1.9
Γ_{44}	$\Xi(1690)^0 K^+$, $\Xi^{*0} \to \Lambda\overline{K}^0$		$(1.6 \pm 0.5) \times 10^{-3}$	
Γ_{45}	$\Sigma^0\pi^+$		(1.29 ± 0.07) %	S=1.1
Γ_{46}	$\Sigma^0\pi^+\eta$		$(7.5 \pm 0.8) \times 10^{-3}$	
Γ_{47}	$\Sigma^+\pi^0$		(1.25 ± 0.10) %	
Γ_{48}	$\Sigma^+\eta$		$(4.4 \pm 2.0) \times 10^{-3}$	
Γ_{49}	$\Sigma^+\eta'$		(1.5 ± 0.6) %	
Γ_{50}	$\Sigma^+\pi^+\pi^-$		(4.50 ± 0.25) %	S=1.3
Γ_{51}	$\Sigma^+\rho^0$		< 1.7 %	CL=95%
Γ_{52}	$\Sigma^- 2\pi^+$		(1.87 ± 0.18) %	
Γ_{53}	$\Sigma^0\pi^+\pi^0$		(3.5 ± 0.4) %	
Γ_{54}	$\Sigma^+\pi^0\pi^0$		(1.55 ± 0.15) %	
Γ_{55}	$\Sigma^0\pi^- 2\pi^+$		(1.11 ± 0.30) %	
Γ_{56}	$\Sigma^+\pi^+\pi^-\pi^0$		—	
Γ_{57}	$\Sigma^+\omega$	[a]	(1.70 ± 0.21) %	
Γ_{58}	$\Sigma^-\pi^0 2\pi^+$		(2.1 ± 0.4) %	
Γ_{59}	$\Sigma^+ K^+ K^-$		$(3.5 \pm 0.4) \times 10^{-3}$	S=1.1
Γ_{60}	$\Sigma^+\phi$	[a]	$(3.9 \pm 0.6) \times 10^{-3}$	S=1.1
Γ_{61}	$\Xi(1690)^0 K^+$, $\Xi^{*0} \to \Sigma^+ K^-$		$(1.02 \pm 0.25) \times 10^{-3}$	
Γ_{62}	$\Sigma^+ K^+ K^-$ nonresonant		$< 8 \times 10^{-4}$	CL=90%
Γ_{63}	$\Xi^0 K^+$		$(5.5 \pm 0.7) \times 10^{-3}$	
Γ_{64}	$\Xi^- K^+\pi^+$		$(6.2 \pm 0.6) \times 10^{-3}$	S=1.1
Γ_{65}	$\Xi(1530)^0 K^+$		$(4.3 \pm 0.9) \times 10^{-3}$	S=1.1

Hadronic modes with a hyperon: $S = 0$ final states

Γ_{66}	ΛK^+		$(6.1 \pm 1.2) \times 10^{-4}$	
Γ_{67}	$\Lambda K^+\pi^+\pi^-$		$< 5 \times 10^{-4}$	CL=90%
Γ_{68}	$\Sigma^0 K^+$		$(5.2 \pm 0.8) \times 10^{-4}$	
Γ_{69}	$\Sigma^0 K^+\pi^+\pi^-$		$< 2.6 \times 10^{-4}$	CL=90%
Γ_{70}	$\Sigma^+ K^+\pi^-$		$(2.1 \pm 0.6) \times 10^{-3}$	
Γ_{71}	$\Sigma^+ K^*(892)^0$	[a]	$(3.5 \pm 1.0) \times 10^{-3}$	
Γ_{72}	$\Sigma^- K^+\pi^+$		$< 1.2 \times 10^{-3}$	CL=90%

Doubly Cabibbo-suppressed modes

Γ_{73}	$p K^+\pi^-$		$(1.11 \pm 0.18) \times 10^{-4}$

Semileptonic modes

Γ_{74}	$\Lambda e^+\nu_e$		(3.6 ± 0.4) %
Γ_{75}	$\Lambda\mu^+\nu_\mu$		(3.5 ± 0.5) %

Inclusive modes

Γ_{76}	e^+ anything		(3.95 ± 0.35) %
Γ_{77}	p anything		(50 ± 16) %
Γ_{78}	n anything		(50 ± 16) %
Γ_{79}	Λ anything		$(38.2 {}^{+2.9}_{-2.4})$ %
Γ_{80}	K^0_S anything		(9.9 ± 0.7) %
Γ_{81}	3prongs		(24 ± 8) %

$\Delta C = 1$ weak neutral current ($C1$) modes, or Lepton Family number (LF), or Lepton number (L), or Baryon number (B) violating modes

Γ_{82}	$p e^+ e^-$	$C1$	$< 5.5 \times 10^{-6}$	CL=90%
Γ_{83}	$p\mu^+\mu^-$ non-resonant	$C1$	$< 7.7 \times 10^{-8}$	CL=90%
Γ_{84}	$p e^+\mu^-$	LF	$< 9.9 \times 10^{-6}$	CL=90%
Γ_{85}	$p e^-\mu^+$	LF	$< 1.9 \times 10^{-5}$	CL=90%
Γ_{86}	$\overline{p} 2e^+$	L,B	$< 2.7 \times 10^{-6}$	CL=90%
Γ_{87}	$\overline{p} 2\mu^+$	L,B	$< 9.4 \times 10^{-6}$	CL=90%
Γ_{88}	$\overline{p} e^+\mu^+$	L,B	$< 1.6 \times 10^{-5}$	CL=90%
Γ_{89}	$\Sigma^-\mu^+\mu^+$	L	$< 7.0 \times 10^{-4}$	CL=90%

[a] This branching fraction includes all the decay modes of the final-state resonance.

CONSTRAINED FIT INFORMATION

An overall fit to 41 branching ratios uses 62 measurements and one constraint to determine 21 parameters. The overall fit has a $\chi^2 = 47.4$ for 42 degrees of freedom.

The following *off-diagonal* array elements are the correlation coefficients $\langle \delta x_i \delta x_j \rangle / (\delta x_i \cdot \delta x_j)$, in percent, from the fit to the branching fractions, $x_i \equiv \Gamma_i/\Gamma_{\rm total}$. The fit constrains the x_i whose labels appear in this array to sum to one.

x_2	54									
x_7	46	55								
x_{10}	44	64	39							
x_{11}	51	61	40	60						
x_{28}	54	66	44	42	43					
x_{30}	45	61	41	38	36	65				
x_{32}	51	37	28	41	60	45	36			
x_{43}	16	22	14	14	14	26	19	12		
x_{45}	51	55	38	37	40	74	58	44	20	
x_{47}	38	39	30	25	29	34	33	23	10	29
x_{50}	51	88	50	60	61	59	55	39	20	50
x_{52}	5	9	5	6	6	6	6	3	2	5
x_{55}	13	14	9	12	15	13	11	20	4	12
x_{57}	19	30	18	23	26	19	18	18	6	16
x_{59}	23	41	23	28	28	27	25	18	9	23
x_{60}	19	32	19	22	23	22	20	14	7	18
x_{63}	8	15	8	10	9	10	9	6	3	8
x_{64}	29	39	25	25	25	51	35	24	14	38
x_{65}	6	11	6	7	7	7	7	4	2	6
	x_1	x_2	x_7	x_{10}	x_{11}	x_{28}	x_{30}	x_{32}	x_{43}	x_{45}

x_{50}	36								
x_{52}	4	8							
x_{55}	7	14	1						
x_{57}	14	29	3	5					
x_{59}	17	45	4	6	13				
x_{60}	13	37	3	5	11	16			
x_{63}	6	13	1	2	5	6	5		
x_{64}	19	34	4	7	11	16	13	6	
x_{65}	4	10	1	2	3	4	4	2	4
	x_{47}	x_{50}	x_{52}	x_{55}	x_{57}	x_{59}	x_{60}	x_{63}	x_{64}

Λ_c^+ BRANCHING RATIOS

A few really obsolete results have been omitted.

Hadronic modes with a p: $S = -1$ final states

$\Gamma(pK^0_S)/\Gamma_{\rm total}$ — Γ_1/Γ

VALUE (%)	EVTS	DOCUMENT ID		TECN	COMMENT
1.59±0.08 OUR FIT Error includes scale factor of 1.1.					
1.52±0.08±0.03	1243	ABLIKIM	16	BES3	$e^+e^- \to \Lambda_c\overline{\Lambda}_c$, 4.599 GeV

$\Gamma(pK^0_S)/\Gamma(pK^-\pi^+)$ — Γ_1/Γ_2

Measurements given as a $\overline{K}^0$ ratio have been divided by 2 to convert to a K^0_S ratio.

VALUE	EVTS	DOCUMENT ID		TECN	COMMENT
0.254±0.012 OUR FIT Error includes scale factor of 1.4.					
0.234±0.020 OUR AVERAGE					
0.23 ±0.01 ±0.02	1025	ALAM	98	CLE2	$e^+e^- \approx \Upsilon(4S)$
0.22 ±0.04 ±0.03	133	AVERY	91	CLEO	e^+e^- 10.5 GeV
0.28 ±0.09 ±0.07	45	ANJOS	90	E691	γBe 70–260 GeV
0.31 ±0.08 ±0.02	73	ALBRECHT	88C	ARG	e^+e^- 10 GeV

$\Gamma(pK^-\pi^+)/\Gamma_{\rm total}$ — Γ_2/Γ

VALUE (%)	EVTS	DOCUMENT ID		TECN	COMMENT
6.28±0.32 OUR FIT Error includes scale factor of 1.4.					
6.3 ±0.5 OUR AVERAGE Error includes scale factor of 2.0.					
5.84±0.27±0.23	6.3k	ABLIKIM	16	BES3	$e^+e^- \to \Lambda_c\overline{\Lambda}_c$, 4.599 GeV
$6.84 \pm 0.24 {}^{+0.21}_{-0.27}$	1.4k	[1] ZUPANC	14	BELL	$e^+e^- \to D^{(*)-}\overline{p}\pi^+$ recoil
• • • We do not use the following data for averages, fits, limits, etc. • • •					
5.0 ±1.3		[2] PDG	02		See footnote

[1] This ZUPANC 14 value is the FIRST-EVER model-independent measurement of a Λ_c^+ branching fraction.

[2] See the note by P. Burchat, "Λ_c^+ Branching Fractions," in any edition of the Review from 2002 through 2014 for how this value was obtained. It is now obsolete.

$\Gamma(p\overline{K}^*(892)^0)/\Gamma(pK^-\pi^+)$ — Γ_3/Γ_2

Unseen decay modes of the $\overline{K}^*(892)^0$ are included.

VALUE	EVTS	DOCUMENT ID		TECN	COMMENT
0.31±0.04 OUR AVERAGE					
0.29±0.04±0.03		[1] AITALA	00	E791	$\pi^- N$, 500 GeV
$0.35 {}^{+0.06}_{-0.07} \pm 0.03$	39	BOZEK	93	NA32	π^- Cu 230 GeV
0.42±0.24	12	BASILE	81B	CNTR	$pp \to \Lambda_c^+ e^- X$
• • • We do not use the following data for averages, fits, limits, etc. • • •					
0.35±0.11		BARLAG	90D	NA32	See BOZEK 93

[1] AITALA 00 makes a coherent 5-dimensional amplitude analysis of 946 ± 38 $\Lambda_c^+ \to pK^-\pi^+$ decays.

Downloaded from https://academic.oup.com/ptep/article/2022/8/083C01/6651666 by KIT Library user on 27 September 2022

$\Gamma(\Delta(1232)^{++}K^-)/\Gamma(pK^-\pi^+)$ — Γ_4/Γ_2

VALUE	EVTS	DOCUMENT ID		TECN	COMMENT
0.17±0.04 OUR AVERAGE Error includes scale factor of 1.1.					
0.18±0.03±0.03		[1] AITALA	00	E791	π^- N, 500 GeV
$0.12^{+0.04}_{-0.05}\pm0.05$	14	BOZEK	93	NA32	π^- Cu 230 GeV
0.40±0.17	17	BASILE	81B	CNTR	$pp\to\Lambda_c^+e^-X$

[1] AITALA 00 makes a coherent 5-dimensional amplitude analysis of 946 ± 38 $\Lambda_c^+\to pK^-\pi^+$ decays.

$\Gamma(\Lambda(1520)\pi^+)/\Gamma(pK^-\pi^+)$ — Γ_5/Γ_2

Unseen decay modes of the $\Lambda(1520)$ are included.

VALUE	EVTS	DOCUMENT ID		TECN	COMMENT
0.35±0.08 OUR AVERAGE					
0.34±0.08±0.05		[1] AITALA	00	E791	π^- N, 500 GeV
$0.40^{+0.18}_{-0.13}\pm0.09$	12	BOZEK	93	NA32	π^- Cu 230 GeV

[1] AITALA 00 makes a coherent 5-dimensional amplitude analysis of 946 ± 38 $\Lambda_c^+\to pK^-\pi^+$ decays.

$\Gamma(pK^-\pi^+\text{nonresonant})/\Gamma(pK^-\pi^+)$ — Γ_6/Γ_2

VALUE	EVTS	DOCUMENT ID		TECN	COMMENT
0.55±0.06 OUR AVERAGE					
0.55±0.06±0.04		[1] AITALA	00	E791	π^- N, 500 GeV
$0.56^{+0.07}_{-0.09}\pm0.05$	71	BOZEK	93	NA32	π^- Cu 230 GeV

[1] AITALA 00 makes a coherent 5-dimensional amplitude analysis of 946 ± 38 $\Lambda_c^+\to pK^-\pi^+$ decays.

$\Gamma(pK_S^0\pi^0)/\Gamma_{total}$ — Γ_7/Γ

VALUE (%)	EVTS	DOCUMENT ID		TECN	COMMENT
1.97±0.13 OUR FIT Error includes scale factor of 1.1.					
1.87±0.13±0.05	558	ABLIKIM	16	BES3	$e^+e^-\to\Lambda_c\overline{\Lambda}_c$, 4.599 GeV

$\Gamma(pK_S^0\pi^0)/\Gamma(pK^-\pi^+)$ — Γ_7/Γ_2

Measurements given as a $\overline{K}^0$ ratio have been divided by 2 to convert to a K_S^0 ratio.

VALUE	EVTS	DOCUMENT ID		TECN	COMMENT
0.314±0.018 OUR FIT					
0.33 ±0.03 ±0.04	774	ALAM	98	CLE2	$e^+e^-\approx\Upsilon(4S)$

$\Gamma(nK_S^0\pi^+)/\Gamma_{total}$ — Γ_8/Γ

VALUE (%)	EVTS	DOCUMENT ID		TECN	COMMENT
1.82±0.23±0.11	83	ABLIKIM	17H	BES3	e^+e^- at 4.6 GeV

$\Gamma(p\overline{K}^0\eta)/\Gamma(pK^-\pi^+)$ — Γ_9/Γ_2

VALUE	EVTS	DOCUMENT ID		TECN	COMMENT
0.25±0.04±0.04	57	AMMAR	95	CLE2	$e^+e^-\approx\Upsilon(4S)$

$\Gamma(p\overline{K}^0\eta)/\Gamma_{total}$ — Γ_9/Γ

VALUE (%)	EVTS	DOCUMENT ID		TECN	COMMENT
0.828±0.168±0.056	42	[1] ABLIKIM	21H	BES3	e^+e^- at 4.6 GeV

[1] ABLIKIM 21H measures $B(\Lambda_c^+\to pK_S^0\eta)=(0.414\pm0.084\pm0.028)\%$.

$\Gamma(pK_S^0\pi^+\pi^-)/\Gamma_{total}$ — Γ_{10}/Γ

VALUE (%)	EVTS	DOCUMENT ID		TECN	COMMENT
1.60±0.12 OUR FIT Error includes scale factor of 1.1.					
1.53±0.11±0.09	485	ABLIKIM	16	BES3	$e^+e^-\to\Lambda_c\overline{\Lambda}_c$, 4.599 GeV

$\Gamma(pK_S^0\pi^+\pi^-)/\Gamma(pK^-\pi^+)$ — Γ_{10}/Γ_2

Measurements given as a $\overline{K}^0$ ratio have been divided by 2 to convert to a K_S^0 ratio.

VALUE	EVTS	DOCUMENT ID		TECN	COMMENT
0.255±0.015 OUR FIT Error includes scale factor of 1.1.					
0.257±0.031 OUR AVERAGE					
0.26 ±0.02 ±0.03	985	ALAM	98	CLE2	$e^+e^-\approx\Upsilon(4S)$
0.22 ±0.06 ±0.02	83	AVERY	91	CLEO	e^+e^- 10.5 GeV
0.49 ±0.18 ±0.04	12	BARLAG	90D	NA32	π^- 230 GeV

$\Gamma(pK^-\pi^+\pi^0)/\Gamma_{total}$ — Γ_{11}/Γ

VALUE (%)	EVTS	DOCUMENT ID		TECN	COMMENT
4.46±0.30 OUR FIT Error includes scale factor of 1.5.					
4.53±0.23±0.30	1849	ABLIKIM	16	BES3	$e^+e^-\to\Lambda_c\overline{\Lambda}_c$, 4.599 GeV

$\Gamma(pK^-\pi^+\pi^0)/\Gamma(pK^-\pi^+)$ — Γ_{11}/Γ_2

VALUE	EVTS	DOCUMENT ID		TECN	COMMENT
0.71 ±0.04 OUR FIT Error includes scale factor of 2.4.					
0.685±0.019 OUR AVERAGE					
0.685±0.007±0.018	242k	PAL	17	BELL	$e^+e^-\approx\Upsilon(4S),\Upsilon(5S)$
0.67 ±0.04 ±0.11	2.6k	ALAM	98	CLE2	$e^+e^-\approx\Upsilon(4S)$

$\Gamma(pK^*(892)^-\pi^+)/\Gamma(pK_S^0\pi^+\pi^-)$ — Γ_{12}/Γ_{10}

Unseen decay modes of the $K^*(892)^-$ are included.

VALUE	EVTS	DOCUMENT ID		TECN	COMMENT
0.88±0.28	17	ALEEV	94	BIS2	nN 20–70 GeV

$\Gamma(p(K^-\pi^+)_{nonresonant}\pi^0)/\Gamma(pK^-\pi^+)$ — Γ_{13}/Γ_2

VALUE	EVTS	DOCUMENT ID		TECN	COMMENT
0.73±0.12±0.05	67	BOZEK	93	NA32	π^- Cu 230 GeV

$\Gamma(\Delta(1232)\overline{K}^*(892))/\Gamma_{total}$ — Γ_{14}/Γ

VALUE	EVTS	DOCUMENT ID		TECN	COMMENT
seen	35	AMENDOLIA	87	SPEC	γGe-Si

$\Gamma(pK^-2\pi^+\pi^-)/\Gamma(pK^-\pi^+)$ — Γ_{15}/Γ_2

VALUE	DOCUMENT ID		TECN	COMMENT
0.022±0.015	BARLAG	90D	NA32	π^- 230 GeV

$\Gamma(pK^-\pi^+2\pi^0)/\Gamma(pK^-\pi^+)$ — Γ_{16}/Γ_2

VALUE	EVTS	DOCUMENT ID		TECN	COMMENT
0.16±0.07±0.03	15	BOZEK	93	NA32	π^- Cu 230 GeV

Hadronic modes with a p: $S=0$ final states

$\Gamma(p\pi^0)/\Gamma_{total}$ — Γ_{17}/Γ

VALUE	CL%	DOCUMENT ID		TECN	COMMENT
• • • We do not use the following data for averages, fits, limits, etc. • • •					
$<2.7\times10^{-4}$	90	ABLIKIM	17Q	BES3	e^+e^- at 4.6 GeV

$\Gamma(p\pi^0)/\Gamma(pK^-\pi^+)$ — Γ_{17}/Γ_2

VALUE	CL%	EVTS	DOCUMENT ID		TECN	COMMENT
$<1.273\times10^{-3}$	90	7.7k	[1] LI	21	BELL	e^+e^- at $\Upsilon(nS)$

[1] Uses $B(\pi^0\to\gamma\gamma)=0.9882\pm0.0003$.

$\Gamma(p\eta)/\Gamma_{total}$ — Γ_{18}/Γ

Unseen decay modes of the η are included.

VALUE (units 10^{-3})	EVTS	DOCUMENT ID		TECN	COMMENT
• • • We do not use the following data for averages, fits, limits, etc. • • •					
1.24±0.28±0.10	52	ABLIKIM	17Q	BES3	$\eta\to2\gamma$, $\pi^+\pi^0\pi^-$

$\Gamma(p\eta)/\Gamma(pK^-\pi^+)$ — Γ_{18}/Γ_2

VALUE (units 10^{-2})	EVTS	DOCUMENT ID		TECN	COMMENT
2.258±0.077±0.122	7.7k	[1] LI	21	BELL	e^+e^- at $\Upsilon(nS)$

[1] Uses $B(\eta\to\gamma\gamma)=0.3941\pm0.0020$.

$\Gamma(p\omega(782)^0)/\Gamma_{total}$ — Γ_{19}/Γ

VALUE (units 10^{-4})	EVTS	DOCUMENT ID		TECN	COMMENT
• • • We do not use the following data for averages, fits, limits, etc. • • •					
9.4±3.2±2.2	13	AAIJ	18N	LHCB	Seen in $\Lambda_c^+\to p\mu^+\mu^-$

$\Gamma(p\omega(782)^0)/\Gamma(pK^-\pi^+)$ — Γ_{19}/Γ_2

VALUE (units 10^{-2})	EVTS	DOCUMENT ID		TECN	COMMENT
1.32±0.12±0.10	1.8k	[1] LI	21E	BELL	e^+e^- at $\Upsilon(nS)$

[1] LI 21E reconstructs the $\omega(782)$ via $\omega\to\pi^+\pi^-\pi^0$ and $\pi^0\to\gamma\gamma$.

$\Gamma(p\pi^+\pi^-)/\Gamma(pK^-\pi^+)$ — Γ_{20}/Γ_2

VALUE (units 10^{-2})	EVTS	DOCUMENT ID		TECN	COMMENT
7.35±0.24 OUR AVERAGE Error includes scale factor of 1.3.					
7.44±0.08±0.18	20k	AAIJ	18V	LHCB	$\Lambda_b^0\to\Lambda_c^+\mu^-X$
6.70±0.48±0.25	495	ABLIKIM	16U	BES3	e^+e^- at 4.599 GeV
6.9 ±3.6	5	BARLAG	90D	NA32	π^- 230 GeV

$\Gamma(pf_0(980))/\Gamma(pK^-\pi^+)$ — Γ_{21}/Γ_2

Unseen decay modes of the $f_0(980)$ are included.

VALUE	DOCUMENT ID		TECN	COMMENT
0.055±0.036	BARLAG	90D	NA32	π^- 230 GeV

$\Gamma(p2\pi^+2\pi^-)/\Gamma(pK^-\pi^+)$ — Γ_{22}/Γ_2

VALUE	DOCUMENT ID		TECN	COMMENT
0.036±0.023	BARLAG	90D	NA32	π^- 230 GeV

$\Gamma(pK^+K^-)/\Gamma(pK^-\pi^+)$ — Γ_{23}/Γ_2

VALUE (units 10^{-2})	EVTS	DOCUMENT ID		TECN	COMMENT
1.70±0.04 OUR AVERAGE					
1.70±0.03±0.03	3.4k	AAIJ	18V	LHCB	$\Lambda_b^0\to\Lambda_c^+\mu^-X$
1.4 ±0.2 ±0.2	676	ABE	02C	BELL	$e^+e^-\approx\Upsilon(4S)$
3.9 ±0.9 ±0.7	214	ALEXANDER	96C	CLE2	$e^+e^-\approx\Upsilon(4S)$
• • • We do not use the following data for averages, fits, limits, etc. • • •					
9.6 ±2.9 ±1.0	30	FRABETTI	93H	E687	γBe, $\overline{E}_\gamma$ 220 GeV
4.8 ±2.7		BARLAG	90D	NA32	π^- 230 GeV

$\Gamma(p\phi)/\Gamma(pK^-\pi^+)$ — Γ_{24}/Γ_2

Unseen decay modes of the ϕ are included.

VALUE (units 10^{-2})	EVTS	DOCUMENT ID		TECN	COMMENT
1.70±0.21 OUR AVERAGE					
1.81±0.33±0.13	44	ABLIKIM	16U	BES3	e^+e^- at 4.599 GeV
1.5 ±0.2 ±0.2	345	ABE	02C	BELL	$e^+e^-\approx\Upsilon(4S)$
2.4 ±0.6 ±0.3	54	ALEXANDER	96C	CLE2	$e^+e^-\approx\Upsilon(4S)$
• • • We do not use the following data for averages, fits, limits, etc. • • •					
4.0 ±2.7		BARLAG	90D	NA32	π^- 230 GeV

Downloaded from https://academic.oup.com/ptep/article/2022/8/083C01/6651666 by KIT Library user on 27 September 2022

$\Gamma(pK^+K^-\text{non-}\phi)/\Gamma(pK^-\pi^+)$ — Γ_{25}/Γ_2

VALUE (units 10^{-3})	EVTS	DOCUMENT ID		TECN	COMMENT
8.4 ±1.8 OUR AVERAGE					
9.36±2.22±0.71	38	ABLIKIM	16U	BES3	e^+e^- at 4.599 GeV
7 ±2 ±2	344	ABE	02C	BELL	$e^+e^- \approx \Upsilon(4S)$

$\Gamma(p\phi\pi^0)/\Gamma(pK^-\pi^+)$ — Γ_{26}/Γ_2

VALUE (units 10^{-3})	DOCUMENT ID		TECN	COMMENT
$1.538\pm0.641^{+0.077}_{-0.100}$	PAL	17	BELL	$e^+e^- \approx \Upsilon(4S),\Upsilon(5S)$

$\Gamma(pK^+K^-\pi^0\text{nonresonant})/\Gamma_{\text{total}}$ — Γ_{27}/Γ

VALUE	CL%	DOCUMENT ID		TECN	COMMENT
$<6.3\times10^{-5}$	90	PAL	17	BELL	$e^+e^- \approx \Upsilon(4S),\Upsilon(5S)$

Hadronic modes with a hyperon: $S=-1$ final states

$\Gamma(\Lambda\pi^+)/\Gamma_{\text{total}}$ — Γ_{28}/Γ

VALUE (%)	EVTS	DOCUMENT ID		TECN	COMMENT
1.30±0.07 OUR FIT Error includes scale factor of 1.1.					
1.24±0.07±0.03	706	ABLIKIM	16	BES3	$e^+e^- \to \Lambda_c\overline{\Lambda}_c$, 4.599 GeV

$\Gamma(\Lambda\pi^+)/\Gamma(pK^-\pi^+)$ — Γ_{28}/Γ_2

VALUE	EVTS	DOCUMENT ID		TECN	COMMENT
0.207±0.009 OUR FIT Error includes scale factor of 1.2.					
0.204±0.019 OUR AVERAGE					
0.217±0.013±0.020	750	LINK	05F	FOCS	γ nucleus, $\overline{E}_\gamma\approx180$ GeV
0.18 ±0.03 ±0.04		ALBRECHT	92	ARG	$e^+e^-\approx10.4$ GeV
0.18 ±0.03 ±0.03	87	AVERY	91	CLEO	e^+e^- 10.5 GeV

$\Gamma(\Lambda(1670)\pi^+,\ \Lambda(1670)\to\eta\Lambda)/\Gamma(pK^-\pi^+)$ — Γ_{29}/Γ_2

VALUE (units 10^{-2})	EVTS	DOCUMENT ID		TECN	COMMENT
5.54±0.29±0.73	9.7k	LEE	21A	BELL	$e^+e^- \approx \Upsilon(\text{nS})$

$\Gamma(\Lambda\pi^+\pi^0)/\Gamma_{\text{total}}$ — Γ_{30}/Γ

VALUE (%)	EVTS	DOCUMENT ID		TECN	COMMENT
7.1 ±0.4 OUR FIT Error includes scale factor of 1.1.					
7.01±0.37±0.19	1497	ABLIKIM	16	BES3	$e^+e^- \to \Lambda_c\overline{\Lambda}_c$, 4.599 GeV

$\Gamma(\Lambda\pi^+\pi^0)/\Gamma(pK^-\pi^+)$ — Γ_{30}/Γ_2

VALUE	EVTS	DOCUMENT ID		TECN	COMMENT
1.12±0.05 OUR FIT Error includes scale factor of 1.1.					
0.73±0.09±0.16	464	AVERY	94	CLE2	$e^+e^- \approx \Upsilon(3S),\Upsilon(4S)$

$\Gamma(\Lambda\rho^+)/\Gamma(pK^-\pi^+)$ — Γ_{31}/Γ_2

VALUE	CL%	DOCUMENT ID		TECN	COMMENT
<0.95	95	AVERY	94	CLE2	$e^+e^- \approx \Upsilon(3S),\Upsilon(4S)$

$\Gamma(\Lambda\pi^-2\pi^+)/\Gamma_{\text{total}}$ — Γ_{32}/Γ

VALUE (%)	EVTS	DOCUMENT ID		TECN	COMMENT
3.64±0.29 OUR FIT Error includes scale factor of 1.4.					
3.81±0.24±0.18	609	ABLIKIM	16	BES3	$e^+e^- \to \Lambda_c\overline{\Lambda}_c$, 4.599 GeV

$\Gamma(\Lambda\pi^-2\pi^+)/\Gamma(pK^-\pi^+)$ — Γ_{32}/Γ_2

VALUE	EVTS	DOCUMENT ID		TECN	COMMENT
0.58 ±0.04 OUR FIT Error includes scale factor of 1.9.					
0.522±0.032 OUR AVERAGE					
0.508±0.024±0.024	1356	LINK	05F	FOCS	γ nucleus, $\overline{E}_\gamma\approx180$ GeV
0.65 ±0.11 ±0.12	289	AVERY	91	CLEO	e^+e^- 10.5 GeV
0.82 ±0.29 ±0.27	44	ANJOS	90	E691	γBe 70–260 GeV
0.94 ±0.41 ±0.13	10	BARLAG	90D	NA32	π^- 230 GeV
0.61 ±0.16 ±0.04	105	ALBRECHT	88C	ARG	e^+e^- 10 GeV

$\Gamma(\Sigma(1385)^+\pi^+\pi^-,\ \Sigma^{*+}\to\Lambda\pi^+)/\Gamma(\Lambda\pi^-2\pi^+)$ — Γ_{33}/Γ_{32}

VALUE	DOCUMENT ID		TECN	COMMENT
0.28±0.10±0.08	LINK	05F	FOCS	γ nucleus, $\overline{E}_\gamma\approx180$ GeV

$\Gamma(\Sigma(1385)^-2\pi^+,\ \Sigma^{*-}\to\Lambda\pi^-)/\Gamma(\Lambda\pi^-2\pi^+)$ — Γ_{34}/Γ_{32}

VALUE	DOCUMENT ID		TECN	COMMENT
0.21±0.03±0.02	LINK	05F	FOCS	γ nucleus, $\overline{E}_\gamma\approx180$ GeV

$\Gamma(\Lambda\pi^+\rho^0)/\Gamma(\Lambda\pi^-2\pi^+)$ — Γ_{35}/Γ_{32}

VALUE	DOCUMENT ID		TECN	COMMENT
0.40±0.12±0.12	LINK	05F	FOCS	γ nucleus, $\overline{E}_\gamma\approx180$ GeV

$\Gamma(\Sigma(1385)^+\rho^0,\ \Sigma^{*+}\to\Lambda\pi^+)/\Gamma(\Lambda\pi^-2\pi^+)$ — Γ_{36}/Γ_{32}

VALUE	DOCUMENT ID		TECN	COMMENT
0.14±0.09±0.07	LINK	05F	FOCS	γ nucleus, $\overline{E}_\gamma\approx180$ GeV

$\Gamma(\Lambda\pi^-2\pi^+\text{nonresonant})/\Gamma(\Lambda\pi^-2\pi^+)$ — Γ_{37}/Γ_{32}

VALUE	CL%	DOCUMENT ID		TECN	COMMENT
<0.3	90	LINK	05F	FOCS	γ nucleus, $\overline{E}_\gamma\approx180$ GeV

$\Gamma(\Lambda\pi^-\pi^0 2\pi^+\text{total})/\Gamma(pK^-\pi^+)$ — Γ_{38}/Γ_2

VALUE	EVTS	DOCUMENT ID		TECN	COMMENT
0.36±0.09±0.09	50	[1] CRONIN-HEN.	03	CLE3	$e^+e^- \approx \Upsilon(4S)$

[1] CRONIN-HENNESSY 03 finds this channel to be dominantly $\Lambda\eta\pi^+$ and $\Lambda\omega\pi^+$; see below.

$\Gamma(\Lambda\pi^+\eta)/\Gamma_{\text{total}}$ — Γ_{39}/Γ

VALUE (units 10^{-2})	EVTS	DOCUMENT ID		TECN	COMMENT
1.84±0.21±0.15	154	ABLIKIM	19Y	BES3	e^+e^- at 4.6 GeV

$\Gamma(\Lambda\pi^+\eta)/\Gamma(pK^-\pi^+)$ — Γ_{39}/Γ_2

Unseen decay modes of the η are included.

VALUE	EVTS	DOCUMENT ID		TECN	COMMENT
0.295±0.014 OUR AVERAGE					
0.293±0.003±0.014	51k	LEE	21A	BELL	$e^+e^- \approx \Upsilon(\text{nS})$
0.41 ±0.17 ±0.10	11	CRONIN-HEN.	03	CLE3	$e^+e^- \approx \Upsilon(4S)$
0.35 ±0.05 ±0.06	116	AMMAR	95	CLE2	$e^+e^- \approx \Upsilon(4S)$

$\Gamma(\Sigma(1385)^+\eta)/\Gamma_{\text{total}}$ — Γ_{40}/Γ

VALUE (units 10^{-2})	EVTS	DOCUMENT ID		TECN	COMMENT
0.91±0.18±0.09	54	ABLIKIM	19Y	BES3	e^+e^- at 4.6 GeV

$\Gamma(\Sigma(1385)^+\eta)/\Gamma(pK^-\pi^+)$ — Γ_{40}/Γ_2

Unseen decay modes of the $\Sigma(1385)^+$ and η are included.

VALUE	EVTS	DOCUMENT ID		TECN	COMMENT
0.190±0.016 OUR AVERAGE					
0.192±0.006±0.016	29k	LEE	21A	BELL	$e^+e^- \approx \Upsilon(\text{nS})$
0.17 ±0.04 ±0.03	54	AMMAR	95	CLE2	$e^+e^- \approx \Upsilon(4S)$

$\Gamma(\Lambda\pi^+\omega)/\Gamma(pK^-\pi^+)$ — Γ_{41}/Γ_2

Unseen decay modes of the ω are included.

VALUE	EVTS	DOCUMENT ID		TECN	COMMENT
0.24±0.06±0.06	32	CRONIN-HEN.	03	CLE3	$e^+e^- \approx \Upsilon(4S)$

$\Gamma(\Lambda\pi^-\pi^0 2\pi^+,\ \text{no}\ \eta\ \text{or}\ \omega)/\Gamma(pK^-\pi^+)$ — Γ_{42}/Γ_2

VALUE	CL%	DOCUMENT ID		TECN	COMMENT
<0.13	90	CRONIN-HEN.	03	CLE3	$e^+e^- \approx \Upsilon(4S)$

$\Gamma(\Lambda K^+\overline{K}^0)/\Gamma(pK^-\pi^+)$ — Γ_{43}/Γ_2

VALUE	EVTS	DOCUMENT ID		TECN	COMMENT
0.090±0.017 OUR FIT Error includes scale factor of 1.9.					
0.131±0.020 OUR AVERAGE					
0.142±0.018±0.022	251	LINK	05F	FOCS	γ nucleus, $\overline{E}_\gamma\approx180$ GeV
0.12 ±0.02 ±0.02	59	AMMAR	95	CLE2	$e^+e^- \approx \Upsilon(4S)$

$\Gamma(\Xi(1690)^0K^+,\ \Xi^{*0}\to\Lambda\overline{K}^0)/\Gamma(\Lambda K^+\overline{K}^0)$ — Γ_{44}/Γ_{43}

VALUE	EVTS	DOCUMENT ID		TECN	COMMENT
0.28±0.07 OUR AVERAGE					
0.32±0.10±0.04	84±24	LINK	05F	FOCS	γ nucleus, $\overline{E}_\gamma\approx180$ GeV
0.26±0.08±0.03	93	ABE	02C	BELL	$e^+e^- \approx \Upsilon(4S)$

$\Gamma(\Lambda K^+\overline{K}^0)/\Gamma(\Lambda\pi^+)$ — Γ_{43}/Γ_{28}

VALUE	EVTS	DOCUMENT ID		TECN	COMMENT
0.44 ±0.08 OUR FIT Error includes scale factor of 2.0.					
0.395±0.026±0.036	460 ± 30	AUBERT	07U	BABR	$e^+e^- \approx \Upsilon(4S)$

$\Gamma(\Sigma^0\pi^+)/\Gamma_{\text{total}}$ — Γ_{45}/Γ

VALUE (%)	EVTS	DOCUMENT ID		TECN	COMMENT
1.29±0.07 OUR FIT Error includes scale factor of 1.1.					
1.27±0.08±0.03	522	ABLIKIM	16	BES3	$e^+e^- \to \Lambda_c\overline{\Lambda}_c$, 4.599 GeV

$\Gamma(\Sigma^0\pi^+)/\Gamma(pK^-\pi^+)$ — Γ_{45}/Γ_2

VALUE	EVTS	DOCUMENT ID		TECN	COMMENT
0.206±0.010 OUR FIT Error includes scale factor of 1.2.					
0.20 ±0.04 OUR AVERAGE					
0.21 ±0.02 ±0.04	196	AVERY	94	CLE2	$e^+e^- \approx \Upsilon(3S),\Upsilon(4S)$
0.17 ±0.06 ±0.04		ALBRECHT	92	ARG	$e^+e^-\approx10.4$ GeV

$\Gamma(\Sigma^0\pi^+)/\Gamma(\Lambda\pi^+)$ — Γ_{45}/Γ_{28}

VALUE	EVTS	DOCUMENT ID		TECN	COMMENT
0.99 ±0.04 OUR FIT					
0.98 ±0.05 OUR AVERAGE					
0.977±0.015±0.051	33k	AUBERT	07U	BABR	$e^+e^- \approx \Upsilon(4S)$
1.09 ±0.11 ±0.19	750	LINK	05F	FOCS	γ nucleus, $\overline{E}_\gamma\approx180$ GeV

$\Gamma(\Sigma^0\pi^+\eta)/\Gamma(pK^-\pi^+)$ — Γ_{46}/Γ_2

VALUE	EVTS	DOCUMENT ID		TECN	COMMENT
0.120±0.006±0.010	17k	LEE	21A	BELL	$e^+e^- \approx \Upsilon(\text{nS})$

$\Gamma(\Sigma^+\pi^0)/\Gamma_{\text{total}}$ — Γ_{47}/Γ

VALUE (%)	EVTS	DOCUMENT ID		TECN	COMMENT
1.25±0.10 OUR FIT					
1.18±0.10±0.03	309	ABLIKIM	16	BES3	$e^+e^- \to \Lambda_c\overline{\Lambda}_c$, 4.599 GeV

Downloaded from https://academic.oup.com/ptep/article/2022/8/083C01/6651666 by KIT Library user on 27 September 2022

$\Gamma(\Sigma^+\pi^0)/\Gamma(pK^-\pi^+)$ — Γ_{47}/Γ_2

VALUE	EVTS	DOCUMENT ID		TECN	COMMENT
0.199±0.015 OUR FIT					
0.20 ±0.03 ±0.03	93	KUBOTA	93	CLE2	$e^+e^- \approx \Upsilon(4S)$

$\Gamma(\Sigma^+\eta)/\Gamma(pK^-\pi^+)$ — Γ_{48}/Γ_2

Unseen decay modes of the η are included.

VALUE	EVTS	DOCUMENT ID		TECN	COMMENT
0.11±0.03±0.02	26	AMMAR	95	CLE2	$e^+e^- \approx \Upsilon(4S)$

$\Gamma(\Sigma^+\eta)/\Gamma(\Sigma^+\pi^0)$ — Γ_{48}/Γ_{47}

VALUE	EVTS	DOCUMENT ID		TECN	COMMENT
0.35±0.16±0.02	15	[1] ABLIKIM	19X	BES3	e^+e^- at 4.6 GeV

[1] ABLIKIM 19X report evidence for the observation of the decay $\Lambda_c^+ \to \Sigma^+\eta$ at 2.5σ significance.

$\Gamma(\Sigma^+\eta')/\Gamma(\Sigma^+\omega)$ — Γ_{49}/Γ_{57}

VALUE	EVTS	DOCUMENT ID		TECN	COMMENT
0.86±0.34±0.04	13	[1] ABLIKIM	19X	BES3	e^+e^- at 4.6 GeV

[1] ABLIKIM 19X report evidence for the observation of the decay $\Lambda_c^+ \to \Sigma^+\eta'$ at 3.2σ significance.

$\Gamma(\Sigma^+\pi^+\pi^-)/\Gamma_{total}$ — Γ_{50}/Γ

VALUE (%)	EVTS	DOCUMENT ID		TECN	COMMENT
4.50±0.25 OUR FIT	Error includes scale factor of 1.3.				
4.25±0.24±0.20	1156	ABLIKIM	16	BES3	$e^+e^- \to \Lambda_c\overline{\Lambda}_c$, 4.599 GeV

$\Gamma(\Sigma^+\pi^+\pi^-)/\Gamma(pK^-\pi^+)$ — Γ_{50}/Γ_2

VALUE	EVTS	DOCUMENT ID		TECN	COMMENT
0.716±0.019 OUR FIT					
0.720±0.024 OUR AVERAGE					
0.719±0.003±0.024	2.7M	BERGER	18	BELL	$e^+e^- \approx \Upsilon(4S)$
0.74 ±0.07 ±0.09	487	KUBOTA	93	CLE2	$e^+e^- \approx \Upsilon(4S)$
• • • We do not use the following data for averages, fits, limits, etc. • • •					
0.72 ±0.14	47 ± 9	VAZQUEZ-JA...08		SELX	Σ^- nucleus, 600 GeV
0.54 $^{+0.18}_{-0.15}$	11	BARLAG	92	NA32	π^-Cu 230 GeV

$\Gamma(\Sigma^+\rho^0)/\Gamma(pK^-\pi^+)$ — Γ_{51}/Γ_2

VALUE	CL%	DOCUMENT ID		TECN	COMMENT
<0.27	95	KUBOTA	93	CLE2	$e^+e^- \approx \Upsilon(4S)$

$\Gamma(\Sigma^-2\pi^+)/\Gamma_{total}$ — Γ_{52}/Γ

VALUE (%)	EVTS	DOCUMENT ID		TECN	COMMENT
1.87±0.18 OUR FIT					
1.81±0.17±0.09	161	ABLIKIM	17Y	BES3	e^+e^- at 4.6 GeV

$\Gamma(\Sigma^-2\pi^+)/\Gamma(pK^-\pi^+)$ — Γ_{52}/Γ_2

VALUE	EVTS	DOCUMENT ID		TECN	COMMENT
0.297±0.030 OUR FIT	Error includes scale factor of 1.1.				
0.314±0.067	30 ± 6	VAZQUEZ-JA...08		SELX	Σ^- nucleus, 600 GeV

$\Gamma(\Sigma^-2\pi^+)/\Gamma(\Sigma^+\pi^+\pi^-)$ — Γ_{52}/Γ_{50}

VALUE	EVTS	DOCUMENT ID		TECN	COMMENT
0.42±0.04 OUR FIT	Error includes scale factor of 1.1.				
0.53±0.15±0.07	56	FRABETTI	94E	E687	γBe, $\overline{E}_\gamma$ 220 GeV

$\Gamma(\Sigma^0\pi^+\pi^0)/\Gamma(pK^-\pi^+)$ — Γ_{53}/Γ_2

VALUE	EVTS	DOCUMENT ID		TECN	COMMENT
0.56 ±0.05 OUR AVERAGE	Error includes scale factor of 1.5.				
0.575±0.005±0.036	2.7M	BERGER	18	BELL	$e^+e^- \approx \Upsilon(4S)$
0.36 ±0.09 ±0.10	117	AVERY	94	CLE2	$e^+e^- \approx \Upsilon(3S), \Upsilon(4S)$

$\Gamma(\Sigma^+\pi^0\pi^0)/\Gamma(pK^-\pi^+)$ — Γ_{54}/Γ_2

VALUE	EVTS	DOCUMENT ID		TECN	COMMENT
0.247±0.006±0.019	925k	BERGER	18	BELL	$e^+e^- \approx \Upsilon(4S)$

$\Gamma(\Sigma^0\pi^-2\pi^+)/\Gamma(pK^-\pi^+)$ — Γ_{55}/Γ_2

VALUE	EVTS	DOCUMENT ID		TECN	COMMENT
0.18±0.05 OUR FIT					
0.21±0.05±0.05	90	AVERY	94	CLE2	$e^+e^- \approx \Upsilon(3S), \Upsilon(4S)$

$\Gamma(\Sigma^0\pi^-2\pi^+)/\Gamma(\Lambda\pi^-2\pi^+)$ — Γ_{55}/Γ_{32}

VALUE	EVTS	DOCUMENT ID		TECN	COMMENT
0.31±0.08 OUR FIT					
0.26±0.06±0.09	480	LINK	05F	FOCS	γ nucleus, $\overline{E}_\gamma \approx 180$ GeV

$\Gamma(\Sigma^+\omega)/\Gamma_{total}$ — Γ_{57}/Γ

VALUE (%)	EVTS	DOCUMENT ID		TECN	COMMENT
1.70±0.21 OUR FIT					
1.56±0.20±0.07	157	ABLIKIM	16	BES3	$e^+e^- \to \Lambda_c\overline{\Lambda}_c$, 4.599 GeV

$\Gamma(\Sigma^+\omega)/\Gamma(pK^-\pi^+)$ — Γ_{57}/Γ_2

Unseen decay modes of the ω are included.

VALUE	EVTS	DOCUMENT ID		TECN	COMMENT
0.271±0.031 OUR FIT					
0.54 ±0.13 ±0.06	107	KUBOTA	93	CLE2	$e^+e^- \approx \Upsilon(4S)$

$\Gamma(\Sigma^-\pi^02\pi^+)/\Gamma_{total}$ — Γ_{58}/Γ

VALUE (%)	EVTS	DOCUMENT ID		TECN	COMMENT
2.11±0.33±0.14	88	ABLIKIM	17Y	BES3	e^+e^- at 4.6 GeV

$\Gamma(\Sigma^+K^+K^-)/\Gamma(pK^-\pi^+)$ — Γ_{59}/Γ_2

VALUE	EVTS	DOCUMENT ID		TECN	COMMENT
0.056±0.006 OUR FIT					
0.070±0.011±0.011	59	AVERY	93	CLE2	$e^+e^- \approx 10.5$ GeV

$\Gamma(\Sigma^+K^+K^-)/\Gamma(\Sigma^+\pi^+\pi^-)$ — Γ_{59}/Γ_{50}

VALUE	EVTS	DOCUMENT ID		TECN	COMMENT
0.078±0.008 OUR FIT					
0.074±0.009 OUR AVERAGE					
0.076±0.007±0.009	246	ABE	02C	BELL	$e^+e^- \approx \Upsilon(4S)$
0.071±0.011±0.011	103	LINK	02G	FOCS	γ nucleus, ≈ 180 GeV

$\Gamma(\Sigma^+\phi)/\Gamma(pK^-\pi^+)$ — Γ_{60}/Γ_2

Unseen decay modes of the ϕ are included.

VALUE	EVTS	DOCUMENT ID		TECN	COMMENT
0.062±0.009 OUR FIT					
0.069±0.023±0.016	26	AVERY	93	CLE2	$e^+e^- \approx 10.5$ GeV

$\Gamma(\Sigma^+\phi)/\Gamma(\Sigma^+\pi^+\pi^-)$ — Γ_{60}/Γ_{50}

Unseen decay modes of the ϕ are included.

VALUE	EVTS	DOCUMENT ID		TECN	COMMENT
0.087±0.012 OUR FIT					
0.086±0.012 OUR AVERAGE					
0.085±0.012±0.012	129	ABE	02C	BELL	$e^+e^- \approx \Upsilon(4S)$
0.087±0.016±0.006	57	LINK	02G	FOCS	γ nucleus, ≈ 180 GeV

$\Gamma(\Xi(1690)^0K^+, \Xi^{*0} \to \Sigma^+K^-)/\Gamma(\Sigma^+\pi^+\pi^-)$ — Γ_{61}/Γ_{50}

VALUE	EVTS	DOCUMENT ID		TECN	COMMENT
0.023±0.005 OUR AVERAGE					
0.023±0.005±0.005	75	ABE	02C	BELL	$e^+e^- \approx \Upsilon(4S)$
0.022±0.006±0.006	34	LINK	02G	FOCS	γ nucleus, ≈ 180 GeV

$\Gamma(\Sigma^+K^+K^-\text{nonresonant})/\Gamma(\Sigma^+\pi^+\pi^-)$ — Γ_{62}/Γ_{50}

VALUE	CL%	DOCUMENT ID		TECN	COMMENT
<0.018	90	ABE	02C	BELL	$e^+e^- \approx \Upsilon(4S)$
• • • We do not use the following data for averages, fits, limits, etc. • • •					
<0.028	90	LINK	02G	FOCS	γ nucleus, ≈ 180 GeV

$\Gamma(\Xi^0K^+)/\Gamma_{total}$ — Γ_{63}/Γ

VALUE (units 10^{-3})	EVTS	DOCUMENT ID		TECN	COMMENT
5.5 ±0.7 OUR FIT					
5.90±0.86±0.39	68	ABLIKIM	18Y	BES3	e^+e^- at 4.6 GeV

$\Gamma(\Xi^0K^+)/\Gamma(pK^-\pi^+)$ — Γ_{63}/Γ_2

VALUE	EVTS	DOCUMENT ID		TECN	COMMENT
0.088±0.012 OUR FIT					
0.078±0.013±0.013	56	AVERY	93	CLE2	$e^+e^- \approx 10.5$ GeV

$\Gamma(\Xi^-K^+\pi^+)/\Gamma(pK^-\pi^+)$ — Γ_{64}/Γ_2

VALUE	EVTS	DOCUMENT ID		TECN	COMMENT
0.099±0.009 OUR FIT					
0.098±0.021 OUR AVERAGE	Error includes scale factor of 1.3. See the ideogram below.				
0.14 ±0.03 ±0.02	34	ALBRECHT	95B	ARG	$e^+e^- \approx 10.4$ GeV
0.079±0.013±0.014	60	AVERY	93	CLE2	$e^+e^- \approx 10.5$ GeV
0.15 ±0.04 ±0.03	30	AVERY	91	CLEO	e^+e^- 10.5 GeV

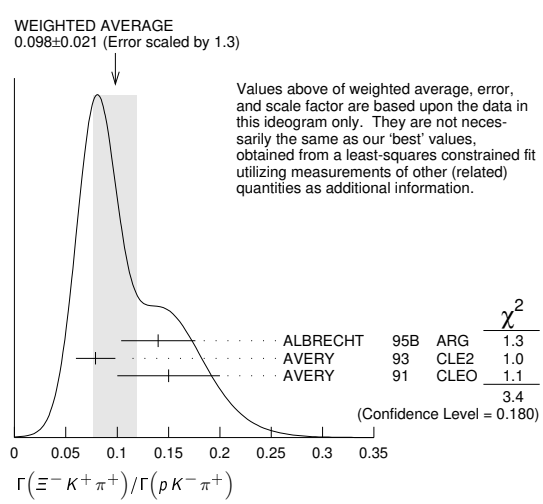

Downloaded from https://academic.oup.com/ptep/article/2022/8/083C01/6651666 by KIT Library user on 27 September 2022

$\Gamma(\Xi^- K^+ \pi^+)/\Gamma(\Lambda\pi^+)$ — Γ_{64}/Γ_{28}

VALUE	EVTS	DOCUMENT ID		TECN	COMMENT
0.48 ±0.04 OUR FIT					
0.480±0.016±0.039	2665 ± 84	AUBERT	07U	BABR	$e^+e^- \approx \Upsilon(4S)$

$\Gamma(\Xi(1530)^0 K^+)/\Gamma_{total}$ — Γ_{65}/Γ

VALUE (units 10^{-3})	EVTS	DOCUMENT ID		TECN	COMMENT
4.3 ±0.9 OUR FIT Error includes scale factor of 1.1.					
5.02±0.99±0.31	60	ABLIKIM	18Y	BES3	e^+e^- at 4.6 GeV

$\Gamma(\Xi(1530)^0 K^+)/\Gamma(pK^-\pi^+)$ — Γ_{65}/Γ_2

VALUE	EVTS	DOCUMENT ID		TECN	COMMENT
0.068±0.014 OUR FIT Error includes scale factor of 1.1.					
0.053±0.016±0.010	24	AVERY	93	CLE2	$e^+e^- \approx 10.5$ GeV
• • • We do not use the following data for averages, fits, limits, etc. • • •					
0.05 ±0.02 ±0.01	11	ALBRECHT	95B	ARG	$e^+e^- \approx 10.4$ GeV

Hadronic modes with a hyperon: $S = 0$ final states

$\Gamma(\Lambda K^+)/\Gamma(\Lambda\pi^+)$ — Γ_{66}/Γ_{28}

VALUE	EVTS	DOCUMENT ID		TECN	COMMENT
0.047±0.009 OUR AVERAGE Error includes scale factor of 1.8.					
0.044±0.004±0.003	1162±101	AUBERT	07U	BABR	$e^+e^- \approx \Upsilon(4S)$
0.074±0.010±0.012	265	ABE	02C	BELL	$e^+e^- \approx \Upsilon(4S)$

$\Gamma(\Lambda K^+\pi^+\pi^-)/\Gamma(\Lambda\pi^+)$ — Γ_{67}/Γ_{28}

VALUE	CL%	DOCUMENT ID		TECN	COMMENT
$<4.1\times10^{-2}$	90	AUBERT	07U	BABR	$e^+e^- \approx \Upsilon(4S)$

$\Gamma(\Sigma^0 K^+)/\Gamma(\Sigma^0\pi^+)$ — Γ_{68}/Γ_{45}

VALUE	EVTS	DOCUMENT ID		TECN	COMMENT
0.040±0.006 OUR AVERAGE					
0.038±0.005±0.003	366 ± 52	AUBERT	07U	BABR	$e^+e^- \approx \Upsilon(4S)$
0.056±0.014±0.008	75	ABE	02C	BELL	$e^+e^- \approx \Upsilon(4S)$

$\Gamma(\Sigma^0 K^+\pi^+\pi^-)/\Gamma(\Sigma^0\pi^+)$ — Γ_{69}/Γ_{45}

VALUE	CL%	DOCUMENT ID		TECN	COMMENT
$<2.0\times10^{-2}$	90	AUBERT	07U	BABR	$e^+e^- \approx \Upsilon(4S)$

$\Gamma(\Sigma^+ K^+\pi^-)/\Gamma(\Sigma^+\pi^+\pi^-)$ — Γ_{70}/Γ_{50}

VALUE	EVTS	DOCUMENT ID		TECN	COMMENT
0.047±0.011±0.008	105	ABE	02C	BELL	$e^+e^- \approx \Upsilon(4S)$

$\Gamma(\Sigma^+ K^*(892)^0)/\Gamma(\Sigma^+\pi^+\pi^-)$ — Γ_{71}/Γ_{50}

Unseen decay modes of the $K^*(892)^0$ are included.

VALUE	EVTS	DOCUMENT ID		TECN	COMMENT
0.078±0.018±0.013	49	LINK	02G	FOCS	γ nucleus, ≈ 180 GeV

$\Gamma(\Sigma^- K^+\pi^+)/\Gamma(\Sigma^+ K^*(892)^0)$ — Γ_{72}/Γ_{71}

VALUE	CL%	DOCUMENT ID		TECN	COMMENT
<0.35	90	LINK	02G	FOCS	γ nucleus, ≈ 180 GeV

Doubly Cabibbo-suppressed modes

$\Gamma(pK^+\pi^-)/\Gamma(pK^-\pi^+)$ — Γ_{73}/Γ_2

VALUE (units 10^{-3})	EVTS	DOCUMENT ID		TECN	COMMENT
1.77±0.27 OUR AVERAGE Error includes scale factor of 1.9.					
1.65±0.15±0.05	392	AAIJ	18V	LHCB	$\Lambda_b^0 \to \Lambda_c^+ \mu^- X$
2.35±0.27±0.21	3379	YANG	16	BELL	At or near Υs

Semileptonic modes

$\Gamma(\Lambda e^+\nu_e)/\Gamma_{total}$ — Γ_{74}/Γ

VALUE (%)	EVTS	DOCUMENT ID		TECN	COMMENT
3.63±0.38±0.20	104	ABLIKIM	15Y	BES3	567 pb^{-1}, 4.599 GeV

$\Gamma(\Lambda e^+\nu_e)/\Gamma(e^+ \text{anything})$ — Γ_{74}/Γ_{76}

VALUE (%)	EVTS	DOCUMENT ID		TECN	COMMENT
91.9±12.5±5.4	214	ABLIKIM	18AF	BES3	e^+e^- 4.6 GeV

$\Gamma(\Lambda e^+\nu_e)/\Gamma(pK^-\pi^+)$ — Γ_{74}/Γ_2

VALUE	DOCUMENT ID		TECN	COMMENT
• • • We do not use the following data for averages, fits, limits, etc. • • •				
0.43±0.08	[1,2] BERGFELD	94	CLE2	$e^+e^- \approx \Upsilon(4S)$
0.38±0.14	[2,3] ALBRECHT	91G	ARG	$e^+e^- \approx 10.4$ GeV

[1] BERGFELD 94 measures $\sigma(e^+e^- \to \Lambda_c^+ X)\cdot B(\Lambda_c^+ \to \Lambda e^+\nu_e) = (4.87 \pm 0.28 \pm 0.69)$ pb.

[2] To extract $\Gamma(\Lambda_c^+ \to \Lambda e^+\nu_e)/\Gamma(\Lambda_c^+ \to pK^-\pi^+)$, we use $\sigma(e^+e^- \to \Lambda_c^+ X)\cdot B(\Lambda_c \to pK^-\pi^+) = (11.2 \pm 1.3)$ pb, which is the weighted average of measurements from ARGUS (ALBRECHT 96E) and CLEO (AVERY 91).

[3] ALBRECHT 91G measures $\sigma(e^+e^- \to \Lambda_c^+ X)\cdot B(\Lambda_c^+ \to \Lambda e^+\nu_e) = (4.20 \pm 1.28 \pm 0.71)$ pb.

$\Gamma(\Lambda\mu^+\nu_\mu)/\Gamma_{total}$ — Γ_{75}/Γ

VALUE (%)	EVTS	DOCUMENT ID		TECN	COMMENT
3.49±0.46±0.27	79	ABLIKIM	17D	BES3	e^+e^- at 4.6 GeV

$\Gamma(\Lambda\mu^+\nu_\mu)/\Gamma(pK^-\pi^+)$ — Γ_{75}/Γ_2

VALUE	DOCUMENT ID		TECN	COMMENT
• • • We do not use the following data for averages, fits, limits, etc. • • •				
0.40±0.09	[1,2] BERGFELD	94	CLE2	$e^+e^- \approx \Upsilon(4S)$
0.35±0.20	[2,3] ALBRECHT	91G	ARG	$e^+e^- \approx 10.4$ GeV

[1] BERGFELD 94 measures $\sigma(e^+e^- \to \Lambda_c^+ X)\cdot B(\Lambda_c^+ \to \Lambda\mu^+\nu_\mu) = (4.43 \pm 0.51 \pm 0.64)$ pb.

[2] To extract $\Gamma(\Lambda_c^+ \to \Lambda\mu^+\nu_\mu)/\Gamma(\Lambda_c^+ \to pK^-\pi^+)$, we use $\sigma(e^+e^- \to \Lambda_c^+ X)\cdot B(\Lambda_c \to pK^-\pi^+) = (11.2 \pm 1.3)$ pb, which is the weighted average of measurements from ARGUS (ALBRECHT 96E) and CLEO (AVERY 91).

[3] ALBRECHT 91G measures $\sigma(e^+e^- \to \Lambda_c^+ X)\cdot B(\Lambda_c^+ \to \Lambda\mu^+\nu_\mu) = (3.91 \pm 2.02 \pm 0.90)$ pb.

$\Gamma(\Lambda\mu^+\nu_\mu)/\Gamma(\Lambda e^+\nu_e)$ — Γ_{75}/Γ_{74}

VALUE	DOCUMENT ID		TECN	COMMENT
• • • We do not use the following data for averages, fits, limits, etc. • • •				
0.96±0.16±0.04	[1] ABLIKIM	17D	BES3	e^+e^- at 4.6 GeV

[1] This is the ratio of the ABLIKIM 17D $\Lambda\mu^+\nu_e$ branching fraction and the ABLIKIM 15Y $\Lambda e^+\nu_e$ branching fraction (see above), and so is not an independent measurement.

Inclusive modes

$\Gamma(e^+ \text{anything})/\Gamma_{total}$ — Γ_{76}/Γ

VALUE (%)	EVTS	DOCUMENT ID		TECN	COMMENT
3.95±0.34±0.09	214	ABLIKIM	18AF	BES3	e^+e^- 4.6 GeV

$\Gamma(p \text{ anything})/\Gamma_{total}$ — Γ_{77}/Γ

VALUE	DOCUMENT ID		TECN	COMMENT
0.50±0.08±0.14	[1] CRAWFORD	92	CLEO	e^+e^- 10.5 GeV

[1] This CRAWFORD 92 value includes protons from Λ decay. The value is model dependent, but account is taken of this in the systematic error.

$\Gamma(n \text{ anything})/\Gamma_{total}$ — Γ_{78}/Γ

VALUE	DOCUMENT ID		TECN	COMMENT
0.50±0.08±0.14	[1] CRAWFORD	92	CLEO	e^+e^- 10.5 GeV

[1] This CRAWFORD 92 value includes neutrons from Λ decay. The value is model dependent, but account is taken of this in the systematic error.

$\Gamma(\Lambda \text{ anything})/\Gamma_{total}$ — Γ_{79}/Γ

VALUE (%)	EVTS	DOCUMENT ID		TECN	COMMENT
$38.2^{+2.8}_{-2.2}\pm0.9$	700	ABLIKIM	18E	BES3	e^+e^- at 4.6 GeV

$\Gamma(K_S^0 \text{ anything})/\Gamma_{total}$ — Γ_{80}/Γ

VALUE (%)	EVTS	DOCUMENT ID		TECN	COMMENT
9.9±0.6±0.4	478	ABLIKIM	20AJ	BES3	e^+e^- at 4.6 GeV

$\Gamma(3\text{prongs})/\Gamma_{total}$ — Γ_{81}/Γ

VALUE	DOCUMENT ID	TECN	COMMENT
0.24±0.07±0.04	KAYIS-TOPAK.03	CHRS	ν_μ emulsion, $\overline{E}$=27 GeV

Rare or forbidden modes

$\Gamma(pe^+e^-)/\Gamma_{total}$ — Γ_{82}/Γ

A test for the ΔC=1 weak neutral current. Allowed by higher-order electroweak interactions.

VALUE	CL%	EVTS	DOCUMENT ID		TECN	COMMENT
$<5.5\times10^{-6}$	90	4.0 ± 7.1	LEES	11G	BABR	$e^+e^- \approx \Upsilon(4S)$

$\Gamma(p\mu^+\mu^- \text{non-resonant})/\Gamma_{total}$ — Γ_{83}/Γ

A test for the ΔC=1 weak neutral current. Allowed by higher-order electroweak interactions.

VALUE	CL%	DOCUMENT ID		TECN	COMMENT
$<7.7\times10^{-8}$	90	AAIJ	18N	LHCB	Ratio to $p\phi$, $\phi \to \mu^+\mu^-$
• • • We do not use the following data for averages, fits, limits, etc. • • •					
$<4.4\times10^{-5}$	90	LEES	11G	BABR	$e^+e^- \approx \Upsilon(4S)$
$<3.4\times10^{-4}$	90	KODAMA	95	E653	π^- emulsion 600 GeV

$\Gamma(pe^+\mu^-)/\Gamma_{total}$ — Γ_{84}/Γ

A test of lepton family-number conservation.

VALUE	CL%	EVTS	DOCUMENT ID		TECN	COMMENT
$<9.9\times10^{-6}$	90	−0.7±3.0	LEES	11G	BABR	$e^+e^- \approx \Upsilon(4S)$

$\Gamma(pe^-\mu^+)/\Gamma_{total}$ — Γ_{85}/Γ

A test of lepton family-number conservation.

VALUE	CL%	EVTS	DOCUMENT ID		TECN	COMMENT
$<19\times10^{-6}$	90	6.2 ± 4.9	LEES	11G	BABR	$e^+e^- \approx \Upsilon(4S)$

Downloaded from https://academic.oup.com/ptep/article/2022/8/083C01/6651666 by KIT Library user on 27 September 2022

$\Gamma(\overline{p}2e^+)/\Gamma_{total}$ — Γ_{86}/Γ

A test of lepton- and baryon-number conservation.

VALUE	CL%	EVTS	DOCUMENT ID		TECN	COMMENT
$<2.7\times10^{-6}$	90	-1.5 ± 4.5	LEES	11G	BABR	$e^+e^-\approx\Upsilon(4S)$

$\Gamma(\overline{p}2\mu^+)/\Gamma_{total}$ — Γ_{87}/Γ

A test of lepton- and baryon-number conservation and of lepton family-number conservation.

VALUE	CL%	EVTS	DOCUMENT ID		TECN	COMMENT
$<9.4\times10^{-6}$	90	0.0 ± 2.2	LEES	11G	BABR	$e^+e^-\approx\Upsilon(4S)$

$\Gamma(\overline{p}e^+\mu^+)/\Gamma_{total}$ — Γ_{88}/Γ

A test of lepton- and baryon-number conservation and of lepton family-number conservation.

VALUE	CL%	EVTS	DOCUMENT ID		TECN	COMMENT
$<16\times10^{-6}$	90	10.1 ± 6.8	LEES	11G	BABR	$e^+e^-\approx\Upsilon(4S)$

$\Gamma(\Sigma^-\mu^+\mu^+)/\Gamma_{total}$ — Γ_{89}/Γ

A test of lepton-number conservation.

VALUE	CL%	EVTS	DOCUMENT ID		TECN	COMMENT
$<7.0\times10^{-4}$	90	0	KODAMA	95	E653	π^- emulsion 600 GeV

Λ_c^+ DECAY PARAMETERS

See the note on "Baryon Decay Parameters" in the neutron Listings.

α FOR $\Lambda_c^+ \to \Lambda\pi^+$

VALUE	EVTS	DOCUMENT ID		TECN	COMMENT
-0.84 ± 0.09 OUR AVERAGE					
$-0.80\pm0.11\pm0.02$		ABLIKIM	19AX	BES3	e^+e^- at 4.6 GeV
$-0.78\pm0.16\pm0.19$		LINK	06A	FOCS	γ A, $\overline{E}_\gamma\approx$ 180 GeV
$-0.94\pm0.21\pm0.12$	414	[1] BISHAI	95	CLE2	$e^+e^-\approx\Upsilon(4S)$
-0.96 ± 0.42		ALBRECHT	92	ARG	$e^+e^-\approx$ 10.4 GeV
$-1.1\ \pm0.4$	86	AVERY	90B	CLEO	$e^+e^-\approx$ 10.6 GeV

[1] BISHAI 95 actually gives $\alpha=-0.94^{+0.21+0.12}_{-0.06-0.06}$, chopping the errors at the physical limit -1.0. However, for $\alpha\approx-1.0$, some experiments should *get* unphysical values ($\alpha<-1.0$), and for averaging with other measurements such values (or errors that extend below -1.0) should *not* be chopped.

α FOR $\Lambda_c^+ \to \Sigma^+\pi^0$

VALUE	EVTS	DOCUMENT ID		TECN	COMMENT
-0.55 ± 0.11 OUR AVERAGE					
$-0.57\pm0.10\pm0.07$		ABLIKIM	19AX	BES3	e^+e^- at 4.6 GeV
$-0.45\pm0.31\pm0.06$	89	BISHAI	95	CLE2	$e^+e^-\approx\Upsilon(4S)$

α FOR $\Lambda_c^+ \to \Sigma^0\pi^+$

VALUE	DOCUMENT ID		TECN	COMMENT
$-0.73\pm0.17\pm0.07$	ABLIKIM	19AX	BES3	e^+e^- at 4.6 GeV

α FOR $\Lambda_c^+ \to \Lambda\ell^+\nu_\ell$

The experiments don't cover the complete (or same incomplete) $M(\Lambda\ell^+)$ range, but we average them together anyway.

VALUE	EVTS	DOCUMENT ID		TECN	COMMENT
-0.86 ± 0.04 OUR AVERAGE					
$-0.86\pm0.03\pm0.02$	3201	[1] HINSON	05	CLEO	$e^+e^-\approx\Upsilon(4S)$
$-0.91\pm0.42\pm0.25$		[2] ALBRECHT	94B	ARG	$e^+e^-\approx$ 10 GeV
• • • We do not use the following data for averages, fits, limits, etc. • • •					
$-0.82^{+0.09+0.06}_{-0.06-0.03}$	700	[3] CRAWFORD	95	CLE2	See HINSON 05
$-0.89^{+0.17+0.09}_{-0.11-0.05}$	350	[4] BERGFELD	94	CLE2	See CRAWFORD 95

[1] HINSON 05 measures the form-factor ratio $R\equiv f_2/f_1$ for $\Lambda_c^+\to\Lambda e^+\nu_e$ events to be $-0.31\pm0.05\pm0.04$ and the pole mass to be $2.21\pm0.08\pm0.14$ GeV/c^2, and from these calculates α, averaged over q^2, where $\langle q^2\rangle=0.67$ (GeV/c)^2.

[2] ALBRECHT 94B uses Λe^+ and $\Lambda\mu^+$ events in the mass range $1.85<M(\Lambda\ell^+)<2.20$ GeV.

[3] CRAWFORD 95 measures the form-factor ratio $R\equiv f_2/f_1$ for $\Lambda_c^+\to\Lambda e^+\nu_e$ events to be $-0.25\pm0.14\pm0.08$ and from this calculates α, averaged over q^2, to be the above.

[4] BERGFELD 94 uses Λe^+ events.

α FOR $\Lambda_c^+ \to pK_S^0$

VALUE	DOCUMENT ID		TECN	COMMENT
$0.18\pm0.43\pm0.14$	ABLIKIM	19AX	BES3	e^+e^- at 4.6 GeV

$\Lambda_c^+, \overline{\Lambda}_c^-$ *CP*-VIOLATING DECAY ASYMMETRIES

$(\alpha+\overline{\alpha})/(\alpha-\overline{\alpha})$ in $\Lambda_c^+\to\Lambda\pi^+, \overline{\Lambda}_c^-\to\overline{\Lambda}\pi^-$

This is zero if *CP* is conserved.

VALUE	DOCUMENT ID		TECN	COMMENT
$-0.07\pm0.19\pm0.24$	LINK	06A	FOCS	γ A, $\overline{E}_\gamma\approx$ 180 GeV

$(\alpha+\overline{\alpha})/(\alpha-\overline{\alpha})$ in $\Lambda_c^+\to\Lambda e^+\nu_e, \overline{\Lambda}_c^-\to\overline{\Lambda}e^-\overline{\nu}_e$

This is zero if *CP* is conserved.

VALUE	DOCUMENT ID		TECN	COMMENT
$0.00\pm0.03\pm0.02$	HINSON	05	CLEO	$e^+e^-\approx\Upsilon(4S)$

$A_{CP}(\Lambda X)$ in $\Lambda_c\to\Lambda X, \overline{\Lambda}_c\to\overline{\Lambda}X$

VALUE (%)	EVTS	DOCUMENT ID		TECN	COMMENT
$2.1^{+7.0}_{-6.6}\pm1.6$	700	ABLIKIM	18E	BES3	e^+e^- at 4.6 GeV

$\Delta A_{CP}=A_{CP}(\Lambda_c^+\to pK^+K^-)-A_{CP}(\Lambda_c^+\to p\pi^+\pi^-)$

VALUE (%)	DOCUMENT ID		TECN	COMMENT
$0.30\pm0.91\pm0.61$	[1] AAIJ	18R	LHCB	pp 7, 8 TeV

[1] AAIJ 18R applies phase-space-dependent weights to the $\Lambda_c^+\to p\pi^+\pi^-$ sample to align its kinematics with the $\Lambda_c^+\to pK^+K^-$ sample.

Λ_c^+ REFERENCES

We have omitted some papers that have been superseded by later experiments. The omitted papers may be found in our 1992 edition (Physical Review **D45**, 1 June, Part II) or in earlier editions.

ABLIKIM 21H PL B817 136327 M. Ablikim et al. (BESIII Collab.)
ABLIKIM 21N PR D103 L091101 M. Ablikim et al. (BESIII Collab.) J
LEE 21A PR D103 052005 J.Y. Lee et al. (BELLE Collab.)
LI 21 PR D103 072004 S.X. Li et al. (BELLE Collab.)
LI 21E PR D104 072008 S.X. Li et al. (BELLE Collab.)
ABLIKIM 20AJ EPJ C80 935 M. Ablikim et al. (BESIII Collab.)
AAIJ 19AG PR D100 032001 R. Aaij et al. (LHCb Collab.)
ABLIKIM 19AX PR D100 072004 M. Ablikim et al. (BESIII Collab.)
ABLIKIM 19X CP C43 083002 M. Ablikim et al. (BESIII Collab.)
ABLIKIM 19Y PR D99 032010 M. Ablikim et al. (BESIII Collab.)
AAIJ 18N PR D97 091101 R. Aaij et al. (LHCb Collab.)
AAIJ 18R JHEP 1803 182 R. Aaij et al. (LHCb Collab.)
AAIJ 18V JHEP 1803 043 R. Aaij et al. (LHCb Collab.)
ABLIKIM 18AF PRL 121 251801 M. Ablikim et al. (BESIII Collab.)
ABLIKIM 18E PRL 121 062003 M. Ablikim et al. (BESIII Collab.)
ABLIKIM 18Y PL B783 200 M. Ablikim et al. (BESIII Collab.)
BERGER 18 PR D98 112006 M. Berger et al. (BELLE Collab.)
ABLIKIM 17D PL B767 42 M. Ablikim et al. (BESIII Collab.)
ABLIKIM 17H PRL 118 112001 M. Ablikim et al. (BESIII Collab.)
ABLIKIM 17Q PR D95 111102 M. Ablikim et al. (BESIII Collab.)
ABLIKIM 17Y PL B772 388 M. Ablikim et al. (BESIII Collab.)
PAL 17 PR D96 051102 B. Pal et al. (BELLE Collab.)
ABLIKIM 16 PRL 116 052001 M. Ablikim et al. (BESIII Collab.)
ABLIKIM 16U PRL 117 232002 M. Ablikim et al. (BESIII Collab.)
YANG 16 PRL 117 011801 S.B. Yang et al. (BELLE Collab.)
ABLIKIM 15Y PRL 115 221805 M. Ablikim et al. (BESIII Collab.)
ZUPANC 14 PRL 113 042002 A. Zupanc et al. (BELLE Collab.)
LEES 11G PR D84 072006 J.P. Lees et al. (BABAR Collab.)
VAZQUEZ-JA... 08 PL B666 299 E. Vazquez-Jauregui et al. (SELEX Collab.)
AUBERT 07U PR D75 052002 B. Aubert et al. (BABAR Collab.)
LINK 06A PL B634 165 J.M. Link et al. (FNAL FOCUS Collab.)
AUBERT,B 05S PR D72 052006 B. Aubert et al. (BABAR Collab.)
HINSON 05 PRL 94 191801 J.W. Hinson et al. (CLEO Collab.)
LINK 05F PL B624 22 J.M. Link et al. (FNAL FOCUS Collab.)
CRONIN-HEN... 03 PR D67 012001 D. Cronin-Hennessy et al. (CLEO Collab.)
KAYIS-TOPAK... 03 PR B555 156 A. Kayis-Topaksu et al. (CERN CHORUS Collab.)
ABE 02C PL B524 33 K. Abe et al. (KEK BELLE Collab.)
LINK 02C PRL 88 161801 J.M. Link et al. (FNAL FOCUS Collab.)
LINK 02G PL B540 25 J.M. Link et al. (FNAL FOCUS Collab.)
PDG 02 PR D66 010001 K. Hagiwara et al. (PDG Collab.)
KUSHNIR... 01 PRL 86 5243 A. Kushnirenko et al. (FNAL SELEX Collab.)
MAHMOOD 01 PRL 86 2232 A.H. Mahmood et al. (CLEO Collab.)
AITALA 00 PL B471 449 E.M. Aitala et al. (FNAL E791 Collab.)
ALAM 98 PR D57 4467 M.S. Alam et al. (CLEO Collab.)
ALBRECHT 96E PRPL 276 223 H. Albrecht et al. (ARGUS Collab.)
ALEXANDER 96C PR D53 1013 J.P. Alexander et al. (CLEO Collab.)
ALBRECHT 95B PL B342 397 H. Albrecht et al. (ARGUS Collab.)
AMMAR 95 PRL 74 3534 R. Ammar et al. (CLEO Collab.)
BISHAI 95 PL B350 256 M. Bishai et al. (CLEO Collab.)
CRAWFORD 95 PRL 75 624 G. Crawford et al. (CLEO Collab.)
KODAMA 95 PL B345 85 K. Kodama et al. (FNAL E653 Collab.)
ALBRECHT 94B PL B326 320 H. Albrecht et al. (ARGUS Collab.)
ALEEV 94 PAN 57 1370 A.N. Aleev et al. (Serpukhov BIS-2 Collab.)
Translated from YF 57 1443.
AVERY 94 PL B325 257 P. Avery et al. (CLEO Collab.)
BERGFELD 94 PL B323 219 T. Bergfeld et al. (CLEO Collab.)
FRABETTI 94E PL B328 193 P.L. Frabetti et al. (FNAL E687 Collab.)
AVERY 93 PRL 71 2391 P. Avery et al. (CLEO Collab.)
BOZEK 93 PL B312 247 A. Bozek et al. (CERN NA32 Collab.)
FRABETTI 93D PRL 70 1755 P.L. Frabetti et al. (FNAL E687 Collab.)
FRABETTI 93H PL B314 477 P.L. Frabetti et al. (FNAL E687 Collab.)
KUBOTA 93 PRL 71 3255 Y. Kubota et al. (CLEO Collab.)
ALBRECHT 92 PL B274 239 H. Albrecht et al. (ARGUS Collab.)
BARLAG 92 PL B283 465 S. Barlag et al. (ACCMOR Collab.)
CRAWFORD 92 PR D45 752 G. Crawford et al. (CLEO Collab.)
JEZABEK 92 PL B286 175 M. Jezabek, K. Rybicki, R. Rylko (CRAC)
ALBRECHT 91G PL B269 234 H. Albrecht et al. (ARGUS Collab.)
AVERY 91 PR D43 3599 P. Avery et al. (CLEO Collab.)
ALVAREZ 90 ZPHY C47 539 M.P. Alvarez et al. (CERN NA14/2 Collab.)
ALVAREZ 90B PL B246 256 M.P. Alvarez et al. (CERN NA14/2 Collab.)
ANJOS 90 PR D41 801 J.C. Anjos et al. (FNAL E691 Collab.)
AVERY 90B PRL 65 2842 P. Avery et al. (CLEO Collab.)
BARLAG 90D ZPHY C48 29 S. Barlag et al. (ACCMOR Collab.)
FRABETTI 90 PL B251 639 P.L. Frabetti et al. (FNAL E687 Collab.)
BARLAG 89 PL B218 374 S. Barlag et al. (ACCMOR Collab.)
AGUILAR-... 88B ZPHY C40 321 M. Aguilar-Benitez et al. (LEBC-EHS Collab.)
Also PL B189 254 M. Aguilar-Benitez et al. (LEBC-EHS Collab.)
Also PL B199 462 M. Aguilar-Benitez et al. (LEBC-EHS Collab.)
Also SJNP 48 833 M. Begalli et al. (LEBC-EHS Collab.)
Translated from YAF 48 1310.
ALBRECHT 88C PL B207 109 H. Albrecht et al. (ARGUS Collab.)
ANJOS 88B PRL 60 1379 J.C. Anjos et al. (FNAL E691 Collab.)
AMENDOLIA 87 ZPHY C36 513 S.R. Amendolia et al. (CERN NA1 Collab.)
JONES 87 ZPHY C36 593 G.T. Jones et al. (CERN WA21 Collab.)
BOSETTI 82 PL 109B 234 P.C. Bosetti et al. (AACH3, BONN, CERN+)
BASILE 81B NC 62A 14 M. Basile et al. (CERN, BGNA, PGIA, FRAS)
CALICCHIO 80 PL 93B 521 M. Calicchio et al. (BARI, BIRM, BRUX+)

OTHER RELATED PAPERS

MIGLIOZZI 99 PL B462 217 P. Migliozzi et al.
DUNIETZ 98 PR D58 094010 I. Dunietz

Downloaded from https://academic.oup.com/ptep/article/2022/8/083C01/6651666 by KIT Library user on 27 September 2022

$\Lambda_c(2595)^+$

$I(J^P) = 0(\frac{1}{2}^-)$ Status: ***

The $\Lambda_c^+\pi^+\pi^-$ mode is largely, and perhaps entirely, $\Sigma_c\pi$, which is just at threshold; since the Σ_c has $J^P = 1/2^+$, the J^P here is almost certainly $1/2^-$. This result is in accord with the theoretical expectation that this is the charm counterpart of the strange $\Lambda(1405)$.

$\Lambda_c(2595)^+$ MASS

The mass is obtained from the $\Lambda_c(2595)^+$–Λ_c^+ mass-difference measurements below.

VALUE (MeV)	DOCUMENT ID
2592.25±0.28 OUR FIT	

$\Lambda_c(2595)^+ - \Lambda_c^+$ MASS DIFFERENCE

VALUE (MeV)	EVTS	DOCUMENT ID		TECN	COMMENT
305.79±0.24 OUR FIT					
305.79±0.14±0.20	3.5k	AALTONEN	11H	CDF	$p\overline{p}$ at 1.96 TeV
• • • We do not use the following data for averages, fits, limits, etc. • • •					
305.6 ±0.3		[1] BLECHMAN	03		Threshold shift
309.7 ±0.9 ±0.4	19	ALBRECHT	97	ARG	$e^+e^- \approx$ 10 GeV
309.2 ±0.7 ±0.3	14 ± 4.5	FRABETTI	96	E687	γBe, $\overline{E}_\gamma \approx$ 220 GeV
307.5 ±0.4 ±1.0	112 ± 17	EDWARDS	95	CLE2	$e^+e^- \approx$ 10.5 GeV

[1] BLECHMAN 03 finds that a more sophisticated treatment than a simple Breit-Wigner for the proximity of the threshold of the dominant decay, $\Sigma_c(2455)\pi$, lowers the $\Lambda_c(2595)^+ - \Lambda_c^+$ mass difference by 2 or 3 MeV. The analysis of AALTONEN 11H bears this out.

$\Lambda_c(2595)^+$ WIDTH

VALUE (MeV)	EVTS	DOCUMENT ID		TECN	COMMENT
2.59±0.30±0.47	3.5k	[2] AALTONEN	11H	CDF	$p\overline{p}$ at 1.96 TeV
• • • We do not use the following data for averages, fits, limits, etc. • • •					
$2.9\ ^{+2.9}_{-2.1}\ ^{+1.8}_{-1.4}$	19	ALBRECHT	97	ARG	$e^+e^- \approx$ 10 GeV
$3.9\ ^{+1.4}_{-1.2}\ ^{+2.0}_{-1.0}$	112 ± 17	EDWARDS	95	CLE2	$e^+e^- \approx$ 10.5 GeV

[2] AALTONEN 11H treats the three charged modes $\Lambda_c(2595)^+ \to \Sigma_c(2455)^{++}\pi^-$, $\Sigma_c(2455)^+\pi^0$, $\Sigma_c(2455)^0\pi^+$ separately in terms of a common coupling constant h_2 and obtains $h_2^2 = 0.36 \pm 0.08$. From this the width is determined.

$\Lambda_c(2595)^+$ DECAY MODES

$\Lambda_c^+\pi\pi$ and its submode $\Sigma_c(2455)\pi$ — the latter just barely — are the only strong decays allowed to an excited Λ_c^+ having this mass; and the submode seems to dominate.

	Mode	Fraction (Γ_i/Γ)
Γ_1	$\Lambda_c^+\pi^+\pi^-$	[a] —
Γ_2	$\Sigma_c(2455)^{++}\pi^-$	24 ± 7 %
Γ_3	$\Sigma_c(2455)^0\pi^+$	24 ± 7 %
Γ_4	$\Lambda_c^+\pi^+\pi^-$ 3-body	18 ± 10 %
Γ_5	$\Lambda_c^+\pi^0$	[b] not seen
Γ_6	$\Lambda_c^+\gamma$	not seen

[a] See AALTONEN 11H, Fig. 8, for the calculated ratio of $\Lambda_c^+\pi^0\pi^0$ and $\Lambda_c^+\pi^+\pi^-$ partial widths as a function of the $\Lambda_c(2595)^+ - \Lambda_c^+$ mass difference. At our value of the mass difference, the ratio is about 4.

[b] A test that the isospin is indeed 0, so that the particle is indeed a Λ_c^+.

$\Lambda_c(2595)^+$ BRANCHING RATIOS

$\Gamma(\Sigma_c(2455)^{++}\pi^-)/\Gamma(\Lambda_c^+\pi^+\pi^-)$ — Γ_2/Γ_1

VALUE	DOCUMENT ID		TECN	COMMENT
0.36±0.10 OUR AVERAGE				
0.37±0.12±0.13	ALBRECHT	97	ARG	$e^+e^- \approx$ 10 GeV
0.36±0.09±0.09	EDWARDS	95	CLE2	$e^+e^- \approx$ 10.5 GeV

$\Gamma(\Sigma_c(2455)^0\pi^+)/\Gamma(\Lambda_c^+\pi^+\pi^-)$ — Γ_3/Γ_1

VALUE	DOCUMENT ID		TECN	COMMENT
0.37±0.10 OUR AVERAGE				
0.29±0.10±0.11	ALBRECHT	97	ARG	$e^+e^- \approx$ 10 GeV
0.42±0.09±0.09	EDWARDS	95	CLE2	$e^+e^- \approx$ 10.5 GeV

$[\Gamma(\Sigma_c(2455)^{++}\pi^-) + \Gamma(\Sigma_c(2455)^0\pi^+)]/\Gamma(\Lambda_c^+\pi^+\pi^-)$ — $(\Gamma_2+\Gamma_3)/\Gamma_1$

VALUE	CL%	DOCUMENT ID		TECN	COMMENT
• • • We do not use the following data for averages, fits, limits, etc. • • •					
$0.66\ ^{+0.13}_{-0.16}$±0.07		ALBRECHT	97	ARG	$e^+e^- \approx$ 10 GeV
>0.51	90	[3] FRABETTI	96	E687	γBe, $\overline{E}_\gamma \approx$ 220 GeV

[3] The results of FRABETTI 96 are consistent with this ratio being 100%.

$\Gamma(\Lambda_c^+\pi^0)/\Gamma(\Lambda_c^+\pi^+\pi^-)$ — Γ_5/Γ_1

$\Lambda_c^+\pi^0$ decay is forbidden by isospin conservation if this state is in fact a Λ_c.

VALUE	CL%	DOCUMENT ID		TECN	COMMENT
<3.53	90	EDWARDS	95	CLE2	$e^+e^- \approx$ 10.5 GeV

$\Gamma(\Lambda_c^+\gamma)/\Gamma(\Lambda_c^+\pi^+\pi^-)$ — Γ_6/Γ_1

VALUE	CL%	DOCUMENT ID		TECN	COMMENT
<0.98	90	EDWARDS	95	CLE2	$e^+e^- \approx$ 10.5 GeV

$\Lambda_c(2595)^+$ REFERENCES

AALTONEN	11H	PR D84 012003	T. Aaltonen *et al.*	(CDF Collab.)
BLECHMAN	03	PR D67 074033	A.E. Blechman *et al.*	(JHU, FLOR)
ALBRECHT	97	PL B402 207	H. Albrecht *et al.*	(ARGUS Collab.)
FRABETTI	96	PL B365 461	P.L. Frabetti *et al.*	(FNAL E687 Collab.)
EDWARDS	95	PRL 74 3331	K.W. Edwards *et al.*	(CLEO Collab.)

$\Lambda_c(2625)^+$

$I(J^P) = 0(\frac{3}{2}^-)$ Status: ***

The spin-parity has not been measured but is expected to be $3/2^-$: this is presumably the charm counterpart of the strange $\Lambda(1520)$.

$\Lambda_c(2625)^+$ MASS

The mass is obtained from the $\Lambda_c(2625)^+$–Λ_c^+ mass-difference measurements below.

VALUE (MeV)	EVTS	DOCUMENT ID		TECN	COMMENT
2628.11±0.19 OUR FIT Error includes scale factor of 1.1.					
• • • We do not use the following data for averages, fits, limits, etc. • • •					
2626.6 ±0.5 ±1.5	42 ± 9	ALBRECHT	93F	ARG	See ALBRECHT 97

$\Lambda_c(2625)^+ - \Lambda_c^+$ MASS DIFFERENCE

VALUE (MeV)	EVTS	DOCUMENT ID		TECN	COMMENT
341.65±0.13 OUR FIT Error includes scale factor of 1.1.					
341.65±0.15 OUR AVERAGE Error includes scale factor of 1.3. See the ideogram below.					
341.65±0.04±0.12	6.2k	AALTONEN	11H	CDF	$p\overline{p}$ at 1.96 TeV
342.1 ±0.5 ±0.5	51	ALBRECHT	97	ARG	$e^+e^- \approx$ 10 GeV
342.2 ±0.2 ±0.5	245 ± 19	EDWARDS	95	CLE2	$e^+e^- \approx$ 10.5 GeV
340.4 ±0.6 ±0.3	40 ± 9	FRABETTI	94	E687	γBe, $\overline{E}_\gamma$ = 220 GeV

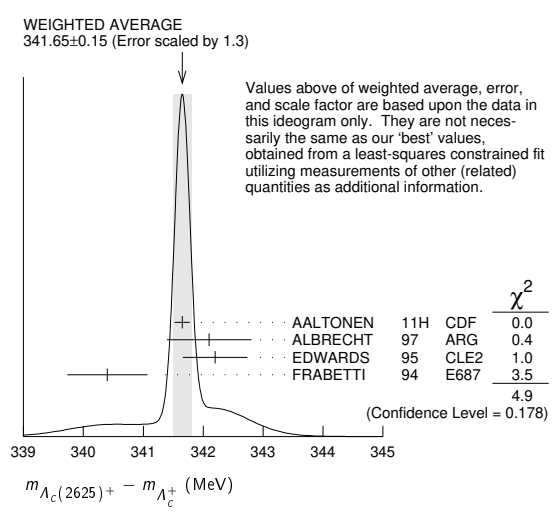

$\Lambda_c(2625)^+$ WIDTH

VALUE (MeV)	CL%	EVTS	DOCUMENT ID		TECN	COMMENT
<0.97	90	6.2k	AALTONEN	11H	CDF	$p\overline{p}$ at 1.96 TeV
• • • We do not use the following data for averages, fits, limits, etc. • • •						
<1.9	90	245 ± 19	EDWARDS	95	CLE2	$e^+e^- \approx$ 10.5 GeV
<3.2	90		ALBRECHT	93F	ARG	$e^+e^- \approx \Upsilon(4S)$

Downloaded from https://academic.oup.com/ptep/article/2022/8/083C01/6651666 by KIT Library user on 27 September 2022

$\Lambda_c(2625)^+$ DECAY MODES

$\Lambda_c^+ \pi\pi$ and its submode $\Sigma(2455)\pi$ are the only strong decays allowed to an excited Λ_c^+ having this mass.

	Mode	Fraction (Γ_i/Γ)	Confidence level
Γ_1	$\Lambda_c^+ \pi^+ \pi^-$	$\approx 67\%$	
Γ_2	$\Sigma_c(2455)^{++} \pi^-$	<5	90%
Γ_3	$\Sigma_c(2455)^0 \pi^+$	<5	90%
Γ_4	$\Lambda_c^+ \pi^+ \pi^-$ 3-body	large	
Γ_5	$\Lambda_c^+ \pi^0$	[a] not seen	
Γ_6	$\Lambda_c^+ \gamma$	not seen	

[a] A test that the isospin is indeed 0, so that the particle is indeed a Λ_c^+.

$\Lambda_c(2625)^+$ BRANCHING RATIOS

$\Gamma(\Sigma_c(2455)^{++}\pi^-)/\Gamma(\Lambda_c^+\pi^+\pi^-)$ — Γ_2/Γ_1

VALUE	CL%	DOCUMENT ID		TECN	COMMENT
<0.08	90	EDWARDS	95	CLE2	$e^+e^- \approx$ 10.5 GeV

$\Gamma(\Sigma_c(2455)^0\pi^+)/\Gamma(\Lambda_c^+\pi^+\pi^-)$ — Γ_3/Γ_1

VALUE	CL%	DOCUMENT ID		TECN	COMMENT
<0.07	90	EDWARDS	95	CLE2	$e^+e^- \approx$ 10.5 GeV

$[\Gamma(\Sigma_c(2455)^{++}\pi^-) + \Gamma(\Sigma_c(2455)^0\pi^+)]/\Gamma(\Lambda_c^+\pi^+\pi^-)$ — $(\Gamma_2+\Gamma_3)/\Gamma_1$

VALUE	CL%	EVTS	DOCUMENT ID		TECN	COMMENT
• • • We do not use the following data for averages, fits, limits, etc. • • •						
<0.36	90		FRABETTI	94	E687	γBe, $\overline{E}_\gamma$ = 220 GeV
0.46 ± 0.14		21	ALBRECHT	93F	ARG	$e^+e^- \approx \Upsilon(4S)$

$\Gamma(\Lambda_c^+\pi^+\pi^-$ 3-body$)/\Gamma(\Lambda_c^+\pi^+\pi^-)$ — Γ_4/Γ_1

VALUE	EVTS	DOCUMENT ID		TECN	COMMENT
• • • We do not use the following data for averages, fits, limits, etc. • • •					
0.54 ± 0.14	16	ALBRECHT	93F	ARG	$e^+e^- \approx \Upsilon(4S)$

$\Gamma(\Lambda_c^+\pi^0)/\Gamma(\Lambda_c^+\pi^+\pi^-)$ — Γ_5/Γ_1

$\Lambda_c^+\pi^0$ decay is forbidden by isospin conservation if this state is in fact a Λ_c.

VALUE	CL%	DOCUMENT ID		TECN	COMMENT
<0.91	90	EDWARDS	95	CLE2	$e^+e^- \approx$ 10.5 GeV

$\Gamma(\Lambda_c^+\gamma)/\Gamma(\Lambda_c^+\pi^+\pi^-)$ — Γ_6/Γ_1

VALUE	CL%	DOCUMENT ID		TECN	COMMENT
<0.52	90	EDWARDS	95	CLE2	$e^+e^- \approx$ 10.5 GeV

$\Lambda_c(2625)^+$ REFERENCES

AALTONEN	11H	PR D84 012003	T. Aaltonen *et al.*	(CDF Collab.)
ALBRECHT	97	PL B402 207	H. Albrecht *et al.*	(ARGUS Collab.)
EDWARDS	95	PRL 74 3331	K.W. Edwards *et al.*	(CLEO Collab.)
FRABETTI	94	PRL 72 961	P.L. Frabetti *et al.*	(FNAL E687 Collab.)
ALBRECHT	93F	PL B317 227	H. Albrecht *et al.*	(ARGUS Collab.)

$\Lambda_c(2765)^+$ or $\Sigma_c(2765)$

$I(J^P) = ?(?^?)$ Status: *

OMITTED FROM SUMMARY TABLE

A broad, statistically significant peak (997^{+141}_{-129} events) seen in $\Lambda_c^+\pi^+\pi^-$. However, nothing at all is known about its quantum numbers, including whether it is a Λ_c^+ or a Σ_c, or whether the width might be due to overlapping states.

$\Lambda_c(2765)^+$ MASS

The mass is obtained from the $\Lambda_c(2765)^+ - \Lambda_c^+$ mass-difference measurement below.

VALUE (MeV)	DOCUMENT ID
2766.6±2.4 OUR FIT	

$\Lambda_c(2765)^+ - \Lambda_c^+$ MASS DIFFERENCE

VALUE (MeV)	EVTS	DOCUMENT ID		TECN	COMMENT
480.1±2.4 OUR FIT					
480.1±2.4	997^{+141}_{-129}	ARTUSO	01	CLE2	$e^+e^- \approx \Upsilon(4S)$

$\Lambda_c(2765)^+$ WIDTH

VALUE (MeV)	DOCUMENT ID		TECN	COMMENT
50	ARTUSO	01	CLE2	$e^+e^- \approx \Upsilon(4S)$

$\Lambda_c(2765)^+$ DECAY MODES

	Mode	Fraction (Γ_i/Γ)
Γ_1	$\Lambda_c^+\pi^+\pi^-$	seen

$\Lambda_c(2765)^+$ REFERENCES

ARTUSO	01	PRL 86 4479	M. Artuso *et al.*	(CLEO Collab.)

$\Lambda_c(2860)^+$

$I(J^P) = 0(\frac{3}{2}^+)$ Status: ***

$\Lambda_c(2860)^+$ MASS

VALUE (MeV)	DOCUMENT ID		TECN	COMMENT
$\mathbf{2856.1^{+2.0}_{-1.7} \pm 0.5^{+1.1}_{-5.6}}$	[1] AAIJ	17s	LHCB	in $\Lambda_b^0 \to D^0 p \pi^-$

[1] The third AAIJ 17s uncertainty comes from modeling the resonant shape of the nearby $\Lambda_c(2880)^+$ and the background (non-resonant) amplitudes.

$\Lambda_c(2860)^+$ WIDTH

VALUE (MeV)	DOCUMENT ID		TECN	COMMENT
$\mathbf{67.6^{+10.1}_{-8.1} \pm 1.4^{+5.9}_{-20.0}}$	[1] AAIJ	17s	LHCB	in $\Lambda_b^0 \to D^0 p \pi^-$

[1] The third AAIJ 17s uncertainty comes from modeling the resonant shape of the nearby $\Lambda_c(2880)^+$ and the background (non-resonant) amplitudes.

$\Lambda_c(2860)^+$ DECAY MODES

	Mode	Fraction (Γ_i/Γ)
Γ_1	$D^0 p$	seen

$\Lambda_c(2860)^+$ BRANCHING RATIOS

$\Gamma(D^0 p)/\Gamma_{total}$ — Γ_1/Γ

VALUE	DOCUMENT ID		TECN	COMMENT
seen	AAIJ	17s	LHCB	in $\Lambda_b^0 \to D^0 p \pi^-$

$\Lambda_c(2860)^+$ REFERENCES

AAIJ	17S	JHEP 1705 030	R. Aaij *et al.*	(LHCb Collab.) JP

$\Lambda_c(2880)^+$

$I(J^P) = 0(\frac{5}{2}^+)$ Status: ***

A narrow peak seen in $\Lambda_c^+\pi^+\pi^-$ and in pD^0. It is not seen in pD^+, and therefore it is a Λ_c^+ and not a Σ_c.

$\Lambda_c(2880)^+$ MASS

VALUE (MeV)	EVTS	DOCUMENT ID		TECN	COMMENT
2881.63±0.24 OUR FIT					
2881.62±0.24 OUR AVERAGE					
$2881.75 \pm 0.29 \pm 0.07^{+0.14}_{-0.20}$		[1] AAIJ	17s	LHCB	in $\Lambda_b^0 \to D^0 p \pi^-$
$2881.9 \pm 0.1 \pm 0.5$	2.8k	AUBERT	07	BABR	in pD^0
$2881.2 \pm 0.2 \pm 0.4$	690	MIZUK	07	BELL	in $\Sigma_c(2455)^{0,++}\pi^\pm$

[1] The third AAIJ 17s uncertainty comes from modeling the resonant shape of the $\Lambda_c(2880)^+$ and the background (non-resonant) amplitudes.

$\Lambda_c(2880)^+ - \Lambda_c^+$ MASS DIFFERENCE

VALUE (MeV)	EVTS	DOCUMENT ID		TECN	COMMENT
595.17±0.28 OUR FIT					
596 ±1 ±2	350	ARTUSO	01	CLE2	in $\Lambda_c^+\pi^+\pi^-$

$\Lambda_c(2880)^+$ WIDTH

VALUE (MeV)	CL%	EVTS	DOCUMENT ID		TECN	COMMENT
$\mathbf{5.6^{+0.8}_{-0.6}}$ **OUR AVERAGE**						
$5.43^{+0.77}_{-0.71} \pm^{+0.81}_{-0.29}$			[2] AAIJ	17s	LHCB	in $\Lambda_b^0 \to D^0 p \pi^-$
$5.8 \pm 1.5 \pm 1.1$		2.8k	AUBERT	07	BABR	in pD^0
$5.8 \pm 0.7 \pm 1.1$		690	MIZUK	07	BELL	in $\Sigma_c(2455)^{0,++}\pi^\pm$

Downloaded from https://academic.oup.com/ptep/article/2022/8/083C01/6651666 by KIT Library user on 27 September 2022

• • • We do not use the following data for averages, fits, limits, etc. • • •

<8	90	ARTUSO	01	CLEO	in $\Lambda_c^+ \pi^+ \pi^-$

[2] AAIJ 17S reports $5.43^{+0.77}_{-0.71} \pm 0.29^{+0.75}_{-0.00}$ MeV value where the third uncertainty comes from modeling the resonant shape of the $\Lambda_c(2880)^+$ and the background (non-resonant) amplitudes. We have combined in quadrature the systematic uncertainties.

$\Lambda_c(2880)^+$ DECAY MODES

	Mode	Fraction (Γ_i/Γ)
Γ_1	$\Lambda_c^+ \pi^+ \pi^-$	seen
Γ_2	$\Sigma_c(2455)^{0,++} \pi^\pm$	seen
Γ_3	$\Sigma_c(2520)^{0,++} \pi^\pm$	seen
Γ_4	$p D^0$	seen

$\Lambda_c(2880)^+$ BRANCHING RATIOS

$\Gamma(\Sigma_c(2455)^{0,++}\pi^\pm)/\Gamma(\Lambda_c^+\pi^+\pi^-)$ — Γ_2/Γ_1

VALUE	EVTS	DOCUMENT ID		TECN	COMMENT
0.392±0.031 OUR AVERAGE		Error includes scale factor of 1.3.			
0.404±0.021±0.014		MIZUK	07	BELL	in $\Sigma_c(2455)^{0,++} \pi^\pm$
0.31 ±0.06 ±0.03	96	ARTUSO	01	CLE2	$e^+e^- \approx \Upsilon(4S)$

$\Gamma(\Sigma_c(2520)^{0,++}\pi^\pm)/\Gamma(\Lambda_c^+\pi^+\pi^-)$ — Γ_3/Γ_1

VALUE	CL%	DOCUMENT ID		TECN	COMMENT
0.091±0.025±0.010		MIZUK	07	BELL	in $\Sigma_c(2455)^{0,++} \pi^\pm$
• • • We do not use the following data for averages, fits, limits, etc. • • •					
<0.11	90	ARTUSO	01	CLE2	$e^+e^- \approx \Upsilon(4S)$

$\Gamma(\Sigma_c(2520)^{0,++}\pi^\pm)/\Gamma(\Sigma_c(2455)^{0,++}\pi^\pm)$ — Γ_3/Γ_2

VALUE	DOCUMENT ID		TECN	COMMENT
• • • We do not use the following data for averages, fits, limits, etc. • • •				
0.225±0.062±0.025	[3] MIZUK	07	BELL	in $\Sigma_c(2455)^{0,++} \pi^\pm$

[3] This MIZUK 07 ratio is redundant with MIZUK 07 ratios given above.

$\Lambda_c(2880)^+$ REFERENCES

AAIJ	17S	JHEP 1705 030	R. Aaij *et al.*	(LHCb Collab.) JP
AUBERT	07	PRL 98 012001	B. Aubert *et al.*	(BABAR Collab.)
MIZUK	07	PRL 98 262001	R. Mizuk *et al.*	(BELLE Collab.)
ARTUSO	01	PRL 86 4479	M. Artuso *et al.*	(CLEO Collab.)

$\Lambda_c(2940)^+$

$I(J^P) = 0(\frac{3}{2}^-)$ Status: ***

A narrow peak seen in $p D^0$ and in $\Lambda_c^+ \pi^+ \pi^-$. It is not seen in $p D^+$, and therefore it is a Λ_c^+ and not a Σ_c. $J^P = 3/2^-$ is favored, but not certain.

$\Lambda_c(2940)^+$ MASS

VALUE (MeV)	EVTS	DOCUMENT ID		TECN	COMMENT
$2939.6^{+1.3}_{-1.5}$ OUR AVERAGE					
$2944.8^{+3.5}_{-2.5} \pm 0.4^{+0.1}_{-4.6}$		[1] AAIJ	17S	LHCB	in $\Lambda_b^0 \to D^0 p \pi^-$
2939.8±1.3±1.0	2.2k	AUBERT	07	BABR	in $p D^0$
$2938.0 \pm 1.3^{+2.0}_{-4.0}$	220	MIZUK	07	BELL	in $\Sigma_c(2455)^{0,++} \pi^\pm$

[1] The third AAIJ 17S uncertainty comes from modeling the resonant shape of the nearby $\Lambda_c(2880)^+$ and the background (non-resonant) amplitudes.

$\Lambda_c(2940)^+$ WIDTH

VALUE (MeV)	EVTS	DOCUMENT ID		TECN	COMMENT
20^{+6}_{-5} OUR AVERAGE					
$27.7^{+8.2}_{-6.0} \pm 0.9^{+5.2}_{-10.4}$		[2] AAIJ	17S	LHCB	in $\Lambda_b^0 \to D^0 p \pi^-$
17.5±5.2± 5.9	2.2k	AUBERT	07	BABR	in $p D^0$
$13^{+8}_{-5} {}^{+27}_{-7}$	220	MIZUK	07	BELL	in $\Sigma_c(2455)^{0,++} \pi^\pm$

[2] The third AAIJ 17S uncertainty comes from modeling the resonant shape of the nearby $\Lambda_c(2880)^+$ and the background (non-resonant) amplitudes.

$\Lambda_c(2940)^+$ DECAY MODES

	Mode	Fraction (Γ_i/Γ)
Γ_1	$p D^0$	seen
Γ_2	$\Sigma_c(2455)^{0,++} \pi^\pm$	seen

$\Lambda_c(2940)^+$ REFERENCES

AAIJ	17S	JHEP 1705 030	R. Aaij *et al.*	(LHCb Collab.) JP
AUBERT	07	PRL 98 012001	B. Aubert *et al.*	(BABAR Collab.)
MIZUK	07	PRL 98 262001	R. Mizuk *et al.*	(BELLE Collab.)

$\Sigma_c(2455)$

$I(J^P) = 1(\frac{1}{2}^+)$ Status: ****

The angular distribution of $B^- \to \Sigma_c(2455)^0 \overline{p}$ favors $J = 1/2$ (as the quark model predicts). $J = 3/2$ is excluded by more than four standard deviations; see AUBERT 08BN.

$\Sigma_c(2455)$ MASSES

The masses are obtained from the mass-difference measurements that follow.

$\Sigma_c(2455)^{++}$ MASS

VALUE (MeV)	DOCUMENT ID
2453.97±0.14 OUR FIT	

$\Sigma_c(2455)^+$ MASS

VALUE (MeV)	DOCUMENT ID
$2452.65^{+0.22}_{-0.16}$ OUR FIT	

$\Sigma_c(2455)^0$ MASS

VALUE (MeV)	DOCUMENT ID
2453.75±0.14 OUR FIT	

$\Sigma_c(2455) - \Lambda_c^+$ MASS DIFFERENCES

$m_{\Sigma_c(2455)^{++}} - m_{\Lambda_c^+}$

VALUE (MeV)	EVTS	DOCUMENT ID		TECN	COMMENT
167.510± 0.017 OUR FIT					
167.510± 0.022 OUR AVERAGE					
167.51 ± 0.01 ±0.02	36k	LEE	14	BELL	e^+e^- at $\Upsilon(4S)$
167.44 ± 0.04 ±0.12	13.8k	AALTONEN	11H	CDF	$p\overline{p}$ at 1.96 TeV
167.4 ± 0.1 ±0.2	2k	ARTUSO	02	CLE2	$e^+e^- \approx \Upsilon(4S)$
167.35 ± 0.19 ±0.12	461	LINK	00C	FOCS	γ A, $\overline{E}_\gamma$ 180 GeV
167.76 ± 0.29 ±0.15	122	AITALA	96B	E791	$\pi^- N$, 500 GeV
167.6 ± 0.6 ±0.6	56	FRABETTI	96	E687	γBe, $\overline{E}_\gamma \approx$ 220 GeV
168.2 ± 0.3 ±0.2	126	CRAWFORD	93	CLE2	$e^+e^- \approx \Upsilon(4S)$
167.8 ± 0.4 ±0.3	54	BOWCOCK	89	CLEO	e^+e^- 10 GeV
168.2 ± 0.5 ±1.6	92	ALBRECHT	88D	ARG	e^+e^- 10 GeV
167.4 ± 0.5 ±2.0	46	DIESBURG	87	SPEC	nA ~ 600 GeV
• • • We do not use the following data for averages, fits, limits, etc. • • •					
167 ± 1	2	JONES	87	HBC	νp in BEBC
166 ± 1	1	BOSETTI	82	HBC	See JONES 87
168 ± 3	6	BALTAY	79	HLBC	ν Ne-H in 15-ft
166 ±15	1	CAZZOLI	75	HBC	νp in BNL 7-ft

$m_{\Sigma_c(2455)^+} - m_{\Lambda_c^+}$

VALUE (MeV)	EVTS	DOCUMENT ID		TECN	COMMENT
$166.19^{+0.16}_{-0.08}$ OUR FIT					
$166.19^{+0.15}_{-0.08}$ OUR AVERAGE					
$166.17 \pm 0.05^{+0.16}_{-0.07}$		YELTON	21	BELL	e^+e^- at $\Upsilon(nS)$
166.4 ±0.2 ±0.3	661	AMMAR	01	CLE2	$e^+e^- \approx \Upsilon(4S)$
• • • We do not use the following data for averages, fits, limits, etc. • • •					
168.5 ±0.4 ±0.2	111	CRAWFORD	93	CLE2	See AMMAR 01
168 ±3	1	CALICCHIO	80	HBC	νp in BEBC-TST

$m_{\Sigma_c(2455)^0} - m_{\Lambda_c^+}$

VALUE (MeV)	EVTS	DOCUMENT ID		TECN	COMMENT
167.290±0.017 OUR FIT					
167.290±0.022 OUR AVERAGE					
167.29 ±0.01 ±0.02	32k	LEE	14	BELL	e^+e^- at $\Upsilon(4S)$
167.28 ±0.03 ±0.12	15.9k	AALTONEN	11H	CDF	$p\overline{p}$ at 1.96 TeV
167.2 ±0.1 ±0.2	2k	ARTUSO	02	CLE2	$e^+e^- \approx \Upsilon(4S)$
167.38 ±0.21 ±0.13	362	LINK	00C	FOCS	γ A, $\overline{E}_\gamma$ 180 GeV
167.38 ±0.29 ±0.15	143	AITALA	96B	E791	$\pi^- N$, 500 GeV
167.8 ±0.6 ±0.2		ALEEV	96	SPEC	n nucleus, 50 GeV/c
166.6 ±0.5 ±0.6	69	FRABETTI	96	E687	γBe, $\overline{E}_\gamma \approx$ 220 GeV
167.1 ±0.3 ±0.2	124	CRAWFORD	93	CLE2	$e^+e^- \approx \Upsilon(4S)$
168.4 ±1.0 ±0.3	14	ANJOS	89D	E691	γBe 90–260 GeV
• • • We do not use the following data for averages, fits, limits, etc. • • •					
167.9 ±0.5 ±0.3	48	[1] BOWCOCK	89	CLEO	e^+e^- 10 GeV
167.0 ±0.5 ±1.6	70	[1] ALBRECHT	88D	ARG	e^+e^- 10 GeV
178.2 ±0.4 ±2.0	85	[2] DIESBURG	87	SPEC	nA ~ 600 GeV
163 ±2	1	AMMAR	86	EMUL	νA

Downloaded from https://academic.oup.com/ptep/article/2022/8/083C01/6651666 by KIT Library user on 27 September 2022

[1] This result enters the fit through $m_{\Sigma_c^{++}} - m_{\Sigma_c^0}$ given below.

[2] See the note on DIESBURG 87 in the $m_{\Sigma_c^{++}} - m_{\Sigma_c^0}$ section below.

$\Sigma_c(2455)$ MASS DIFFERENCES

$m_{\Sigma_c(2455)^{++}} - m_{\Sigma_c(2455)^0}$

VALUE (MeV)	DOCUMENT ID		TECN	COMMENT
0.220±0.013 OUR FIT				
0.221±0.014 OUR AVERAGE				
0.22 ±0.01 ±0.01	LEE	14	BELL	e^+e^- at $\Upsilon(4S)$
0.2 ±0.1 ±0.1	ARTUSO	02	CLE2	$e^+e^- \approx \Upsilon(4S)$
− 0.03 ±0.28 ±0.11	LINK	00C	FOCS	γ A, $\overline{E}_\gamma$ 180 GeV
0.38 ±0.40 ±0.15	AITALA	96B	E791	$\pi^- N$, 500 GeV
1.1 ±0.4 ±0.1	CRAWFORD	93	CLE2	$e^+e^- \approx \Upsilon(4S)$
− 0.1 ±0.6 ±0.1	BOWCOCK	89	CLEO	e^+e^- 10 GeV
1.2 ±0.7 ±0.3	ALBRECHT	88D	ARG	$e^+e^- \sim$ 10 GeV
• • • We do not use the following data for averages, fits, limits, etc. • • •				
−10.8 ±2.9	[3] DIESBURG	87	SPEC	nA ∼ 600 GeV

[3] DIESBURG 87 is completely incompatible with the other experiments, which is surprising since it agrees with them about $m_{\Sigma_c(2455)^{++}} - m_{\Lambda_c^+}$. We go with the majority here.

$m_{\Sigma_c(2455)^+} - m_{\Sigma_c(2455)^0}$

VALUE (MeV)	DOCUMENT ID		TECN	COMMENT
$-1.10^{+0.16}_{-0.08}$ OUR FIT				
• • • We do not use the following data for averages, fits, limits, etc. • • •				
1.4 ±0.5 ±0.3	CRAWFORD	93	CLE2	See AMMAR 01

$\Sigma_c(2455)$ WIDTHS

$\Sigma_c(2455)^{++}$ WIDTH

VALUE (MeV)	EVTS	DOCUMENT ID		TECN	COMMENT
$1.89^{+0.09}_{-0.18}$ OUR AVERAGE Error includes scale factor of 1.1.					
$1.84\pm0.04^{+0.07}_{-0.20}$	36k	LEE	14	BELL	e^+e^- at $\Upsilon(4S)$
2.34±0.13±0.45	13.8k	AALTONEN	11H	CDF	$p\overline{p}$ at 1.96 TeV
2.3 ±0.2 ±0.3	2k	ARTUSO	02	CLE2	$e^+e^- \approx \Upsilon(4S)$
$2.05^{+0.41}_{-0.38}\pm0.38$	1110	LINK	02	FOCS	γ A, $\overline{E}_\gamma \approx$ 180 GeV

$\Sigma_c(2455)^+$ WIDTH

VALUE (MeV)	CL%	EVTS	DOCUMENT ID		TECN	COMMENT
2.3±0.3±0.3			YELTON	21	BELL	e^+e^- at Υ(nS)
• • • We do not use the following data for averages, fits, limits, etc. • • •						
<4.6	90	661	AMMAR	01	CLE2	$e^+e^- \approx \Upsilon(4S)$

$\Sigma_c(2455)^0$ WIDTH

VALUE (MeV)	EVTS	DOCUMENT ID		TECN	COMMENT
$1.83^{+0.11}_{-0.19}$ OUR AVERAGE Error includes scale factor of 1.2.					
$1.76\pm0.04^{+0.09}_{-0.21}$	32k	LEE	14	BELL	e^+e^- at $\Upsilon(4S)$
1.65±0.11±0.49	15.9k	AALTONEN	11H	CDF	$p\overline{p}$ at 1.96 TeV
2.6 ±0.5 ±0.3		AUBERT	08BN	BABR	$B^- \to \overline{p}\Lambda_c^+\pi^-$
2.5 ±0.2 ±0.3	2k	ARTUSO	02	CLE2	$e^+e^- \approx \Upsilon(4S)$
$1.55^{+0.41}_{-0.37}\pm0.38$	913	LINK	02	FOCS	γ A, $\overline{E}_\gamma \approx$ 180 GeV

$\Sigma_c(2455)$ DECAY MODES

$\Lambda_c^+\pi$ is the only strong decay allowed to a Σ_c having this mass.

	Mode	Fraction (Γ_i/Γ)
Γ_1	$\Lambda_c^+\pi$	≈ 100 %

$\Sigma_c(2455)$ REFERENCES

YELTON	21	PR D104 052003	J. Yelton *et al.*	(BELLE Collab.)
LEE	14	PR D89 091102	S.-H. Lee *et al.*	(BELLE Collab.)
AALTONEN	11H	PR D84 012003	T. Aaltonen *et al.*	(CDF Collab.)
AUBERT	08BN	PR D78 112003	B. Aubert *et al.*	(BABAR Collab.)
ARTUSO	02	PR D65 071101	M. Artuso *et al.*	(CLEO Collab.)
LINK	02	PL B525 205	J.M. Link *et al.*	(FNAL FOCUS Collab.)
AMMAR	01	PRL 86 1167	R. Ammar *et al.*	(CLEO Collab.)
LINK	00C	PL B488 218	J.M. Link *et al.*	(FNAL FOCUS Collab.)
AITALA	96B	PL B379 292	E.M. Aitala *et al.*	(FNAL E791 Collab.)
ALEEV	96	JINRRC 3-77 31	A.N. Aleev *et al.*	(Serpukhov EXCHARM Collab.)
FRABETTI	96	PL B365 461	P.L. Frabetti *et al.*	(FNAL E687 Collab.)
CRAWFORD	93	PRL 71 3259	G. Crawford *et al.*	(CLEO Collab.)
ANJOS	89D	PRL 62 1721	J.C. Anjos *et al.*	(FNAL E691 Collab.)
BOWCOCK	89	PRL 62 1240	T.J.V. Bowcock *et al.*	(CLEO Collab.)
ALBRECHT	88D	PL B211 489	H. Albrecht *et al.*	(ARGUS Collab.)
DIESBURG	87	PRL 59 2711	M. Diesburg *et al.*	(FNAL E400 Collab.)
JONES	87	ZPHY C36 593	G.T. Jones *et al.*	(CERN WA21 Collab.)
AMMAR	86	JETPL 43 515	R. Ammar *et al.*	(ITEP)
		Translated from ZETFP 43 401.		
BOSETTI	82	PL 109B 234	P.C. Bosetti *et al.*	(AACH3, BONN, CERN+)
CALICCHIO	80	PL 93B 521	M. Calicchio *et al.*	(BARI, BIRM, BRUX+)
BALTAY	79	PRL 42 1721	C. Baltay *et al.*	(COLU, BNL)
CAZZOLI	75	PRL 34 1125	E.G. Cazzoli *et al.*	(BNL)

$\Sigma_c(2520)$

$I(J^P) = 1(\frac{3}{2}^+)$ Status: ***

Seen in the $\Lambda_c^+\pi^\pm$ mass spectrum. The natural assignment is that this is the $J^P = 3/2^+$ excitation of the $\Sigma_c(2455)$, the charm counterpart of the $\Sigma(1385)$, but neither J nor P has been measured.

$\Sigma_c(2520)$ MASSES

The masses are obtained from the mass-difference measurements that follow.

$\Sigma_c(2520)^{++}$ MASS

VALUE (MeV)	EVTS	DOCUMENT ID		TECN	COMMENT
$2518.41^{+0.22}_{-0.18}$ OUR FIT Error includes scale factor of 1.1.					
• • • We do not use the following data for averages, fits, limits, etc. • • •					
2530 ±5 ±5	6	[1] AMMOSOV	93	HLBC	$\nu p \to \mu^- \Sigma_c(2530)^{++}$

[1] AMMOSOV 93 sees a cluster of 6 events and estimates the background to be 1 event.

$\Sigma_c(2520)^+$ MASS

VALUE (MeV)	DOCUMENT ID
$2517.4^{+0.7}_{-0.5}$ OUR FIT	

$\Sigma_c(2520)^0$ MASS

VALUE (MeV)	DOCUMENT ID
2518.48±0.20 OUR FIT Error includes scale factor of 1.1.	

$\Sigma_c(2520)$ MASS DIFFERENCES

$m_{\Sigma_c(2520)^{++}} - m_{\Lambda_c^+}$

VALUE (MeV)	EVTS	DOCUMENT ID		TECN	COMMENT
$231.95^{+0.18}_{-0.12}$ OUR FIT Error includes scale factor of 1.3.					
231.95±0.16 OUR AVERAGE Error includes scale factor of 1.6. See the ideogram below.					
231.99±0.10±0.02	44k	LEE	14	BELL	e^+e^- at $\Upsilon(4S)$
230.73±0.56±0.16	8.8k	AALTONEN	11H	CDF	$p\overline{p}$ at 1.96 TeV
231.5 ±0.4 ±0.3	1.3k	ATHAR	05	CLEO	e^+e^-, 9.4–11.5 GeV
234.5 ±1.1 ±0.8	677	BRANDENB...	97	CLE2	$e^+e^- \approx \Upsilon(4S)$

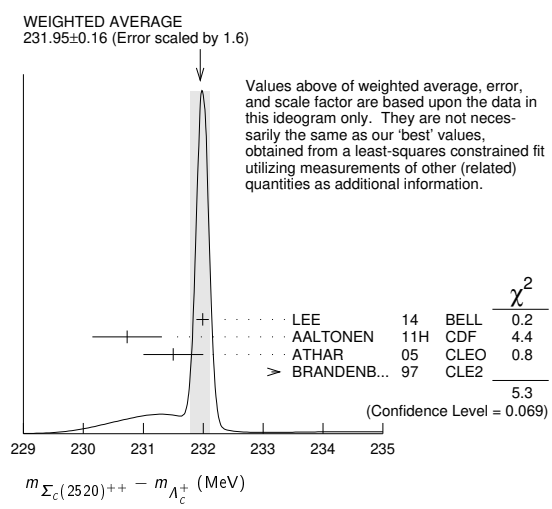

$m_{\Sigma_c(2520)^+} - m_{\Lambda_c^+}$

VALUE (MeV)	EVTS	DOCUMENT ID		TECN	COMMENT
$230.9^{+0.7}_{-0.5}$ OUR FIT					
$230.9^{+0.7}_{-0.5}$ OUR AVERAGE					
$230.9\pm0.5^{+0.5}_{-0.1}$		YELTON	21	BELL	e^+e^- at Υ(nS)
231.0±1.1±2.0	327	AMMAR	01	CLE2	$e^+e^- \approx \Upsilon(4S)$

$m_{\Sigma_c(2520)^0} - m_{\Lambda_c^+}$

VALUE (MeV)	EVTS	DOCUMENT ID		TECN	COMMENT
$232.02^{+0.16}_{-0.14}$ OUR FIT Error includes scale factor of 1.3.					
232.02±0.17 OUR AVERAGE Error includes scale factor of 1.5. See the ideogram below.					
231.98±0.11±0.04	41k	LEE	14	BELL	e^+e^- at $\Upsilon(4S)$
232.88±0.43±0.16	9.0k	AALTONEN	11H	CDF	$p\overline{p}$ at 1.96 TeV
231.4 ±0.5 ±0.3	1.3k	ATHAR	05	CLEO	e^+e^-, 9.4–11.5 GeV
232.6 ±1.0 ±0.8	504	BRANDENB...	97	CLE2	$e^+e^- \approx \Upsilon(4S)$

Downloaded from https://academic.oup.com/ptep/article/2022/8/083C01/6651666 by KIT Library user on 27 September 2022

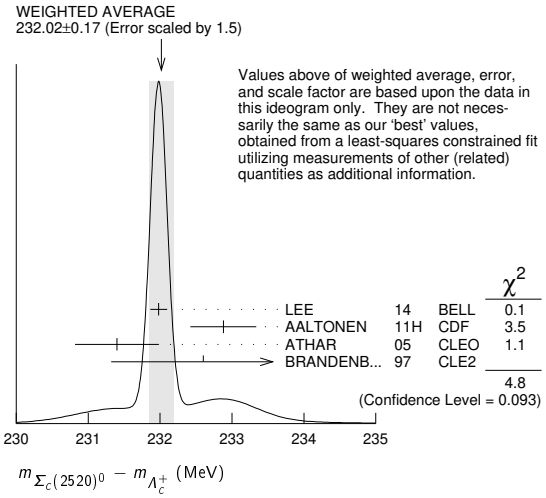

$m_{\Sigma_c(2520)^{++}} - m_{\Sigma_c(2520)^0}$

VALUE (MeV)	EVTS	DOCUMENT ID		TECN	COMMENT
0.01±0.15±0.03	44/41k	LEE	14	BELL	e^+e^- at $\Upsilon(4S)$
• • • We do not use the following data for averages, fits, limits, etc. • • •					
0.1 ±0.8 ±0.3		[2] ATHAR	05	CLEO	e^+e^-, 9.4–11.5 GeV
1.9 ±1.4 ±1.0		[3] BRANDENB...	97	CLE2	$e^+e^- \approx \Upsilon(4S)$

[2] This ATHAR 05 result is redundant with measurements in earlier entries.
[3] This BRANDENBURG 97 result is redundant with measurements in earlier entries.

$\Sigma_c(2520)$ WIDTHS

$\Sigma_c(2520)^{++}$ WIDTH

VALUE (MeV)	EVTS	DOCUMENT ID		TECN	COMMENT
$14.78^{+0.30}_{-0.40}$ OUR AVERAGE					
$14.77\pm0.25^{+0.18}_{-0.30}$	44k	LEE	14	BELL	e^+e^- at $\Upsilon(4S)$
15.03±2.12±1.36	8.8k	AALTONEN	11H	CDF	$p\overline{p}$ at 1.96 TeV
$14.4\ ^{+1.6}_{-1.5}\ \pm1.4$	1.3k	ATHAR	05	CLEO	e^+e^-, 9.4–11.5 GeV
$17.9\ ^{+3.8}_{-3.2}\ \pm4.0$	677	BRANDENB...	97	CLE2	$e^+e^- \approx \Upsilon(4S)$

$\Sigma_c(2520)^+$ WIDTH

VALUE (MeV)	CL%	EVTS	DOCUMENT ID		TECN	COMMENT
$17.2^{+2.3+3.1}_{-2.1-0.7}$			YELTON	21	BELL	e^+e^- at $\Upsilon(nS)$
• • • We do not use the following data for averages, fits, limits, etc. • • •						
<17	90	327	AMMAR	01	CLE2	$e^+e^- \approx \Upsilon(4S)$

$\Sigma_c(2520)^0$ WIDTH

VALUE (MeV)	EVTS	DOCUMENT ID		TECN	COMMENT
$15.3\ ^{+0.4}_{-0.5}$ OUR AVERAGE					
$15.41\pm0.41^{+0.20}_{-0.32}$	41k	LEE	14	BELL	e^+e^- at $\Upsilon(4S)$
12.51±1.82±1.37	9.0k	AALTONEN	11H	CDF	$p\overline{p}$ at 1.96 TeV
$16.6\ ^{+1.9}_{-1.7}\ \pm1.4$	1.3k	ATHAR	05	CLEO	e^+e^-, 9.4–11.5 GeV
$13.0\ ^{+3.7}_{-3.0}\ \pm4.0$	504	BRANDENB...	97	CLE2	$e^+e^- \approx \Upsilon(4S)$

$\Sigma_c(2520)$ DECAY MODES

$\Lambda_c^+\pi$ is the only strong decay allowed to a Σ_c having this mass.

	Mode	Fraction (Γ_i/Γ)
Γ_1	$\Lambda_c^+\pi$	≈ 100 %

$\Sigma_c(2520)$ REFERENCES

YELTON	21	PR D104 052003	J. Yelton *et al.*	(BELLE Collab.)
LEE	14	PR D89 091102	S.-H. Lee *et al.*	(BELLE Collab.)
AALTONEN	11H	PR D84 012003	T. Aaltonen *et al.*	(CDF Collab.)
ATHAR	05	PR D71 051101	S.B. Athar *et al.*	(CLEO Collab.)
AMMAR	01	PRL 86 1167	R. Ammar *et al.*	(CLEO Collab.)
BRANDENB...	97	PRL 78 2304	G. Brandenburg *et al.*	(CLEO Collab.)
AMMOSOV	93	JETPL 58 247	V.V. Ammosov *et al.*	(SERP)
		Translated from ZETFP 58 241.		

$\Sigma_c(2800)$

$I(J^P) = 1(?^?)$ Status: ***

Seen in the $\Lambda_c^+\pi^+$, $\Lambda_c^+\pi^0$, and $\Lambda_c^+\pi^-$ mass spectra.

$\Sigma_c(2800)$ MASSES

The charged ++ and + masses are obtained from the mass-difference measurements that follow. The neutral mass is dominated by the mass-difference measurement, but is pulled up somewhat by the less well-determined but considerably higher direct-mass measurement. It is possible, in fact, that AUBERT 08BN is seeing a different Σ_c.

$\Sigma_c(2800)^{++}$ MASS

VALUE (MeV)	DOCUMENT ID
$2801\ ^{+4}_{-6}$ OUR FIT	

$\Sigma_c(2800)^+$ MASS

VALUE (MeV)	DOCUMENT ID
$2792\ ^{+14}_{-5}$ OUR FIT	

$\Sigma_c(2800)^0$ MASS

VALUE (MeV)	DOCUMENT ID		TECN	COMMENT
$2806\ ^{+5}_{-7}$ OUR FIT Error includes scale factor of 1.3.				
2846±8±10	AUBERT	08BN	BABR	$B^- \to \overline{p}\Lambda_c^+\pi^-$

$\Sigma_c(2800)$ MASS DIFFERENCES

$m_{\Sigma_c(2800)^{++}} - m_{\Lambda_c^+}$

VALUE (MeV)	EVTS	DOCUMENT ID		TECN	COMMENT
$514\ ^{+4}_{-6}$ OUR FIT					
$514.5^{+3.4+2.8}_{-3.1-4.9}$	2810^{+1090}_{-775}	MIZUK	05	BELL	$e^+e^- \approx \Upsilon(4S)$

$m_{\Sigma_c(2800)^+} - m_{\Lambda_c^+}$

VALUE (MeV)	EVTS	DOCUMENT ID		TECN	COMMENT
$505\ ^{+14}_{-5}$ OUR FIT					
$505.4^{+5.8+12.4}_{-4.6-2.0}$	1540^{+1750}_{-1050}	MIZUK	05	BELL	$e^+e^- \approx \Upsilon(4S)$

$m_{\Sigma_c(2800)^0} - m_{\Lambda_c^+}$

VALUE (MeV)	EVTS	DOCUMENT ID		TECN	COMMENT
$519\ ^{+5}_{-7}$ OUR FIT Error includes scale factor of 1.3.					
$515.4^{+3.2+2.1}_{-3.1-6.0}$	2240^{+1300}_{-740}	MIZUK	05	BELL	$e^+e^- \approx \Upsilon(4S)$

$\Sigma_c(2800)$ WIDTHS

$\Sigma_c(2800)^{++}$ WIDTH

VALUE (MeV)	EVTS	DOCUMENT ID		TECN	COMMENT
75^{+18+12}_{-13-11}	2810^{+1090}_{-775}	MIZUK	05	BELL	$e^+e^- \approx \Upsilon(4S)$

$\Sigma_c(2800)^+$ WIDTH

VALUE (MeV)	EVTS	DOCUMENT ID		TECN	COMMENT
62^{+37+52}_{-23-38}	1540^{+1750}_{-1050}	MIZUK	05	BELL	$e^+e^- \approx \Upsilon(4S)$

$\Sigma_c(2800)^0$ WIDTH

VALUE (MeV)	EVTS	DOCUMENT ID		TECN	COMMENT
$72\ ^{+22}_{-15}$ OUR AVERAGE					
$86\ ^{+33}_{-22}\ \pm12$		AUBERT	08BN	BABR	$B^- \to \overline{p}\Lambda_c^+\pi^-$
$61\ ^{+18+22}_{-13-13}$	2240^{+1300}_{-740}	MIZUK	05	BELL	$e^+e^- \approx \Upsilon(4S)$

$\Sigma_c(2800)$ DECAY MODES

	Mode	Fraction (Γ_i/Γ)
Γ_1	$\Lambda_c^+\pi$	seen

$\Sigma_c(2800)$ REFERENCES

AUBERT	08BN	PR D78 112003	B. Aubert *et al.*	(BABAR Collab.)
MIZUK	05	PRL 94 122002	R. Mizuk *et al.*	(BELLE Collab.)

Downloaded from https://academic.oup.com/ptep/article/2022/8/083C01/6651666 by KIT Library user on 27 September 2022

Ξ_c^+

$I(J^P) = \frac{1}{2}(\frac{1}{2}^+)$ Status: ***

Neither of J or P has actually been measured.

Ξ_c^+ MASS

The fit uses the Ξ_c^+ and Ξ_c^0 mass and mass-difference measurements.

VALUE (MeV)	EVTS	DOCUMENT ID		TECN	COMMENT
2467.71 ± 0.23 OUR FIT Error includes scale factor of 1.3.					
2467.95 ± 0.19 OUR AVERAGE					
2467.97 ± 0.14 ± 0.17	3.8k	[1] AAIJ	14Z	LHCB	pp at 7, 8 TeV
2468.00 ± 0.18 ± 0.51	5.1k	AALTONEN	14B	CDF	$p\overline{p}$ at 1.96 TeV
2468.1 ± 0.4 $^{+0.2}_{-1.4}$	4.9k	[2] LESIAK	05	BELL	e^+e^-, $\Upsilon(4S)$
2465.8 ± 1.9 ± 2.5	90	FRABETTI	98	E687	γ Be, $\overline{E}_\gamma$= 220 GeV
2467.0 ± 1.6 ± 2.0	147	EDWARDS	96	CLE2	$e^+e^- \approx \Upsilon(4S)$
2465.1 ± 3.6 ± 1.9	30	ALBRECHT	90F	ARG	e^+e^- at $\Upsilon(4S)$
2467 ± 3 ± 4	23	ALAM	89	CLEO	e^+e^- 10.6 GeV
2466.5 ± 2.7 ± 1.2	5	BARLAG	89C	ACCM	π^- Cu 230 GeV
• • • We do not use the following data for averages, fits, limits, etc. • • •					
2464.4 ± 2.0 ± 1.4	30	FRABETTI	93B	E687	See FRABETTI 98
2459 ± 5 ±30	56	[3] COTEUS	87	SPEC	nA $\simeq$ 600 GeV
2460 ±25	82	BIAGI	83	SPEC	Σ^-Be 135 GeV

[1] AAIJ 14Z systematic error includes in quadrature the 0.14 MeV uncertainty from the m(Λ_c^+) mass value.

[2] The systematic error was (wrongly) given the other way round in LESIAK 05; see the erratum.

[3] Although COTEUS 87 claims to agree well with BIAGI 83 on the mass and width, there appears to be a discrepancy between the two experiments. BIAGI 83 sees a single peak (stated significance about 6 standard deviations) in the $\Lambda K^-\pi^+\pi^+$ mass spectrum. COTEUS 87 sees *two* peaks in the same spectrum, one at the Ξ_c^+ mass, the other 75 MeV lower. The latter is attributed to $\Xi_c^+ \to \Sigma^0 K^-\pi^+\pi^+ \to (\Lambda\gamma)K^-\pi^+\pi^+$, with the γ unseen. The *combined* significance of the double peak is stated to be 5.5 standard deviations. But the absence of any trace of a lower peak in BIAGI 83 seems to us to throw into question the interpretation of the lower peak of COTEUS 87.

Ξ_c^+ MEAN LIFE

VALUE (10^{-15} s)	EVTS	DOCUMENT ID		TECN	COMMENT
453 ± 5 OUR AVERAGE					
454 ± 5 ± 2	56k	[1] AAIJ	19AG	LHCB	$\Xi_c^+ \to pK^-\pi^+$
503 ± 47 ± 18	250	MAHMOOD	02	CLE2	$e^+e^- \approx \Upsilon(4S)$
439 ± 22 ± 9	532	LINK	01D	FOCS	γ nucleus, $\overline{E}_\gamma \approx$ 180 GeV
340 $^{+70}_{-50}$ ± 20	56	FRABETTI	98	E687	γ Be, $\overline{E}_\gamma$= 220 GeV
400 $^{+180}_{-120}$ ±100	102	COTEUS	87	SPEC	nA $\simeq$ 600 GeV
480 $^{+210}_{-150}$ $^{+200}_{-100}$	53	BIAGI	85C	SPEC	Σ^-Be 135 GeV
• • • We do not use the following data for averages, fits, limits, etc. • • •					
410 $^{+110}_{-80}$ ± 20	30	FRABETTI	93B	E687	See FRABETTI 98
200 $^{+110}_{-60}$	6	BARLAG	89C	ACCM	π^- (K^-) Cu 230 GeV

[1] AAIJ 19AG reports [Ξ_c^+ MEAN LIFE] / [$D^\pm$ MEAN LIFE] = 0.4392 ± 0.0034 ± 0.0028 which we multiply by our best value $D^\pm$ MEAN LIFE = (1.033 ± 0.005) × 10^{-12} s. Our first error is their experiment's error and our second error is the systematic error from using our best value.

Ξ_c^+ DECAY MODES

Branching fractions marked with a footnote, e.g. [a], have been corrected for decay modes not observed in the experiments. For example, the submode fraction $\Xi_c^+ \to \Sigma^+\overline{K}^*(892)^0$ seen in $\Xi_c^+ \to \Sigma^+K^-\pi^+$ has been multiplied up to include $\overline{K}^*(892)^0 \to \overline{K}^0\pi^0$ decays.

	Mode		Fraction (Γ_i/Γ)	Scale factor/ Confidence level
	Cabibbo-favored ($S = -2$) decays			
Γ_1	$p2K_S^0$		$(2.5\pm1.3)\times10^{-3}$	
Γ_2	$\Lambda\overline{K}^0\pi^+$		—	
Γ_3	$\Sigma(1385)^+\overline{K}^0$	[a]	(2.9±2.0) %	
Γ_4	$\Lambda K^-2\pi^+$		(9 ±4) $\times10^{-3}$	
Γ_5	$\Lambda\overline{K}^*(892)^0\pi^+$	[a]	< 5 $\times10^{-3}$	CL=90%
Γ_6	$\Sigma(1385)^+K^-\pi^+$	[a]	< 6 $\times10^{-3}$	CL=90%
Γ_7	$\Sigma^+K^-\pi^+$		(2.7±1.2) %	
Γ_8	$\Sigma^+\overline{K}^*(892)^0$	[a]	(2.3±1.1) %	
Γ_9	$\Sigma^0K^-2\pi^+$		(8 ±5) $\times10^{-3}$	
Γ_{10}	$\Xi^0\pi^+$		(1.6±0.8) %	
Γ_{11}	$\Xi^-2\pi^+$		(2.9±1.3) %	
Γ_{12}	$\Xi(1530)^0\pi^+$	[a]	< 2.9 $\times10^{-3}$	CL=90%
Γ_{13}	$\Xi(1620)^0\pi^+$		seen	
Γ_{14}	$\Xi(1690)^0\pi^+$		seen	
Γ_{15}	$\Xi^0\pi^+\pi^0$		(6.7±3.5) %	
Γ_{16}	$\Xi^0\pi^-2\pi^+$		(5.0±2.6) %	
Γ_{17}	$\Xi^0e^+\nu_e$		(7 ±4) %	
Γ_{18}	$\Omega^-K^+\pi^+$		(2.0±1.5) $\times10^{-3}$	
	Cabibbo-suppressed decays			
Γ_{19}	$pK^-\pi^+$		(6.2±3.0) $\times10^{-3}$	S=1.5
Γ_{20}	$p\overline{K}^*(892)^0$	[a]	(3.3±1.7) $\times10^{-3}$	
Γ_{21}	$\Sigma^+\pi^+\pi^-$		(1.4±0.8) %	
Γ_{22}	$\Sigma^-2\pi^+$		(5.1±3.4) $\times10^{-3}$	
Γ_{23}	$\Sigma^+K^+K^-$		(4.3±2.5) $\times10^{-3}$	
Γ_{24}	$\Sigma^+\phi$	[a]	< 3.2 $\times10^{-3}$	CL=90%
Γ_{25}	$\Xi(1690)^0K^+$, $\Xi^0 \to \Sigma^+K^-$		< 1.3 $\times10^{-3}$	CL=90%
Γ_{26}	$p\phi(1020)$		(1.2±0.6) $\times10^{-4}$	

[a] This branching fraction includes all the decay modes of the final-state resonance.

Ξ_c^+ BRANCHING RATIOS

Cabibbo-favored ($S = -2$) decays

$\Gamma(p2K_S^0)/\Gamma(\Xi^-2\pi^+)$ — Γ_1/Γ_{11}

VALUE	EVTS	DOCUMENT ID		TECN	COMMENT
0.087±0.016±0.014	168 ± 27	LESIAK	05	BELL	e^+e^-, $\Upsilon(4S)$

$\Gamma(\Sigma(1385)^+\overline{K}^0)/\Gamma(\Xi^-2\pi^+)$ — Γ_3/Γ_{11}

Unseen decay modes of the $\Sigma(1385)^+$ are included.

VALUE	EVTS	DOCUMENT ID		TECN	COMMENT
1.00±0.49±0.24	20	LINK	03E	FOCS	< 1.72, 90% CL

$\Gamma(\Lambda K^-2\pi^+)/\Gamma(\Xi^-2\pi^+)$ — Γ_4/Γ_{11}

VALUE	EVTS	DOCUMENT ID		TECN	COMMENT
0.323±0.033 OUR AVERAGE					
0.32 ±0.03 ±0.02	1177 ± 55	LESIAK	05	BELL	e^+e^-, $\Upsilon(4S)$
0.28 ±0.06 ±0.06	58	LINK	03E	FOCS	γ nucleus, $\overline{E}_\gamma \approx$ 180 GeV
0.58 ±0.16 ±0.07	61	BERGFELD	96	CLE2	$e^+e^- \approx \Upsilon(4S)$

$\Gamma(\Lambda\overline{K}^*(892)^0\pi^+)/\Gamma(\Lambda K^-2\pi^+)$ — Γ_5/Γ_4

Unseen decay modes of the $\overline{K}^*(892)^0$ are included.

VALUE	CL%	DOCUMENT ID		TECN	COMMENT
<0.5	90	BERGFELD	96	CLE2	$e^+e^- \approx \Upsilon(4S)$

$\Gamma(\Sigma(1385)^+K^-\pi^+)/\Gamma(\Lambda K^-2\pi^+)$ — Γ_6/Γ_4

Unseen decay modes of the $\Sigma(1385)^+$ are included.

VALUE	CL%	DOCUMENT ID		TECN	COMMENT
<0.7	90	BERGFELD	96	CLE2	$e^+e^- \approx \Upsilon(4S)$

$\Gamma(\Sigma^+K^-\pi^+)/\Gamma(\Xi^-2\pi^+)$ — Γ_7/Γ_{11}

VALUE	EVTS	DOCUMENT ID		TECN	COMMENT
0.94±0.10 OUR AVERAGE					
0.91±0.11±0.04	251	LINK	03E	FOCS	γ nucleus, $\overline{E}_\gamma \approx$ 180 GeV
0.92±0.20±0.07		[1] JUN	00	SELX	Σ^- nucleus, 600 GeV
1.18±0.26±0.17	119	BERGFELD	96	CLE2	$e^+e^- \approx \Upsilon(4S)$

[1] This JUN 00 result is redundant with other results given below.

$\Gamma(\Sigma^+\overline{K}^*(892)^0)/\Gamma(\Xi^-2\pi^+)$ — Γ_8/Γ_{11}

Unseen decay modes of the $\overline{K}^*(892)^0$ are included.

VALUE	EVTS	DOCUMENT ID		TECN	COMMENT
0.81±0.15 OUR AVERAGE					
0.78±0.16±0.06	119	LINK	03E	FOCS	γ nucleus, $\overline{E}_\gamma \approx$ 180 GeV
0.92±0.27±0.14	61	BERGFELD	96	CLE2	$e^+e^- \approx \Upsilon(4S)$

$\Gamma(\Sigma^0K^-2\pi^+)/\Gamma(\Lambda K^-2\pi^+)$ — Γ_9/Γ_4

VALUE	EVTS	DOCUMENT ID		TECN	COMMENT
0.84±0.36	47	[1] COTEUS	87	SPEC	nA $\simeq$ 600 GeV

[1] See, however, the note on the COTEUS 87 Ξ_c^+ mass measurement.

$\Gamma(\Xi^0\pi^+)/\Gamma(\Xi^-2\pi^+)$ — Γ_{10}/Γ_{11}

VALUE	EVTS	DOCUMENT ID		TECN	COMMENT
0.55±0.13±0.09	39	EDWARDS	96	CLE2	$e^+e^- \approx \Upsilon(4S)$

$\Gamma(\Xi^-2\pi^+)/\Gamma_{total}$ — Γ_{11}/Γ

VALUE (units 10^{-2})	EVTS	DOCUMENT ID		TECN	COMMENT
2.86±1.21±0.38	24	[1] LI	19C	BELL	$e^+e^- \approx \Upsilon(4S)$

Downloaded from https://academic.oup.com/ptep/article/2022/8/083C01/6651666 by KIT Library user on 27 September 2022

• • • We do not use the following data for averages, fits, limits, etc. • • •

seen	131	BERGFELD	96	CLE2	$e^+e^- \approx \Upsilon(4S)$
seen	160	AVERY	95	CLE2	$e^+e^- \approx \Upsilon(4S)$
seen	30	FRABETTI	93B	E687	γBe, $\overline{E}_\gamma$= 220 GeV
seen	30	ALBRECHT	90F	ARG	e^+e^- at $\Upsilon(4S)$
seen	23	ALAM	89	CLEO	e^+e^- 10.6 GeV

[1] LI 19C report a significance of 6.8 σ for the observation of this decay mode, observed in Ξ_c^+ from $\overline{B}^0 \to \overline{\Lambda}_c^- \Xi_c^+$.

$\Gamma(\Xi(1530)^0\pi^+)/\Gamma(\Xi^-2\pi^+)$ — Γ_{12}/Γ_{11}

Unseen decay modes of the $\Xi(1530)^0$ are included.

VALUE	CL%	DOCUMENT ID		TECN	COMMENT
<0.1	90	LINK	03E	FOCS	γ nucleus, $\overline{E}_\gamma \approx 180$ GeV

• • • We do not use the following data for averages, fits, limits, etc. • • •

<0.2	90	BERGFELD	96	CLE2	$e^+e^- \approx \Upsilon(4S)$

$\Gamma(\Xi(1620)^0\pi^+)/\Gamma_{total}$ — Γ_{13}/Γ

VALUE	DOCUMENT ID		TECN	COMMENT
seen	SUMIHAMA	19	BELL	e^+e^- mostly at $\Upsilon(4S)$

$\Gamma(\Xi(1690)^0\pi^+)/\Gamma_{total}$ — Γ_{14}/Γ

VALUE	DOCUMENT ID		TECN	COMMENT
seen	SUMIHAMA	19	BELL	e^+e^- mostly at $\Upsilon(4S)$

$\Gamma(\Xi^0\pi^+\pi^0)/\Gamma(\Xi^-2\pi^+)$ — Γ_{15}/Γ_{11}

VALUE	EVTS	DOCUMENT ID		TECN	COMMENT
2.34±0.57±0.37	81	EDWARDS	96	CLE2	$e^+e^- \approx \Upsilon(4S)$

$\Gamma(\Xi(1530)^0\pi^+)/\Gamma(\Xi^0\pi^+\pi^0)$ — Γ_{12}/Γ_{15}

VALUE	CL%	DOCUMENT ID		TECN	COMMENT

• • • We do not use the following data for averages, fits, limits, etc. • • •

<0.3	90	EDWARDS	96	CLE2	$e^+e^- \approx \Upsilon(4S)$

$\Gamma(\Xi^0\pi^-2\pi^+)/\Gamma(\Xi^-2\pi^+)$ — Γ_{16}/Γ_{11}

VALUE	EVTS	DOCUMENT ID		TECN	COMMENT
1.74±0.42±0.27	57	EDWARDS	96	CLE2	$e^+e^- \approx \Upsilon(4S)$

$\Gamma(\Xi^0 e^+\nu_e)/\Gamma(\Xi^-2\pi^+)$ — Γ_{17}/Γ_{11}

VALUE	EVTS	DOCUMENT ID		TECN	COMMENT
$2.3\pm0.6^{+0.3}_{-0.6}$	41	ALEXANDER	95B	CLE2	$e^+e^- \approx \Upsilon(4S)$

$\Gamma(\Omega^-K^+\pi^+)/\Gamma(\Xi^-2\pi^+)$ — Γ_{18}/Γ_{11}

VALUE	EVTS	DOCUMENT ID		TECN	COMMENT
0.07±0.03±0.03	14	LINK	03E	FOCS	< 0.12, 90% CL

$\Gamma(pK^-\pi^+)/\Gamma_{total}$ — Γ_{19}/Γ

VALUE (units 10^{-3})	EVTS	DOCUMENT ID		TECN	COMMENT
6.2 ±3.0 OUR AVERAGE	Error includes scale factor of 1.5.				
11.35±0.02±3.87	1.6M	[1] AAIJ	20AH	LHCB	pp at 13 TeV
4.5 ±2.1 ±0.7	24	[2] LI	19C	BELL	$e^+e^- \approx \Upsilon(4S)$

[1] AAIJ 20AH extracts $B(\Xi_c^+ \to pK^-\pi^+)$ assuming production fraction ratios $f_{\Xi_c^0}/f_{\Lambda_c^+} = (9.7 \pm 0.9 \pm 3.1) \times 10^{-2}$ (from AAIJ 19AB plus heavy quark symmetry arguments) as well as $f_{\Xi_c^0}/f_{\Xi_c^+} = 1.00 \pm 0.01$, and uses the input $B(\Lambda_c^+ \to pK^-\pi^+) = (6.23 \pm 0.33) \times 10^{-2}$. Its correlation with $B(\Xi_c^0 \to \Lambda_c^+\pi^-)$, as measured in AAIJ 20AH, is 0.414.

[2] LI 19C report a significance of 4.4 σ for the observation of this decay mode, observed in Ξ_c^+ from $\overline{B}^0 \to \overline{\Lambda}_c^- \Xi_c^+$.

Cabibbo-suppressed decays

$\Gamma(pK^-\pi^+)/\Gamma(\Xi^-2\pi^+)$ — Γ_{19}/Γ_{11}

VALUE	EVTS	DOCUMENT ID		TECN	COMMENT
0.21 ±0.04 OUR AVERAGE					
0.194±0.054	47 ± 11	VAZQUEZ-JA...08		SELX	Σ^- nucleus, 600 GeV
0.234±0.047±0.022	202	LINK	01B	FOCS	γ nucleus

• • • We do not use the following data for averages, fits, limits, etc. • • •

0.20 ±0.04 ±0.02	76	JUN	00	SELX	See VAZQUEZ-JAUREGUI 08

$\Gamma(p\overline{K}^*(892)^0)/\Gamma(pK^-\pi^+)$ — Γ_{20}/Γ_{19}

Unseen decay modes of the $\overline{K}^*(892)^0$ are included.

VALUE	DOCUMENT ID		TECN	COMMENT
0.54±0.09±0.05	LINK	01B	FOCS	γ nucleus

$\Gamma(\Sigma^+\pi^+\pi^-)/\Gamma(\Xi^-2\pi^+)$ — Γ_{21}/Γ_{11}

VALUE	EVTS	DOCUMENT ID		TECN	COMMENT
0.48±0.20	21 ± 8	VAZQUEZ-JA...08		SELX	Σ^- nucleus, 600 GeV

$\Gamma(\Sigma^-2\pi^+)/\Gamma(\Xi^-2\pi^+)$ — Γ_{22}/Γ_{11}

VALUE	EVTS	DOCUMENT ID		TECN	COMMENT
0.18±0.09	10 ± 4	VAZQUEZ-JA...08		SELX	Σ^- nucleus, 600 GeV

$\Gamma(\Sigma^+K^+K^-)/\Gamma(\Sigma^+K^-\pi^+)$ — Γ_{23}/Γ_7

VALUE	EVTS	DOCUMENT ID		TECN	COMMENT
0.16±0.06±0.01	17	LINK	03E	FOCS	γ nucleus, $\overline{E}_\gamma \approx 180$ GeV

$\Gamma(\Sigma^+\phi)/\Gamma(\Sigma^+K^-\pi^+)$ — Γ_{24}/Γ_7

Unseen decay modes of the ϕ are included.

VALUE	CL%	DOCUMENT ID		TECN	COMMENT
<0.12	90	LINK	03E	FOCS	γ nucleus, $\overline{E}_\gamma \approx 180$ GeV

$\Gamma(p\phi(1020))/\Gamma(pK^-\pi^+)$ — Γ_{26}/Γ_{19}

VALUE (units 10^{-3})	EVTS	DOCUMENT ID		TECN	COMMENT
19.8±0.7±0.9±0.2	3.4k	[1] AAIJ	19I	LHCB	pp at 8 TeV

[1] The last uncertainty is due to the uncertainty in the $\phi \to K^+K^-$ branching fraction.

$\Gamma(\Xi(1690)^0K^+\times B(\Xi(1690)^0 \to \Sigma^+K^-))/\Gamma(\Sigma^+K^-\pi^+)$ — Γ_{25}/Γ_7

VALUE	CL%	DOCUMENT ID		TECN	COMMENT
<0.05	90	LINK	03E	FOCS	γ nucleus, $\overline{E}_\gamma \approx 180$ GeV

Ξ_c^+ REFERENCES

AAIJ	20AH	PR D102 071101	R. Aaij et al.	(LHCb Collab.)
AAIJ	19AB	PR D99 052006	R. Aaij et al.	(LHCb Collab.)
AAIJ	19AG	PR D100 032001	R. Aaij et al.	(LHCb Collab.)
AAIJ	19I	JHEP 1904 084	R. Aaij et al.	(LHCb Collab.)
LI	19C	PR D100 031101	Y.B. Li et al.	(BELLE Collab.)
SUMIHAMA	19	PRL 122 072501	M. Sumihama et al.	(BELLE Collab.)
AAIJ	14Z	PRL 113 032001	R. Aaij et al.	(LHCb Collab.)
AALTONEN	14B	PR D89 072014	T. Aaltonen et al.	(CDF Collab.)
VAZQUEZ-JA...	08	PL B666 299	E. Vazquez-Jauregui et al.	(SELEX Collab.)
LESIAK	05	PL B605 237	T. Lesiak et al.	(BELLE Collab.)
Also		PL B617 198 (errat.)	T. Lesiak et al.	(BELLE Collab.)
LINK	03E	PL B571 139	J.M. Link et al.	(FNAL FOCUS Collab.)
MAHMOOD	02	PR D65 031102	A.H. Mahmood et al.	(CLEO Collab.)
LINK	01B	PL B512 277	J.M. Link et al.	(FNAL FOCUS Collab.)
LINK	01D	PL B523 53	J.M. Link et al.	(FNAL FOCUS Collab.)
JUN	00	PRL 84 1857	S.Y. Jun et al.	(FNAL SELEX Collab.)
FRABETTI	98	PL B427 211	P.L. Frabetti et al.	(FNAL E687 Collab.)
BERGFELD	96	PL B365 431	T. Bergfeld et al.	(CLEO Collab.)
EDWARDS	96	PL B373 261	K.W. Edwards et al.	(CLEO Collab.)
ALEXANDER	95B	PRL 74 3113	J. Alexander et al.	(CLEO Collab.)
Also		PRL 75 4155 (erratum)	J. Alexander et al.	(CLEO Collab.)
AVERY	95	PRL 75 4364	P. Avery et al.	(CLEO Collab.)
FRABETTI	93B	PRL 70 1381	P.L. Frabetti et al.	(FNAL E687 Collab.)
ALBRECHT	90F	PL B247 121	H. Albrecht et al.	(ARGUS Collab.)
ALAM	89	PL B226 401	M.S. Alam et al.	(CLEO Collab.)
BARLAG	89C	PL B233 522	S. Barlag et al.	(ACCMOR Collab.)
COTEUS	87	PRL 59 1530	P. Coteus et al.	(FNAL E400 Collab.)
BIAGI	85C	PL 150B 230	S.F. Biagi et al.	(CERN WA62 Collab.)
BIAGI	83	PL 122B 455	S.F. Biagi et al.	(CERN WA62 Collab.)

Ξ_c^0

$I(J^P) = \frac{1}{2}(\frac{1}{2}^+)$ Status: ****

Neither J or P has actually been measured.

Ξ_c^0 MASS

The fit uses the Ξ_c^0 and Ξ_c^+ mass and mass-difference measurements.

VALUE (MeV)	EVTS	DOCUMENT ID		TECN	COMMENT
2470.44±0.28 OUR FIT	Error includes scale factor of 1.2.				
$2470.99^{+0.30}_{-0.50}$ OUR AVERAGE					
2470.85±0.24±0.55	3.4k	AALTONEN	14B	CDF	$p\overline{p}$ at 1.96 TeV
2471.0 ±0.3 $^{+0.2}_{-1.4}$	8.6k	[1] LESIAK	05	BELL	e^+e^-, $\Upsilon(4S)$
2470.0 ±2.8 ±2.6	85	FRABETTI	98B	E687	γ Be, $\overline{E}_\gamma$ = 220 GeV
2469 ±2 ±3	9	HENDERSON	92B	CLEO	Ω^-K^+
2472.1 ±2.7 ±1.6	54	ALBRECHT	90F	ARG	e^+e^- at $\Upsilon(4S)$
2473.3 ±1.9 ±1.2	4	BARLAG	90	ACCM	π^- (K^-) Cu 230 GeV
2472 ±3 ±4	19	ALAM	89	CLEO	e^+e^- 10.6 GeV

• • • We do not use the following data for averages, fits, limits, etc. • • •

2462.1 ±3.1 ±1.4	42	[2] FRABETTI	93C	E687	See FRABETTI 98B
2471 ±3 ±4	14	AVERY	89	CLEO	See ALAM 89

[1] The systematic error was (wrongly) given the other way round in LESIAK 05.

[2] The FRABETTI 93C mass is well below the other measurements.

$\Xi_c^0 - \Xi_c^+$ MASS DIFFERENCE

VALUE (MeV)	EVTS	DOCUMENT ID		TECN	COMMENT
2.72±0.23 OUR FIT	Error includes scale factor of 1.1.				
2.91±0.26 OUR AVERAGE					
2.85±0.30±0.04	5.1/3.4k	AALTONEN	14B	CDF	$p\overline{p}$ at 1.96 TeV
2.9 ±0.5		LESIAK	05	BELL	e^+e^-, $\Upsilon(4S)$
7.0 ±4.5 ±2.2		ALBRECHT	90F	ARG	e^+e^- at $\Upsilon(4S)$
6.8 ±3.3 ±0.5		BARLAG	90	ACCM	π^- (K^-) Cu 230 GeV
5 ±4 ±1		ALAM	89	CLEO	$\Xi_c^0 \to \Xi^-\pi^+$, $\Xi_c^+ \to \Xi^-\pi^+\pi^+$

Downloaded from https://academic.oup.com/ptep/article/2022/8/083C01/6651666 by KIT Library user on 27 September 2022

Ξ_c^0 MEAN LIFE

VALUE (10^{-15} s)	EVTS	DOCUMENT ID		TECN	COMMENT
151.9± 2.4 OUR AVERAGE					
153.4± 2.4±0.7	22k	[1] AAIJ	19AG	LHCB	$\Xi_c^0 \to p K^- K^- \pi^+$
$118 \; ^{+14}_{-12} \pm 5$	110	LINK	02H	FOCS	γ nucleus, ≈ 180 GeV
$101 \; ^{+25}_{-17} \pm 5$	42	FRABETTI	93C	E687	γ Be, $\overline{E}_\gamma$= 220 GeV
$82 \; ^{+59}_{-30}$	4	BARLAG	90	ACCM	π^- (K^-) Cu 230 GeV

[1] AAIJ 19AG reports [Ξ_c^0 MEAN LIFE] / [$D^\pm$ MEAN LIFE] = 0.1485 ± 0.0017 ± 0.0016 which we multiply by our best value $D^\pm$ MEAN LIFE = (1.033 ± 0.005) × 10^{-12} s. Our first error is their experiment's error and our second error is the systematic error from using our best value.

Ξ_c^0 DECAY MODES

	Mode	Fraction (Γ_i/Γ)	Scale factor
	Cabibbo-favored decays		
Γ_1	$p K^- K^- \pi^+$	(4.8 ±1.2) × 10^{-3}	1.1
Γ_2	$p K^- \overline{K}^*(892)^0$, $\overline{K}^{*0} \to K^- \pi^+$	(2.0 ±0.6) × 10^{-3}	
Γ_3	$p K^- K^- \pi^+$ (no $\overline{K}^{*0}$)	(3.0 ±0.9) × 10^{-3}	
Γ_4	ΛK_S^0	(3.2 ±0.7) × 10^{-3}	
Γ_5	$\Lambda K^- \pi^+$	(1.45±0.33) %	1.1
Γ_6	$\Lambda \overline{K}^*(892)^0$	(2.6 ±0.7) × 10^{-3}	
Γ_7	$\Lambda \overline{K}^0 \pi^+ \pi^-$	seen	
Γ_8	$\Lambda K^- \pi^+ \pi^+ \pi^-$	seen	
Γ_9	$\Sigma^0 K_S^0$	(5.4 ±1.6) × 10^{-4}	
Γ_{10}	$\Sigma^+ K^-$	(1.8 ±0.4) × 10^{-3}	
Γ_{11}	$\Sigma^0 \overline{K}^*(892)^0$	(9.8 ±2.3) × 10^{-3}	
Γ_{12}	$\Sigma^+ K^*(892)^-$	(4.9 ±1.4) × 10^{-3}	
Γ_{13}	$\Xi^- \pi^+$	(1.43±0.32) %	1.1
Γ_{14}	$\Xi^- \pi^+ \pi^+ \pi^-$	(4.8 ±2.3) %	
Γ_{15}	$\Xi^0 K^+ K^-$		
Γ_{16}	$\Xi^0 \phi$, $\phi \to K^+ K^-$	(5.1 ±1.3) × 10^{-4}	
Γ_{17}	$\Xi^0 K^+ K^-$ nonresonant	(5.6 ±1.4) × 10^{-4}	
Γ_{18}	$\Omega^- K^+$	(4.2 ±1.0) × 10^{-3}	
Γ_{19}	$\Xi^- e^+ \nu_e$	(1.04±0.24) %	
Γ_{20}	$\Xi^- \mu^+ \nu_\mu$	(1.01±0.25) %	
	Cabibbo-suppressed decays		
Γ_{21}	$\Lambda_c^+ \pi^-$	(5.5 ±1.8) × 10^{-3}	
Γ_{22}	$\Xi^- K^+$	(3.9 ±1.2) × 10^{-4}	
Γ_{23}	$\Lambda K^+ K^-$ (no ϕ)	(4.1 ±1.4) × 10^{-4}	
Γ_{24}	$\Lambda \phi$	(4.9 ±1.5) × 10^{-4}	

CONSTRAINED FIT INFORMATION

An overall fit to 5 branching ratios uses 6 measurements and one constraint to determine 4 parameters. The overall fit has a χ^2 = 1.4 for 3 degrees of freedom.

The following *off-diagonal* array elements are the correlation coefficients $\langle \delta x_i \delta x_j \rangle / (\delta x_i \cdot \delta x_j)$, in percent, from the fit to the branching fractions, $x_i \equiv \Gamma_i/\Gamma_{total}$. The fit constrains the x_i whose labels appear in this array to sum to one.

x_5	68	
x_{13}	89	76
	x_1	x_5

Ξ_c^0 BRANCHING RATIOS

Cabibbo-favored (S = −2) decays

$\Gamma(p K^- K^- \pi^+)/\Gamma_{total}$ — Γ_1/Γ

VALUE (%)	EVTS	DOCUMENT ID		TECN	COMMENT
0.48±0.12 OUR FIT	Error includes scale factor of 1.1.				
0.58±0.23±0.05	17 ± 5	LI	19A	BELL	$e^+ e^-$ at $\Upsilon(4S)$

$\Gamma(p K^- K^- \pi^+)/\Gamma(\Xi^- \pi^+)$ — Γ_1/Γ_{13}

VALUE	EVTS	DOCUMENT ID		TECN	COMMENT
0.339±0.035 OUR FIT					
0.34 ±0.04 OUR AVERAGE					
0.33 ±0.03 ±0.03	1908 ± 62	LESIAK	05	BELL	$e^+ e^-$, $\Upsilon(4S)$
0.35 ±0.06 ±0.03	148 ± 18	DANKO	04	CLEO	$e^+ e^-$

$\Gamma(p K^- \overline{K}^*(892)^0, \overline{K}^{*0} \to K^- \pi^+)/\Gamma(\Xi^- \pi^+)$ — Γ_2/Γ_{13}

VALUE	DOCUMENT ID		TECN	COMMENT
0.14±0.03±0.01	DANKO	04	CLEO	$e^+ e^-$

$\Gamma(p K^- K^- \pi^+ (\text{no } \overline{K}^{*0}))/\Gamma(\Xi^- \pi^+)$ — Γ_3/Γ_{13}

VALUE	DOCUMENT ID		TECN	COMMENT
0.21±0.04±0.02	DANKO	04	CLEO	$e^+ e^-$

$\Gamma(\Lambda K_S^0)/\Gamma(\Xi^- \pi^+)$ — Γ_4/Γ_{13}

VALUE	EVTS	DOCUMENT ID		TECN	COMMENT
0.225±0.013 OUR AVERAGE					
0.229±0.008±0.012	5.6k	LI	21F	BELL	$e^+ e^-$ at Υ(nS)
0.21 ±0.02 ±0.02	465 ± 37	LESIAK	05	BELL	$e^+ e^-$, $\Upsilon(4S)$

$\Gamma(\Lambda K^- \pi^+)/\Gamma_{total}$ — Γ_5/Γ

VALUE (%)	EVTS	DOCUMENT ID		TECN	COMMENT
1.45±0.33 OUR FIT	Error includes scale factor of 1.1.				
1.17±0.37±0.09	24 ± 6	LI	19A	BELL	$e^+ e^-$ at $\Upsilon(4S)$

$\Gamma(\Lambda K^- \pi^+)/\Gamma(\Xi^- \pi^+)$ — Γ_5/Γ_{13}

VALUE	EVTS	DOCUMENT ID		TECN	COMMENT
1.02±0.15 OUR FIT	Error includes scale factor of 1.2.				
1.07±0.12±0.07	2979 ± 211	LESIAK	05	BELL	$e^+ e^-$, $\Upsilon(4S)$

$\Gamma(\Lambda \overline{K}^*(892)^0)/\Gamma(\Xi^- \pi^+)$ — Γ_6/Γ_{13}

VALUE	EVTS	DOCUMENT ID		TECN	COMMENT
0.18±0.02±0.01	4k	JIA	21	BELL	$e^+ e^-$ at Υ(nS)

$\Gamma(\Lambda \overline{K}^0 \pi^+ \pi^-)/\Gamma_{total}$ — Γ_7/Γ

VALUE	DOCUMENT ID		TECN	COMMENT
seen	FRABETTI	98B	E687	γ Be, $\overline{E}_\gamma$ = 220 GeV

$\Gamma(\Lambda K^- \pi^+ \pi^+ \pi^-)/\Gamma_{total}$ — Γ_8/Γ

VALUE	DOCUMENT ID		TECN	COMMENT
seen	FRABETTI	98B	E687	γ Be, $\overline{E}_\gamma$ = 220 GeV

$\Gamma(\Sigma^0 K_S^0)/\Gamma(\Xi^- \pi^+)$ — Γ_9/Γ_{13}

VALUE (units 10^{-2})	EVTS	DOCUMENT ID		TECN	COMMENT
3.8±0.6±0.4	279	LI	21F	BELL	$e^+ e^-$ at Υ(nS)

$\Gamma(\Sigma^+ K^-)/\Gamma(\Xi^- \pi^+)$ — Γ_{10}/Γ_{13}

VALUE (units 10^{-2})	EVTS	DOCUMENT ID		TECN	COMMENT
12.3±0.7±1.0	889	LI	21F	BELL	$e^+ e^-$ at Υ(nS)

$\Gamma(\Sigma^0 \overline{K}^*(892)^0)/\Gamma(\Xi^- \pi^+)$ — Γ_{11}/Γ_{13}

VALUE	EVTS	DOCUMENT ID		TECN	COMMENT
0.69±0.03±0.03	6.3k	JIA	21	BELL	$e^+ e^-$ at Υ(nS)

$\Gamma(\Sigma^+ K^*(892)^-)/\Gamma(\Xi^- \pi^+)$ — Γ_{12}/Γ_{13}

VALUE	EVTS	DOCUMENT ID		TECN	COMMENT
0.34±0.06±0.02	373	JIA	21	BELL	$e^+ e^-$ at Υ(nS)

$\Gamma(\Xi^- \pi^+)/\Gamma_{total}$ — Γ_{13}/Γ

VALUE (%)	EVTS	DOCUMENT ID		TECN	COMMENT
1.43±0.32 OUR FIT	Error includes scale factor of 1.1.				
1.80±0.50±0.14	45 ± 7	LI	19A	BELL	$e^+ e^-$ at $\Upsilon(4S)$

$\Gamma(\Xi^- \pi^+)/\Gamma(\Xi^- \pi^+ \pi^+ \pi^-)$ — Γ_{13}/Γ_{14}

VALUE	DOCUMENT ID		TECN	COMMENT
0.30±0.12±0.05	ALBRECHT	90F	ARG	$e^+ e^-$ at $\Upsilon(4S)$

$\Gamma(\Omega^- K^+)/\Gamma(\Xi^- \pi^+)$ — Γ_{18}/Γ_{13}

VALUE	EVTS	DOCUMENT ID		TECN	COMMENT
0.294±0.018±0.016	650	AUBERT,B	05M	BABR	$e^+ e^- \approx \Upsilon(4S)$

$\Gamma(\Xi^0 \phi, \phi \to K^+ K^-)/\Gamma(\Xi^- \pi^+)$ — Γ_{16}/Γ_{13}

VALUE	EVTS	DOCUMENT ID		TECN	COMMENT
0.036±0.004±0.002	311	[1] MCNEIL	21	BELL	$e^+ e^-$ at Υ(nS)

[1] MCNEIL 21 assumes an azimuthally symmetric amplitude model to recover resonant and nonresonant contributions to $\Xi_c^0 \to \Xi^0 K^+ K^-$.

$\Gamma(\Xi^0 K^+ K^- \text{nonresonant})/\Gamma(\Xi^- \pi^+)$ — Γ_{17}/Γ_{13}

VALUE	EVTS	DOCUMENT ID		TECN	COMMENT
0.039±0.004±0.002	311	[1] MCNEIL	21	BELL	$e^+ e^-$ at Υ(nS)

[1] MCNEIL 21 assumes an azimuthally symmetric amplitude model to recover resonant and nonresonant contributions to $\Xi_c^0 \to \Xi^0 K^+ K^-$.

$\Gamma(\Xi^- e^+ \nu_e)/\Gamma(\Xi^- \pi^+)$ — Γ_{19}/Γ_{13}

VALUE	EVTS	DOCUMENT ID		TECN	COMMENT
0.730±0.021±0.039		[1] LI	21C	BELL	$e^+ e^-$ at 10.52, 10.58 GeV
• • • We do not use the following data for averages, fits, limits, etc. • • •					
1.38 ±0.14 ±0.22		ACHARYA	21A	ALCE	pp at 13 TeV
$3.1 \pm 1.0 \; ^{+0.3}_{-0.5}$	54	ALEXANDER	95B	CLE2	$e^+ e^- \approx \Upsilon(4S)$
0.96 ±0.43 ±0.18	18	[2] ALBRECHT	93B	ARG	$e^+ e^- \approx$ 10.4 GeV

[1] LI 21C measures ratio B($\Xi_c^0 \to \Xi^- e^+ \nu_e$) / B($\Xi_c^0 \to \Xi^- \mu^+ \nu_\mu$) = 1.03 ± 0.05 ± 0.07.

[2] This ALBRECHT 93B value is the average of the ($\Xi^- e^+$ anything)/$\Xi^- \pi^+$ and ($\Xi^- \mu^+$ anything)/$\Xi^- \pi^+$ ratios. Here we average it with the $\Xi^- e^+ \nu_e/\Xi^- \pi^+$ ratio.

Downloaded from https://academic.oup.com/ptep/article/2022/8/083C01/6651666 by KIT Library user on 27 September 2022

$\Gamma(\Xi^- \mu^+ \nu_\mu)/\Gamma(\Xi^- \pi^+)$ — Γ_{20}/Γ_{13}

VALUE	DOCUMENT ID		TECN	COMMENT
0.708±0.033±0.056	[1] LI	21C	BELL	e^+e^- at 10.52, 10.58 GeV

[1] LI 21C measures ratio $B(\Xi_c^0 \to \Xi^- e^+ \nu_e)$ / $B(\Xi_c^0 \to \Xi^- \mu^+ \nu_\mu) = 1.03 \pm 0.05 \pm 0.07$.

$\Gamma(\Xi^- e^+ \nu_e)/\Gamma(\Xi^- \mu^+ \nu_\mu)$ — Γ_{19}/Γ_{20}

VALUE	DOCUMENT ID		TECN	COMMENT
• • • We do not use the following data for averages, fits, limits, etc. • • •				
1.03±0.05±0.07	[1] LI	21C	BELL	e^+e^- at 10.52, 10.58 GeV

[1] LI 21C value is not independent from other quoted measurements.

Cabibbo-suppressed decays

$\Gamma(\Lambda_c^+ \pi^-)/\Gamma_{total}$ — Γ_{21}/Γ

VALUE (units 10^{-3})	EVTS	DOCUMENT ID		TECN	COMMENT
5.5±0.2±1.8	6.3k	[1] AAIJ	20AH	LHCB	pp at 13 TeV

[1] AAIJ 20AH extracts $B(\Xi_c^0 \to \Lambda_c^+ \pi^-)$ using two different normalization modes: $\Lambda_c^+ \to p K^- \pi^+$ and $\Xi_c^+ \to p K^- \pi^+$. The mean value of both results, taking their correlations into account, is presented as the final result. The measurement assumes production fraction ratios $f_{\Xi_c^0}/f_{\Lambda_c^+} = (9.7 \pm 0.9 \pm 3.1) \times 10^{-2}$ (from AAIJ 19AB plus heavy quark symmetry arguments) as well as $f_{\Xi_c^0}/f_{\Xi_c^+} = 1.00 \pm 0.01$. It further uses the inputs $B(\Lambda_c^+ \to p K^- \pi^+) = (6.23 \pm 0.33) \times 10^{-2}$ and $B(\Xi_c^+ \to p K^- \pi^+) = (4.5 \pm 2.1 \pm 0.7) \times 10^{-3}$ (from LI 19C). Its correlation with $B(\Xi_c^+ \to p K^- \pi^+)$, as measured in AAIJ 20AH, is 0.414.

$\Gamma(\Xi^- K^+)/\Gamma(\Xi^- \pi^+)$ — Γ_{22}/Γ_{13}

VALUE (units 10^{-2})	EVTS	DOCUMENT ID		TECN	COMMENT
2.75±0.51±0.25	314 ± 58	CHISTOV	13	BELL	$e^+e^- \approx \Upsilon(4S)$

$\Gamma(\Lambda K^+ K^- (\text{no}\,\phi))/\Gamma(\Xi^- \pi^+)$ — Γ_{23}/Γ_{13}

VALUE (units 10^{-2})	EVTS	DOCUMENT ID		TECN	COMMENT
2.86±0.61±0.37	510 ± 110	CHISTOV	13	BELL	$e^+e^- \approx \Upsilon(4S)$

$\Gamma(\Lambda\phi)/\Gamma(\Xi^- \pi^+)$ — Γ_{24}/Γ_{13}

VALUE (units 10^{-2})	EVTS	DOCUMENT ID		TECN	COMMENT
3.43±0.58±0.32	316 ± 54	CHISTOV	13	BELL	$e^+e^- \approx \Upsilon(4S)$

Ξ_c^0 DECAY PARAMETERS

See the note on "Baryon Decay Parameters" in the neutron Listings.

α FOR $\Xi_c^0 \to \Xi^- \pi^+$

VALUE	EVTS	DOCUMENT ID		TECN	COMMENT
−0.64±0.05±0.01		LI	21C	BELL	e^+e^- at 10.52, 10.58 GeV
• • • We do not use the following data for averages, fits, limits, etc. • • •					
$-0.56 \pm 0.39^{+0.10}_{-0.09}$	138	CHAN	01	CLE2	$e^+e^- \approx \Upsilon(4S)$

α FOR $\overline{\Xi}_c^0 \to \overline{\Xi}^+ \pi^-$

VALUE	DOCUMENT ID		TECN	COMMENT
0.61±0.05±0.01	LI	21C	BELL	e^+e^- at 10.52, 10.58 GeV

α FOR $\Xi_c^0 \to \Lambda \overline{K}^*(892)^0$

VALUE	EVTS	DOCUMENT ID		TECN	COMMENT
0.15±0.22±0.04	4k	[1] JIA	21	BELL	e^+e^- at Υ(nS)

[1] JIA 21 measures $\alpha(\Xi_c^0 \to \Lambda \overline{K}^*(892)^0)\ \alpha(\Lambda \to p\pi^-) = 0.115 \pm 0.164 \pm 0.031$, and uses $\alpha(\Lambda \to p\pi^-) = 0.747 \pm 0.010$.

α FOR $\Xi_c^0 \to \Sigma^+ K^*(892)^-$

VALUE	EVTS	DOCUMENT ID		TECN	COMMENT
−0.52±0.30±0.02	373	[1] JIA	21	BELL	e^+e^- at Υ(nS)

[1] JIA 21 measures $\alpha(\Xi_c^0 \to \Sigma^+ \overline{K}^*(892)^-)\ \alpha(\Sigma^+ \to p\pi^0) = 0.514 \pm 0.295 \pm 0.012$, and uses $\alpha(\Sigma^+ \to p\pi^0) = -0.980 \pm 0.017$.

Ξ_c^0 REFERENCES

ACHARYA	21A	PRL 127 272001	S. Acharya et al.	(ALICE Collab.)
JIA	21	JHEP 2106 160	S. Jia et al.	(BELLE Collab.)
LI	21C	PRL 127 121803	Y.B. Li et al.	(BELLE Collab.)
LI	21F	PR D105 L011102	Y. Li et al.	(BELLE Collab.)
MCNEIL	21	PR D103 112002	J.T. McNeil et al.	(BELLE Collab.)
AAIJ	20AH	PR D102 071101	R. Aaij et al.	(LHCb Collab.)
AAIJ	19AB	PR D99 052006	R. Aaij et al.	(LHCb Collab.)
AAIJ	19AG	PR D100 032001	R. Aaij et al.	(LHCb Collab.)
LI	19A	PRL 122 082001	Y.B. Li et al.	(BELLE Collab.)
LI	19C	PR D100 031101	Y.B. Li et al.	(BELLE Collab.)
AALTONEN	14B	PR D89 072014	T. Aaltonen et al.	(CDF Collab.)
CHISTOV	13	PR D88 071103	R. Chistov et al.	(BELLE Collab.)
AUBERT,B	05M	PRL 95 142003	B. Aubert et al.	(BABAR Collab.)
LESIAK	05	PL B605 237	T. Lesiak et al.	(BELLE Collab.)
Also		PL B617 198 (errat.)	T. Lesiak et al.	(BELLE Collab.)
DANKO	04	PR D69 052004	I. Danko et al.	(CLEO Collab.)
LINK	02H	PL B541 211	J.M. Link et al.	(FNAL FOCUS Collab.)
CHAN	01	PR D63 111102	S. Chan et al.	(CLEO Collab.)
FRABETTI	98B	PL B426 403	P.L. Frabetti et al.	(FNAL E687 Collab.)
ALEXANDER	95B	PRL 74 3113	J. Alexander et al.	(CLEO Collab.)
Also		PRL 75 4155 (erratum)	J. Alexander et al.	(CLEO Collab.)
ALBRECHT	93B	PL B303 368	H. Albrecht et al.	(ARGUS Collab.)
FRABETTI	93C	PRL 70 2058	P.L. Frabetti et al.	(FNAL E687 Collab.)
HENDERSON	92B	PL B283 161	S. Henderson et al.	(CLEO Collab.)
ALBRECHT	90F	PL B247 121	H. Albrecht et al.	(ARGUS Collab.)
BARLAG	90	PL B236 495	S. Barlag et al.	(ACCMOR Collab.)
ALAM	89	PL B226 401	M.S. Alam et al.	(CLEO Collab.)
AVERY	89	PRL 62 863	P. Avery et al.	(CLEO Collab.)

$\Xi_c^{\prime +}$

$I(J^P) = \frac{1}{2}(\frac{1}{2}^+)$ Status: ***

The $\Xi_c^{\prime +}$ and $\Xi_c^{\prime 0}$ presumably complete the SU(3) sextet whose other members are the Σ_c^{++}, Σ_c^+, Σ_c^0, and Ω_c^0: see Fig. 5 in the "Quark Model" review. The quantum numbers given above come from this presumption but have not been measured.

$\Xi_c^{\prime +}$ MASS

The mass is obtained from the mass-difference measurement that follows.

VALUE (MeV)	DOCUMENT ID
2578.2±0.5 OUR FIT Error includes scale factor of 1.1.	

$\Xi_c^{\prime +} - \Xi_c^+$ MASS DIFFERENCE

VALUE (MeV)	EVTS	DOCUMENT ID		TECN	COMMENT
110.5±0.4 OUR FIT					
110.5±0.1±0.4	7k	YELTON	16	BELL	e^+e^-, Υ regions
• • • We do not use the following data for averages, fits, limits, etc. • • •					
107.8±1.7±2.5	25	JESSOP	99	CLE2	$e^+e^- \approx \Upsilon(4S)$

$\Xi_c^{\prime +} - \Xi_c^{\prime 0}$ MASS DIFFERENCE

VALUE (MeV)	DOCUMENT ID		TECN	COMMENT
−0.5±0.6 OUR FIT				
• • • We do not use the following data for averages, fits, limits, etc. • • •				
−0.8±0.1±0.5	YELTON	16	BELL	7055 and 11,560 evts

$\Xi_c^{\prime +}$ DECAY MODES

The $\Xi_c^{\prime +}$–Ξ_c^+ mass difference is too small for any strong decay to occur.

	Mode	Fraction (Γ_i/Γ)
Γ_1	$\Xi_c^+ \gamma$	seen

$\Xi_c^{\prime +}$ REFERENCES

YELTON	16	PR D94 052011	J. Yelton et al.	(BELLE Collab.)
JESSOP	99	PRL 82 492	C.P. Jessop et al.	(CLEO Collab.)

$\Xi_c^{\prime 0}$

$I(J^P) = \frac{1}{2}(\frac{1}{2}^+)$ Status: ***

The $\Xi_c^{\prime 0}$ and $\Xi_c^{\prime +}$ presumably complete the SU(3) sextet whose other members are the Σ_c^{++}, Σ_c^+, Σ_c^0, and Ω_c^0: see Fig. 5 in the "Quark Model" review. The quantum numbers given above come from this presumption but have not been measured.

$\Xi_c^{\prime 0}$ MASS

The mass is obtained from the mass-difference measurement that follows.

VALUE (MeV)	DOCUMENT ID
2578.7±0.5 OUR FIT	

$\Xi_c^{\prime 0} - \Xi_c^0$ MASS DIFFERENCE

VALUE (MeV)	EVTS	DOCUMENT ID		TECN	COMMENT
108.3±0.4 OUR FIT					
108.3±0.1±0.4	11.5k	YELTON	16	BELL	e^+e^-, Υ regions
• • • We do not use the following data for averages, fits, limits, etc. • • •					
107.0±1.4±2.5	28	JESSOP	99	CLE2	$e^+e^- \approx \Upsilon(4S)$

Downloaded from https://academic.oup.com/ptep/article/2022/8/083C01/6651666 by KIT Library user on 27 September 2022

$\Xi_c'^0$ DECAY MODES

The $\Xi_c'^0 - \Xi_c^0$ mass difference is too small for any strong decay to occur.

	Mode	Fraction (Γ_i/Γ)
Γ_1	$\Xi_c^0\gamma$	seen

$\Xi_c'^0$ REFERENCES

YELTON	16	PR D94 052011	J. Yelton *et al.*	(BELLE Collab.)
JESSOP	99	PRL 82 492	C.P. Jessop *et al.*	(CLEO Collab.)

$\Xi_c(2645)$

$I(J^P) = \frac{1}{2}(\frac{3}{2}^+)$ Status: ***

The natural assignment is that this is the $J^P = 3/2^+$ excitation of the Ξ_c in the same SU(4) multiplet as the $\Delta(1232)$, but the quantum numbers have not been measured.

$\Xi_c(2645)$ MASSES

$\Xi_c(2645)^+$ MASS

VALUE (MeV)	EVTS	DOCUMENT ID		TECN	COMMENT
2645.10±0.30 OUR FIT	Error includes scale factor of 1.2.				
2645.6 ±0.2 $^{+0.6}_{-0.8}$	578 ± 32	LESIAK	08	BELL	$e^+e^- \approx \Upsilon(4S)$

$\Xi_c(2645)^0$ MASS

VALUE (MeV)	EVTS	DOCUMENT ID		TECN	COMMENT
2646.16±0.25 OUR FIT	Error includes scale factor of 1.3.				
2645.7 ±0.2 $^{+0.6}_{-0.7}$	611 ± 32	LESIAK	08	BELL	$e^+e^- \approx \Upsilon(4S)$

$\Xi_c(2645) - \Xi_c$ MASS DIFFERENCES

$m_{\Xi_c(2645)^+} - m_{\Xi_c^0}$

VALUE (MeV)	EVTS	DOCUMENT ID		TECN	COMMENT
174.67±0.09 OUR FIT					
174.66±0.06±0.07	1260	YELTON	16	BELL	e^+e^- in Υ regions
• • • We do not use the following data for averages, fits, limits, etc. • • •					
177.1 ±0.5 ±1.1	47	FRABETTI	98B	E687	γ Be, $\overline{E}_\gamma$ = 220 GeV
174.3 ±0.5 ±1.0	34	GIBBONS	96	CLE2	$e^+e^- \approx \Upsilon(4S)$

$m_{\Xi_c(2645)^0} - m_{\Xi_c^+}$

VALUE (MeV)	EVTS	DOCUMENT ID		TECN	COMMENT
178.45±0.10 OUR FIT					
178.46±0.07±0.07	975	YELTON	16	BELL	e^+e^- in Υ regions
• • • We do not use the following data for averages, fits, limits, etc. • • •					
178.2 ±0.5 ±1.0	55	AVERY	95	CLE2	$e^+e^- \approx \Upsilon(4S)$

$\Xi_c(2645)^+ - \Xi_c(2645)^0$ MASS DIFFERENCE

VALUE (MeV)	DOCUMENT ID		TECN	COMMENT
−1.06±0.27 OUR FIT Error includes scale factor of 1.1.				
• • • We do not use the following data for averages, fits, limits, etc. • • •				
−0.85±0.09±0.49	YELTON	16	BELL	1260 and 975 evts
−0.1 ±0.3 ±0.6	LESIAK	08	BELL	≈ 600 evts each

$\Xi_c(2645)$ WIDTHS

$\Xi_c(2645)^+$ WIDTH

VALUE (MeV)	CL%	EVTS	DOCUMENT ID		TECN	COMMENT
2.14±0.19 OUR AVERAGE Error includes scale factor of 1.1.						
2.06±0.13±0.13		1260	YELTON	16	BELL	e^+e^- in Υ regions
2.6 ±0.2 ±0.4		3.7k	KATO	14	BELL	e^+e^- $\Upsilon(1S)$-$\Upsilon(5S)$
• • • We do not use the following data for averages, fits, limits, etc. • • •						
<3.1	90		GIBBONS	96	CLE2	$e^+e^- \approx \Upsilon(4S)$

$\Xi_c(2645)^0$ WIDTH

VALUE (MeV)	CL%	EVTS	DOCUMENT ID		TECN	COMMENT
2.35±0.18±0.13		975	YELTON	16	BELL	e^+e^- in Υ regions
• • • We do not use the following data for averages, fits, limits, etc. • • •						
<5.5	90	55	AVERY	95	CLE2	$e^+e^- \approx \Upsilon(4S)$

$\Xi_c(2645)$ DECAY MODES

$\Xi_c\pi$ is the only strong decay allowed to a Ξ_c resonance having this mass.

	Mode	Fraction (Γ_i/Γ)
Γ_1	$\Xi_c^0\pi^+$	seen
Γ_2	$\Xi_c^+\pi^-$	seen

$\Xi_c(2645)$ REFERENCES

YELTON	16	PR D94 052011	J. Yelton *et al.*	(BELLE Collab.)
KATO	14	PR D89 052003	Y. Kato *et al.*	(BELLE Collab.)
LESIAK	08	PL B665 9	T. Lesiak *et al.*	(BELLE Collab.)
FRABETTI	98B	PL B426 403	P.L. Frabetti *et al.*	(FNAL E687 Collab.)
GIBBONS	96	PRL 77 810	L.K. Gibbons *et al.*	(CLEO Collab.)
AVERY	95	PRL 75 4364	P. Avery *et al.*	(CLEO Collab.)

$\Xi_c(2790)$

$I(J^P) = \frac{1}{2}(\frac{1}{2}^-)$ Status: ***

Seen in $\Xi_c'\pi$ decays. The simplest assignment, based on the mass, width, and decay mode, is that this belongs in the same SU(4) multiplet as the $\Lambda(1405)$ and the $\Lambda_c(2595)^+$, but the spin and parity have not been measured.

$\Xi_c(2790)$ MASSES

The masses are obtained from the mass-difference measurements that follow.

$\Xi_c(2790)^+$ MASS

VALUE (MeV)	DOCUMENT ID
2791.9±0.5 OUR FIT	

$\Xi_c(2790)^0$ MASS

VALUE (MeV)	DOCUMENT ID
2793.9±0.5 OUR FIT	

$\Xi_c(2790) - \Xi_c'$ MASS DIFFERENCES

$m_{\Xi_c(2790)^+} - m_{\Xi_c^0}$

VALUE (MeV)	EVTS	DOCUMENT ID		TECN	COMMENT
213.20±0.22 OUR FIT					
213.2 ±0.2 ±0.1		YELTON	16	BELL	2231 and 11,560 evts
• • • We do not use the following data for averages, fits, limits, etc. • • •					
211.2 ±1.3 ±1.0	18	CSORNA	01	CLEO	$e^+e^- \approx \Upsilon(4S)$

$m_{\Xi_c(2790)^0} - m_{\Xi_c'^+}$

VALUE (MeV)	EVTS	DOCUMENT ID		TECN	COMMENT
215.70±0.22 OUR FIT					
215.7 ±0.2 ±0.1		YELTON	16	BELL	1241 and 7055 evts
• • • We do not use the following data for averages, fits, limits, etc. • • •					
216.2 ±1.3 ±1.0	14	CSORNA	01	CLEO	$e^+e^- \approx \Upsilon(4S)$

$\Xi_c(2790)^+ - \Xi_c(2790)^0$ MASS DIFFERENCE

VALUE (MeV)	DOCUMENT ID		TECN	COMMENT
−2.0±0.7 OUR FIT				
• • • We do not use the following data for averages, fits, limits, etc. • • •				
−3.3±0.4±0.5	YELTON	16	BELL	2231 and 1241 evts

$\Xi_c(2790)$ WIDTHS

$\Xi_c(2790)^+$ WIDTH

VALUE (MeV)	CL%	EVTS	DOCUMENT ID		TECN	COMMENT
8.9±0.6±0.8		2231	YELTON	16	BELL	e^+e^-, Υ regions
• • • We do not use the following data for averages, fits, limits, etc. • • •						
<15	90		CSORNA	01	CLEO	$e^+e^- \approx \Upsilon(4S)$

$\Xi_c(2790)^0$ WIDTH

VALUE (MeV)	CL%	EVTS	DOCUMENT ID		TECN	COMMENT
10.0±0.7±0.8		1241	YELTON	16	BELL	e^+e^-, Υ regions
• • • We do not use the following data for averages, fits, limits, etc. • • •						
<12	90		CSORNA	01	CLEO	$e^+e^- \approx \Upsilon(4S)$

$\Xi_c(2790)$ DECAY MODES

	Mode	Fraction (Γ_i/Γ)
Γ_1	$\Xi_c'\pi$	seen
Γ_2	$\Xi_c^0\gamma$	
Γ_3	$\Xi_c^+\gamma$	

$\Xi_c(2790)$ BRANCHING RATIOS

$\Gamma(\Xi_c'\pi)/\Gamma_{total}$ — Γ_1/Γ

VALUE	DOCUMENT ID		TECN	COMMENT
seen	YELTON	16	BELL	e^+e^-, Υ regions
seen	CSORNA	01	CLEO	$e^+e^- \approx \Upsilon(4S)$

Downloaded from https://academic.oup.com/ptep/article/2022/8/083C01/6651666 by KIT Library user on 27 September 2022

$\Gamma(\Xi_c^0\gamma)/\Gamma(\Xi_c'\pi)$ — Γ_2/Γ_1

VALUE	EVTS	DOCUMENT ID		TECN	CHG	COMMENT
0.13±0.03±0.02	401	[1] YELTON	20	BELL	0	e^+e^- at $\Upsilon(4S)$

[1] Assumes $B(\Xi_c'^+ \to \Xi_c^+\gamma) = 100\%$, noting no strong decay of the Ξ_c' is permitted in the available phase space. YELTON 20 measures $B(\Xi_c(2790)^0 \to \Xi_c^0\gamma)/B(\Xi_c(2790)^0 \to \Xi_c'^+\pi^- \to \Xi_c^+\gamma\pi^-)$.

$\Gamma(\Xi_c^+\gamma)/\Gamma(\Xi_c'\pi)$ — Γ_3/Γ_1

VALUE	CL%	DOCUMENT ID		TECN	CHG	COMMENT
<0.06	90	[1] YELTON	20	BELL	+	e^+e^- at $\Upsilon(4S)$

[1] Assumes $B(\Xi_c'^0 \to \Xi_c^0\gamma) = 100\%$, noting no strong decay of the Ξ_c' is permitted in the available phase space. YELTON 20 measures $B(\Xi_c(2790)^+ \to \Xi_c^+\gamma)/B(\Xi_c(2790)^+ \to \Xi_c'^0\pi^+ \to \Xi_c^0\gamma\pi^+)$.

$\Xi_c(2790)$ REFERENCES

YELTON	20	PR D102 071103	J. Yelton *et al.*	(BELLE Collab.)
YELTON	16	PR D94 052011	J. Yelton *et al.*	(BELLE Collab.)
CSORNA	01	PRL 86 4243	S.E. Csorna *et al.*	(CLEO Collab.)

$\Xi_c(2815)$

$I(J^P) = \frac{1}{2}(\frac{3}{2}^-)$ Status: ***

Seen in both $\Xi_c'\pi$ and $\Xi_c\pi\pi$ decays. The simplest assignment is that this belongs to the same SU(4) multiplet as the $\Lambda(1520)$ and the $\Lambda_c(2625)$, but the spin and parity have not been measured.

$\Xi_c(2815)$ MASSES

The masses are obtained from the mass-difference measurements that follow.

$\Xi_c(2815)^+$ MASS

VALUE (MeV)	EVTS	DOCUMENT ID		TECN	COMMENT
2816.51±0.25 OUR FIT	Error includes scale factor of 1.2.				
• • • We do not use the following data for averages, fits, limits, etc. • • •					
2817.0 ±1.2 $^{+0.7}_{-0.8}$	73 ± 10	LESIAK	08	BELL	$e^+e^- \approx \Upsilon(4S)$

$\Xi_c(2815)^0$ MASS

VALUE (MeV)	EVTS	DOCUMENT ID		TECN	COMMENT
2819.79±0.30 OUR FIT	Error includes scale factor of 1.1.				
• • • We do not use the following data for averages, fits, limits, etc. • • •					
2820.4 ±1.4 $^{+0.9}_{-1.0}$	48 ± 8	LESIAK	08	BELL	$e^+e^- \approx \Upsilon(4S)$

$\Xi_c(2815) - \Xi_c$ MASS DIFFERENCES

$m_{\Xi_c(2815)^+} - m_{\Xi_c^+}$

VALUE (MeV)	EVTS	DOCUMENT ID		TECN	COMMENT
348.80±0.10 OUR FIT					
348.80±0.08±0.06	941	YELTON	16	BELL	e^+e^-, Υ regions
• • • We do not use the following data for averages, fits, limits, etc. • • •					
348.6 ±0.6 ±1.0	20	ALEXANDER	99B	CLE2	$e^+e^- \approx \Upsilon(4S)$

$m_{\Xi_c(2815)^0} - m_{\Xi_c^0}$

VALUE (MeV)	EVTS	DOCUMENT ID		TECN	COMMENT
349.35±0.11 OUR FIT					
349.35±0.08±0.07	1258	YELTON	16	BELL	e^+e^-, Υ regions
• • • We do not use the following data for averages, fits, limits, etc. • • •					
347.2 ±0.7 ±2.0	9	ALEXANDER	99B	CLE2	$e^+e^- \approx \Upsilon(4S)$

$\Xi_c(2815)^+ - \Xi_c(2815)^0$ MASS DIFFERENCE

$m_{\Xi_c(2815)^+} - m_{\Xi_c(2815)^0}$

VALUE (MeV)	DOCUMENT ID		TECN	COMMENT
−3.27±0.27 OUR FIT				
• • • We do not use the following data for averages, fits, limits, etc. • • •				
−3.47±0.12±0.48	YELTON	16	BELL	941 and 1258 evts
−3.4 ±1.9 ±0.9	LESIAK	08	BELL	73 & 48 events

$\Xi_c(2815)$ WIDTHS

$\Xi_c(2815)^+$ WIDTH

VALUE (MeV)	CL%	EVTS	DOCUMENT ID		TECN	COMMENT
2.43±0.20±0.17		941	YELTON	16	BELL	e^+e^-, Υ regions
• • • We do not use the following data for averages, fits, limits, etc. • • •						
<3.5	90		ALEXANDER	99B	CLE2	$e^+e^- \approx \Upsilon(4S)$

$\Xi_c(2815)^0$ WIDTH

VALUE (MeV)	CL%	EVTS	DOCUMENT ID		TECN	COMMENT
2.54±0.18±0.17		1258	YELTON	16	BELL	e^+e^-, Υ regions
• • • We do not use the following data for averages, fits, limits, etc. • • •						
<6.5	90		ALEXANDER	99B	CLE2	$e^+e^- \approx \Upsilon(4S)$

$\Xi_c(2815)$ DECAY MODES

The $\Xi_c\pi\pi$ modes are consistent with being entirely via $\Xi_c(2645)\pi$.

	Mode	Fraction (Γ_i/Γ)
Γ_1	$\Xi_c'\pi$	seen
Γ_2	$\Xi_c(2645)\pi$	seen
Γ_3	$\Xi_c^0\gamma$	seen
Γ_4	$\Xi_c^+\gamma$	

$\Gamma(\Xi_c'\pi)/\Gamma_{total}$ — Γ_1/Γ

VALUE	DOCUMENT ID		TECN	COMMENT
seen	YELTON	16	BELL	e^+e^-, Υ regions
seen	ALEXANDER	99B	CLE2	$e^+e^- \approx \Upsilon(4S)$

$\Gamma(\Xi_c(2645)\pi)/\Gamma_{total}$ — Γ_2/Γ

VALUE	DOCUMENT ID		TECN	COMMENT
seen	YELTON	16	BELL	e^+e^-, Υ regions
seen	LESIAK	08	BELL	$e^+e^- \approx \Upsilon(4S)$

$\Gamma(\Xi_c^0\gamma)/\Gamma(\Xi_c(2645)\pi)$ — Γ_3/Γ_2

VALUE	EVTS	DOCUMENT ID		TECN	CHG	COMMENT
0.41±0.05±0.03	222	[1] YELTON	20	BELL	0	e^+e^- at $\Upsilon(4S)$

[1] Assumes $B(\Xi_c(2645)^+ \to \Xi_c^0\pi^+) = 100\%$, which is the only strong decay of the $\Xi_c(2645)$ permitted in the available phase space. YELTON 20 measures $B(\Xi_c(2815)^0 \to \Xi_c^0\gamma)/B(\Xi_c(2815)^0 \to \Xi_c(2645)^+\pi^- \to \Xi_c^0\pi^+\pi^-)$.

$\Gamma(\Xi_c^+\gamma)/\Gamma(\Xi_c(2645)\pi)$ — Γ_4/Γ_2

VALUE	CL%	DOCUMENT ID		TECN	CHG	COMMENT
<0.09	90	[1] YELTON	20	BELL	+	e^+e^- at $\Upsilon(4S)$

[1] Assumes $B(\Xi_c(2645)^0 \to \Xi_c^+\pi^-) = 100\%$, which is the only strong decay of the $\Xi_c(2645)$ permitted in the available phase space. YELTON 20 measures $B(\Xi_c(2815)^+ \to \Xi_c^+\gamma)/B(\Xi_c(2815)^+ \to \Xi_c(2645)^0\pi^+ \to \Xi_c^+\pi^-\pi^+)$.

$\Xi_c(2815)$ REFERENCES

YELTON	20	PR D102 071103	J. Yelton *et al.*	(BELLE Collab.)
YELTON	16	PR D94 052011	J. Yelton *et al.*	(BELLE Collab.)
LESIAK	08	PL B665 9	T. Lesiak *et al.*	(BELLE Collab.)
ALEXANDER	99B	PRL 83 3390	J.P. Alexander *et al.*	(CLEO Collab.)

$\Xi_c(2923)$

$I(J^P) = ?(?^?)$ Status: **

OMITTED FROM SUMMARY TABLE

$\Xi_c(2923)$ MASSES

$\Xi_c(2923)^0$ MASS

VALUE (MeV)	EVTS	DOCUMENT ID		TECN	COMMENT
2923.04±0.25±0.24	5.4k	[1] AAIJ	20X	LHCB	pp at 13 TeV

[1] AAIJ 20X reports 2923.04 ± 0.25 ± 0.20 ± 0.14 MeV where the last uncertainty is due to the Λ_c^+ mass.

$\Xi_c(2923)$ WIDTHS

$\Xi_c(2923)^0$ WIDTH

VALUE (MeV)	EVTS	DOCUMENT ID		TECN	COMMENT
7.1±0.8±1.8	5.4k	AAIJ	20X	LHCB	pp at 13 TeV

$\Xi_c(2923)$ DECAY MODES

	Mode	Fraction (Γ_i/Γ)
Γ_1	$\Lambda_c^+ K^-$	seen

$\Xi_c(2923)$ BRANCHING RATIOS

$\Gamma(\Lambda_c^+ K^-)/\Gamma_{total}$ — Γ_1/Γ

VALUE	EVTS	DOCUMENT ID		TECN	COMMENT
seen	5.4k	AAIJ	20X	LHCB	pp at 13 TeV

$\Xi_c(2923)$ REFERENCES

AAIJ	20X	PRL 124 222001	R. Aaij *et al.*	(LHCb Collab.)

Downloaded from https://academic.oup.com/ptep/article/2022/8/083C01/6651666 by KIT Library user on 27 September 2022

$\Xi_c(2930)$

$I(J^P) = ?(?^?)$ Status: **

OMITTED FROM SUMMARY TABLE

$\Xi_c(2930)$ MASSES

$\Xi_c(2930)^+$ MASS

VALUE (MeV)	EVTS	DOCUMENT ID		TECN	COMMENT
2942.3±4.4±1.5	21	LI	18D	BELL	e^+e^- at $\Upsilon(4S)$

$\Xi_c(2930)^0$ MASS

VALUE (MeV)	EVTS	DOCUMENT ID		TECN	COMMENT
2938.55±0.21± 0.22	10.4k	[1] AAIJ	20X	LHCB	pp at 13 TeV
• • • We do not use the following data for averages, fits, limits, etc. • • •					
$2928.9 \pm 3.0 \,^{+0.9}_{-12.0}$	61	LI	18A	BELL	e^+e^- at $\Upsilon(4S)$
$2931 \pm 3 \pm 5$	34	AUBERT	08H	BABR	$\Upsilon(4S) \to B\overline{B}$

[1] AAIJ 20X reports 2938.55 ± 0.21 ± 0.17 ± 0.14 MeV where the last uncertainty is due to the Λ_c^+ mass. Observes that the broader resonance at 2930 MeV seen in $B^- \to K^-\Lambda_c^+\overline{\Lambda}_c^-$ by LI 18A and AUBERT 08H resolves into two narrower peaks at approximately 2939 MeV and 2923 MeV.

$\Xi_c(2930)^+ - \Xi_c(2930)^0$ MASS DIFFERENCE

VALUE (MeV)	EVTS	DOCUMENT ID		TECN	COMMENT
• • • We do not use the following data for averages, fits, limits, etc. • • •					
$13.4 \pm 5.3 \,^{+1.7}_{-12.1}$	21	[1] LI	18D	BELL	e^+e^- at $\Upsilon(4S)$

[1] This LI 18D value is not independent of the mass measurements.

$\Xi_c(2930)$ WIDTHS

$\Xi_c(2930)^+$ WIDTH

VALUE (MeV)	EVTS	DOCUMENT ID		TECN	COMMENT
14.8±8.8±2.5	21	LI	18D	BELL	e^+e^- at $\Upsilon(4S)$

$\Xi_c(2930)^0$ WIDTH

VALUE (MeV)	EVTS	DOCUMENT ID		TECN	COMMENT
10.2±0.8± 1.1	10.4k	[1] AAIJ	20X	LHCB	pp at 13 TeV
• • • We do not use the following data for averages, fits, limits, etc. • • •					
$19.5 \pm 8.4 \,^{+5.9}_{-7.9}$	61	LI	18A	BELL	e^+e^- at $\Upsilon(4S)$
$36 \pm 7 \pm 11$	34	AUBERT	08H	BABR	$\Upsilon(4S) \to B\overline{B}$

[1] AAIJ 20X observes that the broader resonance at 2930 MeV seen in $B^- \to K^-\Lambda_c^+\overline{\Lambda}_c^-$ by LI 18A and AUBERT 08H resolves into two narrower peaks at approximately 2939 MeV and 2923 MeV.

$\Xi_c(2930)$ DECAY MODES

	Mode	Fraction (Γ_i/Γ)
Γ_1	$\Lambda_c^+ K^-$	seen
Γ_2	$\Lambda_c^+ K_S^0$	seen

$\Xi_c(2930)$ BRANCHING RATIOS

$\Gamma(\Lambda_c^+ K^-)/\Gamma_{total}$ — Γ_1/Γ

VALUE	EVTS	DOCUMENT ID		TECN	COMMENT
seen	10.4k	AAIJ	20X	LHCB	pp at 13 TeV
seen	61	LI	18A	BELL	Significance 5.1 std
seen	34	AUBERT	08H	BABR	e^+e^- at $\Upsilon(4S)$

$\Gamma(\Lambda_c^+ K_S^0)/\Gamma_{total}$ — Γ_2/Γ

VALUE	EVTS	DOCUMENT ID		TECN	COMMENT
seen	21	LI	18D	BELL	Significance 4.1 std

$\Xi_c(2930)$ REFERENCES

AAIJ	20X	PRL 124 222001	R. Aaij *et al.*	(LHCb Collab.)
LI	18A	EPJ C78 252	Y.B. Li *et al.*	(BELLE Collab.)
LI	18D	EPJ C78 928	Y.B. Li *et al.*	(BELLE Collab.)
AUBERT	08H	PR D77 031101	B. Aubert *et al.*	(BABAR Collab.)

$\Xi_c(2970)$

$I(J^P) = \frac{1}{2}(\frac{1}{2}^+)$ Status: ***

was $\Xi_c(2980)$

$J^P = 1/2^+$ is favored by MOON 21.

$\Xi_c(2970)$ MASSES

$\Xi_c(2970)^+$ MASS

VALUE (MeV)	EVTS	DOCUMENT ID		TECN	COMMENT
2964.3±1.5 OUR FIT Error includes scale factor of 3.9.					
2967.1±1.4 OUR AVERAGE Error includes scale factor of 2.0. See the ideogram below.					
$2966.0 \pm 0.8 \pm 0.2$	0.9k	YELTON	16	BELL	$e^+e^- \to \Upsilon(4S), \Upsilon(5S)$ and continuum
$2974.9 \pm 1.5 \pm 2.1$	244 ± 39	KATO	14	BELL	e^+e^- $\Upsilon(1S)$ to $\Upsilon(5S)$
$2969.3 \pm 2.2 \pm 1.7$	756 ± 206	AUBERT	08J	BABR	$e^+e^- \approx$ 10.58 GeV
$2967.7 \pm 2.3 \,^{+1.1}_{-1.2}$	78 ± 13	LESIAK	08	BELL	$e^+e^- \approx \Upsilon(4S)$
• • • We do not use the following data for averages, fits, limits, etc. • • •					
$2978.5 \pm 2.1 \pm 2.0$	405 ± 51	CHISTOV	06	BELL	See KATO 14

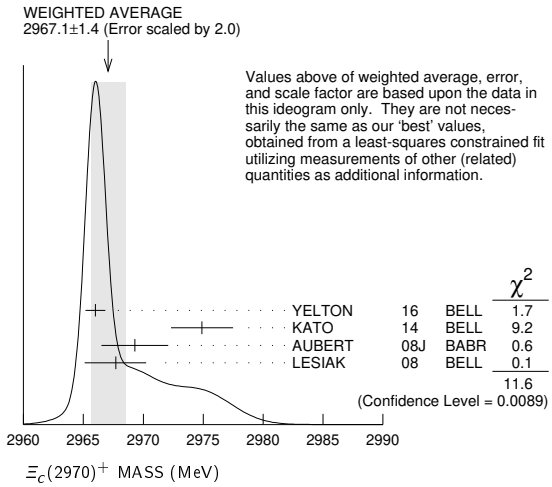

$\Xi_c(2970)^0$ MASS

The evidence is statistically weaker for this charge state.

VALUE (MeV)	EVTS	DOCUMENT ID		TECN	COMMENT
2967.1 ±1.7 OUR FIT Error includes scale factor of 6.7.					
2965.9 ±2.2 OUR AVERAGE Error includes scale factor of 7.4.					
$2964.88 \pm 0.26 \pm 0.20$	11.7k	[1] AAIJ	20X	LHCB	pp at 13 TeV
$2970.8 \pm 0.7 \pm 0.2$	1.4k	YELTON	16	BELL	$e^+e^- \to \Upsilon(4S)$, $\Upsilon(5S)$, continuum
$2972.9 \pm 4.4 \pm 1.6$	67 ± 44	AUBERT	08J	BABR	$e^+e^- \approx$ 10.58 GeV
$2965.7 \pm 2.4 \,^{+1.1}_{-1.2}$	57 ± 13	LESIAK	08	BELL	$e^+e^- \approx \Upsilon(4S)$
$2977.1 \pm 8.8 \pm 3.5$	42 ± 24	CHISTOV	06	BELL	$e^+e^- \approx \Upsilon(4S)$

[1] AAIJ 20X reports 2964.88 ± 0.26 ± 0.14 ± 0.14 MeV where the last uncertainty is due to the Λ_c^+ mass. Further studies are required to establish whether the narrow resonance at 2965 MeV is a different baryon from the narrow resonance at 2970 MeV seen by YELTON 16.

$\Xi_c(2970) - \Xi_c$ MASS DIFFERENCES

$m_{\Xi_c(2970)^+} - m_{\Xi_c^+}$

VALUE (MeV)	EVTS	DOCUMENT ID		TECN	COMMENT
496.6±1.5 OUR FIT Error includes scale factor of 3.7.					
498.1±0.8±0.2	916	YELTON	16	BELL	e^+e^-, Υ regions

$m_{\Xi_c(2970)^0} - m_{\Xi_c^0}$

VALUE (MeV)	EVTS	DOCUMENT ID		TECN	COMMENT
496.7±1.8 OUR FIT Error includes scale factor of 5.3.					
499.9±0.7±0.2	1.4k	YELTON	16	BELL	e^+e^-, Υ regions

$\Xi_c(2970)^+ - \Xi_c(2970)^0$ MASS DIFFERENCE

VALUE (MeV)	DOCUMENT ID		TECN	COMMENT
−2.8±1.9 OUR FIT Error includes scale factor of 4.8.				
−4.8±0.1±0.5	YELTON	16	BELL	916 and 1443 evts

$\Xi_c(2970)$ WIDTHS

$\Xi_c(2970)^+$ WIDTH

VALUE (MeV)	EVTS	DOCUMENT ID		TECN	COMMENT
$\mathbf{20.9 \,^{+2.4}_{-3.5}}$ **OUR AVERAGE** Error includes scale factor of 1.2.					
$28.1 \pm 2.4 \,^{+1.0}_{-5.0}$	916	YELTON	16	BELL	e^+e^-, Υ regions
$14.8 \pm 2.5 \pm 4.1$	244 ± 39	KATO	14	BELL	e^+e^- $\Upsilon(1S)$ to $\Upsilon(5S)$
$27 \pm 8 \pm 2$	756 ± 206	AUBERT	08J	BABR	$e^+e^- \approx$ 10.58 GeV
$18 \pm 6 \pm 3$	78 ± 13	LESIAK	08	BELL	$e^+e^- \approx \Upsilon(4S)$
• • • We do not use the following data for averages, fits, limits, etc. • • •					
$43.5 \pm 7.5 \pm 7.0$	405 ± 51	CHISTOV	06	BELL	See KATO 14

$\Xi_c(2970)^0$ WIDTH

VALUE (MeV)	EVTS	DOCUMENT ID		TECN	COMMENT
$14.1 \pm 0.9 \pm 1.3$	11.7k	[1] AAIJ	20X	LHCB	pp at 13 TeV
$30.3 \pm 2.3 \,^{+1.0}_{-1.8}$	1443	YELTON	16	BELL	e^+e^-, Υ regions

Downloaded from https://academic.oup.com/ptep/article/2022/8/083C01/6651666 by KIT Library user on 27 September 2022

• • • We do not use the following data for averages, fits, limits, etc. • • •

31 ±7 ±8	67 ± 44	AUBERT	08J	BABR	$e^+e^- \approx$ 10.58 GeV
15 ±6 ±3	57 ± 13	LESIAK	08	BELL	$e^+e^- \approx \Upsilon(4S)$

[1] Further studies are required to establish whether the narrow resonance at 2965 MeV is a different baryon from the narrow resonance at 2970 MeV seen by YELTON 16.

$\Xi_c(2970)$ DECAY MODES

	Mode	Fraction (Γ_i/Γ)
Γ_1	$\Lambda_c^+ \overline{K}\pi$	seen
Γ_2	$\Sigma_c(2455)\overline{K}$	seen
Γ_3	$\Lambda_c^+ \overline{K}$	not seen
Γ_4	$\Lambda_c^+ K^-$	seen
Γ_5	$\Xi_c 2\pi$	seen
Γ_6	$\Xi_c' \pi$	seen
Γ_7	$\Xi_c(2645)\pi$	seen

$\Xi_c(2970)$ BRANCHING RATIOS

$\Gamma(\Lambda_c^+ \overline{K}\pi)/\Gamma_{total}$ — Γ_1/Γ

VALUE	DOCUMENT ID		TECN	COMMENT
seen	AUBERT	08J	BABR	$e^+e^- \approx \Upsilon(4S)$
seen	CHISTOV	06	BELL	$e^+e^- \approx \Upsilon(4S)$

$\Gamma(\Lambda_c^+ K^-)/\Gamma_{total}$ — Γ_4/Γ

VALUE	EVTS	DOCUMENT ID		TECN	COMMENT
seen	11.7k	[1] AAIJ	20X	LHCB	pp at 13 TeV

[1] Further studies are required to establish whether the narrow resonance at 2965 MeV is a different baryon from the narrow resonance at 2970 MeV seen by YELTON 16.

$\Gamma(\Sigma_c(2455)\overline{K})/\Gamma(\Lambda_c^+ \overline{K}\pi)$ — Γ_2/Γ_1

VALUE	DOCUMENT ID		TECN	COMMENT
0.55±0.07±0.13	AUBERT	08J	BABR	$e^+e^- \approx \Upsilon(4S)$

$\Gamma(\Xi_c' \pi)/\Gamma_{total}$ — Γ_6/Γ

VALUE	DOCUMENT ID		TECN	COMMENT
seen	YELTON	16	BELL	e^+e^-, Υ regions

$\Gamma(\Xi_c(2645)\pi)/\Gamma_{total}$ — Γ_7/Γ

VALUE	DOCUMENT ID		TECN	COMMENT
seen	LESIAK	08	BELL	$e^+e^- \approx \Upsilon(4S)$

$\Gamma(\Xi_c' \pi)/\Gamma(\Xi_c(2645)\pi)$ — Γ_6/Γ_7

VALUE	EVTS	DOCUMENT ID		TECN	COMMENT
$1.67\pm0.29^{+0.15}_{-0.09}\pm0.25$	778	[1] MOON	21	BELL	e^+e^- at Υ(nS)

[1] Measurement of the ratio of $\Xi_c(2970)^+ \to \Xi_c(2645)^0\pi^+$ versus $\Xi_c(2970)^+ \to \Xi_c'^0\pi^+$. The last uncertainty is from possible isospin-symmetry-breaking effects. MOON 21 determines from an angular analysis of the $\Xi_c^+\pi^+\pi^-$ final state that the spin of the $\Xi_c(2970)^+$ is strongly compatible with $J = 1/2$, assuming domination by the lowest partial wave in $\Xi_c(2970)^+ \to \Xi_c(2645)^0\pi^+$. When further combined with the size of this ratio, MOON 21 determines from heavy quark symmetry that the spin-parity of the $\Xi_c(2970)^+$ is favored to be $J^P = 1/2^+$, with light degrees of freedom in the 0^+ state.

$\Xi_c(2970)$ REFERENCES

MOON	21	PR D103 L111101	T.J. Moon *et al.*	(BELLE Collab.) JP
AAIJ	20X	PRL 124 222001	R. Aaij *et al.*	(LHCb Collab.)
YELTON	16	PR D94 052011	J. Yelton *et al.*	(BELLE Collab.)
KATO	14	PR D89 052003	Y. Kato *et al.*	(BELLE Collab.)
AUBERT	08J	PR D77 012002	B. Aubert *et al.*	(BABAR Collab.)
LESIAK	08	PL B665 9	T. Lesiak *et al.*	(BELLE Collab.)
CHISTOV	06	PRL 97 162001	R. Chistov *et al.*	(BELLE Collab.)

$\Xi_c(3055)$

$I(J^P) = ?(?^?)$ Status: ***

$\Xi_c(3055)$ MASSES

$\Xi_c(3055)^+$ MASS

VALUE (MeV)	EVTS	DOCUMENT ID		TECN	COMMENT
3055.9±0.4	894	KATO	16	BELL	e^+e^- Υ region
• • • We do not use the following data for averages, fits, limits, etc. • • •					
3058.1±1.0±2.1	199 ± 46	KATO	14	BELL	See KATO 16
3054.2±1.2±0.5	218 ± 95	AUBERT	08J	BABR	$e^+e^- \approx$ 10.58 GeV

$\Xi_c(3055)$ WIDTHS

$\Xi_c(3055)^+$ WIDTH

VALUE (MeV)	EVTS	DOCUMENT ID		TECN	COMMENT
7.8±1.2± 1.5		KATO	16	BELL	e^+e^- Υ region
• • • We do not use the following data for averages, fits, limits, etc. • • •					
9.7±3.4± 3.3	199 ± 46	KATO	14	BELL	e^+e^- $\Upsilon(1S)$ to $\Upsilon(5S)$
17 ±6 ±11	218 ± 95	AUBERT	08J	BABR	$e^+e^- \approx$ 10.58 GeV

$\Xi_c(3055)$ DECAY MODES

	Mode	Fraction (Γ_i/Γ)
Γ_1	$\Sigma^{++}K^-$	seen
Γ_2	ΛD^+	seen

$\Xi_c(3055)$ BRANCHING RATIOS

$\Gamma(\Lambda D^+)/\Gamma(\Sigma^{++}K^-)$ — Γ_2/Γ_1

VALUE	DOCUMENT ID		TECN	COMMENT
5.09±1.01±0.76	KATO	16	BELL	721 and 103 evts

$\Xi_c(3055)$ REFERENCES

KATO	16	PR D94 032002	Y. Kato *et al.*	(BELLE Collab.)
KATO	14	PR D89 052003	Y. Kato *et al.*	(BELLE Collab.)
AUBERT	08J	PR D77 012002	B. Aubert *et al.*	(BABAR Collab.)

$\Xi_c(3080)$

$I(J^P) = \frac{1}{2}(?^?)$ Status: ***

$\Xi_c(3080)$ MASSES

$\Xi_c(3080)^+$ MASS

VALUE (MeV)	EVTS	DOCUMENT ID		TECN	COMMENT
3077.2±0.4 OUR AVERAGE					
3077.9±0.9	596	KATO	16	BELL	e^+e^- Υ region
3077.0±0.4±0.2	403 ± 60	AUBERT	08J	BABR	$e^+e^- \approx$ 10.58 GeV
• • • We do not use the following data for averages, fits, limits, etc. • • •					
3076.9±0.3±0.2	210 ± 30	KATO	14	BELL	See KATO 16
3076.7±0.9±0.5	326 ± 40	CHISTOV	06	BELL	See KATO 14

$\Xi_c(3080)^0$ MASS

VALUE (MeV)	EVTS	DOCUMENT ID		TECN	COMMENT
3079.9±1.4 OUR AVERAGE Error includes scale factor of 1.3.					
3079.3±1.1±0.2	90 ± 27	AUBERT	08J	BABR	$e^+e^- \approx$ 10.58 GeV
3082.8±1.8±1.5	67 ± 20	CHISTOV	06	BELL	$e^+e^- \approx \Upsilon(4S)$

$\Xi_c(3080)$ WIDTHS

$\Xi_c(3080)^+$ WIDTH

VALUE (MeV)	EVTS	DOCUMENT ID		TECN	COMMENT
3.6±1.1 OUR AVERAGE Error includes scale factor of 1.5.					
3.0±0.7±0.4	596	KATO	16	BELL	e^+e^- Υ region
5.5±1.3±0.6	403 ± 60	AUBERT	08J	BABR	$e^+e^- \approx$ 10.58 GeV
• • • We do not use the following data for averages, fits, limits, etc. • • •					
2.4±0.9±1.6	210 ± 30	KATO	14	BELL	See KATO 16
6.2±1.2±0.8	326 ± 40	CHISTOV	06	BELL	See KATO 14

$\Xi_c(3080)^0$ WIDTH

VALUE (MeV)	EVTS	DOCUMENT ID		TECN	COMMENT
5.6±2.2 OUR AVERAGE					
5.9±2.3±1.5	90 ± 27	AUBERT	08J	BABR	$e^+e^- \approx$ 10.58 GeV
5.2±3.1±1.8	67 ± 20	CHISTOV	06	BELL	$e^+e^- \approx \Upsilon(4S)$

$\Xi_c(3080)$ DECAY MODES

	Mode	Fraction (Γ_i/Γ)
Γ_1	$\Lambda_c^+ \overline{K}\pi$	seen
Γ_2	$\Sigma_c(2455)\overline{K}$	seen
Γ_3	$\Sigma_c(2455)^{++}K^-$	seen
Γ_4	$\Sigma_c(2520)^{++}K^-$	seen
Γ_5	$\Sigma_c(2455)\overline{K} + \Sigma_c(2520)\overline{K}$	seen
Γ_6	$\Lambda_c^+ \overline{K}$	not seen
Γ_7	$\Lambda_c^+ \overline{K}\pi^+\pi^-$	not seen
Γ_8	ΛD^+	seen

$\Xi_c(3080)$ BRANCHING RATIOS

$\Gamma(\Sigma_c(2455)\overline{K})/\Gamma(\Lambda_c^+ \overline{K}\pi)$ — Γ_2/Γ_1

VALUE	DOCUMENT ID		TECN	COMMENT
0.45±0.06 OUR AVERAGE				
0.45±0.05±0.05	AUBERT	08J	BABR	in $\Lambda_c^+ K^-\pi^+$
0.44±0.12±0.07	AUBERT	08J	BABR	in $\Lambda_c^+ K_S^0\pi^-$

Downloaded from https://academic.oup.com/ptep/article/2022/8/083C01/6651666 by KIT Library user on 27 September 2022

$\Gamma(\Sigma_c(2520)^{++}K^-)/\Gamma(\Sigma_c(2455)^{++}K^-)$ — Γ_4/Γ_3

VALUE	DOCUMENT ID		TECN	COMMENT
1.07±0.27±0.04	KATO	16	BELL	234 and 176 evts

$[\Gamma(\Sigma_c(2455)\overline{K}) + \Gamma(\Sigma_c(2520)\overline{K})]/\Gamma(\Lambda_c^+\overline{K}\pi)$ — Γ_5/Γ_1

VALUE	DOCUMENT ID		TECN	COMMENT
0.89±0.12 OUR AVERAGE				
0.95±0.14±0.06	AUBERT	08J	BABR	in $\Lambda_c^+ K^-\pi^+$
0.78±0.21±0.05	AUBERT	08J	BABR	in $\Lambda_c^+ K_S^0\pi^-$

$\Gamma(\Lambda D^+)/\Gamma(\Sigma_c(2455)^{++}K^-)$ — Γ_8/Γ_3

VALUE	DOCUMENT ID		TECN	COMMENT
1.29±0.30±0.15	KATO	16	BELL	186 and 176 evts

$\Xi_c(3080)$ REFERENCES

KATO	16	PR D94 032002	Y. Kato *et al.*	(BELLE Collab.)
KATO	14	PR D89 052003	Y. Kato *et al.*	(BELLE Collab.)
AUBERT	08J	PR D77 012002	B. Aubert *et al.*	(BABAR Collab.)
CHISTOV	06	PRL 97 162001	R. Chistov *et al.*	(BELLE Collab.)

$\Xi_c(3123)$

$I(J^P) = ?(?^?)$ Status: *

OMITTED FROM SUMMARY TABLE

A peak in the $\Sigma_c(2520)^{++}K^- \to \Lambda_c^+ K^-\pi^+$ mass spectrum with a significance of 3.6 standard deviations. KATO 14 finds no evidence for this state.

$\Xi_c(3123)$ MASSES

$\Xi_c(3123)^+$ MASS

VALUE (MeV)	EVTS	DOCUMENT ID		TECN	COMMENT
3122.9±1.3±0.3	101 ± 35	AUBERT	08J	BABR	$e^+e^- \approx$ 10.58 GeV

$\Xi_c(3123)$ WIDTHS

$\Xi_c(3123)^+$ WIDTH

VALUE (MeV)	EVTS	DOCUMENT ID		TECN	COMMENT
4.4±3.4±1.7	101 ± 35	AUBERT	08J	BABR	$e^+e^- \approx$ 10.58 GeV

$\Xi_c(3123)$ REFERENCES

KATO	14	PR D89 052003	Y. Kato *et al.*	(BELLE Collab.)
AUBERT	08J	PR D77 012002	B. Aubert *et al.*	(BABAR Collab.)

Ω_c^0

$I(J^P) = 0(\frac{1}{2}^+)$ Status: ***

The quantum numbers have not been measured, but are simply assigned in accord with the quark model, in which the Ω_c^0 is the *ssc* ground state. No absolute branching fractions have been measured.

Ω_c^0 MASS

VALUE (MeV)	EVTS	DOCUMENT ID		TECN	COMMENT
2695.2± 1.7 OUR FIT	Error includes scale factor of 1.3.				
$2695.2^{+1.8}_{-1.6}$ OUR AVERAGE	Error includes scale factor of 1.3. See the ideogram below.				
2693.6± $0.3^{+1.8}_{-1.5}$	725	SOLOVIEVA	09	BELL	$\Omega^-\pi^+$ in $e^+e^- \to \Upsilon(4S)$
2694.6± 2.6±1.9	40	[1] CRONIN-HEN..	01	CLE2	$e^+e^- \approx$ 10.6 GeV
2699.9± 1.5±2.5	42	[2] FRABETTI	94H	E687	γBe, $\overline{E}_\gamma$= 221 GeV
• • • We do not use the following data for averages, fits, limits, etc. • • •					
2705.9± 3.3±2.0	10	[3] FRABETTI	93	E687	γBe, $\overline{E}_\gamma$= 221 GeV
2719.0± 7.0±2.5	11	[4] ALBRECHT	92H	ARG	$e^+e^- \approx$ 10.6 GeV
2740 ±20	3	BIAGI	85B	SPEC	Σ^-Be 135 GeV/c

[1] CRONIN-HENNESSY 01 sees 40.4 ± 9.0 events in a sum over five channels.
[2] FRABETTI 94H claims a signal of 42.5 ± 8.8 $\Sigma^+K^-K^-\pi^+$ events. The background is about 24 events.
[3] FRABETTI 93 claims a signal of 10.3 ± 3.9 $\Omega^-\pi^+$ events above a background of 5.8 events.
[4] ALBRECHT 92H claims a signal of 11.5 ± 4.3 $\Xi^-K^-\pi^+\pi^+$ events. The background is about 5 events.

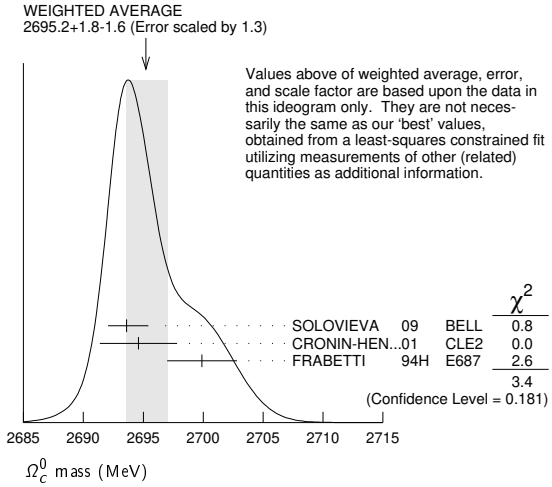

Ω_c^0 MEAN LIFE

VALUE (10^{-15} s)	EVTS	DOCUMENT ID		TECN	COMMENT
268±24±10	978	[1] AAIJ	18J	LHCB	$pK^-K^-\pi^+$
• • • We do not use the following data for averages, fits, limits, etc. • • •					
72±11±11	64	LINK	03C	FOCS	$\Omega^-\pi^+$, $\Xi^-K^-\pi^+\pi^+$
55^{+13+18}_{-11-23}	86	ADAMOVICH	95B	WA89	$\Omega^-\pi^-\pi^+\pi^+$, $\Xi^-K^-\pi^+\pi^+$
86^{+27}_{-20}±28	25	FRABETTI	95D	E687	$\Sigma^+K^-K^-\pi^+$

[1] AAIJ 18J, with nearly five times more events that the previous three experiments combined, gets a lifetime that is nearly four times larger than the average of those experiments, (69 ± 12) × 10^{-15} s. We go with the larger data sample.

Ω_c^0 DECAY MODES

No absolute branching fractions have been measured. The following are branching *ratios* relative to $\Omega^-\pi^+$.

	Mode	Fraction (Γ_i/Γ)	Confidence level
	Cabibbo-favored ($S = -3$) decays — relative to $\Omega^-\pi^+$		
Γ_1	$\Omega^-\pi^+$	**DEFINED AS 1**	
Γ_2	$\Omega^-\pi^+\pi^0$	1.80±0.33	
Γ_3	$\Omega^-\rho^+$	>1.3	90%
Γ_4	$\Omega^-\pi^-2\pi^+$	0.31±0.05	
Γ_5	$\Omega^-e^+\nu_e$	2.4 ±1.2	
Γ_6	$\Xi^0\overline{K}^0$	1.64±0.29	
Γ_7	$\Xi^0K^-\pi^+$	1.20±0.18	
Γ_8	$\Xi^0\overline{K}^{*0}$, $\overline{K}^{*0} \to K^-\pi^+$	0.68±0.16	
Γ_9	$\Omega(2012)^-\pi^+$, $\Omega(2012)^- \to \Xi^0K^-$	0.12±0.05	
Γ_{10}	$\Xi^-\overline{K}^0\pi^+$	2.12±0.28	
Γ_{11}	$\Omega(2012)^-\pi^+$, $\Omega(2012)^- \to \Xi^-\overline{K}^0$	0.12±0.06	
Γ_{12}	$\Xi^-K^-2\pi^+$	0.63±0.09	
Γ_{13}	$\Xi(1530)^0K^-\pi^+$, $\Xi^{*0} \to \Xi^-\pi^+$	0.21±0.06	
Γ_{14}	$\Xi^-\overline{K}^{*0}\pi^+$	0.34±0.11	
Γ_{15}	$pK^-K^-\pi^+$	seen	
Γ_{16}	$\Sigma^+K^-K^-\pi^+$	<0.32	90%
Γ_{17}	$\Lambda\overline{K}^0\overline{K}^0$	1.72±0.35	

Ω_c^0 BRANCHING RATIOS

A few early but now obsolete measurements have been omitted. See K.A. Olive, et al. (Particle Data Group), Chinese Physics **C38** 070001 (2014).

$\Gamma(\Omega^-\pi^+\pi^0)/\Gamma(\Omega^-\pi^+)$ — Γ_2/Γ_1

VALUE	EVTS	DOCUMENT ID		TECN	COMMENT
1.80±0.33 OUR AVERAGE	Error includes scale factor of 1.9.				
2.00±0.17±0.11	403	YELTON	18	BELL	$e^+e^- \to \Upsilon(4S)$, +higher
1.27±0.31±0.11	64	AUBERT	07AH	BABR	$e^+e^- \approx \Upsilon(4S)$

Downloaded from https://academic.oup.com/ptep/article/2022/8/083C01/6651666 by KIT Library user on 27 September 2022

$\Gamma(\Omega^-\rho^+)/\Gamma(\Omega^-\pi^+\pi^0)$ — Γ_3/Γ_2

VALUE	CL%	DOCUMENT ID		TECN	COMMENT
>0.71	90	[1] YELTON	18	BELL	$e^+e^- \to \Upsilon(4S)$, +higher

[1] This submode fraction is evaluated from a background-subtracted signal in a mass plot. Result ignores interference effects and systematic uncertainties, which YELTON 18 claim are both small.

$\Gamma(\Omega^-\pi^-2\pi^+)/\Gamma(\Omega^-\pi^+)$ — Γ_4/Γ_1

VALUE	EVTS	DOCUMENT ID		TECN	COMMENT
0.31±0.05 OUR AVERAGE					
0.32±0.05±0.02	108	YELTON	18	BELL	$e^+e^- \to \Upsilon(4S)$, +higher
0.28±0.09±0.01	25	AUBERT	07AH	BABR	$e^+e^- \approx \Upsilon(4S)$

$\Gamma(\Omega^-\pi^+)/\Gamma(\Omega^-e^+\nu_e)$ — Γ_1/Γ_5

VALUE	EVTS	DOCUMENT ID		TECN	COMMENT
0.41±0.19±0.04	11	AMMAR	02	CLE2	$e^+e^- \approx \Upsilon(4S)$

$\Gamma(\Xi^0\overline{K}^0)/\Gamma(\Omega^-\pi^+)$ — Γ_6/Γ_1

VALUE	EVTS	DOCUMENT ID		TECN	COMMENT
1.64±0.26±0.12	98	YELTON	18	BELL	$e^+e^- \to \Upsilon(4S)$, +higher

$\Gamma(\Xi^0K^-\pi^+)/\Gamma(\Omega^-\pi^+)$ — Γ_7/Γ_1

VALUE	EVTS	DOCUMENT ID		TECN	COMMENT
1.20±0.16±0.08	168	YELTON	18	BELL	$e^+e^- \to \Upsilon(4S)$, +higher

$\Gamma(\Xi^0\overline{K}^{*0}, \overline{K}^{*0} \to K^-\pi^+)/\Gamma(\Xi^0K^-\pi^+)$ — Γ_8/Γ_7

VALUE	EVTS	DOCUMENT ID		TECN	COMMENT
0.57±0.10	95	[1] YELTON	18	BELL	$e^+e^- \to \Upsilon(4S)$, +higher

[1] This submode fraction is evaluated from a background-subtracted signal in a mass plot. Result ignores interference effects and systematic uncertainties, which YELTON 18 claim are both small.

$\Gamma(\Omega(2012)^-\pi^+, \Omega(2012)^- \to \Xi^0K^-)/\Gamma(\Xi^0K^-\pi^+)$ — Γ_9/Γ_7

VALUE (units 10^{-2})	EVTS	DOCUMENT ID		TECN	COMMENT
9.6±3.2±1.8	28	[1] LI	21D	BELL	e^+e^- at $\Upsilon(nS)$

[1] LI 21D reports the significance of the $\Omega(2012)$ signal is 4.2 σ including systematic uncertainties. Also measures $B(\Omega_c^0 \to \Omega(2012)^-\pi^+,\ \Omega(2012)^- \to (\overline{K}\Xi)^-)/B(\Omega_c^0 \to \Xi^0K^-\pi^+) = 0.220 \pm 0.059 \pm 0.035$.

$\Gamma(\Xi^-\overline{K}^0\pi^+)/\Gamma(\Omega^-\pi^+)$ — Γ_{10}/Γ_1

VALUE	EVTS	DOCUMENT ID		TECN	COMMENT
2.12±0.24±0.14	349	YELTON	18	BELL	$e^+e^- \to \Upsilon(4S)$, +higher

$\Gamma(\Omega(2012)^-\pi^+, \Omega(2012)^- \to \Xi^-\overline{K}^0)/\Gamma(\Xi^-\overline{K}^0\pi^+)$ — Γ_{11}/Γ_{10}

VALUE (units 10^{-2})	EVTS	DOCUMENT ID		TECN	COMMENT
5.5±2.8±0.7	18	[1] LI	21D	BELL	e^+e^- at $\Upsilon(nS)$

[1] LI 21D reports the significance of the $\Omega(2012)$ signal is 4.2σ including systematic uncertainties. Also measures $B(\Omega_c^0 \to \Omega(2012)^-\pi^+,\ \Omega(2012)^- \to (\overline{K}\Xi)^-)/B(\Omega_c^0 \to \Xi^0K^-\pi^+) = 0.220 \pm 0.059 \pm 0.035$.

$\Gamma(\Xi^-K^-2\pi^+)/\Gamma(\Omega^-\pi^+)$ — Γ_{12}/Γ_1

VALUE	EVTS	DOCUMENT ID		TECN	COMMENT
0.63±0.09 OUR AVERAGE	Error includes scale factor of 1.4.				
0.68±0.07±0.03	278	YELTON	18	BELL	$e^+e^- \to \Upsilon(4S)$, +higher
0.46±0.13±0.03	45	AUBERT	07AH	BABR	$e^+e^- \approx \Upsilon(4S)$

$\Gamma(\Xi(1530)^0K^-\pi^+, \Xi^{*0} \to \Xi^-\pi^+)/\Gamma(\Xi^-K^-2\pi^+)$ — Γ_{13}/Γ_{12}

VALUE	EVTS	DOCUMENT ID		TECN	COMMENT
0.33±0.09	74	[1] YELTON	18	BELL	$e^+e^- \to \Upsilon(4S)$, +higher

[1] This submode fraction is evaluated from a background-subtracted signal in a mass plot. Result ignores interference effects and systematic uncertainties, which YELTON 18 claim are both small.

$\Gamma(\Xi^-\overline{K}^{*0}\pi^+)/\Gamma(\Xi^-K^-2\pi^+)$ — Γ_{14}/Γ_{12}

VALUE	EVTS	DOCUMENT ID		TECN	COMMENT
0.55±0.16	136	[1] YELTON	18	BELL	$e^+e^- \to \Upsilon(4S)$, +higher

[1] This submode fraction is evaluated from a background-subtracted signal in a mass plot. Result ignores interference effects and systematic uncertainties, which YELTON 18 claim are both small.

$\Gamma(pK^-K^-\pi^+)/\Gamma_{total}$ — Γ_{15}/Γ

VALUE	DOCUMENT ID		TECN	COMMENT
seen	AAIJ	16O	LHCB	pp at 7, 8 TeV

$\Gamma(\Sigma^+K^-K^-\pi^+)/\Gamma(\Omega^-\pi^+)$ — Γ_{16}/Γ_1

VALUE	CL%	EVTS	DOCUMENT ID		TECN	COMMENT
<0.32	90	17	YELTON	18	BELL	$e^+e^- \to \Upsilon(4S)$, +higher

$\Gamma(\Lambda\overline{K}^0\overline{K}^0)/\Gamma(\Omega^-\pi^+)$ — Γ_{17}/Γ_1

VALUE	EVTS	DOCUMENT ID		TECN	COMMENT
1.72±0.32±0.14	95	YELTON	18	BELL	$e^+e^- \to \Upsilon(4S)$, +higher

Ω_c^0 REFERENCES

LI	21D	PR D104 052005	Y.B. Li *et al.*	(BELLE Collab.)
AAIJ	18J	PRL 121 092003	R. Aaij *et al.*	(LHCb Collab.)
YELTON	18	PR D97 032001	J. Yelton *et al.*	(BELLE Collab.)
AAIJ	16O	PR D93 092007	R. Aaij *et al.*	(LHCb Collab.)
PDG	14	CP C38 070001	K. Olive *et al.*	(PDG Collab.)
SOLOVIEVA	09	PL B672 1	E. Solovieva *et al.*	(BELLE Collab.)
AUBERT	07AH	PRL 99 062001	B. Aubert *et al.*	(BABAR Collab.)
LINK	03C	PL B561 41	J.M. Link *et al.*	(FNAL FOCUS Collab.)
AMMAR	02	PRL 89 171803	R. Ammar *et al.*	(CLEO Collab.)
CRONIN-HEN...	01	PRL 86 3730	D. Cronin-Hennessy *et al.*	(CLEO Collab.)
ADAMOVICH	95B	PL B358 151	M.I. Adamovich *et al.*	(CERN WA89 Collab.)
FRABETTI	95D	PL B357 678	P.L. Frabetti *et al.*	(FNAL E687 Collab.)
FRABETTI	94H	PL B338 106	P.L. Frabetti *et al.*	(FNAL E687 Collab.)
FRABETTI	93	PL B300 190	P.L. Frabetti *et al.*	(FNAL E687 Collab.)
ALBRECHT	92H	PL B288 367	H. Albrecht *et al.*	(ARGUS Collab.)
BIAGI	85B	ZPHY C28 175	S.F. Biagi *et al.*	(CERN WA62 Collab.)

$\Omega_c(2770)^0$

$I(J^P) = 0(\frac{3}{2}^+)$ Status: ***

The natural assignment is that this goes with the $\Sigma_c(2520)$ and $\Xi_c(2645)$ to complete the lowest mass $J^P = \frac{3}{2}^+$ SU(3) sextet, part of the SU(4) 20-plet that includes the $\Delta(1232)$. But J and P have not been measured.

$\Omega_c(2770)^0$ MASS

The mass is obtained from the mass-difference measurement that follows.

VALUE (MeV)	DOCUMENT ID
2765.9±2.0 OUR FIT Error includes scale factor of 1.2.	

$\Omega_c(2770)^0 - \Omega_c^0$ MASS DIFFERENCE

VALUE (MeV)	EVTS	DOCUMENT ID		TECN	COMMENT
$70.7^{+0.8}_{-0.9}$ OUR FIT					
$70.7^{+0.8}_{-1.0}$ OUR AVERAGE					
$70.7\pm0.9^{+0.1}_{-0.9}$	54 ± 9	SOLOVIEVA	09	BELL	$\Omega_c^0\gamma$ in $e^+e^- \to \Upsilon(4S)$
70.8±1.0±1.1	105 ± 22	AUBERT,BE	06I	BABR	$e^+e^- \approx \Upsilon(4S)$

$\Omega_c(2770)^0$ DECAY MODES

The $\Omega_c(2770)^0$–Ω_c^0 mass difference is too small for any strong decay to occur.

	Mode	Fraction (Γ_i/Γ)
Γ_1	$\Omega_c^0\gamma$	presumably 100%

$\Omega_c(2770)^0$ REFERENCES

SOLOVIEVA	09	PL B672 1	E. Solovieva *et al.*	(BELLE Collab.)
AUBERT,BE	06I	PRL 97 232001	B. Aubert *et al.*	(BABAR Collab.)

$\Omega_c(3000)^0$

$I(J^P) = ?(?^?)$ Status: ***

$\Omega_c(3000)^0$ MASS

VALUE (MeV)	EVTS	DOCUMENT ID		TECN	COMMENT
3000.41±0.22 OUR AVERAGE					
3000.7 ±1.0 ±0.2	38	YELTON	18B	BELL	e^+e^- at $\Upsilon(4S)$
3000.4 ±0.2 ±0.1	1.3k	AAIJ	17AH	LHCB	pp at 7, 8, 13 TeV
• • • We do not use the following data for averages, fits, limits, etc. • • •					
2999.2 ±0.9 ±$0.9^{+0.19}_{-0.22}$	24	[1] AAIJ		21AC	LHCB	pp at 7, 8, 13 TeV

[1] Measured via $\Omega_b^- \to \Omega_c^{**0}\pi^- \to \Xi_c^+K^-\pi^-$. The third uncertainty is due to the uncertainty in the Ξ_c^+ mass.

$\Omega_c(3000)^0$ WIDTH

VALUE (MeV)	EVTS	DOCUMENT ID		TECN	COMMENT
4.5±0.6±0.3	1.3k	AAIJ	17AH	LHCB	pp at 7, 8, 13 TeV
• • • We do not use the following data for averages, fits, limits, etc. • • •					
4.8±2.1±2.5	24	AAIJ	21AC	LHCB	pp at 7, 8, 13 TeV

$\Omega_c(3000)^0$ DECAY MODES

	Mode	Fraction (Γ_i/Γ)
Γ_1	$\Xi_c^+K^-$	seen

Downloaded from https://academic.oup.com/ptep/article/2022/8/083C01/6651666 by KIT Library user on 27 September 2022

$\Omega_c(3000)^0$ BRANCHING RATIOS

$\Gamma(\Xi_c^+ K^-)/\Gamma_{total}$ — Γ_1/Γ

VALUE	EVTS	DOCUMENT ID		TECN	COMMENT
seen	24	[1] AAIJ	21AC	LHCB	pp at 7, 8, 13 TeV
seen	38	[2] YELTON	18B	BELL	e^+e^- at $\Upsilon(4S)$
seen	1.3k	[3] AAIJ	17AH	LHCB	pp at 7, 8, 13 TeV

[1] AAIJ 21AC report a significance of 6.2 σ.
[2] YELTON 18B report a significance of 3.9 σ
[3] AAIJ 17AH report a significance of 20.4 σ.

$\Omega_c(3000)^0$ REFERENCES

AAIJ	21AC	PR D104 L091102	R. Aaij *et al.*	(LHCb Collab.)
YELTON	18B	PR D97 051102	J. Yelton *et al.*	(BELLE Collab.)
AAIJ	17AH	PRL 118 182001	R. Aaij *et al.*	(LHCb Collab.)

$\Omega_c(3050)^0$

$I(J^P) = ?(?^?)$ Status: ***

AAIJ 21AC rejects $J = 1/2$ hypothesis at 2.2 σ.

$\Omega_c(3050)^0$ MASS

VALUE (MeV)	EVTS	DOCUMENT ID		TECN	COMMENT
3050.19±0.13 OUR AVERAGE					
$3050.1 \pm 0.3 \pm 0.2^{+0.19}_{-0.22}$	33	[1] AAIJ	21AC	LHCB	pp at 7, 8, 13 TeV
$3050.2 \pm 0.4 \pm 0.2$	28	YELTON	18B	BELL	e^+e^- at $\Upsilon(4S)$
$3050.2 \pm 0.1 \pm 0.1$	970	AAIJ	17AH	LHCB	pp at 7, 8, 13 TeV

[1] Measured via $\Omega_b^- \to \Omega_c^{**0}\pi^- \to \Xi_c^+ K^-\pi^-$. The third uncertainty is due to the uncertainty in the Ξ_c^+ mass.

$\Omega_c(3050)^0$ WIDTH

VALUE (MeV)	CL%	DOCUMENT ID		TECN	COMMENT
<1.2	95	AAIJ	17AH	LHCB	pp at 7, 8, 13 TeV
• • • We do not use the following data for averages, fits, limits, etc. • • •					
<1.6	95	AAIJ	21AC	LHCB	pp at 7, 8, 13 TeV

$\Omega_c(3050)^0$ DECAY MODES

	Mode	Fraction (Γ_i/Γ)
Γ_1	$\Xi_c^+ K^-$	seen

$\Omega_c(3050)^0$ BRANCHING RATIOS

$\Gamma(\Xi_c^+ K^-)/\Gamma_{total}$ — Γ_1/Γ

VALUE	EVTS	DOCUMENT ID		TECN	COMMENT
seen	33	[1] AAIJ	21AC	LHCB	pp at 7, 8, 13 TeV
seen	28	[2] YELTON	18B	BELL	e^+e^- at $\Upsilon(4S)$
seen	970	[3] AAIJ	17AH	LHCB	pp at 7, 8, 13 TeV

[1] AAIJ 21AC report a significance of 9.9 σ.
[2] YELTON 18B report a significance of 4.6 σ
[3] AAIJ 17AH report a significance of 20.4 σ.

$\Omega_c(3050)^0$ REFERENCES

AAIJ	21AC	PR D104 L091102	R. Aaij *et al.*	(LHCb Collab.)
YELTON	18B	PR D97 051102	J. Yelton *et al.*	(BELLE Collab.)
AAIJ	17AH	PRL 118 182001	R. Aaij *et al.*	(LHCb Collab.)

$\Omega_c(3065)^0$

$I(J^P) = ?(?^?)$ Status: ***

AAIJ 21AC rejects $J = 1/2$ hypothesis at 3.6 σ.

$\Omega_c(3065)^0$ MASS

VALUE (MeV)	EVTS	DOCUMENT ID		TECN	COMMENT
3065.54±0.26 OUR AVERAGE					
$3065.9 \pm 0.4 \pm 0.4^{+0.19}_{-0.22}$	51	[1] AAIJ	21AC	LHCB	pp at 7, 8, 13 TeV
$3064.9 \pm 0.6 \pm 0.2$	82	YELTON	18B	BELL	e^+e^- at $\Upsilon(4S)$
$3065.6 \pm 0.1 \pm 0.3$	1.74k	AAIJ	17AH	LHCB	pp at 7, 8, 13 TeV

[1] Measured via $\Omega_b^- \to \Omega_c^{**0}\pi^- \to \Xi_c^+ K^-\pi^-$. The third uncertainty is due to the uncertainty in the Ξ_c^+ mass.

$\Omega_c(3065)^0$ WIDTH

VALUE (MeV)	EVTS	DOCUMENT ID		TECN	COMMENT
3.3±0.6 OUR AVERAGE Error includes scale factor of 1.5.					
$1.7 \pm 1.0 \pm 0.5$	51	AAIJ	21AC	LHCB	pp at 7, 8, 13 TeV
$3.5 \pm 0.4 \pm 0.2$	1.74k	AAIJ	17AH	LHCB	pp at 7, 8, 13 TeV

$\Omega_c(3065)^0$ DECAY MODES

	Mode	Fraction (Γ_i/Γ)
Γ_1	$\Xi_c^+ K^-$	seen

$\Omega_c(3065)^0$ BRANCHING RATIOS

$\Gamma(\Xi_c^+ K^-)/\Gamma_{total}$ — Γ_1/Γ

VALUE	EVTS	DOCUMENT ID		TECN	COMMENT
seen	51	[1] AAIJ	21AC	LHCB	pp at 7, 8, 13 TeV
seen	82	YELTON	18B	BELL	e^+e^- at $\Upsilon(4S)$
seen	1.74k	[2] AAIJ	17AH	LHCB	pp at 7, 8, 13 TeV

[1] AAIJ 21AC report a significance of 11.9 σ.
[2] AAIJ 17AH report a significance of 23.9 σ.

$\Omega_c(3065)^0$ REFERENCES

AAIJ	21AC	PR D104 L091102	R. Aaij *et al.*	(LHCb Collab.)
YELTON	18B	PR D97 051102	J. Yelton *et al.*	(BELLE Collab.)
AAIJ	17AH	PRL 118 182001	R. Aaij *et al.*	(LHCb Collab.)

$\Omega_c(3090)^0$

$I(J^P) = ?(?^?)$ Status: ***

$\Omega_c(3090)^0$ MASS

VALUE (MeV)	EVTS	DOCUMENT ID		TECN	COMMENT
3090.1±0.5 OUR AVERAGE					
$3091.0 \pm 1.1 \pm 1.0^{+0.19}_{-0.22}$	41	[1] AAIJ	21AC	LHCB	pp at 7, 8, 13 TeV
$3089.3 \pm 1.2 \pm 0.2$	87	YELTON	18B	BELL	e^+e^- at $\Upsilon(4S)$
$3090.2 \pm 0.3 \pm 0.5$	2.0k	AAIJ	17AH	LHCB	pp at 7, 8, 13 TeV

[1] Measured via $\Omega_b^- \to \Omega_c^{**0}\pi^- \to \Xi_c^+ K^-\pi^-$. The third uncertainty is due to the uncertainty in the Ξ_c^+ mass.

$\Omega_c(3090)^0$ WIDTH

VALUE (MeV)	EVTS	DOCUMENT ID		TECN	COMMENT
8.7±1.0±0.8	2.0k	AAIJ	17AH	LHCB	pp at 7, 8, 13 TeV
• • • We do not use the following data for averages, fits, limits, etc. • • •					
$7.4 \pm 3.1 \pm 2.8$	41	AAIJ	21AC	LHCB	pp at 7, 8, 13 TeV

$\Omega_c(3090)^0$ DECAY MODES

	Mode	Fraction (Γ_i/Γ)
Γ_1	$\Xi_c^+ K^-$	seen

$\Omega_c(3090)^0$ BRANCHING RATIOS

$\Gamma(\Xi_c^+ K^-)/\Gamma_{total}$ — Γ_1/Γ

VALUE	EVTS	DOCUMENT ID		TECN	COMMENT
seen	41	[1] AAIJ	21AC	LHCB	pp at 7, 8, 13 TeV
seen	87	YELTON	18B	BELL	e^+e^- at $\Upsilon(4S)$
seen	2.0k	[2] AAIJ	17AH	LHCB	pp at 7, 8, 13 TeV

[1] AAIJ 21AC report a significance of 7.8 σ.
[2] AAIJ 17AH report a significance of 21.1 σ.

$\Omega_c(3090)^0$ REFERENCES

AAIJ	21AC	PR D104 L091102	R. Aaij *et al.*	(LHCb Collab.)
YELTON	18B	PR D97 051102	J. Yelton *et al.*	(BELLE Collab.)
AAIJ	17AH	PRL 118 182001	R. Aaij *et al.*	(LHCb Collab.)

Downloaded from https://academic.oup.com/ptep/article/2022/8/083C01/6651666 by KIT Library user on 27 September 2022

$\Omega_c(3120)^0$

$I(J^P) = ?(?^?)$ Status: ***

$\Omega_c(3120)^0$ MASS

VALUE (MeV)	EVTS	DOCUMENT ID		TECN	COMMENT
3119.1±0.3±0.9±0.3	480	[1] AAIJ	17AH	LHCB	pp at 7, 8, 13 TeV

[1] The third error is the uncertainty on the Ξ_c^+ mass. (AAIJ 17AH gave $^{+0.3}_{-0.5}$ MeV here, but as of 2018 it is ±0.3.)

$\Omega_c(3120)^0$ WIDTH

VALUE (MeV)	CL%	DOCUMENT ID		TECN	COMMENT
<2.6	95	AAIJ	17AH	LHCB	pp at 7, 8, 13 TeV

$\Omega_c(3120)^0$ DECAY MODES

	Mode	Fraction (Γ_i/Γ)
Γ_1	$\Xi_c^+ K^-$	seen

$\Omega_c(3120)^0$ BRANCHING RATIOS

$\Gamma(\Xi_c^+ K^-)/\Gamma_{total}$ — Γ_1/Γ

VALUE	DOCUMENT ID		TECN	COMMENT
seen	[1] AAIJ	17AH	LHCB	pp at 7, 8, 13 TeV

[1] AAIJ 17AH report a significance of 10.4 σ.

$\Omega_c(3120)^0$ REFERENCES

AAIJ 17AH PRL 118 182001 R. Aaij et al. (LHCb Collab.)

Downloaded from https://academic.oup.com/ptep/article/2022/8/083C01/6651666 by KIT Library user on 27 September 2022

DOUBLY CHARMED BARYONS ($C = +2$)

$\Xi_{cc}^{++} = ucc$, $\Xi_{cc}^{+} = dcc$, $\Omega_{cc}^{+} = scc$

Ξ_{cc}^{+}

$I(J^P) = ?(?^?)$ Status: *

OMITTED FROM SUMMARY TABLE

Nominally the isospin partner of the Ξ_{cc}^{++} (ccu). While the SELEX experiment (MATTSON 02, OCHERASHVILI 05) claimed an observation of this state, subsequent searches by BABAR (AUBERT,B 06D), Belle (CHISTOV 06, KATO 14), and LHCb (AAIJ 13CD, AAIJ 20AX) did not find any significant signal or evidence for the Ξ_{cc}^{+}. However, AAIJ 21AE reports that its search for $\Xi_{cc}^{+} \to \Xi_c^{+}\pi^+\pi^-$, when combined with a prior search for $\Xi_{cc}^{+} \to \Lambda_c^{+}K^-\pi^+$ decays in AAIJ 20AX, yields a signal at 2.9 σ global significance (4.0 σ local).

Ξ_{cc}^{+} MASS

VALUE (MeV)	EVTS	DOCUMENT ID		TECN	COMMENT
3518.9±0.9 OUR AVERAGE					
3518 ±3	6	[1] OCHERASHVI..05		SELX	Σ^- nucleus ≈ 600 GeV
3519 ±1	16	[2] MATTSON	02	SELX	Σ^- nucleus ≈ 600 GeV
• • • We do not use the following data for averages, fits, limits, etc. • • •					
3623.0±1.4	368 ± 193	[3] AAIJ	21AE	LHCB	pp at 7, 8, 13 TeV

[1] OCHERASHVILI 05 claims "an excess of 5.62 events over ... 1.38 ± 0.13 events" for a significance of 4.8 σ in pD^+K^- events.

[2] MATTSON 02 claims "an excess of 15.9 events over an expected background of 6.1 ± 0.5 events, a statistical significance of 6.3 σ" in the $\Lambda_c^+K^-\pi^+$ invariant-mass spectrum. The probability that the peak is a fluctuation increases from 1.0×10^{-6} to 1.1×10^{-4} when the number of bins searched is considered.

[3] Uncertainties are statistical only. Because of undetermined systematic uncertainties in the extraction of this result it cannot be considered a mass measurement. AAIJ 21AE performs a combined fit to its $\Xi_{cc}^{+} \to \Xi_c^{+}\pi^+\pi^-$ data and the $\Xi_{cc}^{+} \to \Lambda_c^{+}K^-\pi^+$ data from AAIJ 20AX, finding a global significance of 2.9 σ (4.0 σ local).

Ξ_{cc}^{+} MEAN LIFE

VALUE (10^{-15} s)	CL%	DOCUMENT ID		TECN	COMMENT
• • • We do not use the following data for averages, fits, limits, etc. • • •					
<33	90	MATTSON	02	SELX	Σ^- nucleus, ≈ 600 GeV

Ξ_{cc}^{+} DECAY MODES

	Mode	Fraction (Γ_i/Γ)
Γ_1	$\Lambda_c^+K^-\pi^+$	not seen
Γ_2	$\Xi_c^+\pi^+\pi^-$	not seen
Γ_3	pD^+K^-	

$\Gamma(pD^+K^-)/\Gamma(\Lambda_c^+K^-\pi^+)$ — Γ_3/Γ_1

VALUE	EVTS	DOCUMENT ID		TECN	COMMENT
• • • We do not use the following data for averages, fits, limits, etc. • • •					
0.36±0.21	6	OCHERASHVI..05		SELX	Σ^- ≈ 600 GeV

$\Gamma(\Lambda_c^+K^-\pi^+)/\Gamma_{total}$ — Γ_1/Γ

VALUE	DOCUMENT ID		TECN	COMMENT
not seen	[1] AAIJ	20AX	LHCB	pp at 7, 8, 13 TeV

[1] No significant signal is observed in the mass range 3.4–3.8 GeV

$\Gamma(\Xi_c^+\pi^+\pi^-)/\Gamma_{total}$ — Γ_2/Γ

VALUE	CL%	EVTS	DOCUMENT ID		TECN	COMMENT
not seen	95	145 ± 139	[1] AAIJ	21AE	LHCB	pp at 7, 8, 13 TeV

[1] No significant signal is seen in the mass range 3.4–3.8 GeV . AAIJ 21AE performs a combined fit to its $\Xi_{cc}^{+} \to \Xi_c^{+}\pi^+\pi^-$ data and the $\Xi_{cc}^{+} \to \Lambda_c^{+}K^-\pi^+$ data from AAIJ 20AX, finding a global significance of 2.9 σ (4.0 σ local).

Ξ_{cc}^{+} REFERENCES

AAIJ	21AE	JHEP 2112 107	R. Aaij *et al.*	(LHCb Collab.)
AAIJ	20AX	SCPMA 63 221062	R. Aaij *et al.*	(LHCb Collab.)
KATO	14	PR D89 052003	Y. Kato *et al.*	(BELLE Collab.)
AAIJ	13CD	JHEP 1312 090	R. Aaij *et al.*	(LHCb Collab.)
AUBERT,B	06D	PR D74 011103	B. Aubert *et al.*	(BABAR Collab.)
CHISTOV	06	PRL 97 162001	R. Chistov *et al.*	(BELLE Collab.)
OCHERASHVI...05		PL B628 18	A. Ocherashvili *et al.*	(FNAL SELEX Collab.)
MATTSON	02	PRL 89 112001	M. Mattson *et al.*	(FNAL SELEX Collab.)

Ξ_{cc}^{++}

$I(J^P) = ?(?^?)$ Status: ***

Ξ_{cc}^{++} MASS

VALUE (MeV)	EVTS	DOCUMENT ID		TECN	COMMENT
3621.55±0.23±0.30	2k	[1] AAIJ	20J	LHCB	pp at 13 TeV
• • • We do not use the following data for averages, fits, limits, etc. • • •					
3620.6 ±1.5 ±0.4 ±0.3	91	[2] AAIJ	18BA	LHCB	pp at 13 TeV
3621.40±0.72±0.27±0.14	313	[3] AAIJ	17BC	LHCB	pp at 13 TeV

[1] AAIJ 20J combines mass measurements 3621.53 ± 0.24 ± 0.29 MeV from $\Xi_{cc}^{++} \to \Lambda_c^+K^-\pi^+\pi^+$ and 3621.95 ± 0.60 ± 0.49 MeV from $\Xi_{cc}^{++} \to \Xi_c^+\pi^+$. Supersedes AAIJ 18BA and AAIJ 17BC.

[2] The third error in AAIJ 18BA value is from the uncertainty of the Ξ_c^+ mass.

[3] The third error in AAIJ 17BC value is from the uncertainty of the Λ_c^+ mass. The width of the signal is 6.6 ± 0.8 MeV, consistent with the experimental resolution.

Ξ_{cc}^{++} MEAN LIFE

VALUE (10^{-15} s)	EVTS	DOCUMENT ID		TECN	COMMENT
256^{+24}_{-22}±14	304	AAIJ	18G	LHCB	pp at 13 TeV

Ξ_{cc}^{++} DECAY MODES

	Mode	Fraction (Γ_i/Γ)
Γ_1	$\Lambda_c^+K^-\pi^+\pi^+$	seen
Γ_2	$\Xi_c^+\pi^+$, $\Xi_c^+ \to pK^-\pi^+$	seen
Γ_3	$D^+pK^-\pi^+$	

$\Gamma(\Lambda_c^+K^-\pi^+\pi^+)/\Gamma_{total}$ — Γ_1/Γ

VALUE	DOCUMENT ID		TECN	COMMENT
seen	AAIJ	17BC	LHCB	12 std significance

$\Gamma(\Xi_c^+\pi^+, \Xi_c^+ \to pK^-\pi^+)/\Gamma_{total}$ — Γ_2/Γ

VALUE	EVTS	DOCUMENT ID		TECN	COMMENT
seen	91	AAIJ	18BA	LHCB	5.9 std significance

$\Gamma(\Xi_c^+\pi^+, \Xi_c^+ \to pK^-\pi^+)/\Gamma(\Lambda_c^+K^-\pi^+\pi^+)$ — Γ_2/Γ_1

VALUE (units 10^{-3})	DOCUMENT ID		TECN	COMMENT
2.2±0.6±0.1	[4] AAIJ	18BA	LHCB	Ratio 91 over 289 events

[4] AAIJ 18BA reports $[\Gamma(\Xi_{cc}^{++} \to \Xi_c^+\pi^+, \Xi_c^+ \to pK^-\pi^+)/\Gamma(\Xi_{cc}^{++} \to \Lambda_c^+K^-\pi^+\pi^+)] / [B(\Lambda_c^+ \to pK^-\pi^+)] = (3.5 \pm 0.9 \pm 0.3) \times 10^{-2}$ which we multiply by our best value $B(\Lambda_c^+ \to pK^-\pi^+) = (6.28 \pm 0.32) \times 10^{-2}$. Our first error is their experiment's error and our second error is the systematic error from using our best value.

$\Gamma(D^+pK^-\pi^+)/\Gamma(\Lambda_c^+K^-\pi^+\pi^+)$ — Γ_3/Γ_1

VALUE	CL%	DOCUMENT ID		TECN	COMMENT
$<1.7 \times 10^{-2}$	90	AAIJ	19AO	LHCB	pp at 13 TeV

Ξ_{cc}^{++} REFERENCES

AAIJ	20J	JHEP 2002 049	R. Aaij *et al.*	(LHCb Collab.)
AAIJ	19AO	JHEP 1910 124	R. Aaij *et al.*	(LHCb Collab.)
AAIJ	18BA	PRL 121 162002	R. Aaij *et al.*	(LHCb Collab.)
AAIJ	18G	PRL 121 052002	R. Aaij *et al.*	(LHCb Collab.)
AAIJ	17BC	PRL 119 112001	R. Aaij *et al.*	(LHCb Collab.)

Downloaded from https://academic.oup.com/ptep/article/2022/8/083C01/6651666 by KIT Library user on 27 September 2022

BOTTOM BARYONS
($B = -1$)

$\Lambda_b^0 = udb$, $\Xi_b^0 = usb$, $\Xi_b^- = dsb$, $\Omega_b^- = ssb$

Λ_b^0

$I(J^P) = 0(\frac{1}{2}^+)$ Status: ***

In the quark model, a Λ_b^0 is an isospin-0 udb state. The lowest Λ_b^0 ought to have $J^P = 1/2^+$. None of I, J, or P have actually been measured.

Λ_b^0 MASS

$m_{\Lambda_b^0}$

VALUE (MeV)	EVTS	DOCUMENT ID		TECN	COMMENT
5619.60± 0.17 OUR AVERAGE					
5619.62± 0.16± 0.13		[1] AAIJ	17AM	LHCB	pp at 7, 8 TeV
5619.30± 0.34		[2] AAIJ	14AA	LHCB	pp at 7 TeV
5620.15± 0.31± 0.47		[3] AALTONEN	14B	CDF	$p\overline{p}$ at 1.96 TeV
5619.7 ± 0.7 ± 1.1		[3] AAD	13U	ATLS	pp at 7 TeV
5621 ± 4 ± 3		[4] ABE	97B	CDF	$p\overline{p}$ at 1.8 TeV
5668 ± 16 ± 8	4	[5] ABREU	96N	DLPH	$e^+e^- \to Z$
5614 ± 21 ± 4	4	[5] BUSKULIC	96L	ALEP	$e^+e^- \to Z$
• • • We do not use the following data for averages, fits, limits, etc. • • •					
5619.65± 0.17± 0.17		[6] AAIJ	16Y	LHCB	Repl. by AAIJ 17AM
5619.44± 0.13± 0.38		[3] AAIJ	13AV	LHCB	Repl. by AAIJ 17AM
5619.19± 0.70± 0.30		[3] AAIJ	12E	LHCB	Repl. by AAIJ 13AV
5619.7 ± 1.2 ± 1.2		[7] ACOSTA	06	CDF	Repl. by AALTONEN 14B
not seen		[8] ABE	93B	CDF	Repl. by ABE 97B
5640 ± 50 ±30	16	[9] ALBAJAR	91E	UA1	$p\overline{p}$ 630 GeV
5640 $^{+100}_{-210}$	52	BARI	91	SFM	$\Lambda_b^0 \to pD^0\pi^-$
5650 $^{+150}_{-200}$	90	BARI	91	SFM	$\Lambda_b^0 \to \Lambda_c^+\pi^+\pi^-\pi^-$

[1] Uses $\Lambda_b^0 \to \chi_{c1}pK^-$, $\Lambda_b^0 \to \chi_{c2}pK^-$, $\Lambda_b^0 \to J/\psi\Lambda$, $\Lambda_b^0 \to p\psi(2S)K^-$, $\Lambda_b^0 \to pJ/\psi\pi^+\pi^-K^-$, and $\Lambda_b^0 \to pJ/\psi K^-$ decays.

[2] Uses exclusively reconstructed final states $\Lambda_b^0 \to \Lambda_c^+D_s^-$, $\Lambda_c^+D^-$ and $\overline{B}^0 \to D^+D_s^-$ decays. The uncertainty includes both statistical and systematic contributions.

[3] Uses $\Lambda_b^0 \to J/\psi\Lambda$ fully reconstructed decays.

[4] ABE 97B observed 38 events with a background of 18 ± 1.6 events in the mass range 5.60–5.65 GeV/c^2, a significance of > 3.4 standard deviations.

[5] Uses 4 fully reconstructed Λ_b events.

[6] Uses $\Lambda_b^0 \to p\psi(2S)K^-$, $\Lambda_b^0 \to pJ/\psi\pi^+\pi^-K^-$, and $\Lambda_b^0 \to pJ/\psi K^-$ decays.

[7] Uses exclusively reconstructed final states containing a $J/\psi \to \mu^+\mu^-$ decays.

[8] ABE 93B states that, based on the signal claimed by ALBAJAR 91E, CDF should have found 30 ± 23 $\Lambda_b^0 \to J/\psi(1S)\Lambda$ events. Instead, CDF found not more than 2 events.

[9] ALBAJAR 91E claims 16 ± 5 events above a background of 9 ± 1 events, a significance of about 5 standard deviations.

$m_{\Lambda_b^0} - m_{B^0}$

VALUE (MeV)	DOCUMENT ID		TECN	COMMENT
339.2±1.4±0.1	[1] ACOSTA	06	CDF	$p\overline{p}$ at 1.96 TeV

[1] Uses exclusively reconstructed final states containing $J/\psi \to \mu^+\mu^-$ decays.

$m_{\Lambda_b^0} - m_{B^+}$

VALUE (MeV)	DOCUMENT ID		TECN	COMMENT
339.72±0.28 OUR AVERAGE				
339.72±0.24±0.18	[1] AAIJ	14AA	LHCB	pp at 7 TeV
339.71±0.71±0.09	[2] AAIJ	12E	LHCB	pp at 7 TeV

[1] Uses exclusively reconstructed final states $\Lambda_b^0 \to \Lambda_c^+D_s^-$, $\Lambda_c^+D^-$ and $\overline{B}^0 \to D^+D_s^-$ decays.

[2] Uses exclusively reconstructed final states containing $J/\psi \to \mu^+\mu^-$ decays.

Λ_b^0 MEAN LIFE

See b-baryon Admixture section for data on b-baryon mean life average over species of b-baryon particles.

"OUR EVALUATION" is an average using rescaled values of the data listed below. The average and rescaling were performed by the Heavy Flavor Averaging Group (HFLAV) and are described at https://hflav.web.cern.ch/. The averaging/rescaling procedure takes into account correlations between the measurements and asymmetric lifetime errors.

VALUE (10^{-12} s)	EVTS	DOCUMENT ID		TECN	COMMENT
1.471±0.009 OUR EVALUATION					
1.477±0.027±0.009		[1] SIRUNYAN	18BY	CMS	pp at 8 TeV
1.415±0.027±0.006		[2] AAIJ	14E	LHCB	pp at 7 TeV
1.479±0.009±0.010		[3] AAIJ	14U	LHCB	pp at 7, 8 TeV
1.565±0.035±0.020		[2] AALTONEN	14B	CDF	$p\overline{p}$ at 1.96 TeV
1.449±0.036±0.017		[2] AAD	13U	ATLS	pp at 7 TeV
1.503±0.052±0.031		[2] CHATRCHYAN	13AC	CMS	pp at 7 TeV
1.303±0.075±0.035		[2] ABAZOV	12U	D0	$p\overline{p}$ at 1.96 TeV
1.401±0.046±0.035		[4] AALTONEN	10B	CDF	$p\overline{p}$ at 1.96 TeV
1.27 $^{+0.35}_{-0.29}$ ±0.09		ABREU	95S	DLPH	Excess $p\mu^-$, decay lengths
• • • We do not use the following data for averages, fits, limits, etc. • • •					
1.482±0.018±0.012		[5] AAIJ	13BB	LHCB	Repl. by AAIJ 14U
1.537±0.045±0.014		[2] AALTONEN	11	CDF	Repl. by AALTONEN 14B
1.218 $^{+0.130}_{-0.115}$ ±0.042		[2] ABAZOV	07S	D0	Repl. by ABAZOV 12U
1.290 $^{+0.119}_{-0.110}$ $^{+0.087}_{-0.091}$		[6] ABAZOV	07U	D0	$p\overline{p}$ at 1.96 TeV
1.593 $^{+0.083}_{-0.078}$ ±0.033		[2] ABULENCIA	07A	CDF	Repl. by AALTONEN 11
1.22 $^{+0.22}_{-0.18}$ ±0.04		[2] ABAZOV	05C	D0	Repl. by ABAZOV 07S
1.11 $^{+0.19}_{-0.18}$ ±0.05		[7] ABREU	99W	DLPH	$e^+e^- \to Z$
1.29 $^{+0.24}_{-0.22}$ ±0.06		[7] ACKERSTAFF	98G	OPAL	$e^+e^- \to Z$
1.21 ±0.11		[7] BARATE	98D	ALEP	$e^+e^- \to Z$
1.32 ±0.15 ±0.07		[8] ABE	96M	CDF	$p\overline{p}$ at 1.8 TeV
1.19 $^{+0.21}_{-0.18}$ $^{+0.07}_{-0.08}$		ABREU	96D	DLPH	Repl. by ABREU 99W
1.14 $^{+0.22}_{-0.19}$ ±0.07	69	AKERS	95K	OPAL	Repl. by ACKERSTAFF 98G
1.02 $^{+0.23}_{-0.18}$ ±0.06	44	BUSKULIC	95L	ALEP	Repl. by BARATE 98D

[1] Measured using $\Lambda_b^0 \to J/\psi\Lambda$ decays.

[2] Measured mean life using fully reconstructed $\Lambda_b^0 \to J/\psi\Lambda$ decays.

[3] Used $\Lambda_b^0 \to J/\psi pK^-$ decays.

[4] Measured mean life using fully reconstructed $\Lambda_b^0 \to \Lambda_c^+\pi^-$ decays.

[5] Measured the lifetime ratio of decays $\Lambda_b^0 \to J/\psi pK^-$ to $B^0 \to J/\psi\pi^+K^-$ to be 0.976 ± 0.012 ± 0.006 with τ_{B^0} = 1.519 ± 0.007 ps.

[6] Measured using semileptonic decays $\Lambda_b^0 \to \Lambda_c^+\mu\nu X$ and $\Lambda_c^+ \to K_S^0 p$.

[7] Measured using $\Lambda_c\ell^-$ and $\Lambda\ell^+\ell^-$.

[8] Excess $\Lambda_c\ell^-$, decay lengths.

$\tau_{\Lambda_b^0}/\tau_{\overline{\Lambda}_b^0}$

VALUE	DOCUMENT ID		TECN	COMMENT
0.940±0.035±0.006	[1] AAIJ	14E	LHCB	pp at 7 TeV

[1] Measured using $\Lambda_b^0 \to J/\psi\Lambda$ decays.

$\tau_{\Lambda_b^0}/\tau_{B^0}$ MEAN LIFE RATIO

$\tau_{\Lambda_b^0}/\tau_{B^0}$ (direct measurements)

"OUR EVALUATION" has been obtained by the Heavy Flavor Averaging Group (HFLAV) by including both B^0 and B^+ decays.

VALUE	DOCUMENT ID		TECN	COMMENT
0.964±0.007 OUR EVALUATION				
0.970±0.009 OUR AVERAGE	Error includes scale factor of 1.4. See the ideogram below.			
0.978±0.018±0.006	[1] SIRUNYAN	18BY	CMS	pp at 8 TeV
0.929±0.018±0.004	[1] AAIJ	14E	LHCB	pp at 7 TeV
0.974±0.006±0.004	[2] AAIJ	14U	LHCB	pp at 7, 8 TeV
0.960±0.025±0.016	[3] AAD	13U	ATLS	pp at 7 TeV
0.864±0.052±0.033	[4,5] ABAZOV	12U	D0	$p\overline{p}$ at 1.96 TeV
1.020±0.030±0.008	[4] AALTONEN	11	CDF	$p\overline{p}$ at 1.96 TeV
• • • We do not use the following data for averages, fits, limits, etc. • • •				
0.976±0.012±0.006	[6] AAIJ	13BB	LHCB	Repl. by AAIJ 14U
0.811 $^{+0.096}_{-0.087}$ ±0.034	[4,5] ABAZOV	07S	D0	Repl. by ABAZOV 12U
1.041±0.057	[7] ABULENCIA	07A	CDF	Repl. by AALTONEN 11
0.87 $^{+0.17}_{-0.14}$ ±0.03	[7] ABAZOV	05C	D0	Repl. by ABAZOV 07S

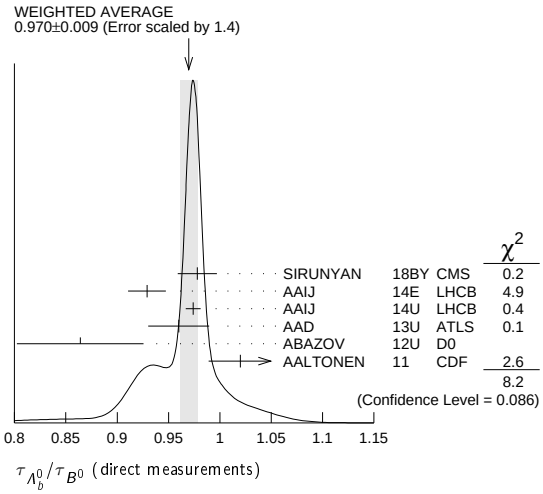

Downloaded from https://academic.oup.com/ptep/article/2022/8/083C01/6651666 by KIT Library user on 27 September 2022

[1] Measured using $\Lambda_b^0 \to J/\psi\Lambda$ and $B^0 \to J/\psi K^*(892)^0$ decays.
[2] Used $\Lambda_b^0 \to J/\psi p K^-$ and $B^0 \to J/\psi K^*(892)^0$ decays.
[3] Measured with $\Lambda_b^0 \to J/\psi(\mu^+\mu^-)\,\Lambda^0(p\pi^-)$ decays.
[4] Uses fully reconstructed $\Lambda_b \to J/\psi\Lambda$ decays.
[5] Uses $B^0 \to J/\psi K_S^0$ decays for denominator.
[6] Measures $1/\tau_{\Lambda_b^0} - 1/\tau_{B^0}$ and uses $\tau_{B^0} = 1.519 \pm 0.007$ ps to extract lifetime ratio.
[7] Measured mean life ratio using fully reconstructed decays.

Λ_b^0 DECAY MODES

The branching fractions B(b-baryon $\to \Lambda\ell^-\overline{\nu}_\ell$anything) and B($\Lambda_b^0 \to \Lambda_c^+\ell^-\overline{\nu}_\ell$anything) are not pure measurements because the underlying measured products of these with B($b \to b$-baryon) were used to determine B($b \to b$-baryon), as described in the note "Production and Decay of b-Flavored Hadrons."

For inclusive branching fractions, *e.g.*, $\Lambda_b \to \overline{\Lambda}_c$anything, the values usually are multiplicities, not branching fractions. They can be greater than one.

	Mode		Fraction (Γ_i/Γ)	Scale factor/ Confidence level
Γ_1	$J/\psi(1S)\Lambda \times$ B($b \to \Lambda_b^0$)		$(5.8 \pm 0.8) \times 10^{-5}$	
Γ_2	$J/\psi(1S)\Lambda$			
Γ_3	$J/\psi(1S)\Lambda\phi$			
Γ_4	$\psi(2S)\Lambda$			
Γ_5	$pD^0\pi^-$		$(6.3 \pm 0.6) \times 10^{-4}$	
Γ_6	$\Lambda_c(2860)^+\pi^-$, $\Lambda_c^+ \to D^0 p$			
Γ_7	$\Lambda_c(2880)^+\pi^-$, $\Lambda_c^+ \to D^0 p$			
Γ_8	$\Lambda_c(2940)^+\pi^-$, $\Lambda_c^+ \to D^0 p$			
Γ_9	pD^0K^-		$(4.6 \pm 0.8) \times 10^{-5}$	
Γ_{10}	pDK^-, $D \to K^-\pi^+$			
Γ_{11}	pDK^-, $D \to K^+\pi^-$			
Γ_{12}	$pJ/\psi\pi^-$		$(2.6 {}^{+0.5}_{-0.4}) \times 10^{-5}$	
Γ_{13}	$p\pi^- J/\psi$, $J/\psi \to \mu^+\mu^-$		$(1.6 \pm 0.8) \times 10^{-6}$	
Γ_{14}	$pJ/\psi K^-$		$(3.2 {}^{+0.6}_{-0.5}) \times 10^{-4}$	
Γ_{15}	$p\eta_c(1S)K^-$		$(1.06 \pm 0.26) \times 10^{-4}$	
Γ_{16}	$P_c(4312)^+K^-$, $P_c(4312)^+ \to p\eta_c(1S)$		$< 2.5 \times 10^{-5}$	CL=95%
Γ_{17}	$P_c(4380)^+K^-$, $P_c \to pJ/\psi$	[a]	$(2.7 \pm 1.4) \times 10^{-5}$	
Γ_{18}	$P_c(4450)^+K^-$, $P_c \to pJ/\psi$	[a]	$(1.3 \pm 0.4) \times 10^{-5}$	
Γ_{19}	$\chi_{c1}(1P)pK^-$		$(7.6 {}^{+1.5}_{-1.3}) \times 10^{-5}$	
Γ_{20}	$\chi_{c1}(1P)p\pi^-$		$(5.0 {}^{+1.3}_{-1.1}) \times 10^{-6}$	
Γ_{21}	$\chi_{c2}(1P)pK^-$		$(7.9 {}^{+1.6}_{-1.4}) \times 10^{-5}$	
Γ_{22}	$\chi_{c2}(1P)p\pi^-$		$(4.8 \pm 1.9) \times 10^{-6}$	
Γ_{23}	$pJ/\psi(1S)\pi^+\pi^-K^-$		$(6.6 {}^{+1.3}_{-1.1}) \times 10^{-5}$	
Γ_{24}	$p\psi(2S)K^-$		$(6.6 {}^{+1.2}_{-1.0}) \times 10^{-5}$	
Γ_{25}	$\chi_{c1}(3872)pK^-$		$(3.2 \pm 1.4) \times 10^{-5}$	
Γ_{26}	$\chi_{c1}(3872)\Lambda(1520)$		$(1.9 \pm 0.9) \times 10^{-5}$	
Γ_{27}	$\psi(2S)p\pi^-$		$(7.5 {}^{+1.6}_{-1.4}) \times 10^{-6}$	
Γ_{28}	$p\overline{K}^0\pi^-$		$(1.3 \pm 0.4) \times 10^{-5}$	
Γ_{29}	pK^0K^-		$< 3.5 \times 10^{-6}$	CL=90%
Γ_{30}	$\Lambda_c^+\pi^-$		$(4.9 \pm 0.4) \times 10^{-3}$	S=1.2
Γ_{31}	$\Lambda_c^+K^-$		$(3.56 \pm 0.28) \times 10^{-4}$	S=1.2
Γ_{32}	$\Lambda_c^+a_1(1260)^-$		seen	
Γ_{33}	$\Lambda_c^+D^-$		$(4.6 \pm 0.6) \times 10^{-4}$	
Γ_{34}	$\Lambda_c^+D_s^-$		(1.10 ± 0.10) %	
Γ_{35}	$\Lambda_c^+\pi^+\pi^-\pi^-$		$(7.6 \pm 1.1) \times 10^{-3}$	S=1.1
Γ_{36}	$\Lambda_c(2595)^+\pi^-$, $\Lambda_c(2595)^+ \to \Lambda_c^+\pi^+\pi^-$		$(3.4 \pm 1.4) \times 10^{-4}$	
Γ_{37}	$\Lambda_c(2625)^+\pi^-$, $\Lambda_c(2625)^+ \to \Lambda_c^+\pi^+\pi^-$		$(3.3 \pm 1.3) \times 10^{-4}$	
Γ_{38}	$\Sigma_c(2455)^0\pi^+\pi^-$, $\Sigma_c^0 \to \Lambda_c^+\pi^-$		$(5.7 \pm 2.2) \times 10^{-4}$	
Γ_{39}	$\Sigma_c(2455)^{++}\pi^-\pi^-$, $\Sigma_c^{++} \to \Lambda_c^+\pi^+$		$(3.2 \pm 1.5) \times 10^{-4}$	
Γ_{40}	$\Lambda_c^+K^+K^-\pi^-$		$(1.02 \pm 0.11) \times 10^{-3}$	
Γ_{41}	$\Lambda_c^+p\overline{p}\pi^-$		$(2.63 \pm 0.27) \times 10^{-4}$	
Γ_{42}	$\Sigma_c(2455)^0p\overline{p}$, $\Sigma_c^0 \to \Lambda_c^+\pi^-$		$(2.3 \pm 0.5) \times 10^{-5}$	
Γ_{43}	$\Sigma_c(2520)^0p\overline{p}$, $\Sigma_c(2520)^0 \to \Lambda_c^+\pi^-$		$(3.1 \pm 0.7) \times 10^{-5}$	
Γ_{44}	$\Lambda K^0 2\pi^+ 2\pi^-$			
Γ_{45}	$\Lambda_c^+\ell^-\overline{\nu}_\ell$anything	[b]	(10.9 ± 2.2) %	
Γ_{46}	$\Lambda_c^+\ell^-\overline{\nu}_\ell$		$(6.2 {}^{+1.4}_{-1.3})$ %	
Γ_{47}	$\Lambda_c^+\pi^+\pi^-\ell^-\overline{\nu}_\ell$		(5.6 ± 3.1) %	
Γ_{48}	$\Lambda_c(2595)^+\ell^-\overline{\nu}_\ell$		$(7.9 {}^{+4.0}_{-3.5}) \times 10^{-3}$	
Γ_{49}	$\Lambda_c(2625)^+\ell^-\overline{\nu}_\ell$		$(1.3 {}^{+0.6}_{-0.5})$ %	
Γ_{50}	$\Sigma_c(2455)^0\pi^+\ell^-\overline{\nu}_\ell$			
Γ_{51}	$\Sigma_c(2455)^{++}\pi^-\ell^-\overline{\nu}_\ell$			
Γ_{52}	ph^-	[c]	$< 2.3 \times 10^{-5}$	CL=90%
Γ_{53}	$p\pi^-$		$(4.5 \pm 0.8) \times 10^{-6}$	
Γ_{54}	pK^-		$(5.4 \pm 1.0) \times 10^{-6}$	
Γ_{55}	pD_s^-		$< 4.8 \times 10^{-4}$	CL=90%
Γ_{56}	$p\mu^-\overline{\nu}_\mu$		$(4.1 \pm 1.0) \times 10^{-4}$	
Γ_{57}	$\Lambda\mu^+\mu^-$		$(1.08 \pm 0.28) \times 10^{-6}$	
Γ_{58}	$p\pi^-\mu^+\mu^-$		$(6.9 \pm 2.5) \times 10^{-8}$	
Γ_{59}	$pK^-e^+e^-$		$(3.1 \pm 0.6) \times 10^{-7}$	
Γ_{60}	$pK^-\mu^+\mu^-$		$(2.6 {}^{+0.5}_{-0.4}) \times 10^{-7}$	
Γ_{61}	$\Lambda\gamma$		$(7.1 \pm 1.7) \times 10^{-6}$	
Γ_{62}	$\Lambda\eta$		$(9 {}^{+7}_{-5}) \times 10^{-6}$	
Γ_{63}	$\Lambda\eta'(958)$		$< 3.1 \times 10^{-6}$	CL=90%
Γ_{64}	$\Lambda\pi^+\pi^-$		$(4.6 \pm 1.9) \times 10^{-6}$	
Γ_{65}	$\Lambda K^+\pi^-$		$(5.6 \pm 1.2) \times 10^{-6}$	
Γ_{66}	ΛK^+K^-		$(1.60 \pm 0.22) \times 10^{-5}$	
Γ_{67}	$\Lambda\phi$		$(9.8 \pm 2.6) \times 10^{-6}$	
Γ_{68}	$p\pi^-\pi^+\pi^-$		$(2.10 \pm 0.22) \times 10^{-5}$	
Γ_{69}	$pK^-K^+\pi^-$		$(4.0 \pm 0.6) \times 10^{-6}$	
Γ_{70}	$pK^-\pi^+\pi^-$		$(5.0 \pm 0.5) \times 10^{-5}$	
Γ_{71}	$pK^-K^+K^-$		$(1.26 \pm 0.13) \times 10^{-5}$	

[a] P_c^+ is a pentaquark-charmonium state.
[b] Not a pure measurement. See note at head of Λ_b^0 Decay Modes.
[c] Here h^- means π^- or K^-.

CONSTRAINED FIT INFORMATION

An overall fit to 10 branching ratios uses 12 measurements and one constraint to determine 7 parameters. The overall fit has a $\chi^2 = 10.8$ for 6 degrees of freedom.

The following *off-diagonal* array elements are the correlation coefficients $\langle \delta x_i \delta x_j \rangle / (\delta x_i \cdot \delta x_j)$, in percent, from the fit to the branching fractions, $x_i \equiv \Gamma_i/\Gamma_{total}$. The fit constrains the x_i whose labels appear in this array to sum to one.

	x_{30}	x_{31}	x_{35}	x_{46}	x_{53}
x_{31}	92				
x_{35}	46	43			
x_{46}	13	12	6		
x_{53}	0	0	0	0	
x_{54}	0	0	0	0	82

Λ_b^0 BRANCHING RATIOS

$\Gamma(J/\psi(1S)\Lambda \times$ B($b \to \Lambda_b^0$)$)/\Gamma_{total}$ — Γ_1/Γ

VALUE (units 10^{-5})	EVTS	DOCUMENT ID		TECN	COMMENT
5.8 ± 0.8 OUR AVERAGE					
$6.01 \pm 0.60 \pm 0.58 \pm 0.28$		[1] ABAZOV	11O	D0	$p\overline{p}$ at 1.96 TeV
$4.7 \pm 2.3 \pm 0.2$		[2] ABE	97B	CDF	$p\overline{p}$ at 1.8 TeV
• • • We do not use the following data for averages, fits, limits, etc. • • •					
180 ± 60 ± 90	16	ALBAJAR	91E	UA1	$p\overline{p}$ at 630 GeV

[1] ABAZOV 11O uses B($B^0 \to J/\psi K_S^0$) × B($b \to B^0$) = $(1.74 \pm 0.08) \times 10^{-4}$ to obtain the result. The $(\pm 0.08) \times 10^{-4}$ uncertainty of this product is listed as the last uncertainty of the measurement, $(\pm 0.28) \times 10^{-5}$.

[2] ABE 97B reports [B($\Lambda_b^0 \to J/\psi\Lambda$) × B($b \to \Lambda_b^0$)] / [B($B^0 \to J/\psi K_S^0$) × B($b \to B^0$)] = $0.27 \pm 0.12 \pm 0.05$. We multiply by our best value B($B^0 \to J/\psi K_S^0$) × B($b \to B^0$) = $(1.74 \pm 0.08) \times 10^{-4}$. Our first error is their experiment error and our second error is the systematic error from using our best value.

Downloaded from https://academic.oup.com/ptep/article/2022/8/083C01/6651666 by KIT Library user on 27 September 2022

$\Gamma(\psi(2S)\Lambda)/\Gamma(J/\psi(1S)\Lambda)$ — Γ_4/Γ_2

VALUE	DOCUMENT ID		TECN	COMMENT
0.508±0.023 OUR AVERAGE				
0.513±0.023±0.019	[1] AAIJ	19F	LHCB	pp at 7, 8 TeV
0.50 ±0.03 ±0.02	[2] AAD	15CH	ATLS	pp at 8 TeV

[1] AAIJ 19F uses $B(J/\psi \to \mu^+\mu^-) = (5.961 \pm 0.033) \times 10^{-2}$ and $B(\psi(2S) \to e^+e^-) = (7.93 \pm 0.17) \times 10^{-3}$ from PDG 18 with assumption of lepton universality. AAIJ 19F reports this result as $0.513 \pm 0.023 \pm 0.016 \pm 0.011$, where the last uncertainty is the contribution due to the external input of branching fractions used in the analysis.

[2] AAD 15CH uses $B(J/\psi \to \mu^+\mu^-) = (5.961 \pm 0.033) \times 10^{-2}$ and $B(\psi(2S) \to \mu^+\mu^-) = (7.89 \pm 0.17) \times 10^{-3}$ from PDG 14 with assumption of lepton universality.

$\Gamma(J/\psi(1S)\Lambda\phi)/\Gamma(\psi(2S)\Lambda)$ — Γ_3/Γ_4

VALUE (units 10^{-2})	DOCUMENT ID		TECN	COMMENT
8.26±0.90±0.69	SIRUNYAN	20H	CMS	pp at 13 TeV

$\Gamma(pD^0\pi^-)/\Gamma_{total}$ — Γ_5/Γ

VALUE	EVTS	DOCUMENT ID		TECN	COMMENT
• • • We do not use the following data for averages, fits, limits, etc. • • •					
seen	52	BARI	91	SFM	$D^0 \to K^-\pi^+$
seen		BASILE	81	SFM	$D^0 \to K^-\pi^+$

$\Gamma(\Lambda_c(2860)^+\pi^-, \Lambda_c^+ \to D^0 p)/\Gamma(\Lambda_c(2880)^+\pi^-, \Lambda_c^+ \to D^0 p)$ — Γ_6/Γ_7

VALUE	DOCUMENT ID		TECN	COMMENT
$\mathbf{4.54^{+0.51}_{-0.39}{}^{+0.21}_{-0.59}}$	AAIJ	17S	LHCB	pp at 7, 8 TeV

$\Gamma(\Lambda_c(2940)^+\pi^-, \Lambda_c^+ \to D^0 p)/\Gamma(\Lambda_c(2880)^+\pi^-, \Lambda_c^+ \to D^0 p)$ — Γ_8/Γ_7

VALUE	DOCUMENT ID		TECN	COMMENT
$\mathbf{0.83^{+0.31}_{-0.10}{}^{+0.18}_{-0.43}}$	AAIJ	17S	LHCB	pp at 7, 8 TeV

$\Gamma(pD^0K^-)/\Gamma(pD^0\pi^-)$ — Γ_9/Γ_5

VALUE (units 10^{-2})	DOCUMENT ID		TECN	COMMENT
$\mathbf{7.3\pm0.8^{+0.5}_{-0.6}}$	AAIJ	14H	LHCB	pp at 7 TeV

$\Gamma(pDK^-, D \to K^-\pi^+)/\Gamma(pDK^-, D \to K^+\pi^-)$ — Γ_{10}/Γ_{11}

VALUE	DOCUMENT ID		TECN	COMMENT
$\mathbf{7.1\pm0.8^{+0.4}_{-0.3}}$	[1] AAIJ	21AD	LHCB	pp at 7, 8, 13 TeV

[1] Measured in the full phase space.

$\Gamma(pJ/\psi\pi^-)/\Gamma(pJ/\psi K^-)$ — Γ_{12}/Γ_{14}

VALUE (units 10^{-2})	DOCUMENT ID		TECN	COMMENT
8.24±0.25±0.42	AAIJ	14K	LHCB	pp at 7, 8 TeV

$\Gamma(pJ/\psi K^-)/\Gamma_{total}$ — Γ_{14}/Γ

VALUE (units 10^{-4})	DOCUMENT ID		TECN	COMMENT
$\mathbf{3.17\pm0.04^{+0.57}_{-0.45}}$	[1] AAIJ	16A	LHCB	pp at 7, 8 TeV

[1] AAIJ 16A reported the measurement of $(3.17 \pm 0.04 \pm 0.07 \pm 0.34^{+0.45}_{-0.28}) \times 10^{-4}$ where the first uncertainty is statistical, the second is systematic, the third is due to the branching fraction of $B^0 \to J/\psi K^*(892)^0$, and the fourth is due to the knowledge of f_{Λ_b}/f_d. We combined in quadrature second to fourth uncertainties to a total systematic uncertainty.

$\Gamma(p\eta_c(1S)K^-)/\Gamma(pJ/\psi K^-)$ — Γ_{15}/Γ_{14}

VALUE	DOCUMENT ID		TECN	COMMENT
0.333±0.050±0.037	[1] AAIJ	20AK	LHCB	pp at 13 TeV

[1] AAIJ 20AK reported the measurement of $0.333 \pm 0.050 \pm 0.019 \pm 0.032$, where the last uncertainty is due uncertainties of the used branching fractions of $J/\psi \to p\overline{p}$ and $\eta_c \to p\overline{p}$ decays. We combined in quadrature the systematic uncertainties.

$\Gamma(P_c(4312)^+K^-, P_c(4312)^+ \to p\eta_c(1S))/\Gamma(p\eta_c(1S)K^-)$ — Γ_{16}/Γ_{15}

VALUE	CL%	DOCUMENT ID		TECN	COMMENT
<0.24	95	AAIJ	20AK	LHCB	pp at 13 TeV

$\Gamma(P_c(4380)^+K^-, P_c \to pJ/\psi)/\Gamma_{total}$ — Γ_{17}/Γ

P_c^+ is a pentaquark-charmonium state.

VALUE (units 10^{-5})	DOCUMENT ID		TECN	COMMENT
$\mathbf{2.66\pm0.22^{+1.41}_{-1.38}}$	[1] AAIJ	16A	LHCB	pp at 7, 8 TeV

[1] AAIJ 16 total systematic includes the uncertainties on $f(P_c^+)$ and $B(\Lambda_b \to pJ/\psi K^-)$.

$\Gamma(P_c(4450)^+K^-, P_c \to pJ/\psi)/\Gamma_{total}$ — Γ_{18}/Γ

P_c^+ is a pentaquark-charmonium state.

VALUE (units 10^{-5})	DOCUMENT ID		TECN	COMMENT
$\mathbf{1.30\pm0.16^{+0.42}_{-0.39}}$	[1] AAIJ	16A	LHCB	pp at 7, 8 TeV

[1] AAIJ 16 total systematic includes the uncertainties on $f(P_c^+)$ and $B(\Lambda_b \to pJ/\psi K^-)$.

$\Gamma(\chi_{c1}(1P)pK^-)/\Gamma(pJ/\psi K^-)$ — Γ_{19}/Γ_{14}

VALUE	DOCUMENT ID		TECN	COMMENT
0.239±0.019±0.007	[1] AAIJ	17AM	LHCB	pp at 7, 8 TeV

[1] AAIJ 17AM reports $0.242 \pm 0.014 \pm 0.016$ from a measurement of $[\Gamma(\Lambda_b^0 \to \chi_{c1}(1P)pK^-)/\Gamma(\Lambda_b^0 \to pJ/\psi K^-)] \times [B(\chi_{c1}(1P) \to \gamma J/\psi(1S))]$ assuming $B(\chi_{c1}(1P) \to \gamma J/\psi(1S)) = (33.9 \pm 1.2) \times 10^{-2}$, which we rescale to our best value $B(\chi_{c1}(1P) \to \gamma J/\psi(1S)) = (34.3 \pm 1.0) \times 10^{-2}$. Our first error is their experiment's error and our second error is the systematic error from using our best value.

$\Gamma(\chi_{c1}(1P)p\pi^-)/\Gamma(\chi_{c1}(1P)pK^-)$ — Γ_{20}/Γ_{19}

VALUE (units 10^{-2})	DOCUMENT ID		TECN	COMMENT
6.59±1.01±0.22	AAIJ	21R	LHCB	pp at 13 TeV

$\Gamma(\chi_{c2}(1P)pK^-)/\Gamma(pJ/\psi K^-)$ — Γ_{21}/Γ_{14}

VALUE	DOCUMENT ID		TECN	COMMENT
0.250±0.025±0.007	[1] AAIJ	17AM	LHCB	pp at 7, 8 TeV

[1] AAIJ 17AM reports $0.248 \pm 0.02 \pm 0.017$ from a measurement of $[\Gamma(\Lambda_b^0 \to \chi_{c2}(1P)pK^-)/\Gamma(\Lambda_b^0 \to pJ/\psi K^-)] \times [B(\chi_{c2}(1P) \to \gamma J/\psi(1S))]$ assuming $B(\chi_{c2}(1P) \to \gamma J/\psi(1S)) = (19.2 \pm 0.7) \times 10^{-2}$, which we rescale to our best value $B(\chi_{c2}(1P) \to \gamma J/\psi(1S)) = (19.0 \pm 0.5) \times 10^{-2}$. Our first error is their experiment's error and our second error is the systematic error from using our best value.

$\Gamma(\chi_{c2}(1P)pK^-)/\Gamma(\chi_{c1}(1P)pK^-)$ — Γ_{21}/Γ_{19}

VALUE	DOCUMENT ID		TECN	COMMENT
1.06±0.05±0.04±0.04	[1] AAIJ	21R	LHCB	pp at 13 TeV

[1] The first uncertainty is statistical, the second is systematic and the third is related to the uncertainties in the branching fractions of the $\chi_{cJ} \to J/\psi\gamma$ decays.

$\Gamma(\chi_{c2}(1P)p\pi^-)/\Gamma(\chi_{c1}(1P)p\pi^-)$ — Γ_{22}/Γ_{20}

VALUE	DOCUMENT ID		TECN	COMMENT
0.95±0.30±0.04±0.04	[1] AAIJ	21R	LHCB	pp at 13 TeV

[1] Evidence for the $\Lambda_b^0 \to \chi_{c2}p\pi^-$ decay is obtained with a significance of 3.5 standard deviations. The first uncertainty is statistical, the second is systematic and the third is related to the uncertainties in the branching fractions of the $\chi_{cJ} \to J/\psi\gamma$ decays.

$\Gamma(pJ/\psi(1S)\pi^+\pi^-K^-)/\Gamma(pJ/\psi K^-)$ — Γ_{23}/Γ_{14}

VALUE	DOCUMENT ID		TECN	COMMENT
0.2086±0.0096±0.0134	[1] AAIJ	16Y	LHCB	pp at 7, 8 TeV

[1] Excludes $\psi(2S) \to J/\psi\pi^+\pi^-$.

$\Gamma(p\psi(2S)K^-)/\Gamma(pJ/\psi K^-)$ — Γ_{24}/Γ_{14}

VALUE	DOCUMENT ID		TECN	COMMENT
0.2070±0.0076±0.0059	[1] AAIJ	16Y	LHCB	pp at 7, 8 TeV

[1] AAIJ 16Y reports a measurement of $0.2070 \pm 0.0076 \pm 0.0046 \pm 0.0037$ where the third uncertainty is due to the knowledge of J/ψ and $\psi(2S)$ branching fractions. We have combined both systematic uncertainties in quadrature.

$\Gamma(\chi_{c1}(3872)\Lambda(1520))/\Gamma(\chi_{c1}(3872)pK^-)$ — Γ_{26}/Γ_{25}

VALUE	DOCUMENT ID		TECN	COMMENT
0.58±0.15	AAIJ	19AN	LHCB	pp at 7, 8, 13 TeV

$\Gamma(\chi_{c1}(3872)pK^-)/\Gamma(p\psi(2S)K^-)$ — Γ_{25}/Γ_{24}

VALUE	DOCUMENT ID		TECN	COMMENT
0.49±0.10±0.16	[1] AAIJ	19AN	LHCB	pp at 7, 8, 13 TeV

[1] AAIJ 19AN reports $[\Gamma(\Lambda_b^0 \to \chi_{c1}(3872)pK^-)/\Gamma(\Lambda_b^0 \to p\psi(2S)K^-)] \times [B(\chi_{c1}(3872) \to \pi^+\pi^-J/\psi(1S))]$ / $[B(\psi(2S) \to J/\psi(1S)\pi^+\pi^-)] = (5.4 \pm 1.1 \pm 0.2) \times 10^{-2}$ which we multiply or divide by our best values $B(\chi_{c1}(3872) \to \pi^+\pi^-J/\psi(1S)) = (3.8 \pm 1.2) \times 10^{-2}$, $B(\psi(2S) \to J/\psi(1S)\pi^+\pi^-) = (34.68 \pm 0.30) \times 10^{-2}$. Our first error is their experiment's error and our second error is the systematic error from using our best values.

$\Gamma(\psi(2S)p\pi^-)/\Gamma(p\psi(2S)K^-)$ — Γ_{27}/Γ_{24}

VALUE (%)	DOCUMENT ID		TECN	COMMENT
11.4±1.3±0.2	AAIJ	18AF	LHCB	pp at 7, 8, 13 TeV

$\Gamma(p\overline{K}^0\pi^-)/\Gamma_{total}$ — Γ_{28}/Γ

VALUE (units 10^{-5})	DOCUMENT ID		TECN	COMMENT
1.26±0.19±0.36	[1] AAIJ	14Q	LHCB	pp at 7 TeV

[1] Used the normalizing mode branching fraction value of $B(B^0 \to K^0\pi^+\pi^-) = (4.96 \pm 0.20) \times 10^{-5}$.

$\Gamma(pK^0K^-)/\Gamma_{total}$ — Γ_{29}/Γ

VALUE	CL%	DOCUMENT ID		TECN	COMMENT
$<3.5 \times 10^{-6}$	90	AAIJ	14Q	LHCB	pp at 7 TeV

$\Gamma(\Lambda_c^+\pi^-)/\Gamma_{total}$ — Γ_{30}/Γ

VALUE (units 10^{-3})	EVTS	DOCUMENT ID		TECN	COMMENT
4.9 ±0.4 OUR FIT Error includes scale factor of 1.2.					
4.8 ±0.5 OUR AVERAGE Error includes scale factor of 1.5.					
$4.60^{+0.31}_{-0.30} \pm 0.14$		[1] AAIJ	14I	LHCB	pp at 7 TeV
$5.97 \pm 0.28 \pm 0.81$		[2] AAIJ	14Q	LHCB	pp at 7 TeV
8.8 ±2.8 ±1.5		[3] ABULENCIA	07B	CDF	$p\overline{p}$ at 1.96 TeV

Downloaded from https://academic.oup.com/ptep/article/2022/8/083C01/6651666 by KIT Library user on 27 September 2022

• • • We do not use the following data for averages, fits, limits, etc. • • •

seen	3	ABREU	96N	DLPH	$\Lambda_c^+ \to p K^- \pi^+$
seen	4	BUSKULIC	96L	ALEP	$\Lambda_c^+ \to p K^- \pi^+$, $p \overline{K}^0$, $\Lambda \pi^+ \pi^+ \pi^-$

[1] AAIJ 14I reports $(4.30 \pm 0.03 {}^{+0.12}_{-0.11} \pm 0.26 \pm 0.21) \times 10^{-3}$ from a measurement of $[\Gamma(\Lambda_b^0 \to \Lambda_c^+ \pi^-)/\Gamma_{\rm total}] \times [B(B^0 \to D^- \pi^+)]$ assuming $B(B^0 \to D^- \pi^+) = (2.68 \pm 0.13) \times 10^{-3}$, which we rescale to our best value $B(B^0 \to D^- \pi^+) = (2.51 \pm 0.08) \times 10^{-3}$. Our first error is their experiment's error and our second error is the systematic error from using our best value. Uses information on $f_{\rm baryon}/f_d$ from measurement in semileptonic decays by the same authors.

[2] Obtained using the branching fraction of $\Lambda_c^+ \to p K^- \pi^+$ decay.

[3] The result is obtained from $(f_{\rm baryon}/f_{\rm d})$ $(B(\Lambda_b^0 \to \Lambda_c^+ \pi^-)/B(\overline{B}^0 \to D^+ \pi^-)) = 0.82 \pm 0.08 \pm 0.11 \pm 0.22$, assuming $f_{\rm baryon}/f_{\rm d} = 0.25 \pm 0.04$ and $B(\overline{B}^0 \to D^+ \pi^-) = (2.68 \pm 0.13) \times 10^{-3}$.

$\Gamma(p D^0 \pi^-)/\Gamma(\Lambda_c^+ \pi^-)$ — Γ_5/Γ_{30}

VALUE	DOCUMENT ID		TECN	COMMENT
$0.128 \pm 0.007 {}^{+0.006}_{-0.007}$	[1] AAIJ	14H	LHCB	pp at 7 TeV

[1] AAIJ 14H reports $[\Gamma(\Lambda_b^0 \to p D^0 \pi^-)/\Gamma(\Lambda_b^0 \to \Lambda_c^+ \pi^-)] \times [B(D^0 \to K^- \pi^+)] / [B(\Lambda_c^+ \to p K^- \pi^+)] = (8.06 \pm 0.23 \pm 0.35) \times 10^{-2}$ which we multiply or divide by our best values $B(D^0 \to K^- \pi^+) = (3.947 \pm 0.030) \times 10^{-2}$, $B(\Lambda_c^+ \to p K^- \pi^+) = (6.28 \pm 0.32) \times 10^{-2}$. Our first error is their experiment's error and our second error is the systematic error from using our best values.

$\Gamma(\Lambda_c^+ K^-)/\Gamma_{\rm total}$ — Γ_{31}/Γ

VALUE (units 10^{-4})	DOCUMENT ID		TECN	COMMENT
3.56±0.28 OUR FIT	Error includes scale factor of 1.2.			
3.55±0.44±0.50	[1] AAIJ	14Q	LHCB	pp at 7 TeV

[1] Obtained using the branching fraction of $\Lambda_c^+ \to p K^- \pi^+$ decay.

$\Gamma(\Lambda_c^+ K^-)/\Gamma(\Lambda_c^+ \pi^-)$ — Γ_{31}/Γ_{30}

VALUE (units 10^{-2})	DOCUMENT ID		TECN	COMMENT
7.31±0.22 OUR FIT				
7.31±0.16±0.16	AAIJ	14H	LHCB	pp at 7 TeV

$\Gamma(\Lambda_c^+ a_1(1260)^-)/\Gamma_{\rm total}$ — Γ_{32}/Γ

VALUE	EVTS	DOCUMENT ID		TECN	COMMENT
seen	1	ABREU	96N	DLPH	$\Lambda_c^+ \to p K^- \pi^+$, $a_1^- \to \rho^0 \pi^- \to \pi^+ \pi^- \pi^-$

$\Gamma(\Lambda_c^+ D_s^-)/\Gamma_{\rm total}$ — Γ_{34}/Γ

VALUE (units 10^{-2})	DOCUMENT ID		TECN	COMMENT
1.1±0.1	[1] AAIJ	14AA	LHCB	pp at 7 TeV

[1] Uses $B(\overline{B}^0 \to D^+ D_s^-) = (7.2 \pm 0.8) \times 10^{-3}$ and their measured $B(\Lambda_b^0 \to \Lambda_c^+ \pi^-))/B(\overline{B}^0 \to D^+ \pi^-)$ values.

$\Gamma(\Lambda_c^+ D^-)/\Gamma(\Lambda_c^+ D_s^-)$ — Γ_{33}/Γ_{34}

VALUE	DOCUMENT ID		TECN	COMMENT
0.042±0.003±0.003	AAIJ	14AA	LHCB	pp at 7 TeV

$\Gamma(\Lambda_c^+ \pi^+ \pi^- \pi^-)/\Gamma_{\rm total}$ — Γ_{35}/Γ

VALUE (units 10^{-3})	EVTS	DOCUMENT ID		TECN	COMMENT
7.6±1.1 OUR FIT	Error includes scale factor of 1.1.				
$14.8 {}^{+3.8}_{-3.1} \pm 1.1$		[1] AALTONEN	12A	CDF	$p\overline{p}$ at 1.96 TeV

• • • We do not use the following data for averages, fits, limits, etc. • • •

seen	90	BARI	91	SFM	$\Lambda_c^+ \to p K^- \pi^+$

[1] AALTONEN 12A reports $[\Gamma(\Lambda_b^0 \to \Lambda_c^+ \pi^+ \pi^- \pi^-)/\Gamma_{\rm total}] / [B(\Lambda_b^0 \to \Lambda_c^+ \pi^-)] = 3.04 \pm 0.33 {}^{+0.70}_{-0.55}$ which we multiply by our best value $B(\Lambda_b^0 \to \Lambda_c^+ \pi^-) = (4.9 \pm 0.4) \times 10^{-3}$. Our first error is their experiment's error and our second error is the systematic error from using our best value.

$\Gamma(\Lambda_c^+ \pi^+ \pi^- \pi^-)/\Gamma(\Lambda_c^+ \pi^-)$ — Γ_{35}/Γ_{30}

VALUE	DOCUMENT ID		TECN	COMMENT
1.57±0.21 OUR FIT				
1.43±0.16±0.13	AAIJ	11E	LHCB	pp at 7 TeV

$\Gamma(\Lambda_c(2595)^+ \pi^-, \Lambda_c(2595)^+ \to \Lambda_c^+ \pi^+ \pi^-)/\Gamma(\Lambda_c^+ \pi^+ \pi^- \pi^-)$ — Γ_{36}/Γ_{35}

VALUE (units 10^{-2})	DOCUMENT ID		TECN	COMMENT
$4.4 \pm 1.7 {}^{+0.6}_{-0.4}$	AAIJ	11E	LHCB	pp at 7 TeV

$\Gamma(\Lambda_c(2625)^+ \pi^-, \Lambda_c(2625)^+ \to \Lambda_c^+ \pi^+ \pi^-)/\Gamma(\Lambda_c^+ \pi^+ \pi^- \pi^-)$ — Γ_{37}/Γ_{35}

VALUE (units 10^{-2})	DOCUMENT ID		TECN	COMMENT
4.3±1.5±0.4	AAIJ	11E	LHCB	pp at 7 TeV

$\Gamma(\Sigma_c(2455)^0 \pi^+ \pi^-, \Sigma_c^0 \to \Lambda_c^+ \pi^-)/\Gamma(\Lambda_c^+ \pi^+ \pi^- \pi^-)$ — Γ_{38}/Γ_{35}

VALUE (units 10^{-2})	DOCUMENT ID		TECN	COMMENT
7.4±2.4±1.2	AAIJ	11E	LHCB	pp at 7 TeV

$\Gamma(\Sigma_c(2455)^{++} \pi^- \pi^-, \Sigma_c^{++} \to \Lambda_c^+ \pi^+)/\Gamma(\Lambda_c^+ \pi^+ \pi^- \pi^-)$ — Γ_{39}/Γ_{35}

VALUE (units 10^{-2})	DOCUMENT ID		TECN	COMMENT
4.2±1.8±0.7	AAIJ	11E	LHCB	pp at 7 TeV

$\Gamma(\Lambda_c^+ K^+ K^- \pi^-)/\Gamma(\Lambda_c^+ D_s^-)$ — Γ_{40}/Γ_{34}

VALUE (units 10^{-2})	DOCUMENT ID		TECN	COMMENT
9.26±0.29±0.53	[1] AAIJ	21B	LHCB	pp at 7 and 8 TeV

[1] AAIJ 21B systematic uncertainty includes the contribution from the $D_s^- \to K^+ K^- \pi^-$ branching fraction.

$\Gamma(\Lambda_c^+ p \overline{p} \pi^-)/\Gamma(\Lambda_c^+ \pi^-)$ — Γ_{41}/Γ_{30}

VALUE (units 10^{-2})	DOCUMENT ID		TECN	COMMENT
5.40±0.23±0.32	AAIJ	18AW	LHCB	pp at 7 and 8 TeV

$\Gamma(\Sigma_c(2455)^0 p \overline{p}, \Sigma_c^0 \to \Lambda_c^+ \pi^-)/\Gamma(\Lambda_c^+ p \overline{p} \pi^-)$ — Γ_{42}/Γ_{41}

VALUE (units 10^{-2})	DOCUMENT ID		TECN	COMMENT
8.9±1.5±0.6	AAIJ	18AW	LHCB	pp at 7 and 8 TeV

$\Gamma(\Sigma_c(2520)^0 p \overline{p}, \Sigma_c(2520)^0 \to \Lambda_c^+ \pi^-)/\Gamma(\Lambda_c^+ p \overline{p} \pi^-)$ — Γ_{43}/Γ_{41}

VALUE	DOCUMENT ID		TECN	COMMENT
0.119±0.020±0.014	AAIJ	18AW	LHCB	pp at 7 and 8 TeV

$\Gamma(\Lambda K^0 2\pi^+ 2\pi^-)/\Gamma_{\rm total}$ — Γ_{44}/Γ

VALUE	EVTS	DOCUMENT ID		TECN	COMMENT
• • • We do not use the following data for averages, fits, limits, etc. • • •					
seen	4	[1] ARENTON	86	FMPS	$\Lambda K_S^0 2\pi^+ 2\pi^-$

[1] See the footnote to the ARENTON 86 mass value.

$\Gamma(\Lambda_c^+ \ell^- \overline{\nu}_\ell \text{anything})/\Gamma_{\rm total}$ — Γ_{45}/Γ

The values and averages in this section serve only to show what values result if one assumes our $B(b \to b\text{-baryon})$. They cannot be thought of as measurements since the underlying product branching fractions were also used to determine $B(b \to b\text{-baryon})$ as described in the note on "Production and Decay of b-Flavored Hadrons."

VALUE	EVTS	DOCUMENT ID		TECN	COMMENT
0.109±0.022 OUR AVERAGE					
0.102±0.019±0.013		[1] BARATE	98D	ALEP	$e^+ e^- \to Z$
$0.14 {}^{+0.05}_{-0.04} \pm 0.02$	29	[2] ABREU	95S	DLPH	$e^+ e^- \to Z$
• • • We do not use the following data for averages, fits, limits, etc. • • •					
0.090±0.022±0.012	55	[3] BUSKULIC	95L	ALEP	Repl. by BARATE 98D
0.18 ±0.07 ±0.02	21	[4] BUSKULIC	92E	ALEP	$\Lambda_c^+ \to p K^- \pi^+$

[1] BARATE 98D reports $[\Gamma(\Lambda_b^0 \to \Lambda_c^+ \ell^- \overline{\nu}_\ell \text{anything})/\Gamma_{\rm total}] \times [B(\overline{b} \to b\text{-baryon})] = 0.0086 \pm 0.0007 \pm 0.0014$ which we divide by our best value $B(\overline{b} \to b\text{-baryon}) = (8.4 \pm 1.1) \times 10^{-2}$. Our first error is their experiment's error and our second error is the systematic error from using our best value. Measured using $\Lambda_c \ell^-$ and $\Lambda \ell^+ \ell^-$.

[2] ABREU 95S reports $[\Gamma(\Lambda_b^0 \to \Lambda_c^+ \ell^- \overline{\nu}_\ell \text{anything})/\Gamma_{\rm total}] \times [B(\overline{b} \to b\text{-baryon})] = 0.0118 \pm 0.0026 {}^{+0.0031}_{-0.0021}$ which we divide by our best value $B(\overline{b} \to b\text{-baryon}) = (8.4 \pm 1.1) \times 10^{-2}$. Our first error is their experiment's error and our second error is the systematic error from using our best value.

[3] BUSKULIC 95L reports $[\Gamma(\Lambda_b^0 \to \Lambda_c^+ \ell^- \overline{\nu}_\ell \text{anything})/\Gamma_{\rm total}] \times [B(\overline{b} \to b\text{-baryon})] = 0.00755 \pm 0.0014 \pm 0.0012$ which we divide by our best value $B(\overline{b} \to b\text{-baryon}) = (8.4 \pm 1.1) \times 10^{-2}$. Our first error is their experiment's error and our second error is the systematic error from using our best value.

[4] BUSKULIC 92E reports $[\Gamma(\Lambda_b^0 \to \Lambda_c^+ \ell^- \overline{\nu}_\ell \text{anything})/\Gamma_{\rm total}] \times [B(\overline{b} \to b\text{-baryon})] = 0.015 \pm 0.0035 \pm 0.0045$ which we divide by our best value $B(\overline{b} \to b\text{-baryon}) = (8.4 \pm 1.1) \times 10^{-2}$. Our first error is their experiment's error and our second error is the systematic error from using our best value. Superseded by BUSKULIC 95L.

$\Gamma(\Lambda_c^+ \ell^- \overline{\nu}_\ell)/\Gamma_{\rm total}$ — Γ_{46}/Γ

VALUE	DOCUMENT ID		TECN	COMMENT
$0.062 {}^{+0.014}_{-0.013}$ OUR FIT				
$0.050 {}^{+0.011}_{-0.008} {}^{+0.016}_{-0.012}$	[1] ABDALLAH	04A	DLPH	$e^+ e^- \to Z^0$

[1] Derived from a combined likelihood and event rate fit to the distribution of the Isgur-Wise variable and using HQET. The slope of the form factor is measured to be $\rho^2 = 2.03 \pm 0.46 {}^{+0.72}_{-1.00}$.

$\Gamma(\Lambda_c^+ \ell^- \overline{\nu}_\ell)/\Gamma(\Lambda_c^+ \pi^-)$ — Γ_{46}/Γ_{30}

VALUE	DOCUMENT ID		TECN	COMMENT
$12.8 {}^{+3.0}_{-2.7}$ OUR FIT				
$16.6 \pm 3.0 {}^{+2.8}_{-3.6}$	AALTONEN	09E	CDF	$p\overline{p}$ at 1.96 TeV

Downloaded from https://academic.oup.com/ptep/article/2022/8/083C01/6651666 by KIT Library user on 27 September 2022

$\Gamma(\Lambda_c^+ \pi^+ \pi^- \ell^- \overline{\nu}_\ell)/\Gamma_{total}$ — Γ_{47}/Γ

VALUE	DOCUMENT ID		TECN	COMMENT
$0.056^{+0.031}_{-0.030}$	[1] ABDALLAH	04A	DLPH	$e^+ e^- \to Z^0$

[1] Derived from the fraction of $\Gamma(\Lambda_b^0 \to \Lambda_c^+ \ell^- \overline{\nu}_\ell)$ / ($\Gamma(\Lambda_b^0 \to \Lambda_c^+ \ell^- \overline{\nu}_\ell) + \Gamma(\Lambda_b^0 \to \Lambda_c^+ \pi^+ \pi^- \ell^- \overline{\nu}_\ell)$) $= 0.47^{+0.10}_{-0.08}{}^{+0.07}_{-0.06}$.

$\Gamma(\Lambda_c^+ \ell^- \overline{\nu}_\ell)/[\Gamma(\Lambda_c^+ \ell^- \overline{\nu}_\ell) + \Gamma(\Lambda_c^+ \pi^+ \pi^- \ell^- \overline{\nu}_\ell)]$ — $\Gamma_{46}/(\Gamma_{46}+\Gamma_{47})$

VALUE	DOCUMENT ID		TECN	COMMENT
$0.47^{+0.10}_{-0.08}{}^{+0.07}_{-0.06}$	ABDALLAH	04A	DLPH	$e^+ e^- \to Z^0$

$\Gamma(\Lambda_c(2595)^+ \ell^- \overline{\nu}_\ell)/\Gamma(\Lambda_c^+ \ell^- \overline{\nu}_\ell)$ — Γ_{48}/Γ_{46}

VALUE	DOCUMENT ID		TECN	COMMENT
$0.126 \pm 0.033^{+0.047}_{-0.038}$	[1] AALTONEN	09E	CDF	$p\overline{p}$ at 1.96 TeV

[1] AALTONEN 09E assumes isospin conservation for $\Lambda_c(2595) \to \Lambda_c \pi^+ \pi^+$ and $\Lambda_c(2595) \to \Lambda_c \pi^0 \pi^0$. Significant isospin violation from thresholds in $\Lambda_c(2595) \to \Sigma_c(2455)\pi \to \Lambda_c \pi\pi$ may alter the recovered ratio.

$\Gamma(\Lambda_c(2625)^+ \ell^- \overline{\nu}_\ell)/\Gamma(\Lambda_c^+ \ell^- \overline{\nu}_\ell)$ — Γ_{49}/Γ_{46}

VALUE	DOCUMENT ID		TECN	COMMENT
$0.210 \pm 0.042^{+0.071}_{-0.050}$	AALTONEN	09E	CDF	$p\overline{p}$ at 1.96 TeV

$[\frac{1}{2}\Gamma(\Sigma_c(2455)^0 \pi^+ \ell^- \overline{\nu}_\ell) + \frac{1}{2}\Gamma(\Sigma_c(2455)^{++} \pi^- \ell^- \overline{\nu}_\ell)]/\Gamma(\Lambda_c^+ \ell^- \overline{\nu}_\ell)$ — $(\frac{1}{2}\Gamma_{50}+\frac{1}{2}\Gamma_{51})/\Gamma_{46}$

VALUE	DOCUMENT ID		TECN	COMMENT
$0.054 \pm 0.022^{+0.021}_{-0.018}$	AALTONEN	09E	CDF	$p\overline{p}$ at 1.96 TeV

$\Gamma(p h^-)/\Gamma_{total}$ — Γ_{52}/Γ

VALUE	CL%	DOCUMENT ID		TECN	COMMENT
$<2.3 \times 10^{-5}$	90	[1] ACOSTA	05O	CDF	$p\overline{p}$ at 1.96 TeV

[1] Assumes $f_\Lambda / f_d = 0.25$, and equal momentum distribution for Λ_b and B mesons.

$\Gamma(p\pi^-)/\Gamma_{total}$ — Γ_{53}/Γ

VALUE (units 10^{-6})	CL%	DOCUMENT ID		TECN	COMMENT
4.5 ± 0.8 OUR FIT					
4.0 ± 0.9 ± 0.5		[1] AALTONEN	09C	CDF	$p\overline{p}$ at 1.96 TeV
• • • We do not use the following data for averages, fits, limits, etc. • • •					
<50	90	[2] BUSKULIC	96V	ALEP	$e^+ e^- \to Z$

[1] AALTONEN 09C reports $[\Gamma(\Lambda_b^0 \to p\pi^-)/\Gamma_{total}]$ / $[B(B^0 \to K^+\pi^-)] \times [B(\overline{b} \to b\text{-baryon})]$ / $[B(\overline{b} \to B^0)] = 0.042 \pm 0.007 \pm 0.006$ which we multiply or divide by our best values $B(B^0 \to K^+\pi^-) = (1.96 \pm 0.05) \times 10^{-5}$, $B(\overline{b} \to b\text{-baryon}) = (8.4 \pm 1.1) \times 10^{-2}$, $B(\overline{b} \to B^0) = (40.8 \pm 0.7) \times 10^{-2}$. Our first error is their experiment's error and our second error is the systematic error from using our best values.

[2] BUSKULIC 96V assumes PDG 96 production fractions for B^0, B^+, B_s, b baryons.

$\Gamma(pK^-)/\Gamma_{total}$ — Γ_{54}/Γ

VALUE (units 10^{-6})	CL%	DOCUMENT ID		TECN	COMMENT
5.4 ± 1.0 OUR FIT					
6.3 ± 1.1 ± 0.8		[1] AALTONEN	09C	CDF	$p\overline{p}$ at 1.96 TeV
• • • We do not use the following data for averages, fits, limits, etc. • • •					
<360	90	[2] ADAM	96D	DLPH	$e^+ e^- \to Z$
< 50	90	[3] BUSKULIC	96V	ALEP	$e^+ e^- \to Z$

[1] AALTONEN 09C reports $[\Gamma(\Lambda_b^0 \to pK^-)/\Gamma_{total}]$ / $[B(B^0 \to K^+\pi^-)] \times [B(\overline{b} \to b\text{-baryon})]$ / $[B(\overline{b} \to B^0)] = 0.066 \pm 0.009 \pm 0.008$ which we multiply or divide by our best values $B(B^0 \to K^+\pi^-) = (1.96 \pm 0.05) \times 10^{-5}$, $B(\overline{b} \to b\text{-baryon}) = (8.4 \pm 1.1) \times 10^{-2}$, $B(\overline{b} \to B^0) = (40.8 \pm 0.7) \times 10^{-2}$. Our first error is their experiment's error and our second error is the systematic error from using our best values.

[2] ADAM 96D assumes $f_{B^0} = f_{B^-} = 0.39$ and $f_{B_s} = 0.12$.

[3] BUSKULIC 96V assumes PDG 96 production fractions for B^0, B^+, B_s, b baryons.

$\Gamma(p\pi^-)/\Gamma(pK^-)$ — Γ_{53}/Γ_{54}

VALUE	DOCUMENT ID		TECN	COMMENT
0.84 ± 0.09 OUR FIT				
0.86 ± 0.08 ± 0.05	AAIJ	12AR	LHCB	pp at 7 TeV

$\Gamma(pD_s^-)/\Gamma_{total}$ — Γ_{55}/Γ

VALUE	CL%	DOCUMENT ID		TECN	COMMENT
$<4.8 \times 10^{-4}$	90	AAIJ	14Q	LHCB	pp at 7 TeV

$\Gamma(p\mu^-\overline{\nu}_\mu)/\Gamma_{total}$ — Γ_{56}/Γ

VALUE (units 10^{-4})	DOCUMENT ID		TECN	COMMENT
4.1 ± 1.0	[1] AAIJ	15BG	LHCB	pp at 8 TeV

[1] The ratio of $B(\Lambda_b^0 \to p\mu^-\overline{\nu}_\mu)$ to $B(\Lambda_b^0 \to \Lambda_c^+ \mu^-\overline{\nu}_\mu)$ is measured within a restricted q^2 region. Combined with theoretical calculations of the form factors and the previously measured value of $|V_{cb}|$, the first $|V_{ub}| = (3.27 \pm 0.15 \pm 0.16 \pm 0.06) \times 10^{-3}$ measurement from the Λ_b decay is obtained, consistent with the exclusively measured world averages.

$\Gamma(p\mu^-\overline{\nu}_\mu)/\Gamma(\Lambda_c^+ \ell^- \overline{\nu}_\ell)$ — Γ_{56}/Γ_{46}

VALUE (units 10^{-2})	DOCUMENT ID		TECN	COMMENT
• • • We do not use the following data for averages, fits, limits, etc. • • •				
$1.0 \pm 0.04 \pm 0.08$	[1] AAIJ	15BG	LHCB	pp at 8 TeV

[1] This measurement is a ratio of $\Gamma(\Lambda_b^0 \to p\mu^-\overline{\nu}_\mu)[q^2 > 15\ \text{GeV}/c^2]$ to $\Gamma(\Lambda_b^0 \to \Lambda_c^+ \mu^-\overline{\nu}_\mu)[q^2 > 7\ \text{GeV}/c^2]$ within a restricted q^2 region. Combined with theoretical calculations of the form factors and the previously measured value of $|V_{cb}|$, the first $|V_{ub}| = (3.27 \pm 0.15 \pm 0.16 \pm 0.06) \times 10^{-3}$ measurement from the Λ_b decay is obtained, consistent with the exclusively measured world averages.

$\Gamma(\Lambda\mu^+\mu^-)/\Gamma_{total}$ — Γ_{57}/Γ

VALUE (units 10^{-7})	DOCUMENT ID		TECN	COMMENT
10.8 ± 2.8 OUR AVERAGE				
9.6 ± 1.6 ± 2.5	[1] AAIJ	13AJ	LHCB	pp at 7 TeV
17.3 ± 4.2 ± 5.5	AALTONEN	11AI	CDF	$p\overline{p}$ at 1.96 TeV

[1] Uses $B(\Lambda_b^0 \to J/\psi\Lambda) = (6.2 \pm 1.4) \times 10^{-4}$. This measurement comes from the sum of the differential rates in q^2 regions excluding those corresponding to J/ψ and $\psi(2S)$ ([8.68,10.09] and [12.86, 14.18] GeV^2/c^4).

$\Gamma(p\pi^-\mu^+\mu^-)/\Gamma_{total}$ — Γ_{58}/Γ

VALUE (units 10^{-8})	DOCUMENT ID		TECN	COMMENT
$6.9 \pm 1.9^{+1.7}_{-1.5}$	[1] AAIJ	17P	LHCB	pp at 7, 8 TeV

[1] Excludes J/ψ and $\psi(2S)$ decays to $\mu^+\mu^-$.

$\Gamma(p\pi^-\mu^+\mu^-)/\Gamma(p\pi^- J/\psi, J/\psi \to \mu^+\mu^-)$ — Γ_{58}/Γ_{13}

VALUE (units 10^{-2})	DOCUMENT ID		TECN	COMMENT
4.4 ± 1.2 ± 0.7	[1] AAIJ	17P	LHCB	pp at 7, 8 TeV

[1] The $p\pi^-\mu^+\mu^-$ mode excludes J/ψ and $\psi(2S)$ decays to $\mu^+\mu^-$.

$\Gamma(pK^- e^+ e^-)/\Gamma_{total}$ — Γ_{59}/Γ

VALUE (units 10^{-6})	DOCUMENT ID		TECN	COMMENT
$0.310 \pm 0.040^{+0.054}_{-0.047}$	[1,2] AAIJ	20M	LHCB	pp at 7, 8, 13 TeV

[1] Measured over $0.1 < q^2 < 6.0$ GeV/c^2, and $m_{pK} < 2.6$ GeV/c^2.

[2] The first uncertainty is the statistical uncertainty and the second is the combination of all systematic uncertainties including those related to the normalization of $\Lambda_b^0 \to J/\psi p K^-$.

$\Gamma(pK^-\mu^+\mu^-)/\Gamma_{total}$ — Γ_{60}/Γ

VALUE (units 10^{-6})	DOCUMENT ID		TECN	COMMENT
$0.265 \pm 0.014^{+0.049}_{-0.039}$	[1,2] AAIJ	20M	LHCB	pp at 7, 8, 13 TeV

[1] Measured over $0.1 < q^2 < 6.0$ GeV/c^2, and $m_{pK} < 2.6$ GeV/c^2.

[2] The first uncertainty is the statistical uncertainty and the second is the combination of all systematic uncertainties including those related to the normalization of $\Lambda_b^0 \to J/\psi p K^-$.

$\Gamma(pK^-\mu^+\mu^-)/\Gamma(pK^- e^+ e^-)$ — Γ_{60}/Γ_{59}

VALUE	DOCUMENT ID		TECN	COMMENT
$0.86^{+0.14}_{-0.11} \pm 0.05$	[1] AAIJ	20M	LHCB	pp at 7, 8, 13 TeV

[1] Measured over $0.1 < q^2 < 6.0$ GeV/c^2, and $m_{pK} < 2.6$ GeV/c^2.

$\Gamma(pK^- e^+ e^-)/\Gamma(pJ/\psi K^-)$ — Γ_{59}/Γ_{14}

VALUE (units 10^{-4})	DOCUMENT ID		TECN	COMMENT
$9.8^{+1.4}_{-1.3} \pm 0.8$	[1] AAIJ	20M	LHCB	pp at 7, 8, 13 TeV

[1] Measured over $0.1 < q^2 < 6.0$ GeV/c^2, and $m_{pK} < 2.6$ GeV/c^2.

$\Gamma(pK^-\mu^+\mu^-)/\Gamma(pJ/\psi K^-)$ — Γ_{60}/Γ_{14}

VALUE (units 10^{-4})	DOCUMENT ID		TECN	COMMENT
8.4 ± 0.4 ± 0.4	[1] AAIJ	20M	LHCB	pp at 7, 8, 13 TeV

[1] Measured over $0.1 < q^2 < 6.0$ GeV/c^2, and $m_{pK} < 2.6$ GeV/c^2.

$\Gamma(\Lambda\gamma)/\Gamma_{total}$ — Γ_{61}/Γ

VALUE (units 10^{-6})	CL%	DOCUMENT ID		TECN	COMMENT
7.1 ± 1.5 ± 0.9		[1] AAIJ	19Z	LHCB	pp at 13 TeV
• • • We do not use the following data for averages, fits, limits, etc. • • •					
<1300	90	ACOSTA	02G	CDF	$p\overline{p}$ at 1.8 TeV

[1] AAIJ 19Z normalized to $B^0 \to K^{*0}\gamma$ and used an integrated luminosity of 1.7 fb^{-1}.

$\Gamma(\Lambda\eta)/\Gamma_{total}$ — Γ_{62}/Γ

VALUE (units 10^{-6})	DOCUMENT ID		TECN	COMMENT
$9^{+7}_{-5} \pm 1$	[1] AAIJ	15AH	LHCB	pp at 7, 8 TeV

[1] AAIJ 15AH reports $[\Gamma(\Lambda_b^0 \to \Lambda\eta)/\Gamma_{total}]$ / $[B(B^0 \to \eta' K^0)] = 0.142^{+0.11}_{-0.08}$ which we multiply by our best value $B(B^0 \to \eta' K^0) = (6.6 \pm 0.4) \times 10^{-5}$. Our first error is their experiment's error and our second error is the systematic error from using our best value. The single uncertainty quoted with the original measurement combines in quadrature statistical and systematic uncertainties.

Downloaded from https://academic.oup.com/ptep/article/2022/8/083C01/6651666 by KIT Library user on 27 September 2022

$\Gamma(\Lambda\eta'(958))/\Gamma_{total}$ — Γ_{63}/Γ

VALUE	CL%	DOCUMENT ID		TECN	COMMENT
$<3.1\times10^{-6}$	90	[1] AAIJ	15AH	LHCB	pp at 7, 8 TeV

[1] AAIJ 15AH reports $[\Gamma(\Lambda_b^0 \to \Lambda\eta'(958))/\Gamma_{total}]$ / $[B(B^0 \to \eta' K^0)] < 0.047$ which we multiply by our best value $B(B^0 \to \eta' K^0) = 6.6\times10^{-5}$.

$\Gamma(\Lambda\pi^+\pi^-)/\Gamma(\Lambda_c^+\pi^-)$ — Γ_{64}/Γ_{30}

VALUE (units 10^{-4})	DOCUMENT ID		TECN	COMMENT
$9.5\pm3.8\pm0.5$	[1] AAIJ	16W	LHCB	pp at 7, 8 TeV

[1] AAIJ 16W reports $[\Gamma(\Lambda_b^0 \to \Lambda\pi^+\pi^-)/\Gamma(\Lambda_b^0 \to \Lambda_c^+\pi^-)]$ / $[B(\Lambda_c^+ \to \Lambda\pi^+)] = (7.3 \pm 1.9 \pm 2.2)\times10^{-2}$ which we multiply by our best value $B(\Lambda_c^+ \to \Lambda\pi^+) = (1.30 \pm 0.07)\times10^{-2}$. Our first error is their experiment's error and our second error is the systematic error from using our best value.

$\Gamma(\Lambda K^+\pi^-)/\Gamma(\Lambda_c^+\pi^-)$ — Γ_{65}/Γ_{30}

VALUE (units 10^{-4})	DOCUMENT ID		TECN	COMMENT
$11.6\pm2.3\pm0.6$	[1] AAIJ	16W	LHCB	pp at 7, 8 TeV

[1] AAIJ 16W reports $[\Gamma(\Lambda_b^0 \to \Lambda K^+\pi^-)/\Gamma(\Lambda_b^0 \to \Lambda_c^+\pi^-)]$ / $[B(\Lambda_c^+ \to \Lambda\pi^+)] = (8.9 \pm 1.2 \pm 1.3)\times10^{-2}$ which we multiply by our best value $B(\Lambda_c^+ \to \Lambda\pi^+) = (1.30 \pm 0.07)\times10^{-2}$. Our first error is their experiment's error and our second error is the systematic error from using our best value.

$\Gamma(\Lambda K^+K^-)/\Gamma(\Lambda_c^+\pi^-)$ — Γ_{66}/Γ_{30}

VALUE (units 10^{-3})	DOCUMENT ID		TECN	COMMENT
$3.29\pm0.35\pm0.17$	[1] AAIJ	16W	LHCB	pp at 7, 8 TeV

[1] AAIJ 16W reports $[\Gamma(\Lambda_b^0 \to \Lambda K^+K^-)/\Gamma(\Lambda_b^0 \to \Lambda_c^+\pi^-)]$ / $[B(\Lambda_c^+ \to \Lambda\pi^+)] = (25.3 \pm 1.9 \pm 1.9)\times10^{-2}$ which we multiply by our best value $B(\Lambda_c^+ \to \Lambda\pi^+) = (1.30 \pm 0.07)\times10^{-2}$. Our first error is their experiment's error and our second error is the systematic error from using our best value.

$\Gamma(\Lambda\phi)/\Gamma_{total}$ — Γ_{67}/Γ

VALUE (units 10^{-6})	DOCUMENT ID		TECN	COMMENT
$9.8\pm2.1^{+1.6}_{-1.5}$	[1] AAIJ	16J	LHCB	pp at 7, 8 TeV

[1] AAIJ 16J reports $[\Gamma(\Lambda_b^0 \to \Lambda\phi)/\Gamma_{total}]$ / $[B(B^0 \to K^0\phi)] \times [B(\overline{b} \to b\text{-baryon})]$ / $[B(\overline{b} \to B^0)] = 0.275 \pm 0.055 \pm 0.020$ which we multiply or divide by our best values $B(B^0 \to K^0\phi) = (7.3 \pm 0.7)\times10^{-6}$, $B(\overline{b} \to b\text{-baryon}) = (8.4 \pm 1.1)\times10^{-2}$, $B(\overline{b} \to B^0) = (40.8 \pm 0.7)\times10^{-2}$. Our first error is their experiment's error and our second error is the systematic error from using our best values.

$\Gamma(p\pi^-\pi^+\pi^-)/\Gamma(\Lambda_c^+\pi^-)$ — Γ_{68}/Γ_{30}

VALUE (units 10^{-3})	DOCUMENT ID		TECN	COMMENT
$4.30\pm0.24^{+0.22}_{-0.23}$	[1] AAIJ	18Q	LHCB	pp at 7, 8 TeV

[1] AAIJ 18Q reports $[\Gamma(\Lambda_b^0 \to p\pi^-\pi^+\pi^-)/\Gamma(\Lambda_b^0 \to \Lambda_c^+\pi^-)]$ / $[B(\Lambda_c^+ \to pK^-\pi^+)] = (6.85 \pm 0.19 \pm 0.08 \pm 0.32)\times10^{-2}$ which we multiply by our best value $B(\Lambda_c^+ \to pK^-\pi^+) = (6.28 \pm 0.32)\times10^{-2}$. Our first error is their experiment's error and our second error is the systematic error from using our best value.

$\Gamma(pK^-K^+\pi^-)/\Gamma(\Lambda_c^+\pi^-)$ — Γ_{69}/Γ_{30}

VALUE (units 10^{-3})	DOCUMENT ID		TECN	COMMENT
$0.83\pm0.10\pm0.04$	[1] AAIJ	18Q	LHCB	pp at 7, 8 TeV

[1] AAIJ 18Q reports $[\Gamma(\Lambda_b^0 \to pK^-K^+\pi^-)/\Gamma(\Lambda_b^0 \to \Lambda_c^+\pi^-)]$ / $[B(\Lambda_c^+ \to pK^-\pi^+)] = (1.32 \pm 0.09 \pm 0.09 \pm 0.10)\times10^{-2}$ which we multiply by our best value $B(\Lambda_c^+ \to pK^-\pi^+) = (6.28 \pm 0.32)\times10^{-2}$. Our first error is their experiment's error and our second error is the systematic error from using our best value.

$\Gamma(pK^-\pi^+\pi^-)/\Gamma(\Lambda_c^+\pi^-)$ — Γ_{70}/Γ_{30}

VALUE (units 10^{-3})	DOCUMENT ID		TECN	COMMENT
$10.3\pm0.5\pm0.5$	[1] AAIJ	18Q	LHCB	pp at 7, 8 TeV

[1] AAIJ 18Q reports $[\Gamma(\Lambda_b^0 \to pK^-\pi^+\pi^-)/\Gamma(\Lambda_b^0 \to \Lambda_c^+\pi^-)]$ / $[B(\Lambda_c^+ \to pK^-\pi^+)] = (16.4 \pm 0.3 \pm 0.2 \pm 0.7)\times10^{-2}$ which we multiply by our best value $B(\Lambda_c^+ \to pK^-\pi^+) = (6.28 \pm 0.32)\times10^{-2}$. Our first error is their experiment's error and our second error is the systematic error from using our best value.

$\Gamma(pK^-K^+K^-)/\Gamma(\Lambda_c^+\pi^-)$ — Γ_{71}/Γ_{30}

VALUE (units 10^{-3})	DOCUMENT ID		TECN	COMMENT
$2.58\pm0.15^{+0.13}_{-0.14}$	[1] AAIJ	18Q	LHCB	pp at 7, 8 TeV

[1] AAIJ 18Q reports $[\Gamma(\Lambda_b^0 \to pK^-K^+K^-)/\Gamma(\Lambda_b^0 \to \Lambda_c^+\pi^-)]$ / $[B(\Lambda_c^+ \to pK^-\pi^+)] = (4.11 \pm 0.12 \pm 0.06 \pm 0.19)\times10^{-2}$ which we multiply by our best value $B(\Lambda_c^+ \to pK^-\pi^+) = (6.28 \pm 0.32)\times10^{-2}$. Our first error is their experiment's error and our second error is the systematic error from using our best value.

PARTIAL BRANCHING FRACTIONS IN $\Lambda_b \to \Lambda\mu^+\mu^-$

$B(\Lambda_b \to \Lambda\mu^+\mu^-)$ ($q^2 < 2.0$ GeV$^2/c^4$)

VALUE (units 10^{-7})	DOCUMENT ID		TECN	COMMENT
0.71 ± 0.27 OUR AVERAGE				
$0.72^{+0.24}_{-0.22}\pm0.14$	[1] AAIJ	15AE	LHCB	pp at 7, 8 TeV
$0.15\pm2.01\pm0.05$	AALTONEN	11AI	CDF	$p\overline{p}$ at 1.96 TeV
• • • We do not use the following data for averages, fits, limits, etc. • • •				
$0.56\pm0.76\pm0.80$	[2] AAIJ	13AJ	LHCB	Repl. by AAIJ 15AE

[1] AAIJ 15AE measurement covers $0.1 < q^2 < 2.0$ GeV$^2/c^4$.
[2] Uses $B(\Lambda_b^0 \to J/\psi\Lambda) = (6.2 \pm 1.4)\times10^{-4}$.

$B(\Lambda_b \to \Lambda\mu^+\mu^-)$ ($2.0 < q^2 < 4.3$ GeV$^2/c^4$)

VALUE (units 10^{-7})	DOCUMENT ID		TECN	COMMENT
$0.28\ ^{+0.28}_{-0.21}$ OUR AVERAGE				
$0.253^{+0.276}_{-0.207}\pm0.046$	[1] AAIJ	15AE	LHCB	pp at 7, 8 TeV
$1.8\ \pm1.7\ \pm0.6$	AALTONEN	11AI	CDF	$p\overline{p}$ at 1.96 TeV
• • • We do not use the following data for averages, fits, limits, etc. • • •				
$0.71\ \pm0.60\ \pm0.23$	[2] AAIJ	13AJ	LHCB	Repl. by AAIJ 15AE

[1] AAIJ 15AE measurement covers $2.0 < q^2 < 4.0$ GeV$^2/c^4$.
[2] Uses $B(\Lambda_b^0 \to J/\psi\Lambda) = (6.2 \pm 1.4)\times10^{-4}$.

$B(\Lambda_b \to \Lambda\mu^+\mu^-)$ ($q^2 < 4.3$ GeV$^2/c^4$)

VALUE (units 10^{-7})	DOCUMENT ID		TECN	COMMENT
$2.7\pm2.5\pm0.9$	AALTONEN	11AI	CDF	$p\overline{p}$ at 1.96 TeV

$B(\Lambda_b \to \Lambda\mu^+\mu^-)$ ($4.0 < q^2 < 6.0$ GeV$^2/c^4$)

VALUE (units 10^{-7})	DOCUMENT ID		TECN	COMMENT
$0.04^{+0.18}_{-0.00}\pm0.02$	AAIJ	15AE	LHCB	pp at 7, 8 TeV

$B(\Lambda_b \to \Lambda\mu^+\mu^-)$ ($1.0 < q^2 < 6.0$ GeV$^2/c^4$)

VALUE (units 10^{-7})	DOCUMENT ID		TECN	COMMENT
$0.47^{+0.31}_{-0.27}$ OUR AVERAGE				
$0.45^{+0.30}_{-0.25}\pm0.10$	[1] AAIJ	15AE	LHCB	pp at 7 and 8 TeV
$1.3\ \pm2.1\ \pm0.4$	AALTONEN	11AI	CDF	$p\overline{p}$ at 1.96 TeV

[1] AAIJ 15AE measurement covers $1.1 < q^2 < 6.0$ GeV$^2/c^4$.

$B(\Lambda_b \to \Lambda\mu^+\mu^-)$ ($6.0 < q^2 < 8.0$ GeV$^2/c^4$)

VALUE (units 10^{-7})	DOCUMENT ID		TECN	COMMENT
$0.50^{+0.24}_{-0.22}\pm0.10$	AAIJ	15AE	LHCB	pp at 7, 8 TeV

$B(\Lambda_b \to \Lambda\mu^+\mu^-)$ ($4.3 < q^2 < 8.68$ GeV$^2/c^4$)

VALUE (units 10^{-7})	DOCUMENT ID		TECN	COMMENT
$0.5\ \pm0.7$ OUR AVERAGE				
$0.66\pm0.74\pm0.18$	[1] AAIJ	13AJ	LHCB	pp at 7 TeV
$-0.2\ \pm1.6\ \pm0.1$	AALTONEN	11AI	CDF	$p\overline{p}$ at 1.96 TeV

[1] Uses $B(\Lambda_b^0 \to J/\psi\Lambda) = (6.2 \pm 1.4)\times10^{-4}$.

$B(\Lambda_b \to \Lambda\mu^+\mu^-)$ ($10.09 < q^2 < 12.86$ GeV$^2/c^4$)

VALUE (units 10^{-7})	DOCUMENT ID		TECN	COMMENT
$2.2\ \pm0.6$ OUR AVERAGE				
$2.08^{+0.42}_{-0.39}\pm0.42$	[1] AAIJ	15AE	LHCB	pp at 7, 8 TeV
$3.0\ \pm1.5\ \pm1.0$	AALTONEN	11AI	CDF	$p\overline{p}$ at 1.96 TeV
• • • We do not use the following data for averages, fits, limits, etc. • • •				
$1.55\pm0.58\pm0.55$	[2] AAIJ	13AJ	LHCB	Repl. by AAIJ 15AE

[1] AAIJ 15AE measurement covers $11.0 < q^2 < 12.5$ GeV$^2/c^4$.
[2] Uses $B(\Lambda_b^0 \to J/\psi\Lambda) = (6.2 \pm 1.4)\times10^{-4}$.

$B(\Lambda_b \to \Lambda\mu^+\mu^-)$ ($14.18 < q^2 < 16.0$ GeV$^2/c^4$)

VALUE (units 10^{-7})	DOCUMENT ID		TECN	COMMENT
$1.7\ \pm0.5$ OUR AVERAGE Error includes scale factor of 1.1.				
$2.04^{+0.35}_{-0.33}\pm0.42$	[1] AAIJ	15AE	LHCB	pp at 7, 8 TeV
$1.0\ \pm0.7\ \pm0.3$	AALTONEN	11AI	CDF	$p\overline{p}$ at 1.96 TeV
• • • We do not use the following data for averages, fits, limits, etc. • • •				
$1.44\pm0.44\pm0.42$	[2] AAIJ	13AJ	LHCB	Repl. by AAIJ 15AE

[1] AAIJ 15AE measurement covers $15.0 < q^2 < 16.0$ GeV$^2/c^4$.
[2] Uses $B(\Lambda_b^0 \to J/\psi\Lambda) = (6.2 \pm 1.4)\times10^{-4}$.

$B(\Lambda_b \to \Lambda\mu^+\mu^-)$ ($16.0 < q^2$ GeV$^2/c^4$)

VALUE (units 10^{-7})	DOCUMENT ID		TECN	COMMENT
$7.0\ \pm1.9\ \pm2.2$	AALTONEN	11AI	CDF	$p\overline{p}$ at 1.96 TeV
• • • We do not use the following data for averages, fits, limits, etc. • • •				
$4.73\pm0.77\pm1.25$	[1,2] AAIJ	13AJ	LHCB	Repl. by AAIJ 15AE

[1] Uses $B(\Lambda_b^0 \to J/\psi\Lambda) = (6.2 \pm 1.4)\times10^{-4}$.
[2] Requires $16.00 < q^2 < 20.30$ GeV$^2/c^4$.

Downloaded from https://academic.oup.com/ptep/article/2022/8/083C01/6651666 by KIT Library user on 27 September 2022

$B(\Lambda_b \to \Lambda\mu^+\mu^-)$ $(18.0 < q^2 < 20.0\ GeV^2/c^4)$

VALUE (units 10^{-7})	DOCUMENT ID		TECN	COMMENT
2.44±0.28±0.50	AAIJ	15AE	LHCB	pp at 7, 8 TeV

$B(\Lambda_b \to \Lambda\mu^+\mu^-)$ $(15.0 < q^2 < 20.0\ GeV^2/c^4)$

VALUE (units 10^{-7})	DOCUMENT ID		TECN	COMMENT
6.00±0.45±1.25	AAIJ	15AE	LHCB	pp at 7, 8 TeV

CP VIOLATION

A_{CP} is defined as

$$A_{CP} = \frac{B(\Lambda_b^0 \to f) - B(\overline{\Lambda}_b^0 \to \overline{f})}{B(\Lambda_b^0 \to f) + B(\overline{\Lambda}_b^0 \to \overline{f})},$$

the CP-violation asymmetry of exclusive Λ_b^0 and $\overline{\Lambda}_b^0$ decay.

$A_{CP}(\Lambda_b \to p\pi^-)$

VALUE	DOCUMENT ID		TECN	COMMENT
−0.025±0.029 OUR AVERAGE	Error includes scale factor of 1.2.			
−0.035±0.017±0.020	AAIJ	18AX	LHCB	pp at 7 and 8 TeV
0.06 ±0.07 ±0.03	AALTONEN	14P	CDF	$p\overline{p}$ at 1.96 TeV
• • • We do not use the following data for averages, fits, limits, etc. • • •				
0.03 ±0.17 ±0.05	AALTONEN	11N	CDF	Repl. by AALTONEN 14P

$A_{CP}(\Lambda_b \to pK^-)$

VALUE	DOCUMENT ID		TECN	COMMENT
−0.025±0.022 OUR AVERAGE				
−0.020±0.013±0.019	AAIJ	18AX	LHCB	pp at 7 and 8 TeV
−0.10 ±0.08 ±0.04	AALTONEN	14P	CDF	$p\overline{p}$ at 1.96 TeV
• • • We do not use the following data for averages, fits, limits, etc. • • •				
0.37 ±0.17 ±0.03	AALTONEN	11N	CDF	Repl. by AALTONEN 14P

$A_{CP}(\Lambda_b \to DpK^-)$

VALUE	DOCUMENT ID		TECN	COMMENT
$\mathbf{0.12 \pm 0.09^{+0.02}_{-0.03}}$	[1] AAIJ	21AD	LHCB	pp at 7, 8, 13 TeV

[1] A_{CP} is measured from $(B(\Lambda_b^0 \to [K^+\pi^-]_D pK^-) - B(\overline{\Lambda}_b^0 \to [K^-\pi^+]_D \overline{p}K^+))/(B(\Lambda_b^0 \to [K^+\pi^-]_D pK^-) + B(\overline{\Lambda}_b^0 \to [K^-\pi^+]_D \overline{p}K^+))$ in the full phase space.

$\Delta A_{CP}(pK^-/\pi^-)$

$\Delta A_{CP} \equiv A_{CP}(pK^-) - A_{CP}(p\pi^-)$

VALUE	DOCUMENT ID		TECN	COMMENT
0.014±0.022±0.010	AAIJ	18AX	LHCB	pp at 7 and 8 TeV

$A_{CP}(\Lambda_b \to p\overline{K}^0\pi^-)$

VALUE	DOCUMENT ID		TECN	COMMENT
0.22±0.13±0.03	AAIJ	14Q	LHCB	pp at 7 TeV

$\Delta A_{CP}(J/\psi p\pi^-/K^-)$

$\Delta A_{CP} \equiv A_{CP}(J/\psi p\pi^-) - A_{CP}(J/\psi pK^-)$

VALUE (units 10^{-2})	DOCUMENT ID		TECN	COMMENT
5.7±2.4±1.2	AAIJ	14K	LHCB	pp at 7, 8 TeV

$A_{CP}(\Lambda_b \to \Lambda K^+\pi^-)$

VALUE	DOCUMENT ID		TECN	COMMENT
−0.53±0.23±0.11	[1] AAIJ	16W	LHCB	pp at 7, 8 TeV

[1] Measured relative to $\Lambda_b^0 \to \Lambda_c^+\pi^-$ decay.

$A_{CP}(\Lambda_b \to \Lambda K^+K^-)$

VALUE	DOCUMENT ID		TECN	COMMENT
−0.28±0.10±0.07	[1] AAIJ	16W	LHCB	pp at 7, 8 TeV

[1] Measured relative to $\Lambda_b^0 \to \Lambda_c^+\pi^-$ decay.

$\Delta A_{CP}(\Lambda_b^0 \to pK^-\mu^+\mu^-)$

$\Delta A_{CP} \equiv A_{CP}(pK^-\mu^+\mu^-) - A_{CP}(pK^-J/\psi)$

VALUE (units 10^{-2})	DOCUMENT ID		TECN	COMMENT
−3.5±5.0±0.2	AAIJ	17T	LHCB	pp at 7, 8 TeV

$\Delta A_{CP}(\Lambda_b^0 \to p\pi^-\pi^+\pi^-)$

$\Delta A_{CP} \equiv A_{CP}(\Lambda_b^0 \to p\pi^-\pi^+\pi^-) - A_{CP}(\Lambda_b^0 \to (\Lambda_c^+ \to p\pi^-\pi^+)\pi^-)$

VALUE (units 10^{-2})	DOCUMENT ID		TECN	COMMENT
1.1±2.5±0.6	[1] AAIJ	19AH	LHCB	pp at 7 and 8 TeV

[1] Full phase space.

$\Delta A_{CP}(\Lambda_b^0 \to (p\pi^-\pi^+\pi^-)_{LBM})$

$\Delta A_{CP} \equiv A_{CP}(\Lambda_b^0 \to (p\pi^-\pi^+\pi^-)_{LBM}) - A_{CP}(\Lambda_b^0 \to (\Lambda_c^+ \to p\pi^-\pi^+)\pi^-)$. Two-body low invariant-mass region (LBM): $m(p\pi^-) < 2000$MeV and $m(\pi^+\pi^-) < 1640$ MeV.

VALUE (units 10^{-2})	DOCUMENT ID		TECN	COMMENT
3.7±4.1±0.5	[1] AAIJ	19AH	LHCB	pp at 7 and 8 TeV

[1] Measurement done with $m(p\pi^-) < 2000$ MeV/c^2 and $m(\pi^+\pi^-) < 1640$ MeV/c^2.

$\Delta A_{CP}(\Lambda_b^0 \to pa_1(1260)^-)$

$\Delta A_{CP} \equiv A_{CP}(\Lambda_b^0 \to pa_1(1260)^-) - A_{CP}(\Lambda_b^0 \to (\Lambda_c^+ \to p\pi^-\pi^+)\pi^-)$. $419 < m(\pi^+\pi^-\pi^+) < 1500$ MeV.

VALUE (units 10^{-2})	DOCUMENT ID		TECN	COMMENT
−1.5±4.2±0.6	AAIJ	19AH	LHCB	pp at 7 and 8 TeV

$\Delta A_{CP}(\Lambda_b^0 \to N(1520)^0\rho(770)^0)$

$\Delta A_{CP} \equiv A_{CP}(\Lambda_b^0 \to N(1520)^0\rho(770)^0) - A_{CP}(\Lambda_b^0 \to (\Lambda_c^+ \to p\pi^-\pi^+)\pi^-)$. $1078 < m(p\pi^-) < 1800$ MeV and $m(\pi^+\pi^-) < 1100$ MeV.

VALUE (units 10^{-2})	DOCUMENT ID		TECN	COMMENT
2.0±4.9±0.4	AAIJ	19AH	LHCB	pp at 7 and 8 TeV

$\Delta A_{CP}(\Lambda_b^0 \to \Delta(1232)^{++}\pi^-\pi^-)$

$\Delta A_{CP} \equiv A_{CP}(\Lambda_b^0 \to \Delta(1232)^{++}\pi^-\pi^-) - A_{CP}(\Lambda_b^0 \to (\Lambda_c^+ \to p\pi^-\pi^+)\pi^-)$. $1078 < m(p\pi^+) < 1432$ MeV.

VALUE (units 10^{-2})	DOCUMENT ID		TECN	COMMENT
0.1±3.2±0.6	AAIJ	19AH	LHCB	pp at 7 and 8 TeV

$\Delta A_{CP}(\Lambda_b^0 \to pK^-\pi^+\pi^-)$

$\Delta A_{CP} \equiv A_{CP}(\Lambda_b^0 \to pK^-\pi^+\pi^-) - A_{CP}(\Lambda_b^0 \to (\Lambda_c^+ \to pK^-\pi^+)\pi^-)$

VALUE (units 10^{-2})	DOCUMENT ID		TECN	COMMENT
3.2±1.1±0.6	[1] AAIJ	19AH	LHCB	pp at 7 and 8 TeV

[1] Full phase space.

$\Delta A_{CP}(\Lambda_b^0 \to (pK^-\pi^+\pi^-)_{LBM})$

$\Delta A_{CP} \equiv A_{CP}(\Lambda_b^0 \to (pK^-\pi^+\pi^-)_{LBM}) - A_{CP}(\Lambda_b^0 \to (\Lambda_c^+ \to pK^-\pi^+)\pi^-)$. Two-body low invariant-mass region (LBM): $m(pK^-) < 2000$ MeV and $m(\pi^+\pi^-) < 1640$ MeV.

VALUE (units 10^{-2})	DOCUMENT ID		TECN	COMMENT
3.5±1.5±0.5	[1] AAIJ	19AH	LHCB	pp at 7 and 8 TeV

[1] Measurement done with $m(pK^-) < 2000$ MeV/c^2 and $m(\pi^+\pi^-) < 1640$ MeV/c^2.

$\Delta A_{CP}(\Lambda_b^0 \to N(1520)^0K^*(892)^0)$

$\Delta A_{CP} \equiv A_{CP}(\Lambda_b^0 \to N(1520)^0K^*(892)^0) - A_{CP}(\Lambda_b^0 \to (\Lambda_c^+ \to pK^-\pi^+)\pi^-)$. $1078 < m(p\pi^-) < 1800$ MeV and $750 < m(\pi^+K^-) < 1100$ MeV.

VALUE (units 10^{-2})	DOCUMENT ID		TECN	COMMENT
5.5±2.5±0.5	AAIJ	19AH	LHCB	pp at 7 and 8 TeV

$\Delta A_{CP}(\Lambda_b^0 \to \Lambda(1520)\rho(770)^0)$

$\Delta A_{CP} \equiv A_{CP}(\Lambda_b^0 \to \Lambda(1520)\rho(770)^0) - A_{CP}(\Lambda_b^0 \to (\Lambda_c^+ \to pK^-\pi^+)\pi^-)$. $1460 < m(pK^-) < 1580$ MeV and $m(\pi^+\pi^-) < 1100$ MeV.

VALUE (units 10^{-2})	DOCUMENT ID		TECN	COMMENT
0.6±6.0±0.5	AAIJ	19AH	LHCB	pp at 7 and 8 TeV

$\Delta A_{CP}(\Lambda_b^0 \to \Delta(1232)^{++}K^-\pi^-)$

$\Delta A_{CP} \equiv A_{CP}(\Lambda_b^0 \to \Delta(1232)^{++}K^-\pi^-) - A_{CP}(\Lambda_b^0 \to (\Lambda_c^+ \to pK^-\pi^+)\pi^-)$. $1078 < m(p\pi^+) < 1432$ MeV.

VALUE (units 10^{-2})	DOCUMENT ID		TECN	COMMENT
4.4±2.6±0.6	AAIJ	19AH	LHCB	pp at 7 and 8 TeV

$\Delta A_{CP}(\Lambda_b^0 \to pK_1(1410)^-)$

$\Delta A_{CP} \equiv A_{CP}(\Lambda_b^0 \to pK_1(1410)^-) - A_{CP}(\Lambda_b^0 \to (\Lambda_c^+ \to pK^-\pi^+)\pi^-)$. $1200 < m(K^-\pi^+\pi^-) < 1600$ MeV.

VALUE (units 10^{-2})	DOCUMENT ID		TECN	COMMENT
4.7±3.5±0.8	AAIJ	19AH	LHCB	pp at 7 and 8 TeV

$\Delta A_{CP}(\Lambda_b^0 \to pK^-K^+\pi^-)$

$\Delta A_{CP} \equiv A_{CP}(\Lambda_b^0 \to pK^-K^+\pi^-) - A_{CP}(\Lambda_b^0 \to (\Lambda_c^+ \to pK^-\pi^+)\pi^-)$

VALUE (units 10^{-2})	DOCUMENT ID		TECN	COMMENT
−6.9±4.9±0.8	[1] AAIJ	19AH	LHCB	pp at 7 and 8 TeV

[1] Full phase space.

$\Delta A_{CP}(\Lambda_b^0 \to pK^-K^+K^-)$

$\Delta A_{CP} \equiv A_{CP}(\Lambda_b^0 \to pK^-K^+K^-) - A_{CP}(\Lambda_b^0 \to (\Lambda_c^+ \to pK^-\pi^+)\pi^-)$

VALUE (units 10^{-2})	DOCUMENT ID		TECN	COMMENT
0.2±1.8±0.6	[1] AAIJ	19AH	LHCB	pp at 7 and 8 TeV

[1] Full phase space.

$\Delta A_{CP}(\Lambda_b^0 \to \Lambda(1520)\phi(1020))$

$\Delta A_{CP} \equiv A_{CP}(\Lambda_b^0 \to \Lambda(1520)\phi(1020)) - A_{CP}(\Lambda_b^0 \to (\Lambda_c^+ \to pK^-\pi^+)\pi^-)$. $1460 < m(pK^-) < 1600$ MeV and $1005 < m(K^+K^-) < 1040$ MeV.

VALUE (units 10^{-2})	DOCUMENT ID		TECN	COMMENT
4.3±5.6±0.4	AAIJ	19AH	LHCB	pp at 7 and 8 TeV

$\Delta A_{CP}(\Lambda_b^0 \to (pK^-)_{highmass}\ \phi(1020))$

$\Delta A_{CP} \equiv A_{CP}(\Lambda_b^0 \to (pK^-)_{highmass}\ \phi(1020)) - A_{CP}(\Lambda_b^0 \to (\Lambda_c pK^-\pi^+)\pi^-)$. $m(pK^-) > 1600$ MeV and $1005 < m(K^+K^-) < 1040$ MeV.

VALUE (units 10^{-2})	DOCUMENT ID		TECN	COMMENT
−0.7±3.3±0.7	[1] AAIJ	19AH	LHCB	pp at 7 and 8 TeV

[1] Measurement done with $m(pK^-) > 1600$ MeV/c^2.

Downloaded from https://academic.oup.com/ptep/article/2022/8/083C01/6651666 by KIT Library user on 27 September 2022

$\Delta A_{CP}(\Lambda_b^0 \to (pK^-K^+K^-)_{LBM})$

$\Delta A_{CP} \equiv A_{CP}(\Lambda_b^0 \to (pK^-K^+K^-)_{LBM}) - A_{CP}(\Lambda_b^0 \to (\Lambda_c^+ \to pK^-\pi^+)\pi^-)$. Two-body low invariant-mass region (LBM): m(pK^-) < 2000 MeVand m(K^+K^-) < 1675 MeV.

VALUE (units 10^{-2})	DOCUMENT ID		TECN	COMMENT
2.7±2.3±0.6	[1] AAIJ	19AH	LHCB	pp at 7 and 8 TeV

[1] Measurement done with $m(pK^-) < 2000$ MeV/c^2 and $m(K^+K^-) < 1675$ MeV/c^2.

CP AND *T* VIOLATION PARAMETERS

Measured values of the triple-product asymmetry parameters, odd under time-reversal, are defined as $A_{c(s)}(\Lambda/\phi) = (N^+_{c(s)} - N^-_{c(s)})$ / (sum) where $N^+_{c(s)}$, $N^-_{c(s)}$ are the number of Λ or ϕ candidates for which the cos(Φ) and sin(Φ) observables are positive and negative, respectively. Angles cos(Φ) and sin(Φ) are defined as in LEITNER 07.

$A_c(\Lambda)$

VALUE	DOCUMENT ID		TECN	COMMENT
−0.22±0.12±0.06	AAIJ	16J	LHCB	pp at 7, 8 TeV

$A_s(\Lambda)$

VALUE	DOCUMENT ID		TECN	COMMENT
0.13±0.12±0.05	AAIJ	16J	LHCB	pp at 7, 8 TeV

$A_c(\phi)$

VALUE	DOCUMENT ID		TECN	COMMENT
−0.01±0.12±0.03	AAIJ	16J	LHCB	pp at 7, 8 TeV

$A_s(\phi)$

VALUE	DOCUMENT ID		TECN	COMMENT
−0.07±0.12±0.01	AAIJ	16J	LHCB	pp at 7, 8 TeV

$a_{CP}(\Lambda_b^0 \to p\pi^-\pi^+\pi^-)$

Observable calculated as half of the difference between triple products for Λ_b^0 and $\overline{\Lambda}_b^0$, which is sensitive to *CP* violation.

VALUE (%)	DOCUMENT ID		TECN	COMMENT
−0.7 ±0.7 ±0.2	[1] AAIJ	20AB	LHCB	pp at 7, 8, 13 TeV
• • • We do not use the following data for averages, fits, limits, etc. • • •				
1.15±1.45±0.32	[2] AAIJ	17H	LHCB	Repl. by AAIJ 20AB

[1] Used both triple product asymmetries and the unbinned energy test method.
[2] Measured over full phase space of the decay.

$a_{CP}(\Lambda_b^0 \to pK^-\pi^+\pi^-)$

Observable calculated as half of the difference between triple products for Λ_b^0 and $\overline{\Lambda}_b^0$, which is sensitive to *CP* violation.

VALUE (%)	DOCUMENT ID		TECN	COMMENT
−0.81±0.84±0.31	[1] AAIJ	18AG	LHCB	pp at 7, 8 TeV

[1] Measured over full phase space of the decay.

$a_{CP}(\Lambda_b^0 \to pK^-K^+\pi^-)$

Observable calculated as half of the difference between triple products for Λ_b^0 and $\overline{\Lambda}_b^0$, which is sensitive to *CP* violation.

VALUE (%)	DOCUMENT ID		TECN	COMMENT
−0.93±4.54±0.42	[1] AAIJ	17H	LHCB	pp at 7, 8 TeV

[1] Measured over full phase space of the decay.

$a_{CP}(\Lambda_b^0 \to pK^-K^+K^-)$

Observable calculated as half of the difference between triple products for Λ_b^0 and $\overline{\Lambda}_b^0$, which is sensitive to *CP* violation.

VALUE (%)	DOCUMENT ID		TECN	COMMENT
1.12±1.51±0.32	[1] AAIJ	18AG	LHCB	pp at 7, 8 TeV

[1] Measured over full phase space of the decay.

$a_{CP}(\Lambda_b^0 \to pK^-\mu^+\mu^-)$

VALUE (%)	DOCUMENT ID		TECN	COMMENT
1.2±5.0±0.7	AAIJ	17T	LHCB	pp at 7, 8 TeV

P VIOLATION PARAMETERS

Observables calculated as average of the triple products for Λ_b^0 and $\overline{\Lambda}_b^0$, which is sensitive to parity violation.

$a_P(\Lambda_b^0 \to p\pi^-\pi^+\pi^-)$

VALUE (%)	DOCUMENT ID		TECN	COMMENT
−4.0 ±0.7 ±0.2	[1] AAIJ	20AB	LHCB	pp at 7, 8, 13 TeV
• • • We do not use the following data for averages, fits, limits, etc. • • •				
−3.71±1.45±0.32	[2] AAIJ	17H	LHCB	Repl. by AAIJ 20AB

[1] Used both triple product asymmetries and the unbinned energy test method.
[2] Measured over full phase space of the decay.

$a_P(\Lambda_b^0 \to pK^-\pi^+\pi^-)$

VALUE (%)	DOCUMENT ID		TECN	COMMENT
−0.60±0.84±0.31	[1] AAIJ	18AG	LHCB	pp at 7, 8 TeV

[1] Measured over full phase space of the decay.

$a_P(\Lambda_b^0 \to pK^-K^+\pi^-)$

VALUE (%)	DOCUMENT ID		TECN	COMMENT
3.62±4.54±0.42	[1] AAIJ	17H	LHCB	pp at 7, 8 TeV

[1] Measured over full phase space of the decay.

$a_P(\Lambda_b^0 \to pK^-K^+K^-)$

VALUE (%)	DOCUMENT ID		TECN	COMMENT
−1.56±1.51±0.32	[1] AAIJ	18AG	LHCB	pp at 7, 8 TeV

[1] Measured over full phase space of the decay.

$a_P(\Lambda_b^0 \to pK^-\mu^+\mu^-)$

VALUE (%)	DOCUMENT ID		TECN	COMMENT
−4.8±5.0±0.7	AAIJ	17T	LHCB	pp at 7, 8 TeV

Λ_b^0 DECAY PARAMETERS

See the note on "Baryon Decay Parameters" in the neutron Listings.

α decay parameter for $\Lambda_b \to J/\psi\Lambda$

VALUE	DOCUMENT ID		TECN	COMMENT
−0.017±0.026 OUR AVERAGE				
$-0.022^{+0.027}_{-0.026}$	[1] AAIJ	20O	LHCB	pp at 7, 8, 13 TeV
−0.14 ±0.14 ±0.10	[2] SIRUNYAN	18R	CMS	pp at 7, 8 TeV
0.30 ±0.16 ±0.06	[3] AAD	14L	ATLS	pp at 7 TeV
• • • We do not use the following data for averages, fits, limits, etc. • • •				
0.05 ±0.17 ±0.07	[4] AAIJ	13AG	LHCB	Repl. by AAIJ 20O

[1] Extracted using a Bayesian analysis. The most probable value is given as −0.022, with a 68% credibility interval [-0.048, 0.005]. Transverse polarizations of Λ_b^0 of −0.004 (68% credibility interval [-0.064, 0.051]), 0.001 (68% credibility interval [-0.035, 0.045]), and 0.032 (68% credibility interval [-0.011, 0.065]) are also reported at 7 TeV, 8 TeV and 13 TeV, respectively. Note that both statistical and systematic uncertainties are included.
[2] An angular analysis of $\Lambda_b \to J/\psi\Lambda$ decay is performed. Note that the sign of α in CMS definition is the opposite to that used by AAIJ 13AG and AAD 14L. Λ_b transverse production polarization of 0.00 ± 0.06 ± 0.06 is also reported, as well as squares of the helicity amplitudes.
[3] An angular analysis of $\Lambda_b \to J/\psi\Lambda$ decay is performed and magnitudes of all helicity amplitudes are also reported.
[4] An angular analysis of $\Lambda_b \to J/\psi\Lambda$ decay is performed and a Λ_b transverse production polarization of 0.06 ± 0.07 ± 0.02 is also reported.

$f_L(\mu\mu)$ longitudinal polarization fraction in $\Lambda_b \to \Lambda\mu^+\mu^-$

VALUE	DOCUMENT ID		TECN	COMMENT
$\mathbf{0.61^{+0.11}_{-0.14}\pm0.03}$	[1] AAIJ	15AE	LHCB	pp at 7, 8 TeV

[1] AAIJ 15AE measurement covers 15.0 < q^2 < 20.0 GeV^2/c^4.

FORWARD-BACKWARD ASYMMETRIES

The forward-backward assymmetry is defined as $A_{FB}(\Lambda_b^0)$ = [N(F) − N(B)] / [N(F) + N(B)], where the forward (F) direction corresponds to a particle (Λ_b^0 or Λ_b^-) sharing valence quark flavors with a beam particle with the same sign of rapidity.

$A_{FB}(\Lambda_b^0 \to J/\psi\Lambda)$

VALUE	DOCUMENT ID		TECN	COMMENT
0.04±0.07±0.02	[1] ABAZOV	15I	D0	pp at 1.96 TeV

[1] The measured asymmetry integrated over rapidity y in the range of 0.1 < |y| < 2.0.

$A^\ell_{FB}(\mu\mu)$ in $\Lambda_b \to \Lambda\mu^+\mu^-$

VALUE	DOCUMENT ID		TECN	COMMENT
−0.39±0.04±0.01	[1] AAIJ	18AP	LHCB	pp at 7, 8, 13 TeV
• • • We do not use the following data for averages, fits, limits, etc. • • •				
−0.05±0.09±0.03	[2] AAIJ	15AE	LHCB	Repl. by AAIJ 18AP.

[1] The measurement covers 15.0 < q^2 < 20.0 GeV^2/c^4.
[2] AAIJ 15AE measurement covers 15.0 < q^2 < 20.0 GeV^2/c^4.

$\Delta(A^\ell_{FB}(\mu\mu))$ in $\Lambda_b \to \Lambda\mu^+\mu^-$

Difference of asymmetries $A^\ell_{FB}(\mu\mu)$ in $\Lambda_b \to \Lambda\mu^+\mu^-$ between Λ_b and $\overline{\Lambda}_b$ decays

VALUE	DOCUMENT ID		TECN	COMMENT
−0.05±0.09±0.03	AAIJ	18AO	LHCB	pp at 7, 8 TeV

$A^h_{FB}(p\pi)$ in $\Lambda_b \to \Lambda(p\pi)\mu^+\mu^-$

VALUE	DOCUMENT ID		TECN	COMMENT
−0.30±0.05±0.02	[1] AAIJ	18AP	LHCB	pp at 7, 8, 13 TeV
• • • We do not use the following data for averages, fits, limits, etc. • • •				
−0.29±0.07±0.03	[2] AAIJ	15AE	LHCB	Repl. by AAIJ 18AP.

[1] The measurement covers 15.0 < q^2 < 20.0 GeV^2/c^4.
[2] AAIJ 15AE measurement covers 15.0 < q^2 < 20.0 GeV^2/c^4.

$A^{\ell h}_{FB}$ in $\Lambda_b \to \Lambda\mu^+\mu^-$

VALUE	DOCUMENT ID		TECN	COMMENT
0.25±0.04±0.01	[1] AAIJ	18AP	LHCB	pp at 7, 8, 13 TeV

[1] The measurement covers 15.0 < q^2 < 20.0 GeV^2/c^4.

Downloaded from https://academic.oup.com/ptep/article/2022/8/083C01/6651666 by KIT Library user on 27 September 2022

$\Lambda_b^0 - \overline{\Lambda}_b^0$ Production Asymmetry

$$A_P(\Lambda_b^0) = [\sigma(\Lambda_b^0) - \sigma(\overline{\Lambda}_b^0)] \,/\, [\sigma(\Lambda_b^0) + \sigma(\overline{\Lambda}_b^0)]$$

$A_P(\Lambda_b^0)$

VALUE (units 10^{-2})	DOCUMENT ID		TECN	COMMENT
1.4 ±0.4 OUR AVERAGE	Error includes scale factor of 1.8.			
1.92±0.35	[1] AAIJ	21AJ	LHCB	pp at 7 TeV
1.09±0.29	[1] AAIJ	21AJ	LHCB	pp at 8 TeV
−0.11±2.53±1.08	[2] AAIJ	17BF	LHCB	pp at 7 TeV
3.44±1.61±0.76	[2] AAIJ	17BF	LHCB	pp at 8 TeV

[1] Integrated over the kinematic range $2 < p_T < 27$ GeV/c and $2.15 < y < 4.10$.

[2] Indirect determination in kinematic range $2 < p_T < 30$ GeV/c and $2.1 < \eta < 4.5$ from production asymmetries of B^+, B^0 and B_s^0.

Λ_b^0 REFERENCES

AAIJ	21AD	PR D104 112008	R. Aaij et al.	(LHCb Collab.)
AAIJ	21AJ	JHEP 2110 060	R. Aaij et al.	(LHCb Collab.)
AAIJ	21B	PL B815 136172	R. Aaij et al.	(LHCb Collab.)
AAIJ	21R	JHEP 2105 095	R. Aaij et al.	(LHCb Collab.)
AAIJ	20AB	PR D102 051101	R. Aaij et al.	(LHCb Collab.)
AAIJ	20AK	PR D102 112012	R. Aaij et al.	(LHCb Collab.)
AAIJ	20M	JHEP 2005 040	R. Aaij et al.	(LHCb Collab.)
AAIJ	20O	JHEP 2006 110	R. Aaij et al.	(LHCb Collab.)
SIRUNYAN	20H	PL B802 135203	A.M. Sirunyan et al.	(CMS Collab.)
AAIJ	19AH	EPJ C79 745	R. Aaij et al.	(LHCb Collab.)
AAIJ	19AN	JHEP 1909 028	R. Aaij et al.	(LHCb Collab.)
AAIJ	19F	JHEP 1903 126	R. Aaij et al.	(LHCb Collab.)
AAIJ	19Z	PRL 123 031801	R. Aaij et al.	(LHCb Collab.)
AAIJ	18AF	JHEP 1808 131	R. Aaij et al.	(LHCb Collab.)
AAIJ	18AG	JHEP 1808 039	R. Aaij et al.	(LHCb Collab.)
AAIJ	18AO	JHEP 1809 145 (errat.)	R. Aaij et al.	(LHCb Collab.)
AAIJ	18AP	JHEP 1809 146	R. Aaij et al.	(LHCb Collab.)
AAIJ	18AW	PL B784 101	R. Aaij et al.	(LHCb Collab.)
AAIJ	18AX	PL B787 124	R. Aaij et al.	(LHCb Collab.)
AAIJ	18Q	JHEP 1802 098	R. Aaij et al.	(LHCb Collab.)
PDG	18	PR D98 030001	M. Tanabashi et al.	(PDG Collab.)
SIRUNYAN	18BY	EPJ C78 457	A.M. Sirunyan et al.	(CMS Collab.)
SIRUNYAN	18R	PR D97 072010	A.M. Sirunyan et al.	(CMS Collab.)
AAIJ	17AM	PRL 119 062001	R. Aaij et al.	(LHCb Collab.)
AAIJ	17BF	PL B774 139	R. Aaij et al.	(LHCb Collab.)
AAIJ	17H	NATP 13 391	R. Aaij et al.	(LHCb Collab.)
AAIJ	17P	JHEP 1704 029	R. Aaij et al.	(LHCb Collab.)
AAIJ	17S	JHEP 1705 030	R. Aaij et al.	(LHCb Collab.)
AAIJ	17T	JHEP 1706 108	R. Aaij et al.	(LHCb Collab.)
AAIJ	16	JHEP 1601 012	R. Aaij et al.	(LHCb Collab.)
AAIJ	16A	CP C40 011001	R. Aaij et al.	(LHCb Collab.)
AAIJ	16J	PL B759 282	R. Aaij et al.	(LHCb Collab.)
AAIJ	16W	JHEP 1605 081	R. Aaij et al.	(LHCb Collab.)
AAIJ	16Y	JHEP 1605 132	R. Aaij et al.	(LHCb Collab.)
AAD	15CH	PL B751 63	G. Aad et al.	(ATLAS Collab.)
AAIJ	15AE	JHEP 1506 115	R. Aaji et al.	(LHCb Collab.)
Also		JHEP 1809 145 (errat.)	R. Aaij et al.	(LHCb Collab.)
AAIJ	15AH	JHEP 1509 006	R. Aaij et al.	(LHCb Collab.)
AAIJ	15BG	NATP 11 743	R. Aaij et al.	(LHCb Collab.)
ABAZOV	15I	PR D91 072008	V.M. Abazov et al.	(D0 Collab.)
AAD	14L	PR D89 092009	G. Aad et al.	(ATLAS Collab.)
AAIJ	14AA	PRL 112 202001	R. Aaij et al.	(LHCb Collab.)
AAIJ	14E	JHEP 1404 114	R. Aaij et al.	(LHCb Collab.)
AAIJ	14H	PR D89 032001	R. Aaij et al.	(LHCb Collab.)
AAIJ	14I	JHEP 1408 143	R. Aaij et al.	(LHCb Collab.)
AAIJ	14K	JHEP 1407 103	R. Aaij et al.	(LHCb Collab.)
AAIJ	14Q	JHEP 1404 087	R. Aaij et al.	(LHCb Collab.)
AAIJ	14U	PL B734 122	R. Aaij et al.	(LHCb Collab.)
AALTONEN	14B	PR D89 072014	T. Aaltonen et al.	(CDF Collab.)
AALTONEN	14P	PRL 113 242001	T. Aaltonen et al.	(CDF Collab.)
PDG	14	CP C38 070001	K. Olive et al.	(PDG Collab.)
AAD	13U	PR D87 032002	G. Aad et al.	(ATLAS Collab.)
AAIJ	13AG	PL B724 27	R. Aaij et al.	(LHCb Collab.)
AAIJ	13AJ	PL B725 25	R. Aaij et al.	(LHCb Collab.)
AAIJ	13AV	PRL 110 182001	R. Aaij et al.	(LHCb Collab.)
AAIJ	13BB	PRL 111 102003	R. Aaij et al.	(LHCb Collab.)
CHATRCHYAN	13AC	JHEP 1307 163	S. Chatrchyan et al.	(CMS Collab.)
AAIJ	12AR	JHEP 1210 037	R. Aaij et al.	(LHCb Collab.)
AAIJ	12E	PL B708 241	R. Aaij et al.	(LHCb Collab.)
AALTONEN	12A	PR D85 032003	T. Aaltonen et al.	(CDF Collab.)
ABAZOV	12U	PR D85 112003	V.M. Abazov et al.	(D0 Collab.)
AAIJ	11E	PR D84 092001	R. Aaij et al.	(LHCb Collab.)
Also		PR D85 039904 (errat.)	R. Aaij et al.	(LHCb Collab.)
AALTONEN	11	PRL 106 121804	T. Aaltonen et al.	(CDF Collab.)
AALTONEN	11AI	PRL 107 201802	T. Aaltonen et al.	(CDF Collab.)
AALTONEN	11N	PRL 106 181802	T. Aaltonen et al.	(CDF Collab.)
ABAZOV	11O	PR D84 031102	V.M. Abazov et al.	(D0 Collab.)
AALTONEN	10B	PRL 104 102002	T. Aaltonen et al.	(CDF Collab.)
AALTONEN	09C	PRL 103 031801	T. Aaltonen et al.	(CDF Collab.)
AALTONEN	09E	PR D79 032001	T. Aaltonen et al.	(CDF Collab.)
ABAZOV	07S	PRL 99 142001	V.M. Abazov et al.	(D0 Collab.)
ABAZOV	07U	PRL 99 182001	V.M. Abazov et al.	(D0 Collab.)
ABULENCIA	07A	PRL 98 122001	A. Abulencia et al.	(FNAL CDF Collab.)
ABULENCIA	07B	PRL 98 122002	A. Abulencia et al.	(FNAL CDF Collab.)
LEITNER	07	NPBPS 174 169	O. Leitner, Z.J. Ajaltouni	
ACOSTA	06	PRL 96 202001	D. Acosta et al.	(CDF Collab.)
ABAZOV	05C	PRL 94 102001	V.M. Abazov et al.	(D0 Collab.)
ACOSTA	05O	PR D72 051104	D. Acosta et al.	(CDF Collab.)
ABDALLAH	04A	PL B585 63	J. Abdallah et al.	(DELPHI Collab.)
ACOSTA	02G	PR D66 112002	D. Acosta et al.	(CDF Collab.)
ABREU	99W	EPJ C10 185	P. Abreu et al.	(DELPHI Collab.)
ACKERSTAFF	98G	PL B426 161	K. Ackerstaff et al.	(OPAL Collab.)
BARATE	98D	EPJ C2 197	R. Barate et al.	(ALEPH Collab.)
ABE	97B	PR D55 1142	F. Abe et al.	(CDF Collab.)
ABE	96M	PRL 77 1439	F. Abe et al.	(CDF Collab.)
ABREU	96D	ZPHY C71 199	P. Abreu et al.	(DELPHI Collab.)
ABREU	96N	PL B374 351	P. Abreu et al.	(DELPHI Collab.)
ADAM	96D	ZPHY C72 207	W. Adam et al.	(DELPHI Collab.)
BUSKULIC	96L	PL B380 442	D. Buskulic et al.	(ALEPH Collab.)
BUSKULIC	96V	PL B384 471	D. Buskulic et al.	(ALEPH Collab.)
PDG	96	PR D54 1	R. M. Barnett et al.	(PDG Collab.)
ABREU	95S	ZPHY C68 375	P. Abreu et al.	(DELPHI Collab.)
AKERS	95K	PL B353 402	R. Akers et al.	(OPAL Collab.)
BUSKULIC	95L	PL B357 685	D. Buskulic et al.	(ALEPH Collab.)
ABE	93B	PR D47 2639	F. Abe et al.	(CDF Collab.)
BUSKULIC	92E	PL B294 145	D. Buskulic et al.	(ALEPH Collab.)
ALBAJAR	91E	PL B273 540	C. Albajar et al.	(UA1 Collab.)
BARI	91	NC 104A 1787	G. Bari et al.	(CERN R422 Collab.)
ARENTON	86	NP B274 707	M.W. Arenton et al.	(ARIZ, NDAM, VAND)
BASILE	81	LNC 31 97	M. Basile et al.	(CERN R415 Collab.)

$\Lambda_b(5912)^0$

$J^P = \frac{1}{2}^-$ Status: ***

Quantum numbers are based on quark model expectations.

$\Lambda_b(5912)^0$ MASS

VALUE (MeV)	DOCUMENT ID		TECN	COMMENT
5912.19±0.17 OUR AVERAGE				
5912.19±0.03±0.17	[1] AAIJ	20Q	LHCB	pp at 7, 8, 13 TeV
5912.32±0.12±0.17	[2] SIRUNYAN	20K	CMS	pp at 13 TeV
• • • We do not use the following data for averages, fits, limits, etc. • • •				
5912.20±0.13±0.17	[3,4] AAIJ	12AL	LHCB	Repl. by AAIJ 20Q

[1] AAIJ 20Q measures $m(\Lambda_b(5912)^0) - m(\Lambda_b^0) = 292.589 \pm 0.029 \pm 0.010$ MeV. We have adjusted the measurement to our best value of $m(\Lambda_b^0) = 5619.60 \pm 0.17$ MeV. Our first error is their experiment's error and our second error is the systematic error from using our best values.

[2] SIRUNYAN 20K measures $m(\Lambda_b(5912)^0) - m(\Lambda_b^0) = 292.72 \pm 0.12 \pm 0.01$ MeV. We have adjusted the measurement to our best value of $m(\Lambda_b^0) = 5619.60 \pm 0.17$ MeV. Our first error is their experiment's error and our second error is the systematic error from using our best values.

[3] Observed in $\Lambda_b(5912)^0 \to \Lambda_b^0 \pi^+ \pi^-$ decays with 17.6 ± 4.8 candidates with a significance of 5.2 sigma.

[4] AAIJ 12AL measures $m(\Lambda_b(5912)^0) - m(\Lambda_b^0) = 292.60 \pm 0.12 \pm 0.04$ MeV. We have adjusted the measurement to our best value of $m(\Lambda_b^0) = 5619.60 \pm 0.17$ MeV. Our first error is their experiment's error and our second error is the systematic error from using our best values.

$\Lambda_b(5912)^0$ WIDTH

VALUE (MeV)	CL%	DOCUMENT ID		TECN	COMMENT
<0.25	90	AAIJ	20Q	LHCB	pp at 7, 8, 13 TeV
• • • We do not use the following data for averages, fits, limits, etc. • • •					
<0.66	90	AAIJ	12AL	LHCB	Repl. by AAIJ 20Q

$\Lambda_b(5912)^0$ DECAY MODES

	Mode	Fraction (Γ_i/Γ)
Γ_1	$\Lambda_b^0 \pi^+ \pi^-$	seen

$\Lambda_b(5912)^0$ BRANCHING RATIOS

$\Gamma(\Lambda_b^0 \pi^+ \pi^-)/\Gamma_{total}$ — Γ_1/Γ

VALUE	DOCUMENT ID		TECN	COMMENT
seen	AAIJ	20Q	LHCB	pp at 7, 8, 13 TeV
seen	SIRUNYAN	20K	CMS	pp at 13 TeV
seen	AAIJ	12AL	LHCB	pp at 7 TeV

$\Lambda_b(5912)^0$ REFERENCES

AAIJ	20Q	JHEP 2006 136	R. Aaij et al.	(LHCb Collab.)
SIRUNYAN	20K	PL B803 135345	A.M. Sirunyan et al.	(CMS Collab.)
AAIJ	12AL	PRL 109 172003	R. Aaij et al.	(LHCb Collab.)

$\Lambda_b(5920)^0$

$J^P = \frac{3}{2}^-$ Status: ***

Quantum numbers are based on quark model expectations.

$\Lambda_b(5920)^0$ MASS

VALUE (MeV)	DOCUMENT ID		TECN	COMMENT
5920.09±0.17 OUR AVERAGE				
5920.09±0.02±0.17	[1] AAIJ	20Q	LHCB	pp at 7, 8, 13 TeV
5920.16±0.07±0.17	[2] SIRUNYAN	20K	CMS	pp at 13 TeV
• • • We do not use the following data for averages, fits, limits, etc. • • •				
5919.4 ±0.5 ±0.2	[3,4] AALTONEN	13V	CDF	$p\overline{p}$ at 1.96 TeV
5920.00±0.09±0.17	[5,6] AAIJ	12AL	LHCB	Repl. by AAIJ 20Q

[1] AAIJ 20Q measures $m(\Lambda_b(5920)^0) - m(\Lambda_b^0) = 300.492 \pm 0.019 \pm 0.010$ MeV. We have adjusted the measurement to our best value of $m(\Lambda_b^0) = 5619.60 \pm 0.17$ MeV. Our first error is their experiment's error and our second error is the systematic error from using our best values.

[2] SIRUNYAN 20K measures $m(\Lambda_b(5920)^0) - m(\Lambda_b^0) = 300.56 \pm 0.07 \pm 0.01$ MeV. We have adjusted the measurement to our best value of $m(\Lambda_b^0) = 5619.60 \pm 0.17$ MeV. Our first error is their experiment's error and our second error is the systematic error from using our best values.

Downloaded from https://academic.oup.com/ptep/article/2022/8/083C01/6651666 by KIT Library user on 27 September 2022

[3] Measured in $\Lambda_b(5920)^0 \to \Lambda_b^0 \pi^+ \pi^-$ decays with $17.3^{+5.3}_{-4.6}$ events, with a significance of 3.5 sigma.
[4] AALTONEN 13V measures $m(\Lambda_b(5920)^0) - m(\Lambda_b^0) - 2m(\pi) = 20.68 \pm 0.35 \pm 0.30$ MeV. We have adjusted the measurement to our best values of $m(\Lambda_b^0) = 5619.60 \pm 0.17$ MeV and $m(\pi) = 139.57039 \pm 0.00018$ MeV. Our first error is their experiment's error and our second error is the systematic error from using our best values.
[5] Observed in $\Lambda_b(5920)^0 \to \Lambda_b^0 \pi^+ \pi^-$ decays with 52.5 ± 8.1 candidates with a significance of 10.2 sigma.
[6] AAIJ 12AL measures $m(\Lambda_b(5920)^0) - m(\Lambda_b^0) = 300.40 \pm 0.08 \pm 0.04$ MeV. We have adjusted the measurement to our best value of $m(\Lambda_b^0) = 5619.60 \pm 0.17$ MeV. Our first error is their experiment's error and our second error is the systematic error from using our best values.

$\Lambda_b(5920)^0$ WIDTH

VALUE (MeV)	CL%	DOCUMENT ID		TECN	COMMENT
<0.19	90	AAIJ	20Q	LHCB	pp at 7, 8, 13 TeV
• • • We do not use the following data for averages, fits, limits, etc. • • •					
<0.63	90	AAIJ	12AL	LHCB	Repl. by AAIJ 20Q

$\Lambda_b(5920)^0$ DECAY MODES

	Mode	Fraction (Γ_i/Γ)
Γ_1	$\Lambda_b^0 \pi^+ \pi^-$	seen

$\Lambda_b(5920)^0$ BRANCHING RATIOS

$\Gamma(\Lambda_b^0 \pi^+ \pi^-)/\Gamma_{total}$ — Γ_1/Γ

VALUE	DOCUMENT ID		TECN	COMMENT
seen	AAIJ	20Q	LHCB	pp at 7, 8, 13 TeV
seen	SIRUNYAN	20K	LHCB	pp at 13 TeV
seen	AALTONEN	13V	CDF	$p\overline{p}$ at 1.96 TeV
seen	AAIJ	12AL	LHCB	pp at 7 TeV

$\Lambda_b(5920)^0$ REFERENCES

AAIJ	20Q	JHEP 2006 136	R. Aaij *et al.*	(LHCb Collab.)
SIRUNYAN	20K	PL B803 135345	A.M. Sirunyan *et al.*	(CMS Collab.)
AALTONEN	13V	PR D88 071101	T. Aaltonen *et al.*	(CDF Collab.)
AAIJ	12AL	PRL 109 172003	R. Aaij *et al.*	(LHCb Collab.)

$\Lambda_b(6070)^0$

$J^P = \frac{1}{2}^+$ Status: ***

Quantum numbers are based on quark model expectations.

$\Lambda_b(6070)^0$ MASS

VALUE (MeV)	DOCUMENT ID		TECN	COMMENT
6072.3±2.9±0.2	[1] AAIJ	20Q	LHCB	pp at 7, 8, 13 TeV

[1] AAIJ 20Q measures $m(\Lambda_b(6070)^0) - m(\Lambda_b^0) = 452.7 \pm 2.9 \pm 0.5$ MeV. We have adjusted the measurement to our best value of $m(\Lambda_b^0) = 5619.60 \pm 0.17$ MeV. Our first error is their experiment's error and our second error is the systematic error from using our best values.

$\Lambda_b(6070)^0$ WIDTH

VALUE (MeV)	DOCUMENT ID		TECN	COMMENT
72±11±2	AAIJ	20Q	LHCB	pp at 7, 8, 13 TeV

$\Lambda_b(6070)^0$ DECAY MODES

	Mode	Fraction (Γ_i/Γ)
Γ_1	$\Lambda_b^0 \pi^+ \pi^-$	seen

$\Lambda_b(6070)^0$ BRANCHING RATIOS

$\Gamma(\Lambda_b^0 \pi^+ \pi^-)/\Gamma_{total}$ — Γ_1/Γ

VALUE	DOCUMENT ID		TECN	COMMENT
seen	AAIJ	20Q	LHCB	pp at 7, 8, 13 TeV

$\Lambda_b(6070)^0$ REFERENCES

AAIJ	20Q	JHEP 2006 136	R. Aaij *et al.*	(LHCb Collab.)

$\Lambda_b(6146)^0$

$J^P = \frac{3}{2}^+$ Status: ***

Quantum numbers are based on quark model expectations.

$\Lambda_b(6146)^0$ MASS

$\Lambda_b(6146)^0$ MASS

VALUE (MeV)	DOCUMENT ID		TECN	COMMENT
6146.2 ±0.4 OUR AVERAGE				
6146.5 ±2.1 ±0.2	[1] SIRUNYAN	20K	CMS	pp at 13 TeV
6146.17±0.33±0.27	[2] AAIJ	19AJ	LHCB	pp at 7, 8, 13 TeV

[1] SIRUNYAN 20K measures $m(\Lambda_b(6146)^0) - m(\Lambda_b^0) = 526.9 \pm 1.9 \pm 0.8$ MeV. We have adjusted the measurement to our best value of $m(\Lambda_b^0) = 5619.60 \pm 0.17$ MeV. Our first error is their experiment's error and our second error is the systematic error from using our best values.
[2] Observed in $\Lambda_b^0 \pi^+ \pi^-$ mode.

$m_{\Lambda_b(6146)^0} - m_{\Lambda_b^0}$

VALUE (MeV)	DOCUMENT ID		TECN	COMMENT
526.55±0.33±0.10	[1] AAIJ	19AJ	LHCB	pp at 7, 8, 13 TeV

[1] Observed in $\Lambda_b^0 \pi^+ \pi^-$ mode.

$\Lambda_b(6146)^0$ WIDTH

VALUE (MeV)	DOCUMENT ID		TECN	COMMENT
2.9±1.3±0.3	[1] AAIJ	19AJ	LHCB	pp at 7, 8, 13 TeV

[1] Observed in $\Lambda_b^0 \pi^+ \pi^-$ mode.

$\Lambda_b(6146)^0$ DECAY MODES

	Mode	Fraction (Γ_i/Γ)
Γ_1	$\Lambda_b^0 \pi^+ \pi^-$	seen

$\Lambda_b(6146)^0$ BRANCHING RATIOS

$\Gamma(\Lambda_b^0 \pi^+ \pi^-)/\Gamma_{total}$ — Γ_1/Γ

VALUE	DOCUMENT ID		TECN	COMMENT
seen	SIRUNYAN	20K	LHCB	pp at 13 TeV
seen	AAIJ	19AJ	LHCB	pp at 7, 8, 13 TeV

$\Lambda_b(6146)^0$ REFERENCES

SIRUNYAN	20K	PL B803 135345	A.M. Sirunyan *et al.*	(CMS Collab.)
AAIJ	19AJ	PRL 123 152001	R. Aaij *et al.*	(LHCb Collab.)

$\Lambda_b(6152)^0$

$J^P = \frac{5}{2}^+$ Status: ***

Quantum numbers are based on quark model expectations.

$\Lambda_b(6152)^0$ MASS

$\Lambda_b(6152)^0$ MASS

VALUE (MeV)	DOCUMENT ID		TECN	COMMENT
6152.5 ±0.4 OUR AVERAGE				
6152.7 ±1.2 ±0.2	[1] SIRUNYAN	20K	CMS	pp at 13 TeV
6152.51±0.26±0.27	[2] AAIJ	19AJ	LHCB	pp at 7, 8, 13 TeV

[1] SIRUNYAN 20K measures $m(\Lambda_b(6152)^0) - m(\Lambda_b^0) = 533.1 \pm 1.1 \pm 0.4$ MeV. We have adjusted the measurement to our best value of $m(\Lambda_b^0) = 5619.60 \pm 0.17$ MeV. Our first error is their experiment's error and our second error is the systematic error from using our best values.
[2] Observed in $\Lambda_b^0 \pi^+ \pi^-$ mode.

$m_{\Lambda_b(6152)^0} - m_{\Lambda_b^0}$

VALUE (MeV)	DOCUMENT ID		TECN	COMMENT
532.89±0.26±0.10	[1] AAIJ	19AJ	LHCB	pp at 7, 8, 13 TeV

[1] Observed in $\Lambda_b^0 \pi^+ \pi^-$ mode.

$m_{\Lambda_b(6152)^0} - m_{\Lambda_b(6146)^0}$

VALUE (MeV)	DOCUMENT ID		TECN	COMMENT
6.34±0.32±0.02	AAIJ	19AJ	LHCB	pp at 7, 8, 13 TeV

$\Lambda_b(6152)^0$ WIDTH

VALUE (MeV)	DOCUMENT ID		TECN	COMMENT
2.1±0.8±0.3	[1] AAIJ	19AJ	LHCB	pp at 7, 8, 13 TeV

[1] Observed in $\Lambda_b^0 \pi^+ \pi^-$ mode.

$\Lambda_b(6152)^0$ DECAY MODES

	Mode	Fraction (Γ_i/Γ)
Γ_1	$\Lambda_b^0 \pi^+ \pi^-$	seen

Downloaded from https://academic.oup.com/ptep/article/2022/8/083C01/6651666 by KIT Library user on 27 September 2022

$\Lambda_b(6152)^0$ BRANCHING RATIOS

$\Gamma(\Lambda_b^0\pi^+\pi^-)/\Gamma_{total}$ — Γ_1/Γ

VALUE	DOCUMENT ID		TECN	COMMENT
seen	SIRUNYAN	20K	LHCB	pp at 13 TeV
seen	AAIJ	19AJ	LHCB	pp at 7, 8, 13 TeV

$\Lambda_b(6152)^0$ REFERENCES

SIRUNYAN	20K	PL B803 135345	A.M. Sirunyan *et al.*	(CMS Collab.)
AAIJ	19AJ	PRL 123 152001	R. Aaij *et al.*	(LHCb Collab.)

Σ_b

$I(J^P) = 1(\frac{1}{2}^+)$ Status: ***
I, J, P need confirmation.

In the quark model Σ_b^+, Σ_b^0, Σ_b^- are an isotriplet (uub, udb, ddb) state. The lowest Σ_b ought to have $J^P = 1/2^+$. None of I, J, or P have actually been measured.

Σ_b MASS

Σ_b^+ MASS

VALUE (MeV)	DOCUMENT ID		TECN	COMMENT
5810.56±0.25 OUR AVERAGE				
5810.55±0.11±0.23	[1] AAIJ	19A	LHCB	pp at 7, 8 TeV
5811.3 $^{+0.9}_{-0.8}$ ±1.7	[2] AALTONEN	12F	CDF	$p\overline{p}$ at 1.96 TeV
• • • We do not use the following data for averages, fits, limits, etc. • • •				
5807.8 $^{+2.0}_{-2.2}$ ±1.7	[3] AALTONEN	07K	CDF	Repl. by AALTONEN 12F

[1] Measured using fully reconstructed $\Lambda_b^0 \to \Lambda_c^+\pi^-$ and $\Lambda_c^+ \to pK^-\pi^+$ decays.
[2] Measured using fully reconstructed $\Lambda_b^0 \to \Lambda_c^+\pi^-$ and $\Lambda_c^+ \to K^-\pi^+$ decays.
[3] Observed four $\Lambda_b^0\pi^\pm$ resonances in the fully reconstructed decay mode $\Lambda_b^0 \to \Lambda_c^+\pi^-$, where $\Lambda_c^+ \to pK^-\pi^+$.

Σ_b^- MASS

VALUE (MeV)	DOCUMENT ID		TECN	COMMENT
5815.64±0.27 OUR AVERAGE				
5815.64±0.14±0.24	[1] AAIJ	19A	LHCB	pp at 7, 8 TeV
5815.5 $^{+0.6}_{-0.5}$ ±1.7	[2] AALTONEN	12F	CDF	$p\overline{p}$ at 1.96 TeV
• • • We do not use the following data for averages, fits, limits, etc. • • •				
5815.2 ±1.0 ±1.7	[3] AALTONEN	07K	CDF	Repl. by AALTONEN 12F

[1] Measured using fully reconstructed $\Lambda_b^0 \to \Lambda_c^+\pi^-$ and $\Lambda_c^+ \to pK^-\pi^+$ decays.
[2] Measured using fully reconstructed $\Lambda_b^0 \to \Lambda_c^+\pi^-$ and $\Lambda_c^+ \to K^-\pi^+$ decays.
[3] Observed four $\Lambda_b^0\pi^\pm$ resonances in the fully reconstructed decay mode $\Lambda_b^0 \to \Lambda_c^+\pi^-$, where $\Lambda_c^+ \to pK^-\pi^+$.

$m_{\Sigma_b^+} - m_{\Sigma_b^-}$

VALUE (MeV)	DOCUMENT ID		TECN	COMMENT
−5.06±0.18 OUR AVERAGE				
−5.09±0.18±0.01	[1] AAIJ	19A	LHCB	pp at 7, 8 TeV
−4.2 $^{+1.1}_{-1.0}$ ±0.1	[2] AALTONEN	12F	CDF	$p\overline{p}$ at 1.96 TeV

[1] Measured using fully reconstructed $\Lambda_b^0 \to \Lambda_c^+\pi^-$ and $\Lambda_c^+ \to pK^-\pi^+$ decays.
[2] Measured using fully reconstructed $\Lambda_b^0 \to \Lambda_c^+\pi^-$ and $\Lambda_c^+ \to K^-\pi^+$ decays.

Σ_b WIDTH

Σ_b^+ WIDTH

VALUE (MeV)	DOCUMENT ID		TECN	COMMENT
5.0 ±0.5 OUR AVERAGE				
4.83±0.31±0.37	[1] AAIJ	19A	LHCB	pp at 7, 8 TeV
9.7 $^{+3.8}_{-2.8}$ $^{+1.2}_{-1.1}$	[2] AALTONEN	12F	CDF	$p\overline{p}$ at 1.96 TeV

[1] Measured using fully reconstructed $\Lambda_b^0 \to \Lambda_c^+\pi^-$ and $\Lambda_c^+ \to pK^-\pi^+$ decays.
[2] Measured using fully reconstructed $\Lambda_b^0 \to \Lambda_c^+\pi^-$ and $\Lambda_c^+ \to K^-\pi^+$ decays.

Σ_b^- WIDTH

VALUE (MeV)	DOCUMENT ID		TECN	COMMENT
5.3 ±0.5 OUR AVERAGE				
5.33±0.42±0.37	[1] AAIJ	19A	LHCB	pp at 7, 8 TeV
4.9 $^{+3.1}_{-2.1}$ ±1.1	[2] AALTONEN	12F	CDF	$p\overline{p}$ at 1.96 TeV

[1] Measured using fully reconstructed $\Lambda_b^0 \to \Lambda_c^+\pi^-$ and $\Lambda_c^+ \to pK^-\pi^+$ decays.
[2] Measured using fully reconstructed $\Lambda_b^0 \to \Lambda_c^+\pi^-$ and $\Lambda_c^+ \to K^-\pi^+$ decays.

Σ_b DECAY MODES

	Mode	Fraction (Γ_i/Γ)
Γ_1	$\Lambda_b^0\pi$	dominant

Σ_b BRANCHING RATIOS

$\Gamma(\Lambda_b^0\pi)/\Gamma_{total}$ — Γ_1/Γ

VALUE	DOCUMENT ID		TECN	COMMENT
dominant	AALTONEN	07K	CDF	$p\overline{p}$ at 1.96 TeV

Σ_b REFERENCES

AAIJ	19A	PRL 122 012001	R. Aaij *et al.*	(LHCb Collab.)
AALTONEN	12F	PR D85 092011	T. Aaltonen *et al.*	(CDF Collab.)
AALTONEN	07K	PRL 99 202001	T. Aaltonen *et al.*	(CDF Collab.)

Σ_b^*

$I(J^P) = 1(\frac{3}{2}^+)$ Status: ***
I, J, P need confirmation.

I, J, P need confirmation. Quantum numbers shown are quark-model predictions.

Σ_b^* MASS

Σ_b^{*+} MASS

VALUE (MeV)	DOCUMENT ID		TECN	COMMENT
5830.32±0.27 OUR AVERAGE				
5830.28±0.14±0.24	[1] AAIJ	19A	LHCB	pp at 7, 8 TeV
5832.1 ±0.7 $^{+1.7}_{-1.8}$	[2] AALTONEN	12F	CDF	$p\overline{p}$ at 1.96 TeV

[1] Measured using fully reconstructed $\Lambda_b^0 \to \Lambda_c^+\pi^-$ and $\Lambda_c^+ \to pK^-\pi^+$ decays.
[2] Measured using fully reconstructed $\Lambda_b^0 \to \Lambda_c^+\pi^-$ and $\Lambda_c^+ \to K^-\pi^+$ decays.

Σ_b^{*-} MASS

VALUE (MeV)	DOCUMENT ID		TECN	COMMENT
5834.74±0.30 OUR AVERAGE				
5834.73±0.17±0.25	[1] AAIJ	19A	LHCB	pp at 7, 8 TeV
5835.1 ±0.6 $^{+1.7}_{-1.8}$	[2] AALTONEN	12F	CDF	$p\overline{p}$ at 1.96 TeV

[1] Measured using fully reconstructed $\Lambda_b^0 \to \Lambda_c^+\pi^-$ and $\Lambda_c^+ \to pK^-\pi^+$ decays.
[2] Measured using fully reconstructed $\Lambda_b^0 \to \Lambda_c^+\pi^-$ and $\Lambda_c^+ \to K^-\pi^+$ decays.

$m_{\Sigma_b^{*+}} - m_{\Sigma_b^{*-}}$

VALUE (MeV)	DOCUMENT ID		TECN	COMMENT
−4.37±0.33 OUR AVERAGE Error includes scale factor of 1.6.				
−4.45±0.22±0.01	[1] AAIJ	19A	LHCB	pp at 7, 8 TeV
−3.0 $^{+1.0}_{-0.9}$ ±0.1	[2] AALTONEN	12F	CDF	$p\overline{p}$ at 1.96 TeV

[1] Measured using fully reconstructed $\Lambda_b^0 \to \Lambda_c^+\pi^-$ and $\Lambda_c^+ \to pK^-\pi^+$ decays.
[2] Measured using fully reconstructed $\Lambda_b^0 \to \Lambda_c^+\pi^-$ and $\Lambda_c^+ \to K^-\pi^+$ decays.

$m_{\Sigma_b^{*+}} - m_{\Sigma_b^+}$

VALUE	DOCUMENT ID		TECN	COMMENT
19.73±0.18±0.01	[1] AAIJ	19A	LHCB	pp at 7, 8 TeV

[1] Measured using fully reconstructed $\Lambda_b^0 \to \Lambda_c^+\pi^-$ and $\Lambda_c^+ \to pK^-\pi^+$ decays.

$m_{\Sigma_b^{*-}} - m_{\Sigma_b^-}$

VALUE	DOCUMENT ID		TECN	COMMENT
19.09±0.22±0.02	[1] AAIJ	19A	LHCB	pp at 7, 8 TeV

[1] Measured using fully reconstructed $\Lambda_b^0 \to \Lambda_c^+\pi^-$ and $\Lambda_c^+ \to pK^-\pi^+$ decays.

Σ_b^* WIDTH

Σ_b^{*+} WIDTH

VALUE (MeV)	DOCUMENT ID		TECN	COMMENT
9.4 ±0.5 OUR AVERAGE				
9.34±0.47±0.26	[1] AAIJ	19A	LHCB	pp at 7, 8 TeV
11.5 $^{+2.7}_{-2.2}$ $^{+1.0}_{-1.5}$	[2] AALTONEN	12F	CDF	$p\overline{p}$ at 1.96 TeV

[1] Measured using fully reconstructed $\Lambda_b^0 \to \Lambda_c^+\pi^-$ and $\Lambda_c^+ \to pK^-\pi^+$ decays.
[2] Measured using fully reconstructed $\Lambda_b^0 \to \Lambda_c^+\pi^-$ and $\Lambda_c^+ \to K^-\pi^+$ decays.

Σ_b^{*-} WIDTH

VALUE (MeV)	DOCUMENT ID		TECN	COMMENT
10.4 ±0.8 OUR AVERAGE Error includes scale factor of 1.3.				
10.68±0.60±0.33	[1] AAIJ	19A	LHCB	pp at 7, 8 TeV

Downloaded from https://academic.oup.com/ptep/article/2022/8/083C01/6651666 by KIT Library user on 27 September 2022

$7.5\ ^{+2.2}_{-1.8}\ ^{+0.9}_{-1.4}$	[2] AALTONEN	12F	CDF	$p\overline{p}$ at 1.96 TeV

[1] Measured using fully reconstructed $\Lambda_b^0 \to \Lambda_c^+ \pi^-$ and $\Lambda_c^+ \to p K^- \pi^+$ decays.
[2] Measured using fully reconstructed $\Lambda_b^0 \to \Lambda_c^+ \pi^-$ and $\Lambda_c^+ \to K^- \pi^+$ decays.

$m_{\Sigma_b^*} - m_{\Sigma_b}$

VALUE (MeV)	DOCUMENT ID		TECN	COMMENT
$\mathbf{21.2^{+2.0}_{-1.9}{}^{+0.4}_{-0.3}}$	[1] AALTONEN	07K	CDF	$p\overline{p}$ at 1.96 TeV

[1] Observed four $\Lambda_b^0 \pi^\pm$ resonances in the fully reconstructed decay mode $\Lambda_b^0 \to \Lambda_c^+ \pi^-$, where $\Lambda_c^+ \to p K^- \pi^+$. Assumes $m_{\Sigma_b^{*+}} - m_{\Sigma_b^+} = m_{\Sigma_b^{*-}} - m_{\Sigma_b^-}$

Σ_b^* DECAY MODES

	Mode	Fraction (Γ_i/Γ)
Γ_1	$\Lambda_b^0 \pi$	dominant

Σ_b^* BRANCHING RATIOS

$\Gamma(\Lambda_b^0 \pi)/\Gamma_{total}$ — Γ_1/Γ

VALUE	DOCUMENT ID		TECN	COMMENT
dominant	AALTONEN	07K	CDF	$p\overline{p}$ at 1.96 TeV

Σ_b^* REFERENCES

AAIJ	19A	PRL 122 012001	R. Aaij *et al.*	(LHCb Collab.)
AALTONEN	12F	PR D85 092011	T. Aaltonen *et al.*	(CDF Collab.)
AALTONEN	07K	PRL 99 202001	T. Aaltonen *et al.*	(CDF Collab.)

$\Sigma_b(6097)^+$

$J^P = ?^?$ Status: ***

$\Sigma_b(6097)^+$ MASS

VALUE (MeV)	DOCUMENT ID		TECN	COMMENT
6095.8±1.7±0.4	[1] AAIJ	19A	LHCB	pp at 7, 8 TeV

[1] Measured using fully reconstructed $\Lambda_b^0 \to \Lambda_c^+ \pi^-$ and $\Lambda_c^+ \to p K^- \pi^+$ decays.

$m_{\Sigma_b(6097)^\pm} - m_{\Sigma_b(6097)^-}$

VALUE	DOCUMENT ID		TECN	COMMENT
-2.2 +-2.4 +-0.3 MeV	[1] AAIJ	19A	LHCB	pp at 7, 8 TeV

[1] Measured using fully reconstructed $\Lambda_b^0 \to \Lambda_c^+ \pi^-$ and $\Lambda_c^+ \to p K^- \pi^+$ decays.

$\Sigma_b(6097)^+$ WIDTH

VALUE (MeV)	DOCUMENT ID		TECN	COMMENT
31.0±5.5±0.7	[1] AAIJ	19A	LHCB	pp at 7, 8 TeV

[1] Measured using fully reconstructed $\Lambda_b^0 \to \Lambda_c^+ \pi^-$ and $\Lambda_c^+ \to p K^- \pi^+$ decays.

$\Sigma_b(6097)^+$ DECAY MODES

	Mode	Fraction (Γ_i/Γ)
Γ_1	$\Lambda_b \pi^+ \times B(b \to \Sigma_b(6097)^+)$	seen

$\Sigma_b(6097)^+$ BRANCHING RATIOS

$\Gamma(\Lambda_b \pi^+ \times B(b \to \Sigma_b(6097)^+))/\Gamma_{total}$ — Γ_1/Γ

VALUE	DOCUMENT ID		TECN	COMMENT
seen	AAIJ	19A	LHCB	pp at 7, 8 TeV

$\Sigma_b(6097)^+$ REFERENCES

AAIJ	19A	PRL 122 012001	R. Aaij *et al.*	(LHCb Collab.)

$\Sigma_b(6097)^-$

$J^P = ?^?$ Status: ***

$\Sigma_b(6097)^-$ MASS

VALUE (MeV)	DOCUMENT ID		TECN	COMMENT
6098.0±1.7±0.5	[1] AAIJ	19A	LHCB	pp at 7, 8 TeV

[1] Measured using fully reconstructed $\Lambda_b^0 \to \Lambda_c^+ \pi^-$ and $\Lambda_c^+ \to p K^- \pi^+$ decays.

$\Sigma_b(6097)^-$ WIDTH

VALUE (MeV)	DOCUMENT ID		TECN	COMMENT
28.9±4.2±0.9	[1] AAIJ	19A	LHCB	pp at 7, 8 TeV

[1] Measured using fully reconstructed $\Lambda_b^0 \to \Lambda_c^+ \pi^-$ and $\Lambda_c^+ \to p K^- \pi^+$ decays.

$\Sigma_b(6097)^-$ DECAY MODES

	Mode	Fraction (Γ_i/Γ)
Γ_1	$\Lambda_b \pi^- \times B(b \to \Sigma_b(6097)^-)$	seen

$\Sigma_b(6097)^-$ BRANCHING RATIOS

$\Gamma(\Lambda_b \pi^- \times B(b \to \Sigma_b(6097)^-))/\Gamma_{total}$ — Γ_1/Γ

VALUE	DOCUMENT ID		TECN	COMMENT
seen	AAIJ	19A	LHCB	pp at 7, 8 TeV

$\Sigma_b(6097)^-$ REFERENCES

AAIJ	19A	PRL 122 012001	R. Aaij *et al.*	(LHCb Collab.)

Ξ_b^-

$I(J^P) = \frac{1}{2}(\frac{1}{2}^+)$ Status: ***
I, J, P need confirmation.

In the quark model, Ξ_b^0 and Ξ_b^- are an isodoublet (usb, dsb) state; the lowest Ξ_b^0 and Ξ_b^- ought to have $J^P = 1/2^+$. None of I, J, or P have actually been measured.

Ξ_b^- MASS

Ξ_b^- MASS

VALUE (MeV)	DOCUMENT ID		TECN	COMMENT
5797.0 ± 0.6 OUR AVERAGE Error includes scale factor of 1.7. See the ideogram below.				
5796.70± 0.39± 0.23	AAIJ	19AB	LHCB	pp at 7, 8 and 13 TeV
5797.72± 0.46± 0.31	[1] AAIJ	14BJ	LHCB	pp at 7, 8 TeV
5793.4 ± 1.8 ± 0.7	[2] AALTONEN	14B	CDF	$p\overline{p}$ at 1.96 TeV
5774 ±11 ±15	[3] ABAZOV	07K	D0	$p\overline{p}$ at 1.96 TeV
• • • We do not use the following data for averages, fits, limits, etc. • • •				
5795.8 ± 0.9 ± 0.4	[4] AAIJ	13AV	LHCB	Repl. by AAIJ 19AB
5796.7 ± 5.1 ± 1.4	[5] AALTONEN	11X	CDF	Repl. by AALTONEN 14B
5790.9 ± 2.6 ± 0.8	[6] AALTONEN	09AP	CDF	Repl. by AALTONEN 14B
5792.9 ± 2.5 ± 1.7	[7] AALTONEN	07A	CDF	Repl. by AALTONEN 09AP

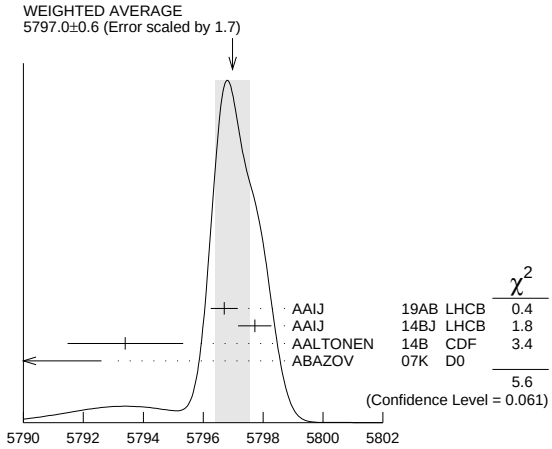

[1] Reconstructed in $\Xi_b^- \to \Xi_c^0 \pi^-$, $\Xi_c^0 \to p K^- K^- \pi^+$ decays. Reference Λ_b^0 mass 5619.30 ± 0.34 MeV from AAIJ 14AA.
[2] Uses $\Xi_b^- \to J/\psi \Xi^-$ and $\Xi_c^0 \pi^-$ decays.
[3] Observed in $\Xi_b^- \to J/\psi \Xi^-$ decays with $15.2 \pm 4.4^{+1.9}_{-0.4}$ candidates, a significance of 5.5 sigma.
[4] Measured in $\Xi_b^- \to J/\psi \Xi^-$ decays.
[5] Measured in $\Xi_b^- \to \Xi_c^0 \pi^-$ with $25.8^{+5.5}_{-5.2}$ candidates.
[6] Measured in $\Xi_b^- \to J/\psi \Xi^-$ decays with 66^{+14}_{-9} candidates.
[7] Observed in $\Xi_b^- \to J/\psi \Xi^-$ decays with 17.5 ± 4.3 candidates, a significance of 7.7 sigma.

Downloaded from https://academic.oup.com/ptep/article/2022/8/083C01/6651666 by KIT Library user on 27 September 2022

$m_{\Xi_b^-} - m_{\Lambda_b^0}$

VALUE (MeV)	DOCUMENT ID		TECN	COMMENT
177.46±0.31 OUR AVERAGE	Error includes scale factor of 1.3.			See the ideogram below.
177.71±0.24±0.16	[1] AAIJ	21	LHCB	pp at 7, 8, 13 TeV
177.08±0.47±0.16	[2] AAIJ	17BE	LHCB	pp at 7, 8 TeV
176.2 ±0.9 ±0.1	[3] AAIJ	13AV	LHCB	pp at 7 TeV
• • • We do not use the following data for averages, fits, limits, etc. • • •				
177.73±0.33±0.14	[4] AAIJ	17BE	LHCB	pp at 7, 8 TeV
178.36±0.46±0.16	[1,5] AAIJ	14BJ	LHCB	Repl. by AAIJ 2021

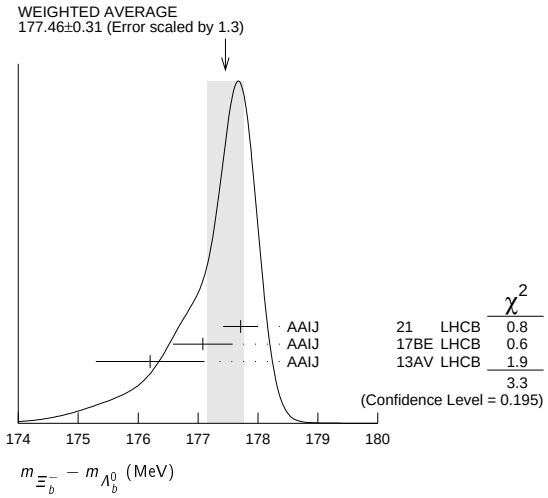

[1] Reconstructed in $\Xi_b^- \to \Xi_c^0 \pi^-$, $\Xi_c^0 \to p K^- K^- \pi^+$ decays.Reference decays $\Lambda_b^0 \to \Lambda_c^+ \pi^-$ were used.

[2] Reconstructed in $\Xi_b^- \to J/\psi \Lambda K^-$ decays. Reference decays $\Lambda_b^0 \to J/\psi \Lambda$ were used.

[3] Reconstructed in $\Xi_b^- \to J/\psi \Xi^-$ decays.

[4] Combination of the original statistically independent measurements of AAIJ 17BE and AAIJ 14BJ taking into account correlation between systematic uncertainties.

[5] Combined with AAIJ 17BE.

$m_{\Xi_b^-} - m_{\Xi_b^0}$

VALUE (MeV)	DOCUMENT ID		TECN	COMMENT
5.9 ±0.6 OUR AVERAGE				
5.92±0.60±0.23	[1] AAIJ	14BJ	LHCB	pp at 7, 8 TeV
3.1 ±5.6 ±1.3	[2] AALTONEN	11X	CDF	$p\overline{p}$ at 1.96 TeV

[1] Reconstructed in $\Xi_b^- \to \Xi_c^0 \pi^-$, $\Xi_c^0 \to p K^- K^- \pi^+$ decays. Uses $m(\Xi_b^0) - m(\Lambda_b^0) = 172.44 \pm 0.39 \pm 0.17$ MeV from AAIJ 14Z.

[2] Derived from measurements in $\Xi_b^0 \to \Xi_c^+ \pi^-$ and $\Xi_b^- \to J/\psi \Xi^-$ from AALTONEN 09AP taking correlated systematic uncertainties into account.

Ξ_b^- MEAN LIFE

"OUR EVALUATION" is an average using rescaled values of the data listed below. The average and rescaling were performed by the Heavy Flavor Averaging Group (HFLAV) and are described at https://hflav.web.cern.ch/. The averaging/rescaling procedure takes into account correlations between the measurements and asymmetric lifetime errors.

Ξ_b^- MEAN LIFE

VALUE (10^{-12} s)	DOCUMENT ID		TECN	COMMENT
1.572±0.040 OUR EVALUATION				
1.57 ±0.04 OUR AVERAGE	Error includes scale factor of 1.1.			
1.599±0.041±0.022	[1] AAIJ	14BJ	LHCB	pp at 7, 8 TeV
$1.55 \pm^{0.10}_{0.09} \pm 0.03$	[2] AAIJ	14T	LHCB	pp at 7, 8 TeV
1.36 ±0.15 ±0.02	AALTONEN	14B	CDF	$p\overline{p}$ at 1.96 TeV
• • • We do not use the following data for averages, fits, limits, etc. • • •				
$1.56 \pm^{0.27}_{0.25} \pm 0.02$	[3] AALTONEN	09AP	CDF	Repl. by AALTONEN 14B

[1] Reconstructed in $\Xi_b^- \to \Xi_c^0 \pi^-$, $\Xi_c^0 \to p K^- K^- \pi^+$ decays. Reference Λ_b^0 lifetime $1.479 \pm 0.009 \pm 0.010$ ps from AAIJ 14U.

[2] Measured in $\Xi_b^- \to J/\psi \Xi^-$ decays.

[3] Measured in $\Xi_b^- \to J/\psi \Xi^-$ decays with $66 \pm^{14}_{9}$ candidates.

MEAN LIFE RATIOS

$\tau_{\Xi_b^-} / \tau_{\Lambda_b^0}$ mean life ratio

VALUE	DOCUMENT ID		TECN	COMMENT
1.089±0.026±0.011	[1] AAIJ	14BJ	LHCB	pp at 7, 8 TeV

[1] Reconstructed in $\Xi_b^- \to \Xi_c^0 \pi^-$, $\Xi_c^0 \to p K^- K^- \pi^+$ decays. Reference $\Lambda_b^0 \to \Lambda_c^+ \pi^-$.

$\tau_{\Xi_b^-} / \tau_{\Xi_b^0}$ mean life ratio

VALUE	DOCUMENT ID		TECN	COMMENT
1.083±0.032±0.016	[1] AAIJ	14BJ	LHCB	pp at 7, 8 TeV

[1] Reconstructed in $\Xi_b^- \to \Xi_c^0 \pi^-$, $\Xi_c^0 \to p K^- K^- \pi^+$ decays. Uses Ξ_b^0 measurements from AAIJ 14Z.

Ξ_b^- DECAY MODES

	Mode	Fraction (Γ_i/Γ)
Γ_1	$J/\psi \Xi^- \times B(b \to \Xi_b^-)$	$(1.02 \pm^{0.26}_{0.21}) \times 10^{-5}$
Γ_2	$J/\psi \Lambda K^- \times B(b \to \Xi_b^-)$	$(2.5 \pm 0.4) \times 10^{-6}$
Γ_3	$p K^- K^- \times B(b \to \Xi_b^-)$	$(3.7 \pm 0.8) \times 10^{-8}$
Γ_4	$p K^- K^-$	seen
Γ_5	$p \pi^- \pi^-$	
Γ_6	$p K^- \pi^-$	seen
Γ_7	$\Lambda_b^0 \pi^- \times B(b \to \Xi_b^-)/B(b \to \Lambda_b^0)$	$(5.7 \pm 2.0) \times 10^{-4}$
Γ_8	$\Xi_c^0 \pi^-$	seen
Γ_9	$\Sigma(1385) K^-$	$(2.6 \pm 2.3) \times 10^{-7}$
Γ_{10}	$\Lambda(1405) K^-$	$(1.9 \pm 1.2) \times 10^{-7}$
Γ_{11}	$\Lambda(1520) K^-$	$(7.6 \pm 3.2) \times 10^{-7}$
Γ_{12}	$\Lambda(1670) K^-$	$(4.5 \pm 2.3) \times 10^{-7}$
Γ_{13}	$\Sigma(1775) K^-$	$(2.2 \pm 1.5) \times 10^{-7}$
Γ_{14}	$\Sigma(1915) K^-$	$(2.6 \pm 2.5) \times 10^{-7}$

Ξ_b^- BRANCHING RATIOS

$\Gamma(J/\psi \Xi^- \times B(b \to \Xi_b^-))/\Gamma_{total}$ — Γ_1/Γ

VALUE (units 10^{-4})	DOCUMENT ID		TECN	COMMENT
$0.102 \pm^{0.026}_{0.021}$ OUR AVERAGE				
$0.098 \pm^{0.023}_{0.016} \pm 0.014$	[1] AALTONEN	09AP	CDF	$p\overline{p}$ at 1.96 TeV
0.16 ±0.07 ±0.02	[2] ABAZOV	07K	D0	$p\overline{p}$ at 1.96 TeV

[1] AALTONEN 09AP reports $[\Gamma(\Xi_b \to J/\psi \Xi^- \times B(b \to \Xi_b^-))/\Gamma_{total}] / [B(\Lambda_b^0 \to J/\psi(1S)\Lambda \times B(b \to \Lambda_b^0))] = 0.167 \pm^{0.037}_{0.025} \pm 0.012$ which we multiply by our best value $B(\Lambda_b^0 \to J/\psi(1S)\Lambda \times B(b \to \Lambda_b^0)) = (5.8 \pm 0.8) \times 10^{-5}$. Our first error is their experiment's error and our second error is the systematic error from using our best value.

[2] ABAZOV 07K reports $[\Gamma(\Xi_b \to J/\psi \Xi^- \times B(b \to \Xi_b^-))/\Gamma_{total}] / [B(\Lambda_b^0 \to J/\psi(1S)\Lambda \times B(b \to \Lambda_b^0))] = 0.28 \pm 0.09 \pm^{0.09}_{0.08}$ which we multiply by our best value $B(\Lambda_b^0 \to J/\psi(1S)\Lambda \times B(b \to \Lambda_b^0)) = (5.8 \pm 0.8) \times 10^{-5}$. Our first error is their experiment's error and our second error is the systematic error from using our best value.

$\Gamma(J/\psi \Lambda K^- \times B(b \to \Xi_b^-))/\Gamma_{total}$ — Γ_2/Γ

VALUE (units 10^{-6})	DOCUMENT ID		TECN	COMMENT
2.45±0.19±0.35	[1,2] AAIJ	17BE	LHCB	pp at 7 and 8 TeV

[1] AAIJ 17BE reports $[\Gamma(\Xi_b \to J/\psi \Lambda K^- \times B(b \to \Xi_b^-))/\Gamma_{total}] / [B(\Lambda_b^0 \to J/\psi(1S)\Lambda \times B(b \to \Lambda_b^0))] = (4.19 \pm 0.29 \pm 0.15) \times 10^{-2}$ which we multiply by our best value $B(\Lambda_b^0 \to J/\psi(1S)\Lambda \times B(b \to \Lambda_b^0)) = (5.8 \pm 0.8) \times 10^{-5}$. Our first error is their experiment's error and our second error is the systematic error from using our best value.

[2] Integrated over the b-baryon transverse momentum $p_T < 25$ GeV and rapidity $2.0 < y < 4.5$.

$\Gamma(p K^- K^- \times B(b \to \Xi_b^-))/\Gamma_{total}$ — Γ_3/Γ

VALUE (units 10^{-8})	DOCUMENT ID		TECN	COMMENT
3.7±0.8±0.2	[1] AAIJ	17F	LHCB	pp at 7, 8 TeV

[1] AAIJ 17F reports $[\Gamma(\Xi_b \to p K^- K^- \times B(\overline{b} \to \Xi_b))/\Gamma_{total}] / [B(B^+ \to K^+ K^- K^+)] / [B(\overline{b} \to B^+)] = (2.65 \pm 0.35 \pm 0.47) \times 10^{-3}$ which we multiply by our best values $B(B^+ \to K^+ K^- K^+) = (3.40 \pm 0.14) \times 10^{-5}$, $B(\overline{b} \to B^+) = (40.8 \pm 0.7) \times 10^{-2}$. Our first error is their experiment's error and our second error is the systematic error from using our best values.

$\Gamma(p K^- K^-)/\Gamma_{total}$ — Γ_4/Γ

VALUE (units 10^{-6})	DOCUMENT ID		TECN	COMMENT
2.3±0.9	[1] AAIJ	21AH	LHCB	pp at 7, 8, 13 TeV

[1] Obtained using the ratio of fragmentation and branching fractions relative to the $B^- \to K^+ K^- K^-$ decay.

$\Gamma(p \pi^- \pi^-)/\Gamma(p K^- K^-)$ — Γ_5/Γ_4

VALUE	CL%	DOCUMENT ID		TECN	COMMENT
<0.56	90	[1] AAIJ	17F	LHCB	pp at 7, 8 TeV

[1] Measures the ratio as $0.28 \pm 0.16 \pm 0.13$.

$\Gamma(p K^- \pi^-)/\Gamma(p K^- K^-)$ — Γ_6/Γ_4

VALUE	DOCUMENT ID		TECN	COMMENT
0.98±0.27±0.09	AAIJ	17F	LHCB	pp at 7, 8 TeV

Downloaded from https://academic.oup.com/ptep/article/2022/8/083C01/6651666 by KIT Library user on 27 September 2022

$\Gamma(\Lambda_b^0\pi^- \times B(b \to \Xi_b^-)/B(b \to \Lambda_b^0))/\Gamma_{total}$ — Γ_7/Γ

VALUE (units 10^{-4})	DOCUMENT ID		TECN	COMMENT
$5.7 \pm 1.8^{+0.8}_{-0.9}$	[1] AAIJ	15BA	LHCB	pp at 7, 8 TeV

[1] A signal is reported with a significance of 3.2 standard deviations in the decay chain of $\Xi_b^- \to \Lambda_b^0\pi^-$, $\Lambda_b^0 \to \Lambda_c^+\pi^-$, and $\Lambda_c^+ \to pK^-\pi^+$.

$\Gamma(\Xi_c^0\pi^-)/\Gamma_{total}$ — Γ_8/Γ

VALUE	DOCUMENT ID		TECN	COMMENT
seen	AAIJ	16O	LHCB	pp at 7, 8 TeV

$\Gamma(\Sigma(1385)K^-)/\Gamma_{total}$ — Γ_9/Γ

VALUE (units 10^{-6})	DOCUMENT ID		TECN	COMMENT
$0.26 \pm 0.11 \pm 0.20$	[1] AAIJ	21AH	LHCB	pp at 7, 8 and 13 TeV

[1] Obtained from an amplitude analysis of quasi-two-body contributions to the $\Xi_b^- \to RK^-$ decay, with $R \to pK^-$.

$\Gamma(\Lambda(1405)K^-)/\Gamma_{total}$ — Γ_{10}/Γ

VALUE (units 10^{-6})	DOCUMENT ID		TECN	COMMENT
$0.19 \pm 0.06 \pm 0.10$	[1] AAIJ	21AH	LHCB	pp at 7, 8 and 13 TeV

[1] Obtained from an amplitude analysis of quasi-two-body contributions to the $\Xi_b^- \to RK^-$ decay, with $R \to pK^-$.

$\Gamma(\Lambda(1520)K^-)/\Gamma_{total}$ — Γ_{11}/Γ

VALUE (units 10^{-6})	DOCUMENT ID		TECN	COMMENT
$0.76 \pm 0.09 \pm 0.31$	[1] AAIJ	21AH	LHCB	pp at 7, 8 and 13 TeV

[1] Obtained from an amplitude analysis of quasi-two-body contributions to the $\Xi_b^- \to RK^-$ decay, with $R \to pK^-$.

$\Gamma(\Lambda(1670)K^-)/\Gamma_{total}$ — Γ_{12}/Γ

VALUE (units 10^{-6})	DOCUMENT ID		TECN	COMMENT
$0.45 \pm 0.07 \pm 0.22$	[1] AAIJ	21AH	LHCB	pp at 7, 8 and 13 TeV

[1] Obtained from an amplitude analysis of quasi-two-body contributions to the $\Xi_b^- \to RK^-$ decay, with $R \to pK^-$.

$\Gamma(\Sigma(1775)K^-)/\Gamma_{total}$ — Γ_{13}/Γ

VALUE (units 10^{-6})	DOCUMENT ID		TECN	COMMENT
$0.22 \pm 0.08 \pm 0.13$	[1] AAIJ	21AH	LHCB	pp at 7, 8 and 13 TeV

[1] Obtained from an amplitude analysis of quasi-two-body contributions to the $\Xi_b^- \to RK^-$ decay, with $R \to pK^-$.

$\Gamma(\Sigma(1915)K^-)/\Gamma_{total}$ — Γ_{14}/Γ

VALUE (units 10^{-6})	DOCUMENT ID		TECN	COMMENT
$0.26 \pm 0.09 \pm 0.23$	[1] AAIJ	21AH	LHCB	pp at 7, 8 and 13 TeV

[1] Obtained from an amplitude analysis of quasi-two-body contributions to the $\Xi_b^- \to RK^-$ decay, with $R \to pK^-$.

P VIOLATION ASYMMETRY

$A_P(\Xi_b)$, $\Xi_b^- - \Xi_b^+$ production asymmetry

$$A_P(\Xi_b) = [\sigma(\Xi_b^-) - \sigma(\Xi_b^+)]/[\sigma(\Xi_b^-) + \sigma(\Xi_b^+)]$$

VALUE (units 10^{-2})	DOCUMENT ID		TECN	COMMENT
-2 ± 4 OUR AVERAGE				
$1.1 \pm 5.6 \pm 1.9$	[1,2] AAIJ	19AB	LHCB	pp at 7 and 8 TeV
$-3.9 \pm 4.9 \pm 2.5$	[1,2] AAIJ	19AB	LHCB	pp at 13 TeV

[1] Baryon kinematic range $p_T < 20$ GeV/c and $2 < \eta < 6$.
[2] Measured using previous measurements of $A_P(\Lambda_b)$ in AAIJ 17BF.

CP VIOLATION in Ξ_b deays

$$A_{CP}(\Xi_b) = [B(\Xi_b^- \to f) - B(\Xi_b^+ \to \overline{f})]/\text{Sum}$$

$A_{CP}(\Xi_b^- \to \Sigma(1385)K^-)$

VALUE	DOCUMENT ID		TECN	COMMENT
$(-27 \pm 34 \pm 73) \times 10^{-2}$	AAIJ	21AH	LHCB	pp at 7, 8, 13 TeV

$A_{CP}(\Xi_b^- \to \Lambda(1405)K^-)$

VALUE	DOCUMENT ID		TECN	COMMENT
$(-1 \pm 24 \pm 32) \times 10^{-2}$	AAIJ	21AH	LHCB	pp at 7, 8, 13 TeV

$A_{CP}(\Xi_b^- \to \Lambda(1520)K^-)$

VALUE	DOCUMENT ID		TECN	COMMENT
$(-5 \pm 9 \pm 8) \times 10^{-2}$	AAIJ	21AH	LHCB	pp at 7, 8, 13 TeV

$A_{CP}(\Xi_b^- \to \Lambda(1670)K^-)$

VALUE	DOCUMENT ID		TECN	COMMENT
$(3 \pm 14 \pm 10) \times 10^{-2}$	AAIJ	21AH	LHCB	pp at 7, 8, 13 TeV

$A_{CP}(\Xi_b^- \to \Sigma(1775)K^-)$

VALUE	DOCUMENT ID		TECN	COMMENT
$(-47 \pm 26 \pm 14) \times 10^{-2}$	AAIJ	21AH	LHCB	pp at 7, 8, 13 TeV

$A_{CP}(\Xi_b^- \to \Sigma(1915)K^-)$

VALUE	DOCUMENT ID		TECN	COMMENT
$(11 \pm 26 \pm 22) \times 10^{-2}$	AAIJ	21AH	LHCB	pp at 7, 8, 13 TeV

Ξ_b^- REFERENCES

AAIJ	21	PR D103 012004	R. Aaij et al.	(LHCb Collab.)
AAIJ	21AH	PR D104 052010	R. Aaij et al.	(LHCb Collab.)
AAIJ	19AB	PR D99 052006	R. Aaij et al.	(LHCb Collab.)
AAIJ	17BE	PL B772 265	R. Aaij et al.	(LHCb Collab.)
AAIJ	17BF	PL B774 139	R. Aaij et al.	(LHCb Collab.)
AAIJ	17F	PRL 118 071801	R. Aaij et al.	(LHCb Collab.)
AAIJ	16O	PR D93 092007	R. Aaij et al.	(LHCb Collab.)
AAIJ	15BA	PRL 115 241801	R. Aaij et al.	(LHCb Collab.)
AAIJ	14AA	PRL 112 202001	R. Aaij et al.	(LHCb Collab.)
AAIJ	14BJ	PRL 113 242002	R. Aaij et al.	(LHCb Collab.)
AAIJ	14T	PL B736 154	R. Aaij et al.	(LHCb Collab.)
AAIJ	14U	PL B734 122	R. Aaij et al.	(LHCb Collab.)
AAIJ	14Z	PRL 113 032001	R. Aaij et al.	(LHCb Collab.)
AALTONEN	14B	PR D89 072014	T. Aaltonen et al.	(CDF Collab.)
AAIJ	13AV	PRL 110 182001	R. Aaij et al.	(LHCb Collab.)
AALTONEN	11X	PRL 107 102001	T. Aaltonen et al.	(CDF Collab.)
AALTONEN	09AP	PR D80 072003	T. Aaltonen et al.	(CDF Collab.)
AALTONEN	07A	PRL 99 052002	T. Aaltonen et al.	(CDF Collab.)
ABAZOV	07K	PRL 99 052001	V.M. Abazov et al.	(D0 Collab.)

Ξ_b^0

$I(J^P) = \frac{1}{2}(\frac{1}{2}^+)$ Status: ***
I, J, P need confirmation.

In the quark model, Ξ_b^0 and Ξ_b^- are an isodoublet (usb, dsb) state; the lowest Ξ_b^0 and Ξ_b^- ought to have $J^P = 1/2^+$. None of I, J, or P have actually been measured.

Ξ_b^0 MASS

Ξ_b^0 MASS

VALUE (MeV)	DOCUMENT ID		TECN	COMMENT
5791.9 ±0.5 OUR AVERAGE				
$5794.3 \pm 2.4 \pm 0.7$	AAIJ	14H	LHCB	pp at 7 TeV
$5791.80 \pm 0.39 \pm 0.31$	[1] AAIJ	14Z	LHCB	pp at 7, 8 TeV
$5788.7 \pm 4.3 \pm 1.4$	[2] AALTONEN	14B	CDF	$p\overline{p}$ at 1.96 TeV
• • • We do not use the following data for averages, fits, limits, etc. • • •				
$5787.8 \pm 5.0 \pm 1.3$	[3] AALTONEN	11X	CDF	Repl. by AALTONEN 14B

[1] Uses $\Xi_b^0 \to \Xi_c^+\pi^-$ and $\Xi_c^+ \to pK^-\pi^+$ decays. The measurement comes from the mass difference of Ξ_b^0 and Λ_b^0.
[2] Uses $\Xi_b^0 \to \Xi_c^+\pi^-$ decays.
[3] Measured in $\Xi_b^0 \to \Xi_c^+\pi^-$ with $25.3^{+5.6}_{-5.4}$ candidates.

$m_{\Xi_b^0} - m_{\Lambda_b^0}$

VALUE (MeV)	DOCUMENT ID		TECN	COMMENT
172.5 ±0.4 OUR AVERAGE				
$174.8 \pm 2.4 \pm 0.5$	AAIJ	14H	LHCB	pp at 7 TeV
$172.44 \pm 0.39 \pm 0.17$	[1] AAIJ	14Z	LHCB	pp at 7, 8 TeV

[1] Uses $\Xi_b^0 \to \Xi_c^+\pi^-$ and $\Xi_c^+ \to pK^-\pi^+$ decays.

Ξ_b^0 MEAN LIFE

"OUR EVALUATION" is an average using rescaled values of the data listed below. The average and rescaling were performed by the Heavy Flavor Averaging Group (HFLAV) and are described at https://hflav.web.cern.ch/. The averaging/rescaling procedure takes into account correlations between the measurements and asymmetric lifetime errors.

Ξ_b^0 MEAN LIFE

VALUE (10^{-12} s)	DOCUMENT ID		TECN	COMMENT
1.480±0.030 OUR EVALUATION				
$1.477 \pm 0.026 \pm 0.019$	[1] AAIJ	14Z	LHCB	pp at 7, 8 TeV

[1] Uses $\Xi_b^0 \to \Xi_c^+\pi^-$ and $\Xi_c^+ \to pK^-\pi^+$ decays. The measurement comes from the value of relative lifetime of Ξ_b^0 to Λ_b^0.

τ_{mix} $(1/2\pi)$ times the oscillation period

VALUE (s)	DOCUMENT ID		TECN	COMMENT
$>13 \times 10^{-12}$	[1] AAIJ	17BH	LHCB	pp at 7, 8 TeV

[1] Uses Ξ_b^{*-} and $\Xi_b^{\prime -}$ decays to $\Xi_b^0\pi^-$, where $\Xi_b^0 \to \Xi_c^+\pi^-$, $\Xi_c^+ \to pK^-\pi^+$.

Ξ_b^0 DECAY MODES

	Mode	Fraction (Γ_i/Γ)	Confidence level
Γ_1	$pD^0K^- \times B(b \to \Xi_b^0)$	$(1.7 \pm 0.5) \times 10^{-6}$	
Γ_2	$p\overline{K}^0\pi^- \times B(b \to \Xi_b^0)/B(\overline{b} \to B^0)$	$< 1.6 \times 10^{-6}$	90%

Downloaded from https://academic.oup.com/ptep/article/2022/8/083C01/6651666 by KIT Library user on 27 September 2022

Γ_3	$pK^0K^- \times B(b \to \Xi_b^0)/B(\overline{b} \to B^0)$	< 1.1	$\times 10^{-6}$	90%
Γ_4	$\Lambda\pi^+\pi^- \times B(b \to \Xi_b^0)/B(b \to \Lambda_b^0)$	< 1.7	$\times 10^{-6}$	90%
Γ_5	$\Lambda K^-\pi^+ \times B(b \to \Xi_b^0)/B(b \to \Lambda_b^0)$	< 8	$\times 10^{-7}$	90%
Γ_6	$\Lambda K^+K^- \times B(b \to \Xi_b^0)/B(b \to \Lambda_b^0)$	< 3	$\times 10^{-7}$	90%
Γ_7	$J/\psi\Lambda$	seen		
Γ_8	$J/\psi\Xi^0$	seen		
Γ_9	$\Lambda_c^+K^- \times B(b \to \Xi_b^0)$	$(6 \pm 4) \times 10^{-7}$		
Γ_{10}	$pK^-\pi^+\pi^- \times B(b \to \Xi_b^0)/B(b \to \Lambda_b^0)$	$(1.9 \pm 0.4) \times 10^{-6}$		
Γ_{11}	$pK^-K^-\pi^+ \times B(b \to \Xi_b^0)/B(b \to \Lambda_b^0)$	$(1.71 \pm 0.31) \times 10^{-6}$		
Γ_{12}	$pK^-K^+K^- \times B(b \to \Xi_b^0)/B(b \to \Lambda_b^0)$	$(1.7 \pm 1.0) \times 10^{-7}$		

Ξ_b^0 BRANCHING RATIOS

$\Gamma(pD^0K^- \times B(b \to \Xi_b^0))/\Gamma_{total}$ — Γ_1/Γ

VALUE (units 10^{-6})	DOCUMENT ID		TECN	COMMENT
1.7±0.4±0.4	[1] AAIJ	14H	LHCB	pp at 7 TeV

[1] AAIJ 14H reports $[\Gamma(\Xi_b \to pD^0K^- \times B(\overline{b} \to \Xi_b))/\Gamma_{total}]$ / $[B(\overline{b} \to b\text{-baryon})]$ / $[B(\Lambda_b^0 \to pD^0K^-)] = 0.44 \pm 0.09 \pm 0.06$ which we multiply by our best values $B(\overline{b} \to b\text{-baryon}) = (8.4 \pm 1.1) \times 10^{-2}$, $B(\Lambda_b^0 \to pD^0K^-) = (4.6 \pm 0.8) \times 10^{-5}$. Our first error is their experiment's error and our second error is the systematic error from using our best values.

$\Gamma(p\overline{K}^0\pi^-) \times B(b \to \Xi_b^0)/B(\overline{b} \to B^0))/\Gamma_{total}$ — Γ_2/Γ

VALUE	CL%	DOCUMENT ID		TECN	COMMENT
$<1.6 \times 10^{-6}$	90	AAIJ	14Q	LHCB	pp at 7 TeV

$\Gamma(pK^0K^- \times B(b \to \Xi_b^0)/B(\overline{b} \to B^0))/\Gamma_{total}$ — Γ_3/Γ

VALUE	CL%	DOCUMENT ID		TECN	COMMENT
$<1.1 \times 10^{-6}$	90	AAIJ	14Q	LHCB	pp at 7 TeV

$\Gamma(\Lambda\pi^+\pi^- \times B(b \to \Xi_b^0)/B(b \to \Lambda_b^0))/\Gamma_{total}$ — Γ_4/Γ

VALUE	CL%	DOCUMENT ID		TECN	COMMENT
$<1.7 \times 10^{-6}$	90	AAIJ	16W	LHCB	pp at 7, 8 TeV

$\Gamma(\Lambda K^-\pi^+ \times B(b \to \Xi_b^0)/B(b \to \Lambda_b^0))/\Gamma_{total}$ — Γ_5/Γ

VALUE	CL%	DOCUMENT ID		TECN	COMMENT
$<0.8 \times 10^{-6}$	90	AAIJ	16W	LHCB	pp at 7, 8 TeV

$\Gamma(\Lambda K^+K^- \times B(b \to \Xi_b^0)/B(b \to \Lambda_b^0))/\Gamma_{total}$ — Γ_6/Γ

VALUE	CL%	DOCUMENT ID		TECN	COMMENT
$<0.3 \times 10^{-6}$	90	AAIJ	16W	LHCB	pp at 7, 8 TeV

$\Gamma(J/\psi\Lambda)/\Gamma(J/\psi\Xi^0)$ — Γ_7/Γ_8

VALUE (units 10^{-3})	DOCUMENT ID		TECN	COMMENT
8.2±2.1±0.9	[1] AAIJ	20U	LHCB	pp at 7, 8 and 13 TeV

[1] The Cabibbo suppressed $\Xi_b \to J/\psi\Lambda$ decay is observed for the first time.

$\Gamma(\Lambda_c^+K^- \times B(b \to \Xi_b^0))/\Gamma(pD^0K^- \times B(b \to \Xi_b^0))$ — Γ_9/Γ_1

VALUE	DOCUMENT ID		TECN	COMMENT
0.36±0.19±0.02	[1] AAIJ	14H	LHCB	pp at 7 TeV

[1] AAIJ 14H reports $[\Gamma(\Xi_b \to \Lambda_c^+K^- \times B(\overline{b} \to \Xi_b))/\Gamma(\Xi_b \to pD^0K^- \times B(\overline{b} \to \Xi_b))] \times [B(\Lambda_c^+ \to pK^-\pi^+)]$ / $[B(D^0 \to K^-\pi^+)] = 0.57 \pm 0.22 \pm 0.21$ which we multiply or divide by our best values $B(\Lambda_c^+ \to pK^-\pi^+) = (6.28 \pm 0.32) \times 10^{-2}$, $B(D^0 \to K^-\pi^+) = (3.947 \pm 0.030) \times 10^{-2}$. Our first error is their experiment's error and our second error is the systematic error from using our best values.

$\Gamma(pK^-\pi^+\pi^- \times B(b \to \Xi_b^0)/B(b \to \Lambda_b^0))/\Gamma_{total}$ — Γ_{10}/Γ

VALUE (units 10^{-6})	DOCUMENT ID		TECN	COMMENT
1.90±0.35±0.17	[1] AAIJ	18Q	LHCB	pp at 7, 8 TeV

[1] AAIJ 18Q reports $[\Gamma(\Xi_b \to pK^-\pi^+\pi^- \times B(b \to \Xi_b^0)/B(b \to \Lambda_b^0))/\Gamma_{total}]$ / $[B(\Lambda_c^+ \to pK^-\pi^+)]$ / $[B(\Lambda_b^0 \to \Lambda_c^+\pi^-)] = (6.2 \pm 0.8 \pm 0.2 \pm 0.8) \times 10^{-3}$ which we multiply by our best values $B(\Lambda_c^+ \to pK^-\pi^+) = (6.28 \pm 0.32) \times 10^{-2}$, $B(\Lambda_b^0 \to \Lambda_c^+\pi^-) = (4.9 \pm 0.4) \times 10^{-3}$. Our first error is their experiment's error and our second error is the systematic error from using our best values.

$\Gamma(pK^-K^-\pi^+ \times B(b \to \Xi_b^0)/B(b \to \Lambda_b^0))/\Gamma_{total}$ — Γ_{11}/Γ

VALUE (units 10^{-6})	DOCUMENT ID		TECN	COMMENT
1.71±0.27±0.15	[1] AAIJ	18Q	LHCB	pp at 7, 8 TeV

[1] AAIJ 18Q reports $[\Gamma(\Xi_b \to pK^-K^-\pi^+ \times B(b \to \Xi_b^0)/B(b \to \Lambda_b^0))/\Gamma_{total}]$ / $[B(\Lambda_c^+ \to pK^-\pi^+)]$ / $[B(\Lambda_b^0 \to \Lambda_c^+\pi^-)] = (5.6 \pm 0.6 \pm 0.4 \pm 0.5) \times 10^{-3}$ which we multiply by our best values $B(\Lambda_c^+ \to pK^-\pi^+) = (6.28 \pm 0.32) \times 10^{-2}$, $B(\Lambda_b^0 \to \Lambda_c^+\pi^-) = (4.9 \pm 0.4) \times 10^{-3}$. Our first error is their experiment's error and our second error is the systematic error from using our best values.

$\Gamma(pK^-K^+K^- \times B(b \to \Xi_b^0)/B(b \to \Lambda_b^0))/\Gamma_{total}$ — Γ_{12}/Γ

VALUE (units 10^{-6})	DOCUMENT ID		TECN	COMMENT
0.17±0.09±0.02	[1,2] AAIJ	18Q	LHCB	pp at 7, 8 TeV

[1] AAIJ 18Q reports $[\Gamma(\Xi_b \to pK^-K^+K^- \times B(b \to \Xi_b^0)/B(b \to \Lambda_b^0))/\Gamma_{total}]$ / $[B(\Lambda_c^+ \to pK^-\pi^+)]$ / $[B(\Lambda_b^0 \to \Lambda_c^+\pi^-)] = (0.57 \pm 0.28 \pm 0.08 \pm 0.10) \times 10^{-3}$ which we multiply by our best values $B(\Lambda_c^+ \to pK^-\pi^+) = (6.28 \pm 0.32) \times 10^{-2}$, $B(\Lambda_b^0 \to \Lambda_c^+\pi^-) = (4.9 \pm 0.4) \times 10^{-3}$. Our first error is their experiment's error and our second error is the systematic error from using our best values.

[2] AAIJ 18Q sees excess with a significance of 2.3σ. Using $B(\Lambda_b^0 \to \Lambda_c^+\pi^-) = (0.430 \pm 0.036) \times 10^{-2}$ and $B(\Lambda_c^+ \to pK^-\pi^+) = (6.46 \pm 0.24) \times 10^{-2}$ the authors set two sided limit [0.11–0.25] at 90% C.L.

P AND CP VIOLATION ASYMMETRIES

$a_P(\Xi_b^0 \to pK^-K^-\pi^+)$

Observable calculated as average of the triple products for Ξ_b^0 and $\overline{\Xi}_b^0$, which is sensitive to parity violation.

VALUE (%)	DOCUMENT ID		TECN	COMMENT
−3.04±5.19±0.36	[1] AAIJ	18AG	LHCB	pp at 7, 8 TeV

[1] Measured over full phase space of the decay.

$a_{CP}(\Xi_b^0 \to pK^-K^-\pi^+)$

Observable calculated as half of the difference between triple products for Ξ_b^0 and $\overline{\Xi}_b^0$, which is sensitive to CP violation.

VALUE (%)	DOCUMENT ID		TECN	COMMENT
−3.58±5.19±0.36	[1] AAIJ	18AG	LHCB	pp at 7, 8 TeV

[1] Measured over full phase space of the decay.

$\Delta A_{CP}(\Xi_b^0 \to pK^-\pi^+\pi^-)$

$\Delta A_{CP} \equiv A_{CP}(\Xi_b^0 \to pK^-\pi^+\pi^-) - A_{CP}(\Xi_b^0 \to (\Xi_c^+ \to pK^-\pi^+)\pi^-)$

VALUE (units 10^{-2})	DOCUMENT ID		TECN	COMMENT
−17±11±1	[1] AAIJ	19AH	LHCB	pp at 7 and 8 TeV

[1] Full phase space.

$\Delta A_{CP}(\Xi_b^0 \to pK^-\pi^+K^-)$

$\Delta A_{CP} \equiv A_{CP}(\Xi_b^0 \to pK^-\pi^+K^-) - A_{CP}(\Xi_b^0 \to (\Xi_c^+ \to pK^-\pi^+)\pi^-)$

VALUE (units 10^{-2})	DOCUMENT ID		TECN	COMMENT
−6.8±8.0±0.8	[1] AAIJ	19AH	LHCB	pp at 7 and 8 TeV

[1] Full phase space.

Ξ_b^0 REFERENCES

AAIJ	20U	PRL 124 111802	R. Aaij *et al.*	(LHCb Collab.)
AAIJ	19AH	EPJ C79 745	R. Aaij *et al.*	(LHCb Collab.)
AAIJ	18AG	JHEP 1808 039	R. Aaij *et al.*	(LHCb Collab.)
AAIJ	18Q	JHEP 1802 098	R. Aaij *et al.*	(LHCb Collab.)
AAIJ	17BH	PRL 119 181807	R. Aaij *et al.*	(LHCb Collab.)
AAIJ	16W	JHEP 1605 081	R. Aaij *et al.*	(LHCb Collab.)
AAIJ	14H	PR D89 032001	R. Aaij *et al.*	(LHCb Collab.)
AAIJ	14Q	JHEP 1404 087	R. Aaij *et al.*	(LHCb Collab.)
AAIJ	14Z	PRL 113 032001	R. Aaij *et al.*	(LHCb Collab.)
AALTONEN	14B	PR D89 072014	T. Aaltonen *et al.*	(CDF Collab.)
AALTONEN	11X	PRL 107 102001	T. Aaltonen *et al.*	(CDF Collab.)

$\Xi_b'(5935)^-$

$J^P = \frac{1}{2}^+$ Status: ***

$\Xi_b'(5935)^-$ MASS

VALUE (MeV)	DOCUMENT ID		TECN	COMMENT
5935.02±0.02±0.05	[1] AAIJ	15H	LHCB	pp at 7, 8 TeV

[1] Not independent of the mass difference measurement below. Observed in $\Xi_b^0\pi^-$ channel with $\Xi_b^0 \to \Xi_c^+\pi^-$ and $\Xi_c^+ \to pK^-\pi^+$.

$m_{\Xi_b'(5935)^-} - m_{\Xi_b^0} - m_{\pi^-}$

VALUE (MeV)	DOCUMENT ID		TECN	COMMENT
3.653±0.018±0.006	[2] AAIJ	15H	LHCB	pp at 7, 8 TeV

[2] Observed in $\Xi_b^0\pi^-$ channel with $\Xi_b^0 \to \Xi_c^+\pi^-$ and $\Xi_c^+ \to pK^-\pi^+$.

Downloaded from https://academic.oup.com/ptep/article/2022/8/083C01/6651666 by KIT Library user on 27 September 2022

$\Xi'_b(5935)^-$ WIDTH

VALUE (MeV)	CL%	DOCUMENT ID		TECN	COMMENT
<0.08	95	[3] AAIJ	15H	LHCB	pp at 7, 8 TeV

[3] Observed in $\Xi_b^0\pi^-$ channel with $\Xi_b^0 \to \Xi_c^+\pi^-$ and $\Xi_c^+ \to pK^-\pi^+$.

$\Xi'_b(5935)^-$ DECAY MODES

	Mode	Fraction (Γ_i/Γ)
Γ_1	$\Xi_b^0\pi^- \times B(\overline{b} \to \Xi'_b(5935)^-)/B(\overline{b} \to \Xi_b^0)$	(11.8±1.8) %

$\Xi'_b(5935)^-$ BRANCHING RATIOS

$\Gamma(\Xi_b^0\pi^- \times B(\overline{b} \to \Xi'_b(5935)^-)/B(\overline{b} \to \Xi_b^0))/\Gamma_{total}$ — Γ_1/Γ

VALUE	DOCUMENT ID		TECN	COMMENT
0.118±0.017±0.007	[4] AAIJ	15H	LHCB	pp at 7, 8 TeV

[4] Observed in $\Xi_b^0\pi^-$ channel with $\Xi_b^0 \to \Xi_c^+\pi^-$ and $\Xi_c^+ \to pK^-\pi^+$.

$\Xi'_b(5935)^-$ REFERENCES

AAIJ 15H PRL 114 062004 R. Aaij et al. (LHCb Collab.)

$\Xi_b(5945)^0$

$J^P = \frac{3}{2}^+$ Status: ***

Quantum numbers are based on quark model expectations.

$\Xi_b(5945)^0$ MASS

VALUE (MeV)	DOCUMENT ID		TECN	COMMENT
5952.3±0.6 OUR AVERAGE				
5952.3±0.1±0.6	[1] AAIJ	16AE	LHCB	pp at 7, 8 TeV
5951.4±0.8±0.6	[2] CHATRCHYAN	12S	CMS	pp at 7 TeV, 5.3 fb^{-1}

[1] AAIJ 16AE measures $m(\Xi_b(5945)^0) - m(\Xi_b^-) - m(\pi^+) = 15.727 \pm 0.068 \pm 0.023$ MeV. We have adjusted the measurement to our best values of $m(\Xi_b^-) = 5797.0 \pm 0.6$ MeV, $m(\pi^+) = 139.57039 \pm 0.00018$ MeV. Our first error is their experiment's error and our second error is the systematic error from using our best values.

[2] CHATRCHYAN 12S measures $m(\Xi_b(5945)^0) - m(\Xi_b^-) - m(\pi^+) = 14.84 \pm 0.74 \pm 0.28$ MeV. We have adjusted the measurement to our best values of $m(\Xi_b^-) = 5797.0 \pm 0.6$ MeV, $m(\pi^+) = 139.57039 \pm 0.00018$ MeV. Our first error is their experiment's error and our second error is the systematic error from using our best values.

$\Xi_b(5945)^0$ WIDTH

VALUE (MeV)	DOCUMENT ID		TECN	COMMENT
0.90±0.16±0.08	[3] AAIJ	16AE	LHCB	pp at 7, 8 TeV
• • • We do not use the following data for averages, fits, limits, etc. • • •				
2.1 ±1.7	[4] CHATRCHYAN	12S	CMS	pp at 7 TeV, 5.3 fb^{-1}

[3] Measured using $\Xi_b(5945)^0 \to \Xi_b^-\pi^+$, $\Xi_b^- \to \Xi_c^0\pi^-$, $\Xi_c^0 \to pK^-K^-\pi^+$ decays.
[4] Systematic uncertainty not evaluated.

$\Xi_b(5945)^0$ DECAY MODES

	Mode	Fraction (Γ_i/Γ)
Γ_1	$\Xi_b^-\pi^+$	seen

$\Xi_b(5945)^0$ BRANCHING RATIOS

$\Gamma(\Xi_b^-\pi^+)/\Gamma_{total}$ — Γ_1/Γ

VALUE	DOCUMENT ID		TECN	COMMENT
seen	AAIJ	16AE	ATLS	pp at 7, 8 TeV
seen	CHATRCHYAN	12S	CMS	pp at 7 TeV, 5.3 fb^{-1}

$\Xi_b(5945)^0$ REFERENCES

AAIJ 16AE JHEP 1605 161 R. Aaij et al. (LHCb Collab.)
CHATRCHYAN 12S PRL 108 252002 S. Chatrchyan et al. (CMS Collab.)

$\Xi_b(5955)^-$

$J^P = \frac{3}{2}^+$ Status: ***

$\Xi_b(5955)^-$ MASS

VALUE (MeV)	DOCUMENT ID		TECN	COMMENT
5955.33±0.12±0.05	[1] AAIJ	15H	LHCB	pp at 7, 8 TeV

[1] Not independent of the mass difference measurement below. Observed in $\Xi_b^0\pi^-$ channel with $\Xi_b^0 \to \Xi_c^+\pi^-$ and $\Xi_c^+ \to pK^-\pi^+$.

$m_{\Xi_b(5955)^-} - m_{\Xi_b^0} - m_{\pi^-}$

VALUE (MeV)	DOCUMENT ID		TECN	COMMENT
23.96±0.12±0.06	[1] AAIJ	15H	LHCB	pp at 7, 8 TeV

[1] Observed in $\Xi_b^0\pi^-$ channel with $\Xi_b^0 \to \Xi_c^+\pi^-$ and $\Xi_c^+ \to pK^-\pi^+$.

$\Xi_b(5955)^-$ WIDTH

VALUE (MeV)	DOCUMENT ID		TECN	COMMENT
1.65±0.31±0.10	[1] AAIJ	15H	LHCB	pp at 7, 8 TeV

[1] Observed in $\Xi_b^0\pi^-$ channel with $\Xi_b^0 \to \Xi_c^+\pi^-$ and $\Xi_c^+ \to pK^-\pi^+$.

$\Xi_b(5955)^-$ DECAY MODES

	Mode	Fraction (Γ_i/Γ)
Γ_1	$\Xi_b^0\pi^- \times B(\overline{b} \to \Xi_b^*(5955)^-)/B(\overline{b} \to \Xi_b^0)$	(20.7±3.5) %

$\Xi_b(5955)^-$ BRANCHING RATIOS

$\Gamma(\Xi_b^0\pi^- \times B(\overline{b} \to \Xi_b^*(5955)^-)/B(\overline{b} \to \Xi_b^0))/\Gamma_{total}$ — Γ_1/Γ

VALUE	DOCUMENT ID		TECN	COMMENT
0.207±0.032±0.015	[1] AAIJ	15H	LHCB	pp at 7, 8 TeV

[1] Observed in $\Xi_b^0\pi^-$ channel with $\Xi_b^0 \to \Xi_c^+\pi^-$ and $\Xi_c^+ \to pK^-\pi^+$.

$\Xi_b(5955)^-$ REFERENCES

AAIJ 15H PRL 114 062004 R. Aaij et al. (LHCb Collab.)

$\Xi_b(6100)^-$

$J^P = \frac{3}{2}^-$ Status: ***
J, P need confirmation.

$\Xi_b(6100)^-$ MASS

VALUE (MeV)	DOCUMENT ID		TECN	COMMENT
6100.3±0.2±0.6	[1] SIRUNYAN	21F	CMS	pp at 13 TeV

[1] Observed in $\Xi_b(6100)^- \to \Xi_b^-\pi^+\pi^-$ decays.

$m_{\Xi_b(6100)^-} - m_{\Xi_b^-} - 2\, m_{\pi^\pm}$

VALUE (MeV)	DOCUMENT ID		TECN	COMMENT
24.14±0.22±0.09	[1] SIRUNYAN	21F	CMS	pp at 13 TeV

[1] Observed in $\Xi_b(6100)^- \to \Xi_b^-\pi^+\pi^-$ decays.

$\Xi_b(6100)^-$ WIDTH

VALUE (MeV)	CL%	DOCUMENT ID		TECN	COMMENT
<1.9	95	[1] SIRUNYAN	21F	CMS	pp at 13 TeV

[1] Observed in $\Xi_b(6100)^- \to \Xi_b^-\pi^+\pi^-$ decays.

$\Xi_b(6100)^-$ DECAY MODES

	Mode	Fraction (Γ_i/Γ)
Γ_1	$\Xi_b^-\pi^+\pi^-$	seen

$\Xi_b(6100)^-$ BRANCHING RATIOS

$\Gamma(\Xi_b^-\pi^+\pi^-)/\Gamma_{total}$ — Γ_1/Γ

VALUE	EVTS	DOCUMENT ID		TECN	COMMENT
seen	60	SIRUNYAN	21F	CMS	pp at 13 TeV

$\Xi_b(6100)^-$ REFERENCES

SIRUNYAN 21F PRL 126 252003 A.M. Sirunyan et al. (CMS Collab.)

$\Xi_b(6227)^-$

$J^P = ?^?$ Status: ***

$\Xi_b(6227)^-$ MASS

VALUE (MeV)	DOCUMENT ID		TECN	COMMENT
6227.9±0.9±0.2	[1] AAIJ	21	LHCB	pp at 7, 8, 13 TeV

Downloaded from https://academic.oup.com/ptep/article/2022/8/083C01/6651666 by KIT Library user on 27 September 2022

• • • We do not use the following data for averages, fits, limits, etc. • • •

6226.9±2.0±0.4	[2,3] AAIJ	18H	LHCB	Repl. by AAIJ 2021

[1] AAIJ 21 measures $m(\Xi_b(6227)^-) - m(\Lambda_b^0) = 608.3 \pm 0.8 \pm 0.4$ MeV. We have adjusted the measurement to our best value of $m(\Lambda_b^0) = 5619.60 \pm 0.17$ MeV. Our first error is their experiment's error and our second error is the systematic error from using our best values.
[2] Uses $\Lambda_b^0 K^-$ and $\Xi_b^0 \pi^-$ modes.
[3] Measures mass difference $m(\Xi_b(6227)^-) - m(\Lambda_b^0) = 607.3 \pm 2.0 \pm 0.3$ MeV and uses $m(\Lambda_b^0) = 5619.58 \pm 0.17$ MeV.

$\Xi_b(6227)^-$ WIDTH

VALUE (MeV)	DOCUMENT ID		TECN	COMMENT
19.9±2.1±1.5	[1] AAIJ	21	LHCB	pp at 7, 8, 13 TeV
• • • We do not use the following data for averages, fits, limits, etc. • • •				
18.1±5.4±1.8	[2] AAIJ	18H	LHCB	Repl. by AAIJ 2021

[1] Uses $\Lambda_b^0 K^-$ decays.
[2] Uses $\Lambda_b^0 K^-$ and $\Xi_b^0 \pi^-$ modes.

$\Xi_b(6227)^-$ DECAY MODES

	Mode	Fraction (Γ_i/Γ)	Scale factor
Γ_1	$\Lambda_b^0 K^- \times$ B($b \to \Xi_b(6227)$)/B($b \to \Lambda_b^0$)	$(3.20 \pm 0.35) \times 10^{-3}$	
Γ_2	$\Xi_b^0 \pi^- \times$ B($b \to \Xi_b(6227)$)/B($b \to \Xi_b^0$)	(2.8 ±1.1) %	1.8

$\Xi_b(6227)^-$ BRANCHING RATIOS

$\Gamma(\Lambda_b^0 K^- \times B(b \to \Xi_b(6227))/B(b \to \Lambda_b^0))/\Gamma_{total}$ — Γ_1/Γ

VALUE (units 10^{-3})	DOCUMENT ID		TECN	COMMENT
3.20±0.35 OUR AVERAGE				
3.0 ±0.3 ±0.4	AAIJ	18H	LHCB	pp at 7, 8 TeV
3.4 ±0.3 ±0.4	AAIJ	18H	LHCB	pp at 13 TeV

$\Gamma(\Xi_b^0 \pi^- \times B(b \to \Xi_b(6227))/B(b \to \Xi_b^0))/\Gamma_{total}$ — Γ_2/Γ

VALUE (units 10^{-3})	DOCUMENT ID		TECN	COMMENT
28±11 OUR AVERAGE Error includes scale factor of 1.8.				
47±10±7	AAIJ	18H	LHCB	pp at 7, 8 TeV
22± 6±3	AAIJ	18H	LHCB	pp at 13 TeV

$\Xi_b(6227)^-$ REFERENCES

AAIJ 21 PR D103 012004 R. Aaij et al. (LHCb Collab.)
AAIJ 18H PRL 121 072002 R. Aaij et al. (LHCb Collab.)

$\Xi_b(6227)^0$

$J^P = ?^?$ Status: ***

$\Xi_b(6227)^0$ MASS

VALUE (MeV)	DOCUMENT ID		TECN	COMMENT
$6226.8^{+1.4}_{-1.5} \pm 0.6$	[1,2] AAIJ	21	LHCB	pp at 7, 8, 13 TeV

[1] AAIJ 21 measures $m(\Xi_b(6227)^0) - m(\Xi_b^-) = 429.8^{+1.4}_{-1.5} \pm 0.3$ MeV. We have adjusted the measurement to our best value of $m(\Xi_b^-) = 5797.0 \pm 0.6$ MeV. Our first error is their experiment's error and our second error is the systematic error from using our best values.
[2] Uses $\Xi_b^- \pi^+$ decays.

$\Xi_b(6227)^0$ WIDTH

VALUE (MeV)	DOCUMENT ID		TECN	COMMENT
$18.6^{+5.0}_{-4.1} \pm 1.4$	[1] AAIJ	21	LHCB	pp at 7, 8, 13 TeV

[1] Uses $\Xi_b^- \pi^+$ decays.

$\Xi_b(6227)^0$ DECAY MODES

	Mode	Fraction (Γ_i/Γ)
Γ_1	$\Xi_b^- \pi^+ \times$ B($b \to \Xi_b(6227)^0$)/B($b \to \Xi_b^-$)	(4.5±0.9) %

$\Xi_b(6227)^0$ BRANCHING RATIOS

$\Gamma(\Xi_b^- \pi^+ \times B(b \to \Xi_b(6227)^0)/B(b \to \Xi_b^-))/\Gamma_{total}$ — Γ_1/Γ

VALUE (%)	DOCUMENT ID		TECN	COMMENT
4.5±0.8±0.4	AAIJ	21	LHCB	pp at 7, 8, 13 TeV

$\Xi_b(6227)^0$ REFERENCES

AAIJ 21 PR D103 012004 R. Aaij et al. (LHCb Collab.)

Ξ_{bc}^0

$J^P = \frac{1}{2}^+$

OMITTED FROM SUMMARY TABLE

Ξ_{bc}^0 DECAY MODES

	Mode	Fraction (Γ_i/Γ)	Confidence level
Γ_1	$D^0 p K^- \times$ B($b \to \Xi_{bc}^0$)/B($b \to \Lambda_b$)	$<1.4 \times 10^{-5}$	95%

Ξ_{bc}^0 BRANCHING RATIOS

$\Gamma(D^0 p K^- \times B(b \to \Xi_{bc}^0)/B(b \to \Lambda_b))/\Gamma_{total}$ — Γ_1/Γ

VALUE	CL%	DOCUMENT ID		TECN	COMMENT
$<1.4 \times 10^{-5}$	95	[1,2] AAIJ	20AM	LHCB	pp at 13 TeV

[1] AAIJ 20AM reports upper limits for [$\Gamma(\Xi_{bc}^0 \to D^0 p K^- \times B(b \to \Xi_{bc}^0)/B(b \to \Lambda_b))/\Gamma_{total}$] / [$B(\Lambda_b^0 \to p D^0 K^-)$] $< 3.0 \times 10^{-1}$–1.7×10^{-2} for the considered Ξ_{bc}^0 mass and lifetime hypotheses ranging from 6.7 to 7.2 GeV and from 100 to 500 fs. We use the 3.0×10^{-1} limit for the quoted result.
[2] AAIJ 20AM reports [$\Gamma(\Xi_{bc}^0 \to D^0 p K^- \times B(b \to \Xi_{bc}^0)/B(b \to \Lambda_b))/\Gamma_{total}$] / [$B(\Lambda_b^0 \to p D^0 K^-)$] $< 3.0 \times 10^{-1}$ which we multiply by our best value $B(\Lambda_b^0 \to p D^0 K^-) = 4.6 \times 10^{-5}$.

Ξ_{bc}^0 REFERENCES

AAIJ 20AM JHEP 2011 095 R. Aaij et al. (LHCb Collab.)

Ω_b^-

$I(J^P) = 0(\frac{1}{2}^+)$ Status: ***
I, J, P need confirmation.

In the quark model Ω_b^- is ssb ground state. None of its quantum numbers has been measured.

Ω_b^- MASS

VALUE (MeV)	DOCUMENT ID		TECN	COMMENT
6045.2 ± 1.2 OUR AVERAGE				
6044.30± 1.20± 1.12	[1] AAIJ	21AC	LHCB	pp at 7, 8, 13 TeV
6045.1 ± 3.2 ± 0.8	[2] AAIJ	16O	LHCB	pp at 7, 8 TeV
6047.5 ± 3.8 ± 0.6	[3] AALTONEN	14B	CDF	$p\overline{p}$ at 1.96 TeV
6046.0 ± 2.2 ± 0.5	[4] AAIJ	13AV	LHCB	pp at 7 TeV
• • • We do not use the following data for averages, fits, limits, etc. • • •				
6054.4 ± 6.8 ± 0.9	[5] AALTONEN	09AP	CDF	Repl. by AALTONEN 14B
6165 ±10 ±13	[6] ABAZOV	08AL	D0	$p\overline{p}$ at 1.96 TeV

[1] Uses $\Omega_b^- \to \Xi_c^+ K^- \pi^-$ and $\Xi_c^+ \to p K^- \pi^+$ decays. Reports the value of 6044.3 ± 1.2 ± $1.1^{+0.19}_{-0.22}$ MeV where the last uncertainty is due to the mass of Ξ_c^+. We have combined the two systematic uncertainties in quadrature.
[2] Reconstructed in $\Omega_b^- \to \Omega_c^0 \pi^-$, $\Omega_c^0 \to p K^- K^- \pi^+$ decays. Reference Ξ_b^- mass 5797.72 ± 0.6 MeV from AAIJ 14B.
[3] Uses $\Omega_b^- \to J/\psi \Omega^-$ and $\Omega_c^0 \pi^-$ decays, with the first evidence for $\Omega_b^- \to \Omega_c^0 \pi^-$ at 3.3 σ significance.
[4] Measured in $\Omega_b^- \to J/\psi \Omega^-$ with 19 ± 5 events.
[5] Observed in $\Omega_b^- \to J/\psi \Omega^-$ decays with 16^{+6}_{-4} candidates, a significance of 5.5 sigma from a combined mass-lifetime fit.
[6] Observed in $\Omega_b^- \to J/\psi \Omega^-$ decays with 17.8 ± 4.9 ± 0.8 candidates, a significance of 5.4 sigma.

$m_{\Omega_b^-} - m_{\Lambda_b^0}$

VALUE (MeV)	DOCUMENT ID		TECN	COMMENT
426.4±2.2±0.4	AAIJ	13AV	LHCB	pp at 7 TeV

$m_{\Omega_b^-} - m_{\Xi_b^-}$

VALUE (MeV)	DOCUMENT ID		TECN	COMMENT
247.3±3.2±0.5	[1] AAIJ	16O	LHCB	pp at 7, 8 TeV

Downloaded from https://academic.oup.com/ptep/article/2022/8/083C01/6651666 by KIT Library user on 27 September 2022

[1] Uses $\Omega_b^- \to \Omega_c^0 \pi^-$, $\Omega_c^0 \to p K^- K^- \pi^+$ and $\Xi_b^- \to \Xi_c^0 \pi^-$, $\Xi_c^0 \to p K^- K^- \pi^+$ decays.

Ω_b MEAN LIFE

"OUR EVALUATION" has been provided by the Heavy Flavor Averaging Group (HFLAV, https://hflav.web.cern.ch/).

VALUE (10^{-12} s)	DOCUMENT ID		TECN	COMMENT
$1.64^{+0.18}_{-0.17}$ OUR EVALUATION				
$1.65^{+0.18}_{-0.16}$ OUR AVERAGE				
$1.78 \pm 0.26 \pm 0.05 \pm 0.06$	[1] AAIJ	16O	LHCB	pp at 7, 8 TeV
$1.54^{+0.26}_{-0.21} \pm 0.05$	[2] AAIJ	14T	LHCB	pp at 7, 8 TeV
$1.66^{+0.53}_{-0.40} \pm 0.02$	[2] AALTONEN	14B	CDF	$p\overline{p}$ at 1.96 TeV
• • • We do not use the following data for averages, fits, limits, etc. • • •				
$1.13^{+0.53}_{-0.40} \pm 0.02$	[3] AALTONEN	09AP	CDF	Repl. by AALTONEN 14B

[1] Measured in $\Omega_b^- \to \Omega_c^0 \pi^-$, $\Omega_c^0 \to p K^- K^- \pi^+$ decays relative to $\Xi_b^- \to \Xi_c^0 \pi^-$, $\Xi_c^0 \to p K^- K^- \pi^+$ decays with reference Ξ_b^- mean life 1.599 ± 0.06 ps from AAIJ 14B.

[2] Measured in $\Omega_b^- \to J/\psi \Omega^-$ decays.

[3] Observed in $\Omega_b^- \to J/\psi \Omega^-$ decays with 16^{+6}_{-4} candidates, a significance of 5.5 sigma from a combined mass-lifetime fit.

$\tau(\Omega_b^-)/\tau(\Xi_b^-)$ mean life ratio

VALUE	DOCUMENT ID		TECN	COMMENT
$1.11 \pm 0.16 \pm 0.03$	[1] AAIJ	16O	LHCB	pp at 7, 8 TeV

[1] Uses $\Omega_b^- \to \Omega_c^0 \pi^-$, $\Omega_c^0 \to p K^- K^- \pi^+$ and $\Xi_b^- \to \Xi_c^0 \pi^-$, $\Xi_c^0 \to p K^- K^- \pi^+$ decays.

Ω_b^- DECAY MODES

	Mode	Fraction (Γ_i/Γ)	Confidence level
Γ_1	$J/\psi \Omega^- \times B(b \to \Omega_b)$	$(2.9^{+1.1}_{-0.8}) \times 10^{-6}$	
Γ_2	$p K^- K^- \times B(\overline{b} \to \Omega_b)$	$< 2.3 \times 10^{-9}$	90%
Γ_3	$p \pi^- \pi^- \times B(\overline{b} \to \Omega_b)$	$< 1.5 \times 10^{-8}$	90%
Γ_4	$p K^- \pi^- \times B(\overline{b} \to \Omega_b)$	$< 7 \times 10^{-9}$	90%
Γ_5	$\Omega_c^0 \pi^-$	seen	
Γ_6	$\Omega_c^0 \pi^-$, $\Omega_c^0 \to p K^- K^- \pi^+$	seen	
Γ_7	$\Xi_c^+ K^- \pi^-$	seen	

Ω_b^- BRANCHING RATIOS

$\Gamma(J/\psi \Omega^- \times B(b \to \Omega_b))/\Gamma_{total}$ — Γ_1/Γ

VALUE (units 10^{-4})	DOCUMENT ID		TECN	COMMENT
$0.029^{+0.011}_{-0.008}$ OUR AVERAGE				
$0.026^{+0.010}_{-0.007} \pm 0.004$	[1] AALTONEN	09AP	CDF	$p\overline{p}$ at 1.96 TeV
$0.08 \pm 0.04 \pm 0.02$	[2] ABAZOV	08AL	D0	$p\overline{p}$ at 1.96 TeV

[1] AALTONEN 09AP reports $[\Gamma(\Omega_b^- \to J/\psi \Omega^- \times B(b \to \Omega_b))/\Gamma_{total}] / [B(\Lambda_b^0 \to J/\psi(1S) \Lambda \times B(b \to \Lambda_b^0))] = 0.045^{+0.017}_{-0.012} \pm 0.004$ which we multiply by our best value $B(\Lambda_b^0 \to J/\psi(1S) \Lambda \times B(b \to \Lambda_b^0)) = (5.8 \pm 0.8) \times 10^{-5}$. Our first error is their experiment's error and our second error is the systematic error from using our best value.

[2] ABAZOV 08AL reports $[\Gamma(\Omega_b^- \to J/\psi \Omega^- \times B(b \to \Omega_b))/\Gamma_{total}] / [B(\Xi_b \to J/\psi \Xi^- \times B(b \to \Xi_b^-))] = 0.80 \pm 0.32^{+0.14}_{-0.22}$ which we multiply by our best value $B(\Xi_b \to J/\psi \Xi^- \times B(b \to \Xi_b^-)) = (1.02^{+0.26}_{-0.21}) \times 10^{-5}$. Our first error is their experiment's error and our second error is the systematic error from using our best value.

$\Gamma(p K^- K^- \times B(\overline{b} \to \Omega_b))/\Gamma_{total}$ — Γ_2/Γ

VALUE (units 10^{-5})	CL%	DOCUMENT ID		TECN	COMMENT
$< 2.3 \times 10^{-4}$	90	[1] AAIJ	21AH	LHCB	pp at 7, 8, 13 TeV
• • • We do not use the following data for averages, fits, limits, etc. • • •					
$< 2.5 \times 10^{-4}$	90	[2] AAIJ	17F	LHCB	pp at 7, 8 TeV

[1] AAIJ 21AH reports $[\Gamma(\Omega_b^- \to p K^- K^- \times B(\overline{b} \to \Omega_b))/\Gamma_{total}] / [B(\Xi_b^- \to p K^- K^- \times B(b \to \Xi_b^-))] < 62 \times 10^{-3}$ which we multiply by our best value $B(\Xi_b^- \to p K^- K^- \times B(b \to \Xi_b^-)) = 3.7 \times 10^{-8}$.

[2] AAIJ 17F reports $[\Gamma(\Omega_b^- \to p K^- K^- \times B(\overline{b} \to \Omega_b))/\Gamma_{total}] / [B(B^+ \to K^+ K^- K^+)] / [B(\overline{b} \to B^+)] < 18 \times 10^{-5}$ which we multiply by our best values $B(B^+ \to K^+ K^- K^+) = 3.40 \times 10^{-5}$, $B(\overline{b} \to B^+) = 40.8 \times 10^{-2}$.

$\Gamma(p \pi^- \pi^- \times B(\overline{b} \to \Omega_b))/\Gamma_{total}$ — Γ_3/Γ

VALUE (units 10^{-5})	CL%	DOCUMENT ID		TECN	COMMENT
$< 1.5 \times 10^{-3}$	90	[1] AAIJ	17F	LHCB	pp at 7, 8 TeV

[1] AAIJ 17F reports $[\Gamma(\Omega_b^- \to p \pi^- \pi^- \times B(\overline{b} \to \Omega_b))/\Gamma_{total}] / [B(B^+ \to K^+ K^- K^+)] / [B(\overline{b} \to B^+)] < 109 \times 10^{-5}$ which we multiply by our best values $B(B^+ \to K^+ K^- K^+) = 3.40 \times 10^{-5}$, $B(\overline{b} \to B^+) = 40.8 \times 10^{-2}$.

$\Gamma(p K^- \pi^- \times B(\overline{b} \to \Omega_b))/\Gamma_{total}$ — Γ_4/Γ

VALUE (units 10^{-5})	CL%	DOCUMENT ID		TECN	COMMENT
$< 7 \times 10^{-4}$	90	[1] AAIJ	17F	LHCB	pp at 7, 8 TeV

[1] AAIJ 17F reports $[\Gamma(\Omega_b^- \to p K^- \pi^- \times B(\overline{b} \to \Omega_b))/\Gamma_{total}] / [B(B^+ \to K^+ K^- K^+)] / [B(\overline{b} \to B^+)] < 51 \times 10^{-5}$ which we multiply by our best values $B(B^+ \to K^+ K^- K^+) = 3.40 \times 10^{-5}$, $B(\overline{b} \to B^+) = 40.8 \times 10^{-2}$.

$\Gamma(\Omega_c^0 \pi^-)/\Gamma_{total}$ — Γ_5/Γ

VALUE	DOCUMENT ID		TECN	COMMENT
seen	AAIJ	16O	LHCB	pp at 7, 8 TeV

$\Gamma(\Xi_c^+ K^- \pi^-)/\Gamma(\Omega_c^0 \pi^-, \Omega_c^0 \to p K^- K^- \pi^+)$ — Γ_7/Γ_6

VALUE (units 10^2)	DOCUMENT ID		TECN	COMMENT
$2.2 \pm 0.2 \pm 1.0$	[1] AAIJ	21AC	LHCB	pp at 7, 8, 13 TeV

[1] AAIJ 21AC reports $[\Gamma(\Omega_b^- \to \Xi_c^+ K^- \pi^-)/\Gamma(\Omega_b^- \to \Omega_c^0 \pi^-, \Omega_c^0 \to p K^- K^- \pi^+)] \times [B(\Xi_c^+ \to p K^- \pi^+)] = 1.35 \pm 0.11 \pm 0.05$ which we divide by our best value $B(\Xi_c^+ \to p K^- \pi^+) = (6.2 \pm 3.0) \times 10^{-3}$. Our first error is their experiment's error and our second error is the systematic error from using our best value.

Ω_b^- REFERENCES

AAIJ	21AC	PR D104 L091102	R. Aaij *et al.*	(LHCb Collab.)
AAIJ	21AH	PR D104 052010	R. Aaij *et al.*	(LHCb Collab.)
AAIJ	17F	PRL 118 071801	R. Aaij *et al.*	(LHCb Collab.)
AAIJ	16O	PR D93 092007	R. Aaij *et al.*	(LHCb Collab.)
AAIJ	14B	PL B728 234	R. Aaij *et al.*	(LHCb Collab.)
AAIJ	14T	PL B736 154	R. Aaij *et al.*	(LHCb Collab.)
AALTONEN	14B	PR D89 072014	T. Aaltonen *et al.*	(CDF Collab.)
AAIJ	13AV	PRL 110 182001	R. Aaij *et al.*	(LHCb Collab.)
AALTONEN	09AP	PR D80 072003	T. Aaltonen *et al.*	(CDF Collab.)
ABAZOV	08AL	PRL 101 232002	V.M. Abazov *et al.*	(D0 Collab.)

$\Omega_b(6316)^-$

$I(J^P) = ?(?^?)$ Status: *
I, J, P need confirmation.

OMITTED FROM SUMMARY TABLE

$\Omega_b(6316)^-$ MASS

VALUE (MeV)	DOCUMENT ID		TECN	COMMENT
$6315.6 \pm 0.3 \pm 0.5$	[1] AAIJ	20T	LHCB	pp at 7, 8, 13 TeV

[1] AAIJ 20T measures $m(\Omega_b(6316)^-) - m(\Xi_b^0) = 523.74 \pm 0.31 \pm 0.07$ MeV. We have adjusted the measurement to our best values of $m(\Xi_b^0) = 5791.9 \pm 0.5$ MeV. Our first error is their experiment's error and our second error is the systematic error from using our best values.

$\Omega_b(6316)^-$ WIDTH

VALUE (MeV)	CL%	DOCUMENT ID		TECN	COMMENT
< 4.2	95	AAIJ	20T	LHCB	pp at 7, 8, 13 TeV

$\Omega_b(6316)^-$ DECAY MODES

	Mode	Fraction (Γ_i/Γ)
Γ_1	$\Xi_b^0 K^-$	seen

$\Omega_b(6316)^-$ BRANCHING RATIOS

$\Gamma(\Xi_b^0 K^-)/\Gamma_{total}$ — Γ_1/Γ

VALUE	DOCUMENT ID		TECN	COMMENT
seen	[1] AAIJ	20T	LHCB	pp at 7, 8, 13 TeV

[1] AAIJ 20T establishes the decay at 2.1 σ significance level.

$\Omega_b(6316)^-$ REFERENCES

AAIJ	20T	PRL 124 082002	R. Aaij *et al.*	(LHCb Collab.)

Downloaded from https://academic.oup.com/ptep/article/2022/8/083C01/6651666 by KIT Library user on 27 September 2022

$\Omega_b(6330)^-$

$I(J^P) = ?(?^?)$ Status: *
I, J, P need confirmation.

OMITTED FROM SUMMARY TABLE

$\Omega_b(6330)^-$ MASS

VALUE (MeV)	DOCUMENT ID		TECN	COMMENT
6330.3±0.3±0.5	[1] AAIJ	20T	LHCB	pp at 7, 8, 13 TeV

[1] AAIJ 20T measures $m(\Omega_b(6330)^-)-m(\Xi_b^0) = 538.40 \pm 0.28 \pm 0.07$ MeV. We have adjusted the measurement to our best values of $m(\Xi_b^0) = 5791.9 \pm 0.5$ MeV. Our first error is their experiment's error and our second error is the systematic error from using our best values.

$\Omega_b(6330)^-$ WIDTH

VALUE (MeV)	CL%	DOCUMENT ID		TECN	COMMENT
<4.7	95	AAIJ	20T	LHCB	pp at 7, 8, 13 TeV

$\Omega_b(6330)^-$ DECAY MODES

	Mode	Fraction (Γ_i/Γ)
Γ_1	$\Xi_b^0 K^-$	seen

$\Omega_b(6330)^-$ BRANCHING RATIOS

$\Gamma(\Xi_b^0 K^-)/\Gamma_{total}$ — Γ_1/Γ

VALUE	DOCUMENT ID		TECN	COMMENT
seen	[1] AAIJ	20T	LHCB	pp at 7, 8, 13 TeV

[1] AAIJ 20T establishes the decay at 2.6 σ significance level.

$\Omega_b(6330)^-$ REFERENCES

AAIJ 20T PRL 124 082002 R. Aaij et al. (LHCb Collab.)

$\Omega_b(6340)^-$

$I(J^P) = ?(?^?)$ Status: *
I, J, P need confirmation.

OMITTED FROM SUMMARY TABLE

$\Omega_b(6340)^-$ MASS

VALUE (MeV)	DOCUMENT ID		TECN	COMMENT
6339.7±0.3±0.5	[1] AAIJ	20T	LHCB	pp at 7, 8, 13 TeV

[1] AAIJ 20T measures $m(\Omega_b(6340)^-)-m(\Xi_b^0) = 547.81 \pm 0.26 \pm 0.05$ MeV. We have adjusted the measurement to our best values of $m(\Xi_b^0) = 5791.9 \pm 0.5$ MeV. Our first error is their experiment's error and our second error is the systematic error from using our best values.

$\Omega_b(6340)^-$ WIDTH

VALUE (MeV)	CL%	DOCUMENT ID		TECN	COMMENT
<1.8	95	AAIJ	20T	LHCB	pp at 7, 8, 13 TeV

$\Omega_b(6340)^-$ DECAY MODES

	Mode	Fraction (Γ_i/Γ)
Γ_1	$\Xi_b^0 K^-$	seen

$\Omega_b(6340)^-$ BRANCHING RATIOS

$\Gamma(\Xi_b^0 K^-)/\Gamma_{total}$ — Γ_1/Γ

VALUE	DOCUMENT ID		TECN	COMMENT
seen	AAIJ	20T	LHCB	pp at 7, 8, 13 TeV

$\Omega_b(6340)^-$ REFERENCES

AAIJ 20T PRL 124 082002 R. Aaij et al. (LHCb Collab.)

$\Omega_b(6350)^-$

$I(J^P) = ?(?^?)$ Status: *
I, J, P need confirmation.

OMITTED FROM SUMMARY TABLE

$\Omega_b(6350)^-$ MASS

VALUE (MeV)	DOCUMENT ID		TECN	COMMENT
6349.8±0.4±0.5	[1] AAIJ	20T	LHCB	pp at 7, 8, 13 TeV

[1] AAIJ 20T measures $m(\Omega_b(6350)^-)-m(\Xi_b^0) = 557.98 \pm 0.35 \pm 0.05$ MeV. We have adjusted the measurement to our best values of $m(\Xi_b^0) = 5791.9 \pm 0.5$ MeV. Our first error is their experiment's error and our second error is the systematic error from using our best values.

$\Omega_b(6350)^-$ WIDTH

VALUE (MeV)	CL%	DOCUMENT ID		TECN	COMMENT
<3.2	95	AAIJ	20T	LHCB	pp at 7, 8, 13 TeV

$\Omega_b(6350)^-$ DECAY MODES

	Mode	Fraction (Γ_i/Γ)
Γ_1	$\Xi_b^0 K^-$	seen

$\Omega_b(6350)^-$ BRANCHING RATIOS

$\Gamma(\Xi_b^0 K^-)/\Gamma_{total}$ — Γ_1/Γ

VALUE	DOCUMENT ID		TECN	COMMENT
seen	AAIJ	20T	LHCB	pp at 7, 8, 13 TeV

$\Omega_b(6350)^-$ REFERENCES

AAIJ 20T PRL 124 082002 R. Aaij et al. (LHCb Collab.)

b-baryon ADMIXTURE (Λ_b, Ξ_b, Ω_b)

b-baryon ADMIXTURE MEAN LIFE

Each measurement of the b-baryon mean life is an average over an admixture of various b baryons which decay weakly. Different techniques emphasize different admixtures of produced particles, which could result in a different b-baryon mean life. More b-baryon flavor specific channels are not included in the measurement.

VALUE (10^{-12} s)	EVTS	DOCUMENT ID		TECN	COMMENT
• • • We do not use the following data for averages, fits, limits, etc. • • •					
$1.218^{+0.130}_{-0.115}\pm0.042$		[1] ABAZOV	07S	D0	Repl. by ABAZOV 12U
$1.22\ ^{+0.22}_{-0.18}\ \pm0.04$		[1] ABAZOV	05C	D0	Repl. by ABAZOV 07S
$1.16\ \pm0.20\ \pm0.08$		[2] ABREU	99W	DLPH	$e^+e^-\to Z$
$1.19\ \pm0.14\ \pm0.07$		[3] ABREU	99W	DLPH	$e^+e^-\to Z$
$1.14\ \pm0.08\ \pm0.04$		[4] ABREU	99W	DLPH	$e^+e^-\to Z$
$1.11\ ^{+0.19}_{-0.18}\ \pm0.05$		[5] ABREU	99W	DLPH	$e^+e^-\to Z$
$1.29\ ^{+0.24}_{-0.22}\ \pm0.06$		[5] ACKERSTAFF	98G	OPAL	$e^+e^-\to Z$
$1.20\ \pm0.08\ \pm0.06$		[6] BARATE	98D	ALEP	$e^+e^-\to Z$
$1.21\ \pm0.11$		[5] BARATE	98D	ALEP	$e^+e^-\to Z$
$1.32\ \pm0.15\ \pm0.07$		[7] ABE	96M	CDF	$p\overline{p}$ at 1.8 TeV
$1.46\ ^{+0.22}_{-0.21}\ ^{+0.07}_{-0.09}$		ABREU	96D	DLPH	Repl. by ABREU 99W
$1.10\ ^{+0.19}_{-0.17}\ \pm0.09$		[5] ABREU	96D	DLPH	$e^+e^-\to Z$
$1.16\ \pm0.11\ \pm0.06$		[5] AKERS	96	OPAL	$e^+e^-\to Z$
$1.27\ ^{+0.35}_{-0.29}\ \pm0.09$		ABREU	95S	DLPH	Repl. by ABREU 99W
$1.05\ ^{+0.12}_{-0.11}\ \pm0.09$	290	BUSKULIC	95L	ALEP	Repl. by BARATE 98D
$1.04\ ^{+0.48}_{-0.38}\ \pm0.10$	11	[8] ABREU	93F	DLPH	Excess $\Lambda\mu^-$, decay lengths
$1.05\ ^{+0.23}_{-0.20}\ \pm0.08$	157	[9] AKERS	93	OPAL	Excess $\Lambda\ell^-$, decay lengths
$1.12\ ^{+0.32}_{-0.29}\ \pm0.16$	101	[10] BUSKULIC	92I	ALEP	Excess $\Lambda\ell^-$, impact parameters

[1] Measured mean life using fully reconstructed $\Lambda_b^0 \to J/\psi\Lambda$ decays.
[2] Measured using $\Lambda\ell^-$ decay length.
[3] Measured using $p\ell^-$ decay length.
[4] This ABREU 99W result is the combined result of the $\Lambda\ell^-$, $p\ell^-$, and excess $\Lambda\mu^-$ impact parameter measurements.
[5] Measured using $\Lambda_c\ell^-$ and $\Lambda\ell^+\ell^-$.
[6] Measured using the excess of $\Lambda\ell^-$, lepton impact parameter.

Downloaded from https://academic.oup.com/ptep/article/2022/8/083C01/6651666 by KIT Library user on 27 September 2022

[7] Measured using $\Lambda_c \ell^-$.
[8] ABREU 93F superseded by ABREU 96D.
[9] AKERS 93 superseded by AKERS 96.
[10] BUSKULIC 92I superseded by BUSKULIC 95L.

b-baryon ADMIXTURE DECAY MODES (Λ_b, Ξ_b, Ω_b)

These branching fractions are actually an average over weakly decaying b-baryons weighted by their production rates at the LHC, LEP, and Tevatron, branching ratios, and detection efficiencies. They scale with the b-baryon production fraction B($b \to$ b-baryon).

The branching fractions B(b-baryon $\to \Lambda \ell^- \overline{\nu}_\ell$ anything) and B($\Lambda_b^0 \to \Lambda_c^+ \ell^- \overline{\nu}_\ell$ anything) are not pure measurements because the underlying measured products of these with B($b \to$ b-baryon) were used to determine B($b \to$ b-baryon), as described in the note "Production and Decay of b-Flavored Hadrons."

For inclusive branching fractions, *e.g.*, $B \to D^\pm$ anything, the values usually are multiplicities, not branching fractions. They can be greater than one.

	Mode	Fraction (Γ_i/Γ)	Scale factor
Γ_1	$p\mu^-\overline{\nu}$ anything	$(5.8^{+2.3}_{-2.0})$ %	
Γ_2	$p\ell\overline{\nu}_\ell$ anything	(5.6 ± 1.2) %	
Γ_3	p anything	(70 ± 22) %	
Γ_4	$\Lambda\ell^-\overline{\nu}_\ell$ anything	(3.8 ± 0.6) %	
Γ_5	$\Lambda\ell^+\nu_\ell$ anything	(3.2 ± 0.8) %	
Γ_6	Λ anything	(39 ± 7) %	
Γ_7	$\Xi^-\ell^-\overline{\nu}_\ell$ anything	$(4.6 \pm 1.4) \times 10^{-3}$	1.2

b-baryon ADMIXTURE (Λ_b, Ξ_b, Ω_b) BRANCHING RATIOS

$\Gamma(p\mu^-\overline{\nu}\text{anything})/\Gamma_{\text{total}}$ — Γ_1/Γ

VALUE (%)	EVTS	DOCUMENT ID		TECN	COMMENT
$5.8^{+2.2}_{-1.9} \pm 0.8$	125	[1] ABREU	95S	DLPH	$e^+e^- \to Z$

[1] ABREU 95S reports [$\Gamma(b\text{-baryon} \to p\mu^-\overline{\nu}\text{anything})/\Gamma_{\text{total}}$] × [B($\overline{b} \to$ b-baryon)] = $0.0049 \pm 0.0011^{+0.0015}_{-0.0011}$ which we divide by our best value B($\overline{b} \to$ b-baryon) = $(8.4 \pm 1.1) \times 10^{-2}$. Our first error is their experiment's error and our second error is the systematic error from using our best value.

$\Gamma(p\ell\overline{\nu}_\ell\text{anything})/\Gamma_{\text{total}}$ — Γ_2/Γ

VALUE (%)	DOCUMENT ID		TECN	COMMENT
$5.6 \pm 0.9 \pm 0.7$	[1] BARATE	98V	ALEP	$e^+e^- \to Z$

[1] BARATE 98V reports [$\Gamma(b\text{-baryon} \to p\ell\overline{\nu}_\ell\text{anything})/\Gamma_{\text{total}}$] × [B($\overline{b} \to$ b-baryon)] = $(4.72 \pm 0.66 \pm 0.44) \times 10^{-3}$ which we divide by our best value B($\overline{b} \to$ b-baryon) = $(8.4 \pm 1.1) \times 10^{-2}$. Our first error is their experiment's error and our second error is the systematic error from using our best value.

$\Gamma(p\ell\overline{\nu}_\ell\text{anything})/\Gamma(p\text{anything})$ — Γ_2/Γ_3

VALUE (%)	DOCUMENT ID		TECN	COMMENT
$8.0 \pm 1.2 \pm 1.4$	BARATE	98V	ALEP	$e^+e^- \to Z$

$\Gamma(\Lambda\ell^-\overline{\nu}_\ell\text{anything})/\Gamma_{\text{total}}$ — Γ_4/Γ

The values and averages in this section serve only to show what values result if one assumes our B($b \to$ b-baryon). They cannot be thought of as measurements since the underlying product branching fractions were also used to determine B($b \to$ b-baryon) as described in the note on "Production and Decay of b-Flavored Hadrons."

VALUE (%)	EVTS	DOCUMENT ID		TECN	COMMENT
3.8±0.6 OUR AVERAGE					
$3.9 \pm 0.5 \pm 0.5$		[1] BARATE	98D	ALEP	$e^+e^- \to Z$
$3.5 \pm 0.4 \pm 0.5$		[2] AKERS	96	OPAL	Excess of $\Lambda\ell^-$ over $\Lambda\ell^+$
$3.6 \pm 0.9 \pm 0.5$	262	[3] ABREU	95S	DLPH	Excess of $\Lambda\ell^-$ over $\Lambda\ell^+$
$7.3 \pm 1.4 \pm 1.0$	290	[4] BUSKULIC	95L	ALEP	Excess of $\Lambda\ell^-$ over $\Lambda\ell^+$
• • • We do not use the following data for averages, fits, limits, etc. • • •					
seen	157	[5] AKERS	93	OPAL	Excess of $\Lambda\ell^-$ over $\Lambda\ell^+$
$8.3 \pm 2.5 \pm 1.1$	101	[6] BUSKULIC	92I	ALEP	Excess of $\Lambda\ell^-$ over $\Lambda\ell^+$

[1] BARATE 98D reports [$\Gamma(b\text{-baryon} \to \Lambda\ell^-\overline{\nu}_\ell\text{anything})/\Gamma_{\text{total}}$] × [B($\overline{b} \to$ b-baryon)] = $0.00326 \pm 0.00016 \pm 0.00039$ which we divide by our best value B($\overline{b} \to$ b-baryon) = $(8.4 \pm 1.1) \times 10^{-2}$. Our first error is their experiment's error and our second error is the systematic error from using our best value. Measured using the excess of $\Lambda\ell^-$, lepton impact parameter.

[2] AKERS 96 reports [$\Gamma(b\text{-baryon} \to \Lambda\ell^-\overline{\nu}_\ell\text{anything})/\Gamma_{\text{total}}$] × [B($\overline{b} \to$ b-baryon)] = $0.00291 \pm 0.00023 \pm 0.00025$ which we divide by our best value B($\overline{b} \to$ b-baryon) = $(8.4 \pm 1.1) \times 10^{-2}$. Our first error is their experiment's error and our second error is the systematic error from using our best value.

[3] ABREU 95S reports [$\Gamma(b\text{-baryon} \to \Lambda\ell^-\overline{\nu}_\ell\text{anything})/\Gamma_{\text{total}}$] × [B($\overline{b} \to$ b-baryon)] = $0.0030 \pm 0.0006 \pm 0.0004$ which we divide by our best value B($\overline{b} \to$ b-baryon) = $(8.4 \pm 1.1) \times 10^{-2}$. Our first error is their experiment's error and our second error is the systematic error from using our best value.

[4] BUSKULIC 95L reports [$\Gamma(b\text{-baryon} \to \Lambda\ell^-\overline{\nu}_\ell\text{anything})/\Gamma_{\text{total}}$] × [B($\overline{b} \to$ b-baryon)] = $0.0061 \pm 0.0006 \pm 0.0010$ which we divide by our best value B($\overline{b} \to$ b-baryon) = $(8.4 \pm 1.1) \times 10^{-2}$. Our first error is their experiment's error and our second error is the systematic error from using our best value.

[5] AKERS 93 superseded by AKERS 96.

[6] BUSKULIC 92I reports [$\Gamma(b\text{-baryon} \to \Lambda\ell^-\overline{\nu}_\ell\text{anything})/\Gamma_{\text{total}}$] × [B($\overline{b} \to$ b-baryon)] = $0.0070 \pm 0.0010 \pm 0.0018$ which we divide by our best value B($\overline{b} \to$ b-baryon) = $(8.4 \pm 1.1) \times 10^{-2}$. Our first error is their experiment's error and our second error is the systematic error from using our best value. Superseded by BUSKULIC 95L.

$\Gamma(\Lambda\ell^+\nu_\ell\text{anything})/\Gamma(\Lambda\text{anything})$ — Γ_5/Γ_6

VALUE (units 10^{-2})	DOCUMENT ID		TECN	COMMENT
8.0±1.2±0.8	ABBIENDI	99L	OPAL	$e^+e^- \to Z$
• • • We do not use the following data for averages, fits, limits, etc. • • •				
$7.0 \pm 1.2 \pm 0.7$	ACKERSTAFF	97N	OPAL	Repl. by ABBIENDI 99L

$\Gamma(\Lambda\text{anything})/\Gamma_{\text{total}}$ — Γ_6/Γ

VALUE (%)	DOCUMENT ID		TECN	COMMENT
39± 7 OUR AVERAGE				
$42 \pm 6 \pm 5$	[1] ABBIENDI	99L	OPAL	$e^+e^- \to Z$
$27^{+15}_{-9} \pm 3$	[2] ABREU	95C	DLPH	$e^+e^- \to Z$
• • • We do not use the following data for averages, fits, limits, etc. • • •				
$47 \pm 7 \pm 6$	[3] ACKERSTAFF	97N	OPAL	Repl. by ABBIENDI 99L

[1] ABBIENDI 99L reports [$\Gamma(b\text{-baryon} \to \Lambda\text{anything})/\Gamma_{\text{total}}$] × [B($\overline{b} \to$ b-baryon)] = $0.035 \pm 0.0032 \pm 0.0035$ which we divide by our best value B($\overline{b} \to$ b-baryon) = $(8.4 \pm 1.1) \times 10^{-2}$. Our first error is their experiment's error and our second error is the systematic error from using our best value.

[2] ABREU 95C reports $0.28^{+0.17}_{-0.12}$ from a measurement of [$\Gamma(b\text{-baryon} \to \Lambda\text{anything})/\Gamma_{\text{total}}$] × [B($\overline{b} \to$ b-baryon)] assuming B($\overline{b} \to$ b-baryon) = 0.08 ± 0.02, which we rescale to our best value B($\overline{b} \to$ b-baryon) = $(8.4 \pm 1.1) \times 10^{-2}$. Our first error is their experiment's error and our second error is the systematic error from using our best value.

[3] ACKERSTAFF 97N reports [$\Gamma(b\text{-baryon} \to \Lambda\text{anything})/\Gamma_{\text{total}}$] × [B($\overline{b} \to$ b-baryon)] = $0.0393 \pm 0.0046 \pm 0.0037$ which we divide by our best value B($\overline{b} \to$ b-baryon) = $(8.4 \pm 1.1) \times 10^{-2}$. Our first error is their experiment's error and our second error is the systematic error from using our best value.

$\Gamma(\Xi^-\ell^-\overline{\nu}_\ell\text{anything})/\Gamma_{\text{total}}$ — Γ_7/Γ

VALUE (units 10^{-3})	DOCUMENT ID		TECN	COMMENT
4.6±1.4 OUR AVERAGE Error includes scale factor of 1.2.				
$3.6 \pm 1.2 \pm 0.5$	[1] ABDALLAH	05C	DLPH	$e^+e^- \to Z^0$
$6.4 \pm 1.6 \pm 0.8$	[2] BUSKULIC	96T	ALEP	Excess $\Xi^-\ell^-$ over $\Xi^-\ell^+$
• • • We do not use the following data for averages, fits, limits, etc. • • •				
$7.0 \pm 2.8 \pm 0.9$	[3] ABREU	95V	DLPH	Repl. by ABDALLAH 05C

[1] ABDALLAH 05C reports [$\Gamma(b\text{-baryon} \to \Xi^-\ell^-\overline{\nu}_\ell\text{anything})/\Gamma_{\text{total}}$] × [B($\overline{b} \to$ b-baryon)] = $(3.0 \pm 1.0 \pm 0.3) \times 10^{-4}$ which we divide by our best value B($\overline{b} \to$ b-baryon) = $(8.4 \pm 1.1) \times 10^{-2}$. Our first error is their experiment's error and our second error is the systematic error from using our best value.

[2] BUSKULIC 96T reports [$\Gamma(b\text{-baryon} \to \Xi^-\ell^-\overline{\nu}_\ell\text{anything})/\Gamma_{\text{total}}$] × [B($\overline{b} \to$ b-baryon)] = $(5.4 \pm 1.1 \pm 0.8) \times 10^{-4}$ which we divide by our best value B($\overline{b} \to$ b-baryon) = $(8.4 \pm 1.1) \times 10^{-2}$. Our first error is their experiment's error and our second error is the systematic error from using our best value.

[3] ABREU 95V reports [$\Gamma(b\text{-baryon} \to \Xi^-\ell^-\overline{\nu}_\ell\text{anything})/\Gamma_{\text{total}}$] × [B($\overline{b} \to$ b-baryon)] = $(5.9 \pm 2.1 \pm 1.0) \times 10^{-4}$ which we divide by our best value B($\overline{b} \to$ b-baryon) = $(8.4 \pm 1.1) \times 10^{-2}$. Our first error is their experiment's error and our second error is the systematic error from using our best value.

b-baryon ADMIXTURE (Λ_b, Ξ_b, Ω_b) REFERENCES

ABAZOV	12U	PR D85 112003	V.M. Abazov *et al.*	(D0 Collab.)
ABAZOV	07S	PRL 99 142001	V.M. Abazov *et al.*	(D0 Collab.)
ABAZOV	05C	PRL 94 102001	V.M. Abazov *et al.*	(D0 Collab.)
ABDALLAH	05C	EPJ C44 299	J. Abdallah *et al.*	(DELPHI Collab.)
ABBIENDI	99L	EPJ C9 1	G. Abbiendi *et al.*	(OPAL Collab.)
ABREU	99W	EPJ C10 185	P. Abreu *et al.*	(DELPHI Collab.)
ACKERSTAFF	98G	PL B426 161	K. Ackerstaff *et al.*	(OPAL Collab.)
BARATE	98D	EPJ C2 197	R. Barate *et al.*	(ALEPH Collab.)
BARATE	98V	EPJ C5 205	R. Barate *et al.*	(ALEPH Collab.)
ACKERSTAFF	97N	ZPHY C74 423	K. Ackerstaff *et al.*	(OPAL Collab.)
ABE	96M	PRL 77 1439	F. Abe *et al.*	(CDF Collab.)
ABREU	96D	ZPHY C71 199	P. Abreu *et al.*	(DELPHI Collab.)
AKERS	96	ZPHY C69 195	R. Akers *et al.*	(OPAL Collab.)
BUSKULIC	96T	PL B384 449	D. Buskulic *et al.*	(ALEPH Collab.)
ABREU	95C	PL B347 447	P. Abreu *et al.*	(DELPHI Collab.)
ABREU	95S	ZPHY C68 375	P. Abreu *et al.*	(DELPHI Collab.)
ABREU	95V	ZPHY C68 541	P. Abreu *et al.*	(DELPHI Collab.)
BUSKULIC	95L	PL B357 685	D. Buskulic *et al.*	(ALEPH Collab.)
ABREU	93F	PL B311 379	P. Abreu *et al.*	(DELPHI Collab.)
AKERS	93	PL B316 435	R. Akers *et al.*	(OPAL Collab.)
BUSKULIC	92I	PL B297 449	D. Buskulic *et al.*	(ALEPH Collab.)

Downloaded from https://academic.oup.com/ptep/article/2022/8/083C01/6651666 by KIT Library user on 27 September 2022

EXOTIC BARYONS

See the related review(s):

Pentaquarks

$P_c(4312)^+$

Status: *

$P_c(4312)^+$ MASS

VALUE (MeV)	DOCUMENT ID		TECN	COMMENT
$4311.9 \pm 0.7^{+6.8}_{-0.6}$	AAIJ	19W	LHCB	pp at 7, 8, 13 TeV

$P_c(4312)^+$ WIDTH

VALUE (MeV)	DOCUMENT ID		TECN	COMMENT
$9.8 \pm 2.7^{+3.7}_{-4.5}$	AAIJ	19W	LHCB	pp at 7, 8, 13 TeV

$P_c(4312)^+$ DECAY MODES

	Mode	Fraction (Γ_i/Γ)
Γ_1	$J/\psi p$	seen

$P_c(4312)^+$ BRANCHING RATIOS

$\Gamma(J/\psi p)/\Gamma_{total}$ — Γ_1/Γ

VALUE	DOCUMENT ID		TECN	COMMENT
seen	AAIJ	19W	LHCB	pp at 7, 8, 13 TeV

$P_c(4312)^+$ REFERENCES

AAIJ 19W PRL 122 222001 R. Aaij et al. (LHCb Collab.)

$P_c(4380)^+$

Status: *

A resonance seen in $\Lambda_b^0 \to P_c^+ K^-$, then $P_c \to J/\psi p$, with a significance of 9 standard deviations. The $J/\psi p$ quark content is $uudc\overline{c}$, a pentaquark. See also the $P_c(4450)^+$. In the best amplitude fit, the two states have opposite parity, one having $J = 3/2$, the other $J = 5/2$.

Extraction of the pentaquark signals requires some understanding of the dominant $K^- p$ background. AAIJ 15P used a model-dependent approach. AAIJ 16AG reanalyzed the data making minimal assumptions about the $K^- p$ background, and thus confirmed the strong significance of the pentaquark signals.

$P_c(4380)^+$ MASS

VALUE (MeV)	DOCUMENT ID		TECN	COMMENT
4380±8±29	AAIJ	15P	LHCB	pp at 7, 8 TeV

$P_c(4380)^+$ WIDTH

VALUE (MeV)	DOCUMENT ID		TECN	COMMENT
205±18±86	AAIJ	15P	LHCB	pp at 7, 8 TeV

$P_c(4380)^+$ DECAY MODES

	Mode	Fraction (Γ_i/Γ)
Γ_1	$J/\psi p$	seen

$P_c(4380)^+$ BRANCHING RATIOS

$\Gamma(J/\psi p)/\Gamma_{total}$ — Γ_1/Γ

VALUE	DOCUMENT ID		TECN	COMMENT
seen	AAIJ	15P	LHCB	pp at 7, 8 TeV

$P_c(4380)^+$ REFERENCES

AAIJ 16AG PRL 117 082002 R. Aaij et al. (LHCb Collab.)
AAIJ 15P PRL 115 072001 R. Aaij et al. (LHCb Collab.)

$P_c(4440)^+$

Status: *

$P_c(4440)^+$ MASS

VALUE (MeV)	DOCUMENT ID		TECN	COMMENT
$4440.3 \pm 1.3^{+4.1}_{-4.7}$	AAIJ	19W	LHCB	pp at 7, 8, 13 TeV

$P_c(4440)^+$ WIDTH

VALUE (MeV)	DOCUMENT ID		TECN	COMMENT
$20.6 \pm 4.9^{+8.7}_{-10.1}$	AAIJ	19W	LHCB	pp at 7, 8, 13 TeV

$P_c(4440)^+$ DECAY MODES

	Mode	Fraction (Γ_i/Γ)
Γ_1	$J/\psi p$	seen

$P_c(4440)^+$ BRANCHING RATIOS

$\Gamma(J/\psi p)/\Gamma_{total}$ — Γ_1/Γ

VALUE	DOCUMENT ID		TECN	COMMENT
seen	[1] POPOV	21	D0	$p\overline{p}$ at 1.96 TeV
seen	AAIJ	19W	LHCB	pp at 7, 8, 13 TeV

[1] Search for J/ψ inclusive production in association with a charged particle, assumed to be a proton. POPOV 21 observes a resonant signal consistent with a superposition of the $P_c(4440)^+$ and $P_c(4457)^+$, using masses and widths measured by AAIJ 19W, at significance of 3σ.

$P_c(4440)^+$ REFERENCES

POPOV 21 PAN 83 1383 A.V. Popov et al. (D0 Collab.)
AAIJ 19W PRL 122 222001 R. Aaij et al. (LHCb Collab.)

$P_c(4457)^+$

Status: *

was $P_c(4450)$

A resonance seen in $\Lambda_b^0 \to P_c^+ K^-$, then $P_c \to J/\psi p$, with a significance of 12 standard deviations. The $J/\psi p$ quark content is $uudc\overline{c}$, a pentaquark. See also the $P_c(4380)^+$. In the best amplitude fit, the two states have opposite parity, one having $J = 3/2$, the other $J = 5/2$.

Extraction of the pentaquark signals requires some understanding of the dominant $K^- p$ background. AAIJ 15P used a model-dependent approach. AAIJ 16AG reanalyzed the data making minimal assumptions about the $K^- p$ background, and thus confirmed the strong significance of the pentaquark signals.

$P_c(4457)^+$ MASS

VALUE (MeV)	DOCUMENT ID		TECN	COMMENT
$4457.3 \pm 0.6^{+4.1}_{-1.7}$	AAIJ	19W	LHCB	pp at 7, 8, 13 TeV
• • • We do not use the following data for averages, fits, limits, etc. • • •				
4449.8±1.7±2.5	[1] AAIJ	15P	LHCB	Repl. by AAIJ 19W

[1] Considering $P_c(4440)$ and $P_c(4457)$ as a single resonance.

$P_c(4457)^+$ WIDTH

VALUE (MeV)	DOCUMENT ID		TECN	COMMENT
$6.4 \pm 2.0^{+5.7}_{-1.9}$	AAIJ	19W	LHCB	pp at 7, 8, 13 TeV
• • • We do not use the following data for averages, fits, limits, etc. • • •				
39 ±5 ±19	[1] AAIJ	15P	LHCB	Repl. by AAIJ 19W

[1] Considering $P_c(4440)$ and $P_c(4457)$ as a single resonance.

$P_c(4457)^+$ DECAY MODES

	Mode	Fraction (Γ_i/Γ)
Γ_1	$J/\psi p$	seen

$P_c(4457)^+$ BRANCHING RATIOS

$\Gamma(J/\psi p)/\Gamma_{total}$ — Γ_1/Γ

VALUE	DOCUMENT ID		TECN	COMMENT
seen	[1] POPOV	21	D0	$p\overline{p}$ at 1.96 TeV

Downloaded from https://academic.oup.com/ptep/article/2022/8/083C01/6651666 by KIT Library user on 27 September 2022

seen	AAIJ	19W	LHCB	pp at 7, 8, 13 TeV
seen	AAIJ	15P	LHCB	pp at 7, 8 TeV

[1] Search for J/ψ inclusive production in association with a charged particle, assumed to be a proton. POPOV 21 observes a resonant signal consistent with a superposition of the $P_c(4440)^+$ and $P_c(4457)^+$, using masses and widths measured by AAIJ 19W, at significance of 3σ.

$P_c(4457)^+$ REFERENCES

POPOV	21	PAN 83 1383	A.V. Popov *et al.*	(D0 Collab.)
AAIJ	19W	PRL 122 222001	R. Aaij *et al.*	(LHCb Collab.)
AAIJ	16AG	PRL 117 082002	R. Aaij *et al.*	(LHCb Collab.)
AAIJ	15P	PRL 115 072001	R. Aaij *et al.*	(LHCb Collab.)

Downloaded from https://academic.oup.com/ptep/article/2022/8/083C01/6651666 by KIT Library user on 27 September 2022

Magnetic Monopole Searches 2185
Supersymmetric Particle Searches 2187
Technicolor 2238
Quark and Lepton Compositeness 2239
Extra Dimensions 2243
WIMP and Dark Matter Searches 2249
Other Particle Searches 2263

SEARCHES IN OTHER SECTIONS

Neutral Higgs Bosons, Searches for 1187
Charged Higgs Bosons ($H^{\pm}$ and $H^{\pm\pm}$), Searches for 1196
New Heavy Bosons 1200
Axions (A^0) and Other Very Light Bosons 1217
Heavy Charged Lepton Searches 1272
Double-β Decay 1284
Heavy Neutral Leptons, Searches for 1307
b' (Fourth Generation) Quark 1337
t' (Fourth Generation) Quark 1339
Free Quark Searches 1341

Related Reviews in Volume 1

85. Extra dimensions (rev.) 983
86. W'-boson searches (rev.) 991
87. Z'-boson searches (rev.) 995
88. Supersymmetry: theory (rev.) 1000
89. Supersymmetry: experiment (rev.) 1019
90. Axions and other similar particles (rev.) 1038
91. Quark and lepton compositeness, searches for (rev.) . . 1055
92. Dynamical electroweak symmetry 1061
breaking: implications of the H^0 (rev.)
93. Grand unified theories 1076
94. Leptoquarks (rev.) 1090
95. Magnetic monopoles (rev.) 1093

Downloaded from https://academic.oup.com/ptep/article/2022/8/083C01/6651666 by KIT Library user on 27 September 2022

Downloaded from https://academic.oup.com/ptep/article/2022/8/083C01/6651666 by KIT Library user on 27 September 2022

See key on page 1127

SEARCHES not in other sections

Magnetic Monopole Searches

See the related review(s):
Magnetic Monopoles

Monopole Production Cross Section — Accelerator Searches

X-SECT (cm^2)	MASS (GeV)	CHG (g)	ENERGY (GeV)	BEAM	DOCUMENT ID		TECN
<3 E-38	750–1910	1–5	13000	pp	[1] ACHARYA	21	INDU
<1.3E−40	200–4000	1	13000	pp	[2] AAD	20G	ATLS
<5.6E−40	500–4000	2	13000	pp	[2] AAD	20G	ATLS
	200–5000	2	13000	pp	[3] ACHARYA	19B	INDU
	200–5000	1	13000	pp	[4] ACHARYA	18A	INDU
<2.5E−37	200–6000	1	13000	pp	[5] ACHARYA	17	INDU
<2E−37	200–6000	2	13000	pp	[5] ACHARYA	17	INDU
<4E−37	200–5000	3	13000	pp	[5] ACHARYA	17	INDU
<1.5E−36	400–4000	4	13000	pp	[5] ACHARYA	17	INDU
<7E−36	1000–3000	5	13000	pp	[5] ACHARYA	17	INDU
<5E−40	200–2500	0.5–2.0	8000	pp	[6] AAD	16AB	ATLS
<2E−37	100–3500	1	8000	pp	[7] ACHARYA	16	INDU
<2E−37	100–3500	2	8000	pp	[7] ACHARYA	16	INDU
<6E−37	500–3000	3	8000	pp	[7] ACHARYA	16	INDU
<7E−36	1000–2000	4	8000	pp	[7] ACHARYA	16	INDU
<1.6E−38	200–1200	1	7000	pp	[8] AAD	12CS	ATLS
<5E−38	45–102	1	206	e^+e^-	[9] ABBIENDI	08	OPAL
<0.2E−36	200–700	1	1960	$p\overline{p}$	[10] ABULENCIA	06K	CNTR
< 2.E−36		1	300	e^+p	[11,12] AKTAS	05A	INDU
< 0.2 E−36		2	300	e^+p	[11,12] AKTAS	05A	INDU
< 0.09E−36		3	300	e^+p	[11,12] AKTAS	05A	INDU
< 0.05E−36		≥ 6	300	e^+p	[11,12] AKTAS	05A	INDU
< 2.E−36		1	300	e^+p	[11,13] AKTAS	05A	INDU
< 0.2E−36		2	300	e^+p	[11,13] AKTAS	05A	INDU
< 0.07E−36		3	300	e^+p	[11,13] AKTAS	05A	INDU
< 0.06E−36		≥ 6	300	e^+p	[11,13] AKTAS	05A	INDU
< 0.6E−36	>265	1	1800	$p\overline{p}$	[14] KALBFLEISCH	04	INDU
< 0.2E−36	>355	2	1800	$p\overline{p}$	[14] KALBFLEISCH	04	INDU
< 0.07E−36	>410	3	1800	$p\overline{p}$	[14] KALBFLEISCH	04	INDU
< 0.2E−36	>375	6	1800	$p\overline{p}$	[14] KALBFLEISCH	04	INDU
< 0.7E−36	>295	1	1800	$p\overline{p}$	[15,16] KALBFLEISCH	00	INDU
< 7.8E−36	>260	2	1800	$p\overline{p}$	[15,16] KALBFLEISCH	00	INDU
< 2.3E−36	>325	3	1800	$p\overline{p}$	[15,17] KALBFLEISCH	00	INDU
< 0.11E−36	>420	6	1800	$p\overline{p}$	[15,17] KALBFLEISCH	00	INDU
<0.65E−33	<3.3	≥ 2	11A	^{197}Au	[18,19] HE	97	
<1.90E−33	<8.1	≥ 2	160A	^{208}Pb	[18,19] HE	97	
<3.E−37	<45.0	1.0	88–94	e^+e^-	PINFOLD	93	PLAS
<3.E−37	<41.6	2.0	88–94	e^+e^-	PINFOLD	93	PLAS
<7.E−35	<44.9	0.2–1.0	89–93	e^+e^-	KINOSHITA	92	PLAS
<2.E−34	<850	≥ 0.5	1800	$p\overline{p}$	BERTANI	90	PLAS
<1.2E−33	<800	≥ 1	1800	$p\overline{p}$	PRICE	90	PLAS
<1.E−37	<29	1	50–61	e^+e^-	KINOSHITA	89	PLAS
<1.E−37	<18	2	50–61	e^+e^-	KINOSHITA	89	PLAS
<1.E−38	<17	<1	35	e^+e^-	BRAUNSCH...	88B	CNTR
<8.E−37	<24	1	50–52	e^+e^-	KINOSHITA	88	PLAS
<1.3E−35	<22	2	50–52	e^+e^-	KINOSHITA	88	PLAS
<9.E−37	<4	<0.15	10.6	e^+e^-	GENTILE	87	CLEO
<3.E−32	<800	≥ 1	1800	$p\overline{p}$	PRICE	87	PLAS
<3.E−38		<3	29	e^+e^-	FRYBERGER	84	PLAS
<1.E−31		1,3	540	$p\overline{p}$	AUBERT	83B	PLAS
<4.E−38	<10	<6	34	e^+e^-	MUSSET	83	PLAS
<8.E−36	<20		52	pp	[20] DELL	82	CNTR
<9.E−37	<30	<3	29	e^+e^-	KINOSHITA	82	PLAS
<1.E−37	<20	<24	63	pp	CARRIGAN	78	CNTR
<1.E−37	<30	<3	56	pp	HOFFMANN	78	PLAS
			62	pp	[20] DELL	76	SPRK
<4.E−33			300	p	[20] STEVENS	76B	SPRK
<1.E−40	<5	<2	70	p	[21] ZRELOV	76	CNTR
<2.E−30			300	n	[20] BURKE	75	OSPK
<1.E−38			8	ν	[22] CARRIGAN	75	HLBC
<5.E−43	<12	<10	400	p	EBERHARD	75B	INDU
<2.E−36	<30	<3	60	pp	GIACOMELLI	75	PLAS
<5.E−42	<13	<24	400	p	CARRIGAN	74	CNTR
<6.E−42	<12	<24	300	p	CARRIGAN	73	CNTR
<2.E−36		1	0.001	γ	[21] BARTLETT	72	CNTR
<1.E−41	<5		70	p	GUREVICH	72	EMUL
<1.E−40	<3	<2	28	p	AMALDI	63	EMUL
<2.E−40	<3	<2	30	p	PURCELL	63	CNTR
<1.E−35	<3	<4	28	p	FIDECARO	61	CNTR
<2.E−35	<1	1	6	p	BRADNER	59	EMUL

[1] ACHARYA 21 search for dyons at LHC. Using a production model limits (we report the lowest) are set for dyons with magnetic charge up to 5 gD, electric charges up to 200 e and spins 0, 1/2, 1. The corresponding mass limits for magnetic monopoles are in the range 870–2040 GeV for magnetic charges in the same range.

[2] AAD 20G give limits for Drell-Yan production with spin-0 and spin-1/2 monopoles. The above limit is for spin = 0 at mass = 3 TeV.

[3] ACHARYA 19B limits both β-dependent and β-independent on monopoles with spins 0, 1/2, and 1 and with magnetic charges ranging from one to five times the Dirac charge in mass ranges between 200 GeV and 5000 GeV.

[4] ACHARYA 18A provide limits on monopoles with spins 0, 1/2, and 1 and with magnetic charges ranging from two to five times the Dirac charge.

[5] The search was sensitive to monopoles which had stopped in aluminium trapping volumes. Monopoles with spins 0 and 1/2 were considered; mass-dependent spin 1/2 monopole limits are quoted here.

[6] AAD 16AB model-independent 95% CL limits estimated using a fiducial region of approximately constant acceptance. Limits are mass-dependent.

[7] ACHARYA 16 limits at 95% CL estimated using a Drell-Yan-like production mechanism for scalar monopoles.

[8] AAD 12CS searched for monopoles as highly ionising objects. The cross section limits are based on an assumed Drell Yan-like production process for spin 1/2 monopoles. The limits are mass- and scenario-dependent.

[9] ABBIENDI 08 assume production of spin 1/2 monopoles with effective charge $g\beta$ (n=1), via $e^+e^- \rightarrow \gamma^* \rightarrow M\overline{M}$, so that the cross section is proportional to $(1 + \cos^2\theta)$. There is no z information for such highly saturated tracks, so a parabolic track in the jet chamber is projected onto the xy plane. Charge per hit in the chamber produces a clean separation of signal and background.

[10] ABULENCIA 06K searches for high-ionizing signals in CDF central outer tracker and time-of-flight detector. For Drell-Yan $M\overline{M}$ production, the cross section limit implies $M > 360$ GeV at 95% CL.

[11] AKTAS 05A model-dependent limits as a function of monopole mass shown for arbitrary mass of 60 GeV. Based on search for stopped monopoles in the H1 Al beam pipe.

[12] AKTAS 05A limits with assumed elastic spin 0 monopole pair production.

[13] AKTAS 05A limits with assumed inelastic spin 1/2 monopole pair production.

[14] KALBFLEISCH 04 reports searches for stopped magnetic monopoles in Be, Al, and Pb samples obtained from discarded material from the upgrading of DØ and CDF. A large-aperture warm-bore cryogenic detector was used. The approach was an extension of the methods of KALBFLEISCH 00. Cross section results moderately model dependent; interpretation as a mass lower limit depends on possibly invalid perturbation expansion.

[15] KALBFLEISCH 00 used an induction method to search for stopped monopoles in pieces of the DØ (FNAL) beryllium beam pipe and in extensions to the drift chamber aluminum support cylinder. Results are model dependent.

[16] KALBFLEISCH 00 result is for aluminum.

[17] KALBFLEISCH 00 result is for beryllium.

[18] HE 97 used a lead target and barium phosphate glass detectors. Cross-section limits are well below those predicted via the Drell-Yan mechanism.

[19] This work has also been reinterpreted in the framework of monopole production via the thermal Schwinger process (GOULD 17); this gives rise to lower mass limits.

[20] Multiphoton events.

[21] Cherenkov radiation polarization.

[22] Re-examines CERN neutrino experiments.

Monopole Production — Other Accelerator Searches

MASS (GeV)	CHG (g)	SPIN	ENERGY (GeV)	BEAM	DOCUMENT ID		TECN
> 610	≥ 1	0	1800	$p\overline{p}$	[1] ABBOTT	98K	D0
> 870	≥ 1	1/2	1800	$p\overline{p}$	[1] ABBOTT	98K	D0
>1580	≥ 1	1	1800	$p\overline{p}$	[1] ABBOTT	98K	D0
> 510			88–94	e^+e^-	[2] ACCIARRI	95C	L3

[1] ABBOTT 98K search for heavy pointlike Dirac monopoles via central production of a pair of photons with high transverse energies.

[2] ACCIARRI 95C finds a limit $B(Z \rightarrow \gamma\gamma\gamma) < 0.8 \times 10^{-5}$ (which is possible via a monopole loop) at 95% CL and sets the mass limit via a cross section model.

Monopole Flux — Cosmic Ray Searches

"Caty" in the charge column indicates a search for monopole-catalyzed nucleon decay.

FLUX (cm^{-2}sr^{-1}s^{-1})	MASS (GeV)	CHG (g)	COMMENTS ($\beta = v/c$)	DOCUMENT ID		TECN
<2E-19		1	0.86< β <0.995	[1] ABBASI	22	ICCB
<2E-14	>5E8		6E-4< β <5E-3	[2] ACERO	21	NOVA
<1E-17		Caty	1E-5 < β <1E-3	[3] GAPONENKO	21	BAIK
<1.5E−18		1	β >0.6	[4] ALBERT	17	ANTR
<2.5E−21		1	1E8< γ <1E13	[5] AAB	16	AUGE
<1.55E-18			β >0.51	[6] AARTSEN	16B	ICCB
<1E-17		Caty	1E-3< β <1E-2	[7] AARTSEN	14	ICCB
<3E-18		1	β >0.8	[8] ABBASI	13	ICCB
<1.3E-17		1	β >0.625	[9] ADRIAN-MAR..	12A	ANTR
<6E-28	<1E17	Caty	1E-5< β <0.04	[10] UENO	12	SKAM
<1E-19		**1**	**γ >1E10**	[11] DETRIXHE	11	ANIT
<3.8E-17		1	β >0.76	[8] ABBASI	10A	ICCB
<1.3E−15	1E4<M<5E13	1	β >0.05	[12] BALESTRA	08	PLAS
<0.65E−15	>5E13	1	β >0.05	[12] BALESTRA	08	PLAS
<1E−18		**1**	**γ >1 E8**	[11] HOGAN	08	RICE
<1.4E−16		**1**	**1.1E−4 < β <1**	[13] AMBROSIO	02B	MCRO
<3E−16		Caty	1.1E−4 < β <5E−3	[14] AMBROSIO	02C	MCRO
<1.5E−15		1	5E−3 < β < 0.99	[15] AMBROSIO	02D	MCRO
<1E−15		1	1.1×10^{-4}–0.1	[16] AMBROSIO	97	MCRO
<5.6E−15		1	(0.18–3.0)E−3	[17] AHLEN	94	MCRO
<2.7E−15		Caty	$\beta \sim 1 \times 10^{-3}$	[18] BECKER-SZ...	94	IMB
<8.7E−15		1	>2.E−3	THRON	92	SOUD
<4.4E−12		1	all β	GARDNER	91	INDU

Downloaded from https://academic.oup.com/ptep/article/2022/8/083C01/6651666 by KIT Library user on 27 September 2022

<7.2E−13		1	all β		HUBER	91	INDU
<3.7E−15	>E12	1	β=1.E−4	[19]	ORITO	91	PLAS
<3.2E−16	>E10	1	$\beta > 0.05$	[19]	ORITO	91	PLAS
<3.2E−16	>E10−E12	2, 3		[19]	ORITO	91	PLAS
<3.8E−13		1	all β		BERMON	90	INDU
<5.E−16		Caty	β <1.E−3	[18]	BEZRUKOV	90	CHER
<1.8E−14		1	β >1.1E−4	[20]	BUCKLAND	90	HEPT
<1E−18			3.E−4 < β <1.5E−3	[21]	GHOSH	90	MICA
<7.2E−13		1	all β		HUBER	90	INDU
<5.E−12	>E7	1	3.E−4 < β <5.E−3		BARISH	87	CNTR
<1.E−13		Caty	1.E−5 < β <1	[18]	BARTELT	87	SOUD
<1.E−10		1	all β		EBISU	87	INDU
<2.E−13			1.E−4 < β <6.E−4		MASEK	87	HEPT
<2.E−14			4.E−5 < β <2.E−4		NAKAMURA	87	PLAS
<2.E−14			1.E−3 < β <1		NAKAMURA	87	PLAS
<5.E−14			9.E−4 < β <1.E−2		SHEPKO	87	CNTR
<2.E−13			4.E−4 < β <1		TSUKAMOTO	87	CNTR
<5.E−14		1	all β	[22]	CAPLIN	86	INDU
<5.E−12		1			CROMAR	86	INDU
<1.E−13		1	7.E−4 < β		HARA	86	CNTR
<7.E−11		1	all β		INCANDELA	86	INDU
<1.E−18			4.E−4 < β <1.E−3	[21]	PRICE	86	MICA
<5.E−12		1			BERMON	85	INDU
<6.E−12		1			CAPLIN	85	INDU
<6.E−10		1			EBISU	85	INDU
<3.E−15		Caty	5.E−5 ≤ β ≤ 1.E−3	[18]	KAJITA	85	KAMI
<2.E−21		Caty	β <1.E−3	[18,23]	KAJITA	85	KAMI
<3.E−15		Caty	1.E−3 < β <1.E−1	[18]	PARK	85B	CNTR
<5.E−12		1	1.E−4 < β <1		BATTISTONI	84	NUSX
<7.E−12		1			INCANDELA	84	INDU
<7.E−13		1	3.E−4 < β	[20]	KAJINO	84	CNTR
<2.E−12		1	3.E−4 < β <1.E−1		KAJINO	84B	CNTR
<6.E−13		1	5.E−4 < β <1		KAWAGOE	84	CNTR
<2.E−14			1.E−3 < β	[18]	KRISHNA...	84	CNTR
<4.E−13		1	6.E−4 < β <2.E−3		LISS	84	CNTR
<1.E−16			3.E−4 < β <1.E−3	[21]	PRICE	84	MICA
<1.E−13		1	1.E−4 < β		PRICE	84B	PLAS
<4.E−13		1	6.E−4 < β <2.E−3		TARLE	84	CNTR
				[24]	ANDERSON	83	EMUL
<4.E−13		1	1.E−2 < β <1.E−3		BARTELT	83B	CNTR
<1.E−12		1	7.E−3 < β <1		BARWICK	83	PLAS
<3.E−13		1	1.E−3 < β <4.E−1		BONARELLI	83	CNTR
<3.E−12		Caty	5.E−4 < β <5.E−2	[18]	BOSETTI	83	CNTR
<4.E−11		1			CABRERA	83	INDU
<5.E−15		1	1.E−2 < β <1		DOKE	83	PLAS
<8.E−15		Caty	1.E−4 < β <1.E−1	[18]	ERREDE	83	IMB
<5.E−12		1	1.E−4 < β <3.E−2		GROOM	83	CNTR
<2.E−12			6.E−4 < β <1		MASHIMO	83	CNTR
<1.E−13		1	β=3.E−3		ALEXEYEV	82	CNTR
<2.E−12		1	7.E−3 < β <6.E−1		BONARELLI	82	CNTR
6.E−10		1	all β	[25]	CABRERA	82	INDU
<2.E−11			1.E−2 < β <1.E−1		MASHIMO	82	CNTR
<2.E−15			concentrator		BARTLETT	81	PLAS
<1.E−13	>1		1.E−3 < β		KINOSHITA	81B	PLAS
<5.E−11	<E17		3.E−4 < β <1.E−3		ULLMAN	81	CNTR
<2.E−11			concentrator		BARTLETT	78	PLAS
1.E−1	>200	2		[26]	PRICE	75	PLAS
<2.E−13		>2			FLEISCHER	71	PLAS
<1.E−19		>2	obsidian, mica		FLEISCHER	69C	PLAS
<5.E−15	<15	<3	concentrator		CARITHERS	66	ELEC
<2.E−11		<1–3	concentrator		MALKUS	51	EMUL

[1] ABBASI 22 search was based on Cherenkov light detection in an array of optical modules in the Antarctic ice cap. Limits are speed-dependent.

[2] ACERO 21 employ NOvA experiment to set reported 90% CL upper limit on the cosmic monopoles flux for velocity $6 \times 10^{-4} < \beta < 5 \times 10^{-3}$ and mass $> 5 \times 10^{8}$ GeV.

[3] GAPONENKO 21 use data of NT200 two-year operation at Baikal to give speed-dependent limits for different assumed catalysis cross sections. Reported limit is for $\sigma = 10$ mb.

[4] ALBERT 17 limits were estimated using a Cherenkov light in an array of optical modules under the Mediterranean Sea. The limits are for MM masses between 10^{10} and 10^{14} GeV. The limits are speed-dependent.

[5] AAB 16 search was made with a set of telescopes sampling the longitudinal profile of fluorescence light emitted by extensive air showers. Limits are speed dependent.

[6] AARTSEN 16B was based on a Cherenkov signature in an array of optical modules which were sunk in the Antarctic ice cap. Limits are speed-dependent.

[7] Beyond the monopole speed, the limits of AARTSEN 14 depend on the catalysis cross section (σ) which corresponds to the monopole radiating $\bar{l}$ times the light per track length compared to the Cherenkov light from a single electrically charged, relativistic particle. The values quoted here correspond to $\sigma = 1$ barn or $\bar{l} = 30$.

[8] ABBASI 13 and ABBASI 10A were based on a Cherenkov signature in an array of optical modules which were sunk in the Antarctic ice cap. Limits are speed-dependent.

[9] ADRIAN-MARTINEZ 12A measurements were based on a Cherenkov signature in an underwater telescope in the Western Mediterranean Sea. Limits are speed-dependent.

[10] The limits from UENO 12 depend on the monopole speed and are also sensitive to assumed values of monopole mass and the catalysis cross section.

[11] HOGAN 08 and DETRIXHE 11 limits on relativistic monopoles are based on nonobservation of radio Cherenkov signals at the South Pole. Limits are speed-dependent.

[12] BALESTRA 08 exposed of nuclear track detector modules totaling 400 m^2 for 4 years at the Chacaltaya Laboratory (5230 m) in search for intermediate-mass monopoles with $\beta >$ 0.05. The analysis is mainly based on three CR39 modules. For $M > 5 \times 10^{13}$ GeV there can be upward-going monopoles as well, hence the flux limit is half that obtained for less massive monopoles. Previous experiments (e.g. MACRO and OHYA (ORITO 91)) had set limits only for $M > 1 \times 10^{9}$ GeV.

[13] AMBROSIO 02B direct search final result for $m \geq 10^{17}$ GeV, based upon 4.2 to 9.5 years of running, depending upon the subsystem. Limit with CR39 track-etch detector extends the limit from $\beta = 4 \times 10^{-5}$ (3.1×10^{-16} cm^{-2} sr^{-1} s^{-1}) to $\beta = 1 \times 10^{-4}$ (2.1×10^{-16} cm^{-2} sr^{-1} s^{-1}). Limit curve in paper is piecewise continuous due to different detection techniques for different β ranges.

[14] AMBROSIO 02C limit for catalysis of nucleon decay with catalysis cross section of $\approx$ 1 mb. The flux limit increases by $\sim$ 3 at the higher β limit, and increases to 1×10^{-14} cm^{-2} sr^{-1} s^{-1} if the catalysis cross section is 0.01 mb. Based upon 71193 hr of data with the streamer detector, with an acceptance of 4250 m^2 sr.

[15] AMBROSIO 02D result for "more than two years of data." Ionization search using several subsystems. Limit curve as a function of β not given. Included in AMBROSIO 02B.

[16] AMBROSIO 97 global MACRO 90%CL is 0.78×10^{-15} at $\beta = 1.1 \times 10^{-4}$, goes through a minimum at 0.61×10^{-15} near $\beta = (1.1–2.7) \times 10^{-3}$, then rises to 0.84×10^{-15} at β=0.1. The global limit in this region is below the Parker bound at 10^{-15}. Less stringent limits are established for $4 \times 10^{-5} < \beta < 1 \times 10^{-4}$. Limits set by various triggers and different subdetectors are given in the paper. All limits assume a catalysis cross section smaller than a few mb.

[17] AHLEN 94 limit for dyons extends down to β=0.9E−4 and a limit of 1.3E−14 extends to β = 0.8E−4. Also see comment by PRICE 94 and reply of BARISH 94. One loophole in the AHLEN 94 result is that in the case of monopoles catalyzing nucleon decay, relativistic particles could veto the events. See AMBROSIO 97 for additional results.

[18] Catalysis of nucleon decay; sensitive to assumed catalysis cross section.

[19] ORITO 91 limits are functions of velocity. Lowest limits are given here.

[20] Used DKMPR mechanism and Penning effect.

[21] Assumes monopole attaches fermion nucleus.

[22] Limit from combining data of CAPLIN 86, BERMON 85, INCANDELA 84, and CABRERA 83. For a discussion of controversy about CAPLIN 86 observed event, see GUY 87. Also see SCHOUTEN 87.

[23] Based on lack of high- energy solar neutrinos from catalysis in the sun.

[24] Anomalous long-range α (^{4}He) tracks.

[25] CABRERA 82 candidate event has single Dirac charge within ±5%.

[26] ALVAREZ 75, FLEISCHER 75, and FRIEDLANDER 75 explain as fragmenting nucleus. EBERHARD 75 and ROSS 76 discuss conflict with other experiments. HAGSTROM 77 reinterprets as antinucleus. PRICE 78 reassesses.

Monopole Flux — Astrophysics

FLUX ($cm^{-2}sr^{-1}s^{-1}$)	MASS (GeV)	CHG (g)	COMMENTS (β = v/c)	DOCUMENT ID		TECN
<1.3E−20			faint white dwarf	[1] FREESE	99	ASTR
<1.E−16	E17	1	galactic field	[2] ADAMS	93	COSM
<1.E−23			Jovian planets	[1] ARAFUNE	85	ASTR
<1.E−16	E15		solar trapping	BRACCI	85B	ASTR
<1.E−18		1		[1] HARVEY	84	COSM
<3.E−23			neutron stars	KOLB	84	ASTR
<7.E−22			pulsars	[1] FREESE	83B	ASTR
<1.E−18	<E18	1	intergalactic field	[1] REPHAELI	83	COSM
<1.E−23			neutron stars	[1] DIMOPOUL...	82	COSM
<5.E−22			neutron stars	[1] KOLB	82	COSM
<5.E−15	>E21		galactic halo	SALPETER	82	COSM
<1.E−12	E19	1	β=3.E−3	[3] TURNER	82	COSM
<1.E−16		1	galactic field	PARKER	70	COSM

[1] Catalysis of nucleon decay.

[2] ADAMS 93 limit based on "survival and growth of a small galactic seed field" is 10^{-16} $(m/10^{17}$ GeV) cm^{-2} s^{-1} sr^{-1}. Above 10^{17} GeV, limit 10^{-16} $(10^{17}$ GeV$/m)$ cm^{-2} s^{-1} sr^{-1} (from requirement that monopole density does not overclose the universe) is more stringent.

[3] Re-evaluates PARKER 70 limit for GUT monopoles.

Monopole Density — Matter Searches

DENSITY	CHG (g)	MATERIAL	DOCUMENT ID		TECN
<9.8E−5/gram	≥ 1	Polar rock	BENDTZ	13	INDU
<6.9E−6/gram	>1/3	Meteorites and other	JEON	95	INDU
<2.E−7/gram	>0.6	Fe ore	[1] EBISU	87	INDU
<4.6E−6/gram	> 0.5	deep schist	KOVALIK	86	INDU
<1.6E−6/gram	> 0.5	manganese nodules	[2] KOVALIK	86	INDU
<1.3E−6/gram	> 0.5	seawater	KOVALIK	86	INDU
>1.E+14/gram	>1/3	iron aerosols	MIKHAILOV	83	SPEC
<6.E−4/gram		air, seawater	CARRIGAN	76	CNTR
<5.E−1/gram	>0.04	11 materials	CABRERA	75	INDU
<2.E−4/gram	>0.05	moon rock	ROSS	73	INDU
<6.E−7/gram	<140	seawater	KOLM	71	CNTR
<1.E−2/gram	<120	manganese nodules	FLEISCHER	69	PLAS
<1.E−4/gram	>0	manganese	FLEISCHER	69B	PLAS
<2.E−3/gram	<1–3	magnetite, meteor	GOTO	63	EMUL
<2.E−2/gram		meteorite	PETUKHOV	63	CNTR

[1] Mass 1×10^{14}–1×10^{17} GeV.

[2] KOVALIK 86 examined 498 kg of schist from two sites which exhibited clear mineralogical evidence of having been buried at least 20 km deep and held below the Curie temperature.

Downloaded from https://academic.oup.com/ptep/article/2022/8/083C01/6651666 by KIT Library user on 27 September 2022

Monopole Density — Astrophysics

DENSITY	CHG (g)	MATERIAL	DOCUMENT ID		TECN
<1.E−9/gram	1	sun, catalysis	[1] ARAFUNE	83	COSM
<6.E−33/nucl	1	moon wake	SCHATTEN	83	ELEC
<2.E−28/nucl		earth heat	CARRIGAN	80	COSM
<2.E−4/prot		42cm absorption	BRODERICK	79	COSM
<2.E−13/m^3		moon wake	SCHATTEN	70	ELEC

[1] Catalysis of nucleon decay.

REFERENCES FOR Magnetic Monopole Searches

ABBASI	22	PRL 128 051101	R. Abbasi *et al.*	(IceCube Collab.)
ACERO	21	PR D103 012007	M.A. Acero *et al.*	(NOvA Collab.)
ACHARYA	21	PRL 126 071801	B. Acharya *et al.*	(MoEDAL Collab.)
GAPONENKO	21	PAN 84 287	O.N. Gaponenko	(ASCI)
AAD	20G	PRL 124 031802	G. Add *et al.*	(ATLAS Collab.)
ACHARYA	19B	PRL 123 021802	B. Acharya *et al.*	(MoEDAL Collab.)
ACHARYA	18A	PL B782 510	B. Acharya *et al.*	(MoEDAL Collab.)
ACHARYA	17	PRL 118 061801	B. Acharya *et al.*	(MoEDAL Collab.)
ALBERT	17	JHEP 1707 054	A. Albert *et al.*	(ANTARES Collab.)
GOULD	17	PRL 119 241601	O. Gould, A. Rajantie	
AAB	16	PR D94 082002	A. Aab *et al.*	(Pierre Auger Collab.)
AAD	16AB	PR D93 052009	G. Aad *et al.*	(ATLAS Collab.)
AARTSEN	16B	EPJ C76 133	M.G. Aartsen *et al.*	(IceCube Collab.)
ACHARYA	16	JHEP 1608 067	B. Acharya *et al.*	(MoEDAL Collab.)
AARTSEN	14	EPJ C74 2938	M.G. Aartsen *et al.*	(IceCube Collab.)
Also		EPJ C79 124 (errat.)	M.G. Aartsen *et al.*	(IceCube Collab.)
ABBASI	13	PR D87 022001	R. Abbasi *et al.*	(IceCube Collab.)
BENDTZ	13	PRL 110 121803	K. Bendtz *et al.*	
AAD	12CS	PRL 109 261803	G. Aad *et al.*	(ATLAS Collab.)
ADRIAN-MAR...	12A	ASP 35 634	S. Adrian-Martinez *et al.*	(ANTARES Collab.)
UENO	12	ASP 36 131	K. Ueno *et al.*	(Super-Kamiokande Collab.)
DETRIXHE	11	PR D83 023513	M. Detrixhe *et al.*	(ANITA Collab.)
ABBASI	10A	EPJ C69 361	R. Abbasi *et al.*	(IceCube Collab.)
ABBIENDI	08	PL B663 37	G. Abbiendi *et al.*	(OPAL Collab.)
BALESTRA	08	EPJ C55 57	S. Balestra *et al.*	(SLIM Collab.)
HOGAN	08	PR D78 075031	D.P. Hogan *et al.*	(KANS, NEBR, DELA)
ABULENCIA	06K	PRL 96 201801	A. Abulencia *et al.*	(CDF Collab.)
AKTAS	05A	EPJ C41 133	A. Aktas *et al.*	(H1 Collab.)
KALBFLEISCH	04	PR D69 052002	G.R. Kalbfleisch *et al.*	(OKLA)
AMBROSIO	02B	EPJ C25 511	M. Ambrosio *et al.*	(MACRO Collab.)
AMBROSIO	02C	EPJ C26 163	M. Ambrosio *et al.*	(MACRO Collab.)
AMBROSIO	02D	ASP 18 27	M. Ambrosio *et al.*	(MACRO Collab.)
KALBFLEISCH	00	PRL 85 5292	G.R. Kalbfleisch *et al.*	
FREESE	99	PR D59 063007	K. Freese, E. Krasteva	
ABBOTT	98K	PRL 81 524	B. Abbott *et al.*	(D0 Collab.)
AMBROSIO	97	PL B406 249	M. Ambrosio *et al.*	(MACRO Collab.)
HE	97	PRL 79 3134	Y.D. He	(UCB)
ACCIARRI	95C	PL B345 609	M. Acciarri *et al.*	(L3 Collab.)
JEON	95	PRL 75 1443	H. Jeon, M.J. Longo	(MICH)
Also		PRL 76 159 (erratum)	H. Jeon, M.J. Longo	
AHLEN	94	PRL 72 608	S.P. Ahlen *et al.*	(MACRO Collab.)
BARISH	94	PRL 73 1306	B.C. Barish, G. Giacomelli, J.T. Hong	(CIT+)
BECKER-SZ...	94	PR D49 2169	R.A. Becker-Szendy *et al.*	(IMB Collab.)
PRICE	94	PRL 73 1305	P.B. Price	(UCB)
ADAMS	93	PRL 70 2511	F.C. Adams *et al.*	(MICH, FNAL)
PINFOLD	93	PL B316 407	J.L. Pinfold *et al.*	(ALBE, HARV, MONT+)
KINOSHITA	92	PR D46 881	K. Kinoshita *et al.*	(HARV, BGNA, REHO)
THRON	92	PR D46 4846	J.L. Thron *et al.*	(SOUDAN-2 Collab.)
GARDNER	91	PR D44 622	R.D. Gardner *et al.*	(STAN)
HUBER	91	PR D44 636	M.E. Huber *et al.*	(STAN)
ORITO	91	PRL 66 1951	S. Orito *et al.*	(ICEPP, WASCR, NIHO, ICRR)
BERMON	90	PRL 64 839	S. Bermon *et al.*	(IBM, BNL)
BERTANI	90	EPL 12 613	M. Bertani *et al.*	(BGNA, INFN)
BEZRUKOV	90	SJNP 52 54	L.B. Bezrukov *et al.*	(INRM)
		Translated from YAF 52 86.		
BUCKLAND	90	PR D41 2726	K.N. Buckland *et al.*	(UCSD)
GHOSH	90	EPL 12 25	D.C. Ghosh, S. Chatterjea	(JADA)
HUBER	90	PRL 64 835	M.E. Huber *et al.*	(STAN)
PRICE	90	PRL 65 149	P.B. Price, J. Guiru, K. Kinoshita	(UCB, HARV)
KINOSHITA	89	PL B228 543	K. Kinoshita *et al.*	(HARV, TISA, KEK+)
BRAUNSCH...	88B	ZPHY C38 543	R. Braunschweig *et al.*	(TASSO Collab.)
KINOSHITA	88	PRL 60 1610	K. Kinoshita *et al.*	(HARV, TISA, KEK+)
BARISH	87	PR D36 2641	B.C. Barish, G. Liu, C. Lane	(CIT)
BARTELT	87	PR D36 1990	J.E. Bartelt *et al.*	(Soudan Collab.)
Also		PR D40 1701 (erratum)	J.E. Bartelt *et al.*	(Soudan Collab.)
EBISU	87	PR D36 3359	T. Ebisu, T. Watanabe	(KOBE)
Also		JP G11 883	T. Ebisu, T. Watanabe	(KOBE)
GENTILE	87	PR D35 1081	T. Gentile *et al.*	(CLEO Collab.)
GUY	87	NAT 325 463	J. Guy	(LOIC)
MASEK	87	PR D35 2758	G.E. Masek *et al.*	(UCSD)
NAKAMURA	87	PL B183 395	S. Nakamura *et al.*	(INUS, WASCR, NIHO)
PRICE	87	PRL 59 2523	P.B. Price, R. Guoxiao, K. Kinoshita	(UCB, HARV)
SCHOUTEN	87	JP E20 850	J.C. Schouten *et al.*	(LOIC)
SHEPKO	87	PR D35 2917	M.J. Shepko *et al.*	(TAMU)
TSUKAMOTO	87	EPL 3 39	T. Tsukamoto *et al.*	(ICRR)
CAPLIN	86	NAT 321 402	A.D. Caplin *et al.*	(LOIC)
Also		JP E20 850	J.C. Schouten *et al.*	(LOIC)
Also		NAT 325 463	J. Guy	(LOIC)
CROMAR	86	PRL 56 2561	M.W. Cromar, A.F. Clark, F.R. Fickett	(NBSB)
HARA	86	PRL 56 553	T. Hara *et al.*	(ICRR, KYOT, KEK, KOBE+)
INCANDELA	86	PR D34 2637	J. Incandela *et al.*	(CHIC, FNAL, MICH)
KOVALIK	86	PR A33 1183	J.M. Kovalik, J.L. Kirschvink	(CIT)
PRICE	86	PRL 56 1226	P.B. Price, M.H. Salamon	(UCB)
ARAFUNE	85	PR D32 2586	J. Arafune, M. Fukugita, S. Yanagita	(ICRR, KYOTU+)
BERMON	85	PRL 55 1850	S. Bermon *et al.*	(IBM)
BRACCI	85B	NP B258 726	L. Bracci, G. Fiorentini, G. Mezzorani	(PISA+)
Also		LNC 42 123	L. Bracci, G. Fiorentini	(PISA)
CAPLIN	85	NAT 317 234	A.D. Caplin *et al.*	(LOIC)
EBISU	85	JP G11 883	T. Ebisu, T. Watanabe	(KOBE)
KAJITA	85	JPSJ 54 4065	T. Kajita *et al.*	(ICRR, KEK, NIIG)
PARK	85B	NP B252 261	H.S. Park *et al.*	(IMB Collab.)
BATTISTONI	84	PL 133B 454	G. Battistoni *et al.*	(NUSEX Collab.)
FRYBERGER	84	PR D29 1524	D. Fryberger *et al.*	(SLAC, UCB)
HARVEY	84	NP B236 255	J.A. Harvey	(PRIN)
INCANDELA	84	PRL 53 2067	J. Incandela *et al.*	(CHIC, FNAL, MICH)
KAJINO	84	PRL 52 1373	F. Kajino *et al.*	(ICRR)
KAJINO	84B	JP G10 447	F. Kajino *et al.*	(ICRR)
KAWAGOE	84	LNC 41 315	K. Kawagoe *et al.*	(TOKY)
KOLB	84	APJ 286 702	E.W. Kolb, M.S. Turner	(FNAL, CHIC)
KRISHNA...	84	PL 142B 99	M.R. Krishnaswamy *et al.*	(TATA, OSKC+)
LISS	84	PR D30 884	T.M. Liss, S.P. Ahlen, G. Tarle	(UCB, IND+)
PRICE	84	PRL 52 1265	P.B. Price *et al.*	(ROMA, UCB, IND+)
PRICE	84B	PL 140B 112	P.B. Price	(CERN)
TARLE	84	PRL 52 90	G. Tarle, S.P. Ahlen, T.M. Liss	(UCB, MICH+)
ANDERSON	83	PR D28 2308	S.N. Anderson *et al.*	(WASH)
ARAFUNE	83	PL 133B 380	J. Arafune, M. Fukugita	(ICRR, KYOTU)
AUBERT	83B	PRL 50 655	B. Aubert *et al.*	(CERN, LAPP)
BARTELT	83B	PRL 50 655	J.E. Bartelt *et al.*	(MINN, ANL)
BARWICK	83	PR D28 2338	S.W. Barwick, K. Kinoshita, P.B. Price	(UCB)
BONARELLI	83	PL 126B 137	R. Bonarelli, P. Capiluppi, I. d'Antone	(BGNA)
BOSETTI	83	PL 133B 265	P.C. Bosetti *et al.*	(AACH3, HAWA, TOKY)
CABRERA	83	PRL 51 1933	B. Cabrera *et al.*	(STAN)
DOKE	83	PL 129B 370	T. Doke *et al.*	(WASU, RIKK, TTAM, RIKEN)
ERREDE	83	PRL 51 245	S.M. Errede *et al.*	(IMB Collab.)
FREESE	83B	PRL 51 1625	K. Freese, M.S. Turner, D.N. Schramm	(CHIC)
GROOM	83	PRL 50 573	D.E. Groom *et al.*	(UTAH, STAN)
MASHIMO	83	PL 128B 327	T. Mashimo *et al.*	(ICEPP)
MIKHAILOV	83	PL 130B 331	V.F. Mikhailov	(KAZA)
MUSSET	83	PL 128B 333	P. Musset, M. Price, E. Lohrmann	(CERN, HAMB)
REPHAELI	83	PL 121B 115	Y. Rephaeli, M.S. Turner	(CHIC)
SCHATTEN	83	PR D27 1525	K.H. Schatten	(NASA)
ALEXEYEV	82	LNC 35 413	E.N. Alekseev *et al.*	(INRM)
BONARELLI	82	PL 112B 100	R. Bonarelli *et al.*	(BGNA)
CABRERA	82	PRL 48 1378	B. Cabrera	(STAN)
DELL	82	NP B209 45	G.F. Dell *et al.*	(BNL, ADEL, ROMA)
DIMOPOUL...	82	PL 119B 320	S. Dimopoulos, J. Preskill, F. Wilczek	(HARV+)
KINOSHITA	82	PRL 48 77	K. Kinoshita, P.B. Price, D. Fryberger	(UCB+)
KOLB	82	PRL 49 1373	E.W. Kolb, S.A. Colgate, J.A. Harvey	(LASL, PRIN)
MASHIMO	82	JPSJ 51 3067	T. Mashimo, K. Kawagoe, M. Koshiba	(INUS)
SALPETER	82	PRL 49 1114	E.E. Salpeter, S.L. Shapiro, I. Wasserman	(CORN)
TURNER	82	PR D26 1296	M.S. Turner, E.N. Parker, T.J. Bogdan	(CHIC)
BARTLETT	81	PR D24 612	D.F. Bartlett *et al.*	(COLO, GESC)
KINOSHITA	81B	PR D24 1707	K. Kinoshita, P.B. Price	(UCB)
ULLMAN	81	PRL 47 289	J.D. Ullman	(LEHM, BNL)
CARRIGAN	80	NAT 288 348	R.A. Carrigan	(FNAL)
BRODERICK	79	PR D19 1046	J.J. Broderick *et al.*	(VPI)
BARTLETT	78	PR D18 2253	D.F. Bartlett, D. Soo, M.G. White	(COLO, PRIN)
CARRIGAN	78	PR D17 1754	R.A. Carrigan, B.P. Strauss, G. Giacomelli	(FNAL+)
HOFFMANN	78	LNC 23 357	H. Hoffmann *et al.*	(CERN, ROMA)
PRICE	78	PR D18 1382	P.B. Price *et al.*	(UCB, HOUS)
HAGSTROM	77	PRL 38 729	R. Hagstrom	(LBL)
CARRIGAN	76	PR D13 1823	R.A. Carrigan, F.A. Nezrick, B.P. Strauss	(FNAL)
DELL	76	LNC 15 269	G.F. Dell *et al.*	(CERN, BNL, ROMA, ADEL)
ROSS	76	LBL-4665	R.R. Ross	(LBL)
STEVENS	76B	PR D14 2207	D.M. Stevens *et al.*	(VPI, BNL)
ZRELOV	76	CZJP B26 1306	V.P. Zrelov *et al.*	(JINR)
ALVAREZ	75	LBL-4260	L.W. Alvarez	(LBL)
BURKE	75	PL 60B 113	D.L. Burke *et al.*	(MICH)
CABRERA	75	Thesis	B. Cabrera	(STAN)
CARRIGAN	75	NP B91 279	R.A. Carrigan, F.A. Nezrick	(FNAL)
Also		PR D3 56	R.A. Carrigan, F.A. Nezrick	(FNAL)
EBERHARD	75	PR D11 3099	P.H. Eberhard *et al.*	(LBL, MPIM)
EBERHARD	75B	LBL-4289	P.H. Eberhard	(LBL)
FLEISCHER	75	PRL 35 1412	R.L. Fleischer, R.N.F. Walker	(GESC, WUSL)
FRIEDLANDER	75	PRL 35 1167	M.W. Friedlander	(WUSL)
GIACOMELLI	75	NC 28A 21	G. Giacomelli *et al.*	(BGNA, CERN, SACL+)
PRICE	75	PRL 35 487	P.B. Price *et al.*	(UCB, HOUS)
CARRIGAN	74	PR D10 3867	R.A. Carrigan, F.A. Nezrick, B.P. Strauss	(FNAL)
CARRIGAN	73	PR D8 3717	R.A. Carrigan, F.A. Nezrick, B.P. Strauss	(FNAL)
ROSS	73	PR D8 698	R.R. Ross *et al.*	(LBL, SLAC)
Also		PR D4 3260	P.H. Eberhard *et al.*	(LBL, SLAC)
Also		SCI 167 701	L.W. Alvarez *et al.*	(LBL, SLAC)
BARTLETT	72	PR D6 1817	D.F. Bartlett, M.D. Lahana	(COLO)
GUREVICH	72	PL 38B 549	I.I. Gurevich *et al.*	(KIAE, NOVO, SERP)
Also		JETP 34 917	L.M. Barkov, I.I. Gurevich, M.S. Zolotorev	(KIAE+)
		Translated from ZETF 61 1721.		
Also		PL 31B 394	I.I. Gurevich *et al.*	(KIAE, NOVO, SERP)
FLEISCHER	71	PR D4 24	R.L. Fleischer *et al.*	(GESC)
KOLM	71	PR D4 1285	H.H. Kolm, F. Villa, A. Odian	(MIT, SLAC)
PARKER	70	APJ 160 383	E.N. Parker	(CHIC)
SCHATTEN	70	PR D1 2245	K.H. Schatten	(NASA)
FLEISCHER	69	PR 177 2029	R.L. Fleischer *et al.*	(GESC, FSU)
FLEISCHER	69B	PR 184 1393	R.L. Fleischer *et al.*	(GESC, UNCS, GSCO)
FLEISCHER	69C	PR 184 1398	R.L. Fleischer, P.B. Price, R.T. Woods	(GESC)
Also		JAP 41 958	R.L. Fleischer *et al.*	(GESC)
CARITHERS	66	PR 149 1070	W.C.J. Carithers, R.J. Stefanski, R.K. Adair	
AMALDI	63	NC 28 773	E. Amaldi *et al.*	(ROMA, UCSD, CERN)
GOTO	63	PR 132 387	E. Goto, H.H. Kolm, K.W. Ford	(TOKY, MIT, BRAN)
PETUKHOV	63	NP 49 87	V.A. Petukhov, M.N. Yakimenko	(LEBD)
PURCELL	63	PR 129 2326	E.M. Purcell *et al.*	(HARV, BNL)
FIDECARO	61	NC 22 657	M. Fidecaro, G. Finocchiaro, G. Giacomelli	(CERN)
BRADNER	59	PR 114 603	H. Bradner, W.M. Isbell	(LBL)
MALKUS	51	PR 83 899	W.V.R. Malkus	(CHIC)

OTHER RELATED PAPERS

GROOM	86	PRPL 140 323	D.E. Groom	(UTAH)
Review				

Supersymmetric Particle Searches

The exclusion of particle masses within a mass range (m_1, m_2) will be denoted with the notation "none $m_1 - m_2$" in the VALUE column of the following Listings. The latest unpublished results are described in the "Supersymmetry: Experiment" review.

See the related review(s):

Supersymmetry, Part I (Theory)

Supersymmetry, Part II (Experiment)

CONTENTS:

$\widetilde{\chi}^0_1$ (Lightest Neutralino) mass limit

– Accelerator limits for stable $\widetilde{\chi}^0_1$

– Bounds on $\widetilde{\chi}^0_1$ from dark matter searches

– $\widetilde{\chi}^0_1$-p elastic cross section

Spin-dependent interactions

Spin-independent interactions

– Other bounds on $\widetilde{\chi}^0_1$ from astrophysics and cosmology

– Unstable $\widetilde{\chi}^0_1$ (Lightest Neutralino) mass limit

$\widetilde{\chi}^0_2$, $\widetilde{\chi}^0_3$, $\widetilde{\chi}^0_4$ (Neutralinos) mass limits

$\widetilde{\chi}^\pm_1$, $\widetilde{\chi}^\pm_2$ (Charginos) mass limits

Downloaded from https://academic.oup.com/ptep/article/2022/8/083C01/6651666 by KIT Library user on 27 September 2022

Long-lived $\widetilde{\chi}^{\pm}$ (Chargino) mass limit
$\widetilde{\nu}$ (Sneutrino) mass limit
Charged sleptons
— R-parity conserving $\widetilde{e}$ (Selectron) mass limit
— R-partiy violating $\widetilde{e}$ (Selectron) mass limit
— R-parity conserving $\widetilde{\mu}$ (Smuon) mass limit
— R-parity violating $\widetilde{\mu}$ (Smuon) mass limit
— R-parity conserving $\widetilde{\tau}$ (Stau) mass limit
— R-parity violating $\widetilde{\tau}$ (Stau) mass limit
— Long-lived $\widetilde{\ell}$ (Slepton) mass limit
$\widetilde{q}$ (Squark) mass limit
— R-parity conserving $\widetilde{q}$ (Squark) mass limit
— R-parity violating $\widetilde{q}$ (Squark) mass limit
Long-lived $\widetilde{q}$ (Squark) mass limit
$\widetilde{b}$ (Sbottom) mass limit
— R-parity conserving $\widetilde{b}$ (Sbottom) mass limit
— R-parity violating $\widetilde{b}$ (Sbottom) mass limit
$\widetilde{t}$ (Stop) mass limit
— R-parity conserving $\widetilde{t}$ (Stop) mass limit
— R-parity violating $\widetilde{t}$ (Stop) mass limit
Heavy $\widetilde{g}$ (Gluino) mass limit
— R-parity conserving heavy $\widetilde{g}$ (Gluino) mass limit
— R-parity violating heavy $\widetilde{g}$ (Gluino) mass limit
Long-lived $\widetilde{g}$ (Gluino) mass limit
Light $\widetilde{G}$ (Gravitino) mass limits from collider experiments
Supersymmetry miscellaneous results

The results shown below, unless stated otherwise, are based on the Minimal Supersymmetric Standard Model (MSSM), as described in the Note on Supersymmetry. Unless otherwise indicated, this includes the assumption of common gaugino and scalar masses at the scale of Grand Unification (GUT), and use of the resulting relations in the spectrum and decay branching ratios. Unless otherwise indicated, it is also assumed that R-parity (R) is conserved and that:

1) The $\widetilde{\chi}^0_1$ is the lighest supersymmetric particle (LSP),
2) $m_{\widetilde{f}_L} = m_{\widetilde{f}_R}$, where $\widetilde{f}_{L,R}$ refer to the scalar partners of left- and right-handed fermions.

Limits involving different assumptions are identified in the Comments or in the Footnotes, in particular also the many simplified models, see definitions below. We summarize here the notations used in this Chapter to characterize some of the most common deviations from the MSSM (for further details, see the Note on Supersymmetry).

Theories with R-parity violation (RPV) are characterized by a superpotential of the form: $\lambda_{ijk} L_i L_j e^c_k + \lambda'_{ijk} L_i Q_j d^c_k + \lambda''_{ijk} u^c_i d^c_j d^c_k$, where i, j, k are generation indices. The presence of any of these couplings is often identified in the following by the symbols $LL\overline{E}$, $LQ\overline{D}$, and $\overline{U}\overline{D}\overline{D}$. Mass limits in the presence of RPV will often refer to "direct" and "indirect" decays. Direct refers to RPV decays of the particle in consideration. Indirect refers to cases where RPV appears in the decays of the LSP. The LSP need not be the $\widetilde{\chi}^0_1$.

In several models, most notably in theories with so-called Gauge Mediated Supersymmetry Breaking (GMSB), the gravitino ($\widetilde{G}$) is the LSP. It is usually much lighter than any other massive particle in the spectrum, and $m_{\widetilde{G}}$ is then neglected in all decay processes involving gravitinos. In these scenarios, particles other than the neutralino are sometimes considered as the next-to-lighest supersymmetric particle (NLSP), and are assumed to decay to their even-R partner plus $\widetilde{G}$. If the lifetime is short enough for the decay to take place within the detector, $\widetilde{G}$ is assumed to be undetected and to give rise to missing energy ($\not{E}$) or missing transverse energy ($\not{E}_T$) signatures.

When needed, specific assumptions on the eigenstate content of $\widetilde{\chi}^0$ and $\widetilde{\chi}^{\pm}$ states are indicated, using the notation $\widetilde{\gamma}$ (photino), $\widetilde{H}$ (higgsino), $\widetilde{W}$ (wino), and $\widetilde{Z}$ (zino) to signal that the limit of pure states was used. The term gaugino is also used, to generically indicate wino-like charginos and zino-like neutralinos.

In the listings we have made use of the following abbreviations for simplified models employed by the experimental collaborations in supersymmetry searches published in the past year.

WARNING: Experimental lower mass limits determined within simplified models are to be treated with extreme care as they might not be directly applicable to realistic models. This is outlined in detail in the publications and we recommend consulting them before using bounds. For example, branching ratios, typically fixed to specific values in simplified models, can vary substantially in more elaborate models.

Simplified Models Table

Tglu1A: gluino pair production with $\tilde{g} \to q\bar{q}\tilde{\chi}^0_1$.

Tglu1B: gluino pair production with $\tilde{g} \to qq'\tilde{\chi}^{\pm}_1$, $\tilde{\chi}^{\pm}_1 \to W^{\pm}\tilde{\chi}^0_1$.

Tglu1C: gluino pair production with a 2/3 probability of having a $\tilde{g} \to qq'\tilde{\chi}^{\pm}_1$, $\tilde{\chi}^{\pm}_1 \to W^{\pm}\tilde{\chi}^0_1$ decay and a 1/3 probability of having a $\tilde{g} \to qq\tilde{\chi}^0_2$, $\tilde{\chi}^0_2 \to Z^{\pm}\tilde{\chi}^0_1$ decay.

Tglu1D: gluino pair production with one gluino decaying to $q\bar{q}'\tilde{\chi}^{\pm}_1$ with $\tilde{\chi}^{\pm}_1 \to W^{\pm} + \tilde{G}$, and the other gluino decaying to $q\bar{q}\tilde{\chi}^0_1$ with $\tilde{\chi}^0_1 \to \gamma + \tilde{G}$.

Tglu1E: gluino pair production with $\tilde{g} \to qq'\tilde{\chi}^{\pm}_1$, $\tilde{\chi}^{\pm}_1 \to W^{\pm}\tilde{\chi}^0_2$ and $\tilde{\chi}^0_2 \to Z^{\pm}\tilde{\chi}^0_1$ where $m_{\tilde{\chi}^{\pm}_1} = (m_{\tilde{g}} + m_{\tilde{\chi}^0_1})/2$, $m_{\tilde{\chi}^0_2} = (m_{\tilde{\chi}^{\pm}_1} + m_{\tilde{\chi}^0_1})/2$.

Tglu1F: gluino pair production with $\tilde{g} \to qq'\tilde{\chi}^{\pm}_1$ or $\tilde{g} \to qq\tilde{\chi}^0_2$ with equal branching ratios, where $\tilde{\chi}^{\pm}_1$ decays through an intermediate scalar tau lepton or sneutrino to $\tau\nu\tilde{\chi}^0_1$ and where $\tilde{\chi}^0_2$ decays through an intermediate scalar tau lepton or sneutrino to $\tau^+\tau^-\tilde{\chi}^0_1$ or $\nu\bar{\nu}\tilde{\chi}^0_1$; the mass hierarchy is such that $m_{\tilde{\chi}^{\pm}_1} \sim m_{\tilde{\chi}^0_2} = (m_{\tilde{g}} + m_{\tilde{\chi}^0_1})/2$ and $m_{\tilde{\tau},\tilde{\nu}} = (m_{\tilde{\chi}^{\pm}_1} + m_{\tilde{\chi}^0_1})/2$.

Tglu1G: gluino pair production with $\tilde{g} \to q\bar{q}\tilde{\chi}^0_2$, and $\tilde{\chi}^0_2$ decaying through an intermediate slepton or sneutrino to $l^+l^-\tilde{\chi}^0_1$ or $\nu\bar{\nu}\tilde{\chi}^0_1$ where $m_{\tilde{\chi}^0_2} = (m_{\tilde{g}} + m_{\tilde{\chi}^0_1})/2$ and $m_{\tilde{\ell},\tilde{\nu}} = (m_{\tilde{\chi}^0_2} + m_{\tilde{\chi}^0_1})/2$.

Tglu1H: gluino pair production with $\tilde{g} \to q\bar{q}\tilde{\chi}^0_2$, and $\tilde{\chi}^0_2 \to \tilde{\chi}^0_1 Z^{0(*)}$.

Tglu1I: gluino pair production with $\tilde{g} \to q\bar{q}\tilde{\chi}^0_2$, and $\tilde{\chi}^0_2 \to \tilde{\chi}^0_1 H$.

Tglu1J: gluino pair production with $\tilde{g} \to q\bar{q}\tilde{\chi}^0_2$, and $\mathrm{BR}(\tilde{\chi}^0_2 \to \tilde{\chi}^0_1 Z^{0(*)}) = \mathrm{BR}(\tilde{\chi}^0_2 \to \tilde{\chi}^0_1 H) = 0.5$.

Tglu1LL gluino pair production where $\tilde{g} \to q\bar{q}\tilde{\chi}^0_1$ happens with 1/3 probability and $\tilde{g} \to q\bar{q}\tilde{\chi}^{\pm}_1$ happens with 2/3 probability. The $\tilde{\chi}^{\pm}_1$ is assumed to be few hundreds of MeV heavier than the $\tilde{\chi}^0_1$, and decays to $\tilde{\chi}^0_1$ via a pion.

Tglu2A: gluino pair production with $\tilde{g} \to b\bar{b}\tilde{\chi}^0_1$.

Tglu3A: gluino pair production with $\tilde{g} \to t\bar{t}\tilde{\chi}^0_1$.

Tglu3B: gluino pair production with $\tilde{g} \to t\bar{\tilde{t}}$ where $\tilde{t}$ decays exclusively to $t\tilde{\chi}^0_1$.

Tglu3C: gluino pair production with $\tilde{g} \to t\bar{\tilde{t}}$ where $\tilde{t}$ decays exclusively to $c\tilde{\chi}^0_1$.

Tglu3D: gluino pair production with $\tilde{g} \to t\bar{b}\tilde{\chi}^{\pm}_1$ with $\tilde{\chi}^{\pm}_1 \to W^{\pm}\tilde{\chi}^0_1$.

Tglu3E: gluino pair production where the gluino decays 25% of the time through $\tilde{g} \to t\bar{t}\tilde{\chi}^0_1$, 25% of the time through $\tilde{g} \to b\bar{b}\tilde{\chi}^0_1$ and 50% of the time through $\tilde{g} \to t\bar{b}\tilde{\chi}^{\pm}_1$ with $\tilde{\chi}^{\pm}_1 \to W^{\pm}\tilde{\chi}^0_1$.

Tglu3F: gluino pair production with wino-like couplings to electroweakinos, that is: $\tilde{g} \to t\bar{t}\tilde{\chi}^0_{1,2}$ with BR 17%, $\tilde{g} \to b\bar{b}\tilde{\chi}^0_{1,2}$ with BR 17%, $\tilde{g} \to t\bar{t}\tilde{\chi}^{\pm}_1$ with BR 66%.

Tglu3G: gluino pair production with higgsino-like couplings to electroweakinos, that is: $\tilde{g} \to t\bar{t}\tilde{\chi}^0_{1,2}$ with BR 50%, $\tilde{g} \to t\bar{t}\tilde{\chi}^{\pm}_1$ with BR 50%.

Tglu4A: gluino pair production with one gluino decaying to $q\bar{q}'\tilde{\chi}^{\pm}_1$ with $\tilde{\chi}^{\pm}_1 \to W^{\pm} + \tilde{G}$, and the other gluino decaying to $q\bar{q}\tilde{\chi}^0_1$ with $\tilde{\chi}^0_1 \to \gamma + \tilde{G}$.

Downloaded from https://academic.oup.com/ptep/article/2022/8/083C01/6651666 by KIT Library user on 27 September 2022

Tglu4B: gluino pair production with gluinos decaying to $q\bar{q}\tilde{\chi}_1^0$ and $\tilde{\chi}_1^0 \to \gamma + \tilde{G}$.
Tglu4C: gluino pair production with gluinos decaying to $\tilde{g} \to q\bar{q}\tilde{\chi}_1^0$ and $\tilde{\chi}_1^0 \to Z + \tilde{G}$.
Tglu4D: gluino pair production with $\tilde{g} \to q\bar{q}\tilde{\chi}_1^0$ where the $\tilde{\chi}_1^0$ decays with equal probability to $\tilde{\chi}_1^0 \to \gamma + \tilde{G}$ or to $\tilde{\chi}_1^0 \to H + \tilde{G}$.
Tglu4E: gluino pair production with $\tilde{g} \to b\bar{b}\tilde{\chi}_1^0$ where the $\tilde{\chi}_1^0$ decays with equal probability to $\tilde{\chi}_1^0 \to \gamma + \tilde{G}$ or to $\tilde{\chi}_1^0 \to Z + \tilde{G}$.
Tglu4F: gluino pair production with $\tilde{g} \to t\bar{t}\tilde{\chi}_1^0$ where the $\tilde{\chi}_1^0$ decays with equal probability to $\tilde{\chi}_1^0 \to \gamma + \tilde{G}$ or to $\tilde{\chi}_1^0 \to Z + \tilde{G}$.
Tglu1RPV: gluino pair production with $\tilde{g} \to uds$ via RPV coupling λ''_{112}.
Tglu2RPV: gluino pair production with $\tilde{g} \to (tbd, tbs)$ via RPV coupling λ''_{313} or λ''_{323}.

Tsqk1: squark pair production with $\tilde{q} \to q\tilde{\chi}_1^0$.
Tsqk1LL squark pair production where $\tilde{q} \to q\tilde{\chi}_1^0$ and $\tilde{q} \to q'\tilde{\chi}_1^\pm$ each happen with 50% probability. The $\tilde{\chi}_1^\pm$ is assumed to be few hundreds of MeV heavier than the $\tilde{\chi}_1^0$, and decays to $\tilde{\chi}_1^0$ via a pion.
Tsqk2: squark pair production with $\tilde{q} \to q\tilde{\chi}_2^0$ and $\tilde{\chi}_2^0 \to Z + \tilde{\chi}_1^0$.
Tsqk2A: squark pair production with $\tilde{q} \to q\tilde{\chi}_2^0$, where one of the $\tilde{\chi}_2^0 \to Z^{(*)}\tilde{\chi}_1^0 \to f\bar{f}\tilde{\chi}_1^0$ and the other $\tilde{\chi}_2^0 \to \tilde{\ell}\ell^+ \to \ell^+\ell^-\tilde{\chi}_1^0$.
Tsqk3: squark pair production with $\tilde{q} \to q'\tilde{\chi}_1^\pm$, $\tilde{\chi}_1^\pm \to W^\pm\tilde{\chi}_1^0$ (like Tglu1B but for squarks)
Tsqk4: squark pair production with squarks decaying to $q\tilde{\chi}_1^0$ and $\tilde{\chi}_1^0 \to \gamma + \tilde{G}$.
Tsqk4A: squark pair production with one squark decaying to $q\tilde{\chi}_1^\pm$ with $\tilde{\chi}_1^\pm \to W^\pm + \tilde{G}$, and the other squark decaying to $q\tilde{\chi}_1^0$ with $\tilde{\chi}_1^0 \to \gamma + \tilde{G}$.
Tsqk4B: squark pair production with squarks decaying to $q\tilde{\chi}_1^0$ and $\tilde{\chi}_1^0 \to \gamma + \tilde{G}$.

Tstop1: stop pair production with $\tilde{t} \to t\tilde{\chi}_1^0$.
Tstop1LL stop pair production where $\tilde{t} \to t\tilde{\chi}_1^0$ and $\tilde{t} \to b\tilde{\chi}_1^\pm$ each happen with 50% probability. The $\tilde{\chi}_1^\pm$ is assumed to be few hundreds of MeV heavier than the $\tilde{\chi}_1^0$, and decays to $\tilde{\chi}_1^0$ via a pion.
Tstop2: stop pair production with $\tilde{t} \to b\tilde{\chi}_1^\pm$ with $\tilde{\chi}_1^\pm \to W^\pm\tilde{\chi}_1^0$.
Tstop3: stop pair production with the subsequent four-body decay $\tilde{t} \to bff'\tilde{\chi}_1^0$ where f represents a lepton or a quark.
Tstop4: stop pair production with $\tilde{t} \to c\tilde{\chi}_1^0$.
Tstop5: stop pair production with $\tilde{t} \to b\bar{\nu}\tilde{\tau}$ with $\tilde{\tau} \to \tau\tilde{G}$.
Tstop6: stop pair production with $\tilde{t} \to t + \tilde{\chi}_2^0$, where $\tilde{\chi}_2^0 \to Z + \tilde{\chi}_1^0$ or $H + \tilde{\chi}_1^0$ each with BR 50%.
Tstop7: stop pair production with $\tilde{t}_2 \to \tilde{t}_1 + H/Z$, where $\tilde{t}_1 \to t + \tilde{\chi}_1^0$.
Tstop8: stop pair production with equal probability of the stop decaying via $\tilde{t} \to t\tilde{\chi}_1^0$ or via $\tilde{t} \to b\tilde{\chi}_1^\pm$ with $\tilde{\chi}_1^\pm \to W^\pm\tilde{\chi}_1^0$.
Tstop9: stop pair production with equal probability of the stop decaying via $\tilde{t} \to c\tilde{\chi}_1^0$ or via the four-body decay $\tilde{t} \to bff'\tilde{\chi}_1^0$ where f represents a lepton or a quark.
Tstop10: stop pair production with $\tilde{t} \to b\tilde{\chi}_1^\pm$ and $\tilde{\chi}_1^\pm \to W^{\pm *}\tilde{\chi}_1^0 \to (f\bar{f}') + \tilde{\chi}_1^0$ with a virtual W-boson.
Tstop11: stop pair production with $\tilde{t} \to b\tilde{\chi}_1^\pm$ with $\tilde{\chi}_1^\pm$ decaying through an intermediate slepton to $l\nu\tilde{\chi}_1^0$
Tstop12: stop pair production with $\tilde{t} \to t\tilde{\chi}_1^0$ and $\tilde{\chi}_1^0 \to \gamma + \tilde{G}$
Tstop13: stop pair production with $\tilde{t} \to t\tilde{\chi}_1^0$ where the $\tilde{\chi}_1^0$ can decay with equal probability to $\tilde{\chi}_1^0 \to \gamma + \tilde{G}$ or to $\tilde{\chi}_1^0 \to Z + \tilde{G}$.
Tstop14: stop pair production with wino-like couplings to electroweakinos, that is: $\tilde{t} \to t\tilde{\chi}_{1,2}^0$ with BR 33%, $\tilde{g} \to b\tilde{\chi}_1^\pm$ with BR 67%.
Tstop15: stop pair production with higgsino-like couplings to electroweakinos, that is: $\tilde{t} \to t\tilde{\chi}_{1,2}^0$ with BR 50%, $\tilde{g} \to b\tilde{\chi}_1^\pm$ with BR 50%.
Tstop1RPV: stop pair production with $\tilde{t} \to \bar{b}\bar{s}$ via RPV coupling λ''_{323}.
Tstop2RPV: stop pair production with $\tilde{t} \to b\ell$, via RPV coupling λ'_{i33}.
Tstop3RPV: stop pair production with $\tilde{t} \to q\mu$, via RPV coupling λ'_{23k}.
Tstop4RPV: stop pair production with $\tilde{t} \to b\tilde{\chi}_1^\pm$, $\tilde{\chi}_1^\pm \to bbs$ via RPV coupling λ''_{323}.
Tstop5RPV: stop pair production with $\tilde{t} \to t\tilde{\chi}_{1,2}^0$, $\tilde{\chi}_{1,2}^0 \to tbs$ via RPV coupling λ''_{323}.

Tsbot1: sbottom pair production with $\tilde{b} \to b\tilde{\chi}_1^0$.
Tsbot2: sbottom pair production with $\tilde{b} \to t\chi_1^-$, $\chi_1^- \to W^-\tilde{\chi}_1^0$.
Tsbot3: sbottom pair production with $\tilde{b} \to b\tilde{\chi}_2^0$, where one of the $\tilde{\chi}_2^0 \to Z^{(*)}\tilde{\chi}_1^0 \to f\bar{f}\tilde{\chi}_1^0$ and the other $\tilde{\chi}_2^0 \to \tilde{\ell}\ell^+ \to \ell^+\ell^-\tilde{\chi}_1^0$.
Tsbot4: sbottom pair production with $\tilde{b} \to b\tilde{\chi}_2^0$, with $\tilde{\chi}_2^0 \to H\tilde{\chi}_1^0$

Tchi1chi1A: electroweak pair and associated production of nearly mass-degenerate charginos $\tilde{\chi}_1^\pm$ and neutralinos $\tilde{\chi}_1^0$, where $\tilde{\chi}_1^\pm$ decays to $\tilde{\chi}_1^0$ plus soft radiation, and where one of the $\tilde{\chi}_1^0$ decays to $\gamma + \tilde{G}$ while the other one decays to $Z/H + \tilde{G}$ (with equal probability).
Tchi1chi1B: electroweak pair production of charginos $\tilde{\chi}_1^\pm$, where $\tilde{\chi}_1^\pm$ decays through an intermediate slepton or sneutrino to $l\nu\tilde{\chi}_1^0$ and where the slepton or sneutrino mass is 5%, 25%, 50%, 75% and 95% of the $\tilde{\chi}_1^\pm$ mass.
Tchi1chi1C: electroweak pair production of charginos $\tilde{\chi}_1^\pm$, where $\tilde{\chi}_1^\pm$ decays through an intermediate slepton or sneutrino to $l\nu\tilde{\chi}_1^0$ and where $m_{\tilde{\ell},\tilde{\nu}} = (m_{\tilde{\chi}_1^\pm} + m_{\tilde{\chi}_1^0})/2$.
Tchi1chi1D: electroweak associated pair production of charginos $\tilde{\chi}_1^\pm$, where $\tilde{\chi}_1^\pm$ decays through an intermediate scalar tau lepton or sneutrino to $\tau\nu\tilde{\chi}_1^0$ and where $m_{\tilde{\tau}}, m_{\tilde{\nu}} = (m_{\tilde{\chi}_1^\pm} + m_{\tilde{\chi}_1^0})/2$.
Tchi1chi1F: electroweak pair and associated production of nearly mass-degenerate charginos $\tilde{\chi}_1^\pm$ and neutralinos $\tilde{\chi}_1^0$ (*i.e.* $\tilde{\chi}_1^\pm\tilde{\chi}_1^\pm$ and $\tilde{\chi}_1^\pm\tilde{\chi}_1^0$ production) where the $\tilde{\chi}_1^\pm$ decays exclusively to $\tilde{\chi}_1^0$ plus soft radiation and the $\tilde{\chi}_1^0$ decays to $\gamma/Z + \tilde{G}$.
Tchi1chi1G: electroweak pair production of charginos $\tilde{\chi}_1^\pm$, which are nearly mass-degenerate with neutralinos $\tilde{\chi}_1^0$. The $\tilde{\chi}_1^\pm$ decays either to $W^\pm + \tilde{G}$, or to $\tilde{\chi}_1^0$ plus soft radiation. The $\tilde{\chi}_1^0$ decays exclusively to $\gamma + \tilde{G}$.
Tchi1chi1H: electroweak pair production of charginos $\tilde{\chi}_1^\pm$, with $\tilde{\chi}_1^\pm \to W^\pm + \tilde{\chi}_1^0$ and $W^\pm \to \ell^\pm + \nu$.
Tchi1chi1I: electroweak pair production of charginos $\tilde{\chi}_1^\pm$ with $\tilde{\chi}_1^\pm \to W^\pm\tilde{\chi}_1^0$ and $W^\pm \to q\bar{q}'$.

Tchi1n1A: electroweak associated production of mass-degenerate charginos $\tilde{\chi}_1^\pm$ and neutralinos $\tilde{\chi}_1^0$, where $\tilde{\chi}_1^\pm$ decays exclusively to $W^\pm + \tilde{G}$ and $\tilde{\chi}_1^0$ decays exclusively to $\gamma + \tilde{G}$.
Tchi1n2A: electroweak associated production of mass-degenerate charginos $\tilde{\chi}_1^\pm$ and neutralinos $\tilde{\chi}_2^0$, where $\tilde{\chi}_1^\pm$ decays through an intermediate slepton or sneutrino to $l\nu\tilde{\chi}_1^0$ and where $\tilde{\chi}_2^0$ decays through an intermediate slepton or sneutrino to $l^+l^-\tilde{\chi}_1^0$ or $\nu\bar{\nu}\tilde{\chi}_1^0$.
Tchi1n2B: electroweak associated production of mass-degenerate charginos $\tilde{\chi}_1^\pm$ and neutralinos $\tilde{\chi}_2^0$, where $\tilde{\chi}_1^\pm$ decays through an intermediate slepton or sneutrino to $l\nu\tilde{\chi}_1^0$ and where $\tilde{\chi}_2^0$ decays through an intermediate slepton or sneutrino to $l^+l^-\tilde{\chi}_1^0$ or $\nu\bar{\nu}\tilde{\chi}_1^0$ and where the slepton or sneutrino mass is 5%, 25%, 50%, 75% and 95% of the $\tilde{\chi}_1^\pm$ mass.
Tchi1n2C: electroweak associated production of mass-degenerate charginos $\tilde{\chi}_1^\pm$ and neutralinos $\tilde{\chi}_2^0$, where $\tilde{\chi}_1^\pm$ decays through an intermediate slepton or sneutrino to $l\nu\tilde{\chi}_1^0$ and where $\tilde{\chi}_2^0$ decays through an intermediate slepton or sneutrino to $l^+l^-\tilde{\chi}_1^0$ or $\nu\bar{\nu}\tilde{\chi}_1^0$ and where $m_{\tilde{\ell},\tilde{\nu}} = (m_{\tilde{\chi}_1^\pm} + m_{\tilde{\chi}_1^0})/2$.
Tchi1n2D: electroweak associated production of mass-degenerate charginos $\tilde{\chi}_1^\pm$ and neutralinos $\tilde{\chi}_2^0$, where $\tilde{\chi}_1^\pm$ decays through an intermediate scalar tau lepton or sneutrino to $\tau\nu\tilde{\chi}_1^0$ and where $\tilde{\chi}_2^0$ decays through an intermediate scalar tau lepton or sneutrino to $\tau^+\tau^-\tilde{\chi}_1^0$ or $\nu\bar{\nu}\tilde{\chi}_1^0$ and where $m_{\tilde{\tau},\tilde{\nu}} = (m_{\tilde{\chi}_1^\pm} + m_{\tilde{\chi}_1^0})/2$.
Tchi1n2E: electroweak associated production of mass-degenerate charginos $\tilde{\chi}_1^\pm$ and neutralinos $\tilde{\chi}_2^0$, where $\tilde{\chi}_1^\pm \to W^\pm + \tilde{\chi}_1^0$ and $\tilde{\chi}_2^0 \to H + \tilde{\chi}_1^0$.
Tchi1n2F: electroweak associated production of mass-degenerate wino-like charginos $\tilde{\chi}_1^\pm$ and neutralinos $\tilde{\chi}_2^0$, where $\tilde{\chi}_1^\pm$ decays through an intermediate $W^{\pm *}$ to $l\nu\tilde{\chi}_1^0$ and where $\tilde{\chi}_2^0$ decays through an intermediate Z^* to $l^+l^-\tilde{\chi}_1^0$ or $\nu\bar{\nu}\tilde{\chi}_1^0$.
Tchi1n2Fa: electroweak associated production of mass-degenerate wino-like charginos $\tilde{\chi}_1^\pm$ and neutralinos $\tilde{\chi}_2^0$, where $\tilde{\chi}_1^\pm$ decays through an intermediate $W^{\pm *}$ to $q\bar{q}\tilde{\chi}_1^0$ and where $\tilde{\chi}_2^0$ decays through an intermediate Z^* to $l^+l^-\tilde{\chi}_1^0$ or $\nu\bar{\nu}\tilde{\chi}_1^0$.
Tchi1n2Fb: electroweak associated production of mass-degenerate wino-like charginos $\tilde{\chi}_1^\pm$ and neutralinos $\tilde{\chi}_2^0$, where $\tilde{\chi}_1^\pm$ decays through an intermediate $W^{(*)}$ to $q\bar{q}\tilde{\chi}_1^0$ and where $\tilde{\chi}_2^0$ decays through an intermediate $Z^{(*)}$ to $q\bar{q}\tilde{\chi}_1^0$.
Tchi1n2G: electroweak associated production of Higgsino-like charginos $\tilde{\chi}_1^\pm$ and neutralinos $\tilde{\chi}_2^0$, and electroweak associated production of $\tilde{\chi}_2^0$ and $\tilde{\chi}_1^0$, where $m_{\tilde{\chi}_1^\pm} = (m_{\tilde{\chi}_2^0} + m_{\tilde{\chi}_1^0})/2$ and where $\tilde{\chi}_1^\pm$

Downloaded from https://academic.oup.com/ptep/article/2022/8/083C01/6651666 by KIT Library user on 27 September 2022

decays through an intermediate $W^{\pm *}$ to $q\bar{q}\tilde{\chi}^0_1$ and where $\tilde{\chi}^0_2$ decays through an intermediate Z^* to $l^+l^-\tilde{\chi}^0_1$.

Tchi1n2Ga: electroweak associated production of Higgsino-like charginos $\tilde{\chi}^\pm_1$ and neutralinos $\tilde{\chi}^0_2$, and electroweak associated production of $\tilde{\chi}^0_2$ and $\tilde{\chi}^0_1$, where $m_{\tilde{\chi}^\pm_1} = (m_{\tilde{\chi}^0_2} + m_{\tilde{\chi}^0_1})/2$ and where $\tilde{\chi}^\pm_1$ decays through an intermediate $W^{\pm *}$ to $l\nu\tilde{\chi}^0_1$ and where $\tilde{\chi}^0_2$ decays through an intermediate Z^* to $l^+l^-\tilde{\chi}^0_1$.

Tchi1n2H: electroweak associated production of mass-degenerate charginos $\tilde{\chi}^\pm_1$ and neutralinos $\tilde{\chi}^0_2$, where $\tilde{\chi}^\pm_1$ decays through an intermediate slepton or sneutrino to $l\nu\tilde{\chi}^0_1$ and where $\tilde{\chi}^0_2$ decays through an intermediate scalar tau lepton or sneutrino to $\tau^+\tau^-\tilde{\chi}^0_1$ or $\nu\bar{\nu}\tilde{\chi}^0_1$.

Tchi1n2I: electroweak associated production of mass-degenerate charginos $\tilde{\chi}^\pm_1$ and neutralinos $\tilde{\chi}^0_2$, where $\tilde{\chi}^\pm_1$ decays to $W^\pm + \tilde{\chi}^0_1$ and where $\tilde{\chi}^0_2$ decays 50% of the time to $Z + \tilde{\chi}^0_1$ and 50% of the time to $H + \tilde{\chi}^0_1$.

Tchi1n12_GGM: in the framework of General Gauge Mediation (GGM): electroweak pair and associated production of nearly mass-degenerate charginos $\tilde{\chi}^\pm_1$ and neutralinos $\tilde{\chi}^0_1$, $\tilde{\chi}^0_2$ (*i.e.* $\tilde{\chi}^\pm_1\tilde{\chi}^\pm_1$, $\tilde{\chi}^\pm_1\tilde{\chi}^0_1$ and $\tilde{\chi}^\pm_1\tilde{\chi}^0_2$ production) where the $\tilde{\chi}^\pm_1$ decays exclusively to $W^\pm + \tilde{G}$, the $\tilde{\chi}^0_2$ decays to $Z/H + \tilde{G}$ and the $\tilde{\chi}^0_1$ decays to $\gamma/Z + \tilde{G}$. The branching ratios depend on the composition of the gauge eigenstates of the neutralinos in the GGM scenario.

TwinoLSPBL: Electroweak pair production of wino-like $\tilde{\chi}^\pm_1$ and $\tilde{\chi}^0_1$ (i.e. $\tilde{\chi}^\pm_1\tilde{\chi}^\pm_1$ and $\tilde{\chi}^0_1\tilde{\chi}^0_1$). The $\tilde{\chi}^\pm_1$ can decay via bi-linear RPV into $Z\ell$, $H\ell$ or $W\nu$; the $\tilde{\chi}^0_1$ can decay into $Z\nu$, $H\nu$ or $W\ell$.

Tn1n1A: electroweak pair and associated production of nearly mass-degenerate Higgsino-like charginos $\tilde{\chi}^\pm_1$ and neutralinos $\tilde{\chi}^0_1$ and $\tilde{\chi}^0_2$, where $\tilde{\chi}^\pm_1$ and $\tilde{\chi}^0_2$ decay to $\tilde{\chi}^0_1$ plus soft radiation and where both of the $\tilde{\chi}^0_1$ decay to $H + \tilde{G}$.

Tn1n1B: electroweak pair and associated production of nearly mass-degenerate Higgsino-like charginos $\tilde{\chi}^\pm_1$ and neutralinos $\tilde{\chi}^0_1$ and $\tilde{\chi}^0_2$, where $\tilde{\chi}^\pm_1$ and $\tilde{\chi}^0_2$ decay to $\tilde{\chi}^0_1$ plus soft radiation and where the $\tilde{\chi}^0_1$ decays 50% of the time to $H + \tilde{G}$ and 50 % of the time to $Z + \tilde{G}$.

Tn1n1C: electroweak pair and associated production of nearly mass-degenerate Higgsino-like charginos $\tilde{\chi}^\pm_1$ and neutralinos $\tilde{\chi}^0_1$ and $\tilde{\chi}^0_2$, where $\tilde{\chi}^\pm_1$ and $\tilde{\chi}^0_2$ decay to $\tilde{\chi}^0_1$ plus soft radiation and where both of the $\tilde{\chi}^0_1$ decay to $Z + \tilde{G}$.

Tn1n1D: electroweak pair and associated production of nearly mass-degenerate Higgsino-like charginos $\tilde{\chi}^\pm_1$ and neutralinos $\tilde{\chi}^0_1$, $\tilde{\chi}^0_2$.

Tn1n1E: electroweak pair and associated production of nearly mass-degenerate wino-like charginos $\tilde{\chi}^\pm_1$ and neutralinos $\tilde{\chi}^0_1$.

Tn2n3A: electroweak associated production of mass-degenerate neutralinos $\tilde{\chi}^0_2$ and $\tilde{\chi}^0_3$, where $\tilde{\chi}^0_2$ and $\tilde{\chi}^0_3$ decay through intermediate sleptons to $l^+l^-\tilde{\chi}^0_1$ and where the slepton mass is 5%, 25%, 50%, 75% and 95% of the $\tilde{\chi}^0_2$ mass.

Tn2n3B: electroweak associated production of mass-degenerate neutralinos $\tilde{\chi}^0_2$ and $\tilde{\chi}^0_3$, where $\tilde{\chi}^0_2$ and $\tilde{\chi}^0_3$ decay through intermediate sleptons to $l^+l^-\tilde{\chi}^0_1$ and where $m_{\tilde{\ell}} = (m_{\tilde{\chi}^0_2} + m_{\tilde{\chi}^0_1})/2$.

TWinoBinoA: electroweak pair production of mass-degenerate wino-like doublet $(\tilde{\chi}^0_2, \tilde{\chi}^\pm_1)$ (including all pair-production mechanisms) decaying into a bino singlet $(\tilde{\chi}^0_1)$. Decays happen via Standard Model bosons, assumed to decay via hadrons.

TWinoHinoA: electroweak pair production of mass-degenerate wino-like doublet $(\tilde{\chi}^0_3, \tilde{\chi}^\pm_2)$ (including all possible pair-production mechanisms) decaying into a quasi-mass-degenerate Higgsino triplet $(\tilde{\chi}^0_1, \tilde{\chi}^0_2, \tilde{\chi}^\pm_1)$. Decays happen via Standard Model bosons, assumed to decay via hadrons.

THinoBinoA: electroweak pair production of quasi-mass-degenerate higgsino-like triplet $(\tilde{\chi}^0_2, \tilde{\chi}^0_3, \tilde{\chi}^\pm_1)$ (including all possible pair-production mechanisms) decaying into a bino singlet $(\tilde{\chi}^0_1)$. Decays happen via Standard Model bosons, assumed to decay via hadrons.

HinoWinoA: electroweak pair production of quasi-mass-degenerate higgsino-like triplet $(\tilde{\chi}^0_2, \tilde{\chi}^0_2, \tilde{\chi}^\pm_2)$ (including all possible pair-production mechanisms) decaying into a mass-degenerate wino doublet $(\tilde{\chi}^0_1, \tilde{\chi}^\pm_1)$. Decays happen via Standard Model bosons, assumed to decay via hadrons.

$\tilde{\chi}^0_1$ (Lightest Neutralino) mass limit

$\tilde{\chi}^0_1$ is often assumed to be the lightest supersymmetric particle (LSP). See also the $\tilde{\chi}^0_2$, $\tilde{\chi}^0_3$, $\tilde{\chi}^0_4$ section below.

We have divided the $\tilde{\chi}^0_1$ listings below into five sections:

1) Accelerator limits for stable $\tilde{\chi}^0_1$,
2) Bounds on $\tilde{\chi}^0_1$ from dark matter searches,
3) $\tilde{\chi}^0_1 - p$ elastic cross section (spin-dependent, spin-independent interactions),
4) Other bounds on $\tilde{\chi}^0_1$ from astrophysics and cosmology, and
5) Unstable $\tilde{\chi}^0_1$ (Lightest Neutralino) mass limit.

Accelerator limits for stable $\tilde{\chi}^0_1$

Unless otherwise stated, results in this section assume spectra, production rates, decay modes, and branching ratios as evaluated in the MSSM, with gaugino and sfermion mass unification at the GUT scale. These papers generally study production of $\tilde{\chi}^0_i\tilde{\chi}^0_j$ ($i \geq 1$, $j \geq 2$), $\tilde{\chi}^+_1\tilde{\chi}^-_1$, and (in the case of hadronic collisions) $\tilde{\chi}^+_1\tilde{\chi}^0_2$ pairs. The mass limits on $\tilde{\chi}^0_1$ are either direct, or follow indirectly from the constraints set by the non-observation of $\tilde{\chi}^\pm_1$ and $\tilde{\chi}^0_2$ states on the gaugino and higgsino MSSM parameters M_2 and μ. In some cases, information is used from the nonobservation of slepton decays.

Obsolete limits obtained from e^+e^- collisions up to $\sqrt{s}$=184 GeV have been removed from this compilation and can be found in the 2000 Edition (The European Physical Journal **C15** 1 (2000)) of this Review. $\Delta m = m_{\tilde{\chi}^0_2} - m_{\tilde{\chi}^0_1}$.

VALUE (GeV)	CL%	DOCUMENT ID		TECN	COMMENT
none 450–930	95	[1] AAD	21AX	ATLS	jets + large-R jets + $\not{E}_T$, Tn1n1C
none 200–320	95	[2] AAD	21BF	ATLS	$\ell^\pm$ + b-jets + many jets, Tn1n1D, RPV, λ''_{323} electroweakino decay, degenerate Higgsino triplet
none 200–370	95	[2] AAD	21BF	ATLS	$\ell^\pm$ + b-jets + many jets, Tn1n1E, RPV, λ''_{323} electroweakino decay, degenerate Wino doublet
		[3] DREINER	09	THEO	
>40	95	[4] ABBIENDI	04H	OPAL	all $\tan\beta$, Δm >5 GeV, m_0 >500 GeV, $A_0 = 0$
>42.4	95	[5] HEISTER	04	ALEP	all $\tan\beta$, all Δm, all m_0
>39.2	95	[6] ABDALLAH	03M	DLPH	all $\tan\beta$, $m_{\tilde{\nu}}$ >500 GeV
>46	95	[7] ABDALLAH	03M	DLPH	all $\tan\beta$, all Δm, all m_0
>32.5	95	[8] ACCIARRI	00D	L3	$\tan\beta > 0.7$, $\Delta m > 3$ GeV, all m_0
• • • We do not use the following data for averages, fits, limits, etc. • • •					
		[9] AAD	14K	ATLS	
>24		[10] CALIBBI	13		thermal relic abundance, MSSM particle content

[1] AAD 21AX searched in 139 fb^{-1} of pp collisions at $\sqrt{s} = 13$ TeV for pair production of electroweakinos decaying to the LSP via the emission of Standard Model bosons (Higgs, W, Z) decaying into hadrons. The final state in all cases characterised by the presence of $\not{E}_T$, jets, and large-R jets tagged according to the boson of interest. Different assumptions (Higgsino, Wino, Bino) are made for the pair produced electroweakinos and for the LSP multiplet. No significant excess above the Standard Model predictions is observed. Limits are set on the electroweakino masses as a function of the model parameters (in particular $m_{\tilde{\chi}^0_1}$). See Fig. 16.

[2] AAD 21BF searched in 139 fb^{-1} of pp collisions at $\sqrt{s} = 13$ TeV for pair production of gluinos, stops, electroweakinos decaying RPV either directly or indirectly via the LSP. The final state in all cases is one or two leptons, many jets (up to fifteen) and b-jets. Different models with different branching fractions of the gluino or stop follow from the assumptions on the nature of the electroweakinos. No significant excess above the Standard Model predictions is observed. Limits are set on the *gluino*, $\tilde{t}_1$, electroweakino masses as a function of the $\tilde{\chi}^0_1$ mass in several scenarios of gluino, stop and electroweakino pair production.

[3] DREINER 09 show that in the general MSSM with non-universal gaugino masses there exists no model-independent laboratory bound on the mass of the lightest neutralino. An essentially massless χ^0_1 is allowed by the experimental and observational data, imposing some constraints on other MSSM parameters, including M_2, μ and the slepton and squark masses.

[4] ABBIENDI 04H search for charginos and neutralinos in events with acoplanar leptons+jets and multi-jet final states in the 192–209 GeV data, combined with the results on leptonic final states from ABBIENDI 04. The results hold for a scan over the parameter space covering the region $0 < M_2 < 5000$ GeV, $-1000 < \mu < 1000$ GeV and $\tan\beta$ from 1 to 40. This limit supersedes ABBIENDI 00H.

[5] HEISTER 04 data collected up to 209 GeV. Updates earlier analysis of selectrons from HEISTER 02E, includes a new analysis of charginos and neutralinos decaying into stau and uses results on charginos with initial state radiation from HEISTER 02J. The limit is based on the direct search for charginos and neutralinos, the constraints from the slepton search and the Higgs mass limits from HEISTER 02 using a top mass of 175 GeV, interpreted in a framework with universal gaugino and sfermion masses. Assuming the mixing in the stau sector to be negligible, the limit improves to 43.1 GeV. Under the assumption of MSUGRA with unification of the Higgs and sfermion masses, the limit improves to 50 GeV, and reaches 53 GeV for $A_0 = 0$. These limits include and update the results of BARATE 01.

[6] ABDALLAH 03M uses data from $\sqrt{s} = 192$–208 GeV. A limit on the mass of $\tilde{\chi}^0_1$ is derived from direct searches for neutralinos combined with the chargino search. Neutralinos are searched in the production of $\tilde{\chi}^0_1\tilde{\chi}^0_2$, $\tilde{\chi}^0_1\tilde{\chi}^0_3$, as well as $\tilde{\chi}^0_2\tilde{\chi}^0_3$ and $\tilde{\chi}^0_2\tilde{\chi}^0_4$ giving rise to

Downloaded from https://academic.oup.com/ptep/article/2022/8/083C01/6651666 by KIT Library user on 27 September 2022

cascade decays, and $\tilde{\chi}_1^0\tilde{\chi}_2^0$ and $\tilde{\chi}_1^0\tilde{\chi}_2^0$, followed by the decay $\tilde{\chi}_2^0 \rightarrow \tilde{\tau}\tau$. The results hold for the parameter space defined by values of $M_2 < 1$ TeV, $|\mu| \leq 2$ TeV with the $\tilde{\chi}_1^0$ as LSP. The limit is obtained for $\tan\beta = 1$ and large m_0, where $\tilde{\chi}_2^0\tilde{\chi}_4^0$ and chargino pair production are important. If the constraint from Higgs searches is also imposed, the limit improves to 49.0 GeV in the m_h^{max} scenario with m_t=174.3 GeV. These limits update the results of ABREU 00J.

[7] ABDALLAH 03M uses data from $\sqrt{s}$ = 192–208 GeV. An indirect limit on the mass of $\tilde{\chi}_1^0$ is derived by constraining the MSSM parameter space by the results from direct searches for neutralinos (including cascade decays and $\tilde{\tau}\tau$ final states), for charginos (for all Δm_+) and for sleptons, stop and sbottom. The results hold for the full parameter space defined by values of $M_2 < 1$ TeV, $|\mu| \leq 2$ TeV with the $\tilde{\chi}_1^0$ as LSP. Constraints from the Higgs search in the m_h^{max} scenario assuming m_t=174.3 GeV are included. The limit is obtained for $\tan\beta \geq 5$ when stau mixing leads to mass degeneracy between $\tilde{\tau}_1$ and $\tilde{\chi}_1^0$ and the limit is based on $\tilde{\chi}_2^0$ production followed by its decay to $\tilde{\tau}_1\tau$. In the pathological scenario where m_0 and $|\mu|$ are large, so that the $\tilde{\chi}_2^0$ production cross section is negligible, and where there is mixing in the stau sector but not in stop nor sbottom, the limit is based on charginos with soft decay products and an ISR photon. The limit then degrades to 39 GeV. See Figs. 40–42 for the dependence of the limit on $\tan\beta$ and $m_{\tilde{\nu}}$. These limits update the results of ABREU 00W.

[8] ACCIARRI 00D data collected at $\sqrt{s}$=189 GeV. The results hold over the full parameter space defined by $0.7 \leq \tan\beta \leq 60$, $0 \leq M_2 \leq 2$ TeV, $m_0 \leq 500$ GeV, $|\mu| \leq 2$ TeV The minimum mass limit is reached for $\tan\beta$=1 and large m_0. The results of slepton searches from ACCIARRI 99W are used to help set constraints in the region of small m_0. The limit improves to 48 GeV for $m_0 \gtrsim 200$ GeV and $\tan\beta \gtrsim 10$. See their Figs. 6–8 for the $\tan\beta$ and m_0 dependence of the limits. Updates ACCIARRI 98F.

[9] AAD 14K sets limits on the χ-nucleon spin-dependent and spin-independent cross sections out to $m_\chi = 10$ TeV.

[10] CALIBBI 13 use the fact that if the relic abundance of $\tilde{\chi}_1^0$ does not overclose the universe, scalar lepton and Higgsino masses must be relatively small. Using 8 TeV ATLAS constraints on the scalar tau mass and on invisible Higgs decays, they estimate a lower bound for the $\tilde{\chi}_1^0$ mass.

Bounds on $\tilde{\chi}_1^0$ from dark matter searches

These papers generally exclude regions in the $M_2 - \mu$ parameter plane assuming that $\tilde{\chi}_1^0$ is the dominant form of dark matter in the galactic halo. These limits are based on the lack of detection in laboratory experiments, telescopes, or by the absence of a signal in underground neutrino detectors. The latter signal is expected if $\tilde{\chi}_1^0$ accumulates in the Sun or the Earth and annihilates into high-energy ν's.

VALUE	DOCUMENT ID		TECN
• • • We do not use the following data for averages, fits, limits, etc. • • •			
	[1] ABDALLAH	21	HESS
	[2] ABAZAJIAN	20	FLAT
	[3] ABDALLAH	20	HESS
	[4] ABE	20G	SKAM
	[5] ALBERT	20	HAWC
	[6] ALBERT	20A	ANTR
	[7] ALBERT	20C	ANIC
	[8] ALVAREZ	20	FLAT
	[9] HOOF	20	FLAT
	[10] DI-MAURO	19	FLAT
	[11] JOHNSON	19	FLAT
	[12] LI	19D	FLAT
	[13] ABDALLAH	18	HESS
	[14] AHNEN	18	MGIC
	[15] ALBERT	18B	HAWC
	[16] ALBERT	18C	HAWC
	[17] AARTSEN	17	ICCB
	[18] AARTSEN	17A	ICCB
	[19] AARTSEN	17C	ICCB
	[20] ARCHAMBAU..	17	VRTS
	[21] ADRIAN-MAR..	16	ANTR
	[22] AHNEN	16	MGFL
	[23] AVRORIN	16	BAIK
	[24] CIRELLI	16	THEO
	[24] LEITE	16	THEO
	[25] ACKERMANN	15	FLAT
	[26] ACKERMANN	15A	FLAT
	[27] ACKERMANN	15B	FLAT
	[28] BUCKLEY	15	THEO
	[29] CHOI	15	SKAM
	[30] ALEKSIC	14	MGIC
	[31] AVRORIN	14	BAIK
	[32] AARTSEN	13C	ICCB
	[33] BERGSTROM	13	COSM
	[34] BOLIEV	13	BAKS
	[33] JIN	13	ASTR
	[33] KOPP	13	COSM
	[35] ACKERMANN	10	FLAT
	[36] ACHTERBERG	06	AMND
	[37] ACKERMANN	06	AMND
	[38] DEBOER	06	RVUE
	[39] DESAI	04	SKAM
	[39] AMBROSIO	99	MCRO
	[40] LOSECCO	95	RVUE
	[41] MORI	93	KAMI
	[42] BOTTINO	92	COSM
	[43] BOTTINO	91	RVUE
	[44] GELMINI	91	COSM
	[45] KAMIONKOW..	91	RVUE
	[46] MORI	91B	KAMI
none 4–15 GeV	[47] OLIVE	88	COSM

[1] ABDALLAH 21 places constraints on the dark matter annihilation cross section for annihilations into gamma-rays from the dwarf irregular galaxy WLM for masses between 0.15 to 10 TeV.

[2] ABAZAJIAN 20 sets constraints on the dark matter annihilation from gamma-ray searches from Fermi LAT observations of the Galactic center.

[3] ABDALLAH 20 places constraints on the dark matter annihilation cross section for annihilations into gamma-rays from Milky Way dwarf galaxy satellites for masses between 0.2 to 40 TeV.

[4] ABE 20G is based on SuperKamiokande data taken from 1996 to 2016 searching for neutrinos produced from dark matter annihilations in the galactic center or halo. They place constraints on the dark matter-nucleon scattering cross section for dark matter masses between 1 GeV and 10 TeV.

[5] ALBERT 20 sets limits on the annihilation cross section of dark matter with mass between 1 and 100 TeV from gamma-ray observations of the local dwarf spheroidal galaxies.

[6] ALBERT 20A set limits on the dark matter annihilation cross section from neutrinos observations in the Galactic center using 11 years of ANTARES data.

[7] ALBERT 20C set limits on the dark matter annihilation cross section from neutrinos observations in the Galactic center combining Antares and IceCube data.

[8] ALVAREZ 20 set limits on the dark matter annihilation from gamma-ray searches from Fermi LAT observations in the directions of dwarf spheroidal galaxies.

[9] HOOF 20 set limits on the dark matter annihilation from gamma-ray searches from Fermi LAT observations in the directions of dwarf spheroidal galaxies.

[10] DI-MAURO 19 sets limits on the dark matter annihilation from gamma-ray searches in M31 and M33 galaxies using Fermi LAT data.

[11] JOHNSON 19 sets limits on p-wave dark matter annihilations in the galactic center using Fermi data.

[12] LI 19D sets limits on dark matter annihilation cross sections searching for line-like signals in the all-sky Fermi data.

[13] ABDALLAH 18 places constraints on the dark matter annihilation cross section for annihilations into gamma-rays in the Galactic center for masses between 300 GeV to 70 TeV. This updates ABDALLAH 16.

[14] AHNEN 18 uses observations of the dwarf satellite galaxy Ursa Major II to obtain upper limits on annihilation cross sections for dark matter in various channels for masses between 0.1–100 TeV.

[15] ALBERT 18B sets limits on the annihilation cross section of dark matter with mass between 1 and 100 TeV from gamma-ray observations of the Andromeda galaxy.

[16] ALBERT 18C sets limits on the spin-dependent coupling of dark matter to protons from dark matter annihilation in the Sun.

[17] AARTSEN 17 is based on data collected during 327 days of detector livetime with IceCube. They looked for interactions of ν's resulting from neutralino annihilations in the Earth over a background of atmospheric neutrinos and set 90% CL limits on the spin independent neutralino-proton cross section for neutralino masses in the range 10–10000 GeV.

[18] AARTSEN 17A is based on data collected during 532 days of livetime with the IceCube 86-string detector including the DeepCore sub-array. They looked for interactions of ν's from neutralino annihilations in the Sun over a background of atmospheric neutrinos and set 90% CL limits on the spin dependent neutralino-proton cross section for neutralino masses in the range 10–10000 GeV. This updates AARTSEN 16C.

[19] AARTSEN 17C is based on 1005 days of running with the IceCube detector. They set a limit on the annihilation cross section for dark matter with masses between 10–1000 GeV annihilating in the Galactic center assuming an NFW profile. The limit is of 1.2×10^{23} $cm^3 s^{-1}$ in the $\tau^+\tau^-$ channel. Supercedes AARTSEN 15E.

[20] ARCHAMBAULT 17 performs a joint statistical analysis of four dwarf galaxies with VERITAS looking for gamma-ray emission from neutralino annihilation. They set limits on the neutralino annihilation cross section.

[21] ADRIAN-MARTINEZ 16 is based on data from the ANTARES neutrino telescope. They looked for interactions of ν's from neutralino annihilations in the Sun over a background of atmospheric neutrinos and set 90% CL limits on the muon neutrino flux. They also obtain limits on the spin dependent and spin independent neutralino-proton cross section for neutralino masses in the range 50 to 5,000 GeV. This updates ADRIAN-MARTINEZ 13.

[22] AHNEN 16 combines 158 hours of Segue 1 observations with MAGIC with 6 year observations of 15 dwarf satellite galaxies by Fermi-LAT to set limits on annihilation cross sections for dark matter masses between 10 GeV and 100 TeV.

[23] AVRORIN 16 is based on 2.76 years with Lake Baikal neutrino telescope. They derive 90% upper limits on the annihilation cross section from dark matter annihilations in the Galactic center.

[24] CIRELLI 16 and LEITE 16 derive bounds on the annihilation cross section from radio observations.

[25] ACKERMANN 15 is based on 5.8 years of data with Fermi-LAT and search for monochromatic gamma-rays in the energy range of 0.2–500 GeV from dark matter annihilations. This updates ACKERMANN 13A.

[26] ACKERMANN 15A is based on 50 months of data with Fermi-LAT and search for dark matter annihilation signals in the isotropic gamma-ray background as well as galactic subhalos in the energy range of a few GeV to a few tens of TeV.

[27] ACKERMANN 15B is based on 6 years of data with Fermi-LAT observations of Milky Way dwarf spheroidal galaxies. Set limits on the annihilation cross section from m_χ = 2 GeV to 10 TeV. This updates ACKERMANN 14.

[28] BUCKLEY 15 is based on 5 years of Fermi-LAT data searching for dark matter annihilation signals from Large Magellanic Cloud.

[29] CHOI 15 is based on 3903 days of SuperKamiokande data searching for neutrinos produced from dark matter annihilations in the sun. They place constraints on the dark matter-nucleon scattering cross section for dark matter masses between 4–200 GeV.

[30] ALEKSIC 14 is based on almost 160 hours of observations of Segue 1 satellite dwarf galaxy using the MAGIC telescopes between 2011 and 2013. Sets limits on the annihilation cross section out to $m_\chi = 10$ TeV.

[31] AVRORIN 14 is based on almost 2.76 years with Lake Baikal neutrino telescope. They derive 90% upper limits on the fluxes of muons and muon neutrinos from dark matter annihilations in the Sun.

Downloaded from https://academic.oup.com/ptep/article/2022/8/083C01/6651666 by KIT Library user on 27 September 2022

[32] AARTSEN 13C is based on data collected during 339.8 effective days with the IceCube 59-string detector. They looked for interactions of ν_μ's from neutralino annihilations in nearby galaxies and galaxy clusters. They obtain limits on the neutralino annihilation cross section for neutralino masses in the range 30–100, 000 GeV.

[33] BERGSTROM 13, JIN 13, and KOPP 13 derive limits on the mass and annihilation cross section using AMS-02 data. JIN 13 also sets a limit on the lifetime of the dark matter particle.

[34] BOLIEV 13 is based on data collected during 24.12 years of live time with the Bakson Underground Scintillator Telescope. They looked for interactions of ν_μ's from neutralino annihilations in the Sun over a background of atmospheric neutrinos and set 90% CL limits on the muon flux. They also obtain limits on the spin dependent and spin independent neutralino-proton cross section for neutralino masses in the range 10–1000 GeV.

[35] ACKERMANN 10 place upper limits on the annihilation cross section with $b\overline{b}$ or $\mu^+\mu^-$ final states.

[36] ACHTERBERG 06 is based on data collected during 421.9 effective days with the AMANDA detector. They looked for interactions of ν_μs from the centre of the Earth over a background of atmospheric neutrinos and set 90 % CL limits on the muon flux. Their limit is compared with the muon flux expected from neutralino annihilations into W^+W^- and $b\overline{b}$ at the centre of the Earth for MSSM parameters compatible with the relic dark matter density, see their Fig. 7.

[37] ACKERMANN 06 is based on data collected during 143.7 days with the AMANDA-II detector. They looked for interactions of ν_μs from the Sun over a background of atmospheric neutrinos and set 90 % CL limits on the muon flux. Their limit is compared with the muon flux expected from neutralino annihilations into W^+W^- in the Sun for SUSY model parameters compatible with the relic dark matter density, see their Fig. 3.

[38] DEBOER 06 interpret an excess of diffuse Galactic gamma rays observed with the EGRET satellite as originating from π^0 decays from the annihilation of neutralinos into quark jets. They analyze the corresponding parameter space in a supergravity inspired MSSM model with radiative electroweak symmetry breaking, see their Fig. 3 for the preferred region in the $(m_0, m_{1/2})$ plane of a scenario with large $\tan\beta$.

[39] AMBROSIO 99 and DESAI 04 set new neutrino flux limits which can be used to limit the parameter space in supersymmetric models based on neutralino annihilation in the Sun and the Earth.

[40] LOSECCO 95 reanalyzed the IMB data and places lower limit on $m_{\widetilde{\chi}^0_1}$ of 18 GeV if the LSP is a photino and 10 GeV if the LSP is a higgsino based on LSP annihilation in the sun producing high-energy neutrinos and the limits on neutrino fluxes from the IMB detector.

[41] MORI 93 excludes some region in M_2–μ parameter space depending on $\tan\beta$ and lightest scalar Higgs mass for neutralino dark matter $m_{\widetilde{\chi}^0} > m_W$, using limits on upgoing muons produced by energetic neutrinos from neutralino annihilation in the Sun and the Earth.

[42] BOTTINO 92 excludes some region M_2-μ parameter space assuming that the lightest neutralino is the dark matter, using upgoing muons at Kamiokande, direct searches by Ge detectors, and by LEP experiments. The analysis includes top radiative corrections on Higgs parameters and employs two different hypotheses for nucleon-Higgs coupling. Effects of rescaling in the local neutralino density according to the neutralino relic abundance are taken into account.

[43] BOTTINO 91 excluded a region in $M_2-\mu$ plane using upgoing muon data from Kamioka experiment, assuming that the dark matter surrounding us is composed of neutralinos and that the Higgs boson is not too heavy.

[44] GELMINI 91 exclude a region in $M_2-\mu$ plane using dark matter searches.

[45] KAMIONKOWSKI 91 excludes a region in the M_2–μ plane using IMB limit on upgoing muons originated by energetic neutrinos from neutralino annihilation in the sun, assuming that the dark matter is composed of neutralinos and that $m_{H^0_1} \lesssim$ 50 GeV. See Fig. 8 in the paper.

[46] MORI 91B exclude a part of the region in the M_2–μ plane with $m_{\widetilde{\chi}^0_1} \lesssim$ 80 GeV using a limit on upgoing muons originated by energetic neutrinos from neutralino annihilation in the earth, assuming that the dark matter surrounding us is composed of neutralinos and that $m_{H^0_1} \lesssim$ 80 GeV.

[47] OLIVE 88 result assumes that photinos make up the dark matter in the galactic halo. Limit is based on annihilations in the sun and is due to an absence of high energy neutrinos detected in underground experiments. The limit is model dependent.

$\widetilde{\chi}^0_1$-p elastic cross section

Experimental results on the $\widetilde{\chi}^0_1$-p elastic cross section are evaluated at $m_{\widetilde{\chi}^0_1}$=100 GeV. The experimental results on the cross section are often mass dependent. Therefore, the mass and cross section results are also given where the limit is strongest, when appropriate. Results are quoted separately for spin-dependent interactions (based on an effective 4-Fermi Lagrangian of the form $\overline{\chi}\gamma^\mu\gamma^5\chi\overline{q}\gamma_\mu\gamma^5 q$) and spin-independent interactions ($\overline{\chi}\chi\overline{q}q$). For calculational details see GRIEST 88B, ELLIS 88D, BARBIERI 89C, DREES 93B, ARNOWITT 96, BERGSTROM 96, and BAER 97 in addition to the theory papers listed in the Tables. For a description of the theoretical assumptions and experimental techniques underlying most of the listed papers, see the review on "Dark matter" in this "Review of Particle Physics," and references therein. Most of the following papers use galactic halo and nuclear interaction assumptions from (LEWIN 96).

Spin-dependent interactions

VALUE (pb)	CL%	DOCUMENT ID		TECN	COMMENT
• • • We do not use the following data for averages, fits, limits, etc. • • •					
$< 4 \times 10^{-5}$	90	[1] AMOLE	19	PICO	C_3F_8
$< 5 \times 10^{-4}$	90	[2] APRILE	19A	XE1T	Xe
$< 7 \times 10^{-4}$	90	[3] XIA	19A	PNDX	Xe
$< 8 \times 10^{-4}$	90	[4] AKERIB	17A	LUX	Xe
< 0.28	90	[5] BATTAT	17	DRFT	CS_2; CF_4
< 0.027	90	[6] BEHNKE	17	PICA	C_4F_{10}
$< 5 \times 10^{-4}$	90	[7] AMOLE	16	PICO	CF_3I
$< 6.8 \times 10^{-3}$	90	[8] APRILE	16B	X100	Xe
$< 6.3 \times 10^{-3}$	90	[9] FELIZARDO	14	SMPL	C_2ClF_5
< 0.01	90	[10] AKIMOV	12	ZEP3	Xe
$< 7 \times 10^{-3}$		[11] BEHNKE	12	COUP	CF_3I
$< 8.5 \times 10^{-3}$		[12] FELIZARDO	12	SMPL	C_2ClF_5
< 0.016	90	[13] KIM	12	KIMS	CsI
5×10^{-10} to 10^{-5}	95	[14] BUCHMUEL...	11B	THEO	
< 1	90	[15] ANGLE	08A	XE10	Xe
< 0.055		[16] BEDNYAKOV	08	HDMS	Ge
< 0.33	90	[17] BEHNKE	08	COUP	CF_3I
< 5		[18] AKERIB	06	CDMS	Ge
< 2		[19] SHIMIZU	06A	CNTR	CaF_2
< 0.4		[20] ALNER	05	NAIA	NaI Spin Dep.
< 2		[21] BARNABE-HE...	05	PICA	C
2×10^{-11} to 1×10^{-4}		[22] ELLIS	04	THEO	$\mu > 0$
< 0.8		[23] AHMED	03	NAIA	NaI Spin Dep.
< 40		[24] TAKEDA	03	BOLO	NaF Spin Dep.
< 10		[25] ANGLOHER	02	CRES	Saphire
8×10^{-7} to 2×10^{-5}		[26] ELLIS	01C	THEO	$\tan\beta \leq 10$
< 3.8		[27] BERNABEI	00D	DAMA	Xe
< 0.8		SPOONER	00	UKDM	NaI
< 4.8		[28] BELLI	99C	DAMA	F
<100		[29] OOTANI	99	BOLO	LiF
< 0.6		BERNABEI	98C	DAMA	Xe
< 5		[28] BERNABEI	97	DAMA	F

[1] The strongest limit is $< 2.5 \times 10^{-5}$ pb at $m_\chi = 25$ GeV. This updates AMOLE 17.

[2] The strongest limit is $< 2 \times 10^{-4}$ pb at $m_\chi = 30$ GeV. For scatterings on neutrons, the strongest limit is $< 6.3 \times 10^{-6}$ at $m_\chi = 30$ GeV.

[3] The strongest limit is $< 4.4 \times 10^{-4}$ pb at $m_\chi = 40$ GeV. This updates FU 17.

[4] The strongest limit is 5×10^{-4} pb at $m_\chi = 35$ GeV. The limit for scattering on neutrons is 3×10^{-5} pb at 100 GeV and is 1.6×10^{-5} pb at 35 GeV. This updates AKERIB 16A.

[5] Directional recoil detector. This updates DAW 12.

[6] This result updates ARCHAMBAULT 12. The strongest limit is 0.013 pb at $m_\chi = 20$ GeV.

[7] The strongest limit is 5×10^{-4} pb at $m_\chi = 80$ GeV.

[8] The strongest limit is 5.2×10^{-3} pb at 50 GeV. The limit for scattering on neutrons is 2.8×10^{-4} pb at 100 GeV and the strongest limit is 2.0×10^{-4} pb at 50 GeV. This updates APRILE 13.

[9] The strongest limit is 0.0043 pb and occurs at $m_\chi = 35$ GeV. FELIZARDO 14 also presents limits for the scattering on neutrons. At $m_\chi = 100$ GeV, the upper limit is 0.13 pb and the strongest limit is 0.066 pb at $m_\chi = 35$ GeV.

[10] This result updates LEBEDENKO 09A. The strongest limit is 8×10^{-3} pb at $m_\chi = 50$ GeV. Limit applies to the neutralino neutron elastic cross section.

[11] The strongest limit is 6×10^{-3} at $m_\chi = 60$ GeV.

[12] The strongest limit is 5.7×10^{-3} at $m_\chi = 35$ GeV.

[13] This result updates LEE 07A. The strongest limit is at $m_\chi = 80$ GeV.

[14] Predictions for the spin-dependent elastic cross section based on a frequentist approach to electroweak observables in the framework of $N = 1$ supergravity models with radiative breaking of the electroweak gauge symmetry.

[15] The strongest limit is 0.6 pb and occurs at m_χ= 30 GeV. The limit for scattering on neutrons is 0.01 pb at m_χ= 100 GeV, and the strongest limit is 0.0045 pb at m_χ= 30 GeV.

[16] Limit applies to neutron elastic cross section.

[17] The strongest upper limit is 0.25 pb and occurs at $m_\chi \simeq 40$ GeV.

[18] The strongest upper limit is 4 pb and occurs at $m_\chi \simeq$ 60 GeV. The limit on the neutron spin-dependent elastic cross section is 0.07 pb. This latter limit is improved in AHMED 09, where a limit of 0.02 pb is obtained at $m_\chi = 100$ GeV. The strongest limit in AHMED 09 is 0.018 pb and occurs at $m_\chi = 60$ GeV.

[19] The strongest upper limit is 1.2 pb and occurs at $m_\chi \simeq$ 40 GeV. The limit on the neutron spin-dependent cross section is 35 pb.

[20] The strongest upper limit is 0.35 pb and occurs at $m_\chi \simeq$ 60 GeV.

[21] The strongest upper limit is 1.2 pb and occurs $m_\chi \simeq$ 30 GeV.

[22] ELLIS 04 calculates the χp elastic scattering cross section in the framework of N=1 supergravity models with radiative breaking of the electroweak gauge symmetry, but without universal scalar masses. In the case of universal squark and slepton masses, but non-universal Higgs masses, the limit becomes 2×10^{-4}, see ELLIS 03E.

[23] The strongest upper limit is 0.75 pb and occurs at $m_\chi \approx 70$ GeV.

[24] The strongest upper limit is 30 pb and occurs at $m_\chi \approx$ 20 GeV.

[25] The strongest upper limit is 8 pb and occurs at $m_\chi \simeq 30$ GeV.

[26] ELLIS 01C calculates the χ-p elastic scattering cross section in the framework of N=1 supergravity models with radiative breaking of the electroweak gauge symmetry. In models with nonuniversal Higgs masses, the upper limit to the cross section is 6×10^{-4}.

[27] The strongest upper limit is 3 pb and occurs at $m_\chi \simeq 60$ GeV. The limits are for inelastic scattering $X^0 + {}^{129}Xe \rightarrow X^0 + {}^{129}Xe^*$ (39.58 keV).

[28] The strongest upper limit is 4.4 pb and occurs at $m_\chi \simeq 60$ GeV.

[29] The strongest upper limit is about 35 pb and occurs at $m_\chi \simeq 15$ GeV.

Downloaded from https://academic.oup.com/ptep/article/2022/8/083C01/6651666 by KIT Library user on 27 September 2022

Spin-independent interactions

VALUE (pb)	CL%	DOCUMENT ID		TECN	COMMENT
• • • We do not use the following data for averages, fits, limits, etc. • • •					
$< 6.5 \times 10^{-11}$	90	[1] MENG	21B	PNDX	Xe
$< 5 \times 10^{-10}$	90	[2] WANG	20G	PNDX	Xe
$< 2.5 \times 10^{-8}$	90	[3] ABE	19	XMAS	Xe
$< 3.9 \times 10^{-9}$	90	[4] AJAJ	19	DEAP	Ar
$< 2 \times 10^{-8}$	90	[5] AMOLE	19	PICO	C_3F_8
$< 2.25 \times 10^{-6}$	90	[6] ADHIKARI	18	C100	NaI
$< 1.14 \times 10^{-8}$	90	[7] AGNES	18A	DS50	Ar
$< 1.6 \times 10^{-8}$	90	[8] AGNESE	18A	CDMS	Ge
$< 9 \times 10^{-11}$	90	[9] APRILE	18	XE1T	Xe
$< 1.8 \times 10^{-10}$	90	[10] AKERIB	17	LUX	Xe
$< 1.5 \times 10^{-9}$	90	[11] APRILE	16B	X100	Xe
$< 1.5 \times 10^{-9}$	90	[12] AKERIB	14	LUX	Xe
10^{-11}–10^{-7}	95	[13] BUCHMUEL...	14A	THEO	
$< 4.6 \times 10^{-6}$	90	[14] FELIZARDO	14	SMPL	C_2ClF_5
10^{-11}–10^{-8}	95	[15] ROSZKOWSKI	14	THEO	
$< 2.2 \times 10^{-6}$	90	[16] AGNESE	13	CDMS	Si
$< 5 \times 10^{-8}$	90	[17] AKIMOV	12	ZEP3	Xe
1.6×10^{-6}; 3.7×10^{-5}		[18] ANGLOHER	12	CRES	$CaWO_4$
3×10^{-12} to 3×10^{-9}	95	[19] BECHTLE	12	THEO	
$< 1.6 \times 10^{-7}$		[20] BEHNKE	12	COUP	CF_3I
$< 2.3 \times 10^{-7}$	90	[21] KIM	12	KIMS	CsI
$< 3.3 \times 10^{-8}$	90	[22] AHMED	11A		Ge
$< 4.4 \times 10^{-8}$	90	[23] ARMENGAUD	11	EDE2	Ge
$< 1 \times 10^{-7}$	90	[24] ANGLE	08	XE10	Xe
$< 1 \times 10^{-6}$	90	BENETTI	08	WARP	Ar
$< 7.5 \times 10^{-7}$	90	[25] ALNER	07A	ZEP2	Xe
$< 2 \times 10^{-7}$		[26] AKERIB	06A	CDMS	Ge
$<90 \times 10^{-7}$		ALNER	05	NAIA	NaI Spin Indep.
$<12 \times 10^{-7}$		[27] ALNER	05A	ZEPL	
$<14 \times 10^{-7}$		SANGLARD	05	EDEL	Ge
$< 4 \times 10^{-7}$		[28] AKERIB	04	CDMS	Ge
2×10^{-11} to 1.5×10^{-7}	95	[29] BALTZ	04	THEO	
2×10^{-11} to 8×10^{-6}		[30,31] ELLIS	04	THEO	$\mu > 0$
$< 5 \times 10^{-8}$		[32] PIERCE	04A	THEO	
$< 2 \times 10^{-5}$		[33] AHMED	03	NAIA	NaI Spin Indep.
$< 3 \times 10^{-6}$		[34] AKERIB	03	CDMS	Ge
2×10^{-13} to 2×10^{-7}		[35] BAER	03A	THEO	
$< 1.4 \times 10^{-5}$		[36] KLAPDOR-K...	03	HDMS	Ge
$< 6 \times 10^{-6}$		[37] ABRAMS	02	CDMS	Ge
1×10^{-12} to 7×10^{-6}		[30] KIM	02B	THEO	
$< 3 \times 10^{-5}$		[38] MORALES	02B	CSME	Ge
$< 1 \times 10^{-5}$		[39] MORALES	02C	IGEX	Ge
$< 1 \times 10^{-6}$		BALTZ	01	THEO	
$< 3 \times 10^{-5}$		[40] BAUDIS	01	HDMS	Ge
$< 7 \times 10^{-6}$		[41] BOTTINO	01	THEO	
$< 1 \times 10^{-8}$		[42] CORSETTI	01	THEO	$\tan\beta \leq 25$
5×10^{-10} to 1.5×10^{-8}		[43] ELLIS	01C	THEO	$\tan\beta \leq 10$
$< 4 \times 10^{-6}$		[42] GOMEZ	01	THEO	
2×10^{-10} to 1×10^{-7}		[42] LAHANAS	01	THEO	
$< 3 \times 10^{-6}$		ABUSAIDI	00	CDMS	Ge, Si
$< 6 \times 10^{-7}$		[44] ACCOMANDO	00	THEO	
		[45] BERNABEI	00	DAMA	NaI
2.5×10^{-9} to 3.5×10^{-8}		[46] FENG	00	THEO	$\tan\beta$=10
$< 1.5 \times 10^{-5}$		MORALES	00	IGEX	Ge
$< 4 \times 10^{-5}$		SPOONER	00	UKDM	NaI
$< 7 \times 10^{-6}$		BAUDIS	99	HDMO	^{76}Ge
$< 7 \times 10^{-6}$		BERNABEI	98C	DAMA	Xe

[1] Commissioning Run for PandaX-4T. The strongest limit is 3.8×10^{-11} pb at $m_\chi = 40$ GeV.

[2] WANG 20G strongest limit is 2.2×10^{-10} pb at 30 GeV using 132 ton-day full exposure of PandaX-II. This updates CUI 17A, though the results here provide weaker constraints.

[3] The strongest upper limit is 2.2×10^{-8} pb at 60 GeV.

[4] This updates AMAUDRUZ 18.

[5] This updates AMOLE 16.

[6] The strongest limit is 2.05×10^{-6} at m = 60 GeV.

[7] The strongest limit is 1.09×10^{-8} pb at $m_\chi = 126$ GeV. This updates AGNES 15.

[8] The strongest limit is 1.0×10^{-8} pb at $m_\chi = 46$ GeV. This updates AGNESE 15B.

[9] Based on 278.8 days of data collection. The strongest limit is 4.1×10^{-11} pb at $m_\chi = 30$ GeV. This updates APRILE 17G.

[10] AKERIB 17. The strongest limit is 1.1×10^{-10} pb at 50 GeV. This updates AKERIB 16.

[11] The strongest limit is 1.1×10^{-9} pb at 50 GeV. This updates APRILE 12.

[12] The strongest upper limit is 7.6×10^{-10} at $m_\chi = 33$ GeV.

[13] Predictions for the spin-independent elastic cross section based on a frequentist approach to electroweak observables in the framework of $N = 1$ supergravity models with radiative breaking of the electroweak gauge symmetry using the 20 fb^{-1} 8 TeV and the 5 fb^{-1} 7 TeV LHC data and the LUX data.

[14] The strongest limit is 3.6×10^{-6} pb and occurs at $m_\chi = 35$ GeV. Felizardo 2014 updates Felizardo 2012.

[15] Predictions for the spin-independent elastic cross section based on a Bayesian approach to electroweak observables in the framework of $N = 1$ supergravity models with radiative breaking of the electroweak gauge symmetry using the 20 fb^{-1} LHC data and LUX.

[16] AGNESE 13 presents 90% CL limits on the elastic cross section for masses in the range 7–100 GeV using the Si based detector. The strongest upper limit is 1.8×10^{-6} pb at $m_\chi = 50$ GeV. This limit is improved to 7×10^{-7} pb in AGNESE 13A.

[17] This result updates LEBEDENKO 09. The strongest limit is 3.9×10^{-8} pb at $m_\chi = 52$ GeV.

[18] ANGLOHER 12 presents results of 730 kg days from the CRESST-II dark matter detector. They find two maxima in the likelihood function corresponding to best fit WIMP masses of 25.3 and 11.6 GeV with elastic cross sections of 1.6×10^{-6} and 3.7×10^{-5} pb respectively, see their Table 4. The statistical significance is more than 4σ. ANGLOHER 12 updates ANGLOHER 09

[19] Predictions for the spin-independent elastic cross section based on a frequentist approach to electroweak observables in the framework of $N = 1$ supergravity models with radiative breaking of the electroweak gauge symmetry using the 5 fb^{-1} LHC data and XENON100.

[20] The strongest limit is 1.4×10^{-7} at $m_\chi = 60$ GeV.

[21] This result updates LEE 07A. The strongest limit is 2.1×10^{-7} at $m_\chi = 70$ GeV.

[22] AHMED 11A gives combined results from CDMS and EDELWEISS. The strongest limit is at $m_\chi = 90$ GeV.

[23] ARMENGAUD 11 updates result of ARMENGAUD 10. Strongest limit at $m_\chi = 85$ GeV.

[24] The strongest upper limit is 5.1×10^{-8} pb and occurs at $m_\chi \simeq 30$ GeV. The values quoted here are based on the analysis performed in ANGLE 08 with the update from SORENSEN 09.

[25] The strongest upper limit is 6.6×10^{-7} pb and occurs at $m_\chi \simeq 65$ GeV.

[26] AKERIB 06A updates the results of AKERIB 05. The strongest upper limit is 1.6×10^{-7} pb and occurs at $m_\chi \approx 60$ GeV.

[27] The strongest upper limit is also close to 1.0×10^{-6} pb and occurs at $m_\chi \simeq 70$ GeV. BENOIT 06 claim that the discrimination power of ZEPLIN-I measurement (ALNER 05A) is not reliable enough to obtain a limit better than 1×10^{-3} pb. However, SMITH 06 do not agree with the criticisms of BENOIT 06.

[28] AKERIB 04 is incompatible with BERNABEI 00 most likely value, under the assumption of standard WIMP-halo interactions. The strongest upper limit is 4×10^{-7} pb and occurs at $m_\chi \simeq 60$ GeV.

[29] Predictions for the spin-independent elastic cross section in the framework of $N = 1$ supergravity models with radiative breaking of the electroweak gauge symmetry.

[30] KIM 02 and ELLIS 04 calculate the χp elastic scattering cross section in the framework of N=1 supergravity models with radiative breaking of the electroweak gauge symmetry, but without universal scalar masses.

[31] In the case of universal squark and slepton masses, but non-universal Higgs masses, the limit becomes 2×10^{-6} (2×10^{-11} when constraint from the BNL g–2 experiment are included), see ELLIS 03E. ELLIS 05 display the sensitivity of the elastic scattering cross section to the π-Nucleon Σ term.

[32] PIERCE 04A calculates the χp elastic scattering cross section in the framework of models with very heavy scalar masses. See Fig. 2 of the paper.

[33] The strongest upper limit is 1.8×10^{-5} pb and occurs at $m_\chi \approx 80$ GeV.

[34] Under the assumption of standard WIMP-halo interactions, Akerib 03 is incompatible with BERNABEI 00 most likely value at the 99.98% CL. See Fig. 4.

[35] BAER 03A calculates the χp elastic scattering cross section in several models including the framework of N=1 supergravity models with radiative breaking of the electroweak gauge symmetry.

[36] The strongest upper limit is 7×10^{-6} pb and occurs at $m_\chi \simeq 30$ GeV.

[37] ABRAMS 02 is incompatible with the DAMA most likely value at the 99.9% CL. The strongest upper limit is 3×10^{-6} pb and occurs at $m_\chi \simeq 30$ GeV.

[38] The strongest upper limit is 2×10^{-5} pb and occurs at $m_\chi \simeq 40$ GeV.

[39] The strongest upper limit is 7×10^{-6} pb and occurs at $m_\chi \simeq 46$ GeV.

[40] The strongest upper limit is 1.8×10^{-5} pb and occurs at $m_\chi \simeq 32$ GeV

[41] BOTTINO 01 calculates the χ-p elastic scattering cross section in the framework of the following supersymmetric models: N=1 supergravity with the radiative breaking of the electroweak gauge symmetry, N=1 supergravity with nonuniversal scalar masses and an effective MSSM model at the electroweak scale.

[42] Calculates the χ-p elastic scattering cross section in the framework of N=1 supergravity models with radiative breaking of the electroweak gauge symmetry.

[43] ELLIS 01C calculates the χ-p elastic scattering cross section in the framework of N=1 supergravity models with radiative breaking of the electroweak gauge symmetry. ELLIS 02B find a range 2×10^{-8}–1.5×10^{-7} at $\tan\beta$=50. In models with nonuniversal Higgs masses, the upper limit to the cross section is 4×10^{-7}.

[44] ACCOMANDO 00 calculate the χ-p elastic scattering cross section in the framework of minimal N=1 supergravity models with radiative breaking of the electroweak gauge symmetry. The limit is relaxed by at least an order of magnitude when models with nonuniversal scalar masses are considered. A subset of the authors in ARNOWITT 02 updated the limit to $< 9 \times 10^{-8}$ ($\tan\beta < 55$).

[45] BERNABEI 00 search for annual modulation of the WIMP signal. The data favor the hypothesis of annual modulation at 4σ and are consistent, for a particular model framework quoted there, with m_{χ^0}=44^{+12}_{-9} GeV and a spin-independent χ^0-proton cross section of $(5.4 \pm 1.0) \times 10^{-6}$ pb. See also BERNABEI 01 and BERNABEI 00C.

[46] FENG 00 calculate the χ-p elastic scattering cross section in the framework of N=1 supergravity models with radiative breaking of the electroweak gauge symmetry with a particular emphasis on focus point models. At $\tan\beta$=50, the range is 8×10^{-8}–4×10^{-7}.

Other bounds on $\tilde{\chi}^0_1$ from astrophysics and cosmology

Most of these papers generally exclude regions in the $M_2 - \mu$ parameter plane by requiring that the $\tilde{\chi}^0_1$ contribution to the overall cosmological density is less than some maximal value to avoid overclosure of the Universe. Those not based on the cosmological density are indicated. Many of these papers also include LEP and/or other bounds.

VALUE	DOCUMENT ID		TECN	COMMENT
>46 GeV	[1] ELLIS	00	RVUE	

Downloaded from https://academic.oup.com/ptep/article/2022/8/083C01/6651666 by KIT Library user on 27 September 2022

• • • We do not use the following data for averages, fits, limits, etc. • • •

	[2] ATHRON	17B	COSM	
	[3] BECHTLE	16	COSM	
	[4] BAGNASCHI	15	COSM	
	[5] BUCHMUEL...	14	COSM	
	[6] BUCHMUEL...	14A	COSM	
	[7] ROSZKOWSKI	14	COSM	
	[8] CABRERA	13	COSM	
	[9] ELLIS	13B	COSM	
	[8] STREGE	13	COSM	
	[5] AKULA	12	COSM	
	[5] ARBEY	12A	COSM	
	[5] BAER	12	COSM	
	[10] BALAZS	12	COSM	
	[11] BECHTLE	12	COSM	
	[12] BESKIDT	12	COSM	
> 18 GeV	[13] BOTTINO	12	COSM	
	[5] BUCHMUEL...	12	COSM	
	[5] CAO	12A	COSM	
	[5] ELLIS	12B	COSM	
	[14] FENG	12B	COSM	
	[5] KADASTIK	12	COSM	
	[10] STREGE	12	COSM	
	[15] BUCHMUEL...	11	COSM	
	[16] ROSZKOWSKI	11	COSM	
	[17] ELLIS	10	COSM	
	[18] BUCHMUEL...	09	COSM	
	[19] DREINER	09	THEO	
	[20] BUCHMUEL...	08	COSM	
	[16] ELLIS	08	COSM	
	[21] CALIBBI	07	COSM	
	[22] ELLIS	07	COSM	
	[23] ALLANACH	06	COSM	
	[24] DE-AUSTRI	06	COSM	
	[16] BAER	05	COSM	
	[25] BALTZ	04	COSM	
> 6 GeV	[13,26] BELANGER	04	THEO	
	[27] ELLIS	04B	COSM	
	[28] PIERCE	04A	COSM	
	[29] BAER	03	COSM	
> 6 GeV	[13] BOTTINO	03	COSM	
	[29] CHATTOPAD...	03	COSM	
	[30] ELLIS	03	COSM	
	[16] ELLIS	03B	COSM	
	[29] ELLIS	03C	COSM	
	[29] LAHANAS	03	COSM	
	[31] LAHANAS	02	COSM	
	[32] BARGER	01C	COSM	
	[33] ELLIS	01B	COSM	
	[30] BOEHM	00B	COSM	
	[34] FENG	00	COSM	
< 600 GeV	[35] ELLIS	98B	COSM	
	[36] EDSJO	97	COSM	Co-annihilation
	[37] BAER	96	COSM	
	[16] BEREZINSKY	95	COSM	
	[38] FALK	95	COSM	*CP*-violating phases
	[39] DREES	93	COSM	Minimal supergravity
	[40] FALK	93	COSM	Sfermion mixing
	[39] KELLEY	93	COSM	Minimal supergravity
	[41] MIZUTA	93	COSM	Co-annihilation
	[42] LOPEZ	92	COSM	Minimal supergravity, m_0=A=0
	[43] MCDONALD	92	COSM	
	[44] GRIEST	91	COSM	
	[45] NOJIRI	91	COSM	Minimal supergravity
	[46] OLIVE	91	COSM	
	[47] ROSZKOWSKI	91	COSM	
	[48] GRIEST	90	COSM	
	[46] OLIVE	89	COSM	
none 100 eV – 15 GeV	SREDNICKI	88	COSM	$\tilde{\gamma}$; $m_{\tilde{f}}$=100 GeV
none 100 eV–5 GeV	ELLIS	84	COSM	$\tilde{\gamma}$; for $m_{\tilde{f}}$=100 GeV
	GOLDBERG	83	COSM	$\tilde{\gamma}$
	[49] KRAUSS	83	COSM	$\tilde{\gamma}$
	VYSOTSKII	83	COSM	$\tilde{\gamma}$

[1] ELLIS 00 updates ELLIS 98. Uses LEP e^+e^- data at $\sqrt{s}$=202 and 204 GeV to improve bound on neutralino mass to 51 GeV when scalar mass universality is assumed and 46 GeV when Higgs mass universality is relaxed. Limits on tanβ improve to > 2.7 ($\mu > 0$), > 2.2 ($\mu < 0$) when scalar mass universality is assumed and > 1.9 (both signs of μ) when Higgs mass universality is relaxed.

[2] ATHRON 17B places constraints on the SUSY parameter space in the framework of $N = 1$ supergravity models with radiative breaking of the electroweak gauge symmetry using all Run I and the 13 fb^{-1} 13 TeV Run II LHC searches and other experimental data.

[3] BECHTLE 16 places constraints on the SUSY parameter space in the framework of $N = 1$ supergravity models with radiative breaking of the electroweak gauge symmetry using all Run I LHC searches.

[4] BAGNASCHI 15 places constraints on the SUSY parameter space in the framework of $N = 1$ supergravity models with radiative breaking of the electroweak gauge symmetry using all Run I LHC searches.

[5] Implications of the LHC result on the Higgs mass and on the SUSY parameter space in the framework of $N = 1$ supergravity models with radiative breaking of the electroweak gauge symmetry.

[6] BUCHMUELLER 14A places constraints on the SUSY parameter space in the framework of $N = 1$ supergravity models with radiative breaking of the electroweak gauge symmetry using indirect experimental searches using the 20 fb^{-1} 8 TeV and the 5 fb^{-1} 7 TeV LHC and the LUX data.

[7] ROSZKOWSKI 14 places constraints on the SUSY parameter space in the framework of $N = 1$ supergravity models with radiative breaking of the electroweak gauge symmetry using Bayesian statistics and indirect experimental searches using the 20 fb^{-1} LHC and the LUX data.

[8] CABRERA 13 and STREGE 13 place constraints on the SUSY parameter space in the framework of $N = 1$ supergravity models with radiative breaking of the electroweak gauge symmetry with and without non-universal Higgs masses using the 5.8 fb^{-1}, $\sqrt{s}$ = 7 TeV ATLAS supersymmetry searches and XENON100 results.

[9] ELLIS 13B place constraints on the SUSY parameter space in the framework of $N = 1$ supergravity models with radiative breaking of the electroweak gauge symmetry with and without Higgs mass universality. Models with universality below the GUT scale are also considered.

[10] BALAZS 12 and STREGE 12 place constraints on the SUSY parameter space in the framework of $N = 1$ supergravity models with radiative breaking of the electroweak gauge symmetry using the 1 fb^{-1} LHC supersymmetry searches, the 5 fb^{-1} Higgs mass constraints, both with $\sqrt{s}$ = 7 TeV, and XENON100 results.

[11] BECHTLE 12 places constraints on the SUSY parameter space in the framework of $N = 1$ supergravity models with radiative breaking of the electroweak gauge symmetry using indirect experimental searches, using the 5 fb^{-1} LHC and XENON100 data.

[12] BESKIDT 12 places constraints on the SUSY parameter space in the framework of $N = 1$ supergravity models with radiative breaking of the electroweak gauge symmetry using indirect experimental searches, the 5 fb^{-1} LHC and the XENON100 data.

[13] BELANGER 04 and BOTTINO 12 (see also BOTTINO 03, BOTTINO 03A and BOTTINO 04) do not assume gaugino or scalar mass unification.

[14] FENG 12B places constraints on the SUSY parameter space in the framework of $N = 1$ supergravity models with radiative breaking of the electroweak gauge symmetry and large sfermion masses using the 1 fb^{-1} LHC supersymmetry searches, the 5 fb^{-1} LHC Higgs mass constraints both with $\sqrt{s}$ = 7 TeV, and XENON100 results.

[15] BUCHMUELLER 11 places constraints on the SUSY parameter space in the framework of $N = 1$ supergravity models with radiative breaking of the electroweak gauge symmetry using indirect experimental searches and including supersymmetry breaking relations between A and B parameters.

[16] Places constraints on the SUSY parameter space in the framework of N=1 supergravity models with radiative breaking of the electroweak gauge symmetry but non-Universal Higgs masses.

[17] ELLIS 10 places constraints on the SUSY parameter space in the framework of $N = 1$ supergravity models with radiative breaking of the electroweak gauge symmetry with universality above the GUT scale.

[18] BUCHMUELLER 09 places constraints on the SUSY parameter space in the framework of $N = 1$ supergravity models with radiative breaking of the electroweak gauge symmetry using indirect experimental searches.

[19] DREINER 09 show that in the general MSSM with non-universal gaugino masses there exists no model-independent laboratory bound on the mass of the lightest neutralino. An essentially massless χ^0_1 is allowed by the experimental and observational data, imposing some constraints on other MSSM parameters, including M_2, μ and the slepton and squark masses.

[20] BUCHMUELLER 08 places constraints on the SUSY parameter space in the framework of $N = 1$ supergravity models with radiative breaking of the electroweak gauge symmetry using indirect experimental searches.

[21] CALIBBI 07 places constraints on the SUSY parameter space in the framework of $N = 1$ supergravity models with radiative breaking of the electroweak gauge symmetry with universality above the GUT scale including the effects of right-handed neutrinos.

[22] ELLIS 07 places constraints on the SUSY parameter space in the framework of $N = 1$ supergravity models with radiative breaking of the electroweak gauge symmetry with universality below the GUT scale.

[23] ALLANACH 06 places constraints on the SUSY parameter space in the framework of $N = 1$ supergravity models with radiative breaking of the electroweak gauge symmetry.

[24] DE-AUSTRI 06 places constraints on the SUSY parameter space in the framework of $N = 1$ supergravity models with radiative breaking of the electroweak gauge symmetry.

[25] BALTZ 04 places constraints on the SUSY parameter space in the framework of $N = 1$ supergravity models with radiative breaking of the electroweak gauge symmetry.

[26] Limit assumes a pseudo scalar mass < 200 GeV. For larger pseudo scalar masses, m_χ > 18(29) GeV for tanβ = 50(10). Bounds from WMAP, $(g-2)_\mu$, $b \to s\gamma$, LEP.

[27] ELLIS 04B places constraints on the SUSY parameter space in the framework of N=1 supergravity models with radiative breaking of the electroweak gauge symmetry including supersymmetry breaking relations between A and B parameters. See also ELLIS 03D.

[28] PIERCE 04A places constraints on the SUSY parameter space in the framework of models with very heavy scalar masses.

[29] BAER 03, CHATTOPADHYAY 03, ELLIS 03C and LAHANAS 03 place constraints on the SUSY parameter space in the framework of N=1 supergravity models with radiative breaking of the electroweak gauge symmetry based on WMAP results for the cold dark matter density.

[30] BOEHM 00B and ELLIS 03 place constraints on the SUSY parameter space in the framework of minimal N=1 supergravity models with radiative breaking of the electroweak gauge symmetry. Includes the effect of χ-$\tilde{t}$ co-annihilations.

[31] LAHANAS 02 places constraints on the SUSY parameter space in the framework of minimal N=1 supergravity models with radiative breaking of the electroweak gauge symmetry. Focuses on the role of pseudo-scalar Higgs exchange.

[32] BARGER 01C use the cosmic relic density inferred from recent CMB measurements to constrain the parameter space in the framework of minimal N=1 supergravity models with radiative breaking of the electroweak gauge symmetry.

[33] ELLIS 01B places constraints on the SUSY parameter space in the framework of minimal N=1 supergravity models with radiative breaking of the electroweak gauge symmetry. Focuses on models with large tanβ.

[34] FENG 00 explores cosmologically allowed regions of MSSM parameter space with multi-TeV masses.

[35] ELLIS 98B assumes a universal scalar mass and radiative supersymmetry breaking with universal gaugino masses. The upper limit to the LSP mass is increased due to the inclusion of $\chi - \tilde{\tau}_R$ coannihilations.

Downloaded from https://academic.oup.com/ptep/article/2022/8/083C01/6651666 by KIT Library user on 27 September 2022

[36] EDSJO 97 included all coannihilation processes between neutralinos and charginos for any neutralino mass and composition.

[37] Notes the location of the neutralino Z resonance and h resonance annihilation corridors in minimal supergravity models with radiative electroweak breaking.

[38] Mass of the bino (=LSP) is limited to $m_{\widetilde{B}} \lesssim 350$ GeV for $m_t = 174$ GeV.

[39] DREES 93, KELLEY 93 compute the cosmic relic density of the LSP in the framework of minimal N=1 supergravity models with radiative breaking of the electroweak gauge symmetry.

[40] FALK 93 relax the upper limit to the LSP mass by considering sfermion mixing in the MSSM.

[41] MIZUTA 93 include coannihilations to compute the relic density of Higgsino dark matter.

[42] LOPEZ 92 calculate the relic LSP density in a minimal SUSY GUT model.

[43] MCDONALD 92 calculate the relic LSP density in the MSSM including exact tree-level annihilation cross sections for all two-body final states.

[44] GRIEST 91 improve relic density calculations to account for coannihilations, pole effects, and threshold effects.

[45] NOJIRI 91 uses minimal supergravity mass relations between squarks and sleptons to narrow cosmologically allowed parameter space.

[46] Mass of the bino (=LSP) is limited to $m_{\widetilde{B}} \lesssim 350$ GeV for $m_t \leq 200$ GeV. Mass of the higgsino (=LSP) is limited to $m_{\widetilde{H}} \lesssim 1$ TeV for $m_t \leq 200$ GeV.

[47] ROSZKOWSKI 91 calculates LSP relic density in mixed gaugino/higgsino region.

[48] Mass of the bino (=LSP) is limited to $m_{\widetilde{B}} \lesssim 550$ GeV. Mass of the higgsino (=LSP) is limited to $m_{\widetilde{H}} \lesssim 3.2$ TeV.

[49] KRAUSS 83 finds $m_{\widetilde{\gamma}}$ not 30 eV to 2.5 GeV. KRAUSS 83 takes into account the gravitino decay. Find that limits depend strongly on reheated temperature. For example a new allowed region $m_{\widetilde{\gamma}}$ = 4–20 MeV exists if $m_{\text{gravitino}}$ <40 TeV. See figure 2.

Unstable $\widetilde{\chi}^0_1$ (Lightest Neutralino) mass limit

Unless otherwise stated, results in this section assume spectra and production rates as evaluated in the MSSM. Unless otherwise stated, the goldstino or gravitino mass $m_{\widetilde{G}}$ is assumed to be negligible relative to all other masses. In the following, $\widetilde{G}$ is assumed to be undetected and to give rise to a missing energy ($\not{E}$) signature.

Some earlier papers are now obsolete and have been omitted. They were last listed in our PDG 14 edition: K. Olive, *et al.* (Particle Data Group), Chinese Physics **C38** 070001 (2014) (http://pdg.lbl.gov).

VALUE (GeV)	CL%	DOCUMENT ID		TECN	COMMENT
> 540	95	[1] AAD	21Y	ATLS	$\geq 4\ell$, Tchi1n12-GGM, $\widetilde{\chi}^0_1 \rightarrow Z\widetilde{G}$
none 7–50	95	[2] AAIJ	21V	LHCB	$e^{\pm}\mu^{\mp}$, RPV $\widetilde{\chi}^0_1 \rightarrow e^{\pm}\mu^{\mp}\nu$, 2 ps $< \tau <$ 50 ps
>1100	95	[3] SIRUNYAN	21AF	CMS	long-lived $\widetilde{\chi}^0_1$, RPV $\widetilde{\chi}^0_1 \rightarrow tbs$, λ''_{323} coupling, 0.6 mm $< c\tau <$ 70 mm
> 800	95	[4] SIRUNYAN	21M	CMS	$\ell^{\pm}\ell^{\mp} + \not{E}_T$, Tn1n1C
> 650	95	[4] SIRUNYAN	21M	CMS	$\ell^{\pm}\ell^{\mp} + \not{E}_T$, Tn1n1B
> 380	95	[5] AAD	20AN	ATLS	$2\gamma + \not{E}_T$,Tn1n1A, GMSB
> 525	95	[6] SIRUNYAN	19CA	CMS	$\widetilde{\chi}^0_1 \rightarrow \gamma\widetilde{G}$, GMSB, SPS8, $c\tau$=1 m
> 290	95	[7] SIRUNYAN	19CI	CMS	$\geq 1\ H\ (\rightarrow \gamma\gamma)$ + jets + $\not{E}_T$, Tn1n1A, GMSB
> 230	95	[7] SIRUNYAN	19CI	CMS	$\geq 1\ H\ (\rightarrow \gamma\gamma)$ + jets + $\not{E}_T$, Tn1n1B , GMSB
> 930	95	[8] SIRUNYAN	19K	CMS	γ + lepton + $\not{E}_T$, Tchi1n1A
none 130–230, 290–880	95	[9] AABOUD	18CK	ATLS	$2H\ (\rightarrow bb)+\not{E}_T$,Tn1n1A, GMSB
> 295	95	[10] AABOUD	18Z	ATLS	$\geq 4\ell$, GMSB, Tn1n1C
> 180	95	[11] SIRUNYAN	18AO	CMS	$\ell^{\pm}\ell^{\pm}$ or $\geq 3\ell$, Tn1n1A
> 260	95	[11] SIRUNYAN	18AO	CMS	$\ell^{\pm}\ell^{\pm}$ or $\geq 3\ell$, Tn1n1B
> 450	95	[11] SIRUNYAN	18AO	CMS	$\ell^{\pm}\ell^{\pm}$ or $\geq 3\ell$, Tn1n1C
> 750	95	[12] SIRUNYAN	18AP	CMS	Combination of searches, GMSB, Tn1n1A
> 650	95	[12] SIRUNYAN	18AP	CMS	Combination of searches, GMSB, Tn1n1B
> 690	95	[12] SIRUNYAN	18AP	CMS	Combination of searches, GMSB, Tn1n1C
> 500	95	[13] SIRUNYAN	18AR	CMS	$\ell^{\pm}\ell^{\mp}$+ jets +$\not{E}_T$, GMSB, Tn1n1B
> 650	95	[13] SIRUNYAN	18AR	CMS	$\ell^{\pm}\ell^{\mp}$+ jets +$\not{E}_T$, GMSB, Tn1n1C
none 230–770	95	[14] SIRUNYAN	18O	CMS	$2\ H\ (\rightarrow bb) + \not{E}_T$, Tn1n1A, GMSB
> 205	95	[15] SIRUNYAN	18X	CMS	$\geq 1\ H\ (\rightarrow \gamma\gamma)$ + jets + $\not{E}_T$, Tn1n1A, GMSB
> 130	95	[15] SIRUNYAN	18X	CMS	$\geq 1\ H\ (\rightarrow \gamma\gamma)$ + jets + $\not{E}_T$, Tn1n1B , GMSB
> 380	95	[16] KHACHATRY...	14L	CMS	$\widetilde{\chi}^0_1 \rightarrow Z\widetilde{G}$ simplified models, GMSB, RPV
• • • We do not use the following data for averages, fits, limits, etc. • • •					
		[17] AAD	20D		$\widetilde{q} \rightarrow q\widetilde{\chi}^0_1$, $\widetilde{\chi}^0_1 \rightarrow \ell\ell\nu$, RPV, λ_{121} or $\lambda_{122} \neq 0$
none 300–1000	95	[18] AABOUD	19G	ATLS	$\widetilde{\chi}^0_1 \rightarrow Z\widetilde{G}$ from gluinos as in Tglu1A, GMSB, depending on $c\tau$
		[19] AAIJ	17Z		displaced vertex with associated μ
		[20] KHACHATRY...	16BX	CMS	$\geq 3\ell^{\pm}$, RPV, λ or λ' couplings, wino- or higgsino-like neutralinos
		[21] AAD	14BH	ATLS	$2\gamma + \not{E}_T$, GMSB, SPS8
		[22] AAD	13AP	ATLS	$2\gamma + \not{E}_T$, GMSB, SPS8
none 220–380	95	[23] AAD	13Q	ATLS	$\gamma + b + \not{E}_T$, higgsino-like neutralino, GMSB
		[24] AAD	13R	ATLS	$\widetilde{\chi}^0_1 \rightarrow \mu jj$, RPV, $\lambda'_{211} \neq 0$
		[25] AALTONEN	13I	CDF	$\widetilde{\chi}^0_1 \rightarrow \gamma\widetilde{G}$, $\not{E}_T$, GMSB
> 220	95	[26] CHATRCHYAN	13AH	CMS	$\widetilde{\chi}^0_1 \rightarrow \gamma\widetilde{G}$, GMSB, SPS8, $c\tau$ < 500 mm
		[27] AAD	12CP	ATLS	$2\gamma + \not{E}_T$, GMSB
		[28] AAD	12CT	ATLS	$\geq 4\ell^{\pm}$, RPV
		[29] AAD	12R	ATLS	$\widetilde{\chi}^0_1 \rightarrow \mu jj$, RPV, $\lambda'_{211} \neq 0$
		[30] ABAZOV	12AD	D0	$\widetilde{\chi}^0_1\widetilde{\chi}^0_1 \rightarrow \gamma Z\widetilde{G}\widetilde{G}$, GMSB
		[31] CHATRCHYAN	12BK	CMS	$2\gamma + \not{E}_T$, GMSB
		[32] CHATRCHYAN	11B	CMS	$\widetilde{W}^0 \rightarrow \gamma\widetilde{G}$, $\widetilde{W}^{\pm} \rightarrow \ell^{\pm}\widetilde{G}$, GMSB
> 149	95	[33] AALTONEN	10	CDF	$p\overline{p} \rightarrow \widetilde{\chi}\widetilde{\chi}$, $\widetilde{\chi}=\widetilde{\chi}^0_2$, $\widetilde{\chi}^{\pm}_1$, $\widetilde{\chi}^0_1 \rightarrow \gamma\widetilde{G}$, GMSB
> 175	95	[34] ABAZOV	10P	D0	$\widetilde{\chi}^0_1 \rightarrow \gamma\widetilde{G}$, GMSB
> 125	95	[35] ABAZOV	08F	D0	$p\overline{p} \rightarrow \widetilde{\chi}\widetilde{\chi}$, $\widetilde{\chi}=\widetilde{\chi}^0_2$, $\widetilde{\chi}^{\pm}_1$, $\widetilde{\chi}^0_1 \rightarrow \gamma\widetilde{G}$, GMSB
		[36] ABULENCIA	07H	CDF	RPV, $LL\overline{E}$
> 96.8	95	[37] ABBIENDI	06B	OPAL	$e^+e^- \rightarrow \widetilde{B}\widetilde{B}$, $(\widetilde{B} \rightarrow \widetilde{G}\gamma)$
		[38] ABDALLAH	05B	DLPH	$e^+e^- \rightarrow \widetilde{G}\widetilde{\chi}^0_1$, $(\widetilde{\chi}^0_1 \rightarrow \widetilde{G}\gamma)$
> 96	95	[39] ABDALLAH	05B	DLPH	$e^+e^- \rightarrow \widetilde{B}\widetilde{B}$, $(\widetilde{B} \rightarrow \widetilde{G}\gamma)$

[1] AAD 21Y searched in 139 fb^{-1} of pp collisions at $\sqrt{s}$ = 13 TeV for supersymmetry in events with four or more leptons (electrons, muons and tau-leptons). No significant excess above the Standard Model expectations is observed. Limits are set on Tchi1n12-GGM, and RPV models similar to Tchi1n2l, Tglu1A (with $q = u, d, s, c, b$, with equal branching fractions), and $\widetilde{\ell}_L/\widetilde{\nu} \rightarrow \ell/\nu\widetilde{\chi}^0_1$ (mass-degenerate $\widetilde{\ell}_L$ and $\widetilde{\nu}$ of all 3 generations), all with $\widetilde{\chi}^0_1 \rightarrow \ell^{\pm}\ell^{\mp}\nu$ via λ_{12k} or λ_{i33} (where $i,k \in 1,2$), see their Figure 11.

[2] AAIJ 21V searched in 5.38 fb^{-1} of pp collisions at $\sqrt{s}$ = 13 TeV for long-lived particles (LLP) decaying to $e^{\pm}\mu^{\mp}\nu$. The LLP can be a $\widetilde{\chi}^0_1$ in RPV SUSY, or a right-handed neutrino, and can be produced in pairs, in the decay of the Higgs boson, or from charged current processes. No significant excess above the Standard Model expectations is observed. Limits are set on the cross section times branching ratio for all three production mechanisms, see their Figures 6–8.

[3] SIRUNYAN 21AF searched in 140 fb^{-1} of pp collisions at $\sqrt{s}$ = 13 TeV for supersymmetry in events with with two displaced vertices from long-lived particles decaying into multijet or dijet final states. No significant excess above the Standard Model expectations is observed. Limits are set on the gluino mass in the simplified model Tglu2RPV with λ''_{323} coupling, on the $\widetilde{\chi}^0_1$ mass in an RPV model with $\widetilde{\chi}^0_1$ pair production and the RPV decay $\widetilde{\chi}^0_1 \rightarrow tbs$ with λ''_{323} coupling and on the $\widetilde{t}$ mass in an RPV model with top squark pair production and the RPV decay $\widetilde{t} \rightarrow \overline{d}_i\overline{d}_j$ with λ''_{3ij} coupling, see their Figure 7.

[4] SIRUNYAN 21M searched in 137 fb^{-1} of pp collisions at $\sqrt{s}$ = 13 TeV for supersymmetry in events with two opposite-sign same-flavor leptons (electrons, muons) and $\not{E}_T$. No significant excess above the Standard Model expectations is observed. Limits are set on the gluino mass in the simplified model Tglu4C, see their Figure 10, on the $\widetilde{\chi}^0_2$ and $\widetilde{\chi}^{\pm}_1$ mass in Tchi1n2Fa, see their Figure 11, on the $\widetilde{\chi}^0_1$ mass in Tn1n1C and Tn1n1B for $m_{\widetilde{\chi}^0_2}=m_{\widetilde{\chi}^{\pm}_1}=m_{\widetilde{\chi}^0_1}$, see their Figure 12. Limits are also set on the light squark mass for the simplified model Tsqk2A, on the sbottom mass in Tsbot3, see their Figure 13, and on the slepton mass in direct electroweak pair production of mass-degenerate left- and right-handed sleptons (selectrons and smuons), see their Figure 14.

[5] AAD 20AN searched in 139 fb^{-1} of pp collisions at $\sqrt{s}$ = 13 TeV for events with two photons and missing transverse momentum. Events are further categorised in terms of lepton or jet multiplicity. No significant excess over the expected background is observed. Limits at 95% C.L. are set on the Higgsino mass in the T1n1n1A simplified model, see their Figure 11.

[6] SIRUNYAN 19CA searched in 77.4 fb^{-1} of pp collisions at $\sqrt{s}$ = 13 TeV for events containing delayed photons in both single and diphoton plus $\not{E}_T$ final states. No excess is observed above the background expected from Standard Model processes. The results are used to set 95% C.L. exclusion limits in the context of GMSB, using the SPS8 benchmark model. For neutralino proper decay lengths of 0.1, 1, 10, and 100 m, masses up to about 320, 525, 360, and 215 GeV are excluded, respectively. See their Fig. 5. The searches involve the simplified models Tglu1D, Tglu4A,B,C, Tsqk4,4A,4B.

[7] SIRUNYAN 19CI searched in 77.5 fb^{-1} of pp collisions at $\sqrt{s}$ = 13 TeV for events with one or more high-momentum Higgs bosons, decaying to pairs of photons, jets and $\not{E}_T$. No significant excess above the Standard Model expectations is observed. Limits are set on the sbottom mass in the Tsbot4 simplified model, see Figure 3, and on the wino mass in the Tchi1n2E simplified model, see their Figure 4. Limits are also set on the higgsino mass in the Tn1n1A and Tn1n1B simplified models, see their Figure 5.

[8] SIRUNYAN 19K searched in 35.9 fb^{-1} of pp collisions at $\sqrt{s}$ = 13 TeV for events with a photon, an electron or muon, and large $\not{E}_T$. No significant excess above the Standard Model expectations is observed. In the framework of GMSB, limits are set on the chargino and neutralino mass in the Tchi1n1A simplified model, see their Figure 6. Limits are also set on the gluino mass in the Tglu4A simplified model, and on the squark mass in the Tsqk4A simplified model, see their Figure 7.

[9] AABOUD 18CK searched for events with at least 3 b-jets and large missing transverse energy in two datasets of pp collisions at $\sqrt{s}$ = 13 TeV of 36.1 fb^{-1} and 24.3 fb^{-1} depending on the trigger requirements. The analyses aimed to reconstruct two Higgs bosons decaying to pairs of b-quarks. No significant excess above the Standard Model expectations is observed. Limits are set on the Higgsino mass in the Tn1n1A simplified model, see their Figure 15(a). Constraints are also presented as a function of the BR of Higgsino decaying into an higgs boson and a gravitino, see their Figure 15(b).

[10] AABOUD 18Z searched in 36.1 fb^{-1} of pp collisions at $\sqrt{s}$ = 13 TeV for events containing four or more charged leptons (electrons, muons and up to two hadronically decaying taus). No significant deviation from the expected SM background is observed. Limits are set on the Higgsino mass in simplified models of general gauge mediated supersymmetry Tn1n1A/Tn1n1B/Tn1n1C, see their Figure 9. Limits are also set on the wino, slepton, sneutrino and gluino mass in a simplified model of NLSP pair production with R-parity violating decays of the LSP via λ_{12k} or λ_{i33} to charged leptons, see their Figures 7, 8.

[11] SIRUNYAN 18AO searched in 35.9 fb^{-1} of pp collisions at $\sqrt{s}$ = 13 TeV for direct electroweak production of charginos and neutralinos in events with either two or more leptons (electrons or muons) of the same electric charge, or with three or more leptons, which can include up to two hadronically decaying tau leptons. No significant excess above

Downloaded from https://academic.oup.com/ptep/article/2022/8/083C01/6651666 by KIT Library user on 27 September 2022

the Standard Model expectations is observed. Limits are set on the chargino/neutralino mass in the Tchi1n2A, Tchi1n2H, Tchi1n2D, Tchi1n2E and Tchi1n2F simplified models, see their Figures 14, 15, 16, 17 and 18. Limits are also set on the higgsino mass in the Tn1n1A, Tn1n1B and Tn1n1C simplified models, see their Figure 19.

[12] SIRUNYAN 18AP searched in 35.9 fb^{-1} of pp collisions at $\sqrt{s}$ = 13 TeV for direct electroweak production of charginos and neutralinos by combining a number of previous and new searches. No significant excess above the Standard Model expectations is observed. Limits are set on the chargino/neutralino mass in the Tchi1n2E, Tchi1n2F and Tchi1n2l simplified models, see their Figures 7, 8, 9 an 10. Limits are also set on the higgsino mass in the Tn1n1A, Tn1n1B and Tn1n1C simplified models, see their Figure 11, 12, 13 and 14.

[13] SIRUNYAN 18AR searched in 35.9 fb^{-1} of pp collisions at $\sqrt{s}$ = 13 TeV for events containing two opposite-charge, same-flavour leptons (electrons or muons), jets and $\not{E}_T$. No significant excess above the Standard Model expectations is observed. Limits are set on the gluino mass in the Tglu4C simplified model, see their Figure 7. Limits are also set on the chargino/neutralino mass in the Tchi1n2F simplified models, see their Figure 8, and on the higgsino mass in the Tn1n1B and Tn1n1C simplified models, see their Figure 9. Finally, limits are set on the sbottom mass in the Tsbot3 simplified model, see their Figure 10.

[14] SIRUNYAN 18O searched in 35.9 fb^{-1} of pp collisions at $\sqrt{s}$ = 13 TeV for events with two Higgs bosons, decaying to pairs of b-quarks, and large $\not{E}_T$. No significant excess above the Standard Model expectations is observed. Limits are set on the Higgsino mass in the T1n1n1A simplified model, see their Figure 9.

[15] SIRUNYAN 18X searched in 35.9 fb^{-1} of pp collisions at $\sqrt{s}$ = 13 TeV for events with one or more high-momentum Higgs bosons, decaying to pairs of photons, jets and $\not{E}_T$. The razor variables (M_R and R^2) are used to categorise the events. No significant excess above the Standard Model expectations is observed. Limits are set on the sbottom mass in the Tsbot4 simplified model and on the wino mass in the Tchi1n2E simplified model, see their Figure 5. Limits are also set on the higgsino mass in the Tn1n1A and Tn1n1B simplified models, see their Figure 6.

[16] KHACHATRYAN 14L searched in 19.5 fb^{-1} of pp collisions at $\sqrt{s}$ = 8 TeV for evidence of direct pair production of neutralinos with Higgs or Z-bosons in the decay chain, leading to HH, HZ and ZZ final states with missing transverse energy. The decays of 16–20. a Higgs boson to a b-quark pair, to a photon pair, and to final states with leptons are considered in conjunction with hadronic and leptonic decay modes of the Z and W bosons. No significant excesses over the expected SM backgrounds are observed. The results are interpreted in the context of GMSB simplified models where the decays $\widetilde{\chi}^0_1 \rightarrow H\widetilde{G}$ or $\widetilde{\chi}^0_1 \rightarrow Z\widetilde{G}$ take place either 100% or 50% of the time, see Figs. 16–20.

[17] AAD 20D searched in 32.8 fb^{-1} of pp collisions at $\sqrt{s}$ = 13 TeV for events containing an oppositely charge lepton pair (ee, $\mu\mu$ or $e\mu$) coming from long-lived neutralinos decaying through the R-parity-violating decay $\widetilde{\chi}^0_1 \rightarrow \ell\ell\nu$ with $\lambda_{121} \neq 0$ or $\lambda_{122} \neq 0$. No excess over the expected background is observed. Limits are derived for decay lengths of the neutralino between 1 mm and 10 m in a scenario where a squark-antisquark pair is produced, with the squark decaying to a quark and a $\widetilde{\chi}^0_1$, with either $\widetilde{\chi}^0_1 \rightarrow ee\nu/e\mu\nu$ ($\lambda_{121} \neq 0$) or $\widetilde{\chi}^0_1 \rightarrow e\mu\nu/\mu\mu\nu$ ($\lambda_{122} \neq 0$), see their Figures 4 and 5.

[18] AABOUD 19G searched in 32.9 fb^{-1} of pp collisions at $\sqrt{s}$ = 13 TeV for evidence of neutralinos decaying into a Z-boson and a gravitino, in events characterized by the presence of dimuon vertices with displacements from the pp interaction point in the range of 1400 cm. Neutralinos are assumed to be produced in the decay chain of gluinos as in Tglu1A models. No significant excess is observed in the number of vertices relative to the predicted background. In GGM with a gluino mass of 1100 GeV, neutralino masses in the range 300–1000 GeV are excluded for certain values of $c\tau$, see their Figure 7.

[19] AAIJ 17Z searched in 1 fb^{-1} of pp collisions at $\sqrt{s}$ = 7 TeV and in 2 fb^{-1} of pp collisions at $\sqrt{s}$ = 8 TeV for events containing a displaced vertex with one associated high transverse momentum μ. No excess is observed above the background expected from Standard Model processes. The results are used to set 95% C.L. upper limits on the cross section times branching fractions of pair-produced neutralinos decaying non-promptly into a muon and two quarks. Long-lived particles in a mass range 23–198 GeV are considered, see their Fig. 5 and Fig. 6.

[20] KHACHATRYAN 16BX searched in 19.5 fb^{-1} of pp collisions at $\sqrt{s}$ = 8 TeV for events containing 3 or more leptons coming from the electroweak production of wino- or higgsino-like neutralinos, assuming non-zero R-parity-violating leptonic couplings λ_{122}, λ_{123}, and λ_{233} or semileptonic couplings λ'_{131}, λ'_{233}, λ'_{331}, and λ'_{333}. No excess over the expected background is observed and limits are derived on the neutralino mass, see Figs. 24 and 25.

[21] AAD 14BH searched in 20.3 fb^{-1} of pp collisions at $\sqrt{s}$ = 8 TeV for events containing non-pointing photons in a diphoton plus missing transverse energy final state. No excess is observed above the background expected from Standard Model processes. The results are used to set 95% C.L. exclusion limits in the contact of gauge-mediated supersymmetric breaking models, with the lightest neutralino being the next-to-lightest supersymmetric particle and decaying with a lifetime in the range from 0.25 ns to about 100 ns into a photon and a gravitino. For limits on the NLSP lifetime versus Λ plane, for the SPS8 model, see their Fig. 7.

[22] AAD 13AP searched in 4.8 fb^{-1} of pp collisions at $\sqrt{s}$ = 7 TeV for events containing non-pointing photons in a diphoton plus missing transverse energy final state. No excess is observed above the background expected from Standard Model processes. The results are used to set 95% C.L. exclusion limits in the context of gauge-mediated supersymmetric breaking models, with the lightest neutralino being the next-to-lightest supersymmetric particle and decaying with a lifetime in excess of 0.25 ns into a photon and a gravitino. For limits in the NLSP lifetime versus Λ plane, for the SPS8 model, see their Fig. 8.

[23] AAD 13Q searched in 4.7 fb^{-1} of pp collisions at $\sqrt{s}$ = 7 TeV for events containing a high-p_T isolated photon, at least one jet identified as originating from a bottom quark, and high missing transverse momentum. Such signatures may originate from supersymmetric models with gauge-mediated supersymmetry breaking in events in which one of a pair of higgsino-like neutralinos decays into a photon and a gravitino while the other decays into a Higgs boson and a gravitino. No significant excess above the expected background was found and limits were set on the neutralino mass in a generalized GMSB model (GGM) with a higgsino-like neutralino NLSP, see their Fig. 4. Intermediate neutralino masses between 220 and 380 GeV are excluded at 95% C.L, regardless of the squark and gluino masses, purely on the basis of the expected weak production.

[24] AAD 13R looked in 4.4 fb^{-1} of pp collisions at $\sqrt{s}$ = 7 TeV for events containing new, heavy particles that decay at a significant distance from their production point into a final state containing a high-momentum muon and charged hadrons. No excess over the expected background is observed and limits are placed on the production cross-section of neutralinos via squarks for various $m_{\widetilde{q}}$, $m_{\widetilde{\chi}^0_1}$ in an R-parity violating scenario with $\lambda'_{211} \neq 0$, as a function of the neutralino lifetime, see their Fig. 6.

[25] AALTONEN 13I searched in 6.3 fb^{-1} of $p\overline{p}$ collisions at $\sqrt{s}$ = 1.96 TeV for events containing $\not{E}_T$ and a delayed photon that arrives late in the detector relative to the time expected from prompt production. No evidence of delayed photon production is observed.

[26] CHATRCHYAN 13AH searched in 4.9 fb^{-1} of pp collisions at $\sqrt{s}$ = 7 TeV for events containing $\not{E}_T$ and a delayed photon that arrives late in the detector relative to the time expected from prompt production. No significant excess above the expected background was found and limits were set on the pair production of $\widetilde{\chi}^0_1$ depending on the neutralino proper decay length, see Fig. 8. Supersedes CHATRCHYAN 12BK.

[27] AAD 12CP searched in 4.8 fb^{-1} of pp collisions at $\sqrt{s}$ = 7 TeV for events with two photons and large $\not{E}_T$ due to $\widetilde{\chi}^0_1 \rightarrow \gamma\widetilde{G}$ decays in a GMSB framework. No significant excess above the expected background was found and limits were set on the neutralino mass in a generalized GMSB model (GGM) with a bino-like neutralino NLSP, see Figs. 6 and 7. The other sparticle masses were decoupled, tanβ = 2 and $c\tau_{NLSP}$ < 0.1 mm. Also, in the framework of the SPS8 model, limits are presented in Fig. 8.

[28] AAD 12CT searched in 4.7 fb^{-1} of pp collisions at $\sqrt{s}$ = 7 TeV for events containing four or more leptons (electrons or muons) and either moderate values of missing transverse momentum or large effective mass. No significant excess is found in the data. Limits are presented in a simplified model of R-parity violating supersymmetry in which charginos are pair-produced and then decay into a W-boson and a $\widetilde{\chi}^0_1$, which in turn decays through an RPV coupling into two charged leptons ($e^\pm e^\mp$ or $\mu^\pm\mu^\mp$) and a neutrino. In this model, limits are set on the neutralino mass as a function of the chargino mass, see Fig. 3a. Limits are also set in an R-parity violating mSUGRA model, see Fig. 3b.

[29] AAD 12R looked in 33 pb^{-1} of pp collisions at $\sqrt{s}$ = 7 TeV for events containing new, heavy particles that decay at a significant distance from their production point into a final state containing a high-momentum muon and charged hadrons. No excess over the expected background is observed and limits are placed on the production cross-section of neutralinos via squarks for various ($m_{\widetilde{q}}$, $m_{\widetilde{\chi}^0_1}$) in an R-parity violating scenario with $\lambda'_{211} \neq 0$, as a function of the neutralino lifetime, see their Fig. 8. Superseded by AAD 13R.

[30] ABAZOV 12AD looked in 6.2 fb^{-1} of pp collisions at $\sqrt{s}$ = 1.96 TeV for events with a photon, a Z-boson, and large $\not{E}_T$ in the final state. This topology corresponds to a GMSB model where pairs of neutralino NLSPs are either pair produced promptly or from decays of other supersymmetric particles and then decay to either $Z\widetilde{G}$ or $\gamma\widetilde{G}$. No significant excess over the SM expectation is observed and a limit at 95% C.L. on the cross section is derived as a function of the effective SUSY breaking scale Λ, see Fig. 3. Assuming N_{mes} = 2, M_{mes} = 3 Λ, tanβ = 3, μ = 0.75 M_1, and C_{grav} = 1, the model is excluded at 95% C.L. for values of Λ < 87 TeV.

[31] CHATRCHYAN 12BK searched in 2.23 fb^{-1} of pp collisions at $\sqrt{s}$ = 7 TeV for events with two photons and large $\not{E}_T$ due to $\widetilde{\chi}^0_1 \rightarrow \gamma\widetilde{G}$ decays in a GMSB framework. No significant excess above the expected background was found and limits were set on the pair production of $\widetilde{\chi}^0_1$ depending on the neutralino lifetime, see Fig. 6.

[32] CHATRCHYAN 11B looked in 35 pb^{-1} of pp collisions at $\sqrt{s}$=7 TeV for events with an isolated lepton (e or μ), a photon and $\not{E}_T$ which may arise in a generalized gauge mediated model from the decay of Wino-like NLSPs. No evidence for an excess over the expected background is observed. Limits are derived in the plane of squark/gluino mass versus Wino mass (see Fig. 4). Mass degeneracy of the produced squarks and gluinos is assumed.

[33] AALTONEN 10 searched in 2.6 fb^{-1} of $p\overline{p}$ collisions at $\sqrt{s}$ = 1.96 TeV for diphoton events with large $\not{E}_T$. They may originate from the production of $\widetilde{\chi}^\pm$ in pairs or associated to a $\widetilde{\chi}^0_2$, decaying into $\widetilde{\chi}^0_1$ which itself decays in GMSB to $\gamma\widetilde{G}$. There is no excess of events beyond expectation. An upper limit on the cross section is calculated in the GMSB model as a function of the $\widetilde{\chi}^0_1$ mass and lifetime, see their Fig. 2. A limit is derived on the $\widetilde{\chi}^0_1$ mass of 149 GeV for $\tau_{\widetilde{\chi}^0_1} \ll 1$ ns, which improves the results of previous searches.

[34] ABAZOV 10P looked in 6.3 fb^{-1} of $p\overline{p}$ collisions at $\sqrt{s}$ = 1.96 TeV for events with at least two isolated γs and large $\not{E}_T$. These could be the signature of $\widetilde{\chi}^0_2$ and $\widetilde{\chi}^\pm_1$ production, decaying to $\widetilde{\chi}^0_1$ and finally $\widetilde{\chi}^0_1 \rightarrow \gamma\widetilde{G}$ in a GMSB framework. No significant excess over the SM expectation is observed, and a limit at 95% C.L. on the cross section is derived for N_{mes} = 1, tanβ = 15 and μ > 0, see their Fig. 2. This allows them to set a limit on the effective SUSY breaking scale Λ > 124 TeV, from which the excluded $\widetilde{\chi}^0_1$ mass range is obtained.

[35] ABAZOV 08F looked in 1.1 fb^{-1} of $p\overline{p}$ collisions at $\sqrt{s}$ = 1.96 TeV for diphoton events with large $\not{E}_T$. They may originate from the production of $\widetilde{\chi}^\pm$ in pairs or associated to a $\widetilde{\chi}^0_2$, decaying to a $\widetilde{\chi}^0_1$ which itself decays promptly in GMSB to $\widetilde{\chi}^0_1 \rightarrow \gamma\widetilde{G}$. No significant excess was found compared to the background expectation. A limit is derived on the masses of SUSY particles in the GMSB framework for M = 2Λ, N = 1, tanβ = 15 and μ > 0, see Figure 2. It also excludes Λ < 91.5 TeV. Supersedes the results of ABAZOV 05A. Superseded by ABAZOV 10P.

[36] ABULENCIA 07H searched in 346 pb^{-1} of $p\overline{p}$ collisions at $\sqrt{s}$ = 1.96 TeV for events with at least three leptons (e or μ) from the decay of $\widetilde{\chi}^0_1$ via $LL\overline{E}$ couplings. The results are consistent with the hypothesis of no signal. Upper limits on the cross-section are extracted and a limit is derived in the framework of mSUGRA on the masses of $\widetilde{\chi}^0_1$ and $\widetilde{\chi}^\pm_1$, see e.g. their Fig. 3 and Tab. II.

[37] ABBIENDI 06B use 600 pb^{-1} of data from $\sqrt{s}$ = 189–209 GeV. They look for events with diphotons + $\not{E}$ final states originating from prompt decays of pair-produced neutralinos in a GMSB scenario with $\widetilde{\chi}^0_1$ NLSP. Limits on the cross-section are computed as a function of m($\widetilde{\chi}^0_1$), see their Fig. 14. The limit on the $\widetilde{\chi}^0_1$ mass is for a pure Bino state assuming a prompt decay, with lifetimes up to 10^{-9}s. Supersedes the results of ABBIENDI 04N.

[38] ABDALLAH 05B use data from $\sqrt{s}$ = 180–209 GeV. They look for events with single photons + $\not{E}$ final states. Limits are computed in the plane (m($\widetilde{G}$) , m($\widetilde{\chi}^0_1$)), shown in their Fig. 9b for a pure Bino state in the GMSB framework and in Fig. 9c for a no-scale supergravity model. Supersedes the results of ABREU 00Z.

[39] ABDALLAH 05B use data from $\sqrt{s}$ = 130–209 GeV. They look for events with diphotons + $\not{E}$ final states and single photons not pointing to the vertex, expected in GMSB when

Downloaded from https://academic.oup.com/ptep/article/2022/8/083C01/6651666 by KIT Library user on 27 September 2022

the $\widetilde{\chi}^0_1$ is the NLSP. Limits are computed in the plane (m($\widetilde{G}$), m($\widetilde{\chi}^0_1$)), see their Fig. 10. The lower limit is derived on the $\widetilde{\chi}^0_1$ mass for a pure Bino state assuming a prompt decay and $m_{\widetilde{e}_R} = m_{\widetilde{e}_L} = 2\ m_{\widetilde{\chi}^0_1}$. It improves to 100 GeV for $m_{\widetilde{e}_R} = m_{\widetilde{e}_L} = 1.1\ m_{\widetilde{\chi}^0_1}$. and the limit in the plane (m($\widetilde{\chi}^0_1$), m($\widetilde{e}_R$)) is shown in Fig. 10b. For long-lived neutralinos, cross-section limits are displayed in their Fig 11. Supersedes the results of ABREU 00Z.

$\widetilde{\chi}^0_2$, $\widetilde{\chi}^0_3$, $\widetilde{\chi}^0_4$ (Neutralinos) mass limits

Neutralinos are unknown mixtures of photinos, z-inos, and neutral higgsinos (the supersymmetric partners of photons and of Z and Higgs bosons). The limits here apply only to $\widetilde{\chi}^0_2$, $\widetilde{\chi}^0_3$, and $\widetilde{\chi}^0_4$. $\widetilde{\chi}^0_1$ is the lightest supersymmetric particle (LSP); see $\widetilde{\chi}^0_1$ Mass Limits. It is not possible to quote rigorous mass limits because they are extremely model dependent; i.e. they depend on branching ratios of various $\widetilde{\chi}^0$ decay modes, on the masses of decay products ($\widetilde{e}$, $\widetilde{\gamma}$, $\widetilde{q}$, $\widetilde{g}$), and on the $\widetilde{e}$ mass exchanged in $e^+e^- \rightarrow \widetilde{\chi}^0_i \widetilde{\chi}^0_j$. Limits arise either from direct searches, or from the MSSM constraints set on the gaugino and higgsino mass parameters M_2 and μ through searches for lighter charginos and neutralinos. Often limits are given as contour plots in the $m_{\widetilde{\chi}^0} - m_{\widetilde{e}}$ plane vs other parameters. When specific assumptions are made, e.g, the neutralino is a pure photino ($\widetilde{\gamma}$), pure z-ino ($\widetilde{Z}$), or pure neutral higgsino ($\widetilde{H}^0$), the neutralinos will be labelled as such.

Limits obtained from e^+e^- collisions at energies up to 136 GeV, as well as other limits from different techniques, are now superseded and have not been included in this compilation. They can be found in the 1998 Edition (The European Physical Journal **C3** 1 (1998)) of this Review. Some later papers are now obsolete and have been omitted. They were last listed in our PDG 14 edition: K. Olive, *et al.* (Particle Data Group), Chinese Physics **C38** 070001 (2014) (http://pdg.lbl.gov).

VALUE (GeV)	CL%	DOCUMENT ID		TECN	COMMENT
> 640	95	[1] AAD	21BG	ATLS	$3\ell + \not{E}_T$, Tchi1n2F, wino cross section, $m_{\widetilde{\chi}^0_1} = 0$ GeV
> 300	95	[1] AAD	21BG	ATLS	$3\ell + \not{E}_T$, Tchi1n2F, wino cross section, $m_{\widetilde{\chi}^0_2} - m_{\widetilde{\chi}^0_1} = m_Z$
> 240	95	[1] AAD	21BG	ATLS	$3\ell + \not{E}_T$, Tchi1n2F, wino cross section, $m_{\widetilde{\chi}^0_2} - m_{\widetilde{\chi}^0_1} = 10$ GeV
> 195	95	[1] AAD	21BG	ATLS	$3\ell + \not{E}_T$, Tchi1n2Ga, higgsino cross section, $m_{\widetilde{\chi}^0_2} - m_{\widetilde{\chi}^0_1} = 10$ GeV
> 190	95	[1] AAD	21BG	ATLS	$3\ell + \not{E}_T$, Tchi1n2E, wino cross section, $m_{\widetilde{\chi}^0_1} = 0$ GeV
>1600	95	[2] AAD	21Y	ATLS	$\geq 4\ell$, RPV Tchi1n2l with $\widetilde{\chi}^0_1 \rightarrow \ell^\pm \ell^\mp \nu$, $\lambda_{12k} \neq 0$, $m_{\widetilde{\chi}^0_1} =$ 1200 GeV
>1100	95	[2] AAD	21Y	ATLS	$\geq 4\ell$, RPV Tchi1n2l with $\widetilde{\chi}^0_1 \rightarrow \ell^\pm \ell^\mp \nu$, $\lambda_{i33} \neq 0$, $m_{\widetilde{\chi}^0_1} =$ 1000 GeV
> 750	95	[3] SIRUNYAN	21M	CMS	$\ell^\pm \ell^\mp + \not{E}_T$, Tchi1n2Fa , $m_{\widetilde{\chi}^0_1} <$ 100 GeV
none 400–820	95	[4] TUMASYAN	21C	CMS	1 $\ell^\pm$ + 2b-jets + $\not{E}_T$, Tchi1n2E, $\widetilde{\chi}^0_1 = 200$ GeV
none 160–820	95	[4] TUMASYAN	21C	CMS	1 $\ell^\pm$ + 2b-jets + $\not{E}_T$, Tchi1n2E, $\widetilde{\chi}^0_1 = 0$ GeV
> 380	95	[5] AAD	20AN	ATLS	$2\gamma + \not{E}_T$,Tn1n1A, GMSB
> 193	95	[6] AAD	20I	ATLS	2ℓ (soft), jets, $\not{E}_T$; Tchi1n2Ga, higgsino, $m_{\widetilde{\chi}^0_2} - m_{\widetilde{\chi}^0_1} = 9.3$ GeV
> 240	95	[7] AAD	20I	ATLS	2ℓ (soft), jets, $\not{E}_T$; Tchi1n2Fa, wino, $m_{\widetilde{\chi}^0_2} - m_{\widetilde{\chi}^0_1} = 7$ GeV
> 345	95	[8] AAD	20K	ATLS	$3\ell + \not{E}_T$, Tchi1n2F, $m_{\widetilde{\chi}^0_1} = 0$ GeV
> 740	95	[9] AAD	20R	ATLS	1ℓ + 2b-jets + $\not{E}_T$, Tchi1n2E, $m_{\widetilde{\chi}^0_1} = 0$ GeV
> 290	95	[10] SIRUNYAN	20AU	CMS	soft τ + jet + $\not{E}_T$, Tchi1n2D, wino, $m_{\widetilde{\chi}^\pm_1} - m_{\widetilde{\chi}^0_1} = 50$ GeV
> 680	95	[11] AABOUD	19AU	ATL	0, 1, 2 or more ℓ, H ($\rightarrow \gamma\gamma$, bb, WW^*, ZZ^*, $\tau\tau$) (various searches), Tchi1n2E, $m_{\widetilde{\chi}^0_1}$=0 GeV
> 112	95	[12] SIRUNYAN	19BU	CMS	$pp \rightarrow \widetilde{\chi}^+_1 \widetilde{\chi}^0_2$ + 2 jets, $\widetilde{\chi}^0_2 \rightarrow \ell^+ \ell^- \widetilde{\chi}^0_1$, heavy sleptons, $m_{\widetilde{\chi}^0_2} - m_{\widetilde{\chi}^0_1} = 1$ GeV, $m_{\widetilde{\chi}^0_2} = m_{\widetilde{\chi}^+_1}$
> 215	95	[12] SIRUNYAN	19BU	CMS	$pp \rightarrow \widetilde{\chi}^+_1 \widetilde{\chi}^0_2$ + 2 jets, $\widetilde{\chi}^0_2 \rightarrow \ell^+ \ell^- \widetilde{\chi}^0_1$, heavy sleptons, $m_{\widetilde{\chi}^0_2} - m_{\widetilde{\chi}^0_1} = 30$ GeV, $m_{\widetilde{\chi}^0_2} = m_{\widetilde{\chi}^+_1}$
> 760	95	[13] AABOUD	18AY	ATLS	$2\tau + \not{E}_T$, Tchi1n2D and $\widetilde{\tau}_L$-only, $m_{\widetilde{\chi}^0_1} = 0$ GeV
>1125	95	[14] AABOUD	18BT	ATLS	$2,3\ell + \not{E}_T$, Tchi1n2C, $m_{\widetilde{\chi}^0_1}$=0 GeV
> 580	95	[15] AABOUD	18BT	ATLS	$2,3\ell + \not{E}_T$, Tchi1n2F, $m_{\widetilde{\chi}^0_1}$=0 GeV
none 130–230, 290–880	95	[16] AABOUD	18CK	ATLS	$2H$ ($\rightarrow bb$)$+\not{E}_T$,Tn1n1A, GMSB
none 220–600	95	[17] AABOUD	18CO	ATLS	$2,3\ell + \not{E}_T$, recursive jigsaw, Tchi1n2F, $m_{\widetilde{\chi}^0_1} = 0$ GeV
> 145	95	[18] AABOUD	18R	ATLS	2ℓ (soft) + $\not{E}_T$, Tchi1n2G, higgsino, $m_{\widetilde{\chi}^0_2} - m_{\widetilde{\chi}^0_1} = 5$ GeV
> 175	95	[19] AABOUD	18R	ATLS	2ℓ (soft) + $\not{E}_T$, Tchi1n2F, wino, $m_{\widetilde{\chi}^0_2} - m_{\widetilde{\chi}^0_1} = 10$ GeV
>1060	95	[20] AABOUD	18U	ATLS	$2\ \gamma + \not{E}_T$, GGM,Tchi1chi1A, any NLSP mass
> 167	95	[21] SIRUNYAN	18AJ	CMS	2ℓ (soft) + $\not{E}_T$, Tchi1n2G, higgsino, $m_{\widetilde{\chi}^0_2} - m_{\widetilde{\chi}^0_1} = 15$ GeV
> 710	95	[22] SIRUNYAN	18DP	CMS	$2\tau + \not{E}_T$, Tchi1n2D, $m_{\widetilde{\chi}^0_1} = 0$ GeV
none 220–490	95	[23] SIRUNYAN	17AW	CMS	1ℓ+ 2 b-jets + $\not{E}_T$, Tchi1n2E, $m_{\widetilde{\chi}^0_1} = 0$ GeV
> 600	95	[24] AAD	16AA	ATLS	$3,4\ell + \not{E}_T$, Tn2n3A, $m_{\widetilde{\chi}^0_1}$=0GeV
> 670	95	[24] AAD	16AA	ATLS	$3,4\ell + \not{E}_T$,Tn2n3B,$m_{\widetilde{\chi}^0_1} < 200$GeV
> 250	95	[25] AAD	15BA	ATLS	$m_{\widetilde{\chi}^\pm_1} = m_{\widetilde{\chi}^0_2}$, $m_{\widetilde{\chi}^0_1} = 0$ GeV
> 380	95	[26] AAD	14H	ATLS	$\widetilde{\chi}^\pm_1 \widetilde{\chi}^0_2 \rightarrow \tau^\pm \nu \widetilde{\chi}^0_1 \tau^\pm \tau^\mp \widetilde{\chi}^0_1$, simplified model, $m_{\widetilde{\chi}^\pm_1} = m_{\widetilde{\chi}^0_2}$, $m_{\widetilde{\chi}^0_1} = 0$ GeV
> 700	95	[26] AAD	14H	ATLS	$\widetilde{\chi}^\pm_1 \widetilde{\chi}^0_2 \rightarrow \ell^\pm \nu \widetilde{\chi}^0_1 \ell^\pm \ell^\mp \widetilde{\chi}^0_1$, simplified model, $m_{\widetilde{\chi}^\pm_1} = m_{\widetilde{\chi}^0_2}$, $m_{\widetilde{\chi}^0_1} = 0$ GeV
> 345	95	[26] AAD	14H	ATLS	$\widetilde{\chi}^\pm_1 \widetilde{\chi}^0_2 \rightarrow W \widetilde{\chi}^0_1 Z \widetilde{\chi}^0_1$, simplified model, $m_{\widetilde{\chi}^\pm_1} = m_{\widetilde{\chi}^0_2}$, $m_{\widetilde{\chi}^0_1} = 0$ GeV
> 148	95	[26] AAD	14H	ATLS	$\widetilde{\chi}^\pm_1 \widetilde{\chi}^0_2 \rightarrow W \widetilde{\chi}^0_1 H \widetilde{\chi}^0_1$, simplified model, $m_{\widetilde{\chi}^\pm_1} = m_{\widetilde{\chi}^0_2}$, $m_{\widetilde{\chi}^0_1} = 0$ GeV
> 620	95	[27] AAD	14X	ATLS	$\geq 4\ell^\pm$, $\widetilde{\chi}^0_{2,3} \rightarrow \ell^\pm \ell^\mp \widetilde{\chi}^0_1$, $m_{\widetilde{\chi}^0_1} = 0$ GeV
		[28] AAD	13	ATLS	$3\ell^\pm + \not{E}_T$, pMSSM, SMS
		[29] CHATRCHYAN	12BJ	CMS	$\geq 2\ \ell$, jets + $\not{E}_T$, $pp \rightarrow \widetilde{\chi}^\pm_1 \widetilde{\chi}^0_2$
> 62.4	95	[30] ABREU	00W	DLPH	$\widetilde{\chi}^0_2$, $1 \leq \tan\beta \leq 40$, all Δm, all m_0
> 99.9	95	[30] ABREU	00W	DLPH	$\widetilde{\chi}^0_3$, $1 \leq \tan\beta \leq 40$, all Δm, all m_0
> 116.0	95	[30] ABREU	00W	DLPH	$\widetilde{\chi}^0_4$, $1 \leq \tan\beta \leq 40$, all Δm, all m_0
• • • We do not use the following data for averages, fits, limits, etc. • • •					
> 310	95	[31] AAD	20AN	ATLS	$2\gamma + \not{E}_T$, Tchi1n2E, $m_{\widetilde{\chi}^0_1}$=0 GeV
none 180–355	95	[32] AAD	14G	ATLS	$\widetilde{\chi}^\pm_1 \widetilde{\chi}^0_2 \rightarrow W \widetilde{\chi}^0_1 Z \widetilde{\chi}^0_1$, simplified model, $m_{\widetilde{\chi}^\pm_1} = m_{\widetilde{\chi}^0_2}$, $m_{\widetilde{\chi}^0_1} = 0$ GeV
		[33] KHACHATRY...14I		CMS	$\widetilde{\chi}^0_2 \rightarrow (Z,\ H) \widetilde{\chi}^0_1\ \widetilde{\ell}\ell$, simplified model
		[34] AAD	12AS	ATLS	$3\ell^\pm + \not{E}_T$, pMSSM
		[35] AAD	12T	ATLS	$\ell^\pm \ell^\pm + \not{E}_T$, $pp \rightarrow \widetilde{\chi}^\pm_1 \widetilde{\chi}^0_2$

[1] AAD 21BG searched in 139 fb^{-1} of pp collisions at $\sqrt{s} = 13$ TeV for pair production $\widetilde{\chi}^0_2 \widetilde{\chi}^\pm_1$ in final states with three leptons, with and without assuming the presence of a $Z \rightarrow \ell\ell$ decay. No significant excess above the Standard Model predictions is observed. Limits are set on the $\widetilde{\chi}^0_2$ and $\widetilde{\chi}^\pm_1$ mass in Tchi1n2E, Tchi1n2F and Tchi1n2Ga. See their Fig. 16.

[2] AAD 21Y searched in 139 fb^{-1} of pp collisions at $\sqrt{s} = 13$ TeV for supersymmetry in events with four or more leptons (electrons, muons and tau-leptons). No significant excess above the Standard Model expectations is observed. Limits are set on Tchi1n12-GGM, and RPV models similar to Tchi1n2l, Tglu1A (with $q = u, d, s, c, b$, with equal branching fractions), and $\widetilde{\ell}_L/\widetilde{\nu} \rightarrow \ell/\nu \widetilde{\chi}^0_1$ (mass-degenerate $\widetilde{\ell}_L$ and $\widetilde{\nu}$ of all 3 generations), all with $\widetilde{\chi}^0_1 \rightarrow \ell^\pm \ell^\mp \nu$ via λ_{12k} or λ_{i33} (where $i,k \in 1,2$), see their Figure 11.

[3] SIRUNYAN 21M searched in 137 fb^{-1} of pp collisions at $\sqrt{s} = 13$ TeV for supersymmetry in events with two opposite-sign same-flavor leptons (electrons, muons) and $\not{E}_T$. No significant excess above the Standard Model expectations is observed. Limits are set on the gluino mass in the simplified model Tglu4C, see their Figure 10, on the $\widetilde{\chi}^0_2$ and $\widetilde{\chi}^\pm_1$ mass in Tchi1n2Fa, see their Figure 11, on the $\widetilde{\chi}^0_1$ mass in Tn1n1C and Tn1n1B for $m_{\widetilde{\chi}^0_2} = m_{\widetilde{\chi}^\pm_1} = m_{\widetilde{\chi}^0_1}$, see their Figure 12. Limits are also set on the light squark mass for the simplified model Tsqk2A, on the sbottom mass in Tsbot3, see their Figure 13, and on the slepton mass in direct electroweak pair production of mass-degenerate left- and right-handed sleptons (selectrons and smuons), see their Figure 14.

[4] TUMASYAN 21C searched in 137 fb^{-1} of pp collisions at $\sqrt{s} = 13$ TeV for supersymmetry in events with with one lepton, a Higgs boson decaying to a pair of bottom quarks, and large $\not{E}_T$. No significant excess above the Standard Model expectations is observed. Lower limits are set on the masses of $\widetilde{\chi}^0_2$ and $\widetilde{\chi}^\pm_1$ in the simplified model Tchi1n2E, see their Figure 6.

[5] AAD 20AN searched in 139 fb^{-1} of pp collisions at $\sqrt{s} = 13$ TeV for events with two photons and missing transverse momentum. Events are further categorised in terms of lepton or jet multiplicity. No significant excess over the expected background is observed. Limits at 95% C.L. are set on the Higgsino mass in the T1n1n1A simplified model, see their Figure 11.

Downloaded from https://academic.oup.com/ptep/article/2022/8/083C01/6651666 by KIT Library user on 27 September 2022

[6] AAD 20I reported on ATLAS searches for electroweak production in models with compressed mass spectra as Tchi1n2Ga. A dataset of pp collisions at $\sqrt{s}$ = 13 TeV corresponding to an integrated luminosity of 139 fb^{-1} was used. Events with $\not{E}_T$, two same-flavour, opposite-charge, low-transverse-momentum leptons, and jets from initial-state radiation or characteristic of vector-boson fusion production are selected. Constraints at 95% C.L. are placed in Higgsino models on the mass of the $\widetilde{\chi}^0_2$ (the $\widetilde{\chi}^\pm_1$ mass is halfway between the $\widetilde{\chi}^0_2$ and $\widetilde{\chi}^0_1$ masses) at 193 GeV for a mass splitting between $\widetilde{\chi}^0_2$ and $\widetilde{\chi}^0_1$ of 9.3 GeV and extend down to a mass splitting of 2.4 GeV at the LEP chargino mass limit. See their Fig. 14(a).

[7] AAD 20I reported on ATLAS searches for electroweak production in models with compressed mass spectra as Tchi1n2Fa. A dataset of pp collisions at $\sqrt{s}$ = 13 TeV corresponding to an integrated luminosity of 139 fb^{-1} was used. Events with $\not{E}_T$, two same-flavour, opposite-charge, low-transverse-momentum leptons, and jets from initial-state radiation or characteristic of vector-boson fusion production are selected. Constraints at 95% C.L. are placed in Wino-Bino models on the mass of the $\widetilde{\chi}^0_2$ (degenerate with $\widetilde{\chi}^\pm_1$) at 240 GeV for a mass splitting between $\widetilde{\chi}^0_2$ and $\widetilde{\chi}^0_1$ of 7 GeV and extend down to a mass splitting of 1.5 GeV at the LEP chargino mass limit of 92.4 GeV. See their Fig. 14(b,c).

[8] AAD 20K reported on a search for electroweak production in models with mass splittings near the electroweak scale as Tchi1n2F and exploiting three-lepton final state events with an emulated recursive jigsaw reconstruction method. The analysis uses a dataset of pp collisions at $\sqrt{s}$ = 13 TeV corresponding to an integrated luminosity of 139 fb^{-1}. Exclusion limits at 95% C.L. are derived on next-to-lightest neutralinos and charginos with masses up to 345 GeV for a massless lightest neutralino, see their Fig. 7.

[9] AAD 20R searched for electroweak production in the model Tchi1n2E, selecting events with a pair of b-tagged jets consistent with those from a Higgs boson decay, either an electron or a muon from the W boson decay and $\not{E}_T$. The analysis uses a dataset of pp collisions at $\sqrt{s}$ = 13 TeV corresponding to an integrated luminosity of 139 fb^{-1}. Exclusion limits at 95% C.L. are derived on next-to-lightest neutralinos and charginos with masses up to 740 GeV for a massless lightest neutralino, assuming pure wino cross-sections. See their Fig. 6.

[10] SIRUNYAN 20AU searched in 77.2 fb^{-1} of pp collisions at $\sqrt{s}$ = 13 TeV for events containing one soft, hadronically decaying tau lepton, one energetic jet from initial-state radiation, and large $\not{E}_T$. No excess over the expected background is observed. Limits are derived on the wino mass in the Tchi1n2D simplified model, see their Figure 2.

[11] AABOUD 19AU searched in 36.1 fb^{-1} of pp collisions at $\sqrt{s}$ = 13 TeV for direct electroweak production of charginos and next-to-lightest neutralinos decaying into lightest neutralinos and a W and a Higgs boson, respectively. Fully hadronic, semileptonic, diphoton, and multilepton (electrons, muons) final states with missing transverse momentum are considered in this search. Observations are consistent with the Standard Model expectations, and 95% confidence-level limits of up to 680 GeV on the chargino/next-to-lightest neutralino masses are set (Tchi1n2E model). See their Figure 14 for an overlay of exclusion contours from all searches.

[12] SIRUNYAN 19BU searched for pair production of gauginos via vector boson fusion assuming the gaugino spectrum is compressed, in 35.9 fb^{-1} of pp collisions at $\sqrt{s}$ = 13 TeV. The final states explored included zero leptons plus two jets, one lepton plus two jets, and one hadronic tau plus two jets. A similar bound is obtained in the light slepton limit.

[13] AABOUD 18AY searched in 36.1 fb^{-1} of pp collisions at $\sqrt{s}$ = 13 TeV for direct electroweak production of charginos and neutralinos as in Tchi1n2D models, in events characterised by the presence of at least two hadronically decaying tau leptons and large missing transverse energy. No significant deviation from the expected SM background is observed. Assuming decays via intermediate $\widetilde{\tau}_L$ and $m_{\widetilde{\chi}^\pm_1} = m_{\widetilde{\chi}^0_2}$, the observed limits rule out $\widetilde{\chi}^0_2$ masses up to 760 GeV for a massless $\widetilde{\chi}^0_1$. See their Fig.7 (right). Interpretations are also provided in Fig 8 (bottom) for different assumptions on the ratio between $m_{\widetilde{\tau}}$ and $m_{\widetilde{\chi}^0_2} + m_{\widetilde{\chi}^0_1}$.

[14] AABOUD 18BT searched in 36.1 fb^{-1} of pp collisions at $\sqrt{s}$ = 13 TeV for direct electroweak production of charginos, chargino and next-to-lightest neutralinos and sleptons in events with two or three leptons (electrons or muons), with or without jets, and large missing transverse energy. No significant excess above the Standard Model expectations is observed. Limits are set on the next-to-lightest neutralino mass up to 1100 GeV for massless $\widetilde{\chi}^0_1$ in the Tchi1n2C simplified model exploiting the 3ℓ signature, see their Figure 8(c).

[15] AABOUD 18BT searched in 36.1 fb^{-1} of pp collisions at $\sqrt{s}$ = 13 TeV for direct electroweak production of charginos, chargino and next-to-lightest neutralinos and sleptons in events with two or three leptons (electrons or muons), with or without jets, and large missing transverse energy. No significant excess above the Standard Model expectations is observed. Limits are set on the next-to-lightest neutralino mass up to 580 GeV for massless $\widetilde{\chi}^0_1$ in the Tchi1n2F simplified model exploiting the 2ℓ+2 jets and 3ℓ signatures, see their Figure 8(d).

[16] AABOUD 18CK searched for events with at least 3 b-jets and large missing transverse energy in two datasets of pp collisions at $\sqrt{s}$ = 13 TeV of 36.1 fb^{-1} and 24.3 fb^{-1} depending on the trigger requirements. The analyses aimed to reconstruct two Higgs bosons decaying to pairs of b-quarks. No significant excess above the Standard Model expectations is observed. Limits are set on the Higgsino mass in the T1n1n1A simplified model, see their Figure 15(a). Constraints are also presented as a function of the BR of Higgsino decaying into an higgs boson and a gravitino, see their Figure 15(b).

[17] AABOUD 18CO searched in 36.1 fb^{-1} of pp collisions at $\sqrt{s}$ = 13 TeV for direct electroweak production of mass-degenerate charginos and next-to-lightest neutralinos in events with two or three leptons (electrons or muons), with or without jets, and large missing transverse energy. The search channels are based on recursive jigsaw reconstruction. Limits are set on the next-to-lightest neutralinos mass up to 600 GeV for massless neutralinos in the Tchi1n2F simplified model exploiting the statistical combination of 2ℓ+2 jets and 3ℓ channels. Next-to-lightest neutralinos masses below 220 GeV are not excluded due to an excess of events above the SM prediction in the dedicated regions. See their Figure 13(d).

[18] AABOUD 18R searched in 36.1 fb^{-1} of pp collisions at $\sqrt{s}$ = 13 TeV for electroweak production in scenarios with compressed mass spectra in final states with two low-momentum leptons and missing transverse momentum. The data are found to be consistent with the SM prediction. Results are interpreted in Tchi1n2G higgsino models, and $\widetilde{\chi}^0_2$ masses are excluded up to 145 GeV for $m_{\widetilde{\chi}^0_2} - m_{\widetilde{\chi}^0_1}$ = 5 GeV. The exclusion limits extend down to mass splittings of 2.5 GeV, see their Fig. 10 (top). Results are also interpreted in terms of exclusion bounds on the production cross-sections for the NUHM2 scenario as a function of the universal gaugino mass $m_{1/2}$ and $m_{\widetilde{\chi}^0_2} - m_{\widetilde{\chi}^0_1}$, see their Fig. 12.

[19] AABOUD 18R searched in 36.1 fb^{-1} of pp collisions at $\sqrt{s}$ = 13 TeV for electroweak production in scenarios with compressed mass spectra in final states with two low-momentum leptons and missing transverse momentum. The data are found to be consistent with the SM prediction. Results are interpreted in Tchi1n2F wino models, and $\widetilde{\chi}^0_2$ masses are excluded up to 175 GeV for $m_{\widetilde{\chi}^0_2} - m_{\widetilde{\chi}^0_1}$ = 10 GeV. The exclusion limits extend down to mass splittings of 2 GeV, see their Fig. 10 (bottom). Results are also interpreted in terms of exclusion bounds on the production cross-sections for the NUHM2 scenario as a function of the universal gaugino mass $m_{1/2}$ and $m_{\widetilde{\chi}^0_2} - m_{\widetilde{\chi}^0_1}$, see their Fig. 12.

[20] AABOUD 18U searched in 36.1 fb^{-1} of pp collisions at $\sqrt{s}$ = 13 TeV in events with at least one isolated photon, possibly jets and significant transverse momentum targeting generalised models of gauge-mediated SUSY breaking. No significant excess of events is observed above the SM prediction. Results of the diphoton channel are interpreted in terms of lower limits on the masses of gauginos Tchi1chi1A models, which reach as high as 1.3 TeV. Gaugino masses below 1060 GeV are excluded for any NLSP mass, see their Fig. 10.

[21] SIRUNYAN 18AJ searched in 35.9 fb^{-1} of pp collisions at $\sqrt{s}$ = 13 TeV for events containing two low-momentum, oppositely charged leptons (electrons or muons) and $\not{E}_T$. No excess over the expected background is observed. Limits are derived on the wino mass in the Tchi1n2F simplified model, see their Figure 5. Limits are also set on the stop mass in the Tstop10 simplified model, see their Figure 6. Finally, limits are set on the Higgsino mass in the Tchi1n2G simplified model, see Figure 8 and in the pMSSM, see Figure 7.

[22] SIRUNYAN 18DP searched in 35.9 fb^{-1} of pp collisions at $\sqrt{s}$ = 13 TeV for direct electroweak production of charginos and neutralinos or of chargino pairs in events with a tau lepton pair and significant missing transverse momentum. Both hadronic and leptonic decay modes are considered for the tau lepton. No significant excess above the Standard Model expectations is observed. Limits are set on the chargino mass in the Tchi1chi1D and Tchi1n2 simplified models, see their Figures 14 and 15. Also, excluded stau pair production cross sections are shown in Figures 11, 12, and 13.

[23] SIRUNYAN 17AW searched in 35.9 fb^{-1} of pp collisions at $\sqrt{s}$ = 13 TeV for events with a charged lepton (electron or muon), two jets identified as originating from a b-quark, and large $\not{E}_T$. No significant excess above the Standard Model expectations is observed. Limits are set on the mass of the chargino and the next-to-lightest neutralino in the Tchi1n2E simplified model, see their Figure 6.

[24] AAD 16AA summarized and extended ATLAS searches for electroweak supersymmetry in final states containing several charged leptons, $\not{E}_T$, with or without hadronic jets, in 20 fb^{-1} of pp collisions at $\sqrt{s}$ = 8 TeV. The paper reports the results of new interpretations and statistical combinations of previously published analyses, as well as new analyses. Exclusion limits at 95% C.L. are set on mass-degenerate $\widetilde{\chi}^0_2$ and $\widetilde{\chi}^0_3$ masses in the Tn2n3A and Tn2n3B simplified models. See their Fig. 15.

[25] AAD 15BA searched in 20.3 fb^{-1} of pp collisions at $\sqrt{s}$ = 8 TeV for electroweak production of charginos and neutralinos decaying to a final state containing a W boson and a 125 GeV Higgs boson, plus missing transverse momentum. No excess beyond the Standard Model expectation is observed. Exclusion limits are derived in simplified models of direct chargino and next-to-lightest neutralino production, with the decays $\widetilde{\chi}^\pm_1 \rightarrow W^\pm\widetilde{\chi}^0_1$ and $\widetilde{\chi}^0_2 \rightarrow H\widetilde{\chi}^0_1$ having 100% branching fraction, see Fig. 8. A combination of the multiple final states for the Higgs decay yields the best limits (Fig. 8d).

[26] AAD 14H searched in 20.3 fb^{-1} of pp collisions at $\sqrt{s}$ = 8 TeV for electroweak production of charginos and neutralinos decaying to a final sate with three leptons and missing transverse momentum. No excess beyond the Standard Model expectation is observed. Exclusion limits are derived in simplified models of direct chargino and next-to-lightest neutralino production, with decays to the lightest neutralino via either all three generations of leptons, staus only, gauge bosons, or Higgs bosons, see Fig. 7. An interpretation in the pMSSM is also given, see Fig. 8.

[27] AAD 14X searched in 20.3 fb^{-1} of pp collisions at $\sqrt{s}$ = 8 TeV for events with at least four leptons (electrons, muons, taus) in the final state. No significant excess above the Standard Model expectations is observed. Limits are set on the neutralino mass in an R-parity conserving simplified model where the decay $\widetilde{\chi}^0_{2,3} \rightarrow \ell^\pm\ell^\mp\widetilde{\chi}^0_1$ takes place with a branching ratio of 100%, see Fig. 10.

[28] AAD 13 searched in 4.7 fb^{-1} of pp collisions at $\sqrt{s}$ = 7 TeV for charginos and neutralinos decaying to a final state with three leptons (e and μ) and missing transverse energy. No excess beyond the Standard Model expectation is observed. Exclusion limits are derived in the phenomenological MSSM, see Fig. 2 and 3, and in simplified models, see Fig. 4. For the simplified models with intermediate slepton decays, degenerate $\widetilde{\chi}^\pm_1$ and $\widetilde{\chi}^0_2$ masses up to 500 GeV are excluded at 95% C.L. for very large mass differences with the $\widetilde{\chi}^0_1$. Supersedes AAD 12AS.

[29] CHATRCHYAN 12BJ searched in 4.98 fb^{-1} of pp collisions at $\sqrt{s}$ = 7 TeV for direct electroweak production of charginos and neutralinos in events with at least two leptons, jets and missing transverse momentum. No significant excesses over the expected SM backgrounds are observed and 95% C.L. limits on the production cross section of $\widetilde{\chi}^\pm_1\widetilde{\chi}^0_2$ pair production were set in a number of simplified models, see Figs. 7 to 12. Most limits are for exactly 3 jets.

[30] ABREU 00W combines data collected at $\sqrt{s}$=189 GeV with results from lower energies. The mass limit is obtained by constraining the MSSM parameter space with gaugino and sfermion mass universality at the GUT scale, using the results of negative direct searches for neutralinos (including cascade decays and $\widetilde{\tau}\tau$ final states) from ABREU 01, for charginos from ABREU 00J and ABREU 00T (for all $\Delta m_\perp$), and for charged sleptons from ABREU 01B. The results hold for the full parameter space defined by all values of M_2 and $|\mu| \leq 2$ TeV with the $\widetilde{\chi}^0_1$ as LSP.

[31] AAD 20AN searched in 139 fb^{-1} of pp collisions at $\sqrt{s}$ = 13 TeV for events with two photons and missing transverse momentum. Events are further categorised in terms of lepton or jet multiplicity. No significant excess over the expected background is observed. Limits at 95% C.L. are derived in Tchi1n2E simplified models. Next-to-lightest neutralinos and charginos with masses up to 310 GeV for a massless lightest neutralino are excluded. See their Fig. 10.

[32] AAD 14G searched in 20.3 fb^{-1} of pp collisions at $\sqrt{s}$ = 8 TeV for electroweak production of chargino-neutralino pairs, decaying to a final sate with two leptons (e and μ) and missing transverse momentum. No excess beyond the Standard Model expectation is

Downloaded from https://academic.oup.com/ptep/article/2022/8/083C01/6651666 by KIT Library user on 27 September 2022

observed. Exclusion limits are derived in simplified models of chargino and next-to-lightest neutralino production, with decays to the lightest neutralino via gauge bosons, see Fig. 7. An interpretation in the pMSSM is also given, see Fig. 10.

[33] KHACHATRYAN 14I searched in 19.5 fb^{-1} of pp collisions at $\sqrt{s}$ = 8 TeV for electroweak production of charginos and neutralinos decaying to a final state with three leptons (e or μ) and missing transverse momentum, or with a Z-boson, dijets and missing transverse momentum. No excess beyond the Standard Model expectation is observed. Exclusion limits are derived in simplified models, see Figs. 12–16.

[34] AAD 12AS searched in 2.06 fb^{-1} of pp collisions at $\sqrt{s}$ = 7 TeV for charginos and neutralinos decaying to a final state with three leptons (e and μ) and missing transverse energy. No excess beyond the Standard Model expectation is observed. Exclusion limits are derived in the phenomenological MSSM, see Fig. 2 (top), and in simplified models, see Fig. 2 (bottom).

[35] AAD 12T looked in 1 fb^{-1} of pp collisions at $\sqrt{s}$ = 7 TeV for the production of supersymmetric particles decaying into final states with missing transverse momentum and exactly two isolated leptons (e or μ). Same-sign dilepton events were separately studied. Additionally, in opposite-sign events, a search was made for an excess of same-flavor over different-flavor lepton pairs. No excess over the expected background is observed and limits are placed on the effective production cross section of opposite-sign dilepton events with $\not{E}_T$ > 250 GeV and on same-sign dilepton events with $\not{E}_T$ > 100 GeV. The latter limit is interpreted in a simplified electroweak gaugino production model.

$\widetilde{\chi}_1^+$, $\widetilde{\chi}_2^+$ (Charginos) mass limits

Charginos are unknown mixtures of w-inos and charged higgsinos (the supersymmetric partners of W and Higgs bosons). A lower mass limit for the lightest chargino ($\widetilde{\chi}_1^\pm$) of approximately 45 GeV, independent of the field composition and of the decay mode, has been obtained by the LEP experiments from the analysis of the Z width and decays. These results, as well as other now superseded limits from e^+e^- collisions at energies below 136 GeV, and from hadronic collisions, can be found in the 1998 Edition (The European Physical Journal **C3** 1 (1998)) of this Review.

Unless otherwise stated, results in this section assume spectra, production rates, decay modes and branching ratios as evaluated in the MSSM, with gaugino and sfermion mass unification at the GUT scale. These papers generally study production of $\widetilde{\chi}_1^0\widetilde{\chi}_2^0$, $\widetilde{\chi}_1^+\widetilde{\chi}_1^-$ and (in the case of hadronic collisions) $\widetilde{\chi}_1^\pm\widetilde{\chi}_2^0$ pairs, including the effects of cascade decays. The mass limits on $\widetilde{\chi}_1^\pm$ are either direct, or follow indirectly from the constraints set by the non-observation of $\widetilde{\chi}_2^0$ states on the gaugino and higgsino MSSM parameters M_2 and μ. For generic values of the MSSM parameters, limits from high-energy e^+e^- collisions coincide with the highest value of the mass allowed by phase-space, namely $m_{\widetilde{\chi}_1^\pm} \lesssim \sqrt{s}/2$. The still unpublished combination of the results of the four LEP collaborations from the 2000 run of LEP2 at $\sqrt{s}$ up to $\simeq$ 209 GeV yields a lower mass limit of 103.5 GeV valid for general MSSM models. The limits become however weaker in certain regions of the MSSM parameter space where the detection efficiencies or production cross sections are suppressed. For example, this may happen when: (i) the mass differences $\Delta m_+ = m_{\widetilde{\chi}_1^\pm} - m_{\widetilde{\chi}_1^0}$ or $\Delta m_\nu = m_{\widetilde{\chi}_1^\pm} - m_{\widetilde{\nu}}$ are very small, and the detection efficiency is reduced; (ii) the electron sneutrino mass is small, and the $\widetilde{\chi}_1^\pm$ production rate is suppressed due to a destructive interference between s and t channel exchange diagrams. The regions of MSSM parameter space where the following limits are valid are indicated in the comment lines or in the footnotes.

Some earlier papers are now obsolete and have been omitted. They were last listed in our PDG 14 edition: K. Olive, *et al.* (Particle Data Group), Chinese Physics **C38** 070001 (2014) (http://pdg.lbl.gov).

VALUE (GeV)	CL%	DOCUMENT ID		TECN	COMMENT
>1080	95	[1] AAD	21AX	ATLS	jets + large-R jets + $\not{E}_T$, TWinoBinoA, nearly independent of B($\widetilde{\chi}_2^0 \to Z\widetilde{\chi}_1^0$), $m_{\widetilde{\chi}_1^0}$ = 0 GeV
>1060	95	[1] AAD	21AX	ATLS	jets + large-R jets + $\not{E}_T$, TWinoHinoA, tan β = 10, μ > 0, $m_{\widetilde{\chi}_1^0}$ = 0 GeV
> 900	95	[1] AAD	21AX	ATLS	jets + large-R jets + $\not{E}_T$, THinoBinoA, nearly independent of B($\widetilde{\chi}_2^0 \to Z\widetilde{\chi}_1^0$), $m_{\widetilde{\chi}_1^0}$ = 0 GeV
> 900	95	[1] AAD	21AX	ATLS	jets + large-R jets + $\not{E}_T$, THinoWinoA, tan β = 10, μ > 0, $m_{\widetilde{\chi}_1^0}$ = 0 GeV
>1060	95	[1] AAD	21AX	ATLS	jets + large-R jets + $\not{E}_T$, Tchi1n2E, full hadronic final state, $m_{\widetilde{\chi}_1^0}$ = 0 GeV
> 960	95	[1] AAD	21AX	ATLS	jets + large-R jets + $\not{E}_T$, Tchi1n2Fb, $m_{\widetilde{\chi}_1^0}$ = 0 GeV
none 620–740	95	[1] AAD	21AX	ATLS	jets + large-R jets + $\not{E}_T$, Tchi1chi1l, $m_{\widetilde{\chi}_1^0}$ = 0 GeV
> 640	95	[2] AAD	21BG	ATLS	3ℓ+ $\not{E}_T$, Tchi1n2F, wino cross section, $m_{\widetilde{\chi}_1^0}$ = 0 GeV
> 300	95	[2] AAD	21BG	ATLS	3ℓ+ $\not{E}_T$, Tchi1n2F, wino cross section, $m_{\widetilde{\chi}_2^0} - m_{\widetilde{\chi}_1^0} = m_Z$
> 240	95	[2] AAD	21BG	ATLS	3ℓ+ $\not{E}_T$, Tchi1n2F, wino cross section, $m_{\widetilde{\chi}_2^0} - m_{\widetilde{\chi}_1^0}$ = 10 GeV
> 190	95	[2] AAD	21BG	ATLS	3ℓ+ $\not{E}_T$, Tchi1n2E, wino cross section, $m_{\widetilde{\chi}_1^0}$ = 0 GeV
>1100	95	[3] AAD	21E	ATLS	3ℓ, $Z\ell$ resonances, TwinoLSPBL, RPV, B($\widetilde{\chi}_1^\pm \to Ze$) = B($\widetilde{\chi}_1^0 \to Z\nu$) = 1
>1050	95	[3] AAD	21E	ATLS	3ℓ, $Z\ell$ resonances, TwinoLSPBL, RPV, B($\widetilde{\chi}_1^\pm \to Z\mu$) = B($\widetilde{\chi}_1^0 \to Z\nu$) = 1
> 625	95	[3] AAD	21E	ATLS	3ℓ, $Z\ell$ resonances, TwinoLSPBL, RPV, B($\widetilde{\chi}_1^\pm \to Z\tau$) = B($\widetilde{\chi}_1^0 \to Z\nu$) = 1
> 975	95	[3] AAD	21E	ATLS	3ℓ, $Z\ell$ resonances, TwinoLSPBL, RPV, B($\widetilde{\chi}_1^\pm \to Z\ell$) = B($\widetilde{\chi}_1^0 \to Z\nu$) = 1 and ℓ = e,μ,τ
>1600	95	[4] AAD	21Y	ATLS	$\geq$ 4ℓ, RPV Tchi1n2l with $\widetilde{\chi}_1^0 \to \ell^\pm\ell^\mp\nu$, $\lambda_{12k} \neq 0$, $m_{\widetilde{\chi}_1^0}$ = 1200 GeV
>1100	95	[4] AAD	21Y	ATLS	$\geq$ 4ℓ, RPV Tchi1n2l with $\widetilde{\chi}_1^0 \to \ell^\pm\ell^\mp\nu$, $\lambda_{i33} \neq 0$, $m_{\widetilde{\chi}_1^0}$ = 1000 GeV
> 750	95	[5] SIRUNYAN	21M	CMS	$\ell^\pm\ell^\mp$ + $\not{E}_T$, Tchi1n2Fa, $m_{\widetilde{\chi}_1^0}$ < 100 GeV
none 400–820	95	[6] TUMASYAN	21C	CMS	1 $\ell^\pm$ + 2b-jets + $\not{E}_T$, Tchi1n2E, $\widetilde{\chi}_1^0$ = 200 GeV
none 160–820	95	[6] TUMASYAN	21C	CMS	1 $\ell^\pm$ + 2b-jets + $\not{E}_T$, Tchi1n2E, $\widetilde{\chi}_1^0$ = 0 GeV
> 380	95	[7] AAD	20AN	ATLS	2γ + $\not{E}_T$,Tn1n1A, GMSB
> 240	95	[8] AAD	20I	ATLS	2ℓ (soft), jets, $\not{E}_T$; Tchi1n2Fa, wino, $m_{\widetilde{\chi}_1^\pm} - m_{\widetilde{\chi}_1^0}$ = 7 GeV
> 345	95	[9] AAD	20K	ATLS	3ℓ+$\not{E}_T$, Tchi1n2F, $m_{\widetilde{\chi}_1^0}$ = 0 GeV
> 420	95	[10] AAD	20O	ATLS	2ℓ+$\not{E}_T$, Tchi1chi1H, $m_{\widetilde{\chi}_1^0}$=0 GeV
>1000	95	[11] AAD	20O	ATLS	2ℓ+$\not{E}_T$, Tchi1chi1C, $m_{\widetilde{\chi}_1^0}$=0 GeV
> 740	95	[12] AAD	20R	ATLS	1ℓ + 2b-jets + $\not{E}_T$, Tchi1n2E, $m_{\widetilde{\chi}_1^0}$ = 0 GeV
> 290	95	[13] SIRUNYAN	20AU	CMS	soft τ + jet + $\not{E}_T$, Tchi1n2D, wino, $m_{\widetilde{\chi}_1^\pm} - m_{\widetilde{\chi}_1^0}$ = 50 GeV
>1050	95	[14] SIRUNYAN	20B	CMS	$\geq$ 1γ + $\not{E}_T$, Tchi1chi1F, $\widetilde{\chi}_1^0 \to \gamma\widetilde{G}$
> 825	95	[14] SIRUNYAN	20B	CMS	$\geq$ 1γ + $\not{E}_T$, Tchi1chi1G, $\widetilde{\chi}_1^\pm \to \widetilde{\chi}_1^0$ + soft
> 840	95	[14] SIRUNYAN	20B	CMS	$\geq$ 1γ + $\not{E}_T$, Tchi1n12-GGM, 120 GeV < $m_{\widetilde{\chi}_1^0}$ < 720 GeV
> 680	95	[15] AABOUD	19AU	ATL	0, 1, 2 or more ℓ, H ($\to \gamma\gamma$, bb, WW^*, ZZ^*,$\tau\tau$) (various searches), Tchi1n2E, $m_{\widetilde{\chi}_1^0}$=0 GeV
> 112	95	[16] SIRUNYAN	19BU	CMS	$pp \to \widetilde{\chi}_1^+\widetilde{\chi}_2^0$+2 jets, $\widetilde{\chi}_1^+ \to \ell^+\nu\widetilde{\chi}_1^0$, heavy sleptons, $m_{\widetilde{\chi}_1^+} - m_{\widetilde{\chi}_1^0}$ = 1 GeV, $m_{\widetilde{\chi}_1^+} = m_{\widetilde{\chi}_2^0}$
> 215	95	[16] SIRUNYAN	19BU	CMS	$pp \to \widetilde{\chi}_1^+\widetilde{\chi}_2^0$ + 2 jets, $\widetilde{\chi}_1^+ \to \ell^+\nu\widetilde{\chi}_1^0$, heavy sleptons, $m_{\widetilde{\chi}_1^+} - m_{\widetilde{\chi}_1^0}$ = 30 GeV, $m_{\widetilde{\chi}_1^+} = m_{\widetilde{\chi}_2^0}$
> 235	95	[17] SIRUNYAN	19CI	CMS	$\geq$ 1 H ($\to \gamma\gamma$) + jets + $\not{E}_T$, Tchi1n2E, $m_{\widetilde{\chi}_1^0}$ = 1 GeV
> 930	95	[18] SIRUNYAN	19K	CMS	γ + lepton + $\not{E}_T$, Tchi1n1A
> 630	95	[19] AABOUD	18AY	ATLS	2τ+$\not{E}_T$, Tchi1chi1D and $\widetilde{\tau}_L$-only, $m_{\widetilde{\chi}_1^0}$ = 0 GeV
> 760	95	[20] AABOUD	18AY	ATLS	2τ+$\not{E}_T$, Tchi1n2D and $\widetilde{\tau}_L$-only, $m_{\widetilde{\chi}_1^0}$ = 0 GeV
> 740	95	[21] AABOUD	18BT	ATLS	2ℓ+$\not{E}_T$, Tchi1chi1C, $m_{\widetilde{\chi}_1^0}$=0 GeV
>1125	95	[22] AABOUD	18BT	ATLS	2,3ℓ+$\not{E}_T$, Tchi1n2C, $m_{\widetilde{\chi}_1^0}$=0 GeV
> 580	95	[23] AABOUD	18BT	ATLS	2,3ℓ+$\not{E}_T$, Tchi1n2F, $m_{\widetilde{\chi}_1^0}$=0 GeV
none 130–230, 290–880	95	[24] AABOUD	18CK	ATLS	2H ($\to bb$)+$\not{E}_T$,Tn1n1A, GMSB
none 220–600	95	[25] AABOUD	18CO	ATLS	2,3ℓ + $\not{E}_T$, recursive jigsaw, Tchi1n2F, $m_{\widetilde{\chi}_1^0}$ = 0 GeV
> 175	95	[26] AABOUD	18R	ATLS	2ℓ (soft) + $\not{E}_T$, Tchi1n2F, wino, $m_{\widetilde{\chi}_1^\pm} - m_{\widetilde{\chi}_1^0}$ = 10 GeV
> 145	95	[27] AABOUD	18R	ATLS	2ℓ (soft) + $\not{E}_T$, Tchi1n2G, higgsino, $m_{\widetilde{\chi}_1^\pm} - m_{\widetilde{\chi}_1^0}$ = 5 GeV
>1060	95	[28] AABOUD	18U	ATLS	2γ + $\not{E}_T$, GGM, Tchi1chi1A, any NLSP mass

Downloaded from https://academic.oup.com/ptep/article/2022/8/083C01/6651666 by KIT Library user on 27 September 2022

>1400	95	[29] AABOUD	18Z	ATLS	$\geq 4\ell$, RPV, $\lambda_{12k} \neq 0$, $m_{\widetilde{\chi}^0_1} >$ 500 GeV
>1320	95	[29] AABOUD	18Z	ATLS	$\geq 4\ell$, RPV, $\lambda_{12k} \neq 0$, $m_{\widetilde{\chi}^0_1} > 50$ GeV
> 980	95	[29] AABOUD	18Z	ATLS	$\geq 4\ell$, RPV, $\lambda_{j33} \neq 0$, 400 GeV $<$ $m_{\widetilde{\chi}^0_1} <$ 700 GeV
> 980	95	[30] SIRUNYAN	18AA	CMS	$\geq 1\gamma + \not{E}_T$, GGM, wino-like $\widetilde{\chi}^0_2\widetilde{\chi}^\pm_1$ pair production, nearly degenerate wino and bino masses
> 780	95	[30] SIRUNYAN	18AA	CMS	$\geq 1\gamma + \not{E}_T$, Tchi1n1A
> 950	95	[30] SIRUNYAN	18AA	CMS	$\geq 1\gamma + \not{E}_T$, Tchi1chi1A
> 230	95	[31] SIRUNYAN	18AJ	CMS	2ℓ (soft) $+ \not{E}_T$, Tchi1n2F, wino, $m_{\widetilde{\chi}^0_2} - m_{\widetilde{\chi}^0_1} = 20$ GeV
>1150	95	[32] SIRUNYAN	18AO	CMS	$\ell^\pm\ell^\pm$ or $\geq 3\ell$, Tchi1n2A, $m_{\widetilde{\ell}} = m_{\widetilde{\nu}} = m_{\widetilde{\chi}^0_1} + 0.5\ (m_{\widetilde{\chi}^\pm_1} - m_{\widetilde{\chi}^0_1})$, $m_{\widetilde{\chi}^0_1} = 0$ GeV
>1120	95	[32] SIRUNYAN	18AO	CMS	$\ell^\pm\ell^\pm$ or $\geq 3\ell$, Tchi1n2A, $m_{\widetilde{\ell}} = m_{\widetilde{\nu}} = m_{\widetilde{\chi}^0_1} + 0.05\ (m_{\widetilde{\chi}^\pm_1} - m_{\widetilde{\chi}^0_1})$, $m_{\widetilde{\chi}^0_1} = 0$ GeV
>1050	95	[32] SIRUNYAN	18AO	CMS	$\ell^\pm\ell^\pm$ or $\geq 3\ell$, Tchi1n2A, $m_{\widetilde{\ell}} = m_{\widetilde{\nu}} = m_{\widetilde{\chi}^0_1} + 0.95\ (m_{\widetilde{\chi}^\pm_1} - m_{\widetilde{\chi}^0_1})$, $m_{\widetilde{\chi}^0_1} = 0$ GeV
>1080	95	[32] SIRUNYAN	18AO	CMS	$\ell^\pm\ell^\pm$ or $\geq 3\ell$, Tchi1n2H, $m_{\widetilde{\ell}} = m_{\widetilde{\chi}^0_1} + 0.5\ (m_{\widetilde{\chi}^\pm_1} - m_{\widetilde{\chi}^0_1})$, $m_{\widetilde{\chi}^0_1} = 0$ GeV
>1030	95	[32] SIRUNYAN	18AO	CMS	$\ell^\pm\ell^\pm$ or $\geq 3\ell$, Tchi1n2H, $m_{\widetilde{\ell}} = m_{\widetilde{\chi}^0_1} + 0.05\ (m_{\widetilde{\chi}^\pm_1} - m_{\widetilde{\chi}^0_1})$, $m_{\widetilde{\chi}^0_1} = 0$ GeV
>1050	95	[32] SIRUNYAN	18AO	CMS	$\ell^\pm\ell^\pm$ or $\geq 3\ell$, Tchi1n2H, $m_{\widetilde{\ell}} = m_{\widetilde{\chi}^0_1} + 0.95\ (m_{\widetilde{\chi}^\pm_1} - m_{\widetilde{\chi}^0_1})$, $m_{\widetilde{\chi}^0_1} = 0$ GeV
> 625	95	[32] SIRUNYAN	18AO	CMS	$\ell^\pm\ell^\pm$ or $\geq 3\ell$, Tchi1n2D, $m_{\widetilde{\tau}} = m_{\widetilde{\chi}^0_1} + 0.5\ (m_{\widetilde{\chi}^\pm_1} - m_{\widetilde{\chi}^0_1})$, $m_{\widetilde{\chi}^0_1} = 0$ GeV
> 180	95	[32] SIRUNYAN	18AO	CMS	$\ell^\pm\ell^\pm$ or $\geq 3\ell$, Tchi1n2E, $m_{\widetilde{\chi}^0_1} =$ 0 GeV
> 450	95	[32] SIRUNYAN	18AO	CMS	$\ell^\pm\ell^\pm$ or $\geq 3\ell$, Tchi1n2F, $m_{\widetilde{\chi}^0_1} =$ 0 GeV
> 480	95	[33] SIRUNYAN	18AP	CMS	Combination of searches, Tchi1n2E, $m_{\widetilde{\chi}^0_1} = 0$ GeV
> 650	95	[33] SIRUNYAN	18AP	CMS	Combination of searches, Tchi1n2F, $m_{\widetilde{\chi}^0_1} = 0$ GeV
> 535	95	[33] SIRUNYAN	18AP	CMS	Combination of searches, Tchi1n2l, $m_{\widetilde{\chi}^0_1} = 0$ GeV
none 160–610	95	[34] SIRUNYAN	18AR	CMS	$\ell^\pm\ell^\mp$ + jets $+ \not{E}_T$, Tchi1n2F, $m_{\widetilde{\chi}^0_1} = 0$ GeV
none 170–200	95	[35] SIRUNYAN	18DN	CMS	$\ell^\pm\ell^\mp$, Tchi1chi1E, $m_{\widetilde{\chi}^0_1} = 1$ GeV
> 810	95	[35] SIRUNYAN	18DN	CMS	$\ell^\pm\ell^\mp$, Tchi1chi1C, $m_{\widetilde{\chi}^0_1} = 0$ GeV
> 630	95	[36] SIRUNYAN	18DP	CMS	$2\tau + \not{E}_T$, Tchi1chi1D, $m_{\widetilde{\chi}^0_1} = 0$ GeV
> 710	95	[36] SIRUNYAN	18DP	CMS	$2\tau + \not{E}_T$, Tchi1n2D, $m_{\widetilde{\chi}^0_1} = 0$ GeV
> 170	95	[37] SIRUNYAN	18X	CMS	$\geq 1\ H\ (\rightarrow\ \gamma\gamma)$ + jets $+ \not{E}_T$, Tchi1n2E, $m_{\widetilde{\chi}^0_1} <$ 25 GeV
> 420	95	[38] KHACHATRY...	17L	CMS	$2\tau + \not{E}_T$, Tchi1chi1C and $\widetilde{\tau}$-only, $m_{\widetilde{\chi}^0_1} = 0$ GeV
none 220–490	95	[39] SIRUNYAN	17AW	CMS	1ℓ + 2b-jets $+ \not{E}_T$, Tchi1n2E, $m_{\widetilde{\chi}^0_1} = 0$ GeV
> 500	95	[40] AAD	16AA	ATLS	$2\ell^\pm + \not{E}_T$, Tchi1chi1B, $m_{\widetilde{\chi}^0_1} = 0$ GeV
> 220	95	[40] AAD	16AA	ATLS	$2\ell^\pm + \not{E}_T$, Tchi1chi1C, low Δm for $\widetilde{\chi}^\pm_1$, $\widetilde{\chi}^0_1$
> 700	95	[41] AAD	16AA	ATLS	$3,4\ell + \not{E}_T$, Tchi1n2B, $m_{\widetilde{\chi}^0_1} = 0$ GeV
> 700	95	[41] AAD	16AA	ATLS	$3,4\ell + \not{E}_T$, Tchi1n2C, $m_{\widetilde{\ell}} = m_{\widetilde{\chi}^0_1} +$ 0.5 (or 0.95) $(m_{\widetilde{\chi}^\pm_1} - m_{\widetilde{\chi}^0_1})$
> 400	95	[41] AAD	16AA	ATLS	2 hadronic $\tau + \not{E}_T$ & $3\ell + \not{E}_T$ combination, Tchi1n2D, $m_{\widetilde{\chi}^0_1} = 0$ GeV
> 540	95	[42] KHACHATRY...	16R	CMS	$\geq 1\gamma + 1\ e$ or $\mu + \not{E}_T$, Tchi1n1A
> 250	95	[43] AAD	15BA	ATLS	$m_{\widetilde{\chi}^\pm_1} = m_{\widetilde{\chi}^0_2}$, $m_{\widetilde{\chi}^0_1} = 0$ GeV
> 590	95	[44] AAD	15CA	ATLS	$\geq 2\ \gamma + \not{E}_T$, GGM, bino-like NLSP, any NLSP mass
none 124–361	95	[44] AAD	15CA	ATLS	$\geq 1\ \gamma + e,\mu + \not{E}_T$, GGM, wino-like NLSP
> 700	95	[45] AAD	14H	ATLS	$\widetilde{\chi}^\pm_1\widetilde{\chi}^0_2 \rightarrow \ell^\pm\nu\widetilde{\chi}^0_1\ell^\pm\ell^\mp\widetilde{\chi}^0_1$, simplified model, $m_{\widetilde{\chi}^\pm_1} = m_{\widetilde{\chi}^0_2}$, $m_{\widetilde{\chi}^0_1} = 0$ GeV
> 345	95	[45] AAD	14H	ATLS	$\widetilde{\chi}^\pm_1\widetilde{\chi}^0_2 \rightarrow W\widetilde{\chi}^0_1 Z\widetilde{\chi}^0_1$, simplified model, $m_{\widetilde{\chi}^\pm_1} = m_{\widetilde{\chi}^0_2}$, $m_{\widetilde{\chi}^0_1} = 0$ GeV
> 148	95	[45] AAD	14H	ATLS	$\widetilde{\chi}^\pm_1\widetilde{\chi}^0_2 \rightarrow W\widetilde{\chi}^0_1 H\widetilde{\chi}^0_1$, simplified model, $m_{\widetilde{\chi}^\pm_1} = m_{\widetilde{\chi}^0_2}$, $m_{\widetilde{\chi}^0_1} = 0$ GeV
> 380	95	[45] AAD	14H	ATLS	$\widetilde{\chi}^\pm_1\widetilde{\chi}^0_2 \rightarrow \tau^\pm\nu\widetilde{\chi}^0_1\tau^\pm\tau^\mp\widetilde{\chi}^0_1$, simplified model, $m_{\widetilde{\chi}^\pm_1} = m_{\widetilde{\chi}^0_2}$, $m_{\widetilde{\chi}^0_1} = 0$ GeV
> 750	95	[46] AAD	14X	ATLS	RPV, $\geq 4\ell^\pm$, $\widetilde{\chi}^\pm_1 \rightarrow W^{(*)\pm}\widetilde{\chi}^0_1$, $\widetilde{\chi}^0_1 \rightarrow \ell^\pm\ell^\mp\nu$
> 210	95	[47] KHACHATRY...	14L	CMS	$\widetilde{\chi}^0_2 \rightarrow H\widetilde{\chi}^0_1$ and $\widetilde{\chi}^\pm_1 \rightarrow W^\pm\widetilde{\chi}^0_1$ simplified models, $m_{\widetilde{\chi}^0_2} = m_{\widetilde{\chi}^\pm_1}$, $m_{\widetilde{\chi}^0_1} = 0$ GeV
		[48] AAD	13	ATLS	$3\ell^\pm + \not{E}_T$, pMSSM, SMS
		[49] AAD	13B	ATLS	$2\ell^\pm + \not{E}_T$, pMSSM, SMS
> 540	95	[50] AAD	12CT	ATLS	$\geq 4\ell^\pm$, RPV, $m_{\widetilde{\chi}^0_1} >$ 300 GeV
		[51] CHATRCHYAN	12BJ	CMS	$\geq 2\ \ell$, jets $+ \not{E}_T$, $pp \rightarrow \widetilde{\chi}^\pm_1\widetilde{\chi}^0_2$
> 94	95	[52] ABDALLAH	03M	DLPH	$\widetilde{\chi}^\pm_1$, $\tan\beta \leq 40$, $\Delta m_+ >$3 GeV,all m_0
• • • We do not use the following data for averages, fits, limits, etc. • • •					
> 310	95	[53] AAD	20AN	ATLS	$2\gamma + \not{E}_T$, Tchi1n2E, $m_{\widetilde{\chi}^0_1}$=0 GeV
> 570	95	[54] KHACHATRY...	16AA	CMS	$\geq 1\gamma$ + jets $+ \not{E}_T$, Tchi1chi1A
> 680	95	[54] KHACHATRY...	16AA	CMS	$\geq 1\gamma$ + jets $+ \not{E}_T$, Tchi1n1A
> 710	95	[54] KHACHATRY...	16AA	CMS	$\geq 1\gamma$ + jets $+ \not{E}_T$, GGM, $\widetilde{\chi}^0_2\widetilde{\chi}^\pm_1$ pair production, wino-like NLSP
>1000	95	[55] KHACHATRY...	16R	CMS	$\geq 1\gamma + 1\ e$ or $\mu + \not{E}_T$, Tglu1F, $m_{\widetilde{\chi}^\pm_1} = m_{\widetilde{\chi}^0_2} >$ 200 GeV
> 307	95	[56] KHACHATRY...	16Y	CMS	1,2 soft $\ell^\pm$+jets$+\not{E}_T$, Tchi1n2A, $m_{\widetilde{\chi}^\pm_1} - m_{\widetilde{\chi}^0_1}$=20 GeV
> 410	95	[57] AAD	14AV	ATLS	$\geq\ 2\ \tau + \not{E}_T$, direct $\widetilde{\chi}^\pm_1\widetilde{\chi}^0_2$, $\widetilde{\chi}^\pm_1\widetilde{\chi}^\mp_1$ production, $m_{\widetilde{\chi}^0_2} = m_{\widetilde{\chi}^\pm_1}$, $m_{\widetilde{\chi}^0_1} = 0$ GeV
> 345	95	[58] AAD	14AV	ATLS	$\geq 2\ \tau + \not{E}_T$, direct $\widetilde{\chi}^\pm_1\widetilde{\chi}^\mp_1$ production, $m_{\widetilde{\chi}^0_1} = 0$ GeV
none 100–105, 120–135, 145–160	95	[59] AAD	14G	ATLS	$\widetilde{\chi}^\pm_1\widetilde{\chi}^\mp_1 \rightarrow \ell^+\nu\widetilde{\chi}^0_1\ell^-\overline{\nu}\widetilde{\chi}^0_1$, simplified model, $m_{\widetilde{\chi}^0_1} = 0$ GeV
none 140–465	95	[59] AAD	14G	ATLS	$\widetilde{\chi}^\pm_1\widetilde{\chi}^\mp_1 \rightarrow \ell^+\nu\widetilde{\chi}^0_1\ell^-\overline{\nu}\widetilde{\chi}^0_1$, simplified model, $m_{\widetilde{\chi}^0_1} = 0$ GeV
none 180–355	95	[59] AAD	14G	ATLS	$\widetilde{\chi}^\pm_1\widetilde{\chi}^0_2 \rightarrow W\widetilde{\chi}^0_1 Z\widetilde{\chi}^0_1$, simplified model, $m_{\widetilde{\chi}^\pm_1} = m_{\widetilde{\chi}^0_2}$, $m_{\widetilde{\chi}^0_1} = 0$ GeV
> 168	95	[60] AALTONEN	14	CDF	$3\ell^\pm + \not{E}_T$, $\widetilde{\chi}^\pm_1 \rightarrow \ell\nu\widetilde{\chi}^0_1$, mSUGRA with m_0=60 GeV
		[61] KHACHATRY...	14I	CMS	$\widetilde{\chi}^\pm_1 \rightarrow W\widetilde{\chi}^0_1$, $\ell\widetilde{\nu}$, $\widetilde{\ell}\nu$, simplified model
		[62] AALTONEN	13Q	CDF	$\widetilde{\chi}^\pm_1 \rightarrow \tau X$, simplified gravity- and gauge-mediated models
		[63] AAD	12AS	ATLS	$3\ell^\pm + \not{E}_T$, pMSSM
		[64] AAD	12T	ATLS	$\ell^\pm\ell^\mp + \not{E}_T$, $\ell^\pm\ell^\pm + \not{E}_T$, $pp \rightarrow \widetilde{\chi}^\pm_1\widetilde{\chi}^0_2$
		[65] CHATRCHYAN	11B	CMS	$\widetilde{W}^0 \rightarrow \gamma\widetilde{G}$, $\widetilde{W}^\pm \rightarrow \ell^\pm\widetilde{G}$,GMSB
> 163	95	[66] CHATRCHYAN	11V	CMS	$\tan\beta$=3, m_0=60 GeV, A_0=0, μ >0

[1] AAD 21AX searched in 139 fb^{-1} of pp collisions at $\sqrt{s}$ = 13 TeV for pair production of electroweakinos decaying to the LSP via the emission of Standard Model bosons (Higgs, W, Z) decaying into hadrons. The final state in all cases characterised by the presence of $\not{E}_T$, jets, and large-R jets tagged according to the boson of interest. Different assumptions (Higgsino, Wino, Bino) are made for the pair produced electroweakinos and for the LSP multiplet. No significant excess above the Standard Model predictions is observed. Limits are set on the electroweakino masses as a function of the model parameters (in particular $m_{\widetilde{\chi}^0_1}$). See Figs. 12, 14, 15.

[2] AAD 21BG searched in 139 fb^{-1} of pp collisions at $\sqrt{s}$ = 13 TeV for pair production $\widetilde{\chi}^0_2\widetilde{\chi}^\pm_1$ in final states with three leptons, with and without assuming the presence of a $Z \rightarrow \ell\ell$ decay. No significant excess above the Standard Model predictions is observed. Limits are set on the $\widetilde{\chi}^0_2$ and $\widetilde{\chi}^\pm_1$ mass in Tchi1n2E, Tchi1n2F and Tchi1n2Ga. See their Fig. 16.

Downloaded from https://academic.oup.com/ptep/article/2022/8/083C01/6651666 by KIT Library user on 27 September 2022

[3] AAD 21E searched in 139 fb^{-1} of pp collisions at $\sqrt{s}$ = 13 TeV for production of wino-like $\widetilde{\chi}^{\pm}_1\widetilde{\chi}^{\pm}_1$ and $\widetilde{\chi}^{\pm}_1\widetilde{\chi}^{0}_1$, followed by the RPV decay of $\widetilde{\chi}^{\pm}_1$ into $Z\ell$, $H\ell$ or $W\nu$ and of $\widetilde{\chi}^{0}_1$ into $Z\nu$, $H\nu$ or $W\ell$, in events with three leptons, looking for $Z\ell$ resonances. No significant excess above the Standard Model predictions is observed. Limits are set on the common $m_{\widetilde{\chi}^{\pm}_1}/m_{\widetilde{\chi}^{0}_1}$ mass in the TwinoLSPRPV simplified model, as a function of the common $\widetilde{\chi}^{\pm}_1/\widetilde{\chi}^{0}_1$ branching fraction to a Z boson. See Figure 9.

[4] AAD 21Y searched in 139 fb^{-1} of pp collisions at $\sqrt{s}$ = 13 TeV for supersymmetry in events with four or more leptons (electrons, muons and tau-leptons). No significant excess above the Standard Model expectations is observed. Limits are set on Tchi1n12-GGM, and RPV models similar to Tchi1n2l, Tglu1A (with q = u, d, s, c, b, with equal branching fractions), and $\widetilde{\ell}_L/\widetilde{\nu} \rightarrow \ell/\nu\widetilde{\chi}^{0}_1$ (mass-degenerate $\widetilde{\ell}_L$ and $\widetilde{\nu}$ of all 3 generations), all with $\widetilde{\chi}^{0}_1 \rightarrow \ell^{\pm}\ell^{\mp}\nu$ via λ_{12k} or λ_{i33} (where $i,k \in 1,2$), see their Figure 11.

[5] SIRUNYAN 21M searched in 137 fb^{-1} of pp collisions at $\sqrt{s}$ = 13 TeV for supersymmetry in events with two opposite-sign same-flavor leptons (electrons, muons) and $\not{E}_T$. No significant excess above the Standard Model expectations is observed. Limits are set on the gluino mass in the simplified model Tglu4C, see their Figure 10, on the $\widetilde{\chi}^{0}_2$ and $\widetilde{\chi}^{\pm}_1$ mass in Tchi1n2Fa, see their Figure 11, on the $\widetilde{\chi}^{0}_1$ mass in Tn1n1C and Tn1n1B for $m_{\widetilde{\chi}^{0}_2}=m_{\widetilde{\chi}^{\pm}_1}=m_{\widetilde{\chi}^{0}_1}$, see their Figure 12. Limits are also set on the light squark mass for the simplified model Tsqk2A, on the sbottom mass in Tsbot3, see their Figure 13, and on the slepton mass in direct electroweak pair production of mass-degenerate left- and right-handed sleptons (selectrons and smuons), see their Figure 14.

[6] TUMASYAN 21C searched in 137 fb^{-1} of pp collisions at $\sqrt{s}$ = 13 TeV for supersymmetry in events with with one lepton, a Higgs boson decaying to a pair of bottom quarks, and large $\not{E}_T$. No significant excess above the Standard Model expectations is observed. Lower limits are set on the masses of $\widetilde{\chi}^{0}_2$ and $\widetilde{\chi}^{\pm}_1$ in the simplified model Tchi1n2E, see their Figure 6.

[7] AAD 20AN searched in 139 fb^{-1} of pp collisions at $\sqrt{s}$ = 13 TeV for events with two photons and missing transverse momentum. Events are further categorised in terms of lepton or jet multiplicity. No significant excess over the expected background is observed. Limits at 95% C.L. are set on the Higgsino mass in the T1n1n1A simplified model, see their Figure 11.

[8] AAD 20I reported on ATLAS searches for electroweak production in models with compressed mass spectra as Tchi1n2Fa. A dataset of pp collisions at $\sqrt{s}$ = 13 TeV corresponding to an integrated luminosity of 139 fb^{-1} was used. Events with $\not{E}_T$, two same-flavour, opposite-charge, low-transverse-momentum leptons, and jets from initial-state radiation or characteristic of vector-boson fusion production are selected. Constraints at 95% C.L. are placed on the mass of the $\widetilde{\chi}^{\pm}_1$ (degenerate with $\widetilde{\chi}^{0}_2$) at 240 GeV for a mass splitting between $\widetilde{\chi}^{\pm}_1$ and $\widetilde{\chi}^{0}_1$ of 7 GeV and extend down to a mass splitting of 1.5 GeV at the LEP chargino mass limit of 92.4 GeV. See their Fig. 14(b,c).

[9] AAD 20K reported on a search for electroweak production in models with mass splittings near the electroweak scale as Tchi1n2F and exploiting three-lepton final state events with an emulated recursive jigsaw reconstruction method. The analysis uses a dataset of pp collisions at $\sqrt{s}$ = 13 TeV corresponding to an integrated luminosity of 139 fb^{-1}. Exclusion limits at 95% C.L. are derived on next-to-lightest neutralinos and charginos with masses up to 345 GeV for a massless lightest neutralino, see their Fig. 7.

[10] AAD 20O reported on a search for electroweak production in models with charginos and sleptons decaying into final states with exactly two oppositely charged leptons and missing transverse momentum. A dataset of pp collisions at $\sqrt{s}$ = 13 TeV corresponding to an integrated luminosity of 139 fb^{-1} was used. Exclusion limits at 95% C.L. are derived on $m_{\widetilde{\chi}^{\pm}_1}$ decaying according to the Tchi1chi1H simplified model. Chargino masses up to 420 GeV are excluded for a massless lightest neutralino, see their Fig. 7(a).

[11] AAD 20O reported on a search for electroweak production in models with charginos and sleptons decaying into final states with exactly two oppositely charged leptons and missing transverse momentum. A dataset of pp collisions at $\sqrt{s}$ = 13 TeV corresponding to an integrated luminosity of 139 fb^{-1} was used. Exclusion limits at 95% C.L. are derived on $m_{\widetilde{\chi}^{\pm}_1}$ decaying according to the Tchi1chi1C simplified model. Chargino masses up to 1000 GeV are excluded for a massless lightest neutralino, see their Fig. 7(b).

[12] AAD 20R searched for electroweak production in the model Tchi1n2E, selecting events with a pair of b-tagged jets consistent with those from a Higgs boson decay, either an electron or a muon from the W boson decay and $\not{E}_T$. The analysis uses a dataset of pp collisions at $\sqrt{s}$ = 13 TeV corresponding to an integrated luminosity of 139 fb^{-1}. Exclusion limits at 95% C.L. are derived on next-to-lightest neutralinos and charginos with masses up to 740 GeV for a massless lightest neutralino, assuming pure wino cross-sections. See their Fig. 6.

[13] SIRUNYAN 20AU searched in 77.2 fb^{-1} of pp collisions at $\sqrt{s}$ = 13 TeV for events containing one soft, hadronically decaying tau lepton, one energetic jet from initial-state radiation, and large $\not{E}_T$. No excess over the expected background is observed. Limits are derived on the wino mass in the Tchi1n2D simplified model, see their Figure 2.

[14] SIRUNYAN 20B searched in 35.9 fb^{-1} of pp collisions at $\sqrt{s}$ = 13 TeV for events with at least one photon and large $\not{E}_T$. No significant excess above the Standard Model expectations is observed. Limits are set on chargino masses in a general gauge-mediated SUSY breaking (GGM) scenario Tchi1n12-GGM, see Figure 4. Limits are also set on the NLSP mass in the Tchi1chi1F and Tchi1chi1G simplified models, see their Figure 5. Finally, limits are set on the gluino mass in the Tglu4A simplified model, see Figure 6.

[15] AABOUD 19AU searched in 36.1 fb^{-1} of pp collisions at $\sqrt{s}$ = 13 TeV for direct electroweak production of charginos and next-to-lightest neutralinos decaying into lightest neutralinos and a W, and a Higgs boson, respectively. Fully hadronic, semileptonic, diphoton, and multilepton (electrons, muons) final states with missing transverse momentum are considered in this search. Observations are consistent with the Standard Model expectations, and 95% confidence-level limits of up to 680 GeV on the chargino/next-to-lightest neutralino masses are set (Tchi1n2E model). See their Figure 14 for an overlay of exclusion contours from all searches.

[16] SIRUNYAN 19BU searched for pair production of gauginos via vector boson fusion assuming the gaugino spectrum is compressed, in 35.9 fb^{-1} of pp collisions at $\sqrt{s}$ = 13 TeV. The final states explored included zero leptons plus two jets, one lepton plus two jets, and one hadronic tau plus two jets. A similar bound is obtained in the light slepton limit.

[17] SIRUNYAN 19CI searched in 77.5 fb^{-1} of pp collisions at $\sqrt{s}$ = 13 TeV for events with one or more high-momentum Higgs bosons, decaying to pairs of photons, jets and $\not{E}_T$. No significant excess above the Standard Model expectations is observed. Limits are set on the sbottom mass in the Tsbot4 simplified model, see Figure 3, and on the wino mass in the Tchi1n2E simplified model, see their Figure 4. Limits are also set on the higgsino mass in the Tn1n1A and Tn1n1B simplified models, see their Figure 5.

[18] SIRUNYAN 19K searched in 35.9 fb^{-1} of pp collisions at $\sqrt{s}$ = 13 TeV for events with a photon, an electron or muon, and large $\not{E}_T$. No significant excess above the Standard Model expectations is observed. In the framework of GMSB, limits are set on the chargino and neutralino mass in the Tchi1n1A simplified model, see their Figure 6. Limits are also set on the gluino mass in the Tglu4A simplified model, and on the squark mass in the Tsqk4A simplified model, see their Figure 7.

[19] AABOUD 18AY searched in 36.1 fb^{-1} of pp collisions at $\sqrt{s}$ = 13 TeV for direct electroweak production of charginos as in Tchi1chi1D models in events characterised by the presence of at least two hadronically decaying tau leptons and large missing transverse energy. No significant deviation from the expected SM background is observed. In the Tchi1chi1D model, assuming decays via intermediate $\widetilde{\tau}_L$, the observed limits rule out $\widetilde{\chi}^{\pm}_1$ masses up to 630 GeV for a massless $\widetilde{\chi}^{0}_1$. See their Fig.7 (left). Interpretations are also provided in Fig 8 (top) for different assumptions on the ratio between $m_{\widetilde{\tau}}$ and $m_{\widetilde{\chi}^{\pm}_1}$ + $m_{\widetilde{\chi}^{0}_1}$.

[20] AABOUD 18AY searched in 36.1 fb^{-1} of pp collisions at $\sqrt{s}$ = 13 TeV for direct electroweak production of charginos and neutralinos as in Tchi1n2D models, in events characterised by the presence of at least two hadronically decaying tau leptons and large missing transverse energy. No significant deviation from the expected SM background is observed. Assuming decays via intermediate $\widetilde{\tau}_L$ and $m_{\widetilde{\chi}^{\pm}_1} = m_{\widetilde{\chi}^{0}_2}$, the observed limits rule out $\widetilde{\chi}^{\pm}_1$ masses up to 760 GeV for a massless $\widetilde{\chi}^{0}_1$. See their Fig.7 (right). Interpretations are also provided in Fig 8 (bottom) for different assumptions on the ratio between $m_{\widetilde{\tau}}$ and $m_{\widetilde{\chi}^{\pm}_1} + m_{\widetilde{\chi}^{0}_1}$.

[21] AABOUD 18BT searched in 36.1 fb^{-1} of pp collisions at $\sqrt{s}$ = 13 TeV for direct electroweak production of charginos, chargino and next-to-lightest neutralinos and sleptons in events with two or three leptons (electrons or muons), with or without jets and large missing transverse energy. No significant excess above the Standard Model expectations is observed. Limits are set on the chargino mass up to 750 GeV for massless neutralinos in the Tchi1chi1C simplified model exploiting 2ℓ + 0 jets signatures, see their Figure 8(a).

[22] AABOUD 18BT searched in 36.1 fb^{-1} of pp collisions at $\sqrt{s}$ = 13 TeV for direct electroweak production of charginos, chargino and next-to-lightest neutralinos and sleptons in events with two or three leptons (electrons or muons), with or without jets, and large missing transverse energy. No significant excess above the Standard Model expectations is observed. Limits are set on the chargino mass up to 1100 GeV for massless neutralinos in the Tchi1n2C simplified model exploiting 3ℓ signature, see their Figure 8(c).

[23] AABOUD 18BT searched in 36.1 fb^{-1} of pp collisions at $\sqrt{s}$ = 13 TeV for direct electroweak production of charginos, chargino and next-to-lightest neutralinos and sleptons in events with two or three leptons (electrons or muons), with or without jets, and large missing transverse energy. No significant excess above the Standard Model expectations is observed. Limits are set on the chargino mass up to 580 GeV for massless neutralinos in the Tchi1n2F simplified model exploiting 2ℓ+2 jets and 3ℓ signatures, see their Figure 8(d).

[24] AABOUD 18CK searched for events with at least 3 b-jets and large missing transverse energy in two datasets of pp collisions at $\sqrt{s}$ = 13 TeV of 36.1 fb^{-1} and 24.3 fb^{-1} depending on the trigger requirements. The analyses aimed to reconstruct two Higgs bosons decaying to pairs of b-quarks. No significant excess above the Standard Model expectations is observed. Limits are set on the Higgsino mass in the T1n1n1A simplified model, see their Figure 15(a). Constraints are also presented as a function of the BR of Higgsino decaying into an higgs boson and a gravitino, see their Figure 15(b).

[25] AABOUD 18CO searched in 36.1 fb^{-1} of pp collisions at $\sqrt{s}$ = 13 TeV for direct electroweak production of mass-degenerate charginos and next-to-lightest neutralinos in events with two or three leptons (electrons or muons), with or without jets, and large missing transverse energy. The search channels are based on recursive jigsaw reconstruction. Limits are set on the chargino mass up to 600 GeV for massless neutralinos in the Tchi1n2F simplified model exploiting the statistical combination of 2ℓ+2 jets and 3ℓ channels. Chargino masses below 220 GeV are not excluded due to an excess of events above the SM prediction in the dedicated regions. See their Figure 13(d).

[26] AABOUD 18R searched in 36.1 fb^{-1} of pp collisions at $\sqrt{s}$ = 13 TeV for electroweak production in scenarios with compressed mass spectra in final states with two low-momentum leptons and missing transverse momentum. The data are found to be consistent with the SM prediction. Results are interpreted in Tchi1n2G wino models and $\widetilde{\chi}^{\pm}_1$ masses are excluded up to 175 GeV for $m_{\widetilde{\chi}^{\pm}_1} - m_{\widetilde{\chi}^{0}_1}$ = 10 GeV. The exclusion limits extend down to mass splittings of 2 GeV, see their Fig. 10 (bottom).

[27] AABOUD 18R searched in 36.1 fb^{-1} of pp collisions at $\sqrt{s}$ = 13 TeV for electroweak production in scenarios with compressed mass spectra in final states with two low-momentum leptons and missing transverse momentum. The data are found to be consistent with the SM prediction. Results are interpreted in Tchi1n2G higgsino models and $\widetilde{\chi}^{\pm}_1$ masses are excluded up to 145 GeV for $m_{\widetilde{\chi}^{\pm}_1}$ - $m_{\widetilde{\chi}^{0}_1}$ = 5 GeV. The exclusion limits extend down to mass splittings of 2.5 GeV, see their Fig. 10 (top).

[28] AABOUD 18U searched in 36.1 fb^{-1} of pp collisions at $\sqrt{s}$ = 13 TeV in events with at least one isolated photon, possibly jets and significant transverse momentum targeting generalised models of gauge-mediated SUSY breaking. No significant excess of events is observed above the SM prediction. Results of the diphoton channel are interpreted in terms of lower limits on the masses of gauginos Tchi1chi1A models, which reach as high as 1.3 TeV. Gaugino masses below 1060 GeV are excluded for any NLSP mass, see their Fig. 10.

[29] AABOUD 18Z searched in 36.1 fb^{-1} of pp collisions at $\sqrt{s}$ = 13 TeV for events containing four or more charged leptons (electrons, muons and up to two hadronically decaying taus). No significant deviation from the expected SM background is observed. Limits are set on the Higgsino mass in simplified models of general gauge mediated supersymmetry Tn1n1A/Tn1n1B/Tn1n1C, see their Figure 9. Limits are also set on the wino, slepton, sneutrino and gluino mass in a simplified model of NLSP pair production with R-parity violating decays of the LSP via λ_{12k} or λ_{i33} to charged leptons, see their Figures 7, 8.

[30] SIRUNYAN 18AA searched in 35.9 fb^{-1} of pp collisions at $\sqrt{s}$ = 13 TeV for events with at least one photon and large $\not{E}_T$. No significant excess above the Standard Model expectations is observed. Limits are set on wino masses in a general gauge-mediated SUSY breaking (GGM) scenario with bino-like $\widetilde{\chi}^{0}_1$ and wino-like $\widetilde{\chi}^{\pm}_1$ and $\widetilde{\chi}^{0}_2$, see Figure

Downloaded from https://academic.oup.com/ptep/article/2022/8/083C01/6651666 by KIT Library user on 27 September 2022

7. Limits are also set on the NLSP mass in the Tchi1n1A and Tchi1chi1A simplified models, see their Figure 8. Finally, limits are set on the gluino mass in the Tglu4A and Tglu4B simplified models, see their Figure 9, and on the squark mass in the Tskq4A and Tsqk4B simplified models, see their Figure 10.

[31] SIRUNYAN 18AJ searched in 35.9 fb^{-1} of pp collisions at $\sqrt{s}$ = 13 TeV for events containing two low-momentum, oppositely charged leptons (electrons or muons) and $\not{E}_T$. No excess over the expected background is observed. Limits are derived on the wino mass in the Tchi1n2F simplified model, see their Figure 5. Limits are also set on the stop mass in the Tstop10 simplified model, see their Figure 6. Finally, limits are set on the Higgsino mass in the Tchi1n2G simplified model, see Figure 8 and in the pMSSM, see Figure 7.

[32] SIRUNYAN 18AO searched in 35.9 fb^{-1} of pp collisions at $\sqrt{s}$ = 13 TeV for direct electroweak production of charginos and neutralinos in events with either two or more leptons (electrons or muons) of the same electric charge, or with three or more leptons, which can include up to two hadronically decaying tau leptons. No significant excess above the Standard Model expectations is observed. Limits are set on the chargino/neutralino mass in the Tchi1n2A, Tchi1n2H, Tchi1n2D, Tchi1n2E and Tchi1n2F simplified models, see their Figures 14, 15, 16, 17 and 18. Limits are also set on the higgsino mass in the Tn1n1A, Tn1n1B and Tn1n1C simplified models, see their Figure 19.

[33] SIRUNYAN 18AP searched in 35.9 fb^{-1} of pp collisions at $\sqrt{s}$ = 13 TeV for direct electroweak production of charginos and neutralinos by combining a number of previous and new searches. No significant excess above the Standard Model expectations is observed. Limits are set on the chargino/neutralino mass in the Tchi1n2E, Tchi1n2F and Tchi1n2l simplified models, see their Figures 7, 8, 9 an 10. Limits are also set on the higgsino mass in the Tn1n1A, Tn1n1B and Tn1n1C simplified models, see their Figure 11, 12, 13 and 14.

[34] SIRUNYAN 18AR searched in 35.9 fb^{-1} of pp collisions at $\sqrt{s}$ = 13 TeV for events containing two opposite-charge, same-flavour leptons (electrons or muons), jets and $\not{E}_T$. No significant excess above the Standard Model expectations is observed. Limits are set on the gluino mass in the Tglu4C simplified model, see their Figure 7. Limits are also set on the chargino/neutralino mass in the Tchi1n2F simplified models, see their Figure 8, and on the higgsino mass in the Tn1n1B and Tn1n1C simplified models, see their Figure 9. Finally, limits are set on the sbottom mass in the Tsbot3 simplified model, see their Figure 10.

[35] SIRUNYAN 18DN searched in 35.9 fb^{-1} of pp collisions at $\sqrt{s}$ = 13 TeV for direct electroweak production of charginos and for pair production of top squarks in events with two leptons (electrons or muons) of the opposite electric charge. No significant excess above the Standard Model expectations is observed. Limits are set on the chargino mass in the Tchi1chi1C and Tchi1chi1E simplified models, see their Figure 8. Limits are also set on the stop mass in the Tstop1 and Tstop2 simplified models, see their Figure 9.

[36] SIRUNYAN 18DP searched in 35.9 fb^{-1} of pp collisions at $\sqrt{s}$ = 13 TeV for direct electroweak production of charginos and neutralinos or of chargino pairs in events with a tau lepton pair and significant missing transverse momentum. Both hadronic and leptonic decay modes are considered for the tau lepton. No significant excess above the Standard Model expectations is observed. Limits are set on the chargino mass in the Tchi1chi1D and Tchi1n2 simplified models, see their Figures 14 and 15. Also, excluded stau pair production cross sections are shown in Figures 11, 12, and 13.

[37] SIRUNYAN 18X searched in 35.9 fb^{-1} of pp collisions at $\sqrt{s}$ = 13 TeV for events with one or more high-momentum Higgs bosons, decaying to pairs of photons, jets and $\not{E}_T$. The razor variables (M_R and R^2) are used to categorise the events. No significant excess above the Standard Model expectations is observed. Limits are set on the sbottom mass in the Tsbot4 simplified model and on the wino mass in the Tchi1n2E simplified model, see their Figure 5. Limits are also set on the higgsino mass in the Tn1n1A and Tn1n1B simplified models, see their Figure 6.

[38] KHACHATRYAN 17L searched in about 19 fb^{-1} of pp collisions at $\sqrt{s}$ = 8 TeV for events with two τ (at least one decaying hadronically) and $\not{E}_T$. In the Tchi1chi1C model, assuming decays via intermediate $\tilde{\tau}$ or $\tilde{\nu}_\tau$ with equivalent mass, the observed limits rule out $\tilde{\chi}^{\pm}_1$ masses up to 420 GeV for a massless $\tilde{\chi}^0_1$. See their Fig.5.

[39] SIRUNYAN 17AW searched in 35.9 fb^{-1} of pp collisions at $\sqrt{s}$ = 13 TeV for events with a charged lepton (electron or muon), two jets identified as originating from a b-quark, and large $\not{E}_T$. No significant excess above the Standard Model expectations is observed. Limits are set on the mass of the chargino and the next-to-lightest neutralino in the Tchi1n2E simplified model, see their Figure 6.

[40] AAD 16AA summarized and extended ATLAS searches for electroweak supersymmetry in final states containing several charged leptons, $\not{E}_T$, with or without hadronic jets, in 20 fb^{-1} of pp collisions at $\sqrt{s}$ = 8 TeV. The paper reports the results of new interpretations and statistical combinations of previously published analyses, as well as new analyses. Exclusion limits at 95% C.L. are set on the $\tilde{\chi}^{\pm}_1$ mass in the Tchi1chi1B and Tchi1chi1C simplified models. See their Fig. 13.

[41] AAD 16AA summarized and extended ATLAS searches for electroweak supersymmetry in final states containing several charged leptons, $\not{E}_T$, with or without hadronic jets, in 20 fb^{-1} of pp collisions at $\sqrt{s}$ = 8 TeV. The paper reports the results of new interpretations and statistical combinations of previously published analyses, as well as new analyses. Exclusion limits at 95% C.L. are set on mass-degenerate $\tilde{\chi}^{\pm}_1$ and $\tilde{\chi}^0_2$ masses in the Tchi1n2B, Tchi1n2C, and Tchi1n2D simplified models. See their Figs. 16, 17, and 18. Interpretations in phenomenological-MSSM, two-parameter Non Universal Higgs Masses (NUHM2), and gauge-mediated symmetry breaking (GMSB) models are also given in their Figs. 20, 21 and 22.

[42] KHACHATRYAN 16R searched in 19.7 fb^{-1} of pp collisions at $\sqrt{s}$ = 8 TeV for events with one or more photons, one electron or muon, and $\not{E}_T$. No significant excess above the Standard Model expectations is observed. Limits are set on wino masses in a general gauge-mediated SUSY breaking model (GGM), for a wino-like neutralino NLSP scenario, see Fig. 5. Limits are also set in the Tglu1D and Tchi1n1A simplified models, see Fig. 6. The Tchi1n1A limit is reduced to 340 GeV for a branching ratio reduced by the weak mixing angle.

[43] AAD 15BA searched in 20.3 fb^{-1} of pp collisions at $\sqrt{s}$ = 8 TeV for electroweak production of charginos and neutralinos decaying to a final state containing a W boson and a 125 GeV Higgs boson, plus missing transverse momentum. No excess beyond the Standard Model expectation is observed. Exclusion limits are derived in simplified models of direct chargino and next-to-lightest neutralino production, with the decays $\tilde{\chi}^{\pm}_1 \rightarrow W^{\pm}\tilde{\chi}^0_1$ and $\tilde{\chi}^0_2 \rightarrow H\tilde{\chi}^0_1$ having 100% branching fraction, see Fig. 8. A combination of the multiple final states for the Higgs decay yields the best limits (Fig. 8d).

[44] AAD 15CA searched in 20.3 fb^{-1} of pp collisions at $\sqrt{s}$ = 8 TeV for events with one or more photons and $\not{E}_T$, with or without leptons (e, μ). No significant excess above the Standard Model expectations is observed. Limits are set on wino masses in the general gauge-mediated SUSY breaking model (GGM), for wino-like NLSP, see Fig. 9, 12

[45] AAD 14H searched in 20.3 fb^{-1} of pp collisions at $\sqrt{s}$ = 8 TeV for electroweak production of charginos and neutralinos decaying to a final sate with three leptons and missing transverse momentum. No excess beyond the Standard Model expectation is observed. Exclusion limits are derived in simplified models of direct chargino and next-to-lightest neutralino production, with decays to the lightest neutralino via either all three generations of leptons, staus only, gauge bosons, or Higgs bosons, see Fig. 7. An interpretation in the pMSSM is also given, see Fig. 8.

[46] AAD 14X searched in 20.3 fb^{-1} of pp collisions at $\sqrt{s}$ = 8 TeV for events with at least four leptons (electrons, muons, taus) in the final state. No significant excess above the Standard Model expectations is observed. Limits are set on the wino-like chargino mass in an R-parity violating simplified model where the decay $\tilde{\chi}^{\pm}_1 \rightarrow W^{(*)\pm}\tilde{\chi}^0_1$, with $\tilde{\chi}^0_1 \rightarrow \ell^{\pm}\ell^{\mp}\nu$, takes place with a branching ratio of 100%, see Fig. 8.

[47] KHACHATRYAN 14L searched in 19.5 fb^{-1} of pp collisions at $\sqrt{s}$ = 8 TeV for evidence of chargino-neutralino $\tilde{\chi}^{\pm}_1\tilde{\chi}^0_2$ pair production with Higgs or W-bosons in the decay chain, leading to HW final states with missing transverse energy. The decays of a Higgs boson to a photon pair are considered in conjunction with hadronic and leptonic decay modes of the W bosons. No significant excesses over the expected SM backgrounds are observed. The results are interpreted in the context of simplified models where the decays $\tilde{\chi}^0_2 \rightarrow H\tilde{\chi}^0_1$ and $\tilde{\chi}^{\pm}_1 \rightarrow W^{\pm}\tilde{\chi}^0_1$ take place 100% of the time, see Figs. 22–23.

[48] AAD 13 searched in 4.7 fb^{-1} of pp collisions at $\sqrt{s}$ = 7 TeV for charginos and neutralinos decaying to a final state with three leptons (e and μ) and missing transverse energy. No excess beyond the Standard Model expectation is observed. Exclusion limits are derived in the phenomenological MSSM, see Fig. 2 and 3, and in simplified models, see Fig. 4. For the simplified models with intermediate slepton decays, degenerate $\tilde{\chi}^{\pm}_1$ and $\tilde{\chi}^0_2$ masses up to 500 GeV are excluded at 95% C.L. for very large mass differences with the $\tilde{\chi}^0_1$. Supersedes AAD 12AS.

[49] AAD 13B searched in 4.7 fb^{-1} of pp collisions at $\sqrt{s}$ = 7 TeV for gauginos decaying to a final state with two leptons (e and μ) and missing transverse energy. No excess beyond the Standard Model expectation is observed. Limits are derived in a simplified model of wino-like chargino pair production, where the chargino always decays to the lightest neutralino via an intermediate on-shell charged slepton, see Fig. 2(b). Chargino masses between 110 and 340 GeV are excluded at 95% C.L. for $m_{\tilde{\chi}^0_1}$ = 10 GeV. Exclusion limits are also derived in the phenomenological MSSM, see Fig. 3.

[50] AAD 12CT searched in 4.7 fb^{-1} of pp collisions at $\sqrt{s}$ = 7 TeV for events containing four or more leptons (electrons or muons) and either moderate values of missing transverse momentum or large effective mass. No significant excess is found in the data. Limits are presented in a simplified model of R-parity violating supersymmetry in which charginos are pair-produced and then decay into a W-boson and a $\tilde{\chi}^0_1$, which in turn decays through an RPV coupling into two charged leptons ($e^{\pm}e^{\mp}$ or $e^{\pm}\mu^{\mp}$) and a neutrino. In this model, chargino masses up to 540 GeV are excluded at 95% C.L. for $m_{\tilde{\chi}^0_1}$ above 300 GeV, see Fig. 3a. The limit deteriorates for lighter $\tilde{\chi}^0_1$. Limits are also set in an R-parity violating mSUGRA model, see Fig. 3b.

[51] CHATRCHYAN 12BJ searched in 4.98 fb^{-1} of pp collisions at $\sqrt{s}$ = 7 TeV for direct electroweak production of charginos and neutralinos in events with at least two leptons, jets and missing transverse momentum. No significant excesses over the expected SM backgrounds are observed and 95% C.L. limits on the production cross section of $\tilde{\chi}^{\pm}_1\tilde{\chi}^0_2$ pair production were set in a number of simplified models, see Figs. 7 to 12.

[52] ABDALLAH 03M uses data from $\sqrt{s}$ = 192–208 GeV to obtain limits in the framework of the MSSM with gaugino and sfermion mass universality at the GUT scale. An indirect limit on the mass of charginos is derived by constraining the MSSM parameter space by the results from direct searches for neutralinos (including cascade decays), for charginos and for sleptons. These limits are valid for values of M_2 < 1 TeV, $|\mu| \leq$ 2 TeV with the $\tilde{\chi}^0_1$ as LSP. Constraints from the Higgs search in the m_h^{max} scenario assuming m_t= 174.3 GeV are included. The quoted limit applies if there is no mixing in the third family or when $m_{\tilde{\tau}_1} - m_{\tilde{\chi}^0_1} > 6$ GeV. If mixing is included the limit degrades to 90 GeV. See Fig. 43 for the mass limits as a function of tanβ. These limits update the results of ABREU 00W.

[53] AAD 20AN searched in 139 fb^{-1} of pp collisions at $\sqrt{s}$ = 13 TeV for events with two photons and missing transverse momentum. Events are further categorised in terms of lepton or jet multiplicity. No significant excess over the expected background is observed. Limits at 95% C.L. are derived in Tchi1n2E simplified models. Next-to-lightest neutralinos and charginos with masses up to 310 GeV for a massless lightest neutralino are excluded. See their Fig. 10.

[54] KHACHATRYAN 16AA searched in 7.4 fb^{-1} of pp collisions at $\sqrt{s}$ = 8 TeV for events with one or more photons, hadronic jets and $\not{E}_T$. No significant excess above the Standard Model expectations is observed. Limits are set on wino masses in the general gauge-mediated SUSY breaking model (GGM), for a wino-like neutralino NLSP scenario and with the wino mass fixed at 10 GeV above the bino mass, see Fig. 4. Limits are also set in the Tchi1chi1A and Tchi1n1A simplified models, see Fig. 3.

[55] KHACHATRYAN 16R searched in 19.7 fb^{-1} of pp collisions at $\sqrt{s}$ = 8 TeV for events with one or more photons, one electron or muon, and $\not{E}_T$. No significant excess above the Standard Model expectations is observed. Limits are also set in the Tglu1F simplified model, see Fig. 6.

[56] KHACHATRYAN 16Y searched in 19.7 fb^{-1} of pp collisions at $\sqrt{s}$ = 8 TeV for events with one or two soft isolated leptons, hadronic jets, and $\not{E}_T$. No significant excess above the Standard Model expectations is observed. Limits are set on the $\tilde{\chi}^{\pm}_1$ mass (which is degenerate with the $\tilde{\chi}^0_2$) in the Tchi1n2A simplified model, see Fig. 4.

[57] AAD 14AV searched in 20.3 fb^{-1} of pp collisions at $\sqrt{s}$ = 8 TeV for the direct production of charginos, neutralinos and staus in events containing at last two hadronically decaying τ-leptons, large missing transverse momentum and low jet activity. The quoted limit was derived for direct $\tilde{\chi}^{\pm}_1\tilde{\chi}^0_2$ and $\tilde{\chi}^{\pm}_1\tilde{\chi}^{\mp}_1$ production with $\tilde{\chi}^0_2 \rightarrow \tilde{\tau}\tau \rightarrow \tau\tau\tilde{\chi}^0_1$ and $\tilde{\chi}^{\pm}_1 \rightarrow \tilde{\tau}\nu(\tilde{\nu}_\tau\tau) \rightarrow \tau\nu\tilde{\chi}^0_1$, $m_{\tilde{\chi}^0_2} = m_{\tilde{\chi}^{\pm}_1}$, $m_{\tilde{\tau}} = 0.5\ (m_{\tilde{\chi}^{\pm}_1} + m_{\tilde{\chi}^0_1})$, $m_{\tilde{\chi}^0_1} = 0$ GeV. No excess over the expected SM background is observed. Exclusion limits are set in simplified models of $\tilde{\chi}^{\pm}_1\tilde{\chi}^{\mp}_1$ and $\tilde{\chi}^{\pm}_1\tilde{\chi}^0_2$ pair production, see their Figure 7. Upper limits on the cross section and signal strength for direct di-stau production are derived, see Figures 8 and 9. Also, limits are derived in a pMSSM model where the only light slepton is the $\tilde{\tau}_R$, see Figure 10.

Downloaded from https://academic.oup.com/ptep/article/2022/8/083C01/6651666 by KIT Library user on 27 September 2022

[58] AAD 14AV searched in 20.3 fb^{-1} of pp collisions at $\sqrt{s}$ = 8 TeV for the direct production of charginos, neutralinos and staus in events containing at last two hadronically decaying τ-leptons, large missing transverse momentum and low jet activity. The quoted limit was derived for direct $\widetilde{\chi}_1^\pm\widetilde{\chi}_1^\mp$ production with $\widetilde{\chi}_1^\pm \rightarrow \widetilde{\tau}\nu(\widetilde{\nu}_\tau\tau) \rightarrow \tau\nu\widetilde{\chi}_1^0$, $m_{\widetilde{\tau}}$ = 0.5 ($m_{\widetilde{\chi}_1^\pm} + m_{\widetilde{\chi}_1^0}$), $m_{\widetilde{\chi}_1^0}$ = 0 GeV. No excess over the expected SM background is observed. Exclusion limits are set in simplified models of $\widetilde{\chi}_1^\pm\widetilde{\chi}_1^\mp$ and $\widetilde{\chi}_1^\pm\widetilde{\chi}_2^0$ pair production, see their Figure 7. Upper limits on the cross section and signal strength for direct di-stau production are derived, see Figures 8 and 9. Also, limits are derived in a pMSSM model where the only light slepton is the $\widetilde{\tau}_R$, see Figure 10.

[59] AAD 14G searched in 20.3 fb^{-1} of pp collisions at $\sqrt{s}$ = 8 TeV for electroweak production of chargino pairs, or chargino-neutralino pairs, decaying to a final sate with two leptons (e and μ) and missing transverse momentum. No excess beyond the Standard Model expectation is observed. Exclusion limits are derived in simplified models of chargino pair production, with chargino decays to the lightest neutralino via either sleptons or gauge bosons, see Fig 5.; or in simplified models of chargino and next-to-lightest neutralino production, with decays to the lightest neutralino via gauge bosons, see Fig. 7. An interpretation in the pMSSM is also given, see Fig. 10.

[60] AALTONEN 14 searched in 5.8 fb^{-1} of $p\overline{p}$ collisions at $\sqrt{s}$ = 1.96 TeV for evidence of chargino and next-to-lightest neutralino associated production in final states consisting of three leptons (electrons, muons or taus) and large missing transverse momentum. The results are consistent with the Standard Model predictions within 1.85 σ. Limits on the chargino mass are derived in an mSUGRA model with m_0 = 60 GeV, tanβ = 3, A_0 = 0 and μ >0, see their Fig. 2.

[61] KHACHATRYAN 14I searched in 19.5 fb^{-1} of pp collisions at $\sqrt{s}$ = 8 TeV for electroweak production of chargino pairs decaying to a final state with opposite-sign lepton pairs (e or μ) and missing transverse momentum. No excess beyond the Standard Model expectation is observed. Exclusion limits are derived in simplified models, see Fig. 18.

[62] AALTONEN 13Q searched in 6.0 fb^{-1} of $p\overline{p}$ collisions at $\sqrt{s}$ = 1.96 TeV for evidence of chargino-neutralino associated production in like-sign dilepton final states. One lepton is identified as the hadronic decay of a tau lepton, while the other is an electron or muon. Good agreement with the Standard Model predictions is observed and limits are set on the chargino-neutralino cross section for simplified gravity- and gauge-mediated models, see their Figs. 2 and 3.

[63] AAD 12AS searched in 2.06 fb^{-1} of pp collisions at $\sqrt{s}$ = 7 TeV for charginos and neutralinos decaying to a final state with three leptons (e and μ) and missing transverse energy. No excess beyond the Standard Model expectation is observed. Exclusion limits are derived in the phenomenological MSSM, see Fig. 2 (top), and in simplified models, see Fig. 2 (bottom).

[64] AAD 12T looked in 1 fb^{-1} of pp collisions at $\sqrt{s}$ = 7 TeV for the production of supersymmetric particles decaying into final states with missing transverse momentum and exactly two isolated leptons (e or μ). Opposite-sign and same-sign dilepton events were separately studied. Additionally, in opposite-sign events, a search was made for an excess of same-flavor over different-flavor lepton pairs. No excess over the expected background is observed and limits are placed on the effective production cross section of opposite-sign dilepton events with $\not{E}_T$ > 250 GeV and on same-sign dilepton events with $\not{E}_T$ > 100 GeV. The latter limit is interpreted in a simplified electroweak gaugino production model as a lower chargino mass limit.

[65] CHATRCHYAN 11B looked in 35 pb^{-1} of pp collisions at $\sqrt{s}$=7 TeV for events with an isolated lepton (e or μ), a photon and $\not{E}_T$ which may arise in a generalized gauge mediated model from the decay of Wino-like NLSPs. No evidence for an excess over the expected background is observed. Limits are derived in the plane of squark/gluino mass versus Wino mass (see Fig. 4). Mass degeneracy of the produced squarks and gluinos is assumed.

[66] CHATRCHYAN 11V looked in 35 pb^{-1} of pp collisions at $\sqrt{s}$ = 7 TeV for events with $\geq$ 3 isolated leptons (e, μ or τ), with or without jets and $\not{E}_T$. No evidence for an excess over the expected background is observed. Limits are derived in the CMSSM (m_0, $m_{1/2}$) plane for tanβ = 3 (see Fig. 5).

Long-lived $\widetilde{\chi}^\pm$ (Chargino) mass limit

Limits on charginos which leave the detector before decaying.

VALUE (GeV)	CL%	DOCUMENT ID		TECN	COMMENT
> 884	95	[1] SIRUNYAN	20N	CMS	$\widetilde{\chi}^\pm \rightarrow \widetilde{\chi}_1^0\pi^\pm$, wino LSP, AMSB, tan$\beta$ = 5, μ > 0, τ = 3 ns
> 474	95	[1] SIRUNYAN	20N	CMS	$\widetilde{\chi}^\pm \rightarrow \widetilde{\chi}_1^0\pi^\pm$, wino LSP, AMSB, tan$\beta$ = 5, μ > 0, τ = 0.2 ns
> 750	95	[1] SIRUNYAN	20N	CMS	$\widetilde{\chi}^\pm \rightarrow \widetilde{\chi}_1^0\pi^\pm$, higgsino LSP, AMSB, tanβ=5, μ >0,τ=3ns
> 175	95	[1] SIRUNYAN	20N	CMS	$\widetilde{\chi}^\pm \rightarrow \widetilde{\chi}_1^0\pi^\pm$, higgsino LSP, AMSB, tanβ=5,μ >0,τ=0.05ns
>1090	95	[2] AABOUD	19AT	ATLS	long-lived $\widetilde{\chi}_1^\pm$ mAMSB
> 460	95	[3] AABOUD	18AS	ATLS	$\widetilde{\chi}^\pm \rightarrow \widetilde{\chi}_1^0\pi^\pm$, lifetime 0.2 ns, $m_{\widetilde{\chi}^\pm} - m_{\widetilde{\chi}_1^0}$ = 160 MeV
> 715	95	[4] SIRUNYAN	18BR	CMS	$\widetilde{\chi}^\pm \rightarrow \widetilde{\chi}_1^0\pi^\pm$, AMSB, tan$\beta$ = 5 and μ > 0, τ = 3 ns
> 695	95	[4] SIRUNYAN	18BR	CMS	$\widetilde{\chi}^\pm \rightarrow \widetilde{\chi}_1^0\pi^\pm$, AMSB, tan$\beta$ = 5 and μ > 0, τ = 7 ns
> 505	95	[4] SIRUNYAN	18BR	CMS	$\widetilde{\chi}^\pm \rightarrow \widetilde{\chi}_1^0\pi^\pm$, AMSB, tan$\beta$ = 5, μ > 0, 0.5 ns > τ > 60 ns
> 620	95	[5] AAD	15AE	ATLS	stable $\widetilde{\chi}^\pm$
> 534	95	[6] AAD	15BM	ATLS	stable $\widetilde{\chi}^\pm$
> 239	95	[6] AAD	15BM	ATLS	$\widetilde{\chi}^\pm \rightarrow \widetilde{\chi}_1^0\pi^\pm$, lifetime 1 ns, $m_{\widetilde{\chi}^\pm} - m_{\widetilde{\chi}_1^0}$ = 0.14 GeV
> 482	95	[6] AAD	15BM	ATLS	$\widetilde{\chi}^\pm \rightarrow \widetilde{\chi}_1^0\pi^\pm$, lifetime 15 ns, $m_{\widetilde{\chi}^\pm} - m_{\widetilde{\chi}_1^0}$ = 0.14 GeV
> 103	95	[7] AAD	13H	ATLS	long-lived $\widetilde{\chi}^\pm \rightarrow \widetilde{\chi}_1^0\pi^\pm$, mAMSB, $\Delta m_{\widetilde{\chi}_1^0}$ = 160 MeV
> 92	95	[8] AAD	12BJ	ATLS	long-lived $\widetilde{\chi}^\pm \rightarrow \pi^\pm\widetilde{\chi}_1^0$, mAMSB
> 171	95	[9] ABAZOV	09M	D0	$\widetilde{H}$
> 102	95	[10] ABBIENDI	03L	OPAL	$m_{\widetilde{\nu}}$ >500 GeV
none 2–93.0	95	[11] ABREU	00T	DLPH	$\widetilde{H}^\pm$ or $m_{\widetilde{\nu}} > m_{\widetilde{\chi}^\pm}$
• • • We do not use the following data for averages, fits, limits, etc. • • •					
> 260	95	[12] KHACHATRY...	15AB	CMS	$\widetilde{\chi}_1^\pm \rightarrow \widetilde{\chi}_1^0\pi^\pm$,$\tau_{\widetilde{\chi}_1^\pm}$=0.2ns, AMSB
> 800	95	[13] KHACHATRY...	15AO	CMS	long-lived $\widetilde{\chi}_1^\pm$, mAMSB, τ >100ns
> 100	95	[13] KHACHATRY...	15AO	CMS	long-lived $\widetilde{\chi}_1^\pm$, mAMSB, τ > 3 ns
	95	[14] KHACHATRY...	15W	CMS	long-lived $\widetilde{\chi}^0$, $\widetilde{q} \rightarrow q\widetilde{\chi}^0$, $\widetilde{\chi}^0 \rightarrow \ell^+\ell^-\nu$, RPV
> 270	95	[15] AAD	13BD	ATLS	disappearing-track signature, AMSB
> 278	95	[16] ABAZOV	13B	D0	long-lived $\widetilde{\chi}^\pm$, gaugino-like
> 244	95	[16] ABAZOV	13B	D0	long-lived $\widetilde{\chi}^\pm$, higgsino-like

[1] SIRUNYAN 20N searched in 101 fb^{-1} of pp collisions at $\sqrt{s}$ = 13 TeV for direct electroweak production of long-lived charginos in events containing isolated tracks with missing hits in the outer layer of the silicon tracker and little or no associated calorimetric energy deposits (disappearing tracks). No significant excess above the Standard Model expectations is observed. In an AMSB context and assuming a wino LSP, limits are set on the cross section of direct chargino production through $pp \rightarrow \widetilde{\chi}^\pm\widetilde{\chi}^\mp$ and $pp \rightarrow \widetilde{\chi}^\pm\widetilde{\chi}_1^0$, assuming B($\widetilde{\chi}^\pm \rightarrow \widetilde{\chi}_1^0\pi^\pm$) = 100%, as a function of the chargino mass and mean proper lifetime, see Figure 2. In the case of a Higgsino LSP, limits are set on the cross section of direct chargino production through $pp \rightarrow \widetilde{\chi}^\pm\widetilde{\chi}^\mp$ and $pp \rightarrow \widetilde{\chi}^\pm\widetilde{\chi}_{1,2}^0$, assuming B($\widetilde{\chi}^\pm \rightarrow \widetilde{\chi}_1^0\pi^\pm$) = 95.5%, B($\widetilde{\chi}^\pm \rightarrow \widetilde{\chi}_1^0e^\pm$) = 3%, B($\widetilde{\chi}^\pm \rightarrow \widetilde{\chi}_1^0\mu^\pm$) = 1.5%, as a function of the chargino mass and mean proper lifetime, see Figure 3.

[2] AABOUD 19AT searched in 36.1 fb^{-1} of pp collisions at $\sqrt{s}$ = 13 TeV for metastable R-hadrons. Multiple search strategies for a wide range of lifetimes, corresponding to path lengths of a few meters, are defined. No significant deviations from the expected Standard Model background are observed. Results are interpreted in terms of direct electroweak production of long-lived charginos in the context of mAMSB scenarios. Chargino masses are excluded at 95% C.L. below 1090 GeV. See their Figure 10 (right).

[3] AABOUD 18AS searched in 36.1 fb^{-1} of pp collisions at $\sqrt{s}$ = 13 TeV for direct electroweak production of long-lived charginos in the context of AMSB or phenomenological MSSM scenarios with wino-like LSP. Events with a disappearing track due to a low-momentum pion accompanied by at least one jet with high transverse momentum from initial-state radiation are considered. No significant excess above the Standard Model expectations is observed. Exclusion limits are set at 95% confidence level on the mass of charginos for different chargino lifetimes. For a pure wino with a lifetime of about 0.2 ns, corresponding to a mass-splitting between the charged and neutral wino of around 160 MeV, chargino masses up to 460 GeV are excluded, see their Fig. 8.

[4] SIRUNYAN 18BR searched in 38.4 fb^{-1} of pp collisions at $\sqrt{s}$ = 13 TeV for direct electroweak production of long-lived charginos in events containing isolated tracks with missing hits in the outer layer of the silicon tracker and little or no associated calorimetric energy deposits (disappearing tracks). No significant excess above the Standard Model expectations is observed. In an AMSB context, limits are set on the cross section of direct chargino production through $pp \rightarrow \widetilde{\chi}^\pm\widetilde{\chi}^\mp$ and $pp \rightarrow \widetilde{\chi}^\pm\widetilde{\chi}_1^0$, assuming BR($\widetilde{\chi}^\pm \rightarrow \widetilde{\chi}_1^0\pi^\pm$) = 100%, as a function of the chargino mass and mean proper lifetime, see Figures 3, 4 and 5.

[5] AAD 15AE searched in 19.1 fb^{-1} of pp collisions at $\sqrt{s}$ = 8 TeV for heavy long-lived charged particles, measured through their specific ionization energy loss in the ATLAS pixel detector or their time-of-flight in the ALTAS muon system. In the absence of an excess of events above the expected backgrounds, limits are set on stable charginos, see Fig. 10.

[6] AAD 15BM searched in 18.4 fb^{-1} of pp collisions at $\sqrt{s}$ = 8 TeV for stable and metastable non-relativistic charged particles through their anomalous specific ionization energy loss in the ATLAS pixel detector. In absence of an excess of events above the expected backgrounds, limits are set on stable charginos (see Table 5) and on metastable charginos decaying to $\widetilde{\chi}_1^0\pi^\pm$, see Fig. 11.

[7] AAD 13H searched in 4.7 fb^{-1} of pp collisions at $\sqrt{s}$ = 7 TeV for direct electroweak production of long-lived charginos in the context of AMSB scenarios. The search is based on the signature of a high-momentum isolated track with few associated hits in the outer part of the tracking system, arising from a chargino decay into a neutralino and a low-momentum pion. The p_T spectrum of the tracks was found to be consistent with the SM expectations. Constraints on the lifetime and the production cross section were obtained, see Fig. 6. In the minimal AMSB framework with tanβ = 5, and μ > 0, a chargino having a mass below 103 (85) GeV for a chargino-neutralino mass splitting $\Delta m_{\widetilde{\chi}_1^0}$ of 160 (170) MeV is excluded at the 95% C.L. See Fig. 7 for more precise bounds.

[8] AAD 12BJ looked in 1.02 fb^{-1} of pp collisions at $\sqrt{s}$ = 7 TeV for signatures of decaying charginos resulting in isolated tracks with few associated hits in the outer region of the tracking system. The p_T spectrum of the tracks was found to be consistent with the SM expectations. Constraints on the lifetime and the production cross section were obtained. In the minimal AMSB framework with $m_{3/2}$ < 32 TeV, m_0 < 1.5 TeV, tanβ = 5, and μ > 0, a chargino having a mass below 92 GeV and a lifetime between 0.5 ns and 2 ns is excluded at the 95% C.L. See their Fig. 8 for more precise bounds.

[9] ABAZOV 09M searched in 1.1 fb^{-1} of $p\overline{p}$ collisions at $\sqrt{s}$ = 1.96 TeV for events with direct production of a pair of charged massive stable particles identified by their TOF. The number of the observed events is consistent with the predicted background. The data are used to constrain the production cross section as a function of the $\widetilde{\chi}_1^\pm$ mass, see their Fig. 2. The quoted limit improves to 206 GeV for gaugino-like charginos.

[10] ABBIENDI 03L used e^+e^- data at $\sqrt{s}$ = 130–209 GeV to select events with two high momentum tracks with anomalous dE/dx. The excluded cross section is compared to the theoretical expectation as a function of the heavy particle mass in their Fig. 3. The bounds are valid for colorless fermions with lifetime longer than 10^{-6} s. Supersedes the results from ACKERSTAFF 98P.

[11] ABREU 00T searches for the production of heavy stable charged particles, identified by their ionization or Cherenkov radiation, using data from $\sqrt{s}$= 130 to 189 GeV. These limits include and update the results of ABREU 98P.

[12] KHACHATRYAN 15AB searched in 19.5 fb^{-1} of pp collisions at $\sqrt{s}$ = 8 TeV for events containing tracks with little or no associated calorimeter energy deposits and with missing hits in the outer layers of the tracking system (disappearing-track signature). Such disappearing tracks can result from the decay of charginos that are nearly mass degenerate with the lightest neutralino. The number of observed events is in agreement with the background expectation. Limits are set on the cross section of electroweak chargino production in terms of the chargino mass and mean proper lifetime, see Fig. 4. In the minimal AMSB model, a chargino mass below 260 GeV is excluded at 95% C.L., see their Fig. 5.

Downloaded from https://academic.oup.com/ptep/article/2022/8/083C01/6651666 by KIT Library user on 27 September 2022

[13] KHACHATRYAN 15O searched in 18.8 fb^{-1} of pp collisions at $\sqrt{s}$ = 8 TeV for evidence of long-lived charginos in the context of AMSB and pMSSM scenarios. The results are based on a previously published search for heavy stable charged particles at 7 and 8 TeV. In the minimal AMSB framework with tanβ = 5 and $\mu \geq 0$, constraints on the chargino mass and lifetime were placed, see Fig. 5. Charginos with a mass below 800 (100) GeV are excluded at the 95% C.L. for lifetimes above 100 ns (3 ns). Constraints are also placed on the pMSSM parameter space, see Fig. 3.

[14] KHACHATRYAN 15W searched in up to 20.5 fb^{-1} of pp collisions at $\sqrt{s}$ = 8 TeV for evidence of long-lived neutralinos produced through $\tilde{q}$-pair production, with $\tilde{q} \rightarrow q\tilde{\chi}^0$ and $\tilde{\chi}^0 \rightarrow \ell^+\ell^-\nu$ (RPV: $\lambda_{121}, \lambda_{122} \neq 0$). 95% C.L. exclusion limits on cross section times branching ratio are set as a function of mean proper decay length of the neutralino, see Figs. 6 and 9.

[15] AAD 13BD searched in 20.3 fb^{-1} of pp collisions at $\sqrt{s}$ = 8 TeV for events containing tracks with no associated hits in the outer region of the tracking system resulting from the decay of charginos that are nearly mass degenerate with the lightest neutralino, as is often the case in AMSB scenarios. No significant excess above the background expectation is observed for candidate tracks with large transverse momentum. Constraints on chargino properties are obtained and in the minimal AMSB model, a chargino mass below 270 GeV is excluded at 95% C.L., see their Fig. 7.

[16] ABAZOV 13B looked in 6.3 fb^{-1} of $p\overline{p}$ collisions at $\sqrt{s}$ = 1.96 TeV for charged massive long-lived particles in events with muon-like particles that have both speed and ionization energy loss inconsistent with muons produced in beam collisions. In the absence of an excess, limits are set at 95% C.L. on gaugino- and higgsino-like charginos, see their Table 20 and Fig. 23.

$\tilde{\nu}$ (Sneutrino) mass limit

The limits may depend on the number, $N(\tilde{\nu})$, of sneutrinos assumed to be degenerate in mass. Only $\tilde{\nu}_L$ (not $\tilde{\nu}_R$) is assumed to exist. It is possible that $\tilde{\nu}$ could be the lightest supersymmetric particle (LSP).

We report here, but do not include in the Listings, the limits obtained from the fit of the final results obtained by the LEP Collaborations on the invisible width of the Z boson ($\Delta\Gamma_{\rm inv.}$ < 2.0 MeV, LEP-SLC 06): $m_{\tilde{\nu}}$ > 43.7 GeV ($N(\tilde{\nu})$=1) and $m_{\tilde{\nu}}$ > 44.7 GeV ($N(\tilde{\nu})$=3) .

Some earlier papers are now obsolete and have been omitted. They were last listed in our PDG 14 edition: K. Olive, *et al.* (Particle Data Group), Chinese Physics **C38** 070001 (2014) (http://pdg.lbl.gov).

VALUE (GeV)	CL%	DOCUMENT ID		TECN	COMMENT
>3400	95	[1] AABOUD	18CM	ATLS	RPV, $\tilde{\nu}_\tau \rightarrow e\mu$, $\lambda_{312} = \lambda_{321}$ = 0.07, λ'_{311} = 0.11
>2900	95	[2] AABOUD	18CM	ATLS	RPV, $\tilde{\nu}_\tau \rightarrow e\tau$, $\lambda_{313} = \lambda_{331}$ = 0.07, λ'_{311} = 0.11
>2600	95	[3] AABOUD	18CM	ATLS	RPV, $\tilde{\nu}_\tau \rightarrow \mu\tau$, $\lambda_{323} = \lambda_{332}$ = 0.07, λ'_{311} = 0.11
>1060	95	[4] AABOUD	18Z	ATLS	RPV, $\geq 4\ell$, $\lambda_{12k} \neq 0$, $m_{\tilde{\chi}^0_1}$ = 600 GeV (mass-degenerate left-handed sleptons and sneutrinos of all 3 generations)
> 780	95	[4] AABOUD	18Z	ATLS	RPV, $\geq 4\ell$, $\lambda_{i33} \neq 0$, $m_{\tilde{\chi}^0_1}$ = 300 GeV (mass-degenerate left-handed sleptons and sneutrinos of all 3 generations)
>1700	95	[5] SIRUNYAN	18AT	CMS	RPV, $\tilde{\nu}_\tau \rightarrow e\mu$, $\lambda_{132} = \lambda_{231}$ = λ'_{311} = 0.01
>3800	95	[5] SIRUNYAN	18AT	CMS	RPV, $\tilde{\nu}_\tau \rightarrow e\mu$, $\lambda_{132} = \lambda_{231}$ = λ'_{311} = 0.1
>2300	95	[6] AABOUD	16P	ATLS	RPV, $\tilde{\nu}_\tau \rightarrow e\mu$, λ'_{311} = 0.11
>2200	95	[6] AABOUD	16P	ATLS	RPV, $\tilde{\nu}_\tau \rightarrow e\tau$, λ'_{311} = 0.11
>1900	95	[6] AABOUD	16P	ATLS	RPV, $\tilde{\nu}_\tau \rightarrow \mu\tau$, λ'_{311} = 0.11
> 400	95	[7] AAD	14X	ATLS	RPV, $\geq 4\ell^\pm$, $\tilde{\nu} \rightarrow \nu\tilde{\chi}^0_1$, $\tilde{\chi}^0_1 \rightarrow \ell^\pm\ell^\mp\nu$
		[8] AAD	11Z	ATLS	RPV, $\tilde{\nu}_\tau \rightarrow e\mu$
> 94	95	[9] ABDALLAH	03M	DLPH	1 $\leq$ tanβ $\leq$ 40, $m_{\tilde{e}_R} - m_{\tilde{\chi}^0_1}$ >10 GeV
> 84	95	[10] HEISTER	02N	ALEP	$\tilde{\nu}_e$, any Δm
> 41	95	[11] DECAMP	92	ALEP	$\Gamma(Z \rightarrow$ invisible); $N(\tilde{\nu})$=3, model independent
• • • We do not use the following data for averages, fits, limits, etc. • • •					
		[12] SIRUNYAN	19AO		RPV, $\mu^\pm\mu^\pm + \geq$ 2jets, $\lambda'_{211} \neq 0$, $\tilde{\nu}_\mu \rightarrow \mu\tilde{\chi}^\pm_1$, $\tilde{\chi}^\pm_1 \rightarrow \mu q\overline{q}q\overline{q}$
>1280	95	[13] KHACHATRY...	16BE	CMS	RPV, $\tilde{\nu}_\tau \rightarrow e\mu$, $\lambda_{132} = \lambda_{231}$ = λ'_{311} = 0.01
>2300	95	[13] KHACHATRY...	16BE	CMS	RPV, $\tilde{\nu}_\tau \rightarrow e\mu$, $\lambda_{132} = \lambda_{231}$ = 0.07, λ'_{311} = 0.11
>2000	95	[14] AAD	15O	ATLS	RPV ($e\mu$), $\tilde{\nu}_\tau$, λ'_{311} = 0.11, λ_{i3k} = 0.07
>1700	95	[14] AAD	15O	ATLS	RPV ($\tau\mu$, $e\tau$), $\tilde{\nu}_\tau$, λ'_{311} = 0.11, λ_{i3k} = 0.07
		[15] AAD	13AI	ATLS	RPV, $\tilde{\nu}_\tau \rightarrow e\mu$, $e\tau$, $\mu\tau$
		[16] AAD	11H	ATLS	RPV, $\tilde{\nu}_\tau \rightarrow e\mu$
		[17] AALTONEN	10Z	CDF	RPV, $\tilde{\nu}_\tau \rightarrow e\mu$, $e\tau$, $\mu\tau$
		[18] ABAZOV	10M	D0	RPV, $\tilde{\nu}_\tau \rightarrow e\mu$
> 95	95	[19] ABDALLAH	04H	DLPH	AMSB, μ > 0
> 37.1	95	[20] ADRIANI	93M	L3	$\Gamma(Z \rightarrow$ invisible); $N(\tilde{\nu})$=1
> 36	95	ABREU	91F	DLPH	$\Gamma(Z \rightarrow$ invisible); $N(\tilde{\nu})$=1
> 31.2	95	[21] ALEXANDER	91F	OPAL	$\Gamma(Z \rightarrow$ invisible); $N(\tilde{\nu})$=1

[1] AABOUD 18CM searched in 36.1 fb^{-1} of pp collisions at $\sqrt{s}$ = 13 TeV for heavy particles decaying into $e\mu$, $e\tau$, $\mu\tau$ final state. No significant deviation from the expected SM background is observed. Limits are set on the mass of a stau neutrino with R-parity-violating couplings. For $\tilde{\nu}_\tau \rightarrow e\mu$, masses below 3.4 TeV are excluded at 95% CL, see their Figure 4(b). Upper limits on the RPV couplings $|\lambda_{312}|$ versus $|\lambda'_{311}|$ are also performed, see their Figure 8(a-b).

[2] AABOUD 18CM searched in 36.1 fb^{-1} of pp collisions at $\sqrt{s}$ = 13 TeV for heavy particles decaying into an $e\mu$, $e\tau$, $\mu\tau$ final state. No significant deviation from the expected SM background is observed. Limits are set on the mass of a stau neutrino with R-parity-violating couplings. For $\tilde{\nu}_\tau \rightarrow e\tau$, masses below 2.9 TeV are excluded at 95% CL, see their Figure 5(b). Upper limits on the RPV couplings $|\lambda_{313}|$ versus $|\lambda'_{311}|$ are also performed, see their Figure 8(c).

[3] AABOUD 18CM searched in 36.1 fb^{-1} of pp collisions at $\sqrt{s}$ = 13 TeV for heavy particles decaying into an $e\mu$, $e\tau$, $\mu\tau$ final state. No significant deviation from the expected SM background is observed. Limits are set on the mass of a stau neutrino with R-parity-violating couplings. For $\tilde{\nu}_\tau \rightarrow \mu\tau$, masses below 2.6 TeV are excluded at 95% CL, see their Figure 6(b). Upper limits on the RPV couplings $|\lambda_{323}|$ versus $|\lambda'_{311}|$ are also performed, see their Figure 8(d).

[4] AABOUD 18Z searched in 36.1 fb^{-1} of pp collisions at $\sqrt{s}$ = 13 TeV for events containing four or more charged leptons (electrons, muons and up to two hadronically decaying taus). No significant deviation from the expected SM background is observed. Limits are set on the Higgsino mass in simplified models of general gauge mediated supersymmetry Tn1n1A/Tn1n1B/Tn1n1C, see their Figure 9. Limits are also set on the wino, slepton, sneutrino and gluino mass in a simplified model of NLSP pair production with R-parity violating decays of the LSP via λ_{12k} or λ_{i33} to charged leptons, see their Figures 7, 8.

[5] SIRUNYAN 18AT searched in 35.9 fb^{-1} of pp collisions at $\sqrt{s}$ = 13 TeV for heavy resonances decaying into $e\mu$ final states. No significant excess above the Standard Model expectation is observed and 95% C.L. exclusions are placed on the cross section times branching ratio for the R-parity-violating production and decay of a supersymmetric tau sneutrino, see their Fig. 3.

[6] AABOUD 16P searched in 3.2 fb^{-1} of pp collisions at $\sqrt{s}$ = 13 TeV for events with different flavour dilepton pairs ($e\mu$, $e\tau$, $\mu\tau$) from the production of $\tilde{\nu}_\tau$ via an RPV λ'_{311} coupling and followed by a decay via $\lambda_{312} = \lambda_{321}$ = 0.07 for $e + \mu$, via $\lambda_{313} = \lambda_{331}$ = 0.07 for $e + \tau$ and via $\lambda_{323} = \lambda_{332}$ = 0.07 for $\mu + \tau$. No evidence for a dilepton resonance over the SM expectation is observed, and limits are derived on $m_{\tilde{\nu}}$ at 95% CL, see their Figs. 2(b), 3(b), 4(b), and Table 3.

[7] AAD 14X searched in 20.3 fb^{-1} of pp collisions at $\sqrt{s}$ = 8 TeV for events with at least four leptons (electrons, muons, taus) in the final state. No significant excess above the Standard Model expectations is observed. Limits are set on the sneutrino mass in an R-parity violating simplified model where the decay $\tilde{\nu} \rightarrow \nu\tilde{\chi}^0_1$, with $\tilde{\chi}^0_1 \rightarrow \ell^\pm\ell^\mp\nu$, takes place with a branching ratio of 100%, see Fig. 9.

[8] AAD 11Z looked in 1.07 fb^{-1} of pp collisions at $\sqrt{s}$ = 7 TeV for events with one electron and one muon of opposite charge from the production of $\tilde{\nu}_\tau$ via an RPV λ'_{311} coupling and followed by a decay via λ_{312} into $e + \mu$. No evidence for an (e, μ) resonance over the SM expectation is observed, and a limit is derived in the plane of λ'_{311} versus $m_{\tilde{\nu}}$ for three values of λ_{312}, see their Fig. 2. Masses $m_{\tilde{\nu}}$ < 1.32 (1.45) TeV are excluded for λ'_{311} = 0.10 and λ_{312} = 0.05 (λ'_{311} = 0.11 and λ_{312} = 0.07).

[9] ABDALLAH 03M uses data from $\sqrt{s}$ = 192–208 GeV to obtain limits in the framework of the MSSM with gaugino and sfermion mass universality at the GUT scale. An indirect limit on the mass is derived by constraining the MSSM parameter space by the results from direct searches for neutralinos (including cascade decays) and for sleptons. These limits are valid for values of M_2 < 1 TeV, $|\mu| \leq$ 1 TeV with the $\tilde{\chi}^0_1$ as LSP. The quoted limit is obtained when there is no mixing in the third family. See Fig. 43 for the mass limits as a function of tanβ. These limits update the results of ABREU 00W.

[10] HEISTER 02N derives a bound on $m_{\tilde{\nu}_e}$ by exploiting the mass relation between the $\tilde{\nu}_e$ and $\tilde{e}$, based on the assumption of universal GUT scale gaugino and scalar masses $m_{1/2}$ and m_0 and the search described in the $\tilde{e}$ section. In the MSUGRA framework with radiative electroweak symmetry breaking, the limit improves to $m_{\tilde{\nu}_e}$ >130 GeV, assuming a trilinear coupling A_0=0 at the GUT scale. See Figs. 5 and 7 for the dependence of the limits on tanβ.

[11] DECAMP 92 limit is from Γ(invisible)/$\Gamma(\ell\ell)$ = 5.91 ± 0.15 (N_ν = 2.97 ± 0.07).

[12] SIRUNYAN 19AO searched in 35.9 fb^{-1} of pp collisions at $\sqrt{s}$ = 13 TeV for events containing two same-sign muons and at last two jets, originating from resonant production of second-generation sleptons ($\tilde{\mu}_L$, $\tilde{\nu}_\mu$) via the R-parity violating coupling λ'_{211} to quarks. No significant excess above the Standard Model expectations is observed. Upper limits on cross sections are derived in the context of two simplified models, see their Figure 4. The cross section limits are translated into limits on λ'_{211} for a modified CMSSM, see their Figure 5.

[13] KHACHATRYAN 16BE searched in 19.7 fb^{-1} of pp collisions at $\sqrt{s}$ = 8 TeV for evidence of narrow resonances decaying into $e\mu$ final states. No significant excess above the Standard Model expectation is observed and 95% C.L. exclusions are placed on the cross section times branching ratio for the production of an R-parity-violating supersymmetric tau sneutrino, see their Fig. 3.

[14] AAD 15O searched in 20.3 fb^{-1} of pp collisions at $\sqrt{s}$ = 8 TeV for evidence of heavy particles decaying into $e\mu$, $e\tau$ or $\mu\tau$ final states. No significant excess above the Standard Model expectation is observed, and 95% C.L. exclusions are placed on the cross section times branching ratio for the production of an R-parity-violating supersymmetric tau sneutrino, applicable to any sneutrino flavour, see their Fig. 2.

[15] AAD 13AI searched in 4.6 fb^{-1} of pp collisions at $\sqrt{s}$ = 7 TeV for evidence of heavy particles decaying into $e\mu$, $e\tau$ or $\mu\tau$ final states. No significant excess above the Standard Model expectation is observed, and 95% C.L. exclusions are placed on the cross section times branching ratio for the production of an R-parity-violating supersymmetric tau sneutrino, see their Fig. 2. For couplings λ'_{311} = 0.10 and λ_{i3k} = 0.05, the lower limits on the $\tilde{\nu}_\tau$ mass are 1610, 1110, 1100 GeV in the $e\mu$, $e\tau$, and $\mu\tau$ channels, respectively.

Downloaded from https://academic.oup.com/ptep/article/2022/8/083C01/6651666 by KIT Library user on 27 September 2022

[16] AAD 11H looked in 35 pb^{-1} of pp collisions at $\sqrt{s}$ = 7 TeV for events with one electron and one muon of opposite charge from the production of $\widetilde{\nu}_\tau$ via an RPV λ'_{311} coupling and followed by a decay via λ_{312} into $e + \mu$. No evidence for an excess over the SM expectation is observed, and a limit is derived in the plane of λ'_{311} versus $m_{\widetilde{\nu}}$ for several values of λ_{312}, see their Fig. 2. Superseded by AAD 11Z.

[17] AALTONEN 10Z searched in 1 fb^{-1} of $p\overline{p}$ collisions at $\sqrt{s}$ = 1.96 TeV for events from the production $d\overline{d} \rightarrow \widetilde{\nu}_\tau$ with the subsequent decays $\widetilde{\nu}_\tau \rightarrow e\mu$, $\mu\tau$, $e\tau$ in the MSSM framework with RPV. Two isolated leptons of different flavor and opposite charges are required, with τs identified by their hadronic decay. No statistically significant excesses are observed over the SM background. Upper limits on λ'^2_{311} times the branching ratio are listed in their Table III for various $\widetilde{\nu}_\tau$ masses. Limits on the cross section times branching ratio for λ'_{311} = 0.10 and λ_{i3k} = 0.05, displayed in Fig. 2, are used to set limits on the $\widetilde{\nu}_\tau$ mass of 558 GeV for the $e\mu$, 441 GeV for the $\mu\tau$ and 442 GeV for the $e\tau$ channels.

[18] ABAZOV 10M looked in 5.3 fb^{-1} of $p\overline{p}$ collisions at $\sqrt{s}$ = 1.96 TeV for events with exactly one pair of high p_T isolated $e\mu$ and a veto against hard jets. No evidence for an excess over the SM expectation is observed, and a limit at 95% C.L. on the cross section times branching ratio is derived, see their Fig. 3. These limits are translated into limits on couplings as a function of $m_{\widetilde{\nu}_\tau}$ as shown on their Fig. 4. As an example, for $m_{\widetilde{\nu}_\tau}$ = 100 GeV and $\lambda_{312} \leq 0.07$, couplings $\lambda'_{311} > 7.7 \times 10^{-4}$ are excluded.

[19] ABDALLAH 04H use data from LEP 1 and $\sqrt{s}$ = 192–208 GeV. They re-use results or re-analyze the data from ABDALLAH 03M to put limits on the parameter space of anomaly-mediated supersymmetry breaking (AMSB), which is scanned in the region 1< $m_{3/2}$ <50 TeV, 0< m_0 <1000 GeV, 1.5<tanβ <35, both signs of μ. The constraints are obtained from the searches for mass degenerate chargino and neutralino, for SM-like and invisible Higgs, for leptonically decaying charginos and from the limit on non-SM Z width of 3.2 MeV. The limit is for m_t = 174.3 GeV (see Table 2 for other m_t values). The limit improves to 114 GeV for μ < 0.

[20] ADRIANI 93M limit from $\Delta\Gamma(Z)$(invisible)< 16.2 MeV.

[21] ALEXANDER 91F limit is for one species of $\widetilde{\nu}$ and is derived from Γ(invisible, new)/$\Gamma(\ell\ell)$ < 0.38.

Charged sleptons

This section contains limits on charged scalar leptons ($\widetilde{\ell}$, with ℓ=e,μ,τ). Studies of width and decays of the Z boson (use is made here of $\Delta\Gamma_{\rm inv}$ < 2.0 MeV, LEP 00) conclusively rule out $m_{\widetilde{\ell}_R}$ < 40 GeV (41 GeV for $\widetilde{\ell}_L$) , independently of decay modes, for each individual slepton. The limits improve to 43 GeV (43.5 GeV for $\widetilde{\ell}_L$) assuming all 3 flavors to be degenerate. Limits on higher mass sleptons depend on model assumptions and on the mass splitting Δm= $m_{\widetilde{\ell}} - m_{\widetilde{\chi}^0_1}$. The mass and composition of $\widetilde{\chi}^0_1$ may affect the selectron production rate in e^+e^- collisions through t-channel exchange diagrams. Production rates are also affected by the potentially large mixing angle of the lightest mass eigenstate $\widetilde{\ell}_1$=$\widetilde{\ell}_R$ sinθ_ℓ + $\widetilde{\ell}_L$ cosθ_ℓ. It is generally assumed that only $\widetilde{\tau}$ may have significant mixing. The coupling to the Z vanishes for θ_ℓ=0.82. In the high-energy limit of e^+e^- collisions the interference between γ and Z exchange leads to a minimal cross section for θ_ℓ=0.91, a value which is sometimes used in the following entries relative to data taken at LEP 2. When limits on $m_{\widetilde{\ell}_R}$ are quoted, it is understood that limits on $m_{\widetilde{\ell}_L}$ are usually at least as strong.

Possibly open decays involving gauginos other than $\widetilde{\chi}^0_1$ will affect the detection efficiencies. Unless otherwise stated, the limits presented here result from the study of $\widetilde{\ell}^+\widetilde{\ell}^-$ production, with production rates and decay properties derived from the MSSM. Limits made obsolete by the recent analyses of e^+e^- collisions at high energies can be found in previous Editions of this Review.

For decays with final state gravitinos ($\widetilde{G}$), $m_{\widetilde{G}}$ is assumed to be negligible relative to all other masses.

R-parity conserving $\widetilde{e}$ (Selectron) mass limit

Some earlier papers are now obsolete and have been omitted. They were last listed in our PDG 14 edition: K. Olive, *et al.* (Particle Data Group), Chinese Physics **C38** 070001 (2014) (http://pdg.lbl.gov).

VALUE (GeV)	CL%	DOCUMENT ID		TECN	COMMENT
>700	95	[1] SIRUNYAN	21M	CMS	$\ell^\pm\ell^\mp + \not{E}_T$, $m_{\widetilde{\ell}_R} = m_{\widetilde{\ell}_L}$ and $\widetilde{\ell}$=$\widetilde{e}$, $\widetilde{\mu}$, $m_{\widetilde{\chi}^0_1}$ = 0 GeV
>700	95	[2] AAD	20O	ATLS	2ℓ+$\not{E}_T$, $m_{\widetilde{\ell}_R} = m_{\widetilde{\ell}_L}$ and $\widetilde{\ell}$=$\widetilde{e}$, $\widetilde{\mu}$, $m_{\widetilde{\chi}^0_1}$=0 GeV
>250	95	[3] SIRUNYAN	19AW	CMS	$\ell^\pm\ell^\mp + \not{E}_T$, $\widetilde{e}_R$, $m_{\widetilde{\chi}^0_1}$ = 0 GeV
>310	95	[3] SIRUNYAN	19AW	CMS	$\ell^\pm\ell^\mp + \not{E}_T$, $\widetilde{e}_L$, $m_{\widetilde{\chi}^0_1}$ = 0 GeV
>350	95	[3] SIRUNYAN	19AW	CMS	$\ell^\pm\ell^\mp + \not{E}_T$, $m_{\widetilde{e}_R} = m_{\widetilde{e}_L}$, $m_{\widetilde{\chi}^0_1}$ = 0 GeV
>290	95	[3] SIRUNYAN	19AW	CMS	$\ell^\pm\ell^\mp + \not{E}_T$, $\widetilde{\ell}_R$ and $\widetilde{\ell}$=$\widetilde{e}$, $\widetilde{\mu}$, $m_{\widetilde{\chi}^0_1}$ = 0 GeV
>400	95	[3] SIRUNYAN	19AW	CMS	$\ell^\pm\ell^\mp + \not{E}_T$, $\widetilde{\ell}_L$ and $\widetilde{\ell}$=$\widetilde{e}$, $\widetilde{\mu}$, $m_{\widetilde{\chi}^0_1}$ = 0 GeV
>450	95	[3] SIRUNYAN	19AW	CMS	$\ell^\pm\ell^\mp + \not{E}_T$, $m_{\widetilde{\ell}_R} = m_{\widetilde{\ell}_L}$ and $\widetilde{\ell}$=$\widetilde{e}$, $\widetilde{\mu}$, $m_{\widetilde{\chi}^0_1}$ = 0 GeV
>500	95	[4] AABOUD	18BT	ATLS	$2\ell + \not{E}_T$, $m_{\widetilde{\ell}_R} = m_{\widetilde{\ell}_L}$ and $\widetilde{\ell}$=$\widetilde{e}$, $\widetilde{\mu}$, $\widetilde{\tau}$, with $m_{\widetilde{\chi}^0_1}$ = 0 GeV
>190	95	[5] AABOUD	18R	ATLS	2ℓ (soft) + $\not{E}_T$, $m_{\widetilde{e}} = m_{\widetilde{\mu}}$, $m_{\widetilde{e}} - m_{\widetilde{\chi}^0_1}$ = 5 GeV
		[6] CHATRCHYAN	14R	CMS	$\geq 3\ell^\pm$, $\widetilde{\ell} \rightarrow \ell^\pm\tau^\mp\tau^\mp\widetilde{G}$ simplified model, GMSB, stau (N)NLSP scenario
		[7] AAD	13B	ATLS	$2\ell^\pm + \not{E}_T$, SMS, pMSSM
> 97.5		[8] ABBIENDI	04	OPAL	$\widetilde{e}_R$,Δm > 11 GeV, $\lvert\mu\rvert$ >100 GeV, tanβ=1.5
> 94.4		[9] ACHARD	04	L3	$\widetilde{e}_R$,Δm > 10 GeV, $\lvert\mu\rvert$ >200 GeV, tan$\beta \geq 2$
> 71.3		[9] ACHARD	04	L3	$\widetilde{e}_R$, all Δm
none 30–94	95	[10] ABDALLAH	03M	DLPH	Δm>15 GeV, $\widetilde{e}^+_R\widetilde{e}^-_R$
> 94	95	[11] ABDALLAH	03M	DLPH	$\widetilde{e}_R$,1 $\leq$ tan$\beta \leq$ 40, Δm >10 GeV
> 95	95	[12] HEISTER	02E	ALEP	Δm > 15 GeV, $\widetilde{e}^+_R\widetilde{e}^-_R$
> 73	95	[13] HEISTER	02N	ALEP	$\widetilde{e}_R$, any Δm
>107	95	[13] HEISTER	02N	ALEP	$\widetilde{e}_L$, any Δm
• • • We do not use the following data for averages, fits, limits, etc. • • •					
>101	95	[14] AAD	20I	ATLS	2ℓ (soft), jets, $\not{E}_T$, $\widetilde{e}_R$ only, $m_{\widetilde{e}_R} - m_{\widetilde{\chi}^0_1}$ = 7.5 GeV
>169	95	[15] AAD	20I	ATLS	2ℓ (soft), jets, $\not{E}_T$, $\widetilde{e}_L$ only, $m_{\widetilde{e}_L} - m_{\widetilde{\chi}^0_1}$ = 7.1 GeV
none 90–325	95	[16] AAD	14G	ATLS	$\widetilde{\ell}\widetilde{\ell} \rightarrow \ell^+\widetilde{\chi}^0_1\ell^-\widetilde{\chi}^0_1$, simplified model, $m_{\widetilde{\ell}_L} = m_{\widetilde{\ell}_R}$, $m_{\widetilde{\chi}^0_1}$ = 0 GeV
		[17] KHACHATRY...14I		CMS	$\widetilde{\ell} \rightarrow \ell\widetilde{\chi}^0_1$, simplified model

[1] SIRUNYAN 21M searched in 137 fb^{-1} of pp collisions at $\sqrt{s}$ = 13 TeV for supersymmetry in events with two opposite-sign same-flavor leptons (electrons, muons) and $\not{E}_T$. No significant excess above the Standard Model expectations is observed. Limits are set on the gluino mass in the simplified model Tglu4C, see their Figure 10, on the $\widetilde{\chi}^0_2$ and $\widetilde{\chi}^\pm_1$ mass in Tchi1n2Fa, see their Figure 11, on the $\widetilde{\chi}^0_1$ mass in Tn1n1C and Tn1n1B for $m_{\widetilde{\chi}^0_2}$=$m_{\widetilde{\chi}^\pm_1}$=$m_{\widetilde{\chi}^0_1}$, see their Figure 12. Limits are also set on the light squark mass for the simplified model Tsqk2A, on the sbottom mass in Tsbot3, see their Figure 13, and on the slepton mass in direct electroweak pair production of mass-degenerate left- and right-handed sleptons (selectrons and smuons), see their Figure 14.

[2] AAD 20O reported on a search for electroweak production in models with charginos and sleptons decaying into final states with exactly two oppositely charged leptons and missing transverse momentum. A dataset of pp collisions at $\sqrt{s}$ = 13 TeV corresponding to an integrated luminosity of 139 fb^{-1} was used. Light-flavour sleptons $\widetilde{e}$ and $\widetilde{\mu}$ are constrained at 95% C.L. to have masses above 700 GeV for massless lightest neutralino, see their Fig. 7(c). Exclusion limits are also set for selectrons and smuons separately, considering either right- or left-handed components, by including only the di-electron and di-muon same-flavour signal regions defined in the search, see their Fig. 8.

[3] SIRUNYAN 19AW searched in 35.9 fb^{-1} of pp collisions at $\sqrt{s}$ = 13 TeV for direct electroweak pair production of selectrons or smuons in events with two leptons (electrons or muons) of the opposite electric charge and same flavour, no jets and large $\not{E}_T$. No significant excess above the Standard Model expectations is observed. Limits are set on the selectron mass assuming left-handed, right-handed or both left- and right-handed (mass degenerate) production, see their Figure 6. Similarly, limits are set on the smuon mass, see their Figure 7. Limits are also set on slepton masses under the assumption that the selectron and smuon are mass degenerate, see their Figure 5.

[4] AABOUD 18BT searched in 36.1 fb^{-1} of pp collisions at $\sqrt{s}$ = 13 TeV for direct electroweak production of charginos, chargino and next-to-lightest neutralinos and sleptons in events with two or three leptons (electrons or muons), with or without jets, and large missing transverse energy. No significant excess above the Standard Model expectations is observed. Limits are set on the slepton mass up to 500 GeV for massless $\widetilde{\chi}^0_1$, assuming degeneracy of $\widetilde{e}$, $\widetilde{\mu}$, and $\widetilde{\tau}$ and exploiting the 2ℓ signature, see their Figure 8(b).

[5] AABOUD 18R searched in 36.1 fb^{-1} of pp collisions at $\sqrt{s}$ = 13 TeV for electroweak production in scenarios with compressed mass spectra in final states with two low-momentum leptons and missing transverse momentum. The data are found to be consistent with the SM prediction. Results are interpreted in slepton pair production models with a fourfold degeneracy assumed in selectron and smuon masses. The $\widetilde{e}$ masses are excluded up to 190 GeV for $m_{\widetilde{e}} - m_{\widetilde{\chi}^0_1}$ = 5 GeV. The exclusion limits extend down to mass splittings of 1 GeV, see their Fig. 11.

[6] CHATRCHYAN 14R searched in 19.5 fb^{-1} of pp collisions at $\sqrt{s}$ = 8 TeV for events with at least three leptons (electrons, muons, taus) in the final state. No significant excess above the Standard Model expectations is observed. Limits are set on the slepton mass in a stau (N)NLSP simplified model (GMSB) where the decay $\widetilde{\ell} \rightarrow \ell^\pm\tau^\pm\tau^\mp\widetilde{G}$ takes place with a branching ratio of 100%, see Fig. 8.

[7] AAD 13B searched in 4.7 fb^{-1} of pp collisions at $\sqrt{s}$ = 7 TeV for sleptons decaying to a final state with two leptons (e and μ) and missing transverse energy. No excess beyond the Standard Model expectation is observed. Limits are derived in a simplified model of direct left-handed slepton pair production, where left-handed slepton masses between 85 and 195 GeV are excluded at 95% C.L. for $m_{\widetilde{\chi}^0_1}$ = 20 GeV. See also Fig. 2(a). Exclusion limits are also derived in the phenomenological MSSM, see Fig. 3.

[8] ABBIENDI 04 search for $\widetilde{e}_R\widetilde{e}_R$ production in acoplanar di-electron final states in the 183–208 GeV data. See Fig. 13 for the dependence of the limits on $m_{\widetilde{\chi}^0_1}$ and for the limit at tanβ=35 This limit supersedes ABBIENDI 00G.

[9] ACHARD 04 search for $\widetilde{e}_R\widetilde{e}_L$ and $\widetilde{e}_R\widetilde{e}_R$ production in single- and acoplanar di-electron final states in the 192–209 GeV data. Absolute limits on $m_{\widetilde{e}_R}$ are derived from a scan over the MSSM parameter space with universal GUT scale gaugino and scalar masses $m_{1/2}$ and m_0, 1 $\leq$ tan$\beta \leq$ 60 and $-2 \leq \mu \leq 2$ TeV. See Fig. 4 for the dependence of the limits on $m_{\widetilde{\chi}^0_1}$. This limit supersedes ACCIARRI 99W.

[10] ABDALLAH 03M looked for acoplanar dielectron $+\not{E}$ final states at $\sqrt{s}$ = 189–208 GeV. The limit assumes μ=$-$200 GeV and tanβ=1.5 in the calculation of the production cross

Downloaded from https://academic.oup.com/ptep/article/2022/8/083C01/6651666 by KIT Library user on 27 September 2022

section and B($\tilde{e} \rightarrow e\tilde{\chi}^0_1$). See Fig. 15 for limits in the ($m_{\tilde{e}_R}$, $m_{\tilde{\chi}^0_1}$) plane. These limits include and update the results of ABREU 01

[11] ABDALLAH 03M uses data from $\sqrt{s}$ = 192–208 GeV to obtain limits in the framework of the MSSM with gaugino and sfermion mass universality at the GUT scale. An indirect limit on the mass is derived by constraining the MSSM parameter space by the results from direct searches for neutralinos (including cascade decays) and for sleptons. These limits are valid for values of M_2 <1 TeV, $|\mu| \leq 1$ TeV with the $\tilde{\chi}^0_1$ as LSP. The quoted limit is obtained when there is no mixing in the third family. See Fig. 43 for the mass limits as a function of tanβ. These limits update the results of ABREU 00W.

[12] HEISTER 02E looked for acoplanar dielectron + $\not{E}_T$ final states from e^+e^- interactions between 183 and 209 GeV. The mass limit assumes $\mu < -200$ GeV and tanβ=2 for the production cross section and B($\tilde{e} \rightarrow e\tilde{\chi}^0_1$)=1. See their Fig. 4 for the dependence of the limit on Δm. These limits include and update the results of BARATE 01.

[13] HEISTER 02N search for $\tilde{e}_R\tilde{e}_L$ and $\tilde{e}_R\tilde{e}_R$ production in single- and acoplanar di-electron final states in the 183–208 GeV data. Absolute limits on $m_{\tilde{e}_R}$ are derived from a scan over the MSSM parameter space with universal GUT scale gaugino and scalar masses $m_{1/2}$ and m_0, $1 \leq$ tan$\beta \leq 50$ and $-10 \leq \mu \leq 10$ TeV. The region of small $|\mu|$, where cascade decays are important, is covered by a search for $\tilde{\chi}^0_1\tilde{\chi}^0_3$ in final states with leptons and possibly photons. Limits on $m_{\tilde{e}_L}$ are derived by exploiting the mass relation between the $\tilde{e}_L$ and $\tilde{e}_R$, based on universal m_0 and $m_{1/2}$. When the constraint from the mass limit of the lightest Higgs from HEISTER 02 is included, the bounds improve to $m_{\tilde{e}_R}$ >77(75) GeV and $m_{\tilde{e}_L}$ >115(115) GeV for a top mass of 175(180) GeV. In the MSUGRA framework with radiative electroweak symmetry breaking, the limits improve further to $m_{\tilde{e}_R}$ >95 GeV and $m_{\tilde{e}_L}$ >152 GeV, assuming a trilinear coupling A_0=0 at the GUT scale. See Figs. 4, 5, 7 for the dependence of the limits on tanβ.

[14] AAD 20I reported on ATLAS searches for slepton pair production in models with compressed mass spectra. A dataset of pp collisions at $\sqrt{s}$ = 13 TeV corresponding to an integrated luminosity of 139 fb^{-1} was used. Events with $\not{E}_T$, two same-flavour, opposite-charge, low-transverse-momentum leptons, and jets from initial-state radiation or characteristic of vector-boson fusion production are selected. Light-flavour sleptons $\tilde{e}$ and $\tilde{\mu}$ are constrained at 95% C.L. to have masses above 251 GeV for a mass splitting slepton$-\tilde{\chi}^0_1$ of 10 GeV, with constraints extending down to mass splittings of 550 MeV at the LEP slepton limits (73 GeV), see their Fig. 16(a). If only selectrons are considered, and $\tilde{e} = \tilde{e}_R$, masses below 101 GeV are excluded for mass splitting $\tilde{e}_R$, $\tilde{\chi}^0_1$ of 7.5 GeV. See their Fig. 16(b).

[15] AAD 20I reported on ATLAS searches for slepton pair production in models with compressed mass spectra. A dataset of pp collisions at $\sqrt{s}$ = 13 TeV corresponding to an integrated luminosity of 139 fb^{-1} was used. Events with $\not{E}_T$, two same-flavour, opposite-charge, low-transverse-momentum leptons, and jets from initial-state radiation or characteristic of vector-boson fusion production are selected. Light-flavour sleptons $\tilde{e}$ and $\tilde{\mu}$ are constrained at 95% C.L. to have masses above 251 GeV for a mass splitting slepton$-\tilde{\chi}^0_1$ of 10 GeV, with constraints extending down to mass splittings of 550 MeV at the LEP slepton limits (73 GeV). See their Fig. 16(a). If only selectron are considered, and $\tilde{e} = \tilde{e}_L$, masses below 169 GeV are excluded for mass splitting $\tilde{e}_L$, $\tilde{\chi}^0_1$ of 7.1 GeV. See their Fig. 16(b).

[16] AAD 14G searched in 20.3 fb^{-1} of pp collisions at $\sqrt{s}$ = 8 TeV for electroweak production of slepton pairs, decaying to a final sate with two leptons (e and μ) and missing transverse momentum. No excess beyond the Standard Model expectation is observed. Exclusion limits are derived in simplified models of slepton pair production, see Fig. 8. An interpretation in the pMSSM is also given, see Fig. 10.

[17] KHACHATRYAN 14I searched in 19.5 fb^{-1} of pp collisions at $\sqrt{s}$ = 8 TeV for electroweak production of slepton pairs decaying to a final state with opposite-sign lepton pairs (e or μ) and missing transverse momentum. No excess beyond the Standard Model expectation is observed. Exclusion limits are derived in simplified models, see Fig. 18.

R-partiy violating $\tilde{e}$ (Selectron) mass limit

Some earlier papers are now obsolete and have been omitted. They were last listed in our PDG 14 edition: K. Olive, *et al.* (Particle Data Group), Chinese Physics **C38** 070001 (2014) (http://pdg.lbl.gov).

VALUE (GeV)	CL%	DOCUMENT ID		TECN	COMMENT
>1200	95	[1] AAD	21Y	ATLS	$\geq 4\ell$, $\lambda_{12k} \neq 0$, $m_{\tilde{\chi}^0_1} = 900$ GeV (mass-degenerate $\tilde{\ell}_L$ and $\tilde{\nu}$ of all 3 generations)
> 870	95	[1] AAD	21Y	ATLS	$\geq 4\ell$, $\lambda_{i33} \neq 0$, $m_{\tilde{\chi}^0_1} = 450$ GeV (mass-degenerate $\tilde{\ell}_L$ and $\tilde{\nu}$ of all 3 generations)
>1065	95	[2] AABOUD	18Z	ATLS	$\geq 4\ell$, $\lambda_{12k} \neq 0$, $m_{\tilde{\chi}^0_1} = 600$ GeV (mass-degenerate left-handed sleptons and sneutrinos of all 3 generations)
> 780	95	[2] AABOUD	18Z	ATLS	$\geq 4\ell$, $\lambda_{i33} \neq 0$, $m_{\tilde{\chi}^0_1} = 300$ GeV (mass-degenerate left-handed sleptons and sneutrinos of all 3 generations)
> 410	95	[3] AAD	14X	ATLS	$\geq 4\ell^{\pm}$, $\tilde{\ell} \rightarrow l\tilde{\chi}^0_1$, $\tilde{\chi}^0_1 \rightarrow \ell^{\pm}\ell^{\mp}\nu$
• • • We do not use the following data for averages, fits, limits, etc. • • •					
> 89	95	[4] ABBIENDI	04F	OPAL	$\tilde{e}_L$
> 92	95	[5] ABDALLAH	04M	DLPH	$\tilde{e}_R$, indirect, Δm >5 GeV

[1] AAD 21Y searched in 139 fb^{-1} of pp collisions at $\sqrt{s}$ = 13 TeV for supersymmetry in events with four or more leptons (electrons, muons and tau-leptons). No significant excess above the Standard Model expectations is observed. Limits are set on Tchi1n12-GGM, and RPV models similar to Tchi1n2l, Tglu1A (with $q = u, d, s, c, b$, with equal branching fractions), and $\tilde{\ell}_L/\tilde{\nu} \rightarrow \ell/\nu\tilde{\chi}^0_1$ (mass-degenerate $\tilde{\ell}_L$ and $\tilde{\nu}$ of all 3 generations), all with $\tilde{\chi}^0_1 \rightarrow \ell^{\pm}\ell^{\mp}\nu$ via λ_{12k} or λ_{i33} (where $i,k \in 1,2$), see their Figure 11.

[2] AABOUD 18Z searched in 36.1 fb^{-1} of pp collisions at $\sqrt{s}$ = 13 TeV for events containing four or more charged leptons (electrons, muons and up to two hadronically decaying taus). No significant deviation from the expected SM background is observed. Limits are set on the Higgsino mass in simplified models of general gauge mediated supersymmetry Tn1n1A/Tn1n1B/Tn1n1C, see their Figure 9. Limits are also set on the wino, slepton, sneutrino and gluino mass in a simplified model of NLSP pair production with R-parity violating decays of the LSP via λ_{12k} or λ_{i33} to charged leptons, see their Figures 7, 8.

[3] AAD 14X searched in 20.3 fb^{-1} of pp collisions at $\sqrt{s}$ = 8 TeV for events with at least four leptons (electrons, muons, taus) in the final state. No significant excess above the Standard Model expectations is observed. Limits are set on the slepton mass in an R-parity violating simplified model where the decay $\tilde{\ell} \rightarrow \ell\tilde{\chi}^0_1$, with $\tilde{\chi}^0_1 \rightarrow \ell^{\pm}\ell^{\mp}\nu$, takes place with a branching ratio of 100%, see Fig. 9.

[4] ABBIENDI 04F use data from $\sqrt{s}$ = 189–209 GeV. They derive limits on sparticle masses under the assumption of RPV with $LL\overline{E}$ or $LQ\overline{D}$ couplings. The results are valid for tanβ = 1.5, $\mu = -200$ GeV, with, in addition, $\Delta m \geq 5$ GeV for indirect decays via $LQ\overline{D}$. The limit quoted applies to direct decays via $LL\overline{E}$ or $LQ\overline{D}$ couplings. For indirect decays, the limits on the $\tilde{e}_R$ mass are respectively 99 and 92 GeV for $LL\overline{E}$ and $LQ\overline{D}$ couplings and $m_{\tilde{\chi}^0} = 10$ GeV and degrade slightly for larger $\tilde{\chi}^0_1$ mass. Supersedes the results of ABBIENDI 00.

[5] ABDALLAH 04M use data from $\sqrt{s}$ = 192–208 GeV to derive limits on sparticle masses under the assumption of RPV with $LL\overline{E}$ or $\overline{UDD}$ couplings. The results are valid for $\mu = -200$ GeV, tanβ = 1.5, $\Delta m \geq 5$ GeV and assuming a BR of 1 for the given decay. The limit quoted is for indirect $\overline{UDD}$ decays using the neutralino constraint of 39.5 GeV for $LL\overline{E}$ and of 38.0 GeV for $\overline{UDD}$ couplings, also derived in ABDALLAH 04M. For indirect decays via $LL\overline{E}$ the limit improves to 95 GeV if the constraint from the neutralino is used and to 94 GeV if it is not used. For indirect decays via $\overline{UDD}$ couplings it remains unchanged when the neutralino constraint is not used. Supersedes the result of ABREU 00U.

R-parity conserving $\tilde{\mu}$ (Smuon) mass limit

VALUE (GeV)	CL%	DOCUMENT ID		TECN	COMMENT
>700	95	[1] SIRUNYAN	21M	CMS	$\ell^{\pm}\ell^{\mp} + \not{E}_T$, $m_{\tilde{\ell}_R} = m_{\tilde{\ell}_L}$ and $\tilde{\ell}$=$\tilde{e}$, $\tilde{\mu}$, $m_{\tilde{\chi}^0_1} = 0$ GeV
>150	95	[2] AAD	20I	ATLS	2ℓ (soft), jets, $\not{E}_T$, $\tilde{\mu}_R$ only, $m_{\tilde{\mu}_R} - m_{\tilde{\chi}^0_1} = 8.2$ GeV
>216	95	[3] AAD	20I	ATLS	2ℓ (soft), jets, $\not{E}_T$, $\tilde{\mu}_L$ only, $m_{\tilde{\mu}_L} - m_{\tilde{\chi}^0_1} = 10$ GeV
>700	95	[4] AAD	20O	ATLS	2ℓ+$\not{E}_T$, $m_{\tilde{\ell}_R} = m_{\tilde{\ell}_L}$ and $\tilde{\ell}$=$\tilde{e}$, $\tilde{\mu}$, $m_{\tilde{\chi}^0_1}$=0 GeV
>210	95	[5] SIRUNYAN	19AW	CMS	$\ell^{\pm}\ell^{\mp} + \not{E}_T$, $\tilde{\mu}_R$, $m_{\tilde{\chi}^0_1} = 0$ GeV
>280	95	[5] SIRUNYAN	19AW	CMS	$\ell^{\pm}\ell^{\mp} + \not{E}_T$, $\tilde{\mu}_L$, $m_{\tilde{\chi}^0_1} = 0$ GeV
>290	95	[5] SIRUNYAN	19AW	CMS	$\ell^{\pm}\ell^{\mp} + \not{E}_T$, $\tilde{\ell}_R$ and $\tilde{\ell}$=$\tilde{e}$, $\tilde{\mu}$, $m_{\tilde{\chi}^0_1} = 0$ GeV
>400	95	[5] SIRUNYAN	19AW	CMS	$\ell^{\pm}\ell^{\mp} + \not{E}_T$, $\tilde{\ell}_L$ and $\tilde{\ell}$=$\tilde{e}$, $\tilde{\mu}$, $m_{\tilde{\chi}^0_1} = 0$ GeV
>450	95	[5] SIRUNYAN	19AW	CMS	$\ell^{\pm}\ell^{\mp} + \not{E}_T$, $m_{\tilde{\ell}_R} = m_{\tilde{\ell}_L}$ and $\tilde{\ell}$=$\tilde{e}$, $\tilde{\mu}$, $m_{\tilde{\chi}^0_1} = 0$ GeV
>310	95	[5] SIRUNYAN	19AW	CMS	$\ell^{\pm}\ell^{\mp} + \not{E}_T$, $m_{\tilde{\mu}_R} = m_{\tilde{\mu}_L}$, $m_{\tilde{\chi}^0_1} = 0$ GeV
>190	95	[6] AABOUD	18R	ATLS	2ℓ (soft) + $\not{E}_T$, $m_{\tilde{e}} = m_{\tilde{\mu}}$, $m_{\tilde{\mu}} - m_{\tilde{\chi}^0_1} = 5$ GeV
		[7] CHATRCHYAN	14R	CMS	$\geq 3\ell^{\pm}$, $\tilde{\ell} \rightarrow \ell^{\pm}\tau^{\mp}\tau^{\mp}\tilde{G}$ simplified model, GMSB, stau (N)NLSP scenario
		[8] AAD	13B	ATLS	$2\ell^{\pm} + \not{E}_T$, SMS, pMSSM
> 91.0		[9] ABBIENDI	04	OPAL	Δm >3 GeV, $\tilde{\mu}^+_R\tilde{\mu}^-_R$, $\lvert\mu\rvert$ >100 GeV, tanβ=1.5
> 86.7		[10] ACHARD	04	L3	Δm >10 GeV, $\tilde{\mu}^+_R\tilde{\mu}^-_R$, $\lvert\mu\rvert$ >200 GeV, tan$\beta \geq 2$
none 30–88	95	[11] ABDALLAH	03M	DLPH	Δm >5 GeV, $\tilde{\mu}^+_R\tilde{\mu}^-_R$
> 94	95	[12] ABDALLAH	03M	DLPH	$\tilde{\mu}_R$,1 $\leq$ tan$\beta \leq$ 40, Δm >10 GeV
> 88	95	[13] HEISTER	02E	ALEP	Δm > 15 GeV, $\tilde{\mu}^+_R\tilde{\mu}^-_R$
• • • We do not use the following data for averages, fits, limits, etc. • • •					
>500	95	[14] AABOUD	18BT	ATLS	$2\ell + \not{E}_T$, $m_{\tilde{\ell}_R} = m_{\tilde{\ell}_L}$ and $\tilde{\ell}$=$\tilde{e}$, $\tilde{\mu}$, $\tilde{\tau}$, with $m_{\tilde{\chi}^0_1} = 0$ GeV
none 90–325	95	[15] AAD	14G	ATLS	$\tilde{\ell}\tilde{\ell} \rightarrow \ell^+\tilde{\chi}^0_1\ell^-\tilde{\chi}^0_1$, simplified model, $m_{\tilde{\ell}_L} = m_{\tilde{\ell}_R}$, $m_{\tilde{\chi}^0_1} = 0$ GeV
		[16] KHACHATRY...	14I	CMS	$\tilde{\ell} \rightarrow \ell\tilde{\chi}^0_1$, simplified model
> 80	95	[17] ABREU	00V	DLPH	$\tilde{\mu}_R\tilde{\mu}_R$ ($\tilde{\mu}_R \rightarrow \mu\tilde{G}$), $m_{\tilde{G}}$ >8 eV

[1] SIRUNYAN 21M searched in 137 fb^{-1} of pp collisions at $\sqrt{s}$ = 13 TeV for supersymmetry in events with two opposite-sign same-flavor leptons (electrons, muons) and $\not{E}_T$. No significant excess above the Standard Model expectations is observed. Limits are set on the gluino mass in the simplified model Tglu4C, see their Figure 10, on the $\tilde{\chi}^0_2$ and $\tilde{\chi}^{\pm}_1$ mass in Tchi1n2Fa, see their Figure 11, on the $\tilde{\chi}^0_1$ mass in Tn1n1C and Tn1n1B for $m_{\tilde{\chi}^0_2}$=$m_{\tilde{\chi}^{\pm}_1}$=$m_{\tilde{\chi}^0_1}$, see their Figure 12. Limits are also set on the light squark mass for the simplified model Tsqk2A, on the sbottom mass in Tsbot3, see their Figure 13, and on the slepton mass in direct electroweak pair production of mass-degenerate left- and right-handed sleptons (selectrons and smuons), see their Figure 14.

Downloaded from https://academic.oup.com/ptep/article/2022/8/083C01/6651666 by KIT Library user on 27 September 2022

[2] AAD 20I reported on ATLAS searches for slepton pair production in models with compressed mass spectra. A dataset of pp collisions at $\sqrt{s}$ = 13 TeV corresponding to an integrated luminosity of 139 fb^{-1} was used. Events with $\not{E}_T$, two same-flavour, opposite-charge, low-transverse-momentum leptons, and jets from initial-state radiation or characteristic of vector-boson fusion production are selected. Light-flavour sleptons $\tilde{e}$ and $\tilde{\mu}$ are constrained at 95% C.L. to have masses above 251 GeV for a mass splitting slepton$-\tilde{\chi}^0_1$ of 10 GeV, with constraints extending down to mass splittings of 550 MeV at the LEP slepton limits (73 GeV). See their Fig. 16(a). If only smuon are considered, and $\tilde{\mu} = \tilde{\mu}_R$, masses below 150 GeV are excluded for mass splitting $\tilde{\mu}_R$, $\tilde{\chi}^0_1$ of 8.2 GeV. See their Fig. 16(b).

[3] AAD 20I reported on ATLAS searches for slepton pair production in models with compressed mass spectra. A dataset of pp collisions at $\sqrt{s}$ = 13 TeV corresponding to an integrated luminosity of 139 fb^{-1} was used. Events with $\not{E}_T$, two same-flavour, opposite-charge, low-transverse-momentum leptons, and jets from initial-state radiation or characteristic of vector-boson fusion production are selected. Light-flavour sleptons $\tilde{e}$ and $\tilde{\mu}$ are constrained at 95% C.L. to have masses above 251 GeV for a mass splitting slepton$-\tilde{\chi}^0_1$ of 10 GeV, with constraints extending down to mass splittings of 550 MeV at the LEP slepton limits (73 GeV). See their Fig. 16(a). If only smuon are considered, and $\tilde{\mu} = \tilde{\mu}_L$, masses below 216 GeV are excluded for mass splitting $\tilde{\mu}_L$, $\tilde{\chi}^0_1$ of 10 GeV. See their Fig. 16(b).

[4] AAD 20O reported on a search for electroweak production in models with charginos and sleptons decaying into final states with exactly two oppositely charged leptons and missing transverse momentum. A dataset of pp collisions at $\sqrt{s}$ = 13 TeV corresponding to an integrated luminosity of 139 fb^{-1} was used. Light-flavour sleptons $\tilde{e}$ and $\tilde{\mu}$ are constrained at 95% C.L. to have masses above 700 GeV for massless lightest neutralino, see their Fig. 7(c). Exclusion limits are also set for selectrons and smuons separately, considering either right- or left-handed components, by including only the di-electron and di-muon same-flavour signal regions defined in the search, see their Fig. 8.

[5] SIRUNYAN 19AW searched in 35.9 fb^{-1} of pp collisions at $\sqrt{s}$ = 13 TeV for direct electroweak pair production of selectrons or smuons in events with two leptons (electrons or muons) of the opposite electric charge and same flavour, no jets and large $\not{E}_T$. No significant excess above the Standard Model expectations is observed. Limits are set on the selectron mass assuming left-handed, right-handed or both left- and right-handed (mass degenerate) production, see their Figure 6. Similarly, limits are set on the smuon mass, see their Figure 7. Limits are also set on slepton masses under the assumption that the selectron and smuon are mass degenerate, see their Figure 5.

[6] AABOUD 18R searched in 36.1 fb^{-1} of pp collisions at $\sqrt{s}$ = 13 TeV for electroweak production in scenarios with compressed mass spectra in final states with two low-momentum leptons and missing transverse momentum. The data are found to be consistent with the SM prediction. Results are interpreted in slepton pair production models with a fourfold degeneracy assumed in selectron and smuon masses. The $\tilde{\mu}$ masses are excluded up to 190 GeV for $m_{\tilde{\mu}} - m_{\tilde{\chi}^0_1}$ = 5 GeV. The exclusion limits extend down to mass splittings of 1 GeV, see their Fig. 11.

[7] CHATRCHYAN 14R searched in 19.5 fb^{-1} of pp collisions at $\sqrt{s}$ = 8 TeV for events with at least three leptons (electrons, muons, taus) in the final state. No significant excess above the Standard Model expectations is observed. Limits are set on the slepton mass in a stau (N)NLSP simplified model (GMSB) where the decay $\tilde{\ell} \rightarrow \ell^{\pm}\tau^{\pm}\tau^{\mp}\tilde{G}$ takes place with a branching ratio of 100%, see Fig. 8.

[8] AAD 13B searched in 4.7 fb^{-1} of pp collisions at $\sqrt{s}$ = 7 TeV for sleptons decaying to a final state with two leptons (e and μ) and missing transverse energy. No excess beyond the Standard Model expectation is observed. Limits are derived in a simplified model of direct left-handed slepton pair production, where left-handed slepton masses between 85 and 195 GeV are excluded at 95% C.L. for $m_{\tilde{\chi}^0_1}$ = 20 GeV. See also Fig. 2(a). Exclusion limits are also derived in the phenomenological MSSM, see Fig. 3.

[9] ABBIENDI 04 search for $\tilde{\mu}_R\tilde{\mu}_R$ production in acoplanar di-muon final states in the 183–208 GeV data. See Fig. 14 for the dependence of the limits on $m_{\tilde{\chi}^0_1}$ and for the limit at tanβ=35. Under the assumption of 100% branching ratio for $\tilde{\mu}_R \rightarrow \mu\tilde{\chi}^0_1$, the limit improves to 94.0 GeV for $\Delta m > 4$ GeV. See Fig. 11 for the dependence of the limits on $m_{\tilde{\chi}^0_1}$ at several values of the branching ratio. This limit supersedes ABBIENDI 00G.

[10] ACHARD 04 search for $\tilde{\mu}_R\tilde{\mu}_R$ production in acoplanar di-muon final states in the 192–209 GeV data. Limits on $m_{\tilde{\mu}_R}$ are derived from a scan over the MSSM parameter space with universal GUT scale gaugino and scalar masses $m_{1/2}$ and m_0, $1 \leq$ tan$\beta \leq 60$ and $-2 \leq \mu \leq 2$ TeV. See Fig. 4 for the dependence of the limits on $m_{\tilde{\chi}^0_1}$. This limit supersedes ACCIARRI 99W.

[11] ABDALLAH 03M looked for acoplanar dimuon $+\not{E}$ final states at $\sqrt{s}$ = 189–208 GeV. The limit assumes B($\tilde{\mu} \rightarrow \mu\tilde{\chi}^0_1$) = 100%. See Fig. 16 for limits on the ($m_{\tilde{\mu}_R}$, $m_{\tilde{\chi}^0_1}$) plane. These limits include and update the results of ABREU 01.

[12] ABDALLAH 03M uses data from $\sqrt{s}$ = 192–208 GeV to obtain limits in the framework of the MSSM with gaugino and sfermion mass universality at the GUT scale. An indirect limit on the mass is derived by constraining the MSSM parameter space by the results from direct searches for neutralinos (including cascade decays) and for sleptons. These limits are valid for values of $M_2 < 1$ TeV, $|\mu| \leq 1$ TeV with the $\tilde{\chi}^0_1$ as LSP. The quoted limit is obtained when there is no mixing in the third family. See Fig. 43 for the mass limits as a function of tanβ. These limits update the results of ABREU 00W.

[13] HEISTER 02E looked for acoplanar dimuon + $\not{E}_T$ final states from e^+e^- interactions between 183 and 209 GeV. The mass limit assumes B($\tilde{\mu} \rightarrow \mu\tilde{\chi}^0_1$)=1. See their Fig. 4 for the dependence of the limit on Δm. These limits include and update the results of BARATE 01.

[14] AABOUD 18BT searched in 36.1 fb^{-1} of pp collisions at $\sqrt{s}$ = 13 TeV for direct electroweak production of charginos, chargino and next-to-lightest neutralinos and sleptons in events with two or three leptons (electrons or muons), with or without jets, and large missing transverse energy. No significant excess above the Standard Model expectations is observed. Limits are set on the slepton mass up to 500 GeV for massless $\tilde{\chi}^0_1$, assuming degeneracy of $\tilde{e}$, $\tilde{\mu}$, and $\tilde{\tau}$ and exploiting the 2ℓ signature, see their Figure 8(b).

[15] AAD 14G searched in 20.3 fb^{-1} of pp collisions at $\sqrt{s}$ = 8 TeV for electroweak production of slepton pairs, decaying to a final sate with two leptons (e and μ) and missing transverse momentum. No excess beyond the Standard Model expectation is observed. Exclusion limits are derived in simplified models of slepton pair production, see Fig. 8. An interpretation in the pMSSM is also given, see Fig. 10.

[16] KHACHATRYAN 14I searched in 19.5 fb^{-1} of pp collisions at $\sqrt{s}$ = 8 TeV for electroweak production of slepton pairs decaying to a final state with opposite-sign lepton pairs (e or μ) and missing transverse momentum. No excess beyond the Standard Model expectation is observed. Exclusion limits are derived in simplified models, see Fig. 18.

[17] ABREU 00V use data from $\sqrt{s}$= 130–189 GeV to search for tracks with large impact parameter or visible decay vertices. Limits are obtained as function of $m_{\tilde{G}}$, after combining these results with the search for slepton pair production in the SUGRA framework from ABREU 01 to cover prompt decays and on stable particle searches from ABREU 00Q. For limits at different $m_{\tilde{G}}$, see their Fig. 12.

R-parity violating $\tilde{\mu}$ (Smuon) mass limit

VALUE (GeV)	CL%	DOCUMENT ID		TECN	COMMENT
>1200	95	[1] AAD	21Y	ATLS	$\geq 4\ell$, $\lambda_{12k} \neq 0$, $m_{\tilde{\chi}^0_1}$ = 900 GeV (mass-degenerate $\tilde{\ell}_L$ and $\tilde{\nu}$ of all 3 generations)
> 870	95	[1] AAD	21Y	ATLS	$\geq 4\ell$, $\lambda_{i33} \neq 0$, $m_{\tilde{\chi}^0_1}$ = 450 GeV (mass-degenerate $\tilde{\ell}_L$ and $\tilde{\nu}$ of all 3 generations)
> 780	95	[2] AABOUD	18Z	ATLS	$\geq 4\ell$, $\lambda_{i33} \neq 0$, $m_{\tilde{\chi}^0_1}$=300 GeV (mass-degenerate left-handed sleptons and sneutrinos of all 3 generations)
>1060	95	[2] AABOUD	18Z	ATLS	$\geq 4\ell$, $\lambda_{12k} \neq 0$, $m_{\tilde{\chi}^0_1}$=600 GeV (mass-degenerate left-handed sleptons and sneutrinos of all 3 generations)
> 410	95	[3] AAD	14X	ATLS	RPV, $\geq 4\ell^{\pm}$, $\tilde{\ell} \rightarrow \ell\tilde{\chi}^0_1$, $\tilde{\chi}^0_1 \rightarrow \ell^{\pm}\ell^{\mp}\nu$
• • • We do not use the following data for averages, fits, limits, etc. • • •					
		[4] SIRUNYAN	19AO		$\mu^{\pm}\mu^{\pm}$ + $\geq$ 2jets, $\lambda'_{211} \neq 0$, $\tilde{\mu}_L \rightarrow \mu\tilde{\chi}^0_1$, $\tilde{\chi}^0_1 \rightarrow \mu q\overline{q}$
> 87	95	[5] ABDALLAH	04M	DLPH	RPV, $\tilde{\mu}_R$, indirect, Δm >5 GeV
> 81	95	[6] HEISTER	03G	ALEP	RPV, $\tilde{\mu}_L$

[1] AAD 21Y searched in 139 fb^{-1} of pp collisions at $\sqrt{s}$ = 13 TeV for supersymmetry in events with four or more leptons (electrons, muons and tau-leptons). No significant excess above the Standard Model expectations is observed. Limits are set on Tchi1n12-GGM, and RPV models similar to Tchi1n2l, Tglu1A (with q = u, d, s, c, b, with equal branching fractions), and $\tilde{\ell}_L/\tilde{\nu} \rightarrow \ell/\nu\tilde{\chi}^0_1$ (mass-degenerate $\tilde{\ell}_L$ and $\tilde{\nu}$ of all 3 generations), all with $\tilde{\chi}^0_1 \rightarrow \ell^{\pm}\ell^{\mp}\nu$ via λ_{12k} or λ_{i33} (where $i,k \in 1,2$), see their Figure 11.

[2] AABOUD 18Z searched in 36.1 fb^{-1} of pp collisions at $\sqrt{s}$ = 13 TeV for events containing four or more charged leptons (electrons, muons and up to two hadronically decaying taus). No significant deviation from the expected SM background is observed. Limits are set on the Higgsino mass in simplified models of general gauge mediated supersymmetry Tn1n1A/Tn1n1B/Tn1n1C, see their Figure 9. Limits are also set on the wino, slepton, sneutrino and gluino mass in a simplified model of NLSP pair production with R-parity violating decays of the LSP via λ_{12k} or λ_{i33} to charged leptons, see their Figures 7, 8.

[3] AAD 14X searched in 20.3 fb^{-1} of pp collisions at $\sqrt{s}$ = 8 TeV for events with at least four leptons (electrons, muons, taus) in the final state. No significant excess above the Standard Model expectations is observed. Limits are set on the slepton mass in an R-parity violating simplified model where the decay $\tilde{\ell} \rightarrow \ell\tilde{\chi}^0_1$, with $\tilde{\chi}^0_1 \rightarrow \ell^{\pm}\ell^{\mp}\nu$, takes place with a branching ratio of 100%, see Fig. 9.

[4] SIRUNYAN 19AO searched in 35.9 fb^{-1} of pp collisions at $\sqrt{s}$ = 13 TeV for events containing two same-sign muons and at last two jets, originating from resonant production of second-generation sleptons ($\tilde{\mu}_L$, $\tilde{\nu}_{\mu}$) via the R-parity violating coupling λ'_{211} to quarks. No significant excess above the Standard Model expectations is observed. Upper limits on cross sections are derived in the context of two simplified models, see their Figure 4. The cross section limits are translated into limits on λ'_{211} for a modified CMSSM, see their Figure 5.

[5] ABDALLAH 04M use data from $\sqrt{s}$ = 192–208 GeV to derive limits on sparticle masses under the assumption of RPV with $LL\overline{E}$ or $\overline{UDD}$ couplings. The results are valid for μ = -200 GeV, tanβ = 1.5, Δm > 5 GeV and assuming a BR of 1 for the given decay. The limit quoted is for indirect $\overline{UDD}$ decays using the neutralino constraint of 39.5 GeV for $LL\overline{E}$ and of 38.0 GeV for $\overline{UDD}$ couplings, also derived in ABDALLAH 04M. For indirect decays via $LL\overline{E}$ the limit improves to 90 GeV if the constraint from the neutralino is used and remains at 87 GeV if it is not used. For indirect decays via $\overline{UDD}$ couplings it degrades to 85 GeV when the neutralino constraint is not used. Supersedes the result of ABREU 00U.

[6] HEISTER 03G searches for the production of smuons in the case of RPV prompt decays with $LL\overline{E}$, $LQ\overline{D}$ or $\overline{UDD}$ couplings at $\sqrt{s}$ = 189–209 GeV. The search is performed for direct and indirect decays, assuming one coupling at a time to be non-zero. The limit holds for direct decays mediated by RPV $LQ\overline{D}$ couplings and improves to 90 GeV for indirect decays (for Δm > 10 GeV). Limits are also given for $LL\overline{E}$ direct ($m_{\tilde{\mu}R}$ > 87 GeV) and indirect decays ($m_{\tilde{\mu}R}$ > 96 GeV for $m(\tilde{\chi}^0_1)$ > 23 GeV from BARATE 98S) and for $\overline{UDD}$ indirect decays ($m_{\tilde{\mu}R}$ > 85 GeV for Δm > 10 GeV). Supersedes the results from BARATE 01B.

R-parity conserving $\tilde{\tau}$ (Stau) mass limit

Some earlier papers are now obsolete and have been omitted. They were last listed in our PDG 14 edition: K. Olive, *et al.* (Particle Data Group), Chinese Physics **C38** 070001 (2014) (http://pdg.lbl.gov).

VALUE (GeV)	CL%	DOCUMENT ID		TECN	COMMENT
none 120–390	95	[1] AAD	20H		2 hadronic $\tau + \not{E}_T$, $\tilde{\tau}_{R/L} \rightarrow \tau\tilde{\chi}^0_1$, $m_{\tilde{\chi}^0_1}$ = 0 GeV

Downloaded from https://academic.oup.com/ptep/article/2022/8/083C01/6651666 by KIT Library user on 27 September 2022

none 90–150	95	[2] SIRUNYAN	20P	CMS	$2\,\tau+\not{E}_T$, $\tau_h\tau_h$ and $\ell\tau_h$, $m_{\widetilde{\tau}_R}=m_{\widetilde{\tau}_L}$, $m_{\widetilde{\chi}^0_1}=1$ GeV
$>$ 85.2		[3] ABBIENDI	04	OPAL	$\Delta m>6$ GeV, $\theta_\tau=\pi/2$, $\lvert\mu\rvert>100$ GeV, $\tan\beta$=1.5
$>$ 78.3		[4] ACHARD	04	L3	$\Delta m>15$ GeV, $\theta_\tau=\pi/2$, $\lvert\mu\rvert>200$ GeV,$\tan\beta\geq 2$
$>$ 81.9	95	[5] ABDALLAH	03M	DLPH	$\Delta m>15$ GeV, all θ_τ
$>$ 79	95	[6] HEISTER	02E	ALEP	$\Delta m>15$ GeV, $\theta_\tau=\pi/2$
$>$ 76	95	[6] HEISTER	02E	ALEP	$\Delta m>15$ GeV, θ_τ=0.91
• • • We do not use the following data for averages, fits, limits, etc. • • •					
$>$500	95	[7] AABOUD	18BT	ATLS	$2\ell+\not{E}_T$, $m_{\widetilde{\ell}_R}=m_{\widetilde{\ell}_L}$, $\widetilde{\ell}=\widetilde{e}$, $\widetilde{\mu}$, $\widetilde{\tau}$, $m_{\widetilde{\chi}^0_1}=0$ GeV
	95	[8] KHACHATRY...	17L	CMS	$2\,\tau+\not{E}_T$, $\widetilde{\tau}_L\rightarrow\tau\widetilde{\chi}^0_1$, $m_{\widetilde{\chi}^0_1}=0$ GeV
none 109	95	[9] AAD	16AA	ATLS	2 hadronic $\tau+\not{E}_T$, $\widetilde{\tau}_{R/L}\rightarrow\tau\widetilde{\chi}^0_1$, $m_{\widetilde{\chi}^0_1}=0$ GeV
		[10] AAD	12AF	ATLS	2τ + jets + $\not{E}_T$, GMSB
		[11] AAD	12AG	ATLS	$\geq 1\tau_h$ + jets + $\not{E}_T$, GMSB
		[12] AAD	12CM	ATLS	$\geq 1\tau$ + jets + $\not{E}_T$, GMSB
$>$ 87.4	95	[13] ABBIENDI	06B	OPAL	$\widetilde{\tau}_R\rightarrow\tau\widetilde{G}$, all $\tau(\widetilde{\tau}_R)$
$>$ 68	95	[14] ABDALLAH	04H	DLPH	AMSB, $\mu>0$
none $m_\tau-$ 26.3	95	[5] ABDALLAH	03M	DLPH	$\Delta m>m_\tau$, all θ_τ

[1] AAD 20H presented ATLAS searches for direct production for $\widetilde{\tau}$ in final states with two hadronically decaying leptons and $\not{E}_T$. The analysis uses a dataset of pp collisions at $\sqrt{s}=13$ TeV corresponding to an integrated luminosity of 139 fb^{-1}. Exclusion limits at 95% C.L. are derived in scenarios of direct production of $\widetilde{\tau}$ pairs with each $\widetilde{\tau}$ decaying into a τ and the lightest neutralino $\widetilde{\chi}^0_1$ in simplified models where the $\widetilde{\tau}_R$ and $\widetilde{\tau}_L$ mass eigenstates are degenerate. Stau masses from 120GeV to 390GeV are excluded for a massless lightest neutralino, see their Fig. 7(a). If $\widetilde{\tau}_L$-only pair production is considered, the exclusion region extends between 155 GeV to 310 GeV, see their Fig. 7(b).

[2] SIRUNYAN 20P searched in 77.2 fb^{-1} of pp collisions at $\sqrt{s}=13$ TeV for direct pair production of tau sleptons in events with a tau lepton pair and significant missing transverse momentum. Final states with two double hadronic decay of the tau leptons are considered, as well as where one of the tau leptons decays into an electron or a muon. No significant excess above the Standard Model expectations is observed. Limits are set on the stau mass in a simplified models where two tau sleptons are pair produced and decay to a tau lepton and the lightest neutralino, assuming either only left-handed stau production, see Figure 8, or assuming degenerate left- and right-handed stau production, see Figure 9.

[3] ABBIENDI 04 search for $\widetilde{\tau}\widetilde{\tau}$ production in acoplanar di-tau final states in the 183–208 GeV data. See Fig. 15 for the dependence of the limits on $m_{\widetilde{\chi}^0_1}$ and for the limit at $\tan\beta$=35. Under the assumption of 100% branching ratio for $\widetilde{\tau}_R\rightarrow\tau\widetilde{\chi}^0_1$, the limit improves to 89.8 GeV for $\Delta m>8$ GeV. See Fig. 12 for the dependence of the limits on $m_{\widetilde{\chi}^0_1}$ at several values of the branching ratio and for their dependence on θ_τ. This limit supersedes ABBIENDI 00G.

[4] ACHARD 04 search for $\widetilde{\tau}\widetilde{\tau}$ production in acoplanar di-tau final states in the 192–209 GeV data. Limits on $m_{\widetilde{\tau}_R}$ are derived from a scan over the MSSM parameter space with universal GUT scale gaugino and scalar masses $m_{1/2}$ and m_0, $1\leq\tan\beta\leq 60$ and $-2\leq\mu\leq 2$ TeV. See Fig. 4 for the dependence of the limits on $m_{\widetilde{\chi}^0_1}$.

[5] ABDALLAH 03M looked for acoplanar ditaus $+\not{E}$ final states at $\sqrt{s}=130$–208 GeV. A dedicated search was made for low mass $\widetilde{\tau}$s decoupling from the Z^0. The limit assumes B($\widetilde{\tau}\rightarrow\tau\widetilde{\chi}^0_1$) = 100%. See Fig. 20 for limits on the ($m_{\widetilde{\tau}}$,$m_{\widetilde{\chi}^0_1}$) plane and as function of the $\widetilde{\chi}^0_1$ mass and of the branching ratio. The limit in the low-mass region improves to 29.6 and 31.1 GeV for $\widetilde{\tau}_R$ and $\widetilde{\tau}_L$, respectively, at $\Delta m>m_\tau$. The limit in the high-mass region improves to 84.7 GeV for $\widetilde{\tau}_R$ and $\Delta m>15$ GeV. These limits include and update the results of ABREU 01.

[6] HEISTER 02E looked for acoplanar ditau $+\not{E}_T$ final states from e^+e^- interactions between 183 and 209 GeV. The mass limit assumes B($\widetilde{\tau}\rightarrow\tau\widetilde{\chi}^0_1$)=1. See their Fig. 4 for the dependence of the limit on Δm. These limits include and update the results of BARATE 01.

[7] AABOUD 18BT searched in 36.1 fb^{-1} of pp collisions at $\sqrt{s}=13$ TeV for direct electroweak production of charginos, chargino and next-to-lightest neutralinos and sleptons in events with two or three leptons (electrons or muons), with or without jets, and large missing transverse energy. No significant excess above the Standard Model expectations is observed. Limits are set on the slepton mass up to 500 GeV for massless $\widetilde{\chi}^0_1$, assuming degeneracy of $\widetilde{e}$, $\widetilde{\mu}$, and $\widetilde{\tau}$ and exploiting the 2ℓ signature, see their Figure 8(b).

[8] KHACHATRYAN 17L searched in about 19 fb^{-1} of pp collisions at $\sqrt{s}=8$ TeV for events with two τ (at least one decaying hadronically) and $\not{E}_T$. Results were interpreted to set constraints on the cross section for production of $\widetilde{\tau}_L$ pairs for $m_{\widetilde{\chi}^0_1}$=1 GeV. No mass constraints are set, see their Fig. 7.

[9] AAD 16AA summarized and extended ATLAS searches for electroweak supersymmetry in final states containing several charged leptons, $\not{E}_T$, with or without hadronic jets, in 20 fb^{-1} of pp collisions at $\sqrt{s}=8$ TeV. The paper reports 95% C.L. exclusion limits on the cross-section for production of $\widetilde{\tau}_R$ and $\widetilde{\tau}_L$ pairs for various $m_{\widetilde{\chi}^0_1}$, using the 2 hadronic $\tau+\not{E}_T$ analysis. The $m_{\widetilde{\tau}_{R/L}}=109$ GeV is excluded for $m_{\widetilde{\chi}^0_1}=0$ GeV, with the constraints being stronger for $\widetilde{\tau}_R$. See their Fig. 12.

[10] AAD 12AF searched in 2 fb^{-1} of pp collisions at $\sqrt{s}=7$ TeV for events with two tau leptons, jets and large $\not{E}_T$ in a GMSB framework. No significant excess above the expected background was found and an upper limit on the visible cross section for new phenomena is set. A 95% C.L. lower limit of 32 TeV on the mGMSB breaking scale Λ is set for $M_{mess}=250$ TeV, $N_S=3$, $\mu>0$ and $C_{grav}=1$, independent of $\tan\beta$.

[11] AAD 12AG searched in 2.05 fb^{-1} of pp collisions at $\sqrt{s}=7$ TeV for events with at least one hadronically decaying tau lepton, jets, and large $\not{E}_T$ in a GMSB framework. No significant excess above the expected background was found and an upper limit on the visible cross section for new phenomena is set. A 95% C.L. lower limit of 30 TeV on the mGMSB breaking scale Λ is set for $M_{mess}=250$ TeV, $N_S=3$, $\mu>0$ and $C_{grav}=1$, independent of $\tan\beta$. For large values of $\tan\beta$, the limit on Λ increases to 43 TeV.

[12] AAD 12CM searched in 4.7 fb^{-1} of pp collisions at $\sqrt{s}$=7 TeV for events with at least one tau lepton, zero or one additional light lepton (e/μ) jets, and large $\not{E}_T$ in a GMSB framework. No significant excess above the expected background was found and an upper limit on the visible cross section for new phenomena is set. A 95% C. L. lower limit of 54 TeV on the mGMSB breaking scale Λ is set for $M_{mess}=250$ TeV, $N_S=3$, $\mu>0$ and $C_{grav}=1$, for $\tan\beta>20$. Here the $\widetilde{\tau}_1$ is the NLSP.

[13] ABBIENDI 06B use 600 pb^{-1} of data from $\sqrt{s}=189$–209 GeV. They look for events from pair-produced staus in a GMSB scenario with $\widetilde{\tau}$ NLSP including prompt $\widetilde{\tau}$ decays to ditaus $+\not{E}$ final states, large impact parameters, kinked tracks and heavy stable charged particles. Limits on the cross-section are computed as a function of m($\widetilde{\tau}$) and the lifetime, see their Fig. 7. The limit is compared to the $\sigma\cdot BR^2$ from a scan over the GMSB parameter space.

[14] ABDALLAH 04H use data from LEP 1 and $\sqrt{s}=192$–208 GeV. They re-use results or re-analyze the data from ABDALLAH 03M to put limits on the parameter space of anomaly-mediated supersymmetry breaking (AMSB), which is scanned in the region $1<m_{3/2}<50$ TeV, $0<m_0<1000$ GeV, $1.5<\tan\beta<35$, both signs of μ. The constraints are obtained from the searches for mass degenerate chargino and neutralino, for SM-like and invisible Higgs, for leptonically decaying charginos and from the limit on non-SM Z width of 3.2 MeV. The limit is for $m_t=174.3$ GeV (see Table 2 for other m_t values). The limit improves to 75 GeV for $\mu<0$.

R-parity violating $\widetilde{\tau}$ (Stau) mass limit

Some earlier papers are now obsolete and have been omitted. They were last listed in our PDG 14 edition: K. Olive, *et al.* (Particle Data Group), Chinese Physics **C38** 070001 (2014) (http://pdg.lbl.gov).

VALUE (GeV)	CL%	DOCUMENT ID		TECN	COMMENT
$>$1200	95	[1] AAD	21Y	ATLS	$\geq 4\ell$, $\lambda_{12k}\neq 0$, $m_{\widetilde{\chi}^0_1}=$ 900 GeV (mass-degenerate $\widetilde{\ell}_L$ and $\widetilde{\nu}$ of all 3 generations)
$>$ 870	95	[1] AAD	21Y	ATLS	$\geq 4\ell$, $\lambda_{i33}\neq 0$, $m_{\widetilde{\chi}^0_1}=450$ GeV (mass-degenerate $\widetilde{\ell}_L$ and $\widetilde{\nu}$ of all 3 generations)
$>$1060	95	[2] AABOUD	18Z	ATLS	$\geq 4\ell$, $\lambda_{12k}\neq 0$, $m_{\widetilde{\chi}^0_1}=600$ GeV (mass-degenerate left-handed sleptons and sneutrinos of all 3 generations)
$>$ 780	95	[2] AABOUD	18Z	ATLS	$\geq 4\ell$, $\lambda_{i33}\neq 0$, $m_{\widetilde{\chi}^0_1}=300$ GeV (mass-degenerate left-handed sleptons and sneutrinos of all 3 generations)
$>$ 90	95	[3] ABDALLAH	04M	DLPH	$\widetilde{\tau}_R$, indirect, $\Delta m>5$ GeV
• • • We do not use the following data for averages, fits, limits, etc. • • •					
$>$ 74	95	[4] ABBIENDI	04F	OPAL	$\widetilde{\tau}_L$

[1] AAD 21Y searched in 139 fb^{-1} of pp collisions at $\sqrt{s}=13$ TeV for supersymmetry in events with four or more leptons (electrons, muons and tau-leptons). No significant excess above the Standard Model expectations is observed. Limits are set on Tchi1n12-GGM, and RPV models similar to Tchi1n2l, Tglu1A (with $q=u$, d, s, c, b, with equal branching fractions), and $\widetilde{\ell}_L/\widetilde{\nu}\rightarrow\ell/\nu\widetilde{\chi}^0_1$ (mass-degenerate $\widetilde{\ell}_L$ and $\widetilde{\nu}$ of all 3 generations), all with $\widetilde{\chi}^0_1\rightarrow\ell^\pm\ell^\mp\nu$ via λ_{12k} or λ_{i33} (where $i,k\in 1,2$), see their Figure 11.

[2] AABOUD 18Z searched in 36.1 fb^{-1} of pp collisions at $\sqrt{s}=13$ TeV for events containing four or more charged leptons (electrons, muons and up to two hadronically decaying taus). No significant deviation from the expected SM background is observed. Limits are set on the Higgsino mass in simplified models of general gauge mediated supersymmetry Tn1n1A/Tn1n1B/Tn1n1C, see their Figure 9. Limits are also set on the wino, slepton, sneutrino and gluino mass in a simplified model of NLSP pair production with R-parity violating decays of the LSP via λ_{12k} or λ_{i33} to charged leptons, see their Figures 7, 8.

[3] ABDALLAH 04M use data from $\sqrt{s}=192$–208 GeV to derive limits on sparticle masses under the assumption of RPV with $LL\overline{E}$ couplings. The results are valid for $\mu=-200$ GeV, $\tan\beta=1.5$, $\Delta m>5$ GeV and assuming a BR of 1 for the given decay. The limit quoted is for indirect decays using the neutralino constraint of 39.5 GeV, also derived in ABDALLAH 04M. For indirect decays via $LL\overline{E}$ the limit decreases to 86 GeV if the constraint from the neutralino is not used. Supersedes the result of ABREU 00U.

[4] ABBIENDI 04F use data from $\sqrt{s}=189$–209 GeV. They derive limits on sparticle masses under the assumption of RPV with $LL\overline{E}$ or $LQ\overline{D}$ couplings. The results are valid for $\tan\beta=1.5$, $\mu=-200$ GeV, with, in addition, $\Delta m>5$ GeV for indirect decays via $LQ\overline{D}$. The limit quoted applies to direct decays with $LL\overline{E}$ couplings and improves to 75 GeV for $LQ\overline{D}$ couplings. The limit on the $\widetilde{\tau}_R$ mass for indirect decays is 92 GeV for $LL\overline{E}$ couplings at $m_{\widetilde{\chi}^0}=10$ GeV and no exclusion is obtained for $LQ\overline{D}$ couplings. Supersedes the results of ABBIENDI 00.

Long-lived $\widetilde{\ell}$ (Slepton) mass limit

Limits on scalar leptons which leave detector before decaying. Limits from Z decays are independent of lepton flavor. Limits from continuum e^+e^- annihilation are also independent of flavor for smuons and staus. Selectron limits from e^+e^- collisions in the continuum depend on MSSM parameters because of the additional neutralino exchange contribution.

VALUE (GeV)	CL%	DOCUMENT ID		TECN	COMMENT
$>$720	95	[1] AAD	21AL	ATLS	2ℓ displaced, long-lived $\widetilde{e},\widetilde{e}\rightarrow e\,\widetilde{G}$, $m_{\widetilde{e}_R}=m_{\widetilde{e}_L}$, $\tau_{\widetilde{e}}=0.1$ ns
$>$680	95	[1] AAD	21AL	ATLS	2ℓ displaced, long-lived $\widetilde{\mu},\widetilde{\mu}\rightarrow\mu\,\widetilde{G}$, $m_{\widetilde{\mu}_R}=m_{\widetilde{\mu}_L}$, $\tau_{\widetilde{\mu}}=0.1$ ns
$>$340	95	[1] AAD	21AL	ATLS	2ℓ displaced, long-lived $\widetilde{\tau},\widetilde{\tau}\rightarrow\tau\,\widetilde{G}$, mixing $\sin\theta_{\widetilde{\tau}}=0.95$, $\tau_{\widetilde{\tau}}=0.1$ ns

Downloaded from https://academic.oup.com/ptep/article/2022/8/083C01/6651666 by KIT Library user on 27 September 2022

>820	95	[1] AAD	21AL	ATLS	2ℓ displaced, long-lived $\widetilde{\ell},\widetilde{\ell} \rightarrow \ell\widetilde{G}$, $m_{\widetilde{\ell}_R} = m_{\widetilde{\ell}_L}$, $m_{\widetilde{e}} = m_{\widetilde{\mu}} = m_{\widetilde{\tau}}$, $\tau_{\widetilde{\ell}} = 0.1$ ns
>430	95	[2] AABOUD	19AT	ATLS	long-lived $\widetilde{\tau}$, GMSB
>490	95	[3] KHACHATRY...	16BW	CMS	long-lived $\widetilde{\tau}$ from inclusive production, mGMSB SPS line 7 scenario
>240	95	[3] KHACHATRY...	16BW	CMS	long-lived $\widetilde{\tau}$ from direct pair production, mGMSB SPS line 7 scenario
>440	95	[4] AAD	15AE	ATLS	mGMSB, M_{mess} = 250 TeV, N_5 = 3, $\mu > 0$, C_{grav} = 5000, tanβ = 10
>385	95	[4] AAD	15AE	ATLS	mGMSB, M_{mess} = 250 TeV, N_5 = 3, $\mu > 0$, C_{grav} = 5000, tanβ = 50
>286	95	[4] AAD	15AE	ATLS	direct $\widetilde{\tau}$ production
none 124–309	95	[5] AAIJ	15BD	LHCB	long-lived $\widetilde{\tau}$, mGMSB, SPS7
> 98	95	[6] ABBIENDI	03L	OPAL	$\widetilde{\mu}_R$, $\widetilde{\tau}_R$
none 2–87.5	95	[7] ABREU	00Q	DLPH	$\widetilde{\mu}_R$, $\widetilde{\tau}_R$
> 81.2	95	[8] ACCIARRI	99H	L3	$\widetilde{\mu}_R$, $\widetilde{\tau}_R$
> 81	95	[9] BARATE	98K	ALEP	$\widetilde{\mu}_R$, $\widetilde{\tau}_R$
• • • We do not use the following data for averages, fits, limits, etc. • • •					
>300	95	[10] AAD	13AA	ATLS	long-lived $\widetilde{\tau}$, GMSB, tanβ = 5–20
		[11] ABAZOV	13B	D0	long-lived $\widetilde{\tau}$, 100 <$m_{\widetilde{\tau}}$ <300 GeV
>339	95	[12,13] CHATRCHYAN	13AB	CMS	long-lived $\widetilde{\tau}$, direct $\widetilde{\tau}_1$ pair prod., minimal GMSB, SPS line 7
>500	95	[12,14] CHATRCHYAN	13AB	CMS	long-lived $\widetilde{\tau}$, $\widetilde{\tau}_1$ from direct pair prod. and from decay of heavier SUSY particles, minimal GMSB, SPS line 7
>314	95	[15] CHATRCHYAN	12L	CMS	long-lived $\widetilde{\tau}$, $\widetilde{\tau}_1$ from decay of heavier SUSY particles, minimal GMSB, SPS line 7
>136	95	[16] AAD	11P	ATLS	stable $\widetilde{\tau}$, GMSB scenario, tanβ=5

[1] AAD 21AL searched in 139 fb^{-1} of pp collisions at $\sqrt{s}$ = 13 TeV for pair production of long-lived sleptons in events with highly displaced leptons. No significant excess above the Standard Model predictions is observed. Limits are set on $m_{\widetilde{e}}$, $m_{\widetilde{\mu}}$, $m_{\widetilde{\tau}}$ as a function of the slepton lifetime, assuming the $\widetilde{\ell} \rightarrow \ell\widetilde{G}$ decay and mass-degenerate $\widetilde{\ell}_L$ and $\widetilde{\ell}_R$. See Figures 2.

[2] AABOUD 19AT searched in 36.1 fb^{-1} of pp collisions at $\sqrt{s}$ = 13 TeV for metastable and stable R-hadrons. Multiple search strategies for a wide range of lifetimes, corresponding to path lengths of a few meters, are defined. No significant deviations from the expected Standard Model background are observed. Results are interpreted in terms of exclusion limits on long-lived stau in the context of GMSB models. Lower limits on the mass for direct production of staus are set at 430 GeV, see their Fig. 10 (left).

[3] KHACHATRYAN 16BW searched in 2.5 fb^{-1} of pp collisions at $\sqrt{s}$ = 13 TeV for events with heavy stable charged particles, identified by their anomalously high energy deposits in the silicon tracker and/or long time-of-flight measurements by the muon system. No evidence for an excess over the expected background is observed. Limits are derived for pair production of tau sleptons as a function of mass, depending on their direct or inclusive production in a minimal GMSB scenario along the Snowmass Points and Slopes (SPS) line 7, see Fig. 4 and Table 7.

[4] AAD 15AE searched in 19.1 fb^{-1} of pp collisions at $\sqrt{s}$ = 8 TeV for heavy long-lived charged particles, measured through their specific ionization energy loss in the ATLAS pixel detector or their time-of-flight in the ALTAS muon system. In the absence of an excess of events above the expected backgrounds, limits are set on stable $\widetilde{\tau}$ sleptons in various scenarios, see Figs. 5-7.

[5] AAIJ 15BD searched in 3.0 fb^{-1} of pp collisions at $\sqrt{s}$ = 7 and 8 TeV for evidence of Drell-Yan pair production of long-lived $\widetilde{\tau}$ particles. No evidence for such particles is observed and 95% C.L. upper limits on the cross section of $\widetilde{\tau}$ pair production are derived, see Fig. 7. In the mGMSB, assuming the SPS7 benchmark scenario $\widetilde{\tau}$ masses between 124 and 309 GeV are excluded at 95% C.L.

[6] ABBIENDI 03L used e^+e^- data at $\sqrt{s}$ = 130–209 GeV to select events with two high momentum tracks with anomalous dE/dx. The excluded cross section is compared to the theoretical expectation as a function of the heavy particle mass in their Fig. 3. The limit improves to 98.5 GeV for $\widetilde{\mu}_L$ and $\widetilde{\tau}_L$. The bounds are valid for colorless spin 0 particles with lifetimes longer than 10^{-6} s. Supersedes the results from ACKERSTAFF 98P.

[7] ABREU 00Q searches for the production of pairs of heavy, charged stable particles in e^+e^- annihilation at $\sqrt{s}$= 130–189 GeV. The upper bound improves to 88 GeV for $\widetilde{\mu}_L$, $\widetilde{\tau}_L$. These limits include and update the results of ABREU 98P.

[8] ACCIARRI 99H searched for production of pairs of back-to-back heavy charged particles at $\sqrt{s}$=130–183 GeV. The upper bound improves to 82.2 GeV for $\widetilde{\mu}_L$, $\widetilde{\tau}_L$.

[9] The BARATE 98K mass limit improves to 82 GeV for $\widetilde{\mu}_L$,$\widetilde{\tau}_L$. Data collected at $\sqrt{s}$=161–184 GeV.

[10] AAD 13AA searched in 4.7 fb^{-1} of pp collisions at $\sqrt{s}$ = 7 TeV for events containing long-lived massive particles in a GMSB framework. No significant excess above the expected background was found. A 95% C.L. lower limit of 300 GeV is placed on long-lived $\widetilde{\tau}$'s in the GMSB model with M_{mess} = 250 TeV, N_S = 3, $\mu > 0$, tanβ = 5–20. The lower limit on the GMSB breaking scale Λ was found to be 99–110 TeV, for tanβ values between 5 and 40, see Fig. 4 (top). Also, directly produced long-lived sleptons, or sleptons decaying to long-lived ones, are excluded at 95% C.L. up to a $\widetilde{\tau}$ mass of 278 GeV for models with slepton splittings smaller than 50 GeV.

[11] ABAZOV 13B looked in 6.3 fb^{-1} of $p\overline{p}$ collisions at $\sqrt{s}$ = 1.96 TeV for charged massive long-lived particles in events with muon-like particles that have both speed and ionization energy loss inconsistent with muons produced in beam collisions. In the absence of an excess, limits are set at 95% C.L. on the production cross section of stau leptons in the mass range 100–300 GeV, see their Table 20 and Fig. 23.

[12] CHATRCHYAN 13AB looked in 5.0 fb^{-1} of pp collisions at $\sqrt{s}$ = 7 TeV and in 18.8 fb^{-1} of pp collisions at $\sqrt{s}$ = 8 TeV for events with heavy stable particles, identified by their anomalous dE/dx in the tracker or additionally requiring that it be identified as muon in the muon chambers, from pair production of $\widetilde{\tau}_1$'s. No evidence for an excess over the expected background is observed. Supersedes CHATRCHYAN 12L.

[13] CHATRCHYAN 13AB limits are derived for pair production of $\widetilde{\tau}_1$ as a function of mass in minimal GMSB scenarios along the Snowmass Points and Slopes (SPS) line 7 (see Fig. 8 and Table 7). The limit given here is valid for direct pair $\widetilde{\tau}_1$ production.

[14] CHATRCHYAN 13AB limits are derived for the production of $\widetilde{\tau}_1$ as a function of mass in minimal GMSB scenarios along the Snowmass Points and Slopes (SPS) line 7 (see Fig. 8 and Table 7). The limit given here is valid for the production of $\widetilde{\tau}_1$ from both direct pair production and from the decay of heavier supersymmetric particles.

[15] CHATRCHYAN 12L looked in 5.0 fb^{-1} of pp collisions at $\sqrt{s}$ = 7 TeV for events with heavy stable particles, identified by their anomalous dE/dx in the tracker or additionally requiring that it be identified as muon in the muon chambers, from pair production of $\widetilde{\tau}_1$'s. No evidence for an excess over the expected background is observed. Limits are derived for the production of $\widetilde{\tau}_1$ as a function of mass in minimal GMSB scenarios along the Snowmass Points and Slopes (SPS) line 7 (see Fig. 3). The limit given here is valid for the production of $\widetilde{\tau}_1$ in the decay of heavier supersymmetric particles.

[16] AAD 11P looked in 37 pb^{-1} of pp collisions at $\sqrt{s}$ = 7 TeV for events with two heavy stable particles, reconstructed in the Inner tracker and the Muon System and identified by their time of flight in the Muon System. No evidence for an excess over the SM expectation is observed. Limits on the mass are derived, see Fig. 3, for $\widetilde{\tau}$ in a GMSB scenario and for sleptons produced by electroweak processes only, in which case the limit degrades to 110 GeV.

$\widetilde{q}$ (Squark) mass limit

For $m_{\widetilde{q}}$ > 60–70 GeV, it is expected that squarks would undergo a cascade decay via a number of neutralinos and/or charginos rather than undergo a direct decay to photinos as assumed by some papers. Limits obtained when direct decay is assumed are usually higher than limits when cascade decays are included.

Limits from e^+e^- collisions depend on the mixing angle of the lightest mass eigenstate $\widetilde{q}_1 = \widetilde{q}_R \sin\theta_q + \widetilde{q}_L \cos\theta_q$. It is usually assumed that only the sbottom and stop squarks have non-trivial mixing angles (see the stop and sbottom sections). Here, unless otherwise noted, squarks are always taken to be either left/right degenerate, or purely of left or right type. Data from Z decays have set squark mass limits above 40 GeV, in the case of $\widetilde{q} \rightarrow q\widetilde{\chi}_1$ decays if $\Delta m = m_{\widetilde{q}} - m_{\widetilde{\chi}^0_1} \gtrsim 5$ GeV. For smaller values of Δm, current constraints on the invisible width of the Z ($\Delta\Gamma_{\rm inv}$ < 2.0 MeV, LEP 00) exclude $m_{\widetilde{u}_{L,R}}$ <44 GeV, $m_{\widetilde{d}_R}$ <33 GeV, $m_{\widetilde{d}_L}$ <44 GeV and, assuming all squarks degenerate, $m_{\widetilde{q}}$ <45 GeV.

Some earlier papers are now obsolete and have been omitted. They were last listed in our PDG 14 edition: K. Olive, *et al.* (Particle Data Group), Chinese Physics **C38** 070001 (2014) (http://pdg.lbl.gov).

R-parity conserving $\widetilde{q}$ (Squark) mass limit

VALUE (GeV)	CL%	DOCUMENT ID		TECN	COMMENT
>1400	95	[1] AAD	21AK	ATLS	$\ell^\pm$ + jets + $\not{E}_T$, Tsqk3, 4 degenerate light $\widetilde{q}_\ell$, $m_{\widetilde{\chi}^\pm_1} = (m_{\widetilde{q}} + m_{\widetilde{\chi}^0_1})/2$, $m_{\widetilde{\chi}^0_1}$ < 200 GeV
>1040	95	[1] AAD	21AK	ATLS	$\ell^\pm$ + jets + $\not{E}_T$, Tsqk3, 1 light $\widetilde{q}_\ell$, $m_{\widetilde{\chi}^\pm_1} = (m_{\widetilde{q}} + m_{\widetilde{\chi}^0_1})/2$, $m_{\widetilde{\chi}^0_1}$ < 200 GeV
> 925	95	[2] AAD	21F	ATLS	≥ 1 jet + $\not{E}_T$, Tsqk1, $m_{\widetilde{q}} - m_{\widetilde{\chi}^0_1}$ = 5 GeV
> 550	95	[2] AAD	21F	ATLS	≥ 1 jet + $\not{E}_T$, Tstop3, $m_{\widetilde{t}} - m_{\widetilde{\chi}^0_1}$ = 5 GeV
> 550	95	[2] AAD	21F	ATLS	≥ 1 jet + $\not{E}_T$, Tstop4, $m_{\widetilde{t}} - m_{\widetilde{\chi}^0_1}$ = 5 GeV
> 545	95	[2] AAD	21F	ATLS	≥ 1 jet + $\not{E}_T$, Tsbot1, $m_{\widetilde{b}} - m_{\widetilde{\chi}^0_1}$ = 5 GeV
>1850	95	[3] AAD	21L	ATLS	jets + $\not{E}_T$, Tsqk1, 8 degenerate $\widetilde{q}$, $m_{\widetilde{\chi}^0_1}$ = 0 GeV
>1220	95	[3] AAD	21L	ATLS	jets + $\not{E}_T$, Tsqk1, 1 non-degenerate $\widetilde{q}$, $m_{\widetilde{\chi}^0_1}$ = 0 GeV
>1310	95	[3] AAD	21L	ATLS	jets + $\not{E}_T$, Tsqk3, 4 degenerate $\widetilde{q}_l$, $m_{\widetilde{\chi}^\pm_1} = (m_{\widetilde{q}} + m_{\widetilde{\chi}^0_1})/2$, $m_{\widetilde{\chi}^0_1}$ = 0 GeV
>3000	95	[3] AAD	21L	ATLS	jets + $\not{E}_T$, combined $\widetilde{g}\widetilde{g}$, $\widetilde{g}\,\widetilde{q}$, $\widetilde{q}\widetilde{q}$ production, $\widetilde{g} \rightarrow q q' \widetilde{\chi}^0_1$, $\widetilde{q} \rightarrow q\widetilde{\chi}^0_1$, $m_{\widetilde{q}} = m_{\widetilde{g}}$, $m_{\widetilde{\chi}^0_1}$ = 0 GeV
>1800	95	[4] SIRUNYAN	21M	CMS	$\ell^\pm\ell^\pm$ + $\not{E}_T$, Tsqk2A, $m_{\widetilde{\chi}^0_2}$ = 1500 GeV, $m_{\widetilde{\chi}^0_1}$ = 100 GeV
>1590	95	[5] SIRUNYAN	19AG	CMS	2γ +$\not{E}_T$, Tsqk4B, 500 GeV <$m_{\widetilde{\chi}^0_1}$ < 1500 GeV
>1130	95	[6] SIRUNYAN	19CH	CMS	jets+$\not{E}_T$, Tsqk1, 1 light flavour, $m_{\widetilde{\chi}^0_1}$ = 0 GeV
>1630	95	[6] SIRUNYAN	19CH	CMS	jets+$\not{E}_T$, Tsqk1, 8 degenerate light flavours, $m_{\widetilde{\chi}^0_1}$ = 0 GeV
>1430	95	[7] SIRUNYAN	19K	CMS	$\gamma + \ell + \not{E}_T$, Tsqk4A, $m_{\widetilde{\chi}^0_1}$ = 1200 GeV

Downloaded from https://academic.oup.com/ptep/article/2022/8/083C01/6651666 by KIT Library user on 27 September 2022

>1200	95	[8] AABOUD	18BJ	ATLS	$\ell^\pm\ell^\mp$ + jets + $\not{E}_T$, Tsqk2, $m_{\widetilde{\chi}^0_1}$ = 1 GeV, any $m_{\widetilde{\chi}^0_2}$
> 850	95	[9] AABOUD	18BV	ATLS	c-jets+$\not{E}_T$, Tsqk1 (charm only), $m_{\widetilde{\chi}^0_1}$ = 0 GeV
> 710	95	[10] AABOUD	18I	ATLS	≥ 1 jets+$\not{E}_T$, Tsqk1, $m_{\widetilde{q}} \sim m_{\widetilde{\chi}^0_1}$
>1820	95	[11] AABOUD	18U	ATLS	2 γ + $\not{E}_T$, GGM, Tsqk4B, any NLSP mass
>1550	95	[12] AABOUD	18V	ATLS	jets+$\not{E}_T$, Tsqk1, $m_{\widetilde{\chi}^0_1}$ = 0 GeV
>1150	95	[13] AABOUD	18V	ATLS	jets+$\not{E}_T$, Tsqk3, $m_{\widetilde{\chi}^\pm_1}$ = 0.5 ($m_{\widetilde{q}}$ + $m_{\widetilde{\chi}^0_1}$), $m_{\widetilde{\chi}^0_1}$ = 0 GeV
>1650	95	[14] SIRUNYAN	18AA	CMS	≥ 1γ + $\not{E}_T$, Tsqk4A
>1750	95	[14] SIRUNYAN	18AA	CMS	≥ 1γ + $\not{E}_T$, Tsqk4B
> 675	95	[15] SIRUNYAN	18AY	CMS	jets+$\not{E}_T$, Tsqk1, 1 light flavor state, $m_{\widetilde{\chi}^0_1}$ = 0 GeV
>1320	95	[15] SIRUNYAN	18AY	CMS	jets+$\not{E}_T$,Tsqk1,8 degenerate light flavor states, $m_{\widetilde{\chi}^0_1}$ = 0 GeV
>1220	95	[16] AABOUD	17AR	ATLS	1ℓ+jets+$\not{E}_T$, Tsqk3, $m_{\widetilde{\chi}^0_1}$ = 0 GeV
>1000	95	[17] AABOUD	17N	ATLS	2 same-flavour, opposite-sign ℓ + jets + $\not{E}_T$, Tsqk2, $m_{\widetilde{\chi}^0_1}$ = 0 GeV
>1150	95	[18] KHACHATRY...	17P	CMS	1 or more jets+$\not{E}_T$, Tsqk1, 4(flavor) x 2(isospin) = 8 mass degenerate states, $m_{\widetilde{\chi}^0_1}$ = 0 GeV
> 575	95	[18] KHACHATRY...	17P	CMS	1 or more jets+$\not{E}_T$, Tsqk1, one light flavor state, $m_{\widetilde{\chi}^0_1}$ = 0 GeV
>1370	95	[19] KHACHATRY...	17V	CMS	2 γ + $\not{E}_T$, GGM, Tsqk4, any NLSP mass
>1600	95	[20] SIRUNYAN	17AY	CMS	γ + jets+$\not{E}_T$, Tsqk4B, $m_{\widetilde{\chi}^0_1}$ = 0 GeV
>1370	95	[20] SIRUNYAN	17AY	CMS	γ + jets+$\not{E}_T$, Tsqk4A, $m_{\widetilde{\chi}^0_1}$ = 0 GeV
>1050	95	[21] SIRUNYAN	17AZ	CMS	≥ 1 jets+$\not{E}_T$, Tsqk1, single light flavor state, $m_{\widetilde{\chi}^0_1}$ = 0 GeV
>1550	95	[21] SIRUNYAN	17AZ	CMS	≥ 1 jets+$\not{E}_T$, Tsqk1, 4(flavor) x 2(isospin) = 8 degenerate mass states, $m_{\widetilde{\chi}^0_1}$ = 0 GeV
>1390	95	[22] SIRUNYAN	17P	CMS	jets+$\not{E}_T$, Tsqk1, 4(flavor) x 2(isospin) = 8 degenerate mass states, $m_{\widetilde{\chi}^0_1}$ = 0 GeV
> 950	95	[22] SIRUNYAN	17P	CMS	jets+$\not{E}_T$, Tsqk1, one light flavor state, $m_{\widetilde{\chi}^0_1}$ = 0 GeV
> 608	95	[23] AABOUD	16D	ATLS	≥ 1 jet + $\not{E}_T$, Tsqk1, $m_{\widetilde{q}}-m_{\widetilde{\chi}^0_1}$ = 5 GeV
>1030	95	[24] AABOUD	16N	ATLS	≥ 2 jets + $\not{E}_T$, Tsqk1, $m_{\widetilde{\chi}^0_1}$ = 0 GeV
> 600	95	[25] KHACHATRY...	16BS	CMS	jets + $\not{E}_T$, Tsqk1, single light squark, $m_{\widetilde{\chi}^0_1}$ = 0 GeV
>1260	95	[25] KHACHATRY...	16BS	CMS	jets + $\not{E}_T$, Tsqk1, 8 degenerate light squarks, $m_{\widetilde{\chi}^0_1}$ = 0 GeV
> 850	95	[26] AAD	15BV	ATLS	jets + $\not{E}_T$, $\widetilde{q} \rightarrow q\widetilde{\chi}^0_1$, $m_{\widetilde{\chi}^0_1}$ = 100 GeV
> 250	95	[27] AAD	15CS	ATLS	photon + $\not{E}_T$, $pp \rightarrow \widetilde{q}\widetilde{q}^*\gamma$, $\widetilde{q} \rightarrow q\widetilde{\chi}^0_1$, $m_{\widetilde{q}} - m_{\widetilde{\chi}^0_1} = m_c$
> 490	95	[28] AAD	15K	ATLS	$\widetilde{c} \rightarrow c\widetilde{\chi}^0_1$, $m_{\widetilde{\chi}^0_1}$ < 200 GeV
> 875	95	[29] KHACHATRY...	15AF	CMS	$\widetilde{q} \rightarrow q\widetilde{\chi}^0_1$, simplified model, 8 degenerate light $\widetilde{q}$, $m_{\widetilde{\chi}^0_1}$ = 0
> 520	95	[29] KHACHATRY...	15AF	CMS	$\widetilde{q} \rightarrow q\widetilde{\chi}^0_1$, simplified model, single light squark, $m_{\widetilde{\chi}^0_1}$ = 0
>1450	95	[29] KHACHATRY...	15AF	CMS	CMSSM, tanβ = 30, $A_0 = -2\max(m_0, m_{1/2})$, μ > 0
> 850	95	[30] AAD	14AE	ATLS	jets + $\not{E}_T$, $\widetilde{q} \rightarrow q\widetilde{\chi}^0_1$ simplified model, mass degenerate first and second generation squarks, $m_{\widetilde{\chi}^0_1}$ = 0 GeV
> 440	95	[30] AAD	14AE	ATLS	jets + $\not{E}_T$, $\widetilde{q} \rightarrow q\widetilde{\chi}^0_1$ simplified model, single light-flavour squark, $m_{\widetilde{\chi}^0_1}$ = 0 GeV
>1700	95	[30] AAD	14AE	ATLS	jets + $\not{E}_T$, mSUGRA/CMSSM, $m_{\widetilde{q}} = m_{\widetilde{g}}$
> 800	95	[31] CHATRCHYAN	14AH	CMS	jets + $\not{E}_T$, $\widetilde{q} \rightarrow q\widetilde{\chi}^0_1$ simplified model, $m_{\widetilde{\chi}^0_1}$ = 50 GeV
> 780	95	[32] CHATRCHYAN	14I	CMS	multijets + $\not{E}_T$, $\widetilde{q} \rightarrow q\widetilde{\chi}^0_1$ simplified model, $m_{\widetilde{\chi}^0_1}$ < 200 GeV
>1360	95	[33] AAD	13L	ATLS	jets + $\not{E}_T$, CMSSM, $m_{\widetilde{g}} = m_{\widetilde{q}}$
>1200	95	[34] AAD	13Q	ATLS	γ+b+$\not{E}_T$,higgsino-like neutralino, $m_{\widetilde{\chi}^0_1}$ > 220 GeV, GMSB
		[35] CHATRCHYAN	13	CMS	$\ell^\pm\ell^\mp$ + jets + $\not{E}_T$, CMSSM
>1250	95	[36] CHATRCHYAN	13G	CMS	0,1,2, ≥ 3 b-jets + $\not{E}_T$, CMSSM, $m_{\widetilde{q}} = m_{\widetilde{g}}$
>1430	95	[37] CHATRCHYAN	13H	CMS	2γ + ≥ 4 jets + low $\not{E}_T$, stealth SUSY model
> 750	95	[38] CHATRCHYAN	13T	CMS	jets + $\not{E}_T$, $\widetilde{q} \rightarrow q\widetilde{\chi}^0_1$ simplified model, $m_{\widetilde{\chi}^0_1}$= 0 GeV
> 820	95	[39] AAD	12AX	ATLS	ℓ +jets +$\not{E}_T$, CMSSM, $m_{\widetilde{q}}$=$m_{\widetilde{g}}$
>1200	95	[40] AAD	12CJ	ATLS	$\ell^\pm$+jets+$\not{E}_T$, CMSSM, $m_{\widetilde{q}}$=$m_{\widetilde{g}}$
> 870	95	[41] AAD	12CP	ATLS	2γ +$\not{E}_T$, GMSB, bino NLSP, $m_{\widetilde{\chi}^0_1}$ > 50 GeV
> 950	95	[42] AAD	12W	ATLS	jets + $\not{E}_T$, CMSSM, $m_{\widetilde{q}} = m_{\widetilde{g}}$
		[43] CHATRCHYAN	12	CMS	e, μ, jets, razor, CMSSM
> 760	95	[44] CHATRCHYAN	12AE	CMS	jets + $\not{E}_T$, $\widetilde{q} \rightarrow q\widetilde{\chi}^0_1$, $m_{\widetilde{\chi}^0_1}$ < 200 GeV
>1110	95	[45] CHATRCHYAN	12AT	CMS	jets + $\not{E}_T$, CMSSM
>1180	95	[45] CHATRCHYAN	12AT	CMS	jets + $\not{E}_T$, CMSSM, $m_{\widetilde{q}}$=$m_{\widetilde{g}}$
• • • We do not use the following data for averages, fits, limits, etc. • • •					
>1080	95	[46] AABOUD	18V	ATLS	jets+$\not{E}_T$, Tsqk5, $(m_{\widetilde{\chi}^0_2}-m_{\widetilde{\chi}^0_1})/(m_{\widetilde{q}}-m_{\widetilde{\chi}^0_1})$ < 0.95, $m_{\widetilde{\chi}^0_1}$ = 60 GeV
> 300	95	[47] KHACHATRY...	16BT	CMS	19-parameter pMSSM model, global Bayesian analysis, flat prior
	95	[48] AAD	15AI	ATLS	$\ell^\pm$ + jets + $\not{E}_T$
>1650	95	[26] AAD	15BV	ATLS	jets + $\not{E}_T$, $m_{\widetilde{g}} = m_{\widetilde{q}}$, $m_{\widetilde{\chi}^0_1}$ = 1 GeV
> 790	95	[26] AAD	15BV	ATLS	jets + $\not{E}_T$, $\widetilde{q} \rightarrow qW\widetilde{\chi}^0_1$, $m_{\widetilde{\chi}^0_1}$ = 100 GeV
> 820	95	[26] AAD	15BV	ATLS	2 or 3 leptons + jets, $\widetilde{q}$ decays via sleptons, $m_{\widetilde{\chi}^0_1}$ = 100 GeV
> 850	95	[26] AAD	15BV	ATLS	τ, $\widetilde{q}$ decays via staus, $m_{\widetilde{\chi}^0_1}$ = 50 GeV
> 700	95	[49] KHACHATRY...	15AR	CMS	$\widetilde{q} \rightarrow q\widetilde{\chi}^0_1$, $\widetilde{\chi}^0_1 \rightarrow \widetilde{S}g$, $\widetilde{S} \rightarrow S\widetilde{G}$, $S \rightarrow gg$, $m_{\widetilde{S}}$ = 100 GeV, m_S = 90 GeV
> 550	95	[49] KHACHATRY...	15AR	CMS	$\ell^\pm$, $\widetilde{q} \rightarrow q\widetilde{\chi}^\pm_1$, $\widetilde{\chi}^\pm_1 \rightarrow \widetilde{S}W^\pm$, $\widetilde{S} \rightarrow S\widetilde{G}$, $S \rightarrow gg$, $m_{\widetilde{S}}$ = 100 GeV, m_S = 90 GeV
>1500	95	[50] KHACHATRY...	15AZ	CMS	≥ 2 γ, ≥ 1 jet, (Razor), bino-like NLSP, $m_{\widetilde{\chi}^0_1}$ = 375 GeV
>1000	95	[50] KHACHATRY...	15AZ	CMS	≥ 1 γ, ≥ 2 jet, wino-like NLSP, $m_{\widetilde{\chi}^0_1}$ = 375 GeV
> 670	95	[51] AAD	14E	ATLS	$\ell^\pm\ell^\pm(\ell^\mp)$ + jets, $\widetilde{q} \rightarrow q'\widetilde{\chi}^\pm_1$, $\widetilde{\chi}^\pm_1 \rightarrow W^{(*)\pm}\widetilde{\chi}^0_2$, $\widetilde{\chi}^0_2 \rightarrow Z^{(*)}\widetilde{\chi}^0_1$ simplified model, $m_{\widetilde{\chi}^0_1}$ < 300 GeV
> 780	95	[51] AAD	14E	ATLS	$\ell^\pm\ell^\pm(\ell^\mp)$ + jets, $\widetilde{q} \rightarrow q'\widetilde{\chi}^\pm_1/\widetilde{\chi}^0_2$, $\widetilde{\chi}^\pm_1 \rightarrow \ell^\pm\nu\widetilde{\chi}^0_1$, $\widetilde{\chi}^0_2 \rightarrow \ell^\pm\ell^\mp(\nu\nu)\widetilde{\chi}^0_1$ simplified model
> 700	95	[52] CHATRCHYAN	13AO	CMS	$\ell^\pm\ell^\mp$ + jets + $\not{E}_T$, CMSSM, m_0 < 700 GeV
>1350	95	[53] CHATRCHYAN	13AV	CMS	jets (+ leptons) + $\not{E}_T$, CMSSM, $m_{\widetilde{g}} = m_{\widetilde{q}}$
> 800	95	[54] CHATRCHYAN	13W	CMS	≥ 1 photons + jets + $\not{E}_T$, GGM, wino-like NLSP, $m_{\widetilde{\chi}^0_1}$ = 375 GeV
>1000	95	[54] CHATRCHYAN	13W	CMS	≥ 2 photons + jets + $\not{E}_T$, GGM, bino-like NLSP, $m_{\widetilde{\chi}^0_1}$ = 375 GeV
> 340	95	[55] DREINER	12A	THEO	$m_{\widetilde{q}} \sim m_{\widetilde{\chi}^0_1}$
> 650	95	[56] DREINER	12A	THEO	$m_{\widetilde{q}} = m_{\widetilde{g}} \sim m_{\widetilde{\chi}^0_1}$

[1] AAD 21AK searched in 139 fb^{-1} of pp collisions at $\sqrt{s}$ = 13 TeV for pair production of gluinos and squarks in events with a single isolated electron or muon, originating from the decay of a W boson, multiple jets and significant $\not{E}_T$. No significant excess above the Standard Model expectations is observed. Limits are set on the gluino mass in the Tglu1B simplified model and on the squark mass in the Tsqk3 simplified model, see their Figure 8.

[2] AAD 21F searched in 139 fb^{-1} of pp collisions at $\sqrt{s}$ = 13 TeV for pair production of squarks in events with a high-p_T jet and $\not{E}_T$. No significant excess above the Standard Model predictions is observed. Limits are set on the $\widetilde{t}$ mass in the Tstop3 and Tstop4, on the $\widetilde{b}$ mass in the Tsbot1, and on the $\widetilde{q}$ mass in the Tsqk1 simplified model (four-flavour, two chirality states degeneracy).

Downloaded from https://academic.oup.com/ptep/article/2022/8/083C01/6651666 by KIT Library user on 27 September 2022

[3] AAD 21L searched in 139 fb^{-1} of pp collisions at $\sqrt{s}$ = 13 TeV for pair production of gluinos and squarks in events with jets, large missing transverse momentum but no electrons or muons. No significant excess above the Standard Model expectations is observed. Limits are set on the gluino mass in the Tglu1A and Tglu1B simplified models, on the squark mass in the Tsqk1 and Tsqk3 simplified models and in a simplified model for gluino-squark production, see their Figures 13-17.

[4] SIRUNYAN 21M searched in 137 fb^{-1} of pp collisions at $\sqrt{s}$ = 13 TeV for supersymmetry in events with two opposite-sign same-flavor leptons (electrons, muons) and $\not{E}_T$. No significant excess above the Standard Model expectations is observed. Limits are set on the gluino mass in the simplified model Tglu4C, see their Figure 10, on the $\widetilde{\chi}^0_2$ and $\widetilde{\chi}^\pm_1$ mass in Tchi1n2Fa, see their Figure 11, on the $\widetilde{\chi}^0_1$ mass in Tn1n1C and Tn1n1B for $m_{\widetilde{\chi}^0_2}=m_{\widetilde{\chi}^\pm_1}=m_{\widetilde{\chi}^0_1}$, see their Figure 12. Limits are also set on the light squark mass for the simplified model Tsqk2A, on the sbottom mass in Tsbot3, see their Figure 13, and on the slepton mass in direct electroweak pair production of mass-degenerate left- and right-handed sleptons (selectrons and smuons), see their Figure 14.

[5] SIRUNYAN 19AG searched in 35.9 fb^{-1} of pp collisions at $\sqrt{s}$ = 13 TeV for events with two photons and large $\not{E}_T$. No significant excess above the Standard Model expectations is observed. Limits are set on the gluino mass in the Tglu4B simplified model and on the squark mass in the Tsqk4B simplified model, see their Figure 3.

[6] SIRUNYAN 19CH searched in 137 fb^{-1} of pp collisions at $\sqrt{s}$ = 13 TeV for events containing multiple jets and large $\not{E}_T$. No significant excess above the Standard Model expectations is observed. Limits are set on the gluino mass in the Tglu1A, Tglu1C, Tglu2A and Tglu3A simplified models, see their Figure 13. Limits are also set on squark, sbottom and stop masses in the Tsqk1, Tsbot1, Tstop1 simplified models, see their Figure 14.

[7] SIRUNYAN 19K searched in 35.9 fb^{-1} of pp collisions at $\sqrt{s}$ = 13 TeV for events with a photon, an electron or muon, and large $\not{E}_T$. No significant excess above the Standard Model expectations is observed. In the framework of GMSB, limits are set on the chargino and neutralino mass in the Tchi1n1A simplified model, see their Figure 6. Limits are also set on the gluino mass in the Tglu4A simplified model, and on the squark mass in the Tsqk4A simplified model, see their Figure 7.

[8] AABOUD 18BJ searched in 36.1 fb^{-1} of pp collisions at $\sqrt{s}$ = 13 TeV in events with two opposite-sign charged leptons (electrons and muons), jets and missing transverse momentum, with various requirements to be sensitive to signals with different kinematic endpoint values in the dilepton invariant mass distribution. The data are found to be consistent with the SM expectation. Results are interpreted in the Tsqk2 model in case of $m_{\widetilde{\chi}^0_1}$ = 1 GeV: for any $m_{\widetilde{\chi}^0_2}$, squark masses below 1200 GeV are excluded, see their Fig. 14(b).

[9] AABOUD 18BV searched in 36.1 fb^{-1} of pp collisions at $\sqrt{s}$ = 13 TeV for events with at least one jet identified as c-jet, large missing transverse energy and no leptons. Good agreement is observed between the number of events in data and Standard Model predictions. The results are translated into exclusion limits in Tsqk1 models considering only $\widetilde{c}_1$. In scenarios with massless neutralinos, scharm masses below 850 GeV are excluded. If the differences of the $\widetilde{c}_1$ and $\widetilde{\chi}^0_1$ masses is below 100 GeV, scharm masses below 500 GeV are excluded. See their Fig.6 and Fig.7.

[10] AABOUD 18I searched in 36.1 fb^{-1} of pp collisions at $\sqrt{s}$ = 13 TeV for events with at least one jet with a transverse momentum above 250 GeV and no leptons. Good agreement is observed between the number of events in data and Standard Model predictions. The results are translated into exclusion limits in Tsqk1 models. In the compressed scenario with similar squark and neutralino masses, squark masses below 710 GeV are excluded. See their Fig.10(b).

[11] AABOUD 18U searched in 36.1 fb^{-1} of pp collisions at $\sqrt{s}$ = 13 TeV in events with at least one isolated photon, possibly jets and significant transverse momentum targeting generalised models of gauge-mediated SUSY breaking. No significant excess of events is observed above the SM prediction. Results are interpreted in terms of lower limits on the masses of squark in Tsqk4B models. Masses below 1820 GeV are excluded for any NLSP mass, see their Fig. 9.

[12] AABOUD 18V searched in 36.1 fb^{-1} of pp collisions at $\sqrt{s}$ = 13 TeV in events with no charged leptons, jets and missing transverse momentum. The data are found to be consistent with the SM expectation. Results are interpreted in the Tsqk1 model: squark masses below 1550 GeV are excluded for massless LSP, see their Fig. 13(a).

[13] AABOUD 18V searched in 36.1 fb^{-1} of pp collisions at $\sqrt{s}$ = 13 TeV in events with no charged leptons, jets and missing transverse momentum. The data are found to be consistent with the SM expectation. Results are interpreted in the Tsqk3 model. Assuming that $m_{\widetilde{\chi}^\pm_1}$ = 0.5 ($m_{\widetilde{q}}$ + $m_{\widetilde{\chi}^0_1}$), squark masses below 1150 GeV are excluded for massless LSP, see their Fig. 14(a). Exclusions are also shown assuming $m_{\widetilde{\chi}^0_1}$ = 60 GeV, see their Fig. 14(b).

[14] SIRUNYAN 18AA searched in 35.9 fb^{-1} of pp collisions at $\sqrt{s}$ = 13 TeV for events with at least one photon and large $\not{E}_T$. No significant excess above the Standard Model expectations is observed. Limits are set on wino masses in a general gauge-mediated SUSY breaking (GGM) scenario with bino-like $\widetilde{\chi}^0_1$ and wino-like $\widetilde{\chi}^\pm_1$ and $\widetilde{\chi}^0_2$, see Figure 7. Limits are also set on the NLSP mass in the Tchi1n1A and Tchi1chi1A simplified models, see their Figure 8. Finally, limits are set on the gluino mass in the Tglu4A and Tglu4B simplified models, see their Figure 9, and on the squark mass in the Tskq4A and Tsqk4B simplified models, see their Figure 10.

[15] SIRUNYAN 18AY searched in 35.9 fb^{-1} of pp collisions at $\sqrt{s}$ = 13 TeV for events containing one or more jets and significant $\not{E}_T$. No significant excess above the Standard Model expectations is observed. Limits are set on the gluino mass in the Tglu1A, Tglu2A and Tglu3A simplified models, see their Figure 3. Limits are also set on squark, sbottom and stop masses in the Tsqk1, Tsbot1, Tstop1 and Tstop4 simplified models, see their Figure 3. Finally, limits are set on long-lived gluino masses in a Tglu1A simplified model where the gluino is metastable or long-lived with proper decay lengths in the range 10^{-3} mm $< c\tau < 10^5$ mm, see their Figure 4.

[16] AABOUD 17AR searched in 36.1 fb^{-1} of pp collisions at $\sqrt{s}$ = 13 TeV for events with one isolated lepton, at least two jets and large missing transverse momentum. No significant excess above the Standard Model expectations is observed. Limits up to 1.25 TeV are set on the 1st and 2nd generation squark masses in Tsqk3 simplified models, with x = ($m_{\widetilde{\chi}^\pm_1}-m_{\widetilde{\chi}^0_1}$) / ($m_{\widetilde{q}}-m_{\widetilde{\chi}^0_1}$) = 1/2. Similar limits are obtained for variable x and fixed neutralino mass, $m_{\widetilde{\chi}^0_1}$ = 60 GeV. See their Figure 13.

[17] AABOUD 17N searched in 14.7 fb^{-1} of pp collisions at $\sqrt{s}$ = 13 TeV for events with 2 same-flavour, opposite-sign leptons (electrons or muons), jets and large missing transverse momentum. The results are interpreted as 95% C.L. limits in Tsqk2 models, assuming $m_{\widetilde{\chi}^0_1}$ = 0 GeV and $m_{\widetilde{\chi}^0_2}$ = 600 GeV. See their Fig. 12 for exclusion limits as a function of $m_{\widetilde{\chi}^0_2}$.

[18] KHACHATRYAN 17P searched in 2.3 fb^{-1} of pp collisions at $\sqrt{s}$ = 13 TeV for events with one or more jets and large $\not{E}_T$. No significant excess above the Standard Model expectations is observed. Limits are set on the gluino mass in the Tglu1A, Tglu2A, Tglu3A, Tglu3B, Tglu3C and Tglu3D simplified models, see their Figures 7 and 8. Limits are also set on the squark mass in the Tsqk1 simplified model, see their Fig. 7, and on the sbottom mass in the Tsbot1 simplified model, see Fig. 8. Finally, limits are set on the stop mass in the Tstop1, Tstop3, Tstop4, Tstop6 and Tstop7 simplified models, see Fig. 8.

[19] KHACHATRYAN 17V searched in 2.3 fb^{-1} of pp collisions at $\sqrt{s}$ = 13 TeV for events with two photons and large $\not{E}_T$. No significant excess above the Standard Model expectations is observed. Limits are set on the gluino and squark mass in the context of general gauge mediation models Tglu4B and Tsqk4, see their Fig. 4.

[20] SIRUNYAN 17AY searched in 35.9 fb^{-1} of pp collisions at $\sqrt{s}$ = 13 TeV for events with at least one photon, jets and large $\not{E}_T$. No significant excess above the Standard Model expectations is observed. Limits are set on the gluino mass in the Tglu4A and Tglu4B simplified models, and on the squark mass in the Tskq4A and Tsqk4B simplified models, see their Figure 6.

[21] SIRUNYAN 17AZ searched in 35.9 fb^{-1} of pp collisions at $\sqrt{s}$ = 13 TeV for events with one or more jets and large $\not{E}_T$. No significant excess above the Standard Model expectations is observed. Limits are set on the gluino mass in the Tglu1A, Tglu2A, Tglu3A simplified models, see their Figures 6. Limits are also set on the squark mass in the Tsqk1 simplified model (for single light squark and for 8 degenerate light squarks), on the sbottom mass in the Tsbot1 simplified model and on the stop mass in the Tstop1 simplified model, see their Fig. 7. Finally, limits are set on the stop mass in the Tstop2, Tstop4 and Tstop8 simplified models, see Fig. 8.

[22] SIRUNYAN 17P searched in 35.9 fb^{-1} of pp collisions at $\sqrt{s}$ = 13 TeV for events with multiple jets and large $\not{E}_T$. No significant excess above the Standard Model expectations is observed. Limits are set on the gluino mass in the Tglu1A, Tglu1C, Tglu2A, Tglu3A and Tglu3D simplified models, see their Fig. 12. Limits are also set on the squark mass in the Tsqk1 simplified model, on the stop mass in the Tstop1 simplified model, and on the sbottom mass in the Tsbot1 simplified model, see Fig. 13.

[23] AABOUD 16D searched in 3.2 fb^{-1} of pp collisions at $\sqrt{s}$ = 13 TeV for events with an energetic jet and large missing transverse momentum. The results are interpreted as 95% C.L. limits on masses of first and second generation squarks decaying into a quark and the lightest neutralino in scenarios with $m_{\widetilde{q}} - m_{\widetilde{\chi}^0_1} < 25$ GeV. See their Fig. 6.

[24] AABOUD 16N searched in 3.2 fb^{-1} of pp collisions at $\sqrt{s}$ = 13 TeV for events containing hadronic jets, large $\not{E}_T$, and no electrons or muons. No significant excess above the Standard Model expectations is observed. First- and second-generation squark masses below 1030 GeV are excluded at the 95% C.L. decaying to quarks and a massless lightest neutralino. See their Fig. 7a.

[25] KHACHATRYAN 16BS searched in 2.3 fb^{-1} of pp collisions at $\sqrt{s}$ = 13 TeV for events with at least one energetic jet , no isolated leptons, and significant $\not{E}_T$, using the transverse mass variable M_{T2} to discriminate between signal and background processes. No significant excess above the Standard Model expectations is observed. Limits are set on the squark mass in the Tskq1 simplified model, both in the assumption of a single light squark and of 8 degenerate squarks, see Fig. 11 and Table 3.

[26] AAD 15BV summarized and extended ATLAS searches for gluinos and first- and second-generation squarks in final states containing jets and missing transverse momentum, with or without leptons or b-jets in the $\sqrt{s}$ = 8 TeV data set collected in 2012. The paper reports the results of new interpretations and statistical combinations of previously published analyses, as well as new analyses. Exclusion limits at 95% C.L. are set on the squark mass in several R-parity conserving models. See their Figs. 9, 11, 18, 22, 24, 27, 28.

[27] AAD 15CS searched in 20.3 fb^{-1} of pp collisions at $\sqrt{s}$ = 8 TeV for evidence of pair production of squarks, decaying into a quark and a neutralino, where a photon was radiated either from an initial-state quark, from an intermediate squark, or from a final-state quark. No evidence was found for an excess above the expected level of Standard Model background and a 95% C.L. exclusion limit was set on the squark mass as a function of the squark-neutralino mass difference, see Fig. 19.

[28] AAD 15K searched in 20.3 fb^{-1} of pp collisions at $\sqrt{s}$ = 8 TeV for events containing at least two jets, where the two leading jets are each identified as originating from c-quarks, and large missing transverse momentum. No excess of events above the expected level of Standard Model background was found. Exclusion limits at 95% C.L. are set on the mass of superpartners of charm quarks ($\widetilde{c}$). Assuming that the decay $\widetilde{c} \rightarrow c\widetilde{\chi}^0_1$ takes place 100% of the time, a scalar charm mass below 490 GeV is excluded for $m_{\widetilde{\chi}^0_1} < 200$ GeV. For more details, see their Fig. 2.

[29] KHACHATRYAN 15AF searched in 19.5 fb^{-1} of pp collisions at $\sqrt{s}$ = 8 TeV for events with at least two energetic jets and significant $\not{E}_T$, using the transverse mass variable M_{T2} to discriminate between signal and background processes. No significant excess above the Standard Model expectations is observed. Limits are set on the squark mass in simplified models where the decay $\widetilde{q} \rightarrow q\widetilde{\chi}^0_1$ takes place with a branching ratio of 100%, both for the case of a single light squark or 8 degenerate squarks, see Fig. 12. See also Table 5. Exclusions in the CMSSM, assuming tanβ = 30, $A_0 = -2$ max(m_0, $m_{1/2}$) and $\mu > 0$, are also presented, see Fig. 15.

[30] AAD 14AE searched in 20.3 fb^{-1} of pp collisions at $\sqrt{s}$ = 8 TeV for strongly produced supersymmetric particles in events containing jets and large missing transverse momentum, and no electrons or muons. No excess over the expected SM background is observed. Exclusion limits are derived in simplified models containing squarks that decay via $\widetilde{q} \rightarrow q\widetilde{\chi}^0_1$, where either a single light state or two degenerate generations of squarks are assumed, see Fig. 10.

[31] CHATRCHYAN 14AH searched in 4.7 fb^{-1} of pp collisions at $\sqrt{s}$ = 7 TeV for events with at least two energetic jets and significant $\not{E}_T$, using the razor variables (M_R and R^2) to discriminate between signal and background processes. No significant excess above the Standard Model expectations is observed. Limits are set on squark masses in simplified models where the decay $\widetilde{q} \rightarrow q\widetilde{\chi}^0_1$ takes place with a branching ratio of 100%, see Fig. 28. Exclusions in the CMSSM, assuming tanβ = 10, A_0 = 0 and $\mu > 0$, are also presented, see Fig. 26.

[32] CHATRCHYAN 14I searched in 19.5 fb^{-1} of pp collisions at $\sqrt{s}$ = 8 TeV for events containing multijets and large $\not{E}_T$. No excess over the expected SM background is observed. Exclusion limits are derived in simplified models containing squarks that decay via $\widetilde{q} \rightarrow q\widetilde{\chi}^0_1$, where either a single light state or two degenerate generations of squarks are assumed, see Fig. 7a.

Downloaded from https://academic.oup.com/ptep/article/2022/8/083C01/6651666 by KIT Library user on 27 September 2022

[33] AAD 13L searched in 4.7 fb^{-1} of pp collisions at $\sqrt{s}$ = 7 TeV for the production of squarks and gluinos in events containing jets, missing transverse momentum and no high-p_T electrons or muons. No excess over the expected SM background is observed. In mSUGRA/CMSSM models with tanβ = 10, A_0 = 0 and μ > 0, squarks and gluinos of equal mass are excluded for masses below 1360 GeV at 95% C.L. In a simplified model containing only squarks of the first two generations, a gluino octet and a massless neutralino, squark masses below 1320 GeV are excluded at 95% C.L. for gluino masses below 2 TeV. See Figures 10–15 for more precise bounds.

[34] AAD 13Q searched in 4.7 fb^{-1} of pp collisions at $\sqrt{s}$ = 7 TeV for events containing a high-p_T isolated photon, at least one jet identified as originating from a bottom quark, and high missing transverse momentum. Such signatures may originate from supersymmetric models with gauge-mediated supersymmetry breaking in events in which one of a pair of higgsino-like neutralinos decays into a photon and a gravitino while the other decays into a Higgs boson and a gravitino. No significant excess above the expected background was found and limits were set on the squark mass as a function of the neutralino mass in a generalized GMSB model (GGM) with a higgsino-like neutralino NLSP, see their Fig. 4. For neutralino masses greater than 220 GeV, squark masses below 1020 GeV are excluded at 95% C.L.

[35] CHATRCHYAN 13 looked in 4.98 fb^{-1} of pp collisions at $\sqrt{s}$ = 7 TeV for events with two opposite-sign leptons (e, μ, τ), jets and missing transverse energy. No excess beyond the Standard Model expectation is observed. Exclusion limits are derived in the mSUGRA/CMSSM model with tanβ = 10, A_0 = 0 and μ > 0, see Fig. 6.

[36] CHATRCHYAN 13G searched in 4.98 fb^{-1} of pp collisions at $\sqrt{s}$ = 7 TeV for the production of squarks and gluinos in events containing 0,1,2, $\geq$ 3 b-jets, missing transverse momentum and no electrons or muons. No excess over the expected SM background is observed. In mSUGRA/CMSSM models with tanβ = 10, A_0 = 0, and μ > 0, squarks and gluinos of equal mass are excluded for masses below 1250 GeV at 95% C.L. Exclusions are also derived in various simplified models, see Fig. 7.

[37] CHATRCHYAN 13H searched in 4.96 fb^{-1} of pp collisions at $\sqrt{s}$ = 7 TeV for events with two photons, $\geq$ 4 jets and low $\not{E}_T$ due to $\tilde{q} \rightarrow \gamma\tilde{\chi}^0_1$ decays in a stealth SUSY framework, where the $\tilde{\chi}^0_1$ decays through a singlino ($\tilde{S}$) intermediate state to $\gamma S \tilde{G}$, with the singlet state S decaying to two jets. No significant excess above the expected background was found and limits were set in a particular R-parity conserving stealth SUSY model. The model assumes $m_{\tilde{\chi}^0_1}$ = 0.5 $m_{\tilde{q}}$, $m_{\tilde{S}}$ = 100 GeV and m_S = 90 GeV. Under these assumptions, squark masses less than 1430 GeV were excluded at the 95% C.L.

[38] CHATRCHYAN 13T searched in 11.7 fb^{-1} of pp collisions at $\sqrt{s}$ = 8 TeV for events with at least two energetic jets and significant $\not{E}_T$, using the α_T variable to discriminate between processes with genuine and misreconstructed $\not{E}_T$. No significant excess above the Standard Model expectations is observed. Limits are set on squark masses in simplified models where the decay $\tilde{q} \rightarrow q\tilde{\chi}^0_1$ takes place with a branching ratio of 100%, assuming an eightfold degeneracy of the masses of the first two generation squarks, see Fig. 8 and Table 9. Also limits in the case of a single light squark are given.

[39] AAD 12AX searched in 1.04 fb^{-1} of pp collisions at $\sqrt{s}$ = 7 TeV for supersymmetry in events containing jets, missing transverse momentum and one isolated electron or muon. No excess over the expected SM background is observed and model-independent limits are set on the cross section of new physics contributions to the signal regions. In mSUGRA/CMSSM models with tanβ = 10, A_0 = 0 and μ > 0, squarks and gluinos of equal mass are excluded for masses below 820 GeV at 95% C.L. Limits are also set on simplified models for squark production and decay via an intermediate chargino and on supersymmetric models with bilinear R-parity violation. Supersedes AAD 11G.

[40] AAD 12CJ searched in 4.7 fb^{-1} of pp collisions at $\sqrt{s}$ = 7 TeV for events containing one or more isolated leptons (electrons or muons), jets and $\not{E}_T$. The observations are in good agreement with the SM expectations and exclusion limits have been set in number of SUSY models. In the mSUGRA/CMSSM model with tanβ = 10, A_0 = 0, and μ > 0, 95% C.L. exclusion limits have been derived for $m_{\tilde{q}}$ < 1200 GeV, assuming equal squark and gluino masses. In minimal GMSB, values of the effective SUSY breaking scale Λ < 50 TeV are excluded at 95% C.L. for tanβ < 45. Also exclusion limits in a number of simplified models have been presented, see Figs. 10 and 12.

[41] AAD 12CP searched in 4.8 fb^{-1} of pp collisions at $\sqrt{s}$ = 7 TeV for events with two photons and large $\not{E}_T$ due to $\tilde{\chi}^0_1 \rightarrow \gamma\tilde{G}$ decays in a GMSB framework. No significant excess above the expected background was found and limits were set on the squark mass as a function of the neutralino mass in a generalized GMSB model (GGM) with a bino-like neutralino NLSP. The other sparticle masses were decoupled, tanβ = 2 and $c\tau_{NLSP}$ < 0.1 mm. Also, in the framework of the SPS8 model, a 95% C.L. lower limit was set on the breaking scale Λ of 196 TeV.

[42] AAD 12W searched in 1.04 fb^{-1} of pp collisions at $\sqrt{s}$ = 7 TeV for the production of squarks and gluinos in events containing jets, missing transverse momentum and no electrons or muons. No excess over the expected SM background is observed. In mSUGRA/CMSSM models with tanβ = 10, A_0 = 0 and μ > 0, squarks and gluinos of equal mass are excluded for masses below 950 GeV at 95% C.L. In a simplified model containing only squarks of the first two generations, a gluino octet and a massless neutralino, squark masses below 875 GeV are excluded at 95% C.L.

[43] CHATRCHYAN 12 looked in 35 pb^{-1} of pp collisions at $\sqrt{s}$ = 7 TeV for events with e and/or μ and/or jets, a large total transverse energy, and $\not{E}_T$. The event selection is based on the dimensionless razor variable R, related to the $\not{E}_T$ and M_R, an indicator of the heavy particle mass scale. No evidence for an excess over the expected background is observed. Limits are derived in the CMSSM (m_0, $m_{1/2}$) plane for tanβ = 3, 10 and 50 (see Fig. 7 and 8). Limits are also obtained for Simplified Model Spectra.

[44] CHATRCHYAN 12AE searched in 4.98 fb^{-1} of pp collisions at $\sqrt{s}$ = 7 TeV for events with at least three jets and large missing transverse momentum. No significant excesses over the expected SM backgrounds are observed and 95% C.L. limits on the production cross section of squarks in a scenario where $\tilde{q} \rightarrow q\tilde{\chi}^0_1$ with a 100% branching ratio, see Fig. 3. For $m_{\tilde{\chi}^0_1}$ < 200 GeV, values of $m_{\tilde{q}}$ below 760 GeV are excluded at 95% C.L. Also limits in the CMSSM are presented, see Fig. 2.

[45] CHATRCHYAN 12AT searched in 4.73 fb^{-1} of pp collisions at $\sqrt{s}$ = 7 TeV for the production of squarks and gluinos in events containing jets, missing transverse momentum and no electrons or muons. No excess over the expected SM background is observed. In mSUGRA/CMSSM models with tanβ = 10, A_0 = 0 and μ > 0, squarks with masses below 1110 GeV are excluded at 95% C.L. Squarks and gluinos of equal mass are excluded for masses below 1180 GeV at 95% C.L. Exclusions are also derived in various simplified models, see Fig. 6.

[46] AABOUD 18V searched in 36.1 fb^{-1} of pp collisions at $\sqrt{s}$ = 13 TeV in events with no charged leptons, jets and missing transverse momentum. The data are found to be consistent with the SM expectation. Results are interpreted in the Tsqk5 model. Squark masses below 1100 GeV are excluded if $(m_{\tilde{\chi}^0_2} - m_{\tilde{\chi}^0_1})/(m_{\tilde{q}} - m_{\tilde{\chi}^0_1})$ < 0.95 and $m_{\tilde{\chi}^0_1}$ = 60 GeV, see their Fig. 16(a).

[47] KHACHATRYAN 16BT performed a global Bayesian analysis of a wide range of CMS results obtained with data samples corresponding to 5.0 fb^{-1} of pp collisions at $\sqrt{s}$ = 7 TeV and in 19.5 fb^{-1} of pp collisions at $\sqrt{s}$ = 8 TeV. The set of searches considered, both individually and in combination, includes those with all-hadronic final states, same-sign and opposite-sign dileptons, and multi-lepton final states. An interpretation was given in a scan of the 19-parameter pMSSM. No scan points with a gluino mass less than 500 GeV survived and 98% of models with a squark mass less than 300 GeV were excluded.

[48] AAD 15AI searched in 20 fb^{-1} of pp collisions at $\sqrt{s}$ = 8 TeV for events containing at least one isolated lepton (electron or muon), jets, and large missing transverse momentum. No excess of events above the expected level of Standard Model background was found. Exclusion limits at 95% C.L. are set on the squark masses in the CMSSM/mSUGRA, see Fig. 15, in the NUHMG, see Fig. 16, and in various simplified models, see Figs. 19–21.

[49] KHACHATRYAN 15AR searched in 19.7 of fb^{-1} of pp collisions at $\sqrt{s}$ = 8 TeV for events containing jets, either a charged lepton or a photon, and low missing transverse momentum. No significant excess above the Standard Model expectations is observed. Limits are set on the squark mass in a stealth SUSY model where the decays $\tilde{q} \rightarrow q\tilde{\chi}^{\pm}_1$, $\tilde{\chi}^{\pm}_1 \rightarrow \tilde{S}W^{\pm}$, $\tilde{S} \rightarrow S\tilde{G}$ and $S \rightarrow gg$, with $m_{\tilde{S}}$ = 100 GeV and m_S = 90 GeV, take place with a branching ratio of 100%. See Fig. 6 for γ or Fig. 7 for $\ell^{\pm}$ analyses.

[50] KHACHATRYAN 15AZ searched in 19.7 fb^{-1} of pp collisions at $\sqrt{s}$ = 8 TeV for events with either at least one photon, hadronic jets and $\not{E}_T$ (single photon channel) or with at least two photons and at least one jet and using the razor variables. No significant excess above the Standard Model expectations is observed. Limits are set on gluino masses in the general gauge-mediated SUSY breaking model (GGM), for both a bino-like and wino-like neutralino NLSP scenario, see Fig. 8 and 9.

[51] AAD 14E searched in 20.3 fb^{-1} of pp collisions at $\sqrt{s}$ = 8 TeV for strongly produced supersymmetric particles in events containing jets and two same-sign leptons or three leptons. The search also utilises jets originating from b-quarks, missing transverse momentum and other variables. No excess over the expected SM background is observed. Exclusion limits are derived in simplified models containing gluinos and squarks, see Figures 5 and 6. In the $\tilde{q} \rightarrow q'\tilde{\chi}^{\pm}_1$, $\tilde{\chi}^{\pm}_1 \rightarrow W^{(*)\pm}\tilde{\chi}^0_2$, $\tilde{\chi}^0_2 \rightarrow Z^{(*)}\tilde{\chi}^0_1$ simplified model, the following assumptions have been made: $m_{\tilde{\chi}^{\pm}_1}$ = 0.5 $m_{\tilde{\chi}^0_1}$ + $m_{\tilde{g}}$, $m_{\tilde{\chi}^0_2}$ = 0.5 ($m_{\tilde{\chi}^0_1}$ + $m_{\tilde{\chi}^{\pm}_1}$). In the $\tilde{q} \rightarrow q'\tilde{\chi}^{\pm}_1$ or $\tilde{q} \rightarrow q'\tilde{\chi}^0_2$, $\tilde{\chi}^{\pm}_1 \rightarrow \ell^{\pm}\nu\tilde{\chi}^0_1$ or $\tilde{\chi}^0_2 \rightarrow \ell^{\pm}\ell^{\mp}(\nu\nu)\tilde{\chi}^0_1$ simplified model, the following assumptions have been made: $m_{\tilde{\chi}^{\pm}_1} = m_{\tilde{\chi}^0_2}$ = 0.5 ($m_{\tilde{\chi}^0_1}$ + $m_{\tilde{q}}$), $m_{\tilde{\chi}^0_1}$ < 460 GeV. Limits are also derived in the mSUGRA/CMSSM, bRPV and GMSB models, see their Fig. 8.

[52] CHATRCHYAN 13AO searched in 4.98 fb^{-1} of pp collisions at $\sqrt{s}$ = 7 TeV for events with two opposite-sign isolated leptons accompanied by hadronic jets and $\not{E}_T$. No significant excesses over the expected SM backgrounds are observed and 95% C.L. exclusion limits are derived in the mSUGRA/CMSSM model with tanβ = 10, A_0 = 0 and μ > 0, see Fig. 8.

[53] CHATRCHYAN 13AV searched in 4.7 fb^{-1} of pp collisions at $\sqrt{s}$ = 7 TeV for new heavy particle pairs decaying into jets (possibly b-tagged), leptons and $\not{E}_T$ using the Razor variables. No significant excesses over the expected SM backgrounds are observed and 95% C.L. exclusion limits are derived in the mSUGRA/CMSSM model with tanβ = 10, A_0 = 0 and μ > 0, see Fig. 3. The results are also interpreted in various simplified models, see Fig. 4.

[54] CHATRCHYAN 13W searched in 4.93 fb^{-1} of pp collisions at $\sqrt{s}$ = 7 TeV for events with one or more photons, hadronic jets and $\not{E}_T$. No significant excess above the Standard Model expectations is observed. Limits are set on squark masses in the general gauge-mediated SUSY breaking model (GGM), for both a wino-like and bino-like neutralino NLSP scenario, see Fig. 5.

[55] DREINER 12A reassesses constraints from CMS (at 7 TeV, $\sim$ 4.4 fb^{-1}) under the assumption that the fist and second generation squarks and the lightest SUSY particle are quasi-degenerate in mass (compressed spectrum).

[56] DREINER 12A reassesses constraints from CMS (at 7 TeV, $\sim$ 4.4 fb^{-1}) under the assumption that the first and second generation squarks, the gluino, and the lightest SUSY particle are quasi-degenerate in mass (compressed spectrum).

R-parity violating $\tilde{q}$ (Squark) mass limit

VALUE (GeV)	CL%	DOCUMENT ID		TECN	COMMENT
none 100–720	95	[1] SIRUNYAN	18EA	CMS	2 large jets with four-parton substructure, $\tilde{q} \rightarrow 4q$
>1600	95	[2] KHACHATRY...	16BX	CMS	$\tilde{q} \rightarrow q\tilde{\chi}^0_1$, $\tilde{\chi}^0_1 \rightarrow \ell\ell\nu$, λ_{121} or $\lambda_{122} \neq 0$, $m_{\tilde{g}}$ = 2400 GeV
>1000	95	[3] AAD	15CB	ATLS	jets, $\tilde{q} \rightarrow q\tilde{\chi}^0_1$, $\tilde{\chi}^0_1 \rightarrow \ell q q$, $m_{\tilde{\chi}^0_1}$ = 108 GeV and 2.5 < $c\tau_{\tilde{\chi}^0_1}$ < 200 mm
		[4] AAD	12AX	ATLS	ℓ +jets +$\not{E}_T$, CMSSM, $m_{\tilde{q}}$=$m_{\tilde{g}}$
		[5] CHATRCHYAN	12AL	CMS	$\geq \ell^{\pm}$

[1] SIRUNYAN 18EA searched in 38.2 fb^{-1} of pp collisions at $\sqrt{s}$ = 13 TeV for the pair production of resonances, each decaying to at least four quarks. Reconstructed particles are clustered into two large jets of similar mass, each consistent with four-parton substructure. No statistically significant excess over the Standard Model expectation is observed. Limits are set on the squark and gluino mass in RPV supersymmetry models where squarks (gluinos) decay, through intermediate higgsinos, to four (five) quarks, see their Figure 4.

[2] KHACHATRYAN 16BX searched in 19.5 fb^{-1} of pp collisions at $\sqrt{s}$ = 8 TeV for events containing 4 leptons coming from R-parity-violating decays of $\tilde{\chi}^0_1 \rightarrow \ell\ell\nu$ with $\lambda_{121} \neq 0$ or $\lambda_{122} \neq 0$. No excess over the expected background is observed. Limits are derived on the gluino, squark and stop masses, see Fig. 23.

[3] AAD 15CB searched for events containing at least one long-lived particle that decays at a significant distance from its production point (displaced vertex, DV) into two leptons or into five or more charged particles in 20.3 fb^{-1} of pp collisions at $\sqrt{s}$ = 8 TeV. The dilepton signature is characterised by DV formed from at least two lepton candidates.

Downloaded from https://academic.oup.com/ptep/article/2022/8/083C01/6651666 by KIT Library user on 27 September 2022

Four different final states were considered for the multitrack signature, in which the DV must be accompanied by a high-transverse momentum muon or electron candidate that originates from the DV, jets or missing transverse momentum. No events were observed in any of the signal regions. Results were interpreted in SUSY scenarios involving R-parity violation, split supersymmetry, and gauge mediation. See their Fig. 14–20.

[4] AAD 12AX searched in 1.04 fb^{-1} of pp collisions at $\sqrt{s}$ = 7 TeV for supersymmetry in events containing jets, missing transverse momentum and one isolated electron or muon. No excess over the expected SM background is observed and model-independent limits are set on the cross section of new physics contributions to the signal regions. In mSUGRA/CMSSM models with tanβ = 10, A_0 = 0 and μ > 0, squarks and gluinos of equal mass are excluded for masses below 820 GeV at 95% C.L. Limits are also set on simplified models for squark production and decay via an intermediate chargino and on supersymmetric models with bilinear R-parity violation. Supersedes AAD 11G.

[5] CHATRCHYAN 12AL looked in 4.98 fb^{-1} of pp collisions at $\sqrt{s}$ = 7 TeV for anomalous production of events with three or more isolated leptons. Limits on squark and gluino masses are set in RPV SUSY models with leptonic $LL\overline{E}$couplings, λ_{123} > 0.05, and hadronic $\overline{UDD}$ couplings, λ''_{112} > 0.05 , see their Fig. 5. In the $\overline{UDD}$ case the leptons arise from supersymmetric cascade decays. A very specific supersymmetric spectrum is assumed. All decays are prompt.

Long-lived $\widetilde{q}$ (Squark) mass limit

The following are bounds on long-lived scalar quarks, assumed to hadronise into hadrons with lifetime long enough to escape the detector prior to a possible decay. Limits may depend on the mixing angle of mass eigenstates: $\widetilde{q}_1 = \widetilde{q}_L \cos\theta_q + \widetilde{q}_R \sin\theta_q$. The coupling to the Z^0 boson vanishes for up-type squarks when θ_u=0.98, and for down type squarks when θ_d=1.17.

VALUE (GeV)	CL%	DOCUMENT ID		TECN	COMMENT
>1250	95	[1] AABOUD	19AT	ATLS	$\widetilde{b}$ R-hadrons
>1340	95	[2] AABOUD	19AT	ATLS	$\widetilde{t}$ R-hadrons
>1600	95	[3] SIRUNYAN	19BH	CMS	long-lived $\widetilde{t}$, RPV, $\widetilde{t} \rightarrow \overline{d}\,\overline{d}$, 10 mm < c$\tau$ < 110 mm
>1350	95	[3] SIRUNYAN	19BH	CMS	long-lived $\widetilde{t}$, RPV, $\widetilde{t} \rightarrow b\ell$, 7 mm < c$\tau$ < 110 mm
> 805	95	[4] AABOUD	16B	ATLS	$\widetilde{b}$ R-hadrons
> 890	95	[5] AABOUD	16B	ATLS	$\widetilde{t}$ R-hadrons
>1040	95	[6] KHACHATRY...	16BW	CMS	$\widetilde{t}$ R-hadrons, cloud interaction model
>1000	95	[6] KHACHATRY...	16BW	CMS	$\widetilde{t}$ R-hadrons, charge-suppressed interaction model
> 845	95	[7] AAD	15AE	ATLS	$\widetilde{b}$ R-hadron, stable, Regge model
> 900	95	[7] AAD	15AE	ATLS	$\widetilde{t}$ R-hadron, stable, Regge model
>1500	95	[7] AAD	15AE	ATLS	$\widetilde{g}$ decaying to 300 GeV stable sleptons, LeptoSUSY model
> 751	95	[8] AAD	15BM	ATLS	$\widetilde{b}$ R-hadron, stable, Regge model
> 766	95	[8] AAD	15BM	ATLS	$\widetilde{t}$ R-hadron, stable, Regge model
> 525	95	[9] KHACHATRY...	15AK	CMS	$\widetilde{t}$ R-hadrons, 10 μs< τ <1000 s
> 470	95	[9] KHACHATRY...	15AK	CMS	$\widetilde{t}$ R-hadrons, 1 μs< τ <1000 s
• • • We do not use the following data for averages, fits, limits, etc. • • •					
> 683	95	[10] AAD	13AA	ATLS	$\widetilde{t}$, R-hadrons, generic interaction model
> 612	95	[11] AAD	13AA	ATLS	$\widetilde{b}$, R-hadrons, generic interaction model
> 344	95	[12] AAD	13BC	ATLS	R-hadrons, $\widetilde{t} \rightarrow b\widetilde{\chi}^0_1$, Regge model, lifetime between 10^{-5} and 10^3 s, $m_{\widetilde{\chi}^0_1}$ = 100 GeV
> 379	95	[13] AAD	13BC	ATLS	R-hadrons, $\widetilde{t} \rightarrow t\widetilde{\chi}^0_1$, Regge model, lifetime between 10^{-5} and 10^3 s, $m_{\widetilde{\chi}^0_1}$ = 100 GeV
> 935	95	[14] CHATRCHYAN	13AB	CMS	long-lived $\widetilde{t}$ forming R-hadrons, cloud interaction model

[1] AABOUD 19AT searched in 36.1 fb^{-1} of pp collisions at $\sqrt{s}$ = 13 TeV for metastable and stable R-hadrons. Multiple search strategies for a wide range of lifetimes, corresponding to path lengths of a few meters, are defined. No significant deviations from the expected Standard Model background are observed. Sbottom R-hadrons are excluded at 95% C.L. for masses below 1250 GeV. Less stringent constraints are achieved with the muon-spectrometer agnostic analysis. See their Figure 9 (bottom-left).

[2] AABOUD 19AT searched in 36.1 fb^{-1} of pp collisions at $\sqrt{s}$ = 13 TeV for metastable and stable R-hadrons. Multiple search strategies for a wide range of lifetimes, corresponding to path lengths of a few meters, are defined. No significant deviations from the expected Standard Model background are observed. Stop R-hadrons are excluded at 95% C.L. for masses below 1340 GeV. Similar constraints are achieved with the muon-spectrometer agnostic analysis. See their Figure 9 (bottom-right).

[3] SIRUNYAN 19BH searched in 35.9 fb^{-1} of pp collisions at $\sqrt{s}$ = 13 TeV for long-lived particles decaying into jets, with each long-lived particle having a decay vertex well displaced from the production vertex. The selected events are found to be consistent with standard model predictions. Limits are set on the gluino mass in a GMSB model where the gluino is decaying via $\widetilde{g} \rightarrow g\widetilde{G}$, see their Figure 4 and in an RPV model of supersymmetry where the gluino is decaying via $\widetilde{g} \rightarrow \widetilde{t}\,\overline{b}\,\overline{s}$, see their Figures 5. Limits are also set on the stop mass in two RPV models, see their Figure 6 (for $\widetilde{t} \rightarrow b\ell$ decays) and Figure 7 (for $\widetilde{t} \rightarrow \overline{d}\,\overline{d}$ decays).

[4] AABOUD 16B searched in 3.2 fb^{-1} of pp collisions at $\sqrt{s}$ = 13 TeV for long-lived R-hadrons using observables related to large ionization losses and slow propagation velocities, which are signatures of heavy charged particles traveling significantly slower than the speed of light. Exclusion limits at 95% C.L. are set on the long-lived sbottom masses exceeding 805 GeV. See their Fig. 5.

[5] AABOUD 16B searched in 3.2 fb^{-1} of pp collisions at $\sqrt{s}$ = 13 TeV for long-lived R-hadrons using observables related to large ionization losses and slow propagation velocities, which are signatures of heavy charged particles traveling significantly slower than the speed of light. Exclusion limits at 95% C.L. are set on the long-lived stop masses exceeding 890 GeV. See their Fig. 5.

[6] KHACHATRYAN 16BW searched in 2.5 fb^{-1} of pp collisions at $\sqrt{s}$ = 13 TeV for events with heavy stable charged particles, identified by their anomalously high energy deposits in the silicon tracker and/or long time-of-flight measurements by the muon system. No evidence for an excess over the expected background is observed. Limits are derived for pair production of top squarks as a function of mass, depending on the interaction model, see Fig. 4 and Table 7.

[7] AAD 15AE searched in 19.1 fb^{-1} of pp collisions at $\sqrt{s}$ = 8 TeV for heavy long-lived charged particles, measured through their specific ionization energy loss in the ATLAS pixel detector or their time-of-flight in the ALTAS muon system. In the absence of an excess of events above the expected backgrounds, limits are set R-hadrons in various scenarios, see Fig. 11. Limits are also set in LeptoSUSY models where the gluino decays to stable 300 GeV leptons, see Fig. 9.

[8] AAD 15BM searched in 18.4 fb^{-1} of pp collisions at $\sqrt{s}$ = 8 TeV for stable and metastable non-relativistic charged particles through their anomalous specific ionization energy loss in the ATLAS pixel detector. In absence of an excess of events above the expected backgrounds, limits are set on stable bottom and top squark R-hadrons, see Table 5.

[9] KHACHATRYAN 15AK looked in a data set corresponding to fb^{-1} of pp collisions at $\sqrt{s}$ = 8 TeV, and a search interval corresponding to 281 h of trigger lifetime, for long-lived particles that have stopped in the CMS detector. No evidence for an excess over the expected background in a cloud interaction model is observed. Assuming the decay $\widetilde{t} \rightarrow t\widetilde{\chi}^0_1$ and lifetimes between 1 μs and 1000 s, limits are derived on $\widetilde{t}$ production as a function of $m_{\widetilde{\chi}^0_1}$, see Figs. 4 and 7. The exclusions require that $m_{\widetilde{\chi}^0_1}$ is kinematically consistent with the minimum values of the jet energy thresholds used.

[10] AAD 13AA searched in 4.7 fb^{-1} of pp collisions at $\sqrt{s}$ = 7 TeV for events containing colored long-lived particles that hadronize forming R-hadrons. No significant excess above the expected background was found. Long-lived R-hadrons containing a $\widetilde{t}$ are excluded for masses up to 683 GeV at 95% C.L in a general interaction model. Also, limits independent of the fraction of R-hadrons that arrive charged in the muon system were derived, see Fig. 6.

[11] AAD 13AA searched in 4.7 fb^{-1} of pp collisions at $\sqrt{s}$ = 7 TeV for events containing colored long-lived particles that hadronize forming R-hadrons. No significant excess above the expected background was found. Long-lived R-hadrons containing a $\widetilde{b}$ are excluded for masses up to 612 GeV at 95% C.L in a general interaction model. Also, limits independent of the fraction of R-hadrons that arrive charged in the muon system were derived, see Fig. 6.

[12] AAD 13BC searched in 5.0 fb^{-1} of pp collisions at $\sqrt{s}$ = 7 TeV and in 22.9 fb^{-1} of pp collisions at $\sqrt{s}$ = 8 TeV for bottom squark R-hadrons that have come to rest within the ATLAS calorimeter and decay at some later time to hadronic jets and a neutralino. In absence of an excess of events above the expected backgrounds, limits are set on sbottom masses for the decay $\widetilde{b} \rightarrow b\widetilde{\chi}^0_1$, for different lifetimes, and for a neutralino mass of 100 GeV, see their Table 6 and Fig 10.

[13] AAD 13BC searched in 5.0 fb^{-1} of pp collisions at $\sqrt{s}$ = 7 TeV and in 22.9 fb^{-1} of pp collisions at $\sqrt{s}$ = 8 TeV for bottom squark R-hadrons that have come to rest within the ATLAS calorimeter and decay at some later time to hadronic jets and a neutralino. In absence of an excess of events above the expected backgrounds, limits are set on stop masses for the decay $\widetilde{t} \rightarrow t\widetilde{\chi}^0_1$, for different lifetimes, and for a neutralino mass of 100 GeV, see their Table 6 and Fig 10.

[14] CHATRCHYAN 13AB looked in 5.0 fb^{-1} of pp collisions at $\sqrt{s}$ = 7 TeV and in 18.8 fb^{-1} of pp collisions at $\sqrt{s}$ = 8 TeV for events with heavy stable particles, identified by their anomalous dE/dx in the tracker or additionally requiring that it be identified as muon in the muon chambers, from pair production of $\widetilde{t}_1$'s. No evidence for an excess over the expected background is observed. Limits are derived for pair production of stops as a function of mass in the cloud interaction model (see Fig. 8 and Table 6). In the charge-suppressed model, the limit decreases to 818 GeV.

$\widetilde{b}$ (Sbottom) mass limit

Limits in e^+e^- depend on the mixing angle of the mass eigenstate $\widetilde{b}_1 = \widetilde{b}_L \cos\theta_b + \widetilde{b}_R \sin\theta_b$. Coupling to the Z vanishes for $\theta_b \sim 1.17$. As a consequence, no absolute constraint in the mass region $\lesssim$40 GeV is available in the literature at this time from e^+e^- collisions. In the Listings below, we use $\Delta m = m_{\widetilde{b}_1} - m_{\widetilde{\chi}^0_1}$.

Some earlier papers are now obsolete and have been omitted. They were last listed in our PDG 14 edition: K. Olive, *et al.* (Particle Data Group), Chinese Physics **C38** 070001 (2014) (http://pdg.lbl.gov).

R-parity conserving $\widetilde{b}$ (Sbottom) mass limit

VALUE (GeV)	CL%	DOCUMENT ID		TECN	COMMENT
> 850	95	[1] AAD	21AM	ATLS	$\tau^\pm$'s + b-jets + $\not{E}_T$, Tsbot4, $m_{\widetilde{\chi}^0_2} - m_{\widetilde{\chi}^0_1}$ = 130 GeV, $m_{\widetilde{\chi}^0_2}$ < 180 GeV
>1270	95	[2] AAD	21S	ATLS	b-jets + $\not{E}_T$, Tsbot1, $m_{\widetilde{\chi}^0_1}$=0 GeV
> 660	95	[2] AAD	21S	ATLS	b-jets + $\not{E}_T$, Tsbot1,$m_{\widetilde{b}_1} - m_{\widetilde{\chi}^0_1}$ = 10 GeV
>1600	95	[3] SIRUNYAN	21M	CMS	$\ell^\pm\ell^\mp$ + $\not{E}_T$, Tsbot3, $m_{\widetilde{\chi}^0_2}$ = 1500 GeV, $m_{\widetilde{\chi}^0_1}$ = 100 GeV
> 750	95	[4] AAD	20V	ATLS	same-sign $\ell^\pm\ell^\pm$ + jets, Tsbot2, $m_{\widetilde{\chi}^\pm_1} = m_{\widetilde{\chi}^0_1}$ + 100 GeV, $m_{\widetilde{\chi}^0_1} \sim$ 50 GeV
> 850	95	[5] SIRUNYAN	20T	CMS	same-sign $\ell^\pm\ell^\pm$ or $\geq 3\ell^\pm$ + jets, Tsbot2, $m_{\widetilde{\chi}^\pm_1}$ < 800 GeV, $m_{\widetilde{\chi}^0_1}$ = 50 GeV
>1500	95	[6] AAD	19H	ATLS	$\geq$ 3 b-jets + $\not{E}_T$, Tsbot4, $\geq$ 1 $h(\rightarrow b\overline{b})$, $m_{\widetilde{\chi}^0_1}$ = 60 GeV
>1300	95	[7] AAD	19H	ATLS	$\geq$ 3 b-jets+$\not{E}_T$, Tsbot4, $\geq$ 1$h(\rightarrow b\overline{b})$, $m_{\widetilde{\chi}^0_2} = m_{\widetilde{\chi}^0_1}$ +130 GeV

Downloaded from https://academic.oup.com/ptep/article/2022/8/083C01/6651666 by KIT Library user on 27 September 2022

>1220	95	[8] SIRUNYAN	19CH	CMS	jets+$\not{E}_T$, Tsbot1, $m_{\widetilde{\chi}^0_1}$ = 0 GeV
> 530	95	[9] SIRUNYAN	19CI	CMS	≥ 1 H ($\rightarrow \gamma\gamma$) + jets + $\not{E}_T$, Tsbot4, $m_{\widetilde{\chi}^0_2} = m_{\widetilde{\chi}^0_1}$ + 130 GeV, $m_{\widetilde{\chi}^0_1}$ = 1 GeV
> 430	95	[10] AABOUD	18I	ATLS	≥ 1 jets+$\not{E}_T$, Tsbot1, $m_{\widetilde{b}} - m_{\widetilde{\chi}^0_1} \sim m_b$
> 840	95	[11] SIRUNYAN	18AL	CMS	≥ 3$\ell^\pm$ + jets + $\not{E}_T$, Tsbot2, $m_{\widetilde{\chi}^0_1}$ = 50 GeV
> 975	95	[12] SIRUNYAN	18AR	CMS	$\ell^\pm\ell^\mp$ + jets + $\not{E}_T$, Tsbot3, $m_{\widetilde{\ell}}$= ($m_{\widetilde{\chi}^0_2}$+$m_{\widetilde{\chi}^0_1}$)/2, $m_{\widetilde{\chi}^0_1}$= 100 GeV
>1060	95	[13] SIRUNYAN	18AY	CMS	jets+$\not{E}_T$, Tsbot1, $m_{\widetilde{\chi}^0_1}$ = 0 GeV
>1230	95	[14] SIRUNYAN	18B	CMS	jets+$\not{E}_T$, Tsbot1, $m_{\widetilde{\chi}^0_1}$ = 0 GeV
> 420	95	[15] SIRUNYAN	18X	CMS	≥ 1 H ($\rightarrow \gamma\gamma$) + jets + $\not{E}_T$, Tsbot4, $m_{\widetilde{\chi}^0_2} = m_{\widetilde{\chi}^0_1}$ + 130 GeV, $m_{\widetilde{\chi}^0_1}$ < 225 GeV
> 700	95	[16] AABOUD	17AJ	ATLS	same-sign $\ell^\pm\ell^\pm$ / 3 ℓ + jets + $\not{E}_T$, Tsbot2, $m_{\widetilde{\chi}^0_1}$ = 0 GeV
> 950	95	[17] AABOUD	17AX	ATLS	2 b-jets+$\not{E}_T$, Tsbot1, $m_{\widetilde{\chi}^0_1}$ = 0 GeV
> 880	95	[18] AABOUD	17AX	ATLS	2 b-jets + $\not{E}_T$, mixture Tsbot1 and Tsbot2 BR=50%, $m_{\widetilde{\chi}^0_1}$ = 0 GeV, $m_{\widetilde{\chi}^\pm_1} - m_{\widetilde{\chi}^0_1}$ = 1 GeV
> 315	95	[19] KHACHATRY...	17A	CMS	2 VBF jets + $\not{E}_T$, Tsbot1, $m_{\widetilde{b}} - m_{\widetilde{\chi}^0_1}$ = 5 GeV
> 450	95	[20] KHACHATRY...	17AW	CMS	≥ 3$\ell^\pm$, 2 jets, Tsbot2, $m_{\widetilde{\chi}^0_1}$ = 50 GeV, $m_{\widetilde{\chi}^\pm_1}$ = 200 GeV
> 800	95	[21] KHACHATRY...	17P	CMS	1 or more jets+$\not{E}_T$, Tsbot1, $m_{\widetilde{\chi}^0_1}$ = 0 GeV
>1175	95	[22] SIRUNYAN	17AZ	CMS	≥ 1 jets+$\not{E}_T$, Tsbot1, $m_{\widetilde{\chi}^0_1}$ = 0 GeV
> 890	95	[23] SIRUNYAN	17K	CMS	jets+$\not{E}_T$, Tsbot1, $m_{\widetilde{\chi}^0_1}$ = 0 GeV
> 810	95	[24] SIRUNYAN	17S	CMS	same-sign $\ell^\pm\ell^\pm$ + jets + $\not{E}_T$, Tsbot2, $m_{\widetilde{\chi}^0_1}$ = 50 GeV, $m_{\widetilde{\chi}^\pm_1}$ = 100 GeV
> 323	95	[25] AABOUD	16D	ATLS	≥ 1 jet + $\not{E}_T$, Tsbot1, $m_{\widetilde{b}_1} - m_{\widetilde{\chi}^0_1}$ = 5 GeV
> 840	95	[26] AABOUD	16Q	ATLS	2 b-jets + $\not{E}_T$, Tsbot1, $m_{\widetilde{\chi}^0_1}$ = 100 GeV
> 540	95	[27] AAD	16BB	ATLS	2 same-sign/3ℓ + jets + $\not{E}_T$, Tsbot2, $m_{\widetilde{\chi}^0_1}$ < 55 GeV
> 680	95	[28] KHACHATRY...	16BJ	CMS	same-sign $\ell^\pm\ell^\pm$, Tsbot2, $m_{\widetilde{\chi}^\pm_1}$ < 550 GeV, $m_{\widetilde{\chi}^0_1}$ = 50 GeV
> 500	95	[28] KHACHATRY...	16BJ	CMS	same-sign $\ell^\pm\ell^\pm$, Tsbot2, $m_{\widetilde{b}} - m_{\widetilde{\chi}^\pm_1}$ <100 GeV, $m_{\widetilde{\chi}^0_1}$=50 GeV
> 880	95	[29] KHACHATRY...	16BS	CMS	jets + $\not{E}_T$, Tsbot1, $m_{\widetilde{\chi}^0_1}$ = 0 GeV
> 550	95	[30] KHACHATRY...	16BY	CMS	opposite-sign $\ell^\pm\ell^\pm$, Tsbot3, $m_{\widetilde{\chi}^0_1}$ = 100 GeV
> 600	95	[31] AAD	15CJ	ATLS	$\widetilde{b} \rightarrow b\widetilde{\chi}^0_1$, $m_{\widetilde{\chi}^0_1}$ < 250 GeV
> 440	95	[31] AAD	15CJ	ATLS	$\widetilde{b} \rightarrow t\widetilde{\chi}^\pm_1$, $\widetilde{\chi}^\pm_1 \rightarrow W^{(*)}\widetilde{\chi}^0_1$, $m_{\widetilde{\chi}^0_1}$ = 60 GeV, $m_{\widetilde{b}} - m_{\widetilde{\chi}^\pm_1} < m_t$
none 300–650	95	[31] AAD	15CJ	ATLS	$\widetilde{b} \rightarrow \widetilde{b}b\widetilde{\chi}^0_2$, $\widetilde{\chi}^0_2 \rightarrow h\widetilde{\chi}^0_1$, $m_{\widetilde{\chi}^0_1}$ = 60 GeV, $m_{\widetilde{\chi}^0_2}$ > 250 GeV
> 640	95	[32] KHACHATRY...	15AF	CMS	$\widetilde{b} \rightarrow b\widetilde{\chi}^0_1$, $m_{\widetilde{\chi}^0_1}$ = 0
> 650	95	[33] KHACHATRY...	15AH	CMS	$\widetilde{b} \rightarrow b\widetilde{\chi}^0_1$, $m_{\widetilde{\chi}^0_1}$ = 0
> 250	95	[33] KHACHATRY...	15AH	CMS	$\widetilde{b} \rightarrow b\widetilde{\chi}^0_1$, $m_{\widetilde{b}} - m_{\widetilde{\chi}^0_1}$ < 10 GeV
> 570	95	[34] KHACHATRY...	15I	CMS	$\widetilde{b} \rightarrow t\widetilde{\chi}^\pm_1$, $\widetilde{\chi}^\pm_1 \rightarrow W^\pm\widetilde{\chi}^0_1$, $m_{\widetilde{\chi}^0_1}$ =50 GeV, 150<$m_{\widetilde{\chi}^\pm_1}$ <300 GeV
> 255	95	[35] AAD	14T	ATLS	$\widetilde{b}_1 \rightarrow b\widetilde{\chi}^0_1$, $m_{\widetilde{b}_1} - m_{\widetilde{\chi}^0_1} \approx m_b$
> 400	95	[36] CHATRCHYAN	14AH	CMS	jets + $\not{E}_T$, $\widetilde{b} \rightarrow b\widetilde{\chi}^0_1$ simplified model, $m_{\widetilde{\chi}^0_1}$ = 50 GeV
		[37] CHATRCHYAN	14R	CMS	≥ 3$\ell^\pm$, $\widetilde{b} \rightarrow t\widetilde{\chi}^\pm_1$, $\widetilde{\chi}^\pm_1 \rightarrow W^\pm\widetilde{\chi}^0_1$ simplified model, $m_{\widetilde{\chi}^0_1}$ = 50 GeV
		[38] KHACHATRY...	15AD	CMS	$\ell^\pm\ell^\mp$ + jets + $\not{E}_T$, $\widetilde{b} \rightarrow b\ell^\pm\ell^\mp\widetilde{\chi}^0_1$
none 340–600	95	[39] AAD	14AX	ATLS	≥ 3 b-jets + $\not{E}_T$, $\widetilde{b} \rightarrow b\widetilde{\chi}^0_2$ simplified model with $\widetilde{\chi}^0_2 \rightarrow h\widetilde{\chi}^0_1$, $m_{\widetilde{\chi}^0_1}$=60 GeV, $m_{\widetilde{\chi}^0_2}$=300 GeV
> 440	95	[40] AAD	14E	ATLS	$\ell^\pm\ell^\pm(\ell^\mp)$ + jets, $\widetilde{b}_1 \rightarrow t\widetilde{\chi}^\pm_1$ with $\widetilde{\chi}^\pm_1 \rightarrow W^{(*)\pm}\widetilde{\chi}^0_1$ simplified model, $m_{\widetilde{\chi}^\pm_1} = 2\, m_{\widetilde{\chi}^0_1}$
> 500	95	[41] CHATRCHYAN	14H	CMS	same-sign $\ell^\pm\ell^\pm$, $\widetilde{b} \rightarrow t\widetilde{\chi}^\pm_1$, $\widetilde{\chi}^\pm_1 \rightarrow W^\pm\widetilde{\chi}^0_1$ simplified model, $m_{\widetilde{\chi}^\pm_1}$ = 2 GeV, $m_{\widetilde{\chi}^0_1}$ = 100 GeV
> 620	95	[42] AAD	13AU	ATLS	2 b-jets + $\not{E}_T$, $\widetilde{b}_1 \rightarrow b\widetilde{\chi}^0_1$, $m_{\widetilde{\chi}^0_1}$ < 120 GeV
> 550	95	[43] CHATRCHYAN	13AT	CMS	jets + $\not{E}_T$, $\widetilde{b} \rightarrow b\widetilde{\chi}^0_1$ simplified model, $m_{\widetilde{\chi}^0_1}$= 50 GeV
> 600	95	[44] CHATRCHYAN	13T	CMS	jets + $\not{E}_T$, $\widetilde{b} \rightarrow b\widetilde{\chi}^0_1$ simplified model, $m_{\widetilde{\chi}^0_1}$= 0 GeV
> 450	95	[45] CHATRCHYAN	13V	CMS	same-sign $\ell^\pm\ell^\pm$ + ≥ 2 b-jets, $\widetilde{b} \rightarrow t\widetilde{\chi}^\pm_1$, $\widetilde{\chi}^\pm_1 \rightarrow W^\pm\widetilde{\chi}^0_1$ simplified model, $m_{\widetilde{\chi}^0_1}$ = 50 GeV
> 390	95	[46] AAD	12AN	ATLS	$\widetilde{b}_1 \rightarrow b\widetilde{\chi}^0_1$, simplified model, $m_{\widetilde{\chi}^0_1}$ < 60 GeV
		[47] CHATRCHYAN	12AI	CMS	$\ell^\pm\ell^\pm$ + b-jets + $\not{E}_T$
> 410	95	[48] CHATRCHYAN	12BO	CMS	$\widetilde{b}_1 \rightarrow b\widetilde{\chi}^0_1$, simplified model, $m_{\widetilde{\chi}^0_1}$ = 50 GeV
> 294	95	[49] AAD	11K	ATLS	stable $\widetilde{b}$
		[50] AAD	11O	ATLS	$\widetilde{g} \rightarrow \widetilde{b}_1 b$, $\widetilde{b}_1 \rightarrow b\widetilde{\chi}^0_1$, $m_{\widetilde{\chi}^0_1}$=60 GeV
		[51] CHATRCHYAN	11D	CMS	$\widetilde{b},\widetilde{t} \rightarrow b$
> 230	95	[52] AALTONEN	10R	CDF	$\widetilde{b}_1 \rightarrow b\widetilde{\chi}^0_1$, $m_{\widetilde{\chi}^0_1}$ < 70 GeV
> 247	95	[53] ABAZOV	10L	D0	$\widetilde{b}_1 \rightarrow b\widetilde{\chi}^0_1$, $m_{\widetilde{\chi}^0_1}$ = 0 GeV

• • • We do not use the following data for averages, fits, limits, etc. • • •

[1] AAD 21AM searched in 139 fb^{-1} of pp collisions at $\sqrt{s}$ = 13 TeV for pair production of bottom squarks in events with hadronically decaying $\tau^\pm$-leptons, b-tagged jets, and large $\not{E}_T$. No significant excess above the Standard Model expectations is observed. Limits are set on the bottom squark mass in the Tsbot4 simplified model, assuming $m_{\widetilde{\chi}^0_2} - m_{\widetilde{\chi}^0_1}$ = 130 GeV, see their Figure 8.

[2] AAD 21S searched in 139 fb^{-1} of pp collisions at $\sqrt{s}$ = 13 TeV for pair production of sbottoms, LQ or dark matter in events with b-jets and $\not{E}_T$, also using dedicated secondary-vertex-finding techniques. No significant excess above the Standard Model predictions is observed. Limits are set on $m_{\widetilde{b}_1}$ in the Tsbot1 simplified model, on the LQ masses depending on the BR in $b\nu$, on scalar and pseudoscalar dark matter mediator masses. See Figures 8, 9, 10.

[3] SIRUNYAN 21M searched in 137 fb^{-1} of pp collisions at $\sqrt{s}$ = 13 TeV for supersymmetry in events with two opposite-sign same-flavor leptons (electrons, muons) and $\not{E}_T$. No significant excess above the Standard Model expectations is observed. Limits are set on the gluino mass in the simplified model Tglu4C, see their Figure 10, on the $\widetilde{\chi}^0_2$ and $\widetilde{\chi}^\pm_1$ mass in Tchi1n2Fa, see their Figure 11, on the $\widetilde{\chi}^0_1$ mass in Tn1n1C and Tn1n1B for $m_{\widetilde{\chi}^0_2}$=$m_{\widetilde{\chi}^\pm_1}$=$m_{\widetilde{\chi}^0_1}$, see their Figure 12. Limits are also set on the light squark mass for the simplified model Tsqk2A, on the sbottom mass in Tsbot3, see their Figure 13, and on the slepton mass in direct electroweak pair production of mass-degenerate left- and right-handed sleptons (selectrons and smuons), see their Figure 14.

[4] AAD 20V searched in 139 fb^{-1} of pp collisions at $\sqrt{s}$ = 13 TeV for events with two same-sign charged leptons (electrons or muons) and jets. No significant excess above the Standard Model expectations is observed. Exclusion limits at 95% C.L. are set on the bottom squark masses in the Tsbot2 simplified model for $m_{\widetilde{\chi}^\pm_1} = m_{\widetilde{\chi}^0_1}$ + 100 GeV, see their Fig. 8(a).

[5] SIRUNYAN 20T searched in 137 fb^{-1} of pp collisions at $\sqrt{s}$ = 13 TeV for events with at least two jets, and two isolated same-sign or three or more charged leptons (electrons or muons). No significant excess above the Standard Model expectations is observed. Limits are set on the gluino mass in the Tglu3A, Tglu3B, Tglu3C and Tglu3D simplified models, see their Figure 7, and in the Tglu1C and Tglu1B simplified models, see their Figures 8 and 9. Limits are also set on the sbottom mass in the Tsbot2 simplified model, see their Figure 10, and on the stop mass in the Tstop7 simplified model, see their Figure 11. Finally, limits are set on the gluino mass in RPV simplified models where the gluino decays either via $\widetilde{g} \rightarrow q q \overline{q}\,\overline{q}$ + $e/\mu/\tau$ or via $\widetilde{g} \rightarrow t b s$, see Figure 12.

[6] AAD 19H searched in 139 fb^{-1} of pp collisions at $\sqrt{s}$ = 13 TeV for events with no charged leptons, three or more b-jets, and large $\not{E}_T$. Higgs boson candidates are reconstructed as b-jet pairs. No significant excess above the Standard Model expectations is observed. Limits up to 1500 GeV are set on the sbottom mass in the Tsbot4 simplified model, see Figure 8(a), for fixed $m_{\widetilde{\chi}^0_1}$ = 60 GeV and for $m_{\widetilde{\chi}^0_2}$ up to 1200 GeV.

[7] AAD 19H searched in 139 fb^{-1} of pp collisions at $\sqrt{s}$ = 13 TeV for events with no charged leptons, three or more b-jets, and large $\not{E}_T$. Higgs boson candidates are reconstructed as b-jet pairs. No significant excess above the Standard Model expectations is observed. Limits up to 1300 GeV are set on the sbottom mass in the Tsbot4 simplified model, see Figure 8(b), for $m_{\widetilde{\chi}^0_2} = m_{\widetilde{\chi}^0_1}$ + 130 GeV and $m_{\widetilde{\chi}^0_2}$ from 200 to 750 GeV.

[8] SIRUNYAN 19CH searched in 137 fb^{-1} of pp collisions at $\sqrt{s}$ = 13 TeV for events containing multiple jets and large $\not{E}_T$. No significant excess above the Standard Model expectations is observed. Limits are set on the gluino mass in the Tglu1A, Tglu1C, Tglu2A and Tglu3A simplified models, see their Figure 13. Limits are also set on squark,

Downloaded from https://academic.oup.com/ptep/article/2022/8/083C01/6651666 by KIT Library user on 27 September 2022

sbottom and stop masses in the Tsqk1, Tsbot1, Tstop1 simplified models, see their Figure 14.

[9] SIRUNYAN 19CI searched in 77.5 fb^{-1} of pp collisions at $\sqrt{s}$ = 13 TeV for events with one or more high-momentum Higgs bosons, decaying to pairs of photons, jets and $\not{E}_T$. No significant excess above the Standard Model expectations is observed. Limits are set on the sbottom mass in the Tsbot4 simplified model, see Figure 3, and on the wino mass in the Tchi1n2E simplified model, see their Figure 4. Limits are also set on the higgsino mass in the Tn1n1A and Tn1n1B simplified models, see their Figure 5.

[10] AABOUD 18I searched in 36.1 fb^{-1} of pp collisions at $\sqrt{s}$ = 13 TeV for events with at least one jet with a transverse momentum above 250 GeV and no leptons. Good agreement is observed between the number of events in data and Standard Model predictions. The results are translated into exclusion limits in Tsbot1 models. In the compressed scenario with sbottom and neutralino masses differing by m_b, sbottom masses below 430 GeV are excluded. For $m_{\widetilde{\chi}^0_1}$ = 0 they exclude sbottom masses up to 610 GeV. See their Fig.10(a).

[11] SIRUNYAN 18AL searched in 35.9 fb^{-1} of pp collisions at $\sqrt{s}$ = 13 TeV for events with at least three charged leptons, in any combination of electrons and muons, jets and significant $\not{E}_T$. No significant excess above the Standard Model expectations is observed. Limits are set on the gluino mass in the Tglu3A and Tglu1C simplified models, see their Figure 5. Limits are also set on the sbottom mass in the Tsbot2 simplified model, see their Figure 6, and on the stop mass in the Tstop7 simplified model, see their Figure 7.

[12] SIRUNYAN 18AR searched in 35.9 fb^{-1} of pp collisions at $\sqrt{s}$ = 13 TeV for events containing two opposite-charge, same-flavour leptons (electrons or muons), jets and $\not{E}_T$. No significant excess above the Standard Model expectations is observed. Limits are set on the gluino mass in the Tglu4C simplified model, see their Figure 7. Limits are also set on the chargino/neutralino mass in the Tchi1n2F simplified model, see their Figure 8, and on the neutralino mass in the Tn1n1B and Tn1n1C simplified models, see their Figure 9. Finally, limits are set on the sbottom mass in the Tsbot3 simplified model, see their Figure 10.

[13] SIRUNYAN 18AY searched in 35.9 fb^{-1} of pp collisions at $\sqrt{s}$ = 13 TeV for events containing one or more jets and significant $\not{E}_T$. No significant excess above the Standard Model expectations is observed. Limits are set on the gluino mass in the Tglu1A, Tglu2A and Tglu3A simplified models, see their Figure 3. Limits are also set on squark, sbottom and stop masses in the Tsqk1, Tsbot1, Tstop1 and Tstop4 simplified models, see their Figure 3. Finally, limits are set on long-lived gluino masses in a Tglu1A simplified model where the gluino is metastable or long-lived with proper decay lengths in the range 10^{-3} mm $< c\tau < 10^5$ mm, see their Figure 4.

[14] SIRUNYAN 18B searched in 35.9 fb^{-1} of pp collisions at $\sqrt{s}$ = 13 TeV for the pair production of third-generation squarks in events with jets and large $\not{E}_T$. No significant excess above the Standard Model expectations is observed. Limits are set on the sbottom mass in the Tsbot1 simplified model, see their Figure 5, and on the stop mass in the Tstop4 simplified model, see their Figure 6.

[15] SIRUNYAN 18X searched in 35.9 fb^{-1} of pp collisions at $\sqrt{s}$ = 13 TeV for events with one or more high-momentum Higgs bosons, decaying to pairs of photons, jets and $\not{E}_T$. The razor variables (M_R and R^2) are used to categorise the events. No significant excess above the Standard Model expectations is observed. Limits are set on the sbottom mass in the Tsbot4 simplified model and on the wino mass in the Tchi1n2E simplified model, see their Figure 5. Limits are also set on the higgsino mass in the Tn1n1A and Tn1n1B simplified models, see their Figure 6.

[16] AABOUD 17AJ searched in 36.1 fb^{-1} of pp collisions at $\sqrt{s}$ = 13 TeV for events with two same-sign or three leptons, jets and large missing transverse momentum. No significant excess above the Standard Model expectations is observed. Limits up to 700 GeV are set on the bottom squark mass in Tsbot2 simplified models assuming $m_{\widetilde{\chi}^0_1}$ = 0 GeV. See their Figure 4(d).

[17] AABOUD 17AX searched in 36 fb^{-1} of pp collisions at $\sqrt{s}$ = 13 TeV for events containing two jets identified as originating from b-quarks and large missing transverse momentum. No excess of events above the expected level of Standard Model background was found. Exclusion limits at 95% C.L. are set on the masses of bottom squarks. In the Tsbot1 simplified model, a $\widetilde{b}_1$ mass below 950 GeV is excluded for $m_{\widetilde{\chi}^0_1}$ = 0 (<420) GeV. See their Fig. 7(a).

[18] AABOUD 17AX searched in 36 fb^{-1} of pp collisions at $\sqrt{s}$ = 13 TeV for events containing two jets identified as originating from b-quarks and large missing transverse momentum, with or without leptons. No excess of events above the expected level of Standard Model background was found. Exclusion limits at 95% C.L. are set on the masses of bottom squarks. Assuming 50% BR for Tsbot1 and Tsbot2 simplified models, a $\widetilde{b}_1$ mass below 880 (860) GeV is excluded for $m_{\widetilde{\chi}^0_1}$ = 0 (<250) GeV. See their Fig. 7(b).

[19] KHACHATRYAN 17A searched in 18.5 fb^{-1} of pp collisions at $\sqrt{s}$ = 8 TeV for events with two forward jets, produced through vector boson fusion, and missing transverse momentum. No significant excess above the Standard Model expectations is observed. A limit is set on sbottom masses in the Tsbot1 simplified model, see Fig. 3.

[20] KHACHATRYAN 17AW searched in 2.3 fb^{-1} of pp collisions at $\sqrt{s}$ = 13 TeV for events with at least three charged leptons, in any combination of electrons and muons, and significant $\not{E}_T$. No significant excess above the Standard Model expectations is observed. Limits are set on the gluino mass in the Tglu3A and Tglu1C simplified models, and on the sbottom mass in the Tsbot2 simplified model, see their Figure 4.

[21] KHACHATRYAN 17P searched in 2.3 fb^{-1} of pp collisions at $\sqrt{s}$ = 13 TeV for events with one or more jets and large $\not{E}_T$. No significant excess above the Standard Model expectations is observed. Limits are set on the gluino mass in the Tglu1A, Tglu2A, Tglu3A, Tglu3B, Tglu3C and Tglu3D simplified models, see their Figures 7 and 8. Limits are also set on the squark mass in the Tsqk1 simplified model, see their Fig. 7, and on the sbottom mass in the Tsbot1 simplified model, see Fig. 8. Finally, limits are set on the stop mass in the Tstop1, Tstop3, Tstop4, Tstop6 and Tstop7 simplified models, see Fig. 8.

[22] SIRUNYAN 17AZ searched in 35.9 fb^{-1} of pp collisions at $\sqrt{s}$ = 13 TeV for events with one or more jets and large $\not{E}_T$. No significant excess above the Standard Model expectations is observed. Limits are set on the gluino mass in the Tglu1A, Tglu2A, Tglu3A simplified models, see their Figures 6. Limits are also set on the squark mass in the Tsqk1 simplified model (for single light squark and for 8 degenerate light squarks), on the sbottom mass in the Tsbot1 simplified model and on the stop mass in the Tstop1 simplified model, see their Fig. 7. Finally, limits are set on the stop mass in the Tstop2, Tstop4 and Tstop8 simplified models, see Fig. 8.

[23] SIRUNYAN 17K searched in 2.3 fb^{-1} of pp collisions at $\sqrt{s}$ = 13 TeV for direct production of stop or sbottom pairs in events with multiple jets and significant $\not{E}_T$. A second search also requires an isolated lepton and is combined with the all-hadronic search. No significant excess above the Standard Model expectations is observed. Limits are set on the stop mass in the Tstop1, Tstop8 and Tstop4 simplified models, see their Figures 7, 8 and 9 (for the Tstop4 limits, only the results of the all-hadronic search are used). Limits are also set on the sbottom mass in the Tsbot1 simplified model, see Fig. 10 (also here, only the results of the all-hadronic search are used).

[24] SIRUNYAN 17S searched in 35.9 fb^{-1} of pp collisions at $\sqrt{s}$ = 13 TeV for events with two isolated same-sign leptons, jets, and large $\not{E}_T$. No significant excess above the Standard Model expectations is observed. Limits are set on the mass of the gluino mass in the Tglu3A, Tglu3B, Tglu3C, Tglu3D and Tglu1B simplified models, see their Figures 5 and 6, and on the sbottom mass in the Tsbot2 simplified model, see their Figure 6.

[25] AABOUD 16D searched in 3.2 fb^{-1} of pp collisions at $\sqrt{s}$ = 13 TeV for events with an energetic jet and large missing transverse momentum. The results are interpreted as 95%C.L. limits on mass of sbottom decaying into a b-quark and the lightest neutralino in scenarios with $m_{\widetilde{b}_1} - m_{\widetilde{\chi}^0_1}$ between 5 and 20 GeV. See their Fig. 6.

[26] AABOUD 16Q searched in 3.2 fb^{-1} of pp collisions at $\sqrt{s}$ = 13 TeV for events containing two jets identified as originating from b-quarks and large missing transverse momentum. No excess of events above the expected level of Standard Model background was found. Exclusion limits at 95% C.L. are set on the masses of third-generation squarks. Assuming that the decay $\widetilde{b}_1 \rightarrow b\widetilde{\chi}^0_1$ (Tsbot1) takes place 100% of the time, a $\widetilde{b}_1$ mass below 840 (800) GeV is excluded for $m_{\widetilde{\chi}^0_1}$ < 100 (360) GeV. Differences in mass above 100 GeV between the $\widetilde{b}_1$ and the $\widetilde{\chi}^0_1$ are excluded up to a $\widetilde{b}_1$ mass of 500 GeV. For more details, see their Fig. 4.

[27] AAD 16BB searched in 3.2 fb^{-1} of pp collisions at $\sqrt{s}$ = 13 TeV for events with exactly two same-sign leptons or at least three leptons, multiple hadronic jets, b-jets, and $\not{E}_T$. No significant excess over the Standard Model expectation is found. Exclusion limits at 95% C.L. are set on the sbottom mass for the Tsbot2 model, assuming $m_{\widetilde{\chi}^\pm_1} = m_{\widetilde{\chi}^0_1}$ + 100 GeV. See their Fig. 4c.

[28] KHACHATRYAN 16BJ searched in 2.3 fb^{-1} of pp collisions at $\sqrt{s}$ = 13 TeV for events with two isolated same-sign dileptons and jets in the final state. No significant excess above the Standard Model expectations is observed. Limits are set on the sbottom mass in the Tsbot2 simplified model, see Fig. 6.

[29] KHACHATRYAN 16BS searched in 2.3 fb^{-1} of pp collisions at $\sqrt{s}$ = 13 TeV for events with at least one energetic jet , no isolated leptons, and significant $\not{E}_T$, using the transverse mass variable M_{T2} to discriminate between signal and background processes. No significant excess above the Standard Model expectations is observed. Limits are set on the sbottom mass in the Tsbot1 simplified model, see Fig. 11 and Table 3.

[30] KHACHATRYAN 16BY searched in 2.3 fb^{-1} of pp collisions at $\sqrt{s}$ = 13 TeV for events with two opposite-sign, same-flavour leptons, jets, and missing transverse momentum. No significant excess above the Standard Model expectations is observed. Limits are set on the gluino mass in the Tglu4C simplified model, see Fig. 4, and on sbottom masses in the Tsbot3 simplified model, see Fig. 5.

[31] AAD 15CJ searched in 20 fb^{-1} of pp collisions at $\sqrt{s}$ = 8 TeV for evidence of third generation squarks by combining a large number of searches covering various final states. Limits on the sbottom mass are shown, either assuming the $\widetilde{b} \rightarrow b\widetilde{\chi}^0_1$ decay, see Fig. 11, or assuming the $\widetilde{b} \rightarrow t\widetilde{\chi}^\pm_1$ decay, with $\widetilde{\chi}^\pm_1 \rightarrow W^{(*)}\widetilde{\chi}^0_1$, see Fig. 12a, or assuming the $\widetilde{b} \rightarrow b\widetilde{\chi}^0_2$ decay, with $\widetilde{\chi}^0_2 \rightarrow h\widetilde{\chi}^0_1$, see Fig. 12b. Interpretations in the pMSSM are also discussed, see Figures 13–15.

[32] KHACHATRYAN 15AF searched in 19.5 fb^{-1} of pp collisions at $\sqrt{s}$ = 8 TeV for events with at least two energetic jets and significant $\not{E}_T$, using the transverse mass variable M_{T2} to discriminate between signal and background processes. No significant excess above the Standard Model expectations is observed. Limits are set on the sbottom mass in simplified models where the decay $\widetilde{b} \rightarrow b\widetilde{\chi}^0_1$ takes place with a branching ratio of 100%, see Fig. 12. See also Table 5. Exclusions in the CMSSM, assuming tanβ = 30, $A_0 = -2$ max(m_0, $m_{1/2}$) and μ > 0, are also presented, see Fig. 15.

[33] KHACHATRYAN 15AH searched in 19.4 or 19.7 fb^{-1} of pp collisions at $\sqrt{s}$ = 8 TeV for events containing either a fully reconstructed top quark, or events containing dijets requiring one or both jets to originate from b-quarks, or events containing a mono-jet. No significant excess above the Standard Model expectations is observed. Limits are set on the sbottom mass in simplified models where the decay $\widetilde{b} \rightarrow b\widetilde{\chi}^0_1$ takes place with a branching ratio of 100%, see Fig. 12. Limits are also set in a simplified model where the decay $\widetilde{b} \rightarrow c\widetilde{\chi}^0_1$ takes place with a branching ratio of 100%, see Fig. 12.

[34] KHACHATRYAN 15I searched in 19.5 fb^{-1} of pp collisions at $\sqrt{s}$ = 8 TeV for events in which b-jets and four W-bosons are produced. Five individual search channels are combined (fully hadronic, single lepton, same-sign dilepton, opposite-sign dilepton, multilepton). No significant excess above the Standard Model expectations is observed. Limits are set on the sbottom mass in a simplified model where the decay $\widetilde{b} \rightarrow t\widetilde{\chi}^\pm_1$, with $\widetilde{\chi}^\pm_1 \rightarrow W^\pm\widetilde{\chi}^0_1$, takes place with a branching ratio of 100%, see Fig. 7.

[35] AAD 14T searched in 20.3 fb^{-1} of pp collisions at $\sqrt{s}$ = 8 TeV for monojet-like events. No excess of events above the expected level of Standard Model background was found. Exclusion limits at 95% C.L. are set on the masses of third-generation squarks in simplified models which assume that the decay $\widetilde{b}_1 \rightarrow b\widetilde{\chi}^0_1$ takes place 100% of the time, see Fig. 12.

[36] CHATRCHYAN 14AH searched in 4.7 fb^{-1} of pp collisions at $\sqrt{s}$ = 7 TeV for events with at least two energetic jets and significant $\not{E}_T$, using the razor variables (M_R and R^2) to discriminate between signal and background processes. A second analysis requires at least one of the jets to be originating from a b-quark. No significant excess above the Standard Model expectations is observed. Limits are set on sbottom masses in simplified models where the decay $\widetilde{b} \rightarrow b\widetilde{\chi}^0_1$ takes place with a branching ratio of 100%, see Figs. 28 and 29. Exclusions in the CMSSM, assuming tanβ = 10, A_0 = 0 and μ >0, are also presented, see Fig. 26.

[37] CHATRCHYAN 14R searched in 19.5 fb^{-1} of pp collisions at $\sqrt{s}$ = 8 TeV for events with at least three leptons (electrons, muons, taus) in the final state. No significant excess above the Standard Model expectations is observed. Limits are set on the gluino mass in a simplified model where the decay $\widetilde{b} \rightarrow t\widetilde{\chi}^\pm_1$, with $\widetilde{\chi}^\pm_1 \rightarrow W^\pm\widetilde{\chi}^0_1$, takes place with a branching ratio of 100%, see Fig. 11.

[38] KHACHATRYAN 15AD searched in 19.4 fb^{-1} of pp collisions at $\sqrt{s}$ = 8 TeV for events with two opposite-sign same flavor isolated leptons featuring either a kinematic edge, or a peak at the Z-boson mass, in the invariant mass spectrum. No evidence for a statistically significant excess over the expected SM backgrounds is observed and 95% C.L. exclusion limits are derived in a simplified model of sbottom pair production where the sbottom decays into a b-quark, two opposite-sign dileptons and a neutralino LSP,

Downloaded from https://academic.oup.com/ptep/article/2022/8/083C01/6651666 by KIT Library user on 27 September 2022

through an intermediate state containing either an off-shell Z-boson or a slepton, see Fig. 8.

[39] AAD 14AX searched in 20.1 fb^{-1} of pp collisions at $\sqrt{s}$ = 8 TeV for the strong production of supersymmetric particles in events containing either zero or at last one high high-p_T lepton, large missing transverse momentum, high jet multiplicity and at least three jets identified as originating from b-quarks. No excess over the expected SM background is observed. Limits are derived in mSUGRA/CMSSM models with tanβ = 30, $A_0 = -2\ m_0$ and $\mu > 0$, see their Fig. 14. Also, exclusion limits are set in simplified models containing scalar bottom quarks, where the decay $\widetilde{b} \rightarrow b\widetilde{\chi}^0_2$ and $\widetilde{\chi}^0_2 \rightarrow h\widetilde{\chi}^0_1$ takes place with a branching ratio of 100%, see their Figures 11.

[40] AAD 14E searched in 20.3 fb^{-1} of pp collisions at $\sqrt{s}$ = 8 TeV for strongly produced supersymmetric particles in events containing jets and two same-sign leptons or three leptons. The search also utilises jets originating from b-quarks, missing transverse momentum and other variables. No excess over the expected SM background is observed. Exclusion limits are derived in simplified models containing bottom, see Fig. 7. Limits are also derived in the mSUGRA/CMSSM, bRPV and GMSB models, see their Fig. 8.

[41] CHATRCHYAN 14H searched in 19.5 fb^{-1} of pp collisions at $\sqrt{s}$ = 8 TeV for events with two isolated same-sign dileptons and jets in the final state. No significant excess above the Standard Model expectations is observed. Limits are set on the sbottom mass in a simplified models where the decay $\widetilde{b} \rightarrow t\widetilde{\chi}^{\pm}_1$, $\widetilde{\chi}^{\pm}_1 \rightarrow W^{\pm}\widetilde{\chi}^0_1$ takes place with a branching ratio of 100%, with varying mass of the $\widetilde{\chi}^{\pm}_1$, for $m_{\widetilde{\chi}^0_1}$ = 50 GeV, see Fig. 6.

[42] AAD 13AU searched in 20.1 fb^{-1} of pp collisions at $\sqrt{s}$ = 8 TeV for events containing two jets identified as originating from b-quarks and large missing transverse momentum. No excess of events above the expected level of Standard Model background was found. Exclusion limits at 95% C.L. are set on the masses of third-generation squarks. Assuming that the decay $\widetilde{b}_1 \rightarrow b\widetilde{\chi}^0_1$ takes place 100% of the time, a $\widetilde{b}_1$ mass below 620 GeV is excluded for $m_{\widetilde{\chi}^0_1} < 120$ GeV. For more details, see their Fig. 5.

[43] CHATRCHYAN 13AT provides interpretations of various searches for supersymmetry by the CMS experiment based on 4.73–4.98 fb^{-1} of pp collisions at $\sqrt{s}$ = 7 TeV in the framework of simplified models. Limits are set on the sbottom mass in a simplified models where sbottom quarks are pair-produced and the decay $\widetilde{b} \rightarrow b\widetilde{\chi}^0_1$ takes place with a branching ratio of 100%, see Fig. 4.

[44] CHATRCHYAN 13T searched in 11.7 fb^{-1} of pp collisions at $\sqrt{s}$ = 8 TeV for events with at least two energetic jets and significant $\not{E}_T$, using the α_T variable to discriminate between processes with genuine and misreconstructed $\not{E}_T$. No significant excess above the Standard Model expectations is observed. Limits are set on sbottom masses in simplified models where the decay $\widetilde{b} \rightarrow b\widetilde{\chi}^0_1$ takes place with a branching ratio of 100%, see Fig. 8 and Table 9.

[45] CHATRCHYAN 13V searched in 10.5 fb^{-1} of pp collisions at $\sqrt{s}$ = 8 TeV for events with two isolated same-sign dileptons and at least two b-jets in the final state. No significant excess above the Standard Model expectations is observed. Limits are set on the bottom mass in a simplified models where the decay $\widetilde{b} \rightarrow t\widetilde{\chi}^{\pm}_1$, $\widetilde{\chi}^{\pm}_1 \rightarrow W^{\pm}\widetilde{\chi}^0_1$ takes place with a branching ratio of 100%, with varying mass of the $\widetilde{\chi}^{\pm}_1$, for $m_{\widetilde{\chi}^0_1}$ = 50 GeV, see Fig. 4.

[46] AAD 12AN searched in 2.05 fb^{-1} of pp collisions at $\sqrt{s}$ = 7 TeV for scalar bottom quarks in events with large missing transverse momentum and two b-jets in the final state. The data are found to be consistent with the Standard Model expectations. Limits are set in an R-parity conserving minimal supersymmetric scenario, assuming B($\widetilde{b}_1 \rightarrow b\widetilde{\chi}^0_1$) = 100%, see their Fig. 2.

[47] CHATRCHYAN 12AI looked in 4.98 fb^{-1} of pp collisions at $\sqrt{s}$ = 7 TeV for events with two same-sign leptons (e, μ), but not necessarily same flavor, at least 2 b-jets and missing transverse energy. No excess beyond the Standard Model expectation is observed. Exclusion limits are derived in a simplified model for sbottom pair production, where the sbottom decays through $\widetilde{b}_1 \rightarrow t\widetilde{\chi}_1 W$, see Fig. 8.

[48] CHATRCHYAN 12BO searched in 4.7 fb^{-1} of pp collisions at $\sqrt{s}$ = 7 TeV for scalar bottom quarks in events with large missing transverse momentum and two b-jets in the final state. The data are found to be consistent with the Standard Model expectations. Limits are set in an R-parity conserving minimal supersymmetric scenario, assuming B($\widetilde{b}_1 \rightarrow b\widetilde{\chi}^0_1$) = 100%, see their Fig. 2.

[49] AAD 11K looked in 34 pb^{-1} of pp collisions at $\sqrt{s}$ = 7 TeV for events with heavy stable particles, identified by their anomalous dE/dx in the tracker or time of flight in the tile calorimeter, from pair production of $\widetilde{b}$. No evidence for an excess over the SM expectation is observed and limits on the mass are derived for pair production of sbottom, see Fig. 4.

[50] AAD 11O looked in 35 pb^{-1} of pp collisions at $\sqrt{s}$ = 7 TeV for events with jets, of which at least one is a b-jet, and $\not{E}_T$. No excess above the Standard Model was found. Limits are derived in the ($m_{\widetilde{g}}$, $m_{\widetilde{b}_1}$) plane (see Fig. 2) under the assumption of 100% branching ratios and $\widetilde{b}_1$ being the lightest squark. The quoted limit is valid for $m_{\widetilde{b}_1} <$ 500 GeV. A similar approach for $\widetilde{t}_1$ as the lightest squark with $\widetilde{g} \rightarrow \widetilde{t}_1 t$ and $\widetilde{t}_1 \rightarrow b\widetilde{\chi}^{\pm}_1$ with 100% branching ratios leads to a gluino mass limit of 520 GeV for $130 < m_{\widetilde{t}_1} <$ 300 GeV. Limits are also derived in the CMSSM (m_0, $m_{1/2}$) plane for tanβ = 40, see Fig. 4, and in scenarios based on the gauge group SO(10).

[51] CHATRCHYAN 11D looked in 35 pb^{-1} of pp collisions at $\sqrt{s}$ = 7 TeV for events with $\geq$ 2 jets, at least one of which is b-tagged, and $\not{E}_T$, where the b-jets are decay products of $\widetilde{t}$ or $\widetilde{b}$. No evidence for an excess over the expected background is observed. Limits are derived in the CMSSM (m_0, $m_{1/2}$) plane for tanβ = 50 (see Fig. 2).

[52] AALTONEN 10R searched in 2.65 fb^{-1} of $p\overline{p}$ collisions at $\sqrt{s}$ = 1.96 TeV for events with $\not{E}_T$ and exactly two jets, at least one of which is b-tagged. The results are in agreement with the SM prediction, and a limit on the cross section of 0.1 pb is obtained for the range of masses $80 < m_{\widetilde{b}_1} < 280$ GeV assuming that the sbottom decays exclusively to $b\widetilde{\chi}^0_1$. The excluded mass region in the framework of conserved R_p is shown in a plane of ($m_{\widetilde{b}_1}$, $m_{\widetilde{\chi}^0_1}$), see their Fig.2.

[53] ABAZOV 10L looked in 5.2 fb^{-1} of $p\overline{p}$ collisions at $\sqrt{s}$ = 1.96 TeV for events with at least 2 b-jets and $\not{E}_T$ from the production of $\widetilde{b}_1\widetilde{b}_1$. No evidence for an excess over the SM expectation is observed, and a limit on the cross section is derived under the assumption of 100% branching ratio. The excluded mass region in the framework of conserved R_p is shown in a plane of ($m_{\widetilde{b}_1}$,$m_{\widetilde{\chi}^0_1}$), see their Fig. 3b. The exclusion also extends to $m_{\widetilde{\chi}^0_1}$ = 110 GeV for $160 < m_{\widetilde{b}_1} < 200$ GeV.

R-parity violating $\widetilde{b}$ (Sbottom) mass limit

VALUE (GeV)	CL%	DOCUMENT ID		TECN	COMMENT
>307	95	[1] KHACHATRY...16BX		CMS	RPV, $\widetilde{b} \rightarrow t\,d$ or $t\,s$, λ''_{332} or λ''_{331} coupling
• • • We do not use the following data for averages, fits, limits, etc. • • •					
		[2] AAD	14E	ATLS	$\ell^{\pm}\ell^{\pm}(\ell^{\mp})$ + jets, $\widetilde{b}_1 \rightarrow t\widetilde{\chi}^{\pm}_1$ with $\widetilde{\chi}^{\pm}_1 \rightarrow W^{(*)\pm}\widetilde{\chi}^0_1$ simplified model, $m_{\widetilde{\chi}^{\pm}_1} = 2\ m_{\widetilde{\chi}^0_1}$

[1] KHACHATRYAN 16BX searched in 19.5 fb^{-1} of pp collisions at $\sqrt{s}$ = 8 TeV for events containing 2 leptons coming from R-parity-violating decays of supersymmetric particles. No excess over the expected background is observed. Limits are derived on the sbottom mass, assuming the RPV $\widetilde{b} \rightarrow t\,d$ or $\widetilde{b} \rightarrow t\,s$ decay, see Fig. 15.

[2] AAD 14E searched in 20.3 fb^{-1} of pp collisions at $\sqrt{s}$ = 8 TeV for strongly produced supersymmetric particles in events containing jets and two same-sign leptons or three leptons. The search also utilises jets originating from b-quarks, missing transverse momentum and other variables. No excess over the expected SM background is observed. Exclusion limits are derived in simplified models containing bottom, see Fig. 7. Limits are also derived in the mSUGRA/CMSSM, bRPV and GMSB models, see their Fig. 8.

$\widetilde{t}$ (Stop) mass limit

Limits depend on the decay mode. In e^+e^- collisions they also depend on the mixing angle of the mass eigenstate $\widetilde{t}_1 = \widetilde{t}_L\cos\theta_t + \widetilde{t}_R\sin\theta_t$. The coupling to the Z vanishes when θ_t = 0.98. In the Listings below, we use $\Delta m \equiv m_{\widetilde{t}_1} - m_{\widetilde{\chi}^0_1}$ or $\Delta m \equiv m_{\widetilde{t}_1} - m_{\widetilde{\nu}}$, depending on relevant decay mode. See also bounds in "$\widetilde{q}$ (Squark) MASS LIMIT."

Some earlier papers are now obsolete and have been omitted. They were last listed in our PDG 14 edition: K. Olive, *et al.* (Particle Data Group), Chinese Physics **C38** 070001 (2014) (http://pdg.lbl.gov).

R-parity conserving $\widetilde{t}$ (Stop) mass limit

VALUE (GeV)	CL%	DOCUMENT ID		TECN	COMMENT
>1400	95	[1] AAD	21AW	ATLS	$\tau^{\pm}$ + jets + b-jets + $\not{E}_T$, Tstop5, $m_{\widetilde{\tau}_1}$ = 1200 GeV
>1200	95	[2] AAD	21O	ATLS	$\ell^{\pm}$ + jet + $\not{E}_T$, Tstop1, $m_{\widetilde{\chi}^0_1}$ = 0 GeV
> 710	95	[2] AAD	21O	ATLS	$\ell^{\pm}$ + jet + $\not{E}_T$, Tstop1, $m_{\widetilde{\chi}^0_1}$ = 580 GeV
> 640	95	[2] AAD	21O	ATLS	$\ell^{\pm}$ + jet + $\not{E}_T$, Tstop3, $m_{\widetilde{\chi}^0_1}$ = 580 GeV
>1000	95	[3] AAD	21P	ATLS	$\ell^{\pm}\ell^{\mp}$ + jets + $\not{E}_T$, Tstop1, $m_{\widetilde{\chi}^0_1}$ = 0 GeV
> 600	95	[3] AAD	21P	ATLS	$\ell^{\pm}\ell^{\mp}$ + jets + $\not{E}_T$, Tstop2, $m_{\widetilde{\chi}^0_1}$ = 500 GeV
> 550	95	[3] AAD	21P	ATLS	$\ell^{\pm}\ell^{\mp}$ + jets + $\not{E}_T$, Tstop3, $m_{\widetilde{\chi}^0_1}$ = 500 GeV
>1310	95	[4] SIRUNYAN	21AD	CMS	jets + $\not{E}_T$, Tstop1, $m_{\widetilde{\chi}^0_1} < 300$ GeV
>1170	95	[4] SIRUNYAN	21AD	CMS	jets + $\not{E}_T$, Tstop2, $m_{\widetilde{\chi}^{\pm}_1} = (m_{\widetilde{t}} + m_{\widetilde{\chi}^0_1})/2$, $m_{\widetilde{\chi}^0_1} < 100$ GeV
>1150	95	[4] SIRUNYAN	21AD	CMS	jets + $\not{E}_T$, Tstop1 (50%) or Tstop2 (50%), $m_{\widetilde{\chi}^{\pm}_1} - m_{\widetilde{\chi}^0_1}$ = 5 GeV, $m_{\widetilde{\chi}^0_1}$ = 100 GeV
> 640	95	[4] SIRUNYAN	21AD	CMS	jets + $\not{E}_T$, Tstop3, $m_{\widetilde{t}} - m_{\widetilde{\chi}^0_1}$ = 50 GeV
> 620	95	[4] SIRUNYAN	21AD	CMS	jets + $\not{E}_T$, Tstop3, 10 GeV < $m_{\widetilde{t}} - m_{\widetilde{\chi}^0_1}$ < 60 GeV
> 740	95	[4] SIRUNYAN	21AD	CMS	jets + $\not{E}_T$, Tstop2, $m_{\widetilde{t}} - m_{\widetilde{\chi}^0_1}$ = 80 GeV
> 720	95	[4] SIRUNYAN	21AD	CMS	jets + $\not{E}_T$, Tstop2, 40 GeV < $m_{\widetilde{t}} - m_{\widetilde{\chi}^0_1}$ < 80 GeV
> 595	95	[4] SIRUNYAN	21AD	CMS	jets + $\not{E}_T$, Tstop2, $m_{\widetilde{t}} - m_{\widetilde{\chi}^0_1}$ = 10 GeV
> 630	95	[4] SIRUNYAN	21AD	CMS	jets + $\not{E}_T$, Tstop4, $m_{\widetilde{t}} - m_{\widetilde{\chi}^0_1}$ = 20 GeV
none 200–920	95	[5] SIRUNYAN	21B	CMS	$\ell^{\pm}\ell^{\mp}$ + b-jets + $\not{E}_T$, Tstop1, $m_{\widetilde{\chi}^0_1}$ = 0 GeV
none 250–810		[5] SIRUNYAN	21B	CMS	$\ell^{\pm}\ell^{\mp}$ + b-jets + $\not{E}_T$, Tstop2, $m_{\widetilde{\chi}^{\pm}_1} = (m_{\widetilde{t}} + m_{\widetilde{\chi}^0_1})/2$, $m_{\widetilde{\chi}^0_1}$ = 0 GeV

Downloaded from https://academic.oup.com/ptep/article/2022/8/083C01/6651666 by KIT Library user on 27 September 2022

>1300	95	[5] SIRUNYAN	21B	CMS	$\ell^\pm\ell^\mp$+b-jets+$\not{E}_T$, Tstop11, $m_{\widetilde{\chi}^\pm_1}$=($m_{\widetilde{t}}$ + $m_{\widetilde{\chi}^0_1}$)/2, $m_{\widetilde{\ell}}$ = ($m_{\widetilde{\chi}^\pm_1}$- $m_{\widetilde{\chi}^0_1}$)/2 + $m_{\widetilde{\chi}^0_1}$, $m_{\widetilde{\chi}^0_1}$ = 0
none 400–1180	95	[5] SIRUNYAN	21B	CMS	$\ell^\pm\ell^\mp$+b-jets+$\not{E}_T$, Tstop11, $m_{\widetilde{\chi}^\pm_1}$=($m_{\widetilde{t}}$ + $m_{\widetilde{\chi}^0_1}$)/2, $m_{\widetilde{\ell}}$ = 0.05 ($m_{\widetilde{\chi}^\pm_1}$- $m_{\widetilde{\chi}^0_1}$) + $m_{\widetilde{\chi}^0_1}$, $m_{\widetilde{\chi}^0_1}$ =0
>1400	95	[5] SIRUNYAN	21B	CMS	$\ell^\pm\ell^\mp$+b-jets+$\not{E}_T$, Tstop11, $m_{\widetilde{\chi}^\pm_1}$=($m_{\widetilde{t}}$ + $m_{\widetilde{\chi}^0_1}$)/2, $m_{\widetilde{\ell}}$ = 0.95 ($m_{\widetilde{\chi}^\pm_1}$- $m_{\widetilde{\chi}^0_1}$) + $m_{\widetilde{\chi}^0_1}$, $m_{\widetilde{\chi}^0_1}$ =0
>1325	95	[6] TUMASYAN	21I	CMS	$\geq$ 2 jets + $\not{E}_T$ + 0,1,2 ℓ, Tstop1, $m_{\widetilde{\chi}^0_1}$ = 0 GeV
>1150	95	[6] TUMASYAN	21I	CMS	$\geq$ 2 jets + $\not{E}_T$ + 0,1,2 ℓ, Tstop1, $m_{\widetilde{\chi}^0_1}$ = 700 GeV
>1260	95	[6] TUMASYAN	21I	CMS	$\geq$ 2 jets + $\not{E}_T$ + 0,1,2 ℓ, Tstop2, $m_{\widetilde{\chi}^0_1}$ = 0 GeV
>1000	95	[6] TUMASYAN	21I	CMS	$\geq$ 2 jets + $\not{E}_T$ + 0,1,2 ℓ, Tstop2, $m_{\widetilde{\chi}^0_1}$ <575 GeV
>1175	95	[6] TUMASYAN	21I	CMS	$\geq$ 2 jets + $\not{E}_T$ + 0,1,2 ℓ, Tstop1 (50%) or Tstop2 (50%), $m_{\widetilde{\chi}^0_1}$ = 0 GeV
>1000	95	[6] TUMASYAN	21I	CMS	$\geq$ 2 jets + $\not{E}_T$ + 0,1,2 ℓ, Tstop1 (50%) or Tstop2 (50%), $\widetilde{\chi}^0_1$ = 570 GeV
none 145–295	95	[6] TUMASYAN	21I	CMS	$\ell^\pm\ell^\mp$ + jets + $\not{E}_T$, Tstop1, $\lvert m_{\widetilde{t}} - m_{\widetilde{\chi}^0_1} - 175\ \text{GeV}\rvert$ < 30 GeV
none, 170–230	95	[7] AABOUD	20	ATLS	$e^\pm\mu^\mp$ + $\geq$ 1b-jet, Tstop1, $m_{\widetilde{\chi}^0_1}$ = 0.5 GeV
none, 170–220	95	[7] AABOUD	20	ATLS	$e^\pm\mu^\mp$ + $\geq$ 1b-jet, Tstop1, $m_{\widetilde{\chi}^0_1}$ < 62 GeV
>1220	95	[8] AAD	20AS	ATLS	$\ell^\pm\ell^\mp$ or 2 b-jets and $\not{E}_T$, Tstop6, $m_{\widetilde{\chi}^0_2}$=900 GeV
> 860	95	[9] AAD	20AS	ATLS	$\ell^\pm\ell^\mp$ or 2 b-jets and $\not{E}_T$, $\widetilde{t}_2$ with $\widetilde{t}_2 \rightarrow \widetilde{t}_1 Z$, $\widetilde{t}_1 \rightarrow b f f' \widetilde{\chi}^0_1$, $\Delta m(\widetilde{t}_1, \widetilde{\chi}^0_1)$ = 40 GeV
none 400–1250	95	[10] AAD	20S	ATLS	jets+$\not{E}_T$, Tstop1, $m_{\widetilde{\chi}^0_1}$=0 GeV
none 300–660	95	[11] AAD	20S	ATLS	jets+$\not{E}_T$, Tstop3, $m_{\widetilde{\chi}^0_1}$=0 GeV
> 765	95	[12] AAD	20V	ATLS	same-sign $\ell^\pm\ell^\pm$ + jets, $\widetilde{t}_1 \rightarrow t\widetilde{\chi}^0_2$, $\widetilde{\chi}^0_2 \rightarrow \widetilde{\chi}^\pm_1 W$, $\widetilde{\chi}^\pm_1 \rightarrow \widetilde{\chi}^0_1 W$, $m_{\widetilde{\chi}^\pm_1} \sim m_{\widetilde{\chi}^0_1}$
>1200	95	[13] SIRUNYAN	20AH	CMS	$\ell^\pm$ + jet + $\not{E}_T$, Tstop1, $m_{\widetilde{\chi}^0_1}$ = 0 GeV
>1175	95	[13] SIRUNYAN	20AH	CMS	$\ell^\pm$ + jet + $\not{E}_T$, Tstop1, $m_{\widetilde{\chi}^0_1}$ < 425 GeV
none 230–1140	95	[13] SIRUNYAN	20AH	CMS	$\ell^\pm$ + jet + $\not{E}_T$, Tstop2, $m_{\widetilde{\chi}^\pm_1}$ = ($m_{\widetilde{t}}$ + $m_{\widetilde{\chi}^0_1}$)/2, $m_{\widetilde{\chi}^0_1}$ = 0 GeV
>1100	95	[13] SIRUNYAN	20AH	CMS	$\ell^\pm$ + jet + $\not{E}_T$, Tstop2, $m_{\widetilde{\chi}^\pm_1}$ = ($m_{\widetilde{t}}$ + $m_{\widetilde{\chi}^0_1}$)/2, 50 < $m_{\widetilde{\chi}^0_1}$ < 425 GeV
>1070	95	[13] SIRUNYAN	20AH	CMS	$\ell^\pm$ + jet + $\not{E}_T$, Tstop8, $m_{\widetilde{\chi}^\pm_1}$ − $m_{\widetilde{\chi}^0_1}$ = 5 GeV, $m_{\widetilde{\chi}^0_1}$ = 0 GeV
>1050	95	[13] SIRUNYAN	20AH	CMS	$\ell^\pm$ + jet + $\not{E}_T$, Tstop8, $m_{\widetilde{\chi}^\pm_1}$ − $m_{\widetilde{\chi}^0_1}$ = 5 GeV, $m_{\widetilde{\chi}^0_1}$ < 350 GeV
> 730	95	[14] SIRUNYAN	20T	CMS	same-sign $\ell^\pm\ell^\pm$ or $\geq 3\ell^\pm$ + jets, Tstop7, $m_{\widetilde{t}_1} - m_{\widetilde{\chi}^0_1}$ = 175 GeV, $m_{\widetilde{t}_1}$ = 200 GeV, B($\widetilde{t}_2 \rightarrow \widetilde{t}_1 H$) = 100%
> 890	95	[14] SIRUNYAN	20T	CMS	same-sign $\ell^\pm\ell^\pm$ or $\geq 3\ell^\pm$ + jets, Tstop7, $m_{\widetilde{t}_1} - m_{\widetilde{\chi}^0_1}$ = 175 GeV, $m_{\widetilde{t}_1}$ = 200 GeV, B($\widetilde{t}_2 \rightarrow \widetilde{t}_1 Z$) = 100%
> 760	95	[14] SIRUNYAN	20T	CMS	same-sign $\ell^\pm\ell^\pm$ or $\geq 3\ell^\pm$ + jets, Tstop7, $m_{\widetilde{t}_1} - m_{\widetilde{\chi}^0_1}$ = 175 GeV, $m_{\widetilde{t}_1}$ = 200 GeV, B($\widetilde{t}_2 \rightarrow \widetilde{t}_1 Z$) = B($\widetilde{t}_2 \rightarrow \widetilde{t}_1 H$) = 50%
>1100	95	[15] SIRUNYAN	20U	CMS	$\tau^\pm\tau^\mp$ + b-jets + $\not{E}_T$, Tstop11, $m_{\widetilde{\chi}^\pm_1}$ = 0.5 ($m_{\widetilde{t}}$ + $m_{\widetilde{\chi}^0_1}$), $m_{\widetilde{\tau}}$ = 0.5 $m_{\widetilde{\chi}^\pm_1}$, $m_{\widetilde{\chi}^0_1}$ = 0
>1110	95	[16] SIRUNYAN	19AU	CMS	γ + jets + b-jets + $\not{E}_T$, Tstop13, $m_{\widetilde{\chi}^0_1}$ = 1 GeV
>1230	95	[16] SIRUNYAN	19AU	CMS	γ + jets + b-jets + $\not{E}_T$, Tstop13, $m_{\widetilde{\chi}^0_1}$ = 800 GeV
>1190	95	[17] SIRUNYAN	19CH	CMS	jets+$\not{E}_T$, Tstop1, $m_{\widetilde{\chi}^0_1}$= 0 GeV
>1140	95	[18] SIRUNYAN	19S	CMS	1 or 2 ℓ + jets + $\not{E}_T$, Tstop1, $m_{\widetilde{\chi}^0_1}$ < 200 GeV
> 208	95	[19] SIRUNYAN	19U	CMS	$e^\pm\mu^\mp$ + $\geq$ 1b-jet, Tstop1, $m_{\widetilde{t}_1} - m_{\widetilde{\chi}^0_1}$= 175 GeV
> 235	95	[19] SIRUNYAN	19U	CMS	$e^\pm\mu^\mp$ + $\geq$ 1b-jet, Tstop1, $m_{\widetilde{t}_1} - m_{\widetilde{\chi}^0_1}$= 182.5 GeV
> 242	95	[19] SIRUNYAN	19U	CMS	$e^\pm\mu^\mp$ + $\geq$ 1b-jet, Tstop1, $m_{\widetilde{t}_1} - m_{\widetilde{\chi}^0_1}$= 167.5 GeV
> 940	95	[20] AABOUD	18AQ	ATLS	1ℓ+jets+$\not{E}_T$, Tstop1, $m_{\widetilde{\chi}^0_1}$ = 0 GeV
> 270	95	[21] AABOUD	18AQ	ATLS	1ℓ+jets+$\not{E}_T$, Tstop3, $m_{\widetilde{t}} - m_{\widetilde{\chi}^0_1}$ = 20 GeV
> 840	95	[22] AABOUD	18AQ	ATLS	1ℓ+jets+$\not{E}_T$, Tstop2, $m_{\widetilde{t}} - m_{\widetilde{\chi}^\pm_1}$ = 10 GeV
> 500	95	[23] AABOUD	18BV	ATLS	c-jets+$\not{E}_T$, Tstop4, $m_{\widetilde{t}} - m_{\widetilde{\chi}^0_1}$ < 100 GeV
> 850	95	[24] AABOUD	18BV	ATLS	c-jets+$\not{E}_T$, Tstop4, $m_{\widetilde{\chi}^0_1}$ = 0 GeV
> 390	95	[25] AABOUD	18I	ATLS	$\geq$ 1 jets+$\not{E}_T$, Tstop3, $m_{\widetilde{t}} \sim m_{\widetilde{\chi}^0_1}$
> 430	95	[26] AABOUD	18I	ATLS	$\geq$ 1 jets+$\not{E}_T$, Tstop4, $m_{\widetilde{t}} - m_{\widetilde{\chi}^0_1}$ = 5 GeV
>1160	95	[27] AABOUD	18Y	ATLS	2ℓ ($\geq$ 1 hadronic τ) + b-jets + $\not{E}_T$, Tstop5, $m_{\widetilde{\tau}} \sim$ 800 GeV
> 450	95	[28] SIRUNYAN	18AJ	CMS	2ℓ (soft) + $\not{E}_T$, Tstop10, $m_{\widetilde{\chi}^\pm_1}$ = ($m_{\widetilde{t}}$ + $m_{\widetilde{\chi}^0_1}$)/2, $m_{\widetilde{t}_1} - m_{\widetilde{\chi}^0_1}$ = 40 GeV
> 720	95	[29] SIRUNYAN	18AL	CMS	$\geq 3\ell^\pm$ + jets + $\not{E}_T$, Tstop7, $m_{\widetilde{t}_1}$ - $m_{\widetilde{\chi}^0_1}$ = 175 GeV, $m_{\widetilde{t}_1}$ = 200 GeV, BR($\widetilde{t}_2 \rightarrow \widetilde{t}_1 H$) = 100%
> 780	95	[29] SIRUNYAN	18AL	CMS	$\geq 3\ell^\pm$ + jets + $\not{E}_T$, Tstop7, $m_{\widetilde{t}_1}$ - $m_{\widetilde{\chi}^0_1}$ = 175 GeV, $m_{\widetilde{t}_1}$ = 200 GeV, BR($\widetilde{t}_2 \rightarrow \widetilde{t}_1 Z$) = 100%
> 710	95	[29] SIRUNYAN	18AL	CMS	$\geq 3\ell^\pm$ + jets + $\not{E}_T$, Tstop7, $m_{\widetilde{t}_1}$ - $m_{\widetilde{\chi}^0_1}$ = 175 GeV, $m_{\widetilde{t}_1}$ = 200 GeV, BR($\widetilde{t}_2 \rightarrow \widetilde{t}_1 Z$) = BR($\widetilde{t}_2 \rightarrow \widetilde{t}_1 H$) = 50%
> 730	95	[30] SIRUNYAN	18AN	CMS	1 or 2 γ + ℓ + jets, GGM, Tstop12, $m_{\widetilde{\chi}^0_1}$ = 150 GeV
> 650	95	[30] SIRUNYAN	18AN	CMS	1 or 2 γ + ℓ + jets, GGM, Tstop12, $m_{\widetilde{\chi}^0_1}$ = 500 GeV
>1000	95	[31] SIRUNYAN	18AY	CMS	jets+$\not{E}_T$, Tstop1, $m_{\widetilde{\chi}^0_1}$=0 GeV
> 500	95	[31] SIRUNYAN	18AY	CMS	jets+$\not{E}_T$,Tstop4,$m_{\widetilde{\chi}^0_1}$=420 GeV
> 510	95	[32] SIRUNYAN	18B	CMS	jets+$\not{E}_T$, Tstop4, $m_{\widetilde{t}} - m_{\widetilde{\chi}^0_1}$ = 10 GeV
> 800	95	[33] SIRUNYAN	18C	CMS	$\ell^\pm\ell^\mp$ + b-jets + $\not{E}_T$, Tstop1, $m_{\widetilde{\chi}^0_1}$ = 0
> 750	95	[33] SIRUNYAN	18C	CMS	$\ell^\pm\ell^\mp$ + b-jets + $\not{E}_T$, Tstop2, $m_{\widetilde{\chi}^\pm_1}$ = ($m_{\widetilde{t}}$ + $m_{\widetilde{\chi}^0_1}$)/2, $m_{\widetilde{\chi}^0_1}$ = 0
>1050	95	[33] SIRUNYAN	18C	CMS	Combination of all-hadronic, 1 $\ell^\pm$ and $\ell^\pm\ell^\mp$ searches, Tstop1, $m_{\widetilde{\chi}^0_1}$ = 0

Downloaded from https://academic.oup.com/ptep/article/2022/8/083C01/6651666 by KIT Library user on 27 September 2022

>1000	95	[33] SIRUNYAN	18C	CMS	Combination of all-hadronic, 1 $\ell^\pm$ and $\ell^\pm\ell^\mp$ searches, Tstop2, $m_{\widetilde{\chi}^\pm_1} = (m_{\widetilde{t}} + m_{\widetilde{\chi}^0_1})/2$, $m_{\widetilde{\chi}^0_1} = 0$
>1200	95	[33] SIRUNYAN	18C	CMS	$\ell^\pm\ell^\mp$ + b-jets + $\not{E}_T$, Tstop11, $m_{\widetilde{\chi}^\pm_1} = 0.5\ (m_{\widetilde{t}} + m_{\widetilde{\chi}^0_1})$, $m_{\widetilde{\ell}} = 0.5\ m_{\widetilde{\chi}^\pm_1}$, $m_{\widetilde{\chi}^0_1} = 0$
>1300	95	[33] SIRUNYAN	18C	CMS	$\ell^\pm\ell^\mp$ + b-jets + $\not{E}_T$, Tstop11, $m_{\widetilde{\chi}^\pm_1} = 0.5\ (m_{\widetilde{t}} + m_{\widetilde{\chi}^0_1})$, $m_{\widetilde{\ell}} = 0.95\ m_{\widetilde{\chi}^\pm_1}$, $m_{\widetilde{\chi}^0_1} = 0$
none 460–1060	95	[33] SIRUNYAN	18C	CMS	$\ell^\pm\ell^\mp$ + b-jets + $\not{E}_T$, Tstop11, $m_{\widetilde{\chi}^\pm_1} = 0.5\ (m_{\widetilde{t}} + m_{\widetilde{\chi}^0_1})$, $m_{\widetilde{\ell}} = 0.05\ m_{\widetilde{\chi}^\pm_1}$, $m_{\widetilde{\chi}^0_1} = 0$
>1020	95	[34] SIRUNYAN	18D	CMS	top quark (hadronically decaying) + jets + $\not{E}_T$, Tstop1, $m_{\widetilde{\chi}^0_1} = 0$ GeV
> 420	95	[35] SIRUNYAN	18DI	CMS	$\ell^\pm$ + jet + $\not{E}_T$, Tstop3, $m_{\widetilde{t}_1} - m_{\widetilde{\chi}^0_1} = 10$ GeV
> 560	95	[35] SIRUNYAN	18DI	CMS	$\ell^\pm$ + jet + $\not{E}_T$, Tstop3, $m_{\widetilde{t}_1} - m_{\widetilde{\chi}^0_1} = 80$ GeV
> 540	95	[35] SIRUNYAN	18DI	CMS	$\ell^\pm$, Tstop10, $m_{\widetilde{\chi}^\pm_1} = (m_{\widetilde{t}} + m_{\widetilde{\chi}^0_1})/2$, $m_{\widetilde{t}_1} - m_{\widetilde{\chi}^0_1} = 40$ GeV
> 590	95	[35] SIRUNYAN	18DI	CMS	Combination of all-hadronic and 1 $\ell^\pm$ searches, Tstop3, $m_{\widetilde{t}_1} - m_{\widetilde{\chi}^0_1} = 30$ GeV
> 670	95	[35] SIRUNYAN	18DI	CMS	Combination of all-hadronic and 1 $\ell^\pm$ searches, Tstop10, $m_{\widetilde{\chi}^\pm_1} = (m_{\widetilde{t}} + m_{\widetilde{\chi}^0_1})/2$, $m_{\widetilde{t}_1} - m_{\widetilde{\chi}^0_1} = 60$ GeV
> 450	95	[36] SIRUNYAN	18DN	CMS	$\ell^\pm\ell^\mp$, Tstop1, $m_{\widetilde{t}_1} - m_{\widetilde{\chi}^0_1} = m_W$
none 225–325	95	[36] SIRUNYAN	18DN	CMS	$\ell^\pm\ell^\mp$, Tstop2, $m_{\widetilde{\chi}^\pm_1} = (m_{\widetilde{t}} + m_{\widetilde{\chi}^0_1})/2$, $m_{\widetilde{t}} - m_{\widetilde{\chi}^0_1} = 2\ m_W$
none 210–690	95	[36] SIRUNYAN	18DN	CMS	$\ell^\pm\ell^\mp$, Tstop1, $m_{\widetilde{\chi}^0_1} = 0$ GeV
none 250–600	95	[36] SIRUNYAN	18DN	CMS	$\ell^\pm\ell^\mp$, Tstop2, $m_{\widetilde{\chi}^\pm_1} = (m_{\widetilde{t}} + m_{\widetilde{\chi}^0_1})/2$, $m_{\widetilde{\chi}^0_1} = 0$ GeV
> 700	95	[37] AABOUD	17AJ	ATLS	same-sign $\ell^\pm\ell^\pm$ / 3 ℓ + jets + $\not{E}_T$, Tstop11, $m_{\widetilde{\chi}^0_2} = m_{\widetilde{\chi}^0_1}$ + 100 GeV
> 880	95	[38] AABOUD	17AX	ATLS	b-jets+$\not{E}_T$, mixture Tstop1 and Tstop2 with BR=50%, $m_{\widetilde{\chi}^0_1}$ = 0 GeV, $m_{\widetilde{\chi}^\pm_1}$ - $m_{\widetilde{\chi}^0_1}$ = 1 GeV
none 250–1000	95	[39] AABOUD	17AY	ATLS	jets+$\not{E}_T$, Tstop1, $m_{\widetilde{\chi}^0_1} = 0$ GeV
none 450–850	95	[40] AABOUD	17AY	ATLS	jets+$\not{E}_T$, mixture of Tstop1 and Tstop2 with BR=50%, $m_{\widetilde{\chi}^\pm_1} - m_{\widetilde{\chi}^0_1} = 1$ GeV
> 720	95	[41] AABOUD	17BE	ATLS	$\ell^\pm\ell^\mp$ + $\not{E}_T$, Tstop1, $m_{\widetilde{\chi}^0_1} = 0$ GeV
> 400	95	[42] AABOUD	17BE	ATLS	$\ell^\pm\ell^\mp$ + $\not{E}_T$, Tstop3, $m_{\widetilde{t}_1} - m_{\widetilde{\chi}^0_1} = 40$ GeV
> 430	95	[43] AABOUD	17BE	ATLS	$\ell^\pm\ell^\mp$ + $\not{E}_T$, Tstop1 (offshell t), $m_{\widetilde{t}_1} - m_{\widetilde{\chi}^0_1} \sim m_W$
> 700	95	[44] AABOUD	17BE	ATLS	$\ell^\pm\ell^\mp$ + $\not{E}_T$, Tstop2, $m_{\widetilde{t}_1} - m_{\widetilde{\chi}^\pm_1} = 10$ GeV, $m_{\widetilde{\chi}^0_1} = 0$ GeV
> 750	95	[45] KHACHATRY...17		CMS	jets+$\not{E}_T$,Tstop1,$m_{\widetilde{\chi}^0_1}$=100GeV
none 250–740	95	[46] KHACHATRY...17AD		CMS	jets+b-jets+$\not{E}_T$, Tstop1, $m_{\widetilde{\chi}^0_1} = 0$ GeV
> 610	95	[47] KHACHATRY...17AD		CMS	jets+b-jets+$\not{E}_T$, mixture Tstop1 and Tstop2 with BR=50%, $m_{\widetilde{\chi}^0_1} = 60$ GeV
> 590	95	[48] KHACHATRY...17P		CMS	1 or more jets+$\not{E}_T$, Tstop8, $m_{\widetilde{\chi}^\pm_1} - m_{\widetilde{\chi}^0_1} = 5$ GeV, $m_{\widetilde{\chi}^0_1} = 100$ GeV
none 280–640	95	[48] KHACHATRY...17P		CMS	1 or more jets+$\not{E}_T$, Tstop1, $m_{\widetilde{\chi}^0_1} = 0$ GeV
> 350	95	[48] KHACHATRY...17P		CMS	1 or more jets+$\not{E}_T$, Tstop4, 10 GeV < $m_{\widetilde{t}_1} - m_{\widetilde{\chi}^0_1}$ < 80 GeV
> 280	95	[48] KHACHATRY...17P		CMS	1 or more jets+$\not{E}_T$, Tstop3, 10 GeV < $m_{\widetilde{t}_1} - m_{\widetilde{\chi}^0_1}$ < 80 GeV
> 320	95	[48] KHACHATRY...17P		CMS	1 or more jets+$\not{E}_T$, Tstop9, 10 GeV < $m_{\widetilde{t}_1} - m_{\widetilde{\chi}^0_1}$ < 80 GeV
> 240	95	[49] KHACHATRY...17S		CMS	jets+$\not{E}_T$, Tstop4, $m_{\widetilde{t}} - m_{\widetilde{\chi}^0_1} = 10$ GeV
> 225	95	[50] KHACHATRY...17S		CMS	jets+$\not{E}_T$, Tstop3, $m_{\widetilde{t}} - m_{\widetilde{\chi}^0_1} = 10$ GeV
> 325	95	[51] KHACHATRY...17S		CMS	jets+$\not{E}_T$, Tstop2, $m_{\widetilde{\chi}^\pm_1} = 0.25\ m_{\widetilde{t}} + 0.75\ m_{\widetilde{\chi}^0_1}$, $m_{\widetilde{\chi}^0_1} = 225$ GeV
> 400	95	[52] KHACHATRY...17S		CMS	jets+$\not{E}_T$, Tstop2, $m_{\widetilde{\chi}^\pm_1} = 0.75\ m_{\widetilde{t}} + 0.25\ m_{\widetilde{\chi}^0_1}$, $m_{\widetilde{\chi}^0_1} = 0$ GeV
> 500	95	[53] KHACHATRY...17S		CMS	jets+$\not{E}_T$, Tstop1, $m_{\widetilde{\chi}^0_1} = 0$ GeV
>1120	95	[54] SIRUNYAN	17AS	CMS	1ℓ+jets+$\not{E}_T$, Tstop1, $m_{\widetilde{\chi}^0_1} = 0$ GeV
>1000	95	[54] SIRUNYAN	17AS	CMS	1ℓ+jets+$\not{E}_T$, Tstop2, $m_{\widetilde{\chi}^\pm_1} = (m_{\widetilde{t}} + m_{\widetilde{\chi}^0_1})/2$, $m_{\widetilde{\chi}^0_1} = 0$ GeV
> 980	95	[54] SIRUNYAN	17AS	CMS	1ℓ+jets+$\not{E}_T$, Tstop8, $m_{\widetilde{\chi}^\pm_1} - m_{\widetilde{\chi}^0_1} = 5$ GeV, $m_{\widetilde{\chi}^0_1} = 0$ GeV
>1040	95	[55] SIRUNYAN	17AT	CMS	jets+$\not{E}_T$, Tstop1, $m_{\widetilde{\chi}^0_1} = 0$ GeV
> 750	95	[55] SIRUNYAN	17AT	CMS	jets+$\not{E}_T$, Tstop2, $m_{\widetilde{\chi}^\pm_1} = (m_{\widetilde{t}} + m_{\widetilde{\chi}^0_1})/2$, $m_{\widetilde{\chi}^0_1} = 0$ GeV
> 940	95	[55] SIRUNYAN	17AT	CMS	jets+$\not{E}_T$, Tstop8, $m_{\widetilde{\chi}^\pm_1} - m_{\widetilde{\chi}^0_1} = 5$ GeV, $m_{\widetilde{\chi}^0_1} = 100$ GeV
> 540	95	[55] SIRUNYAN	17AT	CMS	jets+$\not{E}_T$, Tstop3, 10 GeV < $m_{\widetilde{t}_1} - m_{\widetilde{\chi}^0_1}$ < 80 GeV
> 480	95	[55] SIRUNYAN	17AT	CMS	jets+$\not{E}_T$, Tstop4, 10 GeV < $m_{\widetilde{t}_1} - m_{\widetilde{\chi}^0_1}$ < 80 GeV
> 530	95	[55] SIRUNYAN	17AT	CMS	jets+$\not{E}_T$, Tstop10, $m_{\widetilde{\chi}^\pm_1} = (m_{\widetilde{t}} + m_{\widetilde{\chi}^0_1})/2$, 10 GeV < $m_{\widetilde{t}_1} - m_{\widetilde{\chi}^0_1}$ < 80 GeV
>1070	95	[56] SIRUNYAN	17AZ	CMS	$\geq$ 1 jets+$\not{E}_T$, Tstop1, $m_{\widetilde{\chi}^0_1} = 0$ GeV
> 900	95	[56] SIRUNYAN	17AZ	CMS	$\geq$ 1 jets+$\not{E}_T$, Tstop2, $m_{\widetilde{\chi}^\pm_1} = (m_{\widetilde{t}} + m_{\widetilde{\chi}^0_1})/2$, $m_{\widetilde{\chi}^0_1} = 0$ GeV
>1020	95	[56] SIRUNYAN	17AZ	CMS	$\geq$ 1jets+$\not{E}_T$, Tstop8, $m_{\widetilde{\chi}^\pm_1} - m_{\widetilde{\chi}^0_1} = 5$ GeV, $m_{\widetilde{\chi}^0_1} = 100$ GeV
> 540	95	[56] SIRUNYAN	17AZ	CMS	$\geq$ 1 jets+$\not{E}_T$, Tstop4, 10 GeV < $m_{\widetilde{t}_1} - m_{\widetilde{\chi}^0_1}$ < 80 GeV
none 280–830	95	[57] SIRUNYAN	17K	CMS	0, 1 $\ell^\pm$+jets+$\not{E}_T$ (combination), Tstop1, $m_{\widetilde{\chi}^0_1} = 0$ GeV
> 700	95	[57] SIRUNYAN	17K	CMS	0, 1 $\ell^\pm$+jets+$\not{E}_T$ (combination), Tstop8, $m_{\widetilde{\chi}^\pm_1} - m_{\widetilde{\chi}^0_1} = 5$ GeV, $m_{\widetilde{\chi}^0_1} = 100$ GeV
> 160	95	[57] SIRUNYAN	17K	CMS	jets+$\not{E}_T$, Tstop4, 10 < $m_{\widetilde{t}} - m_{\widetilde{\chi}^0_1}$ < 80 GeV
none 230–960	95	[58] SIRUNYAN	17P	CMS	jets+$\not{E}_T$, Tstop1, $m_{\widetilde{\chi}^0_1} = 0$ GeV
> 990	95	[58] SIRUNYAN	17P	CMS	jets+$\not{E}_T$, Tsbot1, $m_{\widetilde{\chi}^0_1} = 0$ GeV
> 323	95	[59] AABOUD	16D	ATLS	$\geq$ 1 jet + $\not{E}_T$, Tstop4, $m_{\widetilde{t}_1} - m_{\widetilde{\chi}^0_1} = 5$ GeV
none, 745–780	95	[60] AABOUD	16J	ATLS	1 $\ell^\pm$ + $\geq$ 4 jets + $\not{E}_T$, Tstop1, $m_{\widetilde{\chi}^0_1} = 0$ GeV
> 490–650	95	[61] AAD	16AY	ATLS	2ℓ (including hadronic τ) + $\not{E}_T$, Tstop5, 87 GeV< $m_{\widetilde{\tau}} < m_{\widetilde{t}_1}$
> 700	95	[62] KHACHATRY...16AV		CMS	1 or 2 $\ell^\pm$+jets+b-jets+$\not{E}_T$, Tstop1, $m_{\widetilde{\chi}^0_1}$ < 250 GeV
> 700	95	[62] KHACHATRY...16AV		CMS	1 or 2 $\ell^\pm$+jets+b-jets $\not{E}_T$, Tstop2, $m_{\widetilde{\chi}^0_1} = 0$ GeV, $m_{\widetilde{\chi}^\pm_1} = 0.75\ m_{\widetilde{t}_1} + 0.25\ m_{\widetilde{\chi}^0_1}$
> 775	95	[63] KHACHATRY...16BK		CMS	jets+$\not{E}_T$,Tstop1,$m_{\widetilde{\chi}^0_1}$ <200GeV
> 620	95	[63] KHACHATRY...16BK		CMS	jets+$\not{E}_T$, Tstop2, $m_{\widetilde{\chi}^0_1}$=0 GeV
> 800	95	[64] KHACHATRY...16BS		CMS	jets+$\not{E}_T$, Tstop1, $m_{\widetilde{\chi}^0_1}$=0 GeV

Downloaded from https://academic.oup.com/ptep/article/2022/8/083C01/6651666 by KIT Library user on 27 September 2022

> 316	95	[65] KHACHATRY...16Y	CMS		1 or 2 soft $\ell^{\pm}$ + jets + $\not{E}_T$, Tstop3, $m_{\widetilde{t}}-m_{\widetilde{\chi}^0_1}$=25 GeV
> 250	95	[66] AAD	15CJ	ATLS	$B(\widetilde{t} \to c\widetilde{\chi}^0_1)+B(\widetilde{t} \to b f f' \widetilde{\chi}^0_1) = 1$, $m_{\widetilde{t}}-m_{\widetilde{\chi}^0_1} = 10$ GeV
> 270	95	[66] AAD	15CJ	ATLS	$\widetilde{t} \to c\widetilde{\chi}^0_1$, $m_{\widetilde{t}} - m_{\widetilde{\chi}^0_1}$=80 GeV
none, 200–700	95	[66] AAD	15CJ	ATLS	$\widetilde{t} \to t\widetilde{\chi}^0_1$, $m_{\widetilde{\chi}^0_1} = 0$
> 500	95	[66] AAD	15CJ	ATLS	$B(\widetilde{t} \to t\widetilde{\chi}^0_1) + B(\widetilde{t} \to b\widetilde{\chi}^{\pm}_1) = 1$, $\widetilde{\chi}^{\pm}_1 \to W^{(*)}\widetilde{\chi}^0_1$, $m_{\widetilde{\chi}^{\pm}_1} = 2m_{\widetilde{\chi}^0_1}$, $m_{\widetilde{\chi}^0_1} < 160$ GeV
> 600	95	[66] AAD	15CJ	ATLS	$\widetilde{t}_2 \to Z\widetilde{t}_1$, $m_{\widetilde{t}_1} - m_{\widetilde{\chi}^0_1} = 180$ GeV, $m_{\widetilde{\chi}^0_1} = 0$
> 600	95	[66] AAD	15CJ	ATLS	$\widetilde{t}_2 \to h\widetilde{t}_1$, $m_{\widetilde{t}_1} - m_{\widetilde{\chi}^0_1} = 180$ GeV, $m_{\widetilde{\chi}^0_1} = 0$
none, 172.5–191	95	[67] AAD	15J	ATLS	$\widetilde{t} \to t\widetilde{\chi}^0_1$, $m_{\widetilde{\chi}^0_1} = 1$ GeV
> 450	95	[68] KHACHATRY...15AF	CMS		$\widetilde{t} \to t\widetilde{\chi}^0_1$, $m_{\widetilde{\chi}^0_1} = 0$, $m_{\widetilde{t}} > m_t + m_{\widetilde{\chi}^0_1}$
> 560	95	[69] KHACHATRY...15AH	CMS		$\widetilde{t} \to t\widetilde{\chi}^0_1$, $m_{\widetilde{\chi}^0_1} = 0$, $m_{\widetilde{t}} > m_t + m_{\widetilde{\chi}^0_1}$
> 250	95	[70] KHACHATRY...15AH	CMS		$\widetilde{t} \to c\widetilde{\chi}^0_1$, $m_{\widetilde{t}}-m_{\widetilde{\chi}^0_1}$ <10 GeV
> 730	95	[71] KHACHATRY...15X	CMS		$\widetilde{t} \to t\widetilde{\chi}^0_1$, $m_{\widetilde{\chi}^0_1} = 100$ GeV, $m_{\widetilde{t}} > m_t + m_{\widetilde{\chi}^0_1}$
none 400–645	95	[71] KHACHATRY...15X	CMS		$\widetilde{t} \to t\widetilde{\chi}^0_1$ or $\widetilde{t} \to b\widetilde{\chi}^{\pm}_1$, $m_{\widetilde{\chi}^0_1} = 100$ GeV, $m_{\widetilde{\chi}^{\pm}_1} - m_{\widetilde{\chi}^0_1} = 5$ GeV
none 270–645	95	[72] AAD	14AJ	ATLS	≥ 4 jets + $\not{E}_T$, $\widetilde{t}_1 \to t\widetilde{\chi}^0_1$, $m_{\widetilde{\chi}^0_1} < 30$ GeV
none 250–550	95	[72] AAD	14AJ	ATLS	≥ 4 jets + $\not{E}_T$, $B(\widetilde{t}_1 \to b\widetilde{\chi}^{\pm}_1) = 50$ %, $m_{\widetilde{\chi}^{\pm}_1} = 2\, m_{\widetilde{\chi}^0_1}$, $m_{\widetilde{\chi}^0_1} < 60$ GeV
none 210–640	95	[73] AAD	14BD	ATLS	$\ell^{\pm}$ + jets + $\not{E}_T$, $\widetilde{t}_1 \to t\widetilde{\chi}^0_1$, $m_{\widetilde{\chi}^0_1} = 0$ GeV
> 500	95	[73] AAD	14BD	ATLS	$\ell^{\pm}$ + jets + $\not{E}_T$, $\widetilde{t}_1 \to b\widetilde{\chi}^{\pm}_1$, $m_{\widetilde{\chi}^{\pm}_1} = 2\, m_{\widetilde{\chi}^0_1}$, 100 GeV < $m_{\widetilde{\chi}^0_1}$ < 150 GeV
none 150–445	95	[74] AAD	14F	ATLS	$\ell^{\pm}\ell^{\mp}$ final state, $\widetilde{t}_1 \to b\widetilde{\chi}^{\pm}_1$, $m_{\widetilde{t}_1} - m_{\widetilde{\chi}^{\pm}_1} = 10$ GeV, $m_{\widetilde{\chi}^0_1} = 1$ GeV
none 215–530	95	[74] AAD	14F	ATLS	$\ell^{\pm}\ell^{\mp}$ final state, $\widetilde{t}_1 \to t\widetilde{\chi}^0_1$, $m_{\widetilde{\chi}^0_1} = 1$ GeV
> 270	95	[75] AAD	14T	ATLS	$\widetilde{t}_1 \to c\widetilde{\chi}^0_1$, $m_{\widetilde{\chi}^0_1} = 200$ GeV
> 240	95	[75] AAD	14T	ATLS	$\widetilde{t}_1 \to c\widetilde{\chi}^0_1$, $m_{\widetilde{t}_1}-m_{\widetilde{\chi}^0_1}$ <85 GeV
> 255	95	[75] AAD	14T	ATLS	$\widetilde{t}_1 \to b f f' \widetilde{\chi}^0_1$, $m_{\widetilde{t}_1} - m_{\widetilde{\chi}^0_1} \approx m_b$
> 400	95	[76] CHATRCHYAN	14AH	CMS	jets + $\not{E}_T$, $\widetilde{t} \to t\widetilde{\chi}^0_1$ simplified model, $m_{\widetilde{\chi}^0_1} = 50$ GeV
		[77] CHATRCHYAN	14R	CMS	$\geq 3\ell^{\pm}$, $\widetilde{t} \to (b\widetilde{\chi}^{\pm}_1/t\widetilde{\chi}^0_1)$, $\widetilde{\chi}^{\pm}_1 \to (q q'/\ell\nu)\widetilde{\chi}^0_1$, $\widetilde{\chi}^0_1 \to (H/Z)\widetilde{G}$, GMSB, natural higgsino NLSP scenario
• • • We do not use the following data for averages, fits, limits, etc. • • •					
> 850	95	[78] AABOUD	17AF	ATLS	2ℓ+jets+b-jets+$\not{E}_T$, Tstop6, $m_{\widetilde{\chi}^0_1} = 0$
> 800	95	[79] AABOUD	17AF	ATLS	2ℓ+jets+b-jets+$\not{E}_T$, Tstop7 with 100% decays via Z, $m_{\widetilde{\chi}^0_1} = 50$ GeV
> 880	95	[80] AABOUD	17AF	ATLS	2ℓ+jets+b-jets+$\not{E}_T$, Tstop7 with 100% decays via higgs, $m_{\widetilde{\chi}^0_1} = 50$ GeV
		[81] AABOUD	17AY	ATLS	jets+$\not{E}_T$, pMSSM-inspired
> 230		ROLBIECKI	15	THEO	WW xsection, $\widetilde{t}_1 \to b W \widetilde{\chi}^0_1$, $m_{\widetilde{t}_1} \simeq m_b + m_W + m_{\widetilde{\chi}^0_1}$
> 600	95	[82] AAD	14B	ATLS	Z+b $\not{E}_T$, $\widetilde{t}_2 \to Z\widetilde{t}_1$, $\widetilde{t}_1 \to t\widetilde{\chi}^0_1$, $m_{\widetilde{\chi}^0_1} < 200$ GeV
> 540	95	[82] AAD	14B	ATLS	Z+b $\not{E}_T$, $\widetilde{t}_1 \to t\widetilde{\chi}^0_1$, $\widetilde{\chi}^0_1 \to Z\widetilde{G}$, natural GMSB, 100 GeV < $m_{\widetilde{\chi}^0_1}$ < $m_{\widetilde{t}_1}$−10 GeV
> 360	95	[83] CHATRCHYAN	14U	CMS	$\widetilde{t}_1 \to b\widetilde{\chi}^{\pm}_1 r$, $\widetilde{\chi}^{\pm}_1 \to f f' \widetilde{\chi}^0_1$, $\widetilde{\chi}^0_1 \to H\widetilde{G}$ simplified model, $m_{\widetilde{\chi}^{\pm}_1} - m_{\widetilde{\chi}^0_1} = 5$ GeV, GMSB
> 215	95	CZAKON	14		$\widetilde{t} \to t\chi^0_1$, $m_{\chi^0_1} < 10$ GeV
		[84] KHACHATRY...14C	CMS		$\widetilde{t}_2 \to H\widetilde{t}_1$ or $t_2 \to Z\widetilde{t}_1$ simplified model

[1] AAD 21AW searched in 139 fb^{-1} of pp collisions at $\sqrt{s}$ = 13 TeV for pair production of stops in events with one or two hadronically decaying τ leptons, jets, b-jets and $\not{E}_T$. No significant excess above the Standard Model predictions is observed. Limits are set on the $\widetilde{t}_1$ mass as a function of the $\widetilde{\tau}_1$ in the Tstop5 scenario. See their Fig. 8.

[2] AAD 21O searched in 139 fb^{-1} of pp collisions at $\sqrt{s}$ = 13 TeV for pair production of top squarks in events with one electron or muon, jets, and large missing transverse momentum. No significant excess above the Standard Model expectations is observed. Limits are set on the top squark mass in the Tstop1 and Tstop3 simplified models and dark matter models, see their Figures 13, 14 and 15.

[3] AAD 21P searched in 139 fb^{-1} of pp collisions at $\sqrt{s}$ = 13 TeV for pair production of top squarks in events with two opposite-sign leptons, jets, and large missing transverse momentum. No significant excess above the Standard Model expectations is observed. Limits are set on the top squark mass in the Tstop1, Tstop2, and Tstop3 simplified models, see their Figures 14.

[4] SIRUNYAN 21AD searched in 137 fb^{-1} of pp collisions at $\sqrt{s}$ = 13 TeV for supersymmetry in events with multiple jets, no leptons, and large $\not{E}_T$. No significant excess above the Standard Model expectations is observed. Limits are set on the top squark mass in the simplified models Tstop1, Tstop2 with $m_{\widetilde{\chi}^{\pm}_1} = (m_{\widetilde{t}} + m_{\widetilde{\chi}^0_1})/2$, and a 50:50 mixture of these with $m_{\widetilde{\chi}^{\pm}_1} - m_{\widetilde{\chi}^0_1} = 5$ GeV, see their Figure 8. Limits are also set on the top squark mass for 10 GeV < $m_{\widetilde{t}} - m_{\widetilde{\chi}^{\pm}_1}$ < 80 GeV in the simplified models Tstop2, Tstop 3, and Tstop4, see their Figure 9. For indirect top squark production, limits are set on the gluino mass in the simplified models Tglu3A, Tglu3C with $m_{\widetilde{t}} - m_{\widetilde{\chi}^0_1} = 20$ GeV, and Tglu3D with $m_{\widetilde{\chi}^{\pm}_1} - m_{\widetilde{\chi}^0_1} = 5$ GeV, see their Figure 10.

[5] SIRUNYAN 21B searched in 137 fb^{-1} of pp collisions at $\sqrt{s}$ = 13 TeV for the pair production of top squarks in events with two oppositely charged leptons (electrons or muons), jets identified as originating from a b-quark and significant $\not{E}_T$. No significant excess above the Standard Model expectations is observed. Limits are set on the stop mass in the Tstop1, Tstop2 and Tstop11 simplified models, see their Figures 6 and 7.

[6] TUMASYAN 21I searched in 137 fb^{-1} of pp collisions at $\sqrt{s}$ = 13 TeV for evidence of top squarks in events with at least two jets and large $\not{E}_T$, categorized into events with 0, 1, or 2 leptons. No significant excess above the Standard Model expectations is observed. Limits are set on the top squark mass in the simplified model Tstop1 in the top corridor $\left|m_{\widetilde{t}} - m_{\widetilde{\chi}^0_1} - 175\ \text{GeV}\right| < 30$ GeV using dilepton events, see their Figure 7. Limits are also set for a combination of earlier searches with 0, 1, and 2 leptons in the models Tstop1, Tstop2 and a 50:50 mixture of these models, see their Figure 9. The results are interpreted in an alternative signal model of dark matter production via a spin-0 mediator in association with a top quark pair as well.

[7] AABOUD 20 searched in 36.1 fb^{-1} of pp collisions at $\sqrt{s}$ = 13 TeV for events containing one electron-muon pair with opposite charge. The search targets a region of parameter space where the kinematics of top squark pair production and top quark pair production is very similar and makes use of the double-differential angular distributions of the leptons. No excess above the Standard Model expectations is observed. Limits are set on the stop mass in the Tstop1 model, see Figures 16 and 17.

[8] AAD 20AS searched in 139 fb^{-1} of pp collisions at $\sqrt{s}$ = 13 TeV for evidence of top squarks in events containing either a pair of jets consistent with SM Higgs boson decay into b-quarks or a same-flavour opposite-sign dilepton pair with an invariant mass consistent with a Z boson. No significant excess over the expected background is observed. Limits at 95% C.L. are set in Tstop6 simplified model. Assuming $m_{\widetilde{\chi}^0_1} = 0$ GeV, $\widetilde{t}_1$ masses up to 1220 GeV are excluded for $m_{\widetilde{\chi}^0_2}$ around 900 GeV. Limits reduce down to $\widetilde{t}_1$ masses up to 900 GeV for $m_{\widetilde{\chi}^0_2}$=130 GeV. See their Fig. 10. Limits are presented also in case of $B(\widetilde{\chi}^0_2 \to \widetilde{\chi}^0_1 h) = 0$ and 1, see their Fig. 11.

[9] AAD 20AS searched in 139 fb^{-1} of pp collisions at $\sqrt{s}$ = 13 TeV for evidence of top squarks in events containing either a pair of jets consistent with SM Higgs boson decay into b-quarks or a same-flavour opposite-sign dilepton pair with an invariant mass consistent with a Z boson. No significant excess over the expected background is observed. Limits at 95% C.L. are set in simplified model featuring $\widetilde{t}_2$ pair production, $\widetilde{t}_2 \to \widetilde{t}_1 Z$ and $\widetilde{t}_1 \to b f f' \widetilde{\chi}^0_1$. Assuming $m_{\widetilde{\chi}^0_1} = 300$ GeV, and a mass difference between $\widetilde{t}_1$ and $\widetilde{\chi}^0_1$ of 40 GeV, $\widetilde{t}_2$ masses up to 860 GeV are excluded. See their Fig. 12.

[10] AAD 20S searched in 139 fb^{-1} of pp collisions at $\sqrt{s}$ = 13 TeV for events containing multiple jets and large $\not{E}_T$. No significant excess above the Standard Model expectations is observed. Exclusion limits at 95% C.L. are set on top squark masses in the Tstop1 model up to 1250 GeV for lightest neutralino masses below 200 GeV. Additional constraints are set in the case where $m_{\widetilde{t}} - m_{\widetilde{\chi}^0_1} \sim m_t$ for which top squark masses in the range 300–630 GeV are excluded. See their Fig. 13.

[11] AAD 20S searched in 139 fb^{-1} of pp collisions at $\sqrt{s}$ = 13 TeV for events containing multiple jets and large $\not{E}_T$. No significant excess above the Standard Model expectations is observed. Exclusion limits at 95% C.L. are set on top squark masses in the Tstop3 model in the range 300–660 GeV. In case $m_{\widetilde{t}} - m_{\widetilde{\chi}^0_1} \sim 5$ GeV or above, $m_{\widetilde{t}}$ below 500 GeV are excluded. See their Fig. 13(b).

[12] AAD 20V searched in 139 fb^{-1} of pp collisions at $\sqrt{s}$ = 13 TeV for events with two same-sign charged leptons (electrons or muons) and jets. No significant excess above the Standard Model expectations is observed. Exclusion limits at 95% C.L. are set on the top squark mass up to 765 GeV assuming $\widetilde{t}_1 \to t\widetilde{\chi}^0_2$ with $\widetilde{\chi}^0_2 \to \widetilde{\chi}^{\pm}_1 W$ and $\widetilde{\chi}^{\pm}_1 \to \widetilde{\chi}^0_1 W$. Masses of the charginos and lightest neutralinos are set as $m_{\widetilde{\chi}^0_1} = m_{\widetilde{t}_1} - 275$ GeV, $m_{\widetilde{\chi}^0_2} = m_{\widetilde{\chi}^0_1} + 100$ GeV and $m_{\widetilde{\chi}^{\pm}_1} \sim m_{\widetilde{\chi}^0_1}$. See their Fig. 8(b).

Downloaded from https://academic.oup.com/ptep/article/2022/8/083C01/6651666 by KIT Library user on 27 September 2022

[13] SIRUNYAN 20AH searched in 137 fb^{-1} of pp collisions at $\sqrt{s}$ = 13 TeV for pair production of top squarks in events with a single isolated electron or muon, multiple jets and large $\not{E}_T$. No significant excess above the Standard Model expectations is observed. Limits are set on the stop mass in the Tstop1, Tstop2 and Tstop8 simplified models, see Figures 6, 7 and 8, respectively.

[14] SIRUNYAN 20T searched in 137 fb^{-1} of pp collisions at $\sqrt{s}$ = 13 TeV for events with at least two jets, and two isolated same-sign or three or more charged leptons (electrons or muons). No significant excess above the Standard Model expectations is observed. Limits are set on the gluino mass in the Tglu3A, Tglu3B, Tglu3C and Tglu3D simplified models, see their Figure 7, and in the Tglu1C and Tglu1B simplified models, see their Figures 8 and 9. Limits are also set on the sbottom mass in the Tsbot2 simplified model, see their Figure 10, and on the stop mass in the Tstop7 simplified model, see their Figure 11. Finally, limits are set on the gluino mass in RPV simplified models where the gluino decays either via $\tilde{g} \rightarrow q q \overline{q} \overline{q} + e/\mu/\tau$ or via $\tilde{g} \rightarrow t b s$, see Figure 12.

[15] SIRUNYAN 20U searched in 77.2 fb^{-1} of pp collisions at $\sqrt{s}$ = 13 TeV for the pair production of top squarks in events with two hadronically decaying taus, jets identified as originating from a b-quark and large $\not{E}_T$. No significant excess above the Standard Model expectations is observed. Limits are set on the stop mass in the Tstop11 simplified model assuming the final state leptons are taus. Different values of the scalar tau mass are considered; the impact on the lower bound is negligible.

[16] SIRUNYAN 19AU searched in 35.9 fb^{-1} of pp collisions at $\sqrt{s}$ = 13 TeV for events with at last one photon, jets, some of which are identified as originating from b-quarks, and large $\not{E}_T$. No significant excess above the Standard Model expectations is observed. In the framework of GMSB, limits are set on the gluino mass in the Tglu4C, Tglu4D and Tglu4E simplified models, and on the top squark mass in the Tstop13 simplified model, see their Figure 5.

[17] SIRUNYAN 19CH searched in 137 fb^{-1} of pp collisions at $\sqrt{s}$ = 13 TeV for events containing multiple jets and large $\not{E}_T$. No significant excess above the Standard Model expectations is observed. Limits are set on the gluino mass in the Tglu1A, Tglu1C, Tglu2A and Tglu3A simplified models, see their Figure 13. Limits are also set on squark, sbottom and stop masses in the Tsqk1, Tsbot1, Tstop1 simplified models, see their Figure 14.

[18] SIRUNYAN 19S searched in 35.9 fb^{-1} of pp collisions at $\sqrt{s}$ = 13 TeV for events with zero or one charged leptons, jets and $\not{E}_T$. The razor variables (M_R and R^2) are used to categorize the events. No significant excess above the Standard Model expectations is observed. Limits are set on the gluino mass in the Tglu3A and Tglu3C simplified models, see Figures 22 and 23, and on the stop mass in the Tstop1 simplified model, see their Figure 24.

[19] SIRUNYAN 19U searched in 35.9 fb^{-1} of pp collisions at $\sqrt{s}$ = 13 TeV for events containing one electron-muon pair with opposite charge. The search targets a region of parameter space where the kinematics of top squark pair production and top quark pair production is very similar, due to the mass difference between the top squark and the neutralino being close to the top quark mass. No excess above the Standard Model expectations is observed. Limits are set on the stop mass in the Tstop1 model, with $m_{\tilde{t}_1} - m_{\tilde{\chi}^0_1}$ close to m_t, see Figure 5.

[20] AABOUD 18AQ searched in 36.1 fb^{-1} of pp collisions at $\sqrt{s}$ = 13 TeV for top squark pair production in final states with one isolated electron or muon, several energetic jets, and missing transverse momentum. No significant excess over the Standard Model prediction is observed. In case of Tstop1 models, top squark masses up to 940 GeV are excluded assuming $m_{\tilde{\chi}^0_1}$ = 0 GeV, see their Fig. 20. If the top quark is not on-shell (3-body) decay, exclusions up to 500 GeV are obtained for $m_{\tilde{\chi}^0_1}$ = 300 GeV. Exclusions as a function of $m_{\tilde{t}_1} - m_{\tilde{\chi}^0_1}$ are given in their Fig. 21.

[21] AABOUD 18AQ searched in 36.1 fb^{-1} of pp collisions at $\sqrt{s}$ = 13 TeV for top squark pair production in final states with one isolated electron or muon, several energetic jets, and missing transverse momentum. No significant excess over the Standard Model prediction is observed. In case of Tstop3 models (4-body), top squark masses up to 370 GeV are excluded for $m_{\tilde{t}} - m_{\tilde{\chi}^0_1}$ as low as 20 GeV. Top squark masses below 195 GeV are excluded for all $m_{\tilde{\chi}^0_1}$, see their Fig. 20 and Fig. 21.

[22] AABOUD 18AQ searched in 36.1 fb^{-1} of pp collisions at $\sqrt{s}$ = 13 TeV for top squark pair production in final states with one isolated electron or muon, several energetic jets, and missing transverse momentum. No significant excess over the Standard Model prediction is observed. In case of Tstop2 models, top squark masses up to 840 GeV are excluded for $m_{\tilde{t}} - m_{\tilde{\chi}^\pm_1}$ = 10 GeV. See their Fig. 23. Exclusion limits for this decay mode are presented also in the context of Higgsino-LSP phenomenological MSSM models, where $m_{\tilde{\chi}^\pm_1} - m_{\tilde{\chi}^0_1}$ = 5 GeV, see their Fig 26.

[23] AABOUD 18BV searched in 36.1 fb^{-1} of pp collisions at $\sqrt{s}$ = 13 TeV for events with at least one jet identified as c-jet, large missing transverse energy and no leptons. Good agreement is observed between the number of events in data and Standard Model predictions. The results are translated into exclusion limits in Tstop4 models. In scenarios with differences of the stop and neutralino masses below 100 GeV, stop masses below 500 GeV are excluded. See their Fig.6 and Fig.7.

[24] AABOUD 18BV searched in 36.1 fb^{-1} of pp collisions at $\sqrt{s}$ = 13 TeV for events with at least one jet identified as c-jet, large missing transverse energy and no leptons. Good agreement is observed between the number of events in data and Standard Model predictions. The results are translated into exclusion limits in Tstop1 models. In scenarios with massless neutralinos, top squark masses below 850 GeV are excluded. See their Fig.6.

[25] AABOUD 18I searched in 36.1 fb^{-1} of pp collisions at $\sqrt{s}$ = 13 TeV for events with at least one jet with a transverse momentum above 250 GeV and no leptons. Good agreement is observed between the number of events in data and Standard Model predictions. The results are translated into exclusion limits in Tstop3 models. Stop masses below 390 GeV are excluded for $m_{\tilde{t}} - m_{\tilde{\chi}^0_1} = m_b$. See their Fig.9(b).

[26] AABOUD 18I searched in 36.1 fb^{-1} of pp collisions at $\sqrt{s}$ = 13 TeV for events with at least one jet with a transverse momentum above 250 GeV and no leptons. Good agreement is observed between the number of events in data and Standard Model predictions. The results are translated into exclusion limits in Tstop4 models. In scenarios with differences of the stop and neutralino masses around 5 GeV, stop masses below 430 GeV are excluded. See their Fig.9(a).

[27] AABOUD 18Y searched in 36.1 fb^{-1} of pp collisions at $\sqrt{s}$ = 13 TeV for direct pair production of top squarks in final states with two tau leptons, b-jets, and missing transverse momentum. At least one hadronic τ is required. No significant deviation from the SM predictions is observed in the data. The analysis results are interpreted in Tstop5 models with a nearly massless gravitino. Top squark masses up to 1.16 TeV and tau slepton masses up to 1 TeV are excluded, see their Fig 7.

[28] SIRUNYAN 18AJ searched in 35.9 fb^{-1} of pp collisions at $\sqrt{s}$ = 13 TeV for events containing two low-momentum, oppositely charged leptons (electrons or muons) and $\not{E}_T$. No excess over the expected background is observed. Limits are derived on the wino mass in the Tchi1n2F simplified model, see their Figure 5. Limits are also set on the stop mass in the Tstop10 simplified model, see their Figure 6. Finally, limits are set on the Higgsino mass in the Tchi1n2G simplified model, see Figure 8 and in the pMSSM, see Figure 7.

[29] SIRUNYAN 18AL searched in 35.9 fb^{-1} of pp collisions at $\sqrt{s}$ = 13 TeV for events with at least three charged leptons, in any combination of electrons and muons, jets and significant $\not{E}_T$. No significant excess above the Standard Model expectations is observed. Limits are set on the gluino mass in the Tglu3A and Tglu1C simplified models, see their Figure 5. Limits are also set on the sbottom mass in the Tsbot2 simplified model, see their Figure 6, and on the stop mass in the Tstop7 simplified model, see their Figure 7.

[30] SIRUNYAN 18AN searched in 19.7 fb^{-1} of pp collisions at $\sqrt{s}$ = 8 TeV for events containing one or two photons and a pair of top quarks from the decay of a pair of top squark in a natural gauge-mediated scenario. The final state consists of a lepton (electron or muon), jets and one or two photons. No significant excess above the Standard Model expectations is observed. Limits are set on the stop mass in the Tstop12 simplified model, see their Figure 6.

[31] SIRUNYAN 18AY searched in 35.9 fb^{-1} of pp collisions at $\sqrt{s}$ = 13 TeV for events containing one or more jets and significant $\not{E}_T$. No significant excess above the Standard Model expectations is observed. Limits are set on the gluino mass in the Tglu1A, Tglu2A and Tglu3A simplified models, see their Figure 3. Limits are also set on squark, sbottom and stop masses in the Tsqk1, Tsbot1, Tstop1 and Tstop4 simplified models, see their Figure 3. Finally, limits are set on long-lived gluino masses in a Tglu1A simplified model where the gluino is metastable or long-lived with proper decay lengths in the range 10^{-3} mm $< c\tau < 10^5$ mm, see their Figure 4.

[32] SIRUNYAN 18B searched in 35.9 fb^{-1} of pp collisions at $\sqrt{s}$ = 13 TeV for the pair production of third-generation squarks in events with jets and large $\not{E}_T$. No significant excess above the Standard Model expectations is observed. Limits are set on the sbottom mass in the Tsbot1 simplified model, see their Figure 5, and on the stop mass in the Tstop4 simplified model, see their Figure 6.

[33] SIRUNYAN 18C searched in 35.9 fb^{-1} of pp collisions at $\sqrt{s}$ = 13 TeV for the pair production of top squarks in events with two oppositely charged leptons (electrons or muons), jets identified as originating from a b-quark and large $\not{E}_T$. No significant excess above the Standard Model expectations is observed. Limits are set on the stop mass in the Tstop1, Tstop2 and Tstop11 simplified models, see their Figures 11 and 12. The Tstop1 and Tstop2 results are combined with complementary searches in the all-hadronic and single lepton channels, see their Figures 13 and 14.

[34] SIRUNYAN 18D searched in 35.9 fb^{-1} of pp collisions at $\sqrt{s}$ = 13 TeV for events containing identified hadronically decaying top quarks, no leptons, and $\not{E}_T$. No significant excess above the Standard Model expectations is observed. Limits are set on the stop mass in the Tstop1 simplified model, see their Figure 8, and on the gluino mass in the Tglu3A, Tglu3B, Tglu3C and Tglu3E simplified models, see their Figure 9.

[35] SIRUNYAN 18DI searched in 35.9 fb^{-1} of pp collisions at $\sqrt{s}$ = 13 TeV for pair production of top squarks in events with a low transverse momentum lepton (electron or muon), a high-momentum jet and significant missing transverse momentum. No significant excess above the Standard Model expectations is observed. Limits are set on the stop mass in the Tstop3 and Tstop10 simplified models, see their Figures 7 and 8. A combination of this search with the all-hadronic search is presented in Figure 9.

[36] SIRUNYAN 18DN searched in 35.9 fb^{-1} of pp collisions at $\sqrt{s}$ = 13 TeV for direct electroweak production of charginos and for pair production of top squarks in events with two leptons (electrons or muons) of the opposite electric charge. No significant excess above the Standard Model expectations is observed. Limits are set on the chargino mass in the Tchi1chi1C and Tchi1chi1E simplified models, see their Figure 8. Limits are also set on the stop mass in the Tstop1 and Tstop2 simplified models, see their Figure 9.

[37] AABOUD 17AJ searched in 36.1 fb^{-1} of pp collisions at $\sqrt{s}$ = 13 TeV for events with two same-sign or three leptons, jets and large missing transverse momentum. No significant excess above the Standard Model expectations is observed. Limits up to 700 GeV are set on the top squark mass in Tstop11 simplified models, assuming $m_{\tilde{\chi}^0_1} = m_{\tilde{t}} - 275$ GeV and $m_{\tilde{\chi}^0_2} = m_{\tilde{\chi}^0_1} + 100$ GeV. See their Figure 4(e).

[38] AABOUD 17AX searched in 36 fb^{-1} of pp collisions at $\sqrt{s}$ = 13 TeV for events containing two jets identified as originating from b-quarks and large missing transverse momentum, with or without leptons. No excess of events above the expected level of Standard Model background was found. Exclusion limits at 95% C.L. are set on the masses of top squarks. Assuming 50% BR for Tstop1 and Tstop2 simplified models, a $\tilde{t}_1$ mass below 880 (860) GeV is excluded for $m_{\tilde{\chi}^0_1}$ = 0 (<250) GeV. See their Fig. 7(b).

[39] AABOUD 17AY searched in 36.1 fb^{-1} of pp collisions at $\sqrt{s}$ = 13 TeV for events with at least four jets and large missing transverse momentum. No significant excess above the Standard Model expectations is observed. Limits in the range 250–1000 GeV are set on the top squark mass in Tstop1 simplified models. For the first time, additional constraints are set for the region $m_{\tilde{t}_1} \sim m_t + m_{\tilde{\chi}^0_1}$, with exclusion of the $\tilde{t}_1$ mass range 235–590 GeV. See their Figure 8.

[40] AABOUD 17AY searched in 36.1 fb^{-1} of pp collisions at $\sqrt{s}$ = 13 TeV for events with at least four jets and large missing transverse momentum. No significant excess above the Standard Model expectations is observed. Limits in the range 450-850 GeV are set on the top squark mass in a mixture of Tstop1 and Tstop2 simplified models with BR=50% and assuming $m_{\tilde{\chi}^\pm_1} - m_{\tilde{\chi}^0_1}$ = 1 GeV and $m_{\tilde{\chi}^0_1} < 240$ GeV. Constraints are given for various values of the BR. See their Figure 9.

[41] AABOUD 17BE searched in 36.1 fb^{-1} of pp collisions at $\sqrt{s}$ = 13 TeV for events with two opposite-charge leptons (electrons and muons) and large missing transverse momentum. No significant excess above the Standard Model expectations is observed. Limits up to 720 GeV are set on the top squark mass in Tstop1 simplified models, assuming massless neutralinos. See their Figure 9 (2-body area).

[42] AABOUD 17BE searched in 36.1 fb^{-1} of pp collisions at $\sqrt{s}$ = 13 TeV for events with two opposite-charge leptons (electrons and muons) and large missing transverse momentum. No significant excess above the Standard Model expectations is observed. Limits up to 400 GeV are set on the top squark mass in Tstop3 simplified models, assuming $m_{\tilde{t}_1} - m_{\tilde{\chi}^0_1}$ = 40 GeV. See their Figure 9 (4-body area).

[43] AABOUD 17BE searched in 36.1 fb^{-1} of pp collisions at $\sqrt{s}$ = 13 TeV for events with two opposite-charge leptons (electrons and muons) and large missing transverse momentum. No significant excess above the Standard Model expectations is observed.

Downloaded from https://academic.oup.com/ptep/article/2022/8/083C01/6651666 by KIT Library user on 27 September 2022

Limits up to 430 GeV are set on the top squark mass in Tstop1 simplified models where top quarks are offshell, assuming $m_{\tilde{t}_1} - m_{\tilde{\chi}^0_1}$ close to the W mass. See their Figure 9 (3-body area).

[44] AABOUD 17BE searched in 36.1 fb^{-1} of pp collisions at $\sqrt{s}$ = 13 TeV for events with two opposite-charge leptons (electrons and muons) and large missing transverse momentum. No significant excess above the Standard Model expectations is observed. Limits up to 700 GeV are set on the top squark mass in Tstop2 simplified models, assuming $m_{\tilde{t}_1} - m_{\tilde{\chi}^\pm_1}$ = 10 GeV and massless neutralinos. See their Figure 10.

[45] KHACHATRYAN 17 searched in 2.3 fb^{-1} of pp collisions at $\sqrt{s}$ = 13 TeV for events containing four or more jets, no more than one lepton, and missing transverse momentum, using the razor variables (M_R and R^2) to discriminate between signal and background processes. No evidence for an excess over the expected background is observed. Limits are derived on the stop mass in the Tstop1 simplified model, see Fig. 17.

[46] KHACHATRYAN 17AD searched in 2.3 fb^{-1} of pp collisions at $\sqrt{s}$ = 13 TeV for events containing at least four jets (including b-jets), missing transverse momentum and tagged top quarks. No evidence for an excess over the expected background is observed. Top squark masses in the range 250–740 GeV and neutralino masses up to 240 GeV are excluded at 95% C.L. See Fig. 12.

[47] KHACHATRYAN 17AD searched in 2.3 fb^{-1} of pp collisions at $\sqrt{s}$ = 13 TeV for events containing at least four jets (including b-jets), missing transverse momentum and tagged top quarks. No evidence for an excess over the expected background is observed. Limits are derived on the $\tilde{t}$ mass in simplified models that are a mixture of Tstop1 and Tstop2 with branching fractions 50% for each of the two decay modes: top squark masses of up to 610 GeV and neutralino masses up to 190 GeV are excluded at 95% C.L. The $\tilde{\chi}^\pm_1$ and the $\tilde{\chi}^0_1$ are assumed to be nearly degenerate in mass, with a 5 GeV difference between their masses. See Fig. 12.

[48] KHACHATRYAN 17P searched in 2.3 fb^{-1} of pp collisions at $\sqrt{s}$ = 13 TeV for events with one or more jets and large $\not{E}_T$. No significant excess above the Standard Model expectations is observed. Limits are set on the gluino mass in the Tglu1A, Tglu2A, Tglu3A, Tglu3B, Tglu3C and Tglu3D simplified models, see their Figures 7 and 8. Limits are also set on the squark mass in the Tsqk1 simplified model, see their Fig. 7, and on the sbottom mass in the Tsbot1 simplified model, see Fig. 8. Finally, limits are set on the stop mass in the Tstop1, Tstop3, Tstop4, Tstop6 and Tstop7 simplified models, see Fig. 8.

[49] KHACHATRYAN 17S searched in 18.5 fb^{-1} of pp collisions at $\sqrt{s}$ = 8 TeV for events containing multiple jets and missing transverse momentum, using the α_T variable to discriminate between signal and background processes. No evidence for an excess over the expected background is observed. Limits are derived on the stop mass in the Tstop4 model: for $\Delta m = m_{\tilde{t}} - m_{\tilde{\chi}^0_1}$ equal to 10 and 80 GeV, masses of stop below 240 and 260 GeV are excluded, respectively. See their Fig.3.

[50] KHACHATRYAN 17S searched in 18.5 fb^{-1} of pp collisions at $\sqrt{s}$ = 8 TeV for events containing multiple jets and missing transverse momentum, using the α_T variable to discriminate between signal and background processes. No evidence for an excess over the expected background is observed. Limits are derived on the stop mass in the Tstop3 model: for $\Delta m = m_{\tilde{t}} - m_{\tilde{\chi}^0_1}$ equal to 10 and 80 GeV, masses of stop below 225 and 130 GeV are excluded, respectively. See their Fig.3.

[51] KHACHATRYAN 17S searched in 18.5 fb^{-1} of pp collisions at $\sqrt{s}$ = 8 TeV for events containing multiple jets and missing transverse momentum, using the α_T variable to discriminate between signal and background processes. No evidence for an excess over the expected background is observed. Limits are derived on the stop mass in the Tstop2 model: assuming $m_{\tilde{\chi}^\pm_1} = 0.25\ m_{\tilde{t}} + 0.75\ m_{\tilde{\chi}^0_1}$, masses of stop up to 325 GeV and masses of the neutralino up to 225 GeV are excluded. See their Fig.3.

[52] KHACHATRYAN 17S searched in 18.5 fb^{-1} of pp collisions at $\sqrt{s}$ = 8 TeV for events containing multiple jets and missing transverse momentum, using the α_T variable to discriminate between signal and background processes. No evidence for an excess over the expected background is observed. Limits are derived on the stop mass in the Tstop2 model: assuming $m_{\tilde{\chi}^\pm_1} = 0.75\ m_{\tilde{t}} + 0.25\ m_{\tilde{\chi}^0_1}$, masses of stop up to 400 GeV are excluded for low neutralino masses. See their Fig.3.

[53] KHACHATRYAN 17S searched in 18.5 fb^{-1} of pp collisions at $\sqrt{s}$ = 8 TeV for events containing multiple jets and missing transverse momentum, using the α_T variable to discriminate between signal and background processes. No evidence for an excess over the expected background is observed. Limits are derived on the stop mass in the Tstop1 model: assuming masses of stop up to 500 GeV and masses of the neutralino up to 105 GeV are excluded. See their Fig.3.

[54] SIRUNYAN 17AS searched in 35.9 fb^{-1} of pp collisions at $\sqrt{s}$ = 13 TeV for events with a single lepton (electron or muon), jets, and large $\not{E}_T$. No significant excess above the Standard Model expectations is observed. Limits are set on the stop mass in the Tstop1, Tstop2 and Tstop8 simplified models, see their Figures 5, 6 and 7.

[55] SIRUNYAN 17AT searched in 35.9 fb^{-1} of pp collisions at $\sqrt{s}$ = 13 TeV for direct production of top squarks in events with jets and large $\not{E}_T$. No significant excess above the Standard Model expectations is observed. Limits are set on the stop mass in the Tstop1, Tstop2 , Tstop3, Tstop4, Tstop8 and Tstop10 simplified models, see their Figures 9 to 14.

[56] SIRUNYAN 17AZ searched in 35.9 fb^{-1} of pp collisions at $\sqrt{s}$ = 13 TeV for events with one or more jets and large $\not{E}_T$. No significant excess above the Standard Model expectations is observed. Limits are set on the gluino mass in the Tglu1A, Tglu2A, Tglu3A simplified models, see their Figures 6. Limits are also set on the squark mass in the Tsqk1 simplified model (for single light squark and for 8 degenerate light squarks), on the sbottom mass in the Tsbot1 simplified model and on the stop mass in the Tstop1 simplified model, see their Fig. 7. Finally, limits are set on the stop mass in the Tstop2, Tstop4 and Tstop8 simplified models, see Fig. 8.

[57] SIRUNYAN 17K searched in 2.3 fb^{-1} of pp collisions at $\sqrt{s}$ = 13 TeV for direct production of stop or sbottom pairs in events with multiple jets and significant $\not{E}_T$. A second search also requires an isolated lepton and is combined with the all-hadronic search. No significant excess above the Standard Model expectations is observed. Limits are set on the stop mass in the Tstop1, Tstop8 and Tstop4 simplified models, see their Figures 7, 8 and 9 (for the Tstop4 limits, only the results of the all-hadronic search are used). Limits are also set on the sbottom mass in the Tsbot1 simplified model, see Fig. 10 (also here, only the results of the all-hadronic search are used).

[58] SIRUNYAN 17P searched in 35.9 fb^{-1} of pp collisions at $\sqrt{s}$ = 13 TeV for events with multiple jets and large $\not{E}_T$. No significant excess above the Standard Model expectations is observed. Limits are set on the gluino mass in the Tglu1A, Tglu1C, Tglu2A, Tglu3A and Tglu3D simplified models, see their Fig. 12. Limits are also set on the squark mass in the Tsqk1 simplified model, on the stop mass in the Tstop1 simplified model, and on the sbottom mass in the Tsbot1 simplified model, see Fig. 13.

[59] AABOUD 16D searched in 3.2 fb^{-1} of pp collisions at $\sqrt{s}$ = 13 TeV in events with an energetic jet and large missing transverse momentum. The results are interpreted as 95% C.L. limits on mass of stop decaying into a charm-quark and the lightest neutralino in scenarios with $m_{\tilde{t}_1} - m_{\tilde{\chi}^0_1}$ between 5 and 20 GeV. See their Fig. 5.

[60] AABOUD 16J searched in 3.2 fb^{-1} of pp collisions at $\sqrt{s}$ = 13 TeV in final states with one isolated electron or muon, jets, and missing transverse momentum. For the direct stop pair production model where the stop decays via top and lightest neutralino, the results exclude at 95% C.L. stop masses between 745 GeV and 780 GeV for a massless $\tilde{\chi}^0_1$. See their Fig. 8.

[61] AAD 16AY searched in 20 fb^{-1} of pp collisions at $\sqrt{s}$ = 8 TeV for events with either two hadronically decaying tau leptons, one hadronically decaying tau and one light lepton, or two light leptons. No significant excess over the Standard Model expectation is found. Exclusion limits at 95% C.L. on the mass of top squarks decaying via $\tilde{\tau}$ to a nearly massless gravitino are placed depending on $m_{\tilde{\tau}}$ which is ranging from the 87 GeV LEP limit to $m_{\tilde{t}_1}$. See their Figs. 9 and 10.

[62] KHACHATRYAN 16AV searched in 19.7 fb^{-1} of pp collisions at $\sqrt{s}$ = 8 TeV for events with one or two isolated leptons, hadronic jets, b-jets and $\not{E}_T$. No significant excess above the Standard Model expectations is observed. Limits are set on the stop mass in the Tstop1 and Tstop2 simplified models, see Fig. 11.

[63] KHACHATRYAN 16BK searched in 18.9 fb^{-1} of pp collisions at $\sqrt{s}$ = 8 TeV for events with hadronic jets and $\not{E}_T$. No significant excess above the Standard Model expectations is observed. Limits are set on the stop mass in the Tstop1 and Tstop2 simplified models, see Fig. 16.

[64] KHACHATRYAN 16BS searched in 2.3 fb^{-1} of pp collisions at $\sqrt{s}$ = 13 TeV for events with at least one energetic jet , no isolated leptons, and significant $\not{E}_T$, using the transverse mass variable M_{T2} to discriminate between signal and background processes. No significant excess above the Standard Model expectations is observed. Limits are set on the stop mass in the Tstop1 simplified model, see Fig. 11 and Table 3.

[65] KHACHATRYAN 16Y searched in 19.7 fb^{-1} of pp collisions at $\sqrt{s}$ = 8 TeV for events with one or two soft isolated leptons, hadronic jets, and $\not{E}_T$. No significant excess above the Standard Model expectations is observed. Limits are set on the stop mass in the Tstop3 simplified model, see Fig. 3.

[66] AAD 15CJ searched in 20 fb^{-1} of pp collisions at $\sqrt{s}$ = 8 TeV for evidence of third generation squarks by combining a large number of searches covering various final states. Stop decays with and without charginos in the decay chain are considered and summaries of all ATLAS Run 1 searches for direct stop production can be found in Fig. 4 (no intermediate charginos) and Fig. 7 (intermediate charginos). Limits are set on stop masses in compressed mass regions regions, with $B(\tilde{t} \rightarrow c\tilde{\chi}^0_1) + B(\tilde{t} \rightarrow bff'\tilde{\chi}^0_1) = 1$, see Fig. 5. Limits are also set on stop masses assuming that both the decay $\tilde{t} \rightarrow t\tilde{\chi}^0_1$ and $\tilde{t} \rightarrow b\tilde{\chi}^\pm_1$ are possible, with both their branching rations summing up to 1, assuming $\tilde{\chi}^\pm_1 \rightarrow W^{(*)}\tilde{\chi}^0_1$ and $m_{\tilde{\chi}^\pm_1} = 2\ m_{\tilde{\chi}^0_1}$, see Fig. 6. Limits on the mass of the next-to-lightest stop $\tilde{t}_2$, decaying either to $Z\tilde{t}_1$, $h\tilde{t}_1$ or $t\tilde{\chi}^0_1$, are also presented, see Figs. 9 and 10.Interpretations in the pMSSM are also discussed, see Figs 13–15.

[67] AAD 15J interpreted the measurement of spin correlations in $t\bar{t}$ production using 20.3 fb^{-1} of pp collisions at $\sqrt{s}$ = 8 TeV in exclusion limits on the pair production of light $\tilde{t}_1$ squarks with masses similar to the top quark mass. The $\tilde{t}_1$ is assumed to decay through $\tilde{t}_1 \rightarrow t\tilde{\chi}^0_1$ with predominantly right-handed top and a 100% branching ratio. The data are found to be consistent with the Standard Model expectations and masses between the top quark mass and 191 GeV are excluded, see their Fig. 2

[68] KHACHATRYAN 15AF searched in 19.5 fb^{-1} of pp collisions at $\sqrt{s}$ = 8 TeV for events with at least two energetic jets and significant $\not{E}_T$, using the transverse mass variable M_{T2} to discriminate between signal and background processes. No significant excess above the Standard Model expectations is observed. Limits are set on the stop mass in simplified models where the decay $\tilde{t} \rightarrow t\tilde{\chi}^0_1$ takes place with a branching ratio of 100%, see Fig. 12. See also Table 5. Exclusions in the CMSSM, assuming tanβ = 30, $A_0 = -2\ \max(m_0, m_{1/2})$ and $\mu > 0$, are also presented, see Fig. 15.

[69] KHACHATRYAN 15AH searched in 19.4 or 19.7 fb^{-1} of pp collisions at $\sqrt{s}$ = 8 TeV for events containing either a fully reconstructed top quark, or events containing dijets requiring one or both jets to originate from b-quarks, or events containing a mono-jet. No significant excess above the Standard Model expectations is observed. Limits are set on the stop mass in simplified models where the decay $\tilde{t} \rightarrow t\tilde{\chi}^0_1$ takes place with a branching ratio of 100%, see Fig. 9. Limits are also set in simplified models where the decays $\tilde{t} \rightarrow t\tilde{\chi}^0_1$ and $\tilde{t} \rightarrow b\tilde{\chi}^\pm_1$, with $m_{\tilde{\chi}^\pm_1}$ - $m_{\tilde{\chi}^0_1}$ = 5 GeV, each take place with a branching ratio of 50%, see Fig. 10, or with other fractions, see Fig. 11. Finally, limits are set in a simplified model where the decay $\tilde{t} \rightarrow c\tilde{\chi}^0_1$ takes place with a branching ratio of 100%, see Figs. 9, 10 and 11.

[70] KHACHATRYAN 15AH searched in 19.4 or 19.7 fb^{-1} of pp collisions at $\sqrt{s}$ = 8 TeV for events containing either a fully reconstructed top quark, or events containing dijets requiring one or both jets to originate from b-quarks, or events containing a mono-jet. No significant excess above the Standard Model expectations is observed. Limits are set on the stop mass in simplified models where the decay $\tilde{t} \rightarrow t\tilde{\chi}^0_1$ takes place with a branching ratio of 100%, see Fig. 9. Limits are also set in simplified models where the decays $\tilde{t} \rightarrow t\tilde{\chi}^0_1$ and $\tilde{t} \rightarrow b\tilde{\chi}^\pm_1$, with $m_{\tilde{\chi}^\pm_1} - m_{\tilde{\chi}^0_1}$ = 5 GeV, each take place with a branching ratio of 50%, see Fig. 10, or with other fractions, see Fig. 11. Finally, limits are set in a simplified model where the decay $\tilde{t} \rightarrow c\tilde{\chi}^0_1$ takes place with a branching ratio of 100%, see Figs. 9, 10, and 11.

[71] KHACHATRYAN 15X searched in 19.3 fb^{-1} of pp collisions at $\sqrt{s}$ = 8 TeV for events with at least two energetic jets, at least one of which is required to originate from a b quark, possibly a lepton, and significant $\not{E}_T$, using the razor variables (M_R and R^2) to discriminate between signal and background processes. No significant excess above the Standard Model expectations is observed. Limits are set on the stop mass in simplified models where the decay $\tilde{t} \rightarrow t\tilde{\chi}^0_1$ and the decay $\tilde{t} \rightarrow b\tilde{\chi}^\pm_1$, with $m_{\tilde{\chi}^\pm_1} - m_{\tilde{\chi}^0_1}$ = 5 GeV, take place with branching ratios varying between 0 and 100%, see Figs. 15, 16 and 17.

[72] AAD 14AJ searched in 20.1 fb^{-1} of pp collisions at $\sqrt{s}$ = 8 TeV for events containing four or more jets and large missing transverse momentum. No excess of events above

Downloaded from https://academic.oup.com/ptep/article/2022/8/083C01/6651666 by KIT Library user on 27 September 2022

the expected level of Standard Model background was found. Exclusion limits at 95% C.L. are set on the masses of third-generation squarks in simplified models which either assume that the decay $\widetilde{t}_1 \rightarrow t\widetilde{\chi}^0_1$ takes place 100% of the time, see Fig. 8, or that this decay takes place 50% of the time, while the decay $\widetilde{t}_1 \rightarrow b\widetilde{\chi}^{\pm}_1$ takes place the other 50% of the time, see Fig. 9.

[73] AAD 14BD searched in 20 fb^{-1} of pp collisions at $\sqrt{s}$ = 8 TeV for events containing one isolated lepton, jets and large missing transverse momentum. No excess of events above the expected level of Standard Model background was found. Exclusion limits at 95% C.L. are set on the masses of third-generation squarks in simplified models which either assume that the decay $\widetilde{t}_1 \rightarrow t\widetilde{\chi}^0_1$ takes place 100% of the time, see Fig. 15, or the decay $\widetilde{t}_1 \rightarrow b\widetilde{\chi}^{\pm}_1$ takes place 100% of the time, see Fig. 16–22. For the mixed decay scenario, see Fig. 23.

[74] AAD 14F searched in 20.3 fb^{-1} of pp collisions at $\sqrt{s}$ = 8 TeV for events containing two leptons (e or μ), and possibly jets and missing transverse momentum. No excess of events above the expected level of Standard Model background was found. Exclusion limits at 95% C.L. are set on the masses of third-generation squarks in simplified models which either assume that the decay $\widetilde{t}_1 \rightarrow b\widetilde{\chi}^{\pm}_1$ takes place 100% of the time, see Figs. 14–17 and 20, or that the decay $\widetilde{t}_1 \rightarrow t\widetilde{\chi}^0_1$ takes place 100% of the time, see Figs. 18 and 19.

[75] AAD 14T searched in 20.3 fb^{-1} of pp collisions at $\sqrt{s}$ = 8 TeV for monojet-like and c-tagged events. No excess of events above the expected level of Standard Model background was found. Exclusion limits at 95% C.L. are set on the masses of third-generation squarks in simplified models which assume that the decay $\widetilde{t}_1 \rightarrow c\widetilde{\chi}^0_1$ takes place 100% of the time, see Fig. 9 and 10. The results of the monojet-like analysis are also interpreted in terms of stop pair production in the four-body decay $\widetilde{t}_1 \rightarrow b f f' \widetilde{\chi}^0_1$, see Fig. 11.

[76] CHATRCHYAN 14AH searched in 4.7 fb^{-1} of pp collisions at $\sqrt{s}$ = 7 TeV for events with at least two energetic jets and significant $\not{E}_T$, using the razor variables (M_R and R^2) to discriminate between signal and background processes. A second analysis requires at least one of the jets to be originating from a b-quark. No significant excess above the Standard Model expectations is observed. Limits are set on sbottom masses in simplified models where the decay $\widetilde{t} \rightarrow t\widetilde{\chi}^0_1$ takes place with a branching ratio of 100%, see Figs. 28 and 29. Exclusions in the CMSSM, assuming tanβ = 10, A_0 = 0 and μ >0, are also presented, see Fig. 26.

[77] CHATRCHYAN 14R searched in 19.5 fb^{-1} of pp collisions at $\sqrt{s}$ = 8 TeV for events with at least three leptons (electrons, muons, taus) in the final state. No significant excess above the Standard Model expectations is observed. Limits are set on the stop mass in a natural higgsino NLSP simplified model (GMSB) where the decay $\widetilde{t} \rightarrow b\widetilde{\chi}^{\pm}_1$, with $\widetilde{\chi}^{\pm}_1 \rightarrow (q q'/\ell\nu) H,\ Z\widetilde{G}$, takes place with a branching ratio of 100% (the particles between brackets have a soft p_T spectrum), see Figs. 4–6.

[78] AABOUD 17AF searched in 36 fb^{-1} of pp collisions at $\sqrt{s}$ = 13 TeV for evidence of top squarks in events containing 2 leptons, jets, b-jets and $\not{E}_T$. In Tstop6 model, assuming $m_{\widetilde{\chi}^0_1}$ = 0 GeV, $\widetilde{t}_1$ masses up to 850 GeV are excluded for $m_{\widetilde{\chi}^0_2}$ > 200 GeV.

[79] AABOUD 17AF searched in 36 fb^{-1} of pp collisions at $\sqrt{s}$ = 13 TeV for evidence of $\widetilde{t}_2$ in events containing 2 leptons, jets, b-jets and $\not{E}_T$. In Tstop7 model, assuming $m_{\widetilde{\chi}^0_1}$ = 50 GeV and 100% decays via Z boson, $\widetilde{t}_2$ masses up to 800 GeV are excluded. Exclusion limits are also shown as a function of the $\widetilde{t}_2$ branching ratios in their Figure 7.

[80] AABOUD 17AF searched in 36 fb^{-1} of pp collisions at $\sqrt{s}$ = 13 TeV for evidence of $\widetilde{t}_2$ in events containing 2 leptons, jets, b-jets and $\not{E}_T$. In Tstop7 model, assuming $m_{\widetilde{\chi}^0_1}$ = 50 GeV and 100% decays via higgs boson, $\widetilde{t}_2$ masses up to 880 GeV are excluded. Exclusion limits are also shown as a function of the $\widetilde{t}_2$ branching ratios in their Figure 7.

[81] AABOUD 17AY searched in 36.1 fb^{-1} of pp collisions at $\sqrt{s}$ = 13 TeV for events with at least four jets and large missing transverse momentum. No significant excess above the Standard Model expectations is observed. Limits are set on the top squark mass assuming three pMSSM-inspired models. The first one, referred to as Higgsino LSP model, assumes $m_{\widetilde{\chi}^{\pm}_1} - m_{\widetilde{\chi}^0_1}$ = 5 GeV and $m_{\widetilde{\chi}^0_2} - m_{\widetilde{\chi}^0_1}$ = 10 GeV, with a mixture of decay modes as in Tstop1, Tstop2 and Tstop6. See their Figure 10. The second and third models are referred to as Wino NLSP and well-tempered pMSSM models, respectively. See their Figure 11 and Figure 12, and text for details on assumptions.

[82] AAD 14B searched in 20.3 fb^{-1} of pp collisions at $\sqrt{s}$ = 8 TeV for events containing a Z boson, with or without additional leptons, plus jets originating from b-quarks and significant missing transverse momentum. No excess over the expected SM background is observed. Limits are derived in simplified models featuring $\widetilde{t}_2$ production, with $\widetilde{t}_2 \rightarrow Z\widetilde{t}_1$, $\widetilde{t}_1 \rightarrow t\widetilde{\chi}^0_1$ with a 100% branching ratio, see Fig. 4, and in the framework of natural GMSB, see Fig. 6.

[83] CHATRCHYAN 14U searched in 19.7 fb^{-1} of pp collisions at $\sqrt{s}$ = 8 TeV for evidence of direct pair production of top squarks, with Higgs bosons in the decay chain. The search is performed using a selection of events containing two Higgs bosons, each decaying to a photon pair, missing transverse energy and possibly b-quark jets. No significant excesses over the expected SM backgrounds are observed. The results are interpreted in the context of a "natural SUSY" simplified model where the decays $\widetilde{t}_1 \rightarrow b\widetilde{\chi}^{\pm}_1$, with $\widetilde{\chi}^{\pm}_1 \rightarrow f f' \widetilde{\chi}^0_1$, and $\widetilde{\chi}^0_1 \rightarrow H\widetilde{G}$, all happen with 100% branching ratio, see Fig. 4.

[84] KHACHATRYAN 14C searched in 19.5 fb^{-1} of pp collisions at $\sqrt{s}$ = 8 TeV for evidence of direct pair production of top squarks, with Higgs or Z-bosons in the decay chain. The search is performed using a selection of events containing leptons and b-quark jets. No significant excesses over the expected SM backgrounds are observed. The results are interpreted in the context of a simplified model with pair production of a heavier top-squark mass eigenstate $\widetilde{t}_2$ decaying to a lighter top-squark eigenstate $\widetilde{t}_1$ via either $\widetilde{t}_2 \rightarrow H\widetilde{t}_1$ or $\widetilde{t}_2 \rightarrow Z\widetilde{t}_1$, followed in both cases by $\widetilde{t}_1 \rightarrow t\widetilde{\chi}^0_1$. The interpretation is performed in the region where the mass difference between the $\widetilde{t}_1$ and $\widetilde{\chi}^0_1$ is approximately equal to the top-quark mass, which is not probed by searches for direct $\widetilde{t}_1$ pair production, see Figs. 5 and 6. The analysis excludes top squarks with masses $m_{\widetilde{t}_2}$ < 575 GeV and $m_{\widetilde{t}_1}$ < 400 GeV at 95% C.L.

R-parity violating $\widetilde{t}$ (Stop) mass limit

VALUE (GeV)	CL%	DOCUMENT ID		TECN	COMMENT
>1100	95	[1] AAD	21BF	ATLS	$\ell^{\pm}$ + b-jets + many jets, Tstop14, λ''_{323} electroweakino decay, 500 GeV < $m_{\widetilde{\chi}^0_1}$ < 800 GeV
>1150	95	[1] AAD	21BF	ATLS	$\ell^{\pm}$ + b-jets + many jets, Tstop15, λ''_{323} electroweakino decay, 600 GeV < $m_{\widetilde{\chi}^0_1}$ < 900 GeV
>1300	95	[1] AAD	21BF	ATLS	$\ell^{\pm}$ + b-jets + many jets, Tstop1, λ''_{323}, electroweakino decay, 500 GeV < $m_{\widetilde{\chi}^0_1}$ < 1000 GeV
>1600	95	[2] SIRUNYAN	21AF	CMS	long-lived $\widetilde{t}$, $\widetilde{t} \rightarrow \overline{d}\,\overline{d}$, λ''_{3i3} coupling, 0.4 mm < $c\tau$ < 80 mm
>1600	95	[3] SIRUNYAN	21U	CMS	long-lived $\widetilde{t}$, $\widetilde{t} \rightarrow b\overline{\ell}$, 5 < $c\tau$ < 240 mm
>1600	95	[3] SIRUNYAN	21U	CMS	long-lived $\widetilde{t}$, $\widetilde{t} \rightarrow d\overline{\ell}$, λ'_{x31} coupling, 3 < $c\tau$ < 360 mm
>1600	95	[3] SIRUNYAN	21U	CMS	long-lived $\widetilde{t}$, $\widetilde{t} \rightarrow \overline{d}\,\overline{d}$, η''_{311} coupling, 2 < $c\tau$ < 1320 mm
> 670	95	[4] SIRUNYAN	21V	CMS	$\ell^{\pm}$ + $\geq$ 7 jets, Tstop1 with $\widetilde{\chi}^0_1 \rightarrow q q q$, λ''_{abc} coupling, a,b,c $\in$ 1,2
> 870	95	[4] SIRUNYAN	21V	CMS	$\ell^{\pm}$ + $\geq$ 7 jets, stealth SYY model
>1700	95	[5] AAD	20M	ATLS	$\widetilde{t} \rightarrow q\mu$, long-lived, Tstop3RPV, τ = 0.1 ns
>1150	95	[6] SIRUNYAN	19BI	ATLS	$\widetilde{t} \rightarrow b\mu$, long-lived, Tstop2RPV, $c\tau$ = 0.1 cm
>1100	95	[7] SIRUNYAN	19BJ	CMS	$\widetilde{t} \rightarrow b e$, Tstop2RPV, prompt
none 100–410	95	[8] AABOUD	18BB	ATLS	4 jets, Tstop1RPV with $\widetilde{t} \rightarrow d s$, λ''_{312} coupling
none 100–470, 480–610	95	[9] AABOUD	18BB	ATLS	4 jets, Tstop1RPV, λ''_{323} coupling
$\geq$ 600–1500	95	[10] AABOUD	18P	ATLS	2ℓ + b-jets, Tstop2RPV, depending on λ'_{i33} coupling (i = 1, 2, 3)
>1130	95	[11] SIRUNYAN	18AD	CMS	$\widetilde{t} \rightarrow b\ell$, long-lived, $c\tau$ = 70–100 mm
> 550	95	[11] SIRUNYAN	18AD	CMS	$\widetilde{t} \rightarrow b\ell$, long-lived, $c\tau$ = 1–1000 mm
>1400	95	[12] SIRUNYAN	18DV	CMS	long-lived $\widetilde{t}$, $\widetilde{t} \rightarrow \overline{d}\,\overline{d}$, 0.6 mm < $c\tau$ < 80 mm
none 80–520	95	[13] SIRUNYAN	18DY	CMS	2, 4 jets, Tstop3RPV, λ''_{312} coupling
none 80–270, 285–340, 400–525	95	[13] SIRUNYAN	18DY	CMS	2 , 4 jets, Tstop1RPV, λ''_{323} coupling
>1200	95	[14] AABOUD	17AI	ATLS	$\geq$ 1ℓ+ $\geq$ 8 jets, Tstop1 with $\widetilde{\chi}^0_1 \rightarrow t b s$, λ''_{323} coupling, $m_{\widetilde{\chi}^0_1}$=500 GeV
none, 100–315	95	[15] AAD	16AM	ATLS	2 large-radius jets, Tstop1RPV
none, 200–350	95	[16] KHACHATRY...	15L	CMS	$\widetilde{t} \rightarrow q q$, $\lambda''_{312} \neq 0$
none, 200–385	95	[16] KHACHATRY...	15L	CMS	$\widetilde{t} \rightarrow q b$, $\lambda''_{323} \neq 0$
> 740	95	[17] KHACHATRY...	14T	CMS	τ + b-jets, $LQ\overline{D}$, $\lambda'_{333} \neq 0$, $\widetilde{t} \rightarrow \tau b$ simplified model
> 580	95	[17] KHACHATRY...	14T	CMS	τ + b-jets, $LQ\overline{D}$, $\lambda'_{3jk} \neq 0$ ($j \neq$ =3), $\widetilde{t} \rightarrow \widetilde{\chi}^{\pm} b$, $\widetilde{\chi}^{\pm} \rightarrow q q \tau^{\pm}$ simplified model
• • • We do not use the following data for averages, fits, limits, etc. • • •					
> 770	95	[18] AAD	21B	ATLS	$\geq$ 8 jets, $\geq$ 5 b-jets,Tstop4RPV
> 890	95	[19] KHACHATRY...	16AC	CMS	$e^+ e^-$+ $\geq$ 5 jets; $\widetilde{t} \rightarrow b\widetilde{\chi}^{\pm}_1$; $\widetilde{\chi}^{\pm}_1 \rightarrow \ell^{\pm} jj$, λ'_{ijk}
>1000	95	[19] KHACHATRY...	16AC	CMS	$\mu^+ \mu^-$+ $\geq$ 5 jets; $\widetilde{t} \rightarrow b\widetilde{\chi}^{\pm}_1$; $\widetilde{\chi}^{\pm}_1 \rightarrow \ell^{\pm} jj$, λ'_{ijk}
> 950	95	[20] KHACHATRY...	16BX	CMS	$\widetilde{t} \rightarrow t\widetilde{\chi}^0_1$, $\widetilde{\chi}^0_1 \rightarrow \ell\ell\nu$, λ_{121} or $\lambda_{122} \neq 0$
> 790	95	[21] KHACHATRY...	15E	CMS	$\widetilde{t}_1 \rightarrow b\ell$, $c\tau$ = 2 cm

[1] AAD 21BF searched in 139 fb^{-1} of pp collisions at $\sqrt{s}$ = 13 TeV for pair production of gluinos, stops, electroweakinos decaying RPV either directly or indirectly via the LSP. The final state in all cases is one or two leptons, many jets (up to fifteen) and b-jets. Different models with different branching fractions of the gluino or stop follow from the assumptions on the nature of the electroweakinos. No significant excess above the Standard Model predictions is observed. Limits are set on the *gluino*, $\widetilde{t}_1$, electroweakino masses as a function of the $\widetilde{\chi}^0_1$ mass in several scenarios of gluino, stop and electroweakino pair production.

Downloaded from https://academic.oup.com/ptep/article/2022/8/083C01/6651666 by KIT Library user on 27 September 2022

[2] SIRUNYAN 21AF searched in 140 fb^{-1} of pp collisions at $\sqrt{s}$ = 13 TeV for supersymmetry in events with with two displaced vertices from long-lived particles decaying into multijet or dijet final states. No significant excess above the Standard Model expectations is observed. Limits are set on the gluino mass in the simplified model Tglu2RPV with λ''_{323} coupling, on the $\widetilde{\chi}^0_1$ mass in an RPV model with $\widetilde{\chi}^0_1$ pair production and the RPV decay $\widetilde{\chi}^0_1 \rightarrow tbs$ with λ''_{323} coupling and on the $\widetilde{t}$ mass in an RPV model with top squark pair production and the RPV decay $\widetilde{t} \rightarrow \overline{d}_i \overline{d}_j$ with λ''_{3ij} coupling, see their Figure 7.

[3] SIRUNYAN 21U searched in 132 fb^{-1} of pp collisions at $\sqrt{s}$ = 13 TeV for supersymmetry in events with displaced tracks and displaced vertices associated with a dijet system. No significant excess above the Standard Model expectations is observed. Limits are set on long-lived gluinos in an RPC GMSB SUSY model of gluino pair production, with $\widetilde{g} \rightarrow g\widetilde{G}$, see their Figure 9, in Tglu1A in a mini-split model, see their Figure 10, and in an RPV model of gluino pair production, with $\widetilde{g} \rightarrow tbs$ with coupling λ''_{323}, see their Figure 11. Limits are also set on long-lived top squarks in Tstop2RPV, see their Figure 12, in an RPV model with $\widetilde{t} \rightarrow d\overline{\ell}$ and λ'_{x31} coupling, see their Figure 13, and in a dynamical RPV model with $\widetilde{t} \rightarrow \overline{d}\overline{d}$ via a nonholomorphic RPV coupling η''_{311}, see their Figure 14. The best mass limit is achieved in all cases at cτ = 30 mm.

[4] SIRUNYAN 21V searched in 137 fb^{-1} of pp collisions at $\sqrt{s}$ = 13 TeV for supersymmetry in events with one charged lepton ($e^{\pm}$ or $\mu^{\pm}$) and $\geq$ 7 jets. No significant excess above the Standard Model expectations is observed. Limits are set on an RPV SUSY model like Tstop1 with the additional decay $\widetilde{\chi}^0_1 \rightarrow qqq$ with coupling λ''_{abc}, with $a,b,c \in 1,2$, and on a stealth SUSY model called SYY, with one scalar particle S with even R-parity and its superpartner $\widetilde{S}$, both singlets under all SM interactions, and with a portal mediated by loop interactions involving a new vectorlike messenger field (Y), where pair produced top squarks decay as $\widetilde{t} \rightarrow tg\widetilde{S}$, and $\widetilde{S} \rightarrow \widetilde{G}S$, and $S \rightarrow gg$, see their Figure 6 and 7.

[5] AAD 20M searched for long-lived particles decaying into hadrons and at least one muon in events containing a displaced muon track and a displaced vertex. The analysis uses a dataset of pp collisions at $\sqrt{s}$ = 13 TeV corresponding to an integrated luminosity of 136 fb^{-1}. Using the Tstop3RPV simplified model, top squarks with masses up to 1.7 TeV are excluded for a lifetime of 0.1 ns, and masses below 1.3 TeV are excluded for lifetimes between 0.01 ns and 30 ns, see their Fig. 7. The dependence on the RPV coupling λ_{23k} multiplied by cosθ_t, with θ_t the mixing angle between the left- and right-handed $\widetilde{t}$ squarks, is also shown, see their Fig. 7.

[6] SIRUNYAN 19BI searched in 35.9 fb^{-1} of pp collisions at $\sqrt{s}$ = 13 TeV in final states with two muons and two jets, or with one muon, two jets, and missing transverse momentum. Limits are set in a model of pair-produced, prompt or long-lived top squarks with R-parity violating decays to a b-quark and a lepton (Tstop2RPV), branching fraction of $\widetilde{t} \rightarrow b\mu$ equal to 1/3 and cτ between 0.1 cm and 10 cm in the case of long-lived top squarks. See their Fig. 10.

[7] SIRUNYAN 19BJ searched in 35.9 fb^{-1} of pp collisions at $\sqrt{s}$ = 13 TeV in final states with two electrons and two jets, or with one electron, two jets, and missing transverse momentum. Limits are set in a model of pair-produced, prompt top squarks with R-parity violating decays to a b-quark and a lepton (Tstop2RPV), assuming branching fraction of $\widetilde{t} \rightarrow be$ equal to 1/3 and cτ = 0 cm. See their Fig.10.

[8] AABOUD 18BB searched in 36.7 fb^{-1} of pp collisions at $\sqrt{s}$ = 13 TeV for massive colored resonances which are pair-produced and decay into two jets. No significant deviation from the background prediction is observed. Results are interpreted in a SUSY simplified model as Tstop1RPV with $\widetilde{t} \rightarrow ds$. Top squarks with masses in the range 100–410 GeV are excluded, see their Figure 9(a). The λ''_{312} coupling is assumed to be sufficiently large for the decays to be prompt, but small enough to neglect the single-top-squark resonant production through RPV couplings.

[9] AABOUD 18BB searched in 36.7 fb^{-1} of pp collisions at $\sqrt{s}$ = 13 TeV for massive coloured resonances which are pair-produced and decay into two jets. No significant deviation from the background prediction is observed. Results are interpreted in Tstop1RPV. Top squarks with masses in the range 100–470 GeV or 480–610 GeV are excluded, see their Figure 9(b). The λ''_{323} coupling is assumed to be sufficiently large for the decays to be prompt, but small enough to neglect the single-top-squark resonant production through RPV couplings.

[10] AABOUD 18P searched in 36.1 fb^{-1} of pp collisions at $\sqrt{s}$ = 13 TeV for pair-produced top squarks that decay through RPV λ'_{i33} (i = 1, 2, 3) couplings to a final state with two leptons and two jets, at least one of which is identified as a b-jet. No significant excess is observed over the SM background. In the Tstop2RPV model, lower limits on the top squark masses between 600 and 1500 GeV are set depending on the branching fraction to be, $b\mu$, and $b\tau$ final states. See their Figs 6 and 7.

[11] SIRUNYAN 18AD searched in 2.6 fb^{-1} of pp collisions at $\sqrt{s}$ = 13 TeV for long-lived particles by exploiting the multiplicity of displaced jets to search for the presence of signal decays occurring at distances between 1 and 1000 mm. Limits are set in a model of pair-produced, long-lived top squarks with R-parity violating decays to a b-quark and a lepton, see their Figure 3.

[12] SIRUNYAN 18DV searched in 38.5 fb^{-1} of pp collisions at $\sqrt{s}$ = 13 TeV for long-lived particles in events with multiple jets and two displaced vertices composed of many tracks. No events with two well-separated high-track-multiplicity vertices were observed. Limits are set on the stop and the gluino mass in RPV models of supersymmetry where the stop (gluino) is decaying solely into dijet (multijet) final states, see their Figures 6 and 7.

[13] SIRUNYAN 18DY searched in 35.9 fb^{-1} of pp collisions at $\sqrt{s}$ = 13 TeV for the pair production of resonances, each decaying to two quarks. The search is conducted separately in a boosted (two-jet) and resolved (four-jet) jet topology. The mass spectra are found to be consistent with the Standard Model expectations. Limits are set on the stop mass in the Tstop3RPV and Tstop1RPV simplified models, see their Figure 11.

[14] AABOUD 17AI searched in 36.1 fb^{-1} of pp collisions at $\sqrt{s}$ = 13 TeV for events with one or more isolated lepton, at least eight jets, either zero or many b-jets, for evidence of R-parity violating decays of the top squark. No significant excess above the Standard Model expectations is observed. Limits up to 1.25 (1.10) TeV are set on the top squark mass in R-parity-violating supersymmetry models where $\widetilde{t}_1$ decays for a bino LSP as: $\widetilde{t} \rightarrow t\widetilde{\chi}^0_1$ and for a higgsino LSP as $\widetilde{t} \rightarrow t\widetilde{\chi}^0_{1,2}/b\widetilde{\chi}^+_1$. These is followed by the decays through the non-zero λ''_{323} coupling $\widetilde{\chi}^0_{1,2} \rightarrow tbs$, $\widetilde{\chi}^{\pm}_1 \rightarrow bbs$. See their Figure 10 and text for details on model assumptions.

[15] AAD 16AM searched in 17.4 fb^{-1} of pp collisions at $\sqrt{s}$ = 8 TeV for events containing two large-radius hadronic jets. No deviation from the background prediction is observed. Top squarks with masses between 100 and 315 GeV are excluded at 95% C.L. in the hypothesis that they both decay via R-parity violating coupling λ''_{323} to b- and s-quarks. See their Fig. 10.

[16] KHACHATRYAN 15L searched in 19.4 fb^{-1} of pp collisions at $\sqrt{s}$ = 8 TeV for pair production of heavy resonances decaying to pairs of jets in four jet events. No significant excess above the Standard Model expectations is observed. Limits are set on the stop mass in R-parity-violating supersymmetry models where $\widetilde{t} \rightarrow qq$ ($\lambda''_{312} \neq 0$), see Fig. 6 (top) and $\widetilde{t} \rightarrow qb$ ($\lambda''_{323} \neq 0$), see Fig. 6 (bottom).

[17] KHACHATRYAN 14T searched in 19.7 fb^{-1} of pp collisions at $\sqrt{s}$ = 8 TeV for events with τ-leptons and b-quark jets, possibly with extra light-flavour jets. No excess above the Standard Model expectations is observed. Limits are set on stop masses in RPV SUSY models with $LQ\overline{D}$ couplings, in two simplified models. In the first model, the decay $\widetilde{t} \rightarrow \tau b$ is considered, with $\lambda'_{333} \neq 0$, see Fig. 3. In the second model, the decay $\widetilde{t} \rightarrow \widetilde{\chi}^{\pm} b$, with the subsequent decay $\widetilde{\chi}^{\pm} \rightarrow qq\tau^{\pm}$ is considered, with $\lambda'_{3jk} \neq 0$ and the mass splitting between the top squark and the charging chosen to be 100 GeV, see Fig. 4.

[18] AAD 21B searched in 139 fb^{-1} of pp collisions at $\sqrt{s}$ = 13 TeV for events with at least eight jets and at least 5 b-jets, for evidence of R-parity violating decays of the top squark. No significant excess above the Standard Model expectations is observed. Limits up to 950 GeV are set on the top squark mass in Tstop4RPV simplified model. See their Figure 7 for more detailed mass bounds.

[19] KHACHATRYAN 16AC searched in 19.7 fb^{-1} of pp collisions at $\sqrt{s}$ = 8 TeV for events with low missing transverse momentum, two oppositely charged electrons or muons, and at least five jets, at least one of which is a b-jet, for evidence of R-parity violating, charging-mediated decays of the top squark. No significant excess above the Standard Model expectations is observed. Limits are set on the stop mass in R-parity-violating supersymmetry models where $\widetilde{t} \rightarrow b\widetilde{\chi}^{\pm}_1$ with $\widetilde{\chi}^{\pm}_1 \rightarrow \ell^{\pm} jj$, $\lambda'_{ijk} \neq 0$ ($i,j,k \leq 2$), and with $m_{\widetilde{t}} - m_{\widetilde{\chi}^{\pm}_1}$ = 100 GeV, see Fig. 3.

[20] KHACHATRYAN 16BX searched in 19.5 fb^{-1} of pp collisions at $\sqrt{s}$ = 8 TeV for events containing 4 leptons coming from R-parity-violating decays of $\widetilde{\chi}^0_1 \rightarrow \ell\ell\nu$ with $\lambda_{121} \neq 0$ or $\lambda_{122} \neq 0$. No excess over the expected background is observed. Limits are derived on the gluino, squark and stop masses, see Fig. 23.

[21] KHACHATRYAN 15E searched for long-lived particles decaying to leptons in 19.7 fb^{-1} of pp collisions at $\sqrt{s}$ = 8 TeV. Events were selected with an electron and muon with opposite charges and each with transverse impact parameter values between 0.02 and 2 cm. Limits are set on SUSY benchmark models with pair production of top squarks decaying into an $e\mu$ final state via RPV interactions. See their Fig. 2

Heavy $\widetilde{g}$ (Gluino) mass limit

For $m_{\widetilde{g}}$ > 60–70 GeV, it is expected that gluinos would undergo a cascade decay via a number of neutralinos and/or charginos rather than undergo a direct decay to photinos as assumed by some papers. Limits obtained when direct decay is assumed are usually higher than limits when cascade decays are included.

Some earlier papers are now obsolete and have been omitted. They were last listed in our PDG 14 edition: K. Olive, *et al.* (Particle Data Group), Chinese Physics **C38** 070001 (2014) (http://pdg.lbl.gov).

R-parity conserving heavy $\widetilde{g}$ (Gluino) mass limit

VALUE (GeV)	CL%	DOCUMENT ID		TECN	COMMENT
>2200	95	[1] AAD	21AK	ATLS	$\ell^{\pm}$ + jets + $\not{E}_T$, Tglu1B, $m_{\widetilde{\chi}^{\pm}_1} = (m_{\widetilde{g}} + m_{\widetilde{\chi}^0_1})/2$, $m_{\widetilde{\chi}^0_1}$ < 400 GeV
none 1300–2050	95	[1] AAD	21AK	ATLS	$\ell^{\pm}$ + jets + $\not{E}_T$, Tglu1B, $m_{\widetilde{\chi}^{\pm}_1} = (m_{\widetilde{g}} + m_{\widetilde{\chi}^0_1})/2$, $m_{\widetilde{\chi}^0_1}$ < 1000 GeV
>2300	95	[2] AAD	21L	ATLS	jets + $\not{E}_T$, Tglu1A, $m_{\widetilde{\chi}^0_1}$ < 200 GeV
>3000	95	[2] AAD	21L	ATLS	jets + $\not{E}_T$, combined $\widetilde{g}\widetilde{g}$, $\widetilde{g}\,\widetilde{q}$, $\widetilde{q}\widetilde{q}$ production, $\widetilde{g} \rightarrow qq'\widetilde{\chi}^0_1$, $\widetilde{q} \rightarrow q\widetilde{\chi}^0_1$, $m_{\widetilde{q}} = m_{\widetilde{g}}$, $m_{\widetilde{\chi}^0_1}$ = 0 GeV
>2200	95	[2] AAD	21L	ATLS	jets + $\not{E}_T$, Tglu1B, $m_{\widetilde{\chi}^0_1}$ = 0 GeV
>1400	95	[3] AAD	21X	ATLS	jets in empty bunch crossings, Tglu1A, long-lived R-hadron, $m_{\widetilde{\chi}^0_1}$ = 100 GeV, 10^{-5} s < $\tau_{R-hadron}$ < 10^3 s
> 870	95	[3] AAD	21X	ATLS	jets in empty bunch crossings, Tglu1A, long-lived R-hadron, $m_{\widetilde{g}} - m_{\widetilde{\chi}^0_1}$ = 100 GeV, 10^{-5} s < $\tau_{R-hadron}$ < 10^3 s
>2260	95	[4] SIRUNYAN	21AD	CMS	jets + $\not{E}_T$, Tglu3A, $m_{\widetilde{\chi}^0_1}$ < 1050 GeV
>2150	95	[4] SIRUNYAN	21AD	CMS	jets + $\not{E}_T$, Tglu3C, $m_{\widetilde{\chi}^0_1}$ = 600 GeV, $m_{\widetilde{t}} - m_{\widetilde{\chi}^0_1}$ = 20 GeV
>2250	95	[4] SIRUNYAN	21AD	CMS	jets + $\not{E}_T$, Tglu3D, $m_{\widetilde{\chi}^0_1}$ = 700 GeV, $m_{\widetilde{\chi}^{\pm}_1} - m_{\widetilde{\chi}^0_1}$ = 5 GeV
>1870	95	[5] SIRUNYAN	21M	CMS	$\ell^{\pm}\ell^{\mp}$ + $\not{E}_T$, Tglu4C, $m_{\widetilde{\chi}^0_1}$ = 1100 GeV

Downloaded from https://academic.oup.com/ptep/article/2022/8/083C01/6651666 by KIT Library user on 27 September 2022

>1980	95	[6] AAD	20AL	ATLS	8 or more jets + $\not{E}_T$, Tglu1E, $m_{\widetilde{\chi}^0_1}$ = 100 GeV
>1820	95	[6] AAD	20AL	ATLS	8 or more jets + $\not{E}_T$, Tglu3A, $m_{\widetilde{\chi}^0_1}$ = 100 GeV
>1600	95	[7] AAD	20V	ATLS	same-sign $\ell^\pm\ell^\pm$ + jets, Tglu1E, $m_{\widetilde{\chi}^0_1}$ = 100 GeV
>1975	95	[8] SIRUNYAN	20B	CMS	$\geq 1\gamma + \not{E}_T$, Tglu4A, BR($\widetilde{g} \rightarrow qq\widetilde{\chi}^\pm_1$)=0.5, $m_{\widetilde{\chi}^0_1} \simeq m_{\widetilde{g}}$
>1920	95	[9] SIRUNYAN	20BJ	CMS	jets+$\not{E}_T$, Tglu1H, $m_{\widetilde{g}} - m_{\widetilde{\chi}^0_2}$ = 50 GeV, $m_{\widetilde{\chi}^0_1}$ = 1 GeV
>2150	95	[10] SIRUNYAN	20E	CMS	1ℓ+jets, Tglu3A, $m_{\widetilde{\chi}^0_1}$ <700 GeV
>2050	95	[10] SIRUNYAN	20E	CMS	1ℓ+jets, Tglu3A, $m_{\widetilde{\chi}^0_1}$ <1100GeV
>1650	95	[10] SIRUNYAN	20E	CMS	1ℓ + jets, Tglu3C, $m_{\widetilde{t}_1} - m_{\widetilde{\chi}^0_1}$= 175 GeV, $m_{\widetilde{\chi}^0_1}$ < 1150 GeV
>1700	95	[11] SIRUNYAN	20T	CMS	same-sign $\ell^\pm\ell^\pm$ or $\geq 3\ell^\pm$ + jets, Tglu3A, $m_{\widetilde{\chi}^0_1}$ = 0 GeV
>1610	95	[11] SIRUNYAN	20T	CMS	same-sign $\ell^\pm\ell^\pm$ or $\geq 3\ell^\pm$ + jets, Tglu3B, $m_{\widetilde{t}_1} - m_{\widetilde{\chi}^0_1}$= 175 GeV, $m_{\widetilde{\chi}^0_1}$ = 0 GeV
>1300	95	[11] SIRUNYAN	20T	CMS	same-sign $\ell^\pm\ell^\pm$ or $\geq 3\ell^\pm$ + jets, Tglu3C, $m_{\widetilde{t}_1} - m_{\widetilde{\chi}^0_1}$= 20 GeV, $m_{\widetilde{\chi}^0_1}$ = 0 GeV
>1500	95	[11] SIRUNYAN	20T	CMS	same-sign $\ell^\pm\ell^\pm$ or $\geq 3\ell^\pm$ + jets, Tglu3D, $m_{\widetilde{\chi}^\pm_1} = m_{\widetilde{\chi}^0_1}$ + 5 GeV, $m_{\widetilde{\chi}^0_1}$ = 0 GeV
>1350	95	[11] SIRUNYAN	20T	CMS	same-sign $\ell^\pm\ell^\pm$ or $\geq 3\ell^\pm$ + jets, Tglu1C, $m_{\widetilde{\chi}^0_2} = m_{\widetilde{\chi}^\pm_1}$ = $(m_{\widetilde{g}} + m_{\widetilde{\chi}^0_1})/2$, $m_{\widetilde{\chi}^0_1}$ = 0 GeV
>1250	95	[11] SIRUNYAN	20T	CMS	same-sign $\ell^\pm\ell^\pm$ or $\geq 3\ell^\pm$ + jets, Tglu1C, $m_{\widetilde{\chi}^0_2} = m_{\widetilde{\chi}^\pm_1}$= $m_{\widetilde{\chi}^0_1}$+20 GeV, $m_{\widetilde{\chi}^0_1}$=0 GeV
>1425	95	[11] SIRUNYAN	20T	CMS	same-sign $\ell^\pm\ell^\pm$ or $\geq 3\ell^\pm$ + jets, Tglu1B, $m_{\widetilde{\chi}^\pm_1}$ = $(m_{\widetilde{g}} + m_{\widetilde{\chi}^0_1})/2$, $m_{\widetilde{\chi}^0_1}$ = 0 GeV
>1425	95	[11] SIRUNYAN	20T	CMS	same-sign $\ell^\pm\ell^\pm$ or $\geq 3\ell^\pm$ + jets, Tglu1B, $m_{\widetilde{\chi}^\pm_1} = m_{\widetilde{\chi}^0_1}$ + 20 GeV, $m_{\widetilde{\chi}^0_1}$ = 0 GeV
>2000	95	[12] AABOUD	19I	ATL	$\geq$ 2 jets + 1 or 2 $\tau + \not{E}_T$, Tglu1F, $m_{\widetilde{\chi}^0_1}$ = 100 GeV
>1860	95	[13] SIRUNYAN	19AG	CMS	2$\gamma + \not{E}_T$, Tglu4B, 500 GeV <$m_{\widetilde{\chi}^0_1}$ < 1500 GeV
>1920	95	[14] SIRUNYAN	19AU	CMS	γ +jets + b-jets + $\not{E}_T$, Tglu4D, $m_{\widetilde{\chi}^0_1}$ = 127 GeV
>1950	95	[14] SIRUNYAN	19AU	CMS	γ + jets + b-jets + $\not{E}_T$, Tglu4E, $m_{\widetilde{\chi}^0_1}$ = 1 GeV
>1800	95	[14] SIRUNYAN	19AU	CMS	γ + jets + b-jets + $\not{E}_T$, Tglu4F, $m_{\widetilde{\chi}^0_1}$ = 1 GeV
>2090	95	[14] SIRUNYAN	19AU	CMS	γ + jets + b-jets + $\not{E}_T$, Tglu4D, $m_{\widetilde{\chi}^0_1}$ = 1200 GeV
>2120	95	[14] SIRUNYAN	19AU	CMS	γ + jets + b-jets + $\not{E}_T$, Tglu4E, $m_{\widetilde{\chi}^0_1}$ = 1200 GeV
>1970	95	[14] SIRUNYAN	19AU	CMS	γ + jets + b-jets + $\not{E}_T$, Tglu4F, $m_{\widetilde{\chi}^0_1}$ = 1200 GeV
>1700	95	[15] SIRUNYAN	19CE	CMS	2 jets, Stealth SUSY, Tglu1A and $\widetilde{\chi}^0_1 \rightarrow \widetilde{S}\,\gamma\,(\widetilde{S} \rightarrow S\,\widetilde{G})$, $m_{\widetilde{\chi}^0_1}$ = 200 GeV
>2000	95	[16] SIRUNYAN	19CH	CMS	jets+$\not{E}_T$, Tglu1A, $m_{\widetilde{\chi}^0_1}$ = 0 GeV
>2030	95	[16] SIRUNYAN	19CH	CMS	jets+$\not{E}_T$, Tglu1C, $m_{\widetilde{\chi}^\pm_1}$=$m_{\widetilde{\chi}^0_2}$= 0.5($m_{\widetilde{g}}$+$m_{\widetilde{\chi}^0_1}$), $m_{\widetilde{\chi}^0_1}$ = 0 GeV
>2270	95	[16] SIRUNYAN	19CH	CMS	jets+$\not{E}_T$, Tglu2A, $m_{\widetilde{\chi}^0_1}$ = 0 GeV
>2180	95	[16] SIRUNYAN	19CH	CMS	jets+$\not{E}_T$, Tglu3A, $m_{\widetilde{\chi}^0_1}$ = 0 GeV
>1750	95	[17] SIRUNYAN	19K	CMS	$\gamma+\ell+\not{E}_T$, Tglu4A, $m_{\widetilde{\chi}^0_1}$ = 1500 GeV
>2000	95	[18] SIRUNYAN	19S	CMS	1 or 2 ℓ + jets + $\not{E}_T$, Tglu3A, $m_{\widetilde{\chi}^0_1}$ < 700 GeV
>1900	95	[18] SIRUNYAN	19S	CMS	1 or 2 ℓ + jets + $\not{E}_T$, Tglu3C, 150 GeV < $m_{\widetilde{\chi}^0_1}$ < 950 GeV
>1970	95	[19] AABOUD	18AR	ATLS	jets+ $\geq$ 3b-jets+$\not{E}_T$, Tglu3A, $m_{\widetilde{\chi}^0_1}$ < 300 GeV
>1920	95	[20] AABOUD	18AR	ATLS	jets+ $\geq$ 3b-jets+$\not{E}_T$, Tglu2A, $m_{\widetilde{\chi}^0_1}$ < 600 GeV
>1650	95	[21] AABOUD	18AS	ATLS	$\geq$ 4 jets and disappearing tracks from $\widetilde{\chi}^\pm \rightarrow \widetilde{\chi}^0_1\pi^\pm$, modified Tglu1A or Tglu1B, $\widetilde{\chi}^\pm$ lifetime 0.2 ns, $m_{\widetilde{\chi}^\pm}$ = 460 GeV
>1850	95	[22] AABOUD	18BJ	ATLS	$\ell^\pm\ell^\mp$ + jets + $\not{E}_T$, Tglu1G, $m_{\widetilde{\chi}^0_1}$ = 100 GeV
>1650	95	[23] AABOUD	18BJ	ATLS	$\ell^\pm\ell^\mp$ + jets + $\not{E}_T$, Tglu1H, $m_{\widetilde{\chi}^0_1}$ = 100 GeV
>2150	95	[24] AABOUD	18U	ATLS	2 $\gamma + \not{E}_T$, GGM, Tglu4B, any NLSP mass
>1600	95	[25] AABOUD	18U	ATLS	γ + jets + $\not{E}_T$, GGM higgsino-bino, mix of Tglu4B and Tglu4C, any NLSP mass
>2030	95	[26] AABOUD	18V	ATLS	jets+$\not{E}_T$, Tglu1A, $m_{\widetilde{\chi}^0_1}$ = 0 GeV
>1980	95	[27] AABOUD	18V	ATLS	jets+$\not{E}_T$, Tglu1B, $m_{\widetilde{\chi}^\pm_1}$=0.5($m_{\widetilde{g}}$+$m_{\widetilde{\chi}^0_1}$), $m_{\widetilde{\chi}^0_1}$ = 0 GeV
>1750	95	[28] AABOUD	18V	ATLS	jets+$\not{E}_T$, Tglu1C, $m_{\widetilde{\chi}^0_1}$ = 1 GeV, any $m_{\widetilde{\chi}^0_2}$ > 100 GeV
>2000	95	[29] SIRUNYAN	18AA	CMS	$\geq 1\gamma + \not{E}_T$, Tglu4A
>2100	95	[29] SIRUNYAN	18AA	CMS	$\geq 1\gamma + \not{E}_T$, Tglu4B
>1800	95	[30] SIRUNYAN	18AC	CMS	1ℓ+jets, Tglu3A, $m_{\widetilde{\chi}^0_1}$ <650 GeV
>1700	95	[30] SIRUNYAN	18AC	CMS	1ℓ+jets, Tglu3A,$m_{\widetilde{\chi}^0_1}$ <1040 GeV
>1900	95	[30] SIRUNYAN	18AC	CMS	1ℓ + jets, Tglu1B, $m_{\widetilde{\chi}^\pm_1}$ = ($m_{\widetilde{g}}$ + $m_{\widetilde{\chi}^0_1}$)/2, $m_{\widetilde{\chi}^0_1}$ < 300 GeV
>1250	95	[30] SIRUNYAN	18AC	CMS	1ℓ + jets, Tglu1B, $m_{\widetilde{\chi}^\pm_1}$ = ($m_{\widetilde{g}}$ + $m_{\widetilde{\chi}^0_1}$)/2, $m_{\widetilde{\chi}^0_1}$ < 950 GeV
>1610	95	[31] SIRUNYAN	18AL	CMS	$\geq 3\ell^\pm$ + jets + $\not{E}_T$, Tglu3A, $m_{\widetilde{\chi}^0_1}$ = 0 GeV
>1160	95	[31] SIRUNYAN	18AL	CMS	$\geq 3\ell^\pm$ + jets + $\not{E}_T$, Tglu1C, $m_{\widetilde{\chi}^0_2} = m_{\widetilde{\chi}^\pm_1}$ = ($m_{\widetilde{g}}$ + $m_{\widetilde{\chi}^0_1}$)/2, $m_{\widetilde{\chi}^0_1}$ = 0 GeV
>1500	95	[32] SIRUNYAN	18AR	CMS	$\ell^\pm\ell^\mp$ + jets + $\not{E}_T$, GMSB, Tglu4C, $m_{\widetilde{\chi}^0_1}$ = 100 GeV
>1770	95	[32] SIRUNYAN	18AR	CMS	$\ell^\pm\ell^\mp$ + jets + $\not{E}_T$, GMSB, Tglu4C, $m_{\widetilde{\chi}^0_1}$ = 1400 GeV
>1625	95	[33] SIRUNYAN	18AY	CMS	jets+$\not{E}_T$, Tglu1A, $m_{\widetilde{\chi}^0_1}$ = 0 GeV
>1825	95	[33] SIRUNYAN	18AY	CMS	jets+$\not{E}_T$, Tglu2A, $m_{\widetilde{\chi}^0_1}$ = 0 GeV
>1625	95	[33] SIRUNYAN	18AY	CMS	jets+$\not{E}_T$, Tglu3A, $m_{\widetilde{\chi}^0_1}$ = 0 GeV
>2040	95	[34] SIRUNYAN	18D	CMS	top quark (hadronically decaying) + jets + $\not{E}_T$, Tglu3A, $m_{\widetilde{\chi}^0_1}$ = 0 GeV
>1930	95	[34] SIRUNYAN	18D	CMS	top quark (hadronically decaying) + jets + $\not{E}_T$, Tglu3B, $m_{\widetilde{t}_1} - m_{\widetilde{\chi}^0_1}$ = 175 GeV, $m_{\widetilde{\chi}^0_1}$ = 200 GeV
>1690	95	[34] SIRUNYAN	18D	CMS	top quark (hadronically decaying) + jets + $\not{E}_T$, Tglu3C, $m_{\widetilde{t}_1} - m_{\widetilde{\chi}^0_1}$ = 20 GeV, $m_{\widetilde{\chi}^0_1}$ = 0 GeV
>1990	95	[34] SIRUNYAN	18D	CMS	top quark (hadronically decaying) + jets + $\not{E}_T$, Tglu3E, $m_{\widetilde{\chi}^\pm_1}$ = $m_{\widetilde{\chi}^0_1}$ + 5 GeV, $m_{\widetilde{\chi}^0_1}$ = 100 GeV
>2010	95	[35] SIRUNYAN	18M	CMS	$\geq 1\ H\ (\rightarrow\ bb) + \not{E}_T$, Tglu1I
>1825	95	[35] SIRUNYAN	18M	CMS	$\geq 1\ H\ (\rightarrow\ bb) + \not{E}_T$, Tglu1J
>1750	95	[36] AABOUD	17AJ	ATLS	same-sign $\ell^\pm\ell^\pm$ / 3 ℓ + jets + $\not{E}_T$, Tglu3A, $m_{\widetilde{\chi}^0_1}$ = 100 GeV
>1570	95	[37] AABOUD	17AJ	ATLS	same-sign $\ell^\pm\ell^\pm$ / 3 ℓ + jets + $\not{E}_T$, Tglu1E, $m_{\widetilde{\chi}^0_1}$ = 100 GeV
>1860	95	[38] AABOUD	17AJ	ATLS	same-sign $\ell^\pm\ell^\pm$ / 3 ℓ + jets + $\not{E}_T$, Tglu1G, $m_{\widetilde{\chi}^0_1}$ = 200 GeV
>2100	95	[39] AABOUD	17AR	ATLS	1ℓ+jets+$\not{E}_T$, Tglu1B, $m_{\widetilde{\chi}^0_1}$ = 0 GeV
>1740	95	[40] AABOUD	17AR	ATLS	1ℓ+jets+$\not{E}_T$, Tglu1E, $m_{\widetilde{\chi}^0_1}$ = 0 GeV
>1800	95	[41] AABOUD	17AY	ATLS	jets+$\not{E}_T$, Tglu3A, $m_{\widetilde{t}_1} - m_{\widetilde{\chi}^0_1}$ = 5 GeV
>1800	95	[42] AABOUD	17AZ	ATLS	$\geq$ 7 jets+$\not{E}_T$, large R-jets and/or b-jets, Tglu1E, $m_{\widetilde{\chi}^0_1}$ = 100 GeV

Downloaded from https://academic.oup.com/ptep/article/2022/8/083C01/6651666 by KIT Library user on 27 September 2022

>1540	95	[43] AABOUD	17AZ	ATLS	$\geq$ 7 jets+$\not{E}_T$, large R-jets and/or b-jets, Tglu3A, $m_{\widetilde{\chi}^0_1}$ = 0 GeV
>1340	95	[44] AABOUD	17N	ATLS	2 same-flavor, opposite-sign ℓ + jets + $\not{E}_T$, Tglu1H, $m_{\widetilde{\chi}^0_1}$ = 0 GeV
>1310	95	[45] AABOUD	17N	ATLS	2 same-flavor, opposite-sign ℓ + jets + $\not{E}_T$, Tglu1H, $m_{\widetilde{\chi}^0_2}$ = $(m_{\widetilde{g}}+m_{\widetilde{\chi}^0_1})/2$, $m_{\widetilde{\chi}^0_1}$ < 400 GeV
>1700	95	[46] AABOUD	17N	ATLS	2 same-flavor, opposite-sign ℓ + jets + $\not{E}_T$, Tglu1G, $m_{\widetilde{\chi}^0_1}$ ~ 1 GeV
>1400	95	[47] KHACHATRY...17		CMS	jets+$\not{E}_T$,Tglu1A,$m_{\widetilde{\chi}^0_1}$=200GeV
>1650	95	[47] KHACHATRY...17		CMS	jets+$\not{E}_T$,Tglu2A,$m_{\widetilde{\chi}^0_1}$=200 GeV
>1600	95	[47] KHACHATRY...17		CMS	jets+$\not{E}_T$,Tglu3A,$m_{\widetilde{\chi}^0_1}$=200GeV
>1550	95	[48] KHACHATRY...17AD		CMS	jets+b-jets+$\not{E}_T$, Tglu3A, $m_{\widetilde{\chi}^0_1}$ = 0 GeV
>1450	95	[49] KHACHATRY...17AD		CMS	jets+b-jets+$\not{E}_T$, Tglu3C, 200 < $m_{\widetilde{\chi}^0_1}$ < 400 GeV
>1570	95	[50] KHACHATRY...17AS		CMS	1ℓ, Tglu3A, $m_{\widetilde{\chi}^0_1}$ < 600 GeV
>1500	95	[50] KHACHATRY...17AS		CMS	1ℓ, Tglu3A, $m_{\widetilde{\chi}^0_1}$ < 775 GeV
>1400	95	[50] KHACHATRY...17AS		CMS	1ℓ, Tglu1B, $m_{\widetilde{\chi}^\pm_1}$ = $(m_{\widetilde{g}}$ + $m_{\widetilde{\chi}^0_1})/2$, $m_{\widetilde{\chi}^0_1}$ < 725 GeV
none 1050–1350	95	[50] KHACHATRY...17AS		CMS	1ℓ, Tglu1B, $m_{\widetilde{\chi}^\pm_1}$ = $(m_{\widetilde{g}}$ + $m_{\widetilde{\chi}^0_1})/2$, $m_{\widetilde{\chi}^0_1}$ < 850 GeV
>1175	95	[51] KHACHATRY...17AW		CMS	$\geq 3\ell^\pm$, 2 jets, Tglu3A, $m_{\widetilde{\chi}^0_1}$ = 0 GeV
> 825	95	[51] KHACHATRY...17AW		CMS	$\geq 3\ell^\pm$, 2 jets, Tglu1C, $m_{\widetilde{\chi}^\pm_1}$ = $(m_{\widetilde{g}}$ + $m_{\widetilde{\chi}^0_1})/2$, $m_{\widetilde{\chi}^0_1}$ = 0 GeV
>1350	95	[52] KHACHATRY...17P		CMS	1 or more jets+$\not{E}_T$, Tglu1A, $m_{\widetilde{\chi}^0_1}$ = 0 GeV
>1545	95	[52] KHACHATRY...17P		CMS	1 or more jets+$\not{E}_T$, Tglu2A, $m_{\widetilde{\chi}^0_1}$ = 0 GeV
>1120	95	[52] KHACHATRY...17P		CMS	1 or more jets+$\not{E}_T$, Tglu3A, $m_{\widetilde{\chi}^0_1}$ = 0 GeV
>1300	95	[52] KHACHATRY...17P		CMS	1 or more jets+$\not{E}_T$, Tglu3D, $m_{\widetilde{\chi}^\pm_1}$ = $m_{\widetilde{\chi}^0_1}$ + 5 GeV, $m_{\widetilde{\chi}^0_1}$ = 100 GeV
> 780	95	[52] KHACHATRY...17P		CMS	1 or more jets+$\not{E}_T$, Tglu3B, $m_{\widetilde{t}_1}-m_{\widetilde{\chi}^0_1}$ = 175 GeV, $m_{\widetilde{\chi}^0_1}$ = 50 GeV
> 790	95	[52] KHACHATRY...17P		CMS	1 or more jets+$\not{E}_T$, Tglu3C, $m_{\widetilde{t}_1}-m_{\widetilde{\chi}^0_1}$ = 20 GeV, $m_{\widetilde{\chi}^0_1}$ = 0 GeV
>1650	95	[53] KHACHATRY...17V		CMS	2 γ + $\not{E}_T$, GGM, Tglu4B, any NLSP mass
>1900	95	[54] SIRUNYAN	17AF	CMS	1ℓ+jets+b-jets+$\not{E}_T$, Tglu3A, $m_{\widetilde{\chi}^0_1}$ = 0 GeV
>1600	95	[54] SIRUNYAN	17AF	CMS	1ℓ+jets+b-jets+$\not{E}_T$, Tglu3B, $m_{\widetilde{t}_1}$ − $m_{\widetilde{\chi}^0_1}$ = 175 GeV, $m_{\widetilde{\chi}^0_1}$ = 50 GeV
>1800	95	[55] SIRUNYAN	17AY	CMS	γ + jets+$\not{E}_T$, Tglu4B, $m_{\widetilde{\chi}^0_1}$ = 0 GeV
>1600	95	[55] SIRUNYAN	17AY	CMS	γ + jets+$\not{E}_T$, Tglu4A, $m_{\widetilde{\chi}^0_1}$ = 0 GeV
>1860	95	[56] SIRUNYAN	17AZ	CMS	$\geq$ 1 jets + $\not{E}_T$, Tglu1A, $m_{\widetilde{\chi}^0_1}$ = 0 GeV
>2025	95	[56] SIRUNYAN	17AZ	CMS	$\geq$ 1 jets+$\not{E}_T$, Tglu2A, $m_{\widetilde{\chi}^0_1}$ = 0 GeV
>1900	95	[56] SIRUNYAN	17AZ	CMS	$\geq$ 1 jets+$\not{E}_T$, Tglu3A, $m_{\widetilde{\chi}^0_1}$ = 0 GeV
>1825	95	[57] SIRUNYAN	17P	CMS	jets+$\not{E}_T$, Tglu1A, $m_{\widetilde{\chi}^0_1}$ = 0 GeV
>1950	95	[57] SIRUNYAN	17P	CMS	jets+$\not{E}_T$, Tglu2A, $m_{\widetilde{\chi}^0_1}$ = 0 GeV
>1960	95	[57] SIRUNYAN	17P	CMS	jets+$\not{E}_T$, Tglu3A, $m_{\widetilde{\chi}^0_1}$ = 0 GeV
>1800	95	[57] SIRUNYAN	17P	CMS	jets+$\not{E}_T$, Tglu1C, $m_{\widetilde{\chi}^\pm_1}$ = $m_{\widetilde{\chi}^0_2}$ = $(m_{\widetilde{g}}+m_{\widetilde{\chi}^0_1})/2$, $m_{\widetilde{\chi}^0_1}$ = 0 GeV
>1870	95	[57] SIRUNYAN	17P	CMS	jets+$\not{E}_T$, Tglu3D, $m_{\widetilde{\chi}^\pm_1}$ = $m_{\widetilde{\chi}^0_1}$ + 5 GeV, $m_{\widetilde{\chi}^0_1}$ = 1000 GeV
>1520	95	[58] SIRUNYAN	17S	CMS	same-sign $\ell^\pm\ell^\pm$ + jets + $\not{E}_T$, Tglu3A, $m_{\widetilde{\chi}^0_1}$ = 0 GeV
>1200	95	[58] SIRUNYAN	17S	CMS	same-sign $\ell^\pm\ell^\pm$ + jets + $\not{E}_T$, Tglu3D, $m_{\widetilde{\chi}^\pm_1}$ = $m_{\widetilde{\chi}^0_1}$ + 5 GeV, $m_{\widetilde{\chi}^0_1}$ = 100 GeV
>1370	95	[58] SIRUNYAN	17S	CMS	same-sign $\ell^\pm\ell^\pm$ + jets + $\not{E}_T$, Tglu3B, $m_{\widetilde{t}_1}-m_{\widetilde{\chi}^0_1}$ = 175 GeV, $m_{\widetilde{\chi}^0_1}$ = 50 GeV
>1180	95	[58] SIRUNYAN	17S	CMS	same-sign $\ell^\pm\ell^\pm$ + jets + $\not{E}_T$, Tglu3C, $m_{\widetilde{t}_1}-m_{\widetilde{\chi}^0_1}$ = 20 GeV, $m_{\widetilde{\chi}^0_1}$ = 0 GeV
>1280	95	[58] SIRUNYAN	17S	CMS	same-sign $\ell^\pm\ell^\pm$ + jets + $\not{E}_T$, Tglu1B, $m_{\widetilde{\chi}^\pm_1}$ = $(m_{\widetilde{g}}$ + $m_{\widetilde{\chi}^0_1})/2$, $m_{\widetilde{\chi}^0_1}$ = 0 GeV
>1300	95	[58] SIRUNYAN	17S	CMS	same-sign $\ell^\pm\ell^\pm$ + jets + $\not{E}_T$, Tglu1B, $m_{\widetilde{t}_1}-m_{\widetilde{\chi}^0_1}$ = 20 GeV, $m_{\widetilde{\chi}^0_1}$ = 100 GeV
>1570	95	[59] AABOUD	16AC	ATLS	$\geq$ 2 jets + 1 or 2 τ + $\not{E}_T$, Tglu1F, $m_{\widetilde{\chi}^0_1}$ = 100 GeV
>1460	95	[60] AABOUD	16J	ATLS	1 $\ell^\pm$ + $\geq$ 4 jets + $\not{E}_T$, Tglu3C, $m_{\widetilde{t}_1}-m_{\widetilde{\chi}^0_1}$ = 5 GeV
>1650	95	[61] AABOUD	16M	ATLS	2 γ + $\not{E}_T$, Tglu1D, any NLSP mass
>1510	95	[62] AABOUD	16N	ATLS	$\geq$ 4 jets + $\not{E}_T$, Tglu1A, $m_{\widetilde{\chi}^0_1}$ = 0 GeV
>1500	95	[63] AABOUD	16N	ATLS	$\geq$ 4 jets + $\not{E}_T$, Tglu1B, $m_{\widetilde{\chi}^\pm_1}$ = $(m_{\widetilde{g}}+m_{\widetilde{\chi}^0_1})/2$, $m_{\widetilde{\chi}^0_1}$=200GeV
>1780	95	[64] AAD	16AD	ATLS	0ℓ, $\geq$ 3 b-jets + $\not{E}_T$, Tglu2A, $m_{\widetilde{\chi}^0_1}$ < 800 GeV
>1760	95	[65] AAD	16AD	ATLS	1ℓ, $\geq$ 3 b-jets + $\not{E}_T$, Tglu3A, $m_{\widetilde{\chi}^0_1}$ < 700 GeV
>1300	95	[66] AAD	16BB	ATLS	2 same-sign/3ℓ + jets + $\not{E}_T$, Tglu1D, $m_{\widetilde{\chi}^0_1}$ < 600 GeV
>1100	95	[66] AAD	16BB	ATLS	2 same-sign/3ℓ + jets + $\not{E}_T$, Tglu1E, $m_{\widetilde{\chi}^0_1}$ < 300 GeV
>1200	95	[66] AAD	16BB	ATLS	2 same-sign /3ℓ + jets + $\not{E}_T$, Tglu3A, $m_{\widetilde{\chi}^0_1}$ < 600 GeV
>1600		[67] AAD	16BG	ATLS	1ℓ, $\geq$ 4 jets, $\not{E}_T$, Tglu1B, $m_{\widetilde{\chi}^\pm_1}$= $(m_{\widetilde{g}}$ + $m_{\widetilde{\chi}^0_1})/2$, $m_{\widetilde{\chi}^0_1}$= 100 GeV
>1400	95	[68] AAD	16V	ATLS	$\geq$ 7 to $\geq$ 10 jets + $\not{E}_T$, Tglu1E, $m_{\widetilde{\chi}^0_1}$ < 200 GeV
>1400	95	[68] AAD	16V	ATLS	$\geq$ 7 to $\geq$ 10 jets + $\not{E}_T$, pMSSM M_1 = 60 GeV, M_2 = 3 TeV, tanβ=10, μ < 0
>1100	95	[69] KHACHATRY...16AM		CMS	boosted W+b, Tglu3C, $m_{\widetilde{t}_1}$ − $m_{\widetilde{\chi}^0_1}$ <80GeV,$m_{\widetilde{\chi}^0_1}$ <400GeV
> 700	95	[69] KHACHATRY...16AM		CMS	boosted W+b, Tglu3B, $m_{\widetilde{t}_1}$ − $m_{\widetilde{\chi}^0_1}$=175 GeV, $m_{\widetilde{\chi}^0_1}$=0 GeV
>1050	95	[70] KHACHATRY...16BJ		CMS	same-sign $\ell^\pm\ell^\pm$, Tglu3A, $m_{\widetilde{\chi}^0_1}$ < 800 GeV
>1300	95	[70] KHACHATRY...16BJ		CMS	same-sign $\ell^\pm\ell^\pm$,Tglu3A,$m_{\widetilde{\chi}^0_1}$=0
>1140	95	[70] KHACHATRY...16BJ		CMS	same-sign $\ell^\pm\ell^\pm$, Tglu3B, $m_{\widetilde{t}}$ − $m_{\widetilde{\chi}^0_1}$ = 20 GeV, $m_{\widetilde{\chi}^0_1}$ = 0
> 850	95	[70] KHACHATRY...16BJ		CMS	same-sign $\ell^\pm\ell^\pm$, Tglu3B, $m_{\widetilde{t}}$− $m_{\widetilde{\chi}^0_1}$=20 GeV,$m_{\widetilde{\chi}^0_1}$ <700 GeV
> 950	95	[70] KHACHATRY...16BJ		CMS	same-sign $\ell^\pm\ell^\pm$, Tglu3D, $m_{\widetilde{\chi}^\pm_1}$ = $m_{\widetilde{\chi}^0_1}$ + 5 GeV
>1100	95	[70] KHACHATRY...16BJ		CMS	same-sign $\ell^\pm\ell^\pm$,Tglu1B,$m_{\widetilde{\chi}^\pm_1}$= 0.5($m_{\widetilde{g}}$+$m_{\widetilde{\chi}^0_1}$),$m_{\widetilde{\chi}^0_1}$ <400GeV
> 830	95	[70] KHACHATRY...16BJ		CMS	same-sign $\ell^\pm\ell^\pm$,Tglu1B,$m_{\widetilde{\chi}^\pm_1}$= 0.5($m_{\widetilde{g}}$+$m_{\widetilde{\chi}^0_1}$),$m_{\widetilde{\chi}^0_1}$ <700GeV
>1300	95	[70] KHACHATRY...16BJ		CMS	same-sign $\ell^\pm\ell^\pm$, Tglu3B, $m_{\widetilde{t}}$ − $m_{\widetilde{\chi}^0_1}$ = m_t, $m_{\widetilde{\chi}^0_1}$ = 0
>1050	95	[70] KHACHATRY...16BJ		CMS	same-sign $\ell^\pm\ell^\pm$, Tglu3B, $m_{\widetilde{t}}$ − $m_{\widetilde{\chi}^0_1}$ = m_t, $m_{\widetilde{\chi}^0_1}$ < 800 GeV
>1725	95	[71] KHACHATRY...16BS		CMS	jets + $\not{E}_T$, Tglu1A, $m_{\widetilde{\chi}^0_1}$ = 0
>1750	95	[71] KHACHATRY...16BS		CMS	jets + $\not{E}_T$, Tglu2A, $m_{\widetilde{\chi}^0_1}$ = 0
>1550	95	[71] KHACHATRY...16BS		CMS	jets + $\not{E}_T$, Tglu3A, $m_{\widetilde{\chi}^0_1}$ = 0
>1280	95	[72] KHACHATRY...16BY		CMS	opposite-sign $\ell^\pm\ell^\pm$, Tglu4C, $m_{\widetilde{\chi}^0_1}$ = 1000 GeV

Downloaded from https://academic.oup.com/ptep/article/2022/8/083C01/6651666 by KIT Library user on 27 September 2022

>1030	95	[72] KHACHATRY...16BY	CMS	opposite-sign $\ell^\pm\ell^\pm$, Tglu4C, $m_{\widetilde{\chi}^0_1}=0$ GeV
>1440	95	[73] KHACHATRY...16V	CMS	jets + $\not{E}_T$, Tglu1A, $m_{\widetilde{\chi}^0_1}=0$
>1600	95	[73] KHACHATRY...16V	CMS	jets + $\not{E}_T$, Tglu2A, $m_{\widetilde{\chi}^0_1}=0$
>1550	95	[73] KHACHATRY...16V	CMS	jets + $\not{E}_T$, Tglu3A, $m_{\widetilde{\chi}^0_1}=0$
>1450	95	[73] KHACHATRY...16V	CMS	jets + $\not{E}_T$, Tglu1C, $m_{\widetilde{\chi}^0_1}=0$
> 820	95	[74] AAD 15BG	ATLS	GGM, $\widetilde{g}\to q\overline{q}Z\widetilde{G}$, $\tan\beta=30$, $\mu>600$ GeV
> 850	95	[74] AAD 15BG	ATLS	GGM, $\widetilde{g}\to q\overline{q}Z\widetilde{G}$, $\tan\beta=1.5$, $\mu>450$ GeV
>1150	95	[75] AAD 15BV	ATLS	general RPC $\widetilde{g}$ decays, $m_{\widetilde{\chi}^0_1}<100$ GeV
> 700	95	[76] AAD 15BX	ATLS	$\widetilde{g}\to X\widetilde{\chi}^0_1$, independent of $m_{\widetilde{\chi}^0_1}$
>1290	95	[77] AAD 15CA	ATLS	$\geq 2\gamma+\not{E}_T$, GGM, bino-like NLSP, any NLSP mass
>1260	95	[77] AAD 15CA	ATLS	$\geq 1\gamma+b$-jets $+\not{E}_T$, GGM, higgsino-bino admix. NLSP and $\mu<0$, m(NLSP)>450 GeV
>1140	95	[77] AAD 15CA	ATLS	$\geq 1\gamma+$ jets $+\not{E}_T$, GGM, higgsino-bino admixture NLSP, all $\mu>0$
>1225	95	[78] KHACHATRY...15AF	CMS	$\widetilde{g}\to q\overline{q}\widetilde{\chi}^0_1$, $m_{\widetilde{\chi}^0_1}=0$
>1300	95	[78] KHACHATRY...15AF	CMS	$\widetilde{g}\to b\overline{b}\widetilde{\chi}^0_1$, $m_{\widetilde{\chi}^0_1}=0$
>1225	95	[78] KHACHATRY...15AF	CMS	$\widetilde{g}\to t\overline{t}\widetilde{\chi}^0_1$, $m_{\widetilde{\chi}^0_1}=0$
>1550	95	[78] KHACHATRY...15AF	CMS	CMSSM, $\tan\beta$=30, $m_{\widetilde{g}}=m_{\widetilde{q}}$, $A_0=-2\max(m_0,m_{1/2})$, $\mu>0$
>1150	95	[78] KHACHATRY...15AF	CMS	CMSSM, $\tan\beta$=30, $A_0=-2\max(m_0,m_{1/2})$, $\mu>0$
>1280	95	[79] KHACHATRY...15I	CMS	$\widetilde{g}\to t\overline{t}\widetilde{\chi}^0_1$, $m_{\widetilde{\chi}^0_1}=0$
>1310	95	[80] KHACHATRY...15X	CMS	$\widetilde{g}\to b\overline{b}\widetilde{\chi}^0_1$, $m_{\widetilde{\chi}^0_1}=100$ GeV
>1175	95	[80] KHACHATRY...15X	CMS	$\widetilde{g}\to t\overline{t}\widetilde{\chi}^0_1$, $m_{\widetilde{\chi}^0_1}=100$ GeV
>1330	95	[81] AAD 14AE	ATLS	jets + $\not{E}_T$, $\widetilde{g}\to q\overline{q}\widetilde{\chi}^0_1$ simplified model, $m_{\widetilde{\chi}^0_1}=0$ GeV
>1700	95	[81] AAD 14AE	ATLS	jets + $\not{E}_T$, mSUGRA/CMSSM, $m_{\widetilde{q}}=m_{\widetilde{g}}$
>1090	95	[82] AAD 14AG	ATLS	τ + jets + $\not{E}_T$, natural Gauge Mediation
>1600	95	[82] AAD 14AG	ATLS	τ + jets + $\not{E}_T$, mGMSB, $M_{mess}=250$ GeV, $N_5=3$, $\mu>0$, $C_{grav}=1$
> 640	95	[83] AAD 14X	ATLS	$\geq 4\ell^\pm$, $\widetilde{g}\to q\overline{q}\widetilde{\chi}^0_1$, $\widetilde{\chi}^0_1\to\ell^\pm\ell^\mp\widetilde{G}$, $\tan\beta=30$, GGM
>1000	95	[84] CHATRCHYAN 14AH	CMS	jets + $\not{E}_T$, $\widetilde{g}\to q\overline{q}\widetilde{\chi}^0_1$ simplified model, $m_{\widetilde{\chi}^0_1}=50$ GeV
>1350	95	[84] CHATRCHYAN 14AH	CMS	jets + $\not{E}_T$, CMSSM, $m_{\widetilde{g}}=m_{\widetilde{q}}$
>1000	95	[85] CHATRCHYAN 14AH	CMS	jets + $\not{E}_T$, $\widetilde{g}\to b\overline{b}\widetilde{\chi}^0_1$ simplified model, $m_{\widetilde{\chi}^0_1}=50$ GeV
>1000	95	[86] CHATRCHYAN 14AH	CMS	jets + $\not{E}_T$, $\widetilde{g}\to t\overline{t}\widetilde{\chi}^0_1$ simplified model, $m_{\widetilde{\chi}^0_1}=50$ GeV
>1160	95	[87] CHATRCHYAN 14I	CMS	jets + $\not{E}_T$, $\widetilde{g}\to q\overline{q}\widetilde{\chi}^0_1$ simplified model, $m_{\widetilde{\chi}^0_1}<100$ GeV
>1130	95	[87] CHATRCHYAN 14I	CMS	multijets + $\not{E}_T$, $\widetilde{g}\to t\overline{t}\widetilde{\chi}^0_1$ simplified model, $m_{\widetilde{\chi}^0_1}<100$ GeV
>1210	95	[87] CHATRCHYAN 14I	CMS	multijets + $\not{E}_T$, $\widetilde{g}\to q\overline{q}W/Z\widetilde{\chi}^0_1$ simplified model, $m_{\widetilde{\chi}^0_1}<100$ GeV
>1260	95	[88] CHATRCHYAN 14N	CMS	$1\ell^\pm$+ jets + $\geq 2b$-jets, $\widetilde{g}\to t\overline{t}\widetilde{\chi}^0_1$ simplified model, $m_{\widetilde{\chi}^0_1}$=0 GeV, $m_{\widetilde{t}}>m_{\widetilde{g}}$
		[89] CHATRCHYAN 14R	CMS	$\geq 3\ell^\pm$, $(\widetilde{g}/\widetilde{q})\to q\ell^\pm\ell^\mp\widetilde{G}$ simplified model, GMSB, slepton co-NLSP scenario
		[90] CHATRCHYAN 14R	CMS	$\geq 3\ell^\pm$, $\widetilde{g}\to t\overline{t}\widetilde{\chi}^0_1$ simplified model
• • • We do not use the following data for averages, fits, limits, etc. • • •				
>1500	95	[91] AABOUD 18BJ	ATLS	$\ell^\pm\ell^\mp$ + jets + $\not{E}_T$, Tglu1H, $m_{\widetilde{\chi}^0_1}=1$ GeV, any $m_{\widetilde{\chi}^0_2}$
>1770	95	[92] AABOUD 18V	ATLS	jets+$\not{E}_T$, Tglu1C-like, 1/2 BR per decay mode, any $m_{\widetilde{\chi}^0_2}-m_{\widetilde{\chi}^0_1}$, $m_{\widetilde{\chi}^0_1}=60$ GeV
>1600	95	[93] AABOUD 17AZ	ATLS	$\geq$ 7 jets+$\not{E}_T$, large R-jets and/or b-jets, pMSSM, $m_{\widetilde{\chi}^\pm_1}=200$ GeV
>1600	95	[94] KHACHATRY...16AY	CMS	$1\ell^\pm$ + jets + b-jets + $\not{E}_T$, Tglu3A, $m_{\widetilde{\chi}^0_1}=0$ GeV
> 500	95	[95] KHACHATRY...16BT	CMS	19-parameter pMSSM model, global Bayesian analysis, flat prior
	95	[96] AAD 15AB	ATLS	$\widetilde{g}\to\widetilde{S}g$, $c\tau=1$ m, $\widetilde{S}\to S\widetilde{G}$ and $S\to gg$, BR = 100%
	95	[97] AAD 15AI	ATLS	$\ell^\pm$ + jets + $\not{E}_T$
>1600	95	[75] AAD 15BV	ATLS	pMSSM, $M_1=60$ GeV, $m_{\widetilde{q}}<1500$ GeV
>1280	95	[75] AAD 15BV	ATLS	mSUGRA, $m_0>2$ TeV
>1100	95	[75] AAD 15BV	ATLS	via $\widetilde{\tau}$, natural GMSB, all $m_{\widetilde{\tau}}$
>1330	95	[75] AAD 15BV	ATLS	jets + $\not{E}_T$, $\widetilde{g}\to q\overline{q}\widetilde{\chi}^0_1$, $m_{\widetilde{\chi}^0_1}=1$ GeV
>1500	95	[75] AAD 15BV	ATLS	jets + $\not{E}_T$, $\widetilde{g}\to\widetilde{q}q$, $\widetilde{q}\to q\widetilde{\chi}^0_1$, $m_{\widetilde{\chi}^0_1}=1$ GeV
>1650	95	[75] AAD 15BV	ATLS	jets + $\not{E}_T$, $m_{\widetilde{g}}=m_{\widetilde{q}}$, $m_{\widetilde{\chi}^0_1}=1$ GeV
> 850	95	[75] AAD 15BV	ATLS	jets + $\not{E}_T$, $\widetilde{g}\to g\widetilde{\chi}^0_1$, $m_{\widetilde{\chi}^0_1}<550$ GeV
>1270	95	[75] AAD 15BV	ATLS	jets + $\not{E}_T$, $\widetilde{g}\to q\overline{q}W\widetilde{\chi}^0_1$, $m_{\widetilde{\chi}^0_1}=100$ GeV
>1150	95	[75] AAD 15BV	ATLS	jets + $\ell^\pm\ell^\pm$, $\widetilde{g}\to q\overline{q}WZ\widetilde{\chi}^0_1$, $m_{\widetilde{\chi}^0_1}=100$ GeV
>1320	95	[75] AAD 15BV	ATLS	jets + $\ell^\pm\ell^\pm$, $\widetilde{g}$ decays via sleptons, $m_{\widetilde{\chi}^0_1}=100$ GeV
>1220	95	[75] AAD 15BV	ATLS	τ, $\widetilde{q}$ decays via staus, $m_{\widetilde{\chi}^0_1}=100$ GeV
>1310	95	[75] AAD 15BV	ATLS	b-jets, $\widetilde{g}\to t\overline{t}\widetilde{\chi}^0_1$, $m_{\widetilde{\chi}^0_1}<400$ GeV
>1220	95	[75] AAD 15BV	ATLS	b-jets, $\widetilde{g}\to\widetilde{t}_1 t$ and $\widetilde{t}_1\to t\widetilde{\chi}^0_1$, $m_{\widetilde{T}_1}<1000$ GeV
>1180	95	[75] AAD 15BV	ATLS	b-jets, $\widetilde{g}\to\widetilde{t}_1 t$ and $\widetilde{t}_1\to b\widetilde{\chi}^\pm_1$, $m_{\widetilde{T}_1}<1000$ GeV, $m_{\widetilde{\chi}^0_1}=60$ GeV
>1260	95	[75] AAD 15BV	ATLS	b-jets, $\widetilde{g}\to\widetilde{t}_1 t$ and $\widetilde{g}\to c\widetilde{\chi}^0_1$
>1200	95	[75] AAD 15BV	ATLS	b-jets, $\widetilde{g}\to\widetilde{b}_1 b$ and $\widetilde{b}_1\to b\widetilde{\chi}^0_1$, $m_{\widetilde{b}_1}<1000$ GeV
>1250	95	[75] AAD 15BV	ATLS	b-jets, $\widetilde{g}\to b\overline{b}\widetilde{\chi}^0_1$, $m_{\widetilde{\chi}^0_1}<400$ GeV
none, 750–1250	95	[75] AAD 15BV	ATLS	b-jets, $\widetilde{g}$ decay via offshell $\widetilde{t}_1$ and $\widetilde{b}_1$, $m_{\widetilde{\chi}^0_1}<500$ GeV
>1100	95	[98] AAD 15CB	ATLS	jets, $\widetilde{g}\to qq\widetilde{\chi}^0_1$, $\widetilde{\chi}^0_1\to Z\widetilde{G}$, GGM, $m_{\widetilde{\chi}^0_1}=400$ GeV and $3<c\tau_{\widetilde{\chi}^0_1}<500$ mm
>1400	95	[98] AAD 15CB	ATLS	jets or $\not{E}_T$, $\widetilde{g}\to qq\widetilde{\chi}^0_1$, Split SUSY, $m_{\widetilde{\chi}^0_1}=100$ GeV and $15<c\tau<300$ mm
>1500	95	[98] AAD 15CB	ATLS	$\not{E}_T$, $\widetilde{g}\to qq\widetilde{\chi}^0_1$, Split SUSY, $m_{\widetilde{\chi}^0_1}=100$ GeV and $20<c\tau<250$ mm
		[99] KHACHATRY...15AD	CMS	$\ell^\pm\ell^\mp$ + jets + $\not{E}_T$, GMSB, $\widetilde{g}\to q\overline{q}Z\widetilde{G}$
>1300	95	[100] KHACHATRY...15AZ	CMS	$\geq 2\gamma$, ≥ 1 jet, (Razor), bino-like NLSP, $m_{\widetilde{\chi}^0_1}=375$ GeV
> 800	95	[100] KHACHATRY...15AZ	CMS	$\geq 1\gamma$, ≥ 2 jet, wino-like NLSP, $m_{\widetilde{\chi}^0_1}=375$ GeV
>1280	95	[101] AAD 14AX	ATLS	≥ 3 b-jets + $\not{E}_T$, CMSSM
>1250	95	[101] AAD 14AX	ATLS	≥ 3 b-jets + $\not{E}_T$, $\widetilde{g}\to\widetilde{b}_1 b\widetilde{\chi}^0_1$ simplified model, $\widetilde{b}_1\to b\widetilde{\chi}^0_1$, $m_{\widetilde{\chi}^0_1}=60$ GeV, $m_{\widetilde{b}_1}<900$ GeV
>1190	95	[101] AAD 14AX	ATLS	≥ 3 b-jets + $\not{E}_T$, $\widetilde{g}\to\widetilde{t}_1 t\widetilde{\chi}^0_1$ simplified model, $\widetilde{t}_1\to t\widetilde{\chi}^0_1$, $m_{\widetilde{\chi}^0_1}=60$ GeV, $m_{\widetilde{t}_1}<1000$ GeV
>1180	95	[101] AAD 14AX	ATLS	≥ 3 b-jets + $\not{E}_T$, $\widetilde{g}\to\widetilde{t}_1 t\widetilde{\chi}^0_1$ simplified model, $\widetilde{t}_1\to b\widetilde{\chi}^\pm_1$, $m_{\widetilde{\chi}^\pm_1}=2m_{\widetilde{\chi}^0_1}$, $m_{\widetilde{\chi}^0_1}$=60 GeV, $m_{\widetilde{t}_1}$<1000 GeV
>1250	95	[101] AAD 14AX	ATLS	≥ 3 b-jets + $\not{E}_T$, $\widetilde{g}\to b\overline{b}\widetilde{\chi}^0_1$ simplified model, $m_{\widetilde{\chi}^0_1}<400$ GeV
>1340	95	[101] AAD 14AX	ATLS	≥ 3 b-jets + $\not{E}_T$, $\widetilde{g}\to t\overline{t}\widetilde{\chi}^0_1$ simplified model, $m_{\widetilde{\chi}^0_1}<400$ GeV

Downloaded from https://academic.oup.com/ptep/article/2022/8/083C01/6651666 by KIT Library user on 27 September 2022

>1300	95	[101] AAD	14AX	ATLS	≥ 3 b-jets + $\not{E}_T$, $\widetilde{g} \rightarrow t\overline{t}\widetilde{\chi}_1^{\pm}$ simplified model, $\widetilde{\chi}_1^{\pm} \rightarrow f f' \widetilde{\chi}_1^0$, $m_{\widetilde{\chi}_1^{\pm}} - m_{\widetilde{\chi}_1^0} = 2$ GeV, $m_{\widetilde{\chi}_1^0} < 300$ GeV
> 950	95	[102] AAD	14E	ATLS	$\ell^{\pm}\ell^{\pm}(\ell^{\mp})$ + jets, $\widetilde{g} \rightarrow t\overline{t}\widetilde{\chi}_1^0$ simplified model
>1000	95	[102] AAD	14E	ATLS	$\ell^{\pm}\ell^{\pm}(\ell^{\mp})$ + jets, $\widetilde{g} \rightarrow t\widetilde{t}_1$ with $\widetilde{t}_1 \rightarrow b\widetilde{\chi}_1^{\pm}$ simplified model, $m_{\widetilde{t}_1} < 200$ GeV, $m_{\widetilde{\chi}_1^{\pm}} = 118$ GeV, $m_{\widetilde{\chi}_1^0} = 60$ GeV
> 640	95	[102] AAD	14E	ATLS	$\ell^{\pm}\ell^{\pm}(\ell^{\mp})$ + jets, $\widetilde{g} \rightarrow t\widetilde{t}_1$ with $\widetilde{t}_1 \rightarrow c\widetilde{\chi}_1^0$ simplified model, $m_{\widetilde{t}_1} = m_{\widetilde{\chi}_1^0} + 20$ GeV
> 860	95	[102] AAD	14E	ATLS	$\ell^{\pm}\ell^{\pm}(\ell^{\mp})$ + jets, $\widetilde{g} \rightarrow q q' \widetilde{\chi}_1^{\pm}$, $\widetilde{\chi}_1^{\pm} \rightarrow W^{(*)\pm}\widetilde{\chi}_1^0$ simplified model, $m_{\widetilde{\chi}_1^{\pm}} = 2\, m_{\widetilde{\chi}_1^0}$, $m_{\widetilde{\chi}_1^0} < 400$ GeV
>1040	95	[102] AAD	14E	ATLS	$\ell^{\pm}\ell^{\pm}(\ell^{\mp})$ + jets, $\widetilde{g} \rightarrow q q' \widetilde{\chi}_1^{\pm}$, $\widetilde{\chi}_1^{\pm} \rightarrow W^{(*)\pm}\widetilde{\chi}_2^0$, $\widetilde{\chi}_2^0 \rightarrow Z^{(*)}\widetilde{\chi}_1^0$ simplified model, $m_{\widetilde{\chi}_1^0} < 520$ GeV
>1200	95	[102] AAD	14E	ATLS	$\ell^{\pm}\ell^{\pm}(\ell^{\mp})$ + jets, $\widetilde{g} \rightarrow q q' \widetilde{\chi}_1^{\pm}/\widetilde{\chi}_2^0$, $\widetilde{\chi}_1^{\pm} \rightarrow \ell^{\pm}\nu\widetilde{\chi}_1^0$, $\widetilde{\chi}_2^0 \rightarrow \ell^{\pm}\ell^{\mp}(\nu\nu)\widetilde{\chi}_1^0$ simplified model
>1050	95	[103] CHATRCHYAN	14H	CMS	same-sign $\ell^{\pm}\ell^{\pm}$, $\widetilde{g} \rightarrow t\overline{t}\widetilde{\chi}_1^0$ simplified model, massless $\widetilde{\chi}_1^0$
> 900	95	[104] CHATRCHYAN	14H	CMS	same-sign $\ell^{\pm}\ell^{\pm}$, $\widetilde{g} \rightarrow q q' \widetilde{\chi}_1^{\pm}$, $\widetilde{\chi}_1^{\pm} \rightarrow W^{\pm}\widetilde{\chi}_1^0$ simplified model, $m_{\widetilde{\chi}_1^{\pm}} = 0.5\, m_{\widetilde{g}}$, massless $\widetilde{\chi}_1^0$
>1050	95	[105] CHATRCHYAN	14H	CMS	same-sign $\ell^{\pm}\ell^{\pm}$, $\widetilde{g} \rightarrow b\overline{t}\widetilde{\chi}_1^{\pm}$, $\widetilde{\chi}_1^{\pm} \rightarrow W^{\pm}\widetilde{\chi}_1^0$ simplified model, $m_{\widetilde{\chi}_1^{\pm}} = 300$ GeV, $m_{\widetilde{\chi}_1^0} = 50$ GeV

[1] AAD 21AK searched in 139 fb^{-1} of pp collisions at $\sqrt{s} = 13$ TeV for pair production of gluinos and squarks in events with a single isolated electron or muon, originating from the decay of a W boson, multiple jets and significant $\not{E}_T$. No significant excess above the Standard Model expectations is observed. Limits are set on the gluino mass in the Tglu1B simplified model and on the squark mass in the Tsqk3 simplified model, see their Figure 8.

[2] AAD 21L searched in 139 fb^{-1} of pp collisions at $\sqrt{s} = 13$ TeV for pair production of gluinos and squarks in events with jets, large missing transverse momentum but no electrons or muons. No significant excess above the Standard Model expectations is observed. Limits are set on the gluino mass in the Tglu1A and Tglu1B simplified models, on the squark mass in the Tsqk1 and Tsqk3 simplified models and in a simplified model for gluino-squark production, see their Figures 13-17.

[3] AAD 21X searched in 139 fb^{-1} of pp collisions at $\sqrt{s} = 13$ TeV for the decay of long-lived R-hadrons stopped by the calorimeter, producing high-momentum jets resulting in large out-of-time energy deposits in the calorimeters. These decays are detected using data collected during periods in the LHC bunch structure when collisions are absent. No significant excess above the predicted background is observed. Limits are set on the R-hadron mass in the Tglu1A simplified model ad a function of the R-hadron lifetime, for different $m_{\widetilde{\chi}_1^0}$. See Figures 9, 10.

[4] SIRUNYAN 21AD searched in 137 fb^{-1} of pp collisions at $\sqrt{s} = 13$ TeV for supersymmetry in events with multiple jets, no leptons, and large $\not{E}_T$. No significant excess above the Standard Model expectations is observed. Limits are set on the top squark mass in the simplified models Tstop1, Tstop2 with $m_{\widetilde{\chi}_1^{\pm}} = (m_{\widetilde{t}} + m_{\widetilde{\chi}_1^0})/2$, and a 50:50 mixture of these with $m_{\widetilde{\chi}_1^{\pm}} - m_{\widetilde{\chi}_1^0} = 5$ GeV, see their Figure 8. Limits are also set on the top squark mass for 10 GeV $< m_{\widetilde{t}} - m_{\widetilde{\chi}_1^{\pm}} < 80$ GeV in the simplified models Tstop2, Tstop 3, and Tstop4, see their Figure 9. For indirect top squark production, limits are set on the gluino mass in the simplified models Tglu3A, Tglu3C with $m_{\widetilde{t}} - m_{\widetilde{\chi}_1^0} = 20$ GeV, and Tglu3D with $m_{\widetilde{\chi}_1^{\pm}} - m_{\widetilde{\chi}_1^0} = 5$ GeV, see their Figure 10.

[5] SIRUNYAN 21M searched in 137 fb^{-1} of pp collisions at $\sqrt{s} = 13$ TeV for supersymmetry in events with two opposite-sign same-flavor leptons (electrons, muons) and $\not{E}_T$. No significant excess above the Standard Model expectations is observed. Limits are set on the gluino mass in the simplified model Tglu4C, see their Figure 10, on the $\widetilde{\chi}_2^0$ and $\widetilde{\chi}_1^{\pm}$ mass in Tchi1n2Fa, see their Figure 11, on the $\widetilde{\chi}_1^0$ mass in Tn1n1C and Tn1n1B for $m_{\widetilde{\chi}_2^0} = m_{\widetilde{\chi}_1^{\pm}} = m_{\widetilde{\chi}_1^0}$, see their Figure 12. Limits are also set on the light squark mass for the simplified model Tsqk2A, on the sbottom mass in Tsbot3, see their Figure 13, and on the slepton mass in direct electroweak pair production of mass-degenerate left- and right-handed sleptons (selectrons and smuons), see their Figure 14.

[6] AAD 20AL searched in 139 fb^{-1} of pp collisions at $\sqrt{s} = 13$ TeV for events with 8 or more jets and moderate missing transverse momentum. The selection makes requirements according to the number of b-tagged jets and the scalar sum of masses of large-radius jets. No significant excess above the Standard Model expectations is observed. Limits up to about 2 TeV are set on the gluino mass in Tglu1E simplified model. Limits up to about 1.8 TeV are set on the gluino mass in Tglu3A simplified model. See their Fig. 10(a).

[7] AAD 20V searched in 139 fb^{-1} of pp collisions at $\sqrt{s} = 13$ TeV in final states with same-sign charged leptons (electrons or muons) and jets. No significant excess over the Standard Model expectation is observed. In the Tglu1E model, considering off-shell intermediate W and Z bosons in the decay chains, gluino masses are excluded at 95% C.L. up to 1600 GeV for neutralino masses of 100 GeV or above (up to 1000 GeV). See their Fig. 7(a).

[8] SIRUNYAN 20B searched in 35.9 fb^{-1} of pp collisions at $\sqrt{s} = 13$ TeV for events with at least one photon and large $\not{E}_T$. No significant excess above the Standard Model expectations is observed. Limits are set on chargino masses in a general gauge-mediated SUSY breaking (GGM) scenario Tchi1n12-GGM, see Figure 4. Limits are also set on the NLSP mass in the Tchi1chi1F and Tchi1chi1G simplified models, see their Figure 5. Finally, limits are set on the gluino mass in the Tglu4A simplified model, see Figure 6.

[9] SIRUNYAN 20BJ searched in 137 fb^{-1} of pp collisions at $\sqrt{s} = 13$ TeV for events containing two hadronically decaying, highly energetic Z bosons and large $\not{E}_T$. No significant excess above the Standard Model expectations is observed. Limits are set on the gluino mass in the Tglu1H simplified model, see their Figure 9.

[10] SIRUNYAN 20E searched in 137 fb^{-1} of pp collisions at $\sqrt{s} = 13$ TeV for events with a single electron or muon and multiple jets, including at least one identified as originating from a b-quark, and large $\not{E}_T$. No significant excess above the Standard Model expectations is observed. Limits are set on the gluino mass in the Tglu3A simplified model, see their Fig. 10, and the Tglu3C simplified model, see their Fig. 11.

[11] SIRUNYAN 20T searched in 137 fb^{-1} of pp collisions at $\sqrt{s} = 13$ TeV for events with at least two jets, and two isolated same-sign or three or more charged leptons (electrons or muons). No significant excess above the Standard Model expectations is observed. Limits are set on the gluino mass in the Tglu3A, Tglu3B, Tglu3C and Tglu3D simplified models, see their Figure 7, and in the Tglu1C and Tglu1B simplified models, see their Figures 8 and 9. Limits are also set on the sbottom mass in the Tsbot2 simplified model, see their Figure 10, and on the stop mass in the Tstop7 simplified model, see their Figure 11. Finally, limits are set on the gluino mass in RPV simplified models where the gluino decays either via $\widetilde{g} \rightarrow q q \overline{q}\overline{q} + e/\mu/\tau$ or via $\widetilde{g} \rightarrow t b s$, see Figure 12.

[12] AABOUD 19I searched in 36.1 fb^{-1} of pp collisions at $\sqrt{s} = 13$ TeV in final states with hadronic jets, 1 or two hadronically decaying τ and $\not{E}_T$. In Tglu1F, gluino masses are excluded at 95% C.L. up to 2000 GeV for neutralino masses of 100 GeV or below. Neutralino masses up to 1000 GeV are excluded for all gluino masses below 1400 GeV. See their Fig. 9. Limits are also presented in the context of Gauge-Mediated Symmetry Breaking models: in this case, values of Λ below 110 TeV are excluded at the 95% CL for all values of $\tan\beta$ in the range $2 < \tan\beta < 60$, see their Fig 10.

[13] SIRUNYAN 19AG searched in 35.9 fb^{-1} of pp collisions at $\sqrt{s} = 13$ TeV for events with two photons and large $\not{E}_T$. No significant excess above the Standard Model expectations is observed. Limits are set on the gluino mass in the Tglu4B simplified model and on the squark mass in the Tsqk4B simplified model, see their Figure 3.

[14] SIRUNYAN 19AU searched in 35.9 fb^{-1} of pp collisions at $\sqrt{s} = 13$ TeV for events with at last one photon, jets, some of which are identified as originating from b-quarks, and large $\not{E}_T$. No significant excess above the Standard Model expectations is observed. In the framework of GMSB, limits are set on the gluino mass in the Tglu4C, Tglu4D and Tglu4E simplified models, and on the top squark mass in the Tstop13 simplified model, see their Figure 5.

[15] SIRUNYAN 19CE searched in 35.9 fb^{-1} of pp collisions at $\sqrt{s} = 13$ TeV for new particles decaying to a photon and two gluons in events with at least three large-radius jets of which two have substructure and are composed of a photon and two gluons. No statistically significant excess is observed above the SM background expectation. Upper limits at 95% confidence level on the cross section for gluino pair production are set, using a simplified Tglu1A-like stealth SUSY model. Gluino masses up to 1500-1700 GeV are excluded, depending on the neutralino mass, with the highest exclusion set for $m_{\widetilde{\chi}_1^0} = 200$ GeV. See their Fig 4.

[16] SIRUNYAN 19CH searched in 137 fb^{-1} of pp collisions at $\sqrt{s} = 13$ TeV for events containing multiple jets and large $\not{E}_T$. No significant excess above the Standard Model expectations is observed. Limits are set on the gluino mass in the Tglu1A, Tglu1C, Tglu2A and Tglu3A simplified models, see their Figure 13. Limits are also set on squark, sbottom and stop masses in the Tsqk1, Tsbot1, Tstop1 simplified models, see their Figure 14.

[17] SIRUNYAN 19K searched in 35.9 fb^{-1} of pp collisions at $\sqrt{s} = 13$ TeV for events with a photon, an electron or muon, and large $\not{E}_T$. No significant excess above the Standard Model expectations is observed. In the framework of GMSB, limits are set on the chargino and neutralino mass in the Tchi1n1A simplified model, see their Figure 6. Limits are also set on the gluino mass in the Tglu4A simplified model, and on the squark mass in the Tsqk4A simplified model, see their Figure 7.

[18] SIRUNYAN 19S searched in 35.9 fb^{-1} of pp collisions at $\sqrt{s} = 13$ TeV for events with zero or one charged leptons, jets and $\not{E}_T$. The razor variables (M_R and R^2) are used to categorize the events. No significant excess above the Standard Model expectations is observed. Limits are set on the gluino mass in the Tglu3A and Tglu3C simplified models, see Figures 22 and 23, and on the stop mass in the Tstop1 simplified model, see their Figure 24.

[19] AABOUD 18AR searched in 36.1 fb^{-1} of pp collisions at $\sqrt{s} = 13$ TeV for gluino pair production in events containing large missing transverse momentum and several energetic jets, at least three of which must be identified as originating from b-quarks. No excess is found above the predicted background. In Tglu3A models, gluino masses of less than 1.97 TeV are excluded for $m_{\widetilde{\chi}_1^0}$ below 300 GeV, see their Fig. 10(a). Interpretations are also provided for scenarios where Tglu3A modes mix with Tglu2A and Tglu3D, see their Fig 11.

[20] AABOUD 18AR searched in 36.1 fb^{-1} of pp collisions at $\sqrt{s} = 13$ TeV for gluino pair production in events containing large missing transverse momentum and several energetic jets, at least three of which must be identified as originating from b-quarks. No excess is found above the predicted background. In Tglu2A models, gluino masses of less than 1.92 TeV are excluded for $m_{\widetilde{\chi}_1^0}$ below 600 GeV, see their Fig. 10(b). Interpretations are also provided for scenarios where Tglu2A modes mix with Tglu3A and Tglu3D, see their Fig 11.

[21] AABOUD 18AS searched for in 36.1 fb^{-1} of pp collisions at $\sqrt{s} = 13$ TeV for gluino pair production in the context of AMSB or phenomenological MSSM scenarios with wino-like

Downloaded from https://academic.oup.com/ptep/article/2022/8/083C01/6651666 by KIT Library user on 27 September 2022

LSP and long-lived charginos. Events with a disappearing track due to a low-momentum pion accompanied by at least four jets are considered. No significant excess above the Standard Model expectations is observed. Exclusion limits are set at 95% confidence level on the mass of gluinos for different chargino lifetimes. Gluino masses up to 1.65 TeV are excluded assuming a chargino mass of 460 GeV and lifetime of 0.2 ns, corresponding to a mass-splitting between the charged and neutral wino of around 160 MeV. See their Fig. 9.

[22] AABOUD 18BJ searched in 36.1 fb^{-1} of pp collisions at $\sqrt{s}$ = 13 TeV in events with two opposite-sign charged leptons (electrons and muons), jets and missing transverse momentum, with various requirements to be sensitive to signals with different kinematic endpoint values in the dilepton invariant mass distribution. The data are found to be consistent with the SM expectation. Results are interpreted in the Tglu1G model: gluino masses below 1850 GeV are excluded for $m_{\widetilde{\chi}^0_1}$ = 100 GeV, see their Fig. 12(a).

[23] AABOUD 18BJ searched in 36.1 fb^{-1} of pp collisions at $\sqrt{s}$ = 13 TeV in events with two opposite-sign charged leptons (electrons and muons), jets and missing transverse momentum, with various requirements to be sensitive to signals with different kinematic endpoint values in the dilepton invariant mass distribution. The data are found to be consistent with the SM expectation. Results are interpreted in the Tglu1H model: gluino masses below 1650 GeV are excluded for $m_{\widetilde{\chi}^0_1}$ = 100 GeV, see their Fig. 13(a).

[24] AABOUD 18U searched in 36.1 fb^{-1} of pp collisions at $\sqrt{s}$ = 13 TeV in events with at least one isolated photon, possibly jets and significant transverse momentum targeting generalised models of gauge-mediated SUSY breaking. No significant excess of events is observed above the SM prediction. Results for the di-photon channel are interpreted in terms of lower limits on the masses of gluinos in Tglu4B models, which reach as high as 2.3 TeV. Gluinos with masses below 2.15 TeV are excluded for any NLSP mass, see their Fig. 8.

[25] AABOUD 18U searched in 36.1 fb^{-1} of pp collisions at $\sqrt{s}$ = 13 TeV in events with at least one isolated photon, possibly jets and significant transverse momentum targeting generalised models of gauge-mediated SUSY breaking. No significant excess of events is observed above the SM prediction. Results of the γ + jets + $\not{E}_T$ channel are interpreted in terms of lower limits on the masses of gluinos in GGM higgsino-bino models (mix of Tglu4B and Tglu4C), which reach as high as 2050 GeV. Gluino masses below 1600 GeV are excluded for any NLSP mass provided that $m_{\widetilde{g}}-m_{\widetilde{\chi}^0_1}$ > 50 GeV. See their Fig. 11.

[26] AABOUD 18V searched in 36.1 fb^{-1} of pp collisions at $\sqrt{s}$ = 13 TeV in events with no charged leptons, jets and missing transverse momentum. The data are found to be consistent with the SM expectation. Results are interpreted in the Tglu1A model: gluino masses below 2030 GeV are excluded for massless LSP, see their Fig. 13(b).

[27] AABOUD 18V searched in 36.1 fb^{-1} of pp collisions at $\sqrt{s}$ = 13 TeV in events with no charged leptons, jets and missing transverse momentum. The data are found to be consistent with the SM expectation. Results are interpreted in the Tglu1B model. Assuming that $m_{\widetilde{\chi}^\pm_1}$ = 0.5 ($m_{\widetilde{g}}$ + $m_{\widetilde{\chi}^0_1}$), gluino masses below 1980 GeV are excluded for massless LSP, see their Fig. 14(c). Exclusions are also shown assuming $m_{\widetilde{\chi}^0_1}$ = 60 GeV, see their Fig. 14(d).

[28] AABOUD 18V searched in 36.1 fb^{-1} of pp collisions at $\sqrt{s}$ = 13 TeV in events with no charged leptons, jets and missing transverse momentum. The data are found to be consistent with the SM expectation. Results are interpreted in the Tglu1E model: gluino masses below 1750 GeV are excluded for $m_{\widetilde{\chi}^0_1}$ = 1 GeV and any $m_{\widetilde{\chi}^0_2}$ above 100 GeV, see their Fig. 15. Gluino mass exclusion up to 2 TeV is found for $m_{\widetilde{\chi}^0_2}$ = 1 TeV.

[29] SIRUNYAN 18AA searched in 35.9 fb^{-1} of pp collisions at $\sqrt{s}$ = 13 TeV for events with at least one photon and large $\not{E}_T$. No significant excess above the Standard Model expectations is observed. Limits are set on wino masses in a general gauge-mediated SUSY breaking (GGM) scenario with bino-like $\widetilde{\chi}^0_1$ and wino-like $\widetilde{\chi}^\pm_1$ and $\widetilde{\chi}^0_2$, see Figure 7. Limits are also set on the NLSP mass in the Tchi1n1A and Tchi1chi1A simplified models, see their Figure 8. Finally, limits are set on the gluino mass in the Tglu4A and Tglu4B simplified models, see their Figure 9, and on the squark mass in the Tskq4A and Tsqk4B simplified models, see their Figure 10.

[30] SIRUNYAN 18AC searched in 35.9 fb^{-1} of pp collisions at $\sqrt{s}$ = 13 TeV for events with a single electron or muon and multiple jets. No significant excess above the Standard Model expectations is observed. Limits are set on the gluino mass in the Tglu3A and Tglu1B simplified models, see their Figure 5.

[31] SIRUNYAN 18AL searched in 35.9 fb^{-1} of pp collisions at $\sqrt{s}$ = 13 TeV for events with at least three charged leptons, in any combination of electrons and muons, jets and significant $\not{E}_T$. No significant excess above the Standard Model expectations is observed. Limits are set on the gluino mass in the Tglu3A and Tglu1C simplified models, see their Figure 5. Limits are also set on the sbottom mass in the Tsbot2 simplified model, see their Figure 6, and on the stop mass in the Tstop7 simplified model, see their Figure 7.

[32] SIRUNYAN 18AR searched in 35.9 fb^{-1} of pp collisions at $\sqrt{s}$ = 13 TeV for events containing two opposite-charge, same-flavour leptons (electrons or muons), jets and $\not{E}_T$. No significant excess above the Standard Model expectations is observed. Limits are set on the gluino mass in the Tglu4C simplified model, see their Figure 7. Limits are also set on the chargino/neutralino mass in the Tchi1n2F simplified models, see their Figure 8, and on the higgsino mass in the Tn1n1B and Tn1n1C simplified models, see their Figure 9. Finally, limits are set on the sbottom mass in the Tsbot3 simplified model, see their Figure 10.

[33] SIRUNYAN 18AY searched in 35.9 fb^{-1} of pp collisions at $\sqrt{s}$ = 13 TeV for events containing one or more jets and significant $\not{E}_T$. No significant excess above the Standard Model expectations is observed. Limits are set on the gluino mass in the Tglu1A, Tglu2A and Tglu3A simplified models, see their Figure 3. Limits are also set on squark, sbottom and stop masses in the Tsqk1, Tsbot1, Tstop1 and Tstop4 simplified models, see their Figure 3. Finally, limits are set on long-lived gluino masses in a Tglu1A simplified model where the gluino is metastable or long-lived with proper decay lengths in the range 10^{-3} mm < cτ < 10^5 mm, see their Figure 4.

[34] SIRUNYAN 18D searched in 35.9 fb^{-1} of pp collisions at $\sqrt{s}$ = 13 TeV for events containing identified hadronically decaying top quarks, no leptons, and $\not{E}_T$. No significant excess above the Standard Model expectations is observed. Limits are set on the stop mass in the Tstop1 simplified model, see their Figure 8, and on the gluino mass in the Tglu3A, Tglu3B, Tglu3C and Tglu3E simplified models, see their Figure 9.

[35] SIRUNYAN 18M searched in 35.9 fb^{-1} of pp collisions at $\sqrt{s}$ = 13 TeV for events with one or more high-momentum Higgs bosons, decaying to pairs of b-quarks, and large $\not{E}_T$. No significant excess above the Standard Model expectations is observed. Limits are set on the gluino mass in the Tglu1I and Tglu1J simplified models, see their Figure 3.

[36] AABOUD 17AJ searched in 36.1 fb^{-1} of pp collisions at $\sqrt{s}$ = 13 TeV for events with two same-sign or three leptons, jets and large missing transverse momentum. No significant excess above the Standard Model expectations is observed. Limits up to 1.75 TeV are set on the gluino mass in Tglu3A simplified models in case of off-shell top squarks and for $m_{\widetilde{\chi}^0_1}$ = 100 GeV. See their Figure 4(a).

[37] AABOUD 17AJ searched in 36.1 fb^{-1} of pp collisions at $\sqrt{s}$ = 13 TeV for events with two same-sign or three leptons, jets and large missing transverse momentum. No significant excess above the Standard Model expectations is observed. Limits up to 1.57 TeV are set on the gluino mass in Tglu1E simplified models (2-step models) for $m_{\widetilde{\chi}^0_1}$ = 100 GeV. See their Figure 4(b).

[38] AABOUD 17AJ searched in 36.1 fb^{-1} of pp collisions at $\sqrt{s}$ = 13 TeV for events with two same-sign or three leptons, jets and large missing transverse momentum. No significant excess above the Standard Model expectations is observed. Limits up to 1.86 TeV are set on the gluino mass in Tglu1G simplified models for $m_{\widetilde{\chi}^0_1}$ = 200 GeV. See their Figure 4(c).

[39] AABOUD 17AR searched in 36.1 fb^{-1} of pp collisions at $\sqrt{s}$ = 13 TeV for events with one isolated lepton, at least two jets and large missing transverse momentum. No significant excess above the Standard Model expectations is observed. Limits up to 2.1 TeV are set on the gluino mass in Tglu1B simplified models, with x = ($m_{\widetilde{\chi}^\pm_1}-m_{\widetilde{\chi}^0_1}$) / ($m_{\widetilde{g}}-m_{\widetilde{\chi}^0_1}$) = 1/2.Similar limits are obtained for variable x and fixed neutralino mass, $m_{\widetilde{\chi}^0_1}$ = 60 GeV. See their Figure 13.

[40] AABOUD 17AR searched in 36.1 fb^{-1} of pp collisions at $\sqrt{s}$ = 13 TeV for events with one isolated lepton, at least two jets and large missing transverse momentum. No significant excess above the Standard Model expectations is observed. Limits up to 1.74 TeV are set on the gluino mass in Tglu1E simplified model. Limits up to 1.7 TeV are also set on pMSSM models leading to similar signal event topologies. See their Figure 13.

[41] AABOUD 17AY searched in 36.1 fb^{-1} of pp collisions at $\sqrt{s}$ = 13 TeV for events with at least four jets and large missing transverse momentum. No significant excess above the Standard Model expectations is observed. Limits up to 1.8 TeV are set on the gluino mass in Tglu3A simplified models assuming $m_{\widetilde{t}_1}$ − $m_{\widetilde{\chi}^0_1}$ = 5 GeV. See their Figure 13.

[42] AABOUD 17AZ searched in 36.1 fb^{-1} of pp collisions at $\sqrt{s}$ = 13 TeV for events with at least seven jets and large missing transverse momentum. Selected events are further classified based on the presence of large R-jets or b-jets and no leptons. No significant excess above the Standard Model expectations is observed. Limits up to 1.8 TeV are set on the gluino mass in Tglu1E simplified models. See their Figure 6b.

[43] AABOUD 17AZ searched in 36.1 fb^{-1} of pp collisions at $\sqrt{s}$ = 13 TeV for events with at least seven jets and large missing transverse momentum. Selected events are further classified based on the presence of large R-jets or b-jets and no leptons. No significant excess above the Standard Model expectations is observed. Limits up to 1.54 TeV are set on the gluino mass in Tglu3A simplified models. See their Figure 7a.

[44] AABOUD 17N searched in 14.7 fb^{-1} of pp collisions at $\sqrt{s}$ = 13 TeV in final states with 2 same-flavor, opposite-sign leptons (electrons or muons), jets and large missing transverse momentum. In Tglu1J models, gluino masses are excluded at 95% C.L. up to 1300 GeV for $m_{\widetilde{\chi}^0_1}$ = 0 GeV and $m_{\widetilde{\chi}^0_2}$ = 1100 GeV. See their Fig. 12 for exclusion limits as a function of $m_{\widetilde{\chi}^0_2}$. Limits are also presented assuming $m_{\widetilde{\chi}^0_2}$ = $m_{\widetilde{\chi}^0_1}$ + 100 GeV, see their Fig. 13.

[45] AABOUD 17N searched in 14.7 fb^{-1} of pp collisions at $\sqrt{s}$ = 13 TeV in final states with 2 same-flavor, opposite-sign leptons (electrons or muons), jets and large missing transverse momentum. In Tglu1H models, gluino masses are excluded at 95% C.L. up to 1310 GeV for $m_{\widetilde{\chi}^0_1}$ < 400 GeV and assuming $m_{\widetilde{\chi}^0_2}$ = ($m_{\widetilde{g}}$ + $m_{\widetilde{\chi}^0_1}$)/2. See their Fig. 15.

[46] AABOUD 17N searched in 14.7 fb^{-1} of pp collisions at $\sqrt{s}$ = 13 TeV in final states with 2 same-flavor, opposite-sign leptons (electrons or muons), jets and large missing transverse momentum. In Tglu1G models, gluino masses are excluded at 95% C.L. up to 1700 GeV for small $m_{\widetilde{\chi}^0_1}$. The results probe kinematic endpoints as small as $m_{\widetilde{\chi}^0_2}$ − $m_{\widetilde{\chi}^0_1}$ = ($m_{\widetilde{g}}$ − $m_{\widetilde{\chi}^0_1}$)/2 = 50 GeV. See their Fig. 14.

[47] KHACHATRYAN 17 searched in 2.3 fb^{-1} of pp collisions at $\sqrt{s}$ = 13 TeV for events containing four or more jets, no more than one lepton, and missing transverse momentum, using the razor variables (M_R and R^2) to discriminate between signal and background processes. No evidence for an excess over the expected background is observed. Limits are derived on the gluino mass in the Tglu1A, Tglu2A and Tglu3A simplified models, see Figs. 16 and 17. Also, assuming gluinos decay only via three-body processes involving third-generation quarks plus a neutralino/chargino, and assuming $m_{\widetilde{\chi}^\pm_1}$ = $m_{\widetilde{\chi}^0_1}$ + 5 GeV, a branching ratio-independent limit on the gluino mass is given, see Fig. 16.

[48] KHACHATRYAN 17AD searched in 2.3 fb^{-1} of pp collisions at $\sqrt{s}$ = 13 TeV for events containing at least four jets (including b-jets), missing transverse momentum and tagged top quarks. No evidence for an excess over the expected background is observed. Gluino masses up to 1550 GeV and neutralino masses up to 900 GeV are excluded at 95% C.L. See Fig. 13.

[49] KHACHATRYAN 17AD searched in 2.3 fb^{-1} of pp collisions at $\sqrt{s}$ = 13 TeV for events containing at least four jets (including b-jets), missing transverse momentum and tagged top quarks. No evidence for an excess over the expected background is observed. Gluino masses up to 1450 GeV and neutralino masses up to 820 GeV are excluded at 95% C.L. See Fig. 13.

[50] KHACHATRYAN 17AS searched in 2.3 fb^{-1} of pp collisions at $\sqrt{s}$ = 13 TeV for events with a single electron or muon and multiple jets. No significant excess above the Standard Model expectations is observed. Limits are set on the gluino mass in the Tglu3A and Tglu1B simplified models, see their Fig. 7.

[51] KHACHATRYAN 17AW searched in 2.3 fb^{-1} of pp collisions at $\sqrt{s}$ = 13 TeV for events with at least three charged leptons, in any combination of electrons and muons, and significant $\not{E}_T$. No significant excess above the Standard Model expectations is observed. Limits are set on the gluino mass in the Tglu3A and Tglu1C simplified models, and on the sbottom mass in the Tsbot2 simplified model, see their Figure 4.

[52] KHACHATRYAN 17P searched in 2.3 fb^{-1} of pp collisions at $\sqrt{s}$ = 13 TeV for events with one or more jets and large $\not{E}_T$. No significant excess above the Standard Model expectations is observed. Limits are set on the gluino mass in the Tglu1A, Tglu2A, Tglu3A, Tglu3B, Tglu3C and Tglu3D simplified models, see their Figures 7 and 8. Limits are also set on the squark mass in the Tsqk1 simplified model, see their Fig. 7, and on the sbottom mass in the Tsbot1 simplified model, see Fig. 8. Finally, limits are set on the stop mass in the Tstop1, Tstop3, Tstop4, Tstop6 and Tstop7 simplified models, see Fig. 8.

Downloaded from https://academic.oup.com/ptep/article/2022/8/083C01/6651666 by KIT Library user on 27 September 2022

[53] KHACHATRYAN 17V searched in 2.3 fb^{-1} of pp collisions at $\sqrt{s}$ = 13 TeV for events with two photons and large $\not{E}_T$. No significant excess above the Standard Model expectations is observed. Limits are set on the gluino and squark mass in the context of general gauge mediation models Tglu4B and Tsqk4, see their Fig. 4.

[54] SIRUNYAN 17AF searched in 35.9 fb^{-1} of pp collisions at $\sqrt{s}$ = 13 TeV for events with a single lepton (electron or muon), jets, including at least one jet originating from a b-quark, and large $\not{E}_T$. No significant excess above the Standard Model expectations is observed. Limits are set on the gluino mass in the Tglu3A and Tglu3B simplified models, see their Figure 2.

[55] SIRUNYAN 17AY searched in 35.9 fb^{-1} of pp collisions at $\sqrt{s}$ = 13 TeV for events with at least one photon, jets and large $\not{E}_T$. No significant excess above the Standard Model expectations is observed. Limits are set on the gluino mass in the Tglu4A and Tglu4B simplified models, and on the squark mass in the Tskq4A and Tsqk4B simplified models, see their Figure 6.

[56] SIRUNYAN 17AZ searched in 35.9 fb^{-1} of pp collisions at $\sqrt{s}$ = 13 TeV for events with one or more jets and large $\not{E}_T$. No significant excess above the Standard Model expectations is observed. Limits are set on the gluino mass in the Tglu1A, Tglu2A, Tglu3A simplified models, see their Figures 6. Limits are also set on the squark mass in the Tsqk1 simplified model (for single light squark and for 8 degenerate light squarks), on the sbottom mass in the Tsbot1 simplified model and on the stop mass in the Tstop1 simplified model, see their Fig. 7. Finally, limits are set on the stop mass in the Tstop2, Tstop4 and Tstop8 simplified models, see Fig. 8.

[57] SIRUNYAN 17P searched in 35.9 fb^{-1} of pp collisions at $\sqrt{s}$ = 13 TeV for events with multiple jets and large $\not{E}_T$. No significant excess above the Standard Model expectations is observed. Limits are set on the gluino mass in the Tglu1A, Tglu1C, Tglu2A, Tglu3A and Tglu3D simplified models, see their Fig. 12. Limits are also set on the squark mass in the Tsqk1 simplified model, on the stop mass in the Tstop1 simplified model, and on the sbottom mass in the Tsbot1 simplified model, see Fig. 13.

[58] SIRUNYAN 17S searched in 35.9 fb^{-1} of pp collisions at $\sqrt{s}$ = 13 TeV for events with two isolated same-sign leptons, jets, and large $\not{E}_T$. No significant excess above the Standard Model expectations is observed. Limits are set on the mass of the gluino mass in the Tglu3A, Tglu3B, Tglu3C, Tglu3D and Tglu1B simplified models, see their Figures 5 and 6, and on the sbottom mass in the Tsbot2 simplified model, see their Figure 6.

[59] AABOUD 16AC searched in 3.2 fb^{-1} of pp collisions at $\sqrt{s}$ = 13 TeV in final states with hadronic jets, 1 or two hadronically decaying τ and $\not{E}_T$. In Tglu1F, gluino masses are excluded at 95% C.L. up to 1570 GeV for neutralino masses of 100 GeV or below. Neutralino masses up to 700 GeV are excluded for all gluino masses between 800 GeV and 1500 GeV, while the strongest neutralino-mass exclusion of 750 GeV is achieved for gluino masses around 1400 GeV. See their Fig. 8. Limits are also presented in the context of Gauge-Mediated Symmetry Breaking models: in this case, values of Λ below 92 TeV are excluded at the 95% CL, corresponding to gluino masses below 2000 GeV. See their Fig. 9.

[60] AABOUD 16J searched in 3.2 fb^{-1} of pp collisions at $\sqrt{s}$ = 13 TeV in final states with one isolated electron or muon, hadronic jets, and $\not{E}_T$. Gluino-mediated pair production of stops with a nearly mass-degenerate stop and neutralino are targeted and gluino masses are excluded at 95% C.L. up to 1460 GeV. A 100% of stops decaying via charm + neutralino is assumed. The results are also valid in case of 4-body decays $\tilde{t}_1 \rightarrow f f' b \tilde{\chi}^0_1$. See their Fig. 8.

[61] AABOUD 16M searched in 3.2 fb^{-1} of pp collisions at $\sqrt{s}$ = 13 TeV for events with two photons, hadronic jets and $\not{E}_T$. No significant excess above the Standard Model expectations is observed. Exclusion limits at 95% C.L. are set on gluino masses in the general gauge-mediated SUSY breaking model (GGM), for bino-like NLSP. See their Fig. 3.

[62] AABOUD 16N searched in 3.2 fb^{-1} of pp collisions at $\sqrt{s}$ = 13 TeV for events containing hadronic jets, large $\not{E}_T$, and no electrons or muons. No significant excess above the Standard Model expectations is observed. Gluino masses below 1510 GeV are excluded at the 95% C.L. in a simplified model with only gluinos and the lightest neutralino. See their Fig. 7b.

[63] AABOUD 16N searched in 3.2 fb^{-1} of pp collisions at $\sqrt{s}$ = 13 TeV for events containing hadronic jets, large $\not{E}_T$, and no electrons or muons. No significant excess above the Standard Model expectations is observed. Gluino masses below 1500 GeV are excluded at the 95% C.L. in a simplified model with gluinos decaying via an intermediate $\tilde{\chi}^{\pm}_1$ to two quarks, a W boson and a $\tilde{\chi}^0_1$, for $m_{\tilde{\chi}^0_1}$ = 200 GeV. See their Fig 8.

[64] AAD 16AD searched in 3.2 fb^{-1} of pp collisions at $\sqrt{s}$ = 13 TeV for events containing several energetic jets, of which at least three must be identified as b-jets, large $\not{E}_T$ and no electrons or muons. No significant excess above the Standard Model expectations is observed. For $\tilde{\chi}^0_1$ below 800 GeV, gluino masses below 1780 GeV are excluded at 95% C.L. for gluinos decaying via bottom squarks. See their Fig. 7a.

[65] AAD 16AD searched in 3.2 fb^{-1} of pp collisions at $\sqrt{s}$ = 13 TeV for events containing several energetic jets, of which at least three must be identified as b-jets, large $\not{E}_T$ and one electron or muon. Large-radius jets with a high mass are also used to identify highly boosted top quarks. No significant excess above the Standard Model expectations is observed. For $\tilde{\chi}^0_1$ below 700 GeV, gluino masses below 1760 GeV are excluded at 95% C.L. for gluinos decaying via top squarks. See their Fig. 7b.

[66] AAD 16BB searched in 3.2 fb^{-1} of pp collisions at $\sqrt{s}$ = 13 TeV for events with exactly two same-sign leptons or at least three leptons, multiple hadronic jets, b-jets, and $\not{E}_T$. No significant excess over the Standard Model expectation is found. Exclusion limits at 95% C.L. are set on the gluino mass in various simplified models (Tglu1D, Tglu1E, Tglu3A). See their Figs. 4.a, 4.b, and 4.d.

[67] AAD 16BG searched in 3.2 fb^{-1} of pp collisions at $\sqrt{s}$ = 13 TeV in final states with one isolated electron or muon, hadronic jets, and $\not{E}_T$. The data agree with the SM background expectation in the six signal selections defined in the search, and the largest deviation is a 2.1 standard deviation excess. Gluinos are excluded at 95% C.L. up to 1600 GeV assuming they decay via the lightest chargino to the lightest neutralino as in the model Tglu1B for $m_{\tilde{\chi}^0_1}$=100 GeV, assuming $m_{\tilde{\chi}^{\pm}_1}$=$(m_{\tilde{g}} + m_{\tilde{\chi}^0_1})/2$. See their Fig. 6.

[68] AAD 16V searched in 3.2 fb^{-1} of pp collisions at $\sqrt{s}$ = 13 TeV for events with $\not{E}_T$ various hadronic jet multiplicities from $\geq$ 7 to $\geq$ 10 and with various b-jet multiplicity requirements. No significant excess over the Standard Model expectation is found. Exclusion limits at 95% C.L. are set on the gluino mass in one simplified model (Tglu1E) and a pMSSM-inspired model. See their Fig. 5.

[69] KHACHATRYAN 16AM searched in 19.7 fb^{-1} of pp collisions at $\sqrt{s}$ = 8 TeV for events with highly boosted W-bosons and b-jets, using the razor variables (M_R and R^2) to discriminate between signal and background processes. No significant excess above the Standard Model expectations is observed. Limits are set on the gluino mass in the Tglu3C and Tglu3B simplified models, see Fig. 12.

[70] KHACHATRYAN 16BJ searched in 2.3 fb^{-1} of pp collisions at $\sqrt{s}$ = 13 TeV for events with two isolated same-sign dileptons and jets in the final state. No significant excess above the Standard Model expectations is observed. Limits are set on the gluino mass in the following simplified models: Tglu3A and Tglu3D, see Fig. 4, Tglu3B and Tglu3C, see Fig. 5, and Tglu1B, see Fig. 7.

[71] KHACHATRYAN 16BS searched in 2.3 fb^{-1} of pp collisions at $\sqrt{s}$ = 13 TeV for events with at least one energetic jet , no isolated leptons, and significant $\not{E}_T$, using the transverse mass variable M_{T2} to discriminate between signal and background processes. No significant excess above the Standard Model expectations is observed. Limits are set on the gluino mass in the Tglu1A, Tglu2A and Tglu3A simplified models, see Fig. 10 and Table 3.

[72] KHACHATRYAN 16BY searched in 2.3 fb^{-1} of pp collisions at $\sqrt{s}$ = 13 TeV for events with two opposite-sign, same-flavour leptons, jets, and missing transverse momentum. No significant excess above the Standard Model expectations is observed. Limits are set on the gluino mass in the Tglu4C simplified model, see Fig. 4, and on sbottom masses in the Tsbot3 simplified model, see Fig. 5.

[73] KHACHATRYAN 16V searched in 2.3 fb^{-1} of pp collisions at $\sqrt{s}$ = 13 TeV for events with at least four energetic jets and significant $\not{E}_T$, no identified isolated electron or muon or charged track. No significant excess above the Standard Model expectations is observed. Limits are set on the gluino mass in the Tglu1A, Tglu1C, Tglu2A, and Tglu3A simplified models, see Fig. 8.

[74] AAD 15BG searched in 20.3 fb^{-1} of pp collisions at $\sqrt{s}$ = 8 TeV for events with jets, missing E_T, and two opposite-sign same flavor isolated leptons featuring either a kinematic edge, or a peak at the Z-boson mass, in the invariant mass spectrum. No evidence for a statistically significant excess over the expected SM backgrounds are observed and 95% C.L. exclusion limits are derived in a GGM simplified model of gluino pair production where the gluino decays into quarks, a Z-boson, and a massless gravitino LSP, see Fig. 12. Also, limits are set in simplified models with slepton/sneutrino intermediate states, see Fig. 13.

[75] AAD 15BV summarized and extended ATLAS searches for gluinos and first- and second-generation squarks in final states containing jets and missing transverse momentum, with or without leptons or b-jets in the $\sqrt{s}$ =8 TeV data set collected in 2012. The paper reports the results of new interpretations and statistical combinations of previously published analyses, as well as new analyses. Exclusion limits at 95% C.L. are set on the gluino mass in several R-parity conserving models, leading to a generalized constraint on gluino masses exceeding 1150 GeV for lightest supersymmetric particle masses below 100 GeV. See their Figs. 10, 19, 20, 21, 23, 25, 26, 29-37.

[76] AAD 15BX interpreted the results of a wide range of ATLAS direct searches for supersymmetry, during the first run of the LHC using the $\sqrt{s}$ =7 TeV and $\sqrt{s}$ = 8 TeV data set collected in 2012, within the wider framework of the phenomenological MSSM (pMSSM). The integrated luminosity was up to 20.3 fb^{-1}. From an initial random sampling of 500 million pMSSM points, generated from the 19-parameter pMSSM, a total of 310,327 model points with $\tilde{\chi}^0_1$ LSP were selected each of which satisfies constraints from previous collider searches, precision measurements, cold dark matter energy density measurements and direct dark matter searches. The impact of the ATLAS Run 1 searches on this space was presented, considering the fraction of model points surviving, after projection into two-dimensional spaces of sparticle masses. Good complementarity is observed between different ATLAS analyses, with almost all showing regions of unique sensitivity. ATLAS searches have good sensitivity at LSP mass below 800 GeV.

[77] AAD 15CA searched in 20.3 fb^{-1} of pp collisions at $\sqrt{s}$ = 8 TeV for events with one or more photons, hadronic jets or b-jets and $\not{E}_T$. No significant excess above the Standard Model expectations is observed. Limits are set on gluino masses in the general gauge-mediated SUSY breaking model (GGM), for bino-like or higgsino-bino admixtures NLSP, see Fig. 8, 10, 11

[78] KHACHATRYAN 15AF searched in 19.5 fb^{-1} of pp collisions at $\sqrt{s}$ = 8 TeV for events with at least two energetic jets and significant $\not{E}_T$, using the transverse mass variable M_{T2} to discriminate between signal and background processes. No significant excess above the Standard Model expectations is observed. Limits are set on the gluino mass in simplified models where the decay $\tilde{g} \rightarrow q\overline{q}\tilde{\chi}^0_1$ takes place with a branching ratio of 100%, see Fig. 13(a), or where the decay $\tilde{g} \rightarrow b\overline{b}\tilde{\chi}^0_1$ takes place with a branching ratio of 100%, see Fig. 13(b), or where the decay $\tilde{g} \rightarrow t\overline{t}\tilde{\chi}^0_1$ takes place with a branching ratio of 100%, see Fig. 13(c). See also Table 5. Exclusions in the CMSSM, assuming $\tan\beta$ = 30, $A_0 = -2\max(m_0, m_{1/2})$ and $\mu > 0$, are also presented, see Fig. 15.

[79] KHACHATRYAN 15I searched in 19.5 fb^{-1} of pp collisions at $\sqrt{s}$ = 8 TeV for events in which b-jets and four W-bosons are produced. Five individual search channels are combined (fully hadronic, single lepton, same-sign dilepton, opposite-sign dilepton, multilepton). No significant excess above the Standard Model expectations is observed. Limits are set on the gluino mass in a simplified model where the decay $\tilde{g} \rightarrow t\overline{t}\tilde{\chi}^0_1$ takes place with a branching ratio of 100%, see Fig. 5. Also a simplified model with gluinos decaying into on-shell top squarks is considered, see Fig. 6.

[80] KHACHATRYAN 15X searched in 19.3fb^{-1} of pp collisions at $\sqrt{s}$ = 8 TeV for events with at least two energetic jets, at least one of which is required to originate from a b quark, and significant $\not{E}_T$, using the razor variables (M_R) and R^2) to discriminate between signal and background processes. No significant excess above the Standard Model expectations is observed. Limits are set on the gluino mass in simplified models where the decay $\tilde{g} \rightarrow b\overline{b}\tilde{\chi}^0_1$ and the decay $\tilde{g} \rightarrow t\overline{t}\tilde{\chi}^0_1$ take place with branching ratios varying between 0, 50 and 100%, see Figs. 13 and 14.

[81] AAD 14AE searched in 20.3 fb^{-1} of pp collisions at $\sqrt{s}$ = 8 TeV for strongly produced supersymmetric particles in events containing jets and large missing transverse momentum, and no electrons or muons. No excess over the expected SM background is observed. Exclusion limits are derived in simplified models containing gluinos and squarks, see Figures 5, 6 and 7. Limits are also derived in the mSUGRA/CMSSM with parameters $\tan\beta$ = 30, $A_0 = -2\ m_0$ and $\mu > 0$, see their Fig. 8.

[82] AAD 14AG searched in 20.3 fb^{-1} of pp collisions at $\sqrt{s}$ = 8 TeV for events containing one hadronically decaying τ-lepton, zero or one additional light leptons (electrons or muons), jets and large missing transverse momentum. No excess of events above the expected level of Standard Model background was found. Exclusion limits at 95% C.L. are set in several SUSY scenarios. For an interpretation in the minimal GMSB model, see their Fig. 8. For an interpretation in the mSUGRA/CMSSM with parameters $\tan\beta$ = 30, $A_0 = -2\ m_0$ and $\mu > 0$, see their Fig. 9. For an interpretation in the framework of natural Gauge Mediation, see Fig. 10. For an interpretation in the bRPV scenario, see their Fig. 11.

[83] AAD 14X searched in 20.3 fb^{-1} of pp collisions at $\sqrt{s}$ = 8 TeV for events with at least four leptons (electrons, muons, taus) in the final state. No significant excess above the

Downloaded from https://academic.oup.com/ptep/article/2022/8/083C01/6651666 by KIT Library user on 27 September 2022

Standard Model expectations is observed. Limits are set on the gluino mass in a general gauge-mediation model (GGM) where the decay $\widetilde{g} \rightarrow q\overline{q}\widetilde{\chi}^0_1$, with $\widetilde{\chi}^0_1 \rightarrow \ell^{\pm}\ell^{\mp}\widetilde{G}$, takes place with a branching ratio of 100%, for two choices of $\tan\beta = 1.5$ and 30, see Fig. 11. Also some constraints on the higgsino mass parameter μ are discussed.

[84] CHATRCHYAN 14AH searched in 4.7 fb^{-1} of pp collisions at $\sqrt{s} = 7$ TeV for events with at least two energetic jets and significant $\not{E}_T$, using the razor variables (M_R and R^2) to discriminate between signal and background processes. No significant excess above the Standard Model expectations is observed. Limits are set on sbottom masses in simplified models where the decay $\widetilde{g} \rightarrow q\overline{q}\widetilde{\chi}^0_1$ takes place with a branching ratio of 100%, see Fig. 28. Exclusions in the CMSSM, assuming $\tan\beta = 10$, $A_0 = 0$ and $\mu > 0$, are also presented, see Fig. 26.

[85] CHATRCHYAN 14AH searched in 4.7 fb^{-1} of pp collisions at $\sqrt{s} = 7$ TeV for events with at least two energetic jets and significant $\not{E}_T$, using the razor variables (M_R and R^2) to discriminate between signal and background processes. A second analysis requires at least one of the jets to be originating from a b-quark. No significant excess above the Standard Model expectations is observed. Limits are set on sbottom masses in simplified models where the decay $\widetilde{g} \rightarrow b\overline{b}\widetilde{\chi}^0_1$ takes place with a branching ratio of 100%, see Figs. 28 and 29. Exclusions in the CMSSM, assuming $\tan\beta = 10$, $A_0 = 0$ and $\mu > 0$, are also presented, see Fig. 26.

[86] CHATRCHYAN 14AH searched in 4.7 fb^{-1} of pp collisions at $\sqrt{s} = 7$ TeV for events with at least two energetic jets and significant $\not{E}_T$, using the razor variables (M_R and R^2) to discriminate between signal and background processes. A second analysis requires at least one of the jets to be originating from a b-quark. No significant excess above the Standard Model expectations is observed. Limits are set on sbottom masses in simplified models where the decay $\widetilde{g} \rightarrow t\overline{t}\widetilde{\chi}^0_1$ takes place with a branching ratio of 100%, see Figs. 28 and 29. Exclusions in the CMSSM, assuming $\tan\beta = 10$, $A_0 = 0$ and $\mu > 0$, are also presented, see Fig. 26.

[87] CHATRCHYAN 14I searched in 19.5 fb^{-1} of pp collisions at $\sqrt{s} = 8$ TeV for events containing multijets and large $\not{E}_T$. No excess over the expected SM background is observed. Exclusion limits are derived in simplified models containing gluinos that decay via $\widetilde{g} \rightarrow q\overline{q}\widetilde{\chi}^0_1$ with a 100% branching ratio, see Fig. 7b, or via $\widetilde{g} \rightarrow t\overline{t}\widetilde{\chi}^0_1$ with a 100% branching ratio, see Fig. 7c, or via $\widetilde{g} \rightarrow q\overline{q}W/Z\widetilde{\chi}^0_1$, see Fig. 7d.

[88] CHATRCHYAN 14N searched in 19.3 fb^{-1} of pp collisions at $\sqrt{s} = 8$ TeV for events containing a single isolated electron or muon and multiple jets, at least two of which are identified as originating from a b-quark. No significant excesses over the expected SM backgrounds are observed. The results are interpreted in three simplified models of gluino pair production with subsequent decay into virtual or on-shell top squarks, where each of the top squarks decays in turn into a top quark and a $\widetilde{\chi}^0_1$, see Fig. 4. The models differ in which masses are allowed to vary.

[89] CHATRCHYAN 14R searched in 19.5 fb^{-1} of pp collisions at $\sqrt{s} = 8$ TeV for events with at least three leptons (electrons, muons, taus) in the final state. No significant excess above the Standard Model expectations is observed. Limits are set on the gluino mass in a slepton co-NLSP simplified model (GMSB) where the decay $\widetilde{g} \rightarrow q\ell^{\pm}\ell^{\mp}\widetilde{G}$ takes place with a branching ratio of 100%, see Fig. 8.

[90] CHATRCHYAN 14R searched in 19.5 fb^{-1} of pp collisions at $\sqrt{s} = 8$ TeV for events with at least three leptons (electrons, muons, taus) in the final state. No significant excess above the Standard Model expectations is observed. Limits are set on the gluino mass in a simplified model where the decay $\widetilde{g} \rightarrow t\overline{t}\widetilde{\chi}^0_1$ takes place with a branching ratio of 100%, see Fig. 11.

[91] AABOUD 18BJ searched in 36.1 fb^{-1} of pp collisions at $\sqrt{s} = 13$ TeV in events with two opposite-sign charged leptons (electrons and muons), jets and missing transverse momentum, with various requirements to be sensitive to signals with different kinematic endpoint values in the dilepton invariant mass distribution. The data are found to be consistent with the SM expectation. Results are interpreted in the Tglu1H model in case of $m_{\widetilde{\chi}^0_1} = 1$ GeV: for any $m_{\widetilde{\chi}^0_2}$, gluino masses below 1500 GeV are excluded, see their Fig. 14(a).

[92] AABOUD 18V searched in 36.1 fb^{-1} of pp collisions at $\sqrt{s} = 13$ TeV in events with no charged leptons, jets and missing transverse momentum. The data are found to be consistent with the SM expectation. Results are interpreted in a Tglu1C-like model, assuming 50% BR for each gluino decay mode. Gluino masses below 1770 GeV are excluded for any $m_{\widetilde{\chi}^0_2} - m_{\widetilde{\chi}^0_1}$ and $m_{\widetilde{\chi}^0_1} = 60$ GeV, see their Fig. 16(b).

[93] AABOUD 17AZ searched in 36.1 fb^{-1} of pp collisions at $\sqrt{s} = 13$ TeV for events with at least seven jets and large missing transverse momentum. Selected events are further classified based on the presence of large R-jets or b-jets and no leptons. No significant excess above the Standard Model expectations is observed. Limits are set for pMSSM models with $M_1 = 60$ GeV, $\tan(\beta) = 10$, $\mu < 0$ varying the soft-breaking parameters M_3 and μ. Gluino masses up to 1600 GeV are excluded for $m_{\widetilde{\chi}^{\pm}_1} = 200$ GeV. See their Figure 6a and text for details on the model.

[94] KHACHATRYAN 16AY searched in 2.3 fb^{-1} of pp collisions at $\sqrt{s} = 13$ TeV for events with one isolated high transverse momentum lepton (e or μ), hadronic jets of which at least one is identified as coming from a b-quark, and large $\not{E}_T$. No significant excess above the Standard Model expectations is observed. Limits are set on the gluino mass in the Tglu3A simplified model, see Fig. 10, and in the Tglu3B model, see Fig. 11.

[95] KHACHATRYAN 16BT performed a global Bayesian analysis of a wide range of CMS results obtained with data samples corresponding to 5.0 fb^{-1} of pp collisions at $\sqrt{s} =$ 7 TeV and in 19.5 fb^{-1} of pp collisions at $\sqrt{s} = 8$ TeV. The set of searches considered, both individually and in combination, includes those with all-hadronic final states, same-sign and opposite-sign dileptons, and multi-lepton final states. An interpretation was given in a scan of the 19-parameter pMSSM. No scan points with a gluino mass less than 500 GeV survived and 98% of models with a squark mass less than 300 GeV were excluded.

[96] AAD 15AB searched for the decay of neutral, weakly interacting, long-lived particles in 20.3 fb^{-1} of pp collisions at $\sqrt{s} = 8$ TeV. Signal events require at least two reconstructed vertices possibly originating from long-lived particles decaying to jets in the inner tracking detector and muon spectrometer. No significant excess of events over the expected background was found. Results were interpreted in Stealth SUSY benchmark models where a pair of gluinos decay to long-lived singlinos, $\widetilde{S}$, which in turn each decay to a low-mass gravitino and a pair of jets. The 95% confidence-level limits are set on the cross section $\times$ branching ratio for the decay $\widetilde{g} \rightarrow \widetilde{S}g$, as a function of the singlino proper lifetime ($c\tau$). See their Fig. 10(f)

[97] AAD 15AI searched in 20 fb^{-1} of pp collisions at $\sqrt{s} = 8$ TeV for events containing at least one isolated lepton (electron or muon), jets, and large missing transverse momentum. No excess of events above the expected level of Standard Model background was found. Exclusion limits at 95% C.L. are set on the gluino mass in the CMSSM/mSUGRA, see Fig. 15, in the NUHMG, see Fig. 16, and in various simplified models, see Figs. 18–22.

[98] AAD 15CB searched for events containing at least one long-lived particle that decays at a significant distance from its production point (displaced vertex, DV) into two leptons or into five or more charged particles in 20.3 fb^{-1} of pp collisions at $\sqrt{s} = 8$ TeV. The dilepton signature is characterised by DV formed from at least two lepton candidates. Four different final states were considered for the multitrak signature, in which the DV must be accompanied by a high-transverse momentum muon or electron candidate that originates from the DV, jets or missing transverse momentum. No events were observed in any of the signal regions. Results were interpreted in SUSY scenarios involving R-parity violation, split supersymmetry, and gauge mediation. See their Fig. 12–20.

[99] KHACHATRYAN 15AD searched in 19.4 fb^{-1} of pp collisions at $\sqrt{s} = 8$ TeV for events with two opposite-sign same flavor isolated leptons featuring either a kinematic edge, or a peak at the Z-boson mass, in the invariant mass spectrum. No evidence for a statistically significant excess over the expected SM backgrounds is observed and 95% C.L. exclusion limits are derived in a simplified model of gluino pair production where the gluino decays into quarks, a Z-boson, and a massless gravitino LSP, see Fig. 9.

[100] KHACHATRYAN 15AZ searched in 19.7 fb^{-1} of pp collisions at $\sqrt{s} = 8$ TeV for events with either at least one photon, hadronic jets and $\not{E}_T$ (single photon channel) or with at least two photons and at least one jet and using the razor variables. No significant excess above the Standard Model expectations is observed. Limits are set on gluino masses in the general gauge-mediated SUSY breaking model (GGM), for both a bino-like and wino-like neutralino NLSP scenario, see Fig. 8 and 9.

[101] AAD 14AX searched in 20.1 fb^{-1} of pp collisions at $\sqrt{s} = 8$ TeV for the strong production of supersymmetric particles in events containing either zero or at least one high-p_T lepton, large missing transverse momentum, high jet multiplicity and at least three jets identified as originating from b-quarks. No excess over the expected SM background is observed. Limits are derived in mSUGRA/CMSSM models with $\tan\beta = 30$, $A_0 = -2m_0$ and $\mu > 0$, see their Fig. 14. Also, exclusion limits in simplified models containing gluinos and scalar top and bottom quarks are set, see their Figures 12, 13.

[102] AAD 14E searched in 20.3 fb^{-1} of pp collisions at $\sqrt{s} = 8$ TeV for strongly produced supersymmetric particles in events containing jets and two same-sign leptons or three leptons. The search also utilises jets originating from b-quarks, missing transverse momentum and other variables. No excess over the expected SM background is observed. Exclusion limits are derived in simplified models containing gluinos and squarks, see Figures 5 and 6. In the $\widetilde{g} \rightarrow qq'\widetilde{\chi}^{\pm}_1$, $\widetilde{\chi}^{\pm}_1 \rightarrow W^{(*)\pm}\widetilde{\chi}^0_2$, $\widetilde{\chi}^0_2 \rightarrow Z^{(*)}\widetilde{\chi}^0_1$ simplified model, the following assumptions have been made: $m_{\widetilde{\chi}^{\pm}_1} = 0.5\ m_{\widetilde{\chi}^0_1} + m_{\widetilde{g}}$, $m_{\widetilde{\chi}^0_2} = 0.5\ (m_{\widetilde{\chi}^0_1} + m_{\widetilde{\chi}^{\pm}_1})$, $m_{\widetilde{\chi}^0_1} < 520$ GeV. In the $\widetilde{g} \rightarrow qq'\widetilde{\chi}^{\pm}_1$, $\widetilde{\chi}^{\pm}_1 \rightarrow \ell^{\pm}\nu\widetilde{\chi}^0_1$ or $\widetilde{g} \rightarrow qq'\widetilde{\chi}^0_2$, $\widetilde{\chi}^0_2 \rightarrow \ell^{\pm}\ell^{\mp}(\nu\nu)\widetilde{\chi}^0_1$ simplified model, the following assumptions have been made: $m_{\widetilde{\chi}^{\pm}_1} = m_{\widetilde{\chi}^0_2} = 0.5\ (m_{\widetilde{\chi}^0_1} + m_{\widetilde{g}})$, $m_{\widetilde{\chi}^0_1} < 660$ GeV. Limits are also derived in the mSUGRA/CMSSM, bRPV and GMSB models, see their Fig. 8.

[103] CHATRCHYAN 14H searched in 19.5 fb^{-1} of pp collisions at $\sqrt{s} = 8$ TeV for events with two isolated same-sign dileptons and jets in the final state. No significant excess above the Standard Model expectations is observed. Limits are set on the gluino mass in simplified models where the decay $\widetilde{g} \rightarrow t\overline{t}\widetilde{\chi}^0_1$ takes place with a branching ratio of 100%, or where the decay $\widetilde{g} \rightarrow \widetilde{t}t$, $\widetilde{t} \rightarrow t\widetilde{\chi}^0_1$ takes place with a branching ratio of 100%, with varying mass of the $\widetilde{\chi}^0_1$, or where the decay $\widetilde{g} \rightarrow \widetilde{b}b$, $\widetilde{b} \rightarrow t\widetilde{\chi}^{\pm}_1$, $\widetilde{\chi}^{\pm}_1 \rightarrow W^{\pm}\widetilde{\chi}^0_1$ takes place with a branching ratio of 100%, with varying mass of the $\widetilde{\chi}^{\pm}_1$, see Fig. 5.

[104] CHATRCHYAN 14H searched in 19.5 fb^{-1} of pp collisions at $\sqrt{s} = 8$ TeV for events with two isolated same-sign dileptons and jets in the final state. No significant excess above the Standard Model expectations is observed. Limits are set on the gluino mass in simplified models where the decay $\widetilde{g} \rightarrow qq'\widetilde{\chi}^{\pm}_1$, $\widetilde{\chi}^{\pm}_1 \rightarrow W^{\pm}\widetilde{\chi}^0_1$ takes place with a branching ratio of 100%, with varying mass of the $\widetilde{\chi}^{\pm}_1$ and $\widetilde{\chi}^0_1$, see Fig. 7.

[105] CHATRCHYAN 14H searched in 19.5 fb^{-1} of pp collisions at $\sqrt{s} = 8$ TeV for events with two isolated same-sign dileptons and jets in the final state. No significant excess above the Standard Model expectations is observed. Limits are set on the gluino mass in simplified models where the decay $\widetilde{g} \rightarrow b\overline{t}\widetilde{\chi}^{\pm}_1$, $\widetilde{\chi}^{\pm}_1 \rightarrow W^{\pm}\widetilde{\chi}^0_1$ takes place with a branching ratio of 100%, for two choices of $m_{\widetilde{\chi}^{\pm}_1}$ and fixed $m_{\widetilde{\chi}^0_1}$, see Fig. 6.

R-parity violating heavy $\widetilde{g}$ (Gluino) mass limit

VALUE (GeV)	CL%	DOCUMENT ID		TECN	COMMENT
>2200	95	[1] AAD	21BF	ATLS	$\ell^{\pm}$ + b-jets + many jets, Tglu3F, λ''_{323} electroweakino decay, 500 GeV < $m_{\widetilde{\chi}^0_1}$ < 1600 GeV
>2250	95	[1] AAD	21BF	ATLS	$\ell^{\pm}$ + b-jets + many jets, Tglu3G, λ''_{323} electroweakino decay, 600 GeV < $m_{\widetilde{\chi}^0_1}$ < 1600 GeV
>2200	95	[1] AAD	21BF	ATLS	$\ell^{\pm}$ + b-jets + many jets, Tglu3B, λ''_{323} electroweakino decay, 600 GeV < $m_{\widetilde{\chi}^0_1}$ < 1600 GeV
>1800	95	[1] AAD	21BF	ATLS	$\ell^{\pm}$ + b-jets + many jets, Tglu3B, λ''_{323}, $\widetilde{t}$ decay, $m_{\widetilde{t}}$ < 1200 GeV
>2200	95	[1] AAD	21BF	ATLS	$\ell^{\pm}$ + b-jets + many jets, Tglu1A, λ', $\widetilde{\chi}^0_1$ decay with equal probability into e, μ, ν_e, ν_μ, 400 GeV < $m_{\widetilde{\chi}^0_1}$ < 1700 GeV

Downloaded from https://academic.oup.com/ptep/article/2022/8/083C01/6651666 by KIT Library user on 27 September 2022

>2500	95	[2] AAD	21Y	ATLS	$\geq 4\ell$, Tglu1A with $\widetilde{\chi}^0_1 \to \ell^\pm\ell^\mp\nu$, $\lambda_{12k} \neq 0$, $m_{\widetilde{\chi}^0_1} = 2200$ GeV
>1900	95	[2] AAD	21Y	ATLS	$\geq 4\ell$, Tglu1A with $\widetilde{\chi}^0_1 \to \ell^\pm\ell^\mp\nu$, $\lambda_{i33} \neq 0$, $m_{\widetilde{\chi}^0_1} = 1550$ GeV
>1600	95	[3] AAD	20AL	ATLS	8 or more jets+$\not{E}_T$, Tglu2RPV
>1600	95	[4] AAD	20V	ATLS	same-sign $\ell^\pm\ell^\pm$ + jets, $\widetilde{g} \to t\,b\,d$ simplified model
>2150	95	[5] SIRUNYAN	20T	CMS	same-sign $\ell^\pm\ell^\pm$ or $\geq 3\ell^\pm$ + jets, $\widetilde{g} \to q\,q\,\overline{q}\,\overline{q}$ + $e/\mu/\tau$ simplified model
>1725	95	[5] SIRUNYAN	20T	CMS	same-sign $\ell^\pm\ell^\pm$ or $\geq 3\ell^\pm$+jets, $\widetilde{g} \to t\,b\,s$ simplified model
>1500	95	[6] SIRUNYAN	19F	CMS	$\widetilde{g} \to j\,j\,j$
>2260	95	[7] AABOUD	18Z	ATLS	$\geq 4\ell$, $\lambda_{12k} \neq 0$, $m_{\widetilde{\chi}^0_1} > 1000$ GeV
>1650	95	[7] AABOUD	18Z	ATLS	$\geq 4\ell$, $\lambda_{i33} \neq 0$, $m_{\widetilde{\chi}^0_1} > 500$ GeV
>1610	95	[8] SIRUNYAN	18AK	CMS	$\widetilde{g} \to t\,b\,s$, λ''_{332} coupling
>1690	95	[9] SIRUNYAN	18D	CMS	top quark (hadronically decaying) + jets + $\not{E}_T$, Tglu3C, $m_{\widetilde{t}_1} - m_{\widetilde{\chi}^0_1} = 20$ GeV, $m_{\widetilde{\chi}^0_1} = 0$ GeV
none 100–1410	95	[10] SIRUNYAN	18EA	CMS	2 large jets with four-parton substructure, $\widetilde{g} \to 5q$
>2100	95	[11] AABOUD	17AI	ATLS	$\geq 1\ell$+ ≥ 8 jets, Tglu3A and $\widetilde{\chi}^0_1 \to u\,d\,s$, λ''_{112} coupling, $m_{\widetilde{\chi}^0_1}$=1000 GeV
>1650	95	[12] AABOUD	17AI	ATLS	$\geq 1\ell$+ ≥ 8 jets, $\widetilde{g} \to t\,\widetilde{t}$, $\widetilde{t} \to b\,s$, λ''_{323} coupling, $m_{\widetilde{t}}$=1000 GeV
>1800	95	[13] AABOUD	17AI	ATLS	$\geq 1\ell$+ ≥ 8 jets, Tglu1A and $\widetilde{\chi}^0_1 \to q\,q\,l$, λ' coupling, $m_{\widetilde{\chi}^0_1}$=1000 GeV
>1800	95	[14] AABOUD	17AJ	ATLS	same-sign $\ell^\pm\ell^\pm$ / 3 ℓ + jets + $\not{E}_T$, Tglu3A, λ''_{112} coupling, $m_{\widetilde{\chi}^0_1} = 50$ GeV
>1750	95	[15] AABOUD	17AJ	ATLS	same-sign $\ell^\pm\ell^\pm$ / 3 ℓ + jets + $\not{E}_T$, Tglu1A and $\widetilde{\chi}^0_1 \to q\,q\,\ell$, λ' coupling
>1450	95	[16] AABOUD	17AJ	ATLS	same-sign $\ell^\pm\ell^\pm$ / 3 ℓ + jets + $\not{E}_T$, $\widetilde{g} \to t\,\widetilde{t}_1$ and $\widetilde{t}_1 \to s\,d$, λ''_{321} coupling
>1450	95	[17] AABOUD	17AJ	ATLS	same-sign $\ell^\pm\ell^\pm$ / 3 ℓ + jets + $\not{E}_T$, $\widetilde{g} \to t\,\widetilde{t}_1$ and $\widetilde{t}_1 \to b\,d$, λ''_{313} coupling
> 400	95	[18] AABOUD	17AJ	ATLS	same-sign $\ell^\pm\ell^\pm$ / 3 ℓ + jets + $\not{E}_T$, $\widetilde{d}_R \to t\,b\,(t\,s)$, λ''_{313} (λ''_{321}) coupling
none 625–1375	95	[19] AABOUD	17AZ	ATLS	$\geq$ 7 jets+$\not{E}_T$, large R-jets and/or b-jets, $\widetilde{g} \to t\,\widetilde{t}_1$ and $\widetilde{t}_1 \to b\,s$, λ''_{323} coupling
none 600–650	95	[20] KHACHATRY...	17Y	CMS	$\widetilde{g} \to q\,q\,q\,q\,q$, λ''_{212} coupling, $m_{\widetilde{q}} = 100$ GeV
none 600–1030	95	[20] KHACHATRY...	17Y	CMS	$\widetilde{g} \to q\,q\,q\,q\,q$, λ''_{212} coupling, $m_{\widetilde{q}} = 900$ GeV
none 600–650	95	[20] KHACHATRY...	17Y	CMS	$\widetilde{g} \to q\,q\,q\,q\,b$, λ''_{213} coupling, $m_{\widetilde{q}} = 100$ GeV
none 600–1080	95	[20] KHACHATRY...	17Y	CMS	$\widetilde{g} \to q\,q\,q\,q\,b$, λ''_{213} coupling, $m_{\widetilde{q}} = 900$ GeV
none 600–680	95	[20] KHACHATRY...	17Y	CMS	$\widetilde{g} \to q\,q\,q\,b\,b$, λ''_{212} coupling, $m_{\widetilde{q}} = 100$ GeV
none 600–1080	95	[20] KHACHATRY...	17Y	CMS	$\widetilde{g} \to q\,q\,q\,b\,b$, λ''_{212} coupling, $m_{\widetilde{q}} = 900$ GeV
none 600–650	95	[20] KHACHATRY...	17Y	CMS	$\widetilde{g} \to q\,q\,b\,b\,b$, λ''_{213} coupling, $m_{\widetilde{q}} = 100$ GeV
none 600–1100	95	[20] KHACHATRY...	17Y	CMS	$\widetilde{g} \to q\,q\,b\,b\,b$, λ''_{213} coupling, $m_{\widetilde{q}} = 900$ GeV
>1050	95	[21] KHACHATRY...	16BJ	CMS	same-sign $\ell^\pm\ell^\pm$, Tglu3A, $m_{\widetilde{\chi}^0_1} < 800$ GeV
>1140	95	[21] KHACHATRY...	16BJ	CMS	same-sign $\ell^\pm\ell^\pm$, Tglu3B, $m_{\widetilde{t}} - m_{\widetilde{\chi}^0_1} = 20$ GeV, $m_{\widetilde{\chi}^0_1} = 0$
>1030	95	[22] KHACHATRY...	16BX	CMS	$\widetilde{g} \to t\,b\,s$, λ''_{332} coupling
>1150	95	[23] AAD	15BV	ATLS	general RPC $\widetilde{g}$ decays, $m_{\widetilde{\chi}^0_1} < 100$ GeV
>1350	95	[24] AAD	14X	ATLS	$\geq 4\ell^\pm$, $\widetilde{g} \to q\,\overline{q}\,\widetilde{\chi}^0_1$, $\widetilde{\chi}^0_1 \to \ell^\pm\ell^\mp\nu$
> 650	95	[25] CHATRCHYAN	14P	CMS	$\widetilde{g} \to j\,j\,j$
none 200–835	95	[25] CHATRCHYAN	14P	CMS	$\widetilde{g} \to b\,j\,j$

• • • We do not use the following data for averages, fits, limits, etc. • • •

>1875	95	[26] AABOUD	18CF	ATLS	jets and large R-jets, Tglu2RPV and $\widetilde{\chi}^0_1 \to q\,q\,q$, λ'' coupling, $m_{\widetilde{\chi}^0_1}$=1000 GeV
>1400	95	[27] KHACHATRY...	16BX	CMS	$\widetilde{g} \to q\,q\,\widetilde{\chi}^0_1$, $\widetilde{\chi}^0_1 \to \ell\,\ell\,\nu$, λ_{121} or $\lambda_{122} \neq 0$, $m_{\widetilde{\chi}^0_1} > 400$ GeV
>1600	95	[23] AAD	15BV	ATLS	pMSSM, $M_1 = 60$ GeV, $m_{\widetilde{q}} < 1500$ GeV
>1280	95	[23] AAD	15BV	ATLS	mSUGRA, $m_0 > 2$ TeV
>1100	95	[23] AAD	15BV	ATLS	via $\widetilde{\tau}$, natural GMSB, all $m_{\widetilde{\tau}}$
>1220	95	[23] AAD	15BV	ATLS	b-jets, $\widetilde{g} \to \widetilde{t}_1\,t$ and $\widetilde{t}_1 \to t\,\widetilde{\chi}^0_1$, $m_{\widetilde{T}_1} < 1000$ GeV
>1180	95	[23] AAD	15BV	ATLS	b-jets, $\widetilde{g} \to \widetilde{t}_1\,t$ and $\widetilde{t}_1 \to b\,\widetilde{\chi}^\pm_1$, $m_{\widetilde{T}_1} < 1000$ GeV, $m_{\widetilde{\chi}^0_1} = 60$ GeV
> 880	95	[23] AAD	15BV	ATLS	jets, $\widetilde{g} \to \widetilde{t}_1\,t$ and $\widetilde{t}_1 \to s\,b$, $400 < m_{\widetilde{t}_1} < 1000$ GeV
		[28] AAD	15CB	ATLS	ℓ, $\widetilde{g} \to (e/\mu)\,q\,q$, benchmark gluino, neutralino masses
> 600	95	[28] AAD	15CB	ATLS	$\ell\,\ell/Z$, $\widetilde{g} \to (e\,e/\mu\,\mu/e\,\mu)\,q\,q$, $m_{\widetilde{\chi}^0_1} = 400$ GeV and $0.7 < c\tau_{\widetilde{\chi}^0_1} < 3 \times 10^5$ mm
>1000	95	[29] AAD	15X	ATLS	≥ 10 jets, $\widetilde{g} \to q\,\overline{q}\,\widetilde{\chi}^0_1$, $\widetilde{\chi}^0_1 \to q\,q\,q$, $m_{\widetilde{\chi}^0_1}$=500 GeV
> 917	95	[29] AAD	15X	ATLS	$\geq$ 6,7 jets, $\widetilde{g} \to q\,q\,q$, (light-quark, λ'' couplings)
> 929	95	[29] AAD	15X	ATLS	$\geq$ 6,7 jets, $\widetilde{g} \to q\,q\,q$, (b-quark, λ'' couplings)
>1180	95	[30] AAD	14AX	ATLS	$\geq$ 3 b-jets + $\not{E}_T$, $\widetilde{g} \to \widetilde{t}_1\,t\,\widetilde{\chi}^0_1$ simplified model, $\widetilde{t}_1 \to b\,\widetilde{\chi}^\pm_1$, $m_{\widetilde{\chi}^\pm_1}$=2$m_{\widetilde{\chi}^0_1}$, $m_{\widetilde{\chi}^0_1}$=60 GeV, $m_{\widetilde{t}_1}$<1000 GeV
> 850	95	[31] AAD	14E	ATLS	$\ell^\pm\ell^\pm(\ell^\mp)$ + jets, $\widetilde{g} \to t\,\widetilde{t}_1$ with $\widetilde{t}_1 \to b\,s$ simplified model
> 900	95	[32] CHATRCHYAN	14H	CMS	same-sign $\ell^\pm\ell^\pm$, $\widetilde{g} \to t\,b\,s$ simplified model

[1] AAD 21BF searched in 139 fb^{-1} of pp collisions at $\sqrt{s} = 13$ TeV for pair production of gluinos, stops, electroweakinos decaying RPV either directly or indirectly via the LSP. The final state in all cases is one or two leptons, many jets (up to fifteen) and b-jets. Different models with different branching fractions of the gluino or stop follow from the assumptions on the nature of the electroweakinos. No significant excess above the Standard Model predictions is observed. Limits are set on the *gluino*, $\widetilde{t}_1$, electroweakino masses as a function of the $\widetilde{\chi}^0_1$ mass in several scenarios of gluino, stop and electroweakino pair production.

[2] AAD 21Y searched in 139 fb^{-1} of pp collisions at $\sqrt{s} = 13$ TeV for supersymmetry in events with four or more leptons (electrons, muons and tau-leptons). No significant excess above the Standard Model expectations is observed. Limits are set on Tchi1n12-GGM, and RPV models similar to Tchi1n2l, Tglu1A (with $q = u, d, s, c, b$, with equal branching fractions), and $\widetilde{\ell}_L/\widetilde{\nu} \to \ell/\nu\,\widetilde{\chi}^0_1$ (mass-degenerate $\widetilde{\ell}_L$ and $\widetilde{\nu}$ of all 3 generations), all with $\widetilde{\chi}^0_1 \to \ell^\pm\ell^\mp\nu$ via λ_{12k} or λ_{i33} (where $i,k \in 1,2$), see their Figure 11.

[3] AAD 20AL searched in 139 fb^{-1} of pp collisions at $\sqrt{s} = 13$ TeV for events with 8 or more jets and moderate missing transverse momentum. The selection makes requirements according to the number of b-tagged jets and the scalar sum of masses of large-radius jets. No significant excess above the Standard Model expectations is observed. Exclusion limits at 95% C.L. are set on the gluino mass in RPV simplified models where the gluino decays via $\widetilde{g} \to t\,b\,d$ or $\widetilde{g} \to t\,b\,s$. They extend up to almost 1.6 TeV for a $\widetilde{t}_1$ mass of 900 GeV. See their Fig. 10(c).

[4] AAD 20V searched in 139 fb^{-1} of pp collisions at $\sqrt{s} = 13$ TeV for events with two same-sign charged leptons (electrons or muons) and jets. No significant excess above the Standard Model expectations is observed. Exclusion limits at 95% C.L. are set on the gluino mass in RPV simplified models where the gluino decays via $\widetilde{g} \to t\,b\,d$, see Figure 7(b).

[5] SIRUNYAN 20T searched in 137 fb^{-1} of pp collisions at $\sqrt{s} = 13$ TeV for events with at least two jets, and two isolated same-sign or three or more charged leptons (electrons or muons). No significant excess above the Standard Model expectations is observed. Limits are set on the gluino mass in the Tglu3A, Tglu3B, Tglu3C and Tglu3D simplified models, see their Figure 7, and in the Tglu1C and Tglu1B simplified models, see their Figures 8 and 9. Limits are also set on the sbottom mass in the Tsbot2 simplified model, see their Figure 10, and on the stop mass in the Tstop7 simplified model, see their Figure 11. Finally, limits are set on the gluino mass in RPV simplified models where the gluino decays either via $\widetilde{g} \to q\,q\,\overline{q}\,\overline{q}$ + $e/\mu/\tau$ or via $\widetilde{g} \to t\,b\,s$, see Figure 12.

[6] SIRUNYAN 19F searched in 35.9 fb^{-1} of pp collisions at $\sqrt{s} = 13$ TeV for three-jet resonances produced in the decay of a gluino in R-parity violating supersymmetric models. The mass range from 200 to 2000GeV is explored in four separate mass regions. The observations show agreement with standard model expectations. The results are interpreted within the framework of R-parity violating SUSY, where pair-produced gluinos decay to a six quark final state. Gluino masses below 1500GeV are excluded at 95% C.L. See their Fig.5.

[7] AABOUD 18Z searched in 36.1 fb^{-1} of pp collisions at $\sqrt{s} = 13$ TeV for events containing four or more charged leptons (electrons, muons and up to two hadronically decaying taus). No significant deviation from the expected SM background is observed. Limits are set on the Higgsino mass in simplified models of general gauge mediated supersymmetry Tn1n1A/Tn1n1B/Tn1n1C, see their Figure 9. Limits are also set on the wino, slepton, sneutrino and gluino mass in a simplified model of NLSP pair production with R-parity violating decays of the LSP via λ_{12k} or λ_{i33} to charged leptons, see their Figures 7, 8.

Downloaded from https://academic.oup.com/ptep/article/2022/8/083C01/6651666 by KIT Library user on 27 September 2022

[8] SIRUNYAN 18AK searched in 35.9 fb^{-1} of pp collisions at $\sqrt{s}$ = 13 TeV for events containing a single lepton, large jet and b-quark jet multiplicities, coming from R-parity-violating decays of gluinos. No excess over the expected background is observed. Limits are derived on the gluino mass, assuming the RPV $\widetilde{g} \rightarrow t b s$ decay, see their Figure 9.

[9] SIRUNYAN 18D searched in 35.9 fb^{-1} of pp collisions at $\sqrt{s}$ = 13 TeV for events containing identified hadronically decaying top quarks, no leptons, and $\not{E}_T$. No significant excess above the Standard Model expectations is observed. Limits are set on the stop mass in the Tstop1 simplified model, see their Figure 8, and on the gluino mass in the Tglu3A, Tglu3B, Tglu3C and Tglu3E simplified models, see their Figure 9.

[10] SIRUNYAN 18EA searched in 38.2 fb^{-1} of pp collisions at $\sqrt{s}$ = 13 TeV for the pair production of resonances, each decaying to at least four quarks. Reconstructed particles are clustered into two large jets of similar mass, each consistent with four-parton substructure. No statistically significant excess over the Standard Model expectation is observed. Limits are set on the squark and gluino mass in RPV supersymmetry models where squarks (gluinos) decay, through intermediate higgsinos, to four (five) quarks, see their Figure 4.

[11] AABOUD 17AI searched in 36.1 fb^{-1} of pp collisions at $\sqrt{s}$ = 13 TeV for events with one or more isolated lepton, at least eight jets, either zero or many b-jets, for evidence of R-parity violating decays of the gluino. No significant excess above the Standard Model expectations is observed. Limits up to 2.1 TeV are set on the gluino mass in R-parity-violating supersymmetry models as Tglu3A with LSP decay through the non-zero λ''_{112} coupling as $\widetilde{\chi}^0_1 \rightarrow u d s$. See their Figure 9.

[12] AABOUD 17AI searched in 36.1 fb^{-1} of pp collisions at $\sqrt{s}$ = 13 TeV for events with one or more isolated lepton, at least eight jets, either zero or many b-jets, for evidence of R-parity violating decays of the gluino. No significant excess above the Standard Model expectations is observed. Limits up to 1.65 TeV are set on the gluino mass in R-parity-violating supersymmetry models with $\widetilde{g} \rightarrow t \widetilde{t}$, $\widetilde{t} \rightarrow b s$ through the non-zero λ''_{323} coupling. See their Figure 9.

[13] AABOUD 17AI searched in 36.1 fb^{-1} of pp collisions at $\sqrt{s}$ = 13 TeV for events with one or more isolated lepton, at least eight jets, either zero or many b-jets, for evidence of R-parity violating decays of the gluino. No significant excess above the Standard Model expectations is observed. Limits up to 1.8 TeV are set on the gluino mass in R-parity-violating supersymmetry models as Tglu1A with the LSP decay through the non-zero λ' coupling as $\widetilde{\chi}^0_1 \rightarrow q q \ell$. See their Figure 9.

[14] AABOUD 17AJ searched in 36.1 fb^{-1} of pp collisions at $\sqrt{s}$ = 13 TeV for events with two same-sign or three leptons, jets and large missing transverse momentum. No significant excess above the Standard Model expectations is observed. Limits up to 1.8 TeV are set on the gluino mass in R-parity-violating supersymmetry models as Tglu3A with LSP decaying through the non-zero λ''_{112} coupling as $\widetilde{\chi}^0_1 \rightarrow u d s$. See their Figure 5(d).

[15] AABOUD 17AJ searched in 36.1 fb^{-1} of pp collisions at $\sqrt{s}$ = 13 TeV for events with two same-sign or three leptons, jets and large missing transverse momentum. No significant excess above the Standard Model expectations is observed. Limits up to 1.75 TeV are set on the gluino mass in R-parity-violating supersymmetry models as Tglu1A with LSP decaying through the non-zero λ' coupling as $\widetilde{\chi}^0_1 \rightarrow q q \ell$. See their Figure 5(c).

[16] AABOUD 17AJ searched in 36.1 fb^{-1} of pp collisions at $\sqrt{s}$ = 13 TeV for events with two same-sign or three leptons, jets and large missing transverse momentum. No significant excess above the Standard Model expectations is observed. Limits up to 1.45 TeV are set on the gluino mass in R-parity-violating supersymmetry models where $\widetilde{g} \rightarrow t \widetilde{t}_1$ and $\widetilde{t}_1 \rightarrow s d$ through the non-zero λ''_{321} coupling. See their Figure 5(b).

[17] AABOUD 17AJ searched in 36.1 fb^{-1} of pp collisions at $\sqrt{s}$ = 13 TeV for events with two same-sign or three leptons, jets and large missing transverse momentum. No significant excess above the Standard Model expectations is observed. Limits up to 1.45 TeV are set on the gluino mass in R-parity-violating supersymmetry models where $\widetilde{g} \rightarrow t \widetilde{t}_1$ and $\widetilde{t}_1 \rightarrow b d$ through the non-zero λ''_{313} coupling. See their Figure 5(a).

[18] AABOUD 17AJ searched in 36.1 fb^{-1} of pp collisions at $\sqrt{s}$ = 13 TeV for events with two same-sign or three leptons, jets and large missing transverse momentum. No significant excess above the Standard Model expectations is observed. Limits up to 400 GeV are set on the down type squark ($\widetilde{d}_R$ mass in R-parity-violating supersymmetry models where $\widetilde{d}_R \rightarrow t b$ through the non-zero λ''_{313} coupling or $\widetilde{d}_R \rightarrow t s$ through the non-zero λ''_{321}. See their Figure 5(e) and 5(f).

[19] AABOUD 17AZ searched in 36.1 fb^{-1} of pp collisions at $\sqrt{s}$ = 13 TeV for events with at least seven jets and large missing transverse momentum. Selected events are further classified based on the presence of large R-jets or b-jets and no leptons. No significant excess above the Standard Model expectations is observed. Limits are set for R-parity violating decays of the gluino assuming $\widetilde{g} \rightarrow t \widetilde{t}_1$ and $\widetilde{t}_1 \rightarrow b s$ through the non-zero λ''_{323} couplings. The range 625–1375 GeV is excluded for $m_{\widetilde{t}_1}$ = 400 GeV. See their Figure 7b.

[20] KHACHATRYAN 17Y searched in 19.7 fb^{-1} of pp collisions at $\sqrt{s}$ = 8 TeV for events containing at least 8 or 10 jets, possibly b-tagged, coming from R-parity-violating decays of supersymmetric particles. No excess over the expected background is observed. Limits are derived on the gluino mass, assuming various RPV decay modes, see Fig. 7.

[21] KHACHATRYAN 16BJ searched in 2.3 fb^{-1} of pp collisions at $\sqrt{s}$ = 13 TeV for events with two isolated same-sign dileptons and jets in the final state. No significant excess above the Standard Model expectations is observed. Limits are set on the gluino mass in the following simplified models: Tglu3A and Tglu3D, see Fig. 4, Tglu3B and Tglu3C, see Fig. 5, and Tglu1B, see Fig. 7.

[22] KHACHATRYAN 16BX searched in 19.5 fb^{-1} of pp collisions at $\sqrt{s}$ = 8 TeV for events containing 0 or 1 leptons and b-tagged jets, coming from R-parity-violating decays of supersymmetric particles. No excess over the expected background is observed. Limits are derived on the gluino mass, assuming the RPV $\widetilde{g} \rightarrow t b s$ decay, see Fig. 7 and 10.

[23] AAD 15BV summarized and extended ATLAS searches for gluinos and first- and second-generation squarks in final states containing jets and missing transverse momentum, with or without leptons or b-jets in the $\sqrt{s}$ =8 TeV data set collected in 2012. The paper reports the results of new interpretations and statistical combinations of previously published analyses, as well as new analyses. Exclusion limits at 95% C.L. are set on the gluino mass in several R-parity conserving models, leading to a generalized constraint on gluino masses exceeding 1150 GeV for lightest supersymmetric particle masses below 100 GeV. See their Figs. 10, 19, 20, 21, 23, 25, 26, 29-37.

[24] AAD 14X searched in 20.3 fb^{-1} of pp collisions at $\sqrt{s}$ = 8 TeV for events with at least four leptons (electrons, muons, taus) in the final state. No significant excess above the Standard Model expectations is observed. Limits are set on the gluino mass in an R-parity violating simplified model where the decay $\widetilde{g} \rightarrow q \overline{q} \widetilde{\chi}^0_1$, with $\widetilde{\chi}^0_1 \rightarrow \ell^{\pm} \ell^{\mp} \nu$, takes place with a branching ratio of 100%, see Fig. 8.

[25] CHATRCHYAN 14P searched in 19.4 fb^{-1} of pp collisions at $\sqrt{s}$ = 8 TeV for three-jet resonances produced in the decay of a gluino in R-parity violating supersymmetric models. No excess over the expected SM background is observed. Assuming a 100% branching ratio for the gluino decay into three light-flavour jets, limits are set on the cross section of gluino pair production, see Fig. 7, and gluino masses below 650 GeV are excluded at 95% C.L. Assuming a 100% branching ratio for the gluino decaying to one b-quark jet and two light-flavour jets, gluino masses between 200 GeV and 835 GeV are excluded at 95% C L.

[26] AABOUD 18CF searched in 36.1 fb^{-1} of pp collisions at $\sqrt{s}$ = 13 TeV for events with several jets, possibly b-jets, and large-radius jets for evidence of R-parity violating decays of the gluino. No significant excess above the Standard Model expectations is observed. Limits between 1000 and 1875 GeV are set on the gluino mass in R-parity-violating supersymmetry models as Tglu2RPV with the LSP decay through the non-zero λ'' coupling as $\widetilde{\chi}^0_1 \rightarrow q q q$. The most stringent limit is obtained for $m_{\widetilde{\chi}^0_1}$ = 1000 GeV, the weakest for $m_{\widetilde{\chi}^0_1}$ = 50 GeV. See their Figure 7(b). Figure 7(a) presents results for gluinos directly decaying into 3 quarks, Tglu1RPV.

[27] KHACHATRYAN 16BX searched in 19.5 fb^{-1} of pp collisions at $\sqrt{s}$ = 8 TeV for events containing 4 leptons coming from R-parity-violating decays of $\widetilde{\chi}^0_1 \rightarrow \ell \ell \nu$ with $\lambda_{121} \neq 0$ or $\lambda_{122} \neq 0$. No excess over the expected background is observed. Limits are derived on the gluino, squark and stop masses, see Fig. 23.

[28] AAD 15CB searched for events containing at least one long-lived particle that decays at a significant distance from its production point (displaced vertex, DV) into two leptons or into five or more charged particles in 20.3 fb^{-1} of pp collisions at $\sqrt{s}$ = 8 TeV. The dilepton signature is characterised by DV formed from at least two lepton candidates. Four different final states were considered for the multitrak signature, in which the DV must be accompanied by a high-transverse momentum muon or electron candidate that originates from the DV, jets or missing transverse momentum. No events were observed in any of the signal regions. Results were interpreted in SUSY scenarios involving R-parity violation, split supersymmetry, and gauge mediation. See their Fig. 12–20.

[29] AAD 15X searched in 20.3 fb^{-1} of pp collisions at $\sqrt{s}$ = 8 TeV for events containing large number of jets, no requirements on missing transverse momentum and no isolated electrons or muons. The sensitivity of the search is enhanced by considering the number of b-tagged jets and the scalar sum of masses of large-radius jets in an event. No evidence was found for excesses above the expected level of Standard Model background. Exclusion limits at 95% C.L. are set on the gluino mass assuming the gluino decays to various quark flavors, and for various neutralino masses. See their Fig. 11–16.

[30] AAD 14AX searched in 20.1 fb^{-1} of pp collisions at $\sqrt{s}$ = 8 TeV for the strong production of supersymmetric particles in events containing either zero or at last one high high-p_T lepton, large missing transverse momentum, high jet multiplicity and at least three jets identified as originating from b-quarks. No excess over the expected SM background is observed. Limits are derived in mSUGRA/CMSSM models with tanβ = 30, $A_0 = -2m_0$ and $\mu > 0$, see their Fig. 14. Also, exclusion limits in simplified models containing gluinos and scalar top and bottom quarks are set, see their Figures 12, 13.

[31] AAD 14E searched in 20.3 fb^{-1} of pp collisions at $\sqrt{s}$ = 8 TeV for strongly produced supersymmetric particles in events containing jets and two same-sign leptons or three leptons. The search also utilises jets originating from b-quarks, missing transverse momentum and other variables. No excess over the expected SM background is observed. Exclusion limits are derived in simplified models containing gluinos and squarks, see Figures 5 and 6. In the $\widetilde{g} \rightarrow q q' \widetilde{\chi}^{\pm}_1$, $\widetilde{\chi}^{\pm}_1 \rightarrow W^{(*)\pm} \widetilde{\chi}^0_2$, $\widetilde{\chi}^0_2 \rightarrow Z^{(*)} \widetilde{\chi}^0_1$ simplified model, the following assumptions have been made: $m_{\widetilde{\chi}^{\pm}_1} = 0.5\ m_{\widetilde{\chi}^0_1} + m_{\widetilde{g}}$, $m_{\widetilde{\chi}^0_2} = 0.5\ (m_{\widetilde{\chi}^0_1} + m_{\widetilde{\chi}^{\pm}_1})$, $m_{\widetilde{\chi}^0_1} < 520$ GeV. In the $\widetilde{g} \rightarrow q q' \widetilde{\chi}^{\pm}_1$, $\widetilde{\chi}^{\pm}_1 \rightarrow \ell^{\pm} \nu \widetilde{\chi}^0_1$ or $\widetilde{g} \rightarrow q q' \widetilde{\chi}^0_2$, $\widetilde{\chi}^0_2 \rightarrow \ell^{\pm} \ell^{\mp} (\nu \nu) \widetilde{\chi}^0_1$ simplified model, the following assumptions have been made: $m_{\widetilde{\chi}^{\pm}_1} = m_{\widetilde{\chi}^0_2} = 0.5\ (m_{\widetilde{\chi}^0_1} + m_{\widetilde{g}})$, $m_{\widetilde{\chi}^0_1} < 660$ GeV. Limits are also derived in the mSUGRA/CMSSM, bRPV and GMSB models, see their Fig. 8.

[32] CHATRCHYAN 14H searched in 19.5 fb^{-1} of pp collisions at $\sqrt{s}$ = 8 TeV for events with two isolated same-sign dileptons and jets in the final state. No significant excess above the Standard Model expectations is observed. Limits are set on the gluino mass in simplified models where the R-parity violating decay $\widetilde{g} \rightarrow t b s$ takes place with a branching ratio of 100%, see Fig. 8.

Long-lived $\widetilde{g}$ (Gluino) mass limit

Limits on light gluinos ($m_{\widetilde{g}} < 5$ GeV) were last listed in our PDG 14 edition: K. Olive, *et al.* (Particle Data Group), Chinese Physics **C38** 070001 (2014) (http://pdg.lbl.gov).

VALUE (GeV)	CL%	DOCUMENT ID		TECN	COMMENT
>2500	95	[1] SIRUNYAN	21AF	CMS	long-lived $\widetilde{g}$, Tglu2RPV , λ''_{323} coupling, 0.6 mm < $c\tau$ < 90 mm
>2450	95	[2] SIRUNYAN	21U	CMS	long-lived $\widetilde{g}$, $pp \rightarrow \widetilde{g}\widetilde{g}$, $\widetilde{g} \rightarrow g \widetilde{G}$, GMSB, 6 < $c\tau$ < 550 mm
>2500	95	[2] SIRUNYAN	21U	CMS	long-lived $\widetilde{g}$, $pp \rightarrow \widetilde{g}\widetilde{g}$, $\widetilde{g} \rightarrow q \overline{q} \widetilde{\chi}^0_1$, mini-split, $m_{\widetilde{\chi}^0_1}$ =100 GeV, 7 < $c\tau$ < 360 mm
>2500	95	[2] SIRUNYAN	21U	CMS	long-lived $\widetilde{g}$, $pp \rightarrow \widetilde{g}\widetilde{g}$, $\widetilde{g} \rightarrow t b s$, λ''_{323} coupling, 3 < $c\tau$ < 1000 mm
>1980	95	[3] AABOUD	19AT	ATLS	R-hadrons, Tglu1A, metastable
>2060	95	[4] AABOUD	19C	ATLS	R-hadrons, Tglu1A, $\tau \geq 10$ ns, $m_{\widetilde{\chi}^0_1}$ = 100 GeV
>1890	95	[4] AABOUD	19C	ATLS	R-hadrons, Tglu1A, stable
>2400	95	[5] SIRUNYAN	19BH	CMS	long-lived $\widetilde{g}$, RPV, $\widetilde{g} \rightarrow \overline{t} \overline{b} \overline{s}$, 10 mm < $c\tau$ < 250 mm
>2300	95	[5] SIRUNYAN	19BH	CMS	long-lived $\widetilde{g}$, GMSB, $\widetilde{g} \rightarrow g \widetilde{G}$, 20 mm < $c\tau$ < 110 mm

Downloaded from https://academic.oup.com/ptep/article/2022/8/083C01/6651666 by KIT Library user on 27 September 2022

>2100	95	[6] SIRUNYAN	19BT	CMS	long-lived $\widetilde{g}$, GMSB, $\widetilde{g} \rightarrow g\widetilde{G}$, 0.3 m < c$\tau$ < 30 m
>2500	95	[6] SIRUNYAN	19BT	CMS	long-lived $\widetilde{g}$, GMSB, $\widetilde{g} \rightarrow g\widetilde{G}$, c$\tau$ = 1 m
>1900	95	[6] SIRUNYAN	19BT	CMS	long-lived $\widetilde{g}$, GMSB, $\widetilde{g} \rightarrow g\widetilde{G}$, c$\tau$ = 100 m
>2370	95	[7] AABOUD	18S	ATLS	displaced vertex + $\not{E}_T$, long-lived Tglu1A, $m_{\widetilde{\chi}^0_1}$ = 100 GeV, and τ=0.17 ns
>1600	95	[8] SIRUNYAN	18AY	CMS	jets+$\not{E}_T$, Tglu1A, cτ < 0.1 mm, $m_{\widetilde{\chi}^0_1}$ = 100 GeV
>1750	95	[8] SIRUNYAN	18AY	CMS	jets+$\not{E}_T$, Tglu1A, cτ = 1 mm, $m_{\widetilde{\chi}^0_1}$ = 100 GeV
>1640	95	[8] SIRUNYAN	18AY	CMS	jets+$\not{E}_T$, Tglu1A, cτ = 10 mm, $m_{\widetilde{\chi}^0_1}$ = 100 GeV
>1490	95	[8] SIRUNYAN	18AY	CMS	jets+$\not{E}_T$, Tglu1A, cτ = 100 mm, $m_{\widetilde{\chi}^0_1}$ = 100 GeV
>1300	95	[8] SIRUNYAN	18AY	CMS	jets+$\not{E}_T$, Tglu1A, cτ = 1 m, $m_{\widetilde{\chi}^0_1}$ = 100 GeV
> 960	95	[8] SIRUNYAN	18AY	CMS	jets+$\not{E}_T$, Tglu1A, cτ = 10 m, $m_{\widetilde{\chi}^0_1}$ = 100 GeV
> 900	95	[8] SIRUNYAN	18AY	CMS	jets+$\not{E}_T$, Tglu1A, cτ = 100 m, $m_{\widetilde{\chi}^0_1}$ = 100 GeV
>2200	95	[9] SIRUNYAN	18DV	CMS	long-lived $\widetilde{g}$, RPV, $\widetilde{g} \rightarrow \overline{t}\,\overline{b}\overline{s}$, 0.6 mm < c$\tau$ < 80 mm
>1000	95	[10] KHACHATRY...	17AR	CMS	long-lived $\widetilde{g}$, RPV, $\widetilde{g} \rightarrow t\,\overline{b}\overline{s}$, c$\tau$ = 0.3 mm
>1300	95	[10] KHACHATRY...	17AR	CMS	long-lived $\widetilde{g}$, RPV, $\widetilde{g} \rightarrow t\,\overline{b}\overline{s}$, c$\tau$ = 1.0 mm
>1400	95	[10] KHACHATRY...	17AR	CMS	long-lived $\widetilde{g}$, RPV, $\widetilde{g} \rightarrow t\,\overline{b}\overline{s}$, 2 mm < c$\tau$ < 30 mm
>1580	95	[11] AABOUD	16B	ATLS	long-lived R-hadrons
> 740–1590	95	[12] AABOUD	16C	ATLS	R-hadrons, Tglu1A, $\tau \geq$ 0.4 ns, $m_{\widetilde{\chi}^0_1}$ = 100 GeV
>1570	95	[12] AABOUD	16C	ATLS	R-hadrons, Tglu1A, stable
>1610	95	[13] KHACHATRY...	16BW	CMS	long-lived $\widetilde{g}$ forming R-hadrons, f = 0.1, cloud interaction model
>1580	95	[13] KHACHATRY...	16BW	CMS	long-lived $\widetilde{g}$ forming R-hadrons, f = 0.1, charge-suppressed interaction model
>1520	95	[13] KHACHATRY...	16BW	CMS	long-lived $\widetilde{g}$ forming R-hadrons, f = 0.5, cloud interaction model
>1540	95	[13] KHACHATRY...	16BW	CMS	long-lived $\widetilde{g}$ forming R-hadrons, f = 0.5, charge-suppressed interaction model
>1270	95	[14] AAD	15AE	ATLS	$\widetilde{g}$ R-hadron, generic R-hadron model
>1360	95	[14] AAD	15AE	ATLS	$\widetilde{g}$ decaying to 300 GeV stable sleptons, LeptoSUSY model
>1115	95	[15] AAD	15BM	ATLS	$\widetilde{g}$ R-hadron, stable
>1185	95	[15] AAD	15BM	ATLS	$\widetilde{g} \rightarrow (g/q\overline{q})\widetilde{\chi}^0_1$, lifetime 10 ns, $m_{\widetilde{\chi}^0_1}$ = 100 GeV
>1099	95	[15] AAD	15BM	ATLS	$\widetilde{g} \rightarrow (g/q\overline{q})\widetilde{\chi}^0_1$, lifetime 10 ns, $m_{\widetilde{g}} - m_{\widetilde{\chi}^0_1}$ = 100 GeV
>1182	95	[15] AAD	15BM	ATLS	$\widetilde{g} \rightarrow t\overline{t}\widetilde{\chi}^0_1$, lifetime 10 ns, $m_{\widetilde{\chi}^0_1}$ = 100 GeV
>1157	95	[15] AAD	15BM	ATLS	$\widetilde{g} \rightarrow t\overline{t}\widetilde{\chi}^0_1$, lifetime 10 ns, $m_{\widetilde{g}} - m_{\widetilde{\chi}^0_1}$ = 480 GeV
> 869	95	[15] AAD	15BM	ATLS	$\widetilde{g} \rightarrow (g/q\overline{q})\widetilde{\chi}^0_1$, lifetime 1 ns, $m_{\widetilde{\chi}^0_1}$ = 100 GeV
> 821	95	[15] AAD	15BM	ATLS	$\widetilde{g} \rightarrow (g/q\overline{q})\widetilde{\chi}^0_1$, lifetime 1 ns, $m_{\widetilde{g}} - m_{\widetilde{\chi}^0_1}$ = 100 GeV
> 836	95	[15] AAD	15BM	ATLS	$\widetilde{g} \rightarrow t\overline{t}\widetilde{\chi}^0_1$, lifetime 1 ns, $m_{\widetilde{\chi}^0_1}$ = 100 GeV
> 836	95	[15] AAD	15BM	ATLS	$\widetilde{g} \rightarrow t\overline{t}\widetilde{\chi}^0_1$, lifetime 10 ns, $m_{\widetilde{g}} - m_{\widetilde{\chi}^0_1}$ = 480 GeV
>1000	95	[16] KHACHATRY...	15AK	CMS	$\widetilde{g}$ R-hadrons, 10 μs< τ <1000 s
> 880	95	[16] KHACHATRY...	15AK	CMS	$\widetilde{g}$ R-hadrons, 1 μs< τ <1000 s
• • • We do not use the following data for averages, fits, limits, etc. • • •					
> 985	95	[17] AAD	13AA	ATLS	$\widetilde{g}$, R-hadrons, generic interaction model
> 832	95	[18] AAD	13BC	ATLS	R-hadrons, $\widetilde{g} \rightarrow g/q\overline{q}\widetilde{\chi}^0_1$, generic R-hadron model, lifetime between 10^{-5} and 10^3 s, $m_{\widetilde{\chi}^0_1}$ = 100 GeV
>1322	95	[19] CHATRCHYAN	13AB	CMS	long-lived $\widetilde{g}$ forming R-hadrons, f = 0.1, cloud interaction model
none 200–341	95	[20] AAD	12P	ATLS	long-lived $\widetilde{g} \rightarrow g\widetilde{\chi}^0_1$, $m_{\widetilde{\chi}^0_1}$ = 100 GeV
> 640	95	[21] CHATRCHYAN	12AN	CMS	long-lived $\widetilde{g} \rightarrow g\widetilde{\chi}^0_1$
>1098	95	[22] CHATRCHYAN	12L	CMS	long-lived $\widetilde{g}$ forming R-hadrons, f = 0.1
> 586	95	[23] AAD	11K	ATLS	stable $\widetilde{g}$
> 544	95	[24] AAD	11P	ATLS	stable $\widetilde{g}$, GMSB scenario, tanβ=5
> 370	95	[25] KHACHATRY...11		CMS	long lived $\widetilde{g}$
> 398	95	[26] KHACHATRY...11C		CMS	stable $\widetilde{g}$

[1] SIRUNYAN 21AF searched in 140 fb^{-1} of pp collisions at $\sqrt{s}$ = 13 TeV for supersymmetry in events with with two displaced vertices from long-lived particles decaying into multijet or dijet final states. No significant excess above the Standard Model expectations is observed. Limits are set on the gluino mass in the simplified model Tglu2RPV with λ''_{323} coupling, on the $\widetilde{\chi}^0_1$ mass in an RPV model with $\widetilde{\chi}^0_1$ pair production and the RPV decay $\widetilde{\chi}^0_1 \rightarrow tbs$ with λ''_{323} coupling and on the $\widetilde{t}$ mass in an RPV model with top squark pair production and the RPV decay $\widetilde{t} \rightarrow \overline{d}_i\overline{d}_j$ with λ''_{3ij} coupling, see their Figure 7.

[2] SIRUNYAN 21U searched in 132 fb^{-1} of pp collisions at $\sqrt{s}$ = 13 TeV for supersymmetry in events with displaced tracks and displaced vertices associated with a dijet system. No significant excess above the Standard Model expectations is observed. Limits are set on long-lived gluinos in an RPC GMSB SUSY model of gluino pair production, with $\widetilde{g} \rightarrow g\widetilde{G}$, see their Figure 9, in Tglu1A in a mini-split model, see their Figure 10, and in an RPV model of gluino pair production, with $\widetilde{g} \rightarrow tbs$ with coupling λ''_{323}, see their Figure 11. Limits are also set on long-lived top squarks in Tstop2RPV, see their Figure 12, in an RPV model with $\widetilde{t} \rightarrow d\overline{\ell}$ and λ'_{x31} coupling, see their Figure 13, and in a dynamical RPV model with $\widetilde{t} \rightarrow \overline{d}\overline{d}$ via a nonholomorphic RPV coupling η''_{311}, see their Figure 14. The best mass limit is achieved in all cases at cτ = 30 mm.

[3] AABOUD 19AT searched in 36.1 fb^{-1} of pp collisions at $\sqrt{s}$ = 13 TeV for metastable and stable R-hadrons. Multiple search strategies for a wide range of lifetimes, corresponding to path lengths of a few meters, are defined. No significant deviations from the expected Standard Model background are observed. Gluino R-hadrons with lifetimes of the order of 50 ns are excluded at 95% C.L. for masses below 1980 GeV using the muon-spectrometer agnostic analysis. Using the full-detector search, the observed lower limits on the mass are 2000 GeV. See their Figure 9 (top).

[4] AABOUD 19C searched in 36.1 fb^{-1} of pp collisions at $\sqrt{s}$ = 13 TeV for metastable and stable R-hadrons arising as excesses in the mass distribution of reconstructed tracks with high transverse momentum and large dE/dx. Gluino R-hadrons with lifetimes above 10 ns are excluded at 95% C.L. with lower mass limit range between 1000 GeV and 2060 GeV, see their Figure 5(a). Masses smaller than 1290 GeV are excluded for a lifetime of 1 ns, see their Figure 6. In the case of stable R-hadrons, the lower mass limit is 1890 GeV, see their Figure 5(b).

[5] SIRUNYAN 19BH searched in 35.9 fb^{-1} of pp collisions at $\sqrt{s}$ = 13 TeV for long-lived particles decaying into jets, with each long-lived particle having a decay vertex well displaced from the production vertex. The selected events are found to be consistent with standard model predictions. Limits are set on the gluino mass in a GMSB model where the gluino is decaying via $\widetilde{g} \rightarrow g\widetilde{G}$, see their Figure 4 and in an RPV model of supersymmetry where the gluino is decaying via $\widetilde{g} \rightarrow \overline{t}\,\overline{b}\overline{s}$, see their Figures 5. Limits are also set on the stop mass in two RPV models, see their Figure 6 (for $\widetilde{t} \rightarrow b\ell$ decays) and Figure 7 (for $\widetilde{t} \rightarrow \overline{d}\overline{d}$ decays).

[6] SIRUNYAN 19BT searched in 137 fb^{-1} of pp collisions at $\sqrt{s}$ = 13 TeV for long-lived particles decaying to displaced, nonprompt jets and missing transverse momentum. Candidate signal events are identified using the timing capabilities of the CMS electromagnetic calorimeter. The results of the search are found to be consistent with the background predictions. Limits are set on the gluino mass in a GMSB model where long-lived gluinos are pair produced and decaying via $\widetilde{g} \rightarrow g\widetilde{G}$, see their Figures 4 and 5.

[7] AABOUD 18S searched in 32.8 fb^{-1} of pp collisions at $\sqrt{s}$ = 13 TeV for long-lived gluinos in final states with large missing transverse momentum and at least one high-mass displaced vertex with five or more tracks. The observed yield is consistent with the expected background. Exclusion limits are derived for Tglu1A models predicting the existence of long-lived gluinos reaching roughly m($\widetilde{g}$) = 2000 GeV to 2370 GeV for m($\widetilde{\chi}^0_1$) = 100 GeV and gluino lifetimes between 0.02 and 10 ns, see their Fig. 8. Limits are presented also as a function of the lifetime (for a fixed gluino-neutralino mass difference of 100 GeV) and of the gluino and neutralino masses (for a fixed lifetime of 1 ns). See their Fig. 9 and 10 respectively.

[8] SIRUNYAN 18AY searched in 35.9 fb^{-1} of pp collisions at $\sqrt{s}$ = 13 TeV for events containing one or more jets and significant $\not{E}_T$. No significant excess above the Standard Model expectations is observed. Limits are set on the gluino mass in the Tglu1A, Tglu2A and Tglu3A simplified models, see their Figure 3. Limits are also set on squark, sbottom and stop masses in the Tsqk1, Tsbot1, Tstop1 and Tstop4 simplified models, see their Figure 3. Finally, limits are set on long-lived gluino masses in a Tglu1A simplified model where the gluino is metastable or long-lived with proper decay lengths in the range 10^{-3} mm < cτ < 10^5 mm, see their Figure 4.

[9] SIRUNYAN 18DV searched in 38.5 fb^{-1} of pp collisions at $\sqrt{s}$ = 13 TeV for long-lived particles in events with multiple jets and two displaced vertices composed of many tracks. No events with two well-separated high-track-multiplicity vertices were observed. Limits are set on the stop and the gluino mass in RPV models of supersymmetry where the stop (gluino) is decaying solely into dijet (multijet) final states, see their Figures 6 and 7.

[10] KHACHATRYAN 17AR searched in 17.6 fb^{-1} of pp collisions at $\sqrt{s}$ = 8 TeV for R-parity-violating SUSY in which long-lived neutralinos or gluinos decay into multijet final states. No significant excess above the Standard Model expectations is observed. Limits are set on the gluino mass for a range of mean proper decay lengths (cτ), see their Fig. 7. The upper limits on the production cross section times branching ratio squared (Fig. 7) are also applicable to long-lived neutralinos.

[11] AABOUD 16B searched in 3.2 fb^{-1} of pp collisions at $\sqrt{s}$ = 13 TeV for long-lived R-hadrons using observables related to large ionization losses and slow propagation velocities, which are signatures of heavy charged particles traveling significantly slower than the speed of light. Exclusion limits at 95% C.L. are set on the long-lived gluino masses exceeding 1580 GeV. See their Fig. 5.

[12] AABOUD 16C searched in 3.2 fb^{-1} of pp collisions at $\sqrt{s}$ = 13 TeV for long-lived and stable R-hadrons identified by anomalous specific ionization energy loss in the ATLAS Pixel detector. Gluino R-hadrons with lifetimes above 0.4 ns are excluded at 95% C.L. with lower mass limit range between 740 GeV and 1590 GeV. In the case of stable R-hadrons, the lower mass limit is 1570 GeV. See their Figs. 5 and 6.

Downloaded from https://academic.oup.com/ptep/article/2022/8/083C01/6651666 by KIT Library user on 27 September 2022

[13] KHACHATRYAN 16BW searched in 2.5 fb^{-1} of pp collisions at $\sqrt{s}$ = 13 TeV for events with heavy stable charged particles, identified by their anomalously high energy deposits in the silicon tracker and/or long time-of-flight measurements by the muon system. No evidence for an excess over the expected background is observed. Limits are derived for pair production of gluinos as a function of mass, depending on the interaction model and on the fraction f, of produced gluinos hadronizing into a $\widetilde{g}$ - gluon state, see Fig. 4 and Table 7.

[14] AAD 15AE searched in 19.1 fb^{-1} of pp collisions at $\sqrt{s}$ = 8 TeV for heavy long-lived charged particles, measured through their specific ionization energy loss in the ATLAS pixel detector or their time-of-flight in the ALTAS muon system. In the absence of an excess of events above the expected backgrounds, limits are set R-hadrons in various scenarios, see Fig. 11. Limits are also set in LeptoSUSY models where the gluino decays to stable 300 GeV leptons, see Fig. 9.

[15] AAD 15BM searched in 18.4 fb^{-1} of pp collisions at $\sqrt{s}$ = 8 TeV for stable and metastable non-relativistic charged particles through their anomalous specific ionization energy loss in the ATLAS pixel detector. In absence of an excess of events above the expected backgrounds, limits are set within a generic R-hadron model, on stable gluino R-hadrons (see Table 5) and on metastable gluino R-hadrons decaying to $(g/q\overline{q})$ plus a light $\widetilde{\chi}^0_1$ (see Fig. 7) and decaying to $t\overline{t}$ plus a light $\widetilde{\chi}^0_1$ (see Fig. 9).

[16] KHACHATRYAN 15AK looked in a data set corresponding to 18.6 fb^{-1} of pp collisions at $\sqrt{s}$ = 8 TeV, and a search interval corresponding to 281 h of trigger lifetime, for long-lived particles that have stopped in the CMS detector. No evidence for an excess over the expected background in a cloud interaction model is observed. Assuming the decay $\widetilde{g} \rightarrow g\,\widetilde{\chi}^0_1$ and lifetimes between 1 μs and 1000 s, limits are derived on $\widetilde{g}$ production as a function of $m_{\widetilde{\chi}^0_1}$, see Figs. 4 and 6. The exclusions require that $m_{\widetilde{\chi}^0_1}$ is kinematically consistent with the minimum values of the jet energy thresholds used.

[17] AAD 13AA searched in 4.7 fb^{-1} of pp collisions at $\sqrt{s}$ = 7 TeV for events containing colored long-lived particles that hadronize forming R-hadrons. No significant excess above the expected background was found. Long-lived R-hadrons containing a $\widetilde{g}$ are excluded for masses up to 985 GeV at 95% C.L in a general interaction model. Also, limits independent of the fraction of R-hadrons that arrive charged in the muon system were derived, see Fig. 6.

[18] AAD 13BC searched in 5.0 fb^{-1} of pp collisions at $\sqrt{s}$ = 7 TeV and in 22.9 fb^{-1} of pp collisions at $\sqrt{s}$ = 8 TeV for bottom squark R-hadrons that have come to rest within the ATLAS calorimeter and decay at some later time to hadronic jets and a neutralino. In absence of an excess of events above the expected backgrounds, limits are set on gluino masses for different decays, lifetimes, and neutralino masses, see their Table 6 and Fig. 10.

[19] CHATRCHYAN 13AB looked in 5.0 fb^{-1} of pp collisions at $\sqrt{s}$ = 7 TeV and in 18.8 fb^{-1} of pp collisions at $\sqrt{s}$ = 8 TeV for events with heavy stable particles, identified by their anomalous dE/dx in the tracker or additionally requiring that it be identified as muon in the muon chambers, from pair production of $\widetilde{g}$'s. No evidence for an excess over the expected background is observed. Limits are derived for pair production of gluinos as a function of mass (see Fig. 8 and Table 5), depending on the fraction, f, of formation of $\widetilde{g}$–g (R-gluonball) states. The quoted limit is for f = 0.1, while for f = 0.5 it degrades to 1276 GeV. In the conservative scenario where every hadronic interaction causes it to become neutral, the limit decreases to 928 GeV for f = 0.1.

[20] AAD 12P looked in 31 pb^{-1} of pp collisions at $\sqrt{s}$ = 7 TeV for events with pair production of long-lived gluinos. The hadronization of the gluinos leads to R-hadrons which may stop inside the detector and later decay via $\widetilde{g} \rightarrow g\,\widetilde{\chi}^0_1$ during gaps between the proton bunches. No significant excess over the expected background is observed. From a counting experiment, a limit at 95% C.L. on the cross section as a function of $m_{\widetilde{g}}$ is derived for $m_{\widetilde{\chi}^0_1}$ = 100 GeV, see Fig. 4. The limit is valid for lifetimes between 10^{-5} and 10^3 seconds and assumes the *Generic* matter interaction model for the production cross section.

[21] CHATRCHYAN 12AN looked in 4.0 fb^{-1} of pp collisions at $\sqrt{s}$ = 7 TeV for events with pair production of long-lived gluinos. The hadronization of the gluinos leads to R-hadrons which may stop inside the detector and later decay via $\widetilde{g} \rightarrow g\,\widetilde{\chi}^0_1$ during gaps between the proton bunches. No significant excess over the expected background is observed. From a counting experiment, a limit at 95% C.L. on the cross section as a function of $m_{\widetilde{g}}$ is derived, see Fig. 3. The mass limit is valid for lifetimes between 10^{-5} and 10^3 seconds, for what they call "the daughter gluon energy E_g >" 100 GeV and assuming the *cloud* interaction model for R-hadrons. Supersedes KHACHATRYAN 11.

[22] CHATRCHYAN 12L looked in 5.0 fb^{-1} of pp collisions at $\sqrt{s}$ = 7 TeV for events with heavy stable particles, identified by their anomalous dE/dx in the tracker or additionally requiring that it be identified as muon in the muon chambers, from pair production of $\widetilde{g}$'s. No evidence for an excess over the expected background is observed. Limits are derived for pair production of gluinos as a function of mass (see Fig. 3), depending on the fraction, f, of formation of $\widetilde{g}$–g (R-glueball) states. The quoted limit is for f = 0.1, while for f = 0.5 it degrades to 1046 GeV. In the conservative scenario where every hadronic interaction causes it to become neutral, the limit decreases to 928 GeV for f=0.1. Supersedes KHACHATRYAN 11C.

[23] AAD 11K looked in 34 pb^{-1} of pp collisions at $\sqrt{s}$ = 7 TeV for events with heavy stable particles, identified by their anomalous dE/dx in the tracker or time of flight in the tile calorimeter, from pair production of $\widetilde{g}$. No evidence for an excess over the SM expectation is observed. Limits are derived for pair production of gluinos as a function of mass (see Fig. 4), for a fraction, f = 10%, of formation of $\widetilde{g} - g$ (R-gluonball). If instead of a phase space driven approach for the hadronic scattering of the R-hadrons, a triple-Regge model or a bag-model is used, the limit degrades to 566 and 562 GeV, respectively.

[24] AAD 11P looked in 37 pb^{-1} of pp collisions at $\sqrt{s}$ = 7 TeV for events with heavy stable particles, reconstructed and identified by their time of flight in the Muon System. There is no requirement on their observation in the tracker to increase the sensitivity to cases where gluinos have a large fraction, f, of formation of neutral $\widetilde{g} - g$ (R-gluonball). No evidence for an excess over the SM expectation is observed. Limits are derived as a function of mass (see Fig. 4), for f=0.1. For fractions f = 0.5 and 1.0 the limit degrades to 537 and 530 GeV, respectively.

[25] KHACHATRYAN 11 looked in 10 pb^{-1} of pp collisions at $\sqrt{s}$ = 7 TeV for events with pair production of long-lived gluinos. The hadronization of the gluinos leads to R-hadrons which may stop inside the detector and later decay via $\widetilde{g} \rightarrow g\,\widetilde{\chi}^0_1$ during gaps between the proton bunches. No significant excess over the expected background is observed. From a counting experiment, a limit at 95% C.L. on the cross section times branching ratio is derived for $m_{\widetilde{g}} - m_{\widetilde{\chi}^0_1}$ > 100 GeV, see their Fig. 2. Assuming 100% branching ratio, lifetimes between 75 ns and 3×10^5 s are excluded for $m_{\widetilde{g}}$ = 300 GeV. The $\widetilde{g}$ mass exclusion is obtained with the same assumptions for lifetimes between 10 μs and 1000 s, but shows some dependence on the model for R-hadron interactions with matter, illustrated in Fig. 3. From a time-profile analysis, the mass exclusion is 382 GeV for a lifetime of 10 μs under the same assumptions as above.

[26] KHACHATRYAN 11C looked in 3.1 pb^{-1} of pp collisions at $\sqrt{s}$ = 7 TeV for events with heavy stable particles, identified by their anomalous dE/dx in the tracker or additionally requiring that it be identified as muon in the muon chambers, from pair production of $\widetilde{g}$. No evidence for an excess over the expected background is observed. Limits are derived for pair production of gluinos as a function of mass (see Fig. 3), depending on the fraction, f, of formation of $\widetilde{g} - g$ (R-gluonball). The quoted limit is for f=0.1, while for f=0.5 it degrades to 357 GeV. In the conservative scenario where every hadronic interaction causes it to become neutral, the limit decreases to 311 GeV for f=0.1.

Light $\widetilde{G}$ (Gravitino) mass limits from collider experiments

The following are bounds on light ($\ll$ 1 eV) gravitino indirectly inferred from its coupling to matter suppressed by the gravitino decay constant.

Unless otherwise stated, all limits assume that other supersymmetric particles besides the gravitino are too heavy to be produced. The gravitino is assumed to be undetected and to give rise to a missing energy ($\not{E}$) signature.

Some earlier papers are now obsolete and have been omitted. They were last listed in our PDG 14 edition: K. Olive, *et al.* (Particle Data Group), Chinese Physics **C38** 070001 (2014) (http://pdg.lbl.gov).

VALUE (eV)	CL%	DOCUMENT ID		TECN	COMMENT
• • • We do not use the following data for averages, fits, limits, etc. • • •					
> 3.5 $\times 10^{-4}$	95	[1] AAD	15BH	ATLS	jet + $\not{E}_T$, $pp \rightarrow (\widetilde{q}/\widetilde{g})\,\widetilde{G}$, $m_{\widetilde{q}} = m_{\widetilde{g}}$ = 500 GeV
> 3 $\times 10^{-4}$	95	[1] AAD	15BH	ATLS	jet + $\not{E}_T$, $pp \rightarrow (\widetilde{q}/\widetilde{g})\,\widetilde{G}$, $m_{\widetilde{q}} = m_{\widetilde{g}}$ = 1000 GeV
> 2 $\times 10^{-4}$	95	[1] AAD	15BH	ATLS	jet + $\not{E}_T$, $pp \rightarrow (\widetilde{q}/\widetilde{g})\,\widetilde{G}$, $m_{\widetilde{q}} = m_{\widetilde{g}}$ = 1500 GeV
> 1.09 $\times 10^{-5}$	95	[2] ABDALLAH	05B	DLPH	$e^+e^- \rightarrow \widetilde{G}\,\widetilde{G}\gamma$
> 1.35 $\times 10^{-5}$	95	[3] ACHARD	04E	L3	$e^+e^- \rightarrow \widetilde{G}\,\widetilde{G}\gamma$
> 1.3 $\times 10^{-5}$		[4] HEISTER	03C	ALEP	$e^+e^- \rightarrow \widetilde{G}\,\widetilde{G}\gamma$
>11.7 $\times 10^{-6}$	95	[5] ACOSTA	02H	CDF	$p\overline{p} \rightarrow \widetilde{G}\,\widetilde{G}\gamma$
> 8.7 $\times 10^{-6}$	95	[6] ABBIENDI,G	00D	OPAL	$e^+e^- \rightarrow \widetilde{G}\,\widetilde{G}\gamma$

[1] AAD 15BH searched in 20.3 fb^{-1} of pp collisions at $\sqrt{s}$ = 8 TeV for associated production of a light gravitino and a squark or gluino. The squark (gluino) is assumed to decay exclusively to a quark (gluon) and a gravitino. No evidence was found for an excess above the expected level of Standard Model background and 95% C.L. lower limits were set on the gravitino mass as a function of the squark/gluino mass, both in the case of degenerate and non-degenerate squark/gluino masses, see Figs. 14 and 15.

[2] ABDALLAH 05B use data from $\sqrt{s}$ = 180–208 GeV. They look for events with a single photon + $\not{E}$ final states from which a cross section limit of σ < 0.18 pb at 208 GeV is obtained, allowing a limit on the mass to be set. Supersedes the results of ABREU 00Z.

[3] ACHARD 04E use data from $\sqrt{s}$ = 189–209 GeV. They look for events with a single photon + $\not{E}$ final states from which a limit on the Gravitino mass is set corresponding to $\sqrt{F}$ > 238 GeV. Supersedes the results of ACCIARRI 99R.

[4] HEISTER 03C use the data from $\sqrt{s}$ = 189–209 GeV to search for $\gamma\not{E}_T$ final states.

[5] ACOSTA 02H looked in 87 pb^{-1} of $p\overline{p}$ collisions at $\sqrt{s}$=1.8 TeV for events with a high-E_T photon and $\not{E}_T$. They compared the data with a GMSB model where the final state could arise from $q\overline{q} \rightarrow \widetilde{G}\,\widetilde{G}\gamma$. Since the cross section for this process scales as $1/|F|^4$, a limit at 95% CL is derived on $|F|^{1/2}$ > 221 GeV. A model independent limit for the above topology is also given in the paper.

[6] ABBIENDI,G 00D searches for $\gamma\not{E}$ final states from $\sqrt{s}$=189 GeV.

Supersymmetry miscellaneous results

Results that do not appear under other headings or that make nonminimal assumptions.

Some earlier papers are now obsolete and have been omitted. They were last listed in our PDG 14 edition: K. Olive, *et al.* (Particle Data Group), Chinese Physics **C38** 070001 (2014) (http://pdg.lbl.gov).

VALUE	CL%	DOCUMENT ID		TECN	COMMENT
• • • We do not use the following data for averages, fits, limits, etc. • • •					
		[1] AAD	20C	ATLS	habemus MSSM, m_A–tanβ plane
none 450–1400	95	[2] AAD	20L	ATLS	heavy neutral Higgs bosons, hMSSM, m_A–tanβ plane
>65	95	[3] AABOUD	16AF	ATLS	selected ATLAS searches on EWK sector
none 0–2	95	[4] AAD	16AG	ATLS	dark photon, γ_d, in SUSY- and Higgs-portal models
		[5] AAD	13P	ATLS	dark γ, hidden valley
		[6] AALTONEN	12AB	CDF	hidden-valley Higgs
none 100–185	95	[7] AAD	11AA	ATLS	scalar gluons
		[8] CHATRCHYAN	11E	CMS	$\mu\mu$ resonances
		[9] ABAZOV	10N	D0	γ_D, hidden valley

[1] AAD 20C uses a statistical combination of six final states $b\overline{b}b\overline{b}$, $b\overline{b}WW$, $b\overline{b}\tau\tau$, $WWWW$, $b\overline{b}\gamma\gamma$, and $WW\gamma\gamma$ to search for non-resonant and resonant production of Higgs boson pairs. The search uses 36.1 fb^{-1} of pp collisions data at $\sqrt{s}$ = 13 TeV. Constraints in the habemus Minimal Supersymmetric Standard Model in the (m_A, tanβ) parameter space are placed, see their Figure 7(b).

Downloaded from https://academic.oup.com/ptep/article/2022/8/083C01/6651666 by KIT Library user on 27 September 2022

[2] AAD 20L used 27.8 fb^{-1} of pp collision data at $\sqrt{s}$ = 13 TeV to search for heavy neutral Higgs bosons produced in association with at least one b-quark and decaying into a pair of b-quarks. The data are compatible with SM expectations, yielding no significant excess of events in the mass range 450–1400 GeV, see their Fig. 11. Exclusion limits at 95% C.L. were derived in hMSSM scenarios as a function of m_A and tanβ, see their Fig. 9 and 10.

[3] AABOUD 16AF uses a selection of searches by ATLAS for the electroweak production of SUSY particles studying resulting constraints on dark matter candidates. They use 20 fb^{-1} of pp collisions at $\sqrt{s}$ = 8 TeV. A likelihood-driven scan of an effective model focusing on the gaugino-higgsino and Higgs sector of the pMSSM is performed. The ATLAS searches impact models where $m_{\widetilde{\chi}^0_1}$ < 65 GeV, excluding 86% of them. See their Figs. 2, 4, and 6.

[4] AAD 16AG searches for prompt lepton-jets using 20 fb^{-1} of pp collisions at $\sqrt{s}$ = 8 TeV collected with the ATLAS detector. Lepton-jets are expected from decays of low-mass dark photons in SUSY-portal and Higgs-portal models. No significant excess of events is observed and 95% CL upper limits are computed on the production cross section times branching ratio for two prompt lepton-jets in models predicting 2 or 4 γ_d via SUSY-portal topologies, for γ_d mass values between 0 and 2 GeV. See their Figs 9 and 10. The results are also interpreted in terms of a 90% CL exclusion region in kinetic mixing and dark-photon mass parameter space. See their Fig. 13.

[5] AAD 13P searched in 5 fb^{-1} of pp collisions at $\sqrt{s}$ = 7 TeV for single lepton-jets with at least four muons; pairs of lepton-jets, each with two or more muons; and pairs of lepton-jets with two or more electrons. All of these could be signatures of Hidden Valley supersymmetric models. No statistically significant deviations from the Standard Model expectations are found. 95% C.L. limits are placed on the production cross section times branching ratio of dark photons for several parameter sets of a Hidden Valley model.

[6] AALTONEN 12AB looked in 5.1 fb^{-1} of $p\overline{p}$ collisions at $\sqrt{s}$ = 1.96 TeV for anomalous production of multiple low-energy leptons in association with a W or Z boson. Such events may occur in hidden valley models in which a supersymmetric Higgs boson is produced in association with a W or Z boson, with $H \rightarrow \widetilde{\chi}^0_1 \widetilde{\chi}^0_1$ pair and with the $\widetilde{\chi}^0_1$ further decaying into a dark photon (γ_D) and the unobservable lightest SUSY particle of the hidden sector. As the γ_D is expected to be light, it may decay into a lepton pair. No significant excess over the SM expectation is observed and a limit at 95% C.L. is set on the cross section for a benchmark model of supersymmetric hidden-valley Higgs production.

[7] AAD 11AA looked in 34 pb^{-1} of pp collisions at $\sqrt{s}$ = 7 TeV for events with $\geq$ 4 jets originating from pair production of scalar gluons, each decaying to two gluons. No two-jet resonances are observed over the SM background. Limits are derived on the cross section times branching ratio (see Fig. 3). Assuming 100% branching ratio for the decay to two gluons, the quoted exclusion range is obtained, except for a 5 GeV mass window around 140 GeV.

[8] CHATRCHYAN 11E looked in 35 pb^{-1} of pp collisions at $\sqrt{s}$ = 7 TeV for events with collimated μ pairs (leptonic jets) from the decay of hidden sector states. No evidence for new resonance production is found. Limits are derived and compared to various SUSY models (see Fig. 4) where the LSP, either the $\widetilde{\chi}^0_1$ or a $\widetilde{q}$, decays to dark sector particles.

[9] ABAZOV 10N looked in 5.8 fb^{-1} of $p\overline{p}$ collisions at $\sqrt{s}$ = 1.96 TeV for events from hidden valley models in which a $\widetilde{\chi}^0_1$ decays into a dark photon, γ_D, and the unobservable lightest SUSY particle of the hidden sector. As the γ_D is expected to be light, it may decay into a tightly collimated lepton pair, called lepton jet. They searched for events with $\not{E}_T$ and two isolated lepton jets observable by an opposite charged lepton pair ee, $e\mu$ or $\mu\mu$. No significant excess over the SM expectation is observed, and a limit at 95% C.L. on the cross section times branching ratio is derived, see their Table I. They also examined the invariant mass of the lepton jets for a narrow resonance, see their Fig. 4, but found no evidence for a signal.

REFERENCES FOR Supersymmetric Particle Searches

AAD	21AK	EPJ C81 600	G. Aad *et al.*	(ATLAS Collab.)
AAD	21AL	PRL 127 051802	G. Aad *et al.*	(ATLAS Collab.)
AAD	21AM	PR D104 032014	G. Aad *et al.*	(ATLAS Collab.)
AAD	21AW	PR D104 112005	G. Aad *et al.*	(ATLAS Collab.)
AAD	21AX	PR D104 112010	G. Aad *et al.*	(ATLAS Collab.)
AAD	21B	EPJ C81 11	G. Aad *et al.*	(ATLAS Collab.)
Also		EPJ C81 249 (errat.)	G. Aad *et al.*	(ATLAS Collab.)
AAD	21BF	EPJ C81 1023	G. Aad *et al.*	(ATLAS Collab.)
AAD	21BG	EPJ C81 1118	G. Aad *et al.*	(ATLAS Collab.)
AAD	21E	PR D103 112003	G. Aad *et al.*	(ATLAS Collab.)
AAD	21F	PR D103 112006	G. Aad *et al.*	(ATLAS Collab.)
AAD	21L	JHEP 2102 143	G. Aad *et al.*	(ATLAS Collab.)
AAD	21O	JHEP 2104 174	G. Aad *et al.*	(ATLAS Collab.)
AAD	21P	JHEP 2104 165	G. Aad *et al.*	(ATLAS Collab.)
AAD	21S	JHEP 2105 093	G. Aad *et al.*	(ATLAS Collab.)
AAD	21X	JHEP 2107 173	G. Aad *et al.*	(ATLAS Collab.)
AAD	21Y	JHEP 2107 167	G. Aad *et al.*	(ATLAS Collab.)
AAIJ	21V	EPJ C81 261	R. Aaij *et al.*	(LHCb Collab.)
ABDALLAH	21	PR D103 102002	H. Abdallah *et al.*	(H.E.S.S. Collab.)
MENG	21B	PRL 127 261802	Y. Meng *et al.*	(PandaX-4T Collab.)
SIRUNYAN	21AD	PR D104 052001	A.M. Sirunyan *et al.*	(CMS Collab.)
SIRUNYAN	21AF	PR D104 052011	A.M. Sirunyan *et al.*	(CMS Collab.)
SIRUNYAN	21B	EPJ C81 3	A.M. Sirunyan *et al.*	(CMS Collab.)
SIRUNYAN	21M	JHEP 2104 123	A.M. Sirunyan *et al.*	(CMS Collab.)
SIRUNYAN	21U	PR D104 012015	A.M. Sirunyan *et al.*	(CMS Collab.)
SIRUNYAN	21V	PR D104 032006	A.M. Sirunyan *et al.*	(CMS Collab.)
TUMASYAN	21C	JHEP 2110 045	A. Tumasyan *et al.*	(CMS Collab.)
TUMASYAN	21I	EPJ C81 970	A. Tumasyan *et al.*	(CMS Collab.)
AABOUD	20	EPJ C80 754	M. Aaboud *et al.*	(ATLAS Collab.)
AAD	20AL	JHEP 2010 062	G. Aad *et al.*	(ATLAS Collab.)
AAD	20AN	JHEP 2010 005	G. Aad *et al.*	(ATLAS Collab.)
AAD	20AS	EPJ C80 1080	G. Aad *et al.*	(ATLAS Collab.)
AAD	20C	PL B800 135103	G. Aad *et al.*	(ATLAS Collab.)
AAD	20D	PL B801 135114	G. Aad *et al.*	(ATLAS Collab.)
AAD	20H	PR D101 032009	G. Aad *et al.*	(ATLAS Collab.)
AAD	20I	PR D101 052005	G. Aad *et al.*	(ATLAS Collab.)
AAD	20K	PR D101 072001	G. Aad *et al.*	(ATLAS Collab.)
AAD	20L	PR D102 032004	G. Aad *et al.*	(ATLAS Collab.)
AAD	20M	PR D102 032006	G. Aad *et al.*	(ATLAS Collab.)
AAD	20O	EPJ C80 123	G. Aad *et al.*	(ATLAS Collab.)
AAD	20R	EPJ C80 691	G. Aad *et al.*	(ATLAS Collab.)
AAD	20S	EPJ C80 737	G. Aad *et al.*	(ATLAS Collab.)
AAD	20V	JHEP 2006 046	G. Aad *et al.*	(ATLAS Collab.)
ABAZAJIAN	20	PR D102 043012	K.N. Abazajian *et al.*	(UCI, VPI, TOKY+)
ABDALLAH	20	PR D102 062001	H. Abdallah *et al.*	(H.E.S.S. Collab.)
ABE	20G	PR D102 072002	K. Abe *et al.*	(Super-Kamiokande Collab.)
ALBERT	20	PR D101 103001	A. Albert *et al.*	(HAWC Collab.)
ALBERT	20A	PL B805 135439	A. Albert *et al.*	(ANTARES Collab.)
ALBERT	20C	PR D102 082002	A. Albert *et al.*	(ANTARES and IceCube Collab.)
ALVAREZ	20	JCAP 2009 004	A. Alvarez *et al.*	
HOOF	20	JCAP 2002 012	S. Hoof, A. Geringer-Sameth, R. Trotta	(GOET+)
SIRUNYAN	20AH	JHEP 2005 032	A.M. Sirunyan *et al.*	(CMS Collab.)
SIRUNYAN	20AU	PRL 124 041803	A.M. Sirunyan *et al.*	(CMS Collab.)
SIRUNYAN	20B	PL B801 135183	A.M. Sirunyan *et al.*	(CMS Collab.)
SIRUNYAN	20BJ	JHEP 2009 149	A.M. Sirunyan *et al.*	(CMS Collab.)
SIRUNYAN	20E	PR D101 052010	A.M. Sirunyan *et al.*	(CMS Collab.)
SIRUNYAN	20N	PL B806 135502	A.M. Sirunyan *et al.*	(CMS Collab.)
SIRUNYAN	20P	EPJ C80 189	A.M. Sirunyan *et al.*	(CMS Collab.)
SIRUNYAN	20T	EPJ C80 752	A.M. Sirunyan *et al.*	(CMS Collab.)
SIRUNYAN	20U	JHEP 2002 015	A.M. Sirunyan *et al.*	(CMS Collab.)
WANG	20G	CP C44 125001	Q. Wang *et al.*	(PandaX-II Collab.)
AABOUD	19AT	PR D99 092007	M. Aaboud *et al.*	(ATLAS Collab.)
AABOUD	19AU	PR D100 012006	M. Aaboud *et al.*	(ATLAS Collab.)
AABOUD	19C	PL B788 96	M. Aaboud *et al.*	(ATLAS Collab.)
AABOUD	19G	PR D99 012001	M. Aaboud *et al.*	(ATLAS Collab.)
AABOUD	19I	PR D99 012009	M. Aaboud *et al.*	(ATLAS Collab.)
AAD	19H	JHEP 1912 060	G. Aad *et al.*	(ATLAS Collab.)
ABE	19	PL B789 45	K. Abe *et al.*	(XMASS Collab.)
AJAJ	19	PR D100 022004	R. Ajaj *et al.*	(DEAP-3600 Collab.)
AMOLE	19	PR D100 022001	C. Amole *et al.*	(PICO Collab.)
APRILE	19A	PRL 122 141301	E. Aprile *et al.*	(XENON1T Collab.)
DI-MAURO	19	PR D99 123027	M. Di Mauro *et al.*	
JOHNSON	19	PR D99 103007	C. Johnson *et al.*	
LI	19D	PR D99 123519	S. Li *et al.*	
SIRUNYAN	19AG	JHEP 1906 143	A.M. Sirunyan *et al.*	(CMS Collab.)
SIRUNYAN	19AO	EPJ C79 305	A.M. Sirunyan *et al.*	(CMS Collab.)
SIRUNYAN	19AU	EPJ C79 444	A.M. Sirunyan *et al.*	(CMS Collab.)
SIRUNYAN	19AW	PL B790 140	A.M. Sirunyan *et al.*	(CMS Collab.)
SIRUNYAN	19BH	PR D99 032011	A.M. Sirunyan *et al.*	(CMS Collab.)
SIRUNYAN	19BI	PR D99 032014	A.M. Sirunyan *et al.*	(CMS Collab.)
SIRUNYAN	19BJ	PR D99 052002	A.M. Sirunyan *et al.*	(CMS Collab.)
SIRUNYAN	19BT	PL B797 134876	A.M. Sirunyan *et al.*	(CMS Collab.)
SIRUNYAN	19BU	JHEP 1908 150	A.M. Sirunyan *et al.*	(CMS Collab.)
SIRUNYAN	19CA	PR D100 112003	A.M. Sirunyan *et al.*	(CMS Collab.)
SIRUNYAN	19CE	PRL 123 241801	A.M. Sirunyan *et al.*	(CMS Collab.)
SIRUNYAN	19CH	JHEP 1910 244	A.M. Sirunyan *et al.*	(CMS Collab.)
SIRUNYAN	19CI	JHEP 1911 109	A.M. Sirunyan *et al.*	(CMS Collab.)
SIRUNYAN	19F	PR D99 012010	A.M. Sirunyan *et al.*	(CMS Collab.)
SIRUNYAN	19K	JHEP 1901 154	A.M. Sirunyan *et al.*	(CMS Collab.)
SIRUNYAN	19S	JHEP 1903 031	A.M. Sirunyan *et al.*	(CMS Collab.)
SIRUNYAN	19U	JHEP 1903 101	A.M. Sirunyan *et al.*	(CMS Collab.)
XIA	19A	PL B792 193	J. Xia *et al.*	(PandaX-II Collab.)
AABOUD	18AQ	JHEP 1806 108	M. Aaboud *et al.*	(ATLAS Collab.)
AABOUD	18AR	JHEP 1806 107	M. Aaboud *et al.*	(ATLAS Collab.)
AABOUD	18AS	JHEP 1806 022	M. Aaboud *et al.*	(ATLAS Collab.)
AABOUD	18AY	EPJ C78 154	M. Aaboud *et al.*	(ATLAS Collab.)
AABOUD	18BB	EPJ C78 250	M. Aaboud *et al.*	(ATLAS Collab.)
AABOUD	18BJ	EPJ C78 625	M. Aaboud *et al.*	(ATLAS Collab.)
AABOUD	18BT	EPJ C78 995	M. Aaboud *et al.*	(ATLAS Collab.)
AABOUD	18BV	JHEP 1809 050	M. Aaboud *et al.*	(ATLAS Collab.)
AABOUD	18CF	PL B785 136	M. Aaboud *et al.*	(ATLAS Collab.)
AABOUD	18CK	PR D98 092002	M. Aaboud *et al.*	(ATLAS Collab.)
AABOUD	18CM	PR D98 092008	M. Aaboud *et al.*	(ATLAS Collab.)
AABOUD	18CO	PR D98 092012	M. Aaboud *et al.*	(ATLAS Collab.)
AABOUD	18I	JHEP 1801 126	M. Aaboud *et al.*	(ATLAS Collab.)
AABOUD	18P	PR D97 032003	M. Aaboud *et al.*	(ATLAS Collab.)
AABOUD	18R	PR D97 052010	M. Aaboud *et al.*	(ATLAS Collab.)
AABOUD	18S	PR D97 052012	M. Aaboud *et al.*	(ATLAS Collab.)
AABOUD	18U	PR D97 092006	M. Aaboud *et al.*	(ATLAS Collab.)
AABOUD	18V	PR D97 112001	M. Aaboud *et al.*	(ATLAS Collab.)
AABOUD	18Y	PR D98 032008	M. Aaboud *et al.*	(ATLAS Collab.)
AABOUD	18Z	PR D98 032009	M. Aaboud *et al.*	(ATLAS Collab.)
ABDALLAH	18	PRL 120 201101	H. Abdallah *et al.*	(H.E.S.S. Collab.)
ADHIKARI	18	NAT 564 83	G. Adhikari *et al.*	(COSINE-100 Collab.)
AGNES	18A	PR D98 102006	P. Agnes *et al.*	(DarkSide-50 Collab.)
AGNESE	18A	PRL 120 061802	R. Agnese *et al.*	(SuperCDMS Collab.)
AHNEN	18	JCAP 1803 009	M.L. Ahnen *et al.*	(MAGIC Collab.)
ALBERT	18B	JCAP 1806 043	A. Albert *et al.*	(HAWC Collab.)
ALBERT	18C	PR D98 123012	A. Albert *et al.*	(HAWC Collab.)
AMAUDRUZ	18	PRL 121 071801	P.A. Amaudruz *et al.*	(DEAP-3600 Collab.)
APRILE	18	PRL 121 111302	E. Aprile *et al.*	(XENON1T Collab.)
SIRUNYAN	18AA	PL B780 118	A.M. Sirunyan *et al.*	(CMS Collab.)
SIRUNYAN	18AC	PL B780 384	A.M. Sirunyan *et al.*	(CMS Collab.)
SIRUNYAN	18AD	PL B780 432	A.M. Sirunyan *et al.*	(CMS Collab.)
SIRUNYAN	18AJ	PL B782 440	A.M. Sirunyan *et al.*	(CMS Collab.)
SIRUNYAN	18AK	PL B783 114	A.M. Sirunyan *et al.*	(CMS Collab.)
SIRUNYAN	18AL	JHEP 1802 067	A.M. Sirunyan *et al.*	(CMS Collab.)
SIRUNYAN	18AN	JHEP 1803 167	A.M. Sirunyan *et al.*	(CMS Collab.)
SIRUNYAN	18AO	JHEP 1803 166	A.M. Sirunyan *et al.*	(CMS Collab.)
SIRUNYAN	18AP	JHEP 1803 160	A.M. Sirunyan *et al.*	(CMS Collab.)
SIRUNYAN	18AR	JHEP 1803 076	A.M. Sirunyan *et al.*	(CMS Collab.)
SIRUNYAN	18AT	JHEP 1804 073	A.M. Sirunyan *et al.*	(CMS Collab.)
SIRUNYAN	18AY	JHEP 1805 025	A.M. Sirunyan *et al.*	(CMS Collab.)
SIRUNYAN	18B	PL B778 263	A.M. Sirunyan *et al.*	(CMS Collab.)
SIRUNYAN	18BR	JHEP 1808 016	A.M. Sirunyan *et al.*	(CMS Collab.)
SIRUNYAN	18C	PR D97 032009	A.M. Sirunyan *et al.*	(CMS Collab.)
SIRUNYAN	18D	PR D97 012007	A.M. Sirunyan *et al.*	(CMS Collab.)
SIRUNYAN	18DI	JHEP 1809 065	A.M. Sirunyan *et al.*	(CMS Collab.)
SIRUNYAN	18DN	JHEP 1811 079	A.M. Sirunyan *et al.*	(CMS Collab.)
SIRUNYAN	18DP	JHEP 1811 151	A.M. Sirunyan *et al.*	(CMS Collab.)
SIRUNYAN	18DV	PR D98 092011	A.M. Sirunyan *et al.*	(CMS Collab.)
SIRUNYAN	18DY	PR D98 112014	A.M. Sirunyan *et al.*	(CMS Collab.)
SIRUNYAN	18EA	PRL 121 141802	A.M. Sirunyan *et al.*	(CMS Collab.)
SIRUNYAN	18M	PRL 120 241801	A.M. Sirunyan *et al.*	(CMS Collab.)
SIRUNYAN	18O	PR D97 032007	A.M. Sirunyan *et al.*	(CMS Collab.)
SIRUNYAN	18X	PL B779 166	A.M. Sirunyan *et al.*	(CMS Collab.)
AABOUD	17AF	JHEP 1708 006	M. Aaboud *et al.*	(ATLAS Collab.)
AABOUD	17AI	JHEP 1709 088	M. Aaboud *et al.*	(ATLAS Collab.)
AABOUD	17AJ	JHEP 1709 084	M. Aaboud *et al.*	(ATLAS Collab.)
Also		JHEP 1908 121 (errat.)	M. Aaboud *et al.*	(ATLAS Collab.)
AABOUD	17AR	PR D96 112010	M. Aaboud *et al.*	(ATLAS Collab.)
AABOUD	17AX	JHEP 1711 195	M. Aaboud *et al.*	(ATLAS Collab.)
AABOUD	17AY	JHEP 1712 085	M. Aaboud *et al.*	(ATLAS Collab.)
AABOUD	17AZ	JHEP 1712 034	M. Aaboud *et al.*	(ATLAS Collab.)
AABOUD	17BE	EPJ C77 898	M. Aaboud *et al.*	(ATLAS Collab.)
AABOUD	17N	EPJ C77 144	M. Aaboud *et al.*	(ATLAS Collab.)
AAIJ	17Z	EPJ C77 224	R. Aaij *et al.*	(LHCb Collab.)
AARTSEN	17	EPJ C77 82	M.G. Aartsen *et al.*	(IceCube Collab.)
AARTSEN	17A	EPJ C77 146	M.G. Aartsen *et al.*	(IceCube Collab.)
Also		EPJ C79 214 (errat.)	M.G. Aartsen *et al.*	(IceCube Collab.)
AARTSEN	17C	EPJ C77 627	M.G. Aartsen *et al.*	(IceCube Collab.)
AKERIB	17	PRL 118 021303	D.S. Akerib *et al.*	(LUX Collab.)
AKERIB	17A	PRL 118 251302	D.S. Akerib *et al.*	(LUX Collab.)
AMOLE	17	PRL 118 251301	C. Amole *et al.*	(PICO Collab.)
APRILE	17G	PRL 119 181301	E. Aprile *et al.*	(XENON Collab.)
ARCHAMBAU...	17	PR D95 082001	S. Archambault *et al.*	(VERITAS Collab.)
ATHRON	17B	EPJ C77 824	P. Athron *et al.*	(GAMBIT Collab.)
BATTAT	17	ASP 91 65	J.B.R. Battat *et al.*	(DRIFT-IId Collab.)
BEHNKE	17	ASP 90 85	E. Behnke *et al.*	(PICASSO Collab.)
CUI	17A	PRL 119 181302	X. Cui *et al.*	(PandaX-II Collab.)

Downloaded from https://academic.oup.com/ptep/article/2022/8/083C01/6651666 by KIT Library user on 27 September 2022

FU	17	PRL 118 071301	C. Fu *et al.*	(PandaX-II Collab.)
Also		PRL 120 049902 (errat.)	C. Fu *et al.*	(PandaX-II Collab.)
KHACHATRY...	17	PR D95 012003	V. Khachatryan *et al.*	(CMS Collab.)
KHACHATRY...	17A	PRL 118 021802	V. Khachatryan *et al.*	(CMS Collab.)
KHACHATRY...	17AD	PR D96 012004	V. Khachatryan *et al.*	(CMS Collab.)
KHACHATRY...	17AR	PR D95 012009	V. Khachatryan *et al.*	(CMS Collab.)
KHACHATRY...	17AS	PR D95 012011	V. Khachatryan *et al.*	(CMS Collab.)
KHACHATRY...	17AW	EPJ C77 635	V. Khachatryan *et al.*	(CMS Collab.)
KHACHATRY...	17L	JHEP 1704 018	V. Khachatryan *et al.*	(CMS Collab.)
KHACHATRY...	17P	EPJ C77 294	V. Khachatryan *et al.*	(CMS Collab.)
KHACHATRY...	17S	PL B767 403	V. Khachatryan *et al.*	(CMS Collab.)
KHACHATRY...	17V	PL B769 391	V. Khachatryan *et al.*	(CMS Collab.)
KHACHATRY...	17Y	PL B770 257	V. Khachatryan *et al.*	(CMS Collab.)
SIRUNYAN	17AF	PRL 119 151802	A.M. Sirunyan *et al.*	(CMS Collab.)
SIRUNYAN	17AS	JHEP 1710 019	A.M. Sirunyan *et al.*	(CMS Collab.)
SIRUNYAN	17AT	JHEP 1710 005	A.M. Sirunyan *et al.*	(CMS Collab.)
SIRUNYAN	17AW	JHEP 1711 029	A.M. Sirunyan *et al.*	(CMS Collab.)
SIRUNYAN	17AY	JHEP 1712 142	A.M. Sirunyan *et al.*	(CMS Collab.)
SIRUNYAN	17AZ	EPJ C77 710	A.M. Sirunyan *et al.*	(CMS Collab.)
SIRUNYAN	17K	EPJ C77 327	A.M. Sirunyan *et al.*	(CMS Collab.)
SIRUNYAN	17P	PR D96 032003	A.M. Sirunyan *et al.*	(CMS Collab.)
SIRUNYAN	17S	EPJ C77 578	A.M. Sirunyan *et al.*	(CMS Collab.)
AABOUD	16AC	EPJ C76 683	M. Aaboud *et al.*	(ATLAS Collab.)
AABOUD	16AF	JHEP 1609 175	M. Aaboud *et al.*	(ATLAS Collab.)
AABOUD	16B	PL B760 647	M. Aaboud *et al.*	(ATLAS Collab.)
AABOUD	16C	PR D93 112015	M. Aaboud *et al.*	(ATLAS Collab.)
AABOUD	16D	PR D94 032005	M. Aaboud *et al.*	(ATLAS Collab.)
AABOUD	16J	PR D94 052009	M. Aaboud *et al.*	(ATLAS Collab.)
AABOUD	16M	EPJ C76 517	M. Aaboud *et al.*	(ATLAS Collab.)
AABOUD	16N	EPJ C76 392	M. Aaboud *et al.*	(ATLAS Collab.)
AABOUD	16P	EPJ C76 541	M. Aaboud *et al.*	(ATLAS Collab.)
AABOUD	16Q	EPJ C76 547	M. Aaboud *et al.*	(ATLAS Collab.)
AAD	16AA	PR D93 052002	G. Aad *et al.*	(ATLAS Collab.)
AAD	16AD	PR D94 032003	G. Aad *et al.*	(ATLAS Collab.)
AAD	16AG	JHEP 1602 062	G. Aad *et al.*	(ATLAS Collab.)
AAD	16AM	JHEP 1606 067	G. Aad *et al.*	(ATLAS Collab.)
AAD	16AY	EPJ C76 81	G. Aad *et al.*	(ATLAS Collab.)
AAD	16BB	EPJ C76 259	G. Aad *et al.*	(ATLAS Collab.)
AAD	16BG	EPJ C76 565	G. Aad *et al.*	(ATLAS Collab.)
AAD	16V	PL B757 334	G. Aad *et al.*	(ATLAS Collab.)
AARTSEN	16C	JCAP 1604 022	M.G. Aartsen *et al.*	(IceCube Collab.)
ABDALLAH	16	PRL 117 111301	H. Abdallah *et al.*	(H.E.S.S. Collab.)
ADRIAN-MAR...	16	PL B759 69	S. Adrian-Martinez *et al.*	(ANTARES Collab.)
AHNEN	16	JCAP 1602 039	M.L. Ahnen *et al.*	(MAGIC and Fermi-LAT Collab.)
AKERIB	16	PRL 116 161301	D.S. Akerib *et al.*	(LUX Collab.)
AKERIB	16A	PRL 116 161302	D.S. Akerib *et al.*	(LUX Collab.)
AMOLE	16	PR D93 052014	C. Amole *et al.*	(PICO Collab.)
APRILE	16B	PR D94 122001	E. Aprile *et al.*	(XENON100 Collab.)
AVRORIN	16	ASP 81 12	A.D. Avrorin *et al.*	(BAIKAL Collab.)
BECHTLE	16	EPJ C76 96	P. Bechtle *et al.*	
CIRELLI	16	JCAP 1607 041	M. Cirelli, M. Taoso	(LPNHE, MADE)
KHACHATRY...	16AA	PL B759 479	V. Khachatryan *et al.*	(CMS Collab.)
KHACHATRY...	16AC	PL B760 178	V. Khachatryan *et al.*	(CMS Collab.)
KHACHATRY...	16AM	PR D93 092009	V. Khachatryan *et al.*	(CMS Collab.)
KHACHATRY...	16AV	JHEP 1607 027	V. Khachatryan *et al.*	(CMS Collab.)
KHACHATRY...	16AY	JHEP 1608 122	V. Khachatryan *et al.*	(CMS Collab.)
KHACHATRY...	16BE	EPJ C76 317	V. Khachatryan *et al.*	(CMS Collab.)
KHACHATRY...	16BJ	EPJ C76 439	V. Khachatryan *et al.*	(CMS Collab.)
KHACHATRY...	16BK	EPJ C76 460	V. Khachatryan *et al.*	(CMS Collab.)
KHACHATRY...	16BS	JHEP 1610 006	V. Khachatryan *et al.*	(CMS Collab.)
KHACHATRY...	16BT	JHEP 1610 129	V. Khachatryan *et al.*	(CMS Collab.)
KHACHATRY...	16BW	PR D94 112004	V. Khachatryan *et al.*	(CMS Collab.)
KHACHATRY...	16BX	PR D94 112009	V. Khachatryan *et al.*	(CMS Collab.)
KHACHATRY...	16BY	JHEP 1612 013	V. Khachatryan *et al.*	(CMS Collab.)
KHACHATRY...	16R	PL B757 6	V. Khachatryan *et al.*	(CMS Collab.)
KHACHATRY...	16V	PL B758 152	V. Khachatryan *et al.*	(CMS Collab.)
KHACHATRY...	16Y	PL B759 9	V. Khachatryan *et al.*	(CMS Collab.)
LEITE	16	JCAP 1611 021	N. Leite *et al.*	
AAD	15AB	PR D92 012010	G. Aad *et al.*	(ATLAS Collab.)
AAD	15AE	JHEP 1501 068	G. Aad *et al.*	(ATLAS Collab.)
AAD	15AI	JHEP 1504 116	G. Aad *et al.*	(ATLAS Collab.)
AAD	15BA	EPJ C75 208	G. Aad *et al.*	(ATLAS Collab.)
AAD	15BG	EPJ C75 318	G. Aad *et al.*	(ATLAS Collab.)
Also		EPJ C75 463	G. Aad *et al.*	(ATLAS Collab.)
AAD	15BH	EPJ C75 299	G. Aad *et al.*	(ATLAS Collab.)
Also		EPJ C75 408 (errat.)	G. Aad *et al.*	(ATLAS Collab.)
AAD	15BM	EPJ C75 407	G. Aad *et al.*	(ATLAS Collab.)
AAD	15BV	JHEP 1510 054	G. Aad *et al.*	(ATLAS Collab.)
AAD	15BX	JHEP 1510 134	G. Aad *et al.*	(ATLAS Collab.)
AAD	15CA	PR D92 072001	G. Aad *et al.*	(ATLAS Collab.)
AAD	15CB	PR D92 072004	G. Aad *et al.*	(ATLAS Collab.)
AAD	15CJ	EPJ C75 510	G. Aad	(ATLAS Collab.)
AAD	15CS	PR D91 012008	G. Aad *et al.*	(ATLAS Collab.)
Also		PR D92 059903 (errat.)	G. Aad *et al.*	(ATLAS Collab.)
AAD	15J	PRL 114 142001	G. Aad *et al.*	(ATLAS Collab.)
AAD	15K	PRL 114 161801	G. Aad *et al.*	(ATLAS Collab.)
AAD	15O	PRL 115 031801	G. Aad *et al.*	(ATLAS Collab.)
AAD	15X	PR D91 112016	G. Aad *et al.*	(ATLAS Collab.)
AAIJ	15BD	EPJ C75 595	R. Aaij *et al.*	(LHCb Collab.)
AARTSEN	15E	EPJ C75 492	M.G. Aartsen *et al.*	(IceCube Collab.)
ACKERMANN	15	PR D91 122002	M. Ackermann *et al.*	(Fermi-LAT Collab.)
ACKERMANN	15A	JCAP 1509 008	M. Ackermann *et al.*	(Fermi-LAT Collab.)
ACKERMANN	15B	PRL 115 231301	M. Ackermann *et al.*	(Fermi-LAT Collab.)
AGNES	15	PL B743 456	P. Agnes *et al.*	(DarkSide-50 Collab.)
AGNESE	15B	PR D92 072003	R. Agnese *et al.*	(SuperCDMS Collab.)
BAGNASCHI	15	EPJ C75 500	E.A. Bagnaschi *et al.*	
BUCKLEY	15	PR D91 102001	M.R. Buckley *et al.*	
CHOI	15	PRL 114 141301	K. Choi *et al.*	(Super-Kamiokande Collab.)
KHACHATRY...	15AB	JHEP 1501 096	V. Khachatryan *et al.*	(CMS Collab.)
KHACHATRY...	15AD	JHEP 1504 124	V. Khachatryan *et al.*	(CMS Collab.)
KHACHATRY...	15AF	JHEP 1505 078	V. Khachatryan *et al.*	(CMS Collab.)
KHACHATRY...	15AH	JHEP 1506 116	V. Khachatryan *et al.*	(CMS Collab.)
KHACHATRY...	15AK	EPJ C75 151	V. Khachatryan *et al.*	(CMS Collab.)
KHACHATRY...	15AO	EPJ C75 325	V. Khachatryan *et al.*	(CMS Collab.)
KHACHATRY...	15AR	PL B743 503	V. Khachatryan *et al.*	(CMS Collab.)
KHACHATRY...	15AZ	PR D92 072006	V. Khachatryan *et al.*	(CMS Collab.)
KHACHATRY...	15E	PRL 114 061801	V. Khachatryan *et al.*	(CMS Collab.)
KHACHATRY...	15I	PL B745 5	V. Khachatryan *et al.*	(CMS Collab.)
KHACHATRY...	15L	PL B747 98	V. Khachatryan *et al.*	(CMS Collab.)
KHACHATRY...	15O	PL B748 255	V. Khachatryan *et al.*	(CMS Collab.)
KHACHATRY...	15W	PR D91 052012	V. Khachatryan *et al.*	(CMS Collab.)
KHACHATRY...	15X	PR D91 052018	V. Khachatryan *et al.*	(CMS Collab.)
ROLBIECKI	15	PL B750 247	K. Rolbiecki, J. Tattersall	(MADE, HEID)
AAD	14AE	JHEP 1409 176	G. Aad *et al.*	(ATLAS Collab.)
AAD	14AG	JHEP 1409 103	G. Aad *et al.*	(ATLAS Collab.)
AAD	14AJ	JHEP 1409 015	G. Aad *et al.*	(ATLAS Collab.)
AAD	14AV	JHEP 1410 096	G. Aad *et al.*	(ATLAS Collab.)
AAD	14AX	JHEP 1410 024	G. Aad *et al.*	(ATLAS Collab.)
AAD	14B	EPJ C74 2883	G. Aad *et al.*	(ATLAS Collab.)
AAD	14BD	JHEP 1411 118	G. Aad *et al.*	(ATLAS Collab.)
AAD	14BH	PR D90 112005	G. Aad *et al.*	(ATLAS Collab.)
AAD	14E	JHEP 1406 035	G. Aad *et al.*	(ATLAS Collab.)
AAD	14F	JHEP 1406 124	G. Aad *et al.*	(ATLAS Collab.)
AAD	14G	JHEP 1405 071	G. Aad *et al.*	(ATLAS Collab.)
AAD	14H	JHEP 1404 169	G. Aad *et al.*	(ATLAS Collab.)
AAD	14K	PR D90 012004	G. Aad *et al.*	(ATLAS Collab.)
AAD	14T	PR D90 052008	G. Aad *et al.*	(ATLAS Collab.)
AAD	14X	PR D90 052001	G. Aad *et al.*	(ATLAS Collab.)
AALTONEN	14	PR D90 012011	T. Aaltonen *et al.*	(CDF Collab.)
ACKERMANN	14	PR D89 042001	M. Ackermann *et al.*	(Fermi-LAT Collab.)
AKERIB	14	PRL 112 091303	D.S. Akerib *et al.*	(LUX Collab.)
ALEKSIC	14	JCAP 1402 008	J. Aleksic *et al.*	(MAGIC Collab.)
AVRORIN	14	ASP 62 12	A.D. Avrorin *et al.*	(BAIKAL Collab.)
BUCHMUEL...	14	EPJ C74 2809	O. Buchmueller *et al.*	
BUCHMUEL...	14A	EPJ C74 2922	O. Buchmueller *et al.*	
CHATRCHYAN	14AH	PR D90 112001	S. Chatrchyan *et al.*	(CMS Collab.)
CHATRCHYAN	14H	JHEP 1401 163	S. Chatrchyan *et al.*	(CMS Collab.)
CHATRCHYAN	14I	JHEP 1406 055	S. Chatrchyan *et al.*	(CMS Collab.)
CHATRCHYAN	14N	PL B733 328	S. Chatrchyan *et al.*	(CMS Collab.)
CHATRCHYAN	14P	PL B730 193	S. Chatrchyan *et al.*	(CMS Collab.)
CHATRCHYAN	14R	PR D90 032006	S. Chatrchyan *et al.*	(CMS Collab.)
CHATRCHYAN	14U	PRL 112 161802	S. Chatrchyan *et al.*	(CMS Collab.)
CZAKON	14	PRL 113 201803	M. Czakon *et al.*	(AACH, CAMB, UCB, LBL+)
FELIZARDO	14	PR D89 072013	M. Felizardo *et al.*	(SIMPLE Collab.)
KHACHATRY...	14C	PL B736 371	V. Khachatryan *et al.*	(CMS Collab.)
KHACHATRY...	14I	EPJ C74 3036	V. Khachatryan *et al.*	(CMS Collab.)
KHACHATRY...	14L	PR D90 092007	V. Khachatryan *et al.*	(CMS Collab.)
KHACHATRY...	14T	PL B739 229	V. Khachatryan *et al.*	(CMS Collab.)
PDG	14	CP C38 070001	K. Olive *et al.*	(PDG Collab.)
ROSZKOWSKI	14	JHEP 1408 067	L. Roszkowski, E.M. Sessolo, A.J. Williams	(WINR)
AAD	13	PL B718 841	G. Aad *et al.*	(ATLAS Collab.)
AAD	13AA	PL B720 277	G. Aad *et al.*	(ATLAS Collab.)
AAD	13AI	PL B723 15	G. Aad *et al.*	(ATLAS Collab.)
AAD	13AP	PR D88 012001	G. Aad *et al.*	(ATLAS Collab.)
AAD	13AU	JHEP 1310 189	G. Aad *et al.*	(ATLAS Collab.)
AAD	13B	PL B718 879	G. Aad *et al.*	(ATLAS Collab.)
AAD	13BC	PR D88 112003	G. Aad *et al.*	(ATLAS Collab.)
AAD	13BD	PR D88 112006	G. Aad *et al.*	(ATLAS Collab.)
AAD	13H	JHEP 1301 131	G. Aad *et al.*	(ATLAS Collab.)
AAD	13L	PR D87 012008	G. Aad *et al.*	(ATLAS Collab.)
AAD	13P	PL B719 299	G. Aad *et al.*	(ATLAS Collab.)
AAD	13Q	PL B719 261	G. Aad *et al.*	(ATLAS Collab.)
AAD	13R	PL B719 280	G. Aad *et al.*	(ATLAS Collab.)
AALTONEN	13I	PR D88 031103	T. Aaltonen *et al.*	(CDF Collab.)
AALTONEN	13Q	PRL 110 201802	T. Aaltonen *et al.*	(CDF Collab.)
AARTSEN	13C	PR D88 122001	M.G. Aartsen *et al.*	(IceCube Collab.)
ABAZOV	13B	PR D87 052011	V.M. Abazov *et al.*	(D0 Collab.)
ACKERMANN	13A	PR D88 082002	M. Ackermann *et al.*	(Fermi-LAT Collab.)
ADRIAN-MAR...	13	JCAP 1311 032	S. Adrian-Martinez *et al.*	(ANTARES Collab.)
AGNESE	13	PR D88 031104	R. Agnese *et al.*	(CDMS Collab.)
AGNESE	13A	PRL 111 251301	R. Agnese *et al.*	(CDMS Collab.)
APRILE	13	PRL 111 021301	E. Aprile *et al.*	(XENON100 Collab.)
BERGSTROM	13	PRL 111 171101	L. Bergstrom *et al.*	
BOLIEV	13	JCAP 1309 019	M. Boliev *et al.*	
CABRERA	13	JHEP 1307 182	M. Cabrera, J. Casas, R. de Austri	
CALIBBI	13	JHEP 1310 132	L. Calibbi *et al.*	
CHATRCHYAN	13	PL B718 815	S. Chatrchyan *et al.*	(CMS Collab.)
CHATRCHYAN	13AB	JHEP 1307 122	S. Chatrchyan *et al.*	(CMS Collab.)
CHATRCHYAN	13AH	PL B722 273	S. Chatrchyan *et al.*	(CMS Collab.)
CHATRCHYAN	13AO	PR D87 072001	S. Chatrchyan *et al.*	(CMS Collab.)
CHATRCHYAN	13AT	PR D88 052017	S. Chatrchyan *et al.*	(CMS Collab.)
CHATRCHYAN	13AV	PRL 111 081802	S. Chatrchyan *et al.*	(CMS Collab.)
CHATRCHYAN	13G	JHEP 1301 077	S. Chatrchyan *et al.*	(CMS Collab.)
CHATRCHYAN	13H	PL B719 42	S. Chatrchyan *et al.*	(CMS Collab.)
CHATRCHYAN	13T	EPJ C73 2568	S. Chatrchyan *et al.*	(CMS Collab.)
CHATRCHYAN	13V	JHEP 1303 037	S. Chatrchyan *et al.*	(CMS Collab.)
Also		JHEP 1307 041 (errat.)	S. Chatrchyan *et al.*	(CMS Collab.)
CHATRCHYAN	13W	JHEP 1303 111	S. Chatrchyan *et al.*	(CMS Collab.)
ELLIS	13B	EPJ C73 2403	J. Ellis *et al.*	
JIN	13	JCAP 1311 026	H.-B. Jin, Y.-L. Wu, Y.-F. Zhou	
KOPP	13	PR D88 076013	J. Kopp	
STREGE	13	JCAP 1304 013	C. Strege *et al.*	
AAD	12AF	PL B714 180	G. Aad *et al.*	(ATLAS Collab.)
AAD	12AG	PL B714 197	G. Aad *et al.*	(ATLAS Collab.)
AAD	12AN	PRL 108 181802	G. Aad *et al.*	(ATLAS Collab.)
AAD	12AS	PRL 108 261804	G. Aad *et al.*	(ATLAS Collab.)
AAD	12AX	PR D85 012006	G. Aad *et al.*	(ATLAS Collab.)
Also		PR D87 099903 (errat.)	G. Aad *et al.*	(ATLAS Collab.)
AAD	12BJ	EPJ C72 1993	G. Aad *et al.*	(ATLAS Collab.)
AAD	12CJ	PR D86 092002	G. Aad *et al.*	(ATLAS Collab.)
AAD	12CM	EPJ C72 2215	G. Aad *et al.*	(ATLAS Collab.)
AAD	12CP	PL B718 411	G. Aad *et al.*	(ATLAS Collab.)
AAD	12CT	JHEP 1212 124	G. Aad *et al.*	(ATLAS Collab.)
AAD	12P	EPJ C72 1965	G. Aad *et al.*	(ATLAS Collab.)
AAD	12R	PL B707 478	G. Aad *et al.*	(ATLAS Collab.)
AAD	12T	PL B709 137	G. Aad *et al.*	(ATLAS Collab.)
AAD	12W	PL B710 67	G. Aad *et al.*	(ATLAS Collab.)
AALTONEN	12AB	PR D85 092001	T. Aaltonen *et al.*	(CDF Collab.)
ABAZOV	12AD	PR D86 071701	V.M. Abazov *et al.*	(D0 Collab.)
AKIMOV	12	PL B709 14	D.Yu. Akimov *et al.*	(ZEPLIN-III Collab.)
AKULA	12	PR D85 075001	S. Akula *et al.*	(NEAS, MICH)
ANGLOHER	12	EPJ C72 1971	G. Angloher *et al.*	(CRESST-II Collab.)
APRILE	12	PRL 109 181301	E. Aprile *et al.*	(XENON100 Collab.)
ARBEY	12A	PL B708 162	A. Arbey *et al.*	
ARCHAMBAU...	12	PL B711 153	S. Archambault *et al.*	(PICASSO Collab.)
BAER	12	JHEP 1205 091	H. Baer, V. Barger, A. Mustafayev	(OKLA, WISC+)
BALAZS	12	EPJ C73 2563	C. Balazs *et al.*	
BECHTLE	12	JHEP 1206 098	P. Bechtle *et al.*	
BEHNKE	12	PR D86 052001	E. Behnke *et al.*	(COUPP Collab.)
Also		PR D90 079902 (errat.)	E. Behnke *et al.*	(COUPP Collab.)
BESKIDT	12	EPJ C72 2166	C. Beskidt *et al.*	(KARLE, JINR, ITEP)
BOTTINO	12	PR D85 095013	A. Bottino, N. Fornengo, S. Scopel	(TORI, SOGA)
BUCHMUEL...	12	EPJ C72 2020	O. Buchmueller *et al.*	
CAO	12A	PL B710 665	J. Cao *et al.*	
CHATRCHYAN	12	PR D85 012004	S. Chatrchyan *et al.*	(CMS Collab.)
CHATRCHYAN	12AE	PRL 109 171803	S. Chatrchyan *et al.*	(CMS Collab.)
CHATRCHYAN	12AI	JHEP 1208 110	S. Chatrchyan *et al.*	(CMS Collab.)
CHATRCHYAN	12AL	JHEP 1206 169	S. Chatrchyan *et al.*	(CMS Collab.)
CHATRCHYAN	12AN	JHEP 1208 026	S. Chatrchyan *et al.*	(CMS Collab.)
CHATRCHYAN	12AT	JHEP 1210 018	S. Chatrchyan *et al.*	(CMS Collab.)
CHATRCHYAN	12BJ	JHEP 1211 147	S. Chatrchyan *et al.*	(CMS Collab.)
CHATRCHYAN	12BK	JHEP 1211 172	S. Chatrchyan *et al.*	(CMS Collab.)
CHATRCHYAN	12BO	JHEP 1212 055	S. Chatrchyan *et al.*	(CMS Collab.)
CHATRCHYAN	12L	PL B713 408	S. Chatrchyan *et al.*	(CMS Collab.)
DAW	12	ASP 35 397	E. Daw *et al.*	(DRIFT-IId Collab.)
DREINER	12A	EPL 99 61001	H.K. Dreiner, M. Kramer, J. Tattersall	(BONN+)
ELLIS	12B	EPJ C72 2005	J. Ellis, K. Olive	
FELIZARDO	12	PRL 108 201302	M. Felizardo *et al.*	(SIMPLE Collab.)
FENG	12B	PR D85 075007	J. Feng, K. Matchev, D. Sanford	
KADASTIK	12	JHEP 1205 061	M. Kadastik *et al.*	
KIM	12	PRL 108 181301	S.C. Kim *et al.*	(KIMS Collab.)
STREGE	12	JCAP 1203 030	C. Strege *et al.*	(LOIC, AMST, MADU, GRAN+)
AAD	11AA	EPJ C71 1828	G. Aad *et al.*	(ATLAS Collab.)
AAD	11G	PRL 106 131802	G. Aad *et al.*	(ATLAS Collab.)

Downloaded from https://academic.oup.com/ptep/article/2022/8/083C01/6651666 by KIT Library user on 27 September 2022

AAD	11H	PRL 106 251801	G. Aad *et al.*	(ATLAS Collab.)
AAD	11K	PL B701 1	G. Aad *et al.*	(ATLAS Collab.)
AAD	11O	PL B701 398	G. Aad *et al.*	(ATLAS Collab.)
AAD	11P	PL B703 428	G. Aad *et al.*	(ATLAS Collab.)
AAD	11Z	EPJ C71 1809	G. Aad *et al.*	(ATLAS Collab.)
AHMED	11A	PR D84 011102	Z. Ahmed *et al.*	(CDMS and EDELWEISS Collabs.)
ARMENGAUD	11	PL B702 329	E. Armengaud *et al.*	(EDELWEISS-II Collab.)
BUCHMUEL...	11	EPJ C71 1583	O. Buchmueller *et al.*	
BUCHMUEL...	11B	EPJ C71 1722	O. Buchmueller *et al.*	
CHATRCHYAN	11B	JHEP 1106 093	S. Chatrchyan *et al.*	(CMS Collab.)
CHATRCHYAN	11D	JHEP 1107 113	S. Chatrchyan *et al.*	(CMS Collab.)
CHATRCHYAN	11E	JHEP 1107 098	S. Chatrchyan *et al.*	(CMS Collab.)
CHATRCHYAN	11V	PL B704 411	S. Chatrchyan *et al.*	(CMS Collab.)
KHACHATRY...	11	PRL 106 011801	V. Khachatryan *et al.*	(CMS Collab.)
KHACHATRY...	11C	JHEP 1103 024	V. Khachatryan *et al.*	(CMS Collab.)
ROSZKOWSKI	11	PR D83 015014	L. Roszkowski *et al.*	
AALTONEN	10	PRL 104 011801	T. Aaltonen *et al.*	(CDF Collab.)
AALTONEN	10R	PRL 105 081802	T. Aaltonen *et al.*	(CDF Collab.)
AALTONEN	10Z	PRL 105 191801	T. Aaltonen *et al.*	(CDF Collab.)
ABAZOV	10L	PL B693 95	V.M. Abazov *et al.*	(D0 Collab.)
ABAZOV	10M	PRL 105 191802	V.M. Abazov *et al.*	(D0 Collab.)
ABAZOV	10N	PRL 105 211802	V.M. Abazov *et al.*	(D0 Collab.)
ABAZOV	10P	PRL 105 221802	V.M. Abazov *et al.*	(D0 Collab.)
ACKERMANN	10	JCAP 1005 025	M. Ackermann	(Fermi-LAT Collab.)
ARMENGAUD	10	PL B687 294	E. Armengaud *et al.*	(EDELWEISS-II Collab.)
ELLIS	10	EPJ C69 201	J. Ellis, A. Mustafayev, K. Olive	
ABAZOV	09M	PRL 102 161802	V.M. Abazov *et al.*	(D0 Collab.)
AHMED	09	PRL 102 011301	Z. Ahmed *et al.*	(CDMS Collab.)
ANGLOHER	09	ASP 31 270	G. Angloher *et al.*	(CRESST Collab.)
BUCHMUEL...	09	EPJ C64 391	O. Buchmueller *et al.*	(LOIC, FNAL, CERN+)
DREINER	09	EPJ C62 547	H. Dreiner *et al.*	
LEBEDENKO	09	PR D80 052010	V.N. Lebedenko *et al.*	(ZEPLIN-III Collab.)
LEBEDENKO	09A	PRL 103 151302	V.N. Lebedenko *et al.*	(ZEPLIN-III Collab.)
SORENSEN	09	NIM A601 339	P. Sorensen *et al.*	(XENON10 Collab.)
ABAZOV	08F	PL B659 856	V.M. Abazov *et al.*	(D0 Collab.)
ANGLE	08	PRL 100 021303	J. Angle *et al.*	(XENON10 Collab.)
ANGLE	08A	PRL 101 091301	J. Angle *et al.*	(XENON10 Collab.)
BEDNYAKOV	08	PAN 71 111	V.A. Bednyakov, H.P. Klapdor-Kleingrothaus, I.V. Krivosheina	
		Translated from YAF 71 112.		
BEHNKE	08	SCI 319 933	E. Behnke	(COUPP Collab.)
BENETTI	08	ASP 28 495	P. Benetti *et al.*	(WARP Collab.)
BUCHMUEL...	08	JHEP 0809 117	O. Buchmueller *et al.*	
ELLIS	08	PR D78 075012	J. Ellis, K. Olive, P. Sandick	(CERN, MINN)
ABULENCIA	07H	PRL 98 131804	A. Abulencia *et al.*	(CDF Collab.)
ALNER	07A	ASP 28 287	G.J. Alner *et al.*	(ZEPLIN-II Collab.)
CALIBBI	07	JHEP 0709 081	L. Calibbi *et al.*	
ELLIS	07	JHEP 0706 079	J. Ellis, K. Olive, P. Sandick	(CERN, MINN)
LEE	07A	PRL 99 091301	H.S. Lee *et al.*	(KIMS Collab.)
ABBIENDI	06B	EPJ C46 307	G. Abbiendi *et al.*	(OPAL Collab.)
ACHTERBERG	06	ASP 26 129	A. Achterberg *et al.*	(AMANDA Collab.)
ACKERMANN	06	ASP 24 459	M. Ackermann *et al.*	(AMANDA Collab.)
AKERIB	06	PR D73 011102	D.S. Akerib *et al.*	(CDMS Collab.)
AKERIB	06A	PRL 96 011302	D.S. Akerib *et al.*	(CDMS Collab.)
ALLANACH	06	PR D73 015013	B.C. Allanach *et al.*	
BENOIT	06	PL B637 156	A. Benoit *et al.*	
DE-AUSTRI	06	JHEP 0605 002	R.R. de Austri, R. Trotta, L. Roszkowski	
DEBOER	06	PL B636 13	W. de Boer *et al.*	
LEP-SLC	06	PRPL 427 257	ALEPH, DELPHI, L3, OPAL, SLD and working groups	
SHIMIZU	06A	PL B633 195	Y. Shimizu *et al.*	
SMITH	06	PL B642 567	N.J.T. Smith, A.S. Murphy, T.J. Summer	
ABAZOV	05A	PRL 94 041801	V.M. Abazov *et al.*	(D0 Collab.)
ABDALLAH	05B	EPJ C38 395	J. Abdallah *et al.*	(DELPHI Collab.)
AKERIB	05	PR D72 052009	D.S. Akerib *et al.*	(CDMS Collab.)
ALNER	05	PL B616 17	G.J. Alner *et al.*	(UK Dark Matter Collab.)
ALNER	05A	ASP 23 444	G.J. Alner *et al.*	(UK Dark Matter Collab.)
BAER	05	JHEP 0507 065	H. Baer *et al.*	(FSU, MSU, HAWA)
BARNABE-HE...	05	PL B624 186	M. Barnabe-Heider *et al.*	(PICASSO Collab.)
ELLIS	05	PR D71 095007	J. Ellis *et al.*	
SANGLARD	05	PR D71 122002	V. Sanglard *et al.*	(EDELWEISS Collab.)
ABBIENDI	04	EPJ C32 453	G. Abbiendi *et al.*	(OPAL Collab.)
ABBIENDI	04F	EPJ C33 149	G. Abbiendi *et al.*	(OPAL Collab.)
ABBIENDI	04H	EPJ C35 1	G. Abbiendi *et al.*	(OPAL Collab.)
ABBIENDI	04N	PL B602 167	G. Abbiendi *et al.*	(OPAL Collab.)
ABDALLAH	04H	EPJ C34 145	J. Abdallah *et al.*	(DELPHI Collab.)
ABDALLAH	04M	EPJ C36 1	J. Abdallah *et al.*	(DELPHI Collab.)
Also		EPJ C37 129 (errat.)	J. Abdallah *et al.*	(DELPHI Collab.)
ACHARD	04	PL B580 37	P. Achard *et al.*	(L3 Collab.)
ACHARD	04E	PL B587 16	P. Achard *et al.*	(L3 Collab.)
AKERIB	04	PRL 93 211301	D.S. Akerib *et al.*	(CDMS II Collab.)
BALTZ	04	JHEP 0410 052	E. Baltz, P. Gondolo	
BELANGER	04	JHEP 0403 012	G. Belanger *et al.*	
BOTTINO	04	PR D69 037302	A. Bottino *et al.*	
DESAI	04	PR D70 083523	S. Desai *et al.*	(Super-Kamiokande Collab.)
ELLIS	04	PR D69 015005	J. Ellis *et al.*	
ELLIS	04B	PR D70 055005	J. Ellis *et al.*	
HEISTER	04	PL B583 247	A. Heister *et al.*	(ALEPH Collab.)
PIERCE	04A	PR D70 075006	A. Pierce	
ABBIENDI	03L	PL B572 8	G. Abbiendi *et al.*	(OPAL Collab.)
ABDALLAH	03M	EPJ C31 421	J. Abdallah *et al.*	(DELPHI Collab.)
AHMED	03	ASP 19 691	B. Ahmed *et al.*	(UK Dark Matter Collab.)
AKERIB	03	PR D68 082002	D.S. Akerib *et al.*	(CDMS Collab.)
BAER	03	JCAP 0305 006	H. Baer, C. Balazs	
BAER	03A	JCAP 0309 007	H. Baer *et al.*	
BOTTINO	03	PR D68 043506	A. Bottino *et al.*	
BOTTINO	03A	PR D67 063519	A. Bottino, N. Fornengo, S. Scopel	
CHATTOPAD...	03	PR D68 035005	U. Chattopadhyay, A. Corsetti, P. Nath	
ELLIS	03	ASP 18 395	J. Ellis, K.A. Olive, Y. Santoso	
ELLIS	03B	NP B652 259	J. Ellis *et al.*	
ELLIS	03C	PL B565 176	J. Ellis *et al.*	
ELLIS	03D	PL B573 162	J. Ellis *et al.*	
ELLIS	03E	PR D67 123502	J. Ellis *et al.*	
HEISTER	03C	EPJ C28 1	A. Heister *et al.*	(ALEPH Collab.)
HEISTER	03G	EPJ C31 1	A. Heister *et al.*	(ALEPH Collab.)
KLAPDOR-K...	03	ASP 18 525	H.V. Klapdor-Kleingrothaus *et al.*	
LAHANAS	03	PL B568 55	A. Lahanas, D. Nanopoulos	
TAKEDA	03	PL B572 145	A. Takeda *et al.*	
ABRAMS	02	PR D66 122003	D. Abrams *et al.*	(CDMS Collab.)
ACOSTA	02H	PRL 89 281801	D. Acosta *et al.*	(CDF Collab.)
ANGLOHER	02	ASP 18 43	G. Angloher *et al.*	(CRESST Collab.)
ARNOWITT	02	hep-ph/0211417	R. Arnowitt, B. Dutta	
ELLIS	02B	PL B532 318	J. Ellis, A. Ferstl, K.A. Olive	
HEISTER	02	PL B526 191	A. Heister *et al.*	(ALEPH Collab.)
HEISTER	02E	PL B526 206	A. Heister *et al.*	(ALEPH Collab.)
HEISTER	02J	PL B533 223	A. Heister *et al.*	(ALEPH Collab.)
HEISTER	02N	PL B544 73	A. Heister *et al.*	(ALEPH Collab.)
KIM	02	PL B527 18	H.B. Kim *et al.*	
KIM	02B	JHEP 0212 034	Y.G. Kim *et al.*	
LAHANAS	02	EPJ C23 185	A. Lahanas, V.C. Spanos	
MORALES	02B	ASP 16 325	A. Morales *et al.*	(COSME Collab.)
MORALES	02C	PL B532 8	A. Morales *et al.*	(IGEX Collab.)
ABREU	01	EPJ C19 29	P. Abreu *et al.*	(DELPHI Collab.)
ABREU	01B	EPJ C19 201	P. Abreu *et al.*	(DELPHI Collab.)
BALTZ	01	PRL 86 5004	E. Baltz, P. Gondolo	
BARATE	01	PL B499 67	R. Barate *et al.*	(ALEPH Collab.)
BARATE	01B	EPJ C19 415	R. Barate *et al.*	(ALEPH Collab.)
BARGER	01C	PL B518 117	V. Barger, C. Kao	
BAUDIS	01	PR D63 022001	L. Baudis *et al.*	(Heidelberg-Moscow Collab.)
BERNABEI	01	PL B509 197	R. Bernabei *et al.*	(DAMA Collab.)
BOTTINO	01	PR D63 125003	A. Bottino *et al.*	
CORSETTI	01	PR D64 125010	A. Corsetti, P. Nath	
ELLIS	01B	PL B510 236	J. Ellis *et al.*	
ELLIS	01C	PR D63 065016	J. Ellis, A. Ferstl, K.A. Olive	
GOMEZ	01	PL B512 252	M.E. Gomez, J.D. Vergados	
LAHANAS	01	PL B518 94	A. Lahanas, D.V. Nanopoulos, V. Spanos	
ABBIENDI	00	EPJ C12 1	G. Abbiendi *et al.*	(OPAL Collab.)
ABBIENDI	00G	EPJ C14 51	G. Abbiendi *et al.*	(OPAL Collab.)
ABBIENDI	00H	EPJ C14 187	G. Abbiendi *et al.*	(OPAL Collab.)
Also		EPJ C16 707 (errat.)	G. Abbiendi *et al.*	(OPAL Collab.)
ABBIENDI,G	00D	EPJ C18 253	G. Abbiendi *et al.*	(OPAL Collab.)
ABREU	00J	PL B479 129	P. Abreu *et al.*	(DELPHI Collab.)
ABREU	00Q	PL B478 65	P. Abreu *et al.*	(DELPHI Collab.)
ABREU	00T	PL B485 95	P. Abreu *et al.*	(DELPHI Collab.)
ABREU	00U	PL B487 36	P. Abreu *et al.*	(DELPHI Collab.)
ABREU	00V	EPJ C16 211	P. Abreu *et al.*	(DELPHI Collab.)
ABREU	00W	PL B489 38	P. Abreu *et al.*	(DELPHI Collab.)
ABREU	00Z	EPJ C17 53	P. Abreu *et al.*	(DELPHI Collab.)
ABUSAIDI	00	PRL 84 5699	R. Abusaidi *et al.*	(CDMS Collab.)
ACCIARRI	00D	PL B472 420	M. Acciarri *et al.*	(L3 Collab.)
ACCOMANDO	00	NP B585 124	E. Accomando *et al.*	
BERNABEI	00	PL B480 23	R. Bernabei *et al.*	(DAMA Collab.)
BERNABEI	00C	EPJ C18 283	R. Bernabei *et al.*	(DAMA Collab.)
BERNABEI	00D	NJP 2 15	R. Bernabei *et al.*	(DAMA Collab.)
BOEHM	00B	PR D62 035012	C. Boehm, A. Djouadi, M. Drees	
ELLIS	00	PR D62 075010	J. Ellis *et al.*	
FENG	00	PL B482 388	J.L. Feng, K.T. Matchev, F. Wilczek	
LEP	00	CERN-EP-2000-016	LEP Collabs.	(ALEPH, DELPHI, L3, OPAL, SLD+)
MORALES	00	PL B489 268	A. Morales *et al.*	(IGEX Collab.)
PDG	00	EPJ C15 1	D.E. Groom *et al.*	(PDG Collab.)
SPOONER	00	PL B473 330	N.J.C. Spooner *et al.*	(UK Dark Matter Col.)
ACCIARRI	99H	PL B456 283	M. Acciarri *et al.*	(L3 Collab.)
ACCIARRI	99R	PL B470 268	M. Acciarri *et al.*	(L3 Collab.)
ACCIARRI	99W	PL B471 280	M. Acciarri *et al.*	(L3 Collab.)
AMBROSIO	99	PR D60 082002	M. Ambrosio *et al.*	(Macro Collab.)
BAUDIS	99	PR D59 022001	L. Baudis *et al.*	(Heidelberg-Moscow Collab.)
BELLI	99C	NP B563 97	P. Belli *et al.*	(DAMA Collab.)
OOTANI	99	PL B461 371	W. Ootani *et al.*	
ABREU	98P	PL B444 491	P. Abreu *et al.*	(DELPHI Collab.)
ACCIARRI	98F	EPJ C4 207	M. Acciarri *et al.*	(L3 Collab.)
ACKERSTAFF	98P	PL B433 195	K. Ackerstaff *et al.*	(OPAL Collab.)
BARATE	98K	PL B433 176	R. Barate *et al.*	(ALEPH Collab.)
BARATE	98S	EPJ C4 433	R. Barate *et al.*	(ALEPH Collab.)
BERNABEI	98C	PL B436 379	R. Bernabei *et al.*	(DAMA Collab.)
ELLIS	98	PR D58 095002	J. Ellis *et al.*	
ELLIS	98B	PL B444 367	J. Ellis, T. Falk, K. Olive	
PDG	98	EPJ C3 1	C. Caso *et al.*	(PDG Collab.)
BAER	97	PR D57 567	H. Baer, M. Brhlik	
BERNABEI	97	ASP 7 73	R. Bernabei *et al.*	(DAMA Collab.)
EDSJO	97	PR D56 1879	J. Edsjo, P. Gondolo	
ARNOWITT	96	PR D54 2374	R. Arnowitt, P. Nath	
BAER	96	PR D53 597	H. Baer, M. Brhlik	
BERGSTROM	96	ASP 5 263	L. Bergstrom, P. Gondolo	
LEWIN	96	ASP 6 87	J.D. Lewin, P.F. Smith	
BEREZINSKY	95	ASP 5 1	V. Berezinsky *et al.*	
FALK	95	PL B354 99	T. Falk, K.A. Olive, M. Srednicki	(MINN, UCSB)
LOSECCO	95	PL B342 392	J.M. LoSecco	(NDAM)
ADRIANI	93M	PRPL 236 1	O. Adriani *et al.*	(L3 Collab.)
DREES	93	PR D47 376	M. Drees, M.M. Nojiri	(DESY, SLAC)
DREES	93B	PR D48 3483	M. Drees, M.M. Nojiri	
FALK	93	PL B318 354	T. Falk *et al.*	(UCB, UCSB, MINN)
KELLEY	93	PR D47 2461	S. Kelley *et al.*	(TAMU, ALAH)
MIZUTA	93	PL B298 120	S. Mizuta, M. Yamaguchi	(TOHO)
MORI	93	PR D48 5505	M. Mori *et al.*	(KEK, NIIG, TOKY, TOKA+)
BOTTINO	92	MPL A7 733	A. Bottino *et al.*	(TORI, ZARA)
Also		PL B265 57	A. Bottino *et al.*	(TORI, INFN)
DECAMP	92	PRPL 216 253	D. Decamp *et al.*	(ALEPH Collab.)
LOPEZ	92	NP B370 445	J.L. Lopez, D.V. Nanopoulos, K.J. Yuan	(TAMU)
MCDONALD	92	PL B283 80	J. McDonald, K.A. Olive, M. Srednicki	(LISB+)
ABREU	91F	NP B367 511	P. Abreu *et al.*	(DELPHI Collab.)
ALEXANDER	91F	ZPHY C52 175	G. Alexander *et al.*	(OPAL Collab.)
BOTTINO	91	PL B265 57	A. Bottino *et al.*	(TORI, INFN)
GELMINI	91	NP B351 623	G.B. Gelmini, P. Gondolo, E. Roulet	(UCLA, TRST)
GRIEST	91	PR D43 3191	K. Griest, D. Seckel	
KAMIONKOW...	91	PR D44 3021	M. Kamionkowski	(CHIC, FNAL)
MORI	91B	PL B270 89	M. Mori *et al.*	(Kamiokande Collab.)
NOJIRI	91	PL B261 76	M.M. Nojiri	(KEK)
OLIVE	91	NP B355 208	K.A. Olive, M. Srednicki	(MINN, UCSB)
ROSZKOWSKI	91	PL B262 59	L. Roszkowski	(CERN)
GRIEST	90	PR D41 3565	K. Griest, M. Kamionkowski, M.S. Turner	(UCB+)
BARBIERI	89C	NP B313 725	R. Barbieri, M. Frigeni, G. Giudice	
OLIVE	89	PL B230 78	K.A. Olive, M. Srednicki	(MINN, UCSB)
ELLIS	88D	NP B307 883	J. Ellis, R. Flores	
GRIEST	88B	PR D38 2357	K. Griest	
OLIVE	88	PL B205 553	K.A. Olive, M. Srednicki	(MINN, UCSB)
SREDNICKI	88	NP B310 693	M. Srednicki, R. Watkins, K.A. Olive	(MINN, UCSB)
ELLIS	84	NP B238 453	J. Ellis *et al.*	(CERN)
GOLDBERG	83	PRL 50 1419	H. Goldberg	(NEAS)
KRAUSS	83	NP B227 556	L.M. Krauss	(HARV)
VYSOTSKII	83	SJNP 37 948	M.I. Vysotsky	(ITEP)
		Translated from YAF 37 1597.		

Downloaded from https://academic.oup.com/ptep/article/2022/8/083C01/6651666 by KIT Library user on 27 September 2022

Technicolor

See the related review(s):

Dynamical Electroweak Symmetry Breaking: Implications of the H^0

The latest unpublished results are described in "Dynamical Electroweak Symmetry Breaking" review.

MASS LIMITS for Resonances in Models of Dynamical Electroweak Symmetry Breaking

VALUE (GeV)	CL%	DOCUMENT ID		TECN	COMMENT
• • • We do not use the following data for averages, fits, limits, etc. • • •					
>3900	95	[1] AAD	20AM	ATLS	top-color Z'
		[2] AAD	20W	ATLS	$\rho_T \to W\pi_T \to \ell\nu q\overline{q}$
		[3] AAD	16W	ATLS	color octet vector resonance
>2400	95	[4] KHACHATRY...	16E	CMS	top-color Z'
		[5] AAD	15AB	ATLS	$h \to \pi_V\pi_V$
>1800	95	[6] AAD	15AO	ATLS	top-color Z'
		[7] AAD	15BB	ATLS	$pp \to \rho_T/a_{1T} \to Wh$ or Zh
		[8] AAD	15Q	ATLS	$h \to \pi_V\pi_V$
		[9] AAIJ	15AN	LHCB	$h \to \pi_V\pi_V$
>1140	95	[10] KHACHATRY...	15C	CMS	$\rho_T \to WZ$
		[11] KHACHATRY...	15W	CMS	$H \to \pi_V\pi_V$
none 200–700, 750–890	95	[12] AAD	14AT	ATLS	$pp \to \omega_T \to Z\gamma$
none 275–960	95	[12] AAD	14AT	ATLS	$pp \to a_T \to W\gamma$
		[13] AAD	14V	ATLS	color singlet techni-vector
> 703		[14] AAD	13AN	ATLS	$pp \to a_T \to W\gamma$
> 494		[15] AAD	13AN	ATLS	$pp \to \omega_T \to Z\gamma$
none 500–1740	95	[16] AAD	13AQ	ATLS	top-color Z'
>1300	95	[17] CHATRCHYAN	13AP	CMS	top-color Z'
>2100	95	[16] CHATRCHYAN	13BM	CMS	top-color Z'
		[18] BAAK	12	RVUE	QCD-like technicolor
none 167–687	95	[19] CHATRCHYAN	12AF	CMS	$\rho_T \to WZ$
> 805	95	[16] AALTONEN	11AD	CDF	top-color Z'
> 805	95	[16] AALTONEN	11AE	CDF	top-color Z'
		[20] CHIVUKULA	11	RVUE	top-Higgs
		[21] CHIVUKULA	11A	RVUE	techini-π
		[22] AALTONEN	10I	CDF	$p\overline{p} \to \rho_T/\omega_T \to W\pi_T$
none 208–408	95	[23] ABAZOV	10A	D0	$\rho_T \to WZ$
		[24] ABAZOV	07I	D0	$p\overline{p} \to \rho_T/\omega_T \to W\pi_T$
> 280	95	[25] ABULENCIA	05A	CDF	$\rho_T \to e^+e^-, \mu^+\mu^-$
		[26] CHEKANOV	02B	ZEUS	color octet techni-π
> 207	95	[27] ABAZOV	01B	D0	$\rho_T \to e^+e^-$
none 90–206.7	95	[28] ABDALLAH	01	DLPH	$e^+e^- \to \rho_T$
		[29] AFFOLDER	00F	CDF	color-singlet techni-ρ, $\rho_T \to W\pi_T, 2\pi_T$
> 600	95	[30] AFFOLDER	00K	CDF	color-octet techni-ρ, $\rho_{T8} \to 2\pi_{LQ}$
none 350–440	95	[31] ABE	99F	CDF	color-octet techni-ρ, $\rho_{T8} \to \overline{b}b$
		[32] ABE	99N	CDF	techni-ω, $\omega_T \to \gamma\overline{b}b$
none 260–480	95	[33] ABE	97G	CDF	color-octet techni-ρ, $\rho_{T8} \to$ 2jets

[1] AAD 20AM search for a top-color Z' decaying to $t\overline{t}$ in pp collisions at $\sqrt{s}$ = 13 TeV. The quoted limit is for $\Gamma_{Z'}/M_{Z'}$ = 0.01. The limit becomes $M_{Z'}$ > 4700 GeV for $\Gamma_{Z'}/M_{Z'}$ = 0.03.

[2] AAD 20W search for techni-ρ decaying to $\pi_T W$ in pp collisions at $\sqrt{s}$ = 13 TeV. See their Fig. 5a for limits on $\sigma \cdot B$.

[3] AAD 16W search for color octet vector resonance decaying to bB in pp collisions at $\sqrt{s}$ = 8 TeV. The vector like quark B is assumed to decay to bH. See their Fig.3 and Fig.4 for limits on $\sigma \cdot B$.

[4] KHACHATRYAN 16E search for top-color Z' decaying to $t\overline{t}$. The quoted limit is for $\Gamma_{Z'}/m_{Z'}$ = 0.012. Also exclude $m_{Z'}$ < 2.9 TeV for wider topcolor Z' with $\Gamma_{Z'}/m_{Z'}$ = 0.1.

[5] AAD 15AB search for long-lived hidden valley π_V particles which are produced in pairs by the decay of a scalar boson. π_V is assumed to decay into dijets. See their Fig. 10 for the limit on σB.

[6] AAD 15AO search for top-color Z' decaying to $t\overline{t}$. The quoted limit is for $\Gamma_{Z'}/m_{Z'}$ = 0.012.

[7] AAD 15BB search for minimal walking technicolor (MWT) isotriplet vector and axial-vector resonances decaying to Wh or Zh. See their Fig. 3 for the exclusion limit in the MWT parameter space.

[8] AAD 15Q search for long-lived hidden valley π_V particles which are produced in pairs by the decay of scalar boson. π_V is assumed to decay into dijets. See their Fig. 5 and Fig. 6 for the limit on σB.

[9] AAIJ 15AN search for long-lived hidden valley π_V particles which are produced in pairs by the decay of scalar boson with a mass of 120GeV. π_V is assumed to decay into dijets. See their Fig. 4 for the limit on σB.

[10] KHACHATRYAN 15C search for a vector techni-resonance decaying to WZ. The limit assumes M_{π_T} = (3/4) M_{ρ_T} − 25 GeV. See their Fig.3 for the limit in $M_{\pi_T} - M_{\rho_T}$ plane of the low scale technicolor model.

[11] KHACHATRYAN 15W search for long-lived hidden valley π_V particles which are produced in pairs in the decay of heavy higgs boson H. π_V is assumed to decay into $\ell^+\ell^-$. See their Fig. 7 and Fig. 8 for the limits on σB.

[12] AAD 14AT search for techni-ω and techni-a resonances decaying to $V\gamma$ with $V = W(\to \ell\nu)$ or $Z(\to \ell^+\ell^-)$.

[13] AAD 14V search for vector techni-resonances decaying into electron or muon pairs in pp collisions at $\sqrt{s}$ = 8 TeV. See their table IX for exclusion limits with various assumptions.

[14] AAD 13AN search for vector techni-resonance a_T decaying into $W\gamma$.

[15] AAD 13AN search for vector techni-resonance ω_T decaying into $Z\gamma$.

[16] Search for top-color Z' decaying to $t\overline{t}$. The quoted limit is for $\Gamma_{Z'}/m_{Z'}$ = 0.012.

[17] CHATRCHYAN 13AP search for top-color leptophobic Z' decaying to $t\overline{t}$. The quoted limit is for $\Gamma_{Z'}/m_{Z'}$ = 0.012.

[18] BAAK 12 give electroweak oblique parameter constraints on the QCD-like technicolor models. See their Fig. 28.

[19] CHATRCHYAN 12AF search for a vector techni-resonance decaying to WZ. The limit assumes M_{π_T} = (3/4) M_{ρ_T} − 25 GeV. See their Fig. 3 for the limit in $M_{\pi_T} - M_{\rho_T}$ plane of the low scale technicolor model.

[20] Using the LHC limit on the Higgs boson production cross section, CHIVUKULA 11 obtain a limit on the top-Higgs mass > 300 GeV at 95% CL assuming 150 GeV top-pion mass.

[21] Using the LHC limit on the Higgs boson production cross section, CHIVUKULA 11A obtain a limit on the techinipion mass ruling out the region 110 GeV < m_P < $2m_t$. Existence of color techni-fermions, top-color mechanism, and $N_{TC} \geq$ 3 are assumed.

[22] AALTONEN 10I search for the vector techni-resonances (ρ_T, ω_T) decaying into $W\pi_T$ with $W \to \ell\nu$ and $\pi_T \to b\overline{b}$, $b\overline{c}$, or $b\overline{u}$. See their Fig. 3 for the exclusion plot in $M_{\pi_T} - M_{\rho_T}$ plane.

[23] ABAZOV 10A search for a vector techni-resonance decaying into WZ. The limit assumes $M_{\rho_T} < M_{\pi_T} + M_W$.

[24] ABAZOV 07I search for the vector techni-resonances (ρ_T, ω_T) decaying into $W\pi_T$ with $W \to e\nu$ and $\pi_T \to b\overline{b}$ or $b\overline{c}$. See their Fig. 2 for the exclusion plot in $M_{\pi_T} - M_{\rho_T}$ plane.

[25] ABULENCIA 05A search for resonances decaying to electron or muon pairs in $p\overline{p}$ collisions. at $\sqrt{s}$ = 1.96 TeV. The limit assumes Technicolor-scale mass parameters $M_V = M_A$ = 500 GeV.

[26] CHEKANOV 02B search for color octet techni-π P decaying into dijets in ep collisions. See their Fig. 5 for the limit on $\sigma(ep \to ePX)\cdot B(P \to 2j)$.

[27] ABAZOV 01B searches for vector techni-resonances (ρ_T, ω_T) decaying to e^+e^-. The limit assumes $M_{\rho_T} = M_{\omega_T} < M_{\pi_T} + M_W$.

[28] The limit is independent of the π_T mass. See their Fig. 9 and Fig. 10 for the exclusion plot in the $M_{\rho_T} - M_{\pi_T}$ plane. ABDALLAH 01 limit on the techni-pion mass is M_{π_T} > 79.8 GeV for N_D=2, assuming its point-like coupling to gauge bosons.

[29] AFFOLDER 00F search for ρ_T decaying into $W\pi_T$ or $\pi_T\pi_T$ with $W \to \ell\nu$ and $\pi_T \to \overline{b}b$, $\overline{b}c$. See Fig. 1 in the above Note on "Dynamical Electroweak Symmetry Breaking" for the exclusion plot in the $M_{\rho_T} - M_{\pi_T}$ plane.

[30] AFFOLDER 00K search for the ρ_{T8} decaying into $\pi_{LQ}\pi_{LQ}$ with $\pi_{LQ} \to b\nu$. For $\pi_{LQ} \to c\nu$, the limit is $M_{\rho_{T8}}$ >510 GeV. See their Fig. 2 and Fig. 3 for the exclusion plot in the $M_{\rho_{T8}} - M_{\pi_{LQ}}$ plane.

[31] ABE 99F search for a new particle X decaying into $b\overline{b}$ in $p\overline{p}$ collisions at E_{cm}= 1.8 TeV. See Fig. 7 in the above Note on "Dynamical Electroweak Symmetry Breaking" for the upper limit on $\sigma(p\overline{p} \to X)\times B(X \to b\overline{b})$. ABE 99F also exclude top gluons of width Γ=0.3M in the mass interval 280 <M< 670 GeV, of width Γ=0.5M in the mass interval 340 <M< 640 GeV, and of width Γ=0.7M in the mass interval 375 <M< 560 GeV.

[32] ABE 99N search for the techni-ω decaying into $\gamma\pi_T$. The technipion is assumed to decay $\pi_T \to b\overline{b}$. See Fig. 2 in the above Note on "Dynamical Electroweak Symmetry Breaking" for the exclusion plot in the $M_{\omega_T} - M_{\pi_T}$ plane.

[33] ABE 97G search for a new particle X decaying into dijets in $p\overline{p}$ collisions at E_{cm}= 1.8 TeV. See Fig. 5 in the above Note on "Dynamical Electroweak Symmetry Breaking" for the upper limit on $\sigma(p\overline{p} \to X)\times B(X \to 2j)$.

REFERENCES FOR Technicolor

AAD	20AM	JHEP 2010 061	G. Aad et al.	(ATLAS Collab.)
AAD	20W	JHEP 2006 151	G. Aad et al.	(ATLAS Collab.)
AAD	16W	PL B758 249	G. Aad et al.	(ATLAS Collab.)
KHACHATRY...	16E	PR D93 012001	V. Khachatryan et al.	(CMS Collab.)
AAD	15AB	PR D92 012010	G. Aad et al.	(ATLAS Collab.)
AAD	15AO	JHEP 1508 148	G. Aad et al.	(ATLAS Collab.)
AAD	15BB	EPJ C75 263	G. Aad et al.	(ATLAS Collab.)
AAD	15Q	PL B743 15	G. Aad et al.	(ATLAS Collab.)
AAIJ	15AN	EPJ C75 152	R. Aaij et al.	(LHCb Collab.)
KHACHATRY...	15C	PL B740 83	V. Khachatryan et al.	(CMS Collab.)
KHACHATRY...	15W	PR D91 052012	V. Khachatryan et al.	(CMS Collab.)
AAD	14AT	PL B738 428	G. Aad et al.	(ATLAS Collab.)
AAD	14V	PR D90 052005	G. Aad et al.	(ATLAS Collab.)
AAD	13AN	PR D87 112003	G. Aad et al.	(ATLAS Collab.)
Also		PR D91 119901 (errat.)	G. Aad et al.	(ATLAS Collab.)
AAD	13AQ	PR D88 012004	G. Aad et al.	(ATLAS Collab.)
CHATRCHYAN	13AP	PR D87 072002	S. Chatrchyan et al.	(CMS Collab.)
CHATRCHYAN	13BM	PRL 111 211804	S. Chatrchyan et al.	(CMS Collab.)
Also		PRL 112 119903 (errat.)	S. Chatrchyan et al.	(CMS Collab.)
BAAK	12	EPJ C72 2003	M. Baak et al.	(Gfitter Group)
CHATRCHYAN	12AF	PRL 109 141801	S. Chatrchyan et al.	(CMS Collab.)
AALTONEN	11AD	PR D84 072003	T. Aaltonen et al.	(CDF Collab.)
AALTONEN	11AE	PR D84 072004	T. Aaltonen et al.	(CDF Collab.)
CHIVUKULA	11	PR D84 095022	R.S. Chivukula et al.	
CHIVUKULA	11A	PR D84 115025	R. S. Chivukula et al.	
AALTONEN	10I	PRL 104 111802	T. Aaltonen et al.	(CDF Collab.)
ABAZOV	10A	PRL 104 061801	V.M. Abazov et al.	(D0 Collab.)
ABAZOV	07I	PRL 98 221801	V.M. Abazov et al.	(D0 Collab.)
ABULENCIA	05A	PRL 95 252001	A. Abulencia et al.	(CDF Collab.)
CHEKANOV	02B	PL B531 9	S. Chekanov et al.	(ZEUS Collab.)
ABAZOV	01B	PRL 87 061802	V.M. Abazov et al.	(D0 Collab.)
ABDALLAH	01	EPJ C22 17	J. Abdallah et al.	(DELPHI Collab.)
AFFOLDER	00F	PRL 84 1110	T. Affolder et al.	(CDF Collab.)
AFFOLDER	00K	PRL 85 2056	T. Affolder et al.	(CDF Collab.)
ABE	99F	PRL 82 2038	F. Abe et al.	(CDF Collab.)
ABE	99N	PRL 83 3124	F. Abe et al.	(CDF Collab.)
ABE	97G	PR D55 5263	F. Abe et al.	(CDF Collab.)

Downloaded from https://academic.oup.com/ptep/article/2022/8/083C01/6651666 by KIT Library user on 27 September 2022

Quark and Lepton Compositeness, Searches for

The latest unpublished results are described in the "Quark and Lepton Compositeness" review.

See the related review(s):

Searches for Quark and Lepton Compositeness

CONTENTS:

Scale Limits for Contact Interactions: $\Lambda(eeee)$
Scale Limits for Contact Interactions: $\Lambda(ee\mu\mu)$
Scale Limits for Contact Interactions: $\Lambda(ee\tau\tau)$
Scale Limits for Contact Interactions: $\Lambda(\ell\ell\ell\ell)$
Scale Limits for Contact Interactions: $\Lambda(eeqq)$
Scale Limits for Contact Interactions: $\Lambda(\mu\mu qq)$
Scale Limits for Contact Interactions: $\Lambda(\ell\nu\ell\nu)$
Scale Limits for Contact Interactions: $\Lambda(e\nu qq)$
Scale Limits for Contact Interactions: $\Lambda(qqqq)$
Scale Limits for Contact Interactions: $\Lambda(\nu\nu qq)$
Mass Limits for Excited e (e^*)
— Limits for Excited e (e^*) from Pair Production
— Limits for Excited e (e^*) from Single Production
— Limits for Excited e (e^*) from $e^+e^- \to \gamma\gamma$
— Indirect Limits for Excited e (e^*)
Mass Limits for Excited μ (μ^*)
— Limits for Excited μ (μ^*) from Pair Production
— Limits for Excited μ (μ^*) from Single Production
— Indirect Limits for Excited μ (μ^*)
Mass Limits for Excited τ (τ^*)
— Limits for Excited τ (τ^*) from Pair Production
— Limits for Excited τ (τ^*) from Single Production
Mass Limits for Excited Neutrino (ν^*)
— Limits for Excited ν (ν^*) from Pair Production
— Limits for Excited ν (ν^*) from Single Production
Mass Limits for Excited q (q^*)
— Limits for Excited q (q^*) from Pair Production
— Limits for Excited q (q^*) from Single Production
Mass Limits for Color Sextet Quarks (q_6)
Mass Limits for Color Octet Charged Leptons (ℓ_8)
Mass Limits for Color Octet Neutrinos (ν_8)
Mass Limits for W_8 (Color Octet W Boson)

SCALE LIMITS for Contact Interactions: $\Lambda(eeee)$

Limits are for $\Lambda^{\pm}_{LL}$ only. For other cases, see each reference.

Λ^+_{LL}(TeV)	Λ^-_{LL}(TeV)	CL%	DOCUMENT ID		TECN	COMMENT
>8.3	**>10.3**	95	[1] BOURILKOV	01	RVUE	E_{cm}= 192–208 GeV
• • • We do not use the following data for averages, fits, limits, etc. • • •						
>4.5	>7.0	95	[2] SCHAEL	07A	ALEP	E_{cm}= 189–209 GeV
>5.3	>6.8	95	ABDALLAH	06C	DLPH	E_{cm}= 130–207 GeV
>4.7	>6.1	95	[3] ABBIENDI	04G	OPAL	E_{cm}= 130–207 GeV
>4.3	>4.9	95	ACCIARRI	00P	L3	E_{cm}= 130–189 GeV

[1] A combined analysis of the data from ALEPH, DELPHI, L3, and OPAL.
[2] SCHAEL 07A limits are from R_c, Q^{depl}_{FB}, and hadronic cross section measurements.
[3] ABBIENDI 04G limits are from $e^+e^- \to e^+e^-$ cross section at $\sqrt{s}$ = 130–207 GeV.

SCALE LIMITS for Contact Interactions: $\Lambda(ee\mu\mu)$

Limits are for $\Lambda^{\pm}_{LL}$ only. For other cases, see each reference.

Λ^+_{LL}(TeV)	Λ^-_{LL}(TeV)	CL%	DOCUMENT ID		TECN	COMMENT
>6.6	**>9.5**	95	[1] SCHAEL	07A	ALEP	E_{cm}= 189–209 GeV
> 8.5	>3.8	95	ACCIARRI	00P	L3	E_{cm}= 130–189 GeV
• • • We do not use the following data for averages, fits, limits, etc. • • •						
>7.3	>7.6	95	ABDALLAH	06C	DLPH	E_{cm}= 130–207 GeV
>8.1	>7.3	95	[2] ABBIENDI	04G	OPAL	E_{cm}= 130–207 GeV

[1] SCHAEL 07A limits are from R_c, Q^{depl}_{FB}, and hadronic cross section measurements.
[2] ABBIENDI 04G limits are from $e^+e^- \to \mu\mu$ cross section at $\sqrt{s}$ = 130–207 GeV.

SCALE LIMITS for Contact Interactions: $\Lambda(ee\tau\tau)$

Limits are for $\Lambda^{\pm}_{LL}$ only. For other cases, see each reference.

Λ^+_{LL}(TeV)	Λ^-_{LL}(TeV)	CL%	DOCUMENT ID		TECN	COMMENT
>7.9	>5.8	95	[1] SCHAEL	07A	ALEP	E_{cm}= 189–209 GeV
>7.9	>4.6	95	ABDALLAH	06C	DLPH	E_{cm}= 130–207 GeV
>4.9	**>7.2**	95	[2] ABBIENDI	04G	OPAL	E_{cm}= 130–207 GeV
• • • We do not use the following data for averages, fits, limits, etc. • • •						
>5.4	>4.7	95	ACCIARRI	00P	L3	E_{cm}= 130–189 GeV

[1] SCHAEL 07A limits are from R_c, Q^{depl}_{FB}, and hadronic cross section measurements.
[2] ABBIENDI 04G limits are from $e^+e^- \to \tau\tau$ cross section at $\sqrt{s}$ = 130–207 GeV.

SCALE LIMITS for Contact Interactions: $\Lambda(\ell\ell\ell\ell)$

Lepton universality assumed. Limits are for $\Lambda^{\pm}_{LL}$ only. For other cases, see each reference.

Λ^+_{LL}(TeV)	Λ^-_{LL}(TeV)	CL%	DOCUMENT ID		TECN	COMMENT
>7.9	**> 10.3**	95	[1] SCHAEL	07A	ALEP	E_{cm}= 189–209 GeV
>9.1	>8.2	95	ABDALLAH	06C	DLPH	E_{cm}= 130–207 GeV
• • • We do not use the following data for averages, fits, limits, etc. • • •						
>7.7	>9.5	95	[2] ABBIENDI	04G	OPAL	E_{cm}= 130–207 GeV
			[3] BABICH	03	RVUE	
>9.0	>5.2	95	ACCIARRI	00P	L3	E_{cm}= 130–189 GeV

[1] SCHAEL 07A limits are from R_c, Q^{depl}_{FB}, and hadronic cross section measurements.
[2] ABBIENDI 04G limits are from $e^+e^- \to \ell^+\ell^-$ cross section at $\sqrt{s}$ = 130–207 GeV.
[3] BABICH 03 obtain a bound -0.175 TeV^{-2} $< 1/\Lambda^2_{LL} <$ 0.095 TeV^{-2} (95%CL) in a model independent analysis allowing all of Λ_{LL}, Λ_{LR}, Λ_{RL}, Λ_{RR} to coexist.

SCALE LIMITS for Contact Interactions: $\Lambda(eeqq)$

Limits are for $\Lambda^{\pm}_{LL}$ only. For other cases, see each reference.

Λ^+_{LL}(TeV)	Λ^-_{LL}(TeV)	CL%	DOCUMENT ID		TECN	COMMENT
>23.5	>26.1	95	[1] AAD	21Q	ATLS	$(eeqq)$
>19.5	>24.0	95	[2] SIRUNYAN	21N	CMS	$(eeqq)$
>23.5	>26.1	95	[3] AAD	20AP	ATLS	$(eeqq)$
> 4.5	>12.8	95	[4] ABRAMOWICZ	19	ZEUS	$(eeqq)$
>16.8	>23.9	95	[5] SIRUNYAN	19AC	CMS	$(eeqq)$
>24	**>37**	95	[6] AABOUD	17AT	ATLS	$(eeqq)$
> 8.4	**>10.2**	95	[7] ABDALLAH	09	DLPH	$(eebb)$
> 9.4	**>5.6**	95	[8] SCHAEL	07A	ALEP	$(eecc)$
> 9.4	>4.9	95	[7] SCHAEL	07A	ALEP	$(eebb)$
>23.3	**>12.5**	95	[9] CHEUNG	01B	RVUE	$(eeuu)$
>11.1	**>26.4**	95	[9] CHEUNG	01B	RVUE	$(eedd)$
• • • We do not use the following data for averages, fits, limits, etc. • • •						
> 7.1	>7.1	95	[10] AAD	21AU	ATLS	$(eebs)$
>15.5	>19.5	95	[11] AABOUD	16U	ATLS	$(eeqq)$
>13.5	>18.3	95	[12] KHACHATRY...	15AE	CMS	$(eeqq)$
>16.4	>20.7	95	[13] AAD	14BE	ATLS	$(eeqq)$
> 9.5	>12.1	95	[14] AAD	13E	ATLS	$(eeqq)$
>10.1	>9.4	95	[15] AAD	12AB	ATLS	$(eeqq)$
> 4.2	>4.0	95	[16] AARON	11C	H1	$(eeqq)$
> 3.8	>3.8	95	[17] ABDALLAH	11	DLPH	$(eetc)$
>12.9	>7.2	95	[18] SCHAEL	07A	ALEP	$(eeqq)$
> 3.7	>5.9	95	[19] ABULENCIA	06L	CDF	$(eeqq)$

[1] AAD 21Q limits are from pp collisions at $\sqrt{s}$ = 13 TeV. A frequentist statistical framework is used to remove the prior dependence.
[2] SIRUNYAN 21N limits are from e^+e^- mass distribution in pp collisions at $\sqrt{s}$ = 13 TeV.
[3] AAD 20AP limits are from e^+e^- mass distribution in pp collisions at $\sqrt{s}$ = 13 TeV.
[4] ABRAMOWICZ 19 limits are from Q^2 spectrum measurements of $e^{\pm}p \to e^{\pm}X$.
[5] SIRUNYAN 19AC limits are from e^+e^- mass distribution in pp collisions at $\sqrt{s}$ = 13 TeV.
[6] AABOUD 17AT limits are from pp collisions at $\sqrt{s}$ = 13 TeV. The quoted limit uses a uniform positive prior in $1/\Lambda^2$.
[7] ABDALLAH 09 and SCHAEL 07A limits are from R_b, A^b_{FB}.
[8] SCHAEL 07A limits are from R_c, Q^{depl}_{FB}, and hadronic cross section measurements.
[9] CHEUNG 01B is an update of BARGER 98E.
[10] AAD 21AU search for new phenomena in final states with e^+e^- and one or no b-tagged jets in pp collisions at $\sqrt{s}$ = 13 TeV. The quoted limits assume $g^2_* = 4\pi$.
[11] AABOUD 16U limits are from pp collisions at $\sqrt{s}$ = 13 TeV. The quoted limit uses a uniform positive prior in $1/\Lambda^2$.
[12] KHACHATRYAN 15AE limit is from e^+e^- mass distribution in pp collisions at E_{cm} = 8 TeV.
[13] AAD 14BE limits are from pp collisions at $\sqrt{s}$ = 8 TeV. The quoted limit uses a uniform positive prior in $1/\Lambda^2$.
[14] AAD 13E limis are from e^+e^- mass distribution in pp collisions at E_{cm} = 7 TeV.
[15] AAD 12AB limis are from e^+e^- mass distribution in pp collisions at E_{cm} = 7 TeV.
[16] AARON 11C limits are from Q^2 spectrum measurements of $e^{\pm}p \to e^{\pm}X$.
[17] ABDALLAH 11 limit is from $e^+e^- \to t\overline{t}$ cross section. $\Lambda_{LL} = \Lambda_{LR} = \Lambda_{RL} = \Lambda_{RR}$ is assumed.
[18] SCHAEL 07A limit assumes quark flavor universality of the contact interactions.
[19] ABULENCIA 06L limits are from $p\overline{p}$ collisions at $\sqrt{s}$ = 1.96 TeV.

SCALE LIMITS for Contact Interactions: $\Lambda(\mu\mu qq)$

Λ^+_{LL}(TeV)	Λ^-_{LL}(TeV)	CL%	DOCUMENT ID		TECN	COMMENT
>22.3	>32.7	95	[1] AAD	21Q	ATLS	$(\mu\mu qq)$
>23.3	**> 40.0**	95	[2] SIRUNYAN	21N	CMS	$(\mu\mu qq)$
>22.3	>32.7	95	[3] AAD	20AP	ATLS	$(\mu\mu qq)$
>20.4	>30.4	95	[4] SIRUNYAN	19AC	CMS	$(\mu\mu qq)$
>20	>30	95	[5] AABOUD	17AT	ATLS	$(\mu\mu qq)$

Downloaded from https://academic.oup.com/ptep/article/2022/8/083C01/6651666 by KIT Library user on 27 September 2022

• • • We do not use the following data for averages, fits, limits, etc. • • •

> 8.5	>8.5	95	[6] AAD	21AU	ATLS	($\mu\mu bs$)
>15.8	>21.8	95	[7] AABOUD	16U	ATLS	($\mu\mu qq$)
>12.0	>15.2	95	[8] KHACHATRY...	15AE	CMS	($\mu\mu qq$)
>12.5	>16.7	95	[9] AAD	14BE	ATLS	($\mu\mu qq$)
> 9.6	>12.9	95	[10] AAD	13E	ATLS	($\mu\mu qq$) (isosinglet)
> 9.5	>13.1	95	[11] CHATRCHYAN	13K	CMS	($\mu\mu qq$) (isosinglet)
> 8.0	>7.0	95	[12] AAD	12AB	ATLS	($\mu\mu qq$) (isosinglet)

[1] AAD 21Q limits are from pp collisions at $\sqrt{s}$ = 13 TeV. A frequentist statistical framework is used to remove the prior dependence.
[2] SIRUNYAN 21N limits are from $\mu^+\mu^-$ mass distribution in pp collisions at $\sqrt{s}$ = 13 TeV.
[3] AAD 20AP limits are from $\mu^+\mu^-$ mass distribution in pp collisions at $\sqrt{s}$ = 13 TeV.
[4] SIRUNYAN 19AC limits are from $\mu^+\mu^-$ mass distribution in pp collisions at $\sqrt{s}$ = 13 TeV.
[5] AABOUD 17AT limits are from pp collisions at $\sqrt{s}$ = 13 TeV. The quoted limit uses a uniform positive prior in $1/\Lambda^2$.
[6] AAD 21AU search for new phenomena in final states with $\mu^+\mu^-$ and one or no b-tagged jets in pp collisions at $\sqrt{s}$ = 13 TeV. The quoted limits assume $g_*^2 = 4\pi$.
[7] AABOUD 16U limits are from pp collisions at $\sqrt{s}$ = 13 TeV. The quoted limit uses a uniform positive prior in $1/\Lambda^2$.
[8] KHACHATRYAN 15AE limit is from $\mu^+\mu^-$ mass distribution in pp collisions at E_{cm} = 8 TeV.
[9] AAD 14BE limits are from pp collisions at $\sqrt{s}$ = 8 TeV. The quoted limit uses a uniform positive prior in $1/\Lambda^2$.
[10] AAD 13E limis are from $\mu^+\mu^-$ mass distribution in pp collisions at E_{cm} = 7 TeV.
[11] CHATRCHYAN 13K limis are from $\mu^+\mu^-$ mass distribution in pp collisions at E_{cm} = 7 TeV.
[12] AAD 12AB limis are from $\mu^+\mu^-$ mass distribution in pp collisions at E_{cm} = 7 TeV.

SCALE LIMITS for Contact Interactions: $\Lambda(\ell\nu\ell\nu)$

VALUE (TeV)	CL%	DOCUMENT ID		TECN	COMMENT
>3.10	90	[1] JODIDIO	86	SPEC	$\Lambda^{\pm}_{LR}(\nu_\mu \nu_e \mu e)$
• • • We do not use the following data for averages, fits, limits, etc. • • •					
>3.8		[2] DIAZCRUZ	94	RVUE	$\Lambda^{+}_{LL}(\tau\nu_\tau e\nu_e)$
>8.1		[2] DIAZCRUZ	94	RVUE	$\Lambda^{-}_{LL}(\tau\nu_\tau e\nu_e)$
>4.1		[3] DIAZCRUZ	94	RVUE	$\Lambda^{+}_{LL}(\tau\nu_\tau \mu\nu_\mu)$
>6.5		[3] DIAZCRUZ	94	RVUE	$\Lambda^{-}_{LL}(\tau\nu_\tau \mu\nu_\mu)$

[1] JODIDIO 86 limit is from $\mu^+ \to \overline{\nu}_\mu e^+ \nu_e$. Chirality invariant interactions $L = (g^2/\Lambda^2)$ $[\eta_{LL}\ (\overline{\nu}_{\mu L}\gamma^\alpha\mu_L)\ (\overline{e}_L\gamma_\alpha\nu_{eL}) + \eta_{LR}\ (\overline{\nu}_{\mu L}\gamma^\alpha\nu_{eL}\ (\overline{e}_R\gamma_\alpha\mu_R)]$ with $g^2/4\pi = 1$ and $(\eta_{LL},\eta_{LR}) = (0,\pm1)$ are taken. No limits are given for $\Lambda^{\pm}_{LL}$ with $(\eta_{LL},\eta_{LR}) = (\pm1,0)$. For more general constraints with right-handed neutrinos and chirality nonconserving contact interactions, see their text.
[2] DIAZCRUZ 94 limits are from $\Gamma(\tau \to e\nu\nu)$ and assume flavor-dependent contact interactions with $\Lambda(\tau\nu_\tau e\nu_e) \ll \Lambda(\mu\nu_\mu e\nu_e)$.
[3] DIAZCRUZ 94 limits are from $\Gamma(\tau \to \mu\nu\nu)$ and assume flavor-dependent contact interactions with $\Lambda(\tau\nu_\tau \mu\nu_\mu) \ll \Lambda(\mu\nu_\mu e\nu_e)$.

SCALE LIMITS for Contact Interactions: $\Lambda(e\nu qq)$

VALUE (TeV)	CL%	DOCUMENT ID		TECN
>2.81	95	[1] AFFOLDER	01I	CDF

[1] AFFOLDER 00I bound is for a scalar interaction $\overline{q}_R\, q_L\, \overline{\nu} e_L$.

SCALE LIMITS for Contact Interactions: $\Lambda(qqqq)$

Λ^{+}_{LL}(TeV)	Λ^{-}_{LL}(TeV)	CL%	DOCUMENT ID		TECN	COMMENT
>13.1 none 17.4–29.5	**>21.8**	95	[1] AABOUD	17AK	ATLS	pp dijet angl.
• • • We do not use the following data for averages, fits, limits, etc. • • •						
			[2] AABOUD	18AV	ATLS	$pp \to t\overline{t}t\overline{t}$
>12.8	>17.5	95	[3] SIRUNYAN	18DD	CMS	pp dijet angl.
>11.5	>14.7	95	[4] SIRUNYAN	17F	CMS	pp dijet angl.
>12.0	>17.5	95	[5] AAD	16S	ATLS	pp dijet angl.
			[6] AAD	15AR	ATLS	$pp \to t\overline{t}t\overline{t}$
			[7] AAD	15BY	ATLS	$pp \to t\overline{t}t\overline{t}$
> 8.1	>12.0	95	[8] AAD	15L	ATLS	pp dijet angl.
> 9.0	>11.7	95	[9] KHACHATRY...	15J	CMS	pp dijet angl.
> 5		95	[10] FABBRICHESI	14	RVUE	$q\overline{q}t\overline{t}$

[1] AABOUD 17AK limit is from dijet angular distribution in pp collisions at $\sqrt{s}$ = 13 TeV. u, d, and s quarks are assumed to be composite.
[2] AABOUD 18AV obtain limit on t_R compositeness $2\pi/\Lambda^2_{RR}$ < 1.6 TeV^{-2} at 95% CL from $t\overline{t}t\overline{t}$ production in the pp collisions at E_{cm} = 13 TeV.
[3] SIRUNYAN 18DD limit is from dijet angular distribution in pp collisions at $\sqrt{s}$ = 13 TeV.
[4] SIRUNYAN 17F limit is from dijet angular cross sections in pp collisions at E_{cm} = 13 TeV. All quarks are assumed to be composite.
[5] AAD 16S limit is from dijet angular selections in pp collisions at E_{cm} = 13 TeV. u, d, and s quarks are assumed to be composite.
[6] AAD 15AR obtain limit on the t_R compositeness $2\pi/\Lambda^2_{RR}$ < 6.6 TeV^{-2} at 95% CL from the $t\overline{t}t\overline{t}$ production in the pp collisions at E_{cm} = 8 TeV.
[7] AAD 15BY obtain limit on the t_R compositeness $2\pi/\Lambda^2_{RR}$ < 15.1 TeV^{-2} at 95% CL from the $t\overline{t}t\overline{t}$ production in the pp collisions at E_{cm} = 8 TeV.
[8] AAD 15L limit is from dijet angular distribution in pp collisions at E_{cm} = 8 TeV. u, d, and s quarks are assumed to be composite.
[9] KHACHATRYAN 15J limit is from dijet angular distribution in pp collisions at E_{cm} = 8 TeV. u, d, s, c, and b quarks are assumed to be composite.
[10] FABBRICHESI 14 obtain bounds on chromoelectric and chromomagnetic form factors of the top-quark using $pp \to t\overline{t}$ and $p\overline{p} \to t\overline{t}$ cross sections. The quoted limit on the $q\overline{q}t\overline{t}$ contact interaction is derived from their bound on the chromoelectric form factor.

SCALE LIMITS for Contact Interactions: $\Lambda(\nu\nu qq)$

Limits are for $\Lambda^{\pm}_{LL}$ only. For other cases, see each reference.

Λ^{+}_{LL}(TeV)	Λ^{-}_{LL}(TeV)	CL%	DOCUMENT ID		TECN	COMMENT
>5.0	**>5.4**	95	[1] MCFARLAND	98	CCFR	νN scattering

[1] MCFARLAND 98 assumed a flavor universal interaction. Neutrinos were mostly of muon type.

MASS LIMITS for Excited e (e^*)

Most e^+e^- experiments assume one-photon or Z exchange. The limits from some e^+e^- experiments which depend on λ have assumed transition couplings which are chirality violating ($\eta_L = \eta_R$). However they can be interpreted as limits for chirality-conserving interactions after multiplying the coupling value λ by $\sqrt{2}$; see Note.

Excited leptons have the same quantum numbers as other ortholeptons. See also the searches for ortholeptons in the "Searches for Heavy Leptons" section.

Limits for Excited e (e^*) from Pair Production

These limits are obtained from $e^+e^- \to e^{*+}e^{*-}$ and thus rely only on the (electroweak) charge of e^*. Form factor effects are ignored unless noted. For the case of limits from Z decay, the e^* coupling is assumed to be of sequential type. Possible t channel contribution from transition magnetic coupling is neglected. All limits assume a dominant $e^* \to e\gamma$ decay except the limits from $\Gamma(Z)$.

For limits prior to 1987, see our 1992 edition (Physical Review **D45** S1 (1992)).

VALUE (GeV)	CL%	DOCUMENT ID		TECN	COMMENT
>103.2	95	[1] ABBIENDI	02G	OPAL	$e^+e^- \to e^*e^*$ Homodoublet type
• • • We do not use the following data for averages, fits, limits, etc. • • •					
>102.8	95	[2] ACHARD	03B	L3	$e^+e^- \to e^*e^*$ Homodoublet type

[1] From e^+e^- collisions at $\sqrt{s}$ = 183–209 GeV. $f = f'$ is assumed.
[2] From e^+e^- collisions at $\sqrt{s}$ = 189–209 GeV. $f = f'$ is assumed. ACHARD 03B also obtain limit for $f = -f'$: m_{e^*} > 96.6 GeV.

Limits for Excited e (e^*) from Single Production

These limits are from $e^+e^- \to e^*e$, $W \to e^*\nu$, or $ep \to e^*X$ and depend on transition magnetic coupling between e and e^*. All limits assume $e^* \to e\gamma$ decay except as noted. Limits from LEP, UA2, and H1 are for chiral coupling, whereas all other limits are for nonchiral coupling, $\eta_L = \eta_R = 1$. In most papers, the limit is expressed in the form of an excluded region in the λ–m_{e^*} plane. See the original papers.

For limits prior to 1987, see our 1992 edition (Physical Review **D45** S1 (1992)).

VALUE (GeV)	CL%	DOCUMENT ID		TECN	COMMENT
>5600	95	[1] SIRUNYAN	20AJ	CMS	$pp \to e e^* X$
• • • We do not use the following data for averages, fits, limits, etc. • • •					
>4800	95	[2] AABOUD	19AZ	ATLS	$pp \to e e^* X$
>3900	95	[3] SIRUNYAN	19Z	CMS	$pp \to e e^* X$
>2450	95	[4] KHACHATRY...	16AQ	CMS	$pp \to e e^* X$
>3000	95	[5] AAD	15AP	ATLS	$pp \to e^{(*)} e^* X$
>2200	95	[6] AAD	13BB	ATLS	$pp \to e e^* X$
>1900	95	[7] CHATRCHYAN	13AE	CMS	$pp \to e e^* X$
>1870	95	[8] AAD	12AZ	ATLS	$pp \to e^{(*)} e^* X$

[1] SIRUNYAN 20AJ search for e^* production in $2e2j$ final states in pp collisions at $\sqrt{s}$ = 13 TeV. The quoted limit assumes $\Lambda = m_{e^*}$, $f = f' = 1$. The contact interaction is included. See their Fig.11 for exclusion limits in m_{e^*}–Λ plane.
[2] AABOUD 19AZ search for single e^* production in pp collisions at $\sqrt{s}$ = 13 TeV. The limit quoted above is from $e^* \to eq\overline{q}$ and $e^* \to \nu W$ decays assuming $f = f' = 1$ and $m_{e^*} = \Lambda$. The contact interaction is included in e^* production and decay amplitudes. See their Fig.6 for exclusion limits in $m_{e^*} - \Lambda$ plane.
[3] SIRUNYAN 19Z search for e^* production in $\ell\ell\gamma$ final states in pp collisions at $\sqrt{s}$ = 13 TeV. The quoted limit assumes $\Lambda = m_{e^*}$, $f = f' = 1$. The contact interaction is included in the e^* production and decay amplitudes.
[4] KHACHATRYAN 16AQ search for single e^* production in pp collisions at $\sqrt{s}$ = 8 TeV. The limit above is from the $e^* \to e\gamma$ search channel assuming $f = f' = 1$, $m_{e^*} = \Lambda$. See their Table 7 for limits in other search channels or with different assumptions.
[5] AAD 15AP search for e^* production in evens with three or more charged leptons in pp collisions at $\sqrt{s}$ = 8 TeV. The quoted limit assumes $\Lambda = m_{e^*}$, $f = f' = 1$. The contact interaction is included in the e^* production and decay amplitudes.
[6] AAD 13BB search for single e^* production in pp collisions with $e^* \to e\gamma$ decay. $f = f' = 1$, and e^* production via contact interaction with $\Lambda = m_{e^*}$ are assumed.
[7] CHATRCHYAN 13AE search for single e^* production in pp collisions with $e^* \to e\gamma$ decay. $f = f' = 1$, and e^* production via contact interaction with $\Lambda = m_{e^*}$ are assumed.
[8] AAD 12AZ search for e^* production via four-fermion contact interaction in pp collisions with $e^* \to e\gamma$ decay. The quoted limit assumes $\Lambda = m_{e^*}$. See their Fig. 8 for the exclusion plot in the mass-coupling plane.

Downloaded from https://academic.oup.com/ptep/article/2022/8/083C01/6651666 by KIT Library user on 27 September 2022

Limits for Excited e (e^*) from $e^+e^- \to \gamma\gamma$

These limits are derived from indirect effects due to e^* exchange in the t channel and depend on transition magnetic coupling between e and e^*. All limits are for $\lambda_\gamma = 1$. All limits except ABE 89J and ACHARD 02D are for nonchiral coupling with $\eta_L = \eta_R = 1$. We choose the chiral coupling limit as the best limit and list it in the Summary Table.

For limits prior to 1987, see our 1992 edition (Physical Review **D45** S1 (1992)).

VALUE (GeV)	CL%	DOCUMENT ID		TECN	COMMENT
>356	95	[1] ABDALLAH	04N	DLPH	$\sqrt{s}$= 161–208 GeV
• • • We do not use the following data for averages, fits, limits, etc. • • •					
>310	95	ACHARD	02D	L3	$\sqrt{s}$= 192–209 GeV

[1] ABDALLAH 04N also obtain a limit on the excited electron mass with ee^* chiral coupling, $m_{e^*} > 295$ GeV at 95% CL.

Indirect Limits for Excited e (e^*)

These limits make use of loop effects involving e^* and are therefore subject to theoretical uncertainty.

VALUE (GeV)	DOCUMENT ID		TECN	COMMENT
• • • We do not use the following data for averages, fits, limits, etc. • • •				
	[1] DORENBOS...	89	CHRM	$\overline{\nu}_\mu e \to \overline{\nu}_\mu e$, $\nu_\mu e \to \nu_\mu e$
	[2] GRIFOLS	86	THEO	$\nu_\mu e \to \nu_\mu e$
	[3] RENARD	82	THEO	$g-2$ of electron

[1] DORENBOSCH 89 obtain the limit $\lambda_\gamma^2 \Lambda_{\rm cut}^2/m_{e^*}^2 < 2.6$ (95% CL), where $\Lambda_{\rm cut}$ is the cutoff scale, based on the one-loop calculation by GRIFOLS 86. If one assumes that $\Lambda_{\rm cut} = 1$ TeV and $\lambda_\gamma = 1$, one obtains $m_{e^*} > 620$ GeV. However, one generally expects $\lambda_\gamma \approx m_{e^*}/\Lambda_{\rm cut}$ in composite models.

[2] GRIFOLS 86 uses $\nu_\mu e \to \nu_\mu e$ and $\overline{\nu}_\mu e \to \overline{\nu}_\mu e$ data from CHARM Collaboration to derive mass limits which depend on the scale of compositeness.

[3] RENARD 82 derived from $g-2$ data limits on mass and couplings of e^* and μ^*. See figures 2 and 3 of the paper.

MASS LIMITS for Excited μ (μ^*)

Limits for Excited μ (μ^*) from Pair Production

These limits are obtained from $e^+e^- \to \mu^{*+}\mu^{*-}$ and thus rely only on the (electroweak) charge of μ^*. Form factor effects are ignored unless noted. For the case of limits from Z decay, the μ^* coupling is assumed to be of sequential type. All limits assume a dominant $\mu^* \to \mu\gamma$ decay except the limits from $\Gamma(Z)$.

For limits prior to 1987, see our 1992 edition (Physical Review **D45** S1 (1992)).

VALUE (GeV)	CL%	DOCUMENT ID		TECN	COMMENT
>103.2	95	[1] ABBIENDI	02G	OPAL	$e^+e^- \to \mu^*\mu^*$ Homodoublet type
• • • We do not use the following data for averages, fits, limits, etc. • • •					
>102.8	95	[2] ACHARD	03B	L3	$e^+e^- \to \mu^*\mu^*$ Homodoublet type

[1] From e^+e^- collisions at $\sqrt{s}$ = 183–209 GeV. $f = f'$ is assumed.

[2] From e^+e^- collisions at $\sqrt{s}$ = 189–209 GeV. $f = f'$ is assumed. ACHARD 03B also obtain limit for $f = -f'$: $m_{\mu^*} > 96.6$ GeV.

Limits for Excited μ (μ^*) from Single Production

These limits are from $e^+e^- \to \mu^*\mu$ and depend on transition magnetic coupling between μ and μ^*. All limits assume $\mu^* \to \mu\gamma$ decay. Limits from LEP are for chiral coupling, whereas all other limits are for nonchiral coupling, $\eta_L = \eta_R = 1$. In most papers, the limit is expressed in the form of an excluded region in the $\lambda - m_{\mu^*}$ plane. See the original papers.

For limits prior to 1987, see our 1992 edition (Physical Review **D45** S1 (1992)).

VALUE (GeV)	CL%	DOCUMENT ID		TECN	COMMENT
>5700	95	[1] SIRUNYAN	20AJ	CMS	$pp \to \mu\mu^* X$
• • • We do not use the following data for averages, fits, limits, etc. • • •					
>3800	95	[2] SIRUNYAN	19Z	CMS	$pp \to \mu\mu^* X$
>2800	95	[3] AAD	16BM	ATLS	$pp \to \mu\mu^* X$
>2470	95	[4] KHACHATRY...	16AQ	CMS	$pp \to \mu\mu^* X$
>3000	95	[5] AAD	15AP	ATLS	$pp \to \mu^{(*)}\mu^* X$
>2200	95	[6] AAD	13BB	ATLS	$pp \to \mu\mu^* X$
>1900	95	[7] CHATRCHYAN	13AE	CMS	$pp \to \mu\mu^* X$
>1750	95	[8] AAD	12AZ	ATLS	$pp \to \mu^{(*)}\mu^* X$

[1] SIRUNYAN 20AJ search for μ^* production in $2\mu 2j$ final states in pp collisions at $\sqrt{s}$ = 13 TeV. The quoted limit assumes $\Lambda = m_{\mu^*}$, $f = f' = 1$. The contact interaction is included. See their Fig.11 for exclusion limits in m_{μ^*}–Λ plane.

[2] SIRUNYAN 19Z search for μ^* production in $\ell\ell\gamma$ final states in pp collisions at $\sqrt{s}$ = 13 TeV. The quoted limit assumes $\Lambda = m_{\mu^*}$, $f = f' = 1$. The contact interaction is included in the μ^* production and decay amplitudes.

[3] AAD 16BM search for μ^* production in $\mu\mu jj$ events in pp collisions at $\sqrt{s}$ = 8 TeV. Both the production and decay are assumed to occur via a contact interaction with $\Lambda = m_{\mu^*}$.

[4] KHACHATRYAN 16AQ search for single μ^* production in pp collisions at $\sqrt{s}$ = 8 TeV. The limit above is from the $\mu^* \to \mu\gamma$ search channel assuming $f = f' = 1$, $m_{\mu^*} = \Lambda$. See their Table 7 for limits in other search channels or with different assumptions.

[5] AAD 15AP search for μ^* production in evens with three or more charged leptons in pp collisions at $\sqrt{s}$ = 8 TeV. The quoted limit assumes $\Lambda = m_{\mu^*}$, $f = f' = 1$. The contact interaction is included in the μ^* production and decay amplitudes.

[6] AAD 13BB search for single μ^* production in pp collisions with $\mu^* \to \mu\gamma$ decay. $f = f' = 1$, and μ^* production via contact interaction with $\Lambda = m_{\mu^*}$ are assumed.

[7] CHATRCHYAN 13AE search for single μ^* production in pp collisions with $\mu^* \to \mu\gamma$ decay. $f = f' = 1$, and μ^* production via contact interaction with $\Lambda = m_{\mu^*}$ are assumed.

[8] AAD 12AZ search for μ^* production via four-fermion contact interaction in pp collisions with $\mu^* \to \mu\gamma$ decay. The quoted limit assumes $\Lambda = m_{\mu^*}$. See their Fig. 8 for the exclusion plot in the mass-coupling plane.

Indirect Limits for Excited μ (μ^*)

These limits make use of loop effects involving μ^* and are therefore subject to theoretical uncertainty.

VALUE (GeV)	DOCUMENT ID		TECN	COMMENT
• • • We do not use the following data for averages, fits, limits, etc. • • •				
	[1] RENARD	82	THEO	$g-2$ of muon

[1] RENARD 82 derived from $g-2$ data limits on mass and couplings of e^* and μ^*. See figures 2 and 3 of the paper.

MASS LIMITS for Excited τ (τ^*)

Limits for Excited τ (τ^*) from Pair Production

These limits are obtained from $e^+e^- \to \tau^{*+}\tau^{*-}$ and thus rely only on the (electroweak) charge of τ^*. Form factor effects are ignored unless noted. For the case of limits from Z decay, the τ^* coupling is assumed to be of sequential type. All limits assume a dominant $\tau^* \to \tau\gamma$ decay except the limits from $\Gamma(Z)$.

For limits prior to 1987, see our 1992 edition (Physical Review **D45** S1 (1992)).

VALUE (GeV)	CL%	DOCUMENT ID		TECN	COMMENT
>103.2	95	[1] ABBIENDI	02G	OPAL	$e^+e^- \to \tau^*\tau^*$ Homodoublet type
• • • We do not use the following data for averages, fits, limits, etc. • • •					
>102.8	95	[2] ACHARD	03B	L3	$e^+e^- \to \tau^*\tau^*$ Homodoublet type

[1] From e^+e^- collisions at $\sqrt{s}$ = 183–209 GeV. $f = f'$ is assumed.

[2] From e^+e^- collisions at $\sqrt{s}$ = 189–209 GeV. $f = f'$ is assumed. ACHARD 03B also obtain limit for $f = -f'$: $m_{\tau^*} > 96.6$ GeV.

Limits for Excited τ (τ^*) from Single Production

These limits are from $e^+e^- \to \tau^*\tau$ and depend on transition magnetic coupling between τ and τ^*. All limits assume $\tau^* \to \tau\gamma$ decay. Limits from LEP are for chiral coupling, whereas all other limits are for nonchiral coupling, $\eta_L = \eta_R = 1$. In most papers, the limit is expressed in the form of an excluded region in the $\lambda - m_{\tau^*}$ plane. See the original papers.

VALUE (GeV)	CL%	DOCUMENT ID		TECN	COMMENT
>2500	95	[1] AAD	15AP	ATLS	$pp \to \tau^{(*)}\tau^* X$
• • • We do not use the following data for averages, fits, limits, etc. • • •					
> 180	95	[2] ACHARD	03B	L3	$e^+e^- \to \tau\tau^*$
> 185	95	[3] ABBIENDI	02G	OPAL	$e^+e^- \to \tau\tau^*$

[1] AAD 15AP search for τ^* production in events with three or more charged leptons in pp collisions at $\sqrt{s}$ = 8 TeV. The quoted limit assumes $\Lambda = m_{\tau^*}$, $f = f' = 1$. The contact interaction is included in the τ^* production and decay amplitudes.

[2] ACHARD 03B result is from e^+e^- collisions at $\sqrt{s}$ = 189–209 GeV. $f = f' = \Lambda/m_{\tau^*}$ is assumed. See their Fig. 4 for the exclusion plot in the mass-coupling plane.

[3] ABBIENDI 02G result is from e^+e^- collisions at $\sqrt{s}$ = 183–209 GeV. $f = f' = \Lambda/m_{\tau^*}$ is assumed for τ^* coupling. See their Fig. 4c for the exclusion limit in the mass-coupling plane.

MASS LIMITS for Excited Neutrino (ν^*)

Limits for Excited ν (ν^*) from Pair Production

These limits are obtained from $e^+e^- \to \nu^*\nu^*$ and thus rely only on the (electroweak) charge of ν^*. Form factor effects are ignored unless noted. The ν^* coupling is assumed to be of sequential type unless otherwise noted. All limits assume a dominant $\nu^* \to \nu\gamma$ decay except the limits from $\Gamma(Z)$.

VALUE (GeV)	CL%	DOCUMENT ID		TECN	COMMENT
>1600	95	[1] AAD	15AP	ATLS	$pp \to \nu^*\nu^* X$
• • • We do not use the following data for averages, fits, limits, etc. • • •					
		[2] ABBIENDI	04N	OPAL	
> 102.6	95	[3] ACHARD	03B	L3	$e^+e^- \to \nu^*\nu^*$ Homodoublet type

[1] AAD 15AP search for ν^* pair production in evens with three or more charged leptons in pp collisions at $\sqrt{s}$ = 8 TeV. The quoted limit assumes $\Lambda = m_{\nu^*}$, $f = f' = 1$. The contact interaction is included in the ν^* production and decay amplitudes.

[2] From e^+e^- collisions at $\sqrt{s}$ = 192–209 GeV, ABBIENDI 04N obtain limit on $\sigma(e^+e^- \to \nu^*\nu^*)$ $B^2(\nu^* \to \nu\gamma)$. See their Fig.2. The limit ranges from 20 to 45 fb for $m_{\nu^*} > 45$ GeV.

[3] From e^+e^- collisions at $\sqrt{s}$ = 189–209 GeV. $f = -f'$ is assumed. ACHARD 03B also obtain limit for $f = f'$: $m_{\nu^*_e} > 101.7$ GeV, $m_{\nu^*_\mu} > 101.8$ GeV, and $m_{\nu^*_\tau} > 92.9$ GeV. See their Fig. 4 for the exclusion plot in the mass-coupling plane.

Downloaded from https://academic.oup.com/ptep/article/2022/8/083C01/6651666 by KIT Library user on 27 September 2022

Limits for Excited ν (ν^*) from Single Production

These limits are from $e^+e^- \to \nu\nu^*$, $Z \to \nu\nu^*$, or $ep \to \nu^* X$ and depend on transition magnetic coupling between ν/e and ν^*. Assumptions about ν^* decay mode are given in footnotes.

VALUE (GeV)	CL%	DOCUMENT ID		TECN	COMMENT
>213	95	[1] AARON	08	H1	$ep \to \nu^* X$
• • • We do not use the following data for averages, fits, limits, etc. • • •					
>190	95	[2] ACHARD	03B	L3	$e^+e^- \to \nu\nu^*$
none 50–150	95	[3] ADLOFF	02	H1	$ep \to \nu^* X$
>158	95	[4] CHEKANOV	02D	ZEUS	$ep \to \nu^* X$

[1] AARON 08 search for single ν^* production in ep collisions with the decays $\nu^* \to \nu\gamma$, νZ, eW. The quoted limit assumes $f = -f' = \Lambda/m_{\nu^*}$. See their Fig. 3 and Fig. 4 for the exclusion plots in the mass-coupling plane.

[2] ACHARD 03B result is from e^+e^- collisions at $\sqrt{s}$ = 189–209 GeV. The quoted limit is for ν^*_e. $f = -f' = \Lambda/m_{\nu^*}$ is assumed. See their Fig. 4 for the exclusion plot in the mass-coupling plane.

[3] ADLOFF 02 search for single ν^* production in ep collisions with the decays $\nu^* \to \nu\gamma$, νZ, eW. The quoted limit assumes $f = -f' = \Lambda/m_{\nu^*}$. See their Fig. 1 for the exclusion plots in the mass-coupling plane.

[4] CHEKANOV 02D search for single ν^* production in ep collisions with the decays $\nu^* \to \nu\gamma$, νZ, eW. $f = -f' = \Lambda/m_{\nu^*}$ is assumed for the e^* coupling. CHEKANOV 02D also obtain limit for $f = f' = \Lambda/m_{\nu^*}$: m_{ν^*} >135 GeV. See their Fig. 5c and Fig. 5d for the exclusion plot in the mass-coupling plane.

MASS LIMITS for Excited q (q^*)

Limits for Excited q (q^*) from Pair Production

These limits are mostly obtained from $e^+e^- \to q^*\overline{q}^*$ and thus rely only on the (electroweak) charge of the q^*. Form factor effects are ignored unless noted. Assumptions about the q^* decay are given in the comments and footnotes.

VALUE (GeV)	CL%	DOCUMENT ID		TECN	COMMENT
>338	95	[1] AALTONEN	10H	CDF	$q^* \to tW^-$
• • • We do not use the following data for averages, fits, limits, etc. • • •					
none 700–1200	95	[2] SIRUNYAN	18V	CMS	$pp \to t^*_{3/2}\overline{t}^*_{3/2} \to t\overline{t}gg$
		[3] BARATE	98U	ALEP	$Z \to q^*q^*$
> 45.6	95	[4] ADRIANI	93M	L3	u or d type, $Z \to q^*q^*$
> 41.7	95	[5] BARDADIN-...	92	RVUE	u-type, $\Gamma(Z)$
> 44.7	95	[5] BARDADIN-...	92	RVUE	d-type, $\Gamma(Z)$
> 40.6	95	[6] DECAMP	92	ALEP	u-type, $\Gamma(Z)$
> 44.2	95	[6] DECAMP	92	ALEP	d-type, $\Gamma(Z)$
> 45	95	[7] DECAMP	92	ALEP	u or d type, $Z \to q^*q^*$
> 45	95	[6] ABREU	91F	DLPH	u-type, $\Gamma(Z)$
> 45	95	[6] ABREU	91F	DLPH	d-type, $\Gamma(Z)$

[1] AALTONEN 10H obtain limits on the q^*q^* production cross section in $p\overline{p}$ collisions. See their Fig. 3.

[2] SIRUNYAN 18V search for pair production of spin 3/2 excited top quarks. $B(t^*_{3/2} \to tg) = 1$ is assumed.

[3] BARATE 98U obtain limits on the form factor. See their Fig. 16 for limits in mass-form factor plane.

[4] ADRIANI 93M limit is valid for $B(q^* \to qg)$> 0.25 (0.17) for up (down) type.

[5] BARDADIN-OTWINOWSKA 92 limit based on $\Delta\Gamma(Z)$<36 MeV.

[6] These limits are independent of decay modes.

[7] Limit is for $B(q^* \to qg)+B(q^* \to q\gamma)=1$.

Limits for Excited q (q^*) from Single Production

These limits are from $e^+e^- \to q^*\overline{q}$, $p\overline{p} \to q^*X$, or $pp \to q^*X$ and depend on transition magnetic couplings between q and q^*. Assumptions about q^* decay mode are given in the footnotes and comments.

VALUE (GeV)	CL%	DOCUMENT ID		TECN	COMMENT
>6700 (CL = 95%) OUR LIMIT					
none 2000–6700	95	[1] AAD	20T	ATLS	$pp \to q^*X$, $q^* \to qg$
none 1250–3200	95	[1] AAD	20T	ATLS	$pp \to b^*X$, $b^* \to bg$, $b\gamma$, bZ, tW
none 1800–6300	95	[2] SIRUNYAN	20AI	CMS	$pp \to q^*X$, $q^* \to qg$
none 1500–2600	95	[3] AABOUD	18AB	ATLS	$pp \to b^*X$, $b^* \to bg$
none 1500–5300	95	[4] AABOUD	18BA	ATLS	$pp \to q^*X$, $q^* \to q\gamma$
none 1000–5500	95	[5] SIRUNYAN	18AG	CMS	$pp \to q^*X$, $q^* \to q\gamma$
none 1000–1800	95	[6] SIRUNYAN	18AG	CMS	$pp \to b^*X$, $b^* \to b\gamma$
none 600–6000	95	[7] SIRUNYAN	18BO	CMS	$pp \to q^*X$, $q^* \to qg$
none 1200–5000	95	[8] SIRUNYAN	18P	CMS	$pp \to q^*X$, $q^* \to qW$
none 1200–4700	95	[8] SIRUNYAN	18P	CMS	$pp \to q^*X$, $q^* \to qZ$
>6000	95	[9] AABOUD	17AK	ATLS	$pp \to q^*X$, $q^* \to qg$
• • • We do not use the following data for averages, fits, limits, etc. • • •					
>2600	95	[10] SIRUNYAN	21AG	CMS	$pp \to b^*X$, $b^* \to tW$
none 600–5400	95	[11] KHACHATRY...	17W	CMS	$pp \to q^*X$, $q^* \to qg$
none 1100–2100	95	[12] AABOUD	16	ATLS	$pp \to b^*X$, $b^* \to bg$
>1500	95	[13] AAD	16AH	ATLS	$pp \to b^*X$, $b^* \to tW$
>4400	95	[14] AAD	16AI	ATLS	$pp \to q^*X$, $q^* \to q\gamma$
		[15] AAD	16AV	ATLS	$pp \to q^*X$, $q^* \to Wb$
>5200	95	[16] AAD	16S	ATLS	$pp \to q^*X$, $q^* \to qg$
>1390	95	[17] KHACHATRY...	16I	CMS	$pp \to b^*X$, $b^* \to tW$
>5000	95	[18] KHACHATRY...	16K	CMS	$pp \to q^*X$, $q^* \to qg$
none 500–1600	95	[19] KHACHATRY...	16L	CMS	$pp \to q^*X$, $q^* \to qg$
>4060	95	[20] AAD	15V	ATLS	$pp \to q^*X$, $q^* \to qg$
>3500	95	[21] KHACHATRY...	15V	CMS	$pp \to q^*X$, $q^* \to qg$
>3500	95	[22] AAD	14A	ATLS	$pp \to q^*X$, $q^* \to q\gamma$
>3200	95	[23] KHACHATRY...	14	CMS	$pp \to q^*X$, $q^* \to qW$
>2900	95	[24] KHACHATRY...	14	CMS	$pp \to q^*X$, $q^* \to qZ$
none 700–3500	95	[25] KHACHATRY...	14J	CMS	$pp \to q^*X$, $q^* \to q\gamma$
>2380	95	[26] CHATRCHYAN	13AJ	CMS	$pp \to q^*X$, $q^* \to qW$
>2150	95	[27] CHATRCHYAN	13AJ	CMS	$pp \to q^*X$, $q^* \to qZ$

[1] AAD 20T search for resonances decaying into dijets in pp collisions at $\sqrt{s}$ = 13 TeV. Assume $\Lambda = m_{q^*}$, $f_s = f = f' = 1$.

[2] SIRUNYAN 20AI search for resonances decaying into dijets in pp collisions at $\sqrt{s}$ = 13 TeV. Assume $\Lambda = m_{q^*}$, $f_s = f = f' = 1$.

[3] AABOUD 18AB assume $\Lambda = m_{b^*}$, $f_s = f = f' = 1$. The contact interactions are not included in b^* production and decay amplitudes.

[4] AABOUD 18BA search for first-generation excited quarks (u^* and d^*) with degenerate mass, assuming $\Lambda = m_{q^*}$, $f_s = f = f' = 1$. The contact interactions are not included in q^* production and decay amplitudes.

[5] SIRUNYAN 18AG search for first-generation excited quarks (u^* and d^*) with degenerate mass, assuming $\Lambda = m_{q^*}$, $f_s = f = f' = 1$.

[6] SIRUNYAN 18AG search for excited b quark assuming $\Lambda = m_{q^*}$, $f_s = f = f' = 1$.

[7] SIRUNYAN 18BO assume $\Lambda = m_{q^*}$, $f_s = f = f' = 1$. The contact interactions are not included in q^* production and decay amplitudes.

[8] SIRUNYAN 18P use the hadronic decay of W or Z, assuming $\Lambda = m_{q^*}$, $f_s = f = f' = 1$.

[9] AABOUD 17AK assume $\Lambda = m_{q^*}$, $f_s = f = f' = 1$. The contact interactions are not included in q^* production and decay amplitudes. Only the decay of $q^* \to gu$ and $q^* \to gd$ is simulated as the benchmark signals in the analysis.

[10] SIRUNYAN 21AG search for b^* decaying to tW in pp collisions at $\sqrt{s}$ = 13 TeV. The limit quoted above assumes $\kappa^b_L = g_L = 1$, $\kappa^b_R = g_R = 0$. The limit becomes m_{b^*} > 2.8 TeV (> 3.1 TeV) if we assume $\kappa^b_L = g_L = 0$, $\kappa^b_R = g_R = 1$ ($\kappa^b_L = g_L = \kappa^b_R = g_R = 1$). See their Fig. 5 for limits on $\sigma \cdot B$.

[11] KHACHATRYAN 17W assume $\Lambda = m_{q^*}$, $f_s = f = f' = 1$. The contact interactions are not included in q^* production and decay amplitudes.

[12] AABOUD 16 assume $\Lambda = m_{b^*}$, $f_s = f = f' = 1$. The contact interactions are not included in the b^* production and decay amplitudes.

[13] AAD 16AH search for b^* decaying to tW in pp collisions at $\sqrt{s}$ = 8 TeV. $f_g = f_L = f_R = 1$ are assumed. See their Fig. 12b for limits on $\sigma \cdot B$.

[14] AAD 16AI assume $\Lambda = m_{q^*}$, $f_s = f = f' = 1$.

[15] AAD 16AV search for single production of vector-like quarks decaying to Wb in pp collisions. See their Fig. 8 for the limits on couplings and mixings.

[16] AAD 16S assume $\Lambda = m_{q^*}$, $f_s = f = f' = 1$. The contact interactions are not included in q^* production and decay amplitudes.

[17] KHACHATRYAN 16I search for b^* decaying to tW in pp collisions at $\sqrt{s}$ = 8 TeV. $\kappa^b_L = g_L = 1$, $\kappa^b_R = g_R = 0$ are assumed. See their Fig. 8 for limits on $\sigma \cdot B$.

[18] KHACHATRYAN 16K assume $\Lambda = m_{q^*}$, $f_s = f = f' = 1$. The contact interactions are not included in q^* production and decay amplitudes.

[19] KHACHATRYAN 16L search for resonances decaying to dijets in pp collisions at $\sqrt{s}$ = 8 TeV using the data scouting technique which increases the sensitivity to the low mass resonances.

[20] AAD 15V assume $\Lambda = m_{q^*}$, $f_s = f = f' = 1$. The contact interactions are not included in q^* production and decay amplitudes.

[21] KHACHATRYAN 15V assume $\Lambda = m_{q^*}$, $f_s = f = f' = 1$. The contact interactions are not included in q^* production and decay amplitudes.

[22] AAD 14A assume $\Lambda = m_{q^*}$, $f_s = f = f' = 1$.

[23] KHACHATRYAN 14 use the hadronic decay of W, assuming $\Lambda = m_{q^*}$, $f_s = f = f' = 1$.

[24] KHACHATRYAN 14 use the hadronic decay of Z, assuming $\Lambda = m_{q^*}$, $f_s = f = f' = 1$.

[25] KHACHATRYAN 14J assume $f_s = f = f' = \Lambda / m_{q^*}$.

[26] CHATRCHYAN 13AJ use the hadronic decay of W.

[27] CHATRCHYAN 13AJ use the hadronic decay of Z.

MASS LIMITS for Color Sextet Quarks (q_6)

VALUE (GeV)	CL%	DOCUMENT ID		TECN	COMMENT
>84	95	[1] ABE	89D	CDF	$p\overline{p} \to q_6\overline{q}_6$

[1] ABE 89D look for pair production of unit-charged particles which leave the detector before decaying. In the above limit the color sextet quark is assumed to fragment into a unit-charged or neutral hadron with equal probability and to have long enough lifetime not to decay within the detector. A limit of 121 GeV is obtained for a color decuplet.

MASS LIMITS for Color Octet Charged Leptons (ℓ_8)

$\lambda \equiv m_{\ell_8}/\Lambda$

VALUE (GeV)	CL%	DOCUMENT ID		TECN	COMMENT
>86	95	[1] ABE	89D	CDF	Stable ℓ_8: $p\overline{p} \to \ell_8\overline{\ell}_8$
• • • We do not use the following data for averages, fits, limits, etc. • • •					
		[2] ABT	93	H1	e_8: $ep \to e_8 X$

Downloaded from https://academic.oup.com/ptep/article/2022/8/083C01/6651666 by KIT Library user on 27 September 2022

[1] ABE 89D look for pair production of unit-charged particles which leave the detector before decaying. In the above limit the color octet lepton is assumed to fragment into a unit-charged or neutral hadron with equal probability and to have long enough lifetime not to decay within the detector. The limit improves to 99 GeV if it always fragments into a unit-charged hadron.

[2] ABT 93 search for e_8 production via e-gluon fusion in ep collisions with $e_8 \to eg$. See their Fig. 3 for exclusion plot in the m_{e_8}–Λ plane for m_{e_8} = 35–220 GeV.

MASS LIMITS for Color Octet Neutrinos (ν_8)

$\lambda \equiv m_{\ell_8}/\Lambda$

VALUE (GeV)	CL%	DOCUMENT ID		TECN	COMMENT
>110	90	[1] BARGER	89	RVUE	ν_8: $p\overline{p} \to \nu_8\overline{\nu}_8$
• • • We do not use the following data for averages, fits, limits, etc. • • •					
none 3.8–29.8	95	[2] KIM	90	AMY	ν_8: $e^+e^- \to$ acoplanar jets
none 9–21.9	95	[3] BARTEL	87B	JADE	ν_8: $e^+e^- \to$ acoplanar jets

[1] BARGER 89 used ABE 89B limit for events with large missing transverse momentum. Two-body decay $\nu_8 \to \nu g$ is assumed.

[2] KIM 90 is at E_{cm} = 50–60.8 GeV. The same assumptions as in BARTEL 87B are used.

[3] BARTEL 87B is at E_{cm} = 46.3–46.78 GeV. The limit assumes the ν_8 pair production cross section to be eight times larger than that of the corresponding heavy neutrino pair production. This assumption is not valid in general for the weak couplings, and the limit can be sensitive to its $SU(2)_L \times U(1)_Y$ quantum numbers.

MASS LIMITS for W_8 (Color Octet W Boson)

VALUE (GeV)	DOCUMENT ID		TECN	COMMENT
• • • We do not use the following data for averages, fits, limits, etc. • • •				
	[1] ALBAJAR	89	UA1	$p\overline{p} \to W_8 X$, $W_8 \to Wg$

[1] ALBAJAR 89 give $\sigma(W_8 \to W+\text{jet})/\sigma(W) < 0.019$ (90% CL) for $m_{W_8} > 220$ GeV.

REFERENCES FOR Searches for Quark and Lepton Compositeness

AAD	21AU	PRL 127 141801	G. Aad et al.	(ATLAS Collab.)
AAD	21Q	JHEP 2104 142	G. Aad et al.	(ATLAS Collab.)
SIRUNYAN	21AG	JHEP 2112 106	A.M. Sirunyan et al.	(CMS Collab.)
SIRUNYAN	21N	JHEP 2107 208	A.M. Sirunyan et al.	(CMS Collab.)
AAD	20AP	JHEP 2011 005	G. Aad et al.	(ATLAS Collab.)
AAD	20T	JHEP 2003 145	G. Aad et al.	(ATLAS Collab.)
SIRUNYAN	20AI	JHEP 2005 033	A.M. Sirunyan et al.	(CMS Collab.)
SIRUNYAN	20AJ	JHEP 2005 052	A.M. Sirunyan et al.	(CMS Collab.)
AABOUD	19AZ	EPJ C79 803	M. Aaboud et al.	(ATLAS Collab.)
ABRAMOWICZ	19	PR D99 092006	H. Abramowicz et al.	(ZEUS Collab.)
SIRUNYAN	19AC	JHEP 1904 114	A.M. Sirunyan et al.	(CMS Collab.)
SIRUNYAN	19Z	JHEP 1904 015	A.M. Sirunyan et al.	(CMS Collab.)
AABOUD	18AB	PR D98 032016	M. Aaboud et al.	(ATLAS Collab.)
AABOUD	18AV	JHEP 1807 089	M. Aaboud et al.	(ATLAS Collab.)
AABOUD	18BA	EPJ C78 102	M. Aaboud et al.	(ATLAS Collab.)
SIRUNYAN	18AG	PL B781 390	A.M. Sirunyan et al.	(CMS Collab.)
SIRUNYAN	18BO	JHEP 1808 130	A.M. Sirunyan et al.	(CMS Collab.)
SIRUNYAN	18DD	EPJ C78 789	A.M. Sirunyan et al.	(CMS Collab.)
SIRUNYAN	18P	PR D97 072006	A.M. Sirunyan et al.	(CMS Collab.)
SIRUNYAN	18V	PL B778 349	A.M. Sirunyan et al.	(CMS Collab.)
AABOUD	17AK	PR D96 052004	M. Aaboud et al.	(ATLAS Collab.)
AABOUD	17AT	JHEP 1710 182	M. Aaboud et al.	(ATLAS Collab.)
KHACHATRY...	17W	PL B769 520	V. Khachatryan et al.	(CMS Collab.)
SIRUNYAN	17F	JHEP 1707 013	A.M. Sirunyan et al.	(CMS Collab.)
AABOUD	16	PL B759 229	M. Aaboud et al.	(ATLAS Collab.)
AABOUD	16U	PL B761 372	M. Aaboud et al.	(ATLAS Collab.)
AAD	16AH	JHEP 1602 110	G. Aad et al.	(ATLAS Collab.)
AAD	16AI	JHEP 1603 041	G. Aad et al.	(ATLAS Collab.)
AAD	16AV	EPJ C76 442	G. Aad et al.	(ATLAS Collab.)
AAD	16BM	NJP 18 073021	G. Aad et al.	(ATLAS Collab.)
AAD	16S	PL B754 302	G. Aad et al.	(ATLAS Collab.)
KHACHATRY...	16AQ	JHEP 1603 125	V. Khachatryan et al.	(CMS Collab.)
KHACHATRY...	16I	JHEP 1601 166	V. Khachatryan et al.	(CMS Collab.)
KHACHATRY...	16K	PRL 116 071801	V. Khachatryan et al.	(CMS Collab.)
KHACHATRY...	16L	PRL 117 031802	V. Khachatryan et al.	(CMS Collab.)
AAD	15AP	JHEP 1508 138	G. Aad et al.	(ATLAS Collab.)
AAD	15AR	JHEP 1508 105	G. Aad et al.	(ATLAS Collab.)
AAD	15BY	JHEP 1510 150	G. Aad et al.	(ATLAS Collab.)
AAD	15L	PRL 114 221802	G. Aad et al.	(ATLAS Collab.)
AAD	15V	PR D91 052007	G. Aad et al.	(ATLAS Collab.)
KHACHATRY...	15AE	JHEP 1504 025	V. Khachatryan et al.	(CMS Collab.)
KHACHATRY...	15J	PL B746 79	V. Khachatryan et al.	(CMS Collab.)
KHACHATRY...	15V	PR D91 052009	V. Khachatryan et al.	(CMS Collab.)
AAD	14A	PL B728 562	G. Aad et al.	(ATLAS Collab.)
AAD	14BE	EPJ C74 3134	G. Aad et al.	(ATLAS Collab.)
FABBRICHESI	14	PR D89 074028	M. Fabbrichesi, M. Pinamonti, A. Tonero	
KHACHATRY...	14	JHEP 1408 173	V. Khachatryan et al.	(CMS Collab.)
KHACHATRY...	14J	PL B738 274	V. Khachatryan et al.	(CMS Collab.)
AAD	13BB	NJP 15 093011	G. Aad et al.	(ATLAS Collab.)
AAD	13E	PR D87 015010	G. Aad et al.	(ATLAS Collab.)
CHATRCHYAN	13AE	PL B720 309	S. Chatrchyan et al.	(CMS Collab.)
CHATRCHYAN	13AJ	PL B723 280	S. Chatrchyan et al.	(CMS Collab.)
CHATRCHYAN	13K	PR D87 032001	S. Chatrchyan et al.	(CMS Collab.)
AAD	12AB	PL B712 40	G. Aad et al.	(ATLAS Collab.)
AAD	12AZ	PR D85 072003	G. Aad et al.	(ATLAS Collab.)
AARON	11C	PL B705 52	F. D. Aaron et al.	(H1 Collab.)
ABDALLAH	11	EPJ C71 1555	J. Abdallah et al.	(DELPHI Collab.)
AALTONEN	10H	PRL 104 091801	T. Aaltonen et al.	(CDF Collab.)
ABDALLAH	09	EPJ C60 1	J. Abdallah et al.	(DELPHI Collab.)
AARON	08	PL B663 382	F.D. Aaron et al.	(H1 Collab.)
SCHAEL	07A	EPJ C49 411	S. Schael et al.	(ALEPH Collab.)
ABDALLAH	06C	EPJ C45 589	J. Abdallah et al.	(DELPHI Collab.)
ABULENCIA	06L	PRL 96 211801	A. Abulencia et al.	(CDF Collab.)
ABBIENDI	04G	EPJ C33 173	G. Abbiendi et al.	(OPAL Collab.)
ABBIENDI	04N	PL B602 167	G. Abbiendi et al.	(OPAL Collab.)
ABDALLAH	04N	EPJ C37 405	J. Abdallah et al.	(DELPHI Collab.)
ACHARD	03B	PL B568 23	P. Achard et al.	(L3 Collab.)
BABICH	03	EPJ C29 103	A.A. Babich et al.	
ABBIENDI	02G	PL B544 57	G. Abbiendi et al.	(OPAL Collab.)
ACHARD	02D	PL B531 28	P. Achard et al.	(L3 Collab.)
ADLOFF	02	PL B525 9	C. Adloff et al.	(H1 Collab.)
CHEKANOV	02D	PL B549 32	S. Chekanov et al.	(ZEUS Collab.)
AFFOLDER	01I	PRL 87 231803	T. Affolder et al.	(CDF Collab.)
BOURILKOV	01	PR D64 071701	D. Bourilkov	
CHEUNG	01B	PL B517 167	K. Cheung	
ACCIARRI	00P	PL B489 81	M. Acciarri et al.	(L3 Collab.)
AFFOLDER	00I	PR D62 012004	T. Affolder et al.	(CDF Collab.)
BARATE	98U	EPJ C4 571	R. Barate et al.	(ALEPH Collab.)
BARGER	98E	PR D57 391	V. Barger et al.	
MCFARLAND	98	EPJ C1 509	K.S. McFarland et al.	(CCFR/NuTeV Collab.)
DIAZCRUZ	94	PR D49 2149	J.L. Diaz Cruz, O.A. Sampayo	(CINV)
ABT	93	NP B396 3	I. Abt et al.	(H1 Collab.)
ADRIANI	93M	PRPL 236 1	O. Adriani et al.	(L3 Collab.)
BARDADIN-...	92	ZPHY C55 163	M. Bardadin-Otwinowska	(CLER)
DECAMP	92	PRPL 216 253	D. Decamp et al.	(ALEPH Collab.)
PDG	92	PR D45 S1	K. Hikasa et al.	(KEK, LBL, BOST+)
ABREU	91F	NP B367 511	P. Abreu et al.	(DELPHI Collab.)
KIM	90	PL B240 243	G.N. Kim et al.	(AMY Collab.)
ABE	89B	PRL 62 1825	F. Abe et al.	(CDF Collab.)
ABE	89D	PRL 63 1447	F. Abe et al.	(CDF Collab.)
ABE	89J	ZPHY C45 175	K. Abe et al.	(VENUS Collab.)
ALBAJAR	89	ZPHY C44 15	C. Albajar et al.	(UA1 Collab.)
BARGER	89	PL B220 464	V. Barger et al.	(WISC, KEK)
DORENBOS...	89	ZPHY C41 567	J. Dorenbosch et al.	(CHARM Collab.)
BARTEL	87B	ZPHY C36 15	W. Bartel et al.	(JADE Collab.)
GRIFOLS	86	PL 168B 264	J.A. Grifols, S. Peris	(BARC)
JODIDIO	86	PR D34 1967	A. Jodidio et al.	(LBL, NWES, TRIU)
Also		PR D37 237 (erratum)	A. Jodidio et al.	(LBL, NWES, TRIU)
RENARD	82	PL 116B 264	F.M. Renard	(CERN)

Extra Dimensions

For explanation of terms used and discussion of significant model dependence of following limits, see the "Extra Dimensions" review. Footnotes describe originally quoted limit. δ indicates the number of extra dimensions.

Limits not encoded here are summarized in the "Extra Dimensions" review, where the latest unpublished results are also described.

See the related review(s):

Extra Dimensions

CONTENTS:

Limits on R from Deviations in Gravitational Force Law
Limits on R from On-Shell Production of Gravitons: $\delta = 2$
Mass Limits on M_{TT}
Limits on $1/R = M_c$
Limits on Kaluza-Klein Gravitons in Warped Extra Dimensions
Limits on Kaluza-Klein Gluons in Warped Extra Dimensions
Black Hole Production Limits
– Semiclassical Black Holes
– Quantum Black Holes

Limits on R from Deviations in Gravitational Force Law

This section includes limits on the size of extra dimensions from deviations in the Newtonian $(1/r^2)$ gravitational force law at short distances. Deviations are parametrized by a gravitational potential of the form $V = -(G\, m\, m'/r)\,[1 + \alpha \exp(-r/R)]$. For δ toroidal extra dimensions of equal size, $\alpha = 8\delta/3$. Quoted bounds are for $\delta = 2$ unless otherwise noted.

VALUE (μm)	CL%	DOCUMENT ID		TECN	COMMENT
• • • We do not use the following data for averages, fits, limits, etc. • • •					
		[1] BLAKEMORE	21		Optical levitation
		[2] HEACOCK	21		Neutron scattering
		[3] LEE	20		Torsion pendulum
< 37	95	[4] TAN	20A		Torsion pendulum
		[5] BERGE	18	MICR	Space accelerometer
		[6] FAYET	18A	MICR	Space accelerometer
		[7] KLIMCHITSK...	17A		Torsion oscillator
		[8] XU	13		Nuclei properties
		[9] BEZERRA	11		Torsion oscillator
		[10] SUSHKOV	11		Torsion pendulum
		[11] BEZERRA	10		Microcantilever
		[12] MASUDA	09		Torsion pendulum
		[13] GERACI	08		Microcantilever
		[14] TRENKEL	08		Newton's constant
		[15] DECCA	07A		Torsion oscillator
< 37	95	[16] KAPNER	07		Torsion pendulum
< 47	95	[17] TU	07		Torsion pendulum
		[18] SMULLIN	05		Microcantilever
<130	95	[19] HOYLE	04		Torsion pendulum
		[20] CHIAVERINI	03		Microcantilever
$\lesssim$200	95	[21] LONG	03		Microcantilever
<190	95	[22] HOYLE	01		Torsion pendulum
		[23] HOSKINS	85		Torsion pendulum

[1] BLAKEMORE 21 obtain constraints on non-Newtonian forces with strengths $|\alpha| \gtrsim 10^8$ and length scales $R > 10\ \mu$m. See their Fig. 4 for more details including comparison with previous searches.

[2] HEACOCK 21 obtain constraints on non-Newtonian forces with strengths $10^{18} \lesssim |\alpha| \lesssim 10^{25}$ and length scales $R \simeq$ 0.02–10 nm. See their Figure 3 for more details. This improves the results of HADDOCK 18. These constraints do not place limits on the size of extra flat dimensions.

Downloaded from https://academic.oup.com/ptep/article/2022/8/083C01/6651666 by KIT Library user on 27 September 2022

[3] LEE 20 search for new forces probing a range of $|\alpha| \simeq 0.1$–10^5 and length scales $R \simeq 7$–$90\ \mu$m. For $\delta = 1$ the bound on R is 30 μm. See their Fig. 5 for details on the bound.

[4] TAN 20A search for new forces probing a range of $|\alpha| \simeq 4\times10^{-3}$–$1\times10^{2}$ and length scales $R \simeq 40$–$350\ \mu$m. See their Fig. 6 for details on the bound.

[5] BERGE 18 uses results from the MICROSCOPE experiment to obtain constraints on non-Newtonian forces with strengths $10^{-11} \lesssim |\alpha| \lesssim 10^{-7}$ and length scales $R \gtrsim 10^5$ m. See their Figure 1 for more details. These constraints do not place limits on the size of extra flat dimensions.

[6] FAYET 18A uses results from the MICROSCOPE experiment to obtain constraints on an EP-violating force possibly arising from a new U(1) gauge boson. For $R \gtrsim 10^7$ m the limits are $|\alpha| \lesssim$ a few 10^{-13} to a few 10^{-11} depending on the coupling, corresponding to $|\epsilon| \lesssim 10^{-24}$ for the coupling of the new spin-1 or spin-0 mediator. These constraints do not place limits on the size of extra flat dimensions. This extends the results of FAYET 18.

[7] KLIMCHITSKAYA 17A uses an experiment that measures the difference of Casimir forces to obtain bounds on non-Newtonian forces with strengths $|\alpha| \simeq 10^5$–10^{17} and length scales $R = 0.03$–$10\ \mu$m. See their Fig. 3. These constraints do not place limits on the size of extra flat dimensions.

[8] XU 13 obtain constraints on non-Newtonian forces with strengths $|\alpha| \simeq 10^{34}$–10^{36} and length scales $R \simeq 1$–10 fm. See their Fig. 4 for more details. These constraints do not place limits on the size of extra flat dimensions.

[9] BEZERRA 11 obtain constraints on non-Newtonian forces with strengths $10^{11} \lesssim |\alpha| \lesssim 10^{18}$ and length scales $R = 30$–1260 nm. See their Fig. 2 for more details. These constraints do not place limits on the size of extra flat dimensions.

[10] SUSHKOV 11 obtain improved limits on non-Newtonian forces with strengths $10^7 \lesssim |\alpha| \lesssim 10^{11}$ and length scales $0.4\ \mu\text{m} < R < 4\ \mu$m (95% CL). See their Fig. 2. These bounds do not place limits on the size of extra flat dimensions. However, a model dependent bound of $M_* > 70$ TeV is obtained assuming gauge bosons that couple to baryon number also propagate in $(4+\delta)$ dimensions.

[11] BEZERRA 10 obtain improved constraints on non-Newtonian forces with strengths $10^{19} \lesssim |\alpha| \lesssim 10^{29}$ and length scales $R = 1.6$–14 nm (95% CL). See their Fig. 1. This bound does not place limits on the size of extra flat dimensions.

[12] MASUDA 09 obtain improved constraints on non-Newtonian forces with strengths $10^9 \lesssim |\alpha| \lesssim 10^{11}$ and length scales $R = 1.0$–$2.9\ \mu$m (95% CL). See their Fig. 3. This bound does not place limits on the size of extra flat dimensions.

[13] GERACI 08 obtain improved constraints on non-Newtonian forces with strengths $|\alpha| > 14{,}000$ and length scales $R = 5$–$15\ \mu$m. See their Fig. 9. This bound does not place limits on the size of extra flat dimensions.

[14] TRENKEL 08 uses two independent measurements of Newton's constant G to constrain new forces with strength $|\alpha| \simeq 10^{-4}$ and length scales $R = 0.02$–1 m. See their Fig. 1. This bound does not place limits on the size of extra flat dimensions.

[15] DECCA 07A search for new forces and obtain bounds in the region with strengths $|\alpha| \simeq 10^{13}$–10^{18} and length scales $R = 20$–86 nm. See their Fig. 6. This bound does not place limits on the size of extra flat dimensions.

[16] KAPNER 07 search for new forces, probing a range of $|\alpha| \simeq 10^{-3}$–10^5 and length scales $R \simeq 10$–$1000\ \mu$m. For $\delta = 1$ the bound on R is 44 μm. For $\delta = 2$, the bound is expressed in terms of M_*, here translated to a bound on the radius. See their Fig. 6 for details on the bound.

[17] TU 07 search for new forces probing a range of $|\alpha| \simeq 10^{-1}$–10^5 and length scales $R \simeq 20$–$1000\ \mu$m. For $\delta = 1$ the bound on R is 53 μm. See their Fig. 3 for details on the bound.

[18] SMULLIN 05 search for new forces, and obtain bounds in the region with strengths $\alpha \simeq 10^3$–10^8 and length scales $R = 6$–$20\ \mu$m. See their Figs. 1 and 16 for details on the bound. This work does not place limits on the size of extra flat dimensions.

[19] HOYLE 04 search for new forces, probing α down to 10^{-2} and distances down to 10μm. Quoted bound on R is for $\delta = 2$. For $\delta = 1$, bound goes to 160 μm. See their Fig. 34 for details on the bound.

[20] CHIAVERINI 03 search for new forces, probing α above 10^4 and λ down to 3μm, finding no signal. See their Fig. 4 for details on the bound. This bound does not place limits on the size of extra flat dimensions.

[21] LONG 03 search for new forces, probing α down to 3, and distances down to about 10μm. See their Fig. 4 for details on the bound.

[22] HOYLE 01 search for new forces, probing α down to 10^{-2} and distances down to 20μm. See their Fig. 4 for details on the bound. The quoted bound is for $\alpha \geq 3$.

[23] HOSKINS 85 search for new forces, probing distances down to 4 mm. See their Fig. 13 for details on the bound. This bound does not place limits on the size of extra flat dimensions.

Limits on R from On-Shell Production of Gravitons: $\delta = 2$

This section includes limits on on-shell production of gravitons in collider and astrophysical processes. Bounds quoted are on R, the assumed common radius of the flat extra dimensions, for $\delta = 2$ extra dimensions. Studies often quote bounds in terms of derived parameter; experiments are actually sensitive to the masses of the KK gravitons: $m_{\vec{n}} = |\vec{n}|/R$. See the Review on "Extra Dimensions" for details. Bounds are given in μm for $\delta = 2$.

VALUE (μm)	CL%	DOCUMENT ID		TECN	COMMENT
< 3.8	95	[1] AAD	21F	ATLS	$pp \to jG$
< 0.00016	95	[2] HANNESTAD	03		Neutron star heating
• • • We do not use the following data for averages, fits, limits, etc. • • •					
< 56	95	[3] SIRUNYAN	21A	CMS	$pp \to ZG$
< 4.1	95	[4] TUMASYAN	21D	CMS	$pp \to jG$
		[5] SIRUNYAN	17AQ	CMS	$pp \to \gamma G$
< 90	95	[6] AABOUD	16F	ATLS	$pp \to \gamma G$
		[7] KHACHATRY...	16N	CMS	$pp \to \gamma G$
		[8] AAD	15CS	ATLS	$pp \to \gamma G$
< 127	95	[9] AAD	13C	ATLS	$pp \to \gamma G$
< 34.4	95	[10] AAD	13D	ATLS	$pp \to jj$
< 0.0087	95	[11] AJELLO	12	FLAT	Neutron star γ sources
< 245	95	[12] AALTONEN	08AC	CDF	$p\overline{p} \to \gamma G, jG$
< 615	95	[13] ABAZOV	08S	D0	$p\overline{p} \to \gamma G$
< 0.916	95	[14] DAS	08		Supernova cooling
< 350	95	[15] ABULENCIA,A	06	CDF	$p\overline{p} \to jG$
< 270	95	[16] ABDALLAH	05B	DLPH	$e^+e^- \to \gamma G$
< 210	95	[17] ACHARD	04E	L3	$e^+e^- \to \gamma G$
< 480	95	[18] ACOSTA	04C	CDF	$\overline{p}p \to jG$
< 0.00038	95	[19] CASSE	04		Neutron star γ sources
< 610	95	[20] ABAZOV	03	D0	$\overline{p}p \to jG$
< 0.96	95	[21] HANNESTAD	03		Supernova cooling
< 0.096	95	[22] HANNESTAD	03		Diffuse γ background
< 0.051	95	[23] HANNESTAD	03		Neutron star γ sources
< 300	95	[24] HEISTER	03C	ALEP	$e^+e^- \to \gamma G$
		[25] FAIRBAIRN	01		Cosmology
< 0.66	95	[26] HANHART	01		Supernova cooling
		[27] CASSISI	00		Red giants
<1300	95	[28] ACCIARRI	99S	L3	$e^+e^- \to ZG$

[1] AAD 21F search for $pp \to jG$, using 139 fb^{-1} of data at $\sqrt{s} = 13$ TeV to place lower limits on M_D for two to six extra dimensions (see their Table X), from which this bound on R is derived. This limit supersedes that in AABOUD 18I.

[2] HANNESTAD 03 obtain a limit on R from the heating of old neutron stars by the surrounding cloud of trapped KK gravitons. Limits for all $\delta \leq 7$ are given in their Tables V and VI. These limits supersede those in HANNESTAD 02.

[3] SIRUNYAN 21A search for $pp \to ZG$, using 137 fb^{-1} of data at $\sqrt{s} = 13$ TeV to place lower limits on M_D for two to seven extra dimensions (see their Figure 12), from which this bound on R is derived. These limits supersede those obtained in SIRUNYAN 18BV.

[4] TUMASYAN 21D search for $pp \to jG$, using 137 fb^{-1} of data at $\sqrt{s} = 13$ TeV to place lower limits on M_D for two to seven extra dimensions (see their Table 3), from which this bound on R is derived. This limit supersedes that in SIRUNYAN 18S.

[5] SIRUNYAN 17AQ search for $pp \to \gamma G$, using 12.9 fb^{-1} of data at $\sqrt{s} = 13$ TeV to place limits on M_D for three to six extra dimensions (see their Table 3).

[6] AABOUD 16F search for $pp \to \gamma G$, using 3.2 fb^{-1} of data at $\sqrt{s} = 13$ TeV to place limits on M_D for two to six extra dimensions (see their Figure 9), from which this bound on R is derived.

[7] KHACHATRYAN 16N search for $pp \to \gamma G$, using 19.6 fb^{-1} of data at $\sqrt{s} = 8$ TeV to place limits on M_D for three to six extra dimensions (see their Table 5).

[8] AAD 15CS search for $pp \to \gamma G$, using 20.3 fb^{-1} of data at $\sqrt{s} = 8$ TeV to place lower limits on M_D for two to six extra dimensions (see their Fig. 18).

[9] AAD 13C search for $pp \to \gamma G$, using 4.6 fb^{-1} of data at $\sqrt{s} = 7$ TeV to place bounds on M_D for two to six extra dimensions, from which this bound on R is derived.

[10] AAD 13D search for the dijet decay of quantum black holes in 4.8 fb^{-1} of data produced in pp collisions at $\sqrt{s} = 7$ TeV to place bounds on M_D for two to seven extra dimensions, from which these bounds on R are derived. Limits on M_D for all $\delta \leq 7$ are given in their Table 3.

[11] AJELLO 12 obtain a limit on R from the gamma-ray emission of point γ sources that arise from the photon decay of KK gravitons which are gravitationally bound around neutron stars. Limits for all $\delta \leq 7$ are given in their Table 7.

[12] AALTONEN 08AC search for $p\overline{p} \to \gamma G$ and $p\overline{p} \to jG$ at $\sqrt{s} = 1.96$ TeV with 2.0 fb^{-1} and 1.1 fb^{-1} respectively, in order to place bounds on the fundamental scale and size of the extra dimensions. See their Table III for limits on all $\delta \leq 6$.

[13] ABAZOV 08S search for $p\overline{p} \to \gamma G$, using 1 fb^{-1} of data at $\sqrt{s} = 1.96$ TeV to place bounds on M_D for two to eight extra dimensions, from which these bounds on R are derived. See their paper for intermediate values of δ.

[14] DAS 08 obtain a limit on R from Kaluza-Klein graviton cooling of SN1987A due to plasmon-plasmon annihilation.

[15] ABULENCIA,A 06 search for $p\overline{p} \to jG$ using 368 pb^{-1} of data at $\sqrt{s} = 1.96$ TeV. See their Table II for bounds for all $\delta \leq 6$.

[16] ABDALLAH 05B search for $e^+e^- \to \gamma G$ at $\sqrt{s} = 180$–209 GeV to place bounds on the size of extra dimensions and the fundamental scale. Limits for all $\delta \leq 6$ are given in their Table 6. These limits supersede those in ABREU 00Z.

[17] ACHARD 04E search for $e^+e^- \to \gamma G$ at $\sqrt{s} = 189$–209 GeV to place bounds on the size of extra dimensions and the fundamental scale. See their Table 8 for limits with $\delta \leq 8$. These limits supersede those in ACCIARRI 99R.

[18] ACOSTA 04C search for $\overline{p}p \to jG$ at $\sqrt{s} = 1.8$ TeV to place bounds on the size of extra dimensions and the fundamental scale. See their paper for bounds on $\delta = 4, 6$.

[19] CASSE 04 obtain a limit on R from the gamma-ray emission of point γ sources that arises from the photon decay of gravitons around newly born neutron stars, applying the technique of HANNESTAD 03 to neutron stars in the galactic bulge. Limits for all $\delta \leq 7$ are given in their Table I.

[20] ABAZOV 03 search for $p\overline{p} \to jG$ at $\sqrt{s}$=1.8 TeV to place bounds on M_D for 2 to 7 extra dimensions, from which these bounds on R are derived. See their paper for bounds on intermediate values of δ. We quote results without the approximate NLO scaling introduced in the paper.

[21] HANNESTAD 03 obtain a limit on R from graviton cooling of supernova SN1987a. Limits for all $\delta \leq 7$ are given in their Tables V and VI.

[22] HANNESTAD 03 obtain a limit on R from gravitons emitted in supernovae and which subsequently decay, contaminating the diffuse cosmic γ background. Limits for all $\delta \leq 7$ are given in their Tables V and VI. These limits supersede those in HANNESTAD 02.

[23] HANNESTAD 03 obtain a limit on R from gravitons emitted in two recent supernovae and which subsequently decay, creating point γ sources. Limits for all $\delta \leq 7$ are given in their Tables V and VI. These limits are corrected in the published erratum.

[24] HEISTER 03C use the process $e^+e^- \to \gamma G$ at $\sqrt{s} = 189$–209 GeV to place bounds on the size of extra dimensions and the scale of gravity. See their Table 4 for limits with $\delta \leq 6$ for derived limits on M_D.

[25] FAIRBAIRN 01 obtains bounds on R from over production of KK gravitons in the early universe. Bounds are quoted in paper in terms of fundamental scale of gravity. Bounds depend strongly on temperature of QCD phase transition and range from R< 0.13 μm to 0.001 μm for δ=2; bounds for δ=3,4 can be derived from Table 1 in the paper.

[26] HANHART 01 obtain bounds on R from limits on graviton cooling of supernova SN 1987a using numerical simulations of proto-neutron star neutrino emission.

[27] CASSISI 00 obtain rough bounds on M_D (and thus R) from red giant cooling for δ=2,3. See their paper for details.

[28] ACCIARRI 99S search for $e^+e^- \to ZG$ at $\sqrt{s}$=189 GeV. Limits on the gravity scale are found in their Table 2, for $\delta \leq 4$.

Downloaded from https://academic.oup.com/ptep/article/2022/8/083C01/6651666 by KIT Library user on 27 September 2022

Mass Limits on M_{TT}

This section includes limits on the cut-off mass scale, M_{TT}, of dimension-8 operators from KK graviton exchange in models of large extra dimensions. Ambiguities in the UV-divergent summation are absorbed into the parameter λ, which is taken to be $\lambda = \pm 1$ in the following analyses. Bounds for $\lambda = -1$ are shown in parenthesis after the bound for $\lambda = +1$, if appropriate. Different papers use slightly different definitions of the mass scale. The definition used here is related to another popular convention by $M_{TT}^4 = (2/\pi)\ \Lambda_T^4$, as discussed in the above Review on "Extra Dimensions."

VALUE (TeV)		CL%	DOCUMENT ID		TECN	COMMENT
> 9.02		95	[1] SIRUNYAN	18DD	CMS	$pp \to$ dijet, ang. distrib.
>20.6	**(> 15.7)**	95	[2] GIUDICE	03	RVUE	Dim-6 operators
• • • We do not use the following data for averages, fits, limits, etc. • • •						
> 6.7		95	[3] SIRUNYAN	21N	CMS	$pp \to e^+e^-, \mu^+\mu^-$
> 6.9		95	[4] SIRUNYAN	19AC	CMS	$pp \to e^+e^-, \mu^+\mu^-, \gamma\gamma$
> 7.0	(>5.6)	95	[5] SIRUNYAN	18DU	CMS	$pp \to \gamma\gamma$
> 6.5		95	[6] AABOUD	17AP	ATLS	$pp \to \gamma\gamma$
> 3.8		95	[7] AAD	14BE	ATLS	$pp \to e^+e^-,\ \mu^+\mu^-$
> 3.2		95	[8] AAD	13E	ATLS	$pp \to e^+e^-, \mu^+\mu^-, \gamma\gamma$
			[9] BAAK	12	RVUE	Electroweak
> 0.90	(>0.92)	95	[10] AARON	11C	H1	$e^\pm p \to e^\pm X$
> 1.48		95	[11] ABAZOV	09AE	D0	$p\overline{p} \to$ dijet, ang. distrib.
> 1.45		95	[12] ABAZOV	09D	D0	$p\overline{p} \to e^+e^-, \gamma\gamma$
> 1.1	(> 1.0)	95	[13] SCHAEL	07A	ALEP	$e^+e^- \to e^+e^-$
> 0.898	(> 0.998)	95	[14] ABDALLAH	06C	DLPH	$e^+e^- \to \ell^+\ell^-$
> 0.853	(> 0.939)	95	[15] GERDES	06		$p\overline{p} \to e^+e^-,\ \gamma\gamma$
> 0.96	(> 0.93)	95	[16] ABAZOV	05V	D0	$p\overline{p} \to \mu^+\mu^-$
> 0.78	(> 0.79)	95	[17] CHEKANOV	04B	ZEUS	$e^\pm p \to e^\pm X$
> 0.805	(> 0.956)	95	[18] ABBIENDI	03D	OPAL	$e^+e^- \to \gamma\gamma$
> 0.7	(> 0.7)	95	[19] ACHARD	03D	L3	$e^+e^- \to ZZ$
> 0.82	(> 0.78)	95	[20] ADLOFF	03	H1	$e^\pm p \to e^\pm X$
> 1.28	(> 1.25)	95	[21] GIUDICE	03	RVUE	
> 0.80	(> 0.85)	95	[22] HEISTER	03C	ALEP	$e^+e^- \to \gamma\gamma$
> 0.84	(> 0.99)	95	[23] ACHARD	02D	L3	$e^+e^- \to \gamma\gamma$
> 1.2	(> 1.1)	95	[24] ABBOTT	01	D0	$p\overline{p} \to e^+e^-, \gamma\gamma$
> 0.60	(> 0.63)	95	[25] ABBIENDI	00R	OPAL	$e^+e^- \to \mu^+\mu^-$
> 0.63	(> 0.50)	95	[25] ABBIENDI	00R	OPAL	$e^+e^- \to \tau^+\tau^-$
> 0.68	(> 0.61)	95	[25] ABBIENDI	00R	OPAL	$e^+e^- \to \mu^+\mu^-, \tau^+\tau^-$
			[26] ABREU	00A	DLPH	$e^+e^- \to \gamma\gamma$
> 0.680	(> 0.542)	95	[27] ABREU	00S	DLPH	$e^+e^- \to \mu^+\mu^-, \tau^+\tau^-$
> 15–28		99.7	[28] CHANG	00B	RVUE	Electroweak
> 0.98		95	[29] CHEUNG	00	RVUE	$e^+e^- \to \gamma\gamma$
> 0.29–0.38		95	[30] GRAESSER	00	RVUE	$(g-2)_\mu$
> 0.50–1.1		95	[31] HAN	00	RVUE	Electroweak
> 2.0	(> 2.0)	95	[32] MATHEWS	00	RVUE	$\overline{p}p \to jj$
> 1.0	(> 1.1)	95	[33] MELE	00	RVUE	$e^+e^- \to VV$
			[34] ABBIENDI	99P	OPAL	
			[35] ACCIARRI	99M	L3	
			[36] ACCIARRI	99S	L3	
> 1.412	(> 1.077)	95	[37] BOURILKOV	99		$e^+e^- \to e^+e^-$

[1] SIRUNYAN 18DD use dijet angular distributions in 35.9 fb^{-1} of data from pp collisions at $\sqrt{s} = 13$ TeV to place a lower bound on Λ_T, here converted to M_{TT}. This updates the results of SIRUNYAN 17F.

[2] GIUDICE 03 place bounds on Λ_6, the coefficient of the gravitationally-induced dimension-6 operator $(2\pi\lambda/\Lambda_6^2)(\sum \overline{f}\gamma_\mu\gamma^5 f)(\sum \overline{f}\gamma^\mu\gamma^5 f)$, using data from a variety of experiments. Results are quoted for $\lambda = \pm 1$ and are independent of δ.

[3] SIRUNYAN 21N use 137 (140) fb^{-1} of data from pp collisions at $\sqrt{s} = 13$ TeV in the dielectron (dimuon) channels to place a lower limit on Λ_T, here converted to M_{TT}. Bounds on individual channels can be found in their Table 7.

[4] SIRUNYAN 19AC use 35.9 (36.3) fb^{-1} of data from pp collisions at $\sqrt{s} = 13$ TeV in the dielectron (dimuon) channels to place a lower limit on Λ_T, here converted to M_{TT}. The dielectron and dimuon channels are combined with previous results in the diphoton channel to set the best limit. Bounds on individual channels and different priors can be found in their Table 2. This updates the results in KHACHATRYAN 15AE.

[5] SIRUNYAN 18DU use 35.9 fb^{-1} of data from pp collisions at $\sqrt{s} = 13$ TeV to place lower limits on M_{TT} (equivalent to their M_S). This updates the results of CHATRCHYAN 12R.

[6] AABOUD 17AP use 36.7 fb^{-1} of data from pp collisions at $\sqrt{s} = 13$ TeV to place lower limits on M_{TT} (equivalent to their M_S). This updates the results of AAD 13AS.

[7] AAD 14BE use 20 fb^{-1} of data from pp collisions at $\sqrt{s} = 8$ TeV in the dilepton channel to place lower limits on M_{TT} (equivalent to their M_S).

[8] AAD 13E use 4.9 and 5.0 fb^{-1} of data from pp collisions at $\sqrt{s} = 7$ TeV in the dielectron and dimuon channels, respectively, to place lower limits on M_{TT} (equivalent to their M_S). The dielectron and dimuon channels are combined with previous results in the diphoton channel to set the best limit. Bounds on individual channels and different priors can be found in their Table VIII.

[9] BAAK 12 use electroweak precision observables to place bounds on the ratio Λ_T/M_D as a function of M_D. See their Fig. 22 for constraints with a Higgs mass of 120 GeV.

[10] AARON 11C search for deviations in the differential cross section of $e^\pm p \to e^\pm X$ in 446 pb^{-1} of data taken at $\sqrt{s} = 301$ and 319 GeV to place a bound on M_{TT}.

[11] ABAZOV 09AE use dijet angular distributions in 0.7 fb^{-1} of data from $p\overline{p}$ collisions at $\sqrt{s} = 1.96$ TeV to place lower bounds on Λ_T (equivalent to their M_S), here converted to M_{TT}.

[12] ABAZOV 09D use 1.05 fb^{-1} of data from $p\overline{p}$ collisions at $\sqrt{s} = 1.96$ TeV to place lower bounds on Λ_T (equivalent to their M_s), here converted to M_{TT}.

[13] SCHAEL 07A use e^+e^- collisions at $\sqrt{s} = 189$–209 GeV to place lower limits on Λ_T, here converted to limits on M_{TT}.

[14] ABDALLAH 06C use e^+e^- collisions at $\sqrt{s} \sim 130$–207 GeV to place lower limits on M_{TT}, which is equivalent to their definition of M_s. Bound shown includes all possible final state leptons, $\ell = e, \mu, \tau$. Bounds on individual leptonic final states can be found in their Table 31.

[15] GERDES 06 use 100 to 110 pb^{-1} of data from $p\overline{p}$ collisions at $\sqrt{s} = 1.8$ TeV, as recorded by the CDF Collaboration during Run I of the Tevatron. Bound shown includes a K-factor of 1.3. Bounds on individual e^+e^- and $\gamma\gamma$ final states are found in their Table I.

[16] ABAZOV 05V use 246 pb^{-1} of data from $p\overline{p}$ collisions at $\sqrt{s} = 1.96$ TeV to search for deviations in the differential cross section to $\mu^+\mu^-$ from graviton exchange.

[17] CHEKANOV 04B search for deviations in the differential cross section of $e^\pm p \to e^\pm X$ with 130 pb^{-1} of combined data and Q^2 values up to 40,000 GeV^2 to place a bound on M_{TT}.

[18] ABBIENDI 03D use e^+e^- collisions at $\sqrt{s}$=181–209 GeV to place bounds on the ultraviolet scale M_{TT}, which is equivalent to their definition of M_s.

[19] ACHARD 03D look for deviations in the cross section for $e^+e^- \to ZZ$ from $\sqrt{s} =$ 200–209 GeV to place a bound on M_{TT}.

[20] ADLOFF 03 search for deviations in the differential cross section of $e^\pm p \to e^\pm X$ at $\sqrt{s}$=301 and 319 GeV to place bounds on M_{TT}.

[21] GIUDICE 03 review existing experimental bounds on M_{TT} and derive a combined limit.

[22] HEISTER 03C use e^+e^- collisions at $\sqrt{s}$= 189–209 GeV to place bounds on the scale of dim-8 gravitational interactions. Their $M_s^\pm$ is equivalent to our M_{TT} with $\lambda = \pm 1$.

[23] ACHARD 02 search for s-channel graviton exchange effects in $e^+e^- \to \gamma\gamma$ at $E_{cm} =$ 192–209 GeV.

[24] ABBOTT 01 search for variations in differential cross sections to e^+e^- and $\gamma\gamma$ final states at the Tevatron.

[25] ABBIENDI 00R uses e^+e^- collisions at $\sqrt{s}$= 189 GeV.

[26] ABREU 00A search for s-channel graviton exchange effects in $e^+e^- \to \gamma\gamma$ at E_{cm}= 189–202 GeV.

[27] ABREU 00S uses e^+e^- collisions at $\sqrt{s}$=183 and 189 GeV. Bounds on μ and τ individual final states given in paper.

[28] CHANG 00B derive 3σ limit on M_{TT} of (28,19,15) TeV for δ=(2,4,6) respectively assuming the presence of a torsional coupling in the gravitational action. Highly model dependent.

[29] CHEUNG 00 obtains limits from anomalous diphoton production at OPAL due to graviton exchange. Original limit for δ=4. However, unknown UV theory renders δ dependence unreliable. Original paper works in HLZ convention.

[30] GRAESSER 00 obtains a bound from graviton contributions to $g-2$ of the muon through loops of 0.29 TeV for δ=2 and 0.38 TeV for δ=4,6. Limits scale as $\lambda^{1/2}$. However calculational scheme not well-defined without specification of high-scale theory. See the "Extra Dimensions Review."

[31] HAN 00 calculates corrections to gauge boson self-energies from KK graviton loops and constrain them using S and T. Bounds on M_{TT} range from 0.5 TeV (δ=6) to 1.1 TeV (δ=2); see text. Limits have strong dependence, $\lambda^{\delta+2}$, on unknown λ coefficient.

[32] MATHEWS 00 search for evidence of graviton exchange in CDF and DØ dijet production data. See their Table 2 for slightly stronger δ-dependent bounds. Limits expressed in terms of $\widetilde{M}_S^4 = M_{TT}^4/8$.

[33] MELE 00 obtains bound from KK graviton contributions to $e^+e^- \to VV$ ($V=\gamma, W, Z$) at LEP. Authors use Hewett conventions.

[34] ABBIENDI 99P search for s-channel graviton exchange effects in $e^+e^- \to \gamma\gamma$ at E_{cm}=189 GeV. The limits $G_+ > 660$ GeV and $G_- > 634$ GeV are obtained from combined E_{cm}=183 and 189 GeV data, where $G_\pm$ is a scale related to the fundamental gravity scale.

[35] ACCIARRI 99M search for the reaction $e^+e^- \to \gamma G$ and s-channel graviton exchange effects in $e^+e^- \to \gamma\gamma$, W^+W^-, ZZ, e^+e^-, $\mu^+\mu^-$, $\tau^+\tau^-$, $q\overline{q}$ at E_{cm}=183 GeV. Limits on the gravity scale are listed in their Tables 1 and 2.

[36] ACCIARRI 99S search for the reaction $e^+e^- \to ZG$ and s-channel graviton exchange effects in $e^+e^- \to \gamma\gamma$, W^+W^-, ZZ, e^+e^-, $\mu^+\mu^-$, $\tau^+\tau^-$, $q\overline{q}$ at E_{cm}=189 GeV. Limits on the gravity scale are listed in their Tables 1 and 2.

[37] BOURILKOV 99 performs global analysis of LEP data on e^+e^- collisions at $\sqrt{s}$=183 and 189 GeV. Bound is on Λ_T.

Limits on $1/R = M_c$

This section includes limits on $1/R = M_c$, the compactification scale in models with one TeV-sized extra dimension, due to exchange of Standard Model KK excitations. Bounds assume fermions are not in the bulk, unless stated otherwise. See the "Extra Dimensions" review for discussion of model dependence.

VALUE (TeV)	CL%	DOCUMENT ID		TECN	COMMENT
>4.16	95	[1] AAD	12CC	ATLS	$pp \to \ell\overline{\ell}$
>6.1		[2] BARBIERI	04	RVUE	Electroweak
• • • We do not use the following data for averages, fits, limits, etc. • • •					
		[3] AVNISH	21	RVUE	$pp \to$ multijet
		[4] AABOUD	18AV	ATLS	$pp \to t\overline{t}t\overline{t}$
		[5] AABOUD	18CE	ATLS	$pp \to t\overline{t}t\overline{t}$
>3.8	95	[6] ACCOMANDO	15	RVUE	Electroweak
>3.40	95	[7] KHACHATRY...15T		CMS	$pp \to \ell X$
		[8] CHATRCHYAN	13AQ	CMS	$pp \to \ell X$
>1.38	95	[9] CHATRCHYAN	13W	CMS	$pp \to \gamma\gamma$, δ=6, M_D=5 TeV
>0.715	95	[10] EDELHAUSER	13	RVUE	$pp \to \ell\overline{\ell} + X$
>1.40	95	[11] AAD	12CP	ATLS	$pp \to \gamma\gamma$, δ=6, M_D=5 TeV
>1.23	95	[12] AAD	12X	ATLS	$pp \to \gamma\gamma$, δ=6, M_D=5 TeV
>0.26	95	[13] ABAZOV	12M	D0	$p\overline{p} \to \mu\mu$
>0.75	95	[14] BAAK	12	RVUE	Electroweak
		[15] FLACKE	12	RVUE	Electroweak
>0.43	95	[16] NISHIWAKI	12	RVUE	$H \to WW, \gamma\gamma$
>0.729	95	[17] AAD	11F	ATLS	$pp \to \gamma\gamma$, δ=6, M_D=5 TeV
>0.961	95	[18] AAD	11X	ATLS	$pp \to \gamma\gamma$, δ=6, M_D=5 TeV
>0.477	95	[19] ABAZOV	10P	D0	$p\overline{p} \to \gamma\gamma$, δ=6, M_D=5 TeV
>1.59	95	[20] ABAZOV	09AE	D0	$p\overline{p} \to$ dijet, angular dist.
>0.6	95	[21] HAISCH	07	RVUE	$\overline{B} \to X_s\gamma$
>0.6	90	[22] GOGOLADZE	06	RVUE	Electroweak
>3.3	95	[23] CORNET	00	RVUE	Electroweak
> 3.3–3.8	95	[24] RIZZO	00	RVUE	Electroweak

Downloaded from https://academic.oup.com/ptep/article/2022/8/083C01/6651666 by KIT Library user on 27 September 2022

[1] AAD 12CC use 4.9 and 5.0 fb^{-1} of data from pp collisions at $\sqrt{s}$ = 7 TeV in the dielectron and dimuon channels, respectively, to place a lower bound on the mass of the lightest KK Z/γ boson (equivalent to $1/R = M_c$). The limit quoted here assumes a flat prior corresponding to when the pure Z/γ KK cross section term dominates. See their Section 15 for more details.

[2] BARBIERI 04 use electroweak precision observables to place a lower bound on the compactification scale $1/R$. Both the gauge bosons and the Higgs boson are assumed to propagate in the bulk.

[3] AVNISH 21 perform a study on the ATLAS collaboration search for multiple jets plus missing transverse energy from pp collisions at $\sqrt{s}$ = 13 TeV and integrated luminosity of 139 fb^{-1}, to place constraints on the compactification scale and cutoff scale Λ in universal extra dimension models with Standard Model fields propagating in the bulk.

[4] AABOUD 18AV use 36.1 fb^{-1} of data from pp collisions at $\sqrt{s}$ = 13 TeV in final states with multiple b-jets, to place a lower bound on the compactification scale in a model with two universal extra dimensions. Assuming the radii of the two extra dimensions are equal, a lower limit of 1.8 TeV for the Kaluza-Klein mass is obtained.

[5] AABOUD 18CE use 36.1 fb^{-1} of data from pp collisions at $\sqrt{s}$ = 13 TeV in final states with same-charge leptons and b-jets, to place a lower bound on the compactification scale in a model with two universal extra dimensions. Assuming the radii of the two extra dimensions are equal, a lower limit of 1.45 TeV for the Kaluza-Klein mass is obtained.

[6] ACCOMANDO 15 use electroweak precision observables to place a lower bound on the compactification scale $1/R$. See their Fig. 2 for the bound as a function of $\sin\beta$, which parametrizes the VEV contribution from brane and bulk Higgs fields. The quoted value is for the minimum bound which occurs at $\sin\beta = 0.45$.

[7] KHACHATRYAN 15T use 19.7 fb^{-1} of data from pp collisions at $\sqrt{s}$ = 8 TeV to place a lower bound on the compactification scale $1/R$.

[8] CHATRCHYAN 13AQ use 5.0 fb^{-1} of data from pp collisions at $\sqrt{s}$ = 7 TeV and a further 3.7 fb^{-1} of data at $\sqrt{s}$ = 8 TeV to place a lower bound on the compactification scale $1/R$, in models with universal extra dimensions and Standard Model fields propagating in the bulk. See their Fig. 5 for the bound as a function of the universal bulk fermion mass parameter μ.

[9] CHATRCHYAN 13W use diphoton events with large missing transverse momentum in 4.93 fb^{-1} of data produced from pp collisions at $\sqrt{s}$ = 7 TeV to place a lower bound on the compactification scale in a universal extra dimension model with gravitational decays. The bound assumes that the cutoff scale Λ, for the radiative corrections to the Kaluza-Klein masses, satisfies $\Lambda/M_c = 20$. The model parameters are chosen such that the decay $\gamma^* \rightarrow G\gamma$ occurs with an appreciable branching fraction.

[10] EDELHAUSER 13 use 19.6 and 20.6 fb^{-1} of data from pp collisions at $\sqrt{s}$ = 8 TeV analyzed by the CMS Collaboration in the dielectron and dimuon channels, respectively, to place a lower bound on the mass of the second lightest Kaluza-Klein Z/γ boson (converted to a limit on $1/R = M_c$). The bound assumes Standard Model fields propagating in the bulk and that the cutoff scale Λ, for the radiative corrections to the Kaluza-Klein masses, satisfies $\Lambda/M_c = 20$.

[11] AAD 12CP use diphoton events with large missing transverse momentum in 4.8 fb^{-1} of data produced from pp collisions at $\sqrt{s}$ = 7 TeV to place a lower bound on the compactification scale in a universal extra dimension model with gravitational decays. The bound assumes that the cutoff scale Λ, for the radiative corrections to the Kaluza-Klein masses, satisfies $\Lambda/M_c = 20$. The model parameters are chosen such that the decay $\gamma^* \rightarrow G\gamma$ occurs with an appreciable branching fraction.

[12] AAD 12X use diphoton events with large missing transverse momentum in 1.07 fb^{-1} of data produced from pp collisions at $\sqrt{s}$ = 7 TeV to place a lower bound on the compactification scale in a universal extra dimension model with gravitational decays. The bound assumes that the cutoff scale Λ, for the radiative corrections to the Kaluza-Klein masses, satisfies $\Lambda/M_c = 20$. The model parameters are chosen such that the decay $\gamma^* \rightarrow G\gamma$ occurs with an appreciable branching fraction.

[13] ABAZOV 12M use same-sign dimuon events in 7.3 fb^{-1} of data from $p\overline{p}$ collisions at $\sqrt{s}$ = 1.96 TeV to place a lower bound on the compactification scale $1/R$, in models with universal extra dimensions where all Standard Model fields propagate in the bulk.

[14] BAAK 12 use electroweak precision observables to place a lower bound on the compactification scale $1/R$, in models with universal extra dimensions and Standard Model fields propagating in the bulk. Bound assumes a 125 GeV Higgs mass. See their Fig. 25 for the bound as a function of the Higgs mass.

[15] FLACKE 12 use electroweak precision observables to place a lower bound on the compactification scale $1/R$, in models with universal extra dimensions and Standard Model fields propagating in the bulk. See their Fig. 1 for the bound as a function of the universal bulk fermion mass parameter μ.

[16] NISHIWAKI 12 use up to 2 fb^{-1} of data from the ATLAS and CMS experiments that constrains the production cross section of a Higgs-like particle to place a lower bound on the compactification scale $1/R$ in universal extra dimension models. The quoted bound assumes Standard Model fields propagating in the bulk and a 125 GeV Higgs mass. See their Fig. 1 for the bound as a function of the Higgs mass.

[17] AAD 11F use diphoton events with large missing transverse energy in 3.1 pb^{-1} of data produced from pp collisions at $\sqrt{s}$ = 7 TeV to place a lower bound on the compactification scale in a universal extra dimension model with gravitational decays. The bound assumes that the cutoff scale Λ, for the radiative corrections to the Kaluza-Klein masses, satisfies $\Lambda/M_c = 20$. The model parameters are chosen such that the decay $\gamma^* \rightarrow G\gamma$ occurs with an appreciable branching fraction.

[18] AAD 11X use diphoton events with large missing transverse energy in 36 pb^{-1} of data produced from pp collisions at $\sqrt{s}$ = 7 TeV to place a lower bound on the compactification scale in a universal extra dimension model with gravitational decays. The bound assumes that the cutoff scale Λ, for the radiative corrections to the Kaluza-Klein masses, satisfies $\Lambda/M_c = 20$. The model parameters are chosen such that the decay $\gamma^* \rightarrow G\gamma$ occurs with an appreciable branching fraction.

[19] ABAZOV 10P use diphoton events with large missing transverse energy in 6.3 fb^{-1} of data produced from $p\overline{p}$ collisions at $\sqrt{s}$ = 1.96 TeV to place a lower bound on the compactification scale in a universal extra dimension model with gravitational decays. The bound assumes that the cutoff scale Λ, for the radiative corrections to the Kaluza-Klein masses, satisfies Λ/M_c=20. The model parameters are chosen such that the decay $\gamma^* \rightarrow G\gamma$ occurs with an appreciable branching fraction.

[20] ABAZOV 09AE use dijet angular distributions in 0.7 fb^{-1} of data from $p\overline{p}$ collisions at $\sqrt{s}$ = 1.96 TeV to place a lower bound on the compactification scale.

[21] HAISCH 07 use inclusive $\overline{B}$-meson decays to place a Higgs mass independent bound on the compactification scale $1/R$ in the minimal universal extra dimension model.

[22] GOGOLADZE 06 use electroweak precision observables to place a lower bound on the compactification scale in models with universal extra dimensions. Bound assumes a 115 GeV Higgs mass. See their Fig. 3 for the bound as a function of the Higgs mass.

[23] CORNET 00 translates a bound on the coefficient of the 4-fermion operator $(\overline{\ell}\gamma_\mu\tau^a\ell)(\overline{\ell}\gamma^\mu\tau^a\ell)$ derived by Hagiwara and Matsumoto into a limit on the mass scale of KK W bosons.

[24] RIZZO 00 obtains limits from global electroweak fits in models with a Higgs in the bulk (3.8 TeV) or on the standard brane (3.3 TeV).

Limits on Kaluza-Klein Gravitons in Warped Extra Dimensions

This section places limits on the mass of the first Kaluza-Klein (KK) excitation of the graviton in the warped extra dimension model of Randall and Sundrum. Bounds in parenthesis assume Standard Model fields propagate in the bulk. Experimental bounds depend strongly on the warp parameter, k. See the "Extra Dimensions" review for a full discussion.

Here we list limits for the value of the warp parameter $k/\overline{M}_P$ = 0.1.

VALUE (TeV)	CL%	DOCUMENT ID		TECN	COMMENT
>4.78	95	[1] SIRUNYAN	21N	CMS	$pp \rightarrow G \rightarrow e^+e^-, \mu^+\mu^-$
• • • We do not use the following data for averages, fits, limits, etc. • • •					
		[2] AAD	21AF	ATLS	$pp \rightarrow G \rightarrow ZZ$
>4.5	95	[3] AAD	21AY	ATLS	$pp \rightarrow G \rightarrow \gamma\gamma$
		[4] AAD	20AT	ATLS	$pp \rightarrow G \rightarrow WW,\ ZZ$
		[5] AAD	20C	ATLS	$pp \rightarrow G \rightarrow HH$
		[6] AAD	20T	ATLS	$pp \rightarrow G \rightarrow b\overline{b}$
>2.6	95	[7] SIRUNYAN	20AI	CMS	$pp \rightarrow G \rightarrow jj$
		[8] SIRUNYAN	20F	CMS	$pp \rightarrow G \rightarrow HH$
		[9] SIRUNYAN	20Q	CMS	$pp \rightarrow G \rightarrow WW,\ ZZ$
		[10] AABOUD	19A	ATLS	$pp \rightarrow G \rightarrow HH$
		[11] AABOUD	19O	ATLS	$pp \rightarrow G \rightarrow HH$
		[12] AAD	19D	ATLS	$pp \rightarrow G \rightarrow WW,\ ZZ$
		[13] SIRUNYAN	19	CMS	$pp \rightarrow G \rightarrow HH$
		[14] SIRUNYAN	19BE	CMS	$pp \rightarrow G \rightarrow HH$
		[15] SIRUNYAN	19CF	CMS	$pp \rightarrow G \rightarrow HH$
		[16] AABOUD	18BI	ATLS	$pp \rightarrow G \rightarrow t\overline{t}$
		[17] AABOUD	18CJ	ATLS	$pp \rightarrow G \rightarrow VV, VH, \ell\overline{\ell}$
		[18] AABOUD	18CQ	ATLS	$pp \rightarrow G \rightarrow HH$
		[19] AABOUD	18CW	ATLS	$pp \rightarrow G \rightarrow HH$
		[20] SIRUNYAN	18AF	CMS	$pp \rightarrow G \rightarrow HH$
		[21] SIRUNYAN	18AS	CMS	$pp \rightarrow G \rightarrow ZZ$
		[22] SIRUNYAN	18AX	CMS	$pp \rightarrow G \rightarrow WW$
		[23] SIRUNYAN	18BK	CMS	$pp \rightarrow G \rightarrow ZZ$
		[24] SIRUNYAN	18CW	CMS	$pp \rightarrow G \rightarrow HH$
		[25] SIRUNYAN	18DJ	CMS	$pp \rightarrow G \rightarrow ZZ$
>4.1	95	[26] SIRUNYAN	18DU	CMS	$pp \rightarrow G \rightarrow \gamma\gamma$
		[27] SIRUNYAN	18F	CMS	$pp \rightarrow G \rightarrow HH$
		[28] SIRUNYAN	18I	CMS	$pp \rightarrow G \rightarrow b\overline{b}$
		[29] AAD	16R	ATLS	$pp \rightarrow G \rightarrow WW, ZZ$
		[30] AAD	15AZ	ATLS	$pp \rightarrow G \rightarrow WW$
		[31] AAD	15CT	ATLS	$pp \rightarrow G \rightarrow WW, ZZ$
>2.68	95	[32] AAD	14V	ATLS	$pp \rightarrow G \rightarrow e^+e^-, \mu^+\mu^-$
>1.23 (>0.84)	95	[33] AAD	13A	ATLS	$pp \rightarrow G \rightarrow WW$
>0.94 (>0.71)	95	[34] AAD	13AO	ATLS	$pp \rightarrow G \rightarrow WW$
>2.23	95	[35] AAD	13AS	ATLS	$pp \rightarrow \gamma\gamma, e^+e^-, \mu^+\mu^-$
>0.845	95	[36] AAD	12AD	ATLS	$pp \rightarrow G \rightarrow ZZ$
		[37] AALTONEN	12V	CDF	$p\overline{p} \rightarrow G \rightarrow ZZ$
		[38] BAAK	12	RVUE	Electroweak
		[39] AALTONEN	11G	CDF	$p\overline{p} \rightarrow G \rightarrow ZZ$
>1.058	95	[40] AALTONEN	11R	CDF	$p\overline{p} \rightarrow G \rightarrow e^+e^-, \gamma\gamma$
>0.754	95	[41] ABAZOV	11H	D0	$p\overline{p} \rightarrow G \rightarrow WW$
>0.607		[42] AALTONEN	10N	CDF	$p\overline{p} \rightarrow G \rightarrow WW$
>1.05		[43] ABAZOV	10F	D0	$p\overline{p} \rightarrow G \rightarrow e^+e^-,\ \gamma\gamma$
		[44] AALTONEN	08S	CDF	$p\overline{p} \rightarrow G \rightarrow ZZ$
>0.90		[45] ABAZOV	08J	D0	$p\overline{p} \rightarrow G \rightarrow e^+e^-, \gamma\gamma$
		[46] AALTONEN	07G	CDF	$p\overline{p} \rightarrow G \rightarrow \gamma\gamma$
>0.889		[47] AALTONEN	07H	CDF	$p\overline{p} \rightarrow G \rightarrow e\overline{e}$
>0.785		[48] ABAZOV	05N	D0	$p\overline{p} \rightarrow G \rightarrow \ell\ell, \gamma\gamma$
>0.71		[49] ABULENCIA	05A	CDF	$p\overline{p} \rightarrow G \rightarrow \ell\overline{\ell}$

[1] SIRUNYAN 21N use 137 (140) fb^{-1} of data from pp collisions at $\sqrt{s}$ = 13 TeV to search for dilepton resonances in the dielectron (dimuon) channel. See Table 6 for other limits with warp parameter values $k/\overline{M}_P$ = 0.01 and 0.05. This updates the results of SIRUNYAN 18BB.

[2] AAD 21AF use 139 fb^{-1} of data from pp collisions at $\sqrt{s}$ = 13 TeV to search for ZZ resonances in the $\ell\ell\ell\ell$ and $\ell\ell\nu\overline{\nu}$ final states (ℓ=e, μ). See their Figure 8 for the limit on the cross section times branching fraction as a function of the KK graviton mass, including theoretical values for $k/\overline{M}_P$ = 1. This updates the results of AAD 15AU and AABOUD 18BF.

[3] AAD 21AY use 139 fb^{-1} of data from pp collisions at $\sqrt{s}$ = 13 TeV in the diphoton channel to place a lower limit on the mass of the lightest KK graviton. This updates the results of AABOUD 17AP.

[4] AAD 20AT use 139 fb^{-1} of data from pp collisions at $\sqrt{s}$ = 13 TeV to search for diboson resonances in semileptonic final states ($\ell\nu qq$,$\ell\ell qq$, $\nu\nu qq$). See their Figure 15 for the limit on the cross section times branching fraction as a function of the KK graviton mass. Lower limits on the graviton mass are also given for $k/\overline{M}_P$ = 1. This updates the results of AABOUD 18AK and AABOUD 18AL.

[5] AAD 20C use 36.1 fb^{-1} of data from pp collisions at $\sqrt{s}$ = 13 TeV to search for Higgs boson pair production in the $b\overline{b}b\overline{b}$, $b\overline{b}W^+W^-$, and $b\overline{b}\tau^+\tau^-$ final states. See their Figure 5(b)(c) for limits on the cross section as a function of the KK graviton mass. In the case of $k/\overline{M}_P$ = 1 and 2, gravitons are excluded in the mass range 260–3000 GeV and 260–1760 GeV, respectively.

Downloaded from https://academic.oup.com/ptep/article/2022/8/083C01/6651666 by KIT Library user on 27 September 2022

[6] AAD 20T use 139 fb^{-1} of data from pp collisions at $\sqrt{s}$ = 13 TeV to search for narrow resonances decaying to bottom quark pairs. See their Figure 7 for the limit on the product of the cross section, branching fraction, acceptance and b-tagging efficiency as a function of the KK graviton mass. In the case of $k/\overline{M}_P$ = 0.2, KK gravitons in the mass range 1.25–2.8 TeV are excluded.

[7] SIRUNYAN 20AI use 137 fb^{-1} of data from pp collisions at $\sqrt{s}$ = 13 TeV to search for dijet resonances. See their Figure 6 for the limit on the product of the cross section, branching fraction and acceptance as a function of the KK graviton mass. This updates the results of SIRUNYAN 18BO.

[8] SIRUNYAN 20F use 35.9 fb^{-1} of data from pp collisions at $\sqrt{s}$ = 13 TeV to search for Higgs boson pair production in the $b\overline{b}ZZ$ final state. See their Figure 4 for limits on the cross section times branching fraction as a function of the KK graviton mass, and Figure 5 for limits as a function of $k/\overline{M}_P$.

[9] SIRUNYAN 20Q use 77.3 fb^{-1} of data from pp collisions at $\sqrt{s}$ = 13 TeV to search for diboson resonances with dijet final states. See their Figure 12 for the limit on the cross section times branching fraction as a function of the KK graviton mass, including the theoretical prediction for $k/\overline{M}_P$ = 0.5. This updates the results of SIRUNYAN 18P.

[10] AABOUD 19A use 36.1 fb^{-1} of data from pp collisions at $\sqrt{s}$ = 13 TeV to search for Higgs boson pair production in the $b\overline{b}b\overline{b}$ final state. See their Figure 9 for limits on the cross section times branching fraction as a function of the KK graviton mass. Assuming $k/\overline{M}_P$ = 1, gravitons in the mass range 313–1362 GeV are excluded. This updates the results of AABOUD 16I.

[11] AABOUD 19O use 36.1 fb^{-1} of data from pp collisions at $\sqrt{s}$ = 13 TeV to search for Higgs boson pair production in the $b\overline{b}WW$ final state. See their Figure 12 for limits on the cross section times branching fraction as a function of the KK graviton mass for $k/\overline{M}_P$ = 1 and $k/\overline{M}_P$ = 2.

[12] AAD 19D use 139 fb^{-1} of data from pp collisions at $\sqrt{s}$ = 13 TeV to search for diboson resonances in the all-hadronic final state. See their Figure 9(b) for the limit on the cross section times branching fraction as a function of the KK graviton mass, including theoretical values for $k/\overline{M}_P$ = 1. This updates the results of AABOUD 18F.

[13] SIRUNYAN 19 use 35.9 fb^{-1} of data from pp collisions at $\sqrt{s}$ = 13 TeV to search for Higgs boson pair production in the $\gamma\gamma b\overline{b}$ final state. See their Figure 9 for limits on the cross section times branching fraction as a function of the KK graviton mass. Assuming $k/\overline{M}_P$ = 1, gravitons in the mass range 290–810 GeV are excluded. This updates the result of KHACHATRYAN 16BQ.

[14] SIRUNYAN 19BE use 35.9 fb^{-1} of data from pp collisions at $\sqrt{s}$ = 13 TeV to search for Higgs boson pair production by combining the results from four final states: $b\overline{b}\gamma\gamma$, $b\overline{b}\tau\overline{\tau}$, $b\overline{b}b\overline{b}$, and $b\overline{b}VV$. See their Figure 7 for limits on the cross section times branching fraction as a function of the KK graviton mass.

[15] SIRUNYAN 19CF use 35.9 fb^{-1} of data from pp collisions at $\sqrt{s}$ = 13 TeV to search for Higgs boson pair production in the $b\overline{b}q\overline{q}'\ell\nu$ final state. See their Figure 7 for limits on the cross section times branching fraction as a function of the KK graviton mass, including theoretical values for $k/\overline{M}_P$ = 0.1 and 0.3.

[16] AABOUD 18BI use 36.1 fb^{-1} of data from pp collisions at $\sqrt{s}$ = 13 TeV to search for top-quark pairs decaying into the lepton-plus jets topology. See their Figure 16 for the limit on the KK graviton mass as a function of the cross section times branching fraction, including theoretical values for $k/\overline{M}_P$ = 1.

[17] AABOUD 18CJ combine the searches for heavy resonances decaying into bosonic and leptonic final states from 36.1 fb^{-1} of pp collision data at $\sqrt{s}$ = 13 TeV. The lower limit on the KK graviton mass, with $k/\overline{M}_P$ = 1, is 2.3 TeV.

[18] AABOUD 18CQ use 36.1 fb^{-1} of data from pp collisions at $\sqrt{s}$ = 13 TeV to search for Higgs boson pair production in the $b\overline{b}\tau^+\tau^-$ final state. See their Figure 2 for limits on the cross section times branching fraction as a function of the KK graviton mass. Assuming $k/\overline{M}_P$ = 1, gravitons in the mass range 325–885 GeV are excluded.

[19] AABOUD 18CW use 36.1 fb^{-1} of data from pp collisions at $\sqrt{s}$ = 13 TeV to search for Higgs boson pair production in the $\gamma\gamma b\overline{b}$ final state. See their Figure 7 for limits on the cross section times branching fraction as a function of the KK graviton mass.

[20] SIRUNYAN 18AF use 35.9 fb^{-1} of data from pp collisions at $\sqrt{s}$ = 13 TeV to search for Higgs boson pair production in the $b\overline{b}b\overline{b}$ final state. See their Figure 9 for limits on the cross section times branching fraction as a function of the KK graviton mass, including theoretical values for $k/\overline{M}_P$ = 0.5. This updates the results of KHACHATRYAN 15R.

[21] SIRUNYAN 18AS use 35.9 fb^{-1} of data from pp collisions at $\sqrt{s}$ = 13 TeV to search for ZZ resonances in the $\ell\ell\nu\overline{\nu}$ final state (ℓ=e, μ). See their Figure 5 for the limit on the KK graviton mass as a function of the cross section times branching fraction, including theoretical values for $k/\overline{M}_P$ = 0.1, 0.5, and 1.0.

[22] SIRUNYAN 18AX use 35.9 fb^{-1} of data from pp collisions at $\sqrt{s}$ = 13 TeV to search for WW resonances in $\ell\nu qq$ final states (ℓ=e, μ). See their Figure 6 for the limit on the KK graviton mass as a function of the cross section times branching fraction, including theoretical values for $k/\overline{M}_P$ = 0.5. This updates the results of KHACHATRYAN 14A.

[23] SIRUNYAN 18BK use 35.9 fb^{-1} of data from pp collisions at $\sqrt{s}$ = 13 TeV to search for ZZ resonances in the $\nu\overline{\nu}q\overline{q}$ final state. See their Figure 4 for the limit on the KK graviton mass as a function of the cross section times branching fraction, including theoretical values for $k/\overline{M}_P$ = 0.5 .

[24] SIRUNYAN 18CW use 35.9 fb^{-1} of data from pp collisions at $\sqrt{s}$ = 13 TeV to search for Higgs boson pair production in the $b\overline{b}b\overline{b}$ final state. See their Figure 8 for limits on the cross section times branching fraction as a function of the KK graviton mass, including theoretical values for $k/\overline{M}_P$ = 0.5.

[25] SIRUNYAN 18DJ use 35.9 fb^{-1} of data from pp collisions at $\sqrt{s}$ = 13 TeV to search for ZZ resonances in $2\ell 2q$ final states (ℓ = e, μ). See their Figure 6 for the limit on the KK graviton mass as a function of the cross section times branching fraction. Assuming $k/\overline{M}_P$ = 0.5, a graviton mass is excluded below 925 GeV.

[26] SIRUNYAN 18DU use 35.9 fb^{-1} of data from pp collisions at $\sqrt{s}$ = 13 TeV, in the diphoton channel to place a lower limit on the mass of the lightest KK graviton. See their paper for limits with other warp parameter values $k/\overline{M}_P$ = 0.01 and 0.2. This updates the results of KHACHATRYAN 16M.

[27] SIRUNYAN 18F use 35.9 fb^{-1} of data from pp collisions at $\sqrt{s}$ = 13 TeV to search for Higgs boson pair production in the $b\overline{b}\ell\nu\ell\nu$ final state. See their Figure 7 for limits on the cross section times branching fraction as a function of the KK graviton mass, including theoretical values for $k/\overline{M}_P$ = 0.1.

[28] SIRUNYAN 18I use 19.7 fb^{-1} of data from pp collisions at $\sqrt{s}$ = 8 TeV to search for narrow resonances decaying to bottom quark pairs. See their Figure 3 for the limit on the KK graviton mass as a function of the cross section times branching fraction in the mass range of 325–1200 GeV.

[29] AAD 16R use 20.3 fb^{-1} of data from pp collisions at $\sqrt{s}$ = 8 TeV to place a lower bound on the mass of the lightest KK graviton. See their Figure 4 for the limit on the KK graviton mass as a function of the cross section times branching fraction.

[30] AAD 15AZ use 20.3 fb^{-1} of data from pp collisions at $\sqrt{s}$ = 8 TeV to place a lower bound on the mass of the lightest KK graviton. See their Figure 2 for limits on the KK graviton mass as a function of the cross section times branching ratio.

[31] AAD 15CT use 20.3 fb^{-1} of data from pp collisions at $\sqrt{s}$ = 8 TeV to place a lower bound on the mass of the lightest KK graviton. See their Figures 6b and 6c for the limit on the KK graviton mass as a function of the cross section times branching fraction.

[32] AAD 14V use 20.3 (20.5) fb^{-1} of data from pp collisions at $\sqrt{s}$ = 8 TeV in the dielectron (dimuon) channels to place a lower bound on the mass of the lightest KK graviton. This updates the results of AAD 12CC .

[33] AAD 13A use 4.7 fb^{-1} of data from pp collisions at $\sqrt{s}$ = 7 TeV in the $\ell\nu\ell\nu$ channel, to place a lower bound on the mass of the lightest KK graviton.

[34] AAD 13AO use 4.7 fb^{-1} of data from pp collisions at $\sqrt{s}$ = 7 TeV in the $\ell\nu jj$ channel, to place a lower bound on the mass of the lightest KK graviton.

[35] AAD 13AS use 4.9 fb^{-1} of data from pp collisions at $\sqrt{s}$ = 7 TeV in the diphoton channel to place lower limits on the mass of the lightest KK graviton. The diphoton channel is combined with previous results in the dielectron and dimuon channels to set the best limit. See their Table 2 for warp parameter values $k/\overline{M}_P$ between 0.01 and 0.1. This updates the results of AAD 12Y .

[36] AAD 12AD use 1.02 fb^{-1} of data from pp collisions at $\sqrt{s}$ = 7 TeV to search for KK gravitons in a warped extra dimension decaying to ZZ dibosons in the $lljj$ and $llll$ channels (ℓ=e, μ). The limit is quoted for the combined $lljj + llll$ channels. See their Figure 5 for limits on the cross section $\sigma(G \rightarrow ZZ)$ as a function of the graviton mass.

[37] AALTONEN 12V use 6 fb^{-1} of data from $p\overline{p}$ collisions at $\sqrt{s}$ = 1.96 TeV to search for KK gravitons in a warped extra dimension decaying to ZZ dibosons in the $lljj$ and $llll$ channels (ℓ=e, μ). It provides improved limits over the previous analysis in AALTONEN 11G. See their Figure 16 for limits from all channels combined on the cross section times branching ratio $\sigma(p\overline{p} \rightarrow G^* \rightarrow ZZ)$ as a function of the graviton mass.

[38] BAAK 12 use electroweak precision observables to place a lower bound on the compactification scale $k\,e^{-\pi kR}$, assuming Standard Model fields propagate in the bulk and the Higgs is confined to the IR brane. See their Fig. 27 for more details.

[39] AALTONEN 11G use 2.5–2.9 fb^{-1} of data from $p\overline{p}$ collisions at $\sqrt{s}$ = 1.96 TeV to search for KK gravitons in a warped extra dimension decaying to ZZ dibosons via the $eeee$, $ee\mu\mu$, $\mu\mu\mu\mu$, $eejj$, and $\mu\mu jj$ channels. See their Fig. 20 for limits on the cross section $\sigma(G \rightarrow ZZ)$ as a function of the graviton mass.

[40] AALTONEN 11R uses 5.7 fb^{-1} of data from $p\overline{p}$ collisions at $\sqrt{s}$ = 1.96 TeV in the dielectron channel to place a lower bound on the mass of the lightest graviton. It provides combined limits with the diphoton channel analysis of AALTONEN 11U. For warp parameter values $k/\overline{M}_P$ between 0.01 to 0.1 the lower limit on the mass of the lightest graviton is between 612 and 1058 GeV. See their Table I for more details.

[41] ABAZOV 11H use 5.4 fb^{-1} of data from $p\overline{p}$ collisions at $\sqrt{s}$ = 1.96 TeV to place a lower bound on the mass of the lightest graviton. Their 95% C.L. exclusion limit does not include masses less than 300 GeV.

[42] AALTONEN 10N use 2.9 fb^{-1} of data from $p\overline{p}$ collisions at $\sqrt{s}$ = 1.96 TeV to place a lower bound on the mass of the lightest graviton.

[43] ABAZOV 10F use 5.4 fb^{-1} of data from $p\overline{p}$ collisions at $\sqrt{s}$ = 1.96 TeV to place a lower bound on the mass of the lightest graviton. For warp parameter values of $k/\overline{M}_P$ between 0.01 and 0.1 the lower limit on the mass of the lightest graviton is between 560 and 1050 GeV. See their Fig. 3 for more details.

[44] AALTONEN 08S use $p\overline{p}$ collisions at $\sqrt{s}$ = 1.96 TeV to search for KK gravitons in warped extra dimensions. They search for graviton resonances decaying to four electrons via two Z bosons using 1.1 fb^{-1} of data. See their Fig. 8 for limits on $\sigma \cdot$B$(G \rightarrow ZZ)$ versus the graviton mass.

[45] ABAZOV 08J use $p\overline{p}$ collisions at $\sqrt{s}$ = 1.96 TeV to search for KK gravitons in warped extra dimensions. They search for graviton resonances decaying to electrons and photons using 1 fb^{-1} of data. For warp parameter values of $k/\overline{M}_P$ between 0.01 and 0.1 the lower limit on the mass of the lightest excitation is between 300 and 900 GeV. See their Fig. 4 for more details.

[46] AALTONEN 07G use $p\overline{p}$ collisions at $\sqrt{s}$ = 1.96 TeV to search for KK gravitons in warped extra dimensions. They search for graviton resonances decaying to photons using 1.2 fb^{-1} of data. For warp parameter values of $k/\overline{M}_P$ = 0.1, 0.05, and 0.01 the bounds on the graviton mass are 850, 694, and 230 GeV, respectively. See their Fig. 3 for more details. See also AALTONEN 07H.

[47] AALTONEN 07H use $p\overline{p}$ collisions at $\sqrt{s}$ = 1.96 TeV to search for KK gravitons in warped extra dimensions. They search for graviton resonances decaying to electrons using 1.3 fb^{-1} of data. For a warp parameter value of $k/\overline{M}_P$ = 0.1 the bound on the graviton mass is 807 GeV. See their Fig. 4 for more details. A combined analysis with the diphoton data of AALTONEN 07G yields for $k/\overline{M}_P$ = 0.1 a graviton mass lower bound of 889 GeV.

[48] ABAZOV 05N use $p\overline{p}$ collisions at $\sqrt{s}$ = 1.96 TeV to search for KK gravitons in warped extra dimensions. They search for graviton resonances decaying to muons, electrons or photons, using 260 pb^{-1} of data. For warp parameter values of $k/\overline{M}_P$ = 0.1, 0.05, and 0.01, the bounds on the graviton mass are 785, 650 and 250 GeV respectively. See their Fig. 3 for more details.

[49] ABULENCIA 05A use $p\overline{p}$ collisions at $\sqrt{s}$ = 1.96 TeV to search for KK gravitons in warped extra dimensions. They search for graviton resonances decaying to muons or electrons, using 200 pb^{-1} of data. For warp parameter values of $k/\overline{M}_P$ = 0.1, 0.05, and 0.01, the bounds on the graviton mass are 710, 510 and 170 GeV respectively.

Limits on Kaluza-Klein Gluons in Warped Extra Dimensions

This section places limits on the mass of the first Kaluza-Klein (KK) excitation of the gluon in warped extra dimension models with Standard Model fields propagating in the bulk. Bounds are given for a specific benchmark model with Γ/m = 15.3% where Γ is the width and m the mass of the KK gluon. See the "Extra Dimensions" review for more discussion.

VALUE (TeV)	CL%	DOCUMENT ID		TECN	COMMENT
>3.8	95	[1] AABOUD	18BI	ATLS	$g_{KK} \rightarrow t\overline{t} \rightarrow \ell j$
• • • We do not use the following data for averages, fits, limits, etc. • • •					
		[2] AABOUD	19AS	ATLS	$g_{KK} \rightarrow t\overline{t} \rightarrow jj$
		[3] SIRUNYAN	19AL	CMS	$g_{KK} \rightarrow tT$
>2.5	95	[4] CHATRCHYAN	13BM	CMS	$g_{KK} \rightarrow t\overline{t}$
		[5] CHEN	13A		$\overline{B} \rightarrow X_s\gamma$
>1.5	95	[6] AAD	12BV	ATLS	$g_{KK} \rightarrow t\overline{t} \rightarrow \ell j$

Downloaded from https://academic.oup.com/ptep/article/2022/8/083C01/6651666 by KIT Library user on 27 September 2022

[1] AABOUD 18BI use 36.1 fb^{-1} of data from pp collisions at $\sqrt{s}$ = 13 TeV. This result updates AAD 13AQ.

[2] AABOUD 19AS use 36.1 fb^{-1} of data from pp collisions at $\sqrt{s}$ = 13 TeV. An upper bound of 3.4 TeV is placed on the KK gluon mass for Γ/m = 30%.

[3] SIRUNYAN 19AL use 35.9 fb^{-1} of data from pp collisions at $\sqrt{s}$ = 13 TeV to place limits on a KK gluon decaying to a top quark and a heavy vector-like fermion, T. KK gluon masses between 1.5 and 2.3 TeV and between 2.0 and 2.4 TeV are excluded for T masses of 1.2 and 1.5 TeV, respectively.

[4] CHATRCHYAN 13BM use 19.7 fb^{-1} of data from pp collisions at $\sqrt{s}$ = 8 TeV. Bound is for a width of approximately 15–20% of the KK gluon mass.

[5] CHEN 13A place limits on the KK mass scale for a specific warped model with custodial symmetry and bulk fermions. See their Figures 4 and 5.

[6] AAD 12BV use 2.05 fb^{-1} of data from pp collisions at $\sqrt{s}$ = 7 TeV.

Black Hole Production Limits

Semiclassical Black Holes

VALUE (GeV)	DOCUMENT ID		TECN	COMMENT
• • • We do not use the following data for averages, fits, limits, etc. • • •				
	[1] SIRUNYAN	18DA	CMS	$pp \to$ multijet
	[2] AAD	16N	ATLS	$pp \to$ multijet
	[3] AAD	16O	ATLS	$pp \to \ell + (\ell\ell/\ell j/jj)$
	[4] AAD	13AW	ATLS	$pp \to \mu\mu$

[1] SIRUNYAN 18DA use 35.9 fb^{-1} of data from pp collisions at $\sqrt{s}$ = 13 TeV to search for semiclassical black holes decaying to multijet final states. No excess of events above the expected level of standard model background was observed. Exclusions at 95% CL are set on the mass threshold for black hole production as a function of the higher-dimensional Planck scale for rotating and nonrotating black holes under several model assumptions (ADD, 2, 4, 6 extra dimensions model) in the 7.1–10.3 TeV range. These limits supersede those in SIRUNYAN 17CP.

[2] AAD 16N use 3.6 fb^{-1} of data from pp collisions at $\sqrt{s}$ = 13 TeV to search for semiclassical black hole decays to multijet final states. No excess of events above the expected level of Standard Model background was observed. Exclusion contours at 95% C.L. are set on the mass threshold for black hole production versus higher-dimensional Planck scale for rotating black holes (ADD, 6 extra dimensions model).

[3] AAD 16O use 3.2 fb^{-1} of data from pp collisions at $\sqrt{s}$ = 13 TeV to search for semiclassical black hole decays to high-mass final states with leptons and jets. No excess of events above the expected level of Standard Model background was observed. Exclusion contours at 95% C.L. are set on the mass threshold for black hole production versus higher-dimensional Planck scale for rotating black holes (ADD, 2 to 6 extra dimensions).

[4] AAD 13AW use 20.3 fb^{-1} of data from pp collisions at $\sqrt{s}$ = 8 TeV to search for semiclassical black hole decays to like-sign dimuon final states using large track multiplicity. No excess of events above the expected level of Standard Model background was observed. Exclusion contours at 95% C.L. are set on the mass threshold for black hole production versus higher-dimensional Planck scale in various extra dimensions, rotating and non-rotating models.

Quantum Black Holes

VALUE (GeV)	DOCUMENT ID		TECN	COMMENT
• • • We do not use the following data for averages, fits, limits, etc. • • •				
	[1] AAD	20T	ATLS	$pp \to jj$
	[2] AABOUD	18BA	ATLS	$pp \to \gamma j$
	[3] AABOUD	18CM	ATLS	$pp \to e\mu,\ e\tau,\ \mu\tau$
	[4] SIRUNYAN	18AT	CMS	$pp \to e\mu$
	[5] SIRUNYAN	18DD	CMS	$pp \to$ dijet, ang. distrib.
	[6] SIRUNYAN	17CP	CMS	$pp \to jj$
	[7] KHACHATRY...16BE		CMS	$pp \to e\mu$
	[8] KHACHATRY...15V		CMS	$pp \to jj$
	[9] AAD	14AL	ATLS	$pp \to \ell j$
	[10] AAD	14V	ATLS	$pp \to ee,\ \mu\mu$
	[11] CHATRCHYAN	13A	CMS	$pp \to jj$

[1] AAD 20T use 139 fb^{-1} of data from pp collisions at $\sqrt{s}$ = 13 TeV to search for quantum black hole decays to final states with dijets. No excess of events above the expected level of Standard Model background was observed. Exclusion limits at 95% C.L. are set on mass thresholds for black hole production in an ADD (6 extra dimensions) model. Assuming the black hole mass threshold is equal to the higher-dimensional Planck scale, mass thresholds below 9.4 TeV are excluded. This limit supersedes AABOUD 17AK.

[2] AABOUD 18BA use 36.7 fb^{-1} of data from pp collisions at $\sqrt{s}$ = 13 TeV to search for quantum black hole decays to final states with a photon and a jet. No excess of events above the expected level of Standard Model background was observed. Exclusion limits at 95% C.L. are set on mass thresholds for black hole production in ADD (6 extra dimensions) and RS1 models. Assuming the black hole mass threshold is equal to the Planck scale, mass thresholds below 7.1 TeV and 4.4 TeV are excluded for the ADD and RS1 models, respectively. These limits supersede those in AAD 16AI.

[3] AABOUD 18CM use 36.1 fb^{-1} of data from pp collisions at $\sqrt{s}$ = 13 TeV to search for quantum black hole decays with different-flavor high-mass dilepton final states. No excess of events above the expected level of Standard Model background was observed. Exclusion limits at 95% C.L. are set on mass thresholds for black hole production in ADD (6 extra dimensions) and RS1 models. Assuming the black hole mass threshold is equal to the higher-dimensional Planck scale, mass thresholds below 5.6 (3.4), 4.9 (2.9), and 4.5 (2.6) TeV are excluded in the $e\mu$, $e\tau$ and $\mu\tau$ channels for the ADD (RS1) models, respectively. These limits supersede those in AABOUD 16P.

[4] SIRUNYAN 18AT use 35.9 fb^{-1} of data from pp collisions at $\sqrt{s}$ = 13 TeV to search for quantum black hole decays to $e\mu$ final states. In Figure 4, lower mass limits of 5.3, 5.5 and 5.6 TeV are placed in a model with 4, 5 and 6 extra dimensions, respectively, and a lower mass limit of 3.6 TeV is found for a single warped dimension.

[5] SIRUNYAN 18DD use 35.9 fb^{-1} of data from pp collisions at $\sqrt{s}$ = 13 TeV to search for quantum black hole decays in dijet angular distributions. A lower mass limit of 5.9 (8.2) TeV is placed in the RS (ADD) model with one (six) extra dimension(s).

[6] SIRUNYAN 17CP use 2.3 fb^{-1} of data from pp collisions at $\sqrt{s}$ = 13 TeV to search for quantum black holes decaying to dijet final states. No excess of events above the expected level of standard model background was observed. Limits on the quantum black hole mass threshold are set as a function of the higher-dimensional Planck scale, under the assumption that the mass threshold must exceed the above Planck scale. Depending on the model, mass thresholds in the range up to 5.1–9.0 TeV are excluded.

[7] KHACHATRYAN 16BE use 19.7 fb^{-1} of data from pp collisions at $\sqrt{s}$ = 8 TeV to search for quantum black holes undergoing lepton flavor violating decay to the $e\mu$ final state. No excess of events above the expected level of standard model background was observed. Exclusion limits at 95% CL are set on mass thresholds for black hole production in the ADD (2–6 flat extra dimensions), RS1 (1 warped extra dimension), and a model with a Planck scale at the TeV scale from a renormalization of the gravitational constant (no extra dimensions). Limits on the black hole mass threshold are set assuming that it is equal to the higher-dimensional Planck scale. Mass thresholds for quantum black holes in the range up to 3.15–3.63 TeV are excluded in the ADD model. In the RS1 model, mass thresholds below 2.81 TeV are excluded in the PDG convention for the Schwarzschild radius. In the model with no extra dimensions, mass thresholds below 1.99 TeV are excluded.

[8] KHACHATRYAN 15V use 19.7 fb^{-1} of data from pp collisions at $\sqrt{s}$ = 8 TeV to search for quantum black holes decaying to dijet final states. No excess of events above the expected level of standard model background was observed. Exclusion limits at 95% CL are set on mass thresholds for black hole production in the ADD (2–6 flat extra dimensions) and RS1 (1 warped extra dimension) model. Limits on the black hole mass threshold are set as a function of the higher-dimensional Planck scale, under the assumption that the mass threshold must exceed the above Planck scale. Depending on the model, mass thresholds in the range up to 5.0–6.3 TeV are excluded. This paper supersedes CHATRCHYAN 13AD.

[9] AAD 14AL use 20.3 fb^{-1} of data from pp collisions at $\sqrt{s}$ = 8 TeV to search for quantum black hole decays to final states with high-invariant-mass lepton + jet. No excess of events above the expected level of Standard Model background was observed. Exclusion limits at 95% C.L. are set on mass thresholds for black hole production in an ADD (6 extra dimensions) model. Assuming the black hole mass threshold is equal to the higher-dimensional Planck scale, mass thresholds below 5.3 TeV are excluded.

[10] AAD 14V use 20.3 (20.5) fb^{-1} of data in the dielectron (dimuon) channels from pp collisions at $\sqrt{s}$ = 8 TeV to search for quantum black hole decays involving high-mass dilepton resonances. No excess of events above the expected level of Standard Model background was observed. Exclusion limits at 95% C.L. are set on mass thresholds for black hole production in ADD (6 extra dimensions) and RS1 models. Assuming the black hole mass threshold is equal to the higher-dimensional Planck scale, mass thresholds below 3.65 TeV and 2.24 TeV are excluded for the ADD and RS1 models, respectively.

[11] CHATRCHYAN 13A use 5 fb^{-1} of data from pp collisions at $\sqrt{s}$ = 7 TeV to search for quantum black holes decaying to dijet final states. No excess of events above the expected level of standard model background was observed. Exclusion limits at 95% CL are set on mass thresholds for black hole production in the ADD (2–6 flat extra dimensions) and RS (1 warped extra dimension) model. Limits on the black hole mass threshold are set as a function of the higher-dimensional Planck scale, under assumption that the mass threshold must exceed the above Planck scale. Depending on the model, mass thresholds in the range up to 4.0–5.3 TeV are excluded.

REFERENCES FOR Extra Dimensions

AAD	21AF	EPJ C81 332	G. Aad et al.	(ATLAS Collab.)
AAD	21AY	PL B822 136651	G. Aad et al.	(ATLAS Collab.)
AAD	21F	PR D103 112006	G. Aad et al.	(ATLAS Collab.)
AVNISH	21	PR D103 115011	Avnish et al.	
BLAKEMORE	21	PR D104 L061101	C.P. Blakemore et al.	(STAN)
HEACOCK	21	SCI 373 1239	B. Heacock et al.	(NIST, RIKEN, NAGO+)
SIRUNYAN	21A	EPJ C81 13	A.M. Sirunyan et al.	(CMS Collab.)
Also		EPJ C81 333 (errat.)	A.M. Sirunyan et al.	(CMS Collab.)
SIRUNYAN	21N	JHEP 2107 208	A.M. Sirunyan et al.	(CMS Collab.)
TUMASYAN	21D	JHEP 2111 153	A. Tumasyan et al.	(CMS Collab.)
AAD	20AT	EPJ C80 1165	G. Aad et al.	(ATLAS Collab.)
AAD	20C	PL B800 135103	G. Aad et al.	(ATLAS Collab.)
AAD	20T	JHEP 2003 145	G. Aad et al.	(ATLAS Collab.)
LEE	20	PRL 124 101101	J.G. Lee et al.	(WASH)
SIRUNYAN	20AI	JHEP 2005 033	A.M. Sirunyan et al.	(CMS Collab.)
SIRUNYAN	20F	PR D102 032003	A.M. Sirunyan et al.	(CMS Collab.)
SIRUNYAN	20Q	EPJ C80 237	A.M. Sirunyan et al.	(CMS Collab.)
TAN	20A	PRL 124 051301	W.-H. Tan et al.	
AABOUD	19A	JHEP 1901 030	M. Aaboud et al.	(ATLAS Collab.)
AABOUD	19AS	PR D99 092004	M. Aaboud et al.	(ATLAS Collab.)
AABOUD	19O	JHEP 1904 092	M. Aaboud et al.	(ATLAS Collab.)
AAD	19D	JHEP 1909 091	G. Aad et al.	(ATLAS Collab.)
Also		JHEP 2006 042 (errat.)	G. Aad et al.	(ATLAS Collab.)
SIRUNYAN	19	PL B788 7	A.M. Sirunyan et al.	(CMS Collab.)
SIRUNYAN	19AC	JHEP 1904 114	A.M. Sirunyan et al.	(CMS Collab.)
SIRUNYAN	19AL	EPJ C79 208	A.M. Sirunyan et al.	(CMS Collab.)
SIRUNYAN	19BE	PRL 122 121803	A.M. Sirunyan et al.	(CMS Collab.)
SIRUNYAN	19CF	JHEP 1910 125	A.M. Sirunyan et al.	(CMS Collab.)
AABOUD	18AK	JHEP 1803 042	M. Aaboud et al.	(ATLAS Collab.)
AABOUD	18AL	JHEP 1803 009	M. Aaboud et al.	(ATLAS Collab.)
AABOUD	18AV	JHEP 1807 089	M. Aaboud et al.	(ATLAS Collab.)
AABOUD	18BA	EPJ C78 102	M. Aaboud et al.	(ATLAS Collab.)
AABOUD	18BF	EPJ C78 293	M. Aaboud et al.	(ATLAS Collab.)
AABOUD	18BI	EPJ C78 565	M. Aaboud et al.	(ATLAS Collab.)
AABOUD	18CE	JHEP 1812 039	M. Aaboud et al.	(ATLAS Collab.)
AABOUD	18CJ	PR D98 052008	M. Aaboud et al.	(ATLAS Collab.)
AABOUD	18CM	PR D98 092008	M. Aaboud et al.	(ATLAS Collab.)
AABOUD	18CQ	PRL 121 191801	M. Aaboud et al.	(ATLAS Collab.)
AABOUD	18CW	JHEP 1811 040	M. Aaboud et al.	(ATLAS Collab.)
AABOUD	18F	PL B777 91	M. Aaboud et al.	(ATLAS Collab.)
AABOUD	18I	JHEP 1801 126	M. Aaboud et al.	(ATLAS Collab.)
BERGE	18	PRL 120 141101	J. Berge et al.	(MICROSCOPE Collab.)
FAYET	18	PR D97 055039	P. Fayet	(EPOL)
FAYET	18A	PR D99 055043	P. Fayet	(ENSP, EPOL)
HADDOCK	18	PR D97 062002	C. Haddock et al.	(NAGO, KEK, OSAK+)
SIRUNYAN	18AF	PL B781 244	A.M. Sirunyan et al.	(CMS Collab.)
SIRUNYAN	18AS	JHEP 1803 003	A.M. Sirunyan et al.	(CMS Collab.)
SIRUNYAN	18AT	JHEP 1804 073	A.M. Sirunyan et al.	(CMS Collab.)
SIRUNYAN	18AX	JHEP 1805 088	A.M. Sirunyan et al.	(CMS Collab.)
SIRUNYAN	18BB	JHEP 1806 120	A.M. Sirunyan et al.	(CMS Collab.)
SIRUNYAN	18BK	JHEP 1807 075	A.M. Sirunyan et al.	(CMS Collab.)
SIRUNYAN	18BO	JHEP 1808 130	A.M. Sirunyan et al.	(CMS Collab.)
SIRUNYAN	18BV	EPJ C78 291	A.M. Sirunyan et al.	(CMS Collab.)
SIRUNYAN	18CW	JHEP 1808 152	A.M. Sirunyan et al.	(CMS Collab.)
SIRUNYAN	18DA	JHEP 1811 042	A.M. Sirunyan et al.	(CMS Collab.)
SIRUNYAN	18DD	EPJ C78 789	A.M. Sirunyan et al.	(CMS Collab.)
SIRUNYAN	18DJ	JHEP 1809 101	A.M. Sirunyan et al.	(CMS Collab.)
SIRUNYAN	18DU	PR D98 092001	A.M. Sirunyan et al.	(CMS Collab.)
SIRUNYAN	18F	JHEP 1801 054	A.M. Sirunyan et al.	(CMS Collab.)
SIRUNYAN	18I	PRL 120 201801	A.M. Sirunyan et al.	(CMS Collab.)
SIRUNYAN	18P	PR D97 072006	A.M. Sirunyan et al.	(CMS Collab.)
SIRUNYAN	18S	PR D97 092005	A.M. Sirunyan et al.	(CMS Collab.)
AABOUD	17AK	PR D96 052004	M. Aaboud et al.	(ATLAS Collab.)
AABOUD	17AP	PL B775 105	M. Aaboud et al.	(ATLAS Collab.)

Downloaded from https://academic.oup.com/ptep/article/2022/8/083C01/6651666 by KIT Library user on 27 September 2022

KLIMCHITSK...	17A	PR D95 123013	G.L. Klimchitskaya, V.M. Mostepanenko	
SIRUNYAN	17AQ	JHEP 1710 073	A.M. Sirunyan *et al.*	(CMS Collab.)
SIRUNYAN	17CP	PL B774 279	A.M. Sirunyan *et al.*	(CMS Collab.)
SIRUNYAN	17F	JHEP 1707 013	A.M. Sirunyan *et al.*	(CMS Collab.)
AABOUD	16F	JHEP 1606 059	M. Aaboud *et al.*	(ATLAS Collab.)
AABOUD	16I	PR D94 052002	M. Aaboud *et al.*	(ATLAS Collab.)
AABOUD	16P	EPJ C76 541	M. Aaboud *et al.*	(ATLAS Collab.)
AAD	16AI	JHEP 1603 041	G. Aad *et al.*	(ATLAS Collab.)
AAD	16N	JHEP 1603 026	G. Aad *et al.*	(ATLAS Collab.)
AAD	16O	PL B760 520	G. Aad *et al.*	(ATLAS Collab.)
AAD	16R	PL B755 285	G. Aad *et al.*	(ATLAS Collab.)
KHACHATRY...	16BE	EPJ C76 317	V. Khachatryan *et al.*	(CMS Collab.)
KHACHATRY...	16BQ	PR D94 052012	V. Khachatryan *et al.*	(CMS Collab.)
KHACHATRY...	16M	PRL 117 051802	V. Khachatryan *et al.*	(CMS Collab.)
KHACHATRY...	16N	PL B755 102	V. Khachatryan *et al.*	(CMS Collab.)
AAD	15AU	EPJ C75 69	G. Aad *et al.*	(ATLAS Collab.)
AAD	15AZ	EPJ C75 209	G. Aad *et al.*	(ATLAS Collab.)
Also		EPJ C75 370 (errat.)	G. Aad *et al.*	(ATLAS Collab.)
AAD	15CS	PR D91 012008	G. Aad *et al.*	(ATLAS Collab.)
Also		PR D92 059903 (errat.)	G. Aad *et al.*	(ATLAS Collab.)
AAD	15CT	JHEP 1512 055	G. Aad *et al.*	(ATLAS Collab.)
ACCOMANDO	15	MPL A30 1540010	E. Accomando	(SHMP)
KHACHATRY...	15AE	JHEP 1504 025	V. Khachatryan *et al.*	(CMS Collab.)
KHACHATRY...	15R	PL B749 560	V. Khachatryan *et al.*	(CMS Collab.)
KHACHATRY...	15T	PR D91 092005	V. Khachatryan *et al.*	(CMS Collab.)
KHACHATRY...	15V	PR D91 052009	V. Khachatryan *et al.*	(CMS Collab.)
AAD	14AL	PRL 112 091804	G. Aad *et al.*	(ATLAS Collab.)
AAD	14BE	EPJ C74 3134	G. Aad *et al.*	(ATLAS Collab.)
AAD	14V	PR D90 052005	G. Aad *et al.*	(ATLAS Collab.)
KHACHATRY...	14A	JHEP 1408 174	V. Khachatryan *et al.*	(CMS Collab.)
AAD	13A	PL B718 860	G. Aad *et al.*	(ATLAS Collab.)
AAD	13AO	PR D87 112006	G. Aad *et al.*	(ATLAS Collab.)
AAD	13AQ	PR D88 012004	G. Aad *et al.*	(ATLAS Collab.)
AAD	13AS	NJP 15 043007	G. Aad *et al.*	(ATLAS Collab.)
AAD	13AW	PR D88 072001	G. Aad *et al.*	(ATLAS Collab.)
AAD	13C	PRL 110 011802	G. Aad *et al.*	(ATLAS Collab.)
AAD	13D	JHEP 1301 029	G. Aad *et al.*	(ATLAS Collab.)
AAD	13E	PR D87 015010	G. Aad *et al.*	(ATLAS Collab.)
CHATRCHYAN	13A	JHEP 1301 013	S. Chatrchyan *et al.*	(CMS Collab.)
CHATRCHYAN	13AD	JHEP 1307 178	S. Chatrchyan *et al.*	(CMS Collab.)
CHATRCHYAN	13AQ	PR D87 072005	S. Chatrchyan *et al.*	(CMS Collab.)
CHATRCHYAN	13BM	PRL 111 211804	S. Chatrchyan *et al.*	(CMS Collab.)
Also		PRL 112 119903 (errat.)	S. Chatrchyan *et al.*	(CMS Collab.)
CHATRCHYAN	13W	JHEP 1303 111	S. Chatrchyan *et al.*	(CMS Collab.)
CHEN	13A	CP C37 063102	J-B. Chen *et al.*	(DALI)
EDELHAUSER	13	JHEP 1308 091	L. Edelhauser, T. Flacke, M. Kramer	(AACH, KAIST)
XU	13	JP G40 035107	J. Xu *et al.*	
AAD	12AD	PL B712 331	G. Aad *et al.*	(ATLAS Collab.)
AAD	12BV	JHEP 1209 041	G. Aad *et al.*	(ATLAS Collab.)
AAD	12CC	JHEP 1211 138	G. Aad *et al.*	(ATLAS Collab.)
AAD	12CP	PL B718 411	G. Aad *et al.*	(ATLAS Collab.)
AAD	12X	PL B710 519	G. Aad *et al.*	(ATLAS Collab.)
AAD	12Y	PL B710 538	G. Aad *et al.*	(ATLAS Collab.)
AALTONEN	12V	PR D85 012008	T. Aaltonen *et al.*	(CDF Collab.)
ABAZOV	12M	PRL 108 131802	V.M. Abazov *et al.*	(D0 Collab.)
AJELLO	12	JCAP 1202 012	M. Ajello *et al.*	(Fermi-LAT Collab.)
BAAK	12	EPJ C72 2003	M. Baak *et al.*	(Gfitter Group)
CHATRCHYAN	12R	PRL 108 111801	S. Chatrchyan *et al.*	(CMS Collab.)
FLACKE	12	PR D85 126007	T. Flacke, C. Pasold	(WURZ)
NISHIWAKI	12	PL B707 506	K. Nishiwaki *et al.*	(KOBE, OSAK)
AAD	11F	PRL 106 121803	G. Aad *et al.*	(ATLAS Collab.)
AAD	11X	EPJ C71 1744	G. Aad *et al.*	(ATLAS Collab.)
AALTONEN	11G	PR D83 112008	T. Aaltonen *et al.*	(CDF Collab.)
AALTONEN	11R	PRL 107 051801	T. Aaltonen *et al.*	(CDF Collab.)
AALTONEN	11U	PR D83 011102	T. Aaltonen *et al.*	(CDF Collab.)
AARON	11C	PL B705 52	F. D. Aaron *et al.*	(H1 Collab.)
ABAZOV	11H	PRL 107 011801	V.M. Abazov *et al.*	(D0 Collab.)
BEZERRA	11	PR D83 075004	V.B. Bezerra *et al.*	
SUSHKOV	11	PRL 107 171101	A.O. Sushkov *et al.*	
AALTONEN	10N	PRL 104 241801	T. Aaltonen *et al.*	(CDF Collab.)
ABAZOV	10F	PRL 104 241802	V.M. Abazov *et al.*	(D0 Collab.)
ABAZOV	10P	PRL 105 221802	V.M. Abazov *et al.*	(D0 Collab.)
BEZERRA	10	PR D81 055003	V.B. Bezerra *et al.*	
ABAZOV	09AE	PRL 103 191803	V.M. Abazov *et al.*	(D0 Collab.)
ABAZOV	09D	PRL 102 051601	V.M. Abazov *et al.*	(D0 Collab.)
MASUDA	09	PRL 102 171101	M. Masuda, M. Sasaki	(ICRR)
AALTONEN	08AC	PRL 101 181602	T. Aaltonen *et al.*	(CDF Collab.)
AALTONEN	08S	PR D78 012008	T. Aaltonen *et al.*	(CDF Collab.)
ABAZOV	08J	PRL 100 091802	V.M. Abazov *et al.*	(D0 Collab.)
ABAZOV	08S	PRL 101 011601	V.M. Abazov *et al.*	(D0 Collab.)
DAS	08	PR D78 063011	P.K. Das, V.H.S. Kumar, P.K. Suresh	
GERACI	08	PR D78 022002	A.A. Geraci *et al.*	(STAN)
TRENKEL	08	PR D77 122001	C. Trenkel	
AALTONEN	07G	PRL 99 171801	T. Aaltonen *et al.*	(CDF Collab.)
AALTONEN	07H	PRL 99 171802	T. Aaltonen *et al.*	(CDF Collab.)
DECCA	07A	EPJ C51 963	R.S. Decca *et al.*	
HAISCH	07	PR D76 034014	U. Haisch, A. Weiler	
KAPNER	07	PRL 98 021101	D.J. Kapner *et al.*	
SCHAEL	07A	EPJ C49 411	S. Schael *et al.*	(ALEPH Collab.)
TU	07	PRL 98 201101	L.-C. Tu *et al.*	
ABDALLAH	06C	EPJ C45 589	J. Abdallah *et al.*	(DELPHI Collab.)
ABULENCIA,A	06	PRL 97 171802	A. Abulencia *et al.*	(CDF Collab.)
GERDES	06	PR D73 112008	D. Gerdes *et al.*	
GOGOLADZE	06	PR D74 093012	I. Gogoladze, C. Macesanu	
ABAZOV	05N	PRL 95 091801	V.M. Abazov *et al.*	(D0 Collab.)
ABAZOV	05V	PRL 95 161602	V.M. Abazov *et al.*	(D0 Collab.)
ABDALLAH	05B	EPJ C38 395	J. Abdallah *et al.*	(DELPHI Collab.)
ABULENCIA	05A	PRL 95 252001	A. Abulencia *et al.*	(CDF Collab.)
SMULLIN	05	PR D72 122001	S.J. Smullin *et al.*	
ACHARD	04E	PL B587 16	P. Achard *et al.*	(L3 Collab.)
ACOSTA	04C	PRL 92 121802	D. Acosta *et al.*	(CDF Collab.)
BARBIERI	04	NP B703 127	R. Barbieri *et al.*	
CASSE	04	PRL 92 111102	M. Casse *et al.*	
CHEKANOV	04B	PL B591 23	S. Chekanov *et al.*	(ZEUS Collab.)
HOYLE	04	PR D70 042004	C.D. Hoyle *et al.*	(WASH)
ABAZOV	03	PRL 90 251802	V.M. Abazov *et al.*	(D0 Collab.)
ABBIENDI	03D	EPJ C26 331	G. Abbiendi *et al.*	(OPAL Collab.)
ACHARD	03D	PL B572 133	P. Achard *et al.*	(L3 Collab.)
ADLOFF	03	PL B568 35	C. Adloff *et al.*	(H1 Collab.)
CHIAVERINI	03	PRL 90 151101	J. Chiaverini *et al.*	
GIUDICE	03	NP B663 377	G.F. Giudice, A. Strumia	
HANNESTAD	03	PR D67 125008	S. Hannestad, G.G. Raffelt	
Also		PR D69 029901(errat.)	S. Hannestad, G.G. Raffelt	
HEISTER	03C	EPJ C28 1	A. Heister *et al.*	(ALEPH Collab.)
LONG	03	NAT 421 922	J.C. Long *et al.*	
ACHARD	02	PL B524 65	P. Achard *et al.*	(L3 Collab.)
ACHARD	02D	PL B531 28	P. Achard *et al.*	(L3 Collab.)
HANNESTAD	02	PRL 88 071301	S. Hannestad, G. Raffelt	
ABBOTT	01	PRL 86 1156	B. Abbott *et al.*	(D0 Collab.)
FAIRBAIRN	01	PL B508 335	M. Fairbairn	
HANHART	01	PL B509 1	C. Hanhart *et al.*	
HOYLE	01	PRL 86 1418	C.D. Hoyle *et al.*	
ABBIENDI	00R	EPJ C13 553	G. Abbiendi *et al.*	(OPAL Collab.)
ABREU	00A	PL B491 67	P. Abreu *et al.*	(DELPHI Collab.)
ABREU	00S	PL B485 45	P. Abreu *et al.*	(DELPHI Collab.)
ABREU	00Z	EPJ C17 53	P. Abreu *et al.*	(DELPHI Collab.)
CASSISI	00	PL B481 323	S. Cassisi *et al.*	
CHANG	00B	PRL 85 3765	L.N. Chang *et al.*	
CHEUNG	00	PR D61 015005	K. Cheung	
CORNET	00	PR D61 037701	F. Cornet, M. Relano, J. Rico	
GRAESSER	00	PR D61 074019	M.L. Graesser	
HAN	00	PR D62 125018	T. Han, D. Marfatia, R.-J. Zhang	
MATHEWS	00	JHEP 0007 008	P. Mathews, S. Raychaudhuri, K. Sridhar	
MELE	00	PR D61 117901	S. Mele, E. Sanchez	
RIZZO	00	PR D61 016007	T.G. Rizzo, J.D. Wells	
ABBIENDI	99P	PL B465 303	G. Abbiendi *et al.*	(OPAL Collab.)
ACCIARRI	99M	PL B464 135	M. Acciarri *et al.*	(L3 Collab.)
ACCIARRI	99R	PL B470 268	M. Acciarri *et al.*	(L3 Collab.)
ACCIARRI	99S	PL B470 281	M. Acciarri *et al.*	(L3 Collab.)
BOURILKOV	99	JHEP 9908 006	D. Bourilkov	
HOSKINS	85	PR D32 3084	J.K. Hoskins *et al.*	

WIMP and Dark Matter Searches

We omit papers on CHAMP's, millicharged particles, and other exotic particles.

GALACTIC WIMP SEARCHES

These limits are for weakly-interacting stable particles that may constitute the invisible mass in the galaxy. Unless otherwise noted, a local mass density of 0.3 GeV/cm^3 is assumed; see each paper for velocity distribution assumptions. In the papers the limit is given as a function of the X^0 mass. Here we list limits only for typical mass values of sub-GeV, GeV, 20 GeV, 100 GeV, and 1 TeV. Specific limits on supersymmetric dark matter particles may be found in the Supersymmetry section.

Spin-Independent Cross Section Limits for Dark Matter Particle (X^0) on Nucleon

For m_{X^0} in GeV range

We provide here limits fo m_{X^0} < 5 GeV

VALUE (pb)	CL%	DOCUMENT ID		TECN	COMMENT
• • • We do not use the following data for averages, fits, limits, etc. • • •					
$<2 \times 10^{-7}$	95	[1] AKERIB	21A	LUX	low mass WIMPs
$<5 \times 10^{6}$	90	[2] ALKHATIB	21	SCDM	light DM
$<1 \times 10^{8}$	95	[3] ANDRIAMIR...	21A		sub-GeV DM on nucleon
$<1 \times 10^{-8}$	90	[4] APRILE	21	XE1T	GeV scale DM
$<8 \times 10^{-4}$	90	[5] AGUILAR-AR...	20C	DMIC	WIMP SI scatter on Si
$<8 \times 10^{-4}$	90	[6] AKERIB	20A	LUX	GeV-scale WIMP search
$<1 \times 10^{-2}$	90	[7] ABDELHAME..	19A	CRES	$CaWO_4$
$<5.4 \times 10^{-6}$	90	[8] AGNESE	19A	SCDM	GeV-scale WIMPs on Ge
<1	90	[9] AKERIB	19	LUX	light DM on Xe via Migdal/brem effect
$<1 \times 10^{-6}$	90	[10] AMOLE	19	PICO	C_3F_8
$<1.6 \times 10^{-3}$	90	[11] APRILE	19C	XE1T	DM on Xe
$<1 \times 10^{-7}$	90	[12] APRILE	19D	XE1T	DM on Xe
<0.1	90	[13] ARMENGAUD	19	EDEL	GeV-scale WIMPs on Ge
$<1.6 \times 10^{3}$	90	[14] KOBAYASHI	19	XMAS	annual modulation Xe
$<7 \times 10^{2}$	90	[15] LIU	19B	CDEX	Ge; sub-GeV DM via Migdal
$<7 \times 10^{-7}$	90	[16] AGNES	18	DS50	GeV-scale WIMPs on Ar
$<1.5 \times 10^{-5}$	95	[17] AGNESE	18	SCDM	GeV-scale WIMPs on Ge
$<2 \times 10^{-8}$	90	[18] APRILE	18	XE1T	Xe, SI
$<4.5 \times 10^{-3}$	90	[19] ARNAUD	18	NEWS	low mass WIMP, Ne
$<8 \times 10^{-6}$	90	[20] JIANG	18	CDEX	GeV-scale WIMPs on Ge
$<3 \times 10^{-5}$	90	[21] YANG	18	CDEX	WIMPs on Ge
$<1 \times 10^{-6}$	90	[22] AKERIB	17	LUX	Xe
$<1 \times 10^{2}$	90	[23] ANGLOHER	17A	CRES	GeV-scale WIMPs
$<7 \times 10^{-5}$	90	[24] ANGLOHER	16	CRES	$CaWO_4$
$<3 \times 10^{-5}$	90	[25] APRILE	16	X100	Xe
$<4.3 \times 10^{-4}$	90	[26] ARMENGAUD	16	EDE3	GeV-scale WIMPs on Ge
$<7 \times 10^{-5}$	90	[27] HEHN	16	EDE3	SI WIMP on Ge
$<6 \times 10^{-5}$	90	[28] ZHAO	16	CDEX	GeV-scale WIMPs on Ge
$<1 \times 10^{-4}$	90	[29] AMOLE	15	PICO	C_3F_8
$<8 \times 10^{-5}$	90	[30] XIAO	15	PNDX	WIMPs on Xe
$<3 \times 10^{-5}$	90	[31] AGNESE	14	SCDM	GeV-scale WIMPs
$<1 \times 10^{-3}$	90	[32] AKERIB	14	LUX	WIMP on Xe
$<9 \times 10^{-4}$	90	[33] LI	13B	TEXO	WIMPs on Ge
$<3 \times 10^{-4}$	90	[34] ARCHAMBAU..	12	PICA	C_4F_{10}
$<2 \times 10^{-4}$	90	[35] AALSETH	11	CGNT	GeV WIMPs on Ge
$<5 \times 10^{-4}$	90	[36] AHMED	11B	CDM2	GeV-scale WIMPs on Ge
$<8 \times 10^{-5}$	90	[37] ANGLE	11	XE10	Xe
$<5 \times 10^{-4}$	90	[38] AKERIB	10	CDM2	WIMPs on Ge/Si

[1] AKERIB 21A present new technique for low mass WIMP detection. Require $\sigma^{SI}(p\chi) < 2 \times 10^{-7}$ pb for m(WIMP) 10 GeV.

[2] ALKHATIB 21 search for light DM using SuperCDMS; require $\sigma^{SI}(p\chi) < 5 \times 10^{6}$ for m(DM) = 0.1 GeV.

[3] ANDRIAMIRADO 21A search for upscattered (boosted) sub-GeV DM interacting with proton in PROSPECT detector. No signal observed. Limits placed in $\sigma(\chi N)$ vs. m(DM) plane for m(DM) $\sim$ 1 keV $-$ 0.5 GeV. The listed limit is for m(DM) = 1 keV.

Downloaded from https://academic.oup.com/ptep/article/2022/8/083C01/6651666 by KIT Library user on 27 September 2022

[4] APRILE 21 search for low recoil energy GeV-scale DM in XENON1T with 1.6 keV threshold. No signal in 0.6 t y exposure. Limits placed in $\sigma^{SI}(\chi N)$ vs. m(DM) plane for m(DM) between 3–12 GeV. The listed limit is for m(DM) = 5 GeV.

[5] AGUILAR-AREVALO 20C search for WIMP SI scatter on Si using DAMIC at SNOLab; some excess; limits placed in σ vs m(DM) for m(DM) in 1.2–10 GeV; quoted limit for m(WIMP) = 2 GeV.

[6] AKERIB 20A search for GeV-scale WIMPs via WIMP-nucleon scatter with single photon emission; no signal; limits placed in m(WIMP) vs σ^{SI} plane: for example $\sigma^{SI}(\chi n) < 8 \times 10^{-4}$ pb for m(WIMP) = 2.5 GeV.

[7] ABDELHAMEED 19A search for GeV scale dark matter SI scatter on $CaWO_4$; no signal, limits placed in σ vs. mass plane for m(DM) $\sim$ 0.1–10 GeV. The listed limit is for m(DM) = 1 GeV.

[8] AGNESE 19A search for 1.5–10 GeV WIMP scatter on Ge in CDMSlite dataset. Limits set in a likelihood analysis. No signal was observed. Limit reported for m(χ) = 5 GeV.

[9] AKERIB 19 search for 0.4–5 GeV DM using bremsstrahlung photons and "Migdal" electrons; 1.4×10^4 kg d exposure of liquid Xe; constraint $\sigma^{SI}(\chi N) < 1$ pb for m(χ) = 5 GeV in light scalar mediator model.

[10] AMOLE 19 search for SI WIMP scatter on C_3F_8 in PICO-60 bubble chamber; no signal: set limit for spin independent coupling $\sigma^{SI}(\chi N) < 1 \times 10^{-6}$ pb for m(χ) = 5 GeV.

[11] APRILE 19C search for light DM scatter on Xe via atomic excitation, ionization (Migdal effect) or bremsstrahlung; no signal, limits placed in σ vs. m(DM) plane for m(DM) $\sim$ 0.085–2 GeV. The listed limit is for m(DM) = 1 GeV.

[12] APRILE 19D search for light DM scatter on Xe via ionization to probe SI, SD, and χe cross sections; with 22 t d exposure, limits placed in various σ vs. m(DM) planes. Quoted limit is for m(DM) = 5 GeV.

[13] ARMENGAUD 19search for GeV scale WIMP scatter on Ge; limits placed in $\sigma^{SI}(\chi N)$ vs. m(χ) plane for m(χ) $\sim$ 0.045–10 GeV; quoted limit is for m(χ) = 5 GeV.

[14] KOBAYASHI 19 search for sub-GeV WIMP annual modulation in Xe via brems; no signal; limits placed in $\sigma^{SI}(\chi N)$ vs. m(χ) plane for m $\sim$ 0.3–1 GeV; quoted limit is for m(χ) = 0.5 GeV.

[15] LIU 19B seach for sub-GeV DM using Migdal effect on Ge at CDEX-IB; no signal, require $\sigma^{SI}(\chi N) < 7 \times 10^2$ pb for m(χ) = 0.1 GeV.

[16] AGNES 18 search for 1.8–20 GeV WIMP SI scatter on Ar; quoted limit is for m(χ) = 5 GeV.

[17] AGNESE 18 search for GeV scale WIMPs using CDMSlite; limits placed in $\sigma^{SI}(\chi N)$ vs. m(χ) plane for m $\sim$ 1.5–20 GeV; quoted limit is for m(χ) = 5 GeV.

[18] APRILE 18 search for WIMP scatter on 1 t yr Xe; no signal, limits set in $\sigma(\chi N)$ vs. m(χ) plane for m(χ) $\sim$ 6–1000 GeV; quoted limit is for m = 6 GeV.

[19] ARNAUD 18 search for low mass WIMP scatter on Ne via SPC at NEWS-G; limits set in $\sigma^{SI}(\chi N)$ vs. m(χ) plane for m $\sim$ 0.5–20 GeV; quoted limit is for m = 5 GeV.

[20] JIANG 18 search for GeV scale WIMP scatter on Ge; limits placed in $\sigma^{SI}(\chi N)$ vs. m(χ) plane for m(χ) $\sim$ 3–10 GeV; quoted limit is for m(χ) = 5 GeV.

[21] YANG 18 search for WIMP scatter on Ge; limits placed in $\sigma^{SI}(\chi N)$ vs. m(χ) plane for m(χ) $\sim$ 2–10 GeV; quoted limit is for m(χ) = 5 GeV.

[22] AKERIB 17 search for WIMP scatter on Xe; limits placed in $\sigma^{SI}(\chi N)$ vs. m(χ) plane for m(χ) $\sim$ 5–1 $\times 10^5$ GeV; quoted limit is for m(χ) = 5 GeV.

[23] ANGLOHER 17A search for GeV scale WIMP scatter on Al_2O_3 crystal; limits placed in $\sigma^{SI}(\chi N)$ vs. m(χ) plane for m(χ) $\sim$ 0.15–10 GeV; quoted limit is for m(χ) = 5 GeV.

[24] ANGLOHER 16 search for GeV scale WIMP scatter on $CaWO_4$; limits placed in $\sigma^{SI}(\chi N)$ vs. m(χ) plane for m(χ) $\sim$ 0.5–30 GeV; quoted limit is for m(χ) = 5 GeV.

[25] APRILE 16 search for low mass WIMPs via ionization at XENON100; limits placed in $\sigma^{SI}(\chi N)$ vs m(χ) plane for m $\sim$ 3.5–20 GeV; quoted limit is for m(χ) = 5 GeV.

[26] ARMENGAUD 16 search for GeV scale WIMP scatter on Ge; limits placed in $\sigma^{SI}(\chi N)$ vs. m(χ) plane for m(χ) $\sim$ 4–30 GeV; quoted limit is for m(χ) = 5 GeV.

[27] HEHN 16 search for low mass WIMPs via SI scatter on Ge target using profile likelihood analysis; limits placed in $\sigma^{SI}(\chi N)$ vs. m(χ) plane for m(χ) $\sim$ 4–30 GeV; quoted limit is for m(χ) = 5 GeV.

[28] ZHAO 16 search for GeV-scale WIMP scatter on Ge; limits placed in $\sigma^{SI}(\chi N)$ vs. m(χ) plane for m(χ) $\sim$ 4–30 GeV; quoted limit is for m(χ) = 5 GeV.

[29] AMOLE 15 search for WIMP scatter on C_3F_8 in PICO-2L; limits placed in $\sigma^{SI}(\chi N)$ vs. m(χ) plane for m(χ) $\sim$ 4–25 GeV; quoted limit is for m(χ) = 5 GeV.

[30] XIAO 15 search for WIMP scatter on Xe with PandaX-I; limits placed in $\sigma^{SI}(\chi N)$ vs. m(χ) plane for m(χ) $\sim$ 5–100 GeV; quoted limit is for m(χ) = 5 GeV.

[31] AGNESE 14 search for GeV scale WIMPs SI scatter at SuperCDMS; no signal, limits placed in $\sigma^{SI}(\chi N)$ vs. m(χ) plane for m(χ) $\sim$ 3.5–30 GeV; quoted limit is for m(χ) = 5 GeV.

[32] AKERIB 14 search for WIMP scatter on Xe; limits placed in $\sigma^{SI}(\chi N)$ vs. m(χ) plane for m(χ) $\sim$ 5–5000 GeV. Limit given for m(χ) = 5 GeV.

[33] LI 13B search for WIMP scatter on Ge; limits placed in $\sigma^{SI}(\chi N)$ vs. m(χ) plane for m(χ) $\sim$ 4–100 GeV; quoted limit is for m(χ) = 5 GeV.

[34] ARCHAMBAULT 12 search for low mass WIMP scatter on C_4F_{10}; limits set in $\sigma^{SI}(\chi N)$ vs. m(χ) plane for m $\sim$ 4–12 GeV; quoted limit is for m = 5 GeV.

[35] AALSETH 11 search for GeV-scale SI WIMP scatter on Ge; limits placed on $\sigma^{SI}(\chi N)$ for m(χ) $\sim$ 3.5–100 GeV; quoted limit is for m(χ) = 5 GeV.

[36] AHMED 11B search for GeV scale WIMP scatter on Ge in CDMS II; limits placed in $\sigma^{SD}(\chi n)$ vs. m(χ) plane for m $\sim$ 4–12 GeV.

[37] ANGLE 11 search for GeV scale WIMPs in Xenon-10; limits placed in $\sigma^{SI}(\chi N)$ vs. m(χ) plane for m(χ) $\sim$ 4–20 GeV; quoted limit is for m(χ) = 5 GeV.

[38] AKERIB 10 search for WIMP scatter on Ge/Si in CDMS II; limits place in $\sigma_{SI}(\chi N)$ vs. m(χ) plane for m $\sim$ 3–100 GeV. Limit given for m(DM) = 5 GeV.

For m_{X^0} = 20 GeV

For limits from X^0 annihilation in the Sun, the assumed annihilation final state is shown in parenthesis in the comment.

VALUE (pb)	CL%	DOCUMENT ID		TECN	COMMENT
• • • We do not use the following data for averages, fits, limits, etc. • • •					
$<5 \times 10^{-11}$	90	[1] MENG	21B	PNDX	Xe WIMP search
$<5 \times 10^{-5}$		[2] FELIZARDO	20	SMPL	C_2ClF_5
$<2.2 \times 10^{-10}$	90	[3] WANG	20G	PNDX	Xe TPC
		[4] ANGLOHER	19	CRES	$CaWO_4$
$<7 \times 10^{-5}$	90	[5] KIM	19A	KIMS	NaI
$<3 \times 10^{-7}$	90	[6] KOBAYASHI	19	XMAS	SI WIMP on Xe
		[7] SEONG	19	BELL	$\Upsilon \to \gamma A$, $A \to \chi\chi$
$<3.5 \times 10^{-5}$	90	[8] YANG	19	CDEX	annual modulation Ge
$<2 \times 10^{-7}$	90	[9] ABE	18C	XMAS	X^0- Xe modulation
$<1.44 \times 10^{-5}$	90	[10] ADHIKARI	18	C100	NaI
$<3 \times 10^{-7}$	90	[11] AGNES	18	DS50	X^0-Ar
$<5 \times 10^{-6}$	95	[12] AARTSEN	18	SCDM	Ge
$<4 \times 10^{-8}$	90	[13] AGNESE	18A	SCDM	Ge
$<6 \times 10^{-11}$	90	[14] APRILE	18	XE1T	Xe, SI
$<4.5 \times 10^{-3}$	90	[15] ARNAUD	18	NEWS	GeV WIMPs on Ne
$<2 \times 10^{-6}$	90	[16] AARTSEN	17	ICCB	ν, earth
$<2 \times 10^{-10}$	90	[17] AKERIB	17	LUX	Xe
$<1 \times 10^{-3}$	90	[18] BARBOSA-D...	17	ICCB	NaI
$<1.7 \times 10^{-10}$	90	[19] CUI	17A	PNDX	WIMPs on Xe
$<7.3 \times 10^{-7}$	90	AGNES	16	DS50	Ar
$<1 \times 10^{-5}$	90	[20] AGNESE	16	CDMS	Ge
$<2 \times 10^{-4}$	90	[21] AGUILAR-AR...	16	DMIC	Si CCDs
$<4.5 \times 10^{-5}$	90	[22] ANGLOHER	16	CRES	$CaWO_4$
$<2 \times 10^{-6}$	90	[23] APRILE	16	X100	Xe
$<9.4 \times 10^{-8}$	90	[24] ARMENGAUD	16	EDE3	Ge
$<1.0 \times 10^{-7}$	90	[25] HEHN	16	EDE3	Ge
$<5 \times 10^{-6}$	90	[26] ZHAO	16	CDEX	Ge
$<1 \times 10^{-5}$	90	AGNES	15	DS50	Ar
$<1.5 \times 10^{-6}$	90	[27] AGNESE	15A	CDM2	Ge
$<1.5 \times 10^{-7}$	90	[28] AGNESE	15B	CDM2	Ge
$<2 \times 10^{-6}$	90	[29] AMOLE	15	PICO	C_3F_8
$<1.2 \times 10^{-5}$	90	CHOI	15	SKAM	H, solar ν ($b\overline{b}$)
$<1.19 \times 10^{-6}$	90	CHOI	15	SKAM	H, solar ν ($\tau^+\tau^-$)
$<2 \times 10^{-8}$	90	[30] XIAO	15	PNDX	Xe
$<2.0 \times 10^{-7}$	90	[31] AGNESE	14	SCDM	Ge
$<3.7 \times 10^{-5}$	90	[32] AGNESE	14A	SCDM	Ge
$<1 \times 10^{-9}$	90	[33] AKERIB	14	LUX	Xe
$<2 \times 10^{-6}$	90	[34] ANGLOHER	14	CRES	$CaWO_4$
$<5 \times 10^{-6}$	90	FELIZARDO	14	SMPL	C_2ClF_5
$<8 \times 10^{-6}$	90	[35] LEE	14A	KIMS	CsI
$<2 \times 10^{-4}$	90	[36] LIU	14A	CDEX	Ge
$<1 \times 10^{-5}$	90	[37] YUE	14	CDEX	Ge
$<1.08 \times 10^{-4}$	90	[38] AARTSEN	13	ICCB	H, solar ν ($\tau^+\tau^-$)
$<1.5 \times 10^{-5}$	90	[39] ABE	13B	XMAS	Xe
$<3.1 \times 10^{-6}$	90	[40] AGNESE	13	CDM2	Si
$<3.4 \times 10^{-6}$	90	[41] AGNESE	13A	CDM2	Si
$<2.2 \times 10^{-6}$	90	[42] AGNESE	13A	CDM2	Si
		[43] BERNABEI	13A	DAMA	NaI modulation
$<1.2 \times 10^{-4}$	90	[44] LI	13B	TEXO	Ge
		[45] ZHAO	13	CDEX	Ge
$<1.2 \times 10^{-7}$	90	AKIMOV	12	ZEP3	Xe
		[46] ANGLOHER	12	CRES	$CaWO_4$
$<8 \times 10^{-6}$	90	[47] ANGLOHER	12	CRES	$CaWO_4$
$<7 \times 10^{-9}$	90	[48] APRILE	12	X100	Xe
$<7 \times 10^{-7}$	90	[49] ARMENGAUD	12	EDE2	Ge
		[50] BARRETO	12	DMIC	CCD
$<2 \times 10^{-6}$	90	BEHNKE	12	COUP	CF_3I
$<7 \times 10^{-6}$		[51] FELIZARDO	12	SMPL	C_2ClF_5
$<1.5 \times 10^{-6}$	90	KIM	12	KIMS	CsI
$<5 \times 10^{-5}$	90	[52] AALSETH	11	CGNT	Ge
		[53] AALSETH	11A	CGNT	Ge
$<5 \times 10^{-7}$	90	[54] AHMED	11	CDM2	Ge, inelastic
$<2.7 \times 10^{-7}$	90	[55] AHMED	11A	RVUE	Ge
$<3 \times 10^{-6}$	90	[56] ANGLE	11	XE10	Xe
$<7 \times 10^{-8}$	90	[57] APRILE	11	X100	Xe
		[58] APRILE	11A	X100	Xe, inelastic
$<2 \times 10^{-8}$	90	[48] APRILE	11B	X100	Xe
		[59] HORN	11	ZEP3	Xe
$<2 \times 10^{-7}$	90	AHMED	10	CDM2	Ge
$<1 \times 10^{-5}$	90	[60] AKERIB	10	CDM2	Si, Ge, low threshold
$<1 \times 10^{-7}$	90	APRILE	10	X100	Xe
$<2 \times 10^{-6}$	90	ARMENGAUD	10	EDE2	Ge
$<4 \times 10^{-5}$	90	FELIZARDO	10	SMPL	C_2ClF_3
$<1.5 \times 10^{-7}$	90	[61] AHMED	09	CDM2	Ge
$<2 \times 10^{-4}$	90	[62] LIN	09	TEXO	Ge
		[63] AALSETH	08	CGNT	Ge

[1] MENG 21B search for SI WIMP interaction with 3.7 t Xe and 0.63 t yr exposure. No signal observed. Limits placed in m(DM) vs. σ^{SI} plane.

[2] FELIZARDO 20 presents 2014 SIMPLE bounds on WIMP DM using C_2ClF_5 target .

[3] WANG 20G search for SI WIMP scatter on Xe with 132 t d exposure of PANDAX-II .

[4] ANGLOHER 19 search for low mass WIMP scatter on $CaWO_4$; no signal; limits placed on Wilson coefficients for m(χ) = 0.6–60 GeV.

[5] KIM 19A search for WIMP scatter in NaI KIMS experiment; no signal: require $\sigma^{SI}(\chi n) < 7 \times 10^{-5}$ pb for m(χ) = 20 GeV.

[6] KOBAYASHI 19 search for WIMP scatter in XMASS single-phase liquid Xe detector; no signal; require $\sigma^{SI}(\chi N) < 3 \times 10^{-7}$ pb for m(χ) = 20 GeV.

Downloaded from https://academic.oup.com/ptep/article/2022/8/083C01/6651666 by KIT Library user on 27 September 2022

[7] SEONG 19 search for $\Upsilon \rightarrow \gamma A$, $A \rightarrow \chi\chi$ via CP-odd Higgs; no signal; limits on BF set; model dependent conversion to WIMP-nucleon scattering cross section limits $\sigma^{SI} < 10^{-36}$ cm^2 for m(χ) = 0.01–1 GeV.

[8] YANG 19 search for low mass wimps via annual modulation in Ge; no signal; require $\sigma^{SI}(\chi N) < 3.5 \times 10^{-5}$ pb for m(χ) = 20 GeV.

[9] ABE 18C search for WIMP annual modulation signal for m(WIMP): 6–20 GeV; limits set on SI WIMP-nucleon cross section: see Fig. 6.

[10] ADHIKARI 18 search for WIMP scatter on NaI; no signal; require $\sigma^{SI} < 1.44 \times 10^{-5}$ pb for m(WIMP) = 20 GeV; inconsistent with DAMA/LIBRA result.

[11] AGNES 18 search low mass m(WIMP): 1.8–20 GeV scatter on Ar; limits on SI WIMP-nucleon cross section set in Fig. 8.

[12] AGNESE 18 give limits for $\sigma^{SI}(\chi N)$ for m(WIMP) between 1.5 and 20 GeV using CDMSlite mode data.

[13] AGNESE 18A search for WIMP scatter on Ge at SuperCDMS; 1 event, consistent with expected background; set limit in $\sigma^{SI}(\chi N)$ vs. m(χ) plane for m $\sim$ 10–250 GeV.

[14] APRILE 18 search for WIMP scatter on 1 t yr Xe; no signal, limits placed in $\sigma^{SI}(\chi N)$ vs. m(χ) plane for m(χ) $\sim$ 6–1000 GeV.

[15] ARNAUD 18 search for low mass WIMP scatter on Ne via SPC at NEWS-G; limits set in $\sigma^{SI}(\chi N)$ vs. m(χ) plane for m $\sim$ 0.5–20 GeV.

[16] AARTSEN 17 obtain σ(SI) $< 6 \times 10^{-6}$ pb for m(wimp) = 20 GeV from ν from earth.

[17] AKERIB 17 search for WIMP scatter on Xe; limits placed in $\sigma^{SI}(\chi N)$ vs. m(χ) plane for m(χ) $\sim$ 5–1 $\times 10^5$ GeV.

[18] BARBOSA-DE-SOUZA 17 search for annual modulation of WIMP scatter on NaI using an exposure of 61 kg yr of DM-Ice17 for recoil energy in the 4–20 keV range (DAMA found modulation for recoil energy < 5 keV). No modulation seen. Sensitivity insufficient to distinguish DAMA signal from null.

[19] CUI 17A search for SI WIMP scatter; limits placed in $\sigma^{SI}(\chi N)$ vs. m(χ) plane for m $\sim$ 10–1 $\times 10^4$ GeV using 54 ton-day exposure of Xe.

[20] AGNESE 16 CDMSlite excludes low mass WIMPs 1.6–5.5 GeV and SI scattering cross section depending on m(WIMP); see Fig. 4.

[21] AGUILAR-AREVALO 16 search low mass 1–10 GeV WIMP scatter on Si CCDs; set limits Fig. 11.

[22] ANGLOHER 16 search for GeV scale WIMP scatter on $CaWO_4$; limits placed in $\sigma^{SI}(\chi N)$ vs. m(χ) plane for m(χ) $\sim$ 0.5–30 GeV.

[23] APRILE 16 search for low mass WIMPs via ionization at XENON100; limits placed in $\sigma^{SI}(\chi N)$ vs m(χ) plane for m $\sim$ 3.5–20 GeV.

[24] ARMENGAUD 16 search for GeV scale WIMP scatter on Ge; limits placed in $\sigma^{SI}(\chi N)$ vs. m(χ) plane for m(χ) $\sim$ 4–30 GeV.

[25] HEHN 16 search for low mass WIMPs via SI scatter on Ge target using profile likelihood analysis; limits placed in $\sigma^{SI}(\chi N)$ vs. m(χ) plane for m(χ) $\sim$ 4–30 GeV.

[26] ZHAO 16 search for GeV-scale WIMP scatter on Ge; limits placed in $\sigma^{SI}(\chi N)$ vs. m(χ) plane for m(χ) $\sim$ 4–30 GeV.

[27] AGNESE 15A reanalyse AHMED 11B low threshold data. See their Fig. 12 (left) for improved limits extending down to 5 GeV.

[28] AGNESE 15B reanalyse AHMED 10 data.

[29] See their Fig. 7 for limits extending down to 4 GeV.

[30] XIAO 15 search for WIMP scatter on Xe with PandaX-I; limits placed in $\sigma^{SI}(\chi N)$ vs. m(χ) plane for m(χ) $\sim$ 5–100 GeV.

[31] This limit value is provided by the authors. See their Fig. 4 for limits extending down to m_{X^0} = 3.5 GeV.

[32] This limit value is provided by the authors. AGNESE 14A result is from CDMSlite mode operation with enhanced sensitivity to low mass m_{X^0}. See their Fig. 3 for limits extending down to m_{X^0} = 3.5 GeV (see also Fig. 4 in AGNESE 14).

[33] See their Fig. 5 for limits extending down to m_{X^0} = 5.5 GeV.

[34] See their Fig. 5 for limits extending down to m_{X^0} = 1 GeV.

[35] See their Fig. 5 for limits extending down to m_{X^0} = 5 GeV.

[36] LIU 14A result is based on prototype CDEX-0 detector. See their Fig. 13 for limits extending down to m_{X^0} = 2 GeV.

[37] See their Fig. 4 for limits extending down to m_{X^0} = 4.5 GeV.

[38] AARTSEN 13 search for neutrinos from the Sun arising from the pair annihilation of X^0 trapped by the sun in data taken between June 2010 and May 2011.

[39] See their Fig. 8 for limits extending down to m_{X^0} = 7 GeV.

[40] This limit value is provided by the authors. AGNESE 13 use data taken between Oct. 2006 and July 2007. See their Fig. 4 for limits extending down to m_{X^0} = 7 GeV.

[41] This limit value is provided by the authors. AGNESE 13A use data taken between July 2007 and Sep. 2008. Three candidate events are seen. Assuming these events are real, the best fit parameters are m_{X^0} = 8.6 GeV and $\sigma = 1.9 \times 10^{-5}$ pb.

[42] This limit value is provided by the authors. Limit from combined data of AGNESE 13 and AGNESE 13A. See their Fig. 4 for limits extending down to m_{X^0} = 5.5 GeV.

[43] BERNABEI 13A search for annual modulation of counting rate in the 2–6 keV recoil energy interval, in a 14 yr live time exposure of 1.33 t yr. Find a modulation of 0.0112 $\pm$ 0.0012 counts/(day kg keV) with 9.3 sigma C.L. Find period and phase in agreement with expectations from DM particles.

[44] LI 13B search for WIMP scatter on Ge; limits placed in $\sigma^{SI}(\chi N)$ vs. m(χ) plane for m(χ) $\sim$ 4–100 GeV.

[45] See their Fig. 5 for limits for m_{X^0} = 4–12 GeV.

[46] ANGLOHER 12 observe excess events above the expected background which are consistent with X^0 with mass $\sim$ 25 GeV (or 12 GeV) and spin-independent X^0-nucleon cross section of 2×10^{-6} pb (or 4×10^{-5} pb).

[47] Reanalysis of ANGLOHER 09 data with all three nuclides. See also BROWN 12.

[48] See also APRILE 14A.

[49] See their Fig. 4 for limits extending down to m_{X^0} = 7 GeV.

[50] See their Fig. 13 for cross section limits for m_{X^0} between 1.2 and 10 GeV.

[51] See also DAHL 12 for a criticism.

[52] See their Fig. 4 for limits extending to m_{X^0} = 3.5 GeV.

[53] AALSETH 11A find indications of annual modulation of the data, the energy spectrum being compatible with X^0 mass around 8 GeV. See also AALSETH 13.

[54] AHMED 11 search for X^0 inelastic scattering. See their Fig. 8–10 for limits. The inelastic cross section reduces to the elastic cross section at the limit of zero mass splitting (Fig. 8, left).

[55] AHMED 11A combine CDMS II and EDELWEISS data.

[56] ANGLE 11 show limits down to m_{X^0} = 4 GeV on Fig. 3.

[57] APRILE 11 reanalyze APRILE 10 data.

[58] APRILE 11A search for X^0 inelastic scattering. See their Fig. 2 and 3 for limits. See also APRILE 14A.

[59] HORN 11 perform detector calibration by neutrons. Earlier results are only marginally affected.

[60] See their Fig. 10 and 12 for limits extending to X^0 mass of 1 GeV.

[61] Superseded by AHMED 10.

[62] See their Fig. 6(a) for cross section limits for m_{X^0} extending down to 2 GeV.

[63] See their Fig. 2 for cross section limits for m_{X^0} between 4 and 10 GeV.

For m_{X^0} = 100 GeV

For limits from X^0 annihilation in the Sun, the assumed annihilation final state is shown in parenthesis in the comment.

VALUE (pb)	CL%	DOCUMENT ID		TECN	COMMENT
• • • We do not use the following data for averages, fits, limits, etc. • • •					
$<6 \times 10^{-11}$	90	[1] MENG	21B	PNDX	Xe WIMP search
		[2] ADHIKARI	20	DEAP	Ar
$<5 \times 10^{-5}$		[3] FELIZARDO	20	SMPL	W
$<4.2 \times 10^{-10}$	90	[4] WANG	20G	PNDX	Xe TPC
$<4 \times 10^{-8}$	90	[5] ABE	19	XMAS	Xe
$<3.9 \times 10^{-9}$	90	[6] AJAJ	19	DEAP	Ar
$<2.3 \times 10^{-6}$	90	[7] ADHIKARI	18	C100	NaI
$<1.14 \times 10^{-8}$	90	[8] AGNES	18A	DS50	Ar
$<2 \times 10^{-8}$	90	[9] AGNESE	18A	CDMS	Ge
$<1.2 \times 10^{-8}$	90	[10] AMAUDRUZ	18	DEAP	Ar
$<9.12 \times 10^{-11}$	90	[11] APRILE	18	XE1T	Xe
		[12] REN	18	PNDX	SIDM at PDX-II
$<1.7 \times 10^{-10}$	90	[13] AKERIB	17	LUX	Xe
$<1.2 \times 10^{-10}$	90	[14] APRILE	17G	XE1T	Xe
$<1.2 \times 10^{-10}$	90	[15] CUI	17A	PNDX	Xe
$<2.0 \times 10^{-8}$	90	AGNES	16	DS50	Ar
$<1 \times 10^{-9}$	90	[16] AKERIB	16	LUX	Xe
$<1 \times 10^{-9}$	90	[17] APRILE	16B	X100	Xe
$<2 \times 10^{-8}$	90	[18] TAN	16	PNDX	Xe
$<4 \times 10^{-10}$	90	[19] TAN	16B	PNDX	Xe
$<6 \times 10^{-8}$	90	AGNES	15	DS50	Ar
$<4 \times 10^{-8}$	90	[20] AGNESE	15B	CDM2	Ge
$<7.13 \times 10^{-6}$	90	CHOI	15	SKAM	H, solar ν ($b\overline{b}$)
$<6.26 \times 10^{-7}$	90	CHOI	15	SKAM	H, solar ν ($W^+ W^-$)
$<2.76 \times 10^{-7}$	90	CHOI	15	SKAM	H, solar ν ($\tau^+ \tau^-$)
$<1.5 \times 10^{-8}$	90	[21] XIAO	15	PNDX	Xe
$<1 \times 10^{-9}$	90	AKERIB	14	LUX	Xe
$<4.0 \times 10^{-6}$	90	[22] AVRORIN	14	BAIK	H, solar ν ($W^+ W^-$)
$<1.0 \times 10^{-4}$	90	[22] AVRORIN	14	BAIK	H, solar ν ($b\overline{b}$)
$<1.6 \times 10^{-6}$	90	[22] AVRORIN	14	BAIK	H, solar ν ($\tau^+ \tau^-$)
$<5 \times 10^{-6}$	90	FELIZARDO	14	SMPL	C_2ClF_5
$<6.01 \times 10^{-7}$	90	[23] AARTSEN	13	ICCB	H, solar ν ($W^+ W^-$)
$<3.30 \times 10^{-5}$	90	[23] AARTSEN	13	ICCB	H, solar ν ($b\overline{b}$)
$<1.9 \times 10^{-6}$	90	[24] ADRIAN-MAR..	13	ANTR	H, solar ν ($W^+ W^-$)
$<1.2 \times 10^{-4}$	90	[24] ADRIAN-MAR..	13	ANTR	H, solar ν ($b\overline{b}$)
$<7.6 \times 10^{-7}$	90	[24] ADRIAN-MAR..	13	ANTR	H, solar ν ($\tau^+ \tau^-$)
$<2 \times 10^{-6}$	90	[25] AGNESE	13	CDM2	Si
$<1.6 \times 10^{-6}$	90	[26] BOLIEV	13	BAKS	H, solar ν ($W^+ W^-$)
$<1.9 \times 10^{-5}$	90	[26] BOLIEV	13	BAKS	H, solar ν ($b\overline{b}$)
$<7.1 \times 10^{-7}$	90	[26] BOLIEV	13	BAKS	H, solar ν ($\tau^+ \tau^-$)
$<3.2 \times 10^{-4}$	90	[27] LI	13B	TEXO	WIMPs on Ge
$<1.67 \times 10^{-6}$	90	[28] ABBASI	12	ICCB	H, solar ν ($W^+ W^-$)
$<1.07 \times 10^{-4}$	90	[28] ABBASI	12	ICCB	H, solar ν ($b\overline{b}$)
$<4 \times 10^{-8}$	90	AKIMOV	12	ZEP3	Xe
$<1.4 \times 10^{-6}$	90	[29] ANGLOHER	12	CRES	$CaWO_4$
$<3 \times 10^{-9}$	90	[30] APRILE	12	X100	Xe
$<3 \times 10^{-7}$	90	BEHNKE	12	COUP	CF_3I
$<7 \times 10^{-6}$		FELIZARDO	12	SMPL	C_2ClF_5
$<2.5 \times 10^{-7}$	90	[31] KIM	12	KIMS	CsI
$<2 \times 10^{-4}$	90	AALSETH	11	CGNT	Ge
		[32] AHMED	11	CDM2	Ge, inelastic
$<3.3 \times 10^{-8}$	90	[33] AHMED	11A	RVUE	Ge
		[34] AJELLO	11	FLAT	
$<3 \times 10^{-8}$	90	[35] APRILE	11	X100	Xe
		[36] APRILE	11A	X100	Xe, inelastic
$<1 \times 10^{-8}$	90	[30] APRILE	11B	X100	Xe
$<5 \times 10^{-8}$	90	[37] ARMENGAUD	11	EDE2	Ge
		[38] HORN	11	ZEP3	Xe
$<4 \times 10^{-8}$	90	AHMED	10	CDM2	Ge
$<9 \times 10^{-6}$	90	AKERIB	10	CDM2	Si, Ge, low threshold
		[39] AKIMOV	10	ZEP3	Xe, inelastic
$<5 \times 10^{-8}$	90	APRILE	10	X100	Xe
$<1 \times 10^{-7}$	90	ARMENGAUD	10	EDE2	Ge
$<3 \times 10^{-5}$	90	FELIZARDO	10	SMPL	C_2ClF_3
$<5 \times 10^{-8}$	90	[40] AHMED	09	CDM2	Ge
		[41] ANGLE	09	XE10	Xe, inelastic
$<3 \times 10^{-4}$	90	LIN	09	TEXO	Ge
		[42] GIULIANI	05	RVUE	

Downloaded from https://academic.oup.com/ptep/article/2022/8/083C01/6651666 by KIT Library user on 27 September 2022

[1] MENG 21B search for SI WIMP interaction with 3.7 t Xe and 0.63 t yr exposure. No signal observed. Limits placed in m(DM) vs. σ^{SI} plane.
[2] ADHIKARI 20 search for SI WIMP scatter from Ar in AJAJ 19 data. No signal observed. Limits placed on σ^{p} vs. m(WIMP) for various assumed operators and models.
[3] FELIZARDO 20 presents 2014 SIMPLE bounds on WIMP DM using C_2ClF_5 target .
[4] WANG 20G search for SI WIMP scatter on Xe with 132 t d exposure of PANDAX-II .
[5] ABE 19 search for SI DD in single phase Xe; no signal; require $\sigma^{SI}(\chi p) < 4 \times 10^{-8}$ pb for m(χ) $\sim$ 100 GeV.
[6] AJAJ 19 search for SI WIMP-nucleon scatter with 758 tonne day exposure of single phase liquid Ar; no signal: require $\sigma^{SI}(\chi N) < 3.9 \times 10^{-9}$ pb for m(χ) = 100 GeV.
[7] ADHIKARI 18 search for WIMP scatter on NaI;limit set $\sigma^{SI}(\chi p) < 2.3 \times 10^{-6}$ pb for m(χ) = 100 GeV.
[8] AGNES 18A search for WIMP scatter on 46.4 kg Ar; no signal; require $\sigma^{SI}(\chi N) < 1.14 \times 10^{-8}$ pb for m(χ) = 100 GeV.
[9] AGNESE 18A set limit $\sigma^{SI}(\chi N) < 2 \times 10^{-8}$ pb for m(WIMP) = 100 GeV.
[10] AMAUDRUZ 18 search for WIMP scatter on Ar with DEAP-3600; limits set: $\sigma^{SI}(\chi p) < 1.2 \times 10^{-8}$ pb for m(WIMP) = 100 GeV.
[11] APRILE 18 search for WIMP scatter on 1.3 t liquid Xe; no signal; require $\sigma^{SI}(\chi p) < 9.12 \times 10^{-11}$ pb for m(χ) = 100 GeV.
[12] REN 18 search for self-interacting DM at Panda-X-II with a total exposure of 54 ton day; limits set in m(DM) vs. m(mediator) plane.
[13] AKERIB 17 exclude SI cross section $> 1.7 \times 10^{-10}$ pb for m(WIMP) = 100 GeV. Uses complete LUX data set.
[14] APRILE 17G set limit $\sigma^{SI}(\chi p) < 1.2\ 10^{-10}$ pb for m(WIMP) = 100 GeV using 1 ton fiducial mass Xe TPC. Exposure is 34.2 live days.
[15] CUI 17A search for SI WIMP scatter; limits placed in $\sigma^{SI}(\chi N)$ vs. m(χ) plane for m $\sim$ 10–1 $\times 10^4$ GeV using 54 ton-day exposure of Xe.
[16] AKERIB 16 re-analysis of 2013 data exclude SI cross section $> 1\times10^{-9}$ pb for m(WIMP) = 100 GeV on Xe target.
[17] APRILE 16B combined 447 live days using Xe target exclude σ(SI) $> 1.1 \times 10^{-9}$ pb for m(WIMP) = 50 GeV.
[18] TAN 16 search for WIMP scatter off Xe target; see SI exclusion plot Fig. 6.
[19] TAN 16B search for WIMP-p scatter off Xe target; see Fig. 5 for SI exclusion.
[20] AGNESE 15B reanalyse AHMED 10 data.
[21] XIAO 15 search for WIMP scatter on Xe with PandaX-I; limits placed in $\sigma^{SI}(\chi N)$ vs. m(χ) plane for m(χ) $\sim$ 5–100 GeV.
[22] AVRORIN 14 search for neutrinos from the Sun arising from the pair annihilation of X^0 trapped by the Sun in data taken between 1998 and 2003. See their Table 1 for limits assuming annihilation into neutrino pairs.
[23] AARTSEN 13 search for neutrinos from the Sun arising from the pair annihilation of X^0 trapped by the sun in data taken between June 2010 and May 2011.
[24] ADRIAN-MARTINEZ 13 search for neutrinos from the Sun arising from the pair annihilation of X^0 trapped by the sun in data taken between Jan. 2007 and Dec. 2008.
[25] AGNESE 13 use data taken between Oct. 2006 and July 2007.
[26] BOLIEV 13 search for neutrinos from the Sun arising from the pair annihilation of X^0 trapped by the sun in data taken from 1978 to 2009. See also SUVOROVA 13 for an older analysis of the same data.
[27] LI 13B search for WIMP scatter on Ge; limits placed in $\sigma^{SI}(\chi N)$ vs. m(χ) plane for m(χ) $\sim$ 4–100 GeV.
[28] ABBASI 12 search for neutrinos from the Sun arising from the pair annihilation of X^0 trapped by the Sun. The amount of X^0 depends on the X^0-proton cross section.
[29] Reanalysis of ANGLOHER 09 data with all three nuclides. See also BROWN 12.
[30] See also APRILE 14A.
[31] See their Fig. 6 for a limit on inelastically scattering X^0 for m_{X^0} = 70 GeV.
[32] AHMED 11 search for X^0 inelastic scattering. See their Fig. 8–10 for limits.
[33] AHMED 11A combine CDMS and EDELWEISS data.
[34] AJELLO 11 search for $e^{\pm}$ flux from X^0 annihilations in the Sun. Models in which X^0 annihilates into an intermediate long-lived weakly interacting particles or X^0 scatters inelastically are constrained. See their Fig. 6–8 for limits.
[35] APRILE 11 reanalyze APRILE 10 data.
[36] APRILE 11A search for X^0 inelastic scattering. See their Fig. 2 and 3 for limits. See also APRILE 14A.
[37] Supersedes ARMENGAUD 10. A limit on inelastic cross section is also given.
[38] HORN 11 perform detector calibration by neutrons. Earlier results are only marginally affected.
[39] AKIMOV 10 give cross section limits for inelastically scattering dark matter. See their Fig. 4.
[40] Superseded by AHMED 10.
[41] ANGLE 09 search for X^0 inelastic scattering. See their Fig. 4 for limits.
[42] GIULIANI 05 analyzes the spin-independent X^0-nucleon cross section limits with both isoscalar and isovector couplings. See their Fig. 3 and 4 for limits on the couplings.

For m_{X^0} = 1 TeV

For limits from X^0 annihilation in the Sun, the assumed annihilation final state is shown in parenthesis in the comment.

VALUE (pb)	CL%	DOCUMENT ID		TECN	COMMENT
• • • We do not use the following data for averages, fits, limits, etc. • • •					
$<5 \times 10^{-10}$	90	[1] MENG	21B	PNDX	Xe WIMP search
		[2] ADHIKARI	20	DEAP	Ar
$<4 \times 10^{-9}$	90	[3] WANG	20G	PNDX	Xe TPC
$<3 \times 10^{-6}$	90	[4] YAGUNA	19		Ar; I-spin viol DM
$<3.8 \times 10^{-8}$	90	[5] AGNES	18A	DS50	Ar
$<8.24 \times 10^{-10}$	90	[6] APRILE	18	XE1T	Xe
$<2 \times 10^{-9}$	90	[7] AKERIB	17	LUX	Xe
<0.3	90	[8] CHEN	17E	PNDX	$\chi N \rightarrow \chi^* \rightarrow \chi\gamma$
$<1.2 \times 10^{-9}$	90	[9] CUI	17A	PNDX	SI WIMPs on Xe
$<8.6 \times 10^{-8}$	90	AGNES	16	DS50	Ar
$<2 \times 10^{-7}$	90	AGNES	15	DS50	Ar
$<2 \times 10^{-7}$	90	[10] AGNESE	15B	CDM2	Ge
$<1 \times 10^{-8}$	90	AKERIB	14	LUX	Xe
$<2.2 \times 10^{-6}$	90	[11] AVRORIN	14	BAIK	H, solar ν (W^+W^-)
$<5.5 \times 10^{-5}$	90	[11] AVRORIN	14	BAIK	H, solar ν ($b\overline{b}$)
$<6.8 \times 10^{-7}$	90	[11] AVRORIN	14	BAIK	H, solar ν ($\tau^+\tau^-$)
$<3.46 \times 10^{-7}$	90	[12] AARTSEN	13	ICCB	H, solar ν (W^+W^-)
$<7.75 \times 10^{-6}$	90	[12] AARTSEN	13	ICCB	H, solar ν ($b\overline{b}$)
$<6.9 \times 10^{-7}$	90	[13] ADRIAN-MAR..	13	ANTR	H, solar ν (W^+W^-)
$<1.5 \times 10^{-5}$	90	[13] ADRIAN-MAR..	13	ANTR	H, solar ν ($b\overline{b}$)
$<1.8 \times 10^{-7}$	90	[13] ADRIAN-MAR..	13	ANTR	H, solar ν ($\tau^+\tau^-$)
$<4.3 \times 10^{-6}$	90	[14] BOLIEV	13	BAKS	H, solar ν (W^+W^-)
$<3.4 \times 10^{-5}$	90	[14] BOLIEV	13	BAKS	H, solar ν ($b\overline{b}$)
$<1.2 \times 10^{-6}$	90	[14] BOLIEV	13	BAKS	H, solar ν ($\tau^+\tau^-$)
$<2.12 \times 10^{-7}$	90	[15] ABBASI	12	ICCB	H, solar ν (W^+W^-)
$<6.56 \times 10^{-6}$	90	[15] ABBASI	12	ICCB	H, solar ν ($b\overline{b}$)
$<4 \times 10^{-7}$	90	AKIMOV	12	ZEP3	Xe
$<1.1 \times 10^{-5}$	90	[16] ANGLOHER	12	CRES	$CaWO_4$
$<2 \times 10^{-8}$	90	[17] APRILE	12	X100	Xe
$<2 \times 10^{-6}$	90	BEHNKE	12	COUP	CF_3I
$<4 \times 10^{-6}$		FELIZARDO	12	SMPL	C_2ClF_5
$<1.5 \times 10^{-6}$	90	KIM	12	KIMS	CsI
		[18] AHMED	11	CDM2	Ge, inelastic
$<1.5 \times 10^{-7}$	90	[19] AHMED	11A	RVUE	Ge
$<2 \times 10^{-7}$	90	[20] APRILE	11	X100	Xe
$<8 \times 10^{-8}$	90	[17] APRILE	11B	X100	Xe
$<2 \times 10^{-7}$	90	[21] ARMENGAUD	11	EDE2	Ge
		[22] HORN	11	ZEP3	Xe
$<2 \times 10^{-7}$	90	AHMED	10	CDM2	Ge
$<4 \times 10^{-7}$	90	APRILE	10	X100	Xe
$<6 \times 10^{-7}$	90	ARMENGAUD	10	EDE2	Ge
$<3.5 \times 10^{-7}$	90	[23] AHMED	09	CDM2	Ge

[1] MENG 21B search for SI WIMP interaction with 3.7 t Xe and 0.63 t yr exposure. No signal observed. Limits placed in m(DM) vs. σ^{SI} plane.
[2] ADHIKARI 20 search for SI WIMP scatter from Ar in AJAJ 19 data. No signal observed. Limits placed on σ^{p} vs. m(WIMP) for various assumed operators and models.
[3] WANG 20G search for SI WIMP scatter on Xe with 132 t d exposure of PANDAX-II .
[4] YAGUNA 19 recasts DEAP-3600 single-phase liquid argon results in limit for isospin violating DM; for $f_n/f_p = -0.69$, requires $\sigma^{SI}(\chi p) < 3 \times 10^{-6}$ pb for m(χ) = 1 TeV.
[5] AGNES 18A search for WIMP scatter on 46.4 kg Ar; no signal; require $\sigma^{SI}(\chi N) < 3.8 \times 10^{-8}$ pb for m(χ) = 1 TeV.
[6] APRILE 18 search for WIMP scatter on 1.3 t Xe; no signal seen; require $\sigma^{SI}(\chi p) < 8.24 \times 10^{-10}$ pb for m(χ) = 1 TeV.
[7] AKERIB 17 search for WIMP scatter on Xe using complete LUX data set; limits placed in $\sigma^{SI}(\chi N)$ vs. m(χ) plane for m(χ) $\sim$ 5–1 $\times 10^5$ GeV.
[8] CHEN 17E search for inelastic WIMP scatter on Xe; require $\sigma^{SI}(\chi N) < 0.3$ pb for m(χ) = 1 TeV and (mass difference) = 300 keV.
[9] CUI 17A search for WIMP scatter using 54 ton-day exposure of Xe; limits placed in $\sigma^{SI}(\chi N)$ vs. m(χ) plane for m $\sim$ 10–1 $\times 10^4$ GeV.
[10] AGNESE 15B reanalyse AHMED 10 data.
[11] AVRORIN 14 search for neutrinos from the Sun arising from the pair annihilation of X^0 trapped by the Sun in data taken between 1998 and 2003. See their Table 1 for limits assuming annihilation into neutrino pairs.
[12] AARTSEN 13 search for neutrinos from the Sun arising from the pair annihilation of X^0 trapped by the sun in data taken between June 2010 and May 2011.
[13] ADRIAN-MARTINEZ 13 search for neutrinos from the Sun arising from the pair annihilation of X^0 trapped by the sun in data taken between Jan. 2007 and Dec. 2008.
[14] BOLIEV 13 search for neutrinos from the Sun arising from the pair annihilation of X^0 trapped by the sun in data taken from 1978 to 2009. See also SUVOROVA 13 for an older analysis of the same data.
[15] ABBASI 12 search for neutrinos from the Sun arising from the pair annihilation of X^0 trapped by the Sun. The amount of X^0 depends on the X^0-proton cross section.
[16] Reanalysis of ANGLOHER 09 data with all three nuclides. See also BROWN 12.
[17] See also APRILE 14A.
[18] AHMED 11 search for X^0 inelastic scattering. See their Fig. 8–10 for limits.
[19] AHMED 11A combine CDMS and EDELWEISS data.
[20] APRILE 11 reanalyze APRILE 10 data.
[21] Supersedes ARMENGAUD 10. A limit on inelastic cross section is also given.
[22] HORN 11 perform detector calibration by neutrons. Earlier results are only marginally affected.
[23] Superseded by AHMED 10.

Spin-Dependent Cross Section Limits for Dark Matter Particle (X^0) on Proton

For m_{X^0} in GeV range

We provide here limits fo m_{X^0} < 5 GeV

VALUE (pb)	CL%	DOCUMENT ID		TECN	COMMENT
• • • We do not use the following data for averages, fits, limits, etc. • • •					
$< 8 \times 10^4$	90	[1] ABDELHAME..	20A	CRES	$LiAlO_2$
$< 1 \times 10^6$	95	[2] ABDELHAME..	19	CRES	GeV-scale WIMPs on Li
$< 3 \times 10^{-4}$	90	[3] AMOLE	19	PICO	C_3F_8
$< 1.7 \times 10^4$	90	[4] APRILE	19C	XE1T	light DM on Xe via Migdal/brem effect
$< 8 \times 10^6$	90	[5] ARMENGAUD	19	EDEL	GeV-scale WIMPs on Ge
< 70	90	[6] XIA	19A	PNDX	SD WIMP on Xe
<100	90	[7] AGNESE	18	SCDM	GeV-scale WIMPs on Ge
< 1	90	[8] AKERIB	17A	LUX	Xe
< 0.6	90	[9] FU	17	PNDX	SD WIMP on Xe
< 0.2	90	[10] AMOLE	15	PICO	C_3F_8
$< 1.6 \times 10^{-1}$	90	[11] ARCHAMBAU..	12	PICA	^{19}F

Downloaded from https://academic.oup.com/ptep/article/2022/8/083C01/6651666 by KIT Library user on 27 September 2022

[1] ABDELHAMEED 20A use $LiAlO_2$ target in CRESST to search for SD WIMP scatter on p; no signal; quoted limit is for m(DM) = 1 GeV.

[2] ABDELHAMEED 19 search for SD WIMP scatter on ^{7}Li; limits placed on $\sigma^{SD}(\chi p)$ for m(χ) ~ 0.8–20 GeV; quoted limit is for m(χ) = 1 GeV.

[3] AMOLE 19 search for SD WIMP scatter on C_3F_8 in PICO-60 bubble chamber; no signal: set limit for spin dependent coupling $\sigma^{SD}(\chi p) < 2 \times 10^{-4}$ pb for m(χ) = 5 GeV.

[4] APRILE 19C search for light DM on Xe via Migdal/brem effect; no signal, require $\sigma^{SD}(\chi p) < 1.7 \times 10^4$ pb for m(χ) = 1 GeV.

[5] ARMENGAUD 19 search for GeV scale WIMP scatter on Ge; limits placed in $\sigma^{SD}(\chi p)$ vs. m(χ) plane for m(χ) ~ 0.5–10 GeV; quoted limit is for m(χ) = 5 GeV.

[6] XIA 19A search for WIMP scatter on Xe in PandaX-II; limits placed in $\sigma^{SD}(\chi p)$ vs. m(χ) plane for m(χ) ~ 5–1 × 10^5 GeV; quoted limit is for m(χ) = 5 GeV.

[7] AGNESE 18 search for GeV scale WIMPs with CDMSlite; limits placed in $\sigma^{SD}(\chi p)$ vs. m(χ) plane for m(χ) ~ 1.5–20 GeV; quoted limit is for m(χ) = 5 GeV.

[8] AKERIB 17A search for SD WIMP scatter on Xe using 129.5 kg yr exposure; limits placed in $\sigma^{SD}(\chi p)$ vs. m(χ) plane for m(χ) ~ 6–1 × 10^5 GeV.

[9] FU 17 search for SD WIMP scatter on Xe; limits set in $\sigma^{SD}(\chi p)$ vs. m(χ) plane for m(χ) ~ 4–1 × 10^3 GeV.; quoted limit is for m(χ) = 5 GeV.

[10] AMOLE 15 search for WIMP scatter on C_3F_8 in PICO-2L; limits placed in $\sigma^{SD}(\chi p)$ vs. m(χ) plane for m(χ) ~ 4–1 × 10^4 GeV; quoted limit is for m(χ) = 5 GeV.

[11] ARCHAMBAULT 12 search for SD WIMP scatter in ^{19}F with PICASSO; limits set in $\sigma^{SD}(\chi p)$ vs. m(χ) plane for m ~ 4–500 GeV; quoted limit is for m(χ) = 5 GeV.

For m_{X^0} = 20 GeV

For limits from X^0 annihilation in the Sun, the assumed annihilation final state is shown in parenthesis in the comment.

VALUE (pb)	CL%	DOCUMENT ID		TECN	COMMENT
• • • We do not use the following data for averages, fits, limits, etc. • • •					
< 9 × 10^{-5}	90	[1] AARTSEN	20C	ICCB	SD WIMP on p
< 2 × 10^5	90	[2] ABDELHAME..	20A	CRES	$LiAlO_2$
< 5 × 10^{-3}		[3] FELIZARDO	20	SMPL	WIMPs via SIMPLE
< 3 × 10^5	95	[4] ABDELHAME..	19	CRES	^{7}Li
< 2.5 × 10^{-5}	90	[5] AMOLE	19	PICO	C_3F_8
< 2.5 × 10^{-4}	90	[6] APRILE	19A	XE1T	Xe, SD
< 1 × 10^{-3}	90	[7] XIA	19A	PNDX	SD WIMP on Xe
< 30	95	[8] AGNESE	18	SCDM	Ge
< 1 × 10^{-3}	90	[9] AKERIB	17A	LUX	Xe
< 1.32 × 10^{-2}	90	[10] BEHNKE	17	PICA	C_4F_{10}
< 2 × 10^{-3}	90	[11] FU	17	PNDX	SD WIMP on Xe
< 5 × 10^{-4}	90	[12] AMOLE	16A	PICO	C_3F_8
< 2 × 10^{-6}	90	[13] KHACHATRY..	16AJ	CMS	8 TeV $pp \to Z + \not{E}_T$; $Z \to \ell\overline{\ell}$
< 1.2 × 10^{-3}	90	AMOLE	15	PICO	C_3F_8
< 1.43 × 10^{-3}	90	CHOI	15	SKAM	H, solar ν ($b\overline{b}$)
< 1.42 × 10^{-4}	90	CHOI	15	SKAM	H, solar ν ($\tau^+\tau^-$)
< 5 × 10^{-3}	90	FELIZARDO	14	SMPL	C_2ClF_5
< 1.29 × 10^{-2}	90	[14] AARTSEN	13	ICCB	H, solar ν ($\tau^+\tau^-$)
< 3.17 × 10^{-2}	90	[15] APRILE	13	X100	Xe
< 3 × 10^{-2}	90	[16] ARCHAMBAU..	12	PICA	F (C_4F_{10})
< 6 × 10^{-2}	90	BEHNKE	12	COUP	CF_3I
< 20	90	DAW	12	DRFT	F (CF_4)
< 7 × 10^{-3}		FELIZARDO	12	SMPL	C_2ClF_5
< 0.15	90	KIM	12	KIMS	CsI
< 1 × 10^5	90	[17] AHLEN	11	DMTP	F (CF_4)
< 0.1	90	[17] BEHNKE	11	COUP	CF_3I
< 1.5 × 10^{-2}	90	[18] TANAKA	11	SKAM	H, solar ν ($b\overline{b}$)
< 0.2	90	ARCHAMBAU..	09	PICA	F
< 4	90	LEBEDENKO	09A	ZEP3	Xe
< 0.6	90	ANGLE	08A	XE10	Xe
<100	90	ALNER	07	ZEP2	Xe
< 1	90	LEE	07A	KIMS	CsI
< 20	90	[19] AKERIB	06	CDMS	^{73}Ge, ^{29}Si
< 2	90	SHIMIZU	06A	CNTR	F (CaF_2)
< 0.5	90	ALNER	05	NAIA	NaI
< 1.5	90	BARNABE-HE..	05	PICA	F (C_4F_{10})
< 1.5	90	GIRARD	05	SMPL	F (C_2ClF_5)
< 35	90	MIUCHI	03	BOLO	LiF
< 30	90	TAKEDA	03	BOLO	NaF

[1] AARTSEN 20C place combined IceCube and Pico-60 velocity-independent limits on spin-dependent WIMP-p scatter $\sigma^{SD}(\chi p)$< 9–5 pb for m(WIMP) = 20 GeV assuming dominant annihilation to $\tau\overline{\tau}$.

[2] ABDELHAMEED 20A use $LiAlO_2$ target in CRESST to search for spin-dependent WIMP scatter on p; limits set for m(WIMP): 0.3–30 GeV in Fig. 8. Quoted limit is for M(WIMP) = 30 GeV.

[3] FELIZARDO 20 presents 2014 SIMPLE bounds on WIMP DM using C_2ClF_5 target .

[4] ABDELHAMEED 19 uses Li_2MoO_4 target to set limit for spin dependent coupling $\sigma^{SD}(\chi p) <$ 3. × 10^5 pb for m(χ) = 20 GeV.

[5] AMOLE 19 search for SD WIMP scatter on C_3F_8 in PICO-60 bubble chamber; no signal: set limit for spin dependent coupling $\sigma^{SD}(\chi p) < 2.5 \times 10^{-5}$ pb for m(χ) = 20 GeV.

[6] APRILE 19A search for SD WIMP scatter on 1 t yr Xe; no signal, limits placed in $\sigma^{SD}(\chi p)$ vs. m(χ) plane for m ~ 6–1000 GeV.

[7] XIA 19A search for WIMP scatter on Xe in PandaX-II; limits placed in $\sigma^{SD}(\chi p)$ vs. m(χ) plane for m(χ) ~ 5–1 × 10^5 GeV.

[8] AGNESE 18 give limits for $\sigma^{SD}(p\chi)$ for m(WIMP) between 1.5 and 20 GeV using CDMSlite mode data.

[9] AKERIB 17A search for SD WIMP scatter on Xe using 129.5 kg yr exposure; limits placed in $\sigma^{SD}(\chi p)$ vs. m(χ) plane for m(χ) ~ 6–1 × 10^5 GeV.

[10] BEHNKE 17 show final Picasso results based on 231.4 kg d exposure at SNOLab for WIMP scatter on C_4F_{10} search via superheated droplet; require σ(SD) < 1.32 × 10^{-2} pb for m(WIMP) = 20 GeV.

[11] FU 17 search for SD WIMP scatter on Xe; limits set in $\sigma^{SD}(\chi p)$ vs. m(χ) plane for m(χ) ~ 4–1 × 10^3 GeV.

[12] AMOLE 16A require SD WIMP-p scattering < 5 × 10^{-4} pb for m(WIMP) = 20 GeV; bubbles from C_3F_8 target.

[13] KHACHATRYAN 16AJ require SD WIMP-p < 2 × 10^{-6} pb for m(WIMP) = 20 GeV from $pp \to Z + \not{E}_T$; $Z \to \ell\overline{\ell}$ signal.

[14] AARTSEN 13 search for neutrinos from the Sun arising from the pair annihilation of X^0 trapped by the sun in data taken between June 2010 and May 2011.

[15] The value has been provided by the authors. APRILE 13 note that the proton limits on Xe are highly sensitive to the theoretical model used. See also APRILE 14A.

[16] ARCHAMBAULT 12 search for WIMP scatter on C_4F_{10}; limits set in $\sigma^{SD}(\chi p)$ vs. m(χ) plane for m ~ 4–500 GeV.

[17] Use a direction-sensitive detector.

[18] TANAKA 11 search for neutrinos from the Sun arising from the pair annihilation of X^0 trapped by the Sun. The amount of X^0 depends on the X^0-proton cross section.

[19] See also AKERIB 05.

For m_{X^0} = 100 GeV

For limits from X^0 annihilation in the Sun, the assumed annihilation final state is shown in parenthesis in the comment.

VALUE (pb)	CL%	DOCUMENT ID		TECN	COMMENT
• • • We do not use the following data for averages, fits, limits, etc. • • •					
< 50	90	[1] IKEDA	21	NAGE	directional gas TPC
< 3.34 × 10^{-4}	90	[2] AARTSEN	20C	ICCB	SD WIMP on p
< 6.5 × 10^{-3}		[3] FELIZARDO	20	SMPL	WIMPs via SIMPLE
< 4 × 10^{-5}	90	[4] AMOLE	19	PICO	C_3F_8
< 4 × 10^{-4}	90	[5] APRILE	19A	XE1T	Xe, SD
< 8 × 10^{-4}	90	[6] XIA	19A	PNDX	SD WIMP on Xe
< 8 × 10^{-4}	90	[7] AKERIB	17A	LUX	Xe
< 5 × 10^{-5}	90	[8] AMOLE	17	PICO	C_3F_8
< 3.3 × 10^{-2}	90	[9] APRILE	17A	X100	Xe inelastic
< 2.8 × 10^{-1}	90	[10] BATTAT	17	DRFT	CS_2
< 1.5 × 10^{-3}	90	[11] FU	17	PNDX	Xe
< 0.553–0.019	95	[12] AABOUD	16D	ATLS	$pp \to j + \not{E}_T$
< 1 × 10^{-5}	90	[13] AABOUD	16F	ATLS	$pp \to \gamma + \not{E}_T$
< 1 × 10^{-4}	90	[14] AARTSEN	16C	ICCB	solar ν (W^+W^-)
< 2 × 10^{-4}	90	[15] ADRIAN-MAR..	16	ANTR	solar ν (WW, $b\overline{b}$, $\tau\overline{\tau}$)
< 3 × 10^{-3}	90	[16] AKERIB	16A	LUX	Xe
< 5 × 10^{-4}	90	[17] AMOLE	16	PICO	CF_3I
< 1.5 × 10^{-3}	90	AMOLE	15	PICO	C_3F_8
< 3.19 × 10^{-3}	90	CHOI	15	SKAM	H, solar ν ($b\overline{b}$)
< 2.80 × 10^{-4}	90	CHOI	15	SKAM	H, solar ν (W^+W^-)
< 1.24 × 10^{-4}	90	CHOI	15	SKAM	H, solar ν ($\tau^+\tau^-$)
< 8 × 10^2	90	[18] NAKAMURA	15	NAGE	CF_4
< 1.7 × 10^{-3}	90	[19] AVRORIN	14	BAIK	H, solar ν (W^+W^-)
< 4.5 × 10^{-2}	90	[19] AVRORIN	14	BAIK	H, solar ν ($b\overline{b}$)
< 7.1 × 10^{-4}	90	[19] AVRORIN	14	BAIK	H, solar ν ($\tau^+\tau^-$)
< 6 × 10^{-3}	90	FELIZARDO	14	SMPL	C_2ClF_5
< 2.68 × 10^{-4}	90	[20] AARTSEN	13	ICCB	H, solar ν (W^+W^-)
< 1.47 × 10^{-2}	90	[20] AARTSEN	13	ICCB	H, solar ν ($b\overline{b}$)
< 8.5 × 10^{-4}	90	[21] ADRIAN-MAR..	13	ANTR	H, solar ν (W^+W^-)
< 5.5 × 10^{-2}	90	[21] ADRIAN-MAR..	13	ANTR	H, solar ν ($b\overline{b}$)
< 3.4 × 10^{-4}	90	[21] ADRIAN-MAR..	13	ANTR	H, solar ν ($\tau^+\tau^-$)
< 1.00 × 10^{-2}	90	[22] APRILE	13	X100	Xe
< 7.1 × 10^{-4}	90	[23] BOLIEV	13	BAKS	H, solar ν (W^+W^-)
< 8.4 × 10^{-3}	90	[23] BOLIEV	13	BAKS	H, solar ν ($b\overline{b}$)
< 3.1 × 10^{-4}	90	[23] BOLIEV	13	BAKS	H, solar ν ($\tau^+\tau^-$)
< 7.07 × 10^{-4}	90	[24] ABBASI	12	ICCB	H, solar ν (W^+W^-)
< 4.53 × 10^{-2}	90	[24] ABBASI	12	ICCB	H, solar ν ($b\overline{b}$)
< 7 × 10^{-2}	90	[25] ARCHAMBAU..	12	PICA	F (C_4F_{10})
< 1 × 10^{-2}	90	BEHNKE	12	COUP	CF_3I
< 1.8	90	DAW	12	DRFT	F (CF_4)
< 9 × 10^{-3}		FELIZARDO	12	SMPL	C_2ClF_5
< 2 × 10^{-2}	90	KIM	12	KIMS	CsI
< 2 × 10^3	90	[18] AHLEN	11	DMTP	F (CF_4)
< 7 × 10^{-2}	90	BEHNKE	11	COUP	CF_3I
< 2.7 × 10^{-4}	90	[26] TANAKA	11	SKAM	H, solar ν (W^+W^-)
< 4.5 × 10^{-3}	90	[26] TANAKA	11	SKAM	H, solar ν ($b\overline{b}$)
		[27] FELIZARDO	10	SMPL	C_2ClF_3
< 6 × 10^3	90	[18] MIUCHI	10	NAGE	CF_4
< 0.4	90	ARCHAMBAU..	09	PICA	F
< 0.8	90	LEBEDENKO	09A	ZEP3	Xe
< 1.0	90	ANGLE	08A	XE10	Xe
< 15	90	ALNER	07	ZEP2	Xe
< 0.2	90	LEE	07A	KIMS	CsI
< 1 × 10^4	90	[18] MIUCHI	07	NAGE	F (CF_4)
< 5	90	[28] AKERIB	06	CDMS	^{73}Ge, ^{29}Si
< 2	90	SHIMIZU	06A	CNTR	F (CaF_2)
< 0.3	90	ALNER	05	NAIA	NaI
< 2	90	BARNABE-HE..	05	PICA	F (C_4F_{10})

Downloaded from https://academic.oup.com/ptep/article/2022/8/083C01/6651666 by KIT Library user on 27 September 2022

<100	90	BENOIT	05	EDEL	^{73}Ge
< 1.5	90	GIRARD	05	SMPL	F (C_2ClF_5)
< 0.7		[29] GIULIANI	05A	RVUE	
		[30] GIULIANI	04	RVUE	
		[31] GIULIANI	04A	RVUE	
< 35	90	MIUCHI	03	BOLO	LiF
< 40	90	TAKEDA	03	BOLO	NaF

[1] IKEDA 21 use direction sensitive TPC NEWAGE to search for SD WIMPs. No signal observed. Limits set in $\sigma^{SD}(\chi p)$ vs. m plane; $\sigma^{SD}(\chi p) < 50$ pb for m(DM) = 100 GeV.
[2] AARTSEN 20C place combined IceCube and Pico-60 velocity-independent limits on spin-dependent WIMP-p scatter $\sigma^{SD}(\chi p) < 3.34 \times 10^{-4}$ pb for m(WIMP) = 100 GeV assuming dominant annihilation to $\tau\overline{\tau}$.
[3] FELIZARDO 20 presents 2014 SIMPLE bounds on WIMP DM using C_2ClF_5 target .
[4] AMOLE 19 search for SD WIMP scatter on C_3F_8 in PICO-60 bubble chamber; no signal: set limit for spin dependent coupling $\sigma^{SD}(\chi p) < 4 \times 10^{-5}$ pb for m(χ) = 100 GeV.
[5] APRILE 19A search for SD WIMP scatter on 1 t yr Xe; no signal, limits placed in $\sigma^{SD}(\chi p)$ vs. m(χ) plane for m $\sim$ 6–1000 GeV.
[6] XIA 19A search for WIMP scatter on Xe in PandaX-II; limits placed in $\sigma^{SD}(\chi p)$ vs. m(χ) plane for m(χ) $\sim$ 5–1 $\times 10^5$ GeV.
[7] AKERIB 17A search for SD WIMP scatter on Xe using 129.5 kg yr exposure; limits placed in $\sigma^{SD}(\chi p)$ vs. m(χ) plane for m(χ) $\sim$ 6–1 $\times 10^5$ GeV.
[8] AMOLE 17 require σ(WIMP-p)^{SD} $< 5 \times 10^{-5}$ pb for m(WIMP) = 100 GeV using PICO-60 1167 kg-days exposure at SNOLab.
[9] APRILE 17A require require σ(WIMP-p)(inelastic)^{SD} $< 3.3 \times 10^{-2}$ pb for m(WIMP) = 100 GeV, based on 7640 kg day exposure at LNGS.
[10] BATTAT 17 use directional detection of CS_2 ions to require σ(SD) $< 2.8 \times 10^{-1}$ pb for 100 GeV WIMP with a 55 days exposure at the Boulby Underground Science Facility.
[11] FU 17 from a 33000 kg d exposure at CJPL, PANDAX II derive for m(DM) = 100 GeV, σ^{SD}(WIMP-p) $< 2 \times 10^{-3}$ pb.
[12] AABOUD 16D use ATLAS 13 TeV 3.2 fb^{-1} of data to search for monojet plus missing E_T; agree with SM rates; present limits on large extra dimensions, compressed SUSY spectra and wimp pair production.
[13] AABOUD 16F search for monophoton plus missing E_T events at ATLAS with 13 Tev and 3.2 fb^{-1}; signal agrees with SM background; place limits on SD WIMP-proton scattering vs. mediator mass and large extra dimension models.
[14] AARTSEN 16C search for high energy νs from WIMP annihilation in solar core; limits set on SD WIMP-p scattering (Fig. 8).
[15] ADRIAN-MARTINEZ 16 search for WIMP annihilation into νs from solar core; exclude SD cross section < few 10^{-4} depending on m(WIMP).
[16] AKERIB 16A using 2013 data exclude SD WIMP-proton scattering > 3×10^{-3} pb for m(WIMP) = 100 GeV.
[17] AMOLE 16 use bubble technique on CF_3I target to exclude SD WIMP-p scattering > 5×10^{-4} pb for m(WIMP) = 100 GeV.
[18] Use a direction-sensitive detector.
[19] AVRORIN 14 search for neutrinos from the Sun arising from the pair annihilation of X^0 trapped by the Sun in data taken between 1998 and 2003. See their Table 1 for limits assuming annihilation into neutrino pairs.
[20] AARTSEN 13 search for neutrinos from the Sun arising from the pair annihilation of X^0 trapped by the sun in data taken between June 2010 and May 2011.
[21] ADRIAN-MARTINEZ 13 search for neutrinos from the Sun arising from the pair annihilation of X^0 trapped by the sun in data taken between Jan. 2007 and Dec. 2008.
[22] The value has been provided by the authors. APRILE 13 note that the proton limits on Xe are highly sensitive to the theoretical model used. See also APRILE 14A.
[23] BOLIEV 13 search for neutrinos from the Sun arising from the pair annihilation of X^0 trapped by the sun in data taken from 1978 to 2009. See also SUVOROVA 13 for an older analysis of the same data.
[24] ABBASI 12 search for neutrinos from the Sun arising from the pair annihilation of X^0 trapped by the Sun. The amount of X^0 depends on the X^0-proton cross section.
[25] ARCHAMBAULT 12 search for WIMP scatter on C_4F_{10}; limits set in $\sigma^{SD}(\chi p)$ vs. m(χ) plane for m $\sim$ 4–500 GeV.
[26] TANAKA 11 search for neutrinos from the Sun arising from the pair annihilation of X^0 trapped by the Sun. The amount of X^0 depends on the X^0-proton cross section.
[27] See their Fig. 3 for limits on spin-dependent proton couplings for X^0 mass of 50 GeV.
[28] See also AKERIB 05.
[29] GIULIANI 05A analyze available data and give combined limits.
[30] GIULIANI 04 reanalyze COLLAR 00 data and give limits for spin-dependent X^0-proton coupling.
[31] GIULIANI 04A give limits for spin-dependent X^0-proton couplings from existing data.

For m_{X^0} = 1 TeV

For limits from X^0 annihilation in the Sun, the assumed annihilation final state is shown in parenthesis in the comment.

VALUE (pb)	CL%	DOCUMENT ID		TECN	COMMENT
• • • We do not use the following data for averages, fits, limits, etc. • • •					
<200	90	[1] IKEDA	21	NAGE	directional gas TPC
< 4.81×10^{-3}	90	[2] AARTSEN	20C	ICCB	SD WIMP on p
< 3×10^{-4}	90	[3] AMOLE	19	PICO	C_3F_8
< 4×10^{-3}	90	[4] APRILE	19A	XE1T	Xe, SD
< 5×10^{-3}	90	[5] XIA	19A	PNDX	SD WIMP on Xe
		[6] ALBERT	18C	HAWC	DM annihilation in Sun to long-lived mediator
< 2.05×10^{-5}	90	[7] AARTSEN	17A	ICCB	ν, sun
< 7×10^{-3}	90	[8] AKERIB	17A	LUX	Xe
< 2×10^{-2}	90	[9] FU	17	PNDX	SD WIMP on Xe
		[10] ADRIAN-MAR..	16B	ANTR	solar μ from WIMP annih.
< 1×10^{-2}	90	AMOLE	15	PICO	C_3F_8
< 1.5×10^3	90	NAKAMURA	15	NAGE	CF_4
< 2.7×10^{-3}	90	[11] AVRORIN	14	BAIK	H, solar ν ($W^+ W^-$)
< 6.9×10^{-2}	90	[11] AVRORIN	14	BAIK	H, solar ν ($b\overline{b}$)
< 8.4×10^{-4}	90	[11] AVRORIN	14	BAIK	H, solar ν ($\tau^+\tau^-$)
< 4.48×10^{-4}	90	[12] AARTSEN	13	ICCB	H, solar ν ($W^+ W^-$)
< 1.00×10^{-2}	90	[12] AARTSEN	13	ICCB	H, solar ν ($b\overline{b}$)
< 8.9×10^{-4}	90	[13] ADRIAN-MAR..	13	ANTR	H, solar ν ($W^+ W^-$)
< 2.0×10^{-2}	90	[13] ADRIAN-MAR..	13	ANTR	H, solar ν ($b\overline{b}$)
< 2.3×10^{-4}	90	[13] ADRIAN-MAR..	13	ANTR	H, solar ν ($\tau^+\tau^-$)
< 7.57×10^{-2}	90	[14] APRILE	13	X100	Xe
< 5.4×10^{-3}	90	[15] BOLIEV	13	BAKS	H, solar ν ($W^+ W^-$)
< 4.2×10^{-2}	90	[15] BOLIEV	13	BAKS	H, solar ν ($b\overline{b}$)
< 1.5×10^{-3}	90	[15] BOLIEV	13	BAKS	H, solar ν ($\tau^+\tau^-$)
< 2.50×10^{-4}	90	[16] ABBASI	12	ICCB	H, solar ν ($W^+ W^-$)
< 7.86×10^{-3}	90	[16] ABBASI	12	ICCB	H, solar ν ($b\overline{b}$)
< 8×10^{-2}	90	BEHNKE	12	COUP	CF_3I
< 8	90	DAW	12	DRFT	F (CF_4)
< 6×10^{-2}		FELIZARDO	12	SMPL	C_2ClF_5
< 8×10^{-2}	90	KIM	12	KIMS	CsI
< 8×10^3	90	[17] AHLEN	11	DMTP	F (CF_4)
< 0.4	90	BEHNKE	11	COUP	CF_3I
< 2×10^{-3}	90	[18] TANAKA	11	SKAM	H, solar ν ($b\overline{b}$)
< 2×10^{-2}	90	[18] TANAKA	11	SKAM	H, solar ν ($W^+ W^-$)
< 1×10^{-3}	90	[19] ABBASI	10	ICCB	KK dark matter
< 2×10^4	90	[17] MIUCHI	10	NAGE	CF_4
< 8.7×10^{-4}	90	ABBASI	09B	ICCB	H, solar ν ($W^+ W^-$)
< 2.2×10^{-2}	90	ABBASI	09B	ICCB	H, solar ν ($b\overline{b}$)
< 3	90	ARCHAMBAU..	09	PICA	F
< 6	90	LEBEDENKO	09A	ZEP3	Xe
< 9	90	ANGLE	08A	XE10	Xe
<100	90	ALNER	07	ZEP2	Xe
< 0.8	90	LEE	07A	KIMS	CsI
< 4×10^4	90	[17] MIUCHI	07	NAGE	F (CF_4)
< 30	90	[20] AKERIB	06	CDMS	^{73}Ge, ^{29}Si
< 1.5	90	ALNER	05	NAIA	NaI
< 15	90	BARNABE-HE..	05	PICA	F (C_4F_{10})
<600	90	BENOIT	05	EDEL	^{73}Ge
< 10	90	GIRARD	05	SMPL	F (C_2ClF_5)
<260	90	MIUCHI	03	BOLO	LiF
<150	90	TAKEDA	03	BOLO	NaF

[1] IKEDA 21 use direction sensitive TPC NEWAGE to search for SD WIMPs. No signal observed. Limits set in $\sigma^{SD}(\chi p)$ vs. m plane; $\sigma^{SD}(\chi p) < 200$ pb for m(DM) = 1000 GeV.
[2] AARTSEN 20C place combined IceCube and Pico-60 velocity-independent limits on spin-dependent WIMP-p scatter $\sigma^{SD}(\chi p) < 3 \times 10^{-3}$ pb for m(WIMP) = 1 TeV assuming dominant annihilation to WW.
[3] AMOLE 19 search for SD WIMP scatter on C_3F_8 in PICO-60 bubble chamber; no signal: set limit for spin dependent coupling $\sigma^{SD}(\chi p) < 3 \times 10^{-4}$ pb for m(χ) = 1000 GeV.
[4] APRILE 19A search for SD WIMP scatter on 1 t yr Xe; no signal, limits placed in $\sigma^{SD}(\chi p)$ vs. m(χ) plane for m $\sim$ 6–1000 GeV.
[5] XIA 19A search for WIMP scatter on Xe in PandaX-II; limits placed in $\sigma^{SD}(\chi p)$ vs. m(χ) plane for m(χ) $\sim$ 5–1 $\times 10^5$ GeV.
[6] ALBERT 18C search for DM annihilation in Sun to long-lived mediator (LLM) which decays outside Sun, for DM masses above 1 TeV; assuming LLM, limits set on $\sigma^{SD}(\chi p)$.
[7] AARTSEN 17A search for neutrinos from solar WIMP annihilation into $\tau^+\tau^-$ in 532 days of live time.
[8] AKERIB 17A search for SD WIMP scatter on Xe using 129.5 kg yr exposure; limits placed in $\sigma^{SD}(\chi p)$ vs. m(χ) plane for m(χ) $\sim$ 6–1 $\times 10^5$ GeV.
[9] FU 17 search for SD WIMP scatter on Xe; limits set in $\sigma^{SD}(\chi p)$ vs. m(χ) plane for m(χ) $\sim$ 4–1 $\times 10^3$ GeV.
[10] ADRIAN-MARTINEZ 16B search for secluded DM via WIMP annihilation in solar core into light mediator which later decays to μ or νs; limits presented in Figures 3 and 4.
[11] AVRORIN 14 search for neutrinos from the Sun arising from the pair annihilation of X^0 trapped by the Sun in data taken between 1998 and 2003. See their Table 1 for limits assuming annihilation into neutrino pairs.
[12] AARTSEN 13 search for neutrinos from the Sun arising from the pair annihilation of X^0 trapped by the sun in data taken between June 2010 and May 2011.
[13] ADRIAN-MARTINEZ 13 search for neutrinos from the Sun arising from the pair annihilation of X^0 trapped by the sun in data taken between Jan. 2007 and Dec. 2008.
[14] The value has been provided by the authors. APRILE 13 note that the proton limits on Xe are highly sensitive to the theoretical model used. See also APRILE 14A.
[15] BOLIEV 13 search for neutrinos from the Sun arising from the pair annihilation of X^0 trapped by the sun in data taken from 1978 to 2009. See also SUVOROVA 13 for an older analysis of the same data.
[16] ABBASI 12 search for neutrinos from the Sun arising from the pair annihilation of X^0 trapped by the Sun. The amount of X^0 depends on the X^0-proton cross section.
[17] Use a direction-sensitive detector.
[18] TANAKA 11 search for neutrinos from the Sun arising from the pair annihilation of X^0 trapped by the Sun. The amount of X^0 depends on the X^0-proton cross section.
[19] ABBASI 10 search for ν_μ from annihilations of Kaluza-Klein photon dark matter in the Sun.
[20] See also AKERIB 05.

Downloaded from https://academic.oup.com/ptep/article/2022/8/083C01/6651666 by KIT Library user on 27 September 2022

Spin-Dependent Cross Section Limits for Dark Matter Particle (X^0) on Neutron

For m_{X^0} in GeV range

We provide here limits fo $m_{X^0} < 5$ GeV

VALUE (pb)	CL%	DOCUMENT ID		TECN	COMMENT
• • • We do not use the following data for averages, fits, limits, etc. • • •					
$< 1 \times 10^{8}$	90	[1] ABDELHAME..	20A	CRES	$LiAlO_2$
$< 1 \times 10^{10}$	95	[2] ABDELHAME..	19	CRES	SD low mass DM on Li
$< 2.3 \times 10^{2}$	90	[3] APRILE	19C	XE1T	light DM on Xe via Migdal/brem effect
$< 1 \times 10^{-2}$	90	[4] APRILE	19D	XE1T	light DM on Xe via ionization
$< 4 \times 10^{4}$	90	[5] ARMENGAUD	19	EDEL	GeV-scale WIMPs on Ge
$< 8 \times 10^{-2}$	90	[6] XIA	19A	PNDX	SD WIMP on Xe
< 3	90	[7] AGNESE	18	SCDM	GeV-scale WIMPs on Ge
< 3	90	[8] JIANG	18	CDEX	GeV-scale WIMPs on Ge
< 10	90	[9] YANG	18	CDEX	WIMPs on Ge
$< 1 \times 10^{-1}$	90	[10] AKERIB	17A	LUX	Xe
< 0.1	90	[11] FU	17	PNDX	SD WIMP on Xe
< 20	90	[12] ZHAO	16	CDEX	GeV-scale WIMPs on Ge
<150	90	[13] AHMED	11B	CDM2	GeV-scale WIMPs on Ge

[1] ABDELHAMEED 20A use $LiAlO_2$ target in CRESST to search for SD WIMP scatter; no signal; quoted limit is for m(DM) = 1 GeV.

[2] ABDELHAMEED 19 search for GeV-scale WIMP SD scatter on ^{7}Li crystal; set limit $\sigma^{SD}(\chi n)$ for m(χ) ~ 0.8–20 GeV; quoted limit for m(χ) = 1 GeV.

[3] APRILE 19C search for light DM on Xe via Migdal/bremsstrahlung effect; no signal, require $\sigma^{SD}(\chi n)$ <230 pb for m(χ) = 1 GeV.

[4] APRILE 19D search for light DM scatter on Xe via ionization; no signal, limits placed in σ vs. m(DM) ~ 3–6 GeV; quoted limit is for m(DM) = 5 GeV.

[5] ARMENGAUD 19 search for GeV scale WIMP scatter on Ge; limits placed in $\sigma^{SD}(\chi n)$ vs. m(χ) plane for m(χ) ~ 0.5–10 GeV; quoted limit is for m(χ) = 5 GeV.

[6] XIA 19A search for WIMP scatter on Xe in PandaX-II; limits placed in $\sigma^{SD}(\chi n)$ vs. m(χ) plane for m(χ) ~ 5–1 × 10^5 GeV; quoted limit is for m(χ) = 5 GeV.

[7] AGNESE 18 search for GeV scale WIMPs scatter at CDMSlite; limits placed in $\sigma^{SD}(\chi n)$ vs. m(χ) plane for m ~ 1.5–20 GeV; quoted limit is for m(χ) = 5 GeV.

[8] JIANG 18 search for GeV scale WIMP scatter on Ge; limits placed in $\sigma^{SD}(\chi n)$ vs. m(χ) plane for m(χ) ~ 3–10 GeV; quoted limit is for m(χ) = 5 GeV.

[9] YANG 18 search for WIMP scatter on Ge; limits placed in $\sigma^{SD}(\chi n)$ vs. m(χ) plane for m(χ) ~ 2–10 GeV; quoted limit is for m(χ) = 5 GeV.

[10] AKERIB 17A search for SD WIMP scatter on Xe with 129.5 kg yr exposure; limits placed in $\sigma^{SD}(\chi n)$ vs. m(χ) plane for m(χ) ~ 5–1 × 10^5 GeV; quoted limit is for m(χ) = 5 GeV.

[11] FU 17 search for SD WIMP scatter on Xe; limits set in $\sigma^{SD}(\chi n)$ vs. m(χ) plane for m(χ) ~ 4–1 × 10^3 GeV.; quoted limit is for m(χ) = 5 GeV.

[12] ZHAO 16 search for GeV-scale WIMP scatter on Ge; limits placed in $\sigma^{SD}(\chi n)$ vs. m(χ) plane for m(χ) ~ 4–30 GeV; quoted limit is for m(χ) = 5 GeV.

[13] AHMED 11B search for GeV scale WIMP scatter on Ge in CDMS II; limits placed in $\sigma^{SD}(\chi n)$ vs. m(χ) plane for m ~ 4–12 GeV. Limit given for m(χ) = 5 GeV.

For m_{X^0} = 20 GeV

VALUE (pb)	CL%	DOCUMENT ID		TECN	COMMENT
• • • We do not use the following data for averages, fits, limits, etc. • • •					
$< 5 \times 10^{7}$	90	[1] ABDELHAME..	20A	CRES	$LiAlO_2$
$< 1 \times 10^{-1}$		[2] FELIZARDO	20	SMPL	WIMPs via SIMPLE
$< 8 \times 10^{-6}$	90	[3] APRILE	19A	XE1T	Xe, SD
$< 3 \times 10^{-5}$	90	[4] XIA	19A	PNDX	SD WIMP on Xe
< 1.5	95	[5] AGNESE	18	SCDM	Ge
$< 2.5 \times 10^{-5}$	90	[6] AKERIB	17A	LUX	Xe
$< 7 \times 10^{-5}$	90	[7] FU	17	PNDX	SD WIMP on Xe
< 2	90	[8] ZHAO	16	CDEX	GeV-scale WIMPs on Ge
< 0.09	90	FELIZARDO	14	SMPL	C_2ClF_5
< 8	90	[9] UCHIDA	14	XMAS	^{129}Xe, inelastic
$< 1.13 \times 10^{-3}$	90	[10] APRILE	13	X100	Xe
< 0.02	90	AKIMOV	12	ZEP3	Xe
< 0.06	90	AHMED	09	CDM2	Ge
< 0.04	90	LEBEDENKO	09A	ZEP3	Xe
< 50		[11] LIN	09	TEXO	Ge
$< 6 \times 10^{-3}$	90	ANGLE	08A	XE10	Xe
< 0.5	90	ALNER	07	ZEP2	Xe
< 25	90	LEE	07A	KIMS	CsI
< 0.3	90	[12] AKERIB	06	CDMS	^{73}Ge, ^{29}Si
< 30	90	SHIMIZU	06A	CNTR	F (CaF_2)
< 60	90	ALNER	05	NAIA	NaI
< 20	90	BARNABE-HE..	05	PICA	F (C_4F_{10})
< 10	90	BENOIT	05	EDEL	^{73}Ge
< 4	90	KLAPDOR-K...	05	HDMS	^{73}Ge (enriched)
<600	90	TAKEDA	03	BOLO	NaF

[1] ABDELHAMEED 20A use $LiAlO_2$ target in CRESST to search for SD WIMP scatter on n; limits placed for m(WIMP): 0.3–30 GeV in Fig. 8. Quoted limit is for M(WIMP) = 30 GeV.

[2] FELIZARDO 20 presents 2014 SIMPLE bounds on WIMP DM using C_2ClF_5 target .

[3] APRILE 19A search for SD WIMP scatter on 1 t yr Xe; no signal: limits placed in $\sigma^{SD}(\chi n)$ vs. m(χ) plane for m ~ 6–1000 GeV.

[4] XIA 19A search for WIMP scatter on Xe in PandaX-II; limits placed in $\sigma^{SD}(\chi n)$ vs. m(χ) plane for m(χ) ~ 5–1 × 10^5 GeV.

[5] AGNESE 18 give limits for $\sigma^{SD}(n\chi)$ for m(WIMP) between 1.5 and 20 GeV using CDMSlite mode data.

[6] AKERIB 17A search for SD WIMP scatter on Xe with 129.5 kg yr exposure; limits placed in $\sigma^{SD}(\chi n)$ vs. m(χ) plane for m(χ) ~ 5–1 × 10^5 GeV.

[7] FU 17 search for SD WIMP scatter on Xe; limits set in $\sigma^{SD}(\chi n)$ vs. m(χ) plane for m(χ) ~ 4–1 × 10^3 GeV.

[8] ZHAO 16 search for GeV-scale WIMP scatter on Ge; limits placed in $\sigma^{SD}(\chi n)$ vs. m(χ) plane for m(χ) ~ 4–30 GeV.

[9] Derived limit from search for inelastic scattering $X^0 + {}^{129}Xe \rightarrow X^0 + {}^{129}Xe^*$(39.58 keV).

[10] The value has been provided by the authors. See also APRILE 14A.

[11] See their Fig. 6(b) for cross section limits for m_{X^0} extending down to 2 GeV.

[12] See also AKERIB 05.

For m_{X^0} = 100 GeV

VALUE (pb)	CL%	DOCUMENT ID		TECN	COMMENT
• • • We do not use the following data for averages, fits, limits, etc. • • •					
$< 1.5 \times 10^{-1}$		[1] FELIZARDO	20	SMPL	WIMPs via SIMPLE
$< 1.5 \times 10^{-5}$	90	[2] APRILE	19A	XE1T	Xe, SD
$< 4 \times 10^{-3}$	90	[3] SUZUKI	19	XMAS	^{129}Xe, inelastic
$< 2 \times 10^{-5}$	90	[4] XIA	19A	PNDX	SD WIMP on Xe
$< 2.5 \times 10^{-5}$	90	[5] AKERIB	17A	LUX	Xe
$< 7 \times 10^{-5}$	90	[6] FU	17	PNDX	SD WIMP on Xe
< 0.1	90	FELIZARDO	14	SMPL	C_2ClF_5
< 0.05	90	[7] UCHIDA	14	XMAS	^{129}Xe, inelastic
$< 4.68 \times 10^{-4}$	90	[8] APRILE	13	X100	Xe
< 0.01	90	AKIMOV	12	ZEP3	Xe
		[9] FELIZARDO	10	SMPL	C_2ClF_3
< 0.02	90	AHMED	09	CDM2	Ge
< 0.01	90	LEBEDENKO	09A	ZEP3	Xe
<100	90	LIN	09	TEXO	Ge
< 0.01	90	ANGLE	08A	XE10	Xe
< 0.05	90	[10] BEDNYAKOV	08	RVUE	Ge
< 0.08	90	ALNER	07	ZEP2	Xe
< 6	90	LEE	07A	KIMS	CsI
< 0.07	90	[11] AKERIB	06	CDMS	^{73}Ge, ^{29}Si
< 30	90	SHIMIZU	06A	CNTR	F (CaF_2)
< 10	90	ALNER	05	NAIA	NaI
< 30	90	BARNABE-HE..	05	PICA	F (C_4F_{10})
< 0.7	90	BENOIT	05	EDEL	^{73}Ge
< 0.2		[12] GIULIANI	05A	RVUE	
< 1.5	90	KLAPDOR-K...	05	HDMS	^{73}Ge (enriched)
		[13] GIULIANI	04	RVUE	
		[14] GIULIANI	04A	RVUE	
		[15] MIUCHI	03	BOLO	LiF
<800	90	TAKEDA	03	BOLO	NaF

[1] FELIZARDO 20 presents 2014 SIMPLE bounds on WIMP DM using C_2ClF_5 target .

[2] APRILE 19A search for SD WIMP scatter on 1 t yr Xe; no signal, limits placed in $\sigma^{SD}(\chi n)$ vs. m(χ) plane for m ~ 6–1000 GeV.

[3] SUZUKI 19 search in single phase liquid xenon detector for inelastic scattering $X^0 + {}^{129}Xe \rightarrow X^0 + {}^{129}Xe^*$ (39.58 keV) ; no signal: require $\sigma(\chi n)^{SD} < 4 \times 10^{-3}$ pb for m(χ) = 100 GeV.

[4] XIA 19A search for WIMP scatter on Xe in PandaX-II; limits placed in $\sigma^{SD}(\chi n)$ vs. m(χ) plane for m(χ) ~ 5–1 × 10^5 GeV.

[5] AKERIB 17A search for SD WIMP scatter on Xe with 129.5 kg yr exposure; limits placed in $\sigma^{SD}(\chi n)$ vs. m(χ) plane for m(χ) ~ 5–1 × 10^5 GeV.

[6] FU 17 search for SD WIMP scatter on Xe; limits set in $\sigma^{SD}(\chi n)$ vs. m(χ) plane for m(χ) ~ 4–1 × 10^3 GeV.

[7] UCHIDA 14 derived limit from search for inelastic scattering $X^0 + {}^{129}Xe \rightarrow X^0 + {}^{129}Xe$(39.58 keV).

[8] The value has been provided by the authors. See also APRILE 14A.

[9] See their Fig. 3 for limits on spin-dependent neutron couplings for X^0 mass of 50 GeV.

[10] BEDNYAKOV 08 reanalyze KLAPDOR-KLEINGROTHAUS 05 and BAUDIS 01 data.

[11] See also AKERIB 05.

[12] GIULIANI 05A analyze available data and give combined limits.

[13] GIULIANI 04 reanalyze COLLAR 00 data and give limits for spin-dependent X^0-neutron coupling.

[14] GIULIANI 04A give limits for spin-dependent X^0-neutron couplings from existing data.

[15] MIUCHI 03 give model-independent limit for spin-dependent X^0-proton and neutron cross sections. See their Fig. 5.

For m_{X^0} = 1 TeV

VALUE (pb)	CL%	DOCUMENT ID		TECN	COMMENT
• • • We do not use the following data for averages, fits, limits, etc. • • •					
$< 7 \times 10^{-1}$		[1] FELIZARDO	20	SMPL	WIMPs via SIMPLE
$< 1.2 \times 10^{-4}$	90	[2] APRILE	19A	XE1T	Xe, SD
$< 2 \times 10^{-4}$	90	[3] XIA	19A	PNDX	Xe
$< 2.5 \times 10^{-4}$	90	[4] AKERIB	17A	LUX	Xe
$< 4 \times 10^{-4}$	90	[5] FU	17	PNDX	SD WIMP on Xe
< 0.07	90	FELIZARDO	14	SMPL	C_2ClF_5
< 0.2	90	[6] UCHIDA	14	XMAS	^{129}Xe, inelastic
$< 3.64 \times 10^{-3}$	90	[7] APRILE	13	X100	Xe
< 0.08	90	AKIMOV	12	ZEP3	Xe
< 0.2	90	AHMED	09	CDM2	Ge
< 0.1	90	LEBEDENKO	09A	ZEP3	Xe

Downloaded from https://academic.oup.com/ptep/article/2022/8/083C01/6651666 by KIT Library user on 27 September 2022

< 0.1	90	ANGLE	08A	XE10	Xe
< 0.25	90	[8] BEDNYAKOV	08	RVUE	Ge
< 0.6	90	ALNER	07	ZEP2	Xe
< 30	90	LEE	07A	KIMS	CsI
< 0.5	90	[9] AKERIB	06	CDMS	^{73}Ge, ^{29}Si
< 40	90	ALNER	05	NAIA	NaI
<200	90	BARNABE-HE...	05	PICA	F (C_4F_{10})
< 4	90	BENOIT	05	EDEL	^{73}Ge
< 10	90	KLAPDOR-K...	05	HDMS	^{73}Ge (enriched)
< 4 $\times 10^3$	90	TAKEDA	03	BOLO	NaF

[1] FELIZARDO 20 presents 2014 SIMPLE bounds on WIMP DM using C_2ClF_5 target .
[2] APRILE 19A search for SD WIMP scatter on 1 t yr Xe; no signal, limits placed in $\sigma^{SD}(\chi n)$ vs. m(χ) plane for m $\sim$ 6–1000 GeV.
[3] XIA 19A search for WIMP scatter on Xe in PandaX-II; limits placed in $\sigma^{SD}(\chi n)$ vs. m(χ) plane for m(χ) $\sim$ 5–1 $\times 10^5$ GeV.
[4] AKERIB 17A search for SD WIMP scatter on Xe with 129.5 kg yr exposure; limits placed in $\sigma^{SD}(\chi n)$ vs. m(χ) plane for m(χ) $\sim$ 5–1 $\times 10^5$ GeV.
[5] FU 17 search for SD WIMP scatter on Xe; limits set in $\sigma^{SD}(\chi n)$ vs. m(χ) plane for m(χ) $\sim$ 4–1 $\times 10^3$ GeV.
[6] Derived limit from search for inelastic scattering $X^0 + {}^{129}$Xe* $\rightarrow X^0 + {}^{129}$Xe*(39.58 keV).
[7] The value has been provided by the authors. See also APRILE 14A.
[8] BEDNYAKOV 08 reanalyze KLAPDOR-KLEINGROTHAUS 05 and BAUDIS 01 data.
[9] See also AKERIB 05.

Cross-Section Limits for Dark Matter Particles (X^0) on electron

For m_{X^0} in GeV range

We provide here limits fo m_{X^0} < 5 GeV

VALUE (pb)	CL%	DOCUMENT ID		TECN	COMMENT
• • • We do not use the following data for averages, fits, limits, etc. • • •					
< 10	90	[1] CHENG	21	PNDX	MeV-scale DM on e
		[2] AKERIB	20	LUX	mirror DM with Xe
< 8.7 $\times 10^2$	90	[3] AMARAL	20	SCDM	light DM scatter on e in Si
		[4] APRILE	20	XE1T	excess keV electron recoil in Xe
<100	90	[5] ARNAUD	20	EDEL	MeV DM scatter on e in Ge
< 0.6	90	[6] BARAK	20	SENS	MeV scale DM scatter from e in Si
< 2 $\times 10^6$	90	[7] ABRAMOFF	19	SENS	WIMP-e scatter on Si
		[8] AGUILAR-AR...	19A	DMIC	MeV scale DM scatter on e in Si
< 1 $\times 10^{-4}$	90	[9] APRILE	19D	XE1T	light DM on Xe via ionization
< 9 $\times 10^{-3}$	90	[10] AGNES	18B	DS50	Ar
< 1 $\times 10^4$	90	[11] AGNESE	18B	SCDM	$e\chi$ scatter
< 5 $\times 10^3$	90	[12] CRISLER	18	SENS	Si CCD
		[13] APRILE	17	X100	Xe, annual modulation

[1] CHENG 21 search for MeV-scale DM scatter from e in PANDAX-II. No signal detected. Limits set in $\sigma(\chi e)$ vs. m(DM) plane for two choices of form factors; $\sigma(\chi e)$ < 10 pb for m(χ) = 10 MeV and F_{DM} = 1.
[2] AKERIB 20 search for mirror DM with LUX 95 d $\times$ 118 kg data for mirror e scatter from Xe; no signal, limits placed in kinetic mixing parameter vs. mirror e temperature T $\sim$ 0.1–0.9 keV plane.
[3] AMARAL 20 search SuperCDMS data for low mass DM scatter from e in Si; no signal; quoted limit σ_e < 8.7 $\times 10^2$ pb for m(DM) = 10 MeV with form factor F_{DM} = 1.
[4] APRILE 20 report excess at electron recoil around 2–3 keV in Xe; data compared to unforeseen tritium background, and various signal models (bosonic DM, solar axion, and neutrino magnetic moment).
[5] ARNAUD 20 search for MeV DM scattering from e in Ge; no signal; quoted limit is for m(DM) = 10 MeV with form factor F_{DM} = 1.
[6] BARAK 20 report search for MeV scale DM scatter from e in Si; limits placed in σ_e vs. m(DM) plane; quoted limit is for m(DM) = 10 MeV and form factor F_{DM} = 1.
[7] ABRAMOFF 19 search for MeV-scale WIMP scatter from Si skipper-CCD; limits placed on $\sigma(\chi e)$ for m(χ) $\sim$ 0.5–100 MeV depending on DM form factors. Limit given for m(DM) = 1 MeV.
[8] AGUILAR-AREVALO 19A search for MeV scale DM scatter from e in Si CCDs at SNOLAB; no signal, limits placed in σ(e) vs. m(DM) plane for m(DM) $\sim$ 0.6–100 MeV.
[9] APRILE 19D search for light DM scatter on Xe via ionization; no signal, limits placed in σ on nucleus vs. m(DM) plane for m(DM) $\sim$ 0.02–10 GeV; quoted limit is for m(DM) = 0.2 GeV.
[10] AGNES 18B search for MeV scale WIMP scatter from e in Ar; no signal, limits set in σ_e vs. m(χ) plane for m $\sim$ 20–1000 MeV and two choices of form factor F(DM); quoted limit for m(χ) = 100 MeV and F = 1.
[11] AGNESE 18B search for $e\chi$ scatter in SuperCDMS; limits placed in $\sigma(e\chi)$ vs. m(χ) plane for m $\sim$ 0.3–1 $\times 10^4$ MeV for two assumed form factors and also in m(dark photon) vs. kinetic mixing plane. Limit given for m(χ) = 1 GeV and F=1.
[12] CRISLER 18 search for $\chi e \rightarrow \chi e$ scatter in Si CCD; place limits on MeV DM in σ_e vs. m(χ) plane for m $\sim$ 0.5–1000 MeV for different form factors; quoted limit is for F(DM) = 1 and m(χ) = 10 MeV.
[13] APRILE 17 search for WIMP-e annual modulation signal for recoil energy in the 2.0–5.8 keV interval using 4 years data with Xe. No significant effect seen.

Cross-Section Limits for Dark Matter Particles (X^0) on Nuclei

For m_{X^0} in GeV range

We provide here limits fo m_{X^0} < 5 GeV

For m_{X^0} = 20 GeV

VALUE (nb)	CL%	DOCUMENT ID		TECN	COMMENT
• • • We do not use the following data for averages, fits, limits, etc. • • •					
< 0.03	90	[1] UCHIDA	14	XMAS	^{129}Xe, inelastic
< 0.08	90	[2] ANGLOHER	02	CRES	Al
		[3] BENOIT	00	EDEL	Ge
< 0.04	95	[4] KLIMENKO	98	CNTR	^{73}Ge, inel.
< 0.8		ALESSAND...	96	CNTR	O
< 6		ALESSAND...	96	CNTR	Te
< 0.02	90	[5] BELLI	96	CNTR	^{129}Xe, inel.
		[6] BELLI	96C	CNTR	^{129}Xe
< 4 $\times 10^{-3}$	90	[7] BERNABEI	96	CNTR	Na
< 0.3	90	[7] BERNABEI	96	CNTR	I
< 0.2	95	[8] SARSA	96	CNTR	Na
< 0.015	90	[9] SMITH	96	CNTR	Na
< 0.05	95	[10] GARCIA	95	CNTR	Natural Ge
< 0.1	95	QUENBY	95	CNTR	Na
<90	90	[11] SNOWDEN-...	95	MICA	^{16}O
< 4 $\times 10^3$	90	[11] SNOWDEN-...	95	MICA	^{39}K
< 0.7	90	BACCI	92	CNTR	Na
< 0.12	90	[12] REUSSER	91	CNTR	Natural Ge
< 0.06	95	CALDWELL	88	CNTR	Natural Ge

[1] UCHIDA 14 limit is for inelastic scattering $X^0 + {}^{129}$Xe* $\rightarrow X^0 + {}^{129}$Xe* (39.58 keV).
[2] ANGLOHER 02 limit is for spin-dependent WIMP-Aluminum cross section.
[3] BENOIT 00 find four event categories in Ge detectors and suggest that low-energy surface nuclear recoils can explain anomalous events reported by UKDMC and Saclay NaI experiments.
[4] KLIMENKO 98 limit is for inelastic scattering X^0 ^{73}Ge $\rightarrow X^0$ ^{73}Ge* (13.26 keV).
[5] BELLI 96 limit for inelastic scattering X^0 ^{129}Xe $\rightarrow X^0$ ^{129}Xe*(39.58 keV).
[6] BELLI 96C use background subtraction and obtain σ < 150 pb (< 1.5 fb) (90% CL) for spin-dependent (independent) X^0-proton cross section. The confidence level is from R. Bernabei, private communication, May 20, 1999.
[7] BERNABEI 96 use pulse shape discrimination to enhance the possible signal. The limit here is from R. Bernabei, private communication, September 19, 1997.
[8] SARSA 96 search for annual modulation of WIMP signal. See SARSA 97 for details of the analysis. The limit here is from M.L. Sarsa, private communication, May 26, 1997.
[9] SMITH 96 use pulse shape discrimination to enhance the possible signal. A dark matter density of 0.4 GeV cm^{-3} is assumed.
[10] GARCIA 95 limit is from the event rate. A weaker limit is obtained from searches for diurnal and annual modulation.
[11] SNOWDEN-IFFT 95 look for recoil tracks in an ancient mica crystal. Similar limits are also given for ^{27}Al and ^{28}Si. See COLLAR 96 and SNOWDEN-IFFT 96 for discussion on potential backgrounds.
[12] REUSSER 91 limit here is changed from published (0.04) after reanalysis by authors. J.L. Vuilleumier, private communication, March 29, 1996.

For m_{X^0} = 100 GeV

VALUE (nb)	CL%	DOCUMENT ID		TECN	COMMENT
• • • We do not use the following data for averages, fits, limits, etc. • • •					
< 3.3 $\times 10^{-6}$	90	[1] APRILE	21A	XE1T	^{129}Xe, inelastic
< 3 $\times 10^{-3}$	90	[2] UCHIDA	14	XMAS	^{129}Xe, inelastic
< 0.3	90	[3] ANGLOHER	02	CRES	Al
		[4] BELLI	02	RVUE	
		[5] BERNABEI	02C	DAMA	
		[6] GREEN	02	RVUE	
		[7] ULLIO	01	RVUE	
		[8] BENOIT	00	EDEL	Ge
< 4 $\times 10^{-3}$	90	[9] BERNABEI	00D		^{129}Xe, inelastic
		[10] AMBROSIO	99	MCRO	
		[11] BRHLIK	99	RVUE	
< 8 $\times 10^{-3}$	95	[12] KLIMENKO	98	CNTR	^{73}Ge, inelastic
< 0.08	95	[13] KLIMENKO	98	CNTR	^{73}Ge, inelastic
< 4		ALESSAND...	96	CNTR	O
<25		ALESSAND...	96	CNTR	Te
< 6 $\times 10^{-3}$	90	[14] BELLI	96	CNTR	^{129}Xe, inelastic
		[15] BELLI	96C	CNTR	^{129}Xe
< 1 $\times 10^{-3}$	90	[16] BERNABEI	96	CNTR	Na
< 0.3	90	[16] BERNABEI	96	CNTR	I
< 0.7	95	[17] SARSA	96	CNTR	Na
< 0.03	90	[18] SMITH	96	CNTR	Na
< 0.8	90	[18] SMITH	96	CNTR	I
< 0.35	95	[19] GARCIA	95	CNTR	Natural Ge
< 0.6	95	QUENBY	95	CNTR	Na
< 3	95	QUENBY	95	CNTR	I
< 1.5 $\times 10^2$	90	[20] SNOWDEN-...	95	MICA	^{16}O
< 4 $\times 10^2$	90	[20] SNOWDEN-...	95	MICA	^{39}K
< 0.08	90	[21] BECK	94	CNTR	^{76}Ge
< 2.5	90	BACCI	92	CNTR	Na
< 3	90	BACCI	92	CNTR	I
< 0.9	90	[22] REUSSER	91	CNTR	Natural Ge
< 0.7	95	CALDWELL	88	CNTR	Natural Ge

Downloaded from https://academic.oup.com/ptep/article/2022/8/083C01/6651666 by KIT Library user on 27 September 2022

[1] APRILE 21A search for inelastic DM scatter off ^{129}Xe nuclei with 0.83 t yr exposure. No signal obseved. Limits placed in $\sigma(\chi$Xe) vs. m(DM) plane for WIMP mass between 20 GeV and 10 TeV.
[2] UCHIDA 14 limit is for inelastic scattering $X^0 + {}^{129}$Xe* $\rightarrow X^0 + {}^{129}$Xe*(39.58 keV).
[3] ANGLOHER 02 limit is for spin-dependent WIMP-Aluminum cross section.
[4] BELLI 02 discuss dependence of the extracted WIMP cross section on the assumptions of the galactic halo structure.
[5] BERNABEI 02C analyze the DAMA data in the scenario in which X^0 scatters into a slightly heavier state as discussed by SMITH 01.
[6] GREEN 02 discusses dependence of extracted WIMP cross section limits on the assumptions of the galactic halo structure.
[7] ULLIO 01 disfavor the possibility that the BERNABEI 99 signal is due to spin-dependent WIMP coupling.
[8] BENOIT 00 find four event categories in Ge detectors and suggest that low-energy surface nuclear recoils can explain anomalous events reported by UKDMC and Saclay NaI experiments.
[9] BERNABEI 00D limit is for inelastic scattering $X^0\,^{129}$Xe $\rightarrow X^0\,^{129}$Xe (39.58 keV).
[10] AMBROSIO 99 search for upgoing muon events induced by neutrinos originating from WIMP annihilations in the Sun and Earth.
[11] BRHLIK 99 discuss the effect of astrophysical uncertainties on the WIMP interpretation of the BERNABEI 99 signal.
[12] KLIMENKO 98 limit is for inelastic scattering $X^0\,^{73}$Ge $\rightarrow X^0\,^{73}$Ge* (13.26 keV).
[13] KLIMENKO 98 limit is for inelastic scattering $X^0\,^{73}$Ge $\rightarrow X^0\,^{73}$Ge* (66.73 keV).
[14] BELLI 96 limit for inelastic scattering $X^0\,^{129}$Xe $\rightarrow X^0\,^{129}$Xe*(39.58 keV).
[15] BELLI 96C use background subtraction and obtain $\sigma < 0.35$ pb (< 0.15 fb) (90% CL) for spin-dependent (independent) X^0-proton cross section. The confidence level is from R. Bernabei, private communication, May 20, 1999.
[16] BERNABEI 96 use pulse shape discrimination to enhance the possible signal. The limit here is from R. Bernabei, private communication, September 19, 1997.
[17] SARSA 96 search for annual modulation of WIMP signal. See SARSA 97 for details of the analysis. The limit here is from M.L. Sarsa, private communication, May 26, 1997.
[18] SMITH 96 use pulse shape discrimination to enhance the possible signal. A dark matter density of 0.4 GeV cm^{-3} is assumed.
[19] GARCIA 95 limit is from the event rate. A weaker limit is obtained from searches for diurnal and annual modulation.
[20] SNOWDEN-IFFT 95 look for recoil tracks in an ancient mica crystal. Similar limits are also given for ^{27}Al and ^{28}Si. See COLLAR 96 and SNOWDEN-IFFT 96 for discussion on potential backgrounds.
[21] BECK 94 uses enriched ^{76}Ge (86% purity).
[22] REUSSER 91 limit here is changed from published (0.3) after reanalysis by authors. J.L. Vuilleumier, private communication, March 29, 1996.

For $m_{X^0} = 1$ TeV

VALUE (nb)	CL%	DOCUMENT ID		TECN	COMMENT
• • • We do not use the following data for averages, fits, limits, etc. • • •					
< 0.03	90	[1] UCHIDA	14	XMAS	^{129}Xe, inelastic
< 3	90	[2] ANGLOHER	02	CRES	Al
		[3] BENOIT	00	EDEL	Ge
		[4] BERNABEI	99D	CNTR	SIMP
		[5] DERBIN	99	CNTR	SIMP
< 0.06	95	[6] KLIMENKO	98	CNTR	^{73}Ge, inel.
< 0.4	95	[7] KLIMENKO	98	CNTR	^{73}Ge, inel.
< 40		ALESSAND...	96	CNTR	O
<700		ALESSAND...	96	CNTR	Te
< 0.05	90	[8] BELLI	96	CNTR	^{129}Xe, inel.
< 1.5	90	[9] BELLI	96	CNTR	^{129}Xe, inel.
		[10] BELLI	96C	CNTR	^{129}Xe
< 0.01	90	[11] BERNABEI	96	CNTR	Na
< 9	90	[11] BERNABEI	96	CNTR	I
< 7	95	[12] SARSA	96	CNTR	Na
< 0.3	90	[13] SMITH	96	CNTR	Na
< 6	90	[13] SMITH	96	CNTR	I
< 6	95	[14] GARCIA	95	CNTR	Natural Ge
< 8	95	QUENBY	95	CNTR	Na
< 50	95	QUENBY	95	CNTR	I
<700	90	[15] SNOWDEN-...	95	MICA	^{16}O
$< 1 \times 10^3$	90	[15] SNOWDEN-...	95	MICA	^{39}K
< 0.8	90	[16] BECK	94	CNTR	^{76}Ge
< 30	90	BACCI	92	CNTR	Na
< 30	90	BACCI	92	CNTR	I
< 15	90	[17] REUSSER	91	CNTR	Natural Ge
< 6	95	CALDWELL	88	CNTR	Natural Ge

[1] UCHIDA 14 limit is for inelastic scattering $X^0 + {}^{129}$Xe* $\rightarrow X^0 + {}^{129}$Xe* (39.58 keV).
[2] ANGLOHER 02 limit is for spin-dependent WIMP-Aluminum cross section.
[3] BENOIT 00 find four event categories in Ge detectors and suggest that low-energy surface nuclear recoils can explain anomalous events reported by UKDMC and Saclay NaI experiments.
[4] BERNABEI 99D search for SIMPs (Strongly Interacting Massive Particles) in the mass range 10^3–10^{16} GeV. See their Fig. 3 for cross-section limits.
[5] DERBIN 99 search for SIMPs (Strongly Interacting Massive Particles) in the mass range 10^2–10^{14} GeV. See their Fig. 3 for cross-section limits.
[6] KLIMENKO 98 limit is for inelastic scattering $X^0\,^{73}$Ge $\rightarrow X^0\,^{73}$Ge* (13.26 keV).
[7] KLIMENKO 98 limit is for inelastic scattering $X^0\,^{73}$Ge $\rightarrow X^0\,^{73}$Ge* (66.73 keV).
[8] BELLI 96 limit for inelastic scattering $X^0\,^{129}$Xe $\rightarrow X^0\,^{129}$Xe*(39.58 keV).
[9] BELLI 96 limit for inelastic scattering $X^0\,^{129}$Xe $\rightarrow X^0\,^{129}$Xe*(236.14 keV).
[10] BELLI 96C use background subtraction and obtain $\sigma < 0.7$ pb (< 0.7 fb) (90% CL) for spin-dependent (independent) X^0-proton cross section. The confidence level is from R. Bernabei, private communication, May 20, 1999.
[11] BERNABEI 96 use pulse shape discrimination to enhance the possible signal. The limit here is from R. Bernabei, private communication, September 19, 1997.
[12] SARSA 96 search for annual modulation of WIMP signal. See SARSA 97 for details of the analysis. The limit here is from M.L. Sarsa, private communication, May 26, 1997.
[13] SMITH 96 use pulse shape discrimination to enhance the possible signal. A dark matter density of 0.4 GeV cm^{-3} is assumed.
[14] GARCIA 95 limit is from the event rate. A weaker limit is obtained from searches for diurnal and annual modulation.
[15] SNOWDEN-IFFT 95 look for recoil tracks in an ancient mica crystal. Similar limits are also given for ^{27}Al and ^{28}Si. See COLLAR 96 and SNOWDEN-IFFT 96 for discussion on potential backgrounds.
[16] BECK 94 uses enriched ^{76}Ge (86% purity).
[17] REUSSER 91 limit here is changed from published (5) after reanalysis by authors. J.L. Vuilleumier, private communication, March 29, 1996.

Miscellaneous Results from Underground Dark Matter Searches

VALUE	CL%	DOCUMENT ID		TECN	COMMENT
• • • We do not use the following data for averages, fits, limits, etc. • • •					
		[1] ADHIKARI	22	DEAP	Planck scale DM multiple scatter on Ar
		[2] AKERIB	21B	LUX	limits on WIMP EFT couplings
		[3] AMARE	21	ANAI	annual modulation on NaI
		[4] AGOSTINI	20	HPGE	keV-MeV scale super-WIMP absorption in Ge
		[5] ANDRIANAV...	20	FUNK	hidden photon DM search
		[6] CLARK	20		superheavy MIMP DM
		[7] ABRAMOFF	19	SENS	MeV DM e-Si; dark photon Si absorption
		[8] ADHIKARI	19	C100	annual modulation NaI
		[9] AMARE	19	ANAI	annual modulation NaI
$<6.4 \times 10^{-10}$	90	[10] APRILE	19	XE1T	π (Xe)
		[11] BRINGMANN	19		cosmic ray DM
		[12] BRUNE	19		Majoran DM
		[13] CHOI	19	THEO	290 TeV IceCube ν
		[14] HA	19	C100	inelastic boosted dark γ
		[15] KLOPF	19		$n \rightarrow \chi e^+ e^-$
		[16] AARTSEN	18D	ICCB	relic WIMP $\chi \rightarrow \nu X$
		[17] ABE	18F	XMAS	$A' e \rightarrow A' e$
		[18] AGNES	18B	DS50	Ar
		[19] AGNESE	18B	SCDM	MeV DM e-Si; dark photon Si absorption
		[20] AKERIB	18A	LUX	Xe
		[21] ARMENGAUD	18	EDE3	Ge
		[22] KACHULIS	18	SKAM	boosted DM on e
$<1 \times 10^{-12}$	90	[23] AGUILAR-AR...	17	DMIC	γ' on Si
		[24] APRILE	17	X100	Xe
		[25] APRILE	17D	X100	Xe
		[26] APRILE	17H	X100	keV bosonic DM search
		[27] APRILE	17K	X100	$\chi N \rightarrow \chi^* \rightarrow \chi\gamma$
$<4 \times 10^{-3}$	90	[28] ANGLOHER	16A	CRES	$CaWO_4$
		[29] APRILE	15	X100	Event rate modulation
		[30] APRILE	15A	X100	Electron scattering

[1] ADHIKARI 22 search for multiple scatter of Planck scale DM on Ar using DEAP detector. No signal observed. Limits placed in mass vs. cross section plane for m(DM): 10^7–10^{19} GeV.
[2] AKERIB 21B place limits on 15 WIMP non-relativistic EFT couplings for m(DM): 10–4000 GeV using 3.14 kg d exposure.
[3] AMARE 21 search for WIMP annual modulation signal on NaI target in the Canfranc Underground Laboratory (LSC). With an effective exposure of 313.95 kg y, and a sensitivity of 2.5 σ no signal is observed. Incompatible with DAMA/LIBRA at 3.3 σ level.
[4] AGOSTINI 20 search for keV–MeV scale super-WIMP absorption in Ge in GERDA; no signal; limits placed on keV–MeV scale bosonic superWIMPs in coupling vs. mass plane.
[5] ANDRIANAVALOMAHEFA 20 search for hidden photon DM in eV range; place limits in m(DM) vs ln(χ) plane: exclude coupling $\chi \lesssim 1 \times 10^{-12}$ for m(DM) $\sim$ 2.5–7 eV.
[6] CLARK 20 use Majorana and Xe-1-ton data to constrain superheavy multply interacting dark matter (MIMP) in range m$\sim 10^8$–10^{17} GeV depending on interaction cross section.
[7] ABRAMOFF 19 search for MeV scale DM via DM$-e$ scattering and dark photon DM via absorption in Si; limits set in coupling vs. m(χ) plane and on dark photon in m(A) vs. kinetic mixing parameter plane.
[8] ADHIKARI 19 search for annual modulation signal from WIMP scatter on NaI with 1.7 yr exposure; result consistent with both DAMA/LIBRA and null hypothesis.
[9] AMARE 19 is ANAIS-112 search for WIMP scatter annual modulation on NaI; 157.55 kg yr exposure; result compatible with null hypothesis; confirm goal of reaching sensitivity at 3σ to DAMA/LIBRA result in 5 years.
[10] APRILE 19 search for WIMP-pion scattering in Xe; no signal: require $\sigma(\chi\pi) < 6.4 \times 10^{-10}$ pb for m(χ) = 30 GeV.
[11] BRINGMANN 19 derive theoretically limits on GeV and sub-GeV mass dark matter, in its high energy component generated by interaction with cosmic rays; place limits on σ^{SI} and $\sigma^{SD} < 10^5$ pb.
[12] BRUNE 19 examine possibility of Majoron dark matter; limits placed on Majoron mass vs. coupling from SN1987a and ν-less double beta decay.
[13] CHOI 19 from multimessenger observation finds limit on $\sigma(\nu\chi)$/m(DM) $< 5.1 \times 10^{-23}$ cm^2/GeV based on 290 TeV IceCube neutrino event.
[14] HA 19 search for inelastic boosted MeV scale dark photon using COSINE-100 data; limits placed in m vs. epsilon plane for various mediators.
[15] KLOPF 19 search for DM via $n \rightarrow \chi e^+ e^-$; no signal: limits placed in branching fraction vs. m($e^+ e^-$) plane.
[16] AARTSEN 18D search for long-lived DM particles decaying $\chi \rightarrow \nu X$; no excess seen; for DM masses above 10 TeV, excluding lifetimes shorter than 10^{28} s.

Downloaded from https://academic.oup.com/ptep/article/2022/8/083C01/6651666 by KIT Library user on 27 September 2022

[17] ABE 18F search for keV mass ALPs and hidden photons (HP) scatter on electrons; limits set on mass vs. coupling.

[18] AGNES 18B search for MeV-scale DM scatter on electrons in Ar; no signal; require $\sigma(\chi e) < 9 \times 10^{-3}$ pb for DM form factor F(DM) = 1 and < 300 pb for F(DM) proportional to $1/q^2$ for m(χ) = 100 MeV.

[19] AGNESE 18B search for MeV scale DM via DM-e scattering and dark photon DM via absorption in Si; limits set on MeV DM in coupling vs. m(χ) plane and on dark photon in m(A') vs. kinetic mixing plane.

[20] AKERIB 18A search for annual and diurnal modulation of DM scattering rate on electrons for recoil energy between 2 and 6 keVee; no signal found.

[21] ARMENGAUD 18 search for ALP from the Sun and galactic bosonic DM, interacting in Ge; no signal; limits set for 0.8–500 keV DM particles.

[22] KACHULIS 18 search for an excess of elastically scattered electrons above the atmospheric neutrino background in Super-K; limits placed for simple annihilation or decay in the Sun or galactic center producing "boosted" dark matter.

[23] AGUILAR-AREVALO 17 search for hidden photon DM scatter on Si target CCD; limit kinetic mixing $\kappa < 1 \times 10^{-12}$ for m = 10 eV.

[24] APRILE 17 search for WIMP-e annual modulation signal for recoil energy in the 2.0–5.8 keV interval using 4 years data with Xe. No significant effect seen.

[25] APRILE 17D set limits on 14 WIMP-nucleon different interaction operators. No deviations found using 225 live days in the 6.6–240 keV recoil energy range.

[26] APRILE 17H search for keV bosonic DM via $e\chi \rightarrow e$, looking for electronic recoils with 224.6 live days of data and 34 kg of LXe. Limits set on $\chi e e$ coupling for m(χ) = 8–125 keV.

[27] APRILE 17K search for magnetic inelastic DM via $\chi N \rightarrow \chi^* \rightarrow \chi\gamma$. Limits set in DM magnetic moment vs. mass splitting plane for two DM masses corresponding to the DAMA/LIBRA best fit values.

[28] ANGLOHER 16A require q^2 dependent scattering $< 8 \times 10^{-3}$ pb for asymmetric DM m(WIMP) = 3 GeV on $CaWO_4$ target. It uses a local dark matter density of 0.38 GeV/cm^3.

[29] APRILE 15 search for periodic variation of electronic recoil event rate in the data between Feb. 2011 and Mar. 2012. No significant modulation is found for periods up to 500 days.

[30] APRILE 15A search for X^0 scattering off electrons. See their Fig. 4 for limits on cross section through axial-vector coupling for m_{X^0} between 0.6 GeV and 1 TeV. For m_{X^0} = 2 GeV, σ < 60 pb (90%CL) is obtained.

X^0 Annihilation Cross Section

Limits are on σv for X^0 pair annihilation at threshold.

VALUE (cm^{3}s^{-1})	CL%	DOCUMENT ID		TECN	COMMENT
• • • We do not use the following data for averages, fits, limits, etc. • • •					
$<5 \times 10^{-24}$	95	[1] ABDALLAH	21	HESS	WIMP annihilation in dwarf irregular galaxy
		[2] CIRELLI	21		light DM annihilation producing X-rays
		[3] JOHN	21		cosmic positron spectra limits on leptophilic DM
$<2.5 \times 10^{-27}$	95	[4] ABAZAJIAN	20	FLAT	γ from galactic center
		[5] ABDALLAH	20	HESS	WIMP annihilation in dwarf satellite galaxies
$<1.2 \times 10^{-24}$	90	[6] ABE	20G	SKAM	WIMP annihilation to neutrinos
$<2.2 \times 10^{-24}$	95	[7] ALBERT	20	HAWC	WIMP annihilation to γ
$<5 \times 10^{-24}$	90	[8] ALBERT	20A	ANTR	WIMP annihilation to νs in galactic center
$<1 \times 10^{-23}$	90	[9] ALBERT	20C	ANTR	Antares/IceCube search for WIMP annihilation to νs
$<8 \times 10^{-26}$		[10] ALVAREZ	20	FLAT	dwarf spheroidal; J-distribution
$<2 \times 10^{-26}$	90	[11] HOOF	20	FLAT	WIMP annihilation to γ
		[12] MAZZIOTTA	20	FLAT	DM annihilation in Sun to γ
		[13] ABEYSEKARA	19	HAWC	DM annihilation to γs within galactic substructure
$<0.8 \times 10^{-22}$	95	[14] ALBERT	19B	HAWC	annihilation/decay to γ in M31
$<4 \times 10^{-26}$	95	[15] CHEUNG	19	EDGS	$\chi\chi \rightarrow e^+e^-$ and $b\overline{b}$
$<7 \times 10^{-27}$	95	[16] DI-MAURO	19	FLAT	Fermi-LAT M31 and M33
		[17] JOHNSON	19	FLAT	P-wave DM; Fermi-LAT
$<2 \times 10^{-26}$	95	[18] LI	19D	FLAT	$\chi\chi \rightarrow \gamma$
$<1 \times 10^{-32}$		[19] NG	19		sterile ν decay/annihilation
		[20] QUEIROZ	19		semi-annihilating DM
$<4 \times 10^{-28}$	95	[21] ABDALLAH	18	HESS	$X^0X^0 \rightarrow \gamma X$; galactic halo
$<1 \times 10^{-23}$	95	[22] AHNEN	18	MGIC	$X^0X^0 \rightarrow \gamma X$; Ursa Major II
$<1 \times 10^{-22}$	95	[23] ALBERT	18B	HAWC	$X^0X^0 \rightarrow \gamma X$; Andromeda
$<1 \times 10^{-26}$	95	[24] CHANG	18A		$\chi\chi \rightarrow b\overline{b} \rightarrow \gamma$
		[25] LISANTI	18	THEO	Fermi, γ; galaxy groups
		[26] MAZZIOTTA	18	FLAT	Fermi-LAT CRE data
$<1.2 \times 10^{-23}$	95	[27] AARTSEN	17C	ICCB	$\chi\chi \rightarrow$ neutrinos
$<1 \times 10^{-23}$	90	[28] ALBERT	17A	ANTR	ν, DM annihilation
$<1.32 \times 10^{-25}$	95	[29] ARCHAMBAU..	17	VRTS	γ dwarf galaxies
$<7 \times 10^{-21}$	90	[30] AVRORIN	17	BAIK	cosmic ν
$<1 \times 10^{-28}$		[31] BOUDAUD	17		MeV DM to e^+e^-
		[32] AARTSEN	16D	ICCB	ν, galactic center
$<6 \times 10^{-26}$	95	[33] ABDALLAH	16	HESS	Central Galactic Halo
$<1 \times 10^{-27}$	95	[34] ABDALLAH	16A	HESS	WIMP+WIMP $\rightarrow \gamma\gamma$; galactic center
$<3 \times 10^{-26}$	95	[35] AHNEN	16	MGFL	Satellite galaxy, m(WIMP)=100 GeV
$<1.9 \times 10^{-21}$	90	[36] AVRORIN	16	BAIK	νs from galactic center
$<3 \times 10^{-26}$	95	[37] CAPUTO	16	FLAT	small Magellanic cloud
$<1 \times 10^{-25}$	95	[38] FORNASA	16	FLAT	Fermi-LAT γ-ray anisotropy
$<5 \times 10^{-27}$		[39] LEITE	16		WIMP, radio
$<2 \times 10^{-26}$	95	[40] LI	16	FLAT	dwarf galaxies
$<1 \times 10^{-25}$	95	[41] LI	16A	FLAT	Fermi-LAT; M31
$<1 \times 10^{-26}$		[42] LIANG	16	FLAT	Fermi-LAT, gamma line
$<1 \times 10^{-25}$	95	[43] LU	16	FLAT	Fermi-LAT and AMS-02
$<1 \times 10^{-23}$	95	[44] SHIRASAKI	16	FLAT	extra galactic
		[45] AARTSEN	15C	ICCB	ν, Galactic halo
		[46] AARTSEN	15E	ICCB	ν, Galactic center
		[47] ABRAMOWSKI	15	HESS	Galactic center
		[48] ACKERMANN	15	FLAT	monochromatic γ
		[49] ACKERMANN	15A	FLAT	isotropic γ background
		[50] ACKERMANN	15B	FLAT	Satellite galaxy
		[51] ADRIAN-MAR..	15	ANTR	ν, Galactic center
$<2.90 \times 10^{-26}$	95	[52,53] ACKERMANN	14	FLAT	Satellite galaxy, m = 10 GeV
$<1.84 \times 10^{-25}$	95	[52,54] ACKERMANN	14	FLAT	Satellite galaxy, m = 100 GeV
$<1.75 \times 10^{-24}$	95	[52,54] ACKERMANN	14	FLAT	Satellite galaxy, m = 1 TeV
$<4.52 \times 10^{-24}$	95	[55] ALEKSIC	14	MGIC	Segue 1, m = 1.35 TeV
		[56] AARTSEN	13C	ICCB	Galaxies
		[57] ABRAMOWSKI	13	HESS	Central Galactic Halo
		[58] ACKERMANN	13A	FLAT	Galaxy
		[59] ABRAMOWSKI	12	HESS	Fornax Cluster
		[60] ACKERMANN	12	FLAT	Galaxy
		[61] ACKERMANN	12	FLAT	Galaxy
		[62] ALIU	12	VRTS	Segue 1
$<1 \times 10^{-22}$	90	[63] ABBASI	11C	ICCB	Galactic halo, m=1 TeV
$<3 \times 10^{-25}$	95	[64] ABRAMOWSKI	11	HESS	Near Galactic center, m=1 TeV
$<1 \times 10^{-26}$	95	[65] ACKERMANN	11	FLAT	Satellite galaxy, m=10 GeV
$<1 \times 10^{-25}$	95	[65] ACKERMANN	11	FLAT	Satellite galaxy, m=100 GeV
$<1 \times 10^{-24}$	95	[65] ACKERMANN	11	FLAT	Satellite galaxy, m=1 TeV

[1] ABDALLAH 21 search for WIMP-WIMP annihilation into 2 monoenergetic γ rays in WLM dwarf irregular galaxy using HESS data. No signal. Limits placed in $\langle\sigma v\rangle$ vs. m(WIMP) plane for a mass of 370 GeV.

[2] CIRELLI 21 derive limits on light DM annihilation to ee, $\mu\mu$, $\pi\pi$ that then produce X-rays using data published by INTEGRAL telescope. Limits placed in $\langle\sigma v\rangle$ vs. m(DM) plane for m(DM) = 1–5000 MeV.

[3] JOHN 21 derive limits on leptophilic DM annihilating to positrons by comparing expected spectra to AMS-02 data. The range m(DM): 60–300 GeV appears excluded for this type of model, see Fig. 3.

[4] ABAZAJIAN 20 derive new limits on WIMP annihilation in galactic center (GC): $\sigma \cdot v < 2.5 \times 10^{-27}$ cm^3/s for m(WIMP) = 50 GeV: seems to rule out WIMP explanation for GC γ excess, favouring an astrophysics origin.

[5] ABDALLAH 20 search for WIMP annihilation in newly discovered by DES dwarf satellite galaxies using HESS; limits placed in $\langle\sigma v\rangle$ vs. m(DM) plane depending on annihilation channel and which dwarf satellite.

[6] ABE 20G search Super-Kamiokande data for WIMP annihilation to neutrinos in galactic center/halo; no signal; limits placed in $\langle\sigma v\rangle$ vs. m(DM) plane depending on annihilation channel and m(WIMP). Reported limit for annihilation to $\nu\overline{\nu}$ at 1 GeV.

[7] ALBERT 20 search for TeV-scale WIMP annihilation to $\gamma\gamma$ in dwarf spheroidal galaxies; no signal; limits placed in σv vs m(WIMP) plane: e.g. $\sigma v < 2.2 \times 10^{-24}$ cm^3/s for m(WIMP) = 1 TeV.

[8] ALBERT 20A search for WIMP annihilation to νs in galactic center using Antares; limits placed in $\sigma \cdot$ v vs m(WIMP) plane e.g. $\sigma \cdot$ v < 5×10^{-24} cm^3/s for m(WIMP) = 1 TeV assuming annihilation dominantly to $\tau\overline{\tau}$.

[9] ALBERT 20C report combined Antares + IceCube search for WIMP annihilation to $\tau\overline{\tau}$; for NFW halo profile report $\sigma v < 1 \times 10^{-23}$ cm^3/s for m(WIMP) = 100 GeV.

[10] ALVAREZ 20 use profiling over J-factor distributions and background to derive new limits on $\sigma \cdot$v; e.g. $\sigma \cdot$ v < 8×10^{-26} cm^3/s for m(WIMP) = 100 GeV.

[11] HOOF 20 examine γ rays from 27 dwarf spheroidals using Fermi-LAT data; place limits in $\sigma \cdot$ v vs m(WIMP) plane using profile likelihood and marginalized posterior techniques for DM annihilation to $\tau\overline{\tau}$ and $b\overline{b}$; quoted limit uses first technique and $b\overline{b}$ channel for m(WIMP) = 100 GeV; results rule out WIMP explanation of galactic center excess.

[12] MAZZIOTTA 20 use Fermi-LAT pointed-at-Sun data to search for DM annihilation in the Sun to long-lived mediators decaying into gamma rays, i.e. $\chi\chi \rightarrow \phi\phi \rightarrow 4\gamma$. Limits placed on the SI and SD DM-nucleon cross sections in the σ–DM mass plane for DM masses in the range 3 GeV – 1.8 TeV. Limits are evaluated in both cases of equilibrium and non-equilibrium.

[13] ABEYSEKARA 19 search for γs from DM annihilation in galactic substructures with HAWC; no signal, limits placed in J$\langle\sigma v\rangle$ vs. declination plane for m(DM) $\sim$ 1–108 TeV.

[14] ALBERT 19B search for DM signal from M31 galaxy in μ, τ, t, b, W channels using HAWC for m(DM) $\sim$ 1–100 TeV; no signal, limits placed in $\langle\sigma v\rangle$ vs. m(DM) plane.

[15] CHEUNG 19 derive model-dependent bounds on $\langle\sigma v\rangle$ from EDGES data: $< 4 \times 10^{-26}$ cm^3/s for e^+e^- and $b\overline{b}$ for m(χ) = 100 GeV (including boost factor).

[16] DI-MAURO 19 place limits on WIMP annihilation via Fermi-LAT observation of M31 and M33 galaxies: $\langle\sigma v\rangle < 7 \times 10^{-27}$cm^3/s for m($\chi$) = 20 GeV from M31.

[17] JOHNSON 19 search for γ-rays, 10–600 GeV energy, from P-wave annihilating DM around SgrA* BH using Fermi-LAT; limits set for various models.

[18] LI 19D search for $\chi\chi \rightarrow \gamma$ in Fermi-LAT data; no signal, require $\langle\sigma v\rangle < 2 \times 10^{-26}$ cm^3/s for m(χ) = 100 GeV.

[19] NG 19 search for X-ray line from sterile ν decay/annihilation using NuStar M-31; no signal: limits placed in m(ν) vs mixing angle and $\langle\sigma v\rangle$ vs m(ν).

[20] QUEIROZ 19 examine $\chi\chi \rightarrow \chi SM$ semi-annihilation of DM reaction; limits placed for various assumed SM particles in $\langle\sigma v\rangle$ vs. m(χ) plane.

[21] ABDALLAH 18 search for WIMP WIMP $\rightarrow \gamma X$ in central galactic halo, 10 years of data; limits placed in $\langle\sigma v\rangle$ vs. m(WIMP) plane for m(WIMP): 0.3–70 TeV.

[22] AHNEN 18 search for WIMP WIMP$\rightarrow \gamma X$ from Ursa Major II; limits set in $\langle\sigma v\rangle$ vs. m(WIMP) plane for $b\overline{b}$, W^+W^-, $\tau^+\tau^-$, and $\mu^+\mu^-$ annihilation modes.

[23] ALBERT 18B search for TeV-scale WIMPs with WIMP WIMP $\rightarrow \gamma X$ in Andromeda galaxy using HAWC Observatory; limits set in $\langle\sigma v\rangle$ vs m(WIMP) plane.

Downloaded from https://academic.oup.com/ptep/article/2022/8/083C01/6651666 by KIT Library user on 27 September 2022

[24] CHANG 18A examine $\chi\chi \rightarrow b\overline{b} \rightarrow \gamma$ using Fermi Pass 8 data; no signal; require $\langle\sigma{\cdot}v\rangle < 10^{-26}$ cm^3/s for m(χ) = 50 GeV.

[25] LISANTI 18 examine Fermi Pass 8 γ-ray data from galaxy groups; report m(WMP) > 30 GeV for annihilation in $b\overline{b}$ channel.

[26] MAZZIOTTA 18 examine Fermi-LAT electron and positron spectra searching for features originating from DM particles annihilation into e^+e^- pairs, from 45 GeV to 2 TeV; no signal found, limits are obtained.

[27] AARTSEN 17C use 1005 days of IceCube data to search for $\chi\chi \rightarrow$ neutrinos via various annihilation channels. Limits set.

[28] ALBERT 17A search for DM annihilation to νs using ANTARES data from 2007–2015. No signal. Limits set in $\langle\sigma{\cdot}v\rangle$ vs. m(DM) plane for m(DM) $\sim$ 10–10 $\times$ 10^5 GeV. The listed limit is for m(DM) = 100 TeV.

[29] ARCHAMBAULT 17 set limits for WIMP mass between 100 GeV and 1 TeV on $\langle\sigma{\cdot}v\rangle$ for W^+W^-, ZZ, $b\overline{b}$, $s\overline{s}$, $u\overline{u}$, $d\overline{d}$, $t\overline{t}$, e^+e^-, gg, $c\overline{c}$, hh, $\gamma\gamma$, $\mu^+\mu^-$,$\tau^+\tau^-$ annihilation channels.

[30] AVRORIN 17 find upper limits for the annhilation cross section in various channels for DM particle mass between 30 GeV and 10 TeV. Strongest upper limits coming from the two neutrino channel require $\langle\sigma{\cdot}v\rangle < 6\times10^{-20}$ cm^3/s in dwarf galaxies and $\langle\sigma{\cdot}v\rangle < 7\times10^{-21}$ cm^3/s in LMC for 5 TeV WIMP mass.

[31] BOUDAUD 17 use data from the spacecraft Voyager 1, beyond the heliopause, and from AMS02 on $\chi\chi \rightarrow e^+e^-$ to require $\langle\sigma{\cdot}v\rangle < 1.\times10^{-28}$ cm^3/s for m(χ) = 10 MeV.

[32] AARTSEN 16D search for GeV νs from WIMP annihilation in galaxy; limits set on $\langle\sigma{\cdot}v\rangle$ in Fig. 6, 7.

[33] ABDALLAH 16 require $\langle\sigma{\cdot}v\rangle < 6\times10^{-26}$ cm^3/s for m(WIMP) = 1.5 TeV from 254 hours observation (WW channel) and $< 2\times10^{-26}$ cm^3/s for m(WIMP) = 1.0 TeV in $\tau^+\tau^-$ channel.

[34] ABDALLAH 16A search for line spectra from WIMP + WIMP $\rightarrow \gamma\gamma$ in 18 hr HESS data; rule out previous 130 GeV WIMP hint from Fermi-LAT data.

[35] AHNEN 16 require $\langle\sigma{\cdot}v\rangle < 3\times10^{-26}$ cm^3/s for m(WIMP) = 100 GeV (WW channel).

[36] AVRORIN 16 require $\langle$s.v$\rangle < 1.91\times10^{-21}$ cm^3/s from WIMP annihilation to νs via WW channel for m(WIMP) = 1 TeV.

[37] CAPUTO 16 place limits on WIMPs from annihilation to gamma rays in Small Magellanic Cloud using Fermi-LaT data: $\langle\sigma{\cdot}v\rangle < 3\times10^{-26}$cm^3/s for m(WIMP) = 10 GeV.

[38] FORNASA 16 use anisotropies in the γ-ray diffuse emission detected by Fermi-LAT to bound $\langle\sigma{\cdot}v\rangle < 10^{-25}$cm^3/s for m(WIMP) = 100 GeV in $b\overline{b}$ channel: see Fig. 28. The limit is driven by dark-matter subhalos in the Milky Way and it refers to their Most Constraining Scenario.

[39] LEITE 16 constrain WIMP annihilation via search for radio emissions from Smith cloud; $\langle\sigma{\cdot}v\rangle < 5\times10^{-27}$cm^3/s in ee channel for m(WIMP) = 5 GeV.

[40] LI 16 re-analyze Fermi-LAT data on 8 dwarf spheroidals; set limit $\langle\sigma{\cdot}v\rangle < 2\times10^{-26}$ cm^3/s for m(WIMP) = 100 GeV in $b\overline{b}$ mode with substructures included.

[41] LI 16A constrain $\langle\sigma{\cdot}v\rangle < 10^{-25}$cm^3/s in $b\overline{b}$ channel for m(WIMP) = 100 GeV using Fermi-LAT data from M31; see Fig. 6.

[42] LIANG 16 search dwarf spheroidal galaxies, Large Magellanic Cloud, and Small Magellanic Cloud for γ-line in Fermi-LAT data.

[43] LU 16 re-analyze Fermi-LAT and AMS-02 data; require $\langle\sigma{\cdot}v\rangle < 10^{-25}$cm^3/s for m_m(WIMP) = 1 TeV in $b\overline{b}$ channel .

[44] SHIRASAKI 16 re-anayze Fermi-LAT extra-galactic data; require $\langle\sigma{\cdot}v\rangle < 10^{-23}$cm^3/s for m(WIMP) = 1 TeV in $b\overline{b}$ channel; see Fig. 8.

[45] AARTSEN 15C search for neutrinos from X^0 annihilation in the Galactic halo. See their Figs. 16 and 17, and Table 5 for limits on $\sigma\cdot$v for X^0 mass between 100 GeV and 100 TeV.

[46] AARTSEN 15E search for neutrinos from X^0 annihilation in the Galactic center. See their Figs. 7 and 9, and Table 3 for limits on $\sigma\cdot$v for X^0 mass between 30 GeV and 10 TeV.

[47] ABRAMOWSKI 15 search for γ from X^0 annihilation in the Galactic center. See their Fig. 4 for limits on $\sigma\cdot$v for X^0 mass between 250 GeV and 10 TeV.

[48] ACKERMANN 15 search for monochromatic γ from X^0 annihilation in the Galactic halo. See their Fig. 8 and Tables 2–4 for limits on $\sigma\cdot$v for X^0 mass between 0.2 GeV and 500 GeV.

[49] ACKERMANN 15A search for γ from X^0 annihilation (both Galactic and extragalactic) in the isotropic γ background. See their Fig. 7 for limits on $\sigma\cdot$v for X^0 mass between 10 GeV and 30 TeV.

[50] ACKERMANN 15B search for γ from X^0 annihilation in 15 dwarf spheroidal satellite galaxies of the Milky Way. See their Figs. 1 and 2 for limits on $\sigma\cdot$v for X^0 mass between 2 GeV and 10 TeV.

[51] ADRIAN-MARTINEZ 15 search for neutrinos from X^0 annihilation in the Galactic center. See their Figs. 10 and 11 and Tables 1 and 2 for limits on $\sigma\cdot$v for X^0 mass between 25 GeV and 10 TeV.

[52] ACKERMANN 14 search for γ from X^0 annihilation in 25 dwarf spheroidal satellite galaxies of the Milky Way. See their Tables II–VII for limits assuming annihilation into e^+e^-, $\mu^+\mu^-$, $\tau^+\tau^-$, $u\overline{u}$, $b\overline{b}$, and W^+W^-, for X^0 mass ranging from 2 GeV to 10 TeV.

[53] Limit assuming X^0 pair annihilation into $b\overline{b}$.

[54] Limit assuming X^0 pair annihilation into W^+W^-.

[55] ALEKSIC 14 search for γ from X^0 annihilation in the dwarf spheroidal galaxy Segue 1. The listed limit assumes annihilation into W^+W^-. See their Figs. 6, 7, and 16 for limits on $\sigma\cdot$v for annihilation channels $\mu^+\mu^-$, $\tau^+\tau^-$, $b\overline{b}$, $t\overline{t}$, $\gamma\gamma$, γZ, W^+W^-, ZZ for X^0 mass between 10^2 and 10^4 GeV.

[56] AARTSEN 13C search for neutrinos from X^0 annihilation in nearby galaxies and galaxy clusters. See their Figs. 5–7 for limits on $\sigma\cdot$v for $X^0X^0 \rightarrow \nu\overline{\nu}$, $\mu^+\mu^-$, $\tau^+\tau^-$, and W^+W^- for X^0 mass between 300 GeV and 100 TeV.

[57] ABRAMOWSKI 13 search for monochromatic γ from X^0 annihilation in the Milky Way halo in the central region. Limit on $\sigma\cdot$v between 10^{-28} and 10^{-25} cm^3 s^{-1} (95% CL) is obtained for X^0 mass between 500 GeV and 20 TeV for $X^0X^0 \rightarrow \gamma\gamma$. X^0 density distribution in the Galaxy by Einasto is assumed. See their Fig. 4.

[58] ACKERMANN 13A search for monochromatic γ from X^0 annihilation in the Milky Way. Limit on $\sigma\cdot$v for the process $X^0X^0 \rightarrow \gamma\gamma$ in the range 10^{-29}–10^{-27} cm^3 s^{-1} (95% CL) is obtained for X^0 mass between 5 and 300 GeV. The limit depends slightly on the assumed density profile of X^0 in the Galaxy. See their Tables VII–X and Fig.10. Supersedes ACKERMANN 12.

[59] ABRAMOWSKI 12 search for γ's from X^0 annihilation in the Fornax galaxy cluster. See their Fig. 7 for limits on $\sigma\cdot$v for X^0 mass between 0.1 and 100 TeV for the annihilation channels $\tau^+\tau^-$, $b\overline{b}$, and W^+W^-.

[60] ACKERMANN 12 search for monochromatic γ from X^0 annihilation in the Milky Way. Limit on $\sigma\cdot$v in the range 10^{-28}–10^{-26} cm^{3}s^{-1} (95% CL) is obtained for X^0 mass between 7 and 200 GeV if X^0 annihilates into $\gamma\gamma$. The limit depends slightly on the assumed density profile of X^0 in the Galaxy. See their Table III and Fig. 15.

[61] ACKERMANN 12 search for γ from X^0 annihilation in the Milky Way in the diffuse γ background. Limit on $\sigma\cdot$v of 10^{-24} cm^{3}s^{-1} or larger is obtained for X^0 mass between 5 GeV and 10 TeV for various annihilation channels including W^+W^-, $b\overline{b}$, gg, e^+e^-, $\mu^+\mu^-$, $\tau^+\tau^-$. The limit depends slightly on the assumed density profile of X^0 in the Galaxy. See their Figs. 17–20.

[62] ALIU 12 search for γ's from X^0 annihilation in the dwarf spheroidal galaxy Segue 1. Limit on $\sigma\cdot$v in the range 10^{-24}–10^{-20} cm^{3}s^{-1} (95% CL) is obtained for X^0 mass between 10 GeV and 2 TeV for annihilation channels e^+e^-, $\mu^+\mu^-$, $\tau^+\tau^-$, $b\overline{b}$, and W^+W^-. See their Fig. 3.

[63] ABBASI 11C search for ν_μ from X^0 annihilation in the outer halo of the Milky Way. The limit assumes annihilation into $\nu\nu$. See their Fig. 9 for limits with other annihilation channels.

[64] ABRAMOWSKI 11 search for γ from X^0 annihilation near the Galactic center. The limit assumes Einasto DM density profile.

[65] ACKERMANN 11 search for γ from X^0 annihilation in ten dwarf spheroidal satellite galaxies of the Milky Way. The limit for m = 10 GeV assumes annihilation into $b\overline{b}$, the others W^+W^-. See their Fig. 2 for limits with other final states. See also GERINGER-SAMETH 11 for a different analysis of the same data.

Dark Matter Particle (X^0) Production in Hadron Collisions

Searches for X^0 production in asociation with observable particles (γ, jets, ...) in high energy hadron collisions. If a specific form of effective interaction Lagrangian is assumed, the limits may be translated into limits on X^0-nucleon scattering cross section.

VALUE	DOCUMENT ID		TECN	COMMENT
• • • We do not use the following data for averages, fits, limits, etc. • • •				
	[1] AAD	21AZ	ATLS	DM search in $H\,\not{E}_T \rightarrow \gamma\gamma\,\not{E}_T$
	[2] AAD	21BB	ATLS	DM search in $H\,\not{E}_T \rightarrow b\overline{b}\,\not{E}_T$
	[3] AAD	21D	ATLS	Dark Higgs
	[4] AAD	21F	ATLS	jet + missing momentum
	[5] AAD	21K	ATLS	photon + DM
	[6] AAD	21O	ATLS	ℓ + jets + $\not{E}_T$ to search for t-pairs + DM
	[7] AAD	21P	ATLS	$\ell^+\ell^-$ + jets + $\not{E}_T$
	[8] AAD	21S	ATLS	b-jets + $\not{E}_T$
	[9] SIRUNYAN	21A	CMS	$pp \rightarrow Z\chi\chi$; $Z \rightarrow \ell\overline{\ell}$
	[10] TUMASYAN	21D	CMS	DM search in jets + $\not{E}_T$
	[11] SIRUNYAN	20X	CMS	$pp \rightarrow Z' \rightarrow A(Z')h \rightarrow h + \not{E}_T$
	[12] AABOUD	19AA	ATLS	multi-channel BSM search
	[13] AABOUD	19AI	ATLS	$H \rightarrow \chi\chi$
	[14] AABOUD	19AL	ATLS	$H \rightarrow \chi\chi$
	[15] AABOUD	19Q	ATLS	single t+$\not{E}_T$
	[16] AABOUD	19V	ATLS	review mediator based DM searches
	[17] BANERJEE	19	NA64	$eN \rightarrow eN$+$\not{E}$
	[18] SIRUNYAN	19AN	CMS	$H\chi\chi \rightarrow b\overline{b}\,\not{E}_T$
	[19] SIRUNYAN	19BC	CMS	LQ LQ $\rightarrow \mu j\,\not{E}_T$
	[20] SIRUNYAN	19BO	CMS	$VV \rightarrow Hqq$; $H \rightarrow$ DM
	[21] SIRUNYAN	19C	CMS	$pp \rightarrow t\overline{t}\chi\chi$
	[22] SIRUNYAN	19O	CMS	$pp \rightarrow \gamma\,\not{E}_T$
	[23] SIRUNYAN	19X	CMS	$pp \rightarrow t\overline{t} + \not{p}_T$; $pp \rightarrow t(\overline{t}) + \not{p}_T$
	[24] AABOUD	18	ATLS	$pp \rightarrow Z\chi\chi$; $Z \rightarrow \ell\ell$
	[25] AABOUD	18A	ATLS	$pp \rightarrow t\overline{t}\,\not{E}_T$; $pp \rightarrow b\overline{b}\,\not{E}_T$
	[26] AABOUD	18CA	ATLS	$pp \rightarrow V\chi\chi$; $V \rightarrow jj$
	[27] AABOUD	18I	ATLS	$pp \rightarrow$ jet(s) + $\not{E}_T$
	[28] AGUILAR-AR...	18B	MBNE	$pN \rightarrow \chi X$, $\chi = e$, π, or N
	[29] KHACHATRY...	18	CMS	$pp \rightarrow Z(\ell\ell) + \not{E}_T$
	[30] SIRUNYAN	18BF	CMS	$pp \rightarrow t\,\not{E}_T$
	[31] SIRUNYAN	18BO	CMS	dijet resonance search
	[32] SIRUNYAN	18BV	CMS	$pp \rightarrow Z\,\not{E}_T$
	[33] SIRUNYAN	18C	CMS	$pp \rightarrow t\overline{t}\,\not{E}_T$
	[34] SIRUNYAN	18CU	CMS	$pp \rightarrow Z\,\not{E}_T$
	[35] SIRUNYAN	18DH	CMS	$pp \rightarrow \chi\chi h$; $h \rightarrow \gamma\gamma$ or $\tau\overline{\tau}$
	[36] SIRUNYAN	18S	CMS	$pp \rightarrow$ jets $\not{E}_T$
	[37] AABOUD	17A	ATLS	pp ($H \rightarrow b\overline{b}$ + WIMP pair)
	[38] AABOUD	17AM	ATLS	$pp \rightarrow Z' \rightarrow Ah \rightarrow h(b\overline{b}) + \not{E}_T$
	[39] AABOUD	17AQ	ATLS	$pp \rightarrow h(\gamma\gamma) + \not{E}_T$
	[40] AABOUD	17BD	ATLS	$pp \rightarrow$ jet(s) + $\not{E}_T$
	[41] AABOUD	17R	ATLS	$pp \rightarrow \gamma\not{E}_T$
	[42] AGUILAR-AR...	17A	MBNE	$pN \rightarrow \chi\chi X$; $\chi N \rightarrow \chi N$
	[43] BANERJEE	17	NA64	$eN \rightarrow eN\gamma'$
	[44] KHACHATRY...	17A	CMS	forward jets + $\not{E}_T$
	[45] KHACHATRY...	17F	CMS	$H \rightarrow$ invisibles
	[46] SIRUNYAN	17	CMS	$Z + \not{E}_T$
	[47] SIRUNYAN	17AP	CMS	$pp \rightarrow Z' \rightarrow Ah \rightarrow h + \not{E}_T$
	[48] SIRUNYAN	17AQ	CMS	$pp \rightarrow \gamma + \not{E}_T$
	[49] SIRUNYAN	17BB	CMS	$pp \rightarrow t\overline{t}$+$\not{E}_T$; $pp \rightarrow b\overline{b}$+$\not{E}_T$

Downloaded from https://academic.oup.com/ptep/article/2022/8/083C01/6651666 by KIT Library user on 27 September 2022

[50] SIRUNYAN	17G	CMS	$pp \to j + \not{E}_T$
[51] SIRUNYAN	17U	CMS	$pp \to Z\chi\chi$; $Z \to \ell\overline{\ell}$
[52] AABOUD	16AD	ATLS	(W or $Z \to$ jets) + $\not{E}_T$
[53] AAD	16AF	ATLS	$VV \to$ forward jets $+\not{E}_T$
[54] AAD	16AG	ATLS	ℓ + jets
[55] AAD	16M	ATLS	$pp \to H + \not{E}_T$, $H \to b\overline{b}$
[56] KHACHATRY...	16BZ	CMS	jet(s) + $\not{E}_T$
[57] KHACHATRY...	16CA	CMS	jets + $\not{E}_T$
[58] KHACHATRY...	16N	CMS	$pp \to \gamma + \not{E}_T$
[59] AAD	15AS	ATLS	$b\,(\overline{b}) + \not{E}_T$, $t\overline{t} + \not{E}_T$
[60] AAD	15BH	ATLS	jet + $\not{E}_T$
[61] AAD	15CF	ATLS	$H^0 + \not{E}_T$
[62] AAD	15CS	ATLS	$\gamma + \not{E}_T$
[63] KHACHATRY...	15AG	CMS	$t\overline{t} + \not{E}_T$
[64] KHACHATRY...	15AL	CMS	jet + $\not{E}_T$
[65] KHACHATRY...	15T	CMS	$\ell + \not{E}_T$
[66] AAD	14AI	ATLS	$W + \not{E}_T$
[67] AAD	14BK	ATLS	W, $Z + \not{E}_T$
[68] AAD	14K	ATLS	$Z + \not{E}_T$
[69] AAD	14O	ATLS	$Z + \not{E}_T$
[70] AAD	13AD	ATLS	jet + $\not{E}_T$
[71] AAD	13C	ATLS	$\gamma + \not{E}_T$
[72] AALTONEN	12K	CDF	$t + \not{E}_T$
[73] AALTONEN	12M	CDF	jet + $\not{E}_T$
[74] CHATRCHYAN	12AP	CMS	jet + $\not{E}_T$
[75] CHATRCHYAN	12T	CMS	$\gamma + \not{E}_T$

[1] AAD 21AZ search for DM in $H\,\not{E}_T \to \gamma\gamma\,\not{E}_T$ events with 139 fb^{-1} at 13 TeV. No signal observed. Limits placed for several simplified models.

[2] AAD 21BB search for DM in $H\,\not{E}_T \to b\overline{b}\,\not{E}_T$ events with 139 fb^{-1} at 13 TeV. No signal observed. Limits placed for several simplified models.

[3] AAD 21D search for $VV + \chi\chi$, $V \to q\overline{q}$ with 139 fb^{-1} at 13 TeV LHC. No signal detected. Limits placed in dark Higgs boson mass vs. m(Z') plane. Here VV stand for $W^{\pm}W^{\mp}$, ZZ.

[4] AAD 21F search for monojet recoiling against invisibles with 139 fb^{-1} at 13 TeV LHC. No signal detected. Limits placed in various simplified dark matter models.

[5] AAD 21K search for a photon recoiling against dark matter with 139 fb^{-1} at 13 TeV LHC. No signal detected. Limits placed on parameter space of various simplified models.

[6] AAD 21O search for ℓ + jets + $\not{E}_T$ to search for t-pairs + DM particles with 139 fb^{-1} at LHC 13 TeV LHC. No signal detected. Limits placed in the cross-section vs. mediator mass plane, assuming light DM states.

[7] AAD 21P search for $\ell^+\ell^-$ + jets + $\not{E}_T$ in context of various BSM models with 139 fb^{-1} at 13 TeV LHC. No signal observed. Limits placed in parameter space of dark matter models and SUSY.

[8] AAD 21S search for b-jets + $\not{E}_T$ signal from BSM/DM models with 139 fb^{-1} at 13 TeV LHC. No signal observed. Limits placed on parameter space of DM models.

[9] SIRUNYAN 21A search for DM production in association with leptonically decaying Z boson in 137 fb^{-1} at 13 TeV; no signal; limits set in large variety of simplified DM models.

[10] TUMASYAN 21D search for DM and other exotica at CMS in jets + $\not{E}_T$ events with 137 fb^{-1} at 13 TeV. No signal observed. Limits placed for a variety of simplified models.

[11] SIRUNYAN 20X search for DM in $pp \to Z' \to A(Z')h \to h + \not{E}_T$ in CMS at 13 TeV with 35.9 fb^{-1}; no signal; limits placed in σ^{SI} vs. m(χ), and σ, m(A) and tanβ vs m(Z') for considered DM models.

[12] AABOUD 19AA searches for BSM physics in more than 700 event classes with more than 10^5 regions at 13 TeV with 3.2 fb^{-1}; no significant signal.

[13] AABOUD 19AI searches for vector boson fusion $pp \to Hqq$, $H \to$ invisible at 13 TeV with 36.1 fb^{-1}; no signal: require B($H \to$ invisible) < 0.37 (0.28 expected).

[14] AABOUD 19AL perform search in three different channels for $H \to \chi\chi$ at 7, 8 and 13 TeV; combined result BF($H \to$ invisible) < 0.26 (0.17 expected).

[15] AABOUD 19Q search for single $t + \not{E}_T$ at 13 TeV with 36.1 fb^{-1} of data; no signal; limits set in σ or coupling vs. mass plane for simplified models.

[16] AABOUD 19V review ATLAS results from 7, 8 and 13 TeV searches for mediator-based DM and DE scalar which couples to gravity; no signal: limits set for large variety of simplified models .

[17] BANERJEE 19 search for dark photon via $eN \to eN+\not{E}$ in NA64; no signal, limits placed in kinetic mixing ϵ vs. m(DM) plane for m(DM) $\sim$ 0.001–1 GeV.

[18] SIRUNYAN 19AN search at 13 TeV with 35.9 fb^{-1} for $pp \to H\chi\chi \to b\overline{b}\,\not{E}_T$; no signal: limits set in the context of a 2HDM + pseudoscalar (a) model and a baryonic Z' model.

[19] SIRUNYAN 19BC search for DM via LeptoQuark pair annihilation LQ LQ $\to \mu j\chi\chi \to \mu j\,\not{E}_T$ with 77.4 fb^{-1}, 13 TeV; no signal: limits placed in m(χ) vs. m(LQ) plane. Model dependent limits on DM mass up to 600 GeV depending on m(LQ) placed.

[20] SIRUNYAN 19BO search for vector boson fusion $VV \to qqH$ with $H \to \chi\chi$ at 13 TeV with 38.2 fb^{-1}; no signal: limits placed for several models. Also search for $H \to$ invisible at 7, 8, and 13 TeV; no signal: limit placed on BF < 0.19.

[21] SIRUNYAN 19C search for DM via $pp \to t\overline{t}\chi\chi$ at 13 TeV, 35.9 fb^{-1}; no signal; limits placed on coupling vs. mediator mass for various simplified models.

[22] SIRUNYAN 19O search for $pp \to \gamma$ at 13 TeV with 35.9 fb^{-1}; no signal: limits placed on parameters of various models.

[23] SIRUNYAN 19X search for $pp \to t\overline{t}\,\not{E}_T$ and $pp \to t\,\not{E}_T + ...$ at 13 TeV with 35.9 fb^{-1}; no signal: limits placed on χ production σ for various simplified models with m(χ) = 1 GeV.

[24] AABOUD 18 search for $pp \to Z + \not{E}_T$ with $Z \to \ell\ell$ at 13 TeV with 36.1 fb^{-1} of data. Limits set for simplified models.

[25] AABOUD 18A search for $pp \to t\overline{t}\,\not{E}_T$ or $pp \to b\overline{b}\,\not{E}_T$ at 13 TeV, 36.1 fb^{-1} of data. Limits set for simplified models.

[26] AABOUD 18CA search for $pp \to V\chi\chi$ with $V \to jj$ at 13 TeV, 36.1 fb^{-1}; no signal; limits set in m(DM) vs m(mediator) simplified model plane .

[27] AABOUD 18I search for $pp \to j + \not{E}_T$ at 13 TeV with 36.1 fb^{-1} of data. Limits set for simplified models with pair-produced weakly interacting dark-matter candidates.

[28] AGUILAR-AREVALO 18B search for WIMP production in MiniBooNE p beam dump; no signal; limits set for m(χ) $\sim$ 5–50 MeV in vector portal DM model.

[29] KHACHATRYAN 18 search for $pp \to Z(\ell\ell) + \not{E}_T$; no signal ; limits set on effective dark matter interactions and other exotic physics models .

[30] SIRUNYAN 18BF search for $pp \to t\,\not{E}_T$ at 13 TeV and 36 fb^{-1}; no signal; limits placed on DM models involving a flavor changing neutral current, scalar resonance decaying to top quark and DM.

[31] SIRUNYAN 18BO search for high mass dijet resonances at 13 TeV and 36 fb^{-1}; no signal: limits placed on various models, including simplified DM models involving a spin = 1 Z' mediator.

[32] SIRUNYAN 18BV search for $pp \to Z\,\not{E}_T$ at 13 TeV; no signal, limits placed for various exotic physics models including DM.

[33] SIRUNYAN 18C search for new physics in $pp \to$ final states with two oppositely charged leptons at 13 TeV with 35.9 fb^{-1}. Limits placed on m(mediator) and top squark for various simplified models.

[34] SIRUNYAN 18CU search for $pp \to Z\,\not{E}_T$ at 13 TeV and 2.3 fb^{-1}; no signal: limits placed for various exotic models including DM .

[35] SIRUNYAN 18DH search for $pp \to \chi\chi h$; $h \to \gamma\gamma$ or $\tau\overline{\tau}$ at 13 TeV, 35.9 fb^{-1}; no signal; limits placed on massive boson mediator Z' in the context of Z'+2HDM and baryonic Z' models. Limits also cast in terms of spin-independent WIMP-nucleon cross section for masses 1–200 GeV.

[36] SIRUNYAN 18S search for $pp \to$ jets $\not{E}_T$ at 13 TeV; no signal: limits placed on simplified dark matter models, on the branching ratio of the Higgs boson to invisible particles, and on several other exotic physics models including fermion portal DM.

[37] AABOUD 17A search for $H \to b\overline{b} + \not{E}_T$. See Fig. 4b for limits set on VB mediator vs WIMP mass.

[38] AABOUD 17AM search for $pp \to Z' \to Ah \to h(b\overline{b}) + \not{E}_T$ at 13 TeV. Limits set in m(Z') vs. m(A) plane and on the visible cross section of $h(b\overline{b}) + \not{E}_T$ events in bins of $\not{E}_T$.

[39] AABOUD 17AQ search for WIMP in $pp \to h(\gamma\gamma) + \not{E}_T$ in 36.1 fb^{-1} of data. Limits on the visible cross section are also provided. Model dependent limits on spin independent DM - Nucleon cross-section are also presented, which are more stringent than those from direct searches for DM mass smaller than 2.5 GeV .

[40] AABOUD 17BD search for $pp \to$ jet(s) + $\not{E}_T$ at 13 TeV with 3.2 fb^{-1} of data. Limits set for simplified models. Observables corrected for detector effects can be used to constrain other models.

[41] AABOUD 17R, for an axial vector mediator in the s-channel, excludes m(mediator) $<$ 750–1200 GeV for m(DM) $<$ 230–480 GeV, depending on the couplings.

[42] AGUILAR-AREVALO 17A search for DM produced in 8 GeV proton collisions with steel beam dump followed by DM-nucleon scattering in MiniBooNE detector. Limit placed on DM cross section parameter $Y < 2 \times 10^{-8}$ for $\alpha_D = 0.5$ and for $0.01 < m$(DM) $<$ 0.3 GeV.

[43] BANERJEE 17 search for dark photon invisible decay via $e\,N$ scattering; exclude m(γ') $<$ 100 MeV as an explanation of (g_μ−2) muon anomaly.

[44] KHACHATRYAN 17A search for WIMPs in forward jets + $\not{E}_T$ channel with 18.5 fb^{-1} at 8 TeV; limits set in effective theory model, Fig. 3.

[45] KHACHATRYAN 17F search for $H \to$ invisibles in pp collisions at 7, 8, and 13 TeV; place limits on Higgs portal DM.

[46] SIRUNYAN 17 search for $pp \to Z + \not{E}_T$ with 2.3 fb^{-1} at 13 TeV; no signal seen; limits placed on WIMPs and unparticles.

[47] SIRUNYAN 17AP search for $pp \to Z' \to Ah \to h + \not{E}_T$ with $h \to b\overline{b}$ or $\gamma\gamma$ and $A \to \chi\chi$ with 2.3 fb^{-1} at 13 TeV. Limits set in m(Z') vs. m(A) plane.

[48] SIRUNYAN 17AQ search for $pp \to \gamma + \not{E}_T$ at 13 TeV with 12.9 fb^{-1}. Limits derived for simplified DM models, effective electroweak-DM interaction and Extra Dimensions models.

[49] SIRUNYAN 17BB search for WIMPs via $pp \to t\overline{t}+\not{E}_T$, $pp \to b\overline{b}+\not{E}_T$ at 13 TeV with 2.2 fb^{-1}. Limits derived for various simplified models.

[50] SIRUNYAN 17G search for $pp \to j + \not{E}_T$ with 12.9 fb^{-1} at 13 TeV; limits placed on WIMP mass/mediators in DM simplified models.

[51] SIRUNYAN 17U search for WIMPs/unparticles via $pp \to Z\chi\chi$, $Z \to \ell\overline{\ell}$ at 13 TeV with 2.3 fb^{-1}. Limits derived for various simplified models.

[52] AABOUD 16AD place limits on VVXX effective theory via search for hadronic W or Z plus WIMP pair production. See Fig. 5.

[53] AAD 16AF search for $VV \to (H \to$ WIMP pair) + forward jets with 20.3 fb^{-1} at 8 TeV; set limits in Higgs portal model, Fig. 8 .

[54] AAD 16AG search for lepton jets with 20.3 fb^{-1} of data at 8 TeV; Fig. 13 excludes dark photons around 0.1–1 GeV for kinetic mixing 10^{-6}–10^{-2}.

[55] AAD 16M search with 20.3 fb^{-1} of data at 8 TeV pp collisions; limits placed on EFT model (Fig. 7) and simplified Z' model (Fig. 6).

[56] KHACHATRYAN 16BZ search for jet(s) + $\not{E}_T$ in 19.7 fb^{-1} at 8 TeV; limits set for variety of simplified models.

[57] KHACHATRYAN 16CA search for WIMPs via jet(s) + $\not{E}_T$ using razor variable; require mediator scale $>$ 1 TeV for various effective theories.

[58] KHACHATRYAN 16N search for γ + WIMPs in 19.6 fb^{-1} at 8 TeV; limits set on SI and SD WIMP-p scattering in Fig. 3.

[59] AAD 15AS search for events with one or more bottom quark and missing E_T, and also events with a top quark pair and missing E_T in pp collisions at $E_{\rm cm}$ = 8 TeV with L = 20.3 fb^{-1}. See their Figs. 5 and 6 for translated limits on X^0-nucleon cross section for m = 1–700 GeV.

[60] AAD 15BH search for events with a jet and missing E_T in pp collisions at $E_{\rm cm}$ = 8 TeV with L = 20.3 fb^{-1}. See their Fig. 12 for translated limits on X^0-nucleon cross section for m = 1–1200 GeV.

[61] AAD 15CF search for events with a H^0 ($\to \gamma\gamma$) and missing E_T in pp collisions at $E_{\rm cm}$ = 8 TeV with L = 20.3 fb^{-1}. See paper for limits on the strength of some contact interactions containing X^0 and the Higgs fields.

[62] AAD 15CS search for events with a photon and missing E_T in pp collisions at $E_{\rm cm}$ = 8 TeV with L = 20.3 fb^{-1}. See their Fig. 13 (see also erratum) for translated limits on X^0-nucleon cross section for m = 1–1000 GeV.

[63] KHACHATRYAN 15AG search for events with a top quark pair and missing E_T in pp collisions at $E_{\rm cm}$ = 8 TeV with L = 19.7 fb^{-1}. See their Fig. 8 for translated limits on X^0-nucleon cross section for m = 1–200 GeV.

Downloaded from https://academic.oup.com/ptep/article/2022/8/083C01/6651666 by KIT Library user on 27 September 2022

[64] KHACHATRYAN 15AL search for events with a jet and missing E_T in pp collisions at E_{cm} = 8 TeV with L = 19.7 fb^{-1}. See their Fig. 5 and Tables 4–6 for translated limits on X^0-nucleon cross section for m = 1–1000 GeV.

[65] KHACHATRYAN 15T search for events with a lepton and missing E_T in pp collisions at E_{cm} = 8 TeV with L = 19.7 fb^{-1}. See their Fig. 17 for translated limits on X^0-proton cross section for m = 1–1000 GeV.

[66] AAD 14AI search for events with a W and missing E_T in pp collisions at E_{cm} = 8 TeV with L = 20.3 fb^{-1}. See their Fig. 4 for translated limits on X^0–nucleon cross section for m = 1–1500 GeV.

[67] AAD 14BK search for hadronically decaying W, Z in association with $\not{E}_T$ in 20.3 fb^{-1} at 8 TeV pp collisions. Fig. 5 presents exclusion results for SI and SD scattering cross section. In addition, cross section limits on the anomalous production of W or Z bosons with large missing transverse momentum are also set in two fiducial regions.

[68] AAD 14K search for events with a Z and missing E_T in pp collisions at E_{cm} = 8 TeV with L = 20.3 fb^{-1}. See their Fig. 5 and 6 for translated limits on X^0–nucleon cross section for m = 1–10^3 GeV.

[69] AAD 14O search for ZH^0 production with H^0 decaying to invisible final states. See their Fig. 4 for translated limits on X^0–nucleon cross section for m = 1–60 GeV in Higgs-portal X^0 scenario.

[70] AAD 13AD search for events with a jet and missing E_T in pp collisions at E_{cm} = 7 TeV with L = 4.7 fb^{-1}. See their Figs. 5 and 6 for translated limits on X^0-nucleon cross section for m = 1–1300 GeV.

[71] AAD 13C search for events with a photon and missing E_T in pp collisions at E_{cm} = 7 TeV with L = 4.6 fb^{-1}. See their Fig. 3 for translated limits on X^0-nucleon cross section for m = 1–1000 GeV.

[72] AALTONEN 12K search for events with a top quark and missing E_T in $p\overline{p}$ collisions at E_{cm} = 1.96 TeV with L = 7.7 fb^{-1}. Upper limits on $\sigma(tX^0)$ in the range 0.4–2 pb (95% CL) is given for m_{X^0} = 0–150 GeV.

[73] AALTONEN 12M search for events with a jet and missing E_T in $p\overline{p}$ collisions at E_{cm} = 1.96 TeV with L = 6.7 fb^{-1}. Upper limits on the cross section in the range 2–10 pb (90% CL) is given for m_{X^0} = 1–300 GeV. See their Fig. 2 for translated limits on X^0-nucleon cross section.

[74] CHATRCHYAN 12AP search for events with a jet and missing E_T in pp collisions at E_{cm} = 7 TeV with L = 5.0 fb^{-1}. See their Fig. 4 for translated limits on X^0-nucleon cross section for m_{X^0} = 0.1–1000 GeV.

[75] CHATRCHYAN 12T search for events with a photon and missing E_T in pp collisions at E_{cm} = 7 TeV with L = 5.0 fb^{-1}. Upper limits on the cross section in the range 13–15 fb (90% CL) is given for m_{X^0} = 1–1000 GeV. See their Fig. 2 for translated limits on X^0-nucleon cross section.

REFERENCES FOR WIMP and Dark Matter Searches

ADHIKARI	22	PRL 128 011801	P. Adhikari *et al.*	(DEAP Collab.)
AAD	21AZ	JHEP 2110 013	G. Aad *et al.*	(ATLAS Collab.)
AAD	21BB	JHEP 2111 209	G. Aad *et al.*	(ATLAS Collab.)
AAD	21D	PRL 126 121802	G. Aad *et al.*	(ATLAS Collab.)
AAD	21F	PR D103 112006	G. Aad *et al.*	(ATLAS Collab.)
AAD	21K	JHEP 2102 226	G. Aad *et al.*	(ATLAS Collab.)
AAD	21O	JHEP 2104 174	G. Aad *et al.*	(ATLAS Collab.)
AAD	21P	JHEP 2104 165	G. Aad *et al.*	(ATLAS Collab.)
AAD	21S	JHEP 2105 093	G. Aad *et al.*	(ATLAS Collab.)
ABDALLAH	21	PR D103 102002	H. Abdallah *et al.*	(H.E.S.S. Collab.)
AKERIB	21A	PR D104 012011	D.S. Akerib *et al.*	(LUX Collab.)
AKERIB	21B	PR D104 062005	D.S. Akerib *et al.*	(LUX Collab.)
ALKHATIB	21	PRL 127 061801	I. Alkhatib *et al.*	(SuperCDMS Collab.)
AMARE	21	PR D103 102005	J. Amare *et al.*	(ANAIS Collab.)
ANDRIAMIR...	21A	PR D104 012009	M. Andriamirado *et al.*	(PROSPECT Collab.)
APRILE	21	PRL 126 091301	E. Aprile *et al.*	(XENON1T Collab.)
APRILE	21A	PR D103 063028	E. Aprile *et al.*	(XENON1T Collab.)
CHENG	21	PRL 126 211803	C. Cheng *et al.*	(PandaX-II Collab.)
CIRELLI	21	PR D103 063022	M. Cirelli *et al.*	
IKEDA	21	PTEP 2021 063F01	T. Ikeda *et al.*	(NEWAGE Collab.)
JOHN	21	JCAP 2112 007	I. John, T. Linden	(STOH)
MENG	21B	PRL 127 261802	Y. Meng *et al.*	(PandaX-4T Collab.)
SIRUNYAN	21A	EPJ C81 13	A.M. Sirunyan *et al.*	(CMS Collab.)
Also		EPJ C81 333 (errat.)	A.M. Sirunyan *et al.*	(CMS Collab.)
TUMASYAN	21D	JHEP 2111 153	A. Tumasyan *et al.*	(CMS Collab.)
AARTSEN	20C	EPJ C80 819	M.G. Aartsen *et al.*	(IceCube, PICO Collabs)
ABAZAJIAN	20	PR D102 043012	K.N. Abazajian *et al.*	(UCI, VPI, TOKY+)
ABDALLAH	20	PR D102 062001	H. Abdallah *et al.*	(H.E.S.S. Collab.)
ABDELHAME...	20A	EPJ C80 834	A.H. Abdelhameed *et al.*	(CRESST Collab.)
ABE	20G	PR D102 072002	K. Abe *et al.*	(Super-Kamiokande Collab.)
ADHIKARI	20	PR D102 082001	P. Adhikari *et al.*	(DEAP-3600 Collab.)
AGOSTINI	20	PRL 125 011801	M. Agostini *et al.*	(GERDA Collab.)
AGUILAR-AR...	20C	PRL 125 241803	A. Aguilar-Arevalo	(DAMIC Collab.)
AKERIB	20	PR D101 012003	D.S. Akerib *et al.*	(LUX Collab.)
AKERIB	20A	PR D101 042001	D.S. Akerib *et al.*	(LUX Collab.)
ALBERT	20	PR D101 103001	A. Albert *et al.*	(HAWC Collab.)
ALBERT	20A	PL B805 135439	A. Albert *et al.*	(ANTARES Collab.)
ALBERT	20C	PR D102 082002	A. Albert *et al.*	(ANTARES and IceCube Collab.)
ALVAREZ	20	JCAP 2009 004	A. Alvarez *et al.*	
AMARAL	20	PR D102 091101	D.W. Amaral *et al.*	(SuperCDMS Collab.)
ANDRIANAV...	20	PR D102 042001	A. Andrianavalomahefa *et al.*	(FUNK Collab.)
APRILE	20	PR D102 072004	E. Aprile *et al.*	(XENON Collab.)
ARNAUD	20	PRL 125 141301	Q. Arnaud *et al.*	(EDELWEISS Collab.)
BARAK	20	PRL 125 171802	L. Barak *et al.*	(SENSEI Collab.)
CLARK	20	PR D102 123026	M. Clark *et al.*	(PURD)
Also		PR D104 129903 (errat.)	M. Clark *et al.*	
FELIZARDO	20	IJMP A35 2030005	M. Felizardo	(SIMPLE Collab.)
HOOF	20	JCAP 2002 012	S. Hoof, A. Geringer-Sameth, R. Trotta	(GOET+)
MAZZIOTTA	20	PR D102 022003	M.N. Mazziotta *et al.*	
SIRUNYAN	20X	JHEP 2003 025	A.M. Sirunyan *et al.*	(CMS Collab.)
WANG	20G	CP C44 125001	Q. Wang *et al.*	(PandaX-II Collab.)
AABOUD	19AA	EPJ C79 120	M. Aaboud *et al.*	(ATLAS Collab.)
AABOUD	19AI	PL B793 499	M. Aaboud *et al.*	(ATLAS Collab.)
AABOUD	19AL	PRL 122 231801	M. Aaboud *et al.*	(ATLAS Collab.)
AABOUD	19Q	JHEP 1905 041	M. Aaboud *et al.*	(ATLAS Collab.)
AABOUD	19V	JHEP 1905 142	M. Aaboud *et al.*	(ATLAS Collab.)
ABDELHAME...	19	EPJ C79 630	A.H. Abdelhameed *et al.*	(CRESST Collab.)
ABDELHAME...	19A	PR D100 102002	A.H. Abdelhameed *et al.*	(CRESST Collab.)
ABE	19	PL B789 45	K. Abe *et al.*	(XMASS Collab.)
ABEYSEKARA	19	JCAP 1907 022	A.U. Abeysekara *et al.*	(HAWC Collab.)
ABRAMOFF	19	PRL 122 161801	O. Abramoff *et al.*	(SENSEI Collab.)
ADHIKARI	19	PRL 123 031302	G. Adhikari *et al.*	(COSINE-100 Collab.)
AGNESE	19A	PR D99 062001	R. Agnese *et al.*	(CDMS Collab.)
AGUILAR-AR...	19A	PRL 123 181802	A. Aguilar-Arevalo *et al.*	(DAMIC Collab.)
AJAJ	19	PR D100 022004	R. Ajaj *et al.*	(DEAP-3600 Collab.)
AKERIB	19	PRL 122 131301	D.S. Akerib *et al.*	(LUX Collab.)
ALBERT	19B	JCAP 1904 E01	A. Albert *et al.*	(HAWC Collab.)
AMARE	19	PRL 123 031301	J. Amare *et al.*	(ANAIS Collab.)
AMOLE	19	PR D100 022001	C. Amole *et al.*	(PICO Collab.)
ANGLOHER	19	EPJ C79 43	G. Angloher *et al.*	(CRESST-II Collab.)
APRILE	19	PRL 122 071301	E. Aprile *et al.*	(XENON1T Collab.)
APRILE	19A	PRL 122 141301	E. Aprile *et al.*	(XENON1T Collab.)
APRILE	19C	PRL 123 241803	E. Aprile *et al.*	(XENON1T Collab.)
APRILE	19D	PRL 123 251801	E. Aprile *et al.*	(XENON1T Collab.)
ARMENGAUD	19	PR D99 082003	E. Armengaud *et al.*	(EDELWEISS Collab.)
BANERJEE	19	PRL 123 121801	D. Banerjee *et al.*	(NA64 Collab.)
BRINGMANN	19	PRL 122 171801	T. Bringmann, M. Pospelov	(OSLO, VICT)
BRUNE	19	PR D99 096005	T. Brune, H. Pas	(DORT)
CHEUNG	19	PL B789 137	K. Cheung *et al.*	
CHOI	19	PR D99 083018	K.-Y. Choi, J. Kim, C. Rott	(SUNG)
DI-MAURO	19	PR D99 123027	M. Di Mauro *et al.*	
HA	19	PRL 122 131802	C. Ha *et al.*	(COSINE-100 Collab.)
JOHNSON	19	PR D99 103007	C. Johnson *et al.*	
KIM	19A	JHEP 1903 194	K.W. Kim *et al.*	(KIMS Collab.)
KLOPF	19	PRL 122 222503	M. Klopf *et al.*	(PERKEO II Collab.)
KOBAYASHI	19	PL B795 308	M. Kobayashi *et al.*	(XMASS Collab.)
LI	19D	PR D99 123519	S. Li *et al.*	
LIU	19B	PRL 123 161301	Z.Z. Liu *et al.*	(CDEX Collab.)
NG	19	PR D99 083005	K.C.Y. Ng *et al.*	
QUEIROZ	19	JCAP 1904 048	F.S. Queiroz, C. Siqueira	
SEONG	19	PRL 122 011801	I.S. Seong *et al.*	(BELLE Collab.)
SIRUNYAN	19AN	EPJ C79 280	A.M. Sirunyan *et al.*	(CMS Collab.)
SIRUNYAN	19BC	PL B795 76	A.M. Sirunyan *et al.*	(CMS Collab.)
SIRUNYAN	19BO	PL B793 520	A.M. Sirunyan *et al.*	(CMS Collab.)
SIRUNYAN	19C	PRL 122 011803	A.M. Sirunyan *et al.*	(CMS Collab.)
SIRUNYAN	19O	JHEP 1902 074	A.M. Sirunyan *et al.*	(CMS Collab.)
SIRUNYAN	19X	JHEP 1903 141	A.M. Sirunyan *et al.*	(CMS Collab.)
SUZUKI	19	ASP 110 1	T. Suzuki *et al.*	(XMASS Collab.)
XIA	19A	PL B792 193	J. Xia *et al.*	(PandaX-II Collab.)
YAGUNA	19	JCAP 1904 041	C. Yaguna	
YANG	19	PRL 123 221301	L.T. Yang *et al.*	(CDEX Collab.)
AABOUD	18	PL B776 318	M. Aaboud *et al.*	(ATLAS Collab.)
AABOUD	18A	EPJ C78 18	M. Aaboud *et al.*	(ATLAS Collab.)
AABOUD	18CA	JHEP 1810 180	M. Aaboud *et al.*	(ATLAS Collab.)
AABOUD	18I	JHEP 1801 126	M. Aaboud *et al.*	(ATLAS Collab.)
AARTSEN	18D	EPJ C78 831	M.G. Aartsen *et al.*	(IceCube Collab.)
ABDALLAH	18	PRL 120 201101	H. Abdallah *et al.*	(H.E.S.S. Collab.)
ABE	18C	PR D97 102006	K. Abe *et al.*	(XMASS Collab.)
ABE	18F	PL B787 153	K. Abe *et al.*	(XMASS Collab.)
ADHIKARI	18	NAT 564 83	G. Adhikari *et al.*	(COSINE-100 Collab.)
AGNES	18	PRL 121 081307	P. Agnes *et al.*	(DarkSide-50 Collab.)
AGNES	18A	PR D98 102006	P. Agnes *et al.*	(DarkSide-50 Collab.)
AGNES	18B	PRL 121 111303	P. Agnes *et al.*	(DarkSide-50 Collab.)
AGNESE	18	PR D97 022002	R. Agnese *et al.*	(SuperCDMS Collab.)
AGNESE	18A	PRL 120 061802	R. Agnese *et al.*	(SuperCDMS Collab.)
AGNESE	18B	PRL 121 051301	R. Agnese *et al.*	(SuperCDMS Collab.)
Also		PRL 122 069901 (errat.)	R. Agnese *et al.*	(SuperCDMS Collab.)
AGUILAR-AR...	18B	PR D98 112004	A.A. Aguilar-Arevalo	(MiniBooNE Collab.)
AHNEN	18	JCAP 1803 009	M.L. Ahnen *et al.*	(MAGIC Collab.)
AKERIB	18A	PR D98 062005	D.S. Akerib *et al.*	(LUX Collab.)
ALBERT	18B	JCAP 1806 043	A. Albert *et al.*	(HAWC Collab.)
ALBERT	18C	PR D98 123012	A. Albert *et al.*	(HAWC Collab.)
AMAUDRUZ	18	PRL 121 071801	P.A. Amaudruz *et al.*	(DEAP-3600 Collab.)
APRILE	18	PRL 121 111302	E. Aprile *et al.*	(XENON1T Collab.)
ARMENGAUD	18	PR D98 082004	E. Armengaud *et al.*	(EDELWEISS-III Collab.)
ARNAUD	18	ASP 97 54	Q. Arnaud *et al.*	(NEWS-G Collab.)
CHANG	18A	PR D98 123004	L.J. Chang, M. Lisanti, S. Mishra-Sharma	(PRIN)
CRISLER	18	PRL 121 061803	M. Crisler *et al.*	(SENSEI Collab.)
JIANG	18	PRL 120 241301	H. Jiang *et al.*	(CDEX Collab.)
KACHULIS	18	PRL 120 221301	C. Kachulis *et al.*	(Super-Kamiokande Collab.)
KHACHATRY...	18	PR D97 099903	V. Khachatryan *et al.*	(CMS Collab.)
LISANTI	18	PRL 120 101101	M. Lisanti *et al.*	(PRIN, MIT, MICH)
MAZZIOTTA	18	PR D98 022006	M. Mazziotta *et al.*	(Fermi-LAT Collab.)
REN	18	PRL 121 021304	X. Ren *et al.*	(PandaX-II Collab.)
SIRUNYAN	18BF	JHEP 1806 027	A.M. Sirunyan *et al.*	(CMS Collab.)
SIRUNYAN	18BO	JHEP 1808 130	A.M. Sirunyan *et al.*	(CMS Collab.)
SIRUNYAN	18BV	EPJ C78 291	A.M. Sirunyan *et al.*	(CMS Collab.)
SIRUNYAN	18C	PR D97 032009	A.M. Sirunyan *et al.*	(CMS Collab.)
SIRUNYAN	18CU	JHEP 1801 056	A.M. Sirunyan *et al.*	(CMS Collab.)
SIRUNYAN	18DH	JHEP 1809 046	A.M. Sirunyan *et al.*	(CMS Collab.)
SIRUNYAN	18S	PR D97 092005	A.M. Sirunyan *et al.*	(CMS Collab.)
YANG	18	CP C42 023002	L.T. Yang *et al.*	(CDEX Collab.)
AABOUD	17A	PL B765 11	M. Aaboud *et al.*	(ATLAS Collab.)
AABOUD	17AM	PRL 119 181804	M. Aaboud *et al.*	(ATLAS Collab.)
AABOUD	17AQ	PR D96 112004	M. Aaboud *et al.*	(ATLAS Collab.)
AABOUD	17BD	EPJ C77 765	M. Aaboud *et al.*	(ATLAS Collab.)
AABOUD	17R	EPJ C77 393	M. Aaboud *et al.*	(ATLAS Collab.)
AARTSEN	17	EPJ C77 82	M.G. Aartsen *et al.*	(IceCube Collab.)
AARTSEN	17A	EPJ C77 146	M.G. Aartsen *et al.*	(IceCube Collab.)
Also		EPJ C79 214 (errat.)	M.G. Aartsen *et al.*	(IceCube Collab.)
AARTSEN	17C	EPJ C77 627	M.G. Aartsen *et al.*	(IceCube Collab.)
AGUILAR-AR...	17	PRL 118 141803	A. Aguilar-Arevalo *et al.*	(DAMIC Collab.)
AGUILAR-AR...	17A	PRL 118 221803	A.A. Aguilar-Arevalo *et al.*	(MiniBooNE Collab.)
AKERIB	17	PRL 118 021303	D.S. Akerib *et al.*	(LUX Collab.)
AKERIB	17A	PRL 118 251302	D.S. Akerib *et al.*	(LUX Collab.)
ALBERT	17A	PL B769 249	A. Albert *et al.*	(ANTARES Collab.)
Also		PL B796 253 (errat.)	A. Albert *et al.*	(ANTARES Collab.)
AMOLE	17	PRL 118 251301	C. Amole *et al.*	(PICO Collab.)
ANGLOHER	17A	EPJ C77 637	G. Angloher *et al.*	(CRESST Collab.)
APRILE	17	PRL 118 101101	E. Aprile *et al.*	(XENON100 Collab.)
APRILE	17A	PR D96 022008	E. Aprile *et al.*	(XENON100 Collab.)
APRILE	17D	PR D96 042004	E. Aprile *et al.*	(XENON100 Collab.)
APRILE	17G	PRL 119 181301	E. Aprile *et al.*	(XENON Collab.)
APRILE	17H	PR D96 122002	E. Aprile *et al.*	(XENON100 Collab.)
APRILE	17K	JCAP 1710 039	E. Aprile *et al.*	(XENON100 Collab.)
ARCHAMBAU...	17	PR D95 082001	S. Archambault *et al.*	(VERITAS Collab.)
AVRORIN	17	JETP 125 80	A.D. Avrorin *et al.*	(BAIKAL Collab.)
BANERJEE	17	PRL 118 011802	D. Banerjee *et al.*	(NA64 Collab.)
BARBOSA-D...	17	PR D95 032006	E. Barbosa de Souza *et al.*	(DM17 Collab.)
BATTAT	17	ASP 91 65	J.B.R. Battat *et al.*	(DRIFT-IId Collab.)
BEHNKE	17	ASP 90 85	E. Behnke *et al.*	(PICASSO Collab.)
BOUDAUD	17	PRL 119 021103	M. Boudaud, J. Lavalle, P. Salati	
CHEN	17E	PR D96 102007	X. Chen *et al.*	(PandaX-II Collab.)
CUI	17A	PRL 119 181302	X. Cui *et al.*	(PandaX-II Collab.)
FU	17	PRL 118 071301	C. Fu *et al.*	(PandaX-II Collab.)
Also		PRL 120 049902 (errat.)	C. Fu *et al.*	(PandaX-II Collab.)
KHACHATRY...	17A	PRL 118 021802	V. Khachatryan *et al.*	(CMS Collab.)
KHACHATRY...	17F	JHEP 1702 135	V. Khachatryan *et al.*	(CMS Collab.)
SIRUNYAN	17	JHEP 1703 061	A.M. Sirunyan *et al.*	(CMS Collab.)
SIRUNYAN	17AP	JHEP 1710 180	A.M. Sirunyan *et al.*	(CMS Collab.)
SIRUNYAN	17AQ	JHEP 1710 073	A.M. Sirunyan *et al.*	(CMS Collab.)
SIRUNYAN	17BB	EPJ C77 845	A.M. Sirunyan *et al.*	(CMS Collab.)
SIRUNYAN	17G	JHEP 1707 014	A.M. Sirunyan *et al.*	(CMS Collab.)
SIRUNYAN	17U	JHEP 1709 106	A.M. Sirunyan *et al.*	(CMS Collab.)
AABOUD	16AD	PL B763 251	M. Aaboud *et al.*	(ATLAS Collab.)

Downloaded from https://academic.oup.com/ptep/article/2022/8/083C01/6651666 by KIT Library user on 27 September 2022

AABOUD	16D	PR D94 032005	M. Aaboud *et al.*	(ATLAS Collab.)
AABOUD	16F	JHEP 1606 059	M. Aaboud *et al.*	(ATLAS Collab.)
AAD	16AF	JHEP 1601 172	G. Aad *et al.*	(ATLAS Collab.)
AAD	16AG	JHEP 1602 062	G. Aad *et al.*	(ATLAS Collab.)
AAD	16M	PR D93 072007	G. Aad *et al.*	(ATLAS Collab.)
AARTSEN	16C	JCAP 1604 022	M.G. Aartsen *et al.*	(IceCube Collab.)
AARTSEN	16D	EPJ C76 531	M.G. Aartsen *et al.*	(IceCube Collab.)
ABDALLAH	16	PRL 117 111301	H. Abdallah *et al.*	(H.E.S.S. Collab.)
ABDALLAH	16A	PRL 117 151302	H. Abdallah *et al.*	(H.E.S.S. Collab.)
ADRIAN-MAR...	16	PL B759 69	S. Adrian-Martinez *et al.*	(ANTARES Collab.)
ADRIAN-MAR...	16B	JCAP 1605 016	S. Adrian-Martinez *et al.*	(ANTARES Collab.)
AGNES	16	PR D93 081101	P. Agnes *et al.*	(DarkSide-50 Collab.)
AGNESE	16	PRL 116 071301	R. Agnese *et al.*	(SuperCDMS Collab.)
AGUILAR-AR...	16	PR D94 082006	A. Aguilar-Arevalo *et al.*	(DAMIC Collab.)
AHNEN	16	JCAP 1602 039	M.L. Ahnen *et al.*	(MAGIC and Fermi-LAT Collab.)
AKERIB	16	PRL 116 161301	D.S. Akerib *et al.*	(LUX Collab.)
AKERIB	16A	PRL 116 161302	D.S. Akerib *et al.*	(LUX Collab.)
AMOLE	16	PR D93 052014	C. Amole *et al.*	(PICO Collab.)
AMOLE	16A	PR D93 061101	C. Amole *et al.*	(PICO Collab.)
ANGLOHER	16	EPJ C76 25	G. Angloher *et al.*	(CRESST-II Collab.)
ANGLOHER	16A	PRL 117 021303	G. Angloher *et al.*	(CRESST-II Collab.)
APRILE	16	PR D94 092001	E. Aprile *et al.*	(XENON100 Collab.)
APRILE	16B	PR D94 122001	E. Aprile *et al.*	(XENON100 Collab.)
ARMENGAUD	16	JCAP 1605 019	E. Armengaud *et al.*	(EDELWEISS-III Collab.)
AVRORIN	16	ASP 81 12	A.D. Avrorin *et al.*	(BAIKAL Collab.)
CAPUTO	16	PR D93 062004	R. Caputo *et al.*	
FORNASA	16	PR D94 123005	M. Fornasa *et al.*	(Fermi-LAT Collab.)
HEHN	16	EPJ C76 548	L. Hehn *et al.*	(EDELWEISS-III Collab.)
KHACHATRY...	16AJ	PR D93 052011	V. Khachatryan *et al.*	(CMS Collab.)
KHACHATRY...	16BZ	JHEP 1612 083	V. Khachatryan *et al.*	(CMS Collab.)
Also		JHEP 1708 035 (errat.)	V. Khachatryan *et al.*	(CMS Collab.)
KHACHATRY...	16CA	JHEP 1612 088	V. Khachatryan *et al.*	(CMS Collab.)
KHACHATRY...	16N	PL B755 102	V. Khachatryan *et al.*	(CMS Collab.)
LEITE	16	JCAP 1611 021	N. Leite *et al.*	
LI	16	PR D93 043518	S. Li *et al.*	
LI	16A	JCAP 1612 028	Z. Li *et al.*	
LIANG	16	PR D94 103502	Y.-F. Liang *et al.*	
LU	16	PR D93 103517	B-Q. Lu, H-S. Zong	
SHIRASAKI	16	PR D94 063522	M. Shirasaki *et al.*	
TAN	16	PR D93 122009	T.H. Tan *et al.*	(PandaX Collab.)
TAN	16B	PRL 117 121303	A. Tan *et al.*	(PandaX Collab.)
ZHAO	16	PR D93 092003	W. Zhao *et al.*	(CDEX Collab.)
AAD	15AS	EPJ C75 92	G. Aad *et al.*	(ATLAS Collab.)
AAD	15BH	EPJ C75 299	G. Aad *et al.*	(ATLAS Collab.)
Also		EPJ C75 408 (errat.)	G. Aad *et al.*	(ATLAS Collab.)
AAD	15CF	PRL 115 131801	G. Aad *et al.*	(ATLAS Collab.)
AAD	15CS	PR D91 012008	G. Aad *et al.*	(ATLAS Collab.)
Also		PR D92 059903 (errat.)	G. Aad *et al.*	(ATLAS Collab.)
AARTSEN	15C	EPJ C75 20	M.G. Aartsen *et al.*	(IceCube Collab.)
AARTSEN	15E	EPJ C75 492	M.G. Aartsen *et al.*	(IceCube Collab.)
ABRAMOWSKI	15	PRL 114 081301	A. Abramowski *et al.*	(H.E.S.S. Collab.)
ACKERMANN	15	PR D91 122002	M. Ackermann *et al.*	(Fermi-LAT Collab.)
ACKERMANN	15A	JCAP 1509 008	M. Ackermann *et al.*	(Fermi-LAT Collab.)
ACKERMANN	15B	PRL 115 231301	M. Ackermann *et al.*	(Fermi-LAT Collab.)
ADRIAN-MAR...	15	JCAP 1510 068	S. Adrian-Martinez *et al.*	(ANTARES Collab.)
AGNES	15	PL B743 456	P. Agnes *et al.*	(DarkSide-50 Collab.)
AGNESE	15A	PR D91 052021	R. Agnese *et al.*	(SuperCDMS Collab.)
AGNESE	15B	PR D92 072003	R. Agnese *et al.*	(SuperCDMS Collab.)
AMOLE	15	PRL 114 231302	C. Amole *et al.*	(PICO Collab.)
APRILE	15	PRL 115 091302	E. Aprile *et al.*	(XENON Collab.)
APRILE	15A	SCI 349 851	E. Aprile *et al.*	(XENON Collab.)
CHOI	15	PRL 114 141301	K. Choi *et al.*	(Super-Kamiokande Collab.)
KHACHATRY...	15AG	JHEP 1506 121	V. Khachatryan *et al.*	(CMS Collab.)
KHACHATRY...	15AL	EPJ C75 235	V. Khachatryan *et al.*	(CMS Collab.)
KHACHATRY...	15T	PR D91 092005	V. Khachatryan *et al.*	(CMS Collab.)
NAKAMURA	15	PTEP 2015 4 043F01	K. Nakamura *et al.*	(NEWAGE Collab.)
XIAO	15	PR D92 052004	X. Xiao *et al.*	(PandaX Collab.)
AAD	14AI	JHEP 1409 037	G. Aad *et al.*	(ATLAS Collab.)
AAD	14BK	PRL 112 041802	G. Aad *et al.*	(ATLAS Collab.)
AAD	14K	PR D90 012004	G. Aad *et al.*	(ATLAS Collab.)
AAD	14O	PRL 112 201802	G. Aad *et al.*	(ATLAS Collab.)
ACKERMANN	14	PR D89 042001	M. Ackermann *et al.*	(Fermi-LAT Collab.)
AGNESE	14	PRL 112 241302	R. Agnese *et al.*	(SuperCDMS Collab.)
AGNESE	14A	PRL 112 041302	R. Agnese *et al.*	(SuperCDMS Collab.)
AKERIB	14	PRL 112 091303	D.S. Akerib *et al.*	(LUX Collab.)
ALEKSIC	14	JCAP 1402 008	J. Aleksic *et al.*	(MAGIC Collab.)
ANGLOHER	14	EPJ C74 3184	G. Angloher *et al.*	(CRESST-II Collab.)
APRILE	14A	ASP 54 11	E. Aprile *et al.*	(XENON100 Collab.)
AVRORIN	14	ASP 62 12	A.D. Avrorin *et al.*	(BAIKAL Collab.)
FELIZARDO	14	PR D89 072013	M. Felizardo *et al.*	(SIMPLE Collab.)
LEE	14A	PR D90 052006	H.S. Lee *et al.*	(KIMS Collab.)
LIU	14A	PR D90 032003	S.K. Liu *et al.*	(CDEX Collab.)
UCHIDA	14	PTEP 2014 063C01	H. Uchida *et al.*	(XMASS Collab.)
YUE	14	PR D90 091701	Q. Yue *et al.*	(CDEX Collab.)
AAD	13AD	JHEP 1304 075	G. Aad *et al.*	(ATLAS Collab.)
AAD	13C	PRL 110 011802	G. Aad *et al.*	(ATLAS Collab.)
AALSETH	13	PR D88 012002	C.E. Aalseth *et al.*	(CoGeNT Collab.)
AARTSEN	13	PRL 110 131302	M.G. Aartsen *et al.*	(IceCube Collab.)
AARTSEN	13C	PR D88 122001	M.G. Aartsen *et al.*	(IceCube Collab.)
ABE	13B	PL B719 78	K. Abe *et al.*	(XMASS Collab.)
ABRAMOWSKI	13	PRL 110 041301	A. Abramowski *et al.*	(H.E.S.S. Collab.)
ACKERMANN	13A	PR D88 082002	M. Ackermann *et al.*	(Fermi-LAT Collab.)
ADRIAN-MAR...	13	JCAP 1311 032	S. Adrian-Martinez *et al.*	(ANTARES Collab.)
AGNESE	13	PR D88 031104	R. Agnese *et al.*	(CDMS Collab.)
AGNESE	13A	PRL 111 251301	R. Agnese *et al.*	(CDMS Collab.)
APRILE	13	PRL 111 021301	E. Aprile *et al.*	(XENON100 Collab.)
BERNABEI	13A	EPJ C73 2648	R. Bernabei *et al.*	(DAMA Collab.)
BOLIEV	13	JCAP 1309 019	M. Boliev *et al.*	
LI	13B	PRL 110 261301	H.B. Li *et al.*	(TEXONO Collab.)
SUVOROVA	13	PAN 76 1367	O.V. Suvorova *et al.*	(INRM)
		Translated from YAF 76 1433.		
ZHAO	13	PR D88 052004	W. Zhao *et al.*	(CDEX Collab.)
AALTONEN	12K	PRL 108 201802	T. Aaltonen *et al.*	(CDF Collab.)
AALTONEN	12M	PRL 108 211804	T. Aaltonen *et al.*	(CDF Collab.)
ABBASI	12	PR D85 042002	R. Abbasi *et al.*	(IceCube Collab.)
ABRAMOWSKI	12	APJ 750 123	A. Abramowski *et al.*	(H.E.S.S. Collab.)
ACKERMANN	12	PR D86 022002	M. Ackermann *et al.*	(Fermi-LAT Collab.)
AKIMOV	12	PL B709 14	D.Yu. Akimov *et al.*	(ZEPLIN-III Collab.)
ALIU	12	PR D85 062001	E. Aliu *et al.*	(VERITAS Collab.)
ANGLOHER	12	EPJ C72 1971	G. Angloher *et al.*	(CRESST-II Collab.)
APRILE	12	PRL 109 181301	E. Aprile *et al.*	(XENON100 Collab.)
ARCHAMBAU...	12	PL B711 153	S. Archambault *et al.*	(PICASSO Collab.)
ARMENGAUD	12	PR D86 051701	E. Armengaud *et al.*	(EDELWEISS Collab.)
BARRETO	12	PL B711 264	J. Barreto *et al.*	(DAMIC Collab.)
BEHNKE	12	PR D86 052001	E. Behnke *et al.*	(COUPP Collab.)
Also		PR D90 079902 (errat.)	E. Behnke *et al.*	(COUPP Collab.)
BROWN	12	PR D85 021301	A. Brown *et al.*	(OXF)
CHATRCHYAN	12AP	JHEP 1209 094	S. Chatrchyan *et al.*	(CMS Collab.)
CHATRCHYAN	12T	PRL 108 261803	S. Chatrchyan *et al.*	(CMS Collab.)
DAHL	12	PRL 108 259001	C.E. Dahl, J. Hall, W.H. Lippincott	(CHIC, FNAL)
DAW	12	ASP 35 397	E. Daw *et al.*	(DRIFT-Ild Collab.)
FELIZARDO	12	PRL 108 201302	M. Felizardo *et al.*	(SIMPLE Collab.)
KIM	12	PRL 108 181301	S.C. Kim *et al.*	(KIMS Collab.)
AALSETH	11	PRL 106 131301	C.E. Aalseth *et al.*	(CoGeNT Collab.)
AALSETH	11A	PRL 107 141301	C.E. Aalseth *et al.*	(CoGeNT Collab.)
ABBASI	11C	PR D84 022004	R. Abbasi *et al.*	(IceCube Collab.)
ABRAMOWSKI	11	PRL 106 161301	A. Abramowski *et al.*	(H.E.S.S. Collab.)
ACKERMANN	11	PRL 107 241302	M. Ackermann *et al.*	(Fermi-LAT Collab.)
AHLEN	11	PL B695 124	S. Ahlen *et al.*	(DMTPC Collab.)
AHMED	11	PR D83 112002	Z. Ahmed *et al.*	(CDMS Collab.)
AHMED	11A	PR D84 011102	Z. Ahmed *et al.*	(CDMS and EDELWEISS Collabs.)
AHMED	11B	PRL 106 131302	Z. Ahmed *et al.*	(CDMS Collab.)
AJELLO	11	PR D84 032007	M. Ajello *et al.*	(Fermi-LAT Collab.)
ANGLE	11	PRL 107 051301	J. Angle *et al.*	(XENON10 Collab.)
Also		PRL 110 249901 (errat.)	J. Angle *et al.*	(XENON10 Collab.)
APRILE	11	PR D84 052003	E. Aprile *et al.*	(XENON100 Collab.)
APRILE	11A	PR D84 061101	E. Aprile *et al.*	(XENON100 Collab.)
APRILE	11B	PRL 107 131302	E. Aprile *et al.*	(XENON100 Collab.)
ARMENGAUD	11	PL B702 329	E. Armengaud *et al.*	(EDELWEISS-II Collab.)
BEHNKE	11	PRL 106 021303	E. Behnke *et al.*	(COUPP Collab.)
GERINGER-SA...	11	PRL 107 241303	A. Geringer-Sameth, S.M. Koushiappas	
HORN	11	PL B705 471	M. Horn *et al.*	(ZEPLIN-III Collab.)
TANAKA	11	APJ 742 78	T. Tanaka *et al.*	(Super-Kamiokande Collab.)
ABBASI	10	PR D81 057101	R. Abbasi *et al.*	(IceCube Collab.)
AHMED	10	SCI 327 1619	Z. Ahmed *et al.*	(CDMS II Collab.)
AKERIB	10	PR D82 122004	D.S. Akerib *et al.*	(CDMS II Collab.)
AKIMOV	10	PL B692 180	D.Yu. Akimov *et al.*	(ZEPLIN-III Collab.)
APRILE	10	PRL 105 131302	E. Aprile *et al.*	(XENON100 Collab.)
ARMENGAUD	10	PL B687 294	E. Armengaud *et al.*	(EDELWEISS-II Collab.)
FELIZARDO	10	PRL 105 211301	M. Felizardo *et al.*	(The SIMPLE Collab.)
MIUCHI	10	PL B686 11	K. Miuchi *et al.*	(NEWAGE Collab.)
ABBASI	09B	PRL 102 201302	R. Abbasi *et al.*	(IceCube Collab.)
AHMED	09	PRL 102 011301	Z. Ahmed *et al.*	(CDMS Collab.)
ANGLE	09	PR D80 115005	J. Angle *et al.*	(XENON10 Collab.)
ANGLOHER	09	ASP 31 270	G. Angloher *et al.*	(CRESST Collab.)
ARCHAMBAU...	09	PL B682 185	S. Archambault *et al.*	(PICASSO Collab.)
LEBEDENKO	09A	PRL 103 151302	V.N. Lebedenko *et al.*	(ZEPLIN-III Collab.)
LIN	09	PR D79 061101	S.T. Lin *et al.*	(TEXONO Collab.)
AALSETH	08	PRL 101 251301	C.E. Aalseth *et al.*	(CoGeNT Collab.)
Also		PRL 102 109903 (errat.)	C.E. Aalseth *et al.*	(CoGeNT Collab.)
ANGLE	08A	PRL 101 091301	J. Angle *et al.*	(XENON10 Collab.)
BEDNYAKOV	08	PAN 71 111	V.A. Bednyakov, H.P. Klapdor-Kleingrothaus, I.V. Krivosheina	
		Translated from YAF 71 112.		
ALNER	07	PL B653 161	G.J. Alner *et al.*	(ZEPLIN-II Collab.)
LEE	07A	PRL 99 091301	H.S. Lee *et al.*	(KIMS Collab.)
MIUCHI	07	PL B654 58	K. Miuchi *et al.*	
AKERIB	06	PR D73 011102	D.S. Akerib *et al.*	(CDMS Collab.)
SHIMIZU	06A	PL B633 195	Y. Shimizu *et al.*	
AKERIB	05	PR D72 052009	D.S. Akerib *et al.*	(CDMS Collab.)
ALNER	05	PL B616 17	G.J. Alner *et al.*	(UK Dark Matter Collab.)
BARNABE-HE...	05	PL B624 186	M. Barnabe-Heider *et al.*	(PICASSO Collab.)
BENOIT	05	PL B616 25	A. Benoit *et al.*	(EDELWEISS Collab.)
GIRARD	05	PL B621 233	T.A. Girard *et al.*	(SIMPLE Collab.)
GIULIANI	05	PRL 95 101301	F. Giuliani	
GIULIANI	05A	PR D71 123503	F. Giuliani, T.A. Girard	
KLAPDOR-K...	05	PL B609 226	H.V. Klapdor-Kleingrothaus, I.V. Krivosheina, C. Tomei	
GIULIANI	04	PL B588 151	F. Giuliani, T.A. Girard	
GIULIANI	04A	PRL 93 161301	F. Giuliani	
MIUCHI	03	ASP 19 135	K. Miuchi *et al.*	
TAKEDA	03	PL B572 145	A. Takeda *et al.*	
ANGLOHER	02	ASP 18 43	G. Angloher *et al.*	(CRESST Collab.)
BELLI	02	PR D66 043503	P. Belli *et al.*	
BERNABEI	02C	EPJ C23 61	R. Bernabei *et al.*	(DAMA Collab.)
GREEN	02	PR D66 083003	A.M. Green	
BAUDIS	01	PR D63 022001	L. Baudis *et al.*	(Heidelberg-Moscow Collab.)
SMITH	01	PR D64 043502	D. Smith, N. Weiner	
ULLIO	01	JHEP 0107 044	P. Ullio, M. Kamionkowski, P. Vogel	
BENOIT	00	PL B479 8	A. Benoit *et al.*	(EDELWEISS Collab.)
BERNABEI	00D	NJP 2 15	R. Bernabei *et al.*	(DAMA Collab.)
COLLAR	00	PRL 85 3083	J.I. Collar *et al.*	(SIMPLE Collab.)
AMBROSIO	99	PR D60 082002	M. Ambrosio *et al.*	(Macro Collab.)
BERNABEI	99	PL B450 448	R. Bernabei *et al.*	(DAMA Collab.)
BERNABEI	99D	PRL 83 4918	R. Bernabei *et al.*	(DAMA Collab.)
BRHLIK	99	PL B464 303	M. Brhlik, L. Roszkowski	
DERBIN	99	PAN 62 1886	A.V. Derbin *et al.*	
		Translated from YAF 62 2034.		
KLIMENKO	98	JETPL 67 875	A.A. Klimenko *et al.*	
		Translated from ZETFP 67 835.		
SARSA	97	PR D56 1856	M.L. Sarsa *et al.*	(ZARA)
ALESSAND...	96	PL B384 316	A. Alessandrello *et al.*	(MILA, MILAI, SASSO)
BELLI	96	PL B387 222	P. Belli *et al.*	(DAMA Collab.)
Also		PL B389 783 (erratum)	P. Belli *et al.*	(DAMA Collab.)
BELLI	96C	NC C19 537	P. Belli *et al.*	(DAMA Collab.)
BERNABEI	96	PL B389 757	R. Bernabei *et al.*	(DAMA Collab.)
COLLAR	96	PRL 76 331	J.I. Collar	(SCUC)
SARSA	96	PL B386 458	M.L. Sarsa *et al.*	(ZARA)
Also		PR D56 1856	M.L. Sarsa *et al.*	(ZARA)
SMITH	96	PL B379 299	P.F. Smith *et al.*	(RAL, SHEF, LOIC+)
SNOWDEN-...	96	PRL 76 332	D.P. Snowden-Ifft, E.S. Freeman, P.B. Price	(UCB)
GARCIA	95	PR D51 1458	E. Garcia *et al.*	(ZARA, SCUC, PNL)
QUENBY	95	PL B351 70	J.J. Quenby *et al.*	(LOIC, RAL, SHEF+)
SNOWDEN-...	95	PRL 74 4133	D.P. Snowden-Ifft, E.S. Freeman, P.B. Price	(UCB)
Also		PRL 76 331	J.I. Collar	(SCUC)
Also		PRL 76 332	D.P. Snowden-Ifft, E.S. Freeman, P.B. Price	(UCB)
BECK	94	PL B336 141	M. Beck *et al.*	(MPIK, KIAE, SASSO)
BACCI	92	PL B293 460	C. Bacci *et al.*	(Beijing-Roma-Saclay Collab.)
REUSSER	91	PL B255 143	D. Reusser *et al.*	(NEUC, CIT, PSI)
CALDWELL	88	PRL 61 510	D.O. Caldwell *et al.*	(UCSB, UCB, LBL)

Downloaded from https://academic.oup.com/ptep/article/2022/8/083C01/6651666 by KIT Library user on 27 September 2022

Other Particle Searches

OMITTED FROM SUMMARY TABLE

OTHER PARTICLE SEARCHES

Revised February 2018 by K. Hikasa (Tohoku University).

We collect here those searches which do not appear in any other search categories. These are listed in the following order:

- Concentration of stable particles in matter
- General new physics searches
- Limits on jet-jet resonance in hadron collisions
- Limits on neutral particle production at accelerators
- Limits on charged particles in e^+e^- collisions
- Limits on charged particles in hadron reactions
- Limits on charged particles in cosmic rays
- Searches for quantum black hole production

Note that searches appear in separate sections elsewhere for Higgs bosons (and technipions), other heavy bosons (including W_R, W', Z', leptoquarks, axigluons), axions (including pseudo-Goldstone bosons, Majorons, familons), WIMPs, heavy leptons, heavy neutrinos, free quarks, monopoles, supersymmetric particles, and compositeness.

We no longer list for limits on tachyons and centauros. See our 1994 edition for these limits.

CONCENTRATION OF STABLE PARTICLES IN MATTER

Concentration of Heavy (Charge +1) Stable Particles in Matter

VALUE	CL%	DOCUMENT ID		TECN	COMMENT
• • • We do not use the following data for averages, fits, limits, etc. • • •					
$<4\times10^{-17}$	95	[1] YAMAGATA	93	SPEC	Deep sea water, M=5–1600m_p
$<6\times10^{-15}$	95	[2] VERKERK	92	SPEC	Water, M= 10^5 to 3×10^7 GeV
$<7\times10^{-15}$	95	[2] VERKERK	92	SPEC	Water, M= 10^4, 6×10^7 GeV
$<9\times10^{-15}$	95	[2] VERKERK	92	SPEC	Water, M= 10^8 GeV
$<3\times10^{-23}$	90	[3] HEMMICK	90	SPEC	Water, M = 1000m_p
$<2\times10^{-21}$	90	[3] HEMMICK	90	SPEC	Water, M = 5000m_p
$<3\times10^{-20}$	90	[3] HEMMICK	90	SPEC	Water, M = 10000m_p
$<1.\times10^{-29}$		SMITH	82B	SPEC	Water, M=30–400m_p
$<2.\times10^{-28}$		SMITH	82B	SPEC	Water, M=12–1000m_p
$<1.\times10^{-14}$		SMITH	82B	SPEC	Water, M >1000 m_p
$<(0.2–1.)\times10^{-21}$		SMITH	79	SPEC	Water, M=6–350 m_p

[1] YAMAGATA 93 used deep sea water at 4000 m since the concentration is enhanced in deep sea due to gravity.

[2] VERKERK 92 looked for heavy isotopes in sea water and put a bound on concentration of stable charged massive particle in sea water. The above bound can be translated into into a bound on charged dark matter particle (5×10^6 GeV), assuming the local density, ρ=0.3 GeV/cm^3, and the mean velocity $\langle v\rangle$=300 km/s.

[3] See HEMMICK 90 Fig. 7 for other masses 100–10000 m_p.

Concentration of Heavy Stable Particles Bound to Nuclei

VALUE	CL%	DOCUMENT ID		TECN	COMMENT
• • • We do not use the following data for averages, fits, limits, etc. • • •					
$<2\times10^{-17}$/nucleon	95	[1] AFEK	21		millicharged particle search
$<1.2\times10^{-11}$	95	[2] JAVORSEK	01	SPEC	Au, M= 3 GeV
$<6.9\times10^{-10}$	95	[2] JAVORSEK	01	SPEC	Au, M= 144 GeV
$<1\times10^{-11}$	95	[3] JAVORSEK	01B	SPEC	Au, M= 188 GeV
$<1\times10^{-8}$	95	[3] JAVORSEK	01B	SPEC	Au, M= 1669 GeV
$<6\times10^{-9}$	95	[3] JAVORSEK	01B	SPEC	Fe, M= 188 GeV
$<1\times10^{-8}$	95	[3] JAVORSEK	01B	SPEC	Fe, M= 647 GeV
$<4\times10^{-20}$	90	[4] HEMMICK	90	SPEC	C, M = 100m_p
$<8\times10^{-20}$	90	[4] HEMMICK	90	SPEC	C, M = 1000m_p
$<2\times10^{-16}$	90	[4] HEMMICK	90	SPEC	C, M = 10000m_p
$<6\times10^{-13}$	90	[4] HEMMICK	90	SPEC	Li, M = 1000m_p
$<1\times10^{-11}$	90	[4] HEMMICK	90	SPEC	Be, M = 1000m_p
$<6\times10^{-14}$	90	[4] HEMMICK	90	SPEC	B, M = 1000m_p
$<4\times10^{-17}$	90	[4] HEMMICK	90	SPEC	O, M = 1000m_p
$<4\times10^{-15}$	90	[4] HEMMICK	90	SPEC	F, M = 1000m_p
$<1.5\times10^{-13}$/nucleon	68	[5] NORMAN	89	SPEC	^{206}PbX^-
$<1.2\times10^{-12}$/nucleon	68	[5] NORMAN	87	SPEC	^{56,58}FeX^-

[1] AFEK 21 search for millicharged particles bound to matter using an optomechanical device. No signal was observed. Limits placed in the abundance vs. charge plane (Fig. 3). This is translated to the mass versus charge plane by requiring bound states to be stable.

[2] JAVORSEK 01 search for (neutral) SIMPs (strongly interacting massive particles) bound to Au nuclei. Here M is the effective SIMP mass.

[3] JAVORSEK 01B search for (neutral) SIMPs (strongly interacting massive particles) bound to Au and Fe nuclei from various origins with exposures on the earth's surface, in a satellite, heavy ion collisions, etc. Here M is the mass of the anomalous nucleus. See also JAVORSEK 02.

[4] See HEMMICK 90 Fig. 7 for other masses 100–10000 m_p.

[5] Bound valid up to $m_{X^-}\sim$ 100 TeV.

GENERAL NEW PHYSICS SEARCHES

This subsection lists some of the search experiments which look for general signatures characteristic of new physics, independent of the framework of a specific model.

The observed events are compatible with Standard Model expectation, unless noted otherwise.

VALUE	DOCUMENT ID		TECN	COMMENT
• • • We do not use the following data for averages, fits, limits, etc. • • •				
	[1] ALKHATIB	21A	SCDM	CDMSlite search for fractionally charged relics
	[2] AGUILAR-AR...	20B	CONN	ν elastic scatter on nuclei
	[3] FEDDERKE	20		CHAMPs from white dwarfs
	[4] SIRUNYAN	20A	CMS	SUSY/LQ search with mT2 or long-lived charged particles
	[5] ALCANTARA	19		Auger, superheavy DM
	[6] PORAYKO	18	PPTA	pulsar timing fuzzy DM search
	[7] AAD	15AT	ATLS	$t+\not{E}_T$
	[8] KHACHATRY...	15F	CMS	$t+\not{E}_T$
	[9] AALTONEN	14J	CDF	W + 2 jets
	[10] AAD	13A	ATLS	$WW\to\ell\nu\ell'\nu$
	[11] AAD	13C	ATLS	$\gamma+\not{E}_T$
	[12] AALTONEN	13I	CDF	Delayed $\gamma+\not{E}_T$
	[13] CHATRCHYAN	13	CMS	$\ell^+\ell^-$ + jets + $\not{E}_T$
	[14] AAD	12C	ATLS	$t\bar{t}+\not{E}_T$
	[15] AALTONEN	12M	CDF	jet + $\not{E}_T$
	[16] CHATRCHYAN	12AP	CMS	jet + $\not{E}_T$
	[17] CHATRCHYAN	12Q	CMS	Z + jets + $\not{E}_T$
	[18] CHATRCHYAN	12T	CMS	$\gamma+\not{E}_T$
	[19] AAD	11S	ATLS	jet + $\not{E}_T$
	[20] AALTONEN	11AF	CDF	$\ell^\pm\ell^\pm$
	[21] CHATRCHYAN	11C	CMS	$\ell^+\ell^-$ + jets + $\not{E}_T$
	[22] CHATRCHYAN	11U	CMS	jet + $\not{E}_T$
	[23] AALTONEN	10AF	CDF	$\gamma\gamma+\ell,\not{E}_T$
	[24] AALTONEN	09AF	CDF	$\ell\gamma b\not{E}_T$
	[25] AALTONEN	09G	CDF	$\ell\ell\ell\not{E}_T$

[1] ALKHATIB 21A search for lightly ionizing fractionally charged relics scattering from Ge. No signal observed. Limits plotted in fractional charge f vs. vertical intensity plane for m $\sim$ 5 MeV to 100 TeV.

[2] AGUILAR-AREVALO 20B search for light BSM mediator effect on ν elastic scatter on nuclei; no signal; limits placed in m(mediator) vs. coupling plane for two models of MeV-scale mediators.

[3] FEDDERKE 20 place limits on cosmic relic charged massive particles (CHAMPs) due to their capture and subsequent disruption of old white dwarf stars; limits placed in the m(CHAMP) vs. relic density parameter plane.

[4] SIRUNYAN 20A search for SUSY and LQ production using mT2 or presence of long-lived charged particle; no signal, limits placed in various mass planes for different BSM scenarios and various assumed lifetimes.

[5] ALCANTARA 19 place limits on m(WIMPzilla=X) vs lifetime from upper bound on ultra high energy cosmic rays at Auger experiment: e.g. $\tau(X)<4\times10^{22}$ yr for m(X) = 10^{16} GeV.

[6] PORAYKO 18 search for deviations in the residuals of pulsar timing data using PPTA. No signal observed. Limits set on fuzzy DM with $3\times10^{-24}<$ m(DM) $<2\times10^{-22}$ eV.

[7] AAD 15AT search for events with a top quark and mssing E_T in pp collisions at E_{cm} = 8 TeV with L = 20.3 fb^{-1}.

[8] KHACHATRYAN 15F search for events with a top quark and mssing E_T in pp collisions at E_{cm} = 8 TeV with L = 19.7 fb^{-1}.

[9] AALTONEN 14J examine events with a W and two jets in $p\overline{p}$ collisions at E_{cm} = 1.96 TeV with L = 8.9 fb^{-1}. Invariant mass distributions of the two jets are consistent with the Standard Model expectation.

[10] AAD 13A search for resonant WW production in pp collisions at E_{cm} = 7 TeV with L = 4.7 fb^{-1}.

[11] AAD 13C search for events with a photon and missing $\not{E}_T$ in pp collisions at E_{cm} = 7 TeV with L = 4.6 fb^{-1}.

[12] AALTONEN 13I search for events with a photon and missing E_T, where the photon is detected after the expected timing, in $p\overline{p}$ collisions at E_{cm} = 1.96 TeV with L = 6.3 fb^{-1}. The data are consistent with the Standard Model expectation.

[13] CHATRCHYAN 13 search for events with an opposite-sign lepton pair, jets, and missing E_T in pp collisions at E_{cm} = 7 TeV with L = 4.98 fb^{-1}.

[14] AAD 12C search for events with a $t\bar{t}$ pair and missing $\not{E}_T$ in pp collisions at E_{cm} = 7 TeV with L = 1.04 fb^{-1}.

[15] AALTONEN 12M search for events with a jet and missing E_T in $p\overline{p}$ collisions at E_{cm} = 1.96 TeV with L = 6.7 fb^{-1}.

Downloaded from https://academic.oup.com/ptep/article/2022/8/083C01/6651666 by KIT Library user on 27 September 2022

[16] CHATRCHYAN 12AP search for events with a jet and missing E_T in pp collisions at E_{cm} = 7 TeV with L = 5.0 fb^{-1}.
[17] CHATRCHYAN 12Q search for events with a Z, jets, and missing $\not{E}_T$ in pp collisions at E_{cm} = 7 TeV with L = 4.98 fb^{-1}.
[18] CHATRCHYAN 12T search for events with a photon and missing $\not{E}_T$ in pp collisions at E_{cm} = 7 TeV with L = 5.0 fb^{-1}.
[19] AAD 11S search for events with one jet and missing E_T in pp collisions at E_{cm} = 7 TeV with L = 33 pb^{-1}.
[20] AALTONEN 11AF search for high-p_T like-sign dileptons in $p\overline{p}$ collisions at E_{cm} = 1.96 TeV with L = 6.1 fb^{-1}.
[21] CHATRCHYAN 11C search for events with an opposite-sign lepton pair, jets, and missing E_T in pp collisions at E_{cm} = 7 TeV with L = 34 pb^{-1}.
[22] CHATRCHYAN 11U search for events with one jet and missing E_T in pp collisions at E_{cm} = 7 TeV with L = 36 pb^{-1}.
[23] AALTONEN 10AF search for $\gamma\gamma$ events with e, μ, τ, or missing E_T in $p\overline{p}$ collisions at E_{cm} = 1.96 TeV with L = 1.1–2.0 fb^{-1}.
[24] AALTONEN 09AF search for $\ell\gamma b$ events with missing E_T in $p\overline{p}$ collisions at E_{cm} = 1.96 TeV with L = 1.9 fb^{-1}. The observed events are compatible with Standard Model expectation including $t\overline{t}\gamma$ production.
[25] AALTONEN 09G search for $\mu\mu\mu$ and $\mu\mu e$ events with missing E_T in $p\overline{p}$ collisions at E_{cm} = 1.96 TeV with L = 976 pb^{-1}.

LIMITS ON JET-JET RESONANCES

Heavy Particle Production Cross Section

Limits are for a particle decaying to two hadronic jets.

Units(pb)	CL%	Mass(GeV)	DOCUMENT ID		TECN	COMMENT
• • • We do not use the following data for averages, fits, limits, etc. • • •						
			[1] AAD	20AD	ATLS	pp at 13 TeV, dijet resonance
			[2] AAD	20T	ATLS	dijet resonance search
			[3] AAD	20W	ATLS	dijet resonance plus lepton
			[4] SIRUNYAN	20AI	CMS	dijet resonance search
			[5] AABOUD	19AJ	ATLS	$pp \to \gamma X$, $X \to jj$
			[6] SIRUNYAN	19B	CMS	$pp \to jA$, $A \to b\overline{b}$
			[7] SIRUNYAN	19CD	CMS	$pp \to Z'\gamma$, $Z' \to jj$
			[8] AABOUD	18AD	ATLS	$pp \to Y \to HX \to (bb) + (qq)$
			[9] AABOUD	18CK	ATLS	$pp \to bbb + \not{E}_T$
			[10] AABOUD	18CL	ATLS	$pp \to$ vector-like quarks
			[11] AABOUD	18N	ATLS	$pp \to jj$ resonance
			[12] SIRUNYAN	18DJ	CMS	$pp \to ZZ$ or $WZ \to \ell\overline{\ell}jj$
			[13] SIRUNYAN	18DY	CMS	$pp \to RR$; $R \to jj$
			[14] KHACHATRY...	17W	CMS	$pp \to jj$ resonance
			[15] KHACHATRY...	17Y	CMS	$pp \to (8\text{–}10)\ j + \not{E}_T$
			[16] SIRUNYAN	17F	CMS	$pp \to jj$ angular distribution
			[17] AABOUD	16	ATLS	$pp \to b$ + jet
			[18] AAD	16N	ATLS	$pp \to$ 3 high E_T jets
			[19] AAD	16S	ATLS	$pp \to jj$ resonance
			[20] KHACHATRY...	16K	CMS	$pp \to jj$ resonance
			[21] KHACHATRY...	16L	CMS	$pp \to jj$ resonance
			[22] AAD	13D	ATLS	7 TeV $pp \to$ 2 jets
			[23] AALTONEN	13R	CDF	1.96 TeV $p\overline{p} \to$ 4 jets
			[24] CHATRCHYAN	13A	CMS	7 TeV $pp \to$ 2 jets
			[25] CHATRCHYAN	13A	CMS	7 TeV $pp \to b\overline{b}X$
			[26] AAD	12S	ATLS	7 TeV $pp \to$ 2 jets
			[27] CHATRCHYAN	12BL	CMS	7 TeV $pp \to t\overline{t}X$
			[28] AAD	11AG	ATLS	7 TeV $pp \to$ 2 jets
			[29] AALTONEN	11M	CDF	1.96 TeV $p\overline{p} \to W+$ 2 jets
			[30] ABAZOV	11I	D0	1.96 TeV $p\overline{p} \to W+$ 2 jets
			[31] AAD	10	ATLS	7 TeV $pp \to$ 2 jets
			[32] KHACHATRY...	10	CMS	7 TeV $pp \to$ 2 jets
			[33] ABE	99F	CDF	1.8 TeV $p\overline{p} \to b\overline{b}+$ anything
			[34] ABE	97G	CDF	1.8 TeV $p\overline{p} \to$ 2 jets
<2603	95	200	[35] ABE	93G	CDF	1.8 TeV $p\overline{p} \to$ 2 jets
< 44	95	400	[35] ABE	93G	CDF	1.8 TeV $p\overline{p} \to$ 2 jets
< 7	95	600	[35] ABE	93G	CDF	1.8 TeV $p\overline{p} \to$ 2 jets

[1] AAD 20AD search for weakly supervised dijet resonance in ATLAS with 139 fb^{-1} at 13 TeV; no signal; various limits placed depending on kinematics and production cross section.
[2] AAD 20T search for dijet resonance with or without b-jets at 13 TeV and 139 fb^{-1}; no signal; limits placed in $\sigma \cdot$ BF vs mass plane for various BSM models.
[3] AAD 20W search for dijet resonance plus lepton with ATLAS at 13 TeV and 139 fb^{-1}; no signal; limits placed in $\sigma \cdot$ BF vs. mass plane for various BSM models.
[4] SIRUNYAN 20AI search for dijet resonance in CMS at 13 TeV with 137 fb^{-1}; no signal; limits set in σ vs. mass plane for various BSM models .
[5] AABOUD 19AJ search for low mass dijet resonance in $pp \to \gamma X$, $X \to jj$ at 13 TeV with 79.8 fb^{-1} of data; no signal found; limits placed on Z' model in coupling vs. m(Z') plane.
[6] SIRUNYAN 19B search for low mass resonance $pp \to jA$, $A \to b\overline{b}$ at 13 TeV using 35.9 fb^{-1}; no signal; exclude resonances 50–350 GeV depending on production and decay.
[7] SIRUNYAN 19CD search for $pp \to Z'\gamma$, $Z' \to jj$ with fat jet (jj); no signal, limits placed in m(Z') vs. coupling plane for Z' masses from 10 to 125 GeV.
[8] AABOUD 18AD search for new heavy particle $Y \to HX \to (bb) + (qq)$. No signal observed. Limits set on m(Y) vs. m(X) in the ranges of m(Y) in 1–4 TeV and m(X) in 50–1000 GeV.
[9] AABOUD 18CK search for SUSY Higgsinos in gauge-mediation via $pp \to bbb + \not{E}_T$ at 13 TeV using two complementary analyses with 24.3/36.1 fb^{-1}; no signal is found and Higgsinos with masses between 130 and 230 GeV and between 290 and 880 GeV are excluded at the 95% confidence level.
[10] AABOUD 18CL search for $pp \to$ vector-like quarks $\to$ jets at 13 TeV with 36 fb^{-1}; no signal seen; limits set on various VLQ scenarios. For pure $B \to Hb$ or $T \to Ht$, set the mass limit m > 1010 GeV.
[11] AABOUD 18N search for dijet resonance at Atlas with 13 TeV and 29.3 fb^{-1}; limits set on m(Z') in the mass range of 450–1800 GeV.
[12] SIRUNYAN 18DJ search for $pp \to ZZ$ or $WZ \to \ell\overline{\ell}jj$ resonance at 13 TeV, 35.9 fb^{-1}; no signal; limits set in the 400–4500 GeV mass range, exclusion of W' up to 2270 GeV in the HVT model A, and up to 2330 GeV for HVT model B. WED bulk graviton exclusion up to 925 GeV.
[13] SIRUNYAN 18DY search for $pp \to RR$; $R \to jj$ two dijet resonances at 13 TeV 35.9 fb^{-1}; no signal; limits placed on RPV top-squark pair production.
[14] KHACHATRYAN 17W search for dijet resonance in 12.9 fb^{-1} data at 13 TeV; see Fig. 2 for limits on axigluons, diquarks, dark matter mediators etc.
[15] KHACHATRYAN 17Y search for $pp \to (8\text{–}10)\ j$ in 19.7 fb^{-1} at 8 TeV. No signal seen. Limits set on colorons, axigluons, RPV, and SUSY.
[16] SIRUNYAN 17F measure $pp \to jj$ angular distribution in 2.6 fb^{-1} at 13 TeV; limits set on LEDs and quantum black holes.
[17] AABOUD 16 search for resonant dijets including one or two b-jets with 3.2 fb^{-1} at 13 TeV; exclude excited b^* quark from 1.1–2.1 TeV; exclude leptophilic Z' with SM couplings from 1.1–1.5 TeV.
[18] AAD 16N search for $\geq$ 3 jets with 3.6 fb^{-1} at 13 TeV; limits placed on micro black holes (Fig. 10) and string balls (Fig. 11).
[19] AAD 16S search for high mass jet-jet resonance with 3.6 fb^{-1} at 13 TeV; exclude portions of excited quarks, W', Z' and contact interaction parameter space.
[20] KHACHATRYAN 16K search for dijet resonance in 2.4 fb^{-1} data at 13 TeV; see Fig. 3 for limits on axigluons, diquarks etc.
[21] KHACHATRYAN 16L use data scouting technique to search for jj resonance on 18.8 fb^{-1} of data at 8 TeV. Limits on the coupling of a leptophobic Z' to quarks are set, improving on the results by other experiments in the mass range between 500–800 GeV.
[22] AAD 13D search for dijet resonances in pp collisions at E_{cm} = 7 TeV with L = 4.8 fb^{-1}. The observed events are compatible with Standard Model expectation. See their Fig. 6 and Table 2 for limits on resonance cross section in the range m = 1.0–4.0 TeV.
[23] AALTONEN 13R search for production of a pair of jet-jet resonances in $p\overline{p}$ collisions at E_{cm} = 1.96 TeV with L = 6.6 fb^{-1}. See their Fig. 5 and Tables I, II for cross section limits.
[24] CHATRCHYAN 13A search for qq, qg, and gg resonances in pp collisions at E_{cm} = 7 TeV with L = 4.8 fb^{-1}. See their Fig. 3 and Table 1 for limits on resonance cross section in the range m = 1.0–4.3 TeV.
[25] CHATRCHYAN 13A search for $b\overline{b}$ resonances in pp collisions at E_{cm} = 7 TeV with L = 4.8 fb^{-1}. See their Fig. 8 and Table 4 for limits on resonance cross section in the range m = 1.0–4.0 TeV.
[26] AAD 12S search for dijet resonances in pp collisions at E_{cm} = 7 TeV with L = 1.0 fb^{-1}. See their Fig. 3 and Table 2 for limits on resonance cross section in the range m = 0.9–4.0 TeV.
[27] CHATRCHYAN 12BL search for $t\overline{t}$ resonances in pp collisions at E_{cm} = 7 TeV with L = 4.4 fb^{-1}. See their Fig. 4 for limits on resonance cross section in the range m = 0.5–3.0 TeV.
[28] AAD 11AG search for dijet resonances in pp collisions at E_{cm} = 7 TeV with L = 36 pb^{-1}. Limits on number of events for m = 0.6–4 TeV are given in their Table 3.
[29] AALTONEN 11M find a peak in two jet invariant mass distribution around 140 GeV in W + 2 jet events in $p\overline{p}$ collisions at E_{cm} = 1.96 TeV with L = 4.3 fb^{-1}.
[30] ABAZOV 11I search for two-jet resonances in W + 2 jet events in $p\overline{p}$ collisions at E_{cm} = 1.96 TeV with L = 4.3 fb^{-1} and give limits σ < (2.6–1.3) pb (95% CL) for m = 110–170 GeV. The result is incompatible with AALTONEN 11M.
[31] AAD 10 search for narrow dijet resonances in pp collisions at E_{cm} = 7 TeV with L = 315 nb^{-1}. Limits on the cross section in the range 10–10^3 pb is given for m = 0.3–1.7 TeV.
[32] KHACHATRYAN 10 search for narrow dijet resonances in pp collisions at E_{cm} = 7 TeV with L = 2.9 pb^{-1}. Limits on the cross section in the range 1–300 pb is given for m = 0.5–2.6 TeV separately in the final states qq, qg, and gg.
[33] ABE 99F search for narrow $b\overline{b}$ resonances in $p\overline{p}$ collisions at E_{cm}=1.8 TeV. Limits on $\sigma(p\overline{p} \to X+$ anything$)\times$B($X \to b\overline{b}$) in the range 3–10^3 pb (95%CL) are given for m_X=200–750 GeV. See their Table I.
[34] ABE 97G search for narrow dijet resonances in $p\overline{p}$ collisions with 106 pb^{-1} of data at E_{cm} = 1.8 TeV. Limits on $\sigma(p\overline{p} \to X+$ anything$)\cdot$B($X \to jj$) in the range 10^4–10^{-1} pb (95%CL) are given for dijet mass m=200–1150 GeV with both jets having $|\eta| < 2.0$ and the dijet system having $|\cos\theta^*| < 0.67$. See their Table I for the list of limits. Supersedes ABE 93G.
[35] ABE 93G give cross section times branching ratio into light (d, u, s, c, b) quarks for Γ = 0.02 M. Their Table II gives limits for M = 200–900 GeV and Γ = (0.02–0.2) M.

LIMITS ON NEUTRAL PARTICLE PRODUCTION

Production Cross Section of Radiatively-Decaying Neutral Particle

VALUE (pb)	CL%	DOCUMENT ID		TECN	COMMENT
• • • We do not use the following data for averages, fits, limits, etc. • • •					
		[1] ALBERT	18C	HAWC	γ from Sun
		[2] KHACHATRY...	17D	CMS	$Z\gamma$ resonance
<0.0008	95	[3] AAD	16AI	ATLS	$pp \to \gamma$ + jet
		[4] KHACHATRY...	16M	CMS	$pp \to \gamma\gamma$ resonance
<(0.043–0.17)	95	[5] ABBIENDI	00D	OPAL	$e^+e^- \to X^0Y^0$, $X^0 \to Y^0\gamma$
<(0.05–0.8)	95	[6] ABBIENDI	00D	OPAL	$e^+e^- \to X^0X^0$, $X^0 \to Y^0\gamma$
<(2.5–0.5)	95	[7] ACKERSTAFF	97B	OPAL	$e^+e^- \to X^0Y^0$, $X^0 \to Y^0\gamma$
<(1.6–0.9)	95	[8] ACKERSTAFF	97B	OPAL	$e^+e^- \to X^0X^0$, $X^0 \to Y^0\gamma$

Downloaded from https://academic.oup.com/ptep/article/2022/8/083C01/6651666 by KIT Library user on 27 September 2022

[1] ALBERT 18C search for WIMP annihilation in Sun to long-lived, radiatively decaying mediator; no signal; limits set on $\sigma^{SD}(\chi p)$ assuming long-lived mediator.

[2] KHACHATRYAN 17D search for new scalar resonance decaying to $Z\gamma$ with $Z \to e^+e^-$, $\mu^+\mu^-$ in pp collisions at 8 and 13 TeV; no signal seen.

[3] AAD 16AI search for excited quarks (EQ) and quantum black holes (QBH) in 3.2 fb^{-1} at 13 TeV of data; exclude EQ below 4.4 TeV and QBH below 3.8 (6.2) TeV for RS1 (ADD) models. The visible cross section limit was obtained for 5 TeV resonance with $\sigma_G/M_G = 2\%$.

[4] KHACHATRYAN 16M search for $\gamma\gamma$ resonance using 19.7 fb^{-1} at 8 TeV and 3.3 fb^{-1} at 13 Tev; slight excess at 750 GeV noted; limit set on RS graviton.

[5] ABBIENDI 00D associated production limit is for m_{X^0}= 90–188 GeV, m_{Y^0}=0 at E_{cm}=189 GeV. See also their Fig. 9.

[6] ABBIENDI 00D pair production limit is for m_{X^0} = 45–94 GeV, m_{Y^0}=0 at E_{cm}=189 GeV. See also their Fig. 12.

[7] ACKERSTAFF 97B associated production limit is for m_{X^0} = 80–160 GeV, m_{Y^0}=0 from 10.0 pb^{-1} at E_{cm} = 161 GeV. See their Fig. 3(a).

[8] ACKERSTAFF 97B pair production limit is for m_{X^0} = 40–80 GeV, m_{Y^0}=0 from 10.0 pb^{-1} at E_{cm} = 161 GeV. See their Fig. 3(b).

Heavy Particle Production Cross Section

VALUE (cm^2/N)	CL%	DOCUMENT ID		TECN	COMMENT
• • • We do not use the following data for averages, fits, limits, etc. • • •					
		[1] AAD	21F	ATLS	monojet search
		[2] AAIJ	20AL	LHCB	pp at 13 TeV, dimuon resonance
		[3] SIRUNYAN	20AY	CMS	$\Upsilon(1S)\mu^+\mu^-$ decay states
		[4] SIRUNYAN	20Z	CMS	multilepton BSM search, 13 TeV
		[5] AABOUD	19H	ATLS	di-photon-jet resonance
		[6] AABOUD	19V	ATLS	ATLAS review, mediator-based DM
		[7] SIRUNYAN	19O	CMS	$pp \to \gamma \not{E}_T$
		[8] AABOUD	18CJ	ATLS	$pp \to VV/\ell\ell/\ell\nu$, $V = W,Z,h$
		[9] AABOUD	18CM	ATLS	$pp \to e\mu/e\tau/\mu\tau$
		[10] AAIJ	18AJ	LHCB	$pp \to A' \to \mu^+\mu^-$; dark photon
		[11] BANERJEE	18	NA64	$eZ \to eZX(A')$
		[12] BANERJEE	18A	NA64	$eZ \to eZA'$, $A' \to \chi\chi$
		[13] MARSICANO	18	E137	$e^+e^- \to A'(\gamma)$ visible decay
		[14] SIRUNYAN	18BB	CMS	$pp \to Z' \to \ell^+\ell^-$ at 13 TeV
		[15] SIRUNYAN	18DA	CMS	$pp \to$ Black Hole, string ball, sphaleron
		[16] SIRUNYAN	18DD	CMS	$pp \to jj$
		[17] SIRUNYAN	18DR	CMS	$pp \to b\mu\overline{\mu}$
		[18] SIRUNYAN	18DU	CMS	$pp \to \gamma\gamma$
		[19] SIRUNYAN	18ED	CMS	$pp \to V \to Wh$; $h \to b\overline{b}$; $W \to \ell\nu$
		[20] AABOUD	17B	ATLS	WH, ZH resonance
		[21] AAIJ	17BR	LHCB	$pp \to \pi_V\pi_V$, $\pi_V \to jj$
		[22] AAD	16O	ATLS	$\ell + (\ell$s or jets)
		[23] AAD	16R	ATLS	WW, WZ, ZZ resonance
		[24] KRASZNAHO...	16		p^7Li $\to$ ^{8}Be $\to X(17)N$, $X(17) \to e^+e^-$
		[25] LEES	15E	BABR	e^+e^- collisions
		[26] ADAMS	97B	KTEV	m= 1.2–5 GeV
$< 10^{-36}$–10^{-33}	90	[27] GALLAS	95	TOF	m= 0.5–20 GeV
$<(4$–$0.3) \times 10^{-31}$	95	[28] AKESSON	91	CNTR	m = 0–5 GeV
$<2 \times 10^{-36}$	90	[29] BADIER	86	BDMP	$\tau = (0.05$–$1.) \times 10^{-8}$s
$<2.5 \times 10^{-35}$		[30] GUSTAFSON	76	CNTR	$\tau > 10^{-7}$ s

[1] AAD 21F search for hard monojet production at ATLAS with 139 $^{-1}$ of 13 TeV data. No signal observed. Limits placed on invisible production cross-section recoiling against ISR and interpreted in variety of BSM models.

[2] AAIJ 20AL search for dimuon resonance from promptly decaying X particle; no signal; limits placed on m(X) up to 60 GeV depending on mixing in 2HDM .

[3] SIRUNYAN 20AY measured $\Upsilon(1S)$ pair production cross section and searched for new states decaying into $\Upsilon(1S)\mu^+\mu^-$ at CMS with 13 TeV with 35.9 fb^{-1}. No signal is found and limits are set in $\sigma\cdot$BF vs. mass plane for tetra-b-quarks with masses between 17.5 and 19 GeV and for generic search for narrow resonances with mass between 16.5 and 27 GeV.

[4] SIRUNYAN 20Z search for BSM physics via multilepton production with CMS at 13 TeV with 137 fb^{-1}; no signal is found and limits are set on type-III seesaw and other BSM models.

[5] AABOUD 19H searches for di-photon-jet resonance at 13 TeV and 36.7 fb^{-1} of data; no signal found and limits placed on $\sigma\cdot$BR vs. mass plane for various simplified models.

[6] AABOUD 19V review ATLAS searches for mediator-based DM at 7, 8, and 13 TeV with up to 37 fb^{-1} of data; no signal found and limits set for wide variety of simplified models of dark matter.

[7] SIRUNYAN 19O search for $pp \to \gamma \not{E}_T$ at 13 TeV with 36.1 fb^{-1}; no signal found and limits set for various simplified models.

[8] AABOUD 18CJ make multichannel search for $pp \to VV/\ell\ell/\ell\nu$, $V = W,Z,h$ at 13 TeV, 36.1 fb^{-1}; no signal found; limits placed for several BSM models.

[9] AABOUD 18CM search for lepton-flavor violating resonance in $pp \to e\mu/e\tau/\mu\tau$ at 13 TeV, 36.1 fb^{-1}; no signal is found and limits placed for various BSM models.

[10] AAIJ 18AJ search for prompt and delayed dark photon decay $A' \to \mu^+\mu^-$ at LHCb detector using 1.6 fb^{-1} of pp collisions at 13 TeV; limits on m(A') vs. kinetic mixing are set.

[11] BANERJEE 18 search for dark photon A'/16.7 MeV boson X at NA64 via $eZ \to eZX(A')$; no signal found and limits set on the X-e^- coupling ϵ_e in the range $1.3 \times 10^{-4} \le \epsilon_e \le 4.2 \times 10^{-4}$ excluding part of the allowed parameter space.

[12] BANERJEE 18A search for invisibly decaying dark photons in $eZ \to eZA'$, $A' \to$ invisible; no signal found and limits set on mixing for m(A') < 1 GeV.

[13] MARSICANO 18 search for dark photon $e^+e^- \to A'(\gamma)$ visible decay in SLAC E137 e beam dump data. No signal observed and limits set in ϵ coupling vs m(A') plane, see their figure 7.

[14] SIRUNYAN 18BB search for high mass dilepton resonance; no signal found and exclude portions of p-space of Z', KK graviton models.

[15] SIRUNYAN 18DA search for $pp \to$ Black Hole, string ball, sphaleron via high multiplicity events at 13 TeV, 35.9 fb^{-1}; no signal, require e.g. m(BH) > 10.1 TeV.

[16] SIRUNYAN 18DD search for $pp \to jj$ deviations in dijet angular distribution. No signal observed. Set limits on large extra dimensions, black holes and DM mediators e.g. m(BH) > 5.9–8.2 TeV.

[17] SIRUNYAN 18DR search for dimuon resonance in $pp \to b\mu\overline{\mu}$ at 8 and 13 TeV. Slight excess seen at m($\mu\overline{\mu}$) $\sim$ 28 GeV in some channels.

[18] SIRUNYAN 18DU search for high mass diphoton resonance in $pp \to \gamma\gamma$ at 13 TeV using 35.9 fb^{-1}; no signal; limits placed on RS Graviton, LED, and clockwork.

[19] SIRUNYAN 18ED search for $pp \to V \to Wh$; $h \to b\overline{b}$; $W \to \ell\nu$ at 13 TeV with 35.9 fb^{-1}; no signal; limits set on m(W') > 2.9 TeV.

[20] AABOUD 17B exclude m(W', Z') < 1.49–2.31 TeV depending on the couplings and W'/Z' degeneracy assumptions via WH, ZH search in pp collisions at 13 TeV with 3.2 fb^{-1} of data.

[21] AAIJ 17BR search for long-lived hidden valley pions from Higgs decay. Limits are set on the signal strength as a function of the mass and lifetime of the long-lived particle in their Fig. 4 and Tab. 4.

[22] AAD 16O search for high E_T $\ell + (\ell$s or jets) with 3.2 fb^{-1} at 13 TeV; exclude micro black holes mass < 8 TeV (Fig. 3) for models with two extra dimensions.

[23] AAD 16R search for WW, WZ, ZZ resonance in 20.3 fb^{-1} at 8 TeV data; limits placed on massive RS graviton (Fig. 4).

[24] KRASZNAHORKAY 16 report pLi $\to$ Be $\to e\overline{e}N$ 5σ resonance at 16.7 MeV– possible evidence for nuclear interference or new light boson . However, such nuclear interference was ruled out already by ZANG 17.

[25] LEES 15E search for long-lived neutral particles produced in e^+e^- collisions in the Upsilon region, which decays into e^+e^-, $\mu^+\mu^-$, $e^\pm\mu^\mp$, $\pi^+\pi^-$, K^+K^-, or $\pi^\pm K^\mp$. See their Fig. 2 for cross section limits.

[26] ADAMS 97B search for a hadron-like neutral particle produced in pN interactions, which decays into a ρ^0 and a weakly interacting massive particle. Upper limits are given for the ratio to K_L production for the mass range 1.2–5 GeV and lifetime 10^{-9}–10^{-4} s. See also our Light Gluino Section.

[27] GALLAS 95 limit is for a weakly interacting neutral particle produced in 800 GeV/c pN interactions decaying with a lifetime of 10^{-4}–10^{-8} s. See their Figs. 8 and 9. Similar limits are obtained for a stable particle with interaction cross section 10^{-29}–10^{-33} cm^2. See Fig. 10.

[28] AKESSON 91 limit is from weakly interacting neutral long-lived particles produced in pN reaction at 450 GeV/c performed at CERN SPS. Bourquin-Gaillard formula is used as the production model. The above limit is for $\tau > 10^{-7}$ s. For $\tau > 10^{-9}$ s, $\sigma < 10^{-30}$ cm^{-2}/nucleon is obtained.

[29] BADIER 86 looked for long-lived particles at 300 GeV π^- beam dump. The limit applies for nonstrongly interacting neutral or charged particles with mass >2 GeV. The limit applies for particle modes, $\mu^+\pi^-$, $\mu^+\mu^-$, $\pi^+\pi^-$X, $\pi^+\pi^-\pi^\pm$ etc. See their figure 5 for the contours of limits in the mass-τ plane for each mode.

[30] GUSTAFSON 76 is a 300 GeV FNAL experiment looking for heavy (m >2 GeV) long-lived neutral hadrons in the M4 neutral beam. The above typical value is for m = 3 GeV and assumes an interaction cross section of 1 mb. Values as a function of mass and interaction cross section are given in figure 2.

Production of New Penetrating Non-ν Like States in Beam Dump

VALUE	DOCUMENT ID		TECN	COMMENT
• • • We do not use the following data for averages, fits, limits, etc. • • •				
	[1] ANDREEV	21	NA64	search for new boson X in $eZ \to eZX$
	[2] LOSECCO	81	CALO	28 GeV protons

[1] ANDREEV 21 search for new invisibly decaying boson X in $eZ \to eZX$ at NA64. No signal observed. Limits set in coupling vs. m(X) plane for m(X) $\sim$ 10^{-3} to 1 GeV.

[2] No excess neutral-current events leads to σ(production) $\times$ σ(interaction)$\times$acceptance $< 2.26 \times 10^{-71}$ cm^4/nucleon^2 (CL = 90%) for light neutrals. Acceptance depends on models (0.1 to 4. $\times 10^{-4}$).

LIMITS ON CHARGED PARTICLES IN e^+e^-

Heavy Particle Production Cross Section in e^+e^-

Ratio to $\sigma(e^+e^- \to \mu^+\mu^-)$ unless noted. See also entries in Free Quark Search and Magnetic Monopole Searches.

VALUE	CL%	DOCUMENT ID		TECN	COMMENT
• • • We do not use the following data for averages, fits, limits, etc. • • •					
		[1] KILE	18	ALEP	$e^+e^- \to$ 4 jets
$<1 \times 10^{-3}$	90	[2] ABLIKIM	17AA	BES3	$e^+e^- \to \ell\overline{\ell}\gamma$
		[3] ACKERSTAFF	98P	OPAL	Q=1,2/3, m=45–89.5 GeV
		[4] ABREU	97D	DLPH	Q=1,2/3, m=45–84 GeV
		[5] BARATE	97K	ALEP	Q=1, m=45–85 GeV
$<2 \times 10^{-5}$	95	[6] AKERS	95R	OPAL	Q=1, m= 5–45 GeV
$<1 \times 10^{-5}$	95	[6] AKERS	95R	OPAL	Q=2, m= 5–45 GeV
$<2 \times 10^{-3}$	90	[7] BUSKULIC	93C	ALEP	Q=1, m=32–72 GeV
$<(10^{-2}$–1)	95	[8] ADACHI	90C	TOPZ	Q=1, m=1–16, 18–27 GeV
$<7 \times 10^{-2}$	90	[9] ADACHI	90E	TOPZ	Q = 1, m = 5–25 GeV
$<1.6 \times 10^{-2}$	95	[10] KINOSHITA	82	PLAS	Q=3–180, m <14.5 GeV
$<5.0 \times 10^{-2}$	90	[11] BARTEL	80	JADE	Q=(3,4,5)/3 2–12 GeV

Downloaded from https://academic.oup.com/ptep/article/2022/8/083C01/6651666 by KIT Library user on 27 September 2022

[1] KILE 18 investigate archived ALEPH $e^+e^- \to$ 4 jets data and see 4–5 σ excess at 110 GeV.
[2] ABLIKIM 17AA search for dark photon $A \to \ell\overline{\ell}$ at 3.773 GeV with 2.93 fb^{-1}. Limits are set in ϵ vs m(A) plane.
[3] ACKERSTAFF 98P search for pair production of long-lived charged particles at E_{cm} between 130 and 183 GeV and give limits σ <(0.05–0.2) pb (95%CL) for spin-0 and spin-1/2 particles with m=45–89.5 GeV, charge 1 and 2/3. The limit is translated to the cross section at E_{cm}=183 GeV with the s dependence described in the paper. See their Figs. 2–4.
[4] ABREU 97D search for pair production of long-lived particles and give limits σ <(0.4–2.3) pb (95%CL) for various center-of-mass energies E_{cm}=130–136, 161, and 172 GeV, assuming an almost flat production distribution in cosθ.
[5] BARATE 97K search for pair production of long-lived charged particles at E_{cm} = 130, 136, 161, and 172 GeV and give limits σ <(0.2–0.4) pb (95%CL) for spin-0 and spin-1/2 particles with m=45–85 GeV. The limit is translated to the cross section at E_{cm}=172 GeV with the E_{cm} dependence described in the paper. See their Figs. 2 and 3 for limits on J = 1/2 and J = 0 cases.
[6] AKERS 95R is a CERN-LEP experiment with $W_{cm} \sim m_Z$. The limit is for the production of a stable particle in multihadron events normalized to $\sigma(e^+e^- \to$ hadrons). Constant phase space distribution is assumed. See their Fig. 3 for bounds for $Q = \pm 2/3$, $\pm 4/3$.
[7] BUSKULIC 93C is a CERN-LEP experiment with $W_{cm} = m_Z$. The limit is for a pair or single production of heavy particles with unusual ionization loss in TPC. See their Fig. 5 and Table 1.
[8] ADACHI 90C is a KEK-TRISTAN experiment with W_{cm} = 52–60 GeV. The limit is for pair production of a scalar or spin-1/2 particle. See Figs. 3 and 4.
[9] ADACHI 90E is KEK-TRISTAN experiment with W_{cm} = 52–61.4 GeV. The above limit is for inclusive production cross section normalized to $\sigma(e^+e^- \to \mu^+\mu^-)\cdot\beta(3-\beta^2)/2$, where $\beta = (1 - 4m^2/W_{cm}^2)^{1/2}$. See the paper for the assumption about the production mechanism.
[10] KINOSHITA 82 is SLAC PEP experiment at W_{cm} = 29 GeV using lexan and ^{39}Cr plastic sheets sensitive to highly ionizing particles.
[11] BARTEL 80 is DESY-PETRA experiment with W_{cm} = 27–35 GeV. Above limit is for inclusive pair production and ranges between 1. $\times 10^{-1}$ and 1. $\times 10^{-2}$ depending on mass and production momentum distributions. (See their figures 9, 10, 11).

Branching Fraction of Z^0 to a Pair of Stable Charged Heavy Fermions

VALUE	CL%	DOCUMENT ID		TECN	COMMENT
• • • We do not use the following data for averages, fits, limits, etc. • • •					
$<5 \times 10^{-6}$	95	[1] AKERS	95R	OPAL	m= 40.4–45.6 GeV
$<1 \times 10^{-3}$	95	AKRAWY	90O	OPAL	m = 29–40 GeV

[1] AKERS 95R give the 95% CL limit $\sigma(X\overline{X})/\sigma(\mu\mu) < 1.8\times10^{-4}$ for the pair production of singly- or doubly-charged stable particles. The limit applies for the mass range 40.4–45.6 GeV for $X^{\pm}$ and < 45.6 GeV for $X^{\pm\pm}$. See the paper for bounds for $Q = \pm 2/3$, $\pm 4/3$.

LIMITS ON CHARGED PARTICLES IN HADRONIC REACTIONS

MASS LIMITS for Long-Lived Charged Heavy Fermions

Limits are for spin 1/2 particles with no color and SU(2)$_L$ charge. The electric charge Q of the particle (in the unit of e) is therefore equal to its weak hypercharge. Pair production by Drell-Yan like γ and Z exchange is assumed to derive the limits.

VALUE (GeV)	CL%	DOCUMENT ID		TECN	COMMENT
• • • We do not use the following data for averages, fits, limits, etc. • • •					
		[1] SIRUNYAN	20N	CMS	disappearing track LLP
>660	95	[2] AAD	15BJ	ATLS	$\lvert Q\rvert = 2$
>200	95	[3] CHATRCHYAN	13AB	CMS	$\lvert Q\rvert = 1/3$
>480	95	[3] CHATRCHYAN	13AB	CMS	$\lvert Q\rvert = 2/3$
>574	95	[3] CHATRCHYAN	13AB	CMS	$\lvert Q\rvert = 1$
>685	95	[3] CHATRCHYAN	13AB	CMS	$\lvert Q\rvert = 2$
>140	95	[4] CHATRCHYAN	13AR	CMS	$\lvert Q\rvert = 1/3$
>310	95	[4] CHATRCHYAN	13AR	CMS	$\lvert Q\rvert = 2/3$

[1] SIRUNYAN 20N search for LLPs using disappearing track signature at CMS at 13 TeV with 101 fb^{-1}; no signal; limits placed on long-lived winos and higgsinos from SUSY depending on mass and lifetime: e.g. at 95% CL, for a purely higgsino neurtalino, m(chargino) > 750 (175) GeV for τ = 3 (0.05) ns, and for a purely wino neutralino, m(chargino) > 884 (474) GeV for τ = 3 (0.2) ns.
[2] AAD 15BJ use 20.3 fb^{-1} of pp collisions at E_{cm} = 8 TeV. See paper for limits for $\lvert Q\rvert$ = 3, 4, 5, 6.
[3] CHATRCHYAN 13AB use 5.0 fb^{-1} of pp collisions at E_{cm} = 7 TeV and 18.8 fb^{-1} at E_{cm} = 8 TeV. See paper for limits for $\lvert Q\rvert$ = 3, 4,. . ., 8.
[4] CHATRCHYAN 13AR use 5.0 fb^{-1} of pp collisions at E_{cm} = 7 TeV.

Heavy Particle Production Cross Section

VALUE (nb)	CL%	DOCUMENT ID		TECN	COMMENT
• • • We do not use the following data for averages, fits, limits, etc. • • •					
		[1] SIRUNYAN	21T	CMS	model independent search
		[2] SIRUNYAN	20C	CMS	4t search via multileptons
		[3] AABOUD	19AA	ATLS	BSM search
		[4] AABOUD	19Q	ATLS	single top +MET
		[5] AABOUD	17D	ATLS	anomalous $WWjj$, $WZjj$
		[6] AABOUD	17L	ATLS	m>870 GeV, $Z(\to \nu\nu)tX$
		[7] SIRUNYAN	17B	CMS	tH
		[8] SIRUNYAN	17C	CMS	$Z + (t$ or $b)$
		[9] SIRUNYAN	17J	CMS	$X_{5/3} \to tW$
		[10] AAIJ	15BD	LHCB	m=124–309 GeV
		[11] AAD	13AH	ATLS	$\lvert q\rvert$=(2–6)e, m=50–600 GeV
$<1.2 \times 10^{-3}$	95	[12] AAD	11I	ATLS	$\lvert q\rvert$=10e, m=0.2–1 TeV
$<1.0 \times 10^{-5}$	95	[13,14] AALTONEN	09Z	CDF	m>100 GeV, noncolored
$<4.8 \times 10^{-5}$	95	[13,15] AALTONEN	09Z	CDF	m>100 GeV, colored
$< 0.31–0.04 \times 10^{-3}$	95	[16] ABAZOV	09M	D0	pair production
<0.19	95	[17] AKTAS	04C	H1	m=3–10 GeV
<0.05	95	[18] ABE	92J	CDF	m=50–200 GeV
<30–130		[19] CARROLL	78	SPEC	m=2–2.5 GeV
<100		[20] LEIPUNER	73	CNTR	m=3–11 GeV

[1] SIRUNYAN 21T perform model unspecific search for deviations from SM with CMS at 13 TeV with 35.9^{-1} fb data in numerous signature channels. No deviations from SM found.
[2] SIRUNYAN 20C search for four top-quark production with decay to multileptons at CMS at 13 TeV with 137 fb^{-1}; no signal is found and limits are placed on the Higgs boson oblique parameter in the effective field theory framework (EFT) and the model parameters (tanβ).
[3] AABOUD 19AA search for BSM physics at 13 TeV with 3.2 fb^{-1} in $> 10^5$ regions of > 700 event classes; no significant signal found.
[4] AABOUD 19Q search for single top+MET events at 13 TeV with 36.1 fb^{-1} of data; no signal found and limits set in σ or coupling vs. mass plane for variety of simplified models including DM and vector-like top quark T.
[5] AABOUD 17D search for $WWjj$, $WZjj$ in pp collisions at 8 TeV with 3.2 fb^{-1}; set limits on anomalous couplings.
[6] AABOUD 17L search for the pair production of heavy vector-like T quarks in the $Z(\to \nu\nu)tX$ final state.
[7] SIRUNYAN 17B search for vector-like quark $pp \to TX \to tHX$ in 2.3 fb^{-1} at 13 TeV; no signal seen; limits placed.
[8] SIRUNYAN 17C search for vector-like quark $pp \to TX \to Z + (t$ or $b)$ in 2.3 fb^{-1} at 13 TeV; no signal seen; limits placed.
[9] SIRUNYAN 17J search for $pp \to X_{5/3}X_{5/3} \to tWtW$ with 2.3 fb^{-1} at 13 TeV. No signal seen: m(X) > 1020 (990) GeV for RH (LH) new charge 5/3 quark.
[10] AAIJ 15BD search for production of long-lived particles in pp collisions at E_{cm} = 7 and 8 TeV. See their Table 6 for cross section limits.
[11] AAD 13AH search for production of long-lived particles with $\lvert q\rvert$=(2–6)e in pp collisions at E_{cm} = 7 TeV with 4.4 fb^{-1}. See their Fig. 8 for cross section limits.
[12] AAD 11I search for production of highly ionizing massive particles in pp collisions at E_{cm} = 7 TeV with L = 3.1 pb^{-1}. See their Table 5 for similar limits for $\lvert q\rvert = 6e$ and 17e, Table 6 for limits on pair production cross section.
[13] AALTONEN 09Z search for long-lived charged particles in $p\overline{p}$ collisions at E_{cm} = 1.96 TeV with L = 1.0 fb^{-1}. The limits are on production cross section for a particle of mass above 100 GeV in the region $\lvert\eta\rvert \lesssim 0.7$, p_T > 40 GeV, and 0.4 < β < 1.0.
[14] Limit for weakly interacting charge-1 particle.
[15] Limit for up-quark like particle.
[16] ABAZOV 09M search for pair production of long-lived charged particles in $p\overline{p}$ collisions at E_{cm} = 1.96 TeV with L = 1.1 fb^{-1}. Limit on the cross section of (0.31–0.04) pb (95% CL) is given for the mass range of 60–300 GeV, assuming the kinematics of stau pair production.
[17] AKTAS 04C look for charged particle photoproduction at HERA with mean c.m. energy of 200 GeV.
[18] ABE 92J look for pair production of unit-charged particles which leave detector before decaying. Limit shown here is for m=50 GeV. See their Fig. 5 for different charges and stronger limits for higher mass.
[19] CARROLL 78 look for neutral, $S = -2$ dihyperon resonance in $pp \to 2K^+X$. Cross section varies within above limits over mass range and p_{lab} = 5.1–5.9 GeV/c.
[20] LEIPUNER 73 is an NAL 300 GeV p experiment. Would have detected particles with lifetime greater than 200 ns.

Heavy Particle Production Differential Cross Section

VALUE (cm^{2}sr^{-1}GeV^{-1})	CL%	DOCUMENT ID		TECN	CHG	COMMENT
• • • We do not use the following data for averages, fits, limits, etc. • • •						
$<2.6 \times 10^{-36}$	90	[1] BALDIN	76	CNTR	−	Q= 1, m=2.1–9.4 GeV
$<2.2 \times 10^{-33}$	90	[2] ALBROW	75	SPEC	±	Q= ±1, m=4–15 GeV
$<1.1 \times 10^{-33}$	90	[2] ALBROW	75	SPEC	±	Q= ±2, m=6–27 GeV
$<8. \times 10^{-35}$	90	[3] JOVANOV...	75	CNTR	±	m=15–26 GeV
$<1.5 \times 10^{-34}$	90	[3] JOVANOV...	75	CNTR	±	Q= ±2, m=3–10 GeV
$<6. \times 10^{-35}$	90	[3] JOVANOV...	75	CNTR	±	Q= ±2, m=10–26 GeV
$<1. \times 10^{-31}$	90	[4] APPEL	74	CNTR	±	m=3.2–7.2 GeV
$<5.8 \times 10^{-34}$	90	[5] ALPER	73	SPEC	±	m=1.5–24 GeV
$<1.2 \times 10^{-35}$	90	[6] ANTIPOV	71B	CNTR	−	Q=−, m=2.2–2.8
$<2.4 \times 10^{-35}$	90	[7] ANTIPOV	71C	CNTR	−	Q=−, m=1.2–1.7, 2.1–4
$<2.4 \times 10^{-35}$	90	BINON	69	CNTR	−	Q=−, m=1–1.8 GeV
$<1.5 \times 10^{-36}$		[8] DORFAN	65	CNTR		Be target m=3–7 GeV
$<3.0 \times 10^{-36}$		[8] DORFAN	65	CNTR		Fe target m=3–7 GeV

[1] BALDIN 76 is a 70 GeV Serpukhov experiment. Value is per Al nucleus at θ = 0. For other charges in range −0.5 to −3.0, CL = 90% limit is $(2.6 \times 10^{-36})/\lvert$(charge)$\rvert$ for mass range (2.1–9.4 GeV) $\times \lvert$(charge)$\rvert$. Assumes stable particle interacting with matter as do antiprotons.
[2] ALBROW 75 is a CERN ISR experiment with E_{cm} = 53 GeV. θ = 40 mr. See figure 5 for mass ranges up to 35 GeV.
[3] JOVANOVICH 75 is a CERN ISR 26+26 and 15+15 GeV pp experiment. Figure 4 covers ranges Q = 1/3 to 2 and m = 3 to 26 GeV. Value is per GeV momentum.
[4] APPEL 74 is NAL 300 GeV pW experiment. Studies forward production of heavy (up to 24 GeV) charged particles with momenta 24–200 GeV (−charge) and 40–150 GeV (+charge). Above typical value is for 75 GeV and is per GeV momentum per nucleon.
[5] ALPER 73 is CERN ISR 26+26 GeV pp experiment. p >0.9 GeV, 0.2 < β <0.65.
[6] ANTIPOV 71B is from same 70 GeV p experiment as ANTIPOV 71C and BINON 69.
[7] ANTIPOV 71C limit inferred from flux ratio. 70 GeV p experiment.
[8] DORFAN 65 is a 30 GeV/c p experiment at BNL. Units are per GeV momentum per nucleus.

Downloaded from https://academic.oup.com/ptep/article/2022/8/083C01/6651666 by KIT Library user on 27 September 2022

Long-Lived Heavy Particle Invariant Cross Section

VALUE ($cm^2/GeV^2/N$)	CL%	DOCUMENT ID		TECN	CHG	COMMENT
• • • We do not use the following data for averages, fits, limits, etc. • • •						
$< 5–700 \times 10^{-35}$	90	[1] BERNSTEIN	88	CNTR		
$< 5–700 \times 10^{-37}$	90	[1] BERNSTEIN	88	CNTR		
$<2.5 \times 10^{-36}$	90	[2] THRON	85	CNTR	−	Q= 1, m=4–12 GeV
$<1. \times 10^{-35}$	90	[2] THRON	85	CNTR	+	Q= 1, m=4–12 GeV
$<6. \times 10^{-33}$	90	[3] ARMITAGE	79	SPEC		m=1.87 GeV
$<1.5 \times 10^{-33}$	90	[3] ARMITAGE	79	SPEC		m=1.5–3.0 GeV
		[4] BOZZOLI	79	CNTR	±	Q = (2/3, 1, 4/3, 2)
$<1.1 \times 10^{-37}$	90	[5] CUTTS	78	CNTR		m=4–10 GeV
$<3.0 \times 10^{-37}$	90	[6] VIDAL	78	CNTR		m=4.5–6 GeV

[1] BERNSTEIN 88 limits apply at $x = 0.2$ and $p_T = 0$. Mass and lifetime dependence of limits are shown in the regions: m = 1.5–7.5 GeV and $\tau = 10^{-8}$–2×10^{-6} s. First number is for hadrons; second is for weakly interacting particles.

[2] THRON 85 is FNAL 400 GeV proton experiment. Mass determined from measured velocity and momentum. Limits are for $\tau > 3 \times 10^{-9}$ s.

[3] ARMITAGE 79 is CERN-ISR experiment at E_{cm} = 53 GeV. Value is for $x = 0.1$ and $p_T = 0.15$. Observed particles at m = 1.87 GeV are found all consistent with being antideuterons.

[4] BOZZOLI 79 is CERN-SPS 200 GeV pN experiment. Looks for particle with τ larger than 10^{-8} s. See their figure 11–18 for production cross-section upper limits vs mass.

[5] CUTTS 78 is pBe experiment at FNAL sensitive to particles of $\tau > 5 \times 10^{-8}$ s. Value is for $-0.3 < x < 0$ and $p_T = 0.175$.

[6] VIDAL 78 is FNAL 400 GeV proton experiment. Value is for $x = 0$ and $p_T = 0$. Puts lifetime limit of $< 5 \times 10^{-8}$ s on particle in this mass range.

Long-Lived Heavy Particle Production (σ(Heavy Particle) / $\sigma(\pi)$)

VALUE	EVTS	DOCUMENT ID		TECN	CHG	COMMENT
• • • We do not use the following data for averages, fits, limits, etc. • • •						
$<10^{-8}$		[1] NAKAMURA	89	SPEC	±	Q= (−5/3,±2)
	0	[2] BUSSIERE	80	CNTR	±	Q= (2/3,1,4/3,2)

[1] NAKAMURA 89 is KEK experiment with 12 GeV protons on Pt target. The limit applies for mass $\lesssim$ 1.6 GeV and lifetime $\gtrsim 10^{-7}$ s.

[2] BUSSIERE 80 is CERN-SPS experiment with 200–240 GeV protons on Be and Al target. See their figures 6 and 7 for cross-section ratio vs mass.

Production and Capture of Long-Lived Massive Particles

VALUE (10^{-36} cm^2)	DOCUMENT ID		TECN	COMMENT
• • • We do not use the following data for averages, fits, limits, etc. • • •				
	[1] AAD	21X	ATLS	search for captured LLPs
	[2] ACHARYA	21	INDU	dyons production, capture
<20 to 800	[3] ALEKSEEV	76	ELEC	τ=5 ms to 1 day
<200 to 2000	[3] ALEKSEEV	76B	ELEC	τ=100 ms to 1 day
<1.4 to 9	[4] FRANKEL	75	CNTR	τ=50 ms to 10 hours
<0.1 to 9	[5] FRANKEL	74	CNTR	τ=1 to 1000 hours

[1] AAD 21X search for LLPs which come to rest in ATLAS detector to deposit energy between collisions. No signal observed in 111 fb^{-1} of data. Limits placed in lifetime vs. mass place assuming model with gluino hadrons: e.g. m > 1.4 TeV for $\tau \sim 10^{-5}$ to 10^3 sec.

[2] ACHARYA 21 search for dyons (carrying electric and magnetic charge) and monopoles via production and capture in 6.46 fb^{-1} of 13 TeV LHC data. No signal observed. Limits placed in mass vs. magnetic charge plane.

[3] ALEKSEEV 76 and ALEKSEEV 76B are 61–70 GeV p Serpukhov experiment. Cross section is per Pb nucleus.

[4] FRANKEL 75 is extension of FRANKEL 74.

[5] FRANKEL 74 looks for particles produced in thick Al targets by 300–400 GeV/c protons.

Long-Lived Particle (LLP) Search at Hadron Collisions

Limits are for cross section times branching ratio.

VALUE (fb)	CL%	DOCUMENT ID		TECN	COMMENT
• • • We do not use the following data for averages, fits, limits, etc. • • •					
		[1] AAD	21AL	ATLS	charged LLPs search
		[2] AAD	21BA	ATLS	LLP from higgs decay search
		[3] AAIJ	21V	LHCB	LLP $\to e\mu\nu$ search
		[4] SIRUNYAN	21AF	CMS	LLP search via displaced jets
< 0.07	95	[5] SIRUNYAN	21U	CMS	LLP search via displaced jets
		[6] TUMASYAN	21	CMS	LLP endcap muon detector searches
		[7] AAD	20D	ATLS	$pp \to$ LLPs at 13 TeV
		[8] AAD	20J	ATLS	scalar boson decay to LLPs
		[9] AAD	20M	ATLS	LLP top squark decay to μ
		[10] AAD	20P	ATLS	LLP dark photon search
		[11] AAIJ	20AL	LHCB	pp dimuon resonance
		[12] BALL	20		LLP milli-charged particles at LHC
		[13] AABOUD	19AE	ATLS	pp at 13 TeV
		[14] AABOUD	19AK	ATLS	$pp \to \Phi \to ZZ_d$
		[15] AABOUD	19AM	ATLS	DY multi-charged LLP production
		[16] AABOUD	19AO	ATLS	LLP via displaced jets
		[17] AABOUD	19AT	ATLS	heavy, charged LLPs
		[18] AABOUD	19G	ATLS	LLP decay to $\mu^+\mu^-$
		[19] SIRUNYAN	19BH	CMS	LLP via displaced jets
		[20] SIRUNYAN	19BT	CMS	LLP via displaced jets+MET
		[21] SIRUNYAN	19CA	CMS	LLP $\to \gamma$ search
		[22] SIRUNYAN	19Q	CMS	$pp \to j$ + displaced dark quark jet
		[23] SIRUNYAN	18AW	CMS	Long-lived particle search
		[24] AAIJ	16AR	LHCB	$H \to XX$ LLPs
		[25] KHACHATRY...	16BW	CMS	direct production: HSCPs
<2000	90	[26] BADIER	86	BDMP	$\tau = (0.05–1.) \times 10^{-8}$s

[1] AAD 21AL reports on ATLAS search for long-lived charged particles with 139 fb^{-1} at 13 TeV. No signal observed. Limits placed in lifetime vs. mass plane: e.g. for τ(LLP) $\sim$ 0.1 ns, m(selectron) > 720 GeV.

[2] AAD 21BA search for long-lived particles from ZH production ($H \to b\overline{b}$) with 2 displaced vertices in 139 fb^{-1} of data at 13 TeV. No signal detected. Limits placed in branching fraction vs. lifetime plane.

[3] AAIJ 21V search for $pp \to$ LLP + LLP with LLP$\to e\mu\nu$ in the lifetime range between 2 and 50 ps at LHCb with 5.4 fb^{-1} at 13 TeV. No signal observed. Limits placed in LLP cross section vs. mass or lifetime plane for m(LLP) $\sim$ 7 to 50 GeV.

[4] SIRUNYAN 21AF search for LLPs at CMS via jets with 2 displaced vertices in 140 fb^{-1} of data at 13 TeV. No signal observed. Limits placed for RPV SUSY models in which a long-lived neutralino or gluino decays into a multijet final state with top, bottom, and strange quarks.

[5] SIRUNYAN 21U search for long-lived particles (LLPs) via displaced jets at CMS with LHC13 and 132 fb^{-1}. No signal detected. Limits placed on simplified model production of LLP $X \to q\overline{q}$ with σ < 0.07 fb for m(X) > 500 GeV and cτ $\sim$ 2 to 250 mm.

[6] TUMASYAN 21 search for long-lived particles in CMS muon endcap detector in 137 fb^{-1} of data at 13 TeV. No signal detected. Limits are placed depending on the branching fraction of Higgs boson to LLP decaying to dd, bb, and $\tau^+\tau^-$, depending on proper decay length, and LLP masses.

[7] AAD 20D search for opposite-sign dileptons originating from long-lived particles in pp collisions at 13 Tev with 32.8 fb^{-1}; limits placed in squark cross section vs. cτ plane for RPV SUSY.

[8] AAD 20J search for scalar boson decay to two long-lived particles; no signal; limits placed in BF vs cτ plane for various mass hypotheses. This search is also combined with other ATLAS displaced-jet searches.

[9] AAD 20M search for long-lived top-squarks decay to μ and hadrons; no signal; limits placed in cross section vs. mass and mass vs. lifetime planes .

[10] AAD 20P search for long-lived dark photons produced from the decay of a scalar boson, with each dark photon decaying into displaced collimated leptons or light hadrons at 13 TeV with 36 fb^{-1}; no signal; limits placed in $\sigma \cdot$BF vs. cτ and other planes.

[11] AAIJ 20AL search for long-lived $X \to \mu^+\mu^-$ decays in 5.1 fb^{-1} of LHCb data at 13 TeV; no signal; limits placed on m(X) up to 3 GeV depending on kinetic mixing.

[12] BALL 20 search for long-lived milli-charged particles produced at LHC; limits placed in charge vs. mass plane (Fig. 8).

[13] AABOUD 19AE search for long-lived particles via displaced jets using 10.8 fb^{-1} or 33.0 fb^{-1} data (depending on a trigger) at 13 TeV; no signal found and limits set in branching ratio vs. decay length plane.

[14] AABOUD 19AK searches for long-lived particle Z_d via $pp \to \Phi \to ZZ_d$ at 13 TeV with 36.1 fb^{-1}; no signal found and limits set in $\sigma\times$BR vs. lifetime plane for simplified model.

[15] AABOUD 19AM search for Drell-Yan (DY) production of long-lived multi-charge particles at 13 TeV with 36.1 fb^{-1} of data; no signal found and exclude 50 GeV < m(LLMCP) < 980–1220 GeV for electric charge |q| = (2–7)e.

[16] AABOUD 19AO search for neutral long-lived particles producing displaced jets at 13 TeV with 36.1 fb^{-1} of data; no signal found and exclude regions of $\sigma \cdot$BR vs. lifetime plane for various models.

[17] AABOUD 19AT search for heavy, charged long-lived particles at 13 TeV with 36.1 fb^{-1}; no signal found and upper limits set on masses of various hypothetical particles.

[18] AABOUD 19G search for long-lived particle with decay to $\mu^+\mu^-$ at 13 TeV with 32.9 fb^{-1}; no signal found and limits set in combinations of lifetime, mass and coupling planes for various simplified models.

[19] SIRUNYAN 19BH search for long-lived SUSY particles via displaced jets at 13 TeV with 35.9 fb^{-1}; no signal found and limits placed in mass vs lifetime plane for various hypothetical models.

[20] SIRUNYAN 19BT search for displaced jet(s)+$\not{E}_T$ at 13 TeV with 137 fb^{-1}; no signal found and limits placed in mass vs lifetime plane for gauge mediated SUSY breaking models.

[21] SIRUNYAN 19CA search for gluino/squark decay to long-lived neutralino, decay to γ in GMSB; no signal, limits placed in m(χ) vs. lifetime plane for SPS8 GMSB benchmark point .

[22] SIRUNYAN 19Q search for $pp \to j$ + displaced jet via dark quark with 13 TeV at 16.1 fb^{-1}; no signal found and limits set in mass vs lifetime plane for dark quark/dark pion model.

[23] SIRUNYAN 18AW search for very long lived particles (LLPs) decaying hadronically or to $\mu\overline{\mu}$ in CMS detector; none seen/limits set on lifetime vs. cross section.

[24] AAIJ 16AR search for long lived particles from $H \to XX$ with displaced X decay vertex using 0.62 fb^{-1} at 7 TeV; limits set in Fig. 7.

[25] KHACHATRYAN 16BW search for heavy stable charged particles via ToF with 2.5 fb^{-1} at 13 TeV; require stable m(gluinoball) > 1610 GeV.

[26] BADIER 86 looked for long-lived particles at 300 GeV π^- beam dump. The limit applies for nonstrongly interacting neutral or charged particles with mass >2 GeV. The limit applies for particle modes, $\mu^+\pi^-$, $\mu^+\mu^-$, $\pi^+\pi^-$X, $\pi^+\pi^-\pi^\pm$ etc. See their figure 5 for the contours of limits in the mass-τ plane for each mode.

Long-Lived Heavy Particle Cross Section

VALUE (pb/sr)	CL%	DOCUMENT ID		TECN	COMMENT
• • • We do not use the following data for averages, fits, limits, etc. • • •					
<34	95	[1] RAM	94	SPEC	$1015<m_{X^{++}}<1085$ MeV
<75	95	[1] RAM	94	SPEC	$920<m_{X^{++}}<1025$ MeV

[1] RAM 94 search for a long-lived doubly-charged fermion X^{++} with mass between m_N and m_N+m_π and baryon number +1 in the reaction $pp \to X^{++}n$. No candidate is found. The limit is for the cross section at 15° scattering angle at 460 MeV incident energy and applies for $\tau(X^{++}) \gg 0.1\,\mu$s.

Downloaded from https://academic.oup.com/ptep/article/2022/8/083C01/6651666 by KIT Library user on 27 September 2022

LIMITS ON CHARGED PARTICLES IN COSMIC RAYS

Heavy Particle Flux in Cosmic Rays

VALUE ($cm^{-2}sr^{-1}s^{-1}$)	CL%	EVTS	DOCUMENT ID		TECN	COMMENT
• • • We do not use the following data for averages, fits, limits, etc. • • •						
			[1] ALVIS	18	MAJD	Fractionally charged
$< 1 \times 10^{-8}$	90		[2] AGNESE	15	CDM2	$Q = 1/6$
$\sim 6 \times 10^{-9}$		2	[3] SAITO	90		$Q \simeq 14$, $m \simeq 370 m_p$
$< 1.4 \times 10^{-12}$	90	0	[4] MINCER	85	CALO	$m \geq 1$ TeV
			[5] SAKUYAMA	83B	PLAS	$m \sim 1$ TeV
$< 1.7 \times 10^{-11}$	99	0	[6] BHAT	82	CC	
$< 1. \times 10^{-9}$	90	0	[7] MARINI	82	CNTR	$Q = 1$, $m \sim 4.5 m_p$
$2. \times 10^{-9}$		3	[8] YOCK	81	SPRK	$Q = 1$, $m \sim 4.5 m_p$
		3	[8] YOCK	81	SPRK	Fractionally charged
3.0×10^{-9}		3	[9] YOCK	80	SPRK	$m \sim 4.5\ m_p$
$(4 \pm 1) \times 10^{-11}$		3	GOODMAN	79	ELEC	$m \geq 5$ GeV
$< 1.3 \times 10^{-9}$	90		[10] BHAT	78	CNTR	$m > 1$ GeV
$< 1.0 \times 10^{-9}$		0	BRIATORE	76	ELEC	
$< 7. \times 10^{-10}$	90	0	YOCK	75	ELEC	$Q > 7e$ or $< -7e$
$> 6. \times 10^{-9}$		5	[11] YOCK	74	CNTR	$m > 6$ GeV
$< 3.0 \times 10^{-8}$		0	DARDO	72	CNTR	
$< 1.5 \times 10^{-9}$		0	TONWAR	72	CNTR	$m > 10$ GeV
$< 3.0 \times 10^{-10}$		0	BJORNBOE	68	CNTR	$m > 5$ GeV
$< 5.0 \times 10^{-11}$	90	0	JONES	67	ELEC	m=5–15 GeV

[1] ALVIS 18 search for fractional charged flux of cosmic matter at Majorana demonstrator; no signal observed and limits are set on the flux of lightly ionizing particles for charge as low as e/1000.

[2] See AGNESE 15 Fig. 6 for limits extending down to Q = 1/200.

[3] SAITO 90 candidates carry about 450 MeV/nucleon. Cannot be accounted for by conventional backgrounds. Consistent with strange quark matter hypothesis.

[4] MINCER 85 is high statistics study of calorimeter signals delayed by 20–200 ns. Calibration with AGS beam shows they can be accounted for by rare fluctuations in signals from low-energy hadrons in the shower. Claim that previous delayed signals including BJORNBOE 68, DARDO 72, BHAT 82, SAKUYAMA 83B below may be due to this fake effect.

[5] SAKUYAMA 83B analyzed 6000 extended air shower events. Increase of delayed particles and change of lateral distribution above 10^{17} eV may indicate production of very heavy parent at top of atmosphere.

[6] BHAT 82 observed 12 events with delay $> 2. \times 10^{-8}$ s and with more than 40 particles. 1 eV has good hadron shower. However all events are delayed in only one of two detectors in cloud chamber, and could not be due to strongly interacting massive particle.

[7] MARINI 82 applied PEP-counter for TOF. Above limit is for velocity = 0.54 of light. Limit is inconsistent with YOCK 80 YOCK 81 events if isotropic dependence on zenith angle is assumed.

[8] YOCK 81 saw another 3 events with $Q = \pm 1$ and m about $4.5 m_p$ as well as 2 events with $m > 5.3 m_p$, $Q = \pm 0.75 \pm 0.05$ and $m > 2.8 m_p$, $Q = \pm 0.70 \pm 0.05$ and 1 event with $m = (9.3 \pm 3.) m_p$, $Q = \pm 0.89 \pm 0.06$ as possible heavy candidates.

[9] YOCK 80 events are with charge exactly or approximately equal to unity.

[10] BHAT 78 is at Kolar gold fields. Limit is for $\tau > 10^{-6}$ s.

[11] YOCK 74 events could be tritons.

Superheavy Particle (Quark Matter) Flux in Cosmic Rays

VALUE ($cm^{-2}sr^{-1}s^{-1}$)	CL%	DOCUMENT ID		TECN	COMMENT
• • • We do not use the following data for averages, fits, limits, etc. • • •					
		[1] ADRIANI	15	PMLA	$4 < m < 1.2 \times 10^5\ m_p$
$< 5 \times 10^{-16}$	90	[2] AMBROSIO	00B	MCRO	$m > 5 \times 10^{14}$ GeV
$< 1.8 \times 10^{-12}$	90	[3] ASTONE	93	CNTR	$m \geq 1.5 \times 10^{-13}$ gram
$< 1.1 \times 10^{-14}$	90	[4] AHLEN	92	MCRO	$10^{-10} < m < 0.1$ gram
$< 2.2 \times 10^{-14}$	90	[5] NAKAMURA	91	PLAS	$m > 10^{11}$ GeV
$< 6.4 \times 10^{-16}$	90	[6] ORITO	91	PLAS	$m > 10^{12}$ GeV
$< 2.0 \times 10^{-11}$	90	[7] LIU	88	BOLO	$m > 1.5 \times 10^{-13}$ gram
$< 4.7 \times 10^{-12}$	90	[8] BARISH	87	CNTR	$1.4 \times 10^8 < m < 10^{12}$ GeV
$< 3.2 \times 10^{-11}$	90	[9] NAKAMURA	85	CNTR	$m > 1.5 \times 10^{-13}$ gram
$< 3.5 \times 10^{-11}$	90	[10] ULLMAN	81	CNTR	Planck-mass 10^{19} GeV
$< 7. \times 10^{-11}$	90	[10] ULLMAN	81	CNTR	$m \leq 10^{16}$ GeV

[1] ADRIANI 15 search for relatively light quark matter with charge $Z = 1$–8. See their Figs. 2 and 3 for flux upper limits.

[2] AMBROSIO 00B searched for quark matter ("nuclearites") in the velocity range $(10^{-5}$–$1)\ c$. The listed limit is for $2 \times 10^{-3}\ c$.

[3] ASTONE 93 searched for quark matter ("nuclearites") in the velocity range $(10^{-3}$–$1)\ c$. Their Table 1 gives a compilation of searches for nuclearites.

[4] AHLEN 92 searched for quark matter ("nuclearites"). The bound applies to velocity $< 2.5 \times 10^{-3}\ c$. See their Fig. 3 for other velocity/c and heavier mass range.

[5] NAKAMURA 91 searched for quark matter in the velocity range $(4 \times 10^{-5}$–$1)\ c$.

[6] ORITO 91 searched for quark matter. The limit is for the velocity range $(10^{-4}$–$10^{-3})\ c$.

[7] LIU 88 searched for quark matter ("nuclearites") in the velocity range $(2.5 \times 10^{-3}$–$1)\ c$. A less stringent limit of 5.8×10^{-11} applies for $(1$–$2.5) \times 10^{-3}\ c$.

[8] BARISH 87 searched for quark matter ("nuclearites") in the velocity range $(2.7 \times 10^{-4}$–$5 \times 10^{-3})\ c$.

[9] NAKAMURA 85 at KEK searched for quark-matter. These might be lumps of strange quark matter with roughly equal numbers of u, d, s quarks. These lumps or nuclearites were assumed to have velocity of $(10^{-4}$–$10^{-3})\ c$.

[10] ULLMAN 81 is sensitive for heavy slow singly charge particle reaching earth with vertical velocity 100–350 km/s.

Highly Ionizing Particle Flux

VALUE ($m^{-2}yr^{-1}$)	CL%	EVTS	DOCUMENT ID		TECN	COMMENT
• • • We do not use the following data for averages, fits, limits, etc. • • •						
< 0.4	95	0	KINOSHITA	81B	PLAS	Z/β 30–100

SEARCHES FOR BLACK HOLE PRODUCTION

VALUE	DOCUMENT ID		TECN	COMMENT
• • • We do not use the following data for averages, fits, limits, etc. • • •				
not seen	[1] AABOUD	16P	ATLS	13 TeV $pp \to e\mu, e\tau, \mu\tau$
	[2] AAD	15AN	ATLS	8 TeV $pp \to$ multijets
	[3] AAD	14A	ATLS	8 TeV $pp \to \gamma +$ jet
	[4] AAD	14AL	ATLS	8 TeV $pp \to \ell +$ jet
	[5] AAD	14C	ATLS	8 TeV $pp \to \ell + (\ell$ or jets)
	[6] AAD	13D	ATLS	7 TeV $pp \to 2$ jets
	[7] CHATRCHYAN	13A	CMS	7 TeV $pp \to 2$ jets
	[8] CHATRCHYAN	13AD	CMS	8 TeV $pp \to$ multijets
	[9] AAD	12AK	ATLS	7 TeV $pp \to \ell + (\ell$ or jets)
	[10] CHATRCHYAN	12W	CMS	7 TeV $pp \to$ multijets
	[11] AAD	11AG	ATLS	7 TeV $pp \to 2$ jets

[1] AABOUD 16P set limits on quantum BH production in n = 6 ADD or n = 1 RS models.

[2] AAD 15AN search for black hole or string ball formation followed by its decay to multijet final states, in pp collisions at $E_{cm} = 8$ TeV with $L = 20.3\ fb^{-1}$. See their Figs. 6–8 for limits.

[3] AAD 14A search for quantum black hole formation followed by its decay to a γ and a jet, in pp collisions at $E_{cm} = 8$ TeV with $L = 20\ fb^{-1}$. See their Fig. 3 for limits.

[4] AAD 14AL search for quantum black hole formation followed by its decay to a lepton and a jet, in pp collisions at $E_{cm} = 8$ TeV with $L = 20.3\ fb^{-1}$. See their Fig. 2 for limits.

[5] AAD 14C search for microscopic (semiclassical) black hole formation followed by its decay to final states with a lepton and ≥ 2 (leptons or jets), in pp collisions at $E_{cm} = 8$ TeV with $L = 20.3\ fb^{-1}$. See their Figures 8–11, Tables 7, 8 for limits.

[6] AAD 13D search for quantum black hole formation followed by its decay to two jets, in pp collisions at $E_{cm} = 7$ TeV with $L = 4.8\ fb^{-1}$. See their Fig. 8 and Table 3 for limits.

[7] CHATRCHYAN 13A search for quantum black hole formation followed by its decay to two jets, in pp collisions at $E_{cm} = 7$ TeV with $L = 5\ fb^{-1}$. See their Figs. 5 and 6 for limits.

[8] CHATRCHYAN 13AD search for microscopic (semiclassical) black hole formation followed by its evapolation to multiparticle final states, in multijet (including γ, ℓ) events in pp collisions at $E_{cm} = 8$ TeV with $L = 12\ fb^{-1}$. See their Figs. 5–7 for limits.

[9] AAD 12AK search for microscopic (semiclassical) black hole formation followed by its decay to final states with a lepton and ≥ 2 (leptons or jets), in pp collisions at $E_{cm} = 7$ TeV with $L = 1.04\ fb^{-1}$. See their Fig. 4 and 5 for limits.

[10] CHATRCHYAN 12W search for microscopic (semiclassical) black hole formation followed by its evapolation to multiparticle final states, in multijet (including γ, ℓ) events in pp collisions at $E_{cm} = 7$ TeV with $L = 4.7\ fb^{-1}$. See their Figs. 5–8 for limits.

[11] AAD 11AG search for quantum black hole formation followed by its decay to two jets, in pp collisions at $E_{cm} = 7$ TeV with L = 36 pb^{-1}. See their Fig. 11 and Table 4 for limits.

REFERENCES FOR Other Particle Searches

AAD	21AL	PRL 127 051802	G. Aad *et al.*	(ATLAS Collab.)
AAD	21BA	JHEP 2111 229	G. Aad *et al.*	(ATLAS Collab.)
AAD	21F	PR D103 112006	G. Aad *et al.*	(ATLAS Collab.)
AAD	21X	JHEP 2107 173	G. Aad *et al.*	(ATLAS Collab.)
AAIJ	21V	EPJ C81 261	R. Aaij *et al.*	(LHCb Collab.)
ACHARYA	21	PRL 126 071801	B. Acharya *et al.*	(MoEDAL Collab.)
AFEK	21	PR D104 012004	G. Afek *et al.*	(YALE)
ALKHATIB	21A	PRL 127 081802	I. Alkhatib *et al.*	(SuperCDMS Collab.)
ANDREEV	21	PRL 126 211802	Yu.M. Andreev *et al.*	(NA64 Collab.)
SIRUNYAN	21AF	PR D104 052011	A.M. Sirunyan *et al.*	(CMS Collab.)
SIRUNYAN	21T	EPJ C81 629	A.M. Sirunyan *et al.*	(CMS Collab.)
SIRUNYAN	21U	PR D104 012015	A.M. Sirunyan *et al.*	(CMS Collab.)
TUMASYAN	21	PRL 127 261804	A. Tumasyan *et al.*	(CMS Collab.)
AAD	20AD	PRL 125 131801	G. Aad *et al.*	(ATLAS Collab.)
AAD	20D	PL B801 135114	G. Aad *et al.*	(ATLAS Collab.)
AAD	20J	PR D101 052013	G. Aad *et al.*	(ATLAS Collab.)
AAD	20M	PR D102 032006	G. Aad *et al.*	(ATLAS Collab.)
AAD	20P	EPJ C80 450	G. Aad *et al.*	(ATLAS Collab.)
AAD	20T	JHEP 2003 145	G. Aad *et al.*	(ATLAS Collab.)
AAD	20W	JHEP 2006 151	G. Aad *et al.*	(ATLAS Collab.)
AAIJ	20AL	JHEP 2010 156	R. Aaij *et al.*	(LHCb Collab.)
AGUILAR-AR...	20B	JHEP 2004 054	A. Aguilar-Arevalo *et al.*	(CONNIE Collab.)
BALL	20	PR D102 032002	A.H. Ball *et al.*	(milliQan)
FEDDERKE	20	PR D101 115021	M.A. Fedderke, P.W. Graham, S. Rajendran	(STAN+)
SIRUNYAN	20A	EPJ C80 3	A.M. Sirunyan *et al.*	(CMS Collab.)
SIRUNYAN	20AI	JHEP 2005 033	A.M. Sirunyan *et al.*	(CMS Collab.)
SIRUNYAN	20AY	PL B808 135578	A.M. Sirunyan *et al.*	(CMS Collab.)
SIRUNYAN	20C	EPJ C80 75	A.M. Sirunyan *et al.*	(CMS Collab.)
SIRUNYAN	20N	PL B806 135502	A.M. Sirunyan *et al.*	(CMS Collab.)
SIRUNYAN	20Z	JHEP 2003 051	A.M. Sirunyan *et al.*	(CMS Collab.)
AABOUD	19AA	EPJ C79 120	M. Aaboud *et al.*	(ATLAS Collab.)
AABOUD	19AE	EPJ C79 481	M. Aaboud *et al.*	(ATLAS Collab.)
AABOUD	19AJ	PL B795 56	M. Aaboud *et al.*	(ATLAS Collab.)
AABOUD	19AK	PRL 122 151801	M. Aaboud *et al.*	(ATLAS Collab.)
AABOUD	19AM	PR D99 052003	M. Aaboud *et al.*	(ATLAS Collab.)
AABOUD	19AO	PR D99 052005	M. Aaboud *et al.*	(ATLAS Collab.)
AABOUD	19AT	PR D99 092007	M. Aaboud *et al.*	(ATLAS Collab.)
AABOUD	19G	PR D99 012001	M. Aaboud *et al.*	(ATLAS Collab.)
AABOUD	19H	PR D99 012008	M. Aaboud *et al.*	(ATLAS Collab.)
AABOUD	19Q	JHEP 1905 041	M. Aaboud *et al.*	(ATLAS Collab.)
AABOUD	19V	JHEP 1905 142	M. Aaboud *et al.*	(ATLAS Collab.)
ALCANTARA	19	PR D99 103016	E. Alcantara, L.A. Anchordoqui, J.F. Soriano	
SIRUNYAN	19B	PR D99 012005	A.M. Sirunyan *et al.*	(CMS Collab.)
SIRUNYAN	19BH	PR D99 032011	A.M. Sirunyan *et al.*	(CMS Collab.)
SIRUNYAN	19BT	PL B797 134876	A.M. Sirunyan *et al.*	(CMS Collab.)
SIRUNYAN	19CA	PR D100 112003	A.M. Sirunyan *et al.*	(CMS Collab.)
SIRUNYAN	19CD	PRL 123 231803	A.M. Sirunyan *et al.*	(CMS Collab.)
SIRUNYAN	19O	JHEP 1902 074	A.M. Sirunyan *et al.*	(CMS Collab.)

Downloaded from https://academic.oup.com/ptep/article/2022/8/083C01/6651666 by KIT Library user on 27 September 2022

SIRUNYAN	19Q	JHEP 1902 179	A.M. Sirunyan *et al.*	(CMS Collab.)
AABOUD	18AD	PL B779 24	M. Aaboud *et al.*	(ATLAS Collab.)
AABOUD	18CJ	PR D98 052008	M. Aaboud *et al.*	(ATLAS Collab.)
AABOUD	18CK	PR D98 092002	M. Aaboud *et al.*	(ATLAS Collab.)
AABOUD	18CL	PR D98 092005	M. Aaboud *et al.*	(ATLAS Collab.)
AABOUD	18CM	PR D98 092008	M. Aaboud *et al.*	(ATLAS Collab.)
AABOUD	18N	PRL 121 081801	M. Aaboud *et al.*	(ATLAS Collab.)
AAIJ	18AJ	PRL 120 061801	R. Aaij *et al.*	(LHCb Collab.)
ALBERT	18C	PR D98 123012	A. Albert *et al.*	(HAWC Collab.)
ALVIS	18	PRL 120 211804	S.I. Alvis *et al.*	(MAJORANA Collab.)
BANERJEE	18	PRL 120 231802	D. Banerjee *et al.*	(NA64 Collab.)
BANERJEE	18A	PR D97 072002	D. Banerjee *et al.*	(NA64 Collab.)
KILE	18	JHEP 1810 116	J. Kile, J. von Wimmersperg-Toeller	(LISBT)
MARSICANO	18	PR D98 015031	L. Marsicano *et al.*	
PORAYKO	18	PR D98 102002	N.K. Porayako *et al.*	(PPTA Collab.)
SIRUNYAN	18AW	JHEP 1805 127	A.M. Sirunyan *et al.*	(CMS Collab.)
SIRUNYAN	18BB	JHEP 1806 120	A.M. Sirunyan *et al.*	(CMS Collab.)
SIRUNYAN	18DA	JHEP 1811 042	A.M. Sirunyan *et al.*	(CMS Collab.)
SIRUNYAN	18DD	EPJ C78 789	A.M. Sirunyan *et al.*	(CMS Collab.)
SIRUNYAN	18DJ	JHEP 1809 101	A.M. Sirunyan *et al.*	(CMS Collab.)
SIRUNYAN	18DR	JHEP 1811 161	A.M. Sirunyan *et al.*	(CMS Collab.)
SIRUNYAN	18DU	PR D98 092001	A.M. Sirunyan *et al.*	(CMS Collab.)
SIRUNYAN	18DY	PR D98 112014	A.M. Sirunyan *et al.*	(CMS Collab.)
SIRUNYAN	18ED	JHEP 1811 172	A.M. Sirunyan *et al.*	(CMS Collab.)
AABOUD	17B	PL B765 32	M. Aaboud *et al.*	(ATLAS Collab.)
AABOUD	17D	PR D95 032001	M. Aaboud *et al.*	(ATLAS Collab.)
AABOUD	17L	JHEP 1708 052	M. Aaboud *et al.*	(ATLAS Collab.)
AAIJ	17BR	EPJ C77 812	R. Aaij *et al.*	(LHCb Collab.)
ABLIKIM	17AA	PL B774 252	M. Ablikim *et al.*	(BESIII Collab.)
KHACHATRY...	17D	JHEP 1701 076	V. Khachatryan *et al.*	(CMS Collab.)
KHACHATRY...	17W	PL B769 520	V. Khachatryan *et al.*	(CMS Collab.)
KHACHATRY...	17Y	PL B770 257	V. Khachatryan *et al.*	(CMS Collab.)
SIRUNYAN	17B	JHEP 1704 136	A.M. Sirunyan *et al.*	(CMS Collab.)
SIRUNYAN	17C	JHEP 1705 029	A.M. Sirunyan *et al.*	(CMS Collab.)
SIRUNYAN	17F	JHEP 1707 013	A.M. Sirunyan *et al.*	(CMS Collab.)
SIRUNYAN	17J	JHEP 1708 073	A.M. Sirunyan *et al.*	(CMS Collab.)
ZANG	17	PL B773 159	X. Zang, G.A. Miller	(WASH)
AABOUD	16	PL B759 229	M. Aaboud *et al.*	(ATLAS Collab.)
AABOUD	16P	EPJ C76 541	M. Aaboud *et al.*	(ATLAS Collab.)
AAD	16AI	JHEP 1603 041	G. Aad *et al.*	(ATLAS Collab.)
AAD	16N	JHEP 1603 026	G. Aad *et al.*	(ATLAS Collab.)
AAD	16O	PL B760 520	G. Aad *et al.*	(ATLAS Collab.)
AAD	16R	PL B755 285	G. Aad *et al.*	(ATLAS Collab.)
AAD	16S	PL B754 302	G. Aad *et al.*	(ATLAS Collab.)
AAIJ	16AR	EPJ C76 664	R. Aaij *et al.*	(LHCb Collab.)
KHACHATRY...	16BW	PR D94 112004	V. Khachatryan *et al.*	(CMS Collab.)
KHACHATRY...	16K	PRL 116 071801	V. Khachatryan *et al.*	(CMS Collab.)
KHACHATRY...	16L	PRL 117 031802	V. Khachatryan *et al.*	(CMS Collab.)
KHACHATRY...	16M	PRL 117 051802	V. Khachatryan *et al.*	(CMS Collab.)
KRASZNAHO...	16	PRL 116 042501	A.J. Krasznahorkay *et al.*	(HINR, ANIK+)
AAD	15AN	JHEP 1507 032	G. Aad *et al.*	(ATLAS Collab.)
AAD	15AT	EPJ C75 79	G. Aad *et al.*	(ATLAS Collab.)
AAD	15BJ	EPJ C75 362	G. Aad *et al.*	(ATLAS Collab.)
AAIJ	15BD	EPJ C75 595	R. Aaij *et al.*	(LHCb Collab.)
ADRIANI	15	PRL 115 111101	O. Adriani *et al.*	(PAMELA Collab.)
AGNESE	15	PRL 114 111302	R. Agnese *et al.*	(CDMS Collab.)
KHACHATRY...	15F	PRL 114 101801	V. Khachatryan *et al.*	(CMS Collab.)
LEES	15E	PRL 114 171801	J.P. Lees *et al.*	(BABAR Collab.)
AAD	14A	PL B728 562	G. Aad *et al.*	(ATLAS Collab.)
AAD	14AL	PRL 112 091804	G. Aad *et al.*	(ATLAS Collab.)
AAD	14C	JHEP 1408 103	G. Aad *et al.*	(ATLAS Collab.)
AALTONEN	14J	PR D89 092001	T. Aaltonen *et al.*	(CDF Collab.)
AAD	13A	PL B718 860	G. Aad *et al.*	(ATLAS Collab.)
AAD	13AH	PL B722 305	G. Aad *et al.*	(ATLAS Collab.)
AAD	13C	PRL 110 011802	G. Aad *et al.*	(ATLAS Collab.)
AAD	13D	JHEP 1301 029	G. Aad *et al.*	(ATLAS Collab.)
AALTONEN	13I	PR D88 031103	T. Aaltonen *et al.*	(CDF Collab.)
AALTONEN	13R	PRL 111 031802	T. Aaltonen *et al.*	(CDF Collab.)
CHATRCHYAN	13	PL B718 815	S. Chatrchyan *et al.*	(CMS Collab.)
CHATRCHYAN	13A	JHEP 1301 013	S. Chatrchyan *et al.*	(CMS Collab.)
CHATRCHYAN	13AB	JHEP 1307 122	S. Chatrchyan *et al.*	(CMS Collab.)
CHATRCHYAN	13AD	JHEP 1307 178	S. Chatrchyan *et al.*	(CMS Collab.)
CHATRCHYAN	13AR	PR D87 092008	S. Chatrchyan *et al.*	(CMS Collab.)
AAD	12AK	PL B716 122	G. Aad *et al.*	(ATLAS Collab.)
AAD	12C	PRL 108 041805	G. Aad *et al.*	(ATLAS Collab.)
AAD	12S	PL B708 37	G. Aad *et al.*	(ATLAS Collab.)
AALTONEN	12M	PRL 108 211804	T. Aaltonen *et al.*	(CDF Collab.)
CHATRCHYAN	12AP	JHEP 1209 094	S. Chatrchyan *et al.*	(CMS Collab.)
CHATRCHYAN	12BL	JHEP 1212 015	S. Chatrchyan *et al.*	(CMS Collab.)
CHATRCHYAN	12Q	PL B716 260	S. Chatrchyan *et al.*	(CMS Collab.)
CHATRCHYAN	12T	PRL 108 261803	S. Chatrchyan *et al.*	(CMS Collab.)
CHATRCHYAN	12W	JHEP 1204 061	S. Chatrchyan *et al.*	(CMS Collab.)
AAD	11AG	NJP 13 053044	G. Aad *et al.*	(ATLAS Collab.)
AAD	11I	PL B698 353	G. Aad *et al.*	(ATLAS Collab.)
AAD	11S	PL B705 294	G. Aad *et al.*	(ATLAS Collab.)
AALTONEN	11AF	PRL 107 181801	T. Aaltonen *et al.*	(CDF Collab.)
AALTONEN	11M	PRL 106 171801	T. Aaltonen *et al.*	(CDF Collab.)
ABAZOV	11I	PRL 107 011804	V.M. Abazov *et al.*	(D0 Collab.)
CHATRCHYAN	11C	JHEP 1106 026	S. Chatychyan *et al.*	(CMS Collab.)
CHATRCHYAN	11U	PRL 107 201804	S. Chatychyan *et al.*	(CMS Collab.)
AAD	10	PRL 105 161801	G. Aad *et al.*	(ATLAS Collab.)
AALTONEN	10AF	PR D82 052005	T. Aaltonen *et al.*	(CDF Collab.)
KHACHATRY...	10	PRL 105 211801	V. Khachatryan *et al.*	(CMS Collab.)
Also		PRL 106 029902	V. Khachatryan *et al.*	(CMS Collab.)
AALTONEN	09AF	PR D80 011102	T. Aaltonen *et al.*	(CDF Collab.)
AALTONEN	09G	PR D79 052004	T. Aaltonen *et al.*	(CDF Collab.)
AALTONEN	09Z	PRL 103 021802	T. Aaltonen *et al.*	(CDF Collab.)
ABAZOV	09M	PRL 102 161802	V.M. Abazov *et al.*	(D0 Collab.)
AKTAS	04C	EPJ C36 413	A. Atkas *et al.*	(H1 Collab.)
JAVORSEK	02	PR D65 072003	D. Javorsek II *et al.*	
JAVORSEK	01	PR D64 012005	D. Javorsek II *et al.*	
JAVORSEK	01B	PRL 87 231804	D. Javorsek II *et al.*	
ABBIENDI	00D	EPJ C13 197	G. Abbiendi *et al.*	(OPAL Collab.)
AMBROSIO	00B	EPJ C13 453	M. Ambrosio *et al.*	(MACRO Collab.)
ABE	99F	PRL 82 2038	F. Abe *et al.*	(CDF Collab.)
ACKERSTAFF	98P	PL B433 195	K. Ackerstaff *et al.*	(OPAL Collab.)
ABE	97G	PR D55 5263	F. Abe *et al.*	(CDF Collab.)
ABREU	97D	PL B396 315	P. Abreu *et al.*	(DELPHI Collab.)
ACKERSTAFF	97B	PL B391 210	K. Ackerstaff *et al.*	(OPAL Collab.)
ADAMS	97B	PRL 79 4083	J. Adams *et al.*	(FNAL KTeV Collab.)
BARATE	97K	PL B405 379	R. Barate *et al.*	(ALEPH Collab.)
AKERS	95R	ZPHY C67 203	R. Akers *et al.*	(OPAL Collab.)
GALLAS	95	PR D52 6	E. Gallas *et al.*	(MSU, FNAL, MIT, FLOR)
RAM	94	PR D49 3120	S. Ram *et al.*	(TELA, TRIU)
ABE	93G	PRL 71 2542	F. Abe *et al.*	(CDF Collab.)
ASTONE	93	PR D47 4770	P. Astone *et al.*	(ROMA, ROMAI, CATA, FRAS)
BUSKULIC	93C	PL B303 198	D. Buskulic *et al.*	(ALEPH Collab.)
YAMAGATA	93	PR D47 1231	T. Yamagata, Y. Takamori, H. Utsunomiya	(KONAN)
ABE	92J	PR D46 1889	F. Abe *et al.*	(CDF Collab.)
AHLEN	92	PRL 69 1860	S.P. Ahlen *et al.*	(MACRO Collab.)
VERKERK	92	PRL 68 1116	P. Verkerk *et al.*	(ENSP, SACL, PAST)
AKESSON	91	ZPHY C52 219	T. Akesson *et al.*	(HELIOS Collab.)
NAKAMURA	91	PL B263 529	S. Nakamura *et al.*	
ORITO	91	PRL 66 1951	S. Orito *et al.*	(ICEPP, WASCR, NIHO, ICRR)
ADACHI	90C	PL B244 352	I. Adachi *et al.*	(TOPAZ Collab.)
ADACHI	90E	PL B249 336	I. Adachi *et al.*	(TOPAZ Collab.)
AKRAWY	90O	PL B252 290	M.Z. Akrawy *et al.*	(OPAL Collab.)
HEMMICK	90	PR D41 2074	T.K. Hemmick *et al.*	(ROCH, MICH, OHIO+)
SAITO	90	PRL 65 2094	T. Saito *et al.*	(ICRR, KOBE)
NAKAMURA	89	PR D39 1261	T.T. Nakamura *et al.*	(KYOT, TMTC)
NORMAN	89	PR D39 2499	E.B. Norman *et al.*	(LBL)
BERNSTEIN	88	PR D37 3103	R.M. Bernstein *et al.*	(STAN, WISC)
LIU	88	PRL 61 271	G. Liu, B. Barish	
BARISH	87	PR D36 2641	B.C. Barish, G. Liu, C. Lane	(CIT)
NORMAN	87	PRL 58 1403	E.B. Norman, S.B. Gazes, D.A. Bennett	(LBL)
BADIER	86	ZPHY C31 21	J. Badier *et al.*	(NA3 Collab.)
MINCER	85	PR D32 541	A. Mincer *et al.*	(UMD, GMAS, NSF)
NAKAMURA	85	PL 161B 417	K. Nakamura *et al.*	(KEK, INUS)
THRON	85	PR D31 451	J.L. Thron *et al.*	(YALE, FNAL, IOWA)
SAKUYAMA	83B	LNC 37 17	H. Sakuyama, N. Suzuki	(MEIS)
Also		LNC 36 389	H. Sakuyama, K. Watanabe	(MEIS)
Also		NC 78A 147	H. Sakuyama, K. Watanabe	(MEIS)
Also		NC 6C 371	H. Sakuyama, K. Watanabe	(MEIS)
BHAT	82	PR D25 2820	P.N. Bhat *et al.*	(TATA)
KINOSHITA	82	PRL 48 77	K. Kinoshita, P.B. Price, D. Fryberger	(UCB+)
MARINI	82	PR D26 1777	A. Marini *et al.*	(FRAS, LBL, NWES, STAN+)
SMITH	82B	NP B206 333	P.F. Smith *et al.*	(RAL)
KINOSHITA	81B	PR D24 1707	K. Kinoshita, P.B. Price	(UCB)
LOSECCO	81	PL 102B 209	J.M. LoSecco *et al.*	(MICH, PENN, BNL)
ULLMAN	81	PRL 47 289	J.D. Ullman	(LEHM, BNL)
YOCK	81	PR D23 1207	P.C.M. Yock	(AUCK)
BARTEL	80	ZPHY C6 295	W. Bartel *et al.*	(JADE Collab.)
BUSSIERE	80	NP B174 1	A. Bussiere *et al.*	(BGNA, SACL, LAPP)
YOCK	80	PR D22 61	P.C.M. Yock	(AUCK)
ARMITAGE	79	NP B150 87	J.C.M. Armitage *et al.*	(CERN, DARE, FOM+)
BOZZOLI	79	NP B159 363	W. Bozzoli *et al.*	(BGNA, LAPP, SACL+)
GOODMAN	79	PR D19 2572	J.A. Goodman *et al.*	(UMD)
SMITH	79	NP B149 525	P.F. Smith, J.R.J. Bennett	(RHEL)
BHAT	78	PRAM 10 115	P.N. Bhat, P.V. Ramana Murthy	(TATA)
CARROLL	78	PRL 41 777	A.S. Carroll *et al.*	(BNL, PRIN)
CUTTS	78	PRL 41 363	D. Cutts *et al.*	(BROW, FNAL, ILL, BARI+)
VIDAL	78	PL 77B 344	R.A. Vidal *et al.*	(COLU, FNAL, STON+)
ALEKSEEV	76	SJNP 22 531	G.D. Alekseev *et al.*	(JINR)
		Translated from YAF 22 1021.		
ALEKSEEV	76B	SJNP 23 633	G.D. Alekseev *et al.*	(JINR)
		Translated from YAF 23 1190.		
BALDIN	76	SJNP 22 264	B.Y. Baldin *et al.*	(JINR)
		Translated from YAF 22 512.		
BRIATORE	76	NC 31A 553	L. Briatore *et al.*	(LCGT, FRAS, FREIB)
GUSTAFSON	76	PRL 37 474	H.R. Gustafson *et al.*	(MICH)
ALBROW	75	NP B97 189	M.G. Albrow *et al.*	(CERN, DARE, FOM+)
FRANKEL	75	PR D12 2561	S. Frankel *et al.*	(PENN, FNAL)
JOVANOV...	75	PL 56B 105	J.V. Jovanovich *et al.*	(MANI, AACH, CERN+)
YOCK	75	NP B86 216	P.C.M. Yock	(AUCK, SLAC)
APPEL	74	PRL 32 428	J.A. Appel *et al.*	(COLU, FNAL)
FRANKEL	74	PR D9 1932	S. Frankel *et al.*	(PENN, FNAL)
YOCK	74	NP B76 175	P.C.M. Yock	(AUCK)
ALPER	73	PL 46B 265	B. Alper *et al.*	(CERN, LIVP, LUND, BOHR+)
LEIPUNER	73	PRL 31 1226	L.B. Leipuner *et al.*	(BNL, YALE)
DARDO	72	NC 9A 319	M. Dardo *et al.*	(TORI)
TONWAR	72	JP A5 569	S.C. Tonwar, S. Naranan, B.V. Sreekantan	(TATA)
ANTIPOV	71B	NP B31 235	Y.M. Antipov *et al.*	(SERP)
ANTIPOV	71C	PL 34B 164	Y.M. Antipov *et al.*	(SERP)
BINON	69	PL 30B 510	F.G. Binon *et al.*	(SERP)
BJORNBOE	68	NC B53 241	J. Bjornboe *et al.*	(BOHR, TATA, BERN+)
JONES	67	PR 164 1584	L.W. Jones	(MICH, WISC, LBL, UCLA, MINN+)
DORFAN	65	PRL 14 999	D.E. Dorfan *et al.*	(COLU)

Downloaded from https://academic.oup.com/ptep/article/2022/8/083C01/6651666 by KIT Library user on 27 September 2022

Downloaded from https://academic.oup.com/ptep/article/2022/8/083C01/6651666 by KIT Library user on 27 September 2022